ISSN 1070-4272. Russian Journal of Applied Chemistry, 2006, Vol. 79, No. 1, pp. 1–5. © Pleiades Publishing, Inc., 2006.
Original Russian Text © A.A. Fakeev, A.I. Sukhanovskaya, 2006, published in Zhurnal Prikladnoi Khimii, 2006, Vol. 79, No. 1, pp. 3–7.

INORGANIC SYNTHESIS AND INDUSTRIAL INORGANIC CHEMISTRY

Preparation of Ultrapure Calcium Formate

A. A. Fakeev and A. I. Sukhanovskaya

State Research Institute of Chemicals and Ultrapure Chemical Substances, Moscow, Russia

Received April 15, 2005

Abstract—Crystallization of $Ca(HCOO)_2$ from aqueous solutions was studied and conditions under which an ultrapure product can be obtained were determined.

DOI: 10.1134/S1070427206010010

Calcium formate is a promising material for synthesis of high-temperature superconductors (HTSs) from bismuth, rare-earth elements, thallium, and mercury [1–3]. Substitution of oxides, nitrates, or carbonates by the corresponding formates in solid-phase synthesis markedly simplifies the process and ensures high chemical homogeneity and stoichiometry of the material obtained [4]. In [5], a high efficiency of metal formates in fabrication of films and ceramics from solutions was demonstrated.

In synthesis of HTSs, impurities can strongly affect their structure, phase composition, electrical properties, and strength. It has been shown for the example of the Y–Ba–Cu–O ceramics that particular attention should be given to control over the content of such impurities as ions of iron, nickel, manganese, cobalt, zinc, magnesium, etc. [6, 7].

Calcium formate of pure grades is not manufactured in Russia. Previously, minor amounts of a pure reagent (iron, heavy metals 1×10^{-3} wt % each, chlorides 5×10^{-3} wt %, sulfates 1×10^{-2} wt %) have been manufactured to order [8]. According to catalogs, calcium formate is manufactured in Italy, Germany, Switzerland, the United Kingdom, France, and the United States. Most of the products being manufactured are of the pure grade. Companies in Italy and Switzerland produce a higher-quality formate.

No reports describing synthesis of ultrapure calcium formate could be found in the literature. It has been suggested to obtain the product by the reaction of dilute formic acid with $CaCO_3$, with the subsequent recovery of crystals by evaporation on a water bath and drying in air [9]. A method for synthesis of $Ca(HCOO)_2$ by the reaction of $CaCO_3$ with concentrated HCOOH (90 wt %), evaporation, drying of the resulting crystals, and their triple recrystallization has been described [10], with the quality of the product not specified. A method is known for synthesis of calcium formate by dissolution of $CaCO_3$ is dilute HCOOH (15 wt %), taken in a 43% excess relative to the stoichiometry, with the subsequent evaporation of the solution on a steam bath, separation of the crystals formed, their washing with ethanol, and drying in air successively at room temperature and at 60°C [8].

Of most practical interest among the known methods for deep purification of inorganic substances [11], as applied to $Ca(HCOO)_2$, is its crystallization from aqueous solutions. The compound is comparatively well soluble in water, has a positive temperature coefficient of solubility, and the method for its crystallization from aqueous solutions may be one of the simplest among methods for production of ultrapure calcium formate.

The aim of this study was to develop a procedure for preparing ultrapure calcium formate.

The efficiency of the crystallization purification of calcium formate can be tentatively evaluated using data on phase equilibria in water–salt systems containing this compound. Analysis of the solubility diagrams in the systems $Ca(HCOO)_2$–$M^{n+}(HCOO)_n$–H_2O (M^{n+} is Li^+ [12], K^+ [13], Mg^{2+} [14], Zn^{2+} [15], Cd^{2+} [16], Pb^{2+} [17], Cu^{2+} [18], Y^{3+} [19], Mn^{2+} [20], Ni^{2+} [21], and Cu^{2+} [22]) at 25°C shows that there is no iso- or isodimorphism of the components, with the exception of the system with Cd(II), and, presumably, separation of $Ca(HCOO)_2$ and formates of the above-mentioned elements is possible. Solid solutions are not formed in the systems considered in the region of $Ca(HCOO)_2$ crystallization [12–22], and, consequently, formates of these element will be concentrated in the mother liquor. It would be expected that lithium, potassium, magnesium, zinc, cadmium, lead, cop-

Table 1. Crystal structure of calcium formate and formates of concomitant elements

Compound	Type of crystal lattice	References
α-$Ca(HCOO)_2$	Rhombic, space group *Pbca*	[20]
$Mn(HCOO)_2 \cdot 2H_2O$	Monoclinic, space group $P2_1/c$	[20]
$Cu(HCOO)_2 \cdot 2H_2O$	Monoclinic, space group $P2_1/c$	[18]
$Ni(HCOO)_2 \cdot 2H_2O$	Monoclinic, space group $P2_1/c$	[21]
$Co(HCOO)_2 \cdot 2H_2O$	Monoclinic, space group $P2_1/c$	[24]
$Pb(HCOO)_2$	Rhombic, space group $P2_12_12_1$	[17]
$Mg(HCOO)_2 \cdot 2H_2O$	Monoclinic, space group $P2_1/c$	[14]
$Zn(HCOO)_2 \cdot 2H_2O$	Monoclinic, space group $P2_1/c$	[15]
$Cd(HCOO)_2 \cdot 2H_2O$	Monoclinic, space group $P2_1/c$	[24]
$Fe(HCOO)_2 \cdot .2H_2O$	Monoclinic, pace group $P2_1/c$	[24]

per, manganese, nickel, and yttrium formates will be removed by the subsequent recrystallization of $Ca(HCOO)_2$. No data are available in the literature for water–salt systems containing Ca–Co and Ca–Fe, but, with the solubilities [23] and structure of these formates (Table 1) taken into account, it could be assumed that calcium and cobalt (iron) formates can be separated.

Analysis of published data on the structure of calcium formate and concomitant elements shows that only calcium formate crystallizes in the rhombic crystal system, whereas the other formates form monoclinic crystals. Comparison of the data in Table 1 with the results obtained in studies of the corresponding water–salt systems [14–22] confirms the suggestion that the crystallization method for $Ca(HCOO)_2$ purification is efficient.

With account of the aforesaid, we studied experimentally the crystallization of calcium formate from aqueous solutions. The influence exerted by the yield of $Ca(HCOO)_2$ and by washing of its crystals on the efficiency of the purification process was analyzed.

EXPERIMENTAL

An aqueous solution of $Ca(HCOO)_2$ (200 ml), saturated at 80–85°C, was evaporated on a water bath until crystals were obtained and cooled to 25°C under continuous agitation. The crystals formed were separated and thoroughly squeezed between sheets of a blue-band paper filter under a press to remove the mother liquor, and a sample was taken for analysis. The remaining $Ca(HCOO)_2$ crystals were transferred to a glass vessel for washing, poured over with a calcium formate solution saturated at 25°C (s : l = 1 : 2), the mixture was thoroughly agitated for about 30 min, and the washed crystals were separated and squeezed as described above. Crystals taken for analysis before and after washing were dried at 80°C for about 2 h.

Impurities can be captured in crystallization of $Ca(HCOO)_2$ via adsorption or occlusion of the mother liquor.

The starting $Ca(HCOO)_2$ and crystals before and after washing were analyzed by the atomic-emission method with excitation in an inductively coupled plasma (Baird plasma spectrometer, the United States). The determination error was 10–30%, depending on the properties of an impurity and its content [25].

The results of the analysis were used to calculate the purification coefficients K_p as a ratio of the impurity contents before and after crystallization (washing) [11].

Analysis of the results obtained (Table 2) shows that a change in the degree of crystallization from 0.2 to 0.7 affects only slightly the efficiency of $Ca(HCOO)_2$ purification. For impurities of iron, manganese, and copper ions, the efficiency of the crystallization is virtually the same (K_p = 35–60); additional washing of the crystals positively affects the purification coefficient. In view of the insufficient sensitivity of this analytical technique, it was impossible to determine K_p of $Ca(HCOO)_2$ crystals after washing for all of the impurities studied.

The efficiency of $Ca(HCOO)_2$ crystallization from aqueous solutions was determined using radioactive tracers ^{54}Mn and ^{63}Ni. The experimental procedure was supplemented with spiking of the starting solution with the tracer; the content of manganese and nickel varied from 10^{-3} to 10^{-5} wt %.

The activity of the solutions (crystals were preliminarily dissolved in distilled water) was measured

Table 2. Distribution of impurities in crystallization of calcium formate from aqueous solutions at 25°C

Impurity ion	Degree of $Ca(HCOO)_2$ crystallization	Impurity content, wt %			K_p of crystals	
		before crystallization	after crystallization	after washing	before washing	after washing
Fe	0.2	7×10^{-4}	2×10^{-5}	$<5\times10^{-6}$	35±7	>140
Mn		5×10^{-4}	8×10^{-6}	$<5\times10^{-6}$	62±15	>100
Cu		5×10^{-5}	1×10^{-6}	$<1\times10^{-6}$	50±10	>50
Ni		2×10^{-5}	1×10^{-6}	$<1\times10^{-6}$	20±5	>20
Co		5×10^{-6}	1×10^{-6}	5×10^{-7}	5±1	10
Fe	0.5	7×10^{-4}	2×10^{-5}	$<5\times10^{-6}$	35±8	>140
Mn		5×10^{-4}	1×10^{-5}	$<5\times10^{-6}$	50±10	>100
Cu		5×10^{-5}	1×10^{-6}	$<1\times10^{-6}$	50±10	>50
Ni		2×10^{-5}	1×10^{-6}	$<1\times10^{-6}$	20±5	>20
Co		5×10^{-6}	1×10^{-6}	5×10^{-7}	5±1	10
Fe	0.7	7×10^{-4}	2×10^{-5}	$<5\times10^{-6}$	35±10	>140
Mn		5×10^{-4}	1×10^{-5}	$<5\times10^{-6}$	50±10	>100
Cu		5×10^{-5}	1×10^{-6}	$<1\times10^{-6}$	50±10	>50
Ni		2×10^{-5}	1×10^{-6}	$<1\times10^{-6}$	20±5	>20
Co		5×10^{-6}	1×10^{-6}	5×10^{-7}	5±1	10

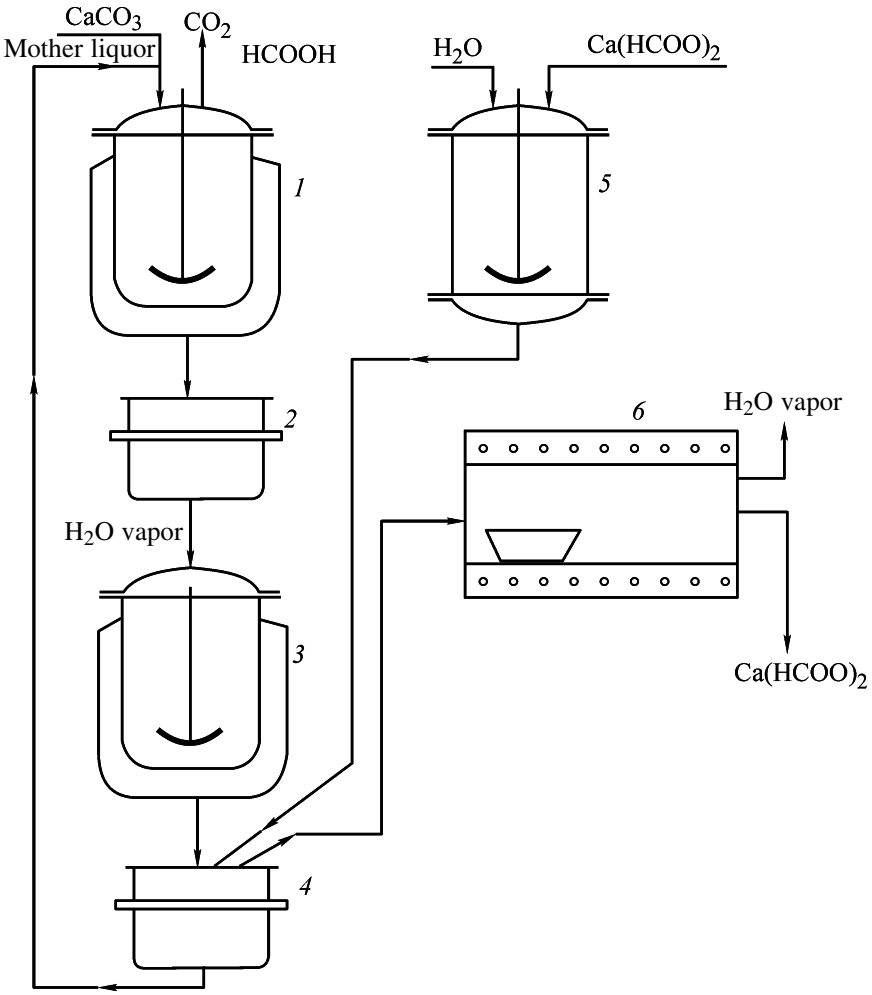
Table 3. Distribution of ^{54}Mn and ^{63}Ni tracers in crystallization of calcium formate from aqueous solutions at 25°C

Initial tracer content, wt %	Degree of $Ca(HCOO)_2$ crystallization	Purification coefficient of crystals			
		^{54}Mn tracer		^{63}Ni tracer	
		before washing	after washing	before washing	after washing
10^{-3}	0.2	50±3	260±7	45±4	300±25
10^{-4}		55±4	260±8	47±5	310±30
10^{-5}		58±4	260±7	45±5	305±30
10^{-3}	0.4	52±4	260±7	43±4	300±30
10^{-4}		55±4	262±7	45±5	305±30
10^{-5}		59±3	268±8	45±4	305±31
10^{-3}	0.7	60±3	270±7	44±4	300±30
10^{-4}		63±4	268±8	44±4	295±30
10^{-5}		66±4	270±8	43±5	295±30

with a BDIS-3-05 transducer with a detector of ^{54}Mn γ-radiation. The accuracy of radiometric measurements of the activity was 2–3 rel %. In studying the behavior of the ^{63}Ni impurity (β-radiation), the activity was measured with a BDIS-3-05 transducer with scintillation grains; the accuracy of radiometric measurements of the activity was about 10 rel %.

The data obtained (Table 3) show that, in crystallization from aqueous solutions, the purification coefficients of $Ca(HCOO)_2$ crystals are about 40–60 for manganese and nickel ions. After washing of the crystals with a saturated solution of $Ca(HCOO)_2$, these coefficients increase to 260–300. In this case, the degree of crystallization (in the range 0.2–0.7) and the impurity content (10^{-3}–10^{-5} wt %) have no essential effect on the purification coefficients.

The purification coefficients obtained by various methods for manganese and nickel ions in $Ca(HCOO)_2$ crystallization are reasonably consistent (Tables 2, 3) and are in good agreement with the data on the structure of formates of the elements under consideration (Table 1).



Flowsheet for synthesis of ultrapure $Ca(HCOO)_2$: (*1*) reactor for production of a $Ca(HCOO)_2$ solution, (*2*) filter for filtration of the solution, (*3*) evaporator for evaporation of the solution, (*4*) filter for separation and washing of $Ca(HCOO)_2$ crystals, (*5*) reactor for preparation of washing $Ca(HCOO)_2$ solution, and (*6*) quartz furnace for drying of crystals.

Thus, the crystallization of calcium formate from aqueous solutions is an efficient method of its purification.

The results obtained in the study were used to develop a flowsheet of a process for synthesis of ultrapure calcium formate. The principal stages of the process are as follows: production of a calcium formate solution and its filtration, evaporation of the solution, crystallization, separation of $Ca(HCOO)_2$ crystals, washing of the crystals with a saturated solution of $Ca(HCOO)_2$, and drying.

Reagent-grade $Ca(HCOO)_2$ was obtained using $CaCO_3$ of analytically pure grade [GOST (State Standard) 4530–76], formic acid of the same grade (GOST 5848–73), and distilled water:

$$CaCO_{3(solid)} + 2HCOOH + H_2O = Ca(HCOO)_{2(solution)} + CO_2 + 2H_2O.$$

A reasonable excess of HCOOH (15% relative to the stoichiometry), necessary for complete dissolution of $CaCO_3$, was chosen empirically. With a lesser excess of HCOOH (5–10%), the dissolution of the $CaCO_3$ powder was incomplete. The solution obtained was filtered ("blue ribbon" paper filter), evaporated, and gradually cooled under vigorous agitation. The resulting crystals of $Ca(HCOO)_2$ were separated, thoroughly washed on the filter with its saturated solution prepared by dissolution of preliminarily purified crystals, squeezed, and dried at 80–90°C. All stages of the process for synthesis of ultrapure $Ca(HCOO)_2$ were tested on a laboratory installation (see figure). The mother liquor produced in the crystallization stage contained (wt %): $Ca(HCOO)_2$ about 13.9, HCOOH 11.9, and H_2O 74.2, according to the results of a chemical analysis. It was thrice recycled into the stage of preparation of the starting

Table 4. Quality of a laboratory sample of $Ca(HCOO)_2$ and best foreign analogs (according to catalogs)

Sample	Content, wt %							
	Fe	Mn	Ni	Co	Cu	Pb	Mg	Zn
Laboratory	0.5	0.5	0.5	0.2	0.1	5	50	5
Pure grade, TU (Technical Specifications) 6-09-11-1149–86, Russia	100							
RPE, C.Erba, Italy	50		25		25	25	200	25
Fluka, Switzerland	50	500	50	50	50	50	5000	50

$Ca(HCOO)_2$ solution and then was removed from the process by precipitation of calcium carbonate with a 10% solution of Na_2CO_3.

Performing the crystallization from acid solutions (~15 wt % excess of HCOOH relative to stoichiometry) ruled out adsorption of cation impurities by the crystals and somewhat raised the yield of the finished product [26].

Analysis of a laboratory sample of the product shows that the method developed yields ultrapure calcium formate of a better quality, compared with the best foreign analogs (Table 4).

CONCLUSIONS

(1) Calcium formate can be purified by crystallization from aqueous solutions.

(2) A procedure for synthesis of ultrapure $Ca(HCOO)_2$ was developed.

REFERENCES

1. Tret'yakov, Yu.D., *Zh. Vses. Khim. O-va. im. D.I. Mendeleeva*, 1989, vol. 34, no. 4, pp. 436–445.
2. Antipov, E.V. and Aleshin, V.A., *Zh. Neorg. Khim.*, 2002, vol. 47, no. 4, pp. 530–539.
3. Chernoplekov, N.A., *Vestn. Ross. Akad. Nauk*, 2001, vol. 71, no. 4, pp. 303–319.
4. Krasil'nikov, V.N., Antsygina, V.V., and Bazuev, G.V., *Zh. Neorg. Khim.*, 1995, vol. 40, no. 7, pp. 1065–1069.
5. Ostroushko, A.A. and Zhuravleva, L.I., *Izv. Vyssh. Uchebn. Zaved., Khim. Khim. Tekhnol.*, 1992, vol. 35, no. 10, pp. 87–90.
6. Azhazha, V.M., Lavrinenko, S.D., Tikhinskii, G.F., and Tokar', I.N., *Vysokochist. Veshch.*, 1990, no. 5, pp. 60–63.
7. Bychkova, M.I., Burkhanov, G.S., and Novikov, I.I., *Vysokochist. Veshch.*, 1991, no. 3, pp. 66–70.
8. *TU* (Technical Specifications) *6-09-11-1149–86: Calcium Formate of Pure Grade.*
9. Lumsden, J.S., *J. Chem. Soc.*, 1902, vol. 81, pp. 350–362.
10. Kendall, J. and Adler, H., *J. Am. Chem. Soc.*, 1921, vol. 43, no. 7, pp. 1470–1481.
11. *Metody polucheniya osobo chistykh neorganicheskikh veshchestv* (Methods for Synthesis of Ultrapure Inorganic Substances), Stepin, B.D., Gorshtein, I.G., Blyum, G.Z., *et al.*, Eds., Leningrad: Khimiya, 1969.
12. Itkina, L.S. and Portnova, S.M., *Zh. Neorg. Khim.*, 1980, vol. 25, no. 4, pp. 1109–1111.
13. Portnova, S.M. and Palitskaya, T.A., *Zh. Neorg. Khim.*, 1994, vol. 39, no. 1, pp. 163–168.
14. Eremeeva, I.L., Kalacheva, V.G., and Shvarts, E.M., *Izv. Akad. Nauk Latv. SSR*, 1977, no. 6, pp. 666–668.
15. Vassileva, V.Z., *Zh. Neorg. Khim.*, 2000, vol. 45, no. 3, pp. 381–383.
16. Vassileva, V.Z., *Coll. Czech. Chem. Commun.*, 1998, vol. 63, no. 12, pp. 2036–2043.
17. Portnova, S.M. and Palitskaya, T.A., *Zh. Neorg. Khim.*, 1989, vol. 34, no. 1, pp. 204–209.
18. Portnova, S.M. and Palitskaya, T.A., *Zh. Neorg. Khim.*, 1992, vol. 37, no. 9, pp. 2126–2131.
19. Portnova, S.M., Balakaeva, I.V., and Krasilov, Yu.I., *Zh. Neorg. Khim.*, 1990, vol. 35, no. 1, pp. 230–236.
20. Fakeev, A.A., Orlova, I.V., and Zhadanov, B.V., *Zh. Neorg. Khim.*, 1996, vol. 41, no. 8, pp. 1379–1381.
21. Fakeev, A.A., Orlova, I.V., and Iskhakova, L.D., *Zh. Prikl. Khim.*, 2000, vol. 73, no. 10, pp. 1581–1584.
22. Fakeev, A.A., Orlova, I.V., Iskhakova, L.D., and Zhadanov, B.V., *Zh. Prikl. Khim.*, 1997, vol. 70, no. 10, pp. 1602–1605.
23. *Spravochnik khimika* (Chemist's Handbook), Nikol'skii, B.P., Ed., Moscow: Khimiya, 1971, vol. 3, pp. 98, 182.
24. Balarew, C., *Z. Kristallogr.*, 1987, vol. 181, pp. 35–82.
25. Chupakhin, M.S., Sukhanovskaya, A.I., Krasil'shchik, V.Z., *et al.*, *Metody analiza khimicheskikh reaktivov* (Methods for Analysis of Chemicals), Moscow: Khimiya, 1984.
26. Dunn, L.J. and Philip, J.C., *J. Chem. Soc.*, 1934, vol. 137, pp. 658–666.

ISSN 1070-4272. Russian Journal of Applied Chemistry, 2006, Vol. 79, No. 1, pp. 6–9. © Pleiades Publishing, Inc., 2006.
Original Russian Text © A.A. Fakeev, 2006, published in Zhurnal Prikladnoi Khimii, 2006, Vol. 79, No. 1, pp. 8–11.

INORGANIC SYNTHESIS AND INDUSTRIAL INORGANIC CHEMISTRY

Behavior of Manganese(II) in Calcium Formate Solutions

A. A. Fakeev

State Research Institute of Chemicals and Ultrapure Chemical Substances, Moscow, Russia

Received February 9, 2005

Abstract—The solubility in the system $Ca(HCOO)_2$–$Mn(HCOO)_2$–H_2O at 25°C was studied by the isothermal method. The behavior of manganese in $Ca(HCOO)_2$ crystallization from aqueous solutions was examined with ^{54}Mn tracer in the concentration range 10^{-3}–10^{-5} wt %.

DOI: 10.1134/S1070427206010022

Practical use of high-temperature superconductors (HTS) is largely determined by the stability of their properties [1, 2]. Passing from the solid-phase technology to synthesis of HTS from aqueous solutions with the use of metal formates, acetates, and oxalates provides high chemical homogeneity and stoichiometry of compositions [3, 4].

Introduction of calcium into HTS based on compounds of bismuth, thallium, rare-earth elements, and mercury improves the properties of these superconductors [3–5].

Use of metal formates in production of HTS imposes stringent requirements upon the content of impurities (iron, manganese, nickel, copper, cobalt, chromium, etc.), which can strongly affect the microstructure, state of grain boundaries, and, in the end, the electrical and mechanical properties of HTS [6, 7].

Calcium formate of pure grades is not manufactured in Russia.

Calcium formate is fairly well soluble in water and has a positive temperature coefficient of solubility; therefore, its crystallization from aqueous solutions may be one of the simplest and most efficient techniques for synthesis of an ultrapure product.

The efficiency of crystallization as the purificaiton method can be tentatively evaluated by data obtained in a study of water–salt systems composed of calcium formate and ions whose content in HTS is limited. As the objects of study served water–salt systems $Ca(HCOO)_2$–$M^n(HCOO)_n$–H_2O at 25°C, where M^n is nickel [8], copper [9], lead [10], magnesium [11], lithium [12], potassium [13], zinc [14], cadmium [15], barium [16], and yttrium [17]. Systems with lithium, magnesium, lead, barium, nickel, zinc, and yttrium ions are of a simple eutonic type, and those with copper, potassium, and cadmium ions are complex systems in which double formates are formed. Analysis of the data obtained shows that there is no interaction between the components in the region of crystallization of calcium formate, and ions will be captured by the forming crystals via adsorption and occlusion of the mother liquor.

In this study, we examined the behavior of manganese(II) in a wide range of its concentrations in calcium formate solutions at 25°C.

EXPERIMENTAL

To judge how manganese(II) behaves in crystallization of calcium formate from aqueous solutions, the ranges of macro- and microconcentrations were examined.

Calcium formate and manganese(II) formate dihydrate were obtained by the reaction of calcium carbonate of ultrapure 7–3 grade [TU (Technical Specifications) 6-09-1990–75] or basic manganese carbonate of analytically pure grade [GOST (State Standard) 7205–77] with formic acid of analytically pure grade (GOST 5847–73). According to the results of chemical and X-ray phase analyses, the compounds obtained were of composition α-$Ca(HCOO)_2$ [18] and $Mn(HCOO)_2 \cdot 2H_2O$ [19].

The content of calcium and manganese jointly present in the macroconcentration range was determined by complexometric titration with a 0.05 M solution of Na_2EDTA with Eriochrome Black T as indicator: the sum of calcium and manganese, at pH 12, and separately manganese, upon precipitation of calcium with a 0.1 M solution of ammonium fluoride.

Table 1. Solubility in the system $Ca(HCOO)_2$–$Mn(HCOO)_2$–H_2O at 25°C

Point no.	Liquid phase, wt %		Solid residue, wt %		Composition of solid phase
	$Ca(HCOO)_2$	$Mn(HCOO)_2$	$Ca(HCOO)_2$	$Mn(HCOO)_2$	
1A	15.6	–	–	–	$Ca(HCOO)_2$
2	15.1	1.0	79.8	0.6	$Ca(HCOO)_2$
3	15.0	1.2	74.0	0.6	$Ca(HCOO)_2$
4E	14.0	2.9	70.0	5.5	$Ca(HCOO)_2$ + $Mn(HCOO)_2 \cdot 2H_2O$
	14.0	2.9	13.1	43.2	$Ca(HCOO)_2$ + $Mn(HCOO)_2 \cdot 2H_2O$
5	12.8	2.8	4.5	46.0	$Mn(HCOO)_2 \cdot 2H_2O$
6	12.6	3.0	4.4	46.6	$Mn(HCOO)_2 \cdot 2H_2O$
7	10.0	3.0	4.2	49.2	$Mn(HCOO)_2 \cdot 2H_2O$
8	9.4	3.5	3.6	51.4	$Mn(HCOO)_2 \cdot 2H_2O$
9	8.4	3.7	3.1	51.2	$Mn(HCOO)_2 \cdot 2H_2O$
10	4.9	4.6	1.7	54.2	$Mn(HCOO)_2 \cdot 2H_2O$
11	0.9	6.3	0.3	56.0	$Mn(HCOO)_2 \cdot 2H_2O$
12B	–	7.7	–	–	$Mn(HCOO)_2 \cdot 2H_2O$

To prevent hydrolysis of manganese(II), hydroxylamine hydrochloride was introduced into the solutions being analyzed [20]. The admissible discrepancy between two parallel determinations was 0.5 rel %, and the total error of analysis, 1.5 rel %.

An X-ray diffraction analysis of the samples was made on a DRON-4-13 diffractometer with CuK_α radiation and semiconductor-purity germanium as internal reference. The X-ray diffraction patterns obtained were processed using the Rapid software package; the reflections were assigned and the lattice constants refined by means of the Powtool software package.

As manganese(II) is susceptible to oxidation in air [21], we tested preliminarily the stability of 2–10% manganese(II) formate solutions in formic acid. The optical spectra of freshly prepared manganese(II) formate solutions in 2.0, 5.0, and 10.0 wt % formic acid and those after 20 days, measured at 350–700 nm on a Specord instrument (Germany) with cell thickness of 1 cm and solution concentration of ~10 wt %, were virtually identical. With account of the aforesaid, an HCOOH concentration of about 2.0 wt % is sufficient for oxidation and hydrolysis of manganese(II) formate to be prevented.

The system $Ca(HCOO)_2$–$Mn(HCOO)_2$–H_2O was studied at 25°C by the isothermal method in special hermetically sealed glass vessels with magnetic stirrers without any liquid seals. The temperature was maintained constant with an accuracy of ±0.1°C [22]. The HCOOH concentration was approximately 2.0 wt %. The starting substances were charged in accordance with the results of a preliminary calculation. The time in which equilibrium was attained was about two days.

The composition of the solid phases was graphically determined by the Schreinemakers method and confirmed by chemical and X-ray techniques.

The data on the solubility in binary systems $Ca(HCOO)_2$–H_2O and $Mn(HCOO)_2$–H_2O were taken from the literature [23, 24].

A study of the solubility in the system $Ca(HCOO)_2$–$Mn(HCOO)_2$–H_2O in a wide range of concentrations of the components at 25°C demonstrated (Table 1) that there is no interaction between the components. Construction of the solubility diagram and an analysis of the solid phases by chemical and X-ray diffraction techniques confirmed the presence of the starting components, $Ca(HCOO)_2$ [18] and $Mn(HCOO)_2$ [19], as solid phases. The composition of the eutonic solution was as follows (wt %): $Ca(HCOO)_2$ 14.0 and $Mn(HCOO)_2$ 2.9. Calcium formate exerts a salting-out effect on manganese(II) formate, reducing its solubility by a factor of nearly 3. The main part of the diagram is occupied by the crystallization branch of the least soluble component, manganese(II) formate.

In the region of crystallization of calcium formate, there is no interaction between the components to give new phases or solid solutions. The capture of manganese(II) ions by crystals of calcium formate may be due to their adsorption on the surface or to occlusion of the mother liquor, and, consequently, a considerable degree of product purification to remove manganese(II) ions would be expected.

Table 2. Distribution of the ^{54}Mn impurity in crystallization of calcium formate from aqueous solutions at 25°C

Initial content of impurity, wt %	Degree of crystallization of $Ca(HCOO)_2$	Purification coefficient of crystals	
		before washing	after washing
10^{-3}	0.2	50 ± 3	260 ± 7
10^{-4}		55 ± 4	260 ± 8
10^{-5}		58 ± 4	260 ± 7
10^{-3}	0.4	52 ± 4	260 ± 7
10^{-4}		55 ± 4	262 ± 7
10^{-5}		59 ± 3	268 ± 8
10^{-3}	0.7	60 ± 3	270 ± 7
10^{-4}		63 ± 4	268 ± 8
10^{-5}		66 ± 4	270 ± 8

The system $Ca(HCOO)_2$–$Mn(HCOO)_2$–H_2O was studied in the range of microconcentrations of manganese(II) by using a radioactive tracer, ^{54}Mn.

^{54}Mn was introduced into a concentrated aqueous solution of calcium formate at 75–80°C, formic acid was added in an amount necessary for creating a concentration of 2.0 wt %, and the mixture was vigorously agitated for 1.0 h. The precipitated $Ca(HCOO)_2$ crystals were separated on a funnel, thoroughly squeezed between sheets of a filter paper to remove the mother liquor, and a sample was taken to measure the activity of the crystals. The squeezed crystals of calcium formate were washed by decantation with an aqueous solution of calcium formate, saturated at room temperature and taken in a 1 : 2 ratio by mass, and the thus washed crystals were squeezed as described above. The content of manganese(II) in solution was varied from 10^{-3} to 10^{-5} wt %, and the degree of crystallization, from 0.2 to 0.7 [25].

The activity of the solutions preliminarily prepared by dissolving the crystals in distilled water was measured with a BDIS-3-05 transducer with a detector of γ-radiation. The accuracy of radiometric measurements was 2–3 rel %. The data obtained in these measurements were used to calculate the purification coefficient as a ratio of the activities before and after crystallization, related to unit mass of calcium formate [25].

As shown by the results obtained (Table 2), a microimpurity of manganese(II) is mainly concentrated in crystallization of calcium formate in the mother liquor. An additional washing of $Ca(HCOO)_2$ crystals with a saturated aqueous solution of calcium formate substantially enhances the purification effect. The concentration of the manganese(II) impurity and the degree of crystallization do not noticeably affect the purification coefficient.

A study of the distribution of manganese(II) in the microconcentration range in crystallization of $Ca(HCOO)_2$ (Table 2) demonstrated that there is no isodimorphism or isomorphism of calcium formate and manganese(II) formate dihydrate. Manganese(II) is captured by crystals of calcium formate via occlusion of the mother liquor [adsorption of manganese(II) on the surface of the crystals is reduced to a minimum in the case of crystallization in an acid medium, HCOOH].

Thus, the results of studying the behavior of manganese(II) in calcium formate solutions in a wide range of concentrations (micro- and macroranges) indicate that there is no interaction between the components, which is accounted for by the difference of the crystal structures of calcium formate and manganese(II) formate dihydrate. $Ca(HCOO)_2$ crystallizes in the rhombic crystal system (space group *Pbca*) [18]; according to refined data, $Mn(COOH)_2 \cdot 2H_2O$ crystallizes in the monoclinic crystal system (space group $P2_1/c$) [26].

According to the data presented above and published data, ions of manganese(II), nickel, copper, magnesium, lithium, potassium, zinc, cadmium, barium, and yttrium [8–17] can find their way into the crystals formed in synthesis of ultrapure calcium formate by crystallization via occlusion of the mother liquor or adsorption. Thorough washing of the precipitate is necessary for removing these impurities. Performing the crystallization of $Ca(HCOO)_2$ in formic acid (2–3 wt %) will virtually rule out adsorption of ions on the crystals.

CONCLUSIONS

(1) The solubility diagram of the system $Ca(HCOO)_2$–$Mn(HCOO)_2$–H_2O was studied in a wide range of concentrations of the components; the system is of a simple eutonic type. The composition of the solid phases was confirmed by the results of chemical and X-ray analyses.

(2) The behavior of ^{54}Mn in crystallization of $Ca(HCOO)_2$ was studied at concentrations in the range 10^{-3}–10^{-5} wt % and the occlusion nature of its capture by the crystals formed was established.

(3) Crystallization from aqueous solutions is a promising method for purification of $Ca(HCOO)_2$.

REFERENCES

1. Tret'yakov, Yu.D., *Zh. Vses. Khim. O-va. im. D.I. Mendeleeva*, 1989, vol. 34, no. 4, pp. 436–445.
2. Chernoplekov, N.A., *Vestn. Ross. Akad. Nauk*, 2001, vol. 71, no. 4, pp. 303–319.
3. Krasil'nikov, V.N., Antsygina, V.V., and Bazuev, G.V., *Zh. Neorg. Khim.*, 1995, vol. 40, no. 7, pp. 1065–1069.
4. Vasil'ev, V.G. and Fotiev, A.A., *Zh. Neorg. Khim.*, 1995, vol. 40, no. 2, pp. 184–186.
5. Lennikov, V.V., Mitina, I.I., Kazin, P.E., and Tret'yakov, Yu.D., *Zh. Neorg. Khim.*, 2000, vol. 45, no. 1, pp. 36–37.
6. Azhazha, V.M., Lavrinenko, S.D., Tikhinskii, G.F., and Tokar', I.N., *Vysokochist. Veshch.*, 1990, no. 5, pp. 60–63.
7. Bychkova, M.I., Burkhanov, G.S., and Novikov, I.I., *Vysokochist. Veshch.*, 1991, no. 3, pp. 66–70.
8. Fakeev, A.A., Orlova, I.V., Iskhakova, L.D., and Zhadanov, B.V., *Zh. Prikl. Khim.*, 2000, vol. 73, no. 10, pp. 1581–1584.
9. Fakeev, A.A., Orlova, I.V., Iskhakova, L.D., and Zhadanov, B.V., *Zh. Prikl. Khim.*, 1997, vol. 70, no. 10, pp. 1602–1605.
10. Portnova, S.M. and Palitskaya, T.A., *Zh. Neorg. Khim.*, 1989, vol. 34, no. 1, pp. 204–209.
11. Eremeeva, I.A., Kalacheva, V.G., and Shvarts, E.M., *Izv. Akad. Nauk Latv. SSR*, 1977, no. 5, pp. 666–668.
12. Itkina, L.S. and Portnova, S.M., *Zh. Neorg. Khim.*, 1980, vol. 25, no. 4, pp. 1109–1111.
13. Portnova, S.M. and Palitskaya, T.A., *Zh. Neorg. Khim.*, 1994, vol. 39, no. 1, pp. 163–168.
14. Vasileva, V.Z., *Zh. Prikl. Khim.*, 2000, vol. 73, no. 3, pp. 381–383.
15. Vassileva, V.Z., *Coll. Czech. Chem. Commun.*, 1998, vol. 83, no. 12, pp. 2036–2043.
16. Vasileva, V.Z., *Zh. Prikl. Khim.*, 2003, vol. 76, no. 8, pp. 1260–1263.
17. Portnova, S.M., Balakaeva, I.V., and Krasilov, Yu.I., *Zh. Neorg. Khim.*, 1990, vol. 35, no. 1, pp. 230–236.
18. Watanabe, T. and Matsui, M., *Acta Crystallogr., Sect. B*, 1978, vol. 34, no. 9, pp. 2731–2736.
19. Osaki, K., Nakai, Y., and Watanabe, T., *J. Phys. Soc. Jpn.*, 1964, vol. 19, no. 5, pp. 717–723.
20. Schwarzenbach, G. und Flaschka, H., *Die Komplexometrische Titration*, Stuttgart: Ferdinand Enke, 1965. Translated under the title *Kompleksonometricheskoe titrovanie*, Moscow: Khimiya, 1970, p. 159.
21. Lavrukhina, A.K. and Yukina, L.B., *Analiticheskaya khimiya margantsa* (Analytical Chemistry of Manganese), Moscow: Nauka, 1974.
22. Fakeev, A.A., Oboznenko, Yu.V., and Stepin, B.D., *Zh. Neorg. Khim.*, 1968, vol. 13, no. 9, pp. 2577–2581.
23. *Spravochnik khimika* (Chemist's Handbook), Nikol'skii, B.P., Ed., Moscow: Khimiya, 1965, p. 187.
24. Balarev, Kh., Stoilova, D., and Vasileva, V., *Dokl. Bolg. Akad. Nauk*, 1982, vol. 35, no. 7, pp. 933–936.
25. *Metody polucheniya osobo chistykh neorganicheskikh veshchestv* (Methods for Synthesis of Ultrapure Inorganic Substances), Stepin, B.D., Gorshtein, I.G., Blyum, G.Z., *et al.*, Eds., Leningrad: Khimiya, 1969.
26. Fakeev, A.A., Akhtamova, A.Sh., Kon'kova, O.V., *et al.*, *Zh. Neorg. Khim.*, 1997, vol. 42, no. 5, pp. 814–817.

ISSN 1070-4272. Russian Journal of Applied Chemistry, 2006, Vol. 79, No. 1, pp. 10–15. © Pleiades Publishing, Inc., 2006.
Original Russian Text © I.V. Zatovskii, N.S. Slobodyanik, T.I. Ushchapivskaya, I.V. Ogorodnik, A.A. Babarik, 2006, published in Zhurnal Prikladnoi Khimii, 2006, Vol. 79, No. 1, pp. 12–17.

INORGANIC SYNTHESIS AND INDUSTRIAL INORGANIC CHEMISTRY

Synthesis of Complex Phosphates with a Langbeinite Structure from Melts

I. V. Zatovskii, N. S. Slobodyanik, T. I. Ushchapivskaya, I. V. Ogorodnik, and A. A. Babarik

Shevchenko Kiev National University, Kiev, Ukraine
Kiev National Agricultural University, Kiev, Ukraine

Received July 26, 2005

Abstract—Phase formation processes were studied and features of the crystallization of complex phosphates with a langbeinite structure from potassium phosphate melts were established. The compounds obtained were characterized by X-ray phase analysis, IR spectroscopy, diffuse reflection spectroscopy, and ESR spectroscopy.

DOI: 10.1134/S1070427206010034

Two structural types, Nasicon and langbeinite, are realized for complex phosphates with a three-dimensional crystal framework $[M_2(PO_4)_3]^{n-}$ [1]. At present phosphates with the Nasicon framework are the most studied, because they are of interest as superionic conductors [1–5] and high-temperature materials with low thermal expansion coefficients [6, 7]. Complex phosphates with the langbeinite-type lattice are first of all considered as promising crystal matrices for immobilization of radioactive and highly toxic wastes with the aim of their further disposal [8], thanks to high chemical and radiation resistance of phosphates with the langbeinite structure.

A three-dimensional anionic crystal framework $[M_2(PO_4)_3]^{n-}$ of the langbeinite type forms relatively large cationic cavities, which can retain cations of various sizes: Na^+, K^+, Rb^+, Cs^+, Ca^{2+}, Sr^{2+}, and Ba^{2+}. Various elements or their pairs can play the role of framework-forming metals: Ti, Fe, Cr, Nb, Y, Zr, Hf, and REE [8–18]. Such a variety of possible combinations stimulates the further search for compounds with practically important and special properties among phosphates with the langbeinite structure.

Complex phosphates, which are structural analogs of langbeinite, were synthesized using various techniques, namely, solid-phase reactions [8–10, 14–16], melt crystallization [11, 18, 19], and hydrothermal synthesis [20]. At the same time, approaches to the target-oriented synthesis of phosphates of this structural type are in the stage of formation and coming into being.

We examined the main regular trends in the phase formation of complex phosphates with a langbeinite-type crystal framework in potassium phosphate melts. The compounds obtained were characterized by X-ray phase analysis (XPA), IR spectroscopy, diffuse reflection spectroscopy, and ESR spectroscopy. The influence of framework-forming different-valence metals on the formation of crystalline phosphates with the langbeinite structure from melts is discussed.

EXPERIMENTAL

We studied phase formation of complex phosphates with the langbeinite structure from melts of the systems K_2O–P_2O_5–TiO_2–$M^{II}O$ (M^{II} = Mn, Ni, Co, Cu, Zn), K_2O–P_2O_5–TiO_2–$M^{III}_2O_3$ (M^{III} = Al, Sc, Cr, Fe, In, Y), and K_2O–P_2O_5–$M^{V}_2O_5$–$M^{III}_2O_3$ (M^{V} = Nb, Ta; M^{III} = Fe, Cr, In, Y). The starting substances for preparing the melts were analytically pure grade KPO_3, $NH_4H_2PO_4$, $K_4P_2O_7 \cdot 4H_2O$, Al_2O_3, Cr_2O_3, In_2O_3, NiO, cobalt subcarbonate (containing 59.1 wt % CoO), CuO, ZnO, and also ultrapure grade TiO_2, Fe_2O_3, Y_2O_3, Nb_2O_5, and Ta_2O_5. In some cases, pure grade dihydrogen phosphates $Cu(H_2PO_4) \cdot 2H_2O$ and $Mn(H_2PO_4)_2 \cdot 2H_2O$ were used.

Potassium/phosphorus ratios (K/P) in the systems were set within the limits from 0.70 to 1.45; the M^{III}/Ti, M^{II}/Ti, and M^{II}/M^{V} ratios were varied discretely from 0.05 to 2.00. Ground charges of the starting components were heated in platinum crucibles

to 1000–1150°C. The resulting melts were kept with intermittent stirring for 3–8 h under isothermal conditions up to complete dissolution of the oxides. The temperature and dissolution time were determined empirically depending on the nature and content of oxides in the system. After homogenization of the melts, their crystallization was carried out by spontaneous cooling at a rate of 10–50 deg h^{-1} to 650–750°C. The solubility of oxides and the phase formation were monitored by intermittent sampling. Melt samples were dissolved in water, and the presence of oxides or crystalline phases was determined by optical microscopy. After the crystallization completion, we decanted the melts leaving the formed phases and washed them to remove the residual flux with hot solutions of inorganic acids. The resulting compounds were washed with double-distilled water and dried in air at 105–120°C.

We carried out the X-ray phase analysis of the crystallization products and recorded the X-ray patterns of the individual compounds on a DRON-3.0 diffractometer using CuK_α radiation (λ = 1.54178 Å). The IR spectra were recorded on Nexus 470 FTIR (Nicolet) and UR-20 spectrometers in the range 400–1500 cm^{-1}; the samples were pelletized with KBr. The ESR spectra of polycrystalline samples were recorded on a PS100.X instrument at room temperature, and the electronic diffuse reflection spectra, on a UV-VIS Specord M-40 spectrophotometer in the range 14000–36000 cm^{-1}.

Complex phosphates with the langbeinite structure in potassium phosphate melts are formed as crystals of tetrahedral or octahedral shape. In most cases, their composition and phase-formation area depend on both K/P and M^{III}/Ti (M^{II}/Ti, M^{III}/M^{V}) ratios in a system and also on particular metal. The optimized conditions of the crystallization of the phosphates isostructural to langbeinite are given in Table 1.

For the systems K_2O–P_2O_5–TiO_2– $M^{II}O$ (M^{II} = Mn, Ni, Co, Cu, Zn), the character and areas of the formation of $K_2Ti_{1.5}M^{II}_{0.5}(PO_4)_3$ phases are similar in the case of manganese, nickel, and cobalt (K/P = 0.9–1.1; M^{II}/Ti = 0.5–2.0, Ti/P = 0.15) and considerably differ for the copper- and zinc-containing systems. The complex phosphate $K_2Cu^{II}_{0.5}Ti_{1.5}(PO_4)_3$ isostructural to langbeinite can be isolated in the pure form only within a narrow temperatures range 900–720°C for the ratios K/P = 0.9–1.0, Cu^{II}/Ti = 0.7–1.5, and Ti/P = 0.12–0.14. Such limits are caused by partial reduction of copper(II) to copper(I) in the melts with ratios K/P < 0.9 and, consequently, by the formation of complex phosphates containing copper(I). At higher (K/P = 1.0–1.2) ratios, three complex phosphates $KTi_2(PO_4)_3$, $K_2Cu^{II}_{0.5}Ti_{1.5}(PO_4)_3$, and $KTiOPO_4$ crystallize simultaneously. A similar pattern is observed for melts of the system K_2O–P_2O_5–TiO_2–ZnO where crystals of the phosphate $K_2Zn_{0.5}Ti_{1.5}(PO_4)_3$ isostructural to langbeinite can be obtained in a mixture with $KTi_2(PO_4)_3$ or $KTiOPO_4$.

The crystallization of complex phosphates with the langbeinite structure in K_2O–P_2O_5–TiO_2–$M^{III}_2O_3$ (M^{III} = Al, Sc, Cr, Fe, In, Y) melts in a wide range of M^{III}/Ti ratios is accompanied by redox processes [19]. Generally, the composition of the resulting complex phosphates is described by the formula $K_{1+y}Ti_{2-x}\cdot M^{III}_x(PO_4)_3$ ($0 < x \le 1$, $0 \le y \le 1$, $y \ge x$), and the resulting compounds contain titanium(III). The formation of a compound with a fixed composition in the melts and the degree of reduction of titanium(IV) to titanium(III) primarily depend on the initial ratios K/P and M^{III}/Ti in the system. A series of compounds $K_{1+y}Ti_{2-x}Al_x(PO_4)_3$ ($0 < x \le 1$, $0 \le y \le 1$, $y \ge x$) obtained by spontaneous crystallization in the melts of the system K_2O–P_2O_5–TiO_2–Al_2O_3 were studied in detail in [21]. It was shown by X-ray photoelectron spectroscopy, X-ray fluorescence analysis, and ESR spectroscopy that the partial reduction $Ti^{4+} \rightarrow Ti^{3+}$ is caused by a rearrangement of the three-dimensional crystal framework with the formation of a langbeinite-type structure when Al^{3+} is incorporated in the double phosphate $KTi_2(PO_4)_3$. In this case, the Ti^{3+} content in the $K_{1+y}Ti_{2-x}Al_x(PO_4)_3$ compounds first increases as the initial Al/Ti ratio in the melt increases from 0.2 to 0.7, and then it decreases in the range of Al/Ti = 0.7–1.5. For Al/Ti ratios higher than 1.5, the phosphate $K_2TiAl(PO_4)_3$ isostructural to langbeinite and containing no titanium(III) crystallizes.

The formation of complex phosphates $K_{1+y}Ti_{2-x}\cdot M^{III}_x(PO_4)_3$ ($0 < x \le 1$, $0 \le y \le 1$, $y \ge x$) in the melts of the systems K_2O–P_2O_5–TiO_2–$M^{III}_2O_3$ (M^{III} = Sc, Cr, Fe, In, Y) occurs similarly. The amount of titanium(III) in the crystal phases first increases and then decreases as the M^{III}/Ti ratio in the melt increases, which is manifested in the intensity of color of the resulting compounds. On reaching a certain "critical" M^{III}/Ti ratio, colorless phosphates of the composition $K_2TiM^{III}(PO_4)_3$ are formed. Numerically this ratio depends on the nature of M(III) (Table 1). At the same time, it should be noted that $K_{1+y}Ti_{2-x}M^{III}_x(PO_4)_3$ phosphates (M^{III} = Cr, Fe, In, Y) can be obtained in the pure state within the limits of M^{III}/Ti ratios from 0.1 to 1.0. At $M^{III} > 1.0$, double diphosphates $KM^{III}P_2O_7$ are formed simultaneously in the melts.

Table 1. Areas and conditions of the crystallization of phosphates with a langbeinite structure from melts

Compound	Ratio of components in a melt	Temperature of crystal formation, °C	Habit and color of crystals
$K_2Ti_{1.5}Mn_{0.5}(PO_4)_3$	K/P = 0.9–1.1, Mn/Ti = 2.0–0.5, Ti/P = 0.25–0.3	950–700	Red-brown tetrahedra with bevel vertices
$K_2Ti_{1.5}Ni_{0.5}(PO_4)_3$	K/P = 0.9–1.1, Ni/Ti = 2.0–0.5, Ti/P = 0.27–0.32	1000–650	Green tetrahedra of regular shape
$K_2Ti_{1.5}Co_{0.5}(PO_4)_3$	K/P = 0.9–1.1, Co/Ti = 2.0–0.5, Ti/P = 0.25–0.3	950–700	Red tetrahedra with bevel vertices or regular octahedra
$K_2Ti_{1.5}Cu_{0.5}(PO_4)_3$	K/P = 0.85–0.95, Cu/Ti = 1.5–0.5, Ti/P = 0.25–0.32	900–720	Grey-blue tetrahedra with elongated vertices
$K_2Ti_{1.5}Zn_{0.5}(PO_4)_3$	K/P = 0.9, Zn/Ti = 2.0, Ti/P = 0.25–0.27	1000–800	Colorless tetrahedra with elongated vertices
$K_{1+y}Ti_{2-x}Al_x(PO_4)_3$ $(0<x\le1,\ 0\le y\le1,\ y\ge x)$	K/P = 0.8–1.15, Al/Ti = 0.2–1.5, Ti/P = 0.15–0.30	1000–750	Regular tetrahedra or octahedra with color from pale blue to dark blue
$K_{1+y}Ti_{2-x}Fe_x(PO_4)_3$ $(0<x\le1,\ 0\le y\le1,\ y\ge x)$	K/P = 1.0–1.2, Fe/Ti = 0.5–1.5, Ti/P = 0.15–0.26	1000–700	Regular tetrahedra with color from pale blue to dark blue
$K_{1+y}Ti_{2-x}Cr_x(PO_4)_3$ $(0<x\le1,\ 0\le y\le1,\ y\ge x)$	K/P = 1.0–1.2, Cr/Ti = 0.5–1.5, Ti/P = 0.15–0.22	1000–800	Gray-green regular tetrahedra
$K_{1+y}Ti_{2-x}In_x(PO_4)_3$ $(0<x\le1,\ 0\le y\le1,\ y\ge x)$	K/P = 1.0–1.15, In/Ti = 0.3–1.0, Ti/P = 0.17–0.26	1000–800	Regular tetrahedra with color from pale blue to dark blue
$K_{1+y}Ti_{2-x}Y_x(PO_4)_3$ $(0<x\le1,\ 0\le y\le1,\ y\ge x)$	K/P = 1.0–1.15, Y/Ti = 0.2–1.0, Ti/P = 0.17–0.25	1000–800	Regular tetrahedra with color from pale blue to dark blue
$K_2Nb_{0.5}Fe_{1.5}(PO_4)_3$	K/P = 0.7–1.1, Fe/Nb = 1.0, Fe/P = 0.28	820–780	Light pink regular tetrahedra
$K_2Ta_{0.5}Fe_{1.5}(PO_4)_3$	K/P = 1.0–1.1, Fe/Ta = 2.0–3.0, Fe/P = 0.37	1000–820	Yellow-brown regular tetrahedra or octahedra
$K_2Ta_{0.5}Cr_{1.5}(PO_4)_3$	K/P = 1.0–1.2, Cr/Ta = 1.0, Cr/P = 0.13	850–780	Dark green regular tetrahedra
$K_2Nb_{0.5}In_{1.5}(PO_4)_3$	K/P = 1.0–1.4, In/Nb = 1.0, In/P = 0.13	820–760	Colorless tetrahedra with bevel vertices
$K_2Ta_{0.5}In_{1.5}(PO_4)_3$	K/P = 1.0–1.4, In/Ta = 1.0, In/P = 0.044	820–760	Colorless tetrahedra with bevel vertices
$K_2Nb_{0.5}Y_{1.5}(PO_4)_3$	K/P = 1.2–1.5, Y/Nb = 1.0, Y/P = 0.19	920–860	Colorless regular tetrahedra
$K_2Ta_{0.5}Y_{1.5}(PO_4)_3$	K/P = 1.2–1.5, Y/Ta = 1.0, Y/P = 0.125	920–860	Colorless regular tetrahedra

The areas of the crystallization of phosphates isostructural to langbeinite correspond to rather narrow ranges of the K/P ratio in the system. In the case of scandium, indium, and yttrium, they are limited to K/P values from 1.00 to 1.15; for iron and chromium, the limits are somewhat wider (K/P = 1.00–1.20); and for aluminum, they are the widest (K/P = 0.9–1.15).

The presence of titanium(III) in the phosphates $K_{1+y}Ti_{2-x}M^{III}_x(PO_4)_3$ ($0 < x \le 1$, $0 \le y \le 1$, $y \ge x$; M^{III} = Sc, Cr, Fe, In, Y) isostructural to langbeinite was confirmed by diffuse reflection and ESR spectroscopy. The diffuse reflection spectra of a series of phosphates (Fig. 1) contain two bands. The first broad band in the region of 17 500–18 800 cm^{-1} corresponds to the one-electron transition $^2T_{2g} \rightarrow {}^2E_g$ in the $[Ti^{3+}O_6]$ chromophore, and the second strong band at 31 000 cm^{-1} is caused by the oxygen-to-metal charge transfer. Slight asymmetry of the first band suggests

possible trigonal distortion of the [TiO_6] polyhedron, resulting in the splitting of the T_{2g} term. The effect of trigonal splitting of the T_{2g} ground term is confirmed by the ESR data, as the ESR spectra of Ti^{3+} complexes are known to be observable at room temperature at an axial distortion in a trigonal-symmetry field [22]. In the case of the series of phosphates under study $K_{1+y}Ti_{2-x}M^{III}_x(PO_4)_3$ ($0 < x \le 1$, $0 \le y \le 1$, $y \ge x$) containing various metals(III) (aluminum, iron, scandium, indium, and yttrium), all ESR spectra at room temperature represent a symmetric singlet with equal parameters: g = 2.001 and ΔH = 110 G.

Regions and conditions of the formation of complex phosphate phases with the langbeinite structure for the melts of the systems K_2O–P_2O_5–$M^V_2O_5$–$M^{III}_2O_3$ (M^V = Nb, Ta; M^{III} = Fe, Cr, In, Y) substantially depend on particular M(III). It was found experimentally that the usual content of M(V) oxides in the systems required for the crystallization of phosphates of this structural type is 12–16 wt % for Nb_2O_5 and 5–10 wt % for Ta_2O_5. The content of M(III) oxides can vary in a rather wide range, 5–20 wt %. The phosphates isostructural to langbeinite are formed as transparent colorless or colored crystals of tetrahedral or octahedral habit (Table 1).

We failed to obtain phosphates isostructural to langbeinite from melts of the system K_2O–P_2O_5–Nb_2O_5–Cr_2O_3. This is caused by the primary formation of kinetically labile $KCrP_2O_7$ on the Cr_2O_3–melt phase boundary. It is practically insoluble and blocks the active oxide surface.

The X-ray patterns of the obtained double phosphates isostructural to langbeinite were analyzed using the least-squares iteration method applied to identity periods of structural models based on the structural data for the compounds $K_2Ti_2(PO_4)_3$ [10, 11, 20], $KBaFe_2(PO_4)_3$ [12], and $K_{1.388}Ti^{4+}_{1.612}Ti^{3+}_{0.273}Al_{0.115}(PO_4)_3$ [23]. The calculated parameters of cubic unit cells of the synthesized phosphates vary within 9.8–11.6 Å depending on the ionic radii of the framework-forming metals (Table 2).

The main absorption bands in the IR spectra of phosphates with the langbeinite structure (Fig. 2) are characteristic of double orthophosphates with a three-dimensional $[M_2(PO_4)_3]^{n-}$ crystal framework [24]. In the frequency range 400–700 cm^{-1}, five absorption bands are usually present, corresponding to δ_s and δ_{as} vibrations of O–P–O and MO_2 groups. The ν_s vibration of the P–O bond is manifested in the spectra as a strong broad band in the frequency range 850–970 cm^{-1}, and the ν_{as} vibration of this bond gives rise

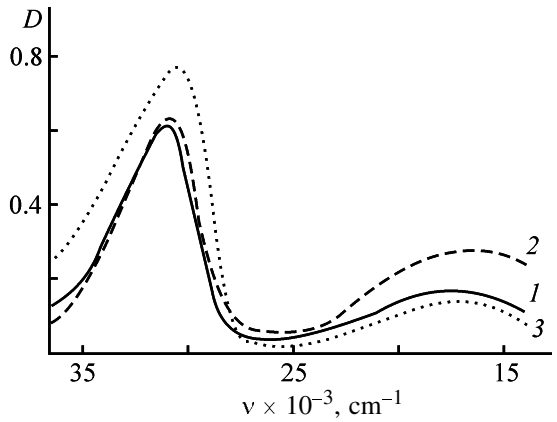


Fig. 1. Diffuse reflection electronic spectra of complex phosphates containing trivalent titanium, isostructural to langbeinite: (*D*) optical density and (ν) wavenumber. (*1*) $K_{1+x}Al_xTi_{1.3}(PO_4)_3$, (*2*) $K_{1.9}Sc_{0.9}Ti_{1.1}(PO_4)_3$, and (*3*) $K_{1.7}In_{0.7}Ti_{1.3}(PO_4)_3$.

to two bands at 1000–1020 and 1100–1130 cm^{-1}. In some cases, an additional band near 1050 cm^{-1} is also observed.

Generally, when considering the processes of the formation of phosphate phases with the langbeinite structure, we should note that the construction of $[M_2(PO_4)_3]^{n-}$ three-dimensional crystal frameworks can be realized with different-valence metals significantly differing in the ionic radius. The ionic radii of M(II) and M(III) for titanium-containing frameworks $[Ti_{1.5}M_{0.5}(PO_4)_3]^{2-}$ and $[Ti^{IV}M^{III}(PO_4)_3]^{2-}$

Table 2. Unit cell parameters of complex phosphates isostructural to langbeinite

Compound	a, Å	V, Å^3
$K_2Mn_{0.5}Ti_{1.5}(PO_4)_3$	9.88	965.1
$K_2Ni_{0.5}Ti_{1.5}(PO_4)_3$	9.82	948.3
$K_2Co_{0.5}Ti_{1.5}(PO_4)_3$	9.83	951.0
$K_2Cu_{0.5}Ti_{1.5}(PO_4)_3$	9.81	946.4
$K_2Zn_{0.5}Ti_{1.5}(PO_4)_3$	9.85	956.6
$K_{1+y}Ti_{2-x}Al_x(PO_4)_3$	9.67–9.77	905.2–932.4
$K_{1+y}Ti_{2-x}Fe_x(PO_4)_3$	9.78–9.84	935.4–952.8
$K_{1+y}Ti_{2-x}Cr_x(PO_4)_3$	9.74–9.82	924.0–947.0
$K_{1+y}Ti_{2-x}In_x(PO_4)_3$	9.86–10.05	958.6–1015.1
$K_{1+y}Ti_{2-x}Y_x(PO_4)_3$	9.92–10.12	976.2–1036.4
$K_2Fe_{1.5}Nb_{0.5}(PO_4)_3$	9.94	982.2
$K_2In_{1.5}Nb_{0.5}(PO_4)_3$	10.13	1039.5
$K_2Y_{1.5}Nb_{0.5}(PO_4)_3$	11.60	1560.9
$K_2Fe_{1.5}Ta_{0.5}(PO_4)_3$	9.84	952.8
$K_2Cr_{1.5}Ta_{0.5}(PO_4)_3$	9.85	955.7
$K_2In_{1.5}Ta_{0.5}(PO_4)_3$	10.01	1003.0
$K_2Y_{1.5}Ta_{0.5}(PO_4)_3$	11.34	1458.3

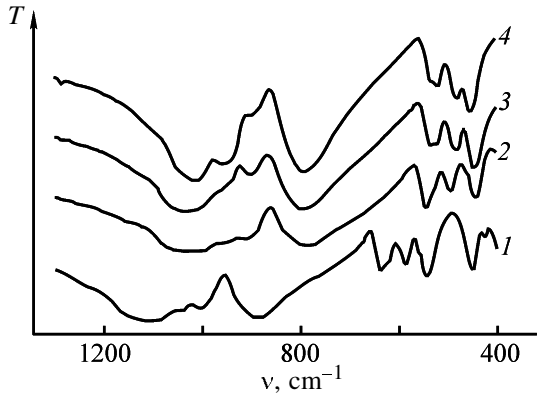


Fig. 2. IR spectra of phosphates isostructural to langbeinite: (*T*) transmittance and (ν) wavenumber. (*1*) $K_2Fe_{1.5}Nb_{0.5}(PO_4)_3$, (*2*) $K_2Cr_{1.5}Nb_{0.5}(PO_4)_3$, (*3*) $K_2In_{1.5}Nb_{0.5}(PO_4)_3$, and (*4*) $K_2Y_{1.5}Nb_{0.5}(PO_4)_3$.

can vary over a wide range: 0.74–0.91 Å from magnesium(II) to manganese(II) and 0.57–0.97 Å from aluminum(III) to yttrium(III) [25]. Correspondingly, the ratios of ionic radii M^{2+} (0.74–0.91)/Ti^{4+} (0.64) = 1.16–1.42 and M^{3+} (0.57–0.97)/Ti^{4+} (0.64) = 0.89–1.52 of the metals forming a three-dimensional framework can differ by a factor of more than 1.5. A similar pattern is also observed with the frameworks $M^{V}_{0.5}M^{III}_{1.5}(PO_4)_3]^{2-}$ (M^V = Nb, Ta) with the ratios M^{3+} (0.67–0.97)/M^{5+} (0.66) = 1.02–1.45. At the same time, the crystallization areas in potassium phosphate melts (ratios K/P, M^{III}/Ti, M^{II}/Ti, and M^{II}/M^V) in phosphates isostructural to langbeinite can considerably differ depending on the nature of different-valence framework-forming metals (Table 1).

CONCLUSIONS

(1) As a result of comprehensive studies of phase formation of complex phosphates with the langbeinite structure in potassium phosphate melts, the crystallization areas (K/P, M^{III}/Ti, M^{II}/Ti, and M^{II}/M^V ratios) and conditions were determined for the following complex phosphates: $K_2Ti_{1.5}M^{II}_{0.5}(PO_4)_3$ (M^{II} = Mn, Ni, Co, Cu, Zn), $K_{1+y}Ti_{2-x}M^{III}_x(PO_4)_3$ ($0 < x \le 1$, $0 \le y \le 1$, $y \ge x$; M^{III} = Al, Sc, Cr, Fe, In, Y), and $K_2M^{V}_{0.5}M^{III}_{1.5}(PO_4)_3$ (M^V = Nb, Ta; M^{III} = Fe, Cr, In, Y).

(2) The complex phosphates obtained were shown by X-ray phase analysis and powder X-ray diffraction to be isostructural; the parameters of their unit cells were calculated.

(3) The compounds synthesized were characterized by IR spectroscopy, diffuse reflection spectroscopy, and ESR spectroscopy.

(4) In the case of langbeinite structures, the ionic radii of different-valence metals forming the $[M_2(PO_4)_3]^{2-}$ three-dimensional crystal framework can differ by a factor of more than 1.5.

REFERENCES

1. Kalinin, V.B. and Stefanovich, S.Yu., *Izv. Akad. Nauk SSSR, Neorg. Mater.*, 1982, vol. 18, no. 9, pp. 1567–1571.
2. Stefanovich, S.Yu. and Kalinin, V.B., *Fiz. Tverd. Tela*, 1981, vol. 23, no. 11, pp. 3509–3512.
3. Alamo, J. and Rodrigo, J.L., *Mater. Res. Bull.*, 1992, vol. 27, pp. 1091–1098.
4. Warhus, U., Maier, J., and Rabenau, A., *J. Solid State Chem.*, 1988, vol. 72, pp. 113–125.
5. Winand, J.M., Rulmont, A., and Tarte, P., *J. Mater. Sci.*, 1990, vol. 25, no. 3, pp. 4008–4013.
6. Govindan Kutty, K.V., Asuvathraman, R., and Mathews, S.K., *Mater. Res. Bull.*, 1994, vol. 29, pp. 1009–1016.
7. Zharinova, M.V., Orlova, A.I., Koryttseva, A.K., *et al.*, *Zh. Neorg. Khim.*, 2004, vol. 49, no. 2, pp. 174–180.
8. Orlova, A.I., Trubach, I.G., Kurazhkovskaya, V.S., *et al.*, *J. Solid State Chem.*, 2003, vol. 173, pp. 314–318.
9. Masse, R., Durif, A., Guitel, J.C., and Tordjman, I., *Bull. Soc. Fr. Miner. Cristallogr.*, 1972, vol. 95, pp. 405–411.
10. Leclaire, A., Benmoussa, A., Borel, M.M., *et al.*, *J. Solid State Chem.*, 1989, vol. 78, pp. 227–231.
11. Zatovsky, I.V., Slobodynik, N.S., Stratiychuk, D.A., *et al.*, *Z. Naturforsch. (b)*, 2000, vol. 55, no. 3/4, pp. 291–298.
12. Battle, P.D., Cheetham, A.K., Harrison, W.T, and Long, G.J., *J. Solid State Chem.*, 1986, vol. 62, pp. 16–25.
13. Battle, P.D., Gibb, T.C., Nixon, C., and Harrison, W.T., *J. Solid State Chem.* 1988, vol. 75, pp. 21–29.
14. Isasi, J. and Daidouh, A., *Solid State Ionics*, 2000, vol. 133, pp. 303–313.
15. Wulff, H., Guth, U., and Loescher, B., *Powder Diffraction*, 1992, vol. 7, pp. 103–107.
16. Guth, U., Loscher, B., Schmidt, P., and Wulff, H., *Solid State Ionics*, 1992, vol. 51, no. 3–4, pp. 183–185.
17. Losilla, E.R., Bruque, S., Aranda, M.A.G., *et al.*, *Solid State Ionics*, 1998, vol. 112, pp. 53–62.
18. Norberg, S.T., *Acta Crystallogr., Sect. B*, 2002, vol. 58, pp. 743–749.

19. Ushchapivskaya, T.I., Synthesis, Structure, and Properties of Phosphates of Uni- and Polyvalent Metals, *Cand. Sci. Dissertation*, Kiev, 2003.
20. Lunezheva, E.S., Maksimov, B.A., Mel'nikov, O.K., and Muradyan, L.A., *Kristallografiya*, 1989, vol. 34, no. 3, pp. 611–614.
21. Shpak, A.L., Korduban, A.M., Trachevskii, V.V., and Slobodyanik, N.S., *Teor. Eksp. Khim.*, 2000, vol. 36, no. 5, pp. 267–280.
22. Gladnev, H.D., *J. Chem. Phys.*, 1965, vol. 42, pp. 1999–2010.
23. Slobodyanik, N.S., Stus', N.V., Nagornyi, P.G., and Kapshuk, A.A., *Zh. Neorg. Khim.*, 1991, vol. 36, no. 11, pp. 2772–2775.
24. Tananaev, I.V., *Atlas infrakrasnykh spektrov fosfatov. Dvoinye mono- i difosfaty* (Atlas of Infrared Spectra of Phosphates. Double Mono- and Diphosphates), Moscow: Nauka, 1990.
25. Vainshtein, B.K., Fridkin, V.M., and Indenbom, V.L., *Sovremennaya kristallografiya* (Modern Crystallography), Moscow: Nauka, 1979, vol. 2, pp. 75–81.

ISSN 1070-4272. Russian Journal of Applied Chemistry, 2006, Vol. 79, No. 1, pp. 16–19. © Pleiades Publishing, Inc., 2006.
Original Russian Text © I.V. Lazareva, L.G. Gerasimova, R.F. Okhrimenko, M.V. Maslova, 2006, published in Zhurnal Prikladnoi Khimii, 2006, Vol. 79, No. 1, pp. 18–21.

INORGANIC SYNTHESIS AND INDUSTRIAL INORGANIC CHEMISTRY

Reaction of Sphene with Sulfuric Acid Solutions

I. V. Lazareva, L. G. Gerasimova, R. F. Okhrimenko, and M. V. Maslova

Tananaev Institute of Chemistry and Technology of Rare Elements and Mineral Raw Materials, Kola Scientific Center, Russian Academy of Sciences, Apatity, Murmansk oblast, Russia

Received October 11, 2005

Abstract—The kinetics of titanium(IV) extraction from sphene with boiling 4–6 M sulfuric acid was studied. The rate constants of the sphene dissolution were determined. The influence of the particle size of the starting mineral on the rate of its dissolution was established. The feasibility of performing sphene dissolution by a liquid-phase procedure yielding stable titanium-containing sulfate solutions suitable for the synthesis of multifunctional composite materials was examined.

DOI: 10.1134/S1070427206010046

Sulfuric acid breakdown of sphene ($TiSiCaO_5$) is an operation determining the whole subsequent process cycle and, consequently, the ultimate goal of its processing. The conditions of carrying out the operation are most commonly chosen so as to attain the maximal degree of sphene breakdown, which is possible only if the process is carried out under rigid conditions: at a high H_2SO_4 concentration of 70–92 wt % and an elevated temperature of 140–200°C with continuous stirring of the reaction mixture [1–3]. However, in this case the service life of the process equipment becomes shorter and its safe maintenance is complicated. Moreover, the reagent expenditure and, correspondingly, the amount of wastes polluting the environment increase. Sphene reacts with a dilute acid (up to 3 M H_2SO_4) [4] very slowly, and its dissolution is accompanied by the formation of a finely dispersed mixed solid phase containing titanium(IV) and silicon(IV) hydroxides and calcium sulfate dihydrate.

We have chosen 4–6 M H_2SO_4 for this study. As the preliminary tests showed, such a choice, firstly, provides high stability of Ti(IV) in the liquid phase of the heated and cooled reaction mass, secondly, makes the operation of the process equipment easier, and, thridly, provides formation of a versatile titanium-containing intermediate product (as a solution), which serves as the basis for subsequent syntheses of various titanium-containing products [5–7].

To find optimal conditions for processing the mineral concentrate containing sphene, we have carried out a physicochemical study of the reaction of the mineral with H_2SO_4 solutions and have determined the kinetic features of this process.

The subject of the study was a crushed sphene concentrate with various particle size. It contained 94 wt % sphene mineral, which corresponds to the content of TiO_2 in the concentrate of 35–36 wt %. The process temperature was 108–115°C (boiling), and the weight ratio of sphene to sulfuric acid (calculated for monohydrate) in the starting mixture was s : 1 = 1 : (1.2–1.8).

A three-necked flask equipped with a stirrer, a reflux condenser, and a thermometer was charged with H_2SO_4 of a specified concentration, and then sphene was added under stirring. The suspension was heated to boil and stirred for 7 h. Samples of the reaction mixture were taken after heating for 30, 120, 180, 240, 300, and 420 min; in these samples, the liquid and solid phases were separated, and their composition was determined. In the liquid phase we determined the content of $Ti(IV)_{tot}$ and also of $Ti(IV)_{react}$ existing in the form of monomeric sulfate complexes or polymeric complexes with a low degree of polymerization. To determine $Ti(IV)_{tot}$, we boiled an aliquot of the solution with an addition of H_2O_2 and determined the optical density of the resulting colored solution [8–10]. The procedure of determining $Ti(IV)_{react}$ was as follows: 1 ml of H_2O_2 (30 wt %) was added into a volumetric flask filled with H_2SO_4 (5 wt %) almost to a mark, then an aliquot of the test solution was added, and the mixture was brought to the mark with H_2SO_4 (5 wt %) [11]. The optical density of the colored solution of Ti(IV) was determined with a

Changes in the content of $Ti(IV)_{react}$ in the liquid phase

Sphene fraction, μm	c_{acid}, M	Content of Ti(IV), TiO_2, g l^{-1}, in indicated time, min						
		30	120	180	240	300	420	1450
<28	5.5	19.6	57.0	69.5	81.0	86.2	97.2	97.8
<63	5.5	6.4	26.9	38.0	47.8	56.0	75.5	78.0
28–63	5.5	5.6	20.8	27.6	35.0	42.0	52.4	50.0
63–100	5.5	3.6	17.6	24.0	28.0	33.0	42.6	48.0
<100	6.0	10.3	38.4	46.4	54.6	66.0	76.8	78.0
<100	5.0	9.2	26.1	31.0	38.4	47.0	52.2	52.3
<100	4.0	7.8	21.8	30.5	36.0	37.2	46.2	50.0

KFK-2 photocolorimeter. The first colorimetric determination was carried out 1 min after the contact between the analyzed solution and H_2O_2. A cell with the colored solution remained in the device, and the optical density was determined in 2, 4, 6, 8, and 10 min. The TiO_2 content (g l^{-1}) was plotted vs. time (min). The initial linear portion of the curve was extrapolated to the *x*-axis (zero time). The value found by the extrapolation corresponds to the content of $Ti(IV)_{react}$. The changes in its content in the liquid phase of the suspension on its keeping at the boiling point are given in the table. These data almost completely coincide with the $Ti(IV)_{tot}$ concentrations. The solid phase was washed with water and alcohol, and its phase composition was determined with a DRON-2 diffractometer. The samples were examined with an electron microscope.

We ground the sphene concentrate in a ball mill in the dry mode. The ground product was separated into three fractions: <28, 28–63, and 63–100 μm. The specific pore volume determined with a Mikrometric-2000 device substantially increases as the sphene particle size decreases. The deterioration of the structural order of the sphene grains resulting from mechanical action (crushing) enhances the chemical activity of the particles and is accompanied by the ionization and amorphization of the surface [12]. The particle activity is the higher, the smaller are sphene particles. The IR spectra (a Perkin–Elmer FT spectrometer) of the sphene samples with various particle size *D* are not identical. Thus, for smaller particles a band appears in the region of 2500–2550 cm^{-1}, typical for silanol Si–OH groups, and intensification of the band in the region of 1412–1507 cm^{-1} suggests formation of calcium carbonate on the particle surface (Fig. 1). The appearance of new formations in the form of amorphous shells on the surface of the ground sphene particles is confirmed by a photomicrograph (Fig. 2).

The sphene activated by grinding reacts with sulfuric acid of the specified concentrations as follows:

$$CaSiTiO_5 + 2H_2SO_4 = TiOSO_4 + CaSO_4\downarrow + SiO_2 \cdot xH_2O\downarrow + H_2O.$$

In the process, Ti(IV) passes into the liquid phase, and solid reaction products, calcium sulfate and amor-

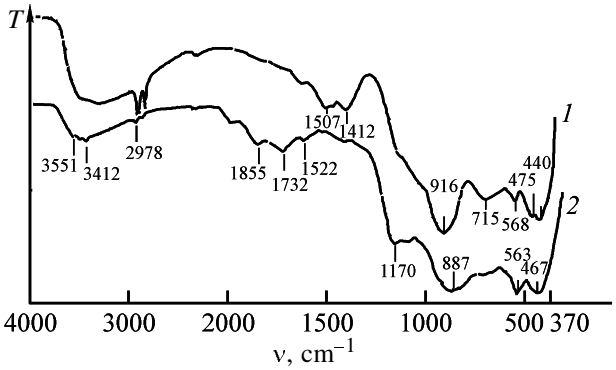


Fig. 1. IR spectra of sphene samples. Particle size, μm: (*1*) <28 and (*2*) 63–100. (*T*) Transmission and (ν) wavenumber.

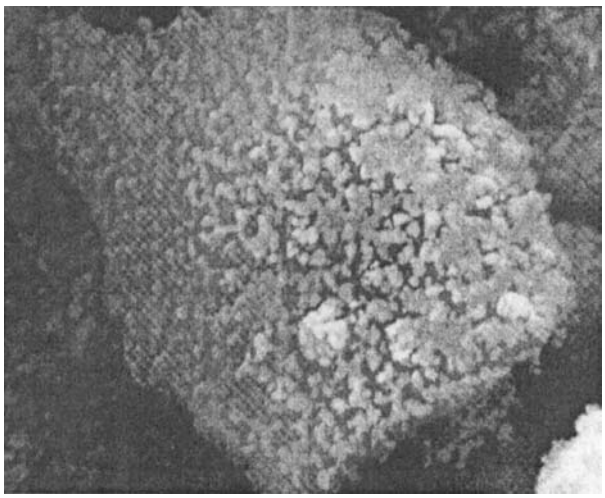


Fig. 2. Photomicrograph of a sphene particle (fraction <28 μm).

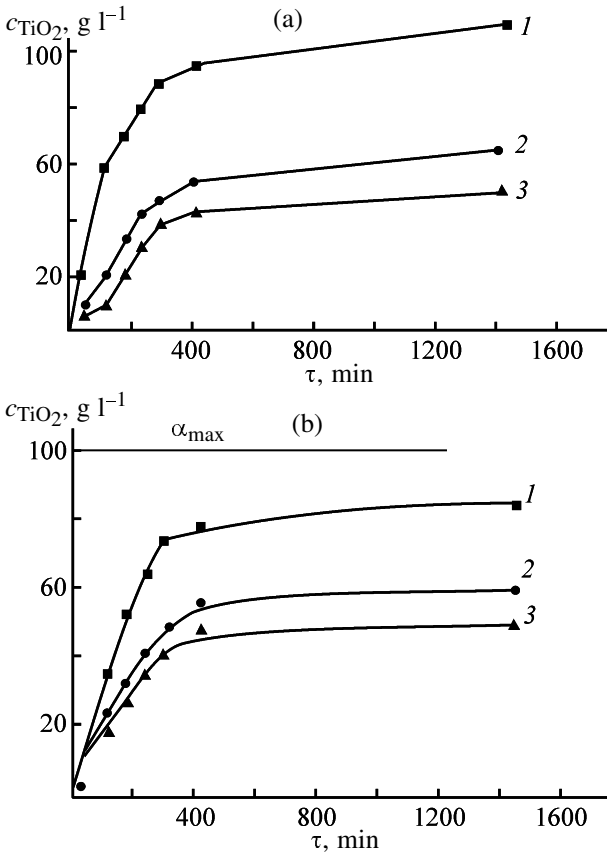


Fig. 3. Titanium extraction into the liquid phase in the course of sphene decomposition: (c_{TiO_2}) titanium concentration in the liquid phase (in terms of TiO_2) and (τ) time. (a) Initial particle size of sphene D < 100 μm. Initial H_2SO_4 concentration c_{in} (M): (*1*) 6, (*2*) 5, and (*3*) 4. (b) $c_{in}(H_2SO_4)$ = 5.5 M; (α_{max}) maximal possible extraction. D, μm: (*1*) <28, (*2*) 28–63, and (*3*) 63–100.

phous $SiO_2 \cdot xH_2O$, are formed. Titanium(IV) is concentrated in the liquid phase owing to its high solubility under the conditions outlined. Since the sphene dissolution is a heterogeneous process and occurs at the liquid (sulfuric acid solution)–solid (sphene particles) interface, its rate can depend not only on sulfuric acid concentration and temperature initiating the crystal disruption, but also on the interface area, i.e., on the particle size.

Figure 3a shows changes in the Ti(IV) content in the suspension liquid phase on its heating at various initial concentrations of sulfuric acid: 4, 5, and 6 M. Figure 3b shows the influence of the sphene particle size. These curves show that, initially, sphene dissolution and Ti(IV) extraction into the liquid phase occur rather actively (stage I). An increase in the H_2SO_4 concentration and, correspondingly, in the temperature accelerates the reaction. As the amount of solid products in the reaction mass increases, the process decelerates. Examination of the solid phase by X-ray phase analysis and electron microscopy shows that the reaction products (amorphous $SiO_2 \cdot xH_2O$ and crystalline $CaSO_4$) are formed as individual phases and also make a porous shell on the surface of sphene particles. The rate of the further Ti(IV) extraction from sphene is determined by the rate of the reagent diffusion through this shell (stage II). Approximately in 5 h, the degree of Ti(IV) passing into the liquid sulfuric acid phase ranges from 35 to 80% depending on the process conditions. The mechanism of dissolution is the same in both stages of the process. Only the rate of Ti(IV) transfer into the liquid phase changes.

To calculate the rate constant K of the sphene dissolution reaction (c = 5.5 M H_2SO_4), we used the known graphic procedure [1, 13, 14]. We constructed $\ln(c_{TiO_2}) = f(\tau)$ plots and determined from them the rate constants (stages I and II) in relation to the initial particle size of sphene. The results are given below:

D, μm	<28	28–63	63–100
K, min^{-1}:			
Stage I	1.8×10^{-2}	1.5×10^{-2}	1.2×10^{-2}
Stage II	5.52×10^{-4}	3.80×10^{-4}	2.29×10^{-4}

In the system under study, Ti(IV) mostly occurs in the form of monomeric titanium(IV) oxosulfate complexes which show a high resistance to polymerization and, consequently, to the solid phase formation.

The sphene particle size affects the kinetics of its dissolution to a greater extent than does variation of the acidity within the range under study. The reaction rate both in the first and in the second stages is the higher, the smaller are sphene particles. However, the rate constant in the first stage increases in total by 30% as the particle size decreases, whereas in the second stage it increases by a factor of almost 2.5. A substantial decrease in the dissolution rate is observed during the process, especially for sphene with larger particles (≥63 μm). This is caused not only by the formation of reaction products on the surface of mineral particles, but also by the necessity of destroying the mineral grains.

CONCLUSIONS

(1) In the range of sulfuric acid concentrations under study, sphene dissolution occurring at the boiling point of the reaction mass is accompanied by transfer of Ti(IV) into the liquid phase and formation of solid reaction products: anhydrous $CaSO_4$ and amorphous silica gel.

(2) Titanium(IV) concentrating in the liquid phase predominantly occurs in the form of monomeric titanium(IV) oxosulfate complexes ensuring high resistance of the system to the formation of a titanium-containing solid phase.

(3) The sphene dissolution in the heterogeneous system is controlled by the diffusion, i.e., by delivery of the reagent through a layer of reaction products on the sphene particle surface.

(4) The fact that the system kept for a long time undergoes no significant changes offers processing advantages; in particular, it allows separation of sphene components present in the liquid and solid phases.

REFERENCES

1. Motov, D.L. and Maksimova, G.K., *Sfen i ego khimicheskaya pererabotka na titanovye pigmenty i napolniteli* (Sphene and Its Chemical Processing into Titanium Pigments and Fillers), Leningrad: Nauka, 1983.
2. Goryachev, A.A. and Dvegubskii, N.S., *Lakokras. Mater. Ikh Primen.*, 1990, no. 4, pp. 30–34.
3. USSR Inventor's Certificate no. 1611909.
4. USSR Inventor's Certificate no. 1331827.
5. RF Patent 2096331.
6. RF Patent 2179528.
7. Gerasimova, L.G., *Pigmenty i napolniteli iz mineral'nogo syr'ya i tekhnogennykh otkhodov* (Pigments and Fillers from Mineral Resources and Process Wastes), Apatity: Kol'skii Nauchn. Tsentr Ross. Akad. Nauk, 2001.
8. Kozachek, N.I., Parakhnevich, A.I., and El'tsova, A.D., *Lakokras. Mater. Ikh Primen.*, 1972, no. 4, pp. 54–56.
9. Kozachek, N.I., Parakhnevich, A.I., and El'tsova, A.D., *Kolloidn. Zh.*, 1973, vol. 35, no. 1, pp. 167–170.
10. Gerasimova, L.G., Motov, D.L., and Kharchenko, R.F., Available from *Zh. Prikl. Khim.*, March 16, 1983, no. 1384-83-DEP.
11. Gerasimova, L.G., Maslova, M.V., Zhdanova, N.M., and Okhrimenko, R.F., *Zh. Prikl. Khim.*, 2001, vol. 74, no. 11, pp. 1734–1736.
12. Bobkov, S.P. *Protsessy v dispersnykh sredakh* (Processes in Disperse Media), Ivanovo: Ivanov. Gos. Tekhnol. Univ., 1997.
13. Zaitsev, O.S., *Khimicheskaya termodinamika k kursu obshchei khimii* (Chemical Thermodynamics for the Course of General Chemistry), Moscow: Mosk. Gos. Univ., 1973.
14. Gerasimova, L.G., Okhrimenko, R.F., Zhdanova, N.M., and Lazareva, I.V., *Lakokras. Mater. Ikh Primen.*, 2001, no. 5, pp. 14–16.

ISSN 1070-4272. Russian Journal of Applied Chemistry, 2006, Vol. 79, No. 1, pp. 20–28. © Pleiades Publishing, Inc., 2006.
Original Russian Text © A.A. Kiprianov, 2006, published in Zhurnal Prikladnoi Khimii, 2006, Vol. 79, No. 1, pp. 22–29.

INORGANIC SYNTHESIS AND INDUSTRIAL INORGANIC CHEMISTRY

Regular Trends in Uptake of Halogens by Alkali Silicate Glasses Containing Two Glass-Forming Components

A. A. Kiprianov

St. Petersburg State University, St. Petersburg, Russia

Received June 23, 2005

Abstract—Oxyhalide alkali silicate glasses M_2O–R_2O_3–SiO_2 + Hal (M = Li, Na, K; R = B, Al; Hal = F, Cl) containing two network-forming components were prepared, and their bulk thermal and electrical properties were studied.

DOI: 10.1134/S1070427206010058

Oxyhalide glasses attract growing interest of biologists [1], medicians [2], and optical [3] and electronics engineers [4]. The addition of halogen-containing components into the starting stock in synthesis of silicate glasses, which was done for a long time exclusively for process purposes [5], allows preparation of the materials with new unique properties.

At the same time, the structure of such glasses containing a mixed anionic constituent virtually is not studied. Simple and evident problems concerning the limiting content of halogen additives that does not cause glass opacification remain unclear. The same can be said about the components favoring fixation of fluorine and chlorine in the silicate network. Data concerning the influence of halide additives on the glass properties, obtained by different authors, are controversial. Most commonly, replacement of the bridging oxygen atom in the silicate tetrahedron by halogen, suggested by the polarization theory which has been proposed more than forty years ago [6], is not confirmed in experiments [7]. Active studies performed in the last years mostly by the high-resolution NMR spectroscopy {^{19}F, ^{27}Al, ^{29}Si MAS-NMR (magic angle spinning), ^{19}F–^{27}Al, ^{19}F–^{29}Si cross-polarization} [1, 8–12], and analysis of their results in particular, show that a variety of fluorine-containing groups derived from network-forming components (silicate, aluminate, and borate), in which the central cation is present in different coordination states, can be formed in the glass structure. At the same time, these and earlier experiments [13, 14] show that fluorine-containing aluminate groups are formed preferentially.

The type of the structural groups is the key parameter affecting the properties of electrode glasses: the character of ion-exchange centers determines the potentiometric behavior of pH- and pM-metric sensors. The halide additives exert a positive effect on the selectivity of cation-exchange glass membranes [15, 16]. This study was performed to interpret the previously obtained results and develop theoretical principles of controllable synthesis of oxyhalide glasses with preset characteristics, including electrode characteristics.

EXPERIMENTAL

As objects of study we chose alkali silicate glasses M_2O–R_2O_3–SiO_2 (M is Li, Na, K; R is Al, B) containing two network-forming components; in their preparation, a part of alkali metal oxides was replaced by the metal halides. In each series of the glasses studied, the ratio of the content of the modifier to the sum of the network-forming cations [M]/([R] + [Si]) (by synthesis) was kept constant. The compositions are given in terms of the known designation: glass-forming oxides and modifiers are given in molar percents and the metal halide, in weight percents. For example, the glass containing by synthesis 26 mol % $Li_2(O,F_2)$, 1 mol % Al_2O_3, and 63 mol % SiO_2, in which a part of alkali metal oxide is replaced by the alkali halide (one Li_2O unit by two LiF units) providing a fluorine content of 4 wt % (in terms of atomic fluorine), is designated as LiAl-2601 + 4 wt % F. This method of designation of the halogen content in glass is the most convenient [17]. The above designation simplifies comparison of the volatile fluorine content by both synthesis and analysis. Moreover, recalculation of the glass compositions in terms of atomic percents shows that the numerical values for fluorine in

weight and atomic percents are reasonably close, i.e., this method is the most useful source of information.

The glasses were synthesized in a laboratory electrical furnace equipped with Silit (silicon carbide) heaters in open platinum crucibles at 1550–1600°C. The total duration of the process including filling of the starting mixture and the synthesis itself was from 5 to 10 h. The glasses were made in the form of rods and pellets. This was done by casting a melt into cooled massive metallic molds with subsequent annealing in a muffle furnace.

The halide content was determined by specially developed methods in all glasses. The fluorine content was determined by the method described in [18] and the chlorine content, by the known Mohr's method [19]. The error of the analysis did not exceed 2–5%.

The thermal characteristics of the glasses (softening point T_w and glass-transition point T_g) were measured in a DBK-5AM vertical quartz dilatometer in the temperature range 20–900°C at a heating rate of 4 deg min^{-1}.

The resistance of the glass pellets (3 cm in diameter, 0.3 cm thick, Aquadag contact area 0.81 cm^2) was measured with an E8-2 ac bridge at a frequency of 100 Hz in the temperature range 100–350°C. The temperature in the cell was maintained constant to within ±0.5°C. The measurement error did not exceed 5%.

The compositions of the glasses synthesized and the results of determining the halide content in them are presented in the table. Most of the glasses synthesized are homogeneous, without visible evidence of phase separation and crystallization. In synthesis of certain compositions, the known opacification properties of fluorine [20] were, however, revealed by the marked opalescence. The opalescence was weak [see table, outward appearance (2)] or strong [(3)]; a portion of glasses synthesized from the starting mixture with the high content of fluorine was milk-white [(4)]. In the glasses synthesized from the starting mixture containing up to 10 wt % chlorides, even weak opacification was not observed. Glasses with a high content of chlorine, however, could not be prepared quantitatively because of spontaneous ejection of melt from the crucible [see table, (5)]; the results of analysis of the remaining glass melt are given in parentheses. The syntheses of these glasses under varied conditions from starting components prepared by different methods gave the same result.

The data of the table confirm the well-known conclusions that the silicate glass synthesis is accompanied by significant loss of halides: from 1/4 to 1/3 of their initial amount evolves into the gas phase. To assess the reproducibility of the results obtained, and, correspondingly, of the fluorine content in the glass,

Glass compositions

Composition of base glass	Fluorine content, wt %		Loss, %	Outward appearance of glasses*
	by synthesis	by analysis		
	Fluorine			
LiAl-2601	0			(1)
	4	1.9	53	(2)
LiB-2601	0			(2)
	4	2.7	33	(4)
LiB-2010	0			(4)
	4	2.6	35	(4)
LiAl-2010	0			(1)
	4	1.6	60	(1)
LiAl-1616	0			(1)
	4	2.6	35	(1)
NaAl-1202	0			(1)
	4	2.4	40	(2)
NaAl-1206	0			(1)
	4	2.8	30	(2)
NaAl-2404	0			(1)
	2	1.1	45	(1)
	4	2.3	43	(1)
	6	3.5	42	(3)
NaAl-2412	0			(1)
	4	2.7	33	(1)
NaAl-2424	0			(1)
	4	2.6	35	(1)
NaAl-2704	0			(1)
	4	2.6	35	(1)
KAl-2010	0			(1)
	4	3.1	23	(1)
KAl-2505	0			(1)
	1	0.7	30	(1)
	2	1.4	30	(1)
	3	2.3	23	(1)
	6	4.5	25	(2)
	9	6.5	28	(4)
	Chlorine			
NaAl-2404	0			(1)
	1	0.7	30	(1)
NaAl-2705	0			(1)
	1	0.7	30	(1)
	2.5	1.3	48	(1)
	5	1.7	66	(1)
	10	(0.8)		(5)
KAl-2705	0			(1)
	5			(5)
	10	(0.49)		(5)

* (1)–(5) For comments, see text.

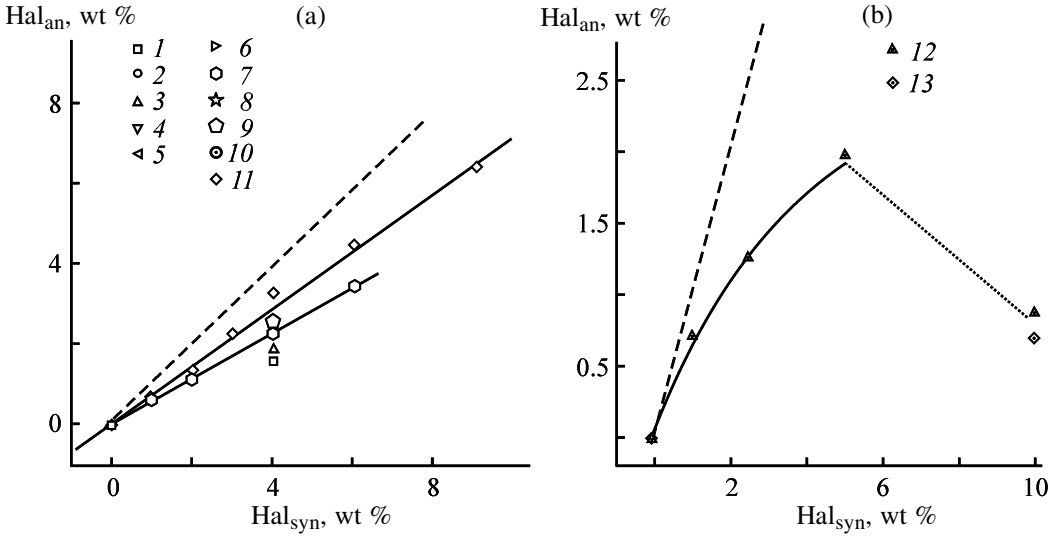


Fig. 1. Dependences of the halogen content Hal_{an} taken up by glass (by analysis) on its content Hal_{syn} introduced into the staring stock in synthesis. (a) Fluorine and (b) chlorine. (a) (*1*) LiAl-2010 (+*x* wt % F), (*2*) LiAl-1616, (*3*) LiAl-2601, (*4*) LiB-2601, (*5*) NaAl-1202, (*6*) NaAl-1206, (*7*) NaAl-2404, (*8*) NaAl-2412, (*9*) NaAl-2424, (*10*) KAl-2010, and (*11*) KAl-2505; (b) (*12*) NaAl-2705 (+*x* wt % Cl) and (*13*) KAl-2705. Correlation coefficients of the linear dependences R_7 = 0.99978, R_{11} = 0.99943. Dashed lines correspond to the maximum content of halogen in the glass.

the chosen compositions were synthesized again: the results of the analyses agreed to within ±0.1 wt % F.

Figures 1a and 1b present the dependences of the halogen content in the glass determined by analysis vs. its content introduced into the starting mixture in synthesis. In the case of fluoride additives, the dependences are linear (a), whereas in the case of chloride additives they tend to flatten out (b). These trends are qualitatively similar to those known from the literature [14, 17, 21].

Undoubtedly, the results obtained reflect certain regular trends responsible for the uptake of halogens by silicate glasses (the correlation coefficients *R* of the linear dependences are given in caption to Fig. 1). At the same time, the mechanism of this process and the type of the newly formed groups cannot be revealed from these dependences. To do this, we studied the bulk thermal and electrical properties of the glasses synthesized.

The dependences of the softening point T_w on the fluorine content taken up by the glass are presented in Fig. 2a. As seen, the known general trend consisting in that the characteristic temperatures of silicate glasses decrease with the introduction of fluorine [17, 21, 22] is observed with the majority of samples. At the same time, for a number of the compositions studied, the fluorine introduction produces an opposite effect, and for certain dependences a pronounced minimum is observed. Similar results reflecting ambiguity of the effect exerted by chlorine on the thermal characteristics of silicate glasses are presented in [23].

The electrical characteristics of the glasses synthesized are plotted in Fig. 2b. As in the previous case, the dependences describing the resistivity $\log \rho_{20}$ of glasses vs. the fluorine content in them show no common trend.

The data obtained do not principally differ from those known from the literature. However, the method of their presentation is purely demonstrational and does not reveal true effects exerted by halogens on the properties of silicate glasses. Undoubtedly, analysis of the dependences obtained is also complicated by the fact that the true compositions of the glasses studied (by analysis) do not coincide with those ascribed to them (by synthesis), because a portion of components in the form of halides actively vaporizes in the course of the synthesis.

The subsequent treatment of our results was largely formal. The oxyfluoride glasses synthesized were divided onto four groups according to the degree of opacification. The photographs of some samples are shown in Fig. 3.

The X-ray phase analysis of the chosen glasses revealed X-ray amorphous glassy phase in glasses (1) whose phase composition was homogeneous by visual observation. At the same time, the opacification of

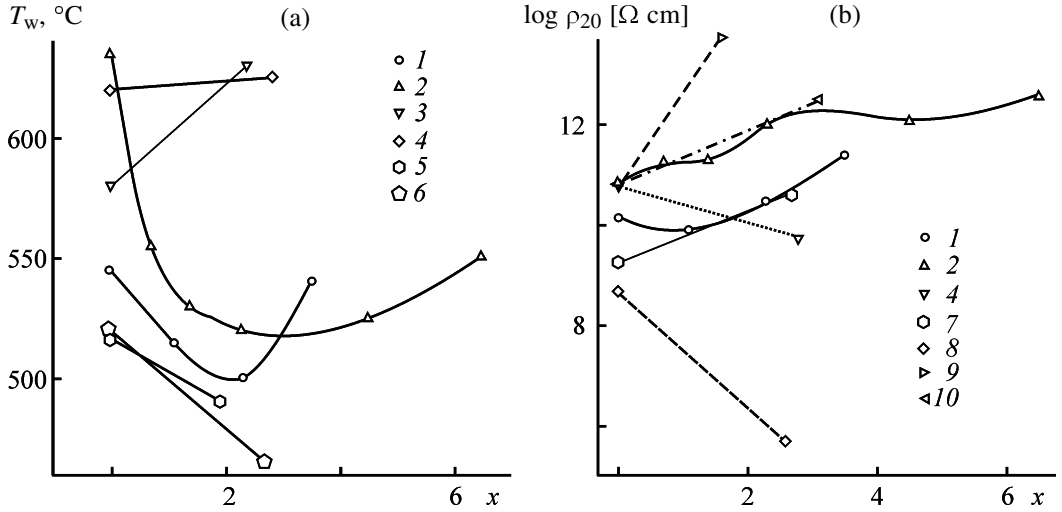


Fig. 2. Dependences of the (a) softening point T_w and (b) logarithm of the resistivity $\log \rho_{20}$ on fluorine content x (wt %, by analysis) for ternary alkali silicate glasses. (*1*) NaAl-2404 (+x wt % F), (*2*) KAl-2505, (*3*) NaAl-1202, (*4*) NaAl-1206, (*5*) LiAl-2601, (*6*) LiB-2601, (*7*) NaAl-2412, (*8*) NaAl-2424, (*9*) LiAl-2010, and (*10*) KAl-2010.

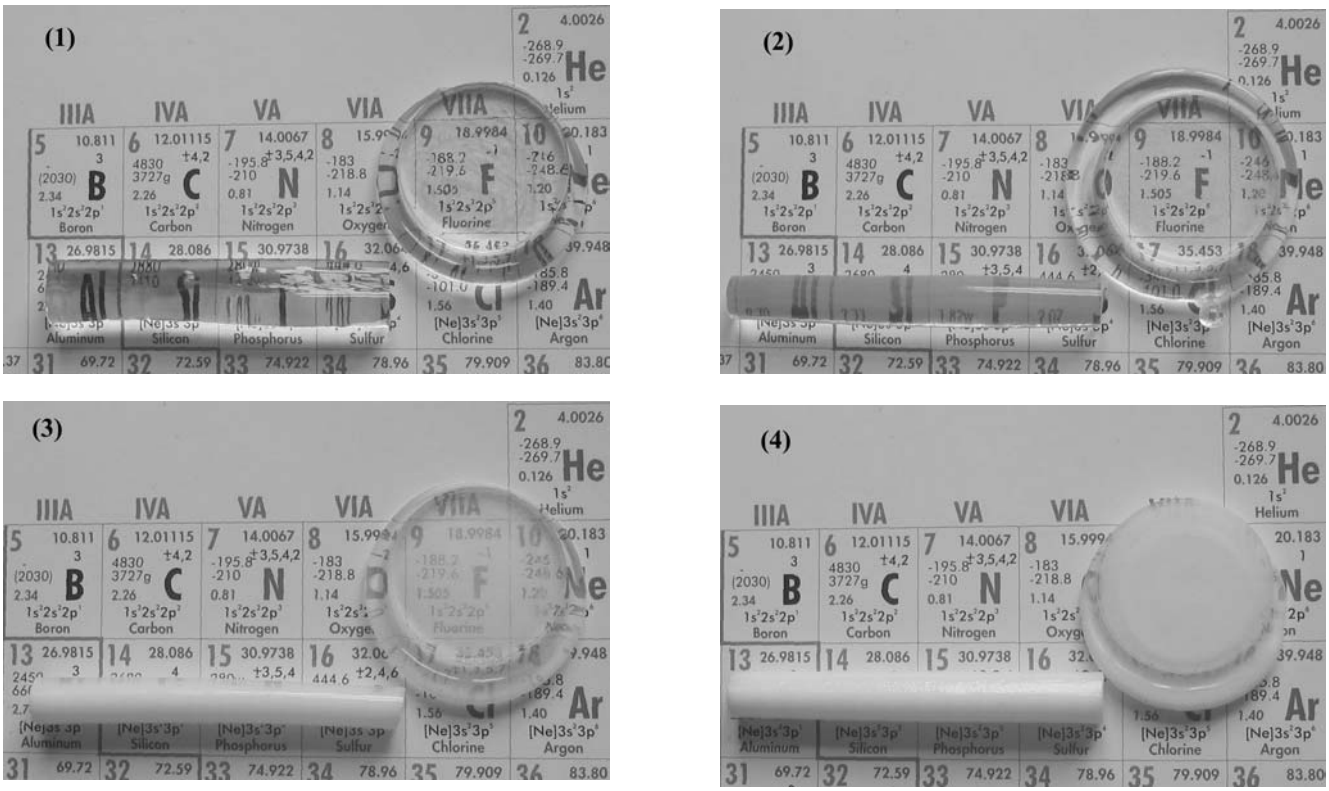


Fig. 3. Appearance of the glass samples with different degrees of opacification. Glass (see table): (1) transparent, (2) weakly opalescent, (3) strongly opalescent, and (4) milk-white.

sodium aluminosilicate glasses is due to the separation of sodium fluoride, whereas that of potassium aluminosilicate glasses, due to the separation of cryolite $3KF \cdot AlF_3$. The latter result is in line with the conclusions of [24] consisting in that the above fluorides are major components of the crystalline phase of opaque (opalescent) glasses. The photomicrographs of the glasses confirm the presence of this crystalline phase dispersed in the glass matrix [25].

The previously performed studies, including those

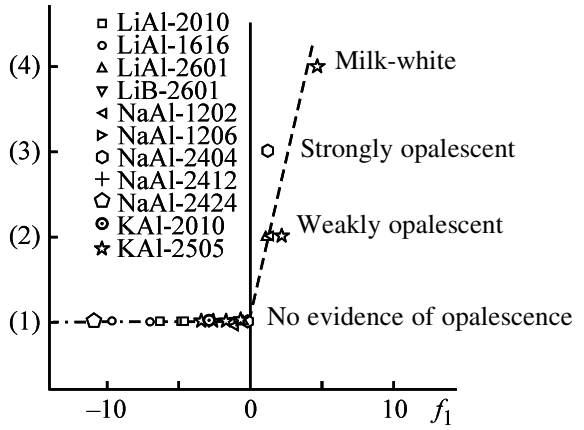


Fig. 4. Outward appearance of the glass as a function of the difference in the content of fluorine and second network-forming oxide f_1 = [F, at. %] – [R, at. %].

concerning the electrode properties of oxyhalide glasses containing two glass-forming components [15, 16], suggest that fluorine enters the aluminate constituent of the glass network with the formation of strong acid groups. To support this suggestion, in view of development of a formal semiquantitative method suitable for interpretation of the results obtained, we present the dependence of the degree of the glass opacification on the difference between the contents of fluorine and aluminum introduced in the glass synthesis (f_1 = [F, at. %] – [Al, at. %]) (Fig. 4). The vertical line at $f_1 = 0$ is a boundary where the contents of the aluminate groups and the halogen atoms are equal; on the left-hand side ($f_1 < 0$) are located glasses with excess sites and on the right-hand side, glasses with excess halide atoms. As seen, all glasses with the inhomogeneous phase composition are located in the right-hand side of the graphs at $f_1 > 1$. It may be suggested that glass opacification, i.e., formation of the separate fluoride phase from the evolution of excess fluorine, is typical of compositions wherein the substitution of one of bridging oxygens in each aluminate tetrahedra by nonbridging fluorine $[AlO_{4/2}]^- \rightarrow [AlO_{3/2}F]^-$ (first step) is complete in the course of melting and the second step $[AlO_{3/2}F]^- \rightarrow [AlO_{2/2}F_2]^-$ starts developing. The forming doubly substituted groups containing two bridging oxygen atoms lose their network-forming properties and serve as a source of the crystallization of the corresponding fluorides (MF or $3MF \cdot AlF_3$).

The results of studying the bulk thermal and electrical properties of the glasses, taking into account the revealed regular trends, are shown in Fig. 5. As argument was chosen the ratio of the fluorine and aluminum contents introduced in the glass synthesis; when their contents are equal, $f_2 = 1$. As seen, the softening point T_w decreases with the incorporation of fluorine into the glass structure (Fig. 5a). This is due to the substitution of one bridging oxygen by nonbridging fluorine, which weakens the glass framework. An increase in T_w at the high content of halogen

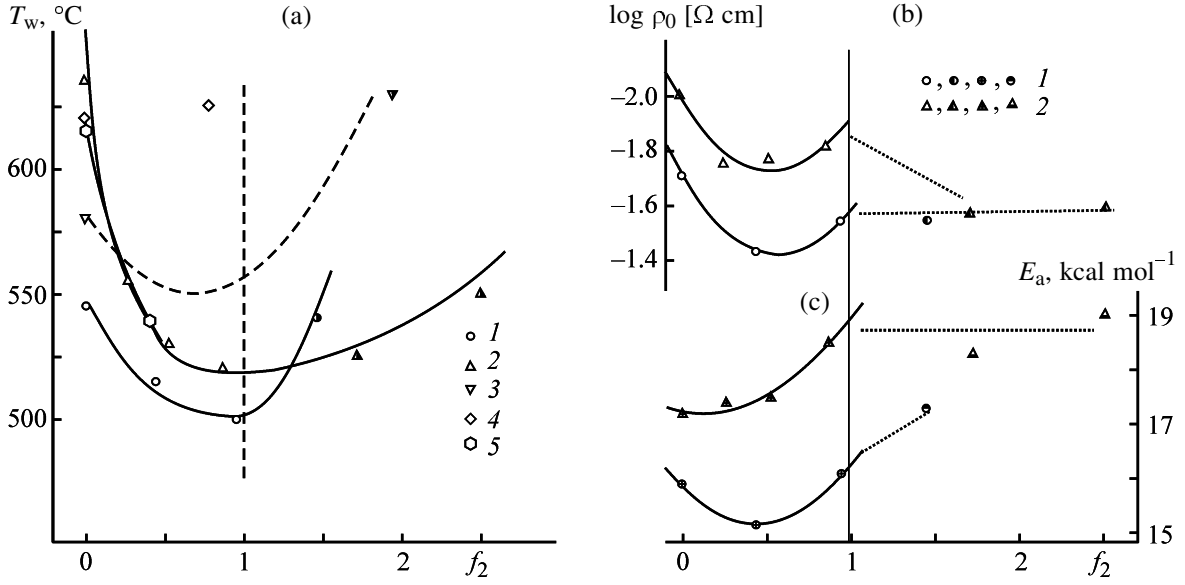


Fig. 5. Dependences of the (a) softening point T_w, (b) ogarithm of the preexponential term $\log \rho_0$, and (c) activation energy of electrical conductivity E_a on the ratio of the fluorine content introduced into the glass to the content of the second network-forming component f_2 = [F, at. %]/[R, at. %]. (*1*) NaAl-2404 (+*x* wt % F), (*2*) KAl-2505, (*3*) NaAl-1202, (*4*) NaAl-1206, and (*5*) NaAl-2412.

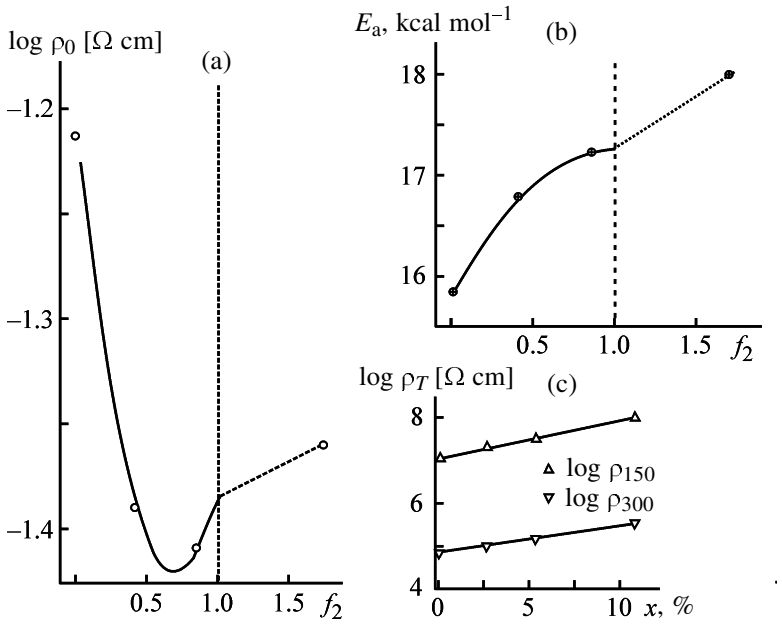


Fig. 6. Dependences of the (a) preexponential term $\log \rho_0$ and (b) activation energy of electrical conductivity E_a on the ratio of fluorine content introduced into a glass containing (wt %) 20 Na_2O, 10 Al_2O_3, 9 ZnO, 6 B_2O_3, 55 SiO_2 + x F_2 to the content of the second network-forming component f_2 = [F, at. %]/[Al + B, at. %]. (c) Data of [26]. (*x*) Amount of F added.

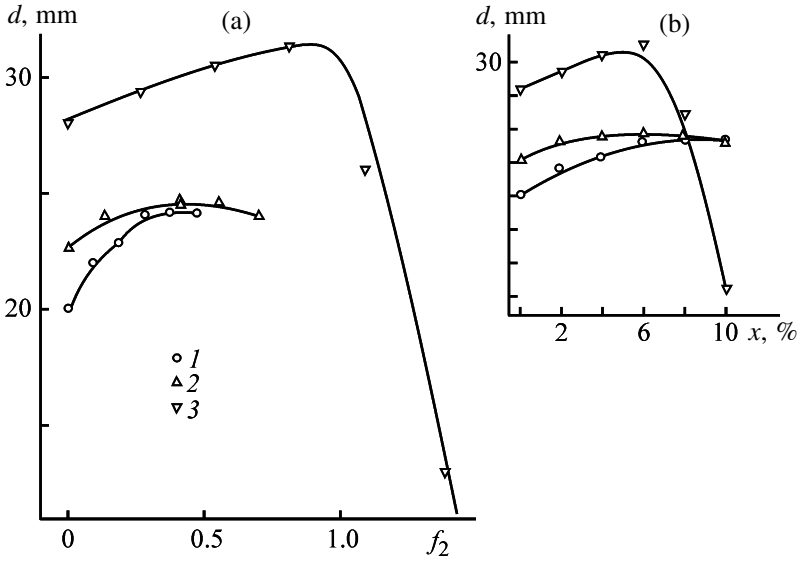


Fig. 7. (a) Flowability data from [27] for three series of yNa_2O–zB_2O_3–$(100 - y - z)SiO_2$ (mol %) glasses containing sodium fluoride, plotted vs. the ratio of the fluorine content introduced into the glass to the content of the second network-forming oxide f_2 = [F, at. %]/[B, at. %]), and (b) the same data plotted vs. fluorine content x. For explanations, see text. (*d*) Drop diameter. (*1*) Series I: y = 12.5, z = 37.5; (*2*) series II: $y = z$ = 25; (*3*) series III: y = 37.5, z = 12.5.

is due to the cardinal transformation of the glass structure owing to the crystallization of excess fluorides.

The electrical conductivity parameters, i.e., the logarithm of the preexponential term ρ_0 in the $\rho = \rho_0 \exp(E_a/RT)$ dependence, where ρ is the resistivity, and the activation energy of conductivity, presented in the new coordinates for different glasses, also became reasonable (Fig. 5b). Variations with the halogen content are regular at $f_2 < 1$, i.e., in the region of macrohomogeneous glass compositions; on passing to inhomogeneous compositions, the characteristics change, and this change is determined by the type of the crystallizing compound and by the phase ratio.

To confirm the common character of the suggested description, we have processed the available data obtained by other researchers (Figs. 6, 7). To a first ap-

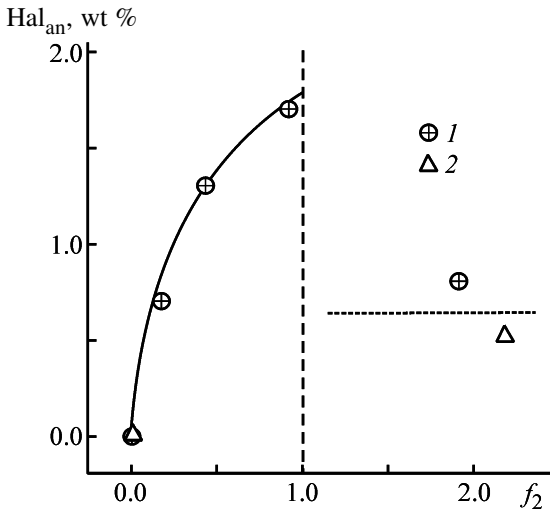


Fig. 8. Fluorine content by analysis Hal$_{an}$ in (*1*) NaAl-2705 + *x* wt % Cl and (*2*) KAl-2705 + *x* wt % Cl glasses as a function of the ratio of the chlorine content in the glass to the content of the second network-forming oxide f_2 = [Cl, at. %]/[R, at. %].

proximation, the dependences of the electrical conductivity parameters reported in [26] for the series of glasses containing (wt %): 20 Na_2O, 10 Al_2O_3, 9 ZnO, 6 B_2O_3, 55 SiO_2 + xF_2 (the composition NaAlZnB-21$_3$05$_2$07$_3$05$_7$ + *x* wt % F) (Fig. 6c) coincide with our dependences (Fig. 5b). It should be noted that, according to input data, to $f_2 > 1$ corresponds an opal glass containing 10.8 wt % fluorine.

Belyaev and Belyi [27] studied the fusibility and flowability of fusible enamel frits of various basicites containing fluorine (for compositions, see caption to Fig. 7). The target characteristics was determined from the diameter of drop formed by heating a small bar of glass powder (10 mm in diameter, 8 mm high) at 800°C for 5 min (the results are reproduced in Fig. 7b). The authors ascribed the observed decrease in fusibility of base glasses to their crystallization caused by surrounding of sodium with fluorine. The input data plotted in the new coordinates in Fig. 7a suggest that the crystallization and, consequently, the deteriorated flowability are revealed in compositions with $f_2 > 1$, i.e., in glasses formed from the melts, in which the substitution of bridging oxygens for fluorine in borate tetrahedra proceeded up to the formation of doubly substituted groups $[BO_{2/2}F_2]^-$.

The most convincing argument in favor of the concept proposed are results of processing of our data for glasses with the chloride additives. The data of Fig. 1b in the form of the dependences of the chlorine content taken up by glass on the structure-sensitive function f_2 are demonstrated in Fig. 8. It is seen that, as in the case of fluoride additives, fixation of chlorine in the glass-forming matrix occurs only as long as the content of the aluminate tetrahedra exceeds the content of the halogen atoms introduced into the melt. At the same time, contrary to the case of fluorine whose excess is separated into the crystalline phase, it is likely that the increased content of chlorine results in the formation of doubly substituted aluminum oxychloride groups $[AlO_{2/2}Cl_2]^-$, which easily lose oxygen atoms and release volatile $AlCl_3$.[1] The possibility of formation of these multiply substituted groups was predicted in [6] based on the fact that the polarizability of chloride anion is higher than that of fluoride anion and is comparable to that of oxygen. Therefore, the probability that chlorine replaces more than one oxygen in the aluminum coordination sphere is considerably higher than in the case of fluorine [6]. Apparently, it is the accumulation of a large amount of gaseous aluminum chloride that caused the above-noted ejection of the glass melt from the crucible [see table, (5)].

Our suggestions on the formation of $[RO_{3/2}Hal]^-$ groups by halogens with the second network-forming oxide do not contradict the conclusions made elsewhere. For example, Callow [17] noted a decrease in the opalescence with the replacement of a portion of SiO_2 by Al_2O_3, and Parker *et al.* [14] noted a slight increase in fixation of fluorine with increasing content of aluminum oxide in the alkali silicate glass. The latter fact is attributed in [14, 17] to an increase in the melt viscosity with the introduction of aluminum oxide, on the one hand, and to a decrease in the fluoride activity and, correspondingly, volatility, owing to fixation of alkali metal cation in the aluminate tetrahedron, on the other hand. According to the data of [29], agreement has been achieved concerning the formation of Al–F bond in aluminosilicate glasses. The fact that halogen forms bonds preferentially with aluminum (i.e., with the second network-forming oxide) is confirmed by a variety of the NMR spectra in which Si–F bonds are manifested only weakly [11] or are absent [1]. At the same time, the reason of this preference and the types of the groups formed remain unclear. Based on analysis of the high-resolution NMR spectra (^{19}F, ^{27}Al, ^{29}Si MAS-NMR, ^{19}F–^{27}Al, ^{19}F–^{29}Si cross-polarization) of the jadeite, cryolite, and albite glasses containing the fluoride additives, it is concluded in [1, 12] that fluorine forms bonds with the three main groups, [4]Al, [5]Al, and [6]Al, which differ in the coordination states of aluminum, with the AlF_6^{3-} octahedral complexes being major. Schaller

[1] $T_{subl}(AlCl_3)$ = 179.9°C, whereas $T_{boil}(AlF_3)$ = 1529°C [28].

et al. [12] also suggest that bridging Al–F–Al bonds, mixed octahedral aluminum complexes containing fluorine and oxygen [6] $Al(F,O)_n$, and tetrahedral complexes AlF_4^- can be formed. As a result of these structural transformations, aluminum loses network-forming properties and, according to the authors' data, converts into a modifying ion.

Liu and Nekvasil [29, 30] made a critical review supported by the model calculations, concerning the suggestions made in the literature on the formation of fluorine-containing groups in silicate glasses. It is convincingly demonstrated that the analysis of the above NMR spectra should be revised. For all the tetrahedral aluminum fragments, the calculated positions of the peaks are in good agreement with the experiment, demonstrating that any AlF_4^- group, $[AlF_3O_{1/2}]^-$, $[AlF_2O_{2/2}]^-$, or $[AlFO_{3/2}]$, or all these groups simultaneously, can be present in a glass. Moreover, the analysis showed that the experimental data [1, 12] do not distinguish the above groups. These conclusions coincide with those made in [8] that the four-coordinate aluminum groups $[AlO_xF_y]_n$ are major halogen-containing fragments in $CaO \cdot CaF_2 \cdot Al_2O_3 \cdot 2SiO_2$ glass. It should be noted that no data are available in the literature concerning the formation of oxychloride aluminate groups in a glass or melt.

Thus, the results obtained extend our views on the fixation of halogens (both fluorine and chlorine) in the groups involving the second network-forming oxide (both aluminum and boron) and clearly demonstrate that the groups formed are $[RO_{3/2}Hal]^-$ (R is Al or B and Hal, F or Cl).

CONCLUSIONS

(1) The results of a study of the bulk thermal and electrical characteristics of a series of alkali silicate oxyhalide glasses containing the second network-forming agent, with account made of the synthesis conditions and tendency to crystallize, showed that the halogen (F, Cl) is selectively fixed by the second network-forming oxide with the formation of mixed tetrahedra $[RO_{3/2}Hal]^-$, with substitution of one bridging oxygen.

(2) Exceess of the halide content introduced during the glass synthesis over the content of the second network-forming oxide results in the formation of doubly substituted groups $[RO_{2/2}Hal_2]^-$, which serve as source of crystallization of the corresponding fluorides in the case of fluorine or are converted into highly volatile $AlCl_3$ in the case of chlorine.

REFERENCES

1. Kohn, S.C., Dupree, R., Mortuza, M.G., and Henderson, C.M.B., *Am. Mineral*., 1991, vol. 76, pp. 309–312.
2. Vogel, W., Holand, W., Naumann, K., and Gummel, J., *J. Non-Cryst. Solids*, 1986, vol. 80, pp. 34–51.
3. Lucas, J., Smektala, F., and Adam, J.L., *J. Fluorine Chem*., 2002, vol. 114, no. 2, pp. 113–118.
4. Kim, J.-H., Seo, S.-H., Yun, S.-M., and Chang, H.-Y., *Appl. Phys. Lett*., 1996, vol. 68, pp. 1507–1509.
5. Bezborodov, M.A., *Sintez i stroenie silikatnykh stekol* (Synthesis and Structure of Silicate Glasses), Minsk: Nauka i Tekhnika, 1968.
6. Rabinovich, E.M., *Izv. Akad. Nauk SSSR, Neorg. Mater*., 1967, vol. 3, no. 5, pp. 855–859.
7. Hill, R., Wood, D., and Thomas, M., *J. Mater. Sci*., 1999, vol. 34, pp. 1767–1774.
8. Stamboulis, A., Hill, R.G., and Law, R.W., *J. Non-Cryst. Solids*, 2004, vol. 333, pp. 101–107.
9. Stebbins, J.F., and Zeng, Q., *J. Non-Cryst. Solids*, 2000, vol. 262, pp. 1–5.
10. Kiczenski, T.J., Du Lin-Shu, and Stebbins, J.F., *J. Non-Cryst. Solids*, 2004, vol. 337, pp. 142–149.
11. Zeng, Q., and Stebbins, J.F., *Am. Mineral*., 2000, vol. 85, pp. 863–867.
12. Schaller, T., Dingwell, D.B., Keppler, H., *et al*., *Geochim. Cosmochim. Acta*, 1992, vol. 56, pp. 701–707.
13. Mysen, B.O., and Virgo, D., *Contrib. Mineral. Petrol*., 1985, vol. 91, pp. 205–220.
14. Parker, J.M., Al-Dulaimy, J.A.M., and Juma, Q.A., *Glass Technol*., 1984, vol. 25, no. 4, pp. 180–187.
15. Kiprianov, A.A. and Karpukhina, N.G., *Fiz. Khim. Stekla*, 2001, vol. 27, no. 1, pp. 101–107.
16. Kiprianov, A.A., and Cherepanov, P.V., *Trudy III nauchnoi sessii Nauchnogo tsentra po khimii Sankt-Peterburga* (Proc. III Sci. Session of Scientific Center for Chemistry, St. Petersburg), St. Petersburg, 2004, pp. 102–103.
17. Callow, R.J., *J. Soc. Glass Technol*., 1949, vol. 33, no. 153, pp. 255–266.
18. Kiprianov, A.A., and Karpukhina, N.G., *Zh. Prikl. Khim*., 1997, vol. 70, no. 7, pp. 1206–1208.
19. Skoog, D.A., and West, D.M., *Fundamentals of Analytical Chemistry*, New York: Holt, Rinehardt, and Winston, 1976, 3rd ed.
20. Juma, Q.A. and Parker, J.M., *Advances in Ceramics*, Beall, G.H., Ed., Am. Ceram. Soc, 1982, vol. 4, pp. 218–323.
21. Hirayama, C., and Camp, F.E., *Glass Technol*., 1969, vol. 10, no. 5, pp. 123–127.

22. Mathur, A., and Pye, I.D., *Glastechn. Ber*., 1989, vol. 62, no. 4, pp. 135–141.
23. Siwadamrongpong, S., Koide, M., and Matusita, K., *J. Non-Cryst. Solids*, 2004, vol. 347, pp. 114–120.
24. Sil'vestrovich, S.I., and Rabinovich, E.M., *Zh. Prikl. Khim*., 1959, vol. 32, no. 8, pp. 1690–1695.
25. Karpukhina, N.G., Study of Bulk and Electrode Properties of Halide-Containing Alkali Silicate Glasses, *Cand. Sci. Dissertation*, St. Petersburg, 2001.
26. Mazurin, O.V., and Molchanova, E.V., *Tr. Leningr. Tekhnol. Inst*., 1955, no. 34, pp. 48–52.
27. Belyaev, G.I., and Belyi, Ya.I., *Steklo Keram*., 1965, no. 4, pp. 34–36.
28. *Spravochnik khimika* (Chemist's Reference Book), Nikol'skii, B.P., Ed., Moscow: Goskhimizdat, 1964, vol. 2.
29. Liu, Y., and Nekvasil, H., *Am. Mineral*., 2002, vol. 87, pp. 339–346.
30. Liu, Y., and Nekvasil, H., *Am. Mineral*., 2001, vol. 86, pp. 491–497.

ISSN 1070-4272. Russian Journal of Applied Chemistry, 2006, Vol. 79, No. 1, pp. 29–33. © Pleiades Publishing, Inc., 2006.
Original Russian Text © M.V. Charykova, I.I. Bornyakova, Yu.S. Polekhovskii, N.A. Charykov, E.V. Kustova, O.V. Arapov, 2006, published in Zhurnal Prikladnoi Khimii, 2006, Vol. 79, No. 1, pp. 30–34.

INORGANIC SYNTHESIS AND INDUSTRIAL INORGANIC CHEMISTRY

Chemical Composition of Extracts from Shungite and "Shungite Water"

M. V. Charykova, I. I. Bornyakova, Yu. S. Polekhovskii, N. A. Charykov, E. V. Kustova, and O. V. Arapov

St. Petersburg State University, St. Petersburg, Russia
Innovations at Leningrad Institutes and Enterprises, Private Company, St. Petersburg, Russia

Received October 26, 2005

Abstract—A chemical analysis of aqueous extracts from shungite-III from the Zazhogino deposit (Republic of Karelia) and of natural water contacting with shungite rocks was made. The chemical composition and bactericide properties of "shungite water" were studied.

DOI: 10.1134/S107042720601006X

At present shungite-based preparations are widely used in cosmetology and medicine. In particular, evidence concerning the unique therapeutic-prophylactic properties of water infusion of shungite, shungite-based skin preparations, baths with shungite, and shungite rubble and pebble for massage is given in monographs [1, 2] and numerous advertising issues.

The aim of this study was to examine the chemical composition and selected properties of water that was brought in contact in both laboratory and natural conditions. Our study involved model experiments on leaching of shungite with distilled water, sampling and chemical analysis of samples of natural water that was in contact with shungite rock, and analysis of the chemical composition and bactericidal properties of "shungite water."

As the object of laboratory studies served shungite-III, a material based on shungite rock from the Zazhogino deposit (Republic of Karelia). Shungites (shungite rock) from the Zazhogino deposit are, on the average, composed of 30% carbon and 70% silicates [3]. As regards the content of carbon, they belong to a third variety of shungite rock (shungite-III) [3] or to maxovites [4]. The following microimpurities were found in these shungites: Fe, Ti, V, Ni, Cu, and Zn, mainly in the sulfide (pyrite, pyrrhotine, sphalerite) and oxide (e.g., rutile) mineral forms.

Table 1 lists the concentrations of a number of microelements in an averaged sample of shungite-III, determined by quantitative emission analysis (Central Analytical Laboratory, Karpinskii Russian Research Geological Institute). The content of the rock-forming oxides is as follows (wt %): Al_2O_3 3.5, MgO 4.0, CaO 0.12, Na_2O 0.3, K_2O 1.8, and TiO_2 0.4.

The aqueous extracts were prepared and chemically analyzed as follows. Model experiments on determination of water-soluble forms of shungite microcomponents were performed at room temperature under static conditions: weighed portions of three different fractions of shungite (<0.25 mm, 0.25–1 mm, and 1–3 mm) were poured over with distilled water in a 1 : 5 ratio and the resulting mixtures were thoroughly agitated for 1 h, were allowed to stand for three days (as shown in [5], this time is sufficient for the water-soluble fractions to virtually completely pass from shungite into water), and then were filtered through a "blue band" paper filter. The aqueous extracts, natural water, and shungite water were analyzed by the ICP ES technique at the Laboratory of the Center for Research and Water Quality Monitoring, Vodokanal State Unitary Enterprise. The results obtained are listed in Table 2. The concentrations of Na, Ti, Ag,

Table 1. Concentrations of microelements in shungite-III

Element	Concentration, mg kg^{-1}	Element	Concentration, mg kg^{-1}
Fe	25 000	Zn	311
Cr	58.4	Pb	70.2
Co	10.6	Ni	181
Cu	111	Mn	98.9

Table 2. Chemical composition of aqueous extracts from shungite

Element	Concentration, mg l^{-1}, in an aqueous extract from indicated fraction, mm			Concentration, mg kg^{-1}, of a water-soluble form in indicated shungite fraction, mm		
	<0.25	0.25–1	1–3	<0.25	0.25–1	1–3
Al	100	85	58	500	426	290
Ba	0.010	0.010	0.013	0.050	0.050	0.065
Be	0.013	0.010	0.007	0.065	0.050	0.034
Ca	21	5.4	3.8	105	27.1	19.0
Cd	0.55	0.47	0.40	2.75	2.36	2.00
Co	1.3	1.0	0.83	6.50	5.01	4.16
Cr	0.024	0.036	0.038	0.120	0.180	0.190
Cu	13	8.7	5.2	65.0	43.6	26.0
Fe	260	250	190	1300	1250	951
K	2.0	2.3	2.7	10.0	11.5	13.5
Mg	46	33	29	230	165	145
Mn	1.6	1.0	0.74	8.00	5.01	3.71
Mo	0.0013	0.0014	0.0016	0.007	0.007	0.008
Ni	26	20	16	130	100	80.1
Pb	0.0045	0.0047	0.036	0.023	0.024	0.180
Se	0.33	0.24	0.19	1.65	1.20	0.951
Si	22	11	7.2	110	55.1	36.0
Sr	0.068	0.013	0.0084	0.340	0.065	0.042
V	0.043	0.11	0.17	0.215	0.551	0.851
Zn	59	56	45	295	281	225
Na	<5.0	<5.0	<5.0	<25	<25	<25
Ti	<0.001	<0.001	<0.001	<0.005	<0.005	<0.005
pH	3.15	3.1	3.1			

As, B, and Sb are below the detection limit. The concentrations of microelements in aqueous extracts, recalculated to their content in shungite, give notion of the fraction of water-soluble forms of separate components relative to their total content (Table 2). It can be seen from the data presented that some elements (Fe, Al, Zn) are present in the aqueous extracts in rather high concentrations; probably, their hydrolysis may be a reason for the substantial decrease in the pH of distilled water after its interaction with shungite.

The chemical elements contained in the shungite samples studied can be conditionally divided into three groups. To the first group belong elements that the least actively pass into an aqueous extract. For these elements, the fraction of water-soluble forms relative to their total content in a solid sample is exceedingly low: tenths of a percent for Na, Cr, Mo, V; hundredths of a percent for K, Pb; and even less for Ti, Ba. For these elements, either no changes at all with the degree of shungite grinding are observed in their concentrations in aqueous extracts or this dependence is very weak. The only exception is lead, but the difference revealed (nearly an order of magnitude) is due to some local contamination. For the second group of elements (Al, Ca, Mg, Fe, Mn, and Be), the fraction of water-soluble elements relative to their total content in shungite is several percents (10–12% at most). A clearly pronounced increase in their concentrations in aqueous extracts with the degree of shungite grinding is observed. The same dependence is preserved for elements belonging to the third group (Cu, Co, Ni, and Zn), but these elements differ in that they pass into an aqueous solution to a considerably greater extent than the others: The fraction of water-soluble forms relative to their total content in shungite is several tens of percent and reaches values of 60–90% in the case of leaching of the <0.25-mm fraction. Similarly to Fe, these elements are present in shungite mainly as sulfides, which turn into more soluble mineral forms under oxidizing conditions.

In addition to laboratory experiments, samples of natural water directly contacting with shungite rock or of water from reservoirs lying close to shungite deposits were taken. The results of their chemical analyses are listed in Table 3. Sample no. 1 was taken from a well at the Maksovo open pit, where under-

Table 3. Results of a chemical analysis of samples of natural water

Element	Concentration in a sample, mg l^{-1}					MPC, mg l^{-1}
	no. 1	no. 2	no. 3	no. 4	no. 5	
Al	220	11	0.036	0.037	0.012	0.5
Ba	0.032	0.025	0.220	0.130	0.130	0.1
Be	0.014	0.002	<0.0001	<0.0001	<0.0001	0.0002
Ca	46	68	50	41	51	
Cd	1.9	0.065	<0.0001	<0.0001	<0.0001	0.001
Co	2.6	0.36	<0.001	<0.001	<0.001	0.1
Cr	1.5	<0.001	<0.001	<0.001	<0.001	0.5
Cu	20	2.3	<0.001	0.001	<0.001	1.0
Fe	2600	0.890	0.430	0.320	0.170	0.3
K	1.1	10	2.7	4.6	4.7	
Mg	74	94	20	17	23	
Mn	8.2	3.5	0.047	0.026	0.0099	0.1
Mo	0.19	<0.001	<0.001	<0.001	<0.001	0.25
Na	14	3.1	8.7	5.7	5.6	200.0
Ni	48	4.1	0.001	0.005	0.002	0.1
Pb	0.034	0.001	0.002	0.002	0.003	0.03
Se	1.7	0.023	<0.005	<0.005	<0.005	0.01
Si	15	9.4	4.2	1.9	2.2	10.0
Sn	0.016	<0.005	<0.005	<0.005	<0.005	
Sr	0.073	0.091	0.063	0.053	0.054	7.0
Ti	0.17	0.0031	<0.001	<0.001	<0.001	0.1
V	3.1	<0.001	<0.001	<0.001	<0.001	0.1
Zn	230	6.2	0.004	0.018	0.003	1.0
Ag	<0.005	<0.005	<0.005	<0.005	<0.005	0.05
As	9.8	<0.005	<0.005	<0.005	<0.005	0.05
B	<0.01	0.013	<0.01	<0.01	<0.01	0.5
Sb	<0.005	<0.005	<0.005	<0.005	<0.005	0.05
Tl	<0.005	<0.005	<0.005	<0.005	<0.005	0.0001

ground water is in direct contact with shungite rock. The water of this sample was distinguished by dark color, muddiness, and large content of a suspended shungite material. Sample no. 2 was taken on the territory of the Zazhogino deposit from a sedimentation tank for technical water used to wash shungite. The water was also distinguished by muddiness and rather large content of a suspended material. Finally, sample no. 3 was taken from the Tsarevka River at a distance of approximately 500 m from the Zazhogino deposit. The water was slightly muddy and yellowish. Sample nos. 4 and 5 were taken from rivers running close to the Maksovo deposit: Kelei River (about 4 km from Tolvuya settlement and 0.5 km from the Maksovo deposit) and at the mouth of the Tsarevka River (Lake Onega, near Tolvuya settlement). Both these rivers flow past several shungite bedrocks. It can be seen from Table 3 that the fundamental aspects revealed in analysis of aqueous extracts from shungite are only valid for sample no. 1, i.e., for water that has been in prolonged contact with shungite rock and contains a large amount of a suspended shungite material. Compared with the others, this sample is distinguished by an exceedingly high concentration of iron and very high content of aluminum, zinc, nickel, and copper. Sample no. 2 is also characterized by increased concentrations of a number of microcomponents (Al, Cd, Co, Mn, Ni, Zn), because this water basin lies in the industrial zone and is subject to a strong technological impact. In the rest of the samples, i.e., in water from small rivers running near Zazhogino and Maksovo deposits, the maximum permissible concentrations for potable and household water [6] are not exceeded. Thus, under natural conditions, water is not enriched with microelements from shungite to any noticeable extent without its direct and prolonged contact with ground shungite rock.

Table 4. Results of a chemical analysis of shungite water

Element	Concentration, mg l^{-1}, in sample		Upper permissible consumption level, mg day^{-1}
	I	II	
V	0.82	0.42	0.1
Ca	30.0	27.0	2500
Fe	710	330	45.0
Mg	130.0	80.0	800
Cd	1.3	0.75	N/r*
K	1.6	3.4	3500
Co	2.7	1.3	0.03
Na	28.0	21.0	N/r
Mn	2.5	1.7	11.0
Se	0.49	0.25	0.15
Cu	9.8	5.8	5.0
B	0.092	0.066	6.0
Mo	0.046	0.0014	0.2
Si	10.0	5.9	10.0
As	0.074	0.020	N/r
Ti	0.019	0.0019	N/r
Ni	49.0	29.0	N/r
Be	0.016	0.010	N/r
Pb	0.20	0.69	N/r
Ba	0.015	0.022	N/r
Ag	<0.005	<0.005	0.07
Al	150.0	97.0	N/r
Sb	<0.005	<0.005	N/r
Tl	<0.005	<0.005	N/r
Cr	0.25	0.11	0.25
Sr	0.13	0.12	N/r
Zn	180.0	90.0	40.0

* No regulations.

Table 5. Results of a microbiological analysis of shungite water

Sample	Coli index	Total microbe number, colony-forming units cm^{-3}
Water from the Neva River		
before treatment	2.4×10^6	4.4×10^5
after treatment	<10	<10

To analyze the chemical composition and properties of shungite water by the methods described in [2, 7], two samples were prepared. The first method consisted in the following: a well-washed 15-g shungite sample was poured over with 25 ml of ordinary tap water and the mixture was kept at room temperature for three days. After this time, the mixture was filtered. The second sample was prepared in the same way, but, prior to being kept for three days, the mixture was boiled for 20 min. The results of chemical analyses are listed in Table 4. The same table presents for comparison values of the upper permissible consumption level of some elements, which is "the highest daily consumption level that does not exert any unfavorable influence on the health of all members of a population. When the consumption exceeds this level, the risk of unfavorable consequences becomes higher" [8].

To study the bactericidal properties of shungite and shungite water, two samples were prepared. The first sample was taken from the Neva River for comparative analysis, and the second was composed of the same water subjected to treatment with shungite by the first of the two techniques described above. The bactericidal properties of shungite water prepared by the second technique (with preliminary boiling of shungites) were not studied because most of bacteria perish in boiling, irrespective of the influence exerted on them by shungite. The study was performed[1] using the method of sanitary-microbiological analysis of water from surface reservoirs (no. 2285–91; January 19, 1981), which included determination of two basic components: total microbial number (colony-forming units cm^{-3}) and Coli index.

The results obtained are listed in Table 5. It is clearly seen that, upon interaction with shungite, water that could be named "dirty" with confidence becomes microbiologically clean. In view of the previously obtained data on leaching-out of various chemical elements, including heavy metals, from shungite, it may be suggested that just the increased concentrations of these elements are among the reasons for the bactericidal properties of shungite and shungite water.

CONCLUSIONS

(1) The interaction of ground shungite with water gives a solution with rather high concentrations of a number of microelements, including heavy matals. The shungite water prepared in accordance with techniques described in the literature exhibits bactericidal properties.

(2) The concentrations of microcomponents in aqueous extracts from shungite-III are rather high and frequently exceed the maximum permissible concentrations for potable and household water.

[1] The study was performed at the St. Petersburg Certification Center, TEST-Sankt-Peterburg Federal State Institution.

ACKNOWLEDGMENTS

The study was supported by the Federal Scientific and Technical Target Program "Research and Development in Priority Areas of Science and Technology" for the years 2002–2006 (State Contract no. 0.2.467.11.7005 of May 23, 2005).

REFERENCES

1. Rys'ev, O.A., *Shungit – kamen' zdorov'ya* (Shungite, a Health Stone), St. Petersburg: Tessa, 2001.
2. Doronina, Yu.A., *Shungit – kamen'-zagadka* (Shungite, an Enigma Stone), St. Petersburg: Nevskii Prospekt, 2001.
3. Sokolov, V.A., Kalinin, Yu.K., and Dyukkiev, E.F., *Shungity – novoe uglerodistoe syr'e* (Shungites, a New Kind of Carbon Raw Materials), Petrozavodsk: Karel'sk. Filial Akad. Nauk SSSR, 1984.
4. Filippov, M.M., *Shungitonosnye porody Karelii* (Shungite Rock of Karelia), Petrozavodsk: Karel'sk. Nauchn. Tsentr Ross. Akad. Nauk, 2004.
5. Goncharov, G.N., Kalinin, A.I., and Skorobogatov, G.A., *Zh. Obshch. Khim.*, 1993, vol. 64, no. 2, pp. 203–207.
6. Bespamyatnov, G.P. and Krotov, Yu.A., *Predel'no dopustimye kontsentratsii khimicheskikh veshchestv v okruzhayushchei srede: Spravochnik* (Maximum Permissible Concentrations of Chemical Substances in the Environment: Reference Book), Leningrad: Khimiya, 1985.
7. Orlov, A.D., *Shungit – kamen' chistoi vody* (Shungite, a Pure-Water Stone), St. Petersburg: Dilya, 2004.
8. *MR* (Methodological Recommendations) *2.3.1.19 150–04: Recommended Consumption Levels of Nutritional and Biologically Active Substances*, Moscow, 2004.

ISSN 1070-4272. Russian Journal of Applied Chemistry, 2006, Vol. 79, No. 1, pp. 34–37. © Pleiades Publishing, Inc., 2006.
Original Russian Text © E.D. Totchasov, M.Yu. Nikiforov, G.A. Al'per, 2006, published in Zhurnal Prikladnoi Khimii, 2006, Vol. 79, No. 1, pp. 35–38.

PHYSICOCHEMICAL STUDIES OF SYSTEMS AND PROCESSES

Calculation of Heat Capacity of Systems *n*-Alkanol–*n*-Alkane

E. D. Totchasov, M. Yu. Nikiforov, and G. A. Al'per

Institute of Chemistry of Solutions, Russian Academy of Sciences, Ivanovo, Russia

Received January 13, 2005; in final form, August 2005

Abstract—A method was suggested for calculating the molar heat capacity of *n*-alkanol–*n*-alkane solutions with account of the molecular association by the free-volume theory from data on the viscosity of these systems.

DOI: 10.1134/S1070427206010071

The heat capacity belongs to the most important thermodynamic properties of a solution. The study of heat capacity is urgent from both applied (to calculate the thermal regimes of reactors and choose heat carriers) and basic viewpoint (in view of the role of the heat capacity in solution thermodynamics) [1].

For *n*-alkanol–*n*-alkane mixtures, the heat capacity has been studied to a considerably lesser extent than other physicochemical properties. Therefore, the calculation of the heat capacity by using quantitative property–property relationships is an urgent problem. In our previous study [2], a method was suggested for calculating the viscosity of *n*-alkanol–*n*-alkane solutions with account of the molecular association by the free-volume theory. In this study, we used the data on viscosity of *n*-alkanol–*n*-alkane solutions to calculate their heat capacity with account of the molecular association by the free-volume theory. The calculation method was tested with the experimentally studied [3] 1-pentanol–*n*-decane system and with systems ethanol–*n*-heptane, 1-propanol–*n*-heptane, 1-propanol–*n*-hexane, 1-butanol–*n*-heptane, and 1-butanol–*n*-decane, for which the heat capacity and viscosity values required for the calculation are available from the literature [3–8].

One of the semiempirical methods for describing the viscosity of liquids that obviate fitting parameters is the free-volume theory relating the viscosity to the so-called reduced volume $\tilde{V}$ [9]:

$$\Delta\ln\eta = \frac{1}{\tilde{V} - 1} - \frac{x_A}{\tilde{V}_A - 1} - \frac{x_B}{\tilde{V}_B - 1}, \quad (1)$$

where $\Delta\ln\eta = \ln\eta - x_A\ln\eta_A - x_B\ln\eta_B$, η_A and η_B are the dynamic viscosities of components A and B, respectively; $\tilde{V} = V/V^*$, $\tilde{V}_A = V_A/V_A^*$, and $\tilde{V}_B = V_B/V_B^*$ are the reduced volumes of the solution and of components A and B, respectively; x_A and x_B are the mole fractions of components A and B, respectively; V, V_A, and V_B are the molar volumes of the solution and of components A and B, respectively; V^*, V_A^*, and V_B^* are the volumes of the solution occupied by the liquid molecule (the occupied volume) and of components A and B, respectively.

The free-volume concept, applicable to both thermodynamic and kinetic properties, makes it possible to find a quantitative relationship between the heat capacity and viscosity of liquid mixtures. The excess molar volume V^E($V^E = V - V_A x_A - V_B x_B$) incorporates the chemical term V^E_{chem} and the physical term V^E_{phys} [10].

$$V^E = V^E_{chem} - V^E_{phys}, \quad (2)$$

$$V^E_{chem} = \tilde{V}V^E_{assoc} = \tilde{V}\Delta V^0(1 - K\varphi_A)/S = H^E_{assoc}(\Delta V^0/\Delta H^0)\tilde{V}, \quad (3)$$

where S is the average degree of association; K, association constant of 1-alkanol; φ_A, volume fraction of 1-alkanol; and H^E, enthalpy of mixing.

The standard enthalpy of association ΔH^0 for *n*-alkanols is taken as –25.1 kJ mol^{-1}, and the change in the volume in association, as $\Delta V^0 = -5.6$ cm^3 mol^{-1} [10]. The subscript assoc at the excess thermodynamic quantity stands for the association processes.

In any accepted molecular association model, it is preferable to calculate the parameter

$$(\partial V^E_{assoc}/\partial T) = (C^E_p)_{assoc}(\Delta V^0/\Delta H^0) \quad (4)$$

from the experimental viscosity values rather than from those obtained from theoretical models. Analysis of a large body of the experimental data [11] showed that the dependences of C_p^E on the composition in *n*-alkanol–*n*-alkane solutions are determined solely by the chemical term $(C_p^E)_{assoc}$ (except for the areas with small *n*-alkane concentration); the same is true for $(\partial V^E/\partial T)$. Then,

$$(\partial V^E_{chem}/\partial T)_p = \tilde{V} C_p^E (\Delta V^0/\Delta H^0) + (\partial \tilde{V}^E_{chem}/\partial T) H^E_{assoc} (\Delta V^0/\Delta H^0). \quad (5)$$

Compared to the first term, the second term is smaller by an order of magnitude. As a result, we obtain

$$(\partial V^E_{chem}/\partial T)_p \cong \tilde{V} C_p^E (\Delta V^0/\Delta H^0). \quad (6)$$

For C_p^E with account of relation (6) we have

$$C_p^E = \frac{V^* \Delta H^0 [\alpha - V^{-1}(x_A \alpha_A V_A + x_B \alpha_B V_B)]}{\Delta V^0}, \quad (7)$$

where α, α_A, and α_B are the volume expansion coefficients of the solution, *n*-alkanol, and *n*-alkane, respectively.

For pure solvents, the α values are known, whereas for mixtures, as a rule, they are lacking. To calculate the volume expansion coefficient in terms of the Flory theory [12], it is necessary to know the reduced volume of solution $\tilde{V}$, which can be determined by substituting the dynamic viscosity values in formula (1). Then, from the known value of $\tilde{V}$ we can calculate α of the solution by the formula

$$\alpha = \frac{3(1 - \tilde{V}^{1/3})}{(3\tilde{V}^{1/3} - 4)T}. \quad (8)$$

To calculate the occupied volume of the solution V^* by formula (7), we used the Kretschmer–Wiebe's model of continuous association [10]. This model takes into account that the alcohol molecules form chains of associates $A_n + A_1 \rightleftarrows A_{n+1}$, where the length of the chain *n* can acquire infinitely large values ($n \div \infty$), with the association constant satisfying the relation $K_n = [(n + 1)/n]K$. In view of the fact that the occupied volume is physically an additive parameter, for the binary mixture, taking into account the 1-alkanol association, we obtain

$$V^* = (V^*_{A_1} + \Delta V^0 K \varphi_{A_1}) x_A + V^*_B x_B, \quad (9)$$

where V^*_A is the mole fraction of a hypothetical liquid of monomers and φ_{A_1} is the volume fraction of the monomers in the mixture, which is determined by the relation

$$\varphi_{A_1} = [2K\varphi_A + 1 - (4K\varphi_A + 1)^{1/2}]/2K^2\varphi_A. \quad (10)$$

The V^*_{A1} and K values were taken from [10]. They are presented in Table 1 along with other properties of 1-alkanols and *n*-alkanes.

Table 1. Properties and parameters of pure components at T = 298.15 K [10]

Component	K	V	$V^*_{A_1}$	V^*
		$cm^3\ mol^{-1}$		
Ethanol	317	58.66	52.19	46.90
1-Propanol	197	75.12	66.32	61.09
1-Butanol	175	91.98	80.89	75.70
1-Pentanol	153	108.7	95.27	90.10
n-Hexane	–	131.6	–	99.34
n-Heptane	–	144.5	–	111.5
n-Decane	–	195.9	–	155.9

Substituting the α and V^* values calculated by formulas (8) and (9), respectively, in formula (7), we will determine C_p^E of the solution and, from this quantity, the molar heat capacity:

$$C_p = C_p^E + C_{p_A} x_A + C_{p_B} x_B, \quad (11)$$

where C_{p_A} and C_{p_B} are the molar heat capacities of 1-alkanol and *n*-alkane, respectively.

As example, we will calculate the molar heat capacity for the system 1-propanol–*n*-hexane at the mole fraction x_A = 0.102.

(1) Using formula (10), we determine the mole fraction of 1-propanol monomers in the system φ_{A_1} (for 1-propanol K = 197 at T = 298.15 K [10], φ_A = 0.061):

$$\varphi_{A_1} = \frac{2K\varphi_A + 1 - (4K\varphi_A + 1)^{1/2}}{2K^2\varphi_A} = 0.004727.$$

(2) Using formula (9), we calculate the occupied volume of the binary mixture at T = 298.15 K (for 1-propanol, $V^*_{A_1}$ = 66.32 [10], ΔV^0 = –5.6 [10], V^*_B = 99.34 $cm^3\ mol^{-1}$ [10]):

$$V^* = (V^*_{A_1} + \Delta V^0 K \varphi_{A_1}) x_A + V^*_B x_B = 95.440\ cm^3\ mol^{-1}.$$

(3) Using formula (8), we determine the reduced

Table 2. Experimental and calculated molar heat capacities C_p for different systems at T = 298.15 K

x_A, mole fraction	C_p(exp)	C_p(calc)
	J mol^{-1} K^{-1}	
1-Butanol (A)–*n*-decane (B)		
0.213	298.51 [4]	299.01
0.463	264.46 [4]	264.94
0.510	257.59 [4]	257.94
0.585	246.43 [4]	246.65
0.874	198.00 [4]	197.45
1-Pentanol (A)–*n*-decane (B)		
0.185	304.99 [3]	304.57
0.336	296.99 [3]	296.66
0.560	274.70 [3]	274.49
0.653	262.20 [3]	262.01
0.841	233.00 [3]	232.96
Ethanol (A)–*n*-heptane (B)		
0.0997	223.80 [5]	223.73
0.1915	215.11 [5]	215.36
0.2606	207.65 [5]	208.07
0.3249	200.42 [5]	200.49
0.4012	191.59 [5]	191.78
0.4930	181.22 [5]	181.28
0.6006	166.54 [5]	166.67
0.6997	153.51 [5]	153.36
0.8010	139.90 [5]	139.63
1-Propanol (A)–*n*-heptane (B)		
0.0919	227.98 [5]	228.28
0.2269	219.53 [5]	220.36
0.3400	210.93 [5]	211.41
0.4038	205.72 [5]	206.19
0.5210	195.01 [5]	195.33
0.5980	187.34 [5]	187.74
0.6616	180.83 [5]	180.98
0.7849	167.93 [5]	167.95
0.8790	157.35 [5]	157.41
1-Butanol (A)–*n*-heptane (B)		
0.0852	230.91 [5]	231.05
0.1620	228.91 [5]	228.98
0.2260	226.57 [5]	226.64
0.3751	219.84 [5]	219.87
0.4869	213.96 [5]	214.01
0.5924	207.48 [5]	207.48
0.6828	201.28 [5]	201.32
0.7617	195.48 [5]	195.45
1-Propanol (A)–*n*-hexane (B)		
0.1020	207.29 [6]	207.54
0.2020	203.40 [6]	203.96
0.2885	198.38 [6]	198.55
0.5032	183.95 [6]	184.04
0.6477	172.89 [6]	173.58
0.8011	161.39 [6]	161.36

volumes of 1-propanol and *n*-hexane (the volume expansion coefficient taking into account the association is α_A = 0.000914 K^{-1} for 1-propanol [10] and α_B = 0.001385 K^{-1} for *n*-hexane [10]; T = 298.15 K):

$$\tilde{V}_A = [\alpha_A T/3(1 + \alpha_A T) + 1]^3 = 1.22980,$$

$$\tilde{V}_B = [\alpha_B T/3(1 + \alpha_B T) + 1]^3 = 1.32165.$$

(4) We determine the reduced volume of the solution by relationship (1) (for a given composition, $\Delta\ln\eta$ = –0.1224 [13]):

$$\tilde{V} = \frac{1 + \Delta\ln\eta + x_A/(\tilde{V}_A - 1) + x_B/(\tilde{V}_B - 1)}{\Delta\ln\eta + x_A/(\tilde{V}_A - 1) + x_B/(\tilde{V}_B - 1)} = 1.32120.$$

(5) Using relationship (8), we calculate the volume expansion coefficient of the solution:

$$\alpha = \frac{3(1 - \tilde{V}^{1/3})}{(3\tilde{V}^{1/3} - 4)T} = 0.0013825.$$

(6) Using formula (7), we determine C_p^E (J mol^{-1} K^{-1}) of the solution (ΔH^0 = –25.1 kJ mol^{-1} [10]; the 1-propanol–*n*-hexane solution of the given composition at T = 298.15 K has the molar volume V = 126.022 cm^3 mol^{-1} [13], α = 0.0013825 K^{-1}):

$$C_p^E = \frac{V^*\Delta H^0[\alpha - V^{-1}(x_A\alpha_A V_A + x_B\alpha_B V_B)]}{\Delta V^0}$$

$$= 12.055 \text{ J mol}^{-1}\text{ K}^{-1}.$$

(7) By formula (11), we determine the molar heat capacity of the given solution (at T = 298.15 K, 1-propanol has the molar heat capacity C_{pA} = 143.9 J mol^{-1} K^{-1} [6] and *n*-hexane, C_{pB} = 201.34 J mol^{-1} K^{-1} [6]):

$$C_p = C_p^E + C_{pA}x_A + C_{pB}x_B = 207.54 \text{ J mol}^{-1}\text{ K}^{-1}.$$

CONCLUSIONS

(1) The calculated heat capacities are in good agreement with the experimental data (Table 2). The average error in calculating the heat capacity is 0.046 and the maximum error, 0.31%. The relationship between the heat capacity and viscosity of nonelectrolyte systems was studied for the first time by the example of 1-alkanol–*n*-alkane solution. In other words, a method was suggested for calculating the heat capacity of 1-alkanol–*n*-alkane systems from data on their viscosity.

(2) For practical purposes, the heat capacity of nonelectrolyte systems can be calculated from data on their properties.

REFERENCES

1. Belousov, V.P., Morachevskii, A.G., and Panov, M.Yu., *Teplovye svoistva rastvorov neelektrolitov* (Thermal Properties of Nonelectrolyte Solutions), Leningrad: Khimiya, 1981.
2. Totchasov, E.D., Nikiforov, M.Yu., Luk'yanchikova, I.A., and Al'per, G.A., *Zh. Prikl. Khim.*, 2001, vol. 74, no. 5, pp. 797–804.
3. Totchasov, E.D., Luk'yanchikova, I.A., Nikiforov, M.Yu., and Al'per, G.A., *Zh. Fiz. Khim.*, 2000, vol. 74, no. 2, pp. 225–228.
4. Kehiaian, H.V., and Renon, H., *Measurement, Evaluation and Prediction of Phase Equilibria: Studies in Modern Thermodynamics*, Amsterdam: Elsevier, 1986, part 6.
5. Tanaka, R., Toyama, S., and Murakami, S., *J. Chem. Thermodyn.*, 1986, vol. 18, no. 1, pp. 63–73.
6. Kalinowska, B., Jedlinska, J., Steski, J., and Woycicki W., *J. Chem. Thermodyn.*, 1981, vol. 13, pp. 357–366.
7. Papaioannou, D., and Panayiotou, C., *J. Chem. Eng. Data*, 1994, vol. 39, no. 3, pp. 463–466.
8. Franjo, C., Jimenes, E., Iglesias, T.P., *et al.*, *J. Chem. Eng. Data*, 1995, vol. 40, no. 1, pp. 68–70.
9. Cohen, M.H., and Turnbull, D., *J. Chem. Phys.*, 1959, vol. 31, no. 5, pp. 1164–1169.
10. Heintz, A., *Ber. Bunsenges. Phys. Chem.*, 1985, vol. 89, no. 2, pp. 172–181.
11. Treszczanowicz, A.J., Kiyohara, O., and Benson, G.C., *J. Chem. Thermodyn.*, 1981, vol. 13, pp. 253–260.
12. Flory, P.J., Orwoll, R.A., and Vrij, A., *J. Am. Chem. Soc.*, 1964, vol. 86, no. 17, pp. 3507–3514.
13. Orge, B., Iglesias, M., Rodriguez, A., *et al.*, *Fluid Phase Equil.*, 1997, vol. 133, pp. 213–227.

ISSN 1070-4272. Russian Journal of Applied Chemistry, 2006, Vol. 79, No. 1, pp. 38–42. © Pleiades Publishing, Inc., 2006.
Original Russian Text © V.P. Korolev, N.L. Smirnova, N.A. Litova, 2006, published in Zhurnal Prikladnoi Khimii, 2006, Vol. 79, No. 1, pp. 39–43.

PHYSICOCHEMICAL STUDIES OF SYSTEMS AND PROCESSES

Calorimetric Study of Solvation of Alkanes with Mixtures of Acetone or 1,4-Dioxane with 1-Octanol at 25°C

V. P. Korolev, N. L. Smirnova, and N. A. Litova

Institute of Chemistry of Solutions, Russian Academy of Sciences, Ivanovo, Russia
Ivanovo State University of Chemical Engineering, Ivanovo, Russia

Received July 27, 2005

Abstract—Heats of solution of cyclohexane and squalane in mixtures of 1-octanol with acetone or 1,4-dioxane within the entire range of compositions were measured calorimetrically. The enthalpies of solution of cyclohexane, squalane, and hexadecane in the mixtures of acetone or 1,4-dioxane with 1-octanol show linear correlation. Enthalpies of solvation of propane, decane, and eicosane in these mixtures were calculated.

DOI: 10.1134/S1070427206010083

Alkanes are the simplest organic compounds. Only a few papers concern the thermochemistry of solution of alkanes in binary nonaqueous solvents [1–6]. In this study, we took a cyclic alkane, cyclohexane, and a branched alkane, squalane (2,6,10,15,19,23-hexamethyltetracosane), which is a liquid (mp 38°C) with a high molecular weight and a low volatility; this simplifies the calorimetric experiment. Squalane is widely used in gas–liquid chromatography as a stationary phase [7–9], in medicine for treatment of burns [10], and as a constituent of pharmaceuticals, perfumes, and cosmetics.

We took as one of solvents 1-octanol, which, along with octane, chloroform, and propylene glycol dipelargonate, constitutes the so-called "critical quartet" [11, 12] used to provide better correlation of the distribution coefficients of biologically active substances (including medicinal preparations) between water and nonaqueous solvent with their ability to penetrate through cell membranes. 1,4-Dioxane, similarly to ethers, has low dielectric constant and in this respect can be classed with low-polarity solvents. However, the standard heats of solution of alkanes in dioxane and ethers differ very strongly. For instance, for hexadecane in dibutyl ether it is as low as 1.80 kJ mol^{-1} [13], whereas in dioxane it is by an order of magnitude higher [4, 14, 15]. Thus, dioxane and ethers are located at the opposite ends of the solvency scale with respect to alkanes. Acetone as an object of the investigation was taken because of its wide application.

In this study, we measured the enthalpies of solution of cyclohexane and squalane in mixtures of acetone or 1,4-dioxane with 1-octanol.

EXPERIMENTAL

Integral heats of solution were measured on an ampule-type variable-temperature calorimeter equipped with an isothermal jacket and 60 cm^3 reaction vessel. The procedure of the calorimetric experiment was the same as in [16, 17]. The thermometric and thermal sensitivities of the device were 5×10^{-6} deg and 5×10^{-3} J per mm of the recorder scale, respectively.

The solvents used were purified as in [18]. The water content in 1-octanol was monitored by Fischer titration [19] and was no more than 0.03 wt %. Chromatographically pure grade cyclohexane and squalane (Merck) were used without additional purification.

The arithmetical mean heats of solution ($\Delta_s H^m$) were taken as standard enthalpies of solution of the compounds ($\Delta_s H^0$) (Table 1), because the difference between these values was within the limits of the experimental error, which was estimated at 2–3%.

The standard enthalpies of solution of cyclohexane in 1-octanol that we measured well coincide with the published value, 1.88 kJ mol^{-1} [20]. To check the squalane quality, we measured the enthalpy of its solution in chloroform and CCl_4. The data obtained are in good agreement with the published values [21] (in parentheses): 11.10 ± 0.08 (11.12 ± 0.05) and 4.84 ± 0.08 (4.67 ± 0.08) kJ mol^{-1}, respectively.

The data obtained are listed in Table 1. They were

Table 1. Enthalpies of solution (ΔH^m, kJ mol^{-1}) of cyclohexane and squalane in mixtures of acetone or 1,4-dioxane with 1-octanol at 25°C

Alkane	Acetone–1-octanol			1,4-Dioxane–1-octanol		
	X_2	$m\times 10^3$, mol kg^{-1}	$\Delta_s H^m$, J mol^{-1}	X_2	$m\times 10^3$, mol kg^{-1}	$\Delta_s H^m$, kJ mol^{-1}
Cyclohexane	0.00	44	7.11	0.00	21	5.51
		90	7.15		40	5.55
	0.201	48	4.62	0.200	60	4.32
		120	4.55		166	4.29
	0.499	84	3.99	0.499	64	2.72
		170	3.89		140	2.71
	0.799	67	1.98	0.800	68	1.96
		119	1.93		157	1.92
	1.00	17	1.58			
		32	1.62			
Squalane	0.00	19	26.92	0.00	5	28.01
		23	27.12		5	27.80
		37	27.10		13	27.68
	0.204	6	16.98	0.200	6	16.64
		9	17.01		12	16.62
	0.372	8	11.44	0.392	6	11.12
		8	11.28		7	11.03
	0.620	5	7.46	0.587	8	7.47
		12	7.34		8	7.44
	0.798	7	5.80	0.791	12	5.56
		13	5.93		18	5.48
	1.00	13	4.68			
		16	4.76			
		31	4.66			

* (X_2) Mole fraction of 1-octanol; (m) molality, mol per kg of solvent.

Table 2. Coefficients of polynomials $\Delta H^0 = A_0 + A_1X_2 + (A_2 + A_3X_2)X_1X_2$ describing the enthalpies of solution of cyclohexane and squalane in mixed solvents at 25°C

System	A_0	A_1	A_2	A_3	S,* kJ mol^{-1}
Acetone–1-octanol (cyclohexane)	6.83	–5.23	–3.28	–	0.50
1,4-Dioxane–1-octanol (cyclohexane)	5.55	–3.93	–3.22	–	0.06
Acetone–1-octanol (squalane)	27.06	–22.35	–39.63	23.66	0.14
1,4-Dioxane–1-octanol (squalane)	27.76	–23.11	–43.80	26.76	0.25

* (S) Standard deviation.

approximated by Eqs. (1)–(3):

$$\Delta_s H^0 = A_0 + A_1X_2 + A_2X_1X_2, \quad (1)$$

$$\Delta_s H^0 = A_0 + A_1X_2 + (A_2 + A_3X_1X_2)X_1X_2, \quad (2)$$

$$\Delta_s H^0 = B_0 + B_1\Phi_2 + B_2\Phi_1\Phi_2, \quad (3)$$

where X_2 and Φ_2 are mole and volume fractions of 1-octanol, respectively. The coefficients of these equations are listed in Tables 2 and 3.

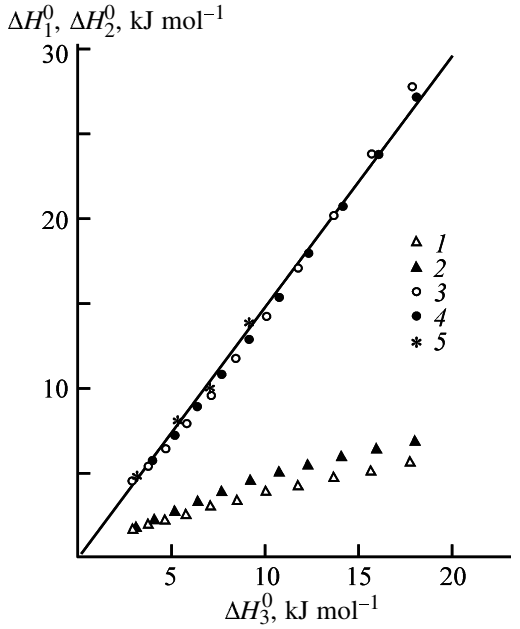
In Eqs. (1)–(3), the sum of the first and second terms is equal to the additive value of the enthalpy of solution, and the third term is equal to excess enthalpy of solution, described by the Redlich–Kister equation [22]. Representation of the experimental data in the form of approximating function allows estimation of the smoothness of the experimental dependences, reproducibility of measurements, and random error; it also allows compact storage of the experimental data (22).

Table 3. Coefficients of polynomials $\Delta H^0 = B_0 + B_1\Phi_2 + B_2\Phi_1\Phi_2$ describing the enthalpies of solution of squalane in the mixed solvents at 25°C

System	B_0	B_1	B_2	S, kJ mol^{-1}
Acetone–1-octanol	27.14	–22.55	–11.40	0.29
1,4-Dioxane–1-octanol	27.83	–23.18	–17.53	0.13

As seen from Tables 2 and 3, transition from mole to volume fractions allows the power of the approximation function in the case of squalane to be decreased without noticeable worsening of the description. For hexadecane in the mixed solvents [5, 6], transition from X to Φ also leads to improvement of description and decrease in the polynomial power. However, for cyclohexane, probably because of small size or cyclic structure of its molecule, transition from mole to volume fractions does not improve the description of the experiment. Therefore, in further calculations, we used Eq. (1) for cyclohexane and Eq. (3) for squalane.

A linear correlation between the enthalpies of solution of squalane and cyclohexane in isomeric butanols and in 1-octanol was found in [23]. It is of interest to examine similar dependences for solvents considered in this study. The correlations of the enthalpies of solution of cyclohexane and squalane with those of hexadecane are shown in the figure. The enthalpies of solution of cyclohexane in the mixtures studied (including their separate components) were calculated by Eq. (1) with the coefficients taken in Table 2. The enthalpies of solution of squalane were calculated by Eq. (3) with the coefficients from Table 3. The enthalpies of solution of hexadecane in acetone–1-octanol and 1,4-dioxane–1-octanol mixtures (step 0.1 volume fraction), including separate components of the mixed solvent, were calculated by Eq. (3) with the coefficients taken from [5, 6]. As seen from the figure, the correlation between the enthalpies of solution of squalane and those of hexadecane in acetone–1-octanol and 1,4-dioxane–1-octanol mixtures is linear (correlation coefficient R 0.9974). The points corresponding to the enthalpies of solution of squalane in *n*-OctOH, *n*-BuOH, *i*-BuOH, and *t*-BuOH [23] also fall on this line. Data on the enthalpies of solution of hexadecane in the above alcohols were taken from [24, 25]. The linear correlations of the enthalpies of solution of cyclohexane in acetone–1-octanol (R = 0.942) and in 1-octanol–1,4-dioxane (R = 0.995) are different.



Correlation of the enthalpies of solution of cyclohexane ΔH_1^0 in (*1*) 1,4-dioxane–1-octanol and (*2*) acetone–1-octanol mixtures, squalane ΔH_2^0 in (*3*) 1,4-dioxane–1-octanol and (*4*) acetone–1-octanol mixtures, and (*5*) squalane in *n*-OctOH, *n*-BuOH, *i*-BuOH, and *t*-BuOH with those of hexadecane ΔH_3^0. (*1–4*) Calculated by Eqs. (1) and (3); (*5*) experimental.

Stephenson and Fuchs [13] found that the enthalpies of solvation ($\Delta_{solv}H^0$) of *n*-alkanes (C_5–C_{16}) in various solvents are linear functions of the number of carbon atoms in the alkane molecule (N_C). Using the experimental data from [13–15, 26], they obtained linear correlations (4)–(6) of the enthalpies of solvation (kJ mol^{-1}) of *n*-alkanes in acetone, 1,4-dioxane, and 1-octanol, respectively, with N_C of alkane:

$$\Delta_{solv}H^0 = -1.0 - 3.86N_C;\ R = 0.9999,\ S = 0.25, \quad (4)$$

$$\Delta_{solv}H^0 = -0.6 - 3.88N_C;\ R = 0.9999,\ S = 0.09, \quad (5)$$

$$\Delta_{solv}H^0 = -1.7 - 4.80N_C;\ R = 0.9999,\ S = 0.10. \quad (6)$$

We obtained linear correlations of the enthalpies of solution of two linear (C_{11} and C_{16}) and one branched (C_{30}) alkanes in acetone with those in 1,4-dioxane:

$$\Delta_s H^0(Me_2CO) = -0.98\Delta_s H^0(C_4H_8O_2);\ R = 0.9995,$$

$$S = 0.23. \quad (7)$$

Table 4. Calculated enthalpies of solvation of alkanes by binary solvents at 25°C

Φ_2*	Acetone–1-octanol			1,4-Dioxane–1-octanol		
	$\Delta_{solv}H^0$, kJ mol^{-1}					
	C_3H_8	$C_{10}H_{22}$	$C_{20}H_{42}$	C_3H_8	$C_{10}H_{22}$	$C_{20}H_{42}$
0.0	–12.4	–39.5	–78.1	–12.4	–39.6	–78.3
0.1	–12.9	–40.8	–80.7	–13.0	–41.0	–81.1
0.2	–13.4	–42.1	–83.1	–13.5	–42.4	–83.8
0.3	–13.8	–43.3	–85.5	–13.9	–43.7	–86.2
0.4	–14.2	–44.4	–87.6	–14.3	–44.9	–88.4
0.5	–14.6	–45.5	–89.6	–14.7	–45.9	–90.5
0.6	–14.9	–46.5	–91.5	–15.1	–46.9	–92.3
0.7	–15.2	–47.4	–93.2	–15.4	–47.7	–94.0
0.8	–15.5	–48.2	–94.8	–15.6	–48.5	–95.4
0.9	–15.8	–48.9	–96.3	–15.9	–49.1	–96.7
1.0	–16.0	–49.6	–97.6	–16.1	–49.7	–97.7

* (Φ_2) Mole fraction of 1-octanol.

Using Eqs. (4)–(6), we calculated the enthalpies of solvation of propane, decane, and eicosane in acetone, 1,4-dioxane, and 1-octanol and then found linear correlations of the enthalpies of solvation of propane [Eq. (8)], decane [Eq. (9)], and eicosane [Eq. (10)] in acetone–1-octanol and 1,4-dioxane–1-octanol mixtures with the enthalpies of solution of hexadecane in the same mixtures:

$$\Delta_{solv}H^0 = -16.78 + 0.243\Delta_sH^0;\ R = 0.9941,\ S = 0.33; \quad (8)$$

$$\Delta_{solv}H^0 = -51.66 + 0.678\Delta_sH^0;\ R = 0.9990,\ S = 0.30; \quad (9)$$

$$\Delta_{solv}H^0 = -101.50 + 1.30\Delta_sH^0;\ R = 0.9998,\ S = 0.26. \quad (10)$$

Equations (4)–(6) and (8)–(10) allow calculation of the enthalpies of solvation of alkanes over the entire range of compositions of acetone–1-octanol and 1,4-dioxane–1-octanol mixtures without carrying out the experiment. The results of the calculation for propane, decane, and eicosane are listed in Table 4. Propane is a gas and eicosane (C_{20}) is solid under the common conditions, which complicates the comparative calorimetric experiment. Therefore, we calculated the enthalpies of solvation (but not solution). We calculated the enthalpies of solvation by Eq. (11)

$$\Delta_{solv}H^0 = \Delta_sH^0 - \Delta_vH^0, \quad (11)$$

where Δ_vH^0 is the enthalpy of vaporization. The required data on the heats of vaporization were taken from [27].

CONCLUSIONS

(1) Enthalpies of solution of cyclohexane and squalane in mixtures of acetone or 1,4-dioxane with 1-octanol were determined experimentally.

(2) Linear dependences between the enthalpies of solution of branched (squalane), cyclic (cyclohexane), and linear (hexadecane) alkanes in the above mixtures were found.

(3) Enthalpies of solvation of propane, decane, and eicosane in the mixtures studied were calculated.

REFERENCES

1. Krishnan, C.V. and Friedman, H.L., *J. Phys. Chem.*, 1971, vol. 75, no. 23, pp. 3598–3606.
2. Kondo, Y., Ytton, M., and Kusabayashi, S., *J. Chem. Soc., Faraday Trans. I*, 1982, vol. 78, no. 9, pp. 2793–2806.
3. Kondo, Y., Uematsu, R., Nakamura, Y., *et al.*, *J. Chem. Soc., Faraday Trans. I*, 1988, vol. 84, no. 1, pp. 111–116.
4. Litova, N.A., Potokina, N.L., Bushuev, Yu.G., and Korolev, V.P., *Zh. Obshch. Khim.*, 1998, vol. 68, no. 2, pp. 239–243.
5. Potokina, N.L. and Korolev, V.P., *Zh. Obshch. Khim.*, 2001, vol. 71, no. 11, pp. 1775–1784.
6. Smirnova, N.L. and Korolev, V.P., *Zh. Fiz. Khim.*, 2004, vol. 78, no. 3, pp. 417–423.
7. Layla, A., *J. Chem. Eng. Data*, 1998, vol. 31, no. 4, pp. 122–126.

8. Cruickshank, A., Everett, D.H., and Westaway, M.T., *J. Chem, Soc., Faraday Trans. II*, 1965, vol. 61, pp. 235–243.
9. Nabivach, V.M., *Zh. Fiz. Khim.*, 1992, vol. 66, no. 3, p. 824.
10. US Patent 5210101.
11. Pugh, W.J., Roberts, M.S., and Hadgraft, J., *Int. J. Pharm.*, 1996, vol. 138, p. 149.
12. Leahy, D.E., Morris, J.J., and Taylor, P.J., *J. Chem. Soc., Perkin Trans. II*, 1992, p. 723.
13. Stephenson, W.K. and Fuchs, R., *Can. J. Chem.*, 1985, vol. 63, no. 2, pp. 349–352.
14. Solomonov, B.N., Antipin, I.S., Gorbachuk, V.V., and Konovalov, A.I., *Zh. Obshch. Khim.*, 1982, vol. 52, no. 10, pp. 2154–2160.
15. Kulikov, M.V., Kropotova, M.Yu., and Korolev, V.P., *Zh. Obshch. Khim.*, 1997, vol. 67, no. 12, pp. 1953–1958.
16. Manin, N.G., Korolev, V.P., and Krestov, G.A., *Zh. Obshch. Khim.*, 1991, vol. 61, no. 6, pp. 1301–1305.
17. Korolev, V.P., Batov, D.V., Vandyshev, V.N., and Krestov, G.A., *Zh. Fiz. Khim.*, 1983, vol. 57, no. 1, pp. 253–254.
18. Weissberger, A. and Proskauer, E.S., *Organic Solvents. Physical Properties and Methods of Purification*, Riddick, J.A., and Toops, E.E., Eds., New York: Interscience, 1955.
19. Klimova, V.A., *Osnovnye mikrometody analiza organicheskikh soedinenii* (Main Micromethods of Analysis of Organic Compounds), Moscow: 1967.
20. Stephenson, W.K., and Fuchs, R., *Can. J. Chem.*, 1985, vol. 63, no. 9, pp. 336–341.
21. Burchfield, T.E. and Bertrand, G.L., *J. Solution Chem.*, 1975, vol. 4, no. 3, pp. 205–214.
22. Perelygin, I.S., Kimtis, L.L., Chizhik, V.I., *et al.*, *Eksperimental'nye metody khimii rastvorov: spektroskopiya i kalorimetriya* (Experimental Methods of Solution Chemistry: Spectroscopy and Calorimetry), Moscow: Nauka, 1995.
23. Litova, N.A. and Korolev, V.P., *Zh. Obshch. Khim.*, 2001, vol. 71, no. 5, pp. 749–753.
24. Batov, D.V., Potkina, N.L., and Korolev, V.P., *Zh. Obshch. Khim.*, 1998, vol. 68, no. 10, pp. 1630–1637.
25. Potkina, N.L., Litova, N.A., and Korolev, V.P., *Izv. Ross. Akad. Nauk, Ser. Khim.*, 1999, vol. 48, no. 2, pp. 271–273.
26. Kropotova, M.Yu., Kulikov, M.V., and Korolev, V.P., *Zh. Obshch. Khim.*, 1996, vol. 66, no. 9, pp. 1424–1428.
27. Nicolic, A.D., *J. Solution Chem.*, 1993, vol. 22, no. 3, pp. 253–262.

ISSN 1070-4272. Russian Journal of Applied Chemistry, 2006, Vol. 79, No. 1, pp. 43–49. © Pleiades Publishing, Inc., 2006.
Original Russian Text © R.G. Makitra, G.G. Midyana, E.Ya. Pal'chikova, 2006, published in Zhurnal Prikladnoi Khimii, 2006, Vol. 79, No. 1, pp. 44–50.

PHYSICOCHEMICAL STUDIES OF SYSTEMS AND PROCESSES

Regular Trends in Distribution of Substituted Benzoic Acids between Organic Solvents and Water

R. G. Makitra, G. G. Midyana, and E. Ya. Pal'chikova

Institute of Geology and Geochemistry of Fossil Fuels, National Academy of Sciences of Ukraine, Lviv, Ukraine
Division of Physical Chemistry of Fossil Fuels, Litvinenko Institute of Phyiscal Organic and Coal Chemistry, National Academy of Sciences of Ukraine, Lviv, Ukraine

Received April 5, 2005

Abstract—The influence of physicochemical properties of organic solvents on the distribution constants of aromatic carboxylic acids between the organic and aqueous phases was examined.

DOI: 10.1134/S1070427206010095

Substituted benzoic acids are intermediates in the synthesis of numerous organic compounds, including precursors of dyes and drugs. As a rule, syntheses of substituted benzoic acids or particular steps (nitration, reduction) are performed in the aqueous phase. Therefore, recovery of substituted benzoic acids from the aqueous phase with organic solvents is important from both technological and environmental viewpoints. Although available data on the distribution constants K_d of substituted benzoic acids between organic and aqueous phases are numerous, no reliable quantitative relationships between K_d and physicochemical characteristics of the extractants are known. Such relationships would allow prediction of K_d for other solvents, not tested experimentally, and thus would allow purposeful choice of appropriate solvents for the extraction.

We showed in [1, 2] that the logarithms of the distribution constants of substituted aliphatic acids between organic and aqueous phases, $\log K_d$, do not correlate with their dissociation constants, pK. It was appropriate to check whether such a correlation takes place with aromatic acids. The pK values for a series of substituted benzoic acids and their distribution constants ($\log K_d$) in the systems with the most extensively studied organic solvents (*n*-octanol, chloroform, toluene) [3, 4] are given in Table 1. It is seen that, whereas K of *ortho*-substituted benzoic acids is in most cases higher by an order of magnitude than K of their *meta* and *para* isomers, there are no definite trends in the distribution constants: the *meta* and *para* isomers are extracted in some cases better and in other cases worse than the *ortho* isomers.

Table 1. Distribution constants of aromatic acids between organic and aqueous phases

ArCOOH	pK	$\log K_d$ for indicated solvent		
		toluene	*n*-octanol	$CHCl_3$
Benzoic acid	4.18	0.017	1.785	0.021 (0.439)
o-NH_2	4.95	–0.155	1.152	–0.155
m-NH_2	4.74	–	–0.161	–0.398
p-NH_2	4.85	–	0.663	–0.046
o-Cl	2.94	0.279	1.980	0.890
m-Cl	3.82	1.114	2.681	1.919
p-Cl	3.99	1.255	2.653	1.699
o-NO_2	2.17	–0.319	1.459	–0.194
m-NO_2	3.45	0.090	1.830	0.415
p-NO_2	3.44	0.511	1.890	0.880
o-Br	2.85	–	–	0.903
m-Br	3.90	–	2.869	2.041
p-Br	3.97	–	2.857	–
o-I	2.86	–	2.398	–
m-I	3.86	–	3.114	–
p-I	3.93	–	3.021	–
o-OH	3.00	0.417	2.260	0.342
m-OH	4.08	–1.201	1.505	–1.523
p-OH	4.58		1.580	–2.000
o-OCH_3	4.09	0.362	–	1.653
m-OCH_3	4.09	–	2.021	–
p-OCH_3	–	–	0.462	0.146
o-CH_3	3.92	1.146	–	1.875
m-CH_3	4.27	1.100	2.371	1.756
p-CH_3	4.36	1.204	2.270	1.806

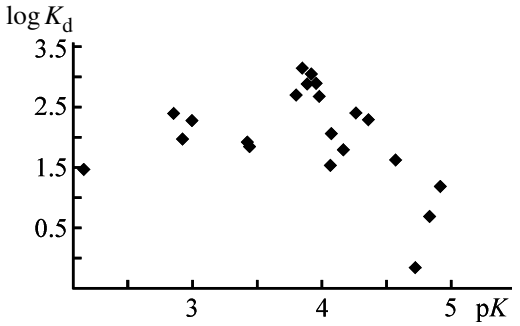


Fig. 1. log K_d of aromatic acids in the octanol–water system vs. their pK.

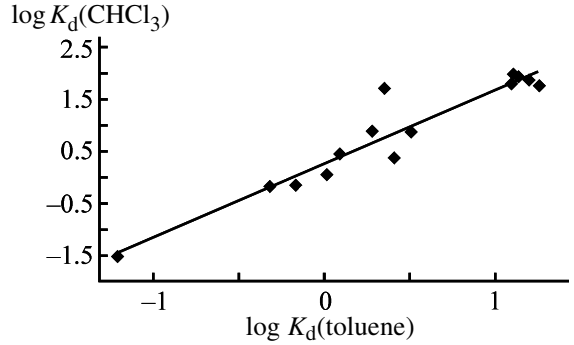


Fig. 2. Correlation between log K_d of carboxylic acids in the chloroform–water and toluene–water systems.

Figure 1 shows that there is no correlation between log K_d of acids in the octanol–water system and their pK. With other organic solvents, such correlation is lacking also. At the same time, it is interesting that, whereas the log K_d values in the systems with octanol and $CHCl_3$ do not correlate with each other, an approximate linear correlation does exist between the data for two aprotic solvents, toluene and $CHCl_3$ (Fig. 2).

We found in [1] that the correlation of K_d of aliphatic carboxylic acids between water and organic solvents with the properties of these solvents can be described by a five-parameter equation

$$\log K_d = a_0 + 4a_1\frac{n^2 - 1}{n^2 + 2} + a_2\frac{\varepsilon - 1}{2\varepsilon + 1} + a_3\delta^2 + a_4B + a_5E_T, \quad (1)$$

where n is the refractive index and ε, dielectric permittivity of the organic solvents (parameters determining their polarizability and polarity and responsible for the nonspecific solvation of a substrate); B, Palm basicity [5] and E_T, Reichardt electrophilicity [6] (parameters determining the capability of a solvent for acid–base interactions, i.e., for specific solvation); and δ^2, Hildebrand solubility parameter squared [parameter characterizing the cohesion (self-association) energy of a solvent, proportional to the energy required for penetration of a foreign molecule into the solvent structure, i.e., for formation of a cavity in the liquid].

We found that the major influence on log K_d of aliphatic acids is exerted by two characteristics of extractants: basicity B and polarity function $f(\varepsilon)$. The major solvation process controlling the transfer of an acid to the organic phase is its interaction with basic solvents with the formation of a complex; the solvent polarity positively affects this process. Formation of such complexes in extraction of phenols with basic solvents was confirmed by UV spectrophotometry and refractometry [7]. Therefore, the influence of properties of a solvent on its extraction power with respect to aliphatic carboxylic acids in most cases can be described with acceptable accuracy by a two-parameter equation

$$\log K_d = a_0 + a_2 f(\varepsilon) + a_4 B. \quad (2)$$

At the same time, we showed in [1] that the coefficients a_0, a_2, and a_4, characterizing the contribution of particular solvation processes to K_d of aliphatic acids, correlate with some of their parameters. Namely, a_4 linearly decreases, with a satisfactory accuracy, with an increase in pK; a_2 decreases with an increase in the Kirkwood parameter $(\varepsilon - 1)/(2\varepsilon + 1)$; a_0 grows with an increase in the molar volume of acids V_m (which is approximately proportional to their molar weight).

In the case of aromatic acids, the applicability of Eqs. (1) and (2) to K_d values with different extractants was proved for benzoic and salicylic acids [8, 9]; therefore, it was interesting to check the applicability of these equations to other aromatic acids and the existence of relationships like (2) with characteristics of the acids. The distribution of aminobenzoic acids was studied in most detail in [3, 4, 10, 11]. The distribution constants K_d of *o*-aminobenzoic acid between water and 38 organic solvents are given in Table 2. This data set can be described with a fairly high multiple correlation coefficient $R = 0.920$ by Eq. (1) supplemented with one more term taking into account the solvent molar volume V_m. Since for some extractants the K_d values given in different papers differ appreciably, we selected their optimal values best fitting the general equation. After such a selection, R increased insignificantly, to 0.927. To attain $R > 0.95$, which is considered as satisfactory level according to recommendations of the Group for Correlation Analysis in Chemistry (CAC IUPAC) [12], we excluded from the calculations the most deviating data for isopropyl

alcohol and dichloroethane. It should be noted here that, when constructing multiparameter equations describing the influence of various properties of solvents on an experimentally measured quantity (reaction rate constants, spectral shifts, or, as in our case, distribution constants), the adequacy of the equations obtained is commonly assessed by the multiple correlation coefficient R itself, rather than by R^2 [13]. Thus, we obtained an adequate equation for 36 extractants:

$$\log K_d = 1.72 - (4.44 \pm 2.18) f(n^2) + (4.21 \pm 1.13) f(\varepsilon) + (6.80 \pm 0.89) \times 10^{-3} B - (0.08 \pm 0.03) E_T + (1.64 \pm 1.67) \times 10^{-3} \delta^2 + (1.32 \pm 1.41) \times 10^{-3} V_m, \quad (3)$$

$$N = 36, \ R = 0.959, \ \text{rms error } s = \pm 0.235.$$

In this case, the decisive parameter is the solvent basicity B, with which $\log K_b$ correlates with the pair correlation coefficient $r = 0.910$ for 36 solvents. The coefficients at some terms of the regression equation (e.g., V_m, δ^2) have large rms deviations, sometimes exceeding their absolute values, which indicates that these terms are insignificant. Therefore, the significance of particular terms of the equation was checked, according to [12], by their alternate exclusion with the calculation of R for the equations with the smaller number of terms. By so doing, we found that V_m and δ^2 are insignificant and the significance of $f(n^2)$ is low. Finally, $\log K_d$ of *o*-aminobenzoic acid is adequately described by a three-parameter equation

$$\log K_d = 0.51 + (2.97 \pm 1.00) f(\varepsilon) + (7.62 \pm 0.66) \times 10^{-3} B - (0.05 \pm 0.02) E_T, \quad (4)$$

$$N = 36, \ R = 0.953, \ s = \pm 0.250.$$

The decisive influence of $f(\varepsilon)$, B, and, to a lesser extent, E_T is consistent with the relatively high coefficients r of correlations of $\log K_d$ with these parameters: 0.754, 0.910, and 0.704, respectively, whereas with the remaining parameters r is within 0.2–0.4. Generalization of the data with a two-parameter equation including the basicity and polarity parameters only is, however, unsatisfactory, because R becomes lower than 0.95 and the standard deviation of the coeficient at the Kirkwood parameter becomes larger than the absolute value of this coefficient, i.e., this factor becomes insignificant. However, the corresponding equation (5) allows comparison with the related two-parameter equations for other acids, including aliphatic acids [1]:

$$\log K_d = -0.54 + (0.65 \pm 0.72) f(\varepsilon) + (6.93 \pm 0.70) \times 10^{-3} B, \quad (5)$$

$$N = 36, \ R = 0.940, \ s = \pm 0.281.$$

The $\log K_d$ values calculated by Eq. (4) and their deviations from the experimental values, $\Delta \log K_d = \log K_{exp} - \log K_{calc}$, are given in Table 2. Except the data for the two excluded solvents, $\Delta \log K_d$ is within $s = \pm 0.250$ or only slightly exceeds this level.

Data on the distribution of other substituted benzoic acids for which the available data are sufficient for statistical treatment can also be satisfactorily fitted by an equation of type (1); as a rule, the decisive influence on $\log K_d$ is exerted by the solvent basicity. In what follows, we present the coefficients r_B of pair correlation of $\log K_d$ with the solvent basicity and also, for comparison with aliphatic acids, the two-parameter equations $\log K_d = f(\varepsilon, B)$, even when their coefficients R are lower than the value of 0.95 recommended in [12], i.e., when these equations are not quite adequate. Table 3 presents the $\log K_d$ values from [3, 4] for *p*- and *m*-amino- and *m*-hydroxybenzoic acids, and also for *m*-chloro- and *m*-nitrobenzoic acids, although the available K_d values for them are fewer.

For *p*-aminobenzoic acid, R for the whole set of 22 solvents is as low as 0.912, but after exclusion of data for dichloromethane and nitrobenzene we obtain an adequate equation:

$$\log K_d = -4.99 + (7.54 \pm 4.95) f(n^2) + (19.09 \pm 1.98) f(\varepsilon) + (4.53 \pm 1.34) \times 10^{-3} B - (0.02 \pm 0.04) E_T - (7.30 \pm 2.79) \times 10^{-3} \delta^2 - (9.33 \pm 2.90) \times 10^{-3} V_m, \quad (6)$$

$$N = 20, \ R = 0.969, \ s = \pm 0.267.$$

In this case, the polarizability and (in contrast to *m*-aminobenzoic acid) electrophilicity factors are insignificant:

$$\log K_d = -3.46 + (17.38 \pm 1.65) f(\varepsilon) + (2.91 \pm 1.15) \times 10^{-3} B - (6.41 \pm 1.10) \times 10^{-3} \delta^2 - (7.14 \pm 2.11) \times 10^{-3} V_m, \quad (7)$$

$$R = 0.962, \ s = \pm 0.298, \ r_B = 0.612.$$

Here the structural factors δ^2 and V_m are also significant; the correlation coefficient R of Eq. (8) obtained upon their exclusion is unacceptably low:

$$\log K_d = -4.46 + (11.30 \pm 1.98) f(\varepsilon) + (2.70 \pm 1.40) \times 10^{-3} B, \quad (8)$$

$$R = 0.878, \ s = \pm 0.519.$$

Table 2. Experimental and calculated [Eq. (4)] distribution constants K_d of *o*-aminobenzoic acid

Extractant	$\log K_d$		$\Delta\log K_d$
	experiment	calculation	
n-Pentane	–0.0506	–0.4842	–0.4335
n-Hexane	–0.2218	–0.4659	–0.2440
n-Heptane	–0.1024	–0.4577	–0.3554
n-Octane	–0.4437	–0.4487	–0.0050
Isooctane	–0.4089	–0.4124	–0.0034
n-Nonane	–0.4089	–0.4348	–0.0259
n-Decane	–0.6198	–0.4274	0.1924
Cyclohexane	–0.5229	–0.4119	0.1110
Benzene	–0.1549	–0.1303	0.0246
Toluene	–0.1549	–0.0068	0.1481
o-Xylene	0.0414	0.0976	0.0562
p-Xylene	–0.0506	0.0768	0.1274
m-Xylene	0.0000	0.0964	0.0964
Ethylbenzene	0.0000	–0.0066	–0.0066
Butanol	1.0607	1.1591	0.0984
Isobutanol	1.1761	1.2321	0.0560
n-Pentanol	1.4082	1.2127	–0.1955
Hexanol	1.2601	1.2261	–0.0340
Heptanol	1.1903	1.2354	0.0451
Octanol	1.1523	1.2165	0.0643
Nonanol	1.0607	1.1988	0.1381
Decanol	1.0000	1.1849	0.1849
Trichloromethane (chloroform)	–0.1549	–0.2463	–0.0914
CCl_4	–0.9208	–0.4157	0.5051
Tribromomethane	0.4314	–0.0756	–0.5070
1,2-Dichloroethane*	1.0899	0.0351	–1.0548
Chlorobenzene	–0.1549	0.0760	0.2309
1,2,4-Trichlorobenzene	0.0792	0.0361	–0.0431
Bromobenzene	–0.0506	0.0730	0.1236
Iodobenzene	–0.4437	–0.0184	0.4253
Nitrobenzene	0.1761	0.4134	0.2373
Diethyl ether	1.4314	1.8993	0.4680
Isopropyl ether*	0.7793	2.0618	1.2624
Chlorex [$(ClCH_2CH_2)_2O$]	1.7324	1.1498	–0.5826
Butyl acetate	1.3010	0.8974	–0.4036
Amyl acetate	1.2788	1.1492	–0.1295
Isoamyl acetate	1.3010	1.1741	–0.1269
Tributyl phosphate	2.4900	2.3442	–0.1457

* Data for these solvents were excluded from further calculations.

With *m*-aminobenzoic acid, large number of factors should be taken into account also. For the whole set of 17 extractants, $R = 0.872$, and a satisfactory correlation is obtained after exclusion of data for $CHBr_3$ and benzene:

$$\log K_d = 6.17 - (47.16 \pm 5.81) f(n^2) + (24.31 \pm 1.68) f(\varepsilon) - (7.52 \pm 1.10) \times 10^{-3} B - (0.11 \pm 0.03) E_T + (0.32 \pm 2.05) \times 10^{-3} \delta^2 + (14.41 \pm 3.30) \times 10^{-3} V_m, \quad (9)$$

$$N = 15,\ R = 0.987,\ s = \pm 0.150,\ r_B = 0.680.$$

In contrast to other benzoic acids, here the coefficient at the basicity parameter B is negative and the coefficients at parameters of nonspecific solvation are very large in absolute values. As in the case of *p*-aminobenzoic acid, the electrophilicity parameter E_T is insignificant here, and the correlation coefficient of the five-parameter equation obtained after its exclusion remains essentially the same ($R = 0.987$), but further exclusion of any term makes the correlation inadequate (R becomes less than 0.95). For the two-parameter equation $\log K_d = f(\varepsilon, B)$, R is as low as 0.774. At the same time, the coefficient at B becomes positive, and the coefficient at $f(\varepsilon)$ drastically decreases:

$$\log K_d = -2.67 + (4.82 \pm 2.21) f(\varepsilon) + (3.85 \pm 1.68) \times 10^{-3} B, \quad (10)$$

$$R = 0.774,\ s = \pm 0.591.$$

With the other three acids, the results obtained were considerably better. The equation obtained for *m*-hydroxybenzoic acid resembles that obtained for *o*-aminobenzoic acid. For the whole set of 15 extractants, R of the five-parameter equation is 0.944, and exclusion of the most deviating data for *o*-nitrotoluene leads to a six-parameter equation with $R = 0.991$, with the desicive influence of the basicity factor ($r_B = 0.946$):

$$\log K_d = 1.33 + (4.91 \pm 3.13) f(n^2) + (9.12 \pm 1.48) f(\varepsilon) + (21.97 \pm 1.63) \times 10^{-3} B - (0.10 \pm 0.04) E_T - (7.46 \pm 2.07) \times 10^{-3} \delta^2 - (1.21 \pm 0.03) \times 10^{-3} V_m, \quad (11)$$

$$R = 0.991,\ s = \pm 0.178.$$

As in the previous case, the parameters $f(n^2)$ and V_m are essentially insignificant, as well as δ^2. The distribution of *m*-hydroxybenzoic acid can be satisfactorily described by simplified equations

$$\log K_d = 0.43 + (7.12 \pm 2.02) f(\varepsilon) + (18.41 \pm 0.02) \times 10^{-3} B - (0.13 \pm 0.06) E_T, \quad (12)$$

$$R = 0.976,\ s = \pm 0.30;$$

Table 3. Distribution constants of substituted benzoic acids between organic and aqueous phases [3, 4]

Solvent	K_d with indicated substituents in acid				
	p-NH_2	*m*-NH_2	*m*-OH	*m*-Cl	*m*-NO_2
n-Hexane	–	–	–2.5229	–	–
n-Heptane	–	–	–2.5229	–	0.0600
n-Octane	–	0.0600	–	–	–
Cyclohexane	–3.3372	0.0012	–2.0458	0.4100	–
Benzene	–1.5229	0.1000	–1.0862	1.6200	1.5000
n-Butanol	0.8998	–	–	–	–
Isobutanol	–	–	1.3979	–	–
n-Pentanol	0.8751	1.2000	–	–	–
n-Hexanol	0.8325	1.0000	–	–	–
n-Heptanol	0.7993	0.8700	–	–	–
n-Octanol	0.6628	0.6800	1.5051	67.6000	67.0000
n-Nonanol	0.4771	0.5400	–	–	–
n-Decanol	0.3802	–	–	–	–
Toluene	–	–	–1.2007	1.2300	1.2000
o-Nitrotoluene	–	–	–0.4202	–	–
m-Xylene	–	–	–	–	1.0800
Chloroform	–0.0458	0.4000	–1.4949	2.6000	2.6000
Bromoform	–0.6990	0.1000	–	–	–
Dichloromethane	–0.8861	–	–	–	–
Tetrachloromethane	–	–	–	1.4200	–
1,2-Dichloroethane	0.8325	2.3000	–0.7212	–	–
Bromobenzene	–	–	–1.3372	–	–
Chlorobenzene	–	–	–1.2366	–	–
Nitrobenzene	–0.1549	0.3000	–0.3872	–	–
Ethyl acetate	1.1987	–	–	–	–
Propyl acetate		–	–	–	–
n-Butyl acetate		1.8000	1.4914	–	–
n-Amyl acetate		1.1000	–	–	–
Isoamyl acetate		0.8900	–	–	–
Diethyl ether		1.5000	–	93.3000	98.0000
Dibutyl ether		–	–	–	–
Tributyl phosphate		28.8000	–	–	–

$$\log K_d = 0.76 + (2.93 \pm 1.08) f(\varepsilon) + (13.99 \pm 1.50) \times 10^{-3} B, \quad (13)$$

$$R = 0.966, \; s = \pm 0.36.$$

The distribution of *m*-chloro- and *m*-nitrobenzoic acids was studied with seven extractants only; therefore, the equations obtained for them are less reliable. Nevertheless, positive results were obtained. For *m*-chlorobenzoic acid, we obtained a six-parameter equation with $R = 0.999$, but a two-parameter equation is also quite adequate:

$$\log K_d = -0.85 + (3.20 \pm 1.13) f(\varepsilon) + (5.90 \pm 0.86) \times 10^{-3} B, \quad (14)$$

$$N = 7, \; R = 0.983, \; s = \pm 0.167.$$

The decisive effect is exerted by the basicity (pair correlation coefficient of $\log K_d$ with B $r_B = 0.960$).

Similar result was obtained for *m*-nitrobenzoic acid: for the six-parameter equation, $R = 0.999$; the polarizability and molar volume factors are essentially insignificant (for the four-parameter equation, $R = 0.996$); the two-parameter equation is also quite adequate:

$$\log K_d = -1.71 + (5.29 \pm 1.92) f(\varepsilon) + (6.43 \pm 1.55) \times 10^{-3} B, \quad (15)$$

$$N = 7, \; R = 0.964, \; s = \pm 0.297, \; r_B = 0.916.$$

For a number of other acids, K_d is known with 4–6 extractants only [3, 4], which makes construction of

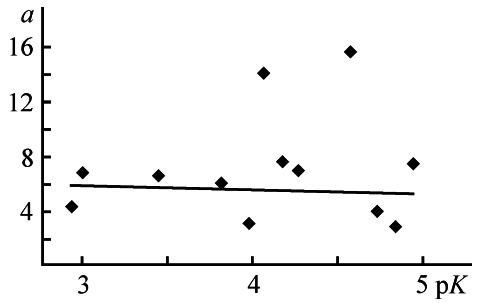


Fig. 3. Coefficient a_4 of equations of type (2) for distribution of aromatic acids vs. their dissociation constant pK.

an equation of type (1) impossible. However, the influence of the major factors, $f(\varepsilon)$ and B, can be evaluated by an equation of type (2), although such equations will be less reliable statistically. Below we give for each acid the K_d values with the examined solvents, the corresponding equation of type (2), and the coefficient r_B. For comparison, we also give two-parameter equations for unsubstituted benzoic and 2-hydroxybenzoic (salicylic) acids, calculated on the basis of data from [8, 9].

Benzoic acid, 36 solvents [8]:

$$\log K_d = -1.15 + (2.56 \pm 0.66) f(\varepsilon) + (7.54 \pm 0.68) \times 10^{-3} B, \quad (16)$$

$$N = 36,\ R = 0.957,\ s = \pm 0.277,\ r_B = 0.936.$$

o-Hydroxybenzoic (salicylic) acid, 28 solvents [9]:

$$\log K_d = -0.671 + (2.63 \pm 1.01) f(\varepsilon) + (6.57 \pm 0.95) \times 10^{-3} B, \quad (17)$$

$$N = 28,\ R = 0.931,\ s \pm 0.344,\ r_B = 0.911.$$

p-Hydroxybenzoic acid: K_d 0.6 (ethylbenzene), 0.01 (chloroform), 26.0 (diethyl ether), 27.0 (isobutanol), 38.0 (*n*-octanol):

$$\log K_d = -0.567 + (3.71 \pm 2.52) f(\varepsilon) + (15.56 \pm 1.82) \times 10^{-3} B, \quad (18)$$

$$N = 5,\ R = 0.979,\ s = \pm 0.349,\ r_B = 0.967.$$

o-Chlorobenzoic acid: K_d 0.41 (cyclohexane), 1.90 (toluene), 1.02 (*m*-xylene), 8.00 ($CHCl_3$), 94.00 (diethyl ether), 95.00 (*n*-octanol):

$$\log K_d = -1.67 + (6.60 \pm 1.22) f(\varepsilon) + (4.28 \pm 0.93) \times 10^{-3} B, \quad (19)$$

$$N = 6,\ R = 0.984,\ s = \pm 0.180,\ r_B = 0.885.$$

m-Chlorobenzoic acid: K_d 0.41 (*n*-hexane), 1.62 (benzene), 2.6 (chloroform), 1.23 (toluene), CCl_4 (1.42), 93.3 (diethyl ether), 67.6 (*n*-octanol):

$$\log K_d = -0.85 + (3.20 \pm 1.13) f(\varepsilon) + (5.90 \pm 0.86) \times 10^{-3} B, \quad (20)$$

$$N = 7,\ R = 0.983,\ s = \pm 0.276,\ r_B = 0.960.$$

p-Chlorobenzoic acid: K_d 2.09 (benzene), 7.58 (chloroform), 3.24 (toluene), 77.6 (*n*-octanol):

$$\log K_d = -0.86 + (4.73 \pm 0.38) f(\varepsilon) + (3.01 \pm 0.37) \times 10^{-3} B, \quad (21)$$

$$N = 4,\ R = 0.997,\ s = \pm 0.05,\ r_B = 0.873.$$

m-Toluic acid: K_d 4.5 (cyclohexane), 12.6 (toluene), 57 (chloroform), 235 (*n*-octanol):

$$\log K_d = -0.528 + (0.72 \pm 0.15) f(\varepsilon) + (6.49 \pm 0.15) \times 10^{-3} B, \quad (22)$$

$$N = 4,\ R = 0.999,\ s = \pm 0.02,\ r_B = 0.997.$$

These equations show that the distribution factors of aromatic acids between organic and aqueous phases can be satisfactorily described in most cases by two-parameter linear equations taking into account the polarity and basicity of the organic solvent, with the influence of basicity being decisive. Certain differences observed with aminobenzoic acids are probably caused by possible simultaneous solvation of the amino group capable of hydrogen bonding. The coefficients at both terms of the equation are positive (i.e., the extraction increases with an increase in the parameters) and vary depending on the acid in the following ranges: at $f(\varepsilon)$, 0.7–11; at $10^{-3}B$, 3–15.5 (for the majority of acids, 4–7). The absolute term a_0 is negative. However, we failed to obtain, as for aliphatic acids [1], explicit correlations of these coefficients with such characteristics of acids as the molar volume and ε. Aromatic acids are crystalline, and the ε values for them are, as a rule, unknown, as well as the densities required for determination of the molar volume. An attempt to construct a correlation of a_4 with pK of acids failed also (Fig. 3). This may be due to the occurrence in aromatic acids of some effects that are absent in aliphatic acids: conjugation of lone electron pairs of the carbonyl oxygen atom with the π-electron ring, possible hydrogen bonding with *o*-amino or *o*-hydroxy groups with the formation of an energetically favorable cyclic structure, steric effects, etc.

The conclusion that the acid–base interactions and extractant polarity are the decisive factors in the extraction of aromatic acids is consistent with the con-

clusions made by Okada *et al.* [10], who studied the distribution of *p*-aminobenzoic acid between the organic and aqueous phases. In experiments on the extraction of this acid with mixtures of cyclohexane with *n*-octanol, they confirmed the lack of linear correlation between $\log K_d$ and ε of the mixtures and concluded that the extraction is influenced by various solvation factors acting simultaneously.

CONCLUSIONS

(1) The distribution constants of substituted aromatic acids between organic and aqueous phases show no linear correlation with any extractant characteristic taken separately. These quantities can be satisfactorily generalized only with multiparameter equations taking into account various properties of the extractants.

(2) The major factor governing the degree of recovery of acids with organic extractants is the Palm basicity of the extractant.

REFERENCES

1. Makitra, R.G., Midyana, G.G., and Gavenko, V.O., *Ukr. Khim. Zh.*, 2004, vol. 70, no. 8, pp. 105–109.
2. Makitra, R.G., *Zh. Obshch. Khim.*, 2003, vol. 73, no. 8, pp. 1244–1252.
3. Korenman, Ya.I., *Koeffitsienty raspredeleniya organicheskikh soedinenii* (Distribution Constants of Organic Compounds), Voronezh: Voronezh. Univ., 1992.
4. Korenman, I.M., *Konstanty raspredeleniya organicheskikh veshchestv mezhdu dvumya zhidkimi fazami* (Distribution Constants of Organic Substances between Two Liquid Phases), Gor'kii: Gor'kov. Univ., 1975–1979, issues 1–5.
5. Koppel, I.A. and Paju, A.I., *Reakts. Sposobn. Org. Soedin.*, 1974, vol. 11, no. 1(39), pp. 121–138.
6. Reichardt, Ch., *Solvents and Solvent Effects in Organic Chemistry*, Weinheim: VCH, 1988.
7. Filippov, I.V., Karpacheva, S.M., and Konysheva, L.V., *Zh. Prikl. Khim.*, 1967, vol. 40, no. 3, pp. 621–627.
8. Makitra, R.G., Pirig, Ya.N., Vasyutin, Ya.M., and Midyana, G.G., *Zh. Obshch. Khim.*, 1994, vol. 64, no. 5, pp. 722–730.
9. Makitra, R.G., Khita, S.I., Vasyutyn, Ya.M., *et al.*, *Zh. Obshch. Khim.*, 1995, vol. 65, no. 5, pp. 752–755.
10. Okada, S., Nakahara, H., Yomota, C., and Mochida, K., *Chem. Pharm. Bull.*, 1985, vol. 33, no. 11, pp. 4916–4922.
11. Korenman, I.M., Gur'ev, I.A., and Denisov, G.S., *Zh. Fiz. Khim.*, 1976, vol. 50, no. 2, pp. 401–404.
12. Makitra, R.G., *Ukr. Khim. Zh.*, 1992, vol. 58, no. 2, pp. 228–229.
13. Koppel, I.A., Palm, V.A., Chapman, N.B., and Shorter, J., *Advances in Linear Free Energy Relationships*, London: Plenum, 1972.

ISSN 1070-4272. Russian Journal of Applied Chemistry, 2006, Vol. 79, No. 1, pp. 50–55. © Pleiades Publishing, Inc., 2006.
Original Russian Text © I.B. Dmitrieva, K.P. Tikhomolova, A.S. Chukhno, 2006, published in Zhurnal Prikladnoi Khimii, 2006, Vol. 79, No. 1, pp. 51–56.

SORPTION AND ION-EXCHANGE PROCESSES

Adsorption of Tetrazole on Ni(II) and Fe(III) Oxides

I. B. Dmitrieva, K. P. Tikhomolova, and A. S. Chukhno

St. Petersburg Academy of Pharmaceutical Chemistry, St. Petersburg, Russia
Research Institute of Chemistry, St. Petersburg State University, St. Petersburg, Russia

Received April 6, 2005

Abstract—Kinetics of evolution of the electrosurface (electrokinetic potential and pH at isoelectric point) and adsorption properties is studied in the systems aqueous tetrazole–metal oxide (NiO or Fe_2O_3) in long-term experiments with variation of the tetrazole concentration and solution pH.

DOI: 10.1134/S1070427206010101

This paper continues a series of studies considering the features of adsorption of azoles on the surface of transition metal oxides [1–5] and concerns adsorption of tetrazole on NiO and Fe_2O_3.

Previously we demonstrated [3, 4] that the electrokinetic potential ζ of NiO, Fe_2O_3, and $NiFeO_4$ surfaces in aqueous tetrazole solutions starts to change practically immediately after bringing the phases in contact, and its evolution in time is rather complex. We concluded that, first, the interaction between tetrazole molecules (both in the molecular and ionic forms) with surface sites of the oxide surface undoubtely occurs, and second, neither the Gouy–Chapman model (nonspecific adsorption), nor the theory of adsorption of organic surfactants can adequately reproduce this interaction. Our results revealed that adsorption of tetrazole and other ligands is caused primarily by the adsorbent–adsorbate donor–acceptor interaction. The facts that ζ changes over a long time and that the ζ vs. t_c dependence (t_c is the contacting time) is rather complex suggest several steps of transformation of the adsorbate in the adsorption layer. In this case, the mechanism of each step (naturally, except for the first one) does not necessarily involve the formation of donor–acceptor bonds.

In this study we examined the kinetics of evolution of the parameters referred to the bulk of the aqueous phase, such as the tetrazole concentration c and pH, and also of those characterizing the oxide surface (electrokinetic potential ζ and pH at the isoelectric point pH_{IEP}). The adsorption of tetrazole per unit surface area Γ was determined from the difference $\Delta c = c - c_0$, where c_0 is the tetrazole concentration in the initial solution, and the specific surface area of the adsorbent s_{sp}. In the experiments we varied the solution pH and c_0. For c_0, we selected two values, 1×10^{-3} and 1×10^{-4} M. For each of these concentrations, we selected two pH values, that established in the system naturally (solution no. 1) and pH 3 (solution no. 2). In the latter case, pH 3 was adjusted and then maintained throughout the experiment by adding an acid or an alkali. The initial pH in solution no. 1 was 3.9 and 5.3 at $c_0 = 1 \times 10^{-3}$ and 1×10^{-4} M, respectively. In addition to the working (tetrazole-containing) solutions we used reference (tetrazole-free) solutions with the same ionic strength, which was adjusted by adding HCl, KCl, and KOH.

All the chemicals used in the study were of analytically pure grade. The solutions were prepared in distilled water [conductivity $(1–2) \times 10^{-6}$ S cm^{-1}].

The metal oxides were prepared as fine powders. Their characteristics were the same as in the corresponding experiments described in [6].

Figure 1 shows the ζ vs. t_c dependence for NiO dispersions in tetrazole solutions of two different concentrations (1×10^{-3} and 1×10^{-4} M) and with different pH values. There was no way to depict data obtained at small t_c using the time scale acceptable for presentation of the data obtained in 7-day experiments. Therefore, in the plot, the ζ values corresponding to $t_c = 0$, in fact, correspond to $t_c = 0.02–0.2$ h. The exact initial ζ values ($t_c = 0$) are equal to those in the corresponding reference solutions (see caption to Fig. 1). Note that, in the reference solutions, ζ remained unchanged throughout prolonged experiments.

Data presented in Fig. 1 are consistent with those reported previously [3, 4]. In all the dispersions, after bringing the phases in contact, initially positive ζ

rapidly increases. Then it passes through a maximum and decreases during a long time. Finally, either ζ remains practically unchanged (in most cases) or increases again (NiO; $c_0 = 10^{-3}$ M) but at a lower rate than initially. The fact that some differences are observed between the results obtained in this study and those reported previously [3, 4], particularly, in the tetrazole concentration at which the characteristic trends are more clearly pronounced, can be attributed to high sensitivity of the electrokinetic properties to the batch of the adsorbent and phase ratio (in this study, both the batch of the oxide and phase ratio were different from those used previously).

Note also that the ζ values at $t_c = 0$ and $t_c = 0.02$–0.2 h, referred to NiO dispersions in solution no. 1, are close to those in the reference solutions at the same pH, while for the dispersions in solution no. 2, ζ in tetrazole-containing solutions is mostly considerably lower. Furthermore, in the NiO dispersions the factors of the tetrazole concentration and pH play certain role, which is not the case in the Fe_2O_3 dispersions. The pH_{IEP} values in tetrazole-containing dispersions ($c_0 = 10^{-3}$ M), measured at $t_c = 24$ h, are 5.4 and 5.7 for NiO and Fe_2O_3, respectively. In the reference solutions, the corresponding values are 7.5 and 6.1. Thus, introduction of tetrazole in concentration of 10^{-3} M shifts pH_{IEP} of both oxides toward lower values, the effect being more pronounced for NiO.

Figure 2 shows the Γ vs. t_c dependences obtained for the dispersions of both oxides at a tetrazole concentration of 10^{-3} M and pH of the liquid phase corresponding to solution nos. 1 and 2. Comparison of Figs. 1 and 2 (adsorbent NiO) shows that the corresponding dependences of ζ vs. t_c and Γ vs. t_c are close in shape. In solution no. 1, the parameters ζ and Γ rapidly increase at small t_c, then they increase at a lower rate, and, finally, flatten out at large t_c. In solution no. 2 the curves run more smoothly, but the similarity remains. In the case of Fe_2O_3, the corresponding curves are similar in shape also.

Note here that there is no need in analysis of the observed differences in the positions of the extrema in the ζ vs. t_c and Γ vs. t_c curves, since the phase ratios in the electrokinetic and adsorption experiments were different.

Figure 3 shows the Γ vs. t_c dependences obtained for the dispersions of both oxides, but at a tetrazole concentration of 10^{-4} M. At this lower tetrazole concentration, the trends in ζ and Γ remain similar, even being less pronounced than at $c_0 = 10^{-3}$ M.

It should be pointed out that the effect of adsorbent

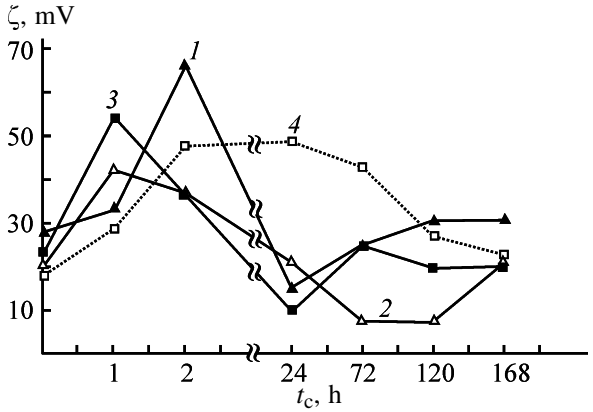


Fig. 1. Electrokinetic potential ζ of NiO as a function of the contacting time t_c. c_0 (M): (*1, 3*) 10^{-3} and (*2, 4*) 10^{-4}. (*1, 2*) Solution no. 1 and (*3, 4*) solution no. 2. ζ (mV) in the corresponding reference solutions: (*1*) +32, (*2*) +17, (*3*) +37, and (*4*) +39.

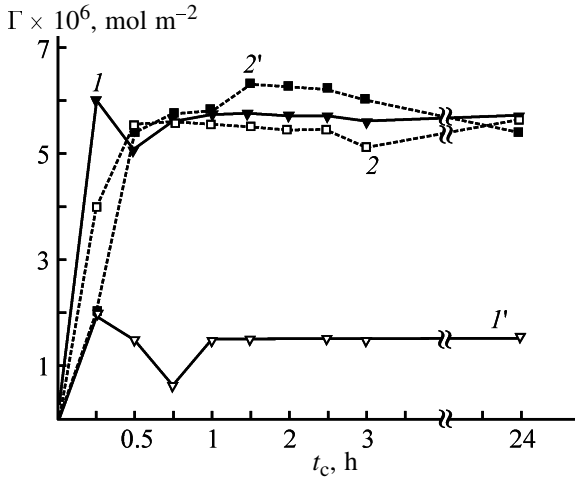


Fig. 2. Adsorption of tetrazole Γ as a function of the contacting time t_c at $c_0 = 10^{-3}$ M: (*1, 2*) NiO and (*1'*, *2'*) Fe_2O_3. (*1, 1'*) Solution no. 1 and (*2, 2'*) solution no. 2.

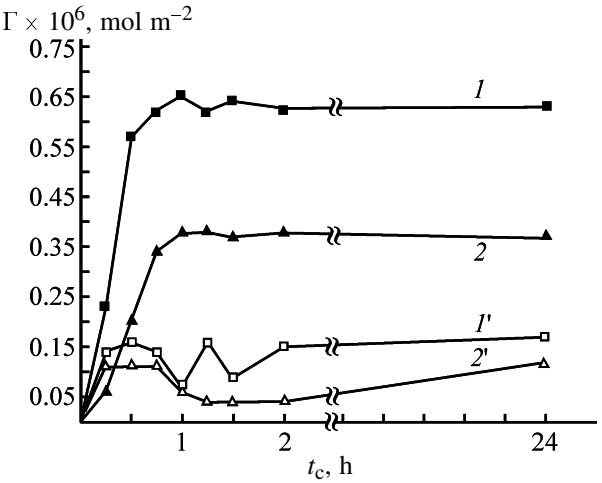


Fig. 3. Adsorption of tetrazole Γ as a function of the contacting time t_c at $c_0 = 10^{-4}$ M: (*1, 2*) NiO and (*1'*, *2'*) Fe_2O_3. (*1, 2'*) Solution no. 1 and (*2, 1'*) solution no. 2.

pH in oxide dispersions in tetrazole solutions at various contacting times

c, M	pH at indicated t_c, h													
	NiO							Fe_2O_3						
	0.02–0.2	1	2	24	72	120	168	0.02–0.2	1	2	24	72	120	168
1×10^{-3}	3.9	4.3	4.4	5.1	4.7	6.5	6.9	4.1	4.2	4.3	4.1	4.0	4.0	4.1
1×10^{-4}	5.3	5.8	6.0	6.7	7.2	7.4	7.4	5.0	5.0	5.0	5.0	5.1	5.0	5.0

on the adsorption of tetrazole is clearly pronounced in the dispersions with an aqueous phase corresponding to solution no. 1 (Figs. 2 and 3), but not at pH 3 (Fig. 2), which can be attributed to the differences in the hydrolytic behavior of iron and nickel. The OH^- group occurring in the surface complex as a result of hydrolysis is a more tightly bound ligand as compared to tetrazole. In contrast to Ni(II), Fe(III) has a strong tendency to hydrolysis at pH realized in solution no. 1. At pH 3 neither surface Fe(III) nor Ni(II) are hydrolyzed.

Data on pH at various contacting times of the oxides with various tetrazole solutions are given in the table. Note here that, at the moment of contacting the oxides with tetrazole solutions, in all cases, pH is lower than pH_{IEP} of the oxides in the reference solutions. Thus, initially (at t_c of about several minutes), the oxide surface was positively charged in all the systems.

The table shows that significant changes in pH occurred only in the NiO dispersions. In the Fe_2O_3 dispersions, pH does not depend on t_c.

All the results obtained suggest specific nature of the processes initiated by introduction of tetrazole into the adsorption layer at the surface of both oxides: increase in the initially positive ζ after addition of tetrazole into the aqueous phase; shift of pH_{IEP}; nonmonotonic run of the kinetic curves of all the characteristic parameters; and long time required to establish the steady state.

Since the trends of the selected characteristic parameters were demonstrated to be more clearly pronounced in NiO dispersions, let us further analyze surface processes occurring on this adsorbent.

The rather complex kinetic curves of ζ and Γ obtained with tetrazole are qualitatively similar to those obtained previously [3, 4]. For example, the observed distinct growth of the initially positive ζ in the initial stage of the experiment is equally typical of both tetrazole and 1,3-diazole.

In the case of 1,3-diazole solutions with a high concentration of the cationic species, the increase in the initially positive ζ on the NiO surface was attributed to the adsorption of long chains of the cations having a large total positive charge. The same interpretation could be applied to the NiO dispersions in aqueous tetrazole solutions at pH 3 (solution no. 2), as containing sufficient amounts of tetrazole in the cationic form. Therefore, in this case, the mechanisms of the surface reactions are similar to those occurring in adsorption of diazole [3, 4].

However, it is clearly seen from even superficial comparison of the properties of the tetrazole and 1,3-diazole solutions that the adsorption mechanisms are significantly different for the dispersions in solution no. 1.

In this case, the fraction of the cationic form of 1,3-diazole is 10–40%, while for tetrazole, this fraction is very small or lacking at all. Furthermore, in this solution, 50–60% of tetrazole occurs in the anionic form (at $c = 1 \times 10^{-4}$ M). It is known that large associates are preferentially formed from cationic azole species, and anionic species do not form associates at all. Therefore, the observed initial growth of the positive ζ in solution no. 1 cannot be attributed to the adsorption of positively charged associates.

Figure 4 shows the suggested mechanisms of successive processes occurring with ionic and molecular species and with associates of tetrazole in the surface layer in the systems with solution no. 1.

As known [7–11], the π system of tetrazole consists of six delocalized π electrons (p_z electron of the carbon atom, p_z^2 lone pair of the pyrrole nitrogen, and p_z electrons of the pyridine nitrogen atoms). The pyridine nitrogens N^2, N^3, and N^4 have lone pairs potentially capable of forming donor–acceptor bonds, and the pyrrole nitrogen (N_1) is responsible for acid–base interactions. At the same time, the tetrazole molecule exhibits distinct aromaticity, which is considerably higher than that in 1,3-diazole. Formation of the

anionic form (deprotonation) increases the electron density on all the atoms of the tetrazole ring. Therefore, the aromaticity of the tetrazolate anion is even higher as compared to the neutral molecule, approaching that of the benzene ring.

When tetrazolate anions, neutral species, and their associates enter the surface layer under the action of Coulombic forces and also as a result of diffusion, they can be fixed on the positively charged oxide surface by virtue of their π-donor capacity (Fig. 4a). The anions add a negative charge, while neutral molecules and associates do not change the potential of the surface layer. In this first stage, the major amount of tetrazole is accumulated in the adsorption layer, and in the other stages, successive transformations of adsorbed tetrazole species take place.

Strong nonuniform surface field polarizes tetrazole, thus increasing the charge localization on separate atoms. In this case, the negative charge on an atom could be preferentially localized on the pyrrole nitrogen (N^1), resulting in electrostatic bonding between N^1 and the positively charged area of the oxide surface (Fig. 4b). In the next stage, all other nitrogen atoms are involved in donor–acceptor bonding with the surface nickel atom (Fig. 4c), which is accompanied by change in the spatial orientation of the adsorbed tetrazole molecule.

The increase in the positive charge in the period t_c = 0.2–2.0 h can be attributed to, e.g., decreasing contribution of the negative charge, i.e., relative increase of the positive charge, by virtue of the ligand exchange of a part of the OH^- groups for neutral tetrazole molecules, as demonstrated by the observed increase in pH (see table).

The increase in pH, in its turn, results in increasing content of tetrazole in the anionic form in the bulk of solution, thus increasing the adsorption of the anions and decreasing ζ potential.

Finally, the above-considered scheme refers to single "portion" of the substance that entered the adsorption layer. In fact, the system is in a dynamic equilibrium, and the experiment demonstrates some statistically averaged pattern. In the course of the experiment, this scheme is multiply realized in the system with successively altered contribution of separate stages.

Let us apply this scheme to analyze the ζ vs. t_c and Γ vs. t_c dependences obtained in the experiments with NiO at $c_0 = 10^{-3}$ M (solution no. 1). It follows from the aforementioned that pH of the initial tetrazole solution was 3.9. According to the speciation diagram

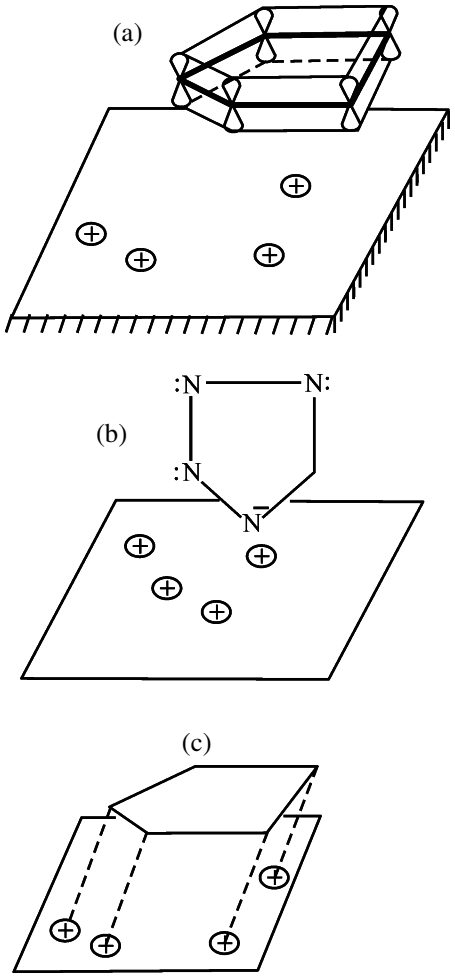


Fig. 4. Scheme of successive processes occurring in the surface layer upon adsorption of the tetrazole anion: (a) fixation on the surface via the π system of tetrazole, (b) electrostatic bonding with localization of the charge on the heterocycle, and (c) donor–acceptor bonding.

estimated from K_a and K_{BH^+} [12], the concentration of cationic species in this solution is extremely low. The surface potential is positive and rather high. It is obvious that, under these conditions, any significant adsorption of the cationic form is quite improbable. Noticeable amounts of neutral and anionic species could be adsorbed via π interaction and via π and Coulombic interactions, respectively. At small t_c, the concentration of the anionic species is low (even being somewhat higher than 7%), and that of the neutral species is high. It is known that introduction of a very low concentration of anions into the electrical double layer cannot significantly decrease the absolute value of ζ (in our experiments ζ remained practically unchanged at t_c < 1 h). The observed considerable growth of ζ at t_c from 1 to 2 h is due to the

fact that, in this period, reorientation and polarization of the adsorbed molecules contribute significantly. The subsequent decrease in ζ suggests that the bulk of solution contains large amount of anionic species (about 50% at pH 5.1) which are actively adsorbed on the surface. With increasing coverage of the surface with adsorbed anions, the further accumulation of the anionic species in the adsorption layer decelerates and then completely ceases after reaching the limiting coverage. The increase in ζ after passing the minimum, as was suggested above, is caused by the ligand exchange of the OH^- groups for the neutral tetrazole species, which is consistent with the increase in pH in this stage like that in the first stage.

The drift of pH_{IEP} to the left suggests that, at least at the final stage of the experiment, it is the anionic form of tetrazole that is adsorbed specifically.

The scheme suggested in this study is also applicable to the systems with $c_0 = 10^{-4}$ M. In this case we obtained the dependences characterized by the lack of the initial flat section and by considerably smoother other sections. The lack of the initial section is quite natural in the systems with a considerably lower concentration of the neutral form as compared to the systems with $c_0 = 10^{-3}$ M. The above-described scheme involving successive processes manifested in particular sections of the ζ vs. t_c curves can be equally used for interpretation of the Γ vs. t_c curves (Figs. 2 and 3).

The results obtained in the systems with Fe_2O_3 are consistent with the suggested scheme also. Generally, the ζ vs. t_c and Γ vs. t_c dependences are similar to those in the systems with NiO, although the positions of the maxima and minima in the curves as well as the levels of particular sections of the curves depend on the adsorbent. The shift of pH_{IEP} is considerably smaller in the Fe_2O_3 suspensions, which is consistent with our previous conclusions [3, 4] that, first, in the case of azoles as ligands, Fe(III) is a weaker acceptor than Ni(II), and second, that hydrolysis of iron increases with increasing pH, while nickel is not hydrolyzed at both pH values used in this study. The fact of considerably lower Γ in the system with Fe_2O_3 at $c_0 = 10^{-3}$ M (solution no. 1; Fig. 2, curve *1*') as compared to solution no. 2 (Fig. 2, curve *2*') also can be attributed to the features of hydrolytic behavior of Fe(III).

To conclude, as expected, the sorption mechanism is controlled primarily by the state of tetrazole molecules in solution.

CONCLUSIONS

(1) In NiO and Fe_2O_3 dispersions in aqueous tetrazole solutions with the initial tetrazole concentration $c_0 = 10^{-3}$ M, at the equilibrium (naturally established) solution pH, the dependences of the electrokinetic potential ζ on the contacting time t_c initially increase, pass through a maximum after a short time after bringing the phases in contact, and then pass through a minimum with increasing t_c. In the NiO dispersions, such an extremal run of the dependences is more clearly pronounced as compared to the Fe_2O_3 dispersions.

(2) The dependences of the tetrazole adsorption Γ on the contacting time are generally similar to the ζ vs. t_c dependences. The limiting Γ is considerably higher in the NiO suspensions.

(3) In the investigated dispersions in aqueous tetrazole solutions, pH_{IEP} shifts to more acidic range relative to the values obtained in HCl and KOH solutions. The shift is larger in the case of NiO (about 2 pH units) as compared to Fe_2O_3 (0.4 pH unit).

(4) The features of the ζ vs. t_c and Γ vs. t_c curves obtained at lower tetrazole concentration ($c_0 = 10^{-4}$ M) are generally the same, but less pronounced.

ACKNOWLEDGMENTS

The study was supported by the grant of the President of the Russian Federation for Support of Leading Scientific Schools (no. NSh-789.2003.3) and by the Russian Foundation for Basic Research (project no. 03-03-32418).

REFERENCES

1. Dmitrieva, I.B., Tikhomolova, K.P., Ivanova, M.V., and Antonova, I.G., *Kolloidn. Zh.*, 1997, vol. 59, no. 6, pp. 747–750.
2. Tikhomolova, K.P., Dmitrieva, I.B., and Ivanova, M.V., *Zh. Prikl. Khim.*, 1998, vol. 71, no. 4, pp. 536–543.
3. Tikhomolova, K.P., Dmitrieva, I.B., Ivanova, M.V., and Koldobskii, G.I., *Zh. Prikl. Khim.*, 2000, vol. 73, no. 3, pp. 391–396.
4. Tikhomolova, K.P., Dmitrieva, I.B., Ivanova, M.V., and Koldobskii, G.I., *Zh. Prikl. Khim.*, 2000, vol. 73, no. 7, pp. 1094–1098.
5. Dmitrieva, I.B. and Chukhno, A.S., in *Informatsionnye tekhnologii v ekonomike, promyshlennosti i obrazovanii: Sbornik nauchnykh trudov* (Information

Technologies in Economics, Industry, and Education: Collection of Scientific Works), Novokuznetsk, 2003, issue 6, pp. 62–65.

6. Dmitrieva, I.B., Tikhomolova, K.P., and Chukhno, A.S., *Zh. Prikl. Khim.*, 2005, vol. 78, no. 5, pp. 741–746.
7. Sadimenko, A.P., Garnovskii, A.D., Shteiner, V.N., and Osipov, O.A., *Khim. Geterotsikl. Soedin.*, 1983, no. 10, pp. 1299–1310.
8. Paquette, L.A., *Principles of Modern Heterocyclic Chemistry*, New York: Benjamin, 1968.
9. Ostrovskii, V.A., Panina, N.S., Koldobskii, G.I., *et al.*, *Zh. Org. Khim.*, 1979, vol. 15, no. 4, pp. 844–847.
10. Ostrovskii, V.A., Erusalimskii, G.B., and Shcherbinin, M.V., *Zh. Org. Khim.*, 1995, vol. 31, no. 9, pp. 1422–1431.
11. Ostrovskii, V.A., Koldobskii, G.I., Gidaspov, B.V., and Osokina, E.N., *Zh. Org. Khim.*, 1977, vol. 13, no. 11, pp. 2421–2425.
12. Ostrovskii, V.A., Erusalimskii, G.B., and Shcherbinin, M.V., *Zh. Org. Khim.*, 1993, vol. 29, no. 7, pp. 1297–1302.

ISSN 1070-4272. Russian Journal of Applied Chemistry, 2006, Vol. 79, No. 1, pp. 56–59. © Pleiades Publishing, Inc., 2006.
Original Russian Text © L.S. Banyan, 2006, published in Zhurnal Prikladnoi Khimii, 2006, Vol. 79, No. 1, pp. 57–61.

SORPTION AND ION-EXCHANGE PROCESSES

Packing for High-Performance Liquid Chromatography Based on Microspheric Particles of (Urea–Formaldehyde Resin)–Silica Gel Composite

L. S. Banyan

Yerevan State University, Yerevan, Armenia

Received June 7, 2005

Abstract—Preparation of uniform microspheric particles of the (urea–formaldehyde resin)–silica gel composite was studied. The suitability of this composite modified with C_{18} groups as packing for reversed-phase high-performance liquid chromatography was evaluated. The sorbent was modified using either octadecyldimethylchlorosilane or polymers containing C_{18} groups, and the columns packed with the resulting sorbent were studied. The experimental results showed that the polymeric modification allows efficient shielding of the surface silanol groups.

DOI: 10.1134/S1070427206010113

Uniform microspheric particles find expanding application in preparation of sorbents and supports for chromatography, and thus the reproducibility of their structural characteristics, primarily determined by reproducibility of the particle size, is of particular importance. Therefore, development of new procedures for preparing microspheric supports for high-performance liquid chromatography HPLC (both porous and non-porous) is an urgent problem [1–3].

Iler *et al*. [4, 5] suggested a new procedure for preparing uniform urea–formaldehyde resin microspheres based on formation of coacervates as liquid micrometer-size drops in the course of polymerization of urea and formaldehyde in acidic silica sol. Oligomers form coacervates bound by hydrogen bonds, which contain silica or other hydrophilic colloidal particles. Microspheric particles with the diameter varying from 0.2 to 20 μm (5–10 μm on the average) are prepared using colloidal silica particles (5–500 nm size) whose parameters are easily controlled. The advantages of the above procedure for preparing (urea–formaldehyde resin)–silica gel (UFR–SG) microspheres [4, 5] are as follows: (1) it yields uniform microspheric particles and thus eliminates fractionation problems and (2) it allows control of the particle size in the course of polycondensation by changing content of colloidal silica in the system.

Airapetyan *et al*. [6, 7] studied the effect of colloidal silica in the course of formation of uniform UFR–SG particles.

The resulting UFR–SG particles can be used as nonporous support for HPLC because they meet such chromatographic requirements as rigid silica skeleton and uniformity of the microspheric particle size (1.5–2.0 μm) typical for nonporous packing. The difference in the particle size does not exceed 10% [8–11].

The suitability of the urea–formaldehyde resin packing as HPLC sorbent was discussed in [12, 13]. Monolithic tube of urea–formaldehyde resin prepared *in situ* is used as a new support for affinity chromatography. This monolithic UFR tube consists of agglomerates of 2-μm particles of irregular shape and is characterized by biporosity. Cibacron Blue dye [12] is used as affine ligand grafted to the support surface [12].

A stationary phase for HPLC in which microspheric particles (3–5 μm in diameters) are formed by condensation of hexamethylenetetramine with urea in the presence of zirconyl chloride was reported in [13].

EXPERIMENTAL

Preparation of microspheric UFR–SG particles. Microspheric UFR–SG particles were prepared under the conditions presented in Table 1. First, urea was dissolved in concentrated hydrochloric acid. Then, the mixture was diluted with distilled water, and the required amounts of silica sol and formaldehyde (Table 1) were added. The volume of silica sol (20%

Table 1. Preparation of UFR and UFR–SG microspheres

Sample no.	Reaction mixture				Total volume of reaction mixture, ml	Time of formation of new phase, min	Particle size, μm	Pore volume, $cm^3\ g^{-1}$	Content of SiO_2 in UFR–SG, wt %
	HCl (conc.), ml	urea, g	Formalin, ml	silica sol					
1	30.0	22.5	30	95	300	10	5.0	0.028	50
2	27.5	22.5	35	90	350	3.0	2.5	0.056	45
3	35.0	22.5	35	15	300	0.5	2.5	0.165	15
4	30.0	22.5	30	15	250	1.6	2.5	0.078	13
5	40.0	22.5	35	15	250	1.3	2.0	0.071	16
6	35.0	22.5	35	10	300	0.5	3.0	0.133	8
7	35.0	22.5	35	0	250	1.2	3.0	0.174	0
8	45.0	22.5	35	0	250	0.4	5.0	0.159	0

SiO_2) was varied in the 0–90 ml range. As colloidal silica, we used stabilized silica sol prepared by the procedure given elsewhere [14]. After addition of all the components, the reaction mixture was stirred for 20–30 s. Depending on the amount of silica sol, the microspheric particles with the particle size varied from 1.0 to 15 μm were obtained. After storage of the resulting particles in the mother liquor for approximately 1 h, they were decanted, washed with distilled water and acetone on the filter, and dried in an oven at 120°C for 2 h.

Modification of the microsphere surface with silanes. Modification of the packing with silanes such as octadecyldimethylchlorosilane (ODCS) and trimethylchlorosilane (TMCS) was performed in accordance with the procedure given in [14]. The microspheric support (10 g) after drying at 120°C for 2 h was placed in a three-necked flask equipped with a thermometer and a stirrer, toluene (250 ml) was added, and the mixture was heated with stirring to reflux (105°C). Then, ODCS (5 ml) and pyridine (2 ml, after refluxing for 30 min) were added, the mixture was refluxed for 8 h. The reaction mixture was cooled to room temperature, and the sorbent was decanted, washed with acetone, water–acetone (1 : 1 v/v) mixture, and acetone on the filter, and dried at 120°C in air. Additional silanization with TMCS was performed by the procedure given above.

Modification of the filler surface with polymers. Copolymers of octadecyl methacrylate (ODMA) and methyl methacrylate (MMA) were prepared by the procedure presented in [11]. Octadecyl methacrylate (3.0 g) was mixed with MMA (3 ml) and polymerization initiator dicumyl peroxide (DCP, 0.05 g). The mixture was heated to reflux in a flask equipped with a reflux condenser until a viscous mass formed, after which the heating was terminated. The resulting oligomer was dissolved in *n*-pentane. The polymeric coating was deposited on the sorbent surface by the following procedure. Microspheric particles (5 g) were added to the solution containing oligomer (1.25 g) and DCP (40 mg) in pentane (15 ml), and the solvent was removed on a rotary evaporator. The dried powder was placed in a sealed flask and exposed to thermal treatment in accordance with the following schedule: The sample was first heated to 100°C over a period of 1 h, then the temperature was increased to 130°C in 1 h, and the sample was kept at this temperature for 2 h. The resulting powder was washed with toluene : dioxane (1/1 v/v) and acetone and dried in an oven at 120°C. The pore characteristics were determined by sorption of benzene vapor.

The HPLC analysis was performed on an HPLC device equipped with a Waters 600S controller, Waters 427 pump, and UV–VIS detector.

Some chromatographic parameters of the columns packed with the UFR–SG and UFR microspheres obtained are listed in Table 2. As can be seen, in the case of microspheric UFR–SG particles with significant content of silica (45–60 wt %), both silanes and polymeric agents act as effective modifiers. It should be noted that polymeric modification provides complete shielding of all the silanol groups on the filler surface, which is confirmed by retention times of pyridine and phenol. The pyridine peak appears before the phenol peak, which confirms the absence of interaction of the silanol groups on the filler surface with pyridine molecules.

Certain decrease in the silica content in the system does not noticeably affect the modification. To obtain polymer-modified sorbents (e.g., sample no. 4), the sample first was modified with vinylchlorosilane and then the polymeric ODMA–MAA layer was de-

Table 2. Main chromatographic properties of the columns packed with UFR–SG and UFR microspheres

Run no.	Packing based on sample no.*	Column, mm	Modifying agent	Retention time, min				Mobile phase	Pressure, bar
				uracil	pyridine	phenol	toluene		
1	1	150 × 4.6	ODCS, TMCS	1.71	–	1.69	2.20	30/70	126
2	2	50 × 4.6	Poly-ODMA–MMA	0.59	0.66	0.68	0.78	30/70	104
3	3	″	Poly-ODMA–MMA	0.52	0.54	0.66	1.02	30/70	114
4	3	″	″	0.59	0.64	1.00	1.48	30/70	74
5	3	″	″	0.53	0.60	0.75	2.10	30/70	86
6	4	″	″	0.70	0.71	0.64	0.68	30/70	95
7	4	″	″	0.57	0.68	0.72	1.25	30/70	78
8	4	″	″	0.53	0.67	0.69	1.42	30/70	92
9	6	″	″	0.68	0.69	0.63	0.63	30/70	96
10	7	150 × 4.6	″	1.65	1.41	1.53	3.01	30/70	132
11	8	″	TMCS	1.90	1.40	–	1.55	30/70	91
12	8	″	γ-APTES	1.96	1.39	–	1.28	50/50	100
13	8	50 × 4.6	Poly-ODMA–MMA	0.58	0.77	0.64	0.93	30/70	83

* Sample numbers are the same as in Table 1.

posited. The chromatographic parameters of the columns packed with microspheres modified with various agents are listed in Table 2.

In the case of polymeric modification, the effect of further decrease in the silica content is minor, which is confirmed by the data on polymeric coating of UFR microspheric particles (Table 2, sample nos. 6–8). Our chromatographic studies showed that these systems can be used as nonporous packing for reversed-phase HPLC (RP–HPLC).

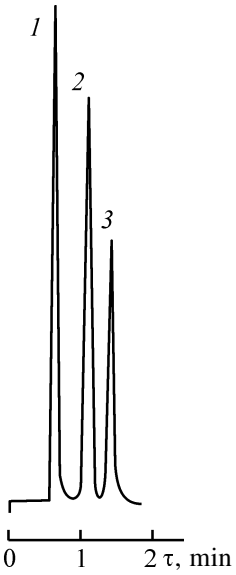


Fig. 1. Chromatographic pattern of the uracil–phenol–toluene model system obtained using the column packed with UFR–SG–C_{18}(TMCS) (Table 2, run no. 1). Components: (*1*) uracil, (*2*) phenol, and (*3*) toluene.

The chromatogram of the uracil–phenol–toluene model system, obtained using the column packed with UFR–SG–C_{18}(TMCS), is shown in Fig. 1. As can be seen, UFR–SG microspheres can be efficiently modified with silanes, i.e., the microsphere surface still contains significant amount of silanol groups capable of covalent bonding with alkyl groups. In the case of model solutions containing pyridine, strong tailing and delay of the pyridine peak are observed.

In the absence of silica, the results of modifying UFR microspheric particles with silanes were unsatisfactory. The resulting samples exhibited insufficient hydrophobic properties and the columns packed with them exhibited no features required of RP–HPLC (Table 2). After modification with trimethylchlorosilane, the retention times of toluene and uracil were 1.55 and 1.9 min, respectively; i.e., this sorbent is unsuitable for RP–HPLC. Similar results were obtained by modification with γ-aminopropyltriethoxysilane (γ-APTES); the toluene peak appeared before those of uracil and pyridine. However, after modification with the polymer (poly-ODMA–MMA), the column packed with the resulting microspheres became suitable for RP–HPLC.

The chromatographic pattern of the uracil–pyridine–phenol–toluene model system obtained using the column packed with UFR–SG–poly-ODMA–MMA is shown in Fig. 2. As can be seen, UFR–SG microspheres after polymeric modification exhibit no tailing and no strong retention of pyridine. This confirms that the polymeric modification provides complete shielding of all the silanol groups on the packing surface.

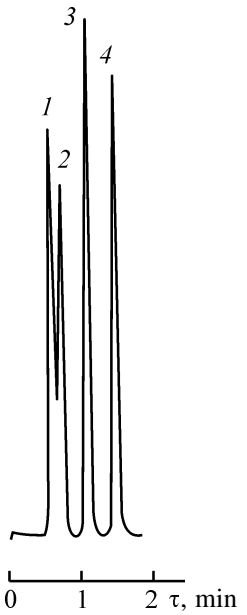


Fig. 2. Chromatographic pattern of the uracil–pyridine–phenol–toluene model system obtained using the column packed with UFR–SG–poly-ODMA–MMA (Table 2, run no. 4). Components: (*1*) uracil, (*2*) pyridine, (*3*) phenol, and (*4*) toluene.

Previously we showed that UFR microspheric particles are easily modified with polymers; this approach eliminates silanol interactions. In the case of UFR–SG, polymeric modification also eliminates silanol interaction (Table 2).

Moreover, the UFR and UFR–SG systems can be successfully used as nonporous packing for RP–HPLC. Comparison of the chromatographic parameters showed that after polymeric modification the retention time of toluene decreases. This is probably due to decreasing surface area of the sorbent (when the polymeric component fills the pores) or to insufficient amount of the C_{18} groups on the sorbent surface. However, our calculations showed that the amount of these groups on the surface is even greater than that at common modification with octadecyldimethylchlorosilane.

CONCLUSIONS

(1) Microspheric particles formed in the (urea–formaldehyde resin)–silica gel system after modification with octadecyldimethylchlorosilane and additional treatment with trimethylchlorosilane are suitable as packing for reversed-phase high-performance liquid chromatography.

(2) Modification with polymers provides efficient shielding of the surface of microspheres formed in the urea–formaldehyde resin system in the presence of silica gel and without it. Efficient shielding of the silanol groups is confirmed by the retention times of pyridine and phenol in the course of chromatographic analysis of the model system.

REFERENCES

1. Majors, R.E., *LG–GC Int*., 1998, April, pp. 7–21.
2. Majors, R.E., *LG–GC Int*., 1998, April, pp. 220–239.
3. Dolan, J.W., *LG–GC Int*., 1998, May, pp. 292–297.
4. US Patent 4010247, 1977.
5. Iler, R.K., *The Chemistry of Silica*, New York: Wiley–Interscience, 1979.
6. Airapetyan, S.S. and Khachatryan, A.G., *Kolloidn. Zh*., 2004, vol. 66, no. 1, pp. 1–3.
7. Airapetyan, S.S. and Khachatryan, A.G., *Kolloidn. Zh*., 2004, vol. 66, no. 4 pp. 451–454.
8. Micra Catalogue, 1997.
9. US Patent 4893369, 1991.
10. US Patent 5304364, 1992.
11. Hanson, M. and Unger, K.K., *LG–GC Int*., 1996, pp. 650–656.
12. Sun, X. and Chai, Z., *J. Chromatogr., Ser. A*, 2002, vol. 943, no. 2, pp. 209–216.
13. Lei, S., Yu., S., and Zhao, C., *J. Chromatogr. Sci*., 2001, vol. 39, no. 7, pp. 280–286.
14. Hayrapetyan, S.S. and Khachatryan, H.G., *Micropor. Mesopor. Mater*., 2005, vol. 78, nos. 2–3, pp. 151–157.
15. Neue, U.D., *Encyclopedia of Analytical Chemistry*, Meyers, R.A., Ed., Chichester: Wiley, 2000, pp. 11450–11472.

ISSN 1070-4272. Russian Journal of Applied Chemistry, 2006, Vol. 79, No. 1, pp. 60–63. © Pleiades Publishing, Inc., 2006.
Original Russian Text © V.V. Sidorchuk, 2006, published in Zhurnal Prikladnoi Khimii, 2006, Vol. 79, No. 1, pp. 62–65.

SORPTION AND ION-EXCHANGE PROCESSES

Hydrothermal Modification of Silica in the Form of a Hydrogel–Xerogel

V. V. Sidorchuk

Institute of Sorption and Problems of Endoecology, National Academy of Sciences of Ukraine, Kiev, Ukraine

Received May 18, 2005

Abstract—The influence exerted by the conditions of hydrothermal treatment of silicas in the form of a gel–xerogel on the pore structure and mechanical properties of the adsorbents obtained was studied.

DOI: 10.1134/S1070427206010125

Two methods for hydrothermal modification of silicas are known: in the form of (i) moist true gel or coagel (sediment) and (ii) dry xerogel [1–3]. Exhibiting common patterns in variation of the pore structure parameters (decrease in the specific surface area and expansion of pores with an increase in temperature [4]), both the methods have their own specific features. For example, treatment of moist gels leads to a significant increase in the pore volume (up to 3 $cm^3\ g^{-1}$), whereas in modification of dry xerogels, this quantity remains unchanged. As a result, the pore size increases to a considerably greater extent in the first case, compared with the second. This, in turn, leads to a poorer mechanical strength of silicas treated as moist gels, compared with those processed in the form of dry xerogels [1, 5–8].

It is known that the strength of a porous body is determined by the strength of unit contacts between primary particles, p_1, and their number on a unit cross-section area, Q_S, which directly depends on the pore volume [1, 9]. Sorption, catalysis, and chromatography frequently require supports that simultaneously have large volume and size of pores and a high mechanical strength [10]. In this study, an attempt was made to combine the advantages of the two above-mentioned alternatives of hydrothermal modification of silica gels: they were treated as a moist hydrogel during a part of time (to achieve a more pronounced increase in the volume and size of pores) and as a dry xerogel during the rest of the time (in order to strengthen the skeleton).

EXPERIMENTAL

As a model serve aerosilogel prepared by the procedure described in [8]: by dispersing an aerosil of A-300 brand in a dispersion medium (distilled water or 2% aqueous ammonia) at an s : l ratio equal to 0.20. The resulting gel was subjected to a hydrothermal treatment at 100–400°C for 5 h either in a moist state or as a dry xerogel (in both cases, an amount of water, necessary for creating an equilibrium pressure of its vapor, was introduced onto the bottom of an autoclave). In addition, a moist gel was modified as follows: it was introduced into the autoclave in an amount that contains a portion of water whose evaporation leads to establishment in the autoclave of an equilibrium pressure at a chosen temperature (modification in the form of a gel–xerogel). As a result, the gel was treated as a moist gel for a certain time (until water was completely evaporated) and as a dry xerogel during the rest of the time. A dry xerogel requiring no drying was discharged from the autoclave. It is known that, in the case of modification of a hydrogel and xerogel with introduction of water to the bottom of an autoclave, the result is determined exclusively by the duration of the isothermal period, being independent of the heating rate [4]. At the same time, when the treatment of a moist gel involves only water contained in the gel itself (treatment of a gel–xerogel), the rate at which the autoclave is heated to a prescribed temperature strongly affects the results obtained, because it predetermines the duration of modification in the form of a moist gel. Both fast (in 0.5 h) and slow (in 2 h) heating modes were used.

The specific surface area S ($m^2\ g^{-1}$) of aerosilogels was found by measuring the thermal desorption of argon with a GKh-1 gas meter, the total pore volume V_Σ ($cm^3\ g^{-1}$) was determined by impregnation with water, and the average pore diameter was calculated using the formula $d_p = 4V_\Sigma 10^3/S$ (nm). The mech-

Table 1. Effect of the mode of hydrothermal treatment on the pore structure of aerosilogels (heating in 2 h)

Gel				Gel–xerogel			Xerogel		
T, °C	S, $m^2\ g^{-1}$	V_Σ, $cm^3\ g^{-1}$	d_p, nm	S, $m^2\ g^{-1}$	V_Σ, $cm^3\ g^{-1}$	d_p, nm	S, $m^2\ g^{-1}$	V_Σ, $cm^3\ g^{-1}$	d_p, nm
20	293	1.40	19.0	293	1.40	19.0	293	1.40	19.0
150	–	–	–	–	–	–	145	1.40	38.5
200	164	1.66	40.5	154	1.54	40.0	92	1.41	61.0
250	148	1.86	50.5	69	1.70	98.5	60	1.40	93.5
300	93	2.14	92.0	44	1.97	179.0	54	1.39	104.0
350	59	2.74	189.0	19	2.25	473.5	32	1.40	175.0
400	35	2.37	271.0	13	2.45	754.0	20	1.40	280.0

Table 2. Effect of the conditions of hydrothermal treatment on the strength of unit contacts of aerosilogels

Aerosilogel	$p_1 \times 10^{10}$, Pa, at indicated T, °C						
	20	150	200	250	300	350	400
Gel, water	1.6	–	6.5	8.3	29.0	154.0	177.0
Gel–xerogel:							
water, 2 h	1.6	–	10.0	132.0	380.0	1650.0	2485.0
water, 0.5 h	1.6	–	61.0	235.0	410.0	720.0	3000.0
2% ammonia, 2 h	3.0	–	190.0	–	910.0	–	4000.0
Xerogel, water	1.6	14.2	51.0	152.0	194.0	660.0	1195.0

anical strength of cylindrical grains, P_m (MPa) was measured with an MP-2S device.

The strength of unit contacts, p_1 (Pa), was calculated by the formula [9]

$$p_1 = P_m/Q_s, \quad (1)$$

and the number of contacts on a unit cross section, Q_s (cm^{-2}), by the formula [11]

$$Q_s = 7.32 \times 10^{10} S^2/V_\Sigma^{2/3}. \quad (2)$$

The manner in which the porous structure parameters of aerosilogels vary in different types of hydrothermal treatment, presented in Table 1, is well consistent with the patterns known for silica sorbents [1–4, 8, 11]: as temperature increases, the specific surface area decreases, pores expand, and the pore volume grows (for gels) or remains constant (for xerogels). As would be expected, tendencies characteristic of treatments in the form of a gel and a xerogel are combined in modification in the form of a gel–xerogel. The decrease in the specific surface area in combined treatment is the most pronounced at temperatures $T \geq 300$°C, and at $T \leq 250$°C the pore size exceeds the corresponding values in treatment of a gel and a xerogel. These experimental data are not quite understandable in terms of the commonly accepted mechanisms of changes in the porous structure in hydrothermal modification of silicas [4].

The most interesting results presented in Table 2 and Figs. 1–3 were obtained for changes in the mech-

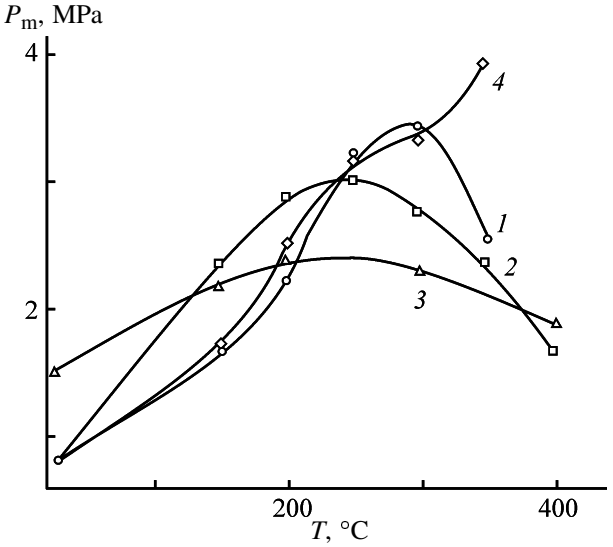


Fig. 1. Mechanical strength P_m of gels-xerogels vs. temperature T of hydrothermal treatment: (*1*) water, heating in 2 h; (*2*) water, heating in 0.5 h; and (*3*) 2% ammonia solution, heating in 0.5 h.

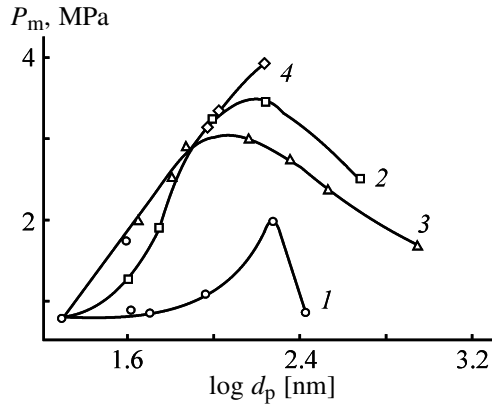


Fig. 2. Mechanical strength P_m of gels-xerogels vs. average pore size d_p in hydrothermal treatment of moist aerosilogels. (*1*) Gel, (*2*) gel–xerogel (heating in 2 h), (*3*) gel–xerogel (heating in 0.5 h), and (*4*) xerogel.

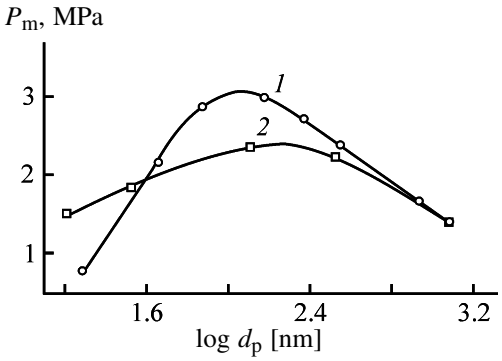


Fig. 3. Mechanical strength P_m of xerogels vs. average pore size d_p in hydrothermal treatment in the form of a gel–xerogel at fast heating (in 0.5 h). Medium: (*1*) water and (*2*) 2% ammonia solution.

anical strength of aerosilogels in the course of hydrothermal treatment by different methods. For example, the mechanical strength steadily increases with temperature only in treatment of a xerogel, whereas in all the other methods, the P_m–T dependence has an extremum, as also does the dependence of P_m on the pore size (Figs. 2, 3). A similar pattern has been observed in hydrothermal treatment of other silicas [1, 5–8] and was attributed to possible thinning of pore walls for very coarsely porous samples formed at high temperatures.

Only at temperatures exceeding 250–300°C (depending on the rate of autoclave heating), the mechanical strength of samples modified in the form of a xerogel exceeds the value of P_m for aerosilogels treated in the form of a gel–xerogel. In the case of fast heating and treatment in the range 150–200°C, the value of P_m for samples modified in the form of a gel–xerogel exceeds by 20–25% the similar parameter for samples processed as a xerogel. Figures 2 and 3 show that, up to a pore size of 100 nm, the silicas obtained by hydrothermal treatment of a gel–xerogel are as strong as the samples modified in the form of a xerogel and substantially exceed in strength the aerosilogels treated as a gel, even though having considerably larger V_Σ than xerogels (Table 1) and, accordingly, smaller Q_s.

In all cases, the strength of unit contacts (Table 2), calculated by formulas (1) and (2), steadily increases with temperature, but does so for the gel to the least extent, because the gel has the least close-packed structure and mass transfer in its treatment is predominantly directed from the surface of fine particles to that of coarse particles, rather than to places of their contact [2, 4]. Therefore, coagulation-type, i.e., the least strong contacts between particles exist in gels [2, 9].

The maximum rise in the strength of unit contacts was recorded in treatment as a gel–xerogel, especially for samples obtained with a 2% ammonia solution. In this case, mass transfer directed to places of contact between particles markedly exceeds that for the gel [3, 4, 8], which leads to formation of strong phase contacts between particles [9].

An unexpected result among those under consideration is the smaller value of p_1 for the most close-packed structure (xerogel), for which the intensity of mass transfer to places of contact between particles must be the highest. The strength of a porous body depends not only on the parameters appearing in formula (1), but also on the presence of mechanical stresses in the structure [9, 10]. Therefore, it may be assumed that the mode of hydrothermal treatment of a gel–xerogel, which, as already noted, is accompanied by mild drying (at a smaller humidity gradient between the gel and the medium), prevents build-up of stress at places of interparticle contacts. This is also confirmed by the data reported in [12].

CONCLUSIONS

(1) A new mode of hydrothermal treatment of silica adsorbents, modification in the form of a gel–xerogel, was considered. This mode enables the following. First, it is possible to combine hydrothermal treatment of a gel and a xerogel and sample drying in a single process. Second, thanks to this combining, the advantages of each separate modification method can be used and thereby it is possible to control in a substantially wider range the specific surface area and the volume and size of pores. As a result, samples

simultaneously having a large pore volume, small specific surface area, and sufficiently high mechanical strength can be obtained.

(2) A technical and economical disadvantage of this treatment technique consists in that the output capacity of the process at temperatures below 300°C is not high, because the filling of the autoclave with the gel does not exceed 25%. Therefore, it is better to use the hydrothermal modification of a gel–xerogel at temperatures $T \geq 300$°C.

REFERENCES

1. Dzis'ko, V.A., Tarasova, D.V., and Vishnyakova, G.P., *Kinet. Katal.*, 1967, vol. 8, no. 1, pp. 193–197.
2. Fenelonov, V.B., Tarasova, D.V., and Gavrilov, V.Yu., *Izv. Sib. Otd. Akad. Nauk SSSR, Ser. Khim. Nauk*, 1978, issue 4, no. 9, pp. 116–129.
3. Iler, R.K., *The Chemistry of Silica*, New York: Wiley–Interscience, 1979.
4. Leboda, R., Charmas, B., and Sidorchuk, V.V., *Adsorp. Sci. Technol.*, 1997, vol. 15, no. 3, pp. 189–214.
5. Leboda, R., Charmas, B., and Sidorchuk, V.V., *Adsorp. Sci. Technol.*, 1997, vol. 15, no. 3, pp. 215–230.
6. Chertov, V.M., Tsyrina, V.V., and Shamrikov, V.M., *Zh. Prikl. Khim.*, 1991, vol. 64, no. 1, pp. 12–16.
7. Chertov, V.M., Tsyrina, V.V., Shamrikov, V.M., and Malkiman, V.I., *Izv. Akad. Nauk SSSR, Neorg. Mater.*, 1991, vol. 27, no. 4, pp. 752–754.
8. Maidannik, D.G., Sidorchuk, V.V.. and Tertykh, V.A., *Zh. Prikl. Khim.*, 1993, vol. 66, no. 9, pp. 2054–2058.
9. Shchukin, E.D., Amelina, E.A., and Kontorovich, S.I., *Kolloidn. Zh.*, 1978, vol. 40, no. 5, pp. 938–945.
10. Sidorchuk, V.V. and Tertykh, V.A., *Khim. Tekhnol.*, 1989, no. 4, pp. 3–15.
11. Maidannik, D.G., Sidorchuk, V.V., and Tertykh, V.A., *Zh. Prikl. Khim.*, 1995, vol. 68, no. 2, pp. 232–235.
12. Danilov, O.L. and Leonchik, B.I., *Inzh.-Fiz. Zh.*, 1967, vol. 13, no. 3, pp. 283–288.

ISSN 1070-4272. Russian Journal of Applied Chemistry, 2006, Vol. 79, No. 1, pp. 64–68. © Pleiades Publishing, Inc., 2006.
Original Russian Text © V.V. Sidorchuk, 2006, published in Zhurnal Prikladnoi Khimii, 2006, Vol. 79, No. 1, pp. 66–70.

SORPTION AND ION-EXCHANGE PROCESSES

Changes in the Pore Structure of Silica in Chemical Modification with Organic Compounds

V. V. Sidorchuk

Institute of Sorption and Problems of Endoecology, National Academy of Sciences of Ukraine, Kiev, Ukraine

Received May 18, 2005

Abstract—Changes in the pore structure of silica adsorbents in their chemical modification with organic compounds of various kinds by gas- and liquid-phase processes, as well as those under conditions of high pressure of the reagents, were studied.

DOI: 10.1134/S1070427206010137

It is believed that changes in the parameters of the pore structure of silicas in their chemical modification is determined by the degree of grafting, size of the molecule of a modifying reagent, and structure of a modifying bed [1, 2]. In the process, the specific surface area S, total pore volume V_Σ, and pore size d, as a rule, decrease. In [2], an equation is given for calculating the specific surface area of modified silica after chemisorption of aliphatic linear reagents. This equation can be used to calculate the decrease in the specific surface area, ΔS, upon modification via shileding of the surface of the starting silica. The calculated value of ΔS depends on the nature and structure of the modifier molecule. At the same time, the value of ΔS can be found from experimental data as the difference of the specific surface areas of the starting and modified silicas:

$$\Delta S = S_0 - S, \quad (1)$$

where S_0 is the specific surface area of the starting silica, and S, that of modified silica; both the quantities are experimentally measured.

In most cases, the calculated decrease in the specific surface area, ΔS, is markedly lower than that measured experimentally. This may be due to the fact that the influence exerted on the decrease in the specific surface area of silica by processes of mass transfer of silica itself, which are possible in pore bodies at elevated temperatures, is disregarded. For example, mass transfer is the main mechanism by which the pore structure of silicas of varied origin changes (primarily, this refers to the specific surface area) in treatment in aqueous media, especially under hydrothermal conditions [2–4].

Although the solubility of silicon dioxide in organic media is considerably lower than that in water [3], it is clearly impossible to disregard mass transfer of silica in its modification with organic compounds. This is so because many liquid-phase, and especially gas-phase, modification processes are performed at elevated temperatures (100–400°C and higher) [2, 5], when mass transfer via surface self-diffusion of silica is possible. It is not advisable to disregard the influence exerted on mass transfer processes by water desorbed from the surface in the course of modification and by that released in surface reactions. This is of particular importance in the presence of nitrogen-containing organic bases, which are frequently used as catalysts for modification processes [5]. It is necessary to primarily take into account the mass transfer of silica in modification under the conditions of a high pressure in the autoclave [6]. In view of the aforesaid, the total decrease in the specific surface area of silica, ΔS, in the course of its chemical modification should be, in the general case, a sum of at least two terms:

$$\Delta S = \Delta S_{chem} + \Delta S_{mass}, \quad (2)$$

where ΔS_{mass} is the change in the specific surface area associated with mass-transfer processes, and ΔS_{chem} is that associated with shielding of the surface by a grafted layer.

Equations (1), (2) and experimental data make it possible to evaluate each component of the change in the specific surface area in chemical modification. For example, ΔS_{chem} can be found if mass transfer of silica is excluded in modification.

In the authors' opinion, use of the specific surface area of silica in calculating the surface concentration

Table 1. Change in of the adsorption-structural characteristics of aerosilogel in relation to the modification conditions

Sample no.	Modification conditions	S	S_{corr}	v_Σ, $cm^3\ g^{-1}$	μ, μmol m^{-2}
		$m^2\ g^{-1}$			
1	Starting	336	336	1.36	–
2	Keeping in autoclave at 250°C	328	328	1.36	–
3	l/ph, 117°C, *n*-butanol	270	308	1.18	2.32
4	l/ph, 123°C, hexamethyldisiloxane	151	203	1.12	2.56
5	l/ph, 56°C, acetone	335	335	1.36	–
6	l/ph, 62°C, hexane	338	338	1.36	–
7	l/ph, 135°C, chlorobenzene	334	334	1.36	–
8	g/ph, 300°C, *n*-butanol	242	287	1.22	2.86
9	g/ph, 450°C, *n*-butanol	211	263	1.17	3.61
10	g/ph, 150°C, hexamethyldisiloxane	250	305	1.16	1.96
11	g/ph, 450°C, hexamethyldisiloxane	213	231	1.14	0.75
12	g/ph, 300°C, acetone	333	333	1.35	–
13	g/ph, 300°C, hexane	337	337	1.36	–
14	g/ph, 300°C, chlorobenzene	332	332	1.35	–
15	g/ph, 450°C, hexamethyldisiloxane	260	292	1.20	1.03
16	P = 40 atm, 250°C, *n*-butanol	182	255	1.17	5.33
17	P = 42 atm, 250°C, hexamethyldisiloxane	116	152	1.11	2.37
18	P = 100 atm, 250°C, acetone	275	275	1.36	–
19	P = 77 atm, 250°C, hexane	266	266	1.35	–
20	P = 51 atm, 250°C, chlorobenzene	252	252	1.34	–

of grafted groups (μmol m^{-2}) is unjustified. If the modification processes occur without mass transfer of silica, the specific surface area of the starting silica should be used. If, however, the mass transfer of silica does occur in modification, it is necessary to use a corrected value of the specific surface area, which takes into account the decrease in the specific surface area of the starting silica via mass transfer:

$$S_{corr} = S_0 - \Delta S_{mass} \quad (3)$$

or, with account of Eqs. (1) and (2),

$$S_{corr} = S + \Delta S_{chem}. \quad (4)$$

It is just the quantity S_{corr}, rather than S_0 or S_{chem} (frequently suggested in the literature [2, 5]), that is preferable for calculation of the surface concentration μ (μM) of grafted groups:

$$\mu = c \times 10^3 / S_{corr}, \quad (5)$$

where c is the concentration of grafted groups (μmol g^{-1}).

EXPERIMENTAL

The study was concerned with changes in the pore structure parameters of a model silica, aerosilogel prepared using the procedure described in [7], in the course of its modification with organic compounds of varied nature by ordinary gas- and liquid-phase processes [5] and also under conditions of a high pressure of reagents in the autoclave [6]. The starting aerosilogel was preliminarily dried in air at 150°C for 4 h (for liquid-phase and autoclave processes) or thermally treated in a vacuum at 150°C for 2 h at a residual pressure of 10^{-3} Torr (for gas-phase processes).

All the compounds were purified and dried prior to being used for modification. The specific surface area of the starting (S_0) and modified (S) silicas was measured by the method based on thermal desorption of argon on a GKh-1 gas meter, the total pore volume V_Σ was found by impregnation with ethanol [8], and the pore size distribution was determined on a PA-3M mercury porosimeter. The course of surface reactions was monitored qualitatively by measuring IR spectra on an IKS-29 spectrophotometer in the range 4200–1400 cm^{-1}, and quantitatively, by derivatographic analysis on a Q-1500D instrument in the temperature range 20–1000°C and a heating rate of 10 deg min^{-1} [9, 10], and also by elemental analysis on a Carlo Erba CHN Mod 1106 elemental analyzer.

Table 1 lists data on modification of the aerosilogel with various organic compounds in several ways. It can be seen that, for ordinary gas-phase (g/ph) and

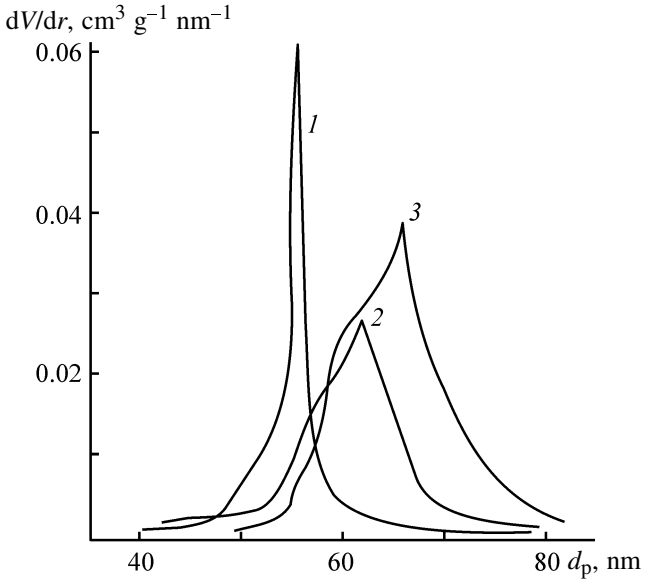


Fig. 1. Pore size distribution, according to data of mercury porosimetry, for (*1*) starting aerosilogel and (*2, 3*) aerosilogels treated in the autoclave with hexane at (*2*) 200 and (*3*) 300°C. (*V*) Pore volume, (d_p) pore diameter, and (*r*) pore radius.

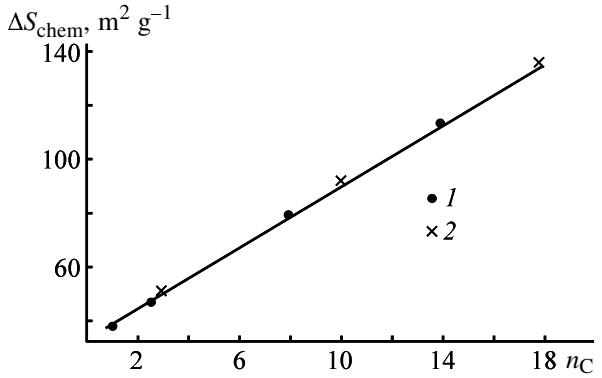


Fig. 2. Specific surface area ΔS_{chem} containing 1 mmol of a grafted substance vs. the length n_C of the hydrocarbon chain of the modifier. (*1*) Aliphatic alcohols and (*2*) alkylchlorosilanes according to [1].

liquid-phase (l/ph) processes, S and V_Σ decrease only in those cases when chemical modification of the surface occurs. When this is not the case, S and V_Σ remain virtually constant, despite the rather high treatment temperature, which is exemplified by gas-phase modification in a quartz cell (sample nos. 12–14; it should be noted that the pressure of modifier vapor in gas-phase processes did not exceed 100 mm Hg). At the same time, treatment in an autoclave even with such compounds, chemically inert toward the silica surface, as hexane, acetone, or chlorobenzene (sample nos. 18–20) leads to a rather significant decrease in the specific surface area at a constant V_Σ (modifier vapor pressure 40–100 atm). The change in the pore structure of the aerosilogel upon its modification with hexane is also indicated by the distribution curves of pore volume with pore size, measured using mercury porosimetry (Fig. 1): it can be seen that the curves are shifted into the region of larger pore radii. In this case, there is no grafting of organic fragments to the surface (according to the data furnished by IR spectroscopy and derivatography). Therefore, the decrease in S and also a change in the type of pore volume distribution respect to pore sizes should be attributed to rearrangement of the skeleton of silica via mass transfer. The strongest decrease in the specific surface area is observed when aerosilogel is modified with hexamethyldisilazane (sample nos. 4, 10, 17), whose interaction with silanol groups on the surface yields ammonia, which intensifies the mass transfer [3].

In order to rule out the mass transfer of silica, an aerosilogel sample preliminarily hydrothermally treated at 250°C was subjected to chemical modification in an autoclave at 250°C. It is known that treatment under more severe, in particular, hydrothermal, conditions precludes mass transfer in a subsequent treatment under milder conditions [11]. In this case, $\Delta S_{mass} = 0$ and $\Delta S_{chem} = S_0 - S$. As a result, we obtained the dependence of ΔS_{chem} per 1 mmol of a grafted alcohol on its chain length (C_1–C_{14}) (Fig. 2). The line constructed is also a good fit to the points calculated using the data of [1] for silicas modified with alkylchlorosilanes with a length of the hydrocarbon chain C_3, C_{10}, and C_{18}. Hence follows the conclusion that the plot in Fig. 2 can be used with a satisfactory accuracy for evaluating ΔS_{chem} in treatment of silica with any linear multifunctional modifier.

Similarly, experiments on modification of aerosilogel samples hydrothermally treated at 250°C with trimethylchlorosilane, trimethyliodosilane, hexamethyldisiloxane, and hexamethyldisilazane show that grafting of 1 mmol of trimethylsilyl groups to the silica surface leads to a decrease in the specific surface area of silica by 105 ± 5 $m^2\ g^{-1}$.

The resulting values of ΔS_{chem} were used to calculate S_{corr} and the concentration of grafted groups per unit surface area (Table 1). The values of μ calculated by Eq. (1) using the values of S_{corr} were 10–30% higher than those obtained using the specific surface area S_0 of the starting silica and 10–30% lower than those obtained with the specific surface area S of modified samples.

In order to verify the results of calculation of ΔS_{chem}, chemical modification in the autoclave was also performed for aerosilogels preliminarily treated

Table 2. Changes in the adsorption-structural characteristics in chemical modification in an autoclave of aerosilogels preliminarily treated under hydrothermal conditions

Sample no.	Modification conditions*	S, $m^2\ g^{-1}$	S_{corr}, $m^2\ g^{-1}$	v_Σ, $cm^3\ g^{-1}$	d_p, nm	μ, μmol m^{-2}
1	HTT 200°C, 3 h	115	115	1.36	53.0	–
2	Sample no. 1 + 200°C, *n*-butanol	88	116	1.23	43.0	5.60
3	Sample no. 2 + hydrolysis	112	112	1.35	52.5	–
4	Sample no. 1 + 250°C, *n*-butanol	70	109	1.15	41.5	5.96
5	Sample no. 4 + TT 450°C	113	113	1.35	55.0	–
6	Sample no. 4 + hydrolysis	114	114	1.35	54.0	–
7	Sample no. 1 + 300°C, *n*-butanol	71	104	1.19	47.0	5.58
8	Sample no. 7 + TT 450°C	98	98	1.36	57.0	–
9	Sample no. 7 + hydrolysis	104	104	1.34	56.0	–
10	HTT 150°C 3 h	133	133	1.36	46.5	–
11	Sample no. 10 + 150°C, *n*-butanol	100	123	1.29	40.0	3.41
12	Sample no. 11 + TT 450°C	120	120	1.35	48.0	–
13	Sample no. 11 + hydrolysis	125	125	1.37	48.5	–
14	Sample no. 10 + 150°C, hexamethyldisilazane	70	102	1.17	37.0	2.96
15	Sample no. 14 + TT 700°C	105	105	1.34	50.5	–
16	Sample no. 10 + 250°C, *n*-butanol	70	111	1.18	38.0	6.20
17	Sample no. 16 + TT 450°C	117	117	1.35	48.0	–
18	Sample no. 16 + hydrolysis	110	110	1.35	49.0	–
19	Sample no. 10 + 250°C, hexamethyldisilazane	46	84	1.23	44.0	4.28
20	Sample no. 19 + TT 700°C	90	90	1.36	61.0	–

* HTT and TT are hydrothermal and thermal treatments, respectively.

under hydrothermal conditions at 150 and 200°C (Table 2). Butoxy groups were removed from the silica surface after chemical modification either by mild hydrolysis (by boiling in water in the presence of ammonia) or by thermal decomposition in air at 450°C. Trimethylsilyl groups were removed by thermal decomposition in air at 700°C (the temperatures of thermal decomposition were found from derivatographic measurements). In this way we restored the surface onto which the modifiers were grafted. The data obtained indicate the following.

(1) If the temperature of chemical modification with *n*-butanol does not exceed that of hydrothermal treatment by more than 50°C, then there is virtually no mass transfer of silica in the course of modification and, after removal of butoxy groups, the specific surface area virtually coincides with the value of S for the sample before modification (compare sample nos. 1, 3, 5, 6 and 10, 12, 13).

(2) If, however, the temperature of chemical modification exceeds that of preliminary hydrothermal treatment by 100°C, the former process may involve an additional decrease in the specific surface area via mass transfer of silicon (compare sample nos. 1, 8, 9, and 10, 17, 18).

(3) In chemical modification with hexamethyldisilazane, during which ammonia is liberated, mass transfer of silica apparently occurs at any of the temperatures studied (compare sample nos. 10, 15, 20).

The change in the most probable pore size (Table 2), calculated from porosimetric data, confirms the above reasoning.

The following experimental fact should be mentioned in conclusion: chemical modification is necessarily accompanied by a decrease in the pore volume (Tables 1, 2). At the same time, it is known that treatment in the absence of chemical modifiers does not change the pore volume of silica xerogels. The magnitude of the decrease in V_Σ is proportional to the degree of grafting and to the molar volume of modifier; however, an additional study is necessary for establishing a clearly pronounced relationship. It should only be added here that the decrease in the total pore volume of silicas is a good indicator of their chemical modification, and the V_Σ measurement itself is a simple express technique for establishing the fact of grafting of a modifier to the surface.

CONCLUSIONS

(1) The results obtained in the study point to an important contribution made by mass transfer of silica to the decrease in its specific surface area in chemical modification with organic compounds, especially under conditions of a high pressure of reagents.

(2) A more precise calculation of the concentration of grafted groups per unit surface area requires, in addition to measuring the specific surface area of modified silica, also estimating the extent to which the specific surface area decreases via shielding of the surface by the grafted layer. It is shown that the following support can be used for this purpose: silica treated under hydrothermal conditions at a temperature exceeding by 100–150°C that of the reaction of chemical modification.

REFERENCES

1. Berendsen, G.E., Pikaart, K.A., and Galan, L. de, *J. Liq. Chromatogr.*, 1980, vol. 3, no. 10, pp. 1437–1464.
2. *Modifitsirovannye kremnezemy v adsorbtsii, katalize, khromatografii* (Modified Silicas in Adsorption, Catalysis, and Cromatography), Lisichkin, G.V., Ed., Moscow: Khimiya, 1986.
3. Iler, R.K., *The Chemistry of Silica*, New York: Wiley–Interscience, 1979.
4. Leboda, R., Charmas, B., and Sidorchuk, V.V., *Adsorp. Sci. Technol.*, 1997, vol. 15, no. 3, pp. 189–214.
5. Tertykh, V.A. and Belyakova, L.A., *Khimicheskie reaktsii s uchastiem poverkhnosti kremnezema* (Chemical Reactions Involving the Surface of Silica), Kiev: Naukova Dumka, 1991.
6. Sidorchuk, V.V., Tertykh, V.A., Leboda, R., and Hubicki, Z., *Adsorp. Sci. Technol.*, 1995, vol. 12, no. 3, pp. 231–238.
7. Maidannik, D.G., Sidorchuk, V.V., and Tertykh, V.A., *Zh. Prikl. Khim.*, 1993, vol. 66, no. 9, pp. 2054–2058.
8. *Adsorbtsiya organicheskikh veshchestv iz vody* (Adsorption of Organic Substances from Water), Koganovskii, A.M., Ed., Leningrad: Khimiya, 1990.
9. Leboda, R., *J. Therm. Anal.*, 1978, vol. 13, no. 2, pp. 213–220.
10. Belyakova, L.A., Tertykh, V.A., and Bortun, A.I., *Khim. Tekhnol.*, 1987, no. 2, pp. 3–8.
11. Chertov, V.M., Litvin, V.I., and Tsyrina, V.V., *Ukr. Khim. Zh.*, 1985, vol. 51, no. 6, pp. 926–928.

ISSN 1070-4272. Russian Journal of Applied Chemistry, 2006, Vol. 79, No. 1, pp. 69–73. © Pleiades Publishing, Inc., 2006.
Original Russian Text © E.M. Rakhman'ko, A.L. Gulevich, T.N. Kiiko, V.A. Kovalevich, 2006, published in Zhurnal Prikladnoi Khimii, 2006, Vol. 79, No. 1, pp. 71–76.

SORPTION AND ION-EXCHANGE PROCESSES

Effect of Solvating Additives on Anion-Exchange Extraction of Trichloroacetate Anions from Aqueous Solutions with Trinonyloctadecylammonium Picrate in Toluene

E. M. Rakhman'ko, A. L. Gulevich, T. N. Kiiko, and V. A. Kovalevich

Belarussian State University, Minsk, Belarus

Received October 10, 2005

Abstract—The solvation effect of trifluoroacetophenone derivatives on anion-exchange extraction of trichloroacetate anions from aqueous phase with trinonyloctadecylammonium picrate in toluene was studied.

DOI: 10.1134/S1070427206010149

Solutions of higher quaternary ammonium salts (QASs) in organic solvents immiscible with water efficiently extract various anions from aqueous phase by the anion-exchange mechanism [1]. The extractability of anions from aqueous solutions in these systems is quantitatively characterized by the concentration equilibrium constant $K_{Cl^-}^{An^-}$ of the anion-exchange reaction

$$R_4N^+Cl^-_{org} + An^-_{aq} \rightleftarrows R_4N^+An^-_{org} + Cl^-_{aq}.$$

It is known that the order of extractability of anions of various kinds with liquid anion exchangers does not depend on the organic solvent [1]. Therefore, the relative extractability of anions in their series can be changed either by going to another liquid anion exchanger [2] or by adding some additional solvating agent [3]. For example, even small additions of hexyl *p*-trifluoroacetylbenzoate (approximately 10^{-2} M) increase the extraction constant of carboxylate anions R–COO$^-$ with QASs in organic solvents by several orders of magnitude [4].

In this study we examined the effect of trifluoroacetophenone derivatives of various structures on anion-exchange extraction of trichloroacetate anions from aqueous phase with a quaternary ammonium picrate in toluene and determined the extraction and solvation constants and the average solvation numbers.

EXPERIMENTAL

We studied the extraction of trichloroacetate (TCA) anions from aqueous sodium trichloroacetate with a liquid anion exchanger, trinonyloctadecylammonim $[(C_9H_{19})_3C_{18}H_{37}N^+]$ picrate, TNODA Pic, in toluene. The extraction was carried out in test tubes with ground-glass stoppers at the volume ratio of the organic and aqueous phases of 1 : 1 at 293 ± 1 K. After completion of the extraction, the aqueous phase was separated and filtered. The content of picrate anions in the filtered solutions was determined spectrophotometrically on an SF-26 spectrophotometer [5].

The ion-exchange extraction of TCA$^-$ anions from aqueous phase with TNODA Pic in toluene can be described by equation of the following heterogeneous reaction:

$$R_4N^+Pic^-_{org} + TCA^-_{aq} \rightleftarrows R_4N^+TCA^-_{org} + Pic^-_{aq}. \quad (1)$$

The concentration constant of this reaction $K_{Pic^-}^{TCA^-}$ was calculated by the equation

$$K_{Pic^-}^{TCA^-} = \frac{[Pic^-]^2}{(c_{0,R_4N^+Pic^-} - [Pic^-])(c_{0,TCA^-} - [Pic^-])}, \quad (2)$$

where $c_{0,R_4N^+Pic^-}$ is the initial TNODA Pic concentration and c_{0,TCA^-}, the initial trichloroacetate anion concentration in the aqueous phase.

On addition of the solvating agent S to the organic phase, TNODA TCA is selectively solvated with S molecules by the reaction

$$R_4N^+TCA^- + pS \rightleftarrows R_4N^+TCA^-\cdots pS. \quad (3)$$

whereas TNODA Pic is not solvated [6].

The constant $K_{Pic^-}^{TCA^-}$ [Eq. (2)] does not take into account the solvation of the extracted TCA anions by reaction (3) (Eq. 1). Therefore, this constant is considered to be an apparent quantity and hereinafter is denoted as $\tilde{K}_{Pic^-}^{TCA^-}$.

Logarithms of the apparent anion-exchange extraction constants, logarithms of the solvation constants, and average solvation numbers of TCA anions in their extraction from aqueous phase with TNODA Pic in toluene in the presence of solvating additives S (10^{-2} M)

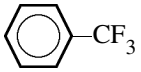
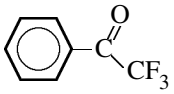
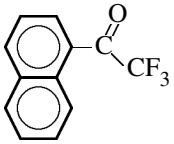
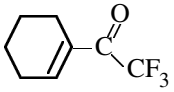
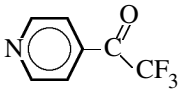
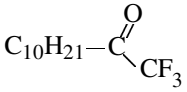
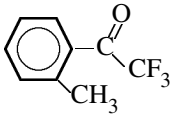
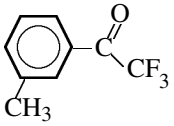
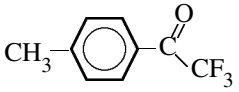
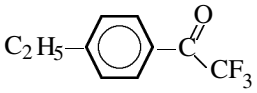
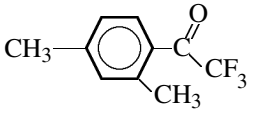
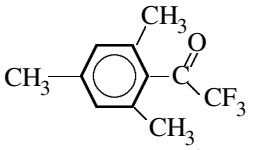
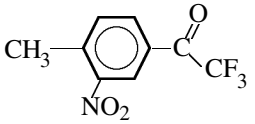
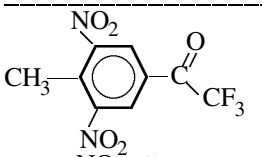
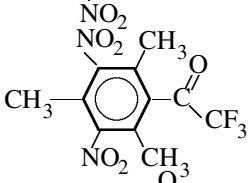
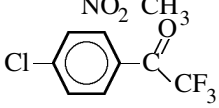
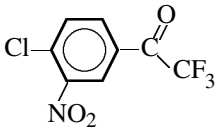
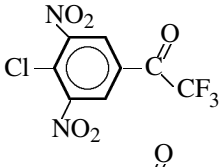
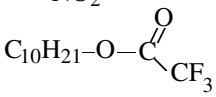
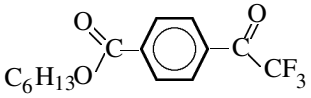
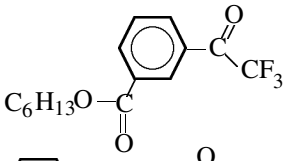
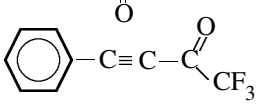
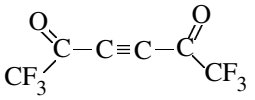
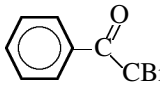
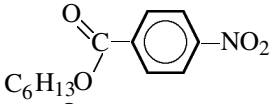
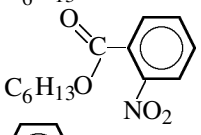
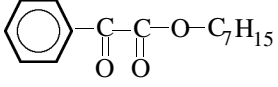
Solvating additive		$\log \tilde{K}_{Pic^-}^{TCA^-}$	$\Delta\log \tilde{K}_{Pic^-}^{TCA^-}$	$\log K_s \pm \delta$	$\bar{p} \pm \delta$
No additive		–4.67	0	–	–
	S1	–4.67	0	–	–
	S2	–4.15	0.52	2.35 ± 0.06	0.99 ± 0.04
	S3	–4.57	0.10	1.70 ± 0.28	1.01 ± 0.37
	S4	–4.59	0.08	–	–
	S5	–4.66	0	–	–
	S6	–4.71	0	–	–
	S7	–4.59	0.08	1.54 ± 0.42	1.07 ± 0.46
	S8	–4.38	0.29	2.04 ± 0.35	1.01 ± 0.23
	S9	–4.41	0.26	1.61 ± 0.54	0.81 ± 0.35
	S10	–4.40	0.27	1.83 ± 0.11	0.96 ± 0.07
	S11	–4.46	0.21	–	–
	S12	–4.49	0.18	–	–
	S13	–2.91	1.76	3.46 ± 0.28	0.92 ± 0.10

Table (Contd.)

Solvating additive		$\log \tilde{K}_{Pic^-}^{TCA^-}$	$\Delta\log \tilde{K}_{Pic^-}^{TCA^-}$	$\log K_s \pm \delta$	$\bar{p} \pm \delta$
	S14	–1.85	2.82	4.79 ± 0.38	0.93 ± 0.10
	S15	–4.69	0	–	–
	S16	–3.67	1.00	2.73 ± 0.55	0.99 ± 0.25
	S17	–2.27	2.40	4.61 ± 0.38	1.07 ± 0.12
	S18	–1.71	2.96	4.99 ± 0.47	0.93 ± 0.12
	S19	–4.70	0	–	–
	S20	–3.32	1.35	3.20 ± 0.37	1.05 ± 0.14
	S21	–3.76	0.91	3.06 ± 0.60	1.11 ± 0.27
	S22	–4.02	0.65	2.31 ± 0.07	0.88 ± 0.04
	S23	–4.48	0.19	1.55 ± 0.58	0.93 ± 0.27
	S24	–4.72	0	–	–
	S25	–4.69	0	–	–
	S26	–4.70	0	–	–
	S27	–4.70	0	–	–

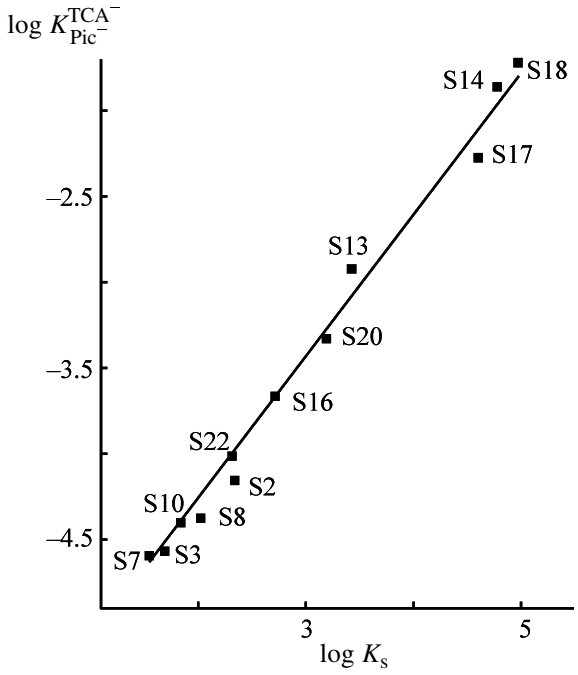


Fig. 1. Correlation between the logarithms of the anion-exchange extraction constants of TCA^- anions from the aqueous phase with TNODA Pic in toluene containing various organic additives and logarithms of the solvation constant K_s of TCA anions.

The relation between the concentration anion-exchange extraction constants $K_{Pic^-}^{TCA^-}$, the apparent anion-exchange extraction constants $\tilde{K}_{Pic^-}^{TCA^-}$, solvation constants K_s, and average solvation number p is described by the following bilogarithmic equation:

$$\log(\tilde{K}_{Cr^-}^{An^-}/K_{Cr^-}^{An^-} - 1) = \log K_s + p\log[S]. \quad (4)$$

The parameters K_s and p calculated by Eq. (4) using the special computer program [7] are listed in the table.

Analysis of the results listed in the table shows that the additives (trifluoroacetophenone derivatives) increasing the anion-exchange extraction of trichloroacetate anions are characterized by the following structural features.

(1) All the additives contain the CF_3 groups. This is seen from the fact that, in going from trifluoroacetophenone (structure S2) to tribromoacetophenone (structure S24), the effect of additive on the extraction completely disappears.

(2) The CF_3 group is a fragment of the trifluoroacetyl group –CO–CF_3. This requirement is confirmed by the fact that trifluoromethylbenzene (structure SI) does not affect the anion-exchange equilibrium. The molecules containing the carbonyl (structure S27) or ester (structures S25 and S26) groups only do not enhance the anion-exchange extraction either:

(3) The additives containing trifluoroacetyl group bound to saturated hydrocarbon radical directly (structure S6) or via the ester oxygen atom (S19 structure) do not affect the extraction constant.

(4) Di(trifluoroacetyl)acetylene containing two trifluoroacetyl groups linked by the C≡C group (structure S23) slightly increases the extraction constant (by 0.2 logarithmic units). This effect considerably increases (to 0.65 logarithmic units) if one of the trifluoacetyl groups is replaced by the benzene ring (structure S22). The binding of benzene ring directly to the trifluoroacetyl group (structure S2) does not noticeably change this effect ($\Delta\log K = 0.52$).

These results show that the organic additives increasing extraction of TCA anions must contain the trifluoroacetyl group and the benzene ring. The simplest molecule of this kind is trifluoroacetophenone (structure S2). The solvation efficiency of this additive can be increased by substituting the hydrogen atoms of the benzene ring by appropriate substituent.

We found that the complete substitution of hydrogen atoms in the trifluoroacetophenone benzene ring by the methyl and nitro groups (structure S15) results in disappearance of the solvation effect. This result shows that the hydrogen atoms of the benzene ring contribute to solvation of the trichloroaceate anion with trifluoroacetophenone. The similar effect was first reported in [8].

Table shows that, for all the additives, the average solvation number is approximately 1. These data also show (Fig. 1) that the logarithms of the apparent ion-exchange extraction constants linearly correlate with the logarithms of the solvation constants. This correlation is described by the equation

$$\log K_{Pic^-}^{TCA^-} = (-5.91 \pm 0.08) + (0.83 \pm 0.03)\log K_s,\ r = 0.994.$$

Figure 2 shows that the logarithms of the anion-exchange extraction constants linearly correlate with the sum of the Hammett σ-constants of substituents in solvating agents (*m*- and *p*-substituted trifluoroacetophenone). As expected, the maximal increase in extraction occurs for solvating agent of structure S18 having three substituens: *p*-chlorine and two *m*-nitro groups. In the presence of this additive, the extractive power of TNODA Pic with respect to TCA anions exceeds that in the presence of hexyl *p*-trifluoroacetylbenzoate, unsubstituted trifluoroacetophenone, and TNODA Pic in toluene by a factor of 1.61, 2.44, and 2.96, respectively.

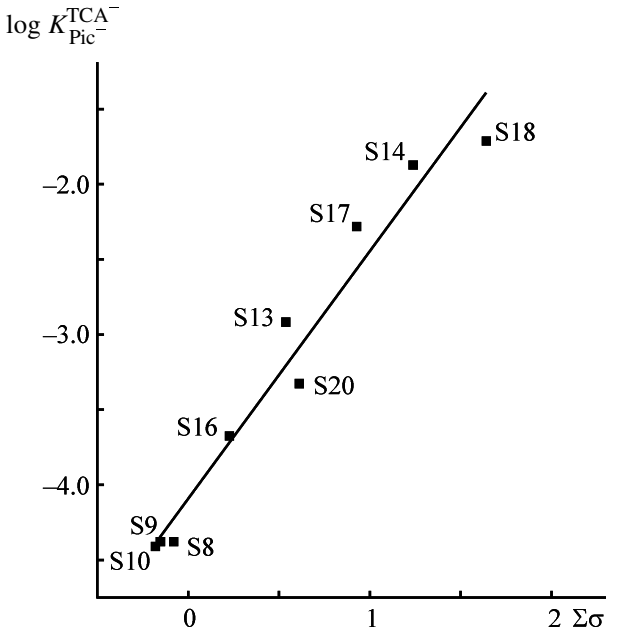


Fig. 2. Correlation between the logarithms of the anion-exchange extraction constants of TCA^- anions from the aqueous phase with TNODA Pic in toluene containing various organic additives and sum of the Hammett σ constants of substituents in the organic additives. Regression equation $\log K_{Pic^-}^{TCA^-} = 4.10 + 1.65\Sigma\sigma$.

The Hammett equation $\log K = \log K_0 + \rho\Sigma\sigma$ contains the parameter ρ reflecting the sensitivity of the anion-exchange equilibrium to variation in the trifluoroacethophenone electrophilicity. We found that, for the extraction systems under consideration, $\rho = 1.65 \pm 0.13$. We believe that high ρ value in our systems is caused by low toluene polarity; it is consistent with the data on ρ values for anion-exchange equilibria in chlorobenzene ($\rho = 1.89 \pm 0.04$) and methyl butyl ketone ($\rho = 1.71 \pm 0.06$) reported in [3].

The introduction of Cl and NO_2 electron-acceptor groups into the benzene ring of trifluoroacetophenone sharply increases the anion-exchange extraction of trichloroacetate anions. We believe that this effect is caused by the fact that the introduced substituents, exhibiting strong negative inductive effect (*–I*), increase the electrophilicity of the carbon atoms of the carbonyl groups in trifluoroacetophenone molecules and, as a result, enhance their solvating power with respect to TCA anions.

We found that substituted trifluoroacetophenones are strong solvating agents increasing the extraction of trichloroacetate by three orders of magnitude even at their low content (10^{-2} M). Taking into account that the anion-exchange extraction constant increases in the direct proportion with increasing concentration of the solvating additive, we can increase the anion-exchange extraction constant to five orders of magnitude by increasing the solvating agent concentration.

CONCLUSIONS

(1) Among 27 trifluoroacetophenone derivatives and related compounds tested as solvating additives in extraction of trifluoroacetate anions with trinonyloctadecylammonium picrate in toluene, only those containing the trichloroacetyl group bound to the benzene ring increase the extraction, provided that the benzene ring contains unsubstituted H atoms. The introduction of nitro groups and chlorine atoms into the benzene ring of the solvating additives increases this effect.

(2) Logarithms of anion-exchange extraction constants of trichloroacetate with trinonyloctadecylammonium picrate in toluene vary in direct proportion with the solvation constant of trichloroacetate with solvating additives.

(3) The apparent anion-exchange extraction constants of trichloroacetate with TNODA Pic in toluene linearly depend on the sum of the Hammett σ-constants of the solvating additives.

REFERENCES

1. Rakhman'ko, E.M., Physicochemical Principles of Analytical Application of Extraction with Salts of Higher Quaternary Ammonium Salts, *Doctoral Dissertation*, Minsk, 1994.
2. Pomelenok, E.V., Influence of Steric Accessibility of the Exchange Centers of Higher Quaternary Ammonium Salts on the Selectivity of Anion-Exchange Extraction, *Cand. Sci. Dissertation*, Minsk, 2004.
3. Karavan, V.S., Nikiforov, V.A., and Ampilogova, N.A., *Zh. Anal. Khim.*, 1989, vol. 44, no. 5, pp. 914–916.
4. Gulevich, A.L., Rakhman'ko, E.M., and Podterob, A.P., *Zh. Fiz. Khim. Rastv.*, 1996, vol. 70, no. 12, pp. 2192–2193.
5. Starobinets, G.L., Rakhman'ko, E.M., and Soroka, Zh.S., *Zh. Neorg. Khim.*, 1978, vol. 23, no. 6, p. 1628.
6. Podterob, A.P., Extraction of Substituted Benzoate Anions with Higher Quaternary Ammonium Salts and Its Analytical Application, *Cand. Sci. Dissertation*, Minsk, 1997.
7. Gulevich, A.L., Anion-Exchange Extraction of Organic Anions with Higher Quaternary Ammonium Salts and Its Analytical Application, *Doctoral Dissertation*, Minsk, 1997.
8. Rakhman'ko, E.M., Gulevich, A.L., Podterob, A.P., and Senin, P.V., *Zh. Anal. Khim.*, 1998, vol. 53, no. 4, pp. 1–4.

ISSN 1070-4272. Russian Journal of Applied Chemistry, 2006, Vol. 79, No. 1, pp. 74–78. © Pleiades Publishing, Inc., 2006.
Original Russian Text © N.N. Kostyuk, T.A. Dik, A.G. Trebnikov, 2006, published in Zhurnal Prikladnoi Khimii, 2006, Vol. 79, No. 1, pp. 77–81.

APPLIED ELECTROCHEMISTRY AND CORROSION PROTECTION OF METALS

Anodic Oxidation of Gadolinium Metal in the Presence of Thenoyltrifluoroacetone

N. N. Kostyuk, T. A. Dik, and A. G. Trebnikov

Sevchenko Institute of Applied Physical Problems, Belarussian State University, Minsk, Belarus

Received June 22, 2005

Abstract—The possibility of preparing gadolinium chelates of various compositions by electrolysis of a nonaqueous solution containing thenoyltrifluoroacetone was examined.

DOI: 10.1134/S1070427206010150

Anodic dissolution of rare-earth metals and alloys in nonaqueous media in the presence of β-diketones yields β-diketonates [1–10]. The advantages of the electrochemical procedure for preparing rare-earth chelates are as follows: the process is one-step, no by-products are formed, and hydration and hydrolysis are excluded. Anodic dissolution of *f* elements allows preparation of chelates of metals in various valence states [4–7, 9, 11, 12], which is particularly valuable, as it becomes possible to prepare under common conditions coordination compounds of rare-earth elements in lower oxidation states [4–7, 9].

The electrolyses performed in [1–12] involved no profound changes in the chemical composition of β-diketones. The cathodic reduction was accompanied only by transition of the β-diketone to the acido form due to elimination of the proton from the γ-position. At the same time, under certain conditions acetylacetone can be electrochemically converted into a tetraketone (3,4-diacetylhexane-2,5-dione) [13]. This reaction opens prospects for one-step electrochemical synthesis of complex metal chelates with tetraketones. One of typical β-diketones is thenoyltrifluoroacetone; electrochemical preparation of its complexes with such *d* elements as Cr, Co, and Cu was reported in [14–16]. At the same time, the behavior of thenoyltrifluoroacetone in the course of electrolysis with a uranium anode is not unambiguous. For example, Matassa *et al.* [11] failed to prepare electrochemically uranyl thenoyltrifluoroacetonate; this fact suggests that the β-diketone could undergo electrochemical transformations in the presence of an *f* element.

In this study we attempted one-step electrochemical synthesis of a gadolinium tetraketonate starting from thenoyltrifluoroacetone. The choice of Gd was governed by the stability of its trivalent state under the conditions of the anodic oxidation [6], which makes the reaction pathway more predictable.

EXPERIMENTAL

Tetraethylammonium bromide and thenoyltrifluoroacetone [1,1,1-trifluoro-4-(2-thienyl)-2,4-butanedione, HTTA] of analytically pure grade was recrystallized twice from ethanol and stored in a vacuum desiccator over phosphorus pentoxide. The IR absorption spectra were recorded on a Specord IR75 spectrophotometer in the range 4000–400 cm^{-1}; samples were taken as mulls in mineral oil or as films prepared from acetone solutions. The mass spectra were recorded with an MKh-1320 mass spectrometer. The metal content in the substances was determined gravimetrically after calcination of weighed portions to Gd_2O_3 [6].

Electrolysis of a 0.2 M solution of thenoyltrifluoroacetone in acetonitrile was performed in a diaphragmless cylindrical cell with direct current at a voltage of 3 V under argon. The initial current density was 10 mA cm^{-2}. The cathode (nickel foil) was arranged along the internal lateral surface of the cell. The gadolinium anode was arranged in the cell center. The ratio of the cathode and anode surface areas was 28 : 1. The electrochemical synthesis procedure is described in more detail elsewhere [1–12].

Devices for thermal studies [thermogravimetric (TG) analysis, isothermal heating] were described in [7]. Isothermal heating of samples was performed under argon.

During 180-min electrolysis, 420 C of the electricity was passed. The solution remained transparent

Table 1. Gadolinium chelates with thenoyltrifluoroacetone derivatives

Substance no.	Chelate			Gd content, wt %	
	formula	weight, g	current efficiency, %	found	calculated
1	$[Gd\{(TTA^*)_2\}_3]$	1.85	85.8	10.6	10.59
2	$[(Gd\{(TTA^*)_2\}_{2.75}]$	0.4	21.8	11.6	11.45
3	$[Gd\{(TTA^*)_2\}_{2.25}]$	0.9	–	14.0	13.64

Note: $(TTA^*)_2$ denotes 1,1,1,6,6,6-hexafluoro-3,4-di(2-thienylcarbonyl)hexane-2,5-dione.

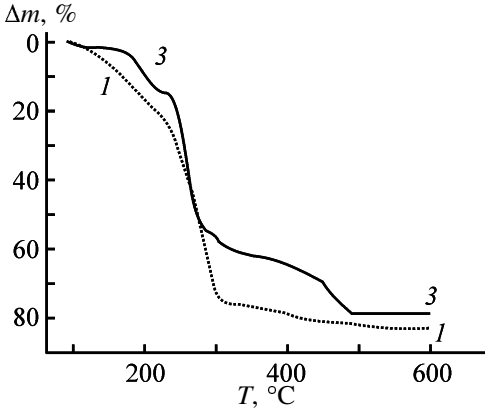
throughout the process. The current density decreased to 1.6 mA cm^{-2}, which is presumably caused by formation of weakly dissociating chelates in the solution. The anode weight loss was 0.609 g, which corresponded to 267% current efficiency by Gd(III) and suggests simultaneous chemical dissolution of Gd in the course of the electrolysis. Similar electrochemical behavior of some rare-earth metals was observed in other studies [7–10, 15].

The mother liquor obtained was evaporated to a slurry and treated with diethyl ether. The residue after evaporation of the ether was partially soluble in benzene. Thus, we obtained substance 1 insoluble in benzene and substance 2 soluble in benzene (after the solvent evaporation). Substance 3 was obtained by treatment of substance 1 with water. The analytical data, current efficiencies, and presumed compositions of the complexes are given in Table 1.

The gadolinium : thenoyltrifluoroacetone ratio in the first chelate is 1 : 6. If TTA remained unchanged in the course of electrolysis, such a ratio would correspond to the composition $Gd(TTA)_3 \cdot 3HTTA$. Weakly bound neutral β-diketone molecules are usually removed from complexes in the first step of thermolysis [1, 2, 4–10, 14, 15]. The TG curves of chelates 1 and 3 (Table 1) are shown in the figure. The curves have no pronounced plateaus that could be expected for adducts (stability of the intermediate desolvated form). The pattern of thermal decomposition is complex, with weak inflections in the TG curves, but the process occurs in one step. The most pronounced inflection is observed in the initial portion of the TG curves at 150–170°C. Therefore, we performed a series of isothermal heatings at 140, 145, 150, and 155°C. The weight loss was 1.3, 1.4, 1.6, and 2.2%, respectively. Thus, under isothermal conditions, we also failed to obtain a stable intermediate corresponding to elimination of a large neutral ligand.

The IR spectrum of $[Gd\{(TTA^*)_2\}_3]$ (Table 2) contains strong bands in the range of CO and CC stretching vibrations at 1700–1500 cm^{-1}. The absorption bands in the range 1560–1500 cm^{-1} suggest formation of a quasiaromatic chelate ring [17–23]. The bathochromic shift of the C=O bands caused by a decrease in the C=O bond multiplicity reaches 105–83 cm^{-1} (the C=O strecthing vibrations in HTTA are manifested at 1660 and 1638 cm^{-1}). The very strong band at 1595 cm^{-1} with a shoulder at 1630 cm^{-1} can be assigned to C=O groups of thenoyltrifluoroacetone coordinated without formation of a quasiaromatic chelate, i.e., without transformation of the ligand into the acido form [18, 20–23]. As expected, the bathochromic shift in this case is considerably smaller: 65–8 cm^{-1}. The complex shape of the band at 1595 cm^{-1} indicates that the neutral CO groups are coordinated to the central atom to a different extent. An alternative explanation of the weaker bathochromic shift may be hydrogen bonding of the carbonyl groups in the enol form of the β-diketone [24]. The presence of the enol form is confirmed by a broad strong band at 3650–3050 cm^{-1} (OH stretching vibrations, Table 2), taking into account that the synthesis was performed in acetonitrile under anhydrous conditions.

As noted above, substance 3 (Table 1) was obtained by treatment of $[Gd\{(TTA^*)_2\}_3]$ with water. Usually β-diketonates of *f* elements are susceptible to hydration and hydrolysis [25–27]. However, the IR



TG curves of gadolinium chelates (curve nos. are substance nos. in Table 1): (Δ*m*) weight loss and (*T*) temperature.

Table 2. Vibration frequencies of gadolinium chelates and their assignment

Frequency, cm^{-1}		Assignment
$[Gd\{(TTA^*)_2\}_3]$	$[Gd\{(TTA^*)_2\}_{2.25}]$	
3650–3050 vs		$\nu(OH)$
2950 sh	3000–2800 w	$\nu(CH)$
2915 m		
2840 w		
1693		
1680		
1630 sh	1630 vw	$\nu(CO)_{coord}$
	1605 sh	
1595 vs	1597 vs	
1555 vw	1554 w	$\nu(CO)_{chel}$, $\nu(CC)_{chel}$
1532 s	1528 s	
1515 w	1515 s	
1500 m	1502 m	
1450 w	1469 w	$\nu(CO)_{chel}$, $\delta(CCH_\gamma)$
1405 s	1407 s	$\nu(CO)_{chel}$, $\nu(CC)_{chel}$, $\delta(CCH_\gamma)$, $\nu(CC)$
1347 m	1348 s	$\delta(CF_3)$, $\nu(CC)$, δ_{chel}
1297 vs	1295 vs	$\nu(CF)$, $\delta(CF_3)$
1241 w	1240 w	
1222 w	1224 w	
1175 s	1171 m	$\nu(CO)_{chel}$, $\delta(CCH_\gamma)$
1125 s	1125 s	$\nu(CF)$, $\delta(CF_3)$
1070 vw	1073 vw	$\delta(C{=}CH)$, $\nu(CC)$,
1050 w	1050 w	$\nu(CO)$
925 w	921 w	$\nu(CC)_{chel}$, $\nu(CO)_{chel}$, δ_{chel}
850 w	850 w	$\nu(CS)$, $\delta(C{=}CH)$
780 m	775 m	$\delta(CH_\gamma)_{out\text{-}of\text{-}plane}$, $\nu(CF)$, $\delta(CF_3)$
710 m	712 w	$\delta(CH)$, $\delta_{chel\,out\text{-}of\text{-}plane}$
673 vw	672 w	$\nu(GdO)$, $\nu(CC)$, $\nu(CO)_{chel}$, $\delta(CF_3)$
635 w	624 w	$\delta(CSC)$, $\delta(C{=}CH)$
575 w	571 w	$\delta_{chel\,out\text{-}of\text{-}plane}$, $\nu(CC)_{chel}$, $\nu(CO)_{chel}$

Table 3. Mass spectrum of $[Gd\{(TTA^*)_2\}_3]$

m/z	Relative intensity, %	Assignment (calculated *m/z*)
154	12.0	$[HL-C_3H_3-CO-H]^+$ (154)
155	6.0	$[HL-C_3H_3-CO]^+$ (155)
160	6.0	$[HL-CHS-CH_3-2H]^+$ (160)
188	7.2	$[HL-F-CH_3]^+$ (188)
201	28.8	$[LF-C_3H_3]^+$ (201)
202	16.7	$[L-F]^+$ (202)
203	10.3	$[HL-F]^+$ (203)
206	10.0	$[L-H-CH_2]^+$ (206)
207	10.3	$[HL-H-CH_2]^+$ (207)
208	10.5	$[HL-CH_2]^+$ (208)
219	10.5	$[L-2H]^+$ (219)
220	100	$[L-H]^+$ (220)
223	16.5	$[HL_2^*-L]^+$ (223)
224	6.0	$[HL_2^*F-L-CH_3-2H]^+$ (224)
230	23.0	$[HLF_2-L-CO-2H]^+$ (230)
244	5.0	$[L_2^*-CF_3-C_3HS-CHS-CH_3]^+$ (244)
248	13.0	$[L_2^*-C_4H_3SCO-C_4H_3S]^+$ (248)
249	9.6	$[HL_2^*-C_4H_3SCO-C_4H_3S]^+$ (249)
297	10.0	$[L_2^*-C_4H_3S-2CF]^+$ (297)
309	16.7	$[L_2^*-C_4H_3S-CF_2]^+$ (309)
310	6.0	$[HL_2^*-C_4H_3S-CF_2]^+$ (310)
313	26.2	$[HL_2^*-C_4H_3SCæ-F]^+$ (313)
314	9.1	$[H_2L_2^*-C_4H_3SCO-F]^+$ (314)
327	12.5	$[L_2^*-C_4H_3S-CF]^+$ (327)
331	96.6	$[L_2^*-C_4H_3SCO]^+$ (331)
332	21.5	$[HL_2^*-C_4H_3SCO]^+$ (332)
355	6.0	$[HL_2^*-CF_3]^+$ or $[H_2L_2^*-F-CF_3]^+$ (355)
404	8.4	$[L_2^*-2F]^+$ (404)
405	8.4	$[HL_2^*-2F]^+$ (405)
423	94.3	$[L_2^*-F]^+$ (423)
426	11.8	$[HL_2^*-F]^+$ (426)
442	25.3	$[L_2^*]^+$ (442)

* L denotes TTA, and L_2^*, 1,1,1,6,6,6-hexafluoro-3,4-di(2-thienylcarbonyl)hexane-2,5-dione.

spectrum of $[Gd\{(TTA^*)_2\}_{2.25}]$ shows no absorption in the range 4000–3000 cm^{-1} (Table 2). In the range 1650–1580 cm^{-1}, there is a strong band with a maximum at 1597 cm^{-1} with a well-defined shoulder at 1605 cm^{-1}. On the whole, the IR spectrum of $[Gd\{(TTA^*)_2\}_{2.25}]$ in this range resembles the spectrum of $[Gd\{(TTA^*)_2\}_3]$ with the only difference that the shoulder at 1630 cm^{-1} in the spectrum of the latter is manifested as a very weak band in the spectrum of the former. The spectra of these two substances differ more significantly in the range 1560–1500 cm^{-1} corresponding to stretching vibrations of the CO and CC groups of the quasiaromatic ring. In the spectrum of $[Gd\{(TTA^*)_2\}_{2.25}]$, the bands are appreciably stronger than in the spectrum of $[Gd\{(TTA^*)_2\}_3]$, though their positions are essentially the same. The absorption patterns of these two compounds in the other ranges are virtually identical (Table 2).

Comparison of the IR spectra of $[Gd\{(TTA^*)_2\}_3]$ and $[Gd\{(TTA^*)_2\}_{2.25}]$ shows that treatment of the former chelate with water does not result in its hydration and hydrolysis but results in removal of a part of

the ligand occurring in the enol form. The strong CF_3 vibration bands at 1300–1100 cm^{-1} in the spectra of the complexes (Table 2) indicate that the electrochemical synthesis leaves the CF_3 groups intact. As judged from the spectra, the thienyl group remains intact also (bands at 1050, 850, 624 cm^{-1} [19]).

The mass spectra of $[Gd\{(TTA^*)_2\}_3]$ are given in Table 3. No metal-containing ions, which could be reliably identified by a characteristic isotopic pattern [28], were detected. The heaviest ions observed in the mass spectrum correspond to the doubled weight of thenoyltrifluoroacetone (minus two hydrogen atoms): 443, 442, and 441. These peaks indicate that thenoyltrifluoroacetone underwent dimerization in the course of electrolysis. The further fragmentation pattern of the dimer shows that it contains intact thienyl and CF_3 groups (Table 3), which is consistent with the IR data. The whole set of the data obtained (spectroscopy, elemental analysis, thermolysis) suggest that HTTA underwent dimerization by coupling of the γ-C atoms with elimination of γ-H atoms. The resulting 1,1,1,6,6,6-hexafluoro-3,4-di(2-thienylcarbonyl)hexane-2,5-dione $[(TTA^*)_2]$ can potentially form two chelate rings via enolization of the two remaining γ-H protons. However, apparently, the removal of the second proton will be hindered, in particular, because of the electrostatic effect of the arising negative charge. This assumption allows us to account for formation of complexes with lower ligand content and fractional ligand-to-metal ratios on treatment of $[Gd\{(TTA^*)_2\}_3]$ with various solvents (Table 1).

The lack of metal-containing fragments in the mass spectrum of $[Gd\{(TTA^*)_2\}_3]$ is due to the capability of the ligand for complexation in two opposite directions, which is confirmed by the IR data (strong donor–acceptor interaction without transition into the acido form). This should result in polymerization of the chelate due to strong binding of the metal with ligands of adjacent chelate fragments. Whereas a metal atom is bonded at least with four ligand molecules (three in the acido form and one from the surrounding of the adjacent metal by the donor–acceptor mechanism; in this case, the coordination number is 8, which is typical of rare-earth metals [25]), not all the ligands will be bonded with two metal atoms (excess coordination capacity, steric hindrance caused by branched structure), which is confirmed by detection of the enol form. Therefore, under conditions of the mass-spectrometric experiment, the complex will decompose with the elimination of the least bonded ligands, rather than pass into the gas phase.

CONCLUSIONS

(1) Electrolysis of an acetonitrile solution containing thenoyltrifluoroacetone with a gadolinium anode allows preparation of $[Gd\{(TTA^*)_2\}_3]$ and $[Gd\{(TTA^*)_2\}_{2.75}]$, where $(TTA^*)_2$ is 1,1,1,6,6,6-hexafluoro-3,4-di(2-thienylcarbonyl)hexane-2,5-dione. Treatment of the former compound with water yields $[Gd\{(TTA^*)_2\}_{2.25}]$.

(2) The compounds obtained contain no neutral ligands, and the peripheral CF_3 and thienyl groups remain intact. The ligand interacts with the metal with the formation of a quasiaromatic chelate ring, i.e., via transition into the acido form. The remaining neutral part of the tetraketone interacts with the adjacent Gd atoms.

(3) Not all the available carbonyl groups are involved in donor–acceptor interactions, because of steric hindrance and deficiency of metal atoms. Therefore, some of these groups are enolized. The compounds obtained, when treated with water, lose only a part of the ligand occurring in the enol form and are not hydrated or hydrolyzed; such a behavior is untypical of β-diketonates.

REFERENCES

1. Kostyuk, N.N., Shirokii, V.L., Dik, T.A., *et al.*, *Koord. Khim.*, 1991, vol. 17, no. 11, pp. 1573–1575.
2. Kostyuk, N.N., Shirokii, V.L., Vinokurov, I.I., and Maier, N.A., *Zh. Obshch. Khim.*, 1994, vol. 64, no. 9, pp. 1432–1434.
3. Tsodikov, M.V., Bukhtenko, O.V., Elert, O.G., *et al.*, *Izv. Ross. Akad. Nauk, Ser. Khim.*, 1995, no. 8, pp. 1454–1458.
4. Kostyuk, N.N., Dik, T.A., and Trebnikov, A.G., in *Materialy Mezhdunarodnoi nauchno-tekhnicheskoi konferentsii "Razrabotka importozameshchayushchikh tekhnologii i materialov v khimicheskoi promyshlennosti"* (Proc. Int. Scientific and Technical Conf. "Development of Technologies and Materials for Chemical Industry Aimed to Replace Imported Products"), Minsk, October 20–22, 1999, pp. 283–285.
5. Kostyuk, N.N., Dik, T.A., Trebnikov, A.G., *et al.*, in *Materialy Mezhdunarodnoi nauchno-tekhnicheskoi konferentsii "Razrabotka importozameshchayushchikh tekhnologii i materialov v khimicheskoi promyshlennosti"* (Proc. Int. Scientific and Technical Conf. "Development of Technologies and Materials for Chemical Industry Aimed to Replace Imported Products"), Minsk, October 20–22, 1999, pp. 285–287.
6. Kostyuk, N.N. and Dik, T.A., *Vybranyya navukovyya pratsy Belaruskaga dzyarzhaunaga univ.* (Selected

Scientific Works of the Belarussian State Univ.), Svirydav, V.V., Ed., Minsk: BDU, 2001, pp. 282–298.

7. Kostyuk, N.N., Dik, T.A., Trebnikov, A.G., and Shirokii, V.L., *Elektrokhimiya*, 2003, vol. 39, no. 11, pp. 1371–1375.
8. Kostyuk, N.N., Dik, T.A., Tereshko, N.V., and Trebnikov, A.G., *Elektrokhimiya*, 2003, vol. 39, no. 11, pp. 1376–1379.
9. Kostyuk, N.N., Dik, T.A., and Trebnikov, A.G., *Dokl. Nats. Akad. Navuk Bel.*, 2004, vol. 48, no. 1, pp. 60–64.
10. Kostyuk, N.N., Dik, T.A., Tereshko, N.V., and Trebnikov, A.G., *Radiokhimiya*, 2004, vol. 46, no. 6, pp. 510–512.
11. Matassa, L., Kumar, N., and Tuck, D.G., *Inorg. Chim. Acta*, 1985, vol. 109, no. 1, pp. 19–21.
12. Kostyuk, N.N., Kolevich, T.A., Shirokii, V.L., and Umreiko, D.S., *Koord. Khim.*, 1989, vol. 15, no. 12, pp. 1704–1707.
13. USSR Inventor's Certificate no. 1773902 A1.
14. Shirokii, V.L., Vinokurov, I.I., Sedova, L.G., *et al.*, *Zh. Obshch. Khim.*, 2000, vol. 70, no. 4, pp. 597–599.
15. Kostyuk, N.N., *Cand. Sci. Dissertation*, Minsk, 1993.
16. Shirokii, V.L., Vinokurov, I.I., Kostyuk, N.N., *et al.*, *Zh. Obshch. Khim.*, 1996, vol. 66, no. 2, pp. 184–188.
17. Bellamy, L.J., *The Infra-Red Spectra of Complex Molecules*, New York: Wiley, 1957.
18. Nakamoto, K., *Infrared and Raman Spectra of Inorganic and Coordination Compounds*, New York: Wiley, 1986.
19. Sverdlov, L.M., Kovner, M.A., and Krainov, E.P., *Kolebatel'nye spektry mnogoatomnykh molekul* (Vibrational Spectra of Polyatomic Molecules), Moscow: Nauka, 1970.
20. Kradenov, K.V. and Kolesov, B.A., *Analiz normal'nykh kolebanii β-diketonatov medi(II)* (Normal Mode Analysis of Copper(II) β-Diketonates), Novosibirsk, 1986, Available from VINITI, no. 8696-V86.
21. Kradenov, K.V. and Kolesov, B.A., *Raschet raspredeleniya potentsial'noi energii po estestvennym kolebatel'nym koordinatam na primere β-diketonatov medi(II)* (Calculation of the Potential Energy Distribution over Natural Vibration Coordinates, with Copper(II) β-Diketonates as Example), Novosibirsk, 1986, Available from VINITI, no. 8695-V86.
22. Dik, T.A., Kostyuk, N.N., and Umreiko, D.S., *Zh. Prikl. Spektrosk.*, 1991, vol. 54, no. 5, pp. 736–739.
23. Dik, T.A., Kostyuk, N.N., and Umreiko, D.S., *Zh. Prikl. Spektrosk.*, 1993, vol. 58, nos. 1–2, pp. 178–183.
24. Neiland, O.Ya., Stradyn', Ya.P., Silin'sh, E.A., *et al.*, *Stroenie i tautomernye prevrashcheniya β-dikarbonil'nykh soedinenii* (Structure and Tautomeric Transformations of β-Dicarbonyl Compounds), Riga: Zinatne, 1977.
25. Suglobov, D.N., Sidorenko, G.V., and Legin, E.K., *Letuchie organicheskie i kompleksnye soedineniya f-elementov* (Volatile Organic and Coordination Compounds of *f* Elements), Moscow: Energoatomizdat, 1987.
26. Martynenko, L.I., Murav'eva, I.A., Khalmurzaev, I.K., and Spitsyn, V.I., *Izv. Akad. Nauk SSSR, Ser. Khim.*, 1984, no. 6, pp. 1207–1211.
27. Martynenko, L.I., Murav'eva, I.A., Khalmurzaev, I.K., and Spitsyn, V.I., *Izv. Akad. Nauk SSSR, Ser. Khim.*, 1984, no. 3, pp. 489–495.
28. *Fizicheskaya entsiklopediya* (Physical Encyclopedia), Moscow: Sov. Entsiklopediya, 1990, vol. 2.

ISSN 1070-4272. Russian Journal of Applied Chemistry, 2006, Vol. 79, No. 1, pp. 79–81. © Pleiades Publishing, Inc., 2006.
Original Russian Text © G.N. Al'tshuler, A.A. Evdoshenko, E.V. Ostapova, 2006, published in Zhurnal Prikladnoi Khimii, 2006, Vol. 79, No. 1, pp. 82–84.

APPLIED ELECTROCHEMISTRY AND CORROSION PROTECTION OF METALS

Electrochemical Properties of a Network Polymer Based on Tetra(sulfonatophenyl)-*meta*-cyclophanoctol

G. N. Al'tshuler, A. A. Evdoshenko, and E. V. Ostapova

Kemerovo Division, Institute of Solid State Chemistry and Mechanochemistry, Siberian Division, Russian Academy of Sciences, Kemerovo, Russia

Received August 2, 2005

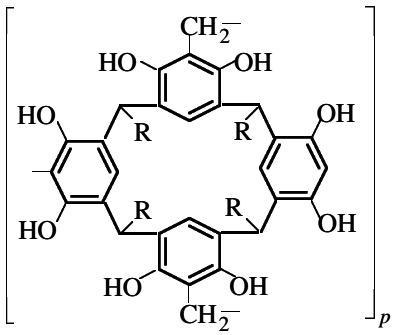
Abstract—Conductivity of the network polymer based on tetra(sulfonatophenyl)-*meta*-cyclophanoctol in the H^+, Na^+, Cu^{2+}, Zn^{2+}, and Ni^{2+} forms is studied, and the self-diffusion coefficients and activation energies of diffusion of the metal cations in the polymer phase are estimated.

DOI: 10.1134/S1070427206010162

High-performance fuel cells could be developed only on the basis of novel materials, which should be highly efficient and selective catalysts of cathodic oxidation of fuel and anodic reduction of oxygen. The use of such materials in fabricating electrodes should increase the exchange current and decrease the energy loss for polarization of the oxygen electrode. Finely dispersed Pt-group metals were suggested as catalysts of electrode reactions. Also it seems promising to use finely dispersed "soft" transition metals such as copper and nickel. Optimal distribution of a liquid and gas in the electrode material should also improve the performance of fuel cells. Therefore, its structure should be porous, and it should contain hydrophilic fragments in combination with hydrophobized active layers [1].

Network polymers based on calixarenes, particularly, *meta*-cyclophanoctols, show promise as the matrix in developing composite materials for electrodes of a new generation of fuel cells. Thanks to the presence of the hydrophobic belt formed by the arene fragments and also of the hydrophilic substituents in the immobilized *meta*-cyclophanoctols, the structure of the calixarene-containing polymers contains both hydrophilic and hydrophobic layers. It is known [2] that calixarene-based network polymers are cation exchangers. They can be charged with various metal ions, and the metal concentration in the polymer can be varied over a wide range. To determine the kinetic characteristics of redox reactions in the systems containing polymeric materials based on *meta*-cyclophanoctols, it is necessary to have available information on the electrochemical properties of immobilized *meta*-cyclophanoctols, particularly, on the dependences of the ionic conductivity of the polymers on their counterion composition and temperature.

In this study we measured the conductivity of the network polymer based on *cis*-tetra(sulfonatophenyl)-*meta*-cyclophanoctol



R = $PhSO_3H$,

and estimated the self-diffusion coefficients and activation energies of diffusion of Na^+, Cu^{2+}, Zn^{2+}, and Ni^{2+} in the polymer phase over the temperature range 298–333 K.

EXPERIMENTAL

The network polymer based on *cis*-tetra(sulfonatophenyl)-*meta*-cyclophanoctol was obtained as spherical granules 0.05–0.5 mm in diameter by catalytic resol polycondensation of *cis*-tetraphenyl-*meta*-cyclophanoctol with formaldehyde, followed by treatment with concentrated sulfuric acid [3]. The dynamic ion-exchange capacity of the polymer was determined by passing 0.1 N NaCl through a column packed with the polymer in the H form or of 0.05 N $CuCl_2$, $ZnCl_2$, and $NiCl_2$ through a bed of the polymer in the Na

Conductivity of the polymer $\bar{\chi}$ and self-diffusion coefficient $\bar{D}_i$, activation energy of diffusion $\bar{E}_a$, and entropy constituent of the free energy of diffusion $d\exp(\Delta S^{\neq}/2R)$ of cations in the polymer phase at 298 K

Cation	$\bar{\chi} \times 10^4$, Ω^{-1} cm^{-1}	$\bar{D}_i \times 10^6$, cm^2 s^{-1}	$\bar{E}_a$, kJ mol^{-1}	$d\exp(\Delta S^{\neq}/2R)$
H^+	1150 ± 11	N. d*	N. d	N. d
Na^+	106 ± 1.0	4.69 ± 0.09	18.7 ± 0.2	2.3 ± 0.1
Zn^{2+}	53 ± 0.5	1.08 ± 0.02	19.0 ± 2.1	1.2 ± 0.5
Cu^{2+}	43 ± 0.5	0.88 ± 0.02	16.6 ± 1.6	0.6 ± 0.2
Ni^{2+}	40 ± 0.5	0.82 ± 0.02	16.3 ± 1.5	0.7 ± 0.2

* (N. d.) Not determined. It is difficult to estimate t_i for H^+ because of possible penetration of a Donnan electrolyte to the polymer phase.

form (to 100% breakthrough of the metal ion). The volume dynamic ion-exchange capacity of the polymer in the H and Na forms was found to be 0.53 and 0.59 g-equiv l^{-1}, respectively, and in the Cu^{2+}, Ni^{2+}, and Zn^{2+} forms, 0.65 g-equiv l^{-1}.

The conductivity of the polymer itself was estimated from the experimental conductivity of the interface polymer/equilibrium electrolyte solution and that of the equilibrium electrolyte near the isoelectric point using the semiempirical relationship [5]. The concentration of the isoelectric HCl solution in equilibrium with the H form of the polymer approached 0.5 g-equiv l^{-1}. In the cases of cationic forms of the polymer, the concentration of the equilibrium solutions of the corresponding metal chlorides was no more than 0.1 g-equiv l^{-1}. The conductivities of the polymer/electrolyte interfacial layer and of the electrolyte solutions were measured at 1000 and 4000 Hz using a measuring system representing an ac bridge equipped with a dual-beam oscillograph as an amplitude-phase balance indicator, switched to the diagonal of the bridge. An audio-frequency oscillator, having a fine adjustment of the frequency and output voltage amplitude, equipped with an output transformer with a grounded point and fully balanced halfparts of the output winding, was switched to another diagonal of the bridge. The grade of accuracy of the devices constituting the measuring system is 0.2. The interfacial conductivity was measured using a specially designed cell with a mobile Pt electrode [6]. The conductivity of the equilibrium solution was measured separately using a conductometric sensor with platinized Pt electrodes. The conductometric cell and sensor were calibrated using standard KCl solutions.

The ionic conductivity of swollen cation exchangers, including the investigated polymer, strongly depends on the mobile counterion [7]. The table shows the conductivity of the network polymer based on *cis*-tetra(sulfonatophenyl)-*meta*-cyclophanoctol in the H^+, Na^+, Cu^{2+}, Ni^{2+}, and Zn^{2+} forms.

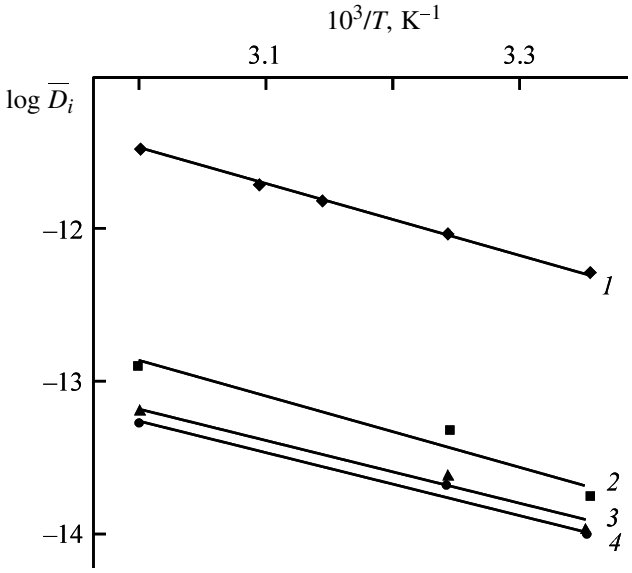
The conductivity of the investigated polymer is well comparable with that of nonaqueous electrolytes in lithium power sources [8], solid sodium aluminate proposed as an electrolyte for chemical power sources [1], and ordinary ion-exchange resins [6]. The conductivity of various cationic forms of the polymer increases in the order $Ni^{2+} < Cu^{2+} < Zn^{2+} < Na^+ \ll H^+$. The observed considerably higher conductivity of the H form can be attributed to the relay mechanism of charge transfer in the systems containing H^+. Furthermore, the conductivity of the H form could be significantly increased by virtue of the Donnan electrolyte as a result of rather high concentration of the isoconducting HCl solution in equilibrium with the polymer in the H form.

The conductivity of the polymer is directly related to the self-diffusion coefficient of the cation through the well-known Nernst–Einstein equation:

$$D_i = \frac{RT}{zF^2}\frac{\bar{\chi} t_i}{\bar{c}_R}, \quad (1)$$

where D_i is the self-diffusion coefficient of the ion; R, gas constant; T, temperature; z, ionic charge; F, Faraday number; $\bar{\chi}$, conductivity of the polymer phase; $\bar{c}_R$, volume ion-exchange capacity of the polymer; and t_i, transport number of the counterion.

In the polymer phase, the ionic groups are tightly bound to the polymer matrix and are not involved in charge transfer. Mobile species are counterions and ions penetrating to the polymer phase as a result of the Donnan effect. Since the salt concentration in the solutions in equilibrium with the polymer was no more than 0.1 g-equiv l^{-1}, charge transfer in the polymer studied proceeds essentially by the metal ions ($t_i \to 1$). The self-diffusion coefficient of the cations in the polymer phase (see table), estimated by Eq. (1), increases with decreasing cationic charge. The counterions are electrostatically attracted to the charges fixed on the polymer matrix. It is logical to suggest



Dependence of $\log \bar{D}_i$ vs. $1/T$ for self-diffusion of (*1*) Na^+, (*2*) Zn^{2+}, (*3*) Cu^{2+}, and (*4*) Ni^{2+} in the network polymer based on *cis*-tetra(sulfonatophenyl)-*meta*-cyclophanoctol.

that, with decreasing cationic charge, the electrostatic interaction between the fixed ion and counterion weakens, thus decreasing the activation energy and increasing the self-diffusion coefficient of the counterion in the polymer phase.

The figure shows the temperature dependences of the logarithms of the self-diffusion coefficients of the cations in the polymer phase. The dependences are linear (r 0.98–0.99), suggesting that the activation energies of diffusion of the cations can be estimated from the slope of the Arrhenius curves. As seen from the table, the activation energy of diffusion of Na^+, Cu^{2+}, Zn^{2+}, and Ni^{2+} in the polymer studied is 16–19 kJ mol^{-1} at 298–333 K, i.e., no clearly pronounced dependence on the cationic charge is observed.

The Eyring equation relates the diffusion coefficient to the activation energy E_a and activation entropy $\Delta S^{\neq}$ of the process:

$$\bar{D}_i = ea^2 \frac{kT}{h} \exp(\Delta S^{\neq}/R) \exp(-E_a/RT), \qquad (2)$$

where d is the jumping distance of the ion in diffusion; k, Boltzmann constant; and h, Planck constant.

Comparison of the self-diffusion coefficients of the cations with the entropy term (see table) shows that a decrease in $\bar{D}_i$ on passing from Na^+ to the double-charged cations is accompanied by a decrease in the entropy term, which is probably due to partial localization of the diffusing species in the vicinity of the ionic groups of the polymer.

CONCLUSIONS

(1) The conductivity at 298 K of the network polymer based on tetra(sulfonatophenyl)-*meta*-cyclophanoctol in the Cu^{2+}, Zn^{2+}, and Ni^{2+} forms is found to be 0.004–0.005 Ω^{-1} cm^{-1}, increasing to 0.01 and 0.115 Ω^{-1} cm^{-1} for the Na^+ and H^+ forms, respectively.

(2) The self-diffusion coefficient of the metal cations in the polymer phase increases on passing from the double-charged cations to Na^+, which is due to an increase in the entropy constituent of the free energy of activation of diffusion.

REFERENCES

1. Bagotskii, V.S., *Zh. Vses. Khim. O-va. im. D.I. Mendeleeva*, 1971, vol. 16, no. 6, pp. 685–690.
2. Altshuler, H., Sapozhnikova, L., Ostapova, E., *et al.*, *Solvent Extr. Ion Exch.*, 2002, vol. 20, no. 2, pp. 263–271.
3. Altshuler, H., Ostapova, E., Fedyaeva, O., *et al.*, *Macromol. Symp.*, 2002, vol. 181, pp. 1–4.
4. Marhol, M., *Ion Exchangers in Analytical Chemistry. Their Properties and Use in Inorganic Chemistry*, Prague: Academia, 1982.
5. Gnusin, N.P., Grebenyuk, V.D., and Fomin, A.G., *Elektrokhimiya*, 1966, vol. 2, no. 4, pp. 479–486.
6. Nikolaev, N.I. and Filimonova, F.M., in *Issledovanie svoistv ionoobmennykh materialov* (Studying Properties of Ion-Exchange Materials), Moscow: Nauka, 1964, p. 188.
7. Helfferich, F., *Ionenaustauscher*, Weinheim: Chemie, 1959.
8. Kolosnitsyn, V.S., Dukhanin, G.P., Dumler, S.A., *et al.*, *Zh. Prikl. Khim.*, 2005, vol. 78, no. 1, pp. 3–20.

ISSN 1070-4272. Russian Journal of Applied Chemistry, 2006, Vol. 79, No. 1, pp. 82–84. © Pleiades Publishing, Inc., 2006.
Original Russian Text © N.A. Dobrovinskaya, E.I. Dobkina, S.M. Kuznetsova, 2006, published in Zhurnal Prikladnoi Khimii, 2006, Vol. 79, No. 1, pp. 85–87.

CATALYSIS

Influence of Concentration and Amount of Spent Sulfuric Acid on the Degree of Its Catalytic Decomposition

N. A. Dobrovinskaya, E. I. Dobkina, and S. M. Kuznetsova

St. Petersburg State Technological Institute, St. Petersburg, Russia

Received June 9, 2005

Abstract—The influence of the concentration, composition, and amount of spent sulfuric acid on final characteristics of its thermocatalytic decomposition was studied.

DOI: 10.1134/S1070427206010174

Spent sulfuric acid (SSA) containing small amounts of organic impurities (usually no more than 2–4 wt %) is formed in certain large-capacity processes, such as alkylation and production of synthetic alcohols [1]. Thermocatalytic decomposition in a fluidized bed at 750–850°C yielding sulfur dioxide suitable for the further processing into sulfuric acid by classic schemes [2] seems to be the most promising for the regeneration of such SSA.

Thus, the final aim of the SSA thermolysis is the production of commercial acid of standard concentrations, and the content of sulfur dioxide in the gases from the decomposition is the factor determining the feasibility of their further processing. To reach the maximal productivity of catalytic reactors of the SO_2 oxidation to SO_3, it is recommended [2] to maintain the 7.0–7.5 vol % concentration of sulfur dioxide at the reactor input in the case of single contact and 9–10 vol % in the case of double contact.

It was shown in [3] that it is appropriate to carry out the thermocatalytic decomposition on supported iron–copper oxide catalysts using silica-modified γ-Al_2O_3 as support.

EXPERIMENTAL

All experiments were carried out with the above-mentioned catalyst. The content of sulfur dioxide in the decomposition products of spent SSA from the production of methyl ethyl ketone (MEK) is plotted in Fig. 1 vs. SSA concentration. The starting acid containing 43 wt % monohydrate was evaporated to 63, 72, and 85 wt % monohydrate. The amount of organic impurities in the evaporated acid was 1.6, 1.7, and 1.8 wt %, respectively (1.5 wt % in the starting SSA); their effect on the sulfuric acid thermolysis is negligible [4].

It is seen from Fig. 1 that, in the range of loads with respect to SSA under study, the required concentration of sulfur dioxide is reached in thermolysis of the acid containing no less than 70 wt % monohydrate. To obtain a gas with an SO_2 content sufficient for the subsequent industrial oxidation, it is appropriate to carry out the thermocatalytic SSA decomposition at high loads with respect to the acid. However, an increase in these loads can lead to the catalyst deactivation owing to coking of its surface. Figure 2 shows that the decrease in the activity when the optimal load with respect to SSA is considerably exceeded is different for acid samples containing different amounts of organic impurities.

When SSA from alkylation, containing 3.0 wt % hydrocarbons, is decomposed, the degree of decomposition β gradually decreases as the specific load

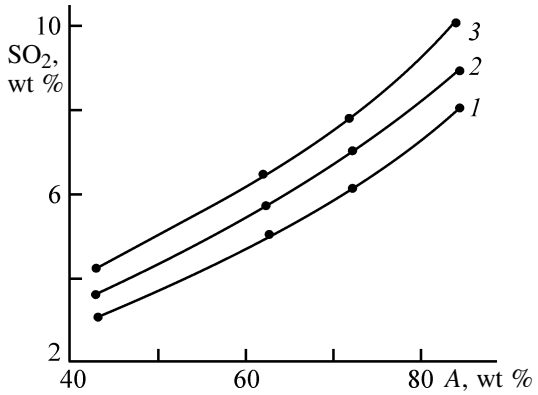


Fig. 1. SO_2 concentration in decomposition products of SSA from MEK production as a function of the monohydrate content A in the acid. Load with respect to SSA, kg h^{-1}: (*1*) 0.04, (*2*) 0.05, and (*3*) 0.06.

with respect to SSA increases and sharply decreases when the load exceeds 1500 kg h^{-1} m^{-3} (Fig. 2, curve *1a*). As L_{sp} growths further, β of 5–7% remains almost unchanged. Obviously, owing to the coking, the further SSA decomposition proceeds not catalytically, but under the action of a high temperature and of reducing agents present in SSA.

The pore structure of the catalyst was examined by porosimetry and scanning electron microscopy (SEM). The results obtained agree well with variations in the activity at a substantial growth of specific loads with respect to the acid. The fresh catalyst is characterized by a rather wide pore-size distribution, from 3 to 400 nm (Fig. 3, curve *1*); pores with radii of 5–10 nm dominate. During 100-h operation of the catalyst in the decomposition of alkylation SSA at L_{sp} = 900 kg h^{-1} m^{-3}, its pores increase in size practically over the whole range, the amount of thin pores decreases by 35–40%, and the total volume of pores, by 7–8% (Fig. 3, curve *2*).

As the process under study is kinetically controlled [3, 5], coke should be evenly distributed over the volume of catalyst grains [6]. In fact, the porogram of the sample coked at SSA feeding rate of 1700 kg h^{-1} m^{-3} (Fig. 3, curve *3*) indicates that coke is deposited inside pores of practically all sizes, the majority of thin pores being completely plugged. The total volume of pores decreases in this case by approximately 30%.

Electron microscopic examination confirmed that coke is distributed in the volume of the catalyst granules. For comparison we also studied the regenerated catalyst. The regeneration was carried out in an air flow at 550–600°C up to complete termination of the release of carbon oxides into the gas phase. In this case, the activity of the regenerated sample was restored to 98–100% (Fig. 2, curve *1b*).

The electron microscopic examination shows that clearly distinctive pore entrances on the surface of the starting catalyst appear to be completely blocked because of coking. After the regeneration, the pores become clearly visible again. Their amount and size increase as a result of the transformation of the support structure in the course of operation.

A similar pattern is also observed on chips of the sample granules. Pore sizes in the starting and coked catalysts are practically equal, whereas, according to the data of mercury porosimetry, they increase in the spent sample (Fig. 3, curve *2*). Obviously, the coke deposited on pore walls decreases their effective radii.

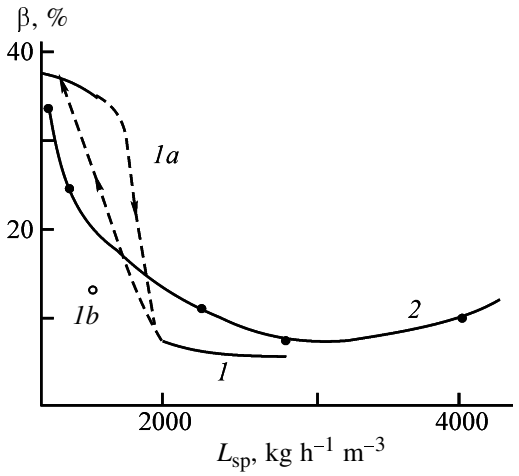


Fig. 2. Degree of decomposition β as a function of the specific load with respect to SSA L_{sp}. The catalyst operated for 100 h in the decomposition process; (*1a*) SSA form alkylation (85 wt % monohydrate, 1.7 wt % organic impurities), (*1b*) SSA form alkylation (after regeneration), and (*2*) SSA from MEK production (72 wt % monohydrate, 1.7 wt % organic impurities).

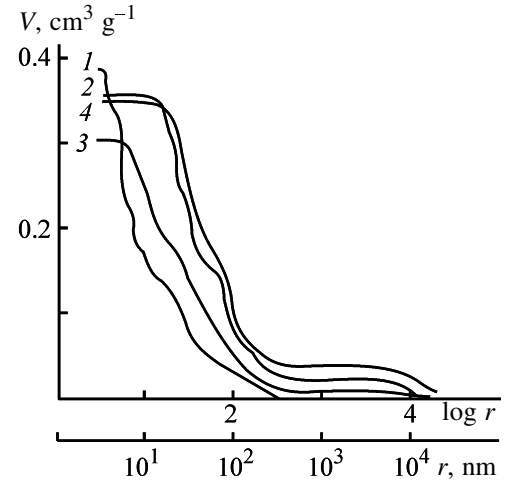


Fig. 3. Porograms of the catalyst: (*V*) total pore volume and (*r*) pore radius. Catalyst: (*1*) starting, (*2*) after operation for 100 h with SSA from alkylation, (*3*) coked at high loads with respect to SSA from alkylation, and (*4*) after operation at high loads with respect to SSA from MEK production.

After removal of coke deposits in the course of the regeneration, larger pores are seen, which became coarser in the course of the catalyst operation.

As the specific load with respect to SSA from MEK production (1.7 wt % organic substances) increasees, the degree of decomposition becomes more uniform (Fig. 2, curve *2*), which is attributable to insufficient residence time of such amount of the acid

in the bed, rather than to blocking of the catalyst active centers by coke. The study of the pore structure of the catalyst that operated at high loads with respect to SSA from MEK production has shown that the coking of the catalyst surface is insignificant, if any (Fig. 3, curve *4*). This is proved by the fact that a decrease in the specific load results in the restoration of the initial degree of SSA decomposition.

When L_{sp} exceeds 2700 kg h^{-1} m^{-3}, β starts to increase. This is apparently associated with the appearance of carbon monoxide in the reaction zone owing to incomplete oxidation of organic impurities. According to numerous papers, the amount of CO can become sufficient for the reaction $SO_3 + CO = SO_2 + CO_2$ to make an appreciable contribution to the SSA decomposition. However, these high loads with respect to SSA are not justified from the process viewpoint, because of a low degree of SSA decomposition. According to our experimental results, at the real loads of 400–900 kg h^{-1} m^{-3} both in the case of SSA from alkylation and SSA form MEK production, organic impurities are oxidized completely and the catalyst is not coked.

CONCLUSION

A quantitative relationship was found between the specific load in the thermocatalytic decomposition of spent sulfuric acid and the degree of its decomposition.

REFERENCES

1. Kirillova, Zh.V., Metelitsa, T.M., and Neipert, K.V., *Ispol'zovanie otrabotannoi sernoi kisloty v SSSR i za rubezhom* (Use of Spent Sulfuric Acid in the USSR and Abroad), Moscow: NIITEKhIM, 1984.
2. Amelin, A.G., *Tekhnologiya sernoi kisloty* (Technology of Sulfuric Acid), Moscow: Khimiya, 1983.
3. Dobrovinskaya, N.A., Dobkina, E.I., and Kuznetsova, S.M., *Zh. Prikl. Khim.*, 2004, vol. 77, no. 1, pp. 36–42.
4. Syurkaev, A.A., Shenfel'd, B.E., and Dobrovinskaya, N.A., *Zh. Prikl. Khim.*, 1990, vol. 63, no. 2, pp. 426–429.
5. Gel'man, E.I., Thermocatalytic Decomposition of Spent Sulfuric Acid with a Low Content of Organic Impurities, *Cand. Sci. (Chem.) Dissertation*, Leningrad, 1989.
6. Hughes, R., Dakessian, V., and Brito-Alayon, A., *Sadhana*, 1987, vol. 10, nos. 1–2, pp. 87–98.

ISSN 1070-4272. Russian Journal of Applied Chemistry, 2006, Vol. 79, No. 1, pp. 85–88. © Pleiades Publishing, Inc., 2006.
Original Russian Text © V.S. Tkach, D.S. Suslov, M. Gomboogiin, G.V. Ratovskii, F.K. Shmidt, 2006, published in Zhurnal Prikladnoi Khimii, 2006, Vol. 79, No. 1, pp. 88–91.

CATALYSIS

Isomerization of Alkenes in the Presence of $Pd(acac)_2$–BF_3OEt_2 Catalytic System

V. S. Tkach, D. S. Suslov, M. Gomboogiin, G. V. Ratovskii, and F. K. Shmidt

Irkutsk State University, Irkutsk, Russia
Mongolian State University, Ulan-Bator, Mongolian Republic

Received October 20, 2005

Abstract—Positional isomerization of alkenes was studied in the presence of $Pd(acac)_2$ + $20BF_3OEt_2$ catalytic system. The reactivity of alkenes decreases in the following order: 1-hexene > 1-heptene > 2-methyl-1-pentene > 4-methyl-2-pentene (*cis* + *trans*).

DOI: 10.1134/S1070427206010186

Systems containing bis(acetylacetonato)palladium $Pd(acac)_2$ and trifluoroboron etherate are efficient catalysts of dimerization of vinylaromatic hydrocarbons, e.g., selective dimerization of styrene [1, 2], telomerization of diene hydrocarbons with secondary amines [3, 4], and di- and oligomerization of ethylene and propylene [5–7]. These systems exhibit relatively high catalytic activity in positional isomerization of 1-hexene [8]. Isomerization of alkenes in the presence of Pd(II) complexes as catalysts has been extensively studied. Different isomerization mechanisms were proposed. The following processes are believed to be key steps of isomerization: (a) oxidative addition of alkene to Pd(II) to form allylpalladium(IV) hydride [9], (b) formation of carbenium ion by reaction of Pd(II) with alkene coordinated to the transition metal [10], (c) reversible addition of olefin to Pd(II) hydrides without a change in the Pd oxidation state [11]. Akenes like 1-hexene play a critical role in formation of Pd–H bonds in reactive complexes (RC) formed in the presence of $Pd(acac)_2$–BF_3OEt_2 catalytic system. Probably, the composition of these square-planar complexes is $HPd(L,L')BF_4$, where L is unsaturated hydrocarbon and L' = L or PR_3 [12].

Here we experimentally studied isomerization of alkenes in the presence of $Pd(acac)_2$–BF_3OEt_2 catalytic system, as influenced by various factors including the composition of the catalyst, preparation conditions of RC, and the solvent. With the positional isomerization of alkenes as an example, we intended to gain insight into the mechanism of transformation of unsaturated hydrocarbons including alkenes and vinylaromatic and diene hydrocarbons in the presence of bis(acetylacetonato)palladium–boron trifluoride etherate catalytic system.

EXPERIMENTAL

Isomerization of alkenes was performed under argon in a glass reactor equipped with a magnetic stirrer. A solution of appropriate alkene and $Pd(acac)_2$ was allowed to stand at 10°C for 15 min. The isomerization was initiated by addition of BF_3OEt_2. An aliquot (1 ml) of the reaction mixture was taken at regular intervals and placed into a test tube containing 3% aqueous hydrochloric acid to decompose the catalyst. The organic layer was separated and dried over calcium chloride. The isomerization products in the sample were analyzed by gas–liquid chromatography (GLC) on Tsvet-100M and Chrom-42M chromatographs equipped with a flame-ionization detector and a 100-m copper column with an internal diameter of 0.5 mm. We used vacuum oil as the stationary phase. The inlet pressure of the carrier gas was 0.6×10^5 Pa. The column temperature was 45°C.

Synthesis of $Pd(acac)_2$. To a solution of KOH (0.7310 g, 13.028×10^{-3} mol) in 15 ml of H_2O in a beaker was added acacH (1.2423 g, 12.408×10^{-3} mol). The mixture was heated at 45±5°C. A transparent solution of acacK was obtained.

To an aqueous solution (50 ml) of KCl (0.8830 g, 11.844×10^{-3} mol) in another beaker was added $PdCl_2$ (1.0000 g, 5.64×10^{-3} mol). The mixture was heated at 45±5°C with stirring until the brown precipitate completely dissolved to form a brown solution. The solution was filtered while hot.

The solutions were mixed at 45±5°C. The yellow precipitate was filtered off on a Büchner funnel, washed 5–7 times with 100-ml portions of H_2O, and dried at 50°C. $Pd(acac)_2$ was recrystallized from ace-

Table 1. Time dependence of the composition of 1-hexene isomerization products formed in benzene in the presence of $Pd(acac)_2$ + $20BF_3OEt_2$ catalytic system prepared and kept under Ar without the substrate for 30 min. 283 K, c_{Pd} = 1.47×10^{-3} M, $c_{1\text{-hexene}}$ = 0.941 M

Time, min	Composition of isomerization products, wt %			
	1-hexene	2-hexene (*trans*)	2-hexene (*cis*)	3-hexene (*cis* + *trans*)
1	91.6	7.9	0.5	–
2	78.8	20.9	0.5	–
3	42.6	54.2	3.2	–
5	–	94.5	5.5	–
8	–	79.3	12.4	8.3
15	–	78.7	8.5	12.8

tone by heating on a water bath. The precipitate was filtered off on a Büchner funnel and dried at 50°C (P = 10 mm Hg). Yield 83%.

Found (%): Pd 34.85, C 39.49, H 4.59.
$Pd(acac)_2$.
Calculated (%): Pd 34.87, C 39.47, H 4.61.

The solvents were treated by the standard procedures used in oranometallic chemistry [13].

The kinetic curves of 1-hexene isomerization in the presence of $Pd(acac)_2$ + $20BF_3OEt_2$ catalytic system are shown in Fig. 1. Curves *2* and *3* corresponding to fractions of *trans*-2-hexene and *cis*-1-hexene, respectively, do not pass through the origin when extrapolated. This can be due to a short induction period of the first step of 1-hexene isomerization, when 1-hexene is involved in formation of catalytically active palladium complexes. Under the experimental conditions (Fig. 1), the 1-hexene conversion into the isomerization products in 10–12 min is more than 15000 mol per mole of $Pd(acac)_2$. The major isomerization product (up to 62%) is *trans*-2-hexene.

When $Pd(acac)_2$ and BF_3OEt_2 react for 30 min in the absence of 1-hexene, i.e., when the conditions of formation of AC change, the rate of 1-hexene isomerization decreases by a factor of approximately 3. However, in this case the selectivity of isomerization into *trans*-2-hexene increases to 94.7% (Table 1).

The study of kinetic features of 1-hexene isomerization in the presence of $Pd(acac)_2$ + $20BF_3OEt_2$ system [8] showed that this process is of the first and zero order with respect to the catalysts and 1-hexene, respectively.

In the presence of PPh_3 (P/Pd = 1), the reaction is of the first and third order with respect to 1-hexene and the catalyst, respectively. Introduction of trivalent phosphorus compounds into the $Pd(acac)_2$ + $20BF_3OEt_2$ catalytic system decelerates isomerization

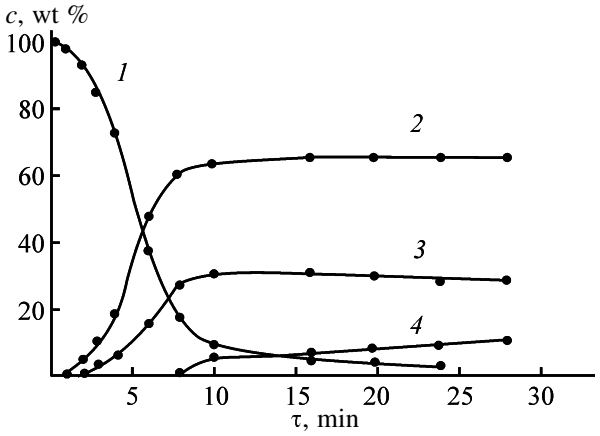


Fig. 1. Composition of 1-hexene isomerization products formed in benzene in the presence of $Pd(acac)_2$ + $20BF_3OEt_2$ at 293 K as a function of time τ: (*1*) 1-hexene, (*2*) *trans*-2-hexene, (*3*) *cis*-2-hexene, and (*4*) 3-hexene. c_{Pd} = 2.74×10^{-3} M, $c_{1\text{-hexene}}$ = 4.113 M.

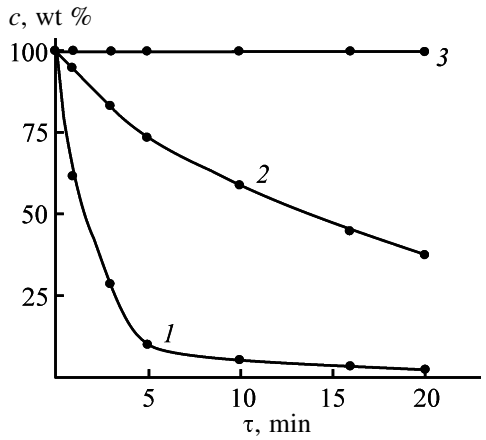


Fig. 2. Concentration of 1-hexene in benzene at 288 K in the presence of $Pd(acac)_2$ + PPh_3 + $20BF_3OEt_2$ catalytic system as a function of time τ. P/Pd: (*1*) 1, (*2*) 1.5, and (*3*) 2. c_{Pd} = 1.47×10^{-3} M, $c_{1\text{-hexene}}$ = 0.941 M.

Table 2. Composition of the products of 1-hexene isomerization performed for 10 min in the presence of $Pd(acac)_2$ + $20BF_3OEt_2$ catalytic system containing different phosphines PR_3

Time, min	Composition of isomerization products, wt %			
	1-hexene	2-hexene (*trans*)	2-hexene (*cis*)	3-hexene (*cis* + *trans*)
PPh_3	–	60.8	29.3	9.9
$P(n\text{-}Bu)_3$	–	55.6	34.3	10.1
$P(Cy)_3$	–	53.5	33.7	12.8

Table 3. Composition of the products of 1-hexene isomerization in the presence of $Pd(acac)_2$ + PPh_3 + $20BF_3OEt_2$ catalytic system at different reaction times and different initial concentration of 1-hexene

Time, min	Composition of isomerization products, wt %							
	1-hexene		2-hexene (*trans*)		2-hexene (*cis*)		3-hexene (*cis* + *trans*)	
	1*	2*	1	2	1	2	1	2
1	93.0	100.0	7.0	–	–	–	–	–
2	68.5	78.2	20.5	16.5	11.0	5.3	–	–
3	53.0	75.4	28.8	19.3	18.2	5.3	–	–
5	36.9	47.4	44.1	26.2	19.0	26.4	–	–
10	12.7	16.6	61.4	42.6	22.6	37.4	3.4	–
20	–	–	69.1	48.2	24.4	44.4	6.5	7.4

* $c_{1\text{-hexene}}$: (*1*) 1.89 and (*2*) 0.236 M.

of 1-hexene. The palladium catalyst is completely deactivated when the P/Pd atomic ratio increases to 2 (Fig. 2).

The structure type of trivalent phosphorous compounds has virtually no effect on the selectivity of 1-hexene isomerization (Table 2).

However, in the presence of PR_3, the ratio of *cis* and *trans* isomers of 2-hexene substantially depends on the initial concentration of 1-hexene (Table 3).

When the 1-hexene : palladium ratio changes from 1286 to 160, the ratio of *trans* and *cis* isomers of 2-hexene decreases approximately from 3 to 1.

The catalytic activity of the examined system strongly depends on the solvent. The catalytic activity increases with an increase in the polarity of the solvent in the following series: heptane + benzene (1 : 1 vol : vol) < benzene < toluene < isopropylbenzene. The catalytic activity of $Pd(acac)_2$ + PPh_3 + $20BF_3OEt_2$ system in isomerization of 1-hexene in toluene is slightly higher than that in more polar isopropylbenzene (Fig. 3). This can be due to competitive coordination of 1-hexene and the solvent to RC of palladium.

The isomerization rate decreases when the length of the hydrocarbon chain and the number of substituents at the double bond increase in the series 1-hexene, 1-heptene, 2-methyl-1-pentene, *cis* + *trans*-4-methyl-2-pentene (Fig. 4). This is typical for coordination isomerization of alkenes in the presence of transition metal complexes.

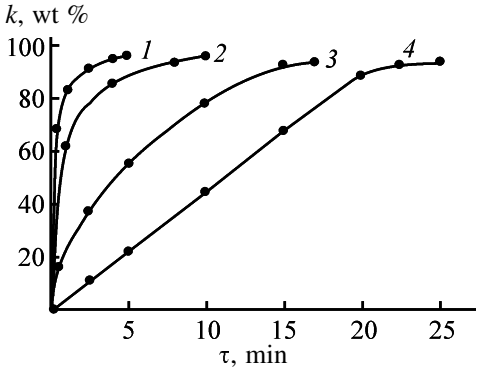


Fig. 3. Conversion of 1-hexene *k* into its isomers in the presence of $Pd(acac)_2$ + PPh_3 + $20BF_3OEt_2$ catalytic system at 283 K in (*1*) toluene, (*2*) isopropylbenzene, (*3*) benzene, and (*4*) benzene + heptane (1 : 1 vol/vol), $c_{Pd} = 1.47 \times 10^{-3}$ M, $c_{1\text{-hexene}} = 0.471$ M.

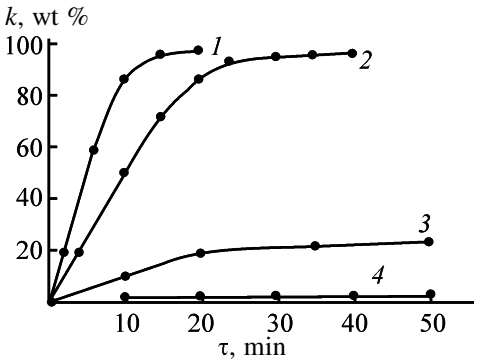


Fig. 4. Conversion k of (*1*) 1-hexene, (*2*) 1-heptene, (*3*) 2-methyl-1-pentene, and (*4*) *cis* + *trans*-4-methyl-2-pentene into their isomers in the presence of $Pd(acac)_2 + PPh_3 + 20BF_3OEt_2$ catalytic system at 283 K in benzene. $c_{Pd} = 1.47 \times 10^{-3}$ M, $c_{olefin} = 0.941$ M.

CONCLUSIONS

(1) The $Pd(acac)_2$–BF_3OEt_2 system shows high catalytic activity in positional isomerization of α-alkenes. The conversion of 1-hexene into the isomerization products under the optimal conditions (B/Pd = 20/1, $c_{Pd} = 1.47 \times 10^{-3}$ M, T = 293 K, benzene) within 10–12 min is 15000 mol g-at.$^{-1}$ of Pd. The *trans*-2-hexene content in the isomerization products is up to 62 %.

(2) The catalytic activity of the system decreases when its components are allowed to react with each other for 30 min in the absence of 1-hexene. In this case, however, the selectivity of 1-hexene isomerization into *trans*-2-hexene can be as high as 94.5%.

(3) In the presence of trivalent phosphorus compounds, the rate of α-alkene isomerization decreases, reaching zero value for 1-hexene at P/Pd = 2. The inhibiting effect can be due to blocking of the coordination vacancies of Pd in the RC. The BF_4 ligand should occupy the fourth coordination site in the AC to form Pd–F · BF_3 bond. The composition of the resulting charge-transfer complex is $HPd(L_2)FBF_3$, where L is alkene.

REFERENCES

1. Tkach, V.S., Myagmarsuren Gomboo, Mesyef, M., and Shmidt, F.K., *React. Kinet. Catal. Lett*., 1999, vol. 66, no. 2, pp. 281–287.
2. Myagmarsuren Gomboo, Tkach, V.S., Shmidt, F.K., *et al*., *J. Mol. Catal. A: Chem*., 2005, vol. 235, pp. 154–160.
3. Keit, W., Röper, M., and Scheren, A., *J. Mol. Catal. A: Chem*., 1983, vol. 20, p. 139.
4. Chernyshev, M.L., Tkach, V.S., Dmitrieva, T.V., *et al*., *Kinet. Katal*., 1997, vol. 38, no. 4, p. 575.
5. USSR Inventor's Certificate no. 961193.
6. USSR Inventor's Certificate no. 1160631.
7. Myagmarsuren Gomboo, Tkach, V.S., Suslov, D.S., and Shmidt, F.K., *React. Kinet. Catal. Lett*., 2005, vol. 85, no. 1, pp. 197–203.
8. Myagmarsuren Gomboo, Tkach, V.S., and Shmidt, F.K., *React. Kinet. Catal. Lett*., 2004, vol. 83, no. 2, pp. 337–343.
9. Cramer, R. and Linsday, R.V., *J. Am. Chem. Soc*., 1966, vol. 88, p. 3534.
10. Harrod, J.F. and Chalk, A.J., *J. Am. Chem. Soc*., 1966, vol. 88, p. 3491.
11. Sen, A., and Ta-Wang Lai, *Inorg. Chem*., 1981, vol. 20, p. 4036.
12. Tkach, V.S., Ratovskii, G.V., Gomboogiin, M., *et al*., *Koord. Khim*., 2000, vol. 26, no. 3, pp. 219–228.
13. Gordon, A.J. and Ford, R.A., *The Chemist's Companion*, New York: Wiley, 1972. Translated under the title *Sputnik khimika*, Moscow: Mir, 1976, pp. 438–448.

ISSN 1070-4272. Russian Journal of Applied Chemistry, 2006, Vol. 79, No. 1, pp. 89–92. © Pleiades Publishing, Inc., 2006.
Original Russian Text © E.V. Pyatnitsyna, M.M. El'chaninov, A.P. Savost'yanov, 2006, published in Zhurnal Prikladnoi Khimii, 2006, Vol. 79, No. 1, pp. 92–95.

CATALYSIS

Catalytic Hydrogenation of 2-Butyne-1,4-diol to 2-Butene-1,4-diol at Atmospheric Pressure in the Liquid Phase

E. V. Pyatnitsyna, M. M. El'chaninov, and A. P. Savost'yanov

South-Russian State Technical University, Novocherkassk, Rostov oblast, Russia

Received October 10, 2005

Abstract—Selective hydrogenation of 2-butyne-1,4-diol to 2-butene-1,4-diol on suspended palladium and Raney nickel catalysts at atmospheric pressure was studied. The optimal parameters of this reaction were determined. Samples containing 90% 2-butene-1,4-diol were prepared.

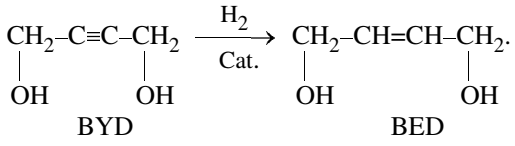
DOI: 10.1134/S1070427206010198

2-Butene-1,4-diol (BED) is used to produce valuable materials such as Endosulfan (insecticide) [1], polyesters [2], alkyd resins [3], butadiene rubber [4], and plasticizers [4] for various branches of industry and medicine. However, this monomer was not produced in Russia. Selective preparation of this monomer by hydrogenation of 2-butyne-1,4-diol (BYD) is of great practical interest.

Here we studied selective hydrogenation of BYD to BED on suspended catalysts at atmospheric pressure.

EXPERIMENTAL

Hydrogenation of BED to BYD was performed in an aqueous suspensions on fine powders of palladium catalysts containing 0.8 and 2.0% Pd and on Raney nickel:



2-Butyne-1,4-diol was reduced in a 100-ml long-necked reactor fixed on a shaker. To maintain the required temperature of the reactor and buret, thermostated water was passed through their jackets. A weighed portion of BYD (1.32 g), water (20 ml), and calculated amount of finely divided catalyst were placed in the reactor. The reaction completion was judged from the volume of hydrogen absorbed, which was measured with a 300-ml gas buret. The palladium catalysts (0.8 and 2.0 wt % Pd supported by OUB carbon) was prepared by impregnation of the support with hydrochloric acid solution of palladium(II) chloride, followed by reduction to metallic Pd with formaldehyde [5]. The selective W-6 nickel catalyst was prepared by leaching a nickel–aluminum Raney alloy with a solution of sodium hydroxide (20 wt %) [6].

The hydrogenation products were analyzed on a Tsvet chromatograph using a 2000 × 3-mm column. The carrier gas was nitrogen; the column temperature was 60–200°C. The support was Chromaton Super (0.16–0.20 mm); the stationary phase was polyethylene glycol 15000.

To determine the best hydrogenation conditions, we studied the composition of the hydrogenation products as influenced by the temperature in the range from 30 to 70°C and the catalyst amount in the reaction mixture in the range from 10 to 100% relative to BYD. The results are summarized in Tables 1 and 2. Chromatographic analysis of the products showed that the target product is formed with 93–94% selectivity on both palladium catalysts, especially at 40–50°C, after absorption of hydrogen in the amount corresponding to reduction of one π bond. When the Pd/C-2 catalyst with higher metal content was used, the weight fraction of BED did not noticeably change. At 30 and 60–70°C, the selectivity decreases. This is due, in the first case, to a low reaction rate and, in the second case, to an increase in the partial pressure of water vapor and fast dehydration, isomerization, and exhaustive hydrogenation.

Hydrogenation on a Raney Ni is slower. The BED content in the reaction product is 73–76%. Under these conditions, γ-hydroxybutyraldehyde (HBA), isomerization product of BED, is formed in a large amount. This compound is dehydrated and hydro-

Table 1. Composition of the hydrogenation products of BYD at different weight fractions of the catalysts in the reaction mixture

Catalyst	Hydrogenation conditions*				Composition of hydrogenation products, wt %				
	catalyst fraction, wt %	τ, min	V_t	V_{exp}	BTN	HBA	BAD	BED	BYD
			cm^3						
Pd/C-0.8	10	138	461.4	442.2	0.9	1.1	2.2	94.9	0.9
	20	118	459.4	450.0	1.5	1.6	1.9	94.6	0.4
	50	95	459.4	455.2	3.8	2.2	2.9	90.9	0.2
	75	84	461.4	455.5	4.0	5.1	5.6	85.3	–
	100	72	462.8	458.5	4.6	7.1	8.1	80.2	–
Pd/C-2	10	132	469.8	455.7	0.8	1.2	2.4	94.5	1.1
	20	117	467.7	458.8	1.7	1.4	2.5	94.4	–
	50	92	468.4	467.5	4.2	3.7	2.8	89.3	–
	75	80	464.2	462.5	4.5	5.4	6.8	83.3	–
	100	65	466.3	470.5	4.8	7.5	8.4	79.3	–
Raney Ni	10	315	464.2	451.7	4.1	13.9	1.4	76.3	4.3
	20	228	465.6	465.0	5.8	15.1	3.9	75.2	–
	50	183	462.8	460.9	7.4	13.7	5.7	73.2	–
	75	150	464.2	465.6	8.7	10.1	8.5	72.7	–
	100	122	465.6	466.0	10.4	7.6	11.9	70.7	–

* (V_t) Theoretical volume of hydrogen absorbed, corrected for the reaction conditions; (V_{exp}) experimental volume of hydrogen absorbed; (τ) hydrogenation time.

Table 2. Composition of the products of BYD hydrogenation on the suspended catalysts at different temperatures

Catalyst	Hydrogenation conditions*				Composition of hydrogenation products, wt %				
	T, °C	τ, min	V_t	V_{exp}	BTN	HBA	BAD	BED	BYD
			cm^3						
Pd/C-0.8	30	165	401.8	397.5	1.7	0.3	2.0	89.1	6.9
	40	130	427.8	423.3	1.5	1.7	2.7	93.5	0.6
	50	99	464.2	462.3	1.8	1.3	2.4	94.2	0.3
	60	95	525.0	519.5	3.9	1.9	4.2	90.7	0.2
	70	72	629.3	620.0	5.7	3.4	7.5	82.0	1.4
Pd/C-2	30	160	399.6	384.7	1.5	0.4	2.2	89.2	6.7
	40	127	426.8	420.5	2.8	1.6	2.9	92.7	–
	50	94	466.3	463.0	1.7	1.4	2.5	94.4	–
	60	90	526.8	520.3	3.7	2.1	3.9	90.3	–
	70	75	623.3	615.0	5.5	3.7	8.2	81.0	1.6
Raney Ni	30	230	404.6	392.0	5.3	16.2	1.8	76.7	–
	50	212	469.8	461.5	5.7	14.6	4.3	75.4	–
	70	195	629.3	615.5	6.2	12.7	6.6	73.2	1.3

genated to form *n*-butanol (BTN). In addition, the hydrogenation product of BED, butane-1,4-diol (BAD), is accumulated.

We studied how the weight fraction of the catalysts in the reaction mixture affects the composition of the hydrogenation products formed at 50°C. The results are presented in Table 2. As seen from Table 2, the yield of the target product is maximal at the weight fraction of the palladium catalyst from 10 to 20%. When the catalyst content increases to 50–100%, the reaction is accelerated by a factor of 2 but the selectivity of BED formation decreases owing to side reac-

Table 3. Time dependence of the composition of the products of BYD hydrogenation at 40°C

τ, min	V_{exp}, cm^3	Composition of hydrogenation products, wt %				
		BTN	HBA	BAD	BED	BYD
15	49.9	0.5	0.1	Absent	14.5	85.1
30	100.0	1.5	0.1	Absent	29.1	69.5
45	132.5	2.0	0.2	0.6	42.3	54.9
60	180.5	2.4	0.5	0.8	50.9	45.4
75	245.0	2.4	0.5	0.9	64.5	31.7
90	275.2	2.4	0.5	0.9	74.7	21.5
105	335.9	2.9	0.8	1.1	82.8	12.4
120	370.4	3.3	1.1	1.2	88.3	6.1
135	432.0	3.9	1.5	1.4	93.2	Absent

tions yielding BTN, HBA, and BAD is significant amounts. The hydrogenation is also accelerated by a factor of approximately 3 with increasing the weight fraction of the Raney nickel catalyst. In this case, the BED yield significantly decreases owing to formation of large amounts of the by-products including BAD. It should be noted that the weight fraction of HBA decreases with increasing the concentration of Raney Ni catalyst. This fact indicates that HBA is reduced to BAD in the presence of this catalyst.

We studied how the composition (wt %) of products of BYD hydrogenation at 40°C in the presence of Pd/C-0/8 depends on the reaction time (Table 3, Fig. 1). Analysis of the kinetic curves shows that the BED concentration is maximal at the time of complete consumption of BYD. Isomerization and dehydration occur simultaneously with formation of BED. The product of BED hydrogenation is formed in 30 min.

Thus, BYD is selectively hydrogenated to BED on the suspended palladium catalysts at atmospheric pressure when the process is stopped after consumption of 1 mol of hydrogen. Based on this result, we proposed a procedure for laboratory preparation of BED. For this purpose we used a solution of 2-butyne-1,4-diol [TU (Technical Specifications) 64-5-52–79; distilled water [GOST (State Standard) 6709–72]; hydrogen (technical grade, GOST 3022–80); catalyst Pd/C-0.8.

A weighed portion of catalyst (75 g) and 25 wt % aqueous solution of BYD (1.5 l) were placed in a 2-l three-necked flask equipped with a stirrer, a bubbler, and a tube connected with a Woulfe bottle for moni-

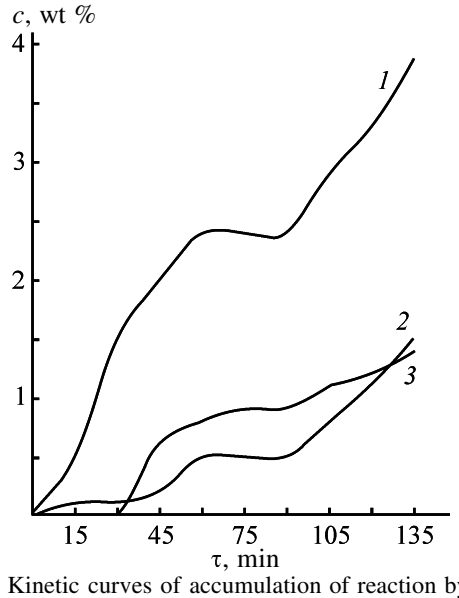


Fig. 1. Kinetic curves of accumulation of reaction by-products (*1*) BTN, (*2*) HBA, and (*3*) BAD at 40°C. (*c*) Concentration and (τ) time; the same for Fig. 2.

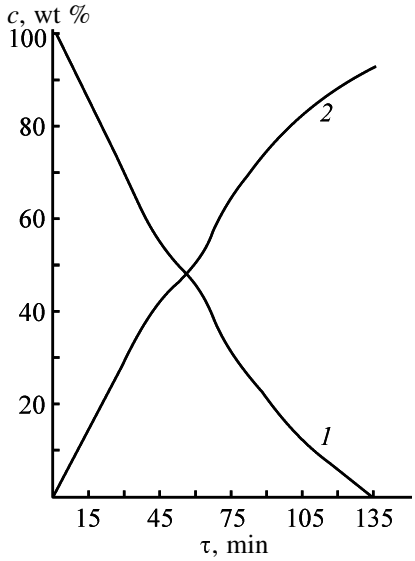


Fig. 2. Kinetic curves of (*1*) BYD consumption and (*2*) accumulation of BED at 40°C.

toring the evolved gas. The reaction mixture was heated to 50–60°C, the stirrer was switched on, and hydrogen bubbling was started. The composition of the hydrogenation products was determined on a Tsvet-104 chromatograph with a flame ionization detector. Th reaction was stopped when the intensity of the peak on unchanged BYD was no higher than 0.2–0.5%. Then the reaction mixture was filtered on a Büchner funnel. Water was removed from the filtrate in a water-jet pump vacuum with heating on a water bath. The residue was distilled with a dephlegmator in a vacuum of an RVN-20 pump (3 mm Hg). The BED yield was 276.2 g (~72%); bp 230–235°C at 760 mm Hg.

CONCLUSION

As shown by chromatographic analysis, 2-butyne-1,4-diol can be selectively hydrogenated to 2-butene-1,4-diol in the liquid phase on suspended finely divided palladium catalysts at atmospheric pressure in the batch mode at a fixed amount of hydrogen absorbed.

REFERENCES

1. Mel'nikov, N.N., *Khimiya i tekhnologiya pestitsidov* (Chemistry and Technology of Pesticides), Moscow: Khimiya, 1974.
2. JPN. Patent 49-48291.
3. FRG Patent 2414341.
4. Sokol'skii, D.V., Pak, A.M., and Ten, E.I., Abstracts of Papers, *IV Vsesouznaya konferentsiya po khimii atsetilena* (IV All-Union Conf. on Acetylene Chemistry), vol. 3: *Polimerizatsiya atsetilenovykh soedinenii: Kataliticheskoe vosstanovlenie i tekhnologiya atsetilena i ego proizvodnykh* (Polymerization of Acetylene Compounds: Catalytic Reduction and Technology of Acetylene and Its Derivatives), Alma-Ata: Inst. Khim. Nauk Akad. Nauk Kaz. SSSR, 1972, pp. 254–259.
5. Mandel'shtam, T.V., Ioffe, B.V., Artsybasheva, Yu.P., and Bolotov, B.A., *Sovremennye metody organicheskogo sinteza* (Modern Procedures of Organic Synthesis), Leningrad: Leningr. Gos. Univ., 1974.
6. Adkins, H. and Billica, H.R., *J. Am. Chem. Soc.*, 1955, vol. 70, p. 695.

ISSN 1070-4272. Russian Journal of Applied Chemistry, 2006, Vol. 79, No. 1, pp. 93–97. © Pleiades Publishing, Inc., 2006.
Original Russian Text © Yu.V. Tsarev, V.V. Kashnikov, S.V. Krupin, V.V. Kostrov, 2006, published in Zhurnal Prikladnoi Khimii, 2006, Vol. 79, No. 1, pp. 96–99.

PROCESSES AND EQUIPMENT OF CHEMICAL INDUSTRY

Simulation of the Electrocatalytic Oxidation of Acetone in a Fixed Catalyst Bed

Yu. V. Tsarev, V. V. Kashnikov, S. V. Krupin, and V. V. Kostrov

Ivanovo State University of Chemical Engineering, Ivanovo, Russia

Received October 26, 2004; in final form, June 2005

Abstract—Catalytic oxidation of acetone on samples of a copper-containing catalyst with an ac electric field applied to the catalyst bed was simulated. The distribution of temperature across the catalyst bed was studied at varied delivered specific electric power, and kinetic parameters of the catalyst samples were determined.

DOI: 10.1134/S1070427206010204

Solution of the problems of environment protection requires that gas discharges should be purified to remove volatile organic compounds (VOCs). Organization of a system for detoxication of VOC discharges and its design constitute a complicated scientific and technological problem. In this study, the major attention is given to simulation of electrocatalytic detoxication of hydrocarbon-containing gases on copper-containing catalysts and to determination of their kinetic parameters.

The catalyst was prepared from technical-grade carbon of PM-750 brand by mixing the carbon with copper hydroxo carbonate. Then a plasticizer (10% solution of polyvinyl alcohol) was added to the resulting mixture and it was formed at the optimal forming moisture content to give grains 0.5–1.0 mm in diameter, which were calcined in a flow of CO_2 at 350°C. As a model gas system we studied a mixture constituted by air and 1–2 g m^{-3} of acetone. The concentration of acetone in the gas–air mixture was determined nephelometrically on a KFK-2MP photoelectrocolorimeter at a wavelength of 320 nm [1]. The conversion of acetone on the catalyst samples synthesized was found in an isothermal plug-flow reactor. During the tests, an ac electric voltage was applied across the catalyst bed. The total specific surface area of the catalyst was measured on a Tsvet-211 sorption meter by the procedure described in [2]. The surface area of the catalysts was determined by selective low-temperature chemisorption of helium. The chemisorption measurements were performed in the pulsed mode at –136°C.

In view of the fact that application of an electric field across the catalyst bed may lead to its prolonged heating, it was suggested to use a nonstationary model describing the catalytic reactor [3]. A two-phase model was chosen. The following assumptions were made to enable solution of the system of equations: (1) the longitudinal and radial transfer was disregarded in the balance equations for the gas phase; (2) absence of temperature gradients in a grain was allowed; (3) the process was considered in the absence of heat transfer across a reactor wall; and (4) the concentration gradients in a grain were considered to be absent.

With account of these assumptions, it was suggested to solve the following system of differential equations to describe the electrocatalytic oxidation in a catalyst bed with application of an ac electric field to this bed:

$$\frac{\partial T}{\partial \tau} = \frac{\alpha S}{C_p \rho_a}(\theta - T) - U\frac{\partial T}{\partial \varepsilon}, \quad (1)$$

$$\frac{\partial \theta}{\partial \tau} = \frac{1}{C_c \rho_c}\left[-\alpha_{cm} S_m(\theta - T_{env})/V_r + P_m + \lambda\frac{\partial^2 \theta}{\partial \varepsilon^2} - \alpha S(\theta - T) + Q k_0 \exp(-E_a/RT)(1 - X_c)\right], \quad (2)$$

$$\frac{\partial X_c}{\partial \tau} = \beta(X_c - X_g) - U\frac{\partial X_g}{\partial \varepsilon}, \quad (3)$$

$$\frac{\partial X_c}{\partial \tau} = k_0 \exp(-E_a/RT)(1 - X_c) - \beta(X_c - X_g), \quad (4)$$

where T is temperature in the gas phase (K); θ, tem-

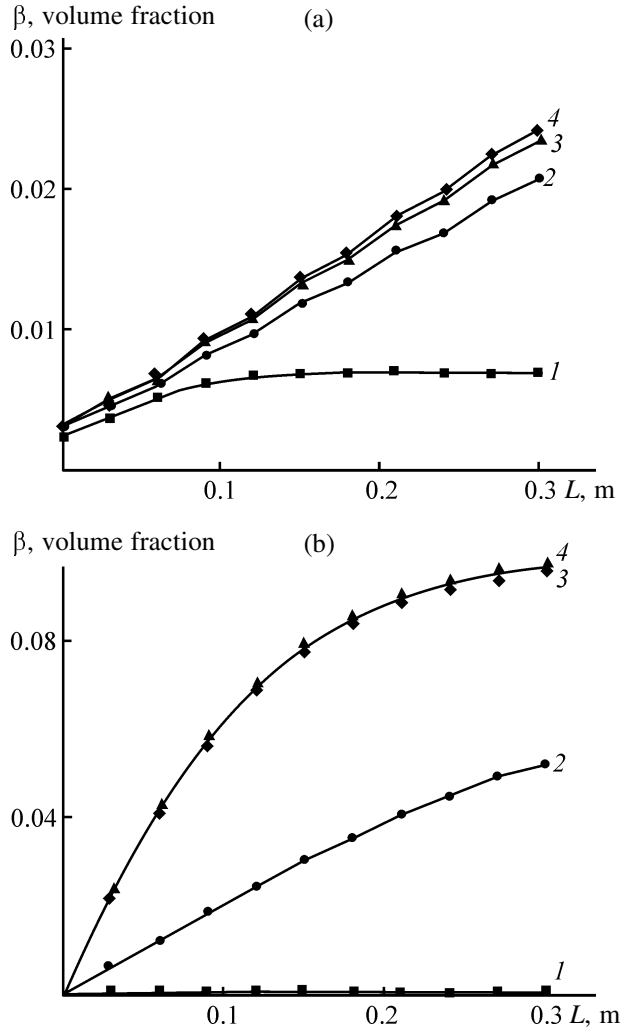


Fig. 1. Calculated distribution of the conversions β along the reactor length L for a delivered specific power of (a) 0.02 and (b) 2.00 W cm^{-3}. Time during which the gas–air mixture was passed (s): (*1*, *2*) 100, (*3*) 600, and (*4*) 1200.

perature in the catalyst grain (K); X_c, degree of purification in a catalyst grain (fraction units); X_g, degree of purification in a gas flow (fraction units); τ, running time elapsed from the time origin (s); α, coefficient of heat transfer from the outer surface of grains to the flow (W m^{-1} K^{-1}); S, volume-related specific surface area of the catalyst (m^2 m^{-3}); C_p, specific heat of air (kJ kg^{-1} K^{-1}); ρ_a, density of air (kg m^{-3}); U, true gas-flow velocity in the reactor (m s^{-1}); ε, running reactor height (m); C_c, specific heat of the catalyst (kJ kg^{-1} K^{-1}); ρ_c, apparent density of the catalyst (kg m^{-3}); λ, effective coefficient of heat conductivity via the bed "skeleton" (W m^{-1} s^{-1}); Q, amount of heat released in the course of the reaction, related to the volume of the gas flow at the initial concentration of the reagent (kJ m^{-2} K^{-1}); k_0, preexponential factor of the reaction rate constant (s^{-1}); E_a, activation energy of the reaction on the catalyst (kJ m^{-1} K^{-1}); β, coefficient of mass transfer from the flow to the surface of catalyst grains (W m^{-2} K^{-1}); P_m, power of heating of the catalyst bed by the electric current, related to the unit volume of the catalyst (W m^{-3}); α_{cm}, coefficient of heat transfer from the catalyst bed to the environment (W m^{-2} K^{-1}); S_m, surface area of heat exchange between the reactor and the environment (m^2); V_r, reactor volume (m^3); and T_{env}, environment temperature (K).

The preexponential factor k_0 and the activation energy E_a make it possible to account for the activity of the catalyst to which an electric field is applied. The system of differential equations enables analysis of the process under nonstationary conditions and evaluation of the time in which the system attains a steady state.

Equation (1) describes the heat balance in the gas phase. Equation (2) represents the heat balance in the catalyst bed, and Eqs. (3) and (4), material balance in the gas phase and in the catalyst bed, respectively. Equations (2) and (4) use as a kinetic term a first-order equation that describes the majority of processes of deep oxidation of organic compounds [3].

One (gas) phase is constituted by the flow of reagents moving across the catalyst bed, and the other (solid) is formed by the catalyst bed in which the reaction occurs. The heat transfer caused by the arising temperature gradients is distributed among the phases. A similar transfer of substance occurs only in the reagent flow. In this model, both phases are quasi-homogeneous, and, therefore, each point within the catalyst bed is represented by two sets of substance concentrations and temperatures.

To consider completely defined the problem of describing the oxidation of acetone in a catalyst bed to which an electric field is applied, it is necessary to specify the initial and boundary conditions.

Initial conditions:

$$\text{at } \tau = 0\text{: } T = T_{in},\ \theta = T_{in},\ X_c = 0,\ X_g = 0.$$

Boundary conditions:

$$\text{at } \varepsilon = 0\text{: } T = T_{inl},\ X_g = X_{inl} = 0,\ \partial\theta/\partial\varepsilon = 0,\ \partial X_c/\partial\varepsilon = 0;$$

$$\text{at } \varepsilon = h\text{: } \partial T/\partial\varepsilon = 0,\ \partial\theta/\partial\varepsilon = 0,\ \partial X_g/\partial\varepsilon = 0,\ \partial X_c/\partial\varepsilon = 0.$$

The heat- and mass-transfer coefficients α and β were found from the corresponding criterion equations

[4]. It was recommended in [5] to take the effective coefficient for the catalyst bed skeleton as 10 times the heat conductivity coefficient of air. The variation of the thermal properties of the gas phase (air, to a first approximation) with temperature was accounted for using nomographic data [6, 7]. The coefficient of heat transfer from the reactor to the environment was found using the data of [8]. The temperature dependence of the specific heat and of the heat effect of the reaction was neglected in the case under consideration.

The chosen system of equations was solved by the approximate numerical net-point method (finite-difference method). It was suggested in [5] to use an implicit scheme, with nonlinear constraints in a given temporal layer excluded (it is suggested to take nonlinear terms from the preceding temporal layer). The chosen system of differential equations (1)–(4) was solved by the explicit net-point method [9]. Heat effect of the reaction, Q_R = 1785 kJ mol^{-1} [10]; molecular weight of acetone, M = 58 g mol^{-1}. The molar volumes of the gases were used to calculate the diffusion coefficients [6].

A program in the Object Pascal language was developed in the visual-oriented programming environment Delphi version 6. The program calculates the distribution of temperature and degree of purification across the bed profile in a catalyst grain and in the flow for a given instant of time. The results of a calculation by the program for the time of passing the gas–air mixture in the range from 1 to 1200 s and delivered specific power of electric current ranging from 0.02 to 2.00 W cm^{-3} are presented in Figs. 1–3.

Figures 1a and 1b show the distributions of acetone conversion along the reactor length for different times of passing the gas–air mixture across the catalyst bed. The results of the simulation suggest that the process reaches the steady state 10–20 min after the beginning of reactor operation. This time becomes shorter as the delivered specific power increases. For example, for a delivered specific power of 2 W cm^{-3} in Fig. 1b, the distributions of acetone conversion along the reactor length for times of 600 and 1200 s virtually coincide, whereas for a delivered specific power of 0.02 W cm^{-3} in Fig. 1a, no coincidence is observed for the corresponding distributions. It can also be noted (Fig. 3) that, as the delivered specific power is raised from 0.02 to 1 W cm^{-3}, the temperature in the catalyst bed may increase from 25 to 200°C. This makes a contribution to the rise in the acetone conversion on the catalyst (Fig. 2).

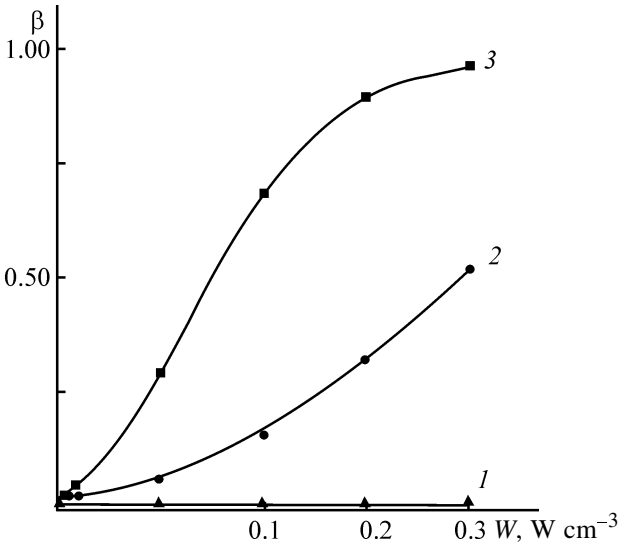


Fig. 2. Calculated conversion β of acetone vs. the delivered specific power W. Time of passing the gas–air mixture (s): (*1, 2*) 100 and (*3*) 600; the same for Fig. 3.

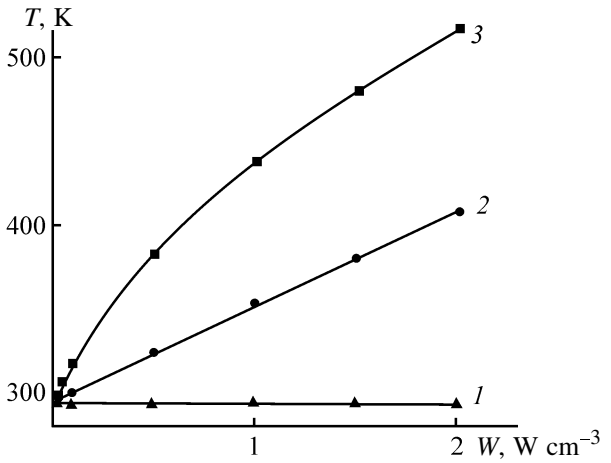


Fig. 3. Calculated dependence of the temperature T of the gas–air mixture at the exit from the catalyst bed on the delivered specific power W.

Points in Fig. 4 represent the experimental values of the acetone conversion in relation to the delivered specific power, which were obtained for a time of passing the gas–air mixture across the catalyst bed exceeding 1200 s, for catalyst samples with varied percentage content of copper oxide. These experimental values are in good agreement with the calculated dependences of the acetone conversion on a copper-containing catalyst on the delivered specific power for a time of 1200 s (solid lines).

The table lists the calculated rms deviations of the experimental values from those calculated in terms of the model. The strongest deviation is observed for catalyst samples containing copper(II) oxide at

Activation energy E_a and preexponential factor k_0 for catalyst samples, and the root-mean-square deviation S of experimental data from the calculation results

Parameter	CuO content, wt %				
	0	10	20	40	60
k_0, s^{-1}	0.3	3.0	13.0	283.0	686.0
E_a, kJ mol^{-1}	4.6	7.0	10.0	16.7	18.3
S, %	6.4	11.7	8.1	5.4	1.0

delivered specific power of electric current exceeding 2 W cm^{-3}. This is due to the fact that the air space in the catalyst bed is ionized under the experimental conditions at the given specific power of electric current. As a result, acetone can be oxidized under the given conditions not only on the catalyst surface, but also in the air space between catalyst grains, which is reflected on the degree of acetone oxidation [11].

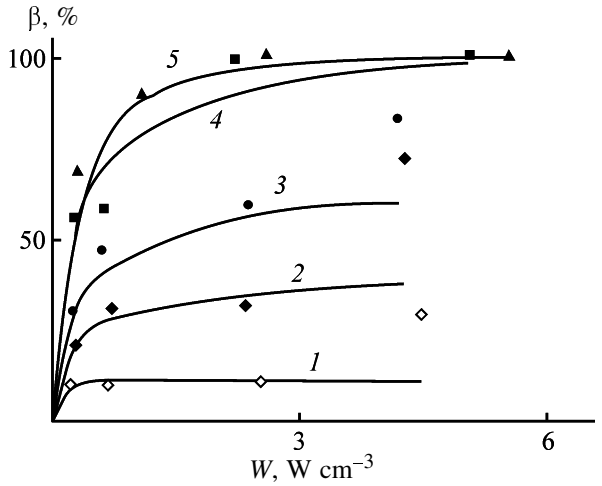


Fig. 4. Experimental (points) and calculated (lines) conversions β of acetone vs. the delivered specific power W of electric current. Content of CuO in the catalyst (wt %): (*1*) 0, (*2*) 10, (*3*) 20, (*4*) 40, and (*5*) 60; the same for Fig. 5.

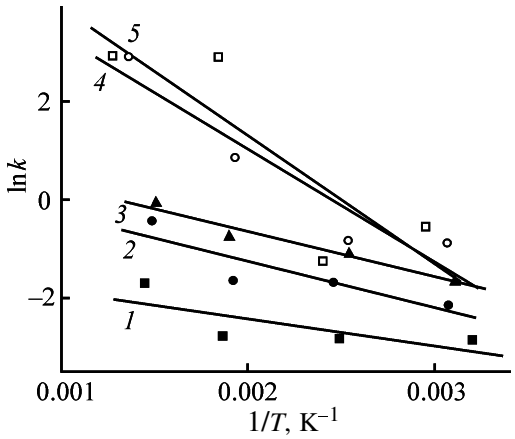


Fig. 5. Logarithm of the rate constant k vs. temperature T.

Figure 5 shows kinetic dependences calculated and plotted for catalyst samples with varied percentage content of copper oxide. The table lists the calculated kinetic parameters of the catalyst samples. The samples with a copper oxide content of less than 40% exhibit an activation energy lower than that for samples containing 40 and 60% CuO and a smaller preexponential factor. On the whole, it could be noted that the percentage of copper oxide introduced into a catalyst affects its behavior in acetone oxidation under the conditions of an applied electric field.

CONCLUSIONS

(1) The developed model of the reactor made it possible to describe how the system constituted by a catalyst bed, electric current, and gas–air mixture behaves with time.

(2) The mathematical model was used to determine the possibility of attainment of steady conditions in the oxidation of acetone, which is important for carrying out a kinetic study.

(3) The chosen mathematical model made it possible to calculate kinetic parameters of the catalyst samples synthesized.

REFERENCES

1. Peregud, E.A. and Gernet, E.V., *Khimicheskii analiz vozdukha promyshlennykh predpriyatii* (Chemical Analysis of Air at Industrial Plants), Leningrad: Khimiya, 1970.
2. Buyanova, N.E., *et al.*, *Opredelenie udel'noi poverkhnosti katalizatora* (Determination of the Specific Surface Area of a Catalyst), Moscow: Khimiya, 1973.
3. *Ekologiya i kataliz: Sbornik nauchnykh trudov* (Ecology and Catalysis: Coll. of Sci. Works), Il'in, V.P. and Matros, Yu.Sh., Executive Eds., Novosibirsk: Nauka, 1990.
4. Aerov, M.A. and Todes, O.M., *Gidravlicheskie i teplovye osnovy raboty apparatov so statsionarnym i kipyashchim zernistym sloem* (Hydraulic and Thermal Foundations of the Operation of Apparatus with Fixed and Fluidized Grainy Beds), Leningrad: Khimiya, 1968.
5. Beskov, V.S. and Flokk, V., *Modelirovanie kataliticheskikh protsessov i reaktorov* (Simulation of Catalytic Processes and Reactors), Moscow: Khimiya, 1991.
6. Pavlov, K.F., Romankov, P.G., and Noskov, A.A., *Primery i zadachi po kursu protsessov i apparatov*

khimicheskoi tekhnologii (Problems for the Course of Processes and Apparatus of Chemical Technology), Leningrad: Khimiya, 1987, 10th ed.

7. *Spravochnik khimika* (Chemist's Handbook), Nikol'skii, B.P., Ed., Moscow: Khimiya, 1968, 2nd ed., vol. 5.
8. Lebedev, V.Ya., *Raschet i proektirovanie teploispol'zuyushchego oborudovaniya* (Calculation and Design of Heat-Employing Apparatus), Ivanovo: Ivanovsk. Khimiko-Tekhnol. Inst., 1994.
9. Samarskii, A.A. and Nikolaev, E.S., *Metody resheniya setochnykh uravnenii* (Methods for Calculation of Net Equations), Moscow: Nauka, 1978.
10. *Kratkii spravochnik fiziko-khimicheskikh velichin* (Concise Reference Book of Physicochemical Constants), Ravdel', A.A. and Ponomareva, A.M., Eds., St. Petersburg: Spetsial'naya Literatura, 1998, 9th ed.
11. Matros, Yu.Sh., *Nestatsionarnye protsessy v kataliticheskikh reaktorakh* (Nonstationary Processes in Catalytic Reactors), Novosibirsk: Nauka, 1982.

ISSN 1070-4272. Russian Journal of Applied Chemistry, 2006, Vol. 79, No. 1, pp. 98–102. © Pleiades Publishing, Inc., 2006.
Original Russian Text © N.M. Karpyak, R.G. Makitra, G.A. Marshalok, E.Ya. Pal'chikova, 2006, published in Zhurnal Prikladnoi Khimii, 2006, Vol. 79, No. 1, pp. 100–104.

ORGANIC SYNTHESIS AND INDUSTRIAL ORGANIC CHEMISTRY

Solvent Effect on the Rate of Cycloaddition of Isoprene to Maleic Anhydride

N. M. Karpyak, R. G. Makitra, G. A. Marshalok, and E. Ya. Pal'chikova

L'vivs'ka Politekhnika National University, Lviv, Ukraine
Institute of Geology and Geochemistry of Fossil Fuels, National Academy of Sciences of Ukraine, Lviv, Ukraine

Received May 25, 2005

Abstract—The solvent effect on the rate of the reaction of isoprene with maleic anhydride was studied; the total effect of the solvent polarity and cohesion energy density was revealed.

DOI: 10.1134/S1070427206010216

The Diels–Alder cycloaddition discovered in 1916 [1] is a route to valuable drugs, e.g., phencamphamine psychotropic agent, cyclothiazide diuretic, etc. [2]. The same mechanism is operative in dimerization of cyclopentadiene catalyzed by sulfuric acid with the formation of so-called Satdecanol, a raw material for production of valuable unsaturated polyesters, and in the reaction of cyclopentadiene with maleic anhydride, whose product is a raw material for production of various epoxy resins [3]. Although the rate of this reaction can vary depending on the structure of the reactants within the range covering several orders of magnitude [4], it is also affected by other factors: temperature, pressure, and solvent. Therefore, optimization of the reaction conditions, in particular, proper choice of solvent, is very important.

The kinetics of the Diels–Alder cycloaddition in various media was examined in numerous papers; many of them concern the reaction of dienes with maleic anhydride. The solvent effect on this reaction is so strong that the reaction rates in different solvents can differ by several orders of magnitude, and in some cases even different products can be obtained [5–8]. However, there is still no general concept accounting for the solvent effect on the kinetics of this reaction. Attempts to construct adequate one-parameter correlations of the rate constants of a Diels–Alder reaction with such solvent properties as cohesion energy density [9], polarity [10, 11], or Gutmann acceptor number AN [12] failed: with a relatively large set of solvents, numerous deviations from the suggested linear correlations were observed. Frish *et al.* [13] examined the possibility of correlating the kinetic data obtained for a series of reactions in different media using the concept of so-called corresponding states. According to this approach, the difference between the activation free energies of a process performed in two different media, determined from the logarithms of the corresponding reaction rates, will be proportional to the quotient from division of the difference of the critical temperatures of these solvents by the difference of their critical volumes. However, an attempt to correlate the data on the rate constants k of the reaction of maleic anhydride with isoprene in ten solvents using this concept failed also: the differences between the calculated and experimental $\log k$ values in some cases exceeded 50% [13]. The lack of a general correlation between the cycloaddition rate and any single characteristic of solvents suggests the complexity of solvation processes occurring in the system.

EXPERIMENTAL

It is generally appropriate to consider the solvent effect on physicochemical processes in terms of the linear free energy relationship taking into account various types of interaction, primarily specific and nonspecific solvation [14]:

$$\Delta G = \sum \Delta g_i. \quad (1)$$

Therefore, in this study, to correlate data on the solvent effect on the rate of addition of dienes to maleic anhydride, we used the Koppel–Palm equation [14] supplemented with additional terms taking into

Table 1. Experimental [11] and calculated [Eq. (4)] logarithms of the rate constants (l mol^{-1} s^{-1}) of the reaction of isoprene with maleic anhydride in various solvents at 30.3°C

Solvent no.	Solvent	$\log(k_{exp} \times 10^5)$	$\log(k_{calc} \times 10^5)$	$\Delta \log k$
1	Benzene	1.2430	1.2368	–0.0062
2	Anisole	1.4014	1.3316	–0.0698
3	Dipropyl ether	0.6998	0.7205	0.0206
4	Chlorobenzene	1.4014	1.3895	–0.0119
5	*m*-Dichlorobenzene	1.5185	1.6072	0.0877
6	*o*-Dichlorobenzene	1.8241	1.7700	–0.0541
7	Benzonitrile	1.5353	1.6447	0.1094
8	Nitrobenzene	1.7235	1.6676	–0.0559
9	Nitromethane	1.5211	1.5002	–0.0210

account the solvent structure [15]:

$$\log k = a_0 + a_1\frac{n^2-1}{n^2+2} + a_2\frac{\varepsilon-1}{2\varepsilon+1} + a_3B + aE_T + a_5\delta^2 + a_6V_m, \quad (2)$$

where n is the refractive index and ε, dielectric permittivity of solvents (parameters determining their polarizability and polarity and responsible for the nonspecific solvation of a substrate); B, Palm basicity [14] and E_T, Reichardt electrophilicity [6] (parameters determining the capability of a solvent for acid–base interactions, i.e., for specific solvation); δ^2, Hildebrand solubility parameter squared (parameter characterizing the cohesion energy of a solvent); and V_m, molar volume of solvents reflecting the possible effect of structural factors.

The solvent characteristics were taken from [14, 16, 17], and the calculation procedures, according to recommendations of the Group for Correlation Analysis in Chemistry at IUPAC [18].

The rates of cycloaddition of isoprene to maleic anhydride were determned in numerous studies [7, 9, 10, 13], but only in a few solvents. The most representative data set is given in [11]: The rate constants of the reaction of isoprene with maleic anhydride were determined in the range 0–100.3°C in ten solvents; for nine of them, all the characteristics required for calculation by Eq. (2) are available from the literature. The rate constants of the reaction at 30.3°C (reactant concentrations 0.5 M), taken from [11], are given in Table 1. Calculations with Eq. (2) show that these data are fitted by a six-parameter equation

$$\log(k\times10^5) = 8.82 + (3.13\pm0.78)f(n^2) + (7.89\pm1.79)f(\varepsilon) + (0.84\pm0.59)\times10^{-3}B - (0.34\pm0.08)E_T + (6.52\pm1.43)\times10^{-3}\delta^2 - (1.11\pm0.41)\times10^{-2}V_m. \quad (3)$$

Its multiple correlation coefficient, $R = 0.991$, meets the reliability criterion recommended in [18] ($R \geq 0.95$); the rms error s is ± 0.04. However, low coefficients r of pair correlation between $\log k$ and separate parameters, ranging from 0.4 to 0.7, do not allow us to assess directly the influence of these parameters on $\log k$. Therefore, in accordance with [14], the significance of particular terms of Eq. (3) was assessed by their alternate exclusion with construction of correlations with the remaining parameters and calculation of the corresponding coefficients R. If R decreases insignificantly upon exclusion of a parameter, this factor can be regarded as insignificant. Using this procedure, we found that the factors of basicity B ($R = 0.988$) and molar volume V_m ($R = 0.982$) are actually insignificant. The solvent effect on the reaction rate can be described with an acceptable accuracy by a four-parameter equation

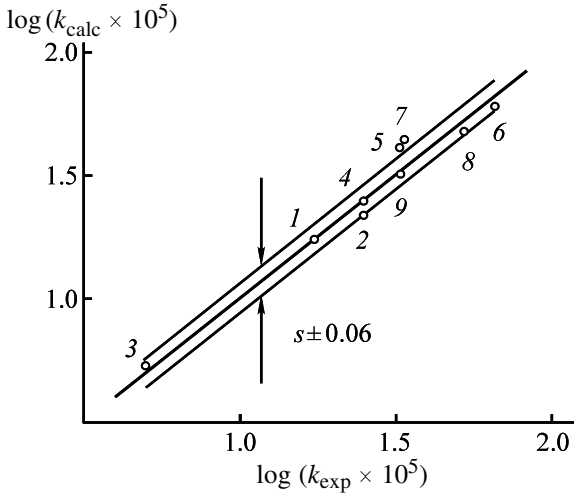
$$\log(k\times10^5) = 4.19 + (3.72\pm1.07)f(n^2) + (3.85\pm1.12)f(\varepsilon) - (0.21\pm0.06)E_T + (6.14\pm1.38)\times10^{-3}\delta^2, \quad (4)$$

$$R = 0.981,\ s = \pm0.06.$$

Further exclusion of any of the remaining terms of Eq. (4) impairs the correlation more significantly: R decreases to approximately 0.95 or even 0.93 (with exclusion of δ^2). Nevertheless, according to the Fisher test, the three-parameter correlation taking into account the most significant factors (polarity, electrophilicity, cohesion energy density of solvents) is still adequate:

$$\log(k\times10^5) = 9.00 + (6.91\pm1.08)f(\varepsilon) - (0.37\pm0.06)E_T + (9.56\pm1.53)\times10^{-3}\delta^2, \quad (5)$$

$$R = 0.951,\ s = \pm0.10.$$



Correlation between the experimental [11] and calculated [Eq. (4)] logaritms of rate constants. Point nos. are solvent nos. in Table 1.

Thus, the solvent effect on the reaction rate is the sum of the favorable effects of the solvent self-association and nonspecific solvation of the reaction complex and negative effect of the capability of the solvent for electrophilic solvation. The latter effect is easy to understand: According to [5], the diene synthesis involving transfer of excess π electrons from a diene to a dienophile presumably occurs via charge-transfer complex. This assumption is supported by the frequently observed strong transient coloration of the reaction mixture. It is known that acid (in particular, tetrafluorophthalic) anhydrides form charge-transfer complexes with π-electron donors such as aromatic hydrocarbons [19]. Apparently, solvents capable of electrophilic solvation (having high E_T) can solvate the diene molecule. As a result, the concentration of the free diene decreases and the reaction decelerates because of competition between maleic anhydride and electrophilic solvent for the diene molecule.

Table 2. Experimental [11] rate constants k of the reaction of isoprene with maleic anhydride at 0, 60.3, and 100.3°C and the activation energies E_a

Solvent	$k \times 10^5$, l mol^{-1} s^{-1}, at indicated temperature, °C			E_a,* kcal mol^{-1}
	0	60.3	100.3	
Benzene	1.62	104	762	12.3
Anisole	2.59	166	1290	12.6
Isopropyl ether	–	43.8	411	14.2
Veratrole	–	215	–	12.7
Chlorobenzene	2.36	143	1220	12.6
m-Dichlorobenzene	–	230	–	12.5
o-Dichlorobenzene	7.62	367	2670	11.8
Benzonitrile	3.17	223	–	13.0
Nitrobenzene	4.89	292	2220	12.3
Nitromethane	3.09	210	1330	12.3

* The activation energies are given in kcal mol^{-1} in accordance with [11].

The log k values calculated by Eq. (4) and their deviations from the experimental data, $\Delta\log k = \log k_{calc} - \log k_{exp}$, are given in Table 1, and in the figure the $\log k_{calc}$ values are plotted vs. $\log k_{exp}$. As seen, almost all the $\Delta\log k$ values fall within the error corridor $s \pm 0.06$ or lie only slightly beyond it.

Dewar and Pyron [11] also determined the reaction rate constants at 60.3 (nine solvents), 0, and 100.3°C (seven solvents), and also the activation energies of the process. Their results are given in Table 2. Correlation of these data gave equations in which the coefficients at particular terms have the same sign as in Eq. (4) and only slightly differ in the absolute value.

At 0°C,

$$\log(k \times 10^5) = 6.80 + (6.48 \pm 0.81) f(\varepsilon) - (0.31 \pm 0.06) E_T + (7.11 \pm 1.57) \times 10^{-3} \delta^2, \quad (6)$$

$$R = 0.965, \; s = \pm 0.06;$$

at 60.3°C,

$$\log(k \times 10^5) = 8.53 + (6.02 \pm 0.74) f(\varepsilon) - (0.37 \pm 0.04) E_T + (7.95 \pm 1.04) \times 10^{-3} \delta^2, \quad (7)$$

$$R = 0.969, \; s = \pm 0.07;$$

and at 100.3°C,

$$\log(k \times 10^5) = 9.13 + (5.41 \pm 1.03) f(\varepsilon) - (0.29 \pm 0.06) E_T + (7.16 \pm 1.52) \times 10^{-3} \delta^2, \quad (8)$$

$$R = 0.934, \; s = \pm 0.09.$$

Since data for 0 and 100.3°C were obtained for a smaller number of solvents, the corresponding correlations are less reliable statistically. Nevertheless, we obtained excellent correlation coefficients for the six-parameter equation: 0°C, R = 0.998; 60.3°C, R = 0.988; and 100.3°C, R = 0.999. In all the three cases, three-parameter equations (6)–(8), $\log k = f(\varepsilon, E_T, \delta^2)$, are also sufficiently adequate.

In all the cases, further exclusion of any of the remaining parameters fully breaks the correlation (R

Table 3. Experimental [9] and calculated [Eq. (12)] logarithms of the rate constants of the reaction of isoprene with maleic anhydride in various solvents (relative to benzene)

Solvent	$[\log(k_{solv}/k_{C_6H_6})]_{exp}$	$[\log(k_{solv}/k_{C_6H_6})]_{calc}$	$\Delta\log(k_{solv}/k_{C_6H_6})$
Dipropyl ether	–0.7450	–0.7008	0.0442
Hexane	–0.5950	–0.7074	–0.1124
n-Butyl chloride	–0.4430	–0.3525	0.0905
Ethyl acetate	–0.3330	–0.3201	0.0129
Benzene	0.0000	0.1214	0.1214
m-Dichlorobenzene	0.1700	0.2077	0.0377
Chlorobenzene	0.1000	0.1808	0.0808
o-Dichlorobenzene	0.4800	0.2694	–0.2106
Anisole	0.0690	0.1172	0.0482
Nitrobenzene	0.4190	0.4275	0.0085
Dichloromethane	0.3160	0.1528	–0.1632
Nitromethane	0.4980	0.5400	0.0420

becomes as low as 0.5–0.6). At the same time, in accordance with the low rms deviation s, calculation by Eqs. (6)–(8) gives the $\log k$ values that only slightly differ from the experimental values. It is interesting that, with increasing temperature, the absolute term a_0 determining the reaction rate in the absence of solvation tends to increase (with a deviation at 30.3°C) and the coefficient at $f(\varepsilon)$ (i.e., the significance of the nonspecific solvation of the reaction complex) tends to decrease. The coefficients at E_T and δ^2 remain approximately constant. It should be noted here that a theoretical calculation by Eq. (8) for the same reaction in toluene gives $\log(k \times 10^5) = 2.96$, which is reasonably consistent with the experimental value $k = 600 \times 10^{-5}$ l mol^{-1} s^{-1} [$\log(k \times 10^5) \approx 2.78$] determined in [4] for the same solvent at 100°C. The deviation, $\Delta\log(k \times 10^5)$, is 0.18, i.e., it exceeds the rms error of Eq. (8), $s = \pm 0.09$, by a factor of only 2. This result confirms the validity of our calculations, the more so as the kinetic studies in [4, 11] were performed in different concentration ranges.

Correlation of the activation energies also gives consistent results. The solvent effect on E_a is adequately described by a six-parameter equation

$$E_a = -16.67 - (2.16 \pm 2.76)f(n^2) - (21.91 \pm 6.32)f(\varepsilon) - (2.15 \pm 2.08) \times 10^{-3}B + (1.05 \pm 0.29)E_T - (16.67 \pm 2.08) \times 10^{-3}\delta^2 + (0.65 \pm 0.01)V_m, \quad (9)$$

$$R = 0.974, \; s = \pm 0.27.$$

In Eq. (9), the signs at particular terms are opposite to those in the equations for $\log k$, i.e., the solvation factors favoring the reaction simultaneously decrease its activation barrier. In this case, also, the parameters B and n^2 are essentially insignificant. For adequate description of the solvent effects on E_a, it is sufficient to use a four-parameter equation

$$E_a = -1273 - (18.86 \pm 2.78)f(\varepsilon) + (0.90 \pm 0.10)E_T - (14.43 \pm 3.44) \times 10^{-3}\delta^2 + (3.93 \pm 0.93) \times 10^{-2}V_m, \quad (10)$$

$$R = 0.968, \; s = \pm 0.69.$$

However, in this case the molar volume is also significant: its exclusion actually breaks the correlation ($R = 0.910$).

Whereas in [11] the reaction was mainly studied in aromatic solvents, except aliphatic dipropyl ether and nitromethane, in [9] the aromatic and aliphatic solvents were equal in number. However, Wong and Eckert reported not the absolute rate constants but the logarithms of the rate constants of the reactions in solvents relative to benzene, for which the relative rate constant was taken as unity. These quantities, $\log(k_{solv}/k_{C_6H_6})$, are given in Table 3 and are correlated with Eq. (2). With the six-parameter equation, an excellent correlation was obtained, with the same signs at all the parameters as in Eq. (3) except the sign at the basicity parameter, which was shown to be insignificant:

$$\log(k_{solv}/k_{C_6H_6}) = 2.60 + (3.07 \pm 0.82)f(n^2) + (3.97 \pm 1.02)f(\varepsilon) - (0.69 \pm 0.28) \times 10^{-3}B - (0.13 \pm 0.04)E_T + (3.01 \pm 0.51) \times 10^{-3}\delta^2 - (8.91 \pm 1.90)V_m, \quad (11)$$

$$R = 0.989, \; s = \pm 0.06.$$

In this case, also, the parameter B can be excluded:

$$\log(k_{solv}/k_{C_6H_6}) = 2.58 + (3.72 \pm 0.96) f(n^2)$$
$$+ (3.78 \pm 1.27) f(\varepsilon) - (0.13 \pm 0.05) E_T + (2.96 \pm 0.63) \times 10^{-3} \delta^2$$
$$- (1.03 \pm 0.22) \times 10^{-3} V_m, \quad (12)$$
$$R = 0.983, \; s = \pm 0.08.$$

However, in contrast to the previous case, here the parameters of the electrophilic solvation and solvent polarity are also insignificant. Their exclusion decreases R to 0.970, whereas the exclusion of the molar volume decreases the correlation coefficient more significantly, to 0.950. This difference may be cuased by different nature of solvents included in this set. Below we give a three-parameter equation adequately describing the data in Table 3:

$$\log(k_{solv}/k_{C_6H_6}) = 1.68 + (5.77 \pm 0.89) f(n^2)$$
$$+ (1.75 \pm 0.46) \times 10^{-3} \delta^2 - (0.56 \pm 0.21) \times 10^{-2} V_m, \quad (13)$$
$$R = 0.989, \; s = \pm 0.06.$$

The $\log(k_{solv}/k_{C_6H_6})$ values calculated by this equation and their deviation from the experimental values are also given in Table 3.

CONCLUSIONS

(1) The dependence of the rate of cycloaddition of isoprene to maleic anhydride on the solvent properties can be adequately described only by multiparameter equations taking into account various solvation processes.

(2) The capability of a solvent for self-association and nonspecific solvation favors the cycloaddition, whereas the capability for electrophilic solvation exerts a negative effect.

REFERENCES

1. Diels, O. and Alder, K., *Lieb. Ann.*, 1928, vol. 460, no. 1, pp. 98–110.
2. Shvaika, O., *Osnovi sintezu likarskikh rechovin ta ikh promizhnikh produktiv* (Principles of Synthesis of Drugs and Their Intermediates), Donetsk: Nats. Akad. Nauk Ukr., 2004, 2nd ed., pp. 246–298.
3. Wataru Koga, *Neftekhim. Rubezh.*, 1968, no. 2, pp. 16–20.
4. Blankenburg, B., Fiedler, H., Hampel, M., *et al.*, *J. Prakt. Chem.*, 1974, vol. 316, no. 5, pp. 804–816.
5. Kletzel, M.S., *Organic Reactions*, Adams, R., Ed., New York: Wiley, 1942. Translated under the title *Organicheskie reaktsii*, Moscow: Inostrannaya Literatura, 1951, issue 4, pp. 7–86.
6. Reichardt, Ch., *Solvents and Solvent Effects in Organic Chemistry*, Weinheim: VCH, 2003.
7. Soula, J.C., Lombroso, D., Hellin, M., and Coussemant, F., *Bull. Soc. Chim. Fr.*, 1966, no. 10, pp. 2051–2056.
8. Piatek, A., Chapuis, C., and Jurczak, J., *J. Phys. Org. Chem.*, 2003, vol. 16, no. 10, pp. 700–708.
9. Wong, K.F. and Eckert, C.A., *Ind. Eng. Chem. Process Des. Devel.*, 1963, vol. 8, no. 4, pp. 568–573.
10. Grieger, R.A. and Eckert, C.A., *Trans. Faraday Soc.*, 1977, vol. 66, no. 7, pp. 2579–2584.
11. Dewar, J.C. and Pyron, R.S., *J. Am. Chem. Soc.*, 1970, vol. 92, no. 10, pp. 3098–3103.
12. Corsico Coda, A., Desimoni, G., Ferrari, E., *et al.*, *Tetrahedron*, 1984, vol. 40, no. 9, pp. 1611–1615.
13. Frish, H.L., Bak, T.A., and Webster, E.R., *J. Phys. Chem.*, 1962, vol. 66, no. 11, pp. 2101–2107.
14. Palm, V.A., *Osnovy kolichestvennoi teorii organicheskikh reaktsii* (Principles of the Quantitative Theory of Organic Reactions), Leningrad: Khimiya, 1977.
15. Makitra, R.G., Zaglad'ko, E.A., Turovskii, A.A., and Zaikov, G.E., *Zh. Prikl. Khim.*, 2004, vol. 77, no. 2, pp. 324–327.
16. Makitra, R.G., Pirig, Ya.N., and Kivelyuk, R.B., Available from VINITI, Moscow, 1985, no. 628–V86.
17. Abboud, J.L.M. and Notario, R., *Pure Appl. Chem.*, 1999, vol. 71, no. 4, p. 645.
18. Makitra, R.G., *Ukr. Khim. Zh.*, 1992, vol. 58, no. 3, pp. 260–261.
19. Makitra, R.G. and Pirig, Ya.N., *Ukr. Khim. Zh.*, 1986, vol. 52, no. 9, pp. 907–911.

ISSN 1070-4272. Russian Journal of Applied Chemistry, 2006, Vol. 79, No. 1, pp. 103–106. © Pleiades Publishing, Inc., 2006.
Original Russian Text © Yu.G. Khabarov, N.D. Kamakina, L.V. Gusakov, V.A. Veshnyakov, 2006, published in Zhurnal Prikladnoi Khimii, 2006, Vol. 79, No. 1, pp. 105–108.

ORGANIC SYNTHESIS AND INDUSTRIAL ORGANIC CHEMISTRY

A New Spectrophotometric Method for Determination of Furfural and Pentoses

Yu. G. Khabarov, N. D. Kamakina, L. V. Gusakov, and V. A. Veshnyakov

Arkhangelsk State Technical University, Arkhangelsk, Russia

Received October 20, 2005

Abstract—A spectrophotometric method for determination of furfural and pentoses based on their color reaction with sulfuric acid in the presence of mercury(II) was developed.

DOI: 10.1134/S1070427206010228

Furfural (furan-2-carbaldehyde) is a heterocyclic aldehyde exhibiting a series of valuable chemical properties. Furfural is readily formed from pentoses under heating in an acid medium. This reaction can also be used for spectrophotometric determination of pentoses.

Analytical determination of furfural and carbohydrates is an important problem. A number of chromatographic [1, 2], spectrophotometric (IR [3], UV [4], visible [5, 6]), and polarographic [7] methods were developed recently.

Use of UV spectroscopy for determination of furfural is based on its light absorption at 272–278 nm [8, 9]. However, as applied to aqueous process solutions, this procedure is often complicated by the presence of other substances also absorbing light in this region. The selectivity with respect to furfural can be elevated by the chemical reaction forming products with higher extinction coefficients.

It was found that the reaction of furfural and pentoses with sulfuric acid in the presence of mercury(II) acetate gives unidentified products with a very intense absorption band at 238 nm (Figs. 1a, 1b). The absorption spectrum of the product of the xylose reaction with sulfuric acid in the presence of Hg(II) completely coincides with that of the product of arabinose reaction.

EXPERIMENTAL

Chemically pure grade *L*-(+)-arabinose, glacial acetic acid, and mercury(II) acetate, analytically pure grade *D*-xylose, and pure grade concentrated sulfuric

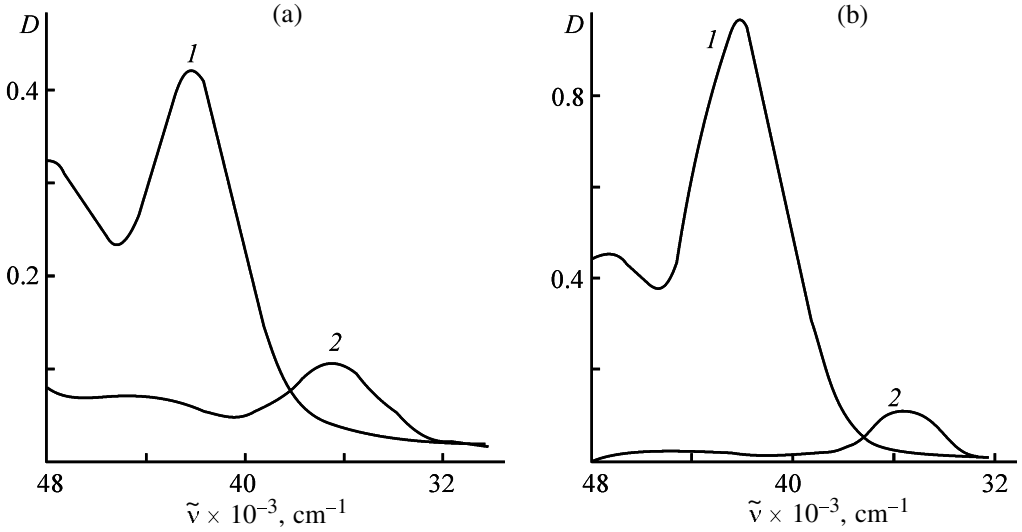


Fig. 1. Absorption spectra of the reaction product formed from (a) furfural and (b) arabinol (*1*) with addition of mercury(II) acetate and (*2*) without it. (*D*) Optical density and ($\tilde{\nu}$) wavenumber.

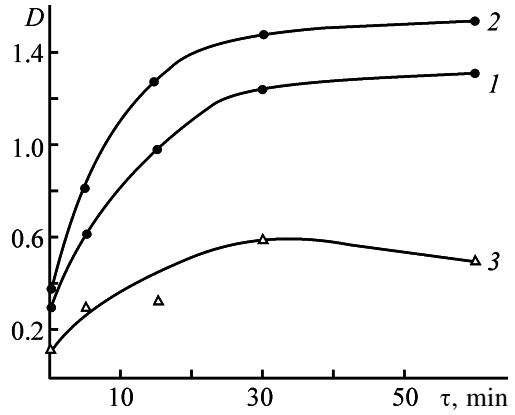


Fig. 2. Solution optical density D at 238 nm as a function of the reaction time τ. (*1*) *L*-(+)-Arabinose, (*2*) *D*-xylose, and (*3*) furfural; the same for Fig. 3.

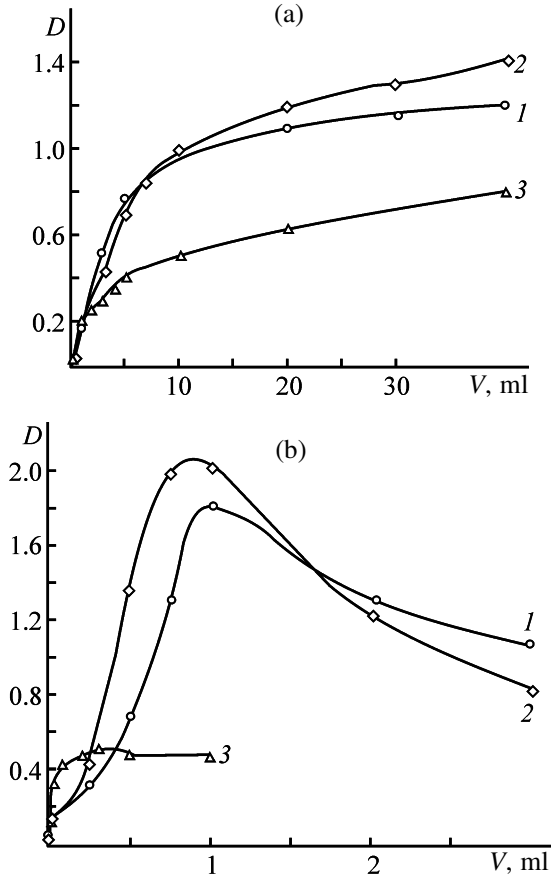


Fig. 3. Optical density D at 238 nm of the reaction product as a function of the consumption V (a) mercury(II) acetate and (b) concentrated sulfuric acid.

acid were used. Furfural was twice distilled; the 160–161°C fraction was taken.

Aqueous solution of mercury(II) acetate was prepared by dissolution of 4.00 g of the salt in a 200-ml volumetric flask with addition of 5 ml of glacial acetic acid to suppress hydrolysis.

To perform a photometric reaction, an approximately 100-mg weighed portion of furfural was dissolved in water in a 25-ml volumetric flask (solution no. 1). In the case of the reaction with pentoses, similar solution was prepared in a 100-ml volumetric flask by dissolving in water an approximately 1-g pentose sample (weighed with a 0.0001-g error). Then, aliquots of a solution no. 1 and a solution of mercury(II) acetate were introduced into a 50-ml volumetric flask, and water was added to the mark (solution no. 2). After that, 1 ml of solution no. 2 and a definite volume of concentrated sulfuric acid were mixed in a test tube. The test tube was heated for a definite time on a boiling water bath, the reaction mixture was transferred into a 100-ml volumetric flask, and water was added to the mark.

The absorption spectra were recorded on a Specord M40 spectrophotometer within the 48 000–30 000 cm^{-1} range relative to water. The optical density of solutions at 238 nm was measured on an SF-46 spectrophotometer relative to water.

The influence of the time of the photometric reaction was studied at a consumption of solutions of Hg(II) acetate of 5 ml and H_2SO_4 of 0.3 ml and heating time of 0, 5, 15, 30, and 60 min.

With increasing the reaction time, the absorption spectra substantially change. The intensity of the furfural band at 278 nm decreases, whereas the optical density at 238 nm increases. The dependences of D_{238} on reaction time are shown in Fig. 2.

As seen, 30-min heating is optimal for the photometric reaction.

The influence of the Hg(II) acetate concentration was studied with addition of 1, 2, 3, 4, 5, 10, 20, and 40 ml of the Hg(II) acetate solution and 0.3 ml of H_2SO_4; the reaction time was 30 min. The dependence of D_{238} on the Hg(II) acetate concentration is shown in Fig. 3a.

As seen, the solution optical density increases with increase in the volume of the added Hg(II) acetate solution from 1 to 5 ml and then decreases. Therefore, the optimal volume of the mercury(II) acetate solution is 5 ml.

The influence of H_2SO_4 amount on optical density of the solutions for photometry was studied with addition of 5 ml of Hg(II) acetate and heating for 30 min; 0.03, 0.1, 0.2, 0.3, 0.5, 1, 2, or 3 ml of concentrated H_2SO_4 was added (Fig. 3b). As seen, sulfuric acid

Table 1. Coefficients of calibration equations

Compound	Coefficients of calibration equations $D_{238} = a + bC$		Coefficient of pair correlation, R^2
	a	b	
L-(+)-Arabinose	0.1032	0.4271	0.997
D-Xylose	0.1155	0.4219	0.995
Furfural	0.0677	0.5059	0.999

Table 2. Estimation of reproducibility of furfural and pentose determination

Introduced, mg l^{-1}	Optical density at 238 nm				rms deviation	Variation coefficient, %
	D_1	D_2	D_3	D_{av}		
			L-(+)-Arabinose			
0	0.070	0.070	0.070	0.070	0.000	0.0
0.40	0.265	0.270	0.260	0.265	0.005	1.9
1.20	0.635	0.660	0.650	0.648	0.013	1.9
2.00	0.985	0.990	0.990	0.988	0.003	0.3
2.80	1.325	1.340	1.310	1.325	0.015	1.1
3.60	1.610	1.570	1.600	1.593	0.021	1.3
			D-Xylose			
0.00	0.105	0.100	–	0.103	0.004	3.5
0.20	0.175	0.180	–	0.178	0.004	2.0
0.40	0.275	0.260	–	0.268	0.011	4.0
0.59	0.355	0.375	–	0.365	0.014	3.9
1.02	0.585	0.560	–	0.573	0.018	3.1
1.39	0.725	0.730	–	0.728	0.004	0.5
2.01	1.000	1.025	–	1.013	0.018	1.8
3.01	1.350	1.320	–	1.335	0.021	1.6
			Furfural			
0.4536	0.336	0.295	0.303	0.311	0.021	6.9
0.9312	0.559	0.525	0.522	0.535	0.020	3.8
1.3088	0.728	0.741	0.715	0.728	0.013	1.8

strongly affects the optical density (by a factor of 6–8 after addition of one drop of sulfuric acid). The optical density passes through a maximum at 0.3–1 ml of sulfuric acid.

Thus, addition of 0.3–1 ml of concentrated sulfuric acid into a photometric solution is optimal in the analytical method developed.

To construct the calibration plots and assess the reproducibility of the results, we performed experiments under the optimal conditions found: amount of mercury(II) acetate solution 5 ml, that of H_2SO_4 0.3 ml, and heating time 30 min. Three replicate analyses were performed. From the data obtained, we calculated the coefficients of the calibration diagrams and the pair correlation coefficients using the least-squares method [10] (Table 1).

The dependences of the optical densities on furfural or pentose concentrations are linear, which is confirmed by high values of the pair correlation coefficient R^2. The optical density of the product of the photometric reaction obeys the Bouguer–Lambert–Beer law. The calibration diagrams for xylose and arabinose are virtually the same (Table 2).

The error of the concentration determination was estimated using furfural and pentose solutions with

Table 3. Accuracy of determination of furfural and pentoses

D_{238}	Concentration, mg g^{-1}		Absolute error, mg g^{-1}	Accuracy, %
	introduced	found		
		L-(+)-Arabinose		
0.543	0.99	1.03	0.04	96
1.003	2.00	2.11	0.10	95
1.392	3.00	3.02	0.02	99
		D-Xylose		
0.180	0.22	0.15	–0.07	69
0.550	1.02	1.04	0.02	98
1.200	2.51	2.56	0.05	98
		Furfural		
0.322	0.45	0.50	0.05	89
0.488	0.83	0.83	–0.00	99
0.663	1.18	1.18	–0.00	99
0.891	1.60	1.63	0.03	98

the known concentrations. The optical density of each solution was measured three times (Table 3).

CONCLUSION

A new highly sensitive photometric method was developed for determination of furfural and pentoses with high precision and reproducibility.

REFERENCES

1. Karmil'chik, A.Ya., Stonkus, V.V., and Korchagova, E.Kh., *Zh. Anal. Khim.*, 1971, vol. 26, no. 6, p. 1231.
2. Karmil'chik, A.Ya, Stonkus, V.V., Korchagova, E.Kh., and Bubovich, V.I., *Gidrolizn. Lesokhim. Prom-st.*, 1972, no. 4, pp. 17–18.
3. Maisaiya, D.D., in *Referat. Mater. Gidrolizn. Proizv.*, 1970, no. 6, pp. 13–16.
4. Demikhovskii, S.Z., *Gidrolizn. Lesokhim. Prom-st.*, 1961, no. 7, pp. 20–21.
5. Korenman, I.M., *Metody opredeleniya organicheskikh soedinenii* (Methods of Determination of Organic Compounds) Moscow: Khimiya, 1975.
6. Jacquemain, R. and Remy, M.C., *Bull. Soc. Chim. Fr.*, 1964, no. 6, pp. 1207–1210.
7. Davidek, J., *Nature*, 1963, vol. 197, pp. 378–379.
8. Silverstein, R.M., Bassler, G.C., and Morrill, T.C., *Spectrometric Identification of Organic Compounds*, New York: Wiley, 1974.
9. Rao, C.N.R., *Ultra-Violet and Visible Spectroscopy: Chemical Applications*, London: Butterworth, 1961.
10. Doerfel, K., *Statistik in der analytischen Chemie*, Leipzig: Leuna-Merseburg, 1966.

ISSN 1070-4272. Russian Journal of Applied Chemistry, 2006, Vol. 79, No. 1, pp. 107–116. © Pleiades Publishing, Inc., 2006.
Original Russian Text © V.P. Talzi, 2006, published in Zhurnal Prikladnoi Khimii, 2006, Vol. 79, No. 1, pp. 109–118.

ORGANIC SYNTHESIS AND INDUSTRIAL ORGANIC CHEMISTRY

A ^{13}C and ^{1}H NMR Analysis of Perfumes

V. P. Talzi

Institute of Problems of Hydrocarbon Processing, Siberian Division, Russian Academy of Sciences, Omsk, Russia

Received September 28, 2005

Abstract—Composition of a series of formulations used in Russia for production of various perfumes, among them car air fresheners, was studied by ^{13}C and ^{1}H NMR. The main components were identified, approximate compositions of several perfumes were determined, and spectral data are given. These spectral data can be used for prompt analysis for composition of commercial odorants with the aim of monitoring their quality and hygienic characteristics.

DOI: 10.1134/S107042720601023X

In Russia, the range of perfume goods was extended in the past few years. In production of many air fresheners, deodorants, and eau de Colognes, imported mixtures of very limited set of chemicals, not much complicated in composition, are used. Data on the chemical composition of the perfumes can be useful for monitoring of their quality and analysis of their hygienic characteristics.

In some cases, a prompt analysis of aromatizers (odorants) can be performed by ^{13}C NMR on the condition that a part of experiments on the analysis of the chemicals available in Russia has been already performed and the signals in the ^{13}C NMR spectra of these chemicals were assigned to the specific components. It is just this part of experiments that we performed based on analysis of the ^{13}C NMR spectra of approximately 30 commercial concentrated fragrance compounds used for production of perfume goods, among them car air fresheners. The composition of odorants can be quantitatively estimated from their ^{1}H NMR spectra by the common procedures [1] on the condition that the compounds entering into their composition give signals not overlapping with signals of other components. These signals were found for the most of the compounds frequently entering into the composition of odorants (Table 1), which allowed determination of approximate formulation of several commercial perfumes.

Table 2 presents the approximate composition of several commercial odorants obtained with consideration of data listed in Table 1. The numbers of compounds whose composition seems to be determined most reliably are underlined.

Although the modern software for simulation of NMR spectra on the basis of a given structure is available and efficient, it gives the calculated spectra practically completely coinciding with the experimental spectra only if the corresponding spectrum from the catalog (atlas) is present in the inner database of the software. Otherwise, large differences in the chemical shifts of signals in actual and calculated spectra can take place, which is usually of minor importance for the spectrum of an individual compound but can substantially complicate the analysis of a mixture. Therefore, the data on actual NMR spectra of components of commercial odorants, summarized in this paper, is extremely useful for determination of their composition by NMR spectroscopy. The NMR spectra of the perfumes in hand usually contain signals of tens of different substances, and therefore, their qualitative and quantitative analysis based solely on NMR spectra seems to be laborious and unreliable; however, the following factors simplify the problem.

As mentioned above, the components of odorants in hand are usually fairly simple in structure and well-known organic substances from a limited set. Data on these substances are available from reference books [2].

For four samples, we succeeded in receiving the producer formulas, which allowed us, in spite of serious discrepancies between the declared and actual compositions, to identify several important and frequently occurring components of odorants and, hence, to simplify the analysis of mixtures.

Successful analysis of perfumes is favored by the fact that some samples contain only three or four

Table 1. Assignment of signals in the NMR spectra of odorants to individual components

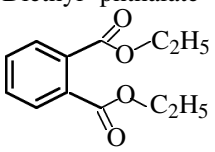
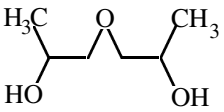
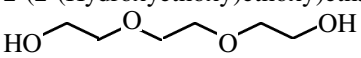
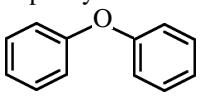
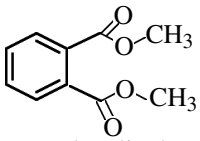
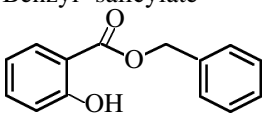
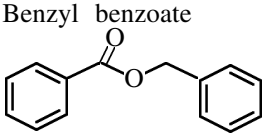
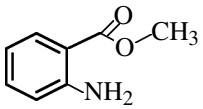
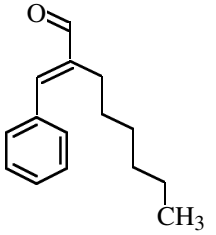
Compound	Structure, name	NMR signals; chemical shifts, δ, ppm	
		^{13}C*	^{1}H**
1	Diethyl phthalate 	166.5(+), 132.4, 130.6, 128.6, 60.9(+), 13.9	Quadruplet 4.3 (4)
2	Dipropylene glycol  A mixture of dimers and trimers	76.96, 76.68(+), 76.26(+), 75.89, 74.97, 73.89(+), 73.25(+), 72.21, 66.67, 66.15, 66.00, 65.86(+), 65.73(+), 19.17, 19.07, 16.02	Two signals in the ranges 3.8–4.0 and 3.0–3.6 (12) [in formula (1) I_i is the total intensity of these signals, M_i = 136 (recalculated to dimer)]
3	2-(2-(Hydroxyethoxy)ethoxy)ethanol 	74.2(+), 70.8(+), 70.6(+), 66.3(+) 61.4(+), 15.3	Quadruplet 3.5 (2)
4	Diphenyl ether 	157.23(+), 125.46, 122.88, 118.65	Narrow multiplet 7.2 (2)
5	Isopropyl laurate $C_{11}H_{23}COOCH(CH_3)_2$	172.3(+), 67.3, 34.3(+), 31.8(+), 29.5(+), 29.4(+), 29.3(+), 24.8(+), 22.1(+), 22.0	Triplet 2.2(2)
6	Dimethyl phthalate 	167.2(+), 132.6, 130.8, 128.5, 51.5	Singlet 3.6 (6)
7	Benzyl salicylate 	169.51(+), 161.92(+), 135.36, 135.27(+), 130.83, 129.81, 129.35, 127.68, 118.64, 117.72, 112.13(+), 66.54(+)	Singlet 5.3 (2)
8	Benzyl benzoate 	165.36(+), 135.99(+), 132.61, 129.41, 128.24, 127.85, 129.31(+), 65.93(+)	Doublet 8.0 (2); singlet 5.3 (2)
9	Methyl 2-aminobenzoate 	168.5(+), 152.3(+), 134.9, 131.3, 117.2, 116.0, 110.3(+)	Doublet 6.7 (1); singlet 3.8(3)
10	2-Hexyl-3-phenylpropenal 	193.93, 148.63, 143.20(+), 134.97(+), 129.83, 129.11, 128.50, 31.38(+), 29.42(+), 28.07(+), 26.35(+), 22.60(+), 13.89	Triplet 2.5(2); singlet 9.4 (1)

Table 1. (Contd.)

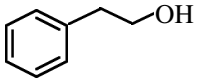
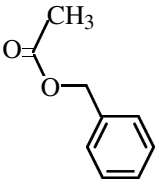
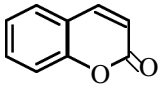
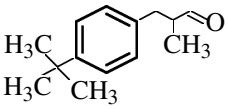
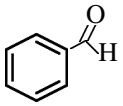
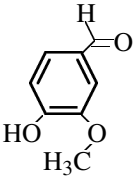
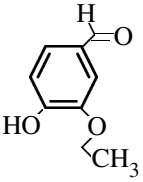
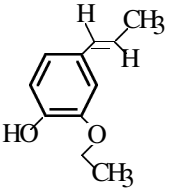
Compound	Structure, name	NMR signals; chemical shifts, δ, ppm	
		^{13}C*	^{1}H**
11	2-Phenylethanol 	138.87(+), 128.60, 128.40, 125.82, 62.90(+), 39.27(+)	Triplet 2.8 (2)
12	Benzyl acetate 	170.50(+), 136.50(+), 128.34, 128.05, 66.40(+), 20.70	Singlet 5.0 (2); narrow multiplet 7.3(5)
13	Coumarin 	159.71(+), 154.20(+), 143.08, 128.0, 125.49, 124.90, 116.39, 118.76	Doublet 6.3 (1); Doublet 7.8 (1)
14	3-(4-*tert*-Butylphenyl)-2-methylpropanal 	203.14, 150.21(+), 137.18(+), 46.98, 38.35(+), 14.29	Singlet 9.5 (1)
15	Benzaldehyde 	192.5, 136.7(+), 134.6, 129.80, 129.20	Singlet 9.95 (1)
16	Vanillin 	189.46, 152.56(+), 147.73(+), 129.24(+), 127.40, 114.81, 109.35, 53.58	Singlet 9.84 (1); doublet 7.0 (1); singlet 3.9 (3)
17	Ethyl vanillin 	189.8, 152.45(+), 147.74(+), 130.62(+), 127.66, 114.74, 110.13, 64.11(+), 14.35	Singlet 9.79 (1); doublet 7.0 (1); quadruplet 4.0 (2)
18	Isoeugenol 	147.07(+), 146.84(+), 131.88(+), 131.21, 124.46, 121.74, 116.50, 110.29, 18.20, 55.30	Narrow multiplet 6.7 (1); complex doublet 1.7 (3)

Table 1. (Contd.)

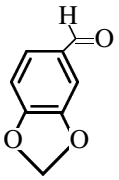
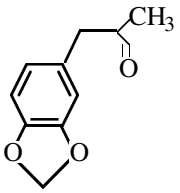
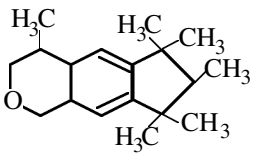
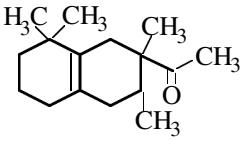
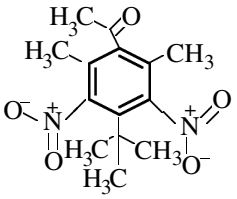
Compound	Structure, name	NMR signals; chemical shifts, δ, ppm	
		^{13}C*	^{1}H**
19	Heliotropin (piperonal) 	190.1, 153.20(+), 148.63(+), 132.10, 128.20, 108.49, 107.00, 102.50(+)	Singlet 6.0 (2); singlet 9.76 (1)
20	Piperonylpropanal (pional) 	108.59, 107.37, 102.32(+)	
21	Propyl acetate $CH_3COOCH_2CH_2CH_3$	171.2(+), 65.70(+), 22.12(+), 20.82, 10.23	Singlet 1.96 (3)
22	Isoamyl acetate $CH_3COO(CH_2)_2CH(CH_3)_2$	171.0(+), 61.4(+), 37.5(+), 25.2, 22.8, 22.2	Singlet 2.0 (3)
23	*n*-Amyl butyrate n-$C_3H_7COO(CH_2)_4CH_3$	174.1(+), 64.3(+), 36.7(+), 29.2(+), 28.7(+), 23.2(+), 18.5(+), 14.2, 13.8	Triplet 2.2 (2)
24	Galaxolide (1,3,4,6,7,8-hexahydro-4,6,6,7,8,8-hexamethylcyclopentano-γ-benzopyran) 	149.27(+), 148.72(+), 136.85(+), 132.40(+), 121.19, 117.94, 71.00(+), 68.31(+), 54.27, 44.21(+), 44.09(+), 32.07, 29.01, 25.54, 19.02, 8.38	Singlet 6.63 (1); singlet 6.90 (10)
25	Ambralux [1-(2,3,8,8-tetramethyl-1,2,3,4,5,6,7,8-octahydronaphthalen-2-yl)ethanone] 	217.21(+), 55.42, 50.95, 38.40(+), 37.83, 36.99(+), 31.90(+), 27.54(+), 26.95, 26.05, 25.47(+), 23.54, 22.25(+), 22.19(+), 17.38, 16.83	Singlet 1.96 (3)
26	Unidentified ketone, a component with musk odor	212.1(+), 33.3(+), 33.2(+), 32.9(+), 27.3(+), 26.4(+), 26.5(+), 24.0(+)	
27	Musk ketone 	200.43(+), 125.88(+), 162.08(+), 142.21(+), 31.14	

Table 1. (Contd.)

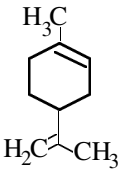
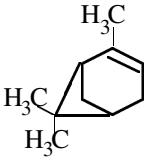
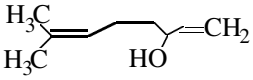
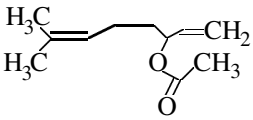
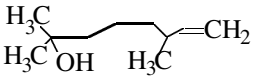
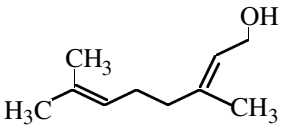
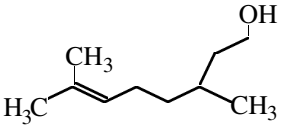
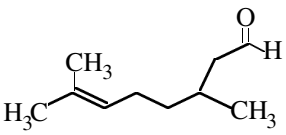
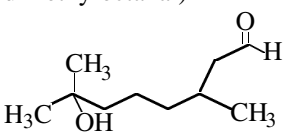
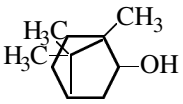
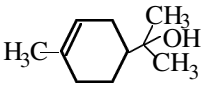
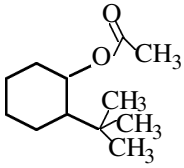
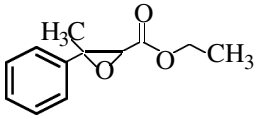
Compound	Structure, name	NMR signals; chemical shifts, δ, ppm	
		^{13}C*	^{1}H**
28	Limonene (diterpene) 	149.07(+), 132.84(+), 120.62, 108.55(+), 40.88, 30.41(+), 30.59(+), 27.71(+), 23.26, 20.56	Singlet 4.6 (1)
29	α-Pinene 	143.35(+), 116.20, 47.21, 41.20, 38.15(+), 31.50(+), 25.50, 23.10, 20.80	
30	Linalool 	145.38, 130.36(+), 124.29, 111.28(+), 72.49(+), 42.36(+), 25.50, 25.00, 22.71(+), 18.62	Singlet 5.77 (0.25)
31	Linalyl acetate 	169.67(+), 141.81(+), 131.48(+), 124.00, 112.24(+), 82.49(+), 39.34(+), 25.85, 25.21, 25.211(+), 21.97, 17.51	Singlet 5.98 (0.25)
32	Dihydromyrcenol 	144.48, 112.96(+), 70.00(+), 43.93(+), 37.69, 37.29(+), 29.01, 28.98, 20.56	A group of signals 5.54–5.75 (1)
33	Geraniol (rhodinol) 	137.67(+), 133.17(+), 124.83, 124.13, 58.43(+), 39.39(+), 26.49(+), 25.25, 18.72	Broad triplet 5.35 (2)
34	Citronellol (3,7-dimethyl-6-octenol) 	129.9(+), 124.9, 60.07(+), 39.30(+), 37.12(+), 29.07, 25.34(+), 25.56, 19.42, 17.45	
35	Citronellal (3,7-dimethyl-6-octenal) 	202.2, 131.50(+), 124.10, 51.00(+), 37.10(+), 27.80, 25.60(+), 25.40, 19.80, 17.40	
36	Hydroxycitronellal (7-hydroxy-3,7-dimethyloctanal) 	201.59, 69.90(+), 50.62(+), 43.64(+), 37.28(+), 31.45(+), 29.80, 27.17, 20.16	Singlet 9.5(1)

Table 1. (Contd.)

Compound	Structure, name	NMR signals; chemical shifts, δ, ppm	
		^{13}C*	^{1}H**
37	Borneol (isoborneol) 	80.06, 48.40(+), 46.90(+), 44.94, 38.57(+), 33.64(+), 26.92(+), 19.93, 19.71, 11.13	Singlet 5.77 (0.25)
38	α-Terpinol 	135.27(+), 120.50, 72.30(+), 45.10, 30.90(+), 27.37(+), 24.00(+), 27.01, 25.01	
39	2-*tert*-Butylcyclohexyl acetate 	168.84(+), 70.70, 49.92, 32.00(+), 31.21(+), 27.51, 26.32(+), 21.76(+), 21.02, 20.00(+)	Singlet 0.85 (9)
40	Ethyl 2,3-epoxy-3-methyl-3-phenylpropionate (a mixture of *cis* and *trans* isomers) 	166.6(+), 166.5(+), 141.5(+), 140.3(+), 129.0, 125.3, 124.8, 61.4(+), 61.2, 60.5, 60.5(+), 60.4(+), 24.7, 21.2, 16.8, 14.2, 14.1	Two singlets at 1.61(3) and 1.70(3); their total intensity corresponds to the total concentration of *cis* and *trans* isomers of 40; singlets at 3.27(1) and 3.50(1) can be used in a similar way

* The most typical signals are underlined; sign (+) corresponds to the signals of carbon atoms with even number of protons (including zero).

** Used for quantitative estimations of concentrations of components; the number of protons N_i entering into formula (1) is shown in parentheses.

components. In addition, the compound odor, sometimes reflected in its commercial name, can give additional information on its composition.

The components of odorants identified by ^{13}C NMR are listed below. The corresponding signals in the ^{13}C NMR spectra are presented in Table 1 without assignment, otherwise it would be too large. In identification of components the signals were assigned as usual, considering their multiplicity without proton decoupling, which gives information on the number of protons directly bonded to carbon atoms in the compound being analyzed. With the above-mentioned well-known software for simulation of NMR spectra, structural formulas of the compounds, and the list of the signals corresponding to this compound (Table 1), as a rule, assignment of signals becomes a simple procedure. In some cases, Table 1 does not contain all signals of the spectra since a part of these signals is not observed due to overlapping with the signals of other components or because of other reasons. These components are included in Table 1 only with consideration of additional data obtained from the sanitary certificates mentioned above.

In Table 1 we also give the corresponding absorption ranges not overlapping with other signals, when these signals were identified in the ^{1}H NMR spectra of odorants; from their integral intensities, the quantitative content of one or other component can be estimated. The number of protons in the molecule of the component contributing into absorption in the above ranges of the spectrum is also given. This number should be known for determination of the weight fraction of the component by the formula

$$c_i = I_i M_i / N_i, \quad (1)$$

where c_i is the weight fraction of component i; M_i is its molecular weight; I_i is the integral intensity of the

Table 2. Approximate composition of some commercial odorants

Component no.	Composition of odorant, wt %										
	1	2	3	4	5	6	7	8	9	10	11
1	25	15	68	17		41				36	25
2	5	15		41				65	32	31	27
3							63				
4					33						
5						20					
7	25	41		15				10			
8					2	10					
9							4				
10	3			7					13	8	
11	9	2	7								
13		8	5			7					6
14				3							
15							20				
16		5				5	2				15
17		11				15					
18						2					2
19							2				
22							6				
23							5				
24	15		15							4	
25										3	3
27	2										
28								2	30	3	
30	7		6					10		12	10
31				5				8		3	12
32				3	4			5	20		
33	7	2									
34	1	1									
36	1		4								
37				6	61						
38			5	3					5		

^{1}H NMR signal chosen for determination of the concentration of the ith component; and N_i is the number of protons in the component molecule, contributing to the intensity I_i.

The following data on the composition of odorants are grouped according to chemical classification of components or their destination. Typically, the majority of compounds and, in some cases, practically all compounds entering into the composition of odorants can be identified from the NMR spectra. Only in one case of 30, attempts to determine the chemical composition failed, since components of this formulation are likely not individual chemical compounds but are, for example, mixtures of terpenylcyclohexanols of the type of Sandalidol fragrance compound [2].

Solvents. The solvents, diethyl phthalate 1 and dipropylene glycol 2 [1], most frequently used in production of odorants, can be easily identified, since these chemicals and their NMR spectra are available. Many of the perfume samples contain both substances 1 and 2 or at least one of these substances. In some samples, the total concentration of solvents 1 and 2 exceeds 80%. Only three samples of odorants contain, instead of compounds 1 and 2, other solvents, 2-[2-(hydroxyethoxy)ethoxy]ethanol 3, diphenyl ether (diphenyl oxide) 4, and isopropyl ether of unidentified fatty acid, e.g., isopropyl laurate or stearate 5. In one of the samples, a part of substance 1 is substituted by dimethyl phthalate 6. In several samples, along with compounds 1 and 2, additional unidentified solvents, possibly acetates of polyols, such as ethylene glycol and glycerol, were used. Identification of the solvents is usually simplified by higher intensity of their

signals in the NMR spectra. In preparation of a series of perfume goods, the odorants in hand are dissolved in 70% aqueous ethanol.

Aromatic esters, alcohols, and aldehydes. It is well known that the widely used components of perfumes are odor fixers having a weak balsamic odor, such as, e.g., esters of salicylic and benzoic acids [2]. We found that benzyl salicylate 7 is contained in a significant concentration (more than 30%) in several samples of the odorants studied. In the ^{13}C NMR spectra of almost all the perfumes, none of the signals of compound 7 overlap with the signals of the other components. Futhermore, compound 7 is mentioned in the sanitary certificates for odorants. It was reported that salicylates in the composition of perfumes play also the role of stabilizers inhibiting polymerization and oxidation of olefin and aldehyde components [2].

Benzyl benzoate 8 was added into some compositions instead of 7. This compound corresponds to the most downfield signal in the ^{1}H NMR spectra of odorants, except the signal of aldehyde protons at approximately 8.0 ppm.

In a series of esters of aromatic carboxylic acids used in perfumery, methyl 2-aminobenzoate 9 was found in a small concentration in one of the odorants. Weak ^{13}C NMR signals assigned to 9 coincide with those in the calculated spectrum. In the corresponding ^{1}H NMR spectrum there are signals coinciding with signals of 9 given in atlas [3]. According to reference data, esters of cinnamic acid (cinnamates) are widely used in perfumes [2]. Low-intensity doublets characteristic of olefin protons (7.5 and 6.3 ppm) and the corresponding signals of carbon atoms (153 and 117 ppm) were observed in the spectra of two samples. According to published real spectra [3, 4] these ^{13}C signals correspond to cinnamates, but we failed to assign them to specific cinnamates.

The other artificial derivative of cinnamic acid with jasmine odor, 2-hexyl-3-phenylpropenal 10, not occurring in the nature, was found in a half of the samples studied, in some cases, in significant concentration (approximately 10%) and in mixtures consisting of only three or four components, so that its identity is beyond question. The concentration of aldehyde 10 is the simplest to estimate from the intensity of the signal of its aldehyde proton (δ 9.4 ppm) or triplet of allyl methylene group (δ 2.5 ppm). Hereinafter, we use for fragrance compounds the commonly accepted nonsystematic or trade names given in reference books [2].

Several samples of odorants contain 3-phenylethanol 11, benzyl acetate 12, and coumarin 13, which are well-known perfume chemicals produced on a mass scale [2]. The signals assigned to compounds 11–13, considering data given in sanitary certificates, coincide with those in the corresponding NMR spectra given in reference books [3, 4].

In the sanitary certificate, for two of four odorants the presence of lilialdehyde [3-(4-*tert*-butylphenyl)-2-methylpropanal] 14 (approximately 3%) in their composition was documented. Contrary to aldehyde 10, unambiguously identified by all signals in its spectrum, only two or three ^{13}C NMR signals, not overlapping with the signals of other components, can be assigned to 14 (Table 1).

One of the odorants named "Cherry" contains 25% benzaldehyde 15, whose odor is similar to odor of cherry pits.

Derivatives of phenols. Classic fragrance compounds vanillin and eugenol belong to derivatives of phenols. Vanillin 16 and its homolog with more intensive odor, ethyl vanillin 17 not occurring in the nature, are present in many odorants. In several samples, these components are major, which is reflected in their names, e.g., "Vanilla," so that identification of 16 and 17 presents no problems.

The presence of approximately 1% isoeugenol 18, occurring in the nature in essential oil of eugenol basil, was reliably detected in only two samples. Due to low concentration of this component, its identification required more prolonged analysis than in the case of 16 and 17, in spite of indications on the presence of isoeugenol in several odorants.

The presence of another widely known fragrance from the same series, heliotropin (piperonal) 19, occurring in small amounts (approximately 1%) in several odorants, is simpler to prove by NMR than in the case of 18, due to its highly characteristic NMR spectrum. In particular, the signals of its methylene group with chemical shifts of 102 (^{13}C NMR) and 6.0 ppm (^{1}H NMR) are very specific. In one of the sanitary certificates for an odorant, the presence of a heliotropin derivative with extremely strong flower odor, piperonylpropanal or pional 20, not occurring in the nature, was indicated. Since this odorant was much less concentrated in fragrance components than it was mentioned in the certificate, we failed to record most of the signals of compound 20 other than the signals most typical for the "heliotropin" fragment of its molecule (Table 1).

Aliphatic alcohols, aldehydes, and esters. Among ordinary aliphatic alcohols, aldehydes, and esters,

numerous compounds used as components of perfumes are well known. However, in the available sanitary certificates for odorants, only *n*-butanol and C_{12} fraction of aldehydes are indicated; however, the presence of the latter was not confirmed by the NMR spectra. When the concentration of these components in odorants is low, identification and, the more so, qualitative estimation of these components are difficult due to the closeness of the corresponding signals in the NMR spectra to the signals of compounds of other types. Considering typical spectra of individual compounds, we were able to identify more or less reliably propyl acetate 21, isoamyl acetate 22, and *n*-amyl butyrate 23 in composition of only some samples (Table 1).

Compounds with musk or ambergris odor. Other components of odorants are artificial compounds with musk or ambergris odor, which improve the scent and have also properties to fix odor [2]. Successful identification of these compounds is favored by the presence of the corresponding data in the sanitary certificates. The most frequently occurring and reliably identified compounds of this group in odorants are Galaxolide 24 and Ambralux 25. The ^{13}C NMR spectrum of 24 (Table 1) contains more than ten characteristic signals not overlapping with other signals in the range 8–150 ppm, whose assignment is unambiguous if the stimulated spectrum and spectra of several samples of odorants containing 24 in various concentrations and combinations are available. In the ^{1}H NMR spectrum of 24, there are two characteristic upfield shifted signals of aromatic protons, which allows quantitative determination of the content of this compound.

The ^{13}C NMR spectrum of 25 also contains up to 10 signals in the range 20–217 ppm; however, assignment of these signals is difficult since this substance is a mixture of compounds with various positions of the C=C double bond [2]. These signals were assigned to Ambralux since, according to the sanitary certificate and actually (according to the spectrum), one of the odorants consists by half of compound 25 with the concentrations of other components not exceeding several percents. The signals conclusively corresponding to 25 are listed in Table 1; however, we failed to assign unambiguously these signals to the specific carbon atoms in its molecules. It is difficult to estimate quantitatively the concentration of 25 based on the ^{1}H NMR spectra, since there are no characteristic signals not overlapping with signals of other components of odorants. The singlet of acetyl methyl group at approximately 2 ppm can be used for quantitative estimation of its content if this signal can be reliably assigned to 25 rather than to other acetyl derivatives giving signals in this range.

In one of the samples, instead of 25, unidentified ketone denoted as 26 was used apparently for the same purpose. In spite of the fact that compound 26 was not identified, the signals in the ^{13}C NMR spectrum of the corresponding sample can be assigned to this compound with confidence, since this compound, judging from the intensities of the corresponding signals in the spectrum of the perfume, is in significantly higher concentration than the other components.

Several odorants contain the fourth and the last component from the considered series of compounds that were present in the samples studied, musk ketone 27. This compound is indicated in the sanitary certificate for one of the odorants; the certified composition of this odorant agrees well with the spectral data. This fact, taking into account the other spectra, allowed two or three signals in the ^{13}C NMR spectra of odorants to be unambiguously assigned to 27 (Table 1). In this case, the most characteristic is the signal with a chemical shift of approximately 125 ppm, assigned to aromatic carbon atoms bonded to methyl groups, which, contrary to other carbon atoms of the benzene ring, has a satisfactory intensity (Overhauser effect) and never overlaps with other signals.

Terpenes and terpenoids. Some terpenes, mainly the corresponding alcohols, aldehydes, and ketones (terpenoids), form the most important group of fragrances.

In some samples of odorants, limonene 28 (diterpene), having lemon odor, appears practically as a solvent (concentration higher than 50%), so that its identification and estimation of its concentration from the NMR spectra present no problems (Table 1). The other, no less common, terpene with coniferous odor, forming the basis of turpentine oil, α-pinene 29, was identified from several weak characteristic signals in the ^{13}C MNR spectrum of one of the samples considering data of the sanitary certificate.

Linalool 30, linalyl acetate 31, and dihydromyrcenol 32 (Table 1) are the most abundant and reliably determined qualitatively and quantitatively terpenoids with citric odors. The other well-known fragrances belonging to this class, geraniol 33 with rose odor, citronellol 34, and citronellal 35, can be identified from their complete ^{13}C NMR spectra only in some compounds. More commonly, in the ^{13}C NMR spectra of odorants, only two or three signals belonging to compounds 33–35 can be assigned more or less reli-

ably to terpenoids against the background of signals of other components. It is diffucult to determine the characteristic signals in the ^{1}H NMR spectra of 33–35. Only in some cases these signals can be distinguished among signals of other components (Table 1).

One of the most valuable fragrances is hydroxycitronellal 36 with lime-blossom odor [2]. Taking into account data of the sanitary certificate, compound 36 was unambiguously identified by ^{13}C NMR from all signals of its spectrum (Table 1).

One of the most well-known and available cyclic terpenoids, borneol or isoborneol 37 (particular isomer was not established), having coniferous odor, was identified in two samples. The identification involved no problems, since in one of the odorants with dominant coniferous odor the concentration of 37 exceeds 50% (see the intensities of the corresponding signals in the ^{13}C NMR spectrum). The other well-known cyclic terpinoid, α-terpineol, was tentatively identified in small amount in one of the samples from several characteristic ^{13}C NMR signals (Table 1).

Specific fragrance compounds. Many of the above substances are well-known, find wide use, and are produced on the industrial scale. In two formulations for production of air fresheners, we were able to identify reliably by the ^{1}H and ^{13}C NMR the main components governing their odor, having no natural analogs but included in the reference book [2], ethyl 2,3-epoxy-3-methyl-3-phenylpropionate 39 (strawberry odor) and 2-*tert*-butylcyclohexyl acetate 40 (fruit odor). Successful identification of 39 and 40 was favored by their significant concentration and hence high intensity of the corresponding signals in the NMR spectra. The agreement of the fragments of the odorant spectra assigned to 39 and 40 and the calculated ^{13}C and ^{1}H NMR spectra is sufficient for identification with confidence, the more so as compound 39 is a component of "Strawberry" formulation and compound 40 is a component of "Golden apple" formulation.

EXPERIMENTAL

Samples of commercial odorants produced by various foreign and Russian companies were placed at our disposal by a private company producing car air fresheners.

The ^{1}H and ^{13}C NMR spectra of the samples studied were recorded on a Bruker ACP-200P spectrometer by the standard procedure.

REFERENCES

1. Emsley, J.W., Feeney, J., and Sutcliffe, L.H., *High Resolution Nuclear Magnetic Resonance Spectroscopy*, Oxford: Pergamon, 1965, vol. 1.
2. Kheifits, L.A. and Dashunin, V.M., *Dushistye veshchestva i drugie produkty dlya parfyumerii* (Fragrance Compounds and Other Products for Perfumery), Moscow: Khimiya, 1964.
3. Pouchert, Ch.J. and Campbell, J.R., *The Aldrich Library of NMR Spectra*, 1974.
4. Levy, G.C. and Nelson, G.L., *Carbon-13 Nuclear Magnetic Resonance for Organic Chemists*, New York: Wiley, 1972.

ISSN 1070-4272. Russian Journal of Applied Chemistry, 2006, Vol. 79, No. 1, pp. 117–122. © Pleiades Publishing, Inc., 2006.
Original Russian Text © V.A. Zhorin, B.I. Zapadinskii, M.R. Kiselev, T.P. Puryaeva, 2006, published in Zhurnal Prikladnoi Khimii, 2006, Vol. 79, No. 1, pp. 119–124.

ORGANIC SYNTHESIS AND INDUSTRIAL ORGANIC CHEMISTRY

Structural and Electrophysical Aspects of Phenolphthalein Coloration in Plastic Deformation under High Pressure

V. A. Zhorin, B. I. Zapadinskii, M. R. Kiselev, and T. P. Puryaeva

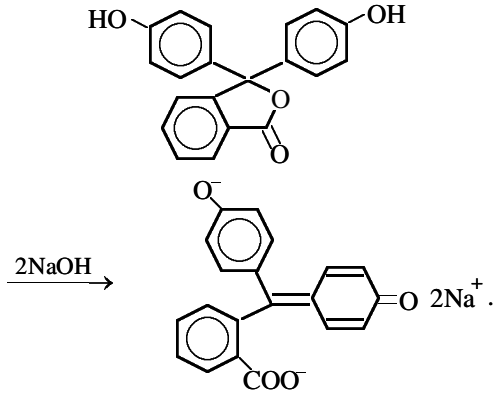
Semenov Institute of Chemical Physics, Russian Academy of Sciences, Moscow, Russia
Institute of Physical Chemistry, Russian Academy of Sciences, Moscow, Russia

Received November 3, 2005

Abstract—The influence exerted on the process of phenolphthalein coloration by the electrophysical conditions under which its pressure treatment is carried out was studied.

DOI: 10.1134/S1070427206010241

A change in the color of various substances in the course of chemical transformations is a well-known phenomenon. A particular place among compounds of this kind is occupied by chemical indicators, i.e., substances that change their color depending on the charge state of the environment. For example, colorless phenolphthalein, a known acid–base indicator, turns pink when the pH of the medium changes from neutral to alkaline. This is due to cleavage of the benzofuran ring to give a quinoid structure:



All the known processes of indicator coloration occur in the liquid phase under ordinary conditions. At the same time, it was reported in [1] that phenolphthalein turns pink when subjected to plastic deformation at a pressure of 5 GPa in a high-pressure apparatus constituted by Bridgman anvils. In this case, no absorption bands characteristic of the quinoid structure could be observed in the IR spectra of samples colored under pressure; the coloration of the sample was preserved at room temperature, but disappeared upon dissolution.

A study of the behavior of phenolphthalein subjected to plastic deformation under a high pressure was continued in [2] and the pressure dependence of the flow stress was obtained in the pressure range 0.5–5 GPa in the form of two virtually linear portions. The slope of the plot with respect to the ordinate axis decreased at a pressure of 1.2–1.5 GPa, so that a bend was formed. The presence of such a bend in the baric dependence was attributed to a polymorphic transition, even though an X-ray diffraction analysis of samples treated both below and above the bend-point pressure demonstrated that, in both cases, the substance was in an X-ray amorphous state upon a pressure treatment. At the same time, an analysis of baric dependences of the flow stress carried out in [3] for numerous organic compounds of varied structure suggested that bends in dependences of this kind reflect electronic processes that occur in various substances in the case of plastic deformation under pressure.

A vast body of experimental data obtained in studies of various aspects of the behavior of solids subjected to plastic deformation under a high pressure indicates that their electrical properties significantly change and the electric charge formed in the course of pressure treatment strongly affects the way in which various properties of the materials being treated are formed. For example, the dielectric constant of various low-molecular-weight organic compounds may increase at a pressure of up to 3–4 GPa by a factor of 2.5–3 [4]; salts and oxides of metals may dissociate under pressure treatment [5]; a high pressure stimulates injection of electrons from the metal of the anvils into pressure-treated insulators [6]; a directed

transport of carriers captured by structural defects, the so-called deformation current, is recorded in the course of plastic deformation [7]; melting parameters of polyethylene and its acoustical characteristics vary with the electrophysical conditions of pressure treatment [8, 9]; presence of charge captured by structural defects in the course of plastic deformation of polymeric samples under a high pressure has been recorded in the form of thermally stimulated currents [10].

In view of the aforesaid, it was of interest to study in more detail the behavior of phenolphthalein directly in the course of plastic deformation under a high pressure and also to analyze some properties of this material after its treatment under a high pressure, keeping in mind the fact that a thin layer of an insulator, phenolphthalein, is in close contact with the metal of which the anvils are made.

EXPERIMENTAL

Phenolphthalein of analytically pure grade was chosen for the study. The samples were treated under pressures of up to 2 GPa on anvils made of CrVMn hardened steel and a hard alloy of the VK6 brand; the diameter of the working surfaces of the anvils was 20 mm. In measurements of deformation currents under pressure, one of the anvils was made of a VK6 hard alloy, and the other, of CrVMn steel [7]. The deformation currents were measured with an M-95 needle microammeter. The coloration of phenolphthalein samples as a result of plastic deformation under pressure was recorded visually. Calorimetric studies were performed on an MAC-2M microcalorimeter at temperatures in the range 25–160°C at a sample heating rate of 8 deg min^{-1}; the mass of the samples was 20 mg. The X-ray diffraction analysis of the samples was carried out on a DRON-2 diffractometer with a monochromated copper radiation in the reflection configuration.

Already the first experiments with phenolphthalein demonstrated that the coloration process has a threshold nature: the colored form of phenolphthalein cannot be obtained at pressures of up to 1–1.1 GPa, with intense coloration of the sample appearing only upon its treatment at pressures of 1.5 GPa and more. Thus, phenolphthalein is not colored before the electronic transition, which is recorded in baric dependences of the flow stress as a bend, and intense coloration appears only at pressures exceeding the bend pressure.

When deformed under pressure, phenolphthalein is colored pink-orange uniformly over the entire working surface of the anvils. At the same time, in the case of a chemical reaction, the degree of conversion depends on the degree of deformation, and the coloration intensity of the samples markedly increases on passing from the central part of the anvils, where the deformations are at a minimum, to the peripheral zone, where they are the strongest.

The coloration of pressure-treated phenolphthalein samples is preserved at room temperature for several days, but disappears completely upon dissolution or upon heating to 70–80°C for 10–15 min. The decolorized substance retains ability to respond to changes in the charge state of the environment: addition of pressure-colored and decolorized phenolphthalein to aqueous solutions of alkalis yielded a standard color reaction.

Thus, the coloration of phenolphthalein in plastic deformation under pressure is a totally reversible process.

The materials of which the anvils were made (CrVMn steel and VK6 hard alloy) differ in the electron work function: for steel, it is lower than that for the hard alloy. This circumstance was reflected in that, at the same pressure and same rotation angles of the anvils, the coloration of samples treated on steel anvils was markedly more intense than that in the case of anvils made of the hard alloy. The result obtained indicates that injected charges can affect the process in which the coloration of an organic substance changes in plastic deformation under pressure without formation of a new product. Thus, the modification of the electrophysical conditions experienced by a sample in the course of its pressure treatment, which is associated with a change in the injecting capacity of the anvils, strongly affects the process in which the coloration varies.

All the results described above were obtained on grounded anvils. In this case, the electric charges whose formation is possible in the course of pressure treatment could leak away from the samples. The simplest way to modify the electrophysical conditions in substance treatment was to insulate the high-pressure cell from the mass of the press, i.e., to prevent leakage of electric charges.

In those cases when phenolphthalein samples were deformed under a pressure of 2 GPa on insulated anvils, the coloration of the samples was considerably less intense than that with grounded anvils.

The difference in coloration intensity in pressure treatment of samples on anvils made of different materials, as well as that on insulated and grounded anvils, point to a strong influence exerted on the

phenolphthalein coloration by the electrophysical conditions in which pressure-induced deformation is carried out.

It is well known that heating of preliminarily polarized polymers activates various kinds of molecular mobility and charge carriers are released from structural traps. In the process, an electric current, the so-called thermally stimulated depolarization current, flows through the samples.

As already mentioned, high pressure strongly intensifies the injection of electrons from the metal of the anvils into insulators subjected to pressure treatment. According to [10], part of electrons injected into a sample can be captured by structural defects and, thus, may remain in the samples after pressure is relieved. On heating such samples in the temperature range 25–130°C, an electric current flowed through the samples. This current was attributed to motion of electrons injected from the metal of the anvils and captured by structural defects of a polymeric sample.

Experiments with samples colored by deformation under a pressure of 2 GPa demonstrated that, on heating to 130°C, an electric current varying around 10^{-8} A flowed through the samples.

The following two processes can be distinguished in pressure treatment of phenolphthalein samples: (1) formation of structural defects on which charges can be localized and (2) injection of electrons from the metal of the anvils into the material of a sample. According to [11], the first of these is virtually pressure-independent in the pressure range 1–6 GPa, being determined by the extent of deformation. The second is enhanced as the pressure at which samples are treated is raised. It should also be noted that, in the course of plastic deformation, part of the structural defects leave the sample, but, at the same time, new defects are formed, i.e., the system is in a dynamic equilibrium. Thus, if the samples are first subjected to plastic deformation under pressure, which leads to coloration, and then pressure is relieved, with the number of injected electrons thereby reduced, but the deformation of the already colored samples is not terminated, i.e., the number of structural defects is maintained constant, then the following will occur. The structural defects with captured electrons will be removed from a sample and the amount of charge in the samples will be considerably smaller than that in the case when the rotation of the anvils is first stopped and then the pressure is relieved.

In the case of phenolphthalein treatment by the "deformation with pressure relieved" scheme, the material of a sample remained uncolored and the thermally stimulated currents were 10^{-11}–10^{-12} A.

As regards the stimulation of the electron injection, the action of only a high pressure of up to 6 GPa is considerably stronger than that of a pressure of 2 GPa. However, solely compression of samples under a pressure of up to 6 GPa without shear deformation caused by anvil rotation yields a very weak pinkish coloration. This may be due to plastic deformation of phenolphthalein crystals in local regions in compaction of a substance under the action of a high pressure.

The coloration of phenolphthalein may change in the presence of an electric charge not only under the action of a high pressure, but also in ordinary conditions. For example, the starting phenolphthalein was wetted with water (5–10 wt %), a pellet was compacted, and it was placed between two nickel electrodes across which a voltage of 45 V was applied. In 5–7 h, the samples started to acquire a color, to become yellow in 15–20 h. The difference in coloration between the samples colored under pressure and in an electrolytic cell is only apparent. The substance obtained after a high-pressure treatment is in the compacted state, but, on being ground in a mortar, it turns yellow-beige.

In the course of plastic deformation, structural defects with captured electrons move within a sample. According to [7], an electric current flows through the samples in pressure-induced deformation of various metals and metal–polymer composites. It was of interest in this context to study the transport of deformation currents in phenolphthalein samples in various modes of pressure treatment. Attempts to measure deformation currents at 0.3–0.5–1 GPa failed, and these currents could be only recorded at a pressure of 1.5 GPa.

At 2 GPa, a current was recorded immediately after the anvil rotation commenced. As the degree of deformation became higher, the current steadily increased to reach the limiting value of $(2–5) \times 10^{-7}$ A at anvil rotation angles of 80°–100°. As the degree of deformation increased further, the current changed only slightly. After the deformation was terminated, the current decreased to zero in several seconds. In the second and subsequent cycles of deformation, the above pattern was totally reproduced, but the deformation current was independent of the direction of anvil rotation.

The direction in which the deformation currents flowed in phenolphthalein samples coincided with that in metal samples subjected to a similar treatment. This

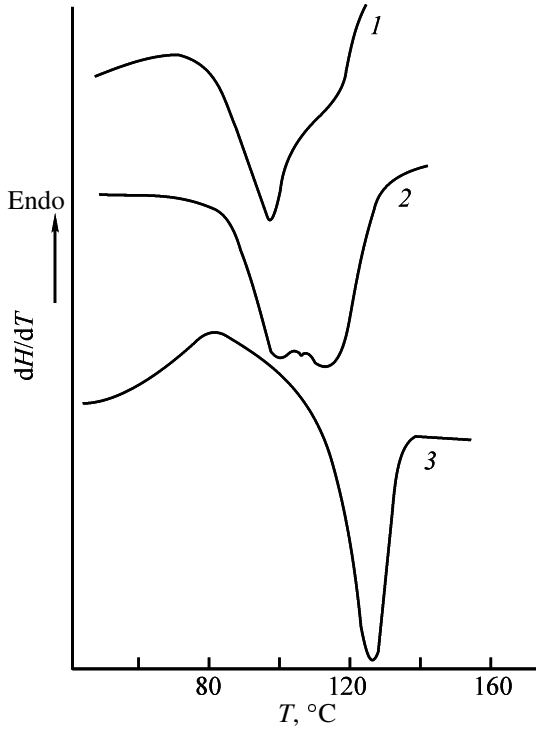


Fig. 1. Thermograms of phenolphthalein samples treated at a pressure of 2 GPa and anvil rotation angles of (*1*) 10, (*2*) 50, and (*3*) 400°C. (*T*) Temperature.

indicates that, as in the case of phenolphthalein, the current is carried by electrons that are, in all probability, injected from the anvils, rather than being intrinsic.

After deformation at 2 GPa, the pressure was reduced to 1 GPa. When relieving the pressure, a current pulse was recorded, whose direction was the opposite to that of the deformation current measured at a pressure of 2 GPa. The reverse current recorded when relieving the pressure strongly depended on the rate at which the pressure was reduced: when this rate was low, no noticeable current surges could be detected. At the same time, when the pressure was relieved rapidly, the current surge could be as large as 10–15% of the deformation current recorded directly in the course of a pressure treatment. In deformation at 1 GPa of a sample colored in treatment at 2 GPa, the maximum current strength was 2.5–3 times smaller than that at 2 GPa, the current flow was unstable, and the current decreased to zero as the extent of deformation increased.

After such a sequence of experimental procedures, the samples were either weakly colored or colorless. Repeated deformation of these samples at 2 GPa gave rise to deformation currents that virtually coincided in direction and magnitude with the current measured at the beginning of such a measurement cycle and led to appearance of a coloration.

The coloration of phenolphthalein and the appearance of deformation currents have a threshold nature. The threshold pressure coincides with the pressure at which a bend is recorded in the baric dependence of the flow pressure.

Together with the electrical measurements performed, of interest was a study by differential scanning calorimetry and X-ray diffraction analysis of specific structural features of phenolphthalein samples deformed at various pressures.

No thermal effects could be recorded in the range from room temperature to 160°C in thermograms of samples of the starting phenolphthalein; a similar situation occurred in the case of samples subjected to plastic deformation at a pressure of 1 GPa or lower.

Solely compression of samples to a pressure of 2 GPa did not lead to any changes in the thermograms. At the same time, rotation of the anvils by 10° at the same pressure led to weak coloration of the samples and to appearance of a low-intensity (enthalpy 4–5 J g^{-1}) bimodal exothermic peak (Fig. 1). As the rotation angle of the anvils was raised to 50°, the intensity of the exothermic process increased to 12–14 J g^{-1}, the ratio of peak intensities changed, but their position on the temperature scale remained constant. The thermograms of samples subjected to deformation at anvil rotation angles of 400° and more strongly differed from those described above: they contained two peaks, a broad endothermic peak at 60–70°C (enthalpy 30–40 J g^{-1}) and an exothermic peak at 127°C (enthalpy 60–70 J g^{-1}). As seen from Fig. 1, the exo- and endothermic peaks appreciably overlap; therefore, these enthalpies are very approximate. Repeated heating of the same samples was not accompanied by any thermal effects.

The coloration of a phenolphthalein sample colored in deformation under a pressure of 2 GPa became substantially less intense after four days; simultaneously, the intensity of the endothermic peak decreased to 10–12 J g^{-1}, and that of the exothermic peak, to 30 J g^{-1}. After coloration of the samples at a pressure of 2 GPa and subsequent treatment by the "deformation with pressure relieved" scheme, the intensity of the endothermic peak was 1.5 J g^{-1}, and that of the exothermic peak, 20 J g^{-1}.

Figure 2 shows an X-ray diffraction pattern of the starting phenolphthalein, which contains a set of narrow peaks of various intensities. Deformation at pressures of 0.7 and 2 GPa led to disintegration of

Scattering angles 2θ, line half-widths *L*, and interplanar spacings *d* for phenolphthalein samples

Sample no.	Starting sample			Treated sample*		
	2θ, deg	*L*	*d*, Å	2θ, deg	*L*	*d*, Å
1	9.05	0.16	9.782	8.89	0.32	9.958
2	11.85	0.25	7.468	11.68	0.53	7.583
3	12.66	0.23	6.986	12.50	0.51	7.075
4	14.11	0.10	6.281	–	–	–
5	14.87	0.30	5.953	14.70	0.61	6.022
6	16.85	0.29	5.258	16.70	0.65	5.315
7	17.98	0.28	4.931	–	–	–
8	18.28	0.39	4.856	18.10	0.91	4.963
9	19.59	0.52	4.534	19.38	0.92	4.582
10	21.63	0.47	4.110	21.35	1.69	4.164
11	22.58	0.43	3.939	–	–	–
12	23.31	0.37	3.814	23.03	0.68	3.863
13	23.96	0.41	3.715	23.73	0.51	3.742
14	25.59	0.31	3.480	25.38	0.48	3.509
15	26.30	0.10	3.390	–	–	–
16	26.93	0.17	3.309	26.58	1.05	3.355

* Sample treated by the "deformation with pressure relieved" scheme.

the crystal structure of phenolphthalein: in both cases, amorphous halos were present in the X-ray diffraction patterns, with weakly pronounced traces of the highest-intensity lines of phenolphthalein discernible on their background.

Heating of the amorphized samples at 90–100°C for 15–20 min led to decoloration of colored samples and had virtually no effect on the crystal structure of the substance. At the same time, storage of the samples for two months at room temperature led to appearance of broad low-intensity lines shifted to smaller diffraction angles, compared with the lines of the starting phenolphthalein, in the X-ray diffraction patterns.

The X-ray diffraction technique was used to study phenolphthalein samples that were first deformed at a pressure of 2 GPa and then treated by the "deformation with pressure relieved" scheme. After a treatment of this kind, the X-ray diffraction patterns of the samples contained, on the background of an amorphous halo, well-pronounced but broadened lines of phenolphthalein shifted to smaller angles (see table, Fig. 2). This indicates that the amorphized substance can restore its crystal structure under the action of plastic deformations. This effect is presumably based on vibrational excitation of molecules in plastic deformation.

To confirm the conclusion that crystallization of amorphous low-molecular-weight substances in plastic deformation is possible, samples of a pressure-treated phenolphthalein were subjected, after their amorphous state was recorded by X-ray diffraction analysis, to treatment by the "deformation with pressure relieved" scheme, with the initial treatment carried out at 1.5–1–0.5 GPa. In all cases, the crystal structure of phenolphthalein was identified by the X-ray diffraction patterns.

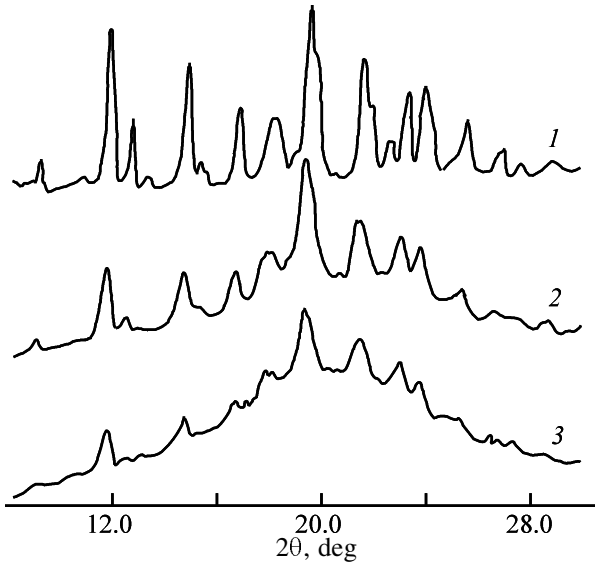


Fig. 2. X-ray diffraction patterns of (*1*) starting phenolphthalein, (*2*) that deformed at a pressure of 2 GPa and then treated by the "deformation with pressure relieved" scheme, and (*3*) amorphous phenolphthalein treated by the "deformation with pressure relieved" scheme. (2θ) Bragg angle.

The possibility that amorphous metallic alloys can crystallize in the course of plastic deformation under a high pressure was reported in [12, 13] on the basis of calorimetric and X-ray diffraction data.

CONCLUSIONS

(1) The coloration of phenolphthalein upon a high-pressure treatment does not involve formation of new products and is totally reversible.

(2) The coloration process has a threshold nature with respect to pressure, is independent of the state of the crystal structure, and correlates with changes in the electronic structure of the substance, caused by the joint action of high pressure and shear deformations.

(3) The coloration of phenolphthalein is strongly affected by charges generated in the samples in the course of their pressure treatment. These charges manifest themselves as deformation currents in deformation and as thermally stimulated currents upon completion of the pressure treatment. The most probable reason for the appearance of charged states in the samples is capture by structural defects of electrons injected into a sample from the metal of the anvil.

(4) The heat effects observed in the thermograms of samples subjected to pressure treatment indicate that relaxation processes occur in the electronic subsystem of the solid.

(5) The crystal structure of phenolphthalein, amorphized under the action of a high pressure, can be restored not only by heating of the samples, but also by their plastic deformation at low pressures.

REFERENCES

1. Larsen, H.A. and Drickamer, H.G., *J. Phys. Chem.*, 1958, vol. 62, no. 1, p. 119.
2. Gonikberg, M.G., Petrov, A.A., Aneli, Dzh.N., *et al.*, *Izv. Akad. Nauk SSSR, Ser. Khim.*, 1968, no. 3, pp. 486–490.
3. Zhorin, V.A., *Zh. Fiz. Khim.*, 2001, vol. 75, no. 10, pp. 1825–1831.
4. Maksimychev, A.V., Zhorin, V.A., Ponomarenko, A.T., and Enikolopyan, N.S. *Dokl. Akad. Nauk SSSR*, 1978, vol. 241, no. 1, pp. 141–143.
5. Zhorin, V.A., Nikiforov, G.A., Khristyuk, A.V., and Enikolopyan, N.S., *Dokl. Akad. Nauk SSSR*, 1983, vol. 271, no. 3, pp. 650–652.
6. Berlin, Yu.A., Beshenko, S.I., Zhorin, V.A., and Enikolopyan, N.S., *Dokl. Akad. Nauk SSSR*, 1982, vol. 262, no. 4, pp. 911–913.
7. Zhorin, V.A., *Vysokomol. Soedin., Ser. A*, 1994, vol. 36, no. 4, pp. 559–579.
8. Zhorin, V.A., Svistunov, V.S., Zelenetskii, A.N., *et al.*, *Vysokomol. Soedin., Ser. A*, 1999, vol. 41, no. 4, pp. 687–694.
9. Zhorin, V.A. and Volkova, A.V., *Vysokomol. Soedin., Ser. A*, 1988, vol. 30, no. 9, pp. 1868–1872.
10. Zhorin, V.A., Lushcheikin, G.A., and Razumovskaya, I.V., *Vysokomol. Soedin., Ser. A*, 2001, vol. 43, no. 12, pp. 2163–2169.
11. Zhorin, V.A., Shashkin, D.P., and Enikolopyan, N.S., *Dokl. Akad. Nauk SSSR*, 1984, vol. 278, no. 1, pp. 144–147.
12. Durochenko, A.M., Zhorin, V.A., and Malinochka, E.Ya., *Metallofizika*, 1986, vol. 8, no. 5, pp. 105–106.
13. Zhorin, V.A., Durochenko, A.M., Malinochka, E.Ya., *et al.*, *Dokl. Akad. Nauk SSSR*, 1985, vol. 284, no. 6, pp. 1400–1402.

ISSN 1070-4272. Russian Journal of Applied Chemistry, 2006, Vol. 79, No. 1, pp. 123–126. © Pleiades Publishing, Inc., 2006.
Original Russian Text © A.A. Sedykh, A.G. Galstyan, 2006, published in Zhurnal Prikladnoi Khimii, 2006, Vol. 79, No. 1, pp. 125–128.

ORGANIC SYNTHESIS AND INDUSTRIAL ORGANIC CHEMISTRY

Oxidation of *p*-Cresol with Ozone in Acetic Anhydride

A. A. Sedykh and A. G. Galstyan

Dal' East-Ukrainian National University, Rubezhnoe Branch, Rubezhnoe, Lugansk oblast, Ukraine

Received July 26, 2005

Abstract—Preparation of aromatic alcohols and aldehydes by oxidation of *p*-cresol with ozone in acetic anhydride in the presence of sulfuric acid, manganese acetate, and potassium bromide was studied. The optimal oxidation conditions were determined.

DOI: 10.1134/S1070427206010253

p-Cresol (*p*-Cr) oxidation products, *p*-hydroxybenzyl alcohol (*p*-HBA) and *p*-hydroxybenzaldehyde (*p*-HBAd), are used in production of synthetic drugs and products of fine organic synthesis [1]. These products are prepared by oxidation of *p*-cresol with sodium dichromate or chromic anhydride in concentrated sulfuric acid [2]. The disadvantages of this procedure are formation of large amounts of difficult to utilize toxic waste and relatively low selectivity. To overcome these disadvantages, environmentally clean oxidizing agent, ozone, can be used.

Ozone is used to oxidize methylbenzenes in acetic acid to the corresponding benzenecarboxylic acids [3]. The possible intermediates, aromatic alcohols and aldehydes, are readily oxidized under these conditions and cannot be isolated.

To decelerate the oxidation at the step of formation of *p*-HBA and *p*-HBAd and to develop a low-waste technology of their production, we studied the reaction of *p*-Cr with ozone in acetic anhydride in the presence of a strong mineral acid. Under these conditions, acetic anhydride is a strong acylating agent and reacts with the intermediate reaction products to form the acetate and acylal derivatives which are more resistant to oxidation [4].

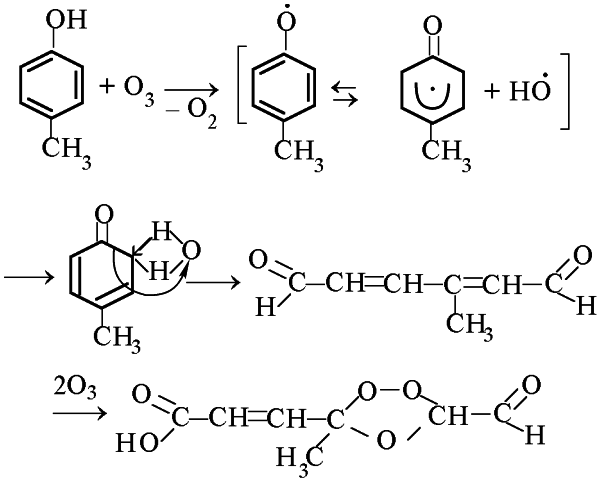
It is known [5] that *p*-Cr readily reacts with ozone in the liquid phase with opening of the aromatic ring to form peroxides ($k = 2 \times 10^3$ l mol^{-1} s^{-1}, CCl_4, 293 K). In acetic acid, one *p*-Cr molecule is consumed per three ozone molecules, which suggests that this process occurs in two steps by Scheme 1 [6].

In the first step, ozone attacks the O–H bond to form the phenoxy radical. Then hydroxy radical is added to phenoxy radical with opening of the aromatic ring. The product reacts with two ozone molecules to form the aliphatic peroxide.

To stabilize the aromatic ring of *p*-cresol, its OH group was acylated. Weighed portions of *p*-Cr and acetic anhydride were loaded in a flask. A mixture of acetic anhydride and phosphoric acid taken in a 10 : 1 weight ratio was added in small portions at 5°C. The reaction mixture was poured into water after 20 min. The oil was separated, washed with a 5% solution of sodium hydroxide and water, and distilled in a vacuum. The yield of *p*-cresyl acetate (*p*-CrA) was 80%.

An ozone–air mixture with an ozone concentration of 4×10^{-4} M was bubbled through a *p*-CrA solution in acetic anhydride. The kinetic experiments showed that the reactivity of *p*-CrA with respect to ozone substantially decreases: the rate constant of this reaction at 20°C is $k = 1.3$ l mol^{-1} s^{-1}. This fact and the stoichiometric coefficient of ozone in this reaction (one ozone molecule per substrate molecule) confirm the change in the oxidation mechanism. In this case, in accordance with the classical concept on ozonolysis of

Scheme 1



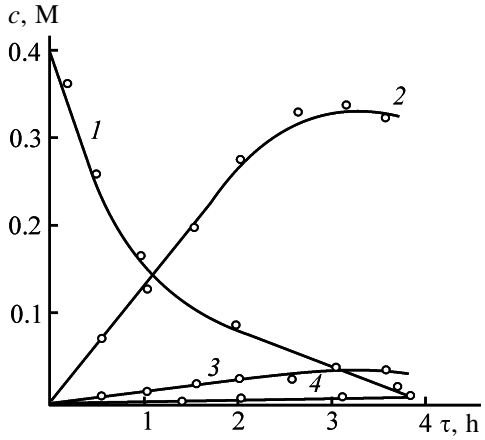


Fig. 1. Kinetic curves of (*1*) *p*-CrA consumption and accumulation of (*2*) peroxides, (*3*) *p*-ABA, and (*4*) *p*-ABDA in oxidation of *p*-CrA with an ozone–air mixture in acetic anhydride at 5°C. $[p\text{-Cr}]_0 = 0.4$, $[H_2SO_4]_0 = 1.2$, $[O_3]_0 = 4 \times 10^{-4}$ M; $v_{air} = 8.3 \times 10^{-3}$ l s^{-1}. (*c*) Concentration and (τ) time; the same for Fig. 2.

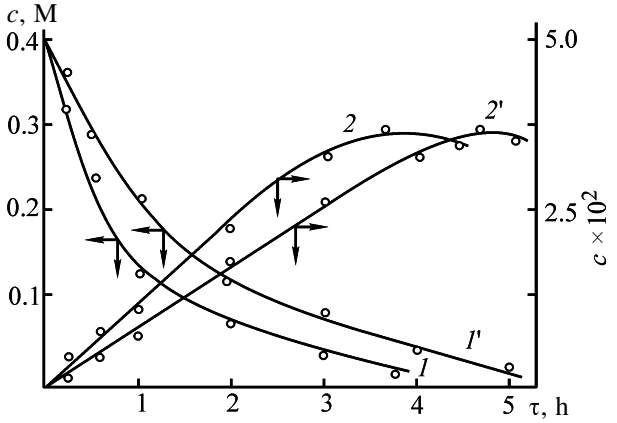
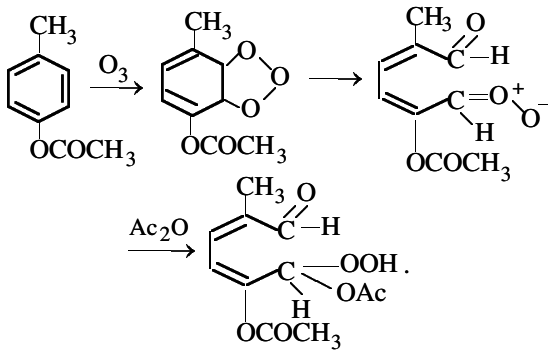


Fig. 2. Rate and selectivity of *p*-CrA oxidation with an ozone–air mixture in acetic anhydride at 5°C in the presence of (*1*, *2*) H_2SO_4 and (*1'*, *2'*) H_3PO_4. $[p\text{-Cr}]_0 = 0.4$, $[acid]_0 = 1.2$, $[O_3]_0 = 4 \times 10^{-4}$ M; $v_{air} = 8.3 \times 10^{-3}$ l s^{-1}. (*1*, *1'*) Consumption of *p*-CrA and (*2*, *2'*) total accumulation of *p*-ABA and *p*-ABDA.

alkylbenzenes [6], ozone attacks the aromatic ring to form peroxide monomers by Scheme 2:

Scheme 2



Under these conditions, virtually no aromatic alcohol and aldehyde are formed. In the presence of acylation catalyst (mineral acid such as sulfuric and phosphoric acid) in the reaction mixture, *p*-HBA and *p*-HBAd do not decompose and are converted into *p*-acetoxybenzyl acetate (*p*-ABA) and *p*-acetoxybenzylidene diacetate (*p*-ABDA) having lower reactivity with respect to ozone. However, under these conditions the total yield of the aromatic products is still as low as 10% (Fig. 1). It should be noted that the selectivity of the oxidation of the methyl group is independent of the type of the mineral acid but the reaction is accelerated in going from phosphoric to sulfuric acid (Fig. 2).

The selectivity of oxidation of the side chain increases in the presence of an oxidation catalyst, variable-valence metal salt [3]. We studied the oxidation of *p*-CrA catalyzed by manganese(II) acetate (Table 1). This reaction is fast and yields mainly *p*-ABA. The oxidation is complete in 1 h at the manganese(II) acetate concentration of 0.18 M and temperature of 5°C. The selectivity of oxidation of the methyl group is 77%; the yield of *p*-ABA and *p*-ABDA is 56 and 21%, respectively (Table 1).

After the oxidation completion, the reaction mixture was diluted with a fivefold volume of water and then was extracted with ether. The organic layer was distilled under atmospheric pressure to remove the ether and then in a vacuum (10 mm Hg) to remove the unchanged *p*-CrA. Th residue was refluxed in 5% NaOH. The resulting *p*-HBA was extracted with ether; the yield based on reacted *p*-CrA was 51%.

The methyl group is selectively oxidized in two steps with ozone in the presence of manganese(II) acetate. Under these conditions, ozone reacts mainly with Mn^{2+} {reaction (1), $k_1 = 4.7 \times 10^3$ [7]; $k_{AcOC_6H_4CH_3\text{-}p+O_3} = 1.3$ l mol^{-1} s^{-1}, our data} to form reactive Mn^{3+} species which rapidly and selectively oxidize the methyl group of *p*-CrA [reaction (2)]:

$$Mn^{2+} + O_3 + H^+ \rightarrow Mn^{3+} + HO^\bullet + O_2, \quad (1)$$

$$AcOC_6H_4CH_3\text{-}p + Mn^{3+} \rightarrow AcOC_6H_4CH_2^\bullet\text{-}p + Mn^{2+} + H^+. \quad (2)$$

For reaction (1) to occur, ozone should be continuously fed into the system. When the ozone supply is stopped, the process is decelerated up to its complete cessation. This fact additionally confirms formation of reactive catalytic species by reaction (1). Since the concentration of molecular oxygen under the experi-

mental conditions is higher by one and half orders of magnitude than that of ozone, the benzyl radical formed by reaction (2) reacts mainly with molecular oxygen by reaction (3) to form the peroxy radical which is converted into *p*-ABA by reactions (4)–(6):

$$AcOC_6H_4CH_2^{\bullet}\text{-}p + O_2 \longrightarrow AcOC_6H_4CH_2O_2^{\bullet}\text{-}p, \quad (3)$$

$$AcOC_6H_4CH_2O_2^{\bullet}\text{-}p + O_3 \longrightarrow AcOC_6H_4CH_2O^{\bullet}\text{-}p + 2O_2, \quad (4)$$

$$AcOC_6H_4CH_2O^{\bullet}\text{-}p + Mn^{2+} \rightarrow AcOC_6H_4CH_2O^{-}\text{-}p + Mn^{3+}, \quad (5)$$

$$AcOC_6H_4CH_2O^{-}\text{-}p + Ac_2O + H^{+} \rightarrow AcOC_6H_4CH_2OAc\text{-}p + AcOH. \quad (6)$$

Introduction of potassium bromide in the system increases the conversion and selectivity of catalytic oxidation of the methyl group of *p*-CrA to 84%. The major reaction product is *p*-ABDA. Its yield reaches 67% (Table 2).

After the reaction completion, the reaction mixture was poured into a glass beaker filled by two thirds with finely divided ice and then was diluted to 100 ml with cold water. The mixture was vigorously stirred until the oil solidified. The solid product was filtered off, washed with cold water, and dried. Concentrated HCl (20 ml), water (20 ml) and alcohol (4 ml) were added to crude *p*-ABDA. The mixture was refluxed with stirring for 1 h. The reaction mixture was cooled, and *p*-HBAd precipitate was filtered off. The yield based on *p*-CrA was 62%.

Potassium bromide reacts with manganese(II) acetate catalyst to form $Mn^{2+}Br^{\bullet}$ which is more reactive than Mn^{3+}:

$$Mn^{2+} + Br^{-} \rightleftarrows Mn^{2+}Br^{-}, \quad (7)$$

$$Mn^{2+}Br^{-} + O_3 \rightarrow Mn^{2+}Br^{\bullet} + HO^{\bullet} + O_2. \quad (8)$$

$Mn^{2+}Br^{\bullet}$ oxidizes the methyl group of *p*-ABA by the following scheme:

$$AcOC_6H_4CH_2OAc\text{-}p + Mn^{2+}Br^{\cdot} \rightarrow AcOC_6H_4C^{\bullet}HOAc\text{-}p + Mn^{2+} + Br^{-} + H^{+}, \quad (9)$$

$$AcOC_6H_4C^{\bullet}HOAc\text{-}p + O_2 \rightarrow AcOC_6H_4C(OO^{\bullet})HOAc\text{-}p, \quad (10)$$

$$AcOC_6H_4C(OO^{\bullet})HOAc\text{-}p + O_3 \rightarrow AcOC_6H_4C(O^{\bullet})HOAc\text{-}p + 2O_2, \quad (11)$$

Table 1. Yield of the products of oxidation of the methyl group in *p*-CrA at 5°C and various concentration of $Mn(OAc)_2$. $[p\text{-Cr}]_0 = 0.4$, $[H_2SO_4]_0 = 1.2$, $[O_3]_0 = 4 \times 10^{-4}$ M; $\tau = 1$ h

$[Mn(OAc)_2]_0$, M	Yield, %	
	p-ABA	*p*-ABDA
0.05	30.1	8.7
0.10	42.4	12.5
0.14	51.3	17.2
0.18	56.1	21.3
0.20	54.2	20.1

Table 2. Yield of the oxidation products of the methyl group in *p*-CrA at 5°C and various KBr concentrations. $[p\text{-Cr}]_0 = 0.4$, $[Mn(OAc)_2]_0 = 0.18$, $[H_2SO_4]_0 = 1.2$, $[O_3]_0 = 4 \times 10^{-4}$ M; $\tau = 50$ min

$[KBr]_0$, M	Yield, %	
	p-ABA	*p*-ABDA
0.02	40.2	39.8
0.06	24.2	51.9
0.08	19.3	60.3
0.10	17.2	67.1
0.12	17.1	66.3

$$AcOC_6H_4C(O^{\bullet})HOAc\text{-}p + Mn^{2+}Br^{-} \rightarrow AcOC_6H_4C(O^{-})HOAc\text{-}p + Mn^{2+}Br^{\bullet}, \quad (12)$$

$$AcOC_6H_4C(O^{-})HOAc\text{-}p + Ac_2O + H^{+} \rightarrow AcOC_6H_4CH(OAc)_2\text{-}p + AcOH. \quad (13)$$

The increase in the oxidative conversion of *p*-CrA in the presence of potassium bromide is due to accumulation of reactive complex $Mn^{2+}Br^{\bullet}$ in the system. Oxidation of *p*-ABA in the presence of this complex is faster than that in the presence of Mn^{3+} [9].

EXPERIMENTAL

Analytically pure grade acetic anhydride and manganese(II) acetate were used as received. Crystalline *p*-Cr was recrystallized repeatedly from water.

The experiments were performed in a glass column with a porous partition. Acetic anhydride (10 ml), *p*-Cr (0.4 M), appropriate mineral acid (1.2 M), and a weighed portion of the catalyst were placed in the

column. The column was thermostated and an ozone–air mixture (ozone concentration 4×10^{-4} M) was passed through at a flow rate of 30 l h^{-1} under the steady operation conditions of the ozonizer. The ozone concentration in the gas phase was determined spectrophotometrically by the absorption in the range 254–290 nm.

The oxidation products were identified and their concentration in the solution was determined by gas–liquid chromatography on an LKhM-80 chromatograph with a flame ionization detector using a 2 m × 4 mm column packed with Chromaton N-AW. The stationary phase was SE-30 in the 5% amount of the support weight. The analysis was performed under the following conditions: vaporizer temperature 250°C; thermostat temperature 180°C; flow rate of the carrier gas (nitrogen) 1.8, hydrogen 1.8, and air 18 l h^{-1}. *p*-Nitrochlorobenzene was used as the internal reference.

CONCLUSION

p-Cresol was oxidized with ozone in acetic anhydride in the presence of mineral acid, manganese(II) acetate, and potassium bromide as catalysts. In the presence of manganese(II) acetate, the reaction can be stopped at the step of formation of *p*-hydroxybenzyl alcohol in the form of the corresponding diacetate (yield 56%). Introduction of potassium bromide into the catalytic system allows preparation of *p*-hydroxybenzaldehyde in the form of triacetate in a 67% yield.

REFERENCES

1. JPN Patent 2 172 940.
2. Weygand–Hilgetag, *Organisch-chemische Experimentierkunst*, Leipzig: Johann Ambrosius Barth, 1964, 3th ed.
3. Galstyan, G.A., Galstyan, T.M., and Mikulenko, L.I., *Kinet. Katal.*, 1994, vol. 35, no. 2, p. 255.
4. Potapenko, E.V. and Galstyan, G.A., *Ukr. Khim. Zh.*, 2000, vol. 66, no. 1, p. 34.
5. Razumovskii, S.D., Globenko, G.M., *et al.*, *Neftekhimiya*, 1972, vol. 12, p. 65.
6. Galstyan, G.A., Tyupalo, N.F. and Razumovskii, S.D., *Ozon i ego reaktsii s aromaticheskimi soedineniyami v zhidkoi faze* (Ozone and Its Reactions with Aromatic Compounds in the Liquid Phase), Lugansk: Vostochno-Ukr. Nats. Univ., 2004.
7. Perepletchikov, M.L., Tarunina, V.N., Tarunin, B.I., and Aleksandrov, Yu.A., *Zh. Obshch. Khim.*, 1985, vol. 55, no. 3, p. 487.
8. Zakharov, I.V. and Galetii, Yu.V., *Neftekhimiya*, 1978, vol. 18, no. 4, p. 615.
9. Potapenko, E.V. and Galstyan, G.A., *Zh. Prikl. Khim.*, 2000, vol. 73, no. 7, p. 1218.

ISSN 1070-4272. Russian Journal of Applied Chemistry, 2006, Vol. 79, No. 1, pp. 127–132. © Pleiades Publishing, Inc., 2006.
Original Russian Text © M.V. Solovskii, A.M. Korchagin, E.B. Tarabukina, E.N. Vlasova, A.A. Shpyrkov, A.I. Amirova, 2006, published in Zhurnal Prikladnoi Khimii, 2006, Vol. 79, No. 1, pp. 129–134.

MACROMOLECULAR CHEMISTRY AND POLYMERIC MATERIALS

Synthesis of Low-Molecular-Weight Copolymers of *N*-Vinylpyrrolidone with 2-Hydroxyethyl Methacrylate and of Polymeric Oxacillin Esters Derived from Them

M. V. Solovskii, A. M. Korchagin, E. B. Tarabukina, E. N. Vlasova, A. A. Shpyrkov, and A. I. Amirova

Institute of Macromolecular Compounds, Russian Academy of Sciences, St. Petersburg, Russia

Received October 10, 2005

Abstract—The radical copolymerization of *N*-vinylpyrrolidone with 2-hydroxyethyl methacrylate in 2-propanol at 60°C, initiated by azobis(isobutyronitrile) and inhibited by mercaptoethanol or terminated after a short period, was studied. The low-molecular-weight copolymers obtained were used to prepare new polymeric forms of Oxacillin antibiotic. The chemical uniformity, composition, and antimicrobial activity of the new derivatives were studied, and the rate of their hydrolysis in saline (pH 7.3) and glycine buffer (pH 2.0) was determined.

DOI: 10.1134/S1070427206010265

In the development of polymeric carriers based on *N*-vinylpyrrolidone (VP) for biologically active substances (BASs) [1], much promise is shown by copolymers of VP with 2-hydroxyethyl methacrylate (HEMA), which are hydrophilic, nontoxic, and biocompatible with a living body.

Previously [2] we studied the copolymerization of VP (M_1) with HEMA (M_2) and determined the compositions and molecular weights of the resulting copolymers. The copolymerization constants obtained, $r_1 = 0.29 \pm 0.02$ and $r_2 = 6.68 \pm 0.34$, showed that HEMA is considerably more active comonomer than VP. As a result, the calculated running composition of the copolymer is enriched in HEMA units at any composition of the starting monomer mixture (Fig. 1). This results in formation of copolymers of nonuniform composition. More compositionally uniform copolymers are formed only in copolymerization of monomer mixtures enriched in VP. The molecular weight (MW) of the resulting VP–HEMA copolymers, 50000–90000 Da, exceeded the limiting MW of synthetic non-biodegradable polymers (40000 Da) [3] passing through kidneys.

The goal of this study was to prepare low-molecular-weight (MW = 20000–30000 Da) VP–HEMA copolymers and to examine the possibility of their use as new polymeric BAS carriers.

To obtain low-molecular-weight copolymers, we performed the copolymerization of VP with HEMA in 2-propanol, initiated by azobis(isobutyronitrile) (AIBN), in the presence of a chain-terminating agent, mercaptoethanol, added in an amount of 0.1–0.2 wt % relative to the sum of the comonomers, or terminated the copolymerization after a short period. The conditions of the synthesis of low-molecular-weight VP–

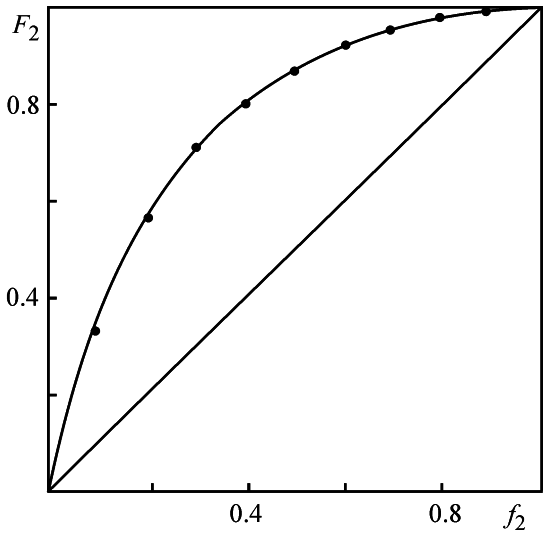
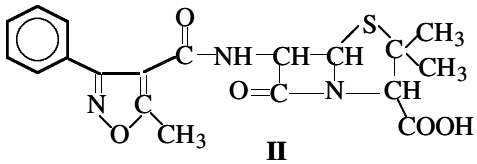


Fig. 1. Running composition of VP (M_1)–HEMA (M_2) copolymers as a function of the composition of the starting monomer mixture: (f_2) mole fraction of HEMA in the starting mixture and (F_2) mole fraction of HEMA units in the VP–HEMA copolymer.

HEMA copolymers **I** and their characteristics (compositions, diffusion coefficients D, sedimentation coefficients S_0, intrinsic viscosities, molecular weights M_{SD}) are given in Table 1. It is seen that, under these conditions, low-molecular-weight (M_{SD} = 16000–31000 Da) VP–HEMA copolymers are obtained in 53–65% yield. With an increase in the mercaptoethanol content in the starting mixture, the yield and MW of the resulting copolymer decrease, which is apparently associated with an increase in the chain termination rate. Copolymers **Ia**–**Ic** are enriched in HEMA units relative to the composition of the starting monomer mixture. This effect becomes more pronounced with a decrease in the polymer yield. Copolymers **Ib** and **Ic** are readily soluble in water and contain a large amount (25.8–29.4 mol %) of hydroxyl-containing HEMA units, which allows their use for modifying Oxacillin antibiotic.

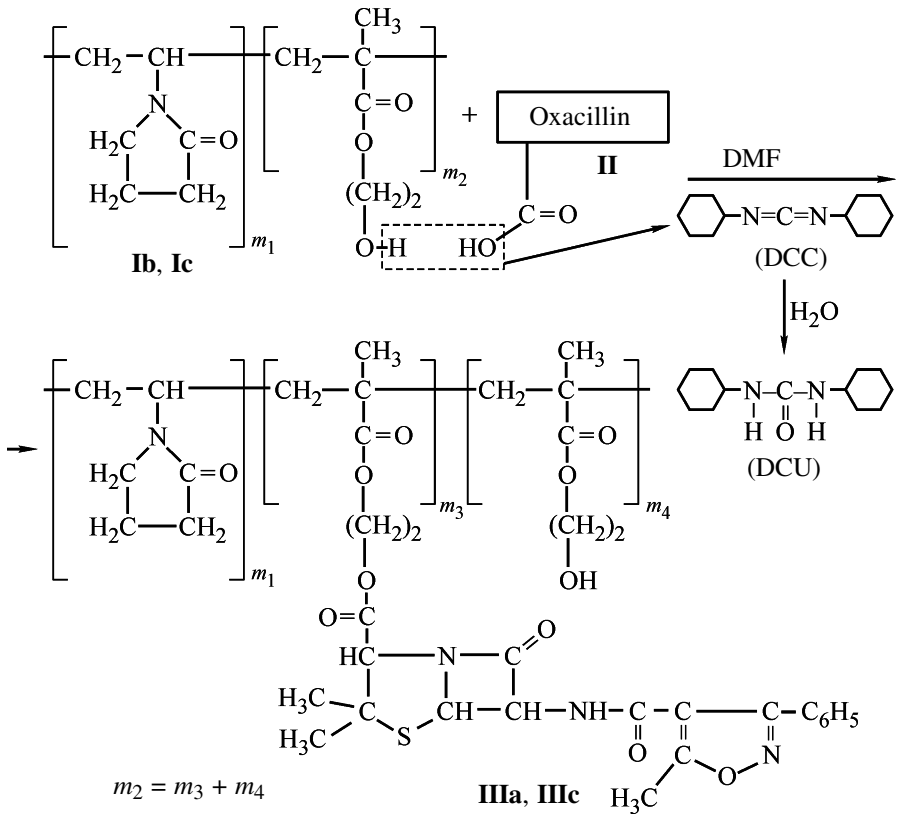
Oxacillin **II** is a semisynthetic penicillin [4] which is effective against penicillinase-forming staphylococci, acid-resistant, and nontoxic; it is widely used in clinical practice in the form of sodium salt:



II

However, the major drawback of Oxacillin is its short therapeutic effect. To maintain the therapeutic concentration of Oxacillin in blood, it should be administered every 4 h. To develop polymeric forms of Oxacillin of prolonged effect, the antibiotic was modified with copolymers **Ib** and **Ic**.

Condensation of Oxacillin with VP–HEMA copolymers **Ib** and **Ic** was performed in DMF at 0–5°C in the presence of a condensing agent, N,N'-dicyclohexylcarbodiimide (DCC). In so doing, the antibiotic was linked to the polymeric carrier by an ester bond:



The evidence of the reaction was formation of an abundant precipitate of the by-product, dicyclohexylurea (DCU).

By gel filtration (Sephadex G-50 [5]) we confirmed the chemical uniformity of condensation products **IIIa** and **IIIb** and the absence of free Oxacillin impurities.

Table 1. Copolymerization of VP with HEMA in 2-propanol at 60°C and properties of copolymers **I** ([AIBN] = 4.5 wt %, $[M_1^0] : [M_2^0]$ molar ratio 80 : 20)

Starting monomer mixture, wt %		Copolymerization time, h	Copolymer	Yield, %	N, %	m_2, mol %	$[\eta]$, dl g^{-1}, 25°C, DMF	$D \times 10^7$, cm^2 s^{-1}	$S_0 \times 10^{13}$, Sv	M_{SD}, Da
$[M_1^0 + M_2^0]$	mercaptoethanol									
7.5	0.2	24	**Ia**	53.4	7.95	33.4	0.07	6.6	1.0	16000
7.5	0.1	24	**Ib**	63.2	8.48	29.4	0.11	4.6	1.2	27000
10.0	–	2	**Ic**	65.0	8.92	25.8	0.13	7.1	1.9	31000

The structure of Oxacillin polyesters **IIIa** and **IIIb** was confirmed by UV and IR spectroscopy and also by quantitative iodometric analysis for penicillins [6]. As seen from Figs. 2 and 3, in the UV spectra of aqueous solutions of Oxacillin sodium salt and polymeric Oxacillin ester **IIIa** there is a shoulder at 230–250 nm, absent in the spectrum of an aqueous solution of the starting polymer **Ic**. This fact confirms the presence of Oxacillin in **IIIa** and allows estimation of the Oxacillin content in the product. Figure 4 shows the IR spectra of VP–HEMA copolymer **Ic** and polymeric Oxacillin ester **IIIa** derived from it. It is seen that a new strong band at about 750 cm^{-1}, absent in the spectrum of **Ic** and belonging to bending vibrations of the –CH= groups of the benzene ring in the Oxacillin molecule, appears in the spectrum of **IIIa**. The stretching vibration band of the ester C=O groups at about 1720 cm^{-1} in the spectrum of **IIIa** is stronger than in the spectrum of **Ic** owing to addition of Oxacillin to **Ic** through an ester bond. Finally, the methyl stretching vibration band at about 2900 cm^{-1} in the IR spectrum of **IIIa** is broadened relative to the corresponding band in the spectrum of **Ic**. This fact is also indicative of the incorporation of Oxacillin containing three CH_3 groups into the polymeric product.

The compositions of polymeric Oxacillin esters **IIIa** and **IIIb** are given in Table 2. It is seen that the Oxacillin content determined spectrophotometrically and iodometrically coincides within the analytical error. This means that Oxacillin is not inactivated in the course of the DCC-induced esterification (the β-lactam ring, actually determined in the iodometric procedure, is preserved).

The content of the incorporated Oxacillin in polyesters **IIIa** and **IIIb** is high (30–33%). The degree of conversion Q of the hydroxy groups of the polymeric carriers in their reaction with Oxacillin, calculated from these data, is 64–66%. This high value of Q indicates that the above-noted microstructural features of the starting VP–HEMA copolymers do not interfere with their reaction with Oxacillin molecules.

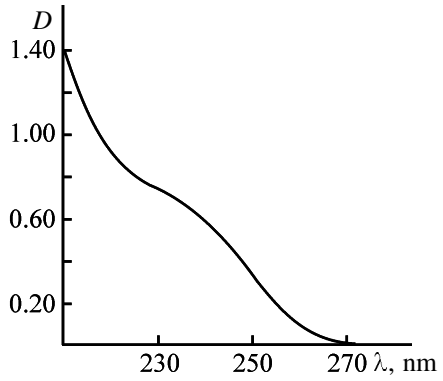


Fig. 2. UV spectrum of an aqueous solution of Oxacillin sodium salt (c = 25.7 μg ml^{-1}): (D) optical density and (λ) wavelength; the same for Fig. 3.

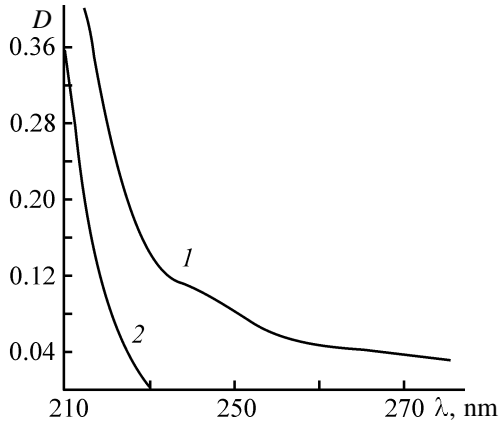


Fig. 3. UV spectra of aqueous solutions of (*1*) polymeric Oxacillin ester **IIIa** (c = 10.9 μg ml^{-1}) and (*2*) starting copolymer **Ic** (c = 19.7 μg ml^{-1}).

We found that polymeric Oxacillin ester **IIIa** exhibits high antimicrobial activity *in vitro*. When taken in concentrations of 3×10^{-3}–3×10^{-4} μg ml^{-1}, it killed standard staphylococcus strains (Table 2).[1]

[1] The authors are grateful to T.S. Potekhina for the determination of the antistaphylococcus activity of Oxacillin sodium salt and polymeric Oxacillin ester **IIIa**.

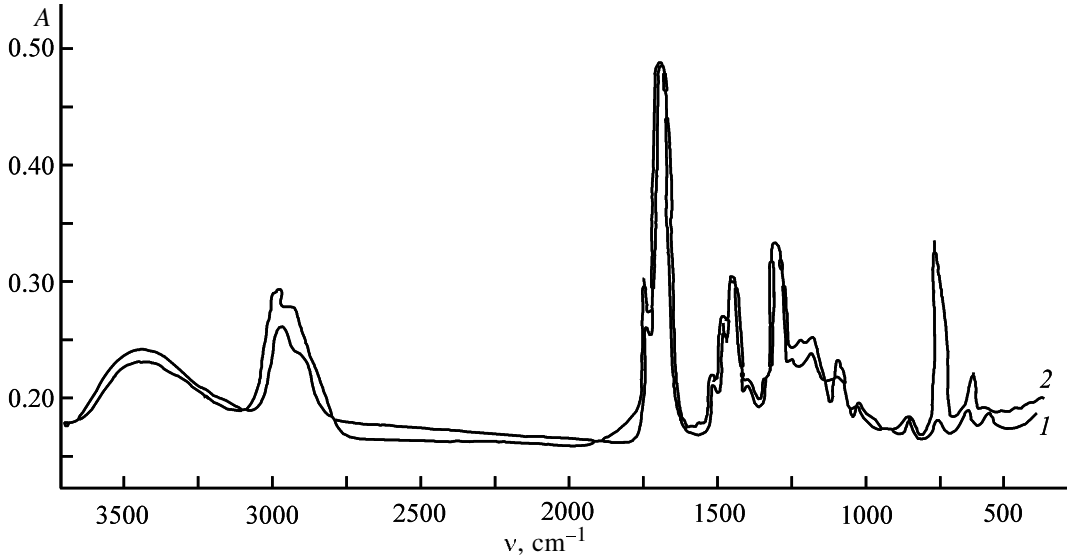


Fig. 4. IR spectra (films prepared from chloroform solution): (*A*) absorption and (ν) wavenumber. (*1*) Copolymer **Ic** and (*2*) polymeric Oxacillin ester **IIIa**.

As Oxacillin is administered parenterally and perorally, it seemed appropriate to estimate by dialysis through a semipermeable cellophane membrane the rate of cleavage of the ester bond between the antibiotic and polymeric carrier in the following model media: (a) saline, pH 7.3, 37°C; (b) glycine buffer solution, pH 2.0, 37°C. We found (Table 3) that the hydrolysis of **IIIa** in both media occurs at a noticeable rate even in the first hours of the reaction. As expected, at pH 2.0 the reaction is faster: 58% of the antibiotic is eliminated in 7 h and 84%, in 24 h. In saline, the degree of hydrolysis of **IIIa** is 44% in 7 h and 69% in 24 h.

The relatively high rate of hydrolysis of **IIIa** at both pH 2.0 and pH 7.3, in combination with the high antimicrobial activity of the preparation, indicate that the chosen approach to development of Oxacillin preparations of prolonged effect for both peroral and parenteral administration shows much promise.

EXPERIMENTAL

N-Vinylpyrrolidone was purified by threefold vacuum distillation from granulated KOH (polymerization inhibitor) in the presence of KU-2 cation-exchange resin sorbing amine impurities present in VP. The fraction boiling at 75–76°C/5–6 mm Hg was collected. Found: n_D^{20} = 1.5110, d_4^{20} = 1.0430 g cm^{-3}. Published data: n_D^{20} = 1.5130, d_4^{20} = 1.0458 g cm^{-3}. Found: molecular refraction R = 31.88 cm^3 mol^{-1}; calculated: R = 31.65 cm^3 mol^{-1}.

2-Hydroxyethyl methacrylate (Fluka) was distilled twice in a vacuum from molecular sieves in the presence of bis(naphthoquinonyl)-*p*-phenylenediamine (polymerization inhibitor). The fraction boiling at 87°C/5 mm Hg was collected. Found: n_D^{25} = 1.4500, d_4^{25} = 1.069 g cm^{-3}. Published data: n_D^{25} = 1.4505,

Table 2. Compositions and antistaphylococcus activity of polymeric Oxacillin esters

Copolymeric carrier	m_2, mol %	Ester	Yield, %	m_3	m_4	Oxacillin content, wt %		MBcC,* μg ml^{-1}	
				mol %		UV spectroscopy	iodometric titration	*St. aureus* 209 P	*St. aureus* 6538 P
Ic	25.8	**IIIa**	39.8	17.0	8.8	31.7	30.1	0.0003	0.003
Ib	29.4	**IIIb**	43.4	18.9	10.5	35.4	32.8	Not determined	
Oxacillin sodium salt (control)							92.5	0.0001	0.001

* (MBcC) Minimal bactericidal concentration recalculated to the Oxacillin content in the preparation.

d_4^{25} = 1.077 g cm^{-3}. Found: R = 32.68 cm^3 mol^{-1}; calculated: R = 32.62.

The initiator, azobis(isobutyronitrile) (AIBN), was recrystallized three times from chloroform–ethanol, 1 : 5. Yield of purified AIBN 76.2%, mp 103°C. Published data: mp 103°C.

Dimethylformamide was purified by the standard procedure [7]. Absolute 2-propanol, DCC (Fluka), and Oxacillin sodium salt (iodometric activity 925 μg mg^{-1}) were used without additional purification.

VP–HEMA copolymer Ib. An 80-ml glass ampule treated with live steam and dried was charged through a funnel with 0.121 g of AIBN and then with a mixture of 2 ml of VP, 0.58 ml of HEMA, 4 μl of mercaptoethanol, and 42 ml of 2-propanol. The ampule was purged with argon, sealed, and placed in a thermostat kept at 60°C. After heating for 24 h, the ampule was removed from the thermostat, cooled, and opened. The viscous transparent polymerization product was poured dropwise with stirring into a beaker containing 300 ml of diethyl ether. The precipitated copolymer was collected on a glass frit, washed with fresh portions of ether, and dried in a vacuum without heating to constant weight. Yield 1.71 g (63.2%). Found: N 8.48%.

Synthesis of Oxacillin from its sodium salt. Oxacillin sodium salt (2.5 g) was dissolved in 30 ml of water. The solution was transferred into a 250-ml separating funnel, and 50 ml of chloroform was added. To the aqueous layer, 1 N HCl was added dropwise, and the contents were shaken until the white precipitate in the aqueous layer disappeared. After the precipitation in the aqueous layer was complete, the acidification was stopped. The chloroform layer was separated, washed with three 30-ml portions of water, and dried over anhydrous sodium sulfate for 1 day at room temperature. The chloroform layer was separated, the solvent was removed on a rotary evaporator, and the residue was dried in a vacuum. Yield 1.78 g (78.4%). Iodometric activity 920 μg mg^{-1}. Found: S 7.84%; calculated: S 7.98%.

Polymeric Oxacillin ester IIIa. VP–HEMA copolymer **Ic** (0.5 g) was dissolved in 5 ml of DMF, and 0.445 g of dry Oxacillin was added. The mixture was stirred at cooling with an ice–salt mixture for 30 min, and a solution of 0.3 g of DCC in 3 ml of DMF was added. The solution was stirred for 2 h with cooling (0–5°C) and then for 5 h at room temperature. The mixture was left overnight in a refrigerator, after which the precipitate of dicyclohexylurea was filtered off, and the solution was poured into acetone to precipitate the reaction product (in so doing, unchanged Oxacillin, which is readily soluble in acetone, remained in the solution). After drying, 0.37 g (39.8%) of the water-soluble polymeric Oxacillin ester was obtained. The bound Oxacillin content was 31.7 wt % according to UV data and 30.1 wt % according to iodometric titration.

Table 3. Hydrolysis of polymeric Oxacillin ester **IIIa** at 37°C

Time from start of reaction, h	Degree of hydrolysis, %	
	pH 7.3	pH 2.0
1	12	27
2	21	36
3	29	44
4	34	47
5	37	50
6	40	54
7	44	58
24	69	84

The UV spectra of aqueous solutions of Oxacillin sodium salt, polymeric Oxacillin esters **IIIa** and **IIIb**, and copolymer **Ic** were recorded on a Specord M-40 spectrophotometer. The IR spectra of copolymer **Ic** and polymeric Oxacillin ester **IIIa** were measured on a Bruker IFS spectrometer; samples were prepared as films from chloroform solutions.

The molecular weights of copolymers **Ia**–**Ic** were determined by a sedimentation–diffusion procedure described elsewhere [2].

Hydrolysis of polymeric Oxacillin ester **IIIa** was studied in glycine buffer (pH 2.0) and saline (pH 7.3) at 37°C using the procedure described in [8].

The iodometric activity of Oxacillin and its polymeric esters was determined according to [6].

The antimicrobial activity of Oxacillin sodium salt and polymeric Oxacillin ester **IIIa** was studied by the method of tenfold serial dilutions in a liquid culture medium (meat–peptone broth, pH 7.0) [4]. The bacteria were grown for 18 h. The microbial load was 5×10^5 microbial bodies per milliliter.

CONCLUSIONS

(1) Conditions were found for preparing low-molecular-weight water-soluble *N*-vinylpyrrolidone–

2-hydroxyethyl methacrylate copolymers with a high (up to 33.4 mol %) content of 2-hydroxyethyl methacrylate units.

(2) From these copolymers, polymeric Oxacillin esters containing 30–33 wt % incorporated antibiotic and showing high antistaphylococcus activity *in vitro* were prepared.

(3) The hydrolysis of the polymeric Oxacillin ester with a molecular weight of 31000 Da at 37°C in model systems (glycine buffer, pH 2.0; saline, pH 7.3) was studied. In both systems, the hydrolysis of the polymeric ester is fairly fast: The degree of hydrolysis in 24 h is 84% in glycine buffer and 69% in saline.

ACKNOWLEDGMENTS

The study was financially supported by a Grant of the RF Ministry of Science and Education for support of leading scientific schools (no. NSh-1823.2003.3).

REFERENCES

1. Panarin, E.F. and Ushakova, V.N., *Polimery meditsinskogo naznacheniya* (Polymers for Medicine), Plate, N.A. and Krentsel', B.A., Eds., Moscow: Inst. Neftekhimicheskogo Sinteza, Ross. Akad. Nauk, 1988, pp. 66–94.
2. Solovskii, M.V., Tarabukina, E.B., Shpyrkov, A.A., *et al.*, *Zh. Prikl. Khim.*, 2005, vol. 78, no. 4, pp. 642–646.
3. Hulme, B. and Hardwicke, I., *Clin. Sci.*, 1968, vol. 34, pp. 515–529.
4. Navashin, S.M. and Fomina, I.P., *Ratsional'naya antibiotikoterapiya* (Rational Therapy with Antibiotics), Moscow: Meditsina, 1982.
5. Solovskii, M.V., Nikol'skaya, N.V., and Zaikina, N.A., *Khim.-Farm. Zh.*, 2005, no. 2, pp. 16–19.
6. Alicino, I.F., *Anal. Chem.*, 1961, vol. 33, pp. 648–649.
7. *Laboratorni technica organicke chemie*, Keil, B., Ed., Prague: Ceskoslov. Akad. Ved, 1963.
8. Solovskii, M.V., Nikol'skaya, N.V., and Zaikina, N.A., *Khim.-Farm. Zh.*, 2002, no. 2, pp. 9–13.

ISSN 1070-4272. Russian Journal of Applied Chemistry, 2006, Vol. 79, No. 1, pp. 133–136. © Pleiades Publishing, Inc., 2006.
Original Russian Text © I.L. Beilin, V.P. Arkhireev, S.S. Galibeev, 2006, published in Zhurnal Prikladnoi Khimii, 2006, Vol. 79, No. 1, pp. 135–138.

MACROMOLECULAR CHEMISTRY AND POLYMERIC MATERIALS

Copolymerization of Cyclic Carbonates with Isocyanates under Anionic Initiation Conditions and Structure of the New Copolymers

I. L. Beilin, V. P. Arkhireev, and S. S. Galibeev

Kazan State Technological University, Kazan, Tatarstan, Russia

Received June 20, 2005

Abstract—The possibility of preparing polyamido esters from propylene carbonate and 2,4-toluene diisocyanate in the presence of *N*-methylpyrrolidone was examined. The mechanism of the reaction of the starting monomers and the structure of the resulting copolymers were determined. The properties of the copolymers were studied.

DOI: 10.1134/S1070427206010277

Along with urethane formation, much attention is given today to homo- and copolymerization of isocyanates under the conditions of anionic initiation. Of particular interest are copolymers of isocyanates with compounds of other classes (aldehydes, ketones, alkenes, etc.) [1]. Such polyamido esters (PAEs) can be used as coatings on glass, steel, and fabric supports, as films, and as fibers [2, 3]. Existing procedures for preparing polycarbonates and their copolymers are complex and time-consuming, require strict observance of the prescribed conditions and also high vacuum or elevated temperatures, and involve the use of organic solvents [4], which negatively affects the cost of the polymer and items thereof. At the same time, these materials have unique properties and in many cases are indispensable. Therefore, an urgent problem is development of procedures for preparing PAEs at atmospheric pressure and moderate temperatures. We showed in [5–7] that isocyanates in the presence of alkali metal lactamates and tertiary amines can induce ring opening in many heterocyclic compounds (lactams, lactones, oxiranes) with the formation of alternating copolymers.

In this study we examined the copolymerization of propylene carbonate (PC), 2,4-toluene diisocyanate (TDI), and *N*-methylpyrrolidone (*N*-MP). The synthesis was performed at 20°C; the monomer ratio in the starting mixture was widely varied. The catalyst (triethylamine, TEA) concentration was 0.01 mol %. The amount of the unchanged monomer was determined by extraction of the polymer in a Soxhlet apparatus for 8 h.

The reaction was monitored by ^{1}H NMR spectroscopy with a Tesla-100 spectrometer operating at 100 MHz (solvent and internal reference acetone-d_6). The middle-IR spectra of the copolymers were recorded on a Bruker FT-IR spectrophotometer; samples were prepared as KBr pellets. The elemental analysis was performed with a CNH-3 analyzer (oxidation at 1050°C). Gel-chromatographic studies were made with a Waters-150 C gel chromatograph equipped with Styrogel HR 10^3–10^6 Å columns at 25°C; eluent THF, flow rate 2 ml min^{-1}.

The reaction rate constants were determined according to [8]. To optimize a kinetic study of the ternary copolymerization, we used the simplex-lattice experimental design. As approximating polynomial we used the third-order Scheffe model.

Thermal analysis of samples was performed on an MOM Q-1500 derivatograph (Hungary) at a heating rate of 3 deg min^{-1}.

To determine the physicomechanical characteristics of the materials based on PC, TDI, and *N*-MP, we prepared films of these materials by chemical forming. As solvent for the monomers we used acetone. The breaking stress σ_b was determined with an MR-500T-2 tensile-testing machine at 20 ± 2°C. The velocity of mobile clamps was 100 mm min^{-1}.

The IR spectrum of the TDI–PC–*N*-MP terpolymer contained absorption bands absent in the spectrum of the starting monomers, cm^{-1}: 1704 and 1412 (stretching vibrations of the carbonyl group in tertiary amides formed by cleavage of the isocyanate group across

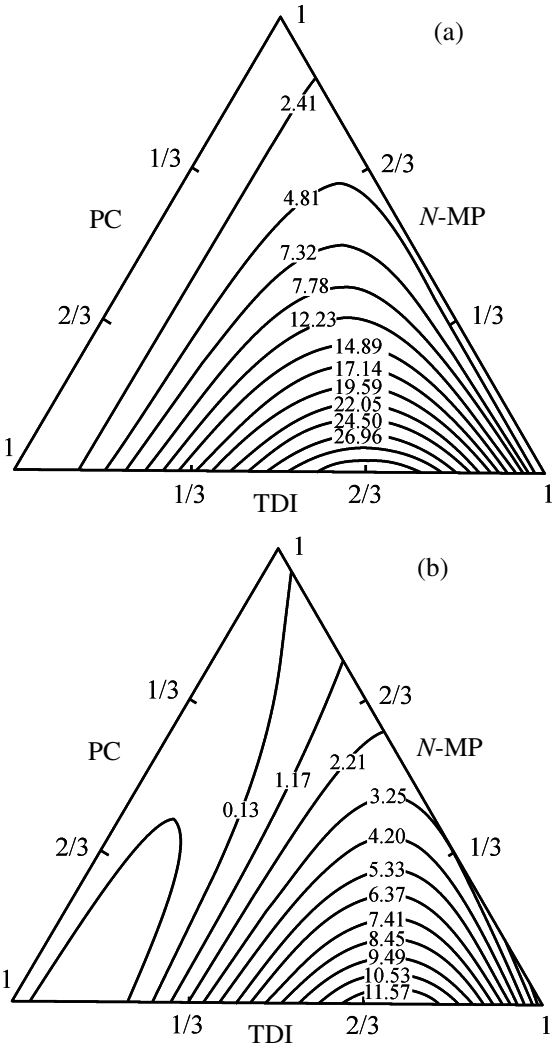


Fig. 1. Lines of (a) equal rates ($\times 10^6$ mol l^{-1} s^{-1}) and (b) equal rate constants ($\times 10^4$ l mol^{-1} s^{-1}) of copolymerization of PC, TDI, and *N*-MP (mole fraction scale).

Table 1. Copolymer yield in the reaction of TDI with PC and *N*-MP

Monomer ratio in the starting mixture, mol %			Yield, wt %
TDI	PC	*N*-MP	
60	20	20	95
40	40	20	84
40	20	40	81
20	40	40	46
20	60	20	48
20	20	60	40

the N=C bond), 1304 (C–N stretching vibrations in amides), 1216 (C–O stretching vibrations in esters), 1066 (C–O–C stretching vibrations in aliphatic esters; this band is indicative of the cleavage of PC), and also 2926 and 2860 (CH stretching vibrations in CH_2 groups). This pattern shows that the copolymerization involved both monomers.

The spectrum does not contain bands at 1692 (C=O stretching vibrations in five-membered lactams), 1270, and 865 cm^{-1} (C–O vibrations in cyclic ethers). Homopolymerization of isocyanates in the presence of tertiary amines is possible, but homopolymerization of PC and *N*-MP under these conditions was not observed. However, the anion generated by cleavage of the isocyanate group is highly reactive and apparently attacks the carbonate or lactam ring, causing its cleavage. The spectrum does not contain bands characteristic of uretidinedione (1780 cm^{-1}) and triisocyanurate (1720 cm^{-1}) rings, which indicates that dimers and trimers of TDI are not formed in the course of the copolymerization [9–11].

The highest rates and rate constants at low (5–10%) conversions (Fig. 1) are observed at the monomer molar ratio in the starting mixture PC : TDI : *N*-MP = 25 : 65 : 10. This kinetic pattern suggests formation of an alternating macromolecule in the copolymerization.

The copolymer is formed in a high yield (Table 1). With an excess of TDI in the starting mixture, polyisocyanate and also (as TDI is a bifunctional agent) branched and partially cross-linked structures are apparently formed on the ends of the macromolecule. This is indirectly confirmed by the fact that the copolymer solubility in organic solvents (dimethylformamide, dimethyl sulfoxide, etc.) becomes worse with an increase in the isocyanate content. With TDI taken in deficiency, excess PC and *N*-MP do not participate in the copolymerization and are removed in the course of the product purification. With a deficiency of one of the heterocycle, after its exhaustion the reaction continues as binary (PC–TDI or *N*-MP–TDI) copolymerization. The number-average molecular weight of the copolymers, according to gel permeation chromatography, is 2900–21 400.

The relative changes in the content of functional groups, monitored by ^1H NMR spectroscopy, apparently determine the composition of the reaction product. At equal excess of both heterocycles relative to TDI in the starting mixture (molar ratio TDI : PC : *N*-MP = 10 : 45 : 45), three carbonate rings are opened per lactam ring. The analytical data (percentage of C, H, N, O) are virtually fully consistent with the assumption that the copolymer contains three PC units

Table 2. Characteristics of the thermal stability of the copolymers obtained*

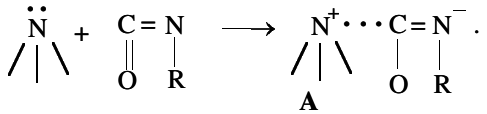
Monomer ratio in starting mixture, mol %			$T_{\Delta m,5}$	$T_{\Delta m,10}$	$T_{\Delta m,50}$	$T_{o.d}$	T_d
TDI	PC	*N*-MP	°C				
100	0	0	294	316	413	288	356
20	0	80	254	281	406	270	325
20	80	0	266	294	404	269	326
20	40	40	288	317	419	310	375
20	60	20	291	322	428	318	386
20	20	60	284	316	415	308	370

* ($T_{\Delta m,5}$, $T_{\Delta m,10}$, $T_{\Delta m,50}$) Temperatures of 5, 10, and 15% weight loss, respectively; ($T_{o.d}$) temperature of degradation onset; and (T_d) degradation temperature.

per *N*-MP unit, with the isocyanate acting as a link:

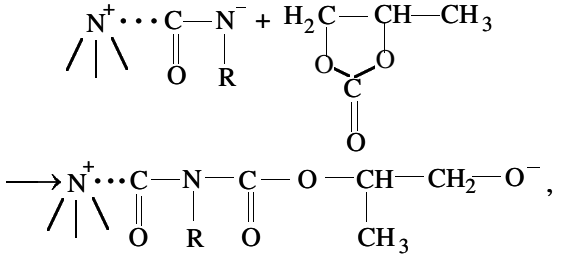
	H	C	N	O	
Found, wt %	6.0	54.4	7.5	32.1	(by difference)
Calculated, wt %	5.7	53.9	7.3	33.1	

Thus, our results in combination with quantum-chemical calculations suggest that the isocyanate component in the ternary system initiates the chain propagation, and PAE is formed by the following mechanism. In the first step (initiation), nucleophilic addition of an anionic catalyst to the electrophilic carbon atom of the isocyanate group yields a charge-transfer complex. This interaction results in a shift of the electron density in the cumulated bond system and formation of anion **A** with the negative charge on N:

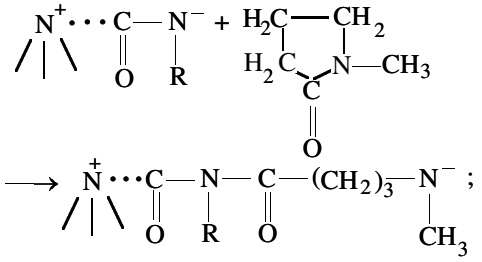


A

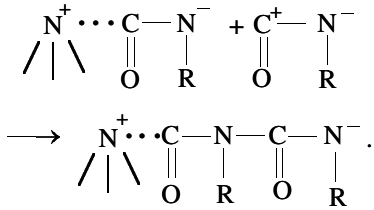
The isocyanate anion adds with the ring opening to propylene carbonate, forming an alkoxide anion:



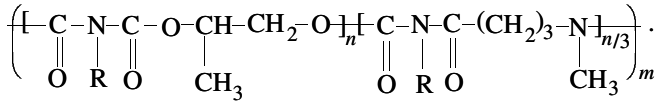
or to the electrophilic carbon atom of lactam:



it can also add to another isocyanate molecule with the formation of a tertiary imide fragment:



The anions formed in the process can further react with isocyanate, PC, or *N*-MP to form an alternating structure which can be represented, to a first approximation, as follows:



The termination in such polymerizing systems occurs, as a rule, by exchange reactions of propagating macroanions with compounds containing a labile hydrogen atom or by chain transfer to the monomer with the formation of terminal amino groups.

The differential thermal and thermogravimetric studies of the copolymers show that their thermal stability depends essentially on the monomer ratio in the starting mixture and is, on the whole, somewhat higher than that of TDI homopolymers and of TDI–PC and TDI–*N*-MP binary copolymers (Table 2).

The feasibility of preparing ready items (including polymer films) by chemical forming is very important. Examination of the strength characteristics of these materials shows that it is possible to prepare materials with the preset properties. In particular, the highest breaking tensile stress of the films, exceeding 40 MPa, was attained at the molar ratio of the components in the starting mixture TDI : PC : *N*-MP ≈ 27 : 67 : 6 (Fig. 2).

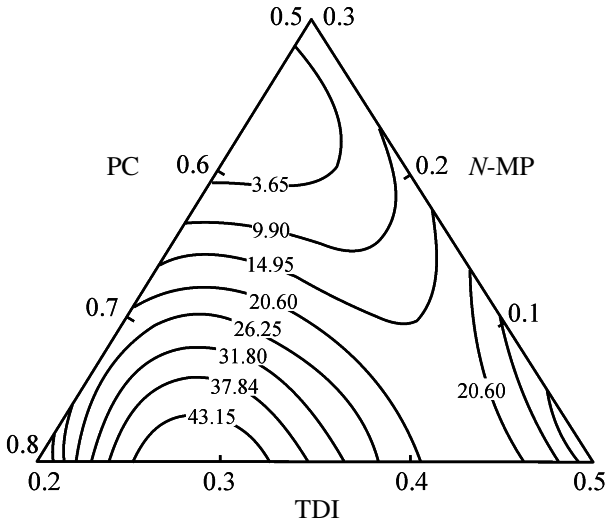


Fig. 2. Composition–property diagram for the breaking tensile stress (MPa) of PC–TDI–*N*-MP copolymers (mole fraction scale).

CONCLUSIONS

(1) Terpolymers of propylene carbonate, 2,4-toluene diisocyanate, and *N*-methylpyrrolidone were prepared in the presence of triethylamine. Although propylene carbonate and *N*-methylpyrrolidone do not homopolymerize under the action of tertiary amines, they readily copolymerize with isocyanates.

(2) The ^{1}H NMR and IR spectra, kinetic data, and elemental analysis suggest that the copolymerization mainly yields high-molecular-weight alternating block copolymers.

(3) The thermal stability (e.g., temperatures of 5, 10, and 50% weight loss; degradation onset and degradation temperatures) and physicomechanical characteristics (e.g., breaking tensile stress of films) of the copolymers can be controlled by varying the monomer ratio in the starting mixture.

REFERENCES

1. *Entsiklopediya polimerov* (Polymer Encyclopedia), Kargin, V.A., Ed., Moscow: Sov. Entsiklopediya, 1974, vol. 2, p. 33.
2. Hopff, H., Müller, A., and Wenger, F., *Die Polyamide*, Berlin: Springer, 1954.
3. Korshak, V.V., *Tekhnologiya plasticheskikh mass* (Technology of Plastics), Moscow: Khimiya, 1985.
4. US Patent 4330481.
5. Spiridonova, R.R. and Galibeev, S.S., *Zh. Prikl. Khim.*, 2003, vol. 76, no. 2, pp. 298–302.
6. Galibeev, S.S., Kochnev, A.M., Spiridonova, R.R., *et al.*, *Plast. Massy*, 2003, no. 8, pp. 17–19.
7. Galibeev, S.S., Arkhireev, V.P., Barnyagina, O.V., *et al.*, *Izv. Vyssh. Uchebn. Zaved., Khim. Khim. Tekhnol.*, 2003, vol. 46, no. 4, pp. 88–90.
8. Sutyagin, V.M., *Eksperimental'nye metody issledovaniya polimerizatsii i sopolimerizatsii* (Experimental Methods for Studying Polymerization and Copolymerization), Tomsk: Tomsk. Politekh. Inst., 1988.
9. Pentin, Yu.A. and Vilkov, L.V., *Fizicheskie metody issledovaniya v khimii* (Physical Methods in Chemistry), Moscow: Mir, 2003.
10. Bellamy, L.J., *The Infra-Red Spectra of Complex Molecules*, New York: Wiley, 1957.
11. *Chemical Applications of Spectroscopy*, West, W., Ed., New York: Interscience, 1956.

ISSN 1070-4272. Russian Journal of Applied Chemistry, 2006, Vol. 79, No. 1, pp. 137–141. © Pleiades Publishing, Inc., 2006.
Original Russian Text © S.E. Mitrofanova, E.N. Girfanova, I.Yu. Averko-Antonovich, E.N. Cherezova, 2006, published in Zhurnal Prikladnoi Khimii, 2006, Vol. 79, No. 1, pp. 139–143.

MACROMOLECULAR CHEMISTRY AND POLYMERIC MATERIALS

New Oligomeric Thioether Antioxidants for Polymers

S. E. Mitrofanova, E. N. Girfanova, I. Yu. Averko-Antonovich, and E. N. Cherezova

Kazan State Technological University, Kazan, Tatarstan, Russia

Received June 20, 2005; in final form, November 2005

Abstract—Polyfunctional oligomeric antioxidants with a sterically hindered phenolic fragment were prepared. The influence of these antioxidants on oxidation and degradation of SKI-3 rubber was analyzed.

DOI: 10.1134/S1070427206010289

Unsaturated nature of rubber macromolecular units makes possible processing of rubbers into articles via vulcanization and preparation of technically valuable structural materials thereof, on the one hand, and is responsible for gradual aging of the material, above all, due to oxidation, on the other. Oxidation follows the radical-chain mechanism [1, 2]. The primary oxidation products of the polymer are polymeric peroxy radicals (PRs) and hydroperoxides (HPs).

Chemically, antioxidative stabilization of polymeric materials consists in scavenging of free radicals and hydroperoxides. The most efficient and widely applied PR scavengers are sterically hindered phenols (SHPs) and aromatic amines [3–5]. Hydroperoxides are decomposed by compounds containing sulfur(II) atoms [6]. The researchers' attention is currently focused on stabilizers whose molecules contain several centers able of decelerating oxidation of polymers. They are attractive because of possible synergism of antioxidation effects [7–9].

It should be taken into account that the use of monomeric antioxidants often causes problems due to their volatility, insufficient solubility, and washing out from polymers. At the same time, a number of studies showed that, with polymeric antioxidants eliminating such problems, the functional groups act less efficiently [9]. Oligomeric antioxidants (OAOs) would apparently be the best choice.

In this study, we developed a procedure for synthesis of OAOs whose molecules contain centers able of inhibiting oxidation via scavenging PRs and HPs and examined their stabilizing performance.

EXPERIMENTAL

As reactants served 4-dimethylaminomethyl-2,6-di-*tert*-butylphenol (Mannich base, MB), mp 93–95°C, and a sulfur-containing oligoether TPM-2 [TU (Technical Specifications) 38 103 636–87; dynamic viscosity 1.9 Pa s at 25°C] with 3.42 wt % terminal SH groups.

The antioxidants were synthesized by the following procedure. A flask equipped with a stirrer, a water-cooled reflux condenser, a thermometer, and a bubbler was charged with TPM-2 and MB (when the reaction was run in a solution, appropriate solvent was added). The amount of MB taken for the reaction was governed by the preset number of the SH groups to enter into the reaction (the calculations were carried out for 100, 75, 50, and 25% conversions of the SH groups in the oligomer). The reaction mixture was stirred at 100–140°C in a nitrogen flow. The reaction was monitored from evolution of dimethylamine absorbed by 0.1 N H_2SO_4 with indicator (Methyl Orange). The completion of the process was judged from ceased evolution of dimethylamine.

The mass fraction of the SH groups was determined by a laboratory technique according to GOST (State Standard) 12 812–80.

The resulting stabilizers were introduced into 5% solutions of SKI-3 (hereinafter, the weight percentage) in toluene and stirred at room temperature until complete homogenization, whereupon the solvent was vacuum-evaporated.

Self-oxidation of the polymer was run by the procedure from [10] under oxygen (p_{O_2} = 250 mm Hg) at 165°C (polymer weighed portion 0.1 g).

The oxidation, degradation, and mass loss temperatures of the polymer were determined by differential thermal (DTA) and thermogravimetric (TGA) analyses on an MOM (Hungary) derivatograph; the heating rate for the samples was 5 deg min^{-1}.

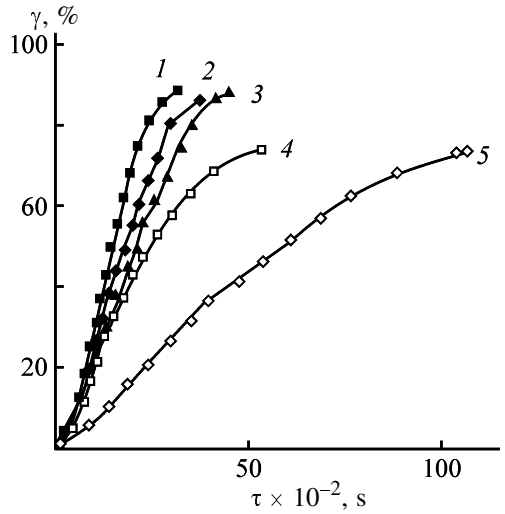


Fig. 1. Influence of temperature on the kinetics of the reaction between TPM-2 and MB in the melt. (γ) Conversion and (τ) time, the same for Fig. 2. Ratio of reacting centers 1 : 1; the same for Fig. 2. Temperature, °C: (*1*) 140, (*2*) 130, (*3*) 120, (*4*) 110, and (*5*) 100.

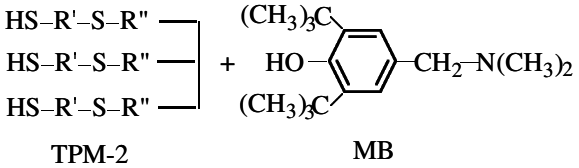
The IR spectra were recorded at 4000–400 cm^{-1} on a 16 PC-FT-IR Perkin–Elmer instrument. To study accumulation of the carbonyl groups from 10% solution of SKI-3 in toluene, containing the stabilizer, we prepared 1.0–1.2-mm-thick films on polyethylene terephthalate support. The films were subjected to thermooxidative aging in air under static conditions at 100°C.

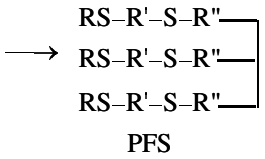
As the base in synthesis of polyfunctional antioxidants served a sulfur-containing polyether with SH terminal groups, TPM-2. This choice was determined by the presence in TPM-2 of sulfide and thiol groups, able of inhibiting oxidation of polymers by decomposing HPs. Also, reactive terminal thiol groups can be used for introduction into the oligomer molecule of a second center of antioxidative stabilization, a PR scavenger (in our case, SHP fragment).

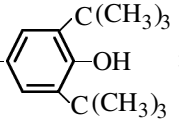
Table 1. Temperature dependence of the rate constant k and preexponential factor A in the reaction between TPM-2 and MB

T, °C	$k \times 10^4$	$A \times 10^4$
	mol l^{-1} s^{-1}	
100	2.3562	2.416
110	4.9218	5.044
120	8.3252	8.526
140	13.9103	14.229

Polyfunctional stabilizers (PFSs) were synthesized by the reaction of TPM-2 and MB:





where R = H, 

;

R' = $CH_2CH_2OCH_2OCH_2CH_2$; and R" = $[CH_2CH\cdot(CH_3)O]_n$.

We chose MB as oxybenzylating agent because of a fairly high reactivity of this class of compounds in substitution of dimethylamino group [11].

To reveal the best conditions for synthesis, we examined how the rate of the reaction between TPM-2 and MB is influenced by the reaction conditions: temperature, presence of the solvent, and solvent polarity. We found that, in melt, this reaction goes at appreciable rate at temperatures above 80°C. Our experimental data showed that the process is substantially accelerated by rising temperature to 120–140°C (Fig. 1).

Based on the kinetic data, we determined the reaction rate constants at different temperatures (Table 1), as well as the preexponential factors and the activation energy of the process, which was estimated at 77.8 kJ mol^{-1}. We found that the reaction between TPM-2 and MB is a first-order reaction with respect to each of the reactants [12].

The activity of 2,6-dialkyl-substituted oxybenzylated agents in reactions with nucleophiles is determined [13] by the possibility of formation at elevated temperature of 2,6-dialkyl-4-hydroxybenzyl carbocation. Under assumption that the reaction goes through deamination, we can suggest that the rate of the process will be affected not only by the temperature but also by the solvent polarity. Our experimental data showed that, in nonpolar solvents (ethylbenzene, decane) at 130°C, the conversion of the reactants attains a maximum within 3–4 h (Fig. 2).

When the process is run in polar solvents (2-buta-

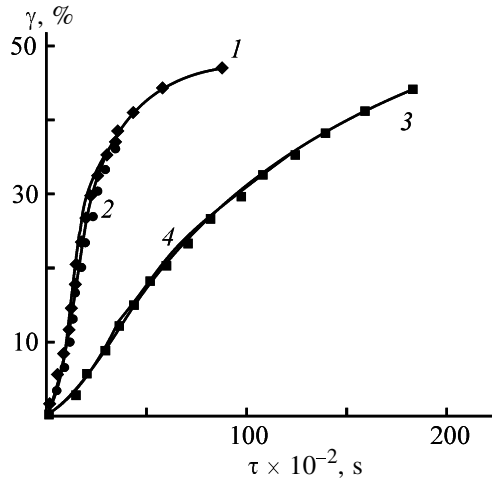


Fig. 2. Kinetics of the reaction between TPM-2 and MB at 130°C as influenced by the solvent polarity. (*1*) DMF, (*2*) 2-butanol, (*3*) decane, and (*4*) ethylbenzene.

nol, DMF), the reaction time is reduced to 1.5 h. The fact that the reaction rate is influenced by the solvent polarity confirms that the reaction goes via a polar transition state.

To elucidate how the number of the SHP fragments introduced into the molecules of PFSs affects their stabilizing performance, we varied the MB proportion in such a way that 25, 50, 75, and 100% of the SH groups of TPM-2 participated in the reaction. The process was run in melt at 120–130°C and was terminated after dimethylamine ceased to evolve. When the process was complete, the chromatogram of the reaction mixture (Silufol-254 plate, eluent benzene : acetone = 5 : 1) did not exhibit a spot characteristic of MB (R_f = 0.1). We determined the content of the SH groups in the resulting PFSs (Table 2). It is seen that the theoretically calculated and experimental data are close, which suggests complete conversion of MB.

The DTA data for PFSs suggest their fairly high stability: The mass loss onset temperature is close to 250°C.

The antioxidative performance of PFSs was studied for SKI-3 rubber samples. To this end, we utilized the manometric method of measuring the induction periods of oxidation of polymers [2], as well as IR spectroscopy, DTA, and TGA.

The manometric method is based on studying the kinetics of thermal oxidation [10]. It is underlain by oxygen absorption by the polymer when heated in air or under oxygen. The induction period is the period before the onset of oxygen absorption by the polymer. Our experimental data showed that, when the concentration of the initial TPM-2 introduced was 1–5 wt parts per 100 wt parts of SKI-3, the induction period before the onset of SKI-3 oxidation increased to a certain extent (Table 3). This suggests that TPM-2 exhibits a weak antioxidative power. Introduction into the TPM-2 molecule of an SHP fragment substantially increases the induction period of the

Table 2. Content of the SH groups in the SHP–S oligomers synthesized

Preset conversion, %, of SH groups in TPM-2	Residual amount of SH groups after reaction with MB, %	
	found	calculated
100	0.00	0.10
75	0.80	0.84
50	1.71	1.75
25	2.56	2.67
0	3.40	3.42

Table 3. Induction periods τ of thermal oxidation of SKI-3 rubber stabilized by PFS. P_{O_2} = 250 mm Hg, T = 165°C

Antioxidant	Wt parts of PFS per 100 wt parts of rubber	τ, min
–	–	30
TPM-2	1	30
	2	40
	3	45
	4	50
	5	55
TPM-2–SHP_{25}*	1	65
	2	95
	3	125
	4	127
	5	128
TPM-2–SHP_{50}*	1	85
	2	115
	3	155
	4	160
	5	160
TPM-2–SHP_{75}*	1	95
	2	105
	3	150
	4	155
	5	155
TPM-2–SHP_{100}*	1	91
	2	100
	3	140
	4	140
	5	140

* Conversion of SH groups 25, 50, 75, and 100%, respectively.

Table 4. Thermal stability of SKI-3 rubber as influenced by the amount of the SHP fragments in the PFS (3 wt parts of SHP–S in TPM-2 per 100 wt parts of rubber)*

Oligomer	T_{ox}	T_d	$T_{m.l.}$, °C			
	°C		onset	5%	10%	50%
TPM-2	225	335	250	309	325	363
TPM-2–SHP_{50}	256	345	250	312	336	378
TPM-2–SHP_{100}	262	350	250	323	345	388

* T_{ox} is the rubber oxidation temperature; T_d, rubber degradation temperature; and $T_{m.l.}$, rubber mass loss temperature.

rubber oxidation. In this connection, two essential points should be mentioned. First, the induction period of SKI-3 oxidation linearly increases with increasing concentration of the antioxidant within 1–3 wt parts per 100 wt parts of the rubber and attains saturation with further increase in the PFS concentration. Second, replacement of all the SH groups in TPM-2 by SHP–S fragments is accompanied by a certain decrease in the induction period of oxidation. This may be due to the synergism of the antioxidative effects in the presence of thiol groups. The antioxidative power of the stabilizer seems to be at a maximum at the 1 : (1–0.5) ratio of the SHP–S to –SH groups in the stabilizer molecule.

The fact that the antioxidative power is improved upon introducing an SHP fragment into the TPM-2 molecule is also demonstrated by the IR spectroscopic monitoring of the SKI-3 oxidation [14]. The IR spectra suggest that thermal oxidation of SKI-3 is accompanied by a decrease in the intensity of absorption near 1666 ($\nu_{C=C}$) and 890 cm^{-1} ($\nu_{H-C=C}$) and appearance of bands at 1720 ($\nu_{C=O}$) and 3475 cm^{-1} (ν_{OH}).

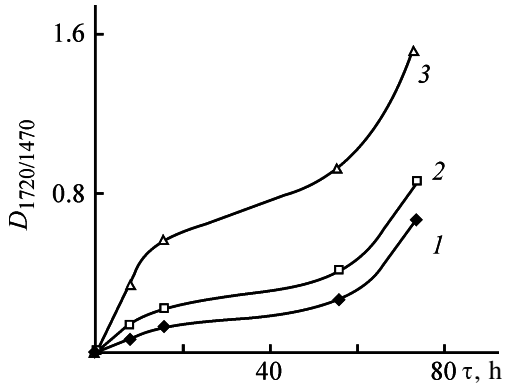


Fig. 3. Ratio of the optical densities D of the absorption bands of the C=O (1720 cm^{-1}) and CH_2 (1470 cm^{-1}) groups as influenced by the oxidation time τ of the SKI-3 films (100°C, air). (*1*) TPM-2–SHP_{100}, (*2*) TPM-2–SHP_{50}, and (*3*) TPM-2 (content of PFS 3 wt parts per 100 wt parts of SKI-3).

With increasing content of the SHP fragments in the PFS oligomer, the time before appearance of the bands at 3475 (ν_{OH}) and 1720 cm^{-1} ($\nu_{C=O}$) tends to increase, and the growth of their intensity is decelerated. As the band characterizing SKI-3 oxidation we chose the absorption band at 1720 cm^{-1}. The band at 1470 cm^{-1} (δ_{CH_3} and δ_{CH_2}) served as internal reference. The extent of the rubber oxidation at the preset thermal oxidation time was estimated from the ratio of the optical densities at 1720 and 1470 cm^{-1}. The experimental results are illustrated by Fig. 3.

The thermal stability of the PFS-containing polymer was estimated by TGA [15]. The rubber stability was estimated from the oxidation and degradation temperatures at which the polymer loses 5, 10, and 50% of the initial mass, as estimated at a constant heating rate.

Our experimental data suggest (Table 4) that, with increasing amount of the SHP fragments introduced into TPM-2, the SKI-3 oxidation temperature increases relative to the rubber free from SHP-S fragments. Introduction of PFS into SKI-3 does not markedly affect the mass loss onset temperature of the rubber, but the mass loss is decelerated.

CONCLUSIONS

(1) Antioxidants for carbon-chain polymers with different ratios of the polymer oxidation inhibition centers, sulfide sulfur and sterically hindered phenolic fragments, were synthesized by the reaction of terminal HS groups of the oligomeric thioether TPM-2 with *N,N*-dimethyl-3,5-di-*tert*-butyl-4-hydroxybenzylamine.

(2) Polyfunctional additions exhibit high antioxidative and themostabilizing power in SKI-3 rubber stabilization. The induction period of thermal oxidation of SKI-3 and the rate of accumulation of the carbonyl groups in the rubber vary with the ratio of the

different inhibition centers, sulfide sulfur : sterically hindered phenolic fragment.

REFERENCES

1. Emanuel', N.M., *Usp. Khim.*, 1979, vol. 48, no. 12, pp. 2113–2158.
2. Denisov, E.T., *Usp. Khim.*, 1978, vol. 47, no. 6, pp. 1090–1118.
3. Gurvich, Ya.A., Zolotarevskaya, L.K., and Kumok, S.T., *Fenol'nye stabilizatory: tematicheskii obzor* (Phenol-Based Stabilizers: Topical Review), Moscow: TsNIITEneftekhim, 1978.
4. Moiseev, V.V., Kosovtsev, V.V., Polukhin, A.N., and Poluektov, I.T., *Kauchuk Rezina*, 1991, no. 1, pp. 10–13.
5. Kavun, S.M., *Kauchuk Rezina*, 1994, no. 5, pp. 32–43.
6. Cherkasova, O.A. and Mukmeneva, N.A., *Zh. Obshch. Khim.*, 1992, vol. 62, no. 10, pp. 2161–2186.
7. Aslanov, A.D., Zolotova, N.V., Denisov, E.T., and Kuliev, F.A., *Neftekhimiya*, 1982, vol. 22, no. 3, pp. 394–399.
8. US Patent 3310587.
9. Emanuel', N.M. and Buchachenko, A.L., *Khimicheskaya fizika molekulyarnogo razrusheniya i stabilizatsii polimerov* (Chemical Physics of Molecular Degradation and Stabilization of Polymers), Moscow: Nauka, 1988.
10. Piotrovskii, K.B. and Tarasova, Z.N., *Starenie i stabilizatsiya sinteticheskikh kauchukov i vulkanizatorov* (Aging and Stabilization of Synthetic Rubbers and Vulcanizers), Moscow: Khimiya, 1980.
11. Tuktarova, L.A., Sterically Hindered Phenolic Mannich Bases, *Cand. Sci. Dissertation*, Ufa, 1984.
12. Bairamov, V.M., *Osnovy khimicheskoi kinetiki i kataliza* (Fundamentals of Chemical Kinetics and Catalysis), Moscow: Akademiya, 2003.
13. Rutman, G.I., Study, Development, and Introduction of a Complex of Phenolic Antioxidants Based on 2,6-Di-*tert*-butylphenol, *Cand. Sci. Dissertation*, Kazan, 1983.
14. Braun, D., Cherdron, H., and Kern, W., *Praktikum der makromolekularen organischen Chemie*, Heidelberg: Alfred Huthig, 1971.
15. Reich, L. and Lewy, D., *Novoe v metodakh issledovaniya polimerov* (Advances in Methods for Studying Polymers), Rogovin, Z.A., Ed., Moscow: Mir, 1968, pp. 129–148.

ISSN 1070-4272. Russian Journal of Applied Chemistry, 2006, Vol. 79, No. 1, pp. 142–145. © Pleiades Publishing, Inc., 2006.
Original Russian Text © V.F. Kurenkov, I.N. Nadezhdin, T.A. Zhelonkina, H.-G. Hartan, F.I. Lobanov, 2006, published in Zhurnal Prikladnoi Khimii, 2006, Vol. 79, No. 1, pp. 144–147.

MACROMOLECULAR CHEMISTRY AND POLYMERIC MATERIALS

Stabilization of Kaolin Suspension in the Presence of Copolymers of Sodium 2-Acrylamido-2-methylpropanesulfonate with *N*-Vinylpyrrolidone

V. F. Kurenkov, I. N. Nadezhdin, T. A. Zhelonkina, H.-G. Hartan, and F. I. Lobanov

Kazan State Technological University, Kazan, Tatarstan, Russia
Stockhausen GmbH Company, Krefeld, Germany
Degussa Eurasia Joint-Stock Company, Moscow, Russia

Received May 25, 2005

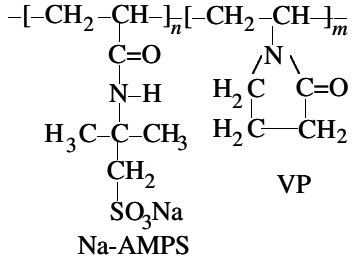
Abstract—The kinetics of sedimentation of kaolin suspension in the presence of copolymers of sodium 2-acrylamido-2-methylpropanesulfonate with *N*-vinylpyrrolidone was studied as influenced by the concentrations, molecular weight, and chemical composition of the copolymer and by the concentration of salts added (NaCl, $CaCl_2$).

DOI: 10.1134/S1070427206010290

Water-soluble polyelectrolytes are widely used to control the stability of dispersion systems [1]. In treatment of natural and waste waters and in concentration and drying of suspensions, the stability of dispersion systems should be decreased and, vice versa, in the case of drilling muds, mortars, and drugs it should be increased. Owing to high flocculation [2], adhesion [3], thickening [4], and complexation properties, copolymers of sodium 2-acrylamido-2-methylpropanesulfonate (Na-AMPS) with *N*-vinylpyrrolidone (VP) show promise for controlling the stability of mineral suspensions. The flocculation properties of Na-AMPS–VP copolymers at their low concentrations ($<2.5 \times 10^{-3}$ wt %) were studied previously using kaolin suspensions, but the data on the stabilization power of these copolymers, which is observed at high concentrations, are lacking. In this study we examined the effect of Na-AMPS–VP copolymers on the stability of kaolin suspensions as influenced by the concentrations, molecular weight (M), and chemical composition of the copolymer and by the concentration of salts added (NaCl, $CaCl_2$).

EXPERIMENTAL

In the experiments we used copolymers of Na-AMPS and VP prepared by radical copolymerization in aqueous solutions by the procedure given in [3]. The resulting polymers were precipitated from aqueous solutions with excess acetone, filtered off, washed with acetone, and dried to constant weight in a vacuum at 50°C. The content of ionic Na-AMPS units in the copolymer of Na-AMPS and VP was determined from the content of sulfur [6]. Since in accordance with the Mark–Houwink equation $M \sim [\eta]$, the molecular weights of the copolymers were calculated from the intrinsic viscosities $[\eta]$ of their solutions, which were measured in a 0.5 M NaCl solution at 30°C on a VPZh-3 capillary viscometer (d_c = 0.43 mm). The properties of copolymers are listed in the table.



The experiments were performed at 20°C with KE-1 brand kaolin (Eleninskoe field), because this dispersion system with the uniform particle size distribution (average particle size 0.2×10^{-6} m) is widely used to evaluate the flocculation properties of water-soluble polymers.

The sedimentation was performed in a 50-ml volumetric cylinder with a ground-glass stopper. The degree of clarification (%) of the kaolin suspension

was determined by the shift of the boundary between the clarified and unclarified fractions of the suspension after mixing by tenfold overturning of the cylinder. The tests were carried out at a concentration of the dispersed phase c_d 5 wt %, which provided distinct boundary between the clarified and unclarified fractions of the suspension in the cylinder in the absence of the copolymer and thus allowed us to compare the rates of sedimentation in the presence of copolymer and without it.

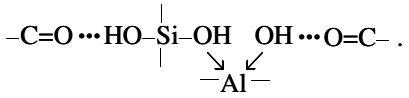
First we studied the effect of the concentration of the dispersed phase c_d (3–10 wt %) on the kaolin sedimentation in the absence of the copolymer. The kinetics of clarification of the kaolin suspension at various c_d is shown in Fig. 1. The sedimentation rate was determined from the slopes of the kinetic curves. As seen from Fig. 1, the rate of kaolin sedimentation decreases with increasing c_d, which is probably due to the effect of hindered sedimentation of the dispersed particles.

The effect of the Na-AMPS–VP flocculant concentration (c_p) on the kaolin suspension sedimentation was studied in the $(0.2–5.0) \times 10^{-3}$ wt % range; here and hereinafter, c_d 5 wt %. The flocculating power D was evaluated as

$$D = (v - v_0)/v_0,$$

where v and v_0 are the sedimentation rates of the kaolin suspension in the presence of the copolymer and without it, respectively.

The dependence of D on c_p is shown in Fig. 2. As seen, the $D = f(c_p)$ dependence passes through a maximum. With increasing c_p in the $(0.2–2.5) \times 10^{-3}$ wt % range, D increases (ascending branch) owing to a decrease in the suspension stability caused by adsorption of the copolymer on the kaolin particles. It is known [7] that the kaolin ($Al_2O_3 \cdot 2SiO_2 \cdot 2H_2O$ with impurities of Fe_2O_3, MnO, Na_2O, K_2O, and TiO_2) particles form hexagons whose basal surfaces are charged negatively at various pH, whereas lateral faces can be either neutral or positively and negatively charged depending on the solution pH. In this study, the experiments were performed at pH 6.8, and adsorption of Na-AMPS–VP copolymer occurred predominantly on the lateral faces of the kaolin particles owing to formation of the hydrogen bonds between the hydroxy groups on the kaolin surface and functional groups of the copolymer:



Properties of Na-AMPS–VP copolymers

Sample no.	Content of ionic units in copolymer, mol %		[η], $cm^3\ g^{-1}$
	Na-AMPS	VP	
1	3.5	96.5	132
2	36.6	63.4	136
3	37.3	62.7	185
4	38.6	61.4	95
5	40.5	59.5	170
6	47.6	52.4	185

In the course of copolymer adsorption, the kaolin particles got bound with macromolecular bridges to form coarse floccules, lost their aggregative stability, and precipitated. As seen from Fig. 2, with further increasing c_p (>2.5×10^{-3} wt %), D decreases (descending branch). This is obviously due to the structuring of the system and attainment of its aggregation and sedimentation stability. Since the flocculation properties at small concentrations of Na-AMPS–VP copoly-

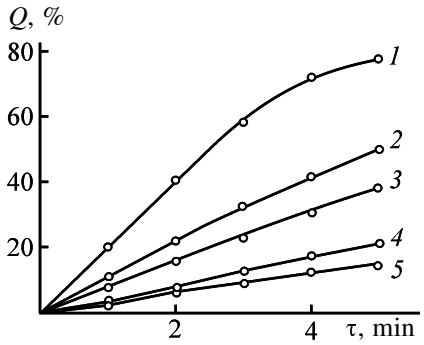


Fig. 1. Degree of clarification of the kaolin suspension Q as a function of time τ. Kaolin content c_d, wt %: (*1*) 3, (*2*) 5, (*3*) 7, (*4*) 9, and (*5*) 10.

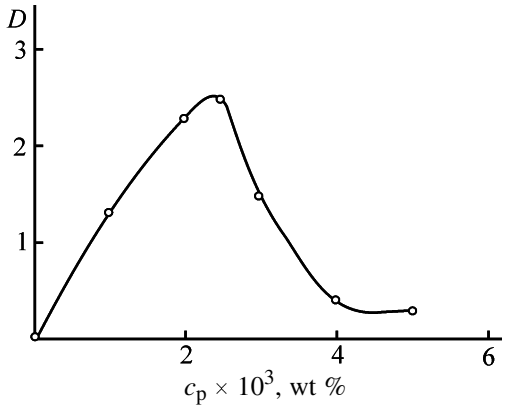


Fig. 2. Flocculation power D as a function of the concentration c_p (wt %) of Na-AMPS copolymer with VP (sample no. 1).

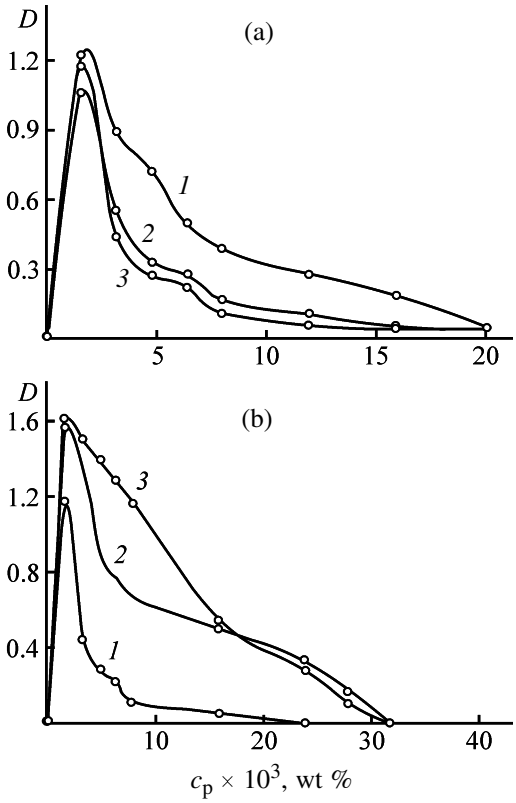


Fig. 3. Flocculation power D as a function of the concentration c_p of Na-AMPS copolymers with various (a) molecular weights M and (b) chemical compositions. Sample nos. (a): (*1*) 3, (*2*) 2, and (*3*) 4; (b): (*1*) 3, (*2*) 5, and (*3*) 6.

mers were studied previously [1], further experiments were performed only at high c_p at which the kaolin suspension is stabilized.

The influence of the chemical composition of the copolymer on the sedimentation of a kaolin suspension was studied using the copolymer samples with similar [η], whereas the content of Na-AMPS units was varied from 37.3 to 47.6 wt % (see table, sample nos. 3, 5, 6). The results of these experiments are shown in Fig. 3a. As seen, at c_p = const the flocculation effect D decreases with decreasing content of the ionic units in the copolymer (Fig. 3a, passing from curve *3* to curve *1*). This effect is observed in a wide concentration range. We assumed that this effect is probably due to a decrease in the effective size $(r^2)^{1/2}$ of macromolecular aggregates owing to weakening of electrostatic repulsion between the similarly charged units along the copolymer chain. This, in turn, decreases the probability of formation of macromolecular bridges between the kaolin particles and thus increases the sedimentation stability of the suspension.

The influence of [η] of Na-AMPS–VP copolymer on D is illustrated in Fig. 3b. The experiments were carried out using the samples of similar compositions, whereas [η] was varied from 95 to 185 $cm^3\ g^{-1}$ (see table, sample nos. 2–4). As seen, at constant c_p, D decreases with increasing [η] in a wide range of c_p (Fig. 3b, passing from curve *3* to curve *1*). Similar effect of the molecular weight of Na-AMPS copolymers with carboxymethyl cellulose at c_p 2.5 wt % on the stabilization of bentonite drilling muds (c 3 wt %) was found previously in [8]. In accordance with [2], at small c_p D increases with increasing M, and, as seen from Fig. 3b, at high c_p D decreases with increasing M. This extremal dependence of D on M well agrees with experimental data on the flocculation of a calcium phosphate suspension in the presence of polyacrylamide [9] and of gold and silver iodide sols in the presence of polyethylene oxide and polyvinyl alcohol [10]. The experimental dependence of the flocculation parameter D on the molecular weight of copolymer M shown in Fig. 3b is predominantly due to the fact that at high c_p the coverage of the kaolin particle surface with copolymer macromolecules increases, and with increasing M the probability of multipoint adsorption of the copolymer on the kaolin particles also increases. The resulting surface layers of the copolymer hinder aggregation of the kaolin particles and thus increase the stability of the kaolin suspension. As seen from Figs. 3a and 3b, the kaolin suspension is stabilized in the c_p range $(2.4–3.2) \times 10^{-2}$ wt %.

In this study we also examined the effect of the ionic strength of the solutions μ (provided by addition of $CaCl_2$ and NaCl) on the sedimentation stability of a kaolin suspension in the presence of Na-AMPS–VP copolymer (sample nos. 3, 5, 6, see table). Our preliminary experiments showed that, in the absence of the copolymer, v_0 slightly decreases with increasing μ, and in further experiments with addition of the copolymer the D values were calculated from v and v_0 determined at similar μ (for both $CaCl_2$ and NaCl). The dependences $D = f(c_p)$ determined in the presence of $CaCl_2$ and NaCl and without them are shown in Fig. 4. As seen from the comparison of experimental data at c_p = const, with increasing μ D increases in a wide range of copolymer concentrations for all the samples studied (Fig. 4, passing from curves *1–3* to curves *4–6* and *7–9*, respectively). It was found [11] that with increasing μ the electrostatic repulsion between the shielded sulfonate anions (Na^+ and Ca^{2+} counterions) along the Na-AMPS–VP copolymer chain decreases. Similarly, the increase in μ decreases the repulsion between the Na-AMPS–VP polyanions and the kaolin surface (ζ potential 4.2 mV); this

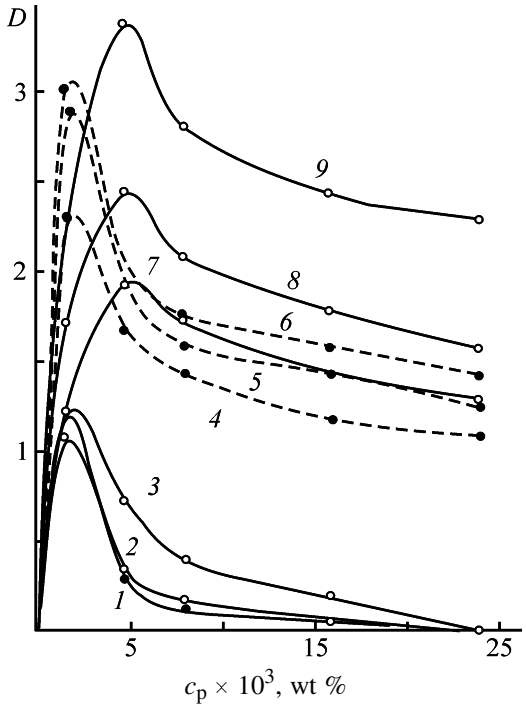


Fig. 4. Flocculation parameter D as influenced by the concentration of Na-AMPS–VP copolymer c_p (*1–3*) in the absence of additives and in the presence of (*4–6*) NaCl (0.5 M) and (*7–9*) $CaCl_2$ (0.5 M). Sample nos.: (*1, 4, 7*) 3, (*2, 5, 8*) 5, and (*3, 6, 9*) 6.

effect prevails over the decrease in D with decreasing $(r^2)^{1/2}$.

As seen from Fig. 4, at μ = const smaller D are observed with $CaCl_2$ as compared to NaCl. This is probably due to stronger binding of Ca^{2+} counterions, as compared to Na^+ cations, with polysulfonate anions [11]. As a result, on substitution of NaCl by $CaCl_2$, $(r^2)^{1/2}$ and the flocculation power of the copolymer both decrease.

CONCLUSIONS

(1) The flocculation effect of copolymers of sodium 2-acrylamido-2-methylpropanesulfonate with *N*-vinylpyrrolidone on a kaolin suspension at a copolymer concentration of $(2–32) \times 10^{-3}$ wt % decreases with increasing concentration and intrinsic viscosity of the copolymer and with decreasing content of 2-acrylamido-2-methylpropanesulfonate units in the copolymer. The kaolin suspension (5 wt %) is completely stabilized at a copolymer concentration of $(2.4–3.2) \times 10^{-2}$ wt %.

(2) The flocculation parameter decreases with a decrease in the ionic strength of the solution (provided by NaCl and $CaCl_2$) and on substitution of NaCl by $CaCl_2$.

REFERENCES

1. Aripov, E.A., Glekel', F.L., and Khamraev, S.S., *Zh. Vses. Khim. O-va. im. D.I. Mendeleeva*, 1989, vol. 34, no. 2, pp. 219–223.
2. Kurenkov, V.F., Sharapova, Z.F., and Khairullin, M.R., *Zh. Prikl. Khim.*, 1999, vol. 72, no. 8, pp. 1374–1378.
3. Shvetsova, S.S., Barkhanova, T.A., Zhelonkina, T.A., and Kurenkov, V.F., *Materialy konferentsii "III Kirpichnikovskie chteniya"* (Proc. Conf. "III Kirpichnikov Lectures"), Kazan: Kazan. Gos. Tekhnol. Univ., 2003, pp. 308–311.
4. Kurenkov, V.F., Sirotkin, R.O., Beryachkova, E.A., and Khairullin, M.R., *Zh. Prikl. Khim.*, 1998, vol. 71, no. 9, pp. 1533–1537.
5. Kurenkov, V.F., Zhelonkina, T.A., and Kovalenko, V.I., *Zh. Prikl. Khim.*, 2005, vol. 78, no. 2, pp. 301–305.
6. Charlot, G., *Les methods de la chimie analytique. Analyse quantitative minerale*, Paris: Masson, 1961, 4th ed.
7. Hocking, M.B., Klimchuk, K.A., and Lowen, S., *J.V.S.–Rev. Macromol. Chem. Phys.*, 1999, vol. 39, no. 2, pp. 177–203.
8. Barabanova, A.I., Gromov, V.F., Teleshov, E.N., *et al.*, *Neft. Khoz.*, 1996, no. 6, pp. 17–20.
9. Healy, T.W. and La Mer, V.K., *J. Colloid Sci.*, 1964, vol. 19, no. 4, pp. 223–232.
10. Solomentseva, I.M., Baran, A.A., Postoronko, A.I., and Kirilenko, O.D., *Ukr. Khim. Zh.*, 1973, vol. 39, no. 8, pp. 785–789.
11. Kurenkov, V.F., Kolesnikova, I.Yu., and Solov'ev, D.A., *Zh. Prikl. Khim.*, 2001, vol. 74, no. 3, pp. 490–493.

ISSN 1070-4272. Russian Journal of Applied Chemistry, 2006, Vol. 79, No. 1, pp. 146–151. © Pleiades Publishing, Inc., 2006.
Original Russian Text © N.P. Prorokova, S.Yu. Vavilova, 2006, published in Zhurnal Prikladnoi Khimii, 2006, Vol. 79, No. 1, pp. 148–153.

MACROMOLECULAR CHEMISTRY AND POLYMERIC MATERIALS

Criteria for Assessing the Leveling Effect of Agents Used for Batch Dyeing of Synthetic Fibrous Materials

N. P. Prorokova and S. Yu. Vavilova

Institute of Chemistry of Solutions, Russian Academy of Sciences, Ivanovo, Russia

Received May 25, 2005

Abstract—Various methods for assessing the performance of levelers in batch dyeing of synthetic fibrous materials were analyzed. Criteria most suitable for technological and scientific applications were chosen.

DOI: 10.1134/S1070427206010307

One of the major indicators of the quality of dyed fibrous materials is uniformity of coloration. The achievement of uniform coloration is hindered by both inhomogeneous properties of the fibrous substrate and the difference in the sorption powers of individual components of mixed dyes. In batch dyeing, nonuniform coloration is also due to fast sorption when the dyeing solution contacts the outer layers of the fibrous material. The solution circulating from the periphery to the center of the material package gets exhausted, and the inner layers get less intensely colored, which requires redistribution of the dye throughout the bulk of the material. This can be avoided by creating dyeing conditions that afford slow sorption and as uniform initial distribution of the dye as possible.

The dye sorption intensity can be varied by varying the temperature rising rate: Slow rising of temperature in the dyeing bath affords uniform distribution of the dye throughout the fibrous substrate. Another important means to achieve more uniform coloration of fibrous materials consists in the use of special surfactant-based agents, levelers. Their action mechanism depends on the type of the surfactants they incorporate (advanced levelers are, for the most part, mixed formulations), the type of the fibrous material, and the dye class [1, 2]. In batch dyeing of synthetic fibrous materials, more uniform coloration is achieved by decelerating the dye sorption due to solubilizing effect of surfactants and further redistribution of the surface-sorbed dye inside the polymer. The former mechanism is universal; it operates in leveling of the coloration of all kinds of fibrous materials with virtually all dyes. The latter mechanism applies only to dyeing of synthetic fibers having a small number of reactive centers and not forming strong bonds with dyes [2]. Designers of textile auxiliary agents often do not take into consideration this mechanism, which deteriorates the performance of levelers they develop for synthetic fibers.

In this study, we analyzed the suitability of various methods for assessing the performance of levelers for batch dyeing of synthetic fibrous materials and chose the criteria most suitable for technological and scientific applications.[1]

EXPERIMENTAL

Uniform application of dyes onto fibrous materials in the first stage of dyeing can be considered as one of the most important prerequisites to uniform coloration. This is most relevant to cases when ionic dyes are used for dyeing of polymers having a large number of reactive centers, for which further redistribution of the dye strongly sorbed by the reactive centers of the fibrous material is a very complex task. The uniformity of distribution of the dye over the fibrous material in the beginning of the dyeing was assessed using the dyeing nonuniformity coefficients K and the leveling power of the agent R. Below, we describe the procedure for estimating the parameters K and R for the case of dyeing of polyamide materials with acid metal complex based dyestuff Dasher Blue Z, using Ivalon K and Lyogen RAM as levelers [3].

This procedure involved dyeing of two samples of a polyamide fibrous material, which were successively charged into the same dyeing bath with a 3-min interval. Total dyeing time 10 min, dyeing bath temperature $98 \pm 2°C$. Dyeing bath composition, %: leveler 1, acetic acid 2, and dye x.

[1] The analysis was carried out for agents developed or studied with participation of the authors.

The dyeing nonuniformity coefficient K was calculated by the formula

$$K = I_1/I_2,$$

where I_1 and I_2 are the coloration intensities of the first and second samples, respectively.

The coloration intensity was determined as the Kubelka–Munk function, based on the reflection coefficients of the colored sample, measured on a Specol-11 instrument. The leveling power R, %, was calculated by the formula

$$R = 100 - \frac{(K_i - 1) \times 100}{K_b},$$

where K_i and K_b are the nonuniformity coefficients for the analyzed and blank samples, respectively.

Table 1 compares the leveling power indicators of Ivalon K and Lyogen RAM. To illustrate how introduction of the leveler into the dyeing system affects the dye sorption and, correspondingly, the K and R parameters, the data in Table 1 are correlated with the uptake curves for the dyestuff Dasher Blue Z [1]. We determined experimentally the uptake curves (the content of the dye on the fibrous material vs. the dyeing time). The amount of the dye in the polymer was determined as the difference between the contents of the dye in the initial dyeing solution and in the residual bath. The dye concentration in solution was determined spectrophotometrically on a Specol-11 instrument in the region where the optical density of the colored solutions linearly varies with the concentration of the dissolved dye. The resulting curves clearly illustrate the run of the sorption process on a fibrous material, but recording them is a time- and labor-consuming procedure. This makes these curves unsuitable for express determination of the leveling power of textile auxiliaries.

Figure 1 shows that introduction of the leveler in the first dyeing stage (0–30°C) decreases the dye sorption by the fibrous material, thereby decreasing the coefficient K (Table 1). It is seen from Fig. 1 that the dye sorption is higher in the case of Lyogen RAM than in the case of Ivalon K, which is consistent with a lower leveling power R of Lyogen RAM (Table 1). Thus, the parameters K and R fairly completely and adequately describe the influence of the agents on the uniformity of dyeing of fibrous materials and can be recommended for estimation of the leveling power and optimal concentration of agents.

The above-described procedure of assessing the uniformity of distribution of the dye in the first dyeing stage can be used for characterizing the processes of dyeing of synthetic fibers at temperatures $T \leq 100$°C. However, this procedure is unsuitable for dyeing under pressure (for example, batch dyeing of polyester fibrous materials is carried out at 130–135°C). We assessed the uniformity of the initial application of the dye onto the polyester material by a more labor-consuming procedure, determination of the moments of the kinetic sorption curves M [4]. They were calculated using our experimental curves of the dye sorption by the first layer of the polyester membrane by the formula [5]

$$M = c_\infty^{-1} \int_0^\infty \tau \frac{\partial c}{\partial \tau} d\tau,$$

where c_∞ is the equilibrium concentration of the dyestuffs in the polymer, g of dye per kg of polymer, and τ, time.

The equilibrium concentration of the dye in the polymer was determined by the multilayer membrane method [5]. To this end, a purified 40×500 mm polyester film was reeled onto a metallic rod 5 mm in diameter. The faces and free end of the roll were

Table 1. Influence of different levelers on the uniformity of dyeing of polyamide knitted fabric with acidic metal-containing dyestuff Dasher Blue Z

Dyeing conditions	K	R, %
Without leveler	3.22 ± 0.09	–
Lyogen RAM	2.39 ± 0.07	56.83 ± 1.70
Ivalon K	2.09 ± 0.06	66.15 ± 1.98

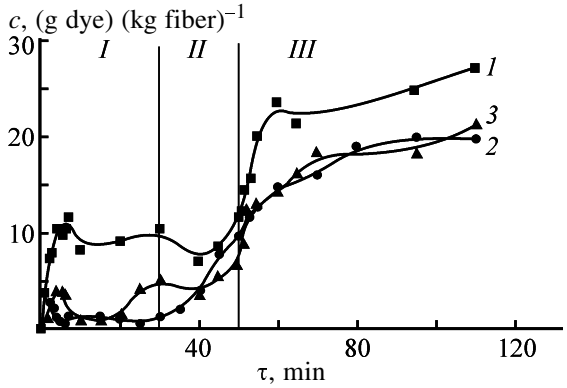


Fig. 1. Uptake curves of dyestuff Dasher Blue Z in the presence of different levelers. (c) Dye concentration on the fiber and (τ) time; the same for Fig. 2. Temperature, °C: (*I*) 0–30, (*II*) 30–50, and (*III*) 50–100. (*1*) Without and (*2, 3*) with leveler: (*2*) Ivalon K and (*3*) Lyogen RAM.

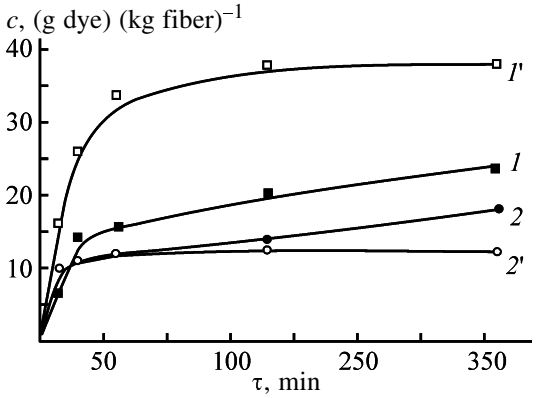


Fig. 2. Kinetic curves of sorption of disperse dyestuffs by the first layer of the polyester membrane when dyed at 135°C. Dyestuff: (*1, 1'*) Disperse Blue 2 PE and (*2, 2'*) Disperse Ruby PE. (*1, 2*) Commercially used technology and (*1', 2'*) 1.5 g l^{-1} of Ivlan-2.

thoroughly sealed. The reeled films were dyed under pressure at 135°C at the bath ratio of 1 : 150 for 360 min. When the treatment was complete, the film was cut across the layers, treated with acetone for 15 min and then with distilled water, and dried. The dye content in each film layer was determined spectrophotometrically.

Figure 2 shows as an example the kinetic curves of sorption by polyester threads of two disperse dyestuffs produced by the Pigment Production Association [4]. We used Disperse Blue 2 PE, an anthraquinone dye with a low leveling power (curves *1, 1'*), and Disperse Ruby PE, an azo dye with a high leveling power (curves *2, 2'*). Polyester threads were dyed at 135°C by the Rapid Color isothermal procedure [6] in the presence of an agent that showed efficient performance in production (a mixture of 1 g l^{-1} of Egonal W4027 leveler with 1 g l^{-1} of carrier, Remol NT) (curves *1, 2*) in the presence of Ivlan-2[2] (intensifying leveler for dyeing Dacron) (curves *1', 2'*).

Using the curves taken at the Ivlan-2 concentrations of 0–3 g l^{-1}, we calculated the sorption moments *M* (see Fig. 3). Since the sorption moment is an integrated characteristic of the process, we cannot state unambiguously that a decrease in *M* favors uniform dyeing, as this can be due not only to deceleration of sorption but also to a decrease in the dye uptake by the fibrous material. A certain decrease in the dyeability of fibrous materials in the presence of levelers is an ordinary drawback of such technologies and can be due to formation of labile complexes between the dye and the surfactant, which degrade incompletely with rising temperature. Formation of such compounds is a prerequisite to deceleration of sorption in the first dyeing stage, but at the same time it decreases the dye uptake by the fibrous material [7].

Thus, in analyzing the data we obtained, it is reasonable to take as the optimal sorption moments the corresponding characteristics of a composition that efficiently performed in production processes. The diagram in Fig. 3 allows the sorption moments of the dyes for different concentrations of the leveler developed to be compared with such characteristics and, thus, the optimal concentrations of the preparation to be estimated. It should be noted that the optimal concentrations depend on dye used: For dyestuff Disperse Dasher Blue 2 PE, the optimal sorption moments are achieved with the solution containing 1.0–2.0 g l^{-1}, and for Disperse Ruby dyestuff, 0.5–2.0 g l^{-1}, of Ivlan-2.

When the uptake of the dye by the fibrous material is decreased, its content in the residual bath increases. We estimated the degree of the dye utilization in the system using the distribution coefficient Γ determined by the Henry–Nernst equation [8]. It characterizes the ratio of the dye concentration in the film dyed for 360 min to that in the residual bath:

$$\Gamma = c_f/c_s,$$

where c_f is the dye concentration in the film, g of dye per kg of film, and c_s, dye concentration in the residual bath, g of dye per kg of solution.

Figure 4 presents the coefficients of distribution of dyestuffs Disperse Blue 2 PE and Disperse Ruby PE between the polyester fibrous material and the dyeing bath at different contents of Ivlan-2 in the bath. It is seen that introduction of any of the levelers decreases to a certain extent the degree of utilization of the dye, but it is possible to choose such concentrations of the preparations at which a decrease in the dyeability will be so insignificant that it will leave virtually unaffected the resulting color characteristics. For example, the uptake by the fibrous material of dyestuff Disperse Blue 2 PE is virtually unaffected by 0.5–1.5 g l^{-1} of Ivlan-2 and that of Disperse Pink PE, by 0.5–2.5 g l^{-1} [4].

It should be noted that leveling of the color in batch dyeing of polyester materials by disperse dyestuffs has specific features. The agent should not only decelerate the dye sorption by the polymer, which underlies the action of levelers for most of dyes and fibrous materials, but also afford major redistribution of the dye sorbed by the polymer [2].

[2] Developed with participation of the authors.

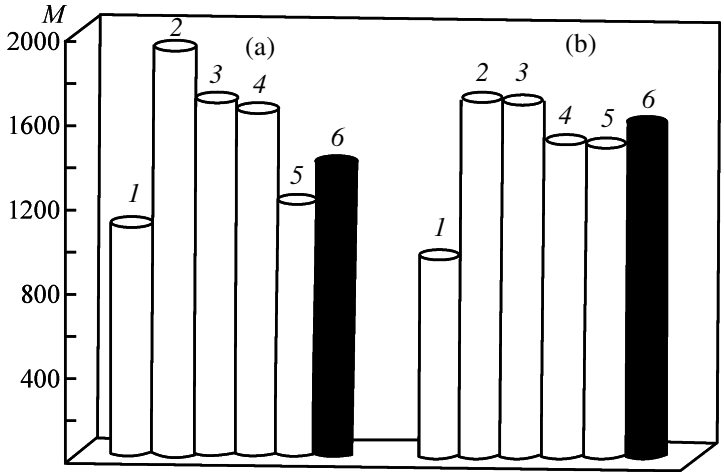


Fig. 3. Moments M of kinetic curves of sorption of dyes for polyester materials in relation to levelers. Dyestuff: (a) Disperse Blue 2 PE and (b) Disperse Ruby PE; the same for Fig. 4. (*1*) Without and (*2–6*) with leveler; (*2–5*) Ivlan-2, g l^{-1}: (*2*) 0.5, (*3*) 1.0, (*4*) 1.5, and (*5*) 2.0; (*6*) Egonal W4027, 1 g l^{-1} + Remol NT, 1 g l^{-1}.

The ability of the agent to afford redistribution of the dye sorbed on the fiber surface into the polymer bulk is estimated quantitatively by the migration method [5, 9]. This method consists in determining the amount of the dye migrating from the colored to uncolored sample in a reel made of two samples of the fabric, twisted together, simulating a nonuniformly colored polyester material. The experiment was carried out in the presence of Ivlan-2 under conditions similar to those in dyeing. The migration effect m was calculated by the formula

$$m = \frac{c_b/c_a}{c_b^0/c_a^0},$$

where c_a^0 and c_a are the contents of the dye in the samples of the preliminarily dyed material in the blank experiment and in the experiment with the leveler added, respectively, and c_b^0 and c_b, contents of the dye in a sample of undyed material in the blank experiment and in the experiment with the leveler added, respectively.

When polyester is dyed by batch high-temperature procedures, sections of the packages with a low density of reel of the fibrous material sorb a larger amount of the dye than sections with a high density. This is especially characteristic of dyeing by isothermal procedures with poorly leveling dyes having a high affinity for the fiber. Special preparations can cause the polyester structure to loosen, which will be responsible for redistribution of the dye in the bulk of the fibrous material owing to migration. However, redistribution of the dye should be uniform, as too high migration intensity deteriorates again the quality of dyeing of the polyester. The dye migration intensity depends on the type of the fibrous material, the leveler and dye used, the leveler concentration, and the temperature of the process. Therefore, theoretical substantiation of the optimal intensity of migration is a very difficult task. In this connection, we can suggest to take a textile auxiliary formulation successfully used in production processes, as a system with optimal characteristics. For example, in dyeing of polyester by Rapid Color high-temperature isothermal procedure, a good performance is demonstrated by a formulation including 1 g l^{-1} of leveler, Egonal W4027, and 1 g l^{-1} of the carrier, Remol NT.

Figure 5 shows how the migration effect m of a disperse dyestuff with a low leveling power, Disperse Blue 2 PE, is affected by the Ivlan-2 concentration at temperatures within 90–135°C. For comparison, we presented the migration effects for the optimal system

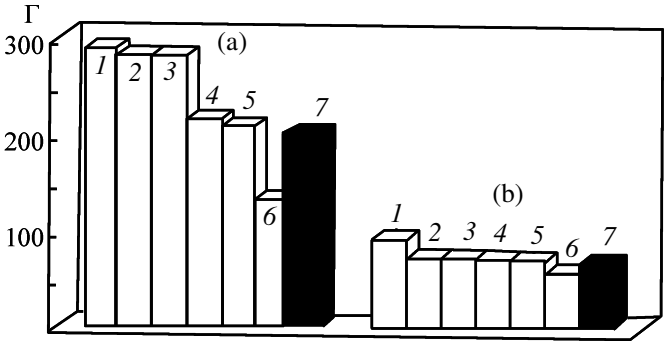


Fig. 4. Dye distribution coefficients Γ in relation to the textile auxiliary agent. (*1*) Without and (*2–7*) with leveler; (*2–6*) Ivlan-2, g l^{-1}: (*2*) 0.5, (*3*) 1.0, (*4*) 1.5, (*5*) 2.0, (*6*) 3.0; (*7*) Egonal W4027, 1 g l^{-1} + Remol NT, 1 g l^{-1}.

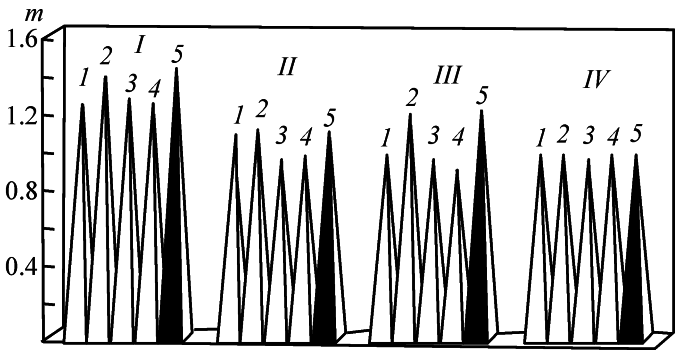


Fig. 5. Migration effect m of the dyestuff Disperse Blue 2 PE in a polyester thread as influenced by the Ivlan-2 concentration. (*1–4*) Ivlan-2, g l^{-1}: (*1*) 0.5, (*2*) 1.0, (*3*) 1.5, and (*4*) 2.0 and (*5*) Egonal W4027, 1 g l^{-1} + Remol NT, 1 g l^{-1}. Temperature, °C: (*I*) 90, (*II*) 115, (*III*) 130, and (*IV*) 135.

(commercially used process). Figure 5 shows that the dye migrates most intensively at 90°C, evidently, due to a purely superficial application of the dye onto the polyester, which is responsible for its easy redistribution. At temperatures above the glass transition point of the polyester (115–135°C), dyes penetrate inside the fibrous material, and the migration intensity decreases. The closest to the optimum are migration effects observed at 135°C and Ivlan-2 concentration of 1.0–1.5 g l^{-1}.

The diffusion coefficients D of the disperse dyestuffs were calculated using the curves of distribution of the dyestuffs over the layers of a multilayer film polyester membrane when dyed for 360 min [5]:

$$X_{c=c_0/2}/(D^{1/2})\tau = 0.964,$$

where $X_{c=c_0/2}$ is the distance to which the dye has penetrated when 50% of the equilibrium sorption is achieved; c, concentration of the dye at the given penetration depth, and τ, dyeing time.

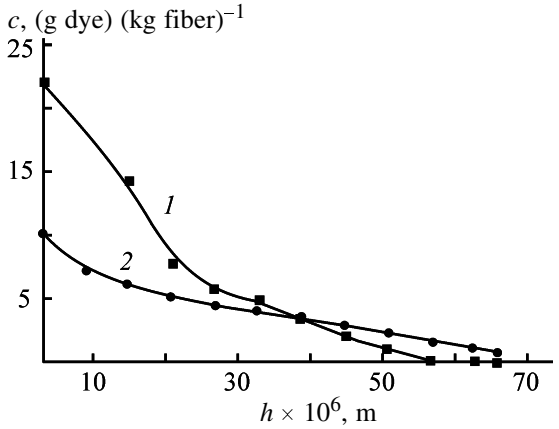


Fig. 6. Curves of redistribution of the dyes over the polyester membrane layers in the presence of 1.5 g l^{-1} of Ivlan-2 at the dyeing temperature of 135°C and dyeing time of 360 min. (*c*) Concentration of the dye on the fiber and *h*, thickness of the polyester membrane layer.

Figure 6 presents as an example the typical curves of distribution of the dyes over the layers of the multilayer polyester membrane in the presence of Ivlan-2. Table 2 lists the calculated diffusion coefficients.

As known, high diffusion coefficients are indicative of possible formation of a nonuniform color on a fibrous material, while a significant decrease in them can cause the dye uptake by the fiber to decrease. The closest to the optimum are the coefficients of diffusion of the dye from a system containing Ivlan-2 in amounts of 1.5 (for Disperse Blue 2 PE) and 0.5–1.0 g l^{-1} (for Disperse Ruby PE).

Analysis of the migration and sorption characteristics of the dye–leveler system for polyester materials shows that, compared to sorption moments and diffusion coefficients, the migration effects determine a narrower range of the leveler concentration, 1–1.5 g l^{-1}, corresponding to highly uniform coloration

Table 2. Coefficients of diffusion of dyes into the polyester film in relation to the levelers

Leveler, g l^{-1}	Diffusion coefficient $D \times 10^{13}$, m s^{-1}, of	
	Disperse Blue 2 PE	Disperse Ruby PE
None	5.7 ± 0.1	11.0 ± 0.2
Ivlan-2:		
0.5	3.5 ± 0.1	7.8 ± 0.1
1.0	8.4 ± 0.1	7.7 ± 0.1
1.5	6.9 ± 0.1	2.1 ± 0.1
2.0	10.9 ± 0.2	3.9 ± 0.1
3.0	3.9 ± 0.1	5.7 ± 0.1
Egonal W 4027, 1 + Remol NT, 1	7.8 ± 0.1	7.4 ± 0.1

of the polyester. This holds for dyes with both high and low leveling powers.

CONCLUSIONS

(1) In batch dyeing of synthetic fibrous materials at temperatures $T \leq 100°C$ in the presence of levelers, such characteristics as the dyeing nonuniformity coefficients K and the leveling power of the agent R fairly completely and adequately describe the influence of the agents on the uniformity of dyeing of fibrous materials. This makes them suitable for assessing the leveling powers of agents and determining their optimal concentration.

(2) In batch dyeing of polyester fibrous materials at 130–135°C, the leveling power of the agents can be completely assessed using the sorption (sorption moment M) and migration (migration effect m and diffusion coefficient D) characteristics. We found that, compared to sorption moments and diffusion coefficients, the migration effects determine a narrower range of the leveler concentration, 1–1.5 g l^{-1}, corresponding to highly uniform coloration of the polyester. Thus, it is more reasonable to use the migration effects for express assessment of the properties of the leveler and determination of its optimal concentration.

(3) In batch dyeing of any synthetic fiber, the degree of utilization of the dye can be assessed using the distribution coefficient Γ.

REFERENCES

1. Belen'kii, L.I., *Zh. Vses. Khim. O-va. im. D.I. Mendeleeva*, 1970, vol. 15, no. 3, pp. 242–249.
2. Smirnova, O.K. and Prorokova, N.P., *Zh. Vses. Khim. O-va. im. D.I. Mendeleeva*, 2002, vol. 46, part 1, pp. 88–95.
3. Prorokova, N.P., Stepanenkova, I.V., Vavilova, S.Yu., and Smirnova, O.K., *Khim. Volokna*, 2001, no. 3, pp. 42–45.
4. Prorokova, N.P., Vavilova, S.Yu., Kalinnikov, Yu.A., and Prorokov, V.N., *Izv. Vyssh. Uchebn. Zaved., Khim. Khim. Tekhnol.*, 2003, vol. 46, no. 5, pp. 38–40.
5. Belen'kii, L.I., Rosinskaya, Ts.Ya., Mel'nikov, B.N., *et al.*, *Tekhnologicheskie raschety v khimicheskoi tekhnologii voloknistykh materialov: Uchebnoe posobie dlya tekstil'nykh vuzov* (Process Calculations in Chemical Technology of Fibrous Materials: Textbook for Textile High Educational Establishments), Belen'kii, L.I., Ed., Moscow: Vysshaya Shkola, 1985.
6. Prorokova, N.P., Vavilova, S.Yu., and Kalinnikov, Yu.A, *Khim. Volokna*, 1996, no. 4, pp. 32–35.
7. Prorokova, N.P. and Vavilova, S.Yu., *Khim. Volokna*, 2003, no. 2, pp. 47–49.
8. Belokurov, S.G., Theoretical Substantiation and Development of the Process of Dyeing of Polyether Textured Threads in Packages, *Cand. Sci. Dissertation*, Ivanovo, 1991.
9. Prorokova, N.P., Vavilova, S.Yu., and Kalinnikov, Yu.A., *Izv. Vyssh. Uchebn. Zaved., Khim. Khim. Tekhnol.*, 2003, vol. 46, no. 1, pp. 108–111.

ISSN 1070-4272. Russian Journal of Applied Chemistry, 2006, Vol. 79, No. 1, pp. 152–155. © Pleiades Publishing, Inc., 2006.
Original Russian Text © V.S. Abramov, V.V. Marusin, 2006, published in Zhurnal Prikladnoi Khimii, 2006, Vol. 79, No. 1, pp. 154–156.

BRIEF COMMUNICATIONS

Deposition of Polysiloxane Films in a Glow Discharge

V. S. Abramov and V. V. Marusin

Institute of Theoretical and Applied Mechanics, Siberian Division, Russian Academy of Sciences, Novosibirsk, Russia

Received January 26, 2005; in final form, November 15, 2005

Abstract—The method of polymerization in the plasma of a dc glow discharge was used to obtain thin-film polysiloxane coatings on metallic substrates. The chemical composition, structure, and deposition rate of the coatings were studied in relation to process parameters.

DOI: 10.1134/S1070427206010319

This study is concerned with deposition of thin organosilicon coatings on metallic substrates by polymerization in the plasma of a glow discharge in a vacuum. Coatings of this kind can be used as antifriction, dielectric, protective, and hydrophobic films. Use of plasma polymerization minimizes the expenditure of materials and makes it possible to obtain thin coatings with a thickness of fractions of a micrometer [1–4]. To solve the problem, a deposition installation and a procedure for measuring the thickness of the coatings obtained were developed. The composition and structure of the coatings were determined by reflection IR spectroscopy.

EXPERIMENTAL

The installation developed in the study is shown schematically in Fig. 1.

The installation includes as a basic unit the working chamber fabricated in the form of a 500 × 300 mm 12Cr18Ni10Ti stainless steel cylinder. The cowling of the chamber has three windows for visual inspection of the process and a hatch with an inner diameter of 250 mm. The lids of the working chamber have apertures for voltage supply to the working electrodes. The 10-mm-thick electrodes are fabricated from D16T aluminum alloy. Systems of parallel electrodes of diameters D 90 and 45 mm are used. An annular hollow, made within the upper electrode, is closed with a tightly fit Teflon cover. The hollow is connected with the lower surface of the electrode by a number of fine (D = 0.8 mm) apertures. The Teflon cover has a pipe for delivery of the monomer vapor into the hollow. This design provides uniform distribution of the monomer vapor over the entire interelectrode space.

The pressure in the working chamber was monitored with a VT-3 thermocouple vacuum gage. The discharge was electrically fed from a UIP-1 versatile power source with a ballast resistor of 6.9 kΩ. The vessel with the starting monomer was connected with the working chamber via a leak. The vessel was heated with an electric heater. The chamber had a special inlet for a wire probe for measuring by the Klagge method the discharge parameters and the thickness of a film being deposited [5].

The 132-24 oligodiethylsiloxane liquid was used as the monomer. Its functional composition was the following: $(C_2H_5)_3SiO_{0.5}$, $(C_2H_5)SiO$, and $C_2H_5SiO_{1.5}$

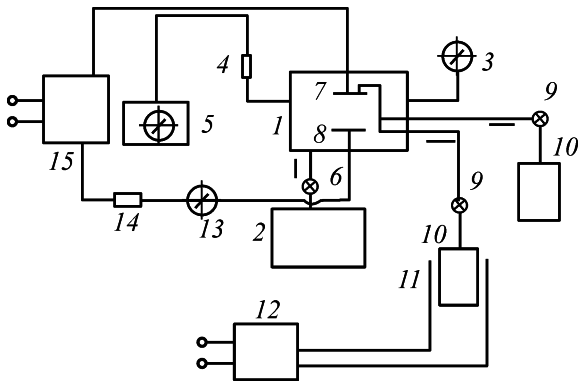


Fig. 1. Schematic of the installation: (*1*) working chamber, (*2*) vacuum pump, (*3*) mechanical vacuum gage, (*4*) thermocouple tube, (*5*) thermocouple vacuum gage, (*6*) evacuation valve, (*7*) upper electrode, (*8*) lower electrode, (*9*) leak, (*10*) vessel with the monomer, (*11*) electric heater, (*12*) laboratory autotransformer, (*13*) milliammeter, (*14*) ballast resistor, and (*15*) power source.

units [6, 7]. This siloxane has a comparatively high partial pressure P of the monomer at room temperature ($P \approx 50$ Pa [6]), which facilitates its feeding into the reactor.

The experiments were carried out as follows. A sample (12Cr18Ni10Ti steel foil strip of thickness 40 μm) was placed on the lower electrode. The small thickness of the sample made it possible to exclude any disturbance of the discharge. The monomer was fed into the interelectrode discharge zone after preliminary evacuation of the reactor. The interelectrode spacing L was varied within the range 10–30 mm, and the ignition voltage in the siloxane vapor was U_i = 450–600 V.

The occurrence of a discharge was visually inspected via windows in the walls of the working chamber.

The coating thickness was determined by weighing. The spectra were measured on a Shimadzu spectrometer. After a spectrum was obtained (100 times with the subsequent averaging), the spectrum of the starting sample was subtracted from that of the coating, the resulting curve was smoothed with a Fourier filter to the fifth frequency, and the spectrum was identified using the database of the Novosibirsk Institute of Organic Chemistry, Siberian Division, Russian Academy of Sciences.

The geometric parameters of the discharge system strongly affect the course of plasmochemical processes that occur in this system. At the critical interelectrode spacing, which depends on the composition of the gas medium, the discharge becomes unstable, and a still smaller spacing, disappears at all [8, 9].

The dependence of the current–voltage (I–U) characteristic of the discharge on the interelectrode spacing was studied in the range L = 10–30 mm. The measurements were made at P = 50 Pa and D = 90 mm. At the interelectrode spacing L = 10 mm, the discharge becomes unstable and spark microdischarge breakdowns of the interelectrode space are observed. At the interelectrode spacing L = 5 mm, there is no discharge in the interelectrode space. The $I(U)$ dependences are linear.

The main results of the experiments are the following: the total thickness of the near-cathode region of the discharge and of the anode space is 5–10 mm for the given gas medium and experimental conditions; as the interelectrode spacing increases, the I–U characteristic of the discharge changes only slightly, i.e., the main voltage drop occurs in the near-cathode region. The voltage drop in the positive column (whose length increases with the interelectrode spacing) is about 20–30 V cm^{-1}.

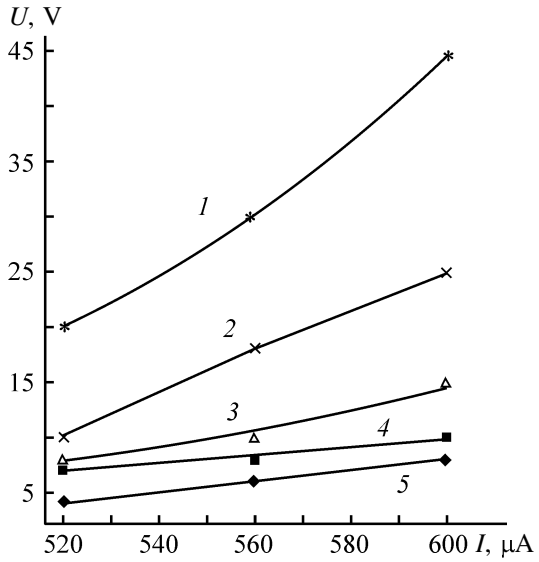


Fig. 2. I–U characteristics of the discharge at different pressures. (U) Voltage and (I) current. P (Pa): (*1*) 100, (*2*) 60, (*3*) 40, (*4*) 25, and (*5*) 15.

The dependence of the I–U characteristic on the pressure P in the chamber was studied at L = 20 mm and D = 90 mm. The results obtained are shown in Fig. 2. It can be seen that the dependence of the I–U characteristic on the pressure P in the working chamber is considerably stronger than that on the interelectrode spacing L. When the pressure is varied within the range 10–40 Pa, the I–U characteristic changes only slightly. If, however, the pressure is raised to 50–100 Pa, the I–U characteristic changes dramatically because of a decrease in the discharge resistance, i.e., an increase in its conductance.

Hence follows that the effect of the electron impact on the dissociation rate and on other plasmochemical processes in the discharge zone changes fundamentally [8, 9].

The rate of coating deposition is determined in plasmochemical processes by the parameters of the working process and by the rate of monomer supply. The following basic processes may occur in this case [10, 11]: (1) homogeneous polymerization in the gas phase, (2) heterogeneous polymerization on the sample surface, and (3) plasmochemical etching of the sample surface.

Depending on a discharge mode, either deposition of a polymer film onto the sample surface or etching of this surface occurred. Three different types of plasma polymerization, depending on the process

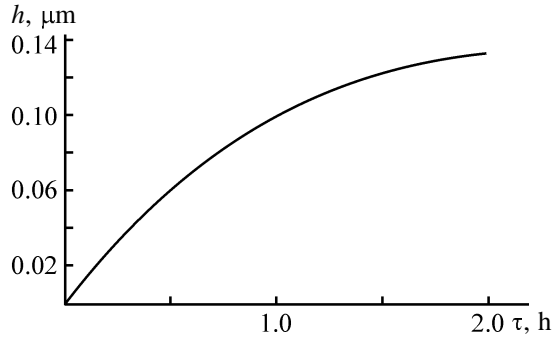


Fig. 3. Polymer film thickness h vs. the deposition time τ.

mode, were revealed in the study. These mode are conditionally termed "mild," "medium," and "severe." The mild process mode has the following parameters: P = 40–50 Pa, I = 8–12 mA, D = 90 mm, j = 0.12–0.19 mA cm^{-2}, L = 20–30 mm, and U = 520–540 V. In each experiment, three samples were placed on the lower electrode, with the arithmetic mean over the three samples taken as the gain in mass. The dependence of the coating thickness on the deposition time is shown in Fig. 3. The film deposition rate is about 0.1 μm h^{-1} in this mode.

It follows from the spectral data obtained that the coating is composed of organosilicon structures containing the starting polysiloxane base and aromatic and unsaturated hydrocarbon units. The low growth rate of the coating (about 0.1 μm h^{-1}) indicates that the polymerization occurs heterogeneously, rather than in the gas phase [1].

The medium process mode has the following parameters: P = 60 Pa, I = 20 mA, D = 90 mm, j = 0.3 mA cm^{-2}, U = 580–600 V, and L = 20–30 mm. When the experiments were performed in this mode, the sample mass decreased, i.e., the sample etching rate exceeded the rate of polymer deposition.

The film deposition rate can be raised by passing to a mode in which the monomer polymerization occurs not only on the electrode surface, but also in the gas phase, with its subsequent deposition onto the surface. For this purpose, it is necessary to make higher the current density and concentration of monomer species in the working zone. Further experiments were performed with electrodes of a smaller (D = 45 mm) diameter. With these electrodes, the third, severe mode could be implemented. This mode has the following parameters: P = 50 Pa, I = 20 mA, j = 1.26 mA cm^{-2}, U = 540 V, L = 20 mm. In this mode, a considerable electrode heating (to above 100°C) was observed.

The results of the experiments consist in the following: (1) the coating deposited in this mode is thicker than that obtained in the mild mode; (2) according to IR data, the specific content of organic units in the coating is considerably lower than that in the preceding experiments. As the deposition mode becomes more severe, the organic component is more intensively removed from the coating.

The coating deposition rate in this mode was about 0.25 μm h^{-1}, i.e., polymerization occurred not only on the sample surface, but also in the gas phase [1, 11]. In this case, the deposition rate of the polymerized product from the gas phase onto the sample surface exceeded that of plasmochemical etching of the surface. As the working pressure was raised to $P \approx$ 120 Pa, and the current, to 40 mA (i.e., to a current density j = 2.5 mA cm^{-2}), no significant increase in the growth rate was observed.

According to the IR data, the resulting coating is mostly composed of SiO_2 (absorption bands of organic compounds are virtually absent). The coating exhibits a high hydrophobicity and it is not wetted by water, methylene chloride, and toluene.

CONCLUSIONS

(1) An installation for deposition of polysiloxane coatings by polymerization in the plasma of a dc glow discharge was developed.

(2) It was shown that raising the working pressure and current density leads to a change of the deposition mechanism from heterogeneous to homogeneous-heterogeneous. The coatings obtained exhibit hydrophobic properties.

REFERENCES

1. Yasuda, H., *Plasma Polymerization*, Orlando: Academic Press, 1985.
2. Hasui, A., *Tekhnika napyleniya* (Deposition Techniques), Moscow: Mashinostroenie, 1975.
3. Danilin, B.S., *Vakuumnaya tekhnika v proizvodstve integral'nykh skhem* (Vacuum Technology in Manufacture of Integrated Circuits), Moscow: Energiya, 1972.
4. Berdichevskii, M.G. and Marusin, V.V., *Nanesenie pokrytii, travlenie i modifitsirovanie polimerov s ispol'zovaniem nizkoental'piinoi neravnovesnoi plazmy* (Deposition of Coatings, Etching and Modification of Polymers with Low-Enthalpy Nonequilibrium Plasma), Novosibirsk: Inst. Teplofiziki, 1993.
5. Ivanov, Yu.A., Lebedev, Yu.A., and Polak, L.S., *Metody kontaktnoi diagnostiki v neravnovesnoi plaz-*

mokhimii (Methods of Contact Diagnostics in Nonequilibrium Plasmochemistry), Moscow: Nauka, 1981.

6. Sobolevskii, M.V., *Oligoorganosiloksany: Svoistva, poluchenie, primenenie* (Oligoorganosiloxanes: Properties, Synthesis, and Use), Moscow: Khimiya, 1985.
7. Sobolevskii, M.V., Muzovskaya, O.A., and Popeleva, G.S., *Svoistva i oblasti primeneniya kremniiorganicheskikh produktov* (Properties and Application Fields of Organosilicon Products), Moscow: Khimiya, 1975.
8. *Khimicheskie reaktsii v nizkotemperaturnoi plazme* (Chemical Reactions in Low-Temperature Plasma), Duchkov, A.B. and Epshtein, I.L., Eds., Moscow: Nauka, 1977.
9. Longmire, C.L, *Elementary Plasma Physics*, New York: Wiley, 1963.
10. Bogatyrev, V.M. and Borisenko, N.V., *Zh. Prikl. Khim.*, 1999, vol. 72, no. 2, pp. 292–298.
11. Osipov, K.A. and Folmanis, G.E., *Osazhdenie plenok iz nizkotemperaturnoi plazmy i ionnykh puchkov* (Deposition of Films from Low-Temperature Plasma and Ion Beams), Moscow: Nauka, 1973.

ISSN 1070-4272. Russian Journal of Applied Chemistry, 2006, Vol. 79, No. 1, pp. 156–158. © Pleiades Publishing, Inc., 2006.
Original Russian Text © A.A. Kabanov, 2006, published in Zhurnal Prikladnoi Khimii, 2006, Vol. 79, No. 1, pp. 157–159.

BRIEF COMMUNICATIONS

Thermal Stability of Limestone with a Medium Content of Iron

A. A. Kabanov

Astaf'ev State Pedagogical University, Krasnoyarsk, Russia

Received August 24, 2005

Abstract—The thermal stabilities of limestone with varied content of iron are compared. The nature of the differences observed is discussed.

DOI: 10.1134/S1070427206010320

The properties and thermal stability of limestone with a high content of iron (0.81 wt %) were considered in [1–3] in comparison with analytically pure grade $CaCO_3 \cdot 0.17H_2O$. Here we compare the thermal stabilities of limestone with a low content of iron and of the same analytically pure grade reagent.

Limestone from the Torgashino deposit in Krasnoyarsk krai was used. After its dispersion, the 0.08-mm fraction was separated by sieving and kept over P_2O_5 for five days. Then the preparation was degassed at 200°C for 6 h. This limestone was taken to be the starting material. The quantitative analysis of the samples was performed in conformity with GOST (State Standard) 4530–76 and 5382–91; a DRON-3 diffractometer served for X-ray diffraction analysis. Mass-spectrometric measurements were made with an MI-1305 ionization spectrometer.

Thermal studies were performed in air with a Q-1500D derivatograph. Mössbauer spectra were measured on an electrodynamic spectrometer based on an AI-5006-3M-V100 analyzer operating in the constant-acceleration mode. The spectra obtained were processed on an ES1022 computer. The ^{57}Co isotope in a chromium matrix, with an activity of 0.5 GBq, served as the source of γ-radiation. Kinetic curves of limestone decomposition were obtained by the volumetric method at 825 ± 0.5°C, with 0.100-g weighed portions used. The procedures used were described in more detail in [1–4].

The chemical composition of limestone is the following (wt %): main substance $CaCO_3$ 93.50, Fe 0.40, (K + Na) 0.11, Si 1.91, Al 0.20, Mg 0.60, and other impurities 3.28. The X-ray phase analysis (Fig. 1) suggested that the starting limestone contains $CaCO_3$ in the calcite modification, goethite FeOOH, and wustite FeO. The content of other crystalline phases is less than 3.16%.

Additional evidence concerning iron minerals was

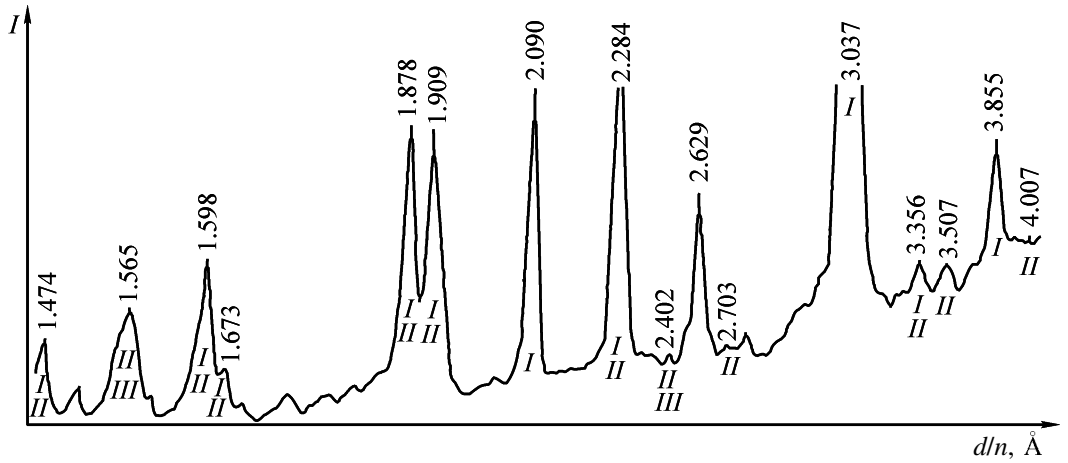


Fig. 1. X-ray diffraction pattern of the starting limestone. (*I*) Absorption intensity and (*d*/*n*) interplanar spacing. (*I*) $CaCO_3$, (*II*) goethite FeOOH, and (*III*) wustite FeO.

obtained by Mössbauer spectrometry on heating the limestone at 825°C (Fig. 2). The shape of the spectrum and its parameters (quadrupole splitting ΔE_Q and isomer chemical shift δE) indicate the following [5]: the doublet of peaks at the center belongs to siderite $FeCO_3$, and broad weak peaks on the periphery of the spectrum, to magnetite Fe_3O_4 and hematite α-Fe_2O_3. It follows from the derivatogram (Fig. 3) that a noticeable change in the mass of the weighed portion of limestone starts in air at 220°C. The decomposition of the preparation is the most pronounced at 860±1°C; the mass of the weighed portion stabilizes at around 879°C. According to the mass-spectrometric data (Fig. 4), the decomposition rate of limestone in a vacuum with a residual pressure of 10^{-6} torr is the highest at 610±1°C. The strong discrepancy between the temperatures of the highest decomposition rate in air and in a vacuum is typical of calcite [6].

The three experimentally obtained peaks of the dehydration rate of limestone (Fig. 4) point to the existence of at least three centers of water localization in limestone. The total content of water in limestone as a whole and at these centers can be judged from the areas delimited by curve *1* (H_2O^+) from above, temperature axis from below, and either the boundaries of the curve or temperature sections of this curve from the right and left (Fig. 4). These areas were calibrated against the mass of water with the use of gravimetric data (Fig. 3, TG curve). The portion of the TG curve below 400°C corresponds to a decrease in the mass of the weighed portion of limestone solely through release of H_2O. However, according to curve *1* in Fig. 4, water is released from limestone beginning at 50°C. Gravimetry fails to detect this water because of the low sensitivity of this technique as compared to mass spectrometry. Therefore, the calibration can be based on the assumption that only 1 mg of H_2O is removed from the starting limestone samples up to 400°C (Fig. 3). This corresponds in Fig. 4 to the area under curve *1*, delimited from the right by the section at T = 400°C. The portion of curve *1* in the range from 50 to 540°C corresponds to dehydration and decomposition of hydrogoethite [7–10]. The X-ray diffraction data (Fig. 1) and the calculations based on the results of chemical analysis and mass-spectrometric data (Fig. 4) confirm this conclusion and yield the formula $FeOOH \cdot 0.7H_2O$. The third peak in Fig. 4 (610°C) corresponds to H_2O from dehydration of calcite [1–4, 6]. The calculation yields the formula $CaCO_3 \cdot 0.02H_2O$. Water is completely removed from the starting limestone only in a vacuum (residual pressure 10^{-6} Torr) at 800°C, when calcite itself completely decomposes also. On the whole, the starting limestone sample contain, according to gravimetric and mass-spectrometric data, 1.20 wt % H_2O.

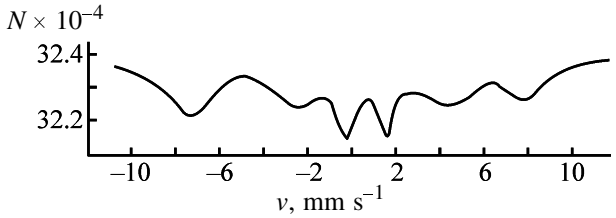


Fig. 2. Mössbauer spectrum of limestone thermally treated at 825°C for 6 h. (*N*) Number of counts per channel and (*v*) motion velocity of the γ-emitter.

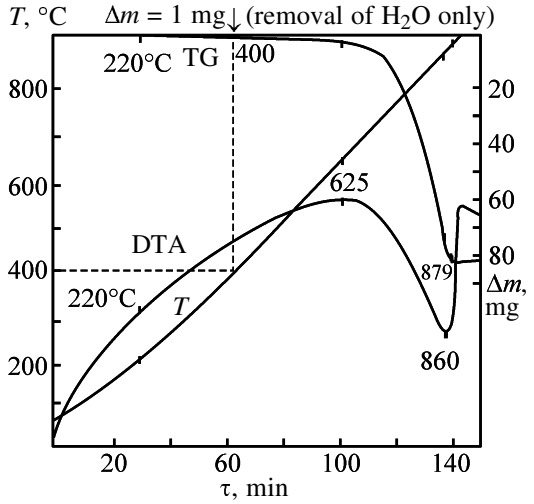


Fig. 3. Derivatogram of the starting limestone: (*T*) temperature, (τ) time, and (Δm) sample weight loss. *M* 0.2 g, $dT/d\tau$ = 6 K min^{-1}.

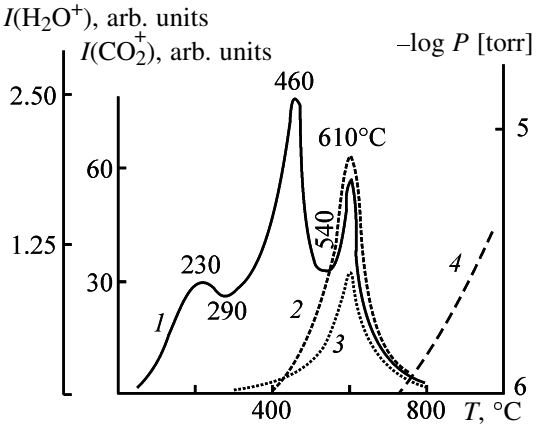


Fig. 4. Mass-spectrometric data for the starting limestone: (*I*) Intensity, (*T*) temperature, and (*P*) pressure in the reaction vessel. *M* = 0.01 g, $dT/d\tau$ = 18.0 K min^{-1}, residual pressure 10^{-6} torr. (*1*) H_2O, (*2*) CO_2, (*3*) log *P*, and (*4*) H_2O signal from the glass of the vessel.

Figure 5 shows for comparison the kinetic curves for the $CaCO_3 \cdot 0.17H_2O$ reagent of analytically pure

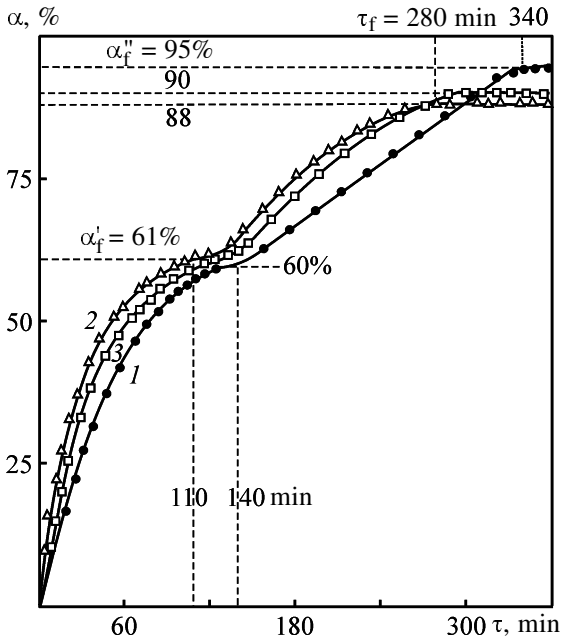


Fig. 5. Kinetic curves for decomposition of (*1*) $CaCO_3 \cdot 0.17H_2O$ reagent and (*2, 3*) limestones at 825 ± 0.5°C. (α) Degree of decomposition of the samples, (τ) time, (α'_f, α''_f) degrees of decomposition to the first and second equilibria, and (τ_f) time in which the second equilibrium is attained. Sample: (*1*) $CaCO_3 \cdot 0.17H_2O$ reagent, (*2*) limestone from the Solomenskoe deposit, and (*3*) that from the Torgashino deposit. (τ) Decomposition time.

grade (curve *1*) and for limestone from the Solomenskoe and Torgashino deposits (curves *2, 3*). All these curves were obtained [2, 4] using the same procedure. It was found that, as regards the shape of the kinetic curve, the Torgashino limestone (curve *3*) is close to that from the Solomenskoe deposit (curve *2*). This similarity is manifested in the decomposition rate, in the time in which the first equilibrium state is attained, and, what is the most important, in the kinetic type of decomposition after that, rather than the diffusion type as in the case of the reagent [2]. The fact that the second equilibrium is reached later for the Torgashino limestone can be attributed to the lower (by a factor of 2) content of iron, which favors slower establishment of the second equilibrium.

Comparison of the chemical and mineralogical compositions of the $CaCO_3 \cdot 0.17H_2O$ reagent and the Solomenskoe [1, 2] and Torgashino varieties of limestone with the shape of the kinetic curves of their decomposition (Fig. 5) suggests that the key factor leading to a decrease in their thermal stability is the presence of iron impurities in the form of various compounds. Previously, this has been established in a study of the decomposition of the $CaCO_3 \cdot 0.17H_2O$ reagent with addition of various iron oxides [11]. The amount of iron in the Solomenskoe limestone is twice that in the Torgashino mineral, and this is, undoubtedly, the basic reason for the difference between curves *2* and *3* in Fig. 5.

CONCLUSIONS

(1) The limestone from the Torgashino deposit contains 1.20 wt % H_2O, which is not removed by drying of dispersed limestone at 200°C for 6 h.

(2) The composition of limestone is the following (wt %): $CaCO_3 \cdot 0.02H_2O$ 94.00, $FeOOH \cdot 0.7H_2O$ 3.52, FeO 0.25, other impurities 2.23.

(3) The Torgashino limestone is close in the kinetics of thermal decomposition at 825°C to that from the Solomenskoe deposit, which is due to the twice lower content of iron in the former.

(4) The lower thermal stability of the Torgashino limestone, compared with the $CaCO_3 \cdot 0.17H_2O$ reagent, is due both to the lower content of water ($CaCO_3 \cdot 0.02H_2O$) and to the considerable content of iron.

REFERENCES

1. Kabanov, A.A., *Zh. Prikl. Khim.*, 2003, vol. 76, no. 7, pp. 1077–1079.
2. Kabanov, A.A., *Zh. Fiz. Khim.*, 2003, vol. 77, no. 11, pp. 1961–1965.
3. Kabanov, A.A., *Zh. Prikl. Khim.*, 2004, vol. 77, no. 9, pp. 1435–1437.
4. Kabanov, A.A., *Zh. Fiz. Khim.*, 2002, vol. 76, no. 2, pp. 227–232.
5. Kündig, W., Lindquist, R., and Constabaris, G., *Magnetic Resonance and Relaxation*, Amsterdam: North-Holland, 1967.
6. Kabanov, A.A., *Zh. Fiz. Khim.*, 2001, vol. 75, no. 4, pp. 746–748.
7. Ischner, B. and Subat, G., *Z. Elektrochem.*, 1962, vol. 66, nos. 8–9, pp. 680–684.
8. Nenitescu, C.D., *Chimie generala*, Bucharest: Tehnica, 1963.
9. Butt, Yu.M. and Timashev, V.V., *Praktikum po khimicheskoi tekhnologii vyazhushchikh materialov* (Manual of Chemical Technology of Binders), Moscow: Vysshaya Shkola, 1973.
10. Glovanoli, R. and Brütsch, R., *Thermochim. Acta*, 1975, vol. 13, pp. 15–36.
11. Kabanov, A.A., *Zh. Fiz. Khim.*, 2002, vol. 76, no. 9, pp. 1719–1721.

ISSN 1070-4272. Russian Journal of Applied Chemistry, 2006, Vol. 79, No. 1, pp. 159–162. © Pleiades Publishing, Inc., 2006.
Original Russian Text © V.V. Pan'kov, O.P. Ol'shevskaya, O.V. Onoprienko, 2006, published in Zhurnal Prikladnoi Khimii, 2006, Vol. 79, No. 1, pp. 160–163.

BRIEF COMMUNICATIONS

Magnetic Properties of Nickel–Zinc Ferrites Synthesized from Liquid Solutions Produced in Chemical and Electrochemical Processing of Metals

V. V. Pan'kov, O. P. Ol'shevskaya, and O. V. Onoprienko

Institute of General and Inorganic Chemistry, National Academy of Sciences of Belarus, Minsk, Belarus

Received October 25, 2005

Abstract—Nickel–zinc ferrite was prepared by coprecipitation from liquid waste formed in chemical and electrochemical processing of metals.

DOI: 10.1134/S1070427206010332

In industry, spent etching solutions for chemical and electrochemical processing of steel articles are converted into a solid phase that is mainly composed of heavy metal hydroxides. In various countries, this solid waste is stored on specially allocated territories and, being exposed there to the atmosphere, contaminates the environment through washing-out of heavy metals. At the same time, spent solutions containing expensive components can serve as valuable secondary raw materials and their use to synthesize ferrites would be a good way to utilize these solutions.

In this context, development of methods for synthesis of valuable products from the liquid waste formed in nickel and zinc plating and from spent solutions produced in electrochemical processing of metals, which would simultaneously eliminate their environment hazard, is, undoubtedly, a matter of current interest. Here we report a method that can be used to obtain highly dispersed powders of nickel–zinc ferrites from these solutions.

Magnetically soft nickel–zinc ferrites having low coercive force and high resistance are extensively used in transformer cores in a wide variety of radioelectronic devices. A promising method for synthesis of nickel–zinc ferrites is coprecipitation, which provides high chemical homogeneity of a magnetic material without repeated grinding and annealing at very high temperatures inherent in the ceramic technology. At the same time, the coprecipitation yields powdered materials whose particle size and stoichiometry can be preset and controlled. Here we report the results obtained in synthesis by coprecipitation of a powdered nickel–zinc ferrite of the composition $Ni_{0.35}Zn_{0.65}\cdot Fe_{1.984}O_{4\pm\gamma}$ from liquid waste formed in nickel and zinc plating, and also from a liquid solution of iron(II) sulfate, produced in chemical processing of steel in its metallurgical manufacture.

EXPERIMENTAL

The waste formed in electrochemical and chemical processing of metals, used in this study, had the following composition (g l^{-1}): (1) $ZnCl_2$ 50–80, $ZnSO_4$ 50–80, NH_4Cl 180–200, additives 35–45, Fe ≤ 0.03; (2) $NiSO_4$ 250–300, NaCl 7–15, Formalin 1.2, 1,4-butynediol 0.15–0.3, Fe ≤ 0.06; and (3) $FeSO_4$ 70–110, H_2SO_4 180.

Samples of a precursor of the ferrite $Ni_{0.35}Zn_{0.65}\cdot Fe_{1.984}O_{4\pm\gamma}$ were obtained by coprecipitation from a mixture of the required amounts of iron sulfate solutions and of the liquid waste from baths for nickel and zinc plating. Preliminarily, complexometry (Na_2EDTA) was used to determine the content of iron (Methylthymol Blue as indicator), nickel (murexide), and zinc (Eriochrome Black). A sodium carbonate solution served as a precipitating agent. A solution containing cations of nickel, zinc, and iron was slowly added to a solution of sodium carbonate, in which the pH was maintained at 9–10 during the precipitation. After the precipitation, the suspension was agitated for 5 h, washed with water to a negative reaction for sulfate and chloride anions, and filtered. Then the precursor was dried in air at 80°C and subjected to thermal treatment in the temperature range 400–950°C. The phase formation was monitored by X-ray phase analysis (CuK_α radiation). Thermogravimetric studies were performed on an MOM Q-1000 derivatograph (Hungary) in the temperature range 20–1000°C.

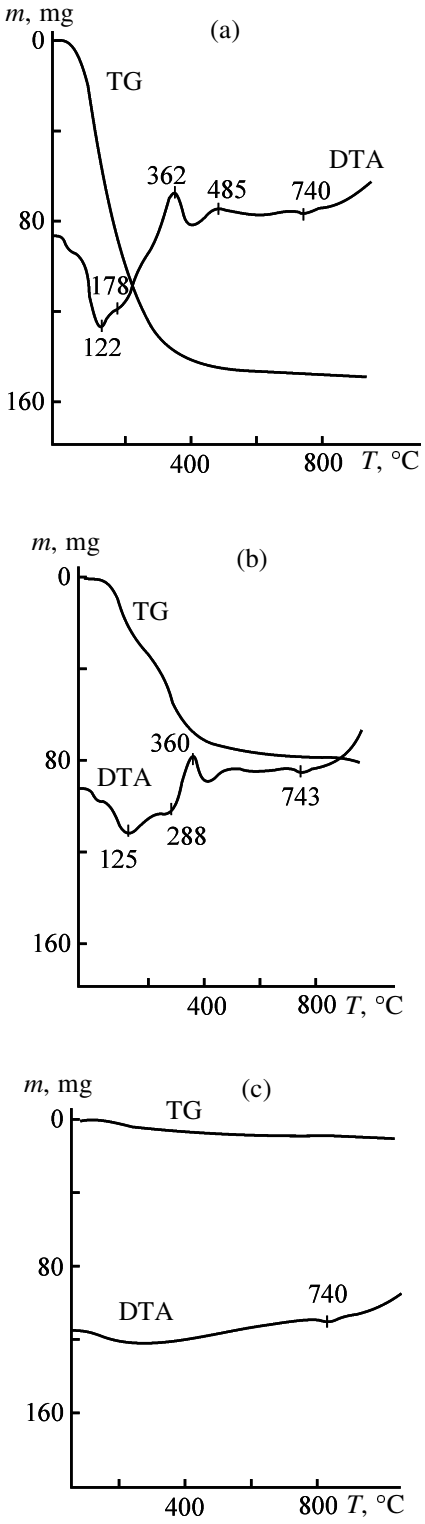


Fig. 1. DTA and TG curves of the precursor of the Ni–Zn ferrite, recorded in air for different samples. (*m*) Weight loss and (*T*) temperature. Sample: (a) dried at 80°C, (b) dried at 180°C, and (c) subjected to preliminary thermal treatment in air at 600°C.

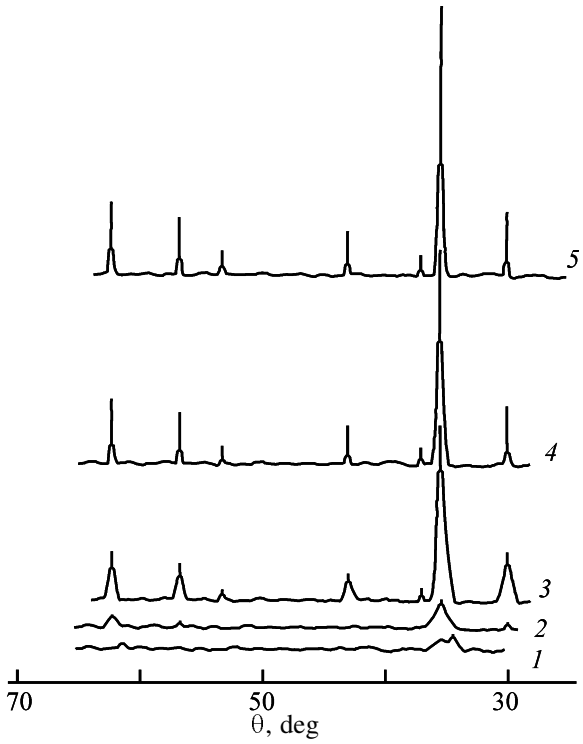


Fig. 2. Powder X-ray diffraction patterns of precursor calcined at different temperatures. (2θ) Bragg angle. *T*, °C: (*1*) 80, (*2*) 400, (*3*) 750, (*4*) 850, and (*5*) 950.

The initial permeability was measured by the induction method with samples fabricated in the form of rings with an outer diameter of 12 mm. The rings were pressed from powders to which polyvinyl alcohol was added and then were sintered at 1100–1250°C. The Curie point was determined from the temperature dependence of the specific saturation magnetization.

The size of powder particles was determined with a SediGraph 5100V2.00 particle size analyzer. The microstructure of the powders and articles fabricated from the nickel–zinc ferrite was determined by scanning electron microscopy on a JEOL 840 instrument with a REVEX (EDS) energy-dispersive analyzer.

The precursor synthesized by precipitation with an aqueous solution of Na_2CO_3 from a mixture of iron(II) solutions and solutions from baths for nickel and zinc plating is composed of a mixture of hydroxides, hydroxo carbonates, and carbonates of iron, nickel, and zinc. Figure 1a shows a derivatogram of a sample dried at 80°C, whence follows that adsorbed water is lost and the starting precursor decomposes with the weight loss in the temperature range 80–400°C. It should be noted that, according to the results of X-ray phase analysis (Fig. 2, curve *1*), the X-ray diffraction pattern of the starting precursor contains

several broadened reflections with maxima at 2.55 and 1.50 Å. This coincides with the X-ray diffraction pattern of the "bilinear" ferrihydrite phase [1], which shows only two broad diffraction bands. A similar X-ray diffraction pattern was observed in [2] for the precursor of the Ni–Zn–Cr ferrite, obtained by coprecipitation from wastes of steel works. This leads to a conclusion that cations of nickel and zinc are captured by the precipitating phase with a structure of ferrihydrite. After this phase decomposes at 360–365°C and the removal of water and carbon dioxide is complete, an exothermic effect appears in the DTA curve (Figs. 1a, 1b). This effect is, in all probability, due to formation of the spinel structure of a poorly crystallized Ni–Zn ferrite. The assignment of the exothermic effect at $T \approx 360$°C to the formation of the spinel phase is supported by the fact that this effect is not observed in the DTA curve of the sample already calcined at 600°C (Fig. 1c) and by the presence of several broad reflections associated with the poorly crystallized spinel phase in the X-ray diffraction pattern of the sample calcined at 400°C for 2 h (Fig. 2, curve *2*). It should be noted that the X-ray diffraction pattern of this sample contains no reflections related to iron oxide. All the DTA curves show a minor, with no weight loss, endothermic effect at $T \approx 740$°C, which cannot be assigned to any process as yet.

We found that the lattice constant of the forming spinel phase varies only slightly with the calcination temperature. This indicates that the composition of the phase with a spinel structure is invariable in the course of its synthesis at so low temperatures, in contrast to the ceramic technique of synthesis of Ni–Zn ferrites, in which the synthesis temperature is considerably higher [3]. In the latter case, the composition of Ni–Zn ferrites is enriched in zinc in early stages of formation.

An increase in the temperature of thermal treatment to 950°C makes higher the intensity of reflections in the X-ray diffraction pattern and leads to their narrowing, which indicates that spinel crystals become larger.

The powders synthesized at 400, 750, 850, and 950°C were used to press toroids (with a 10% solution of polyvinyl alcohol), which were then sintered at 1100, 1200, and 1250°C (3 h). The initial permeability μ was measured for these toroids. The highest initial permeability that could be obtained in sintering at 1250°C was 700 units. Figure 3 shows how the synthesis temperature of the Ni–Zn ferrite and the sintering temperature of the powders affect the permeability of the articles formed. It can be seen that

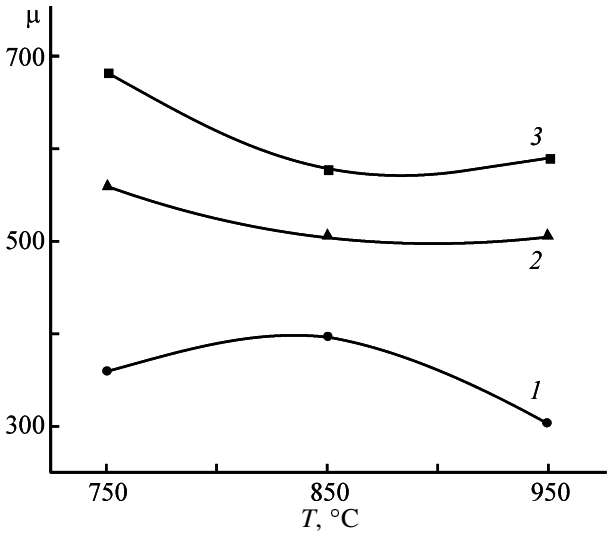


Fig. 3. Initial permeability μ of toroids fabricated from Ni–Zn ferrite vs. temperature T of their synthesis. Sintering temperature (°C): (*1*) 1100, (*2*) 1200, and (*3*) 1250.

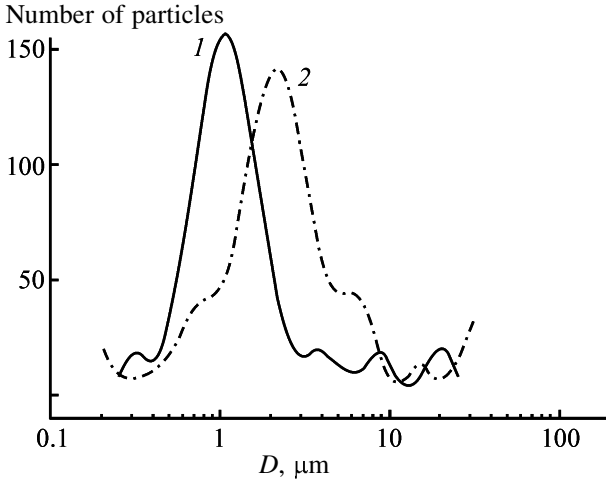


Fig. 4. Particle size (D) distribution of Ni–Zn ferrite powders synthesized at (*1*) 750 and (*2*) 850°C in 2 h.

the sintering temperature strongly affects μ, whereas the synthesis temperature affects μ to a considerably lesser extent in the range 750–950°C. This is presumably due to the fact that the particle size of powders of Ni–Zn ferrites synthesized at 750, 850, and 950°C changes only slightly. The particle size distribution curves show that the average particle size in this temperature range of synthesis is 1.0–2.2 μm (Fig. 4). The slight decrease in the initial permeability, observed as the synthesis temperature is raised, can apparently be attributed to a decrease in the activity of Ni–Zn ferrite powders synthesized at a higher temperature.

The microstructural features of the sintered toroids were studied by scanning electron microscopy of

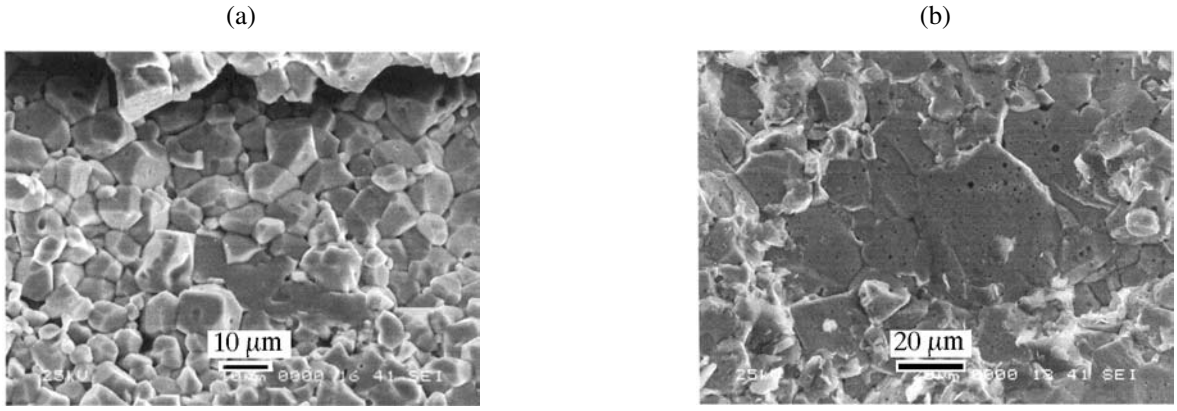


Fig. 5. Microstructure of a cleavage of Ni–Zn ferrite samples sintered at 1250°C. Synthesis duration 2 h. Synthesis temperature, °C: (a) 750 and (b) 950.

cleaved samples. A good uniformity of the grain size was only observed for samples synthesized at 750°C (Fig. 5a). It was found that raising the ferrite synthesis temperature leads to predominant growth of separate grains in sintering and is accompanied by a decrease in the initial permeability for such samples. In all probability, the extent to which the activity of ferrite particles synthesized at temperatures exceeding 750°C decreases varies with the particle size. It is this circumstance that initiates the predominant growth of separate grains in sintering of such powders at 1250°C. The samples synthesized at 950°C and sintered at 1250°C exhibit, in addition, an intragrain porosity (Fig. 5b), which also makes lower the initial permeability.

A typical temperature dependence of the specific saturation magnetization for the $Ni_{0.35}Zn_{0.65}Fe_{1.984} \cdot O_{4\pm\gamma}$ composition is shown in Fig. 6. The shape of the curve points to a rather good homogeneity of the chemical composition of the powder, and the specific saturation magnetization (σ_s = 35 G cm^3 g^{-1}) and the Curie point (θ = 227°C) correspond to the preset composition of the precursor of the Ni–Zn ferrite.

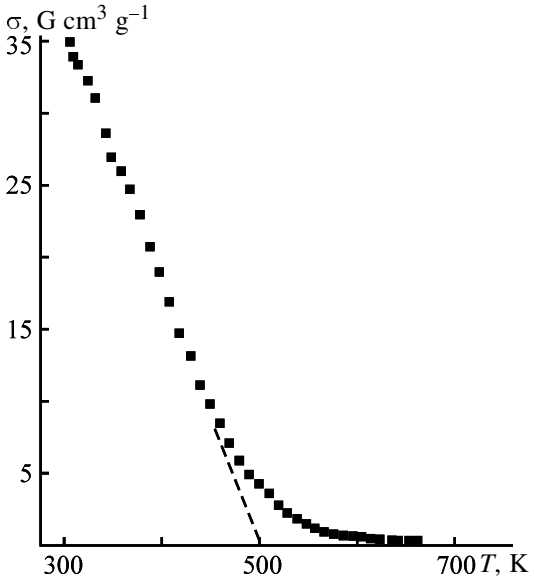


Fig. 6. Specific saturation magnetization σ vs. temperature *T* for the Ni–Zn ferrite. Synthesis temperature 750°C, sintering temperature 1250°C.

CONCLUSIONS

(1) Coprecipitation with an aqueous solution of sodium carbonate from a liquid waste produced in chemical and electrochemical processing of metals yielded a precursor from which a Ni–Zn ferrite of the spinel type is formed even upon heating to 400°C.

(2) Thermal treatment of such a powder at 750°C and sintering at 1250°C make it possible to obtain, without doping, articles with an initial permeability of more than 600 units.

REFERENCES

1. Ueda, M., Shimada, S., and Inagaki, M., *J. Mater. Chem.*, 1993, vol. 3, p. 1199.
2. Lopez-Delgado, A. and Lopes, F., *J. Mater. Res.*, 1999, vol. 14, no. 8, pp. 3427–3432.
3. Pankov, V.V. and Bashkirov, L.A., *J. Solid State Chem.*, 1981, vol. 39, no. 1, pp. 298–308.

ISSN 1070-4272. Russian Journal of Applied Chemistry, 2006, Vol. 79, No. 1, pp. 163–165. © Pleiades Publishing, Inc., 2006.
Original Russian Text © A.P. Yaroshenko, M.V. Savos'kin, V.I. Shologon, R.D. Mysyk, A.N. Magazinskii, 2006, published in Zhurnal Prikladnoi Khimii, 2006, Vol. 79, No. 1, pp. 164–166.

BRIEF COMMUNICATIONS

Synthesis and Properties of Residual Graphite Nitrate Obtained by Treatment of Graphite Nitrate with Water

A. P. Yaroshenko, M. V. Savos'kin, V. I. Shologon, R. D. Mysyk, and A. N. Magazinskii

Litvinenko Institute of Physical Organic Chemistry and Coal Chemistry, National Academy of Sciences of Ukraine, Donetsk, Ukraine

Received October 20, 2005

Abstract—The possibility of obtaining residual graphite nitrate by water treatment of graphite nitrate and its subsequent drying was studied. The expansion coefficients were determined in the temperature range 500–900°C with a step of 100°C for the samples obtained.

DOI: 10.1134/S1070427206010344

Graphite nitrate produced by treatment of graphite with fuming nitric acid is of particular interest for synthesis of flexible graphite and use in the conventional application areas of expandable graphite intercalation compounds [1]. This product is characterized by nearly zero content of sulfur [2], readily undergoes subsequent modification [3], and is effectively expanded when heated to an even relatively low temperature. The manufacture technology of this product is simple and efficient and it employs only a single cheap reagent, fuming nitric acid. However, graphite nitrate is one of the most unstable graphite intercalation compounds and is inconvenient for practical use because of the release of nitric acid introduced into the interlayer space and sorbed on the surface. Graphite nitrate isolated from the reaction mass starts to decompose immediately after being brought in contact with air [4]. The decomposition is accompanied by egress of a part of nitric acid molecules from the interlayer space and, possibly, by ingress of water molecules sorbed from air into the interlayer space [5, 6]. As a result, the so-called residual graphite nitrate is formed [6].

The above-described processes of formation of residual compounds in air are very slow and take several weeks. Attempts to accelerate the process by heating to 50–100°C lead to removal of sorbed nitric acid, but the product itself virtually completely disintegrates and loses its ability to be expanded [5, 6].

It could be assumed *a priori* that residual compounds produced by water treatment of a freshly prepared graphite nitrate must retain a high capacity for expansion and other properties useful for consumers. This study is concerned with the possibility of obtaining practically valuable residual compounds based on graphite nitrate by its water treatment. Natural scaly graphite of the GT-1 brand from the Zaval'evskoe deposit (Ukraine) with an ash content of 5.58 wt % was subjected to oxidation. The bulk of the graphite is represented by two fractions with a particle size of 0.630–0.315 (74.3 wt %) and 0.315–0.200 mm (22.1 wt %). Fuming (98%) nitric acid was used (d = 1.51 g cm^{-3}). The residual graphite nitrate was synthesized at room temperature by the following procedure. A necessary amount of nitric acid was added to 25 g of the starting graphite, and then the reaction mixture was agitated for 10 min under the conditions that provide efficient removal of the forming nitrogen oxides from the reaction mass.

When the reaction was complete, 200 cm^3 of water was poured into the reactor. The reaction mass was agitated for 1 min and then quantitatively transferred to a Büchner funnel and washed with 2 dm^3 of water. The product, washed and squeezed on a filter, was quantitatively transferred to Petri dishes and dried in air to constant weight (about 3 days at 20–30°C). The data on the yield of the product were used to calculate the content m_0 of the intercalant in the product on the assumption that phase oxidation reactions do not occur at room temperature, i.e., the whole amount of carbon from the graphite matrix passes into the final product.

The product obtained, residual graphite nitrate, is a dry loose graphite-like powder with a pH value of

Effect of the expenditure of fuming nitric acid on the intercalant content c and on the expansion coefficient of the final product

Expenditure of HNO_3, g/100 g	c, %	K_v, $cm^3\ g^{-1}$, at indicated expansion temperature, °C				
		500	600	700	800	900
9	1.57	9	11	12	16	21
18	3.25	23	27	33	45	59
27	4.62	41	49	64	98	107
36	6.82	63	87	104	171	203
45	7.17	61	92	139	169	200
54	10.97	55	92	145	180	228
63	11.54	57	96	146	205	231
72	12.13	54	125	160	225	233
81	13.22	59	126	155	217	225
90	15.71	57	128	156	224	232

its water extract falling within the range 2.4–3.3, which makes it convenient for practical use. The product is effectively expanded on heating to give expanded graphite with a bulk density as low as 4 kg m^{-3}.

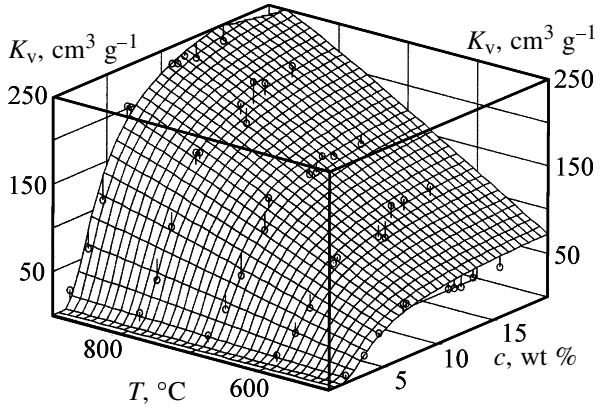


Fig. 1. Expansion coefficient K_v of samples of residual graphite nitrate vs. the intercalant content c and expansion temperature T.

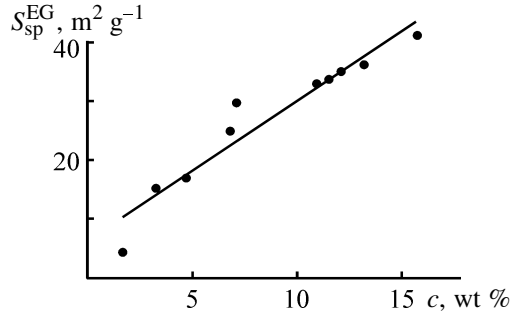


Fig. 2. Specific surface area S_{sp}^{EG} of expanded graphites obtained from samples of residual graphite nitrate at 700°C vs. the content c of the intercalant in these samples.

The expansion coefficient of the products obtained was determined as follows. A weighed portion of the product (m = 0.2–0.3 g) was introduced into a stainless steel cell preliminarily placed in a muffle furnace heated to 500–900°C and was kept there to complete expansion. The cell with the expanded graphite was withdrawn from the furnace, its contents were transferred with caution into a glass volumetric cylinder, and the volume V (cm^3) occupied by the expanded graphite was measured. The expansion coefficient was determined using the formula $K_v = V/m$ as an arithmetic mean of the results of three replicate measurements. The BET specific surface area of samples of expanded graphite, S_{sp}, was found from low-temperature adsorption of argon in conformity with GOST (State Standard) 13144–79. The pH values of water extracts from the samples of residual graphite nitrate were determined in accordance with GOST 17818.6–90.

The table shows how nitric acid in the stage of graphite oxidation affects the intercalant content and the expansion coefficient of the final product at different temperatures.

Figure 1 shows that the expansion coefficient of residual graphite nitrate increases with the content of intercalant in the graphite and with the expansion temperature. In the temperature range studied (500–900°C), the temperature dependences of the expansion coefficient are nearly linear for all values of c and tend to flatten out only at 800–900°C. The dependence of the expansion coefficient on the intercalant content is similar in the entire temperature range studied.

Figure 2 shows that the specific surface area of expanded graphite grows linearly with the intercalant

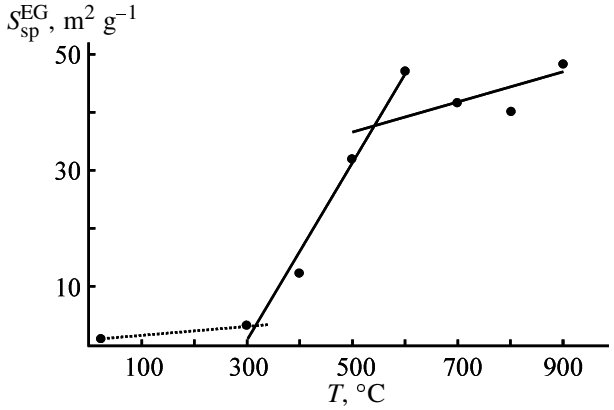


Fig. 3. Specific surface area S_{sp}^{EG} of expanded graphites obtained from a sample of residual graphite nitrate synthesized at an expenditure of fuming nitric acid of 90 g/100 g graphite (c = 15.71 wt %) vs. the expansion temperature T.

content in the starting samples of residual graphite nitrate and reaches a value of about 40 m^2 g^{-1}, which is characteristic of expanded graphite obtained from graphite intercalation compounds in their interaction with acids.

It is appropriate to discuss the plot of the specific surface area of expanded graphite vs. the temperature at which it is obtained (Fig. 3). Three linear portions can be distinguished in this plot. These portions correspond to three temperature ranges: 0–300, 300–550, and 550–900°C. In the first of these, raising the temperature at which the expansion is performed causes only a slight increase in the specific surface area S_{sp}^{EG}. Raising the expansion temperature from 300 to 550°C leads to a steep rise in S_{sp}^{EG} (about 10 m^2 g^{-1}) per 100°C, and in the third temperature range, values of S_{sp}^{EG} grow by only ~2 m^2 g^{-1} per 100°C. Such a run of this dependence can be attributed to the fact that both the starting residual graphite nitrate and expanded graphite prepared from it have virtually zero porosity in the classical understanding of this term. Then the pronounced increase in the specific surface area can occur only via formation of a new open surface.

In the first temperature range, there is no effective expansion of the graphite matrix. Only a pre-expansion occurs to give lens-like particles whose surface area only slightly exceeds that for flat particles of the starting residual graphite nitrate. In this case, the lenses are not ruptured and, as a result, no new surface is formed.

In the second temperature range, the volume of close lenses further increases and they break up to form a new open surface. The fraction of broken-up lenses increases with temperature and, at the end of the second range, virtually all the lenses are broken.

Raising the expansion temperature from 550 to 900°C causes, in all probability, a deeper breakup of the lenses and thereby leads to an additional separation of carbon layers, and just this fact is responsible for the additional gain in the new open surface area.

CONCLUSIONS

(1) Water treatment of graphite nitrate with the subsequent air drying of the resulting product yields residual graphite nitrates that can effectively expand on heating to form expanded graphite. The products obtained are convenient in handling and can find practical use in fire prevention and metallurgy.

(2) The temperature dependences of the expansion coefficient are nearly linear and, depending on the content of intercalate, have the form of ascending curves that level off at approximately 10 wt % intercalate. The maximum expansion coefficient is 230 cm^3 g^{-1}.

(3) The expanded graphite formed when products of this kind are heated compares well in its parameters, bulk density and specific surface area, with that produced from graphite hydrosulfate and can be successfully used as a petroleum sorbent and catalyst support, as well as in manufacture of flexible graphite and articles made of this material.

REFERENCES

1. Yaroshenko, A.P., Popov, A.F., and Shapranov, V.V., *Zh. Prikl. Khim.*, 1994, vol. 67, no. 2, pp. 204–211.
2. Xiling, C., Kemin, S., Jihui, Li, and Jinpeng, L., *Carbon*, 1996, no. 12, pp. 1599–1600.
3. Savos'kin, M.V., Yaroshenko, A.P., Mysyk, R.D., *et al.*, *Teor. Eksp. Khim.*, 2004, no. 2, pp. 89–94.
4. Forsman, W.C., Carl, D.E., and Vogel, F.L., *Mater. Sci. Eng.*, 1981, no. 3, pp. 187–191.
5. Inagaki, M., *Carbon*, 1967, no. 3, pp. 317–318.
6. Fusellier, H., Melin, J., and Herold, A., *Mater. Sci. Eng.*, 1977, pp. 91–94.

ISSN 1070-4272. Russian Journal of Applied Chemistry, 2006, Vol. 79, No. 1, pp. 166–168. © Pleiades Publishing, Inc., 2006.
Original Russian Text © O.V. Arapov, N.D. Abovskii, N.A. Charykov, V.I. Seregin, K.V. Nekrasov, V.I. Gerasimov, 2006, published in Zhurnal Prikladnoi Khimii, 2006, Vol. 79, No. 1, pp. 167–169.

BRIEF COMMUNICATIONS

Distribution of C_{60} and C_{70} Fullerenes in the Extraction System (C_{60} + C_{70})–α-Pinene–Ethanol–H_2O

O. V. Arapov, N. D. Abovskii, N. A. Charykov, V. I. Seregin, K. V. Nekrasov, and V. I. Gerasimov

St. Petersburg State Technological Institute, St. Petersburg, Russia
Innovations of Leningrad Institutes and Enterprises Private Company, St. Petersburg, Russia

Received October 18, 2005

Abstract—The distribution of C_{60} and C_{70} fullerenes in the extraction system (C_{60} + C_{70})–α-pinene– ethanol–H_2O was studied at constant C_{60} to C_{70} ratio and variable total fullerene concentration at 25°C. The relationship between the C_{60} and C_{70} content in ethanol (I) and α-pinene (II) phases is nonlinear over the entire fullerene concentration range.

DOI: 10.1134/S1070427206010356

The development of new high-performance techniques for recovery of fullerenes from their mixtures to obtain relatively cheap commercially available individual fullerenes of high purity is an urgent problem. In this respect, the solvent extraction shows certain advantages as compared to commonly used preparative chromatography.

The first data on distribution of light fullerenes C_{60} and C_{70} in three extraction systems based on *o*-xylene as extractant were reported in [1, 2]. Proceeding with development of extraction system for separation of fullerene mixtures, we looked for a nonaromatic solvent that would readily dissolve fullerenes and form with nonaromatic polar components a multicomponent system with a large area of phase separation. Furthermore, solvated fullerenes (liquid or solid) which can be formed in such an extraction system must be sufficiently readily converted to nonsolvated pure fullerenes.

EXPERIMENTAL

It was found previously that commercial turpentine and turperntine oils containing α-pinene (2,6,6-trimethylbicyclo[3.1.1]hept-2-ene) fairly readily dissolve fullerenes. The treatment of fullerene-containing soot with these solvents allows preparation of organic solutions containing 1.5–2.5 g l^{-1} of C_{60}–C_{70} mixture, which is comparable with the solubility of fullerenes in toluene but is somewhat lower than their solubility in *o*-xylene [3–7].

On mixing α-pinene or its organic solutions with several polar solvents (H_2O, C_2–C_4 *n*-alkanols, diols), two-phase systems are formed without addition of specific phase-separating reagents as it is required in the systems studied in [1, 2]. This feature simplifies the preparation of extraction systems suitable for separation of fullerene mixtures. Since α-pinene is immiscible with water and fullerenes are insoluble in the aqueous phase, the binary pinene–water system is useless for separating fullerene mixtures. At the same time, the two-phase system formed by α-pinene with *n*-alkanol (e.g., ethanol) or *n*-alkanol–water mixture is characterized by more even distribution of all the components (among them fullerenes) and, therefore, can be used for extractive separation of fullerenes. In the case of α-pinene (or α-pinene-based solvent)–ethanol–water system, the lower phase is enriched in α-pinene (hereinafter this phase is referred to as the α-pinene phase) and the upper phase is enriched in ethanol (hereinafter referred to as the ethanol phase). In the course of phase equilibration, the α-pinene phase considerably contracts whereas the ethanol phase volume increases. In our experiments, the final (equilibrium) volume ratio of the ethanol and α-pinene phases was approximately 1 : 2.

It should be noted that commercial nonaromatic solvents (turpentine, turpentine oils, α-pinene) suitable for extractive treatment of fullerenes are much cheaper than chemically pure or analytically pure grade aromatic solvents (e.g., *o*-xylene).

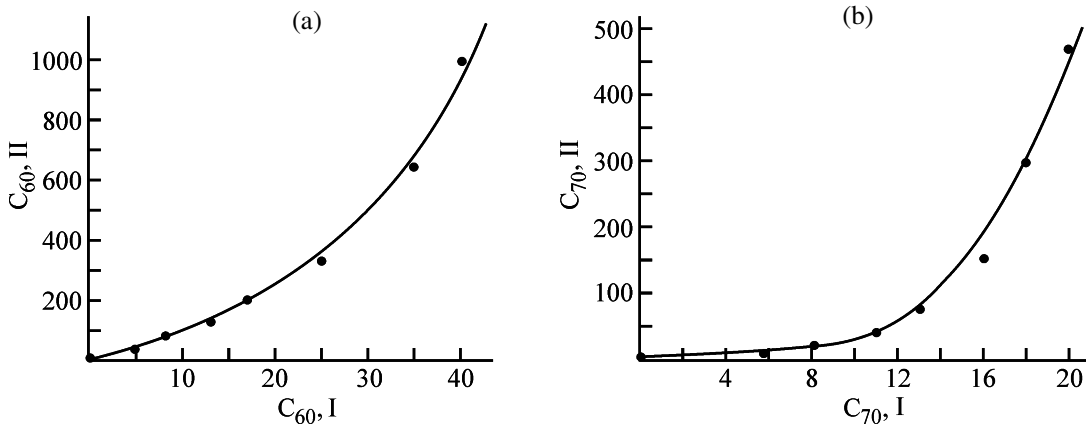


Fig. 1. Distribution of (a) C_{60} and (b) C_{70} between (I) ethanol and (II) α-pinene phases in the system (C_{60} + C_{70} fullerenes)–α-pinene–ethanol–H_2O at 25°C. For comments, see text.

In our experiments we studied the distribution of C_{60} and C_{70} fullerenes in the five-component two-phase system (C_{60} + C_{70} fullerenes)–α-pinene–ethanol–H_2O at 25°C. The extraction equilibria in this system were studied by the technique reported in [1, 2]. The C_{60} + C_{70} mixture was introduced into the extraction system in the form of a solid solution $(C_{60})_{0.68}(C_{70})_{0.32}$ which dissociates into individual fullerenes in the solvating solvents [8]. The equilibrium distribution of fullerenes was attained within 4–6 h. This time was by an order of magnitude shorter than that in the similar systems studied in [1, 2].

The main component contents in the coexisting phases as determined chromatographically was as follows (wt %). α-Pinene phase: α-pinene, 90; ethanol, 5; and water, 5; ethanol phase: α-pinene, 12; ethanol, 62; and water, 26.

Figures 1a and 1b show the distribution of C_{60} and C_{70} between the αpinene and ethanol phases at constant C_{60} content (68 wt %) in the C_{60}–C_{70} mixture and variable total fullerene concentration. The corresponding distribution curves are nonlinear over the entire fullerene concentration range. The similar nonlinear distribution of fullerenes was observed in other extraction systems [1, 2]. In our systems, the maximal C_{60} + C_{70} fullerene concentrations in the α-pinene and ethanol phases were 1400 and ~60 mg l^{-1}, respectively. These values are higher than those in the dimethylformamide-containing system [2] but lower than in the *n*-butylamine- and monoethanolamine-containing systems [1, 2]. Our results show also that in all the systems the α-pinene phase is enriched in C_{60} and C_{70} fullerenes, except for the region of very low C_{70} concentration in the ethanol phase (Fig. 1b).

The C_{60} distribution factor (the fullerene concentration ratio in the α-pinene and ethanol phases) gradually increases from 6.7 to 25 with an increase in the C_{60} + C_{70} concentration in the α-pinene phase from ~40 to 1400 mg l^{-1} (Fig. 1a). The C_{70} distribution factor gradually increases from 0.8 to 2.0 in going from dilute to concentrated solutions of fullerene in the α-pinene phase (Fig. 1b).

The C_{60} distribution factors in our systems are lower than those in the system (C_{60} + C_{70})–*o*-xylene–dimethylformamide and are commensurable with those in the system (C_{60} + C_{70})–toluene–dimethylformamide [2]. The C_{70} distribution factors in our and the above-noted systems [2] are commensurable.

The C_{60}/C_{70} separation factors K_s (the ratio of C_{60} and C_{70} distribution factors) gradually increase from ~8.4 to ~12.5 in going from dilute to concentrated fullerene solutions. It should be noted that in preliminarily studied systems of similar type [1, 2] K_s either remains constant or gradually decreases with increasing the total fullerene content.

Figure 2 shows that C_{60} preferentially accumulates in the α-pinene phase (its relative content ranges from 68 to 87 wt %). At the same time, the ethanol phase is enriched in C_{70} fullerene (its relative content ranges from 35 to 64 wt %). These results show that the aromatic α-pinene phase of lower polarity is enriched in less polarizable (spheroidal) C_{60} fulerene, whereas more polarizable ellipsoidal C_{70} fullerene is accumulated in the more polar phase (amine, monoethanolamine, DMF, ethanol). The similar relationships were preliminarily reported in [1, 2].

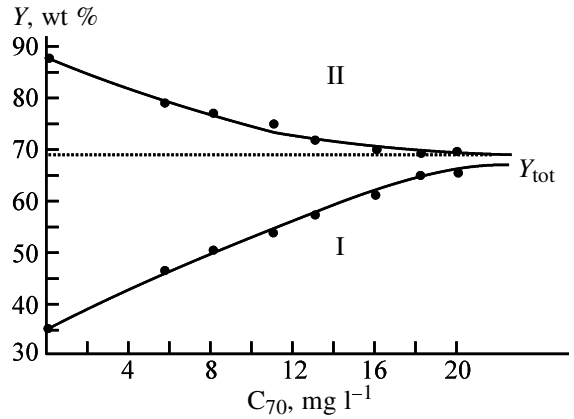


Fig. 2. C_{60} content Y in the $C_{60} + C_{70}$ mixture in (I) ethanol and (II) α-pinene phases vs. the C_{70} content in the ethanol phase in the system ($C_{60} + C_{70}$ fullerenes)–α-pinene–ethanol–H_2O at 25°C. Dotted line: starting $C_{60} + C_{70}$ mixture containing 67.9% C_{60}. Y values corresponding to the zero C_{70} content in the ethanol phase were obtained by extrapolation.

CONCLUSIONS

(1) The distribution of C_{60} and C_{70} in the system ($C_{60} + C_{70}$)–α-pinene–ethanol–H_2O can be used for separation of C_{60} from C_{70}.

(2) The C_{60} distribution factors (fullerene concentration ratio in α-pinene and ethanol phases) gradually increases from 6.7 to 25 with an increase in the $C_{60} + C_{70}$ concentration in the α-pinene phase from ~40 to 1400 mg l^{-1}.

(3) The C_{70} distribution factor gradually increases from 0.8 to 2.0 in going from dilute to concentrated solution of fullerenes in the α-pinene phase.

(4) The C_{60}/C_{70} separation factor K_s (ratio of distribution factors of C_{60} and C_{70}) gradually increases from ~8.4 to ~12.5 in going from dilute to concentrated solutions of fullerenes.

ACKNOWLEDGMENTS

This study was financially supported by the Russian Foundation for Basic Research (project no. 03-05-65 164) and Target Federal Scientific Program "Research and Developments in Priority Lines of Science and Engineering Progress" in 2002–2006 (State Contract no. 02.467.11.7005, May 23, 2005).

REFERENCES

1. Arapov, O.V., Pronkin, A.A., Charykov, N.A., *et al.*, *Zh. Prikl. Khim.*, 2003, vol. 76, no. 1, pp. 39–45.
2. Arapov, O. V., Seregin, V.I., Nekrasov, K.V., *et al.*, *Pis'ma Zh. Tekh. Fiz.*, 2003, vol. 29, no. 3, pp. 74–81.
3. Sivaraman, N., Dhamodaran, R., Kalliapan, I., *et al.*, *J. Electrochem. Soc. Recent Adv. Chem. Phys. Fullerenes Relat. Mater.*, 1994, vol. 94-24, pp. 156–165.
4. Kushch, N.D., Majchrzak, I., Ciesielski, W., *et al.*, *Chem. Phys. Lett.*, 1993, vol. 215, pp. 317–321.
5. Zhou, X. and Gu, Z., *Chin. Bull.*, 1993, vol. 38, pp. 175–181.
6. Zhou, X. and Gu, Z., Wu, J., *et al.*, *Carbon*, 1994, vol. 32, pp. 935–938.
7. Arapov, O.V., Aksel'rod, B.M., Pronkin, A.A., *et al.*, *Zh. Prikl. Khim.*, 2003, vol. 76, no. 1, pp. 35–38.
8. Ponomarev, A.N., Aksel'rod, B.M., Charykov, N.A., *et al.*, *Zh. Fiz. Khim.*, 2000, vol. 74, pp. 2031–2033.

ISSN 1070-4272. Russian Journal of Applied Chemistry, 2006, Vol. 79, No. 1, pp. 169–171. © Pleiades Publishing, Inc., 2006.
Original Russian Text © V.V. Sidorchuk, 2006, published in Zhurnal Prikladnoi Khimii, 2006, Vol. 79, No. 1, pp. 170–172.

BRIEF COMMUNICATIONS

Production of Microspherical Aerosilogels by Spray Drying in a Superheated Steam

V. V. Sidorchuk

Institute of Sorption and Problems of Endoecology, National Academy of Sciences of Ukraine, Kiev, Ukraine

Received May 18, 2005

Abstract—The effect of spray drying of aerosil dispersions in a superheated steam on the formation of microspherical grains and their pore structure was studied.

DOI: 10.1134/S1070427206010368

Modern procedures of liquid chromatography require supports with microspherical grains less than 100 μm in size [1–4]. The preferable technique for synthesis of silica microspheres is spray drying, which combines several important procedures: filtration, drying, and granulation [4–9]. It was noted in [9–11] that drying of suspensions in a superheated steam is advantageous: because of the smaller humidity gradient between the heat carrier and the material being dried, the process occurs in a milder mode, and the fact that the specific heat of steam is 20–30% higher than that of air results in a higher efficiency and rate of drying and lower specific consumption of heat. In [4, 12] we suggested that, in spray drying of silica dispersions with a superheated steam, microspherical particles will be subjected to an additional (even though short-term) hydrothermal (or heat-and-steam) treatment. In the present study we experimentally checked this hypothesis.

It is known that high-purity pyrogenic oxides, and primarily aerosil, are promising for preparation of supports used in catalysis and chromatography. Oxides of this kind can be easily formed as grains and articles of various shapes and dimensions to give uniformly mesoporous structures [4, 13]. Therefore, we examined the influence exerted by the conditions of spray drying of aerosil dispersions in water and ammonia solutions on the properties of the microspherical product, with a superheated steam used as heat carrier.

EXPERIMENTAL

The dispersions studied were prepared from A-175 and A-380 aerosils mixed with distilled water or 2 and 5% ammonia solutions at an aerosil content of 15 wt %, which approximately corresponds to the critical concentration of structurization for these systems [8, 14]. Dispersions with such a content of the solid phase have the best structural-mechanical and rheological parameters for their granulation [8]. The spray drying in a superheated steam with a temperature of 300–600°C was performed on a pilot installation described in [15]. The specific surface area S was measured on a GKh-1 gas meter, using the thermal desorption of argon; and the total pore volume V_Σ, pore size distribution, and the most probable pore diameter d were determined on a PA-3M mercury porosimeter. The granulometric analysis of microspherical aerosilogels was carried out with an Optima microscope (Germany), with the number of grains measured equal to 100–150. The data obtained in these measurements were used to plot the particle-size distribution histograms and to calculate the average grain size D_{av}.

The table lists the structural parameters of the aerosils obtained. It can be seen that even a short-time con-

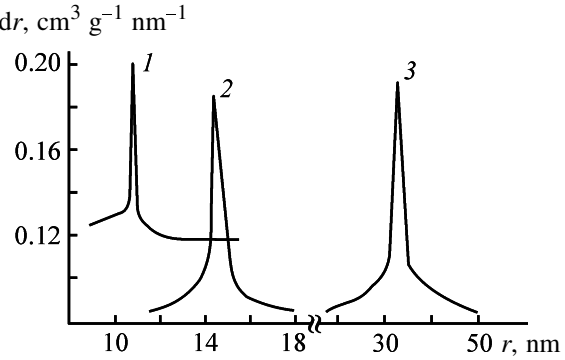


Fig. 1. Distribution of the pore volume with respect to the pore size for aerosilogels (see table). (V) Pore volume and (r) pore radius. Sample no.: (1) 8, (2) 9, and (3) 5.

Effect of the conditions of spray drying on the properties of microspherical aerosilogel

Sample no.	Aerosil	Medium	T, °C	S, $m^2 g^{-1}$	V_Σ, $cm^3 g^{-1}$	d, nm	D_{av}, μm
1	A-175	Water/air*	400	191	1.70	37.2	17.6
2	A-175	Water	400	170	1.82	42.8	12.3
		Ammonia:					
3	A-175	1%	400	154	2.02	54.0	12.4
4	A-175	2%	400	125	2.68	88.5	13.1
5	A-175	5%	400	141	2.48	64.8	12.9
6	A-175	2%	500	98	3.07	122.0	12.8
7	A-175	2%	600	85	3.40	160.0	13.0
8	A-380	Water	400	332	1.65	21.6	13.1
9	A-380	Water	500	314	2.12	28.8	11.2
10	A-380	Water	600	290	2.88	41.5	10.6
		Ammonia:					
11	A-380	2%	400	256	2.21	35.0	8.5
12	A-380	2%	500	240	2.15	34.2	12.4
13	A-380	2%	600	238	2.16	38.1	13.3
14	A-380	5%	600	277	2.01	29.6	9.3

* Dispersion medium, water; heat carrier, air.

tact of aerosilogel grains with steam (residence time of a particle in the drying chamber equal to 15–40 s [9]) leads to rather significant changes in the porosity parameters. This can be attributed to the following: (i) very high temperature of steam; (ii) catalytic effect of ammonia on the mass transfer of silica, which underlies changes in porosity [16]; and (iii) high degree of dispersion spraying and, accordingly, the instantaneous warming-up of its drops over the entire cross section. It can be noted for comparison that the ordinary hydrothermal treatment of silicas at temperatures of 100–300°C, as a rule, requires 3–5 h for an effect of this kind to be achieved [2, 4, 16], and, because of the poor heat conductivity of silica, operation of large semicommercial autoclaves frequently requires a treatment duration of up to 24 h [17] for a product with uniform properties to be obtained.

The patterns of variation of the pore structure, observed as the temperature of the heat carrier (steam) increases, are conventional: the specific surface area decreases and pores grow in volume and size (see table and Fig. 1). At a high ammonia concentration (5%), a minor relative rise in S and the corresponding decrease in V_Σ and d are observed, apparently because of the partial peptization of silica (see table, sample nos. 5 and 14).

It should be noted that use of a steam superheated to 300–600°C, instead of air, provides milder conditions for removal of the liquid from dispersion drops

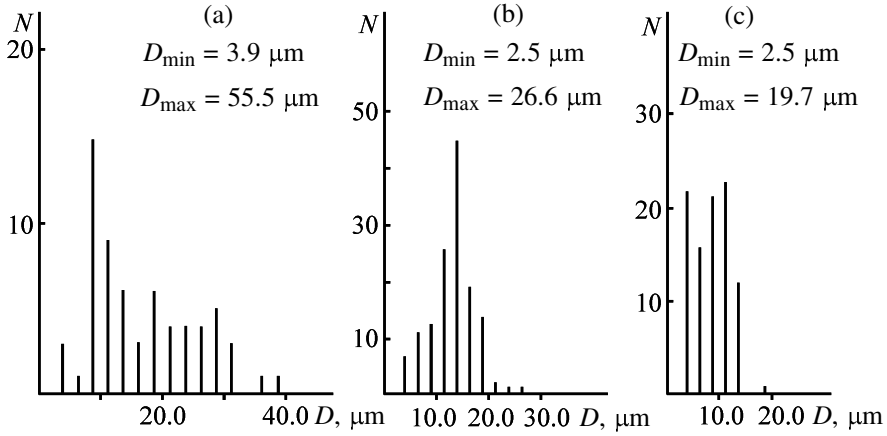


Fig. 2. Histograms of the distribution of the number N of aerosilogel grains with respect to their size D. Sample no.: (a) 1, (b) 5, and (c) 11.

and, consequently, allows the build-up of large stresses in the structure of the forming dry aerosilogel to be avoided. At the same time, the high temperature of the heat carrier and the accordingly high temperature of the intermicellar liquid in the gel result in that the surface tension of this liquid decreases and a very large (>3 $cm^3 g^{-1}$) pore volume in microspherical grains is formed.

According to the table and Fig. 2, the spray drying in a superheated steam leads to formation of finer, and more uniform in size, microspheres, compared with drying with hot air (compare the scatter of grain sizes from D_{min} to D_{max} for both cases). This points to technological advantages of the drying process under consideration.

It should also be added that the heat carrier steam is formed from aerosil dispersions in the course of drying and can be repeatedly used upon condensation to prepare new portions of aerosil dispersions, i.e., the process can be organized as a closed cycle.

CONCLUSION

Use of superheated steam in spray drying of aerosil dispersions makes it possible to obtain a microspherical aerosilogel with a uniform granulometric composition (grain size 10–12 μm). As a result of a hydrothermal treatment, the parameters of the porous structures of the samples vary widely: pore volume, up to 3.4 $cm^3 g^{-1}$, and pore size, up to 160 nm.

REFERENCES

1. Engelhardt, H., *Hochdruck–Flüssigkeits–Chromatographie*, Berlin: Springer, 1977, 2nd ed.
2. *Modifitsirovannye kremnezemy v sorbtsii, katalize i khromatografii* (Modified Silicas in Sorption, Catalysis, and Chromatography), Lisichkin, G.V., Ed., Moscow: Khimiya, 1986.
3. Unger, K.K. and Janzen, R., *J. Chromatogr.*, 1986, vol. 373, pp. 227–264.
4. Sidorchuk, V.V. and Tertykh, V.A., *Khim. Tekhnol.*, 1989, no. 4, pp. 3–15.
5. USSR Inventor's Certificate no. 264 369.
6. UK Patent 1 567 003.
7. USSR Patent 1 836 292.
8. Kotel'nikov, G.R., *Nauchnye osnovy prigotovleniya katalizatorov* (Scientific Foundations of Catalyst Preparation), Novosibirsk: Nauka, 1982, pp. 37–60.
9. Dolinskii, A.A. and Ivanitskii, G.K., *Optimizatsiya protsessov raspylitel'noi sushki* (Optimization of Spray Drying Processes), Kiev: Naukova Dumka, 1984.
10. Danilov, O.L. and Leonchik, B.I., *Inzh.-Fiz. Zh.*, 1967, vol. 13, no. 3, pp. 283–288.
11. Dolinskii, A.A. and Volovik, Yu.I., *Dal'neishee sovershenstvovanie teorii, tekhnologii i tekhniki sushki* (Further Improvement of the Theory and Technology of Drying), Kiev: Naukova Dumka, 1981, pp. 7–8.
12. Ryzhkova, T.S., Maidannik, D.G., and Sidorchuk, V.V., *Dvukhfaznyi potok v energeticheskikh mashinakh i apparatakh* (Two-Phase Flow in Energy-Producing Machines and Apparatus), Leningrad: 1990, vol. 3, pp. 283–284.
13. Despeyroux, B., Deller, K., and Krause, H., *Chem. Ind.*, 1993, vol. 116, no. 10, pp. 48–49.
14. Kruglitskii, N.N., Pakhovchishin, S.V., and Gritsenko, V.F., *Khim. Tekhnol.*, 1977, no. 5, pp. 24–27.
15. Dolinskii, A.A. and Volovik, Yu.I., *Prom. Teplotekh.*, 1980, vol. 2, no. 4, pp. 72–79.
16. Sidorchuk, V.V., Maidannik, D.G., and Tertykh, V.A., *Zh. Prikl. Khim.*, 1991, vol. 64, no. 9, pp. 1870–1873.
17. Kustova, G.L., Development of Uniformly Coarse-Porous Silica Sorbents for Gas Chromatography, *Cand. Sci. Dissertation*, Moscow, 1970.

ISSN 1070-4272. Russian Journal of Applied Chemistry, 2006, Vol. 79, No. 1, pp. 172–173. © Pleiades Publishing, Inc., 2006.
Original Russian Text © A.G. Morachevskii, 2006, published in Zhurnal Prikladnoi Khimii, 2006, Vol. 79, No. 1, pp. 173–174.

BOOK REVIEWS

Usanovich, M.I., *Iz istorii khimii. Ocherki iz zhizni i deyatel'nosti vydayushchikhsya uchenykh* (From the History of Chemistry. Essays about the Life and Activities of Prominent Scientists)

Almaty: Kazakh Univ., 2004, 328 pp.

DOI: 10.1134/S107042720601037X

Professor M.I. Usanovich (1894–1981), a known Russian physical chemist and historian of chemistry, wrote these essays as far back as 1941–1945. However, numerous difficulties encountered when promoting the manuscript, and accusations of underestimation of the role of Russian scientists in the development of the world's chemical science, which were typical of that time, forced the author to give up his attempts to publish the book. Only nowadays, more than 20 years after the scientist's death, his widow, prof. T.N. Sumarokova and a group of Usanovich's disciples could publish this interesting book with the support by the management of Kazakh National University.

The many years' scientific activities of Usanovich were devoted to experimental and theoretical studies of nonaqueous solutions, their physicochemical analysis, and development of the generalized theory of acids and bases. He also wrote a number of papers on the history of chemistry. His investigations in the field of theory of acids and bases made him worldwide known; biographic evidence about the scientist is included in the collection of works *Biografii velikikh khimikov* (Biographies of Outstanding Chemists), Berlin, 1977; Moscow, 1981.

The scientific activities of Usanovich commenced in the autumn of 1918, after he graduated from the natural department of the physicomathematical faculty of the Kiev University, at the biogeochemical laboratory of Academician V.I. Vernadsky (1863–1945), which was among the institutions affiliated with the newly organized Ukrainian Academy of Sciences. Usanovich was a professor at the Tomsk State University in 1930–1934 and headed the chair of physical chemistry at the Central-Asian State University (Tashkent) in 1935–1944 and the chair of physical chemistry at the Kazakh State University in 1944–1981. In 1962, he became academician of the Academy of Sciences of Kazakh SSR. The most important Usanovich's scientific works were included in the collection of works *Issledovaniya v oblasti teorii rastvorov i teorii kislot i osnovanii. Izbrannye trudy* (Investigations in the Theory of Solutions and Theory of Acids and Bases, Selected Works), Alma-Ata: Nauka Kaz. SSR, 1970.

The collection of essays under discussion covers the main events in the history of chemistry from ancient times till the 1940s. People whose biographies are presented in the book are of different ethnic origins and nationalities, but all of them are united by the outstanding contribution to some field of chemistry at a certain period of history. The short author's preface to the collection of essays reads: "The science is international in its origin, because it is a fruit of activities of representatives of all cultured nations and its mission is to serve to the entire humankind." The book comprises 24 brief chapters arranged in historical order.

Chapter I (pp. 15–17) is devoted to the development of chemistry in the Ancient world. The concepts of Aristotle (384–322 B.C.) and Avicenna (980–1037) are presented. Evidence about alchemists of the later time, XIII century, is presented for Albert Magnus, Count Bollstadt (1193–1280), and Roger Bacon (1214–1294). Chapter II (pp. 28–40) discusses works of the most outstanding chemists of the XV and XVI centuries: Paracelsus (1493–1541), Agricola (1494–1555), and van Helmont (1577–1644). Chapter III (pp. 41–44) is concerned with the appearance of the concept of chemical elements. The central position in this chapter is devoted to the life and works of Robert Boyle (1627–1691). Chapter IV (pp. 45–55) presents evidence about the theory of phlogiston and works by H. Stahl (1659–1734), K.W. Scheele (1742–1786), J. Priestley (1733–1804), and H. Cavendish (1731–1810). In chapter V (pp. 56–65), the author analyzes the positive aspects and disadvantages of the theory of phlogiston. The whole chapter VI (pp. 66–76) is devoted to the life and activities of a Russian physical chemist, M.V. Lomonosov (1711–1765). A prominent role in the correct assessment of the scientific achievements of Lomonosov was played by B.N. Menshutkin (1874–1938), who found at the beginning of the

XX century manuscripts of Lomonosov's works, mostly written in Latin, translated these works, and made them accessible to the scientific community. Already in 1904, Menshutkin published a large article "Lomonosov as Physical Chemist" in *Izvestiya Sankt-Peterburgskogo politekhnicheskogo instituta* (Transactions of St. Petersburg Polytechnic Institute), in *Zhurnal russkogo fiziko-khimicheskogo obshchestva* (Journal of the Russian Physicochemical Society), and as a separate edition. The author of these publications was the first to make a full review of all done by Lomonosov in the field of chemistry and physics. In 1911, in connection with the celebration of the 200th anniversary of Lomonosov's birthday, Menshutkin wrote his biography. The many years' studies of the Lomonosov's life and scientific activities culminated in the monograph *Trudy M.V. Lomonosova po fizike i khimii* (M.V. Lomonosov's Works in Physics and Chemistry, 1935).

Chapter VII (pp. 77–84) considers works by C.L. Berthollet (1748–1822) and J.L. Proust (1754–1826), the prolonged polemics between these two about the constancy of composition of substances, and studies by J.B. Richter (1762–1807). Chapter VIII (pp. 85–90) is devoted to the contribution by John Dalton (1766–1844) to the creation of the atomistic theory. Chapter IX (pp. 91–96) describes works by J.L. Gay-Lussac (1778–1850) and A. Avogadro (1776–1856), associated with the further development of the atomic-molecular theory.

Chapter X (pp. 97–104) is devoted to great electrochemists of their time, H. Davy (1778–1829) and M. Faraday (1791–1867). Chapter XI (pp. 105–110) considers works by Swedish scientist J.J. Berzelius (1779–1848), one of the most versatile and successful chemists of the first half of the XIX century. Chapter XII (pp. 111–123) contains evidence about the basic research in the field of organic chemistry. It discusses works by J. Liebig (1803–1873), F. Wöhler (1800–1882), N.N. Zinin (1812–1880), and A.A. Voskresenskii (1809–1880). Chapters XIII (pp. 124–132), XIV (pp. 133–140), and XV (pp. 141–151) continue consideration of the fundamental aspects of organic chemistry, with special attention given to the First International Congress of Chemists in Karlsruhe (Germany) in September 1860, and discuss works by F.A. Kekule (1829–1896), A.M. Butlerov (1828–1886), and C. Schorlemmer (1834–1892).

Chapter XVI (pp. 152–160) is devoted to the origination of the theory of catalysis, to works by L.J. Thenard (1777–1857) and I.V. Dobereiner (1780–1849). Chapter XVII (pp. 161–173) considers thermochemical studies by G.H. Hess (1802–1850), N.N. Beketov (1827–1911), and M. Berthelot (1827–1907). Chapter XVIII (pp. 174–205) is devoted to the life and activities of D.I. Mendeleev, discovery of the Periodic law, and studies of other scientists in the field of systematization of chemical elements. Chapter XIX pays primary attention to the discovery of the phenomenon of radioactivity and works by M. Sklodowska-Curie (1867–1934), P. Curie (1859–1906), and E. Rutherford (1871–1937). Chapter XX (pp. 227–248) considers works by J. van't Hoff (1852–1911) in the field of stereochemistry, studies of the osmotic pressure and chemical affinity by the same scientist, and works by Russian scientists D.P. Konovalov (1856–1929) and N.S. Kurnakov (1860–1941).

Chapter XXI (pp. 249–275) is devoted to the appearance of modern physical chemistry, which is conventionally associated with the beginning of publication of the first specialized journal in this field, *Zeitschrift für physikalische Chemie*, and discussed works by W. Ostwald (1853–1932), S. Arrhenius (1859–1927), N.A. Menshutkin (1842–1907), and I.A. Kablukov (1857–1942). Chapter XXII (pp. 276–282) familiarizes the reader with the life and activities of the founders of modern coordination chemistry, A. Werner (1866–1919) and L.A. Chugaev (1870–1922). Chapter XXIII (pp. 283–297) contains evidence about works of outstanding representatives of the national organic chemistry, academicians A.E. Favorskii (1860–1945), S.V. Lebedev (1874–1934), and N.D. Zelinskii (1861–1953). The primary attention in Chapter XXIV (pp. 298–316) is given to geochemical studies by Academician V.I. Vernadsky (1863–1945) and his disciple and closest associate Academician A.E. Fersman (1883–1945). Of high cognitive value are commentaries by Usanovich to each of the essays.

The book is captivating, interestingly readable, and well published, although the quality of the photographs is, unfortunately, not always satisfactory. The author managed to trace, using essays devoted to the life and activities of separate scientists or groups of scientists, the development of chemistry from ancient times till the middle of the XX century. Among the scientists to whom no essay is devoted for some reason, but who deserve being included, mention should be primarily made of Academician V.N. Ipat'ev (1867–1952), one of the most outstanding chemists of the first half of the XX century.

The book by Usanovich is of indubitable interest for anybody concerned with the history of chemistry and contains an exceedingly valuable evidence for teachers of chemical disciplines at secondary and higher-school institutions, for masters and postgraduate students specialized in chemistry and chemical technology. The book is prefaced by the text "The Word about the Author," written by Prof. Sumarokova.

A. G. Morachevskii

ISSN 1070-4272, Russian Journal of Applied Chemistry, 2006, Vol. 79, No. 2, pp. 175–181. © Pleiades Publishing, Inc., 2006.
Original Russian Text © S. D. Dubrovenskii, N. V. Kulakov, A. A. Malygin, 2006, published in Zhurnal Prikladnoi Khimii, 2006, Vol. 79, No. 2, pp. 177–183.

INORGANIC SYNTHESIS AND INDUSTRIAL INORGANIC CHEMISTRY

Possibility of Quantum Chemical Evaluation of the Probability of Various Chemical Transformations in Syntheses of Phosphorus-, Titanium-, Silicon-, and Vanadium-containing Structures on the Silica Surface

S. D. Dubrovenskii, N. V. Kulakov, and A. A. Malygin

St. Petersburg State Technological Institute, St. Petersburg, Russia

Received July 12, 2005

Abstract—Application of minimum quantum-chemical models for predicting chemical transformations in syntheses of phosphorus-, titanium-, silicon-, and vanadium-containing structures on the silica gel surface by molecular layering is considered. Possible pathways for transformation of the groups synthesized under the action of water vapor and hydrogen chloride are analyzed in terms of the models constructed.

DOI: 10.1134/S1070427206020017

Synthesis of low-dimension systems with prescribed composition and properties on the surface of solid substances can be used in diverse areas of science and technology. The method of molecular layering [1–5] can be used for this purpose. This method consists in alternate cyclic treatment of the surface of a solid matrix carrying chemically active functional groups with low-molecular-weight reagents. As these reagents are commonly used vapors of volatile chlorides: $TiCl_4$ [4], various chlorosilanes [6], $VOCl_3$ [7], $POCl_3$ [8], PCl_3 [9], CrO_2Cl_2 [10], etc. Silica, which has hydroxy groups on its surface, has been the most extensively studied as a substrate for molecular layering. The concentration and mutual positions of these groups depend on the pretreatment temperature and affect the structure and composition of interaction products. As the pretreatment temperature is raised, the content of silanols on the silica surface decreases and the average distance between them increases, which leads, at temperatures above 600°C, to formation of a hydroxy cover mainly composed of isolated OH groups.

In this case, the interaction of a molecular chloride with surface silanols can be represented in the most general case as

$$\equiv\text{Si–OH} + \text{XCl}_n \rightleftarrows \equiv\text{SiO–XCl}_{n-1} + \text{HCl}, \quad (1)$$

where, e.g., X = PO (n = 3), Ti (n = 4), Si (n = 4), and VO (n = 3).

A scheme of this kind is operative in treatment with chlorides of the surface of silica preliminarily calcined at sufficiently high temperatures (600–700°C). On treatment of the products formed by reaction (1) with water vapor

$$\equiv\text{SiO–XCl}_{n-1} + (n-1)\text{H}_2\text{O} \rightleftarrows \equiv\text{SiO–X(OH)}_{n-1} + (n-1)\text{HCl} \quad (2)$$

it is possible to produce a layer of new functional structural units incorporating active hydroxy groups on the surface and to perform by cyclic repetition of processes by schemes (1) and (2) chemical assembly of low-dimension systems of prescribed composition, which are chemically bound to the matrix surface [1–5, 7–11]. With various modifiers XCl_n (X = Ti, VO, CrO_2, PO, Si) used at various stages of molecular layering, it is possible to synthesize multicomponent systems with prescribed alternation of structural units [3]. To ensure in this case the maximum extent of utilization of OH groups in the reactions, the synthesis is performed under an excess of molecular reagents [1–4, 11].

It should be noted that chemical assembly of element-containing nanosystems by the schemes suggested presumes that, under the synthesis conditions, new groups $(\equiv\text{SiO–})_m\text{X(OH)}_{n-m}$ formed in each cycle (1), (2) are stable against H_2O vapor and the gaseous product of reaction (2), hydrogen chloride. How-

ever, experimental data have been reported indicating that element-containing structures may disintegrate under the action of water vapor or hydrogen chloride [7, 12, 13, 15, 16].

For example, a study of the stability of $(\equiv Si–O–)_nECl_{m-n}$ groups (E = VO, Ti, CrO_2, PO) against the action of HCl [7, 12] demonstrated that surface groups may disintegrate under certain conditions under the action of hydrochloric acid to evolve the corresponding chlorides into the gas phase, with the stability against HCl decreasing in the order Ti–V–Cr.

The authors of [14] concluded, based on IR spectroscopic data, that $(\equiv SiO–)TiCl_3$ groups synthesized on the surface of aerosil samples completely disintegrate in the course of vapor-phase hydrolysis.

Of the same opinion are the authors of [14], who observed the formation of bulk titanium oxide in chemisorption of titanium tetrachloride on the silica gel surface, as indicated by X-ray diffraction and NMR spectroscopic data.

In [15], a conclusion was made, on the basis of IR spectral data obtained by *in situ* monitoring and the results of chemical analysis of KSS-4 silica gel samples treated with $TiCl_4$ at 200°C, that titanium-oxochloride groups bound to the surface by a single Si–O–Ti bond may disintegrate. The same authors [16] noted a lesser susceptibility of the Si–O–V bond to disintegration in the stage of vapor-phase hydrolysis compared with titanium-containing groups.

According to the results of various studies, the possible main reason for disintegration in a stage of vapor-phase hydrolysis is water vapor [13, 14] or hydrogen chloride [15], whose corrosive activity is known to increase dramatically in the presence of water.

Therefore, it was of interest to assess the contribution of both water and HCl released in vapor-phase hydrolysis to disintegration of surface structure. In this case, the following reactions are possible:

$$\equiv SiO–XCl_{n-1} + H_2O \rightleftarrows \equiv Si–OH + XCl_{n-1}(OH), \quad (3)$$

$$\equiv SiO–X(OH)_{n-1} + H_2O \rightleftarrows \equiv Si–OH + X(OH)_n, \quad (4)$$

$$\equiv SiO–X(OH)_{n-1} + HCl \rightleftarrows \equiv Si–OH + X(OH)_{n-1}Cl. \quad (5)$$

A combination of experimental studies with model approaches and, in particular, quantum-chemical methods is promising for deeper understanding of the mechanisms of surface chemical processes, interpretation of experimental data, and prognostication of surface nanostructures.

Owing to a large share of covalence of chemical bonds and local nature of interatomic interactions, silica is a convenient object for constructing cluster models [17]. The success in application of cluster models of the silica surface in such processes as sorption of water molecules [18, 19] and dehydroxylation [20], and some studies devoted to the modeling of chemical reaction on the surface of solids [21, 22] give us reason to believe that application of the given approach to molecular layering processes is appropriate.

The main active sites of the silica surface, silanol groups, are modeled with clusters of different sizes, which contain hydrogen atoms as pseudoatoms that saturate ruptured bonds: from the simplest H_3SiOH [18] to structures incorporating several tens of silicon atoms [21–25]. An increase in the cluster size leads, on the one hand, to improvement of the quality of quantum-chemical models and, on the other, to a dramatic increase in the required computer resources. In addition, construction of large clusters requires that structural motifs of some crystalline modification of silica (as a rule, β-cristobalite) should be used [21, 22, 24, 25], which may not quite well correspond to the real surface of the amorphous support.

In addition to choosing the cluster model of active sites for making prognoses, it is also necessary to specify a basis of atomic orbitals and a level of the calculation theory. There is no alternative to nonempirical methods in analysis of chemical structures that include transition elements, beginning from period III of the Periodic Table. In doing so, various authors use Gaussian bases from 3-21G [20, 22] to 6-31G** [21, 24, 26] to construct models.

However, even the widest bases and largest clusters are insufficient for obtaining calculated parameters with accuracy comparable with that of experimental data. Therefore, the quantum-chemical models constructed commonly yield information for comparison of relative changes in characteristics of objects of about the same nature. Because quantitative data on bond lengths and valence angles for element-containing structures obtained in chemical modification of the silica surface cannot be found in the literature, no structural or charge characteristics of the cluster models developed are presented here. Because of this circumstance, the quality of the models and their prognosticating capacity were assessed by comparative analysis of the energy characteristics of structures in-

Table 1. Calculated changes in the total energy, ΔE, in the reactions of formation and vapor-phase hydrolysis of element-containing groups on the silica surface

Scheme	Reaction	ΔE, kJ mol^{-1}, for indicated modifier X			
		PO, $n=3$	Ti, $n=4$	Si, $n=4$	VO, $n=3$
1	$\equiv Si–OH + XCl_n \rightleftarrows \equiv SiO–XCl_{n-1} + HCl$	–167	–137	–137	–130
2	$\equiv SiO–XCl_{n-1} + (n-1)H_2O \rightleftarrows \equiv SiO–X(OH)_{n-1} + (n-1)HCl$	–238	–102	–225	–82
3	$[1/(n-1)]\equiv SiO–XCl_{n-1} + H_2O \rightleftarrows [1/(n-1)]\equiv SiO–X(OH)_{n-1} + HCl$	–118	–34	–75	–41

corporating various modifying elements (P, Ti, Si, V), together with experimental data when possible.

Thus, the development of model approaches, combined with experimental studies, is undoubtedly not only of theoretical, but also of practical interest for solution of problems of applied chemistry, associated with creation of heterogeneous catalysts, sorbents, and fillers for composites with prescribed properties and service characteristics.

The aim of this study was to construct, on the basis of the minimum cluster H_3SiOH and minor basis 3-21G, simplest models of element-containing groups formed on the surface of silica in its successive treatment with a vapor of the chloride of a modifier-element and that of water and to assess their applicability to prognostication of chemical transformations in synthesis by molecular layering.

As objects of study were considered quantum-chemical cluster models of products formed in interaction of volatile chlorides $POCl_3$, $TiCl_4$, $SiCl_4$, and $VOCl_3$ with isolated silanol groups of the silica surface and their possible secondary chemical transformations in reactions with H_2O vapor and HCl. Silanol groups were modeled with the minimum cluster H_3SiOH having the form of an isolated silanol group, which characterizes the surface of silica calcined at a sufficiently high temperature [27]. The models of the interaction products were also in the form of isolated element-containing groups that are bound to the matrix surface by a single Si–O–E bond and do not interact with one another.

Nonempirical quantum-chemical calculations of models of the starting substances and products of chemical reactions on the surface were performed using the restricted Hartree–Fock method and PC GAMESS 6.4 software [28, 29]. The standard set of Gaussian atomic functions 3-21G was used, with the exception of the basis set 3-21G* for the phosphorus atom. All the characteristics are given for models whose structure was determined by minimizing the total potential energy, with a threshold value of the maximum gradient, equal to 10^{-5} Hartree A^{-1}.

The total energy of interaction between nuclei and electrons in the models, obtained by quantum-chemical calculations, served to evaluate the stability of the structures under consideration and the comparative probability of occurrence of surface chemical reactions by schemes (1)–(5). As a measure of the probability of occurrence of chemical reactions served the change in the total energy, ΔE, in accordance with the stoichiometric scheme of a reaction, e.g., for vanadium-containing structures

$$\equiv Si–OH + VOCl_3 \rightleftarrows \equiv SiO–VOCl_2 + HCl, \quad (6)$$

$$\Delta E = E(HCl) + E(H_3SiOVOCl_2) - E(H_3SiOH) - E(VOCl_3), \quad (7)$$

where E is the total energy of interaction between the nuclei and electrons of the structures specified.

This approach, to a certain extent similar to thermodynamic estimations, makes it possible to prognosticate the shift of chemical equilibria by comparing the values of ΔE for chemical reactions. A negative value of ΔE will indicate a preferable shift of the equilibrium toward final products, and a positive value, toward starting substances.

The calculated changes in energy, ΔE, in transformations by schemes (1) and (2) are listed in Table 1. For the reactions of interaction between a molecular chloride and the OH group (1), this quantity can be regarded as the chemical affinity of the corresponding chloride to an isolated silanol group.

It follows from an analysis of the data obtained that, in terms of the quantum-chemical model used,

the affinity is 130–167 kJ mol^{-1} for all the chlorides under consideration. This points to a considerable energy gain as a result of the reaction by scheme (1). The noticeable number of surface silanols not involved in the interaction may be mostly due to steric hindrances [11, 30]. As already mentioned, the calculation level used does not pretend to be chemically accurate, and, therefore, the absolute changes in energy are less reliable than its relative changes in the series of modifies under consideration.

For example, $POCl_3$ exhibits, according to published data, a lower activity than $VOCl_3$ and $TiCl_4$ in the reaction with OH groups on a completely hydroxylated surface of silica, i.e., with adjacent (not isolated) OH groups [7, 8].

At the same time, the presence of an insignificant amount of vanadium-containing functional groups on the surface leads to a dramatic increase in the reactivity of $POCl_3$ both in interaction with free OH groups and in substitution of vanadium atoms by phosphorus in $(Si–O)_nVOCl_{3-n}$ [3].

As follows from the data in Table 1, the energy of formation of the Si–O–E bond, $\Delta E_{Si–O–E}$, in interaction of silanols and chlorides is the highest for phosphorus-oxochloride groups and decreases in the order P–Ti, Si–V. This suggests that the Si–O–P bond is stronger than other bonds, at least with respect to hydrogen chloride. By contrast, the probability of disintegration of vanadium-and-chlorine-containing structures under the action of HCl is the highest among the modifiers considered, in agreement with the results obtained in a study of processes on the silica surface hydroxylated to the maximum possible extent [7, 12].

The calculated data obtained may be of interest for prognostication of chemical transformations in synthesis of multicomponent systems in the course of interaction between silanol groups on the silica surface and a mixture of volatile chlorides. A number of experimental results obtained in studies of chemical interactions in the system constituted by $POCl_3$, $TiCl_4$, $VOCl_3$, and silica gel [30, 31] demonstrated that phosphorus oxochloride displaces titanium-and-chlorine-containing groups from the silica surface, and titanium tetrachloride, in turn, displaces vanadium-and-chlorine-containing groups. This pattern agrees with the calculation results obtained and confirms the prognosticating value of the quantum-chemical models suggested.

As mentioned above, the molecular layering of an oxide monolayer of prescribed thickness involves multiple repetition of reactions (1) and (2). In the process, new reactive OH groups are formed in stage (2). These groups are bound to new atoms X in the functional groups synthesized by scheme (1), rather than to silicon atoms of the starting substrate.

The corresponding energy changes in the formation of an OH group are also negative for all the modifiers (Table 1), which corresponds to energetically favorable processes. Two or three chlorine atoms are present in the element-oxychloride, depending on the nature of a modifying element. Calculation of the change in energy upon substitution of all the chlorine atoms by OH groups gives values that exceed, in the case of phosphorus and silicon (–238 and –225 kJ mol^{-1}, respectively) the changes in energy in reactions (1) (–167 and –137 kJ mol^{-1}). However, for the structures containing titanium and vanadium, these energies are, by contrast, lower than those in reaction (1). It should be noted that the stoichiometries of reactions (1) and (2) are different. For this reason, to ensure a correct comparison of the interactions by schemes (1) and (2), Table 1 lists changes in energy in reaction (2) recalculated per H_2O molecule [Table 1, reaction (3)].

It can be seen in Table 1 that the absolute gain in energy, ΔE, in the formation of the E–OH bond is lower than that in the case of the Si–O–E bond by a factor of 2–4, with the exception of phosphorus-containing groups. Such a result suggests, even with the limited accuracy of quantum-chemical models taken into account, that the extent of the hydrolytic substitution of chlorine atoms by a hydroxo group is lower than that in the case of interaction between chlorides and surface silanols.

It should be noted again that vapor-phase hydrolysis of phosphorus-oxochloride groups must occur with the least pronounced hindrance and the energy of formation of P–OH groups (–118 kJ mol^{-1}) is only slightly lower than that for the Si–O–P bond (–167 kJ mol^{-1}). This process is the least favorable for titanium-containing groups [–34 kJ mol^{-1}, compared with –137 kJ mol^{-1} for reaction (1)], in agreement with published data on incomplete substitution of chlorine atoms by hydroxo groups in vapor-phase hydrolysis of structures of this kind [11]. According to Table 1, silicon- and vanadium-containing groups occupy an intermediate position, i.e., are hydrated more easily than titanium-containing groups, and more difficultly than those containing phosphorus and chlorine.

As already noted, there is a discussion in the literature, concerned with the possibility of rupture of

Table 2. Calculated changes in the total energy, ΔE, in reactions of destruction of element-containing groups on the silica surface

Scheme	Reaction	ΔE, kJ mol^{-1}, for indicated modifier X			
		PO, $n=3$	Ti, $n=4$	Si, $n=4$	VO, $n=3$
3	$\equiv SiO–XCl_{n-1} + H_2O \rightarrow \equiv Si–OH + XCl_{n-1}(OH)$	+38	+36	+49	+39
4	$\equiv SiO–X(OH)_{n-1} + H_2O \rightarrow \equiv Si–OH + X(OH)_n$	+31	+45	+43	+49
5	$\equiv SiO–X(OH)_{n-1} + HCl \rightarrow \equiv Si–OH + X(OH)_{n-1}Cl$	+146	+30	+109	+62

the Si–O–E bond in element-containing surface groups in the course of vapor-phase hydrolysis by reactions (3)–(5), which constitute a set of competitive processes with respect to formation of OH groups bound to the atom of the modifying element [reaction (2)].

Disintegration of element-oxochloride structures in a process of this kind may give as final products silanol groups and hydrated oxides of the corresponding elements. The latter may widely vary in size, from nanoclusters to macroscopic phases. In addition, it is known from the results obtained in studies of transformations of such objects in aqueous solutions that widely diverse variants of compounds differing in both composition and structure are possible, which leads in the given case to severe difficulties in quantum-chemical modeling [32]. Therefore, the present study is only concerned with the initial stages of disintegration, which consist in rupture of Si–O–E bonds in groups formed on the surface in interaction between element chlorides and isolated hydroxy groups of silica.

The possible pathways of the reactions with H_2O vapor (in stage 2) or with HCl (gaseous product of the vapor-phase hydrolysis of chlorine-containing surface structures) can be represented by schemes (3)–(5).

It can be assumed that, from the standpoint of analysis of the energy of such transformations, there undoubtedly exists an uncertainty, because polycondensation, being a spontaneous process, leads to a decrease in the total energy of the system and makes higher the probability of rupture of Si–O–E bonds. At the same time, comparison of the first elementary stages of disintegration for various modifiers can serve as a basis for prognostication of the further behavior of the system.

The calculated changes in the energy of the Si–O–E bond rupture under the action of water vapor (Schemes 3, 4) and hydrogen chloride (Table 2, Scheme 5) are positive in contrast to those in the interaction between chlorides and silanols (Scheme 1) and hydrolytic substitution of chlorine atoms (Scheme 2), i.e., differ not only in magnitude, but also in sign. This suggests that at least the first stages of the disintegration processes are energetically hindered.

Naturally, further polycondensation may lead to another energy pattern of disintegration. In this case, the values listed in Table 2 can be regarded as calculated estimates of the height of energy barriers for destruction reactions, which enables prognostication of the predominant pathways of disintegration of Si–O–E bonds.

From this standpoint, the data in Table 2 demonstrate that the modifiers under consideration behave in strongly different ways. For example, the lowest barrier height is observed for titanium-containing groups in the case of interaction between hydrogen chloride and hydroxylated structures:

$$\equiv SiO–Ti(OH)_3 + HCl \rightarrow \equiv Si–OH + Ti(OH)_3Cl, \quad (8)$$
$$\Delta E \approx +30 \text{ kJ mol}^{-1},$$

whereas for the rest of modifiers, this pathway (Scheme 5) is the least probable (energy barrier 62–146 kJ mol^{-1}). Another competing pathway of the possible destruction of titanium-containing groups is interaction of chlorine-containing structures with water:

$$\equiv SiO–TiCl_3 + H_2O \rightarrow \equiv Si–OH + TiCl_3(OH), \quad (9)$$
$$\Delta E \approx +36 \text{ kJ mol}^{-1},$$

for which the barrier height somewhat exceeds that for reaction (8).

The preferable destruction mechanisms for phosphorus-containing groups are those of interaction with water molecules:

$$\equiv SiO–POCl_2 + H_2O \rightarrow \equiv Si–OH + POCl_2(OH), \quad (10)$$
$$\Delta E \approx +38 \text{ kJ mol}^{-1};$$

$$\equiv SiO–PO(OH)_2 + H_2O \rightarrow \equiv Si–OH + PO(OH)_3, \quad (11)$$
$$\Delta E \approx +31 \text{ kJ mol}^{-1},$$

which is in a quite good agreement with the known concepts of high hygroscopicity of oxygen compounds of phosphorus(V).

Silicon-containing structures are the least susceptible to disintegration, with pathways in which the bonds with the surface of both chlorine-containing and hydroxylated groups are ruptured under the action of water are virtually equally probable:

$$\equiv SiO–SiCl_3 + H_2O \rightarrow \equiv Si–OH + SiCl_3(OH), \quad (12)$$
$$\Delta E \approx +49 \text{ kJ mol}^{-1};$$

$$\equiv SiO–Si(OH)_3 + HCl \rightarrow \equiv Si–OH + Si(OH)_3Cl, \quad (13)$$
$$\Delta E \approx +43 \text{ kJ mol}^{-1}.$$

Finally, the lowest barrier for disintegration of groups containing vanadium corresponds to the reaction of chlorine-containing structures with a molecule of water:

$$\equiv SiO–VOCl_2 + H_2O \rightarrow \equiv Si–OH + VOCl_2(OH), \quad (14)$$
$$\Delta E \approx +39 \text{ kJ mol}^{-1}.$$

It can be noted in summarizing the above reasoning that, in terms of the quantum-chemical models under consideration, the highest stability against disintegration under the action of water vapor or hydrogen chloride would be expected for silicon-containing structures, and the lowest, for those containing titanium. Groups containing phosphorus and vanadium have approximately the same stabilities and occupy an intermediate position among the modifiers. According to the calculated data, a noticeable destruction under the action of hydrogen chloride may only occur for titanium-containing groups.

Thus, according to the results of modeling, destruction of element-containing groups in the stage of vapor-phase hydrolysis is only possible under strongly nonequilibrium conditions of an excess of water vapor or hydrogen chloride or at elevated temperatures sufficient for energy barriers to be overcome. Therefore, of exceedingly high importance is the choice of a synthesis mode, especially in the stage of vapor-phase hydrolysis. A particular significance is assumed by the problem of identification of synthesis products, whose solution can be promoted to a fairly great extent by quantum-chemical modeling.

CONCLUSIONS

(1) Analysis of the results obtained suggests that quantum-chemical modeling of the synthesis of element-containing structures on the silica surface enables high-quality prognostication of the preferable pathways of chemical transformations even with the minimal cluster models and low level of the calculation theory.

(2) The minimum nature of these models makes the approach under consideration accessible to a large number of researchers, because it does not require considerable computing resources. An ordinary personal computer can be used to obtain in several hours or even minutes a prognosis of the development of chemical transformations on the silica surface, which involve new reagents.

(3) The calculations performed for products of synthesis by the method of molecular layering on the silica surface carrying isolated hydroxy groups, i.e., element-containing structures with $POCl_3$, $TiCl_4$, $SiCl_4$, and $VOCl_3$, suggest that the most probable is the pathway that involves chemisorption of molecular chlorides on the silica surface and subsequent hydrolysis. However, disintegration of the structures synthesized is possible under certain conditions (large excess of water or hydrogen chloride in the system). It would be expected that the stability against disintegration under the action of water vapor or hydrogen chloride is the highest for silicon-containing structures and the lowest for titanium-containing groups.

ACKNOWLEDGMENTS

The study was financially supported by the Russian Foundation for Basic Research (project no. 04-03-32048).

REFERENCES

1. Kol'tsov, S.I., *Zh. Prikl. Khim.*, 1969, vol. 42, no. 5, pp. 1023–1028.
2. Aleskovskii, V.B., *Kurs khimii nadmolekulyarnykh soedinenii: Uchebnoe posobie* (A Course of Chemistry of Supramolecular Compounds: Textbook), Leningrad: Len. Gos. Univ., 1996.
3. Malygin, A.A., *Zh. Obshch. Khim.*, 2002, vol. 72, no. 4, pp. 617–632.
4. Malkov, A.A., Sosnov, E.V., Osipenkova, O.V., and Malygin, A.A., *Appl. Surf. Sci.*, 1997, vol. 108, no. 1, pp. 133–139.
5. Leboda, R. and Gun'ko, V.M., *J. Coll. Int. Sci.*, 1999, vol. 218, pp. 23–39.

6. Vainshtein, P.M., Kol'tsov, S.I., Ezhovskii, Yu.K., and Ivanova, E.A., *Zh. Fiz. Khim.*, 1983, vol. 57, no. 7, pp. 1728–1732.
7. Malygin, A.A., Volkova, A.N., Kol'tsov, S.I., and Aleskovskii, V.B., *Zh. Obshch. Khim.*, 1973, vol. 43, no. 7, pp. 1436–1440.
8. Volkova, A.N., Malygin, A.A., Kol'tsov, S.I., and Aleskovskii, V.B., *Zh. Obshch. Khim.*, 1973, vol. 43, no. 4, pp. 724–729.
9. Volkova, A.N., Kol'tsov, S.I., and Aleskovskii, V.B., *Izv. Vyssh. Uchebn. Zaved., Khim. Khim. Tekhnol.*, 1969, vol. 12, no. 3, pp. 247–249.
10. Malygin, A.A., Kol'tsov, S.I., and Aleskovskii, V.B., *Zh. Obshch. Khim.*, 1978, vol. 49, no. 9, pp. 1936–1941.
11. Sosnov, E.A., Malkov, A.A., and Malygin, A.A., *Zh. Prikl. Khim.*, 1988, vol. 61, no. 1, pp. 29–34.
12. Malygin, A.A., Volkova, A.N., Kol'tsov, S.I., and Aleskovskii, V.B., *Zh. Obshch. Khim.*, 1972, vol. 42, no. 11, pp. 2373–2375.
13. Chuiko, A.A., Voronin, E.F., and Tertykh, V.A., *Adsorb. Adsorbent.*, 1983, no. 11, pp. 22–29.
14. Haukka, S., Lakomaa, E.-L., and Root, A., *J. Phys. Chem.*, 1993, vol. 97, pp. 5085–5094.
15. Osipenkova, O.V., Malkov, A.A., and Malygin, A.A., *Zh. Obshch. Khim.*, 1994, vol. 64, no. 4, pp. 549–553.
16. Osipenkova, O.V., Malkov, A.A., and Malygin, A.A., *Zh. Obshch. Khim.*, 1996, vol. 66, no. 1, pp. 7–11.
17. Dunken, H.H. und Lygin, V.I., *Quantchemie der Adsorption an Festkorperoberflachen*, Leipzig: VEB Deutscher Verlag fur Grundstoffindustrie, 1978.
18. Ferrari, A.M., Ugliengo, P., and Garrone, E., *J. Phys. Chem.*, 1993, vol. 97, pp. 2671–2676.
19. Zarko, V.I., Dudnik, V.V., Gun'ko, V.M., and Bogatyreva, V.M., *Zh. Fiz. Khim.*, 1996, vol. 70, no. 10, pp. 1869–1873.
20. Lygin, V.I., *Zh. Fiz. Khim.*, 1997, vol. 71, no. 10, pp. 1735–1742.
21. Ignatov, S.K., Bogatur'yan, A.A., Razuvaev, A.G., *et al.*, *Izv. Akad. Nauk, Ser. Khim.*, 1998, no. 7, pp. 1296–1303.
22. Lygin, V.I., *Zh. Fiz. Khim.*, 2000, vol. 74, no. 8, pp. 1351–1359.
23. Khavryuchenko, V.D., Shcheka, E.F, and Natkanets, I., *Zh. Strukt. Khim.*, 1992, vol. 33, no. 4, pp. 66–75.
24. Civalleri, B., Casassa, S., and Garrone, E., *J. Phys. Chem.*, 1999, vol. 103, pp. 2165–2171.
25. Vigne-Maeder, E. and Saulet, P., *J. Phys. Chem.*, 1997, vol. 101, pp. 8197–8203.
26. Mikheeva, E.P., Kachurovskaya, N.A., and Zhidomirov, G.M., *Kinet. Kataliz*, 2002, vol. 41, no. 2, pp. 245–255.
27. Lygin, V.I., *Zh. Fiz. Khim.*, 1989, vol. 63, no. 2, pp. 289–305.
28. Schmidt, M.W., Baldridge, K.K., Boatz, J.A., *et al.*, *J. Comput. Chem.*, 1993, vol. 14, pp. 1347–1363.
29. Granovsky, Alex A., http:www.clasic.chem.msu.su-gamess. index.html.
30. Evdokimov, A.V., Kol'tsov, S.I., and Malygin, A.A., *Zh. Obshch. Khim.*, 1987, vol. 57, no. 4, pp. 149–152.
31. Evdokimov, A.V., Dubrovenskii, S.D., and Malygin, A.A., *Zh. Obshch. Khim.*, 1999, vol. 69, no. 4, pp. 545–550.
32. Pletnev, R.N., Ivakin, A.A., Kleshev, D.G., *et al.*, *Gidratirovannye oksidy elementov IV i V grupp* (Hydrated Oxides of Group IV and V Elements), Moscow: Nauka, 1986.

ISSN 1070-4272, Russian Journal of Applied Chemistry, 2006, Vol. 79, No. 2, pp. 182–185. © Pleiades Publishing, Inc., 2006.
Original Russian Text © Yu. P. Gladkikh, V. I. Zavrazhina, 2006, published in Zhurnal Prikladnoi Khimii, 2006, Vol. 79, No. 2, pp. 184–187.

INORGANIC SYNTHESIS AND INDUSTRIAL INORGANIC CHEMISTRY

Hydroxylation of the Surface of Calcium Sulfates in Aqueous Media and Processes of Their Solidification

Yu. P. Gladkikh and V. I. Zavrazhina

Shukhov State Technological University, Belgorod, Russia

Received January 26, 2005

Abstract—Mechanisms of hydroxylation of the surface of calcium sulfates and their formulations in aqueous media and processes of their solidification are considered.

DOI: 10.1134/S1070427206020029

Various calcium sulfates, such as calcium sulfate hemihydrate $CaSO_4 \cdot 0.5H_2O$, calcium sulfate dihydrate $CaSO_4 \cdot 2H_2O$, anhydrite $CaSO_4$, estrich gypsum $CaSO_4 \cdot CaO$, and formulations with a number of inorganic and organic compounds, are gypsum binders, which are widely used in building.

The chemistry of calcium sulfate hemihydrate is the best studied. It is known [1] that the structure of the gypsum stone is formed in aqueous media through dissolution of the binder to give calcium and sulfate ions and then calcium sulfate dihydrate, which is less water soluble than calcium sulfate hemihydrate.

$$Ca^{2+} + SO_4^{2-} + 2H_2O \rightarrow CaSO_4 \cdot 2H_2O. \quad (1)$$

According to other data [2], the solidification of gypsum binders occurs by the topochemical mechanism, i.e., water is added directly to solid particles. The solidification reaction in a solidifying mixture of calcium hemihydrate sulfate with water is described by the following scheme:

$$CaSO_4 \cdot 0.5H_2O + 1.5H_2O \rightarrow CaSO_4 \cdot 2H_2O. \quad (2)$$

Thus, there are different explanations of the solidification of gypsum binders in terms of the solution and topochemical mechanisms. However, there are examples [3–5] of solidification of calcium sulfate dihydrate and its formulations with various substances, which cannot be understood in terms of reactions (1) and (2). This indicates that these binders harden by a different mechanism. No other concepts of the solidification of calcium sulfate dihydrate have been formulated. Furthermore, it is impossible to explain satisfactorily the role of some additives of organic compounds in the solidification of gypsum binders and the mechanism of their action on the basis of the available concepts of the processes of solidification of gypsum binders.

Thus, despite the large body of theoretical and experimental data on the solidification of gypsum binders, the existing mechanisms require rethinking.

In this paper, we discuss the hydroxylation of the surface of mixtures of calcium sulfates with water and the condensation mechanism of their solidification. The known procedures for production of gypsum materials, including their preparation from calcium sulfate dihydrate and mixtures of gypsum binders with inorganic and organic additions are considered in terms of this mechanism.

It is known [6, 7] that finely dispersed particles of inorganic solid substances, including gypsum binders, obtained by a mechanical milling and thermal treatment have free unsaturated valence bonds on the surface and possess a free surface energy. When water molecules are adsorbed on surface defects of calcium sulfates these defects are hydrated to calcium sulfate dihydrate and are hydroxylated similarly to defects on the surface of mechanically activated silicon dioxide [7].

When other particles of this kind, with surface defects, are placed in a humid atmosphere or in water, there occurs dissociative adsorption of water molecules on electron-acceptor and electron-donor centers on the surface, formed upon cleavage of crystals. For example, a separate fragment of the surface of calcium

sulfates, gypsum binders $CaSO_4 \cdot nH_2O$ (n = 0–2), formed upon their mechanical dispersion can be represented as $^{\cdot}Ca–(O–SO_2–O–Ca \cdot nH_2O)_x–OSO_2O^{\cdot}$.

Depending on their intensity, duration, thermal treatment, and other factors, physical actions can also cleave a crystal at oxygen–sulfur valence bonds.

The scheme of hydroxylation of a separate unit (fragment) of the surface of calcium sulfate dihydrate is presented below:

$$^{\cdot}Ca–(O–SO_2–O–Ca \cdot 2H_2O)_x–OSO_2O^{\cdot} + HOH \rightarrow HOCa–(OSO_2OCa)_x–OSO_2OH \cdot 2H_2O. \quad (3)$$

In this case, rupture of valence bonds between oxygen atoms and sulfur atom on the hydroxylated surface of calcium sulfates may result in formation of di- and trihydrosulfate groups.

In the presence of a sufficient amount of water in systems constituted by calcium sulfate and water, hydrated ions $Ca^{2+} \cdot nH_2O$, $CaOH^+ \cdot (n - 1)H_2O$, $HSO_4^- \cdot (m - 1)H_2O$, and $SO_4^{2-} \cdot mH_2O$) are also formed.

Calculations performed using the second dissociation constants of calcium hydroxide (4.9×10^{-2}) and sulfuric acid (1.2×10^{-2}) [8] confirm the predominance of hydroxocalcium and hydrosulfate ions in the aqueous phase. For example, the amount of hydroxocalcium ions is five times that of calcium ions, and the amount of hydrosulphate ions is nine times that of sulfate ions.

Thus, depending on the amount of water in a mixture of gypsum binders with water, different systems are formed, which contain different amounts of calcium, sulfate, hydroxylated hydroxocalcium ions and hydrosulfate ions, product of their interaction $HO–CaO–SO_3–OH$, and hydroxylated solid particles, which can react with one another and possess properties of solid polyampholytes [9]. Hydroxylated sulfate groups of solid gypsum particles are of acid nature, and calcium atoms, of basic nature, i.e., hydroxylated solid gypsum particles exhibit amphoteric properties. They can further react both with acids and with bases to form more soluble acid and basic calcium sulfates. Apparently, this interaction is of acid–base, condensation nature, with water molecules released in the condensation reaction. The presence of acid and basic centers on the surface of solid catalysts, including sulfates, has been reported previously [9].

Some of the schemes of condensation processes involving separate fragments of hydroxylated gypsum are presented below:

$$2HO–Ca–(OSO_3Ca \cdot 2H_2O)_x–OSO_2OH \rightarrow HO–Ca–(OSO_3Ca \cdot 2H_2O)_{2x+1}–OSO_2OH + HOH, \quad (4)$$

$$HO–Ca–(OSO_3Ca \cdot 2H_2O)_x–OSO_2OH + Ca(OH)_2 \rightarrow HO–Ca–(OSO_3Ca \cdot 2H_2O)_x–OSO_2O–Ca–OH + HOH, \quad (5)$$

$$HO–Ca–(OSO_3Ca \cdot 2H_2O)_x–OSO_2OH + HO–SO_2–OH \rightarrow HO–SO_2–O–Ca–(OSO_2Ca \cdot 2H_2O)_x–OSO_2OH + HOH. \quad (6)$$

Thus, the acid-base condensation of hydroxylated binders with other hydroxylated particles results in an increase in the molecular weight. The growth of the forming particles leads to the formation of colloids and crystallization in the course of hardening of gypsum binders.

It has been established [3] that mechanochemical activation of a mixture of quicklime with gypsum dihydrate at room temperature yields products of lime addition to gypsum: basic salts, hydroxocalcium sulfates. When brought in contact with mechanically activated and hydroxylated gypsum particles, the forming basic salts can be involved in polycondensation with these particles and with each other, which predetermines their binding power.

We used lump quicklime and a lime dust from the Belgorod Combine of building materials and gypsum stone from the Artemovsk deposit as components of raw mixtures being subjected to mechanical activation. Weighed amounts of quicklime (or lime dust) and of gypsum stone were subjected to a joint milling at room temperature in a VM-4 vibration mill for 1–3 min. This resulted in activation of the mixture to give products of lime addition to gypsum, which was confirmed by X-ray phase analysis and IR spectroscopy [3]. The addition is only possible with the formation of basic salts by the simplified scheme

$$CaSO_4 \cdot 2H_2O + CaO \rightarrow Ca(OH)_2SO_4 \cdot H_2O$$

or in modification of the surface of gypsum or lime. These methods demonstrated that milling of a mixture of gypsum with lime does not result, either, in the formation of calcium sulfate hemihydrate and slaked lime. Quicklime is also absent in the resulting mechanically activated mixture.

Compositions of mixtures and data obtained in sample testing

Composition no.	Content of components, wt %			Water absorption capacity, %	Ultimate strength, MPa	
	quicklime	lime dust	calcium sulfate dihydrate		compression	bending
1	1	–	99	13.0	22	5.4
2	5	–	95	12.0	21	5.4
3	10	–	90	12.2	21	5.5
4	20	–	80	12.6	20	5.4
5	30	–	70	18.6	18.6	5.3
6	–	1	99	10.0	19	–
7	–	2.5	97.5	10.0	18.5	–
8	–	5.0	95	12.0	17	–

To determine the binding power of the mechanically activated mixture, a milled mixture was moistened (w/s = 0.1) and cylindrical samples 20 mm in diameter and height and 50 × 50 × 10 mm plates were compacted under a specific compaction pressure of 20 MPa. The samples were solidified under ordinary atmospheric conditions at room temperature. Their hardness was determined at the age of seven days in conformity with GOST (State Standard) 8462–85.

The water-absorption capacity of the samples was determined from a relative increase in a sample mass after keeping the samples in water at a room temperature for 48 h (see table).

It is seen from the table that the stones obtained from the formulations investigated have a sufficiently high hardness. The low water-absorption capacity of the solid structures formed confirms the (poly)condensation mechanism of solidification of the formulations. If solely more soluble basic salts were formed in solidification, the water-absorption capacity of the gypsum stone would be much higher. The same would take place in the presence of free lime in the structure of the stone.

Condensation processes in solidification of formulations with quicklime for separate units (fragments) of hydroxylated gypsum can be written as follows:

$$\mathrm{HO–Ca–(OSO_3Ca\cdot 2H_2O)_x–OSO_3H + CaO}$$
$$\rightarrow \mathrm{HO–Ca–(OSO_3Ca\cdot 2H_2O)_x–OSO_2–O–Ca–OH.} \quad (7)$$

Water-resistant structures are also formed in contact solidification of calcium sulfate dihydrates in a formulation with an acid oxide, chromic anhydride [4], soda, and cobalt sulfate [5].

$$\mathrm{HO–Ca–(OSO_3Ca\cdot 2H_2O)_x–OSO_3H + CrO_3}$$
$$\rightarrow \mathrm{HO–CrO_2–O–Ca–(OSO_3Ca\cdot 2H_2O)_x–OSO_3H,} \quad (8)$$

$$\mathrm{HO–Ca–(OSO_3Ca\cdot 2H_2O)_x–OSO_3H + Na_2CO_3 + CoSO_4}$$
$$\rightarrow \mathrm{NaO–Co–O–Ca–(O–SO_2–O–Ca\cdot 2H_2O)_x–O–Ca–O–SO_2–O–Na + HOH.} \quad (9)$$

The condensation mechanism of solidification of hydroxylated particles formed by calcium sulfates in aqueous media is confirmed by a large body of experimental data. For example, it is known [9] that the solidification of gypsum binders is terminated upon introduction of methanol into a solidifying system constituted by calcium sulfate hemihydrate and water, which is can be attributed to occurrence of a condensation reaction between hydroxylated particles of calcium sulfates, formed in their mixtures, with water and the alcohol. This results in that surface hydroxyl groups capable of being involved in the condensation reaction disappear and protective (inert) OR groups are formed. The surface of particles is deactivated, with the result that condensation processes in hardening of separate units (fragments) of the binder surface are terminated (crystal water in gypsum is disregarded):

$$\mathrm{HO–Ca–(O–SO_2–O–Ca)_x–O–SO_2–OH + 2ROH}$$
$$\rightarrow \mathrm{R–O–Ca–(O–SO_2–O–Ca)_x–O–SO_2–O–R + HOH.} \quad (10)$$

A similar termination of solidification in the presence of methanol has been observed for other mineral

binders with a polycondensation mechanism of hardening, e.g., for calcium silicates [10].

Another evidence in favor of the occurrence of condensation processes in solidification of gypsum binders is the strong influence of multifunctional additives on the solidification of gypsum binders [11–16]. These are additives of succinic and other polyatomic acids, oxyacids, superplasticizers, ethylene diamine, maleic and phthalic anhydrides, and other substances capable of polycondensation. When a gypsum binders is added to a solidifying system they enter into a chemical interaction of condensation nature with hydroxylated particles of the binder and thus appear in the composition of a gypsum stone, a heteropolymer that contains not only calcium and sulfate ions, but also fragments of the above-mentioned multifunctional additives. In general form, the scheme of these reactions involving a separate unit (fragment) of the surface of a gypsum crystal is as follows:

$$\mathrm{Ca{-}(OSO_2OCa)_{\mathit{x}}{-}OSO_2OH + 2HO{-}R{-}OH}$$
$$\rightarrow \mathrm{HO{-}R{-}O{-}Ca{-}(OSO_2OCa)_{\mathit{x}}{-}OSO_2OR{-}OH + 2HOH}. \quad (11)$$

The above-stated condensation mechanism of solidification of calcium sulfate dihydrate and its formulations is also valid for other calcium sulfates and their formulations with water, because the processes of their solidification first include formation of hydrated and hydroxylated calcium dihydrate, and then, further acid–base condensation of hydroxylated particles.

Thus, the consideration of the solidification processes of gypsum binders in terms of the physical chemistry of solid surfaces, examination of the known experimental data on the solidification of gypsum binders in aqueous media, and establishment of the analogy between solidification processes of gypsum binders and binders with a polycondensation mechanism of solidification indicate that the solidification processes of all calcium sulfates are also of polycondensation nature. This fundamentally changes the chemical nature and chemical processes occurring in solidification of all calcium sulfates.

CONCLUSION

An unconventional condensation mechanism of solidification of gypsum binders and their formulations was suggested and explained for the example of mixtures of calcium sulfate dihydrate with certain inorganic and organic substances.

REFERENCES

1. VolzhenskiI, A.V. and Ferronskaya, A.V., *Gipsovye vyazhushchie i izdeliya* (Gypseous Astringents and Articles), Moscow: Stroiizdat, 1974.
2. Mchedlov-Petrosyan, O.P., *Khimiya neorganicheskikh stroitel'nykh materialov* (Chemistry of Inorganic Building Materials), Moscow: Stroiizdat, 1988.
3. RF Patent 2058955.
4. USSR Inventor's Certificate, no. 1255602.
5. USSR Inventor's Certificate, no. 1451118.
6. Avvakumov, E.G., *Mekhanicheskie metody aktivatsii khimicheskikh protsessov* (Mechanical Methods for Activation of Chemical Processes), Novosibirsk: Nauka, 1986.
7. Kiselev, V.F. and Krylov, O.V., *Adsorbtsionnye protsessy na poverkhnosti poluprovodnikov i dielektrikov* (Adsorption Processes on the Surface of Semiconductors and Insulators), Moscow: Nauka, 1978.
8. Rabinovich, V.A. and Khavin, Z.Ya., *Kratkii spravochnik khimika* (Concise Chemist's Handbook), Rabinovich, V.A., Ed., Leningrad: Khimiya, 1978.
9. Tanabe, K., *Solid Acids and Bases. Their Catalytic Properties*, New York: Academic, 1970.
10. Viker, V., *Trudy VI mezhdunarodnogo kongressa po khimii tsementa* (Proc. VI Int. Congress on Chemistry of Cement), Moscow: Stroiizdat, vol. 2, book 2, 1976.
11. Schwiet, N.E., *Gips*, 1968.
12. Makarov, V.I., Panin, A.I, and Suchkov, V.P., *Stroit. Materialy*, 1974, no. 4, pp. 29–30.
13. Akmalaev, V.A., Improvement of Physicomechanical Properties of Concretes Based on Gypseous Astringents with Addition of a Superplasticizer, *Cand. Sci. Dissertation*, Moscow, 1991.
14. Ratinov, V.B., Ivanitskii, V.V., and Klykova, L.Ya., *Stroit. Materialy*, 1979, no. 1, pp. 28–29.
15. Gordashevskii, P.F., *Stroit. Materialy*, 1964, no. 10, pp. 18–19.
16. Ratinov, V.B. and Rosenberg, T.I., *Dobavki v beton* (Additives to Concrete), Moscow: Stroiizdat, 1989.

ISSN 1070-4272, Russian Journal of Applied Chemistry, 2006, Vol. 79, No. 2, pp. 186–189. © Pleiades Publishing, Inc., 2006.
Original Russian Text © S. M. Azarov, V. N. Makatun, N. V. Kitikova, S. V. Shemchenok, A. I. Rat'ko, 2006, published in Zhurnal Prikladnoi Khimii, 2006, Vol. 79, No. 2, pp. 188–191.

INORGANIC SYNTHESIS AND INDUSTRIAL INORGANIC CHEMISTRY

Phase Formation in the Reaction of Aluminosilicate Ceramics with a Phosphate Binder

S. M. Azarov, V. N. Makatun, N. V. Kitikova, S. V. Shemchenok, and A. I. Rat'ko

Institute of General and Inorganic Chemistry, National Academy of Sciences of Belarus, Minsk, Belarus
Institute of Physicoorganic Chemistry, National Academy of Sciences of Belarus, Minsk, Belarus

Received February 9, 2005

Abstract—The effect of phase formation at the interface between macroscopic agglomerates constituting a porous aliminosilicate ceramic on its properties was studied by physicochemical methods, with an alumino-phosphorous binder used as a modifying agent.

DOI: 10.1134/S1070427206020030

The transformation of acid phosphates of multiply charged ions has been rather well studied in view of their importance for production of construction materials [1–4]. The mode in which viscous phosphate solutions are used as binders or gluing substances in composites and the effect of their application are determined by the nature of the skeleton-forming material.

It has been shown previously [5] that the performance characteristics of sintered macroporous silicate articles can be improved by making interparticle contacts stronger by means of an aluminophosphate binder (APB). This is due to the fact that aluminophosphates have a crystal-chemical affinity to silicate materials containing quartz and its allotropic modifications as skeleton-forming elements. However, an extremal dependence of the strength on the amount of binder introduced would be expected because formation of new phases not bound to the skeleton must have a wedging effect on the structure. Therefore, the aim of this study was physicochemical examination of certain specific features of phase formation at the interface between macroscopic (0.1–1.0 mm) agglomerates.

EXPERIMENTAL

We used as objects of study cylinders with an outer diameter of 60 mm, height of 54 mm, and wall thickness of 3 mm. The cylinders were made of macroporous (pore size >1 μm) ceramics commonly used in filters. The main phases of the starting ceramics are quartz and mullite. We used APB for modification. The flow sheet of production of filter elements, their main characteristics, and a detailed procedure for synthesis of APB have been described previously [5]. We prepared impregnating solutions on the basis of the APB synthesized by diluting a concentrate with water or phosphoric acid solutions. As in the previous study, we used samples treated with formulations with mass ratios APB : H_2O = 1 : 2 (no. 1), APB : 50% solution of H_3PO_4 = 1 : 2 (no. 2), and a 50% solution of H_3PO_4 (no. 3). After the impregnation, the samples were heat treated in air at 20–800°C, with subsequent measurement of their mechanical properties and physicochemical parameters. To study the influence exerted by the amount of APB and free phosphoric acid on the properties of the ceramic, we repeatedly impregnated the cylinders with formulation nos. 2 and 3. To fix the modifier, we dried them at 100°C and then heated at 500°C.

We prepared samples for physicochemical studies by careful (without disintegration of skeleton-forming particles) grinding in an agate mortar to a particle size of 20–40 μm. An X-ray analysis was carried out on a DRON-2 installation with Cu_{K_α} radiation. A differential thermal analysis (DTA) was performed on an MOM derivatograph (Hungary) with heating in air from 20 to 1000°C at a rate of 10 deg min^{-1}. We used corundum with a particle size of 0.5–1.0 mm as a filler inert in this temperature range [4] to prevent foaming of the phosphate binder in the course of heating. The APB : corundum mass ratio was 1 : 4. The IR spectra were recorded on a Midas IR Fourier

spectrometer in the range 400–4000 cm^{-1}. We prepared samples by compaction of pellets with KBr (sample mass 4 mg).

We determined the content of water-soluble substances in the modified cylinders by analysis of water extracts. For this purpose, we boiled the cylinders in distilled water for 0.5 h at a water volume to cylinder mass ratio of 2 : 1. The degree of transfer of the hydrolysis products to the water phase was tentatively estimated by titration of the extracts with a 0.1 N KOH solution, using as indicators methyl orange and phenolphthalein, whose equivalence points correspond to the first and second dissociation constants of phosphoric acid, respectively. The difference in titrant expenditure makes it possible to judge the ratio between purely acidic and substituted components of phosphates passing into the water phase.

No exothermic effects are seen in the DTA curves for the filter samples impregnated with the three formulations, although they occur at about 500°C when pure aluminum dihydrophosphate is heated [6]. This points to the absence of crystallization processes in the composites under study. On heating the modified ceramic after a single impregnation, the main process for all the samples is the removal of chemically bound water, accompanied by an endothermic effect (Fig. 1). In this case, the mass loss is mostly complete at 500°C and constitutes about half of the absorbed amount of APB. For example, the water loss was 1.6% for sample no. 1 (APB/H_2O) with the minimal initial content of the aluminophosphate phase on the ceramic support (3.3%, after keeping at 20°C). For sample no. 2 (APB/H_3PO_4), the content of APB is the highest (15.5%), and the mass loss on heating was 6.7%. For formulation no. 3, the increase in mass after impregnation and mass loss was 9.5 and 4.8%, respectively. According to the X-ray analysis, no new crystalline phases were found in the samples, either, on heating at 500°C within the sensitivity limits of the method.

With another filler, corundum, heat treatment of APB is accompanied by formation of trimetaphosphate, which gives rise to a bend at 500°C in the curve of mass loss [6]. In this case, the final product on heating to 1000°C is aluminum orthophosphate in the form of tridymite [6, 7], the only phase detected by X-ray analysis, with a content of about 12%. This phase may be produced not only via natural transformation of aluminum trimetaphosphate at a sufficiently high temperature (800–1000°C) but also via corrosive pitting of the matrix under the action of products formed in dehydration of free phosphoric acids contained in APB.

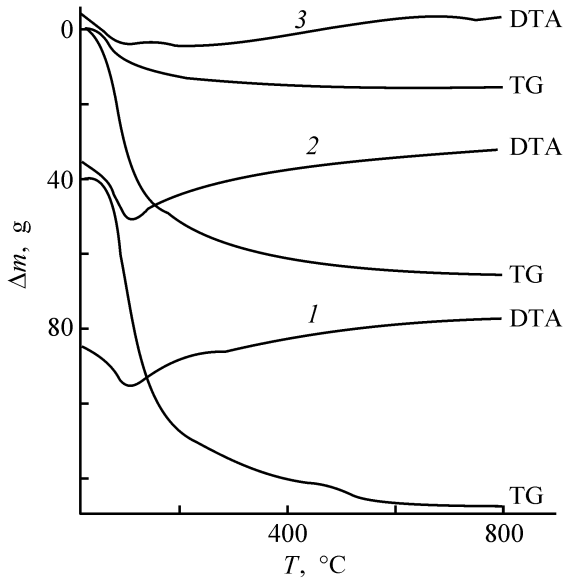


Fig. 1. DTA and TG curves of (*1*) starting APB with corundum and (*2, 3*) modified ceramic. (Δm) Mass loss and (T) temperature. Modifying composition: (*2*) APB/H_3PO_4 and (*3*) APB/H_2O.

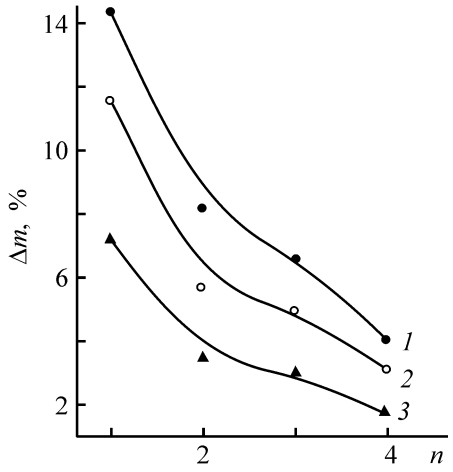


Fig. 2. Mass gain Δm of the aluminophosphate component of impregnated ceramics vs. the number of impregnations, n, at different heat treatment temperatures. Heat treatment temperature (°C): (*1*) 20, (*2*) 100, and (*3*) 500.

We could raise the content of aluminophosphate phase on the ceramic by almost a factor of 2 by repeated impregnation of the matrix, with intermediate heating of the samples at a temperature exceeding that of reversible rehydration, specifically, at 500°C. As a result of four impregnations, the content of deposited aluminophosphate was brought to virtually the maximum possible value of 13.8%. As can seen in Fig. 2, each subsequent impregnation results

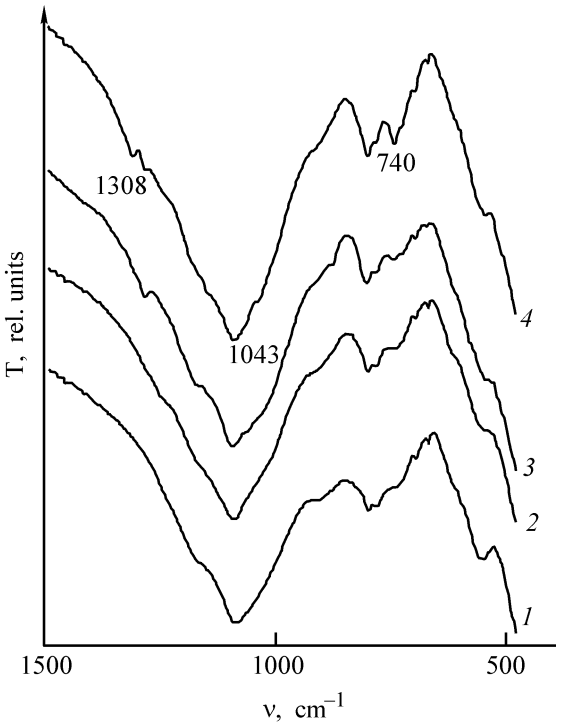


Fig. 3. IR spectra of (*1*) unmodified and (*2*–*4*) modified ceramic heat treated at (*2*, *4*) 800 and (*3*) 500°C. (T) Transmission and (ν) wave number. Number of impregnations: (*2*) 1 and (*3*, *4*) 4.

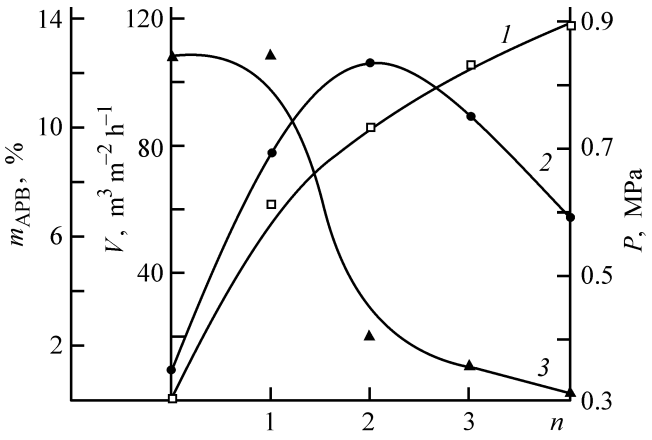


Fig. 4. (*1*) Content of aluminophosphate component, m_{APB}, (*2*) strength *P*, and (*3*) permeability *V* vs. the number of impregnations, *n*.

in a progressively decreasing mass gain. Only in the case of the maximum APB content, weak peaks of aluminum trimetaphosphate are observed in X-ray patterns as a separate phase on the background of the crystalline phases of the starting ceramic on heating at 500°C, and peaks of aluminum orthophosphate with the crystal lattice of tridymite appear at 800°C [6, 7]. Presumably, the appearance of this orthophosphate is associated with secondary reactions of the excess acid with the aluminosilicate matrix.

Because of the mutual overlapping of the absorption frequencies of SiO_4^{4-} and PO_4^{3-} tetrahedra, the vibrational spectroscopy is comparatively poorly informative for identification of new phases in the system under study. Nevertheless, clearly pronounced bands appear at 1308, 1043 (inflection), and 740 cm^{-1} in the spectrum of the sample repeatedly impregnated after a heat treatment at 500°C on the background of the absorption spectrum of silicates (Fig. 3). These bands correspond to the most intensive bands of pure aluminum tri- and tetrapoliphosphates [6] and are absent in the spectrum of a sample impregnated once. The fact that the general character of the IR spectrum is preserved when the heat treatment temperature is raised to 800°C is consistent with the DTA data presented above. The appearance of the band at 740 cm^{-1} may also indicate that APB reacts with the aluminosilicate matrix to give surface silicophosphates [8]. The above-mentioned sequence of transformations of the reactants, revealed by the X-ray and DTA data, together with the IR spectra, is in full agreement with the generally known scheme of transformations of acid aluminophosphates via dihydrotripolyphosphates to give aluminum trimetaphosphate [7, 9].

The formation of a new phase in the intergranular space leads to (i) a natural decrease in porosity and (ii) a less obvious decrease in the strength via loosening of interparticle contacts because of the formation of the crystalline phase. It can be seen in Fig. 4 that, within certain limits of modifier contents, the permeability of the cylinders tested remains almost unchanged at a substantial increase in strength. As expected previously [5], a mechanically strong porous structure can be constructed by creating interparticle contact interactions without any signs of crystallographic phase formation. A similar extremum in the plot of the strength against the binder content was observed for the aluminochromophosphate binder [4]. This, however, occurred for a different reason: the authors of [4] attributed this effect to the formation of a film that prevented gradual removal of the gas phase during the heat treatment, with the result that a porous structure responsible for a decrease in the strength parameters was formed.

A titrimetric analysis of water extracts of modified ceramic cylinders supplements the information obtained and allows a more complete understanding of the occurring chemical reactions. The amount of

Analysis of water extracts of modified ceramics samples

Composition of a modifying solution	Number of impregnations	Heat treatment temperature, °C	Content of the aluminophosphate phase, %	Content of water-soluble compounds in the deposited phase, mg-equiv g^{-1} (%)	
				by methyl orange	by phenolphthalein
APB/H_2O	1	500	1.7	0	0.44 (2.2)
	1	700	1.5	0	0.82 (4.0)
APB/H_3PO_4	1	500	8.1	0.46 (4.5)	1.17 (5.7)
	1	500	8.6	0.73 (7.1)	1.62 (7.9)
	1	700	7.9	0.79 (7.7)	2.48 (12.2)
	1	800	7.9	0.78 (7.6)	2.68 (13.1)
H_3PO_4	1	500	2.2	0.73 (7.2)	3.47 (17.0)
	2	500	14.6	2.08 (20.4)	5.33 (26.1)
	5	500	22.7	2.83 (27.7)	6.44 (31.6)

washed-out phosphorus-containing compounds is directly related to the content of free phosphoric acid in the impregnating solutions (see table).

With a mixture of APB and H_3PO_4 used as a modifying composition at a moderate heat treatment temperature, a certain amount of metaphosphoric acids is always present on the surface of the ceramic. These acids provide the acidity of the surface in operation of the composites in a gas atmosphere, but they are washed-out in an aqueous medium without any substantial decrease in the strength and filtering characteristics of the products. As the content of free phosphoric acid in the modifying solutions decreases, the amount of metaphosphates capable of being hydrolyzed may be decreased, as demonstrated by the negative results of analytical determination of free acids in the samples treated with the modifying solution containing no phosphoric acid, i.e., formulation no. 1.

The results of the analysis of aqueous extracts show a distinct tendency toward a rise in the degree of extraction of phosphorus-containing compounds, observed as the heat treatment temperature increases. This to a certain extent correlates with the fact that peaks do not overlap with the reflections of the matrix appear in the X-ray diffraction patterns. These peaks are close in the interplanar distances to the highest-intensity lines of aluminum orthophosphate in the form of tridymite. With account of the IR spectroscopic data, we believe that, at elevated temperatures, a fraction of tri- and tetrametaphospates in samples enriched in phosphates disintegrates to give orthophosphate and metaphosphoric acids, in agreement with the scheme of transformation suggested in [9].

CONCLUSIONS

(1) Synthesis of mechanically strong silicate composites that preserve their porosity in treatment with aluminophosphate binders should not be accompanied by crystallization processes.

(2) New crystalline phases not only disintegrate the interparticle contacts, but also fill the free volume of a composite, which results both in a loss of mechanical strength and in a decrease in the gas and hydraulic permeability.

REFERENCES

1. Kopeikin, V.A. and Rumyantsev, P.F., *Fiziko-khimicheskie i tekhnologicheskie osnovy zharostoikikh tsementov i betonov* (Physicochemical and Technological Principles of Heat-resistant Cements and Concretes), Moscow: Nauka, 1986.
2. Illarionov, I.E., *Litein. Proizv.*, 1990, no. 3, pp. 16–17.
3. Pilipchatin, L.D., *Ogneupory Tekhn. Keram.*, 1999, no. 7, pp. 25–28.
4. Duderov, Yu.G. and Mel'nikov, A.M., *Ogneupory*, 1980, no. 1, pp. 52–55.
5. Makatun, I.M., Rat'ko, A.I., Azarov, S.M., *et al., Neorg. Mater.*, 2005, vol. 41, no. 1, pp. 88–92.
6. Zharskii, I.M., Vorob'ev, N.I., Mel'nikova, R.Ya., *et al., Svoistva i metody identifikatsii veshchestv v neorganicheskoi tekhnologii* (Properties and Methods for Identification of Substances in Inorganic Technology), Minsk: Belarus. Gos. Univ., 1996.
7. Bobrov, B.S., Zhigun, I.G., Kiseleva, L.V., *et al., Zh. Prikl. Khim.*, 1986, vol. 59, no. 12, pp. 2653–2657.
8. *Fosfaty chetyrekhvalentnykh elementov* (Phosphates of Tetravalent Elements), Tananaev, I.V., Ed., Moscow: Nauka, 1972.
9. *Inorganic Phosphate Materials*, Kanazawa, T., Ed., Tokyo: Kodansha, 1989.

ISSN 1070-4272, Russian Journal of Applied Chemistry, 2006, Vol. 79, No. 2, pp. 190–195. © Pleiades Publishing, Inc., 2006.
Original Russian Text © V. E. Kritskii, B. P. Burylev, E. B. Kritskaya, 2006, published in Zhurnal Prikladnoi Khimii, 2006, Vol. 79, No. 2, pp. 192–197.

PHYSICOCHEMICAL STUDIES OF SYSTEMS AND PROCESSES

Vapor Pressure and Activity of Components of Melts Formed by Manganese Chloride and Chlorides of Alkaline-Earth Metals

V. E. Kritskii, B. P. Burylev, and E. B. Kritskaya

Inter-Oil Produkt OOO, Krasnodar, Russia

Received April 6, 2005

Abstract—The boiling points of melts were measured at different pressures over the melts for certain concentrations of components of the liquid phase in binary systems constituted by manganese chloride and chlorides of alkaline-earth metals. The temperature dependences of the saturated vapor pressure, normal boiling points, and enthalpies of evaporation were calculated. The concentration dependences of the thermodynamic activities of the components of four binary systems were analyzed.

DOI: 10.1134/S1070427206020042

The lack of rich manganese deposits in Russia gives rise to an acute problem of processing of lean manganese ores from West Siberia, Krasnodar krai, etc. Certain deposits are characterized by an increased content of phosphor, and, therefore, to obtain a high-quality metal, it is necessary to perform dephosphorization.

In the case of the economic feasibility of processing by method of the chloride metallurgy [1, 2], a study of systems based on manganese chlorides is a matter of current interest. Compounds of alkaline-earth metals are used in dephosphorization, with preference given to compounds of barium and strontium, including their chlorides [3–6]. In the technological scheme used, the systems $MnCl_2$–MCl_2 (M = Mg, Ca, Sr, Ba) are of practical importance. The binary systems have been studied [7], whereas more complex systems are not understood. Therefore, binary and multicomponent systems are of interest for analysis of real industrial melts. Analysis of the physicochemical properties of systems of this kind is difficult; even more complicated, because of the uncertainty in determining the interparticle interactions, is interpretation of the results obtained. Studies of binary melts in terms of various models and evaluation of parameters of the interparticle interaction will make it possible to reveal strongly interacting systems and assess the possibility of their generalization to multicomponent melts, with weak interactions neglected if necessary.

The aim of this study was to calculate the dependence of the vapor pressure on temperature and composition of binary systems from the results of experimental measurements of the boiling point and to evaluate the interaction parameters for the whole variety of melts in order to obtain expressions that can be used to calculate the thermodynamic activities of the components of melts of manganese chloride and chlorides of alkaline-earth metals.

The experimental procedure is based on measuring the boiling points of chloride systems at different pressures. An experimental setup was assembled for the study from a platinum resistance furnace with transducers measuring with high accuracy the pressure and temperature. The main part of the setup was the furnace in the form of a quartz tube 24 mm in diameter, on which the heater made of a platinum wire 0.5 mm in diameter was wound. The length of the isothermal zone was 100 mm. The furnace worked for a long time in the temperature range from the melting point of the salts to 1450 K. The resistance furnace was placed in another quartz tube 60 mm in diameter with a branch for evacuation of the system. Current was supplied to the heater via the lower part of the tube. The rarefaction was created in the experimental setup with a roughing pump.

The system included a 5-l buffer vessel to eliminate pressure fluctuations occurring because of the irregular operation of the vacuum pump. A leak was installed before the buffer vessel to control the pressure in the vacuum system. This was done at a permanently working vacuum pump by making higher the rate of air delivery to the leak. The rarefaction created in the experimental system was in the range

Table 1. Boiling points T at different pressures P in the $MnCl_2$–MCl_2 systems and melt concentrations

Mole fraction of the alkaline-earth metal, x_{MCl_2}									
0.2		0.4		0.5		0.6		0.8	
P, Pa	T, K	P, Pa	T, K	P, Pa	T, K	P, Pa	T, K	P, Pa	T, K
$MnCl_2$–$MgCl_2$									
10 600	1280	1460	1323	13 320	1327	7600	1250	8270	1331
15 600	1313	19 800	1353	19 530	1361	11 330	1327	1370	1382
22 800	1353	26 000	1378	26 070	1390	17 670	1376	19 330	1423
33 860	1389	35 330	1409			25 200	1405	24 870	1453
48 130	1423					31460	1428		
$MnCl_2$–$CaCl_2$									
		8800	1319			5470	1316	3330	1340
		8800	1314			8800	1371	5930	1402
		12 330	1357			13 070	1419	8930	1457
		18 470	1399			17 200	1450		
		24 530	1432						
$MnCl_2$–$SrCl_2$									
5670	1247	6536	1280	5670	1289	2470	1250	1890	1329
11 530	1311	11 000	1328	9930	1311	4130	1305	1890	1333
17 730	1352	18 930	1371	15 000	1369	4130	1307	3270	1407
24 930	1391	26 260	1398	15 000	1373	6000	1337	4130	1440
32 730	1420	35 400	1423	21 600	1405	9800	1379		
						13930	1437		
$MnCl_2$–$BaCl_2$									
4070	1210	3530	1271	2470	1253	3130	1319	1930	1369
8000	1250	5470	1305	4000	1289	5730	1375	3000	1415
14 800	1350	10 000	1349	7200	1336	8930	1421	5530	1489
21 470	1382	14 530	1390	12 130	1389				
28 660	1416	20 270	1425	18 670	1425				
36 800	1432								

from 100 to 100 000 Pa. The rarefaction produced was measured with a U-shaped sealed mercury vacuum gage connected to the setup directly after the buffer vessel. The accuracy of pressure measurements was ±70 Pa. The resistance furnace was heated with an autotransformer with a reduction gear driven by a low-speed electric motor. The existence of several stages in the gearbox enabled gradual heating of the furnace at a certain prescribed rate. The setup was reliable and, owing to its small volume, rapidly cooled on switching off the current, which enabled fast and multiple experiments.

A substance under study was placed in a quartz test tube 8–10 mm in diameter, which was mounted in the furnace in the middle of the isothermal zone. A thermocouple was introduced from below into a recess at the bottom of the test tube. To prevent the thermocouple from the attack of the medium, its most part was coated with corundum splints. Temperature was measured with a standard platinum–platinum rhodium thermocouple whose cold junctions were thermostated at 273 K. The accuracy of indications of the thermocouple was verified against reference points. The thermal electromotive force of the thermocouple was measured using a complex of measuring, amplifying, and recording devices: electronic dc amplifier I-37 and electronic self-recorder N-37 recording the signal on a 100-mm-wide tape. As starting preparations taken to produce the mixtures served salts of special-purity, chemically pure, and analytically pure grades, which were dehydrated by passing dried gaseous hydrogen chloride through the salts gradually heated to the melting point and kept at this temperature for 2 h. Gaseous hydrogen chloride was obtained by reacting concentrated sulfuric acid with crystalline potassium chloride. The dehydration process was monitored thermographically on a derivatograph and spectroscopically on UR 20 spectrophotometer.

Table 2. Constants of Eq. (1), enthalpies of evaporation, and standard boiling points

x_{MCl_2}	A	$\pm\Delta A$	B	$\pm\Delta B$	$\pm\log P$	ΔH^{ev}, kJ mol^{-1}	T^{sb}	T
							K	
				$MnCl_2$–$MgCl_2$				
0.2	8295	152	10.504	0.115	0.0218	158.8	1509	1280–1423
0.4	8324	95	10.453	0.071	0.0652	159.3	1528	1323–1409
0.5	8533	157	10.597	0.045	0.0112	163.3	1537	1327–1390
0.6	8137	154	10.186	0.114	0.0213	159.7	1571	1290–1428
0.8	7627	118	9.639	0.021	0.0112	145.9	1645	1331–1453
				$MnCl_2$–$CaCl_2$				
0.0	8343	42	10.572	0.031	0.0087	159.7	1499	1250–1428
0.4	7251	127	9.448	0.093	0.0155	138.8	1632	1319–1432
0.6	7044	107	9.086	0.121	0.0325	134.8	1726	1289–1428
0.8	7159	102	8.870	0.088	0.0300	137.0	1852	1340–1457
				$MnCl_2$–$SrCl_2$				
0.2	7778	43	9.993	0.024	0.0074	148.9	1560	1247–1420
0.4	9401	164	1.143	0.121	0.0229	179.9	1532	1280–1423
0.5	9168	198	1.857	0.275	0.0214	175.5	1567	1289–1405
0.6	7560	165	9.426	0.124	0.0326	144.7	1710	1250–1437
0.8	5892	132	7.705	0.096	0.0132	112.8	2183	1329–1440
				$MnCl_2$–$BaCl_2$				
0.2	8949	142	10.800	0.101	0.0290	171.3	1544	1210–1432
0.4	8972	178	10.618	0.132	0.0274	171.7	1599	1271–1425
0.5	8997	96	10.578	0.072	0.0169	172.3	1615	1253–1425
0.6	8366	128	9.840	0.093	0.085	160.1	1731	1289–1421
0.8	7742	185	8.944	0.130	0.0133	148.2	1766	1369–1489

The procedure used to measure the saturated vapor pressure was the following: mixtures were prepared from dehydrated reagents by weighing the components on an analytical balance. Then the weighed portion in a quartz test tube was placed in the resistance furnace and heated to melting. The platinum–platinum rhodium thermocouple was brought to the melt from below. Then the vacuum pump created in the whole system a rarefaction measured with the sealed mercury vacuum gage. After that the sample was gradually heated using the autotransformer with the multistage gearbox. At that instant of time when the external pressure coincided with the saturated vapor pressure over the mixture, a clearly pronounced temperature stop was observed on the tape of the N-37 self-recorder. Just this temperature is the boiling point of the sample. The boiling point was recorded as a well visible stop for 15–20 s. Then the pressure in the system was elevated by 3000–10000 Pa, depending on a system under study, and a detailed measurement was made from the beginning. For each composition, 5–8 measurements were made. The loss of mass of the highly volatile component was 0.01–0.03 g for difficultly volatile systems and 0.08–0.12 g for highly volatile systems, i.e., less than 1% and up to 4% relative to the mass of the weighed portion, respectively. The I-37 amplifier makes it possible to work with a platinum–platinum rhodium thermocouple with a sensitivity of 1 mV per the entire scale of the instrument below 1373 K, and 2.5 mV per scale above 1373 K; the measurement accuracies are ±2 and ±5 K for the lower and upper temperature ranges, respectively.

The experimentally determined boiling points of melts of the systems $MnCl_2$–MCl_2 (M = Mg, Ca, Sr, Ba), listed for constant compositions (x_{MCl_2} is the mole fraction of an alkaline-earth metal) in Table 1, were processed using the least-squares method by the equation

$$\log P = (B \pm \Delta B) - (A \pm \Delta A)/T. \qquad (1)$$

Here, P is the saturated vapor pressure (Pa); T, absolute temperature (K); A and B, constants found by the least-squares procedure; and ΔA and ΔB, confidence intervals for a confidence probability $p = 0.95$.

The values of these quantities are listed for four systems in Table 2, together with the enthalpies of

evaporation ΔH^{ev} and standard boiling points T^{sb} (for P = 101 325 Pa), given by the equations

$$\Delta H^{ev} = 19.14A, \quad (2)$$

$$T^{sb} = A/(B - 5.006). \quad (3)$$

The vapor pressure isotherms plotted using the data from Table 2 characterize the systems studied as systems with a monotonic increase in deviations, in which the share of the chemical interaction grows in going from $MgCl_2$ as additive component to $CaCl_2$, then to $SrCl_2$, and finally to $BaCl_2$. This behavior can be quantitatively described by the mutual exchange energy Q for a binary system composed of components 1 and 2.

The total vapor pressure in the absence of polymerization and complexation is given by

$$P = P_1^0 x_1 f_1 + P_2^0 x_2 f_2, \quad (4)$$

where f_1 and f_2 are the activity coefficients of components 1 and 2, and P_0^1 and P_0^2 are the vapor pressures of pure components; here and hereinafter index 1 refers to $MnCl_2$, and index 2, to $MgCl_2$, $CaCl_2$, $SrCl_2$, and $BaCl_2$ as components being added.

In accordance with the results of [8], the degree of dimerization of manganese chloride is low; the same refers to chlorides of alkaline-earth metals [9]. In the case of applicability of the equations for regular solutions:

$$RT\ln f_1 = Q(1 - x_1)^2, \quad (5)$$

$$RT\ln f_2 = Q(1 - x_2)^2, \quad (6)$$

we obtain for the equimolar composition $x_1 = x_2 = 0.5$:

$$Q = 4RT\ln\frac{2P}{P_1^0 + P_2^0}. \quad (7)$$

The vapor pressures of the pure components are as follows (Pa): $P^0_{MnCl_2}$ = 14 270 [10], $P^0_{MgCl_2}$ = 2570 [9], $P^0_{CaCl_2}$ = 8.1, $P^0_{SrCl_2}$ = 2.5, $P^0_{BaCl_2}$ = 1.6 [9]. From Eq. (7) we obtain for the systems composed of $MnCl_2$ with $MgCl_2$, $CaCl_2$, $SrCl_2$, or $BaCl_2$, Q = +10 790, –7500, –4800, and –19 500 J mol^{-1} for 1300 K.

Because the vapor pressures of calcium, strontium, and barium chlorides are negligible as compared with that of manganese chloride, the activities α of $MnCl_2$ in alloys with Ca, Sr, and Ba chlorides are given by the expression

$$\alpha_{MnCl_2} = P/P^0_{MnCl_2}. \quad (8)$$

We obtain from the data in Table 2

$$\log P - \log P^0_{MnCl_2} = -\frac{\delta A}{T} + \delta B. \quad (9)$$

For an arbitrary composition, we have

$$Q = \frac{19.14T(-\delta A/T + \delta B) - RT\ln x_{MnCl_2}}{(1 - x_{MnCl_2})^2}, \quad (10)$$

and for the equimolar composition at 1300 K

$$Q = 99\,530(-\delta A/1300 + \delta B) + 29\,960. \quad (11)$$

Calculations by the last equations show that the concentration dependences of the activity (and vapor pressure) for the systems $MnCl_2$–MCl_2 are more complex than those described by expressions (5) and (6). Therefore, it is necessary to use for quantitative description equations that take into account the nonadditivity of the energy of a binary solution [11]:

$$RT\ln f_1 = (Q_1 - Q_2)(1 - x_1)^2 + 2Q_2(1 - x_1)^3, \quad (12)$$

$$RT\ln f_2 = (Q_1 + 2Q_2)(1 - x_2)^2 - 2Q_2(1 - x_2)^3, \quad (13)$$

in which constants Q are found from experimental data.

Analysis of the dependences obtained makes it possible to determine how the activities of the components vary with their concentration. To compare the experimental and calculated data, we use the data from Table 1 and the results of calculation by Eq. (4) for 1300 K. We obtain, from Eqs. (5) and (6) for the system $MnCl_2$–$MgCl_2$:

$$\ln f_i = 0.432(1 - x_i)^2. \quad (14)$$

The calculated and experimental values are compared below (1, $MnCl_2$; 2, $MgCl_2$):

x_1	f_1	P_{exp}	P_1	P_2	P_{calc}
0.2	1.890	5917	5393	2136	7529
0.4	1.431	8448	8164	1807	9971
0.5	1.282	10 793	9144	1645	10 789
0.6	1.172	11 218	10 036	1468	11 504
0.8	1.040	13 280	11 876	970	12 846

The strongest difference is observed for two compositions with high content of magnesium chloride. An asymmetry of thermodynamic properties is noticeable for the system $MnCl_2$–$CaCl_2$. Therefore, we have from Eqs. (12) and (13) that $Q_1 = -8150$ and $Q_2 = 7600$ J mol^{-1} and obtain for the activity coefficients

$$\log f_1 = -0.633(1 - x_1)^2 + 0.611(1 - x_1)^3, \quad (15)$$

$$\log f_2 = -0.283(1 - x_2)^2 - 0.611(1 - x_2)^3, \quad (16)$$

where, again, 1 stands for $MnCl_2$, and 2, for $CaCl_2$.

The results of the calculations are presented below:

x_2	α_1	α_2	P_1	P_2	P_{calc}	P_{exp}
0.2	0.763	0.019	10888	0.15	10888	–
0.4	0.520	0.378	7417	3.0	7420	7418
0.5	0.414	0.494	5908	4.0	5948	–
0.6	0.321	0.608	4575	5.0	4580	4651
0.8	0.162	0.818	2307	6.6	2314	2307

A good agreement between the experimental and calculated data is observed.

For the $MnCl_2$–$SrCl_2$ system, the best way to find the activity coefficients was by Eqs. (5) and (6) for $Q = -10000$ J mol^{-1}, whence we have

$$\log f_i = -0.402(1 - x_i)^2. \quad (17)$$

For various compositions, we obtain

x_2	α_2	f_1	P_1	P_{exp}
0.2	0.193	0.964	10998	10231
0.4	0.345	0.862	7381	8156
0.5	0.396	0.793	5659	6378
0.6	0.430	0.717	4089	4080
0.8	0.442	0.553	1578	1488

The partial pressures of strontium chloride somewhat exceed 1 Pa, and, therefore, $P_{calc} \approx P_1$. The agreement between the calculated and experimental data is good, except for the equimolar composition.

For the $MnCl_2$–$BaCl_2$ system, we can take as a first approximation Eqs. (5) and (6) for $Q = -20000$ J mol^{-1}. The best agreement between the experimental and calculated values is achieved with expressions (12) and (13) with $Q_1 = -29730$ J mol^{-1} and $Q_2 = 19280$ J mol^{-1}, whence we have

$$\log f_1 = -1.970(1 - x_1)^2 + 1.550(1 - x_1)^3, \quad (18)$$

$$\log f_2 = 0.355(1 - x_2)^2 - 1.550(1 - x_2)^3, \quad (19)$$

and obtained for various compositions

x_2	α_1	α_2	P_1	P_{exp}
0.2	0.686	0.054	9795	8244
0.4	0.365	0.248	5205	5205
0.5	0.251	0.393	3585	4542
0.6	0.169	0.316	2410	2539
0.8	0.068	0.133	973	974

The strongest difference between the experimental and calculated data is observed for the compositions with x_2 0.2 and 0.5. At other concentrations, the agreement is satisfactory.

Analysis of the results obtained suggests that minor positive deviations from the Raoult law are observed only in the $MnCl_2$–$MgCl_2$ system, whereas small negative deviations from the laws for ideal solutions are characteristic of the systems $MnCl_2$–$CaCl_2$, $MnCl_2$–$SrCl_2$, and $MnCl_2$–$BaCl_2$. The activities of the components steadily decrease at the same concentrations in going from $MnCl_2$–$CaCl_2$ to $MnCl_2$–$SrCl_2$, and further to $MnCl_2$–$BaCl_2$.

The saturated vapor pressures can be prognosticated for the systems studied, using the expression

$$P = \Sigma P_i^0 x_i f_i. \quad (20)$$

The only quantities to be known are the activity coefficients of multicomponent melts. The procedure for determining these coefficients was described in [12].

CONCLUSIONS

(1) The boiling points of chloride melts of manganese and alkaline-earth metals (Mg, Ca, Sr, and Ba) were determined at various pressures in the systems for a wide range of fixed parameters. Metrological characteristics of the experimental setup and the method used were presented.

(2) The pressure dependences of the boiling points were presented for four binary systems $MnCl_2$–$MgCl_2$, $MnCl_2$–$CaCl_2$, $MnCl_2$–$SrCl_2$, and $MnCl_2$–$BaCl_2$ for constant concentrations of the melts. These parameters were used to obtain temperature dependences of the saturated vapor pressure for the given systems. The dependences were approximated with two-parameter expressions, whose constants were found using methods of mathematical statistics.

(3) The experimental data obtained were used to calculate the thermodynamic activities of the components, which were described by equations that take

into account the nonadditivity of the energy of a binary solution. It was shown that the $MnCl_2$–$MgCl_2$ system shows minor positive deviations from ideality, whereas the systems $MnCl_2$–$CaCl_2$, $MnCl_2$–$SrCl_2$, and $MnCl_2$–$BaCl_2$ exhibit moderate negative deviations from ideality, which become more pronounced on passing from the systems with calcium chloride to those with strontium chloride and barium chloride.

(4) It was shown that a model description of the thermodynamic properties of the multicomponent system $MnCl_2$–$MgCl_2$–$CaCl_2$–$SrCl_2$–$BaCl_2$ is possible.

REFERENCES

1. Morozov, I.S., *Primenenie khlora v metallurgii redkikh i tsvetnykh metallov: Fiziko-khimicheskie osnovy* (Use of Chlorine in the Metallurgy of Rare and Nonferrous Metals: Physicochemical Foundations), Moscow: Nauka, 1966.
2. Burylev, B.P., Kritskaya, E.B., and Kostenko, N.B., *Eksperimental'noe issledovanie i modelirovanie davleniya nasyshchennogo para i termodinamicheskikh svoistv rasplavov khloridov na osnove metallov chetvertogo perioda* (Experimental Study and Modeling of Saturated Vapor Pressure and Thermodynamic Properties of Chloride Melts Based on Fourth-Period Metals), Available from VINITI, 2001, Krasnodar, no. 265-V 2001.
3. Burtsev, V.T., Zhuravlev, V.M., Yugov, P.I., and Shetteler, I., *Stal'*, 1991, no. 4, pp. 13–16.
4. Jiang, M.F. and Ichise, E., *Steel Res.*, 1988, vol. 59, no. 9, pp. 375–385.
5. Fujiwara, H. and Iwase, M., *3rd Int. Conf. Molten Slags and Fluxes, Glasgow, June, 27–29, 1988*, London, 1989, pp. 73–76.
6. Burtsev, V.T., Bolgov, V.B., and Serov, G.V., *Metally*, 1989, no. 2, pp. 5–9.
7. Burylev, B.P., Moisov, L.P., and Mil'man, V.M., *Adgez. Raspl. Paika Mater.*, 2003, no. 36, pp. 54–68.
8. Rat'kovskii, I.A., Novikova, L.N., Orekhova, S.E., *et al.*, *Izv. Vyssh. Uchebn. Zaved., Khim. Khim. Tekhnol.*, 1976, vol. 19, no. 3, pp. 407–411.
9. *Termodinamicheskie svoistva individual'nykh veshchestv: Spravochnoe izdanie v 4-kh tomakh* (Thermodynamic Properties of Individual Substances: Reference Book, 4 vols.), Glushko, V.P., Ed., Moscow: Nauka, 1981, vol. 3, book 2.
10. Burylev, B.P. and Mironov, V.L., *Zh. Fiz. Khim.*, 1975, vol. 49, no. 1, pp. 222–223.
11. Burylev, B.P., *Izv. Vyssh. Uchebn. Zaved., Tsv. Metall.*, 1964, no. 4, pp. 65–72.
12. Burylev, B.P., Sryvalin, I.T., and Korpachev, V.G., *Primenenie priblizhennykh metodov dlya rascheta termodinamicheskikh svoistv oksidnykh, metallicheskikh i galogenidnykh system* (Application of Approximate Methods for Calculation of Thermodynamic Properties of Oxide, Metallic, and Halide Systems), Kuban. Gos. Univ., 1986, Krasnodar, Available from ONIITEKhIM, no. 498-khp-86.

ISSN 1070-4272, Russian Journal of Applied Chemistry, 2006, Vol. 79, No. 2, pp. 196–200. © Pleiades Publishing, Inc., 2006.
Original Russian Text © V. M. Lembrikov, V. V. Volkova, G. P. Zhavoronkova, L. V. Konyakhina, 2006, published in Zhurnal Prikladnoi Khimii, 2006, Vol. 79, No. 2, pp. 198–202.

PHYSICOCHEMICAL STUDIES OF SYSTEMS AND PROCESSES

Properties of the Extraction System Constituted by Phosphoric Acid Produced from Khibiny Apatite and Tri-*n*-Butyl Phosphate

V. M. Lembrikov, V. V. Volkova, G. P. Zhavoronkova, and L. V. Konyakhina

Voskresenskii NIUiF (Voskresensk Research Institute of Fertilizers and Phosphoric Acid) Open Joint-Stock Company, Voskresensk, Moscow oblast, Russia

Received June 22, 2005

Abstract—Data on the equilibrium distribution of phosphoric acid among the aqueous and organic phases in extraction of phosphoric acid with tri-*n*-butyl phosphate are presented for the system constituted by phosphoric acid produced from the Khibiny concentrate and by the extracting agent from the industrial system for purification of extraction phosphoric acid at 25–50°C.

DOI: 10.1134/S1070427206020054

Liquid extraction with organic solvents is a promising method for purification of substances and, in particular, that to remove impurities from the extraction phosphoric acid (EPhA). Liquid extraction is used on the industrial scale to purify the apatite EPhA with tri-*n*-butyl phosphate (TBP) as extracting agent [1].

The properties of the following systems have been described in the literature: H_3PO_4–H_2O–TBP at 25°C [2] and 293–343 K [3], and H_3PO_4–H_2SO_4–H_2O–TBP at 293–353 K [4]; the systems were composed of reagent phosphoric acid of pure grade and TBP of technical grade.

The present study is concerned with the distribution of phosphoric acid among the organic and aqueous phases of composition close to that in industrial manufacture of purified phosphoric acid. The experiments were performed at 25–50°C and 255–764 g l^{-1} phosphoric acid in the aqueous phase (in terms of P_2O_5). The choice of the given range of temperatures and concentrations was governed by the real conditions of industrial purification of EPhA. The solutions were prepared by saturating an extracting agent from the industrial system with extraction phosphoric acid. In the concentration of impurities in the aqueous and organic phases, this system corresponds to that in the stage of EPhA extraction in manufacture of purified phosphoric acid.

An evaporated desulfated EPhA produced from the Khibiny apatite concentrate was used in the experiments. The acid had a density of 1.537 g cm^{-3} and the following composition (wt %): P_2O_5 47.5, SO_4^{2-} 0.33, F^- 0.262, and Fe_2O_3 0.21. The extracting agent from the technological system was used for extraction. The temperature in the experiments was maintained constant by thermostating to within ±0.5°C. The content of phosphoric acid in the organic phase was determined by potentiometry [5]. The results of the experiments are presented in Table 1 and Fig. 1.

A mathematical processing of the experimental data demonstrated that the equilibrium contents of P_2O_5 in the organic and aqueous phases are related by an extraction equation similar to the Hand equation [6]:

$$c_{P_2O_5\,org.ph} = a c^{b}_{P_2O_5\,aq.ph}, \quad (1)$$

where $c_{P_2O_5\,org.ph}$ is the content of P_2O_5 in the organic phase (g l^{-1}); $c_{P_2O_5\,aq.ph}$, that in the aqueous phase (g l^{-1}); and a and b, coefficients of the equation.

It should be noted that the re-extraction of phosphoric acid from the extracting agent with water was calculated using the data reported in [3], where equations describing the process were also presented. However, two equations for two different temperature ranges were reported. Therefore, a similar pro-

Table 1. Equilibrium distribution of phosphoric acid among the aqueous and organic phases

Equilibrium content of P_2O_5 in the phases, g l^{-1}		Calculated content of P_2O_5 in the organic phase, g l^{-1}	Δ, %	Equilibrium content of P_2O_5 in the phases, g l^{-1}		Calculated content of P_2O_5 in the organic phase, g l^{-1}	Δ, %
aqueous	organic			aqueous	organic		
25°C				40°C			
370.0	95.3	93.9	1.2	285.8	53.2	56.1	–5.5
605.2	170.1	167.6	1.4	298.8	61.5	59.6	3.0
635.7	178.0	177.7	0.2	325.8	64.8	67.1	–3.5
642.0	181.7	179.7	1.3	399.3	82.1	88.3	–7.6
670.1	194.0	189.0	2.6	440.7	98.5	101.0	–2.5
709.8	215.1	202.3	5.9	544.0	143.4	134.4	6.3
30°C				682.1	174.0	182.6	–4.9
255.8	58.7	56.3	4.1	704.3	189.7	190.7	–0.5
270.5	60.1	60.3	–0.3	738.5	197.9	203.3	–2.7
312.0	70.4	72.0	–2.2	764.3	200.4	213.0	–6.3
403.6	96.3	99.0	–2.8	50°C			
546.8	137.7	144.1	–4.6	298.4	54.0	52.0	3.6
621.8	160.4	169.0	–5.3	300.7	46.9	52.6	–12.1
676.3	172.2	187.5	–8.9	329.8	61.5	60.3	2.0
733.2	190.8	207.2	–8.6	373.7	74.2	72.5	2.3
685.5	189.7	190.6	–0.5	461.3	105.8	98.9	6.5
706.6	195.3	197.9	–1.34	562.7	138.8	132.5	4.5
759.1	220.7	216.3	2.0	654.2	169.2	165.4	2.2
				700.5	181.4	183.0	–0.9
				743.5	193.4	199.8	–3.3
				750.2	200.6	202.4	–0.9

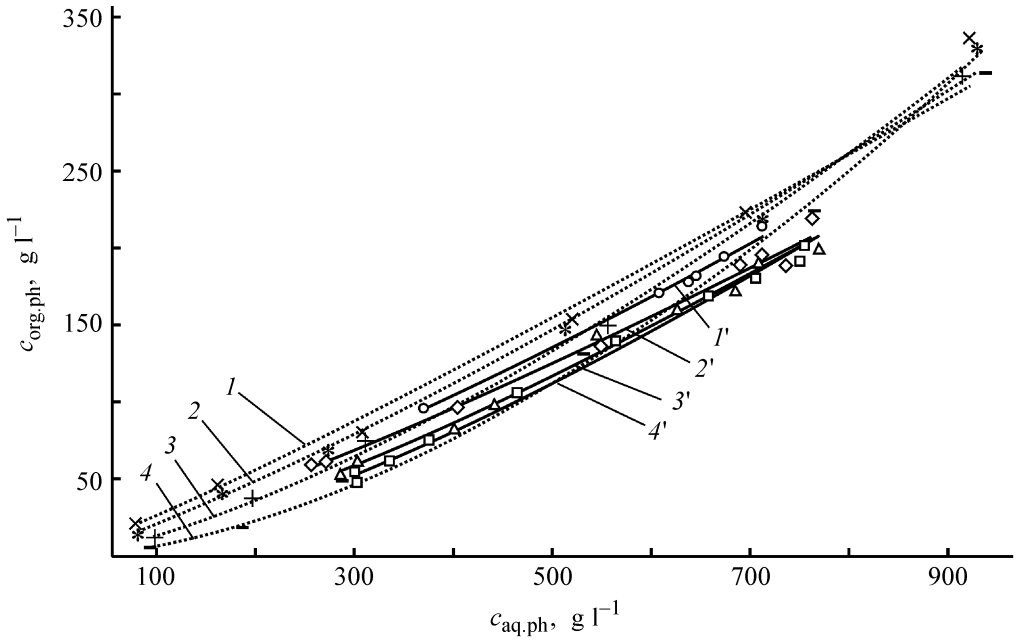


Fig. 1. Equilibrium content of P_2O_5 in the organic phase, $c_{org.ph}$, vs. the content of P_2O_5 in the aqueous phase, $c_{aq.ph}$, for (*1–4*) technical-grade TBP and (*1'–4'*) an extracting agent from the technological system at different temperatures. Extraction temperature (°C): (*1*) 10, (*2*) 20, (*1'*) 25, (*2'*) 30, (*3*, *3'*) 40, (*4'*) 50, and (*4*) 70.

Table 2. Coefficients a and b in Eq. (1) and reliabilities of approximation, R^2

Coefficients of Eq. (1)	Temperature, °C						
	10	20	25	30	40	50	70
				System I			
a	0.146	0.0706	–	–	0.0165	–	0.0024
b	1.1214	1.2303	–	–	1.4485	–	1.7327
R^2	0.9945	0.9978	–	–	0.9973	–	0.9982
				System II			
a	–	–	0.0721	0.0754	0.0264	0.0111	–
b	–	–	1.2136	1.194	1.3512	1.4829	–
R^2	–	–	0.9956	0.9952	0.9934	0.9919	–

Table 3. Coefficients and reliabilities of approximation, R^2, for Eqs. (2) and (3)

System	Coefficients of Eq. (2)		R^2	Coefficients of Eq. (3)		R^2
	n	p		k	m	
I	0.2776	–0.0685	0.9989	0.0102	1.0266	0.9986
II	0.6634	–0.0807	0.9583	0.0118	0.8836	0.9406

cessing of published data [3] was done for the system H_3PO_4–H_2O–TBP. The data used are presented in Fig. 1 (curves *1–3*).

Table 2 lists coefficients a and b and the reliability of approximation, R^2, for each curve. The data of Table 2 were used to plot coefficients a and b against temperature (Fig. 2) for the system H_3PO_4–H_2O–TBP (system I, curve *1*) and for that constituted by apatite EPhA and an extracting agent from the industrial system (system II, curve *2*). The temperature dependences of the coefficients for these systems are similar. The temperature dependence of coefficient a can be described by the equation

$$a = ne^{pT}, \quad (2)$$

and that of coefficient b, by

$$b = kT + m, \quad (3)$$

where T is temperature (°C); n and p, coefficients of Eq. (2); and k and m, those of Eq. (3).

Table 3 lists the coefficients of Eqs. (2) and (3) and the reliability of approximation, R^2, for the system H_3PO_4–H_2O–TBP (I) and for that constituted by apatite EPhA and an extracting agent from the industrial system II.

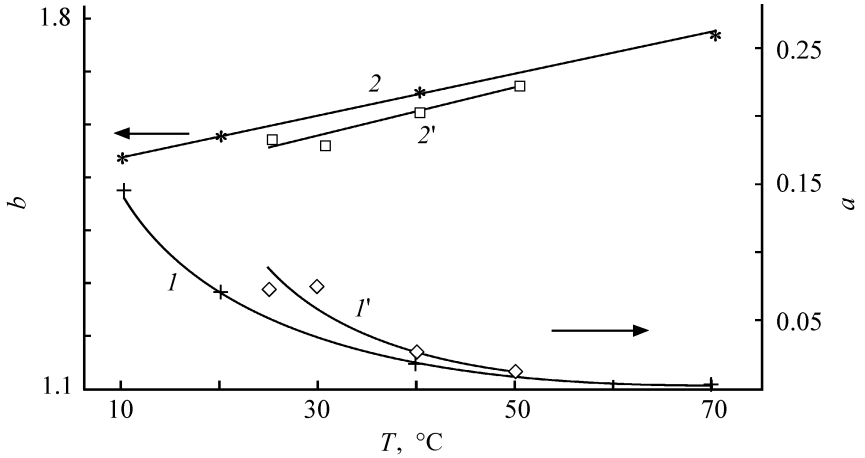


Fig. 2. Coefficients a and b of Eq. (1) vs. temperature T for (*1*, *2*) technical-grade TBP and (*1'*, *2'*) extracting agent from the technological system.

Table 4. Average technological performance parameters of an installation for EPhA purification with TBP in April 2005

T,°C	Parameters of the organic phase				Parameters of the aqueous phase				V_{aq} : V_{org}		Number of stages
	at the column inlet		at the column outlet		at the column inlet		at the column outlet				
	ρ, g cm^{-3}	P_2O_5, g l^{-1}	ρ, g cm^{-3}	P_2O_5, g l^{-1}	ρ, g cm^{-3}	P_2O_5, g l^{-1}	ρ, g cm^{-3}	P_2O_5, g l^{-1}	experiment	calculation	
Stage of extraction											
48	1.002	22.1	1.091	152.0	1.606	834.3	1.294	337.6	0.24	0.263	2.8
Stage of extract washing											
57	1.091	152.0	1.081	130.0	1.000	0.0	1.411	596.4	0.03	0.026	1.0
Stage of re-extraction											
56	1.081	130.0	1.002	22.1	1.000	0.0	1.306	506.7	0.23	0.23	4.4

Consequently, Eq. (1) can be rewritten as

$$c_{P_2O_5\,org.ph} = (ne^{pT})c_{P_2O_5\,aq.ph}^{kT+m}, \quad (4)$$

where T is temperature (°C); n, p, k, and m, coefficients of the equation, which are affected by the degree of contamination of the system by impurities.

Thus, similar equations of the isotherms of extraction and re-extraction of phosphoric acid with tributyl phosphate were obtained for the temperature interval 10–70°C and content of P_2O_5 in the aqueous phase in the range 79 – 930 g l^{-1}:

extraction equation

$$c_{P_2O_5\,org.ph} = (0.6634e^{0.0807T})c_{P_2O_5\,aq.ph}^{0.0118T+0.8836}, \quad (5)$$

and re-extraction equation

$$c_{P_2O_5\,org.ph} = (0.2776e^{0.0685T})c_{P_2O_5\,aq.ph}^{0.0102T+1.0266}. \quad (6)$$

Table 1 lists the contents of P_2O_5 in the organic phases, calculated by Eq. (5) and also presents discrepancies between the experimental and calculated values

$$\Delta = \frac{c_{P_2O_5\,org.ph.exp} - c_{P_2O_5\,org.ph.calc}}{c_{P_2O_5\,org.ph.exp}} \times 100\%.$$

It was found that the discrepancies do not exceed 12.1%.

Using the results obtained to plot the isotherms of extraction and re-extraction makes it possible to determine by the graphical method [7] certain technological parameters of the process of EPhA purification with tributyl phosphate. Figure 3 shows the isotherms of extraction (*1*) and re-extraction (*2*), as well as the working lines (*3–5*) for the industrial process of purification of the apatite EPhA with tributyl phosphate on three pulse columns. The calculations were based on the average monthly performance parameters of the installation in April 2005 (Table 4). During this period of time, the installation worked by the scheme with intermediate washing of the extract with water. The working lines constructed were

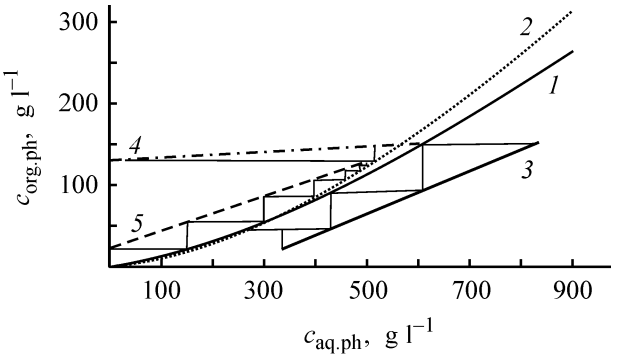


Fig. 3. Isotherms of (*1*) extraction and (*2*) re-extraction and (*3–5*) working lines of the process of extraction purification of EPhA. ($c_{aq.ph}$) Content of P_2O_5 in the aqueous phase and ($c_{org.ph}$) that in the organic phase. Working line of a process: (*3*) extraction, (*4*) washing of the extracting agent, and (*5*) re-extraction.

used to graphically calculate the number of theoretical stages of extraction and re-extraction and to find the theoretical ratio between the volumes of the aqueous and organic phases, $V_{aq} : V_{org}$, equal to the slope of the working line; Table 4 compares the calculated value of this ratio with that observed in practice. It was found that the number of theoretical stages of extraction is 2.8, and that of re-extraction, 5.3.

It should be noted that the extraction isotherm is characterized by lower values of the distribution coefficient of phosphoric acid over the entire range of equilibrium concentrations of the acid. This is due to the fact that the EPhA solution contains various salt impurities, which bind part of H_3PO_4 molecules and make lower the content of free phosphoric acid in solutions [8].

CONCLUSION

It was shown that the dependence of the content of P_2O_5 in the organic phase on that in the aqueous phase can be represented by Eq. (4) whose coefficients are affected by the degree of contamination of the system by impurities.

REFERENCES

1. Lembrikov, V.M., Konyakhina, L.V., Nikitin, V.G., and Volkova, V.V., *Khim. Tekhnol.*, 2004, no. 8, pp. 4–8.
2. Krupatkin, I.L. and Shcherbakova, T.A., *Radiokhimiya*, 1969, vol. 11, no. 4, pp. 378–384.
3. Tokmakova, T.V., Kunin, B.I., Moshkova, V.G., and Konyakhina, L.V., *Zh. Prikl. Khim.*, 1990, vol. 63, no. 3, pp. 679–682.
4. Bogdanova, S.S., Panov, V.P., and Chulkova, E.N., *Zh. Prikl. Khim.*, 1987, vol. 60, no. 1, pp. 47–51.
5. Skornyakova, R.A., Konyakhina, L.V., and Tokmakova, T.V., *Ekspress-informatsiya: Otechestvennyi proizvodstvennyi opyt. Ser. "Metody analiza i kontrolya proizvodstva"* (Express Information: Domestic Industrial Experience, Series "Methods for Industrial Analysis and Monitoring"), Moscow: NIITEKhIM, 1985, no. 6, pp. 20–22.
6. Yagodin, G.A., Kagan, S.Z., Tarasov, V.V., *et al.*, *Osnovy zhidkostnoi ekstraktsii* (Fundamentals of Liquid Extraction), Moscow: Khimiya, 1981.
7. Kasatkin, A.G., *Osnovnye protsessy i apparaty khimicheskoi tekhnologii* (Basic Processes and Apparatus of Chemical Technology), Moscow: Khimiya, 1973.
8. Konyakhina, L.V., Tokmakova, T.V., Moshkova, V.G., and Korneva, Z.N., *Zh. Prikl. Khim.*, 1991, vol. 64, no. 3, pp. 682–684.

ISSN 1070-4272, Russian Journal of Applied Chemistry, 2006, Vol. 79, No. 2, pp. 201–204. © Pleiades Publishing, Inc., 2006.
Original Russian Text © O. V. Arapov, K. N. Semenov, N. A. Charykov, V. I. Seregin, K. V. Nekrasov, V. I. Gerasimov, 2006, published in Zhurnal Prikladnoi Khimii, 2006, Vol. 79, No. 2, pp. 203–206.

PHYSICOCHEMICAL STUDIES OF SYSTEMS AND PROCESSES

Extraction Equilibria in the Fullerene-containing System C_{60}–C_{70}–1,2,4-Trichlorobenzene–Ethanol–H_2O

O. V. Arapov, K. N. Semenov, N. A. Charykov, V. I. Seregin, K. V. Nekrasov, and V. I. Gerasimov

St. Petersburg State Technological Institute, St. Petersburg, Russia

ZAO Innovations of Leningrad Institutes and Enterprises, St. Petersburg, Russia

St. Petersburg State University, St. Petersburg, Russia

Received October 25, 2005

Abstract—The liquid (I)–liquid (II) extraction equilibria in the five-component system fullerene C_{60}–fullerene C_{70}–1,2,4-$C_6H_3Cl_3$–C_2H_5OH–H_2O were studied at 25°C. Isothermal diagrams of distribution of the fullerene components among stratifying liquid phases at a constant content of H_2O were obtained.

DOI: 10.1134/S1070427206020066

This communication continues a series of articles [1–3] devoted to extraction equilibria in systems containing light fullerenes, C_{60} and C_{70}. These papers considered successively the extraction equilibria in the systems constituted by C_{60}, C_{70}, *ortho*-xylene (α-pinene), isobutylamine (dimethylformamide, monoethanolamine, ethanol), and H_2O at 25°C. As a macrocomponent of the extraction system, a solvent, served *ortho*-xylene [1, 2], which has a high ability to dissolve fullerenes and is the most frequently used both to extract fullerenes from fullerene black and to separate C_{60} and C_{70} by means of chromatography [4–6]. In [3], *ortho*-xylene was replaced with a somewhat "weaker" nonaromatic solvent α-pinene, in which the solubility of both the fullerenes, C_{60} and C_{70}, at room temperature is somewhat lower than that in *ortho*-xylene [7]. In [3], as well as in previously studied systems with *ortho*-xylene [1, 2], we could separate C_{60} and C_{70} by means of extraction; however, the efficiency of separation somewhat decreased upon replacement of *ortho*-xylene.

A naturally following next stage of selection of the most effective system of solvents for extraction separation of light fullerenes was our attempt to use other, now "stronger" solvents in which the solubility of fullerenes exceeds that in *ortho*-xylene. The choice was forced to be made among a rather narrow variety of exclusively aromatic solvents: various isomers of trimethylbenzenes, di- and trichlorobenzenes, chloronaphthalene, etc. [8–11]. For convenience in carrying out the experiments (and, further, possibly also in developing the technology), we restricted, from the very beginning, the choice to solvents that are in the liquid state at 25°C. Another fundamentally important issue [naturally, with the exception of harnessing the two-phase equilibrium liquid (I)–liquid (II)] is that it has been impossible to achieve a high solubility in both the liquid phases simultaneously. The exception is provided by the systems constituted by C_{60}, C_{70}, *ortho*-xylene, isobutylamine, and H_2O and by C_{60}, C_{70}, *ortho*-xylene, and monoethanolamine [1]. Unfortunately, the first system was the only one in which C_{60} and C_{70} could not separated at all, and in the second, highly stable and difficultly decomposed compounds of fullerenes with monoethanolamine were formed. In other systems [1–3], one of the phases was always strongly depleted of fullerenes, so that their running concentrations rarely exceeded 100 mg l^{-1}, which is very technologically inconvenient.

We chose as object of study the five-component system C_{60}–C_{70}–1,2,4-$C_6H_3Cl_3$–C_2H_5OH–H_2O at 25°C. The main aromatic solvent 1,2,4-$C_6H_3Cl_3$ has the following properties: this is the only trichlorobenzene that is in the liquid state at room temperature (mp ~17°C). Its isomers, 1,2,3- and 1,3,5-$C_6H_3Cl_3$, melt at 53.5 and 65.5°C, respectively [12]. In practice, we used industrial 1,2,4-$C_6H_3Cl_3$ twice distilled at 212–215°C, which contains, according to the results of a chromatographic analysis, the main product in an amount of 91 wt % and a mixture of 1,2,3- and 1,3,5-$C_6H_3Cl_3$

(9 wt %) (this mixture is not crystallized at 10 ± 1°C during at least 7 days).

1,2,4-$C_6H_3Cl_3$ excellently dissolves C_{60}, C_{70}, and mixtures of these. We could prepare solutions of (C_{60} + C_{70}) with a total concentration of fullerenes, c_{full}, ranging from 20 to 40 g l^{-1}.

Visible and near-UV spectra of fullerenes in 1,2,4-$C_6H_3Cl_3$ are quite ordinary and show absorption peaks at wavelengths of 335 ± 2 and 472 ± 3 nm, which enables spectrophotometric determination of fullerenes in solutions by the conventional technique [13], with an appropriate correction for shifts of the absorption peaks.

1,2,4-$C_6H_3Cl_3$ well dissolves C_2H_5OH and vice versa; their mixtures rapidly stratify upon addition of H_2O to the system (~2 wt %); both the stratifying phases contain high concentrations of 1,2,4-$C_6H_3Cl_3$ and well dissolve fullerenes.

EXPERIMENTAL

An experimental study of the system C_{60}–C_{70}–1,2,4-$C_6H_3Cl_3$–C_2H_5OH–H_2O at 25°C revealed a certain specificity related to the exceedingly high solubility of C_{60} and C_{70} in 1,2,4-$C_6H_3Cl_3$.

To introduce a mixture of fullerenes into the stratifying system, we prepared a diffusion-stable solution of $(C_{60})_{0.83}(C_{70})_{0.17}$. This solid solution was completely dissolved in an excess amount of 1,2,4-$C_6H_3Cl_3$ to give the base liquid solution-1 with concentrations (g l^{-1}): $C_{60}^{base\text{-}1}$ 19.8 and $C_{70}^{base\text{-}1}$ 4.0; with the total concentration of fullerenes, $c_{full}^{base\text{-}1}$ = 23.8 g l^{-1}.

On mixing the base solution with an aliquot amount of C_2H_5OH (abs.) and adding H_2O ($c_W \approx 2.9$ wt %) to cause stratification, solid mixed fullerene solvates instantaneously started to precipitate from both of the stratifying phases. On separating the liquid phases and filtering them off, we obtained a homogeneous predominantly "chlorobenzene" phase, base solution-2, containing (g l^{-1}): $C_{60}^{base\text{-}2}$ 5.6 and $C_{70}^{base\text{-}2}$ 2.3; with the total concentration of fullerenes $c_{full}^{base\text{-}2}$ = 7.9 g l^{-1}.

Base solution-3, whose only distinction was the total absence of fullerenes in the phase, was prepared similarly to solution-2. The last base solution-4 had the form of a predominantly "ethanol" phase in equilibrium with base solution-3. This phase did not contain fullerenes, either.

It should be noted that the following pattern was observed when preparing base solutions-2, -3, and -4: upon mixing, the volume of the trichlorobenzene phase decreased dramatically as compared with the aliquot volume; by contrast, the volume of the ethanol phase increased. Under the experimental conditions, the equilibrium ratio of these volumes was approximately 1.0 : 2.5.

In the first set of experiments, we fixed the composition of the fullerene mixture to be distributed, $(C_{60})_{0.72}(C_{70})_{0.28}$, and the content of H_2O ($c_W \approx$ 2.9 wt %). Further, base solution-3 was mixed with base solution-2 in volume ratios ranging from 100 : 1 to zero, and an aliquot volume of base solution-4 was added to the resulting mixture.

In the second set of experiments, we also fixed the composition of the $(C_{60})_{0.83}(C_{70})_{0.17}$ fullerene mixture to be distributed and the total concentration of fullerenes in a stratifying system. In this case, the content of H_2O in the system, c_W, was varied. First, base solution-1 and 1,2,4-$C_6H_3Cl_3$ were mixed in an approximately 1 : 4 ratio (to preclude precipitation of solid fullerene solvates), then aliquots of C_2H_5OH (abs.) were added to the solutions obtained, and, finally, different amounts of H_2O ($c_W \approx$ 2.3–3.9 wt %) were introduced. In this case, the volumes of the trichlorobenzene phases were again markedly lower than those of the ethanol phases.

The extraction equilibrium was attained in both sets of experiments in 36 h at thermostating to within ±0.03°. After that, the coexisting phases were sampled for analysis.

The phases were analyzed for the content of the fullerene components, C_{60} and C_{70}, as follows: the trichlorobenzene phase, by ordinary spectrophotometry with respect to 1,2,4-$C_6H_3Cl_3$ (at dilutions of 1 : 30 to 1 : 2000 and cuvette width l = 1 cm); aliquots of the ethanol phase were first evaporated to dryness at a temperature of 110°C and a residual pressure of 0.01 mm Hg and then "dry samples" were dissolved in aliquots of *ortho*-xylene and also analyzed by spectrophotometry [13].

The concentrations of the main components of the solvents (1,2,4-C_6H_3Cl, C_2H_5OH, and H_2O) were determined by chromatography [1, 2]. It should be noted that, as regards the macrocomponents, the phase compositions depend on the content of H_2O, c_W. For example, the trichlorobenzene phase virtually did not contain any water in all samples ($c_{H_2O}^{C_6H_3Cl_3} < 1$ wt %), and the content of H_2O in the ethanol phase, $c_{H_2O}^{C_2H_5OH}$, steadily increased from 3.2 to 4.5 wt % as c_W changed from 2.6 to 3.9 wt %. At the same time, the concentrations $c_{C_6H_3Cl_3}^{C_2H_5OH}$ and $c_{C_2H_5OH}^{C_6H_3Cl_3}$ steadily decreased from 21 to 11 and from 11 to 7 wt %, respectively.

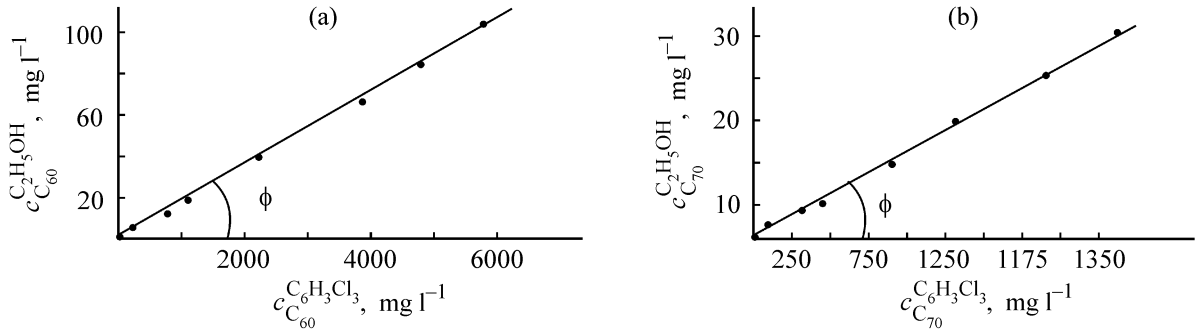


Fig. 1. Diagrams of distribution of fullerenes (a) C_{60} and (b) C_{70} among the ethanol and trichlorobenzene phases in the system C_{60}–C_{70}–1,2,4-trichlorobenzene–C_2H_5OH–H_2O at 25°C. (*c*) Fullerene concentration; (a) $\cot\phi = K_{distr}(C_{60}) = 55.5$ and (b) $\cot\phi = K_{distr}(C_{70}) = 78.7$. For explanation, see text.

Figures 1a and 1b show the distribution diagrams of the fullerene components C_{60} and C_{70} among the trichlorobenzene and ethanol phases for the five-component system C_{60}–C_{70}–1,2,4-$C_6H_3Cl_3$–C_2H_5OH–H_2O at 25°C. The diagrams are plotted for fixed composition of the mixture of fullerenes C_{60} and C_{70} in the system (72 wt % C_{60}) and content of H_2O ($c_W \approx$ 2.9 wt %). As can be seen in Fig. 1, the trichlorobenzene phase is always richer in both the fullerenes than the ethanol phase. The distribution diagrams for C_{60} and C_{70} were virtually rectilinear in the entire concentration range studied, similarly to systems with *ortho*-xylene and isobutylamine [1]. At $c_W \approx 2.9$ wt %, rather high maximum total concentrations of fullerenes in the coexisting phases could be achieved: $c^{C_2H_5OH}_{full} \approx 140$ and $c^{C_6H_3Cl_3}_{full} \approx 7800$ mg l^{-1}.

Figure 2 shows how the relative mass content of C_{60} (in the $C_{60} + C_{70}$ mixture) in the coexisting phases depends on the concentration of C_{60} in the trichlorobenzene phase, also at a fixed c_W (the dashed line represents the composition of a fullerene mixture being distributed: 72 wt % C_{60}). It can be well seen that the ethanol phase is always richer in C_{60} than the trichlorobenzene phase, and the compositions of the phase become closer as the solution concentrations are lowered, beginning at $c^{C_6H_3Cl_3}_{C_{60}} < 700$ mg l^{-1}.

Figure 3 shows the dependence of the concentration of fullerenes C_{60} and C_{70} in the ethanol and trichlorobenzene phases in the system C_{60}–C_{70}–1,2,4-trichlorobenzene–C_2H_5OH–H_2O at 25°C on the content of H_2O in the heterogeneous system, c_W (composition of a fullerene mixture being distributed, Y^{sum} = 83 wt % C_{60}). Figure 4 shows how the relative mass content of C_{60} (in the $C_{60} + C_{70}$ mixture) in the coexisting phases on c_W (the dashed line corresponds to Y^{sum} = 83 wt % C_{60}).

As can be seen in Figs. 3 and 4, the distribution coefficients K_{distr} (ratio between the concentrations in

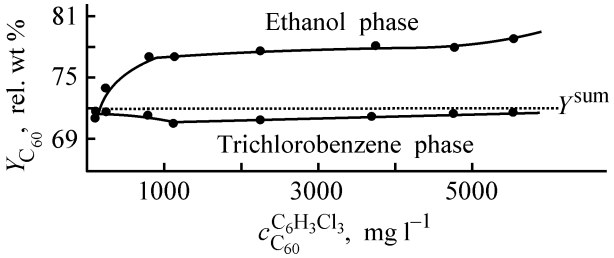


Fig. 2. Relative mass content of C_{60}, $Y_{C_{60}} = [c_{C_{60}}/(c_{C_{60}} + c_{C_{70}})] \times 100$, in the mixture $C_{60} + C_{70}$ in the coexisting phases vs. the concentration of C_{60}, $c^{C_6H_3Cl_3}_{C_{60}}$, in the trichlorobenzene phase in the system C_{60}–C_{70}–1,2,4-trichlorobenzene–C_2H_5OH–H_2O at 25°C. The *dashed line* corresponds to a brutto composition of the fullerene mixture being distributed equal to 72 wt % C_{60}.

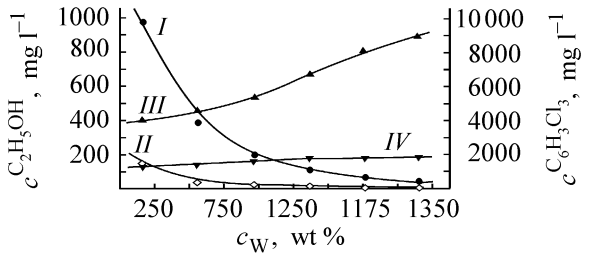


Fig. 3. Concentrations of fullerenes C_{60} and C_{70} in the ethanol and trichlorobenzene phases in the system C_{60}–C_{70}–1,2,4-trichlorobenzene–C_2H_5OH–H_2O at 25°C vs. the content of H_2O in the heterogeneous system, c_W. (*I*) $c^{C_2H_5OH}_{C_{60}}$, (*II*) $c^{C_2H_5OH}_{C_{70}}$, (*III*) $c^{C_6H_3Cl_3}_{C_{60}}$, and (*IV*) $c^{C_6H_3Cl_3}_{C_{70}}$.

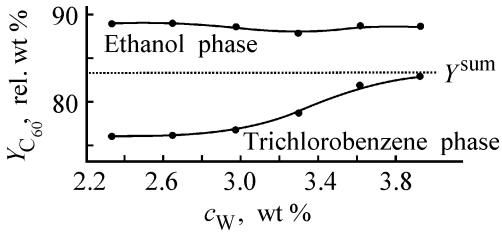


Fig. 4. Relative mass content of C_{60}, $Y_{C_{60}}$, in the $C_{60} + C_{70}$ mixture in coexisting phases vs. c_W. The *dashed line* corresponds to a composition of the fullerene mixture being distributed equal to 83 wt % C_{60}.

the trichlorobenzene and ethanol phases) strongly depend on the content of H_2O in the system, c_W. The coefficients K_{distr} increased with c_W for both the fullerene components. For example, $K_{distr}(C_{60}) \approx 4.2$ and $K_{distr}(C_{70}) \approx 9.3$ rel. units at $c_W \approx 2.3$ wt %; $K_{distr}(C_{60}) \approx 61$ and $K_{distr}(C_{70}) \approx 120$ rel. units at $c_W \approx 3.3$ wt %; and, finally, $K_{distr}(C_{60}) \approx 228$ and $K_{distr}(C_{70}) \approx 360$ rel. units at $c_W \approx 3.9$ wt % (all the figures are given for aliquot ratios of 1,2,4-$C_6H_3Cl_3$ and C_2H_5OH). Simultaneously with an increase in c_W, the content of fullerenes in the ethanol phase critically decreased. For example, the total concentration of C_{60} and C_{70} was as high as 1120 mg l^{-1} at $c_W \approx 2.3$ wt % and decreased to 124 mg l^{-1} at $c_W \approx 3.2$ wt %, whereas at $c_W \approx 3.9$ wt %, $c_{full}^{C_2H_5OH}$ was only 44 mg l^{-1}. In this case, the concentrations of fullerenes in the trichlorobenzene phase, $c_{full}^{C_6H_3Cl_3}$, changed in opposite directions and comparatively slowly and steadily increased from 5350 to 10700 mg l^{-1}. The enrichment coefficients K_{enr} [equal to the ratio of $K_{distr}(C_{70})$ to $K_{distr}(C_{60})$] also varied monotonically, decreasing from 2.2 at $c_W \approx 2.3$ wt % to 1.6 at $c_W \approx 3.9$ wt %.

If the extraction pattern in the system C_{60}–C_{70}–1,2,4-$C_6H_3Cl_3$–C_2H_5OH–H_2O is characterized as a whole, it should be noted that this system somewhat less effectively separates the fullerene components C_{60} and C_{70} as compared with systems with *ortho*-xylene and dimethylformamide, α-pinene, and ethanol [1–3], and more effectively than the system with *ortho*-xylene and isobutylamine [1], although separation is observed in the last system. The only, but very important advantage of the system studied is that the concentrations of fullerenes in both phases are high, compared with those in other systems and reach values of more than 1.1 g l^{-1} for the ethanol phase and more than 7.8 g l^{-1} for the trichlorobenzene phase at the minimum content of H_2O. This fact is exceedingly important for development of an efficient technology for extraction separation of light fullerenes.

CONCLUSIONS

(1) The liquid (I)–liquid (II) extraction equilibria in the five component system constituted by fullerenes C_{60} and C_{70}, 1,2,4-$C_6H_3Cl_3$, C_2H_5OH, and H_2O at 25°C were obtained. As a result, isothermal diagrams of distribution of the fullerene components among the stratifying liquid phases were obtained at a constant content of H_2O. These diagrams were found to be nearly rectilinear for both the fullerene components.

(2) It was shown that the distribution coefficients strongly depend on the content of H_2O in the system, c_W. The coefficients K_{distr} increase with c_W for both the fullerene components.

(3) As c_W increased, the content of fullerenes in the ethanol phase critically decreased, with the concentrations of fullerenes in the trichlorobenzene phase changing in opposite directions.

ACKNOWLEDGMENTS

The study was financially supported by the Russian Foundation for Basic Research (project no. 03-05-65164) and by the Federal Target Scientific-Technical Program "Research and Development in Priority Areas of Science and Technology" for the years 2002–2006 (State contract no. 02.467.11.7005 of May 23, 2005).

REFERENCES

1. Arapov, O.V., Pronkin, A.A., Charykov, N.A., *et al.*, *Zh. Prikl. Khim.*, 2003, vol. 76, no. 1, pp. 39–45.
2. Arapov, O.V., Seregin, V.I., Nekrasov, K.V., *et al.*, *Pis'ma Zh. Tekh. Fiz.*, 2003, vol. 29, no. 3, pp. 74–81.
3. Arapov, O.V., Abovskii, N.D., Charykov, N.A., *et al.*, *Zh. Prikl. Khim.*, 2006, vol. 79, no. 1, pp. 168–170.
4. US Patent 05904852.
5. Chatterjee, K., Parker, D.H., Wurz, P., *et al.*, *J. Org. Chem.*, 1992, vol. 57, pp. 3253–3254.
6. Coustel, N., Bernier, P., Aznar, R., *et al.*, *J. Chem. Soc. Chem. Commun.*, 1992, no. 19, pp. 1402–1403.
7. Ponomarev, A.N., Aksel'rod, B.M., Charykov, N.A., *et al.*, *Zh. Fiz. Khim.*, 2000, vol. 74, pp. 2031–2033.
8. Sivaraman, N., Dhamodaran, R., Kalliapan, I., *et al.*, *J. Electoch. Soc., Recent Adv. in the Chem. & Phys. of Fuller. & Relat. Mater.*, Rouff, R.S., Ed., 1994, vol. 94–24, pp. 156–165.
9. Kushch, N.D., Majchrzak, I., Ciesielski, W., *et al.*, *Chem. Phys. Lett.*, 1993, vol. 215, pp. 317–321.
10. Zhou, X. and Gu, Z., *Chin Bull.*, 1993, vol. 38, pp. 175–181.
11. Zhou, X., Gu, Z., Wu, J., *et al.*, *Carbon*, 1994, vol. 32, pp. 935–938.
12. *Promyshlennye khlororganicheskie produkty* (Industrial Organochlorine Products), Oshin, L.A., Ed., Moscow: Nauka, 1978.
13. Ponomarev, A.N., Yudovich, M.E., Barchenko, V.T., *et al., Optics and Spectroscopy*, 2000, vol. 88, pp. 195–197.

ISSN 1070-4272, Russian Journal of Applied Chemistry, 2006, Vol. 79, No. 2, pp. 205–208. © Pleiades Publishing, Inc., 2006.
Original Russian Text © Yu. V. Shabalina, I. B. Sladkov, 2006, published in Zhurnal Prikladnoi Khimii, 2006, Vol. 79, No. 2, pp. 207–210.

PHYSICOCHEMICAL STUDIES OF SYSTEMS AND PROCESSES

Calculation of the Critical Parameters of Substances by Certain Empirical Relations

Yu. V. Shabalina and I. B. Sladkov

St. Petersburg State Polytechnic University, St. Petersburg, Russia

Received November 22, 2005

Abstract—A large body of statistical data was used to determine the numerical values of constants for five empirical relations between the physicochemical properties of substances for different classes of compounds. The accuracy of calculation of the critical parameters was determined using these relations.

DOI: 10.1134/S1070427206020078

Methods of the theory of thermodynamic similarity are widely used to prognosticate the physicochemical properties of substances [1, 2]. Calculation of physicochemical properties by these methods requires data on the critical parameters of substances. Because experimental data on critical parameters are rather scarce, of practical importance is their determination by calculation.

It was shown in [3, 4] that expressions composed from certain physicochemical parameters retain an approximately same value for different substances, i.e., they can be regarded as constants. Below we present these relations, empirically obtained by us
Quayle equation (I)

$$V_{cr} T_{cr}^{0.3} / \Pi^2 = C_1, \quad (1)$$

Quayle equation (II)

$$\Delta H_b / \Pi P_{cr} = C_2, \quad (2)$$

Egert equation

$$\Delta H_b / (T_{cr} - T_b) = C_3, \quad (3)$$

modified Trouton equation

$$\Delta H_b / RT_{cr} = C_4, \quad (4)$$

and Boutaric equation

$$P_{cr} V_{cr} / T_{cr} = C_5. \quad (5)$$

Here, Π is the parachor ($J^{1/4}$ $cm^{5/2}$ mol^{-1}); T_b, boiling point (K); ΔH_b, enthalpy of evaporation at the boiling point (kJ mol^{-1}); T_{cr}, critical temperature (K); V_{cr}, critical volume (cm^3 mol^{-1}); P_{cr}, critical pressure (MPa); and R, universal gas constant (8.314 J mol^{-1} K^{-1}).

Equations (1)–(5) can be used to calculate the critical parameters if the numerical values of the constants are known. In the first stage of the study, we determined values of constants C_1–C_5 (Table 1). These values were calculated from an array of experimental data obtained in [5–7] for 70 substances.

All the substances we consider can be divided into the following classes of compounds: nonpolar and weakly polar compounds: $SiCl_4$, $GeCl_4$, $SnCl_4$, $TiCl_4$, BBr_3, $SnBr_4$, PBr_3, MoF_6, UF_6, PCl_3O, SCl_2O, ClO_3F, WCl_4O, $SiHBr_3$, $CBrF_3$, CBr_2F_2, $SiBrCl_3$, $SiBr_2Cl_2$, BI_3, and SnI_4; moderately and strongly polar: $SbCl_3$, SbI_3, $BiCl_3$, $SeCl_2$, $TeCl_4$, $SeOF_2$, $SeCl_2O$, CO_2, ClO_2, N_2O, OsO_4, RuO_4, SO_2, Re_2O_7, Tc_2O_7, CSO, HCl, HI, NHF_2, NH_3, N_2H_4, and H_2O; low-boiling: CO, CH_4, CF_4, NF_3, B_2H_6, SiH_4, GeH_4, and PF_3; and organometallic: $Ge(CH_3)_4$, $Ge(CH_3)_3Cl$, $Ge(CH_3)_2Cl_2$, $Ge(CH_3)Cl_3$, $Ge(C_2H_5)_4$, $Ge(C_2H_5)_3Cl$, $Ge(C_2H_5)_2Cl_2$, $Ge(C_2H_5)Cl_3$, $Si(CH_3)_4$, $Si(CH_3)_3Cl$, $Si(CH_3)_2Cl_2$, $Si(CH_3)Cl_3$, $Si(C_2H_5)_4$, $Si(C_2H_5)_3Cl$, $Si(C_2H_5)_2Cl_2$, $Si(C_2H_5)Cl_3$, $Pb(CH_3)_4$, $Pb(C_2H_5)_4$, $Sn(CH_3)_4$, and $Sn(C_2H_5)_4$.

It can be seen from Table 1 that constants C_1, C_2, and C_5 do have virtually identical values for all the classes of substances considered, whereas C_2 and C_5 strongly vary between different classes of compounds. Thus, with Eqs. (1)–(5) used for applied calculations, the necessary numerical values of the constants can

Table 1. Constants C_1–C_5 for various classes of compounds

Constant	Average value of a constant for indicated substances			
	nonpolar and weakly polar	moderately and strongly polar	low-boiling	organometallic
C_1	368	374	348	375
C_2	1.73	1.66	1.56	1.14
C_3	0.15	0.15	0.13	0.11
C_4	6.72	7.03	5.94	4.05
C_5	2.34	2.33	2.41	2.31

Table 2. Accuracy of calculation of the critical parameters by Eqs. (6)–(12)

Parameter	Equation	Average error, %, for indicated substances			
		nonpolar and weakly polar	moderately and strongly polar	low-boiling	organometallic
V_{cr}	(6)	1.4	3.5	5.5	3.6
	(11)	1.4	4.7	1.0	3.2
P_{cr}	(7)	4.6	8.5	7.1	–
	(10)	1.4	4.7	1.0	3.2
T_{cr}	(8)	1.8	4.1	3.6	–
	(9)	2.5	7.7	5.9	–
	(12)	1.4	4.7	1.0	3.2

be chosen from Table 1, with the choice governed by the class of compounds to which a substance under study belongs.

Also, we analyzed the possibility of applying the empirical relations (1)–(5) to calculation of the critical parameters. For this purpose, we rearranged the equations under study in such a way that they were explicitly written in the parameter being determined. It follows from Eq. (1) that

$$V_{cr} = C_1 \Pi^{1.2} / T_{cr}^{0.3}. \quad (6)$$

In principle, relation (1) can be also used to calculate the critical temperature

$$T_{cr} = (C_1 \Pi^{1.2} / V_{cr})^{10/3}.$$

However, a high accuracy of calculation of T_{cr} can hardly be expected, because the input parameters are raised to the power 10/3 and a minor inaccuracy in their determination will lead to a gross error in the calculated value of T_{cr}.

Relation (2) can be used to derive a formula for calculating the critical temperature

$$P_{cr} = \Delta H_b / C_{cr} \Pi. \quad (7)$$

Relation (3) can be used to derive a formule for calculating the critical temperature.

$$T_{cr} = \Delta H_b / C_3 + T_b. \quad (8)$$

The critical temperature can also be calculated using Eq. (4):

$$T_{cr} = \Delta H_b / (C_4 R). \quad (9)$$

Relation (5) can be used to derive formulas for calculating all the critical parameters (P_{cr}, V_{cr}, T_{cr}):

$$P_{cr} = C_5 T_{cr} / V_{cr}, \quad (10)$$

$$V_{cr} = C_5 T_{cr} / P_{cr}, \quad (11)$$

$$T_{cr} = P_{cr} V_{cr} / C_5. \quad (12)$$

The results we obtained in calculating the critical parameters by Eqs. (6)–(12) are listed in Table 2. It can be seen that all the equations provide a high accuracy of prognostication of the critical parameters for nonpolar and weakly polar compounds. Some equations give a satisfactory accuracy for organometal compounds. For substances with a noticeable polarity, only the critical temperature can be predicted with a sufficient accuracy by Eqs. (6) and (8). The rest of the equations provide only a satisfactory accuracy of prognostication. For low-boiling substances, the whole set of critical parameters can be determined with a high accuracy by Eqs. (10)–(12).

For organometal compounds, the inaccuracy of formulas (7)–(9) is rather high (>10%). This can be attributed to the fact that published data for one of the input parameters, ΔH_b, are rather contradictory for organometal compounds and reliable values of this quantity are unknown. For this reason, errors for Eqs. (7)–(9) are not given in Table 2.

In Eqs. (6) and (10)–(12), the critical parameters are calculated one in terms of the others. For poorly studied substances, it is important to have as input parameters the readily accessible properties of a compound, e.g., parameters of the boiling point, T_b and ΔH_b, and the parachor Π. The last parameter is easily calculated using the stoichiometric formula of the compound [5].

Let us rearrange Eqs. (6) and (10)–(12) in order to pass to more accessible input data. We obtain from Eqs. (6) and (8)

$$V_{cr} = C_1 \Pi^{1.2}/(\Delta H_b/C_3 + T_b)^{0.3}. \quad (13)$$

It follows from Eqs. (10), (8), and (13) that

$$P_{cr} = C_5(\Delta H_b/C_3 + T_b)^{1.3}/(C_1 \Pi^{1.2}). \quad (14)$$

We performed a calculation by these formulas for nonpolar and weakly polar substances (Table 3).

It can be seen from the data in Table 3 that the average error of calculation of the critical volume by Eq. (13) is 1.7%, and that for the critical pressure by formula (14), 3.4%. For the case when the initial formulas are used (with the critical parameters as input data), the average error is 1.4% (Table 2). Hence it can be seen that passing to more accessible input data makes somewhat larger the error in calculation of the critical parameters. Table 4 presents recommendations for choice of equations providing the highest accuracy for various classes of compounds.

Comparison of the accuracies of the equations we considered with those for calculation of the critical parameters [5] shows that the accuracy for nonpolar and weakly polar substances is as good as that of the best methods used to prognosticate the critical parameters. For other classes of compounds, the equations considered provide a poorer accuracy than the best of the published methods.

Table 3. Results of calculation of the error in the critical parameters by Eqs. (13) and (14)

Substance	Error, %	
	V_{cr} (13)	P_{cr} (14)
$SiCl_4$	–0.5	0.9
$GeCl_4$	1.0	3.6
$SnCl_4$	–0.6	7.2
$TiCl_4$	–0.7	–2.0
BBr_3	1.3	–3.2
$SnBr_4$	–1.1	4.0
PBr_3	0.2	–1.4
MoF_6	0.3	3.9
UF_6	–1.7	1.9
$POCl_3$	–2.5	4.5
$SOCl_2$	–1.9	–1.5
ClO_3F	5.0	–8.3
WCl_4O	–0.3	3.5
$SiHBr_3$	0.4	1.7
$CBrF_3$	5.2	–5.6
CBr_2F_2	1.2	–1.0
$SiBrCl_3$	–2.0	3.5
$SiBr_2Cl_2$	–2.3	3.6
BI_3	1.4	–1.0
SnI_4	–1.6	6.7
Average error	1.7	3.4

Table 4. Expected error of calculation of the critical parameters by the optimal equations

Parameter	Expected error, %, for indicated substances*		
	nonpolar and weakly polar	moderately and strongly polar	organometallic
T_{cr}	1.4 (12)	4.1 (8)	3.2 (12)
V_{cr}	1.4 (6)	3.5 (6)	3.2 (11)
P_{cr}	1.4 (10)	4.7 (10)	3.2 (10)

* Equation numbers are given in parentheses; at equal accuracies, preference was given to an equation using more accessible input data.

CONCLUSIONS

(1) The accuracy of five empirical relations was analyzed for a data array for 70 substances belonging to different classes of compounds.

(2) It was shown that the empirical relations can be used to calculate the critical parameters if the choice of the numerical values of the constants is governed by the class of compounds to which a substance under study belongs.

(3) It was shown that, for nonpolar and weakly polar substances, the precision of the equations stud-

ied compares well with that of the best methods used to prognosticate the critical parameters.

REFERENCES

1. Filippov, L.P., *Podobie svoistv veshchestv* (Similarity of Properties of Substances), Moscow: Mos. Gos. Univ., 1978.
2. Reid, R.G. and Sherwood, T.K., *The Properties of Gases and Liquids*, New York: McGraw-Hill, 1966.
3. Partington, J.R., *Advanced Treaties of Physical Chemistry*, London: Longman, 1949, vol. 2, pp. 363–370.
4. Viktorov, M.M., *Metody vychisleniya fiziko-khimicheskikh velichin i prikladnye raschety* (Methods for Calculation of Physicochemical Quantities and Applied Calculations), Moscow: Khimiya, 1977.
5. Morachevskii, A.G. and Sladkov, I.B., *Fiziko-khimicheskie svoistva molekulyarnykh neorganicheskikh soedinenii* (Physicochemical Properties of Molecular Inorganic Substances), St. Petersburg: Khimiya, 1996.
6. Kaufman, H.C., *Handbook of Organometallic Compounds*, New York: VNCI, 1961.
7. Razuvaev, G.A., Gribov, B.G., and Domrachev, G.A., *Metalloorganicheskie soedineniya v elektronike* (Organometallic Compounds in Electronics), Moscow: Nauka, 1972.

ISSN 1070-4272, Russian Journal of Applied Chemistry, 2006, Vol. 79, No. 2, pp. 209–212. © Pleiades Publishing, Inc., 2006.
Original Russian Text © N. S. Shoshkova, I. B. Sladkov, 2006, published in Zhurnal Prikladnoi Khimii, 2006, Vol. 79, No. 2, pp. 211–214.

PHYSICOCHEMICAL STUDIES OF SYSTEMS AND PROCESSES

Critical Parameters of Methylbromo- and Ethylbromosilanes

N. S. Shoshkova and I. B. Sladkov

St. Petersburg State Polytechnic University, St. Petersburg, Russia

Received November 22, 2005

Abstract—Critical parameters of nine methylbromo- and ethylbromosilanes were determined.

DOI: 10.1134/S107042720602008X

Tetramethylsilane (TMS) and tetraethylsilane (TES) are widely used in various chemical and metallurgical technologies [1, 2]. In recent years, halogen derivatives of these compounds have also come to demand. These derivatives are numerous, and most of them have been poorly studied. Since experimental determination of physicochemical properties of chemical compounds is frequently difficult, it is important to develop calculation methods for their estimation.

Methods of the thermodynamic similarity theory [3] are widely used to predict physicochemical properties of substances. However, the critical parameters of substances, which are the input data for calculations, are often unknown, which prevents use of such methods. The experimental critical parameters of methylchloro- and ethylchlorosilanes are well known, whereas similar data for bromine derivatives are lacking.

This gap can be filled today by calculating the critical parameters of methylbromo- (MBS) and ethylbromosilanes (EBS) by the equations given in [4–6]. Some of these equations are based on the theory of thermodynamic similarity and, along with physicochemical constants of a substance, contain the main criterion of thermodynamic similarity. Calculation of one of them, ψ, requires data on the boiling point T_b and molar volume V_b at the boiling point of the liquid [4]:

$$\psi = 0.1\ln T_b - 0.122\ln V_b + 0.006.$$

Another criterion, f, is calculated through the parachor Π and T_b [5]:

$$f = \ln T_b - \ln \Pi - 4.$$

In this case, the calculation is based on a single experimental characteristic, boiling point, since, to calculate parachor, we must know only the stoichiometric formula of the compound [4].

We calculated the critical parameters of MBS and EBS by the following equations:

critical temperature

$$T_{cr} = \frac{T_b}{-0.15f + 0.68}, \quad (1)$$

$$T_{cr} = 1.5T_b, \quad (2)$$

$$T_{cr} = \frac{T_b}{0.667 - 0.055f^{0.5}}; \quad (3)$$

critical volume

$$V_{cr} = V_b(2.69 + 0.05f), \quad (4)$$

$$V_{cr} = V_b(2.69 + 1.067\psi), \quad (5)$$

$$V_{cr} = 240.1\frac{\Pi^{1.2}}{T_b^{0.25}}; \quad (6)$$

critical pressure

$$P_{cr} = 0.87T_{cr}/V_b, \quad (7)$$

$$P_{cr} = 1.039T_{cr}/b, \quad (8)$$

where $b = V_b(0.2f + 1.12)$,

$$P_{cr} = \frac{1.185T_{cr}}{V_b(2 - T_b/T_{cr})}. \quad (9)$$

In Eqs. (8) and (9), T_{cr} was calculated by formula (2).

Table 1. Physicochemical properties of substances [4–6]

Substance	T_b, K	V_b, $cm^3\ mol^{-1}$	$\prod$, $J^{1/4}\ cm^{5/2}\ mol^{-1}$	T_{cr}, K	V_{cr}, $cm^3\ mol^{-1}$	P_{cr}, MPa
$SiCl_4$	330.5	121.2	4.30	507.0	326.0	3.73
$SiBr_4$	425.9	143.6	5.30	663.2	382.0	4.01
$SiHBr_3$	392.0	120.5	4.51	609.0	325.1	4.36
$SiHCl_3$	305.2	102.8	3.67	479.0	268.0	4.17
$SiBrCl_3$	353.5	127.6	4.55	540.1	346.1	3.74
$SiBr_2Cl_2$	377.5	132.5	4.81	585.1	364.1	3.81
$SiBr_3Cl$	401.0	137.8	5.05	618.0	384.0	3.85
SiI_4	574.7	182.7	6.94	888.1	495.0	4.24
$Si(CH_3)_4$	300.1	134.8	4.70	448.6	361.0	2.82
$Si(CH_3)_3Cl$	333.2	133.9	4.60	497.8	365.6	3.21
$Si(CH_3)_2Cl_2$	343.5	129.4	4.50	520.4	349.9	3.48
$Si(CH_3)Cl_3$	338.8	125.3	4.40	517.8	339.8	3.51
$Si(C_2H_5)_4$	426.8	215.5	7.46	603.7	585.0	2.60
$Si(C_2H_5)_3Cl$	416.7	188.6	6.67	600.0	520.0	2.84
$Si(C_2H_5)_2Cl_2$	403.6	162.9	5.89	595.8	455.0	3.06
$Si(C_2H_5)Cl_3$	371.6	142.6	5.09	560.8	402.7	3.33

Table 2. Errors of critical parameters calculated by Eqs. (1)–(9)

Substance	Calculation error, %								
	T_{cr}			V_{cr}			P_{cr}		
	(1)	(2)	(3)	(4)	(5)	(6)	(7)	(8)	(9)
$SiCl_4$	0.2	–2.4	1.4	0.4	0.1	–0.6	–2.2	–1.7	–1.5
$SiBr_4$	–0.7	0.4	0.2	1.5	1.3	2.4	–3.7	–0.7	0.1
$SiHBr_3$	1.7	0.8	1.2	0.3	0.4	1.2	–3.4	–1.7	1.2
$SiHCl_3$	0.1	–2.8	0.1	3.7	3.7	2.0	–4.4	–5.8	–3.6
$SiBrCl_3$	0.7	–1.5	1.9	–0.5	–0.8	–1.4	–1.8	–0.5	–0.2
$SiBr_2Cl_2$	–0.6	0.8	0.5	–1.7	–2.0	–1.5	–3.2	0.4	0.8
$SiBr_3Cl$	0.1	1.3	1.1	–3.1	–3.3	–2.5	–2.7	1.3	1.9
SiI_4	0.1	–0.3	0.9	–0.3	–0.5	1.3	–2.9	–0.7	0.1
$Si(CH_3)_4$	–1.6	2.7	0.6	0.4	–0.4	2.3	0.3	9.8	5.0
$Si(CH_3)_3Cl$	1.3	0.8	3.4	–1.2	–1.9	–4.1	0.4	5.4	4.0
$Si(CH_3)_2Cl_2$	1.2	0.5	2.6	–0.2	–0.7	–3.1	–1.0	2.8	2.7
$Si(CH_3)Cl_3$	0.6	2.4	1.8	–0.4	–0.8	–2.5	–1.9	3.6	3.8
$Si(C_2H_5)_4$	4.0	–6.3	6.0	–0.9	–2.6	0.7	6.0	6.0	1.2
$Si(C_2H_5)_3Cl$	2.1	–2.5	4.1	–2.4	–3.6	–0.4	4.2	8.3	3.4
$Si(C_2H_5)_2Cl_2$	0.7	4.0	3.5	–3.6	–4.3	–1.1	1.6	11.7	8.0
$Si(C_2H_5)Cl_3$	0.3	2.7	2.4	–4.5	–5.0	–4.3	–0.6	6.5	1.2
Average error	0.9	2.5	2.0	1.5	2.0	2.0	2.0	4.2	2.7

The first step of the study consisted in confirming the validity of these formulas for calculation of the critical parameters of MBS and EBS. For this purpose, we determined the accuracy of Eqs. (1)–(9) using the related substances with known critical parameters. These substances and the input data for calculation are listed in Table 1, and the results of calculation by Eqs. (1)–(9), in Table 2.

Table 3. Physicochemical properties of methylbromo- and ethylbromosilanes

Substance no.	Substance	T_b, K	V_b, $cm^3\,mol^{-1}$	Π, $J^{1/4}\,cm^{5/2}\,mol^{-1}$	Substance no.	Substance	T_b, K	V_b, $cm^3\,mol^{-1}$	Π, $J^{1/4}\,cm^{5/2}\,mol^{-1}$
1	$Si(CH_3)_3Br$	350.5	138.5	4.85	6	$Si(C_2H_5)_2Br_2$	440.0	181.5	6.38
2	$Si(CH_3)_2Br_2$	384.0	140.0	5.00	7	$SiC_2H_5Br_3$	433.4	164.1	5.84
3	$SiCH_3Br_3$	406.7	141.7	5.15	8	$SiC_2H_5BrCl_2$	392.2	150.2	5.34
4	$SiCH_3BrCl_2$	359.7	133.6	4.65	9	$SiC_2H_5Br_2Cl$	412.7	161.0	5.55
5	$SiCH_3Br_2Cl$	380.7	139.4	4.90					

Table 4. Calculated critical parameters of methylbromo- and ethylbromosilanes

Substance	T_{cr}, K				V_{cr}, $cm^3\,mol^{-1}$				P_{cr}, MPa			
	(1)	(2)	(3)	average	(4)	(5)	(6)	average	(7)	(8)	(9)	average
$Si(CH_3)_3Br$	541.1	525.8	541.1	536	373.4	371.1	369.1	371	3.40	3.45	3.37	3.41
$Si(CH_3)_2Br_2$	601.7	576.0	596.6	591	377.9	376.3	374.2	376	3.74	3.70	3.66	3.72
$SiCH_3Br_3$	642.6	610.1	633.4	629	382.6	381.5	382.2	382	3.95	3.85	3.83	3.88
$SiCH_3BrCl_2$	562.1	539.6	559.6	554	360.7	359.0	348.6	356	3.66	3.62	3.59	3.62
$SiCH_3Br_2Cl$	596.1	571.1	592.3	586	376.3	374.7	366.0	372	3.72	3.67	3.64	3.70
$Si(C_2H_5)_2Br_2$	670.6	660.0	671.8	668	488.2	484.4	484.5	486	3.21	3.34	3.23	3.26
$SiC_2H_5Br_3$	672.3	650.1	669.7	664	442.5	439.8	437.4	440	3.56	3.59	3.52	3.58
$SiC_2H_5BrCl_2$	608.1	588.3	606.0	601	405.0	402.7	402.8	403	3.52	3.55	3.48	3.52
$SiC_2H_5Br_2Cl$	636.9	619.1	638.3	631	434.2	431.1	416.5	427	3.44	3.48	3.42	3.43

It can be seen that the equations used enable fairly reliable prediction of the critical parameters of the substances concerned. We used Eqs. (1)–(9) to calculate the unknown critical parameters of nine MBS and EBS. The input data for the calculations were taken from [4–6] (Table 3). The results are listed in Table 4.

As can be seen, the calculation of critical parameters by various methods gives well coinciding results. Therefore, the averaged values can be recommended (Table 4) (expected error ±2%). Figures 1–3 illustrate the principles of comparative calculation of physicochemical properties. The starting data for the plots were taken from [4, 7, 8]. The well-defined

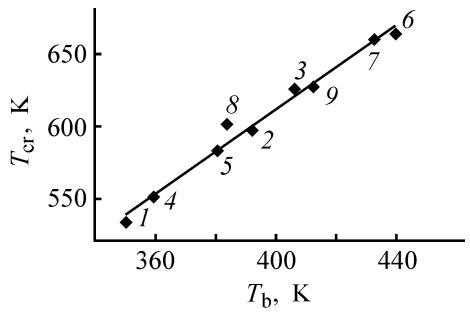


Fig. 1. Critical temperature T_{cr} vs. boiling point T_b for alkylchloro- and alkylbromosilanes. Room-mean-square error s = 0.9%, correlation coefficient r = 0.9916. *Point numbers* are substance numbers in Table 3; the same for Figs. 2 and 3.

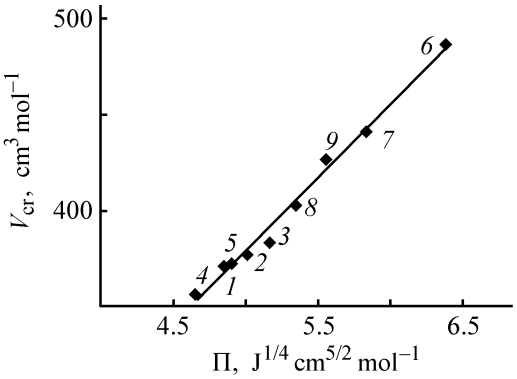


Fig. 2. Critical volume V_{cr} vs. parachor Π for alkylchloro- and alkylbromosilanes. s = 0.9%, r = 0.9962.

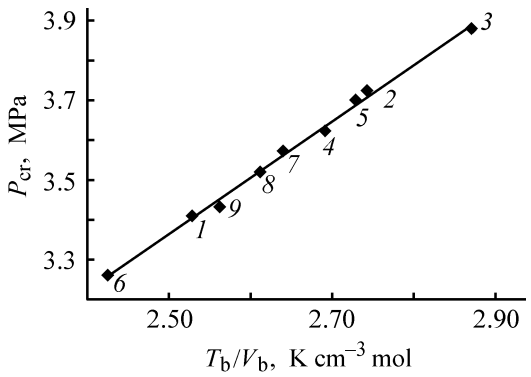


Fig. 3. Critical pressure P_{cr} vs. the ratio T_b/V_b at the boiling point of alkylchloro- and alkylbromosilanes. s = 0.1%, r = 0.9996.

linear dependences in these plots additionally confirm the reliability of the results obtained.

CONCLUSIONS

(1) Critical parameters of nine methylbromo- and ethylbromosilanes were calculated by methods whose reliability was checked on well-studied substances with a similar structure.

(2) The reliability of the results obtained was confirmed by the method of the comparative calculation.

REFERENCES

1. Razuvaev, G.A., Gribov, B.G., and Domrachev, G.A., *Metalloorganicheskie soedineniya v elektronike* (Organometallic Compounds in Electronics), Moscow: Nauka, 1972.
2. Efremov, E.A., Fedorov, V.A., and Grinberg, E.E., *Vysokochist. Veshch.*, 1988, no. 3, pp. 5–43.
3. Reid, R.G., Prausnitz, J.M., and Sherwood, T.K., *The Properties of Gases and Liquids*, New York: McGraw–Hill, 1977.
4. Morachevskii, A.G. and Sladkov, I.B., *Fiziko-khimicheskie svoistva molekulyarnykh neorganicheskikh soedinenii* (Physicochemical Properties of Molecular Inorganic Compounds), Leningrad: Khimiya, 1996.
5. Sladkov, I.B., *Zh. Prikl. Khim.*, 2003, vol. 76, no. 12, pp. 1961–1965.
6. Sladkov, I.B., *Zh. Prikl. Khim.*, 2001, vol. 74, no. 12, pp. 1748–1752.
7. Sladkov, I.B., *Zh. Prikl. Khim.*, 1999, vol. 72, no. 8, pp. 1266–1272.
8. Sladkov, I.B., *Zh. Prikl. Khim.*, 2000, vol. 73, no. 5, pp. 727–732.

ISSN 1070-4272, Russian Journal of Applied Chemistry, 2006, Vol. 79, No. 2, pp. 213–218. © Pleiades Publishing, Inc., 2006.
Original Russian Text © V. P. Korolev, N. L. Smirnova, D. V. Batov, 2006, published in Zhurnal Prikladnoi Khimii, 2006, Vol. 79, No. 2, pp. 215–219.

PHYSICOCHEMICAL STUDIES OF SYSTEMS AND PROCESSES

Calorimetric Study of the Solvation of Benzene and Its Chloro-, Nitro-, and Aminoderivatives by *n*-Hexane, 1-Butanol, and Mixed Solvent *n*-Hexane–1-Butanol

V. P. Korolev, N. L. Smirnova, and D. V. Batov

Institute of Chemistry of Solutions, Russian Academy of Sciences, Ivanovo, Russia

Received June 3, 2005

Abstract—The heats of dissolution of benzene, chlorobenzene, *ortho*-dichlorobenzene, nitrobenzene, and aniline in *n*-hexane and 1-butanol and those of benzene, chlorobenzene, nitrobenzene, and aniline in a mixture of *n*-hexane and 1-butanol were measured by calorimetry at 25°C. The enthalpies of solvation of the compounds were calculated. The correlation between the enthalpies of solvation of the compounds and their molar refraction was studied. The enthalpies of solvation of the compounds and their functional groups by the mixture of *n*-hexane and 1-butanol were considered.

DOI: 10.1134/S1070427206020091

Studies of the solvation of aromatic compounds by individual and mixed solvents are of both theoretical and practical importance. The interest in analysis of energy parameters of solvation of benzene and its derivatives is due to the following. On the one hand, many of these substances are characterized by a nonspecific type of solvation, and on the other, solutions of benzene and its derivatives frequently have fundamentally different properties. For example, the excess volume of an equimolar mixture of benzene and *n*-hexane has a positive value (0.401 $cm^3\ mol^{-1}$) [1], and that of a mixture of chlorobenzene and *n*-hexane is negative (–0.448 $cm^3\ mol^{-1}$) [3]. The excess volume of an equimolar mixture of benzene and 1-butanol is as small as 0.17 $cm^3\ mol^{-1}$ [3]. Thus, the mixture of benzene and *n*-hexane is more nonideal in its volume properties than that of benzene and 1-butanol. It is also of interest that the second derivative of the internal energy with respect to volume at a constant temperature is negative for benzene [2], i.e., benzene can be classed with Van der Waals fluids. At the same time, this derivative is positive for chlorobenzene, nitrobenzene, and aniline [2]. This means that these substances do not belong to Van der Waals fluids. The wide use of aromatic substances in manufacture of plastics, medicines, and dyes also stimulates studies of solvation of these compounds. A particular interest has been expressed recently in analysis of solutions of benzene chloroderivatives. This is due to the fact that these compounds (e.g., *ortho*-dichlorobenzene) are good solvents for fullerenes [4]. Binary mixtures of alcohols with nonpolar solvents, including alkanes, show interesting specific features in the case of minor alcohol additives. In particular, the partial molar specific heats of alcohols in systems of this kind exhibit a clearly pronounced maximum at alcohol content of up to several hundredths of a mole fraction [5].

In the present study, the solvation of benzene, chlorobenzene, *ortho*-dichlorobenzene, and aniline by *n*-hexane and 1-butanol, as well as that of benzene, chlorobenzene, nitrobenzene, and aniline by mixtures of *n*-hexane and 1-butanol, was studied by the thermochemical method. As a result of chloro- and nitrosubstitution in the aromatic ring, the polarizability and dipole moment of the molecules increase. The protons of the amino group favor formation of H-bonds between molecules of aniline and alcohol. A study of the influence exerted by the chemical nature and polarity of molecules on their solvation may be of use for detailing of spectral effects in those cases when aromatic compounds serve as solvatochromic indicators of the solvating capacity of individual [6] and mixed [7] solvents.

Table 1. Enthalpies of dissolution, ΔH^m, of benzene, chlorobenzene, *ortho*-dichlorobenzene, nitrobenzene, and aniline in a mixture of *n*-hexane and 1-butanol at 25°C

x, mole fraction	$m \times 10^3$, mol kg^{-1} solvent	$\Delta_s H^m$, kJ mol^{-1}
	Benzene	
0.00	72	3.15
	145	3.17
0.21	63	3.66
	92	3.67
0.51	52	3.70
	98	3.82
0.80	53	3.31
	88	3.41
1.00	119	2.42
	155	2.39
	Nitrobenzene	
0.00	80	14.58
	152	14.61
0.21	56	10.49
	78	10.37
0.49	89	9.57
	183	9.53
0.80	21	8.30
	52	8.32
1.00	137	7.64
	137	7.44
	Chlorobenzene	
0.00	49	2.94
0.066	43	3.36
0.18	25	3.41
0.50	33	3.16
0.80	49	2.47
0.90	54	2.18
1.00	199	1.31
	199	1.35
	ortho-Dichlorobenzene	
0.00	152	3.35
	213	3.43
1.00	150	1.36
	150	1.37
	Aniline	
0.00	79	10.07
	157	9.63
0.097	76	10.75
	174	10.58
0.21	129	8.68
	245	8.77
0.53	97	6.20
	192	6.18
0.80	129	4.64
	263	4.62
1.00	92	3.29
	122	3.32

* *x*, content of 1-butanol; *m*, molality.

EXPERIMENTAL

The integral heats of dissolution were measured in a calorimeter of the ampule type with variable temperature, with an isothermal sheath and a 60-cm^3 reaction vessel. The calorimeter design was described in the monograph [8]. The thermometric and heat sensitivities of the installation were, respectively, 5×10^{-6} deg and 5×10^{-3} J mm^{-1} of the scale of the recording device.

The compounds used in the study were purified using the methods described in [9]. The content of water in 1-butanol was monitored by titration with the Fischer reagent [10]. It did not exceed 0.1 wt %. Aniline was purified by triple vacuum distillation (according to GLC data, the content of water <0.5 wt %). Benzene, nitrobenzene, chlorobenzene, and *ortho*-chlorobenzene of chemically pure grade "for chromatography" were used without additional purification.

Arithmetic mean values of the heat effects of dissolution, $\Delta_s H^m$ (Table 1) were taken as standard enthalpies of dissolution, $\Delta_s H^0$, of the compounds used in the study. This was done because the difference between these two parameters is within the experimental error, estimated to be 2–3%.

The standard enthalpies of dissolution of aniline and benzene in 1-butanol are in a good agreement with published data, 2.95 [11] and 2.51 kJ mol^{-1} [12], respectively. Also, the enthalpies of solution of benzene, nitrobenzene, and aniline in hexane, obtained in the present study, were compared with the enthalpies of dissolution of these substances in heptane [13] and a directly proportional dependence was obtained ($R^2 = 0.9999$). This fact also confirms the reliability of the experimental data obtained.

Relation (1) was used to calculate the enthalpies of solvation of aromatic compounds by *n*-hexane and 1-butanol.

$$\Delta_{solv} H^0 = \Delta_s H^0 - \Delta_{ev} H^0, \quad (1)$$

where $\Delta_{solv} H^0$ is the standard enthalpy of solvation, and $\Delta_{ev} H^0$, enthalpy of evaporation.

Data on the heats of evaporation of the compounds, necessary for the calculation, were taken from [14] (see Table 2).

Enthalpies of solvation are calculated using different approaches. The semiempirical approach was used in [12] to describe enthalpies of solvation of

hydrocarbons in a number of nonpolar and polar aprotic nonaqueous solvents:

$$\Delta_{solv}H^0 = V_A[p_s - 2(p_A p_s)^{1/2}] - RT. \quad (2)$$

Here p_s and p_A are the densities of the cohesion energy of the solvent (S) and solute (A) [$p = (\Delta_{ev}H^0 - RT)/V_m$], where V_m is the molar volume (Table 2); R, universal gas constant; and T, absolute temperature.

Relation (2) was used to calculate the enthalpies of solvation of CCl_4 by *n*-alkanes and 1-alkanols [15]. The results of calculation were compared with the experimental data. The calculation error increased from *n*-hexane (1%) to *n*-hexadecane (5%). However, the error decreased dramatically from methanol (43%) to 1-decanol (1%). Interestingly, the calculated enthalpies of CCl_4 solvation are less negative than the experimental values in the case of alcohols (with the exception of *tert*-butyl alcohol and decanol), whereas for such solvents as *n*-alkanes, the opposite behavior was observed.

The experimental heats of solvation of aromatic compounds by *n*-hexane or 1-butanol are compared with those calculated by Eq. (2) in Fig. 1.

As would be expected, the calculated and experimental values of $\Delta_{solv}H^0$ for nonpolar or weakly polar compounds (C_6H_6, CCl_4, C_6H_5Cl, $C_6H_4Cl_2$) in solutions in *n*-hexane are in a good agreement. Similar conclusions follow from comparison of the experimental and calculated data for butanol solutions. For nitrobenzene in 1-butanol and aniline in *n*-hexane, Eq. (2) gives unsatisfactory results.

Wide acceptance for analysis of enthalpies of solvation has been gained by correlation approaches. It was shown in [16] that a linear dependence of the enthalpies of solvation of compounds in CCl_4 on the values of their molar refraction (R_m) is observed. This dependence is calculated by the relation

$$R_m = V_m(n^2 - 1)/(n^2 + 2), \quad (3)$$

where n is the refractive index (Table 2).

It was of interest to check whether or not this relation is valid for the systems studied. It was found that there is a tendency for the solvation of the compounds by *n*-hexane and 1-butanol to become more pronounced as R_m grows. However, $\Delta_{solv}H^0$ can be described by the linear dependence (4) with an accuracy close to that in the experiments only for C_6H_6, CCl_4, C_6H_5Cl, and $C_6H_4Cl_2$, with the dependence (4) being common to *n*-hexane and 1-butanol

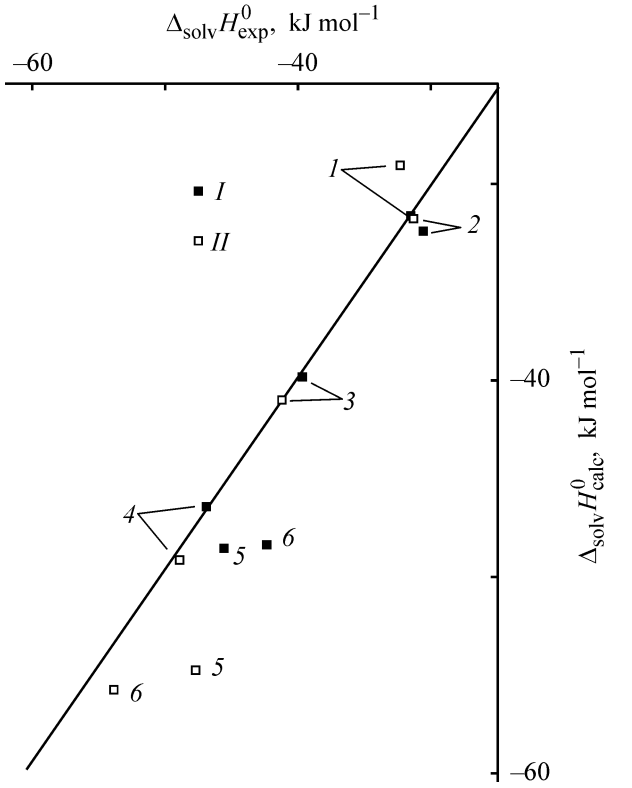


Fig. 1. Experimental enthalpies of solvation by (*I*) *n*-hexane or (*II*) 1-butanol ($\Delta_{solv}H^0_{exp}$) and those calculated by Eq. (2) ($\Delta_{solv}H^0_{calc}$). Substance being solvated: (*1*) CCl_4, (*2*) benzene, (*3*) chlorobenzene, (*4*) *ortho*-dichlorobenzene, (*5*) nitrobenzene, and (*6*) aniline.

$$\Delta_{solv}H^0 = (12.2 \pm 5.7) - (1.64 \pm 0.20)R_m, R\ 0.9991. \quad (4)$$

Table 2. Empirical parameters of compounds [14]*

Compound	n	μ, D	V_m, cm^3 mol^{-1}	$\Delta_{ev}H^0$, kJ mol^{-1}
Benzene	1.4979	0	89.4	33.8
Chlorobenzene	1.5221	1.54	102.2	42.5
ortho-Dichlorobenzene	1.5491	2.27	113.1	50.2
Nitrobenzene	1.5500	4.03	102.7	55.0
Aniline	1.5836	1.51	91.2	56.8
CCl_4	1.4574	0	97.1	32.4
Hexane	1.3723	0.09	131.6	31.6
1-Butanol	1.3973	1.75	92.0	52.4

* n, refractive index; μ, dipole moment; V_m, molar volume; and $\Delta_{ev}H^0$, enthalpy of evaporation.

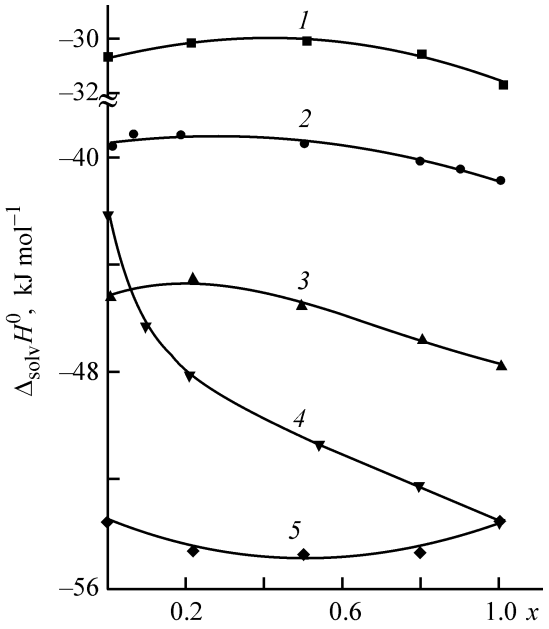


Fig. 2. Enthalpies of solvation ($\Delta_{solv}H^0$) of (*1*) benzene, (*2*) chlorobenzene, (*3*) nitrobenzene, and (*4*) aniline by a mixed solvent composed of *n*-hexane and 1-butanol, and also (*5*) that of aniline by a mixed solvent composed of dihexyl ether and 1-butanol. (*x*) Mole fraction of 1-butanol; the same for Fig. 3.

The only exception from this dependence is the strongly negative enthalpy of solvation of aniline in 1-butanol, which is due to the formation of an intermolecular H-bond. The enthalpies of solvation of $C_6H_5NO_2$ and $C_6H_5NH_2$ in *n*-hexane and $C_6H_5NO_2$ in 1-butanol are also more negative, by approximately 4 kJ mol^{-1}, than those predicted by Eq. (4). Presumably, the small difference between the $\Delta_{solv}H^0$ of the compounds in 1-butanol and *n*-hexane (< 2 kJ mol^{-1}) is due to mutual compensation of the contributions from the intermolecular interaction and void formation in the solvent. The specific relative enthalpies of void formation in *n*-hexane and 1-butanol, calculated in this study by the method described in [17] as the slope rate (k_S) of the linear dependences $\Delta_s H^0 = k_S V_m$ for *n*-alkanes with the use of data from [12, 17–19], were 1.1 and 25.8 J cm^{-3}, respectively. At V_m = 100 cm^3 mol^{-1}, this leads for a difference between the relative enthalpies of void formation by approximately 2.5 kJ mol^{-1}, and between the enthalpies of interaction, by 4 kJ mol^{-1}.

The best results were obtained when the experimental enthalpies of solvation of the substances (Table 2), except aniline, were described separately by linear two-parameter equations for the solvents *n*-hexane (5) and 1-butanol (6), in which μ is the dipole moment (Table 2):

$$\Delta_{solv}H^0 = -(1.19 \pm 0.01)R_m - (1.65 \pm 0.12)\mu, \quad (5)$$

$$R\ 0.9999.$$

$$\Delta_{solv}H^0 = -(1.22 \pm 0.01)R_m - (1.95 \pm 0.16)\mu, \quad (6)$$

$$R\ 0.9999.$$

The negative signs of the coefficients in Eqs. (5), (6) mean that the solvation becomes more exothermic as either R_m or μ increases. The coefficients R_m in Eqs. (5), (6) have the same value, and, therefore, the contribution from R_m will be eliminated for the enthalpy of transfer of the substances studied from *n*-hexane to 1-butanol.

The fact that Eqs. (5), (6) well describe the experimental values of $\Delta_{solv}H^0$ suggests the following. The solvation of aromatic compounds in both polar and nonpolar solvents is determined not only by the dispersion interaction, but also by interactions dependent on the dipole moment. This result contradicts the conclusion made in [16, 17] that neither the dipole moment of the molecule as a whole, nor the moments of the bonds (and, consequently, the orientation and induction interactions affect to any significant extent the enthalpy of nonspecific solvation.

Figure 2 shows how the enthalpies of solvation of benzene, chlorobenzene, nitrobenzene, and aniline by a mixture of *n*-hexane and 1-butanol depend on the composition of this mixture. The same figure presents for comparison the data of [20] for a mixture of dihexyl ether, 1-butanol, and aniline. It can be seen that adding to *n*-hexane a component with a higher solvating capacity, 1-butanol, first ($x < 0.2$) make somewhat lower the exothermicity of solvation of benzene, chlorobenzene, and nitrobenzene, and only then, as the pure alcohol is approached, the solvation becomes more exothermic.

The specific interactions of aniline with 1-butanol dissolved in *n*-hexane lead to a dramatic increase in the exothermicity of aniline solvation at small *x*. Aniline interacts with dihexyl ether as an H-donor, and with 1-butanol both as an H-donor and an H-acceptor. However, the specific interaction of aniline with the alcohol requires that the H-bonds in the solvent should be ruptured. As a result, the enthalpy of aniline solvation by the alcohol becomes equal to the enthalpy of aniline solvation by the ether. It should be noted that aniline is solvated the most exothermically by the equimolar mixture of dihexyl ether and 1-butanol. The ability of the NH_2 group of aniline to

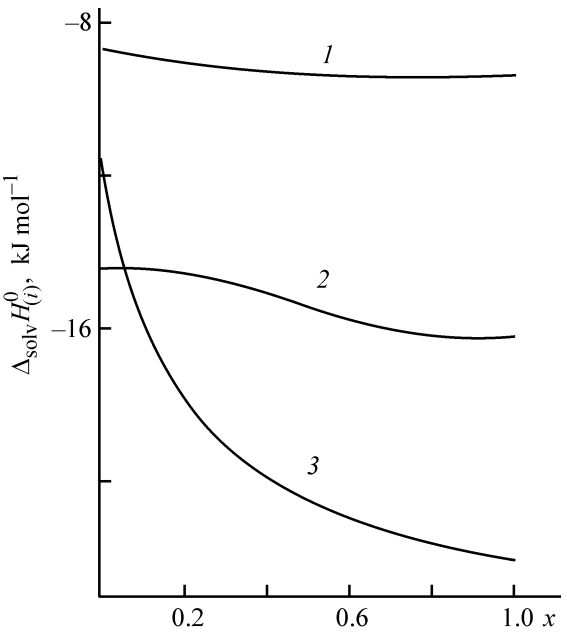


Fig. 3. Contribution of *i*th group to the enthalpies of solvation ($\Delta_{solv}H^0$) of the compounds by a mixed solvent composed of *n*-hexane and 1-butanol. *i*: (*1*) Cl, (*2*) NO_2, and (*3*) NH_2.

be an H-donor and H-acceptor is manifested in this case to the greatest extent.

Figure 3 shows the enthalpies of solvation of the substituents, calculated as the difference of the enthalpies of solvation of the corresponding compounds and benzene. The solvation of the substituents in *n*-hexane is nonspecific. It becomes 3 kJ mol^{-1} more exothermic in going from Cl to NH_2, and the exothermicity increases by additional 3 kJ mol^{-1} in going from NH_2 to NO_2. Already at 5 molecules of the alcohol per 95 molecules of the alkane, the NH_2 and NO_2 groups are solvated similarly. At $x > 0.05$, the solvation of these groups becomes increasingly exothermic in the order Cl, NO_2, and NH_2. In the pure alcohol, the solvation of the NH_2 groups is already 6 kJ mol^{-1} more exothermic than that of NO_2. Thus, the solvation of these groups can be differentiated by varying the composition of the alkane–alcohol mixture.

CONCLUSIONS

(1) The enthalpies of dissolution of benzene, chlorobenzene, *ortho*-dichlorobenzene, nitrobenzene, and aniline in *n*-hexane and 1-butanol, and that of benzene, chlorobenzene, nitrobenzene, and aniline in a mixed solvent composed of *n*-hexane and 1-butanol, were determined experimentally.

(2) Specific features of the solvation of the substances studied by *n*-hexane and 1-butanol were discussed. The correlation of the enthalpies of solvation of the compounds with their molar refraction becomes better if the dipole moments of the molecules are taken into account.

(3) It was found that the composition of the mixture of *n*-hexane and 1-butanol comparatively weakly affects the enthalpies of solvation of benzene, chlorobenzene, and nitrobenzene, whereas the solvation of aniline becomes considerably more exothermic as the content of the alcohol in the mixture increases.

(4) It was shown that the results obtained can be used to supplement the available reference database on heats of solution of aromatic substances in individual and mixed solvents and may be of use in studies of reactions that occur in solutions containing benzene derivatives.

REFERENCES

1. Tardajos, G., Aicart, E., Costas, M., and Patterson, D., *J. Chem. Soc. Faraday Trans. I*, 1986, vol. 82, no. 9, pp. 2977–2987.
2. Dominquez, A., Tardajos, G., Aicart, E., *et al.*, *J. Chem. Soc. Faraday Trans.*, 1993, vol. 89, no. 1, pp. 89–93.
3. Munk, P., Qin, A., and Hoffman, D.E., *Collect. Czech. Commun.*, 1993, vol. 58, pp. 2612–2624.
4. Marcus, Y., *J. Phys. Chem. B*, 2001, vol. 105, pp. 2499.
5. Andreoli-Ball, A., Patterson, D., Costas, M., and Caceres-Alonso, M., *J. Chem. Soc. Faraday Trans. I*, 1988, vol. 84, no. 11, pp. 3991–4012.
6. Kamlet, M.J., Abboud, J.L., and Taft, R.W., *Progr. Phys. Org. Chem.*, 1981, vol. 13, pp. 485–630.
7. Migron, Y. and Marcus, Y., *J. Chem. Soc. Faraday Trans.*, 1991, vol. 87, no. 9, pp. 1339–1343.
8. Belousov, V.P., *Eksperimental'nye metody khimii rastvorov: Spektroskopiya i kalorimetriya* (Experimental Techniques of the Chemistry of Solutions: Spectroscopy and Calorimetry), Moscow: Nauka, 1995.
9. Weisberger, A., Proskauer, E., Riddick J., and Toops, E., *Organicheskie rastvoriteli* (Organic Solvents), Moscow: Inostrannaya Literatura, 1958.
10. Klimova, V.A., *Osnovnye mikrometody analiza organicheskikh soedinenii* (Basic Microscopic Methods for Analysis of Organic Compounds), Moscow: Khimiya, 1967.
11. Manin, N.G., Belichenko, S.Yu., and Korolev, V.P.,

Zh. Obshch. Khim., 2001, vol. 71, no. 5, pp. 743–748.

12. Krishnan, C.V. and Friedman, H.L., *J. Phys. Chem.*, 1971, vol. 75, no. 23, pp. 3598–3606.
13. Stephenson, W.K. and Fuchs, R., *Canad. J. Chem.*, 1985, vol. 63, no. 4, pp. 2529–2535.
14. Marcus, Y., *Ion Solvation*, New York. Willey. 1985.
15. Sivolozhskaya, Yu.A., Potkina, N.L., and Korolev, V.P., *Zh. Obshch. Khim.*, 2000, vol. 70, no. 9, pp. 1492–1498.
16. Solomonov, B.N. and Konovalov, A.I. *Usp. Khim.*, 1991, vol. 60, no. 1, pp. 45–68.
17. Solomonov, B.N., Antipin, I.S., Gorbachuk, V.V., and Konovalov, A.I., *Zh. Obshch. Khim.*, 1982, vol. 52, no. 10, pp. 2154–2160.
18. Stephenson, W.K. and Fuchs, R., *Canad. J. Chem.*, 1985, vol. 63, no. 2, pp. 349–352.
19. Korolev, V.P. Antonova, O.A., Batov, D.V., and Krestov, G.A., *Sbornik nauchnykh trudov IKhNR Ross. Akad. Nauk* (Coll. of Sci. Works of IKhNR, Russian Academy of Sciences), 1990, pp. 104–117.
20. Korolev, V.P. and Potkina, N.L., *Zh. Obshch. Khim.*, 2003, vol. 73, no. 5, pp. 741–746.

ISSN 1070-4272, Russian Journal of Applied Chemistry, 2006, Vol. 79, No. 2, pp. 219–224. © Pleiades Publishing, Inc., 2006.
Original Russian Text © S. S. Stavitskaya, V. M. Vikarchuk, N. N. Tsyba, N. I. Bogdanovich, V. F. Gaevskii, Yu. P. Zaitsev, N. T. Kartel', V. V. Strelko, 2006, published in Zhurnal Prikladnoi Khimii, 2006, Vol. 79, No. 2, pp. 220–225.

SORPTION AND ION-EXCHANGE PROCESSES

Structural and Sorption Characteristics of Carbon Adsorbents from Waste Formed in Wood Processing

S. S. Stavitskaya, V. M. Vikarchuk, N. N. Tsyba, N. I. Bogdanovich, V. F. Gaevskii, Yu. P. Zaitsev, N. T. Kartel', and V. V. Strelko

Institute of Sorption and Endoecological Problems, National Academy of Sciences of Ukraine, Kiev, Ukraine
Arkhangelsk State Technical University, Arkhangelsk, Russia

Received May 13, 2005

Abstract—The structural and sorption characteristics of microporous sorbents from industrial lignin with respect to some toxic substances, Pb^{2+}, Cd^{2+}, Cu^{2+}, and NH_4^+ ions, and also the possibility of accumulation of methane on these carbons were studied. Simple procedures for modification of the carbon surface to improve the sorption power of the carbons were suggested.

DOI: 10.1134/S1070427206020108

Carbon adsorbents from plant raw materials find diverse applications. Lignin, large-tonnage waste from chemical reprocessing of wood, is of doubtless interest as a raw material for carbon production. Procedures for preparation of activated carbons (ACs) from hydrolyzed lignin [1–3], cotton lignin [4], and cellolignin formed as waste in synthesis of furfural by acid-free method of wood hydrolysis [4] have been published. Due to highly developed volume of micropores, the resulting activated carbons have the best adsorption characteristics in comparison with the well-known industrial carbons of AG-3, AR, and UAF brands.

Traditionally, adsorbents from industrial lignin (IL) are produced by its steam and gas activation after precarbonization (pyrolysis).

New methods have been developed for pyrolysis of wastes formed in chemical and mechanical treatment of wood (industrial lignins, wastewater sludges, bark, sawdust, liquors), such as combined process of pyrolysis–steam-and-gas activation, oxidative pyrolysis of high-ash wastes, e.g., wastewater, thermochemical activation at 800–840°C with chemicals used in wood delignification (Na_2SO_4, Na_2CO_3, NaOH) [5–7], and a new method for production of ferromagnetic adsorbents [5, 8, 9].

The aim of this study was to examine some structural sorption and physicochemical characteristics of AC produced by thermochemical activation of IL after its precarbonization[1] [5–9] to find additional possibilities for its use in adsorption technology.

EXPERIMENTAL

The adsorbents synthesized by the procedure described in [8] have a mixed pore structure with predominance of micropores. The volume of micropores with radii r = 10–25 Å in these carbons reaches 1.2 $cm^3\ g^{-1}$, and the volume of mesopores varies in the range 0–0.5 $cm^3\ g^{-1}$.

The carbon sample (approximately 2 kg) was nonuniform in the particle size. The powder fraction (approximately 30%) was sifted off. The sample with particle size from 0.25 to 1.0 mm^2 was used. The pH of the aqueous carbon extract from IL was about 2.5 (Table 1). Therefore, the initial sample was subjected for subsequent testing to additional treatment, washing with hot distilled water until pH of the aqueous extract reached approximately 7 (Table 1) and special oxidation with 25% nitric acid in the liquid phase on a boiling water bath or calcination in an argon flow for 1 h at 700°C [10, 11] (activated sample), with the aim to impart properties of an effective cation or anion exchanger to carbon [10–12] for its

[1] Performed at the Arkhangelsk Hydrolysis Plant.

[2] Sibmitted by staffmembers of the Arkhangelsk State Technical University.

Table 1. Some structural sorption and physicochemical characteristics of carbons from industrial lignin and, for comparison, KAU carbon from natural raw materials

Characteristic	Carbon from IL			KAU
	initial		oxidized	
	activated	washed		
W_s with respect to benzene, $cm^3\ g^{-1}$	1.0	1.4	1.1	0.9
Moisture content, %	30	18	–	10
Ash residue, %	13.4	9.7	6.0	3.0
Bulk density Δ, $g\ cm^{-3}$	–	0.27	0.26	0.36
pH of aqueous extract	2.4	6.0	–	6.5
S_{sp}, $m^2\ g^{-1}$	2000	2100	1450	1010
Sorption, $mg\ g^{-1}$:				
MB	536	670	610	450
OH	20	30	–	–
SEC, $mg\text{-}equiv^{-1}$				
with respect to NaOH	2.7	1.6	3.2	0.1
with respect to HCl	1.0	0.2	0.1	0.35

use in adsorption technology and for environment protection.

The parameters of the carbons studied (Table 1) were evaluated by standard procedures [GOST (State Standard) 6217–74, GOST 4453–74]. We determined the total volume of sorption pores with respect to benzene W_s, moisture content, ash residue, pH of aqueous extract, bulk density Δ, anion-exchange capacity (from sorption of Cl^- ions from 0.01 M aqueous HCl), and cation-exchange capacity (SEC) (from sorption of Na^+ ions from 0.1 N NaOH). A qualitative analysis of pores was based on the adsorption of markers [12]: Methylene Blue (MB, molecular weight 319) and oxyhemoglobin (OH, molecular weight 68 000). Low-temperature (77 K) adsorption of N_2 was used for characterizing the pore structure [13]. BET isotherms of N_2 adsorption and curves of pore radius distribution (Fig. 1) were obtained on a Quantachrome NOVA 2200E high-rate gas sorption analyzer. The specific surface areas S_{sp} of the samples (Table 1) were evaluated by the BET method.

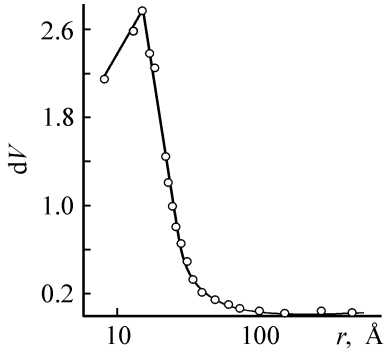


Fig. 1. Curve of differential distribution of pores dV with respect to radius r in the initial carbon prepared from industrial lignin and washed with water.

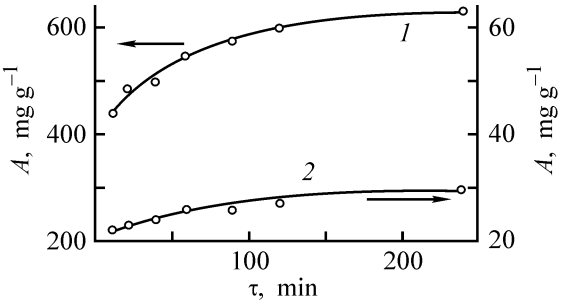


Fig. 2. Kinetics of sorption A of (*1*) Methylene Blue and (*2*) oxyhemoglobin on carbon prepared from industrial lignin and washed with water. Weighed portion of carbon 0.1 g; solution volume 50 ml, T = 20°C. (τ) Process duration.

We found that, similarly to all carbon adsorbents based on lignosulfonates, the carbon studied has a high specific surface area, 1450–2100 $m^2\ g^{-1}$, large volume of sorption area of W_s = 1–1.4 $cm^3\ g^{-1}$, and high clarification power with respect to MB (540–670 $mg\ g^{-1}$).

Table 1 shows that the carbons prepared from IL are highly competitive in structural sorption characteristics and kinetics of absorption of markers (Fig. 2): MB molecules with lower molecular weight are sorbed more readily than OH molecules with higher molecular weight) with well-known granulated sorbents, e.g., carbons from the KAU natural raw materials and can be used for absorption of "small-" and "medium-size" molecules [10].

The presence of a microporous structure in the samples studied is confirmed not only by the behavior in sorption of markers of various molecular weights but also by the low-temperature adsorption of N_2. The sample, indeed, was uniformly microporous with the pore size r = 20 Å, which is a valuable characteristic for practical use.

The experiments showed that the carbon is readily oxidized: upon boiling in nitric acid on a water bath for 1 h, a fairly high ion-exchange capacity (SEC = 3.2 mg-equiv g^{-1}) with predominant content of strongly acidic and phenolic surface groups is reached, whereas, e.g., KAU carbons from pits are oxidized under similar conditions to similar values of SEC only in 15–20 h [10, 11]. It is likely that mineral impurities (ash residue approximately 10%) exert a catalytic effect on the carbon oxidation; similar phenomena have been observed previously [14].

It should be noted that a distinctive feature of activated carbons prepared by thermochemical activation is their capacity for ion exchange. The ion-exchange capacity is acquired without additional oxidative treatment and reaches 1.6 mg-equiv g^{-1} (Table 1). This is apparently caused by the fact that sodium sulfate oxidize the kraft lignin matrix on heating to a temperature above 800°C, with reduction to sulfide and other reduced sulfur compounds [6]. In the process, the content of oxygen-containing acidic groups, responsible for the cation-exchange capacity of the resulting carbon material, increases.

In studying ion exchangers, the amount and quality of individual types of functional groups capable of ion exchange are most frequently estimated from the titration curves [15]. The titration curves of the samples of activated and oxidized carbons from industrial lignin in 0.2 N NaCl with HCl and NaOH are shown in Fig. 3. The integral and differential pH dependences of the Na^+ sorption on the oxidized sample A, evaluated from these titration curves, are shown in Fig. 4. It is seen from Figs. 3 and 4 that the anion exchange on the activated carbon starts, as usually [14, 15], at pH 8.5, and the exchange proceeds on the oxidized sample even at pH 2–2.5; with increasing pH, weaker acidic groups are involved into the exchange. From the most pronounced inflections in the dependence of dA/d pH on pH, we determined the pK values for ionization of three types of functional groups present in the sample studied: 4.7, 9.7, and 10.7, which corresponds to carboxy groups dissociating in the pH range 1–8 and phenolic groups dissociating at pH 8–10 [15].

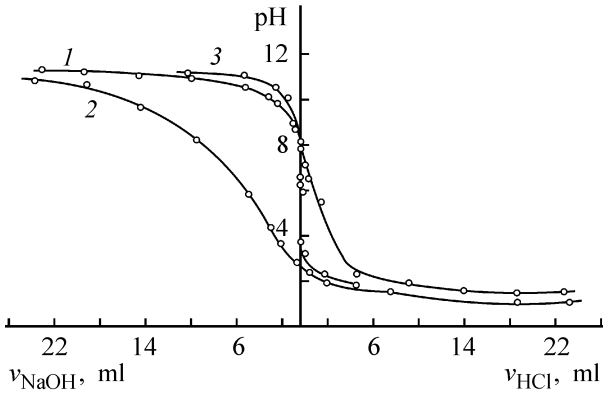


Fig. 3. Curves of pH-potentiometric titration of (*1*) activated and (*2*) oxidized carbon from lignin. (*v*) Amount of HCl and NaOH solutions. (*3*) Blank experiment (without carbon).

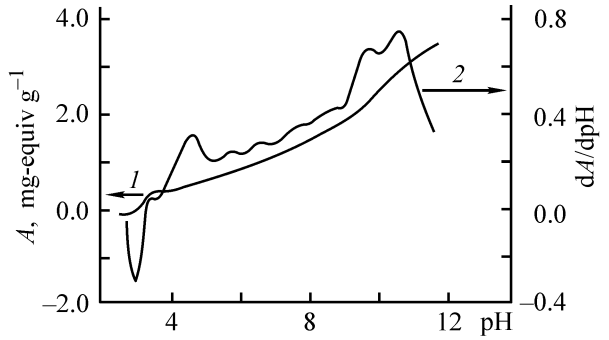


Fig. 4. (*1*) Integral and (*2*) differential pH dependences of the sorption of sodium ions, A, on oxidized sample of carbon from industrial lignin.

The chemical methods used to determine the amount of acidic groups in oxidized carbons from lignin (titration with alkalis with various strengths [16]) confirmed the results of potentiometric titration. It was found that the surface of the carbons studied, with a total exchange capacity of 3.2 mg-equiv g^{-1}, contains strongly acidic carboxy groups in an amount of 1.8 mg-equiv g^{-1} with pK ~ 4 and phenolic groups in an amount of 1.4 mg-equiv g^{-1} (pK ~ 9). Thus, the sample obtained by additional oxidation is a polyfunctional cation exchanger with a widely varying of acidic characteristics of groups responsible for the ion exchange (pK ~ 2–10).

The ion exchange power of the carbons studied is confirmed by the sorption isotherms of toxic metal ions Cu^{2+}, Cd^{2+}, and Pb^{2+} from aqueous solutions of their salts on the initial sample (SEC = 1.6 mg-equiv g^{-1}) in the H form at 20°C (Fig. 5a). The sorption experiments were performed under static conditions. The ratio of the solid and liquid phases was 1 : 250. The initial and equilibrium concentra-

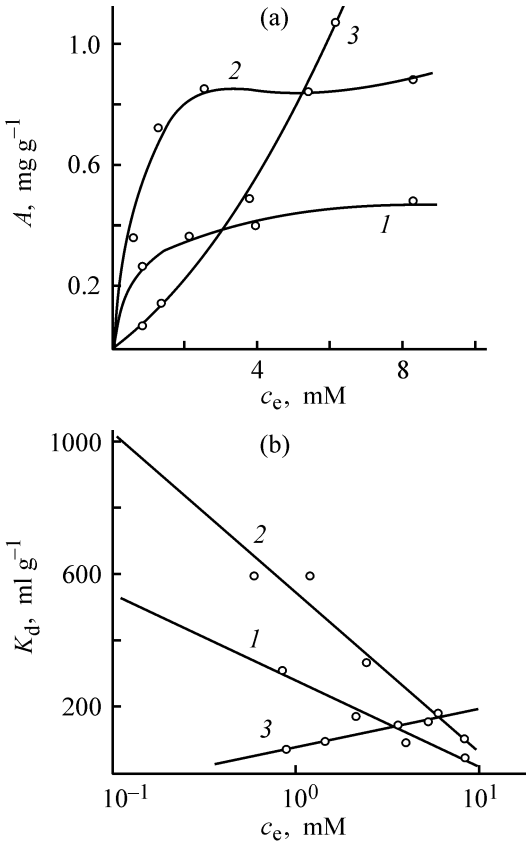


Fig. 5. (a) Sorption isotherms A and (b) dependences of distribution coefficients K_d of (*1*) Cu^{2+}, (*2*) Cd^{2+}, and (*3*) Pb^{2+} ions on the equilibrium concentration c_e for the initial carbon (SEC = 1.6 mg-equiv g^{-1}). Weighed portion of carbon 0.1 g; solution volume 25 ml.

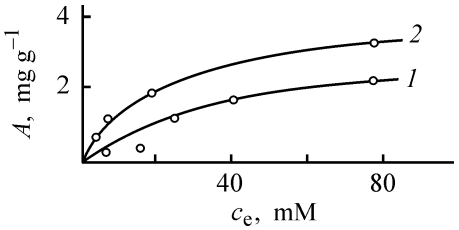


Fig. 6. Sorption isotherm A of ammonium ions on (*1*) H and (*2*) Cu forms of oxidized carbon prepared from lignin. (c_e) Equilibrium concentration of sorbed ion.

tions of metal ions were determined on a KAS-120.1 device [12]. It is seen from Fig. 5a that the sorbability of the ions decreases in the order $Cd^{2+} > Cu^{2+} > Pb^{2+}$. Copper and cadmium ions were best sorbed when the equilibrium concentration c_e was approximately 3 mmol g^{-1}, and the isotherm of lead(II) sorption under the selected conditions did not level off. At $c_e > 6$ mmol g^{-1}, the sorbability order became $Pb^{2+} > Cd^{2+} > Cu^{2+}$.

From the sorption isotherms of the metal ions we evaluated the distribution coefficients K_d (ml g^{-1}) with respect to each ion, brought to the standard conditions: the equilibrium concentration of ions in the solution was 1 mM as in [17]. The concentration dependences of the distribution coefficients of the ions in a wide range of their equilibrium concentrations in solution (from 10^{-1} to 10^{1} mM) are shown in Fig. 5b. The resulting order of sorption selectivity with IL carbons is typical of the majority of oxidized carbons of various origins [15, 17].

Among detrimental products of metabolism are nitrogen-containing substances, which, at increased concentrations, exert toxic effect on a living body: ammonia, uric acid, urea, and creatinine [17]. Removal of these substances from a body is an important and urgent problem [18]. In this context, it was of interest to study how the carbons produced from the cheap raw materials extract some substances mentioned above. The isotherms of sorption of ammonium ions from solutions of ammonium chloride on the H and Cu forms of oxidized carbon produced from lignin (static exchange capacity 3.2 mg-equiv g^{-1}) are shown in Fig. 6. As expected, carbon in the Cu form, in which the content of the modifying ion was 1.2 mg-equiv g^{-1}, absorbed ammonium ions a factor of 2 better than did the carbon in the H form. It is likely that the increase in the sorption capacity with respect to NH_4^+ ions can be favored by possible formation of fairly stable ammonia complexes with copper ions [15] at the surface of Cu form of the oxidized carbon.

Carbon adsorbents attract attention as possible molecular-sieve materials, which can serve as accumulating systems for increasing the capacity of gas cylinders filled with methane to be used as motor fuel. Previously [19, 20] it was shown that addition of carbon sorbents to gas cylinders to be filled with methane allows its accumulation in the same amount at 25–35 atm as in the absence of a sorbent at 150–200 atm.

Absorption of methane on carbon materials was studied on a specially designed volumetric installation. A carbon sample was preliminarily vacuum treated, first at room temperature for 0.5 h and then, at 250°C for 1 h, after which the cooled sample was vacuum treated at room temperature for 0.5 h. The sufface of the carbon prepared by this procedure was saturated with methane (methane accumulation), using multicycle treatment of the sample with methane at room temperature under a gas pressure of 25 atm for 0.5 h and subsequent desorption of CH_4 for a short time (1–2 min) at atmospheric pressure. Five cycles of

Table 2. Adsoption of methane during several cycles of operation on the initial carbon, oxidized sample, and some of its ionic forms

Cycle	Adsorption on samples modified with indicated ions, ml g^{-1}						
	initial carbon	H^+	Li^+	Na^+	K	Rb^+	Cs^+
1	115	10	16	16	7	10	0
2	42	20	0	0	2	0	0
3	0	10	6	17	12	–	4
4	–	0	10	0	8	–	–
5	–	10	10	0	0	–	–
Total	157	50	42	33	29	10	4

adsorption–desorption of methane were performed (Table 2).

For the study we used the initial finely porous washed sample prepared from industrial lignin, the same carbon oxidized with nitric acid (H form), and also K, Na, Li, Rb, and Cs forms of carbon specially modified with ions of the same nature but different sizes. Alkali metal ions were sorbed on carbon material at pH 10–10.5 [14].

The values of methane absorption after each adsorption–desorption cycle on various carbons are listed in Table 2. It follows from Table 2 that CH_4 was best accumulated on the initial carbon and on carbon in the H form; with increasing radius of substituting ion (from Li^+ to Cs^+), the adsorption abruptly decreased. This coincides with theoretical calculations and assumptions [19, 20] that the features of the pore structure and predominant content of micropores play an important role in the process. For example, according to published data [20], to attain the highest affinity for methane, the diameter of micropores of activated carbons should correspond to the sum of the critical diameters of three methane molecules, i.e., approximately 11.2 Å. It is precisely this diameter of slitlike pores at which the closest volume filling of these pores with methane is observed.

It is likely that, in the experiments on directed modification of the carbon surface with cations of various sizes, the diameter of slitlike pores decreases with increasing radius of substituting ions; in this case, the amount of sorbed methane decreases. These studies indicate that the tested samples of carbon sorbents from wastes of forest industry plants show much promise for accumulation of methane.

CONCLUSIONS

(1) The main structural parameters of carbon sorbents based on industrial lignin were determined, and their specific surface area and total volume of sorption pores were found to be $S_{sp} \sim 2000$ m^2 g^{-1} and $W_s \sim 1.4$ cm^3 g^{-1}, respectively. Micropores predominate in these sorbents, and their radius is $r \sim 20$ Å.

(2) The chemical nature of the carbon surface was modified by liquid-phase oxidation (impartment of cation-exchange properties) and high-temperature activation in argon flow (anion-exchange properties).

(3) The ion-exchange power of oxidized carbons from industrial lignin was determined, and isotherms of adsorption of Pb^{2+}, Cu^{2+}, Cd^{2+}, and NH_4^+ ions were obtained.

(4) Owing to their microporous structure, carbon sorbents from wood treatment wastes can efficiently accumulate methane.

REFERENCES

1. Vorozhbitova, L.N., Boikova, G.I., and Seregina, T.A., in *Poluchenie, struktura i svoistva sorbentov* (Synthesis, Structure, and Characteristics of Sorbents), Leningrad: Leningr. Tekhnol. Inst., 1978, pp. 39–46.
2. USSR Inventors' Certificate, no. 971789.
3. Akhmina, E.I., in *Uglerodnye adsorbenty i ikh primenenie v promyshlennosti* (Carbon Adsorbents and Their Use in Industry), Moscow: Nauka, 1983, pp. 48–58.
4. Mukhin, V.M., Tarasov, A.V., and Klushin, V.N., in *Aktivnye ugli Rossii* (Activated Carbons of Russia), Moscow: Metallurgiya, 2000, pp. 50–56.
5. Bogdanovich, N.I., Dobele, G.V., and Kuznetsova, L.N., Abstracts of Papers, *VI Vserossiiskii simpozium "Aktual'nye problemy teorii adsorbtsii i sinteza sorbentov"* (VI All-Russian Symp. "Urgent Problems of Theory of Adsorption and Synthesis of Sorbents"), Moscow: Inst. Fiz. Khim. Ross. Akad. Nauk, 2000, pp. 58–59.
6. Bogdanovich, N.I., Kuznetsova, L.N., Dobele, G.V., and Tsaplina, S.A., Abstracts of Papers, *IX Mezhdunarodnaya konferentsiya "Sovremennoe sostoyanie*

i perspektivy razvitiya teorii adsorbtsii" (IX Int. Conf. "Modern State and Prospects for Development of Adsorption Theory"), Moscow: Inst. Fiz. Khim. Ross. Akad. Nauk, 2001, p. 107.

7. Bogdanovich, N.I.,Kuznetsova, L.N., Dobele, G.V., and Tsaplina, S.A., Abstracts of Papers, *VI Vserossiiskii simpozium "Aktual'nye problemy teorii adsorbtsii i sinteza sorbentov"* (VI All-Russian Symp. "Urgent Problems of Theory of Adsorption and Synthesis of Sorbents")1, Moscow: Inst. Fiz. Khim. Ross. Akad. Nauk, 2000, pp. 54–55.
8. Bogdanovich, N.I., Shevchenko, R.S., Kuznetsova, L.N., and Dobele, G.V., Abstracts of Papers, *VI Vserossiiskii simpozium "Aktual'nye problemy teorii adsorbtsii i sinteza sorbentov"* (VI All-Russian Symp. "Urgent Problems of Theory of Adsorption and Synthesis of Sorbents"), Moscow: Inst. Fiz. Khim. Ross. Akad. Nauk, 2000, pp. 56–57.
9. Bogdanovich, N.I., Dobele, G.V., Kuznetsova, L.N., and Shevchenko, R.S., Abstracts of Papers, *IX Mezhdunarodnaya konferentsiya "Sovremennoe sostoyanie i perspektivy razvitiya teorii adsorbtsii"* (IX Int. Conf. "Modern State and Prospects for Development of Adsorption Theory"), Moscow: Inst. Fiz. Khim. Ross. Akad. Nauk, 2001, p. 108.
10. Kartel', N.T. and Stavitskaya, S.S., *Ukr. Khim. Zh.*, 1998, vol. 64, no. 3, pp. 24–28.
11. Stavitskaya, S.S., Kartel', N.T., and Petrenko, T.P., *Zh. Prikl. Khim.*, 1999, vol. 72, no. 9, pp. 1451–1455.
12. Kel'tsev, N.V., *Osnovy adsorbtsionnoi tekhniki* (Principles of Adsorption Technique), Moscow: Khimiya, 1984.
13. Greg, S.J. and Sing, K.S.W., *Adsorption, Surface Area and Porosity*, London: Academic, 1982, p. 90.
14. Tarkovskaya, I.A., Stavitskaya, S.S., Luk'yanchuk, V.M., and Tikhonova, L.P., *Ukr. Khim. Zh.*, 1998, vol. 64, no. 6, pp. 88–93.
15. Tarkovskaya, I.A., *Okislennyi ugol'* (Oxidized Carbon), Kiev: Naukova Dumka, 1981.
16. Boehm, H.P., *Adv. Catal. Relat. Subj.*, 1966, vol. 66, pp. 179–274.
17. Kartel', N.T., Stavitskaya, S.S., Vikarchuk, V.M., *et al., Teor. Eksp. Khim.*, 2000, vol. 36, no. 1, pp. 53–57.
18. Strelko, V.V., Meleshevich, S.I., Karpenko, G.F., and Petrenko, T.P., *Zh. Prikl. Khim.*, 1998, vol. 71, no. 9, pp. 1448–1451.
19. Sircar, S., Golden, T.C., and Rao, M.V., *Carbon*, 1996, vol. 34, no. 1, pp. 1–12.
20. Parkyns, N.D. and Quinn, D.F., *Porosity in Carbons*, Patrick, J., Ed., New York: Wiley, 1995, pp. 291–298.

ISSN 1070-4272, Russian Journal of Applied Chemistry, 2006, Vol. 79, No. 2, pp. 225–228. © Pleiades Publishing, Inc., 2006.
Original Russian Text © A. M. Akimbaeva, E. E. Ergozhin, 2006, published in Zhurnal Prikladnoi Khimii, 2006, Vol. 79, No. 2, pp. 226–229.

SORPTION AND ION-EXCHANGE PROCESSES

Bentonite-based Phosphoric Acid Organomineral Cationite

A. M. Akimbaeva and E. E. Ergozhin

Bekturov Institute of Chemical Sciences, Ministry of Education and Science of the Republic of Kazakhstan, Almaty, Kazakhstan

Received March 31, 2005

Abstract—The conditions under which bentonite-based phosphoric acid organomineral cationite is obtained were assessed and its acid-base and physicochemical properties were studied.

DOI: 10.1134/S107042720602011X

Until recently, synthetic organic polymers with ionogenic functional groups containing inorganic substances (silica, aluminum oxide, zeolites) have constituted two main classes of ion-exchangers. The wide use of organopolymer sorbents is due to the versatility oftheir action, ease of regeneration, and possibility of widely varying the nature and content of functional groups. The advantages of inorganic ionites include the nonswellability in solvents, mechanical strength, thermal stability, radiation hardness, and, in some cases, unique catalytic properties. Combination of the valuable properties of both classes of sorbents enables development of few-stage methods for synthesis of new effective ion-exchangers with a set of valuable properties. In this context, a necessity arises for creating a new type of materials combining the advantages of these ion exchangers. The materials are obtained by modifying the surface of inorganic substances with organic compounds containing functionally active groups [1]. Of particular importance among these materials are phosphorus-containing organomineral ion-exchangers with a silica matrix, which are used in sorption, concentration, and various types of chromatography [1, 2]. A promising solution in this area is to use natural raw materials and various kinds of industrial waste [3–5].

The aim of the present study was to synthesize a phosphoric acid organomineral cationite based on natural bentonite.

EXPERIMENTAL

Bentonite (Bt), whose main rock-forming mineral is montmorillonite, served as a mineral support. The acid activation of the natural sorbent was done in 20% H_2SO_4 on a boiling water bath in the course of 6 h [6].

After distillation, glycidyl methacrylate (GMA) had the following parameters: $d_4^{20} = 1.0333$, $n_D^{20} = 1.4480$. Slime orthophosphoric acid ($\rho = 1.588$ g cm^{-3}) was taken from the waste of Zhambyl phosphorus plant (Kzakhstan).

The mineral was modified with phosphoric acid in dioxane, with the subsequent polymerization of GMA at 100°C [7]. Then cationite samples were converted from Na^+ to the H-form and back, each time with washing to a neutral reaction of the washing water. The static exchange capacity SEC (mg-equiv g^{-1}) of the final products was determined with a 0.1 N KOH solution [8].

The samples were subjected to potentiometric titration by the method of separate weighed portions. The ionic strength was maintained by adding a certain amount of the electrolyte (KCl). After equilibrium between the cation exchanger and the solution was established, the pH value was measured with an EV-74 ion meter equipped with glass and silver chloride. The results of these measurements were used to plot the curve of potentiometric titration as a graph of pH versus the amount of the titrant.

To determine the chemical and thermal stability of the cationite in the H-form, three weighed portions of the ionite (each 1.0 g in terms of dry substance) were placed in 250-ml round-bottom flasks. The first of these was poured over with a 5 N H_2SO_4 solution (100 ml); the second, with a 5 N NaOH solution (100 ml); and the third, with distilled water (100 ml); after which all the samples were kept at room tem-

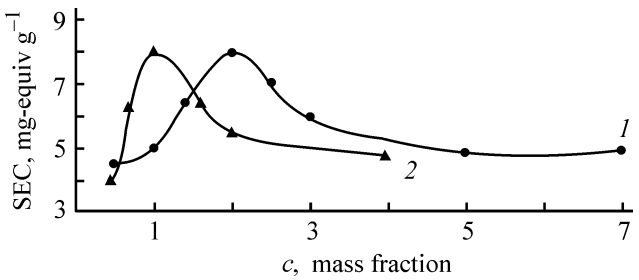


Fig. 1. SEC of the cationite vs. the content c of the modifying agents (modification at 100°C for 3 h). (*1*) H_3PO_4 (Bt : GMA = 1 : 1) and (*2*) GMA (Bt : H_3PO_4 = 1 : 2).

perature for 0.5 h (chemical stability) and on a boiling water bath for 24 h (thermal stability). The mixture was cooled to room temperature, the filtrate was separated from the ionite, and the latter was converted to the H-form and its SEC was determined. The chemical and thermal stability V (%) was calculated by the formula

$$Y = E_1/E_0,$$

where E_0 and E_1 are the SEC (mg-equiv g^{-1}) before and after the treatment of the ionite, respectively.

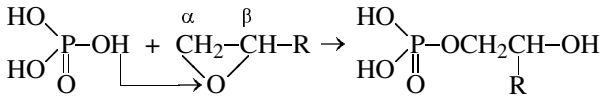
IR spectra of the samples were measured on a UR-20 spectrophotometer in KBr pellets or in thin layer in the spectral range 400–4000 cm^{-1}.

It has been found [9] that the reaction of concentrated H_3PO_4 with kaolin occurs at room temperature via binding of acid molecules by clay particles, whereas at elevated temperature, the structure of the mineral undergoes a deep disintegration [9]. It was shown that the interaction products are partly soluble in water. The best acceptable way to obtain mineral-based sorbents is to use cross-linking agents that can firmly fix functional groups to the support surface.

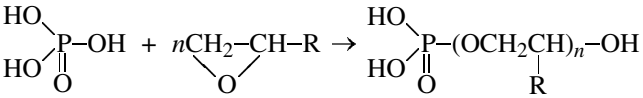
Modification of the bentonite surface with an epoxy compound in the presence of H_3PO_4 promotes involvement of a large number of active centers into condensation and favors uniform cross-linking of polymer chains.

In setting-up the problem, the authors proceeded from the results of previous studies [3–5], in which the possibility of obtaining organomineral products was demonstrated. GMA, which combines an easily polymerizing double bond and a reactive oxirane ring, served as an epoxy compound. Use of monomers of this kind makes it possible to synthesize ionites with a high mechanical strength and a wide variety of functional groups via polymer-analogous transformation of their α-oxide and anhydride groups [10].

It is known that GMA derivatives readily enter into the phosphorylation reaction under rather mild conditions. Adsorption of H_3PO_4 on the clay surface and further polymer-analogous transformation of acid groups under the conditions suggested leads to polymerization of GMA and additional cross-linking of monomer links both via OH groups in the β-position of the epoxy monomer and via surface OH groups of aluminosilicate. In the interaction of glycidyl ethers with H_3PO_4, there occurs [12] a nucleophilic attack of the oxirane ring to give an intermediate associate, which then isomerizes into a phosphoric acid ester. Then the oxide ring is cleaved, the P–O–H bond is transformed into the P–O–C bond, and a hydroxy group appears at the β-carbon atom:



The compounds formed in this case have hydroxy groups in the β-position. These groups can add next molecules of the monomer with an oxide group:



When studying the conditions under which ionites are obtained, it is necessary to take into account factors that affect the exchange properties and physicochemical parameters of the products formed. As the optimality criterion of these parameters serves the value of SEC, which depends on the ratio of the starting components, temperature, and process duration.

A key factor in the synthesis of ionites is the ratio of the starting reagents. The effect of the content of GMA and H_3PO_4 on the ion-exchange properties of the sample studied is illustrated in Fig. 1. It was found that the SEC of the cationites increases from 4.50 to 7.96 mg-equiv g^{-1} (mass ratio Bt : GMA = 1 : 1) as the content of H_3PO_4 in the initial mixture is raised from 0.50 to 2.00 mass parts. A further increase in the amount of H_3PO_4 leads to a decrease in SEC because it impairs the conditions under which the process products are formed.

The ion-exchange and physicochemical properties of the process products are strongly influenced by the amount of an epoxy compound. Its low or high content adversely affects the properties of the sorbent. The content of GMA in the range from 0.5 to 1.0 mass parts leads to an increase in the SEC of cationites from 4.00 to 7.96 mg-equiv g^{-1}. A further

increase in the amount of the epoxy monomer does not make the SEC higher. The study performed revealed the optimal mass ratio Bt : H_3PO_4 : GMA = 1 : 2 : 1.

A necessary condition for ionites with a high exchange capacity and acceptable physicochemical parameters to be obtained is that the optimal process duration and temperature, which strongly affect the basic characteristics of the ionite formed, should be chosen. The influence exerted by the duration of chemical conversion on the exchange properties of the products was studied at 100°C in the range 1–7 h. It was established that the SEC increases from 3.49 to 7.96 mg-equiv g^{-1} in the course of 3 h. A decrease or an increase in this time with respect to that for the material under study makes the SEC lower, which is presumably due, respectively, to degradation of strength properties or densification of the cationite structure. An effective way to improve the exchange properties of the products formed in the process is to raise the temperature of sample modification. It was found that no significant changes in the basic parameters of the products obtained occur above 100°C. Lowering the temperature relative to that specified above leads to a pronounced loss of the SEC of the cationite, to 3.86 mg-equiv g^{-1}. This is due to the low the degree of chemical transformation of active groups in the formation of macromolecules on the bentonite surface. It was found in the study performed that the optimal curing duration and temperature are 3 h and 120°C.

Under industrial conditions, sorbents may come in contact with various aggressive media and aqueous solutions at high temperatures. This may result in chemical destruction of samples, which leads to a decrease in their capacity. The recent achievements in the analysis of the mechanisms and kinetics of destruction of ionites under heating make it possible, in some cases, to choose an appropriate type of an ion exchanger and to prognosticate its service life. The table lists the results obtained in studying the chemical and thermal stability of the organomineral cationite synthesized, which has an exchange capacity for a 0.1 N HCl solution equal to 7.96 mg-equiv g^{-1} and a swelling ability of 3.02 ml g^{-1}. It can be seen that the sorbent samples are rather inert toward the action of 5 N H_2SO_4 and 5 N NaOH. It was found that the SEC of the cationite somewhat increases upon treatment with aggressive solutions (8.02, 8.04 mg-equiv g^{-1}). This is probably due to a facilitated accessibility of active groups upon washing-out of low-molecular-weight impurities, which favors a more complete ion exchange. Treatment with solutions of acids and alkalis at a high temperature also causes a stronger swelling of a cross-linked organic phase of the sorbent, which opens up access to the functional groups that were not involved in the ion exchange before that. Upon a thermal treatment in water for 24 h, the loss of capacity is 3.23%.

Chemical and thermal stability of the phosphoric acid cationite

SEC, mg-equiv g^{-1}, after treatment at 96–98°C		
Stability, %		
5 N H_2SO_4, (0.5 h)	5 M NaOH, (0.5 h)	H_2O (24 h)
8.04 / 101.01	8.02 / 100.81	7.70 / 96.77

An important factor that characterizes the functional groups of the ionites and determines the degree of dissociation is the pH of the medium. The acid–base properties of the cationite were studied by means of potentiometric titration. The run of the curve (Fig. 2) shows two inflections indicating the presence of several types of ionogenic groups. The apparent constants of acid dissociation of the active groups (pK), calculated by the Henderson–Hasselbach equation, are 5.9 and 11.8. These pK values are in a good agreement with published data and correspond to two stages of dissociation of phosphoric acid groups [13].

The IR spectrum of the acid-activated form of natural bentonite (Fig. 3, curve *1*) contains absorption bands associated with stretching and deformation vibrations of the Si–O bond at 472, 520, and 1040 cm^{-1}, and those related to stretching vibrations of Si–O–Al at 790 cm^{-1}. The shoulder at 930 cm^{-1}, which belongs to vibrations of the H–O–Al bond, is characteristic of all layered dioctahedral aluminosilicates.

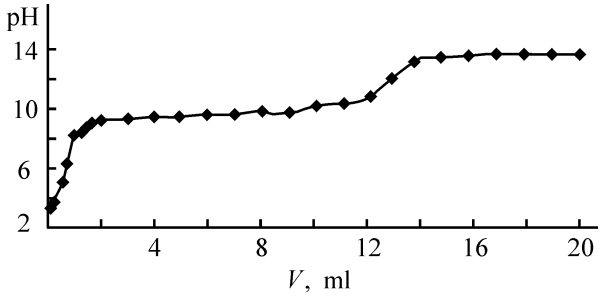


Fig. 2. Potentiometric titration curve for organomineral phosphoric acid cationite. (*V*) Volume of a 0.1 N solution of KOH.

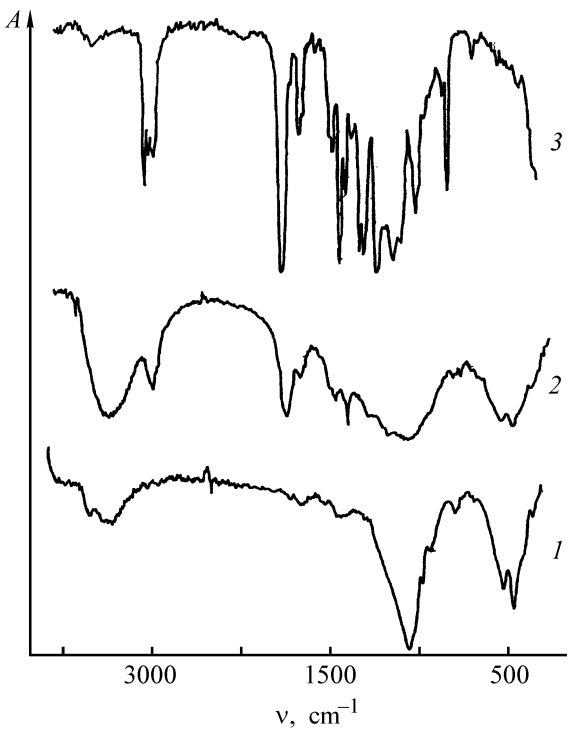


Fig. 3. IR spectrum of bentonite and organomineral phosphoric acid cationite on its base. (*1*) Bentonite, (*2*) cationite, and (*3*) GMA. (*A*) Absorption and (ν) wave number.

In the spectrum of modified bentonite (Fig. 3, curve *2*), the intensity of characteristic absorption bands decreases, compared with that before modification. Absorption bands related to deformation and asymmetric stretching vibrations of the C–H bond appear at 1380, 1440, and 2930 cm^{-1}, respectively. The absorption bands at 1160 and 1270 cm^{-1} are characteristic of stretching vibrations of P=O. Absorption bands associated with antisymmetric stretching vibrations of carbonyl groups appear in the spectrum of the cationite at 1725 cm^{-1}, and the absorption band related to C=C bonds, observed in the spectrum of the starting monomer at 1640 cm^{-1}, disappears. The Characteristic absorption bands associated with deformation and stretching vibrations of the epoxy ring of the starting GMA at 840, 984, and 1272 cm^{-1} (Fig. 3, curve *3*) are not present in the spectrum of modified bentonite, either.

CONCLUSION

Bentonite was modified with H_3PO_4 and then subjected to polymerization with glycidyl methacrylate at 100°C to give a new organomineral phosphoric acid cationite. The optimal conditions of its synthesis in relation to the content of the starting components, temperature, and process duration were found. It was shown that the sorbent obtained is chemically and thermally stable medium-acidity cationite with dissociation constants of 5.9 and 11.8.

REFERENCES

1. *Modifitsirovannye kremnezemy v sorbtsii, katalize i khromatografii* (Modified Silicas in Sorption, Catalysis, and Chromatography), Lisichkin, G.V., Ed., Moscow: Khimiya, 1986.
2. Kholin, Yu.V. and Mernyi, S.A., *Zh. Fiz. Khim.*, 1995, vol. 69, no. 6, pp. 1053–1060.
3. Ergozhin, E.E., Akimbaeva, A.M., Gabdulina, Yu.R., *et al.*, Abstracts of Papers, *XVII Mendeleevskii s'ezda po obshchei i prikladnoi khimii, Kazan, 21–26 sentyabrya 2003 goda* (XVII Mendeleev Congress on General and Applied Chemistry, Kazan, September 2003), Section B, p. 135.
4. Ergozhin, E.E., Akimbaeva, A.M., Gabdulina, Y.R., *et al.*, *The 39th IUPAC Congress and the 86th Conference of the Canadian Society for Chemistry: Chemistry at the Interfaces, August 10–15*, 2003, p. 42.
5. Ergozhin, E.E., Akimbaeva, A.M., Bektenov, N.A., and Gabdulina, Yu.R., *Plast. Massy*, 2002, no. 9, pp. 40–41.
6. Battalova, Sh.B., *Fiziko-khimicheskie osnovy polucheniya i primeneniya katalizatorov i adsorbentov iz bentonitov* (Physcochemical Foundations of Synthesis of Catalysts and Adsorbents from Bentonites and Their Application), Alma-Ata: Nauka, 1986.
7. Ergozhin, E.E., Akimbaeva, A.M., and Gabdulina, Yu.R., *Trudy mezhdunarodnoi nauchno-prakticheskoi konferentsii "Aktual'nye problemy ekologii," 2–3 dekabrya. 2004 goda (Proc. Sci.-Pract. Conf. "Topical Ecological Problems")*, Karaganda: Kar. Gos. Univ. im. E.A. Buketova, 2004, pp. 30–32.
8. Toroptseva, A.M., Belogorodskaya, K.V., and Bondarenko, V.M., *Laboratornyi praktikum po khimii i tekhnologii vysokomolekulyarnykh soedinenii* (Laboratory Course of Chemistry and Technology of Macromolecular Compounds), Leningrad: Khimiya, 1972.
9. Temirova, S.S., Ushanov, B.Zh., Proskurin, A.A., and Sinyaev, V.A., *Izv. Min. Nauki, Akad. Nauk Resp. Kazakhstan, Ser. Khim.*, 1998, no. 2, pp. 67–72.
10. Ergozhin, E.E., Tokmurzin, Zh.T., and Atshabarova, R.B., *Dokl. Akad. Nauk SSSR*, 1987, vol. 294, no. 2, pp. 413–415.
11. Akimbaeva, A.M., Bektenov, N.A., and Ergozhin, E.E., *Plast. Massy*, 2002, no. 11, pp. 29–31.
12. Ergozhin, E.E., Tokmurzin, Zh.T., and Atshabarova, R.B., *Dokl. Akad. Nauk SSSR*, 1987, vol. 294, no. 2, pp. 413–415.
13. Lur'e, Yu.Yu., *Spravochnik po analiticheskoi khimii* (Handbook of Analytical Chemistry), Moscow: Goskhimizdat, 1962.

ISSN 1070-4272, Russian Journal of Applied Chemistry, 2006, Vol. 79, No. 2, pp. 229–235. © Pleiades Publishing, Inc., 2006.
Original Russian Text © A. K. Trofimchuk, V. A. Kuzovenko, I. V. Mel'nik, Yu. L. Zub, 2006, published in Zhurnal Prikladnoi Khimii, 2006, Vol. 79, No. 2, pp. 230–236.

SORPTION AND ION-EXCHANGE PROCESSES

Comparison of the Complexation Abilities of Bifunctional Polysiloxane Xerogels and Chemically Modified Silica Gels

A. K. Trofimchuk, V. A. Kuzovenko, I. V. Mel'nik, and Yu. L. Zub

Taras Shevchenko National University, Kiev, Ukraine

Institute of Surface Chemistry, National Academy of Sciences of Ukraine, Kiev, Ukraine

Received June 20, 2005

Abstract—Complexation of copper(II) on the surface of chemically modified silica gels and polysiloxane xerogels both containing the same functional groups, 3-aminopropyl and 3-mercaptopropyl, was studied. The composition of the complexes formed on the surface of these two classes of sorbents was determined by ESR and electronic spectroscopies.

DOI: 10.1134/S1070427206020121

Chemically modified silica gels (CMSG) and polysiloxane xerogels (PSXG) with a monofunctional surface layer belong to classes of substances that have been rather well studied. However, creating a polyfunctional surface layer on these gels opens up wide prospects for synthesis of new complex-forming sorbents and catalysts because this provides an opportunity to vary not only the nature, but also the molar ratio of functional groups in such a layer. An important role can be played in this case by the type of distribution and by the position of chemical bonds of varied nature, which are covalently bound to the SiO_2 surface and form this multifunctional layer. For example, it has been shown previously in studies of complexation of copper(II) on the surface of a silica gel containing simultaneously 3-aminopropyl and 3-mercaptopropyl groups [1, 2] that several ligand centers containing sulfur or nitrogen atoms are simultaneously involved in complexation at the maximum filling of such a surface. However, no formation of heteroligand complexes of copper with a [N, S] environment was observed on the surface of CMSG of this kind. This is probably due to different spatial positions of grafted ligands in the surface layer [2]. According to [3, 4], 3-aminopropyl groups are arranged horizontally with respect to the silica gel surface, and 3-mercaptopropyl groups and products of their oxidation in interaction with Cu(II), dimercaptopropyl groups, are perpendicular or inclined to the SiO_2 surface.

The aim of this study was to compare (i) processes of complexation of copper(II) on the surface of CMSG and PSXG containing simultaneously the same, 3-aminopropyl and 3-mercaptopropyl, functional groups and (ii) some performance parameters of the sorbents belonging to these two classes.

EXPERIMENTAL

PSXGs with a bifunctional surface layer were produced by the reaction of hydrolytic polycondensation [5]

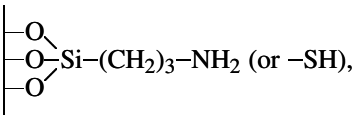
$$\mathrm{Si(OC_2H_5)_4 + (CH_3O)_3Si(CH_2)_3SH + (C_2H_5O)_3Si(CH_2)_3NH_2} \xrightarrow[-\mathrm{ROH}]{+\mathrm{H_2O}} \mathrm{SiO_2/SiO_{3/2}(CH_2)_3SH/SiO_{3/2}(CH_2)_3NH_2}.$$

The following alkoxysilanes manufactured by Aldrich were used as starting substances: $Si(OC_2H_5)_4$ (TEOS, 98%), $(C_2H_5O)_3Si(CH_2)_3NH_2$ (APTES, 99%) and $(CH_3O)_3Si(CH_2)_3SH$ (MPTMS, 95%). To obtain PSXG samples, first 0.096 mol of TEOS was added to 20 cm^3 of methanol under constant agitation, and then MPTMS and APTES taken in molar ratios of 4 : 0, 3 : 1, 1 : 1, and 1 : 3, but in a total amount not exceeding 0.048 mol. Further, 0.264 mol of water was introduced and agitation was terminated [the sample containing only thiol groups was obtained using an aqueous NH_4F solution with F^-/Si = 1/100 (mol)].

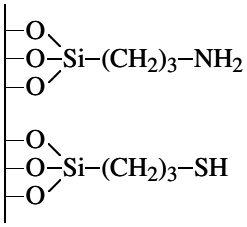
After several minutes, transparent solutions turned into gels, which started to opalesce in the course of time. After 24 h, they were crushed and dried in a vacuum at 90°C for 6 h. Then they were washed with 1 dm^3 of water and again dried under the same conditions.

As the starting substance for synthesis of CMSGs was used Silika 60 silica gel manufactured by Merck, with a specific surface area of 260 $m^2 g^{-1}$ and average pore diameter of 12 nm [3].

Silica gels with a monofunctional layer



and those with various molar ratios of grafted 3-aminopropyl and 3-mercaptopropyl groups in this layer



were synthesized by the same technique: 20 g of a silica gel preliminarily dried at 400°C was placed in a reactor equipped with a stirrer and a reflux with a calcium chloride tube. A 80-cm^3 portion of toluene was added and (under agitation) a modifying agent, APTES or MPTMS, or a mixture of these in varied molar ratio and total amount of 0.05 mol, was introduced. The resulting mixture was brought to boiling under agitation and then synthesis was performed in boiling toluene in the course of 6 h. After that the silica gel was washed in a Soxhlet apparatus, first with toluene and then with acetone for 48 h. The washed product was dried in a vacuum at a residual pressure of 2×10^3 Pa and temperature of 95–100°C.

A silica gel with disulfide (–S–S–) groups was obtained by oxidation of the SH groups of a CMSG-1 sorbent with iodine [3].

The content of amino groups in the thus obtained PSXG and CMSG was determined by back acid–base titration, and that of thiol groups, by back complexometric titration of an excess amount of a standard silver nitrate solution with unithiol in 0.1 M HNO_3. As a metallochromic indicator served di(*para*-sulfophenyl)thiocarbazone [6]. In this way, the concentrations of thiol groups can be determined both on the surface of sorbents with a monofunctional coating and on heteroligand sorbents simultaneously containing SH and NH_2 groups, because Ag^+ ions do not interact with 3-aminopropyl groups in 0.1 M HNO_3.

The structural-adsorption parameters of the samples obtained were determined from isotherms of low-temperature adsorption of nitrogen. The specific surface area was calculated by BET, and the pore size distribution in PSXG, from the pore sizes, using the approach described in [7–9]. All the PSXG and CMSG used had the same granulometric composition, 0.06 – 0.16 mm.

The complexation was studied using aqueous solutions of copper sulfate, prepared from $CuSO_4 \cdot 5H_2O$ (chemically pure). The precise concentrations of the solutions were determined by means of complexometry [10]. The working solutions were prepared by diluting the standard solution with twice-distilled water. The equilibrium concentration of Cu(II) was determined by photometry [11]. The content of copper adsorbed on CMSG or PSXG was found as the difference of its amount in the initial and equilibrium solutions.

The sorption was studied in the static mode (sorbent mass 0.25 g, volume of working solutions 25 cm^3). The suspensions obtained were kept for 24 h with agitation at regular intervals of time. The pH values of the solutions were measured with Ionometr I-130.2m1 pH-meter.

Electronic diffuse-reflectance spectra (EDRS) of the samples were recorded on a Specord M40 spectrophotometer, and ESR spectra, on a 3-cm RE-1306 radiospectrometer at 293 K. The resonance frequency was measured with a Ch3-54 frequency meter with a YaZCh-87 frequency converter. Diphenyl picryl hydrazyl (DPPH, g = 2.0036) and ions of bivalent manganese in a MgO matrix (g = 2.0015) served as calibration samples. The samples were placed in the resonator in ampules 3 mm in diameter. The parameters of the anisotropic spectra were calculated from the positions of lines in the parallel orientation of the g-factor ($g_{\|}$) with an accuracy of 0.005 or evaluated from the positions of lines in the perpendicular orientation of the g-factor ($g_{\perp}$) [12].

As can be seen in Table 1, the functionalized xerogels obtained have close surface areas (214–234 $m^2 g^{-1}$) and total concentrations of functional groups (3.2–4.2 mmol g^{-1}). It is noteworthy that the xerogel containing only 3-mercaptopropyl groups

(PSXG-1) differs from the other xerogels synthesized in lower values of V_s and d_{eff}. In addition, it has, in contrast to bifunctional xerogels, only a single system of mesopores that have size at the boundary between the micro- and mesoscopic ranges. The appearance of these mesopores is, in all probability, due to presence of SH groups, which create a weakly acid medium in synthesis. Attempts to synthesize PSXG-1 with $(n\text{-Bu})_2Sn(O_2CCH_3)_2$ [13–15] as catalyst yielded a xerogel with a specific surface area of less than 1 $m^2\ g^{-1}$; in addition, the time of gelation substantially increased [5]. At the same time, use of alkalis or acids as catalysts in synthesis of PSXG-1 is undesirable because of the possible formation of salts or rapid oxidation of the thiol sulfur. These disadvantages are eliminated if the fluoride ion is used as catalyst [16]. In this case, gelation occurs in the course of several minutes, and the xerogel itself has a developed specific surface area (Table 1). The xerogels with a bifunctional surface layer were synthesized without a catalyst. In this case, the role of a catalyst was played by the amino group, which created an alkaline medium upon introduction of water.

As mentioned above, the starting silica gel used to synthesize CMSG had a specific surface area of 260 $m^2\ g^{-1}$ and average mesopore diameter of 12 nm. In addition, this mesoporous sorbent contained a very small amount of micropores with d = 0.8–1.2 nm (V_{mic} < 0.005 $cm^3\ g^{-1}$), which are inaccessible to large molecules of the modifying agents, including APTES and MPTMS [3]. After modification, the diameter of mesopores somewhat decreases. For example, the curves of pore volume distribution over the effective pore diameters calculated from data on desorption of *n*-hexane vapor with the Thomson–Kelvin equation show peaks at d = 6.0 nm for 3-mercaptopropyl silica gel (CMSG-1) and d = 8.4 nm for 3-aminopropyl silica gel (CMSG-5). The decrease in d for CMSG-1, compared with CMSG-5, is rather due, in the opinion of the authors of [3], to the different orientations of molecules of modifying agents with respect to the SiO_2 surface, which is horizontal in APSG and horizontal or inclined in MPSG. Thus, the structural-adsorption parameters of the CMSG and PSXG samples synthesized are close (Table 1), which is important in comparing their sorption properties.

The concentration of grafted functional groups in CMSG containing 3-aminopropyl and 3-mercaptopropyl groups is about 0.004 mmol m^{-2}, whereas for PSXG with the same functional groups, this concentration is approximately 0.016 mmol m^{-2}, which is an unquestionable advantage of PSXG.

Table 1. Content of functional groups and structural-adsorption parameters of the xerogels and chemically modified silica gels synthesized

Sample	c_{NH_2}	c_{SH}	Structural-adsorption parameters*		
	mmol g^{-1}		S_{sp}, $m^2\ g^{-1}$	V_s, $cm^3\ g^{-1}$	d_{eff}, nm
PSXG-1	–	3.2	216	0.152	3.5
PSXG-2	1.0	3.2	214	0.358	4.0 and 9.8
PSXG-3	2.0	2.1	217	0.302	6.1 and 22.0
PSXG-4	2.4	0.9	234	0.675	3.2 and 16.2
CMSG-1	–	0.93	–	–	–
CMSG-2	0.66	0.33	–	–	–
CMSG-3	0.44	0.33	260	–	12
CMSG-4	0.18	0.81	–	–	–
CMSG-5	0.88	–	–	–	–

* Structural-adsorption parameters for PSXG are given for samples stored for a year.

In sorption of Cu(II) on 3-mercaptopropyl silica gel, copper(II) is reduced to copper(I) and dimercaptodipropyl groups having arch structure, $[\equiv Si(CH_2)_3–S–S–(CH_2)_3Si\equiv]$, are formed. The thus produced Cu(I) ions are bound by the remaining 3-mercaptopropyl groups [17] covalently fixed on the silica gel surface, to form colorless complexes exhibiting low-temperature luminescence [18]. The colorless complexes are also formed via interaction of Cu(I) with dipropyl disulfide groups. Thus, EDRS can furnish information about the composition of the coordination sphere of only Cu(II) complexes. Figure 1 shows EDRS of PSXG-2, PSXG-3, and PSXG-4 samples with different contents of copper sorbed on their

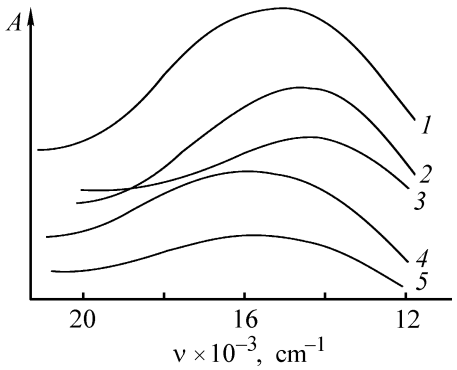


Fig. 1. Electronic reflectance spectra of samples with Cu(II) adsorbed on the PSXG surface. (*A*) Absorption and (ν) wave number. PSXG (mg g^{-1} sorbent): (*1*) PSXG-4, 29; (*2*) PSXG-2, 31; (*3*) PSXG-3, 36; (*4*) PSXG-4, 10; and (*5*) PSXG-2, 10.

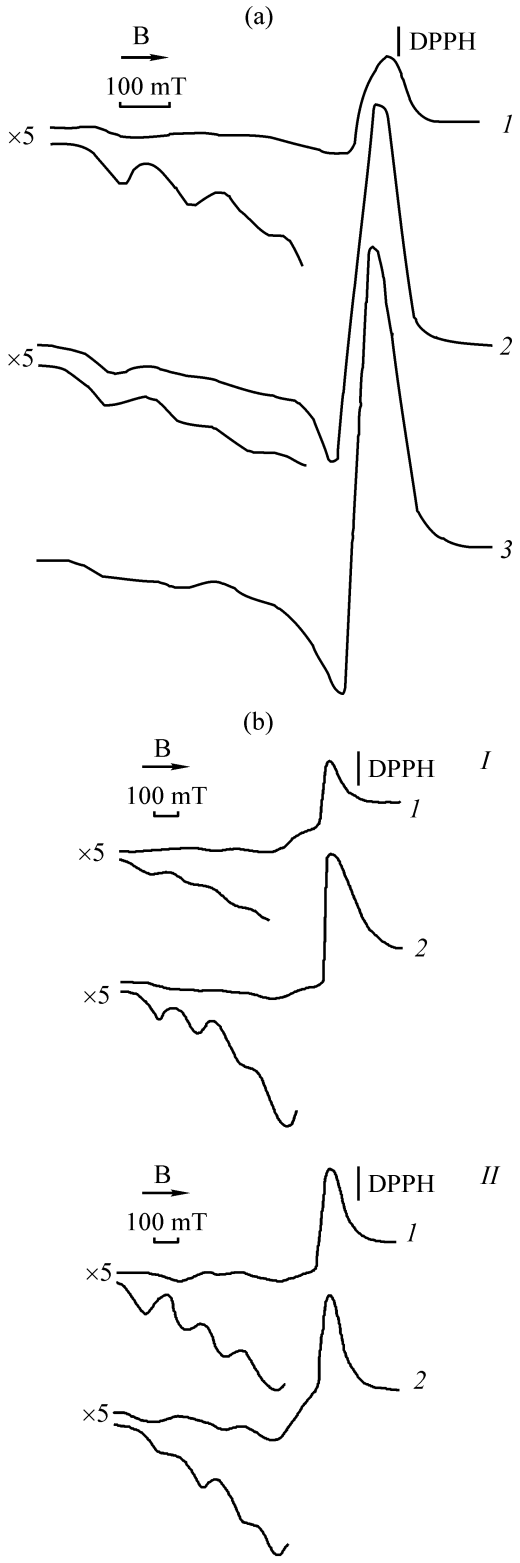


Fig. 2. ESR spectra of Cu(II) complexes on the surface of (a) PSXG and (b) PSXG-1 and CMSG-1. (a) PSXG (mg g^{-1} sorbent): (*1*) PSXG-4, 35; (*2*) PSXG-3, 44; and (*3*) PSXG-2, 36. (b) PSXG (mg g^{-1} sorbent): (*I*) PSXG-1 [(*1*) 10 and (*2*) 43] and (*II*) CMSG-1 [(*1*) 2 and (*2*) 12].

surface. All of them contain a broad band at 14600–16000 cm^{-1}. This band is associated with *d–d* transitions in nitrogen- and oxygen-containing tetragonal complexes of copper(II). In the case of PSXG-2 and PSXG-4, the peak position of this band is shifted to lower frequencies as the filling of their surface by copper(II) ions increases (Fig. 1, curves *5* and *2*, *4* and *1*), However, no shift of this kind is observed for PSXG-3 (Fig. 1, curve *3*).

As is known [19], amine complexes of copper(II) with the nearest environment of the central atom of the [3NO] type exhibit electronic absorption at 16000 cm^{-1}, and complexes of composition [2N2O], absorption at 14500 cm^{-1}. Sulfur-containing complexes of copper(II) exhibit absorption at >25000 cm^{-1} [20]. Therefore, it may be assumed that complexes with coordination sites of Cu[2N2O] and Cu[3NO] types are formed, with predominance of the former, in sorption of copper(II) ions by PSXG containing, together with 3-mercaptopropyl groups, also 3-aminopropyl groups at $c_M < c_L$. As the filling of the PSXG surface by the metal increases, the fraction of complexes containing only two amino groups in the coordination sphere of copper grows. In addition, the composition of the already formed complexes may become simpler in the process: [3NO] $\rightarrow$ [2N2O]. A similar conclusion about the composition of the Cu(II) complexes has been made in a study by EDRS of copper(II) sorption on the surface of heteroligand N,S-CMSGs [1]. However, the observed shift of the band peak in the EDRS of PSXG samples can be explained in another way: complexes with a coordination site of the Cu[2N2O] type are formed already in the initial stages of sorption of copper(II) ions. As the filling of the surface by the metal increases, a tetrahedral distortion of the forming complexes starts to manifest itself, which makes lower the frequency of the *d–d* transitions [21].

Now, the ESR spectra of the Cu(II) complexes formed on the surface of PSXG samples (Fig. 2a, 2b) are considered. All these spectra shown an asymmetry of signals and anisotropy and hyperfine structure of the $g_{\|}$ signal [22]. The shapes of the signals and the calculated parameters of the spectra, presented in Table 2, are characteristic of tetragonal complexes of copper(II). It can be seen from Table 2 that for Cu(II) complexes on the surface of PSXG-2–PSXG-4, the parallel component of the *g*-factor fall within the range 2.242–2.272, and the hyperfine interaction constant takes values of (169–178) $\times 10^{-4}$ cm^{-1}. The shape and parameters of the spectra are characteristic of the coordination environment of Cu(II) of composition [2N2O] [23], which remains unchanged as the content

of 3-aminopropyl groups on the PSXG surface is varied. Consequently, even if Cu[3NO] complexes are formed in the initial stage of copper sorption, their fraction must be insignificant. A similar conclusion concerning the composition of copper(II) complexes on the surface of CMSG can be made on the basis of the parameters of their ESR spectra (Table 1). In this case, however, the concentration of the complexes of composition Cu[3NO] must be even lower because of the difference between the content of functional groups on the surface of CMSG and that on PSXG.

At approximately equal amounts of aminopropyl and mercaptopropyl groups on the surface of silicas, the values of $g_\perp$ for the ESR spectra of copper complexes on the surface of CMSG are somewhat lower than those for copper complexes on PSXG (Table 2). The values of $g_\parallel$ are virtually the same for both types of sorbents. The range of variation of the hyperfine interaction constant for copper complexes on the surface of PSXG is narrower [$(169–178) \times 10^{-4}$ cm^{-1}] than that for complexes on CMSG [$(150–182) \times 10^{-4}$ cm^{-1}].

However, the parameters of the ESR spectra of the copper complexes on CMSG and PSXG do not fall outside the range of values typical of the [2N2O] environment of copper.

It is necessary to consider separately PSXG-1, which contains only 3C-SiC groups. Despite the possibility of Cu(II) reduction to Cu(I) in interaction with SH groups, high-intensity ESR spectra of Cu(II) complexes are observed at c_M, c_L even for PSXG-1 samples (Fig. 2b). The g-factors and values of $A_\parallel$, calculated from these spectra, are characteristic of octahedral oxygen complexes Cu[4O2O], adducts of copper bichelates with a strong axial coordination in the positions 5 and 6 [24], and(or) octahedral complexes of the type of those existing in $CuSO_4 \cdot 5H_2O$ [25, 26]. Complexes of this kind can be formed via coordination of copper(II) with the oxygen atoms of the polysiloxane matrix and water. It is not completely improbable, either, that there is a contribution from physically sorbed copper sulfate. Similar results were obtained in a study of ESR spectra of copper sorbed on the surface of a silica gel modified with 3-mercaptopropyl groups (Table 2).

Thus, a similarity can be noted in the structure of copper(II) complexes formed on the surface of heteroligand (amino thiol) sorbents, irrespective of the method used in their synthesis: sol-gel method in the case of PSXG and chemical modification of the surface for CMSG.

Table 2. Parameters of the ESR spectra of the complexes of Cu(II) ions, formed on the surface of heteroligand sorbents

Sample	Amount of Cu(II) sorbed on the surface, mmol g^{-1} sorbent	$g_\parallel$	$g_\perp$	$A_\parallel$, cm^{-1}
PSXG-1	0.157–0.756	2.362	2.080	139
PSXG-2	0.157–0.661	2.257	2.050	170
PSXG-3	0.157–0.976	2.265	2.058	175
PSXG-4	0.157–0.835	2.255	2.050	178
CMSG-1	0.031–0.183	2.345	2.082	140
CMSG-2	0.060–0.190	2.266	2.048	173
CMSG-3	0.060–0.170	2.265	2.048	177
CMSG-4	0.030–0.090	2.262	2.048	177
CMSG-5	0.062–0.190	2.263	2.048	177

The effect of pH on the sorption of copper(II) by the sorbents under consideration at $c_L^0 \gg c_{Cu}^0$ is illustrated by Fig. 3a. It can be seen (curve *1*) that quantitative sorption of Cu(II) on PSXG-1 is observed

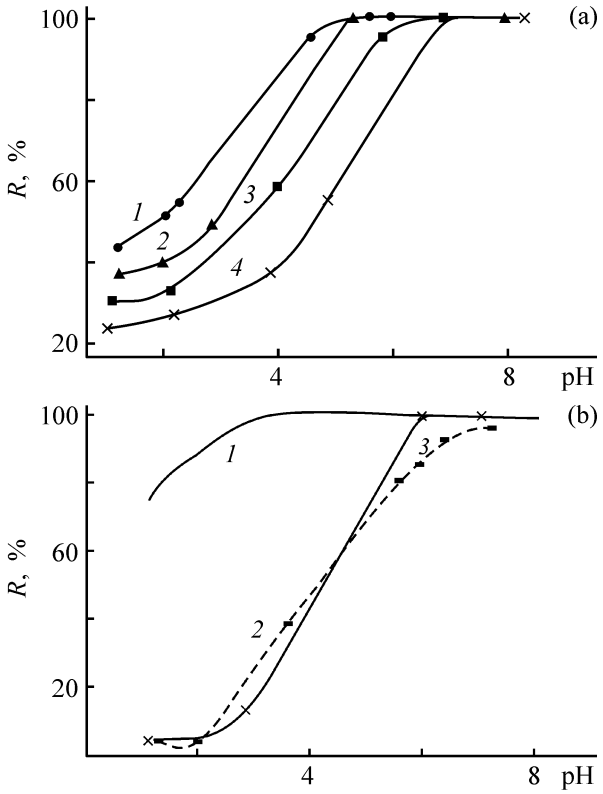


Fig. 3. Recovery of Cu(II), R, vs. the pH of the medium on (a) PSXG and (b) CMSG. (a) V = 25 cm^3, m_{PSXG} = 0.1 g, $c_{Cu(II)}$ = 238 μg/25 cm^3, τ = 24 h. (*1*) PSXG-1, (*2*) PSXG-2, (*3*) PSXG-3, and (*4*) PSXG-4. (b) V = 25 cm^3, m_{CMSG} = 0.2 g, $c_{Cu(II)}$ = 118 μg/25 cm^3, τ = 30 min. (*1*) CMSG-1, (*2*) silica gel with S–S groups, and (*3*) CMSG-5.

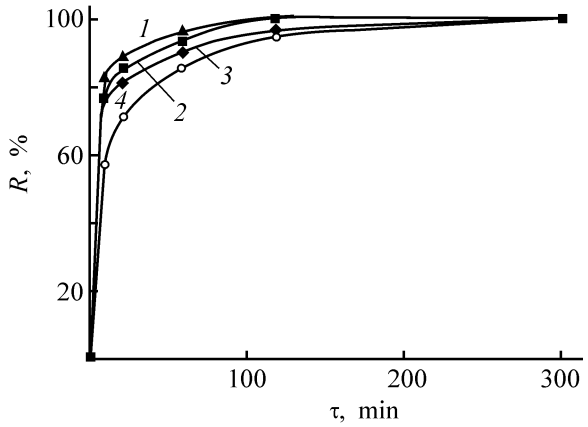


Fig. 4. Kinetic curves of Cu(II) sorption on PSXG. V = 25 cm^3, m_{PSXG} = 0.1 g, $c_{Cu(II)}$ = 238 μg, pH 6. (R) Recovery and (τ) time. (*1*) PSXG-1, (*2*) PSXG-2, (*3*) PSXG-3, and (*4*) PSXG-4.

at pH 5.6. In this case, Cu(II) is reduced to Cu(I) and sorbed either on the remaining (unoxidized) HS groups, or on newly formed S–S groups. As the concentration of NH_2 groups in heteroligand PSXG increases, the pH of 50% sorption of the metal is shifted to a more alkaline region (Fig. 3a, curves *2–4*). This shift indicates that the complexation of copper ions on the surface of the bifunctional xerogels under consideration occurs, as in the case of heteroligand CMSG [3], at several sorption centers to give complexes with different stabilities. The stability of copper complexes with these ligands decreases in the order SH > S–S ≈ NH_2. This is in a good agreement with the type of the dependence $R = f(\text{pH})$ observed for CMSG with the corresponding monofunctional layers (Fig. 3b). If the coordination of copper occurred only at thiol groups (because $c_L^0 \gg c_{Cu}^0$), the above-mentioned shift of the $pH_{50\%}$ would not be observed. The shift of the $pH_{50\%}$ of sorption into the more alkaline region, which occurs as the molar fraction of 3-aminopropyl groups in PSXG becomes larger, indicates that copper complexes are formed on their surface not only with a –SH environment, but also with that of the –S–S– and NH_2 types.

An important criterion for assessing the performance of sorbents is the rate at which the sorption equilibrium is attained. As can be seen in Fig. 4, quantitative recovery of copper(II) is achieved in 5 h, irrespective of the composition of the surface layer of PSXG. In the case of silica gels chemically modified with these groups, the sorption equilibrium is attained in 10 min [1]. Thus, PSXG are strongly inferior to CMSG in their kinetic characteristics. This is, in all probability, due both to difference in the geometric structure of pores in PSXG and CMSG and to a higher concentration of functional groups on the PSXG surface. In the last case, it is assumed that, after first portions of the metal are adsorbed on the PSXG surface, the already formed complexes give rise to additional hindrance to sorption of subsequent portions of the metal.

CONCLUSIONS

(1) Copper(II) is sorbed on the surface of heteroligand chemically modified silica gels and polysiloxane xerogels containing 3-aminopropyl and 3-mercaptopropyl groups via formation of complexes of the same composition, with copper ions surrounded by atoms of sulfur or nitrogen, but there are no copper complexes with heteroligand [S,N] environment.

(2) The specificity of complexation is, in all probability, due to different spatial arrangements of functional groups with respect to the surface of chemically modified silica gels and polysiloxane xerogels: horizontal in the case of 3-aminopropyl groups and vertical (or inclined) for 3-mercaptopropyl groups.

(3) Polysiloxane xerogels severalfold exceed chemically modified silica gels in sorption capacity, but are markedly inferior to the latter in the rate at which the sorption equilibrium is attained.

REFERENCES

1. Trofimchuk, A.K., Kuzovenko, V.A., Kozak, N.V., and Nizel'skii, Yu.N., *Ukr. Khim. Zh.*, 2003, vol. 69, no. 10, pp. 73–76.
2. Trokhimchuk, A.K., Kuzovenko, V.A., and Andrianova, O.B., *Proc. VII Polish–Ukranian Symp. on Theoretical and Experimental Studies of Interfacial Phenomena and Their Technological Applications*, Poland, Lublin: Z.U.P. TEKST, 2003.
3. Tarasevich, Yu.I., Trofimchuk, A.K., Legenchuk, A.V., and Ivanova, Z.G., *Kolloid. Zh.*, 2004, vol. 64, no. 1, pp. 88–94.
4. Okabayashi, H., Izawa, K., Yamamoto, T., *et al., Coll. Polym. Sci.*, 2002, vol. 280, pp. 135–145.
5. Melnyk (Seredyuk), I.V., Zub, Yu.L., Chuiko, A.A., and Van Der Voort, P., *Chem., Phys. Technol. Surf.*, 2002, no. 8, pp. 125–133.
6. Pilipenko, A.T., Arendaryuk, E.N., Ryabushko, O.P., and Batkovskaya, L.A., *Ukr. Khim. Zh.*, 1989, vol. 55, no. 2, pp. 175–179.
7. Gun'ko, V.M. and Do, D.D., *Colloids Surf. A*, 2001, vol. 193, pp. 71.
8. Skubiszewska-Zieba, J., Leboda, R., Seledets, O., and Gun'ko, V.M., *Colloids Surf. A*, 2003, vol. 231, p. 39.
9. Gun'ko, V.M., Skubiszewska-Zieba, J., Leboda, R., *et al., J. Colloid Interface Sci.*, 2004, vol. 269, p. 403.

10. Schwarzenbach, G. und Flaschka, H., *Die Komplexometrische Titration*, Stuttgart: Ferdinand Enke, 1965.
11. Marczenko, Z., *Kolorymetryczne oznaczanie pierwiastkow*, Warszawa: Wydawnictwa Naukowa-techniczne, 1968.
12. Lipatova, T.E. and Nizel'skii, Yu.N., *Uspekhi khimii poliuretanov* (Advances of the Chemistry of Polyurethanes), Kiev: Naukova Dumka, 1972.
13. Khatib, I.S. and Parish, R.V., *J. Organomet. Chem.*, 1989, vol. 369, pp. 9–16.
14. El-Nahhal, I.M., Yang, J.J., Chuang, I.-C., and Maciel, G.E., *J. Non-Cryst. Solids*, 1996, vol. 208, pp. 105–118.
15. McKittrick, M.W. and Christopher, W.J., *Chem. Mater.*, 2003, vol. 15, p. 1132.
16. Corriu, R.J.P. and Leclercq, D., *Recent Angew. Chem., Int. Ed. Engl.*, 1996, vol. 35, pp. 1420–1435.
17. Huang, L., Zingaro, R.A., Meyers, E.A., *et al., Phosphorus, Sulfur and Silicon*, 1995, vol. 105, pp. 175–185.
18. Losev, V.N., Aleinikova, Yu.V., Elsuf'ev, E.V., and Trofimchuk, A.K., *Zh. Anal. Khim.*, 2002, vol. 57, no. 7, pp. 721–725.
19. Volchenskova, I.I., *Teor. Eksp. Khim.*, 1973, vol. 9, no. 5, pp. 627–634.
20. Lever, A.B.P., *Inorganic Electronic Spectroscopy*, Amsterdam: Elsevier, 1984.
21. Yakubovich, T.N., Teslenko, V.V., Zub, Yu.L., and Chuiko, A.A., *Khim. Fiz. Tekhnol. Poverkhn.*, 1997, no. 2, pp. 62–67.
22. Hathaway, B.J. and Billing, D.E., *Coord. Chem. Rev.*, 1970, no. 5, pp. 143–207.
23. Stechenko, O.V., Yakubovich, T.M., Teslenko, V.V., *et al., Ukr. Khim. Zh.*, 2003, vol. 69, no. 1, pp. 19–24.
24. Shklyaev, A.A. and Nizel'skii, Yu.N., *Kataliticheskie svoistva β-diketonatov metallov* (Catalytic Properties of β-Diketonates of Metals), Kiev: Naukova Dumka, 1983.
25. Larin, G.M., *Teor. Eksp. Khim.*, 1968, vol. 4, no. 2, pp. 244–252.
26. Al'tshuler, S.A. and Kozyrev, B.M., *Elektronnyi paramagnitnyi rezonans* (Electronic Paramagnetic Resonance), Moscow: Nauka, 1972.

ISSN 1070-4272, Russian Journal of Applied Chemistry, 2006, Vol. 79, No. 2, pp. 236–240. © Pleiades Publishing, Inc., 2006.
Original Russian Text © L. B. Naumova, L. A. Egorova, A. A. Slivinskaya, 2006, published in Zhurnal Prikladnoi Khimii, 2006, Vol. 79, No. 2, pp. 237–241.

SORPTION AND ION-EXCHANGE PROCESSES

A Study of the Influence of Modifying Iron and Aluminum Chloride Additives on the Water-Absorbing Capacity and Thermal Stability of Peat

L. B. Naumova, L. A. Egorova, and A. A. Slivinskaya

Tomsk State University, Tomsk, Russia

Received December 16, 2005

Abstract—The influence exerted by modifying additives of inorganic nature on the hydrophilicity of peats from the Orlovskoe deposit in Tomsk oblast and on their thermal stability was studied. The acid–base, equilibrium, and kinetic properties of the starting peat samples and those modified with solutions of iron(III) and aluminum chlorides were examined. Their physicochemical parameters were determined: total exchange capacity, acidity by acid and basic groups, relative humidity, distribution coefficients, effective diffusion coefficients, and activation energy. The effect of modifying cations on the thermal decomposition of peat was analyzed.

DOI: 10.1134/S1070427206020133

The wide diversity of the physicochemical properties of peat, one of the most valuable kinds of natural raw materials, has stimulated a wide interest in the problem of its effective use [1–3]. Application of various procedures for processing and modification of peat makes it possible to obtain new polyfunctional materials on its basis. For example, on imparting to peat necessary chemical and physicochemical properties, it is successfully used as a fertilizer in agriculture, in manufacture of building materials, etc. [1, 2]. The high hydrophilicity of some kinds of peat enables their use as sorbents in purification of wastewater to remove various ions, whereas other kinds of peat can serve, owing to their low hydrophilicity, to absorb nonpolar hydrocarbons, such as phenols and petroleum products [4–7]. The last feature is a matter of current interest, because it can be used to solve a wide variety of practical ecological problems and, in particular, to cleanup water and soil after oil spills. The hydrophilicity of peat can be lowered by various treatments [8]. A promising way to obtain peat-containing formulations with prescribed parameters is to introduce modifying additives [9].

The present communication reports the results obtained in a study of the influence exerted by the nature of chemical additives on the water-absorption capacity of peat and on the structural organization of a modified sample in thermal treatment. As objects of study served peats of upland, intermediate, and lowland types from the Orlovskoe deposit. Solutions of aluminum(III) and iron(III) chlorides of various concentrations were used as modifying agents.

It was presumed that introduction of polyvalent metal ions into a water-saturated peat should shift the existing equilibrium and, accordingly, will give rise to ion-exchange processes resulting from the interaction with the functional groups of the organic and inorganic components of peat. Replacement of singly charged ions with those of trivalent nature will alter the structure of the disperse system of peat via cross-linking of associates by the cations introduced and, as a result, will change the water-absorption capacity of peat.

The fact that iron(III) and aluminum ions were chosen as modifying agents is no accident. This is due to the difference in their electronic structure (Al is a *p*-element, and Fe, *d*-element), ionic radius Al^{3+} 0.057 nm, Fe^{3+} 0.067 nm), and capacity for complexation with carboxy groups ($\log K^{Al}_{1,2,3} = 16.3$, $\log K^{Fe}_{1,2,3} = 20.2$).

Thus, it is possible to vary the nature of moisture transfer and thermal destruction processes and the surface activity of the materials obtained by taking into

account the chemical activity of the components introduced and by choosing the modification conditions.

In the study, the acid–base properties of peat were analyzed by means of potentiometric titration. The titration curves were used to calculate the total exchange capacities (TEC) for acid and basic groups and to evaluate the effective ionization constants. The cationic forms were prepared by treating the starting peat samples with aqueous solutions of metal chlorides under static conditions, with vigorous shaking during seven days at a constant ionic strength. To prevent hydrolysis, the peat samples were treated with salts of iron(III) and aluminum at pH 1.8. The concentration range of the metal chloride solutions used in the study was chosen to be 0.100 – 0.025 M (equivalence factor $f = 1/3$). The solution volume was 200 ml, and the weighed portion of peat, 0.5000 g.

The content of metal ions in the equilibrium solution was monitored by complexometry. The difference of the initial and equilibrium concentrations was used to determine the content of a metal in the peat phase. In studying the equilibrium, the distribution coefficients D were calculated. The kinetics of absorption of Fe^{3+} and Al^{3+} ions was studied by the method of limited volume at different temperatures (298, 323, 348 K), concentrations of starting solutions, and peat particle dispersities (r 0.025 and 0.050 cm). The study was carried out in a thermostated vessel, with the solutions agitated with a set of rabbles. After certain intervals of time, t, the solution was separated from the sorbent and analyzed for the content of iron(III) and aluminum ions. Kinetic dependences of the degree of completeness of the process, F, on time t were plotted. The results obtained were processed using the approximate Boyd equation for spherical particles [10].

Because an important role in the manifestation of associate interactions in peat (formation of supramolecular structures [8]) belongs to water, the swelling kinetics of peat samples in their modification with ion(III) and aluminum ions was studied. For this purpose, the relative humidity W (%) of modified peat samples was determined after sorption of ions in each particular case (at a certain time t) by centrifugation [11]. Further, peat samples were dried in drying oven at a temperature of 105°C and the $W(\%) = f(t)$ dependences were plotted.

To evaluate the thermal stability, a thermal analysis of the starting and modified samples was carried out on a Q-1500 derivatograph at a heating rate of 9.5 deg min^{-1} in platinum crucibles.

Table 1. Degrees R of decomposition, TEC, and pK of ionization for the starting peats

Peat	R, %	TEC_{H^+}, mmol g^{-1}	pK_a	TEC_{OH^-}, mmol g^{-1}	pK_b
Upland	5–10	3.67	8.75	2.17	11.80
Intermediate	15–20	3.96	9.60	1.93	10.70
Lowland	25–30	6.33	9.20	1.17	11.05

A study of the acid–base properties of peat samples demonstrated that these samples are high-capacity ampholytes with weakly acid and weakly basic groups (Table 1). The resulting values of TEC for acid and basic groups approach the TEC of synthetic ion exchangers and even somewhat exceed these values.

The TEC for acid groups grows in going from upland to lowland peat, because the latter is more decomposed and, as a result, the amount of humic substances containing COO^- groups in the lowland peat is higher.

The TEC values obtained were used to evaluate the amount of a modifying agent, which should not exceed the total capacity for acid and basic groups. It was as follows: 5.84 mmol g^{-1} for upland peat, 5.89 for intermediate peat, and 7.50 for lowland peat.

The equilibrium parameters of modification of peat samples with solutions of salts of iron(III) and aluminum chlorides are listed in Table 2.

The results obtained indicate (Table 2) that the moisture capacity of peat samples strongly decreases upon sorption of metal ions, compared with the starting samples. The minimum absorption of water is observed at c = 0.049 M for all kinds of peat. Together with a decrease in moisture capacity, these samples show at c = 0.049 M an increase in selectivity (the distribution coefficients D increase). In addition, peat samples change their structure upon centrifugation at a given concentration in solution: on drying they become denser and harder as compared with the starting samples. The experimental data obtained can probably be understood as follows. Absorption of iron(III) ions (c = 0.049 M), probably, creates more favorable conditions for their coordination with the functional groups of peat (mainly with carboxy groups), which causes an increase in the degree of cross-linking of polymer formations and a rise in the structuring of the peat system. The last factor leads to an increase in the viscosity and strength pa-

Table 2. Distribution coefficients D and relative peat humidity W of peats at different concentrations of iron(III) and aluminum chlorides (n = 5, P = 0.95)

Peat	c, M	W_{in}, %	W, %	D
		Iron(III) chloride		
Upland	0.099	92.0 ± 0.4	88.6 ± 0.6	2.8 ± 0.2
	0.071		85.5 ± 0.5	1.9 ± 0.1
	0.049		72.6 ± 0.4	5.9 ± 0.3
	0.024		80.6 ± 0.6	1.5 ± 0.1
Inter-mediate	0.099	88.8 ± 1.1	73.2 ± 0.5	3.7 ± 0.3
	0.071		72.3 ± 0.5	3.0 ± 0.2
	0.049		67.7 ± 0.6	9.0 ± 0.3
	0.024		71.2 ± 0.5	2.7 ± 0.2
Lowland	0.099	82.2 ± 0.6	73.1 ± 0.5	8.5 ± 0.3
	0.071		69.2 ± 0.4	4.3 ± 0.2
	0.049		64.7 ± 0.5	9.9 ± 0.5
	0.024		67.1 ± 0.6	4.0 ± 0.3
		Aluminum(III) chloride		
Upland	0.099	92.0 ± 0.4	88.7 ± 0.4	4.3 ± 0.3
	0.071		82.2 ± 0.2	3.3 ± 0.3
	0.049		79.8 ± 0.3	5.0 ± 0.3
	0.024		81.5 ± 0.3	2.8 ± 0.3
Inter-mediate	0.099	88.8 ± 1.1	72.4 ± 0.4	4.6 ± 0.3
	0.071		65.4 ± 0.4	4.1 ± 0.3
	0.049		60.9 ± 0.3	5.6 ± 0.4
	0.024		63.9 ± 0.6	3.8 ± 0.3
Lowland	0.099	82.2 ± 0.6	67.7 ± 0.5	5.3 ± 0.3
	0.071		65.2 ± 0.2	5.0 ± 0.3
	0.049		58.6 ± 0.2	7.2 ± 0.4
	0.024		63.5 ± 0.3	4.2 ± 0.3

rameters of peat and, as a result, to a decrease in its swelling ability, which is not inconsistent with published data. According to [8], structures of first kind are formed in such cases in the peat phase. At other concentrations, conditions are created for formation of structures of second kind [8]. In the opinion of the authors of the present study, the decrease in the swelling ability of peat samples modified with iron(III) ions is also promoted by the fact that polynuclear dimers of iron are formed in solution at low pH values. Being quadruply charged, these dimers bind, with a high probability, polar active groups on the surface of peat and thereby hinder further penetration of moisture into peat (Table 2).

Aluminum ions, which have a larger hydration shell as compared with iron ions, presumably penetrate in pores in peat, throwing off their hydration shell, and only after that coordinate COO^- groups around them, which leads to a decrease in the swelling ability of peat samples (Table 2) and a possible formation of structures of first kind at $c(AlCl_3)$ = 0.049 M. As stated in [8], further introduction of metal cations leads to such a pronounced development of interassociate bonds that peat particles are transformed to give new associates, which are more compact than the original ones. Such a disordering of the system leads to a decrease in the viscosity and strength of the material and to an increase in its moisture capacity. The so-called new structures, structures of second kind, are formed [8].

The occurrence of structuring in peat, with water molecules involved, is beyond doubt, because it has been confirmed by electron microscopy, electron paramagnetic resonance, and nuclear magnetic resonance [13, 14].

Thus, modification of peat with solutions of iron(III) and aluminum chlorides causes internal transformations in the peat phase and affects the water-absorption capacity of peat. In this case, the supramolecular phases are formed in the same way despite the difference in chemical nature between the modifying ions studied. It should be noted that all kinds of peat studied here exhibit a sufficiently high selectivity with respect to iron(III) and aluminum ions (Table 2).

The kinetics of absorption of iron and aluminum ions was studied using the method of limited volume [10, 11]. An advantage of this method consists in the simplicity of the kinetic experiment, which is performed by sampling at certain intervals of time. This method allows rapid termination of the contact between the phases at any instant of time and reveals the limiting stage of the exchange.

The kinetic problems were solved by plotting the dependence of the degree of completeness of the process, $F = Q_t/Q_\infty$, as a function of the sorption time (Q_t, Q_∞ are the amounts of ions absorbed by peat during a time t elapsed from the beginning of the process and in the equilibrium state, respectively).

As demonstrated by the results of kinetic studies, the exchange rate depends on the concentration of the starting solutions, temperature and peat particle size. This points to a mixed-diffusion mechanism of sorption. It was found, on plotting the kinetic curves in the $-\ln(1 - F) = f(t)$ coordinates, that, in early stages of absorption, the process is limited by outer-sphere diffusion for both iron(III) and aluminum ions. The rate constants R, effective outer-sphere diffusion coefficients D_{eff}, and activation energies E_a of the process were calculated for this region of the ki-

Table 3. Effective diffusion coefficients D_{eff} of Fe^{3+} and Al^{3+} ions activation energies E_a at $c(MCl_3)$ = 0.049 M

Peat	D_{eff}, $cm^2\ s^{-1}$, at indicated T, K			E_a, kJ mol^{-1}
	298	323	348	
		Fe^{3+} ions		
Upland	$(7.2 \pm 0.2) \times 10^{-6}$	$(1.8 \pm 0.1) \times 10^{-5}$	$(2.9 \pm 0.1) \times 10^{-5}$	5.4 ± 0.2
Intermediate	$(6.7 \pm 0.2) \times 10^{-6}$	$(1.4 \pm 0.1) \times 10^{-5}$	$(2.5 \pm 0.1) \times 10^{-5}$	7.9 ± 0.2
Lowland	$(6.3 \pm 0.2) \times 10^{-6}$	$(1.1 \pm 0.1) \times 10^{-5}$	$(2.0 \pm 0.1) \times 10^{-5}$	8.1 ± 0.3
		Al^{3+} ions		
Upland	$(2.0 \pm 0.1) \times 10^{-6}$	$(3.2 \pm 0.1) \times 10^{-6}$	$(1.9 \pm 0.1) \times 10^{-5}$	7.8 ± 0.3
Intermediate	$(1.9 \pm 0.1) \times 10^{-6}$	$(3.0 \pm 0.1) \times 10^{-6}$	$(1.0 \pm 0.1) \times 10^{-5}$	8.6 ± 0.3
Lowland	$(0.8 \pm 0.1) \times 10^{-6}$	$(2.7 \pm 0.2) \times 10^{-6}$	$(0.9 \pm 0.1) \times 10^{-5}$	16.5 ± 0.6

netic dependence (Table 3). As already mentioned, a strong decrease in the swelling ability of peat samples was observed after contact (for 7 days) with salt solutions with a concentration of 0.049 M. Therefore, it was appropriate to calculate the activation energy under the same conditions. E_a was found from the Arrhenius equation. The experimental results are listed in Table 3.

As can be seen from the data in Table 3, the diffusion coefficients of iron(III) and aluminum ions are close to the diffusion coefficients of these ions in solution, and the small values of E_a point to the predominance of the outer-sphere diffusion in the mixed diffusion process. For iron(III) and aluminum ions, these values are close, which confirms the previously made suggestion about the similarity of ion-exchange processes and coordination interactions with the carboxy groups of peat.

An analysis of the kinetic curves of swelling in modification of peats with iron(III) and aluminum ions demonstrated their complex nature, which indicated that internal transformations occur in the peat phase at its various fillings with metal ions. However, despite the complexity of the structuring process, the $W(\%) = f(t)$ curves show a steep decline in swelling ability, irrespective of the concentration of the solutions under study, upon contact for 5 min. This suggests that, already during the first minutes of sorption, supramolecular structures are formed in peat and this process involves the ions being absorbed and water molecules. As a result, the samples acquire an enhanced hardness. A further increase in the time of sorption does not lead to any significant changes in swelling ability and strength parameters.

Thus, the results of the kinetic study suggest that, to obtain hydrophobic peat samples by their modification with solutions of iron(III) and aluminum chlorides, it suffices to perform the process of ion sorption for no more than 5 min.

To study the effect of additives on thermal destruction processes, derivatograms of the starting and modified samples of up- and lowland peat were measured. The results of the thermographic measurements confirmed the suggestion that transformation processes associated with coordination of metal ions with active groups occur in the peat systems. The formation of strong bonds between metal cations and active centers of peats was manifested in that the shape of TG and DTA curves changed upon modification of the starting samples.

Two processes accompanied by loss of mass are revealed for all the samples in the temperature range 20–650°C: the first, low-temperature process involves thermal desorption and removal of water; the second process corresponds to destruction and thermochemical decomposition of the organic component of peat to give gaseous products. The changes in the mass of peat samples are listed in Table 4. Thermogravi-

Table 4. Changes in the mass of initial and modified peat

Peat	Sample	Process 1		Process 2	
		ΔT, °C	Δm, %	ΔT, °C	Δm, %
Upland	Initial	96–232	59.7	303–494	38.6
	Modified:				
	Al^{3+}	89–177	27.7	212–538	44.1
	Fe^{3+}	76–105	14.5	163–527	54.7
Lowland	Initial	84–296	56.3	367–580	37.5
	Modified:				
	Al^{3+}	73–328	63.2	410–580	23.7
	Fe^{3+}	90–343	52.1	428–580	34.8

metric calculations demonstrated that 100 g of lowland peat contains 0.07 mol of aluminum and 0.05 mol of iron.

The observed asymmetry and broadening of DTA peaks indicate that there occur complex processes of destruction of multiphase peat systems.

A comparative analysis of the TG curves of modified and starting peats demonstrated that mineral additives of iron(III) and aluminum chlorides change the temperature range and nature of thermal destruction by modifying the structure of peat. The effect of modifying additives is manifested to a greater extent in the low-temperature region, where thermal desorption of weakly bound water and disintegration of crystal hydrates are observed. The data obtained are consistent with the results of kinetic studies of the swelling ability.

Modification of upland peat with iron(III) and aluminum(III) ions leads to changes in the destruction processes. Apparently, sorbed iron(III) ions form with the active groups of upland peat bonds whose strength approaches that of chemical bonds, which is manifested in clearly pronounced peaks in the DTA and DTG curves at 219°C. The high-temperature disintegration of the sample is identical to the destruction of lowland peat.

Thus, the use of derivatographic data in studies of the equilibrium state and kinetics of absorption of iron(III) and aluminum ions confirmed the suggestion that solid formulations are formed during the first minutes of ion absorption. This makes it possible to rather rapidly obtain hydrophobic peat samples and then use these samples for sorption of nonpolar hydrocarbons. A promising way to obtain a sample of this kind is to use lowland peat modified with solutions of aluminum and iron(III) chlorides.

CONCLUSIONS

(1) The distribution coefficients of Fe^{3+} and Al^{3+} cations in the system constituted by peat and a metal chloride solution, effective diffusion coefficients, activation energy, and relative humidity were used to establish that the hydrophobicity of modified peat samples depends on the concentration of the chloride solutions.

(2) The results of thermographic studies of peat samples modified with solutions of iron(III) and aluminum chlorides suggest that supramolecular structures are formed, constituted not only by various functional groups of peat and metal cations, but also by water molecules. The weakening of the hydrophilic properties of modified peats and the enhancement of their strength can be attributed to the appearance of structures of this kind.

(3) It was shown that the structuring and moisture transfer in peat can be controlled by introduction of modifying additives.

REFERENCES

1. Lishtvan, I.I., *Khim. Tverd. Topl.*, 2002, no. 1, pp. 5–19.
2. Zhukov, V.K., Tomson, A.E., Sokolova, T.V., and Nikolaenkov, A.I., *Prirodopol'zovanie*, 2002, no. 8, pp. 167–182.
3. Bel'kevich, P.I. and Chistova, L.R., *Torf i problema zashchity okruzhayushchei sredy* (Peat and Problems of Environment Protection), Minsk, 1979.
4. Naumova, L.B., Gorlenko, N.P., and Otmakhova, Z.I., *Zh. Prikl. Khim.*, 1995, vol. 68, no. 9, pp. 1461–1465.
5. USSR Inventor's Certificate, no. 806615.
6. Naumova, L.B., Gorlenko, N.P., Otmakhova, Z.I., and Mokrousov, G.M., *Khim. Interes. Ustoich. Razv.*, 1997, no. 5, pp. 609–611.
7. Naumova, L.B., Chashchina, O.V., and Gorlenko, N.P., *Zh. Fiz. Khim.*, 1994, vol. 66, no. 4, pp. 688–691.
8. Lych, P.I., *Gidrofil'nost' torfa* (Hydrophilicity of Peat), Minsk: Nauka i Tekhnika, 1991.
9. Bel'kevich, P.I., Chistova, L.R., *et al., Izv. Akad. Nauk BelSSR, Ser. Khim. Nauk*, 1981, no. 5, pp. 106–108.
10. Helfferich, F., *Ionenaustauscher*, Bd. 1, Weinheim: Chemie, 1959.
11. Marhol, M., *Ion Exchangers in Analytical Chemistry: Their Properties and Use in Inorganic Chemistry*, Prague: Academia, 1982.
12. *Khimicheskaya entsiklopediya* (Chemical Encyclopedia) Moscow: Sov. Entsiklopediya, 1990, vol. 2, p. 671.
13. Bel'kevich, P.I., Chistova, L.R., *et al., Izv. Akad. Nauk BelSSR, Ser. Khim. Nauk*, 1983, no. 2, pp. 28–31.
14. Bel'kevich, P.I., Lych, A.M., Chistova, L.R., *et al., Izv. Akad. Nauk BelSSR, Ser. Khim. Nauk*, 1981, no. 1, pp. 63–67.

ISSN 1070-4272, Russian Journal of Applied Chemistry, 2006, Vol. 79, No. 2, pp. 241–249. © Pleiades Publishing, Inc., 2006.
Original Russian Text © A. G. Morachevskii, Z. I. Vaisgant, V. L. Ugolkov, M. N. Khabachev, E. V. Bochagina, O. A. Kal'ko, Yu. S. Kuznetsova, 2006, published in Zhurnal Prikladnoi Khimii, 2006, Vol. 79, No. 2, pp. 242–250.

APPLIED ELECTROCHEMISTRY AND CORROSION PROTECTION OF METALS

Reduction in Processing of Active Paste from Lead Battery Scrap

A. G. Morachevskii, Z. I. Vaisgant, V. L. Ugolkov, M. N. Khabachev, E. V. Bochagina, O. A. Kal'ko, and Yu. S. Kuznetsova

St. Petersburg State Polytechnic University, St. Petersburg, Russia

El'ta OOO, St. Petersburg, Russia

Grebenshchikov Institute of Silicate Chemistry, Russian Academy of Sciences, St. Petersburg, Russia

Cherepovets State University, Cherepovets, Vologda oblast, Russia

Received January 10, 2006

Abstract—Thermodynamics and mechanism of processes that occur in solid-phase reduction of oxygen compounds of lead are considered.

DOI: 10.1134/S1070427206020145

At present, there is no alternative to use of lead batteries in various vehicles, whose number steadily grows. Utilization of worked-out batteries becomes increasingly economically and ecologically important everywhere. The general situation with collection and processing of lead batteries in Russia and abroad has been the subject of several studies [1–6]. Modern schemes of utilization of battery scrap involve, in most cases, its preliminary cropping (after discharging the electrolyte), with separation into the metallic, oxide-sulfate, and organic fractions. Into the oxide-sulfate fraction passes the active paste of both negative and positive plates of a battery. According to the available results of chemical and X-ray diffraction analyses, the main components of this fraction are PbO_2 (plattnerite, tetragonal modification) and $PbSO_4$ (anglesite), which are present in comparable amounts (Fig. 1) [7, 8]. Also possible is presence of exceedingly small amounts of lead(II) oxide and metallic lead.

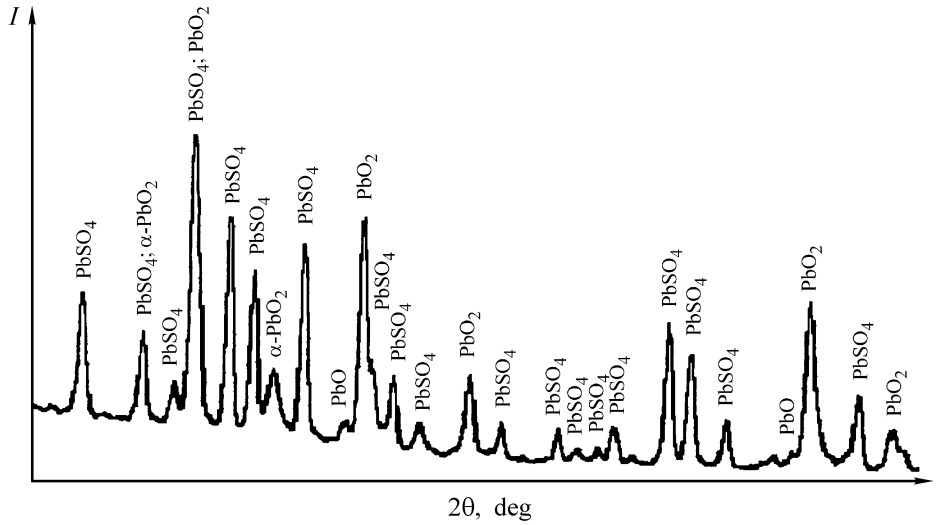


Fig. 1. X-ray diffraction pattern of the starting oxide-sulfate fraction (active paste from the positive and negative plates of lead batteries). (I) Intensity and (2θ) Bragg angle; the same for Figs. 2, 3, and 5.

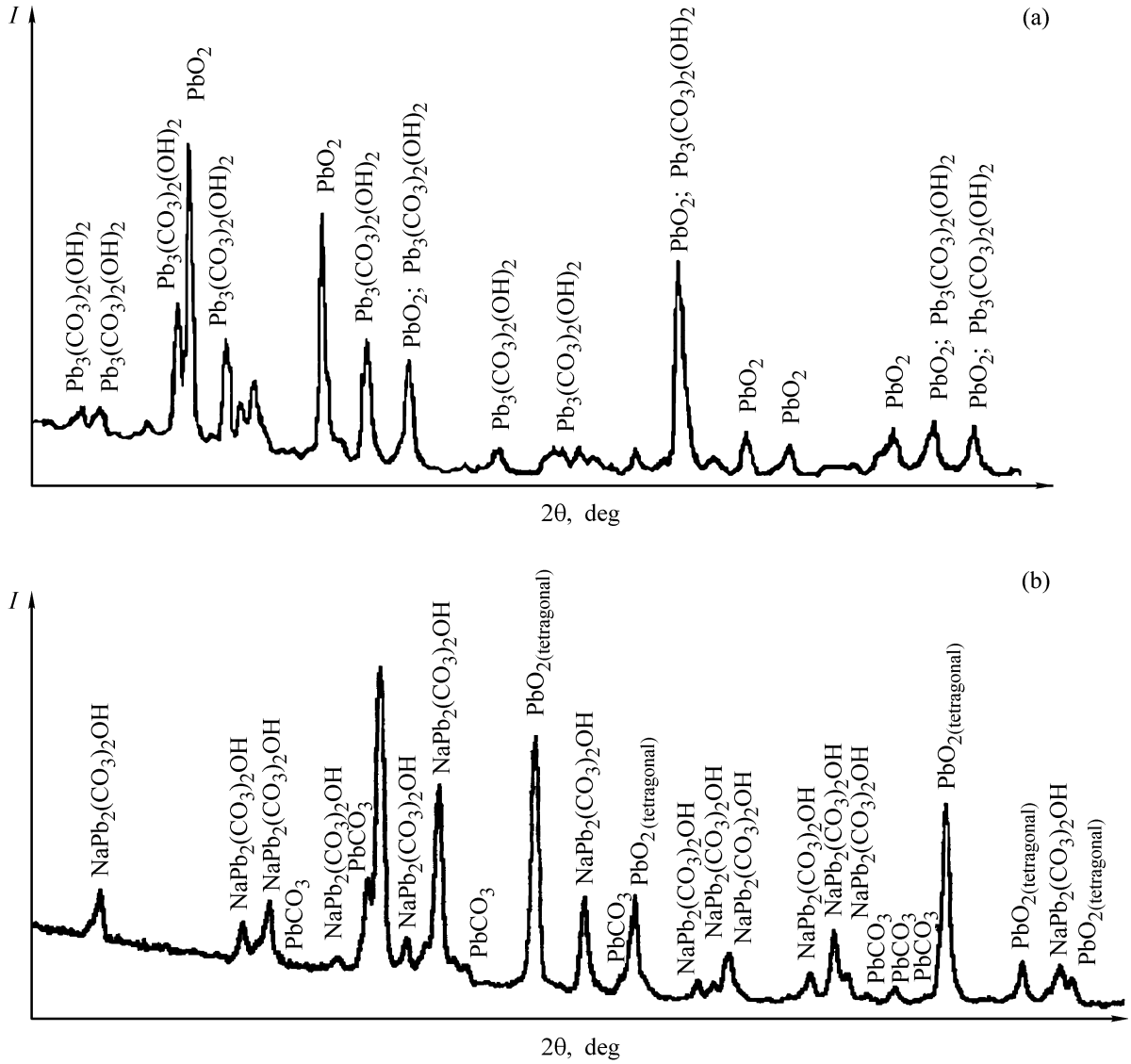


Fig. 2. X-ray diffraction patterns of the oxide-carbonate cake formed in desulfation with sodium carbonate. Formation of (a) hydrocerussite $Pb_3(CO_3)_2(OH)_2$ and (b) $NaPb_2(CO_3)_2OH$.

The presence of lead sulfate substantially complicates the reduction process and leads to appearance of SO_2 in the gas phase and to formation of mattes and slags, whose rational utilization is difficult. To convert $PbSO_4$ into other compounds, it is appropriate to perform a hydrometallurgical procedure (desulfation), which consists in treatment of a crushed oxide-sulfate paste with aqueous solutions of sodium or potassium carbonates o give an oxide-carbonate cake [9, 10]. Aqueous solutions of sodium carbonate are mostly used for this purpose. In desulfation, an excess amount of soda is taken, up to 20% relative to that calculated in accordance of the stoichiometry of the reaction

$$PbSO_4 + Na_2CO_3 = PbCO_3 + Na_2SO_4.$$

Solid to liquid phase ratio s : l = 1 : 4, process temperature 50°C, and duration 1 h under continuous agitation.

Depending on particular process conditions, either hydrocerussite $Pb_3(CO_3)_2(OH)_2$ (Fig. 2a) or the so-called double salt $NaPb_2(CO_3)_2OH$ (Fig. 2b) is formed in desulfation with soda. Both these compounds have rather low solubility products (SP). According to the available rough estimates [9], SP at 25°C is 3.5×10^{-46} for hydrocerussite and 1×10^{-31} for the double salt. It should be noted for comparison that the SP at 25°C for $PbSO_4$ and $PbCO_3$ are 1.6×10^{-8} and 7.4×10^{-14}, respectively. The boundaries of the stability regions of $PbCO_3$, $Pb_3(CO_3)_2(OH)_2$,

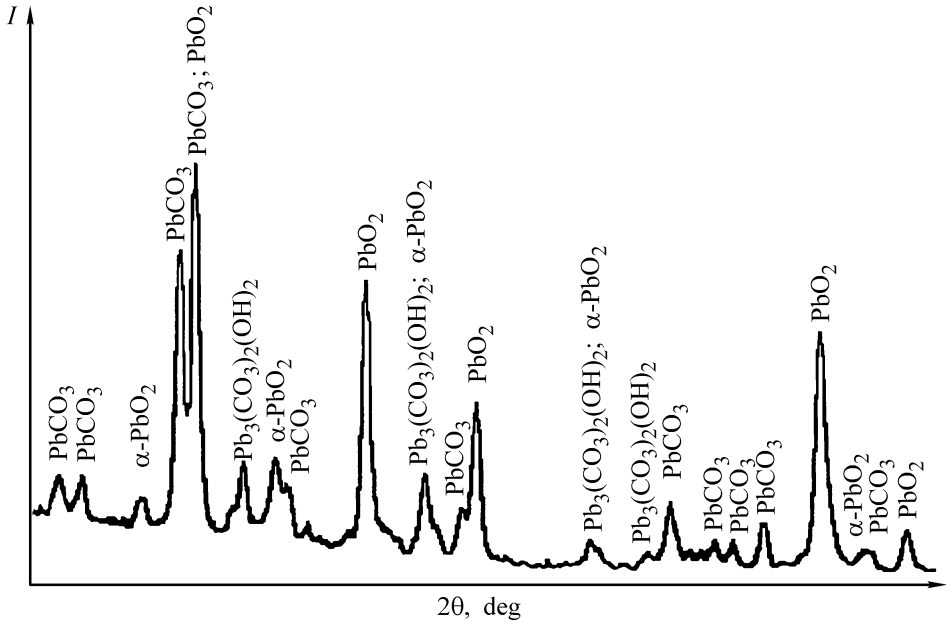


Fig. 3. X-ray diffraction pattern of the oxide-carbonate cake formed in desulfation with potassium carbonate.

$NaPb_2(CO_3)_2OH$ are determined at a given temperature by concentrations of the ions Na^+, $1/2\,CO_3^{2-}$, HCO_3^-, $1/2\,SO_4^{2-}$. The corresponding calculations can be found in [9]. The formation of the double salt from basic lead carbonate (hydrocerussite) can be represented by the reaction

$$2\,[2\,PbCO_3 \cdot Pb(OH)_2] + CO_3^{2-} + HCO_3^- + 3\,Na^+ = 3\,[NaPb_2(CO_3)_2OH] + H_2O.$$

The formation of the same salt from lead carbonate (cerussite) is described by the reaction

$$2PbCO_3 + Na^+ + CO_3^{2-} + H_2O = NaPb_2(CO_3)_2OH + HCO_3^-.$$

Both these reactions can be named "secondary" with respect to the reaction in which hydrocerussite is formed; their occurrence requires that the corresponding compounds should be accumulated. It should be noted that, at a sufficient amount in a sample, the compounds $Pb_3(CO_3)_2(OH)_2$ and $NaPb_2(CO_3)_2OH$ are sufficiently reliably identified by X-ray diffraction analysis.

If potassium carbonate is used for desulfation, no compound similar to the double salt is formed. As can be seen from the X-ray diffraction pattern in Fig. 3, the desulfation products include, together with PbO_2, cerussite and hydrocerussite [7].

Thus, the oxide-carbonate cake formed in desulfation can include, depending on the process conditions, plattnerite PbO_2, cerussite $PbCO_3$, hydrocerussite $Pb_3(CO_3)_2(OH)_2$, and the double salt $NaPb_2(CO_3)_2OH$. Also possible is presence of minor amounts of PbO and $PbSO_4$.

On being heated, the cake decomposes. As is known, lead forms with oxygen a number of oxides: PbO_2, Pb_3O_4, PbO, Pb_2O_3, $Pb_{12}O_{17}$, and $Pb_{12}O_{19}$ [11]. The first three of these exist in two crystalline modifications. It is noted in the monograph by Mostovich and Anisimov [12] that decomposition of PbO_2 to give Pb_3O_4 begins at 280°C and is complete at 400°C. The compound Pb_3O_4 (red lead) also decomposes on further heating, with PbO formed and oxygen evolved. It is emphasized in [12] that all lead oxides that are richer in oxygen than PbO (yellow lead) completely decompose into PbO and O_2 at temperatures exceeding 600°C and the only stable oxide at higher temperatures is PbO.

According to the thermodynamic dependences presented in the reference book by Kulikov [13], the temperature of transition from PbO_2 to Pb_3O_4 is 242°C, and the decomposition temperature of Pb_3O_4, 527°C. According to [14], PbO_2 decomposes in several stages, with the temperatures of formation and decomposition of intermediates affected to a certain extent by the synthesis conditions and structural modification of lead dioxide itself. $Pb_{12}O_{19}$, $Pb_{12}O_{17}$, and Pb_3O_4 are identified as intermediate phases. The following sequence of processes can be adopted in view of the aforesaid: $PbO_2 \rightarrow Pb_{12}O_{19} \rightarrow Pb_{12}O_{17} \rightarrow Pb_3O_4 \rightarrow PbO$.

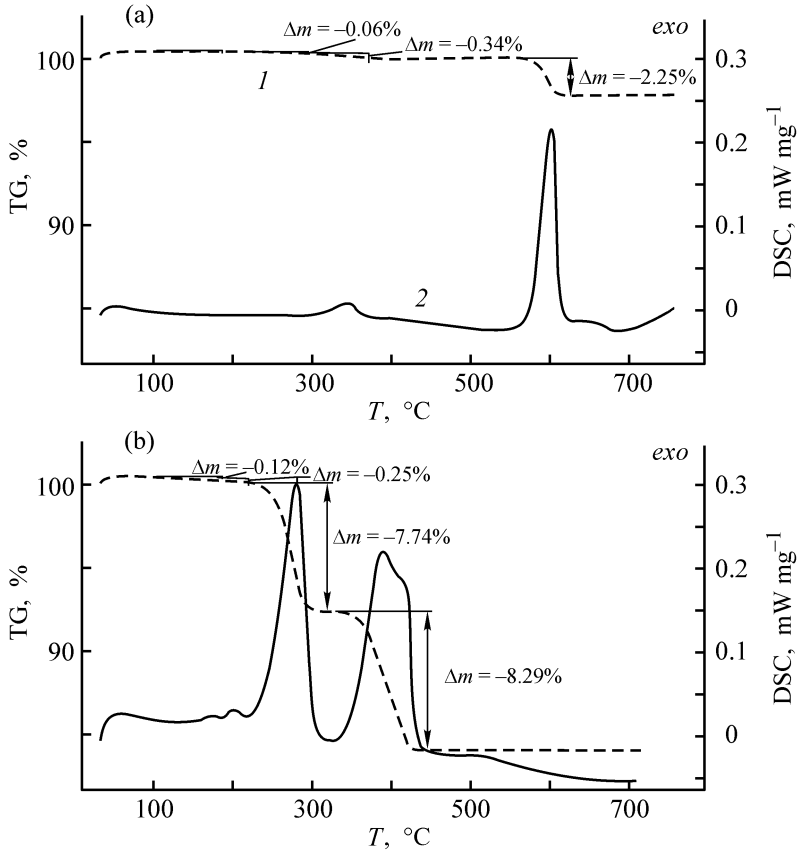


Fig. 4. Curves of (*1*) mass change and (*2*) heat effects, obtained in a comprehensive thermal analysis of (a) Pb_3O_4 and (b) $PbCO_3$.

A comprehensive thermal analysis of the decomposition of Pb_3O_4 demonstrated that its conversion into PbO also occurs in stages. Samples of mass 50 mg, weighed with an accuracy of 0.05 mg, were placed in a corundum crucible of mass 192.5 mg with a corundum cover (cover mass 57.5 mg), heated at a constant rate of 10 deg min^{-1} in the temperature range 20–800°C, and then cooled at the same rate. The experiments were performed on a NETZSCH STA 449 installation for synchronous thermal analysis (Germany).

The analysis included simultaneous determination of the mass of a sample (TG curve) and heat effects accompanying its thermal transformations (DSC curve).

Three steps of mass loss (%) can be distinguished in the TG curve for Pb_3O_4 (Fig. 4a): 0.06 at 237–290°C, 0.34 at 290–368°C, and 2.25 at 553–638°C. The total mass loss was 2.65%, which somewhat exceeds its theoretical value for the process $Pb_3O_4 \rightarrow 3PbO + 1/2O_2$ (2.33%). The DSC curve shows two endothermic effects corresponding to the second and third steps of mass loss. The first step (0.06%) is so small that it virtually cannot be seen in the DSC curve. The endothermic effect peaked at 608°C can be regarded as a characteristic of the transformation of Pb_3O_4 into PbO. At temperatures above 638°C, no changes in mass or in heat effects were observed, which suggests that conversion of Pb_3O_4 to PbO comes to completion at this temperature.

The melting point of PbO is 883°C, and the boiling point, 1470°C. The vapor phase in equilibrium with lead(II) oxide was studied in detail by Kazenas *et al.* [15, 16]. According to their data, the vapor phase is composed at 737–880°C of polymer molecules Pb_nO_n, with n in the range from unity to six. The main component of the sublimation and dissociation products constituting the vapor phase over solid PbO is Pb_4O_4 (61.9% at 747°C). The total vapor pressure over PbO is 5.4×10^{-6} atm at 740°C. The reference book by Gerasimov *et al.* [17] gives a somewhat higher value for the total vapor pressure over solid PbO: 2.35×10^{-5} atm at 750°C.

The available published evidence concerning the decomposition of $PbCO_3$ on heating at a varied content of CO_2 in the gas phase was analyzed in the review [9]. It was established in [18] that cerussite decomposes to PbO at low CO_2 pressures (<1 atm) with only a single intermediate formed:

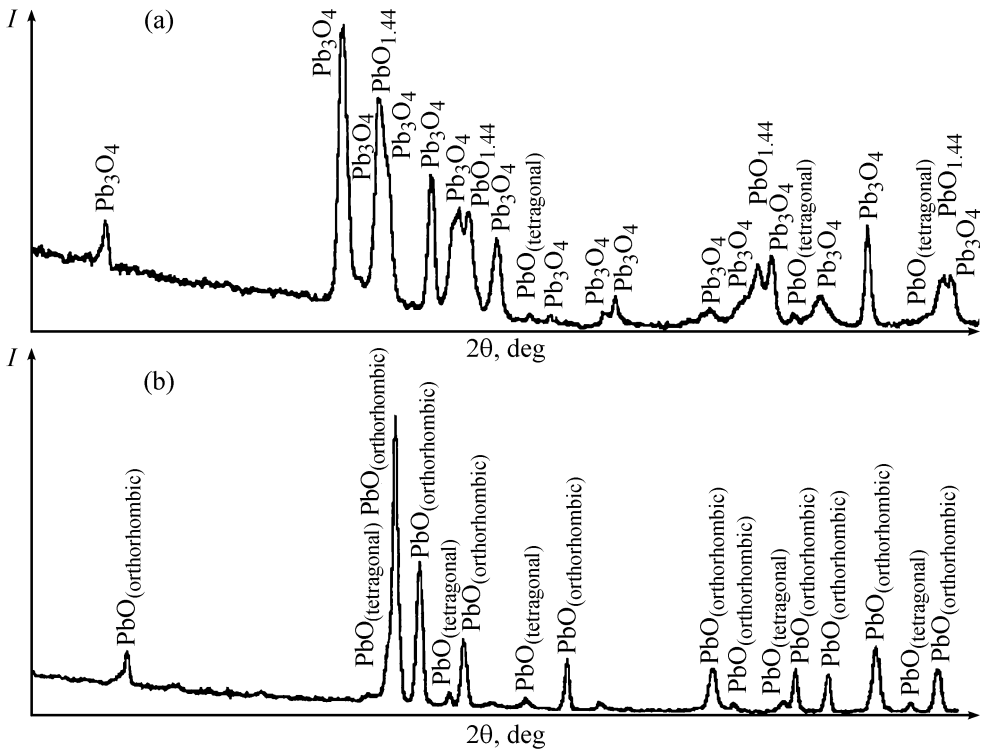


Fig. 5. X-ray diffraction patterns obtained after annealing of the oxide-carbonate cake at (a) 400 and (b) 600°C.

$$PbCO_3 \xrightarrow{200^\circ C} PbCO_3 \cdot 2PbO \xrightarrow{310^\circ C} PbO.$$

At moderate CO_2 pressures (~1 atm), two intermediates are formed [18]:

$$PbCO_3 \xrightarrow{300^\circ C} PbCO_3 \cdot PbO \xrightarrow{310^\circ C} PbCO_3 \cdot 2PbO \xrightarrow{420^\circ C} PbO.$$

The data of [18] confirm the results of an earlier study [19], in which it was noted that the number and composition of intermediates depend on the partial pressure of CO_2 in the gas phase. According to [19], the decomposition of $PbCO_3$ is complete at 430°C.

Four principal steps of mass loss (%) can be distinguished in the TG curve for $PbCO_3$ (Fig. 4b): 0.12 at 150–185°C, 0.25 at 185–220°C, 7.74 at 220–324°C, and 8.29 at 324–455°C. The total mass loss is 16.40%, which virtually coincides with the theoretical mass loss by the solid phase for the reaction $PbCO_3 \rightarrow PbO + CO_2$ (16.47%). The DSC curve shows four endothermic effects corresponding to all the steps of mass loss. The last effect has a double peak, at 392 and 418°C. All these facts point to the complex nature of cerussite decomposition in an experiment carried out in air. The temperatures of the endothermic effects are close to those reported in [18, 19].

Yamaguchi and co-authors studied by various methods the decomposition of hydrocerussite $2PbCO_3 \cdot Pb(OH)_2$ on heating [20]. The DTA curves obtained in air ($P_{CO_2} \ll 1$ atm) show two endothermic peaks, at about 250 and 340°C. The thermogravimetric curves demonstrate mass loss in two temperature ranges: 200–270 and 330–400°C. The results obtained in air suggest the following scheme of hydrocerussite decomposition on heating:

$$2PbCO_3 \cdot Pb(OH)_2 \xrightarrow{200^\circ C} PbCO_3 \cdot PbO \xrightarrow{300^\circ C} PbO.$$

In the first stage, CO_2 and H_2O are released into the gas phase, and in the second stage, only CO_2. Thus, hydrocerussite is stable in air up to a temperature of approximately 280°C, even though it starts to decompose at 200°C. The compound $PbCO_3 \cdot PbO$ is stable in the temperature range 200–400°C, PbO starts to accumulate beginning at 350°C. The existence regions under the experimental conditions of [20] cannot be clearly defined.

Separate heating of PbO and $PbSO_4$ is not accompanied by appearance of any features in the TG and DSC curves. The aforesaid suggests that the only component remaining on heating the oxide-carbonate cake (after desulfation of the active paste) to above 600–620°C is lead(II) oxide PbO. This conclusion is confirmed by X-ray diffraction analysis. Annealing of the oxide-carbonate cake at 400°C for 2 h leads to formation of the oxides Pb_3O_4 (tetragonal lattice) and $PbO_{1.44}$ (*F*-cubic lattice), whose contents are presumably comparable (Fig. 5a). PbO (red, tetra-

Table 1. Thermodynamic characteristics of reactions (1)–(3)

T, K	Reaction (1)		Reaction (2)		Reaction (3)	
	ΔG_T^0	ΔH_T^0	ΔG_T^0	ΔH_T^0	ΔG_T^0	ΔH_T^0
	kJ					
300	51.4	108.6	–68.3	–63.8	119.7	172.0
400	32.2	108.7	–69.8	–64.6	102.0	173.3
500	13.2	108.4	–71.7	–65.2	84.9	173.6
600	–5.9	107.7	–72.1	–65.7	66.2	173.4
700	–25.6	111.8	–73.9	–61.3	48.3	173.1
800	–45.1	108.7	–75.7	–63.7	30.6	172.4
900	–64.1	107.1	–77.1	–64.5	13.0	171.6
1000	–83.0	105.2	–78.4	–65.8	–4.3	171.0

gonal modification, lead ocher) is present in a minor amount. The phase composition of the annealed paste was independent of what compounds were contained in the oxide-carbonate cake: cerussite, hydrocerussite, or the double salt).

Annealing of the cake at 600°C results in that the yellow, orthorhombic modification of PbO (massicot) becomes the main phase. The tetragonal modification of PbO is present in a minor amount (Fig. 5b).

The reduction of PbO with solid carbon may occur by the reactions

$$PbO + C = Pb + CO, \quad (1)$$

$$PbO + CO = Pb + CO_2. \quad (2)$$

An important role in the reduction process is played by the reaction

$$C + CO_2 = 2CO. \quad (3)$$

Table 1 lists the changes in the standard Gibbs energy (ΔG_T^0) and enthalpies of formation (ΔH_T^0), calculated for reactions (1)–(3) in the temperature range 300–1000 K. The calculation was done using data from the reference manual [21]. The experimental ΔG_T^0, obtained for reaction (2) by Tsvetkov *et al.* [22], were close to the calculated values (kJ): –81.0 (973 K) and –82.4 (1023 K).

As is known, according to the most widely accepted concepts of reduction of metal oxides by solid carbon, of fundamental importance in the process is the gas phase, and carbon monoxide CO, rather than solid carbon, is the actual reducing agent [23–25]. However, thermodynamic calculations show that regeneration of CO by reaction (3) cannot proceed to any significant extent at temperatures below 1000 K.

Previously, reduction of individual lead(II) and (IV) oxides by solid carbon has been considered [26]. According to the data obtained, intense reduction of PbO_2 onsets at temperatures of 380–390°C, proceeds with strong heat release, and comes to completion at 400–410°C. The reduction of PbO by carbon begins at higher temperatures, with the onset temperature of the process and its rate being dependent on the amount of the reducing agent introduced. Intense reduction of PbO by solid carbon is in the range 600–700°C [26].

According to Tseft's data [27], reduction of PbO_2 by carbon occurs in several stages: $PbO_2 \rightarrow Pb_2O_3 \rightarrow Pb_3O_4 \rightarrow PbO \rightarrow Pb_2O \rightarrow Pb$.

Reduction of PbO_2 begins at a temperature of 190–210°C, proceeds at a high rate at 360–390°C, then slows down, and then again becomes fast at temperatures exceeding 500°C. The rate of the process was judged by the author of [27] from the volume of gases evolved in unit time.

In [28], the mechanism and kinetics of PbO reduction by carbon were studied in the temperature range 550–700°C. The authors noted that the reduction process is rather slow at 550°C, with only 5% of the initial mass of PbO reacted in 2 h. At the same time, the reaction is virtually complete at 700°C in 20 min. Based on various experimental observations and taking into account that the gas phase is approximately 90% composed of CO_2, the authors of [28] made a number of conclusions concerning the mech-

anism and kinetics of the solid-phase reduction process. Reaction (2) occurs at 600–700°C at a high rate and cannot be the limiting stage of the overall reduction process. As can be seen in Table 2, the thermodynamic characteristics of this reaction are rather favorable for its occurrence. At the same time, the extent of reaction (3) at temperatures below 800°C is not sufficient and, accordingly, cannot provide reaction (2) with the necessary amount of carbon monoxide. During the entire reduction process, its rate is determined by reaction (1). Of key importance is the chemical interaction of solid carbon with lead(II) oxide.

Shafrinskii [29] studied the reduction of cerussite $PbCO_3$ by solid carbon at temperatures of 600–700°C. The author noted that, simultaneously with reduction of $PbCO_3$, there occurs its thermal dissociation to give lead(II) carbonate and oxide as intermediate compounds. Under real industrial conditions, the process of reduction of cerussite must not differ significantly from that of PbO. Complete reduction of lead-containing compounds is favored by their close contact with carbon particles.

Ashin *et al.* [30] studied the kinetics of PbO reduction by graphite at 540–660°C in the atmosphere of argon. Under the experimental conditions, the process rate is strongly affected by temperature: the process is complete in 20 min at 660°C and in no less than 180 min at 580°C. Virtually only a single reaction product, carbon dioxide, was present in effluent gases. The intensity of the reduction process is strongly affected by the degree of grinding of the starting materials. A decrease in the particle size of lead(II) oxide from 1–2 to 0.25–0.50 mm makes the reduction rate approximately three time faster, and passing to a 0.07-mm fraction causes a dramatic acceleration of the process. Grinding of the reducing agent (graphite) intensifies the process to a considerably greater extent than does the corresponding grinding of the oxide. Making larger the relative content of carbon in the PbO + C mixture also rather strongly affects the reduction rate.

The authors of [30] confirmed the concept according to which CO is the primary reaction product under conditions of a comparatively low-temperature reduction of oxides (below 800°C), but it is not regenerated in the course of the process and reaction (3) does not advance. Thus, carbon monoxide cannot act as the main reducing agent and its involvement cannot account for the mechanism of interaction between PbO and carbon at 720–740°C. However, the authors of [30] do not rule out the possibility of sublimation of PbO and interaction of its vapor with carbon. Presence of graphite, which interacts with the PbO vapor, in the stock intensifies the process of sublimation of lead oxide. The whole body of the above evidence concerning the role of carbon in low-temperature solid-phase reduction of metal oxides is in agreement with the approaches used by Elyutin *et al.* [25, 31].

Table 2. Thermodynamic characteristics of reaction (4)

T, K	ΔH_T^0	ΔG_T^0
	kJ	
300	–290.4	–350.2
400	–290.8	–370.6
500	–293.5	–391.0
600	–296.8	–411.5
700	–300.6	–431.9
800	–304.9	–452.4
900	–309.1	–472.5
1000	–313.5	–492.9

Ashin *et al.* [32] also studied the reduction of PbO_2 by graphite at temperatures in the range 320–370°C. At 360–370°C, a steep increase in the process rate was observed, which was due to the occurrence of the reaction

$$3PbO_2 + C = Pb_3O_4 + CO_2. \quad (4)$$

The thermodynamic characteristics of this process are listed in Table 2.

Kinetic curves indicate that the process rate increases with temperature [32]. The thermodynamic characteristics are favorable for occurrence of reaction (4) in the entire range of temperatures considered. The gaseous products formed in reduction of PbO_2 contained, together with CO_2, 5–7 wt % free oxygen.

As noted by Tsvetkov [33], there is no sufficient reason to apply the adsorption-catalytic model to reduction of lead oxides. Autocatalytic phenomena are not characteristic of reactions yielding liquid products.

Electrothermal methods for production of metals and alloys, whose theoretical foundations were considered by Kozhevnikov *et al.* [34], should not be extended to lead oxides because of their comparatively low melting point and high volatility.

In laboratory and enlarged-laboratory conditions, reduction of the oxide-carbonate cake by carbon or carbon-containing materials is nearly complete (yield

of lead ≥95%) at 720–740°C [35, 36]. The occurrence of the process is favored by a higher degree of grinding of both the starting material and the reducing agent. The reduction process is sufficiently ecologically safe, does not require intricate apparatus, and can be performed under low-scale industrial conditions.

CONCLUSION

It is advisable, in processing of lead batteries by their cropping into fractions in order to recover lead from the active paste of positive and negative plates (oxide-sulfate fraction), to perform two successive technological procedures: (i) to convert lead sulfate (anglesite) into carbonate compounds to obtain an oxidecarbonate cake and (ii) to reduce it after drying and grinding with carbon-containing materials at 720–740°C. Both the procedures are sufficiently ecologically safe, do not require intricate apparatus, and can be performed under low-scale industrial conditions. It is advisable to heat the cake at 600°C prior to reduction in order to convert all lead-containing compounds to lead(II) oxide.

REFERENCES

1. Morachevskii, A.G., *Zh. Prikl. Khim.*, 1997, vol. 70, no. 1, pp. 3–15.
2. Morachevskii, A.G., *Zh. Prikl. Khim.*, 2003, vol. 76, no. 9, pp. 1467–1476.
3. Morachevskii, A.G., *Pererabotka vtorichnogo svintsovogo syr'ya: Sovremennoe sostoyanie issledovanii i annotirovannyi ukazatel' literatury za 1997–2001 gg.* (Processing of Secondary Lead: Modern State of Research and Annotated Bibliographic Index for 1997–2001), St. Petersburg: SPbGPU, 2003.
4. Tarasov, A.V., Besser, A.D., Mal'tsev, V.N., and Sorokina, V.S., *Metallurgicheskaya pererabotka vtorichnogo svintsovogo syr'ya* (Metallurgical Processing of Secondary Lead), Tarasov, A.V., Ed., Moscow: Gintsvetmet, 2003.
5. Lamm, K.F., *Erzmetall*, 1998, vol. 51, no. 6, pp. 438–455.
6. Besser, A.D., *Vtor. Resursy*, 2001, nos. 5–6, pp. 53–55.
7. Morachevskii, A.G., Bochagina, E.V., and Khabachev, M.N., *Zh. Prikl. Khim.*, 2003, vol. 76, no. 10, pp. 1748–1750.
8. Chen, T.T. and Dutrizac, J.E., *Hydrometallurgy*, 1996, vol. 40, pp. 223–245.
9. Morachevskii, A.G., *Zh. Prikl. Khim.*, 1998, vol. 71, no. 6, pp. 881–890.
10. Morachevskii, A.G., Vaisgant, Z.I., Bochagina, E.V., and Khabachev, M.N., *Tsv. Met.*, 2002, no. 8, pp. 34–37.
11. Wriedt, H.A., *Bull. Alloy Phase Diagrams*, 1988, vol. 9, no. 2, pp. 106–127.
12. Mostovich, V.Ya. and Anisimov, S.M., *Metallurgiya svintsa* (Metallurgy of Lead), Moscow: Metallurgizdat, 1940.
13. Kulikov, I.S., *Termodinamika oksidov* (Thermodynamics of Oxides), Moscow: Metallurgiya, 1986.
14. Gillibrand, M.I. and Halliwell, B., *J. Inorg. Nucl. Chem.*, 1972, vol. 34, pp. 1143–1159.
15. Kazenas, E.K. and Petrov, A.A., *Metally*, 1996, no. 4, pp. 22–27.
16. Kazenas, E.K. and Tsvetkov, Yu.V., *Isparenie oksidov* (Evaporation of Oxides), Moscow: Nauka, 1997.
17. Gerasimov, Ya.I., Krestovnikov, A.N., and Shakhov, A.S., *Khimicheskaya termodinamika v tsvetnoi metallurgii* (Chemical Thermodynamics in Nonferrous Metallurgy) Moscow: Metallurgizdat, 1961, vol. 2.
18. Yamaguchi, Y., Sawada, Y., Sakurai, O., *et al., Thermochim. Acta*, 1980, vol. 35, no. 3, pp. 307–313.
19. Ball, M.C. and Casson, M.Y., *J. Inorg. Nucl. Chem.*, 1975, vol. 37, no. 11, pp. 2253–2255.
20. Yamaguchi, Y., Sawada, Y., Sakurai, O., *et al., Thermochim. Acta*, 1985, vol. 37, no. 1, pp. 79–88.
21. Barin, I., Knacke, O., and Kubaschewski, O., *Thermochemical Properties of Inorganic Substances: Supplement*, Berlin: Springer, 1977.
22. Tsvetkov, Yu.V., Nesterova, T.E., and Tagirov, I.K., *Metallurgiya tsvetnykh i redkikh metallov* (Metallurgy of Nonferrous and Rare Metals), Moscow: Nauka, 1967, pp. 40–44.
23. Gel'd, P.V., Vlasov, V.G., and Serebrennikov, N.N., *Zh. Prikl. Khim.*, 1952, vol. 25, pp. 121–133.
24. Vol'skii, A.N. and Sergievskaya, E.M., *Teoriya metallurgicheskikh protsessov* (Theory of Metallurgical Processes), Moscow: Metallurgiya, 1968.
25. Elyutin, V.P., Pavlov, Yu.A., Polyakov, V.P., and Shebalov, S.B., *Vzaimodeistvie okislov metallov s uglerodom* (Interaction of Metal Oxides with Carbon), Moscow: Metallurgiya, 1976.
26. Morachevskii, A.G., Kal'ko, O.A., and Vaisgant, Z.I., *Zh. Prikl. Khim.*, 1995, vol. 68, no. 11, pp. 1899–1903.
27. Tseft, A.L. *Trudy Ural'skogo industrial'nogo instituta (Sverdlovsk)* [Trans. Ural Industrial Inst. (Sverdlovsk)], 1944, vol. 18, pp. 45–56.
28. Pavlyuchenko, M.M. and Shelkanovtseva, N.A., *Izv. Akad. Nauk BelSSR, Ser. Fiz.-Tekhn. Nauk*, 1962, no. 3, pp. 46–53.
29. Shafrinskii, Yu.S., To the Chemical Aspect of Reduction of Oxidized Lead-Zinc Ores from Eastern Transbaikalia, *Cand. Sci. Dissertation*, Moscow, 1964.
30. Ashin, A.K., Rostovtsev, S.T., and Kostelov, O.L., *Izv. Vyssh. Uchebn. Zaved., Tsv. Metall.*, 1971, no. 5, pp. 50–53.
31. Elyutin, V.P., Pavlov, B.A., and Polyakov, V.P.,

Izv. Vyssh. Uchebn. Zaved., Chern. Metall., 1966, no. 7, pp. 6–11.

32. Ashin, A.K., Rostovtsev, S.T., and Kostelov, O.L., *Izv. Akad. Nauk SSSR, Metally*, 1971, no. 1, pp. 23–26.
33. Tsvetkov, Yu.V., in *Fizicheskaya khimiya i tekhnologiya v metallurgii* (Physical Chemistry and Technology in Metallurgy), Yekaterinburg: Inst. Metall. Ural. Otd. Ross. Akad. Nauk, 2005, pp. 143–148.
34. Kozhevnikov, G.N., Vorob'ev, V.P., Vodop'yanov, A.G., *et al.*, in *Fizicheskaya khimiya i tekhnologiya v metallurgii* (Physical Chemistry and Technology in Metallurgy), Yekaterinburg: Inst. Metall. Ural. Otd. Ross. Akad. Nauk, 2005, pp. 304–309.
35. Kal'ko, O.A., Behavior of Antimony in Processing of the Active Paste from Lead Battery Scrap, *Cand. Sci. Dissertation*, St. Petersburg, 1996.
36. Morachevskii, A.G., Vaisgant, Z.I., Bochagina, E.V., and Khabachev, M.N., *Materialy IV Vserossiiskoi nauchno-metodicheskoi konferentsii "Fundamental'nye issledovaniya v tekhnicheskikh universitetakh"* (Proc. IV All-Russia Sci.-Methodol. Conf. "Basic Research at Technical Universities"), St. Petersburg: SPb. Gos. Tekhn. Univ., 2000, pp. 126–127.

ISSN 1070-4272, Russian Journal of Applied Chemistry, 2006, Vol. 79, No. 2, pp. 250–255. © Pleiades Publishing, Inc., 2006.
Original Russian Text © Yu. S. Krasnov, G. Ya. Kolbasov, V. N. Zaichenko, 2006, published in Zhurnal Prikladnoi Khimii, 2006, Vol. 79, No. 2, pp. 251–256.

APPLIED ELECTROCHEMISTRY AND CORROSION PROTECTION OF METALS

Kinetics of Coloration of Electrochromic Tungsten Oxide Films Produced by Cathodic Electrodeposition

Yu. S. Krasnov, G. Ya. Kolbasov, and V. N. Zaichenko

Institute of General and Inorganic Chemistry, National Academy of Sciences of the Ukraine, Kiev, Ukraine

Received June 15, 2005

Abstract—The dependence of the kinetic characteristics of electrochromic indicator devices based on films of amorphous tungsten oxide α-WO_3 on the speed of reversible coloration of their working electrode with a film of this kind was studied.

DOI: 10.1134/S1070427206020157

Films of amorphous tungsten oxide α-WO_3 are used in electrochromic devices [1–3]. Their coloration and decoloration in the near-IR and visible spectral ranges occur via double ion–electron injection and extraction [1, 4]. The α-WO_3 electrode is colored on passing the cathode current via capture of electrons injected into the film by free *d*-orbitals of W^{6+} centers, which are thereby reduced to W^{5+} centers and become color centers in α-WO_3. The charge of these electrons in the film bulk is neutralized by mobile singly charged cations H^+, Li^+, or Na^+, which come into the film from the electrolyte and are arranged near oxygen atoms that form bridge and terminal bonds of the types W–O–W and W=O [5, 6]. Extraction of injected carriers from the colored film on reversing the current flow direction in the α-WO_3 electrode leads to its decoloration.

A simple and economical way to obtain α-WO_3 films with well reproducible electrochromic characteristics is cathodic electrodeposition, which is commonly performed from an electrolyte containing soluble peroxotungstates [1, 7–12]. The deposits obtained are commonly X-ray-amorphous [7, 9, 12]; the mechanism of cathodic deposition of α-WO_3 was considered in [7]. In the galvanostatic deposition mode, a linear dependence of the film thickness on the deposition time is observed, but the film retains a smooth uniform surface only to thicknesses not exceeding 1 μm [7, 12]. It has been shown that, because of the high porosity and large content of water molecules, the specific density of the deposit on the cathode is less than half density of crystalline WO_3. Therefore, these films have in the decolorized state a very low optical refractive index, n = 1.6–1.7 (at n = 2.5 for crystalline WO_3).

The coloration of the film begins with the appearance in their optical spectrum of a high-intensity absorption band peaked at $h\omega \leq 1$ eV, but, as current flows at a cathodic shift of the potential of the α-WO_3 electrode, injected electrons start to fill also higher-energy free *d* orbitals of W^{6+} centers with double bonds of the W=O type [12, 13]. α-WO_3 has a nanocluster structure [14, 15] and a decrease in the cluster size enhances the influence exerted by terminal oxygen atoms (terminal double bonds W=O) on the energy position of free *d* orbitals of W^{6+} centers and on the potential of their reduction to W^{5+}, which gives rise to an additional absorption band peaked at $h\omega \approx$ 2 eV [12, 13]. Because of the wide energy scatter of free *d* orbitals of W^+ centers in films of this kind, their successive filling by injected electrons, at a cathodic potential of the α-WO_3 electrode, is accompanied by an increase in the Fermi energy and a reversible shift of the fundamental absorption edge of this amorphous semiconductor to higher photon energies [12, 13]. As a result, films of this kind show a correlation between the concentration of injected carriers, degree of coloration, position of the fundamental absorption edge, Fermi energy, and potential of the α-WO_3 electrode, whose values are also retained on disconnecting the electrode from the power source [12, 13].

This communication reports the results obtained in a study of joint diffusion transport of injected electrodes and protons in a cathodically deposited α-WO_3 at various potentials. The experimental data obtained confirm the nanocluster structure of cathodically deposited α-WO_3 films.

EXPERIMENTAL

α-WO_3 films were produced by cathodic electrodeposition from an aqueous solution of Na_2WO_4 (0.2 M) with addition of 30% hydrogen peroxide (0.13 M) and H_2SO_4 (to pH 1). The deposition was performed in a transparent electrochemical cell with a platinum counter electrode at a constant cathode current density of about 1 mA cm^{-2} and temperature of 23–25°C. The α-WO_3 films were deposited onto a transparent current-conducting SnO_2 film of thickness 0.23 μm on a glass substrate or on a polished surface of sheet tungsten. The design of the electrochemical cell enabled interferometric monitoring of the course of deposition by recording interference patterns simultaneously for two He–Ne laser beams with different angles of incidence on the electrode surface. Computer processing of these diffraction patterns by the procedure described in [12, 16] enabled separate determination of the running values of the thickness and optical refractive index of a growing α-WO_3 layer.

The optical and electrochemical parameters of the electrode fabricated were measured in the transparent electrochemical cell filled with a 1 N solution of H_2SO_4, equipped with a platinum counter electrode and silver chloride reference electrode, relative to which all the potentials E are given. The coloration and decoloration of the α-WO_3 electrodes was achieved by steplike variation of the control potential with an EP-21 potentiostat. The time dependences of the electrode current and intensity of monochromatic light reflected by the α-WO_3 electrode or passed through this electrode were recorded with an automated measuring setup similar to that described previously [17].

In the colored α-WO_3 film, the charge of injected electrons (with a concentration on the order of 10^{21} cm^3) is neutralized by the charge of mobile protons. Because of the large content of water molecules in the structure of a cathodically deposited film, transport of protons in this film occurs via the hydrogen bonds of H_2O molecules (in the form of OH_3^+) [18]. The most probable at so high concentrations of differently charged carriers is the diffusion mechanism of their joint transport in the bulk of α-WO_3. Under nonstationary conditions, the difference between the mobilities of electrons and protons should give rise, by analogy with concentrated solutions of liquid electrolytes, to a diffusion potential, which equalizes the motion velocities of these particles. In this case, the effective coefficient of joint diffusion in the film bulk, D_{eff}, is mainly determined by the motion velocity of the less mobile particle, for which the proton is commonly taken.

Because of the high porosity and large content of water molecules, electrodeposited α-WO_3 films have no potential barrier for protons at the interface with the electrolyte. This makes it possible to assume that a carrier concentration N_0 that is the equilibrium concentration for a given E is rapidly attained at the film surface and to regard the coloration as a diffusion process of joint transport of protons and electrons into a film of finite thickness d from a permanent source with concentration N_0 on the surface. In this case, the common solution to the diffusion equation for the flux (of protons) across the WO_3–electrolyte interface has the form [19]

$$i(t) = (2eN_0D_{eff}d^{-1})\Sigma\exp\{-[(2n + 1)^2\pi^2D_{eff}t(2d)^{-2}]\}, \quad (1)$$

where D_{eff} is the effective coefficient of joint diffusion of protons and electrons; e, elementary charge; and t, time of coloration.

A solution of the same kind is obtained for decoloration. The series (1) rapidly converges and does so the better, the larger t. At $t \geq t_D = 0.25d^2/D$ (t_D is the characteristic time of diffusion) it is possible to retain only the first term of sum, with an error not exceeding 1%. Then, except in the initial stage of coloration or decoloration, the following expression can be written at $t > t_D$

$$\ln|i(t)| = \ln(2eN_0D_{eff}d^{-1}) - \pi^2D_{eff}t(2d)^{-2}, \quad (2)$$

i.e., the dependence $i(t)$ plotted in the coordinates $\ln i(t)$–t is a straight line with a slope $-\pi^2D_{eff}(2d)^{-2}$. Hence, it is possible to find, at a known film thickness d, D_{eff} and N_0, because this straight line intersects the ordinate axis at $\ln(2eN_0D_{eff}d^{-1})$.

Figure 1 shows the experimental time dependences of the current density $|i(t)|$ and normalized intensity of monochromatic light (625 nm) that passed through the electrode. These dependences were obtained in a cycle of coloration–decoloration of an electrode with an α-WO_3 film on glass with a current conducting layer of SnO_2. To minimize the influence exerted on the electrode current by the sheet resistance of the current-conducting substrate, the working area of the α-WO_3 electrode was considerably smaller than that of the SnO_2 layer. The remaining part of the SnO_2 surface was insulated from the electrolyte with a layer of chemically resistant lacquer. The time of the coloration process of the given electrode at λ = 625 nm after a steplike change of its potential E from 0.4 to –0.4 V was about 0.3 s at a transmission contrast of about 80%. At such a rate of electrode coloration, its efficiency was $\Delta D/Q$ = 57 cm^2 C^{-1},

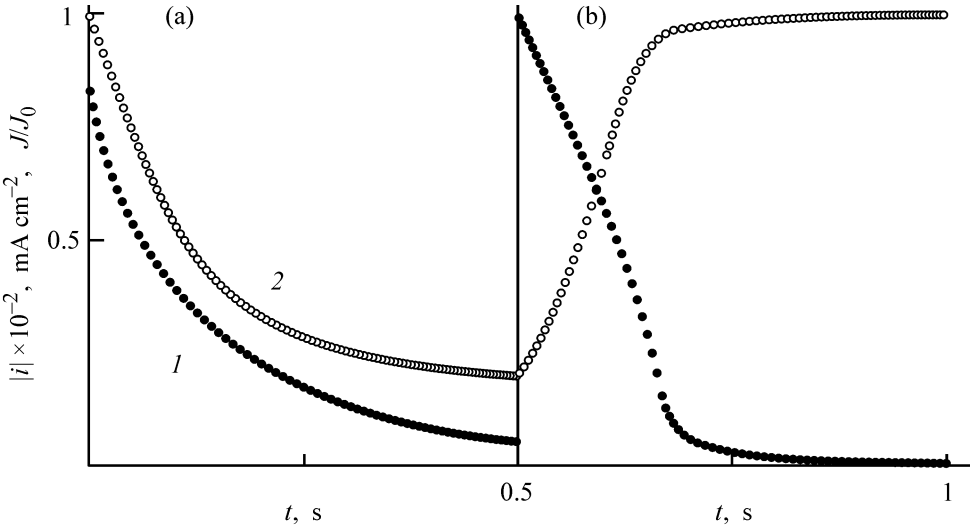


Fig. 1. (*1*) Current i and (*2*) normalized intensity of transmitted light, J/J_0, at λ = 625 nm vs. time t for an electrode with a 343-nm α-WO_3 film (on glass with a SnO_2 layer) in a cycle of coloration–decoloration of this electrode via a steplike change in its potential from 0.4 to –0.4 V. (a) Coloration at E = –0.4 V and (b) decoloration at E = 0.4 V.

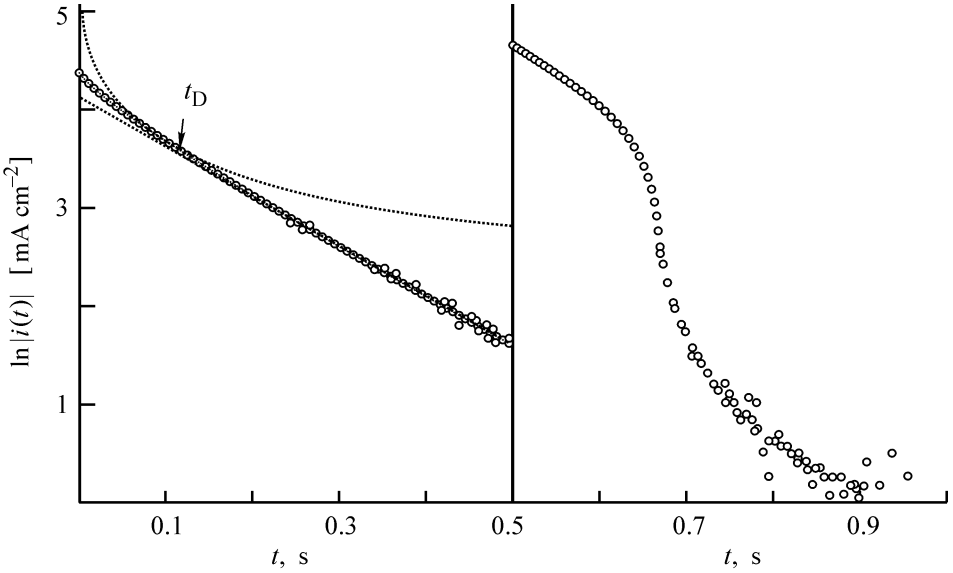


Fig. 2. $\ln|i(t)|$–t dependence for an α-WO_3 electrode with kinetic characteristics shown in Fig. 1. (*i*) Current density. *Dotted line*: expected run of this dependence at the calculated values of D_{eff} and N_0 for the case when $d \to \infty$.

where $D = \log(I_0/I)$ is optical density and Q is the quantity of charge injected into the electrochromic film (at E = –0.4, $Q \approx 12.4$ mC cm^{-2}). These parameters were retained during more than 10 coloration-decoloration cycles. At cathodic potentials exceeding –0.4 V, a part of the electrode current was expended for the reaction of hydrogen evolution, which gradually led to irreversible structural changes in the electrochromic layer and in that of SnO_2.

In Fig. 2, the time dependence of the current $i(t)$ (Fig. 1) is plotted in the $\ln|i(t)|$–t coordinates. At $t >$ 0.12 s, a straight line can be drawn through its experimental points in Fig. 2, which confirms the diffusion mechanism of a concerted motion of protons and electrons from the surface of the α-WO_3 layer toward the interface between this layer and that of SnO_2. The parameters of the electrochromic material, found in accordance with Eq. (2), have the following values: $D_{eff} = 2.38 \times 10^{-9}$ cm^2 s^{-1}, $N_0 = 2.73 \times 10^{21}$ cm^{-3}, t_D = 0.125 s. Because t_D is the time in which protons injected into the film reach the SnO_2 layer, their joint transport with electrons in the film can be regarded as diffusion into a semifinite body from a permanent source with a constant concentration N_0 on its surface.

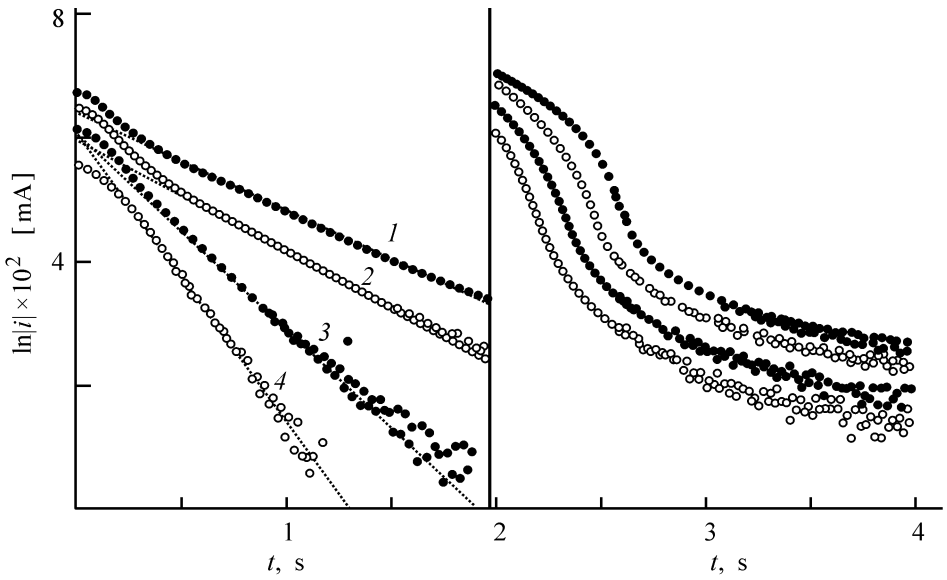


Fig. 3. $\ln|i(t)|$–t dependence for a 0.64-μm α-WO_3 film in its coloration at different control potentials and subsequent decoloration at E = 0.4 V. (*i*) Current. Coloration potential E (V): (*1*) –0.4, (*2*) –0.2, (*3*) –0.1, and (*4*) 0; decoloration at 0.4 V.

In this case, the dependence $i(t) = N_0[D_{\text{eff}}/(\pi t)]^{1/2}$ corresponds to solution to Fick diffusion equations. This dependence is shown in Fig. 2 with account of the value found for N_0. However, the arrangement of experimental points of $i(t)$ in Fig.2 at $t < t_D$ disagrees with this theoretical dependence because the equilibrium carrier concentration N_0 is attained on the film surface only a certain time after the steplike change of the control potential E from 0.4 to –0.4 V, rather than instantaneously.

The decoloration of the film at $E > 0.3$ V occurs faster than the coloration (Fig. 1) because the equilibrium concentration of W^{5+} centers already cannot be attained on its surface. In this case, even a complete disappearance of the color cannot compensate the potential difference applied to the WO_3–electrolyte interface. The uncompensated part of this potential difference creates an electric field, which penetrates into the bulk of the semiconducting α-WO_3 and accelerates transfer of protons into the electrolyte [4]. In this case, the slope rate of the dependence $\ln|i(t)|$–t in the initial and final stages of decoloration is close to that in coloration. In the initial stage of decoloration, this is due to the fact that the penetration depth of the electric field into the film at its surface is as yet small as compared with d. In the final stage of decoloration, the velocity at which carriers are transported to the surface again becomes virtually equal to that of the diffusion transport because of the low electric field strength in the bulk of α-WO_3.

The dependence of D_{eff} on E was determined by changing stepwise the control potential to its various values in coloration and decoloration. In doing so, the use of electrodes in which the α-WO_3 film was deposited on the polished surface of sheet tungsten made it possible to minimize the series resistance for the electrode current. The experimental $i(t)$ dependences obtained on such an electrode with a layer of cathodically deposited α-WO_3 for several coloration potentials are plotted in the $\ln|i(t)|$ coordinates in Fig. 3. At t exceeding 0.4 s, straight lines can be drawn through the experimental points of these dependences. The difference between those values of D_{eff} to which the slopes of straight lines in Fig. 3 correspond and the position of circles in Fig. 4 is due to the dependence of the diffusion coefficient on the coloration potential, whose value in α-WO_3 also sets

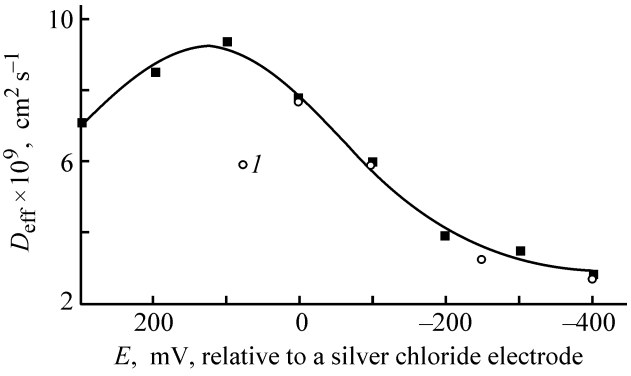


Fig. 4. Coefficient of joint (ambipolar) diffusion of protons and electrons in the bulk of a α-WO_3 film, D_{eff}, vs. the potential E. (*1*) $D_{\text{eff}}(E)$ values found from the slopes of the straight lines in Fig. 3.

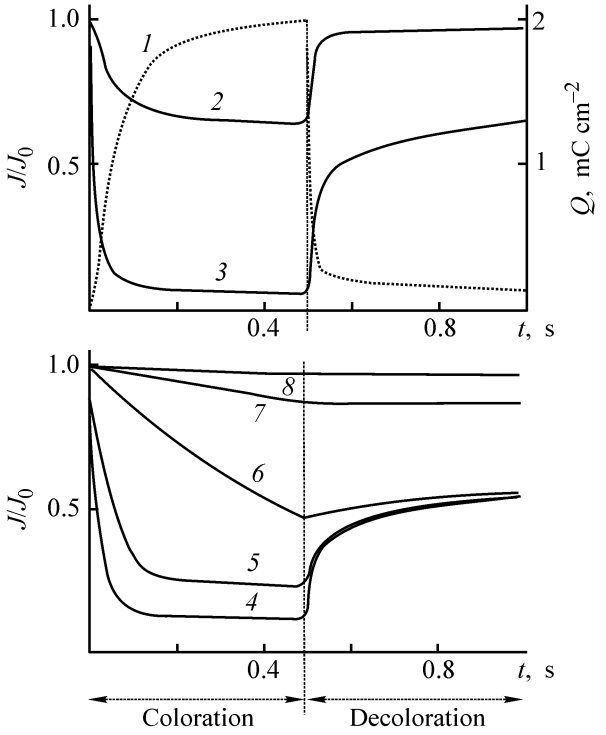


Fig. 5. (*1*) Injected electron charge Q and (*2–8*) normalized intensity of reflected light, J/J_0, at λ of (*2*) 0.6 and (*3–8*) 1.0 μm for an α-WO_3 film on tungsten. Coloration potential E (V): (*1–3*) –0.5, (*4*) –0.3, (*5*) –0.2, (*6*) –0.1, (*7*) –0.05, and (*8*) 0; decoloration at (*1–8*) 0.5 V.

the final concentration of injected carriers, N_0, in the film. At the same time, (1) and (2) are derived from the Fick equation $\partial N/\partial t = D(\partial^2 N/\partial x^2)$ on the assumption that D_{eff} is independent of the concentration of the diffusing substance. If D depends on N, a more general equation $\partial N/\partial t = \partial/\partial x[D(N)(\partial n/\partial x)]$, should be used; however, it is rather difficult to directly solve it in the general form. Therefore, the rest of the points in Fig. 4 correspond to those values of D_{eff} which were obtained from the time dependence of the anode current of this electrode, with the control potential raised stepwise by a small amount (0.1 V). It is assumed that, within each interval of this kind on the potential scale at E between 0.3 and –0.4 V, the variation of D_{eff} with E is small and can be neglected. It was established that, within each of these intervals, the experimental points of the $\ln|i(t)|$ dependences obtained fall on straight lines having the same slope as those for coloration and do not deviate in the course of time from the straight lines because of the dependence of D_{eff} on E.

The dependence of D_{eff} on E, shown in Fig. 4, has a maximum at E of about 0.1 V. A similar D_{eff}–E dependence has been obtained previously in impedance measurements for α-WO_3 films deposited in a vacuum (in their coloration in propylene carbonate containing 1 M $LiClO_4$) [5]. In this study, the decrease in D_{eff}, observed as the concentration of cations increased, was attributed to closure of paths for their motion in the film along bonds of the type W^{6+}=O and O–W^{6+}–O upon reduction of W^{6+} centers to W^{5+}, and the initial rise in D_{eff}, to transition from Li^+ transport within separate clusters to their faster motion over the surface of these clusters, on which the terminal W^{6+}=O bonds are localized. According to [20], a continuous increase in D_{eff} at all values of the control potential is characteristic of WO_3 films produced by the sol-gel method and annealed at 240°C, in the course of their coloration with Li^+. The authors of [20] regard the rise in D_{eff} of this oxide as a result of an increase in its electronic conductivity. Possibly, the rise in D_{eff} in the initial stage of coloration of a cathodically deposited α-WO_3 film in a 1 N H_2SO_4 solution (Fig. 4) is also due to an increase in its electronic conductivity. At the same time, the increase in the (W^{6+}=O)/(O–W^{6+}–O) ratio in the initial stage of film coloration, observed in [5] in Raman scattering measurements, can be attributed to capture of electrons mostly by W^{6+} centers. These centers have no bonds of the W^{6+}=O type, which have a lower energy position of the free *d*-orbital than in centers with W^{6+}=O bonds [12, 13].

Figure 5 shows kinetic dependences obtained on one of the electrodes studied, which had an α-WO_3 film deposited from an electrolyte with acidity raised to pH 2. At $E \geq -0.1$ V, the coloration of the α-WO_3 layer of this electrode is strongly decelerated. This range of coloration potentials E (0.3 to –0.1 V) corresponds to formation of W^{5+} centers within the largest clusters and to appearance of an absorption band peaked at $\lambda \approx 1000$ nm. The extraction of injected electrons captured by these centers is also markedly decelerated in decoloration of the film at E = 0.5 V. Their charge constitutes about 5% of the maximum value of Q in the film at E = –0.5 V, whereas the separation accelerated by the electric field and the removal of most of carriers occur in this case in $t \approx 0.1$ s. It is unlikely that such a pronounced, by several orders of magnitude, change in the carrier mobility in the film between E = –0.1 and –0.2 V could be associated with a change of the pathways of proton transport by the mechanism suggested in [5]. Such a "steplike" change in mobility can be attributed to filling by injected electrons of energy levels that lie on different sides of the "mobility threshold" for electrons in this amorphous semiconductor. The considerable distance between separate large clusters in

the oxide prevents electrons captured by these clusters from being involved in transport phenomena. At $E > 0.1$ V, the probability of an electron hop between clusters of this kind is low, because they are separated by pores filled with water molecules and by smaller nanoclusters with W^{6+} centers having a higher (by 0.3–0.4 eV) energy of the free *d*-orbital. In addition, it is necessary, for the film coloration to begin, that the injected electrons should preliminarily pass across a layer of completely decolorized WO_3 with a low electronic conductivity [20]. Therefore, the initial portion of the *i–t* dependences in Figs. 2 and 3 disagrees with the general solution to the diffusion equations, which is particularly noticeable in the case of coloration at $E = 0$ V (from the position of the experimental points corresponding to the initial stage below the straight line drawn).The steplike increase in the motion velocity of injected carriers in the film, observed at the cathodic potential, presumably corresponds to that energy position of the Fermi level, at which electron transfer occurs across its entire thickness via a macroscopic chain of clusters, between which electrons can move by hopping.

CONCLUSIONS

1) The reversible coloration of cathodically deposited electrochromic α-WO_3 films via joint transport of electrons and protons (in the form of H_3O^+) injected into the film occurs by the diffusion mechanism.

(2) In the course of coloration of the film and cathodic shift of its potential, the effective diffusion coefficient of these mobile carriers first increases to approximately 10^{-8} $cm^2\ s^{-1}$ and then gradually decreases. The occurrence of a maximum in the dependence of this coefficient on the potential of the α-WO_3 electrode at $E \approx 0.1$ V is due to a decrease in the mobility of electrons in the film to values lower than the mobility of protons, observed as the potential of the film is shifted into the anodic region.

(3) Raising the acidity of the initial electrolyte favors deposition of films with an abrupt "mobility threshold" (on the energy scale) for electrons. Its existence is due to the presence of pores and to specific features of the cluster structure of these films, characterized by predominance of small nanoclusters in which most of tungsten atoms have double bonds of the W=O type with terminal oxygen atoms.

REFERENCES

1. Granqvist, C.G., *Handbook of Inorganic Electrochromic Materials*, Amsterdam: Elsevier, 1995.
2. Monk, P.M.S.K., *Handbook of Advanced Electronic and Photonic Materials*, San Diego: Acad., 2001, vol. 7, pp. 105–159.
3. Aegerter, M.A., *Sol-Gel Chromogenic Materials and Devices in Structure and Bonding*, Berlin: Springer, 1996, vol. 85, pp. 149–194.
4. Channin, D.J., Crandall, R.S., Criscimagna, *et al., Display Devices*, Pankove, J.I., Ed., Berlin: Springer, 1980. Translated under the titles *Elektrokhromnye displei na osnove α-WO_3: Displei*, Moscow: Mir, 1982, pp. 228–266.
5. Lee, S.-H., Cheong, H.M., Tracy, S.E., *et al.*, *Electrochim. Acta*, 2001, vol. 46, no. 22, pp. 3415–3419.
6. Kamal, H., Akl, A.A., and Abdel-Hady, K., *Physica B: Condensed Matter*, 2004, vol. 349, nos. 1–4, pp. 192–205.
7. Meulenkamp, E.A., *J. Electrochem. Soc.*, 1997, vol. 144, no. 5, pp. 1664–1671.
8. Shiyanovskaya, I., Hepel, M., and Tewksburry, E., *J. New Mat. Electrochem. Systems*, 2000, no. 3, pp. 241–247.
9. Stevenson, K.J. and Hupp, J.T., *Electrochem. Solid-State Lett.*, 1999, vol. 2, no. 10, pp. 497–500.
10. Habazaki, H., Hayashi, Y., and Konno, H., *Electrochim. Acta*, 2002, vol. 47, no. 9, pp. 4181–4188.
11. Pauporte, T., Bernard, M.C., Soldo-Olivier, Y., and Faure, R., *J. Electrochem. Soc.*, 2004, vol. 151, no. 1, pp. H21–H26.
12. Krasnov, Yu.S. and Kolbasov, G.Ya., *Electrochim. Acta*, 2004, vol. 49, no. 15, pp. 2425–2433.
13. Krasnov, Yu.S. and Kolbasov, G.Ya., *Zh. Prikl. Khim.*, 2002, vol. 75, no. 2, pp. 231–236.
14. Kubo, T. and Nishikitani, Y., *J. Electrochem. Soc.*, 1998, vol. 145, no. 5, pp. 1729–1734.
15. Niklasson, G.A., Klasson, J., and Olsson, E., *Electrochim. Acta*, 2001, vol. 46, no. 13–14, pp. 1967–1971.
16. Vas'ko, A.T., Krasnov, Yu.S., Patsyuk, F.N., and Chumak, S.M., *Ukr. Khim. Zh.*, 1985, vol. 51, no. 2, pp. 152–157.
17. Krasnov, Yu.S., Vas'ko, A.T., Patsyuk, F.N., and Sych, O.A., *Ukr. Khim. Zh.*, 1987, vol. 53, no. 9, pp. 951–956.
18. Georg, A., Graf, W., and Wittwer, V., *Electrochimica Acta*, 2001, vol. 46, nos. 13–14, pp. 2001–2005.
19. Crank, J., *The Mathematics of Diffusion*, London: Oxford Sci., 1992.
20. Avellaneda, C.O. and Bulhões, L.O.S., *Solid State Ionics*, 2003, vol. 165, nos. 1–4, pp. 59–64.

ISSN 1070-4272, Russian Journal of Applied Chemistry, 2006, Vol. 79, No. 2, pp. 256–263. © Pleiades Publishing, Inc., 2006.
Original Russian Text © V. S. Rudnev, D. L. Boguta, P. M. Nedozorov, T. A. Kaidalova, 2006, published in Zhurnal Prikladnoi Khimii, 2006, Vol. 79, No. 2, pp. 257–263.

APPLIED ELECTROCHEMISTRY AND CORROSION PROTECTION OF METALS

Anodic Layers Formed in Polyphosphate Electrolytes on Rectifying Metals

V. S. Rudnev, D. L. Boguta, P. M. Nedozorov, and T. A. Kaidalova

Institute of Chemistry, Far-Eastern Division, Russian Academy of Sciences, Vladivostok, Russia

Received September 9, 2005

Abstract—Results obtained in studying the elemental and phase composition of anodic layers formed on titanium, aluminum, niobium, and zirconium under the action of electric discharges in aqueous electrolytes with hexametaphosphate complexes of Ni(II), Mg(II), and Mn(II) are presented.

DOI: 10.1134/S1070427206020169

It has been shown previously [1–4] that layers containing metal phosphates, along with aluminum oxides, can be formed on the surface of aluminum and its alloys by the method of plasma electrolytic oxidation (PEO)[1] in aqueous electrolytes containing polyphosphate complexes of the metals. Such layers exhibit properties typical of metal phosphates. For example, films containing zinc phosphates can act as biocides [5, 6]. Aluminum–nickel PEO structures on aluminum exhibit a catalytic activity in oxidation of CO to CO_2 [7]. In the general case, composites that are constituted by a metal and a thin layer and contain high-temperature phosphates of doubly, triply, and multiply charged metals have found a wide diversity of applications [8–13].

The composition and thickness of the anodic PEO structures on aluminum depend on the molar ratio n = polyphosphate/M^+ in the electrolyte (Fig. 1), or, in other words, on the state of a solution [1–3]. The coatings formed in true solutions ($n > n_0$) are composed of aluminum oxide and contain insignificant amounts of elements from the electrolyte. The coatings formed in a colloid electrolyte or in an electrolyte that approaches this state ($n < n_0$) are mainly composed of the electrolyte components. According to X-ray phase and thermogravimetric analyses, the elemental composition and mass of the PEO coatings formed in polyphosphate electrolytes with different values of n remain unchanged upon annealing in air at temperatures of up to 1000°C [14–16]. IR spectroscopy has revealed di-, ortho-, and metaphosphate groups in the composition of the layers [15, 16]. Annealing leads to an increase in the content of the crystalline phases in the layers. In this case, complex titanium phosphates, such as $NaTi_2(PO_4)_3$ and $Mn(II)Mn(III)Ti(PO_4)_3$, can crystallize in layers on titanium, in contrast to analogous structures on aluminum [14].

In this communication, we present the results obtained in a study of how the nature of a rectifying metal and an alloy and high-temperature annealing in air affect the composition of PEO layers formed in polyphosphate electrolytes.

EXPERIMENTAL

The coatings were formed on aluminum (99.9%) and its alloys AMTsM, AD1, AD33, D16, AMg6, and V95, a well as on technical grade VT1-00 titanium, niobium of NbTsu brand, and zirconium. We prepared electrolytes using commercial reagents: sodium hexamethaphosphate $Na_6P_6O_{18}$ (30 g l^{-1}), sodium tripolyphosphate $Na_5P_3O_{10}$ (36.1 g l^{-1}), $Mg(CH_3COO)_2 \cdot 4H_2O$, $Ni(CH_3COO)_2 \cdot 4H_2O$, and $Mn(CH_3COO)_2 \cdot 4H_2O$, and distilled water. The molar ratio $n = P_6O_{18}^{6-}/M$ was calculated for the starting reagents. The preparation of the electrolyte and electrodes, the electrochemical cell, and the thyristor power source have been described previously [1–3].

Anodic layers were formed galvanostatically in the course of 10 min (if not specified otherwise) at

[1] Plasma electrolytic oxidation is a method in which anodic layers are formed under the action of electric discharges near the electrode.

Table 1. Elemental composition of coatings formed on various aluminum alloys*

Alloy (main alloying additives, %)	U, V	Content, wt %			
		Al	P	Mg	Na
Aluminum (99.9)	350	5.7	20.4	13.7	0.9
AMTsM (Mg, 1.2–1.8)	343	6.6	22.5	11.6	1.1
AD1 (Fe, 0.3; Si, 0.3)	337	5.3	23.1	11.8	1.0
AD33 (Fe, 0.7; Si, 0.4–0.8; Mg, 0.8–1.2)	342	11.0	22.9	13.3	0.8
V95 (Cu, 1.4–2.0; Zn, 5.0–7.0; Mg, 1.8–2.8)	336	9.6	23.4	11.6	1.1
AMg6 (Mg, 5.8–6.8; Mn, 0.5–0.8)	327	5.3	25.7	14.8	1.1

* The coatings were formed in an electrolyte containing 30 g l^{-1} $Na_6P_6O_{18}$ and $Mg(CH_3COO)_2$, n = 1; U, the final formation potential; data on the alloying additives were taken from [17].

Table 2. Elemental composition of coatings formed on VT1-00 titanium at i = 5 A dm^{-2} for τ = 6 min, according to laser mass-spectrometry

Electrolyte*	n	Content, at. %				
		Ti	M(II)	P	O	C
GMF	–	29.3	–	12.1	57.6	–
GMF + $Mg(Ac)_2$	3	17.9	0.9	19.4	59.6	1.9
	0.5	7.6	6.9	16.7	63.7	4.8
GMF + $Zn(Ac)_2$	3	21.1	0.7	13.4	64	0.6
	0.5	15.9	3.8	11.1	68.3	0.7
GMF + $Ni(Ac)_2$	3	30.6	4.4	17.1	44.9	2.7
	0.5	5.9	14.5	16.8	60.4	2.3
TPF	–	20.1	–	7.6	71.3	0.8
TPF + $Mg(Ac)_2$	3	16.7	0.9	16.8	63.1	2.5
TPF + $Mn(Ac)_2$	3	25.5	2.1	13.5	56.8	2.1
	1	19.7	13.1	14.8	61.8	2.3
TPF + $Ni(Ac)_2$	3	18.8	6.3	13.6	56.1	5

* GMF and TPF are electrolytes containing 30 g l^{-1} $Na_6P_6O_{18}$ and 36.1 g l^{-1} $Na_5P_3O_{10}$, respectively, and Ac = CH_3COO^-.

the effective current density i = 5 A dm^{-2}. Samples of dimensions $10 \times 40 \times 1$ and $40 \times 40 \times 1$ mm were treated. In all cases, a spark discharge appeared on the anode surface during the first minute of the process. The temperature of the electrolyte during the anodizing did not exceed 30°C. The coated samples were washed with distilled water and dried in air. The samples were heated in a muffle furnace at a prescribed temperature for 2 h in air.

The elemental composition of the surface layer of the coatings was determined on a JXA-5A electronic X-ray fluorescence microprobe analyzer (Japan) and on an EMAL-2 laser mass-spectrometer (Russia). The micrographs of the surface were obtained on a LEO-400 electron microscope (France). The phase composition was determined using X-ray diffraction patterns obtained on a DRON-2 diffractometer with Cu_{K_α} radiation (Russia) or on a D8 ADVANCE X-ray diffractometer (Germany) in the Bragg–Bretano configuration with Cu_{K_α} radiation. In the last case, the EVA search software with a PDF-2 database was used in the X-ray phase analysis.

The coating thickness was determined with a VT-201 eddy current thickness meter (Russia).

The data in Table 1 show that the alloying additives in the aluminum alloys affect only slightly the content of the main elements in the coatings, but alter the final potential of coating formation, U. The potential U is at a maximum for coatings formed on pure aluminum. Probably, the coatings are the densest in this case and have the best dielectric characteristics. According to the results of an elemental analysis, the alloying additives are present in the composition of the coating in trace amounts.

The data in Tables 1–3 and Figs. 1, 2 show that the molar ratio n = polyphosphate/M^+ in the elec-

Table 3. Elemental and phase composition of coatings formed on aluminum, titanium, niobium, and zirconium alloys in an electrolyte containing $Na_6P_6O_{18}$ and $Mg(CH_3COO)_2$

Metal	*n*	Coating composition, wt %				XPA
		metal	P	Mg	Na	
AMTsM	1	6.6 (Al)	22.5	11.6	1.1	η-, k-trace; α-Al_2O_3, $AlPO_4$
VT1-00	0.5	13.5 (Ti)	25	6.5	1.1	X.r.a.*
NbTsU	1	23 (Nb)	29.7	9.2	0.8	Amorphous phase
Zr	1	13.6 (Zr)	38.7	19.6	1	Monoclinic ZrO_2; cubic or tetragonal ZrO_2 amorphous phase

* X.r.a., X-ray-amorphous; the same in Tables 4, 5.

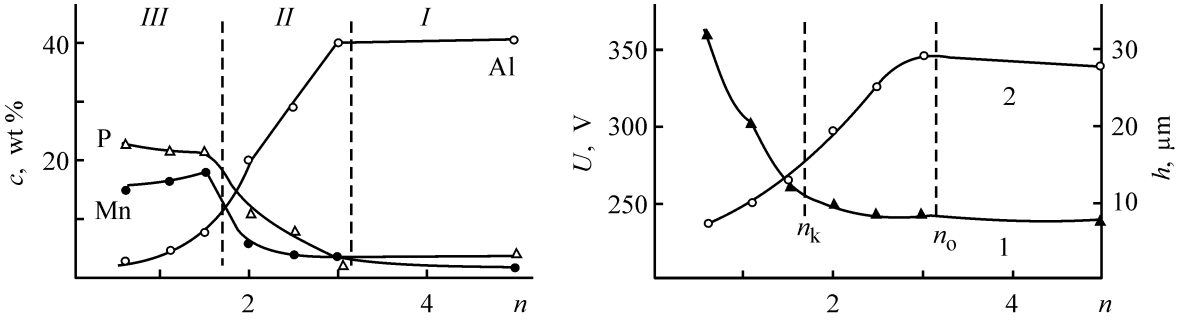


Fig. 1. (*1*) Elemental composition *c* and thickness *h* of anodic layers formed on AMtsM alloy and (*2*) the final potential at the electrode, *U*, vs. the molar ratio *n* = polyphosphate/M^+ in an aqueous electrolyte containing 30 g l^{-1} $Na_6P_6O_{18}$ + $Mn(CH_3COO)_2$. Solution: *I* ($n > n_0$) true, *II* ($n_c < n < n_0$) metastable, and *III* ($n < n_c$) colloidal region.

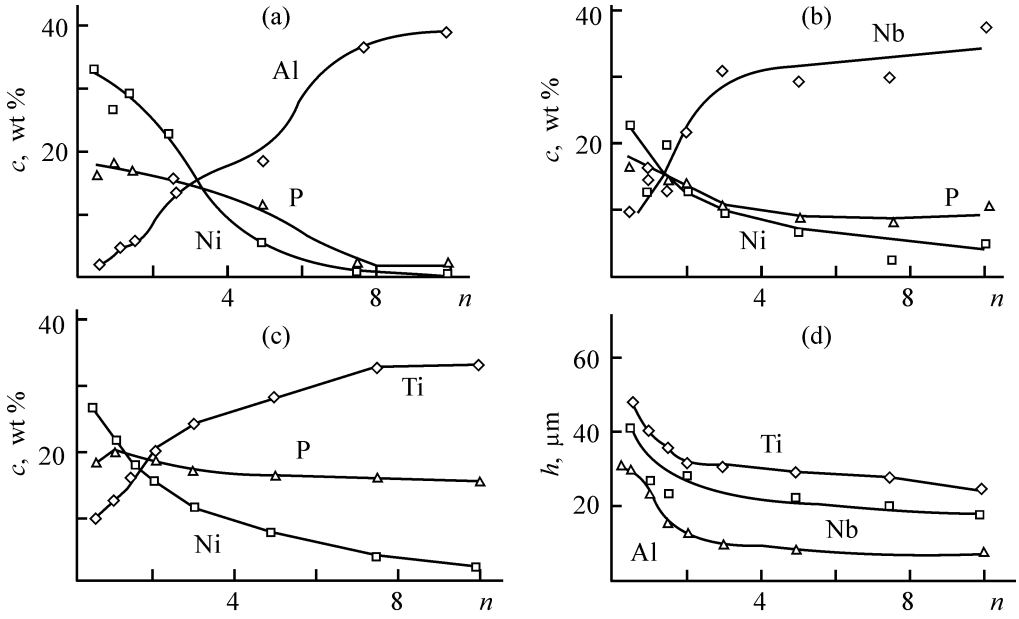


Fig. 2. Effect of the molar ratio *n* = polyphosphate/M^+ on elemental composition of the layers (*c*) formed in an aqueous electrolyte containing 30 g l^{-1} $Na_6P_6O_{18}$ + $Ni(CH_3COO)_2$ on (a) aluminum, (b) niobium, and (c) titanium, and (d) on their thickness *h*.

trolytes affects the elemental composition and thickness of the coatings formed on titanium, niobium, zirconium, and aluminum in similar ways. The main changes in the elemental composition ($\Delta c/\Delta n$) and thickness ($\Delta h/\Delta n$) of the coatings formed on all of the metals studied are observed when the electrolyte approaches the colloid state ($n < 3–6$ transition or metastable region), i.e., the electrolyte components are incorporated in noticeable amounts and the coating thickness grows when the solubility of metal polyphosphate complexes decreases and the solutions are metastable, or hydrated metal polyphosphates are precipitated. Under these conditions, the gain in mass and the coating composition are mostly determined by the products formed in thermolysis of the precipitate and by the high-temperature interactions between the compounds and oxides in the vicinity of electric discharge channels.

At the same time, the nature of a rectifying metal markedly affects the phosphorus content of the layers and their thickness at $n > 2$, i.e., in the case when the films are formed in true solutions and the role of the colloidal precipitate in film formation is insignificant. In the case under study, the metals are arranged in the following order with respect to the phosphorus content in the coatings (wt %) and their thickness: Ti > Nb > Al (Fig. 2). Furthermore, the phosphorus content in the coatings formed on titanium and niobium changes in the transition and colloid regions ($n < 3$) to a lesser extent than that in coatings on aluminum. Presumably, titanium (and to a lesser extent niobium) and their oxides are more susceptible than aluminum and its oxide to formation of phosphate compounds sparingly soluble in water in interaction with the polyphosphate electrolyte in the course of PEO. Apparently, the high content of phosphorus in the coatings formed on titanium is due not only to thermolysis of the precipitate and high-temperature interactions with polyphosphates at places of TiO_2 break-downs, but also to egress of titanium cations into solution to form titanium polyphosphate complexes, which undergo thermolysis at the anode under discharge conditions. Comparison of the data of [18, 19] shows that, in oxidation of titanium and aluminum under the action of electric spark and micro-arc discharges, the titanium concentration in the electrolyte markedly (severalfold) exceeds that of aluminum. A high content of phosphorus (approximately 5–10 wt %) is characteristic of PEO coatings formed on titanium in electrolytes containing water-soluble phosphorus compounds [20, 21]. For PEO structures formed on aluminum and its alloys under the similar conditions, the phosphorus content does not exceed 3–4 wt % [22].

According to the data of laser mass-spectrometry (Table 2), carbon is present in considerable amounts in coatings formed on titanium, and the amount of carbon depends on the nature of a metal cation in the electrolyte. The mechanism of carbon incorporation into the coatings remains unclear.

The composition of the PEO coatings galvanostatically formed at a current density of 5 A dm^{-2} in 6 min on VT1-00 titanium in an aqueous electrolyte containing 30 g l^{-1} $Na_6P_6O_{18}$ and $Mn(CH_3COO)_2$ was studied in [14]. It was found that the original layers are X-ray-amorphous and crystalline phases are formed at annealing temperatures above 650°C. The whole set of results obtained in [14] (thermogravimetric data; constant content of titanium, phosphorus, and manganese in annealing at temperatures of up to 800°C; phase composition and its behavior in the course of annealing) led to a conclusion that coatings formed on titanium in a polyphosphate electrolyte contain sodium and manganese titanophosphates at any n in the polyphosphate electrolyte. For example, the following phases crystallize upon annealing of samples with coatings formed in a polyphosphate electrolyte without Mn(II) acetate (analysis of X-ray diffraction patterns, DRON-2.0): TiO_2 anatase, $NaTi_2(PO_4)_3$, $Na_{0.23}TiO_2$ (bronze-like), and, possibly (weak reflections), titanium diphosphate TiP_2O_7. In coatings formed in an electrolyte containing Mn(II) complexes ($n \le 5$), phosphatotitanates $Mn(II)Mn(III)Ti(PO_4)_3$ and manganese diphosphate $Mn_2P_2O_7$ crystallize in addition to the substances mentioned above. The coatings formed in electrolytes at $n < 1$, i.e., in the solutions with a precipitate, possibly contain Mn_2TiO_4 along with the above phases. As n in the forming electrolyte decreases, which corresponds to a rise in the manganese(II) concentration in the coatings, the crystallinity of the anodic layers and the number of the phases recorded increase.

Similar results were obtained in a study (with a D8 instrument) of the influence exerted by annealing on the phase composition of the coatings formed on titanium in an electrolyte containing 30 g l^{-1} $Na_6P_6O_{18}$ and $Ni(CH_3COO)_2$ (Table 4). The original coatings are either X-ray-amorphous ($n > 5$) or contain the amorphous phase ($n < 2$). TiP_2O_7, $NaTi_2(PO_4)_3$, and TiO_2 (anatase) crystallize above 500°C in films formed in a purely polyphosphate electrolyte (without nickel acetate), in agreement with the results of [14]. Intro-

Table 4. Phase composition of coatings formed on VT1-00 titanium in an electrolyte containing $Na_6P_6O_{18}$ and $Ni(CH_3COO)_2$, as determined on a D8 instrument*

n	Initial coating	Annealing temperature, °C	
		500	800
–	X.r.a.	?TiP_2O_7	TiP_2O_7, $NaTi_2(PO_4)_3$, TiO_2(a)
10	X.r.a.	X.r.a.	TiP_2O_7, $Ni_{0.5}O(TiO)(PO_4)$, $NaTi_2(PO_4)_3$,TiO_2(a)
7.5	X.r.a.	X.r.a.	TiP_2O_7, $Ni_{0.5}O(TiO)(PO_4)$, $NaTi_2(PO_4)_3$, TiO_2(a)
5	X.r.a.	X.r.a.	$NaTi_2(PO_4)_3$, $Na_4(TiO)(PO_4)_2$, $Ni_{0.5}(TiO)(PO_4)$, $Ni_2P_2O_7$
3	X.r.a.	X.r.a.	$NaTi_2(PO_4)_3$, $Na_4(TiO)(PO_4)_2$, $Ni_{0.5}O(TiO)(PO_4)$, $Ni_2P_2O_7$
2	X.r.a.	X.r.a.	$NaTi_2(PO_4)_3$, $Na_4(TiO)(PO_4)_2$, $Ni_{0.5}(TiO)(PO_4)$, $Ni_2P_2O_7$, TiO_2(a)
1.5	a.ph.	a.ph.	$NaTi_2(PO_4)_3$, $Na_4(TiO)(PO_4)_2$, $Ni_{0.5}(TiO)(PO_4)$, $Ni_2P_2O_7$, TiO_2(a)
1	a.ph.	a.ph.	$NaTi_2(PO_4)_3$, $Na_4(TiO)(PO_4)_2$, $Ni_{0.5}(TiO)(PO_4)$, $Ni_2P_2O_7$, TiO_2(a)
0.5	a.ph.	a.ph.	$NaTi_2(PO_4)_3$, $Na_4(TiO)(PO_4)_2$, $Ni_{0.5}(TiO)(PO_4)$, $Ni_2P_2O_7$, $Ti_9P_7O_{35}$

* a.ph., amorphous halo; a, anatase; ?, the phase may be present; the same in Table 5.

Table 5. Phase composition of coatings formed on niobium in an electrolyte containing $Na_6P_6O_{18}$ and $Ni(CH_3COO)_2$, as determined on a D8 instrument

n	Initial coating	Annealing temperature, °C		*n*	Initial coating	Annealing temperature, °C	
		500	800			500	800
–	X.r.a.	Nb_2O_5	Nb_2O_5	2	a.ph.	Nb_2O_5	Nb_2O_5 + $NbO(PO_4)$
10	X.r.a.	Nb_2O_5	Nb_2O_5	1.5	a.ph.	Nb_2O_5	Nb_2O_5 + $NbO(PO_4)$
7.5	X.r.a.	Nb_2O_5	Nb_2O_5 + $NbO(PO_4)$ + $P_2O_5 \cdot 9Nb_2O_5$	1	a.ph.	X.r.a.	Nb_2O_5 + $Ni_2P_2O_7$
5	X.r.a.	Nb_2O_5	Nb_2O_5 + $NbO(PO_4)$ + $P_2O_5 \cdot 9Nb_2O_5$	0.5	a.ph.	X.r.a.	Nb_2O_5 + $Ni_2P_2O_7$
3	X.r.a.	Nb_2O_5	Nb_2O_5 + $NbO(PO_4)$				

duction of nickel acetate, results in that sodium titanophosphate $Na_4(TiO)(PO_4)_2$, nickel titanophosphate $Ni_{0.5}(TiO)(PO_4)$, and nickel diphosphate $Ni_2P_2O_7$ additionally crystallize in the layers. As *n* in the forming electrolyte decreases, the number of the phases recorded grows.

In layers formed on niobium, in contrast to those on titanium, annealing leads to crystallization of a considerably lesser amount of phosphates. These are $NbOPO_4$ and, at $n \le 1$, nickel diphosphate (Table 5). It is noteworthy that annealing of a powdered coating, formed on an aluminum alloy in an electrolyte with Ni(II) polyphosphate complexes at low values of *n* and then detached from the aluminum support, results in the crystallization of Al_2O_3, $NiAl_2O_4$, and $Ni_2P_2O_7$. Consequently, layers with the widest diversity of phosphates are formed on titanium. This is in an agreement with the above-mentioned result that the phosphorus content of PEO layers on titanium exceeds that on other supports.

The study showed that annealing of the samples with coating formed in an electrolyte with polyphosphate complexes of magnesium on niobium and zirconium (Table 3) leads to the following sequence of phase transformations: on niobium

$$\text{Amorphous phase} \xrightarrow{1000^\circ C} Nb_2O_5 + \alpha\text{-}Mg_2P_2O_7$$

and on zirconium:

$$ZrO_2(c) + ZrO_2(m) \xrightarrow{1000^\circ C} ZrO_2(c) + ZrO_2(m) + NaMgPO_4,$$

where c stands for the cubic or tetragonal modification of zirconium oxide, and m, for its monoclinic modification.

The micrographs in Fig. 3 show the surface organization of PEO structures formed on the titanium alloy in an electrolyte containing 30 g l^{-1} $Na_6P_6O_{18}$ and $Ni(CH_3COOO)_2$ at different values of *n*.

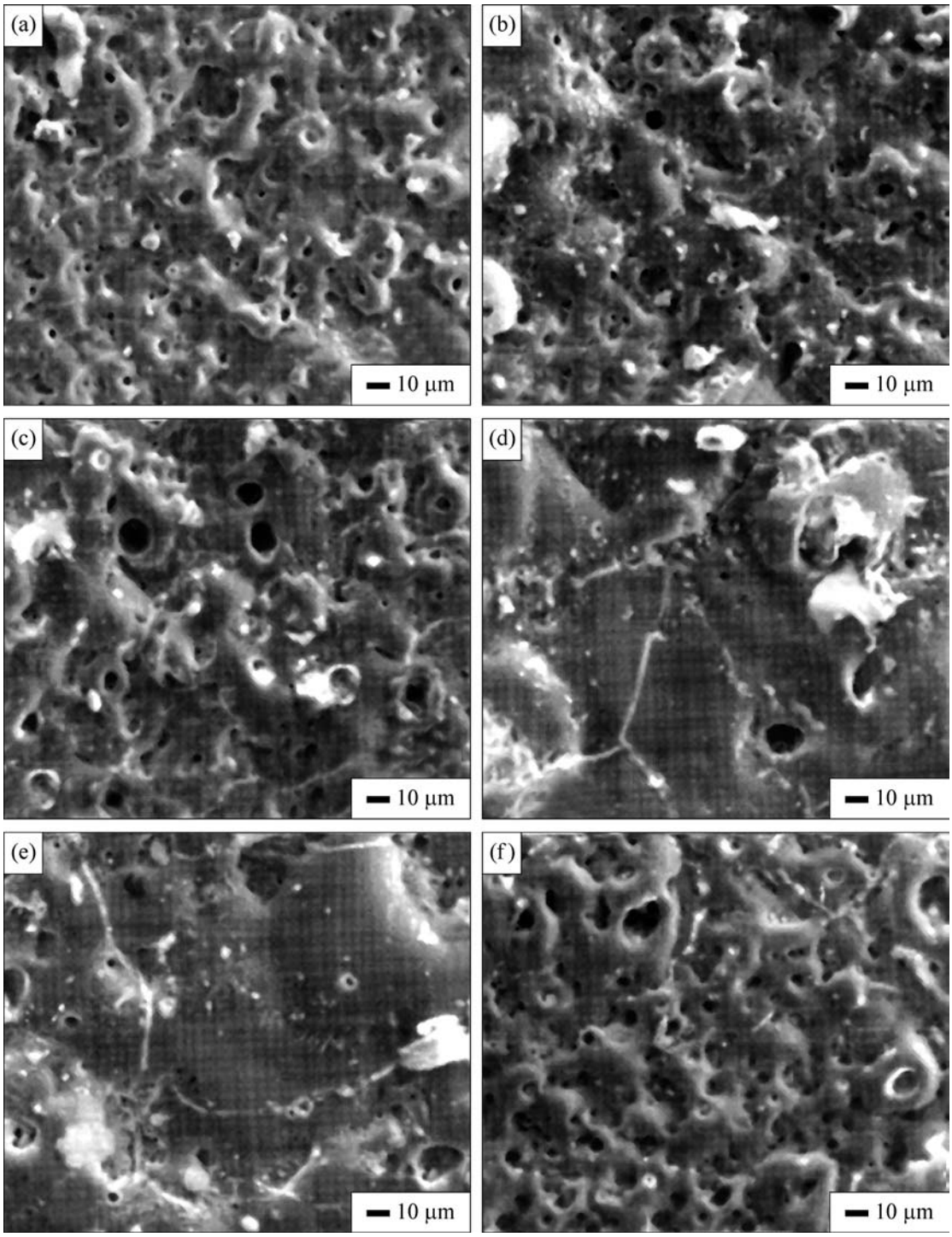


Fig. 3. Surface of PEO structures formed on titanium in an electrolyte containing 30 g l^{-1} $Na_6P_6O_{18}$ + $Ni(CH_3COO)_2$. (a) without $Ni(Ac)_2$; *n*: (b) 7.5; (c) 2, (d) 1.5, (e) 1, and (f) 0.5.

The most uniform and dense, as if partly melted, were coatings obtained at *n* equal to 1 and 1.5, i.e., in the region of transition to a solution with a precipitate. At *n* greater than 1.5 or equal to 0.5, the surfaces have a developed profile and a considerable porosity. It is believed that the pores seen in the micrographs (Fig. 3) are traces of the break-down channels, and the regions surrounding them, subjected to a virtually pulsed heating (the cross-sections of electric discharges vary within 0.01–1.35 mm^2 and

the lifetime of a discharge is ~0.25–3.5 ms [23]) and cooling (the electrolyte has nearly room temperature), contain the highest concentrations of the electrolyte components.

The anodic PEO structures are formed by two basic concurrent processes: (a) electrochemical oxidation on the surface free of discharges and (b) high-temperature synthesis in the breakdown channels. The conditions created in the discharge regions and adjacent zones (high temperature, pressure differences, and electrolyte evaporation) initiate high-temperature reactions involving the electrolyte components, the electrode, and the anode film. These reactions are characteristic of plasmochemistry, hydrothermal synthesis, interactions in melts, solid-phase synthesis, and thermal transformation of precipitates formed from an electrolyte. In these cases, reaction products that are insoluble in the electrolyte remain in the coatings.

The previously obtained results [1–4, 14–16] and our data show that the thermolysis of a precipitate formed in an electrolyte containing metal polyphosphate complexes at $n < 3–6$ makes the main contribution to the formation of PEO layers on rectifying metals and alloys. According to [13, 24–29], annealing at approximately 300°C of the precipitates filtered-off from the solutions containing metal polyphosphate complexes, i.e., hydrated polyphosphates of M(II), M(III), and M(IV), leads to dehydration, rupture of polyphosphate chains or cycles, and formation of a mixture of amorphous or crystalline phosphates of varied structure and degree of condensation. Further heating and prolonged keeping at temperatures of 300 to 900°C (depending on the polyphosphate structure and type of a cation) leads to formation of a high-temperature phosphate characteristic of the given cation in amorphous or crystalline state. For example, for Cu(II), Ni(II), Co(II), Mn(II), and Ba(II), this is a cyclic tetrametaphosphate $M^{II}_2P_4O_{12}$ [26]; for Y(III), Eu(III), and La(III), these are polyphosphates $Ln(PO_3)_3$ [27, 28];, and for Ga and Al, phosphates $M^{III}PO_4$ [29]. A fast cooling of the melt may lead to formation of metaphosphate glasses $M^{II}O \cdot P_2O_5$ or $M^{III}_2O_3 \cdot 3P_2O_5$ [8].

As for the mechanism of thermolysis of polyphosphate complexes in near-breakdown regions on a rectifying anode, it is in part similar to, and partly different from that established in [13, 24–29] in a study of annealing of precipitates formed in the similar solutions. The difference consists in that thermolysis of polyphosphates in anodizing under the action of electrical discharges occurs in specific conditions (parallel deposition and thermolysis in the vapor phase, pulsed changes in pressure and temperature, action of an electric field and illumination). The thermolysis and its products are affected by the nature of the anode metal. Polyphosphates or hightemperature M(II) and M(III) phosphates containing the $AlPO_4$ impurity phase are major thermolysis products formed on aluminum and its alloys (these compounds are also formed in annealing of the precipitates), whereas phosphatotitanates are mostly formed on titanium. In the latter case, polyphosphates or products of their thermolysis intensely interact with titanium or its oxide. Consequently, the thermal transformation mechanism is affected by presence in the reaction regions of rectifying metal, its oxide, and a large number of of other elements: carbon, sodium, alloying additives to rectifying metals and alloys (manganese, iron, magnesium, silicon, etc.). Moreover, it should be kept in mind that the thermolysis of a precipitate from the electrolyte is not the only anode process. In the near-breakdown region there may occur reactions characteristic of plasmochemistry, interactions in melts, solid-phase interactions, and photolysis and electrolysis of water. These processes can also affect the thermolysis mechanism and contribute to the coating formation.

Intense incorporation of the electrolyte components into PEO-coatings in the regions of instability, where the electrolytes containing metal polyphosphates and salts are in the metastable state, suggests that a similar phenomenon can take place in a variety of electrolytes capable of forming precipitates under certain conditions.

CONCLUSIONS

(1) For anodic layers formed on titanium, niobium, and zirconium electrodes in polyphosphate aqueous electrolytes under the action of electrical discharges, the relationship between the concentration of electrolyte components and the elemental composition and thickness of the layers is the same as that for layers formed on aluminum.

(2) For layers formed under similar conditions in electrolytes containing metal polyphosphate complexes, the rectifying metals can be arranged in the following order with respect to the phosphorus content in the layers (wt %) and their thickness: Ti > Nb > Al.

(3) In the course of annealing of the coatings formed on titanium, both metal phosphates incorporated into a polyphosphate complex and metal polyphosphates crystallize.

ACKNOWLEDGMENTS

The study was supported by a grant from the President of the Russian Federation (project no. MK-3559.2004.3).

REFERENCES

1. Rudnev, V.S., Yarovaya, T.P., Boguta, D.L., *et al., Elektrokhimiya*, 2000, vol. 36, no. 12, pp. 1457–1462.
2. Boguta, D.L., Rudnev, V.S., Yarovaya, T.P., *et al., Zh. Prikl. Khim.*, 2000, vol. 73, no. 8, pp. 1296–1300.
3. Rudnev, V.S., Yarovaya, T.P., Boguta, D.L., *et al., J. Electroanal. Chem.*, 2001, vol. 497, nos. 1–2, pp. 150–158.
4. Rudnev, V.S., Gordienko, P.S., Yarovaya, T.P., *et al., Elektrokhimiya*, 1994, vol. 30, no. 7, pp. 914–917.
5. Rudnev, V.S., Yarovaya, T.P., Morozova, V.P., *et al., Zashch. Met.*, 2001, vol. 37, no. 1, pp. 79–84.
6. Rudnev, V.S., Tyrina, L.M., Nikitin, V.M., *et al., Zashch. Met.*, 2003, vol. 39, no. 4, pp. 376–379.
7. Kondrikov, N.B., Rudnev, V.S., Vasil'eva, M.S., *et al.*, Abstracts of Papers, *I Vserossiskaya Konferentsiya "Khimiya dlya avtomobil'nogo transporta-2004"* (I All-Russia Conf. "Chemistry for Auto Transport-2004"), Novosibirsk: Inst. Kataliza, Sib. Otd., Ross. Akad. Nauk, 2004, pp. 67–68.
8. Konstant, Z.A. and Dindune, A.P., *Fosfaty dvukhvalentnykh metallov* (Phosphates of Divalent Metals), Riga: Zinatne, 1987.
9. Bondar', I.A. and Mal'shikov, A.E., *Fosfaty elementov chetvertoi gruppy* (Phosphates of Fourth-Group Elements), St. Petersburg: Nauka, 1992.
10. Litvin, B.N. and Masloboev, V.A., *Redkozemel'nye fosfaty* (Rare-Earth Phosphates), Leningrad: Nauka, 1989.
11. Menon, R., Loo, H.S., Guin, J.A., *et al., Energy Fuels*, 1996, vol. 10, no. 3, pp. 579–586.
12. Mosner, P., Trojan, M., and Kalenda, P., *Sb. Ved. Praci, Vys. Skola Chem. Technol., Pardubice*, 1994, vol. 54, pp. 119–122.
13. Tananaev, I.V., *Zh. Neorg. Khim.*, 1984, vol. 29, no. 2, pp. 467–483.
14. Tyrina, L.M., Rudnev, V.S., Bulanova, S.B., *et al., Zashch. Met.*, 2003, vol. 39, no. 4, pp. 371–375.
15. Boguta, D.L., Formation of Anodic Coatings on Aluminum and Aluminum Alloys in Electrolytes with Polyphosphate Complexes of Metals at Sparking and Breakdown Potentials, *Cand. Sci. Dissertation*, Vladivostok, 2001.
16. Boguta, D.L., Rudnev, V.S., Yarovaya, T.P., *et al., Zh. Prikl. Khim.*, 2002, vol. 75, no. 10, pp. 1639–1642.
17. *Spravochnik metallista* (Metal Worker's Handbook), Rakhshtadt, A.G, and Brostrem, V.A., Eds., Moscow: Mashinostroenie, 1976, vol. 2, pp. 464–498.
18. Li, Y., Shimada, H., Sakaizi, M., *et al., J. Electrochem. Soc.*, 1997, vol. 144, no. 3, pp. 866–876.
19. Marchenoir, J.C., Loup, J.P., and Masson, J., *Thin Solid Films*, 1980, vol. 66, no. 3, pp. 357–369.
20. Gnedenkov, S.V., Gordienko, P.S., Lysenko, L.V., *et al., Fiz. Khim. Obr. Mater.*, 1997, no. 2, pp. 65–69.
21. Gordienko, P.S. and Gnedenkov, S.V., *Mikrodugovoe oksidirovanie titana i ego splavov* (Micro-Arc Oxidizing of Titanium and Its Alloys), Vladivostok: Dal'-nauka, 1997.
22. Rudnev. V.S., Gordienko, P.S., Yarovaya, T.P., *et al., Zh. Prikl. Khim.*, 1994, vol. 67, no. 8, pp. 1279–1282.
23. Yerokhin, A.L., Snizhko, L.O., Gurevina, N.L., *et al., J. Phys. D: Appl. Phys.*, 2003, vol. 36, pp. 2110–2120.
24. Tananaev, I.V., Gruntse, Kh., and Chudinova, N.N., *Izv. Akad. Nauk SSSR, Neorg. Mater.*, 1984, vol. 20, no. 6, pp. 887–900.
25. Lazarevski (Oreshnikova), E.V., Kubasova, L.V., Chudinova, N.N., and Tananaev, I.V., *Izv. Akad. Nauk SSSR*, Neorg. Mater., 1980, vol. 16, no. 1, pp. 120–125.
26. Lazarevski (Oreshnikova), E.V., Kubasova, L.V., Chudinova, N.N., and Tananaev, I.V., *Izv. Akad. Nauk SSSR, Neorg. Mater.*, 1982, vol. 18, no. 9, pp. 1544–1549.
27. Ezhova, Zh.A., Tananaev, I.V., and Koval, E.M., *Zh. Neorg. Khim.*, 1978, vol. 23, no. 11, pp. 2987–2994.
28. Ezhova, Zh.A., Tananaev, I.V., Zorina, L.N., *et al., Izv. Akad. Nauk SSSR, Neorg. Mater.*, 1978, vol. 14, no. 11, pp. 2067–2072.
29. Lazarevski (Oreshnikova), E.V., Kubasova, L.V., Chudinova, N.N., and Tananaev, I.V., *Izv. Akad. Nauk SSSR, Neorg. Mater.*, 1982, vol. 18, no. 9, pp. 1550–1556.

ISSN 1070-4272, Russian Journal of Applied Chemistry, 2006, Vol. 79, No. 2, pp. 264–268. © Pleiades Publishing, Inc., 2006.
Original Russian Text © E. A. Fedorova, E. K. Lysova, 2006, published in Zhurnal Prikladnoi Khimii, 2006, Vol. 79, No. 2, pp. 264–268.

APPLIED ELECTROCHEMISTRY AND CORROSION PROTECTION OF METALS

Chemisorption of Adamantane and Its Derivatives on the Surface of Anodically Polarized Aluminum and Titanium Alloys in Anodizing Electrolytes

E. A. Fedorova and E. K. Lysova

State Technical University, Nizhni Novgorod, Russia

Received July 7, 2005

Abstract—The mechanism of action of adamantane compounds added as modifying agents to anodizing electrolytes was studied. The additives improve the electrically insulating properties of the surface of aluminum and titanium alloys during anodic treatment.

DOI: 10.1134/S1070427206020170

The theoretical and practical interest in surfactants whose molecules contain adamantane structures increases owing to their high lipophilicity [1], thermal stability [2], chemical and electrochemical stability in anodic-treatment processes [3–6], and other distinctive properties [7]. To expand the application areas of adamantane derivatives, it is of importance to reveal the mechanism of their surface activity.

Previously, we have studied the surface activity and adsorption of adamantane and of a number of its derivatives on the untreated and anodically polarized iron, aluminum, and titanium alloys in highly concentrated electropolishing electrolytes, in which ions have virtually no hydration shells [3, 4].

The introduction of adamantane and its derivative, remantadinum, into low-concentrated anodizing solutions based on sulfuric and oxalic acids (up to 0.6 M) appeared to be effective in formation of anodic oxide films (AOF) on aluminum alloys [8].

According to [9], chemisorption from aqueous solutions onto metal oxides cannot take place, because, having a higher affinity for the surface, water molecules hinder adsorption of other compounds. Therefore, the present study is devoted to analysis of surface phenomena at the alloy–solution and AOF–solution interfaces in low-concentrated aqueous solutions for anodizing of aluminum and titanium alloys.

EXPERIMENTAL

Samples of aluminum (AMts, AMg, and D16) and titanium (VT10, VT6, and VT16) alloys were subjected to anodic oxidation in an electrolyzer with a cooling unit and lead cathodes.

Standard anodizing solutions (0.55 M $H_2C_2O_4$ and 0.15 M H_3BO_3 + 0.075 M $Na_2B_4O_7$) were modified by addition in an amount of 1.0–3.0 g l^{-1} of the following organic compounds: adamantane (Ad) $C_{10}H_{16}$, remantadinum (Rem) $C_{10}H_{15}$–NH_2–$C_2H_4 \cdot HCl$ (1-α-aminoethyladamantane hydrochloride), and fluoroderivatives of adamantane, hexafluoropropyl adamantanol $C_{10}H_{15}$–C_3HF_6 (Ad–R_1F_6) and perfluoro-1-propenyl adamantanol $C_{10}H_{15}$–CF=$CFCF_3$ (Ad–R_2F_5).

We used for anodic polarization of electrodes a PI-50-1 potentiostat, LKD-4 *X*–*Y* recorder, three-electrode cell, and saturated silver-chloride reference electrode.

We studied surface phenomena at the alloy–solution, solution–air, and AOF–solution interfaces, using methods for measurement of contact angles with a Wilhelmi plate [4, 10], boundary tension of solutions after Rebinder [4], and surface hardness after Rebinder [3, 9].

We determined the contact angles from the length l of the chords of a drop profile and drop height h, both measured with a reading microscope by the procedure described in [4], with the drop assumed to be spherical:

$$\theta = 2\arctan(2h/l), \quad (1)$$

$$\cos\theta = \frac{(l/2)^2 - h}{(l/2)^2 + h}. \quad (2)$$

Table 1. Electrically insulating properties of oxide films on Al and Ti alloys in relation to addition of remantadinum, adamantane, and its fluoroderivatives to an electrolyte

Alloy brand	Electrolyte composition, g l^{-1}	Process mode		Electrically insulating properties of AOF	
		j_a, A dm^{-2}	τ, min	R_{ins}, 10^{-10} Ω	U_{br}, kV
AMts	50 $H_2C_2O_4$	1.0	60	0.8	2.0
	50 $H_2C_2O_4$, 1.0 Ad	1.0	30	1.0	3.0
AMg	50 $H_2C_2O_4$ + 50 H_2SO_4	2.5	60	1.0	2.7
	50 $H_2C_2O_4$ + 50 H_2SO_4, 3.0 Ad	2.5	60	1.2	4.5
	50 $H_2C_2O_4$, 3.0 Ad	1.0	40	1.7	4.5
AMts	50 $H_2C_2O_4$, 2.0 Ad–R_1F_6	1.0	40	0.8	3.0
	50 $H_2C_2O_4$, 3.0 Rem	1.0	60	0.6	3.0
D16	50 $H_2C_2O_4$, 3.0 Ad	1.0	40	1.0	3.5
VT10	10 H_3BO_3 + 15$Na_2B_4O_7$	10	90	0.0005	1.0
	10 H_3BO_3 + 15 $Na_2B_4O_7$, 2.0 Rem	10	60	0.0010	1.7
VT6	10 H_3BO_3 + 15 $Na_2B_4O_7$, 2.0 Ad–R_2F_5	10	60	0.0003	0.6
VT16	10 H_3BO_3 + 15 $Na_2B_4O_7$	10	90	0.0007	2.0
	10 H_3BO_3 + 15 $Na_2B_4O_7$, 3.0 Rem	10	60	0.0015	3.0

Table 2. Parameters of spreading of a drop of $H_2C_2O_4$ solution (0.55 M) on the surface of AMg alloy in relation to the amount of remantadinum additive introduced into the electrolyte

Rem concentration, g l^{-1}	V_{sp} (±0.2), deg min^{-1}	$\Delta l = l_{running} - l_0$	$\Delta h = h_{running} - h_0$	ΔG^0_{sp}, mJ m^{-2}
		mm		
0.0	3.9	0.70	0.2	29.8
0.2	3.2	0.70	0.1	29.2
1.0	2.9	0.70	0.1	27.0
2.0	2.0	0.45	0.05	24.7
3.0	1.5	0.45	0.03	21.0
4.0	1.5	0.45	0.04	19.0

To establish the presence of adamantane and its derivatives in anodic oxide films formed on the surface of alloys in electrolytes with these compounds added, we used the highly sensitive method of mass-spectrometry, combined with chromatography [11].

The breakdown voltage U_{br} (kV) and the electrical resistance R_{ins} (Ω) of the anodic oxide films, which characterize the dielectric properties of the these coatings, were measured with a UPU-1 voltmeter and an E6-17 megohmmeter, respectively. The porosity of the anodic oxide films formed on aluminum and titanium alloys during anodizing was determined in conformity with GOST (State Standard) 9.302–88 [12].

In aqueous solutions of sulfuric and oxalic acids or their mixtures to be used for anodizing of aluminum alloys and in a boric–borate solution for anodizing of titanium alloys, adamantane and its derivatives improved the electrically insulating properties of the anodic oxide films formed. The maximum resistance and breakdown voltage of anodic oxide films were obtained on aluminum alloys in the presence of an adamantane additive in the oxalic acid solution (Table 1). It was found that R_{ins} and U_{br} of films on anodized titanium alloys VT10 and VT16 increase when Rem, Ad–R_1F_6, and Ad–R_2F_5 are added to the boric-borate electrolyte (Table 1).

On the whole, the resistivity and breakdown voltage of oxide films on alloys of various brands increased by a factor of 1.3–2.3, with the process duration becoming shorter, in the presence of Ad, Rem, Ad–R_1F_6, and Ad–R_2F_5 in anodizing solutions (Table 1). In this case, the porosity of AOF on alloys of various brands decreased by a factor of 1.3–1.5.

The kinetic aspects of spreading of a drop of an oxalic acid solution with and without a remantadinum additive, obtained on an untreated surface of the AMg alloy (Table 2 and Fig. 1), allowed us to estimate changes in drop parameters (chord Δl, height Δh, and

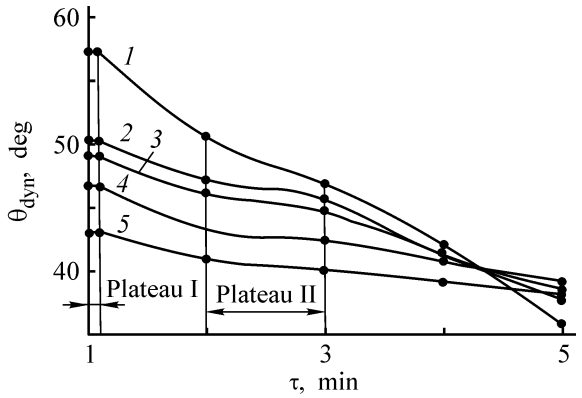


Fig. 1. Kinetic curves for spreading of a drop of an oxalic acid solution on the surface of the AMg alloy. (θ_{dyn}) dynamic contact angle of a solution drop and (τ) spreading time. 0.55 M solution of $H_2C_2O_4$ with a Rem additive (g l^{-1}): (*1*) 0, (*2*) 1.0, (*3*) 2.0, (*4*) 3.0, and (*5*) 4.0.

the rate of its spreading V_{sp}), depending on the Rem concentration and process duration. The presence of Rem in the background solution virtually eliminated spreading of drops in the first 5 min and made it possible to reduce V_{sp} by more than a factor of 2 (Table 2).

In the presence of Rem in the oxalic acid solution, the θ–τ curves have two well-pronounced plateaus characterized by quasi-equilibrium contact angles θ_0 and θ, respectively (Fig. 1). Transition from the quasi-equilibrium state of the surface (plateau I), which reflects the efficiency of competitive adsorption of solution components, to the second portion (plateau II), which characterizes the drop spreading in the viscous diffusion mode, can be evaluated by the driving force of spreading or by the Gibbs energy of spreading, ΔG_{sp} (mJ m^{-2}):

$$\Delta G^0_{sp} = \sigma_{s-g}(\cos\theta_0 - \cos\theta). \quad (3)$$

Here σ_{s-g} is the surface tension at the solution–air interface.

Comparison of the Gibbs energies of spreading of the background solution and that with a Rem additive (Table 2) confirms the hindering effect of the organic additive on the anodic dissolution of the alloy.

We can make the following conclusions on the basis of the experimental and calculated data of Table 2: (i) the decrease in the spreading rate with increasing concentration of remantadinum indicates that the surface chemical reaction and etching processes are hindered by the additive in use; (ii) the $\theta_{din} = F(\tau)$ curves level-off to form a plateau in the presence of Rem in the solution (Fig. 1), which suggests that there is a limiting saturation of the surface layer with remantadinum agglomerates.

The adsorption of Rem on the alloys was determined according to [3] from the surface tension isotherm by graphical differentiation of the dependence $\sigma\cos\theta = f(\ln c)$, using Eq. (4).

$$\Gamma = \frac{d(\cos\theta)\sigma}{dc}\frac{c}{RT}. \quad (4)$$

Here θ is the contact angle of an electrolyte drop and c is the surfactant concentration in solution.

The maximum surface concentration Γ_{max} of Rem in the oxalic acid solution on the AMg alloy was 9.0×10^{-7} mol cm^{-2}. As a rule, the concentrations of $(1–5) \times 10^{-10}$ mol cm^{-2} correspond to a monolayer of an adsorbate on a geometrically smooth surface in the absence of complex intermolecular interactions [10].

Γ_{max} was found in a similar way to be 1.2×10^{-9} mol cm^{-2} for remantadinum in a boric-borate solution on the VT16 alloy.

The resulting overestimated Γ_{max} values, especially on the surface of an aluminum alloy, seem to indicate the following: bulky skeleton agglomerates of surface compounds are formed; there occurs capillary absorption of a solution enriched with an organic substance by the alloy surface and the anodic oxide layer formed; there exists a polymolecular electrolyte layer retaining the saturated solution of an organic substance; and the aging and the subsequent decomposition of supersaturated solutions of organic compound, formed near the electrode surface, are accelerated. Mass-spectrometric data support such a mechanism of action of adamantane additives.

The anodic oxide films formed on the surface of alloys during oxidizing were subjected to cathodic reduction in a 20% H_2SO_4 solution, the solution was neutralized, and then organic components were extracted with methylene chloride. The extracted solution was analyzed in a mass-spectrometer, in which the substance under study was transferred into the gaseous state by electron impact, with the molecules ionized, the resulting ions separated, and their masses and relative amounts recorded in accordance with their mass-to-charge ratio mz^{-1} [11].

Adamantane hydrocarbons markedly differ from other polycyclic hydrocarbons in the nature of their disintegration. They rather readily form a highly stable adamantyl cation $C_{10}H^+_{15}$ characterized by the ratio $mz^{-1} = 135$, as recorded in a mass spectrogram.

In all probability, molecules of adamantane and its derivatives are sorbed on the surface of alloys because of the presence of active species of the adamantyl cation $C_{10}H_{15}^{+}$. Furthermore, remantadinum and electronegative fluoropropyl derivatives of adamantane can be also adsorbed on those parts of the surface which have an excess positive charge owing to the presence of unpaired electrons of nitrogen or fluorine atoms.

An addition of Rem to a boric-borate solution decreased the surface hardness H on the VT16 titanium anode in a wide range of potentials, the effect being the most pronounced at $E > 2.0$ V in the region of oxide formation (Fig. 2). Alternating maxima and minima in the H–E dependence, observed in the additive-free solution, can be accounted for by the presence of several electrocapillary curves [3, 9, 13, 14]. The observed decrease in H values near the peaks of the electrocapillary curves in the presence of remantadinum in the anodizing electrolyte is due to adsorption of Rem molecules on the surface of the anode under study.

Therefore, only organic compounds that form stronger chemical bonds with the surface than the hydrogen bond can be selectively adsorbed on the surface of alloys in the anodically polarized state, with water replaced from the surface.

According to Nechaev's chemisorption theory [15, 16], the adsorption of organic substances on the surface of metals and their oxides from aqueous solutions is determined by the fact that molecules of organic substances have potentials E_i close to the resonance ionization potentials E_r of a metal or an oxide, which actually are sorption characteristics of a solid (a difference of no more than 0.1–0.15 eV between the E_i and E_r values is possible).

The resonance ionization potential of titanium oxide TiO_2 is 9.7 eV [15]; among modifying additions, remantadinum and perfluoro-1-propenyladamantanol have ionization potentials the closest to this value (Table 3). These additives provided the most pronounced improvement of the electrically insulating characteristics of AOF formed on titanium alloys (Table 1).

Thus, we can consider confirmed that the effect of modifying organic additives in anodizing electrolytes on the results of the anodization is due to their adsorption on the surface of both untreated and anodically polarized alloys. However, this fails to reflect the true mechanism of the effect of organic additives, especially if it is considered in the dynamics of a nonequilibrium process of anodic dissolution of alloys in the passive and trans-passive regions.

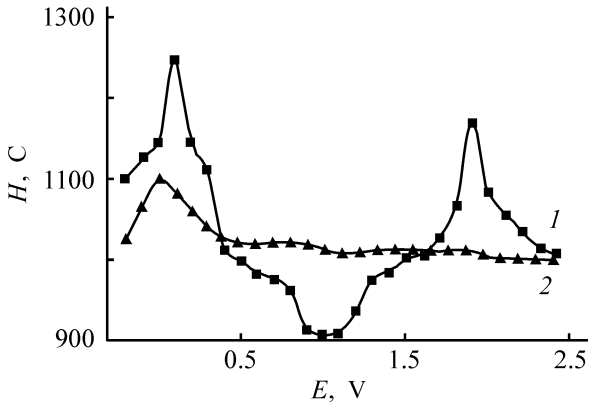


Fig. 2. Dependence of the surface hardness H on the anode potential E of a titanium electrode at 293 K. 0.55 M $H_2C_2O_4$ solution with a Rem additive (g l^{-1}): (*1*) 0, (*2*) 3.0.

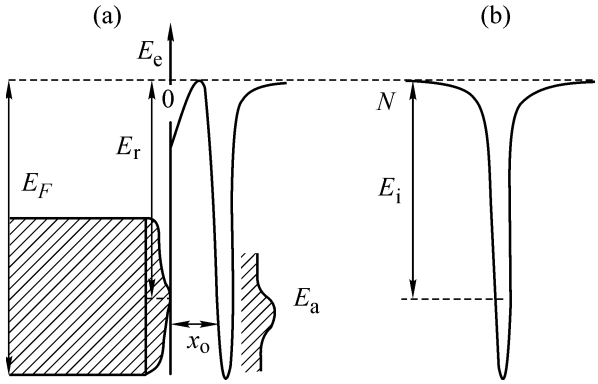


Fig. 3. Schematic of the electron distribution in a system constituted by a metal, oxide film, and adsorbed molecule of an organic substance. (E_e) electron energy, (x_o) distance from the center of an electron orbit to the adsorbent surface, (N) distance to an isolated adsorbent molecule. (a) Adsorbed organic molecule with a shifted electron level $\Delta E = E_a + E_i$, where E_a is the potential of an adsorbed molecule; E_F, position of the Fermi level in the metal; and E_r, resonance ionization potential of the oxide; (b) an isolated molecule with an ionization potential E_i.

Electrons in a molecule of an organic compound in the solution bulk occupy strictly fixed levels with energies determined by the ionization potential E_i (Fig. 3). When an organic molecule approaches

Table 3. Ionization potentials E_i of selected organic compounds [17]

Compound	E_i, eV
$C_{10}H_{16}$	9.25 ± 0.03
$C_{10}H_{15}$–OH	9.23 ± 0.03
$C_{10}H_{15}$–CF=$CFCF_3$	9.55 ± 0.03
$C_{10}H_{15}$–NH_2–C_2H_4 · HCl	9.60 ± 0.03

the surface of the anode, its electron levels are split owing to the interaction of electrons of the adsorbate with those of the adsorbent, with the levels shifted by ΔE [15, 16]. As a result, a set of levels with different energies appears instead of a strictly fixed electron level. The difference between the energies of the system with molecules situated far from an adsorbent surface and directly on the surface determines the adsorption energy E_{ads}.

It has been shown [4] that multiply charged ions of metals entering into the composition of the alloys under study are formed in stages via intermediate formation of monovalent ions (subions): Al^+, Ti^+, V^+, Mo^+, etc., which are further anodically oxidized to the ions Al^{3+}, Ti^{4+}, V^{5+}, and Mo^{6+}.

When the electron wave functions of the adsorbate and adsorbent molecules overlap, there occurs an exchange interaction to form a common electron system. The chemical bond formed in this way is similar in nature to a covalent bond, and the energy gain is determined by the change in the energy of electrons upon the formation of this bond. Both π and σ electrons of the adsorbate can be involved in bond formation.

Thus, we can assume that it is the stage-by-stage anodic dissolution of metals contained in alloys in the series $Ti^+ \rightarrow Ti^{3+} \rightarrow Ti^{4+}$, $Al^+ \rightarrow Al^{3+}$, and others that ensures the strength of the surfactant–AOF chemical bond with an energy exceeding that of the hydrogen bond.

CONCLUSIONS

(1) Additives of remantadinum, adamantane, and its fluoroderivatives in oxalate, sulfuric-oxalate, and boric–borate anodizing electrolytes improve the electrically insulating properties of anodic oxide films on aluminum and titanium alloys: the resistivity and the breakdown voltage of films increases by factors of 1.5–2.3 and 1.3–1.5, respectively; and the porosity decreases by a factor of 1.3–1.5.

(2) The additives have a surface-active effect at the solution–air and solution–alloy interfaces and, being adsorbed on the untreated and anodically polarized surfaces of the alloys, can enter in the composition of the forming oxide layer.

(3) The maximum adsorption of remantadinum on AMg and VT16 alloys was calculated. The high value of Γ_{max} indicates that the adsorption is accompanied by the formation of complex agglomerate structures constituted by remantadinum molecules and metal ions contained in alloys. It is probable that a strong chemisorption of adamantane compounds on the anodically polarized surface of the alloys becomes possible because of the stage-by-stage ionization of various metals contained in the alloys.

REFERENCES

1. Abramzon, A.A. and Golod, E.L., *Zh. Prikl. Khim.*, 1999, vol. 72, no. 2, pp. 327–329.
2. Sevast'yanova, V.V., Krayushkin, M.M., and Yurchenko, A.G., *Fiz. Khim.*, 1970, vol. 39, no. 10, pp. 1721–1753.
3. Fedorova, E.A., Naumov, V.I., and Shul'pina, I.G., *Elektrokhim.*, 1993, vol. 29, no. 5, pp. 585–591.
4. Fedorova, E.A., *Zh. Prikl. Khim.*, 2003, vol. 76, no. 9, pp. 1483–1489.
5. Fedorova, E.A., *Zh. Prikl. Khim.*, 2001, vol. 74, no. 4, pp. 598–602.
6. Fedorova, E.A., *Zh. Prikl. Khim.*, 2001, vol. 74, no. 11, pp. 1775–1779.
7. Bagrii, E.I., *Adamantany: Poluchenie, svoistva, primenenie* (Adamantanes: Preparation, Properties, Application), Moscow: Nauka, 1989.
8. Fedorova, E.A., *Trudy Vserossiskoi Nauchno-prakticheskoi Konferentsii "Sovremennaya Elektrotekhnologiya v Promyshlennosti Rossii"* (Proc. All-Russia Sci.-Pract. Conf. "Modern Electrical Technology in the Industry of Russia"), Tula, 2003, pp. 183–191.
9. Rebinder, P.A. and Venetrem, E.K., *Zh. Fiz. Khim.*, 1945, vol. 19, no. 1, pp. 1–7.
10. Adamson, A.W., *Physical Chemistry of Surfaces*, New York: John Wiley & Sons, 1976.
11. Zaikin, V.G., Varlamov, A.V., Mikaya, A.I., and Prostakov, N.S., *Osnovy mass-spektrometrii organicheskikh soedinenii* (Fundamentals of Mass-Spectrometry of Organic Compounds), Moscow: MAIK Nauka/Interperioidika, 2001.
12. *GOST* (State Standard) *9.302–88: Metallic and Nonmetallic Inorganic Coatings: Monitoring Methods.*
13. Naumov, V.I., Starodubrovskaya, I.N., Izotova, V.V., and Tyurin, Yu.M., *Elektrokhimiya*, 1980, vol. 16, no. 11, pp. 1892–1898.
14. Naumov, V.I., Sazont'eva, T.V., and Tyurin, Yu.M., *Elektrokhimiya*, 1988, vol. 24, no. 9, pp. 1455–1462.
15. Nechaev, E.A., *Khemosorbtsiya organicheskikh veshchestv na oksidakh i metallakh* (Chemisorption of Organic Substance on Oxides and Metals), Khar'kov: Vyshcha Shkola, 1989.
16. Nechaev, E.A., *Elektrokhim.*, 1986, vol. 22, no. 11, pp. 1552–1556.
17. *Energii razryva khimicheskikh svyazei: Potentsialy ionizatsii i srodstvo k elektronu* (Energies of Rupture of Chemical Bonds: Ionization Potentials and Electron Affinity), Kondrat'ev, V.N., Ed., Moscow: Nauka, 1974.

ISSN 1070-4272, Russian Journal of Applied Chemistry, 2006, Vol. 79, No. 2, pp. 269–271. © Pleiades Publishing, Inc., 2006.
Original Russian Text © A. I. Demidov, M. S. Kokhatskaya, 2006, published in Zhurnal Prikladnoi Khimii, 2006, Vol. 79, No. 2, pp. 269–271.

APPLIED ELECTROCHEMISTRY AND CORROSION PROTECTION OF METALS

Effect of the Concentration of Solutions being Titrated on the Shape of Conductometric Titration Curves

A. I. Demidov and M. S. Kokhatskaya

St. Petersburg State Polytechnic University, St. Petersburg, Russia

Received December 29, 2005

Abstract—The influence exerted by the concentration of solution being titrated on the shape of the theoretical curves of conductometric titration was studied. The concentrations at which the equivalence points are clearly observed in the conductometric titration curves were determined.

DOI: 10.1134/S1070427206020182

Conductometric titration is a technique in which the equivalence point is found by measuring the electrical conductivity of a solution being analyzed. The conductivity changes as a result of chemical reactions between the titrant and the substance being determined that occur in the course of titration [1]. Commonly, theoretical curves of conductometric titration are plotted using the electrical conductivities of infinitely diluted solutions [2]. Because the total electrical conductivity of a solution depends on its concentration, the increase in the initial concentration of a solution being titrated affects the shape of a conductometric titration curve. This can impair the accuracy of analysis and make narrower the areas of its applicability [3].

In the study, the influence exerted by the concentration of the solutions being analyzed on the shape of the theoretical curves of conductometric titration was demonstrated for the example of titration of solutions containing sodium hydroxide, sodium carbonate, mixtures of sodium hydroxide and sodium carbonate, and those of sodium carbonate and sodium hydrocarbonate with sulfuric acid. The concentrations at which the equivalence points are clearly manifested in the conductometric titration curves were determined.

The solutions mentioned above were analyzed in processing of worked-out nickel–iron (NI) batteries, in which aqueous sodium hydroxide solutions are the most frequently used as electrolyte. The drawback of alkaline electrolytes is their susceptibility to carbonization, which mainly occurs via absorption of atmospheric carbon(IV) dioxide. In storage of worked-out NI batteries in air, the electrolyte remaining in pores of the active paste undergoes further carbonization. As a result, sodium hydroxide is converted into sodium carbonate, and the carbonate, into hydrocarbonate [4].

The theoretical dependences of the electrical resistivity of the solutions on the number of titrant equivalents were constructed using data from the reference book [5]. In doing so, the dilution of the solution being analyzed during titration was disregarded. The calculation was performed for solutions with an initial concentration of a substance (or substances) to be determined equal to 0.01–0.1 N. The concentration of the titrant was 0.1 N in all cases.

In titrating a sodium hydroxide solution with a standard solution of sulfuric acid, the total electrical conductivity of the solution, χ_Σ, varies as follows:

before the equivalence point, at $0 < y < 1$,

$$\chi_\Sigma = \chi_{NaOH}(1 - y) + \chi_{Na_2SO_4}y,$$

at the equivalence point, at $y = 1$,

$$\chi_\Sigma = \chi_{Na_2SO_4},$$

after the equivalence point, at $1 < y < 2$,

$$\chi_\Sigma = \chi_{Na_2SO_4} + \chi_{H_2SO_4}(y - 1),$$

where χ_{NaOH} is the electrical conductivity of the initial solution of sodium hydroxide; $\chi_{Na_2SO_4}$, electrical

conductivity of the sodium sulfate solution; and y, number of titrant equivalents.

In titrating a sodium carbonate solution with sulfuric acid, the total electrical conductivity of the solution, χ_Σ, varies in the following manner:

before the first equivalence point, at $0 < y < 1$,

$$\chi_\Sigma = \chi_{Na_2CO_3}(1 - y) + \chi_{NaHCO_3}y + \chi_{Na_2SO_4}y,$$

at the first equivalence point, at $y = 1$,

$$\chi_\Sigma = \chi_{NaHCO_3} + \chi_{Na_2SO_4},$$

before the second equivalence point, at $1 < y < 2$,

$$\chi_\Sigma = \chi_{NaHCO_3}(2 - y) + \chi_{Na_2SO_4}y,$$

at the second equivalence point, at $y = 2$,

$$\chi_\Sigma = 2\chi_{Na_2SO_4},$$

after the second equivalence point, at $2 < y < 3$,

$$\chi_\Sigma = 2\chi_{Na_2SO_4} + \chi_{H_2SO_4}(y - 2),$$

where $\chi_{Na_2CO_3}$ and χ_{NaHCO_3} are the electrical conductivities of the initial solution of sodium carbonate and of the solution of sodium hydrocarbonate, respectively.

Before the titration, the total electrical conductivity of a solution containing sodium hydroxide and carbonate is the sum of the electrical conductivities of the solutions of the initial substances $\chi_\Sigma = \chi_{NaOH} + \chi_{Na_2CO_3}$. During titration, the electrical conductivity of the solution varies as follows: before the first equivalence point, at $0 < y < 1$,

$$\chi_\Sigma = 0.5(\chi_{NaOH} + \chi_{Na_2CO_2})(1 - y) + \chi_{NaHCO_3}(y/2) + \chi_{Na_2SO_4}y,$$

at the first equivalence point, at $y = 1$,

$$\chi_\Sigma = 0.5\chi_{NaHCO_3} + \chi_{Na_2SO_4},$$

before the second equivalence point, at $1 < y < 1.5$,

$$\chi_\Sigma = \chi_{NaHCO_3}(1.5 - y) + \chi_{Na_2SO_4}y,$$

at the second equivalence point, at $y = 1.5$,

$$\chi_\Sigma = 1.5\chi_{Na_2SO_4},$$

after the second equivalence point, at $1.5 < y < 2$,

$$\chi_\Sigma = 1.5\chi_{Na_2SO_4} + \chi_{H_2SO_4}(y - 1.5).$$

During the titration of a solution containing sodium carbonate and hydrocarbonate with sulfuric acid, there first occurs the reaction in which sodium hydrocarbonate $NaHCO_3$ and sodium sulfate Na_2SO_4 are formed:

$$Na_2CO_3 + 1/2\,H_2SO_4 \longrightarrow 1/2\,Na_2SO_4 + NaHCO_3.$$

Further, sodium carbonate originally contained in the solution and sodium carbonate produced in titration are neutralized to give sodium sulfate Na_2SO_4:

$$NaHCO_3 + 1/2\,H_2SO_4 \longrightarrow 1/2\,Na_2SO_4 + H_2O + CO_2.$$

Thus, the electrical conductivity of the solution varies during titration as follows:

before the first equivalence point, at $0 < y < 1$,

$$\chi_\Sigma = \chi_{Na_2CO_3}(1 - y) + \chi_{NaHCO_3}(1 + y) + \chi_{Na_2SO_4}y,$$

at the first equivalence point, at $y = 1$,

$$\chi_\Sigma = 2\chi_{NaHCO_3} + \chi_{Na_2SO_4},$$

before the second equivalence point, at $1 < y < 3$,

$$\chi_\Sigma = \chi_{NaHCO_3}(3 - y) + \chi_{Na_2SO_4}y,$$

at the second equivalence point, at $y = 3$,

$$\chi_\Sigma = 3\chi_{Na_2SO_4},$$

after the second equivalence point, at $3 < y < 5$,

$$\chi_\Sigma = 3\chi_{Na_2SO_4} + \chi_{H_2SO_4}(y - 3).$$

The resulting values of the total electrical conductivity were used to construct the theoretical dependences of the electrical resistivity of the solutions on the number of titrant equivalents (Figs. 1a–1d). It can be seen that the curves obtained in titration of dilute solutions show clearly pronounced inflections corresponding to the equivalence points. It was established that the concentrations of a substance (or a mixture of substances) to be determined, at which the equivalence points are clearly observed in the curves of conductometric titration, should not exceed 0.05 N.

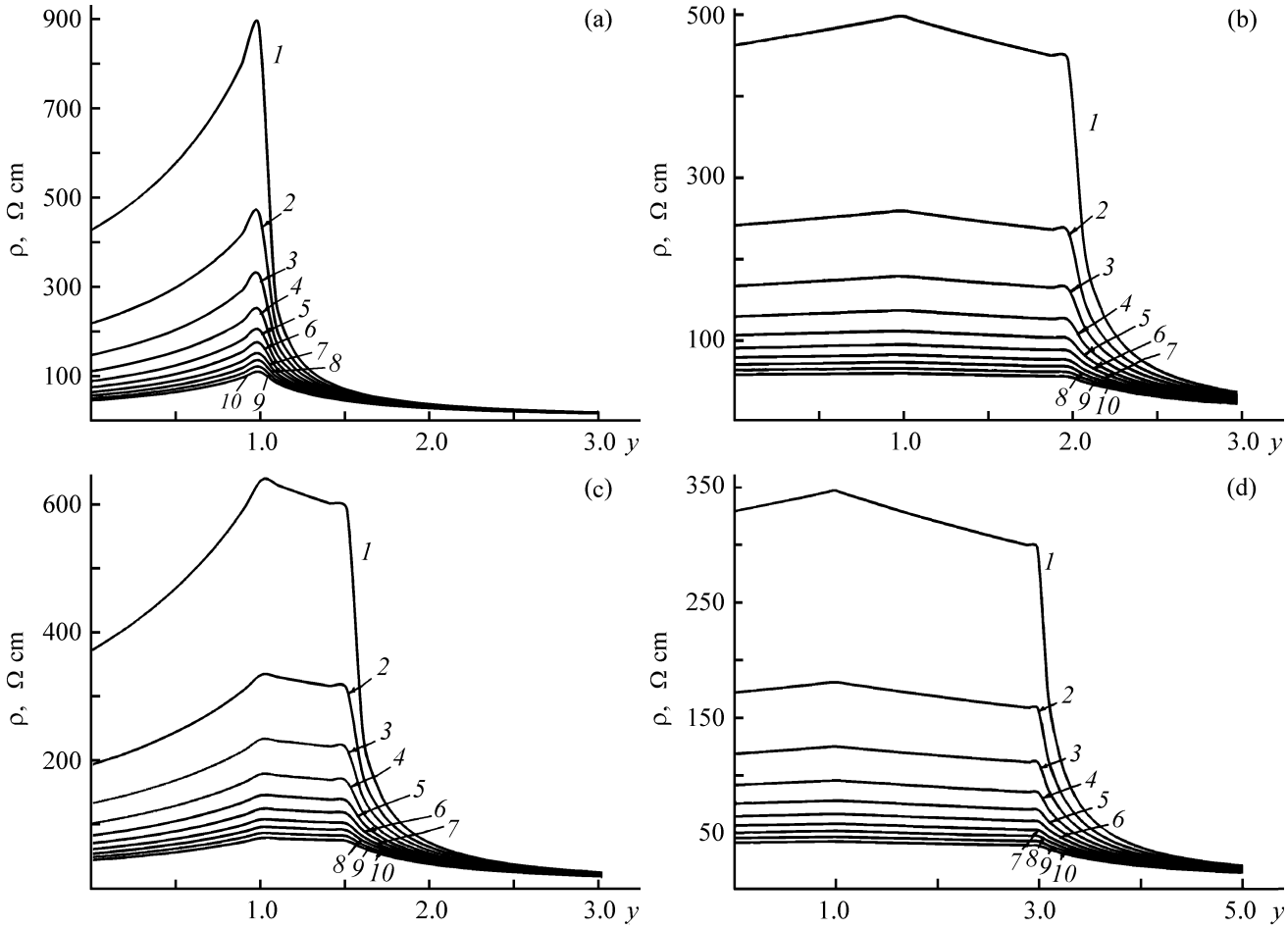


Fig. 1. Theoretical dependence of the electrical resistivity ρ of the solution on the number of titrant equivalents, *y*, in titration of solutions of (a) sodium hydroxide, (b) sodium carbonate, (c) sodium hydroxide and sodium carbonate, and (d) sodium carbonate and sodium hydrocarbonate with 0.1 N H_2SO_4 at 25°C. Concentration (g-equiv l^{-1}): (*1*) 0.01, (*2*) 0.02, (*3*) 0.03, (*4*) 0.04, (*5*) 0.05, (*6*) 0.06, (*7*) 0.07, (*8*) 0.08, (*9*) 0.09, and (*10*) 0.1.

CONCLUSIONS

(1) Theoretical curves of conductometric titration of solutions containing sodium hydroxide, sodium carbonate, mixture of sodium hydroxide and sodium carbonate, and that of sodium carbonate and sodium hydrocarbonate with sulfuric acid were presented and the influence exerted by the concentration of the solutions being analyzed on the shape of the theoretical curves of conductometric titration was demonstrated.

(2) It was found that the concentration of a substance (or a mixture of substances) to be determined, at which the equivalence points are clearly pronounced in the conductometric titration curves, should not exceed 0.05 N.

(3) It was recommended to use conductometric titration to analyze dilute solutions.

REFERENCES

1. Kreshkov, A.P., *Osnovy analiticheskoi khimii: Fizicheskie i fiziko-khimicheskie (instrumental'nye) metody analiza* (Fundamentals of Analytical Chemistry: Physical and Physicochemical (Instrumental) Methods of Analysis), Moscow: Khimiya, 1970, vol. 3.
2. Lopatin, B.A., *Teoreticheskie osnovy elektrokhimicheskikh metodov analiza. Uchebnoe posobie dlya vysshikh uchebnykh zavedenii* (Theoretical Foundations of Electrochemical Analysis. Textbook for Higher-School Students) Moscow: Vysshaya Shkola, 1975.
3. Kazakov, A.V., Kantere, V.M., and Galkin, L.G., *Titrometry* (Titrimeters), Moscow: Mashinostroenie, 1973.
4. Demidov, A.I. and Kokhatskaya, M.S., *Zh. Prikl. Khim.*, 2005, vol. 78, no. 8, pp. 1303–1305.
5. *Spravochnik fizicheskikh, khimicheskikh i tekhnologicheskikh velichin* (Reference Book of Physical, Chemical, and Technological Constants), Martens, L.K., Ed., Moscow: Sov. Entsiklopediya, 1930, vol. 4.

ISSN 1070-4272, Russian Journal of Applied Chemistry, 2006, Vol. 79, No. 2, pp. 272–274. © Pleiades Publishing, Inc., 2006.
Original Russian Text © A. P. Arbatskii, E. P. Traktina, L. A. Smirnova, 2006, published in Zhurnal Prikladnoi Khimii, 2006, Vol. 79, No. 2, pp. 272–274.

APPLIED ELECTROCHEMISTRY AND CORROSION PROTECTION OF METALS

A Titrimetric Study of Chemical Properties of Chitosan

A. P. Arbatskii, E. P. Traktina, and L. A. Smirnova

Nizhni Novgorod State Technical University, Nizhni Novgorod, Russia
Nizhni Novgorod State University, Nizhni Novgorod, Russia

Received October 12, 2005

Abstract—A method for quantitative conductometric titration of chitosan in aqueous hydrochloric and acetic acids was developed. The stoichiometry of complexation of chitosan with Co(II) was studied.

DOI: 10.1134/S1070427206020194

Chitosan, high-molecular-weight polyelectrolyte {poly[β(1-4)-amino-2-deoxy-*D*-glucose]}, is prepared by deacetylation of natural polysaccharide chitin with aqueous alkali. As a rule, the degree of deacetylation ranges from 78 to 92%. Chitosan prepared by this method contains both *D*-glucosamine and *D*-glucosacetamide units. Chitosan and materials on its basis are widely used in various areas: in medicine (dressing), in pharmacology (carriers for drugs of prolonged effect), in aqriculture (encapsulating agents for seed granulation), and in industry (sorbents, selective membranes, flocculants) [1]. The use of chitosan for binding of heavy metals is one of promising areas of its application. Chitosan is coordinated with metals by complicated mechanisms which are poorly understood at present [1]. It is believed that these mechanisms are based on complexation of chitosan macromolecules with metal cations. The binding of metals with chitosan in heterogeneous systems is accompanied by sorption and precipitation, which complicates the elucidation of chitosan-metal interactions. The mechanism of coordination of chitosan with metals in homogeneous solutions is also poorly understood. Only chelation has been discussed, although other kinds of complexation are also possible.

In this study, we developed a technique for quantitative determination of both the chitosan content in solutions and its complexation with cobalt(II).

The main technique used in our experiments was conductometric titration, which allows monitoring of acid-base and coordination interactions in the solutions. This technique is suitable for quantitative determination of the chitosan content in solutions and for study of its complexation with metals. The main aspects of application of conductometric titration to solution of these problems were reported in [2]. The results of conductometric titration are compared with those obtained by pH-metric titration.

EXPERIMENTAL

Solutions of chitosan of a required concentration in 0.1 M aqueous hydrochloric and 0.1 M aqueous acetic acids were used. The molecular weight of chitosan was determined viscometrically in the mixed solvent (0.3 M aqueous CH_3COOH + 0.33 M aqueous NaCl). The viscosity was measured with an Ubbelohde viscosimeter at 21 ± 0.1°C. The chitosan molecular weight was calculated by the equation $[\eta] = KM^{\alpha}$ {$K = 3.41 \times 10^{-3}$ and $\alpha = 1.02$ [3]}.

Solutions of cobalt salts (~1 M) were prepared from their weighed portions in water. The Co(II) concentration was refined by complexometric titration.

The complexation of cobalt with chitosan was studied conductometrically with an Impul's KL-2 conductometer at room temperature. The electrical conductivity of solutions was measured in a conductometric cell with a broadened part [2] at various ratios of cobalt(II) and chitosan. To attain the equilibrium, the solutions were kept for 24 h.

As a rule, solutions of chitosan are prepared in aqueous hydrochloric or aqueous acetic acid. The degree of deacetylation of chitosan was determined by addition of hydrochloric acid, followed by potentiometric back-titration of its excess. The content of monomeric units in chitosan macromolecules was de-

termined by displacement of the amino groups of chitosan with aqueous alkali. This determination can be carried out in both aqueous hydrochloric and aqueous acetic acid media.

Figure 1, curve *1*, shows the conductometric titration curve of a solution of chitosan in aqueous hydrochloric acid. In the initial portion of the titration curve, the electrical conductivity decreases due to neutralization of the excess hydrochloric acid with aqueous sodium hydroxide, and then it increases due to displacement of HCl bound to the primary amino groups of chitosan hydrochloride. The addition of excess aqueous alkali strongly increases the electrical conductivity. The resulting titration curve has two breaks corresponding to the final titration points (FTPs) of free and bound HCl, respectively. The correct positions of these points can be determined by linear extrapolation of the adjacent portions of the titration curve. The chitosan concentration in the solution was determined from the difference between aqueous alkali volumes corresponding to the second and first FTPs, respectively. For comparison, the identical solution of chitosan was titrated with aqueous NaOH potentiometrically. This titration curve also shows two breaks. The chitosan content in the solution was determined by back-titration of a solution corresponding to the first break. We found that the solution of chitosan becomes turbid at pH 9, and chitosan precipitates at higher pH. The chitosan concentration in aqueous HCl, determined by the direct conductometric titration, was 0.0287 ± 0.0006 M ($P = 0.95$, $n = 5$). The degree of deacetylation of chitosan (for monomeric unit with Mr = 161), recalculated to air-dry chitin, was 92.1%. From the pH corresponding to half-displacement with aqueous NaOH of HCl bound with the amino groups of chitosan, we determined the base ionization constant pK_b of the amino groups. This value was found to be 7.7 at 20°C, which is close to published data.

Figure 1, curve *2*, shows conductometric titration curves for solutions of chitosan in aqueous acetic acid. This curve also has two breaks. It is known [2] that the order of titration with strong aqueous alkali of a weak acid in a mixture containing this weak acid and its salt of weak base is governed by the ratio between pK_a of the weak acid and pK_b of the weak base. In our system, this ratio is such that, first, excess acetic acid and then the acetic acid bound to the amino groups of chitosan are titrated with aqueous sodium hydroxide. In the course of titration of the excess acetic acid, the electrical conductivity increases due to the formation of a strong electrolyte (sodium acetate). In the second stage of titration, acetic acid is displaced from chitosan acetate by sodium hydroxide to form

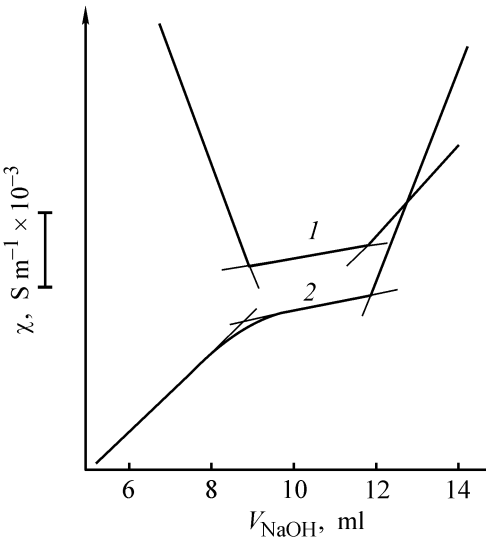


Fig. 1. Conductometric titration curves of solutions of chitosan in (*1*) aqueous hydrochloric and (*2*) aqueous acetic acids with aqueous sodium hydroxide in the coordinates of electrical conductivity χ vs. volume of 0.1 M aqueous NaOH.

sodium acetate. This process also increases the electrical conductivity since the mobility of the chitosan polycation is lower than that of the sodium cation. In this stage of titration, the slope of the plot of the electrical conductivity vs. the volume of aqueous NaOH is smaller than that in titration of excess acetic acid. As a result, the titration curve shows a break corresponding to the completion of neutralization of free acetic acid. Upon further addition of aqueous sodium hydroxide, a second break appears in the titration curve, which corresponds to neutralization of acetic acid bound to the amino groups; it is followed by a steeper increase in the conductivity. Although this break is rounded, its position can be determined sufficiently reliably by extrapolation of the adjacent portions of the titration curve. The chitosan concentration determined from the difference between the volumes of aqueous alkali corresponding to the second and first breaks, was 0.0284 ± 0.0011 M ($P = 0.95$, $n = 5$). We found that, in pH-metric titration of chitosan solutions, the titration curve shows a single break corresponding to titration of a sum of the excess acetic acid and that bound to the amino groups of chitosan. Therefore, determination of chitosan concentration is impossible in this case.

The stoichiometry of coordination of cobalt(II) with chitosan was studied by conductometric titration with aqueous sodium hydroxide of a solution of a cobalt salt in acetic acid in the presence of excess chitosan.

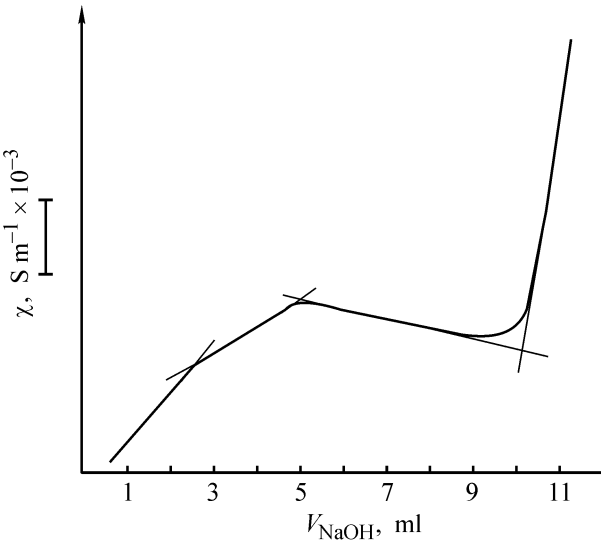


Fig. 2. Conductometric titration curves of solutions containing a chitosan–Co(II) mixture at their molar ratio of 2 : 1 in the coordinates of electrical conductivity χ vs. volume of 0.1 M aqueous NaOH.

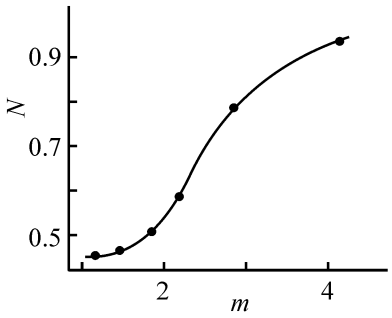


Fig. 3. Number *N* of chitosan moles bound with 1 mol of Co(II) in the chitosan–Co(II) complex vs. chitosan : Co(II) molar ratio *m* in the acetic acid solution.

The titration curve (Fig. 2) consists of four portions. Comparison of the slopes of separate portions of this titration curve with those of the titration curve of chitosan solution containing no Co(II) (Fig. 1, curve *2*) allows elucidation of the main processes occurring in different stages of titration of the Co(II)–chitosan mixture with aqueous NaOH. The first portion of the titration curve reflects the neutralization of the excess acetic acid; the second portion corresponds to titration of the excess chitosan, which is followed by formation of chitosan suspension; and the third portion reflects the superposition of several reactions followed by precipitation of a poorly soluble cobalt hydroxide. This means that, in the final stage of titration, weak chitosan–Co(II) complexes are destroyed and free chitosan is released.

The stoichiometry of coordination of chitosan with cobalt(II) was determined by conductometric back-titration. The excess chitosan was determined from the second portion of the titration curve. The chitosan amount bound to Co(II) was determined as the difference between the total content of chitosan in the system under consideration and its excess. The chitosan concentration in the initial solutions was approximately 0.1 M. In our experiments, all the solutions contained equal amounts of chitosan. The molar ratio of chitosan and Co(II) ranged from 1.33 to 5. Figure 3 shows the number *N* of chitosan molecules bound to Co(II) in the chitosan–Co(II) complexes as a function of the chitosan : Co(II) molar ratio *m* in the solution. It can be seen that, at a more than fourfold excess of chitosan, chitosan–Co(II) complexes containing approximately one Co(II) per chitosan monomeric unit are formed. The deviations from this stoichiometry at smaller excess of chitosan are apparently caused by decomposition of weak chitosan–Co(II) complexes.

CONCLUSIONS

(1) The chitosan concentration and the degree of deacetylation of chitosan can be quantitatively determined with a sufficiently high accuracy by conductometric titration.

(2) The number of chitosan molecules bound to the Co(II) ion is a function of the chitosan to Co(II) molar ratio. At a fourfold excess of chitosan, the chitosan– Co(II) complexes containing approximately one Co(II) ion per chitosan monomeric unit are formed.

REFERENCES

1. *Khitin i khitozan. Poluchenie, svoistva i primenenie* (Chitin and Chitosan. Preparation, Properties and Application), Skryabin, K.G., Vikhoreva, G.A., and Varlamova, V.P., Eds., Moscow: Nauka, 2002.
2. Khudyakova, T.A. and Kreshkov, A.P., *Teoriya i praktika konduktometricheskogo i khronokonduktometricheskogo analiza* (Theory and Practice of Coductometric and Chronoconductometric Analyses), Moscow: Khimiya, 1976.
3. Pogodina, N.V., Pavlova, G.M., and Mel'nikova, A.V., *Vysokomol. Soedin.*, 1982, vol. 28, no. 2, pp. 232–235.

ISSN 1070-4272, Russian Journal of Applied Chemistry, 2006, Vol. 79, No. 2, pp. 275–278. © Pleiades Publishing, Inc., 2006.
Original Russian Text © I. Yu. Vashurina, S. V. Makarov, Yu. A. Kalinnikov, E. A. Vlasova, 2006, published in Zhurnal Prikladnoi Khimii, 2006, Vol. 79, No. 2, pp. 275–278.

CATALYSIS

Humic Acids as Efficient Catalysts for Disproportionation of Peroxide in Alkaline Solutions

I. Yu. Vashurina, S. V. Makarov, Yu. A. Kalinnikov, and E. A. Vlasova

Institute of Chemistry of Solutions, Russian Academy of Sciences, Ivanovo, Russia
Ivanovo State University of Chemical Engineering, Ivanovo, Russia

Received June 16, 2005

Abstract—The influence of sodium salt of humic acids on the reduction of Chrome Green Anthraquinone dye with thiourea dioxide under aerobic and anaerobic conditions was studied.

DOI: 10.1134/S1070427206020200

Sulfur-containing reductants, sodium ditionite $Na_2S_2O_4$ (DTN), sodium hydroxymethanesulfinate $HOCH_2SO_2Na$ (HMS), and thiourea dioxide $(NH_2)_2CSO_2$ (TUDO), are widely used as reductants of vat dyes [1]. The reduction of vat dyes with HMS can be substantially accelereated with catalysts, among which the most commonly used are cobalt dioximates and anthraquinone derivatives [2]. We have shown [3] that the reaction of HMS with a water-soluble model of a vet dye in an alkaline medium is accelerated by humic acids (HAs), a special group of natural organic compounds formed from plant residues; they are the main part of organic matter in the biosphere [4]. In the environment, HAs may act as reductants (they can reduce Fe^{3+}, Sn^{4+}, V^{5+}, Cr^{6+} ions [5]) and as oxidants (due to their quinoid groups capable of reversible reduction) [4]. Quinoid groups may impart to HAs the catalytic properties in various redox reactions.

In this study, we examined the influence of HAs on the reaction of TUDO with superoxide and water-soluble dye Chrome Green Anthraquinone CGA (CI Acid Green 27) as oxidants. Special attention was paid to the effect of oxygen on the dye reduction in the presence of HAs, which was not considered in [3].

EXPERIMENTAL

We used TUDO and HA sodium salt from Aldrich and potassium peroxide from Merck. Technical grade CGA was purified according to [6].

The rate of CGA reduction by excess TUDO was determined by measuring the optical density at the absorption peak of oxidized dye (λ_{max} = 612 nm, ε = 10 870 l mol^{-1} cm^{-1}). Preliminarily, it was verifird that this band is well-resolved from the band of the reduced dye. The CGA concentration was found in the range of validity of the Bouger–Lambert–Beer law.

The rate of DTN formation by TUDO decomposition under aerobic conditions was estimated spectrophotometrically by measuring the optical density at λ_{max} = 315 nm, (ε = 8043 l mol^{-1} cm^{-1} [7]). A Specord M-40 spectrophotometer was used in all kinetic experiments. To eliminate the oxygen effect, the solutions were preliminarily bubbled with Ar for 30 min.

The kinetic curves of CGA reduction by TUDO at various NaOH concentrations in the presence of atmospheric oxygen are shown in Fig. 1. The influence of small HA additions on this process is also illustrated (preliminarily, we found that, under anaerobic conditions and at c_{NaOH} = 0.01–0.5 M, the rate of CGA reduction is independent of HA). It follows from Fig. 1 that at the smallest alkali concentration HA virtually does not affect CGA reduction kinetics, but this influence increases with the alkali concentration.

Most of the kinetic curves in Fig. 1 are linear (this means the zero order with respect to CGA); deviation from linearity is observed only at the final stage of the reaction. When HMS is used as reductant, the kinetic curves are nonlinear and can be well described by first-order equations [3]. The first order with respect to CGA in the reaction of CGA with HMS shows that the initial HMS molecule is involved in the reaction. The zero order with respect to CGA in the reaction of CGA with TUDO shows that

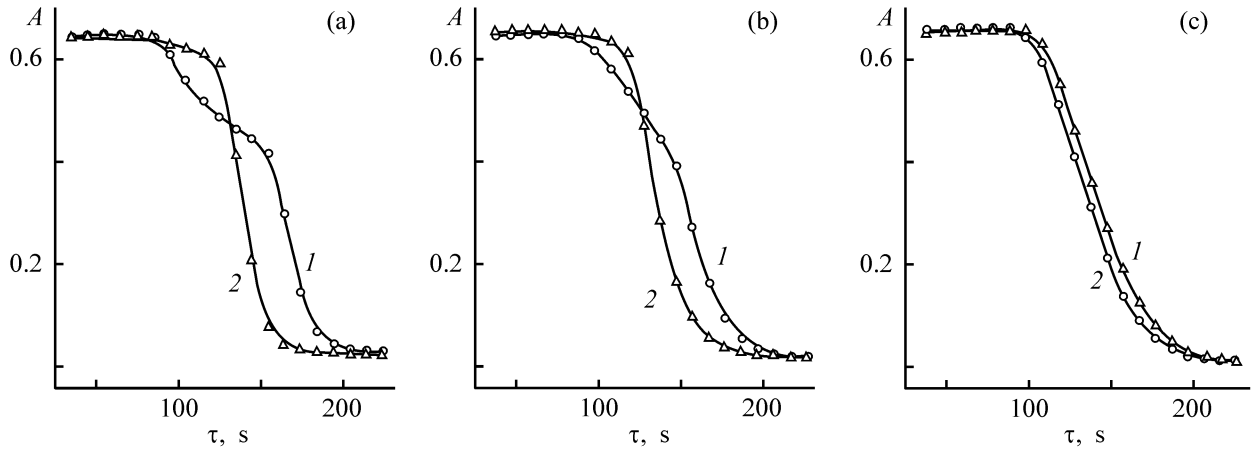


Fig. 1. Influence of solution alkalinity and presence of HA additive on kinetics of CGA reduction by thiourea dioxide at 20°C. $c_{CGA} = 5.98 \times 10^{-5}$ M, $c_{TUDO} = 4.62 \times 10^{-2}$ M, and $c_{HA} = 0.1$ g l^{-1}. (*A*) Optical density of the CGA solution and (τ) time; the same for Figs. 2, 3. c_{NaOH} (M): (a) 0.1, (b) 0.05, and (c) 0.0125. (*1*) Without HAs and (*2*) in the presence of HAs.

the product of its decomposition, rather than TUDO, reacts with oxidant. This product is SO_2^{2-} ion [8] generated by the reaction

$$(NH)_2CSO_2^{2-} + H_2O \rightarrow (NH)_2CO + SO_2^{2-}. \quad (1)$$

In a strongly alkaline solution, TUDO is deprotonated [9], and, therefore, it is represented in reaction (1) as dianion. Reaction (1) determines the overall rate of the CGA reduction.

It is known that the SO_2^{2-} ion rapidly reacts with oxygen to form another strong reductant, radical anion $SO_2^{\cdot-}$ [8]:

$$SO_2^{2-} + O_2 \rightarrow SO_2^{\cdot-} + O_2^{\cdot-}. \quad (2)$$

The reaction of oxygen with SO_2^{2-} ion precedes its reaction with CGA. This gives rise to induction periods in the reduction of CGA, irrespective of pH (Fig. 1). Similar induction periods (conventionally termed first induction periods) have also been observed in reactions of TUDO with other dyes [2]. It was found that the duration of the first induction period depends only on the oxygen concentration, which amounts to 2.4×10^{-4} M in an air-saturated aqueous solution [8], irrespective of the concentrations of active oxygen species (superoxide and peroxide) [10].

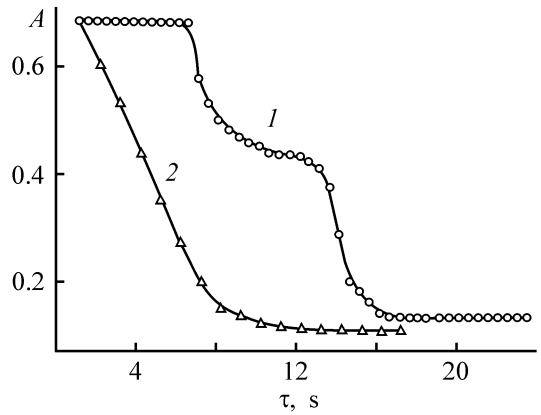


Fig. 2. Influence of atmospheric oxygen on the kinetics of CGA reduction by thiourea dioxide at 20°C. $c_{CGA} = 5.98 \times 10^{-5}$ M, $c_{TUDO} = 1 \times 10^{-3}$ M, $c_{NaOH} = 0.1$ M. (*1*) Without and (*2*) with preliminary bubbling with Ar.

It follows from Fig. 1 that the alkali concentration does not noticeably affect the first induction period. This is natural, since the rate of TUDO decomposition in strongly alkaline solutions [reaction (1)] is independent of pH.

Thus, the mechanisms of HMS and TUDO reactions with CGA substantially differ. The influence of HAs on the CGA reduction by the above sulfur-containing compounds is also manifested differently. The HA additives substantially increase the rate of reduction by HMS [3], whereas in the case of TUDO, their effect is insignificant. The induction period becomes longer when CGA is reduced by TUDO in a strongly alkaline solution in the presence of HA additives and atmospheric oxygen (under anaerobic conditions, the induction period is absent in the presence of HAs). At the same time, the shape of the kinetic curve changes: the curve portion corresponding to a slow decrease in the CGA concentration (conventionally termed second induction period) disappears. It should be noted that both induction periods are absent under anaerobic conditions (Fig. 2). Hence, we may assume that the second induction period is caused by the presence in the reaction mixture of an oxygen reduction product, superoxide [reaction (2)].

To verify this assumption, we examined the effect of potassium superoxide and combination of potassium superoxide with HAs on the shape the kinetic curve of CGA reduction by TUDO in a solution containing 0.5 M NaOH (Fig. 3). The strongly alkaline medium was chosen because disproportionation of the superoxide [reaction (3)] is substantially slower in this case, compared with weakly alkaline or neutral solutions [11]:

$$HO_2^{\cdot} \rightarrow O_2 + H_2O_2. \quad (3)$$

In accordance with Fig. 3, the second induction period in the reduction of CGA, which becomes substantially longer on adding KO_2 (curve *2*), completely disappears in the presence of HAs, whereas the duration of the first induction period increases (curve *3*). This correlation shows that HAs act as superoxide dismutase, i.e., they accelerate the disproportionation of the superoxide.

To confirm this conclusion, we studied the effect of HAs on dithionite formation in alkaline TUDO solutions under aerobic conditions. It was shown in [8] that the $S_2O_4^{2-}$ ion is formed in TUDO alkaline solutions via dimerization of the $SO_2^{\cdot-}$ radical ion generated by reaction (2):

$$2SO_2^{\cdot-} \rightarrow S_2O_4^{2-}. \quad (4)$$

The induction period caused by the reaction of both SO_2^{2-} and $SO_2^{\cdot-}$ with atmospheric oxygen [8] precedes the formation of the $S_2O_4^{2-}$ ion; neither the superoxide nor the peroxide affect the induction period [8, 12].

We found that HA additives make longer the induction period of accumulation of the $S_2O_4^{2-}$ ion in the solution (Fig. 4), i.e., this effect is similar to the effect of CGA reduction under conditions of increasing oxygen concentration [reaction (3)]. It is interesting that an increase in the induction period in the $S_2O_4^{2-}$-vs.-time curves in anaerobic decomposition of TUDO has been observed earlier upon addition of superoxide dismutase [12]. Thus, the data obtained confirmed the accelerating effect of HAs on the disproportionation of the superoxide.

In this context, it should be noted that the catalytic activity of the superoxide dismutase enzyme sharply decreases in alkaline solutions [13]. In this study, we showed that, in contrast to enzymes, the catalytic effect of HAs is fairly high even in 0.5 M NaOH.

Reactions involving the superoxide play an important part in the vital activity of animals and plants [13]. On the one hand, its role as precursor of high reactive hydroxyl radical and singlet oxygen is negative;

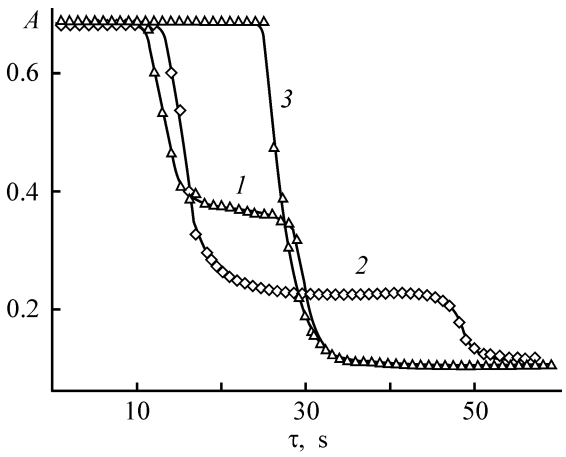


Fig. 3. Reduction of CGA by thiourea dioxide in strongly alkaline solution at 20°C: (*1*) without additives, (*2*) in the presence of KO_2, and (*3*) in the presence of KO_2 and HA. $c_{CGA} = 5.98 \times 10^{-5}$ M, $c_{TUDO} = 1.0 \times 10^{-3}$ M, $c_{NaOH} = 0.5$ M, $c_{KO_2} = 1.0 \times 10^{-4}$ M, and $c_{HA} = 0.1$ g l^{-1}.

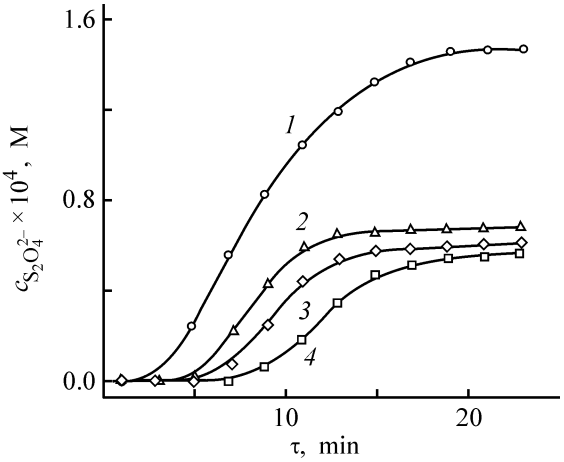


Fig. 4. Influence of HA concentration on the kinetics of $S_2O_4^{2-}$ accumulation in alkaline solution during TUDO decomposition under aerobic conditions at 20°C. $c_{TUDO} = 1.0 \times 10^{-3}$ M, $c_{NaOH} = 0.5$ M, $c_{KO_2} = 1.0 \times 10^{-4}$ M. ($c_{S_2O_4^{2-}}$) Dithionite concentration in the solution and (τ) time. HA concentration (g l^{-1}): (*1*) 0, (*2*) 0.03, (*3*) 0.05, and (*4*) 0.1.

on the other hand, it is involved in processes that prevent tumor development. The mechanisms of superoxide transformations are being actively studied today. Because the biological and medical aspects of chemistry of humic compounds also attract growing attention [14], the catalytic effect of HAs in superoxide disproportionation, found above, is important for determining the biological role of these compounds. This effect may be of interest for industrial processes involving sulfur-containing reductants. For instance, it is known that the reaction of vat dyes with sulfur-con-

taining reductants, especially with TUDO, is accompanied by "overreduction" of dyes [15], which leads to their unproductive consumption. It was found that the fraction of overreduced dye substantially increases with the concentration of active oxygen species [16]. In addition, the rate of decomposition of reductants substantially increases under aerobic conditions. The results of this study show that HA additives can substantially decrease the loss of dyes and reductants.

CONCLUSIONS

(1) The effect of natural humic acids on reduction of water-soluble Chrome Green Anthraquinone dye (CI Acid Green 27) with thiourea dioxide is governed by the presence of atmospheric oxygen in the solution.

(2) Humic acids are efficient catalysts of superoxide disproportionation.

(3) In the technology of dyeing and printing of fibrous materials with vat dyes, addition of humic acids may decrease the consumption of dyes and reductants.

REFERENCES

1. Gordeeva, N.V., Romanova, M.G., and Ratnovskaya, E.D., *Kubovye krasiteli v tekstil'noi promyshlennosti* (Vat Dyes in Textile Industry), Moscow: Legkaya Industriya, 1979.
2. Budanov, V.V. and Makarov, S.V., *Khimiya serosoderzhashchikh vosstanovitelei (rongalit, ditionit, dioksid tiomocheviny)* (Chemistry of Sulfur-containing Reductants (Rongalite, Ditionite, Thiourea Dioxide)), Moscow: Khimiya, 1994.
3. Pogorelova, A.S., Vashurina, I.Yu., and Kalinnikov, Yu.A., *Izv. Vyssh. Uchebn. Zaved., Khim. Khim. Tekhnol.*, 2002, vol. 45, no. 1, pp. 37–41.
4. *Guminovye veshchestva v biosfere* (Humic Substances in the Biosphere), Orlov, D.S., Ed., Moscow: Nauka, 1993.
5. Steelink, S., *Anal. Chem.*, 2002, vol. 74, no. 11, pp. 326A-333A.
6. Vashurina, I.Yu., Association of Active Dyes and Development of Efficient Technology of Dyeing and Crease Resist Processing of Cotton Fabric, *Cand. Sci. Dissertation*, Ivanovo, 1988.
7. McKenna, C.E., Gutheil, V.G., and Song, W., *Biochim. Biophys. Acta*, 1991, vol. 1075, pp. 109–117.
8. Svarovsky, S.A., Simoyi, R.H., and Makarov, S.V., *J. Chem. Soc., Dalton Trans.*, 2000, no. 4, pp. 511–514.
9. Makarov, S.V., *Usp. Khim.*, 2001, vol. 70, no. 10, pp. 995–1006.
10. Naidenko, E.V., Physicochemical Features of Reduction of Oxigen-containing Nitrogen Compounds and Methylviologen with Thiourea Dioxides, *Cand. Sci. Dissertation*, Ivanovo, 2004.
11. Bielski, B.H.J. and Allen, A.O., *J. Phys. Chem.*, 1977, vol. 81, no. 11, pp. 1048–1050.
12. Svarovsky, S.A., Simoyi, R.H., and Makarov, S.V., *J. Phys. Chem. B*, 2001, vol. 105, no. 50, pp. 12634–12643.
13. Bertini, I., Mangani, S., and Viezzoli, M.S., *Adv. Inorg. Chem.*, 1998, vol. 45, pp. 127–249.
14. *Humic Substances: Molecular Details and Applications in Land and Water Conservation*, Ghabbour, E.A. and Davies, G., Eds., New York: Taylor and Francis, 2005.
15. Baumgarte, U., *Rev. Prog. Coloration*, 1987, vol. 17, pp. 32–38.
16. Murav'ev, O.N., Trends of the Effect of the External Factors on Reactivity of Oxygen-containing Organosulfur Reductants, *Cand. Sci. Dissertation*, Ivanovo, 1998.

ISSN 1070-4272, Russian Journal of Applied Chemistry, 2006, Vol. 79, No. 2, pp. 279–283. © Pleiades Publishing, Inc., 2006.
Original Russian Text © Yu. E. Dolgova, V. A. Kudryavtseva, 2006, published in Zhurnal Prikladnoi Khimii, 2006, Vol. 79, No. 2, pp. 279–283.

ENVIRONMENTAL PROBLEMS OF CHEMISTRY AND TECHNOLOGY

Application of New Types of Fibrous Sorbents for Sampling of Dissolved Species of Heavy Metals in Natural Waters

Yu. E. Dolgova and V. A. Kudryavtseva

St. Petersburg Scientific Research Center for Ecological Safety, Russian Academy of Sciences, St. Petersburg, Russia

Received December 2, 2005

Abstract—The article discusses the importance and specific features of the preparatory stages in ecoanalytical monitoring of natural water, aimed to determine the content of heavy metals. A procedure was developed for sampling of dissolved species of heavy metals with sorbents. The influence of humic substances on the sorption of heavy metals was elucidated. The results obtained with the technique suggested are reported.

DOI: 10.1134/S1070427206020212

Analytical monitoring of pollution of natural water is an urgent problem faced by modern hydroecology and environmental analytics. In particular, of special importance is monitoring of the content of heavy metals (HMs) [1] ranking among the most hazardous biologically components of natural water.

The general scheme of ecoanalytical monitoring of any natural object includes the following successive stages: sampling, preservation and transportation of samples, sample preparation, instrumental analysis, and processing and interpretation of the results [2].

Sampling is very important in environmental monitoring; it primarily determines the accuracy of the subsequent analysis. Above all, it is necessary to ensure conditions under which the sample is representative. Of much importance are the specific features of the object and the goal of investigation. There is a need in several replicate measurements, which increases the minimal volume of the sample. Even in the sampling stage, it is necessary to take special measures to avoid contamination. Such measures are typically described in detail either in appropriate techniques or in special manuals of analysis. Careless handling and inappropriate storage may be responsible for changes in the composition of the samples via photolytic or thermal decomposition, chemical reactions, or microbiological transformations.

In many cases, practicians have to preserve the samples, so as to carry out the analysis at a later time [1], rather than under field conditions; this can increase the inaccuracy of the subsequent analysis.

Sample preparation is the first stage of the analytical procedure proper. It is aimed to convert the component being analyzed to a form suitable for analysis by the chosen method, to remove or mask interfering substances, and, in some cases, to precisely adjust the concentration to make the expected content of the component being analyzed close to the middle of the operating range of the analytical method used [3].

Analysis of dissolved species of metals typically requires taking no less than a 1-l isokinetic water sample (or several liters of separate samples taken across the entire river section). The water samples taken should be conserved at the sampling site, and analysis should be carried out within a brief period (not later than in 5–7 days). The use of various conserving agents after sampling of natural water has been reported. To preserve dissolved species of heavy metals, the samples are acidified with nitric acid to pH < 2 or cooled to 3–4°C and stored at this temperature [4], which is technically troublesome. However, sample preservation does not afford a constant composition of a water sample for an infinite period [5]. Bringing samples to stationary analytical laboratories frequently takes a relatively long time, up to several weeks. This inevitably entails loss of dissolved species of heavy metals, e.g., via biochemical processes and sorption on the dishware, which distorts analytical data.

Analytical practice widely uses sorption preconcentration, in particular, in preparation of natural water samples for analysis. The sorption preconcentration has advantages of simplicity and easy performance, high efficiency, rapidity, and possibility of combina-

Table 1. Sorption capacity C of the sorbents

Sorbent	C, mg g^{-1}					
	Cu(II)	Ni(II)	Co(II)	Mn(II)	Pb(II)	Zn(II)
Poliorgs-33n	245	40	40	80	330	100
Poliorgs-34	130	40	40	80	330	66
Poliorgs-35	140	42	80	60	270	74

tion with various analytical methods [6]. For preconcentration of trace elements, certain promise is offered by "filled" fibrous complexing sorbents, i.e., thin polyacrylonitrile fibers retaining a finely ground complexing filling sorbent inside. Such sorbents are distinguished by good kinetic and filtration properties, combined with a high sorption capacity. Complexing sorbents with amidoxime and hydrazidine groups can sorb many transition metals from aqueous solutions [7]. Fibrous sorbents are especially promising for in situ preconcentration of trace elements from natural water.

In this study, we developed a technique for sampling of dissolved species of heavy metals, using fibrous sorbents. A small weighed portion (<0.1 g) of a sorbent allows preconcentration of dissolved species of metals from a large water volume and their further retention without quantitative changes for a long time. The technique we suggest avoids transportation of large water volumes. Without transportation and preservation of liquid samples, the inaccuracy of analysis significantly decreases. Preconcentration of dissolved species of metals by fibrous sorbents even in the sampling stage decreases their detection limits. At the same time, this allows use of less sensitive measuring instrumentation in the subsequent analysis.

EXPERIMENTAL

The initial solutions of metals (0.1 g l^{-1}) were prepared by dissolution of weighed portions of appropriate metals (available from Merck and Aldrich, analytical grade) in a solution of ultrapure nitric acid, pH 2.0 ± 0.1, in twice-distilled water. The working solutions were prepared by dilution of the initial solutions. In implementation of the "introduced–found" procedure, portions of the metal solutions were introduced into model samples close in composition to natural water. The model solutions were prepared using a humic extract isolated from peat. The natural water samples taken were prefiltered across a membrane filter with a pore diameter of 0.45 μm. The concentrations of the metals in solution were determined just before the sorption experiment.

We used a number of sorbents differing in the nature of the reactive groups. Experiments with polyurethane foam showed that it is unsuitable for group sorption of a number of metals (Cd, Pb, Cu, Zn, Fe, Mn) under the conditions suggested in [8, 9]. The content of the metals was determined by atomic absorption on an AAS-30 instrument.[1]

In further experiments we used "filled" sorbents Poliorgs-33n, Poliorgs-34, and Poliorgs-35 exhibiting high sorption capacities (Table 1). Owing to the stability in aqueous media and easy regeneration, these sorbents are suitable for repeated sorption–desorption cycles [7].

Sorption was run under static conditions, by stirring of the model solutions with the sorbent in a shaker (mass ratio of the solid to liquid phase 1 : 2000). The phase contact time in studying the sorption kinetics was varied from 10 min to 3 h. The pH of the solutions studied was kept within 5–6 pH units, since, according to [7, 10], the metals are most completely recovered by the sorbent at these solution acidities. Quantitative desorption was carried out with a 1 M nitric acid solution. The amount of nondesorbed metals was determined by wet ashing of the sorbent.

The content of the metals in the solutions after sorption and in the eluates, as well as in natural water, was determined by the anode stripping voltammetry on an SVA-1BM instrument (Burevestnik Research and Production Enterprise), using a three-electrode cell with carbon-devitrified glass indicator electrode and a platinum auxiliary electrode. As reference elec-

[1] This part of the study was carried out at the Institute of Water and Environmental Problems, Siberian Division, Russian Academy of Sciences.

trode served saturated silver chloride electrode with a salt bridge filled with 0.1 M KNO_3. The accumulation potential was –1.350 V. The accumulation time was varied from 30 to 120 s, depending on the concentration of the components being analyzed in solution. Electric accumulation of the metals was carried out on a rotating indicator mercury-carbon-devitrified-glass disk electrode with a Pentaplast coating, which was followed by the relaxation period. The metal oxidation was performed in the potentiodynamic mode of polarization of the electrode. The linear sweeping of the potential at a rate of 100 mV s^{-1} was carried out until the regeneration potential of the indicator electrode surface of +0.600 V was reached. The concentration of the heavy metals was estimated from the height of the anode current peaks, using the standard addition method.

Our experiments showed that the most suitable sorbent for group concentration of metals is Poliorgs-33n, prepared by treatment of freshly formed polyacrylonitrile fiber with a mixture of hydroxylamine and hydrazine hydrate. Comparison of the patterns of interphase distributions of the metals showed that sorption from the solutions containing a single kind of metal and mixture of metals on Poliorgs-33n sorbent proceeds similarly (Fig. 1). Figure 2 shows that the maximal sorption of all the metals is achieved within 30–40 min, the degree of sorption being 95 ± 5%. Our experiments show that the degree of sorption of the metals remains unchanged at their initial concentrations in the range 5–50 μg l^{-1} (Fig. 3).

One of important and complex stages in studies of natural objects is to ensure the maximal correspondence between the model and real natural samples. Of no less importance is to convert a sample to a form suitable for analysis and to bring it into strict correspondence with the reference samples used, in both the form and chemical composition. In surface waters, characteristic macrocomponents are humic substances (HSs), high-molecular-weight polydisperse compounds containing reactive functional groups of varied nature (phenolic, carboxy, imino, thioether, etc.). All these groups can bind the metal ions into strong compounds like chelates or retain them via coordination bonding [11]. This required a study of the sorption performance of Poliorgs-33n with respect to heavy metals in the presence of HSs, which can interfere with the metal sorption. Our studies of model solutions containing various (specific to different types of natural water) amounts of HSs (0–300 mg l^{-1}) showed that the degree of sorption of heavy metals

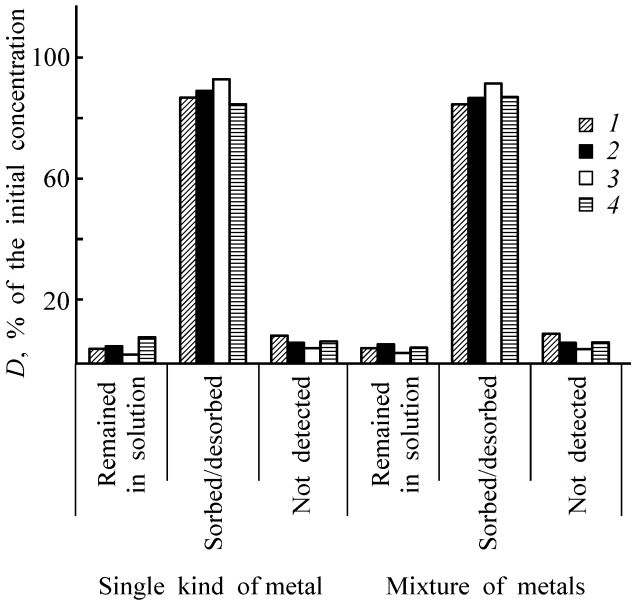


Fig. 1. Interphase distribution D of the metals in sorption on Poliorgs-33n for solutions containing a single kind of metal or a mixture of metals. (*1*) Cu, (*2*) Pb, (*3*) Cd, and (*4*) Mn.

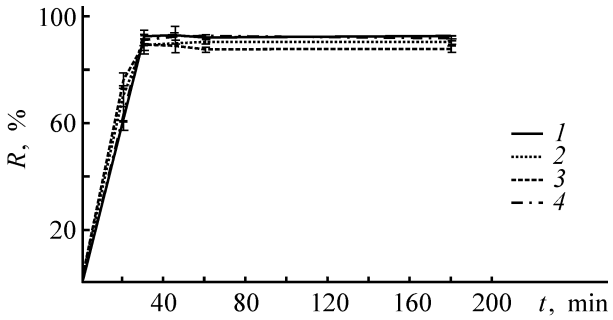


Fig. 2. Degree of sorption of the metals, R, vs. the sorption (phase contact) time t. (*1*) Zn, (*2*) Cd, (*3*) Pb, and (*4*) Cu; the same for Figs. 3 and 4.

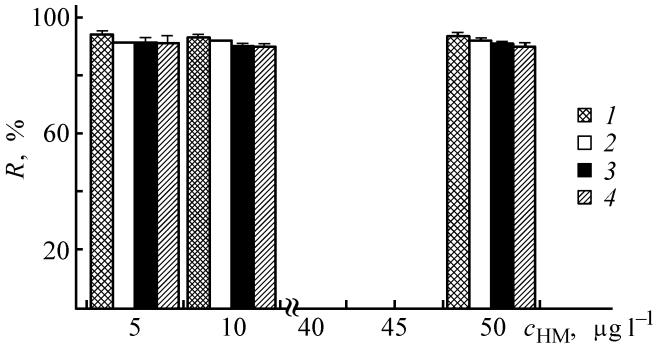


Fig. 3. Degree of sorption, R, vs. the concentration of the metals, c_{HM}, in solution.

Table 2. Content of heavy metals, c_{HM}, in water samples taken from the Neva and Oredezh rivers

Sample no.	Sample*		c_{HM}, μg l^{-1}			
			Zn	Cd	Pb	Cu
Neva river, samples taken on June 17, 2005						
1	Downstream the Lieutenant	a	10.2 ± 0.1	0.52 ± 0.04	1.48 ± 0.06	2.14 ± 0.05
	Shmidt bridge, on the right	b	10.2 ± 0.2	0.50 ± 0.03	1.46 ± 0.04	2.13 ± 0.03
2	Downstream the Birzhevoi	a	3.43 ± 0.09	0.52 ± 0.03	3.14 ± 0.02	3.39 ± 0.05
	bridge, on the left	b	3.42 ± 0.04	0.51 ± 0.01	3.11 ± 0.07	3.37 ± 0.03
3	Upstream the Tuchkov	a	9.4 ± 0.2	0.45 ± 0.07	2.9 ± 0.2	3.03 ± 0.05
	bridge, on the left	b	9.31 ± 0.05	0.43 ± 0.02	2.86 ± 0.07	3.01 ± 0.04
MPC [12]			1000	1	3	1000
Neva river, samples taken on June 29, 2005						
4	Upstream the Tuchkov	a	4.46 ± 0.09	0.38 ± 0.02	3.9 ± 0.2	4.6 ± 0.1
	bridge, on the left	b	4.47 ± 0.06	0.37 ± 0.02	3.8 ± 0.2	4.55 ± 0.07
5	Upstream the Tuchkov	a	1.29 ± 0.06	0.41 ± 0.02	3.91 ± 0.05	2.22 ± 0.06
	bridge, on the right	b	1.27 ± 0.06	0.42 ± 0.01	3.90 ± 0.06	2.19 ± 0.08
MPC [12]			1000	1	3	1000
Oredezh river, samples taken on July 31, 2005						
6	Upstream the Chikinskaya	a	15.4 ± 0.1	1.26 ± 0.01	5.96 ± 0.01	2.87 ± 0.09
	hydropower plant (100 m)	b	15.5 ± 0.5	1.26 ± 0.02	5.98 ± 0.08	2.86 ± 0.05
7	Upstream the Chikinskaya	a	17.5 ± 0.2	1.31 ± 0.06	7.54 ± 0.08	3.64 ± 0.02
	hydropower plant (600 m)	b	17.5 ± 0.3	1.30 ± 0.01	7.57 ± 0.16	3.63 ± 0.01
8	Downstream the Chikinskaya	a	21.6 ± 0.2	1.92 ± 0.04	8.07 ± 0.01	77.5 ± 0.9
	hydropower plant (10 m)	b	21.8 ± 0.8	1.91 ± 0.06	8.06 ± 0.09	78.6 ± 3.6
9	Middle flow, Siverskii	a	19.4 ± 0.8	1.25 ± 0.05	15.3 ± 0.3	40.0 ± 0.4
	settlement	b	19.5 ± 0.5	1.25 ± 0.01	15.2 ± 0.1	40.0 ± 0.8
10	Artesian well	a	18.5 ± 0.2	0.67 ± 0.02	3.44 ± 0.07	6.46 ± 0.01
		b	18.3 ± 0.8	0.67 ± 0.01	3.45 ± 0.09	6.47 ± 0.07
MPC [12]			1000	1	3	1000

* Samples taken (a) by the "classical" procedure and (b) using sorbent.

is independent of the HS concentration (Fig. 4). Comparison of the degrees of sorption of HMs in the presence (Fig. 4) and absence (Fig. 3) of HSs shows that the HMs are completely bound by the sorbent in solutions containing HSs as well. Our results confirm that the technique we suggested for sampling of dissolved species of heavy metals is applicable to various kinds of water, differing in the content of HSs.

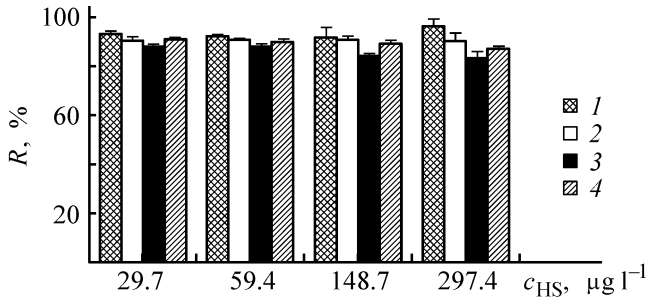


Fig. 4. Degree of sorption R of metals, vs. the concentration of humic substances c_{HS}, in solution.

The technique we developed was tested on real samples of natural water (surface and ground). We took samples from a big river (Neva) and a small river (Oredezh), differing in the aeration and hydrodynamic conditions and in the chemical composition of water. Comparison of the contents of HMs in the samples taken by the "classical" procedure (conservation with acid) and using the sorbent (Table 2) convincingly demonstrated that the technique we suggested does not distort the results of determination of the total content of dissolved species of metals in such complex multicomponent systems as various kinds of

natural water. It is essential that the metals sorbed can be stored on the sorbent for a long time. A 2-month monitoring of the content of HMs on the sorbent showed that, within this period, the concentration remained unchanged. This characteristic of the sorbent seems to be of interest not only for hydrochemistry and environmental analytics, but also for ecological criminology.

CONCLUSIONS

(1) The suitability of fibrous sorbents for sampling and reliable storage before analysis of dissolved species of heavy metals was demonstrated experimentally.

(2) The degrees of sorption of the metals from solutions containing a single kind of metal and a mixture of metals are identical, and the maximal degree of sorption of the metals ($95 \pm 5\%$) is achieved within 40 min.

(3) The maximal degree of sorption of heavy metals is independent of the concentration of humic substances and the concentration of heavy metals in natural water.

ACKNOWLEDGMENTS

The authors are grateful to staff members of the Laboratory of Organic Reagents, Vernadsky Institute of Geochemistry and Analytical Chemistry, Russian Academy of Sciences, for providing the sorbents.

REFERENCES

1. Manahan, S.E., *Environmental Chemistry*, New York: Lewis, 1994.
2. Papina, T.S., *Ekol. Khim.*, 2004, vol. 13, no. 4, pp. 229–235.
3. Markert, B. and Friese, K., *Trace Elements—Their Distribution and Effects in the Environment*, Oxford, 2000.
4. *GOST* (State Standard) *R 51592–2000: Water: General Requirements to Sampling*, 1982.
5. Ramsey, M.H., *Environmental Sampling for Trace Analysis*, Markert, B., Ed., New York: VCH, 1994, pp. 93–112.
6. Zolotov, Yu.A., Tsizin, G.I., Morosanova, E.I., and Dmitrienko, S.G., *Usp. Khim.*, 2005, no. 1, pp. 41–66.
7. Myasoedova, G.V., Nikashina, V.A., Molochnikova, N.P., *et al.*, *Zh. Anal. Khim.*, 2000, no. 6, pp. 611–615.
8. Dmitrienko, S.G. and Zolotov, Yu.A., *Usp. Khim.*, 2002, no. 2, pp. 180–197.
9. Dmitrienko, S.G., *Soros. Obrazovat. Zh.*, 1998, no. 8, pp. 65–70.
10. Myasoedova, G.V., *Fresenius J. Anal. Chem.*, 1991, vol. 341, pp. 586–591.
11. Kudryavtseva, V.A. and Makarova, E.D., *Nauchn. Priborostr.*, 1999, vol. 9, no. 4, p. 73–77.
12. *SanPiN* (Sanitary Regulations and Norms) *no. 42-121-4130–86: Hygienic Norms of Maximal Permissible Concentrations of Harmful Substances in Water of Water Objects Intended for Satisfying Household and Cultural and General Needs*, 1986.

ISSN 1070-4272, Russian Journal of Applied Chemistry, 2006, Vol. 79, No. 2, pp. 284–287. © Pleiades Publishing, Inc., 2006.
Original Russian Text © E. S. Averina, I. A. Gritskova, V. A. Vasnev, L. D. Radnaeva, G. A. Simakova, 2006, published in Zhurnal Prikladnoi Khimii, 2006, Vol. 79, No. 2, pp. 284–287.

ORGANIC SYNTHESIS AND INDUSTRIAL ORGANIC CHEMISTRY

Surfactant Properties of Hydroxyethylated Fats

E. S. Averina, I. A. Gritskova, V. A. Vasnev, L. D. Radnaeva, and G. A. Simakova

Baikal Institute of Nature Management, Siberian Division, Russian Academy of Sciences, Ulan-Ude, Buryatia, Russia
Lomonosov State Academy of Fine Chemical Technology, Moscow, Russia
Buryat State University, Ulan-Ude, Buryatia, Russia
Nesmeyanov Institute of Organoelement Compounds, Russian Academy of Sciences, Moscow, Russia

Received June 29, 2005

Abstract—Surfactant properties of hydroxyethylated fats were studied.

DOI: 10.1134/S1070427206020224

There are obvious advantages of polymeric microspheres as bioligand carriers over particles of the biological origin (bacteria, erythrocytes, etc.). The primary advantage is in the possibility of obtaining monodisperse polymer suspensions with a fixed particle size of polymeric microspheres having surface sites capable of covalent binding to functional groups of the bioligand.

Monodisperse polymeric suspensions are prepared by various methods of heterophase polymerization in the presence of initiators and surfactants. In this case, the stability of the particles with respect to coalescence in the course of polymerization is provided by the structural-mechanical and electrostatic factors.

The polymerization is commonly initiated with potassium persulfate. The presence of ionic fragments of the initiator at the ends of polymeric chains promotes their orientation at the interface with the formation of an electric double layer. To form the structural-mechanical factor of stabilization of the particles in the interfacial layer, surfactants insoluble in water and incompatible with the resulting polymer are used. These are carboxyl-containing [1] and organosilicon [1, 2] surfactants, oligoglycol maleates, etc. [3]. It may be suggested that modified fats of taiga mink (TM), fox (TF), and sea mammals are classified with this type of fats. The last type has already found wide use in various areas of research and in chemical, pharmaceutical, and cosmetic industries. At the same time, the fat of Baikal seal (BS), which is a by-product, obtained in seal-fishing is virtually not used anywhere.

In this study, we examined properties of surfactants synthesized on the basis of hydroxyethylated fats of TM, TF, and BS. The resulting products were used in heterophase polymerization of styrene to prepare monodisperse polymer suspensions.

EXPERIMENTAL

The composition of fats was determined using a Hewlett–Packard 5890-2 gas chromatograph with an HP-5971 mass-spectrometric quadrupole detector. It was demonstrated that BS fat differs from TM and TF fats in a higher content of unsaturated acids C_{20}–C_{22} (Table 1).

Table 1. Composition of BS, TM, and TF fats

Parameter	TM	TF	BS
Acid number	1.3	2.0	0.6
Iodine number	78	70	145
Composition of fatty acids, wt %:			
C_{12}–C_{14}	4.1	4.4	7.1
C_{16}–C_{18}	94.4	95.6	69.7
C_{20}–C_{22}	0.5		23.2
Content of acids, wt %:			
saturated	31.2	34.1	15.5
monounsaturated	59.4	53.9	54.5
polyunsaturated	7.0	9.4	30.0
Degree of hydroxyethylation of modified fats	6(TM-6) 12(TM-12)	6(TF-6) 12(TF-12)	13(PEG-600) 45(PEG-2000) 12(MPEG-550) 42(MPEG-1900)

Table 2. Colloidal-chemical properties of TM- and TF-based surfactants at water/hydrocarbon interface

Surfactant	G, mN m^2 mol^{-1}	σ_{min}, mN m^{-1}	$\Gamma_{max} \times 10^6$, mol m^{-2}	S_{min}, Å	CMC, mM
TM-6	22.7	5.0	2.7	60	1.5
TM-12	32.5	2.0	4.8	36	1.1
TF-6	30.0	2.0	3.6	46	1.0
TF-12	50.0	2.0	4.8	36	0.7

Table 3. Critical micelle concentration of surfactants based on mono- and diesters of BS fatty acids

Ester	CCM $\times 10^4$, M
MPEG-550	0.5–0.8
PEG-600	5.6–6.8
MPEG-1900	7.1–8.3
PEG-2000	7.9–10.2

Di- and monoesters of BS fatty acids and poly(ethylene glycol) (PEG) were synthesized by condensation of the corresponding acyl chlorides with PEG-600 (number of hydroxyethylene groups n = 13) and PEG-2000 (n = 45), and also with poly(ethylene glycol) methyl ethers MPEG-550 (n = 12) and MPEG-1900 (n = 42) in the presence of triethylamine in 1,2-dichloroethane at 30°C for 1 h in an inert atmosphere [4, 5]. The structure of the products was confirmed by IR and ^{1}H NMR spectra.

In the experiments, we used modified TM and TS fats with a degree of hydroxyethylation of 6 (TM-6 and TF-6) and 12% (TM-12 and TF-12)[1].

To optimize the conditions of heterophase polymerization of styrene, we studied the solubility of these products and their colloidal-chemical properties at the hydrocarbon/water interface. The results are summarized in Table 2.

We selected *o*-xylene as a hydrocarbon phase, because its properties are close to those of styrene, i.e., the monomer frequently used in such a research. The solubility of hydroxyethylated fats in *o*-xylene appeared to be sufficiently high (34%). Their solubility in water is considerably lower (mostly 3–5%). The interfacial tension at the *o*-xylene solution of surfactant/water was determined by stalagmometry at a drop formation time of 45–50 and 2 s [6]. The dynamic interfacial tensions were determined to be higher than the corresponding static values (Fig. 1). The surfactants studied demonstrated a high surface activity (G) at the interface, decreasing the interfacial tension σ_{min} to 2–5 mN m^{-1}. The surface activity G was found to be 30–50 mN m^2 mol^{-1} on the average (Table 2).

The limiting adsorptions Γ_{max} and the areas occupied by the molecules in the saturated adsorption layer, estimated by the Gibbs equation, suggest a dense vertical orientation of the surfactant molecules at the water/hydrocarbon interface. The observed small S_{min} (35–60 Å^2) is caused by the orientation of the hydrocarbon chain of the surfactant toward the bulk of the hydrocarbon, and of the hydrophilic polyoxyethylene moiety, toward the aqueous phase.

The surface tension of the aqueous surfactant solutions was measured using the Wilhelmy method [6]. The surfactants based on BS fatty acids and PEG of various molecular weights reduced the surface tension at the water/air interface to 30–42 mN m^{-1}. From the surface tension data, we determined the critical micelle concentrations (CMC). The results show that CMC increases with the number of polyethylene oxide units in the surfactant molecules (Table 3).

The heterophase polymerization of styrene was carried out in dilatometers and in a 1-l reactor at a 1 : 9 styrene to water volume ratio and 80°C to complete conversion of the monomer [7]. As an initiator, we used potassium persulfate (1 wt % based on styrene).

The stability of the styrene emulsions stabilized with the surfactants investigated was characterized by a settling time upon centrifugation at 1500 rpm. It was demonstrated that the stability of styrene emulsions stabilized with TM and TF fats increases with

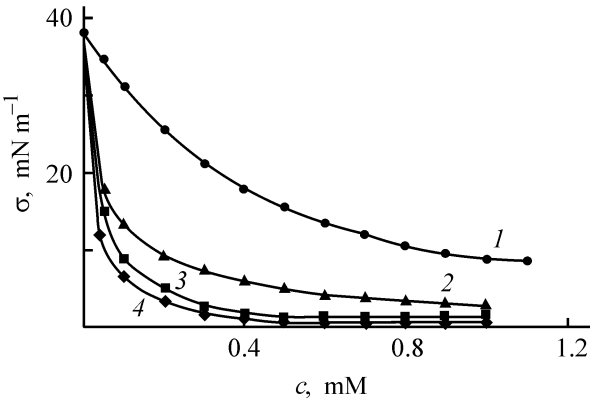


Fig. 1. Dynamic and static interfacial tensions σ vs. the surfactant concentration c (mM): (*1*) TF-6 (σ_{dyn}), (*2*) TF-6 (σ_{st}), (*3*) TF-12 (σ_{dyn}), and (*4*) TF-12 (σ_{st}).

[1] Hydroxyethylated TM and TF fats were synthesized at the Institute for Industrial Chemistry.

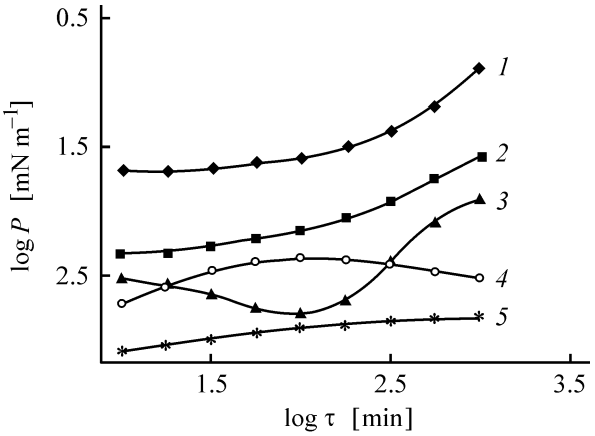


Fig. 2. Logarithmic dependence of the limiting shear stress P on time τ: (*1*) TM-12 + 4 wt % PS, (*2*) TF-12 + 4 wt % PS, (*3*) TM-12, (*4*) TM-6, and (*5*) TF-12.

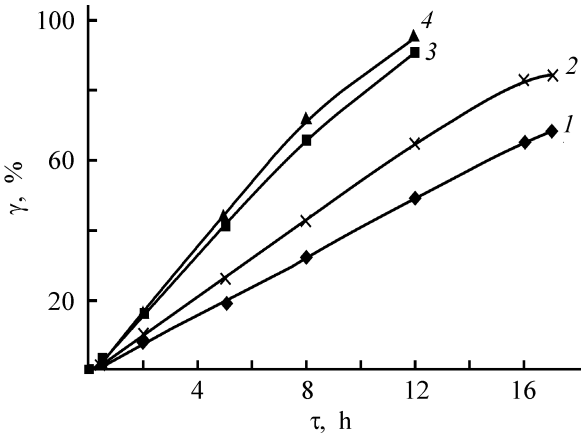


Fig. 3. Conversion γ vs. time τ in polymerization of styrene in the presence of surfactants: (*1*) PEG-600 diesters, (*2*) MPEG-1900 monoesters, (*3*) PEG-2000 diesters, and (*4*) MPEG-550 monoesters.

the degree of hydroxyethylation of the surfactants. With esters of the fatty acids and PEG as stabilizers, the highest stability was observed for the polystyrene suspensions prepared in the presence of monoesters of the fatty acids with MPEG-550 and MPEG-1900.

The dispersity of drops in the styrene emulsions formed by mixing the hydrocarbon and aqueous phases at a stirring rate of 200 rpm was determined to be high by laser spectroscopy (average size of the monomer drops was about 3 μm).

The dispersity of styrene emulsions considerably increased when the phase distribution of the surfactant was nonequilibrium. In this case, the surfactant was added to water, in which it is less soluble than in the organic phase. We observed an intensive mass transfer of the surfactant from the aqueous phase to styrene. As a result of a local decrease in the interfacial tension $\sigma_{1,2}$, a microemulsion with a drop size of 0.2 μm was formed. It should be pointed out that, in preparing emulsion by mixing the surfactant solution in styrene with water, the microemulsion of the monomer is not formed, since the solubility of the surfactant in styrene is much higher than that in water.

The surfactants investigated demonstrated a tendency to form a stable interfacial layer on the drop surface. We measured the limiting shear stress P of the interfacial adsorption layers of hydroxyethylated TM and TF fats, which control the emulsion stability. As can be seen from the log P-vs.-log τ dependences (Fig. 2), P is nearly doubled during the formation of the interfacial layers. Because the polymerization starts and proceeds in the adsorption layers around the particles, the polymer is involved in the formation of the interfacial layer and influences its strength. Figure 2 (curves *1*, *2*) shows data on the strength of the interfacial layers at the surfactant solution/polystyrene interface in the system styrene–water. In the presence of polystyrene, P increases by about an order of magnitude. Therefore, the stability of the styrene emulsions in the presence of the surfactants investigated is primarily caused by the structural-mechanical barrier formed in adsorption of surfactant molecules that can form an ordered layer at the interface. Despite that the surface activity of the surfactant is not high, polystyrene formed in the surface layer promoted formation of a 3*D* structure, i.e., of a gel, in the interfacial layer, thus stabilizing the emulsion particles in the course of polymerization.

Our results allowed optimization of the synthesis of monodisperse polystyrene suspensions, as required for their use as carriers for bioligands.

The conversion-vs.-time curves (Fig. 3) show that the polymerization of styrene proceeds without induction period at a constant rate up to high conversions.

The reaction system was stable throughout the synthesis, which confirms that a strong adsorption layer of the surfactant is formed on the surface of polymer–monomer particles, starting from very low monomer conversion. This is also evidenced by a narrow size distribution of particles of the polystyrene suspension in the course of polymerization. This distribution was studied by electron microscopy and photon correlation spectroscopy. The mean size of particles obtained in the presence of modified TM and TF fats was 0.3 and 0.5 μm, respectively, and that in

Table 4. Characteristics of polystyrene suspensions obtained in the presence of surfactants based on hydroxyethylated BS fatty acids

Surfactants based on mono- and diesters of BS fatty acids with MPEG and PEG	Particle size, μm	Polydispersity factor
PEG-600	0.298	1.00
PEG-2000	0.380	1.02
MPEG-550	0.477	1.02
MPEG-1900	0.258	1.37

Table 5. Characteristics of polystyrene suspensions

Surfactant	Particle size, μm	Polydispersity factor
BS fat	1.021	1.01
PEG-600/BS fat acid diester	0.298	1.00
PEG-2000/BS fat acid diester	0.380	1.02
MPEG-550/BS fat acid monoester	0.477	1.02
MPEG-1990/BS fat acid monoester	0.258	1.37

the presence of surfactants based on BS fat, 0.26–0.48 μm. The polydispersity factor was mostly no more than 1.2, except for the ester of MPEG-1900 and BS fatty acids (Tables 4, 5). The mean molecular weights of the polymers M_n corresponded to the common values observed in polymerization of styrene for particles of this size, being about $(7–8) \times 10^5$.

CONCLUSIONS

(1) Surfactant properties of hydroxyethylated fats containing a mixture of unsaturated fatty acids with a degree of hydroxyethylation of 6 and 12, and also of esters of these acids with poly(ethylene glycols) (MW 600 and 2000) and poly(ethylene glycol) methyl ethers (MW 550 and 1900) with the number of oxyethylene groups from 12 to 45, were studied. The surfactants investigated demonstrate a high surface activity at the hydrocarbon/water interface, which reduces the interfacial tension to 2–5 mN m^{-1}.

(2) Monodisperse polystyrene suspensions (particle size 0.25–0.50 μm) were obtained by heterophase polymerization of styrene in the presence of the surfactants investigated. These suspensions show promise as carriers for bioligands in immunochemical research.

REFERENCES

1. Gritskova, I.A., Zhdanova, A.A., Chirikova, O.V., and Shchegolikhina, O.I., *Dokl. Ross. Akad. Nauk*, 1994, vol. 334, no. 1, pp. 57–61.
2. Gritskova, I.A., Gzhiva, E., Legotski, M., and Krasheninnikova, I.G., *Polimery*, 1991, vol. 36, nos. 11/12, pp. 418–422.
3. Gritskova, I.A., Vorob'eva, N.I., Kadantseva, A.I., and Pravednikov, A.N., *Kolloidn. Zh.*, 1985, no. 2, pp. 394–397.
4. Schönfeldt, N., *Grenzflachenaktive Athylenoxid-Addukte*, Stuttgart: Wissenschaftliche, 1976.
5. Vinogradova, S.V. and Vasnev, V.A., *Polikondensatsionnye protsessy i polimery* (Polycondensation Processes and Polymers), Moscow: Nauka, 2000.
6. Shinoda, K., Nakagawa, T., Tamamushi, B.-I., and Isemura, T., *Colloidal Surfactants. Some Physicochemical Properties*, New York: Academic, 1963.
7. *Uniform Latex Particles*, Bang, L.B., Ed., Indianapolis: Seradyn, 1984.

ISSN 1070-4272, Russian Journal of Applied Chemistry, 2006, Vol. 79, No. 2, pp. 288–292. © Pleiades Publishing, Inc., 2006.
Original Russian Text © V. V. Polyanskova, E. V. Kolyakina, D. F. Grishin, 2006, published in Zhurnal Prikladnoi Khimii, 2006, Vol. 79, No. 2, pp. 288–293.

ORGANIC SYNTHESIS AND INDUSTRIAL ORGANIC CHEMISTRY

Sterically Hindered Nitrogen-containing Compounds in Radical Polymerization of Styrene

V. V. Polyanskova, E. V. Kolyakina, and D. F. Grishin

Research Institute of Chemistry, Lobachevsky Nizhni Novgorod State University, Nizhni Novgorod, Russia

Received November 16, 2005

Abstract—The influence exerted on the radical polymerization of styrene by organic compounds containing a *tert*-butyl group and a nitrogen atom in various oxidation states (*tert*-butylamine, 2-methyl-2-nitrosopropane, 2-methyl-2-nitropropane) was examined.

DOI: 10.1134/S1070427206020235

Controlling the chain propagation step under the conditions of radical initiation and, in particular, performing the polymerization without autoacceleration is a topical problem of the modern synthetic chemistry of macromolecules [1]. By introducing appropriate additives, it is possible to control the chain propagation, perform the process without gelation, and obtain (co)polymers of a definite composition with a relatively narrow molecular-weight distribution, as well as to design specific macromolecules. In polymerization of vinyl monomers, such additives are actively used as nitroxyl radicals and their precursors [1–4], organometallic compounds [5], and some other reactive additives.

In this study, we made a comparative analysis of the performance of sterically hindered nitrogen compounds (2-methyl-2-nitrosopropane, MNP; 2-methyl-2-nitropropane, $ButNO_2$; *tert*-butylamine, TBA) in synthesis of polystyrene (polyST). The choice of these compounds is governed by the fact that, on the one hand, they have the same hydrocarbon skeleton (*tert*-butyl group) and, on the other hand, they contain nitrogen atoms in different oxidation states (amino, nitroso, nitro groups). All these compounds can be expected to form nitroxyl adducts (species controlling the polymerization) directly in the reaction system (*in situ*).

As initiator we chose benzoyl peroxide (BP) traditionally used in commercial syntheses of macromolecules [6].

EXPERIMENTAL

MNP and $ButNO_2$ were prepared by the procedures described in [7, 8]; commercially available TBA was dried over sodium and distilled; BP and solvents were purified by the standard procedures [9, 10]. Styrene (ST) was purified to remove hydroquinone by washing with several portions of 5% alkali (until the monomer became colorless) and then with water to remove residual alkali (until the wash water became neutral), after which it was dried over $CaCl_2$. The dried monomer was distilled under reduced pressure. The physicochemical constants of the compounds used agreed with the reference data.

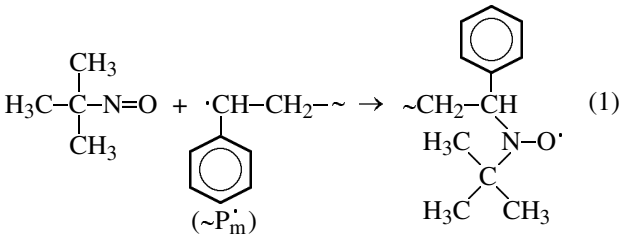
Samples were prepared as follows: The monomer was placed in glass ampules, degassed by threefold freeze–pump–thaw treatment (freezing in liquid N_2), and subjected to polymerization at a residual pressure of 1.3 Pa. The polymerization kinetics was monitored gravimetrically, dilatometrically [11], and thermographically [12].

The molecular weight M of the polymer was determined viscometrically [13] and by gel permeation chromatography with a set of five styrogen columns with pore diameters of 10^5, 3×10^4, 10^4, 10^3, and 250 Å (Waters, the United States). An R-403 differential refractometer (Waters) was used as detector. The eluent was tetrahydrofuran. The device was calibrated with close-cut polystyrene references [14].

To estimate the kinetic parameters of the polymerization of styrene in the presence of nitrogen-containing organic compounds at low conversions, we analyzed the initial portions of the kinetic curves obtained dilatometrically at 60°C. We found that addition of TBA in various concentrations and $ButNO_2$ exerted no significant influence on the initial polymerization rate. The rate of synthesis of the macromolecules somewhat decreased but remained comparable with the rate

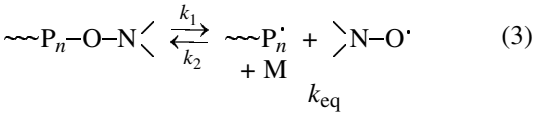
of polymerization initiated by BP without nitrogen-containing additives (Table 1).

At the same time, addition of MNP to the reaction system at the same temperature gives rise to a long induction period (more than 6 h), which may be due to the reaction of the propagating styrene macroradicals ($\sim P_m^{\bullet}$) with the nitroso compound (MNP):



It should be noted that a similar induction period is observed in the polymerization of ST in the presence of 2,2,6,6-tetramethylpiperidine-1-oxyl, the most known and best studied agent for pseudo-living polymerization [15].

As the temperature strongly affects the formation of macromolecules in the presence of nitroxyl radicals [1, 2], it seemed interesting to examine the effect of nitrogen-containing additives on the polymerization of styrene at a higher temperature (100°C), at which the contribution of the reversible inhibition becomes decisive:



We found that at 100°C the kinetics of bulk polymerization of styrene is strongly affected not only by MNP, but also by TBA and $ButNO_2$. Figure 1 shows differential kinetic curves of the ST polymerization in the presence of MNP and $ButNO_2$ at 100°C. It is seen that addition of these nitrogen-containing compounds appreciably reduces the gel effect. It is known [6] that the gel effect is extremely undesirable in the commercial synthesis of polymers, as it favors uncontrollable heat release and spontaneous growth of the molecular weight, which negatively affects the physicomechanical properties of macromolecules.

Table 1. Initial rate v_0 of ST polymerization in the presence of TBA (initiator BP, 1 mol %; reaction temperature 60°C)

Run no.	Addition, mol %	$v_0 \times 10^4$, mol l^{-1} s^{-1}
1	–	1.3
2	TBA:	1.1
3	2	0.9
4	4	0.7
5	8	0.6
6	$ButNO_2$, 3	1.1

It should be noted that the concentration of the additive required to eliminate the autoacceleration up to high conversions is considerably lower with MNP than with $ButNO_2$.

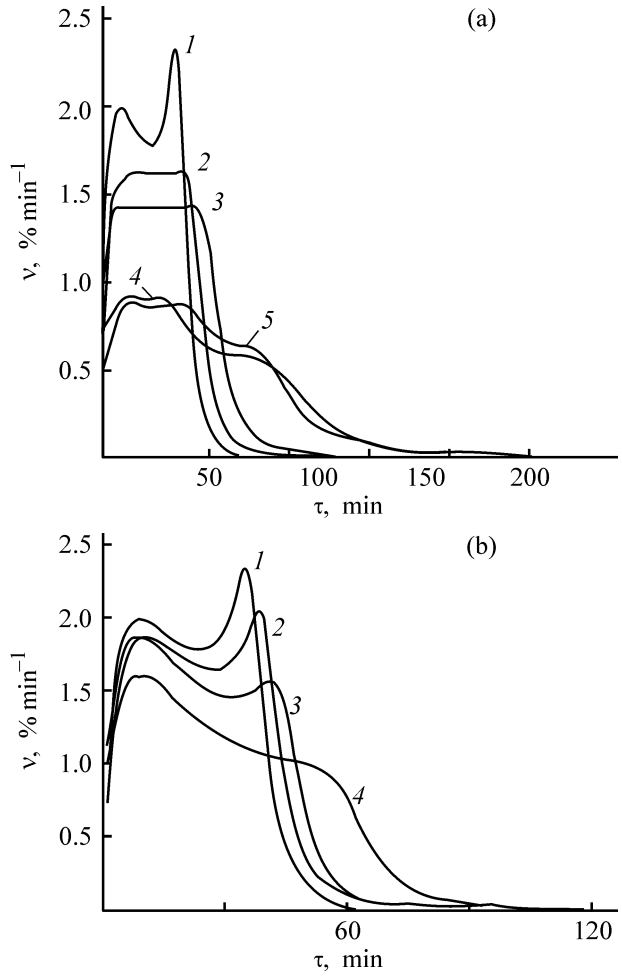


Fig. 1. Differential kinetic curves of the polymerization of ST in the presence of (a) MNP and (b) $ButNO_2$ at 100°C. Initiator BP, 1.0 mol %; the same for Fig. 2. (v) Polymerization rate and (τ) polymerization time. (a) MNP concentration, mol %: (*1*) 0, (*2*) 0.2, (*3*) 0.3, (*4*) 0.5, and (*5*) 0.8. (b) $ButNO_2$ concentration, mol %: (*1*) 0, (*2*) 1, (*3*) 4, and (*4*) 8.

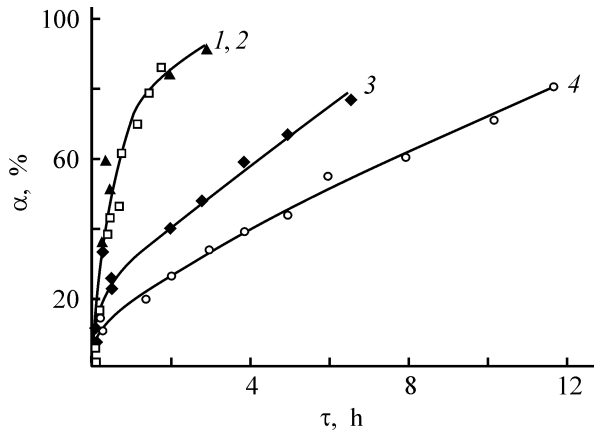


Fig. 2. Integral kinetic curves of the polymerization of ST in the presence of TBA (gravimetric monitoring) at 100°C: (α) conversion and (τ) polymerization time. TBA concentration, mol %: (*1*) 0, (*2*) 1.0, (*3*) 4.0, and (*4*) 8.0.

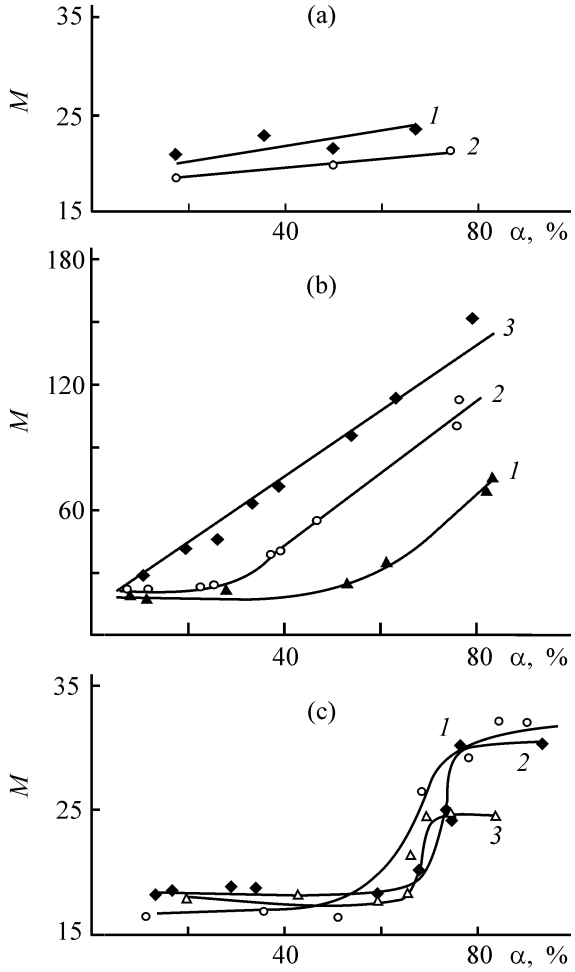


Fig. 3. Molecular weight *M* of polyST vs. conversion α. Initiator BP, 1.0 mol %; polymerization temperature 100°C; the same for Fig. 4. (a) 0.8 mol % MNP; *M*: (*1*) viscosity-average and (*2*) number-average; (b) viscosity-average *M*; TBA concentration, mol %: (*1*) 2.0, (*2*) 4.0, and (*3*) 8.0; (c) viscosity-average *M*; $ButNO_2$ concentration, mol %: (*1*) 0, (*2*) 4.0, and (*3*) 8.0.

As follows from the integral kinetic curves shown in Fig. 2, addition of TBA to the system also leads to a considerable decrease in the overall polymerization rate. The initial rate of the polyST formation in the presence of 1.0–4.0 mol % TBA remains fairly high (~30% conversion in 1 h), but the further reaction is slow. At a higher TBA concentration (8.0 mol %), its inhibiting effect becomes more significant and is manifested already at low conversions.

The molecular-weight characteristics of polyST prepared in the presence of MNP, TBA, and $ButNO_2$ also indirectly suggest that the nitrogen-containing compounds are directly involved in the chain propagation; however, as expected, their effect varies, depending on the compound structure.

We found that the molecular weights of the samples prepared with MNP as a controlling additive linearly increased with the monomer conversion (Fig. 3a), which is one of the evidences of the controlled radical polymerization [1].

The molecular-weight characteristics of polyST synthesized in the presence of TBA showed interesting features. As can be seen from Fig. 3b, on introduction of 8.0 mol % amine, the viscosity-average molecular-weight *M* linearly increases with the conversion, indirectly suggesting the controlled polymerization mechanism. However, with a decrease in the concentration of the additive (to 2–4 mol %), the contribution of the uncontrolled process increases, and, in this case, the curve of *M* vs. conversion consists of two branches with an inflection point characteristic of polymerization with the gel effect. In the initial parts of the curve, *M* of polyST remains approximately constant, but at high conversions it sharply grows. At the amine concentration equal to the initiator concentration (1.0 mol %), TBA exerts no appreciable influence on the molecular-weight characteristics of the polymer, and the dependence of *M* on the conversion is S-shaped, which is typical of the common (uncontrolled) radical polymerization with the gel effect.

In contrast to MNP and TBA, addition of $ButNO_2$ does not noticeably affect the molecular-weight characteristics of the polymer. In particular, the dependences of *M* of polyST samples prepared in the presence of various concentrations of the nitro compound are similar to the case of the common radical initiation (Fig. 3c). At the same time, the polydispersity coefficients of the polymers prepared with the system [$ButNO_2$ + BP] are lower, compared to the samples prepared without additives (Table 2). The above features of the polymerization in the presence of $ButNO_2$

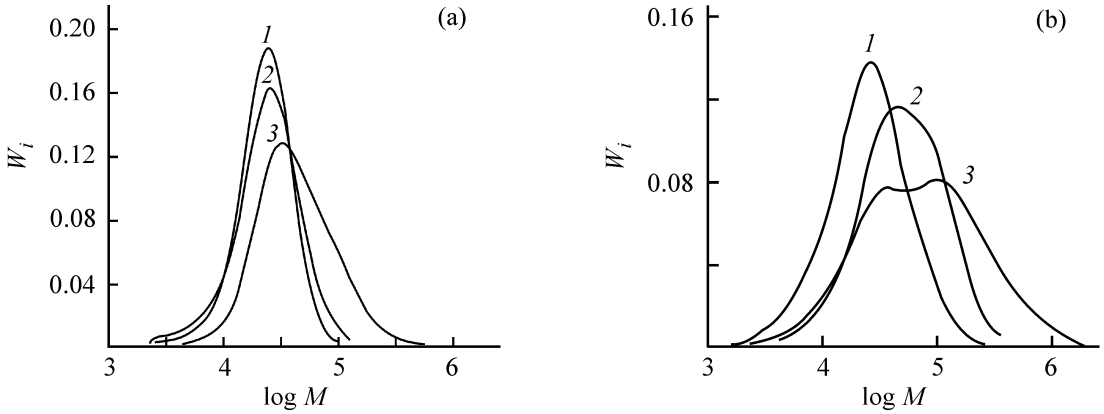


Fig. 4. MWD curves of polyST samples synthesized in the presence of TBA to various conversions. (W_i) weight proportion of the fraction and (log M) logarithm of molecular weight. (a) TBA concentration 1.0 mol %; conversion, %: (*1*) 17, (*2*) 43, and (*3*) 85.7; (b) TBA concentration 4.0 mol %; conversion, %: (*1*) 25, (*2*) 48, and (*3*) 67.

are typical of the processes performed in the presence of weak inhibitors [2, 6].

Taken in combination with published data on the reactivity of nitro compounds [16, 17], our results suggest the following scheme of propagation of the polymeric chain in the presence of $ButNO_2$: The propagating macroradical reacts with the nitro compound to form a nitroxyl spin adduct:

$$\sim\sim P_n^{\cdot} + ButNO_2 \rightarrow But{-}N\begin{matrix}O^{\cdot}\\ \diagdown\\ O{-}P_n\sim\sim\end{matrix} \quad (4)$$

The low-reactive oxygen-centered nitrogen-containing radical formed by this reaction can terminate the second radical chain to form an ether and MNP:

$$But{-}N\begin{matrix}O^{\cdot}\\ \diagdown\\ O{-}P_n\sim\sim\end{matrix} + \sim\sim P_n^{\cdot} \rightarrow But{-}N{=}O + \sim\sim P_nOP_n\sim\sim \quad (5)$$

As shown above, MNP also actively affects the kinetics of radical polymerization of ST.

In synthesis of polyST in the presence of MNP, the polydispersity coefficients of the samples do not noticeably vary with the conversion and amount to 1.3–1.4 (Table 2). These values are appreciably lower than those for the polymer prepared under the comparable conditions of radical initiation but without additives [6].

The effect of TBA on the molecular-weight characteristics of the polymer is determined by the concentration of the additive. When the amine is added in low concentrations (1.0 mol %), the polydispersity coefficients of the polyST synthesized are relatively low, and the molecular-weight distribution (MWD) is unimodal (Fig. 4a). With an increase in the amine concentration, the MWD curves get considerably broadened and become bimodal (Fig. 4b). The polydispersity coefficients of the samples prepared in the presence of 2–8 mol % TBA at high conversions exceed those of the samples prepared without the additives. This may be caused by the occurrence of certain side processes, in particular, of chain transfer to the amine and of other reactions characteristic of such systems. Also, accumulation of 2-methyl-2-nitroprop-

Table 2. Molecular-weight characteristics of polyST synthesized at 100°C (BP concentration 1.0 mol %)

Run no.	Additive, mol %	Conversion, %	$M_n \times 10^{-3}$	$M_w \times 10^{-3}$	M_w/M_n
1	–	91	20	41	2.1
	$ButNO_2$:				
2	4.0	14	12	18	1.5
3	4.0	46	12	18	1.5
4	4.0	75	16	27	1.7
5	8.0	13	12	18	1.5
6	8.0	26	12	18	1.5
7	8.0	74	16	29	1.8
	MNP:				
8	0.8	17	19	26	1.4
9	0.8	50	20	26	1.3
10	0.8	74	22	29	1.3
	TBA:				
11	1.0	17	28	35	1.3
12	1.0	43	31	42	1.5
13	1.0	86	56	107	1.7
14	2.0	28	22	29	1.3
15	2.0	83	31	113	3.6
16	4.0	25	20	35	1.7
17	4.0	66	37	127	3.4
18	8.0	11	36	50	1.4
19	8.0	70	92	265	2.9

ane formed by oxidation of the amine with benzoyl peroxide [18],

$$RNH_2 \xrightarrow{(O)} [RNHOH] \xrightarrow{(O)} [RN(H)O\cdot] \xrightarrow{(O)} RNO_2,$$

and its involvements in the polymerization cannot be ruled out.

With an increase in the amine concentration, the contribution of side processes involving these compounds increases, which results in bimodal MWD and increased polydispersity of the samples.

CONCLUSIONS

(1) 2-Methyl-2-nitrosopropane, *tert*-butylamine, and 2-methyl-2-nitropropane are directly involved in the propagation step in the styrene polymerization initiated by benzoyl peroxide.

(2) Addition of these compounds affects the overall polymerization kinetics by decreasing the reaction rate in the autoacceleration step and controlling the molecular-weight characteristics of polystyrene. 2-Methyl-2-nitrosopropane controls the chain propagation under the conditions of bulk polymerization of styrene more efficiently than do 2-methyl-2-nitro-propane and *tert*-butylamine.

ACKNOWLEDGMENTS

The authors are grateful to M.V. Pavlovskaya and A.Yu. Borisov for participation in certain experiments.

The study was financially supported by the Russian Foundation for Basic Research (project no. 05-03-32688).

REFERENCES

1. Matyjaszewski, K., *Controlled/Living Radical Polymerization*, Oxford: Oxford Univ., 2000.
2. Grishin, D.F. and Semenycheva, L.L., *Usp. Khim.*, 2001, vol. 70, no. 5, p. 486–510.
3. Moad, G. and Rizzardo, E., *Macromolecules*, 1995, vol. 28, no. 26, p. 8722.
4. Benoit, D., Chaplinski, V., Braslau, R., and Hawker, C.J., *J. Am. Chem. Soc.*, 1999, vol. 121, no. 16, p. 3904–3920.
5. Matyjaszewski, K. and Xia, J., *Chem. Rev.*, 2001, vol. 101, p. 2921–2990.
6. Kireev, V.V., *Vysokomolekulyarnye soedineniya* (Macromolecular Compounds), Moscow: Vysshaya Shkola, 1992.
7. Terabe, S. and Konaka, S., *J. Chem. Soc., Perkin Trans. 2*, 1972, no. 14, p. 2163.
8. Kornblum, N., Clutter, R.J., and Jones, W.J., *J. Am. Chem. Soc.*, 1956, vol. 78, no. 16, p. 4003–4004.
9. *Organic Syntheses*, Blatt, A.H., Ed., New York: Wiley, 1944. Translated under the title *Sintezy organicheskikh preparatov*, Moscow: Inostrannaya Literatura, 1949, vol. 2.
10. Weissberger, A. and Proskauer, E.S., *Organic Solvents. Physical Properties and Methods of Purification*, Riddick, J.A. and Toops, E.E., Eds., New York: Interscience, 1955.
11. Emel'yanov, D.N., Panova, G.D., and Ryabov, A.V., *Praktikum po metodam issledovaniya vysokomolekulyarnykh soedinenii* (Practical Course of Methods for Studying Macromolecular Compounds), Gor'kii: Gor'k. Gos. Univ., 1963.
12. Arulin, V.I. and Efimov, L.I., *Tr. Khim. Khim. Tekhnol.*, Gor'kii: Gor'k. Gos. Univ., 1970, issue 2, p. 74–77.
13. Rafikov, S.R., Pavlov, S.A., and Tverdokhlebova, I.I., *Metody opredeleniya molekulyarnykh vesov i polidispersnosti vysokomolekulyarnykh soedinenii* (Methods for Determining Molecular Weights and Polydispersities of Macromolecular Compounds), Moscow: Khimiya, 1963.
14. Belen'kii, B.G. and Vilenchik, L.Z., *Khromatografiya polimerov* (Chromatography of Polymers), Moscow: Khimiya, 1978.
15. Fukuda, T., Goto, A., and Ohno, K., *Macromol. Rapid Commun.*, 2000, vol. 21, p. 151.
16. Hammond, G.S. and Bartlett, P.D., *J. Polym. Sci.*, 1951, vol. 6, p. 617–624.
17. Inamoto, N. and Simamura, O., *J. Org. Chem.*, 1958, vol. 23, no.3, p. 408–410.
18. Gambaryan, S.P. and Kazaryan, L.Z., *Zh. Obshch. Khim.*, 1933, vol. 3, no. 2, p. 222–228.

ISSN 1070-4272, Russian Journal of Applied Chemistry, 2006, Vol. 79, No. 2, pp. 293–296. © Pleiades Publishing, Inc., 2006.
Original Russian Text © A. I. Bol'shakov, D. P. Kiryukhin, 2006, published in Zhurnal Prikladnoi Khimii, 2006, Vol. 79, No. 2, pp. 294–297.

MACROMOLECULAR CHEMISTRY AND POLYMERIC MATERIALS

Low-Temperature Radiation-Initiated Copolymerization of *N*-Vinylpyrrolidone with Acrylic Acid in Glass-Forming Ethanol or Dimethylformamide Solutions

A. I. Bol'shakov and D. P. Kiryukhin

Institute of Problems of Chemical Physics, Russian Academy of Sciences, Chernogolovka, Moscow oblast, Russia

Received August 17, 2005

Abstract—The radiation-initiated copolymerization of *N*-vinylpyrrolidone with acrylic acid at low temperatures in glass-forming ethanol or dimethylformamide solutions was studied. The mechanism of the copolymer formation was elucidated, and conditions were determined for preparing alternating and random block copolymers.

DOI: 10.1134/S1070427206020248

Copolymers of *N*-vinylpyrrolidone (VP) with unsaturated carboxylic acids are used in medicine and biology [1, 2]. In liquid-phase copolymerization, the copolymer composition is determined by the mutual reactivity of the comonomers. As the active monomer is consumed, the resulting copolymer, as a rule, gets enriched with the less reactive monomer, so that the composition of the polymer chains becomes nonuniform. Radiation-chemical initiation makes it possible to accumulate active reaction centers and perform the process in the solid or viscous supercooled state at considerably lower temperatures than with substance initiation. These specific reaction conditions, manifested in a considerable increase in the contact time of the reactants, allow preparation of copolymers whose composition is independent of the conversion and is determined by the composition of the starting mixture [3].

In this study, we examined radiation-initiated copolymerization of VP with acrylic acid (AA) in ethanol or dimethylformamide (DMF) solutions forming a glass at low temperatures.

EXPERIMENTAL

N-Vinylpyrrolidone and acrylic acid were purified by double distillation in a vacuum; ethanol and DMF were not specially purified. The reaction mixtures were placed in glass calorimetric cells, freed from atmospheric oxygen in a vacuum unit, and sealed in a vacuum. Samples were gamma-irradiated from a ^{60}Co source (Gammatok-100 installation) at 77 K. The polymerization was monitored calorimetrically [4]. The irradiated samples were placed in a calorimetric unit precooled to 77 K, and the calorimeter was slowly (at a rate of ~0.35 deg min^{-1}) warmed up. The polymer yield was determined gravimetrically after the removal of the unchanged monomers in a vacuum. The composition of the products was determined by elemental analysis from the nitrogen content in the copolymer.

Figure 1 shows the calorimetric curves of heating of the unirradiated and gamma-irradiated samples of

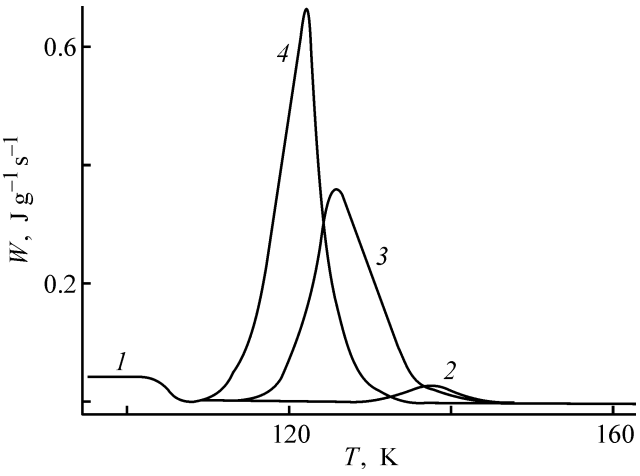


Fig. 1. Calorimetric curves of heating: (*1*) unirradiated solutions of VP, AA, and VP + AA in ethanol; gamma-irradiated solutions of (*2*) VP, (*3*) AA, and (*4*) VP + AA in ethanol. Total concentration of VP, AA, and VP + AA in solution 10 wt %; relative concentration of VP in comonomer mixture 50 mol %; irradiation dose 20 kGy. (*W*) Heat release and (*T*) temperature.

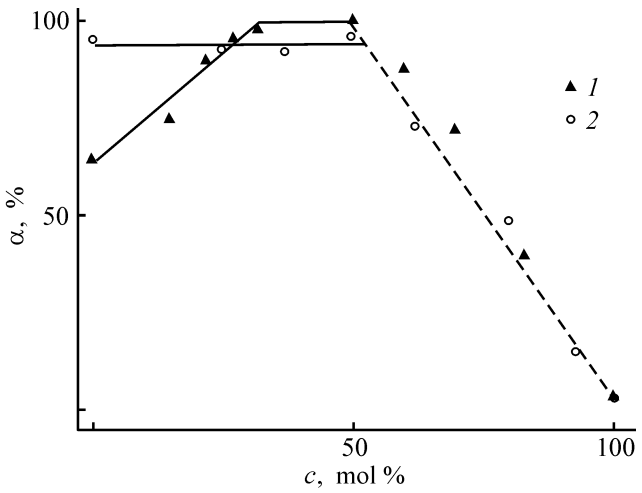


Fig. 2. Copolymer yield α in solutions of VP + AA in (*1*) ethanol and (*2*) DMF as a function of the relative concentration *c* of VP in the comonomer mixture. Total concentration of monomers in solution, wt %: (*1*) 10 and (*2*) 20. Irradiation dose, kGy: (*1*) 20 and (*2*) 2.

VP, AA, and their mixture in ethanol. On cooling to 77 K, these solutions fully transform into a glassy state, and their calorimetric heating curves in the temperature interval 100–105 K exhibit a step corresponding to the transition from a solid glassy state to a supercooled liquid. Then, on warming to 200 K, the calorimeter records no changes associated with the presence or formation of a crystalline phase: The calorimetric heating curves for solutions of VP, AA, and their mixture in ethanol virtually coincide (Fig. 1, curve *1*). Warming of the preliminarily gamma-irradiated (77 K) VP + AA sample is accompanied by heat release after the glass → liquid transition, associated with the formation of VP–AA copolymers (Fig. 1, curve *4*). Hence, in the temperature interval 100–160 K, when the system is in the state of a viscous supercooled liquid, VP efficiently copolymerizes with AA.

It should be noted that the homopolymerization of AA on heating of the preliminarily gamma-irradiated glassy solution of AA in ethanol also occurs after the glass → liquid transition of the system (Fig. 1, curve *3*). The polymer yield steadily increases with the AA content in the solution and reaches 80% at a monomer concentration of about 16 wt % [5].

By contrast, the homopolymerization of VP under these conditions is inefficient. The calorimetric heating curves of the preliminarily gamma-irradiated glassy solutions of VP in ethanol show only slight heat release associated with the VP polymerization (Fig. 1, curve *2*). The polymer yield at an irradiation dose of 20 kGy is as low as ~3%. It has been shown previously [6] that the low chemical activity of VP in the homopolymerization is not associated with the initiation step. The radicals generated by gamma-irradiation, which are stable at 77 K, rapidly take up monomer molecules in the glass → liquid region (R_0 + M → R_p^{VP}) to form active polymerization centers ($R_p^{VP} \approx 0.5R_0$). However, the arising active centers inefficiently take up the like monomer molecules in the course of further heating: The calorimeter records only a slight heat release corresponding to approximately 3% yield of the polymer (Fig. 1, curve *2*).

In copolymerization of VP with AA, addition of low-active VP to the solution should seemingly decrease the polymerization rate and copolymer yield. However, both these quantities actually increase.

Figure 2 shows the dependence of the copolymer yield on the initial comonomer ratio at the total comonomer concentration in ethanol of 10 wt % and irradiation dose of 20 kGy (curve *1*). The yield of the AA homopolymer under these conditions is 65%. On adding VP to a solution of AA in ethanol, the copolymer yield increases with the VP concentration, reaching 100% at 30 mol % content of VP.

The increased reactivity in the VP–AA system and the accordingly higher copolymer yield are attributed to the formation of a 1 : 1 intermolecular complex of AA with VP [7]. Formation of this complex, as noted in [7], makes lower the barriers of intermolecular interactions and accelerates the propagation of the polymer chains.

The ~100% yield of the copolymer is attained at the initial relative VP concentration ranging from 30 to 50 mol %. At a higher VP content, the product yield decreases, reaching 3% with pure VP (Fig. 2, curve *1*).

Then we studied the polymerization of VP and AA and their copolymerization in DMF solutions with a higher glass transition point (T_g ~135 K). The polymerization and copolymerization on warming of preliminarily irradiated solutions of these monomers occur in DMF, as in ethanol, at temperatures above T_g and are not accompanied by product precipitation.

Figure 2 (curve *2*) shows the dependence of the copolymer yield on the relative concentration of VP in a mixture with AA at a total comonomer concentration in DMF solution of 20 wt %, after preliminary irradiation to a dose of 2 kGy. Under these conditions, as in ethanol, the homopolymerization of AA is very efficient (homopolymer yield 90–97%), whereas that of VP is strongly suppressed (3%). However, addition

of VP to a solution of AA in DMF does not decrease the copolymerization rate. The copolymer yield remains constant at a relative VP concentration of up to 50 mol % (Fig. 2, curve *2*). Hence, with an increase in the relative concentration of VP in its mixture with AA to 50 mol %, the propagation of polymer chains is not suppressed.

An increase in the polymerization temperature in the DMF solutions relative to ethanol solutions (by ~30 K) does not appreciably affect the capacity of VP for polymerization. As in the ethanol solution, the monomer conversion does not exceed 3%. As already noted, this is caused by the low activity of the radicals with the terminal VP fragment, R_p^{VP}. Experimental results show that, when involved in copolymerization in both DMF and ethanol solutions, the acrylate radicals R_p^A generated from AA by gamma-irradiation at 77 K readily take up not only the like (AA) monomer molecules (the reaction is fast and the product yield is high), but also less active VP molecules ($R_p^A + VP \rightarrow R_p^{VP}$). As already noted, the resulting R_p^{VP}, does not add VP molecules but actively adds AA molecules. Hence, VP can add to the propagating macroradical mostly as single units, and the polymeric molecule should not contain VP blocks. The polymer chains will propagate until complete exhaustion of AA, after which the propagation should stop.

Formation of random copolymers of the composition corresponding to that of the starting mixture was observed in copolymerization of AA with acrylamide (AM) in glass-forming ethanol solutions [3]. In the viscous supercooled liquid, the time of the mutual contact of the reacting species is considerably longer than that in the gas and liquid phases, and the frequencies of addition of a monomer to the active center of a propagating polymer chain are close to those of translation motion. Under these conditions, the composition of the forming copolymers is determined by the initial concentrations of the comonomers, rather than by their mutual reactivity. It should be noted that the polymerization of AA and AM in glass-forming ethanol solutions is very efficient. In copolymerization of AA with VP, the capacity of one of the comonomers, VP, for polymerization in the supercooled liquid is very low. Then, at the same diffusion mobilities of the comonomers, the polymer chain propagation will stop at the VP concentration exceeding 50 mol %. The excess VP will remain nonpolymerized, and the copolymer yield will decrease with an increase in its concentration. This pattern is actually observed in copolymerization of VP with AA in ethanol and DMF (Fig. 2, curves *1*, *2*).

Content of VP units in copolymers prepared by copolymerization of 20 wt % solutions of VP + AA in DMF at various initial comonomer ratios

VP concentration in starting mixture, mol %	Yield, %	Content of VP units in copolymer, mol %
25.0	93.4	23.8
37.0	94.0	30.6
50.0	96.2	50.4
62.8	73.0	53.4
79.8	39.6	55.5

It follows from the suggested mechanism of copolymerization of VP with AA that at a VP concentration lower than 50 mol % the copolymer composition will correspond to that of the starting comonomer mixture, and the copolymer will consist of –VP–$(AA)_n$– blocks. With an increase in the VP content in the starting mixture, *n* will decrease, and at a VP concentration of 50 mol % *n* will become equal to unity, i.e., a 1 : 1 random copolymer will form. A further increase in the concentration (>50 mol %) will also result in formation of the alternating copolymer, but its yield and molecular weight will be lower, because the chain length will be determined by the relative concentration of low-active VP in the comonomer mixture.

The copolymer yield Γ in the copolymerization of VP with AA at the relative concentration of VP exceeding 50 mol % in ethanol and DMF solutions can be estimated from the initial comonomer concentrations by the expression

$$\Gamma = (N_1M_1 + N_1M_2)/(N_1M_1 + N_2M_2), \qquad (1)$$

where N_1 and N_2, M_1 and M_2 are the amounts (moles) and molecular weights of AA and VP, respectively.

The experimental data on the decrease in the copolymer yields are well described by Eq. (1) [Fig. 2: points, experimental data; dashed line, calculation by formula (1)].

The suggested mechanism of formation of the copolymers is confirmed by the data on the copolymer composition (see table). Indeed, at VP concentrations less than 50 mol %, the copolymer compositions are close to those of the starting mixtures. At VP concentrations exceeding 50 mol %, when the copolymer yield decreases virtually linearly with an increase in the VP content in the starting mixture, the copolymer composition does not noticeably change and is close to 1 : 1.

Thus, our results show that the copolymerization of VP with AA in ethanol and DMF solutions forming a glass at low temperatures allows preparation of alternating and random copolymers of composition determined by the initial comonomer ratio. The mechanism of formation of such copolymers is elucidated, and conditions for their preparation are determined.

CONCLUSIONS

(1) The radiation-initiated copolymerization of *N*-vinylpyrrolidone with acrylic acid in glass-forming ethanol and dimethylformamide solutions was performed. The process occurs after the transition of the systems to the viscous supercooled liquid in the temperature range 100–140 K.

(2) It was found that at the relative concentration of *N*-vinylpyrrolidone less than 50 mol %, the composition of the resulting copolymer corresponds to that of the starting comonomer mixture. At the *N*-vinylpyrrolidone concentration exceeding 50 mol %, an alternating copolymer of *N*-vinylpyrrolidone with acrylic acid is formed.

ACKNOWLEDGMENTS

The authors are grateful to L.S. Kiryukhina for performing the elemental analysis of the polymers.

The study was financially supported by the Russian Foundation for Basic Research and by Ministry of Industry and Science of Moscow oblast (science-city project no. 04-03-97237 r2004).

REFERENCES

1. Plate, N.A. and Vasil'ev, A.E., *Fiziologicheski aktivnye polimery* (Physiologically Active Polymers), Moscow: Nauka, 1986.
2. Panarin, E.F. and Ushakova, V.N., *Sopolimery N-vinilpirrolidona kak nositeli biologicheski aktivnykh veshchestv* (*N*-Vinylpyrrolidone Copolymers as Carriers of Biologically Active Substances), Moscow: Nauka, 1989, pp. 66–95.
3. Bol'shakov, A.I., Mikhailov, A.I., and Barkalov, I.M., *Dokl. Akad. Nauk SSSR*, 1978, vol. 241, no. 6, pp. 1355–1358.
4. Barkalov, I.M. and Kiryukhin, D.P., *Int. Rev. Phys. Chem.*, 1994, vol. 13, no. 2, pp. 337–357.
5. Bol'shakov, A.I., Mikhailov, A.I., and Barkalov, I.M., *Vysokomol. Soedin., Ser. B*, 1976, vol. 19, no. 12, pp. 906–908.
6. Bol'shakov, A.I. and Barkalov, I.M., *Vysokomol. Soedin., Ser. A*, 1991, vol. 33, no. 9, pp. 1828–1833.
7. Usmanov, A.Kh., Turaev, A.S., Nadzhimutdinov, Sh., and Usmanov, Kh.U., *Uzb. Khim. Zh.*, 1975, no. 4, pp. 36–39.

ISSN 1070-4272, Russian Journal of Applied Chemistry, 2006, Vol. 79, No. 2, pp. 297–300. © Pleiades Publishing, Inc., 2006.
Original Russian Text © M. L. Eritsyan, G. V. Akopyan, K. M. Eritsyan, G. G. Galstyan, L. T. Melkonyan, R. A. Karamyan, 2006, published in Zhurnal Prikladnoi Khimii, 2006, Vol. 79, No. 2, pp. 298–301.

MACROMOLECULAR CHEMISTRY AND POLYMERIC MATERIALS

Dynamics of Water Absorption by Copolymers of Acrylic Acid and Its Derivatives

M. L. Eritsyan, G. V. Akopyan, K. M. Eritsyan, G. G. Galstyan, L. T. Melkonyan, and R. A. Karamyan

Abovyan State Pedagogical University, Yerevan, Armenia

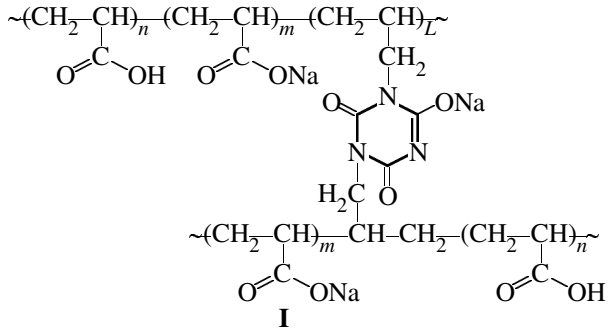
Received April 26, 2006

Abstract—Water absorption by copolymers of acrylic acid, sodium acrylate, and sodium 1,3-diallyl isocyanurate and of acrylic acid, sodium acrylate, acrylamide, and sodium 1,3-diallyl isocyanurate was studied in relation to their composition and the concentration of cross-linking agent.

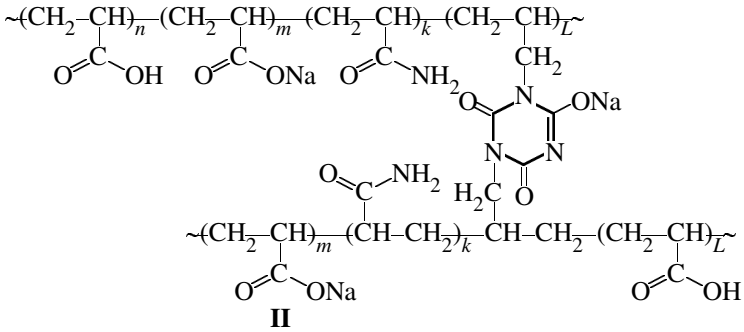
DOI: 10.1134/S107042720602025X

Water absorption by copolymers of acrylic acid and its derivatives has been extensively studied. Acrylate systems absorbing no less than 500 g of water per gram of copolymer were examined in [1–4]. Cross-linked copolymers of various structures exhibiting high absorption capacity (no less than 850 g of water per gram) have been prepared previously [5, 6] from acrylic acid (AA), sodium acrylate (Na-AA), and sodium 1,3-diallyl isocyanurate (Na-DAIC). Similar absorption properties are typical of cross-linked copolymers prepared from AA, Na-AA, Na-DAIC, and acrylamide (AM) [7]. However, data on the rate of water absorption by copolymers based on AA and its reactive hydrophilic derivatives are virtually lacking.

In this study, we measured the rate of water absorption by cross-linked copolymers of AA, Na-AA, and Na-DAIC (**I**) and of AA, Na-AA, Na-DAIC, and AM (**II**), as influenced by the copolymer composition. The structure of the copolymers studied can be represented as:



I



II

Owing to the presence of polar functional and ionic groups, copolymers **I** and **II** are strongly hydrated and swell in water. The maximal (stationary) swelling rate is attained when the cross-linked copolymer fragment is opened to the greatest extent in water and does not hinder free diffusion of water in the intermolecular space of the cross-linked copolymer network. The time required for the maximal opening of the copolymer networks, after which the copolymer swells at a constant rate, can be termed induction period (τ_{in}). It was found that τ_{in} directly depends on both the functional composition of the copolymer and the concentration of the ionic groups.

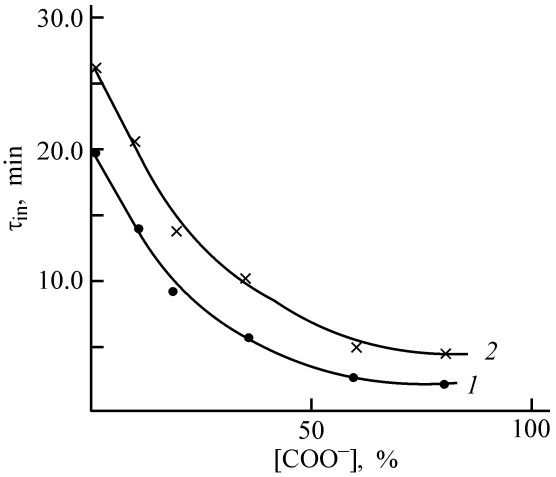


Fig. 1. Induction time of water absorption, τ_{in}, vs. the concentration of COO^- groups [COO^-] in copolymers **I** at concentrations of Na-DAIC equal to (*1*) 1.25×10^{-2} and (*2*) 2.5×10^{-2} M.

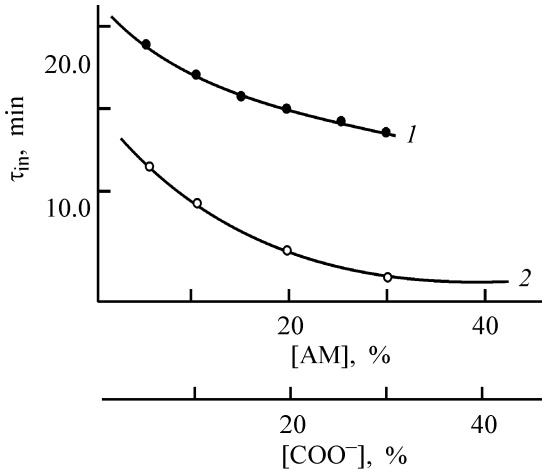


Fig. 2. Induction time of water absorption, τ_{in}, of copolymers **I** and **II** vs. the concentration of (*1*) AM units [AM] in the copolymer chain and (*2*) COO^- groups [COO^-] in the copolymer containing 30% AM units relative to [AA].

The dependence of τ_{in} on the concentration of COO^- groups in copolymer **I** is shown in Fig. 1. It can be seen that, as the concentration of COO^- groups in the copolymer increases, the time in which the stationary rate of water absorption is attained exponentially decreases and then becomes nearly constant at approximately 50% content of the COO^- groups. As can be seen from Fig. 1, τ_{in} depends on the concentration of Na-DAIC; with increasing content of Na-DAIC, the copolymer becomes more compact due to the increased density of cross-linking, which hinders the diffusion of water.

Rate of water absorption as influenced by the composition of the cross-linked copolymers

[COO^-]/[COOH]	V_w, $cm^3\ s^{-1}$, at indicated [Na-DAIC], M	
	1.25×10^{-2}	2.5×10^{-2}
0	3×10^{-3}	1.8×10^{-2}
0.1	6.8×10^{-3}	4.33×10^{-3}
0.2	9.3×10^{-3}	6.8×10^{-3}
0.3	1.75×10^{-2}	1.23×10^{-2}
0.6	5.5×10^{-2}	3.13×10^{-2}
0*	7.6×10^{-3}	5.8×10^{-3}
0.05*	8.1×10^{-3}	6.9×10^{-3}
0.1*	1.2×10^{-3}	8.5×10^{-3}
0.2*	2.1×10^{-2}	1.4×10^{-2}
0.3*	3.2×10^{-2}	2.3×10^{-2}
0.4*	4.5×10^{-2}	3.1×10^{-2}

* Content of AM units in the copolymer 30% relative to [AA].

The data on the stationary rate of water absorption V_w by cross-linked copolymers **I**, as influenced by the [COO^-]/[COOH] molar ratio and the concentration of the cross-linking agent [Na-DAIC], are listed in the table.

It can be seen that, as the concentration of COO^- groups in the copolymer increases by a factor of 6, the rate of water absorption grows by a factor of more than 8 $(5.5 \times 10^{-2})/(6.8 \times 10^{-3})$. As the density of intermolecular cross-links increases, the rate of water absorption decreases. For example, as the concentration of Na-DAIC in the comonomer mixture increases by a factor of 2, the rate of water absorption decreases (on the average) by a factor of 1.5.

Thus, to attain the maximal water absorption by the cross-linked copolymer, it is necessary to provide the optimal ratio of the ionic and hydrophilic groups and their uniform distribution in the copolymer chain and the optimal density of cross-links between the copolymer macromolecules.

Copolymer **II** exhibiting higher water absorption than copolymer **I** seems to be more promising for technical applications. In particular, 1 g of copolymer **II** absorbs up to 1200 g of water.

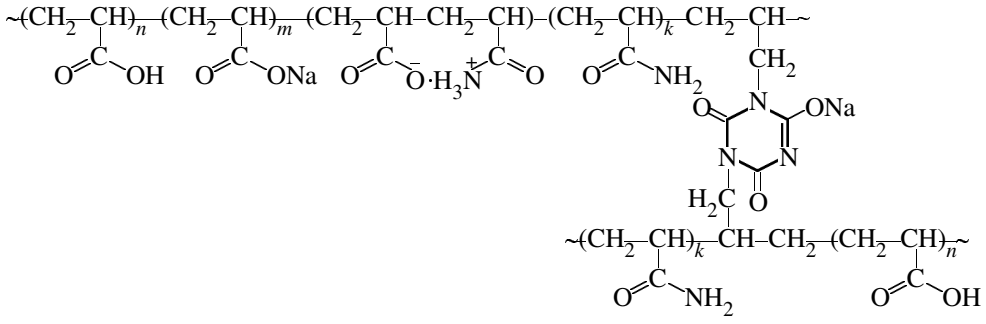
It was found that τ_{in} of copolymer **II** is determined not only by the COO^-/COOH molar ratio, but also exponentially depends on the content of AM units in the copolymer network (Fig. 2).

As can be seen from Fig. 3, τ_{in} decreases as the content of AM units in the copolymer increases. This is

probably due to intermolecular salt formation by interaction of the –COOH and NH_2 groups in the copolymer.

The IR spectra of the copolymers are characterized by absorption in the following ranges ν, cm^{-1}: 763 (*sym*-triazine ring); 1420, 1590–1630 (COO^-); 1490–1530, 1840–1950 ($-C(O)NH_3^+$); 1670–1695 ($-C(O)NH_2$); 1710–1730 (COOH), and 2890–2980 (–CH). The absorption bands at 1490–1530 and 1840–1950 cm^{-1} suggest the presence of the ion pair ($-C(O)N^+H_3^-OOC$).

Based on the above data, the structure of copolymer **II** can be represented as:



The water absorption by copolymer **II** in the linear portion of the kinetic plots is determined by both the COO^-/COOH molar ratio and the content of AM units in the copolymer network. The linear portions of the dependence of the water absorption of copolymer **II** on the concentration of AM units in the copolymer is shown in Fig. 3. Copolymers **II** were prepared at a varied concentration of AM component and [AA] = 1.5, [Na-AA] = 0.45, and [Na-DAIC] = 1.25×10^{-2} M. As can be seen from Fig. 3, copolymer **II** containing 30% AM relative to [AA] exhibit high water absorption capacity.

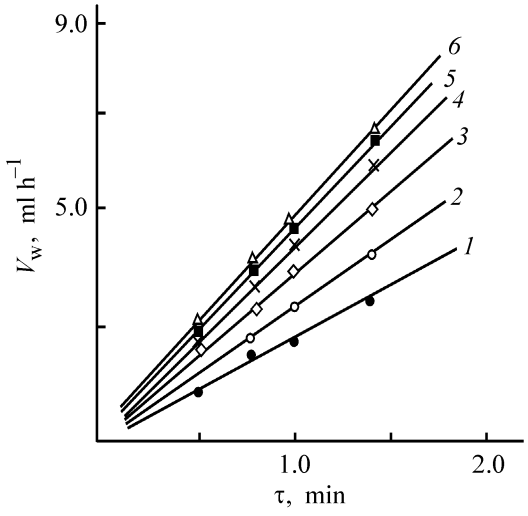


Fig. 3. Water absorption capacity V_w of copolymer **II** vs. time at a varied content of AM units in the copolymer. [AM] relative to [AA], %: (*1*) 5, (*2*) 10, (*3*) 15, (*4*) 20, (*5*) 25, and (*6*) 30.

As the content of the cross-linking agent increases, the density of intermolecular bonds between the macromolecular chains grows thereby decreasing water the absorption capacity of the copolymers.

EXPERIMENTAL

The IR spectra of copolymers were recorded on a UR-20 spectrophotometer. The distilled fraction of acrylic acid (mp 141°C, n_D^{20} 1.4224) was used. Sodium 1,3-diallyl isocyanurate was prepared in accordance with [7]. Acrylamide (mp 85°C) was recrystallized from methanol. Ammonium persulfate was recrystallized from ethanol. Copolymers **I** and **II** were prepared by the procedure described in [6].

To determine the water absorption capacity of copolymers **I** and **II**, a copolymer sample (0.25 g) was placed in a volumetric cylinder (0.5 mm in diameter and 30 cm high); the cylinder was filled with water to the mark and brought to the required temperature. The upwards motion of the boundary of the swollen gel in the course of time was recorded.

CONCLUSIONS

(1) Copolymers of acrylic acid, sodium acrylate, and sodium 1,3-diallyl isocyanurate and of acrylic acid, sodium acrylate, acrylamide, and sodium 1,3-diallyl isocyanurate exhibit a high water absorption capacity.

(2) Water absorption by copolymers increases with the COO^-/COOH molar ratio and the content of acrylamide units in the copolymer.

(3) As the content of the cross-linking agent (sodium 1,3-diallyl isocyanurate) increases, the water absorption capacity of the copolymer decreases.

REFERENCES

1. Doseva, V.N., Shenkev, S.D., Brochkov, Khr.I., *et al.*, *Vysokomol. Soedin., Ser. B*, 2002, vol. 44, no. 8, pp. 1444–1449.
2. Philipova, O.E., Karibyants, N.S., and Starodubtsev, S.E., *Macromolecules*, 1994, vol. 27, no. 9, p. 2398.
3. Karibyants, N.S., Filipovich, O.E., and Starodubtsev, S.G., *Vysokomol. Soedin., Ser. B*, 1995, vol. 37, no. 8, p. 1386.
4. Suleimenov, I.E., Butova, T.V., and Benurov, E.A., *Vysokomol. Soedin., Ser. A*, 2002, vol. 44, no. 9, pp. 1571–1577.
5. Eritsyan, M.L., Galstyan, G.G., and Karamyan, R.A., *Vysokomol. Soedin., Ser. B*, 2003, vol. 45, no. 7, pp. 1202–1204.
6. Armenian Patent Pending P20010115, *Prom. Sobstv.*, 2002, no. 3 (23).
7. Chovnik, L.N., Pazenko, Z.N., Korneev, K.A., and Khamenkova, K.A., *Zh. Org. Khim.*, 1965, vol. 1, no. 10, pp. 742–743.

ISSN 1070-4272, Russian Journal of Applied Chemistry, 2006, Vol. 79, No. 2, pp. 301–305. © Pleiades Publishing, Inc., 2006.
Original Russian Text © V. E. Proskurina, V. A. Myagchenkov, 2006, published in Zhurnal Prikladnoi Khimii, 2006, Vol. 79, No. 2, pp. 302–307.

MACROMOLECULAR CHEMISTRY AND POLYMERIC MATERIALS

Flocculation Activity of Anionic Copolymers of Acrylamide with Respect to Titanium Dioxide Suspension as Influenced by Their Molecular Properties

V. E. Proskurina and V. A. Myagchenkov

Kazan State Technological University, Kazan, Tatarstan, Russia

Received September 21, 2005

Abstract—The kinetics of sedimentation of titanium dioxide suspension in the presence of ionic (anionic) acrylamide copolymers in the mode of free (unrestricted) sedimentation was studied. The effect of concentration and molecular properties of the copolymers on their flocculation activity was evaluated by sedimentation analysis.

DOI: 10.1134/S1070427206020261

An efficient way to improve and intensify various industrial processes and, in particular, those of separation of solid and liquid phases in the course of flocculation, flotation, and filtration in stages of selective concentration or recovery of one of components of the dispersed phased (DP), is to add small amounts of water-soluble synthetic and natural macromolecular flocculants [1]. Among these widely applicable water-soluble polymeric additives, ionic (anionic and cationic) polyacrylamide flocculants (PAAFs) show much promise, because they are relatively available and highly efficient agents controlling the sedimentation stability of various disperse systems (DSs) [2]. The PAAF efficiency is determined by the chemical nature of the alternating units, chemical structure and composition of the copolymer macromolecules, molecular properties and concentration of the flocculant, and a wide set of chemical, physicochemical, and physical properties of the particles of the dispersed phase and the dispersion medium [1, 2].

Among various active factors strongly affecting the sedimentation stability of disperse systems, two parameters of given (co)polymer-flocculant, namely molecular weight and molecular weight polydispersity [3], are the most important. Since the overall effect is determined by a wide set of interrelated active parameters of the system, adequate evaluation of the contribution of each parameter on the flocculation process is possible only for model systems. Ocher, kaolin, and copper oxide are the common standard model DSs for comparative studies of the flocculation properties of water-soluble (co)polymers [1, 2, 4]. The titanium dioxide suspension is used as model DS with high density of DP particles and high charge density on their surface [5, 6]. In comparison with ocher, kaolin, and copper dioxide, titanium dioxide is characterized by more stable average size, size polydispersity, and physicochemical properties at the phase boundary of the TiO_2 particles and a significantly smaller content of impurities and water-soluble inclusions, which allows more reliable evaluation of the effect of the given factors on the flocculation parameters of the system. Therefore, systematic studies of the effect of specific active parameters on the flocculation kinetics of the titanium dioxide suspension are of particular theoretical and practical importance.

In this study, we examined the effect of the molecular weight and molecular weight polydispersity of the ionic (anionic) acrylamide copolymer on the kinetics of TiO_2 suspension flocculation in the mode of free (unrestricted) sedimentation, which is the most convenient for quantitative sedimentation analysis. The effect of molecular properties on the flocculation characteristics of the model and real disperse systems has been examined previously [2, 7, 8]. It should be noted that use of acrylamide copolymer flocculants involves additional severe complications related to the variability of the copolymer composition (β) and compositional heterogeneity. To overcome these problems, samples of copolymers with different molecular weights were prepared by an unconventional technique, ultrasonic degradation across the carbon–carbon skeleton bonds of macromolecules [2, 9].

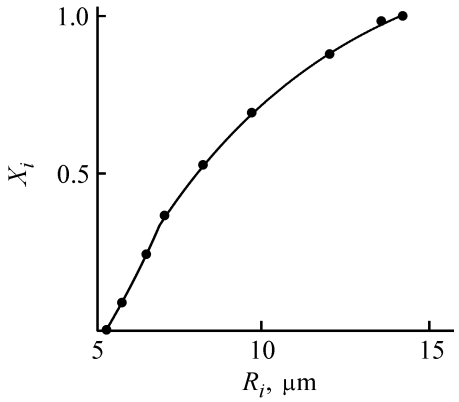


Fig. 1. Integral curve of the particle size distribution of the titanium dioxide dispersed phase (c_d = 0.4%) (X_i) Integral weight fraction of the *i*th fraction and (R_i) particle radius in the *i*th DP fraction.

EXPERIMENTAL

In our study, we used a titanium dioxide suspension [rutile modification, TU (Technical Specifications) 24.1-05762329-001–2003] with the average particle radius $\bar{R} = 8.7 \times 10^{-6}$ m and $\rho = 3.9 \times 10^3$ kg m^{-3}. To obtain more detailed data on the particle size of the system studied, we constructed the integral curve of the DP particle size distribution (Fig. 1), using the results of a sedimentometric analysis in the mode of free (unrestricted) sedimentation. It can be seen that this DS is characterized by a relatively narrow range of particle sizes ($R_{min} = 5.3 \times 10^{-6}$ m and $R_{max} = 14.3 \times 10^{-6}$ m). The flocculation kinetics of the TiO_2 suspension in the presence of acrylamide copolymers in the mode of free sedimentation was determined from accumulation of the precipitate on the pan of a VT-500 torsion balance in a 400-ml cylinder. The optimal working concentration of the dispersed phase (in all the tests, c_d = 0.4%) was determined from the preliminarily analysis of the sedimentation rate of the TiO_2 suspension as influenced by c_d [2]. The required amounts of aqueous solutions of copolymers (the concentration c was varied from 0.01 to 0.1%) were added to the supernatant and, to provide the direct contact between the DP particles and polymer additives, the resulting system was agitated with a perforated (12 holes) disk stirrer, which was slowly shifted within the cylinder 10 times in the vertical direction. Samples of the anionic acrylamide copolymers with various molecular weights M were prepared from a commercial sample of a high-molecular-weight random copolymer of acrylamide and sodium acrylate (DP9-8177 brand, $M = 3.75 \times 10^6$, bulk content of ionic units β 3.7 mol %). Samples with a smaller molecular weight were prepared by ultrasonic degradation in the mild mode in accordance with the procedure described in [9, 10]. The degradation was performed in a 0.1% aqueous solution of the copolymer, using UZDN-2T ultrasonic disperser (22 kHz working frequency) at varied exposure time and ultrasonic treatment power. As can be seen from Table 1, the ultrasonic degradation made it possible to vary the molecular weight of the copolymers in a rather wide range from 7.4×10^4 to 3.75×10^6. It is very important that the parameter β and the composition heterogeneity (CH) remained constant for all the nine copolymer samples studied, similarly to [9, 10]. The molecular weights of the resulting copolymers were calculated from the Staudinger–Mark equation $[\eta] = KM^a$, where $[\eta]$ is the intrinsic viscosity, and K and a are the constants (a = 0.785 and $K = 6.8 \times 10^{-3}$ [11]).

Table 1. Characteristics of samples A1-A9 of the anionic acrylamide copolymers (β = 3.7 mol %) prepared by ultrasonic degradation

Sample no.	Ultrasonic treatment power, W cm^{-2}	Exposure time, min	$[\eta]$, m^3 kg^{-1}	$M \times 10^{-6}$
A1	–	–	0.984	3.75
A2	1.02	6	0.765	2.72
A3	4.4	3	0.628	2.12
A4	4.4	4	0.500	1.59
A5	4.4	7.3	0.319	0.89
A6	8.0	5	0.213	0.53
A7	11.8	4.3	0.155	0.36
A8	15.2	5	0.106	0.22
A9	18.9	4	0.043	0.070

The kinetic data illustrating the effect of the concentration and molecular weight of the polymer (samples A1 and A4) on the sedimentation stability of the titanium dioxide suspension are shown in Figs. 2a and 2b. It can be seen that even insignificant amounts of flocculants (about 5×10^{-6}%), when added to the system, strongly accelerate the sedimentation of the titanium dioxide particles, and as the concentration of the copolymer grows this effect steadily increases. Taking into account the same (negative) sign of charge on the DP particles and copolymer macromolecules, the data given in Fig. 2 suggest the predominantly bridging (rather than that of neutralization type) mechanism of flocculation in the systems studied. Using the kinetic curves, we calculated the flocculation activity λ, i.e., the relative change in the sedimentation rate per unit concentration of the polymeric additive by the following equation [2]:

$$\lambda = (\bar{v}/\bar{v}_0 - 1)/c,$$

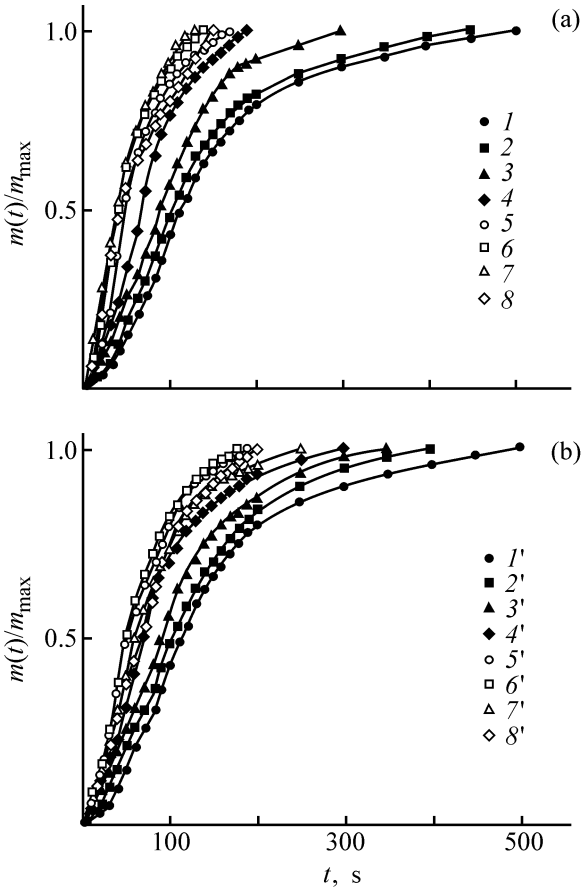


Fig. 2. Kinetic curves of sedimentation of the titanium dioxide suspension in the absence and in the presence of acrylamide copolymer samples (a) A1 ($M = 3.75 \times 10^6$) and (b) A4 (M 1.59×10^6). $c \times 10^4$, wt %: (*1*, *1'*) 0, (*2*, *2'*) 0.05, (*3*, *3'*) 0.15, (*4*, *4'*) 0.35, (*5*, *5'*) 0.74, (*6*, *6'*) 1.53, (*7*, *7'*) 3.05, and (*8*, *8'*) 6.31.

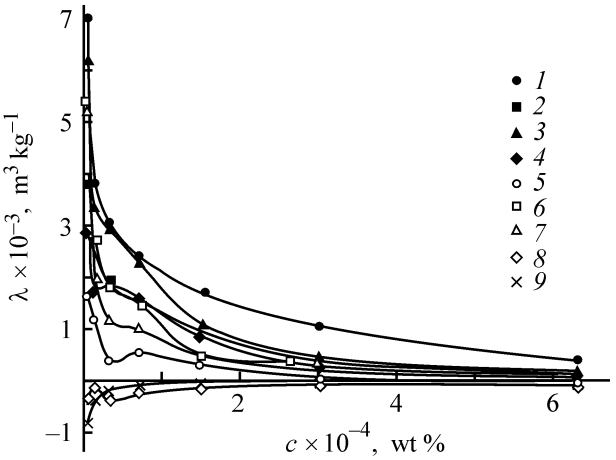


Fig. 3. Flocculation activity λ vs. the concentration c of the anionic acrylamide copolymers A1–A9. $M \times 10^{-6}$: (*1*) 3.75, (*2*) 2.72, (*3*) 2.10, (*4*) 1.59, (*5*) 0.89, (*6*) 0.53, (*7*) 0.36, (*8*) 0.22, and (*9*) 0.07.

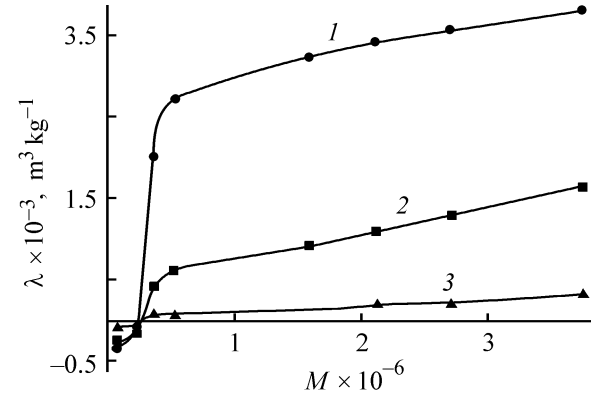


Fig. 4. Flocculation activity λ vs. the molecular weight M of the anionic acrylamide copolymers. $c \times 10^4$, wt %: (*1*) 0.15, (*2*) 1.53, and (*3*) 6.31; the same for Fig. 5.

where $\bar{v}$ and $\bar{v}_0$ are the average rates of sedimentation [at $m(t)/m_{max} = 0.4$] of the titanium dioxide suspension in the presence of flocculant and without it, and c is the concentration of the polymeric additive.

As can be seen from comparative analysis of curves (*2*–*8*) and (*2'*–*8'*) (Figs. 2a and 2b), the flocculation activity increases with the molecular weight of the flocculant.

To obtain more detailed data on the relationship of λ and M, let us consider the experimental dependences of the flocculation activities on the flocculant concentration for all the samples of acrylamide copolymers with various molecular weights shown in Fig. 3. It can be seen that, as the molecular weight decreases and the copolymer concentration increases, the flocculation activity is strongly depressed (curves *1*–*7*). This trend may be due to a decrease in the efficiency of thePAAF macromolecules in floccule formation with increasing concentration of the flocculant [1, 2]. It should be noted that the flocculation activity becomes negative for polymer additives of relatively low molecular weight (curves *8*, *9*), which means that the low-molecular-weight samples (A8 and A9) provide kinetic stabilization of the DP particles.

The quantitative data on the flocculation of the titanium dioxide suspension in the presence of the anionic acrylamide copolymers with various molecular weights are summarized in Fig. 4. In analysis of this data, significant differences in the $\lambda = f(M)$ dependences for curves *1*–*3* (Fig. 4) with relatively low and high ($M > 5 \times 10^5$) molecular weights should be taken into account. In the concentration range studied, the flocculation activity sharply increases for the copolymers with low and intermediate molecular weights,

Table 2. Selected data on the effective size $\bar{R}_{eff}$ of floccules in the presence of anionic acrylamide copolymers and compositions based on them

PAAF	F'	$c \times 10^4$, wt %	$\bar{R}_{eff}$, μm	PAAF	F'	$c \times 10^4$, wt %	$\bar{R}_{eff}$, μm	PAAF	F'	$c \times 10^4$, wt %	$\bar{R}_{eff}$, μm
A1	1	0.15	11.1	A4	1	0.15	10.4	A7	1	0.15	7.94
		1.53	16.5			1.53	14.5			1.53	8.83
		6.31	15.7			6.31	12.6			6.31	7.74
A2	1	0.15	10.1	A5	1	0.15	8.58	A2–A6	1.83	0.15	7.81
		1.53	13.9			1.53	8.12			6.31	20.4
		6.31	11.7			6.31	8.09	A3–A8	2.56	1.53	15.4
A3	1	0.15	10.4	A6	1	0.15	10.1	A3–A9	6.43	1.53	19.5
		1.53	14.3			1.53	12.4			6.31	21.7
		6.31	12.5			6.31	10.9	A1–A5	1.45	6.31	23.2

whereas for copolymers with high molecular weight, λ tends to a constant value out. The decrease in the flocculation activity, observed as the copolymer concentration insreases (passing from curve *1* to curves *2* and *3*)and *M* decreases, is probably due not only to an increase in the stabilization of the DP particles (shown above), but also to a specificity of the processes of adsorption and formation of the structural elements (floccules) from TiO_2 particles and copolymer macromolecules [1, 2]. This is additionally confirmed by selected data, for a series of copolymers, on the effective average size $\bar{R}_{eff}$ of the structural elements formed from DP particles and copolymer macromolecules in the course of flocculation (Table 2). The asymmetry of the floccules was disregarded in calculating the $\bar{R}_{eff}$ values from the data of sedimentometric analysis of the TiO_2 suspensions in the presence of flocculants. As can be seen from Table 2, the DP floccules become significantly coarser in the presence of macromolecular samples A1–A4, whereas for low-molecularweight copolymers A5–A7, $\bar{R}_{eff}$ are typical of floccules of medium size, formed in the absence of the flocculant. Similar results were obtained after preliminarily evaluation of $\bar{R}_{ef}$ of the floccules by microscopy (MBI-3 optical microscope).

The complex nonlinear shape of the $\lambda = f(M)$ dependences found in the experiments indicates that the flocculation activity of the anionic acrylamide copolymers depends not only on the molecular weight of the polymer but also on the polydispersity of the copolymer molecular weight. This conclusion, important in both theoretical and practical aspects, was confirmed by the results of experiments with model ocher system [2, 12]. It was of particular interest to verify this conclusion using another model system (TiO_2) with higher charge density and more stable characteristics of the phase boundary surface.

The copolymers with fixed average molecular weight $\bar{M} = 1.59 \times 10^6$ and various composition polydispersities were prepared using artificial blends of copolymers A1–A9. In the simplest (binary) compositions of copolymers with $M_a > \bar{M}$ and $M_b < \bar{M}$, the weight fractions of the polymer components w_a (for sample with $M = M_a$) and $w_b = 1 - w_a$ (for sample with $M = M_b$) were calculated using the following expression:

$$w_a M_a + (1 - w_a) M_b = \bar{M}.$$

As a quantitative criterion of the molecular weight polydispersity, we used an analog of the Schulz parameter F' [3]:

$$F' = \frac{M_w}{M_n} - 1 = \sum_{i=1}^{k}(w_i M_i) \sum_{i=1}^{k}(w_i / M_i) - 1,$$

where w_i and M_i are the weight fraction and molecular weight of the *i*th sample; *k*, number of fractions in question; and $\bar{M}_w$ and $\bar{M}_n$, weight-average and number-average molecular weights of the copolymer blends, respectively.

In contrast to the "common" calculation of the Schulz parameter *F* using very narrow fractions with $\bar{M}_w = \bar{M}_n$, F' parameter was evaluated using unfractionated copolymer samples for which $\bar{M}_w$ was certainly unequal to $\bar{M}_n$ (obviously, $\bar{M}_w > \bar{M}_n$). The ultrasonic degradation of the copolymer samples is described by dependences of a random degradation without depolymerization [13]. In accordance with the Eniklopov theory for these processes, the copolymer samples are characterized by the molecular weight polydispersity, which virtually coincides with the classical Flory distribution [14] for which $\bar{M}_w/\bar{M}_n = 2$. Since the same relationship of $\bar{M}_w$ and $\bar{M}_n$ is observed for the reference copolymer A4 ($M = 1.59 \times 10^6$), all the calculated data for the analogue of the Schulz parameter F' (including F' for A4) were increased by unity in com-

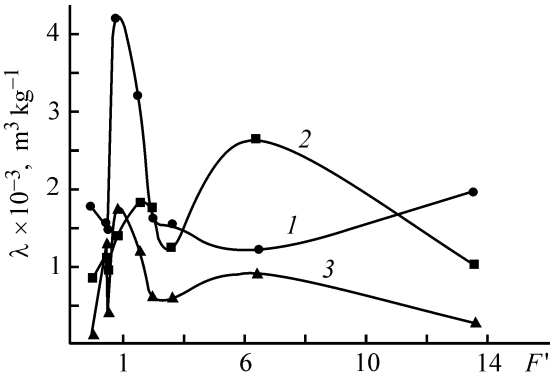


Fig. 5. Flocculation activity λ vs. the F' parameter in the presence of mixed samples of the anionic acrylamide copolymers ($M = 1.59 \times 10^6$).

parison to the calculated F values for the case of uniform copolymer fractions. Apparently, the greater the F and F' parameters, the higher the polydispersity of the polymeric system in question.

Figure 5 illustrates the complex nonmonotonic behavior of the $\lambda = f(F')$ dependences for all the three fixed concentrations of the copolymer blends. Table 2 suggests a certain correlation between $\bar{R}_{\text{eff}}$ and F' for copolymer compositions with $\bar{M} = 1.59 \times 10^6$ and thus indirectly confirms the complex relationships between λ and F'. A strong effect of the flocculant concentration on these dependences is understandable, if we take into account the dynamics and random nature of the processes of segmental adsorption of macromolecules with their subsequent anchor fixation at two particles of the dispersed phase that have approached each other to the critical distance of 0.01–0.1 μm [1, 2, 15, 16]. Rather complex dependences are also typical of the second stage of flocculation, i.e., formation of floccules [1, 16]. On the whole, we can conclude that the control over the molecular weight polydispersity of polymeric flocculants can intensify (or even optimize) the flocculation processes for both model and real disperse systems.

CONCLUSIONS

(1) Nine samples of the anionic copolymer with a wide range of molecular weights and identical composition and compositional heterogeneity were prepared from a random high-molecular-weight copolymer of acrylamide and sodium acrylate with a low degree of hydrolysis (β = 3.7mol %) by ultrasonic degradation of 0.1% aqueous solutions of the copolymer under mild conditions.

(2) The flocculation kinetics was studied at varied molecular weight and concentration of copolymers for the example of negatively charged particles of a disperse system (0.4% suspension of titanium dioxide) in the mode of free (unrestricted) sedimentation. The flocculation activity of the ionic acrylamide copolymers depends not only on the molecular weight of copolymers, but also on the molecular weight polydispersity.

REFERENCES

1. Baran, A.A., *Polimersoderzhashchie dispersnye sistemy* (Polymer-Containing Disperse Systems), Kiev: Naukova Dumka, 1986.
2. Myagchenkov, V.A., Baran, A.A., Bekturov, V.A., and Bulidorova, G.V., *Poliakrilamidnye flokulyanty* (Polyacrylamide Flocculants), Kazan: Kazan. Tekhnol. Univ., 1998.
3. Myagchenkov, V.A. and Frenkel, S.Ya., *Kompozitsionnaya neodnorodnost' polimerov* (Composition Heterogeneity of Polymers), Leningrad: Khimiya, 1988.
4. Zapol'skii, A.K. and Baran, A.A., *Koagulyanty i flokulyanty v protsessakh ochistki vody* (Coagulants and Flocculants in Water Treatment), Leningrad: Khimiya, 1987.
5. Li, D., Zha, S., Pelion, R.H., and Spafford, M., *Colloid Polym. Sci.*, 1999, vol. 277, pp. 108–114.
6. Ma, M. and Zha, S., *Colloid Polym. Sci.*, 1999, vol. 277, pp. 115–122.
7. Myagchenkov, V.A. and Frenkel, S.Ya., *Usp. Khim.*, 1968, vol. 37, no. 12, pp. 2347–2371.
8. Tret'yakov, A.Ya., Barabanov, V.P., and Myagchenkov, V.A., *Kolloidn. Zh.*, 1990, vol. 52, no. 6, pp. 1211–1213.
9. Myagchenkov, V.A., and Krikunenko, O.V., and Churikov, F.I., *Ul'trazvukovaya destruktsiya vodorastvorimykh sopolimerov* (Ultrasound Degradation of Water-Soluble Copolymers), Kazan: Kazan. Tekhnol. Univ., 1998.
10. Myagchenkov, V.A. and Krikunenko, O.V., *Vysokomol. Soedin., Ser. A*, 1995, vol. 37, no. 1, pp. 44–49.
11. Klein, J. and Conrad, K.D., *Makromol. Chem.*, 1978, vol. 179, pp. 1635–1638.
12. Myagchenkov, V.A., Proskurina, V.E., and Gromova, E.Yu., *Khim. Tekhnol. Vody*, 2003, vol. 25, no. 1, pp. 60–68.
13. Berlin, A.A., Vol'fson, S.A., and Eniklopyan, N.S., *Kinetika polimerizatsionnykh protsessov* (Kinetics of Polymerization Processes), Moscow: Khimiya, 1978.
14. Flory, P.J., *Statistical Mechanics of Chain Molecules*, New York: Interscience, 1969.
15. Lipatov, Yu.S., *Kolloidnaya khimiya polimerov* (Colloidal Chemistry of Polymers), Kiev: Naukova Dumka, 1984.
16. Lipatov, Yu.S. and Sergeeva, L.M., *Adsorbtsiya polimerov* (Adsorption of Polymers), Kiev: Naukova Dumka, 1972.

ISSN 1070-4272, Russian Journal of Applied Chemistry, 2006, Vol. 79, No. 2, pp. 306–309. © Pleiades Publishing, Inc., 2006.
Original Russian Text © M. G. Potalitsin, A. A. Babenko, O. S. Alekhin, N. I. Alekseev, O. V. Arapov, N. A. Charykov, K. V. Nekrasov, V. I. Gerasimov, K. N. Semenov, 2006, published in Zhurnal Prikladnoi Khimii, 2006, Vol. 79, No. 2, pp. 308–311.

MACROMOLECULAR CHEMISTRY AND POLYMERIC MATERIALS

Caprolons Modified with Fullerenes and Fulleroid Materials

M. G. Potalitsin, A. A. Babenko, O. S. Alekhin, N. I. Alekseev, O. V. Arapov, N. A. Charykov, K. V. Nekrasov, V. I. Gerasimov, and K. N. Semenov

SUDPLAST-SERVIS, Private Company, St. Petersburg, Russia
St. Petersburg State Technological Institute, St. Petersburg, Russia
St. Petersburg State University, St. Petersburg, Russia

Received May 19, 2005

Abstract—Conditions for the preparation of modified Caprolons were determined and optimized. A number of laboratory and industrial samples was prepared. Their main mechanical, physicochemical, and electrical properties were determined.

DOI: 10.1134/S1070427206020273

Caprolon is a block polyamide. It is used as a structural and antifrictional material. Owing to its unique properties, Caprolon is widely used in shipbuilding, agriculture, power engineering, and chemical, petroleum, pulp and paper, and food industries. Since Caprolon is a strong and lightweight (lighter by a factor of 6–7 than bronze and steel) polymer having low constant of friction, it can be used without lubricants in friction units. It is resistant to hydrocarbons, oils, alcohols, alkalis, and weak acids. In addition, this polymer is nontoxic. In particular, in shipbuilding it is used to produce slide bearings, guides, bushes of friction units, pulleys, blocks and bearing rollers of hoisting devices, body plans, brackets, wheel naves, and other parts for which high impact strength and thermal resistance are required.

The Caprolon properties can be changed by its modification with fillers that are uniformly distributed in the polymeric matrix. Introduction of solid, in particular, powdered fillers allows variation of Caprolon properties in the widest range. These modifiers, when introduced in small amounts (up to several percent), can be nucleating agents and can affect the degree of crystallinity of the polymer. The most efficient is introduction of small amounts of fine (particle size smaller than 10 μm) and ultrafine (particle size smaller than 1 μm) fillers, in particular, of carbon materials. Finely divided graphite is the most widely used as a modifier to improve the hardness, compressive, bending, and electric strength, and other properties of Caprolons [1, 2]. Introduction of graphite changes the strength and electrical properties of Caprolon. In particular, the dielectric constant and dielectric loss tangent increase and the moisture absorption decreases.

It is known [3] that fullerenes and fulleroids (in particular, fullerene-containing soot) strongly affect polymerization of various organic compounds and dramatically change the polymer properties. We suggested that introduction of fullerenes should significantly improve the strength and elasticity of the polymer. The tribological properties of pure fullerenes with respect to metals were studied in [4]. Fullerene-containing soot partly retains these properties. All these factors, along with the reduction of the production cost of fullerene soot and fullerenes, allow us to expect that the consumer properties of Caprolons can be substantially improved by modification with fullerenes without any significant rise in the price of the product.

We tested four types of fullerene materials: (1) C_{60}–C_{70} mixture (weight fraction of C_{60}, C_{70} and higher fullerenes 68, 30, and 2%, respectively); the procedure for determining the fullerene concentration in different phases is described in detail in [5–8]; (2) pure (99.9 wt%) C_{60}; (3) fullerene soot; and (4) washed fullerene soot (fullerene black).

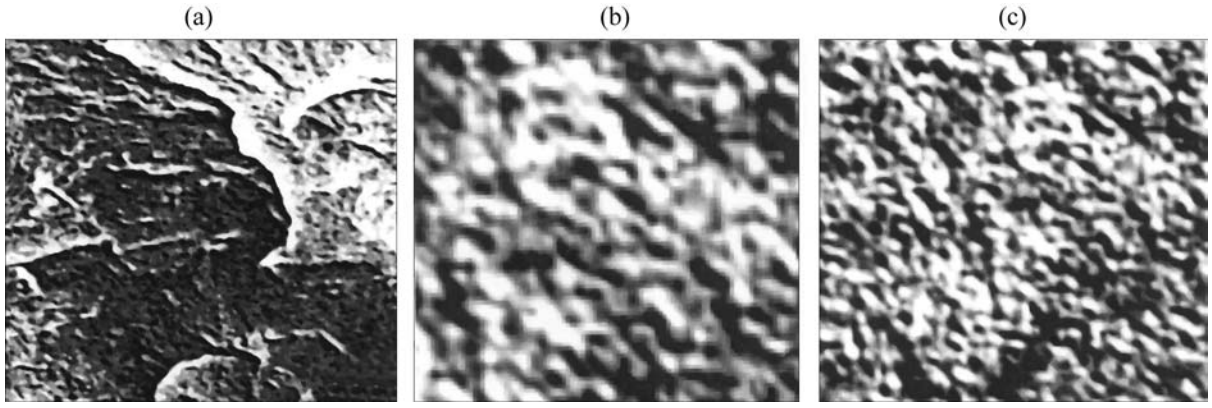


Fig. 1. Electron micrographs of polished sections of (a) unmodified Caprolons, (b) Caprolons modified 0.0017 wt % C_{60} of 99.9 wt % purity, and (c) Caprolons modified with 0.11 wt % fulleren soot. Magnification ×40000.

Fullerene soot (initial product) is a fine carbon powder obtained by arc combustion of graphite electrodes in an inert atmosphere (average particle size 0.5–2.0 μm). Fullerene soot is the main raw material for production of fullerenes. The total fullerene content in the soot is 12.7 wt %. A C_{60}–C_{70} mixture containing up to 2 wt % higher fullerenes (C_{76}, C_{78}, C_{84}, C_{90}) is obtained by extraction of fullerene soot. The washed fullerene soot is the residue formed after extraction of fullerenes. The residual fullerene content in it is not higher than 0.05%. All fullerene products used in this study were prepared at SUDPLAST-SERVIS Private Company (St. Petersburg) by the previously described procedure [9].

Caprolons produced by the modified industrial process, with all of the above substances used as modifiers, are denoted as CMF.

The main starting materials for production of CMF were the same as in the conventional technique for manufacture of Caprolon: caprolactam, metallic sodium (catalyst), 2,4-toluene diisocyanate (TDI) (activator), and argon (inert gas). In the course of CMF synthesis, caprolactam samples were dried in an oven in a vacuum or in air for 2 days. Then calculated amounts of an appropriate fulleroid material were introduced the dry samples. The mixture was stirred until it became visually homogeneous. The mixture was heated to ~100°C and melted in an oven with intermittent stirring. The melt was divided in two equal portions. To one of these portions metallic sodium was added. It completely dissolved in the melt. To the other portion, TDI was added. Both portions were heated in an oven at 130 ± 5°C and mixed in a preheated metallic mold (reactor) with vigorous stirring. The mixture was allowed to stand at the temperature naturally attained in the exothermic polymerization (the maximal temperature rise due to heat release was 10–20°C higher than the oven temperature). The oven was switched off and the mixture was furnace-cooled.

We prepared compact CMF samples containing 0.05 to 1.0 wt % fullerene soot or fullerene black and 0.01 to 0.02 wt % of C_{60} + C_{70} or pure C_{60}. The weight of these samples was 220, 2000–2100, 7900–8100, and 15500–16500 g. The visually homogeneous samples modified with fullerene soot and fullerene are black and gray-green, respectively. The initial unmodified Caprolon is white. The samples were analyzed with a JEM-100S (JEOL) electron microscope at a $(10–100) \times 10^3$ magnification. Typical electron micrographs of chips of CMFs and initial Caprolon are shown in Fig. 1. As can be seen from Fig. 1, modification with both fullerenes and fullerene soot decreases the size of crystal grains and makes the intercrystal spacings narrower and smeared. The structural changes in CMF modified with fullerene soot are more pronounced than those observed upon introduction of fullerenes proper. This is due to the fact that the content of the modifier in the form of a soot is naturally always 1–3 orders of magnitude than that of fullerenes. In particular, the content of the soot and the fullerenes in the samples shown in Fig. 1 is 0.11 and 0.0017 wt %, respectively.

The properties of CMF samples were measured in accordance with GOSTs (State Standards) for study of polyamides, since unmodified Caprolons a polyamide. The average results of 3–10 parallel measurements are summarized in Tables 1 and 2.

As can be seen from Table 1, introduction of even small amounts of fullerene modifiers substantially increases the strength and elasticity of almost all the samples. Modification with metallic additives has a similar effect. However, the fullerene content in the sample is lower by approximately 1–3 orders of magnitude and has virtually no effect on the sample

Table 1. Some mechanical and physicochemical properties of CMF

Property	Unmodified Caprolon	CMF modified with fullerene soot	CMF modified with fullerenes
Moisture absorption (boiling for 24 h), wt %	1.5–2.0	<2.0	<2.0
Brinell hardness* MPa [GOST (State Standard) 4670]	130	135–160	125–150
Ultimate compressive strength, MPa	80–90	120–125	100–110
Charpy impact resilience*, kJ mol^{-1} (GOST 4647)	40	>70	60–70
Yield point under compression*, MPa (GOST 4651)	100–110	110–130	70–90
Density*, g cm^{-3}	1.15–1.16	1.18–1.23	1.16–1.20
Attrition resistance*, mm^3 (GOST 23509–79)	35	<25	<20
Slip coefficient over steel without lubricant*, rel. units (GOST 27492–87)	0.20–0.30	<0.15	<0.10
Relative elongation*, rel. %	15–30	<8	15–25
Softening point under bending, °C	80–100	>105	>100
Melting point, °C	220–225	232	225
Thermal conductivity coefficient at 25°C, W m^{-1} K^{-1}	0.29	<0.20	<0.25

* Measured at 18–25°C.

Table 2. Electrical properties of CMF

Property	Unmodified Caprolon	CMF modified with fullerene soot	CMF modified with fullerenes
ε, rel. units (ν = 1 kHz)	3.0–3.2	3–10	8–20
$\tan\delta \times 10^4$:			
ν = 1 kHz	0.030	0.3–1.2	0.1–0.2
ν = 10 kHz	–	0.03–0.1	0.1
Resistivity, Ω cm	10^{14}	10^{10}–10^{13}	10^8–10^{10}
Electrical strength, kW mm^{-1}	30–35	60–100	>100

density. The determination error of the mechanical properties of CMF, listed in Table 1, ranges from ±5 to ±10 rel %. This accuracy is sufficient to conclude that the mechanical properties of Caprolon strongly change after modification. The slip coefficient over steel and abradability decrease by 40%; the softening and melting points and temperature of thermal degradation in air increase (Fig. 2); thermal conductivity decreases; and the density and moisture absorption do not noticeably change.

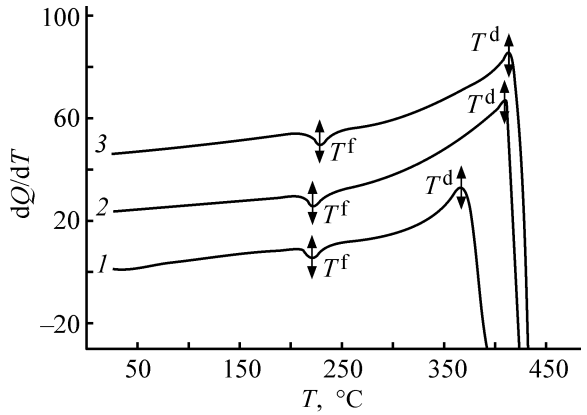


Fig. 2. Thermal analysis curves of (*1*) unmodified Caprolons and Caprolons modified with (*2*) 0.0017 and (*3*) 0.11 wt % C_{60} of 99.9 wt % purity. (T) Temperature, (T^f) melting point, and (T^d) onset temperature of thermolysis on heating in air at a rate of 3 deg min^{-1}.

The electrical properties of CFM, listed in Table 2, show that modification substantially improves the antistatic properties. The decrease in the resistivity of some samples by several orders of magnitude favors accelerated leakage of static electricity. The dielectric constant and hence the breakdown voltage substantially increase.

Thus, use of CMF articles under conditions of contamination with combustible and explosive gases (e.g., in the case of methane outburst in coalbeds) is much safer as compared to that of unmodified Caprolon articles.

CONCLUSIONS

(1) The compatibility of polyamides with fullerene materials was demonstrated for the example of Caprolon.

(2) Modification of Caprolon with small amounts of fullerenes increases the hardness, impact resilience, attrition resistance, and softening and melting points and decreases the moisture absorption and moisture capacity of the samples.

(3) Introduction of fullerenes allows variation of the electrophysical properties (volume and surface conductivity, dielectric constant, and dielectric loss tangents) of the polymers in a wide range.

ACKNOWLEDGMENTS

This study was financially supported by the federal research program "Research and Development in the Priority Fields of Science and Technology" for the years of 2002–2006 (State contract no. 02.467.11.7005, May 23, 2005).

REFERENCES

1. Antropova, N.I., Vlasova, K.N., Samokhvalova, A.V., and Pavlova, G.I., *Kaprolon, ego poluchenie, svoistva i priminenie* (Caprolon, Its Preparation, Properties, and Application), Leningrad: Nauka, 1966.
2. *Entsikopediya polimerov: Spravochnik* (Encyclopedia of Polymers: Handbook), Kabanov, V.A., Ed., Moscow: Sovetskaya Entsikopediya, 1977, vol. 3.
3. Karaulova, E.N. and Bagrii, E.I., *Usp. Khim.*, 1999, no. 11, pp. 979–998.
4. Ginzburg., B.M., Baidakova, M.V., Kirienko, O.F., *et al.*, *Zh. Tekh. Fiz.*, 2000, vol. 70, no. 12, pp. 87–91.
5. Ponomarev, A.N., Yudovich, M.E., Charykov, N.A., and Nikitin, V.A., *Opt. Spectrosc.*, 2000, vol. 88, no. 2, pp. 195–197.
6. Arapov, O.V., Pronkin, A.A., Charykov, N.A., and Seregin, V.I., *Zh. Prikl. Khim.*, 2003, vol. 76, no. 1, pp. 39–45.
7. Strel'nikov, K.B., Pronkin, A.A., and Klepikov, A.A., *Pis'ma Zh. Tekh. Fiz.*, 2003, vol. 29, no. 3, pp. 74–81.
8. Arapov, O.V., Aksel'rod, B.M., Charykov, N.A., *et al.*, *Zh. Prikl. Khim.*, 2003, vol. 76, no. 1, pp. 35–38.
9. RF Patent 39129.

ISSN 1070-4272, Russian Journal of Applied Chemistry, 2006, Vol. 79, No. 2, pp. 310–313. © Pleiades Publishing, Inc., 2006.
Original Russian Text © V. V. Mikheev, R. R. Ivanova, 2006, published in Zhurnal Prikladnoi Khimii, 2006, Vol. 79, No. 2, pp. 312–314.

MACROMOLECULAR CHEMISTRY AND POLYMERIC MATERIALS

Synthesis of Urethane-containing Epoxy Oligomers

V. V. Mikheev and R. R. Ivanova

Kazan State Technological University, Kazan, Tatarstan, Russia

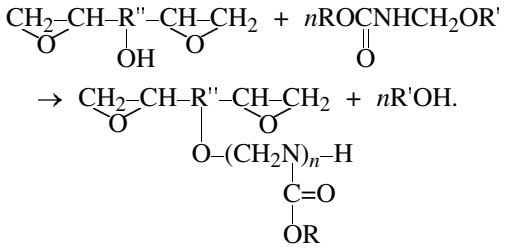
Received November 25, 2005

Abstract—A procedure for preparing urethane-containing epoxy oligomers from reactive monourtheanes was developed.

DOI: 10.1134/S1070427206020285

To improve properties of epoxy polymers and to extend the field of their application, initial epoxy oligomers (EOs) are modified with various functional groups including urethane groups. Urethane groups are usually introduced into EOs using diisocyanates. Urethane-containing EOs are used in practice [1, 2]. However, diisocyanates are expensive and toxic compounds. Therefore, development of a procedure for preparing urethane-containing polymers without using diisocyanates is of interest [3–6].

Here we studied the possibility of preparing urethane-containing epoxy oligomers (UEOs) without using isocyanides by the reaction of EO hydroxy groups with reactive monourethanes (RUs) $ROCONHCH_2OR'$ (R–C_4H_9, C_5H_{11}; R'–*iso*-C_3H_7, C_4H_9):



Reactive monourethanes were prepared in two steps. The first step is reaction of butyl or amyl alcohol with urea to form monourethanes:

$$ROH + H_2NCONH_2 \rightarrow ROCONH_2 + NH_3.$$

To raise the reactivity of monourethanes, *N*-methylol (R' = H) or *N*-alkoxymethylene (R' = *iso*-C_3H_7, C_4H_9) groups were introduced into their structure. *N*-methylolurethanes were prepared by reaction of urethanes with formaldehyde (in the form of paraformaldehyde or Formalin) in an alkaline solution:

$$ROCONH_2 + CH_2O \rightarrow ROCONHCH_2OH.$$

Synthesis of *N*-alkoxymethylurethanes was performed in alcoholic solution at pH 2–3:

$$ROCONH_2 + CH_2O + R'OH \rightarrow ROCONHCH_2OR' + H_2O.$$

The IR spectra of RUs contain the bands of urethane groups at 1260, 1710, and 3320 cm^{-1}. The properties of RUs are listed in Table 1. Reactive mono-

Table 1. Properties of RUs $ROCONHCH_2OR'$

RU	R	R'	Density, g cm^{-3}	Refractive index	*N*, %	
					found	calculated
RU-1	C_4H_9	H	1.075	1.447	9.31	9.52
RU-2	C_5H_{11}	H	1.082	1.448	8.48	8.69
RU-3	C_5H_{11}	*iso*-C_3H_7	1.013	1.445	6.63	6.9
RU-4	C_5H_{11}	C_4H_9	1.021	1.447	6.21	6.45

Table 2. Properties of EOs

EO	M_n	Content, %		EO	M_n	Content, %		EO	M_n	Content, %	
		–CH–CH– (O)	–OH			–CH–CH– (O)	–OH			–CH–CH– (O)	–OH
E-40	620	13.9	2.8	E-41	940	9.1	4.6	E-44	1550	5.5	6.0

Table 3. Properties of UEOs

UEO	Initial monomers		EO : RU, mol : mol	N, %	–CH–CH– (O), wt%	M_n
	EO	RU				
UEO-1	E-40	RU-1	1 : 0.5	0.9	12.8	670
UEO-2	E-40	RU-1	1 : 1	1.9	11.2	770
UEO-3	E-40	RU-2	1 : 1	1.8	11.0	780
UEO-4	E-40	RU-2	1 : 1.5	2.6	10.2	840
UEO-5	E-40	RU-2	1 : 2	2.9	9.3	920
UEO-6	E-40	RU-2	1 : 3	3.7	8.1	1060
UEO-7	E-41	RU-1	1 : 1	1.2	8.1	1060
UEO-8	E-41	RU-1	1 : 3	3.6	7.3	1180
UEO-9	E-41	RU-1	1 : 2	1.6	4.6	1870
UEO-10	E-41	RU-1	1 : 3	2.2	4.3	2000

urethanes colorless and odorless liquids stable in prolonged storage.

We used commercial E-40, E-41, and E-44 oligomers as EOs (Table 2).

Condensation of *N*-methylol and *N*-alkoxymethylene groups with alcohols is catalyzed by acids [7, 8]. Phthalic anhydride is used, in an amount of 1% of the total weight of the reaction mixture, as an acid catalyst for UEO synthesis. The reaction course was monitored by the liberation of the by-product. The oligomerization of RU-1 and RU-2 was faster. In this case, the liberation of water (by-product) in a vacuum started at 90°C and the reaction was complete upon slow warming to 125°C.

When RU-3 and RU-4 were used, isopropanol and isobutanol were liberated only at 130–145°C. The difference in reactivity between RUs is consistent with the known data on the reactivity of other compounds containing *N*-methylol and *N*-alkoxymethylene groups [7]. An attempt to accelerate UEO synthesis by heating above 150°C failed, since the reaction mixture became viscous or even gelatinous under these conditions, owing to the reaction of the epoxy groups with the N–H bonds of urethanes [8].

It is known that compounds containing *N*-methylol and *N*-alkoxymethylene groups not only react with alcohols, but are also capable of self-condensation [7, 9]. This is the case for reactive monouretanes too. Urethane oligomers were synthesized by heating RU-1 and RU-4 in a vacuum at 130–145°C in the presence of catalytic amounts of phthalic anhydride. These compounds are viscous liquids with a molecular weight of 600–800. The reaction can be described by the scheme

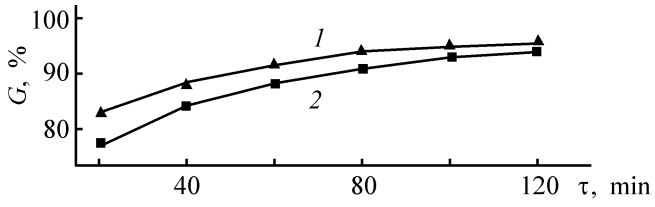
$$n\mathrm{HNCH_2OR'} \rightarrow \mathrm{H(NCH_2)}_n\mathrm{OR'} + (n-1)\mathrm{R'OH}.$$
$$\mathrm{C{=}O} \qquad\qquad \mathrm{C{=}O}$$
$$\mathrm{OR} \qquad\qquad \mathrm{OR}$$

The structure of these oligomers was confirmed by elemental analysis and IR spectroscopy.

Hence, RU can also condense with the OH groups of EO at their molar ratio higher than 1 : 1. Although a molecule of E-40 oligomer contains only one hydroxy group, its UEOs were prepared at the E-40 RU molar ratio from 1 : 0.5 to 1 : 3.

The UEOs derived from E-40 are highly viscous substances; the oligomers derived from E-41 and E-44 are solid. The content of epoxy groups and nitrogen in the oligomers and their molecular weights M_n are listed in Table 3.

The suggested structure of UEOs is confirmed by IR spectroscopy and by the fact that these substances



Content of the gel fraction G in curing of a mixture of UEO-2 with (*1*) diethylenetriamine and (*2*) hexamethylenediamine at 120°C vs. time τ.

are cured to form cross-linked polymers. In going from E-40 to UEO, the band of epoxy group is preserved (900 cm^{-1}), the band of the hydroxy group (3450 cm^{-1}) disappears, and the bands of the urethane group at 1260 and 3330 cm^{-1} appear.

UEOs are readily cured in the presence of aliphatic polyamines. Accumulation of the gel fraction in the course of curing of UEO-2 in the presence of stoichiometric amounts of hexamethylenediamine and diethylenetriamine, which are widely used, [10] as curing agents for EO, is shown in the figure. The high content of the gel fraction (more than 90%) in the curing products suggests that RUs are chemically bound to EO molecules and do not polymerize to form homopolymers.

EXPERIMENTAL

Butyl and amyl urethanes were prepared by refluxing the corresponding alcohols with urea in the presence of catalytic amounts of zinc [9, 11]. RU-1 was prepared as follows. Butyl urethane (58.5 g, 0.5 mol), paraformaldehyde (16.5 g, 0.55 mol), and 0.4 g of 50% aqueous solution of NaOH were placed in a three-necked flask equipped with a stirrer, thermometer, and reflux condenser. The mixture was heated at 55–60°C for 2 h. The resulting liquid was cooled, neutralized, dissolved in chloroform, and washed with water. The organic layer was separated and the solvent was removed in a vacuum. RU-2 was prepared similarly. The synthesis of RU-3 and RU-4 differed in that isopropanol or isobutanol was used as solvent (pH 2–3).

Synthesis of UEO with RU-1 and RU-2 was performed by the following procedure described with an example of RU-1. EO (62 g, 0.1 mol), RU-1 (14.7 g, 0.1 mol), and phthalic anhydride (0.8 g) were placed in a three-necked flask equipped with a stirrer, thermometer, and descending condenser with a condensate receiver. The mixture was slowly heated with stirring at a residual pressure of 0.5 kPa. The onset of water liberation was observed at 90°C. The water condensate was collected in the receiver. Water liberation was complete at 125°C. The reaction mixture was heated at this temperature for 0.5 h and then cooled.

Synthesis of UEO from RU-3 and RU-4 was performed similarly with the exception that the reaction mixture was heated at 130–145°C for 1.5 h.

The content of nitrogen, hydroxy groups, and epoxy groups in the oligomers was determined by the Kjeldahl procedure [12], acetylation procedure [12], and reaction with a solution of hydrochloric acid in acetone [13], respectively. The molecular weight of the oligomers, M_n, was calculated from the content of the epoxy groups. To determine the content of the gel fraction in the course of curing of UEO mixtures, weighed portions of the samples of the reaction mixture were extracted with acetone in a Soxhlet apparatus for 6 h [14].

CONCLUSION

Urethane-containing epoxy oligomers were prepared by reaction of the epoxy oligomers with monourethanes containing *N*-methylol or *N*-alkoxymethylene groups.

REFERENCES

1. Omel'chenko, S.I. and Kadurina, T.I., *Modifitsirovannye poliuretany* (Modified Polyurethanes), Kiev: Naukova Dumka, 1983.
2. Kadurina, T.I., Omel'chenko, S.I., and Stroganov, V.F., *Epoksiuretanovye sistemy: Obzor informatsii. Epoksidnye smoly i materialy na ikh osnove* (Epoxy-urethane Systems: Information Review. Epoxy Resins and Materials on Their Base), Moscow: NIITEKhIM, 1982.
3. Kol'tsov, N.I. and Efremov, V.A., *Soros. Obraz. Zh.*, 2000, no. 9, pp. 31–36.
4. Berlin, A.A., Korolev, G.V., and Kefeli, T.Ya., *Akrilovye oligomery i materialy na ikh osnove* (Acryl Oligomers and Materials on Their Base), Moscow: Khimiya, 1983.
5. Valentine, L.M., *Austr. Occa Proc. News*, 1983, vol. 20, no. 7, pp. 8–17.
6. Berlin, A.A., Varlamova, N.V., and Korshunov, M.A., *Vysokomol. Soedin., Ser. A*, 1980, vol. 22, no. 3, pp. 683–690.
7. Sorokin, M.F., Kochnova, Z.A., and Shode, L.G., *Khimiya i tekhnologiya plenkoobrazuyushchikh veshchestv* (Chemistry and Technology of Film-Forming Agents), Moscow: Khimiya, 1973.

8. Blyakhman, E.M., Litvinova, M.A., and Gvadybadze, A.M., *Vysokomol. Soedin., Ser. B*, 1980, vol. 22, no. 5, pp. 346–349.
9. Virnsha, Z. And Bzhesinskii, Yu., *Aminoplasty* (Aminoplasts), Moscow: Khimiya, 1973.
10. Blagonravova, A.A. and Nepomnyashchii, A.M., *Lakovye epoksidnye smoly* (Varnish Epoxy Resins), Moscow: Khimiya, 1970.
11. Adams, P. and Baron, F.A., *Chem. Rev.*, 1965, vol. 65, no. 5, pp. 567–602.
12. Kalinina, L.S., Motorina, M.A., Nikitina, N.I., *et al.*, *Analiz kondensatsionnykh polimerov* (Analysis of Condensation Polymers), Moscow: Khimiya, 1984.
13. Toroptseva, A.M., Belogorodskaya, K.V., and Bondarenko, V.M., *Laboratornyi praktikum po khimii i tekhnologii vysokomolekylyarnykh soedinenii* (Laboratory Course of Chemistry and Technology of Macromolecular Compounds), Leningrad: Khimiya, 1972.
14. Karyakina, M.I., *Laboratornyi praktikum po ispytaniyu lakokrasochnykh materialov i pokrytii* (Laboratory Course of Testing of Paint and Varnish Materials and Coatings), Moscow: Khimiya, 1977.

ISSN 1070-4272, Russian Journal of Applied Chemistry, 2006, Vol. 79, No. 2, pp. 314–320. © Pleiades Publishing, Inc., 2006.
Original Russian Text © E. V. Solina, V. V. Safonov, T. S. Repina, V. B. Ivanov, 2006, published in Zhurnal Prikladnoi Khimii, 2006, Vol. 79, No. 2, pp. 315–321.

MACROMOLECULAR CHEMISTRY AND POLYMERIC MATERIALS

Kinetic Features of Photocuring of Oligomeric Formulations in the Presence of Disperse Dyes

E. V. Solina, V. V. Safonov, T. S. Repina, and V. B. Ivanov

Kosygin State Textile University, Moscow, Russia
Semenov Institute of Chemical Physics, Russian Academy of Sciences, Moscow, Russia

Received July 22, 2005

Abstract—The kinetics of consumption of double bonds, photoinitiators, and dyes in photocuring of formulations based on oligourethane methacrylate and trimethylolpropane triacrylate was studied. The kinetic parameters and quantum efficiencies of the processes were determined. The contributions from shielding and inhibition to the total polymerization deceleration by the dyes were estimated. The curing of dyed formulation and dye consumption were analyzed in relation to the structural features of the photoinitiators and dyes.

DOI: 10.1134/S1070427206020297

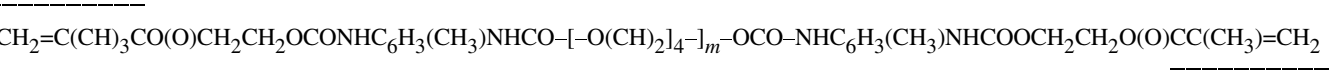
UV-curable dyed oligomer-monomer formulations (so-called UV paints) are widely used in various industries, especially in polygraphy [1–3]. Printing on textile materials with UV paints has a number of environmental and technical benefits, which makes this procedure fairly promising [4, 5]. However, there are no data on how the photocuring of formulations is influenced by textile dyes and on the stability of these dyes during polymerization.

In this study, we elucidated the kinetic relationships in photocuring of dyed formulations and determined the parameters characterizing both the polymerization proper and the consumption of photoinitiators and dyes during polymerization. The primary attention was given to a more detailed analysis of the previously [6] revealed specific features of the process, consisting in that the performance of photoinitiators is affected by the dyes and the consumption of dyes during photocuring of formulations is influenced by the nature of a photoinitiator.

As photopolymerizing binder served a formulation based on oligourethane methacrylate (OUMA) and trimethylolpropane triacrylate (TMPA). The choice of these components was governed by the need to ensure a fairly high adhesion of the resulting polymer to hydrophilic polymer fibers (cotton and viscose), combined with high strength and elasticity. In selection of photoinitiators among aromatic ketones and quinones, as well as among derivatives of thioxanthone and phosphine oxide, we took into account the known data for other photopolymerizing systems [7]. Disperse dyes from various classes with various structures, which are used in textile industry, served as dyes.

EXPERIMENTAL

Oligourethane methacrylate with the formula



$$CH_2=C(CH)_3CO(O)CH_2CH_2OCONHC_6H_3(CH_3)NHCO–[–O(CH)_2]_4–]_m–OCO–NHC_6H_3(CH_3)NHCOOCH_2CH_2O(O)CC(CH_3)=CH_2$$

and a number-average molecular weight M_n = 1400 was prepared from oligotetrahydrofuran with terminal toluene isocyanate groups at the Institute of Chemical Physics, Russian Academy of Sciences. A prototype-commercial sample of TMPA available from Yarsintez Research Institute, Open Joint-Stock Company, as well as commercial samples of 2,6-di-*tert*-butylanthraquinone (Research Institute for Organic Semiproducts and Dyes, Russia), 2-isobutylanthraquinone (Lovson Chemicals, the United Kingdom), and phenylbis(2,4,6-trimethylbenzoyl)phosphine oxide (Irgacure 819, Ciba, Switzerland) were used without further purification. Photoinitiators, 1-chloro-4-propoxythioxanthone, benzophenone, and benzil, were purified by recrystallization from ethanol. Commercial samples of the dyes were purified, when necessary, by

Table 1. Cross-linking parameters for undyed OUMA/TMPA formulations containing 4 wt % photoinitiator

Photoinitiator	A_∞/A_0	$k_p \times 10^3$, s^{-1}	$v_p \times 10^3$, s^{-1}	Φ_p	τ_p, min
Phenylbis(2,4,6-trimethylbenzoyl)phosphine oxide	0.29	360	140	180	3.0
2,6-Di-*tert*-butylanthraquinone	0.42	79	33	35	3.0
2-Isobutylanthraquinone	0.44	20	11	7.8	4.5
1-Chloro-4-propoxythioxanthone	0.41	11	6.4	2.8	5.0
Benzophenone	0.094	2.5	2.2	7.3	9.0
Benzil	1.0	0.68	0.68	1.4	12

recrystallization from acetone or chromatographically. Chemically pure acetone was used without further purification.

Films, 50 μm thick, were cast from acetone solutions on supports made of polyethylene films hydrophilized by a special procedure. The components of the photopolymerizing formulations, OUMA, TMPA, photoinitiators, and dyes, were dosed, i.e., the required amounts of their solutions in acetone with the known concentrations were taken. The resulting films were exposed in air at room temperature ($20 \pm 2°C$) with the light (λ = 365 nm) cut from the total spectrum of a DRSh-1000 Hg lamp with UFS-6 and BS-6 light filters. The degree of cross-linking of the polymerizing formulation was estimated from the decrease in the optical density of the C=C stretching vibration band at 816 cm^{-1}. The extent of photocuring was also judged from the disappearance of the film stickiness [6, 8]. The consumption of the photoinitiators and dyes was monitored by the decrease in the optical density in the UV and visible ranges.

The choice of the film thicknesses, the OUMA/TMPA ratio (75/25 by weight), and the concentrations of the photoinitiators and dyes was governed both by practical (need for a sufficient intensity of color, high curing rate, and good physicomechanical properties) and experimental (need for optimizing the conditions of recording of the reactant concentrations) considerations.

The intensity of incident light for the samples was determined using polyvinyl chloride and polyethylene films containing benzophenone or 2,6-di-*tert*-butylanthraquinone as chemical actinometers. The intensity was calculated from the quantum efficiencies of consumption of benzophenone in polyvinyl chloride and polyethylene, equal to 0.16 [9] and 0.20 [10, 11], respectively.

The initial rates of polymerization (consumption of double bonds) (v_p), conversion of the photoinitiator (v_i), and conversion of dye (v_d), were calculated by differentiation of the experimental kinetic curves.

The absorption spectra in the UV and visible ranges were recorded on a Specord UV-Vis spectrophotometer, and the IR spectra, on a Specord IR-75 spectrophotometer.

When samples containing different photoinitiators are UV-irradiated in the absence of dyes, the double bonds are rapidly consumed (Fig. 1) and a stickiness disappears owing to cross-linking of the formulation (Table 1). The photoinitiators strongly differ in the performance characteristics: phenylbis(2,4,6-trimethylbenzoyl)phosphine oxide and anthraquione and thioxanthone derivatives exhibit the highest (Fig. 1, curves *1*–*4*), and aromatic ketone and diketone (Fig. 1, curves *5*, *6*), the lowest activity. Indeed, Fig. 1 characterizes specifically the activity of the photoinitia-

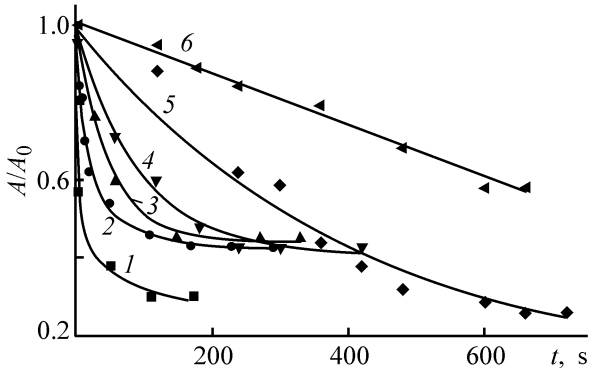


Fig. 1. Kinetic curves of consumption of double bonds (as derived from variation of the optical density at 816 cm^{-1}) for undyed photopolymerizing formulations irradiated in the presence of photoinitiators. Photoinitiator concentration 4 wt %. (A/A_0) Optical density and (t) time; the same for Figs. 2–5. Photoinitiator: (*1*) phenylbis(2,4,6-trimethylbenzoyl)phosphine oxide, (*2*) 2,6-di-*tert*-butylanthraquinone, (*3*) 2-isobutylanthraquinone, (*4*) 1-chloro-4-propoxythioxanthone, (*5*) benzophenone, and (*6*) benzil. (*Points*) Experimental data and (curves) results of calculations (*3*–*6*) by Eq. (1) and (*1*, *2*) by Eq. (2) for the k_p values from Table 1.

Table 2. Performance of 2,6-di-*tert*-butylanthraquinone at different concentrations in undyed formulation

Photoinitiator concentration, %	$v_p \times 10^3$, s^{-1}	Φ_p	$v_i \times 10^3$, s^{-1}	Φ_i	τ_p, min
1	5.9	22	3.5	0.49	10
2	19	35	3.6	0.49	4.5
3	17	23	4.0	0.60	3.5
4	33	35	6.0	0.60	3.0

tors, i.e., their ability to generate free radicals under the given conditions, since the optical densities at the irradiation wavelength of all the samples studied are small and comparable, namely, close to 0.1.

The kinetics of consumption of the double bonds in the cross-linking initiated by 2-isobutylanthraquinone, 1-chloro-4-propoxythioxanthone, benzophenone, or benzil (Fig. 1, curves *3–6*) are satisfactorily fitted by the first-order equation of the type

$$(A_t - A_\infty) = (A_0 - A_\infty)\exp(k_p t). \quad (1)$$

Here, t is the irradiation time; k_p, polymerization constant; A_t, optical density at a given instant of time t; and A_0 and A_∞, optical densities at $t = 0$ and $t \to \infty$, respectively.

The parameter A_∞ was introduced to take into account the kinetic inhibition of the process because of the diffusion limitations at high conversions, when the sample becomes hard.

In the presence of more active photoinitiators, phenylbis(2,4,6-trimethylbenzoyl)phosphine oxide and 2,6-di-*tert*-butylanthraquinone (Fig. 1, curves *1*, *2*), the kinetics of the process is described by the sum of two exponents:

$$(A_t - A_\infty) = (A_0 - A_\infty) \times [a\exp(-k_{p1}t) + (1 - a)\exp(-k_{p2}t)]. \quad (2)$$

Here, a and $(1 - a)$ are the relative contributions from the faster (with k_{p1}) and slower (with k_{p2}) processes, respectively.

We show below that more complex description of the polymerization kinetics in these two systems is due to the need to take into account the consumption of the photoinitiators. It should be noted that, although the k_p constants, relative initial rates v_p, and quantum efficiencies Φ_p of the polymerization differ sharply (by more than two orders of magnitude, Table 1), the times of irradiation until curing is completed, τ_p, differ less strongly (by only a factor of 4).

The consumption rate of double bonds is proportional to the photoinitiator concentration within the experimental error (Table 2), since, as noted above, the optical density at the irradiation wavelength is small. Consequently, the quantum efficiency of the process is constant, 29 ± 7 on the average. This is consistent with the fact that the quantum efficiency of the photoinitiator conversion (0.55 ± 0.06 on the average) is independent of its concentration (Table 2). The time of irradiation until the curing of the formulation is completed naturally, decreases as the photoinitiator concentration increases (Table 2). Considering the shape of the concentration dependence, as well as the crystallization of the photoinitiator in the formulation being cured at relatively high concentrations (≥4 wt %) and the economical aspects, we conclude that the optimal concentration is ca. 3 wt %.

Upon introduction of disperse dyes, the initial polymerization rate v_p, as a rule, significantly decreases and the time of irradiation until curing of the formulation τ_p, typically noticeably increases (Fig. 2, Table 3). The process kinetics is fairly adequately described by Eq. (1) corresponding to a second-order reaction (Fig. 2, curves *1–4*). Only in a single case, namely, in the presence of Yellow K dye, a biexponential dependence of type (2) was observed. The limiting extent of polymerization, defined as A_∞/A_0, changes insignificantly upon introduction of the dye. This is due to the fairly low shielding coefficients at the irradiation wavelength. At the same time, the A_∞/A_0 ratio in curing of dyed formulations, like in the case of undyed formulations, is noticeably larger in a number of cases

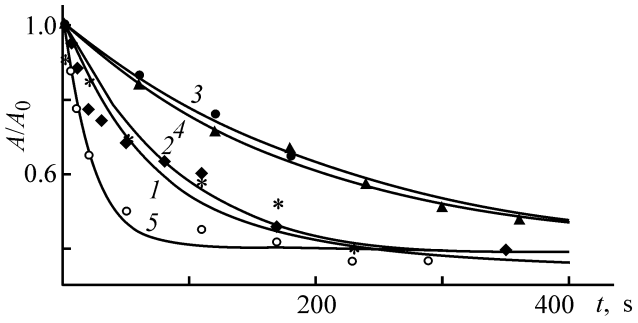


Fig. 2. (*1–4*) Photopolymerization of the formulations containing 3 wt % 2,6-di-*tert*-butylanthraquinone as photoinitiator with different dyes: (*1*) Disperse Blue K, (*2*) Disperse Orange Zh, (*3*) Disperse Red-Brown, and (*4*) Disperse Yellow K and (*5*) consumption of double bonds in the absence of dyes. For dye concentrations, see Table 3.

Table 3. Influence of disperse dyes on the relative initial rate, quantum efficiencies, and time of curing of dyed formulations with 2,6-di-*tert*-butylanthraquinone or phenylbis(2,4,6-trimethylbenzoyl)phosphine oxide (in parentheses) in amount of 3 wt % as initiator

Disperse dye	c, %	A_∞/A_0	$v_p \times 10^3$, s^{-1}	τ_p, min	Φ_p	γ	Φ_{pc}
Yellow Z	1	-	0.23	9	0.087	2.52	0.22
		0.75	(0.28)	(>25)	(0.10)	(3.00)	(0.30)
Yellow 4 Z	0.32	0.32	14	3.5	8.8	1.42	12
		(0.29)	(26)	(4)	(26)	(1.22)	(32)
Yellow 6 Z	0.03	0.41	22	3.5	18	1.0	18
		(0.35)	(19)	(4)	(21)	(1.20)	(25)
Yellow 6 Z PE	0.25	0.44	11	3.5	9.6	1.32	13
		(0.45)	(8.0)	(4)	(9.6)	(1.17)	(11)
Yellow K	1	0.46	18	4	12	1.39	17
		(0.47)	(11)	(6)	(7.3)	(1.25)	(9.1)
Yellow Fast 2K	0.41	0.40	3.2	6	1.7	1.57	2.7
		(0.72)	(2.1)	(>27)	(1.3)	(1.45)	(1.9)
Yellow Fast 4K	0.47	-	0.42	10	0.18	1.99	0.36
		(0.79)	(1.0)	(>24)	(0.5)	(1.70)	(0.85)
Red-brown	0.69	0.37	2.8	7	1.7	1.42	2.4
		(0.45)	(12)	(20)	(8.7)	(1.35)	(12)
Orange Zh	0.33	0.36	6.8	8	4.1	1.44	5.9
		(0.60)	(6.6)	(11)	(7.3)	(1.20)	(8.8)
Pink 2 S PE	1	0.44	10	4.5	26	1.0	26
		(0.45)	(4.3)	(4.5)	(5.0)	(1.17)	(5.85)
Blue K	0.50	0.36	19	6	16	1.30	21
		(0.64)	(22)	(>39)	(24)	(1.20)	(29)
Blue PE	0.50	0.39	18	4	12	1.35	16
		(0.49)	(23)	(17)	(32)	(1.15)	(37)
No dyestuff	–	0.25	30	3.5	29	–	–
		(0.32)	(110)	(3.0)	(175)	–	–

in the presence of phenylbis(2,4,6-trimethylbenzoyl)phosphine oxide than in the presence of 2,6-di-*tert*-butylanthraquinone (Fig. 3). This suggests a general character of the dependence of the limiting extent of polymerization on the structure of the photoinitiator, due to its action mechanism. Photoinitiators decomposing into small radicals under irradiation can migrate by diffusion to significant distances [e.g., phenylbis(2,4,6-trimethylbenzoyl)phosphine oxide]; they cause more profound transformations of the polyfunctional monomer than photoinitiators acting via detachment of the H atom from the environment (e.g., 2,6-di-*tert*-butylanthraquinone) and forming significantly larger radicals.

Detailed analysis of the data in Table 3 reveals three most important features of the photocuring of dyed formulations.

(1) The initial polymerization rates v_p tend to decrease in the presence of a number of dyestuffs more sharply (by two orders of magnitude at a maximum) than increases the irradiation time until curing τ_p (typically severalfold).

(2) The influence of a dye on the polymerization initiated by phenylbis(2,4,6-trimethylbenzoyl)phos-

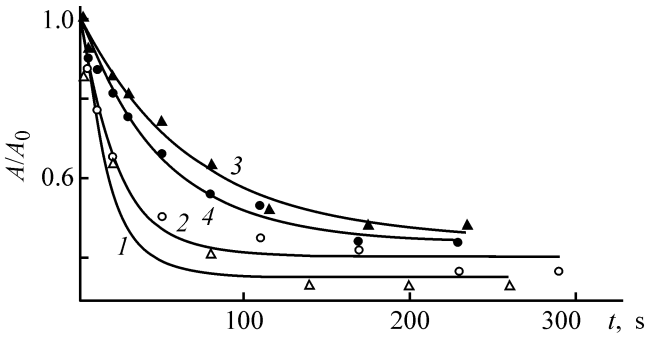


Fig. 3. Photocuring of (*1*, *2*) undyed formulations and (*3*, *4*) formulations containing Disperse Yellow 6Z PE dye (0.25 wt%) in relation to the nature of the photoinitiator. Initiation by (*1*, *3*) phenybis(2,4,6-trimethylbenzoyl)phosphine oxide and (*2*, *4*) 2,6-di-*tert*-butylanthraquinone at the photoinitiator concentration of 3 wt %.

Table 4. Influence of disperse dyestuffs on consumption of 2,6-di-*tert*-butylanthraquinone or phenylbis(2,4,6-trimethylbenzoyl)phosphine oxide (in parentheses) at the photoinitiator concentration of 3 wt %

Disperse dyestuff	c, %	$v_i \times 10^3$, s^{-1}	Φ_i	γ	Φ_{ipc}
Yellow Z	1	0.47	0.020	2.52	0.050
		(1.1)	(0.055)	(3.00)	(0.16)
Yellow 4 Z	0.32	2.7	0.19	1.42	0.27
		(14)	(2.0)	(1.22)	(2.4)
Yellow 6 Z	0.03	53	1.0	1.0	1.0
		(9.6)	(1.5)	(1.20)	1.8
Yellow 6 Z PE	0.25	2.5	0.25	1.32	0.33
		(5.1)	(0.87)	(1.17)	(1.02)
Yellow K	1	1.6	0.11	1.39	0.15
		(7.0)	(0.55)	(1.25)	(0.69)
Yellow Fast 2K	0.41	1.3	0.073	1.57	0.11
		(2.1)	(1.3)	(1.45)	(1.88)
Yellow Fast 4K	0.47	0.63	0.028	1.99	0.056
		(2.6)	(0.18)	(1.70)	(0.31)
Red-brown	0.69	1.1	0.078	1.42	0.11
		(3.0)	(0.31)	(1.35)	(0.42)
Orange Zh	0.33	1.8	0.12	1.44	0.17
		(6.6)	(1.0)	(1.20)	(1.2)
Pink 2 S PE	1	1.8	0.31	1.0	0.31
		(5.2)	(1.9)	(1.17)	(2.2)
Blue K	0.50	1.9	0.17	1.30	0.22
		(5.0)	(0.78)	(1.20)	(0.94)
Blue PE	0.50	1.8	0.14	1.35	0.19
		(8.3)	(1.6)	(1.15)	(1.8)
No dyestuff	–	3.6	0.55	–	
		(8.8)	(2.0)	–	

phine oxide is stronger, compared to initiation by 2,6-di-*tert*-butylanthraquinone.

(3) The activity of the photoinitiators in the presence of dyes may vary so widely that this can change the ratio of their activities: Phenyl-bis(2,4,6-trimethylbenzoyl)phosphine oxide, more active in the absence of dyes, becomes less active than 2,6-di-*tert*-butylanthraquinone in the presence of dyes.

General considerations suggest that one of the main mechanisms by which dyes affect the polymerization is shielding. Table 3 lists the shielding coefficients γ calculated as [12]

$$\gamma = [(A_1 + A_2)/A_1][(1 - 10^{-A_1})/(1 - 10^{-(A_1+A_2)})], \quad (3)$$

where A_1 and A_2 are the optical densities of the undyed samples and samples in the presence of dyes, respectively.

Using these γ parameters, we can calculate the corrected quantum efficiencies of polymerization $\Phi_{pc} = \gamma\Phi_p$. The Φ_{pc} parameters typically slightly exceed the Φ_p parameters (Table 3), since the calculations actually take into account only the amount of light absorbed by the photoinitiator proper, and the dye is regarded as an internal filter only. However, the Φ_{pc} parameters for most of the dyed systems are also substantially lower than the Φ_p parameters for undyed systems. This suggests that, along with shielding (UV absorbers), most of the dyes studied are involved in chemical reactions. It is well known [13] that many disperse dyes and, in particular, azo dyes can react with free radicals, which is one of the main factors making them highly efficient photostabilizers with respect to polydienes. It should be noted that the influence of the dyes on polymerization under the actual conditions fairly well correlates qualitatively with their photoprotection action in polydienes. For example, the photoresistance of polydienes in the presence of azo compounds increases in the following order: 3-methyl-5-*tert*-butyl-6-hydroxyazobenzene (analog of dyestuff Yellow 6 Z) < 4-dimethylamino-4-nitroazobenzene (Disperse Orange Zh) < 4-hydroxy-3-methyl-4-benzeneazo(azobenzene) (Yellow Fast 4K) [13]. The same trend is characteristic of the inhibiting action of these dyes during polymerization (Table 3).

The consumption of the photoinitiators in the presence of dyes (Table 4) is described by dependences of types (1) and (2), characteristic of undyed formulations as well. The inhibition effects for this process are an order of magnitude weaker, compared to polymerization, and do not exceed 7–8 (Table 4). Another feature of this process consists in that the dyes exert comparable influence on the performance of photoinitiators of varied nature (Table 4).

A decrease in the consumption rate of the photoinitiators in the presence of the dyes is only partially due to the shielding effect (Table 4). The action of the dyes, evidently, includes, along with shielding, quenching of excited states of the photoinitiators by the energy transfer mechanism. This, naturally, decelerates the formation of free radicals, thereby decelerating the initiation.

The dye consumption during photocuring of the formulations is also described by equations of types (1) and (2), except for the systems containing Yellow Z or Yellow Fast 4K dyes and 2,6-di-*tert*-butylanthraquinone as photoinitiator.

In the two last-named cases, we observed autocatalytic (S-shaped) curves. The essential features of this process are as follows.

(1) The dye consumption rate and its limiting conversion substantially depend on the dye structure (Fig. 4, Table 5). The least stable are dyes containing amino group (Yellow 4 Z, Yellow 2 K, Orange Zh, Pink 2 S, Blue K, and Blue PE).

(2) The rate and limiting degree of the dye conversion substantially depend on the nature of the photoinitiator as well (Fig. 5, Table 5). For five of the twelve systems studied, dyes are consumed faster in the presence of phenylbis(2,4,6-trimethylbenzoyl)phosphine oxide compared to 2,6-di-*tert*-butylanthraquinone. For four systems (Yellow Z, Yellow Fast 4K, Orange Zh, and Red-Brown dyes), the dye consumption is virtually independent of the nature of the photoinitiator. Only one dye, Pink 2 S, is consumed faster in the presence of 2,6-di-*tert*-butylanthraquinone. Yellow 6 Z and Yellow K dyes are the most stable and are not noticeably consumed in the presence of any of the photoinitiators studied.

There is a qualitative correlation between the conversion rate of the dyes and their influence on the consumption of double bonds. For example, Yellow 4 Z, Yellow 6 Z, Yellow 6 Z PE, and Yellow K dyes are insignificantly consumed themselves in the case of initiation with 2,6-di-*tert*-butylanthraquinone and cause a decrease in the quantum efficiency of conversion of double bonds to only a small extent (Tables 3, 5), unlike Yellow Fast 4 K which is converted fairly rapidly and strongly inhibits the polymerization.

Thus, the influence of disperse dyes on photocuring of oligomer-monomer formulations is due to several simultaneous processes: (1) absorption of photochemically active light (shielding); (2) interaction with the photoinitiator responsible for deceleration of its consumption and, thereby, of initiation; and (3) inhibition of polymerization due to interaction with free radicals, which is also responsible for consumption of the dyes.

Table 5. Dye consumption rates during photocuring of formulations, initiated by 2,6-di-*tert*-butylanthraquinone or phenylbis(2,4,6-trimethylbenzoyl)phosphine oxide (in parentheses) at the photoinitiator concentration of 3 wt %

Disperse dye	c, %	$v_d \times 10^3$, s^{-1}	Φ_d	γ	Φ_{dpc}
Yellow Z	1	0.56 (0.39)	0.0094 (0.0064)	2.52 (3.00)	0.024 (0.019)
Yellow 4 Z	0.32	hs* (30)	hs (0.41)	1.42 (1.22)	hs (0.50)
Yellow 6 Z	0.03	hs (14)	hs (0.032)	1.0 (1.20)	hs (0.038)
Yellow 6 Z P	0.25	hs hs	hs hs	1.32 (1.17)	hs hs
Yellow Fast 2K	0.41	hs (4.9)	hs (0.055)	1.57 (1.45)	hs (0.080)
Yellow Fast 4K	0.47	2.0 (1.5)	0.015 (0.013)	1.99 (1.70)	0.030 (0.027)
Red-brown	0.69	1.6 (0.58)	0.022 (0.0064)	1.42 (1.35)	0.031 (0.0086)
Orange Zh	0.33	2.8 (1.5)	0.026 (0.020)	1.44 (1.20)	0.037 (0.024)
Pink 2 S PE	1	5.1 (0.47)	0.22 (0.14)	1.0 (1.17)	0.22 (0.16)
Blue K	0.50	3.1 (6.9)	0.050 (0.15)	1.30 (1.20)	0.065 (0.18)
Blue PE	0.50	1.4 (10)	0.078 (0.23)	1.35 (1.15)	0.011 (0.26)

* (hs) High stability of dyes.

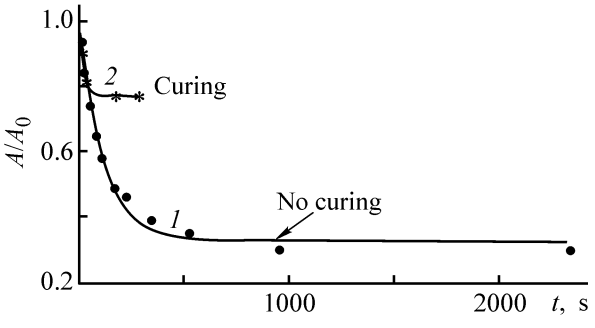


Fig. 4. Variation of the optical density in the region of the absorption maximum of (*1*) Disperse Blue K (0.5% wt %) or (*2*) Disperse Yellow K (1 wt %) dyes in the course of irradiation of the photopolymerizing formulation containing phenylbis(2,4,6-trimethylbenzoyl)phosphine oxide (3 wt %) as photoinitiator.

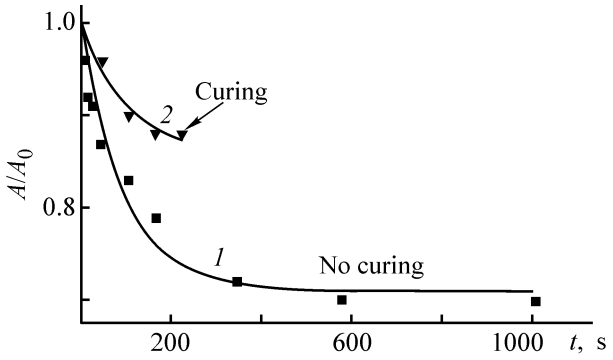


Fig. 5. Consumption of Disperse Blue PE dye (0.5 wt %) in the course of irradiation of the photopolymerizing formulation containing 0.3 wt % of (*1*) phenylbis(2,4,6-trimethylbenzoyl)phosphine oxide and (*2*) 2,6-di-*tert*-butylanthraquinone.

CONCLUSIONS

(1) Kinetic features and kinetic parameters of consumption of double bonds, photoinitiators, and dyes were determined for formulations based on oligourethane methacrylates and trimethylolpropane triacrylate.

(2) The activity of the photoinitiators changes in the presence of dyes.

(3) Consumption of the dyes in photocuring of the formulations depends on the nature of the photoinitiators.

(4) The optimal compositions of the dyed formulations having a fairly high photosensitivity and preserving the color during photocuring were determined.

REFERENCES

1. Volkhonskaya, N.S., *Skrinprinting.RU*, 2004, no. 4, pp. 18–27.
2. Edwards, N. and Little, R., *Polym. Paint Colour J.*, 2005, vol. 195, no. 4487, pp. 35–38.
3. Fachs, A., *Polym. Paint Colour J.*, 2005, vol. 195, no. 4485, pp. 29–34.
4. RU Patent 2037171.
5. WO Patent 98/54399.
6. Solina, E.V., Ivanov, V.B., and Safonov, V.V., *Izv. Vyssh. Uchebn. Zaved., Khim. Khim. Tekhnol.*, 2005, vol. 48, no. 12, pp. 85–87.
7. Monroe, B.M. and Weed, G.C., *Chem. Rev.*, 1993, vol. 39, no. 2, pp. 435–448.
8. Klimova, E.D., Ivashchenko, S.P., Mazyakina, L.M., and Grachev, V.T., *Tekhnologiya poligrafii: fiziko-khimicheskie problemy: Mezhvedomstvennyi Sbornik Nauchnykh Trudov* (Polygraphy Technology: Physicochemical Problems: Interdepartmental Coll. of Scientific Works), Moscow: Mosk. Poligr. Inst., 1991, pp. 81–84.
9. Ivanov, V.B. and Zhuravlev, M.A., *Polym. Photochem.*, 1986, vol. 7, no. 1, pp. 55–64.
10. Zamotaev, P.V., Granchak, V.M., Litsov, N.I., and Kachan, A.A., *Vysokomol. Soedin., Ser. A*, 1985, vol. 27, no. 10, pp. 2072–2078.
11. Charlesby, A., Grace, C.S., and Pilkington, F.B., *Proc. Roy. Soc.*, 1962, vol. 268, no. 2, pp. 202–205.
12. Shlyapintokh, V.Ya., *Photochemical Conversion and Stabilization of Polymers*, Munich: Hanser, 1984.
13. Efremkin, A.F. and Ivanov, V.B., *Polym. Photochem.*, 1984, vol. 4, no. 2, pp. 179–205.

ISSN 1070-4272, Russian Journal of Applied Chemistry, 2006, Vol. 79, No. 2, pp. 321–324. © Pleiades Publishing, Inc., 2006.
Original Russian Text © I. Yu. Vashurina, N. E. Kochkina, Yu. A. Kalinnikov, 2006, published in Zhurnal Prikladnoi Khimii, 2006, Vol. 79, No. 2, pp. 322–325.

MACROMOLECULAR CHEMISTRY AND POLYMERIC MATERIALS

Effect of Peat Humus Acids on the Structure of Sizing Starch Gels

I. Yu. Vashurina, N. E. Kochkina, and Yu. A. Kalinnikov

Institute of Solution Chemistry, Russian Academy of Sciences, Ivanovo, Russia

Received September 13, 2005

Abstract—Influence of peat humus acid microadditions on the structure of starch gels for sizing cotton yarn is studied by rheology.

DOI: 10.1134/S1070427206020303

Sizing is an inherent part of weaving works, consisting in coating of the warp yarn with a polymeric adhesive, such as starch, in order to assist efficient weaving. At the same time, there is strong reason to reduce the starch consumption for sizing. First of all, starch is a valuable raw material for food industry, and the demand for starch steadily grows. Furthermore, both the warp sizing and the fabric desizing processes generate a lot of wastewater containing starch, making wastewater treatment more difficult and expensive (biochemical oxygen demand increases by 0.63 mg O_2 per 1 mg starch).

Previously, we have demonstrated that the starch concentration in the sizing mixture for cotton yarn can be considerably reduced by using humus acid (HA) microadditives [1–3]. Humus acids are natural macromolecular compounds formed by microbial fermentation of plant residues or through purely chemical processes (redox reactions, hydrolysis, and condensation) [4]. The structure of humus acids contains very diverse fragments and functional groups, which causes a broad spectrum of their properties, including the tendency to be involved in intermolecular interactions, catalytic activity in redox reactions, and surfactant properties [5, 6].

Humus acids specifically interact with starch-containing sizing mixtures. As the increasing HA concentration in starch sizing gels increases from 0 to 0.08–0.12%, the relative viscosity of the gels decreases by a factor of tens and hundreds (depending on the starch concentration), reaching values which are only 2–4 times higher than the viscosity of a straight solvent, water. Further increase in the HA concentration abrupt leads to an rise in the viscosity to the point of formation of a glassy mass [2]. The lower the viscosity of the starch–humus hydrogel, the higher its sizing efficiency. For example, hydrogels with the lowest viscosity provide an increase in the tensile stress of 25-tex cotton yarn by 51–57% with a simultaneous decrease in the elasticity loss by 12–20% [3].

It is well known that, if the ordinary starch size acquires such a low viscosity in the course of pulping (suggesting starch dextrinization), it is unsuitable for sizing because it forms a brittle, readily peeling film on the fiber surface [7]. Nevertheless, the films formed from low-viscosity starch-humus gels are well comparable in strength with the starch films [8].

Previously we have demonstrated [9] that one of the reasons for the decrease in the relative viscosity of the starch hydrogel modified with HA microadditives is deeper oxidation of starch by *N*-chlorobenzenesulfonamide, which is a component of the sizing mixture (oxidized group content increases by 50–55%), and the related enhancement of the hydrolysis of the polysaccharide across α-glucoside bonds under the action of NaOH (degree of polymerization of the unit branch of amylopectin decreases from 13.2–15.6 to 11.4–13.6).

At the same time, introduction of 0.1% HA into the starch gels reduces their viscosity severalfold even in the absence of the indicated reagent in the mixture. Therefore, the reasons for the abnormally low viscosity of the gelatinized starch-humus systems consist not only in the chemical modification of the polysaccharide. Evidently, some other mechanism exists, which is responsible for the observed decrease in the relative viscosity of the starch mixture with a simultaneous increase in the sizing efficiency. The high content of HA functional groups that are susceptible to intermolecular interactions suggests that humus acids are in-

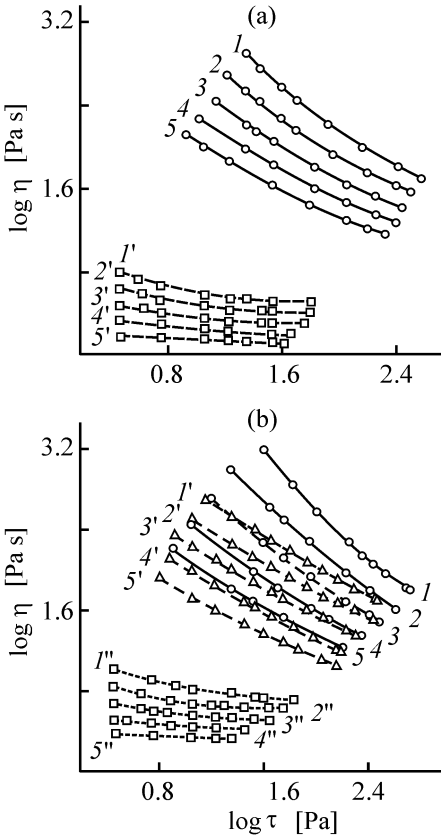


Fig. 1. Viscosity η vs. the shear stress τ in the log–log coordinates: (a) (*1*–*5*) starch and (*1*'–*5*') starch-humus gels; and (b) (*1*–*5*) starch, (*1*'–*5*') dextrinized, and (*1*''–*5*'') starch-humus gels. System composition, %: starch 4, NaOH 0.1, *N*-chlorobenzenesulfonamide 0.05, and HA 0.1. Temperature (°C): (*1*, *1*') 30, (*2*, *2*') 40, (*3*, *3*') 50, (*4*, *4*') 60, and (*5*, *5*') 70.

volved in the formation of a supramolecular structure in the starch gels.

In this study, we examined the influence of humus acids on the structure of sizing starch gels.

EXPERIMENTAL

The starch-based sizing mixture was prepared using the procedure described in [2, 3].

The structure of starch and starch-humus gels was studied rheologically on a Rheotest-2 rotary viscometer with a cylinder-cylinder working unit over the rate range 0.5–437 s^{-1}.

The activation energy of viscous flow of the starch gels, ΔG_{visc}, was estimated from the temperature dependence of the viscosity, using the Frenkel–Eyring equation:

$$\eta = A\exp(\Delta E_{visc}/RT)$$

or

$$\log\eta = \log A + \Delta E_{visc}/RT,$$

where η is the dynamic viscosity of the starch gel; *A*, preexponential factor; *R*, gas constant; and *T*, temperature.

The relative viscosity was measured at 80°C with a VPZh-2 Ostwald viscometer (capillary diameter 1.2 mm).

The degree of polymerization was estimated from data on selective oxidation of starch with sodium periodate [9].

The IR spectra of starch films were recorded at 20°C on an IKS-29 double-beam spectrophotometer.

Figures 1a and 1b show the flow curves for the starch (curves *1*–*5*) and starch-humus gelatinized systems (curves *1*'–*5*') with a polysaccharide concentration of 4 and 5%, respectively, over the temperature range 30–70°C. The results show that, in all the cases, the dependences of the viscosity on the shear stress are incomplete (there is no portion corresponding to the maximal Newtonian viscosity), which is caused by the high molecular weight and flexibility of the polysaccharide macromolecules. At the same time, the curves for the starch gels (curves *1*–*5*) also contain no portions of the minimal Newtonian viscosity, either, while this portion is clearly seen in the curves of the starch-humus gels. This fact suggests a larger length of macromolecules of the gel-forming polymer in the HA-free systems, since a higher shear stress is required to attain the limiting state corresponding to $\eta = \eta_{nm}$. As the temperature rises, all the flow curves become flatter, reflecting the degradation of the structure of gelatinized starch. At the same time, the structurization remains clearly pronounced in the starch gels even at 70°C, whereas it is practically lacking in the starch-humus gels. Therefore, the latter can be regarded as solutions, rather than polysaccharide gels.

To elucidate whether the previously reported [9] decrease in the degree of polymerization of amylopectin is the only factor responsible for the observed degradation of the structure in the starch-humus sizing gels, we performed the following experiment. A HA-free gelatinized starch was subjected to long-term cooking with monitoring of its relative viscosity and the degree of polymerization of amylopectin. For the rheological study we selected a paster (referred to as dextrin paster) with the same degree of polymerization of amylopectin as in the starch-humus gel. Data on the relative viscosity and degree of polymerization of three gelatinized systems with the same

polysaccharide content (ordinary starch, that after dextrinization, and starch-humus gels) are listed in the table.

It is worth noting that the dextrinized gel is characterized not only by the same degree of polymerization of the amylopectin unit branch as the starch-humus gel, but also by the same relative viscosity. By contrast, the behavior of the dextrinized gel under the shear stress strongly differs from that of the starch-humus gel, being closer to the behavior of the ordinary starch gels: at all temperatures, a distinctly pronounced portion corresponding to structured gels is found in the flow curves, and the stage of full breaking of the structure is not attained over the acceptable range of the shear stress (Fig. 1b, curves *1*''–*5*''). Therefore, despite the equally low relative viscosity and similar degree of polymerization of amylopectin, the dextrinized starch gel, like the ordinary starch gel, has a higher degree of structurization as compared to the starch-humus gels. Note that the fact of high degree of structurization in starch gels is well documented [10]. It was demonstrated that the structure of a starch gel consists of supramolecular species, such as globules, colloid particles, and conglomerates, in which the polysaccharide macromolecules are involved in intra- and intermolecular hydrogen bonding. In flowing of the gel out of the capillary of the viscometer, the indicated structural units move in the solvent medium without their breaking, while at high shear rates reached in the experiment even separate globules are broken.

The lack of a stable structure in the starch-humus gels suggests that humus acids (as is known, they are hydrophilic and tend to be involved in an intermolecular interaction) the colloid particles and rupturing of starch by penetrating into these particles interchain hydrogen bonds. Most likely, a fluctuating 3*D* network is formed in this case and this work readily degrades under the shear stress.

The transition of the polymer molecules from one equilibrium state to another by overcoming the intermolecular interaction forces can be characterized by the activation energy of viscous flow ΔE_{visc} [11].

The activation energies estimated for the three systems under consideration at a shear rate ($f = 0.274$ s^{-1}) close to that occirring in the practice of sizing are presented in Fig. 2. It can be seen that the activation energy of viscous flow decreases by 17–20% on passing from ordinary starch to starch-humus gels, thus supporting the suggestion about their fluctuating structure. At the same time, the effect of dextrinization is considerably weaker. For example, the dextrinization resulted in only 7% decrease in ΔG_{visc} in a 5% starch mixture.

Relative viscosity and mean degree of polymerization of amylopectin unit chain in starch gels (composition of starch gel, %: starch 5, NaOH 0.1, and *N*-chlorobenzenesulfonamide 0.05)

System, %	Cooking time, h	η_{rel} at 80°C	DP
Gel:			
ordinary starch	1	37.75	14.4 ± 1.2
dextrinized	7	1.75	12.7 ± 1.0
starch-humus*	1	1.75	12.5 ± 1.1

* HA content 0.1%.

When analyzing the reasons for the decrease in the degree of structurization in starch gels, one more factor should be taken into consideration, namely, the increase in the content of oxidized groups in starch [9]. As is known, oxidized starches are characterized by increased solubility, and their gels, by decreased viscosity, which is caused to a large extent by the dissociation of the carboxy groups formed in the course of oxidation. It is the occurrence of charged groups that is generally accepted as the factor responsible for the nearly tenfold increase in the electrical conductivity of starch after oxidative treatment [10].

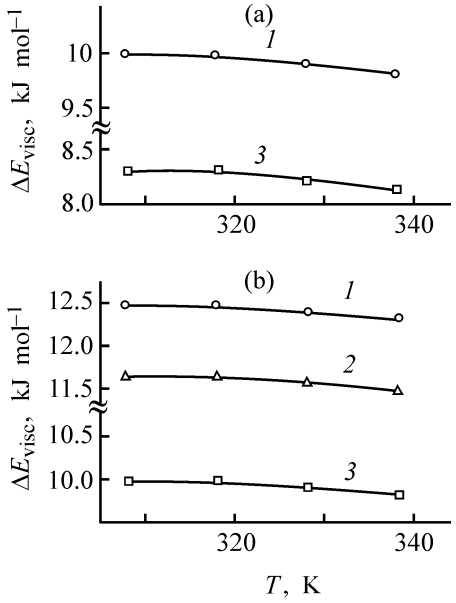


Fig. 2. Activation energy ΔG_{visc} of viscous flow of gelatinized starch mixtures. Component concentration (%): starch (a) 4 and (b) 5, NaOH 0.1, *N*-chlorobenzenesulfonamide 0.05, and HA 0.1. (*T*) Temperature. Systems: (*1*) starch, (*2*) dextrinixed starch, and (*3*) starch-humus gels.

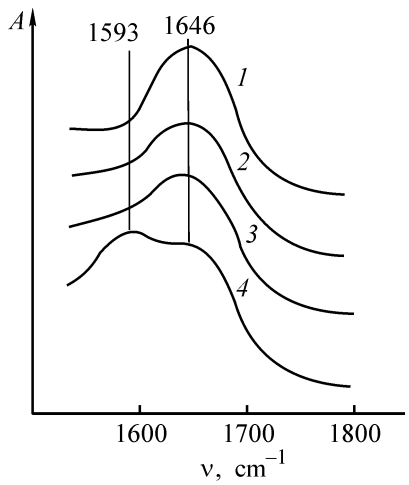


Fig. 3. Infrared spectra of films cast from (*1*) final starch size and (*2–4*) samples of starch-humus sizing mixtures, taken during their cooking. (*A*) Transmission and (ν) wavenumber. Cooking stage at which the samples were taken: (*2*) starch gelling (~67°C), (*3*) viscosity drop stage (~75°C), and (*4*) full fluidification of the sizing mixture (~90°C).

It is notable that, in the presence of HA in the starch gel, such charged groups were found even in the film, as demonstrated by the IR spectra of the films prepared from ordinary starch and starch-humus sizing mixtures (the latter were sampled at different stages of the cooking) (Fig. 3). The band at 1646 cm^{-1} is assigned to the H-bonded carboxy groups of starch, and the band at 1593 cm^{-1}, to the deprotonated carboxy groups [12]. It can be seen that all the carboxy groups are H-bonded in the film formed by the starch size, while ionized groups dominate in the starch-humus film.

CONCLUSIONS

Addition of microamounts of peat humus acids as a second hydrophilic polymer provides extensive structural modification of starch sizing mixtures in the gelation stage, initiating virtually complete degradation of separate colloidal particles of the starch gel. The resulting sizing mixtures better spread over the surface of cotton yarn, ensuring formation of a continuous thin, but sufficiently strong film, thus improving the basic parameters of sizing.

REFERENCES

1. Vashurina, I.Yu., Sharova, I.E., and Kalinnikov, Yu.A., *Tekstiln. Khim.*, 2000, no. 1, pp. 30–34.
2. Kochkina, N.E., Vashurina, I.Yu., and Kalinnikov, Yu.A., *Izv. Vyssh. Uchebn. Zaved., Tekhnol. Tekstil'n. Prom–sti.*, 2004, no. 1, pp. 41–43.
3. Kochkina, N.E., Vashurina, I.Yu., and Kalinnikov, Yu.A., *Izv. Vyssh. Uchebn. Zaved., Tekhnol. Tekstil'n. Prom–sti.*, 2004, no. 2, pp. 39–43.
4. Orlov, D.S., *Gumusovye kisloty pochv i obshchaya teoriya gumifikatsii* (Gumus Acids of Soils and General Theory of Humification), Moscow: Mosk. Gos. Univ., 1990.
5. Syroezhko, A.M., Proskuryakov, V.A., Levanovskii, V.I., *et al.*, Abstracts of Papers, *Vsesoyuznyi Simpozium "Problemy kataliza v uglekhimii"* (All-Union Symp. "Problems of Catalysis in Coal Fuel Chemistry"), Donetsk, 1990, pp. 115–116.
6. Leland, M. and Wandruszka, R. von, *Soil Sci. Soc. Am. J.*, 1999, vol. 63, pp. 1645–1649.
7. Rybakova, V.M., *Tekhnologiya shlikhtovaniya khlopchatobumazhnoi pryazhi* (Sizing Process for Cotton Yarn), Ivanovo: Ivanov. Knizhnoe, 1955.
8. Vashurina, I.Yu., Kochkina, N.E., and Kalinnikov, Yu.A., *Khim. Volokna*, 2004, no. 5, pp. 26–29.
9. Vashurina, I.Yu., Kochkina, N.E., and Kalinnikov, Yu.A., *Tekstil'n. Khim.*, 2004, no. 1, pp. 72–76.
10. Senakhov, A.I., Koval', V.V., and Sadov, F.I., *Zagustki, ikh teoriya i primenenie* (Thickeners: Theory and Applications), Moscow: Legkaya Industriya, 1972.
11. Tager, A.A., *Fiziko-khimiya polimerov* (Physical Chemistry of Polymers), Moscow: Khimiya, 1978.
12. Bellamy, L.J., *The Infra-Red Spectra of Complex Molecules*, New York: Wiley, 1957.

ISSN 1070-4272, Russian Journal of Applied Chemistry, 2006, Vol. 79, No. 2, pp. 325–326. © Pleiades Publishing, Inc., 2006.
Original Russian Text © V. N. Tseluikin, I. S. Chubenko, I. F. Gun'kin, A. Yu. Pankst'yanov, 2006, published in Zhurnal Prikladnoi Khimii, 2006, Vol. 79, No. 2, pp. 326–327.

BRIEF COMMUNICATIONS

Colloidal Dispersion of Fullerene C_{60} Free of Organic Solvents

V. N. Tseluikin, I. S. Chubenko, I. F. Gun'kin, and A. Yu. Pankst'yanov

Engels Technological Institute, Saratov State Technical University, Engels, Saratov oblast, Russia

Received April 13, 2005

Abstract—A new procedure for preparing aqueous colloidal dispersion of C_{60} in water was developed.

DOI: 10.1134/S1070427206020315

Fullerene C_{60} is insoluble in water, which complicates its practical use. However, colloidal aqueous dispersions of fullerenes can be prepared. A large portion of fullerenes in their solution is in the form of clusters [1]. Dispersions of C_{60} are prepared by addition of water to an organic solution of the fullerene, with the subsequent treatment resulting in precipitation of colloidal particles [2–5]. In the process, the organic solvent is not removed from the solution.

The aim of this study was to prepare colloidal dispersions of fullerene C_{60} in water free of admixtures of other solvents.

A water–acetone mixture (1 : 3) containing 5–20 mM of sodium dodecyl sulfate as a stabilizer was prepared. To this mixture, a solution of fullerene C_{60} in chlorobenzene (2.2 mg ml^{-1}) was added dropwise with vigorous stirring on a magnetic stirrer. The resulting yellow homogeneous solution was distilled under atmospheric pressure with vigorous stirring. The first evaporated fraction was acetone. The second fraction was chlorobenzene–water azeotrope. In the course of evaporation of the azeotrope, the fullerene became dispersed in water. Finally, water [refractive index n = 1.3330 (20°C)] was distilled off. Dispersions containing 0.05 to 0.50 g l^{-1} of C_{60} were prepared. Their color varied from yellowish to brown as the fullerene concentration increased. The chlorobenzene band with λ_{max} = 264 nm [6] is absent in the electronic absorption spectrum of the aqueous dispersion of C_{60}. Hence, chlorobenzene was completely removed from the dispersion. It should be noted that the dispersions are highly stable: no coagulation is observed in the course of at least a month. The average particle size of aqueous dispersions of C_{60} was calculated from the turbidity spectrum by the equation [7]

$$r_{av} = \lambda_{av}\alpha/2\pi\mu_0,$$

where λ_{av} is the geometric mean wavelength of the spectral range examined; μ_0, refractive index of the dispersion medium; and α, coefficient dependent on the parameter n ($n = \Delta\log D/\Delta\log\lambda$).

The average size of the colloidal particles is 40 nm.

A yellow homogeneous solution (the initial C_{60} solution in chlorobenzene is violet) is also formed when a C_{60} solution in chlorobenzene is added dropwise with vigorous stirring to a water–acetone mixture (1 : 3) without a stabilizer. The $D(\lambda)$ spectrum dramatically changes under these conditions, i.e., the solvatochromic effect is observed. The $D(\lambda)$ spectrum of a C_{60} solution in chlorobenzene contains bands in the ranges λ = 380–410 and 510–570 nm. In going to a chlorobenzene–water–acetone system, the optical density significantly increases in the whole wavelength range (Fig. 2).

The solvatochromic effect is due to aggregation of fullerenes upon a change in the solvent composition

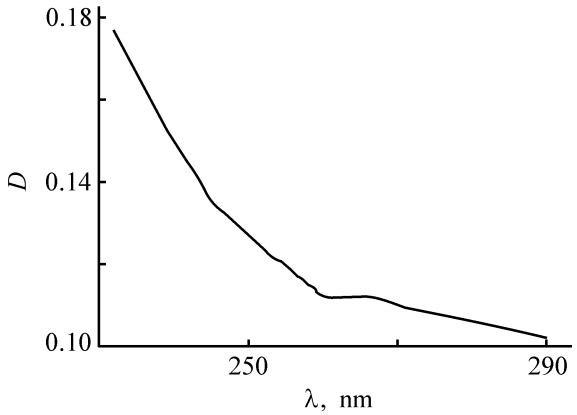


Fig. 1. Absorption spectrum of colloidal dispersion of fullerene C_{60} in water. (D) Optical density and (λ) wavelength. Fullerene concentration 3.5×10^{-3} g l^{-1}.

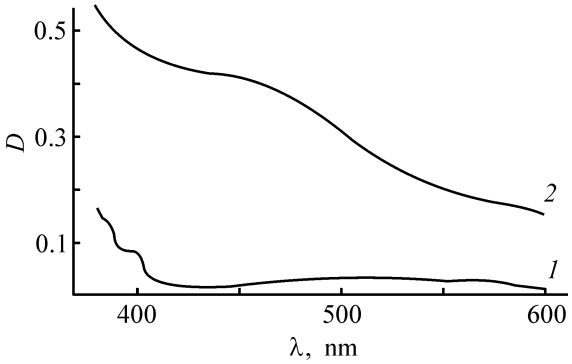


Fig. 2. Absorption spectrum of C_{60} solution in (*1*) chlorobenzene and (*2*) chlorobenzene-water-acetone mixture. (*D*) Optical density and (λ) wavelength. Fullerene concentration 1.6×10^{-5} M.

[1]. The increase in the optical density of the system in the presence of C_{60} is caused not only by light absorption but also by strong light scattering on colloidal fullerene particles. The fact that the optical density of spectrum *2* is significantly higher than that of spectrum *1* (Fig. 2) is due to this effect. When the nonstabilized solution is distilled, no colloidal dispersion is formed and the fullerene coagulates. The stabilization effect can be explained as follows: sodium dodecyl sulfate molecules are sorbed through their hydrocarbon fragments on the surface of C_{60} clusters and their partially dissociated sulfate groups form a charged layer on the surface, thus preventing coagulation. The structure of a colloidal fullerene particle stabilized with sodium dodecyl sulfate can be described by the formula

$$\{n[C_{60}]mC_{12}H_{25}SO_4^-(m - x)Na^+\}xNa^+.$$

Thus, we prepared colloidal solutions of fullerene C_{60} in water free of admixtures of organic solvents.

EXPERIMNETAL

The absorption spectrum of the colloidal dispersion of fullerene C_{60} was recorded in 1-cm quartz cells on an SF-26 spectrophotometer. The reference cell was filled with water. The refractive index was measured on a URL refractometer (model 1). All measurements were performed at $20 \pm 2°C$.

Fullerene C_{60} (99.5 %) was purchased from Merck; sodium dodecyl sulfate was of chemically pure grade. Chlorobenzene was dried over P_2O_5 and distilled; acetone was dried over $CaCl_2$ and subjected to fractional distillation.

CONCLUSIONS

(1) The particle size was determined from the turbidity spectrum.

(2) A solvatochromic effect was observed on adding a C_{60} solution in chlorobenzene to a water–acetone mixture.

REFERENCES

1. Bezmel'nitsyn, V.N., Eletskii, A.V., and Okun', M.V., *Usp. Fiz. Nauk*, 1998, vol. 168, pp. 1195–1220.
2. Andrievsky, G.V., Kosevich, M.V., Vovk, O.M., *et al.*, *Recent Advsances in the Chemistry and Physics of Fullerenes and Related Materials*, Kadish, K.M. and Ruoff, R.S., Eds., Pennington: The Electrochemical Soc. Inc., 1995, pp. 1591–1602.
3. Mchedlov-Petrossyan, N.O., Klochkov, V.K., and Andrievsky, G.A., *J. Chem. Soc., Faraday Trans.*, 1997, vol. 93, pp. 4343–4346.
4. Andrievsky, G.A., Klochkov, V.K., Bordyuh, A.B., and Dovbeshko, G.I., *Chem. Phys. Lett.*, 2002, vol. 364, pp. 8–17.
5. Wei, X., Wu, M., Qi, L., and Xu, Zh., *J. Chem. Soc., Perkin Trans. 2*, 1997, pp. 1389–1393.
6. Sverdlova, O.V., *Elektronnye spektry v organicheskoi khimii* (Electronic Spectra in Organic Chemistry), Leningrad: Khimiya, 1985.
7. Klenin, V.I., Shchegolev, S.Yu., and Lavrushin, V.I., *Kharakteristicheskie funktsii svetorasseyaniya dispersnykh sistem* (Characteristic Functions of Light Scattering of Disperse Systems), Saratov: Saratov. Univ., 1977.

ISSN 1070-4272, Russian Journal of Applied Chemistry, 2006, Vol. 79, No. 2, pp. 327–328. © Pleiades Publishing, Inc., 2006.
Original Russian Text © M. K. Ibraev, A. T. Takibaeva, A. M. Gazaliev, O. A. Nurkenov, S. D. Fazylov, 2006, published in Zhurnal Prikladnoi Khimii, 2006, Vol. 79, No. 2, pp. 328–329.

BRIEF COMMUNICATIONS

Synthesis of Isonicotinic Acid Vinyloxyethylthiosemicarbazide

M. K. Ibraev, A. T. Takibaeva, A. M. Gazaliev, O. A. Nurkenov, and S. D. Fazylov

Institute of Organic Synthesis and Coal Chemistry of the Republic of Kazakhstan, Limited Liability Company, Karaganda, Kazakhstan

Received June 7, 2005

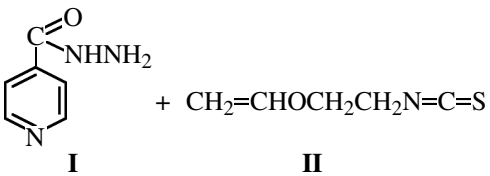
Abstract—The reaction of isonicotinic acid hydrazide with vinyloxyethyl isothiocyanate was studied. The reaction product exhibits antifungal activity toward Candida albicans strain.

DOI: 10.1134/S1070427206020327

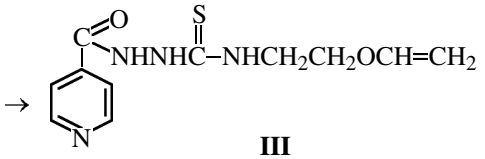
Isonicotinic acid hydrazide **I**, which exhibits strong antitubercular effect and is an antagonist of nicotinamide, the factor of redox processes in a cell, is undoubtedly of interest in a search for new physiologically active substances [1].

Many hydrazine derivatives exhibit a broad spectrum of biological activity, depending on the structure, position, and reactivity of substituents. Therefore, it is of particular interest to prepare hydrazine derivatives from vinyloxyethyl isothiocyanate, because introduction of a sulfur atom into organic molecules decreases their toxicity and gives rise to new types of biological activity [2].

With the aim to search for new bioactive substances and reveal structure–bioactivity relationships, we performed the reaction of isonicotinic acid hydrazide **I** with vinyloxyethyl isothiocyanate **II**. The reaction was performed at equimolar ratio of the reactants in alcohol at 0±5°C with the subsequent heating to 35–40°C:



I **II**



III

Compound **III** obtained from this reaction is a white crystalline substance soluble in organic solvents. Its structure and composition were confirmed by elemental analysis and IR spectroscopy. The IR spectrum of **III** exhibits characteristic absorption bands of N–H, NHCS, CH_2=CH, and C=S stretching vibrations at 3460–3440, 1510–1500, 1645–1640, and 1220–1200 cm^{-1}, respectively. The bending mode of the NH–CO– group is manifested at 1650–1645 cm^{-1}.

Compound **III** was tested for the bactericidal activity against a series of strains, and its antifungal activity against *Candida albicans* strain was revealed.

EXPERIMENTAL

The IR spectrum was recorded on an AVATAR-320 device (KBr pellets).

Isonicotinic acid vinyloxyethylthiosemicarbazide III. A solution of 2.56 g of vinyloxyethyl isothiocyanate **II** in 5 ml of ethanol was slowly added to a solution of 2.74 g of isonicotinic acid hydrazide **I** in 15 ml of ethanol. After the whole amount of **II** was added, the mixture was stirred while heating to 45–55°C over a period of 2–3 h. The solvent was distilled off, and 4.85 g (91%) of isonicotinic acid vinyloxyethylthiosemicarbazide **III** was obtained; mp 193–195°C.

Found, %: C 49.62, H 5.26, N 21.05.
$C_{11}H_{14}N_4O_2S$.
Calculated, %: C 49.56, H 5.22, N 21.0.

The antimicrobial activity of **III** was studied by the procedure described in [3]. The sensitivity of microorganisms to the compound was evaluated by

the method of successive dilutions in a liquid cultural medium. The following strains were used: *S.aureus* 505, *P.vulgaris* 1, *P.aeruginosa* ATC 464, *E.coli* M-17, *B.subtilis* ACCC 6633, *S.agalactiae*, and *C.albicans*. The concentrations of **III** in these tests were 8.0, 4.0, 2.0, 1.0, 0.5, 0.25, and 0.125 mg ml^{-1}. In parallel, we checked the cultural medium and compound **III** for sterility. For the cultivation of *S.aureus* 505, *P.vulgaris* 1, *P.aeruginosa* ATC 464, and *E.coli* M-17, we used the peptone meat agar; for that of *S.agalactiae*, 1% glucose broth; for that of *C.albicans*, Saburo liquid medium; for that of staphylococci, yolk–salt agar; for that of E.coli, the Endo medium; and for that of streptococci, the blood–sugar agar.

The minimal bactericidal concentration was determined by reinoculation to dense cultural media from a liquid cultural medium in which the visible growth was absent. The minimal bacteriostatic concentration was estimated turbidimetrically (SF-26 spectrophotometer) by comparing the intensities of the microorganism growth on liquid cultural media. The cultural medium with the same concentration of **III** as in the given test was used as reference.

We revealed the antifungal activity of **III** against Candida albicans; however, compound **III** showed no antibacterial activity against *S.aureus* 505, *P.vulgaris* 1, *P.aeruginosa* ATC 464, *E.coli* M-17, *B.subtilis* ACCC 6633, and *S.agalactiae* strains. The minimal bactericidal and bacteriostatic concentrations of **III** with respect to *Candida albicans* are 0.25 and 0.125 mg ml^{-1}, respectively.

CONCLUSION

Isonicotinic acid vinyloxyethylthiosemicarbazide was prepared; it exhibits antifungal activity against *Candida albicans* clinical strain.

REFERENCES

1. Mashkovskii, M.D., *Lekarstvennye sredstva* (Drugs), Moscow: Meditsina, 1993.
2. Mel'nikov, N.N., *Pestitsidy. Khimiya, tekhnologiya i primenenie* (Pesticides. Chemistry, Technology, and Use), Moscow: Khimiya, 1987.
3. Navashin, S.M. and Fomina, I.P., *Ratsional'naya antibiotikoterapiya: Spravochnik* (Efficient Therapy with Antibiotics: Handbook), Moscow: Meditsina, 1982.

ISSN 1070-4272, Russian Journal of Applied Chemistry, 2006, Vol. 79, No. 2, pp. 329–330. © Pleiades Publishing, Inc., 2006.
Original Russian Text © M. K. Ibraev, Zh. M. Kozhina, A. M. Gazaliev, S. D. Fazylov, 2006, published in Zhurnal Prikladnoi Khimii, 2006, Vol. 79, No. 2, pp. 330–331.

BRIEF COMMUNICATIONS

Synthesis and Biological Activity of Ethyl [*N*-(Alkylthio)thiocarbonyl]aminoacetates

M. K. Ibraev, Zh. M. Kozhina, A. M. Gazaliev, and S. D. Fazylov

Institute of Organic Synthesis and Coal Chemistry of the Republic of Kazakhstan, Limited Liability Company, Karaganda, Kazakhstan

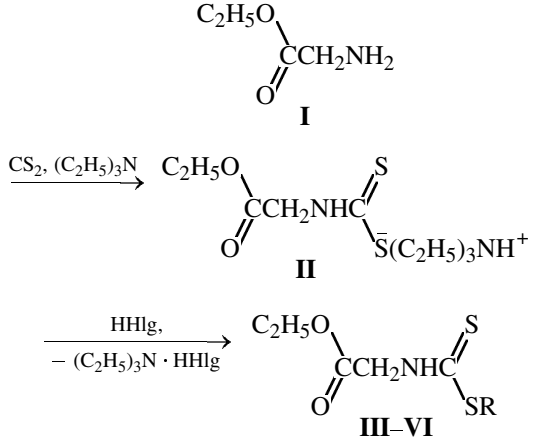
Received June 7, 2005

Abstract—Ethyl [*N*-(alkylthio)thiocarbonyl]aminoacetates were prepared and tested for the fungicidal activity.

DOI: 10.1134/S1070427206020339

Dithiocarbamic acid derivatives exhibit pesticidal [1], fungicidal [2, 3], nematocidal, and herbicidal [4] activity.

With the aim to further study dithiocarbamic acid derivatives, we prepared ethyl [*N*-(alkylthio)thiocarbonyl]aminoacetates **III**–**VI** from ethyl aminoacetate **I** and studied their biological properties:



where R = CH_3 (**III**), C_2H_5 (**IV**), C_3H_7 (**V**), or CH_2=$CHCH_2$ (**VI**); Hlg = I or Br.

The reaction was performed in absolute benzene at 0±5°C with the subsequent heating to 45–50°C. The yields of **III**–**VI** were 75–85%. The yield and the reaction time depend on the size and electron-donor power of the alkyl group in alkyl halide RHlg. The activity of RHlg toward **I** decreases in the following order: CH_3I > C_2H_5Br > C_3H_7Br > CH_2=$CHCH_2Br$. Compounds **III**–**V** are crystalline, and compound **VI** is a viscous oil; compounds **III**–**VI** are soluble in polar organic solvents, but insoluble in water.

The composition and structure of the compounds were confirmed by elemental analysis and IR spectroscopy. The IR spectra contain characteristic bands of stretching vibrations of the N–H, NH–CS, and C=S groups at 3320–3316, 1417–1124, and 1257–1220 cm^{-1}, respectively; also, a strong band of the ester C=O group is observed at 1730–1710 cm^{-1}.

EXPERIMENTAL

Ethyl [*N*-(methylthio)thiocarbonyl]aminoacetate III. A solution of 0.76 g of CS_2 in 10 ml of benzene was slowly added to a solution of 1.47 g of ester **I** and 1.45 g of triethylamine in 30 ml of benzene at 0±5°C. Then a solution of 1.38 g of CH_3I in 10 ml of benzene was slowly added at the same temperature. The mixture was stirred with gentle heating (35–40°C) for 2–3 h. The solvent was distilled off, and 1.54 g (84%) of **III** was obtained; mp 71–72°C.

Found, %: C 36.92, H 5.69, N 7.3.

$C_6H_{11}NO_2S_2$.

Calculated, %: C 36.90, H 5.70, N 7.26.

Esters **IV**–**VI** were prepared similarly.

Ethyl [*N*-(ethylthio)thiocarbonyl]aminoacetate IV. Yield 83%, mp 74–75°C.

Found, %: C 40.61, H 6.18, N 6.34.

$C_7H_{13}NO_2S_2$.

Calculated, %: C 40.63, H 6.10, N 6.30.

Ethyl [*N*-(propylthio)thiocarbonyl]aminoacetate V. Yield 81%, mp 38–40°C.

Found, %: C 43.40, H 6.82, N 6.34.

$C_8H_{15}NO_2S_2$.

Calculated, %: C 43.41, H 6.80, N 6.30.

Ethyl [*N*-(allylthio)thiocarbonyl]aminoacetate VI. Yield 75%.

Found, %: C 43.80, H 5.93, N 6.45.

$C_8H_{13}NO_2S_2$.

Calculated, %: C 43.74, H 5.58, N 6.42.

The fungicidal activity of esters **III**–**VI** was studied as described above. Compounds **III**–**VI** were sterilized by filtration on a Nolgene System apparatus and aseptically introduced into agarized Czapek cultural medium in various concentrations. Phytopathogenic fungi *Fusarium oxysporum* and *Botrytis cinerea* were used as test cultures. The fungicidal activity was evaluated by the intensity of development of the microorganisms on the cultural medium in comparison with the control experiments without addition of **III**–**VI**.

We found that ethyl [*N*-(ethylthio)thiocarbonyl]-aminoacetate **IV** tested in vitro exhibits pronounced fungicidal activity against *Botrytis cinerea* (62–66% growth suppression). Compounds **III**–**VI** also showed pronounced fungicidal activity against *Fusarium oxysporum* (58–65% growth suppression).

CONCLUSIONS

(1) Ethyl [*N*-(alkylthio)thiocarbonyl]aminoacetates were prepared by alkylation of the dithiocarbamic acid derived from glycine.

(2) These compounds showed pronounced fungicidal activity against phytopathogenic fungi *Botrytis cinerea* and *Fusarium oxysporum*.

REFERENCES

1. Mel'nikov, N.N., *Pestitsidy: Khimiya, tekhnologiya i primenenie* (Pesticides: Chemistry, Technology, and Use), Moscow: Khimiya, 1987.
2. JPN Patent 7009.
3. Romanian Patent 58 303.
4. Maksudov, N.Kh. and Safaev, M.A., *Uzb. Khim. Zh.*, 1981, no. 5, pp. 26–28.

ISSN 1070-4272, Russian Journal of Applied Chemistry, 2006, Vol. 79, No. 2, pp. 331–333. © Pleiades Publishing, Inc., 2006.
Original Russian Text © G. I. Elagin, V. L. Mizyuk, L. O. Kobrin, 2006, published in Zhurnal Prikladnoi Khimii, 2006, Vol. 79, No. 2, pp. 332–334.

BRIEF COMMUNICATIONS

Synthesis of *tert*-Alkylperoxy Derivatives of Thiirane and Their Use for Preparing Light-Resistant Polystyrene

G. I. Elagin, V. L. Mizyuk, and L. O. Kobrin

Chernobyl Heroes Cherkassy Institute of Fire Safety, Cherkassy, Ukraine
Ukrainian Academy of Printing, Lviv, Ukraine
Franko Lviv National University, Lviv, Ukraine

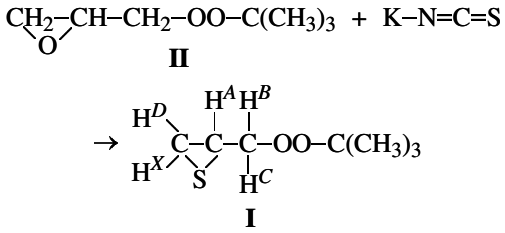
Received June 28, 2005

Abstract—Epithio-substituted primary-tertiary dialkyl peroxides were prepared by treatement of *tert*-alkyl oxiranylmethyl peroxides with potassium thiocyanate and were tested as polymerization initiators in synthesis of light-resistant polystyrene.

DOI: 10.1134/S1070427206020340

It is known that thermal polystyrene is insufficiently light-resistant. Polymerization in the presence of initiators containing a norbornane core [1] yields polystyrene samples whose light resistance exceeds that of the thermal polymer by only 10–15%.

With the aim to prepare polystyrene with enhanced light resistance (containing chemically bound sulfur), we performed polymerization of styrene in the bulk, using an epithio-substituted peroxide, 3-*tert*-butylperoxy-1,2-epithiopropane (**I**), as initiator. Compound **I** was prepared by treatment of 3-*tert*-butylperoxy-1,2-epoxypropane **II** (for the preparation procedure and properties of **II**, see [2–4]) with a suspension of potassium thiocyanate in absolute alcohol:



II

I

Analysis of the epithio-containing polymers obtained shows that the epithio peroxide not only initiates polymerization of styrene by ensuring presence of reactive groups in terminal units but also is grafted to polymeric chains, abstracting a hydrogen atom from them. Incorporation of S(II) in an amount of 0.2–0.5% into the polymer substantially enhances its light resistance (see table).

For light resistance tests, polymer samples were dissolved in benzene and cast to obtain 200–400-μm-thick films, which were irradiated for 17 h in air with the UV light from four LE-60 lamps (60 W each) arranged at a distance of 20 cm from the films and of 4 cm from each other. After the irradiation was complete, the films were dissolved in toluene to obtain 1% solutions (which were then diluted), and the intrinsic viscosity of the polymer samples at 298 K was measured and compared to that of the unirradiated samples. The molecular weight was determined by the Mark–Houwink formula [6].

The 0.29% content of sulfur corresponds to the 0.53% content of epithio groups, or, on the average, to 24.7 epithio groups per polymer macromolecule.

Data on the preparation of light-resistant polystyrene by polymerization of styrene initiated by epithio peroxide **I** are listed in the table.

Depending on the concentration of **I**, the polymerization is accelerated by a factor of 3–10, compared to the thermal polymerization. The light resistance of polystyrene prepared with this initiator depends on the initiator concentration and polymerization time and exceeds the light resistance of thermal polystyrene by 30–40% on the average.

EXPERIMENTAL

The ^{1}H NMR spectra were recorded on a BS-497 spectrometer (operating frequency 100 MHz) in CCl_4,

Rate of styrene conversion and the light resistance of polystyrene obtained under various conditions in the presence of epithio peroxide **I**[*]

T, K	c, M	τ, h	γ, %	Characteristics of polystyrene				ΔM upon irradiation, %
				$[\eta] \times 10^{-2}$, ml g^{-1}		$M \times 10^{-3}$		
				before irradiation	after irradiation	before irradiation	after irradiation	
373	0	3	6.0	1.611	0.950	579.8	269.5	53.5
373	0	6	12.3	1.287	0.840	418.8	225.6	46.1
373	0	15	25.1	1.297	0.631	423.6	149.0	64.8
373	0.025	3	15.3	0.982	0.857	283.0	232.0	17.9
373	0.025	6	22.4	0.994	0.792	288.0	207.2	28.0
373	0.025	15	70.3	1.285	1.182	417.8	370.1	11.4
373	0.050	2	25.2	0.948	0.863	268.9	234.7	12.7
373	0.050	6	53.2	0.852	0.804	230.3	211.7	8.1
373	0.050	15	91.4	1.247	1.005	400.0	292.6	26.8
373	0.100	3	36.2	0.711	0.573	177.2	129.6	26.8
373	0.100	6	57.3	0.806	0.741	212.5	188.1	11.5
373	0.100	15	100.0	0.956	0.901	272.2	249.8	8.2
413	0	8	49.4	0.854	0.687	231.2	168.6	27.1
413	0.050	4	76.3	0.267	0.259	42.85	41.02	4.3
413	0.050	8	100.0	0.277	0.255	45.21	40.10	11.3
413	0.100	4	88.0	0.185	0.185	25.20	25.20	0.0
413	0.100	8	100.0	0.180	0.167	24.20	21.71	10.8

[*] (T) Polymerization temperature, (c) concentration of **I**, (τ) polymerization time, (γ) styrene conversion, (M) molecular weight, and (ΔM) relative decrease in the molecular weight of a film upon irradiation.

with TMS as internal reference; the chemical shifts (ppm) are given in the δ scale.

3-*tert*-Butylperoxy-1,2-epithiopropane I. A reaction flask equipped with a stirrer, liquid seal, and thermometer was charged with a solution of 7.3 g of epoxy peroxide **II** in 25 ml of anhydrous ethanol and with 5.0 g of potassium thiocyanate. The suspension was stirred at 303 K for 40 h; the reaction progress was monitored by TLC on Silufol UV-254 plates (eluent acetone–*p*-xylene, 3 : 20 by volume; development with iodine vapor). After the reaction was complete, the mixture was diluted with 50 ml of water, and epithio peroxide **I** was extracted with diethyl ether (5 × 25 ml). The ether solution was dried over anhydrous magnesium sulfate; the solvent was distilled off at 308–313 K first at ambient pressure and then at a pressure gradually reduced to 10 mm Hg. The residue was chromatographed on a column (100 × 1 cm) with silica gel (eluent benzene). After removing the solvent and keeping for 2–3 h in a vacuum (1–2 mm Hg) at 308–313 K, 4.0 g (49%) of **I** was obtained; d_4^{20} = 1.3590 g cm^{-3}, n_D^{20} = 1.4760, MR_D = 44.25 (calculated MR_D = 44.43).

Found, %: C 53.16, H 8.93, S 19.38; $[O]_{act}$ 9.5; M 158.14.

Calculated, %: C 53.82, H 8.70, S 19.76; $[O]_{act}$ 9.9; M 162.25.

^{1}H NMR spectrum, δ, ppm (J, Hz): 1.22 s (9H, $3CH_3$), 2.18 d.d (1H, H^X, $^3J_{AX}$ 2, $^2J_{DX}$ 5), 2.48 d.d (1H, H^D, $^3J_{AD}$ 6), 3.04 m (1H, H^A), 3.51 d.d (1H, H^C, $^3J_{AC}$ 8, $^2J_{BC}$ 12.5), 4.17 d.d (1H, H^C, $^3J_{AC}$ 4).

Epithio-containing polystyrene. Epithio peroxide **I** (0.81 g) was dissolved in 50 ml of styrene (initiator concentration 1.7 wt %). The solution was charged into ampules under N_2, and the ampules were cooled with dry ice and sealed. The polymerization was performed in the course of 15 h at 373–374 K. Then the ampules were opened, the polymer was dissolved in 100 ml of anhydrous toluene, and the product was precipitated by adding the solution to 100 ml of methanol. The reprecipitation was repeated to remove low-molecular-weight fractions. The product was dried to constant weight in air at 333–343 K. Yield 45.1 g (quantitative), molecular weight 272 200 (determined viscometrically from the intrinsic viscosity in toluene at 298 K [5]).

Found, %: S 0.29.
Calculated, %: S 0.34.

At 373–374 and 413–414 K, in the presence of 3.65–14.6 g of **I**, the yield of the epithio-containing polystyrene was 15–100% (the reaction time was varied).

CONCLUSIONS

(1) Treatment of 3-*tert*-butylperoxy-1,2-epoxypropane with potassium thiocyanate under mild conditions gives an epithio peroxide in ~50% yield. This peroxide can be used as initiator of bulk polymerization of styrene, accelerating it by a factor of 3–10, compared to the thermal polymerization.

(2) Polystyrene prepared in the presence of 3-*tert*-butylperoxy-1,2-epithiopropane surpasses thermal polystyrene in light resistance by 30–40%.

REFERENCES

1. USSR Inventor's Certificate, no. 681 068.
2. USSR Inventor's Certificate, no. 295 755.
3. Elagin, G.I., *Khim. Prom–st. Ukr.*, 2000, no. 3, pp. 37–39.
4. Elagin, G.I. and Protsenko, Yu.V., *Visn. Nats. Univ. "L'vivs'ka Politekh.," Ser.: Khim. Khim. Tekhnol. Org. Rech.*, 2002, vol. 461, pp. 175–180.
5. Shatenshtein, A.I., Virskii, A.P., Pravikova, I.A., *et al., Prakticheskoe rukovodstvo po opredeleniyu molekulyarnykh vesov i molekulyarno-vesovogo raspredeleniya polimerov* (Manual on Determination of Molecular Weights and Molecular-Weight Distribution of Polymers), Moscow: Khimiya, 1964.
6. Lipatov, Yu.S., Nesterov, A.E., Gritsenko, T.M., and Veselovskii, O.A., *Spravochnik po khimii polimerov* (Handbook of Polymer Chemistry), Kiev: Naukova Dumka, 1975.

ISSN 1070-4272, Russian Journal of Applied Chemistry, 2006, Vol. 79, No. 2, pp. 334–335. © Pleiades Publishing, Inc., 2006.
Original Russian Text © Zh. M. Kozhina, M. K. Ibraev, A. M. Gazaliev, S. D. Fazylov, 2006, published in Zhurnal Prikladnoi Khimii, 2006, Vol. 79, No. 2, pp. 335–336.

BRIEF COMMUNICATIONS

Synthesis and Aphicidal Activity of Ethyl *N*-Aroylaminoacetates

Zh. M. Kozhina, M. K. Ibraev, A. M. Gazaliev, and S. D. Fazylov

Institute of Organic Synthesis and Coal Chemistry of the Republic of Kazakhstan, Limited Liability Company, Karaganda, Kazakhstan

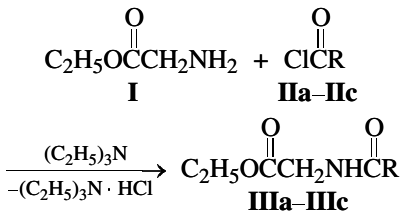
Received June 7, 2005

Abstract—Ethyl aminoacetate was acylated with various aroyl chlorides. The resulting ethyl *N*-aroylacetates were tested for aphicidal activity.

DOI: 10.1134/S1070427206020352

α-Amino acid derivatives and, in particular, *N*-acyl-α-amino acids containing amino and carboxy groups attract steady researchers' interest owing to a broad spectrum of their biological activity [1]. Some of amino acid derivatives exhibit antiphlogistic, antipyretic, antitumor, antiviral, and antibacterial properties, or affect the central nervous system [2, 3].

With the aim to prepare new potentially bioactive substances, we acylated ethyl aminoacetate **I** with carboxylic acid chlorides **IIa**–**IIc**:



where R = C_6H_5 (**a**), *m*-$CH_3C_6H_4$ (**b**), *o*-BrC_6H_4 (**c**).

The reaction was performed in absolute benzene at 0±5°C in the presence of triethylamine as HCl acceptor.

The yields of **IIIa**–**IIIc** depend on the type and position of substituents in the aryl moiety of aroyl chlorides. The electron-donor methyl group in **IIb** slightly decreases the positive charge on the carbonyl carbon atom, compared to unsubstituted benzoyl chloride **IIa**; as a result, the product yield slightly decreases. The *o*-Br substituent in **IIc** also somewhat decreases the product yield, hindering the reaction sterically.

Compounds **IIIa**–**IIIc** are colorless crystalline substances soluble in polar organic solvents and insoluble in water.

The composition and structure of the compounds were confirmed by elemental analysis and IR spectroscopy. The IR spectra of **IIIa**–**IIIc** contain characteristic absorption bands of the amide and carbonyl groups in the ranges 1630–1625 and 1755–1730 cm^{-1}, respectively; the NH group gives rise to a medium-intensity band at 3330–3270 cm^{-1}.

EXPERIMENTAL

The IR spectra were recorded on an AVATAR-320 device (KBr pellets).

The reaction progress and product purity were monitored by TLC.

Ethyl *N*-benzoylaminoacetate IIIa. Benzoyl chloride **IIa** (3.2 g) was slowly added to a solution of 2.4 g of **I** and 2.3 g of triethylamine in absolute benzene at 0±5°C. The mixture was stirred for 3 h. After distilling the solvent off, 3.76 g (90%) of **IIIa** was obtained; mp 59–60°C.

Found, %: C 63.81, H 6.21, N 6.83.
$C_{11}H_{13}NO_3$.
Calculated, %: C 63.76, H 6.28, N 6.76.

Ethyl *N*-(*m*-methylbenzoyl)aminoacetate IIIb was prepared similarly in 89% yield; mp 74–75°C.

Found, %: C 45.24, H 4.46, N 4.93.
$C_{12}H_{15}NO_3$.
Calculated, %: C 46.13, H 4.54, N 4.89.

Ethyl *N*-(*o*-bromobenzoyl)aminoacetate IIIc was prepared similarly in 72% yield; mp 53–54°C.

Found, %: C 65.26, H 6.52, N 6.41.
$C_{11}H_{12}NO_3Br$.
Calculated, %: C 65.15, H 6.78, N 6.33.

The compounds were tested for aphicidal activity in laboratory. Replicate specimens of cucumber and pea plants populated with pests (cucurbit and peach aphids, respectively) were sprayed from an atomizer with solutions of the test compounds of definite concentrations (1 ml) and placed in Petri dishes onto filter paper wetted with water. The pest mortality was evaluated 24 h after the treatment. The biological efficiency was calculated by Abbot's formula [4, 5] and corrected for the death rate in the control experiment performed with water.

The biological efficiency was assessed with cucurbit aphids in a laboratory box in isolated vegetation vessels on cucumber plants populated with the pests. Four replicate runs were performed. Aktellik agent was used as reference. Control runs were performed witn water. The living insects were counted before and 72 h after the treatment (spraying of a plant specimen with 5 ml of a working solution in a single run). The biological efficiency was calculated by Franz's formula [4, 5] taking into account an increase in the number of insects in the control run. In each replicate run, the insects were counted on three leaves of the model plant.

The laboratory assessment of the biological activity showed that treatment with **IIIa** in a concentration of 0.01 wt % reduced the number of cucurbit aphids by 88.3%.

CONCLUSIONS

(1) Ethyl *N*-aroylaminoacetates were prepared by acylation of ethyl aminoacetate with aroyl chlorides.

(2) It was found that ethyl *N*-benzoylaminoacetate exhibits aphicidal activity.

REFERENCES

1. Mikhalkin, A.P., *Usp. Khim.*, 1995, vol. 64, no. 3, pp. 275–290.
2. Agababayan, A.G., Gevorgyan, G.A., and Mndzhoyan, O.L., *Usp. Khim.*, 1982, vol. 51, no. 4, pp. 678– 695.
3. Kovalev, G.V., Rakhimov, A.I., and Ozerov, A.A., *Khim.-Farm. Zh.*, 1990, no. 10, pp. 41– 44.
4. Berin, I.G., *Khimicheskaya zashchita rastenii* (Chemical Protection of Plants), St. Petersburg, 1996.
5. Geshtovt, N.Yu., *Entomopatogennye griby: Biotekhnologicheskie aspekty* (Entomopathogenic Fungi: Biotechnological Aspects), Almaty, 2002.

ISSN 1070-4272, Russian Journal of Applied Chemistry, 2006, Vol. 79, No. 2, pp. 336–338. © Pleiades Publishing, Inc., 2006.
Original Russian Text © R. F. Nafikova, L. A. Mazina, E. I. Nagumanova, V. S. Minkin, R. Ya. Deberdeev, 2006, published in Zhurnal Prikladnoi Khimii, 2006, Vol. 79, No. 2, pp. 337–339.

BRIEF COMMUNICATIONS

Influence of Metal-Containing Lubricants on Characteristics of Polyvinyl Chloride

R. F. Nafikova, L. A. Mazina, E. I. Nagumanova, V. S. Minkin, and R. Ya. Deberdeev

Kaustik Joint-Stock Company, Sterlitamak, Bashkorkostan, Russia
Kazan State Technical University, Kazan, Tatarstan, Russia

Received August 22, 2005

Abstract—The influence of metal-containing lubricants based on monoesters of glycerol and higher isomeric saturated monocarboxylic acids on characteristics of polyvinyl chloride was studied.

DOI: 10.1134/S1070427206020364

Mechanochemical stabilizers or lubricants are the imperative component of polyvinyl chloride formulations, especially those of rigid types [1]. In recovery of polyvinyl chloride (PVC), the presence of lubricants results in a decrease in their internal friction; as a result, the recovery temperature decreases, forming of PVC materials proceeds more smoothly and rapidly, and degradation of PVC decreases. In addition, the distribution of the formulation components becomes easier and the outward appearance of articles is improved.

A wide variety of chemicals are used as lubricants in processing of PVC. They differ in the influence on PVC characteristics, polarity, and compatibility with the polymer.

New metal-containing Vikol lubricants based on higher isomeric saturated monocarboxylic acids (HIAs) are the product of telomerization of ethylene with isobutyric acid.[1]

New metal-containing lubricants are produced in a single stage by the reaction of HIA and glycerol (1 : 1 molar ratio) in the presence of oxides of bivalent metals (Zn, Mg) or their two-component mixture in an amount of 0.6–0.8% relative to the total reaction mass at 180–190°C.

The lubricants traditionally used in industrial processing of PVC are glycerol monoesters based on saturated and unsaturated higher carboxylic acids, predominantly glyceryl monooleates, monostearates, and monorecinoleates [1, 2]. Contrary to acids with normal structure, HIAs have lower freezing points, infinite solubility in organic solvents, and higher viscosity due to the presence of short branchings in their molecules. It was of interest to study how lubricants prepared on the basis of HIAs affect the characteristics of PVC. The Vikol lubricants with various lengths of hydrocarbon chain were obtained and tested in comparison with the well-known surface lubricants, in particular, hydrocarbon wax and Glitserol.

[1] First obtained at the Kaustik Joint-Stock Company.

EXPERIMENTAL

As subjects of the study we used PVC of the S-6358M brand, Vikol metal-containing lubricants, whose characteristics are listed in Table 1, and also commercial Glitserol (ester of glycerol and synthetic fatty acids) and polyethylene wax PV-200. To study the influence of lubricants on the characteristics of PVC, the formulations were prepared as follows: 100 wt parts of suspended PVC, 3 wt parts of tribasic lead sulfate, 1 wt part of calcium stearate, and up to 5 wt parts of lubricant were homogenized in a laboratory mixer at 90°C for 30 min. The resulting mixture was rolled on a PD 320 laboratory roller at 175°C for 5 min. The ultimate tensile strength and the relative elongation were determined on an RMI-250 tensile-testing machine.

As can be seen from Table 1, the samples studied, which differ in the length of the hydrocarbon chain, have different densities, viscosities, and molecular mobilities (judging from the freezing point). It should be noted that these differences in the characteristics of metal-containing additives should affect their compatibility with PVC and, hence, affect the characteristics of the formulations containing these additives.

Table 1. Physicochemical characteristics of Zn-containing lubricants Vikol

Sample no.	Fraction of HIAs	Density at 20°C, g cm^{-3}	Acid number, mg KOH per gram	Temperature, °C		Kinematic viscosity, cSt, at indicated T, °C	
				flash point	freezing point	20	60
1	C_{22}–C_{24}	0.908	3.08	164	–10	328.99	39.3
2	C_{18}–C_{20}	0.937	2.52	145	–13	278.9	31.8
3	C_{12}–C_{14}	1.03	1.64	137	–36	121.14	3.58

The physicomechanical characteristics of rolled films (ultimate tensile strength and relative elongation) with the content of the Vikol lubricant equal to 0.8 wt parts per 100 wt parts of PVC are listed in Table 2 (contents of Glitserol and wax are similar).

As follows from Table 2, a distinctive feature of Vikol lubricants is the increase in the ultimate tensile strength and a certain decrease in the relative elongation of PVC films upon introduction of lubricants into the formulations. The shorter the length of hydrocarbon chain of the Vikol lubricant, the more pronounced this effect. The commonly used lubricants, such as Glitserol and wax, act similarly but to a lesser extent. Thus, at the standard temperature, addition of Vikol lubricants resulted in significant increase in the strength in the glassy state; hence, more rigid PVC films were obtained.

At the same time, the glass transition point T_g estimated on a PTB-1 PZh device from the inflection in the temperature dependence of the sample deformation decreases upon addition of the Vikol lubricant. The T_g values of the PVC formulations with the Vikol content of 1.2 and 5 wt parts per 100 wt parts of PVC are listed in Table 3. For comparison, polyethylene wax did not allow film preparation at its amount in PVC equal to 5 wt parts.

Thus, metal-containing lubricants exert a plasticizing effect on PVC; the performance of lubricants as plasticizers depends on their content in a PVC formulation and on the length of hydrocarbon chain of the Vikol lubricant. In the range of small amounts of lubricants (1.2 wt parts per 100 wt parts of PVC), the performance increases in the order Vikol-1 < Vikol-2 < Vikol-3. With the content of Vikol lubricant equal to 5 wt parts per 100 wt parts of PVC, the effect becomes the opposite. The significant increase in the strength with decreasing relative elongation of rigid PVC films in the presence of small amounts of metal-containing lubricants can be caused by ordering [3] or more complete relaxation of the internal stresses arising in fast cooling of the films [4]. In this case, their plasticizing effect is manifested, judging from the glass transition point of PVC in the presence of the Vikol lubricants (Table 3).

The plasticizing effect of the lubricants studied was also estimated by the broad-line NMR (RYa-2301, operating frequency 16.2 MHz, temperature 23°C) [5]. The molecular mobility of PVC in the presence of the Vikol lubricants was estimated from the second-order momentum of the NMR line ΔH_2^2 (content of Vikol lubricant 0.8 wt parts per 100 wt parts of PVC):

Lubricant type	ΔH_2^2, Oe^2	Lubricant type	ΔH_2^2, Oe^2
Without lubricant	14.4	Vikol no. 3	12.9
Vikol no. 1	13.4	Glitserol	14.1
Vikol no. 2	13.2	Wax PV-200	14.2

Table 2. Physicomechanical characteristics of PVC films containing lubricants

Lubricant type	Ultimate tensile strength, MPa	Relative elongation at break, %
Without lubricant	40	37
Vikol no. 1	51.6	32
Vikol no. 2	59.8	29
Vikol no. 3	72.4	26
Glitserol	44.6	34
Wax PV-200	42.5	35

Table 3. Glass transition point of PVC formulations in the presence of lubricants

Lubricant type	T_g, °C, at indicated lubricant amount, wt parts per 100 wt parts of PVC		
	0	1.2	5.0
Vikol no. 1	81	76	71
Vikol no. 2	81	77	70
Vikol no. 3	81	79	67
Wax PV-200	81	80	–

The data obtained show that all the additives increase the molecular mobility of PVC, i.e., they affect the structure and intermolecular interaction in the PVC samples studied. The increase in the molecular mobility (decrease in ΔH_2^2) is the most significant for Vikol-3, which has the shortest hydrocarbon chain (C_{12}–C_{14}) and, hence, a higher intrinsic molecular mobility. Addition of Glitserol and polyethylene wax decreases ΔH_2^2 only slightly, i.e., their plasticizing effect on PVC is insignificant.

CONCLUSION

A study of the influence of metal-containing lubricants Vikol on characteristics of polyvinyl chloride, judged from the glass transition point and broad-line NMR data, show that small amounts of metal-containing lubricants Vikol exert a plasticizing effect on polyvinyl chloride; the higher the intrinsic mobility of the lubricant, the more pronounced the effect. Due to this fact, formation of the polyvinyl chloride structure is facilitated, and a film material with a higher strength is formed.

REFERENCES

1. Minsker, K.S. and Fedoseeva, G.T., *Destruktsiya i stabilizatsiya polivinilkhlorida* (Degradation and Stabilization of Polyvinyl Chloride), Moscow: Khimiya, 1979.
2. Leaversuch, R.D., *Mod. Plast. Int.*, 1993, vol. 23, no. 9, pp. 60–63.
3. Barshtein, R.S., Kirillovich, V.I., and Nosovskii, Yu.E., *Plastifikatory dlya polimerov* (Plasticizers for Polymers), Moscow: Khimiya, 1982.
4. Kozlov, P.V. and Papkov, S.P., *Fiziko-khimicheskie osnovy plastifikatsii polimerov* (Physicochemical Foundations of Plasticization of Polymers), Moscow: Khimiya, 1982.
5. Slonim, I.Ya. and Lyubimov, A.N., *Yadernyi magnitnyi rezonans v polimerakh* (Nuclear Magnetic Resonance in Polymers), Moscow: Khimiya, 1966.

ISSN 1070-4272, Russian Journal of Applied Chemistry, 2006, Vol. 79, No. 2, pp. 339–341. © Pleiades Publishing, Inc., 2006.
Original Russian Text © O. S. Beusheva, N. P. Mus'ko, M. M. Chemeris, 2006, published in Zhurnal Prikladnoi Khimii, 2006, Vol. 79, No. 2, pp. 340–342.

BRIEF COMMUNICATIONS

The Role of Readily Hydrolyzable Polysaccharides of Larch Wood in Manufacture of Board Materials

O. S. Beusheva, N. P. Mus'ko, and M. M. Chemeris

Polzunov State Technical University, Barnaul, Russia

Received December 21, 2005

Abstract—Role of readily hydrolyzable polysaccharides of larch wood in production of board materials is studied.

DOI: 10.1134/S1070427206020376

The problem of development of environmentally friendly and cost-efficient board materials is now pressing as before. The reason is that thermosetting synthetic resins are mostly used in manufacture of board materials as binders, in addition to a wood filler and adhesive component, e.g., phenol-formaldehyde resol resin.

It was demonstrated in [1, 2] that all components required for production of board materials can be obtained through hydrothermal treatment of wood.

An equally important problem is utilization of large-scale waste of larch wood, which known to have limited application in wood-chemical processing.

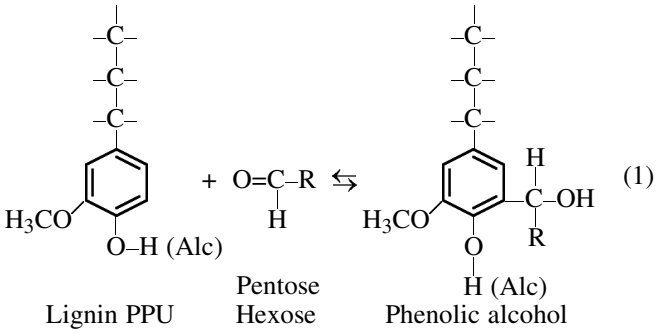
Therefore, we examined in this study the possibility of manufacture of board materials from larch wood exposed to explosive autohydrolysis (EAH).

We examined the effects of temperature and pressure on the behavior of readily hydrolyzable polysaccharides of larch wood in production of board materials by hot pressing.

EXPERIMENTAL

As a raw material for production of boards, we used larch wood chips (25 × 15 × 5 mm) after extraction of bioactive components (arabinogalactan and dihydroquercitrin). Before exposure to explosive autohydrolysis, the chips were treated with water in a 2 : 1 volume ratio [3]. The explosive autohydrolysis was carried out in an autoclave at 220°C for 10 min. Then the resulting lignocarbohydrate material was air-dried, formed into a mat, and hot pressed.

Wood is composed of a complex set of macromolecular compounds, such as cellulose, hemicellulose, and lignin, cross-linked by chemical and hydrogen bonds and also by nonspecific physical interactions. The explosive autohydrolysis strongly modifies the structure of the initial material at the macro- and microlevels. Previously, we have demonstrated [4] that, under hydrothermal conditions, readily hydrolyzable polysaccharides of larch wood are hydrolyzed to give a large amount of reducing agents (RAs). The temperature of 220°C and treatment time of 10 min are the optimal conditions for the hydrolysis, under which the content of readily hydrolyzable polysaccharides in the wood pulp decreases from 22.9 to 3.2%. The content of reducing agents in the resulting aqueous extract is 15.4%. The UV spectra showed that the reaction mixture contains phenolic compounds [5]. Thus, the pulp obtained after explosive autohydrolysis of larch wood contains components that can enter into polycondensation reactions. It may be suggested that, similarly to the reactions of phenols with aldehydes yielding phenol-formaldehyde resins with liberation of water, the *p*-hydroxyphenylpropane units (PPUs) of lignin react with the aldehyde groups of sugars [6, 7]. A simplified scheme of the reaction can be written as



(1)

where R = $C_4H_5(OH)_4$, $C_5H_7(OH)_5$.

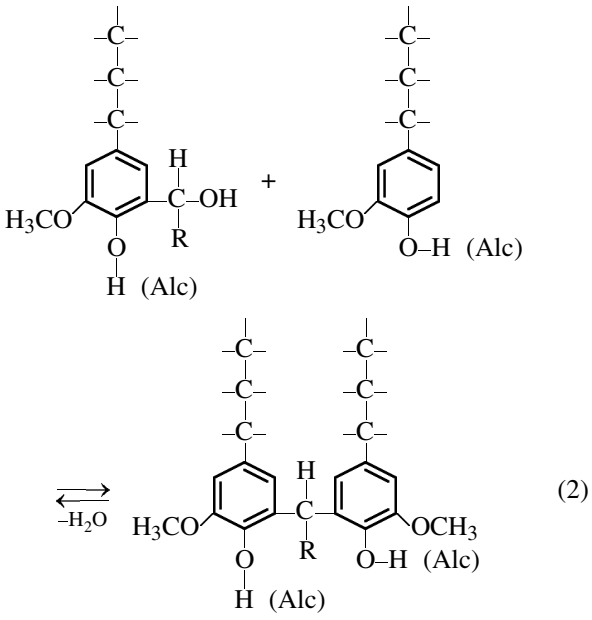
Table 1. Characteristics of board materials from larch wood and of commercial wood chipboards manufactured according to GOST (State Standard) 10632–89.

Parameter	Larch wood chipboards	Commercial chipboards
Density, kg m^{-3}	1200	550–830
Thickness swell, %	10	33–22
Static bending stress, MPa	30	14–16

Table 2. Weight loss in pressing (pressing time 5 min)

Parameter		Weight loss, %
Pressing temperature, °C	100	0.58
(P = 5.2 MPa)	110	0.60
	120	0.63
	130	0.85
	150	1.75
Pressure, MPa	1.2	0.75
(T = 140°C)	2.6	1.25
	5.2	1.58
	6.5	1.75

The resulting phenolic alcohol can enter into the reaction of polycondensation to give thermoplastic resins:



(2)

where R = $C_4H_5(OH)_4$, $C_5H_7(OH)_5$.

If the reaction between the reducing agents and lignin degradation products occurs, this will promote "self-adhesion" of wood particles in the course of hot pressing of wood pulp to give board materials.

The possibility of performing such a process was demonstrated in the preliminary experiments. Table 1 shows selected characteristics of the chipboards thus obtained from larch wood chips in comparison with those of the commercial wood chipboards currently produced in Russia.

As can be seen, the board material from larch wood surpasses the commercial wood chipboards in the basic characteristics. High strength and hydrophobic characteristics, as well as the lack of phenol-formaldehyde resins, make this composite material quite attractive for structural and building applications.

Thus, chemical transformations occurring in the basic components of larch wood in the course of explosive autohydrolysis open prospects for production of board materials without addition of binders.

Upon heating, phenolic alcohols enter into polycondensation to give cross-linked structures serving as a binder in the composite [Scheme (2)].

The formation of insoluble high-molecular-weight compounds (binders) by the reaction between the reducing agents and lignin fragments is confirmed by data on the weight loss in pressing. The weight loss depends on the pressing temperature and pressure (Table 2). The weight loss in the course of pressing can be attributed to the formation of volatile products, among them water.

As the pressing temperature is raised from 100 to 150°C, the weight loss increases from 0.58 to 1.75%.

In hot pressing of the pulp obtained by explosive autohydrolysis, the reducing agents and lignin fragments react to give thermosetting resins serving as binders in the composite. Therefore, the amount of the reducing agents should decrease. The resulting board material was analyzed for the residual reducing agents. The material was powdered and then treated with water to extract water-soluble compounds. The aqueous extract was analyzed for reducing agents. The amount of reducing agents in the wood pulp decreased after pressing as compared to that in the pulp after explosive autohydrolysis (15.4%). As the pressing temperature was raised from 120 to 160°C, the amount of reducing agents decreases from 9.0 to 4.3%

Table 3. Influence of pressing temperature on formation of reducing agents (pressure 5.2 MPa; pressing time 5 min)

Pressing temperature, °C	RA content in board material, %	RAs involved in formation of binders, %
120	9.0	6.4
130	8.7	6.7
140	7.4	8.0
150	5.5	9.9
160	4.3	11.1

Table 4. Influence of pressure on formation of reducing agents (temperature 140°C; pressing time 5 min)

Pressure, MPa	RA content in board material, %	RAs involved in formation of binders, %
1.2	11.8	3.6
2.6	11.2	4.2
3.9	8.9	6.5
5.2	7.4	8.0
6.5	6.8	8.6

(Table 3), suggesting that, in the course of pressing, the polycondensation takes place, and the amount of binders increases with temperature.

The manufacture of board materials involves impact of not only elevated temperature, but also high pressure on the initial mass. Data on the latter effect are listed in Table 4.

An increase in pressure also leads to a decrease in the content of reducing agents in board materials, suggesting their involvement in the formation of binders.

CONCLUSIONS

(1) The possibility of production of board materials from larch wood without addition of binders is demonstrated. These materials surpass commercial chipboards in strength and hydrophobic characteristics.

(2) Pressing of board materials obtained by explosive autohydrolysis of larch wood is accompanied by weight loss and decrease in the content of reducing agents.

REFERENCES

1. Skurydin, Yu.G., Structure and Properties of Composite Materials Obtained from Waste Wood after Explosive Autohydrolysis, *Cand. Sci. Dissertation*, Barnaul, 2000.
2. Kluge, Z.E., Tsekulina, L.V., and Savel'eva, T.G., in *Tekhnologiya modifikatsii drevesiny* (Wood Modification Processes), Riga: Zinatne, 1978, pp. 55–63.
3. Beusheva, O.S., Mus'ko, N.P., and Chemeris, M.M., *Polzunov. Al'manakh. Goriz. Obraz.*, 2003, pp. 17–19.
4. Beusheva, O.S., Mus'ko, N.P., and Chemeris, M.M., *Polzunov. Vestn. Obshch. Prikl. Khim. Ekol.*, 2004, no. 4, pp. 37–39.
5. Beusheva, O.S., Mus'ko, N.P., and Chemeris, M.M., in *Materialy konferentsii "Khimiko-lesnoi kompleks–problemy i resheniya"* (Proc. Conf. "Wood-Chemical Facilities: Problems and Solutions"), Krasnoyarsk, 2003, pp. 27–30.
6. Rubinova, F.Ya. and Nikitin, V.M., *Khim. Drev.*, 1972, no. 11, pp. 97–102.
7. Zakis, G.F., Erin'sh, P.P., Neiberte, B.Ya., and Khokholko, S.V., *Khim. Drev.*, 1990, no. 4, pp. 70–75.

ISSN 1070-4272, Russian Journal of Applied Chemistry, 2006, Vol. 79, No. 2, pp. 342–343. © Pleiades Publishing, Inc., 2006.
Original Russian Text © S. V. Volkov, L. F. Kozin, A. G. Morachevskii, N. F. Zakharchenko, and E. G. Polyakov, 2006, published in Zhurnal Prikladnoi Khimii, 2006, Vol. 79, No. 2, pp. 343–344.

OBITUARY

Oleg Grigor'evich Zarubitskii (1936–2005)

DOI: 10.1134/S1070427206020388

On December 29, 2005, in Kiev, died of severe illness, at the age of 69, Oleg Grigor'evich Zarubitskii. He was a prominent electrochemist, chairman of the Scientific Council of the National Academy of Sciences of the Ukraine for Electrochemistry, Honored scientist and technologist of the Ukraine, doctor of technical science, professor, corresponding member of the National Academy of Sciences of the Ukraine, and head of the Department of electrochemical refining of metals and metalloids (Vernadskii Institute of General and Inorganic Chemistry, National Academy of Sciences of the Ukraine). During many years, until very recently, O.G. Zarubitskii had been an active author of *Zhurnal Prikladnoi Khimii* (Russian Journal of Applied Chemistry, Russian Academy of Sciences).

Zarubitskii was born on July 26, 1931, at a town of Borzna, Chernigov oblast, Ukraine. In 1950, he graduated from the Faculty of chemical engineering of Kiev Polytechnic Institute and, in the same year, commenced his scientific activities at the Institute of General and Inorganic Chemistry, Academy of Sciences of the Ukrainian SSR, where he made a career from an engineer to deputy director for science (1993–2001) and head of a department at the Institute. Zarubitskii was one of the most prominent representatives of the scientific school in electrochemistry of molten salt system, created in the Ukraine by V.A. Plotnikov (1873–1947), V.A. Izbekov (1881–1963), and Yu.K. Delimarskii (1904–1990).

An originally thinking talented scientist, Zarubitskii made a notable contribution to the development of quite a number of areas of high-temperature electrochemistry, his studies had always been closely related the demand of the technological practice. During his entire scientific activities, Zarubitskii paid a considerable attention to study of processes used to produce and refine heavy nonferrous and rare metals in molten electrolytes. Zarubitskii and co-workers were the first in the world to implement on the industrial scale methods for manufacture of bismuth, lead, and indium by electrolysis of molten salts. Zarubitskii was directly involved in the development of worldwide unprecedented apparatus for high-temperature chemical-metallurgical processes: high output capacity diaphragm



electrolyzers and electrolytic baths with bipolar electrodes and thin-layer electrolytes. Zarubitskii and coworkers made a remarkable contribution to investigation of the corrosion resistance of refractories, metals, and alloys used as construction materials in industrial installations that use molten electrolytes. Zarubitskii suggested advanced techniques for chemical, electrochemical, and chemical-thermal treatment of the surface of ferrous and nonferrous metals in ionic melts, performed original studies in the field of electrolytic metallurgy, and developed a technology for electrochemical deactivation of the surface of metals and alloys to remove radioactive contaminations.

Quite a number of Zarubitskii's recent studies were aimed to solve most important energy-related and ecological problems. He suggested an efficient method for production of hydrogen by electrolysis of hydrated melts and developed an economical technique for production of pure amorphous powdered silicon to be used in manufacture of solar cells.

Zarubitskii's scientific legacy is vast. Of particular scientific and practical importance are the monographs *Elektroliticheskoe rafinirovanie tyazhelykh metallov v ionnykh rasplavakh* (Electrolytic Refining of Heavy Metals in Ionic Melts) (together with Delimarskii,

Moscow, 1975) and *Ochistka metallov v rasplavakh shchelochei* (Purification of Metals in Alkali Melts) (Moscow, 1981). Zarubitskii was the author of more than 650 scientific works, including 5 monographs and 230 inventor's certificates and patents. His studies were recognized all over the world and reported at international scientific conferences in numerous countries.

Zarubitskii was distinguished by purposefulness, high working capacity, and position of principle in defending his scientific ideas and views. The Institute of General and Inorganic Chemistry, National Academy of Sciences of the Ukraine, and electrochemists of the Ukraine suffered a severe loss. Oleg Grigor'evich Zarubitskii died in the prime of his creativeness. His colleagues will preserve the memory of this very good person and scientists his ideas and designs will be further developed by his pupils and followers.

S. V. Volkov, L. F. Kozin, A. G. Morachevskii, N. F. Zakharchenko, and E. G. Polyakov

ISSN 1070-4272, Russian Journal of Applied Chemistry, 2006, Vol. 79, No. 2, p. 344. © Pleiades Publishing, Inc., 2006.
Original Russian Text © A. G. Morachevskii, 2006, published in Zhurnal Prikladnoi Khimii, 2006, Vol. 79, No. 2, p. 345.

BOOK REVIEWS

Chekryshkin, Yu.S., Rozdyalovskaya, T.A., and Fedorov, A.A., *Gomogenno-kataliticheskoe glubokoe okislenie galogensoderzhashchikh organicheskikh veshchestv na rasplavakh elektrolitov* (Deep Homogeneous-Catalytic Oxidation of Halogen-containing Organic Substances in Electrolyte Melts),

Yekaterinburg: Ural'sk. Otd. Ross. Akad. Nauk, 2005, 124 pp.

DOI: 10.1134/S107042720602039X

In the brief preface (p. 3), the editor of the book, V.V. Lunin, Academician of the Russian Academy of Sciences, noted that it is the most appropriate, from both the economical and ecological standpoints, to use methods of catalytic hydration and catalytic oxidation in solving the problem of detoxication of halogen-containing waste. In this case, molten formulations containing salts of alkali metals and oxides of some other metals with variable degree of oxidation have important advantages over solid catalysts. Physicochemical characteristics of such melts allow their use in catalytic burning of organic wastes of varied composition and aggregative state. The monograph by Chekryshkin and co-authors presents the results of many years' investigations in the field of application of molten catalysts, which were mostly performed at the Institute of Technical Chemistry, Ural Division, Russian Academy of Sciences, (Perm) and at Perm State Technical University.

The book comprises an introduction, four chapters, conclusion, and bibliographic list. The introduction (pp. 4–7) notes that the development of ecologically safe methods for deactivation of halogen-containing wastes is necessitated by their high toxicity and possibility of their transformation into highly stable dioxins. The first chapter (pp. 8–27) contains general evidence about methods for utilization, detoxication, and elimination of halogen-containing organic substances. The authors rightfully note that the wide diversity of wastes in composition, amount, and territorial distribution makes impossible any versatile technology of their detoxication. Each of the techniques considered in this chapter has its own disadvantages and limitations. In the authors' opinion, the method of deep catalytic oxidation with the use of metal and salt oxides is to be considered an ecologically, economically, and technologically acceptable detoxication technique in the case of comparatively small amounts of highly toxic wastes of complex composition.

The second chapter (pp. 28–79) considers specific features of the use of molten oxides and salts as catalysts for oxidation processes. Particular attention is given to molten formulations containing vanadium(V) oxide and to deep oxidation of halogen-containing organic substances with catalysts of this kind. The reaction of oxidative destruction of halohydrocarbons is initiated by oxygen activated directly by V_2O_5 or by bronzes formed in interaction between V_2O_5 with the starting components of the catalysts (chlorides and carbonates of alkali metals).

The third chapter (pp. 80–104) presents the results of a study of reactions in systems constituted by sodium chloride, oxides of metals with a variable degree of oxidation (V, Cr, Mn, Co, Cu, Mo, Sb), and oxygen. In the presence of oxygen in the reaction medium, metal oxides act as catalysts for oxidation of chlorine atomd by oxygen. A small fourth chapter (pp. 105–108) considers particular examples of catalytic oxidation of a number of complex composites (rubbers, polymers, pesticides, etc.) with the use of molten catalysts. The main results obtained in studying the use of molten catalysts for deep oxidation of organic substances of various compositions and densities are summarized in the conclusion (pp. 109–111). The bibliographic list contains 263 references to works of domestic and foreign authors, mostly published in the last 10 years.

The monograph by Yu.S. Chekryshkin, T.A. Rozdyalovskaya, and A.A. Fedorov reflects the contribution made by the authors and by the scientific schools they represent to the solution of the important economical and ecological problem, utilization of technological and other wastes of complex organic substances. The book is distinguished by originality of formulation of the problem to be solved. It is of interest for researchers and engineers concerned with problems of ecologically and technologically safe elimination of organic substances of widely diverse origin.

A. G. Morachevskii

ISSN 1070-4272. Russian Journal of Applied Chemistry, 2006, Vol. 79, No. 3, pp. 345–350. © Pleiades Publishing, Inc., 2006.
Original Russian Text © A.G. Belous, O.Z. Yanchevskii, A.V. Kramarenko, 2006, published in Zhurnal Prikladnoi Khimii, 2006, Vol. 79, No. 3, pp. 353–357.

INORGANIC SYNTHESIS AND INDUSTRIAL INORGANIC CHEMISTRY

Synthesis of Nanosize Particles of Cobalt and Nickel Oxides from Solutions

A. G. Belous, O. Z. Yanchevskii, and A. V. Kramarenko

Institute of General and Inorganic Chemistry, National Academy of Sciences of Ukraine, Kiev, Ukraine

Received July 4, 2005; in final form, January 2006

Abstract—Rounded nanosize particles of Co_3O_4 and NiO were prepared by precipitation with ammonium carbonate from cobalt and nickel nitrate solutions. Cobalt and nickel oxides and their precursors were characterized by thermal and X-ray phase analyses, electron microscopy, and IR spectroscopy.

DOI: 10.1134/S1070427206030013

Nickel and cobalt oxides and materials based on these compounds possess valuable dielectric, semiconducting, magnetic, and catalytic properties. They are used as electrode materials [1, 2], heterogeneous catalysts [3, 4], and materials for active units of gas sensors [5, 6]. Films of cobalt and nickel oxides can find application in electrochromic devices [7–9]. High-performance ultrahigh-frequency insulators are being developed on the basis of complex oxides of cobalt and nickel [10].

The properties of bulk and film materials largely depend on the morphology and size of particles. Extensive studies of nanosize materials in the last decade have shown that diminishing the particle size to the nanolevel leads to a dramatic increase in the activity of powders, which makes it possible to obtain high-quality materials on their basis.

Nanosize cobalt and nickel oxides are commonly produced by spraying pyrolysis [11–13], organometallic copolymerization [14], sol–gel process [15–17], hydrothermal synthesis [18], solid-state reactions [19], precipitation in microemulsions [20–22], and precipitation with urea [23, 24], carbonates of alkali metals [25, 26], and ammonia [27]. However, most of these methods require special equipment or expensive chemicals. Therefore, development of a comparatively simple method for synthesis of nanosize cobalt and nickel oxides, in which the powders obtained would not be contaminated with reaction products, is a topical task.

The aim of this study was to develop a simple and environmentally safe method for synthesis of nanosize cobalt and nickel oxides and to examine their properties.

EXPERIMENTAL

The synthesis was performed by precipitation from solutions. Chemically pure grade cobalt and nickel nitrates served as starting reagents, and ammonium carbonate of the same grade, as a precipitating agent. Cobalt and nickel carbonates were precipitated both at fixed pH values in the range from 6.2 to 7.8 and with gradual addition of the precipitant to a prescribed pH. At pH values exceeding 8, the precipitates started to appreciably dissolve because of the formation of soluble complexes $[Co(NH_3)_6]^{2+}$ and $[Ni(NH_3)_6]^{2+}$.

The precipitates obtained were transferred onto a porous glass filter and the filtration coefficient K_f (cm s^{-1}) was determined by the Darcy formula [28]

$$K_f = \frac{QL}{SH\tau},$$

where Q is the volume (cm^3) of a filtrate that passed through a precipitate layer of thickness L (cm) and surface area S (cm^2) at a rarefaction H (cm of water column) in a time τ (s).

To improve the reliability of data, the filtration coefficient was calculated for each batch of the precipitate as arithmetic mean of the results of three measurements. The carbonate precipitate was washed to remove NH_4^+ and NO_3^- ions with double-distilled water; the precipitate was twice resuspended, with intermediate washing with the same amount of water. After the second resuspending, cobalt and nickel carbonates were subjected to final washing with distilled water taken in an amount of 20 ml per gram of the precipi-

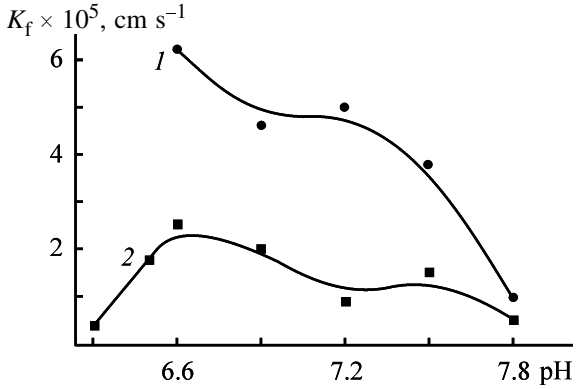


Fig. 1. Filtration coefficients K_f of products formed in precipitation of (*1*) nickel(II) and (*2*) cobalt(II) vs. the pH of precipitation.

tate. For further studies, samples of the precipitates were dried at 70–80°C in air.

Thermal analysis of the precipitation products was made on a Q-1000 OD-102 installation at a heating rate of 5 deg min^{-1}, with aluminum oxide as reference. IR spectra of samples pelletized with KBr were recorded on a Specord M30-1 spectrometer in the range 200–4000 cm^{-1}. X-ray phase analysis was performed with a DRON-3M X-ray diffractometer (CoK_α radiation, λ = 0.178897 nm). The phase composition was identified using the JCPDS (International Committee for Powder Diffraction Standards) database. The morphology of the powders was studied with a JEOL JCXA Superprobe 733 electron microscope (Japan).

The dependences of the filtration coefficients of nickel (light green) and cobalt (lilac-pink) carbonates on the precipitation pH are shown in Fig. 1. The filterability of cobalt precipitation products [K_f = (0.5–2.5) $\times 10^{-5}$ cm s^{-1}] was found to be several times smaller than that of nickel compounds [K_f = (1–6) $\times$ 10^{-5} cm s^{-1}], which may point to their higher dispersity and larger water content. Because both a decrease and an increase in the precipitation pH caused a significant solubility of the precipitate, the optimal precipitation conditions of nickel and cobalt carbonates were pH 7.2 and 7.5, respectively.

Figures 2a and 2b show the IR spectra of the products formed in precipitation of cobalt(II) and nickel(II), respectively, and subjected to thermal treatment at various temperatures. After thermal treatment at 80°C, both the products contain water. This is indicated by strong broad absorption bands with maxima at 3420 and 3410 cm^{-1} [ν(OH)] and by the band at 1630 cm^{-1} [δ(OH)]. The absorption spectrum of cobalt compounds shows a shoulder at 3490 cm^{-1} whose position and shape are characteristic of OH^- groups [29]. According to Bellamy's data [30], hydroxo carbonates have a more complex IR spectrum as compared to carbonates: the absorption band at 1430 cm^{-1}, which is associated with ν(CO) vibrations, is split in two. The number of bands in the range 700–1100 cm^{-1} also increases, which is confirmed by the spectra of the cobalt precipitation product; this feature is manifested by precipitated nickel carbonate to a lesser extent. The broad absorption bands at 370 and 350–425 cm^{-1} for cobalt and nickel products, respectively, are associated with stretching vibrations of the metal–oxygen bond. As the temperature of thermal treatment of cobalt carbonate is raised to 250°C, the bands related to CO_3^{2-} and OH^- groups disappear from the IR spectra, and the band with a maximum at 3420 cm^{-1}, which is associated with ν(OH) vibrations of crystallization water, is shifted to smaller wavenumbers and its intensity markedly decreases. The adsorption doublet at 565 and 660 cm^{-1} indicates that there exist Co^{3+} ions in an octahedral environment, which, combined with the band at 385 cm^{-1} associated with Co^{2+} ions in a tetrahedral environment, corresponds to formation of the spinel Co_3O_4 [31]. At a higher temperature (640°C), cobalt oxide contains no traces of water, and the shift of the absorption bands associated with stretching vibrations of the Co–O bond to 390, 570, and 670 cm^{-1} may indicate that aggregates grow and the number of point defects increases on the surface of a nanocrystal [32].

Nickel carbonate has a higher thermal stability than cobalt carbonate and contains a smaller amount of OH^- groups, and trace amounts of CO_3^{2-} groups (absorption band at 1465 cm^{-1}) are preserved after thermal treatment at 320°C. Another specific feature of the nickel precursor thermally treated at 320°C is that a sharp absorption band appears at 1385 cm^{-1} and the peak of the absorption band of ν(OH) vibrations of crystallization water is shifted to larger, rather than smaller, wavenumbers, to 3460 cm^{-1}. The absorption band of stretching vibrations of the Ni–O bond at 430 cm^{-1} indicates that the individual oxide NiO (bunsenite) exists at 320°C. After thermal treatment at 640°C, only a broad band at 430 cm^{-1}, with shoulders at 485, 512, and 560 cm^{-1}, is observed in the IR spectra of precipitated nickel carbonate, which points to cationic ordering of bunsenite [22]. The narrowing of the band associated with stretching vibrations of the metal–oxygen bond at 640°C indicates that the average size of NiO nanocrystals increases.

The results obtained in thermal analysis of precipitated nickel and cobalt carbonates are presented in Figs. 3a and 3b. Nickel carbonate typically shows two

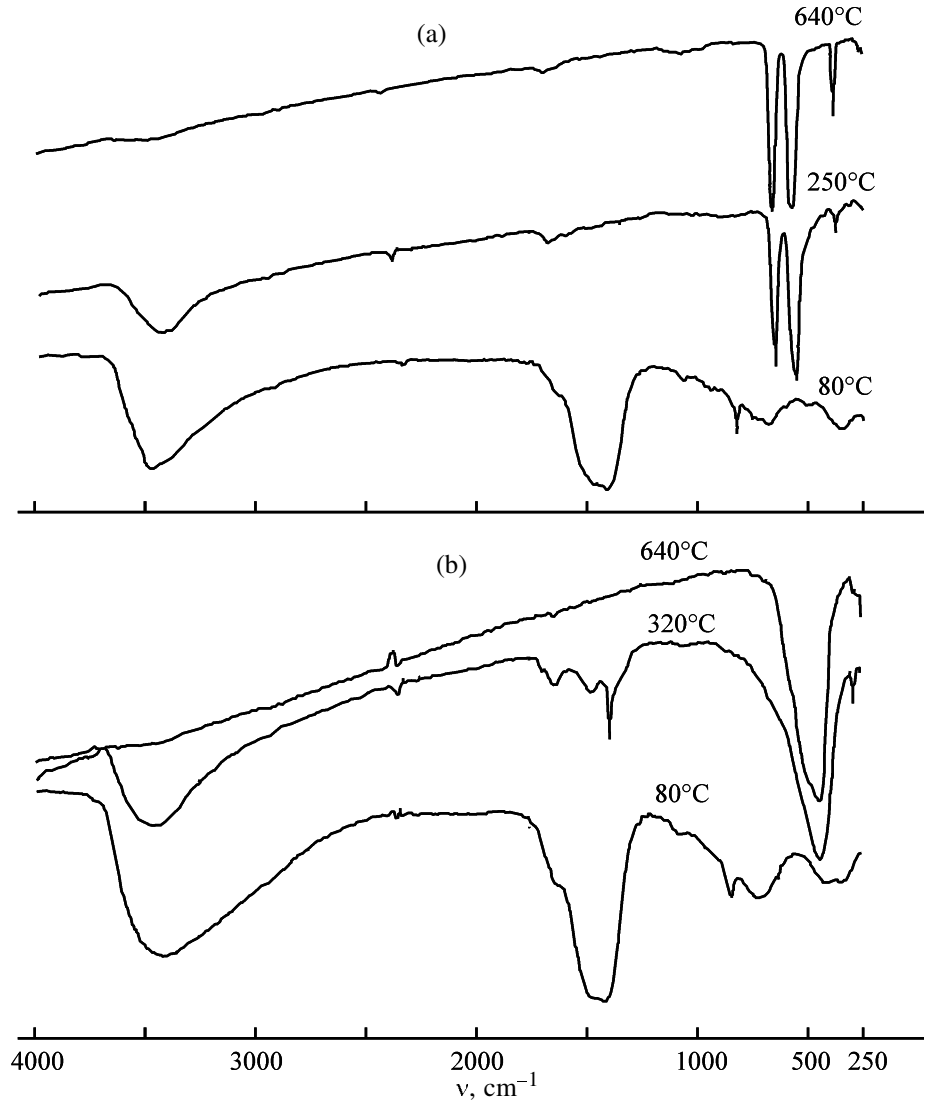


Fig. 2. IR spectra of products formed in precipitation of (a) nickel(II) and (b) cobalt(II) and subjected to thermal treatment at various temperatures for 2 h. pH: (a) 7.5 and (b) 7.2.

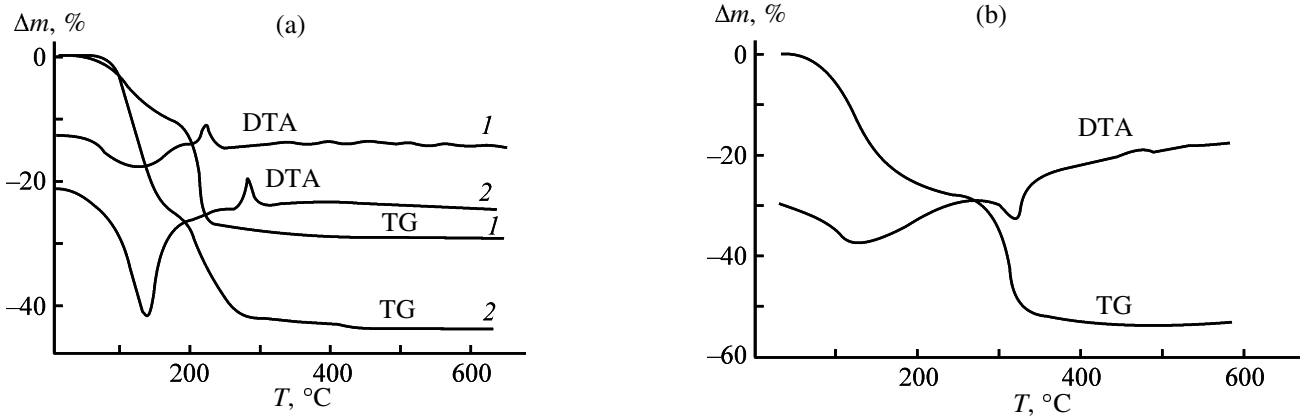


Fig. 3. Thermograms (a) of cobalt carbonate precipitated at (*1*) fixed pH 7.5 and (2) pH increasing to 7.5 in the course of precipitation and (b) of nickel carbonate precipitated at a fixed pH 7.2. (Δm) Weight loss and (T) temperature.

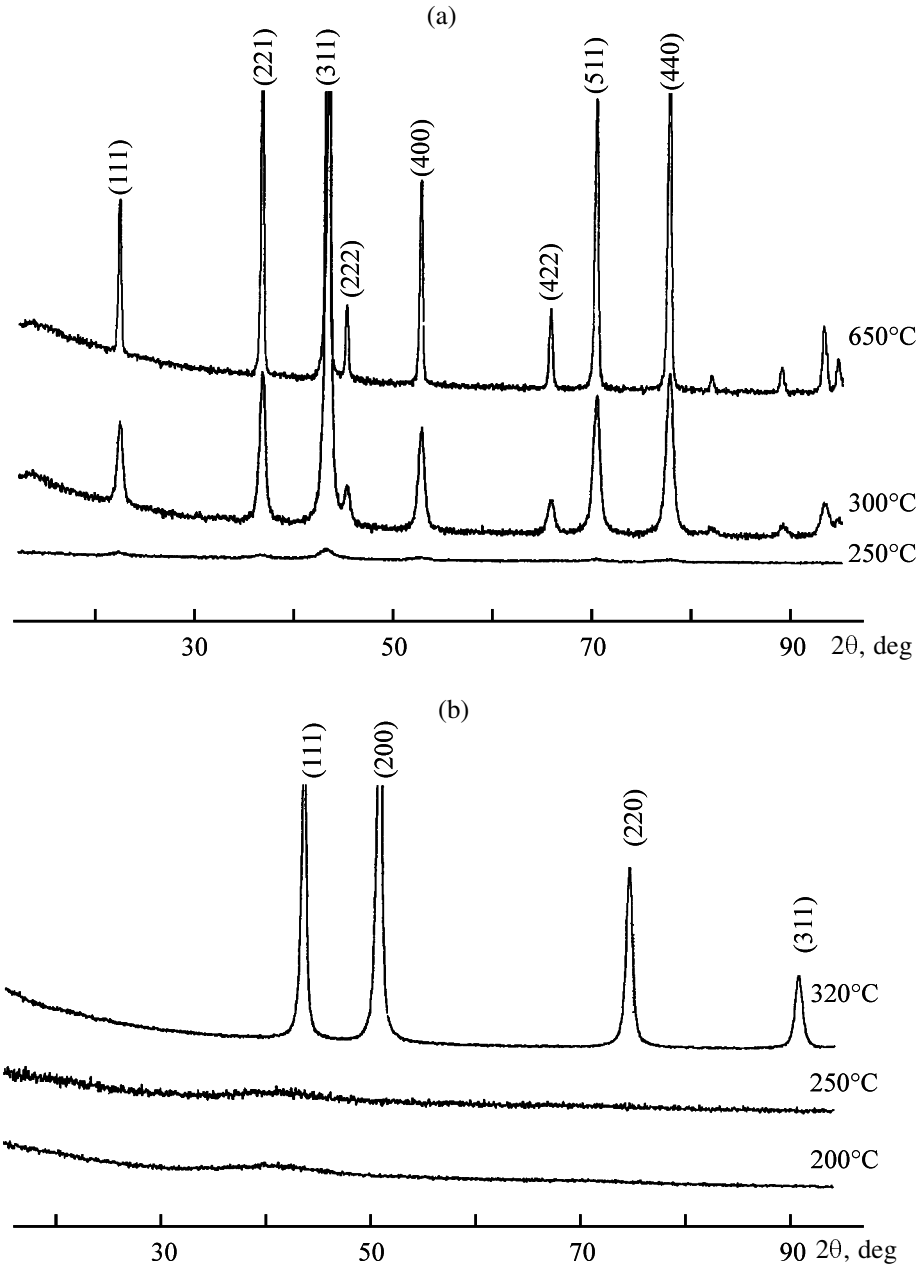


Fig. 4. X-ray diffraction patterns of products formed in precipitation of (a) cobalt(II) and (b) nickel(II) and subjected to thermal treatment at various temperatures for 2 h. (2θ) Bragg angle.

endothermic effects accompanied by weight of loss, with maxima at 120 (removal of absorbed and chemically bound water) and 320°C (removal of carbonate groups). This is in agreement with the data of [21, 23]. According to calculations based on the weight loss, the formula of precipitated nickel carbonate is close to $NiCO_3 \cdot 0.28Ni(OH)_2 \cdot 2.6H_2O$.

Cobalt carbonates precipitated from solution at fixed and varied pH values exhibit a strong difference in behavior under thermal treatment. In the former case, the endo- and exothermic effects have maxima at 120 and 225°C, respectively, whereas in the latter case, these peaks lie at 135 and 290°C, respectively. The shift of the peaks of the thermal effects to lower temperatures in the case of precipitation at a fixed pH value can be attributed to a higher dispersity of particles of the precipitate and to an increase in the content of the basic forms of hydroxo carbonates to give the active blue form of $Co(OH)_2$. At the same time, precipitation at a varying pH value leads to formation of the inactive pink form of $Co(OH)_2$ [34]. In

contrast to the case of nickel carbonate, the decomposition of cobalt carbonate to give Co_3O_4 is accompanied by an exothermic effect, which can be attributed to oxidation of a part of Co^{2+} ions to Co^{3+}. Judging from the results of thermal analysis, the formulas of cobalt carbonates precipitated at fixed and varying pH values can be represented as $CoCO_3 \cdot 0.83Co(OH)_2 \cdot 1.6H_2O$ and $CoCO_3 \cdot 0.75Co(OH)_2 \cdot 2.6H_2O$, respectively.

As can be seen in Figs. 4a and 4b, basic carbonates of cobalt and nickel are X-ray amorphous up to 250°C inclusive. Nevertheless, the presence of diffraction rings in electron diffraction patterns of the samples indicates that a long-range order in the atomic arrangement exists in these samples. The product formed in thermal treatment of cobalt carbonate crystallizes at 300°C to give a single-phase spinel Co_3O_4. All reflections of the Co_3O_4 phase can be identified in the cubic crystal system with a lattice constant a = 0.8052 nm (*Fd*3*m* space group). This is in agreement with the reference data of the JCPDS database [nos. 42-1467 (a = 0.8083 nm) and 43-1003 (a = 0.8084 nm)]. Further increase in temperature to 650°C does not give rise to other phases, but makes the degree of crystallinity of cobalt oxide higher and the lattice constant larger, a = 0.8072 nm; the latter circumstance may be due to an increase in the degree of structure filling by oxygen.

A transition from X-ray amorphous nickel carbonate to crystalline single-phase NiO is observed at 320°C. Nickel oxide (bunsenite) belongs to the cubic crystal system with a lattice constant a = 0.4193 nm (*Fm*3*m* space group), in agreement with the data of the JCPDS database [no. 47-1049 (a = 0.4177 nm)].

The results of thermal and X-ray phase analyses were used to choose, in order to obtain nanosize particles of cobalt and nickel oxides, the minimum possible decomposition temperatures of carbonates of these metals, equal to 300 and 320°C, respectively. According to electron microscopic data, basic cobalt carbonate is composed of needles combined into agglomerates 200–400 nm in size, and basic nickel carbonate, of 200–300-nm agglomerates. Particles of cobalt and nickel oxides, formed in thermal decomposition of basic carbonates, have a rounded shape and are 5–10 nm in size.

CONCLUSIONS

Nanosize particles of cobalt and nickel oxides were synthesized by precipitation from solution, with cobalt and nickel nitrates serving as starting reagents, and ammonium carbonate, as a precipitant agent. Rounded particles of cobalt and nickel oxides 5–10 nm in size were obtained.

REFERENCES

1. Poizot, P., Laruelle, S., Grugeon, S., et al., *Nature* (London), 2000, vol. 407, p. 496.
2. Nuli, Y., Zhao, S., and Qin, Q., *J. Power Sources*, 2003, vol. 14, pp. 113–120.
3. Ahmad, A.S., El-Shobaky, G.A., Al-Noaimi, A.N., et al., *Mater. Lett.*, 1996, vol. 26, pp. 107–112.
4. Curr, M.L., Agostiano, A., Mavelli, F., et al., *Mater. Sci. Eng. C., Biomim. Mater. Sens. Syst.*, 2002, vol. 22, p. 423.
5. Dirksen, J.A., Duval, K., and Ring, T.A., *Sens. Actuators B, Chem.*, 2001, vol. 80, pp. 106–115.
6. Hotovy, I., Huran, J., Spiess, L., et al., *Vacuum*, 2000, vol. 58, pp. 300–307.
7. Svegl, F., Opel, B., Hutchins, M.G., et al., *J. Electrochem. Soc.*, 1996, vol. 143, p. 1532.
8. *Handbook of Inorganic Electrochemical Materials*, Granqist, C.G., Ed., Amsterdam: Elsevier, 1995, pp. 325–334.
9. Miller, E.L. and Rochellau, R.E., *J. Electrochem. Soc.*, 1997, vol. 144, p. 3072.
10. Takanashi, T., *Jpn. J. Appl. Phys.*, 2000, vol. 39, pp. 5637–5641.
11. Jang, Y.I., Wang, H., and Chiang, Y.M., *J. Mater. Chem.*, 1998, vol. 41, p. 2761.
12. Singh, R.N., Koenig, J.F., Poillerate, G., et al., *J. Electrochem. Soc.*, 1990, vol. 137, no. 5, p. 1408.
13. Baydi, M.E., Poillerat, G., Rehspringer, J.L., et al., *Solid State Chem.*, 1994, vol. 109, p. 281.
14. Ahmed, R. and Kofinas, P., *J. Magn. Mater.*, 2004, vol. 9, p. 9.
15. Lakashmi, B., Patrissi, C.J., and Martin, R., *Chem. Mater.*, 1997, vol. 9, p. 2554.
16. Gao, J., Zhao, Y., Yang, W., et al., *J. Univ. Sci. Technol. Beijing*, 2003, vol. 10, no. 1, pp. 54–57.
17. Spinolo, G., Ardizzone, S., and Trasatti, S., *J. Electroanal. Chem.*, 1997, vol. 423, p. 49.
18. Wang, Zh., Chen, X., Zhang, M., et al., *Solid State Sci.*, 2005, vol. 7, pp. 13–15.
19. Yu, J., Jia, D., and Zhen, M., *J. Inorg. Chem.* (China), 1999, vol. 15, no. 1, p. 95.
20. Liu, Y., Wang, G., Xu, C., et al., *Chem. Commun.*, 2002, pp. 1486–1487.
21. Han, D.Y., Yang, H.Y., Shen, C.B., et al., *Powder Technol.*, 2004, vol. 147, pp. 113–116.
22. Xu, G., Hong, K., Liu, S., et al., *J. Cryst. Growth*, 2003, vol. 255, pp. 308–312.

23. Refat, M.S., Teleb, S.M., and Sadeek, S.A., *Spectrochim. Acta, Part A*, 2004, vol. 60, pp. 2803–2805.
24. Wu, L., Wu, Y., Wei, H., et al., *Mater. Lett*., 2004, vol. 58, pp. 2700–2703.
25. François, R. and Imelik, B., *J. Chim. Phys. Phys.-Chim. Biol*., 1954, vol. 51, no. 9, pp. 451–460.
26. Vasserman, I.M., Fomina, E.A., and Brainina, Kh.Z., *Zh. Prikl. Khim*., 1959, vol. 32, no. 12, pp. 2619–2624.
27. Deng, X.Y. and Chen, Z., *Mater. Lett*., 2004, vol. 58, pp. 276–280.
28. Vasserman, I.M., *Khimicheskoe osazhdenie iz rastvorov* (Chemical Precipitation from Solutions), Leningrad: Khimiya, 1980.
29. Nuguist, R.A. and Kagel, R.O., *Infrared Spectra of Inorganic Compounds*, New York: Academic, 1971.
30. Bellamy, L.J., *The Infra-Red Spectra of Complex Molecules*, New York: Wiley, 1957.
31. Figgs, B.N., *Introduction to Ligand Fields*, New York: Interscience, 1996.
32. Preudohome, J. and Tarte, J., *Spectrochim. Acta, Part A*, 1971, vol. 27, p. 1817.
33. Xiang, L., Deng, X.Y., and Jin, Y., *Scripta Mater*., 2002, vol. 47, pp. 219–224.
34. Maksin, V.I., Valuiskaya, E.A., and Standritchuk, O.Z., *Zh. Prikl. Khim*., 1988, vol. 61, no. 1, pp. 24–28.

ISSN 1070-4272. Russian Journal of Applied Chemistry, 2006, Vol. 79, No. 3, pp. 351–355. © Pleiades Publishing, Inc., 2006.
Original Russian Text © N.N. Khimich, O.V. Semashko, E.N. Khimich, M.G. Voronkov, 2006, published in Zhurnal Prikladnoi Khimii, 2006, Vol. 79, No. 3, pp. 358–362.

INORGANIC SYNTHESIS AND INDUSTRIAL INORGANIC CHEMISTRY

Sol–Gel Synthesis of Dispersed ZrO_2 Nanoparticles

N. N. Khimich, O. V. Semashko, E. N. Khimich, and M. G. Voronkov

Institute of Silicate Chemistry, Russian Academy of Sciences, St. Petersburg, Russia
St. Petersburg State University, St. Petersburg, Russia

Received December 27, 2005

Abstract—The influence exerted by the basicity of organic amines on hydrolytic polycondensation of zirconium tetraisopropoxide was studied in order to obtain nanodispersed ZrO_2 particles of various sizes.

DOI: 10.1134/S1070427206030025

Hydrolysis of tetraalkoxysilianes, leading to formation of SiO_2 nanoparticles with a narrow size distribution, has been studied in sufficient detail [1–5]. The influence exerted by the structure of the starting alkoxysilane and an alcohol used as a solvent, concentrations of the alkoxysilane and water, temperature of the sol–gel process, rate of addition of the alkoxysilane, and acidity of the medium has been examined [1–4]. As a result, suspensions of monodisperse SiO_2 particles have become commercially available and found wide use for synthesis of monolithic optical glasses and nanocomposite materials, in optoelectronics, etc. [6, 7]. Hydrosols of particles of this kind form periodic colloid structures, which are unique model systems for fundamental studies of interparticle interaction forces of varied nature [8, 9].

In contrast to the case of tetraalkoxysilanes, the formation of hydrosols of zirconium dioxide in hydrolytic condensation of its alkoxides has been studied to a considerably lesser extent. Let us consider chemical reactions (1)–(6) occurring in this process [10]:

$$Zr(OR)_4 + nH_2O \underset{\text{Etherification (2)}}{\overset{\text{Hydrolysis (1)}}{\rightleftharpoons}} Zr(OH)_n(OR)_{4-n} + n\text{ROH},$$

$$\equiv Zr\text{–}OR + HO\text{–}Zr\equiv \underset{\text{Alcoholysis (4)}}{\overset{\text{Condensation (3)}}{\rightleftharpoons}} \equiv Zr\text{–}O\text{–}Zr\equiv + \text{ROH},$$

$$\equiv Zr\text{–}OH + HO\text{–}Zr\equiv \underset{\text{Hydrolysis (6)}}{\overset{\text{Condensation (5)}}{\rightleftharpoons}} \equiv Zr\text{–}O\text{–}Zr\equiv + H_2O.$$

Despite the apparent similarity of hydrolysis of Si and Zr alkoxides [reaction (1)] and of polycondensation of the forming compounds [reactions (3) and (5)], the formation of ZrO_2 nanoparticles has its distinctive features. This is due, on the one hand, to the tendency for zirconium atoms to increase their coordination number to eight and, on the other, to the markedly higher basicity of the oxygen atom in the ≡Zr–OH group, compared to that in ≡Si–OH (electronegativities of Zr and Si atoms by Pauling are equal to 1.2 and 1.8, respectively). Therefore, zirconium alkoxides have oligomeric structure in contrast to silicon alkoxides, which are monomeric. Zirconium alkoxides contain, as shown in detail for the example of zirconium tetraisopropoxide (ZTIP), alkoxy and oxo fragments in various combinations, with the relative amounts of these fragments dependent both on the preparation technique and on the storage duration of the samples synthesized [11, 12].

Owing to the increased basicity of the oxygen atom in the ≡Zr–OH group, compared to the ≡Si–OH group, the former is more labile in hydrolysis. As a result, the equilibrium of reactions (1) and (2) for zirconium alkoxides is strongly shifted to the right. The condensation reactions (3) and (5) are accompanied by formation of structures that contain a large number of hydroxy groups, which is quite untypical of silicon compounds. The reactions of alcoholysis (4) and hydrolysis (6) of these condensation products, which are responsible for the size ordering of oxide particles and for their growth, occur in the case of zirconium compounds by more complex mechanisms, compared to silicon compounds.

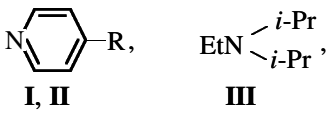
Until now, ZrO_2 hydrosols have been synthesized and the corresponding synthesis mechanisms have been studied in a weakly acidic medium [13–15]. Presumably, the forming suspensions of particles more than 1 μm in size [14] are poorly stable. It may be assumed that the sol–gel method for synthesis of

monodisperse ZrO_2 particles of various sizes by hydrolysis of zirconium tetrabutoxide [15] is seemingly preferable. However, the too complicated experimental procedure and the limited amount of water used for hydrolysis of zirconium tetrabutoxide cast doubt on the completeness of hydrolysis, i.e., on the purity of the oxide synthesized.

The influence exerted by the basicity and nucleophilicity of a number of organic amines on the hydrolysis of tetramethoxysilane (TMOS) and on the polycondensation of the compounds being formed has been studied previously in order to obtain monodisperse SiO_2 particles of prescribed size [5]. The simplicity of this process and of the apparatus involved, as well as the good reproducibility of the results obtained, stimulated studies of the hydrolytic polycondensation of zirconium alkoxides under similar conditions. It was intended to study fundamental aspects of formation of monodisperse ZrO_2 nanoparticles under similar conditions and to develop optimal conditions of their synthesis.

EXPERIMENTAL

The hydrolysis of ZTIP and the polycondensation of the forming compounds were studied under conditions of base catalysis. As catalysts served amines: pyridine (**I**), 4-(dimethylamino)pyridine (**II**), and ethyldiisopropylamine (**III**); as well as tetra-*n*-butylammonium hydroxide (**IV**) $(n\text{-Bu})_4N^+OH^-$:



I, II **III**

where R = H (**I**) and NMe_2 (**II**).

Zirconium tetraisopropxide was synthesized using the previously described method [16, 17] and purified by triple recrystallization from isopropanol. Amines **I** and **III**, preliminarily dried over BaO, were purified by distillation on a 10-TP column; they boiled within 0.2°C range. Amine **II** was recrystallized from ethanol. Hydroxide **IV** (Aldrich) was used without additional purification.

The sol–gel synthesis of ZrO_2 nanoparticles was performed in a glass reactor equipped with a double jacket for introduction of thermostating water, a magnetic stirrer, a dropping funnel, and a reflux condenser. The reactor was charged with ethanol, water, and an amine, and an isopropanol solution of ZTIP was added at 70°C under vigorous stirring in the course of 1 min. The total volume of the solution added was about 20 ml. A total of 12 sol–gel systems were prepared. The molar ratio alkoxide : water : ethanol : amine was $1 : 50 : 200 : X$, with the X values listed below:

Sol–gel system	Amine	X
1a	**I**	1.0
1b	**I**	5.0
1c	**I**	10
1d	**I**	20
1e	**I**	40
2a	**II**	1
2b	**II**	2
2c	**II**	3
2d	**II**	4
3	**III**	1
4	**IV**	1

The particle size in the sol–gel systems obtained was determined with an EM-125 electron microscope at an accelerating voltage of 75 kV. The samples studied were prepared by applying the suspensions obtained onto a carbon-reinforced collodion film substrate.

The choice of compounds **I**–**IV** is due to their different basicities, as characterized by the ionization constants of conjugated acids, pK_a:

$$:NR_3 + H_2O \rightleftarrows HN^+R^- + OH^-. \quad (7)$$

At 20°C, the pK_a values of the compounds used are as follows [18]:

Amine	**I**	**II**	**III**	**IV**
pK_a	5.20	9.70	10.50	15.4

All the experiments performed can be conventionally divided into three groups. To the first of these belong experiments involving hydrolytic polycondensation of ZTIP in the presence of a nucleophilic base of medium strength, 4-(dimethylamino)pyridine (**II**) (sol–gel systems 2a–2e). The second group includes experiments with varied concentration of a weak base, pyridine (**I**) (sol–gel systems 1a–1e). Finally, to the third group belong experiments associated with hydrolysis of ZTIP in the presence of strong organic bases **III** and **IV**.

Figure 1 shows electron micrographs of particles in sol–gel systems 2a, 2c, and 2e. As the concentration of a base in the system increases, the forming ZrO_2 particles become coarser. However, the mechanism of their growth is apparently different from that in formation of SiO_2 particles in hydrolytic polycondensation of TMOS. In the latter case, the coarsening of

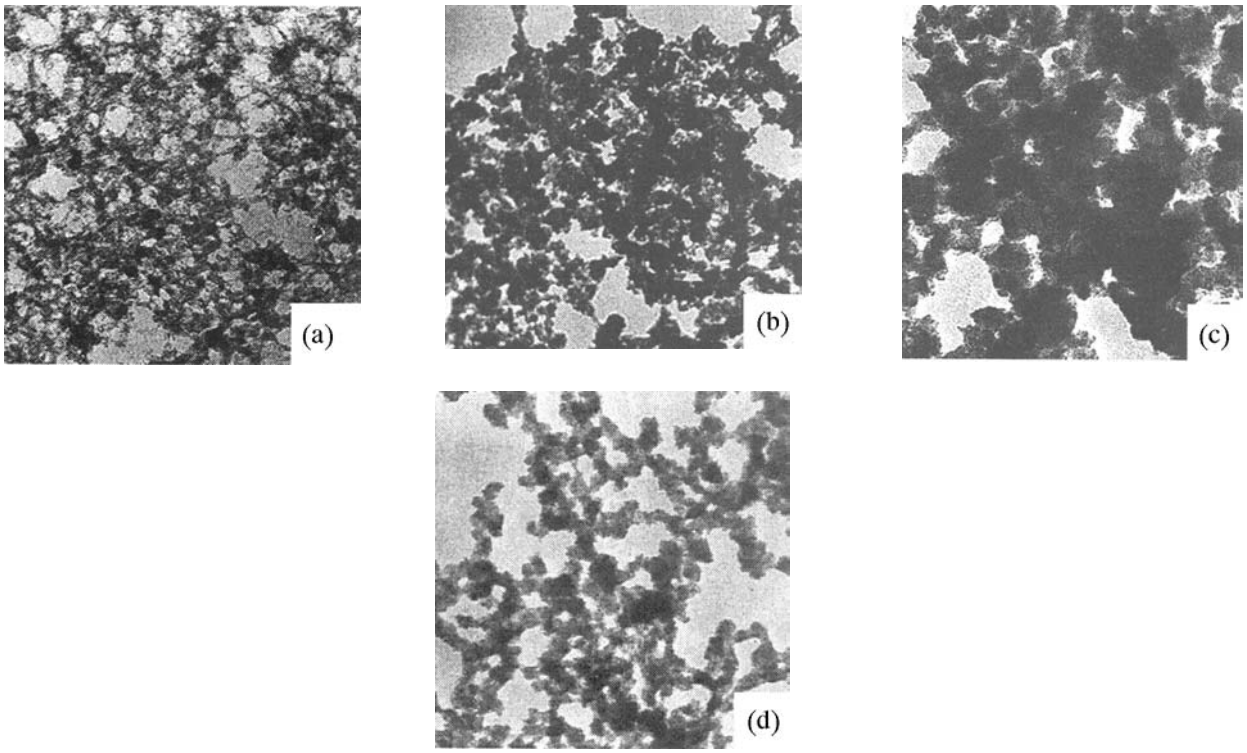
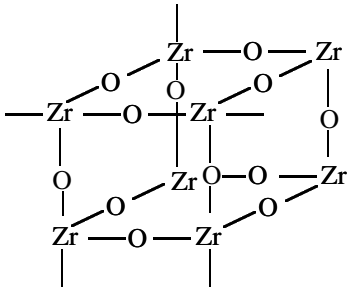


Fig. 1. Electron micrographs of particles in sol–gel systems (a) 2a, (b) 2b, (c) 2c, and (d) 3. Magnification 80000 (125 nm in 1 cm); the same for Figs. 2 and 3.

SiO_2 particles is accompanied by rupture of Si–O–Si bonds at places with an excess surface energy, specifically, at sharp projections and irregularities of the originally formed particles, which results in that they acquire a regular spherical shape [5]. According to Fig. 1, the coarsening of ZrO_2 particles is accompanied by aggregation of particles into a kind of clusters, rather than by growth of each separate particle. This involves sedimentation of the aggregated particles and the subsequent coagulation. As a result, loose nontransparent sediments are formed, with the rate of their formation being proportional to the concentration of the base. On passing from sol–gel system 2a to system 2e, the lifetime of the sol decreases from 10 days to several minutes. The difference between the processes of hydrolytic polycondensation of silicon and zirconium alkoxides can be understood as follows. According to Iler [19], silanols formed in hydrolysis of silicon alkoxides [reaction (1)] enter into condensation reactions (3) and (4). Successive elimination of water or alcohol molecules gives siloxanes of linear, cyclic, or polycyclic structure. After the polymerization is complete, particle of the dispersed phase of SiO_2 are formed and grow in solution. In the process, coarser particles grow by the condensation mechanism via dissolution of fine particles, with virtually only siloxane bonds formed within coarsening particles and silanol groups predominantly situated on the surface of the particles. Such particles with a hydroxylated surface show mutual repulsion and, therefore, cannot aggregate and grow via condensation with molecules of the $Si(OH)_4$ monomer or siloxane oligomers from a true solution [19]. In the case of hydrolytic polycondensation of zirconium alkoxides, the pattern is different. First, formation of linear or cyclic polyzirconoxane bonds $-(Zr-O)_{\overline{n}}$ is not characteristic of zirconium. Second, oxygen compounds of zirconium are never present in hydroxyl-containing solvents in the form of monomeric or low-molecular-weight oligomeric species of the type $[Zr(OH)_4]_n$. Despite that the hydrolysis of the ≡Zr–OR bond is considerably faster than the similar reaction for silicon, the ZrO_2 network



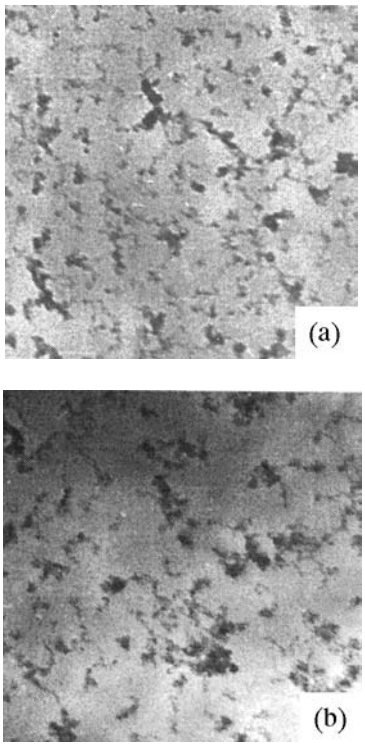


Fig. 2. Electron micrographs of particles in sol–gel systems (a) 1a and (b) 1d.

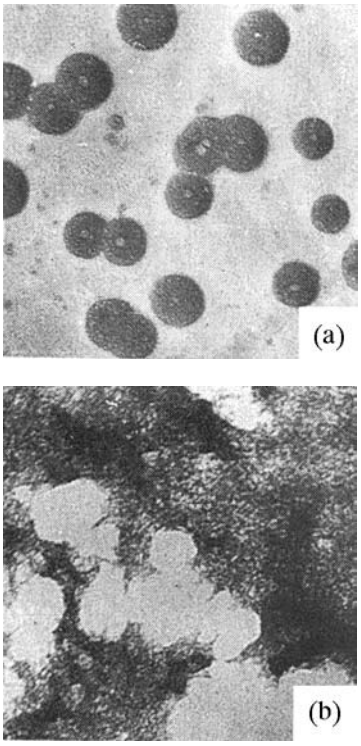


Fig. 3. Electron micrographs of particles in sol–gel system 4 (a) before and (b) after gelation.

does not commonly appear in pure form (in contrast to the case of the siloxane bond). In all cases, polycharged aqua structures, e.g., species of the type $[Zr_4(OH)_8(H_2O)_{16}]^{8+}$ [20], are formed in the course of polymerization. Because of the large number of water molecules in the coordination sphere of a zirconium atom, the content of hydroxy groups on the surface of growing particles is insignificant, which allows their successful aggregation to give jelly-like sediments of hydrated ZrO_2.

The course of the hydrolytic polycondensation of ZTIP is, undoubtedly, strongly affected by the pronounced nucleophilicity of the amine used (amine **II**). In hydrolytic polycondensation of ZTIP in the presence of base **III**, which has low nucleophilicity for steric reasons, but is considerably stronger, the degree of particle aggregation decreases (Fig. 1d).

The degree of aggregation of ZrO_2 particles and their size markedly decrease in the course of a sol–gel process catalyzed by a weak base **I**. The rate of their formation remains equally high, in contrast to the case of hydrolytic polycondensation of tetramethoxysiliane in the presence of pyridine, when many hours' boiling of the reaction mixture is necessary for hardly discernible SiO_2 particles to be formed. The growth of aggregates of ZrO_2 particles is presumably hindered by competition between the nitrogen atoms of pyridine and water molecules for the coordination sphere of a zirconium atom. An increase in the amount of pyridine in the reaction mixture does not make larger the size of the forming aggregates (Fig. 2), but only decreases the time in which a transparent, slightly opalescent gel is formed from tens of days to 1–2 days.

The formation of comparatively spherical ZrO_2 nanoparticles 100–150 nm in diameter (Fig. 3a) was only observed when a very strong base **IV** was used to catalyze the sol–gel process. In contrast to analogous SiO_2 particles, these nanoparticles have a rather loose structure (Fig. 3a) and, in a short time, disintegrate to give a gel-like structure (Fig. 3b).

CONCLUSIONS

(1) The mechanisms of formation and growth of nanodispersed ZrO_2 and SiO_2 particles synthesized by hydrolytic polycondensation of zirconium and silicon alkoxides in the presence of organic bases are different.

(2) The rate of formation of ZrO_2 particles in the sol–gel process of hydrolytic polycondensation of

zirconium tetraisopropoxide is independent of the basicity of the catalysts used.

(3) The coarsening of the ZrO_2 particles being formed occurs via aggregation of finer particles. This makes impossible synthesis of ensembles of monodisperse ZrO_2 particles in a protonic medium in the presence of organic amines.

ACKNOWLEDGMENTS

The study was financially supported by the Russian Foundation for Basic Research (project no. 05-03-32818a).

REFERENCES

1. Stober, W. and Fink, A., *J. Colloid Interface Sci*., 1968, vol. 26, pp. 62–69.
2. Bogush, G.H., Tracy, M.A., and Zukoski, C.F., IV, *J. Non-Cryst. Solids*, 1988, vol. 104, pp. 95–106.
3. So, Jae-Hyun, Yang, Seung-Man, Kim, C., and Hyun, J.C., *Colloids Surf. A: Physicochem. Eng. Aspects*, 2001, vol. 190, pp. 89–98.
4. Sung Kyoo Park, Ki Do Kim, and Hee Taik Kim, *Colloids Surf. A: Physicochem. Eng. Aspects*, 2002, vol. 197, pp. 7–17.
5. Khimich, N.N., Zvyagil'skaya, Yu.V., Zhukov, A.N., and Us'yarov, O.G., *Zh. Prikl. Khim*., 2003, vol. 76, no. 6, pp. 904–908.
6. Petrovskii, G.T., Shashkin, V.S., and Yakhkind, A.K., *Fiz. Khim. Stekla*, 1997, vol. 23, no. 1, pp. 43–53.
7. *Handbook of Sol–Gel Science and Technology*, vol. 3: *Applications of Sol–Gel Technology*, Sumio Sakka, Ed., Boston: Kluwer, 2005.
8. Efremov, I.F., *Periodicheskie kolloidnye struktury* (Periodic Colloid Structures), Leningrad: Khimiya, 1971.
9. Hunter, R.J., *Foundations of Colloid Science*, Oxford: Univ. Press, 2001.
10. *Handbook of Sol–Gel Science and Technology*, vol. 1: *Sol–Gel Processing*, Hiromitsu Kozuku, Ed., Boston: Kluwer, 2005.
11. Vaartstra, B.A., Huffman, J.C., Ggadeff, P.S., et al., *Inorg. Chem*., 1990, vol. 29, pp. 3126–3131.
12. Turevskaya, E.P., Kozlova, N.I., Turova, N.Ya., et al., *Izv. Ross. Akad. Nauk, Ser. Khim*., 1995, no. 4, pp. 752–759.
13. Clearfield, A., *J. Mater. Res*., 1990, vol. 5, no. 1, pp. 161–162.
14. Larbot, A., Fabre, J.-P., Guizard, C., and Cot, L., *J. Am. Ceram. Soc*., 1989, vol. 72, no. 2, pp. 257–261.
15. Ogihara, T., Mizutani, N., and Kato, M., *J. Am. Ceram. Soc*., 1989, vol. 72, no. 3, pp. 421–426.
16. Bradley, D.C. and Wardlaw, W., *J. Chem. Soc*., 1951, pp. 280–285.
17. Bradley, D.C., Mehrotra, R.C., and Wardlaw, W., *J. Chem. Soc*., 1952, pp. 2027–2032.
18. Perrin, D.D., *Dissociation Constants of Organic Bases in Aqueous Solutions*, London: Butterworths, 1965.
19. Iler, R.K., *The Chemistry of Silica: Solubility, Polymerization, Colloid and Surface Properties and Biochemistry of Silica*, New York: Wiley–Interscience, 1979.
20. Stepin, B.D. and Tsvetkov, A.A., *Neorganicheskaya khimiya* (Inorganic Chemistry), Moscow: Vysshaya Shkola, 1994.

ISSN 1070-4272. Russian Journal of Applied Chemistry, 2006, Vol. 79, No. 3, pp. 356–359. © Pleiades Publishing, Inc., 2006.
Original Russian Text © V.N. Pak, E.S. Stromova, B.I. Lobov, A.N. Levkin, 2006, published in Zhurnal Prikladnoi Khimii, 2006, Vol. 79, No. 3, pp. 363–366.

INORGANIC SYNTHESIS AND INDUSTRIAL INORGANIC CHEMISTRY

Specific Features of the Diffusion of Potassium Dichromate Aqueous Solutions in Porous Glass Membranes

V. N. Pak, E. S. Stromova, B. I. Lobov, and A. N. Levkin

Herzen Russian State Pedagogical University, St. Petersburg, Russia

Received October 19, 2005

Abstract—The diffusion coefficients of 0.1 M aqueous solution of potassium dichromate (pH 2–8) in a series of glass membranes with the prevailing pore radii from 4.5 to 70 nm were determined. Characteristic features of variation of the diffusion coefficient were correlated with the calculated content of chromium(VI) anionic species over a wide interval of pH of the solution.

DOI: 10.1134/S1070427206030037

The utility and efficiency of membrane filtration are determined by the relationship between the diffusion coefficients D of the solution components being separated or isolated [1, 2]. In this case, it is often necessary to consider the cases when the form of the dissolved substance depends on pH of the medium. Revealing the possibility and extent of manifestation of such dependences is a specific problem of the chemistry of solutions. Study of the diffusion in membranes can give certain grounds to judge the possibility for structural transformations in transported systems. In this connection, we have considered here the specific features of the diffusion of potassium dichromate aqueous solutions in porous glass membranes. It is universally accepted [3, 4] that in the pH range 2.0–4.5 dichromate anions, $Cr_2O_7^{2-}$, dominate in solutions, whereas in neutral and weakly alkaline media the monomeric chromate species CrO_4^{2-} prevail. A decrease in the acidity in the range 4.5–7.0 could be expected to result in a monotonic increase in the content of chromate ions, which will be accompanied by an increase in the measured diffusion coefficient and in the intensity of the membrane mass transfer as a whole.

First of all, it is necessary to refine the speciation of chromium(VI) in aqueous solutions. This problem remains controversial owing to differences in the pH intervals examined, in the concentrations of solutions under study, and in experimental methods used for detecting the anions. Thus, only monomeric CrO_4^{2-} and $HCrO_4^-$ ions were detected over a wide pH range (1–12) by computer processing of the electronic spectra of dilute potassium dichromate solutions [5]. At the same time, thorough examination of the IR spectra of solutions close in concentrations and pH [6, 7] revealed the presence of dichromate ions $Cr_2O_7^{2-}$ in the amounts reaching 30%, whereas the relationship between the fractions of chromate and dichromate ions was questioned. So far, reliably characterized [8] equilibria (1)–(3) have not been used to judge the influence of pH on the composition of the solutions.

$$H_2CrO_4 \rightleftarrows H^+ + HCrO_4^- \quad (K_1 = 0.16), \qquad (1)$$

$$HCrO_4^- \rightleftarrows H^+ + CrO_4^{2-} \quad (K_2 = 3.2 \times 10^{-7}), \qquad (2)$$

$$2HCrO_4^- \rightleftarrows Cr_2O_7^{2-} + H_2O \quad (K_{dim} = 35.5). \qquad (3)$$

Given the total concentration of the species taking part in equilibria (1) and (2)

$$c = [H_2CrO_4] + [HCrO_4^-] + [CrO_4^{2-}], \qquad (4)$$

their mole fractions can be calculated as

$$\alpha(H_2CrO_4) = \frac{[H^+]^2}{[H^+]^2 + K_1[H^+] + K_1K_2}, \qquad (5)$$

$$\alpha(HCrO_4^-) = \frac{K_1[H^+]}{[H^+]^2 + K_1[H^+] + K_1K_2}, \qquad (6)$$

$$\alpha(CrO_4^{2-}) = \frac{K_1K_2}{[H^+]^2 + K_1[H^+] + K_1K_2}. \qquad (7)$$

With regard to equilibrium (3), the concentration of dichromate ions in the solution is determined as

$$[Cr_2O_7^{2-}] = 0.5[HCrO_4^-]\alpha_{dim}, \quad (8)$$

where α_{dim} is the mole fraction of $HCrO_4^-$ ions that passed into the dimeric form.

Then the equilibrium concentration of $HCrO_4^-$ ions will be $(1 - \alpha_{dim})[HCrO_4^-]$, and the constant of equilibrium (3) will be written in the form

$$K_{dim} = \frac{\alpha_{dim}}{2[HCrO_4^-](1 - \alpha_{dim})^2}. \quad (9)$$

By transforming (9), we obtain quadratic equation (10):

$$\alpha_{dim}^2 - \{2 + 0.5(K_{dim}[HCrO_4^-])^{-1}\}\alpha_{dim} + 1 = 0. \quad (10)$$

As a result, α_{dim} can be found from Eq. (10) by substituting $HCrO_4^-$ concentrations obtained using the mole fraction $\alpha(HCrO_4^-)$ calculated by expression (6) for the pH interval 2–8. The results of our calculation give a quite definite pattern of the behavior of the system (Fig. 1). Thus, the mole fraction of $HCrO_4^-$ appears to be rather low, $\alpha(HCrO_4^-)$ ~0.1, and varies only slightly in the acid region. Chromic acid is formed in noticeable amounts only at a high concentration of protons (pH < 2), whereas the main part of hydrochromate ions, $HCrO_4^-$, passes into the dimeric form of $Cr_2O_7^{2-}$, which appears to dominate over a wide interval of pH 2–6. Approaching the neutral medium is accompanied by abrupt enhancement of the competition between reactions (2) and (3) in favor of the formation of chromate ions CrO_4^{2-}. Therefore, the results given in Fig. 1 refine the known views [3, 4, 8] and make it possible to predict a substantial increase in the fraction of mobile monomeric species in the solution at pH ≥ 6 and an increase in the rate of diffusion transfer in the membranes determined by this fraction.

The procedures for prepaation of membranes from porous glass and for adsorption determination of their structural parameters were published repeatedly [9–13]. The prevailing radii of the pores r_p and the porosity δ of the membranes used in the experiments are given below.

r_p, nm	4.5	19	30	38	45	70
δ, %	26.5	38.9	48.0	42.9	42.6	56.9

When studying the diffusion, we took the membranes as thin (about 1 mm) disks 25 mm in diameter. We fastened them hermetically at the outlets of glass tubes, thus serving as feed cells. These cells were filled with a 0.1 M aqueous solution of $K_2Cr_2O_7$. To

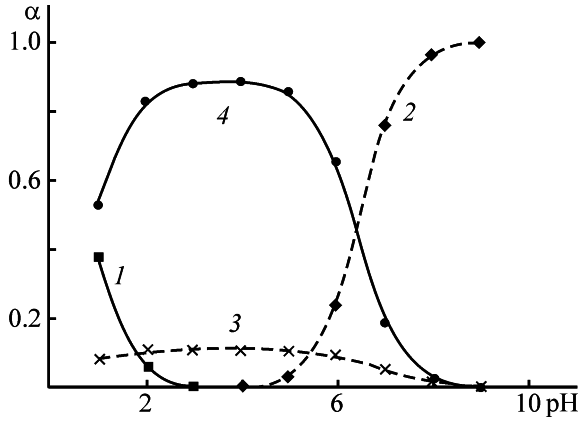


Fig. 1. Plots of equilibrium mole fractions α of (*1*) H_2CrO_4, (*2*) CrO_4^{2-}, and (*3, 4*) $HCrO_4^-$ in (*3*) monomeric and (*4*) dimeric forms vs. pH of the aqueous solution.

fix pH in the range 1–8, we acidified or alkalized the feed solution by adding hydrochloric acid or potassium hydroxide. Potassium dichromate that passed through the membrane was collected in beakers with distilled water, replaced at regular intervals. The concentration of the solutions in the samples did not exceed 10^{-3} M in all the tests, irrespective of pH of the medium and of structural parameters of the membranes in use. The samples were analyzed after bringing pH to 4 to ensure the presence of dichromate ions in them. The content of $Cr_2O_7^{2-}$ was then determined from the optical density at λ = 350 nm with the extinction coefficient ε = 2250 [14]. We carried out the tests under temperature control at 20°C with continuous stirring of the solutions. In all the cases, a steady-state flow through the membranes was attained no later than in 30 min after the beginning of the test. The dependences of the amount of the salt that passed through the membranes on time, *Q*–*t*, were always linear, which allowed us to determine the rates and the diffusion coefficients *D* from the first Fick's law:

$$dQ/d\tau = DS\delta\Delta c/h, \quad (11)$$

where $S\delta$ is the free section of a membrane, which is its geometric area corrected for the porosity; $\Delta c/h$ is the concentration drop at the inlet and outlet of the membrane of thickness *h*.

The resulting dependences of the diffusion coefficient on pH of aqueous 0.1 M solution of $K_2Cr_2O_7$ (Fig. 2) correspond to the steady-state overall transfer of the salt in the glass membranes. The character of *D* variation, the same in all the cases, distinctly reflects the speciation features found above (Fig. 1). In the range of pH 2–6, the diffusion mobility of the electro-

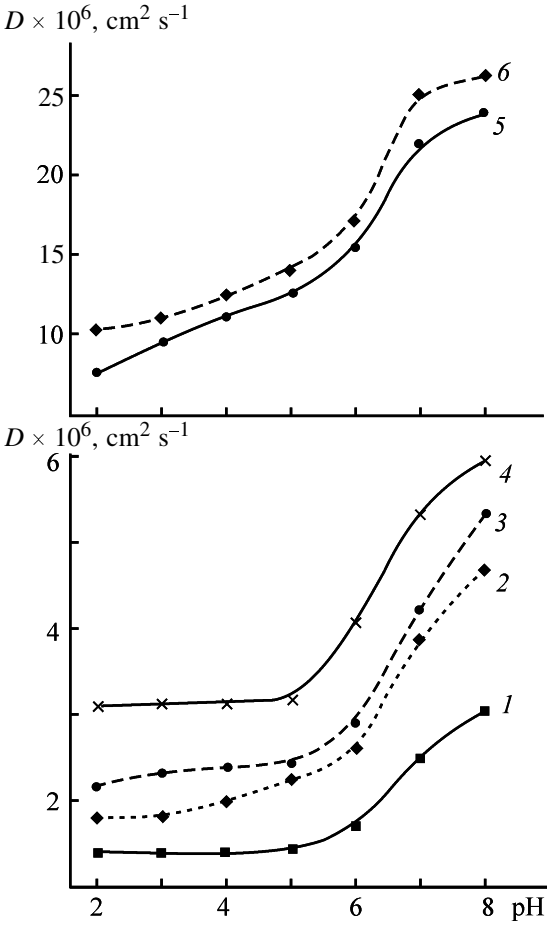


Fig. 2. Effect of pH of 0.1 M aqueous potassium dichromate solution on the diffusion coefficient D in glass membranes. Prevailing radius of membrane pores, nm: (*1*) 4.5, (*2*) 19, (*3*) 30, (*4*) 38, (*5*) 45, and (*6*) 70.

lyte remains almost constant or increases smoothly (in the membranes with pore radii of 45 and 70 nm), which corresponds to the prevalence of the anionic species $Cr_2O_7^{2-}$ in the solution. The further decrease in the acidity of the solution is accompanied by a distinct acceleration of the membrane transport. At pH 6, equilibria (2) and (3) start to rapidly shift toward formation of chromate ions CrO_4^{2-}; their intensive accumulation in the solution results in pronounced acceleration of the diffusion flow through the membranes. We emphasize once more that the diffusion coefficients determined characterize the membrane transfer as a whole. In this case, a substantial (by a factor of 2–3) increase in the diffusion coefficient resulting from pH increase is the consequence not only of higher mobility of CrO_4^{2-} ions compared to $Cr_2O_7^{2-}$ ions, but also of an increase in the number of particles at the membrane inlet, and, hence, in the $\Delta c/h$ gradient in Eq. (11). However, it is hardly possible to estimate the relative contributions of these factors.

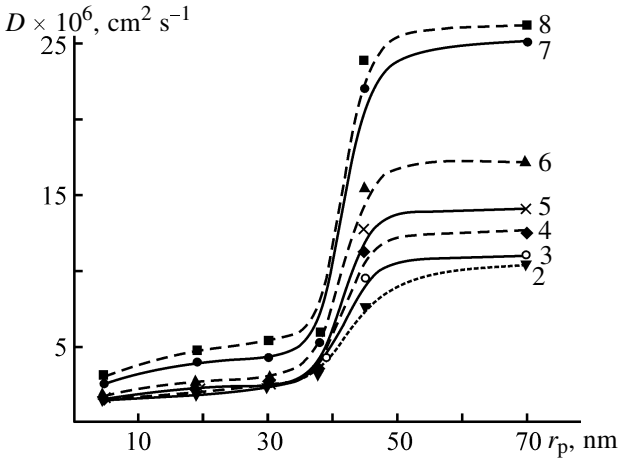


Fig. 3. Plot of diffusion coefficient D of potassium dichromate vs. pore radii r_p of the membranes. The figures at the curves are pH values of the solutions.

When the radius of transport channels of r_p = 45 nm is reached, the rate of diffusion in the glass membranes sharply increases in all the cases. The D–r_p dependences (Fig. 3) suggest that in a narrow interval of the radii of $38 < r_p < 45$ nm the inhibition of diffusion substantially decreases. This feature is most likely determined by the presence in the silica membranes of near-wall boundary layers of solution differing from the bulk of the solution in the structure, concentration, and properties [9–11]. We emphasize that this common factor, despite the difficulties in its detailed description, is distinctly manifested in the temperature dependences of the diffusion transfer of electrolytes [15], in the increased viscosity of boundary layers [1, 16, 17], and in the decreased dielectric permittivity and solvency of the bound water [18, 19]. Consequently, it is believed that low diffusion coefficients of an electrolyte in the pores of radius $r_p \leq$ 38 nm are determined by hindered ion motion in overlapping boundary layers, whereas in the channels of radius r_p = 45 nm a part of the pore solution remote from the silica surface ensures significantly accelerated membrane transfer. As for the uniform shape of the D–r_p curves, it suggests that the effective thickness of the near-wall boundary layer of the solution, in which the diffusion is hindered, remains constant within a wide pH range.

CONCLUSIONS

(1) A decrease in the acidity of an aqueous solution of potassium dichromate to pH ≥ 6 is accom-

panied by a substantial increase in the diffusion coefficient in the porous glass membranes. This feature is in agreement with the calculated pH dependence of the equilibrium composition of the solution.

(2) At any pH of the $K_2Cr_2O_7$ solution, a sharp increase in the diffusion coefficient is observed in the membranes with the pore radii $r_p > 38$ nm. This value can be considered as the effective thickness of the near-wall boundary layer of the solution, in which the diffusion is hindered.

REFERENCES

1. Churaev, N.V., *Fizikokhimiya protsessov massoperenosa v poristykh sredakh* (Physical Chemistry of the Mass Transfer in Porous Media), Moscow: Khimiya, 1990.
2. Nikolaev, N.I., *Diffuziya v membranakh* (Diffusion in Membranes), Moscow: Khimiya, 1980.
3. Cotton, F.A. and Wilkinson, G., *Advanced Inorganic Chemistry*, New York: Interscience, 1966.
4. Slabaugh, W.H. and Parsons, T.D., *General Chemistry*, New York: Wiley, 1976.
5. Sena, M.M., Scarminio, I.S., Collins, K.I., and Collins, C.H., *Talanta*, 2000, vol. 53, no. 2, pp. 453–461.
6. Hoffmann, N.N., Darab, J.C.G., and Fulton, J.L., *J. Phys. Chem*., 2001, vol. 105, no. 10, pp. 1772–1779.
7. Ramsey, J.D., Lin Xia, Kendig, M.W., and McCreery, R.L., *Corrosion Sci*., 2001, vol. 43, no. 8, pp. 1557–1572.
8. Laitinen, G.A., *Khimicheskii analiz* (Chemical Analysis), Moscow: Khimiya, 1996.
9. Voloshina, O.S. and Parsons, T.D., *Obshchaya khimiya* (General Chemistry), Moscow: Mir, 1979, pp. 361–385.
10. Pak, V.N., Nepomnyashchii, A.B., Burkat, T.M., and Mal'kova, S.V., *Zh. Prikl. Khim*., 2002, vol. 75, no. 12, pp. 1959–1962.
11. Pak, V.N., Nepomnyashchii, A.B., and Burkat, T.M., *Zh. Fiz. Khim*., 2003, vol. 77, no. 11, pp. 1979–1982.
12. Mazurin, O.V., Roskova, G.P., Aver'yanov, V.N., and Antropova, T.V., *Dvukhfaznye stekla: struktura, svoistva, primenenie* (Two-Phase Glasses: Structure, Properties, and Application), Leningrad: Nauka, 1991.
13. Burkat, T.M. and Dobychin, D.P., *Fiz. Khim. Stekla*, 1991, vol. 18, no. 5, pp. 129–136.
14. *Spravochnik khimika* (Chemist's Handbook), Nikol'skii, B.P., Ed., Moscow: Khimiya, 1965, vol. 4.
15. Pak, V.N., Nepomnyashchii, A.B., Burkat, T.M., and Kun, Sh.R., *Zh. Fiz. Khim*., 2005, vol. 79, no. 9, pp. 1411–1414.
16. Deryagin, B.V. and Churaev, N.V., *Voda v dispersnykh sistemakh* (Water in Disperse Systems), Deryagin, B.V., Ed., Moscow: Khimiya, 1989, pp. 7–31.
17. Deryagin, B.V., Churaev, N.V., and Muller, V.M., *Poverkhnostnye sily* (Surface Forces), Moscow: Nauka, 1985.
18. Yuzhnovskii, I.R. and Kurylyak, I.I., *Elektrolity* (Electrolytes), Kiev: Naukova Dumka, 1988.
19. Dumanskii, A.V., *Liofil'nost' dispersnykh sistem* (Lyophilicity of Disperse Systems), Kiev: Akad. Nauk Ukr. SSR, 1960.

ISSN 1070-4272. Russian Journal of Applied Chemistry, 2006, Vol. 79, No. 3, pp. 360–362. © Pleiades Publishing, Inc., 2006.
Original Russian Text © V.A. Keskinov, V.V. Lishchuk, A.K. Pyartman, V.E. Skobochkin, 2006, published in Zhurnal Prikladnoi Khimii, 2006, Vol. 79, No. 3, pp. 367–369.

INORGANIC SYNTHESIS AND INDUSTRIAL INORGANIC CHEMISTRY

Mutual Solubility of the Components in Systems RED-1 Diluent–Tri-*n*-butyl Phosphate Solvates of Rare-Earth Element(III) (Nd, Gd, Y, Yb, Lu) Nitrates–Escaid 100 Diluent

V. A. Keskinov, V. V. Lishchuk, A. K. Pyartman, and V. E. Skobochkin

St. Petersburg State Technological Institute (Technical University), St. Petersburg, Russia

Received June 9, 2005

Abstract—Phase diagrams of liquid binary systems RED-1 diluent–tri-*n*-butyl phosphate solvates of rare-earth element(III) (neodymium, gadolinium, yttrium, ytterbium, lutetium) nitrates were studied, and the binodal curves in the ternary systems $[Ln(NO_3)_3(TBP)_3]$ (Ln = Nd and Yb)–RED-1–Escaid 100 were determined at various temperatures.

DOI: 10.1134/S1070427206030049

Extraction of rare-earth elements(III) (REEs) with neutral organophosphorus compounds is widely used in separation and recovery processes. In saturation of the organic phase with coordination solvates of REE(III) nitrates in hydrocarbon diluents, second organic phase (so-called third phase) can be formed [1, 2]. Despite an obvious practical significance for REE separation processes, there are no available quantitative data on the mutual solubility of the components in the system RED-1 diluent–TBP solvates of REE(III) (Nd, Gd, Y, Yb, and Lu) nitrates––Escaid 100 diluent at various temperatures. Our goal was to fill this gap.

The density of the phases was studied by the bottle method. The initial solutions of REE(III) nitrates were prepared by dissolution of the corresponding oxides (ultrapure grade) in nitric acid (ultrapure grade). In the experiments we used vacuum-distilled tri-*n*-butyl phosphate (TBP) (ρ = 0.9727 g cm^{-3} at 298.15 K), RED-1 diluent (99% synthetic paraffin; ρ = 0.7395 g cm^{-3} at 298.15 K; dodecane fraction >50%; aromatics content <0.01 wt %), and Escaid 100 diluent (20 vol % aromatic hydrocarbons in paraffin; ρ = 0.8241 g cm^{-3} at 298.15 K). The coordination solvates $[Ln(NO_3)_3 \cdot (TBP)_3]$ (Ln = Nd, Gd, Y, Yb, and Lu) were prepared by triple extraction from saturated aqueous solutions of REE(III) nitrates [3]. The $[Ln(NO_3)_3(TBP)_3]$ "concentration" in pure solvates was 1.10±0.02 M (ρ = 1.275±0.001 g cm^{-3}). The binodal curves for the binary and ternary systems and the nodes for the binary systems were obtained using the procedure described in [4, 5]. The heterogeneous equilibria were monitored turbidimetrically using a Kernco 966 R instrument and a color filter (λ = 850 nm). The weight fractions of the components were determined to within 0.001–0.002, and the temperature, to within 0.2 K. It was demonstrated in the preliminary experiments that, in mixing the RED-1 solutions with $[Ln(NO_3)_3 \cdot (TBP)_3]$, the change in the volume of the organic phase is within 0.3 vol %. The compositions of the coexisting phases (vol %) were recalculated to the weight fractions taking into account the solution densities. The binodal curves were fitted by third-degree polynomials.

The phase diagrams of the ternary liquid systems, as influenced by the temperature, were constructed using the second-type Roozeboom triangle [rectangular coordinates for two components of the ternary liquid system with reference to the weight fractions (ω_i) of the components (for the third component, $\omega_3 = 1 - \omega_1 - \omega_2$)].

The results show that the $[Ln(NO_3)_3(TBP)_3]$–RED-1 binary systems (Ln = Nd, Gd, Y, Yb, and Lu) are incompletely miscible, forming two separate liquid phases I and II. Phase I is enriched in RED-1, and phase II, in $[Ln(NO_3)_3(TBP)_3]$. Increasing temperature increases the mutual solubility of the components, i.e., the phase separation region decreases (see table).

The binary systems are characterized by the upper critical temperature of solution (mixing) T_{cr} (K):

Phase separation in the systems $[Ln(NO_3)_3(TBP)_3]$–RED-1 at various temperatures

T, K	$[Ln(NO_3)_3(TBP)_3]$, wt fraction	RED-1, wt fraction	Nodes
	Ln = Nd		
296.75	0.965	0.035	1
296.75	0.015	0.985	1
303.15	0.940	0.060	2
303.15	0.047	0.953	2
313.05	0.886	0.114	3
313.05	0.090	0.910	3
322.15	0.161	0.839	4
322.15	0.835	0.165	4
338.65	0.666	0.334	5
338.65	0.302	0.698	5
	Ln = Gd		
298.15	0.064	0.936	1
298.15	0.94	0.060	1
301.75	0.912	0.088	2
301.75	0.079	0.921	2
322.15	0.161	0.839	3
322.15	0.786	0.214	3
342.45	0.302	0.698	4
342.45	0.616	0.384	4
	Ln = Y		
296.15	0.064	0.936	1
296.15	0.939	0.061	1
310.65	0.107	0.893	2
310.65	0.890	0.110	2
325.15	0.161	0.839	3
325.15	0.837	0.163	3
352.15	0.685	0.315	4
352.15	0.301	0.699	4
	Ln = Yb		
296.25	0.940	0.060	1
296.25	0.037	0.963	1
319.15	0.120	0.880	2
319.15	0.173	0.127	2
326.55	0.142	0.839	3
326.55	0.848	0.168	3
357.55	0.725	0.254	4
356.55	0.275	0.735	4
	Ln = Lu		
299.15	0.940	0.060	1
299.15	0.085	0.915	1
314.65	0.122	0.878	2
314.65	0.912	0.088	2
330.15	0.160	0.840	3
330.15	0.873	0.127	3
347.15	0.822	0.178	4
347.15	0.205	0.795	4
362.15	0.801	0.199	5
362.15	0.249	0.751	5

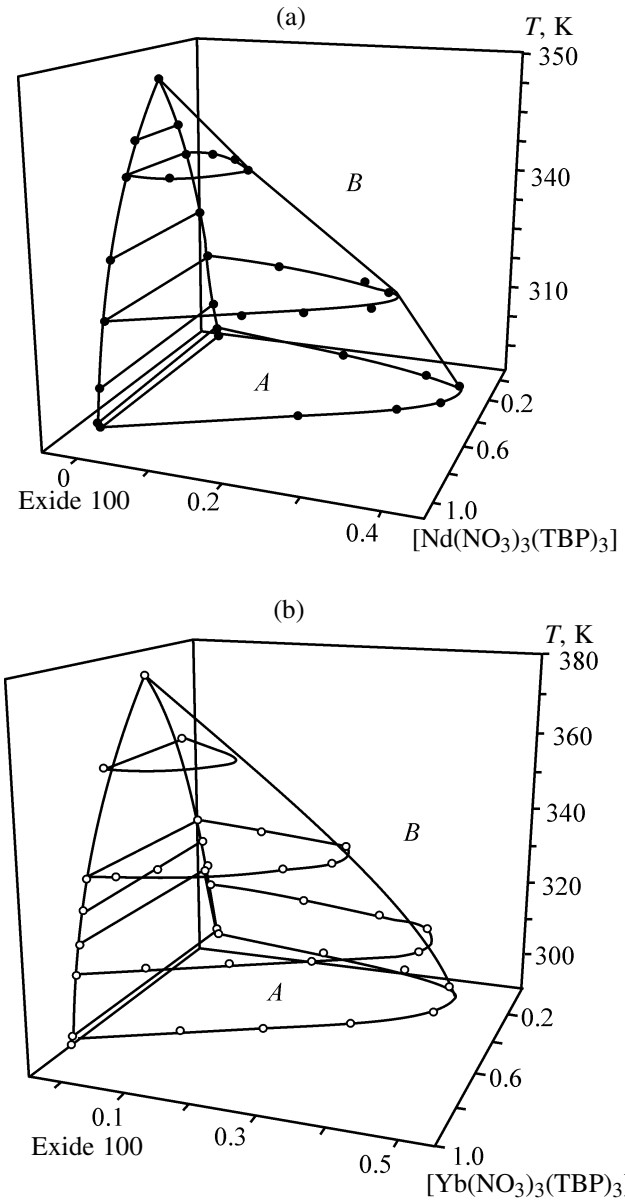


Fig. 1. Phase diagrams of ternary systems (a) $[Nd(NO_3)_3 \cdot (TBP)_3]$–RED-1–Escaid-100 and (b) $[Yb(NO_3)_3(TBP)_3]$–RED-1–Escaid-100. The concentrations are expressed in wt fractions. (*A*) Two-phase and (*B*) homogeneous regions.

346.25 ± 0.5 for the Nd(III) solvate, 349.05 ± 0.5 (Gd), 365.75 ± 0.5 (Y), and 375.55 ± 0.5 (Yb). As for Lu(III), the upper critical temperature of the binary system $[Lu(NO_3)_3(TBP)_3]$–RED-1 lies outside the experimental temperature range (further increase in the temperature above 383.15 K results in evaporation of the solvent from the liquid phase). In this case, T_{cr} was estimated by approximation of the section of the binodal curve by a third-degree polynomial to be 404 K (see table). In the series Nd–Gd–Y–Yb–Lu, the

upper critical temperature of solution for the binary systems increases with decreasing ionic radius of REE(III). The weight fractions of the components at T_{cr} are quite similar: Nd(III) 0.46, Gd(III) 0.45, Y, Yb(III) 0.47, and Lu(III) ~0.5. The observed considerable effect of the lanthanide nature on the upper critical temperature of solution, in our opinion, is caused by the dipole–dipole interaction between the REE solvates, which increases with decreasing ionic radius of REE(III). In the series Nd(III)–Lu(III), the difference in T_{cr} amounts to about 58 K.

The phase diagrams of the ternary systems $[Ln(NO_3)_3(TBP)_3]$–RED-1–Escaid-100 (Ln = Nd and Yb) demonstrate a homogeneous region (*B*) and a two-phase region (*A*) confined by the binodal curves corresponding to a given temperature (Figs. 1a, 1b). The upper critical temperatures of solution of the binary and ternary systems are practically coincident. In the case of $[Nd(NO_3)_3(TBP)_3]$, complete homogenization of the system at low temperature (293–298 K) requires introduction of up to 0.45 wt fraction of Escaid-100, and for $[Yb(NO_3)_3(TBP)_3]$, 0.52 wt fraction.

Finally, practical use of extraction systems based on TBP–RED-1–Escaid-100 mixtures under conditions of saturation of the organic phase with REE(III) nitrates with formation of $[Ln(NO_3)_3(TBP)_3]$ requires partial (about 0.6 wt fraction) replacement of the paraffinic diluent by the diluent containing up to 20% of aromatics. This ensures complete homogenization of the system at low temperatures.

CONCLUSIONS

(1) Binary systems $[Ln(NO_3)_3(TBP)_3]$–RED-1 (Ln = Nd, Gd, Y, Yb, and Lu) separate into two liquid phases I and II. Phase I is enriched in RED-1, and phase II, in $[Yb(NO_3)_3(TBP)_3]$. With increasing temperature the two-phase region decreases, i.e., the miscibility of the components increases.

(2) The binary systems are characterized by the upper critical temperature of solution T_{cr} (K): 346.25 ± 0.5 for the Nd(III) solvate, 349.05 ± 0.5 (Gd), 365.75 ± 0.5 (Y), 375.55 ± 0.5 (Yb), and about 404 (Lu). The upper critical temperature of solution of the binary systems increases in the order Nd < Gd < Y < Yb < Lu, i.e., with decreasing ionic radius of REE(III).

(3) The phase diagrams of the ternary systems $[Ln(NO_3)_3(TBP)_3]$–RED-1–Escaid-100 (Ln = Nd and Yb) demonstrate a homogeneous region and a two-phase region. Complete homogenization of the system at low temperatures (293–298 K) requires introduction of up to 0.6 wt fraction of Escaid-100.

REFERENCES

1. Pyartman, A.K., Kopyrin, A.A., Puzikov, E.A., and Bogatov, K.B., *Radiokhimiya*, 1995, vol. 37, no. 1, pp. 52–55.
2. Nikolotova, Z.I., *Ekstraktsiya neitral'nymi fosfororganicheskimi soedineniyani: Aktinoidy: Spravochnik* (Extraction with Neutral Organophosphorus Compounds: Actinides: A Handbook), Moscow: Energoatomizdat, 1987.
3. *Ekstraktsiya neorganicheskikh veshchestv (Diagrammy rassloeniya, raspredeleniya, vysalivaniya i razdeleniya)* (Extraction of Inorganic Compounds (Phase Separation, Distribution, Salting-out, and Partition Diagrams)), Nikolaev, A.V., Ed., Novosibirsk: Nauka, 1970.
4. Pyartman, A.K., Kudrova, A.V., and Keskinov, V.A., *Zh. Prikl. Khim.*, 2004, vol. 77, no. 4, pp. 560–563.
5. Pyartman, A.K., Kudrova, A.V., and Keskinov, V.A., *Zh. Prikl. Khim.*, 2004, vol. 77, no. 4, pp. 564–567.

ISSN 1070-4272. Russian Journal of Applied Chemistry, 2006, Vol. 79, No. 3, pp. 363–366. © Pleiades Publishing, Inc., 2006.
Original Russian Text © E.A. Zauer, 2006, published in Zhurnal Prikladnoi Khimii, 2006, Vol. 79, No. 3, pp. 370–373.

SORPTION AND ION-EXCHANGE PROCESSES

Sorption of Mercury(II), Zinc(II), and Iron(III) Thiocyanate Complexes on AV-17 Anion Exchanger and KU-2 Cation Exchanger Modified with Rhodamine Zh

E. A. Zauer

Volgograd State Engineering University, Volgograd, Russia

Received March 25, 2005

Abstract—Sorption of anionic mercury(II), zinc(II), and iron(III) thiocyanate complexes on KU-2 cation exchanger modified with Rhodamine Zh and on AV-17-8 strongly basic anion exchanger were studied in relation to the concentration of SCN^- ions and solution pH. Optimal conditions of sorption of metal complexes from dilute solutions were found.

DOI: 10.1134/S1070427206030050

Complex formation is widely used to increase the selectivity of metal ion sorption. Both usual and chemically and surface-modified ion exchangers are used as sorbents [1, 2].

The data on sorption of complex ions with usual and modified ion exchangers are lacking, although they are necessary to optimize sorption preconcentration and separation of elements and to develop technologies of industrial waste management. For instance, sorption of mercury(II) halide complexes with AV-17 anion exchanger was studied in [3]. Sorption of zinc complex ions from chloride solutions on various anion exchangers is described in [4]. Studies on sorption from mixtures of complexes are very few.

In this study, we examined the kinetics of sorption of mercury(II), iron(III), and zinc(II) thiocyanate anionic complexes on AV-17-8 strongly basic anion exchanger and on KU-2 strongly acidic sulfonic cation-exchange resin modified with a basic dye, Rhodamine Zh (RZh).

EXPERIMENTAL

The initial solution of iron(III) was prepared from ferric ammonium sulfate [5] and standardized complexometrically with sulfosalicylic acid [6]. A mercury(II)-containing solution was prepared from mercury sulfate [5] and standardized by complexometric back-titration with Eriochrome Black T indicator [6]. A solution containing Zn(II) was prepared by dissolving metallic zinc (chemically pure grade) in hydrochloric acid [5]. The working solutions were prepared by dilution of the initial solutions with distilled water. AV-17-8 anion exchanger in the chloride form was prepared as in [7].

To obtain modified KU-2 cation exchanger, the initial KU-2 resin in the hydrogen–salt form prepared as in [7] was stored in 0.2% aqueous solution of Rhodamine Zh for 24 h and then separated by filtration, washed with distilled water, and dried. Modification is the ion-exchange reaction

$$RSO_3^-H^+ + RZh^+ \rightarrow RSO_3^-RZh^+ + H^+.$$

It is known that basic dyes form ionic associates with halide and thiocyanate complexes of certain metal ions insoluble in water but soluble in organic solvents (e.g., toluene). This property of dyes is widely used in analytical chemistry for extraction-photometric determination of elements, including mercury(II) and zinc(II) [8, 9].

In this study, ionic associates of elements under consideration were obtained in the phase of the sorbent modified with Rhodamine Zh but not in a solution, and potassium thiocyanate was used as a complexing agent.

To study the sorption kinetics, a 0.50 ± 0.05-g portion of the sorbent was introduced into 100 cm^3 of a solution containing zinc, iron, or mercury after addition of a 25% aqueous solution of potassium thiocyanate. The mixture was stirred with a magnetic stirrer for definite time, and the sorbent was separated, washed with distilled water, and dried.

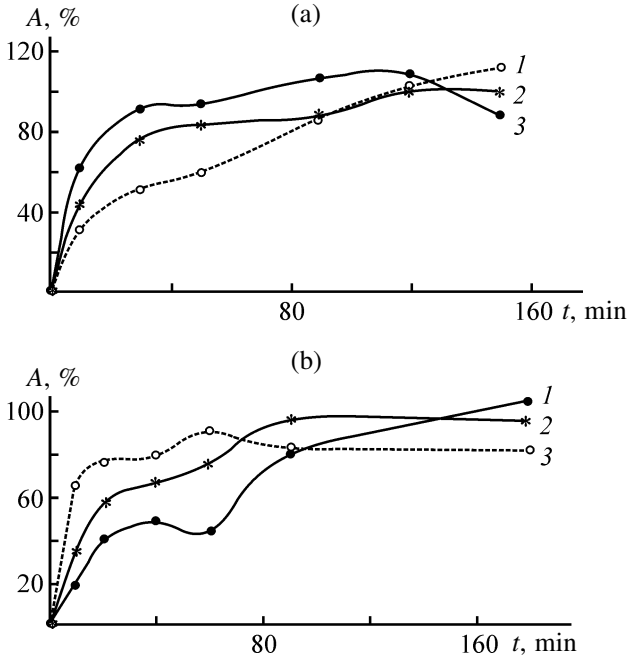


Fig. 1. Kinetics of sorption of (*1*) iron(III), (*2*) zinc(II), and (*3*) mercury(II) thiocyanate complexes from their mixture on (a) modified KU-2 cation exchanger and (b) AV-17 anion exchanger. $C_{KSCN} = 13 \times 10^{-5}$ M. Composition of the mixture of ions (μg cm^{-3}): (a) Fe 3.52, Zn 7.23, Hg 6.27 and (b) Fe 1.55, Zn 7.23, Hg 6.23. (*A*) Degree of sorption and (*t*) time.

Sorption was monitored with a Spektroskan crystal-diffraction scanning X-ray fluorescence spectrometer (Spektron Research and Production Association, St. Petersburg) [10, 11]; the contents of the metals were determined simultaneously on the surface of the solid concentrate at a 40 kV voltage on an X-ray tube with a copper anode at the time of signal accumulation of 40 s. The FeK_α (1936 mÅ), ZnK_α (1435 mÅ), and HgL_α (1241 mÅ) lines were used as analytical lines. The error of mercury, iron, and zinc determination was 3–10 rel. %.

In the presence of SCN^- ions, Hg^{2+}, Zn^{2+} and Fe^{3+} ions form complexes whose compositions depend on the concentration of the complexing ion. Zinc(II) and mercury(II) ions have the general composition $[M(SCN)_n]^{2-n}$ (M is zinc or mercury ion, n = 1–4). Iron(III) forms with thiocyanate ion complexes $[M(SCN)_n]^{3-n}$ (n = 1–6). Among the anionic complexes, the mercury complexes $[Hg(SCN)_3]^-$ ($\log\beta$ = 19.17) and $[Hg(SCN)_4]^{2-}$ ($\log\beta$ = 19.77) are the most stable. The iron {$[Fe(SCN)_4]^-$, $\log\beta$ = 4.53; $[Fe(SCN)_5]^{2-}$, $\log\beta$ = 4.23; $[Fe(SCN)_6]^{3-}$, $\log\beta$ = 3.23} and zinc {$[Zn(SCN)_3]^-$, $\log\beta$ = 2.2; $[Zn(SCN)_4]^{2-}$, $\log\beta$ = 3.7} complexes are moderately stable [12].

Sorption proceeds by the ion-exchange mechanism, when AV-17 anion exchanger is added into the solution containing the above thiocyanate complexes.

When KU-2 ion exchanger modified with Rhodamine Zh is used, the interaction of iron, mercury, or zinc anionic complexes with the dye in the sorbent phase is apparently similar to that in the solution, with the formation of ionic associates of the following composition: for zinc(II) and mercury(II), $(RZh)\cdot[M(SCN)_3]$ and $(RZh)_2[M(SCN)_4]$ and for iron(III), $(RZh)[M(SCN)_4]$, $(RZh)_2[M(SCN)_5]$, and $(RZh)_3\cdot[M(SCN)_6]$.

As seen from Fig. 1a, the rate of sorption of anionic complexes on the cation exchanger modified with Rhodamine Zh decreases in the order $Hg^{2+} > Zn^{2+} > Fe^{3+}$. This coincides with data of [2] showing that the sorbability increases with increasing stability of the complex. The time required to attain complete sorption is 40–60 min with mercury(II) and zinc(II) and 120–150 min with iron(III).

The rate of sorption on AV-17-8 anion exchanger (Fig. 1b) decreases in the same order as on modified KU-2 cation exchanger. The limiting sorption of anionic complexes is reached in 60 min with mercury(II) and in 90–120 min with iron(III) and zinc(II).

The results are presented in Fig. 2a and 2b. At low SCN^- concentrations, cationic iron(III), mercury(II) and zinc(II) complexes, which are not noticeably sorbed, dominate in the solution. As the concentration of SCN^- ions increases, the negatively charged complex ions appear in the solution. They are sorbed on the AV-17 anion exchanger by the ion-exchange reaction and are electrostatically attracted to modified KU-2 cation exchanger with formation of ionic associates with Rhodamine Zh. At a further increase in the SCN^- concentration, the SCN^- ions compete with anionic metal complexes for the sorption sites of the sorbent. However, thiocyanate ions are sorbed more weakly, since their charge is lower as compared to the charges of the complex ions at excess SCN^- ligands.

With the modified sorbent (Fig. 2a), the maximal degree of mercury(II) sorption is attained at a potassium thiocyanate concentration of 1.3×10^{-5} M. The further increase in its concentration does not change the sorption substantially. With Zn^{2+} and Fe^{3+}, the maximal sorption is observed at a KSCN concentration of $(10–13) \times 10^{-5}$ M. Probably, this is connected with the fact that mercury(II), as compared to zinc(II) and iron(III), forms stronger complexes with thiocyanate ions, which are better sorbed with the sorbent.

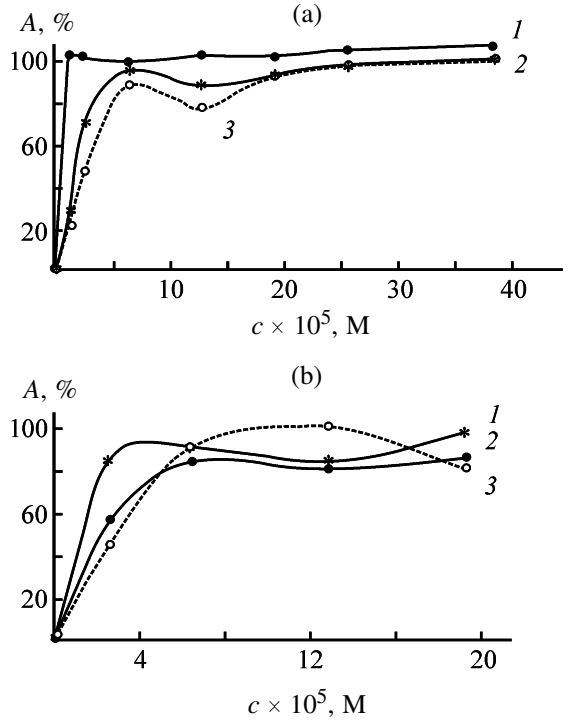


Fig. 2. Influence of KSCN concentration c on the degree of sorption A of (*1*) mercury(II), (*2*) zinc(II), and (*3*) iron(III) thiocyanate complexes on (a) modified KU-2 cation exchanger and (b) AV-17 anion exchanger. Sorption time 2 h. Composition of mixture of ions ($\mu g\ cm^{-3}$): Fe 1.76, Zn 7.23, and Hg 6.27.

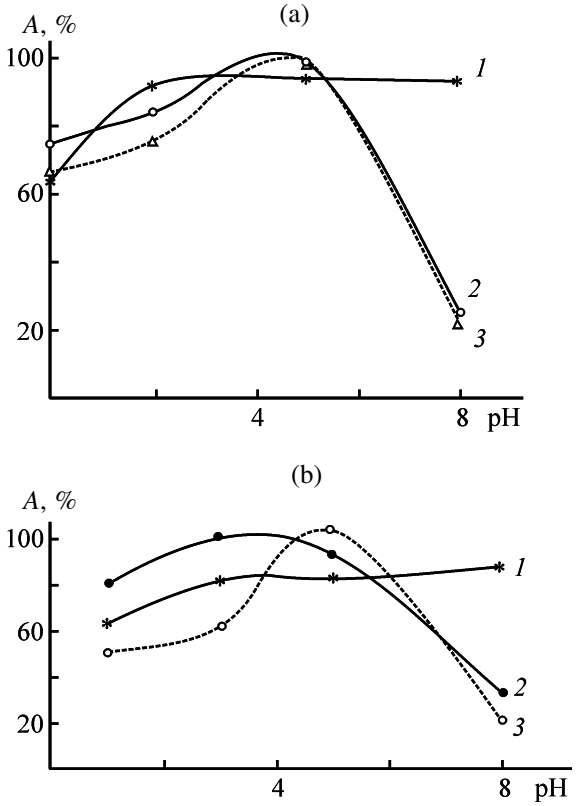


Fig. 3. Influence of solution pH on the degree of sorption A of (*1*) mercury(II), (*2*) zinc(II), and (*3*) iron(III) thiocyanate complexes on (a) modified KU-2 cation exchanger and (b) AV-17 anion exchanger. $c_{KSCN} = 13 \times 10^{-5}$ M, sorption time 2 h. Composition of mixture of ions ($\mu g\ cm^{-3}$): Fe 1.55, Zn 7.23, and Hg 6.27.

The maximal sorption of the metal ions studied on AV-17 resin is reached at a potassium thiocyanate concentration of $(8–13) \times 10^{-5}$ M (Fig. 2b).

Sorption of iron(III) and zinc(II) sharply decreases at pH > 5 on both AV-17 and modified KU-2 resins (Fig. 3a). Probably, this effect is a result of competing reactions of the metal ions with hydroxide ions with formation of hydroxo complexes. With iron(III), these complexes are $[Fe(OH)]^{2+}$ ($\log\beta$ = 11.87) and $[Fe(OH)_2]^{+}$ ($\log\beta$ = 21.17), which predominate in the solution even at pH 5 and prevent penetration of iron into the sorbent phase. In addition, with increasing pH the probability of formation of poorly soluble iron hydroxide $[Fe(OH)_3]^{0}$ increases. Zn^{2+} ions also form with OH^{-} ions hydroxo complexes $[Zn(OH)]^{+}$ ($\log\beta$ = 4.40), $[Zn(OH)_2]^{0}$ ($\log\beta$ = 11.30), $[Zn(OH)_3]^{-}$ ($\log\beta$ = 13.14), and $[Zn(OH)_4]^{2-}$ ($\log\beta$ = 14.66), which are more stable than complexes with thiocyanate ions. In contrast to iron(III) trihydroxide, zinc dihydroxide is amphoteric and forms negatively charged complex ions in the presence of excess hydroxide ions. However, within the pH range studied, cationic zinc complexes prevail; they are not sorbed on the surface of the modified cation exchanger.

At pH > 2 for modified KU-2 cation exchanger and pH > 3 for AV-17 anion exchanger, the acidity of solution does not noticeably affect the sorption of mercury(II), since only the anionic hydroxo complex can be sorbed with the ion exchangers studied among the complexes $[Hg(OH)]^{+}$ ($\log\beta$ = 10.30), $[Hg(OH)_2]^{0}$ ($\log\beta$ = 21.70), and $[Hg(OH)_3]^{-}$ ($\log\beta$ = 21.20) formed under these conditions[12]. Its stability is close to the stability of thiocyanate anionic complexes. Therefore, the decrease in the solution acidity probably causes sorption of mercury in the form of hydroxo but not thiocyanate complexes.

CONCLUSIONS

(1) The shapes of the pH dependences of sorption of mercury(II), iron(III), and zinc(II) with AV-17-8 anion exchanger and KU-2 cation exchanger modified

with Rhodamine Zh are similar. pH substantially affects the sorption of iron(III) and zinc(II) thiocyanate complexes. Sorption of mercury(II) complexes is essentially independent of pH.

(2) The order of sorption on modified cation exchanger and on anion exchanger is the same: initially mercury(II) complex anions, then zinc(II) complexes, and then iron(III) complexes are sorbed.

(3) The optimal conditions of simultaneous sorption of mercury(II), iron(III), and zinc(II) thiocyanate complexes from dilute solutions with modified KU-2 cation exchanger and AV-17-8 anion exchangers are as follows: sorption time 2 h, pH of solutions 4–5, and concentrations of thiocyanate ions $(10–13) \times 10^{-5}$ and $(8–13) \times 10^{-5}$ M in the case of KU-2 and AV-17-8 ion exchangers, respectively.

REFERENCES

1. Zaporozhets, O.A., Gaver, O.M., and Sukhan, V.V., *Usp. Khim.*, 1997, vol. 66, no. 7, pp. 702–712.
2. Marhol, M., *Ion Exchangers in Analytical Chemistry. Their Properties and Use in Inorganic Chemistry*, Prague: Academia, 1982.
3. Leikin, Yu.A., Tarasova, T.I., Tikhonova, L.A., and Musa, N., *Zh. Fiz. Khim.*, 1997, vol. 71, no. 2, pp. 321–323.
4. Skorokhodov, V.I., Radionov, B.K., and Goryaeva, O.Yu., *Zh. Prikl. Khim.*, 2004, vol. 77, no. 9, pp. 1456–1461.
5. Korostylev, P.P., *Prigotovlenie rastvorov dlya khimiko-analiticheskikh rabot* (Preparation of Solutions for Chemical-Analytical Works), Moscow: Nauka, 1964.
6. Schwarzenbach, G. und Flaschka, H., *Die komplexometrische Titration*, Stuttgart: Ferdinand Enke, 1965.
7. *Fiziko-khimicheskie metody analiza: Prakticheskoe rukovodstvo. Uchebnoe posobie dlya vuzov* (Physicochemical Methods of Analysis: Practical Handbook. Textbook for Higher Schools), Aleskovskii, V.B., Ed., Leningrad: Khimiya, 1988.
8. Sandell, E.B., *Colorimetric Determination of Traces of Metals*, New York: Interscience, 1959.
9. Lur'e, Yu.Yu., *Khimicheskii analiz proizvodstvennykh stochnykh vod* (Chemical Analysis of Industrial Wastewaters), Moscow: Khimiya, 1974.
10. Zauer, E.A., Abstracts of Papers, *Ural'skaya konferentsiya po spektroskopii* (XVI Ural Conf. on Spectroscopy), Novoural'sk, September 9–12, 2003, Yekaterinburg, 2003, pp. 110–111.
11. Zauer, E.A., Abstracts of Papers, *Vserossiiskaya konferentsiya "Analitika Rossii"* (All-Russian Conf. "Analytics of Russia"), Moscow, September 27–October 1, 2004, pp. 63–64.
12. Lur'e, Yu.Yu., *Spravochnik po analiticheskoi khimii* (Handbook of Analytical Chemistry), Moscow: Khimiya, 1971.

ISSN 1070-4272. Russian Journal of Applied Chemistry, 2006, Vol. 79, No. 3, pp. 367–371. © Pleiades Publishing, Inc., 2006.
Original Russian Text © D.E. Chirkst, O.V. Cheremisina, M.V. Ivanov, A.A. Chistyakov, I.T. Zhadovskii, 2006, published in Zhurnal Prikladnoi Khimii, 2006, Vol. 79, No. 3, pp. 374–377.

SORPTION AND ION-EXCHANGE PROCESSES

Isotherm of Strontium and Sodium Cation Exchange on Iron–Manganese Nodules

D. E. Chirkst, O. V. Cheremisina, M. V. Ivanov, A. A. Chistyakov, and I. T. Zhadovskii

St. Petersburg State Mining Institute, St. Petersburg, Russia

Received February 17, 2005

Abstract—The isotherm of ion exchange of Sr^{2+} and Na^{+} ions on iron–manganese nodules was obtained. It was suggested to describe the ion exchange by an equation analogous to the Langmuir isotherm equation. The limiting sorption and apparent ion exchange constant were calculated. The effective radius of sorbed strontium ions was determined.

DOI: 10.1134/S1070427206030062

Iron–manganese nodules (IMNs) as natural cation exchangers show promise for the recovery of strontium-90 from radioactively contaminated water and also from reactor conduits.

Radiation pollution of territories near nuclear plants is mainly caused by emergency emissions of cesium-l37 and strontium-90. Strontium is largely sorbed by the mineral component of soils [1–3], and its migratory activity is noticeably higher compared to cesium. A process for treatment of soils contaminated with ^{90}Sr [4] by flushing the soil with solutions of salts of multicharged cations was developed previously on the pilot scale. The study of the ion exchange on IMNs will make it possible to develop a procedure for the removal of strontium-90 from wash waters and also from underground waters.

In this study we examined the isotherm of the exchange of sodium and strontium ions on the IMN surface. As natural IMN samples contain various exchanging cations, iron–manganese nodules were converted to the sodium form.

According to the simplest Helmholtz model, the spatial separation of charges near a surface can be considered as an electrical double layer representing two parallel plates of a charged capacitor separated by a layer of a dispersing medium [5]. One capacitor plate is formed by potential-determining ions fixed on the solid surface and the other, by counterions contained in a liquid. Because of short range of action of adsorption forces, we can distinguish two main parts of an electrical double layer: a dense part (Stern–Helmholtz layer) and a more distant diffuse part (Gouy–Chapman layer). According to the Stern–Graham scheme, the dense part of an electrical double layer consists of internal and external parts. The internal part is formed by partially of completely dehydrated ions specifically adsorbed on the surface in question. The external part consists of hydrated ions, sodium ions in our case, which can exchange with strontium ions according to the Gedroits lyotropic series $Fe^{3+} > Al^{3+} > Cs^{+} > Sr^{2+} > Ca^{2+} > Mg^{2+} > Rb^{+} > K^{+} > Na^{+} > Li^{+}$ [5, 6]. The tendency of the cations to adsorption in this series increases in parallel with the ionic potential, which is equal to the ratio of the charge and radius of the hydrated ion.

It is known that ^{137}Cs is fixed in soils much more strongly than does ^{90}Sr, despite smaller ion charge [6]. As compared to strontium, cesium has a smaller Stokes radius of the hydrated ion. The higher ionic potential of cesium in aqueous solutions compared to strontium is indicated by the fact that the equivalent conductance of cesium ions, equal to 7.72×10^{-3} S m^2 equiv^{-1} at 298 K and infinite dilution, is higher than that of strontium ions, 5.94×10^{-3} S m^2 equiv^{-1} [7]. Owing to higher ionic potential in aqueous solution, cesium ions are bonded more strongly than strontium ions to negatively charged structural fragments on the surface of minerals.

An air-dry IMN sample with granules of size 0.10–0.25 mm was treated with a 5% NaOH solution for 5 days with intermittent stirring. The alkali solution was replaced daily by a fresh solution. The completeness of converting IMN into the sodium form was monitored by reaching the constant activity of Na^{+}

Table 1. Experimental data on the exchange of Na^+ ions for Sr^{2+} ions

c_0	$c_{eq} \times 10^2$	Γ_{Sr}, mol kg^{-1}	$1/\Gamma_{Sr}$	γ_+	c_{Na^+}, M
M					
0.013	0.011	0.129	7.752	0.855	0.026
0.020	0.126	0.187	5.348	0.828	0.037
0.030	0.290	0.271	3.690	0.802	0.054
0.040	0.700	0.329	3.040	0.781	0.066
0.048	1.300	0.346	2.890	0.767	0.069
0.076	3.800	0.395	2.532	0.734	0.088
0.134	9.300	0.411	2.433	0.701	0.082
0.200	15.900	0.409	2.444	0.690	0.082
0.250	20.800	0.417	2.398	0.691	0.083
0.361	32.200	0.390	2.564	0.706	0.078
0.500	45.700	0.429	2.331	0.741	0.086

ions after treating IMN with an alkaline solution. The activity of Na^+ ions in alkaline solutions contacted with IMN and diluted using volumetric glassware to concentrations of 0.001–0.01 mol kg^{-1} was measured with an ion-selective electrode and an Anion ion meter. After that, IMN was multiply washed out with water to pH 7 of the aqueous extract and air-dried.

We studied the ion exchange from 0.013–0.500 M (with respect to Sr^{2+}) model aqueous solutions of $SrCl_2$. The value of sorption Γ_{Sr} (mol kg^{-1}) of strontium ions was determined under static conditions at the ratio of the liquid phase volume to the solid phase weight V/m = 10 ml g^{-1} and at the weight of an IMN sample of 5 g. The sorption value was calculated from the difference of concentrations of the starting (c_0) and equilibrium (c_{eq}) solutions by the formula

$$\Gamma = (c_0 - c_{eq})V/m.$$

A solution of strontium chloride was stirred with an IMN sample by a magnetic stirrer at 400 rpm to reach an equilibrium. The equilibration time required to reach a constant solution concentration was 5–6 h; in the experiments the time of phase contact was no less than 10 h.

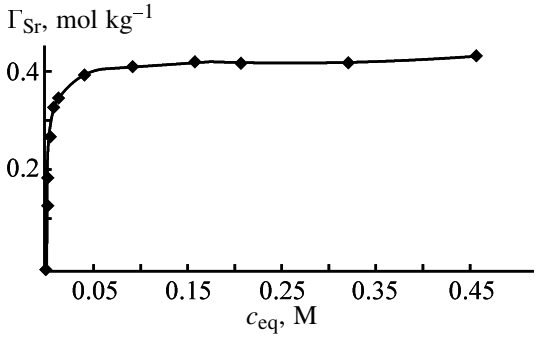


Fig. 1. Isotherm of sorption Γ_{Sr} of strontium cations on the IMN surface. (c_{eq}) Equilibrium concentration of strontium ions.

After experiments, the solution was filtered through a "blue band" filter, the equilibrium concentration of sodium ions was measured with an Anion pH meter equipped with an ion-selective electrode, and that of strontium ions was determined photometrically [8]. Solution aliquots of volume from 2 to 10 ml depending on the strontium(II) content were transferred into a 50-ml flask. The required pH 2.8–3.0 was adjusted by adding 10 ml of acetate buffere solution. Then 25 ml of a 60% aqueous solution of ethanol and 1 ml of a 0.1% solution of Nitroorthanilic C (Nitrochromazo) were added, and the solution in the flask was brought to the mark with distilled water. The strontium(II) content in the solution under study was determined by the intensity of the absorption band of the strontium complex with Nitrochromazo at λ 650 nm. This method allows determination of the strontium(II) content from 2 to 20 μg in 25 ml of solution. Under these conditions, Na^+ and NH_4^+ ions do not hinder up to 100-fold excess; K^+, up to a 30-fold excess; Ca^{2+}, up to 1/5-fold excess; and Mg^{2+}, up to 5-fold excess.

Table 1 shows the initial and equilibrium concentrations of strontium ions c_0 and c_{eq}, sorption values Γ_{Sr}, reciprocals of strontium ions sorption values $1/\Gamma_{Sr}$, equilibrium concentrations of sodium ions c_{Na^+}, and activity coefficients of single-charged cations γ_+ calculated by the Davies equation [9]. The measurements of the equilibrium concentration of sodium ions with an ion-selective electrode confirmed the equivalence of the exchange of sodium and strontium ions. The resulting isotherm of sorption of strontium ions on the IMN surface is given in Fig. 1.

The thermodynamic description of the exchange of strontium and sodium ions was carried out on the assumption of ideality of a solid phase, i.e. without taking into account the activity coefficients of sorbed ions. It was shown in [10] that the ion-exchange isotherm can be described by an equation of the Langmuir isotherm type. We used the linearization procedure suggested earlier [11] for an analog of Langmuir equation.

The equation of mass action law for the ion-exchange reaction

$$2Na^+_{sol} + Sr^{2+}_{aq} \rightleftarrows 2Na^+_{aq} + Sr^{2+}_{sol}$$

is of the form

$$\Gamma = \frac{\Gamma_{Sr^{2+}} a^2_{Na^+}}{\Gamma^2_{Na^+} a_{Sr^{2+}}}, \quad (1)$$

where K is the apparent exchange constant; $\Gamma_{Sr^{2+}}$ and Γ_{Na^+}, values of sorption of ions (mol kg^{-1}); a_{Na^+} and $a_{Sr^{2+}}$, activities of ions in solution (mol kg^{-1}).

The electroneutrality condition implies that the numbers of equivalents of exchanging ions in ion exchange should be equal. Therefore, the limiting sorption of ions should be expressed in equiv kg^{-1}. When calculating the thermodynamic functions by the mass action law, the value of sorption of ions should be expressed in mol kg^{-1}, as ion activities in solution have a dimension of mol kg^{-1} corresponding to the standard state. Thus,

$$\Gamma_\infty = \Gamma_{Na^+} + 2\Gamma_{Sr^{2+}},$$

where Γ_∞ is the limiting sorption of ions (equiv kg^{-1}), and the values of sorption of ions are expressed in mol kg^{-1}.

In view of the aforesaid, Eq. (1) can be reduced to form (2), as in the Debye–Hückel and also in the Davies approximations we have $\gamma_{z^+} = \gamma_+^{2z}$, where z is the cation charge:

$$K = \frac{\Gamma_{Sr^{2+}}[Na^+]^2\gamma_+^2}{\Gamma^2_{Na^+}[Sr^{2+}]\gamma_{2+}} = \frac{\Gamma_{Sr^{2+}} c^2_{Na^+}}{(\Gamma_\infty - 2\Gamma_{Sr^{2+}})^2 c_{eq}\gamma_+^2}. \quad (2)$$

Equation (2) is converted to formula (4) analogous to Langmuir isotherm equation (3).

$$\Gamma = \Gamma_\infty \frac{Ka}{1 + Ka}, \quad (3)$$

$$(\Gamma_{Sr^{2+}})^{1/2} = \Gamma_\infty \frac{(Kc_{eq})^{1/2}\gamma_+}{c_{Na^+} + 2\gamma_+(\Gamma_{Sr^{2+}} Kc_{eq})^{1/2}}, \quad (4)$$

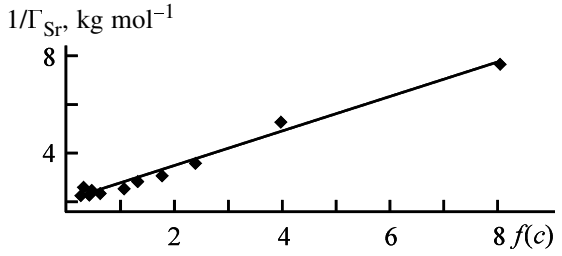


Fig. 2. Linearized isotherm of the exchange of Na^+ and Sr^{2+} ions. ($1/\Gamma_{Sr}$) Reciprocal of sorption of strontium cations; [$f(c)$], function depending on the equilibrium concentrations of sodium ions c_{Na^+} and strontium ions c_{eq}, the sorption value Γ_{Sr}, and the activity coefficients of single-charged cations γ_+ (dimensionless quantity).

where Γ and Γ_∞ are values of sorption and limiting sorption; K, equilibrium constant of the sorption process; and a, activity of sorbed ions.

The linear form of the equation looks like (5).

$$(\Gamma_{Sr^{2+}})^{-1} = \Gamma_\infty^{-1} + c_{Na^+}[\gamma_+\Gamma_\infty(\Gamma_{Sr^{2+}} Kc_{eq})^{1/2}]^{-1}. \quad (5)$$

It is similar to the linear Langmuir equation:

$$\Gamma^{-1} = \Gamma_\infty^{-1} + (\Gamma_\infty Ka)^{-1}.$$

The linear ion-exchange isotherm is shown in Fig. 2. The dependence of the reciprocal of the sorption of strontium ions on the argument

$$f(c) = c_{Na^+}[\gamma_+(\Gamma_{Sr^{2+}} c_{eq})^{1/2}]^{-1}$$

is approximated by the linear equation

$$(\Gamma_{Sr^{2+}})^{-1} = 0.72f(c) + 2.06$$

with $R^2 = 0.98$.

On this basis, using the formula $\Delta G^0_{298} = -RT\ln K$ (T = 298 K), we have calculated the limiting sorption of ions Γ_∞ = 0.97 equiv kg^{-1}, the apparent ion-exchange constant $K_{Na^+/Sr^{2+}}$ = 2.05, and the Gibbs energy of the exchange of strontium ions for sodium ions on the IMN surface ΔG^0_{298} = 1.78 kJ mol^{-1}. The thermodynamic data show that the ion-exchange equilibrium is shifted toward displacement of sodium ions from the IMN surface into the solution by Sr^{2+} ions.

The isotherm of the exchange of strontium and iron(III) ions described by a dependence similar to the Langmuir equation was obtained in [11] for a sample of Cambrian blue clay of the composition $K_2Al_4[Al_2Si_6O_{20}](OH,F)_4$. The resulting apparent exchange constant and the exchange Gibbs energy for

reaction (6) were $K_{Sr^{2+}/Na^+} = 5.28$ and $\Delta G^0_{298} = -4.13$ kJ mol^{-1}.

$$Sr^{2+}_{sol} + 2/3\,Fe^{3+}_{aq} \rightleftarrows Sr^{2+}_{aq} + 2/3\,Fe^{3+}_{sol}. \quad (6)$$

These data show that the equilibrium is shifted toward the displacement of strontium(II) from the solid phase by iron(III) ions.

The limiting sorption of strontium ions on the clay $\Gamma_0 = 0.068$ equiv kg^{-1} [11] is smaller by a factor of 14 than their limiting sorption of 0.97 equiv kg^{-1} on IMN. This is attributable to the fact that the specific surface area of IMN $S_{sp} = 41.81$ m^2 g^{-1} [12] is greater by a factor of 7 than that of Cambrian blue clay, $S_{sp} = 5.86$ m^2 g^{-1} [13], and the capacity of iron–manganese nodules $E = 7.66 \times 10^{-2}$ equiv kg^{-1}, determined by the sorption of Methylene Blue (MG) [12], is greater by a factor of seven than the capacity of the clay with respect to MG, $E = 1.03 \times 10^{-2}$ equiv kg^{-1} [13].

We have estimated the "landing area" of Sr^{2+} ions S_M (m^2) from the IMN specific surface area and limiting sorption of strontium ions of 0.485 mol kg^{-1}:

$$S_M = \frac{S_{sp}}{\Gamma_\infty N_A} = 14.3 \times 10^{-20}\ \text{m}^2,$$

where N is Avogadro's number.

Hence the radius of sorbed Sr^{2+} ions is 213×10^{-12} m or 213 pm, and it is larger than the Stokes crystallographic radius of 113 pm. This fact indicates that strontium ions are sorbed in the hydrated state in the Stern layer on the IMN surface. The found ionic radius of Sr^{2+} on the IMN surface is smaller than the ionic radius of 302 pm for strontium sorbed on the clay [11], which practically coincides with the Stokes ionic radius of Sr^{2+} (309 pm [7]) and is smaller that the radius of Fe^{3+} ions sorbed on a clay from an aqueous solution (348 pm [11]). Apparently, strontium ions are partially dehydrated when sorbed on IMN, and the number of hydration shells is reduced from two in an aqueous solution to one in the Stern layer. This fact indicates that the negative charge density on the IMN surface is higher than on the clay surface.

The Sr^{2+}_{aq} ions have a larger hydrated radius and higher charge than the Na^+ ions. However, the ionic potential, which is proportional to the ratio of the cation charge to the radius of the hydrated ion z/r_{aq}, is higher for Sr^{2+} ions; therefore, they displace Na^+ ions from the IMC surface in the ion-exchange reaction. According to the values of ion-exchange Gibbs energies, cations are ranked in the following order of the replacing power, which correlates with increasing ionic potential z/r_{aq} of hydrated cations:

	Na^+ <	Sr^{2+} <	Fe^{3+}
ΔG^0_{298}, kJ mol^{-1}		–1.78	–4.13 [11]
z/r_{aq}, nm^{-1}	5.46	6.48	8.62 [11]

CONCLUSIONS

(1) The isotherm of ion exchange of Na^+ and Sr^{2+} ions on iron–manganese nodules is described by a dependence analogous to Langmuir equation and can be presented in the linear form with $R^2 = 0.98$.

(2) The apparent ion-exchange constant $K_{Na^+/Sr^{2+}} = 2.05$ and the Gibbs energy of the exchange of strontium ions for sodium ions on the surface of iron–manganese nodules $\Delta G^0_{298} = 1.78$ kJ mol^{-1} were determined. A series of displacing power of ions based on the Gibbs energy of the ion exchange was constructed. It correlates with the growth of ionic potentials.

(3) The "landing area" of strontium ions on the surface of iron–manganese nodules was estimated at 14.3×10^{-20} m^2. The value of 213 pm of the radius of the sorbed cation suggests the sorption in the Stern layer with partial dehydration.

ACKNOWLEDGMENTS

This study was made within the framework of the scientific and technical program of the Federal Agency for Education "Development of the Scientific Potential of Higher School," section 2.1.

REFERENCES

1. Ivanov, Yu.A. and Kashparov, E.A., *Radiokhimiya*, 1992, vol. 34, no. 5, pp. 112–114.
2. Chuveleva, E.A., Firsova, L.A., Milyutin, V.V., et al., *Radiokhimiya*, 1996, vol. 38, no. 6, pp. 554–557.
3. Chirkst, D.E., Chaliyan, K.N., Chaliyan, A.G., et al., *Radiokhimiya*, 1996, vol. 38, no. 1, pp. 88–90.
4. Chirkst, D.E., Litvinova, T.E., Cheremisina, O.V., et al., *Radiokhimiya*, 2001, vol. 43, no. 5, pp. 475–478.
5. Shchukin, E.D. and Pertsov, A.V., *Kolloidnaya khimiya* (Colloid Chemistry), Moscow: Vysshaya Shkola, 2004.
6. Chirkst, D.E., Litvinova, T.E., Cheremisina, O.V., et al., *Radiokhimiya*, 2002, vol. 44, no. 4, pp. 378–381.

7. *Kratkii spravochnik fiziko-khimicheskikh velichin* (Concise Handbook of Physicochemical Quantities), Ravdel', A.A. and Ponomareva, A.M., Eds., Leningrad: Khimiya, 1983.
8. *Analiticheskaya khimiya strontsiya* (Analytical Chemistry of Strontium), Poluektov, N.S. and Mishchenko, V.T., Eds., Moscow: Akad. Nauk SSSR, 1971.
9. Vasil'ev, V.P., *Termodinamicheskie svoistva rastvorov elektrolitov* (Thermodynamic Properties of Electrolyte Solutions), Moscow: Vysshaya Shkola, 1982.
10. Kokotov, Yu.A., and Pasechnik, V.A., *Ravnovesie i kinetika ionnogo obmena* (Equilibrium and Kinetics of Ion Exchange), Leningrad: Khimiya, 1970.
11. Chirkst, D.E., Litvinova, T.E., Cheremisina, O.V., et al., *Zh. Prikl. Khim.*, 2004, vol. 77, no. 5, pp. 580–582.
12. Chirkst, D.E., Cheremisina, O.V., Ivanov M.I., et al., *Zh. Prikl. Khim.*, 2005, vol. 78, no. 4, pp. 599–605.
13. Chirkst, D.E., Krasotkin, I.S., Cheremisina O.V., et al., *Zh. Prikl. Khim.*, 2003, vol. 76, no. 4, pp. 687–689.

ISSN 1070-4272. Russian Journal of Applied Chemistry, 2006, Vol. 79, No. 3, pp. 372–376. © Pleiades Publishing, Inc., 2006.
Original Russian Text © L.Yu. Novoselova, E.E. Sirotkina, E.V. Sergeeva, 2006, published in Zhurnal Prikladnoi Khimii, 2006, Vol. 79, No. 3, pp. 378–382.

SORPTION AND ION-EXCHANGE PROCESSES

Preparation and Study of Properties of Sulfonic Acid Ion Exchangers Based on Polypropylene Fibrous Material

L. Yu. Novoselova, E. E. Sirotkina, and E. V. Sergeeva

Institute of Oil Chemistry, Siberian Division, Russian Academy of Sciences, Tomsk, Russia

Received May 31, 2005; in final form, November 2005

Abstract—The possibility of raising the static exchange capacity of strongly acidic ion-exchange materials produced by grafting of styrene onto polypropylene fibers, with the subsequent sulfonation of the products synthesized, was analyzed. The chemical and osmotic stabilities of the sulfonic cation exchangers obtained and their frost resistance in freeze–thaw cycles were studied.

DOI: 10.1134/S1070427206030074

Chemical modification of materials by grafting of compounds with various functional groups onto their surface can impart to them prescribed properties. Directed control over the thickness, structure, and nature of the grafted layer yields dense or loose, monomeric or polymeric, and mono- or polyfunctional grafted layers. The distribution of molecules in these layers may be statistically uniform, chaotically disordered, or of "islet" type. In each particular case, the most appropriate supports and modifiers should be selected by "successive approximations." The modifiers should contain functional groups imparting the above-mentioned special properties (complexing, hydrophobizing, ion-exchange, catalytic, etc.) to the target product. A functional group is commonly bound to the support surface by the so-called anchor and linker, groups that provide firm fixation of a functional group to the support surface (in the first case) and combine the anchor and functional group into a unit (in the second). Schematically, this structure can be represented as follows: support–anchor–linker–functional group. If compounds containing groups that can form chemical bonds directly with the support surface are used, the modification can be performed in one step. In other cases, it is necessary to carry out the process of modification of a material in a desired direction in steps (two or more), i.e., by the method of surface assembly, which makes it possible to construct complex molecular structures on the surface of a starting material [1–7].

The strong recent rise in the production of nonwoven fibrous materials (NFMs) is due to the simplicity of their manufacture and their efficiency in practical use [8, 9]. NFMs predominate over textiles among technical fibrous materials (FMs) and are more and more frequently used in medicine. Among the methods used to produce NFMs (adhesive-bonding, needle-punching, stitch-bonding, and spun-bonding), the most promising is the last one, whose characteristics provide, in the aggregate, the lowest production cost of the target product. One of the principal tendencies in the manufacture of NFMs is that toward replacement of natural fibers with those synthesized, with increasing share of polypropylene fibers (PPF). These fibers took a leading position, as regards the amount of consumption, as far back as mid-1980s. Polypropylene fibers are regarded as fibers with one of the best values for money because they have low density, high mechanical strength and abrasion resistance, easy fibrillation, etc.

The main application field of NFMs is manufacture of consumer goods and medicinal and technical materials (geotextile, separation, and membrane materials, technical filters for purification of dyes, spinning solvents, and oil-containing emulsions). For example, Remay materials manufactured by Du Pont, which are used to filter oils and air, have a service life 2.5 times that of paper materials and can be easily regenerated. In addition, they are readily corrugated to give cartridge filters because of their rigidity and elasticity. Filtering-protective materials manufactured by Rhône Poulenc and Reifenhäuser companies are made of polypropylene, by needle-punching in the first case and by thermal fixation in the second. Separation and membrane materials are also being manufactured by

Vilene (Japan, Vilene brand), Carl Freudenberg (Germany, Viledon brand), and Saft (France). These NFMs are produced from polypropylene and polyamide with a fiber diameter of 5–15 μm [10–16].

Ion-exchange fibers (IEF) and nonwoven materials on their base, which can be used to treat gas–air and liquid media to remove toxic admixtures, aerosols of acids and alkalis, ions of heavy metals, surfactants, and dyes, have a highly developed surface, good mechanical strength, and chemical and osmotic stabilities. The main advantages of IEFs over granulated ion exchangers in gas and water treatment are the high degree of purification and sorption rate; possibility of production of various textile forms (staple, threads, fabrics, and nonwoven needle-punched or stitch-bonded cloth), which makes wider the choice of apparatus that can be used; possibility of multiple use in sorption–desorption cycles; and low aero- and hydrodynamic resistances [17–19].

Previously, PPFs with surface-grafted compounds (SGCs) have been developed for use as ion exchangers [20–26]. Weakly acidic IEFs were synthesized by grafting of acrylic acid onto PPF, and strongly acidic ones, by sulfonation of styrene-grafted polypropylene fibrous materials. Styrene was grafted in a single step. Further, it was suggested to use the sulfonic cation exchangers obtained to recover metals from water [24, 25].

The aim of this study was to analyze the possibility of improving the capacity characteristics of the sulfonic cation exchangers developed by grafting styrene to PPF in two steps and to examine some properties of the IEFs synthesized. As objects of analysis were chosen such characteristics of IEFs as the chemical and osmotic stability (including the stability in moistening–drying cycles) and frost resistance in freeze–thaw cycles.

EXPERIMENTAL

The starting PPFs were thoroughly washed to remove contaminations and oxidized with atmospheric oxygen (110°C, 30 h) [20]. Styrene was grafted in the presence of initiating agents [benzoyl peroxide (BP) and azobisisobutyronitrile (AIBN)] and without initiators (method 1). After the reaction was complete, the material was washed to remove the possibly formed homopolymer. Then the grafted product was sulfonated with an excess amount of concentrated H_2SO_4 (80°C, 2 h) with preliminary keeping (25°C, 2 h) in 1,2-dichloroethane (DCE) or without it, washed with H_2SO_4 of decreasing concentration, treated with ethanol, and finally washed with distilled water. The washed fiber was dried and its static exchange capacity (SEC) was determined using the standard procedure by titration with an indicator [22].

Further selection of conditions for synthesis of IEF with improved capacity characteristics resulted in the development of a procedure for two-step grafting of styrene (method 2): in the first stage, the starting PPF was treated with styrene without initiator at an elevated temperature; in the second stage, synthesis was performed in ethanol in the presence of an initiator. The conditions under which SGCs were sulfonated and the SEC was determined were the same as those in method 1.

The chemical and osmotic stabilities of IEF (including that to multiple cycles of moistening–drying) and the frost resistance in freeze–thaw cycles were studied. To determine the chemical stability, IEF samples were treated with 5 N H_2SO_4, 1 N HNO_3, and 5 N NaOH solutions (100°C, 6 h). To study the osmotic stability, IEF samples were alternately treated (5 min) with 1 N solutions of HCl and NaOH (the so-called acid-alkaline shock, a total of 100 cycles) and also were subjected to moistening–drying cycles (a total of 30 cycles). In the last case, the materials were moistened with distilled water at 20°C for 5 min and dried in air at 60°C for 1 h. To determine the frost resistance, IEF samples were placed in closed vessels with water and were frozen at –20°C for 22 h and then thawed at 25°C for 2 h (a total of 30 freeze–thaw cycles). The stability of the materials studied to the above treatments was evaluated by changes in their SEC in the course of tests.

The results obtained in the study (Tables 1, 2) confirm some of the previously made assumptions [21, 22]. First, keeping of a grafted product in DCE leads to improved diffusion of the sulfonating agent into the PPF. As a result of swelling of PPF in DCE, the efficiency of sulfonation increases, with the SEC of the final IEF naturally increasing. Thus, it is worth mentioning that the sulfonation conditions affect (as also do the grafting conditions) the type of distribution of functional groups (SO_3H groups in the given case) across the fibrous material. For example, if the duration of sulfonation is decreased or the stage of PPF keeping with SGC in DCE is excluded from the process of manufacture of sulfonic cation exchangers, SO_3H groups are mostly distributed over the surface of a fibrous material even in the case of volume distribution of the grafted copolymer. Thus, researchers can preset the type of distribution of functional groups in a material by choosing conditions of both grafting

Table 1. Conditions of styrene grafting to PPF (in one step) and SEC of IEFs produced by sulfonation of PPF with SGC*

IEF sample no.	C_{St}, wt %	Solvent (initiator)	T_r, °C	τ_r, h	SEC, mg-equiv g^{-1}
1	20	CH_3OH	90	3	0.70
2**	20	CH_3OH	90	3	1.01
3**	80	CH_3OH	90	3	0.66
4**	80	CH_3OH	90	3	1.07***
5**	20	CH_3OH (AIBN)	80	4	1.21
6**	20	CH_3OH (BP)	85	5	1.70
7	20	CH_3OH (BP)	85	5	1.30
8	20	C_2H_5OH	90	3	0.93
9	40	C_2H_5OH	90	3	0.88
10	50	C_2H_5OH	90	3	0.81
11	80	C_2H_5OH	90	3	0.50
12	20	C_2H_5OH (AIBN)	80	4	1.11
13	20	C_2H_5OH (BP)	85	5	1.45
14**	20	C_2H_5OH	90	3	1.10
15**	20	C_2H_5OH (AIBN)	80	4	1.30
16**	20	C_2H_5OH (BP)	85	5	1.85

* C_{St}, concentration of styrene; T_r, reaction temperature; and τ_r, reaction duration.
** IEF samples obtained with products of styrene grafting onto PPF kept in DCE before sulfonation.
*** Experiment with a single washing of the material to remove the homopolymer.

Table 2. Conditions of styrene grafting onto PPF (in two stages) and SEC of the IEF obtained

IEF sample no.	C_{St}, wt %	Solvent (initiator)	T_r, °C	τ_r, h	SEC, mg-equiv g^{-1}
1	100	C_2H_5OH (AIBN)	60	1.5	Impregnation stage
	20		80	1.5	2.14
2	100	C_2H_5OH (AIBN)	60	1.5	Impregnation stage
	10		80	1.5	2.10
3	100	C_2H_5OH (BP)	70	2.0	Impregnation stage
	20		85	2.0	2.23
4	100	C_2H_5OH (BP)	70	2.0	Impregnation stage
	10		85	2.0	2.21
5*	100	C_2H_5OH (AIBN)	60	1.5	Impregnation stage
	20		80	1.5	2.45
6*	100	C_2H_5OH (AIBN)	60	1.5	Impregnation stage
	10		80	1.5	2.41
7*	100	C_2H_5OH (BP)	70	2.0	Impregnation stage
	20		85	2.0	2.54
8*	100	C_2H_5OH (BP)	70	2.0	Impregnation stage
	10		85	2.0	2.52

* IEF samples obtained with products of styrene grafting onto PPF kept in DCE before sulfonation.

and sulfonation (volume or surface sulfonation) and, consequently, can predetermine the nature, rate, and other characteristics of the processes that occur in the subsequent use of the products synthesized. Second, if initiating agents are used to ensure that the graft copolymerization occurs not only under the action of peroxides formed in preliminary oxidation of PPF, but also via chain-transfer reactions, use of BP is somewhat more efficient than that of AIBN.

It can also be seen that performing a two-step grafting of styrene onto PPF makes it possible to reduce the concentration of styrene in the reaction mixture in the second step from 20 to 10 wt % without any decrease in the SEC of IEF (Tables 1, 2). Presumably, the grafting occurs in this case with a higher efficiency for the following reason. Already in the first step (impregnation), the interfiber space of NWM itself, interfibrillar space in separate "threads," and other supra-

Table 3. Changes in the SEC of IEF samples as a result of tests

IEF sample no.*	SEC_{in}, mg-equiv g^{-1}	SEC_{fin}, mg-equiv g^{-1}					
		treatment in aggressive media			treatment with HCl–NaOH	moistening–drying	freeze–thaw
		5 N H_2SO_4	1 N HNO_3	5 N NaOH			
2	2.10	2.12	2.05	2.09	1.99	1.89	1.71
4	2.21	2.18	2.24	2.17	2.16	2.02	1.84
6	2.41	2.38	2.33	2.35	2.25	2.10	1.80
8	2.52	2.40	2.42	2.39	2.36	2.24	1.90

* Sample numbering corresponds to that in Table 2.

molecular structures (in the core, sheath, and surface of fibers) of the starting PPF are saturated with styrene. At the same time, the second stage involves styrene grafting proper over the entire cross section of a fiber, both within inner voids filled with styrene and on the surface of PPF.

The data of Table 2 confirm that production of IEF by two-step grafting is more efficient than the one-step process (Table 1) and leads to an increase in the SEC of the materials synthesized. As already mentioned above, a bulk polystructure is formed, with styrene penetrating through the entire cross section and all macro- and micromorphological formations of the fibrous material in the impregnation step. Presumably, the subsequent synthesis leads to an increase in the amount of grafted copolymer products and, in the end, to a higher SEC of the sulfonic cation exchangers obtained. In addition, the specific features of the mechanism by which the grafting develops in each step are governed by its conditions and primarily by temperature and presence of initiators. For example, an increase in temperature leads to decomposition of the hydroperoxy groups of oxidized PPF [20], which initiates grafting of styrene to PPF. If initiators of radical copolymerization (BP and AIBN) are introduced into the reaction zone, they start to affect these processes by making an additional contribution to the grafting efficiency.

There is no escape from mentioning that the total duration of two-step grafting of styrene to PPF is shorter than that for the single-step grafting. For example, the duration of single-step grafting is 4 (AIBN) and 5 h (BP) (Table 1). Use of two-step techniques makes it possible to reduce the total duration of grafting to 3 h with AIBN and to 4 h with BP (Table 2). Presumably, this is due to the already mentioned intensification of the occurring reactions by preliminary impregnation of the starting PPF with styrene.

Table 3 lists the results obtained in a study of the chemical and osmotic stabilities and frost resistance of some samples of the IEFs obtained, specifically, the effect of these tests on the SEC of the materials.

Table 3 shows that the IEFs synthesized have a high stability against aggressive media (acids and alkalis), which is presumably due to the chemical stability of the polypropylene matrix and sulfo groups and to resistance to washing-out of the grafted copolymer.

The slight decrease in the static exchange capacity of IEF, observed in moistening–drying and freeze–thaw cycles, is presumably due to development of some structural defects in the material. The appearance, development, and accumulation of microcracks may lead to subsequent partial disintegration of an insignificant part of fibers and to their rupture, with the possible removal of a part of the grafted product and the corresponding decrease in the SEC of the material. More demonstrative in this case are frost resistance tests, during which the volume of the aqueous phase changes as a result of freezing and thawing of the samples (in water–ice–water transitions). The stresses generated in the process may lead to partial degradation of the material and to a decrease in its capacity characteristics.

The SEC of ion exchangers as a result of the tests mentioned above may also somewhat decrease because of a certain loosening of the polymeric matrix on keeping PPF with SGC in dichloroethane prior to sulfonation (Table 3, sample nos. 6 and 8). As it frequently occurs, the same treatment of the material (with DCE in the given case) may further have a positive or negative effect. However, choice of the optimal conditions for all the processes makes it possible to obtain, in the end, materials with the necessary prescribed set of properties.

The IEFs studied, which were subjected to multiple

moistening–drying and freeze–thaw cycles, on the whole retain their structure and service characteristics.

CONCLUSIONS

(1) Grafting of styrene to a polypropylene fiber in two steps, including preliminary impregnation of the starting fibrous material with styrene, leads to an increase in the static exchange capacity of sulfonic cation exchangers produced by sulfonation of grafted products.

(2) The sulfonic cation exchangers obtained show a high resistance to acids and alkalis. The slight decrease in their static exchange capacity upon multiple moistening–drying and freeze–thaw cycles is due to the development of certain defects in the materials; nevertheless, they on the whole retain their working characteristics (recovery of metals from water) at a level sufficient for their exploitation.

REFERENCES

1. *Modifitsirovannye kremnezemy v adsorbtsii, katalize i khromatografii* (Modified Silicas in Adsorption, Catalysis, and Chromatography), Lisichkin, G.V., Ed., Moscow: Khimiya, 1986.
2. Radkevich, V.Z., Kistanova, I.E., Soldatov, V.S., and Yegiazarov, Yu.G., *Russ. J. Appl. Chem.*, 2001, vol. 74, no. 9, pp. 1446–1449.
3. Chang, T.C., *Functionalization of Polyolefins*, San Diego: Academic, 2002.
4. Hartley, F.R., *Supported Metal Complexes: A New Generation of Catalysts*, Dordrecht: Reidel, 1989.
5. Yegiazarov, Yu.G., Radkevich, V.Z., Johann, J., et al., *React. Funct. Polym.*, 2000, vol. 44, no. 2, pp. 145–152.
6. Slizhov, Yu.G. and Gavrilenko, M.A., *Primenenie vnutrikompleksnykh soedinenii v gazovoi khromatografii* (Use of Chelates in Gas Chromatography), St. Petersburg: SpetsLit, 2003.
7. Mehrabzadeh, M. and Hossein Nia, K., *J. Appl. Polym. Sci.*, 1999, vol. 72, no. 10, pp. 1257–1265.
8. RF Patent 2 106 898.
9. Sirotkina, E.E., Ivanov, V.G., Glazkov, O.V., et al., *Khim. Inter. Ustoich. Razv.*, 1997, vol. 5, no. 5, pp. 429–437.
10. Perepelkin, K.E., *Struktura i svoistva volokon* (Structure and Properties of Fibers), Moscow: Khimiya, 1985.
11. Genis, A.V., Andrianova, L.N., Semakova, Z.L., and Sindeev, A.A., *Khim. Volokna*, 1989, no. 5, pp. 5–10.
12. Le Thuaut, Ph., Martel, B., Crini, G., et al., *J. Appl. Polym. Sci.*, 2000, vol. 77, no. 10, pp. 2118–2125.
13. Artemenko, S.E., Ponomareva, N.V., and Panova, L.T., *Int. Polym. Sci. Technol.*, 2002, vol. 29, no. 8, pp. 53–54.
14. Mizutani Yukio and Nago Satoshi, *J. Appl. Polym. Sci.*, 1999, vol. 73, no. 8, pp. 1549–1553.
15. Genis, A.V. and Smirnov, A.V., *Plast. Massy*, 2003, no. 5, pp. 13–17.
16. Mansfield, R.G., *Textile World*, 1986, vol. 136, no. 12, pp. 59–62.
17. Soldatov, V.S., *Ion Exchange at the Millenium*, Greig, J.A., Ed., London: Imperial College Press, 2000, pp. 193–200.
18. Soldatov, V.S., Shunkevich, A.A., Elinson, I.S., et al., *Desalination*, 1999, vol. 124, nos. 1–3, pp. 181–192.
19. Soldatov, V.S., Shunkevich, A.A., and Martsinkevich, V.V., *Russ. J. Appl. Chem.*, 2001, vol. 74, no. 9, pp. 1521–1524.
20. Novoselova, L.Yu., *Plast. Massy*, 2002, no. 11, pp. 42–44.
21. Novoselova, L.Yu. and Bordunov, V.V., *Plast. Massy*, 2002, no. 8, pp. 6–8.
22. Novoselova, L.Yu. and Bordunov, V.V., *Plast. Massy*, 2003, no. 8, pp. 9–10.
23. Novoselova, L.Y. and Bordunov, V.V., *Int. Polym. Sci. Technol.*, 2004, vol. 31, no. 4, pp. T/23–26.
24. Novoselova, L.Yu., Mityushkin, M.B., and Vinnichenko, L.I., in *Sovremennye dostizheniya v issledovaniyakh okruzhayushchei sredy i ekologii: Sbornik nauchnykh statei* (Modern Achievements in Studies of the Environment and Ecology: Coll. of Sci. Works), Tomsk: STT, 2004, pp. 82–83.
25. Novoselova, L.Yu. and Bordunov, V.V., in *Sovremennye dostizheniya v issledovaniyakh okruzhayushchei sredy i ekologii: Sbornik nauchnykh statei* (Modern Achievements in Studies of the Environment and Ecology: Coll. of Sci. Works), Tomsk: STT, 2004, pp. 195–197.
26. Novoselova, L.Y. and Bordunov, V.V., *Int. Polym. Sci. Technol.*, 2003, vol. 30, no. 4, pp. T/52–55.

ISSN 1070-4272. Russian Journal of Applied Chemistry, 2006, Vol. 79, No. 3, pp. 377–379. © Pleiades Publishing, Inc., 2006.
Original Russian Text © O.M. Trokhimenko, 2006, published in Zhurnal Prikladnoi Khimii, 2006, Vol. 79, No. 3, pp. 383–386.

SORPTION AND ION-EXCHANGE PROCESSES

Sorption of Molybdoarsenates Reduced by Ascorbic Acid with Polyurethane Foams Based on Ethers, Esters, and Their Copolymers

O. M. Trokhimenko

Shevchenko Kiev National University, Kiev, Ukraine

Received June 20, 2004; in final form, June 2005

Abstract—Sorption of molybdoarsenates reduced by ascorbic acid from aqueous solutions with polyurethane foams based on ethers, esters, and their copolymers was studied in relation to the phase weight ratio and solution acidity.

DOI: 10.1134/S1070427206030086

Preconcentration is required to determine the total content of arsenic or the content of its separate species in the environment by physicochemical methods at concentrations close to the maximum permissible concentration (MPC) [1].

At present, the most widespread extraction methods give way to sorption methods, which provide higher distribution coefficients of microcomponents without using toxic organic solvents [2].

Arsenic(V) as molybdoarsenate is recovered on activated carbon [3] or on membrane nitrocellulose filters in the presence of quaternary ammonium bases [4]. It was shown in [1] that molybdoarsenate is efficiently recovered on an Amberlyte XAD-8 polyacrylate sorbent, or on thin-layer cellulose triacetate filters in the presence of tri-*n*-octylamine. Since polyurethane foams contain ether and amino groups [5, 6], i.e., functional groups of organic solvents recovering heteropoly complexes, they sorb such complexes with phosphorus, silicon [7, 8], and arsenic [9] as central atoms.

There is substantial difference between solvents and sorbents from the practical viewpoint: solvents are individual chemical substances, whereas sorbents are materials. The sorption properties of materials can somewhat vary depending on producer or even from one batch to another [10]. Therefore, the analytical characteristics should be studied for the same batch. In addition, materials based on organic polymers can undergo aging under the action of light, moisture, and air depending on storage conditions.

In this study, we examined sorption of molybdoarsenate reduced with ascorbic acid (RMA) on polyurethane foams based on ethers (PUF-1), esters (PUF-3), and their copolymers (PUF-2). We cannot guarantee the complete repeatability of the results because of the reasons mentioned above. However, general features of the behavior of these sorbents with respect to RMA can be revealed.

EXPERIMENTAL

The stock solution of sodium hydroarsenate [chemically pure grade, 100 μg As(V) in 1 cm^3] was prepared by dissolving an accurately weighed portion of the compound. The other solutions were prepared by dilution of the stock solution. The RMA solutions were prepared in the presence of excess molybdenum(VI) and ascorbic acid [11] taking into account that preliminarily synthesized and isolated heteropoly complexes, when dissolved in water, undergo irreversible acid–base transformations with formation of products with central atom : ligand ratio equal to 1 : 12, 1 : 11, 1 : 9, etc.

Acetone (chemically pure grade) was used to desorb complexes from the PUF surface.

Polyurethane foams based on ethers, esters, and their copolymers of 5-30, 35-98 and ER trademark, respectively, produced by Radikal plant (Kiev) were cut into 3 × 3 × 3 mm cubes and washed with sulfuric acid, water, and acetone before use [8].

Electronic absorption and diffuse reflection spectra were recorded on a Specord M-40 spectrophotometer (Germany).

Sorption was measured in the static mode. A PUF sample [(0.050 – 0.500) ± 0.001 g] was introduced into a beaker with an RMA solution (25–500 cm^3). A PUF cube was pressed to a glass bottom with a spatula to

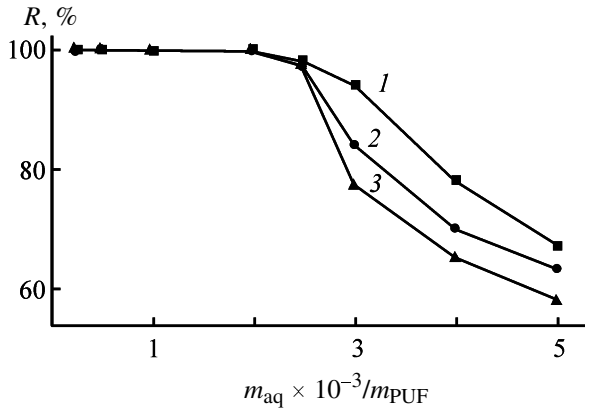


Fig. 1. Influence of phase weight ratio m_{aq}/m_{PUF} on degree of RMA sorption R. 40 μg of As(V), pH 1. Sorbent: (*1*) PUF-1, (*2*) PUF-2, and (*3*) PUF-3; the same for Figs. 2–4.

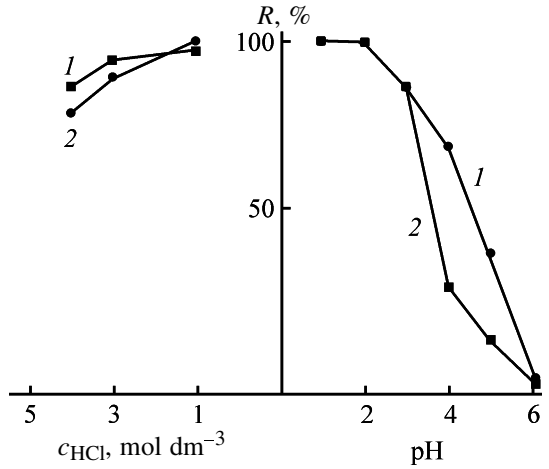


Fig. 2. Influence of solution acidity on the degree R of the recovery of RMA with various sorbents. $c_{As(V)} = 5 \times 10^{-5}$ mol dm^{-3}, $m_{aq}/m_{PUF} = 1000$. (c_{HCl}) HCl concentration.

remove air bubbles, and the solution was agitated with a magnetic stirrer to reach the sorption equilibrium. Then, PUF was separated from the solution, washed with distilled water, and dried between filter paper sheets and then in air. After that, the diffuse reflection spectrum of the sorbent with the sorbate and the absorption spectrum of the acetone desorbate were recorded. The effect of pH on RMA recovery was examined by adding a NaOH solution after complex formation under optimal conditions.

The preliminary experiments showed that the sorption equilibrium between RMA and the sorbent is attained in 10 (PUF-1), 15 (PUF-2), and 20 min (PUF-3).

The effect of the phase weight ratio m_{aq}/m_{PUF} on the RMA recovery was studied at a constant As(V) content. The recovery of the complex was quantitative at $m_{aq}/m_{PUF} < 2500$ (Fig. 1). At a further increase in this ratio, the degree of recovery gradually decreases due to less efficient contact between the sorbent and sorbate.

The state of the reduced heteropoly complexes in the solution depends on the absolute concentration of the central atom and the central atom : ligand ratio, on the type and concentration of the reductant, on pH, and on the solution ionic strength. Under the optimal conditions of formation, RMA is a reduced β-isomer of 12-molybdoarsenate with the formula β-$[AsMo_8^{VI}Mo_4^{V}O_{40}]^{7-}$ [12]. One of the main factors determining the state of the heteropoly complexes and hence their sorbability is the solution acidity.

The dependence of the degree of RMA recovery with polyurethane foams of various types on the solution acidity is shown in Fig. 2. As seen, the recovery of the complex is maximal at pH 0–2, which coincides with the pH range of its maximal extraction with oxygen-containing organic solvents (alcohols, ethers) [2]. In comparison with oxidized molybdoarsenate, RMA is sorbed within a wider pH range [9] due to higher stability with respect to acid and base hydrolysis. Within the entire range of acidity studied, the degree of RMA recovery with PUF-1 is somewhat larger than with PUF-3. This may be due to the fact that the ether groups form H bonds more readily than do ester groups [7, 13]. In addition, ethers are stronger electron donors than esters. This favors stronger donor–acceptor interactions of molybdenum atoms in RMA with oxygen atoms of PUF-1 polyether units. The decrease in the degree of RMA recovery from the acid solutions ($c_{HCl} > 2$ mol dm^{-3}) can be explained by the competition of Cl^- ions in anion-exchange binding of RMS and by partial decomposition of RMA with formation of molybdenum(V, VI) oxycations ($c_{HCl} >$ 4 mol dm^{-3}). A decrease in the recovery at pH 3–5 is caused by deprotonation of the sorbents (rather than by base hydrolysis of the sorbate), since RMA formed under optimal conditions is stable at pH increased to the above values.

Isotherms of RMA sorption are Langmuir-type isotherms (Fig. 3). The limiting sorption a_l and sorption constant K ($n = 5$, $P = 0.95$) calculated from them by the linear form of the Langmuir equation [14] are listed below:

PUF type	a_l, μmol g^{-1}	$K \times 10^{-6}$, dm^3 mol^{-1}
PUF-1	98	1.4
PUF-2	98	0.04
PUF-3	58	0.6

It is seen that a_l for PUF-1 and PUF-2 is actually

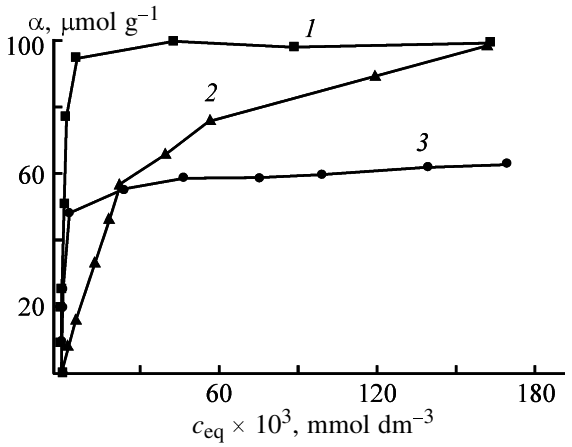


Fig. 3. Sorption isotherms of RMA. m_{aq}/m_{PUF} = 500, T = 293 K. (c_{eq}) RMA equilibrium concentration in aqueous solution and (α) concentration of RMA on PUF.

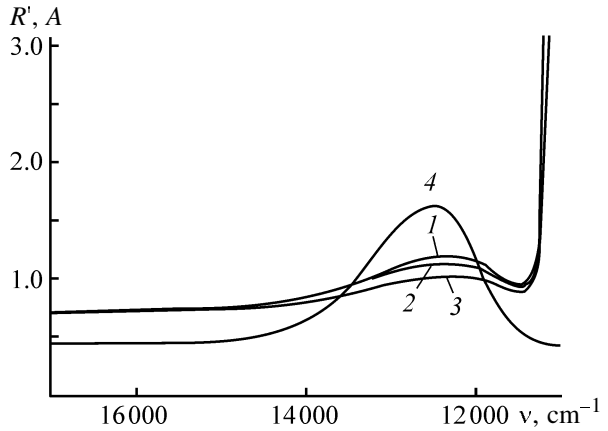


Fig. 4. Diffuse reflection spectra of RMA sorbed on the surface of (*1*) PUF-1, (*2*) PUF-2, and (*3*) PUF-3, and (*4*) its absorption spectrum in aqueous solution. m_{aq}/m_{PUF} = 500; 40 μg of As(V); Specord M-40. (*1–3*) (R') Diffuse reflection, (*4*) (A) optical density, and (ν) wavenumber.

the same, and for PUF-3 it is by a factor 2 lower. The sorption constant K decreases in the order PUF-1 > PUF-3 > PUF-2.

The state of RMA in the polyurethane foam phase was studied by diffuse reflection spectroscopy. The diffuse reflection spectra of RMA sorbed on various types of polyurethane foams and absorption spectrum of RMA aqueous solution are shown in Fig. 4. The band at 13500 cm^{-1} of the latter (Fig. 4, spectrum *4*) transforms into a shoulder, and a new band at ν < 11000 cm^{-1} (Fig. 4, spectra *1–3*) appears when RMA is sorbed on polyurethane foam. Bands within the 16500–12500 cm^{-1} range originate from charge transfer between Mo(V) and Mo(VI). A change in the energy of charge transfer of the complex sorbed on the polyurethane foam surface is indicative of a change in the energy of heteropolyanion molecular orbitals, which, in turn, suggests strong interaction (probably, through H bond) between RMA and the polymeric matrix. RMA is quantitatively recovered with acetone and other oxygen-containing solvents; λ_{max} of desorbates actually coincides with λ_{max} of RMA in aqueous solution.

CONCLUSIONS

(1) Comparative study showed that PUF-1 has higher sorption power with respect to molybdoarsenate reduced with ascorbic acid. This is also characteristic for heteropoly complexes with other central atoms (P, Si).

(2) The recovery of reduced molybdoarsenate by sorption on polyurethane foams is maximal at pH 0–2, and the concentration coefficient is 2.5×10^3.

(3) Isotherms of sorption of reduced molybdoarsenate are Langmuir-type isotherms. The sorption constants decrease in the order PUF-1 > PUF-3 > PUF-3.

REFERENCES

1. Tikhomirova, T.I., Kuznetsova, M.V., Dubovik, D.B., et al., *Zh. Anal. Khim.*, 2000, vol. 55, no. 9, pp. 942–946.
2. Dorokhova, E.N. and Alimarin, I.P., *Usp. Khim.*, 1979, vol. 48, no. 5, pp. 930–952.
3. Kubota, T., Yamaguchi, T., and Okutani, T., *Talanta*, 1998, vol. 46, pp. 1311–1314.
4. Hata, N., Kasahara, I., Taguchi, S., et al., *Analyst*, 1989, vol. 114, pp. 1225–1229.
5. Braun, T., Navratil, Y.D., and Farag, A.B., *Polyurethane Foam Sorbents in Separation Science*, Boca Raton: CRC, 1985.
6. Dmitrienko, S.G. and Zolotov, Yu.A., *Usp. Khim.*, 1999, vol. 68, no. 2, pp. 181–235.
7. Dmitrienko, S.G., Goncharova, L.V., Runov, V.K., et al., *Zh. Fiz. Khim.*, 1997, vol. 71, no. 12, pp. 2227–2231.
8. Trokhimenko, O.M., Sukhan, V.V., and Nabivanets, B.I., *Zh. Obshch. Khim.*, 1999, vol. 69, no. 2, pp. 215–218.
9. Khan, A.S. and Chow, A., *Talanta*, 1984, vol. 31, no. 4, pp. 303–306.
10. Zaitsev, V.N., *Zh. Anal. Khim.*, 2003, vol. 58, no. 7, p. 688.
11. *GOST* (State Standard) *4152–89: Method of Determination of Weight Concentration of Arsenic*, Moscow: Izd. Standartov, 1990, pp. 1–7.
12. Pope, M.T., *Heteropoly and Isopoly Oxometalates*, Berlin: Springer, 1983.
13. Terney, A.L., *Contemporary Organic Chemistry*, Philadelphia: Sandberg, 1980, 2nd ed.
14. *Adsorption from Solution at the Solid/Liquid Interface*, Parfitt, G.D. and Rochester, C.H., Eds., London: Academic, 1983.

ISSN 1070-4272. Russian Journal of Applied Chemistry, 2006, Vol. 79, No. 3, pp. 380–385. © Pleiades Publishing, Inc., 2006.
Published in Russian in Zhurnal Prikladnoi Khimii, 2006, Vol. 79, No. 3, pp. 387–392.

SORPTION AND ION-EXCHANGE PROCESSES

Physicochemical and Rheological Properties of Thickeners Produced from Tunisian Clays[1]

M. Chtourou, M. Trabelsi, S. Baklouti, and M. Hedi Frikha

Laboratory of Applied Chemistry, Sfax, Tunisia
Laboratory of Industrial Chemistry, Sfax, Tunisia

Received October 19, 2004

Abstract—Modification of two samples of Tunisian clays of the type of natural smectites with organic derivatives of ammonium salts was studied. The physicochemical properties of the modified products and the possibility of their use as components of lubricating oils were analyzed.

DOI: 10.1134/S1070427206030098

Natural clays find increasingly wide use. Their application fields include manufacture of ceramics, paints, printing inks, and lubricants [1–3]. Use of natural clays makes it possible not only to reduce the cost of articles, but also to impart to them plasticity and mechanical strength. These properties of clay are associated with the nature and structure of aluminosilicates. Because of their structure, clays can swell in polar solvents, e.g., water. However, they fail to do so in nonpolar solvents and do not acquire new rheological properties [4]. To use clays as thickeners in organic systems, natural hydrophilic materials should be modified by introduction of organic cations. The most widely used of these are cations of salts of quaternary ammonium bases, which contain at least one hydrocarbon chain with 12 to 18 carbon atoms [5–7]. It is the cation exchange of these ions for inorganic ions present on the surface of clay particles that imparts organophilic properties to the clay.

The thus modified organophilic clays are widely used as thickeners in manufacture of paints, printing inks, and lubricants [3, 4]. Introduction of modified clays into lubricants (e.g., into lubricating grease) can change their viscosity, make them pseudoplastic [3], and improve their mechanical properties and stability at elevated temperatures [1, 5–8].

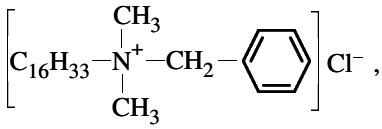
The clays best suitable for modification with organic cations belong to smectites (montmorillonites): bentonite, hectorite, beidellite, stevensite, etc. [8]. These clays have a static exchange capacity (SEC) for cations of no less than 70 mmol-equiv per 100 g [1].

[1] This article was submitted by the authors in English.

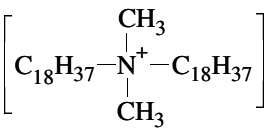
Tunisian clays are widely used in manufacture of ceramic articles [9], but still find use neither in the paint-and-varnish industry, nor in production of lubricants. Here we consider clays suitable for modification with organic cations to enable their use as thickeners. Their physicochemical and rheological properties are studied in comparison with Bentones widely used in the industry. This study is a part of research work devoted to assessment of Tunisian clays.

EXPERIMENTAL

Two clay samples taken in southern Tunisia were chosen for the study. The raw samples were designated as B_{1r} and B_{2r}. The samples were modified with organic cations, using the following ammonium salts (Aldrich): dimethylbenzylhexadecylammonium chloride [BDMHA]Cl and dimethyldioctadecylammonium chloride [DMDOA]Cl:



[BDMHA]Cl



[DMDOA]Cl

The properties of the modified clays were compared with those of industrially modified clay Bentone 34 (RHEOX, Brussels, Belgium). The SEC of the clay samples was determined in the reaction with

bis(ethylenediamine)copper(II) sulfate prepared from copper(II) sulfate and ethylenediamine (both purchased from Aldrich).

The results obtained in a chemical analysis of the clays by the X-ray fluorescence technique are listed in Table 1; the clays studied contain a comparatively small amount of aluminum oxide (9–15 wt %) and are rich in silicon dioxide (40–50 wt %). It should be noted that presence of quartz in a clay impairs its plasticity. The calcination loss by the B_{1r} sample may reach 23%. So large values of the calcination loss are probably observed because of the presence of simple and(or) double carbonates and organic impurities in the clays.

The density ρ of the samples was determined by pycnometry. The specific surface area of the clays under study, S_{sp}, was found by BET on a Flow Sorb II 2300 instrument. The results of these measurements are listed in Table 2.

According to the results obtained, both the clays, B_{1r} and B_{2r}, have a density very close to that of pure montmorillonite (2.0 to 2.4 g cm^{-1}) and a large specific surface area. The value of S_{sp} for sample B_{2r} exceeds that for B_{1r}. Granulometric analysis of the clays (Fig. 1) shows that the constituent particles vary in size from 0.32 to 4.70 μm. However, most of clay particles have sizes falling within a very narrow range 0.32–1.00 μm. The particle sizes of sample B_{2r} are somewhat smaller compared to B_{1r}.

To determine the static exchange capacity of samples B_{1r} and B_{2r}, they were purified to remove mechanical impurities, sieved (~20 μm mesh), and converted into a form saturated with sodium cations. The SEC values of the clay samples were determined by the adsorption of the $[Cu(NH_2CH_2CH_2NH_2)_2]^{2+}$ cation [10]. This cation is highly selective toward clays and forms with them stable compounds [11]. In cation exchange, it can replace in clays most of other cations and even those of heavy metals [12].

In the experiments, 0.3-g samples of purified clays were treated in a 50-ml flask with a $[Cu(NH_2CH_2 \cdot CH_2NH_2)_2]SO_4$ solution of concentration 1.66×10^{-2} M, after which the pH value of the resulting mixture was measured. The adsorption equilibrium was attained in the system in 30 min, and then the mixture was separated by centrifugation. The content of the $[Cu(NH_2CH_2CH_2NH_2)_2]^{2+}$ cation in the supernatant was determined on a spectrophotometer from the absorption in the visible spectral range (550 nm). The SEC of the clays was determined from the difference between the added amount of the Cu(II) complex and that remaining in solution.

Table 1. Chemical composition of the starting clays

Composition	B_{1r}	B_{2r}
SiO_2	40.78	50.87
Al_2O_3	9.2	14.92
MgO	15.9	9.82
Fe_2O_3	2.06	1.36
CaO	5.51	3.28
K_2O	1.98	0.45
Na_2O	2.02	1.86
Calcination loss	22.92	17.37

Table 2. Density ρ and specific surface area S_{sp} of the starting clays

Clay	ρ, g cm^{-3}	S_{sp}, m^2 g^{-1}
B_{1r}	2.34	68.11
B_{2r}	236.0	110.52

Kinetic experiments on exchange of inorganic cations of the clays for organic ammonium cations were carried out by the method that is, in principle, similar to that used to determine the SEC for $[Cu(NH_2CH_2 \cdot CH_2NH_2)_2]^{2+}$. A suspension was prepared from a preliminarily purified clay taken in an amount of 2 wt % relative to the liquid phase (90 vol % H_2O + 10 vol % ethanol). The suspension was placed in a reactor with a reflux condenser and stirrer and was gradually heated to 80°C. After that, a solution of a quaternary ammonium salt (QAS) was added to the suspension. The presence of ethanol in the mixture facilitated dissolution of QAS. The suspension was sampled at regular intervals of time, the samples were separated

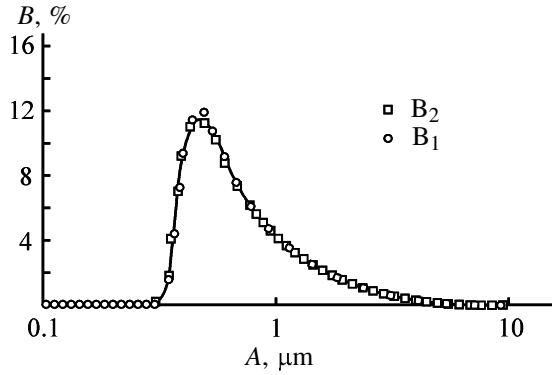


Fig. 1. Rersults of a granulometric analysis of the starting clays. (*B*) Content and (*A*) size of particles.

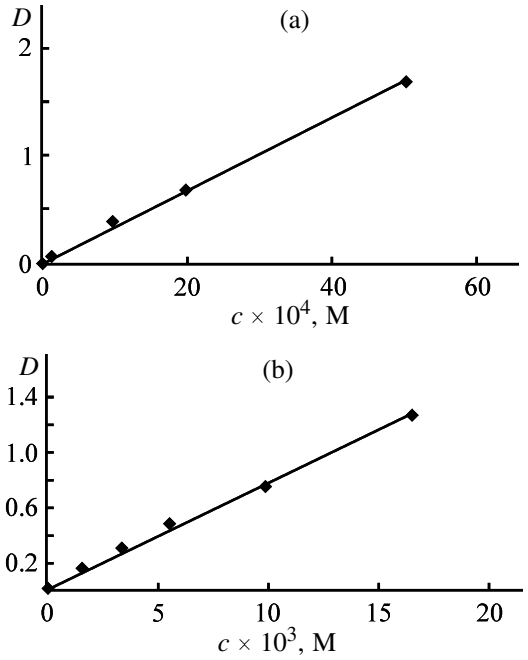


Fig. 2. Calibration plot for UV spectrophotometric determination of the concentration c of (a) $[BDMHA]^+$ and (b) $[Cu(NH_2CH_2CH_2NH_2)_2]^{2+}$ in solution. (D) Optical density. Wavelength λ, nm: (a) 262.5 and (b) 550.

by centrifugation, and the content of QAS was determined in the aqueous-alcoholic phase by two methods: UV spectroscopy and titration. In this way, the running concentration of QAS and the instant of time at which the reaction was complete were determined.

The UV spectroscopic studies of solutions were performed on a Shimadzu UV 2100 spectrophotometer. This method was used to study the kinetics of ion exchange between cations of clays B_{1r} and B_{2r} and the $[BDMHA]^+$ cation, because $[DMDOA]^+$ absorbs neither in the UV nor in the visible spectral range. The calibration plot used to determine the concentration of $[BDMHA]^+$ by UV spectroscopy is shown in Fig. 2a.

The titrimetric determination of the content of $[DMDOA]^+$ was performed by precipitation with a $NaB(C_6H_5)_4$ solution in the presence of Methyl Orange as indicator, in accordance with published recommendations [13].

Table 3. Static exchange capacity of the raw (r) and purified (p) clays

Clay	pH of suspension	Maximum absorbed amount, mmol per 100 g of clay	SEC, mmol-equiv per 100 g of clay
B_{1r}	10.04	32.24	64.48
B_{1p}	10.26	37.80	75.60
B_{2r}	10.26	42.53	85.06
B_{2p}	10.55	49.83	99.66

The IR spectra of modified clays were measured on a JASCO FT-IR 420 instrument. The X-ray phase analysis of the samples was made on a Philips PW 3710 instrument (CuK_α radiation).

The density of the samples was measured on a Helium Accu Pyc V_2 0.3N device.

To determine the rheological properties of the modified clays, the samples were ground in a Fritsch Pulverizer laboratory planetary mill and dispersed with ultrasound in a toluene–ethanol mixture. The resulting suspensions-gels were studied on a Reologica Instruments AB device with a C 40 4 measuring unit.

The composition of the suspensions being analyzed was, in accordance with the recommendations [3, 14], the following (wt %): modified clay 10, ethanol 10, toluene 80.

The static exchange capacity of the clays is the most important factor that predetermined their ability to be modified with organic cations. Clays with higher SEC more strongly swell in organic solvents and, as shown below, have better rheological properties. Figure 2a shows the calibration plot for determining the concentration of $[Cu(NH_2CH_2CH_2NH_2)_2]^{2+}$ ions in solution that is in contact with a clay. The results obtained in determining the SEC of the clays for the bis(ethylenediamine) complex of copper(II) are listed in Table 3. It can be seen that the $[Cu(NH_2CH_2CH_2 \cdot NH_2)_2]^{2+}$ cation is sorbed on the surface of the raw and purified samples of B_1 clays (B_{1r} and B_{1p}, respectively) less effectively than in the case of B_{2r} and B_{2p} samples. For both B_{1p} and B_{2p} samples, the SEC exceeds 70 mmol-equiv per 100 g of clay, which confirms that both the samples are rich in smectite (montmorillonite). Table 3 also shows that purification of clays enhances the adsorption of copper(II). In this case, the SEC increases by approximately 17%. This increase can be attributed to removal of impurities, free quartz and soluble mineral salts, from the clays in the course of their purification.

As follows from Fig. 3a, the rate of cation exchange between clay samples B_{1p} and B_{2p} and the $[BDMHA]^+$ cation is very high. In fact, the degree of replacement of the inorganic cation by the organic cation in 20 min is 90 and 50% for B_{1p} and B_{2p} samples, respectively. That is, the clays exhibit high affinity for organic cations. This primarily refers to B_{1p} sample. The cation exchange leading to modification

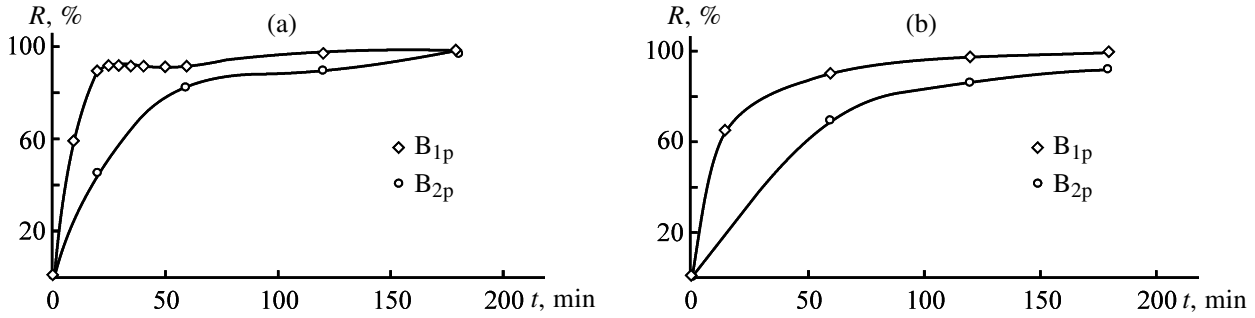


Fig. 3. Degree R of ion exchange with (a) $[BDMHA]^+$ and (b) $[DMDOA]^+$ cation for clays B_{1p} and B_{2p} vs. the time t of contact.

of clay samples with organic ammonium cations is complete in 1 h.

The kinetics of cation exchange between B_{1p} and B_{2p} samples and the $[DMDOA]^+$ cation can be judged from the data in Fig. 3b. Comparison of Figs. 3a and 3b shows that the rate of clay modification with $[BDMHA]^+$ cations is higher than that in the case of the $[DMDOA]^+$ cation. This can be attributed to structural differences between these ions. The $[DMDOA]^+$ cation contains two long hydrocarbon chains C_{18}. According to published data [15], the cation exchange in clays is the fastest when the organic cation contains aromatic groups capable of π-electron interaction with the surface centers of the material. For both the samples, the reaction of their modification with the $[DMDOA]^+$ cation is complete in 3 h.

According to Fig. 3, the saturation of the clays with organic ammonium cations on reaching the above values of SEC corresponds to replacement of approximately 96% of mineral cations with organic cations. Such an exchange makes it possible to raise the degree of hydrophobicity of a clay [16] and its compatibility with organic solvents.

Clays B_{1p} and B_{2p} modified with the organic cations $[BDMHA]^+$ and $[DMDOA]^+$ are designated in what follows as B_1H, B_2H, B_1D, and B_2D, respectively. These clays, obtained under preliminarily determined optimal conditions (time of contact between phases, solution temperature, concentration of an ammonium salt, SEC), were isolated by filtration. Then, they were several times washed on a filter with water and dried at 80–90°C. The products obtained were analyzed by various methods and compared with a commercial sample of Bentone 34.

The IR spectra of modified samples, compared to the raw samples, contain additional peaks (Fig. 4): one at 2851 cm^{-1} and another at about 2920 cm^{-1}. Both these peaks correspond to absorption by aliphatic CH_2 groups of the hydrocarbon chains of the modi-

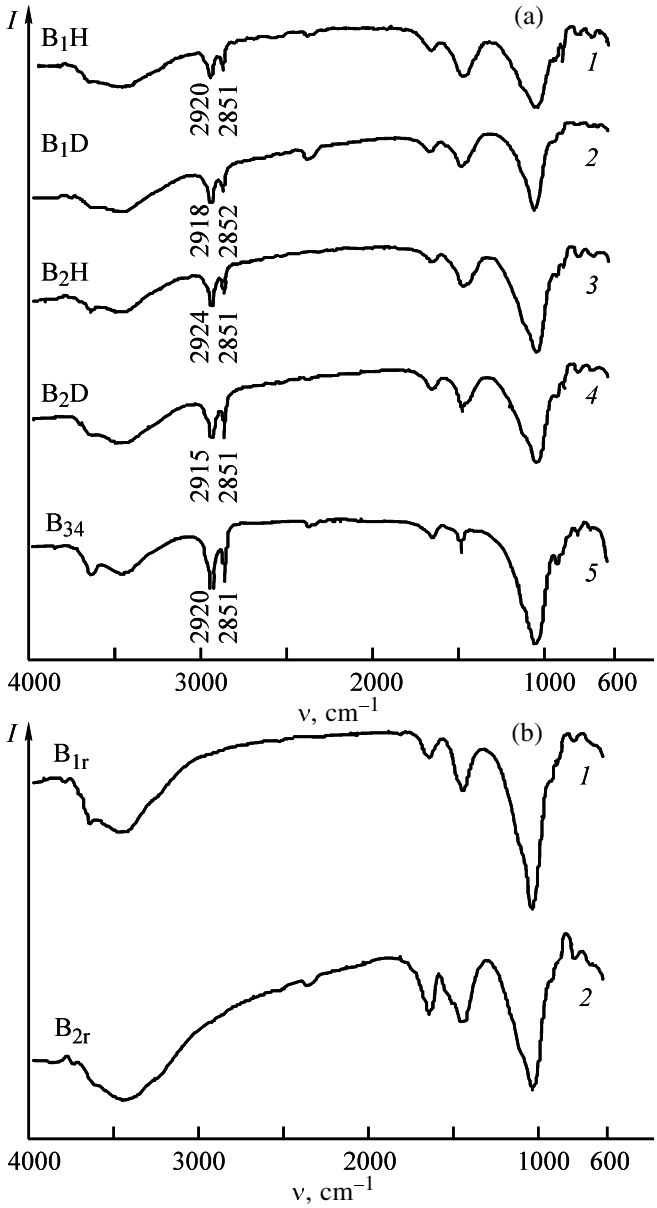


Fig. 4. IR Fourier spectra of clay samples modified with organic cations and those in the raw states. (*I*) Transmission and (ν) wavenumber. Clays: (a) (*1*) B_1H, (*2*) B_1D, (*3*) B_2H, (*4*) B_2D, and (*5*) Bentone 34; (b) (*1*) B_{1r} and (*2*) B_{2r}.

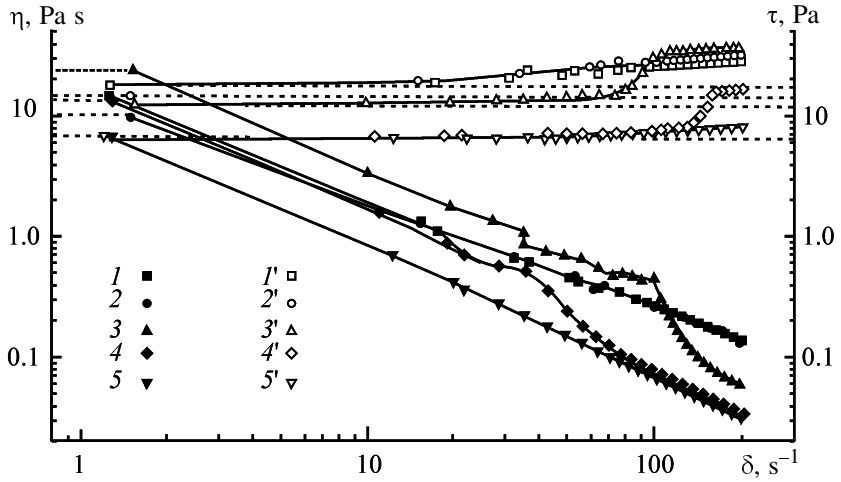


Fig. 5. Rheological characteristics of suspensions of modified clays (η) Dynamic viscosity, (τ) shear stress, and (δ) shear rate. Clay sample: (*1, 1'*) B_{34}, (*2, 2'*) B_2D, (*3, 3'*) B_2H, (*4, 4'*) B_1H, and (*5, 5'*) B_1D. (*1–5*) η and (*1'–5'*) τ.

fying cations [17–19], which confirms that organic cations are present in the clays. The same conclusion can be made on comparing the IR spectra of modified clays with that of Bentone 34.

The results obtained in studying the modified clays by X-ray phase analysis (Table 4) show that the interplanar spacings d_{001} are larger than those in the raw samples. Such an increase would be expected to occur upon intercalation of organic molecules between clay layers [20]. The magnitude of this increase probably corresponds to a monolayer arrangement of adsorbed organic particles [15, 21]. Modified clays, and especially B_1D and B_2D, have interplanar spacings comparable with those of Bentone 34, which is confirmed by their excellent properties in organic media (lubricants and solvents).

The results obtained in determining the densities of the modified clays are listed in Table 4. With the exception of sample B_1H, all other samples had densities close to that of Bentone 34. Comparison of these results with the densities of samples B_{1r} and B_{2r} (Table 1) shows that the density of modified clays decreases upon adsorption of organic cations on those parts of clays which are capable of ion exchange. This conclusion is in agreement with the authors' results that the interplanar spacings in clays increase because of the incorporation of bulky organic cations into their structure.

Table 4. Interplanar spacings *d* of the raw clays and those modified with organic cations and densities ρ of modified clays

Clay	d_{001}	ρ, g cm^{-3}
Raw:		
B_{1r}	15.0	–
B_{2r}	14.6	–
Modified:		
B_1H	17.6	2.002
B_2H	17.3	1.810
B_1D	19.5	1.736
B_2D	19.4	1.717
B_{34}	20.1	1.696

The rheological properties of organic suspensions of the modified clays B_1H, B_2H, B_1D, and B_2D in a toluene–ethanol mixture were compared with those of a suspension of Bentone 34, prepared under the same conditions. Figure 5 shows how the dynamic viscosity η and shear stress τ vary with the shear rate δ for the organic suspensions prepared. All of these are pseudoplastic fluids [15, 22] with dynamic stress values similar to those observed for aqueous suspensions of clays of medium concentration [23]. Such a behavior of the suspension may be associated not only with the formation of a gel of modified clay particles in an organic solvent [16, 24], caused by interparticle interactions, but also with the morphology of clay particles.

The apparent shear stresses (τ_a) for B_1H and B_1D samples (6.85 and 6.59 Pa), on the one hand, and for B_2H and B_2D (13.9 and 14.5 Pa), on the other, are virtually the same. The modified clays B_2D and B_2H are close in τ_a to Bentone 34 sample (18.0 Pa).

The results obtained demonstrate that the nature of a raw clay, morphology and size of its particles, and their specific surface area strongly affect τ_a [15],

depending on an organic ammonium cation adsorbed. This is confirmed by comparison of the specific surface area of the raw clay (Table 1) with its granulometric distribution (Fig. 3). According to published data [25], the area of the solid/liquid phase boundary increases as the particle size becomes smaller, and this makes stronger the interaction between the particles. As a result, the magnitude of the apparent shear stress τ_a increases.

With the exception of sample B_1D, all the other modified clay samples had a viscosity at a very low shear rate, η_{max}, that was comparable with, or exceeded the viscosity of the Bentone 34 suspension. This property is highly important for use of modified clays as thickeners in organic media [3]. The values of η_{max} of B_1H and B_2H clays (modified with the $[BDMHA]^+$ cation) exceeded those for B_1D and B_2D clays (modified with the $[DMDOA]^+$ cation). This phenomenon can be attributed to the specific configuration of adsorbed organic cations in solvents of the alkylbenzene type. The aromatic ring contained in the $[DMDOA]^+$ cation favors gelation [25]. An increase in the mechanical strength of a gel leads to a rise in its dynamic viscosity.

According to the results of this study, modified clays produced from material B_2 have rheological properties, η_{max} and τ_a, satisfactory for their use as thickeners in organic media.

CONCLUSIONS

(1) A study of the modification kinetics of two samples of Tunisian clay demonstrated that their treatment at 80°C with dimethyldioctadecylammonium chloride for 3 h or dimethylhexadecylbenzylammonium chloride for 1 h leads to incorporation of organic ammonium cations into the clay structure. This yields a high SEC for each clay sample and for each modifying cation.

(2) The study of the modified clays revealed their similarity, as regards the physicochemical properties, to products commercially manufactured in Europe, which enables their use as thickeners for lubricants.

ACKNOWLEDGMENTS

The authors thank Prof. N. Attia (Sfax, Tunisia) for help in rheological studies.

REFERENCES

1. US Patent 5 739 087.
2. Murray, H.H., *Appl. Clay. Sci.*, 2000, vol. 17, pp. 207–221.
3. *Peintures et Vernis*, Grandou, P. and Masson, J.C., Eds., Paris: Hermann, 1996.
4. Avci, S., Selection of Rheological Additives for Printing Inks, *Eurocoat Inkmakers Forum During the 2nd European Congr. on Printing Inks*, Nuremberg (Germany), 2003.
5. US Patent 4 664 820.
6. US Patent 4 317 737.
7. US Patent 4 990 272.
8. US Patent 4 406 800.
9. Elfil, H., Srasra, E., and Gogguy, M., *J. Therm. Anal.*, 1995, vol. 44, pp. 663–683.
10. Bergaya, F., *Appl. Clay Sci.*, 1997, vol. 12, pp. 275–280.
11. Maes, A., Peigneur, P., and Cremers, A., *J. Chem. Soc., Faraday Trans.*, 1978, vol. 74, pp. 182–189.
12. Auboiroux, M., Baillif, P., Touray, J., and Bergaya, F., *Appl. Clay Sci.*, 1996, vol. 11, pp. 117–126.
13. Pasto, D. and Johnson, C., *Organic Structure Determination*, New York: Prentice-Hall, 1969.
14. Ben Mansour, L., Benzina, M., and Shoumatski, Y., *Ann. Chim. Sci. Mat.*, 1996, vol. 21, pp. 301–309.
15. Le Pluart, L., *Doctoral Thesis in Materials Sciences*, Lyon (France), 2002.
16. Gherardi, B., Tahani, A., Levitz, P., and Beraya, F., *Appl. Clay Sci.*, 1996, vol. 11, pp. 163–170.
17. Brezesinski, G. and Mohwald, H., *Adv. Colloid Interface Sci.*, 2003, pp. 100–102.
18. Brezesinski, G. and Mohwald, H., *Adv. Colloid Interface Sci.*, 2003, pp. 563–584.
19. Hsu, Y.H., Wang, M.K., Pai, C.W., and Wang, Y.S., *Appl. Clay Sci.*, 2000, vol. 16, pp. 147–159.
20. Lagaly, G., *Solid State Ionics*, 1986, vol. 22, pp. 43–51.
21. Halvaty, V. and Fajnor, V.S., *J. Therm. Anal. Calorim.*, 2002, vol. 67, pp. 113–118.
22. Shi, F.N. and Zheng, X.F., *Int. J. Miner. Process*, 2003, vol. 69, pp. 115–128.
23. Rand, B., Pekenc, E., Goodwin, J.W., and Smith, R., *J. Chem. Soc., Faraday Trans.*, 1980, vol. 76, pp. 225–235.
24. Moraru, V.N., *Appl. Clay Sci.*, 2001, vol. 19, pp. 11–26.
25. Beruto, D.T., Ferrari, A., Barberis, F., and Giordani, M., *J. Eur. Ceram. Soc.*, 2002, vol. 22, pp. 2155–2165.

ISSN 1070-4272. Russian Journal of Applied Chemistry, 2006, Vol. 79, No. 3, pp. 386–389. © Pleiades Publishing, Inc., 2006.
Original Russian Text © A.A. Bachaev, T.E. Kuzina, 2006, published in Zhurnal Prikladnoi Khimii, 2006, Vol. 79, No. 3, pp. 393–396.

APPLIED ELECTROCHEMISTRY AND CORROSION PROTECTION OF METALS

Features of Impregnation of Nickel Metal–Ceramic Porous Supports for Electrodes of Alkaline Batteries

A. A. Bachaev and T. E. Kuzina

Nizhni Novgorod State Technical University, Nizhni Novgorod, Russia

Received November 10, 2005

Abstract—The features of nickel oxidation in impregnation of nickel metal–ceramic porous supports for electrodes of alkaline batteries, which ensure their fabrication in a shorter time, were determined.

DOI: 10.1134/S1070427206030104

Nickel oxide electrodes (NOE) on a nickel metal–ceramic (MC) porous support have high specific characteristics and can be used in a wide range of current densities and temperatures. At the same time, their fabrication is a long power- and labor-consuming process consisting of a number of successive stages [1]. The time and a large number of multicycle stages in fabricating such electrodes are mainly caused by the fact that impregnating porous MC supports in a solution of nickel salts requires long time. The pores of the electrode are filled with a solution of nickel salts in the course of impregnation and then serve for the formation of an active substance. Filling pores takes 5–7% of the impregnation time [2]. The duration of the process is determined by the time necessary for obtaining the active substance by electrochemical oxidation of nickel from the support [3].

Reduction of the impregnation time in fabricating MC NOE should diminish the power consumption and increase the intensity of the process, which is an urgent and practically important problem.

In this study we elucidated the features of nickel oxidation under the impregnation conditions and chose on their basis the routes for reducing the time of fabricating MC NOE.

EXPERIMENTAL

The parameters of nickel etching were determined by analyzing two types of the electrochemical systems: Ni|$Ni(NO_3)_2$|Ni (I) and Pt|$Ni(NO_3)_2$|Ni (II) [4]. The polarization curves of the models studied were obtained in the galvanostatic mode. The progress of nickel oxidation was monitored by the values of the electrode polarizations. In studying the models, we used N0 nickel foil (nickel content 99.9%) and a 30 × 16 × 1-mm smooth platinum plate.

The phase composition of the oxidation products was determined by the X-ray diffraction analysis as in [4]. The densities of the deposit formed on platinum were calculated using the expression for the mass of the unit cell. To do this, the unit cell volume was identified with a crystal lattice constant estimated graphically by the method described in [5].

To test the performance of the system Ni|solution|NiO_x ($x > 1$), a NiO_x ($x > 1$) film was preliminarily deposited on platinum by the procedure described in [6].

The electrodes were fabricated on $30 \times 10 \times 1.6$-mm MC nickel supports with a bulk porosity of 70–75%. Nickel(II) hydroxide in the pores of the MC supports was obtained by the process described in [7, 8]. For impregnation we used $Ni(NO_3)_2$ and $NiSO_4$ solutions.

We analyzed the polarization curves obtained in system I (Fig. 1a) and used the results of the graphical analysis to determine the parameters of the nickel dissolution: the compromise nickel potential was found to be 0.00 V and the current density of the dissolution, 13×10^{-3} mA cm^{-2}. The results obtained in calculating the polarizability of the cathodic and anodic processes showed that nickel is oxidized with a cathodic control. The degree of cathodic control C_c is 75%.

Thus, the oxidation rate of nickel in impregnation of an MC support is determined by the hindrance of the cathodic process. However, studying it on nickel is rather complicated, because the Ni potential established in the system studied is a compromise rather than an equilibrium value. Therefore, it was suggested

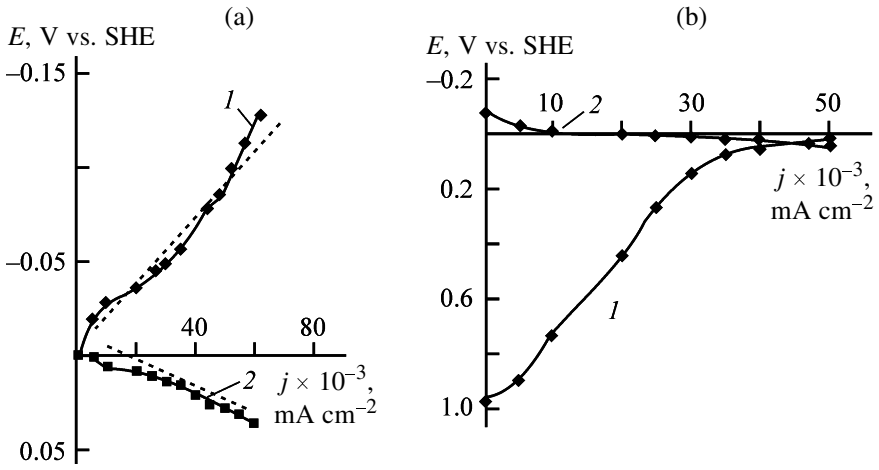


Fig. 1. Diagrams of nickel oxidation, obtained in a $Ni(NO_3)_2$ solution in the systems (a) Ni–Ni and (b) Ni–Pt. T = 80°C, $c_{Ni(NO_3)_2}$ = 950 g l^{-1}, pH 3; the same for Fig. 2. (*E*) Potential and (*j*) current density; the same for Figs. 2 and 3. Curves: (*1*) cathodic and (*2*) anodic.

to study the cathodic processes on a platinum electrode, which allows determination of the potential of a redox system and makes it possible to start a study from this potential. The graphical analysis of the results obtained for system II with a platinum cathode (Fig. 1b) shows that in this case nickel is also oxidized with a cathodic control (degree of cathodic control 92%). The values of the compromise potentials are approximately the same, E_{st} = 0.0 V, which indicates that the model suggested is qualitatively adequate and platinum can be used for studying cathodic processes.

It was shown previously [7] that in a $Ni(NO_3)_2$ solution the rate of reduction of nitrate ions on platinum is limited by their diffusion toward the electrode surface.

When system II, $Ni|Ni(NO_3)_2|Pt$, works under the short-circuit conditions, there occurs a fast decrease in the cathodic current with time. Because nickel is oxidized with a cathodic control, a decrease in the current density is due to the formation of a film of basic nickel compounds on the Pt surface. This film is formed when the pH of the near-electrode layer increases to 7.5 owing to the reduction of the oxidizing agent. According to the X-ray diffraction data, the films formed on Pt have the composition $Ni(NO_3)_2 \cdot Ni(OH)_2$ [4]. The resulting film of basic nickel compounds impedes the diffusion of the oxidizing agent toward the electrode surface. The rate of nickel oxidation in the presence of films on the platinum surface is determined by permeability of the film with respect to the oxidizing agent. Chloride ions are known to exhibit a strong depassivation effect [9].

Addition of $NiCl_2$ into the $Ni(NO_3)_2$ solution (concentration of Cl^- ions 193 g l^{-1}) changed the structure and composition of the above film. According to the X-ray structural analysis, the film formed on Pt at a volume ratio of $Ni(NO_3)_2$ and $NiCl_2$ solutions of 1 : 1 has the chemical composition $Ni(NO_3)_2 \cdot NiCl_2 \cdot Ni(OH)_2$ [4]. The film formed from a solution mixture has a density of 0.93 g cm^{-3}, and that formed from a $Ni(NO_3)_2$ solution, 1.45 g cm^{-3}. Thus, upon impregnation with the first film, the oxidation rate of nickel contained in the MC support is higher.

Examination of the influence of chloride ions showed that the properties of the film formed under the cathodic conditions govern the efficiency of nickel oxidation upon impregnation. The formed film decreases the rate of the process and simultaneously serves as target product, i.e., its growing is necessary for obtaining a large amount of an active substance [8]. In this case, the rate of nickel oxidation can be increased either by eliminating the concentration hindrance or by increasing the oxidizing power of the solution, or by transforming the obtained film into the oxidizing agent.

According to the data of [7], the introduction of 10 g l^{-1} $NaNO_2$ into a $Ni(NO_3)_2$ solution increases its oxidizing power. The $Ni(NO_3)_2$ solution contains, apart from the main oxidizing agent (nitrate ions), other nitrogen compounds having oxidative properties [10]. Therefore, the type of an oxidizing agent in the $Ni(NO_3)_2$ solution was identified by the chronovoltammetric method at a potential sweep rate of 100 mV s^{-1}.

The potentiodynamic curve obtained on Pt in a

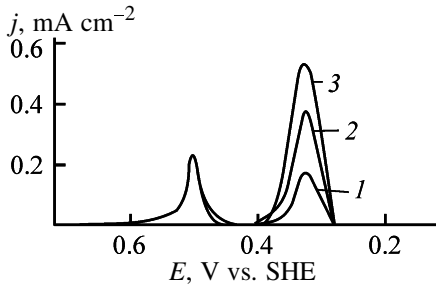


Fig. 2. Chronovoltammograms obtained on Pt in a $Ni(NO_3)_2$ solution (*1*) without additive, (*2*) with 10 g l^{-1} $NaNO_2$, and (*3*) purged with NO_2. V_p = 100 mV s^{-1}.

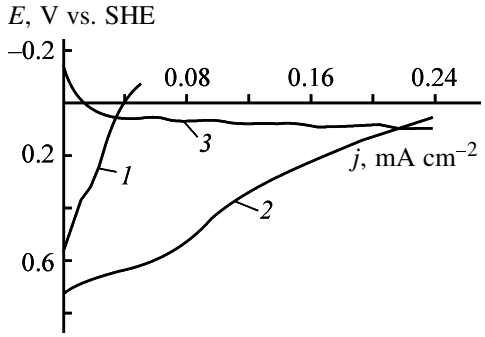


Fig. 3. Diagrams of nickel oxidation obtained in a $NiSO_4$ solution in the system Ni–Pt. $c_{Ni(II)}$ = 200 g l^{-1}, pH 2, T = 80°C. Curves: (*1, 2*) cathodic taken on (*1*) Pt and (*2*) Pt|NiOOH; (*3*) anodic taken on Ni.

$Ni(NO_3)_2$ solution shows at potentials of 0.35–0.1 V two peaks of the limiting current density (Fig. 2). Based on the data of [8, 10], the first peak was associated with reduction of HNO_3 to HNO_2. The latter substance disproportionates in an acid medium at high temperature to give a mixture $2NO_2 \rightleftarrows N_2O_4$ [11], whose components undergo reduction, which is reflected in the presence of the second peak on the curve. The occurrence of this successive transformation is confirmed by the fact that the introduction of sodium nitrite into a $Ni(NO_3)_2$ solution increases by a factor of 4 the current density of the second peak (Fig. 2). Purging a $Ni(NO_3)_2$ solution with NO_2 resulted in a further increase in the current density of the second peak (Fig. 2). All these facts confirm the suggestion that not only NO_3^- ions are responsible for the oxidation of Ni from the MC supports in a $Ni(NO_3)_2$ solution; the main oxidant is the $2NO_2 \rightleftarrows N_2O_4$ mixture.

Thus, to increase the oxidizing power of a $Ni(NO_3)_2$ solution, it is appropriate to introduce nitrites. Their disproportionation should favor the formation of a larger amount of the oxidant, i.e., $2NO_2 \rightleftarrows N_2O_4$ mixture, in the solution. The film formed in a $Ni(NO_3)_2$ solution with $NaNO_2$ added has the composition $Ni(NO_3)_2 \cdot Ni(OH)_2 \cdot NiO_x$ ($x > 1$) [4]. These films are looser than those formed in a $Ni(NO_3)_2$ solution, and, which is the most important, they contain NiO_x ($x > 1$), directly contacting nickel of the support and promoting the nickel oxidation [7].

The fact that the transformation of the film of basic nickel compounds formed on cathodic areas into NiO_x ($x > 1$) increases the oxidation rate of nickel of the porous MC supports [7] is also associated with the change in the composition and structure of the deposit. The time of impregnation of MC supports in the composition suggested decreased to 5 h, whereas in the case of the traditional process, the necessary amount of the active substance in an MC support is accumulated only after 18 h of impregnation in a $Ni(NO_3)_2$ solution. The active substance obtained in pores of MC supports is sufficiently active for operation in an alkaline battery, as indicated by its utilization factor [7].

To confirm the performance of the system Ni|solution|NiO_x ($x > 1$), we studied the similar system in which higher nickel oxides were formed without participation of nitrogen-containing compounds. As oxidant we chose $KMnO_4$, whose oxidative power is comparable with that of a $2NO_2 \rightleftarrows N_2O_4$ mixture. In operation of this system, the rate of nickel dissolution in a $NiSO_4$ solution increased by a factor of 5–6 (Fig. 3), with the control type preserved (C_c = 83%).

Thus, the system Ni|$NiSO_4$|NiO_x ($x > 1$), wherein higher nickel oxides are formed without participation of nitrogen-containing compounds, efficiently operates both in the subsequent impregnation cycles and, probably, in an alkali solution.

The results obtained suggest that the composition of the solution for treatment of the MC supports is as follows: a KOH solution (density 1.22 g cm^{-3}) with a 1% $KMnO_4$ additive. The process temperature is 70–80°C and time, 1 h. The electrodes are treated with a KOH solution containing 1% $KMnO_4$ only in the first cycle. The results showed that the treatment of the electrodes in all the subsequent cycles decreases the coefficient of utilization of the active substance.

When the KOH solution containing $KMnO_4$ is used for treatment, nickel of the MC support is actively oxidized, probably even in an alkali, with the formation of $Ni(OH)_2$ and NiO_x ($x > 1$), which is not the case of the traditional «sulfate» technology [8].

Upon the treatment in a KOH solution containing 1% $KMnO_4$, the basic nickel salts formed in pores of the MC support upon their impregnation in a $NiSO_4$ solution were oxidized. The resulting higher nickel oxides increased twofold the oxidation rate of nickel

contained in the MC supports in the subsequent impregnation cycles. The intermediate oxidation of basic nickel compounds present in pores of the MC supports with a KOH solution containing 1% $KMnO_4$, performed in the first cycle, makes it possible to fabricate the electrodes with a specific capacity of 0.3 A h cm^{-3} after five impregnation cycles.

The total time of fabrication of MC NOE by the method suggested was 18–20 h, which is approximately four times shorter than that of MC NOE fabrication by the traditional sulfate process.

CONCLUSIONS

(1) The revealed features of nickel oxidation in the impregnation of a metal–ceramic support allowed the etching rate to be decreased by a factor of 3–6 and the time of impregnation of nickel oxide electrodes on a metal–ceramic support, to 18–20 h instead of 50–80 h in the traditional processes (depending on solution composition).

(2) The capacity of pilot electrodes is the same as that of electrodes fabricated by the impregnation process applied in the practice.

REFERENCES

1. Dasoyan, M.A., and Novoderezhkin, V.V., *Proizvodstvo elektricheskikh akkumulyatorov* (Manufacture of Electric Batteries), Moscow: Vysshaya Shkola, 1970.
2. Levinzon, L.M., Pozin, Yu.M., and Shtertser, N.I., *Tekhnologiya proizvodstva khimicheskikh istochnikov toka* (Technology for Manufacture of Chemical Power Cells), Moscow: Energoizdat, 1985.
3. Pozin, Yu.M., and Shtertser, N.I., *Zh. Prikl. Khim.*, 1970, vol. 43, no. 7, pp. 1482–1486.
4. Bachaev, A.A., Kuzina, T.E., and Oshurina, L.A., *Zh. Prikl. Khim.*, 2004, vol. 77, no. 6, pp. 948–951.
5. Gorelik, S.S., Skakov, Yu.A., and Rastorguev, L.N., *Rentgenograficheskii i elektronno-opticheskii analiz* (X-ray Diffraction and Electron-Optical Analyses), Moscow: Metallurgiya, 1994.
6. Kuzina, T.E., Bachaev, A.A., and Kargin, S.A., *Usp. Khim. Khim. Tekhnol.*, 2003, vol. 17, no. 9, pp. 75–79.
7. Kuzina, T.E., and Bachaev, A.A., *Zh. Prikl. Khim.*, 2004, vol. 77, no. 9, pp. 1487–1490.
8. Pervushin, Yu.N., A Study in Technology of Fabrication of an MC NOE for Alkaline Battery, *Cand. Sci. Dissertation*, Novocherkassk, 1968.
9. *Prikladnaya elektrokhimiya* (Applied Electrochemistry), Fedot'ev, N.P., Ed., Leningrad: Khimiya, 1967.
10. Gur'yan, L.I., *Okislitel'no-vosstanovitel'nye reaktsii i potentsialy v analiticheskoi khimii* (Redox Reactions and Potentials in Analytical Chemistry), Moscow: Khimiya, 1989.
11. Ugai, Ya.A., *Obshchaya i neorganicheskaya khimiya* (General and Inorganic Chemistry), Moscow: Vysshaya Shkola, 2000.

ISSN 1070-4272. Russian Journal of Applied Chemistry, 2006, Vol. 79, No. 3, pp. 390–396. © Pleiades Publishing, Inc., 2006.
Original Russian Text © V.F. Vakulenko, M.V. Milyukin, V.V. Goncharuk, 2006, published in Zhurnal Prikladnoi Khimii, 2006, Vol. 79, No. 3, pp. 397–403.

ENVIRONMENTAL PROBLEMS OF CHEMISTRY AND TECHNOLOGY

Influence of the Conditions of Photooxidation of Natural Water on the Yield of Carbonyl Compounds

V. F. Vakulenko, M. V. Milyukin, and V. V. Goncharuk

Dumanskii Institute of Colloid Chemistry and Water Chemistry, National Academy of Sciences of Ukraine, Kiev, Ukraine

Received August 3, 2005; in final form, January 2006

Abstract—The yield of carbonyl compounds in treatment of river water and model solutions of humic acid as a function of the ozone uptake and conditions of UV irradiation was analyzed.

DOI: 10.1134/S1070427206030116

Formation and stability of the oxidation by-products is one of insufficiently studied aspects of application of ozone to potable water treatment. The primary products of the ozonolysis of organic impurities contained in natural water are aldehydes, ketones, and carboxylic acids [1, 2]. Ozonation of humic acid (HA) and fulvic acid (FA) solutions [3] and of natural water [1, 2, 4–7] leads to the formation of aliphatic aldehydes C_1–C_{14}, aliphatic carboxylic acids C_1–C_{24}, unsaturated aldehydes, dialdehydes, ketones, keto acids, dibasic aliphatic acids, hydroxy- and dihydroxybenzoic acids, esters, and other products.

Aldehydes, if present in a concentration of 0.2–12.5 μg dm^{-3}, impart to the ozonized water a specific smell (fruit, flower, or less pleasant), which then rapidly disappears [8]. Certain aldehydes and ketones are mutagenes and carcinogenes [2]. In addition, carbonyl compounds and chlorine react with the formation of trihalomethanes and other potentially hazardous organochlorine products. The concentration of some aldehydes and ketones in potable water is regulated on the basis of the Governmental Sanitation Rules and Regulations [9]. The presence of other compounds in water reservoirs is regulated by the maximum permissible concentration (MPC) [10]. The MPCs for aldehydes and ketones in potable water are as follows (mg dm^{-3}): formaldehyde 0.05, acetaldehyde 0.2, benzaldehyde 0.003, propenal 0.02, 2-butenal 0.3, 3-pentanone 0.1, and acetone 2.2. Aliphatic aldehydes C_1–C_{10}, glyoxal, methylglyoxal, and benzaldehyde are included into the list of by-products that are subject to monitoring in potable water in the United States [11].

The presence of 1–80 μg dm^{-3} carbonyl compounds in natural reservoirs results from the biochemical processes of oxidation of organic impurities [2, 4]. In ozonized water their total concentration exceeds many times the natural background [2, 4, 6, 7]. The formation of aldehydes in ozonation of natural water depends on a number of factors such as the structure of natural organic impurities, concentration of total organic carbon (TOC), ozone uptake, temperature, the pH of water, etc. [2–5]. The primary carbonyl compounds formed in ozonation of natural water are formaldehyde, acetaldehyde, glyoxal, and methylglyoxal. Aliphatic aldehydes C_4–C_{10}, benzaldehyde, and other substances are less common and are present in lower concentrations [4, 6].

Presently, the new combined oxidation processes, so-called Advanced Oxidation Processes (AOP), are being actively introduced into practical water treatment. Examples are combined application of ozone and hydrogen peroxide (O_3/H_2O_2) or of ozone and UV irradiation (O_3/UV). The composition of the by-products products formed by the AOP in preparation of potable water is studied insufficiently and the results obtained are controversial [12, 13].

This study is concerned with the composition of carbonyl compounds formed in ozonation, UV irradiation, and in the case of the O_3/UV treatment of river waters. We also studied how the yields of the above compounds are affected by the ozone uptake, conditions of UV irradiation, and by the quality of water.

EXPERIMENTAL

We studied the action of ozone alone and the combined action of ozone and UV radiation under the different irradiation conditions on the water from the

Table 1. Characterization of river water samples and model HA solutions

Water sample no.	T, °C	pH	Color index, deg	A_{254} (1 cm)	COD, mg O_2/dm^3	PO,* mg O_2/dm^3	TOC, mg dm^{-3}
1	20	8.0	42	0.40	35	–	21.2
2	23	8.3	41	0.41	31	15.8	17.9
3	23	8.3	30	0.27	26	13.0	14.7
4**	20	7.2	131	0.58	21	14.7	7.5

* Permanganate oxidizability.
** HA concentration 20.4 mg dm^{-3}.

Dnieper (sample nos. 1, 2) and Desna (sample no. 3) rivers in the summer period, as well as on model solutions of HA (Fluka, sample no. 4) (Table 1). The river water was preliminarily filtered through a paper filter.

The ozonation and joint treatment with ozone and UV radiation of the samples studied was performed on a laboratory installation in a bubbler-type reactor with a plunged UV source arranged in a quartz jacket [14, 15]. The ozonation parameters were recorded with a computer. The irradiation was performed in the continuous or batch mode with a low-pressure DRB-8 mercury-quartz lamp and in the pulse mode with an IFP-800 pulse xenon lamp. The total energy of the UV radiation of the DRB-8 lamp was 1.13 J s^{-1} and that of the IFP-800 pulse lamp, 2.32 J pulse^{-1} (including 1.15 J pulse^{-1} at 200–290 nm) at a pumping energy of 60 W s^{-1}, a pulse time of about 0.1 ms, and a pulse repetition frequency of 2.6 s [16]. The intensity of the UV radiation in the range 200–290 nm was 2.72 mJ cm^{-2} s^{-1} for DRB-8 lamp and 2.76 mJ cm^{-2} pulse^{-1} for IFP-800 lamp (at a total UV intensity of 5.58 mJ cm^{-2} pulse^{-1}). The ozone supply rate was 1.7–2.8 mg dm^{-3} min^{-1}.

In the course of the study, a portion of the solution (V = 0.625 dm^3) was ozonized until a certain amount of ozone (D_{oz}) was taken up. The time of the UV irradiation or O_3/UV treatment of the water was the same as the ozonation time. The UV irradiation of natural waters was done simultaneously with aeration to attain stirring conditions similar to those in ozonation or in the case of O_3/UV treatment. The methods of controlling the oxidation parameters and monitoring the water quality have been reported previously [14, 15].

Carbonyl compounds contained in water immediately after the treatment by the above methods were analyzed in the form of stable 2,4-dinitrophenylhydrazones (2,4-DNPH) and identified by gas chromatography/mass spectrometry (GC/MS) [17, 18]. To determine the amount of 2,4-DNPH by this method [18], we used the Supelco N 4 Carb Method 1004 Mix 2 reference mixture and mixtures of specially synthesized 2,4-DNPHs.

Nine aldehydes (formaldehyde, acetaldehyde, propanal, propenal, methylpropanal, butanal, 2-butenal, 3-methylbutanal, and pentanal) and six ketones (acetone, butanone, 3-methyl-2-butanone, 3-pentanone, 2-pentanone, and 2-hexanone) were identified by GC/MS in river waters and model HA solutions after ozonation and in the case of combined treatment with ozone and UV radiation. The major carbonyl compounds formed under all the treatment conditions used are formaldehyde, acetaldehyde, and acetone. The concentrations of propanal and 2-butenal were also determined by this method. The main problem for the water studied is associated with formaldehyde, since among the carbonyl compounds analyzed its concentration in potable water is regulated most strictly.

In comparison of the results obtained in ozonation of waters taken from different reservoirs or of HAs and FAs isolated from them, the concentrations of the forming oxidation products are given per milligram of TOC or per milligram of ozone taken up. The ratios of the O_3 amount to the TOC concentration in the ozonized waters varied from 0.2 to 3.0 mg mg^{-1} [3, 4]. The studies performed at a number of industrial water supply stations and pilot-plant installations in the United States using different water reservoirs and ozone doses showed [4] that the yields of formaldehyde and the total yield of four major aldehydes C_1–C_3 (formaldehyde, acetaldehyde, glyoxal, and methylglyoxal) in ozonation of natural waters are within 1.1–13.0 and 4.9–30.0 μg mg^{-1} TOC (Table 2). The statistic mean total yield of four major aldehydes in ozonation is approximately 12 μg mg^{-1} TOC, including 5 μg mg^{-1} TOC of formaldehyde. The ozonation of the model FA solutions containing 20 mg dm^{-3} TOC with an ozone amount of 1–3 mg O_3 mg^{-1} TOC produced even higher concentrations of C_1–C_3 aldehydes (~1.5–2.0 μmol mg^{-1} TOC) [3].

Table 2. Yield of carbonyl compounds in ozonation, UV irradiation, and O_3/UV treatment of the water samples studied

Sample no.	Treatment	D_{oz}, mg mg^{-1} TOC	Yield per milligram of TOC, μg				Yield per 1 mg dm^{-3} ozone uptake, μg			
			formaldehyde	acetaldehyde	acetone	total of C_1–C_3 compounds	formaldehyde	acetaldehyde	acetone	total of C_1–C_3 compounds
Potable water (USA) [4]	O_3	0.3–1.5	1.1–13.0	–	–	4.9–30.0	1.2–18.0	–	–	6.0–42.0
1	O_3	0.1–1.7	0.7–5.2	0.8–3.7	0.2–0.9	2.3–8.7	1.7–14.0	1.3–10.2	0.2–4.7	3.5–23.7
	O_3/UV	0.1–1.9	1.4–7.9	1.6–5.0	0.1–0.4	3.5–12.7	2.7–14.4	2.7–18.7	0.1–2.5	5.6–37.1
2	O_3	0.2–0.6	3.4–5.3	3.6–4.6	0.2–0.4	7.8–10.4	8.2–15.3	6.5–17.5	0.7–1.0	15.6–34.0
	O_3/UV	0.2–0.6	2.9–6.6	2.2–3.6	0.1–0.9	6.1–9.8	8.4–23.7	3.5–14.3	0.2–1.5	14.3–39.4
1, 2	UV	0.0	1.5–5.0	0.9–4.7	0.1–0.6	6.1–7.1	–	–	–	–
3	O_3	0.1–0.7	2.0–4.8	4.9–6.0	0.4–0.7	7.3–10.6	4.8–27.0	7.6–44.2	0.9–3.9	15.6–75.0
	O_3/UV	0.1–0.8	1.0–4.3	2.1–5.7	0.1–0.6	3.2–10.6	4.7–12.0	5.2–18.9	0.3–1.8	10.2–26.4
	UV	0.0	2.3–6.3	5.0–7.5	<0.1	7.4–13.8	–	–	–	–
4	O_3	0.3–2.9	0.0–6.6	0.0–12.0	0.0–1.7	0.0–19.0	0.0–3.1	0.0–4.1	0.0–0.8	0.0–6.5
	O_3/UV	0.3–4.2	6.4–18.3	10.6–26.1	0.4–1.6	18.8–34.9	3.0–22.8	3.2–61.5	0.1–4.1	6.3–89.0

The yields of major carbonyl products in oxidation of initial sample nos. 1–4 are presented in Table 2 per milligram of TOC and per 1 mg dm^{-3} ozone uptake. The maximal total yields of formaldehyde, acetaldehyde, acetone, and C_1–C_3 carbonyl compounds in ozonation, UV irradiation, and O_3/UV treatment of the river waters studied (sample nos. 1–3) lie within the interval typical of potable water [4]. At ozone uptakes of 2–12 mg dm^{-3} (0.1–0.8 mg O_3/mg TOC), which are acceptable in potable water treatment, the yields of formaldehyde and acetaldehyde and the total yield of carbonyl compounds C_1–C_3 in ozonation and in O_3/UV treatment of sample nos. 1–3 (1–7, 1–6, and ~2–12 μg mg^{-1} TOC, respectively) do not noticeably exceed the statistic mean values for formaldehyde and the total yield of four major aldehydes in treatment of potable water from other reservoirs [4]. The yield of acetone is lower by approximately an order of magnitude (0.1–0.7 μg mg^{-1} TOC).

In ozonized sample no. 4 (HA solution), aldehydes were observed only after its decolorization, i.e., at D_{oz} > 2 mg mg^{-1} TOC. In this sample, the total yield of formaldehyde and carbonyl compounds per milligram of TOC does not differ from the typical values for river waters (Table 2). The maximal values of the total yields of formaldehyde, acetaldehyde, and major carbonyl compounds (formaldehyde, acetaldehyde, acetone, propanal, and 2-butenal) in the case of O_3/UV treatment of this sample (Table 2) somewhat exceed the values for potable water but are considerably lower than the values observed previously in ozonation of FA solutions [3].

The individual and total yields of carbonyl compounds per 1 mg dm^{-3} ozone uptake in ozonation of sample no. 4 are closer to the minimal values for potable water (Table 2). In the case of O_3/UV treatment of this sample, the maximal yield of acetaldehyde (61.5 and 44.5 μg mg^{-1} O_3) and the maximal total yield of aldehydes and ketones (89.0 and 59.6 μg mg^{-1} O_3) are observed at the minumal uptakes D_{oz} (2.1 and 4.4 mg dm^{-3}, respectively) (Fig. 1b). In the indicated ozone uptake range, this parameter is higher by a factor of at least 2–3 than that observed in the case of O_3/UV treatment at higher ozone uptakes and by an order of magnitude higher than that in ozonation (Table 2).

Also, the yields of formaldehyde and acetaldehyde and the total yield of carbonyl compounds per 1 mg dm^{-3} ozone uptake at D_{oz} < 4 mg dm^{-3} in ozonation and in O_3/UV treatment of river waters are mostly higher by a factor of about 1.5–2.5 as compared to those observed at higher ozone uptakes. Examples are the yield of acetaldehyde and the total yield of carbonyl compounds C_1–C_3 in O_3/UV treatment of sample no. 1 (Fig. 1a) and the yield of all major carbonyl compounds in ozonation of water sample no. 3 (Fig. 2). The total yields of primary carbonyl compounds per 1 mg dm^{-3} ozone uptake in ozonation of sample no. 3 (Figs. 2a, 2b) and in O_3/UV treatment of sample no. 4 (Fig. 1b) are considerably higher than the values typical of potable water only when the ozone uptakes D_{oz} are minimal.

The data obtained show that the O_3/UV treatment in the stage of the decolorization of natural water with

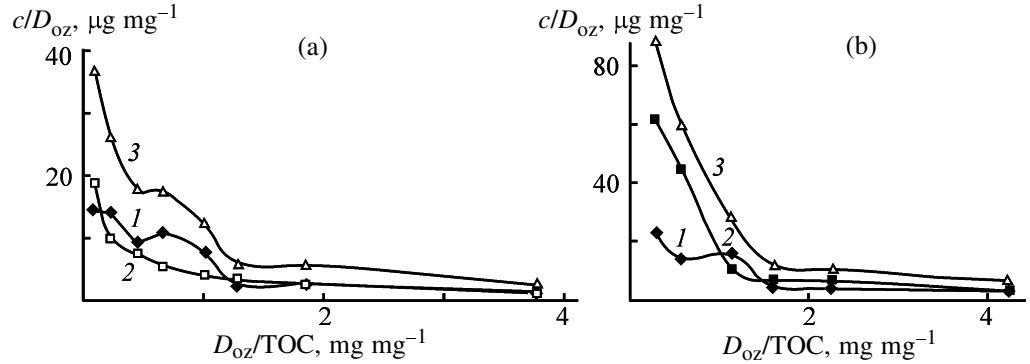


Fig. 1. Yields of (*1*) formaldehyde and (*2*) acetaldehyde, and (*3*) total yield of carbonyl compounds C_1–C_3 per 1 mg dm^{-3} ozone uptake c/D_{oz} vs. the ozone uptake D_{oz}/TOC in O_3/UV treatment of sample (a) no. 1 and (b) no. 4. Ozone feed rate: (a) 2.75 ± 0.05 and (b) 1.8 ± 0.1 mg dm^{-3} min^{-1}; I_{UV} = 2.72 mJ cm^{-2} s^{-1}.

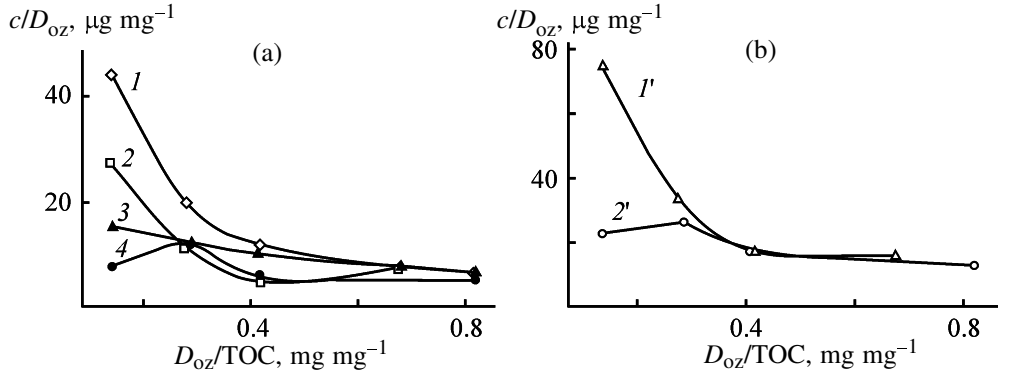


Fig. 2. (a) Yields c/D_{oz} of (*1, 3*) acetaldehyde and (*2, 4*) formaldehyde, and (b) (*1'*, *2'*) total yield of carbonyl compounds C_1–C_3 vs. the ozone uptake D_{oz}/TOC in (*1, 2, 1'*) ozonation and (*3, 4, 2'*) O_3/UV treatment of water sample no. 3. Ozone feed rate 1.95 ± 0.05 mg dm^{-3} min^{-1}, I_{UV} = 2.72 mJ cm^{-2} s^{-1}.

high concentration of HA and FA is undesirable, since it increases the yield of aldehydes in comparison with ozonation.

It has been shown previously [15] that a two-stage oxidation (first, ozonation and then, O_3/UV treatment) ensures more efficient removal of antropogenic microimpurities (pesticides and surfactants) from natural water. The indicated conditions of the treatment also significantly affect the yield of carbonyl products in oxidation of organic impurities (Fig. 3). The UV irradiation of ozonized sample nos. 4 or 1 after the decolorization with ozone ($\tau > 13.5$ and $\tau > 5.0$ min, respectively) significantly decreases both the yields of carbonyl compounds C_1–C_3 (Fig. 3a) and the yield of formaldehyde, which is the most strictly regulated major product, in comparison not only with the continuous combined O_3/UV treatment, but also with ozonation.

The effect exerted by the combined action of ozone and UV radiation on the individual and total yields of carbonyl compounds can differ dramatically, depending on the water source. For example, the O_3/UV treatment of sample no. 3 does not increase the yields of aldehydes in comparison with ozonation at the same ozone doses (Fig. 4b, 4c). The O_3/UV treatment of sample nos. 1 and 2 increases the yield of formaldehyde by a factor of 1.3–2.0 (Figs. 3b, 4a) and the yield of carbonyl compounds, by a factor of 1.3–1.5 (Figs. 3a, 4c).

The yields of carbonyl compounds in the case of the action of UV radiation on the river waters under study differ significantly depending on the radiation source. The radiation of a pulsed IFP-800 xenon lamp in the presence of oxygen increases the formaldehyde yield in sample nos. 2 and 3, whereas using the irradiation jointly with ozonation markedly decreases it in comparison with the case of irradiation with a bactericidal DRB-8 mercury-quartz lamp (Figs. 4a, 4b). The yields of acetaldehyde in the above samples differ by a factor of approximately 1.5–5, depending on the irradiation conditions.

Figure 4 also shows that the yields of formaldehyde in the case of UV irradiation of the water samples studied in the presence of oxygen are close, and frequently, the same as in ozonation and in O_3/UV treatment. For example, the formaldehyde yield in

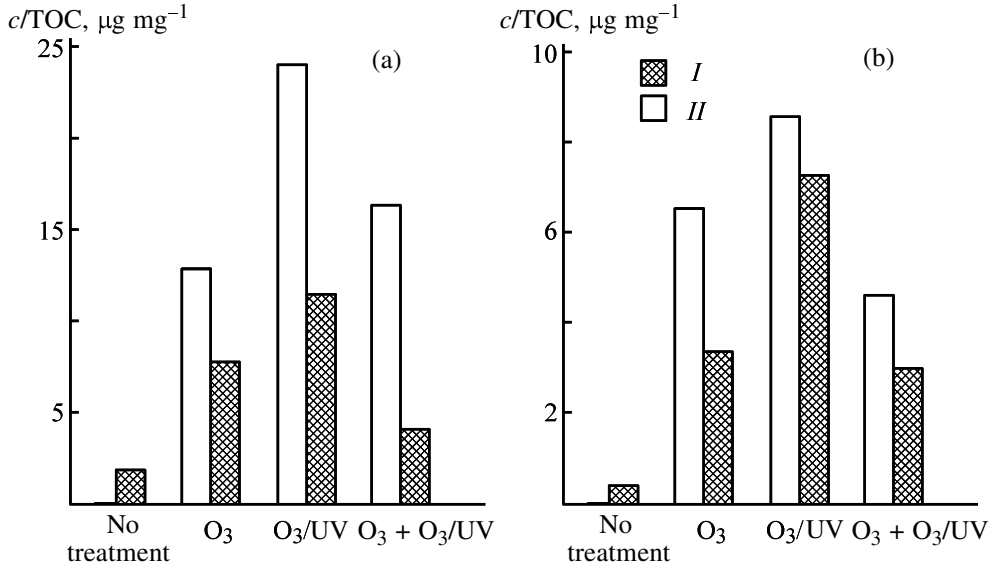


Fig. 3. Effect of ozonation, O_3/UV treatment, and two-stage oxidation (first, ozonation and then, O_3/UV treatment) of water sample (*I*) no. 1 and (*II*) no. 4 on the (a) total yield of carbonyl compounds and (b) yield of formaldehyde per milligram of TOC, *c*/TOC. Total treatment time τ (min) and specific ozone uptake D_{oz}/TOC (mg mg^{-1} TOC): 10.75 and 0.6–0.7 (no. 1), 19.0 and 2.1–2.3 (no. 4).

the combined action of pulsed UV irradiation and an oxidizing agent on water sample no. 2 is virtually independent of the kind of the oxidant (ozone or oxygen) and differs only slightly from the yield in ozonation (Fig. 4a). The yields of acetaldehyde in ozonation and under continuous UV irradiation of water sample no. 3 are equal (Fig. 4b).

Despite the fact that the yields of individual aldehydes differ by a factor of 1.3–6.3, the total yields of carbonyl compounds in two modes of UV irradiation or in O_3/UV treatment of water sample no. 2 are close (Fig. 4b). The individual and total yields of carbonyl compounds in ozonation and in combined treatment with O_3 and continuous UV radiation of water sample no. 3 are virtually equal. The combined treatment of this sample by O_3 and pulsed UV radiation decreases the yields of carbonyl compounds by 10–26% in comparison with the above treatments and by 75% in comparison with the pulsed UV irradiation of this sample in the presence of dissolved oxygen.

Analysis of the combined effect of ozone and UV radiation on the formation of carbonyl compounds in the river waters studied shows that the yield of individual products and the total yield under both conditions of O_3/UV treatment is considerably (by a factor of ~1.3–3.8) lower than their additive value, i.e., in ozonation and in UV irradiation. The additive or synergistic character of the combined action is observed only in a few cases. The additive effect is observed with the yield of formaldehyde in sample no. 2 upon combined treatment with O_3 and continuous UV radiation (Fig. 4a), and the synergistic effect, with the yield of acetone in the same sample irradiated in the pulsed mode.

The data presented show that, apart from oxidant dose and irradiation conditions, the concentration of carbonyl compounds is significantly affected by the quality of natural water, usually differing in the content of organic impurities. It may be suggested that carbonyl compounds are present in natural water as organic impurities of various structures or as various structural fragments of HA and FA. Intense formation of aldehydes at small doses D_{oz} is probably due to the decomposition of readily oxidizable compounds present in natural water or readily oxidizable groups in HA structure. As known, ozone most readily reacts with unsaturated and aromatic organic compounds. Predominance of polysubstituted aromatic nuclei, including polyhydroxy derivatives, and the presence of C=C bonds in aliphatic terminal groups and bridges between aromatic nuclei in the structure of the humic acid under study (Fluka) [19] facilitate its reaction with molecular ozone. The fraction of readily oxidizable compounds (PO/COD) in model HA solutions (0.7) is higher than in the natural waters studied here (0.5–0.6) (Table 1).

At the same time, in ozonation of aromatic compounds the carbonyl compounds C_1–C_3 are formed in the last stage of a complex chain of transformations, consisting of successive cleavage of aromatic nuclei

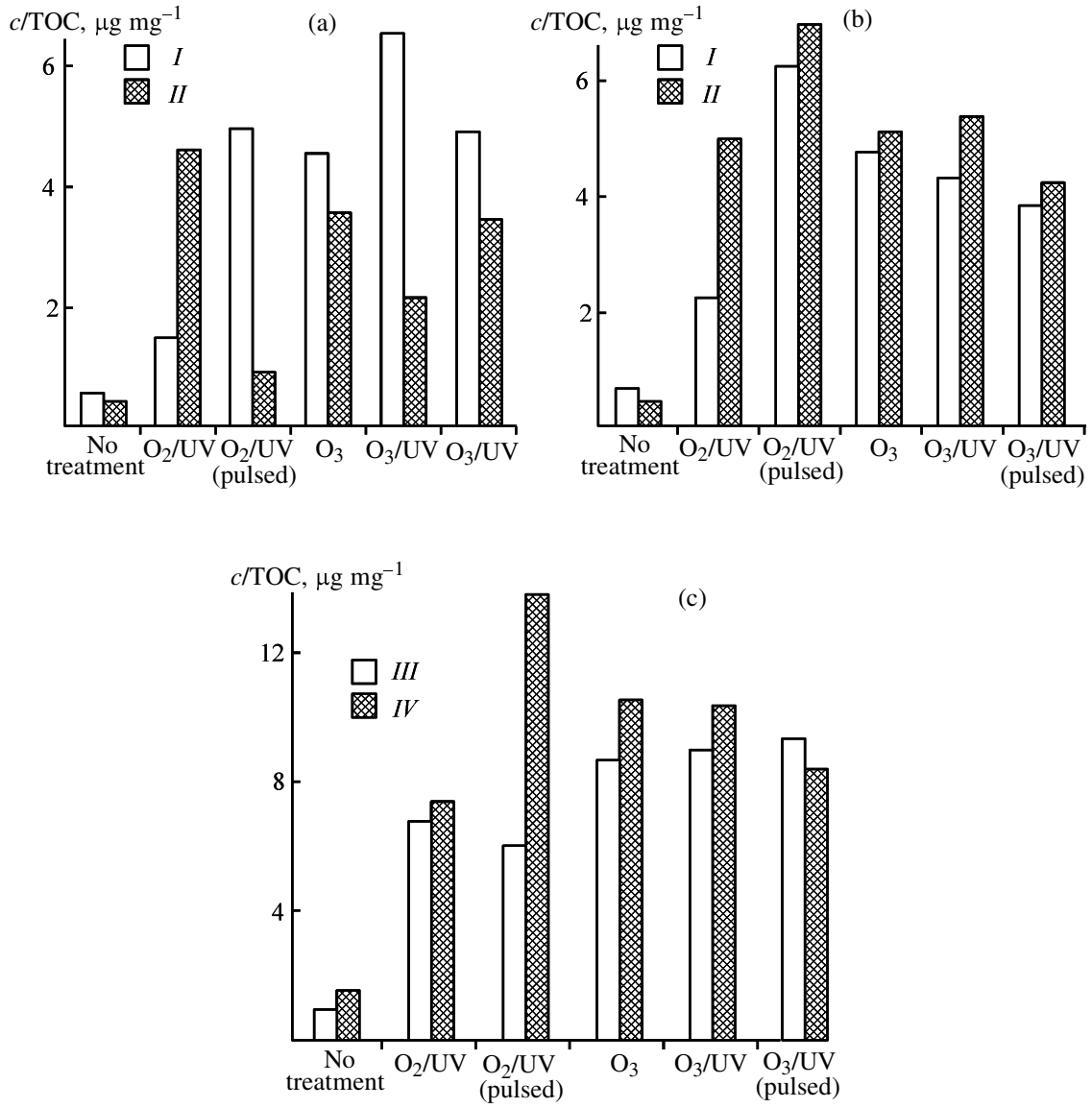


Fig. 4. Comparison of (a, b) yields of (*I*) formaldehyde and (*II*) acetaldehyde and (c) total yields of carbonyl compounds C_1–C_3, *c*/TOC, in ozonation and upon continuous or pulsed UV irradiation in combination with the effect of ozone or oxygen on water sample (a, c) no. 2 and (b, c) no. 3. $D_{oz} = 0.7 \pm 0.1$ mg mg^{-1} TOC, $\tau = 13$ min. (c) Sample: (*III*) no. 2 and (*IV*) no. 3.

and double C=C bonds of the primary products. In O_3/UV treatment, the oxidant species are highly active hydroxy radicals whose reactions are characterized by high rates and nonselectivity. The simultaneous reaction of OH radicals with various structural fragments of HA solutions (Fluka) and the high rates of the reactions predetermine the high yield of carbonyl compounds (per 1 mg dm^{-3} ozone uptake) at small D_{oz}.

Amines, amino acids, unsaturated carboxylic acids, and natural polyphenol compounds (flavones, flavanones, flavonoids, anthocyanes, etc.) should be classed with readily oxidizable compounds contained in natural water. The appearance of propenal and 2-butenal in ozonation and in the case of O_3/UV treatment of the waters studied is likely due to the presence of unsaturated compounds, for example, of higher carboxylic acids (C_{16}–C_{18}) containing two or three C=C bonds. At higher D_{oz}, the formation of aldehydes is associated with profound decomposition of HA and FA. Because the above acids are similar in

nature, the boundaries of the aldehyde yields per milligram of O_3 taken up, obtained for different reservoirs, become considerably narrower.

CONCLUSIONS

(1) Nine aldehydes and six ketones C_1–C_6 were identified by gas chromatography/mass spectrometry in river waters and model humic acid solutions treated with ozone alone and with ozone in combination with UV radiation.

(2) The yields of major carbonyl products (formaldehyde, acetaldehyde, and acetone) formed in oxidation of the samples studied depend on the ozone uptake, conditions of UV irradiation, and quality of water.

(3) The O_3/UV treatment of a natural water containing high concentration of humic and fulvic acids in the stage of decolorization is undesirable, because it results in a higher yield of aldehydes as compared to that in ozonation. It is reasonable to use two-stage oxidation (first, ozonation and then, O_3/UV treatment).

(4) The pulsed O_3/UV treatment of natural water decreases the yield of formaldehyde and the total yield of primary carbonyl compounds C_1–C_3 not only in comparison with the continuous O_3/UV treatment but also with the ozonation.

REFERENCES

1. Richardson, S.D., Thruston, A.D., and Caughran, T.V., *Environ. Sci. Technol.*, 1999, vol. 33, no. 19, pp. 3368–3377.
2. Milyukin, M.V., Goncharuk, V.V., and Vakulenko, V.F., *Khim. Tekhnol. Vody*, 1999, vol. 21, no. 3, pp. 245–258.
3. Andrews, S.A., Huck, P.M., and Coutts, R.T., *Vom Wasser*, 1993, vol. 81, pp. 151–165.
4. Weinberg, H.S., Glaze, W.H., Krasner, S.W., and Sclimenti, M.J., *J. Am. Water Works Assoc.*, 1993, vol. 85, no. 5, pp. 72–85.
5. Paode, R.D., Amy, G.L., Krasner, S.W., et al., *J. Am. Water Works Assoc.*, 1997, vol. 89, no. 6, pp. 79–93.
6. Glaze, W.H., Koga, M., and Cancilla, D., *Environ. Sci. Technol.*, 1989, vol. 23, no. 7, pp. 838–847.
7. Miltner, R.Y., Shukairy, H.T., and Summers, R.S., *J. Am. Water Works Assoc.*, 1992, vol. 84, no. 11, pp. 53–62.
8. Froese, K.L., Wolanski, A., and Hrudey, S.E., *Water Res.*, 1999, vol. 33, no. 6, pp. 1355–1364.
9. *SanPiN* (Sanitation Rules and Regulations) *2.1.4.1074–01: Potable Water. Hygienic Requirements to the Quality of Water from Centralized Systems for Potable Water Supply. Quality Control*, Moscow: Federal'nyi Tsentr Gossanepidnadzora Minzdrava Rossii, 2002.
10. *SanPiN* (Sanitation Rules and Regulations) *4830–88: Sanitation Rules and Regulations for Protection of Surface Waters form Pollution*, Moscow: Minzdrav SSSR, 1988.
11. Richardson, S.D., *Anal. Chem.*, 1999, vol. 71, no. 12, pp. 181R–215R.
12. Ferguson, D.W., McGuire, M.J., Koch, B., et al., *J. Am. Water Works Assoc.*, 1990, vol. 82, no. 4, pp. 181–191.
13. Volk, C., Roche, P., Joret, J.-C., and Paillard, H., *Water Res.*, 1997, vol. 31, no. 3, pp. 650–656.
14. Goncharuk, V.V., Vakulenko, V.F., Sova, A.N., et al., *Khim. Tekhnol. Vody*, 2003, vol. 25, no. 5, pp. 407–427.
15. Goncharuk, V.V., Vakulenko, V.F., Sova, A.N., and Oleinik, L.M., *Khim. Tekhnol. Vody*, 2004, vol. 26, no. 1, pp. 34–49.
16. Goncharuk, V.V., Chornomorets, M.P., Potapchenko, N.G., et al., *Khim. Tekhnol. Vody*, 2002, vol. 24, no. 4, pp. 316–327.
17. Milyukin, M.V., and Gogoman, I.V., *Khim. Tekhnol. Vody*, 1998, vol. 20, no. 6, pp. 569–584.
18. Milyukin, M.V., and Gogoman, I.V., *Khim. Tekhnol. Vody*, 1999, vol. 21, no. 1, pp. 23–29.
19. Ebenga, J.-P., Imbenotte, M., Pommery, J., et al., *Water Res.*, 1986, vol. 20, no. 11, pp. 1383–1392.

ISSN 1070-4272. Russian Journal of Applied Chemistry, 2006, Vol. 79, No. 3, pp. 397–402. © Pleiades Publishing, Inc., 2006.
Original Russian Text © S.V. Efremova, 2006, published in Zhurnal Prikladnoi Khimii, 2006, Vol. 79, No. 3, pp. 404 – 409.

ENVIRONMENTAL PROBLEMS OF CHEMISTRY AND TECHNOLOGY

Water Treatment with a Shungite Sorbent and Biosorbents on Its Base

S. V. Efremova

National Center for Integrated Processing of Mineral Raw Materials of the Republic of Kazakhstan, Almaty, Kazakhstan

Received June 7, 2005; in final form, September 2005

Abstract—Physicochemical and sorption properties of a nonactivated shungite sorbent were studied. The immobilization of yeast cells of *Kluveramyces sp.* (strain 11 K) and *Candida sp*. (strain 10 K) and cells of oil-oxidizing bacterial cultures *Mycobacterium sp.* (strain 119-3 GM) and *Pseudomonas sp.* (strain 51 K) on this sorbent was examined. A comparative analysis of the accumulation of heavy metal ions and degradation of oil by free and immobilized cells of these microorganisms was carried out. The efficiency of application of biosorbents produced on the basis of the shungite support in water treatment to remove heavy metals and oil was studied.

DOI: 10.1134/S1070427206030128

There is a wide variety of materials used as adsorbents to purify water and aqueous solutions: ion-exchange resins, activated carbons, and natural and synthetic zeolites. The practical experience shows that use of natural dispersed materials is the most economically attractive. Numerous examples of their application in particular processes have been reported [1–3]. However, these studies are frequently either not systematic or failing to find wide practical use, and, therefore, a search for new types of raw materials and development of technologies for industrial manufacture of adsorbents on their base remain matters of current interest.

Studies of the sorption properties of shungite rocks from Karelia and their use in treatment of waste and recycled water have been reported [4–7]. Analysis shows that the specific surface area of these materials is comparatively small. However, various methods of modification of the starting rock (with alkali, with alkali under pressure in an autoclave, thermal treatment, etc.) make it possible to improve their sorption properties and to recommend shungite sorbents to be used instead of activated carbons in water treatment to remove mostly organic compounds and, in particular, petroleum products.

Similarly to that from Karelia, the Kazakhstan shungite rock is a multiphase system that contains a mineral component composed of quartzite and aluminosilicates and shungite proper, which differs from the Karelian material in a low degree of structural ordering and high particle dispersity [8–10]. These structural features of the Kazakhstan shungite should, in all probability, positively affect its sorption properties. The fact that a considerable amount of the rock in question is contained, in addition to natural deposits, in wastes formed in mining and dressing of polymetallic ores poses the question of processing of these materials.

Therefore, it was of interest to examine the possibility of using the Kazakhstan shungite rock to produce sorbents that could be used in water treatment to remove various contaminants.

EXPERIMENTAL

The shungite carbon–mineral sorbent (SCMS), whose main adsorption parameters are listed in Table 1, was prepared from a shungite concentrate produced from a homogenized sample of shungite rock[1] ($c \approx 20.0$ wt %) by foam flotation. The concentrate was mixed with an aqueous solution of sugar to the consistency of thick dough. The resulting paste was passed through a worm feeder with holes 0.3 cm in diameter. Grains 0.5–0.8 cm in size were dried in air first at room temperature and then at 110°C for 1 h, and after that were subjected to thermal treatment without access of air at 750°C for 20 min [11, 12].

[1] Bol'shevik deposit, Eastern-Kazakhstan oblast.

Table 1. Principal adsorption properties of carbon sorbents*

Parameter	SCMS	SS	SSA	SSM	SS-750	ACh	BAU-MF
Bulk density, g cm^{-3}	0.4	1.83	1.24	1.23	–	Not rated	
Moisture content, %	1	–	–	–	–	No more than 10	
Ash content, %	10	–	–	–	–	No more than 6	No more than 10
Specific surface area, m^2 g^{-1}	50	6.8	14.0	17.0	9.0	Not rated	
Total porosity for acetone, %	55				31.33	Not rated	
cm^3 g^{-1}		0.35	0.23	0.17			
Total pore volume for water, cm^3 g^{-1}	0.72	0.095	0.106	0.091	0.3	No less than 1.4	Not rated
Adsorption activity toward iodine, %	12					No less than 30	No less than 70
mg g^{-1}		2.4	27.9	24.12	9.84		
Sorption capacity for Methylene Blue, mg g^{-1}	10	19.5	–	–	–	Not rated	

* Shungite sorbent: SS, untreated; SSA activated with steam; SSM, treated with a NaOH solution [6]; SS-750, thermally treated at 750°C [7]; ACh, crushed activated charcoal for removing oil and other impurities from steam condensate; BAU-MF, crushed activated charcoal for adsorption from aqueous media in filtering installations [13].

The activation of the resulting sorbent, recommended in [12], was beyond the scope of this study.

Comparison of the physicochemical properties of SCMS with the characteristics of natural and modified Karelian shungite sorbents and those of activated charcoal shows that nonactivated SCMS is inferior in certain parameters (total pore volume, adsorption activity toward iodine) to commercial activated carbons but greatly surpasses various samples of sorbents produced from Karelian shungite rock in specific surface area and total pore volume (Table 1). In all probability, this is provided by structural features of the Kazakhstan shungite and by the method used to produce SCMS. In this technique, an aqueous solution of sugar serves as a binder, which favors carbonization of the sorbent in thermal treatment without access of air and thereby leads to an increase in its porosity. As regards the pore structure of the sorbent, it follows from experiments on the sorption of iodine, Methylene Blue, and acetone that nonactivated SCMS has a more developed microsctructure than the Karelian sorbents. For example, the pore volume of SCMS is 50 times the volume of micropores in the untreated Karelian shungite sorbent. At the same time, the volume of macropores in SCMS is nearly two times smaller than that in the Karelian sorbent. The volume of mesopores is somewhat larger than that in both untreated and modified Karelian shungite sorbents.

The shungite carbon–mineral sorbent was analyzed for product safety at Kazakh Republican sanitary-epidemiological station. It was found that the activity of natural radionuclides in the sample studied does not exceed the radiation background in various soils; the content of radionuclides in an aqueous extract does not exceed the level established by radiation safety regulations for water; the sorbent meets the sanitary-hygienic requirements.

The shungite carbon–mineral sorbent was tested in water treatment to remove heavy metal ions. The sorption was performed at room temperature by passing through a sorption column (d = 15 mm) at a rate of 75 cm^3 h^{-1} model solutions (pH 6–7) of $Pb(NO_3)_2$, $MnSO_4$, $CdCl_2$, and $ZnCl_2$ containing (mg l^{-1}): Pb^{2+} 0.15, 10; Mn^{2+} 0.15; Cd^{2+} 1, 10, 100; Zn^{2+} 0.15, 1.

The choice of the above solutions is due to the fact that lead(II), cadmium(II), and zinc(II) are the most toxic, and manganese(II) is predominant among heavy metals in the ecosystem of Kazakhstan [14].

The eluted fractions were collected in portions of 150 cm^3 every 2 h during 20 h until the ratio of the volume V of the solution passed to that of the sorbent (V_s) became 75. The content of heavy metal ions in the eluates was monitored with an atomic-adsorption spectrometer. The tests performed made it possible to determine how the sorption capacity of the shungite sorbent depends on the working time of the column and on the nature and concentration of a contaminant. Table 2 shows that SCMS exhibited a high activity in purification of solutions containing 0.15 mg l^{-1} of Pb^{2+} and Zn^{2+} each. Its operation is the most stable

Table 2. Sorption of metal ions by SCMS under dynamic conditions

Working time of column, *h*	Solution volume *V*, cm^3	V/V_s	Degree of recovery (%) of metal ions from their solutions at their indicated concentrations, mg l^{-1}							
			Cd^{2+}			Pb^{2+}		Zn^{2+}		Mn^{2+}
			1.0	10	100	0.15	10	0.15	1.0	0.15
2	150	7.5	91	90	70	100	70	100	92	80
4	300	15	91	90	53	100	20	100	88	80
6	450	22.5	90	90	43	100	20	100	63	80
8	600	30	90	80	38	100	20	100	58	73
10	750	37.5	89	80	38	100	10	87	50	67
12	900	45	89	80	29	100	–	80	45	67
14	1050	52.5	89	80	24	100	–	80	37	60
16	1200	60	87	70	17	100	–	60	37	0
18	1350	67.5	77	70	–	100	–	60	37	–
20	1500	75	76	40	–	100	–	47	37	–

in a wide range of concentrations and large V/V_s in the case of Cd^{2+}.

An important characteristic of any sorbent is its ability to be regenerated and reused. A rather widely adopted way to regenerate natural sorbents used to remove heavy metal ions from water is alkaline treatment [1], which is also recognized as the most efficient method for modification of shungite sorbents [5, 6]. The worked-out SCMS was regenerated by treatment with a 0.4 N NaOH solution (s : l ratio 1 : 10), with boiling at atmospheric pressure for 30 min. In contrast to the autoclave method, such a treatment procedure has virtually no effect on the mechanical characteristics of the sorbent, because SiO_2 is either extracted from the existing pores or from microcracks, without disintegration of the silica skeleton [5]. Regenerated samples were tested in treatment of solutions containing 1.0 and 10 mg l^{-1} of cadmium. It was found that the regenerated material sorbs cadmium(II) from a solution with a concentration of cadmium ions of 10 mg l^{-1} with a lower efficiency than does the initial sorbent. In the case, however, of a solution containing 1 mg l^{-1} Cd^{2+}, the degree of recovery of cadmium(II) ions by a sorbent subjected to alkaline treatment markedly increases and constitutes 100% during the first 10 h of operation of the column. This fact indicates that the sorption capacity of SCMS can be controlled by some kind of modification or by selection of the optimal conditions of the sorption process.

As a method for modification of the sorbent surface can be considered immobilization of cells of microorganisms, e.g., those capable of selective sorption and accumulation of heavy metal ions and of oxidative degradation of oil [15–17].

Yeast cells of *Candida sp*. (strain 10 K) and *Kluveramyces sp*. (strain 11 K) were immobilized on a shungite support in the course of 1, 3, and 24 h (method I). The results obtained demonstrated that SCMS exhibits a higher activity toward cells of strain 10 K, compared with those of strain 11 K; during the first hour, 50 and 18%, respectively, were immobilized. At a longer time of culturing, cells are desorbed from the support surface. For example, the number of immobilized cells decreased to 31% in 3 h and to 25% in 24 h for strain 10 K; in the case of strain 11 K, the respective values were 11 and 6%.

Therefore, the cultures were preliminarily grown for 24 h in a Saburo liquid culture medium (glucose 40 g, peptone 10 g, water 1 l) to the logarithmic phase of active growth. After that the sorbent was introduced into the fermentation medium with these yeast cells, kept there for 24 h, and then separated (method II). The content of yeast cells of strain 11 K, sorbed on the shungite sorbent in this way, exceeded 40%. At the same time, the content of immobilized cells of strain 10 K was about 35%, which was lower than the content of cells fixed by method I during the first hour, but larger than that of cells fixed in 3 and 24 h.

Therefore, samples of modified sorbents were prepared in what follows by culturing of cells of strains 11 K and 10 K with SCMS by method II. The content of cells in finished biosorbents is listed in Table 3.

Table 3. Content of yeast cells adsorbed on the shungite sorbent

Strain	Number of cells in medium		Content of adsorbed cells, %
	without support	with support	
11 K	35.9×10^6	19.1×10^6	47
10 K	12.2×10^6	8.0×10^6	34

The sorption power of the sorbents obtained was studied for the example of aqueous solutions with 1 mg l^{-1} of cadmium and zinc ions each. The sorption of metal ions was observed at room temperature in the static mode at a 1 : 100 mass ratio of the sorbent and the solution being purified. It was found that the maximum degree of solution purification to remove Cd^{2+} and Zn^{2+} is observed after 24 h, with the highest sorption activity exhibited by immobilized cells of strain 11 K; the degrees of absorption by immobilized cells of strains 11 K and 10 K and by SCMS were 56, 55, and 52%, respectively, for cadmium ions, and 60, 55, and 50% for zinc ions.

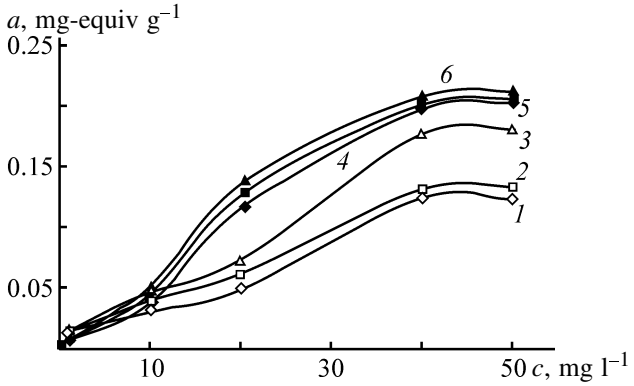


Fig. 1. Isotherms of sorption a of zinc and cadmium ions by shungite biological sorbents. (c) Concentration of metal ions in the solutions being purified. Sorption of Zn^{2+} by (*1*) SCMS, (*2*) immobilized cells of strain 10 K, and (*3*) immobilized cells of strain 11 K and of Cd^{2+} by (*4*) SCMS, (*5*) immobilized cells of strain 10 K, and (*6*) immobilized cells of strain 11 K.

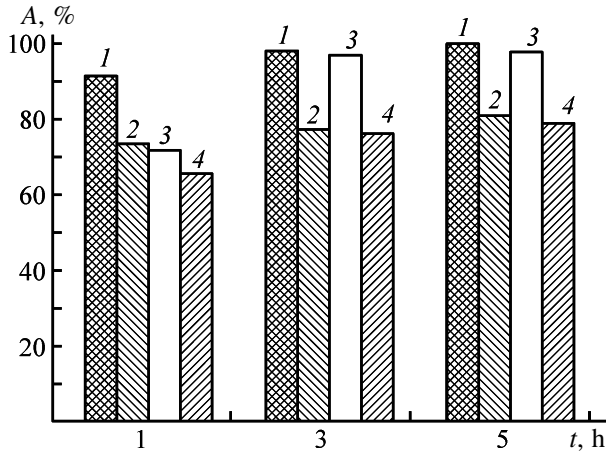


Fig. 2. Dynamics of sorption of cells of *Mycobacterium sp.* (strain 119-3 GM) and *Pseudomonas sp*. (strain 51 K) by granulated and powdered shungite sorbents. (A) Fraction of adsorbed cells and (t) immobilization time. Sorption by granulated sorbent: (*1*) strain 119-3 GM and (*2*) strain 51 K; sorption by powdered sorbent: (*3*) strain 119-3 GM and (*4*) strain 51 K.

Therefore, the absorption of metal ions from solutions with various initial concentrations (0.1 to 50 mg l^{-1} Cd^{2+} and 1 to 50 mg l^{-1} Zn^{2+}) was performed during 24 h. Figure 1 shows sorption isotherms, according to which the fraction of adsorbed ions of the contaminating metals increases with their concentration in solutions, and the sorption capacity of the sorbents tested for metal ions grows in the following order: shungite support, immobilized cells of strain 10 K, immobilized cells of strain 11 K, at a considerably higher sorption affinity for cadmium ions.

Cells of oil-oxidizing bacterial cultures *Mycobacterium* sp. (strain 119-3 GM) and *Pseudomonas sp.* (strain 51 KS) were immobilized on granulated and powdered (without binder) shungite supports in the course of 1, 3, and 5 h. The granulated SCMS (Fig. 2) exhibited a higher activity toward cells of the strains under consideration. Already in 1 h, the fraction of cells adsorbed on its surface reached 90% for strain 119-3 GM and 70% for strain 51 K, whereas for the powdered support, these figures were 72 and 64%, respectively. However, the optimal exposure time for immobilization of the bacterial cultures was 5 h. The fraction of cells of strain 119-3 GM, adsorbed during this interval of time, was 99% for the granulated support and 97% for that in the powdered state; for strain 51 KS, these figures were 80 and 78%, respectively.

On the basis of the results obtained, granulated SCMS was chosen as a support for laboratory experiments on water treatment to remove oil contaminations, and strain 119-3 GM, as hydrocarbon destructor. A shungite sorbent (SCMS) of mass 2 g, pasteurized at 1.5 atm for 1 h, was introduced into a vessel containing 100 cm^3 of a culture medium of the following composition (g): KH_2PO_4 1.0, K_2HPO_4 1.0, $MgSO_4 \cdot 7H_2O$ 0.2, $CaCl_2$ 0.02, $FeSO_4$ 0.002, NH_4NO_3 1.0, and H_2O up to 1 l. As a source of carbon and energy served 3 g of crude oil from the Tengiz oil field. A 10 cm^3 portion of a suspension of *Mycobacterium sp*. cells (strain 119-3 GM, concentration 10^9 cells per cm^3) was introduced into a flask. The culturing was performed on a rocker at 25°C and

a rocking rate of 220 rpm in the course of 3, 5, and 10 days. In a control run, bacterial cells were introduced into a culture medium with oil, but without any sorbent. The residual amount of the hydrocarbon contaminant, measured gravimetrically upon extraction with chloroform, was used to determine the efficiency of its consumption by free and immobilized cells of strain 119-3 GM.

Figure 3 shows that immobilized cells exhibit a stronger oil-oxidizing power than free cells. It should be noted that, after 3 days, the degree of oil oxidation by immobilized cells (78%) was 2.5 times that for free cells (30%). Longer exposure time favors an increase in the degree of degradation of the hydrocarbon contaminant by both immobilized and free cells of the bacterial culture *Mycobacterium sp.* (strain 119-3 GM). For example, the degree of oil degradation in 10 days reaches a value of 86% for immobilized cells of the culture under consideration and 78% for free cells.

A study of the dynamics of redistribution of the biomass of microorganisms in a system constituted by an aqueous medium and a support demonstrated that the fixation of microorganism cells on the shungite sorbent is decelerated in the presence of a hydrocarbon contaminant. As already noted, the fraction of cells adsorbed on the support in an oil-free medium in 1–5 h varied from 90 to 99% (Fig. 2), whereas in a contaminated medium, the fraction of adsorbed cells was only 67% in 3 days, 74% in 5 days, and 93% in 10 days. This behavior can be attributed to the high sorption affinity of SCMS for hydrocarbons, which results in that, in addition to immobilization of microorganisms, adsorption of oil occurs on its surface, with the subsequent degradation of oil by cells of the oil-oxidizing culture fixed on the sorbent. As a result, place for sorption of new portions of microorganism cells and hydrocarbon contaminants is freed, and this leads to an increase in the amount of adsorbed cells of *Mycobacterium sp.* (strain 119-3 GM) and in the degree of oil degradation.

This conclusion was confirmed by a model experiment in an aquarium containing 2 l of artificial Kaspian seawater (pH 8) of the following composition (g l^{-1}): NaCl 2.34, $MgSO_4 \cdot 7H_2O$ 24.6, KCl 1.5, $CaCl_2 \cdot 2H_2O$ 2.9, $FeSO_4$ 0.28, and NH_4Cl 1.0. A 40-g portion of a granulated shungite sorbent, 60 g of oil, and 200 cm^3 of a suspension of *Mycobacterium sp.* cells (strain 119-3 GM) with a concentration of 10^9 cells/cm^3 was introduced into one aquarium, and the same amounts of the contaminant and suspension of microorganism cells, into another. The

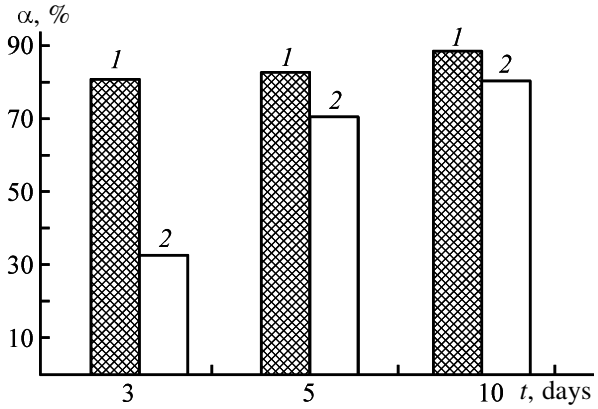


Fig. 3. Oil degradation by cells of the culture *Mycobacterium sp.* (strain 119-3 GM) immobilized on the sorbent and by free cells. (α) Degree of degradation and (*t*) time of degradation. Cells: (*1*) immobilized and (*2*) free.

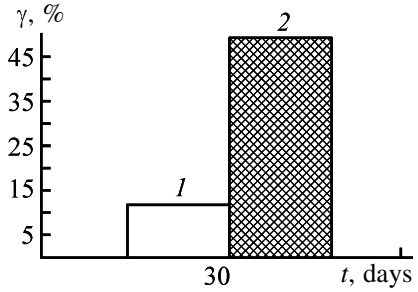


Fig. 4. Oil consumption in an aquarium. (γ) Degree of consumption and (*t*) time of consumption. Cells of strain 119-3 GM: (*1*) free and (*2*) immobilized.

experiment was carried out in the course of 30 days at 22°C without aeration; the degrees of oil consumption by cells of strain 119-3 GM, immobilized on the shungite sorbent and free, were compared. The data obtained (Fig. 4) indicate that the degree of oil consumption by immobilized cells (45%) markedly exceeds that by free cells (7%). Consequently, the shungite support enhances the oxidizing activity of immobilized cells. Adsorbing the hydrocarbon contaminant, it locally disrupts the integrity of the oil spot on the surface of water and thereby improves the aeration, and this enhances the oxidation of oil by immobilized oil-oxidizing microorganisms.

CONCLUSIONS

(1) The physicochemical properties of a nonactivated carbon–mineral sorbent based on Kazakhstan shungite rock were studied in comparison with natural and modified Karelian shungite sorbents and activated charcoals. It was demonstrated that, owing to the structural features of the Kazakhstan shungite and to

the method suggested for producing a carbon–mineral sorbent from this shungite, the sorbent markedly exceeds in sorption characteristics the known Karelian shungite sorbents, being, however, inferior to commercial activated charcoals.

(2) The dynamics of immobilization of cells of yeast cultures *Kluveramyces sp.* (strain 11 K) and *Candida sp.* (strain 10 K) on the shungite sorbent was studied and the optimal immobilization conditions were determined. Immobilized strain 11 K cells exhibit higher sorption aictivity toward heavy metal ions than do immobilized strain 10 K cells and straight shungite sorbent.

(3) It is preferable to use a granulated sorbent as a support for cells of *Mycobacterium sp.* (strain 119-3 GM) and *Pseudomonas sp.* (strain 51 KS).

(4) The possibility of using a shungite sorbent with immobilized oil-oxidizing microorganisms to treat natural water contaminated with oil products was assessed. These biosorbents provide an efficient adsorption-biological water treatment to remove oil.

REFERENCES

1. Tarasevich, Yu.I., *Prirodnye sorbenty v protsessakh ochistki vody* (Natural Sorbents in Water Treatment), Kiev: Naukova Dumka, 1981.
2. Gol'fman, M.I., Tarasova, Yu.V., Shevchenko, T.V., and Mandzii, M.R., *Khim. Prom-st.*, 2002, no. 5, pp. 50–56.
3. Tarasevich, Yu.I., Bondarenko, S.V., Brutko, V.V., et al., *Zh. Prikl. Khim.*, 2003, vol. 76, no. 10, pp. 1619–1624.
4. Kalinin, Yu.K. and Peki, A.S., *Shungity Karelii i puti ikh kompleksnogo ispol'zovaniya* (Karelian Shungites and Ways to Their Integrated Use), Petrozavodsk: Kareliya, 1975.
5. Aunin'sh, E.A., Dyukkiev, E.F., Tupolev, A.G., and Kalinin, Yu.K., *Shungity – novoe uglerodistoe syr'e* (Shungites, New Carbon Raw Material), Petrozavodsk: Kareliya, 1984, pp. 110–124.
6. Lugovskaya, I.G., Theoretical and Experimental Substantiation of Use of Shungite Rock in Treatment of Process Solutions and Discharge Gases, *Cand. Sci. Dissertation*, Moscow, 2001.
7. Krylov, I.O., Lugovskaya, I.G., Anufrieva, S.I., and Krylova, A.V., *Zh. Prikl. Khim.*, 2003, vol. 76, no. 8, pp. 1273–1276.
8. Efremova, S.V., Shungite Carbon as Substitute for Carbon Black as Filler for Composites, *Cand. Sci. Dissertation*, Almaty, 1999.
9. Korolev, Yu.M., Kolesnikov, B.Ya., Efremova, S.V., and Efremov, S.A., *Khim. Tverd. Topl.*, 2000, no. 2, pp. 88–92.
10. Efremova, S.V., Korolev, Yu.M., Nauryzbaev, M.K., and Efremov, S.A., *Khim. Tverd. Topl.*, 2003, no. 1, pp. 11–20.
11. Efremov, S.A., Efremova, S.V., and Kolesnikov, B.Ya., *Materialy Mezhdunarodnoi konferentsii po analiticheskoi khimii, posvyashchennoi 100-letiyu so dnya rozhdeniya chlena-korrespondenta Natsional'noi Akademii Nauk Respubliki Kazakhstan O.A. Songinoi*, Almaty, mai 2001 g. (Proc. Int. Conf. on Analytical Chemistry, Devoted to 100th Anniversary of Birthday of Corresponding Member of the National Academy of Sciences of the Republic of Kazakhstan O.A. Songina, May 2001), Almaty, 2001, p. 52.
12. Kazakhstan Patent 15932.
13. *GOST* (State Standard) *6217–74: Crushed Activated Charcoal*.
14. Romanova, S.M., Musapirova, Z.S., and Kruchenko, S.S., *Vestn. Kaz. Gos. Univ., Ser. Khim.*, 1999, no. 2, pp. 5–11.
15. Davidova, E.G. and Kasparova, S.G., *Mikrobiologiya*, 1992, vol. 61, no. 5, pp. 838–842.
16. Mukasheva, T.D., *Vestn. Kaz. Gos. Univ., Ser. Biol.*, 2001, no. 1 (13), pp. 134–136.
17. Shigaeva, M.Kh., *Vestn. Kaz. Gos. Univ., Ser. Biol.*, 2002, no. 1 (16), pp. 133–137.

ISSN 1070-4272. Russian Journal of Applied Chemistry, 2006, Vol. 79, No. 3, pp. 403–407. © Pleiades Publishing, Inc., 2006.
Original Russian Text © V.P. Zakharov, F.B. Shevlyakov, 2006, published in Zhurnal Prikladnoi Khimii, 2006, Vol. 79, No. 3, pp. 410–414.

PROCESSES AND EQUIPMENT OF CHEMICAL INDUSTRY

Longitudinal Mixing in Fast Liquid-Phase Chemical Reactions in a Two-Phase Mixture

V. P. Zakharov and F. B. Shevlyakov

Bashkir State University, Ufa, Bashkortostan, Russia

Received June 16, 2005; in final form, November 2005

Abstract—The possibility of diminishing the diffusion limitations in the course of fast chemical reactions in liquid–gas systems by varying the reactant ratio and the rate of longitudinal mixing in the liquid phase and at the phase boundary (via changes in the geometry and hydrodynamic parameters of flow in tubular apparatus) was examined.

DOI: 10.1134/S107042720603013X

It is known that the driving force of the process in heat-and-mass exchange in classical apparatus of chemical technology and, consequently, the rate of this process are at a maximum at low coefficients of longitudinal mixing (that along the flow axis) [1]. If the hydrodynamic structure of flow of the reaction mixture approaches the plug-flow mode, this gives rise to the optimal, as regards the time of completion of the process, conditions for most of chemical reactions, which, as a rule, occur under the kinetic control. At the same time, intensive longitudinal mixing is necessary in performing fast liquid-phase chemical reactions in small-size high-output-capacity tubular turbulent apparatus [2]. In this case, the reactor is comparable in size with the region in which the fast chemical reaction occurs, which is essentially small, and longitudinal mixing leads to "smearing" of temperature, with quasi-isothermal conditions created [3]. Raising the rate of longitudinal mixing leads to intensification of the convective heat exchange, which occurs because of the increase in the heat-exchange coefficient of both the reaction mixture and the cooling agent, and to effective heat removal directly from the reaction zone in the case of external thermostating [4].

The previously revealed [5] fundamental aspects of longitudinal mixing in flow of a single-phase reaction mixture in tubular turbulent apparatus enable choice of the optimal conditions for fast liquid-phase chemical reactions in homogeneous media. At the same time, there is no evidence concerning the hydrodynamic mode of flow of two-phase reaction systems in tubular turbulent apparatus, which complicates the choice of the optimal conditions for fast chemical reactions that occur at the phase boundary, in particular in liquid–gas systems. In flow of a gas–liquid mixture in the turbulent mode, the interface is deformed, which should change the hydrodynamic structure of the flow and the conditions of occurrence of fast chemical reactions. A study of the fundamental aspects of the manner in which hydrodynamic structure of the flow of a gas–liquid mixture changes will enable a scientifically substantiated choice of the optimal geometry of an apparatus and of the process mode. In view of the fact that tubular turbulent apparatus are used to perform fast liquid-phase chemical reactions [3], it seemed appropriate to evaluate the longitudinal mixing in a continuous (liquid) phase.

The aim of this study was to analyze the fundamental aspects of variation of the efficiency of longitudinal mixing in the liquid phase in a flow of a two-phase reaction mixture for the example of a gas–liquid flow in tubular apparatus of the diffuser–confuser design.

The coefficient of longitudinal mixing was calculated using the single-parameter diffusion model, which describes the most precisely the curves of distribution over the residence time of the reagents in the reaction zone [5].The key parameter of this model is the Bodenstein number (Peclet number for the case of longitudinal mixing) $\mathrm{Bo} = L^2 w/v_r E$, where w is the flow rate; v_r, reactor volume; E, coefficient of longitudinal mixing; and L, apparatus length. It can be seen that the numerical values of the Bodenstein criterion make it possible to calculate the coefficient of longitudinal mixing E and to evaluate the extent of

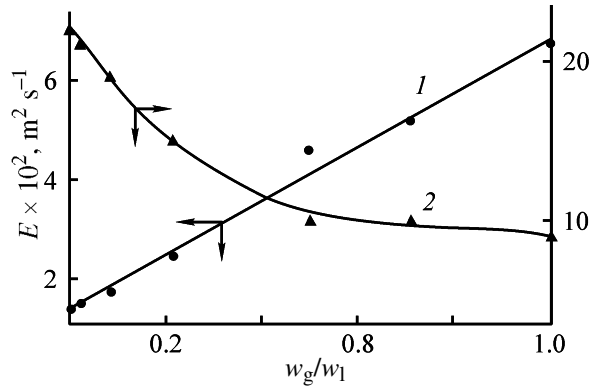


Fig. 1. (*1*) Coefficient of longitudinal mixing E and (*2*) Bodenstein number Bo vs. the ratio of the flow rates of the gas and liquid phases, w_g/w_l. w_l = 160 cm^3 s^{-1}, d_2 = 1.8 mm, d_d/d_c = 1.6.

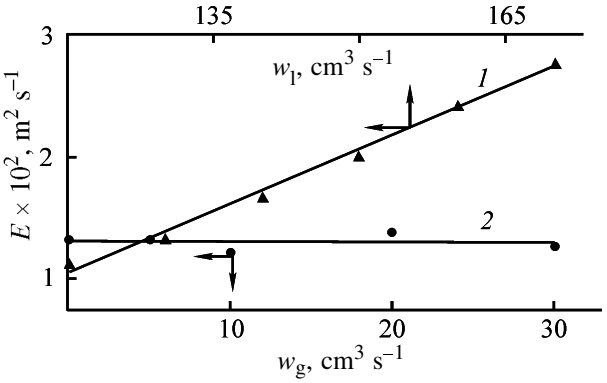


Fig. 2. Coefficient of longitudinal mixing E vs. the flow rate of (*1*) liquid (w_l, w_l/w_g = 5) and (*2*) gas (w_g, w_{l+g} = 160 cm^3 s^{-1}) phases. D_2 = 1.8 mm, d_d/d_c = 1.6.

deviation of the apparatus working mode from the idealized models of mixing (Bo $\to$ 0) and plug flow (Bo $\to \infty$). The design of the tubular turbulent apparatus and the procedure used to measure the curves of response to pulsed introduction of an inert indicator were described in [6].

The experimental setup for a study of the fundamental aspects of flow of two-phase systems comprises a six-section tubular turbulent apparatus of the diffuser–confuser design with inlet of the liquid phase through a coaxial pipe of diameter d_1 = 10 mm and gas feeding through a radially mounted pipe of diameter d_2 (0.8–7 mm). Length of the diffuser–confuser section, L_s = 72 mm; diameter of the wide part of the apparatus (diffuser), d_d = 24 mm; diameter of the narrow part of the apparatus (confuser), d_c = 15–24 mm. Tap water was used as the liquid phase. Its flow rate was measured with a rotameter installed at the line for flow feed into the turbulent apparatus. The flow rate of the gas phase was recorded with a gage installed at the outlet valve of a thick-walled metallic cylinder filled with compressed air (100–150 atm). The frequency curves of the size distribution of drops of the dispersed phase were measured by the method of photographing in high-intensity transmitted light with a SONY DSN-75 digital camera (exposure 1/1000 s, light sensitivity 400 units). To take into account the distortions associated with the bent shape of the apparatus shell, calibrating threads of a known size were introduced into its volume. The calculations used the central part of the longitudinal cross section of the apparatus ($0.75 \times d_d$), in which the discrepancy between the size of the calibration threads, calculated from the image obtained, and the true values was less than 1%. This procedure also made it possible to eliminate the possible image distortions associated with the refractive index of the glass apparatus shell and to take into account the fixed error [7].

As the content of gas in the gas–liquid flow increases, the coefficient of longitudinal mixing E grows (Fig. 1, curve *1*). This leads to a corresponding decrease in the Bodenstein number, with the result that the hydrodynamic structure of the moving reaction mixture approaches the ideal-mixing mode (Fig. 1, curve *2*). Thus, if fast chemical reactions occur under the conditions when a phase boundary exists in the liquid–gas system, including the case of boiling of the reaction mixture, the working mode of the apparatus approaches the ideal mixing mode with a high rate of longitudinal mixing. The high rate of longitudinal mixing results in that the distribution of the residence time of reagents in the reaction zone is broadened, which should be kept in mind when performing fast chemical reactions under real conditions. The coefficient of longitudinal mixing is strongly affected by an increase in the motion velocity of the liquid phase at a fixed gas content of the flow (Fig. 2, curve *1*). At the same time, changes in the ratio of flow rates of the gas and liquid phases, w_g/w_l, at a constant total rate of the gas–liquid flow has virtually no effect on the efficiency of longitudinal mixing (Fig. 2, curve *2*).

The longitudinal mixing in a tubular apparatus can be substantially intensified by changing the geometry of the gas–liquid flow. On passing from a cylindrical apparatus (d_d/d_c = 1) to that of a diffuser–confuser design (d_d/d_c = 3), the coefficient of longitudinal mixing increases by a factor of about 3 (Fig. 3, curve *1*). All other conditions being the same, changing the diameter of the inlet pipe of the gas phase does not affect the rate of longitudinal mixing (Fig. 3, curve *2*).

Generalization of the experimental data obtained made it possible to derive relations that could account for the influence exerted by various process parameters on the rate of longitudinal mixing in a two-phase flow in a tubular turbulent apparatus (Fig. 4). As the volume–surface diameter of particles of the dispersed phase increases to $d_{32} \approx 2$ mm ($d_{32} = \Sigma m_i d_i^3 / \Sigma m_i d_i^2$, where m_i is the number of particles of diameter d_i), the coefficient of longitudinal mixing decreases (Fig. 4, curve *2*). Further coarsening of particles of the dispersed phase has virtually no effect on the rate of mixing of the liquid phase along the apparatus axis. It was found that the coefficient of longitudinal mixing in the liquid phase is largely determined by the number of particles of the dispersed phase. The formation of a gas–liquid flow with a large specific surface area via breakup of the dispersed phase results in that the rate of longitudinal mixing in a continuous medium increases and the working mode of the apparatus closely approaches the ideal-mixing mode (Fig. 4, curve *1*). This makes it possible to create uniform reagent concentration fields directly in the reaction zone in the case of local occurrence of fast chemical processes in liquid–gas systems. If a fast chemical reaction occurs in a single-phase mixture, boiling in the reactor volume, with a two-phase flow formed, will intensify reagent mixing along the apparatus axis.

The competing influence of the particle size in the dispersed phase and the particle number on the rate of longitudinal mixing (Fig. 4) accounts for the dependences obtained in the study (Figs. 1–3). As the gas content of the flow (i.e., the w_g/w_l ratio) increases, particles of the dispersed phase become coarser and their number grows, which intensifies the longitudinal mixing (Fig. 1). Flow of the reaction mixture with a high velocity at a fixed gas content of the flow leads to an increase in the number of particles of the dispersed phase via its breakup and to a rise in the rate of mixing along the apparatus axis (Fig. 2, curve *1*). Apparently, this is the main reason why the reaction zone is "densified" when fast chemical processes are carried out in tubular turbulent apparatus in both single- [3] and two-phase [8] systems. As the residence time of reagents in the reaction zone decreases as the output capacity of the apparatus becomes higher, the yield of the product (process rate) increases, which is determined by intensified homogenization of the reaction mixture, including that in longitudinal mixing. Changing the content of the gas phase at the same total gas–liquid flow rate leads to a slight change in the number of particles of the dispersed phase and, accordingly, in the coefficient of longitudinal mixing (Fig. 2, curve *2*). The rise in the number of particles

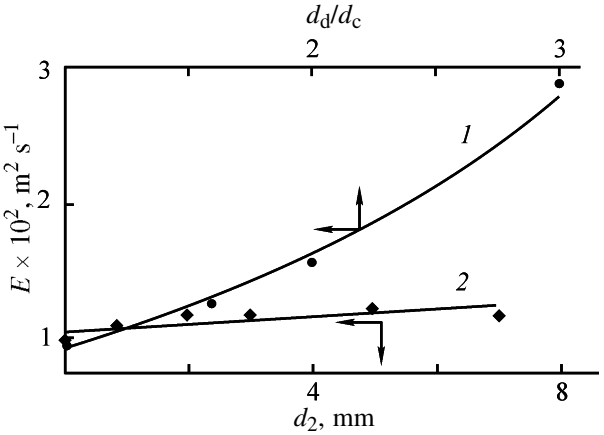


Fig. 3. Coefficient of longitudinal mixing E vs. (*1*) d_d/d_c ratio (d_2 = 3 mm) and (*2*) diameter of the inlet pipe for the gas phase d_2 (d_d/d_c = 2). w_l = 150 cm^3 s^{-1}, w_l/w_g = 3.

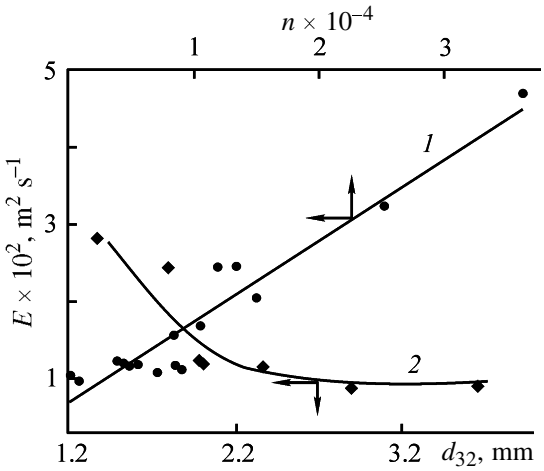


Fig. 4. Generalized dependences of the coefficient of longitudinal mixing E, on (*1*) number n and (*2*) volume–surface diameter d_{32} of particles of the dispersed phase in a gas–liquid flow in a tubular turbulent apparatus.

of the dispersed phase via dispersion predetermines an increase in the rate of longitudinal mixing on passing from a cylindrical apparatus to that of the diffuser–confuser type (Fig. 3, curve *1*).

The hydrodynamic mode of flow of the gas–liquid reaction mixture is affected by the spatial position of a tubular turbulent apparatus of the diffuser–confuser design. In the case of a flow of a single-phase reaction mixture, the position of the apparatus has virtually no effect on the rate of longitudinal mixing (Fig. 5, curve *1*). The gas–liquid flow is characterized by the minimum value of the coefficient of longitudinal mixing at apparatus inclination angles α from –40° to 0°. A vertical position of the tubular apparatus (α = –90°) with a downward direction of the gas–liquid flow determines the maximum value of the coefficient of

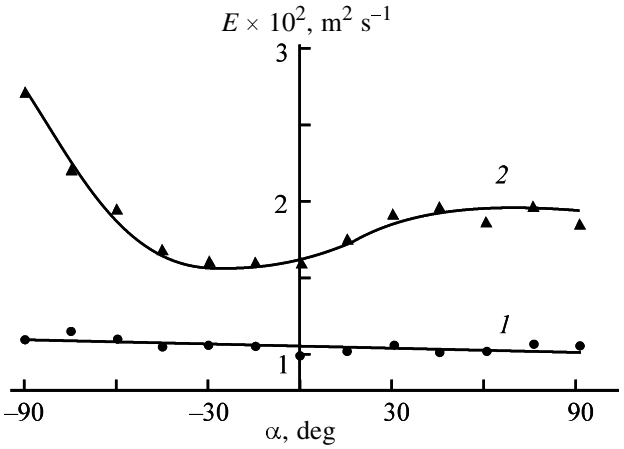


Fig. 5. Coefficient of longitudinal mixing E for (*1*) single- and (*2*) two-phase flows vs. the inclination angle α of the apparatus. d_2 = 3 mm, d_d/d_c = 2, w_l = 170 cm^3 s^{-1}, w_g = 40 cm^3 s^{-1}; position of the apparatus: α = 0°, horizontal; α = 90°, vertically upwards; and α = –90°, vertically downwards.

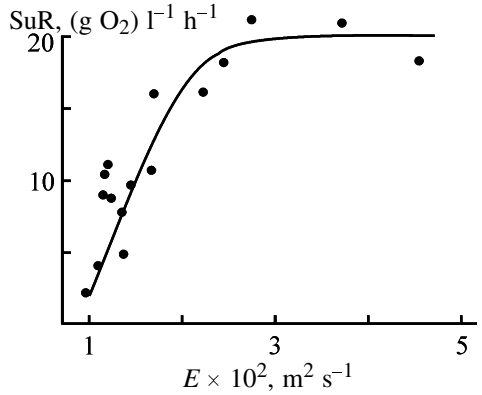


Fig. 6. Generalized dependence of the sulfite number of the reactor SuR on the coefficient of longitudinal mixing E in a gas–liquid (water–air) flow in a tubular turbulent apparatus.

longitudinal mixing. It should be noted that, in this case, the size of particles of the dispersed phase and, accordingly, their number remain unchanged. Apparently, the rate of longitudinal mixing of the gas–liquid flow changes on varying the position of the apparatus by applying to the flowing reaction mixture gravitational forces complicated by strong differences in the density of the constituent components. The dependence of the hydrodynamic mode of flow of the gas–liquid mixture on the position of the apparatus creates additional opportunities for varying the conditions of fast chemical reactions in liquid–gas systems. When carrying out fast chemical reactions in two-phase systems, it is preferable to mount the tubular turbulent apparatus vertically, with the reagents fed from the top. This makes it possible to create an intensive longitudinal mixing and to simplify the discharge of the reaction mixture on terminating the process.

The formation of a reaction mixture with a developed phase boundary and intensive longitudinal mixing in tubular turbulent apparatus predetermines a pronounced increase in the mass-exchange coefficient in the liquid phase. In this case, it becomes possible to effectively diminish the diffusion limitations in the course of fast chemical reactions in liquid–gas systems. This is confirmed by the dependence of the intensity of liquid-phase oxidation, characterized by the "sulfite number of reactor" SuR (amount of oxygen absorbed by unit reaction volume in unit time [8]), on the hydrodynamic structure of flow of the reaction mixture (Fig. 6). It can be seen that raising the coefficient of longitudinal mixing by any of the methods considered in this study leads to an increase in the specific rate of dissolution of atmospheric oxygen in water and, as a result, causes acceleration of the liquid-phase oxidation. In addition, the dependence SuR = $f(E)$ (Fig. 6) has the form of a curve that levels off, and there is no need to make the rate of longitudinal mixing higher than $E = (2–3) \times 10^{-2}$ m^2 s^{-1}.

The fundamental aspects of how the efficiency of longitudinal mixing varies in gas–liquid flows in tubular turbulent apparatus of diffuser–confuser design enable a scientifically substantiated choice of the optimal geometry of the zone of reagent mixing and of the process mode. The formation of disperse systems with a developed phase boundary and, consequently, with a high rate of longitudinal mixing makes it possible to create uniform profiles of reagent concentrations and temperature in a local region in which fast chemical reaction occur and to diminish the diffusion limitations. The correlation between the rate of longitudinal mixing and the efficiency of convective heat exchange in tubular apparatus predetermines the possibility of controlling the process by external thermostating in the course of fast chemical reactions in liquid–gas systems. Apparently, the dependence of the rate of longitudinal mixing in the liquid phase on the particle size of the dispersed phase and particle number, obtained for liquid–gas systems, will be also applicable to description of fast chemical reactions in liquid–liquid and liquid–solid systems.

CONCLUSIONS

(1) The coefficient of longitudinal mixing in the liquid phase in flow of gas–liquid reaction systems in tubular turbulent apparatus of diffuser–confuser

design decreases as particles of the dispersed phase become coarser and is directly proportional to their number.

(2) The rate of a fast (diffusion-controlled) chemical process in a gas–liquid flow depends on the coefficient of longitudinal mixing. Raising the rate of longitudinal mixing in tubular apparatus by changing the geometry and hydrodynamic parameters of flow and the ratio of the reacting components makes it possible to effectively diminish the diffusion limitations in performing fast chemical reactions in liquid–gas systems.

ACKNOWLEDGMENTS

The study was financially supported by the Russian Foundation for Basic Research (project no. 05-03-97903) and by the Foundation for Assistance to National Science.

REFERENCES

1. Ainshtein, V.G., Zakharov, M.K., Nosov, G.A., et al., *Obshchii kurs protsessov i apparatov khimicheskoi tekhnologii* (General Course of Processes and Apparatus of Chemical Technology), Moscow: Logos, 2003, vol. 1.
2. Minsker, K.S., Berlin, Al.Al., Zakharov, V.P., and Zaikov, G.E., *Fast Liquid-Phase Processes in Turbulent Flows*, Netherlands: Brill, 2004.
3. Berlin, Al.Al., Minsker, K.S., and Dyumaev, K.M., *Novye unifitsirovannye energo- i resursosberegayushchie vysokoproizvoditel'nye tekhnologii povyshennoi ekologicheskoi chistoty na osnove trubchatykh turbulentnykh reaktorov* (New Unified Energy- and Resource-Saving High-Output-Capacity Technologies with Improved Environmental Safety, Based on Tubular Turbulent Reactors), Moscow: OAO NIITEKhIM, 1996.
4. Zakharov, V.P., Minsker, K.S., Berlin, Al.Al., and Shevlyakov, F.B., *Teor. Osn. Khim. Tekhnol.*, 2004, vol. 38, no. 5, pp. 528–531.
5. Minsker, K.S., Zakharov, V.P., Shevlyakov, F.B., and Berlin, Al.Al., *Dokl. Ross. Akad. Nauk*, 2003, vol. 392, no. 4, pp. 490–493.
6. Zakharov, V.P., Minsker, K.S., Sadykov, I.V., and Berlin, Al.Al., *Khim. Fiz.*, 2003, vol. 22, no. 3, pp. 34–38.
7. Zakharov, V.P., Mukhametzyanova, A.G., Takhavutdinov, R.G., et al., *Zh. Prikl. Khim.*, 2002, vol. 75, no. 9, pp. 1462–1465.
8. Zakharov, V.P., Minsker, K.S., Shevlyakov, F.B., et al., *Zh. Prikl. Khim.*, 2004, vol. 77, no. 11, pp. 1840–1843.

ISSN 1070-4272. Russian Journal of Applied Chemistry, 2006, Vol. 79, No. 3, pp. 408–410. © Pleiades Publishing, Inc., 2006.
Original Russian Text © M.K. Mamedov, 2006, published in Zhurnal Prikladnoi Khimii, 2006, Vol. 79, No. 3, pp. 415–418.

ORGANIC SYNTHESIS AND INDUSTRIAL ORGANIC CHEMISTRY

Synthesis of Aromatic Alcohols and Their Alkanoic Acid Esters

M. K. Mamedov

Institute of Petrochemical Processes, National Academy of Sciences of Azerbaijan, Baku, Azerbaijan

Received July 26, 2005; in final form, January 2006

Abstract—The reaction of benzene with ethylene and propylene oxides in a helium atmosphere with aluminum chloride as a catalyst and the esterification of the resulting alcohols with saturated monocarboxylic acids in the presence of the heterogeneous catalyst KU-2-8 were studied.

DOI: 10.1134/S1070427206030141

Aldehydes, ketones, and higher alcohols have usually pleasant odor and are synthetic fragrance compounds [1–3]. Some aromatic alcohols and their esters are successfully used in perfume industry as components in preparation of perfume compositions, eau de Colognes, food essences, and odorants for detergents [4–6].

The procedures of synthesis of aromatic alcohols by the reaction of benzene with ethylene and propylene oxides [7, 8], hydrogenation of styrene oxide [9] and cinnamic aldehyde [10], and oxidation of cumene [11] are well known.

Taking account a great practical significance of aromatic alcohols, we developed an efficient procedure of synthesis of 2-phenylethanol and 1-phenyl-2-propanol by hydroxyalkylation of benzene with ethylene and propylene oxides in the presence of aluminum chloride as a catalyst [12].

The reaction proceeds in two steps. In the first step, complexes **A** and hydrogen chloride are formed:

$$C_6H_6 + 3CH_2\overset{O}{\diagdown\diagup}CHR + AlCl_3 \rightarrow \underset{\mathbf{A}}{(C_6H_5CH_2\underset{R}{\underset{|}{C}}HO)_3Al} + 3HCl.$$

In the second step, decomposition of complexes **A** with water yields aromatic alcohols **I** and **II**:

$$\mathbf{A} + H_2O \rightarrow \underset{\mathbf{I, II}}{C_6H_5CH_2\underset{R}{\underset{|}{C}}HOH} + Al(OH)_3,$$

where R is H (**I**) and CH_3 (**II**).

Hydrogen chloride formed in the first step reacts with the initial oxides to give as by-products chlorohydrins **III**–**VI**:

$$HCl + RCHCH_2 \rightarrow \underset{\mathbf{III, IV}}{RCH(OH)CH_2Cl}, \quad \underset{\mathbf{V, VI}}{RCH(Cl)CH_2OH}$$

where R is H (**III, V**), CH_3 (**IV, VI**).

Chlorohydrins **III**–**VI** adversely affect the yield of alcohols **I** and **II**; therefore, to remove hydrogen chloride from the system we used an inert gas (helium); by so doing, we significantly increased the yield of the target products **I** and **II**.

The influence of various factors on the yields of **I** and **II** was studied. We found that the optimum conditions for hydroxyalkylation of benzene are the temperature of 6–7°C, helium flow rate of 2 l min^{-1}, and molar ratio benzene : organic oxide : $AlCl_3$ equal to 5 : 3 : 1. Under these conditions, the yield of alcohols **I** and **II** reaches 90–95% based on organic oxides (compare to the yield of 30–41% for the procedure described in [13]).

To make the process waste-free, hydrogen chloride was passed through aluminum hydroxide to obtain aluminum chloride and helium was purified to remove HCl and repeatedly used in the process.

The composition and structure of **I** and **II** were proved by elemental analysis and IR and ^1H NMR spectra. In the IR spectra the bands at 3300, 3020, 1610, 1500, 745, and 695 cm^{-1} are assigned to the skeleton vibrations of monosubstituted benzene; the absorption at 900 cm^{-1} corresponds to bending modes of the C–H bond; at 1380 cm^{-1}, to methyl groups; at

3440 cm^{-1}, to hydroxy groups; at 1060 cm^{-1}, to primary hydroxy groups; the absorption in the range 1400–1250 cm^{-1} belongs to in-plane bending mode of the bound OH group.

In the ^1H NMR spectra, phenyl protons give signals in the range 6.8–7.28 ppm; methyl protons, at 1.38 ppm; and protons at the tertiary carbon atom and OH group, at 4.75 and 2.60–2.70 ppm, respectively.

With the aim to synthesize esters of the aromatic alcohols synthesized, we studied their esterification with saturated monocarboxylic acids. Contrary to the existing procedures, in this reaction we used a heterogeneous catalyst, ion-exchange resin KU-2-8:

$$\mathbf{I},\ \mathbf{II} + R'COOH \xrightarrow[-H_2O]{\text{KU-2-8}} C_6H_5CH_2\underset{\displaystyle R}{\underset{|}{C}}HOC\overset{\displaystyle O}{\overset{\|}{}}R',$$

VII–XIX

where R is H (**VII**–**XII**), CH_3 (**XIII**–**XIX**); R' is CH_3 (**VII**, **XIII**), C_2H_5 (**VIII**, **XIV**), $CH_3(CH_2)_2$ (**IX**, **XV**), $(CH_3)_2CH$ (**X**, **XIV**), $CH_3(CH_2)_3$ (**XI**, **XVII**), $(CH_3)_2CHCH_2$ (**XII**, **XIX**).

The use of the KU-2-8 catalyst significantly simplifies synthesis of esters (**VI**–**XIX**), since in this case neutralization of the catalyzate, its washing, and drying before distillation are eliminated from the flowsheet.

Removal of water formed in the course of esterification from the system prevents the reverse reaction and significantly increases the yield of the target compounds (to 82–95%).

The structure of the synthesized esters **VI**–**XIX** was proved by the IR spectra. The strong absorption bands at about 1720 and 1200 cm^{-1} suggest the presence of the ester group. In the ^1H NMR spectra, the phenyl protons give a singlet at 7.20 ppm; methyl protons, at 2.10 ppm; and ethylene (CH_2CH_2) protons, at 2.75 and 3.82 ppm.

EXPERIMENTAL

The initial substances were freshly distilled chemically pure grade compounds, whose physicochemical characteristics corresponded to published data [14].

The composition and purity of alcohols **I** and **II** and their esters **VI**–**XIX** were determined by gas–liquid chromatography on an LKhM-8 MD chromatograph; stationary phase polyethylene glycol adipate applied to Sferokhrom (10 wt %), column length 2 m, vaporizer temperature 250°C, column temperature 120–170°C, detector temperature 120–170°C, and current 100 mA. The purity of alcohols **I** and **II** and esters **VI**–**XIX** was 99.0–99.5%.

The IR spectra were recorded on a UR-20 device in CCl_4. The ^1H NMR spectra of solutions of compounds in CCl_4 were recorded on a Tesla BS-487 spectrometer operating at 80 MHz at 25°C; HMDS was used as an internal reference; the accuracy of measuring chemical shifts was ±0.05 ppm.

Hydroxyalkylation of benzene was performed as follows. Benzene was charged into an enameled reactor and anhydrous $AlCl_3$ was added in portions over a period of 1 h; then, a helium from a cylinder was passed through the mixture at a flow rate of 2 l min^{-1}. The released gas was passed through the other reactor containing a suspension of aluminum hydroxide. Then, the calculated amount of ethylene or propylene oxide was fed into the enameled reactor over a period of 3 h. The reaction was carried out at 6–7°C; this temperature was maintained up to the end of the process by passing cooled water through the reactor jacket, since the process is exothermic. After completion of feeding the oxide, the reaction mixture was stirred for 1 h and cold distilled water was added to decompose the resulting complex **A**. In so doing, the upper layer was separated, dried over silica gel, and aromatic alcohols **I** and **II** were isolated by fractional distillation.

2-Phenylethanol (I). From 1560 g of benzene, 528 g of ethylene oxide, and 534 g of $AlCl_3$, 1317.6 g of alcohol **I** was obtained (90%); bp 91–92°C (8 mm Hg), d_4^{20} = 1.0209, n_D^{20} = 1.5306. IR spectrum, ν (cm^{-1}): (CH of phenyl radical) 3330, 3020, 1610, 1500, 900, and 745; (CH_2CH_2) 1440–1470; (OH) 3440, 1060. ^1H NMR spectrum (δ, ppm): (OH) 2.60, (CH_2) 2.85, (CH_2) 3.26, (CH of phenyl radical) 7.20.

Found, %: C 78.45, H 8.25.
$C_8H_{10}O$. Calculated, %: C 78.65, H 8.25.

1-Phenyl-2-propanol (II). From 1170 g of benzene, 522 g of propylene oxide, and 400.5 g of $AlCl_3$, 1138.2 g of alcohol **II** was obtained (93%); bp 92–93°C (2 mm Hg), d_4^{20} = 1.0047, n_D^{20} = 1.5218. IR spectrum, ν (cm^{-1}): (CH of phenyl radical) 3330, 3018, 1605, 900, and 740; (CH_3) 1380, (CH_2 and CH) 1440, 1340; (OH) 3440, 1056. ^1H NMR spectrum (δ, ppm): (OH) 2.60, (CH_2) 1.85, (CH_2) 2.80, (CH) 4.58, (CH of phenyl radical) 7.25.

Found, %: C 79.36, H 8.81.
$C_9H_{12}O$. Calculated, %: C 79.37, H 8.88.

Yield, constants, elemental composition, molecular weight, and odor* of esters **VII**–**XIX**

Compound	Yield, %	bp, °C (10 mm Hg)	d_4^{20}	n_D^{20}	Found, %		Formula	Calculated		*M*	
					C	H		C	H	found	calculated
VII	93	113	1.0181	1.5029	73.04	7.30	$C_{10}H_{12}O_2$	73.14	7.37	164.20	164.20
VIII	92	121	1.0101	1.4904	74.10	7.58	$C_{11}H_{14}O_2$	74.13	7.92	178.10	178.20
IX	91	135	0.9905	1.4905	74.86	8.23	$C_{12}H_{16}O_2$	74.97	8.39	192.20	192.23
X	90	128–129	0.9871	1.4895	74.90	8.26	$C_{12}H_{16}O_2$	74.97	8.39	192.11	192.23
XI	89	138–139	0.9864	1.4982	75.59	8.29	$C_{13}H_{18}O_2$	75.69	8.38	206.21	206.88
XII	89	133–134	0.9791	1.4878	75.61	8.23	$C_{13}H_{18}O_2$	75.69	8.38	206.82	206.28
XIII	93	127	1.0081	1.5180	73.0	7.25	$C_{10}H_{12}O_2$	73.14	7.37	164.10	164.20
XIV	89	138	1.0028	1.5160	74.03	7.89	$C_{11}H_{14}O_2$	74.13	7.92	178.20	178.23
XV	86	146	1.0001	1.5167	74.82	8.27	$C_{12}H_{16}O_2$	74.97	8.39	192.20	192.26
XVI	84	157–158	0.9909	1.5181	75.65	8.62	$C_{13}H_{18}O_2$	75.69	8.80	206.28	206.31
XVII	82	151–152	0.9825	1.5011	75.61	8.69	$C_{13}H_{18}O_2$	75.69	8.80	206.26	206.31
XVIII	83	175–176	0.9806	1.5099	76.25	9.10	$C_{14}H_{20}O_2$	76.33	9.15	220.29	220.31
XIX	82	171–172	0.9800	1.5006	76.28	9.05	$C_{14}H_{20}O_2$	76.33	9.15	220.28	220.31

* Odor: **VII**, fruit (tint of greens); **VIII**, fruit (rose tint); **IX**, fruit (rose tint); **X**, weak fruit; **XI**, delicate fruit; **XII**, apricot (rose tint); **XIV**, grass; **XVI**, weak flower; **XVII**, weak fruit; **XIX**, flower fruit.

Organoleptic tests[1] of the synthesized alcohols show that 2-phenylethanol has rose odor, and 1-phenyl-2-propanol, hyacinth odor.

Esters **VI**–**XIX** of alcohols **I** and **II** (see table) were prepared using a Dean–Stark trap with KU-2-8 catalyst in an amount of 10 wt % based on the raw materials in benzene at 80–85°C. The water release was complete in 4–5 h. The molar ratio of reacting components **I**, **II** : carboxylic acid : solvent was 1 : 1 : 2.

CONCLUSIONS

(1) Aromatic alcohols that are synthetic fragrance compounds were synthesized by hydroxyalkylation of benzene with ethylene and propylene oxides in an inert medium with aluminum chloride as a catalyst (yield 90–93%).

(2) Esterification of the aromatic alcohols synthesized with saturated aliphatic monocarboxylic acids in the presence of a heterogeneous catalyst, KU-2-8 ion-exchange resin, yields esters (yield 82–95%) with pleasant odor, which can be used as a component of perfumes and essences.

[1] Organoleptic tests were performed at the All-Russian Research Institute of Synthetic and Natural Fragrance Compounds (Moscow).

REFERENCES

1. FRG Patent Appl. no. 10226942.
2. FRG Patent Appl. no. 10206771.
3. Challener, C., *Spec. Chem. Mag.*, 2004, vol. 24, no. 6, pp. 32–34.
4. Kheifits, L.A. and Dashunin, V.M., *Dushistye veshchestva i drugie produkty dlya parfumerii* (Fragrance Compounds and Other Products for Perfumery), Moscow: Khimiya, 1994.
5. Clark, C.S., *Perfum. Flavor.*, 1990, vol. 15, pp. 37–44.
6. Bratus, I.N., *Khimiya dushistykh veshchestv* (Chemistry of Fragrance Compounds), Moscow: Agropromizdat, 1992.
7. Cristol, S., Douglass, J., and Meek, J., *J. Am. Chem. Soc.*, 1951, vol. 73, pp. 816–818.
8. USSR Inventors' Certificate no. 433121.
9. Kologrivova, N.E., Shumskaya, I.V., and Kheifits, L.A., *Maslozhir. Prom-st.*, 1983, issue 12, pp. 23–25.
10. French Patent 2015475.
11. US Patent 244700.
12. USSR Inventors' Certificate no. 1778109.
13. Likhterov, V.R. and Etlis, V.S., *Zh. Obshch. Khim.*, 1957, vol. 27, no. 9, pp. 1867–1869.
14. Goronovskii, I.T., Nazarenko, Yu.P., and Nekryach, E.F., *Kratkii spravochnik po khimii* (Brief Handbook on Chemistry), Kiev: Naukova Dumka, 1974.

ISSN 1070-4272. Russian Journal of Applied Chemistry, 2006, Vol. 79, No. 3, pp. 411–415. © Pleiades Publishing, Inc., 2006.
Original Russian Text © V.F. Anikin, N.F. Fed'ko, 2006, published in Zhurnal Prikladnoi Khimii, 2006, Vol. 79, No. 3, pp. 419–423.

ORGANIC SYNTHESIS AND INDUSTRIAL ORGANIC CHEMISTRY

Tetraalkylammonium Salts of Naphthimide and Its Halo and Nitro Derivatives

V. F. Anikin and N. F. Fed'ko

Mechnikov National University, Odessa, Ukraine

Received July 26, 2005

Abstract—Synthesis of tetraalkylammonium salts of naphthimide and its derivatives was studied.

DOI: 10.1134/S1070427206030153

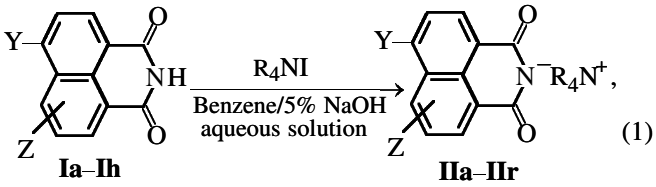
Being efficient phosphors, derivatives of naphthimide {1*H*-benzo[*de*]isoquinoline-1,3(2*H*)dione} are widely used in preparing dyes [1], optical brighteners for natural and synthetic materials [2], day fluorescent pigments [3], blends for crack detection on solid surfaces [4], and active compositions for radioelectronics [5]. Several N-substituted naphthimides are biologically active compounds, which can be used as precursors of antitumor and antiviral preparations [6].

N-Alkylnaphthimides are mainly prepared by one-step acylation of primary amines with the corresponding naphthalic anhydrides. However, side reactions proceeding at the aromatic ring in the course of aminolysis of 4- and 4,5-halo- and nitro-substituted naphthalic anhydrides decrease the yield of the final products. Moreover, because of low solubility of mono- and especially disubstituted anhydrides in organic solvents, acylation should be performed under rather rigid conditions [7].

Since six-membered imide ring in the naphthimide molecule is fairly stable in alkaline solutions, its sodium and potassium salts [8] can be used as nucleophilic reagents. However, the salts of halo- and nitro-substituted naphthimides are also poorly soluble in organic solvents. Certain disadvantages are also typical for acylation of preliminarily prepared potassium and sodium naphthimides under the conditions of phase-transfer catalysis using tetraalkylammonium salts [9, 10]. For example, concentrated alkaline solutions cause hydrolysis of halogenated alkanes.

Assuming that the above disadvantages of known acylation procedures can be eliminated using tetraalkylammonium salts of naphthimide, we developed a new method for preparing these compounds.

The synthesis was performed in benzene–5% NaOH aqueous solution at room temperature by anion exchange and subsequent extraction of the desired salt into the organic solvent; the molar ratio of the corresponding naphthimide and tetraalkylammonium salt was 1.5 : 1. Using this procedure, we prepared tetraalkylammonium naphthimides **IIa**–**IIq**:



Ia–**Ih** **IIa**–**IIr** (1)

I: Y = H, Z = H (**a**), 2-Br (**b**), 3-NO_2 (**c**), 4-Cl (**d**), 4-Br (**e**), 4-NO_2 (**f**), 4-morpholino (**g**); Y = Cl, Z = 4-Cl (**h**); **II**: R = C_8H_{17}, Y = H, Z = H (**a**), 2-Br (**b**), 3-NO_2 (**c**), 4-Cl (**d**), 4-Br (**e**), 4-NO_2 (**f**), 4-morpholino (**g**); Y = Cl, Z = 4-Cl (**h**); R = C_6H_{13}, Y = H, Z = H (**i**), 2-Br (**j**), 3-NO_2 (**k**), 4-Cl (**l**), 4-Br (**m**), 4-NO_2 (**n**); Y = Cl, Z = 4-Cl (**o**); R = C_4H_9, Y = H, Z = H (**p**), 4-Cl (**q**); and Y = Cl, Z = 4-Cl (**r**).

Tetraalkylammonium iodides are available reagents allowing reliable control of the reaction completeness because, in contrast to nitric and hydrochloric acids and to naphthimide, HI acts as a strong acid in the acetic acid solution [11]. This allowed evaluation of the content of tetraalkylammonium naphthimides in the presence of iodide ions in glacial acetic acid using perchloric acid, which is consumed in titration of acetate ions (in amounts equivalent to naphthimide ions) in accordance with the following reactions:

$$\textbf{IIa–IIr} + AcOH \rightarrow \textbf{Ia–Ih} + R_4N^+AcO^-,$$
$$R_4N^+AcO^- + HClO_4 \rightarrow R_4N^+ClO_4^- + AcOH. \quad (2)$$

The degree of anion exchange depends on the structure of the tetraalkylammonium cation. With decreas-

Table 1. Alkylation time τ, yield of naphthimides **IIIa**–**IIIf**, and their melting points

Salt	Alkylating agent	τ, min	Yield, %	mp, °C	References
IId	$C_8H_{17}I$	20	97	79–80	[9]
	C_4H_9I	20	93	92–93	[9]
	$C_8H_{17}Br$	35	98	79.5–80	[9]
	C_4H_9Br	30	95	91.5–93	[9]
	$C_8H_{17}Cl$	45	93	79–80	[9]
	C_4H_9Cl	45	94	91–93	[9]
IIl	$C_8H_{17}Br$	30	98	79–80	[9]
IIq	$C_8H_{17}Br$	30	97	79–80.5	[9]
IIf	$C_8H_{17}Br$	35	96	84–85	[9]
	C_4H_9Br	30	96	97–99	[9]
IIn	$C_8H_{17}Br$	35	95	84.5–85.5	[9]
IIh	$C_8H_{17}Br$	30	96	112–113	[8]
	C_4H_9Br	30	93	175–176	[8]
IIo	$C_8H_{17}Br$	35	95	111.5–113	[8]
IIr	$C_8H_{17}Br$	30	95	112–113	[8]

ing number of carbon atoms bound to the central nitrogen atom of tetraalkylammonium cations, their lipophilicity decreases, thus decreasing the extraction constant. Under similar conditions (vigorous stirring of the reaction mixture for 2 h at room temperature), tetraoctylammonium iodide is converted into the corresponding naphthimide salt in one treatment cycle, whereas the degrees of conversion of tetrahexyl- and tetrabutylammonium iodides are 70 and 45%, respectively. Therefore, in the last two cases the organic phase was separated and repeatedly treated with an aqueous alkaline solution of naphthimide of the same concentration up to complete conversion of the initial salt.

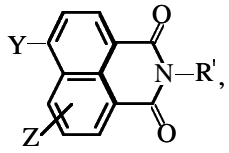
Tetrahexyl- and tetrabutylammonium salts of naphthimide can also be prepared in high yields by conversion of tetraalkylammonium iodide (remaining after extraction) into nitrate using lead or silver nitrate. Nitrate ion is more hydrophilic than iodide [12], and thus its exchange for the naphthimide ion is easier. Since in this case the completeness of extraction of naphthimide ions cannot be monitored because both nitrate and naphthimide anions are titrated with perchloric acid, the reaction completion was judged from the content of unchanged naphthimide in the aqueous phase.

The composition and structure of the resulting compounds **IIa**–**IIr** were determined by elemental analysis and ^{1}H NMR spectroscopy. As compared to the corresponding naphthimides, the signal of aromatic protons in the ^{1}H NMR spectra of the resulting products is shifted upfield and the greatest shielding (by 0.15–0.30 ppm) is observed for protons occurring in the *ortho* and *para* positions to the imide ring. This is probably due to the increased electron density on these carbon atoms owing to the effect of the negatively charged imide fragment and corresponding increase in the shielding constant. The signals of aromatic and aliphatic protons are observed at 7.7–8.9 and 0.8–3.2 ppm, respectively. The spin–spin coupling constants of aromatic protons are typical of naphthimide derivatives [7, 10, 13].

Salts **IIa**–**IIr** are crystalline compounds with distinct melting points (mp); they are readily soluble in polar and nonpolar aprotic solvents and can be stored for a long time. These compounds are convenient reagents for introduction of naphthimide fragment under the mild conditions. For example, *N*-alkylnaphthimides **IIIa**–**IIIf** are formed in nearly quantitative yields in reactions of salts **IId, IIf, IIh, IIl, IIn, IIo, IIq,** and **IIr** with alkylating agents in benzene at 40°C within 25–45 min. Salts of 4-chloro- (**IId, IIm, IIq**), 4-nitro- (**IIf, IIn**), and 4,5-dichloronaphthimides (**IIh, IIo, IIr**) were used to study the possibility of preparing various derivatives of *N*-alkylnaphthimide:

IId, **IIf**, **IIh**, **IIl**, **IIn**, **IIo**, **IIq**, **IIr**

$R'X$, PhH, 40°C $\downarrow -R_4NX$



(3)

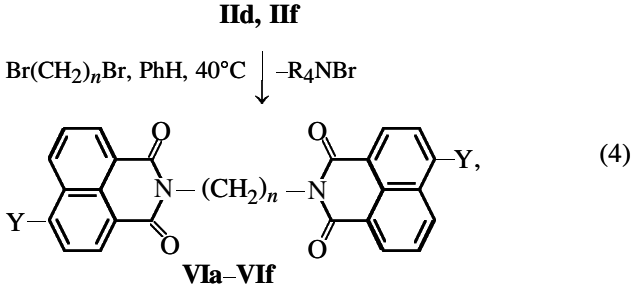
IIIa–**IIIf**

III: Y = H, Z = Cl; R' = C_4H_9 (**a**), C_8H_{17} (**b**); Z = NO_2, R' = C_4H_9 (**c**), C_8H_{17} (**d**); Y = Z = Cl, R' = C_4H_9 (**e**), C_8H_{17} (**f**); X = Cl, Br, I.

The conditions of alkylation of salts **IId, IIf, IIh, IIl, IIn, IIo, IIq**, and **IIr** and the yields and melting points of the resulting products **IIIa**–**IIIf** are given in Table 1. As seen, the reaction rate and yield of *N*-alkylnaphthimides are almost independent of the lengths of hydrocarbon chain in the alkylating agent and tetraalkylammonium cation. On passing from chloro- to iodoalkanes, the reaction rate increases, which agrees with theoretical data [14].

Tetraalkylammonium salts can also be used to prepare bisnaphthimides under mild conditions in high yields. Kupriyan *et al.* [15], when preparing these compounds by alkylation of halogen-substituted

naphthimides with dibromoalkanes under the conditions of phase-transfer catalysis, observed hydrolysis of bromoalkylnaphthimide formed in the first step and a decrease in the yields of the desired bisnaphthimides [from 66% (1,6-dibromohexane) to 24% (1,3-dibromopropane)] with decreasing length of the hydrocarbon chain in the alkylating agent. At the same time, alkylation of tetraoctylammonium salts of 4-chloro- (**IId**) and 4-nitronaphthimide (**IIf**) in benzene proceeds without hydrolysis, with nearly quantitative yields (90–95%) of 4-chloro- (**IVa**–**IVc**) and 4-nitrobisnaphthimides (**IVd**–**IVf**).



(4)

IV, Y = Cl, *n* (**a**) 3, (**b**) 4, (**c**) 6; Y = NO_2, *n* (**d**) 3, (**e**) 4, and (**f**) 6.

EXPERIMENTAL

The ^{1}H NMR spectra were recorded on a Bruker WM-400 device (DMSO-d_6, TMS internal reference). The reaction progress and purity of the resulting compounds were monitored by thin-layer chromatography (TLC) using Silicagel 60 F_{254} plates (Merck), with subsequent UV development.

The starting naphthimides **Ia**–**Ih** were obtained by the procedure presented elsewhere [16]; the required (0.1 M) solution of perchloric acid in glacial acetic acid was prepared; the actual content of perchloric acid was determined by titration with sodium biphthalate [17].

Tetraoctylammonium iodide. Octylamine (26 g), octyl iodide (168 g), and potassium carbonate (55 g) were heated with stirring on a water bath at 90°C for 20 h. After cooling, water was added to the reaction mixture to dissolve inorganic salts, and the product was extracted with chloroform. The organic layer was separated, washed several times with a 10% aqueous ammonia solution and with water, and then dried with sodium sulfate. The solvent was distilled off, and after recrystallization from ethanol tetraoctylammonium iodide was obtained as colorless plates; yield 84 g (70%), mp 121–122°C.

Tetrahexylammonium iodide. Trihexylamine (32.4 g) and hexyl iodide (38.2 g) were heated with stirring on a water bath at 90°C for 18 h. The reaction product was isolated as described above. Tetrahexylammonium iodide was obtained as colorless plates; yield 55.2 g (78%), mp 132–134°C.

Tetraoctylammonium salts of naphthimides IIa–IIh (Table 2). Appropriate finely dispersed naphthimide (1.5 mmol) was mixed with a 5% NaOH aqueous solution (50 ml) and a solution of tetraoctylammonium iodide (1 mmol) in benzene (50 ml). The reaction mixture was vigorously stirred at room temperature for 2 h and filtered. The organic layer was separated, washed with water to neutral reaction, and dried with sodium sulfate; the solvent was distilled off. The aqueous solution was acidified, and unchanged naphthimide was regenerated.

Tetrahexyl- and tetrabutylammonium salts of naphthimides IIi–IIr. *Procedure A.* Appropriate finely dispersed naphthimide (1.5 mmol) was mixed with 5% NaOH aqueous solution (50 ml) and a solution of tetrahexyl- or tetrabutylammonium iodide (1 mmol) in benzene (50 ml). The reaction mixture was vigorously stirred at room temperature for 2 h, filtered, and the organic layer was separated. Then the treatment of the organic phase with aqueous alkaline solution of naphthimide of the same concentration was repeated under similar conditions two times (tetrahexylammonium salts **IIi**–**IIo**) and five times (tetrabutylammonium salts **IIp**–**IIr**). Further treatment of the organic and aqueous layers was performed as described above.

Procedure B. After the first extraction of appropriate naphthimide anion (procedure A), the reaction mixture was mixed with $AgNO_3$ (0.34 g) or $Pb(NO_3)_2$ (0.66 g), and the precipitate was filtered off. Further treatment of the organic and aqueous layers was performed as in procedure A.

To determine the molecular weights of salts **IIa**–**IIr**, a portion of salt **IIa**–**IIr** (0.2 g) was dissolved in acetic acid (25 ml), two drops of Crystalline Violet solution were added, and the resulting solution was titrated with a 0.1 M $HClO_4$ solution up to change of the solution color from violet to blue-green. The molecular weight of compounds **IIa**–**IIr** was evaluated from the following expression:

$$M = m \times 1000/V_a c_m,$$

where m is the weighed portion of salt **IIa**–**IIr** (g), c_m is the concentration of $HClO_4$ solution (M), and V_a is the volume of perchloric acid consumed in titration (ml).

Table 2. Yields, melting points, molecular weights, and elemental analyses of salts **IIa**–**IIr**

Salt	Yield, %	mp, °C	Found/calculated, %				Formula	*M*, found/calculated
			C	H	N	Hlg		
IIa	95	114–116	79.75/79.70	11.23/11.25	4.20/4.22	–/73	$C_{44}H_{74}N_2O_2$	669/663
IIb	94	118.5–120	71.20/71.23	9.95/9.92	3.84/3.78	10.69/10.77	$C_{44}H_{73}BrN_2O_2$	740/742
IIc	95	118–120	74.60/74.64	10.45/10.39	5.98/5.93	–/–	$C_{44}H_{73}N_3O_4$	701/708
IId	97	115–117	75.70/75.77	10.60/10.55	4.00/4.02	5.00/5.08	$C_{44}H_{73}ClN_2O_2$	700/698
IId	96	111.5–113	71.20/71.23	9.95/9.92	3.84/3.78	10.69/10.77	$C_{44}H_{73}BrN_2O_2$	750/742
IIf	94	109–111	74.60/74.64	10.45/10.39	5.98/5.93	–/–	$C_{44}H_{73}N_3O_4$	715/708
IIg	98	110–112	77.08/77.06	10.90/10.91	5.60/5.62	–/–	$C_{48}H_{81}N_3O_3$	750/748
IIh	94	119–121	72.30/72.20	9.95/9.91	3.92/3.83	9.60/9.69	$C_{44}H_{72}Cl_2N_2O_2$	722/732
IIi	99	126–127.5	78.48/78.49	10.65/10.61	5.12/5.09	–/–	$C_{36}H_{58}N_2O_2$	555/551
IIj	95	128–130	68.62/68.66	9.15/9.12	4.40/4.45	12.70/12.69	$C_{36}H_{57}BrN_2O_2$	639/630
IIk	95	126.5–129	72.62/72.57	9.65/9.64	7.12/7.05	–/–	$C_{36}H_{57}N_3O_4$	605/596
IIl	97	123–125	73.90/73.87	9.80/9.82	–/4.79	6.10/6.06	$C_{36}H_{57}ClN_2O_2$	580/585
IIm	96	120–122.5	68.62/68.66	9.15/9.12	4.40/4.45	12.75/12.69	$C_{36}H_{57}BrN_2O_2$	632/630
IIn	98	118–121.5	72.62/72.57	9.65/9.64	7.12/7.05	–/–	$C_{36}H_{57}N_3O_4$	601/596
IIo	95	130–131.5	69.80/69.77	9.15/9.11	4.52/4.52	11.50/11.44	$C_{36}H_{56}Cl_2N_2O_2$	515/508
IIp	98	137–139	76.62/76.67	9.60/9.65	6.40/6.39	–/–	C28H42N2O2	450/439
IIq	97	134–137.5	71.00/71.09	8.70/8.74	5.90/5.92	7.45/7.49	$C_{28}H_{41}ClN_2O_2$	480/473
IIr	96	140–142	66.18/66.26	8.00/7.94	5.64/5.52	13.90/13.97	$C_{28}H_{40}C_{l2}N_2O_2$	503/508

The reactions of tetraalkylammonium salts of naphthimides with alkyl halides (Table 1) were performed as follows. A solution of tetraalkylammonium salt of naphthimide (1 mmol) in benzene (50 ml) was mixed with appropriate alkyl halide (1 mmol). The reaction mixture was stirred at 40°C for 20–45 min, and then the benzene solution was filtered through an alumina bed to remove tetraalkylammonium halide. Then the solvent was evaporated, and the reaction product was recrystallized from ethanol.

To prepare bisnapthimides, a solution of tetraalkylammonium salt of naphthimide (1 mmol) in benzene (50 ml) was mixed with appropriate dibromoalkane (2 mmol). The reaction mixture was stirred at 40°C for 30 min, and the reaction product was filtered off and washed with ethanol; the yields of the final products were 90–95%.

CONCLUSIONS

(1) Tetraalkylammonium salts of naphthimides, which are convenient precursors for introduction of naphthimide fragment, were prepared in high yield (94–99%) by anion exchange and extraction of the desired product into the organic phase.

(2) Tetraalkylammonium salts of naphthimides are alkylated under the mild conditions to form *N*-alkylnaphthimides in high yields (90–98%).

REFERENCES

1. Philipova, T. and Petkov, I., *J. Appl. Polym. Sci.*, 2001, vol. 80, no. 11, pp. 1863–1869.
2. Philipova, T., Grabchev, I., and Petkov, I., *J. Polym. Sci. A: Polym. Chem.*, 1997, vol. 35, no. 6, pp. 1069–1076.
3. He, H., Mortellaro, M.A., Leiner, M.J.P., et al., *Anal. Chem.*, 2003, vol. 75, no. 3, pp. 549–552.
4. Li, C., Du, P., and Tian, H., *Chem. Lett.*, 2003, vol. 32, no. 7, pp. 570–571.
5. Hodgkiss, R.J., Jones, G.W., Long, A., et al., *J. Med. Chem.*, 1991, vol. 34, no. 7, pp. 2268–2274.
6. Pavlov, V.A., Lin, P.K.T., and Rodilla, V., *Chem.-Biol. Interact.*, 2001, vol. 137, no. 1, p. 15–24.
7. Anikin, V.F. and Kupriyan, D.G., *Zh. Org. Khim.*, 2000, vol. 36, no. 11, pp. 1720–1726.

8. Devereux, M.A. and Donahoe, H.B., *J. Org. Chem.*, 1960, vol. 25, no. 3, pp. 457–458.
9. Anikin, V.F., Krasnova, E.A., and Kupriyan, D.G., *Zh. Prikl. Khim.*, 2000, vol. 73, no. 3, pp. 459–462.
10. Anikin, V.F. and Kupriyan, D.G., *Visn. Odes'k. Nats. Univ., Khim.*, 2003, vol. 8, no. 4, pp. 235–242.
11. Koreshkov, A.P., *Analiticheskaya khimiya nevodnykh rastvorov* (Analytical Chemistry of Nonaqueous Solutions), Moscow: Khimiya, 1982.
12. Dehmlow, E.V. and Dehmlow, S.S., *Phase Transfer Catalysis*, Weinheim: Chemie, 1983.
13. Günther, H., *NMR spectroscopy: An Introduction*, Chichester: Wiley, 1980.
14. Carey, F.A. and Sundberg, R.J., *Advanced Organic Chemistry*, part A: *Structure and Mechanisms*, New York: Plenum, 1977.
15. Kupriyan, D.G., Anikin, V.F., Merz, A., and Patsenker, L.D., *Zh. Org. Khim.*, 2004, vol. 40, no. 5, pp. 732–737.
16. Karishin, A.P. and Baklan, V.F., *Zh. Obshch. Khim.*, 1959, vol. 29, no. 9, pp. 3048–3050.
17. Suslennikova, V.M. and Kiseleva, E.K., *Rukovodstvo po prigotovleniyu titrovannykh rastvorov* (Manual on Preparing Titrated Solutions), Leningrad: Khimiya, 1973.

ISSN 1070-4272. Russian Journal of Applied Chemistry, 2006, Vol. 79, No. 3, pp. 416–420. © Pleiades Publishing, Inc., 2006.
Original Russian Text © T.S. Kotel'nikova, S.G. Voronina, A.L. Perkel', 2006, published in Zhurnal Prikladnoi Khimii, 2006, Vol. 79, No. 3, pp. 424–428.

ORGANIC SYNTHESIS AND INDUSTRIAL ORGANIC CHEMISTRY

Formation of Formic Acid and Cyclohexyl Formate in Oxidation of Cyclohexane

T. S. Kotel'nikova, S. G. Voronina, and A. L. Perkel'

Kuznetsk Coal Fields State Technical University, Kemerovo, Russia

Received December 16, 2005

Abstract—The consistency of the suggested mechanisms of formic acid formation with the composition of products formed in the industrial process of cyclohexane oxidation was examined. The role of formic acid in the formation of cyclohexyl esters of mono- and dicarboxylic acids was elucidated.

DOI: 10.1134/S1070427206030165

Mono- and dicarboxylic acids and their cyclohexyl esters are among the main by-products of cyclohexane oxidation to cyclohexanol and cyclohexanone [1, 2]. It is known [1–4] that carboxylic acids are formed by oxidative cleavage of the C–C bond along numerous pathways, mainly in steps following the formation of a ketone. The pathways of formation of formic acid are, apparently, among the least understood. The main pathway of formation of esters derived from secondary alcohols (including cyclohexanol) is alcoholysis of mixed anhydrides of carboxylic acids with secondary alcohols present in the reaction mixture [4–6]. Fast reactions of acyl interchange result in formation of esters containing acyl residues not only from the anhydride initially formed by oxidative degradation (e.g., adipic anhydride), but also from all mono- and dicarboxylic acids present in the reaction medium [4, 6, 7]. Although it was suggested [7] that in alcoholysis of mixed anhydrides two esters are formed with equal probability, irrespective of the structure of the carboxylic acid residue, there are indications [8] that in alcoholysis of mixed formic acid anhydrides the formates are formed preferentially; therefore, increased yield of formates in autooxidation can be expected. This assumption is well consistent with the fact [1] that cyclohexyl formate is the major product among cyclohexyl esters of monocarboxylic acids formed by oxidation of cyclohexane.

This study concerns the pathways of formic acid formation in the industrial process of cyclohexane oxidation to cyclohexanol and cyclohexanone and elucidation of the role of formic acid in ester formation.

EXPERIMENTAL

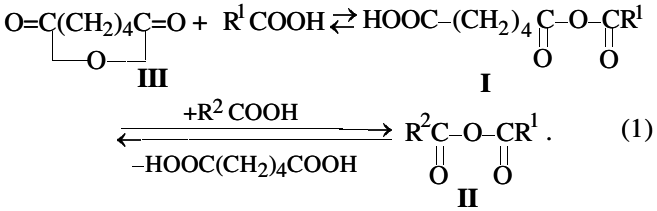
Samples of oxidized cyclohexane (150–155°C, 0.04% cobalt naphthenate, 0.8 MPa) were taken from the oxidation shop of caprolactam production plant of Azot Joint-Stock Company (Kemerovo).

The products of cyclohexane oxidation were determined by GLC. The products were identified by comparison of the retention times of the components with those of reference substances in columns with stationary phases of various polarities. Glutaric acid monoaldehyde was prepared by oxidation of excess glutaraldehyde with aqueous $KMnO_4$ at 0°C. Compounds containing carboxy groups were converted prior to determination to the methyl esters by treatment with diazomethane. Formic acid in cyclohexane oxidation products was determined by a specially developed procedure [8]. After the extraction of water-soluble acids with water from the mixture of oxidation products, these acids were converted to potassium salts by treatment with an alcoholic solution of alkali followed by vacuum evaporation. The dry residue of the salts was treated successively with acetyl chloride and benzyl alcohol in pyridine. Then the content of benzyl formate, corresponding to the concentration of formic acid, was determined. The determination of the total content of mixed anhydrides in oxidized cyclohexane was based on the same principle. Samples were treated with a mixture of formic acid and dodecyl alcohol in pyridine. The amount of dodecyl formate formed in the process (determined by GLC) corresponded to the total content of mixed anhydrides in the sample. Prior to determination of cyclohexanol and cyclohexanone in oxidized cyclohexane, samples

were reduced with triphenylphosphine [9]. The oxidation products were analyzed by GLC using the following stationary phases: Carbowax 6000 on Chromaton N-AW-DMCS 0.250–0.315 mm and 5% XE-60 on Chromaton N-AW 0.20–0.25 mm. Peroxy compounds were determined colorimetrically with a reagent containing Fe^{2+} ions and *N*,*N*-dimethyl-*p*-phenylenediamine [10].

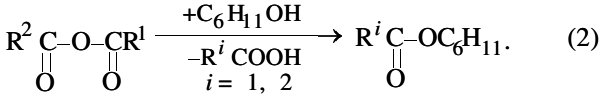
We determined the content of mono- and dicarboxylic acids and their cyclohexyl esters in samples of oxidized cyclohexane taken from the cascade of industrial reactors of the cyclohexane oxidation shop and of recycled cyclohexane (see figure). The qualitative composition of carboxylic acids and cyclohexyl esters is, on the whole, well consistent with published data [1, 2]. The absence of acetic and propionic acids and their esters in oxidized cyclohexane is due to low conversion of cyclohexane. According to [1], these acids appear only at a cyclohexane conversion of 7% and over. We detected for the first time in oxidized cyclohexane glutaric acid monoaldehyde and cyclohexyl ester of adipic acid monoaldehyde. The ratio of the yields of cyclohexyl esters to the content of the corresponding acids in oxidized cyclohexane (Table 1) varies within narrow limits, except for cyclohexyl formate and formic acid. With increasing conversion, this ratio in some cases slightly increases and in other cases slightly decreases. For cyclohexyl formate and formic acid, this ratio is considerably higher than for other mono- and dicarboxylic acids and their cyclohexyl esters.

According to the existing views [4, 6, 7], esters of secondary alcohols are formed in the course of oxidation processes mainly by alcoholysis of mixed anhydrides with secondary alcohols present in the reaction medium. In oxidation of cyclohexane, mixed anhydrides (including those containing a formic acid residue) arise from fast reactions of acyl interchange of adipic anhydride (initial product of oxidative degradation of cyclohexane ring [4]) with carboxylic acids:

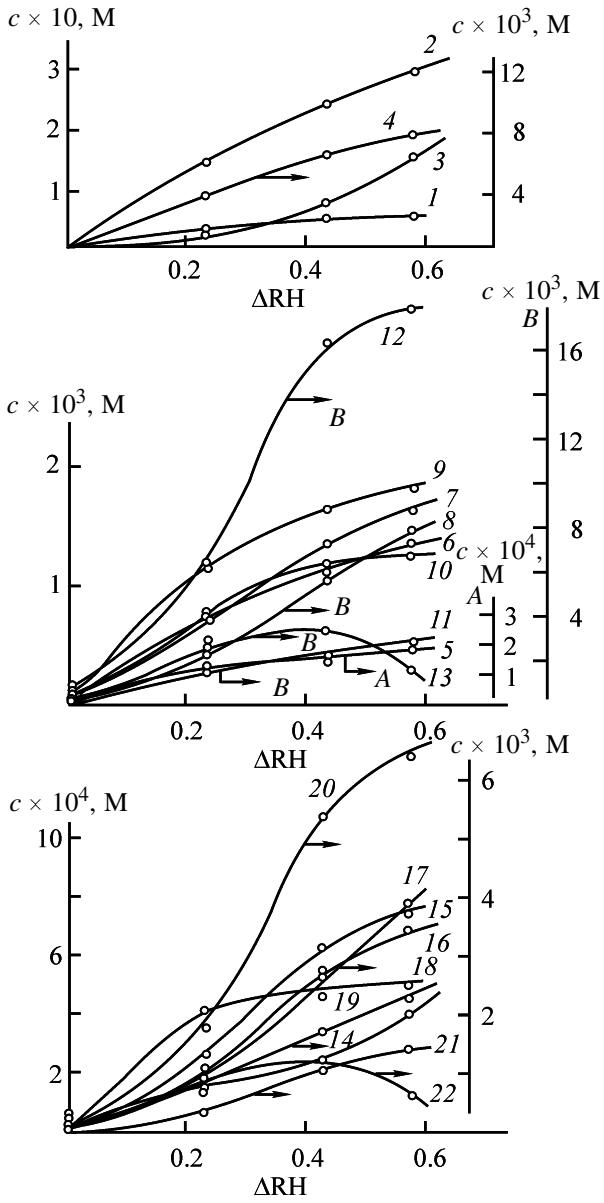


(1)

The reaction of mixed anhydrides with cyclohexanol yields a mixture of esters:



(2)



Content *c* of cyclohexane oxidation products as a function of conversion ΔRH. 150–155°C, 0.8 MPa, 0.04% cobalt naphthenate. (*1*) Peroxy compounds, (*2*) cyclohexanol, (*3*) cyclohexanone, (*4*) adipic anhydride, (*5*) formic acid, (*6*) butyric acid, (*7*) valeric acid, (*8*) caproic acid, (*9*) succinic acid, (*10*) glutaric acid, (*11*) glutaric acid monoaldehyde, (*12*) adipic acid, (*13*) adipic acid monoaldehyde, (*14*) cyclohexyl formate, (*15*) cyclohexyl butyrate, (*16*) cyclohexyl valerate, (*17*) cyclohexyl capronate, (*18*) cyclohexyl hydrogen succinate, (*19*) cyclohexyl hydrogen glutarate, (*20*) cyclohexyl hydrogen adipate, (*21*) dicyclohexyl adipate, and (*22*) cyclohexyl ester of adipic acid monoaldehyde.

Presumably, the reactions of type (2) with mixed anhydrides containing a formic acid residue will preferentially yield cyclohexyl formate:

Table 1. Ratio *B* of yields of cyclohexyl esters of mono- and dicarboxylic acids to the yield of free acids in oxidation of cyclohexane at 150°C to various conversions

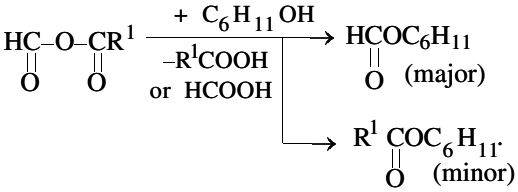
Acid	*B* at indicated conversion,* %		
	1.9	3.2	4.8
Formic	1.25**	1.71**	2.1**
Butyric	0.35**	0.55**	0.56**
Valeric	0.32**	0.41**	0.42**
Capronic	0.41**	0.44**	0.48**
Succinic	0.35	0.28	0.27
Glutaric	0.31**	0.38**	0.45**
Adipic acid monoaldehyde	0.37	0.39	0.4
Adipic***	0.29**	0.33**	0.36**
Cyclohexyl hydrogen adipate****	0.19	0.21	0.23

* Calculated from the total content of oxidation products.
** Minus ester content in recycled cyclohexane.
*** Ratio of the yields of cyclohexyl hydrogen adipate and adipic acid.
**** Ratio of the yields of dicyclohexyl adipate and cyclohexyl hydrogen adipate.

Table 2. Yield of cyclohexyl esters in reactions of carboxylic acids and acetic anhydride with cyclohexanol at 90°C

Acid	Concentration of acid residues, M	Yield of cyclohexyl esters	
		M	mol mol^{-1}*
Formic	1.41	0.64	0.45
Acetic	1.90	0.12	0.06
Propionic	2.18	0.12	0.05
Valeric	1.81	0.07	0.04

* Per mole of starting acid.



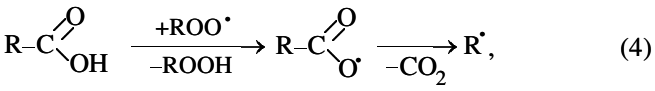
(3)

This assumption is confirmed by the results obtained in the reaction of a mixture of formic, propionic, and valeric acids (for concentrations, see Table 2) and acetic anhydride (0.95 M) with cyclohexanol (4.9 M) in a glass ampule at 90°C. A GLC analysis of the reaction mixture, performed 60 min after the start of the reaction, revealed the presence of cyclohexyl esters of all the acids present in the mixture (Table 2).

Table 2 shows that the yield of the ester per mole of the acid for formic acid is almost an order of magnitude higher than for the other acids. Therefore, reactions (1) and (3) can account for the features of cyclohexyl formate accumulation in the course of cyclohexane oxidation.

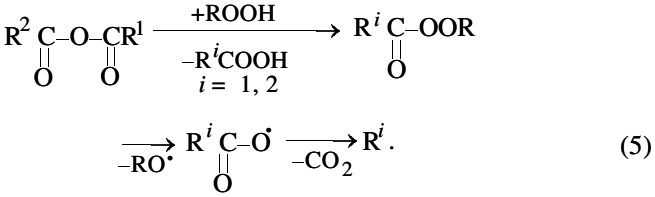
A question naturally arises: Can the increased yield of cyclohexyl formate be partially due to the higher rate of esterification of formic acid with cyclohexanol, compared to other acids formed by cyclohexane oxidation? The initial rate of esterification of formic acid with methanol at 20–40°C is approximately 30 times higher than that of butyric acid [11], which even exceeds the ratio of the rates of formation of the corresponding esters in the alcoholysis of mixed anhydrides (Table 2). This matter undoubtedly requires a special study. At the same time, it should be noted that esterification, in contrast to alcoholysis of anhydrides with alcohols, is reversible and can result not only in formation of etsters in early steps, but also in their hydrolysis if the equilibrium concentration of these compounds will be exceeded as a result of reactions (1) and (3).

The pathways of formation of formic acid in liquid-phase oxidation processes are the least understood, which may be caused by multistep mechanisms of its formation and by problems with analytical determination of this compound [8] because of low sensitivity of a flame ionization detector to formic acid. One of pathways of formic acid formation in the course of cyclohexane oxidation, suggested even in [1], involves successive decarboxylation of monocarboxylic acids, yielding methyl radical and then formic acid. The decarboxylation may occur both with the participation of the peroxy radicals {reactions of type (4) [1, 3]}:



(4)

or via mixed anhydrides [reactions of type (1)], which form peroxy esters in the reactions with hydroperoxides. The homolytic cleavage of peroxy esters can lead to the decarboxylation [4]:



(5)

If reactions (4) and (5) really occur, the reaction products should contain the whole set of monocarboxylic acids from C_6 to C_1, and their content should

decrease with decreasing number of C atoms [1]. As already noted, acetic and propionic acids appear in oxidized cyclohexane only in late oxidation steps, whereas formic acid appears considerably earlier (see figure; Table 1). Therefore, an additional pathway of formation of formic acid was suggested in [1]: from a primary carbon-centered radical formed by reactions of types (4) and (5):

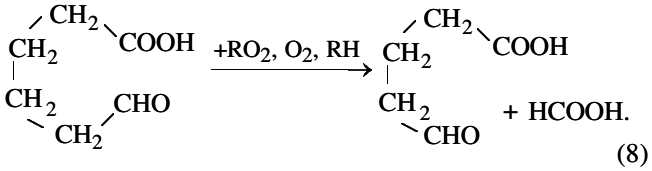
$$R^1\dot{C}H_2 \xrightarrow{+O_2,\ RH} R^1CH_2OOH \xrightarrow[-HO^{\bullet}]{} R^1CH_2O^{\bullet} \xrightarrow[-R^{1\bullet}]{} HCHO \longrightarrow \cdots \longrightarrow HCOOH. \quad (6)$$

However, scheme (6), like schemes (4) and (5), implies multistep formation of formic acid from other monocarboxylic acids and thus its successive, rather than parallel, accumulation, which is inconsistent with the experiment.

Analysis of published data on the mechanisms of oxidation of organic compounds [3] shows that formic acid can form by oxidation of aldehydes at α-CH bonds relative to the carbonyl group [reaction (7), pathway a] [12]:

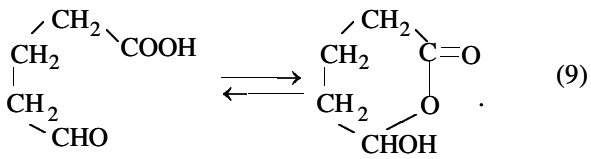
$$RCH_2C(=O)H \xrightarrow{+RO_2,\ O_2,\ RH} \begin{cases} \xrightarrow{(a)} RCH_2C(=O)OOH \\ \xrightarrow{(b)} RCHC(OOH)(=O)H \end{cases} \longrightarrow RCHO + HCOOH. \quad (7)$$

Since one of major aldehyde components of cyclohexane oxidation products is adipic acid monoaldehyde, its oxidative transformations [reaction (7), pathway b] should presumably yield formic acid and glutaric acid monoaldehyde:



(8)

The latter compound was indeed detected in cyclohexane oxidation products; it is accumulated in amounts comparable with those of adipic acid monoaldehyde (see figure, curve *11*). This fact, along with the trend in variation of the adipic acid monoaldehyde content with cyclohexane conversion, typical of intermediates, counts in favor of formation of glutaric acid monoaldehyde by reaction (8). It could be expected that glutaric acid monoaldehyde, in turn, would be oxidized to formic acid and succinic acid monoaldehyde by the reaction of type (8). However, succinic acid monoaldehyde was not detected among cyclohexane oxidation products. Furthermore, the trend in variation of the glutaric acid monoaldehyde content with cyclohexane conversion essentially differs from that observed with adipic acid monoaldehyde (see figure, curves *11*, *13*). This feature may be associated with the possibility of cyclization of 4-acylcarboxylic acids [13] to 5-hydroxy lactones with a stable pyranose ring:



(9)

The cyclization is favored by the presence of free carboxy groups [13]. Presumably, 5-hydroxy-δ-valerolactone is oxidized considerably more difficultly than the open-chain form containing a free aldehyde group. It is known [14] that α-ethylacrolein dimethyl acetal is oxidized with oxygen considerably more difficultly than free α-ethylacrolein.

The hypothesis that formic acid is formed from adipic acid monoaldehyde is also supported by data on the yield of formic acid and some other products in oxidation of neat cyclohexanol and cyclohexanone at 120°C (Table 3).

The ratio of the yields of formic and adipic acids (taking into account their content in the corresponding cyclohexyl esters), calculated from data in Table 3, is 0.54 for cyclohexanol and 0.95 for cyclohexanone.

Table 3. Content of some products in oxidized cyclohexanol and cyclohexanone

Acid	Cyclohexanol	Cyclohexanone
	$c \times 10^3$, M	
Oxygen uptake	82.1	44.6
Formic acid	2.1	3.25
Cyclohexyl formate	2.38	–
Glutaric acid	0.58	0.41
Glutaric acid monoaldehyde	1.25	1.31
Adipic acid	7.52	3.32
Cyclohexyl hydrogen adipate and dicyclohexyl adipate	0.97	–
Adipic acid monoaldehyde	0.82	1.4

The higher yield of formic acid in the oxidation of cyclohexanone, compared to the oxidation of cyclohexanol, correlates with an increase in the content of adipic acid monoadlehyde in going from cyclohexanol to cyclohexanone. Despite milder conditions, the relative yield of formic acid in the oxidation of the alcohol and ketone is appreciably higher than in the oxidation of cyclohexane for which this ratio is about 0.022 (see figure). This fact may be due both to thermal decomposition of formic acid under the conditions of cyclohexane oxidation at elevated temperature and to the loss of formic acid with off-gases under the conditions of the industrial process. It is significant that in all the cases we detected in the reaction mixture glutaric acid monoaldehyde whose formation is not implied by the existing concepts of cyclohexane oxidation.

CONCLUSIONS

(1) In oxidation of cyclohexane under the conditions of the industrial process, the ratio of the yields of cyclohexyl formate and formic acid is considerably higher than the corresponding ratios for the other mono- and dicarboxylic acids and their cyclohexyl esters. The increased relative yield of cyclohexyl formate is due to specific features of alcoholysis of mixed anhydrides containing a formic acid residue.

(2) One of probable pathways of formic acid formation in the oxidation of cyclohexane involves oxidative transformations of adipic acid monoaldehyde, yielding formic acid and glutaric acid monoaldehyde.

ACKNOWLEDGMENTS

The authors are grateful to P.I. Sviridenko (Azot Joint-Stock Company, Kemerovo) for the assistance in taking samples of oxidized cyclohexane.

REFERENCES

1. Berezin, I.V., Denisov, E.T., and Emanuel', N.M., *Okislenie tsiklogeksana* (Oxidation of Cyclohexane), Moscow: Mosk. Gos. Univ., 1962.
2. *Proizvodstvo tsiklogeksanona i adipinovoi kisloty okisleniem tsiklogeksana* (Production of Cyclohexanone and Adipic Acid by Oxidation of Cyclohexane), Furman, M.S. and Gol'dman, A.M., Eds., Moscow: Khimiya, 1967.
3. Denisov, E.T., Mitskevich, N.I., and Agabekov, V.E., *Mekhanizm zhidkofaznogo okisleniya kislorodsoderzhashchikh soedinenii* (Mechanism of Liquid-Phase Oxidation of Oxygen-Containing Compounds), Minsk: Nauka i Tekhnika, 1975.
4. Perkel', A.L., Voronina, S.G., and Freidin, B.G., *Usp. Khim.*, 1994, vol. 63, no. 9, pp. 793–796.
5. Freidin, B.G. and Perkel', A.L., *Zh. Prikl. Khim.*, 1980, vol. 53, no. 4, pp. 861–866.
6. Perkel, A.L., Buneeva, E.I., and Voronina, S.G., *Oxid. Commun.*, 2000, vol. 23, no. 1, pp. 12–28.
7. Perkel', A.L., Freidin, B.G., Neginskaya, R.V., et al., *Zh. Prikl. Khim.*, 1985, vol. 58, no. 7, pp. 1572–1577.
8. Kotel'nikova, T.S., Vdovenko, O.V., Voronina, S.G., and Perkel', A.L., *Zh. Anal. Khim.*, 2006, vol. 61, no. 2, pp. 1–6.
9. Perkel', A.L. and Voronina, S.G., *Zh. Anal. Khim.*, 1998, vol. 53, no. 4, pp. 343–363.
10. Perkel', A.L., Voronina, S.G., and Perkel', R.L., *Zh. Anal. Khim.*, 1991, vol. 46, no. 11, pp. 2283–2286.
11. Smith, H.A., *C. R. Acad. Sci. Paris*, 1964, vol. 61, pp. 254–260.
12. Loury, M., *J. Am. Chem. Soc.*, 1939, vol. 258, no. 1, pp. 238–239.
13. Valters, R.E., *Kol'chato-tsepnaya izomeriya v organicheskoi khimii* (Ring–Chain Isomerism in Organic Chemistry), Riga: Zinatne, 1978.
14. Yatchishin, I.I., Romanyuk, O.I., and Marshalok, G.A., Abstracts of Papers, *Vsesoyuznaya konferentsiya "Kinetika radikal'nykh zhidkofaznykh reaktsii"* (All-Union Conf. "Kinetics of Radical Liquid-Phase Reactions"), Yaroslavl, 1990, p. 115.

ISSN 1070-4272. Russian Journal of Applied Chemistry, 2006, Vol. 79, No. 3, pp. 421–424. © Pleiades Publishing, Inc., 2006.
Original Russian Text © A.I. Rakhimov, N.A. Storozhakova, Khaled Khedar Nasser Akhmed, R.G. Fedunov, 2006, published in Zhurnal Prikladnoi Khimii, 2006, Vol. 79, No. 3, pp. 429–431.

ORGANIC SYNTHESIS AND INDUSTRIAL ORGANIC CHEMISTRY

Catalytic Synthesis of *N*-Benzoyl (*N*-Nitrobenzoyl) Derivatives of ε-Aminocaproic Acid Oligomers

A. I. Rakhimov, N. A. Storozhakova, Khaled Khedar Nasser Akhmed, and R. G. Fedunov

Volgograd State Technical University, Volgograd, Russia
Institute of Chemical Problems of the Environment, Russian Academy of Sciences, Volgograd, Russia

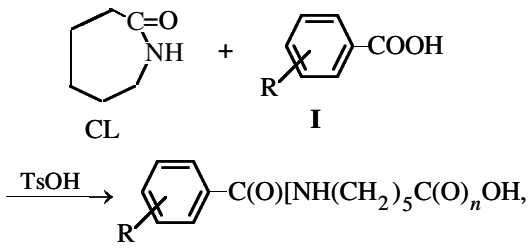
Received August 23, 2005

Abstract—The synthesis of *N*-benzoyl [*N*-(*m*-nitrobenzoyl)] derivatives of ε-aminocaproic acid oligomers by the reaction of ε-caprolactam with benzoic (nitrobenzoic) acid in the presence of *p*-toluenesulfonic acid as catalyst was studied.

DOI: 10.1134/S1070427206030177

It is known that ε-aminocaproic acid oligomers inhibit reproduction of respiratoric viruses. Acid-catalyzed oligomerization of ε-caprolactam with carboxylic acids yields *N*-acyl derivatives of ε-aminocaproic acid oligomers [1–5].

In this study, *N*-benzoyl (BACA) and *N*-nitrobenzoyl (*m*-NBACA) derivatives of ε-aminocaproic acid oligomers were prepared by the reaction of ε-caprolactam (CL) with benzoic (BA) and nitrobenzoic (*m*-NBA) acids in the temperature range 150–210°C. *p*-Toluenesulfonic acid (TsOH) was used as catalyst.



where R = H (BA), *m*-NO_2 (*m*-NBA) (**I**); R' = H (BACA), *m*-NO_2 (*m*-NBACA) (**II**); n =1, 9, 10.

EXPERIMENTAL

The IR spectra (KBr pellets or a mulls in Vaseline oil) were recorded on a Specord M-82 IR spectrometer. The ^{1}H NMR spectra were recorded on a Varian Mercury Plus spectrometer (300 MHz) in DMSO-d_6 with TMS as internal reference. The reagent consumption rate was determined by an ampule technique.

N-Benzoyl derivatives of ε-aminocaproic acid oligomers, R = H (BACA) (**II**). Ampules filled with the reaction mixture (CL 1.9 g, BA 2 g, and TsOH 0.30 g; reactant molar ratio 1 : 1 : 0.1) were kept in a thermostat at 150°C. At 15-min intervals these ampules were successively removed, and chloroform was added. Unchanged CL and BA dissolved in chloroform and were separated from the insoluble residue of BACA oligomer mixture containing oligomers with 9 and 10 monomeric units. To separate these oligomers, the solid residue was mixed with ethanol and heated to boil. The resulting solution was filtered and then cooled. Under these conditions $BACA_{n=10}$ precipitates and $BACA_{n=9}$ remains in ethanol. $BACA_{n=10}$ was separated from $BACA_{n=9}$ by filtration. $BACA_{n=9}$ was isolated from the filtered solution by ethanol evaporation and then recrystallized. $BACA_{n=9}$: yield 0.66 g (35%), mp 165– 167°C. Found, %: N 10.92. Calculated, %: N 11.05. $BACA_{n=10}$: yield 0.85 g (45%), mp 188–190°C. Found, %: N 11.20. Calculated %: N 11.27.

The molecular structures of $BACA_{n=9}$ and $BACA_{n=10}$ were characterized by IR and ^{1}H NMR spectroscopy. The IR spectrum of $BACA_{n=9}$ contains the amide I and amide II absorption bands (1638 and 1584 cm^{-1}, respectively) and the absorption bands of the stretching vibrations of the NH groups at about 3292 cm^{-1}. The IR spectrum of $BACA_{n=10}$ contains the amide I and amide II absorption bands (1636 and 1536 cm^{-1}, respectively) and the absorption band of the stretching vibrations of the NH group at about 3200 cm^{-1}.

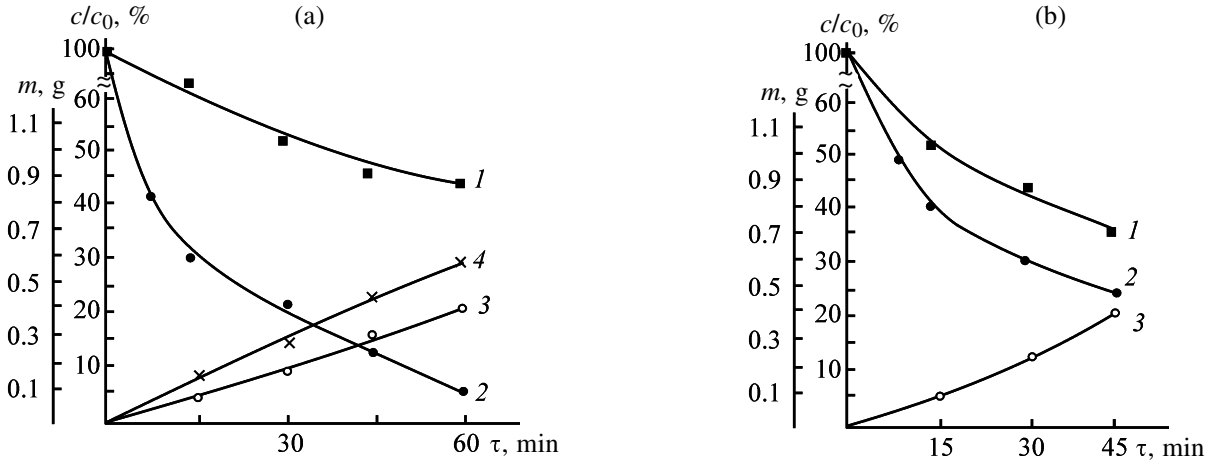


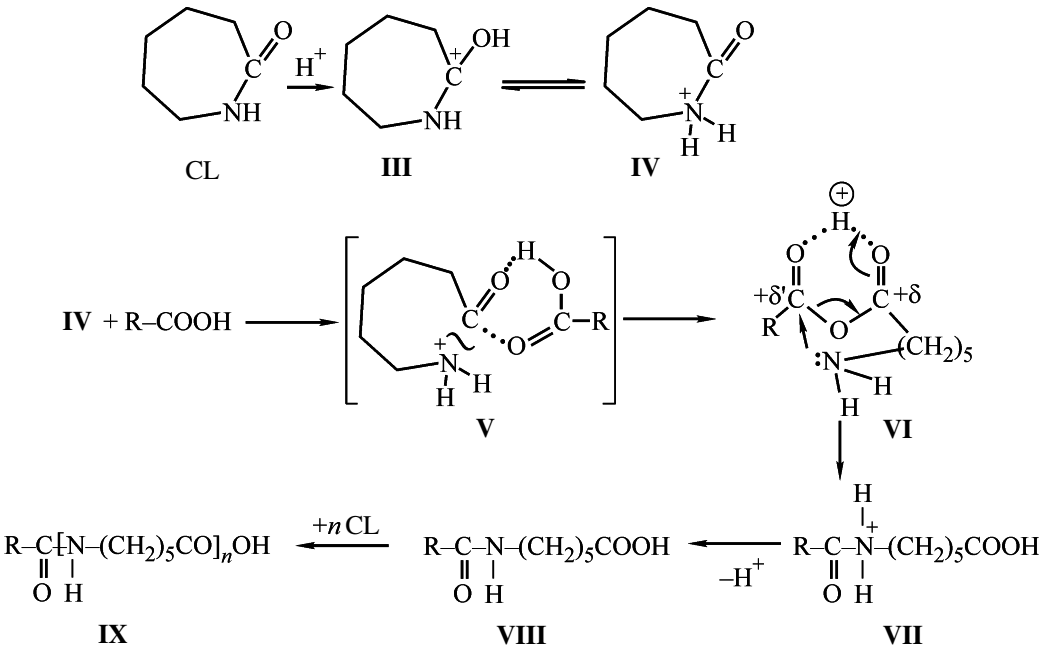
Fig. 1. Time dependence of the reagent consumption (c/c_0) and oligomer formation m in the course of reaction between (a) CL and BA and (b) CL and *m*-NBA. (τ) Time. 150°C (a) (*1*) BA, (*2*) CL, (*3*) $BACA_{n=9}$, and (*4*) $BACA_{n=10}$; (b) (*1*) *m*-NBA, (*2*) CL, and (*3*) *m*-NBACA.

^{1}H NMR spectrum of $BACA_{n=9}$ in DMSO-d_6, δ, ppm: 8.22 s [9H, NH], 2.99 m [18H, CH_2NH], 2.22 m [18H, $CH_2C(O)$], 7.08–7.89 m [5H, Ph], and 1.16–1.98 m [46H, $(CH_2)_{23}$].

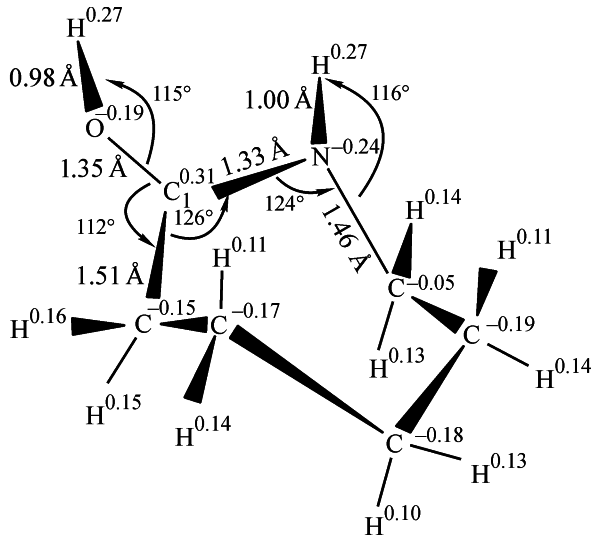
N-(*m*-Nitrobenzoyl)-ε-aminocaproic acid, R = *m*-NO_2 [*m*-NBACA (**II**)], was prepared similarly. After the reaction completion, the product was treated with diethyl ether to remove unchanged CL and *m*-NBA. The insoluble residue was filtered off and then recrystallized from chloroform. *m*-NBACA yield 1.2 g (65%), mp 89–100°C. Found, %: N 9.90. Calculated, %: N 9.96.

^{1}H NMR spectrum of *m*-NBACA in DMSO-d_6, δ, ppm: 8.57 s (H, NH), 3.03 m (2H, CH_2NH), 2.99 m [2H, $CH_2C(O)$], 7.08–8.41 m [4H, Ph], and 1.24–2.98 m [6H, $(CH_2)_3$].

The oligomerization mechanism involving a six-membered intermediate complex of protonated CL with carboxylic acid was suggested:



R = Ph [BA, BACA (**IX**)]; *m*-NO_2Ph [*m*-NBA *m*-NBACA (**VIII**)], n = 9, 10.



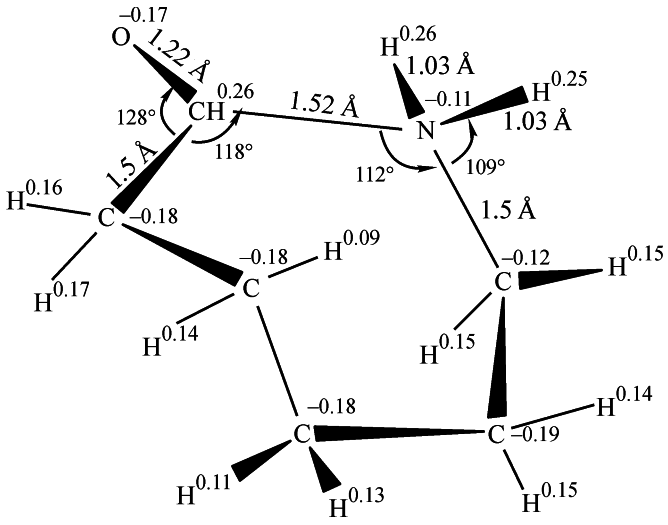


Figure 1 shows the time dependence of c/c_0 (current amount of a reactant relative to its initial amount) and m (oligomer yield, g). In Fig. 1a c/c_0 refers to BA and CL, and m, to $BACA_{n=9}$ and $BACA_{n=10}$. In Fig. 1b, c/c_0 refers to *m*-NBA and CL, and m, to *m*-NBACA.

As seen from these kinetic curves, in the early stage of the reaction, the reactant consumption ratio $V_0(CL)/V_0(m\text{-NBA})$ decreases by a factor of 1.4, whereas the ratio $V_0(CL)/V_0(BA)$ decreases by a factor of 2.

The larger reactant consumption in formation of *m*-NBACA (isolated in 65% yield) can be attributed to acyl rearrangement.

The AM1 quantum-chemical calculations [6] showed that, in the presence of acid catalyst, the activation energy of formation of anhydride via protonation of the amide group of ε-CL (**IV**) is 134 kJ mol^{-1}. The energy gain in acyl rearrangement is no lower than 83.8 kJ mol^{-1}.

The energy of structure **IV** is close to that of structure **III** in which proton is bound to the carbonyl oxygen atom of the ε-CL molecule. However, the protonation of the NH group is accompanied by lengthening of the NC(O) bond from 1.38 Å in **III** to 1.52 Å in **IV**, which facilitates cleavage of the amide ring.

The structural and electronic characteristics of the ε-CL molecule (see below) were calculated with AM technique [1]. Total charge of molecular system (OH cation) Q = 1; bond lengths: $R_{C–C}$ 1.51, $R_{C–H}$ 1.09 Å; bond angles ∠CCC 114°, ∠CCH 109°, $\angle CCC_1$ 112°, ∠CCN 115°; bond order $P_{C_1–N}$ 1.482; total energy E_0 = –33 555 kcal mol^{-1}, and dipole moment μ 3.82 D.

CONCLUSIONS

(1) The rate of consumption of ε-caprolactam and benzoic and *m*-nitrobenzoic acids in the course of synthesis of *N*-benzoyl (*N*-*m*-nitrobenzoyl) derivatives of ε-aminocaproic acid oligomers and the quantum-chemical calculations show that these reactions involve acyl rearrangement in which a mixed anhydride is formed.

(2) The acyl rearrangement is facilitated by appearance of a positive charge on the carbonyl carbon atom of the benzoyl group and an unshared electron pair on the nitrogen atom of the amino group.

(3) Introduction of the electron-acceptor nitro group into the benzoic acid molecule facilitates the acyl rearrangement and, as a result, increases the consumption rate of nitrobenzoic acid.

REFERENCES

1. Storozhakova, N.A., Khalel Khedar Nasser Akhmed, and Rakhimov, A.I., Abstracts of Papers, *Naukoemkie khimicheskie tekhnologii-2004. X Mezhdunarodnaya nauchno-tekhnicheskaya konferentsiya* (High Technologies-2004. X Int. Scientific and Technical Conf.), Moscow, 2004, pp. 325–326.
2. Storozhakova, N.A., Khalel Khedar Nasser Akhmed, and Rakhimov, A.I., *Alicycle 2004. Perspektivy razvitiya khimii i prakticheskogo primeneniya alitsiklicheskikh soedinenii. Mezhdunarodnaya nauchno-tekhni-*

cheskaya konferentsiya (Aliycle 2004. Prospects for Development of Chemistry and Practical Application of Alicyclic Compounds. Int. Scientific and Technical Conf.), Samara, 2004, pp. 63–64.

3. Storozhakova, N.A., Khalel Khedar Nasser Akhmed, and Rakhimov, A.I., Abstracts of Papers, *Kompozit-2004. Perspektivnye polimernye kompozitsionnye materialy. Al'ternativnye tekhnologii. Pererabotka, primenenie, ekologiya. Mezhdunarodnaya nauchno-tekhnicheskaya konferentsiya* (Composites-2004. Promising Polymeric Composite Materials. Alternative Technologies. Processing, Application, and Environmenal Problems. Int. Scientific and Technical Conf.), Saratov–Engels, 2004, pp. 61–62.
4. US Patent 2956068.
5. US Patent 5414099
6. Schmidt, M.W., Baldridge, K.K., Boatz, J.A., et al., *J. Comput. Chem.*, 1993, vol. 4, no. 11, p. 1347.

ISSN 1070-4272. Russian Journal of Applied Chemistry, 2006, Vol. 79, No. 3, pp. 425–429. © Pleiades Publishing, Inc., 2006.
Original Russian Text © A.N. Belyaev, A.V. Vershinin, K.V. Gromov, L.L. Kuznetsov, 2006, published in Zhurnal Prikladnoi Khimii, 2006, Vol. 79, No. 3, pp. 432–436.

ORGANIC SYNTHESIS AND INDUSTRIAL ORGANIC CHEMISTRY

Separation of 2,4'- and 4,4'-Dihydroxydiphenyl Sulfones

A. N. Belyaev, A. V. Vershinin, K. V. Gromov, and L. L. Kuznetsov

St. Petersburg State University of Movie and Television, St. Petersburg, Russia

Received April 27, 2005; in final form January 2006

Abstract—To develop a procedure for separating 2,4'- and 4,4'-dihydroxydiphenyl sulfones, their acidity and solubility in water were studied.

DOI: 10.1134/S1070427206030189

Bisphenol S prepared by the reaction of 2 mol of phenol with 1 mol of sulfuric acid is a mixture of 4,4'- (**I**) and 2,4'-dihydroxydiphenyl sulfone (**II**) with small amounts of 2,4',4"-trihydroxytriphenyl disulfone (**III**) and unidentified colored and colorless impurities.

Previously crude bisphenol S was used for preparing macromolecular components of heat-developable mixtures and photoconductors. At present, only pure sulfones **I** and **II** are used for this purpose. Sulfone **III** does not find practical application so far. Most of the procedures for separating sulfones **I** and **II** are based on their different solubilities in organic solvents. Since only isomer **I** was used in practice, these methods consisted in its separation from concomitant impurities. Isolation of individual sulfones **I** and **II** by treatment of bisphenol S with a boiling mixture of *p*-xylene and isopropanol or methyl ethyl ketone was described in patent [1].

Procedures involving no organic solvents are more convenient for industrial applications. Components of bisphenol S were separated in the form of their monosodium salts [2] by the following procedure. An isomer mixture was dissolved in approximately 2 equiv of aqueous alkali to form the disodium salts readily soluble in water. Only the monosodium salt of **I** was precipitated after partial neutralization of the solution. As stated in patent [2], under these conditions isomer **II** is in the solution in the form of its disodium salt. The suspension was filtered. Monosodium salt of isomer **II** was crystallized after partial neutralization of the filtrate. The salt was separated from the solution. Acidification of an aqueous suspension of this salt gave pure sulfone **II**. Monosodium salts of sulfones **I** and **II** were recovered in 97 and 83% yields respectively, from a mixture containing 79 wt % sulfone **I**, 20 wt % sulfone **II**, and 1 wt % impurities [2]. The purity of both isolated salts was no less than 90%. Thus, this method seems promising for develop a high-performance industrial process for separating isomers **I** and **II** without using organic solvents.

We experimentally tested the procedure described in patent [2]. The results of separation of bisphenol S are presented in Table 1. Isomer **I** was isolated in a yield of 93 wt %, which is close to the yield reported in the patent. However, instead of pure isomer **II** we obtained only a mixture containing 48 wt % target product.

To exclude the possible influence of impurities which can be different in bisphenol used in [2] and in our sample, we prepared a model mixture containing pure isomers **I** and **II** in the ratio equal to that in the bisphenol described in patent [2] (Table 1, run no. 2). The results of separation of this mixture also differed from those reported in the patent.

Since, according to patent [2], monosodium salt of isomer **I** is formed and crystallizes in a solution in which isomer **II** is in the form the disodium salt, the acidity of sulfone **II** should be substantially higher

Table 1. Results of separation of a mixture of dihydroxydiphenyl sulfone isomers

Run no.	Sample	Weight, g	Component content, wt %		
			I	**II**	**III**
1	Bisphenol S	50	82.0	16.5	1.5
	Isomer **I**	40.5	93.2	6.6	0.2
	Isomer **II**	7.9	45.6	48.0	6.4
2	Model mixture	50	80.0	20.0	0.0
	Isomer **I**	42.8	88.3	11.7	0.0
	Isomer **II**	6.9	61.9	38.1	0.0

Table 2. Acidity of isomers **I** and **II** in their 0.004 M aqueous solutions at 22°C

Isomer	Weighed portion, g	V_{equiv},* ml	pK_{a1}	pK_{a2}
I	0.0991	6.13	7.52	8.65
	0.0946	5.87	7.50	8.51
	0.1003	6.21	7.53	8.57
Average	–	–	7.52	8.57
II	0.1043	6.47	7.57	8.79
	0.0915	5.55	7.53	8.83
	0.0974	6.05	7.54	8.86
Average	–	–	7.54	8.83

* V_{equiv} is the equivalent volume of 0.1251 N NaOH.

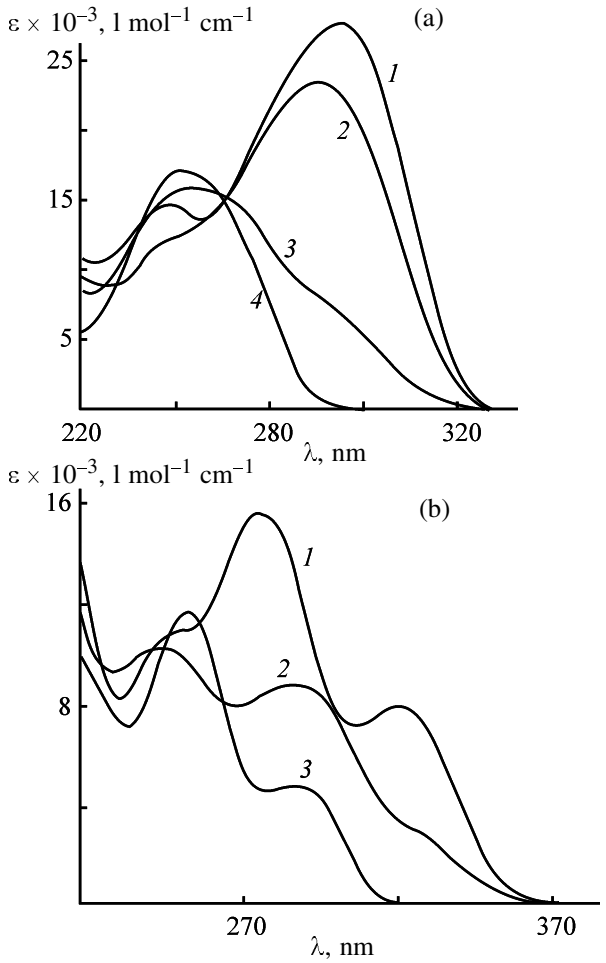


Fig. 1. UV spectra of aqueous solutions of (a) isomer **I** at pH (*1*) 9.95, (*2*) 8.42, (*3*) 7.12, and (*4*) 5.16 and (b) isomer **II** at pH (*1*) 10.12, (*2*) 7.05, and (*3*) 5.24. (ε) Molar extinction coefficient and (λ) wavelength.

than that of sulfone **I**. pK_{a1} and pK_{a2} of sulfone **I** in 71.9 wt % aqueous ethanol at 24°C is 9.01 and 9.93, respectively [3]; in water at 24°C, 7.57 and 8.53, respectively [3]; in 48% aqueous ethanol, 8.79 and 9.41, respectively [4]; and in 70 wt % aqueous ethanol, 8.87 and 10.44, respectively [5].

In addition, the acidity of chlorinated [5] and hydroxymethyl-substituted [6] 4,4'-dihydroxydiphenyl sulfone and 2,2'-dihydroxydiphenyl sulfone [4] is known. No data on acidity of sulfone **II** are reported.

Thus, the published data on isomer **I** are contradictory. This can be due to the influence of the solution composition of the acid properties. Since the acidity of compound **I** in water [3] was measured using an insufficiently pure sample (a mixture of isomers with mp 236–238°C was studied, whereas the mp (melting point) of pure **I** was 249.5°C [7]) and no data on the acidity of sulfone **II** under the comparable conditions were reported, in this study we performed parallel measurements of the acidity of isomers **I** and **II** in an aqueous solution. The potentiometric titration curves of ~0.004 M aqueous solutions of these compounds are similar and typical of dibasic acid. The acidity constants calculated by the Neues procedure [8] are presented in Table 2.

The pK_{a1} (negative logarithm of the dissociation constant for the first step) values of isomers **I** and **II** are almost the same (7.52 and 7.54, respectively). Since the structure of the aromatic ring of the $ArSO_2$ groups insignificantly affects the acidity of the 4-hydroxy group [3], the first dissociation step of compounds **I** and **II** is deprotonation of the 4-hydroxy group. At the same time, the pK_{a2} values of isomers **I** and **II** differ substantially (8.57 and 8.83, respectively). This is due to the fact that the second dissociation step of isomer **I** involves deprotonation of the 4-hydroxy group whereas the second dissociation step of isomer **II** is deprotonation of the 2-hydroxy group.

We found that pK_{a2} of isomer **II** is somewhat larger than that of isomer **I**. This is consistent with the ratio of acidities of other *o*- and *p*-substituted phenols. For example, *o*-nitrophenol is weaker acid than *p*-nitrophenol (pK_a 7.23 and 7.15, respectively [8]).

Our experiments on the influence of the pH on the absorption spectra of aqueous solutions of compounds **I** and **II** additionally confirmed their similar acid properties. Unlike the spectra of the molecular compounds [9], dianions of **I** and **II** strongly absorb in the relatively long-wave range (Fig. 1). The spectrum of dianion **I** contains a band with a maximum at λ = 295 nm (ε = 27400 l mol^{-1} cm^{-1}); two

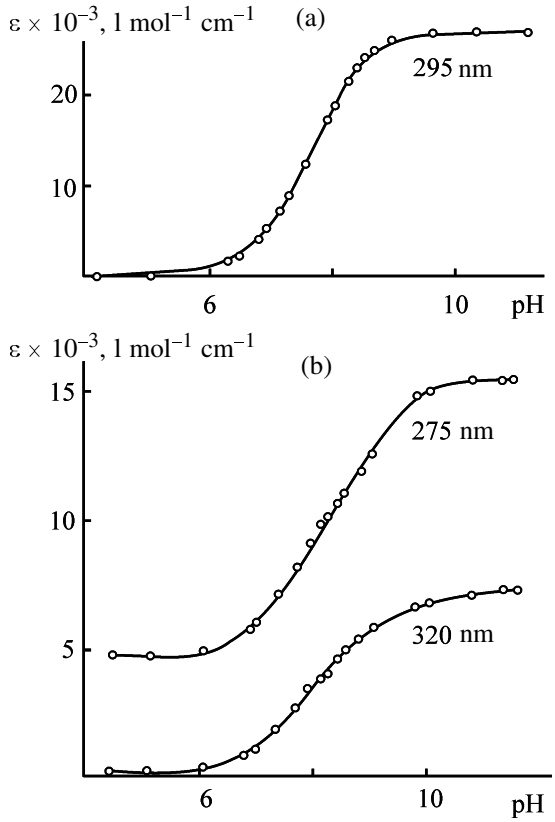


Fig. 2. Molar extinction coefficient ε as a function of pH of solutions of (a) **I** and (b) **II** (analytical wavelengths are indicated).

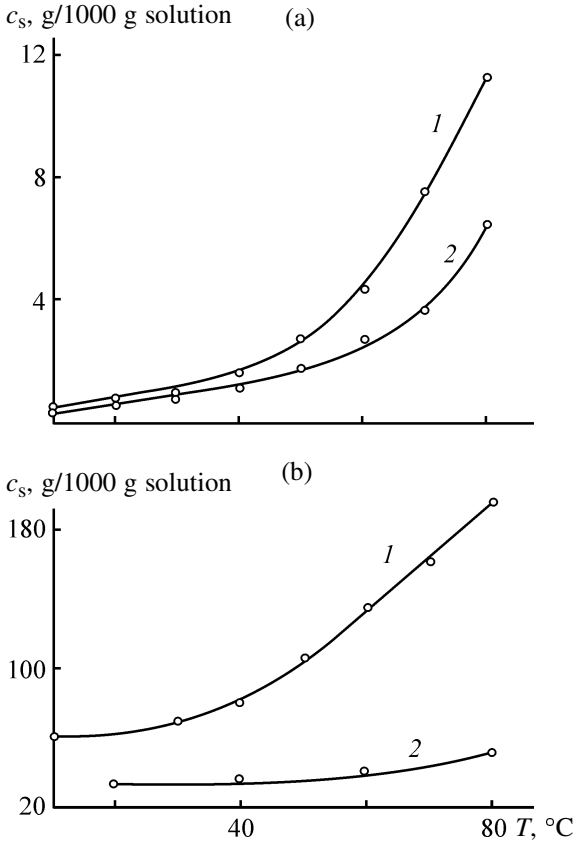


Fig. 3. Solubility c_s of (a) (*1*) sulfone **I** and (*2*) **II** and (b) their monosodium salts as a function of temperature *T*.

bands at λ = 275 nm (ε = 15 400 l mol^{-1} cm^{-1}) and λ = 320 nm (ε = 8000 l mol^{-1} cm^{-1}) are observed in the spectrum of dianion **II**. When pH of solutions of these compounds increases from 6 to 9, the absorption in these ranges increases (Fig. 2). The pH dependence of the molar absorption coefficient has a usual S-shape and reflects an increase in the degree of dissociation with pH. Since the absorption spectra of conjugated acids **I**, **II**, and their mono- and dianions overlap in the whole range, it is impossible to determine pK_{a1} and pK_{a2} from the spectra data. However, the pH of half-neutralization of isomer **I**, calculated from the spectral data, is 7.71. For isomer **II**, this value calculated from the absorption at λ = 275 nm and λ = 320 nm was 8.09 and 8.05, respectively. Thus, these results also show that the acidity of isomer **II** is noticeably lower than that of isomer **I**. Therefore, the statement [2] that monosodium salt of **I** precipitates and the readily water-soluble disodium salt of **II** remains in the solution after acidification of solutions containing disodium salts of **I** and **II** is incorrect.

Selective crystallization of one of the isomers may also be due to its lower solubility. The data on solubility of isomers **I** and **II** are contradictory. Zehenter and Fauzer reported [10] that the solubility of isomer **II** (0.32 g in 100 g of water) at 22°C is higher by a factor of approximately 1.5 than that of isomer **I** (0.24 in 100 g of water). At the same time, isomer **I** was recrystallized from an aqueous solution to remove less soluble isomer **II** [7]. To clarify this point, we studied the solubility of sulfones **I** and **II** in water in a wide temperature range. As seen from Fig. 3, the solubility of isomer **II** at 10–80°C is lower by a factor of 2 than that of isomer **I**. Hence, although the content of isomer **I** in its mixture with isomer **II** is high, it is difficult to isolate isomer **I** by recrystallization from water.

Crystallization of monosodium salt of **I** form an acidified aqueous solution of a mixture of disodium salts of **I** and **II**, described in patent [2], could be due to substantial difference in the solubilities of the monosodium salts of these isomers. Since no data on the solubilities of monosodium salts of **I** and **II** are reported, we determined the concentrations of their saturated aqueous solutions at different temperatures (Fig. 3). As seen from Fig. 3, the solubility of mono-

sodium salt of **II** is lower than that of monosodium salt of **I** in the whole temperature range. These data clarify the experimental results on separation of mixtures of isomers **I** and **II**.

Since separation of sulfone **I** from impurities of isomer **II** was performed by treatment of their ammonium salts [11], we studied the solubility of monoammonium salt of **I** in water at different temperatures. The solubility of this salt in water is noticeably lower than that of the monosodium salt, with the difference being the most pronounced at low temperatures. The solubility c_s (wt %) of the sodium salt at 10, 30, 40, 50, 60, 70, and 80°C is 6.0, 7.0, 8.2, 11.1, 14.6, 16.6, and 20.1, respectively; the solubility of the ammonium salt at 20, 30, 40, 50, 60, and 70°C is 3.4, 3.6, 4.8, 7.1, 11.0, and 15.0, respectively. Thus, isomer **I** can be purified more efficiently in the form of monoammonium salt as compared to its sodium analog.

Thus, separation of isomers **I** and **II** in the form of their monosodium salts based on the difference both in their acidities and in solubilities in water at a usual content of isomer **II** in the mixture (15–20 wt %) is ineffective. However, if the content of isomers **I** and **II** in the mixture substantially differs (~85 and ~2 wt %, respectively), the salts of these compounds can be separated by the procedure described in [11]. This procedure is unsuitable for isolation of pure **II**.

EXPERIMENTAL

Crude bisphenol S was prepared by sulfonation of phenol in the presence of *o*-dichlorobenzene. A 250-ml three-necked flask equipped with a thermometer, a mechanical stirrer with a seal, and a Würtz adapter with a descending condenser was loaded with phenol (120 g) and dichlorobenzene (80 ml). To this solution, 92% sulfuric acid (68 g) was added with stirring at 100–110°C within 10 min. The mixture was kept at 100–110°C for 1 h and then was heated to boil at 140–145°C. The aqueous azeotrope of *o*-dichlorobenzene was separated and the organic layer was returned to the reaction mixture. The temperature of the reaction mixture increased to 180°C within 5 h. Then the reaction mixture was cooled, and *o*-dichlorobenzene was decanted. A solution of sodium hydroxide (51 g) in water (150 ml) was added to the residue. The resulting suspension was heated at 90–95°C with stirring until a solution was formed. The residual organic solvent was separated, and the solution was diluted to 600 ml with distilled water and acidified with 70% sulfuric acid to pH ~3. After cooling of the reaction mixture, the precipitate was filtered off, washed with distilled water, and dried at 110–120°C. The yield of crude bisphenol S containing 82, 16.5, and 1.5 wt % of sulfones **I**, **II**, and **III**, respectively, was 143 g (90%).

Individual isomers I and II were obtained by separation of crude bisphenol using a benzene–acetone mixture by the procedure described in [7]. The melting points of isomer **II** and **I** recrystallized from 5% aqueous ethanol were 185–186 and 248–249°C, respectively, which is close to the published data (186.7 and 249.5°C, respectively [7]).

Monosodium salts of sulfones I and II and monoammonium salt of I were prepared by dissolution of these sulfones in 1 equiv of aqueous solution of the appropriate base on heating. The precipitates of these salts formed on cooling were filtered off and dried at 105–110°C. As determined by UV spectroscopy, the content of the target product was no less than 99.5%.

Chromatographic analysis of crude bisphenol S and the isomer mixtures was performed on a Milikhrom chromatograph using columns packed with Sil 600. A mixture of hexane (40 ml), ethyl acetate (20 ml), acetic acid (2 ml), and trifluoroacetic acid (0.5 ml) was used as the eluent. The wavelength used for detection was λ = 260 mn.

The content of individual isomers in aqueous solutions was determined by their absorption measured in 1-cm quartz cells on an SF-26 spectrophotometer. The molar extinction coefficient of isomers **I** (λ = 295 nm) and **II** (λ = 275 nm) measured in solution with pH 11.0–11.5 was 27400 and 15450 $l\,mol^{-1}\,cm^{-1}$, respectively.

Crude bisphenol S was separated by the procedure in [2]. Crude bisphenol S (50 g) was placed in a 250 ml three-necked flask equipped with a thermometer, a mechanical stirrer, and a reflux condenser. A solution of NaOH (17 g) in water (75 ml) was added. The resulting suspension was refluxed until a solution was formed. 72% sulfuric acid (12.6 g) was added. The suspension was slowly cooled to 40°C. A precipitate of monosodium salt of isomer **I** was filtered off and the liquid phase was thoroughly removed by pressing. The filtrate was heated to 90– 95°C with stirring and acidified to pH 3–4. After cooling, the precipitate of isomer **II** was filtered off, washed with distilled water, and dried at 105–110°C. Isolated monosodium salt of isomer **I** was suspended in distilled water (120 ml). The suspension was heated to 90–95°C with stirring and acidified to pH 4–5. After cooling, the precipitate of isomer **I** was filtered off, washed with distilled water, and dried at 105–110°C.

A mixture containing 80 wt % isomer **I** and 20 wt % isomer **II** was separated similarly.

To determine the solubility of sulfones **I** and **II** and their salts in water, weighed portions of these compounds were mixed with water in a flask equipped with a thermometer and a reflux condenser. The resulting suspensions were heated to a temperature higher by 5–10°C than the required temperature. The system was thermostated with an accuracy of ±0.2°C for 5–6 h with stirring. Samples of the saturated solution were taken with a sampler equipped with a glass frit, placed in a weighing bottle, cooled to room temperature, weighed on an analytical balance with an accuracy of ±0.00005 g, and analyzed spectrophotometrically.

CONCLUSION

The relative acidities of 2,4'- and 4,4'-dihydroxydiphenyl sulfones and the solubilities of their salts do not allow isolation of the pure 2,4'-isomer by precipitation of its monosodium salt but allow removal of impurities of the 2,4'-isomer from 4,4'-dihydroxydiphenyl sulfone.

REFERENCES

1. US Patent 5 399 772.
2. US Patent 5 767 318.
3. Berkman, Ya.P. and Polonskaya, L.A., *Nauchn. Zap. L'vov. Politekh. Inst., Ser. Khim. Tekhnol.*, 1956, no. 22, pp. 49–60.
4. Meyers, C.Y., *Gazz. Chim. Ital.*, 1963, vol. 93, no. 10, pp. 1206–1221.
5. Smirnova, O.V. and Robas, E.Ya., *Zh. Prikl. Khim.*, 1975, vol. 48, no. 3, pp. 578–582.
6. US Patent 3 230 198.
7. Hinkel, L.E. and Summers, G.H.R., *J. Chem. Soc.*, 1949, no. 10, pp. 2854–2856.
8. Albert, A. and Serjeant, E., *Ionization Constants of Acids and Bases. A Laboratory Manual*, New York: Wiley, 1962.
9. Kralovsky, J., Kalhousova, M., and Slosar, P., *Coll. Czech. Chem. Commun.*, 1994, vol. 59, no. 3, pp. 569–574.
10. Zehenter, J. and Fauzer, E., *J. Prakt. Chem.*, 1927, vol. 117, no. 1, pp. 233–244.
11. US Patent 5 097 074.

ISSN 1070-4272. Russian Journal of Applied Chemistry, 2006, Vol. 79, No. 3, pp. 430–432. © Pleiades Publishing, Inc., 2006.
Original Russian Text © V.F. Burdukovskii, D.M. Mognonov, S.O. Botoeva, Zh.P. Mazurevskaya, 2006, published in Zhurnal Prikladnoi Khimii, 2006, Vol. 79, No. 3, pp. 437–439.

ORGANIC SYNTHESIS AND INDUSTRIAL ORGANIC CHEMISTRY

Rearrangement of Polyarylene Benzimidates into Poly(*N*-arylenebenzamides)

V. F. Burdukovskii, D. M. Mognonov, S. O. Botoeva, and Zh. P. Mazurevskaya

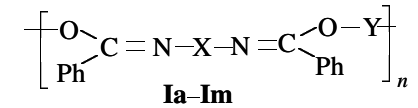
Baikal Institute of Nature Management, Siberian Division, Russian Academy of Sciences, Ulan-Ude, Buryatia, Russia

Received June 8, 2005

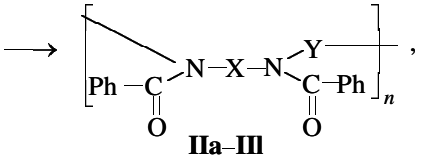
Abstract—The transformation of polyarylene benzimidates prepared by polycondensation of bisphenols with benzimidoyl chlorides in *N*-methyl-2-pyrrolidone into poly(*N*-arylenebenzamides) was studied.

DOI: 10.1134/S1070427206030190

Polyarylene benzimidates (PBIs) prepared by polycondensation of imidoyl chlorides derived from aromatic mono- and dicarboxylic acids with bisphenols [1] exhibit high heat resistance and large interval between the decomposition onset and softening points. Specific features of the imidate bond and available data on its reactivity [2] allowed us to suggest the possibility of the following rearrangement in the polymer chain:



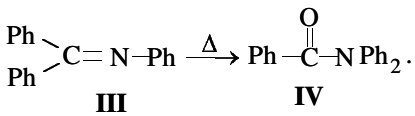
Ia–**Im**



IIa–**III**

Ia, X = *p*-C_6H_4, Y = *m*-C_6H_4; **Ib**, X = *p*-C_6H_4, Y = (*p*-$C_6H_4)_2CMe_2$; **Ic**, X = *p*-C_6H_4, Y = (*p*-$C_6H_4)_2SO_2$; **Id**, X = *m*-C_6H_4, Y = *p*-C_6H_4; **Ie**, X = Y = *m*-C_6H_4; **If**, X = *m*-C_6H_4, Y = (*p*-$C_6H_4)_2CMe_2$; **Ig**, X = *m*-C_6H_4, Y = (*p*-$C_6H_4)_2SO_2$; **Ih**, X = (*p*-$C_6H_4)_2O$, Y = *p*-C_6H_4; **Ii**, X = (*p*-$C_6H_4)_2O$, Y = *m*-C_6H_4; **Ij**, X = (*p*-$C_6H_4)_2O$, Y = (*p*-$C_6H_4)_2SO_2$; **Ik**, X = (*p*-$C_6H_4)_2 \cdot CH_2$, Y = *p*-C_6H_4; **Il**, X = (*p*-$C_6H_4)_2CH_2$, Y = *m*-C_6H_4; **Im**, X = (*p*-$C_6H_4)_2CH_2$, Y = (*p*-$C_6H_4)_2CMe_2$; **IIa**, X = Y = *m*-C_6H_4; **IIb**, X = *p*-C_6H_4, Y = (*p*-$C_6H_4)_2CMe_2$; **IIc**, X = *p*-C_6H_4, Y = (*p*-$C_6H_4)_2SO_2$; **IId**, X = *m*-C_6H_4, Y = *p*-C_6H_4; **IIe**, X = Y = *m*-C_6H_4; **IIf**, X = *m*-C_6H_4, Y = (*p*-$C_6H_4)_2CMe_2$; **IIg**, X = (*p*-$C_6H_4)_2O$, Y = *m*-C_6H_4; **IIh**, X = (*p*-$C_6H_4)_2O$, Y = (*p*-$C_6H_4)_2SO_2$; **IIi**, X = (*p*-$C_6H_4)_2CH_2$, Y = *p*-C_6H_4; **IIj**, X = (*p*-$C_6H_4)_2CH_2$, Y = *m*-C_6H_4; **IIk**, X = (*p*-$C_6H_4)_2CH_2$, Y = (*p*-$C_6H_4)_2CMe_2$; **III**, X = (*p*-$C_6H_4)_2CH_2$, Y = (*p*-$C_6H_4)_2SO_2$.

Initially we studied the rearrangement of a model compound, phenyl *N*-phenylbenzimidate **III**, into *N*,*N*-diphenylbenzamide **IV**, known as Chapman rearrangement [3]:



III **IV**

We found that heating of **III** at 250°C for 13 h leads to its complete transformation into **IV**. The structure of the product was proved by IR and ^{13}C NMR spectroscopy. The IR spectrum of **IV** contains a C=O absorption band at 1657 cm^{-1}, whereas the C–O band at 1210 cm^{-1} is absent. In the ^{13}C NMR spectrum of **IV**, a carbonyl carbon signal appears at 170.53 ppm.

Having obtained the positive result in the model reaction, we examined the possibility of the similar rearrangement in PBIs.

The possibility of thermal rearrangement of the polymers was checked with **Ie** as example (Fig. 1). The first evidences of the transformation in the melt appear in 3 h, after which the reaction accelerates and is complete in 18 h at 86% conversion. The rearrangement in a film and in the glassy state involves a long induction period and therefore takes more than 30 h. The rearrangement of **Ie**, according to viscosity measurements, is not accompanied by significant changes in the molecular weight. The conversion was esti-

mated from the IR spectra (absorption of the imido ester bond).

Figure 1 shows the conversion curves of **If** in nitrobenzene (NB) and diphenyl ether (DPE). The behavior of **If** in these solvents was different. In NB, compound **If** dissolved immediately without swelling, whereas in DPE the dissolution occurred only on heating above 150°C. Nevertheless, at equal other conditions, the rearrangement in DPE was faster.

We found that the molecular weight of PBI did not noticeably affect the kinetic parameters of the reaction.

Our results show that the rearrangement of PBIs into poly(*N*-arylenebenzamides) (PBAs) occurred considerably more readily in the melt and in DPE at 240°C. The conditions for preparing some PBAs are given in Table 1.

For more flexible PBIs **Ie**, **If**, **Il**, and **Im**, the transformation occurs to a greater extent in DPE, and for more rigid PBIs, in the melt.

The structures of PBAs were confirmed by IR spectroscopy: The C=N absorption band in PBIs at 1658 cm^{-1} shifted to 1672 cm^{-1}, and the C–O band at 1220 cm^{-1} virtually disappeared. The most convincing proof is furnished by ^{13}C NMR spectroscopy: In the spectra of PBAs, a signal of the carbonyl carbon atom appears at 174.7 ppm.

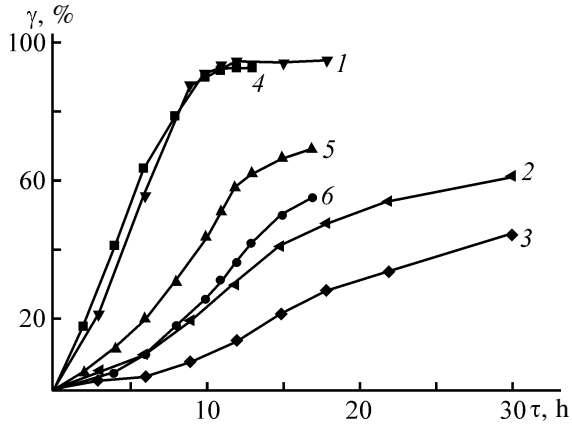
The PBAs obtained, like the starting PBIs, are soluble in DMF, *N*,*N*-dimethylacetamide, DMSO, *m*-cresol, and pyridine, but, in contrast to the starting polymers, dissolve in chloroform only on heating.

The glass transition point of the polymers changes insignificantly upon PBI → PBA rearrangement: from 275–318 to 210–252°C, respectively. The PBAs prepared significantly surpass the PIDs in the heat resistance: The 10% weight loss (TGA in air, 5 deg min^{-1}) is observed at 454–487°C (for the starting PIDs, at 360–415°C).

The PBAs obtained exhibit good film-forming properties; the physicomechanical characteristics of the films are given in Table 2. The properties of the press materials prepared by pressing PBA powders at 70–75 MPa/250–350°C are also given in Table 2.

EXPERIMENTAL

The IR spectra were recorded on Specord IR-75 and UR-20 spectrophotometers (4000–400 cm^{-1}) in KBr. The ^{13}C NMR spectra were taken on a Varian VXR-500S spectrometer (400.0 MHz for ^{1}H) in DMSO-d_6, internal reference TMS.



PBI conversion γ as a function of time τ in (*1*) melt, (*2*) glassy state, (*3*) film, (*4*) DPE at 240°C, (*5*) DPE at 200°C, and (*6*) NB at 200°C.

Dynamic thermogravimetric analysis was performed with a Q-1000 derivatograph in air at a heating rate of 5 deg min^{-1}, with Al_2O_3 as reference. The thermomechanical analysis was performed with a Tsetlin device at a constant load of 0.08 MPa and a heating rate of 100 deg h^{-1}.

Film materials were obtained by casting an 18–20% solution of a polymer in DMF onto a glass support. Physicomechanical tests of film samples were performed according to GOST (State Standard) 14236–81 (COMECON Standard 1490–79), and those of press materials, according to GOSTs 4647–80 and 4648–71.

Phenyl *N*-phenylbenzimidate. A flask equipped with tubes for argon inlet and outlet was charged with

Table 1. Conditions for the rearrangement of PBIs and conversions γ

PBI	In melt			In solution	
	T, °C	τ, h	γ, %	τ, h	γ, %
Ia	340	17	89.7	14	79.2
Ib	290	17	88.3	14	87.1
Ic	320	16	90.2	14	78.8
Id	350	17	89.1	13	87.9
Ie	330	18	86.3	14	89.4
If	260	16	89.6	11	92.8
Ig	290	16	92.0	13	89.6
Ih	340	16	87.4	12	80.2
Ii	340	16	90.5	11	84.5
Ij	300	17	91.3	12	90.3
Ik	320	17	86.7	13	80.5
Il	290	17	90.8	11	94.0
Im	250	17	92.2	10	97.8

Table 2. Physicomechanical properties of PBA films and press materials*

PBA	Films		Press materials	
	σ_t, MPa	ε_b, %	σ_t, MPa	*a*, MPa
IIa	60.7	3.0	60.4	8.2
IIb	39.2	4.6	–	–
IIc	–	–	58.8	6.9
IId	–	–	59.2	6.6
IIe	55.6	3.8	57.5	6.8
IIf	40.8	4.9	–	–
IIg	–	–	62.6	7.3
IIh	42.6	5.5	–	–
IIi	–	–	60.7	8.4
IIj	41.8	4.8	–	–
IIk	39.1	5.0	–	–
III	–	–	59.1	7.1

* (σ_t) Breaking tensile stress, (ε_b) relative break elongation, and (*a*) specific impact resilience.

250 ml of absolute ethanol and 0.3 mol of phenol; 0.25 mol of Na was added in small portions while purging with Ar. After the reaction completion, a solution of 0.25 mol of *N*-phenylbenzimidoyl chloride in dioxane was slowly added. After stirring for 15 h, the mixture was poured onto 300 ml of ice and placed in a freezing chamber for 10 h, after which it was allowed to warm up to room temperature. The precipitate was filtered off and recrystallized from absolute ethanol; yield 87.4%.

Found, %: C 83.18, H 5.90, N 4.95.
$C_{19}H_{15}NO$.
Calculated, %: C 83.52, H 5.49, N 5.13.

***N*,*N*-Diphenylbenzamide** was prepared by rearrangement of phenyl *N*-phenylbenzimidate in an inert atmosphere at 250°C for 13 h; mp 179.5–179.8°C (cf. 179.6°C [4]).

Polyarylene benzimidates were prepared in a 50-ml three-necked flask equipped with a stirrer and with tubes for argon inlet and outlet. A mixture of 0.01 mol of bisphenol with *N*-methyl-2-pyrrolidone was added while purging with argon, and the mixture was homogenized. Then 0.02 mol of triethylamine and 0.01 mol of appropriate imidoyl chloride were added with vigorous stirring. The homogenized reaction mixture was heated to 170–180°C for 17–18 h, after which the product was precipitated by pouring the mixture into 2% aqueous ammonia, filtered off, washed with a 1% solution of sodium bisulfite in water and with water, and dried in a vacuum at 60–70°C to constant weight.

Poly(*N*-arylenebenzamides) were prepared by rearrangement of the corresponding PBIs under Ar in the melt and in DPE (Table 1).

CONCLUSION

Film-forming poly(*N*-arylenebenzamides) were prepared by rearrangement of polyarylene benzimidates in the melt and in diphenyl ether at 240°C. The polymers obtained exhibit good solubility, high resistance to thermal oxidative degradation, and relatively low softening points.

REFERENCES

1. Sanzhizhapov, D.B., Tonevitskii, Yu.V., Mognonov, D.M., and Doroshenko, Yu.E., *Zh. Prikl. Khim.*, 2003, vol. 76, no. 4, pp. 642–646.
2. Sokolov, V.V., Gerasimov, V.D., Savinov, V.M., and Belyakov, V.K., *Termostoikie aromaticheskie poliamidy* (Heat-Resistant Aromatic Polyamides), Moscow: Khimiya, 1975.
3. Vatsuro, K.V. and Mishchenko, G.L., *Imennye reaktsii v organicheskoi khimii* (Named Reactions in Organic Chemistry), Moscow: Khimiya, 1976.
4. Potekhin, A.A., *Svoistva organicheskikh soedinenii: Spravochnik* (Properties of Organic Compounds: Handbook), Leningrad: Khimiya, 1984.

ISSN 1070-4272. Russian Journal of Applied Chemistry, 2006, Vol. 79, No. 3, pp. 433–438. © Pleiades Publishing, Inc., 2006.
Original Russian Text © Yu.N. Sazanov, A.V. Gribanov, 2006, published in Zhurnal Prikladnoi Khimii, 2006, Vol. 79, No. 3, pp. 440–445.

MACROMOLECULAR CHEMISTRY AND POLYMERIC MATERIALS

Cocarbonization of Polymers as a New Concept for Synthesis of Carbon Composites

Yu. N. Sazanov and A. V. Gribanov

Institute of Macromolecular Compounds, Russian Academy of Sciences, St. Petersburg, Russia

Received December 28, 2005

Abstract—Foundations of cocarbonization of a series of carbon-chain and heterochain polymers in the solid phase and in solution were considered; the concept of this process was formulated. The temperature and kinetic parameters of the maximal thermal activity were determined. The possibilities of intermolecular interactions of compatible macromolecular compounds depending on the chemical structure of the initial components of composites and concentration and temperature–time parameters were studied.

DOI: 10.1134/S1070427206030207

An interest in carbonization of polymers arose from studies of synthesis and characteristics of highly heat-resistant polymers and various materials based on these. It was shown [1] that the attainment of high heat resistance requires formation of macromolecules with carbo- and heterocyclic structure, in which the concentration of carbon atoms approaches 100%. Depending on the specific requirements to the materials, polymers can contain various heteroatoms, whose introduction allows preparation of various heat-resistant compounds having unique characteristics.

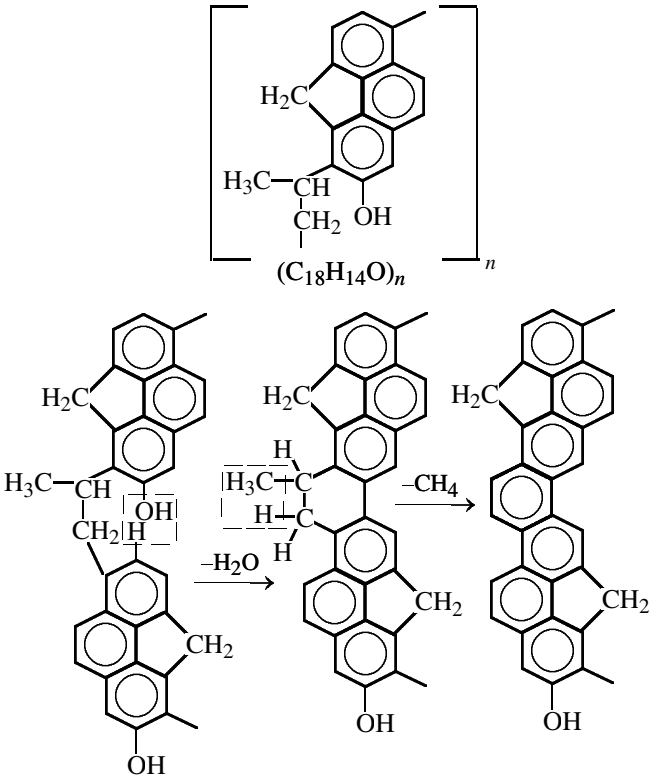
Polymers with carbon-chain, heterochain, and mixed structure, whose heat resistance under certain conditions reaches 500–600°C, were synthesized under laboratory conditions. Many representatives of these polymers are produced on the industrial scale and serve as indispensable materials operating for a long time under extreme thermal conditions [2, 3]. The examples of these polymers are polyphenylenes, cyclic polyacrylonitrile, polyimides, polybenzimidazoles, polybenzoxazoles, polyphenylquinoxalines, and other polyheterocyclic compounds.

During the studies and industrial tests of materials and items based on heat-resistant polymers, problems related to variation of their parameters as a result of thermal overload arose: the characteristics of materials irreversibly changed, which resulted, as a rule, in degradation of polymers and destruction of items based on these.

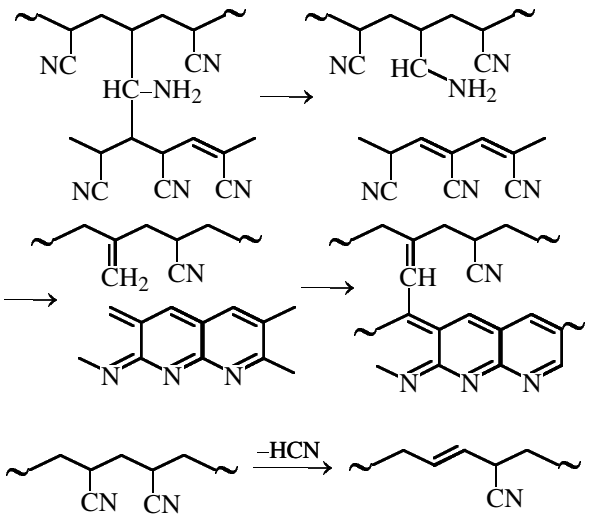
Studies aimed to solving these problems were pursued in two directions: (1) search for pathways of synthesis of new heat-resistant structures, development of various stabilizing agents preventing thermal degradation and composite materials [4–7]; (2) study of the characteristics of polymers altered as a result of thermal overload.

The studies of carbonization of polymers initially concerned carbon fibers based on cellulose hydrate, polyacrylonitrile, and partially carbon and oil distillation residues. It was shown that a number of regular trends well-known in carbon chemistry and coke chemistry are applicable to carbonization of polymers [8]. We can say that the terms "coke" and "coking" were prototypes of the term "carbonization," since they are based on thermochemical reactions related to gradual condensation of organic compounds, formation of rings, their subsequent aggregation [4], and elimination of hydrogen and heteroatoms (oxygen, nitrogen, sulfur, etc.). The similarity of these processes is evident from a comparison of the schemes of transformation of so-called carbon monomer used in coke chemistry (a) and cyclization of polyacrylonitrile (b).

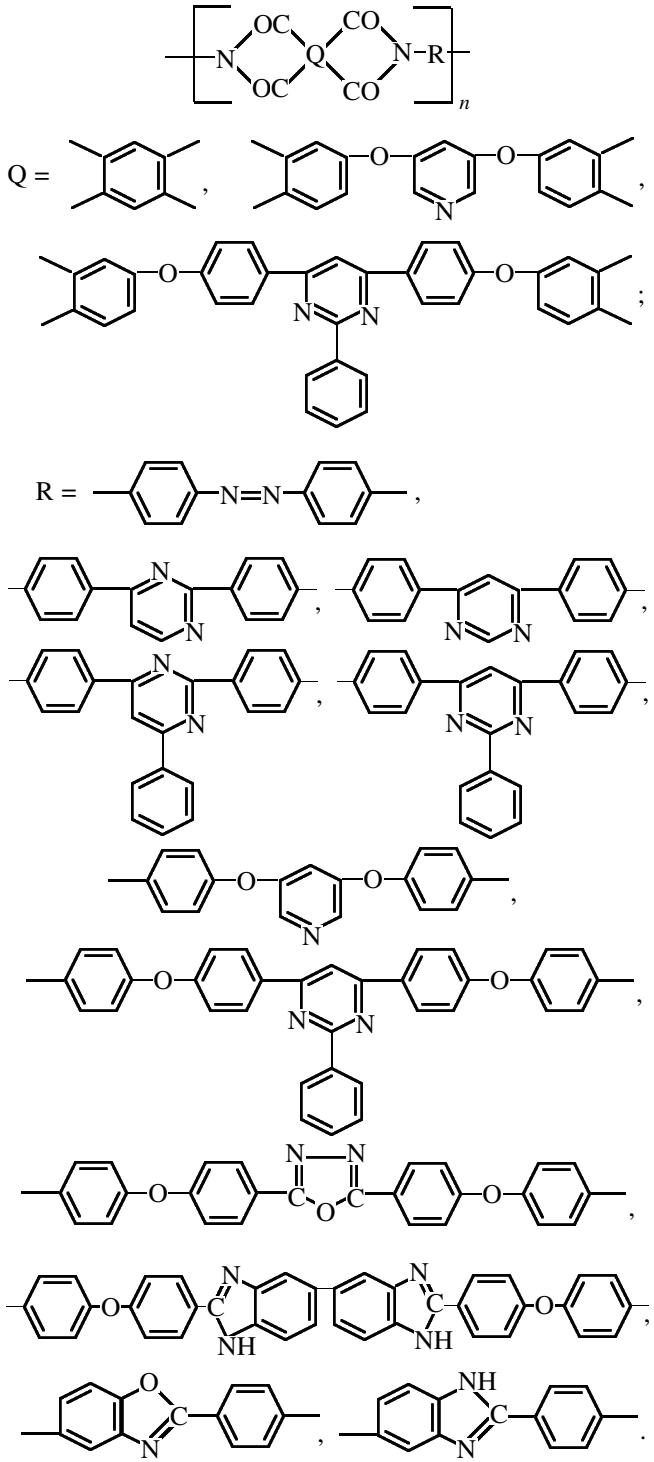
Despite the fact that the residues of carbonized products of cellulose do not exceed 15–20%, carbon fibers based on these are of great practical value especially as highly active sorbents used in medicine. Of even greater value among polymer carbon materials are carbonizates of polyacrylonitrile (PAN); in its carbonization the carbon residue (CR) increases to 60%. The fields of application of carbonized and graphitized PAN are so wide that in dozens of leading branches of industry many of materials and items



Scheme of transformation of carbon monomer to polymer (a)



Scheme of thermochemical cyclization of polyacrylonitrile (b)



Structure of various nitrogen-containing polyimides (c)

based on these are indispensable for numerous structures, devices, and apparatus [9, 10].

Beginning from the 1980s, once the most heat-resistant polymers, polyimides, became commercially available as films and fibers, the need in studying the processes of their carbonization arose. The first studies of the influence of the polyimide unit structure on its thermal stability and some other characteristics showed a certain influence of nitrogen atoms on thermochemical conversion of polyimide to carbonizate

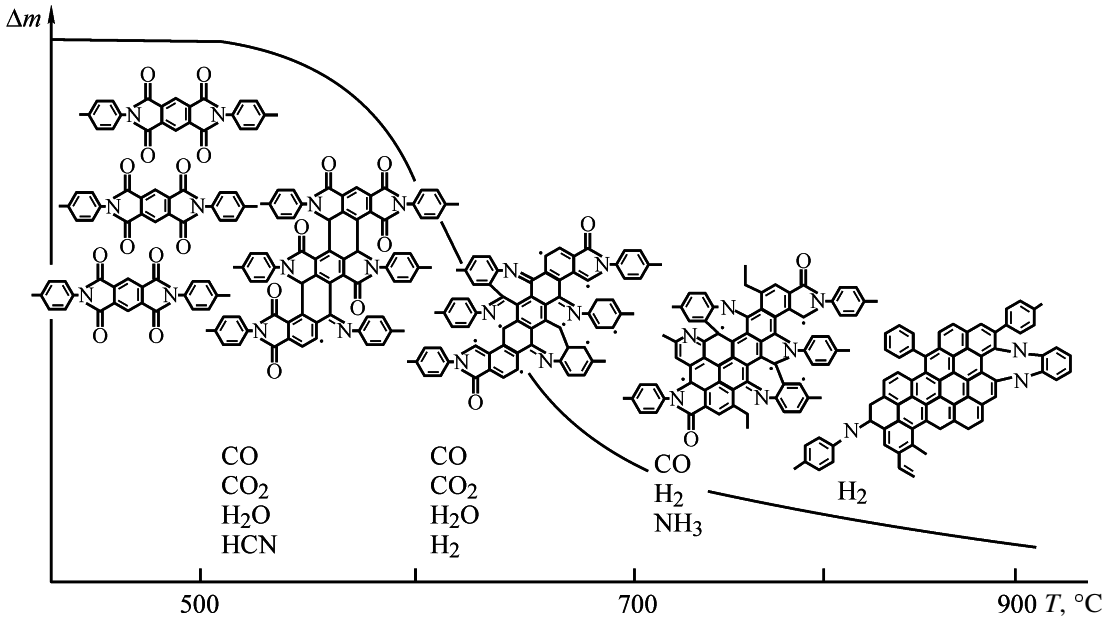


Fig. 1. Schematic thermogram of thermochemical reactions of polyimide PM carbonization in the range 500–900°C. (Δm) Weight loss and (T) thermal treatment temperature; the same for Fig. 3.

at a temperature of 500°C and above. In a series of runs, the yield of coke residue as high as 70–75% was attained; in so doing, a correlation was observed between the ratio of nitrogen atoms and their bonds with neighboring atoms, and on the one hand, and carbon residue (CR), on the other hand [11, 12]. Scheme (c) shows the structures studied, for which it was found that polyimides based on *p*-phenylenediamine, benzoxazole, and pyrimidine derivatives, i.e., polymers containing more nitrogen atoms in the chain, have the highest CR at 900°C. More recent studies [13, 14] showed that nitrogen atom in the polyimide chain plays a crucial role in thermal transformation of this polymer in a wide temperature range. For polyimide PM as example, it was shown that, beginning from the stage of conversion of the polyimide prepolymer into the cyclic polymer, in which nitrogen plays the role of creating factor, up to conversion of the polymer to highly carbonized product above 1200°C, when nitrogen leaves the intermediate cyclic structures (Fig. 1), this atom permanently participates in gradual rearrangement of polyheterocyclic structure to carbocyclic structure. In energy terms, this process is more favorable than the direct carbonization of carbon-chain polymers. The similar "relay" character of thermal transformations of polyimides is observed on introduction of fragments containing pentavalent phosphorus atoms, close in structure to some nitrogen compounds [15].

Further studies on the synthesis of carbonized materials from commercial polyimide film (polyimides PM and VM) involving variation of the conditions of thermal treatment showed that the products with increased content of carbon, exhibiting the stability of shape and increased conductivity, are formed only in a block or thick film under isothermal heating. However, CR values for such a film do not exceed 40–50%.

To minimize the above drawbacks we performed carbonization of copolyimides incorporating, along with the initial dianhydrides of tetracarboxylic acids, two diamines of various isomer compositions based on pyrimidine derivatives. The results of this study [16] showed a noticeable increase in the thermal stability and strength of these polyimides in comparison with polyimide PM. For a series of samples, carbonizates were obtained in a yield of 70–80% with respect to carbon residue. The similar studies were performed with combination of polyimides with other polyheterocyclic compounds. For example, based on phenylquinoxaline, the difference in the structure of the resulting carbonizates depending on the three-dimensional packing of the reactants was revealed [17].

However, the three-dimensional packing of branched polymers does not allow CR to be increased in comparison with PM polymer. The other way of introduction of nitrogen-containing fragments into the polyimide structure was formation of interpolymeric complexes based on common solvent. For this pur-

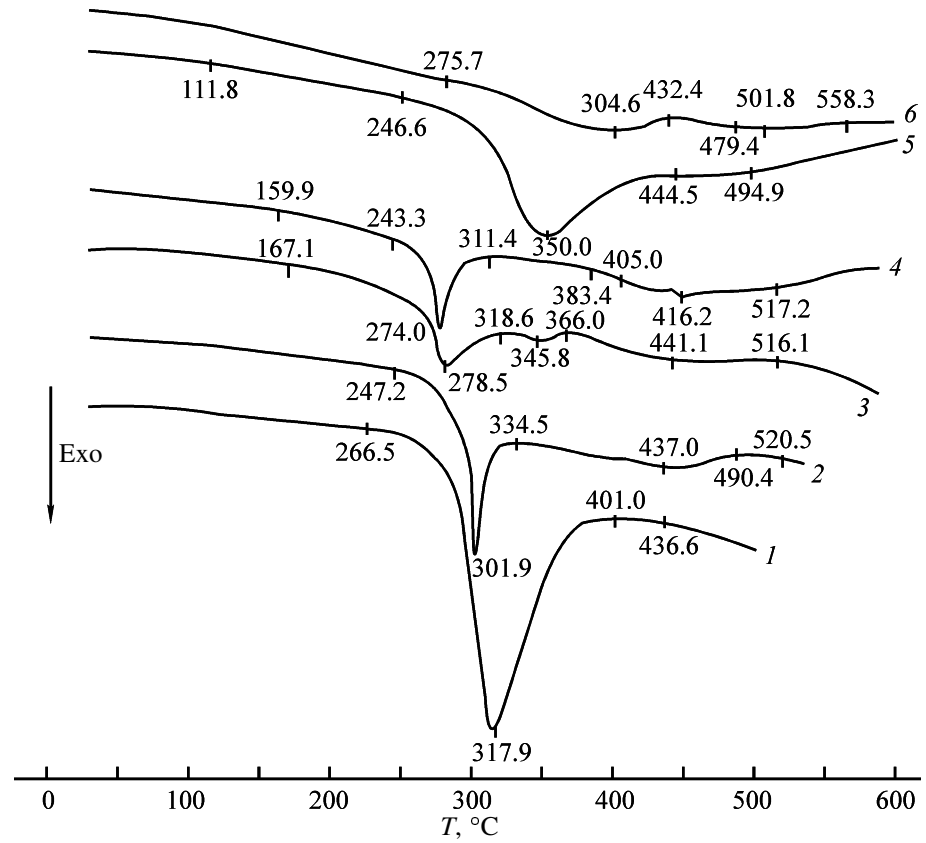


Fig. 2. DSC curves for the samples of PAN, chitin, and PAN + chitin film prepared from DMF. Heating rate 10 deg min^{-1}, weighed portion 5 mg. (*T*) Temperature of thermal treatment. (*1, 2*) PAN powder, (*3, 4*) blend film, and (*5, 6*) chitin powder. (*1, 3, 5*) In air and (*2, 4, 6*) in nitrogen.

pose, the solutions of prepolymers of polyimide PM, polybenzimidazole, polyacrylonitrile (PAN), polyvinylpyridine, polyvinylpyrrolidone, and polyvinyltetrazole in dimethylformamide or dimethylacetamide were used [18–21].

Among the studied polymer pairs polyamido acid–nitrogen-containing polymer, the products of thermal treatment of mixed solutions of polyamido acid (PAA) with PAN are of the most interest for the cocarbonization process. The specific feature of this pair is that the main cyclization reactions of both polyamido acid and polyacrylonitrile are suppressed. Competition of these reactions under ordinary conditions of thermal cyclization prevents formation of copolymer and yields a blend of polyimide with PAN, whose carbonization under subsequent heating does not yield a carbonizate with a new structure different from polyimide and PAN. Only in the case of prolonged heating of a mixture of solvate complexes of the initial polymers at 150–200°C, copolymer can be formed through an interpolymer complex. In some characteristics, this product differs from the initial polymers (increased chemical stability, prolonged thermal stability, improved flexibility and elongation at break). Further heating of this compound at 400–500°C yields a carbonizate whose structure in its spectral characteristics differs from those of both polyimide carbonizate and PAN carbonizate. At 900°C, the carbonized residue retains the shape of the initial material, has metallic luster, conductivity comparable with that of the carbonized polyimide, and CR varying from 60 to 80% depending on the carbonization conditions.

Since synthesis of the above carbonizate presents some problems caused by instability of PAA solutions and prolonged synthesis of the initial copolymer, subsequent experiments on studying cocarbonization were performed with PAN. As the second component of the initial blend we used cellulose and its derivatives. These macromolecular compounds have rich resources and are widely used in industry; thermal degradation and carbonization of these compounds were studied theoretically and experimentally [9, 10]. According to our observations and hypothesis [22] on the role of nitrogen in formation of carbon cyclic-chain structures, we chose nitrogen-containing polysaccharides, chitin and chitosan.

Based on the studies on carbonization of polyimides and their reactions with polymers in a wide temperature range (20–1000°C) in various gaseous media and at various temperature–time modes of thermal treatment, we can postulate the following principles of thermal reactions of polymers (cocarbonization).

(1) Performing cocarbonization in the temperature range in which the reacting polymers exhibit the highest thermal activity (thermal degradation, cross-linking).

(2) Providing conditions favorable for mutual thermochemical cross-linking of polymers.

(3) Using polymers tending to ring formation on the level of polycarbo- and heterocycles.

(4) Using catalytic polymerization and polycondensation applied in chemistry of heat-resistant macromolecular compounds.

(5) Taking into account steric orientation of macromolecules for realization of intermolecular bonds.

The pairs of polymers polyacrylonitrile–chitin and polyacrylonitrile–chitosan, chosen as an example, in their thermochemical characteristics meet the formulated requirements. The DSC curves of the initial polymers PAN and chitin and their blends in various modifications are shown in Fig. 2. It is seen that each of the compounds studied shows the highest thermal reactivity in the same temperature range, 250–400°C (first principle), and thermal effects of formation of carbonizates through interpolymeric complexes suggest the presence of structures different from those of the initial polymers. The TGA data of the same samples (Fig. 3) suggest formation of cocarbonizates (curves *3, 4*) with CR close to that of polyacrylonitrile (70–80%), i.e., the second principle of the cocarbonization concept is realized.

The structure of the initial polymers corresponds to the third principle of the concept. It is well known that in heating the dominating reaction of PAN cross-linking is cyclization, and the initial chitin and chitosan contain glucopyranose rings opening in the above temperature range (250–400°C). In addition, spatial organization of the PAN polymers used is energetically and sterically favorable for their intermolecular interaction (realization of the fifth principle). As regards fourth principle of the concept, it is manifested in the difference in the thermochemical activity of PAN samples synthesized by the radical and anionic mechanisms of acrylonitrile polymerization [22].

The experiments on cocarbonization of polyacrylonitrile with chitin and chitosan and also model studies of the heat resistance and carbonization of cyano derivatives of cellulose [23, 24] confirmed once again the special role of nitrogen atoms in formation of cyclic carbon structures in the early stage of carbonization of nitrogen-containing polymers.

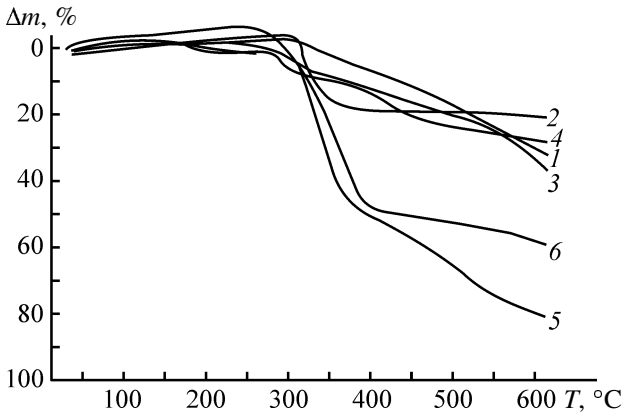


Fig. 3. TG curves for the samples of PAN, chitin, and PAN + chitin film prepared from DMF. The experimental conditions and legend are the same as for Fig. 2.

Thus, the use of the suggested concept of cocarbonization of polymers can promote development and application of new carbon materials.

CONCLUSIONS

(1) A concept of formation of carbon composites, termed cocarbonization of polymers, was suggested. This concept is based on realization of thermochemical reactions of reacting polymers in the range of temperatures of their maximal thermal activity.

(2) The basic principles of cocarbonization are close coincidence of the temperature boundaries of heat resistance, reactions in the diffusion area, and prolonged period of thermal treatment under isothermal conditions.

REFERENCES

1. Bessonov, M.I., Koton, M.M., Kudryavtsev, V.V., and Laius, L.A., *Poliimidy – klass termostoikikh polimerov* (Polyimides: Class of Heat-Resistant Polymers), Leningrad: Nauka, 1983.
2. Koton, M.M. and Sazanov, Yu.N., *Nauka Chelov*., 1986, pp. 278–290.
3. Sazanov, Yu.N., *Zh. Prikl. Khim*., 2001, vol. 74, no. 8, pp. 1217–1234.
4. Sroog, C.E., Endrey, A.I., Abramo, S.V., et al., *J. Polym. Sci., Ser. A*, 1996, vol. 34, no. 11, pp. 2069–2086.

5. Rusanov, A.L., Stadnyuk, T.A., and Müllen, K., *Usp. Khim.*, 1999, vol. 68, no. 8, pp. 760–772.
6. Miichenko, I.P., Mikhailin, Yu.A., and Kostychenko, V.N., *Tekhnol. Konstr. Kompoz. Mater.*, 2000, no. 1, pp. 30–35.
7. Goykhman, M.Ya., Svetlichnyi, V.M., Kudryavtsev, V.V., et al., *Polym. Eng. Sci.*, 1997, vol. 37, no. 8, pp. 1381–1386.
8. Gribanov, A.V. and Sazanov, Yu.N., *Zh. Prikl. Khim.*, 1997, vol. 70, no. 6, pp. 881–902.
9. Fialkov, A.S., *Uglerod, mezhsloevye soedineniya i kompozity na ikh osnove* (Carbon, Intercalation Compounds, and Composites Based on These), Moscow: Aspekt, 1997.
10. Perepelkin, K.E., *Khim. Volokna*, 2003, no. 6, pp. 3–8.
11. Gribanov, A.V., Sazanov, Yu.N., Beloborodova, E.V., and Fedorova, G.N., *Zh. Prikl. Khim.*, 1999, vol. 72, no. 3, pp. 467–473.
12. Gribanov, A.V. and Sazanov, Yu.N., *Zh. Prikl. Khim.*, 2000, vol. 73, no. 3, pp. 465–469.
13. Gribanov, A.V. and Sazanov, Yu.N., *Zh. Prikl. Khim.*, 2000, vol. 73, no. 6, pp. 987–991.
14. Gribanov, A.V. and Sazanov, Yu.N., *Zh. Prikl. Khim.*, 2000, vol. 73, no. 10, pp. 1705–1709.
15. Sazanov, Yu.N., *Zh. Prikl. Khim.*, 2002, vol. 75, no. 1, pp. 98–102.
16. Sazanov, Yu.N., Artem'eva, V.N., Mikhailov, G.M., *et al.*, *Zh. Prikl. Khim.*, 1999, vol. 72, no. 6, pp. 975–982.
17. Gribanov, A.V., Mokeev, M.V., and Sazanov, Yu.N., *Zh. Prikl. Khim.*, 2002, vol. 75, no. 9, pp. 1513–1516.
18. Sazanov, Yu.N., *J. Therm. Anal.*, 1990, vol. 36, no. 2, pp. 361–376.
19. Sazanov, Yu.N., Spirina, T.N., Shibaev, L.A., et al., *J. Therm. Anal.*, 1990, vol. 36, no. 12, pp. 2329–2338.
20. Kosterova, T.A., Sazanov, Yu.N., Shibaev, L.A., and Stepanov, N.G., *Vysokomol. Soedin., Ser. A*, 1991, vol. 33, no. 11, pp. 2392–2397.
21. Sazanov, Yu.N., Kosterova, T.A., Stepanov, N.G., et al., *Vysokomol. Soedin., Ser. B*, 1994, vol. 36, no. 9, pp. 1563–1567.
22. Sazanov, Yu.N., Novoselova, A.V., Amsharov, K.Yu., et al., *Zh. Prikl. Khim.*, 2005, vol. 78, no. 5, pp. 810–814.
23. Sazanov, Yu.N., Nud'ga, L.A., Petrova, V.A., et al., *Zh. Prikl. Khim.*, 2004, vol. 77, no. 8, pp. 1366–1369.
24. Sazanov, Yu.N., Kutsenko, L.I., and Novoselova, A.V., *Zh. Prikl. Khim.*, 2005, vol. 78, no. 4, pp. 652–654.

ISSN 1070-4272. Russian Journal of Applied Chemistry, 2006, Vol. 79, No. 3, pp. 439–444. © Pleiades Publishing, Inc., 2006.
Original Russian Text © E.N. Popova, V.E. Yudin, N.V. Kukarkina, T.A. Kostereva, I.V. Gofman, V.V. Kudryavtsev, 2006, published in Zhurnal Prikladnoi Khimii, 2006, Vol. 79, No. 3, pp. 446–451.

MACROMOLECULAR CHEMISTRY AND POLYMERIC MATERIALS

Heat-Resistant Foamed Organoplastics Based on a Combination of Polyimide Felt, Polyimide Binders, and Montmorillonite Nanoparticles

E. N. Popova, V. E. Yudin, N. V. Kukarkina, T. A. Kostereva, I. V. Gofman, and V. V. Kudryavtsev

Institute of Macromolecular Compounds, Russian Academy of Sciences, St. Petersburg, Russia

Received December 7, 2005

Abstract—A series of foamed organoplastics based on a combination of foamed fully aromatic polyimide binders and Arimid T polyimide felt were prepared. New composite foamed organoplastics reinforced with montmorillonite nanoparticles were prepared using commercially available aromatic monomers.

DOI: 10.1134/S1070427206030219

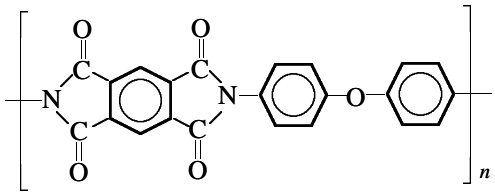
The preparation of strong and light heat-resistant structural materials is one of the most urgent problems of modern engineering. Among these materials the most promising are polymeric composites based on a combination of continuous carbon or organic fibers with heat-resistant polymeric binders. The density of these materials, depending on the kind of filler and its volume fraction, varies, as a rule, from 1100 to 1500 kg m^{-3}. The progressively growing industrial application of highly thermostable composite materials allowed the development of power and fuel-saving technologies and light-weight installations. These materials are successfully used in aircraft industry, ship building, and automobile construction [1].

A great body of data on nanocomposite materials based on a polymeric matrix reinforced with inorganic nanofillers, in particular, montmorillonite (MMT), were published in the last decade. The montmorillonite lamellar structure consists of aluminosilicate layers with a thickness not exceeding 1 nm. Owing to good mechanical and barrier characteristics and high refractoriness [2, 3], composites of this kind are of great scientific and practical interest.

In this study we attempted to prepare lighter polymeric composites based on a combination of polyimide felt and elastic foamed polyimide binder [4–6]. These materials have density ranging from 200 to 500 kg m^{-3}. Their strength and elasticity exceed those of modern foamed polyimides developed in the United States (Skybond, Illmid, Solymide) [7, 8] and of EPPI foamed polyimide produced in Russia [9]. The foamed composites can be prepared with equipment commonly used for preparing carbon-reinforced and organoplastics [10]. It is believed that in future these organoplastics can find wide technical application as efficient heat shielders and light, strong, and nonflammable structural materials [11].

EXPERIMENTAL

In this study the influence of the chemical structure of polyimide binders on the thermomechanical characteristics of foamed composites was examined for foamed composites based on a combination of various polyimide binders (Table 1) and Arimid T polyimide felt prepared from wastes from production of Arimid T polyimide fiber.



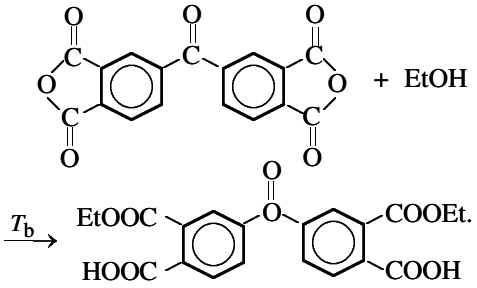
The use of polyimide binders in combination with polyimide fibers of similar chemical and structural type in preparing foamed composites ensures their efficient mutual adhesion and high integrity of the final material. The foamed polyimide binders were prepared from commercially available monomers widely used in production of polyimides: 3,3',4,4'-benzophenonetetracarboxylic acid dianhydride (BP), 3,3',4,4'-(diphenyl

Table 1. Thermomechanical characteristics of foamed composites based on polyimide H complexes

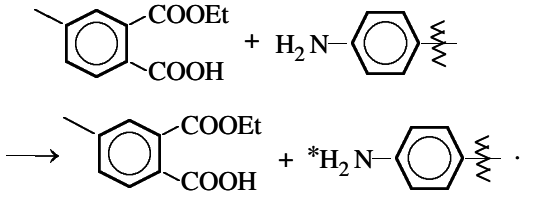
Sample no.	H complex	Solvent	Bending strength, MPa	Modulus of elasticity, MPa		Glass transition point T, °C	Density, kg m^{-3}
				in compression	in shear		
1	BP : *m*-PDA : DADPE	C_2H_5OH	15 ± 3	54	100	235	530
2		C_2H_5OH/H_2O	25 ± 6	176	213	240	530
3	BP : *m*-PDA : DADPM	C_2H_5OH	25 ± 4	159	110	245	520
4		C_2H_5OH/H_2O	2 ± 7	210	198	260	570
5	DPO : *m*-PDA : DADPM	C_2H_5OH	35 ± 5	179	126	236	500
6		C_2H_5OH/H_2O	30 ± 4	180	186	244	500
7	DP : *m*-PDA : DADPM	C_2H_5OH	14 ± 1	155	127	256	520
8	DPO : *m*-PDA : DADPE	C_2H_5OH/H_2O	36 ± 1	213	208	238	520

oxide)tetracarboxylic acid dianhydride (DPO), 3,3',4,4'-diphenyltetracarboxylic acid dianhydride (DP), 4,4'-diaminodiphenylmethane (DADPM), 4,4'-diaminodiphenyl ether (DADPE) and *m*-phenylenediamine (*m*-PDA). Ethyl alcohol and, in some cases, alcohol–water mixtures were used as solvents. It is known that polyimide foamed composites are formed by thermal imidization of H complexes of 3,3',4,4'-(diphenyl oxide)tetracarboxylic acid diesters with aromatic diamines. The chemical reactions and procedures for preparing the initial H complexes were thoroughly analyzed in [12]. The simplified scheme of this process includes three main steps.

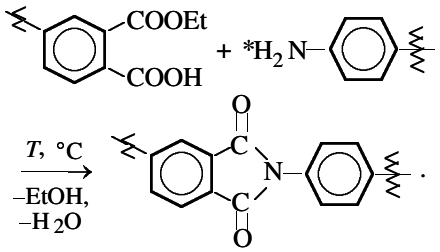
(1) Preparation of 3,3',4,4'-benzophenonetetracarboxylic acid diester (BPE) by esterefication of 3,3',4,4'-benzophenonetetracarboxylic acid dianhydride (BP) with alcohol in solution:



(2) Preparation of H complex of BPE with diamine in the cooled solution.



(3) Conversion of H complexes into polyimide by thermal imidization. In this step, the volatile products (water, alcohol) are evolved to form a porous structure of foamed composite:



To optimize the conditions for preparing foamed composites and ensure efficient impregnation of the prepreg, we studied the rheological features of H complexes. The viscosity of the molten H complexes was measured on a PIRSP flowmeter [13] of cone-plane type (angle at cone apex 1°, cone diameter 40 mm) at 95°C at a constant shear rate of 0.013 s^{-1}. Figure 1a shows the time dependence of viscosity of several molten H complexes prepared under identical conditions in 10% solution of water in ethanol. Comparison of curves *1–3* (Fig. 1) shows how the dianhydride structure affects the initial viscosity of the molten H complex and its subsequent thickening due to thermolysis. It is seen that H complexes under consideration show different impregnation capability. The H-complex based on DPO shows the lowest initial viscosity (approximately 300 Pa s) which in the first 20 min increases only slightly. On the contrary, the viscosity of molten H complex based on BP sharply increases with time. We suggest that this rheological behavior is caused either by structural (ordering of supramolecular structure of H complexes) or chemical (increase in molecular weight of polymer) reasons.

The structural hypothesis is consistent with the dependence of the viscosity of the molten H complexes on the shear rate in the range 0.02–100 s^{-1} (Fig. 1b). The larger slope in the plot of viscosity vs.

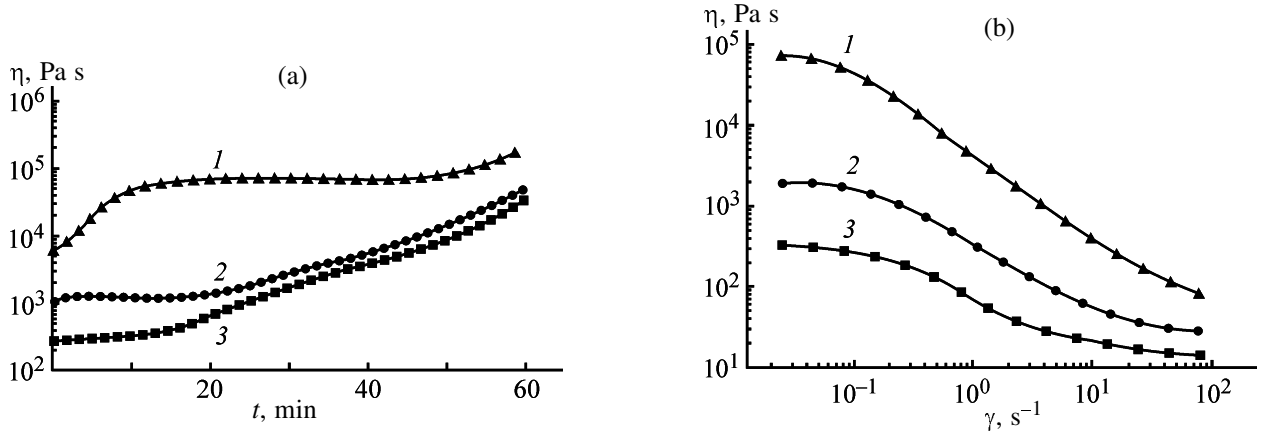


Fig. 1. Dependence of viscosity η of molten H complex on (a) time and (b) shear rate γ at 95°C. (*1*) BP : *m*-PDA : DADPM, (*2*) DP : *m*-PDA : DADPM, and (*3*) DPO : *m*-DPA : DADPM.

shear rate for H complex based on BP dianhydride is indicative of higher ordering of its supramolecular structure at 95°C. At the highest shear rate (about 100 s^{-1}), the viscosity of all the molten H complexes becomes close. We believe that this effect is caused by the fact that the shear stress breaks the supramolecular structure of H complexes. Our results show that only the H complex based on DP allows efficient impregnation of felt at relatively low temperature because this H complex remains low-viscous (~300 Pa s at 95°C) during sufficiently long time (20 min).

The preparation of foamed composite involves two main stages: (1) Preparation of a prepreg based on a combination of polyimide felt and H complex and (2) preparation of foamed composite by hot pressing. A prepreg is prepared by impregnating felt with a molten H complex. This procedure is carried out as follows. An H complex powder is uniformly applied to the felt surface by electrostatic deposition. This intermediate product is placed on an electric plate heated to 120–140°C and rolled for several seconds to ensure uniform distribution of the molten H complex throughout felt. The resulting prepreg is a flexible material suitable for packing into molds. The weight ratio of the H complex and felt in the prepreg is 1 : 1. The multilayer prepreg is packed into a mold of appropriate configuration. The mold is hermetically sealed and placed between slabs of a heated press. Hot pressing is provided by the internal pressure developed in the foaming binder. Therefore, with hermetically sealed molds, a foamed composite can be prepared by heating a prepreg in a thermostat (without external pressure) at 200–220°C for 1–2 h.

This mode of curing and foaming polyimide binders was chosen taking into account that these conditions ensure the maximal degree of imidization for the majority of H complexes. The resulting foamed organoplastics have increased heat-insulating characteristics and high heat resistance. The density of these foam composites can be varied by varying both the degree of felt impregnation with H complex and the number of prepreg layers in a mold. In this study we used four-layered prepreg packing ensuring the preparation of foam composites with approximately equal density of 500 kg m^{-3}.

The failure surface of foamed composites in the zone of its bending was examined with a scanning electron microscope (SEM, Cambridge S-200, the United States). The electron-microscopic pattern of the surface of a foamed composite based on H complex BP : *m*-PDA : DADPM subjected to triple-point bending is shown in Fig. 2. The electron micrograph (Fig. 2c) distinctly shows the porous structure of the composite and uniform distribution of Arimid T fibers throughout the polymeric matrix. Figure 2d shows that the fiber–matrix interface contains specific stitches causing the efficient adhesion. We believe that these interface interactions are responsible for high strength and elasticity of the foamed composite.

The bending tests were carried out with three-point bending technique on a 1958 U-10-1 tensile-testing mashine (distance between supports 30 mm). The tested plates of the foamed composite were 4–5 mm thick and 10 mm wide. The loading rate was 5 mm min^{-1}.

The compression tests of foamed composites was carried out under uniaxial compression on a UTS-10 (Gemany) universal mechanical testing installation. The tested samples were square prisms of 10×10 mm base and 8.5–8.7 mm height. The modulus of elasticity in compression was determined from the initial portion of the loading diagram. The modulus of

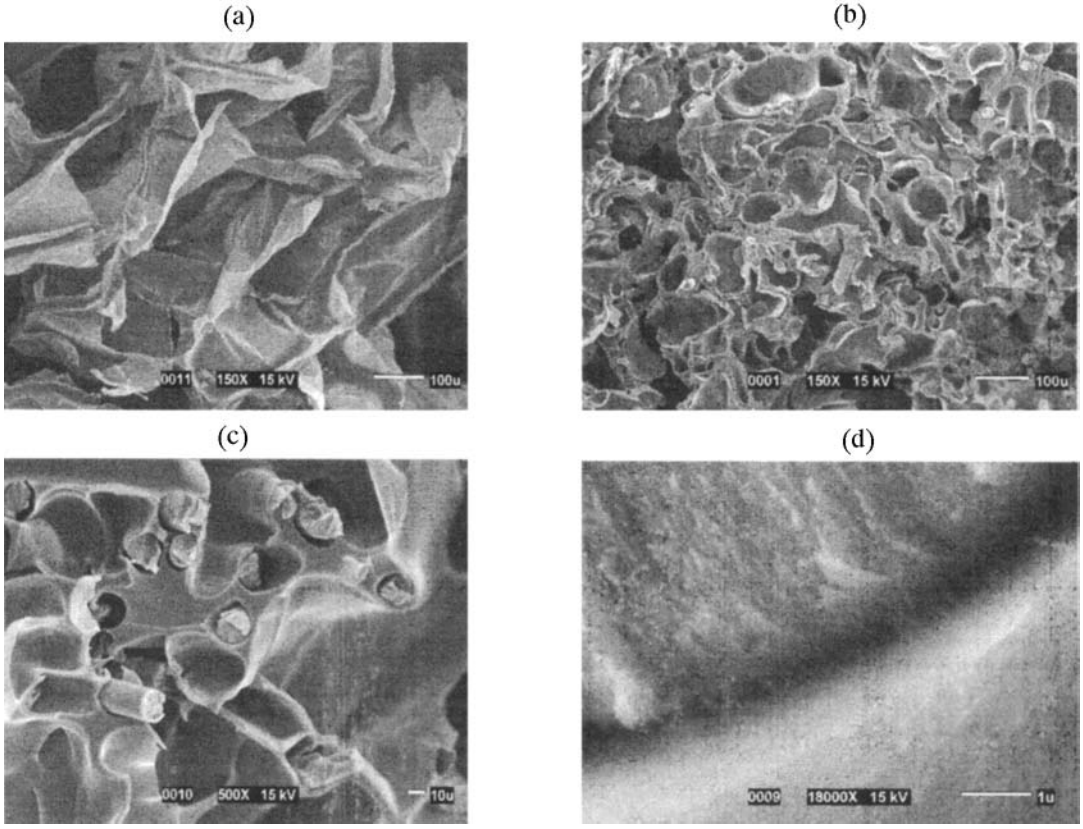


Fig. 2. Electron-microscopic patterns of the failure surface of foamed composites based on BP : *m*-PDA : DADPM H complex. (a) Initial foam and (b–d) failure surface of foamed composite. Magnification: (a, b) × 150, (c) × 500, and (d) 18000.

elasticity in shearing G' and the modulus of shear loss G'' were determined in the temperature range 20–400°C by a method based on free attenuation of torsion vibrations of an MK-003 torsion pendulum developed at the Institute of Macromolecular Compounds, Russian Academy of Sciences. The tested samples were plates of 3 mm thickness, 10 mm width, and 40 mm length. The glass transition point T_g of foamed composites was determined as the temperature corresponding to maximal modulus of shear loss G''. The density of foamed compositions was determined gravimetrically.

The main thermomechanical characteristics of the tested foamed composites are listed in Table 1. These data show that the strength of foamed composites prepared with the H complex based on DPO (sample nos. 5, 6, 8) exceeds that of the foamed composites prepared with the H complex based on BP (sample nos. 1–4). Another advantage of foamed composite based on DPO is decreased softening point. It should be noted that, in a bending test, the foamed composites based on DPO, owing to their higher elasticity, were not broken but only bended. We believe that the better mechanical properties of foamed composites based on DPO dianhydride are mainly due to more efficient impregnation of the felt with molten H complex based on this polyimide binder.

It was found that, in synthesis of foamed composites, the toxic DADPM can be replaced by less toxic and commercially available DADPE [14]. Table 1 shows (sample nos. 6, 8) that this substitution does not deteriorate the mechanical characteristics of foam composites prepared with H complexes based on BPE with addition of water (10 vol %). The composite based on DP (Table 1, sample no. 7) has lower bending strength than the composites based on DPO and BP. At the same time, introduction of DP into the foamed composite matrix considerably increases the glass transition point T_g (Fig. 3).

The optimal thermochemical properties are exhibited by the foamed composite based on DPO : *m*-PDA : DADPE H complex (Table 1, sample no. 8). This composite was subjected to modification with montmorillonite nanoparticles to elucidate their effect on thermomechanical characteristics. Two kinds of

Table 2. Thermomechanical characteristics of foamed composites based on a combination of polyimide H complexes with montmorillonite nanoparticles

Sample no.	H complex	Bending strength, MPa	Modulus of elasticity, MPa		Glass transition point T, °C	Density, kg m^{-3}
			in compression	in shear		
1	BPO : *m*-PDA : DADPE	36 ± 1	213	208	238	520
2	BPO : *m*-PDA : DADPE + 5% MMT	29 ± 1	229	282	238	500
3	DPO : *m*-PDA : DADPE + 5% MMT 15A	17 ± 1	62	123	240	367
4	DPO : *m*-PDA : DADPE + 10% MMT	27 ± 1	264	223	241	505
5	DPO : *m*-PDA : DADPE + 10% MMT 15A	26 ± 1	147	132	241	508

* Solvent C_2H_5OH/H_2O.

montmorillonite were used: (1) untraeated montmorillonite in the Na form and (2) commercially available montmorillonite treated with a quaternary ammonium salt MMT 15A (Cloisite 15A, Southern Clay Products).

In preparation of foamed composites modified with montmorillonite nanoparticles, the latter were introduced under ultrasonic treatment (a Sapfir ultrasonic generator, 40 kHz, 1.5 h, room temperature) into the reaction mixture in an amount of 5 or 10 wt % after completion of formation of H complex.

Thermomechanical characteristics of foamed polyimide composites modified with montmorillonite are listed in Table 2. These results show that introduction of montmorillonite significantly affects the properties of foamed polyimides. The addition of montmorillonite, depending on its kind and content, differently influence the particular thermomechanical properties.

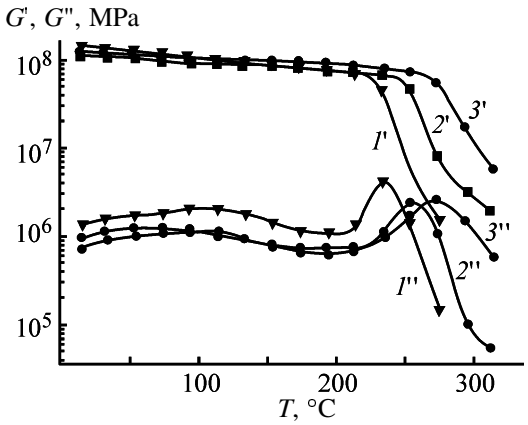


Fig. 3. Temperature dependence of the (*1'–3'*) modulus of elasticity in shear G' and (*1"–3"*) modulus of shear loss $G"$ of foamed composites based on a combination of Arimid T polyimide felt and H complexes based on diamines *m*-PDA and DADPM and dianhydrides. Dianhydride: (*1'*, *1"*) DPO, (*2'*, *2"*) BP, and (*3'*, *3"*) DP.

In our compression tests, the maximal accessible pressure was 90 MPa. Under this pressure, all the samples maintained their integrity. With increasing montmorillonite content from 5 to 10 wt %, the modulus of elasticity in compression of foamed composites modified with untreated montmorillonite increases (Table 2, sample nos. 2, 4). At the same time, the three-point bending test did not show increase in the bending strength. We believe that this result is caused by the fact that the rigid inorganic montmorillonite nanoparticles accumulate stresses, and, as a result, make the composites more brittle. This hypotheses is confirmed by easier brittle failure of the composite modified with nanoparticles as compared to the initial composite (Table 2, sample 1). In shear tests, the modulus of elasticity somewhat increased but only for the composites modified with the untreated montmorillonite (Table 2, samples 2, 4). The addition of montmorillonite did not affect the softening point of the foamed composites.

In contrast to untreated montmorillonite (MMT), MMT 15A nanoparticles exert a plasticizing effect on the foamed composite: the modulus of elasticity in compression decreases by a factor of 4 as compared to initial sample. This modulus somewhat increases with increasing MT concentration to 10% but, nevertheless, remains considerably lower than that of the initial sample. Thus, modification of the foamed composite with untreated montmorillonite MMT is preferable, since this treatment increases the modulus of elasticity, i.e., rigidity.

CONCLUSIONS

(1) Organoplastics of a new kind, based on a combination of foamed polyimide binders and Arimid T polyimide felt, were prepared using commercially available aromatic monomers.

(2) The H complex based on 3,3',4,4'-(diphenyl oxide)tetracarboxylic acid melts to form low-viscous liquid whose viscosity at 95°C remains low and practically constant (300 Pa s) for 20 min.

(3) Thermomechanical characteristics of foamed composites prepared with H complex based on 3,3',4,4'-(diphenyl oxide)tetracarboxylic acid dianhydride exceed those of foamed composites based on 3,3',4,4'-benzophenonetetracarboxylic acid dianhydride by a factor of 1.5. In bending test, the composites based on 3,3',4,4'-(diphenyl oxide)tetracarboxylic acid bend without failure, which makes them promising for preparing new flexible foamed materials.

(4) Modification of foamed polyimide composites with montmorillonite nanoparticles, particularly with untreated montmorillonite, increases their rigidity.

ACKNOWLEDGMENTS

This study was financially supported by the Russian Foundation for Basic Research (project nos. 04-03-32470-a, 04-03-81005-Bel2004-a).

REFERENCES

1. Gagliani, J. and Supkis, D.E., *Acta Austronaut*., 1980, vol. 7, pp. 653–683.
2. Nardo, N.J.Di, *Nanoscale Characterization of Surfaces and Interfaces*, Weinheim: VCH, 1994.
3. Vaia, R.A., Tolle, T.B., Schmitt, G.F., et al., *SAMPE J*., 2001, vol. 37, no. 6, p. 24.
4. Cook, B.A., Yudin, V.E., and Otaigbe, J.U., *J. Mater. Sci. Lett*., 2000, no. 19, pp. 1971–1973.
5. Artem'eva, V.N., Chupano, P.I., Smirnova, E.A., et al., *Zh. Prikl. Khim*., 1990, vol. 63, no. 3, pp. 655–660.
6. Artem'eva, V.N., Kudryavtsev, V.V., Kukarkin, E.N., et al., *Plast. Massy*, 1990, no. 4, pp. 32–34.
7. US Patent 4539336.
8. Serlin, H., Makhart, A.H., and Lavin, E., *Mod. Plast*., 1970, vol. 47, no. 7, pp. 120–122.
9. RF Patent 1824885.
10. Otaigbe, J.U., Yudin, V.E., and Artem'eva, N.N., *Polym. Compos*., 2001, vol. 22, no. 1, pp. 155–164.
11. RF Patent 2081134.
12. Kostereva, T.A., Artem'eva, V.N., Kukarkina, N.V., et al., *Zh. Prikl. Khim*., 2001, vol. 74, no. 1, pp. 118–121.
13. Vinogradov, G.V., Malkin, A.Ya., Plotnikova, E.P., et al., *Vysokomol. Soedin., Ser. A*, 1978, vol. 20, no. 2, pp. 226–230.
14. Artem'eva, V.N., Kostereva, T.A., Kukarkina, N.V., et al., *Zh. Prikl. Khim*., 2002, vol. 75, no. 12, pp. 2036–2041.

ISSN 1070-4272. Russian Journal of Applied Chemistry, 2006, Vol. 79, No. 3, pp. 445–447. © Pleiades Publishing, Inc., 2006.
Original Russian Text © S.V. Ivanov, V.V. Trachevskii, N.V. Stolyarova, L.A. Zozulya, 2006, published in Zhurnal Prikladnoi Khimii, 2006, Vol. 79, No. 3, pp. 452–454.

MACROMOLECULAR CHEMISTRY AND POLYMERIC MATERIALS

Plasmochemical Modification of Polymer Surfaces

S. V. Ivanov, V. V. Trachevskii, N. V. Stolyarova, and L. A. Zozulya

National Aircraft University, National Academy of Science of Ukraine, Kiev, Ukraine

Received December 13, 2005

Abstract—Influence of low-temperature plasma on the polymer surface was studied with the aim of preparing polymers with required surface properties.

DOI: 10.1134/S1070427206030220

The surface properties of most of polymers, even with a high level of bulk physicomechanical parameters, do not meet the industrial, especially aviation, requirements. Polymer composites based on polyurethanes find expanding application. The composites with required performance can be prepared by variation of the polyurethane formulation and by introduction of modifying additives [1–4].

Since urethane formation in a multicomponent system is a complex process, the performances of polyurethanes of different batches, even produced by the same procedures, can differ essentially. In addition, for each particular polyurethane, the composition of the reaction mixture and the type of modifying additive should be optimized.

A feasible procedure for modifying the structure and hence for altering the performances of polymer composites is radiochemical treatment.

Under exposure to ionizing radiation, polymer composites undergo chemical transformations including cross-linking, degradation, and oxidation, which change their physicomechanical parameters. These changes can be negative or positive depending on the radiation dose and the macromolecular structure.

Polymer composites can be modified in a low-temperature plasma [5–10].

A gas-discharge low-temperature plasma affects only the surface layer of a polymer and hence affects bulk physicomechanical properties of the polymer as whole to a lesser extent then do other kinds of radiation. However, the surface transformations of the polymer treated with a low-temperature plasma are stronger. Therefore, treatment of a polymer composite with a low-temperature plasma modifies the surface properties of a composite and has virtually no effect on its main physicomechanical parameters.

Here we studied the effect of a low-temperature gas-discharge plasma on the surface properties of polyurethane composites.

EXPERIMENTAL

We studied a polyurethane composite containing saponified vinyl chloride–vinyl acetate copolymer, urethane prepolymer, and triisocyanate.

The treatment with a low-temperature plasma was performed on a UVN-2M-1 standard vacuum unit. A quartz cylinder 60 mm in diameter was used as the reaction chamber. The reaction chamber was equipped with side inlets for feeding the reaction gas directly in the discharge area. To renew the gas phase in the reactor, its was continuously pumped off through face slits.

A standard generator with a carrier frequency of 40.68 MHz was used as an ac source for the plasma discharge. The maximal power was obtained by varying the output resistance.

The structural transformations of the surface of the polyurethane composites were studied by IR multiple attenuated total internal reflection spectroscopy (IR MATIR), electron microscopy, and NMR. The surface properties of the polyurethane composites were determined from the changes in their adhesion and triboadhesion parameters.

The MATIR spectra were recorded using a conventional unit containing KRS-5 crystals (14 reflections). The apparent thickness of the examined layer calculated by the known equation was 3–5 μm. The electron microscopic studies were performed on an elec-

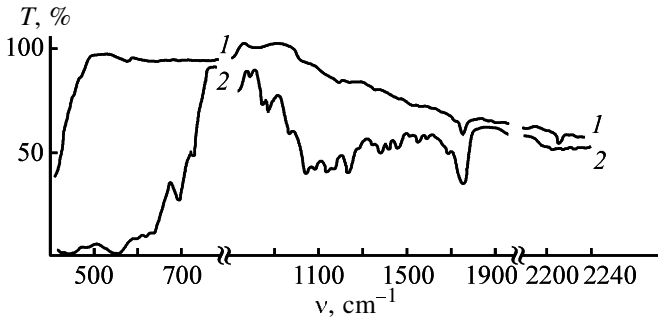


Fig. 1. IR MATIR spectra of the (*1*) initial and (*2*) modified polyurethane composite. (*T*) transmission and (ν) wavenumber.

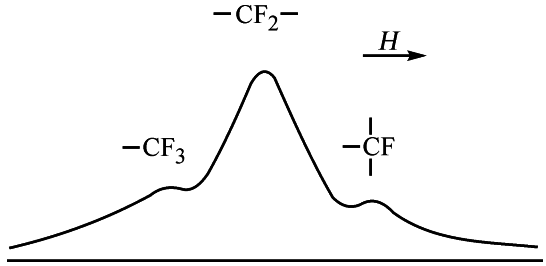


Fig. 2. NMR spectrum of plasmochemically obtained polytetrafluoroethylene.

tron scanning microscope. To increase the picture contrast, a 0.03-μm gold layer was sprayed on the sample surface.

The adhesion was determined as tangential shear strength required for rupture of the adhesion bonds of the polyurethane composite with a model support. These measurements were performed on a special strain-gage unit.

The triboadhesion properties of the polyurethane composites were determined as a change in the transportation strength (F_i and F_f are the initial and final strengths, respectively) as influenced by the number of the passage cycles relative to a stationary counterbody. These experiments were performed on a tribometer under normal (NCC: 40% humidity and 25°C) and extreme (ECC: 98% humidity and 40°C) climatic conditions.

It is known that organic monomers polymerize in a gas-discharge plasma to form cross-linked polymers strongly bound to the support surface.

Plasma polymerization on electrodes was extensively studied. The conditions of plasma polymerization on a polyurethane composite film fixed in the middle of the interelectrode space were studied. To deposit a uniform film, we used a mobile support compensating the nonuniformity of the gas-discharge plasma. The initial monomer was tetrafluoroethylene. We suggested that the antifriction properties of the polymer deposited in plasma from this monomer would be similar to those of Teflon.

Treatment of polyurethane composites in a low-temperature plasma in the presence of tetrafluoroethylene yields a 0.3–0.8-μm film on the support surface. The IR MATIR spectra (Fig. 1) of this coating contain the strong $–CF_2–$ bands at 680, 740, 1242, and 1380 cm^{-1}. In addition, the bands of –CF=, –CF=CF–, $–CF_3$, and SiF_6^{2-} groups were observed at 1230, 1789, 1640, and 540 cm^{-1}, respectively.

These data show that plasma-deposited polytetrafluoroethylene is cross-linked and its structure differs from that of polytetrafluoroethylene formed by polymerization of the double bonds. The branching and cross-linked fragments of the polymer contain the ≡CF groups. The degree of branching and the content of cross-links in the plasma-deposited polymer can be estimated from the content of $–CF_2–$ and ≡CF groups.

Under conditions of gas-discharge polymerization of tetrafluoroethylene, the ≡CF group can be formed without rupture of the C–F bond. This fact suggests that the polymerization involves both addition to the double bonds and rupture of the CF bond. The rupture of this bond is confirmed by the presence of the SiF_6^{2-} band (540 cm^{-1}) in the spectra of the examined polymers. This groups is formed by reaction of fluorine atoms with the glass walls of the reaction chamber.

These data agree well with the results of an ESCA study of plasma-deposited organofluorine polymers [5].

It should also be noted that the band of urethane groups at 1750 cm^{-1} in the spectrum of the polyurethane composites modified in gas-discharge plasma contains a shoulder at 1700 cm^{-1} which can be assigned to CO···HCF hydrogen bonds. This suggests that the plasma-deposited polymer is grafted to the polyurethane matrix.

Our electron microscopic studies show than the surface structure of the polyurethane composite changes after the plasmochemical treatment. The surface of the initial polyurethane composite is loose and highly porous. The number of pores on unit surface is 20 and more; the pore size is 0.7×0.7 μm^2. The surface porosity of the polyurethane composite decreases after the plasmochemical treatment: the number of pores on unit surface decreases to 8 and the pores become narrower: 0.4×0.3 μm^2. This is due to formation of polytetrafluoroethylene film on the composite surface.

The IR and NMR spectra (Fig. 2) of the plasma-deposited coatings show that the polymer with the

Adhesion and triboadhesion properties of polyurethane composites

Sample	Adhesion, N	Triboadhesion					
		NCC			ECC		
		N	F_i, N	F_f, N	N	F_i, N	F_f, N
Initial	2.31	335	1.0	>2, sticking	90	1.2	2.0
Modified	1.32	>4500	1.0	1.26	>1500	1.0	1.2

* F_i and F_f are the initial and final shear strengths, respectively.

maximal content of $-CF_2-$ groups is formed by plasma polymerization of tetrafluoroethylene under the best conditions. As the power increases, the content of the ≡CF groups increases owing to formation of strongly cross-linked polymer. The low fluorine content (C/F ratio) in the polyfluorinated polymer prepared under these conditions substantially decreases its hydrophobicity, which affects the physicochemical (adhesion and triboadhesion) properties of the polymer [6, 8]. In particular, the adhesion of the polyfluorinated polymer to the composite is lower. The wetting angle of water on the surface of the film deposited on the polyurethane composite by plasma polymerization of tetrafluoroethylene under the best conditions is 82°, whereas for the polymer film deposited at a high discharge power (low F/C ratio) this angle is as low as 78°C.

The adhesion and triboadhesion properties of the initial polyurethane composites and the composites modified in gas-discharge low-temperature plasma are presented in the table.

As seen from the table, the adhesion and triboadhesion properties of the polyurethane composite are improved after plasmochemical modification, with the physicomechanical parameters remaining the same.

CONCLUSION

The surface properties of the polyurethane composite can be modified by treatment in gas-discharge low-temperature plasma. The physicochemical properties of the composite which determine its performances remain within the required range.

REFERENCES

1. Lipatov, Yu.S. and Sergeeva, L.M., *Vzaimoproni-kayushchie polimernye setki* (Interpenetrating Polymer Networks), Kiev: Naukova Dumka, 1979.
2. Lipatov, Yu.S., *Fizicheskaya khimiya napolnennykh polimerov* (Physical Chemistry of Filled Polymers), Moscow: Khimiya, 1977.
3. Kercha, Yu.Yu., *Fizicheskaya khimiya poliuretanov* (Physical Chemistry of Polyurethanes), Kiev: Naukova Dumka, 1979.
4. Fedchenko, V.V., Makarova, M.A., and Tereshatov, A.V., Abstracts of Papers, *7-ya Vserossiiskaya nauchno-tekhnicheskaya konferentsiya "Aerokosmicheskaya tekhnika i vysokie tekhnologii-2004"* (7th All-Russian Scientific and Technical Conf. "Aerospace Engineering and High Technologies-2004"), Perm: Perm. Gos. Univ., April 12–14, 2004, p. 144.
5. Yasuda, H., *Plasma Polymerization*, Orlando: Academic Press, 1985.
6. Tkachuk, B.V., and Kolotyrkin, V.M., *Poluchenie tonkikh polimernykh plenok is gazovoi fazy* (Preparation of Thin Polymeric Films from the Gas Phase), Moscow: Khimiya, 1997.
7. Osada, I., *Vysokomol. Soedin., Ser. A*, 1988, vol. 30, no. 9, pp. 1815–1831.
8. Uhaxaku, N., *J. Vac. Sci. Technol.*, 1988, vol. 6, no. 3, pp. 1917–1928.
9. Hermen, D., Bruner, H., and Oehr, C., *Surf. Coat. Technol.*, 2003, vols. 174–175, pp. 253–260.
10. Gamplitskaya, S.A., D'yachkov, A.P., and Ryzhikov, I.A., Abstracts of Papers, *5-ya konf. ITTE OIVT Ross. Akad. Nauk* (5th Conf. of the Inst. of Theoretical and Applied Electrodynamics, Joint Inst. of High Temperatures, Russian Acad. Sci.), Moscow, March 29–April 1, 2004, pp. 18–19.

ISSN 1070-4272. Russian Journal of Applied Chemistry, 2006, Vol. 79, No. 3, pp. 448–452. © Pleiades Publishing, Inc., 2006.
Original Russian Text © O.A. Shamenkova, L.K. Mokeeva, N.A. Kopylova, Yu.D. Semchikov, 2006, published in Zhurnal Prikladnoi Khimii, 2006, Vol. 79, No. 3, pp. 455–459.

MACROMOLECULAR CHEMISTRY AND POLYMERIC MATERIALS

Synthesis of Amphiphilic Block Copolymers Polystyrene–*block*-Polyvinylpyrrolidone from Active Polystyrene

O. A. Shamenkova, L. K. Mokeeva, N. A. Kopylova, and Yu. D. Semchikov

Lobachevsky Nizhni Novgorod State University, Nizhni Novgorod, Russia

Received July 27, 2005

Abstract—A new method was developed for preparing amphiphilic block copolymers polystyrene–*block*-polyvinylpyrrolidone. The colloid-chemical properties of the copolymers were studied by probe microscopy and wetting. The possibility of modifying the properties of surfaces by the block copolymers synthesized and of preparing inverse emulsions based on them was demonstrated.

DOI: 10.1134/S1070427206030232

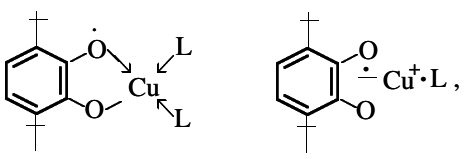
Pseudoliving radical polymerization allows preparation of block copolymers with controllable block length and narrow molecular-weight distribution [1]. However, this process is applicable only to a very limited range of monomers, primarily to so-called inactive monomers (monomers with no π–π conjugation).

Previously we prepared styrene–butyl methacrylate block copolymer based on active polystyrene (PS) containing at the chain end a copper semiquinolate complex activated by UV irradiation [2]. The goal of this study was to reveal the possibility of preparing by this method a block copolymer of styrene (ST) with an inactive water-soluble monomer, *N*-vinylpyrrolidone (VPD). This block copolymer is of doubtless practical interest because of its amphiphilic nature.

EXPERIMENTAL

The commercial monomers were additionally purified prior to use. Styrene was dried over anhydrous sodium sulfate, and VPD, over anhydrous KOH and CaH_2; 0.1 wt % toluene diisocyanate was added to bind the impurities. Then the monomers were distilled under reduced pressure (bp 35°C/0.8 kPa for ST and 78°C/2 kPa for VPD).

Polystyrene (PS) was prepared in the presence of a stable radical, bis(triphenylphosphino)(3,6-di-*tert*-butylbenzo-1,2-semiquinolato)copper(I) (SQCu):



where L is triphenylphosphine.

The SQCu concentration was 1.5×10^{-3} M. AIBN (10^{-2} M) was used as initiator. The mixtures were charged into ampules, deoxygenated by threefold freezing in liquid N_2–pumping–thawing, and the ampules were sealed off. Then the ampules were preheated at 70°C to completion of the induction period, cooled, placed in a thermostat, and UV-irradiated with a PRK lamp at 25°C. The polymerization was performed to 7% conversion. Polystyrene was purified by threefold reprecipitation with methanol from a chloroform solution and dried to constant weight. To perform block copolymerization, 5 wt % solutions of PS and VPD were placed in dilatometric ampules, degassed at a reduced pressure, and exposed to UV radiation at 25°C. The molecular-weight characteristics of the samples were determined by gel permeation chromatography on a Waters chromatograph equipped with a refractometric detector. The supramolecular structure of the polymers was examined by scanning probe microscopy with a Solver Bio NT-MDT device in the continuous mode; weighed portions of the polymers were dissolved in chloroform, the solutions were applied to clean silicon supports, and the specimens were dried at room temperature. The modification of a solid surface with the block copolymers synthesized was studied by the wetting method [3], with measuring the contact angle; a 0.035-g copolymer sample was dissolved in 10 ml of chloroform, and the solution was cast onto a silicon support. Water was used as wetting fluid.

The kinetic curve of VPD polymerization in the presence of active PS is shown in Fig. 1. The poly-

merization involved an induction period (170 min); the mean process rate was 2.2×10^{-5} mol l^{-1} s^{-1}. It should be noted that VPD does not spontaneously polymerize under these conditions. By the copolymerization we obtained two samples (7 and 17% conversion; samples I and II, respectively). Their composition was determined by the Kjeldahl method [4]. The mole fraction of VPD in samples I and II was 0.5 and 0.75, respectively.

Sample II was studied in the most detail. Sequential extraction with methanol and then with cyclohexane in a Soxhlet apparatus showed that this sample contained 2.3% PS, 30.8% polyvinylpyrrolidone (PVPD), and 66.0% block copolymer with the mole fraction of VPD units of 0.65. The following scheme of the block copolymerization can be suggested within the framework of the controlled chain propagation:

$$\text{P–(ST)}_n\text{–SQCu} \overset{h\nu}{\rightleftharpoons} \text{P–(ST)}_n^{\bullet} + \text{SQCu}$$

$$\overset{m\text{VPD}}{\rightleftharpoons} \text{P–(ST)}_n\text{–(VPD)}_m\text{SQCu}.$$

The VPD polymerization is initiated by absorption of a light quantum through reversible dissociation of the macromolecule–semiquinolate complex bond at the end of an active PS macromolecule [P–$(ST)_n$–SQCu(I)]. The PVPD block propagates on the thus generated radical until it recombines with the SQCu molecule.

Let us discuss the cause of formation of homopolymers under these conditions. A GPC analysis of sample II showed that the molecular-weight distribution of the polymer was unimodal; however, despite appreciable conversion, the weight-average molecular weight did not noticeably change relative to the starting active PS (Fig. 2). From the standpoint of pseudo-living block copolymerization, this fact can be attributed only to the parallel occurrence of photochemical degradation. Indeed, Figure 3 shows that, upon UV irradiation of PS in an inert solvent (benzene) for 9 h, the viscosity-average molecular weight of PS decreases by 30%. Irradiation of PVPD in methanol for the same time also decreases its molecular weight, but insignificantly. It was also shown that VPD polymerized upon UV irradiation at 25°C in the presence of PVPD at a rate of 4.9×10^{-4} mol l^{-1} s^{-1}; in the process, the viscosity-average molecular weight of PVPD increased from 96×10^3 to 270×10^3. As VPD does not spontaneously polymerize upon UV irradiation, it can be assumed that the polymerization of VPD is initiated by photochemical degradation of PVPD

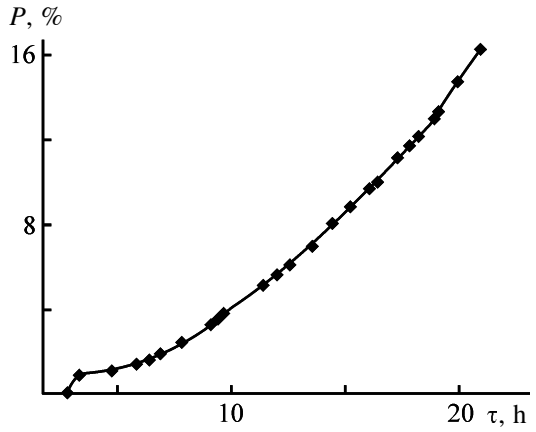


Fig. 1. Conversion P of VDP as a function of time τ in the UV-induced block copolymerization with PS (25°C, PS concentration 5%).

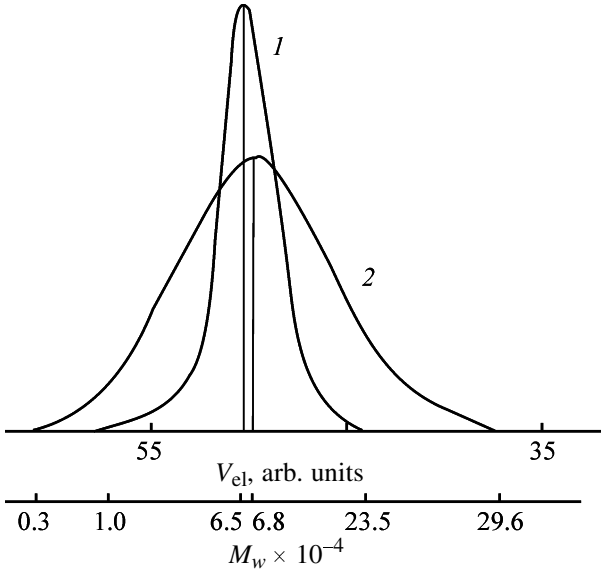


Fig. 2. Gel chromatograms of the (*1*) initial macroinitiator PS and (*2*) product of block copolymerization (sample II). (V_{el}) Eluent volume and (M_w) weight-average molecular weight.

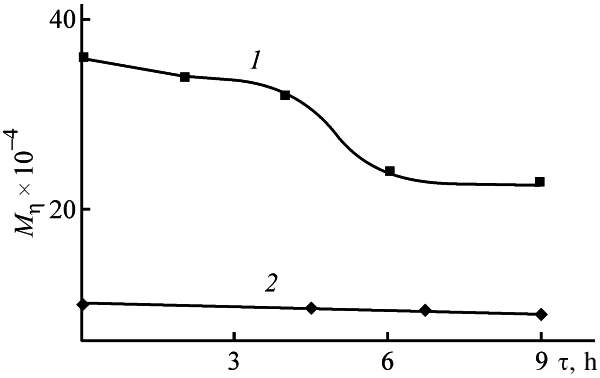
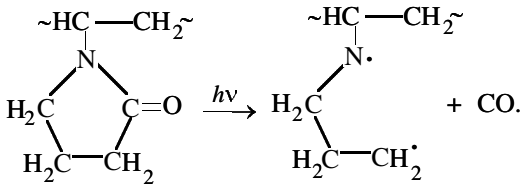
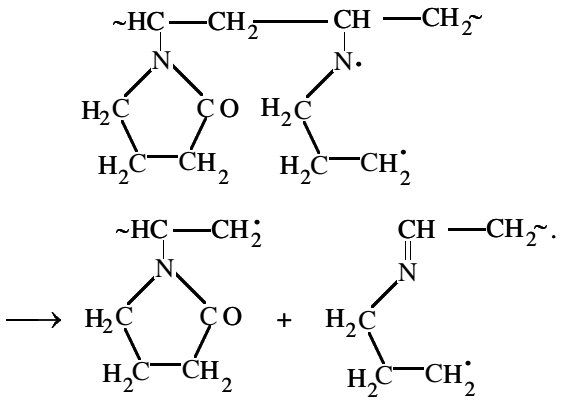


Fig. 3. Viscosity-average molecular weights M_η of (*1*) PS and (*2*) PVPD as functions of UV irradiation time τ. Solvent: (*1*) benzene and (*2*) methanol; 25°C.

(Norrish reaction):



The generated radicals can initiate the process without cleavage of the polymer backbone; also, this reaction can be followed by the chain β-cleavage:



Thus, the general pattern of formation of the block copolymer is as follows. The polymerization of VPD requires the presence of PVPD, which can be formed only by pseudoliving polymerization initiated by active PS. The subsequent polymerization can occur at the expense of degradation of PVPD units.

It is known that the supramolecular structures of block copolymers and homopolymers cardinally differ. Therefore, an obvious evidence of formation of block copolymers is furnished by scanning probe microscopic examination of the surface topography of films prepared from the isolated block copolymer and blends of the homopolymers taken in the corresponding ratio. Figure 4 shows that the topography of the films prepared from the blends (Figs. 4b, 4d) cardinally differs from that of of the films prepared from the block copolymers (Figs. 4a, 4c). Blend films demonstrate complete microphase segregation; at a VPD mole fraction of 0.5 (Fig. 4b), PS is apparently a continuous phase and PVPD forms discrete spherical particles of ~2.3 μm size. This is consistent with the estimated Hildebrand solubility parameter of the solvent and polymers: it is close for $CHCl_3$ and PS [$\delta(PS) = 18.2 \times 10^3$, $\delta(CHCl_3) = 18.6 \times 10^3$ $(J\ m^{-3})^{0.5}$] but significantly different for PVPD [$\delta(PVPD) = 22.2 \times 10^3$ $(J\ m^{-3})^{0.5}$] [5]. The surface topography of a film of a sample prepared in the presence of active PS (Fig. 4a) also contains spherical domains of almost the same size (2.4 μm), but the interphase boundaries are diffuse, up to mutual penetration of the phases.

In the blend with a PVPD mole fraction of 0.75 (Fig. 4d), PVPD is a continuous phase, and PS macromolecules form spherical particles of size 0.4 μm. The topography of sample II of similar composition (Fig. 4c), which is a blend of homopolymers and block copolymer, shows a tendency toward further diffusion of VPD units.

The block copolymer isolated from sample II has a microheterogeneous structure with pronounced supramolecular formations (Fig. 4e). Thus, as expected, films of homopolymer blends, crude block copolymerization products, and isolated block copolymer essentially differ in the topography.

It was interesting to study the surfactant properties of the amphiphilic block copolymer synthesized. For this purpose, we performed two experiments.

Sample II is soluble in chloroform; therefore, it was tested as emulsifier for preparing a water-in-chloroform emulsion. We prepared a 1 wt % solution of the polymer in chloroform, which was then mixed with water in 4 : 1 volume ratio. After shaking the system, the settling took 15 h (without adding the polymer it occurred within 3 s). The lower chloroform layer remained turbid, despite the fact that in the absence of water the sample solution was transparent. This fact is indicative of formation of water-containing micelles (owing to conjugate solubility). Because of a low resolving power of the photocolorimeter, the micelle size was determined after dilution of the system with chloroform to a concentration of 0.03%; it was estimated at 53.7 nm using the tables of characteristic light scattering functions [6].

The possibility of modification of the solid surface was demonstrated by the wetting method with a block copolymer containing 65 mol % VPD units. The silicon support is hydrophilic owing to the presence of OH groups on its surface. In the molecules of the block copolymer, the hydrophilic VPD units are oriented toward the support, and hydrocarbon "tails" of PS are oriented outwards and determine the properties of the surface. As a result, the surface becomes hydrophobic, and the contact angle θ on wetting with water becomes 72°, which is close to the contact angle with PS films (76°). It should be noted that the contact angle of a PVPD film with water is 7°. The blend of a similar composition is characterized by a contact angle of 14°, which differs from the value characteristic of the block copolymer and is one more evidence of formation of a new chemical compound.

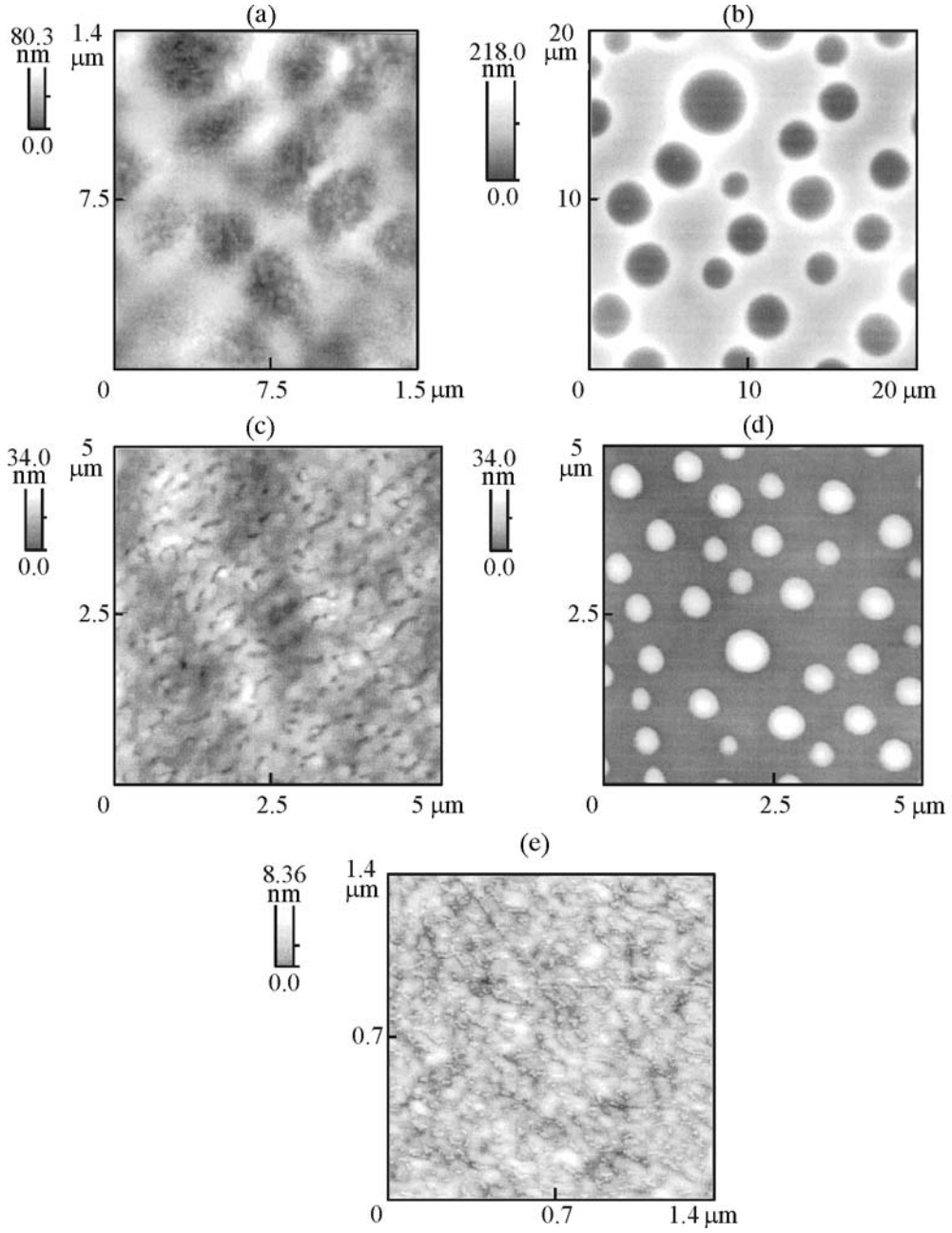


Fig. 4. Topography of the surface of films prepared from (a, b) block copolymerization products [(a) 0.5 PS–0.5 PVPD, (b) 0.25 PS–0.75 PVPD], (c, d) homopolymer blends of respective compositions, and (e) PS–*block*-PVPD copolymer 0.35 PS–0.65 PVPD.

CONCLUSIONS

(1) Amphiphilic copolymers polystyrene–*block*-polyvinylpyrrolidone were prepared by controlled radical polymerization under mild conditions using active polystyrene. The possible effect of the degradation of the macrochain units on formation of the block copolymers was demonstrated.

(2) The supramolecular structure of the surface of films prepared from the copolymers in hand indirectly confirms their block structure.

(3) The block copolymer prepared can be used as an emulsifier and for modification of a solid surface.

ACKNOWLEDGMENTS

The study was financially supported by the Russian Foundation for Basic Research (project no. 04-03-33030) and by the program "Development of the Scientific Potential of Higher School" (project no. 4671).

REFERENCES

1. Zaremskii, M.Yu. and Golubev, V.B., *Vysokomol. Soedin., 2001, vol. 43, no. 9, pp. 1689–1728.*
2. *Shamenkova, O.A., Kopylova, N.A., Semchikov, Yu.D., et al., Vysokomol. Soedin., Ser. B*, 2005, vol. 47, no. 11, pp. 2045–2049.
3. Summ, B.D. and Goryunov, Yu.V., *Fiziko-khimicheskie osnovy smachivaniya i rastekaniya* (Physicochemical Principles of Wetting and Spilling), Moscow: Khimiya, 1976.
4. Houben–Weyl, *Methoden der organischen Chemie*, Stuttgart, 1953, vol. B11.
5. *Entsiklopediya polimerov* (Polymer Encyclopedia), Moscow: Sov. Entsiklopediya, 1977, vol. 3.
6. Klenin, V.I., Shchegolev, S.Yu., and Lavrushin, V.I., *Kharakteristicheskie funktsii svetorasseyaniya dispersnykh sistem* (Characteristic Functions of Light Scattering by Disperse Systems), Saratov: Saratov. Univ., 1977.

ISSN 1070-4272. Russian Journal of Applied Chemistry, 2006, Vol. 79, No. 3, pp. 453–456. © Pleiades Publishing, Inc., 2006.
Original Russian Text © E.V. Anishchenko, N.S. Eremina, N.A. Gavrilenko, G.M. Mokrousov, 2006, published in Zhurnal Prikladnoi Khimii, 2006, Vol. 79, No. 3, pp. 460–463.

MACROMOLECULAR CHEMISTRY AND POLYMERIC MATERIALS

Influence of the Silver Ions on the Physicochemical Properties of Methyl Methacrylate–Methacrylic Acid Copolymer Films

E. V. Anishchenko, N. S. Eremina, N. A. Gavrilenko, and G. M. Mokrousov

Research Institute of Semiconducting Instruments, Tomsk, Russia
Tomsk State University, Tomsk, Russia

Received December 8, 2005

Abstract—The effect of silver ions on the physicochemical properties of methyl methacrylate–methacrylic acid copolymer films, namely, film-forming properties and resistance to fluorine-containing plasma, acid etchers, and temperature, was studied by lithography, derivatography, atomic-force microscopy, and optical spectroscopy. The activation energies were calculated for thermal transformations in the copolymer with and without silver ion additions, when heated in air to 300°C.

DOI: 10.1134/S1070427206030244

Methyl methacrylate–methacrylic acid copolymers form the basis of many positive resists having high resolution powers and good adhesion to metallic and semiconducting supports [1]. However, they exhibit inadequate stability in plasma treatment [2].

This study was aimed to enhance the resistance of methyl methacrylate–methacrylic acid copolymer (MMA–MAA CP) to fluorine-containing CF_4–NH_3 plasma via adding a silver salt. Also, we elucidated how the silver salt affects the film-forming properties and the resistance to acid etchers and temperature and by what mechanism the modifying addition affects the properties of the MMA–MAA CP.

EXPERIMENTAL

Our study was concerned with a commercial solution of MMA–MAA CP in organic solvents, known as ELP-9 electron resist. Silver trifluoroacetate (TFA-Ag) served as modifier. It was prepared by the procedure [3] involving dissolution of freshly precipitated silver oxide in an excess of trifluoroacetic acid and evaporation to dryness of the resulting solution on a water bath, washing of the product with CCl_4 to remove excess acid, drying to constant weight, and storage in a vacuum desiccator in the dark. The silver salt (0.001 to 0.1 mol per liter of the copolymer solution) was introduced by homogenic dissolution via mixing in a WU-4 vibromixer. The resulting solutions were freed from mechanical inclusions by filtration through a polyamide filter with a pore diameter of 0.2 μm.

For lithographic, microscopic, and IR- and UV-spectroscopic studies, thin polymer films (0.4–0.7 μm) were formed by centrifugation on preliminarily degreased supports (silicon and gallium arsenide with a silicon oxide layer applied, optically transparent glasses). For studies of the resistance to high temperatures, thicker copolymer films (14–16 μm) on polyethylene supports were prepared by casting. The resulting coatings were dried at 130, 165, and 180°C (±5°C) for 5, 15, and 30 min, respectively.

The film thickness was determined on an MII-4 interference microscope and a micrometer. The image in the films was formed by exposure to the UV irradiation from a DRKs-500 ultrahigh-pressure mercury–xenon lamp via a quartz template with the element having a minimal size of 0.57 μm, followed by dissolution of the polymer that decomposed under irradiation in a mixture of isopropyl alcohol and methyl ethyl ketone. The quality of the resulting relief was estimated upon exposure to organic solvents, acid etcher for silicon oxide HF–NH_4F–H_2O, CF_4–NH_3 gas mixture (in an Alcatel RDE-300 reactive ionic etching setup). The quantitative characteristic was the time of exposure to an aggressive medium until appearance of defects in the masking layer of the copolymer. The defects were revealed with a Latimet microscope under ×100, ×200, and ×500 magnifications.

The MMA–MAA CP film morphology was studied in a Solver P-47 atomic-force microscope (AFM) in the contact scanning mode. The IR spectra were recorded on a Specord M80 spectrophotometer at 4000–

Characteristics of etching of the polymer films in the CF_4–NH_3 plasma in relation to the content of silver trifluoroacetate in MMA–MAA CP

Content of CF_3COOAg $c \times 10^2$, M	V_{et} (MMA–MAA CP), μm m^{-1}	Etching selectivity V_{et} (SiO_2)/V_{et} (MMA–MAA CP)
–	0.05	1.0
1.0	0.04	1.3
5.0	0.03	1.7
10	0.02	2.5

400 cm^{-1}. The absorption bands were assigned using the reference data [4, 5]. The electronic spectra were recorded on a Specord M40 spectrophotometer at 260–900 nm.

The thermal stability of the polymer films in air was studied with an MOM Q-1500 derivatograph (Hungary) at a heating rate of 6–10 deg min^{-1} in platinum crucibles. We used 100-mg weighed portions of the ground polymer films and silver trifluoroacetate powder. Aluminum oxide served as the reference.

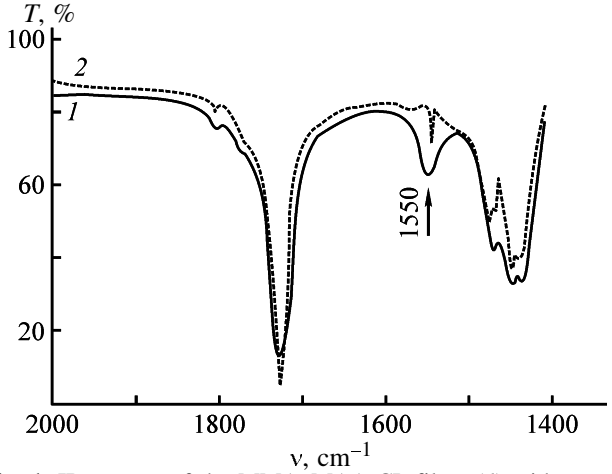


Fig. 1. IR spectra of the MMA–MAA CP films (*1*) without and (*2*) with addition of 0.05 M CF_3COOAg after heat treatment at 180°C. (*T*) Transmission and (ν) wavenumber.

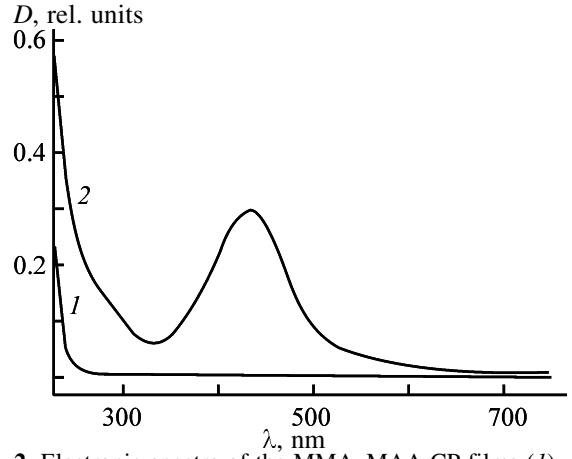


Fig. 2. Electronic spectra of the MMA–MAA CP films (*1*) without and (*2*) with addition of 0.05 M CF_3COOAg after heat treatment at 160°C. (*D*) Absorption and (λ) wavelength.

Our studies showed that the solutions with silver salt additions had good film-forming properties. Films thereof exhibit good adhesion to the support surface and withstand exposures to acid etchers for 10 min and more. This period is required for creation of images in the layers of passivating dielectric coatings (silicon oxide and nitride) and metals (titanium, aluminum, copper, gold) [6]. More precise reproduction of the sizes of the topological elements in production of integrated circuits is provided by reactive ionic etching methods.

The resistance of the silver salt modified MMA–MAA CP to etching in the fluorine-containing plasma increases relative to the initial composition by a factor of 1.3–2.5 (see table). Increased resistance of the copolymer films to an active medium based on CF_4–NH_3 increases the selectivity during etching of silicon oxide, which allows more precise reproduction of the critical sizes of the topological elements of integrated circuits.

The enhanced resistance to plasma, exhibited by the films, can be due to reinforcement of the structure of the polymer via reactions of the functional carbonyl and carboxy groups of the MMA–MAA CP with silver trifluoroacetate. Intermolecular interaction in the polymer–salt system is suggested by the optical spectroscopic data. In the IR spectra of the film with TFA-Ag additions (Fig. 1, curve *1*), the absorption bands at 1530 (asymmetric stretching vibrations of the carboxylate ion) and 1730 cm^{-1} (stretching vibrations of the carbonyl group) [5] exhibit increased intensity and are shifted and broadened. The observed changes in the IR spectra can be due to an increased degree of ionization of the carboxy groups of the macromolecules because of their coordination by the silver ions.

The electronic spectra of the silver salt modified MMA–MAA CP contain an absorption band at 330–600 nm with a maximum at 435 nm (Fig. 2, curve *2*), characteristic for silver compounds [7] and silver nanoparticles in methacrylate matrices [8–10]. Silver nanoparticles in the copolymer films can arise from thermal decomposition of the salt in the presence of the copolymer, e.g., by the scheme

$$4CF_3COOAg \rightarrow 4CO_2\uparrow + C_4F_{10}\uparrow + 2AgF + 2Ag.$$

Evolution of gaseous products from the films and formation of the silver particles on the film surface

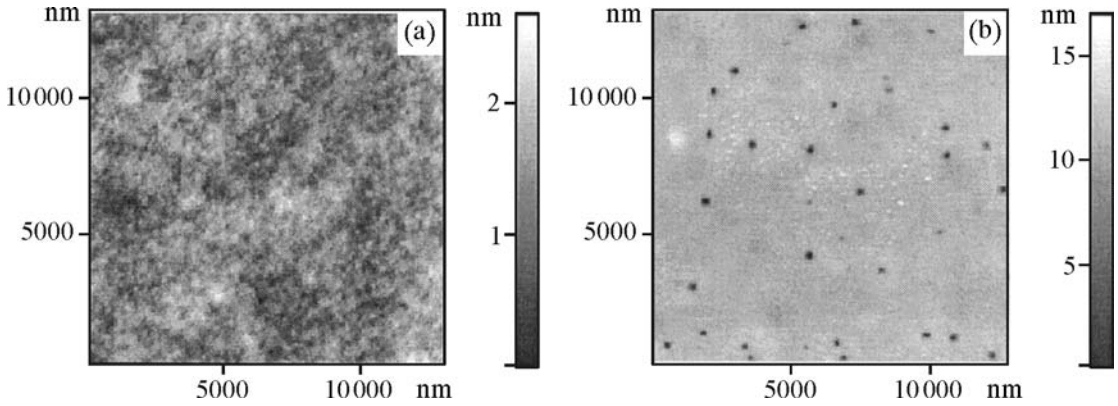


Fig. 3. AFM images of the MMA–MAA CP films (*1*) without and (*2*) with addition of 0.05 M CF_3COOAg after heat treatment at 160°C.

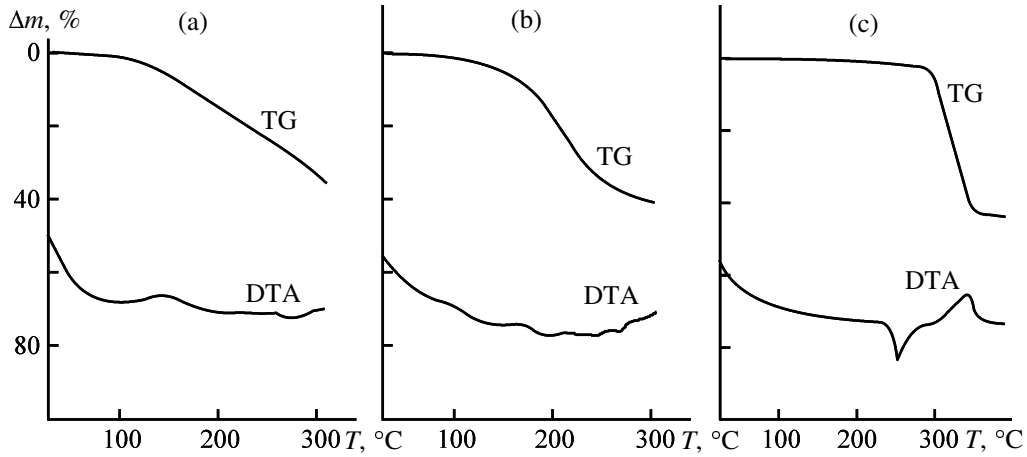


Fig. 4. Derivatograms of (a, b) MMA–MAA CP films (a) without silver trifluoroacetate and (b) containing 1.25×10^{-1} M silver trifluoroacetate and (c) neat silver trifluoroacetate. Heating rate 10 deg min^{-1}. (Δm) Weight loss and (T) heating temperature.

were evidenced by the AFM studies which revealed lustrous silver metal sections, 50–200 nm in size and 1–2 nm in height, around the pits in the films with TFA-Ag additions (Fig. 3b). In films without silver salt additions (Fig. 3a), such phenomena were not observed. Increase in the salt content to 0.1 M favors formation of a uniform lustrous layer over the entire film surface [6].

Thus, the resistance of the silver salt modified copolymer films to the CF_4–NH_3 plasma is due to reinforcement of the polymer structure via formation of additional metal–polymer bonds and formation in the film of silver particles and silver fluoride AgF. The latter can arise from the heat treatment of the modified copolymer and etching in the fluorine-containing plasma [1, 11].

Formation of conducting silver nanoparticles in the bulk and on the surface of the polymer is responsible for electrical conductivity of the polymer material [6]. The MMA–MAA CP films with silver trifluoroacetate (0.1 M) have an electrical conductivity of 1.8×10^{-4} S m^{-1}. This is essential for preventing the charge accumulation and ensuring conditions for discharge during exposure.

Of special interest is the thermal stability of the MMA–MAA CP films with TFA-Ag, specifically, their ability to withstand heating to 200°C. This is essential for preserving the configuration of the image elements during thermal impact (postbaking, ion-plasma processes) [1]. In this connection, we studied how the silver salt affects the resistance of MMA–MAA CP during heating in air to 300°C. The nature of the chemical transformations in the copolymer during heating was judged from the IR spectra.

The MMA–MAA CP without silver salt additions at 60–150°C was characterized by a minor weight loss (to 4 wt %), accompanied by a weak endothermic effect (Fig. 4a). This can be due to removal from the material of low-molecular-weight solvents (butyl acetate, methyl Cellosolve), strongly retained by the

polymer via intermolecular bonds. From the thermogravimetric (TG) data (Fig. 4), we estimated by the Freeman–Carroll method [12, 13] the activation energy of the polymer desolvation at 42.6 kJ mol^{-1}. There were no visible changes in the IR spectra of the copolymer heated to the temperatures mentioned. Further heating to 200°C increases the weight loss to 10%. We showed previously [14] that this is accompanied by appearance of two new absorption bands, at 1760 and 1800 cm^{-1}, in the IR spectra of the copolymer. They suggest formation of anhydride rings by intra- and intermolecular condensation of the ester and carboxy groups, with the elimination of methanol [15]. In the presence of the silver salt, the behavior of the polymer when heated to 250°C remains virtually unchanged (Fig. 4b); at 50–160°C, like in the case of MMA–MAA CP without additions, the residual solvents are removed with the activation energy of 36.4 kJ mol^{-1}. A minor decrease in the activation energy of this process can be due to easier release of the solvents from the copolymer films because of the competing reaction of the silver ion with the reactive centers of MMA–MAA CP. As to silver trifluoroacetate, in the absence of the polymer surrounding it withstands heating in air to 220°C without major changes and decomposes at 250°C (Fig. 4c), possibly, by the above-mentioned scheme. The activation energy of this process was estimated at 167.3 kJ mol^{-1}.

CONCLUSIONS

(1) The additions of silver trifluoroacetate, depending on the content, increase the resistance of methyl methacrylate–methacrylic acid copolymer to fluorine-containing plasma by a factor of 1.3–2.5 and increase the electrical conductivity to 1.8×10^{-4} S m^{-1}.

(2) The changes in the composition of methyl methacrylate–methacrylic acid copolymer and silver trifluoroacetate are due to formation in the bulk of the copolymer of silver particles, followed by formation on the polymer film surface of a metal layer. In the presence of the salt, the basic characteristics of the copolymer are preserved, namely, the ability of forming thin high-quality films, adhesion to various surfaces, ability of forming a masking relief resistant to aggressive acid media, and thermal stability up to 200°C.

ACKNOWLEDGMENTS

The authors are grateful to T.A. Kurmaev for carrying out plasma etching and to K.V. Oskomov for the atomic-force microscopic study of the samples.

REFERENCES

1. Moreau, W.M., *Semiconductor Lithography. Principles, Practices, and Materials*, New York: Plenum, 1988.
2. *Plasma Processing for VLSI*, Einspruch, N.G. and Brown, D.M., Eds., vol. 8 of *VLSI Electronics Macrostructure Science*, New York: Academic, 1984.
3. *Handbuch der präparativen anorganischen Chemie*, Brauer, G., Huber, F., *et al.*, Eds., Stuttgart: Ferdinand Enke, 1978, vol. 2.
4. Kuptsov, A.Kh. and Zhizhin, G.N., *Fur'e-spektry kombinatsionnogo rasseyaniya i infrakrasnogo pogloshcheniya polimerov: Spravochnik* (Fourier Raman and Infrared Absorption Spectra of Polymers: Reference Book), Moscow: Fizmatlit, 2001.
5. Bellamy, L.J., *Advances in Infrared Group Frequencies*, London: Methuen, 1968.
6. Eremina, N.S., Gavrilenko, N.A., Mokrousov, G.M., and Deniskina, O.I., *Zh. Prikl. Khim.*, 1997, vol. 70, no. 9, pp. 1579–1581.
7. *Metody elementoorganicheskoi khimii: Podgruppy medi, skandiya, titana, vanadiya, khroma, margantsa. Lantanoidy i aktinoidy* (Methods of Organometallic Chemistry: Copper, Scandium, Titanium, Vanadium, Chromium, and Manganese Subgroups. Lanthanides and Actinides), Nesmeyanov, A.N. and Kocheshkov, K.A., Eds., Moscow: Nauka, 1974.
8. Sergeev, G.B., *Nanokhimiya* (Nanochemistry), Moscow: Mosk. Gos. Univ., 2003.
9. Yanagihara, N., Tanaka, Y., and Okamoto, H., *Chem. Lett.*, 2001, vol. 30, no. 8, pp. 796–797.
10. Pomogailo, A.D., Rozenberg, A.S., and Uflyand, I.E., *Nanochastitsy metallov v polimerakh* (Nanoparticles of Metals in Polymers), Moscow: Khimiya, 2000.
11. Dikarev, Yu.I., Tsvetkov, S.M., and Surovtsev, I.S., *Kondens. Sredy Mezhfazn. Gran.*, 1999, vol. 1, no. 2, pp. 171–175.
12. Reich, L. and Levi, D.W., *Macromolecular Reviews*, Peterlin, A., Goodman, M., Zimm, H., and Mark, H.F., Eds., New York: Wiley–Interscience, 1967, vol. 1, p. 174.
13. Pavlova, S.A., Zhuravleva, I.V., and Tolchinskii, Yu.I., *Termicheskii analiz organicheskikh i vysokomolekulyarnykh soedinenii* (Thermal Analysis of Organic and Macromolecular Compounds), Moscow: Khimiya, 1983.
14. Anishchenko, E.V., Eremina, N.S., and Mokrousov, G.M., *Elektron. Prom–st.*, 2002, nos. 2–3, pp. 127–129.
15. Frolova, M.I., Oshmarina, L.A., Chervyakova, V.I., and Shmuilevich, S.M., *Akrilovye oligomery: Sinterz, svoistva i primenenie* (Acrylic Polymers: Synthesis, Properties, and Application), Gor'kii: Gor'k. Univ., 1989, pp. 58–91.

ISSN 1070-4272. Russian Journal of Applied Chemistry, 2006, Vol. 79, No. 3, pp. 457–460. © Pleiades Publishing, Inc., 2006.
Original Russian Text © L.A. Kupchik, N.T. Kartel', E.S. Bogdanov, O.V. Bogdanova, M.P. Kupchik, 2006, published in Zhurnal Prikladnoi Khimii, 2006, Vol. 79, No. 3, pp. 464–467.

MACROMOLECULAR CHEMISTRY AND POLYMERIC MATERIALS

Chemical Modification of Pectin to Improve Its Sorption Properties

L. A. Kupchik, N. T. Kartel', E. S. Bogdanov, O. V. Bogdanova, and M. P. Kupchik

Institute of Sorption and Endoecological Problems, National Academy of Science of Ukraine, Kiev, Ukraine
National University of Alimentary Technologies, Kiev, Ukraine

Received June 16, 2005

Abstract—The sorption properties of natural polysaccharide (apple pectin) with respect to heavy metals in a Ringer salt solution were studied as influenced by the procedures and process parameters of its chemical modification.

DOI: 10.1134/S1070427206030256

Pectins are vegetable polymers of *L,D*-galacturonic acid partially esterified with methoxy groups. These polymers are commercial products used as gel-forming agents and fillers in food industry [1–3]. Heavy metal ions react with free carboxy groups of pectins to form difficultly soluble complexes [4–6]. The reactivity of pectins with respect to heavy metal ions strongly depends on the degree of esterification, content of ballast agents, and content of free and bound carboxy groups and can be substantially increased by partial hydrolysis of the ester groups.

Pectins can be modified by saponification catalyzed by mineral acids, bases, salts of weak acids, enzymes, concentrated ammonium systems, and primary aliphatic amines [7–9]. The acid and base (ammonium) hydrolysis are the simplest and most efficient procedures for modifying pectins.

The aim of this study was to develop a procedure for preparing low-esterified pectin with increased sorption capacity for heavy metal ions, which could be used as a detoxicant additive to pharmaceuticals and as a therapeutic and prophylactic agent.

EXPERIMENTAL

We used fresh pomace as the raw material. Wet pectic coagulate was prepared from pomace by the known procedure [10, 11]. The coagulate was saponified with hydrochloric or nitric acid by the following procedure. The coagulate was mixed with an aqueous alcoholic solution of an appropriate acid (the alcohol concentration in the solution was 60–70 wt %) at the coagulate : solution volume ratio of 1 : (3–5). The mixture was heated at 40–50°C for 24–72 h. The precipitate was filtered off and washed with several portions of aqueous alcohol with the alcohol concentration increasing from 60 to 96%. The product was dried at 50°C to constant weight. Saponification of powdered pectins was performed similarly, however, in this case the mixture was heated for 120 min. It should be noted that the treatment of the wet coagulate is faster and is characterized by a lower consumption of alcohol, acid, and energy.

Base (ammonia) saponification of wet pectin coagulate was performed by the following procedure. The coagulate was cooled to 5–7°C and poured over with a mixture of 60% isopropanol and 1.5–1.8 M NH_4OH cooled to 5–7°C. The mixture was kept at 5–7°C for 1–3.2 h. The saponified pectin was filtered off, washed, and dried as in the case of the acid treatment. The content of uronic acid, of free and esterified carboxy groups, and of ballast substances was determined by titration [12]. The degree of esterification was calculated from these data. The degree of esterification of the initial (unmodified) apple pectin was 78.5%. The content of methoxycarbonyl and carboxy groups and of uronic component was 11.9, 3.2, and 64%, respectively. Thus, low-esterified pectin with decreased content of methoxy groups and nonuronic (ballast) compounds (see table) was prepared by acid and ammonia modification of wet or dry apple pectin.

Analytical properties of pectins modified under different conditions

Saponifier, M	τ, h	*T*, °C	Uronic component content, wt %	Content of functional groups, wt %		Degree of esterification β, wt %
				COOH	COOCH	
HNO_3:						
1.44	48	40	63.9	9.18	8.45	47.9
0.72	24	40	51.9	5.66	8.11	58.9
1.20	24	40	64.6	8.11	9.77	54.6
0.96	48	50	63.3	9.29	8.37	47.4
1.40	24	50	63.7	10.02	8.34	45.5
HCl 1.37	24	50	64.1	11.26	5.87	34.4
NH_4OH:						
1.00	2	2	66.9	7.6	9.6	56.0
1.00	3.2	7	50.34	8.9	5.1	36.4
1.00	1	7	61.45	7.8	8.5	52.0

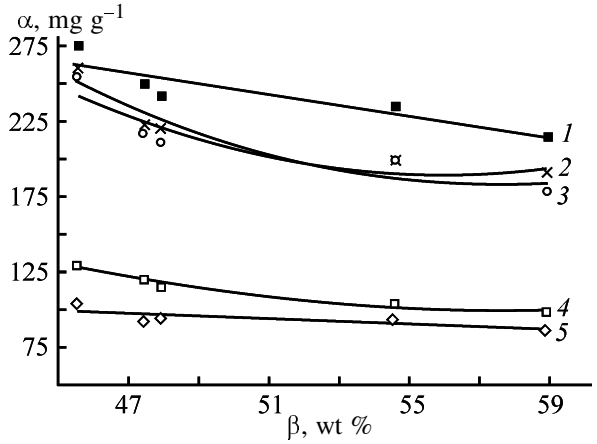


Fig. 1. Sorption capacity of apple pectins α for (*1*) lead(II), (*2*) cadmium(II), (*3*) copper(II), (*4*) nickel(II), and (*5*) strontium(II) as a function of the degree of esterification of the carboxy groups in the pectin β.

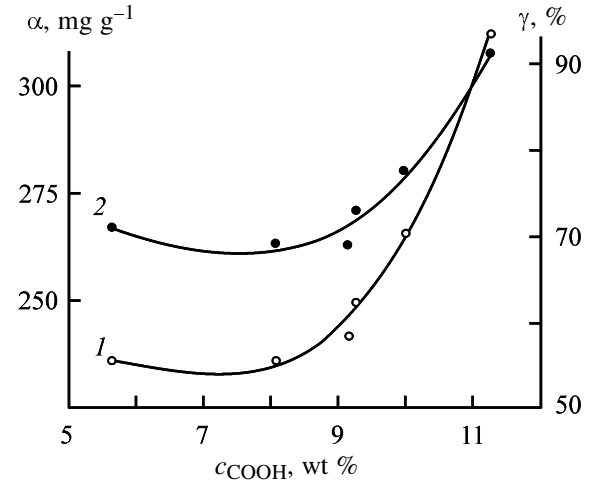


Fig. 2. (*1*) Sorption capacity of pectins α for lead(II) and (*2*) degree of lead sorption from a salt solution γ as functions of the content of free carboxy groups c_{COOH} in the pectin.

The main aim of the modification was to improve the sorption properties of pectin with respect to heavy metal ions. The maximal sorption capacity of modified pectin for lead(II), cadmium(II), nickel(II), copper(II), and strontium(II) ions was experimentally determined by the procedure described in our previous study [13]. The sorption was performed from solutions of appropriate salts of these metals with the initial metal concentration of 1500–1800 mg l^{-1}. A salt mixture simulating the composition of the Ringer's solution was used as the supporting electrolyte. The initial and equilibrium concentrations of heavy metals were measured by atomic absorption spectroscopy on a KAS-120 spectrometer (Selma, Ukraine).

The dependence of the sorption of metal ions by the modified apple pectin on its degree of saponification is shown in Fig. 1. The maximal sorption capacity of unmodified apple pectin for lead(II), cadmium(II), copper(II), nickel(II), and strontium(II), determined under the similar conditions, was 147–180, 61–85, 97–102, 76–89, and 37–43 mg g^{-1}, respectively.

It is seen that the sorption of heavy metal ions from multicomponent salt solutions depends on the degree of esterification of the modified pectin. As the degree of esterification of the carboxy groups decreases, the sorption of lead(II), copper(II), and cadmium(II) from the model salt solutions increases to the greatest extent; the sorption of nickel(II) changes to a lesser extent; and the maximal sorption of strontium(II) remains virtually the same.

To illustrate how the content of free carboxy groups in the modified pectin affects its sorption properties, the dependences of the maximal sorption capacity α (mg g^{-1}) for lead(II) and degree of lead sorption γ (%) from the model solution are shown in Fig. 2. As seen

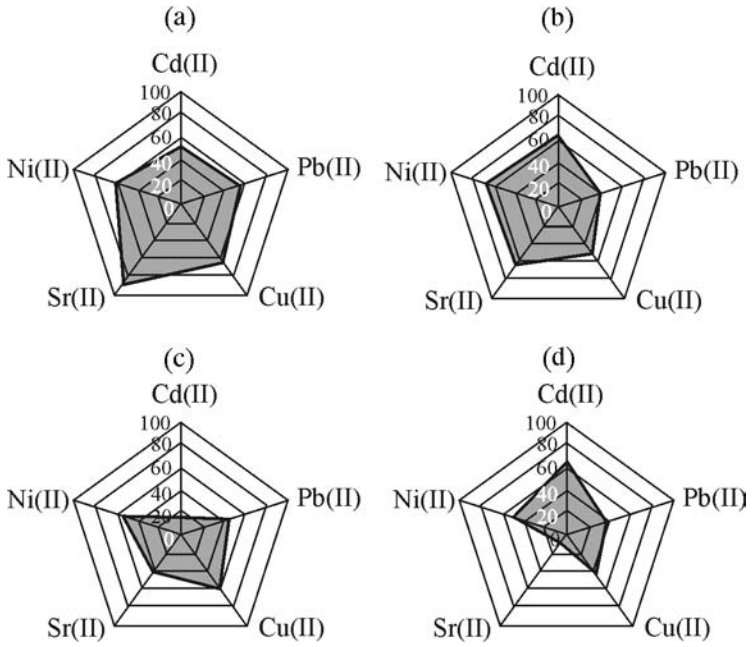


Fig. 3. Degrees of metal sorption from a salt solution γ (%) on (a) initial pectin and pectin modified with (b) HCl, (c) HNO_3, and (d) NH_4OH.

from Fig. 2, the content of free carboxy groups has a critical effect on the sorption properties of pectin. It should be noted that the mechanism of reaction of heavy metal ions with pectin is a matter of discussion. At the qualitative level, this reaction consists in formation of pectates, metal complexes with carboxy groups of the polysaccharide matrix. These compounds contain both chemically bound (coordinated) metal and metal ions occluded by a strongly swollen polysaccharide macromolecule. Ion exchange of metal ions with functional groups of the polysaccharide is also possible.

The degree of sorption of various metal ions by unmodified and modified pectins is shown in Fig. 3. As seen from Fig. 3, the best sorbent for removal of cadmium(II) from biological solutions is pectin modified with HCl; pectin modified with HNO_3 should be used to remove lead(II) and copper(II); and pectin modified with NH_4OH is favorable for removal of strontium(II). When all these ions are present in the solution, pectin saponified with HNO_3 should be used.

Thus, sorption of toxic metal ions (lead, cadmium, etc.) on wet pectin coagulate from multicomponent salt solutions simulating the electrolyte composition of a human body can be substantially increased by partial saponification of methoxycarbonyl groups of pectin by the suggested procedures.

CONCLUSIONS

(1) The content of methoxycarbony groups of wet pectin coagulate can be decreased from 70–75 to 40–45 wt % by saponification with hydrochloric acid, nitric acid, and ammonium hydroxide using the suggested procedures. The content of free carboxy groups after this modification increases from 2–4 to 8–12 wt %.

(2) This chemical modification increases the sorption capacity of the pectins for lead(II), copper(II), and cadmium(II) in multicomponent salt solutions simulating the electrolyte composition of a human body.

REFERENCES

1. Nelina, V.V., *Fiziko-khimicheskie svoistva pektinovykh veshchestv: Razrabotka i sovershenstvovanie tekhnologii pektina i pektinoproduktov* (Physicochemical Properties of Pectin Substances: Development and Improvement of Technologies of Pectins and Pectin-Derived Products), Krasnodar: Kubanskii Gos. Agrarn. Univ., 1996.
2. *Virobnitstvo ta vikoristannya pektiniv v kharchovii promislovosti* (Production and Application of Pectins in Food Industry), Guloi, I.S. and Kupchik, M.P., Eds., Kiev: Shust, 2001.
3. *Proizvodstvo pektina* (Pectin Production), Karpovich, N.S. Ed., Chisinau: Shtiintsa, 1993.

4. *Nauchnye osnovy tekhnologii pektina* (Scientific Foundations of Pectin Technology), Bakasova, Z.B., Ed., Frunze: Ilim, 1988.
5. Kohn, R., *Carbohydr. Polym.*, 1982, vol. 2, no. 4, pp. 273–275.
6. Walter, R.H., *Chemistry and Technology of Pectin*, New York: Academic, 1991.
7. Sinitsya, A., Čopikova, J., and Prutyanov, V., *Carbohydr. Polym.*, 2000, vol. 5, no. 42, pp. 359–368.
8. Black, S.A. and Smit, C.J.B., *J. Food Sci.*, 1972, vol. 37, no. 11, pp. 730–739.
9. El-Nawawi, S.A. and Neikal, Y.A., *Carbohydr. Polym.*, 1995, vol. 27, no. 5, pp. 191–195.
10. Ukrainian Patent 2003076217.
11. Ukrainian Patent 2002097524.
12. Nelina, V.V., Donchenko, L.V., Karpovich, N.L., and Ignat'eva, G.N., *Pektin: Metody kontrolya v pektinovom proizvodstve* (Pectin: Monitoring Methods in Pectin Production), Kiev: Osnova, 1992, pp. 87–89.
13. Kartel, M.T., Kupchik, L.A., and Veisov, V.K., *Chemosphere*, 1999, vol. 38, no. 11, pp. 2591–2596.

ISSN 1070-4272. Russian Journal of Applied Chemistry, 2006, Vol. 79, No. 3, pp. 461–463. © Pleiades Publishing, Inc., 2006.
Original Russian Text © V.P. Greben', I.G. Rodzik, 2006, published in Zhurnal Prikladnoi Khimii, 2006, Vol. 79, No. 3, pp. 468–471.

MACROMOLECULAR CHEMISTRY AND POLYMERIC MATERIALS

Mg/Na Selectivity of Sulfonic Cation-Exchange Membrane Modified with Poly(4-Vinyl-*N*-Propylpyridinium) Bromide

V. P. Greben' and I. G. Rodzik

Institute of Chemistry, Far-Eastern Division, Russian Academy of Sciences, Vladivostok, Russia

Received October 4, 2005

Abstract—Mg/Na selectivity of sulfonic cation-exchange membrane modified with poly(4-vinyl-*N*-propylpyridinium) bromide by surface electrodeposition, influenced by the electrodialysis conditions, is studied.

DOI: 10.1134/S1070427206030268

Cations can be separated by electrodialysis with a cation-exchange membrane using various techniques. The most practicable approach involves complexation of cations of one or several sorts with formation of compounds poorly penetrable through the membrane. In particular, Na and K ions were separated by electrodialysis in the presence of 18-crown-6 as a strong complexant for potassium [1]. Silver was separated from zinc and copper in the presence of EDTA [2]. Malonic, oxalic, and citric acids were used as complexants in separating Cu, Ni, and Co [3]. The drawback of this approach is in a large consumption of chemicals.

Another approach involves bulk or surface modification of the membrane by soaking in solutions of reagents, which are mostly high-molecular-weight cationic surfactants or complexants. For example, impregnation of a cation-exchange membrane with crown ethers increases the permeability with respect to alkali cations as compared to alkaline-earth elements, and also to Na relative to K [4]. Modification with polyethylenimine was used to increase the proton transfer relative to that of divalent cations [5]. The most widely used method is modification of cation-exchange membranes by direct introduction of reagents into the solution to be electrodialyzed. In this case, the modifier, having, as a rule, a positive charge, e.g., cyclodextrin [6], polyethylenimine [7, 8], or crown ether [4], is electrodeposited on the membrane surface from the side of the solution being dialyzed, thus increasing the transmembrane transfer of alkali metals as compared to alkaline-earth elements.

All the above-mentioned methods require regular repeated modification of membranes, because of gradual desorption of modifiers from the surface. Therefore, it is advisable to chemically bind a modifier to the membrane. Takata *et al*. [9] have bound polyethylenimine to the surface of cation-exchange membranes through interaction with sulfochloride groups introduced into the membrane.

In this study we examined the effect of modification of MK-40L membrane with poly(4-vinyl-*N*-propylpyridinium) bromide (PVPPB) on the Mg/Na selectivity of transmembrane transport.

EXPERIMENTAL

The selectivity coefficient of transmembrane transport $P_{Na^+}^{Mg^{2+}}$ is written as

$$P_{Na^+}^{Mg^{2+}} = \bar{t}^{Mg^{2+}} c_{Na^+} / \bar{t}^{Na^+} c_{Mg^{2+}}, \quad (1)$$

where $\bar{t}^{Mg^{2+}}$ and $\bar{t}^{Na^+}$ are the transport numbers of Mg and Na cations across the membrane and $c_{Mg^{2+}}$ and c_{Na^+}, Mg and Na concentrations in the solution (g-equiv l^{-1} or N).

The cell and the procedure of determination of the transport numbers of the cations were the same as in [10]. The middle compartment of the cell between an ideally selective anion-exchange membrane and the investigated cation-exchange membrane was charged with 0.25 N NaCl + 0.25 N $MgCl_2$ with or without addition of PVPPB. Three different procedures were used for modification of the cation-exchange membrane.

(1) The membrane was held for a fixed time in a PVPPB solution, washed with distilled water several times for 3–5 s, and arranged in the cell. The middle compartment was filled with the NaCl and $MgCl_2$

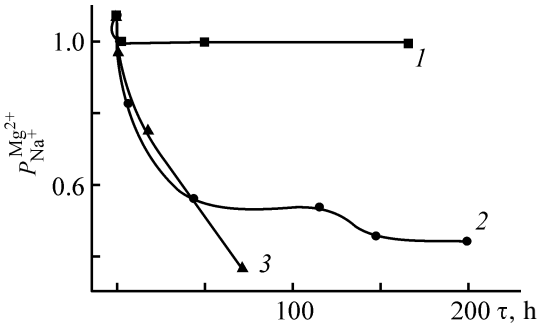


Fig. 1. Selectivity coefficient $P_{Na^+}^{Mg^{2+}}$ as a function of the time of treatment of the cation-exchange membrane in the PVPPB solution τ. Current density (A dm^{-2}): (*1, 2*) 1.0 and (*3*) 2.0. PVPPB concentration (g l^{-1}): (*1*) 0.23 and (*2, 3*) 2.16.

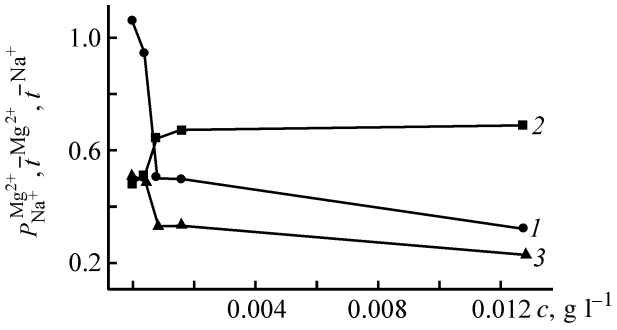


Fig. 2. (*1*) $P_{Na^+}^{Mg^{2+}}$, (*2*) $\bar{t}^{Na^+}$, and (*3*) $\bar{t}^{Mg^{2+}}$ as functions of the PVPPB concentration c in the solution being dialyzed at a current density of 1 A dm^{-2}.

solutions, and electrodialysis was carried out to determine the transmembrane transport numbers of Na and Mg.

(2) The membrane was arranged in the cell. The middle compartment was filled with 0.25 N NaCl + 0.25 N $MgCl_2$ containing a fixed concentration of PVPPB. After electrodialysis the solution was removed, and the compartment was washed with distilled water. All the solutions were combined and analyzed. Then the next run was performed in the same manner.

(3) As in method no. 2, but using PVPPB-free solution in the runs following the first one.

As seen from Fig. 1, increasing time of treatment of the cation-exchange membrane in the PVPPB solution, as well as increasing PVPPB concentration and current density decrease the transmembrane transport of Mg ($P_{Na^+}^{Mg^{2+}}$ decreases).

In the course of soaking in the PVPPB solution, an adsorption layer is formed on the surface of the cation-exchange membrane, which is positively charged, while the polymer matrix (bulk) of the membrane is charged negatively. Therefore, an electrostatic barrier is formed on the membrane surface, whose effect is stronger with respect to double-charged cations as compared to single-charged cations. Most likely, increasing PVPPB concentration and soaking time increase the thickness of the adsorption layer, and increasing current density makes this layer more compact, thus decreasing the transmembrane transport of Mg.

Figure 2 shows how the PVPPB concentration in the dialyzable solution influences the Mg/Na selectivity of the transmembrane transport and the Mg and Na transport numbers in electrodialysis. In the case in hand, a PVPPB film was formed on the membrane surface through migration of PVPPB from the bulk of the solution to the membrane followed by its electrodeposition. It is most likely that, with increasing PVPPB concentration in the solution being dialyzed to 0.0015–0.002 g l^{-1}, the film thickness on the membrane surface increases rapidly, providing the most significant changes in the selectivity coefficient and transport numbers. In the indicated PVPPB concentration range, the sum of the Mg and Na transport numbers approaches unity (0.99 ± 0.01), suggesting the lack of poisoning of the membrane with PVPPB polycations. However, with increasing PVPPB concentration to 0.013 g l^{-1}, this value decreases to 0.92.

The trends in the dependences of the Na and Mg transport numbers and of the selectivity of the transmembrane transport on the current density are similar without (Fig. 3a) and with addition of PVPPB to the solution being dialyzed (Fig. 3b), but their values are strongly different. In both cases, at i < 1 A dm^{-2}, $P_{Na^+}^{Mg^{2+}}$ and transport numbers of Mg and Na increases with increasing current density, but the sum of the Mg and Na transport numbers remains unchanged (0.92 ± 0.01), which can be attributed to some redistribution of Mg and Na fluxes among the membrane areas, depending on the density of functional groups [10] without change in the total transport number of the cations.

Our results show that deposition of a modifier, particularly, PVPPB on the membrane surface can be realized at relatively low modifier concentrations, i.e., its consumption is low. It was interesting to determine the useful life of the PVPPB layer. Figure 4 shows that, in electrodeposition at low PVPPB concentration (0.0016 g l^{-1}), $P_{Na^+}^{Mg^{2+}}$ rapidly increases, and the Na transport number decreases with increasing time of electrodialysis, suggesting small initial thickness of

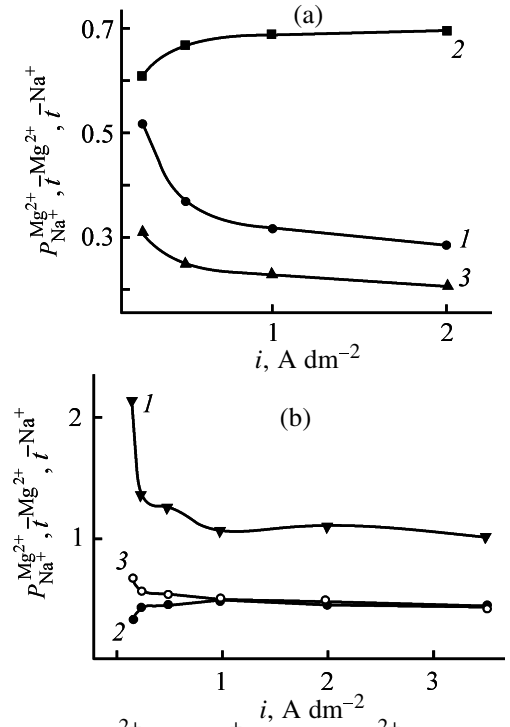


Fig. 3. (*1*) $P_{Na^+}^{Mg^{2+}}$, (*2*) $\bar{t}^{Na^+}$, and (*3*) $\bar{t}^{Mg^{2+}}$ as functions of the current density i. Solution: (a) 0.25 N NaCl + 0.25 N $MgCl_2$ and (b) 0.25 N NaCl + 0.25 N $MgCl_2$ + 0.0128 g l^{-1} PVPPB.

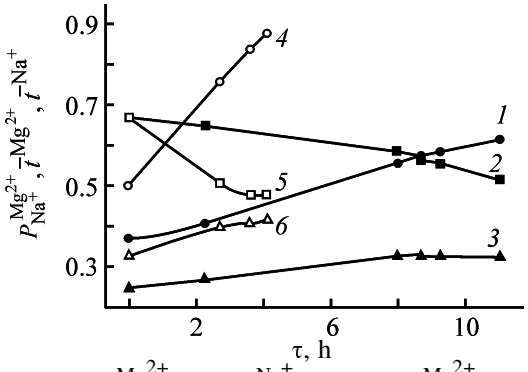


Fig. 4. (*1, 4*) $P_{Na^+}^{Mg^{2+}}$, (*2, 5*) $\bar{t}^{Na^+}$, and (*3, 6*) $\bar{t}^{Mg^{2+}}$ as functions of the electrodialysis time τ with the cation-exchange membrane preliminarily modified by electrodeposition of PVPPB for 30 min. Current density (A dm^{-2}): (*1–3*) 0.5 and (*4–6*) 1. PVPPB concentration (g l^{-1}): (*1–3*) 0.0128 and (*4–6*) 0.0016.

the electrodeposited PVPPB layer. Increasing PVPPB concentration by about an order of magnitude (0.0128 g l^{-1}) results in a considerable decrease in the initial selectivity coefficient, and the dependences of the membrane selectivity and Na transport numbers on the electrodialysis time become weaker.

It should be pointed out that, generally, at optimal conditions, modification of the membrane through addition of PVPPB to the initial solution containing Mg and Na chlorides decreases the membrane selectivity with respect to magnesium by a factor of about 3 (Figs. 2, 4).

CONCLUSIONS

(1) Soaking of the sulfonic cation-exchange membrane in the solution containing poly(4-vinyl-*N*-propylpyridinium) bromide or its electrodeposition on the membrane surface results in the formation of an adsorption layer representing an electrostatic barrier for cations, the effect being stronger with respect to double-charged cations as compared to single-charged cations.

(2) The Mg/Na selectivity of the membrane can be reduced by a factor of about 3 through modification of the membrane with PVPPB.

(3) Over the PVPPB concentration range 0.0015–0.002 g l^{-1} in the solution being dialyzed, the modification significantly decreases the Mg/Na selectivity of the membrane without poisoning.

(4) The Mg/Na selectivity of the sulfonic cation-exchange membrane is studied, as influenced by the current density, electrodialysis time, and PVPPB concentration.

REFERENCES

1. Sata, T., Tanimoto, M., and Matsusaki, K., *Colloid Polym. Sci.*, 2000, vol. 278, no. 1, pp. 57–60.
2. Cherif, A.T., Elmidaoui, A., and Gavach, C., *J. Membr. Sci.*, 1993, vol. 76, no. 1, pp. 39–49.
3. Wang, Jau-Kai and Chang, C.-P., *Desalination*, 2000, vol. 164, no. 3, pp. 269–280.
4. Sata, T., Tanimoto, M., Kawamura, K., and Matsusaki, K., *J. Colloid Interface Sci.*, 1999, vol. 219, no. 2, pp. 310–319.
5. Chapotot, A., Pourcelly, G., Gavach, C., and Lebon, F., *J. Electroanal. Chem.*, 1995, vol. 386, nos. 1–2, pp. 25–37.
6. Sata, T., Kawamura, K., Higa, M., and Matsusaki, K., *J. Membr. Sci.*, 2001, vol. 183, no. 2, pp. 201–212.
7. Sistat, P., Pourselly, G., and Gavach, C., *J. Appl. Electrochem.*, 1997, vol. 27, no. 1, pp. 65–70.
8. Amara, M. and Kerdjoudj, H., *Desalination*, 2003, vol. 155, no. 1, pp. 79–87.
9. Takata, K., Yamamoto, Y., and Sata, T., *J. Membr. Sci.*, 2000, vol. 179, nos. 1–2, pp. 101–107.
10. Greben', V.P. and Rodzik, I.G., *Elektrokhimiya*, 2005, vol. 41, no. 8, pp. 997–1000.

ISSN 1070-4272. Russian Journal of Applied Chemistry, 2006, Vol. 79, No. 3, pp. 464–469. © Pleiades Publishing, Inc., 2006.
Original Russian Text © I.A. Novakov, S.S. Radchenko, A.S. Pastukhov, F.S. Radchenko, 2006, published in Zhurnal Prikladnoi Khimii, 2006, Vol. 79, No. 3, pp. 472–477.

MACROMOLECULAR CHEMISTRY AND POLYMERIC MATERIALS

Water-Soluble Polymer–Colloid Complexes of Aluminum Polyhydroxochloride and Polyethylenimine in Separation of Dispersions at Low pH

I. A. Novakov, S. S. Radchenko, A. S. Pastukhov, and F. S. Radchenko

Volgograd State Technical University, Volgograd, Russia

Received November 8, 2005

Abstract—Interaction of polyethylenimine with aluminum salts in aqueous solutions was studied; in the process, polymer–colloid complexes exhibiting elevated activity in separation of dispersions with low pH are formed.

DOI: 10.1134/S107042720603027X

Polymer–colloid complexes (PCCs) are new specific macromolecular compounds formed by interaction of water-soluble organic polymers with the surface of colloidal particles [1–3]. Though PCCs may have different structures, depending on both the nature of colloidal particles and type of functional groups in the polymer macromolecules, they are all water-soluble. These complexes are of particular importance for flocculation of colloidal dispersions and can be used in treatment of wastewater and in design of closed environmentally safe treatment cycles [4, 5].

Aluminum aquahydroxo complexes are formed as colloidal particles in concentrated aqueous solutions of aluminum pentahydroxochloride (APHC) [6]. It was found [7, 8] that the reaction of APHC with polyacrylamide (PAA) in aqueous solution yields PCCs exhibiting high flocculation activity in separation of model and real aqueous dispersions. Along with PAA, numerous water-soluble polymers with ionizable functional groups [including polyethylenimine (PEI)] can be used to prepare PCCs.

In this study we examined the flocculation properties of the compounds formed in aqueous solutions by APHC colloidal particles with PEI in separation of model and real dispersions.

EXPERIMENTAL

In this study we used APHC prepared by the known procedure [9] (Al^{3+} content 12.8 wt %, Cl^-/Al^{3+} atomic ratio 0.48, pH 4.5, ρ 1330 kg m^{-3}, dry residue 46.8 wt %) and PEI (molecular weight 30 000–40 000) purchased from Serva (the United States).

The composition of PCC of the polymer with APHC was studied with an Ubbelohde viscometer (Cannon, d_c 0.25 mm) at 30 ± 0.1°C. For this purpose, the solution pH was adjusted to 4.5 with 0.1 N HCl; the pH measurements were carried out with a pH-300 pH-meter (Hanna Instruments, the United States) equipped with an HI 1131 combined electrode. Before the viscosity measurements, the solutions were aged for 2 days.

The polymeric complexes were prepared by mixing the aqueous solutions of PEI (1 wt %) and APHC at room temperature; the Al^{3+} : PEI unit ratio was varied from 0.25 to 10.0. To prepare PCC, the resulting solution was stored for 2 days at room temperature.

A model kaolin dispersion (0.8 wt %) was prepared using kaolin [technical grade, GOST (State Standard) 19.608–84] and tap water (pH 7.8) and swollen for 3 h. Before the experiments, the dispersion was thoroughly mixed and poured in 250-ml glass cylinders. Then the required amounts (charges) of the flocculant solution with a concentration from 2 to 20 mg l^{-1} were added, and the resulting suspensions were stirred with disc stirrers for 30 min. After storage for 20 min, the optical density D of the supernatant was measured on a KFK-3 device (λ = 460 nm, l = 1–5 cm). Using the spectrophotometric procedure [9, 10], the clarification effect E_c was calculated as a dimensionless parameter characterizing the flocculation process:

$$E_c = \tau_D^0/\tau_D - 1,$$

where τ_D^0 and τ_D are the supernatant turbidities in

the absence of additives and after flocculant addition, respectively.

The precipitation curves of the kaolin suspension were plotted using the data on changes in the weight of the precipitate accumulated on the pan placed in the suspension using an AUX120 electronic balance with a bottom hook (Shimadzu, Japan). For this purpose, the suspension (600 ml) poured in the cylinder was stirred with the flocculant solution for 30 s with a disc stirrer, and the pan hanged on the hook was submerged in the suspension. Changes in the precipitate weight were recorded in certain periods using a stopwatch.

The rate parameter of the flocculation (flocculation effect) was calculated using the expression given in [11]:

$$D = v/v_0 - 1 = t_0/t - 1,$$

where v and v_0, and t and t_0 are the average precipitation rates and precipitation half-times (Q 0.5) in the presence of the flocculant and without it, respectively.

The constant of the precipitate compaction γ was calculated from the slope of the sedimentation curves at high degrees of clarification ($Q > 0.6$); the curves were plotted in the $\log[Q_{max} - Q(t)] = e^{\gamma t}$ coordinates [12].

The density of the resulting precipitates was calculated from the following equation [13]:

$$\rho_p = \frac{m + [(1 - Q_{max})V_0 - m/\rho]\rho_0}{(1 - Q_{max})V_0}.$$

The flotation of petroleum-containing and dairy wastewaters was performed in a glass column (40 mm in diameter and 350 mm high) stoppered from the bottom with a glass frit (Schott filter no. 4). The wastewater was sampled from a pipe that led to the flotation unit. The emulsion sample (300 cm^3) was placed in the column, and after addition of the reagent solution the column was purged with air supplied from the bottom at a constant rate of 120 $cm^3\ min^{-1}$. After 10 min, a sample was taken from the bottom stopcock of the column and analyzed for the content of petroleum products [14].

The flocculation of the kaolin dispersion was performed in the mode of free (unhindered) sedimentation (content of the dispersed phase c_d 0.8 wt %). As seen from Fig. 1, PEI is characterized by small clarification effect (curve *1*), but after protonation with HCl its flocculation power slightly increases (curve *2*). This is probably due to the opening of the macromolecular globules in the course of ionization of the imine groups. The PEI + APHC compounds exhibit significantly higher flocculation effect, as compared to initial PEI; and the highest effect is attained at Al^{3+}/PEI unit molar ratio of 1.2 (Fig. 1, curve *4*).

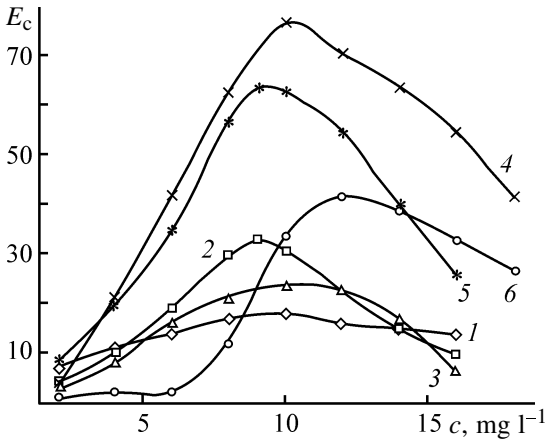


Fig. 1. Clarification effect E_c of a kaolin dispersion (c_d 0.8 wt %) as influenced by the content c and type of the flocculant. (*1*) PEI; (*2*) PEI (pH 4.5); (*3*–*6*) PEI + APHC PCC at Al^{3+}/PEI unit molar ratio of (*3*) 0.8, (*4*) 1.2, (*5*) 1.5, and (*6*) 2.2.

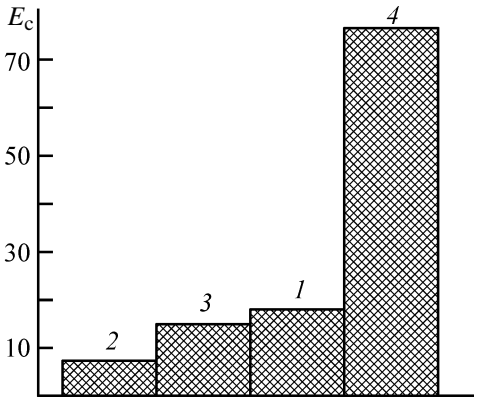


Fig. 2. Clarification effect E_c of a kaolin dispersion (c_d 0.8 wt %) as influenced by the type of the flocculant; Al^{3+}/PEI unit molar ratio 1.2; the same for Fig. 3. (*1*) PEI, (*2*) PEI + $Al_2(SO_4)_3$, (*3*) PEI + $Al(NO_3)_3$, and (*4*) PEI + APHC PCC.

In contrast to APHC, the reactions of PEI with aluminum sulfate and nitrate yield PCCs with a weaker flocculation effect as compared to PEI (Fig. 2). This fact agrees with the ionic-coordination mechanism of formation of the PEI chelate complexes with metal ions, which increases compaction of macromolecules and decreases their flocculation power [15]. In contrast to the complex based on APHC + PAA, formation of the polymer–colloid complexes of APHC and PEI cannot be confirmed by recovery of the product. However, certain increase in the flocculation power of

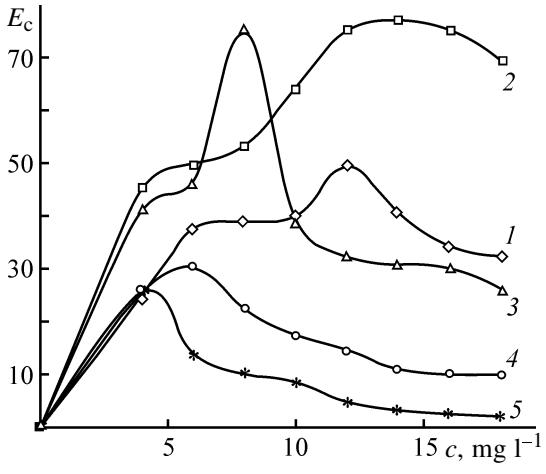


Fig. 3. Clarification effect E_c of a kaolin dispersion (c_d 0.8 wt %) as influenced by the PEI + APHC PCC content c. Solution pH: (*1*) 7.62, (*2*) 6.5, (*3*) 5.5, (*4*) 3.85, and (*5*) 2.

the product of interaction of APHC and PEI in comparison with the individual components indirectly confirms the formation of a PCC.

The data on PCC formation as influenced by the solution pH are of particular importance. To study this effect, PCCs were prepared by mixing the initial components, and then the solution pH was adjusted with 0.1 M HCl. As seen from Fig. 3, the strongest flocculation effect is observed at pH 6.5–5.5 (curves *2, 3*), because in this pH range the macromolecule occurs in the most open conformation [16]. Further acidification of the PCC solution decreases the flocculation effect, probably due to partial degradation of PCC via decomposition of aluminum aquahydroxo complexes [17].

It is known that the performance of an ionic flocculant is determined by the wastewater pH. The data on the clarification effect as influenced by the kaolin dispersion pH (PCC content 6 mg l^{-1} with respect to PEI, Al^{3+}/PEI unit molar ratio 1.2) are given below:

pH	E_c
1.5	2.0
3.0	5.0
4.5	28.4
6.0	30.8
7.4	27.6
9.5	14

As seen, the flocculation effect of PCC is the strongest at pH from 4.5 to 7.5. In this pH range, the PEI macromolecule occurs in the most open conformation, i.e., neutral and acidic solutions are the best for efficient flocculation using PCC.

The kinetics of the dispersion clarification are also of particular importance. The kinetic sedimentation curves of a kaolin suspension in the presence of PEI and PCC at an optimal flocculant content of 8 mg l^{-1} (with respect to polymer) are shown in Fig. 4. As can be seen, the solution pH and PCC composition strongly affect the flocculation kinetics. To obtain more detailed kinetic data, the quantitative parameters [such as the rate parameter of flocculation (flocculation effect) D, the constant of precipitate compaction γ, and the precipitate density ρ_p] were evaluated (Table 1). With decreasing pH to 4.5, the process rate decreases by a factor of 2, but this is accompanied by changes in the precipitate structure, which at the final stage deforms and becomes more compact. Further acidifica-

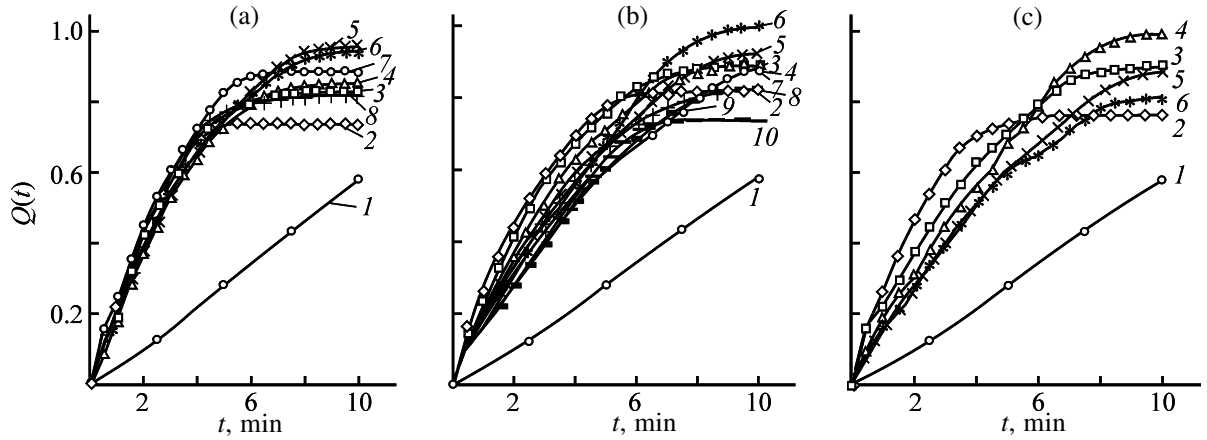


Fig. 4. Kinetic sedimentation curves of the kaolin suspension. (Q) Weight fraction of precipitate and (t) sedimentation time. (a) In the presence of PEI: (*1*) no flocculant; with flocculant at pH (*2*) 10.5, (*3*) 9.0, (*4*) 7.5, (*5*) 6.0, (*6*) 4.5, (*7*) 3.0, and (*8*) 1.5; (b) PCC at pH 4.5: (*1*) no flocculant; with flocculant at Al^{3+}/PEI unit molar ratio: (*2*) 0.25, (*3*) 0.50, (*4*) 0.75, (*5*) 1.00, (*6*) 1.25, (*7*) 1.50, (*8*) 2.00, (*9*) 3.00, and (*10*) 4.00; (c) PCC with Al^{3+}/PEI unit molar ratio of 1.25: (*1*) no flocculant; with flocculant at pH: (*2*) 7.5, (*3*) 6.0, (*4*) 4.5, (*5*) 3.0, and (*6*) 1.5.

Table 1. Flocculation and compaction of kaolin precipitates as influenced by the type of flocculant

Reagent	Solution pH	Al^{3+}/PEI unit molar ratio	*D*	$\gamma \times 10^5$, s^{-1}	ρ, kg m^{-3}
–	–	–	–	–	1011.63
PEI	10.5	0	3.28	4.55	1016.92
	9.0	0	2.95	4.72	1025.61
	7.5	0	2.26	4.76	1029.65
	6.0	0	2.00	4.96	1103.97
	4.5	0	1.88	4.92	1079.44
	3.0	0	2.75	4.91	1038.82
	1.5	0	2.83	4.84	1024.43
PCC	7.5	1.25	3.69	4.75	1018.42
	6.0	1.25	2.01	4.88	1041.87
	4.5	1.25	1.21	5.00	1449.01
	3.0	1.25	1.27	4.92	1038.25
	1.5	1.25	1.42	4.81	1023.14
PCC	4.5	0.25	3.28	4.82	1023.35
	4.5	0.50	2.49	4.96	1036.36
	4.5	0.75	2.33	4.89	1037.46
	4.5	1.00	2.12	4.91	1043.97
	4.5	1.25	1.21	4.98	1449.01
	4.5	1.50	1.27	4.85	1034.05
	4.5	2.00	1.30	4.80	1024.41
	4.5	3.00	1.54	4.77	1023.92
	4.5	4.00	1.73	4.71	1016.57

tion of the initial solutions causes an opposite affect. Our study of the effect of PCC composition on the kinetic parameters of flocculation shows that the most compact precipitate at the smallest rate of the floccule precipitation is formed at the Al^{3+}/PEI unit molar ratio of 1.25.

To explain this behavior of the flocculation system, we examined the effect of the reagent molar ratio on the parameter *F* (Fig. 5):

$$F = \eta_{sp}^{exp}/\eta_{sp}^{cal} - 1,$$

where η_{sp}^{exp} is the specific viscosity of the mixture of PEI and APHC solutions and η_{sp}^{cal} is the sum of the specific viscosities of the individual aqueous solutions of PEI and APHC.

These data show that the interaction of PEI macromolecules with APHC particles proceeds in the entire range of the reagent molar ratios (from 0.25 to 4.0); with increasing Al^{3+}/PEI unit molar ratio from 0 to 1.25, *F* decreases. This confirms formation of PCC; moreover, in the course of addition of APHC to the Al^{3+}/PEI unit molar ratio of 1.25, the reaction mixture contains PCC of the primary composition and excess PEI. In this case, the composition means the number of particles linked with one macromolecule. It should be noted that with formation of PCC of the primary composition the size of the PEI globules decreases, which is confirmed by the decrease in parameter *F*. At Al^{3+}/PEI unit molar ratio of 1.25, all the PEI macromolecules are linked in a polycomplex of the primary composition and this stage is characterized by the smallest parameter *F*. Further increase in the APHC content (Al^{3+}/PEI unit molar ratio >1.25) changes the PCC composition, i.e., the number of APHC particles linked with one macromolecule in-

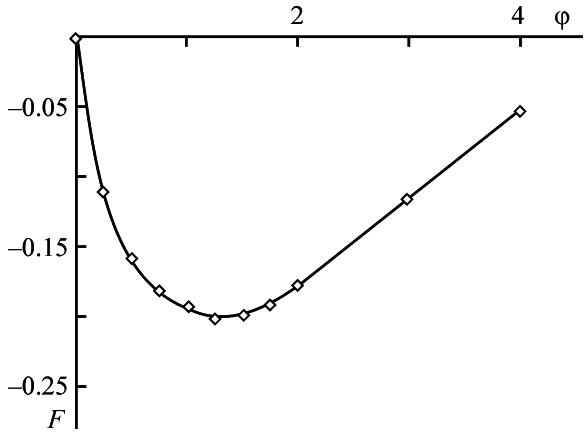


Fig. 5. Parameter *F* as a function of the Al^{3+}/PEI unit molar ratio φ in aqueous solution; PEI content 1 g dl^{-1}, pH 4.5, 30°C.

Table 2. Efficiency of purification of oily wastes as influenced by the reagent composition

Reagent	Al^{3+}/PEI unit molar ratio	Charge, mg l^{-1}	Optical density	Degree of purification
–	–	–	1.210	0
$Al_2(SO_4)_3$	1 : 0	20	0.240	80.1
APHC	1 : 0	20	0.210	82.6
PEI	0 : 1	5	0.446	63.0
PCC-2	2 : 1	5	0.224	81.5
PCC-4	4 : 1	5	0.145	88.0
PCC-6	6 : 1	5	0.110	90.4
PCC-8	8 : 1	5	0.091	92.4
PCC-10	10 : 1	5	0.091	92.4

creases. Simultaneously, the macromolecular globules open owing to electrostatic repulsion between the APHC particles (charged dispersed particles) linked with PEI macromolecule.

The data obtained using the model systems are of particular importance for preliminary evaluation of the PCC flocculation power. Under the real conditions, the reagent performance is determined by the properties of the solution in which it is used as flocculant.

The results of treatment to remove pollutants of wastewaters from an oil refinery containing emulsified oil products (pH 3.5) are listed in Table 2. PCCs with various reagent molar ratios were tested, and the treatment was performed by pressure flotation. For comparison, straight PEI, aluminum sulfate, and APHC were used. As seen, the performance of straight PEI is low. Common inorganic emulsion breakers such as $Al_2(SO_4)_3$ and APHC are more active, but the performance of PCC is significantly higher at even smaller charges. The flocculation activity increases with increasing content of APHC in PCC on passing from PCC-2 to PCC-10, which is due to the appearance of excess particles of aluminum aquahydroxo complexes (not involved in complexation with the polymer), providing degradation of the emulsion particles and their coalescence [18]. The degree of purification also depends on the solution pH (Table 3).

Table 3. Efficiency of purification of oily wastes using PCC-8 flocculant as influenced by the solution pH; reagent charge 6 mg l^{-1}

Wastewater pH*	Optical density**	Degree of purification, %
0.95	0.054	95.5
2.10	0.068	94.3
3.55	0.091	62.4
5.95	0.081	93.3
7.20	0.061	94.8

* The wastewater pH was adjusted with HCl and NaOH solutions.

** Optical density of the initial wastewater 1.210.

As seen from Table 3, owing to high performance in a wide pH range, PCC-8 can be used as specific reagent for treatment of wastewaters with elevated acidity.

The wastewaters from the Volgomyasomoltorg Joint-Stock Company are characterized by high content of the dispersed phase and by complex composition. Similarly to the case of oily wastes, the treatment was performed by pressure flotation. The reagent performance was judged from the degree of purification and such parameters as content of fats and dry residue, chemical oxygen demand (COD), and pH before and after treatment, determined by the procedures given in [19] (Table 4).

Our experimental data show that PCC is more efficient than widely used VPK-402 and KF flocculants and operates at charges smaller by a factor of 4 as compared to weakly basic aluminum oxychloride (AOC) and APHC. It should be noted that PCCs based on PAA and APHC are almost inefficient in dispersions containing fat-and-oil particles, i.e., polymer–colloid complexes of APHC and PEI are the specific reagents for treatment of dairy wastewaters.

CONCLUSIONS

In contrast to other aluminum compounds, aluminum polyhydroxychloride reacts with polyethylenimine in aqueous solutions to form polymer–colloid complexes acting as coagulants destabilizing colloidal and emulsified systems and as cation-active flocculants promoting rapid and complete separation of

Table 4. Efficiency of treatment of wastewaters from the Volgomyasomoltorg Joint-Stock Company as influenced by the type of reagent

Reagent	Charge, mg l^{-1}	Optical density*	Degree of purification, %	pH	COD	Fats	Dry residue
					mg l^{-1}		
Before treatment	–	–	–	5.91	6354	198.75	1648.2
Standard	–	–	–	6.5–8.5	354	25.00	441.5
AOC	25	0.031	94.07	6.48	480	3.15	420.7
APHC	25	0.049	90.63	6.20	360	1.25	465.5
VPK-402	6	0.210	59.85	6.35	862	14.80	793.3
KF	6	0.301	42.44	6.40	911	19.30	933.5
AOC + VPK-402	25 + 6	0.060	88.53	6.52	423	3.48	425.9
PAA	6	0.205	60.80	6.47	887	15.60	813.2
PCC Al^{3+} : PAA = 2	6	0.249	52.39	6.20	556	17.50	853.4
PEI	6	0.148	71.70	6.69	685	10.20	755.3
PCC Al^{3+} : PEI = 1.2	6	0.035	93.31	6.17	416	2.95	403.8

* Optical density of the initial wastewater 0.523.

dispersions. These complexes exhibit high performance in acidic solutions, which is due to conformation behavior of polyethylenimine. The resulting polycomplexes can be used as highly efficient reagents for water treatment.

REFERENCES

1. Averochkina, I.A., Papisov, I.M., and Matvienko, V.N., *Vysokomol. Soedin., Ser. A*, 1993, vol. 35, no. 12, pp. 1986–1990.
2. Sokolov, E., Fengji, Y., Khokhlov, A., et al., *J. Phys. Chem.*, 1998, vol. 102, pp. 7091–7098.
3. Dipankaz, S., Samir Kumar, P., Debabrata, M., et al., *J. Phys. Chem.*, 2000, vol. 104, pp. 6128–6132.
4. GB Patent 2322128.
5. Gordeev-Gavrikov, V.K., Pedashenko, D.D., and Bozhko, L.N., *Zhil. Kommun. Khoz-vo.*, 2001, no. 2, pp. 34–38.
6. Radchenko, S.S., Bykadorov, N.U., Novakov, I.A., et al., *Zh. Prikl. Khim.*, 2002, vol. 75, no. 4, pp. 529–534.
7. Novakov, I.A., Radchenko, F.S., and Papisov, I.M., *Vyskomol. Soedin., Ser. A*, 2003, vol. 45, no. 8, pp. 1340–1344.
8. Novakov, I.A., Radchenko, S.S., and Radchenko, F.S., *Zh. Prikl. Khim.*, 2004, vol. 77, no. 10, pp. 1699–1706.
9. RF Patent 2083495.
10. Chernoberezhskii, Yu.M., Lorentsson, A.V., and Dyagileva, A.B., *Kolloidn. Zh.*, 2000, vol. 62, no. 5, pp. 707–710.
11. Dobrynina, A.F., Faizullina, G.G., Barabanov, V.P., and Manyurov, I.R., *Zh. Prikl. Khim.*, 2002, vol. 75, no. 7, pp. 1131–1134.
12. Myagchenkov, V.A., Proskurina, V.E., and Bulidorova, G.V., *Khim. Tekhnol. Vody*, 2001, vol. 23, no. 5, pp. 453–492.
13. Proskurina, V.E., and Myagchenkov, V.A., *Khim. Tekhnol. Vody*, 2002, vol. 24, no. 3, pp. 215–225.
14. *Kolichestvennyi khimicheskii analiz vod: Metodika vypolneniya izmereniya massovoi kontsentratsii nefteproduktov v probakh pripodnykh i ochishchennykh stochnykh vod* (Qualitative Chemical Analysis of Waters: Procedure of Measurements of the Weight Content of Oily Products in Natural and Purified Wastewaters), PND F 141:2.116–97, Moscow: Gos. Kom. RF po Okhrane Okruzhayushchei Sredy, 1997.
15. Gembitskii, P.A., Zhuk, D.S., and Kargin, V.A., *Polietilenimin* (Polyethylenimine), Moscow: Nauka, 1971.
16. Pastukhov, A.S., Radchenko, S.S., and Radchenko, F.S., *Izv. Volgograd. Gos. Tekh. Univ., Khim. Tekhnol. Elementoorg. Monom. Polim. Mater.*, 2005, no. 2, pp. 86–89.
17. Krivoruchko, O.P., Buyanov, R.A., and Fedotov, M.A., *Kinet. Katal.*, 1978, vol. 19, no. 4, pp. 1070–1072.
18. Skrylev, L.D., Skryleva, T.L., and Nebesnova, T.V., *Izv. Vyssh. Uchebn. Zaved., Khim. Khim. Tekhnol.*, 2001, vol. 44, no. 1, pp. 143–146.
19. Lur'e, Yu.Yu., *Analiticheskaya khimiya promyshlennykh stochnykh vod* (Analytical Chemistry of Industrial Wastewaters), Moscow: Khimiya, 1984.

ISSN 1070-4272. Russian Journal of Applied Chemistry, 2006, Vol. 79, No. 3, pp. 470–474. © Pleiades Publishing, Inc., 2006.
Original Russian Text © I.I. Goncharik, F.F. Mozheiko, A.I. Voitenko, T.P. Kulikova, 2006, published in Zhurnal Prikladnoi Khimii, 2006, Vol. 79, No. 3, pp. 478–482.

MACROMOLECULAR CHEMISTRY AND POLYMERIC MATERIALS

Foaming and Stabilizing Activity of Binary Solutions of Sodium Carboxylates of Different Chain Length

I. I. Goncharik, F. F. Mozheiko, A. I. Voitenko, and T. P. Kulikova

Institute of General and Inorganic Chemistry, Belarussian National Academy of Sciences, Minsk, Belarus

Received April 26, 2005

Abstract—Influence of short-chain soda soap (sodium pentanoate) on the foaming and stabilizing activity of long-chain sodium carboxylates (laurate, myristate, and palmitate) is studied.

DOI: 10.1134/S1070427206030281

Mixtures of sodium salts of homologous carboxylic acids are produced at many chemical works as by-products and wastes: alkaline waste from caprolactam production (adipates), adipose tar (fat work waste), sulfate soap and tall oil (products from distillation of sulfate lye formed in pulping), etc. Generally they are used as foaming agents or collectors in flotation of potash, phosphorite, and other ores.

To understand the effect of these products on flotation, we studied the foaming activity of mixtures consisting of sodium salts of carboxylic acids with different chain length, particularly, of the short-chain pentanoate with long-chain laurate, myristate, and palmitate.

The experimental procedure was as follows. A mixed aqueous solution containing fixed concentrations of reagents (V = 20 ml) was foamed for 30 s in a graduated cylinder. The foaming activity was estimated by the foam volume and lifetime.

For comparison, initially we examined the foaming activity of aqueous solutions of the individual sodium salts of butyric (C_5), octanoic (C_8), lauric (C_{12}), myristic (C_{14}), and palmitic (C_{16}) acids. The foaming activity of these compounds depends on their chain length and concentration (Fig. 1). The foam formation in the solutions considerably increases as the reagent concentration approaches the critical micelle concentration (CMC): 2.28×10^{-2}, 6.96×10^{-3}, and 2.1×10^{-3} M for the laurate, myristate, and palmitate, respectively. The maximum of foaming activity near CMC can be attributed to the completion of the formation of the adsorption layer with the maximal mechanical strength. With a further increase in the reagent concentration above CMC, association (micelle formation) occurs in the bulk of the solution, which decreases the diffusion rate of the molecules to the adsorption layer, thus reducing the foaming activity.

Increase in the length of the hydrocarbon chain in the homologous series of the soaps initially increases their foaming activity from the octanoate to myristate and then decreases on passing to the palmitate (foam head height is 15.5, 18.0, 19.0, and 3.5 cm for the aqueous octanoate, laurate, myristate, and palmitate solutions, respectively). It should be pointed out that the short-chain butyrate and pentanoate do not form foam even in concentrated 25–50% solutions. With increasing chain length, the soap concentration corresponding to the maximal foaming activity decreases from 0.6 M for the octanoate to 2.28×10^{-2} and 6.96×10^{-3} M for the laurate and myristate, respectively.

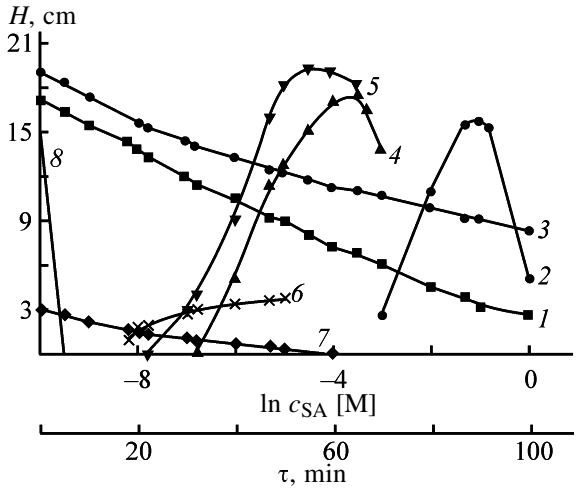


Fig. 1. (*2*, *4–6*) Foaming activity H and (*1*, *3*, *7*, *8*) foam stability τ as functions of the sodium carboxylate concentration c_{SA}: (*1*, *4*) laurate, (*2*, *8*) octanoate, (*3*, *5*) myristate, and (*6*, *7*) palmitate.

The foam stability is among the most important performance characteristics. It was demonstrated that the stability of foam formed by sodium soaps is also controlled by the nature and concentration of the surfactant, approaching the maximum at CMC. For example, for the sodium laurate solutions with the concentrations of 5.6×10^{-3} (below CMC), 2.28×10^{-2} (CMC), and 3.3×10^{-2} M (above CMC), the foam lifetime was found to be 17, 100, and 40 min, respectively.

With increasing chain length in the homologous series of sodium carboxylates, the foam stability increases from the lower carboxylates to the myristate and then decreases. Thus, for the myristate and laurate, the foam head height decreased in 100 min by 50 (Fig. 1, curve *3*) and 83% (Fig. 1, curve *1*), respectively, while with the palmitate the foam fully broke in 50 min (Fig. 1, curve *7*).

We studied the foaming activity of binary solutions of short-chain sodium pentanoate and long-chain sodium soap (laurate, myristate, or palmitate). It was demonstrated that the pentanoate has a positive effect on the foaming activity of the long-chain soaps, depending on their nature and concentration. The dependence of the foaming activity of the laurate, myristate, and palmitate on the pentanoate concentration passes through a maximum, which shifts toward lower pentanoate concentrations on passing from the laurate to the palmitate. For example, at a concentration of the long-chain soap C_{12}, C_{14}, and C_{16} of 5.7×10^{-3}, 2.0×10^{-3}, and 1.6×10^{-3} M, the maximal foaming activity was attained at a pentanoate concentration of 3.2×10^{-2}, 4.0×10^{-3}, and 3.0×10^{-3} M, respectively, and the foam head was 12.0, 5.0, and 4.2 cm against 0.5, 3, and 2.1 cm without the pentanoate.

It should be pointed out that, while for the laurate and myristate this trend is observed over a fairly wide concentration range (up to CMC and even more), in the case of the palmitate, some increase in the foaming activity takes place only below CMC. At higher concentration, addition of the pentanoate decreases the foaming activity (note that in individual pentanoate solutions with the concentrations corresponding to those of the pentanoate additive in the binary solutions studied, no foaming was observed at all).

The positive effect of the short-chain pentanoate on the foaming activity of the long-chain soaps can be attributed to the fact that, when entering the laurate or myristate micelles, the molecules of readily soluble pentanoate weaken the interchain interaction in the micelles and strengthen the electrostatic repulsion

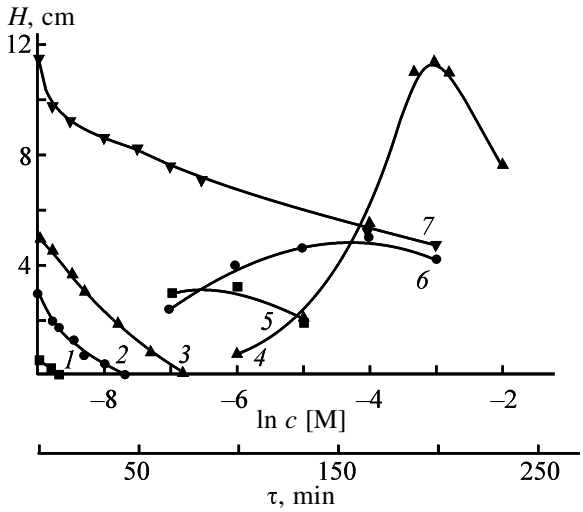


Fig. 2. (*4–6*) Foaming activity H and (*1–3, 7*) foam stability τ as functions of the sodium pentanoate concentration c in the solutions of long-chain sodium carboxylates: (*1, 4, 7*) laurate, (*2, 3, 6*) myristate, and (*5*) palmitate. Curves *1* and *2* were obtained without addition of the pentanoate.

in their surface layer. As a result, the coarse micelles of the poorly soluble long-chain surfactant become more finely dispersed, thus favoring its uniform distribution throughout the bulk of the solution and facilitating the formation of a sufficiently stable adsorption layer at the gas/liquid interface. As for the more hydrophobic palmitate molecules, the effect of the pentanoate is reduced essentially to the role of a supplier of counterions providing coagulation and salting-out of the surfactant at the concentration near its CMC.

Introduction of the pentanoate into the solutions of the long-chain laurate, myristate, and palmitate considerably improves the stability of foam. Figure 2 shows data on the stability in time for the foam formed in the laurate and myristate solutions with addition of the pentanoate. It was demonstrated that, while in the case of individual laurate solution ($c = 5.6 \times 10^{-3}$ M), the foam lifetime was 15 min (Fig. 2, curve *1*), after addition of pentanoate (3.3×10^{-2} M) to this solution, even in 200 min, the foam head decreased only by half (Fig. 2, curve *7*). After addition of pentanoate (1.2×10^{-2} M) to the myristate solution ($c = 2.0 \times 10^{-3}$ M), the foam was broken in 75 min against 48 min without pentanoate (curves *3, 2*) (pentanoate concentrations corresponded to those at which the maximal foaming activity was observed).

Since foam formation often occurs in the presence of some inorganic salts, it was advisable to examine the salt effect on the foaming activity in the laurate–

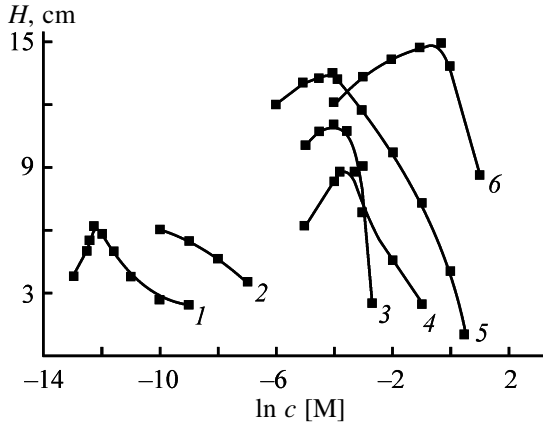


Fig. 3. Foaming activity H of (*1, 4*) myristate–pentanoate and (*2, 3, 5, 6*) laurate–pentanoate binary solutions as a function of the electrolyte concentration c: (*1, 2*) $AlCl_3$, (*3*) KCl, and (*4–6*) NaCl. Pentanoate concentration (M): (*3, 6*) 0.003, (*1, 4*) 0.012, and (*2, 5*) 0.034.

pentanoate and myristate–pentanoate binary solutions. As inorganic salts we used sodium, potassium, and aluminum chlorides. It was demonstrated previously [1] that the foam formation starts at the surfactant bulk concentration c_m corresponding to the saturation of the adsorption layer. It is well known also that, in the presence of electrolytes, this saturation is attained at lower surfactant concentration. Chistyakov and Chernin have shown [2] that, for micelle-forming surfactants, the decrease in c_m with increasing counterion concentration c_i is described by the following relationship:

$$\log c_m = -a \log c_i + \text{const},$$

i.e., increasing electrolyte concentration decreases the surfactant concentration at which the foam formation starts.

Our results show that addition of inorganic electrolytes strongly increases the foaming activity of the investigated surfactants, depending on the nature and concentration of both the surfactants and inorganic salts (Fig. 3). We studied the effect of the NaCl concentration on the foaming activity in 5.6×10^{-3} M laurate and 2.0×10^{-3} M myristate solutions containing 3.0×10^{-3} and 1.2×10^{-2} M pentanoate, respectively. With increasing NaCl concentration, the foaming activity passes through a maximum. In this case, with increasing hydrophobicity of the surfactant, the maximum of the foaming activity is observed at lower electrolyte concentration (0.85 and 0.034 M in the laurate–pentanoate and myristate–pentanoate solutions, respectively). The foam head in these solutions was, respectively, 14.9 and 9.6 cm against 4.7 and 7.1 cm without NaCl.

It was demonstrated in studying the effect of the electrolyte nature on the foaming activity of the sodium soaps that NaCl and KCl, having the same cationic charge, differently influence the foaming and stabilizing properties of the investigated binary solutions. For example, in the laurate–pentanoate system with NaCl, the maximal foaming activity was observed over a wide concentration range (1.8×10^{-2}–1.6 M), whereas with KCl, only near 1.7×10^{-2} M. This is due to different hydrability of the cations (positive for Na^+ and negative for K^+), resulting in different interaction of this cations with the surfactant molecules and micelles. The K^+ ion, having a smaller radius in the hydrated state compared to Na^+, more readily penetrates the Stern layer and more efficiently neutralizes the ionized polar groups of the surfactant, thus facilitating the micelle formation and salting-out.

In the case of trivalent aluminum, the maximal foaming activity was observed at an electrolyte concentration of 4.6×10^{-6} M, which is considerably lower than with the monovalent cations. The reason is that multivalent cations, even taken in low concentration, form complexes with the sodium soaps, initiating aggregation of the micelles followed by salting-out of the surfactant, thus decreasing its foaming activity.

Addition of the inorganic salts into the binary solutions also improves the foam stability (Table 1). For example, addition of NaCl (8.5×10^{-2} M) to the 5.6×10^{-3} M laurate solution containing 3.0×10^{-3} M pentanoate increased the foam lifetime from 20 to 30 min. Increasing pentanoate concentration slightly expands the range of electrolyte concentrations at which foam is formed. For example, at a pentanoate concentration of 3.4×10^{-2} M, after introduction of even 8.5×10^{-2} M NaCl, the foam head height in 2 h remained 85.7% of the initial. The foam formed in the system laurate–pentanoate–water in the presence of KCl taken in concentration corresponding to the maximal foaming activity (3.4×10^{-2} M) is characterized by low stability (8 min).

The increase in the foam stability in the presence of inorganic electrolytes was observed also in the system myristate–pentanoate. For example, the foam formed in the system 2.0×10^{-2} M myristate–5.6×10^{-3} M pentanoate without and with addition of NaCl (3.4×10^{-2} M) was broken in 2 h to 55.5 and 24%, respectively.

As known, the foam break follows the escape of the liquid from it (foam bleeding), which is quantita-

Table 1. Effect of the sodium pentanoate concentration and of inorganic electrolytes on the foaming activity of sodium laurate and myristate (laurate and myristate concentrations 5.6×10^{-3} and 2.0×10^{-2} M, respectively)

Concentration, M × 10²			Foam head, cm		Foam stability in 2 h, %
sodium pentanoate	NaCl	KCl	initial	after 2 h	
Sodium laurate					
0.3	–	–	2	Foam was broken in 20 min	
0.3	8.5	–	15	Foam was broken in 30 min	
3.4	–	–	7	6	64.0
3.4	3.4	–	15	10	67.0
3.4	85.0	–	11	7	85.7
3.4	–	3.4	11	Foam was broken in 8 min	
Sodium myristate					
0.6	–	–	33	1.5	45.5
0.6	3.4	–	11	8.3	76

Table 2. Effect of NaCl and KCl concentrations on W_0 and K_1 for foam formed in the laurate–pentanoate systems (laurate and pentanoate concentrations 5.6×10^{-3} and 3.0×10^{-3} M, respectively)

NaCl			KCl		
concentration × 10², M	$W_0 \times 10^3$, s^{-1}	K_1, m^{-1}	concentration × 10², M	$W_0 \times 10^3$, s^{-1}	K_1, m^{-1}
–	11.0	32.0	–	11.0	32.0
2.1	5.0	45.0	1.7	3.3	39.0
4.3	1.4	31.0	3.4	3.6	39.2
50.0	1.0	32.0	6.7	10.0	27.5
85.0	1.4	31.0	–	–	–

Note: For the laurate solution with $c = 5.6 \times 10^{-3}$, $W_0 = 2.67 \times 10^{-2}$ m s^{-1} and $K_1 = 34.0$ m^{-1}.

tively characterized by the volume of the liquid accumulated below the foam/solution interface in a fixed time, i.e., by the initial rate of foam bleeding W_0. It was interesting to study the effect of the electrolyte (KCl, NaCl) concentration on the foam bleeding rate in the laurate–pentanoate binary solutions. The experimental data were fitted by the following equation [3]:

$$(K_1\tau)/2 = \tau/V' - 1/W_0,$$

where K_1 is a constant; V', volume of the liquid related to the unit cross-section area of the vessel (m^2); W_0, initial rate of foam bleeding (m s^{-1}); and τ, time (s).

The applicability of this equation to foams was demonstrated in [3–5] and in our previous studies. Table 2 shows that addition of the pentanoate to the laurate solution decreases W_0 practically by half from 2.67×10^{-2} to 1.10×10^{-2} m s^{-1}.

Introduction of NaCl and KCl in the laurate–pentanoate system decreases W_0 to 1.4×10^{-3} and 3.3×10^{-3} m s^{-1}, respectively.

To conclude, small concentrations of the electrolytes favor the formation of a more compact adsorption layer of the surfactant at the gas/liquid interface, thus improving the foaming activity of the surfactant solutions and foam stability. Further increase in the inorganic salt concentration results in salting-out of the surfactant and in decrease in its concentration in the solution, foaming activity of the system, and foam stability.

The positive effect of sodium pentanoate and inorganic electrolytes on the foam formation in solutions of long-chain carboxylates is attributed to the facts that the pentanoate tends to be solubilized in the soap micelles and also that introduction of the electrolyte decreases the surfactant concentration corresponding to the saturation of the adsorption layer, thus providing compaction of the adsorption layer

at the gas/liquid interface and increasing the foaming activity and foam stability.

Finally, introduction of the short-chain sodium soap (pentanoate) and inorganic electrolytes into solutions of sodium salts of long-chain carboxylic acids allows control of the foam formation in their solutions.

CONCLUSIONS

(1) The dependence of the foaming activity of long-chain sodium carboxylates (laurate, myristate, and palmitate) on the sodium pentanoate concentration passes through a maximum, which shifts toward lower concentrations on passing from the laurate to palmitate.

(2) Addition of inorganic electrolytes favors the formation and stability of foams formed in binary carboxylate solutions.

(3) Introduction of the electrolytes (KCl, NaCl) into the system sodium pentanoate–water decreases the initial rate of foam bleeding, which is consistent with data on their effect on the foaming.

REFERENCES

1. Tikhomirova, V.K., *Peny: Teoriya i praktika ikh polucheniya* (Foams: Theory and Practice of Foam Formation), Moscow: Khimiya, 1975.
2. Chistyakov, B.E. and Chernin, V.I., *Kolloidn. Zh.*, 1988, vol. 50, no. 1, pp. 187–190.
3. Kruglyakov, P.M. and Taube, P.R., *Zh. Prikl. Khim.*, 1965, vol. 38, pp. 1514–1519.
4. Kruglyakov, P.M. and Taube, P.R., *Zh. Prikl. Khim.*, 1966, vol. 39, pp. 1499–1504.
5. Kruglyakov, P.M. and Taube, P.R., in *Uspekhi kolloidnoi khimii* (Advances in Colloid Chemistry), Moscow: Khimiya, 1973, pp. 304–308.

ISSN 1070-4272. Russian Journal of Applied Chemistry, 2006, Vol. 79, No. 3, pp. 475–479. © Pleiades Publishing, Inc., 2006.
Original Russian Text © A.V. Kalinin, A.N. Reznikov, G.A. Nikolaev, Yu.V. Khoroshavina, A.S. Ramsh, N.K. Skvortsov, 2006, published in Zhurnal Prikladnoi Khimii, 2006, Vol. 79, No. 3, pp. 483–487.

MACROMOLECULAR CHEMISTRY AND POLYMERIC MATERIALS

Synthesis of Poly(dimethyl){methyl[2-(2,2,3-trifluoro-3-trifluoromethylcyclobutyl)ethyl]}siloxane

A. V. Kalinin, A. N. Reznikov, G. A. Nikolaev, Yu. V. Khoroshavina, A. S. Ramsh, and N. K. Skvortsov

Lebedev Research Institute of Synthetic Rubber, State Unitary Enterprise, St. Petersburg, Russia
St. Petersburg State Technological Institute (Technical University), St. Petersburg, Russia

Received June 17, 2005; in final form, December 2005

Abstract—The possibility of preparing a new fluorosiloxane elastomer by hydrolytic copolycondensation of the hydrosilylated derivative of 1-vinyl-2,2,3-trifluoro-3-trifluoromethylcyclobutane with dimethyldichlorosilane was examined.

DOI: 10.1134/S1070427206030293

Development of new elastomers combining high oil and benzine resistance with a low glass transition point remains urgent in the modern chemistry of polymers. Among the best materials having such a set of properties are polyfluoroalkylsiloxanes. However, production of commercial rubbers based on poly(methyl-3,3,3-trifluoropropyl)siloxanes such as SKTFT requires expensive and relatively difficultly accessible 3,3,3-trifluoropropene. Thus, an important task is to develop methods for preparing polymers similar in their characteristics to poly(methyl-3,3,3-trifluoropropyl)siloxane from fluoroalkenes that are more readily available and convenient in handling.

In this respect, one of the most promising compounds is 1-vinyl-2,2,3-trifluoro-3-trifluoromethylcyclobutane **I**, whose preparation by a simple procedure from commercial buta-1,3-diene and hexafluoropropene was described in [1, 2].

Patent [3] reported for the first time on hydrosilylation of fluoroalkene **I** with methyldichlorosilane **II**, giving methyl[2-(2,2,3-trifluoro-3-trifluoromethylcyclobutyl)ethyl]dichlorosilane **III** in 90% yield.

Dichlorolisane **III** was further used for preparing 1,3,5-trimethyl-1,3,5-tris[2-(2,2,3-trifluoro-3-trifluoromethylcyclobutyl)ethyl]cyclotrisiloxane, a monomer in synthesis of the corresponding polysiloxane [4]. Anionic polymerization of the latter yields a high-quality polymer [5], but this method requires isolation of the pure trimer by vacuum distillation [bp 220°C (2 mm Hg)].

The goal of this study was to optimize the process in the hydrosilylation stage, and one of pathways was to choose a catalyst with a high activity and selectivity, as well as to take advantage of the possibility of synthesizing polysiloxanes directly from dichlorosilane **II** without isolation of the high-boiling trimer.

Hydrosilylation of fluoroalkenes was the subject of numerous studies [3, 6–8], most of which mention the commonly used Speier's or Karstedt's catalysts [1, 6, 7]. The only exception is a study by Ojima *et al.* [8] describing in detail hydrosilylation of 3,3,3-trifluoropropene and pentafluorostyrene, catalyzed by palladium, rhodium, and ruthenium complexes. With Rh and Ru catalysts, the reaction proceeds nonselectively, which rules out their practical application.

As shown previously [9–11], the catalytic activity of transition metal complexes in hydrosilylation is substantially affected by the nature of the ligand surrounding, in particular, by the balance of the σ-donor and π-acceptor properties of neutral ligands. In a series of Pt(II) complexes whose ligands have more prominent π-acceptor properties, the catalytic activity in adding hydrosilanes and hydrosiloxanes at the C=C bond tends to increase, as confirmed by kinetic studies [9, 10].

To extend the relationships revealed to reactions of fluoroalkenes, as well as to find new highly efficient catalysts for the process under study, we carried out hydrosilylation of cyclobutane **I** with hydrosilane **II** in the presence of platinum(II) bisphosphine complexes, *cis*-[$PtCl_2L_2$] [L = Et_3P, $Ph_2PCH{=}CH_2$, Ph_3P, *cyclo*-

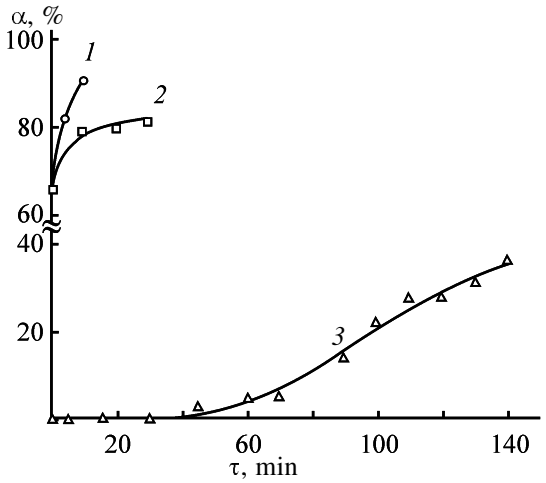
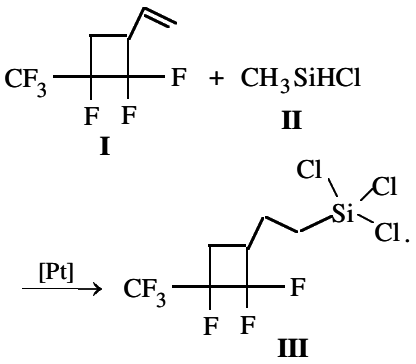


Fig. 1. Kinetic plots for the reaction of cyclobutane **I** and chlorosilane **II** in the presence of Pt(II) complexes. c_{cat} = 4×10^{-4} mol mol^{-1} ≡SiH, T = 50°C. (α) Cyclobutane **I** conversion and (τ) time. (*1*) *cis*-[$PtCl_2(Ph_2PC_6H_9)_2$], (*2*) *cis*-[$PtCl_2(Ph_3P)_2$], and (*3*) *cis*-[$PtCl_2(Ph_2PCH{=}CH_2)_2$].

$C_6H_9PPh_2$ (*cyclo*-C_6H_9 is cyclohex-1-enyl]. The selectivity of the reaction was monitored by ^1H and ^{29}Si NMR spectroscopy.

We found that hydrosilane **II** is added regioselectively; in accordance with the Farmer rule, the only reaction product is methyl[2-(2,2,3-trifluoro-3-trifluoromethylcyclobutyl)ethyl]dichlorosilane **III**, which was isolated from the reaction mixture by vacuum distillation:



The nature of the phosphine in the complex strongly affects its catalytic activity (Fig. 1). We found that, for [$PtCl_2L_2$] complexes, the catalytic activity increases in the ligand series as $Et_3P \ll Ph_2PCH{=}CH_2 \ll Ph_3P < Ph_2PC_6H_9$ and it determined by the combined effect or electronic and steric factors.

Dichlorobis(triethylphosphine)platinum(II) does not noticeably catalyze the reaction under the experimental conditions. With dichlorobis(vinyldiphenylphosphine)platinum(II), there was a significant induction period (30 min), and conversion of cyclobutane **I** within 2 h did not exceed 30%. At the same time, dichlorobis(triphenylphosphine)platinum(II) and dichlorobis(diphenylcyclohex-1-enylphosphine)platinum(II) are very active catalysts.

The ligand "activity series" that we derived shows that the π-acceptor properties of the phosphines are enhanced in going from electron-donating alkyl to alkenyl and aromatic substituents at the phosphorus atom. At the same time, a sharp increase in the catalytic activity in going from the vinyl to a bulky cyclohex-1-enyl substituent suggests a substantial contribution from the steric factors to the catalytic properties of Pt(II) phosphine complexes.

Our kinetic studies showed that the relationships in variation of the catalytic properties of Pt(II) complexes in the reaction of cyclobutane **I** with hydrosilane **II** correspond to those in hydrosilylation of alkenes [9, 10], which facilitates a search for the best reaction catalysts. In the series of the metal complexes considered, the most efficient are dichlorobis(triphenylphosphine)platinum(II) and dichlorobis(diphenylcyclohex-1-enylphosphine)platinum(II).

Patent [5] reports on preparation of polymethyl[2-(2,2,3-trifluoro-3-trifluoromethylcyclobutyl)ethyl]- and polymethyl[2-(2,2,3-trifluoro-2-trifluoromethylcyclobutyl)ethyl]siloxanes by anionic polymerization. It was found that vulcanizates of such a polymer are resistant to swelling in hydrocarbon solvents (somewhat more resistant than those based on SKTFT-100 rubber) and have a high thermal stability (13% weight loss occurs at 430°C) [5]. However, the glass transition point of such material proved to be unacceptably high, from –36 to –32°C. Borisov [12] showed previously with poly(dimethyl)(methylphenyl)siloxane and poly(dimethyl)(diphenyl)siloxane as examples that introduction of dimethylsiloxane units into the macromolecular chain substantially lowers the glass transition point of the polymer. Therefore, in the context of the task of increasing the frost resistance, it was of interest to prepare a polymer with a mixed structure, containing both methyl[2-(2,2,3-trifluoro-3-trifluoromethylcyclobutyl)ethyl]siloxane and dimethylsiloxane units in a ratio such that the fluorine content was as close as possible to that in SKTFT-50 rubber, since this characteristic governs the resistance of the material to nonpolar solvents.

Cazacu *et al*. [13, 14] described a two-step process for preparing mixed polydimethylpolydiphenylsiloxane copolymer by condensation of an equimolar mixture of tetramethyldisiloxanediol in the presence of a polymeric sulfonic acid (Vionit CS-34C). These

silanediols are formed by hydrolysis of the corresponding chlorosilanes, the rate constant of hydrolysis of the Si–Cl bond being virtually independent of the nature of other substituents at the silicon atom [15]. This fact suggested that three different reactions can be integrated into one step (hydrolysis of a mixture of chlorosilanes, condensation of the resulting silanediols and siloxanediols with one another, and opening of the cyclic siloxanes formed by hydrolysis, in the presence of an acid catalyst).

We found that dichlorosilane **III** synthesized by hydrosilylation in the presence of fluoroalkanesulfonic acids enters into the copolycondensation reaction with dimethyldichlorosilane **IV** to form poly(dimethyl)-{methyl[2-(2,2,3-trifluoro-3-trifluoromethylcyclobutyl)ethyl]}siloxane **VI**. According to the ^{29}Si NMR data, it contains about 30% siloxane units with fluorine-containing substituents. To enable vulcanization of the polymer with peroxide initiators, we introduced into the polymer about 0.3% methylvinylsiloxane units. The overall equation of the process can be represented as follows:

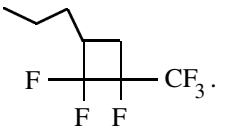
$$x\mathrm{R_FMeSiCl_2} + y\mathrm{Me_2SiCl_2} + z\mathrm{CH_2{=}CH(Me)SiCl_2}$$
III **IV** **V**

$$+ (x + y + z + 1)\mathrm{H_2O}$$

$$\rightarrow \mathrm{HO{-}[(R_FMeSiO)_x(MeOSiO_2)_y(CH_2{=}CH(Me)SiO)_z]{-}H}$$
VI

$$+ 2(x + y + z)\mathrm{HCl},$$

where R_F =



A study of the sample by gel-permeation liquid chromatography showed that it contained about 10% low-molecular-weight cyclic products. The polydispersity index of the polysiloxane was 7.3, and the weight-average molecular weight, 606000.

The resulting polymer is significantly superior to commercial rubbers like SKTFT in the thermal stability. According to thermogravimetric data, for the sample synthesized a 5% weight loss is observed only at 350°C, while for SKTFT-50 rubber even at 270°C a 13% weight loss was observed.

The low-temperature properties of the polymer were studied by the low-temperature dielectric spectroscopy. The maximum in the temperature dependence of the dielectric loss tangent (Fig. 2) corresponds to the temperature of the dielectric α-transition, which is typically 5–10 K higher than the glass transition point of the corresponding polymer [17]. Introduction into the macromolecular chain of a significant number of dimethylsiloxane units, as expected, sharply improved the low-temperature properties relative to the homopolymer. Comparison of our data with the results of similar studies of commercially produced SKTFT-50 rubber (Fig. 2) shows that the polymer that we synthesized is close in the low-temperature properties to SKTFT-50 rubber.

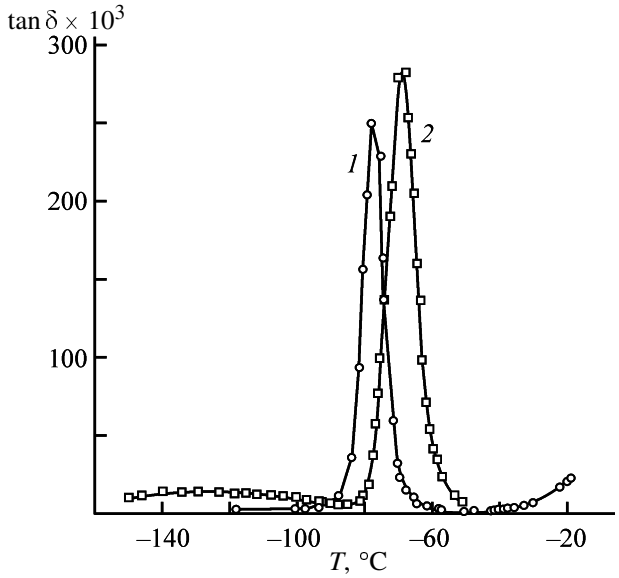


Fig. 2. Temperature dependence of the dielectric loss tangent tan δ for (*1*) SKTFT-50 rubber and (*2*) polysiloxane **VI**.

EXPERIMENTAL

The ^{1}H and ^{29}Si NMR spectra were recorded on a Bruker AC-500 spectrometer (working frequencies 500.142 and 99.361 MHz, respectively) with TMS as internal reference and $CDCl_3$ and $(CD_3)_2CO$ as solvents.

The molecular-weight distribution was determined on a Waters gel chromatograph at 25°C using a column packed with Microstyrogel stationary phase with a permeability of 10000, 500, and 100 Å; mobile phase (THF) flow rate 1 ml min^{-1}.

Thermogravimetric studies were carried out on a Du Pont 951 instrument (heating rate 10 deg min^{-1}).

The dielectric properties of the polysiloxane synthesized were studied with an Orion TR-9701 dielectric bridge using a three-electrode cell temperature-controlled in the range from –150 to 150°C.

Chromatographic analysis was carried out on a Tsvet-100 instrument with a thermal conductivity

detector; stationary phase Chromaton N-AW (0.315–0.400 mm), impregnated with 10% SE-30; carrier gas helium, flow rate 4 $l\,h^{-1}$, bridge current 100 mA; column temperature 150°C.

The kinetics of hydrosilylation of cyclobutane **I** was monitored by chromatographic analysis of the regularly taken samples of the reaction mixture.

Into a temperature-controlled reactor with a magnetic stirrer, 4.9 mmol of cyclobutane **I** and 5.0 mmol of hydrosilane **II** were introduced. When the temperature of the mixture reached 50°C, 20 μl of 0.1 M solution of the catalyst in dichloromethane was added, from which moment the time was counted. The catalyst concentration in the reaction mixture was 4×10^{-4} mol mol^{-1} of hydrosilane **II**.

Dichlorobis(triethylphosphine)platinum(II) and dichlorobis(triphenylphosphine)platinum(II) [18], dichlorobis(vinyldiphenylphosphine)platinum(**II**) [19], and dichlorobis(diphenylcyclohex-1-enylphosphine)-platinum(**II**) [20] were prepared by published procedures.

Methyl[2-(2,2,3-trifluoro-3-trifluoromethylcyclobutyl)ethyl]dichlorosilane III was isolated from the reaction mixture by vacuum distillation, bp 55°C (2 mm Hg), n_D^{20} 1.4039, d_{20}^{20} 1.3573. ^{1}H NMR spectrum, δ, ppm ($CDCl_3$): 0.80 s (3H, CH_3Si); 1.10 t (2H, CH_2Si), J_{HH} 8 Hz; 1.65–2.10 m (2H, CH_2); 2.33 m (1H, CH); 2.65 m (2H, CH_2). ^{29}Si NMR spectrum: δ_{Si} 29.7 ppm.

Found (%): Si 9.05, C 30.02, F 35.60, Cl 22.06, H 3.10.

Calculated (%): Si 9.09, C 30.09, F 35.74, Cl 21.94, H 3.14.

Poly(dimethyl){methyl[2-(2,2,3-trifluoro-3-trifluoromethylcyclobutyl)ethyl]}siloxane VI. Into a four-necked round-bottomed flask equipped with a wide-blade stirrer, glycerol seal, a thermometer, and a dropping funnel, 0.333 mol of dichlorosilane **III**, 0.671 mol of dichlorosilane **IV**, and 3.17 mmol of methylvinyldichlorosilane and then a solution of 0.03 mol of fluoroalkanesulfonic acid in 3 ml of nitromethane were added. To the resulting mixture, a mixture of 1.00 mol of water and 1,2-dimethoxyethane was added dropwise with stirring. Hydrolysis was carried out for 72 h. Then the reaction mixture was stirred in a vacuum (20 mm Hg) for 16 h, dissolved in chloroform, and 0.10 mol of ammonium hydrocarbonate was added to the resulting solution. The solution was stirred for 8 h, the precipitate was separated, the solvent was removed in a water-jet-pump vacuum, and the reaction product was kept in a vacuum oven at 120–150°C and 1.5 mm Hg until frothing ceased. After the treatment, the polymer was once again dissolved in chloroform. To a solution, 0.10 mol of finely pulverized anhydrous sodium hydrocarbonate was added, whereupon the solution was filtered. The polymer was precipitated with ethanol, and the reprecipitated polymer was once again kept in an oven for 6 h at 200°C (1 mm Hg). Yield of polymer **VI** 80%. ^{29}Si NMR spectrum, δ_{Si}, ppm [$(CD_3)_2CO$]: 2.16 [$(CH_3)_2SiO$], 23.8 [$(CH_3)R_FSiO$].

CONCLUSIONS

(1) The cycloaddition product of commercially available buta-1,3-diene and hexafluoropropene, 1-vinyl-2,2,3-trifluoro-3-trifluoromethylcyclobutane, was hydrosilylated with methylchlorosilane to form methyl[2-(2,2,3-trifluoro-3-trifluoromethylcyclobutyl)-ethyl]dichlorosilane. *cis*-Dichlorobis(triphenylphosphine)platinum(II) and *cis*-dichlorobis(diphenylcyclohex-1-enylphosphine)platinum(II) were suggested as efficient hydrosilylation catalysts.

(2) Methyl[2-(2,2,3-trifluoro-3-trifluoromethylcyclobutyl)ethyl]dichlorosilane was used as comonomer in synthesis of poly(dimethyl){methyl[2-(2,2,3-trifluoro-2-trifluoromethylcyclobutyl)ethyl]}siloxane by hydrolytic polycondensation, which eliminates a labor- and power-consuming step of isolation of cyclosiloxanes.

(3) The points of dielectric α-transition of commercial SKTFT-50 rubber and of the elastomer synthesized are close, but the latter is superior in the thermal stability, which makes it promising for production of specialty rubbers.

ACKNOWLEDGMENTS

This study was financially supported by the Russian Foundation for Basic Research (project no. 04-03-32623a).

REFERENCES

1. McBee, E.T., Hsu, C.G., Pierse, O.R., and Roberts, C.W., *J. Am. Chem. Soc.*, 1955, vol. 77, no. 4, pp. 915–917.
2. Banks, R.E., Barlow, M.G., Haszeldine, R.N., and Morton, W.D., *J. Chem. Soc., Perkin Trans. 1*, 1974, no. 11, pp. 1266–1271.
3. RU Patent 2101286.
4. RU Patent 2089554.

5. RU Patent 2078097.
6. US Patent 6291623.
7. Furukawa, Y., Kotera, M., Oharu, K., et al., *Reports Res. Lab., Asahi Glass Co., Ltd.*, 1997, vol. 47, pp. 81–94.
8. Ojima, I., Fuchikami, T., and Yatabe, M., *J. Organomet. Chem.*, 1984, vol. 260, no. 3, pp. 335–346.
9. Skvortsov, N.K., *Zh. Obshch. Khim.*, 1993, vol. 63, no. 5, pp. 961–987.
10. Vekki, D.A. de and Skvortsov, N.K., *Zh. Obshch. Khim.*, 2004, vol. 74, no. 2, pp. 224–233.
11. Reznikov, A.N. and Skvortsov, N.K., *Zh. Obshch. Khim.*, 2004, vol. 74, no. 10, pp. 1639–1643.
12. Borisov, S.N., *Kauchuk Rezina*, 1966, no. 7, pp. 3–8.
13. Cazacu, M., Vlad, A., Marcu, M., et al., *Rev. Roum. Chem.*, 2000, vol. 45, no. 6, pp. 561–566.
14. Cazacu, M., Vlad, A., Marcu, M., and Ragles, C., *Rev. Roum. Chem.*, 2001, vol. 46, no. 8, pp. 919–924.
15. Mileshkevich, V.P., Nikolaev, G.A., Evdokimov, V.F. and Karlin, A.V., *Zh. Obshch. Khim.*, 1971, vol. 41, no. 3, pp. 634–638.
16. Korshak, V.V., *Termostoikie polimery* (Heat-Resistant Polymers), Moscow: Nauka, 1969.
17. Ramsh, A.S., Nikolaev, G.A., and Lobkov, V.D., Abstracts of Papers, *Pervaya Vserossiiskaya konferentsiya po kauchuku i rezine* (First All-Russia Conf. on Rubber and Vulcanized Rubber), Moscow, February 26–28, 2002, pp. 73–75.
18. Colquhoun, H.M., Holton, J., Thomson, D.J., and Twigg, M.V., *New Pathways for Organic Synthesis: Practical Applications of Transitions Metals*, New York: Plenum, 1984.
19. Rahn, J.A., Holt, M.S., Gray, G.A., et al., *Inorg. Chem.*, 1989, vol. 28, no. 2, pp. 217–226.
20. Reznikov, A.N., Krivchun, M.N., Bel'skii, V.K., and Skvortsov, N.K., *Zh. Obshch. Khim.*, 2000, vol. 70, no. 7, pp. 1102–1106.

ISSN 1070-4272. Russian Journal of Applied Chemistry, 2006, Vol. 79, No. 3, pp. 480–483. © Pleiades Publishing, Inc., 2006.
Original Russian Text © O.V. Brovkina, E.D. Shkorina, L.A. Zemnukhova, N.A. Didenko, L.E. Kryukova, 2006, published in Zhurnal Prikladnoi Khimii, 2006, Vol. 79, No. 3, pp. 488–492.

MACROMOLECULAR CHEMISTRY AND POLYMERIC MATERIALS

Bleaching of Buckwheat Straw and Peel with Potassium Peroxoborate

O. V. Brovkina, E. D. Shkorina, L. A. Zemnukhova, N. A. Didenko, and L. E. Kryukova

Institute of Chemistry, Far-Eastern Division, Russian Academy of Sciences, Vladivostok, Russia

Received July 4, 2005

Abstract—The use of potassium peroxoborate for bleaching buckwheat production waste, straw and peal, both untreated and treated with water, mineral acids, sodium hydroxide, and organic solvents, is examined.

DOI: 10.1134/S107042720603030X

Complex utilization of plant raw materials is urgent today. Of special value is renewable waste of cereals, accumulated at plants during corn peeling. Among promising raw materials for preparation of a number of chemical substances is large-tonnage waste from buckwheat production, such as flower shells, peel (BP) or husk, and straw (BS), most of which is currently burned in fields or used as fuel.

Here we continue a study of the waste from buckwheat production as a candidate raw material for chemical industry [1–3] and examine the suitability of potassium peroxoborate (PPB) (whose synthesis procedure was developed previously [4]) for bleaching BP and BS and their residues (after recovery of polysaccharides of various compositions) for pulp production. It should be noted that highly efficient inorganic high-peroxide boron compounds [4] successfully passed laboratory and semicommercial tests as bleaching agents for textile materials (cotton and flax) and mulberry silkworm threads in China.

EXPERIMENTAL

Our study was concerned with BS and BP from various regions of Russia (Primorskii, Krasnodar, and Altai krais, Amur oblast). The straw was ground to 5-cm-long particles, and the peel was separated into fractions, whereupon particles ≥2 mm in size were selected. The raw material was washed with water and dried at 60°C.

We studied how the bleaching agent PPB affects the samples of the initial raw material and its residue after treatment (extraction) with water, mineral acids (1 N HCl, H_2SO_4, HNO_3), sodium hydroxide (0.1 and 1 N solutions), and organic solvents (a chloroform–ethanol mixture, 1 : 1 by volume) at the solid : liquid volume ratio of 1 : 10, extraction time of 1 h, and temperature of 95°C. The raw material residue after extraction of soluble substances was filtered off, washed with water, and dried to constant weight at 60°C.

Table 1 presents the samples of the initial raw ma-

Table 1. BS and BP samples studied*

Raw material	Sample no.	Solvent	Raw material residue, wt %
BS-1	1	–	
	2	H_2O	79.0
	3	1 N HCl	64.0
	4	1 N H_2SO_4	82.0
	5	1 N HNO_3	43.0
	6	$CHCl_3$ + C_2H_5OH (1 : 1)	61.3
	7	0.1 N NaOH	73.0
	8	1 N NaOH	99.0
BS-2	9	0.1 N NaOH	73.0
	10	1 N NaOH	99.0
BS-3	11	0.1 N NaOH	73.0
	12	1 N NaOH	99.0
BP-1	13	–	
	14	H_2O	73.0
	15	1 N HCl	43.0
	16	1 N NaOH	49.0
	17	$CHCl_3$ + C_2H_5OH (1 : 1)	80.5

* BS and BP samples, plant strain, place and time of collection of the raw material: BP-1, Ekaterinoslavka settlement, Amur oblast, 2001; BS-1 and BS-2, town of Ussuriisk, Primorskii krai, Izumrud strain, 2000–2001, respectively; BS-3, town of Ussuriisk, Primoskii krai, strain P-312, 2001.

terial and the weight of its residue after extraction. We determined the composition of the extracts in [2].

The action of PPB containing 20% available oxygen O_{av} on the BS and BP samples under study was examined in relation to pH of the solution (created by the bleaching composition components in the case of PPB and adjusted with alkali in the case of H_2O_2), bleaching agent concentration, and temperature and time of the process. For comparison, we carried out a series of experiments on bleaching of BS and BP with hydrogen peroxide.

The decomposition rate for PPB and H_2O_2 was estimated from the change in the content of O_{av} in solution, determined by permanganatometric titration [5], and calculated as $\ln[c_0/(c_0 - c_x)]$, where c_0 is the initial concentration of available oxygen in solution and $(c_0 - c_x)$, concentration of the available oxygen that did not decompose by the time τ.

The decomposition rate constants of available oxygen in solution were calculated by the rate equation of the first-order reaction [6]. The bleaching power of PPB was determined on a Specol instrument by the technique described in [7] relative to freshly calcined magnesium oxide as the reference. We analyzed the spectrophotometric curves of the reflection coefficient ρ at 400–700 nm and the whitenesses of the raw material samples studied. The results are presented in Figs. 1–4 and Tables 1–3.

Preliminary studies showed that BP (Table 1, sample nos. 13–17) was bleached with PPB much less efficiently than BS, and we chose BS as the primary object of our study.

The initial BS, both ground and nonground (Table 1, sample no. 1), was bleached with PPB and H_2O_2. Figure 1 presents the kinetic curves of thermal decomposition of aqueous solutions of PPB and H_2O_2 during bleaching of BS.

Our data show that, with PPB as the bleaching agent (Fig. 1, curves *1, 2*), decomposition of available oxygen proceeds uniformly at a low rate, which allows a "softer", compared to H_2O_2, bleaching of the raw material (Fig. 1, curves *3, 4*). With PPB as the bleaching agent, the initial concentration of O_{av} within the initial 30 min decreases by 17–27% (Table 2). Further, the decomposition rate of O_{av} remains virtually unchanged. The degree of decomposition of O_{av} within 60 min of bleaching was estimated at 22.7–31.9%.

We calculated the rate constants of O_{av} decomposition in solution and estimated the whiteness of the bleached BP and BS samples (Table 2). The initial

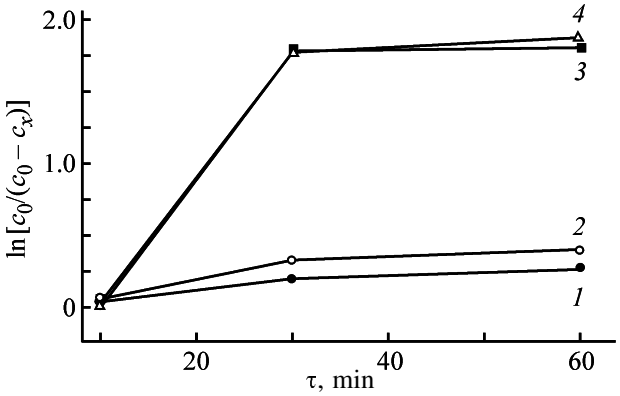


Fig. 1. Kinetic curves of thermal decomposition of O_{av} in solutions containing BS (sample no. 1) in bleaching with (*1, 2*) PPB and (*3, 4*) H_2O_2. (c_0) Initial concentration of O_{av} in solution, (c_x) O_{av} concentration in solution at the moment τ, and (τ) time of bleaching with hydrogen peroxide; the same for Figs. 2 and 3. BS: (*1, 3*) nonground and (*2, 4*) ground.

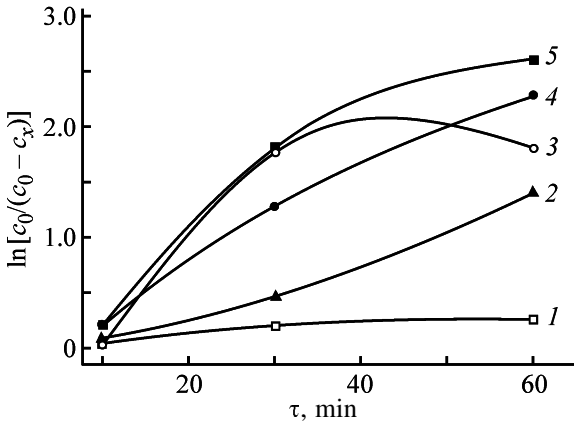


Fig. 2. Kinetic curves of thermal decomposition of O_{av} in solutions containing bleaching agent (PPB or H_2O_2) and the BS residue. Bleaching agent, sample no.: (*1*) PPB, 1; (*2*) PPB, 7 (0.1 N NaOH); (*3*) H_2O_2, 1; (*4*) PPB, 12 (1 N NaOH); and (*5*) H_2O_2, 12 (1 N NaOH).

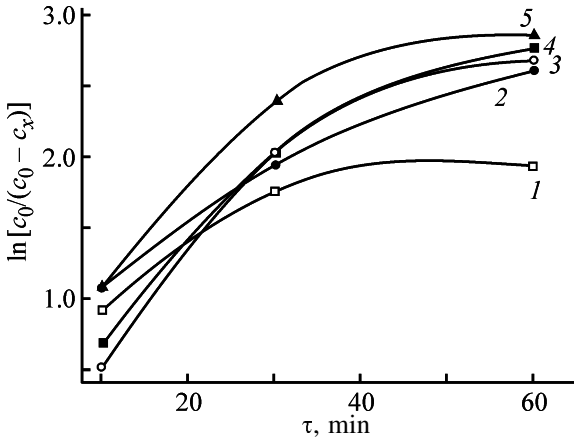


Fig. 3. Kinetic curves of thermal decomposition of O_{av} in solutions containing PPB and BS residue after treatment. Sample no., treating agent: (*1*) 6, organic solvent; (*2*) 4, H_2SO_4; (*3*) 3, HCl; (*4*) 2, H_2O; and (*5*) 5, HNO_3.

Table 2. Bleaching power of PPB and H_2O_2 with respect to BS (T = 95°C, τ = 60 min)

Sample no. in Table 1	Treatment procedure	Bleaching agent	pH	Degree of decomposition of O_{av}			Whiteness, %	$k^* \times 10^4$, s^{-1}		
				10 min	30 min	60 min		10 min	30 min	60 min
1	Initial sample:									
	nonground	PPB	8	3.5	17.02	22.70	68.8	0.6	1.03	0.71
	ground	PPB	8	5.32	27.31	31.92	69.1	0.917	1.77	1.07
	nonground	$H_2O_2 + {}^-OH$	8	0.72	82.98	83.69	45.3	0.23	9.83	5.03
	ground	$H_2O_2 + {}^-OH$	8	0.10	82.98	84.04	58.7	0.05	9.83	5.09
7	0.1 N NaOH	PPB	8	6.38	37.59	76.17	29.0	1.1	2.5	3.97
9	0.1 N NaOH	PPB	8	6.38	37.59	77.31	29.7	1.1	2.61	4.11
11	0.1 N NaOH	PPB	8	7.81	41.14	96.03	30.3	1.35	2.5	8.72
12	0.1 N NaOH	PPB	9	17.73	77.87	98.80	29.9	3.25	8.38	6.33
10	0.1 N NaOH	PPB	9	20.57	79.58	77.52	24.4	3.83	8.83	5.78
12	0.1 N NaOH	PPB	9	17.73	72.80	79.79	23.4	3.25	7.11	6.33
8	0.1 N NaOH	$H_2O_2 + {}^-OH$	9	16.32	83.69	90.92	22.1	2.96	10.05	6.67
10	0.1 N NaOH	$H_2O_2 + {}^-OH$	9	18.44	83.69	91.49	22.8	3.32	10.05	7.03
12	0.1 N NaOH	$H_2O_2 + {}^-OH$	9	17.03	83.69	92.06	20.1	3.1	10.05	7.02

* k is the decomposition rate constant.

Table 3. Buckwheat straw, treated and bleached with PPB and H_2O_2 (T = 95°C, τ = 60 min)

Sample no. in Table 1	Bleaching agent	pH	Degree of decomposition of O_{av}, %			$k \times 10^4$, s^{-1}		
			10 min	30 min	60 min	10 min	30 min	60 min
2	PPB	9	49.36	86.95	93.76	11.33	11.33	7.69
3	PPB	8	40.43	86.95	93.76	8.67	11.33	7.69
4	PPB	8	65.96	90.92	93.76	18.0	13.33	7.69
5	PPB	6	65.96	85.82	93.19	18.0	10.83	7.47
6	PPB	7	60.28	82.98	85.82	15.33	9.83	5.42
2	$H_2O_2 + {}^-OH$	9	18.44	–	95.46	3.33	–	8.58
3	$H_2O_2 + {}^-OH$	9	17.38	–	95.46	3.17	–	8.58
4	$H_2O_2 + {}^-OH$	9	22.34	–	96.03	4.22	–	8.94
5	$H_2O_2 + {}^-OH$	9	36.88	–	86.67	7.67	–	5.58
6	$H_2O_2 + {}^-OH$	9	80.14	–	92.91	27.0	–	7.36

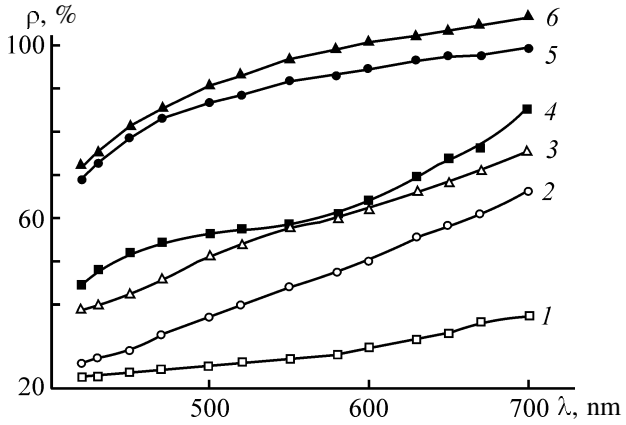


Fig. 4. Spectrophotometric curves of the reflection coefficient ρ for the raw material samples with and without bleaching. (λ) Wavelength. Sample no., bleaching agent: (*1*) 13, none, (*2*) 13, H_2O_2; (*3*) 13, PPB; (*4*) 1, none, (*5*) 1, H_2O_2; and (*6*) 1, PPB.

BS, bleached with PPB, undergoes the most profound oxidation, the whiteness being 69%, and with H_2O_2 the whiteness was no greater than 58%.

Grinding of BS insignificantly accelerated decomposition of O_{av}, leaving the whiteness virtually unaffected (68.8 against 69.1%). Replacement of PPB by H_2O_2 sharply (fivefold) accelerated decomposition of O_{av} (Fig. 1, curves *3* and *4*), with the linear run of the kinetic plots preserved. The degree of decomposition of the available oxygen is 82.98% within the initial 30 min and only slightly changes within the subsequent 30 min. It should be noted that, in this case, grinding of the straw affects the whiteness, namely, increases by 10% (45.3 and 58.7%), leaving the O_{av} decomposition rate virtually unaffected (Table 2).

Figure 2 and Table 2 show how PPB and H_2O_2 affect the BS residue after treatment with alkali solution

(0.1 N for sample nos. 7, 9, 11 in Table 1 and 1 N for sample nos. 8, 10, 12). Like in Fig. 1, the kinetic plots exhibit linear sections, corresponding to decomposition of O_{av} in solution within the initial 30 min. The major loss of O_{av} in solutions with PPB and H_2O_2 was estimated at 72.8–79.6% in the former case and 83.7% in the latter. The degree of decomposition of available oxygen in solutions with PPB and BS residues after hydrolysis of the raw material with 0.1 N NaOH was estimated at 76.2–96.0% (after hydrolysis with 1 N NaOH, 77.5–98.8%) (Table 2). The whitenesses for these samples are close, 29.0–30.3% (after hydrolysis with 1 N NaOH, 23.4–29.9%).

With H_2O_2 as the bleaching agent, the degree of decomposition of O_{av} is higher (92.0%), but the whiteness of the straw does not exceed 20.1–22.8%.

The rate constants of O_{av} decomposition in solutions are independent of the composition of the bleaching agent; they attain a maximum after 30 min and then tend to decrease. In the case of PPB, the rate constant of O_{av} decomposition is 8.5×10^{-4} s^{-1} on the average, and in the case of H_2O_2 it increases to 10.0×10^{-4} s^{-1} (Table 2).

Acid treatment of BS before bleaching with PPB accelerates the O_{av} decomposition in solution compared to the above-mentioned systems. Figure 3 presents the bleaching kinetic curves for BS sample nos. 2–6 (Table 1), and Table 3, the bleaching parameters.

The O_{av} decomposition rate in solution with PPB was at a maximum for the BS residue after extraction with HNO_3 (Fig. 3, curve *5*), and at a minimum, for the BS treated with an organic solvent (Fig. 3, curve *6*). Even within the initial 10 min, the degree of decomposition of O_{av} in solutions for all the systems was 40–66%. The calculated decomposition rate constants (Table 3) suggest that pretreatment of BS with water, acids, or organic solvents decreases this parameter when PPB is used as the bleaching agent.

Going from PPB to H_2O_2 as the bleaching reagent decelerates decomposition of O_{av} in solution with the same BS samples within the initial 10 min: The degree of decomposition of O_{av} was estimated at 17.4–36.9%. However, at the end of the peroxide bleaching (after 60 min) the O_{av} decomposition rate becomes comparable with those of the analogous solutions with PPB, and the degree of decomposition of O_{av} reaches 96%. The O_{av} decomposition rate constants at the end of bleaching of the BS samples with H_2O_2 are close to those for the systems with PPB, namely, 7.2×10^4 and 7.8×10^4 s^{-1}, respectively.

The spectrophotometric curves (Fig. 4) taken for BS and BP before and after bleaching with PPB and H_2O_2 at 400–700 nm suggest that the reflection coefficient ρ of the bleached raw material increases after bleaching. The reflection coefficients for the BS and BP bleached with PPB exceed those attained with H_2O_2.

CONCLUSIONS

(1) The kinetics of thermal decomposition of potassium peroxoborate and hydrogen peroxide during bleaching of buckwheat peel and straw was studied in relation to the kind of the raw material, method of its pretreatment (with water, mineral acid solutions, sodium hydroxide, or a mixture of chloroform with ethanol or its derivatives), and bleaching time. The decomposition rate constant of available oxygen in the case of potassium peroxoborate varies from 10^{-4} for the initial straw to $(7.8–8.7) \times 10^{-4}$ s^{-1} for the straw treated with the solvents, and in the case of hydrogen peroxide, from 5×10^{-4} to 10^{-3} s^{-1}, respectively.

(2) Potassium peroxoborate containing 20% available oxygen is suitable for bleaching of buckwheat straw. The most profound oxidation is characteristic for the initial (untreated) straw, whose whiteness reaches 69.1% (with hydrogen peroxide, 45.3%). The optimal time of bleaching of the straw with hydrogen peroxide was estimated at 30 min.

REFERENCES

1. Sergienko, V.I., Zemnukhova, L.A., Egorov, A.G., et al., *Ross. Khim. Zh.*, 2004, vol. 48, no. 3, pp. 116–122.
2. Zemnukhova, L.A., Tomshich, S.V., Shkorina, E.D., and Klykov, A.G., *Zh. Prikl. Khim.*, 2004, vol. 77, no. 7, pp. 1192–1196.
3. Zemnukhova, L.A., Shkorina, E.D., and Fedorishcheva, G.A., *Zh. Prikl. Khim.*, 2005, vol. 78, no. 2, pp. 329–333.
4. USSR Patent 1 831 843.
5. *GOST* (State Standard) *R 50672–94: Everyday Chemistry Items: A Method for Determination of the Mass Fraction of Available Oxygen: State Standards: Index*, Moscow: Izd. Standartov, 1996. vol. 3.
6. Emanuel', N.M. and Knorre, D.G., *Kurs khimicheskoi kinetiki* (A Course of Chemical Kinetics), Moscow: Vysshaya Shkola, 1984.
7. *OST* (Branch Standard) *6-15-1616–90: Domestic Bleaching Agents: A Procedure for Determination of the Bleaching Power: State Standards: Index*, Moscow: Izd. Standartov, 1996. vol. 3.

ISSN 1070-4272. Russian Journal of Applied Chemistry, 2006, Vol. 79, No. 3, pp. 484–487. © Pleiades Publishing, Inc., 2006.
Original Russian Text © V.P. Nekhoroshev, Yu.P. Turov, A.V. Nekhorosheva, V.D. Ogorodnikov, K.N. Gaevoi, 2006, published in Zhurnal Prikladnoi Khimii, 2006, Vol. 79, No. 3, pp. 493–496.

MACROMOLECULAR CHEMISTRY AND POLYMERIC MATERIALS

Structure of Products of Thermal Oxidative Degradation of Atactic Polypropylene

V. P. Nekhoroshev, Yu. P. Turov, A. V. Nekhorosheva, V. D. Ogorodnikov, and K. N. Gaevoi

Surgut State University, Surgut, Hanty–Mansi Avtonomnyi Okrug, Russia

Received December 9, 2005

Abstract—The structure of oxidized atactic polypropylene was studied.

DOI: 10.1134/S1070427206030311

Previously [1] we reported on preparation of oxidized atactic polypropylene (OAPP) under laboratory conditions and on the properties and applications of this product. Today Ataktika Limited Liability Company (Tomsk) produces OAPP in an amount of 400 t annually on a semicommercial installation by a continuous process of oxidation of atactic polypropylene (APP) melt with atmospheric oxygen.

In this study we analyzed the structure of the polymeric product formed by thermal oxidative degradation (TOD) of APP.

EXPERIMENTAL

APP, a raw material for OAPP production, is a by-product from the polypropylene plant of Tomskneftekhim Limited Liability Company. The properties of the APP-G grade polymer meet TU (Technical Specifications) 2211-056-05 796 653–98 (Table 1).

The viscosity-average molecular weight was calculated from the intrinsic viscosity measured in benzene at 23°C with an Ubbelohde viscometer:

$$[\eta] = 2.7 \times 10^{-4} \overline{M}_{\eta}^{0.71}.$$

The dynamic viscosity of the polymer melt was determined with a programmable Brookfield viscometer. The polydispersity index of the polymers was calculated from the data obtained by centrifugal sedimentation on an MOM analytical ultracentrifuge (for the procedure, see [2]). The amount of impurity isotactic fraction insoluble in boiling heptane was determined by extraction of commercial APP in a Soxhlet apparatus for 6 h. Atactic polypropylene was purified by extraction with heptane at 20°C, followed by repre-

Table 1. Properties of atactic polypropylene

Parameter	Sample			
	no. 1	no. 2	no. 3	no. 4
Viscosity-average molecular weight $M_\eta \times 10^{-3}$	40	36	25	20
Melt viscosity coefficient at 180°C, Pa s	15.0	18.0	0.8	0.2
Ring and ball softening point, °C	125	112	108	105
Needle penetration depth at 25°C, 0.1 mm units	34	40	58	73
Content of impurities, wt %:				
isotactic fraction	40.0	14.0	12.0	9.0
stereoblock fraction	14.0	1.0	18.0	19.0
Polydispersity index M_w/M_n	5.0	5.5	6.0	6.4
Iodine number, g I_2/100 g	0.25	0.28	1.32	1.90
Mean number of double bonds per polymer molecule	0.4	0.4	1.3	1.5

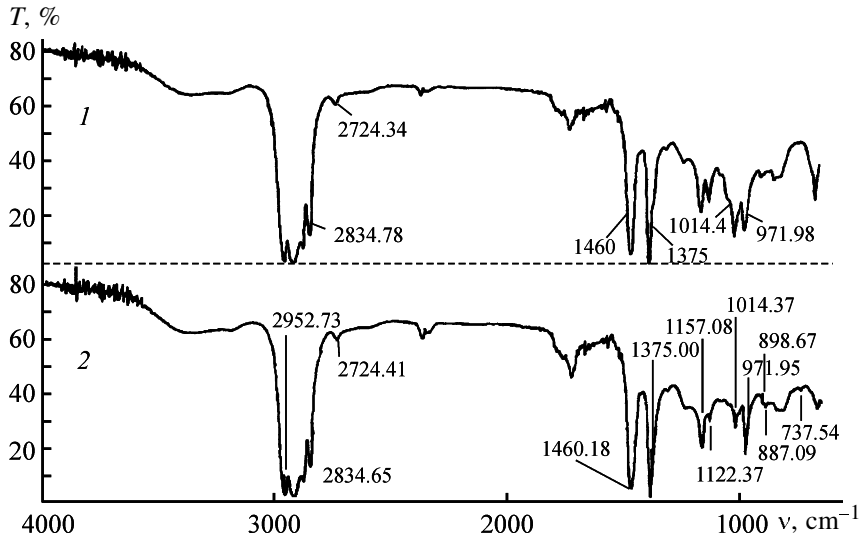


Fig. 1. IR spectra of OAPP: (*T*) transmission and (ν) wavenumber. Oxidation conditions: (*1*) APP sample no. 1, 180°C, 2 h; (*2*) sample no. 4, 250°C, 5 h.

cipitation with alcohol. The content of double bonds was determined by the Kaufman–Baltes method [3] from the iodine number. The IR spectra of APP were recorded on an Impact 410 Nicolet IR Fourier spectrometer using the multiple attenuated total internal reflection (MATIR) technique on a zinc selenide crystal [4]. The polymer was applied to the crystal at 20°C as a film and then kept for 3 h at room temperature.

The content of functional groups in OAPP was determined from the reduced intensities of absorption bands at 1720 (>C=O groups), 3180 (hydrogen-bonded alcoholic OH groups), and 3469 cm^{-1} (non-associated OH groups) [5]. As reference band we used the band at 1460 cm^{-1} whose intensity is insensitive to the OAPP composition and to the structure of its chains but monotonically varies with the sample thickness. The IR spectra of OAPP are shown in Fig. 1.

When calculating the concentrations of carbonyl and hydroxy groups, we used the molar extinction coefficients of 220 and 70 kg mol^{-1} cm^{-1}, respectively [5]. The amount of hydroxy groups at the secondary C atom was determined by acylation with acetic anhydride in pyridine [6].

The kinetic parameters of thermal oxidative degradation of the polymers were determined according to [7] using data obtained with a Q-1000 derivatograph in the range 20–500°C (Table 2).

Oxidized atactic polypropylene was prepared on a semicommercial installation consisting of three series-connected oxidation reactors of bubbler type with a working volume of 180 l and of two separating condensers for isolation of low-molecular-weight condensable liquid degradation products. The synthesis temperature was 150–250°C depending on the grade of OAPP to be obtained and on the properties of the starting polymer; the reaction time was 1.0–8.0 h, and the air flow rate, 0.6–1.9 l min^{-1} kg^{-1}. The yield of low-molecular-weight by-products depends on the oxidation conditions and varies within 0.3–5.0 wt % (Fig. 2). The variation of the molecular weight with time in the course of TOD of commercial APP samples of various quality (Table 1) is shown in Fig. 3.

The composition and properties of commercial APP vary in a wide range (Table 1), which means that the properties of this by-product depend on the grade of the main product, isotactic polypropylene (IPP). Sample nos. 1 and 4 differ in the composition and properties most significantly, and these samples were chosen for further studies. Low-molecular-weight APP has a lower content of the isotactic fraction, a higher content of double bonds, broader molecular-weight distribution, lower softening point, and lower melt viscosity; the latter two properties allow the TOD to be performed at 150°C.

Table 2. Kinetic parameters of thermal oxidative degradation of atactic polypropylene

Parameter	Sample	
	no. 1	no. 2
Activation energy, kJ mol^{-1}	62.4	56.3
Pre-exponential term, s^{-1}	5.0×10^2	1.4×10^2
Thermal effect of reaction, kJ kg^{-1}	–2000	–1306
Apparent reaction order	1.5	1.5

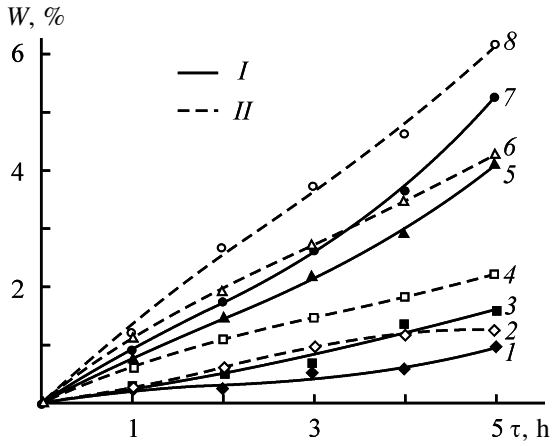
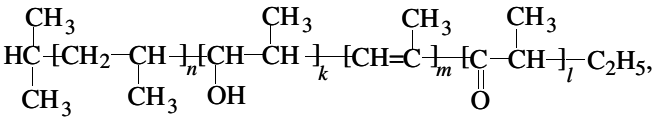


Fig. 2. Yield W of (*I*) low-molecular-weight organic compounds and (*II*) water in APP oxidation. Air flow rate 1.0 l min^{-1} kg^{-1}; the same for Figs. 3–5. (τ) Time; the same for Figs. 3 and 5. Oxidation conditions: (*1*, *2*) APP sample no. 1, 180°C; (*3*, *4*) sample no. 1, 250°C; (*5*, *6*) sample no. 4, 180°C; (*7*, *8*) sample no. 4, 250°C.

Low values of the activation energy and thermal effect of TOD of the lower-molecular-weight polymer confirm significant structural differences between the polymer samples, affecting their reactivity in oxidation (Table 2, sample no. 4).

The IR spectra of OAPP samples (Fig. 1) contain stretching vibration bands of >C=O groups of ketones in the region of 1720 cm^{-1}; at 3400–3200 cm^{-1}, there are characteristic weak broad absorption bands of stretching vibrations of alcoholic OH groups involved in hydrogen bonding and nonassociated OH groups. Weak bands of stretching vibrations of double >C=C< bonds in combination with bending vibration bands at 830, 887, 898, and 971 cm^{-1} are indicative of a high content of vinyl and vinylidene double bonds.

With an increase in the reaction temperature, the yield of water and low-molecular-weight condensable TOD products increases (Fig. 2). The yield of water at 250°C increases to 5.5% owing to dehydration of tertiary alcoholic groups with the formation of olefinic fragments. The reaction temperature and molecular weight of the starting APP affect the structure and properties of OAPP (Fig. 3). The extent of TOD of the polymer is fairly efficiently controlled by the reaction conditions, and three grades of OAPP can be produced (low-oxidized, intermediately oxidized, and highly oxidized) for various applications. The kinetic curves of accumulation of carbonyl and hydroxy groups in the polymer are shown in Figs. 4 and 5. After 1.5-h oxidation, the rate of accumulation of oxygen-containing groups sharply decreases, suggesting that the rates of polymer oxidation and its degradation with the elimination of low-molecular-weight oxygen-containing products (water, ketones) becomes equal. The concentration of hydroxy groups at the tertiary carbon atom considerably decreases with increasing temperature (Fig. 5, curves *1*, *3*), due to their dehydration. The mean content of olefinic double bonds in OAPP increases only slightly (to no more than two bonds per polymer molecule) relative to the starting polymer. The general formula of OAPP obtained on a semicommercial installation by oxidation of a polymer melt at 150–250°C is as follows:



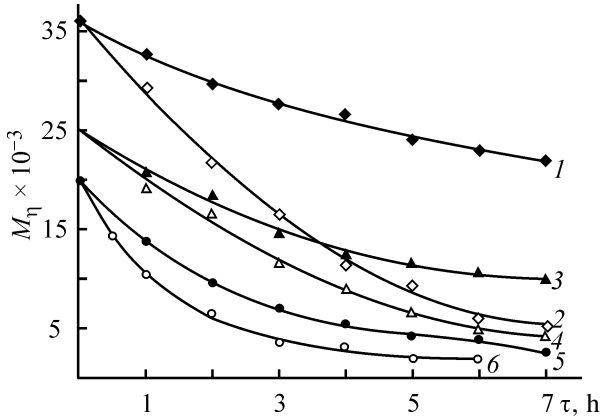


Fig. 3. Variation with time τ of the viscosity-average molecular weight M_η of APP in the course of its thermal oxidative degradation in melt. Oxidation conditions: (*1*, *2*) APP sample no. 2, (*3*, *4*) sample no. 3, and (*5*, *6*) sample no. 4. (*1*, *3*, *5*) 180 and (*2*, *4*, *6*) 250°C.

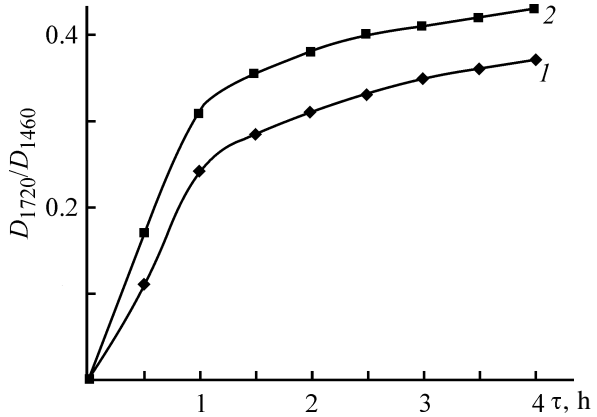


Fig. 4. Kinetic curves of accumulation of carbonyl groups in APP (sample no. 4) in the course of its thermal oxidative degradation. (D_{1720}, D_{1460}) Optical densities at 1720 and 1460 cm^{-1}, respectively; (τ) time. Oxidation temperature, °C: (*1*) 180 and (*2*) 250.

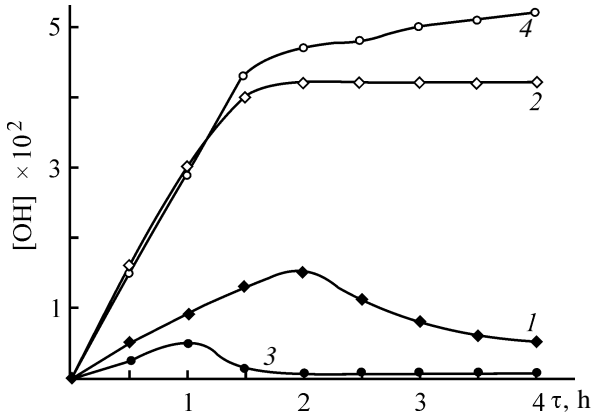


Fig. 5. Kinetic curves of the accumulation of hydroxy groups in APP (sample no. 4) in the course of its thermal oxidative degradation. OH groups: (*1*, *3*) at tertiary and (*2*, *4*) at secondary carbon atoms. Oxidation temperature, °C: (*1*, *2*) 180 and (*3*, *4*) 250.

where n = 123.0–898.0, m = 1.1–2.0, k = 1.0–1.9, l = 1.6–2.0.

Oxidation of APP methylene groups is caused by formation in a polymer melt of active radicals (hydroxy, methyl, primary alkyl), which are low-selective in hydrogen atom abstraction.

CONCLUSIONS

(1) Oxidized atactic polypropylene was prepared under semicommercial conditions by a three-reactor continuous process.

(2) The general formula of oxidized atactic polypropylene prepared by oxidation of atactic polypropylene melt with atmospheric oxygen at 150–250°C was determined.

REFERENCES

1. Nekhoroshev, V.P., Nekhorosheva, A.V., Gossen, L.P., et al., *Zh. Prikl. Khim.*, 2000, vol. 73, no. 6, pp. 996–999.
2. Nekhoroshev, V.P., Gossen, L.P., Balakhonov, E.G., et al., *Plast. Massy*, 1994, no. 2, pp. 71–75.
3. Houben–Weyl, *Methoden der organischen Chemie*, vol. 2: *Analytische Methoden*, Stuttgart: Thieme, 1953.
4. Smith, A.L., *Applied Infrared Spectroscopy: Fundamentals, Techniques, and Analytical Problem-Solving*, New York: Wiley, 1979.
5. Shibryaeva, L.S., Lunis, G.V., Monakhova, T.V., et al., *Khim. Fiz.*, 2002, vol. 21, no. 2, pp. 77–89.
6. Toroptseva, A.M., Belogorodskaya, K.V., and Bondarenko, V.M., *Laboratornyi praktikum po khimii i tekhnologii vysokomolekulyarnykh soedinenii* (Practical Laboratory Course of Chemistry and Technology of Macromolecular Compounds), Leningrad: Khimiya, 1972.
7. Balakhonov, E.G., Isakov, G.N., Nekhoroshev, V.P., et al., *Plast. Massy*, 1985, no. 9, pp. 47–48.

ISSN 1070-4272. Russian Journal of Applied Chemistry, 2006, Vol. 79, No. 3, pp. 488–491. © Pleiades Publishing, Inc., 2006.
Original Russian Text © K.G. Guliev, G.Z. Ponomareva, A.M. Guliev, 2006, published in Zhurnal Prikladnoi Khimii, 2006, Vol. 79, No. 3, pp. 497–500.

MACROMOLECULAR CHEMISTRY AND POLYMERIC MATERIALS

Photosensitivity of Polymers Based on Epoxy-Substituted Vinylphenylcyclopropanes

K. G. Guliev, G. Z. Ponomareva, and A. M. Guliev

Institute of Polymer Materials, National Academy of Sciences of Azerbaijan, Sumgaiyt, Azerbaijan

Received August 9, 2005; in final form, November 2005

Abstract—The capability of polymers synthesized from new monomers, 2-glycidyloxymethyl- and 2-glycidyloxycarbonyl-1-(*p*-vinylphenyl)cyclopropane, to photochemical cross-linking was evaluated from variation of their solubility after UV irradiation. The dependence of the photosensitivity of the polymers on the structure of substituents was studied.

DOI: 10.1134/S1070427206030323

The prospects for practical use of functional polymers, in particular, in negative photoresists, cause an interest in their study. The presence of functional groups and also their chemical nature affect appreciably such important photolithographic parameters of a resist as photosensitivity and resolution [1–7].

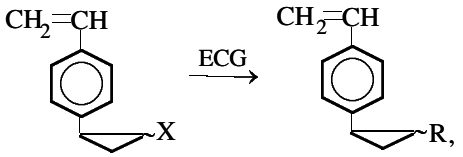
The practice of using some resists in photolithographic processes revealed a number of significant drawbacks, one of which is low photosensitivity. Hence, to improve the photosensitivity and other lithographic characteristics of negative photoresists based on functional polymers, radically new approaches to the synthesis of new monomers and polymers based on these are required.

We studied previously [8] the photochemical characteristics of polymers of functionally 2-substituted cyclopropylstyrenes.

Here we studied how the structure of functional groups affects the photosensitivity of polymers prepared from 2-glycidyloxymethyl- and 2-glycidyloxycarbonyl-1-(*p*-vinylphenyl)cyclopropanes.

The monomer for preparing the polymer was synthesized as follows. First, 2-ethoxycarbonyl-1-(*p*-vinylphenyl)cyclopropane was prepared by the reaction of ethyl diazoacetate with *p*-divinylbenzene in the presence of a catalytic amount of anhydrous $CuSO_4$. Then, 2-ethoxycarbonyl-1-(*p*-vinylphenyl)cyclopropane was saponified to obtain 2-carboxy-1-(*p*-vinylphenyl)cyclopropane and reduced to obtain 2-hydroxymethyl-1-(*p*-vinylphenyl)cyclopropane [9].

To prepare 2-glycidyloxymethyl- and 2-glycidyloxycarbonyl-substituted cyclopropanes, we chose the following pathway:



where X = $-CH_2OH$, $-COOH$;

R = $-CH_2OCH_2-CH(O)-CH_2$ (**I**), $-C(=O)-OCH_2-CH(O)-CH_2$ (**II**).

Chromatographic analysis and spectral data showed that the synthesized monomers I and **II** were mixtures of two individual compounds. We found that these compounds were geometric *cis* and *trans* isomers (ratio *cis* : *trans* = 30 : 70). The purity of the monomers synthesized was monitored by gas-liquid chromatography. In all cases it was 99.9%.

In the IR spectra of **I** and **II**, there are absorption bands at 830–850, 990–1000, 1640–1645, 1035–1045, and 1105–1110 cm^{-1}, characteristic of epoxy ring, vinyl group, three-membered carbon ring, and ether bond, respectively. In addition, in monomer **II** there is an absorption band at 1720 cm^{-1} characteristic of the carbonyl group. The absorption bands at 1500 and 1605 cm^{-1} characteristic of the benzene ring are preserved.

The ^1H NMR spectra of **I** and **II** contain signals characteristic of protons of aromatic ring (δ = 6.60–7.30 ppm), cyclopropane ring (0.65–1.66 ppm), and vinyl group (5.10–6.65 ppm). The epoxy ring protons give signals at 2.30–2.60 ppm (CH_2), and 2.96 ppm

(CH). These results suggest that the reactions in all steps proceed smoothly and with quantitative yields of the target products, leaving the vinyl group and three-membered ring intact.

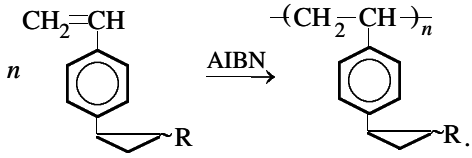
Polymerization of **I** and **II** was performed in the bulk and in benzene solution at 70°C in the presence of azobis(isobutylonitrile) (AIBN).

It was shown that, under the conditions studied, polymerization proceeds via scission of the double bond of the vinyl group to form macromolecules with reactive cyclopropane and epoxy side groups. This fact is confirmed by examination of the structure of the resulting polymers.

A comparison of the IR spectra of the initial monomers and polymers synthesized from them shows that the absorption bands at 990 and 1640 cm^{-1} observed in the spectra of the initial monomers and assigned to the bending and stretching modes of the vinyl bond, respectively, disappear after polymerization. The absorption bands at 1500 and 1605 cm^{-1} and in the range 1035–1045 cm^{-1} characteristic of the benzene ring and cyclopropane group, respectively, are retained during polymerization.

The absorption bands in the spectra of polymers at 1720 and in the ranges 840–850, 1105–1110 cm^{-1}, assigned to vibrations of the C–O, epoxy, and ether groups, are completely retained after the polymerization.

The IR data and elemental analysis suggest that the polymers synthesized have the following structure:



First of all, we should note some features of the structure of the resulting polymers containing two reactive groups, cyclopropane and epoxy, in the side chains of macromolecule. Due to easy rupture of the C–C and C–O bonds under irradiation [10–12], these functional groups impart to the resulting polymers high sensitivity to UV irradiation: under UV irradiation, these polymers easily transform into the insoluble form.

To elucidate the mechanism of photochemical cross-linking, we performed a spectroscopic study. For this purpose, we studied cross-linking of the resulting epoxy and cyclopropane-containing polymers by IR spectroscopy in various stages of UV irradiation. The results of UV irradiation are presented in Table 1.

Table 1. Data on UV irradiation of polymers based on monomers **I** and **II**

Monomer	Amount of polymer, %, after irradiation for indicated time, min				
	1	2	6	10	12
I	17	45	65	88	93
II	23	50	70	91	97

Table 1 shows that the maximal degree of photochemical conversion (the maximal amount of insoluble fractions) is observed with the polymer obtained from monomer **II**. This fact is undoubtedly associated with the structure of the macromolecule: along with cyclopropane and epoxy groups, it contains strongly absorbing carbonyl group, which significantly enhances the uptake of the UV energy.

The spectral analysis of the polymers showed that after UV irradiation the absorption bands characteristic of cyclopropane ring (1030–1040 cm^{-1}) and epoxy fragment (840–850, 917, 1250–1260 cm^{-1}) decrease or disappear. It was shown that the intensities of the absorption bands characteristic of cyclopropane and epoxy fragments decrease to a similar extent during UV irradiation in the initial stages. The clearest results were obtained at irradiation duration of 30 min, when the absorption bands of the above fragments virtually completely disappeared. Since the spectrum of the polymer after irradiation contained no absorption bands corresponding to cyclopropane and epoxy rings, it is evident that these groups participate in the subsequent photochemical reactions and these reactions are apparently resposible for the high capability of the polymer for photochemical cross-linking.

As seen from Table 2, the polymers synthesized have high lithographic characteristics, which allows these polymers to be used as a photosensitive base of photoresists. Thus, our studies demonstrated the possibility of developing a new class of photosensitive materials having high film-forming ability, elasticity, achromatism, and good adhesion characteristics appropriate for formation of photoresist films.

EXPERIMENTAL

2-Glycidyloxymethyl-1-(*p*-vinylphenyl)cyclopropane was prepared in a three-necked flask charged with 14.4 g (0.1 mol) of 2-hydroxymethyl-1-(*p*-vinylphen-

Table 2. Characteristics of polymers based on epoxy-substituted vinylphenylcyclopropanes

Copolymer	Concentration of polymer in benzene, %	Content of microdefects, def cm^{-2}	Film thickness, μm	Exposure time, s	Photosensitivity, $cm^2\ J^{-1}$
I	2	0.20	0.15	20	55.8
	5	0.20	0.15	20	56.7
	6	0.20	0.15	20	52.3
	10	0.25	0.20	20	50.5
II	2	0.15	0.15	20	56.4
	5	0.15	0.15	20	58.4
	6	0.20	0.15	20	53.2
	10	0.20	0.15	20	51.7

yl)cyclopropane in 50 ml of dehydrated ethanol, 0.2 g of hydroquinone, and 8 g (0.2 mol) of powdered sodium hydroxide. Then, 14 g (0.15 mol) of epichlorohydrin (ECH) was added with vigorous stirring. The reaction mixture was stirred for 4 h. The NaCl precipitate was filtered off, and ethyl ether was removed. Then the reaction mixture was distilled to isolate the reaction product: bp 150–153°C at 1 mm Hg, yield 18.86 g (82%), n_D^{20} = 1.5220, d_4^{20} = 1.04, MR_{Dcalc}/MR_{Dfound} = 67.07/67.45.

Found (%): C 78.30, H 7.80.
Calculated (%): C 78.26, H 7.83.

2-Glycidyloxycarbonyl-1-(*p*-vinylphenyl)cyclopropane was prepared in a three-necked flask equipped with a stirrer, a reflux condenser, and a dropping funnel. The flask was charged with 18.8 g (0.1 mol) of 2-carboxy-1-(*p*-vinylphenyl)cyclopropane, 50 ml of anhydrous ether, and 1.2 g of hydroquinone, and 2.3 g (0.1 g-atom) of finely cut sodium metal was added with stirring in a nitrogen atmosphere. After complete dissolution of sodium, 14 g (1.15 mol) of ECH was added dropwise. The mixture was heated to 40°C for 1 h; after reaction completion, NaCl was filtered off, and the ether and unchanged EPC were removed. The residue was distilled in a vacuum; bp 160–162°C at 1 mm Hg, yield 22.21 g (91%), n_D^{20} = 1.5310, d_4^{20} = 1.12, MR_{Dcalc}/MR_{Dfound} = 67.09/67.36.

Found (%): C 78.30, H 7.80.
Calculated (%): C 78.26, H 7.83.

Polymerization was carried out both in the bulk and in a benzene solution in the presence of 0.2 mol % AIBN at 70°C. The resulting polymers were purified by twofold precipitation from a benzene solution with methanol and dried at 30°C in a vacuum (15–20 mm Hg).

After purification, all the polymers obtained are soluble in aromatic and chlorine-containing hydrocarbons and insoluble in alcohols.

The molecular weight was estimated from the intrinsic viscosity determined in benzene in an Ubbelohde viscometer: [η] = 1.05 (**I**) and 1.1 dl g^{-1} (**II**).

The IR spectra of the polymers were recorded on a UR-20 spectrometer.

To study the photochemical cross-linking of polymers, we prepared 2–10% solutions of polymers, which were applied to a glass support (K-8) 60 × 90 mm in size by centrifugation at 2500 rpm. The thickness of the resulting resist film was measured with an MII-4 Linnik microinterferometer. It was 0.15–0.20 μm.

The layer was dried for 10 min at room temperature and for 20 min at 40–45°C at a pressure of 10 mm Hg.

A DRT-220 mercury lamp (current strength 2.2 A) was used as a UV source, the distance from the radiation source was 15 cm, the velocity of moving the exposure meter gate was 720 mm h^{-1}, and the exposure time was 5–20 s. The content of insoluble polymer was determined from the ratio of the polymer weight to the initial weight of the film.

CONCLUSION

New monomers, 2-glycidyloxymethyl- and 2-glycidyloxycarbonyl-1-(*p*-vinylphenyl)cyclopropane, and polymers based on these were synthesized and characterized. The photosensitivity of the resulting polymers and its dependence on the substituent structure were studied. Participation of cyclopropane and epoxy groups in photochemical cross-linking was established.

REFERENCES

1. De Boer Charles, D., *J. Polym. Lett. Ed.*, 1973, vol. 11, no. 1, pp. 25–27.
2. Voskoboinik, G.A., Fedorov, Yu.I., Chernova, G.M., et al., *Vysokomol. Soedin., Ser. B*, 1973, vol. 15, no. 6, pp. 425–428.
3. Vainer, A.Ya. and Dyumaev, K.M., *Khim. Prom-st.*, 1989, no. 7, pp. 483–487.
4. Decker, C., *Prog. Polym. Sci.*, 1996, vol. 21, no. 4, pp. 593–650.
5. Vainer, A.Ya., Dyumaev, K.M., Likhacheva, I.A., et al., *Dokl. Ross. Akad. Nauk*, 2004, vol. 396, no. 3, pp. 362–365.
6. Rames-Lanqlade, Q., Monjiol, P., Sekiquchi, H., et al., *Polymer*, 1997, vol. 21, no. 19, pp. 4965–4972.
7. Hou, H. and Jianq, M., *Eur. Polym. J.*, 1999, vol. 35, no. 11, pp. 1993–2000.
8. Guliev, K.G., Ponomareva, G.Z., Nazaraliev, Kh.G., and Guliev, A.M., *Azerb. Khim. Zh.*, 2004, no. 4, pp. 168–172.
9. Guliev, K.G., Nazaraliev, Kh.G., and Guliev, A.M., *Azerb. Khim. Zh.*, 1999, no. 1, pp. 87–90.
10. Plemenkov, V.V., *Zh. Org. Khim.*, 1997, vol. 33, no. 6, pp. 849–859.
11. Selivanov, G.K., Mozzhukhin, D.D., and Gribov, B.G., *Mikroelektronika*, 1980, vol. 9, no. 6, pp. 317–338.
12. Ito, H., Veda, M., and England, W.P., *Macromolecules*, 1990, vol. 33, no. 9, pp. 2589–2598.

ISSN 1070-4272. Russian Journal of Applied Chemistry, 2006, Vol. 79, No. 3, pp. 492–493. © Pleiades Publishing, Inc., 2006.
Original Russian Text © Yu.P. Perelygin, I.V. Rashevskaya, 2006, published in Zhurnal Prikladnoi Khimii, 2006, Vol. 79, No. 3, pp. 501–503.

BRIEF COMMUNICATIONS

On the Term "pH of the Precipitation Onset of Heavy Metal Hydroxides"

Yu. P. Perelygin and I. V. Rashevskaya

Penza State University, Penza, Russia

Received September 28, 2005; in final form, January 2006

Abstract—It is suggested to take as pH of the precipitation onset of metal hydroxides the pH at which 10% of the initial amount of metal ions has precipitated. An equation for calculating this quantity is presented.

DOI: 10.1134/S1070427206030335

Precipitation of metals in the form of hydroxides is used in hydrometallurgy [1], analytical chemistry [2], and wastewater treatment [3, 4].

The pH values of the onset and completion of the precipitation of hydroxides are determined using the data of the reference book [5]. Whereas by pH of complete precipitation is meant a pH value at which the concentration of metal ions in solution over the precipitate does not exceed 10^{-5} M, the term "pH of the precipitation onset" has no clear definition [5].

In [6], it was suggested to understand by pH of the precipitation onset of metal hydroxides a pH value at which the concentration of metal ions in solution over a precipitated hydroxide is 1 M. However, the initial concentration of the metal ion in solution, which should exceed 1 M, remains unknown and, consequently, it is unclear what part of the initial amount of metal ions has precipitated. In [6], no dependence of pH of the precipitation onset of metal hydroxides on the initial concentration of a salt in solution was demonstrated, whereas in [5], a dependence of this kind was observed.

Thus, the reported pH values of the precipitation onset of hydroxides [5, 6] can hardly be used for practical purposes for the reasons mentioned above. This circumstance initiated the present study.

The concentration of the metal ion in solution, $[M^{+z}]$, over a precipitated metal hydroxide $M(OH)_z$ can be found, if the solubility product (SP) of the metal hydroxide is known, by the equation

$$[M^{+z}] = SP/[OH^-]^z. \quad (1)$$

According to the material balance, the sum of the amounts of the metal ion in the precipitate and solution is equal to the initial amount of the metal ion in solution:

$$c_M V = m/M + [M^{+z}]V, \quad (2)$$

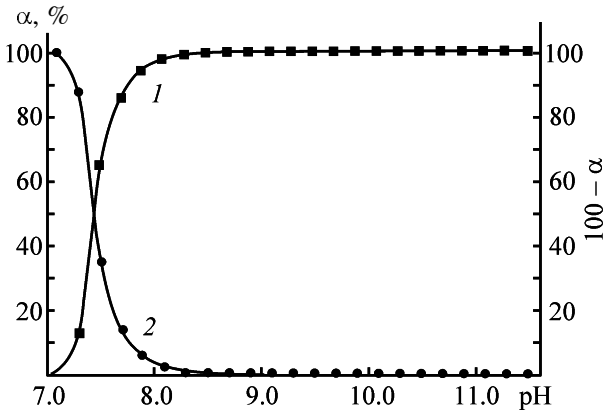
where z is the valence of the metal; V, solution volume; m and M, mass of the precipitate and the molecular weight of the metal hydroxide, respectively; and c_M, initial concentration of the metal ion in solution.

Substituting Eq. (2) into (1) and taking into account that $[OH^-] = K_w/[H^+]$ (K_w is the ionic product of water), we obtain the equation

$$c_M V = m/M + (SP\,V[H^+]^z)/K_w^z. \quad (3)$$

Dividing the left- and right-hand parts of Eq. (3) by the initial amount of the metal ion in solution ($c_M V$), we obtain an equation that can be used to determine the relative fractions of the metal hydroxide [$\alpha = (m/c_M V) \times 100\%$] and metal ion ($100 - \alpha$) in solution as functions of the solution pH:

$$\alpha = [1 - (SP[H^+]^z)/(c_M K_w^z)] \times 100\%. \quad (4)$$



Relative fractions of cadmium ions (*1*) in the precipitate (α) and (*2*) in solution ($100 - \alpha$) vs. pH. Initial concentration of cadmium ions 1 M.

pH values calculated by Eq. (4) and taken from [5, 6]

Hydroxide	pH	
	10% metal hydroxide	[5, 6]
Initial concentration of metal ion 1 M		
$Cd(OH)_2$	7.2	7.2 [5]
$Ni(OH)_2$	6.7	6.7 [5]
$Fe(OH)_2$	6.5	6.5 [5]
$Mn(OH)_2$	7.7	7.8 [5]
$Pb(OH)_2$	6.47	6.4 [6]
$In(OH)_3$	1.7	2.07 [6]
$Cu(OH)_2$	4.5	3.8 [6]
Initial concentration of metal ion 0.01 M		
$Cd(OH)_2$	8.2	8.2 [5]
$Ni(OH)_2$	7.7	7.7 [5]
$Fe(OH)_2$	7.5	7.5 [5]
$Mn(OH)_2$	8.66	8.8 [5]
$Pb(OH)_2$	7.47	–
$In(OH)_3$	2.37	–
$Cu(OH)_2$	5.5	–

Equation (4) is only applicable if $m/M \le c_M V$. As follows from Eq. (4), the relative fraction of the metal ion precipitated in the form of a hydroxide depends on kind of a metal ion, initial concentration of the salt in solution, and pH, which was noted in [5].

The figure shows dependences of the relative fraction of the cadmium ion in the form of an insoluble hydroxide (curve *1*) and as an ion in solution (curve *2*) on the solution pH at an initial concentration of cadmium ions in solution equal to 1 M, calculated using Eq. (4) on a computer by a specially developed software. The solubility products of cadmium hydroxide and other hydroxides were taken from the reference book [5].

Similar curves were obtained for other metals that form no hydroxo complexes.

In view of the aforesaid, we presumably can take as pH of the precipitation onset of metal hydroxides the pH value at which a certain fraction of the initial amount of a metal ion, e.g. 10%, has precipitated. The thus defined pH values, calculated by Eq. (4), and the pH values of the precipitation onset of metal hydroxides from [5, 6] are listed in the table.

Comparison of the data presented in the table shows that the pH values of the precipitation onset of hydroxides, calculated by Eq. (4), and those taken from the reference book [5] virtually coincide, but strongly differ from those reported in [6]. The latter is due to the circumstance noted above: uncertainty in the initial concentration of a metal ion in solution.

Thus, the pH values of the precipitation onset of hydroxides, reported in [5], presumably refer to 10% precipitation of metal ions initially present in the solution.

Equation (4) can also be used to roughly determine pH of the precipitation onset of metal hydroxides for metals that form hydroxo complexes, if we assume that virtually no hydroxo complexes are formed at a given pH.

REFERENCES

1. Vol'dman, G.M. and Zelikman, A.N., *Teoriya gidrometallurgicheskikh protsessov* (Theory of Hydrometallurgical Processes), Moscow: Metallurgiya, 1993.
2. Kreshkov, A.P., *Osnovy analiticheskoi khimii: Teoreticheskie osnovy: Kachestvennyi analiz* (Fundamentals of Analytical Chemistry: Theoretical Foundations: Qualitative Analysis), Moscow: Khimiya, 1965, vol. 1.
3. Proskuryakov, V.A. and Shmidt, L.I., *Ochistka stochnykh vod v khimicheskoi promyshlennosti* (Wastewater Treatment in Chemical Industry), Leningrad: Khimiya, 1977.
4. Vinogradov, S.S., *Ekologicheski bezopasnoe gal'vanicheskoe proizvodstvo* (Environmentally Safe Electroplating Shop), Moscow: Globus, 1998.
5. Lur'e, Yu.Yu., *Spravochnik po analiticheskoi khimii* (Handbook of Analytical Chemistry), Moscow: Khimiya, 1965.
6. Semin, V.D., in *Metallurgiya tsvetnykh metallov: Nauchnye trudy Krasnoyarskogo inst. Tsvetmet* (Metallurgy of Nonferrous Metals: Sci. Works of Krasnoyarsk Tsvetmet Inst.), Krasnoyarsk: Knizhnoe, 1971, no. 4, pp. 190–196.

ISSN 1070-4272. Russian Journal of Applied Chemistry, 2006, Vol. 79, No. 3, pp. 494–496. © Pleiades Publishing, Inc., 2006.
Original Russian Text © I.A. El'kin, S.V. Remizova, E.A. Nadezhina, L.V. Krylova, 2006, published in Zhurnal Prikladnoi Khimii, 2006, Vol. 79, No. 3, pp. 503–505.

BRIEF COMMUNICATIONS

Synthesis of Stabilized Polymeric Sulfur by Rapid Cooling of Sulfur Melts in the Presence of α,α,α,α',α',α'-Hexachloro-*p*-xylene

I. A. El'kin, S. V. Remizova, E. A. Nadezhina, and L. V. Krylova

Central Plant Laboratory, Skoropuskovskii Sintez Limited Liability Company, Skoropuskovskii Settlement, Sergiev Posad, Moscow oblast, Russia

Received April 13, 2005; in final form, February 2006

Abstract—The possibility of raising the yield of stabilized polymeric sulfur by rapid cooling of melts in the presence of previously unstudied complex systems including α,α,α,α',α',α'-hexachloro-*p*-xylene was examined.

DOI: 10.1134/S1070427206030347

Polymeric sulfur (PS) is the simplest inorganic polymer of nonbranched chain structure with $M = 10^3$–10^7, which has low thermodynamic stability. Stabilized polymeric sulfur (SPS) can be successfully used as a lightfast agent in vulcanization of butadiene and isoprene rubbers [1, 2]. The steadily increasing number of publication indicates that the problems associated with optimization of the manufacture of SPS are a matter of current interest [3–7].

There exist three main methods for synthesis of SPS: rapid cooling of a sulfur vapor, reaction between SO_2 and H_2S, and rapid cooling of sulfur melts. The latter method has the lowest selectivity with respect to the target product (no more than 50–55%), compared with values as high as 80–90% for the first two. However, this technique involves considerably lower expenditure of materials and energy, compared with the method of vapor cooling, is environmentally safer, and requires simpler apparatus, compared with the method of reaction between SO_2 and H_2S [2]. The aforesaid suggests that the method of rapid cooling of sulfur melts is rather promising for industrial research, in particular, via use of stabilizing additives. Of interest for a study are systems including α,α,α,α',α',α'-hexachloro-*p*-xylene (HCX) [2–4]; however, published evidence about these systems is scarce.

The aim of this study was to improve the procedure for synthesis of SPN by rapid cooling of sulfur systems by using mixtures of HCX with other substances as stabilizing additives.

EXPERIMENTAL

In the first stage of the study, the main task was to select additives that would enhance the stabilizing effect of HCX in the course of formation of polymeric sulfur.

The experiments were carried out as follows: a mixture of crystalline sulfur (90 wt %), HCX (5%), and an additive (5%) was finely ground in a porcelain mortar. The resulting mixture was transferred into a thin-walled porcelain crucible with a cover, a mechanical stirrer, and a thermometer and heated on an oil bath at 210–215°C for 1 h. The resulting melt was rapidly poured into a mixture of water and ice, so that the temperature of the cooling water did not exceed 10°C in the course of quenching. The degree of hardening was assessed from the consistence of the sample: 3–7 days after the quenching, the sample usually could be finely ground in a porcelain mortar. When a satisfactory result was obtained in grinding, the sample was analyzed for the content of a toluene-insoluble residue (150 ml of toluene was taken per 1.5000 ± 0.1000 g of the product). The resulting yields of an insoluble residue, which characterize the possibility of formation of polymeric sulfur in relation to the type of a stabilizing system, are listed in the table.

The choice of inorganic additives was largely determined by the evidence concerning the favorable effect of silicon oxide [3] and aluminum and zinc chlorides [2]. Probably, the stabilizing action is accounted for in

this case by the possibility of formation of polysulfides of the corresponding elements. A study of the influence exerted by hexamethylenetetramine and *p*-chlorobenzenesulfonic acid (*p*-CBSA) seemed to be of interest because representatives of certain classes of organic substances (aliphatic amines, aromatic sulfo acids, chlorine-substituted alkanes, aromatic compounds) favor formation of organic polysulfides [8]. Urea was used mainly because its thermal decomposition yields ammonia capable of blocking the ends of a polymer chain of sulfur.

To study the influence exerted by an additive introduced together with HCX, an experiment with only HCX was also performed (10 wt % HCX and 90% crystalline sulfur were taken) under conditions similar to those described above. Despite the rather high yield of an insoluble residue (68%) for the method of quenching of sulfuric melts as a whole, such a high content of HCX in the fusion cake is economically unfeasible in view of the strongly and steadily increasing price of HCX. The results obtained for two-component stabilizing systems indicate that the organic additives tested either weaken (urea, to a lesser extent) or enhance (*p*-CBSA) the stabilizing effect of HCX in formation of polymeric sulfur, compared with the inorganic materials used. In the latter case, such an effect of the additive can be accounted for by the probable nucleophilic substitution of the chlorine atom in the benzene ring by the polysulfide residue.

Because the experiment with *p*-CBSA yielded the best result, two experiments were also performed, aimed to determine the optimal ratio of the components of the stabilizing mixture. In particular, an experiment with the following composition (wt %): rhombic sulfur 85, HCX 10, *p*-CBSA 5, made it possible to obtain 74% yield of the insoluble residue, and the experiment with (wt %) rhombic sulfur 85, HCX 5, and *p*-CBSA 10 gave 58%. Thus, HCX plays a considerably more important role in the mixture of the stabilizing components.

Because the main goal is the economical feasibility of synthesis of preparations with a high content of sulfur (the price of *p*-CBSA is nearly an order of magnitude higher than that of urea), the formulation with urea was taken as a basis. A number of formulations of the following initial composition were tested (wt %): crystalline sulfur 85, urea 5, HCX 5, and the third stabilizing additive 5. In this case, the synthesis conditions remained the same as those in a study of two-component stabilizing mixtures.

The choice of the third component for a mixture of additives was governed both by data on the possibility of formation of organic and inorganic polysulfides [8, 9] and by the assumption that some compounds and, in particular, triphenylmethyl chloride, which can form stable radicals in decomposition, could interact with the radical ends of the chain of polymeric sulfur.

Effect of a stabilizing system containing HCX (5 wt %) and additives A (5 wt %) and B (5 wt %) on the content of a toluene-insoluble residue in the product

Additive		Residue, wt %
A	B	
SiO_2	–	40
Al_2O_3	–	43
P_2O_5	–	39
$AlCl_3$	–	47
$FeCl_3$	–	41
$CaCl_2$	–	41
$(CH_2)_6N_4$	–	34
$(NH_2)_2CO$	–	56
$4\text{-}ClC_6H_4SO_3H$	–	71
$(NH_2)_2CO$	Al_2O_3	61
$(NH_2)_2CO$	SiO_2	48
$(NH_2)_2CO$	$CaCl_2$	44
$(NH_2)_2CO$	Na_2SiO_3	43
$(NH_2)_2CO$	$Na_2B_4O_7 \cdot 10H_2O$	43
$(NH_2)_2CO$	$B(OH)_3$	58
$(NH_2)_2CO$	H_2NSO_3H	60
$(NH_2)_2CO$	PhOH	82
$(NH_2)_2CO$	$4\text{-}H_2NC_6H_4SO_3H$	52
$(NH_2)_2CO$	$1,3\text{-}(OH)_2C_6H_4$	48
$(NH_2)_2CO$	$2\text{-}HOC_6H_4COOH$	57
$(NH_2)_2CO$	$C_{14}H_{29}C_6H_4SO_3H$	50
$(NH_2)_2CO$	$C_{14}H_{29}C_6H_4SO_3H$ (2.5 wt %), H_2SO_4 (2.5 wt %)	39
$(NH_2)_2CO$	$4\text{-}HO\text{-}3\text{-}HOOCC_6H_3SO_3H$	84
$(NH_2)_2CO$	Cellulose	34
$(NH_2)_2CO$	α-Pinene	26
$(NH_2)_2CO$	Ph_3CCl	38

The results of these experiments (yields of the toluene-insoluble residue) are listed in the table. In particular, it was found that the highest yields of the insoluble residue are obtained with phenol and 4-hydroxy-3-carboxy-1-benzenesulfonic acid (HCBSA) as the third component (82 and 83 wt %, respectively).

To study more thoroughly the effect of phenol and sulfosalicylic acid, experiments with the corresponding two-component stabilizing systems (i.e., those in the presence of HCX) were carried out by the procedure described above. In this case, the yield of the

insoluble residue decreased to 67% for phenol and to 70% for HCBSA. In addition, the viscosity of the reaction mass significantly increased in the course of synthesis itself, which, in turn, complicated the process of rapid cooling of the fusion cake.

Phenol was used to carry out an experiment with the same relative amounts of the components by the general procedure, but with the time of keeping shortened to 40 min, and an experiment without HCX and urea: phenol 10 wt %, crystalline sulfur 89 wt %, and 1 wt % sodium hydroxide as a promoting additive. The yield of the insoluble residue was 67% in the first experiment and 10% in the second. Apparently, the highest efficiency of formation of polymeric sulfur, which is due to the presence of phenol or sulfosalicylic acid in the reaction mass, is only observed when HCX is used together with urea.

Reducing the time of keeping of the reaction mixture is a negative factor in all cases.

Thus, the method of quenching of sulfur melts containing HCX will, in prospect, successfully compete in selectivity and economical parameters with the technique of rapid cooling of a sulfur vapor and with that involving reaction of hydrogen sulfide with sulfur dioxide.

CONCLUSIONS

α,α,α,α',α',α'-Hexachloro-*p*-xylene is effective as a stabilizing additive in synthesis of polymeric sulfur by rapid cooling of sulfur melts in the presence of *p*-chlorobenzenesulfonic acid, urea, phenol, and 4-hydroxy-3-carboxy-1-benzenesulfonic acid (the yield of stabilized polymeric sulfur is as high as 82–83%).

REFERENCES

1. *Khimicheskie dobavki k polimeram: Spravochnik* (Chemical Additives to Polymers: Reference Book), Maslova, I.P., Ed., Moscow: Khimiya, 1981.
2. Borokhovskii, V.A., Salyuk, A.P., Gordienko, E.G., et al., *Novyi vid khimicheskoi produktsii – polimernaya sera* (New Chemical Product: Polymeric Sulfur), Moscow: Khimiya, 1982.
3. RF Patent 2076843.
4. RF Patent 2142406.
5. RF Patent 2196787.
6. Canadian Patent 2393925.
7. EU Patent 1500630.
8. *Reaktsii sery s organicheskimi soedineniyami* (Reactions of Sulfur with Organic Compounds), Voronkov, M.G., Ed., Novosibirsk: Nauka, 1979.
9. Muller, A., Jaegermann, W., and Enemark, J.H., *Coord. Chem. Rev*. 1982, vol. 46, p. 245.

ISSN 1070-4272. Russian Journal of Applied Chemistry, 2006, Vol. 79, No. 3, pp. 497–498. © Pleiades Publishing, Inc., 2006.
Original Russian Text © A.I. Demidov, M.S. Kokhatskaya, B.V. Chernovets, 2006, published in Zhurnal Prikladnoi Khimii, 2006, Vol. 79, No. 3, pp. 506–507.

BRIEF COMMUNICATIONS

Thermodynamics of Discharge of the Nickel Oxide Electrode

A. I. Demidov, M. S. Kokhatskaya, and B. V. Chernovets

St. Petersburg State Polytechnic University, St. Petersburg, Russia

Received February 15, 2006

Abstract—Standard Gibbs energies and standard potentials of the reactions presumably occurring during discharge of the nickel oxide electrode were calculated.

DOI: 10.1134/S1070427206030359

The nickel–iron battery suggested by Edison in the beginning of the past century [1] belongs to alkaline lamellar batteries. The nickel–iron battery is conventionally described as the following electrochemical system [2]:

$$(-)\,\mathrm{Fe}\,|\mathrm{MOH}|\,\mathrm{NiOOH}\,(+),$$

where Fe is a negative electrode based on iron; MOH, an aqueous solution of KOH or NaOH with LiOH added; and NiOOH, a positive nickel oxide electrode.

As for the nickel oxide electrode, this notation is conventional to a certain extent, as the active material of the positive electrode consists of a mixture of nickel(II) metahydroxides having two structural modifications, β and γ, with graphite as a conducting additive [3]. The oxidation state of nickel in β-NiOOH is 3, and in γ-NiOOH it varies within the limits of 3.32–3.7 [4], i.e., nickel in the γ-phase is present in two oxidation states, 3 and 4. Therefore, reaction (1) occurring on the positive electrode at the potentials of the first section of the discharge curve corresponds only to the β-phase, and for the γ-phase it is conventional.

$$\mathrm{NiOOH} + \mathrm{H_2O} + \mathrm{e} \rightarrow \beta\text{-}\mathrm{Ni(OH)_2} + \mathrm{OH^-}. \quad (1)$$

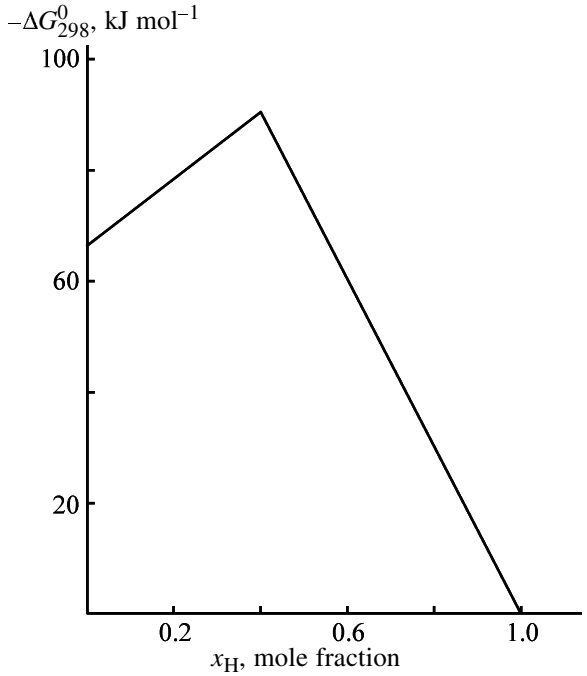
The discharge curve of the nickel oxide electrode contains the second section [3] of an unclear origin. Its potential is lower than the potential of the first section by approximately 0.4 V. Therefore, we decided to calculate the standard Gibbs energies and standard potentials of the reactions presumably occurring during the discharge of the nickel oxide electrode and to compare these values with published data.

In the calculations we used the standard Gibbs energies of formation of $Ni(OH)_2$ and NiO_2 taken from the literature [5] (Table 1). It should be noted that the O : Ni ratio in these compounds is 2, i.e. their compositions lay on the secant of the concentration triangle H–Ni–O drawn from the H vertex to the O–Ni side. The recalculation of the standard Gibbs energies of formation of the compounds per mole of atoms entering into their composition (Table 1) allows us to construct the dependence of the standard Gibbs energy (ΔG^0_{298}) of the quasibinary system $Ni_{0.333}O_{0.66}$–H on the composition x_H (see figure). It should be noted that the standard Gibbs energy found analytically for the compound $Ni_{0.25}O_{0.50}H_{0.25}$ and recalculated to the composition NiOOH agrees well with the value given in [6] for β-NiOOH at the onset of discharge (Table 1). The resulting dependence of the standard Gibbs energy for the quasibinary system $Ni_{0.333}O_{0.66}$–H on the composition allowed us to calculate the standard Gibbs energies of formation of nickel compounds with oxidation states 3.32 ($NiOOH_{0.68}$) and 3.7 ($NiOOH_{0.30}$) (Table 1).

Knowing the standard Gibbs energies of formation of nickel compounds, we have calculated the standard Gibbs energies of reactions (1)–(4) and their standard

Table 1. Standard Gibbs energies of formation of nickel compounds

Compound	ΔG^0_{298}, kJ mol^{-1}	Compound	ΔG^0_{298}, kJ mol^{-1}
NiO_2	–198.7	$Ni_{0.333}O_{0.667}$	–66.2
$NiOOH_{0.30}$	–236.8	$Ni_{0.303}O_{0.606}H_{0.091}$	–71.75
$NiOOH_{0.68}$	–285.1	$Ni_{0.272}O_{0.543}H_{0.185}$	–77.47
NiOOH	–325.8 –325.8 [6]	$Ni_{0.25}O_{0.50}H_{0.25}$	–81.45
$Ni(OH)_2$	–453.1	$Ni_{0.20}O_{0.40}H_{0.40}$	–90.6



Standard Gibbs energy ΔG^0_{298} of the quasibinary system $Ni_{0.333}O_{0.66}$–H as a function of composition x_H.

potentials (Table 2):

$$NiOOH_{0.68} + 1.32H_2O + 1.32e \rightarrow \beta\text{-}Ni(OH)_2 + 1.32OH^-, \quad (2)$$

$$NiOOH_{0.30} + 1.7H_2O + 1.7e \rightarrow \beta\text{-}Ni(OH)_2 + 1.7OH^-, \quad (3)$$

$$NiO_2 + 2H_2O + 2e \rightarrow \beta\text{-}Ni(OH)_2 + 2OH^-. \quad (4)$$

It is seen from Table 2 that the standard potentials of reactions (1)–(4) almost coincide. Thus, our calculations confirm the constancy of the experimental value of the discharge potential of the nickel oxide electrode (the first section of the discharge curve), which is independent of the ratio of β- and γ-phases in its composition [3]. Attempting to understand the origin of the second section of the discharge curve with a constant potential, we assumed that the oxidized and reduced forms of nickel compounds can react with each other, e.g., β-NiOOH can react with β-$Ni(OH)_2$ and NiO_2, with β-$Ni(OH)_2$:

Table 2. Standard Gibbs energies ΔG^0_i and standard potentials E^0_i of reactions (1)–(4)

Reaction	ΔG^0_i, kJ	E^0_i, V
(1)	–47.4	0.491
(2)	–65.5	0.491
(3)	–80.5	0.491
(4)	–94.6	0.490

$$2\beta\text{-}NiOOH + \beta\text{-}Ni(OH)_2 = Ni_3O_4 \cdot 2H_2O, \quad (5)$$

$$NiO_2 + 2\beta\text{-}Ni(OH)_2 = Ni_3O_4 \cdot 2H_2O. \quad (6)$$

The negative values of the standard Gibbs energies of reactions (5) and (6) $\Delta G^0_5 = -81.6$ and $\Delta G^0_6 = -81.4$ kJ indicate that the equilibria of reactions (5) and (6) are shifted toward formation of $Ni_3O_4 \cdot 2H_2O$. In turn, this compound can be reduced during the battery discharge:

$$Ni_3O_4 \cdot 2H_2O + 2H_2O + 2e \rightarrow 3\beta\text{-}Ni(OH)_2 + 2OH^-. \quad (7)$$

The standard potential of reaction (7) describing the second section of the discharge curve with a constant potential is $E^0_7 = 0.068$ V. The difference between the standard potentials of the first and second sections is 0.423 V, which agrees well with the experimental data [3]. Thus, the results of the thermodynamic calculation suggests the possibility of the reaction between the oxidized and reduced forms of nickel compounds and of participation of the reaction product in the electrochemical process.

CONCLUSION

The calculated standard potentials of the reactions presumably occurring during discharge of the nickel oxide electrode are consistent with the experimental constant potentials observed in the discharge curves.

REFERENCES

1. US Patent 678722.
2. Varypaev, V.N., Dasoyan, M.A., and Nikol'skii, V.A., *Khimicheskie istochniki toka* (Chemical Power Sources), Varypaev, V.N., Ed., Moscow: Vysshaya Shkola, 1990.
3. Barde, F., Palacin, M.R., Chabre, Y., et al., *J. Chem. Mater.*, 2004, vol. 16, no. 20, pp. 3936–3948.
4. *Khimicheskie istochniki toka: Spravochnik* (Chemical Current Sources: Handbook), Korovin, N.V. and Skundin, A.M., Eds., Moscow: Mosk. Energeticheskii Inst., 2003.
5. Garrels, R.M. and Christ, Ch.L., *Solutions, Minerals, and Equilibria*, New York: Harper and Row, 1965.
6. Dibrov, I.A., Thermodynamic and Thermoelectric Study of Electrode Processes in Chemical Power Sources, *Doctoral Dissertation*, Leningrad, 1980.

ISSN 1070-4272. Russian Journal of Applied Chemistry, 2006, Vol. 79, No. 3, pp. 499–500. © Pleiades Publishing, Inc., 2006.
Original Russian Text © I.M. Osadchenko, A.P. Tomilov, 2006, published in Zhurnal Prikladnoi Khimii, 2006, Vol. 79, No. 3, pp. 508–509.

BRIEF COMMUNICATIONS

Electrocatalytic Synthesis of Isonipecotic Acid

I. M. Osadchenko and A. P. Tomilov

Volgograd Research and Technological Institute of Meat and Milk Cattle Breeding and Processing of Cattle-Breading Products, Russian Academy of Agricultural Science, Volgograd, Russia
State Research Institute of Organic Chemistry and Technology, Moscow, Russia

Received December 21, 2005

Abstract—An electrocatalytic synthesis of isonipecotic acid was carried out by cathodic reduction of isonicotinic acid in a membrane electrolyzer on a copper cathode activated with Raney nickel in an alkaline medium under mild conditions.

DOI: 10.1134/S1070427206030360

Isonipecotic acid (INPA), 4-piperidinecarboxylic acid, is an important intermediate product in synthesis of biologically active compounds for medicine and veterinary, in particular, it is used for preparing Aceclydine.

It is known [1] that cathodic reduction of heterocyclic compounds, among them pyridine, in an acid medium allows preparation of dihydro derivatives and dimeric products.

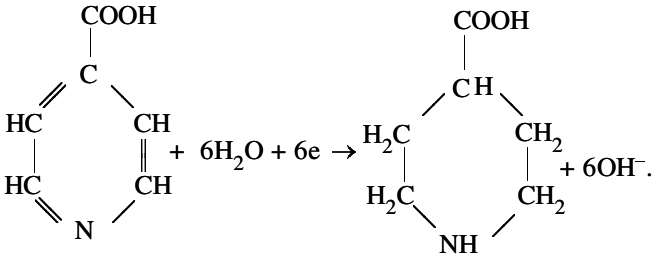
It was reported [2] that, in cathodic reduction of isonicotinic acid anilide in alkaline media on a mercury cathode at controllable potential, this substance is quantitatively converted to its dihydro derivative.

In this study we developed a procedure for exhaustive cathodic reduction of isonicotinic acid (INA).

The cathodic reduction of isonicotinic acid was studied in aqueous alkali on a cathode activated with powdered Raney nickel. An electrolyzer of membrane type was equipped with a nickel anode and a flat horizontal copper cathode. The powdered catalyst was fixed on the cathode surface with a permanent magnet.

15–40 wt % aqueous alkalis were used as anolytes, and 3–10 wt % aqueous alkalis as catholytes. The INA concentration was varied within 5–15%. The catholyte and anolyte were stirred with a mechanical stirrer (50–100 rpm). The catalyst amount on the cathode surface was 5–15 g cm^{-2}. In the course of cathodic reduction, the temperature in the electrolyzer was in the range 20–35°C.

We found that the optimal conditions for cathodic reduction of isonicotinic acid were as follows: initial INA concentration 5–10 wt %, initial sodium hydroxide concentration 5–6 wt % in catholyte and 20–25 wt % in anolyte, temperature 20–30°C, and catalyst content on the cathode surface 8–10 g cm^{-2}. Taking into account that INPA is difficultly separated from INA, in our experiments we ensured quantitative cathodic reduction of INA by passing the electricity in the amount exceeding the calculated value (6 F per mol INA) by 65–70%. The maximal current efficiency for INPA was 60%. We established that cathodic reduction of INA proceeds by the following scheme:



The target product was isolated in the form of INPA hydrochloride which was used in further organic syntheses.

EXPERIMENTAL

Isonicotinic acid, sodium hydroxide, and hydrochloric acid were of the reagent grade.

Electrolyses were performed in a glass cylinder with a lid holding a nickel anode incorporated into a ceramic diaphragm. A hollow copper disk connected to a voltage source was used as a cathode. The electrolyzer was equipped also with a mechanical stirrer and a connecting tube for removing gaseous electrolysis products [3].

The cathodic chamber was loaded with 5% aqueous NaOH (170 cm^3), INA (8.5 g), and Raney nickel (2 g), and the anodic chamber, with 40 cm^3 of 20% aqueous NaOH. The electrolysis was carried out with mild stirring (60 rpm) at 25–30 °C at a current strength of 5 A and a cathodic current density of 8.3 A dm^{-3} (per geometric surface area) for 4.1 h up to completion of hydrogen uptake. After completion of the electrolysis, the catholyte was treated with hydrochloric acid to convert INPA to its poorly soluble hydrochloride derivative. The resulting suspension was cooled and filtered, and the white precipitate of the final product was washed with cold water and dried. Yield of INPA hydrochloride 11.3 g.

Found, %: C 42.80, N 8.29, Cl 21.95.
$C_6H_{12}NCl$.
Calculated, %: C 43.77, N 8.50, Cl 21.55.

The amount of electricity passed through the electrolyzer was 20.5 A h, which exceeds the calculated value by a factor of 1.7. The INPA chemical yield and the corresponding current efficiency were 99 and 60%, respectively.

CONCLUSION

An electrocatalytic synthesis of isonipecotic acid was carried by cathodic reduction of isonicotinic acid on a copper cathode activated with Raney nickel in aqueous alkali with quantitative yield and 60% current efficiency.

REFERENCES

1. Shchennikova, M.K. and Korshunov, I.A., *Zh. Fiz. Khim.*, 1948, vol. 22, pp. 504–508.
2. Lund, H., *Acta Chem. Scand.*, 1963, vol. 17, pp. 2325–2340.
3. Osadchenko, I.M. and Tomilov, A.P., *Elektrokhimiya*, 1997, vol. 33, no. 6, pp. 729–730.

ISSN 1070-4272. Russian Journal of Applied Chemistry, 2006, Vol. 79, No. 3, pp. 501–503. © Pleiades Publishing, Inc., 2006.
Original Russian Text © L.L. Potapova, Z.I. Akulich, Yu.G. Egiazarov, 2006, published in Zhurnal Prikladnoi Khimii, 2006, Vol. 79, No. 3, pp. 510–512.

BRIEF COMMUNICATIONS

Formation of Strongly Basic Functional Groups in Weakly Basic Anion Exchanger at Oxidation of Hydrogen Sulfide on Fe(II)–Ethylenediaminetetraacetate/Anion Exchanger Catalytic System

L. L. Potapova, Z. I. Akulich, and Yu. G. Egiazarov

Institute of Physical Organic Chemistry, Belarussian National Academy of Sciences, Minsk, Belarus

Received November 8, 2005

Abstract—Changes in the nature and concentration of functional groups in the anion exchanger at oxidation of hydrogen sulfide in Fe(II)–ethylenediaminetetraacetate/anion exchanger catalytic system were studied.

DOI: 10.1134/S1070427206030372

As shown previously [1–4], Fe(II)–ethylenediaminetetraacetate (EDTA)/anion exchanger system effectively catalyzes oxidation of hydrogen sulfide with atmospheric oxygen to form H_2O and elemental sulfur. Water formed in the process compensates a decrease in the water content of the catalytic system at its contact with purified air and thus positively affects the process. Sulfur is accumulated in the anion exchanger phase, but its amounts are small, and thus its negative effect on the catalytic system can be decisive only at prolonged operation.

Another factor strongly affects the stability of the system studied. It is known [5, 6] that the oxidation of the reduced chelate containing Fe(II) is accompanied by a side reaction yielding hydrogen peroxide, which, when reacting with $[Fe(II)–EDTA]^{2–}$, generates $OH^•$ radicals:

$$2[Fe(II)–EDTA]^{2–} + O_2 + H_2O \rightarrow 2[Fe(III)–EDTA]^– + H_2O_2 + 2OH^•,$$

$$2[Fe(II)–EDTA]^{2–} + H_2O_2 + H_2O \rightarrow 2[Fe(III)–EDTA]^– + OH^– + OH^•.$$

The $OH^•$ radicals react with the CH_2 group adjacent to the carboxy group in the $EDTA^{4–}$ anion, causing degradation of the complexone in accordance with the following reaction:

$$R'R''NCH_2COO^– + 4OH^• \rightarrow R'R''NH + {}^–OOC–COO^– + 2H_2O + H^+.$$

The methylene groups of the EDTA ethylene bridges can also be oxidized with $OH^•$ radicals.

The possibility of improving the stability of the Fe(II)–EDTA/anion exchanger catalytic system by its modification with anions that exhibit reducing power was studied in [7, 8]. It was found that the strongest stabilization effect is observed when the catalytic system is modified with oxalate ions.

Since organic amines are easily oxidized, it was of particular interest to study the behavior of $OH^•$ radicals with respect to the functional groups of the anion exchanger and to analyze the results of possible oxidative degradation of these functional groups.

EXPERIMENTAL

The catalytic systems were prepared using FIBAN fibrous anion exchangers [9]: FIBAN A-5 weakly basic anion exchanger in the chloride basic form with the exchange capacity (EC) of 4.84 mg-equiv $g^{–1}$ and FIBAN A-6 anion exchanger with strongly and weakly basic amino groups in the chloride basic form (EC_{st} and EC_w 2.19 and 1.18 mg-equiv $g^{–1}$, respectively). A weighed portion of the anion exchanger was kept in a 0.25 M solution of Fe(II)–EDTA (pH 8.0) for 0.5 h. Then the resulting sample was removed from the solution and squeezed with a filter paper.

Hydrogen sulfide was oxidized in a flow tubular reactor at room temperature. A 0.3-g portion of the catalyst (swollen and squeezed) was placed in the reactor and a flow of air containing 0.14 vol % H_2S was passed through the reactor at a rate of

Content and nature of functional groups in the support of Fe(II)–EDTA/anion exchanger catalytic system

Sample	Exchange capacity for amino groups, mg-equiv g^{-1}			EC_{st}/EC_w
	EC_{tot}	EC_w	EC_{st}	
A-5:				
initial	4.84	4.84	–	–
after treatment	4.16	2.78	1.38	0.5
modified with oxalate ions (after experiment)	4.31	3.05	1.26	0.4
A-6:				
initial	3.37	1.18	2.19	1.86
after treatment	2.75	0.92	1.83	1.99

18 ml min^{-1} for 6 h. After the experiment, the sample was taken out and washed with several portions of 0.1 M HCl to remove the complex. The content of amino groups (strongly and weakly basic) in the support samples was determined by the procedure given in [10, 11]. Mass spectrometric analysis of air after its treatment to remove hydrogen sulfide was performed on an MKh 1320 unit.

As seen from the table, the exchange capacity of the support in the Fe(II)–EDTA/anion exchanger system after the experiment is 14–18% smaller than the initial value, which is probably due to partial oxidative degradation of the functional groups of the anion exchanger in the reaction with $OH^{\bullet}$ radicals. The reaction of the amino groups with $OH^{\bullet}$ radicals is confirmed by mass-spectrometric data on the composition of air after its treatment to remove H_2S in the presence of the Fe(II)–EDTA/anion exchanger catalytic system.

The sample studied contained dimethylamine and excess CO_2 relative to its content in air.

It should be noted that in the spent A-5 material the amount of weakly basic groups strongly decreases, whereas new strongly basic groups appeared. Similar phenomenon is observed for A-6 sample: a decrease in EC is accompanied by an increase in the amount of strongly basic centers. These results suggest that in the course of catalytic oxidation of H_2S weakly basic amino groups are alkylated with reactive fragments formed in reactions with available oxygen. This is confirmed by the fact that modification of Fe(II)–EDTA/anion exchanger catalyst with oxalate anion reduces the degradation of the anion exchanger and thus a smaller amount of strongly basic centers is formed.

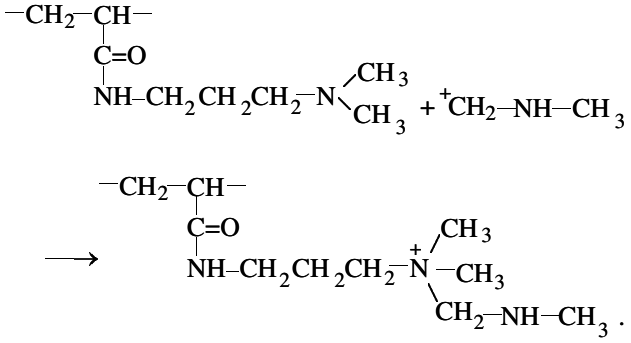
For example, alkylation of the tertiary amino group can proceed according to the scheme given below.

(1) The reaction of $OH^{\bullet}$ radical with amine realized by degradation of the amino group, followed by formation of carbocation:

$$CH_3–NH–CH_3 + OH^{\bullet} \rightarrow {}^{\bullet}CH_2–NH–CH_3 + H_2O,$$

$${}^{\bullet}CH_2–NH–CH_3 + [Fe(III)–EDTA]^{-} \rightarrow {}^{\bullet}CH_2–NH–CH_3 + [Fe(II)–EDTA]^{2-}.$$

(2) Formation of tertiary ammonium compound:



CONCLUSIONS

(1) In the course of oxidation of hydrogen sulfide with molecular oxygen on the Fe(II)–ethylenediaminetetraacetate/anion exchanger catalytic system, the exchange capacity of the anion exchanger decreases, which is due to partial degradation of functional groups in the reaction with available oxygen.

(2) Fragments of organic amines formed by oxidative degradation of functional groups of the anion exchanger can alkylate weakly basic functional groups converting them into the strongly basic centers.

REFERENCES

1. Potapova, L.L., Egiazarov, Yu.G., Soldatov, V.S., and Elinson, I.S., *Dokl. Nats. Akad. Nauk Bel.*, 1998, vol. 42, no. 3, pp. 54–57.

2. Potapova, L.L., Volkovinskaya, T.V., and Yegiazarov, Yu.G., *Russ. J. Phys. Chem.*, 2000, vol. 74, suppl. 3, pp. 564–567.
3. Potapova, L.L., Shunkevich, A.A., Akulich, Z.I., and Egiazarov, Yu.G., *Zh. Prikl. Khim.*, 2000, vol. 73, no. 5, pp. 780–784.
4. Potapova, L.L., Volkovinskaya, T.V., Soldatov, V.S., and Egiazarov, Yu.G., *Zh. Prikl. Khim.*, 2002, vol. 75, no. 8, pp. 1257–1259.
5. Chen, D., Martel, A.E., and McManus, D., *Can. J. Chem.*, 1995, vol. 73, no. 2, pp. 264–274.
6. Chen, D., Motekaitis, R.J., Martell, A.E., and McManus, D., *Can. J. Chem.*, 1993, vol. 71, no. 9, pp. 1524–1531.
7. Potapova, L.L., Volkovinskaya, T.V., and Egiazarov, Yu.G., *Ekotekhnol. Resursosber.*, 2003, no. 1, pp. 33–37.
8. Potapova, L.L., Volkovinskaya, T.V., and Egiazarov, Yu.G., Extended Abstracts, *Mezhdunarodnaya nauchno-tekhnicheskaya konferentsiya "Novye tekhnologii v khimicheskoi promyshlennosti"* (Int. Scientific and Technical Conf. "Novel Technologies in Chemical Industry"), Minsk, November 20–22, 2002, part 2, pp. 246–248.
9. Shunkevich, A.A., Sergeev, G.I., and Elinson, I.S., *Zh. Vses. Khim. O-va. im. D.I. Mendeleeva*, 1990, vol. 35, no. 1, pp. 64–71.
10. Polyanskii, N.G., Gorbunov, G.V., and Polyanskaya, N.L., *Metody issledovaniya ionitov* (Methods for Studying Ion Exchangers), Moscow: Khimiya, 1976.
11. Shtamberg, Yu. and Yurachka, F., *Zh. Prikl. Khim.*, 1962, vol. 35, no. 10, pp. 2295–2302.

ISSN 1070-4272. Russian Journal of Applied Chemistry, 2006, Vol. 79, No. 3, pp. 504–505. © Pleiades Publishing, Inc., 2006.
Original Russian Text © O.V. Bakbardina, N.Zh. Rakhimzhanova, M.A. Gazalieva, S.D. Fazylov, E.Zh. Baimagambetov, 2006, published in Zhurnal Prikladnoi Khimii, 2006, Vol. 79, No. 3, pp. 513–514.

BRIEF COMMUNICATIONS

Synthesis and Biological Activity of Anabasine and Cytisine Derivatives of Monothiooxamides

O. V. Bakbardina, N. Zh. Rakhimzhanova, M. A. Gazalieva, S. D. Fazylov, and E. Zh. Baimagambetov

Institute of Organic Synthesis and Coal Fuel Chemistry of Republic of Kazakhstan, Limited Liability Company, Karaganda, Kazakhstan
Research Institute of Plant Protection, Almaty, Kazakhstan

Received December 1, 2005

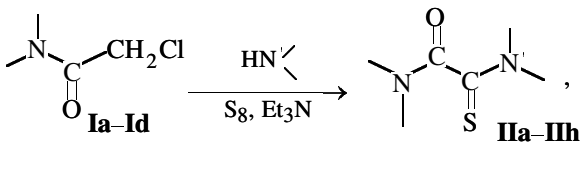
Abstract—Monothiooxamides were synthesized by the reaction of chloroacetamides with elemental sulfur and cyclic amines in the presence of triethylamine. The compounds were tested for fungicidal and aphicidal activity.

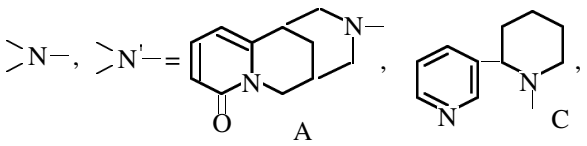
DOI: 10.1134/S1070427206030384

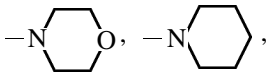
It is known [1] that monothiooxamides contain closely located amide and thioamide groups. Such a combination of the fragments in the structure of derivatives of natural alkaloids can occasionally impart unexpected properties and open new synthetic prospects.

Among the described methods [2, 3], the synthesis of monothiooxamides based on reactions of substituted amides (mainly chloroacetamides) with elemental sulfur and amines is the simplest and most convenient [4]. However, this method (with simultaneous mixing of the reactants) has disadvantages caused by prolonged heating of the reaction mixture; in the process, sulfur reacts with amines to form a complex mixture of products. This substantially complicates preparation and isolation of monothiooxamides.

In order to prepare new potentially bioactive compounds, we synthesized monothiooxamides **IIa**–**IIh** by the reaction of chloroacetamides **Ia**–**Id** with elemental sulfur and amines (cytisine and anabasine) in the presence of triethylamine in dimethylformamide at room temperature (20°C).







where =N– = A (**Ia, IIa, IIe**); C (**Ib, IIb, IIf, IIg**); M (**Ic, IIc**); P (**Id, IId, IIh**); =N'– = A (**IIe**); C (**IIf**); M (**IIa**–**IId**); P (**IIg, IIh**).

A systematic study of S-functionalization of chloroacetamides **Ia**–**Id** showed that the order of mixing the reactants substantially affects the product yields. For instance, preparation of a solution of elemental sulfur in amine beforehand increases the yield of monothiooxamides **IIa**–**IIh** to 64.61%. This is due to the fact that, under the action of amine, eight-membered cyclic molecule of sulfur is cleaved, and polysulfide anions are accumulated in the solution. They substantially facilitate thiolation of the methylene fragment of chloroacetamides **Ia**–**Id**, while in the case of simultaneous introduction of reactants the probability of side reaction of amine alkylation with chloroacetamides **Ia**–**Id** substantially increases.

The physiological properties of the new derivatives synthesized can be of interest. Compounds **IIa**–**IIh** are soluble in many organic solvents.

The structures of compounds **IIa**–**IIh** were determined by IR and ^{1}H NMR spectroscopy, and the composition, by elemental analysis. The IR spectra contain a strong band at 1640 cm^{-1} caused by stretching vibrations of the C=O group and a broad band at 1160 cm^{-1} caused by stretching vibrations of the C=S group.

In the ^{1}H NMR spectra of compounds **IIa**–**IIh**,

Yields, physicochemical constants, and elemental analyses of compounds **IIa**–**IIh**

Compound	Yield, %	bp °C	R_f^*	Found, %			Empirical formula	Calculated, %		
				C	H	N		C	H	N
IIa	64.61	117–118	0.69	58.79	6.05	12.10	$C_{17}H_{21}N_3O_3S$	59.03	6.78	12.73
IIb	50.69	131–132	0.56	60.19	6.58	13.17	$C_{16}H_{21}N_3O_2S$	60.77	6.97	13.48
IIc	53.18	121–122	0.39	49.18	6.55	11.75	$C_{10}H_{16}N_2O_3S$	50.25	7.02	12.48
IId	51.34	115–116	0.78	57.89	7.02	6.14	$C_{11}H_{18}N_2O_2S$	58.48	7.89	6.98
IIe	37.50	116–117	0.74	64.00	5.78	12.44	$C_{24}H_26N_4O_3S$	64.19	5.83	12.37
IIf	37.56	104–105	0.81	67.00	6.60	14.21	$C_{22}H_{26}N_4OS$	67.18	6.57	14.38
IIg	53.25	158–159	0.79	64.35	7.25	13.24	$C_{17}H_{23}N_3OS$	64.44	7.38	13.35
IIh	35.13	188–189	0.72	60.00	8.33	11.67	$C_{12}H_{20}N_2OS$	60.25	8.45	11.49

* Eluent is EtOAc : hexane = 1 : 1.

the chemical shifts of proton signals of the amine (alkaloid) core have typical values [5].

The physicochemical constants and elemental analyses of compounds **IIa**–**IIh** are listed in the table.

Compounds **IIa**–**IIh** were tested for the fungicidal and aphicidal activity. The fungicidal activity was estimated as the intensity of propagation of microorganisms on a cultural medium in comparison with a control (without introduction of compounds studied). We found that 1,2-dianabasinoethan-1-one-2-thione **IIf** *in vitro* has pronounced fungicidal activity with respect to phytopathogenic fungus *Botrytis cinerea* (64–68% suppression).

The aphicidal activity of compounds **IIa**–**IIh** was estimated in laboratory experiments on cucurbit and peach aphids in comparison with Aktellik reference preparation. Laboratory-vegetation experiments showed that 1-anabasino-2-morpholinoethan-1-one-2-thione **IIb** has pronounced aphicidal activity (77.3% suppression for cucurbit aphids at a substance concentration of 0.01%).

The results obtained were confirmed by protocols of biological tests, and compounds **IIf** and **IIb** were recommended for further detailed studies of their applicability in agriculture as pesticides.

EXPERIMENTAL

The IR spectra were recorded on an Avatar-320 spectrometer in KBr pellets, and ^{1}H NMR spectra, on a Tesla BS-587 spectrometer with an operating frequency of 80 MHz in DMSO-d_6 relative to HMDS. The melting points were determined on a Boetius heating stage. The reaction progress and purity of the products were monitored by TLC on Silufol UV-254 plates with EtOAc–hexane, 1 : 1 (by volume) eluent. Chloroacetamides were synthesized by the method described in [6].

Monothiooxamides IIa–IIh. A solution of appropriate amine (0.005 mol) and sulfur (0.16 g, 0.005 mol) in the presence of triethylamine (0.7 g, 0.005 mol) in 10 ml of DMF was added to chloroacetamide **Ia**–**Id** (1.01 g, 0.005 mol). The reaction mixture was stirred at 20°C for 30 min, and then 25 ml of water was added and the precipitate that formed was filtered off. The product was dissolved in acetone (10 ml), and the solution was filtered. After acetone removal, the substance was recrystallized from 95% EtOH.

CONCLUSIONS

(1) Monothiooxamides derived from some alkaloids and their analogs were prepared by S-functionalization of chloroacetamides.

(2) The pronounced fungicidal and aphicidal activities of monothiooxamides containing anabasine and morpholine fragments were revealed.

REFERENCES

1. Mashkovskii, M.D., *Lekarstvennye sredstva* (Drugs), Moscow: Meditsina, 1993.
2. Thiel, W. and Mayer, R., *J. Prakt. Chem*., 1989, p. 331.
3. Milligan, B. and Swan, M., *J. Chem Soc*., 1961, p. 1194.
4. Krayushkin, M.M., Yarovenko, V.N., and Zavarzin, V.N., *Izv. Ross. Akad. Nauk SSSR, Ser. Khim*., 2004, no. 3, pp. 491–501.
5. Gazaliev, A.M., Zhurinov, M.Zh., and Fazylov, S.D., *Novye bioaktivnye proizvodnye alkaloidov* (New Bioactive Derivatives of Alkaloids), Almaty: Gylym, 1992.
6. Vorontsova, O.Yu., Nurkenov, O.A., and Gazaliev, A.M., in *Sintez, prevrashchenie i svoistva sinteticheskikh prirodnykh organicheskikh soedinenii i polimerov: Sbornik nauchnykh trudov* (Synthesis, Transformations, and Properties of Synthetic Natural Organic Compounds and Polymers: Coll. of Scientific Works), Karaganda, 2002, pp. 82–84.

ISSN 1070-4272. Russian Journal of Applied Chemistry, 2006, Vol. 79, No. 3, pp. 506–507. © Pleiades Publishing, Inc., 2006.
Original Russian Text © A.P. Kriven'ko, N.A. Morozova, 2006, published in Zhurnal Prikladnoi Khimii, 2006, Vol. 79, No. 3, pp. 515–516.

BRIEF COMMUNICATIONS

Synthesis of 1,4-Diphenyl-3-phenylimino-1,2-dihydro-1,2,4-triazolium Hydroxide (Nitron)

A. P. Kriven'ko and N. A. Morozova

Chernyshevskii Saratov State University, Saratov, Russia
Institute of Natural Sciences, Saratov State University, Saratov, Russia

Received July 15, 2005; in final form, January 2006

Abstract—1,4-Diphenyl-3-phenylimino-1,2-dihydro-1,2,4-triazolium hydroxide (Nitron) is prepared by the reaction of Pb_3O_4 with diphenylthiourea, followed by the reaction of the obtained diphenylcarbodiimide with phenylhydrazine to form triphenylaminoguanidine, whose heterocyclization yields 1,4-diphenyl-3-phenylimino-1,2-dihydro-1,2,4-triazole, which is subsequently oxidized.

DOI: 10.1134/S1070427206030396

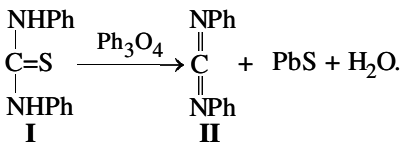
1,4-Diphenyl-3-phenylimino-1,2-dihydro-1,2,4-triazolium hydroxide (Nitron) is a well-known reagent for analysis of nitrate, perchlorate, tungstate, rhuthenate, and iodide anions [1], as well as silicon, germanium, arsenic, and phosphorus [2, 3]. Nitron was used for preparing lithium iodide power sources utilized in manufacture of electrocardiostimulators [4].

The published method of preparation of Nitron [5] allows its synthesis in a yield of ≤20% based on diphenylthiourea **I** because of incomplete conversion in the step of the reaction of phenylhydrazine with diphenylcarbodiimide and formation of a tautomer decreasing the yield and purity of the final product.

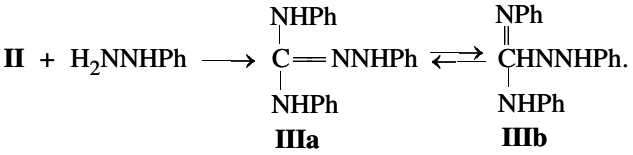
In this study we developed the conditions for synthesis of purer Nitron reagent in higher yields.

EXPERIMENTAL

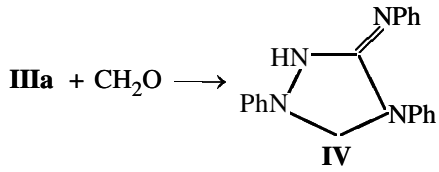
The synthesis includes four steps. First, thiourea is desulfurized with Pb_3O_4 into *N,N*-diphenylcarbodiimide **II**:



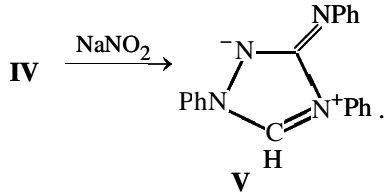
Addition of phenylhydrazine to diimide **II** at 29–31°C yields the desired triphenylaminoguanidine tautomer **IIIa** in 80% yield, which is virtually free of impurity tautomer **IIIb** transforming under the reaction conditions into the ballast "pseudonitron":



Condensation of guanidine **IIIa** with formaldehyde in isopropanol at 55–60°C yields 1,4-diphenyl-3-phenylimino-1,2-dihydro-1,2,4-triazole **IV** in 87–89% yield:



This is followed by oxidation of triazole **IV** into Nitron by the reaction with sodium nitrite; the final product is isolated by reprecipitation from a mixture of acetic acid and 25% ammonia solution:



The resulting Nitron **V** is 98 wt % pure, which corresponds to the analytically pure grade.

The yield of Nitron based on diphenylthiourea was 43%, which is virtually 2 times that reported in [5].

The IR spectra were recorded on an FSM-1201 Fourier spectrometer in Nujol, and the ^1H NMR spec-

tra, on a Varian FT 80A (80 MHz) spectrometer in $CDCl_3$ (with TMS as internal reference).

***N,N*-Diphenylcarbodiimide II.** Thiourea **I** (300 g) in 700 ml of benzene was refluxed with vigorous stirring until water ceased to liberate (Dean–Stark trap), and 300 g of Pb_3O_4 was added in portions. Desulfurization was regarded as complete when water ceased to liberate. The sludge was separated, and diphenylcarbodiimide **II** was taken to the next step without isolation.

Ttriphenylaminoguanidine IIIa. To the solution of diimide **II** (see above), cooled to 10°C, 136 ml of phenylhydrazine was added dropwise so that the temperature in the reaction mixture was about 30°C. Then 100 ml of benzene was distilled off at atmospheric pressure; 300 ml of isopropanol was added to the remaining solution, and the resulting mixture was kept at 0°C for 8–10 h. The crystalline reaction product was filtered off and dried in air; yield 350 g (88%), mp 156–158°C.

1,4-Diphenyl-3-phenylimino-1,2-dihydro-1,2,4-triazole IV. To 200 g of compound **IIIa**, 200 ml of 40% aqueous solution of formaldehyde and 1.0 l of isopropanol were added. The reaction mixture was heated at 55–60°C for 0.5 h and cooled to 22°C. The reaction product was filtered off, washed with 150 ml of isopropanol, and dried in air, which yielded 184 g (89%) of triazole **IV**; mp 126–128°C.

1,4-Diphenyl-3-phenylimino-1,2-dihydro-1,2,4-triazolium hydroxide V. To a solution of 240 g of triazole **IV** in 1 l of isopropanol, glacial acetic acid was added at 65–67°C until complete dissolution of crystalline substance **IV**, which required 200 ml of the acid. Then a solution of 88 g of sodium nitrite in 200 ml of water was added. The reaction was regarded as complete when the color of the solution changed from light green to red. The reaction mass was cooled to room temperature and poured into a 25% aqueous ammonia solution with ice. The resulting finely divided yellow precipitate of Nitron **V** was filtered off and reprecipitated from a mixture of glacial acetic acid and ammonia solution (1 : 3 by volume). The reaction product was dried in a vacuum oven at 50–60°C and a pressure of 0.2 kg cm^{-2}. The yield of Nitron reagent was 176 g (74%), mp 186–188°C (dec.). Published data: mp 189°C (dec.).

Found (%): C 76.89, H 5.20, N 18.01.
$C_{20}H_{16}N_4$.
Calculated (%): C 76.92, H 5.13, N 17.95.

IR spectrum (cm^{-1}): 3052 [$\nu(CH_{arom})$], 2924 [$\nu(CH)$], 572 [$\delta(CH_{arom})$]. ^1H NMR spectrum ($CDCl_3$), δ (ppm): 6.64–7.64 m (16H, Ph, CH).

CONCLUSION

Conditions were developed for synthesis of high-purity (98 wt %) Nitron reagent in the preparative yield of 43% with the use of Pb_3O_4 instead of lead oxide (PbO_2) and 2-propanol instead of ethanol.

REFERENCES

1. Babenko, A.S., Tolmachev, V.N., and Dzizin, A.N., *Ukr. Khim. Zh.*, 1963, vol. 29, no. 7, pp. 702–708.
2. Hahn, H. and Wapen, K., *Z. Anal. Chem.*, 1961, vol. 182, no. 5, pp. 343–357.
3. Canteher, N. and Athanassova, D., *Talanta*, 1973, vol. 20, no. 1, p. 125.
4. USSR Inventor's Certificate 1556486.
5. Buch, M., *Ber.*, 1905, vol. 38, no. 1, pp. 856–866.

ISSN 1070-4272. Russian Journal of Applied Chemistry, 2006, Vol. 79, No. 3, pp. 508–510. © Pleiades Publishing, Inc., 2006.
Original Russian Text © A.M. Gazaliev, O.A. Nurkenov, I.V. Kulakov, A.A. Ainabaev, D.V. Bessonov, 2006, published in Zhurnal Prikladnoi Khimii, 2006, Vol. 79, No. 3, pp. 517–519.

BRIEF COMMUNICATIONS

Synthesis and Fungicidal Activity of Alkaloid-Containing Carbohydrates

A. M. Gazaliev, O. A. Nurkenov, I. V. Kulakov, A. A. Ainabaev, and D. V. Bessonov

Institute of Organic Synthesis and Coal Fuel Chemistry of Kazakhstan Republic, Limited Liability Company, Karaganda, Kazakhstan

Received December 23, 2005

Abstract—*N*-Glycosylamines, triethylammonium salt of xylosyl- and glucosylbenzyldithiocarbamates, and their derivatives containing fragments of alkaloids were synthesized; some of these substances exhibit fungicidal activity.

DOI: 10.1134/S1070427206030402

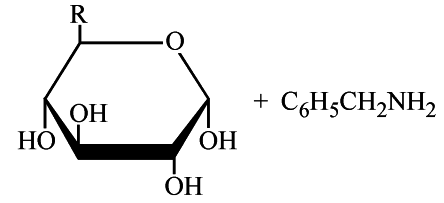
Among numerous substances comprising the environment, carbohydrates and their derivatives occupy an extremely important place and have enormous significance in technology and everyday human activity. Carbohydrates in the form of various derivatives enter into the cell composition of any living body, playing the role of structural material, energy source, substrates, and regulators of specific and biochemical processes [1].

Modified derivatives of monosaccharides are of great scientific and practical interest, since many of these have pronounced biological activity with a wide spectrum of effect. A number of derivatives of monosaccharides find wide use in medicine, e.g., as effective anticancer and antiviral agents [2]. All this stimulates an interest in synthetic chemistry of modification of monosaccharides.

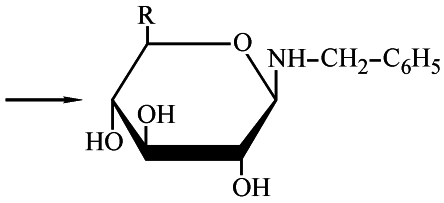
In recent years, *N*-glycosylamides (*N*-glycosides) find expanding application for synthesis of natural glycopeptides, their analogs, and glycoconjugates used in various biological studies. *N*-Glycosylamines are considered as potential pharmaceuticals, since introduction of carbohydrate group into a molecule not only increases the solubility but in some cases alters the biological effect as well [3].

We obtain a series of new carbohydrate-containing derivatives based on xylose and glucose for subsequent study of their reactivity and biological activity.

Condensation of *D*-xylose (**1**) and *D*-glucose (**2**) with benzylamine was performed in alcoholic solution under heating by the procedure described in [4]:



1, **2**



3, **4**

where R is H (**1, 3**), CH_2OH (**2, 4**).

The synthesized xyloxylbenzylamine (**3**) and glucosylbenzylamine (**4**) are hygroscopic white crystalline substances darkening in air. Depending on the synthesis conditions, *N*-glycosides can crystallize with 1 or 0.5 mol of water. When stored in a desiccator over P_2O_5, they become anhydrous.

The IR spectra of the compounds contain an absorption band at 891 ± 7 cm^{-1}, suggesting β-conformation at the anomeric center. Vibrations of the NH group appear in the range 2880–2920 cm^{-1}, and out-of-plane bending modes of the CH group of the aromatic ring, in the ranges 745–755 and 695–705 cm^{-1}. The IR spectra of **3** and **4** show that they contain no C=N bonds, i.e., they are not Schiff bases.

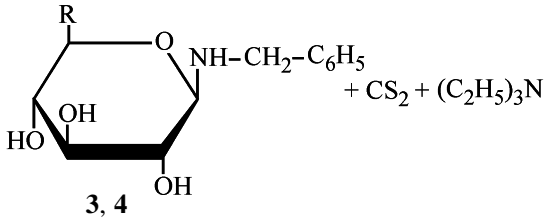
According to published data [5], the absorption in

Physicochemical constants and elemental analyses of compounds **3**–**12**

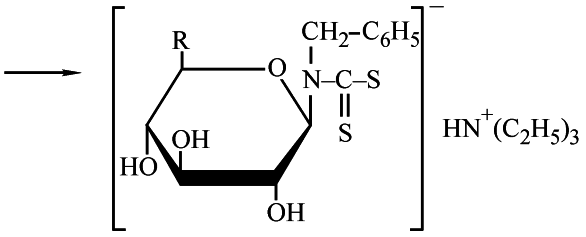
Compound	Yield, %	mp, °C	Found, %			Empirical formula	Calculated, %		
			C	H	N		C	H	N
3	90.2	105–106	60.35	7.18	5.85	$C_{12}H_{17}NO_4$	60.20	7.09	5.80
4	91.8	69–70	58.09	7.02	5.29	$C_{13}H_{19}NO_5$	57.98	7.11	5.20
5	39.7	94–95	54.82	7.79	6.76	$C_{19}H_{32}N_2O_4S_2$	54.76	7.65	6.70
6	41.6	62–63	53.98	7.60	6.33	$C_{20}H_{34}N_2O_5S_2$	53.78	7.67	6.27
7	40.5	129–130	57.26	5.96	8.37	$C_{24}H_{29}N_3O_5S_2$	57.00	5.72	8.32
8	45.3	106–107	56.18	6.12	7.90	$C_{25}H_{33}N_3O_6S_2$	56.05	6.21	7.84
9	57.5	142–143	57.53	6.69	5.93	$C_{23}H_{32}N_2O_5S_2$	57.10	6.63	5.80
10	70.9	68–69	56.55	6.68	5.58	$C_{24}H_{34}N_2O_6S_2$	56.45	6.71	5.49
11	41.8	99–100	57.51	6.79	5.88	$C_{23}H_{32}N_2O_5S_2$	57.10	6.63	5.80
12	51.1	73–74	56.57	6.86	5.59	$C_{24}H_{34}N_2O_6S_2$	56.45	6.71	5.49

the range of 1120–1170 cm^{-1} is characteristic of cyclic forms of carbohydrates, since sugar alcohols having the open-chain structure do not absorb in this range, which is in good agreement with the data obtained.

The synthesized xylosylbenzylamine (**3**) and glucosylbenzylamine (**4**) are fairly reactive compounds. Triethylammonium salts of xylosyl- and glucosylbenzyldithiocarbamates (**5, 6**) were synthesized by the reaction of the corresponding *N*-glycosides with carbon disulfide in ethanol in the presence of triethylamine:



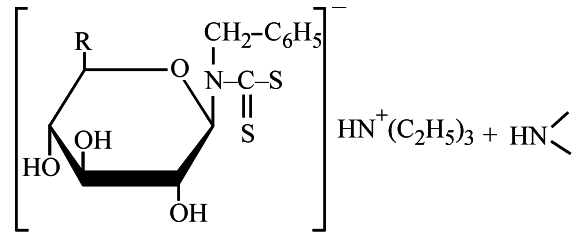
3, **4**



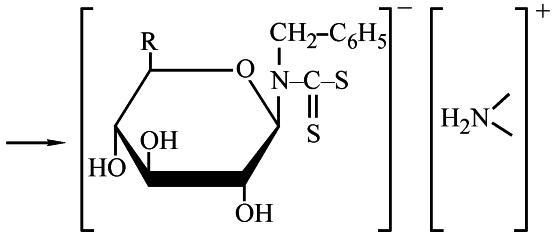
5, **6**

where R is H (**3, 5**), CH_2OH (**4, 6**).

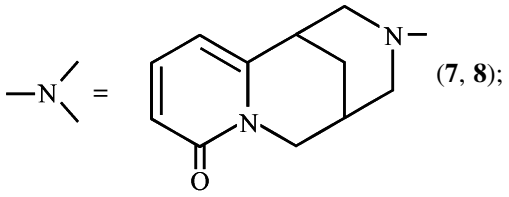
The next stage is substitution of alkaloid fragment for triethylamine by the reaction of triethylammonium xylosyl- and glucosylbenzyldithiocarbamate with alkaloids cytisine, 1-ephedrine, and *d*-pseudoephedrine in alcohol:



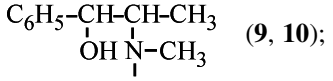
5, **6**



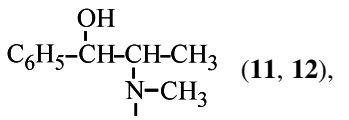
7–**12**



(**7**, **8**);



(**9**, **10**);



(**11**, **12**),

where R is H (**5, 7, 9, 11**); CH_2OH (**6, 8, 10, 12**).

Compounds **7**–**12** are white powders readily soluble in water, ethanol, and DMF and insoluble in hydro-

carbons. The composition and structure of **7**–**12** were confirmed by elemental analysis and IR spectroscopy. The IR spectra of **7**–**12** contain no absorption bands at 844 ± 8 cm^{-1}, which suggests β-conformation of pyranose ring of the compounds synthesized. In the range 2900–2930 cm^{-1}, there are stretching vibration bands of the N–H bond; at 1640–1650 cm^{-1}, the >N–C=O bands; and at 1070–1100 cm^{-1}; the thiocarbonyl group (C=S) bands.

There are contradictory opinions on how the important structural feature of carbohydrates, the presence of pyranose or furanose ring, is manifested in the IR spectrum [6]. The presence of several peaks in the range 1010–1090 cm^{-1} suggests the pyranose form of the glycoside fragment.

The characteristics of **3**–**12** are listed in the table. The spectra of all the compounds studied are characterized by broad strong bands in the range 3250–3400 cm^{-1}, caused by stretching vibrations of OH groups.

Two synthesized compounds **7** and **8** were tested for fungicidal activity. Phytopathogenic fungi *Fusarium oxysporum* and *Botrytis cinerea* were used as test cultures. The fungicidal activity was estimated from the intensity of microorganism development in a nutrient medium in comparison with the reference tests without addition of the compounds studied.

We found that cytisine salts of xylosyl- and glucosylbenzyldithiocarbamates tested *in vitro* have pronounced fungicidal activity against phytopathogenic fungi *Fusarium oxysporum* (72–78 and 69–74% suppression of development, respectively).[1]

The results obtained were recorded in a statement of biological tests.

EXPERIMENTAL

The IR spectra were recorded on an Avatar-320 spectrometer in KBr pellets. Melting points were determined on a Boetius device. The reaction course and purity of the resulting compounds were monitored by thin-layer chromatography on Silufol UV-254 plates in the system isopropanol : ammonia : water = 7 : 2 : 1. The plates were developed with iodine vapor.

Xylosyl- and glucosylbenzylamine (3, 4). To a 0.05 M solution of benzylamine and 8 ml of alcohol, 0.05 M of anhydrous finely ground carbohydrate was added. The mixture was heated on a water bath at 60–65°C for 20 min, then 10 ml of alcohol was added, and the solution was left to crystallize in a refrigerator. In a few hours, the substance completely crystallized. The product was washed with anhydrous ethanol and then with ether and dried in a desiccator upon P_2O_5.

Triethylammonium xylosyl- and glucosylbenzyldithiocarbamates (5, 6). To a 0.01 M solution of xylosyl- or glucosylbenzylamine in 5 ml of ethanol, 0.01 M of triethylamine was added with stirring, after which 0.01 M of carbon sulfide in 10 ml of alcohol was slowly added with cooling (3–5°C), and the mixture was stirred for 60 min at room temperature. After slight cooling, a precipitate formed. The precipitate was washed with anhydrous ethanol and then with anhydrous ether and dried in a desiccator upon P_2O_5.

Cytisine xylosyl- and glucosylbenzyldithiocarbamates (7, 8). To a stirred 0.001 M solution of compound **5** or **6** in 3 ml of ethanol, a 0.001 M solution of cytosine in 5 ml of ethanol was added at room temperature, and the mixture was stirred for 60 min. Then the mixture was heated at 55–58°C for 3 h. The solvent was removed on a water bath. The oily product was triturated with petroleum ether. The resulting powder was washed with diethyl ether.

Compounds **9**–**12** were obtained similarly (see table).

CONCLUSIONS

(1) *N*-Glycosylamines based on xylose and glucose were synthesized.

(2) Triethylammonium xylosyl- and glucosylbenzyldithiocarbamates and their derivatives containing fragments of alkaloids cytisine, 1-ephedrine, and *d*-pseudoephedrine were synthesized.

(3) Cytisine xylosyl- and glucosylbenzyldithiocarbamates exhibit pronounced fungicidal activity.

REFERENCES

1. Kochetkov, N.K., Kudryashov, L.I., and Chlenov, M.A., *Radiatsionnaya khimiya uglevodov* (Radiation Chemistry of Carbohydrates), Moscow: Nauka, 1978.
2. Kochetkov, N.K., Bochkov, A.F., Dmitriev, B.A., et al., *Khimiya uglevodov* (Chemistry of Carbohydrates), Moscow: Khimiya, 1967.
3. Lur'e, S.I. and Shemyakin, M.M., *Zh. Obshch. Khim.*, 1944, vol. 76, nos. 9–10, pp. 935–940.
4. Sorokin, W., *Ber.*, 1887, vol. 20, p. 783.
5. Prima, A.M., Zhbanov, R.G., and Marupov, R., *Zh. Strukt. Khim.*, 1964, vol. 5, no. 6, pp. 845–850.
6. Stepanenko, B.N., *Khimiya i biokhimiya uglevodov (monosakharidy)* (Chemistry and Biochemistry of Carbohydrates (Monosaccharides)), Moscow: Vysshaya Shkola, 1977.

[1] The studies were carried out at the Research Institute of Plant Protection (Almaty, Kazakhstan).

ISSN 1070-4272. Russian Journal of Applied Chemistry, 2006, Vol. 79, No. 3, pp. 511–513. © Pleiades Publishing, Inc., 2006.
Original Russian Text © N.A. Chernyavskaya, D.Yu. Larkin, O.T. Gritsenko, A.I. Chernyavskii, 2006, published in Zhurnal Prikladnoi Khimii, 2006, Vol. 79, No. 3, pp. 520–521.

BRIEF COMMUNICATIONS

Photochemical Vulcanization of Siloxane Rubber with Compounds Containing Silicon–Silicon Bond

N. A. Chernyavskaya, D. Yu. Larkin, O. T. Gritsenko, and A. I. Chernyavskii

Nesmeyanov Institute of Organoelement Compounds, Russian Academy of Sciences, Moscow, Russia
Enikolopov Institute of Synthetic Polymeric Materials, Russian Academy of Sciences, Moscow, Russia

Received November 21, 2005

Abstract—Certain deformation–strength properties of vinyl-containing siloxane rubber cured with oligomeric and polymeric compounds containing silicon–silicon bonds and with dicumyl peroxide were studied.

DOI: 10.1134/S1070427206030414

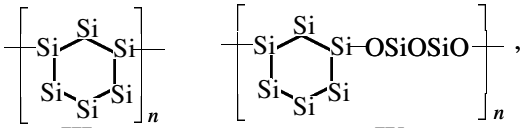
Low mechanical properties are one of disadvantages of organosilicon rubbers exhibiting a wide temperature range of performance. The mechanical properties of organosilicon rubbers can be enchanced by introduction of various modifying additives and crosslinking with various reagents. In particular, dicumyl peroxide is often used to cure siloxane rubbers [1, 2], however, the presence of peroxide initiator or its remainder after vulcanization causes premature aging of the vulcanized composition and impairs its physicomechanical properties.

It was shown that oligoorganosilanes, oligoorganosilane–siloxanes, and polysilane–siloxanes are efficient vulcanizing agents of photolytic curing of siloxane rubbers [3–6]. As a continuation of these studies, we examined photolytic vulcanization of siloxane rubber with oligomeric and polymeric compounds with Si–Si bonds and certain physicomechanical properties of the cured rubber.

EXPERIMENTAL

Liquid siloxane rubber SKTV-0.2MED (synthetic medicinal rubber) containing 0.2% vinyl groups randomly distributed along the chain and terminal hydroxy groups was used to test compounds for the vulcanization power.

Dodecamethylcyclohexasilane $(Me_2Si)_6$ (**I**), low-molecular-weight polydimethylsilane $-(Me_2Si)_n-$ (**II**) (prepared by extraction of high-molecular-weight polydimethylsilane with benzene in a Soxhlet apparatus for 24 h), and two cyclolinear polymers, poly(cyclohexasilane) (**III**) and poly(cyclohexasilane–disiloxane) (**IV**) (methyl groups are not shown)



III **IV**

were used as photoinitiators.

Compounds **I** and **II** were prepared by known methods [7, 8]. Polymers **III** and **IV** were synthesized by a Wurtz-type reaction of 1,3-dichlorodecamethylcyclohexasilane with sodium metal and by its heterofunctional polycondensation with 1,3-dihydroxytetramethyldisiloxane, respectively [9]. Some properties of the polymers prepared are listed in Table 1.

Films 0.5–0.7 mm thick were formed on aluminum foil supports from solutions in toluene and irradiated with light of a DRT-250 high-pressure mercury lamp arranged at a distance of 8 cm. The optimal time of vulcanization was determined from gel fraction content.

Static mechanical properties of the cured films were determined by standard methods on a Autograph AGS-10kNG (Shimadzu) device at room temperature; the sample length was 4 cm, and the extension rate, 4 cm min^{-1}.

Cyclosilane is well compatible with the rubber and forms transparent films. Under UV irradiation, the gel fraction content reaches 92% in 9 min and then changes insignificantly (see figure). Low-molecular-weight polysilane (**II**) gives turbid films, which is apparently caused by microphase segregation of the

Table 1. Yield and molecular-weight* and spectral (UV) characteristics of polymers** **III** and **IV**

Polymer	Yield, %	$M_w \times 10^{-3}$	$M_n \times 10^{-3}$	M_w/M_n	λ_{max}, nm
III	71.2	7.0	2.7	2.59	252, 313
IV	60.5	8.1	4.3	1.88	254

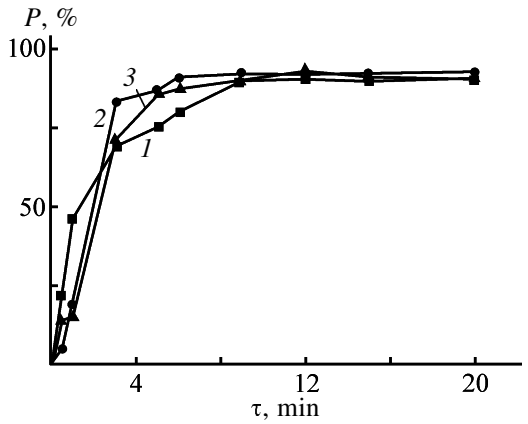
* From data of gel-permeation chromatography.
** 1 wt % of photoinitiator was added.

Table 2. Deformation–strength characteristics of films of cured rubber

Curing agent	Tensile strength, MPa	Modulus of elasticity, MPa	Relative elongation at break, %
I	0.17	0.25	167.0
II	0.20	0.28	168.0
III	0.28	0.37	185.4
IV	0.17	0.26	169.6
Dicumyl peroxide	0.12	0.01	1023.0

components because of their poor compatibility. However, after 3 min of irradiation, the film becomes more transparent, and the gel fraction content sharply increases from 19 to 83%. Polymer **III** gives with rubber very turbid films, which are partially clarified after 7 min of irradiation (the gel fraction content was not determined). Polymer **IV** containing siloxane units is well compatible with the rubber and gives transparent films which are rapidly cured under the action of UV light. Films prepared for studying the static mechanical properties of the compositions were irradiated for 12 min to reach the maximal gel fraction content in the samples with polymeric photoinitiators.

It was found that rubbers cured at room temperature under the action of UV light with oligomeric (**I**, **II**) and polymeric (**III**, **IV**) initiators have better deformation–strength properties as compared to the rubber cured for 6 h at 200°C with dicumyl peroxide (1 wt %) (Table 2). The rubber cured with polymer **III** had the best deformation–strength characteristics: the tensile strength was higher than that of the rubber cured with dicumyl peroxide by a factor of more than 2 and modulus of elasticity, by a factor of more than 35. This is probably caused by the fact that silane photoinitiators provide thicker cross-linking as compared to dicumyl peroxide, which is also confirmed by a decrease in the deformability of the cross-linked rubber when the peroxide is replaced by oligo- and polysilane photoinitiators.



Gel fraction content P in rubber cured with compounds (*1*) **I**, (*2*) **II**, and (*3*) **III** as a function of irradiation time τ.

CONCLUSION

Oligomeric and polymeric compounds with silicon–silicon bond are efficient photoinitiators of curing of vinyl-containing organosilicon rubber: they allow substantial increase in the rubber tensile strength and modulus of elasticity as compared to the rubber cured with dicumyl peroxide by a standard procedure.

REFERENCES

1. Zhdanov, A.A., Levin, V.Yu., Slonimskii, G.L., et al., *Vysokomol. Soedin., Ser. A*, 1983, vol. 25, no. 5, pp. 1030–1034.
2. Zhdanov, A.A., Slonimskii, G.L., Levin, V.Yu., et al., *Vysokomol. Soedin., Ser. A*, 1987, vol. 29, no. 7, pp. 1501–1506.
3. Semenov, V.V. and Cherepennikova, N.F., *Dokl. Akad.*

Nauk SSSR, 1989, vol. 309, no. 1, pp. 119–122.

4. Semenov, V.V., Cherepennikova, N.F., Artemicheva, S.B., and Razuvaev, G.A., *Appl. Organomet. Chem.*, 1990, vol. 4, no. 2, pp. 163–172.
5. Semenov, V.V., Ladilina, E.Yu., Cherepennikova, N.F., and Chesnokova, T.A., *Zh. Prikl. Khim.*, 2002, vol. 75, no. 1, pp. 128–134.
6. Chernyavskii, A.I., Larkin, D.Yu., Buzin, M.I., et al., *Zh. Prikl. Khim.*, 2004, vol. 77, no. 2, pp. 289–293.
7. Chernyavskii, A.I. and Zavin, B.G., *Izv. Ross. Akad. Nauk, Ser. Khim.*, 1997, no. 8, pp. 1513–1517.
8. Chernyavskii, A.I. and Chernyavskaya, N.A., *Izv. Ross. Akad. Nauk, Ser. Khim.*, 2002, no. 9, pp. 1607–1609.
9. Larkin, D.Yu., Chernyavskaya, N.A., and Chernyavskii, A.I., Abstracts of Papers, *Int. Conf. "Modern Trends in Organoelement and Polymer Chemistry,"* Moscow (Russia): Nesmeyanov Inst., May 30–June 4, 2004, report P47.

ISSN 1070-4272. Russian Journal of Applied Chemistry, 2006, Vol. 79, No. 3, pp. 514–515. © Pleiades Publishing, Inc., 2006.
Original Russian Text © G.E. Zaikov, M.I. Artsis, L.L. Madyuskina, 2006, published in Zhurnal Prikladnoi Khimii, 2006, Vol. 79, No. 3, pp. 522–523.

INFORMATION

The 10th European Conference on Fire Retardant Polymers

DOI: 10.1134/S1070427206030426

The 10th European Conference on Fire Retardant Polymers was held from September 7 to 9, 2005 at the Federal Institute for Materials Research and Testing (BAM) in Berlin, Germany.

The conference participants were 250 scientists from 100 research centers of 23 countries including Austria, Belgium, China, France, Germany, Hungary, Iran, Israel, Italy, Japan, the Netherlands, Norway, Poland, Russia, Spain, South Korea, Sweden, Switzerland, Taiwan, the United Kingdom, and the United States.

The Opening Ceremony included the speeches by Prof. M. Hennecke (President, BAM) and Prof. B. Schartel (Conference Chairman, BAM). In his speech Prof. Hennecke proclaimed the motto of the Federal Institute for Materials Research and Testing: "Safety and reliability in chemical and materials technologies." The participants welcome this motto.

The Conference Program included eleven plenary sessions. In Session I (Fundamental Aspects), Prof. M. Lewin gave an overview lecture "Fire Retardancy: Challenges of the Past, Present, and Future" and Prof. R.E. Lyon (the United States) told about the solid state thermochemistry of flaming combustion.

Sessions II and III were devoted to fire retardancy of polymers. In these sessions the participants considered such topics as intumescence of polymers in burning [S. Duquesne, S. Bourbigot, and R. Delobel (France)], fire retarding mechanisms of red phosphorus in polybutylene terephthalate [U. Braun and B. Schartel (Germany)], thermal stability and fire performance of polypropylene loaded with ammonium phosphate microencapsulated by polyurethane shell [S. Giraud, A. Castrovinci, I. Vroman, and G. Camino (Italy)], flame retardant polymers by preformulation [M. Doering, S. Seibold, U. Armold, et al. (Germany)], optimization of flammability and mechanical performances in flame retardant glass reinforced epoxy composites [B.K. Kandola, P. Myler, A.R. Horrocks, et al. (the United Kingdom)], flame retarded epoxy resin system for liquid composite moulding applications [R. Perez, J.K.W. Sandler, V. Alstadt, et al. (Germany)], thermal behavior of covalently bonded phosphorus flame retardant systems [D. Price, L.R. Cunliffe, K.J. Bulett-Pyrah, et al. (the United Kingdom)], and flame retardance of polyacrylonitriles covalently modified with phosphorus-containing groups [J.R. Ebdon, V.L. Crook, B.J. Hunt, et al. (the United Kingdom)].

Session IV (Industrial Application, Regulation and Standardizations) included four presentations. In the invited lecture M. M. Hirschler (the United States) reported on the experience in full scale fire testing of consumer products. The other lectures gave information on epoxy laminates flame retarded with phosphorus-based curing agent and inorganic fillers [S.V. Levchik, V. Buczek, S. Dashevsky (the United States)], new environmentally friendly phosphorus-based flame retardants [S. Horold, O. Schaker (Germany)], and the use of unique type amorphous silicon dioxide as an additive to improve fire retardancy of thermoplastic compounds (G. Schmauks, B. Friede, A. Soerhuus, and J.O. Roszinski).

Session V (Textiles) covered the topics concerning the challenge of replacing halogen flame retardants in textile applications [A.R. Horrocks, P.J. Davies, and B.K. Kandola (the United Kingdom)], optimization of the structure of a polyurethane/clay nanocomposite used as flame-retardant textile coating [M. Rochery, M. Taktak, S. Giraud, et al. (France)], recent advances in flame retardancy of textiles [S. Bourbigot, S. Duquesne, P. Flambard, et al. (France)], and flammability improvement of technical textiles by spunlacing process [X. Flambard, D. Saihi, M. Pochery, et al. (France)].

Session VI (New Materials and New Methods) included five lectures. In the invited lecture J. Gilman, J. Shields, R. Harrisyr, et al. (the United States) told about modern methods for flammability characterization. In other lectures such problems were discussed as evaluation of the effect of nanoclay and aluminium trihydrate in an intumescent formulation by means of a new cone calorimeter test methodology [A. Castrovinci, R. Lyon, R. Walters, et al. (Italy)], development of new halogen-free flame retardant engineering plastics by application of automated optical investigation methods [J.M. Endtner (Germany)]. New ap-

proaches for assessing the performance of intumescent coatings and new method for imparting efficient antidripping properties in flame retarded thermoplastics were considered in the reports presented by the scientists from Germany, Israel, and the Netherlands (M. Bartholmai, B. Shartel, Y. Bar Yaakov, et al.).

Sessions VII and IX concerned the topic "CO, Smoke, and Environmental Aspects." Four lectures were presented in Session VII: Bench-Scale Assessment of Fire Toxicity [T.R. Hull, K. Lebek, K.T. Paul, and D. Price (the United Kingdom)], Effect of Smoke Suppressants on Flammability of Unsaturated Polyester Resin Nanocomposites [S. Nazare, B.K. Kandola, and A.R. Horrocks (the United Kingdom)], Determination of Combustion Toxicity of Electric Cables as a Function of Equivalence Ratio [K. Lebek, T.R. Hull, and D. Price (the United Kingdom)], and Fire-LCA Model: Furniture Including Polyurethane and Textile as Case Study [L. Tange, D. Buszard, C. Blundell, et al. (the Netherlands)].

Five lectures were presented at Session IX, among them Regulations, Harmonization, and Standardization of Fire Testing in the EU—Overview and Trends (J.H. Troizsch), Relevance of SBI Test Results for Fire Safety of Building Constructions [E. Antonatus (Germany)], Modelling Fire Scenarios in Residential Buildings with Respect to the Benefit of Smoke Detectors and Flame Retardants [A. Hofman (Germany)], and IPN Foams with Improved Fire Behavior [A. Lorenzetti (Italy)].

Sessions VIII and X were devoted to nanocomposites. Particularly, Session VIII covered such topics as fire retardancy mechanisms in polymer nanocomposites [B. Schartel, M. Bartholmai, and U. Knoll (Germany)], thermal degradation and flammability of PMMA containing AlOOH submicron particles, Al_2O_3 nanoparticles, and modified montmorillonite [A. Laachachi, M. Cochez, M. Ferriol, et al. (France)], and kinetics of thermal degradation of polymeric nanocomposites [G.E. Zaikov, S.M. Lomakin, I.L. Dubnikova, et al. (Russia)].

Session X included five presentations. The greatest interest has been expressed by the participants in the results reported by Ch.A. Wilkie (the United States) in his invited lecture entitled Nanocomposite Formation as a Component of a Fire Retardant System and also in data on nanostructured flame retardants [G. Beyer (Belgium)]. Other presentations were devoted to comparison of the flame retardant mechanism of nanocomposites in thermoplastic and thermosetting matrices [A. Toldy, G. Marosi, P. Anna, and N. Toth (Hungary)], preparation and combustion properties of nanocomposites based on epoxy resins and organically modified clays [A. Hartwig and D. Putz (Germany)], and physical and flammability properties of polymer/silica and polymer/alumina nanocomposites [F. Yang, I. Bogdanova, and R. Yngard (the United States)].

The last four reports were presented at Session XI: The Emission of Selected Flame Retardants. A Possible Exposure Route [S. Kemmelein, O. Hahn, and O. Jann (Germany)], The EU Regulation: What is the Status for FR Regulation and How Does Industry Respond to It [D. Buszard (the United Kingdom)], Antimony Trioxide as Flame Retardant: Update on Risk Assessment [J.-P. Gaudel and K. Van de Velde (France, Belgium)], and Fire Retardancy of Composites Reinforced by Lignocellulosic Fibers [R. Kozlowski, M. Wladyka-Pizbylak (Poland)].

The Conference also included the Poster Session at which 38 posters were presented, devoted to various aspects of flame retardancy of polymeric materials.

The next XI Conference will be held at the Research Institute in Bolton (the United Kingdom). The organizers of this event are Prof. D. Price and Prof. C.R. Horrocks, world-famous persons in the area of combustion of polymers.

G. E. Zaikov, M. I. Artsis, and L. L. Madyuskina

ISSN 1070-4272. Russian Journal of Applied Chemistry, 2006, Vol. 79, No. 3, p. 516. © Pleiades Publishing, Inc., 2006.
Original Russian Text © A.G. Morachevskii, 2006, published in Zhurnal Prikladnoi Khimii, 2006, Vol. 79, No. 3, p. 524.

BOOK REVIEWS

Kazanbaev, L.A., Kozlov, P.A., Kubasov, V.L., and Travkin, V.F., *Indii. Tekhnologiya polucheniya* (Indium: Manufacture Technology)

Moscow: Ruda i Metally, 2004, 168 pp.

DOI: 10.1134/S1070427206030438

A comparatively close attention has been given to the properties, manufacture, and use of indium and its alloys by the domestic monographic literature. In 1987 was published the monograph by S.P. Yatsenko, *Indii. Svoistva i primenenie* (Indium: Properties and Use) (Moscow: Nauka, 1987, 257 pp.), in which particular attention was paid to indium alloys, their phase diagrams, and physicochemical and thermodynamic properties of the alloys in the solid and liquid states. The vast reference material contained in the monograph still remains important. Yatsenko's book luckily supplemented in those years the already available domestic monographs on coordination chemistry of indium compounds and the indium recovery technology.

Later was published the monograph by P.I. Fedorov and R.Kh. Akchurin *Indii* (Indium) (Moscow: Nauka, MAIK Nauka/Interperiodica, 2000, 276 pp.). This exhaustive monograph for the most part systematically describes the chemical properties of widely diverse classes of indium-containing compounds. A comparatively little attention was given in the book to technological issues. Even though the authors note that Russia occupies one of the leading positions in the world in manufacture of indium, the manufacture technology itself is not detailed.

The monograph by L.A. Kazanbaev and co-authors concentrates the whole attention on the technology of indium recovery from domestic raw materials and methods for refining of the metal. The book comprises three chapters, with bibliographic lists given separately for each chapter. Small Chapter 1 (pp. 5–19, 46 references) contains general evidence about indium and sources of indium-containing raw materials. The content of indium in the Earth's crust is estimated at 1.4×10^{-5} wt % (4×10^{-4} to 5.6×10^{-6}); minerals of indium itself are extremely rare and have no industrial importance. In processing of concentrated ores of nonferrous metals (lead, zinc, tin), indium is accumulated in various products and can be recovered from these products in a number of ways.

Chapter 2 (pp. 20–105, 125 references) is devoted to methods for recovery of indium from various indium-containing raw materials and to manufacture of raw indium. Particular attention is given to indium recovery from products formed in processing of zinc concentrates produced by Chelyabinsk zinc plant. Hydrometallurgical methods in manufacture of raw indium, extraction techniques for recovery of indium from indium-containing solutions, removal of impurities, and production of raw indium by cementation are discussed in most detail. Also discussed are methods for production of raw indium from wastes and industrially produced raw materials.

Chapter 3 (pp. 106–164, 77 references) presents a rather detailed description of methods for production of high-purity indium. As is known, the content of the main component in the raw metal commonly does not exceed 99.0 wt %. At the same time, radio electronics, manufacture of semiconducting compounds and special alloys, and some other fields of technology require indium with a total content of impurities of 10^{-2}–10^{-6}%. The authors consider the whole set of methods for purification of raw indium: chemical purification techniques, refining of indium by successive cementation, physical purification methods, electrolytic methods for production of high-purity indium, and vacuum-thermal distillation purification. In particular detail are discussed electrochemical techniques, including use of diaphragm electrolyzers with molten salt electrolytes. Special attention is given to description of an original method for production of high-purity indium powders.

The monograph by Kazanbaev and co-authors is of a clearly pronounced technological nature and significantly differs in this respect from the other two publications mentioned above. The book is primarily intended for technologists directly engaged in processing of indium-containing materials, production and refining of indium, and manufacture of indium powders. The monograph is based on the results of numerous studies by mostly Russian authors. The book is well published and contains a highly illustrative material.

A. G. Morachevskii

ISSN 1070-4272, Russian Journal of Applied Chemistry, 2006, Vol. 79, No. 4, pp. 517–520. © Pleiades Publishing, Inc., 2006.
Original Russian Text © N. F. Fedorov, M. A. Andreev, A. A. Khartukova, 2006, published in Zhurnal Prikladnoi Khimii, 2006, Vol. 79, No. 4, pp. 529–532.

INORGANIC SYNTHESIS AND INDUSTRIAL INORGANIC CHEMISTRY

Binding Formulations Based on Thermally Treated Serpentinite and Aqueous Salt Solutions

N. F. Fedorov, M. A. Andreev, and A. A. Khartukova

St. Petersburg State Technological Institute (Technical University), St. Petersburg, Russia

Received December 12, 2005

Abstract—Binding properties of thermally treated serpentinite combined with aqueous solutions of chlorides, sulfates, phosphates, and nitrates of a number of Group I–III elements were studied. The influence exerted by the nature of an anion and a salt-forming cation on the absolute value of the strength and its buildup was revealed.

DOI: 10.1134/S107042720604001X

Serpentinite has rather long been attracting researchers' attention as a basis for production of binders. More than half a century ago, Mchedlov-Petrosyan developed a binder named "serpentinite cement" [1, 2]. His work consists in that the starting serpentinite is subjected to thermal treatment at temperatures close to the dissociation temperature (~670°C) and then kept during a time in which the residual water content becomes less than 3 wt %. The product of thermal decomposition is ground to a fineness approximately corresponding to the milling fineness of portland cement and mixed with water. According to Mchedlov-Petrosyan's data [2], confirmed by Kaminskas [3], the serpentinite cement is a hydraulic binder that has a pronounced compressive strength (up to 20 MPa) and is distinguished by a $\sigma_{compr}/\delta_{bend}$ ratio markedly exceeding that of portland cement and other building binders. However, serpentinite has found no practical use, presumably because of the lack of calcinating apparatus with a highly strict control over the thermal treatment temperature.

More effective was combination of a very finely ground and thermally treated serpentinite and phosphoric acid [4], i.e., production of serpentinite phosphate cements.

In our opinion, the number of binders based on serpentinite can be considerably increased. This conclusion follows from [5, 6], where theoretical foundations of a purposeful search for new binders were presented. In accordance with the concept of [5, 6], we assume that the hardening effect will be observed for thermally activated serpentinite combined not only with phosphoric acid, but also with other acids, as well as with aqueous solutions of salts that can react with serpentinite by the oxide–salt scheme, if thermally treated serpentinite is regarded as a mixture of silicon and magnesium oxides, or by the salt–salt scheme, if it is considered to be a "methoserpentinite," i.e., a hypothetical magnesium salt of polysilicic acid. The aim of the present study was to verify this assumption.

EXPERIMENTAL

As the starting material served serpentinite[1] of the following chemical composition (wt %) (as determined by atomic-absorption spectroscopy):

Si	Mg	Fe	Al	Cr	Ni	Mn	Ti	Ca	Na
23.00	25.00	5.70	0.41	0.06	0.17	0.07	0.03	0.11	0.02

A crystal-optical analysis revealed that the mineralogical composition of the rock used includes antigorite, a minor amount of chrysotile, and chromite, brucite, and garnet as impurity phases. The starting serpentinite was thermally treated in a muffle furnace at 750°C to complete dehydration, which was reached in 2 h. The product formed in thermal treatment of serpentinite was ground in a grinder to a milling fineness satisfying the requirements of GOST (State Standard) to portland cement.

[1] Serpentinite from a deposit in Orenburg oblast.

Effect of the type of salt additive on the strength of binding formulations composed of a thermally treated serpentinite and a salt (powder, product formed in grinding of serpentinite thermally treated at 750°C)

Additive	1 : s	Compressive strength, MPa			
		3 days	7 days	14 days	28 days
$NaNO_3$	0.3	5.1	5.2	8.7	9.0
KNO_3	0.3	4.3	4.5	10.4	11.5
NH_4NO_3	0.3	2.0	2.0	2.0	2.1
$Lu(NO_3)_3$	0.3	6.0	9.4	9.4	10.0/18.7*
$Ce(NO_3)_3$	0.3	5.3	8.8	21.3	21/17*
$Eu(NO_3)_3$	0.3	6.0	8.8	8.9	15/35*
$Tl(NO_3)_3$	0.3	3.8	3.8	7.5	8.8/32*
NaCl	0.3	1.8	3.4	4.1	5.0
$MgCl_2$	0.3	1.9	2.3	10.0	10.0
$CaCl_2$	0.3	2.7	4.4	6.5	6.7
NH_4Cl	0.3	1.7	2.4	3.0	3.2
Na_2SO_4	0.3	2.5	3.4	4.0	4.8
$MgSO_4$	0.3	2.8	4.2	5.2	6.2
$(NH)_4SO_4$	0.3	2.0	3.3	4.2	4.2
Na_2HPO_4	0.3	2.9	2.9	3.1	3.2
NaH_2PO_4	0.3	9.5	18.7	19.0	20.0
Na_3PO_4	0.3	1.6	1.9	2.1	2.4
K_2HPO_4	0.3	17.8	35.6	36.0	40.0
KH_2PO_4	0.3	10.0	10.0	13.0	14.0
K_3PO_4	0.3	22.1	40.3	42.9	57.0
Portland cement M 400	0.33	15.0	30.0	–	30.0

* Strength of a sample stored in water.

The binding properties of the formulations composed of a thermally treated serpentinite and a salt were studied by the method of "small" samples. As additives served aqueous solutions of salts (50 wt %) of a number alkali, alkaline-earth, and rare-earth elements at a 1 : s ratio of 0.3. Samples prepared from a paste were stored in air, and those for which preliminary tests revealed stability in water were placed in water after three days of hardening in air and, in 28 days, were tested together with the samples stored in air. The results of the tests are listed in the table.

Analysis of the data obtained shows that, as expected, thermally treated serpentinite is a good basis for preparing binding substances with acid–base type of interaction.

Binding properties were observed in all of the formulations studied. Here, it should be noted that the absolute value of the strength and the type of its buildup are strongly affected by the nature of both the cation and the anion. Among the salt types used (chlorides, sulfates, nitrates, phosphates), the highest strength is observed for phosphate formulations, a somewhat lower strength, for nitrate formulations, and still lower, for sulfate and chloride ones. The following tendency is observed within the same family of formulations: the strength of binding formulations obtained with salts of bivalent metals exceeds that with salts of alkali metals. This tendency is the most clearly pronounced for nitrate cements. Among these cements, those obtained using nitrates of rare-earth metals as additives are distinguished by the following: they have a rather high strength and gain strength in hardening in water. This feature of the binding formulations under consideration seems to be rather remarkable: it opens up a new, previously unknown way to production of hydraulic binders. It should be emphasized that the capacity for hydraulic hardening is observed not only for formulations prepared with nitrates of rare-earth elements as additives, but also for all other nitrate formulations.

In the case when salts of phosphoric acid are used as additives, it is noteworthy that the strength properties are strongly affected not only by the nature of a salt-forming cation (potassium salts provide better strength characteristics than sodium salts), but also by the degree of substitution of hydrogen ions in phosphoric acid. The best results are achieved with sodium and potassium dihydrophosphates mixed with serpentinite.

As is known from the chemistry of binders, the reason for manifestation of binding properties is a chemical interaction, under specific conditions, of compounds constituting, e.g., portland cement or alumina cement, with water. This reaction yields new formations, a hydrated phase [5]. In the binding formulations considered in this study, the binding properties also result from a chemical interaction between thermally treated serpentinite and salts used as additives.

The validity of this statement is confirmed by the results of thermographic and X-ray phase analyses. Figure 1 shows thermograms of europium and calcium nitrates and of cements produced using these salts as additives. It can be seen from Fig. 1 that endothermic effects characteristic of the starting nitrates are totally absent in thermograms of hardened samples. These thermograms show only a single low-temperature endothermic effect characteristic of adsorption-bound and zeolite-like water. The thermograms of hardened samples are virtually identical for dif-

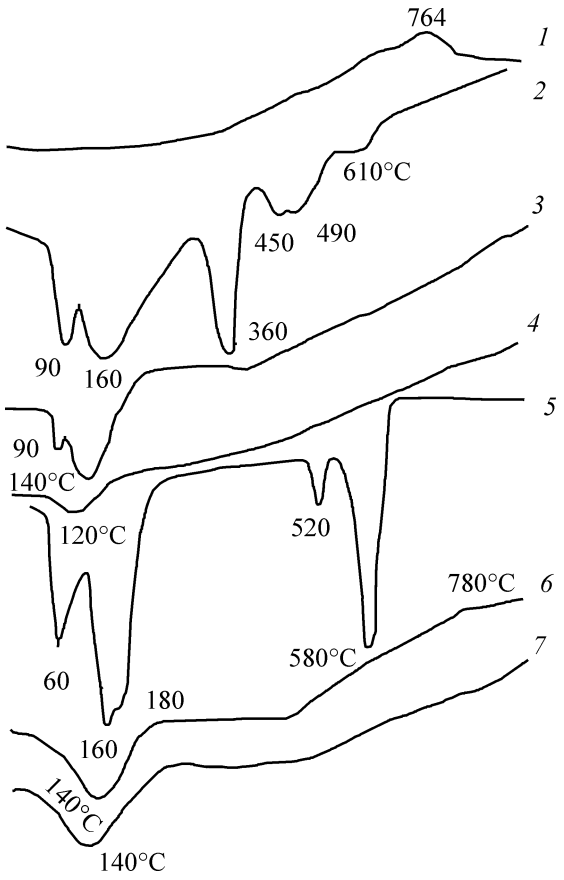


Fig. 1. Thermograms of thermally treated serpentinite, salt additives, and cement stone. (*1*) Thermally treated serpentinite; (*2*) europium nitrate; (*3*) thermally treated serpentinite mixed with a solution of $Eu(NO_3)_3$, storage in air for 28 days; (*4*) thermally treated serpentinite mixed with a solution of $Eu(NO_3)_3$, storage in water for 28 days; (*5*) calcium nitrate; (*6*) thermally treated serpentinite mixed with a solution of $Ca(NO_3)_2$, storage in air for 28 days; and (*7*) thermally treated serpentinite mixed with a solution of $Ca(NO_3)_2$, storage in water for 28 days; the same for Fig. 2.

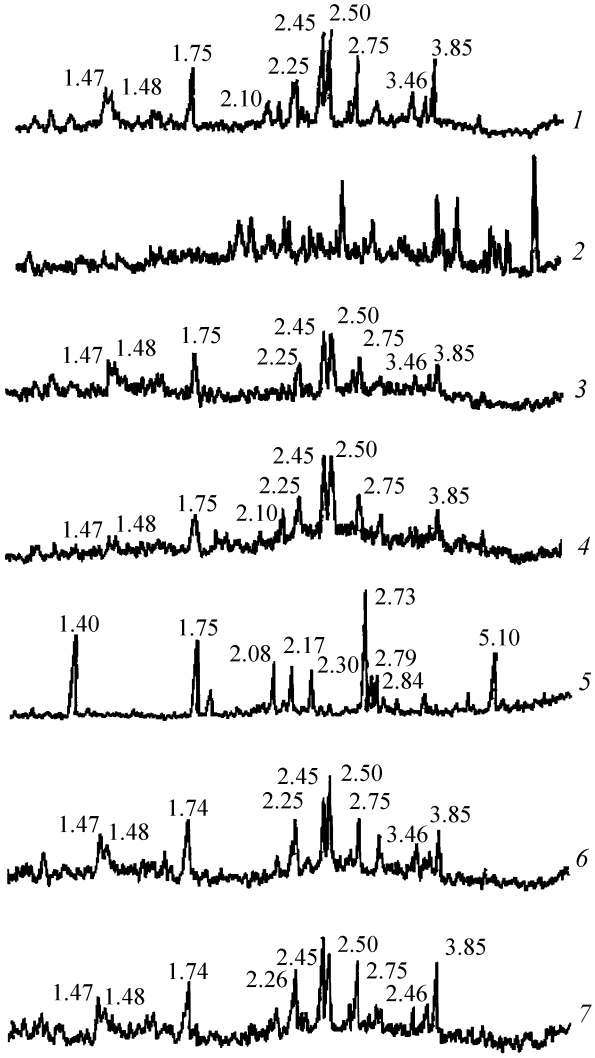


Fig. 2. X-ray diffraction patterns of thermally treated serpentinite, salt additives, and cement stone. Interplanar spacings are indicated in Å.

ferent salt additives, which indicates that cementing phases of the same type are formed in hardening for the whole group of serpentinite–nitrate binding formulations.

The occurrence of a chemical interaction between the salt solution and thermally treated serpentinite is also confirmed by the results of an X-ray phase analysis. It can be seen from Fig. 2, in which X-ray diffraction patterns of the starting salt additives $Ca(NO_2)_2$ and $Eu(NO_3)_3$ and hardened samples are shown, that the starting salts completely disappear in the course of hardening: the main reflections of the salts are not seen in the X-ray diffraction patterns of cement stone, which only contain reflections belonging to thermally treated serpentinite: *d*/*n* 2.45, 2.50, 2.26, 2.74 Å, etc. No reflections indicating that new crystalline formations appear in hardening of nitrate binding formulations. This gives reason to believe that the products formed in hardening of these binding compositions are X-ray amorphous.

CONCLUSIONS

(1) All the formulations under study, composed of thermally treated serpentinite and aqueous solutions of chlorides, sulfates, nitrates, and phosphates of uni-, bi-, and trivalent elements, exhibit binding properties.

(2) The strength properties of the formulations studied are determined by the nature of both the salt-forming cation and the anion. The strength is the highest for the phosphate formulations, somewhat lower for the nitrate binders, and the lowest for the chloride and sulfate binding formulations.

(3) Among the nitrate binding formulations, the strength is the higher, the larger the charge of the salt-forming cation. The highest strength is observed for the cement composed of thermally treated serpentinite and rare-earth nitrates. The presence of rare-earth elements with a large thermal-neutron capture cross-section in these cements makes them suitable for protection from hard radiation.

(4) Binding formulations based on thermally treated serpentinite and aqueous solutions of nitrates are hydraulic binders.

REFERENCES

1. Mchedlov-Petrosyan, O.P., *Sbornik nauchnykh rabot po khimii i tekhnologii silikatov* (Coll. of Sci. Works on Chemistry and Technology of Silicates), Moscow: Promstroiizdat, 1956, pp. 152–153.
2. Mchedlov-Petrosyan, O.P., *Trudy 4-go Soveshchaniya po eksperimental'noi mineralogii i petrografii* (Proc. 4th Symp. on Experimental Mineralogy and Petrography), Moscow, 1952, pp. 98–106.
3. Kaminskas, A.Yu., *Tekhnologiya stroitel'nykh materialov na magnezial'nom syr'e* (Technology of Construction Materials Manufactured from Magnesian Raw Materials), Vil'nyus: Mokslas, 1987.
4. Ter-Grigoryan, M.S., *Fosfatnye vyazhushchie na osnove serpentinite* (Phosphate Binders Based on Serpentinite), Riga: Rizhsk. Politekhn. Inst., 1983.
5. Sychev, M.M., *Neorganicheskie klei* (Inorganic Adhesives), Leningrad: Khimiya, 1974.
6. Fedorov, N.F., *Vvedenie v khimiyu i tekhnologiyu spetsial'nykh vyazhushchikh veshchestv* (Introduction to Chemistry and Technology of Special Binders), Leningrad: Leningr. Tekhnol. Inst. im. Lensoveta, 1976.

ISSN 1070-4272, Russian Journal of Applied Chemistry, 2006, Vol. 79, No. 4, pp. 521–524. © Pleiades Publishing, Inc., 2006.
Original Russian Text © A. S. Brykov, B. V. Danilov, A. V. Larichkov, 2006, published in Zhurnal Prikladnoi Khimii, 2006, Vol. 79, No. 4, pp. 533–536.

INORGANIC SYNTHESIS AND INDUSTRIAL INORGANIC CHEMISTRY

Specific Features of Portland Cement Hydration in the Presence of Sodium Hydrosilicates

A. S. Brykov, B. V. Danilov, and A. V. Larichkov

St. Petersburg State Technological Institute (Technical University), St. Petersburg, Russia

Received June 22, 2005; in final form, December 2005

Abstract—Specific features of hydration of a portland cement with addition of alkaline silicates and the ability of these additives to affect the concentration of hydroxide ions and Ca^{2+} ions in the liquid phase of the cement paste are considered.

DOI: 10.1134/S1070427206040021

The opinion that compounds of alkali metals (sodium and potassium) stimulate the hydration of the main phases of portland cement, at least in early stages of the process, has rather long been established in the literature devoted to cements [1, 2]. There is no common opinion on how their presence affects later stages of hydration, even though most of researchers tend to believe that alkalis adversely affect the final strength and durability of the stone (concrete). In all probability, the aforesaid also refers to alkaline compounds introduced into cement pastes as additives in the form of hydroxides, silicates, and other salts and to alkaline compounds present in the portland cement clinker itself (mostly in the form of sulfates).

Silicates of alkali metals (Na and K), introduced into pastes in the hydrated state, as aqueous solutions, and, more rarely, in the anhydrous state, are well known and find stable use as accelerators of setting and hardening of cement pastes and mortar mixtures [3–5].

The results of previous studies [6, 7] indicate that, depending on the molar ratio SiO_2/M_2O (where M is an alkali metal), alkaline additives introduced into cement pastes in the form of hydrated silicates (HS) differently affect the pH value of the liquid phase, hydration rate of clinker minerals, and morphology of the C–S–H gel formed as a result of hydration.

The aim of the present study was to explain the accelerating effect of HS of alkali metals (K, Na) in early stages of portland cement hydration, using the results of physicochemical studies of the liquid phase of portland cement pastes with addition of sodium silicates with a SiO_2/Na_2O molar ratio of 1 and 2.8.

EXPERIMENTAL

Portland cement of the CEM 1 52.5 NA brand (Aalborg Portland) was used in the study. It had the following mineralogical composition (wt %): C_3S 73, C_2S 16, C_3A 4.5, and C_4AF 1. The parameters of the sodium silicates used (HS1 and HS2) are listed in Table 1.

Table 1. Physicochemical parameters of powdered hydrated sodium silicates*

Parameter	HS1	HS2
SiO_2, wt %	28.5	58.6
Na_2O, wt %	28.7	21.4
Silica ratio	1.0	2.8
H_2O, wt %	42.8	20.0
Particle size, μm	<1600	<250
Dissolution time, min	<5	<5

* HS1, sodium metasilicate pentahydrate $Na_2O \cdot SiO_2 \cdot 5H_2O$ (Akzo PQ Silica Vof, the Netherlands); HS2, $Na_2O \cdot 2.8SiO_2 \cdot 3H_2O$ obtained by microwave dehydration of an aqueous solution of sodium silicate, modified with hydrogen peroxide [8]; white powders.

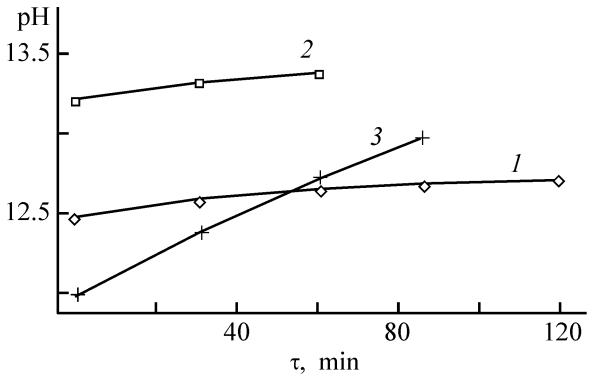


Fig. 1. pH values of pore solutions of cement pastes vs. time τ. Paste: (*1*) control, (*2*) with HS1 additive, and (*3*) with HS2.

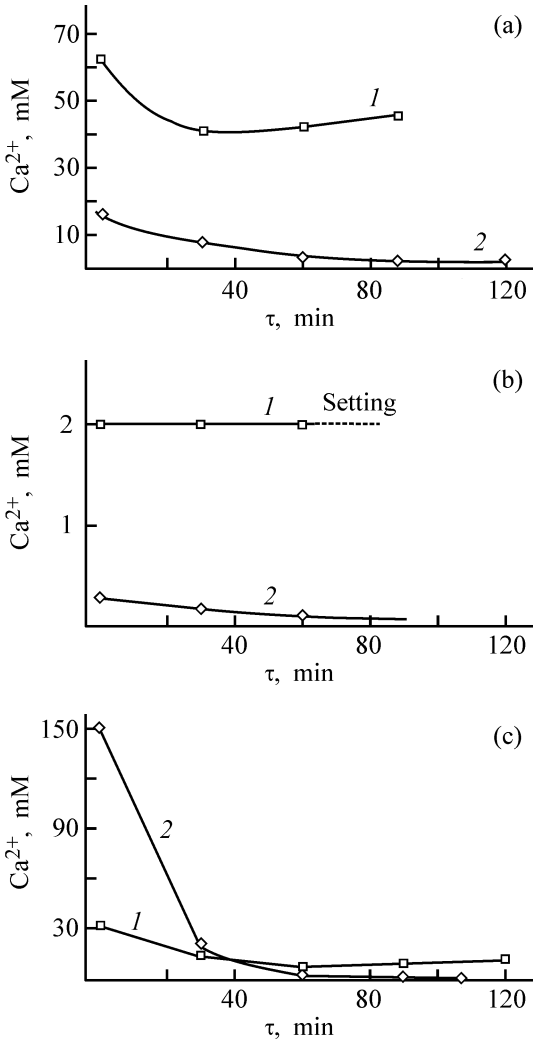


Fig. 2. (*1*) Experimental and (*2*) calculated (equilibrium) Ca^{2+} concentrations in the liquid phase vs. the time τ elapsed from the beginning of cement hydration. Paste: (a) control, (b) with HS1, and (c) with HS2.

To prepare a control (additive-free) paste, cement was mixed with water (w/c = 0.45); in 15 min the paste was sampled and the liquid phase of the sample was separated by centrifugation. Ca(II) was determined in the liquid phase by EDTA titration [9], with subsequent sampling 30, 60, and 90 min after the beginning of hydration.

The HS1 and HS2 additives were calculated in such a way that a constant amount of SiO_2 was introduced into pastes with the additives: 3% relative to the cement mass (which constituted 5 and 10% additives relative to the cement mass, respectively). When preparing the pastes, HS1 and HS2 powders were mixed directly with the cement. The w/c ratio was maintained constant (0.45) for all the formulations. In the case of metasilicate, the water of crystallization contained in its composition was taken into account. The sampling and analysis of the liquid phase were performed as described above.

The pH value of the liquid phase of the cement pastes was measured with a pH-673.M pH-meter.

The equilibrium concentration of Ca^{2+} (M) in a solution saturated with $Ca(OH)_2$ at a steady-state pH value of the paste was calculated using the relation

$$SP_{Ca(OH)_2} = [Ca^{2+}][OH^-]^2 f_{Ca^{2+}} f_{OH^-}^2, \qquad (1)$$

where $SP_{Ca(OH)_2} = 6.5 \times 10^{-6}$ at 20°C [10]; $a_{OH^-} = f_{OH^-}[OH^-] = 10^{-(14-pH)}$ M; and $f_{Ca^{2+}}$, activity coefficient of calcium ions, taken to be 0.44, 0.5, and 0.45 for the control paste and pastes with HS1 and HS2 additives, respectively [10].

The setting times of the pastes under study were determined using the procedure described in [11].

The influence exerted by alkaline silicate additives on the pH value of the liquid phase of the portland cement pastes under study (Fig. 1) is in agreement with the previously obtained results [7].

The calculated equilibrium concentrations of Ca^{2+}, which correspond to a solution saturated with $Ca(OH)_2$ at a steady-state pH value, are presented in Fig. 2. It can be seen from formula (1) and Fig. 2 that the calculated and experimental concentrations of Ca^{2+} are highly sensitive to changes in the pH value.

It should be noted that the highest concentrations of calcium(II) are attained during the first minutes of hydration, after which the content of calcium(II) rather rapidly decreases because of the formation of primary hydrates (Figs. 2a and 2c).

Table 2 lists data on the influence of hydrated sodium silicates on the setting time of cement pastes.

In the pure paste, an induction period begins immediately after a short stage of primary hydration. The duration of this period (up to 1.5–3 h) determines the onset time of setting. A pH value of 12.7 is attained in the system. With the induction period complete and transition to the stage of accelerated hydration, the cement paste loses its plasticity and, after a certain time, acquires initial strength.

An important factor affecting the induction period by supersaturation of the pore solution of the cement paste with calcium ions [with respect to $Ca(OH)_2$] [2, 12]. Immediately after addition of water to the cement, a high concentration of Ca^{2+} and OH^- ions is created in the paste. The supersaturation of the pore solution with calcium ions strongly hinders the dissolution of the clinker phases. In several hours, when the supersaturation reaches values severalfold exceeding the equilibrium concentration of $Ca(OH)_2$, first nuclei of $Ca(OH)_2$ appear. This initiates growth of the C–S–H gel, the supersaturation decreases, and the dissolution of cement particles resumes.

It is of interest, in determining how alkaline silicates affect the hydration of portland cement, to correlate the experimentally determined concentrations of calcium(II) in the pastes with the equilibrium concentrations of calcium(II), which correspond to saturation with $Ca(OH)_2$ at steady-state pH values (Fig. 2).

It can be seen in Fig. 2c that supersaturation is not created originally in a paste with addition of high-silica sodium hydrosilicate HS2: calcium ions that pass into solution are bound by silicate ions of the additive and $[Ca^{2+}]_{exp}$ is considerably lower than the saturation concentration at the corresponding pH value. Further, as the initial pH values of the pastes with addition of water-soluble silicates increase, the equilibrium concentration of Ca^{2+} decreases in accordance with formula (1) and, at a certain stage (at pH 12.5, i.e., approximately 45 min after the instant of mixing of cement with water), the liquid phase in the paste with HS2 will also be a saturated solution. In a pure paste, an induction period begins when the saturation is reached, whereas in a paste with addition of HS2, hydration continues, in all probability, even when the solution becomes supersaturated and the pH value stabilizes at values exceeding that of the pure paste.

While the paste with HS2 is far from supersaturation with Ca^{2+} ions [with respect to $Ca(OH)_2$], the clinker minerals contained in the paste are intensively hydrated and OH^- ions pass into solution to be consumed there for depolymerization and hydrolysis of silicate anions of the additive [6] and for an increase in the pH value of the liquid phase. During this period, hydrated calcium silicates are formed both via precipitation of silicate ions of the additive and via release of silicate and aluminate ions from the clinker. The basicity of the forming calcium silicates continuously varies with the pH value of the liquid phase.

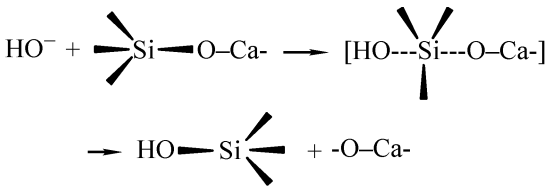
Table 2. Setting time of the cement paste in relation to the type of sodium hydrosilicate added

Sodium hydrosilicate	Setting time, min	
	beginning	end
Without HS (control paste)	95	200
HS1	15	60
HS2	10	45

At a high rate of interaction between hydroxide ions and silicate anions of the additive (e.g., in the case when the HS powder dissolves very rapidly), the period during which a paste has lower pH values than that of the pure paste may be short and virtually unnoticeable.

It is more difficult to understand the acceleration of hydration in a paste with a low-silica (highly alkaline) metasilicate HS1, when pH values exceeding those in an additive-free paste are reached. The concentration of calcium(II) virtually immediately becomes supersaturated [with respect to $Ca(OH)_2$], even though being considerably lower than that in the pure paste (Fig. 2b). The hydration in the pure paste is controlled by crystallization of $Ca(OH)_2$ until the supersaturation is attained. Therefore, it is reasonable to assume that, in the paste with HS1, the onset of intensive hydration is determined by the beginning of crystallization of $Ca(OH)_2$. In this system, the supersaturation of the liquid phase with Ca^{2+} ions [with respect to $Ca(OH)_2$] is so high already in the first minutes of hydration that first nuclei of $Ca(OH)_2$ appear immediately and hydration is initiated. This conclusion is in agreement at least with the known published data according to which additives that make higher the alkalinity of portland cement pastes, including low-silica sodium silicates, accelerate the setting [1, 2, 5], i.e., the concentration of OH^- ions determines the rate of the process. The data in Table 2 also confirm the aforesaid.

It is highly probable that the mechanism by which the main phase of the cement, alite, is hydrated in a strongly alkaline medium includes a primary reaction between the –Si–O–Ca– bond and the hydroxide ion by the type of an S_N2 nucleophilic substitution, with a transition state (bipyramid) formed and the silica tetrahedron inverted [13]:



The rate of this reaction is proportional to the concentration of hydroxide ions.

All the aforesaid is an attempt to explain from a common standpoint the influence exerted by silicates of alkali metals on portland cement pastes during the first hours after the beginning of hydration. Here, account should be taken of the fact that, in later stages, the hydration and fundamental aspects of hardening of pastes with addition of silicates of alkali metals depend on a large number of factors: basicity and morphology of the C–S–H gel being formed and stability of separate hydration products at steady-state pH values.

CONCLUSIONS

(1) The specific features of hydration of a portland cement with addition of silicates of alkali metals are determined in early stages of the process by the ability of these compounds to affect the concentration of hydroxide ions and Ca^{2+} ions in the liquid phase of the cement paste.

(2) Less basic (high-silica) sodium silicates eliminate the supersaturation of the liquid phase with Ca^{2+} [with respect to $Ca(OH)_2$] in the initial stage.

(3) In the presence of highly basic alkaline sodium silicates, the liquid phase becomes supersaturated with Ca^{2+} [with respect to $Ca(OH)_2$] virtually immediately after mixing the cement with water; as a result, hydration is accelerated in both cases, i.e., in the acid and alkaline (with respect to the pure paste) medium.

REFERENCES

1. Jawed, I. and Skalny, J., *Cem. Concr. Res.*, 1978, vol. 8, no. 1, pp. 37–51.
2. Teylor, H.F.W., *Cement Chemistry*, London: Academic, 1990.
3. Larosa-Tompson, J., Gill, P., Scheetz, B.E., and Silsbee, M.R., *Proc. 10th Int. Congr. Chem. Cem.*, Gothenburg, 1997, vol. 3, report 3iii024.
4. Vail, J.G., *Soluble Silicates* (ACS Monograph Series). New York: Reinhold, 1952, vols. 1, 2.
5. US Patent 4 402 749.
6. Aborin, A.V., Brykov, A.S., Danilov, V.V., and Korneev, V.I., *Tsement Ego Primen.*, 2001, no. 3, pp. 40–42.
7. Brykov, A.S., Danilov, V.V., Korneev, V.I., and Larichkov, A.V., *Zh. Prikl. Khim.*, 2002, vol. 75, no. 10, pp. 1612–1614.
8. Brykov, A.S., Danilov, V.V., and Korneev, V.I., *Zh. Prikl. Khim.*, 2000, vol. 73, no. 1, pp. 15–19.
9. *GOST* (State Standard) *5382–91: Cements and Material Produced in Their Manufacture: Methods of Chemical Analysis*.
10. Lur'e, Yu.Yu., *Spravochnik po analiticheskoi khimii* (Handbook of Analytical Chemistry), Moscow: Khimiya, 1989, 6th ed.
11. *GOST* (State Standard) *310.3: Cements: Methods for Determining the Standard Thickness, Setting Time, and Uniformity of Volume Changes*.
12. Tardos, M.E., Skalny, J., and Kalyoncu, R.S., *J. Am. Ceram. Soc.*, 1976, vol. 59, nos. 7–8, pp. 344–347.
13. Tobe, M.L., *Inorganic Reaction Mechanisms*, London: Thomas Nelson & Sons, 1972.

ISSN 1070-4272, Russian Journal of Applied Chemistry, 2006, Vol. 79, No. 4, pp. 525–528. © Pleiades Publishing, Inc., 2006.
Original Russian Text © O. G. Zarubitskii, B. F. Dmitruk, N. F. Zakharchenko, 2006, published in Zhurnal Prikladnoi Khimii, 2006, Vol. 79, No. 4, pp. 537–540.

INORGANIC SYNTHESIS AND INDUSTRIAL INORGANIC CHEMISTRY

Interaction of Graphite with Hydroxide–Salt Melts

O. G. Zarubitskii, B. F. Dmitruk, and N. F. Zakharchenko

Vernadsky Institute of General and Inorganic Chemistry, National Academy of Sciences of the Ukraine, Kiev, Ukraine

Received December 8, 2005

Abstract—The mechanism and kinetics of graphite dissolution in melts based on sodium hydroxide were studied. The effect of various salt additives on the intensity of the occurring reactions is considered. A method recommended for removal of graphite in the form of remainders of molds and mold cores from titanium casts is described.

DOI: 10.1134/S1070427206040033

The existing industrial methods for cleaning the surface of machine and equipment parts to remove operational contaminations are imperfect: they are, as a rule, low-intensive, fail to always provide a satisfactory quality of cleaning, involve manual labor, and cannot rule out health hazard and occurrence of dangerous situations, e.g., inflammation [1]. This, in particular, refers to cleaning of titanium alloy casts to remove remainders of graphite molds and mold rods. Commonly, graphite is removed from casts of this kind manually, with auxiliary cutting tools, with these tools frequently broken; this procedure fails to always provide the due quality of surface cleaning and may cause mechanical damage to articles so that they go to scrap.

The aim of this study was to develop a high-temperature procedure for cleaning the surface of titanium alloy casts to remove graphite rods.

There is no published evidence about systematic studies of the interaction between graphite and hydroxide–salt melts. There have only been reports describing the behavior of carbon electrodes and structural elements in electrochemical processes [2].

EXPERIMENTAL

A derivatographic study of processes occurring in binary C–NaOH, C–KOH, C–$NaNO_3$ systems and ternary mixtures C–NaOH–$NaNO_3$ was carried out. The molar ratio of the components was varied from 5 : 1 to 1 : 4 for the first two systems and from 2 : 1 to 15 : 1 for the third. The molar ratios for the ternary system were 5 : 1 : (0.7, 2.5), 1 : (2–4) : 2, 1 : 2 : 1, and 1 : 1 : 0.5. The measurements were performed on an OD-102 derivatograph at a heating rate of 5.1 deg min^{-1}. The weighed portions of the starting substances were in the range from 0.2 to 1.8 g.

An interaction between the components in mixtures of graphite and sodium and potassium hydroxides is observed even at low temperatures. For example, release of a certain amount of heat begins in the C–2NaOH mixture at approximately 160°C. The process is enhanced as the alkali melts. The quantitative characteristics of the effects observed strongly depend on the ratio of the components. It is noteworthy that oxidation of powdered graphite by atmospheric oxygen begins only at temperatures exceeding 400°C. The processes occurring in C–NaOH mixtures are accompanied by slight changes in the sample weight: the weight loss is due to moisture removal, and the weight gain upon melting of the alkali is associated with oxygen absorption. The thermal and gravimetric effects are considerably more pronounced for mixtures of graphite with potassium hydroxide.

In the C–$NaNO_3$ mixtures, the components interact at a temperature markedly exceeding the melting point of the nitrate. Depending on the component ratio, the beginning of a vigorous reaction is observed in derivatograms at 380–420°C. In mixtures with component ratios of 2 : 1 to 10 : 1, the interaction is markedly enhanced on reaching a temperature of 450°C. At large nitrate contents, the reaction proceeds in a moderate mode.

As follows from the experimental data obtained, the interaction of graphite with sodium and potassium hydroxides is considerably weaker than that in mix-

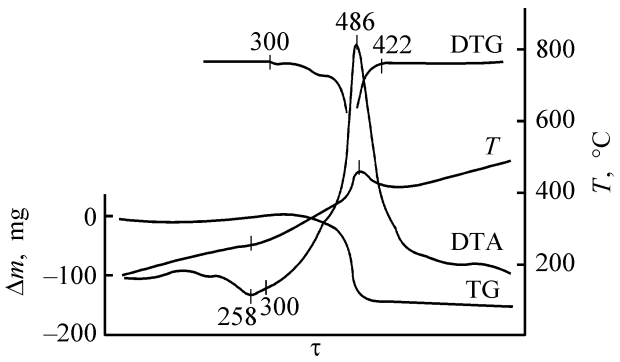


Fig. 1. Derivatogram of the $2NaOH–2NaNO_3$–C mixture. (Δm) Weight loss, (T) temperature, and (τ) time.

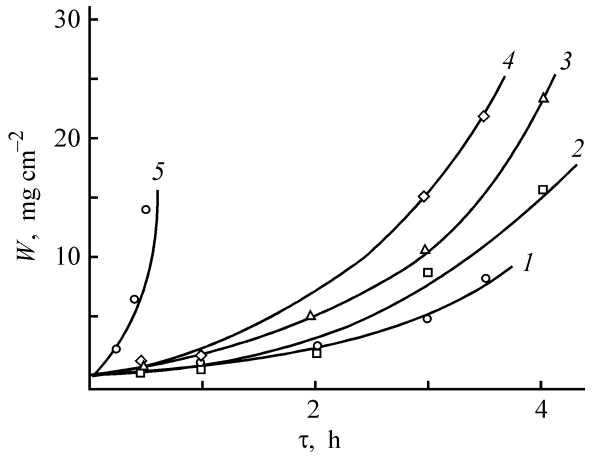


Fig. 2. Amount W of graphite etched away in melts of (*1*) $NaNO_2$, (*2*, *3*) NaOH, and (*4*, *5*) $NaNO_3$. Temperature (°C): (*1*, *2*, *4*) 450 and (*3*, *5*) 500. (τ) Time.

tures of graphite and sodium nitrate. Apparently, atmospheric oxygen is involved in reactions after the melting of the alkali:

$$C + 2MOH + O_2 = M_2CO_3 + H_2O. \quad (1)$$

In the C–NaOH–$NaNO_3$ mixtures, the components intensively interact with carbon at temperatures 80–100°C lower than those in the mixture with sodium nitrate (Fig. 1) and this interaction is accompanied by a considerable weight loss. The values of the weight loss, experimentally determined for the C–2NaOH–$2NaNO_3$ (initial weighed portion of the mixture 1.867 g), correspond to the occurrence of the reaction

$$C + 2NaOH + 2NaNO_3 = Na_2CO_3 + 2NaNO_2 + H_2O. \quad (2)$$

It is noteworthy that the rate of reaction (2) strongly depends on the component ratio. For example, its intensity in the C–4NaOH–$2NaNO_3$ mixture is considerably higher, which can be judged from the abrupt weight loss and a more pronounced rise in temperature.

In addition to carrying out a derivatographic study, the kinetics of graphite etching in molten sodium hydroxide, nitrate, and nitrite and NaOH–$NaNO_3$, NaOH–$NaNO_2$, and KOH–KNO_3 mixtures was examined. The method of isothermal gravimetry of a sample under free-convection conditions was used. Graphite samples (99.9% C) in the form of rods (6–8 cm^2) or plates (10–18 cm^2) were treated in melts at 450 and 500°C. The mass of the melt was 120–140 g. The samples were preliminarily polished to obtain the same surface quality in each case. After treatment in the melt, samples were cooled to room temperature, washed in boiling distilled water for 15–20 min, and calcined at 200°C. In determining the rate of graphite etching in molten NaOH–$NaNO_3$ and NaOH–$NaNO_2$ mixtures, the time of experiment was limited to 20 min and the average value was calculated.

The kinetic curves of graphite etching in the individual melts under study have a shape typical of autocatalytic processes (Fig. 2), which is caused by an increase in the reaction area with time. The kinetic dependences are described by a power equation whose constants are listed in Table 1.

The rate of graphite etching in molten NaOH–$NaNO_3$ and NaOH–$NaNO_2$ mixtures depends to a greater extent on the component ratio. The isotherms of etching rate in these mixtures pass through a maximum (Fig. 3) at a nitrate content of approximately 35% (500°C) and 45% (450°C) in the first system and a nitrite content of 20% at both temperatures in the second system. It is noteworthy that the data for the NaOH–$NaNO_3$ system are in agreement with the results of a derivatographic study of processes in the ternary mixture C–NaOH–$NaNO_3$ in relation to the ratio of the components of the hydroxide–salt phase.

A number of alkaline formulations used to process titanium alloys, namely, to remove scale, are known [3, 4]. However, preliminary experiments demonstrated that formulations of this kind are ineffective or at all unacceptable for removal of graphite present

Table 1. Constants of the power equation $d_0\tau^n$, g cm^{-2} h^{-1}

Melt	T, °C	d_0	n	τ
NaOH	500	1.08	2.3	0–4
$NaNO_3$	500	99.1	3.3	0–1
$NaNO_2$	450	2.02	0.9	0–4

Table 2. Results of industrial tests of the method for cleaning of titanium casts to remove remainders of the graphite-based mold mixture in a melt based on alkali metal hydroxide

Kind of cast	Rod characteristics			Number of simultaneously processed casts	T, °C	Time of complete rod removal, h	Average rate of rod removal, mm h^{-1}
	shape	shape in cross-section, mm	length, mm				
Turbine blade	Straight	5 × 20	120	1	560	7.5	8.0
Pipe	90° bend	d = 8	55	5	540	3.0	9.2
connection	The same	d = 10	40	5	560	2.0	10.0
Adapter		d = 10, 6	70	3	520	4.2	8.3
Flange (6 rods)	Straight	d = 5	10	3	500	0.5	10.0
Base (12 rods)	90° bend	Oval: a = 13, b = 35	27	1	520	1.75	7.7

in the form of remainders of molds and mold rods from titanium casts. It was found experimentally that the intensity of graphite removal in such melts at temperatures lower than 500°C is insufficient, in particular, for long rods. At the same time, treatment at above 500°C may lead to inflammation of articles. For comparison, a melt patented in a number of countries was used [5–7]. The melt contained (wt %): 50–78 sodium hydroxide, 8–20 potassium hydroxide, 9–15 sodium nitrate, and 5–15 sodium chloride. The intensities of graphite (rod) removal and types of corrosion behavior of the titanium alloy were compared for a particular alloy containing the above components in close to the middles of the indicated ranges. The optimal parameters of the process of cast cleaning were found for the VT5 alloy.

The results obtained in the study served as a basis for suggesting a melt containing four components. The melt is based on sodium hydroxide and nitrate. Potassium chloride contained in the melt improves its technological properties and, in addition, serves to prevent inflammation and explosion of potassium nitrate; KCl was introduced in an amount of 4–10 wt %. Making its content higher is undesirable because of a pronounced decrease in the dissolution rate of graphite. New properties are imparted to the melt by sodium orthotitanate. This additive to the alkaline melt exerts the strongest inhibiting influence on the corrosion of titanium. Also, the thermal stability of titanium and its alloys substantially increases. The solubility of sodium orthotitanate in molten sodium hydroxide is limited. For example, it is somewhat higher than 6 wt % at 550°C. The advantage of this salt is that Na_4TiO_4 can be obtained from a titanium waste, and, provided that certain conditions are satisfied, this can be done directly in the alkaline melt.

Comparative experiments demonstrated that the composition containing sodium hydroxide, nitrate, and orthotitanate and potassium chloride has a higher (by a factor of 2.5–10) reactivity toward graphite, and no inflammation is observed at 550°C and a treatment duration providing complete removal of a rod.

The experiments performed suggested as the optimal melt for removal of graphite in the form of remainders of molds and mold rods from titanium casts the following formulations (wt %): sodium nitrate 40–55, potassium chloride 4–10, sodium orthonitrate, 2–6 and sodium hydroxide the rest.

Industrial tests of the technique suggested were carried out at a titanium casting shop of a machine-building plant in an industrial thermal furnace. The melt prepared in a rectangular steel bath had the following composition (wt %): sodium nitrate 48, potassium chloride 5.5, sodium orthotitanate 2.05, and sodium hydroxide the rest.

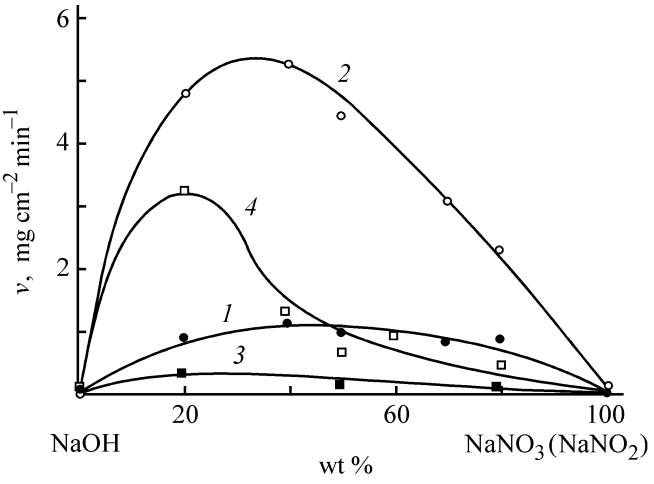


Fig. 3. Isotherms of etching rates v of graphite in molten (*1*, *2*) NaOH–$NaNO_3$ and (*3*, *4*) NaOH–$NaNO_2$. Temperature (°C): (*1*, *3*) 450 and (*2*, *4*) 500.

On melting the mixture and removing moisture at 400–500°C in the course of 1 h, the temperature was elevated to the working point. Casts of a VT5L alloy with remainder of molding sand and graphite rods of variously intricate shapes were cleaned. The removal of rods was periodically monitored in the course of processing. The results of the tests are listed in Table 2. A high rate of rod removal (8–10 mm h^{-1}) was achieved in the tests. A metallographic analysis demonstrated that the surface of the casts remains unchanged, with no corrosion etching occurring, and the mechanical properties of the alloy satisfy the standard requirements.

The advantage of the chemical method for removal of graphite from titanium alloy casts consists in that there is no need for manual labor, the output capacity significantly increases, cutting tools are saved, and the cleaning quality is improved.

CONCLUSIONS

(1) The mechanism and kinetics of graphite dissolution in hydroxide–salt melts and the effect of various salts ($NaNO_3$, $NaNO_2$, KCl, NaCl, Na_4TiO_4, KNO_3) were studied. As a result, an efficient method for removal of graphite in the form of remainder of molds and mold rods from titanium casts was suggested. The optimal melt composition is as follows (wt %): sodium nitrate 40–55, potassium chloride 4–10, sodium orthotitanate 2–6, and sodium hydroxide the rest. The working temperatures of the method are in the range 500–550°C.

(2) The new technique was successfully tested in industry. The tests demonstrated the advantages of the chemical method for removal of graphite from inner hollows of titanium alloy casts.

REFERENCES

1. Morshina, A.P., *Tekhnol. Legk. Splavov: Nauch.-Tekh. Byul. VILS*, Moscow, 1973, no. 2, pp. 110–111.
2. Zarubitskii, O.G., *Ochistka metallov v rasplavakh shchelochei* (Cleaning of Metals in Alkali Melts), Moscow: Metallurgiya, 1981.
3. Usova, V.V., Plotnikova, T.P., and Kushakevich, S.A., *Travlenie titana i ego splavov* (Etching of Titanium and Its Alloys), Moscow: Metallurgiya, 1984.
4. Aleksandrov, V.K., Anoshkin, N.F., Bochvar, G.A., et al., *Polufabrikaty iz titanovykh splavov* (Half-Products Made of Titanium Alloys), Moscow: Metallurgiya, 1979.
5. French Patent 1 477 220.
6. FRG Patent 1 621 556.
7. Swiss Patent 470 491.

ISSN 1070-4272, Russian Journal of Applied Chemistry, 2006, Vol. 79, No. 4, pp. 529–533. © Pleiades Publishing, Inc., 2006.
Original Russian Text © A. S. Brykov, 2006, published in Zhurnal Prikladnoi Khimii, 2006, Vol. 79, No. 4, pp. 541–545.

INORGANIC SYNTHESIS AND INDUSTRIAL INORGANIC CHEMISTRY

Glass Formation and Gelation in the System K_2O–SiO_2–H_2O

A. S. Brykov

St. Petersburg State Technological Institute (Technical University), St. Petersburg, Russia

Received October 24, 2005

Abstract—Systems produced in interaction of colloid SiO_2 particles with potassium hydroxide solutions form, as a result of aging, solid transparent gels and jellies. Depending on the pH value, the systems formed retain the colloid structure or take features of a homogeneous glassy body, with the glass formation possible within a rather large area in the K_2O–SiO_2–H_2O triangle, adjacent to the K_2O–SiO_2 line.

DOI: 10.1134/S1070427206040045

An opinion has strengthened in modern literature that glass formation processes can occur not only in anhydrous silicate systems M_2O–SiO_2 (M = Na, K, Li), but also in ternary systems M_2O–SiO_2–H_2O, with the content of water in these systems varying rather widely [1, 2]. At the same time, when speaking about glass formation, the authors, as a rule, restrict consideration to systems with a molar ratio SiO_2/M_2O (silica ratio) not exceeding 3–4, even though similar processes also occur under certain conditions in higher-silica aqueous silicates and in their solutions with a water content of up to 60–70 wt %. Many of these systems have applied importance as binders (formation of silicate masses, films, and gels).

In the M_2O–SiO_2 system, cooling of melts leads to glass formation at a SiO_2 content exceeding 60% (SiO_2/M_2O molar ratio exceeding 1.5–2) [3]. Aqueous alkaline silicates with a SiO_2/M_2O molar ratio of 2 to 4 (known as liquid glasses) can be obtained by direct dissolution of an alkali silica glass in water, with the subsequent dehydration of the resulting solution to any final content of water. The results of NMR and IR studies of these systems by spectroscopy and other methods underlie the modern concepts of water-containing silicates of alkali metals as systems with an exceedingly complex polymeric structure [4, 5]. At ordinary temperatures, the region in which aqueous sodium silicates with a SiO_2/M_2O molar ratio of about 3 are in a glassy state is limited from above by the water content of 30–40 wt % [2].

In our opinion, glass formation can occur within a rather large region in the ternary system M_2O–SiO_2–H_2O, adjacent to the M_2O–SiO_2 line.

Systems with any value of M_2O/SiO_2, including those exceeding 4–5, can be obtained upon interaction of highly active forms of silica, e.g., SiO_2 particles of colloid size, with solutions of alkalis or silicates of alkali metals (sodium, potassium, or lithium). The content of SiO_2 in the resulting solutions may be 30–50 wt % and more, and the solutions themselves may form, after a certain time, solid or solid-like transparent gels and jellies. Depending on the pH value, the systems being formed retain their colloid structure or acquire features of a homogeneous glassy body. It would be of use to make a general description of these systems and their position in the M_2O–SiO_2–H_2O triangle.

Here we consider systems obtained by mixing of colloid solutions of SiO_2 with potassium hydroxide at SiO_2/K_2O molar ratios in the range from 2 to 100. We restrict our consideration to the most widely occurring commercial stabilized silica sols with a SiO_2 content of 30–50 wt % and a particle size of 7–30 nm.

In contrast to NaOH and LiOH, potassium hydroxide is easily and rapidly assimilated by silica sols in any proportions, which markedly simplifies the preparation of the systems under study.

EXPERIMENTAL

We used in the study commercial monodisperse silica sols with various particles sizes, stabilized with NaOH (Table 1).

Dry KOH was introduced, in an amount necessary to obtain systems with SiO_2/K_2O molar ratios of 2

Table 1. Parameters of silica sols

Silica sol brand, manufacturer	Outward appearance of a silica sol	Particle diameter, nm	Content, wt %		pH
			SiO_2	Na_2O	
Sialit (Silikat ZAO, Russia)	Weakly opalescent	7	29	0.54	10.1
Ludox HS40, Grace Davison, USA	Opalescent	12	40	0.41	9.7
Ludox CL–X, Grace Davison, USA	Strongly opalescent	22	46	0.19	9.1
Levasil 100/45, Bayer, Germany	Milky	30	45	0.23	10.0

to 80–90, into SiO_2 sols under agitation. Accordingly, the K_2O/Na_2O molar ratio in the solution prepared is approximately in the range from 50 to 1 (the lower SiO_2/K_2O, the lesser the extent to which the effect of Na^+ on the properties of the system should be taken into account).

The solutions we prepared were degassed under vacuum for 5 min and stored in hermetically sealed glass ampules for 2–3 months. To accelerate the physicochemical processes occurring in the systems prepared, we stored them at 60°C.

IR spectra of the coagulation structures formed were measured in KBr pellets on a UR-20 spectrophotometer.

The pH values of the solutions prepared were measured with a pH-673M laboratory pH-meter.

Figure 1 show the results of a visual inspection of the state in which systems composed of silica sols and KOH are several months after being prepared.

The IR spectra of the systems under study (the most characteristic band of stretching vibrations of Si–O, peaked at 1000–1150 cm^{-1}) are shown in Fig. 2.

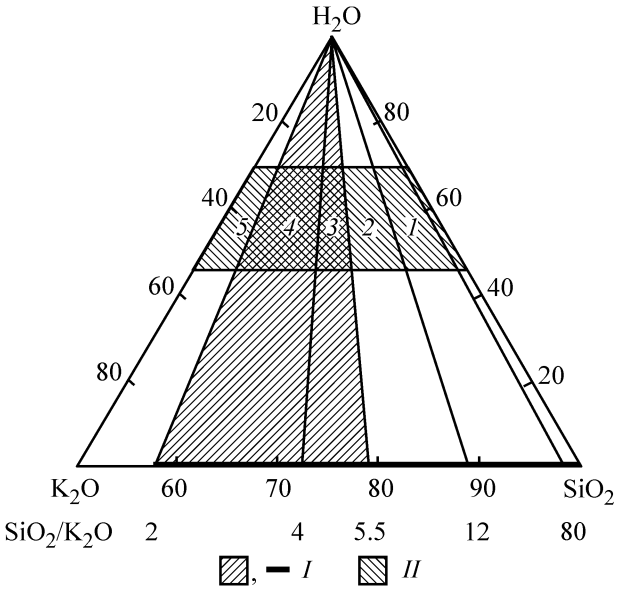


Fig. 1. Structures formed upon interaction of silica sols with KOH: (*1*) brittle gels constituted by SiO_2 colloid particles, (*2*) nontransparent coagulation structures, (*3*) glassy polysilicate jellies, (*4*) viscous liquids (liquid glasses), and (*5*) glassy hydrated silicates. (K_2O, SiO_2) Content (wt %). (*I*) Glass-forming regions in the K_2O–SiO_2 and K_2O–SiO_2–H_2O systems, respectively. (*II*) Range of compositions in the K_2O–SiO_2–H_2O system, produced upon interaction of commercial silica sols with KOH.

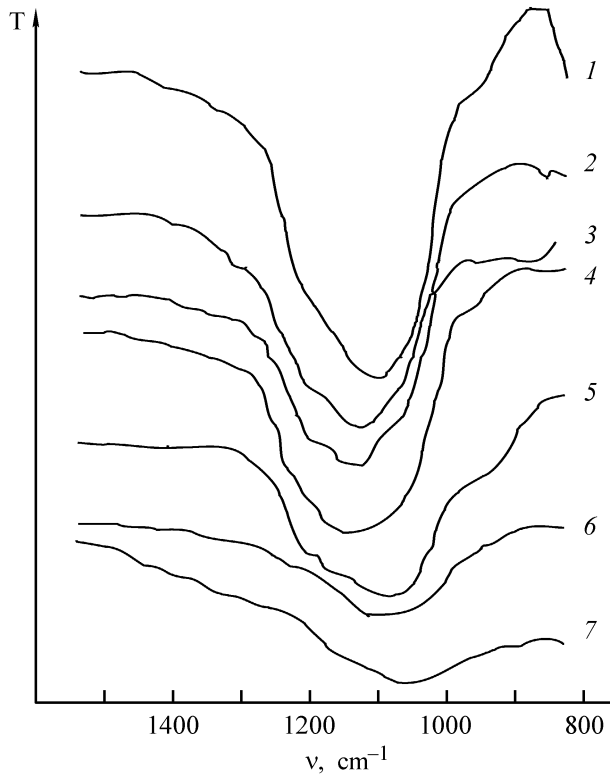


Fig. 2. IR spectra of (*1*) Sialit sol and (*2–7*) gels prepared from this sol. SiO_2/K_2O molar ratio: (*2*) 70, (*3*) 60, (*4*) 25, (*5*) 6, (*6*) 5, and (*7*) 4. (T) Transmission and (ν) wavenumber.

The pH values in these systems in the first day after the preparation (20°C) are listed in Table 2.

As can be seen in Fig. 1, the final states of the systems composed of concentrated silica sols and potassium hydroxide strongly vary with the SiO_2/K_2O ratio. Two regions correspond in this case to a stable state of solid transparent gels.

At small amounts of KOH, for which introduction of potassium hydroxide into a colloid solution of SiO_2 does not lead to an increase in the pH of the whole system to more than 12, brittle (crumbling) gel-like structures are formed. As shown by visual inspection, these structures preserve the optical density of the starting colloid solutions. Gels prepared from sols with particles less than 10 nm in size are transparent, whereas those with coarser particles are slightly turbid or "milky."

Depending on the molar ratio and temperature, the gelation time may be in the range from several hours to several days. The aging of systems of this kind is not accompanied by significant changes in IR absorption spectra (Fig. 2, systems with SiO_2/K_2O = 25, 60, 70) and changes in the pH value. A certain shift of the peak of the absorption band to larger wave numbers points to aggregation of particles and formation of chemical bonds between them.

Apparently, KOH mostly acts in the formation of gels of this type as an electrolyte additive that destabilizes the electrical double layer around silica particles. As a consequence, particles may be fixed with respect to one another at distances sufficient for manifestation of intermolecular attraction forces acting via liquid interlayers and for formation of chemical (siloxane) bonds. When silica sols are mixed with KOH, the system is destabilized and a gel is formed at SiO_2/K_2O molar ratios smaller than 70–90. The stability region of gels of this kind is bounded below by SiO_2/K_2O molar ratios of about 12–25. At a comparatively low content of KOH, conditions are created for slow coagulation, in which new colloid particles are easily attached at ends of chainlike fragments, i.e., at those places where the energy barrier associated with repulsion forces is the lowest. The sol turns into a gel at certain points of contact between particles via formation of an infinite network. Thus, the structure of gels of this type is formed by SiO_2 colloid particles, and, similarly to the starting colloid silica sols, the gels remain heterogeneous, two-phase systems. The same gels are formed upon introduction of electrolytes with pH ≤ 7 into silica sols. The most comprehensive notion of these structures was given by Iler in his monograph [6].

Table 2. Dynamics of variation of the pH value in systems with different SiO_2/K_2O molar ratios

SiO_2/K_2O molar ratio	pH value at indicated time elapsed from the instant of preparation, h		
	first minutes	1	24
5	14.0	12.7	~12.0
12	13.2	12.7	12.2
25	12.9	12.5	12.1
70	11.7	11.6	11.6

As a result of the subsequent processes of shrinking and strain buildup in the silica network, the gels become brittle. In the course of aging of such gels, especially in the case of aging accompanied by dehydration (drying), cracks are formed and split the gel into separate fragments.

Gels of a distinctly different type are formed in aging of systems formed by mixing colloid SiO_2 with potassium hydroxide at SiO_2/K_2O molar ratios ranging from 2–4 to 6. They show a conchoidal fracture characteristic of glasses and, depending on the water content and SiO_2/K_2O ratio, may be more or less hard ?and brittle and are somewhat softened upon moderate heating (up to 60°C). The strength and hardness of the gels formed is the higher, the larger the amount of SiO_2 they contain. In general, these systems have much in common with glasses as regards their physical properties.

High pH values (up to 14) are originally created in systems of this type; subsequently, the alkalinity decreases and stabilizes at pH 11.5–12. In a strongly alkaline aqueous medium (pH > 12), the dissolution of silica particles is accelerated, so that gels become transparent in the course of aging even when prepared from nontransparent or opalescent sols with coarse SiO_2 particles (of the Ludox HS_{40} type).

The IR spectra of these systems significantly differ from the spectra of the starting silica sols and, in the course of time, take the form characteristic of alkali silica systems containing no SiO_2 colloid particles (the high-intensity band of Si–O stretching vibrations at 1125–1150 cm^{-1} is replaced with a broad medium-intensity band peaked at 1050–1100 cm^{-1}).

In our opinion, the dissolution of sol particles is a key process in the formation of gels of the second type. In this case, gelation is a consequence of the formation of a homogeneous spatial structure from residues of silicic acid, which are formed in dissolution of SiO_2 colloid particles under high-alkalinity condi-

tions, are polymerized to a varied extent, and contain various amounts of water. These processes can be considered similar to those occurring in formation and vitrification of silicate melts. At the same time, it is pertinent here to draw analogy with jellification of solutions of some organic polymers, and, therefore, it would be more appropriate to regard gels of this type as jellies.

As is known, the ability of silica-containing melts to form glasses is accounted for by the presence in these melts of 3D silicon–oxygen polymeric structures, whose interaction leads to a considerable increase in the viscosity of the melts in cooling and to their solidification below the glass-transition point, with the disordered structure characteristic of liquids retained.

The of dissolution of compact SiO_2 particles in alkali solutions involves splitting of the siloxane bonds in accordance with the reaction equations

$$\text{Si–O–Si} + \text{OH}^- \rightarrow \text{SiOH} + \text{SiO}^-, \quad (1)$$

$$\text{H}_2\text{O} + \text{SiO}^- \rightarrow \text{Si–OH} + \text{OH}^- \quad (2)$$

and transfer of silica into the liquid phase in the form of ions of silicic acids with various degrees of polymerization. As can be seen from the reaction equations (1) and (2), the polymeric state of the silicon–oxygen structures in the solutions formed depends on the concentration of hydroxide ions and, consequently, on the concentration of the solution and on its silica ratio. The polymeric state of silica becomes more complex as the concentration of SiO_2 and the SiO_2/M_2O molar ratio increase. In higher-silica systems, silica passes into solution in the form of high-polymer ions and whole fragments, which mostly lose the dense amorphous structure of the initial colloid particles [7].

Similarly to glass, the forming polysilicate gel is homogeneous, i.e., is composed, after the dissolution of SiO_2 colloid particles is complete, of a single phase, gelatinized (with an exceedingly high viscosity) lyophilic solution of high-polymer water-containing silica fragments and ions of silica acids.

In an aqueous medium, the extent of destruction of the silicon–oxygen polymeric structure exceeds that in silicate glass-forming melts owing to the high activity of OH^- ions and their permanent regeneration as a result of hydrolysis by Eq. (2). The forming high-polymer ions of silicic acids and cations of alkali metals interact indirectly, via the hydrate sheaths and interlayers of water molecules. This leads to formation of glassy jellies whose state the better corresponds to that of a solid, the lower the content of water they contain. Thus, a high importance is assumed in glass formation in silicate solutions by the nature of the alkali metal cation and its ability to coordinate a certain number of water molecules. It is well known that aqueous solutions of polysilicates of lithium and quaternary ammonium bases exhibit a considerably higher stability against gelation, compared with sodium and potassium polysilicates, in a wide range of silica ratios. Anyway, the boundaries of different regions of state of the $M_2O–SiO_2–H_2O$ system may rather strongly depend on the type of cation.

As the silica ratio increases from 2 to 5–6, i.e., as the polymeric state of silica becomes more complex, the ability of a solution to form glassy structures grows. Systems with a ratio of about 5 readily transform into transparent jellies at a water content of up to 60–70 wt %, whereas systems with a ratio lower than 4, which have a simpler polymeric structure, retain at this concentration the state of a mobile or viscous liquid down to 0°C. Near this temperature the solution crystallizes. Apparently, the glass-formation point of these systems must lie at negative temperatures. At an ordinary temperature, such systems, prepared from commercial silica sols, are to be dehydrated to a water content of 30–40 wt % for transition to the glassy state [2]. Solid transparent glassy films with a SiO_2/K_2O molar ratio of 2 to 5 and water content of about 20 wt % were obtained by dehydration of the corresponding solutions and gels in a closed system over sodium hydroxide. Soluble powders of sodium and potassium silicates, which are glassy hydrates and have a silica ratio of 2 to 3.5 and H_2O content of 15–20 wt %, are industrially manufactured by drying of the corresponding aqueous solutions [1].

Thus, the following pattern is observed for systems with fixed water content and various silica ratios: the larger the silica ratio, the higher the glass-transition point. Raising the content of water at a fixed silica ratio leads to a decrease in the glass-transition point of the system. This pattern is in full agreement with the extent to which the polymeric composition of silicon–oxygen fragments is complex and to which the intermolecular interaction between these fragments in the systems formed is strong.

The jellies and gels formed are thermodynamically unstable nonequilibrium systems. At silica ratio of 3–12, we can only speak about the kinetic stability of these systems, which rapidly decreases as the SiO_2/K_2O molar ratio becomes higher than 5.

The compositions with a SiO_2/K_2O molar ratio of 6 to 11–12 originally form transparent solid gels, which rather rapidly coagulate (especially at elevated temperatures) to give dense nontransparent structures. In some cases, this process is accompanied by syneresis, shrinking of the gel with liberation of a liquid phase. The gels especially readily disintegrate under dehydration or in the presence of mechanical or chemical admixtures. In all probability, certain polymeric varieties of silica appear in this range of silicate ratio, which, in the course of formation, gradually combine into large dense agglomerates or coagulate on incompletely dissolved silica particle, with the result that the system loses transparence. The high alkalinity and, consequently, less complex polymer composition of low-silica aqueous silicates, are the reason for their high stability against coagulation. At silica ratio exceeding 12, i.e., in systems in which the dissolution of colloid particles is slow or virtually does not occur at all, the stability of gels against coagulation also increases.

The above-mentioned boundaries between the gelation regions are rather conventional: transitions from one structure to another are gradual and depend on the temperature and age of a system. The rate of silica dissolution becomes nonzero at pH > 10.7, and the higher the originally created pH values, the faster the dissolution rate of colloid particles [6]. Thus, the only thing to be discussed is what processes predominate in formation of a gel structure. In systems with pH not exceeding 11–11.5, the colloid structure of the solution may be retained for an indefinitely long time. By contrast, SiO_2 particles may dissolve in highly alkaline systems and homogeneous solutions may be formed rather rapidly, depending on the nature and size of colloid particles [7]. In accordance with this circumstance, the systems formed show a gradual transition from solid colloid gels and nontransparent coagulation structures to glassy jellies and viscous liquids.

CONCLUSIONS

(1) In interaction of colloid forms of SiO_2 with KOH solutions, the final state of the systems being formed is determined by whether these systems retain the colloid structure or become homogeneous. Accordingly, a large region in the K_2O–SiO_2–H_2O triangle is occupied by solid gels and glassy jellies.

At small amounts of KOH (an increase in the pH value of the whole system to no more than 12), the structure of gels is constituted by SiO_2 colloid particles and the gels remain heterogeneous, two-phase systems. KOH mostly destabilizes the electrical double layer that envelops silica particles. These particles are fixed with respect to one another by molecular attraction forces acting via liquid interlayers or because of the formation of chemical bonds.

(2) Glassy gels are formed in aging of systems formed by mixing colloid SiO_2 with hydroxides of alkali metals or their aqueous solutions at a SiO_2/K_2O molar ratio of 2 to 6 and initial pH values of about 14. The dissolution of colloid particles, accumulation of silica and silicic acids in forms differing in polymeric state and water content, and predominant involvement of these forms in the formation of the 3D structure distinguishes polysilicate gels from other types of silica hydrogels.

REFERENCES

1. Korneev, V.I. and Danilov, V.V., *Zhidkoe i rastvorimoe steklo* (Liquid and Soluble Glass), St. Petersburg: Stroizdat, 1996.
2. Orlov, Yu.I., *Fiz. Khim. Stekla*, 2002, vol. 28, no. 5, pp. 401–411.
3. Appen, A.A., *Khimiya stekla* (The Chemistry of Glass), Leningrad: Khimiya, 1970.
4. Kinrade, S.D., Knight, C.T., Pole, D.L., and Syvitski, R.T., *Inorg. Chem.*, 1998, vol. 37, no. 17, pp. 4272–4277.
5. Bass, J.L. and Turner, G.L., *J. Phys. Chem. B*, 1997, vol. 101, no. 50, pp. 10638–10644.
6. Iler, R.K., *The Chemistry of Silica*, New York: Wiley–Interscience, 1979.
7. Brykov, A.S., *Kolloidn. Zh.*, 2004, vol. 66, no. 4, pp. 481–486.

ISSN 1070-4272, Russian Journal of Applied Chemistry, 2006, Vol. 79, No. 4, pp. 534–538. © Pleiades Publishing, Inc., 2006.
Original Russian Text © E. P. Lokshin, O. A. Tareeva, T. G. Kashulina, 2006, published in Zhurnal Prikladnoi Khimii, 2006, Vol. 79, No. 4, pp. 546–550.

INORGANIC SYNTHESIS AND INDUSTRIAL INORGANIC CHEMISTRY

Desulfation of Rare-Earth Concentrates

E. P. Lokshin, O. A. Tareeva, and T. G. Kashulina

Tananaev Institute of Chemistry and Technology of Rare Elements and Mineral Resources, Kola Scientific Center, Russian Academy of Sciences, Apatity, Murmansk oblast, Russia

Received December 27, 2005

Abstract—Desulfation of lanthanide concentrates recovered from sulfuric acid solutions of phosphohemihydrate leaching as sulfates and double sulfates with sodium was studied.

DOI: 10.1134/S1070427206040057

Lanthanides are precipitated as sulfates [1] or double sulfates with sodium from solutions obtained by sulfuric acid leaching of phosphohemihydrate and containing 20–30 wt % H_2SO_4, 0.45–0.8 g l^{-1} CaO, and 1.7–3 g l^{-1} ΣLn_2O_3. The resulting concentrates mainly consist of lanthanide and calcium compounds and contain 30–35 wt % ΣLn_2O_3, 8–12.8 wt % CaO (mainly as $CaSO_4 \cdot 0.67H_2O$ according to X-ray phase analysis), and 55–59 wt % SO_4^{2-}. They also contain substantial amount of sodium (4.6–6.4 wt % Na_2O).

To separate lanthanides, preliminary elimination of sulfate ion is required.

In this study, we considered three approaches to separation of sulfate from such concentrates, involving their treatment with solutions of calcium nitrate, sodium carbonate, or sodium hydroxide.

EXPERIMENTAL

Before experiments on desulfation, the lanthanide concentrates were dried at 100°C. The concentrates were not washed to remove residual mother liquor and contained 8–10 wt % free H_2SO_4. A sample of lanthanide sulfate concentrate was treated with appropriate reagents for a definite time at room temperature and continuous stirring. The concentration of lanthanide sum in solutions and precipitates was determined by oxalate gravimetric method [2]. Concentrations of individual lanthanides were determined by atomic emission spectrometry with inductively coupled plasma on a Plasma 400 spectrometer (Perkin–Elmer). The sulfate ion content in solutions was determined gravimetrically by barium sulfate precipitation from solutions neutralized with HCl to pH 7.

We suggested occurrence of the following reactions between lanthanide sulfate and calcium nitrate:

$$Ln_2(SO_4)_3 + 3Ca(NO_3)_2 + 6H_2O = 2Ln(NO_3)_3 + 3CaSO_4 \cdot 2H_2O\downarrow, \quad (1)$$

$$H_2SO_4 + Ca(NO_3)_2 + 2H_2O = CaSO_4 \cdot 2H_2O\downarrow + 2HNO_3, \quad (2)$$

$$NaLn(SO_4)_2 \cdot H_2O + 2Ca(NO_3)_2 \cdot 4H_2O = Ln(NO_3)_3 + NaNO_3 + 2CaSO_4 \cdot 2H_2O\downarrow + 5H_2O. \quad (3)$$

The lanthanide sulfate concentrate was precipitated from leaching solutions with the initial concentration of sulfuric acid $c_{H_2SO_4}$ 22 wt %, by increasing $c_{H_2SO_4}$ to 42–44 wt % [1]. This concentrate was treated under continuous stirring at L : S = 10 with a $Ca(NO_3)_2$ solution, whose amount exceeded by 5% the stoichiometry of reactions (1) and (2). After definite time intervals, samples of the solution were taken, and the contents of lanthanides and calcium were determined. The conversion was estimated from the fraction of lanthanides transferred into the solution.

As seen from Table 1, desulfation of the concentrate proceeded readily: upon the treatment for 60 min, 91.7% of the lanthanides passed into the solution. Further increase in the time of treatment to 180 min did not noticeable change the degree of conversion. The resulting solution contained 41.4 g l^{-1} ΣLn_2O_3 and 9.4 g l^{-1} CaO.

Table 1. Concentrations of lanthanides $c_{\Sigma Ln_2O_3}$ and calcium c_{CaO} in the solution at various times of treatment of the lanthanide sulfate concentrate with a $Ca(NO_3)_2$ solution

Time, min	Concentration in solution, g l^{-1}		Recovery of ΣLn_2O_3 into solution, %	Time, min	Concentration in solution, g l^{-1}		Recovery of ΣLn_2O_3 into solution, %
	$c_{\Sigma Ln_2O_3}$	c_{CaO}			$c_{\Sigma Ln_2O_3}$	c_{CaO}	
10	35.8	11.1	79.5	60	41.3	9.5	91.7
20	36.9	10.8	82.0	90	41.3	9.4	91.8
30	38.1	10.4	84.7	120	41.4	9.4	92.0
40	39.6	10.4	88.1	180	41.4	9.4	92.0
50	41.0	9.5	91.1				

Table 2. Distribution of lanthanides between products of treatment of double lanthanide sulfate concentrate with calcium nitrate solutions

Product	Treatment time, h	$Ca(NO_3)_2$, % of stoichiometry	Recovery of ΣLn_2O_3, %	$c_{\Sigma Ln_2O_3}$ (liquid, g l^{-1}; solid, wt %)
Solution from stage:				
first	1	108.7	22.51	6.10
second	1	108.7	34.23	9.28
third	1	49.5	16.71	8.23
Wash water	–	–	15.75	4.26
$CaSO_4 \cdot xH_2O$	–	–	10.8	2.7
Total	3	267	100	

The elevated content of calcium in the solution containing lanthanides is caused by the higher solubility of calcium sulfate in the nitric acid solution [3] in comparison with its solubility in water and can be decreased by neutralization of free nitric acid formed by reaction (2).

The lanthanide loss is probably caused by isomorphous cocrystallization of double sodium lanthanide sulfates with calcium sulfate [4, 5]. The ΣLn_2O_3 content in $CaSO_4 \cdot 2H_2O$ amounts to no less than 6 wt %. Lanthanides were not leached by treatment of the gypsum formed with sulfuric acid.

To accumulate lanthanides in nitrate solution, we decreased the L : S ratio and used a fresh nitrate solution for conversion of the subsequent portions of lanthanide sulfate concentrate.

Solutions containing 106.5 g l^{-1} ΣLn_2O_3 and 13.9 g l^{-1} CaO were obtained at L : S = 4 in 1 h without decreasing recovery when additional amounts of $Ca(NO_3)_2$ and lanthanide sulfate concentrate were introduced into the solution with $c_{\Sigma Ln_2O_3}$ = 41.4 g l^{-1}. The amount of $Ca(NO_3)_2 \cdot 4H_2O$ added was 2.2–2.3 kg per kilogram of ΣLn_2O_3.

The data on desulfation of the concentrate containing double sodium lanthanide sulfates (55 wt % SO_4^{2-}) are listed in Table 2. The process included three stages. In each stage, after introduction of calcium nitrate solution, the pulp was mixed for 1 h, the solution was separated, and the concentrations of the lanthanide sum and of individual lanthanides were determined. Then, a solution of calcium nitrate was added to the solid phase, and the treatment was continued. The process was performed at V_l : S = 1 : (5–10) with solutions containing 4–5 wt % $Ca(NO_3)_2$. The consumption of $Ca(NO_3)_2$ calculated for reaction (3) was considered as stoichiometric.

As seen, lanthanides pass into the solution from the concentrate containing double sulfates substantially more slowly than from the concentrate prepared by the precipitation from the solution upon addition of sulfuric acid. Although the lanthanide recovery into the solution remained approximately the same (about

Table 3. Ratio of Ln_2O_3 and Ce_2O_3 concentrations in the initial lanthanide concentrate and in nitrate solutions obtained by treatment of the concentrate with calcium nitrate

Ln_2O_3	$Ln_2O_3 : Ce_2O_3$ concentration ratio			
	initial concentrate	solution from indicated stage		
		1	2	3
Y_2O_3	0.0414	0.0382	0.0421	0.0138
La_2O_3	0.276	0.326	0.323	0.337
Ce_2O_3	1	1	1	1
Pr_2O_3	0.147	0.148	0.144	0.153
Nd_2O_3	0.235	0.272	0.279	0.332
Sm_2O_3	0.0425	0.0507	0.0476	0.0612
Eu_2O_3	0.0087	0.0095	0.0096	0.0112
Gd_2O_3	0.0196	0.0229	0.0219	0.0332
Tb_2O_3	0.0035	0.0029	0.0034	0.0023
Dy_2O_3	0.0037	0.0054	0.0056	0.0088
Ho_2O_3	0.0006	0.0006	0.0008	0.0006
Er_2O_3	0.002	0.003	0.0014	0.0012
Yb_2O_3	0.0002	0.00016	0.00015	0.0001

90%), the required time increased from 1 to 3 h and specific consumption of $Ca(NO_3)_3 \cdot 4H_2O$ increased to 7.27 kg per kilogram of ΣLn_2O_3 (for the sulfate concentrate, 2.2–2.3 kg per kilogram of ΣLn_2O_3). As in the previous case, lanthanides did not pass into the solution after treatment of the calcium sulfate formed with sulfuric acid solution ($c_{H_2SO_4}$ = 26 wt %).

The lower lanthanide recovery in the first stage suggests that the conversion is diffusion-controlled.

On the whole, the slower desulfation of the concentrate based on double sulfates is obviously determined by substantially lower solubility of double sodium lanthanide sulfates as compared to the solubility of lanthanide sulfates.

Table 3 shows that individual lanthanides pass into the nitrate solution in the first two stages virtually in proportion to their content in ΣLn_2O_3. Small deviation in the third stage is of no practical interest for separation.

Thus, by desulfation of lanthanide concentrates with calcium nitrate solutions we can obtain solutions of lanthanide nitrates with fairly high concentration, but the lanthanide loss with calcium sulfate is as high as 10–11%. In addition, the resulting solution contains up to 23 g l^{-1} sulfate ion because of the substantial calcium sulfate solubility (9.4–13.8 g l^{-1} CaO). Thus, more efficient desulfation methods should be searched for.

In the further studies, we used concentrates based on double sulfates (hereinafter, lanthanide concentrates) as the form more convenient for recovery.

We studied the treatment of lanthanide sulfate concentrate with a sodium carbonate solution and further dissolution of the resulting carbonate product in nitric acid. We presumed the occurrence of the following reactions:

$$2NaLn(SO_4)_2 \cdot H_2O + 3Na_2CO_3 + (x - 2)H_2O = Ln_2(CO_3)_3 \cdot xH_2O\downarrow + 4Na_2SO_4,\ x = 5-8, \quad (4)$$

$$CaSO_4 \cdot 0.67H_2O + Na_2CO_3 + 4.33H_2O = CaCO_3 \cdot 5H_2O\downarrow + Na_2SO_4, \quad (5)$$

and

$$Ln_2(CO_3)_3 \cdot xH_2O + 6HNO_3 = 2Ln(NO_3)_3 + (3 + x)H_2O + 3CO_2, \quad (6)$$

$$CaCO_3 \cdot 5H_2O + 2HNO_3 = Ca(NO_3)_2 + 6H_2O + CO_2. \quad (7)$$

The lanthanide concentrate contained (wt %): ΣLn_2O_3 34.26, SO_4^{2-} 51.7, and CaO ~10. The main components of the concentrate were double sodium lanthanide sulfates and bassanite $CaSO_4 \cdot 0.67H_2O$. 57.4% of total SO_4^{2-} is bound with double sodium lanthanide sulfate, and 33.2%, with bassanite. About 10% of the sulfate is in the occluded sulfuric acid mother liquor.

The desulfation efficiency was estimated as the fraction of the sulfate transferred into the solution. The treatment with a sodium carbonate solution was performed under stirring. The initial content of Na_2CO_3 was 6 wt %; it was taken in 105% amount relative to the stoichiometry of reactions (4) and (5); L : S = 10. To study the efficiency and kinetics of desulfation, we took samples of solution every 30 min and determined in them the concentrations of sulfate and unchanged sodium carbonate (by titration). The results listed below showed that desulfation decelerated after 0.5 h and stopped after 3 h, in spite of low degree of desulfation (52.7%) reached. The solution and wash water contained no lanthanides:

Time, h	SO_4^{2-} passed into the solution, %	Time, h	SO_4^{2-} passed into the solution, %
0.5	40.7	2.5	51.1
1.0	42.1	3.0	52.7
1.5	47.9	3.5	52.7
2.0	49.4	4.0	52.7

After treatment with sodium carbonate, the solution was separated, and the residue was washed with water and repeatedly treated with a sodium carbonate solution for 1 h (L : S = 10, sodium carbonate consumption 160% relative to the stoichiometric amount corresponding to the residual SO_4^{2-} content). After these procedures, additional 21.7% of the initial SO_4^{2-} content in the concentrate passed into the solution. Because of high crystallization water content in calcium and lanthanide carbonates, the weight of the product obtained was somewhat larger than that of the initial concentrate.

After treatment of the carbonate–sulfate precipitate with 17.5 wt % HNO_3 taken in an amount of 167% relative to the stoichiometry of reactions (6) and (7), only about 44% of the lanthanides contained in the carbonate precipitate passed into the solution. The complete dissolution of the precipitate was attained only after its repeated treatment with nitric acid with addition of hydrogen peroxide.

The consumption per 1 kg of lanthanide sum was as follows: sodium carbonate 1.3 kg and 65 wt % HNO_3 6.7 kg. The sodium carbonate consumption is close to optimal, while the nitric acid consumption can be substantially lowered by using the counterflow mode and precipitating the main part of calcium from nitric acid solutions with sulfuric acid [2]. We can suggest that it will not be higher than 2 kg per kilogram of ΣLn_2O_3.

Lanthanides should not coprecipitate with the gypsum formed, since the nitric acid solutions are virtually sodium-free.

Thus, preliminary treatment of the concentrate with a sodium carbonate solution in combination with the subsequent leaching of the residue with nitric acid allows transfer of lanthanides into the nitric acid solution without losses. However, nitric acid is consumed for dissolution of not only lanthanides, but also calcium, which increases its consumption. The resulting nitric acid solution contains increased concentrations of sulfate ion and calcium.

We assumed that under the action of sodium hydroxide desulfation proceeds by the reactions

$$NaLn(SO_4)_2 \cdot H_2O + 3NaOH + (x - 1)H_2O = Ln(OH)_3 \cdot xH_2O\downarrow + 2Na_2SO_4, \quad (8)$$

$$CaSO_4 \cdot 0.67H_2O + 2NaOH = Ca(OH)_2\downarrow + Na_2SO_4 + 0.67H_2O. \quad (9)$$

In the experiments on desulfation with a sodium hydroxide solution, the chemical procedures were the same as in desulfation with sodium carbonate solutions. A small difference consisted in a somewhat higher content of SO_4^{2-} in the concentrate (59.5 wt %).

A solution containing 3.25 wt % NaOH was used. At L : S = 10, the NaOH excess over the stoichiometry was 30%. As seen from the data on the kinetics of sulfate transfer into the solution, with sodium hydroxide the desulfation proceeded noticeably faster and more completely than with sodium carbonate.

Time, h	SO_4^{2-} passed into the solution, %	Time, h	SO_4^{2-} passed into the solution, %
0.5	86.9	2.0	90.6
1.0	90.6	3.0	90.6
1.5	90.6	4.0	90.6

After the repeated 1-h treatment of the precipitate with NaOH solution, the residual content of SO_4^{2-} ions in the precipitate was 0.12 wt%. Thus, the degree of two-step desulfation of the lanthanide concentrate with an alkali solution was no less than 99.9% (it was taken into account that in this desulfation procedure the weight of the precipitate decreased almost by half). Incomplete desulfation at one-step treatment with a NaOH solution is caused by reversibility of Eqs. (8) and/or (9) or by a decrease in the chemical activity of sodium hydroxide because of partial conversion into sodium carbonate with atmosoheric carbon dioxide. Such a reaction can be noticeable because of small amount of the solution used in the experiment and long reaction time at vigorous stirring. The contribution of this process should decrease at enlargement of the apparatus and its sealing.

As in the case of desulfation with sodium carbonate, the solutions contained no lanthanides.

Calcium hydroxide can be selectively recovered with aqueous ammonium chloride from the lanthanide concentrate after desulfation [6]. To check this assumption, the precipitate that contained hydroxide and carbonate compounds of lanthanides and calcium was calcined at 900°C to decompose calcium carbonate formed in the reaction of the precipitate with atmospheric carbon dioxide. After treatment of the freshly calcined precipitate with an ammonium chloride solution at room temperature, calcium hydroxide formed completely passed into the solution. From this solution, calcium can be precipitated as carbonate with carbon dioxide [6].

In the process, lanthanides were completely concentrated in the precipitate which readily dissolved in the nitric acid. The selective leaching of calcium oxide with ammonium chloride from the concentrate containing 35 wt % Σ Ln_2O_3 and 10 wt % CaO allows a decrease in the nitric acid consumption by one third and preparation of solutions containing lanthanide nitrates only.

CONCLUSIONS

(1) Removal of sulfate ion from lanthanide concentrates precipitated from sulfuric acid leaching solutions in the form of sulfates and double sulfates with sodium by treatment of these concentrates with dilute solutions of calcium nitrate, sodium carbonate, or sodium hydroxide was studied.

(2) From sulfate concentrates treated with calcium nitrate solutions, lanthanides are leached into the solution faster than from concentrates consisting of double sodium lanthanide sulfates. However, about 10% of lanthanides are lost with the gypsum precipitate formed in the process.

(3) After treatment with sodium carbonate solutions, lanthanides completely pass to the carbonate precipitate, but the degree of desulfation is insufficient (less than 75%).

(4) Desulfation with sodium hydroxide solutions is preferred as compared to the other methods studied. This method ensures efficient separation of sulfate and preparation of the hydroxide concentrate readily soluble in nitric acid. This desulfation method allows separation of calcium from the concentrate and involves virtually no loss of lanthanides.

ACKNOWLEDGMENTS

The study was financially supported by the Leading Scientific Schools Foundation (grant no. NSh–1616–2003.03).

REFERENCES

1. RF Patent 2 225 892.
2. Ryabchikov, D.I. and Ryabukhin, V.A., *Analiticheskaya khimiya redkozemel'nykh elementov i ittriya* (Analytical Chenistry of Rare-Earth Elements and Yttrium), Moscow: Nauka, 1966.
3. Vershkova, Yu.A., Tareeva, O.A., Ivlev, K.G. and Lokshin, E.P., *Zh. Prikl. Khim.*, 2003, vol. 76, no. 1, pp. 162–163.
4. Bushuev, N.N., Nabiev, A.G., Petropavlovskii, I.A., and Smirnova, I.S., *Zh. Prikl. Khim.*, 1988, vol. 61, no. 10, pp. 2153–2158.
5. Bobrik, V.M., *Radiokhimiya*, 1977, vol. 19, no. 5, pp. 606–610.
6. Andrianov, A.M., Rusin, N.F., Deineka, G.F., et al., *Zh. Prikl. Khim.*, 1978, vol. 51, no. 7, pp. 1441–1444.

ISSN 1070-4272, Russian Journal of Applied Chemistry, 2006, Vol. 79, No. 4, pp. 539–543. © Pleiades Publishing, Inc., 2006.
Original Russian Text © V. S. Kolosnitsyn, S. P. Kosternova, O. A. Yapryntseva, A. A. Ivashchenko, S. V. Alekseev, 2006, published in Zhurnal Prikladnoi Khimii, 2006, Vol. 79, No. 4, pp. 551–555.

INORGANIC SYNTHESIS AND INDUSTRIAL INORGANIC CHEMISTRY

Recovery of Nickel with Sulfuric Acid Solutions from Spent Catalysts for Steam Conversion of Methane

V. S. Kolosnitsyn, S. P. Kosternova, O. A. Yapryntseva, A. A. Ivashchenko, and S. V. Alekseev

Ishimbai Branch of Ufa State Technical University of Aviation, Ishimbai, Bashkortostan, Russia
Institute of Organic Chemistry, Ufa Scientific Center, Russian Academy of Sciences, Ufa, Bashkortostan, Russia
PALLAD NPF, Salavat, Bashkortostan, Russia

Received May 6, 2005; in final form, December 2005

Abstract—Certain fundamental aspects of leaching-out of nickel with sulfuric acid solutions from spent catalysts for steam conversion of methane under static and dynamic conditions were studied.

DOI: 10.1134/S1070427206040069

At present, a considerable attention is given to the problem of utilization and processing of solid wastes containing nonferrous metals. Wastes of this kind are toxic substances hazardous to the environment, on the one hand, and a valuable chemical raw material, on the other.

A widely occurring type of solid wastes from petrochemical and oil refining industries are spent catalysts, including nickel–alumina catalysts for steam conversion of methane. In the course of operation, the catalysts lose activity as a result of changes in their composition and structure. At high temperatures (600–700°C), the catalyst undergoes sintering and its active surface area decreases.[1] In the course of time, a considerable fraction of nickel cations diffuses from the catalyst surface deep inside alumina, active nickel oxide is converted on alumina into inactive nickel aluminate, and spinel-like compounds, inactive in catalysis, are formed [1, 2].

In some cases, deactivated catalysts are regenerated, but this cannot be done for a large number of catalysts. They are removed from the process and reprocessed.

Commonly, two methods are suggested for recovery of nickel from ores and raw materials of technological origin: pyrometallurgical technique, whose main product is ferronickel obtained at high temperatures, and hydrometallurgical, based on leaching-out of nickel from raw materials with various acids and solutions of ammonia and ammonium salts.

The use of ammonia for leaching-out of nickel relies on the fact that nickel hydroxides readily react with ammonia to give stable complexes of various compositions. This circumstance serves as a basis for recovery of nickel from oxidized ores [3], spent catalysts [4], and worked-out electrodes of nickel–iron batteries [5, 6]:

$$Ni(OH)_2 + 6NH_3 \rightarrow [Ni(NH_3)_6](OH)_2.$$

It was found that addition of ammonium salts to aqueous solutions improves the efficiency of dissolution via the buffer action precluding accumulation of OH^- ions:

$$Ni(OH)_2 + 4NH_3 + 2NH_4Cl \rightarrow [Ni(NH_3)_6]Cl_2 + 2H_2O.$$

It has been suggested to leach-out nickel from oxide raw materials with solutions of $(NH_4)_2SO_4$ and $(NH_4)_2CO_3$ and with mixtures of these at pH 6–8 [7]:

$$NiO + (NH_4)_2SO_4 + 4NH_4OH \rightarrow [Ni(NH_3)_6]SO_4 + 5H_2O.$$

Leaching-out of nickel from ores and raw materials of technological origin with solutions of mineral acids was suggested in [8–12].

However, the leaching methods described in the literature have certain disadvantages. For example, the

[1] The temperature of steam conversion of methane is 800°C.

leaching solutions used are not always harmless: ammonia, which is the most frequently used to leach-out nickel, is a toxic gas. The leaching techniques suggested by certain authors [8, 13] meet technological difficulties. Autoclave leaching requires expensive special apparatus. Use of acid solutions with pH < 1 for leaching-out of nickel complicates the process of selective recovery of nickel from a solid matrix.

Nevertheless, the hydrometallurgical method for nickel recovery, compared with the pyrometallurgical technique, is the most promising because it conforms to the principle of combination of environmental and economical interests (markedly diminishes the number of technological procedures, does not require fuel expenditure for high-temperature processes, minimizes the amount of solid wastes and toxic discharges into the atmosphere). One more advantage of the given technique is that it can recover from leaching solutions, at an appropriate choice of methods used, both metallic nickel (electrolytically) and its salts.

An analysis of published data demonstrated that, despite the wide variety of methods for leaching-out of nickel from raw materials of technological origin, including spent catalysts, the fundamental aspects of nickel recovery by the hydrometallurgical technique are far from being fully understood.

The difficulty encountered in leaching-out of nickel consists in that part of nickel is in the form of compounds that are formed in the course of operation of a catalyst and the composition of these compounds is frequently unknown. Also, a certain part of nickel may be situated deep inside (in pores) catalyst particles, at places inaccessible to the leaching solution. One more difficulty is that, to obtain a product solution enriched with the target component, the leaching solution should be selective with respect to the metal being recovered and should not dissolve the catalyst matrix.

The aim of this study was to examine the fundamental aspects of the process of nickel leaching-out with sulfuric acid from spent nickel–alumina catalysts for methane conversion.

EXPERIMENTAL

In the course of exploitation, a deactivated catalyst is removed from reactors as it loses its activity and is delivered to storage in batches. This gives a mixture of spent catalysts that differ in the content of nickel, degree of coking, porosity, particle shape, and other properties.

As objects of study served spent nickel–alumina catalysts of K-905 and K-87 brands for steam conversion of methane. These catalysts are fabricated by joint precipitation of nickel and aluminum hydroxides, with the subsequent forming and calcination. Therefore, nickel oxide is distributed throughout the catalyst volume.

Grains of K-87 catalyst are gray cylinders about 15 mm in diameter and a height of 14 mm, and those of K-905 catalyst are rings with outer and inner diameters of 15 and 10 mm, respectively, and a height of 14 mm.

An average sample was originally taken from a batch of mixed catalysts. Then the sample was reduced to 100–200 g by the ring-and-cone method [10].

It was noticed that the catalysts differ in outward appearance. It was assumed that the degree of nickel leaching-out from these catalysts will also vary. To elucidate this question, part of catalyst samples were classified into portions: portion 1, dark gray particles of K-905 catalyst; portion 2, gray particles of K-905 catalyst; portion 3, black particles of K-87 particles; and portion 4, gray particles of K-87 catalyst.

The content of nickel in a catalyst was determined by X-ray fluorescence analysis and by complexometric titration.

The X-ray fluorescence analysis was made as follows. A 50-g catalyst sample was calcined in a muffle furnace at 600°C for 2 h and then ground in a ball mill to a dustlike state. The resulting powder was compacted into pellets 10 mm in diameter and 5 mm high.

The catalyst samples were analyzed on a Spectroscan-4 automated X-ray spectrometer (Spektron-OPTEL, St. Petersburg, Russia). The error in nickel determination did not exceed 2.5%.

To determine the content of nickel by complexometric titration, a 150-g catalyst sample was crushed in an agate mortar to a particle size of 2–10 mm, placed in a 500-ml flask, poured over with 300 ml of a 20% sulfuric acid solution, and the mixture was boiled for 20–24 h. Preliminary studies demonstrated that nickel is completely recovered from the catalyst under these conditions.

The thus obtained leaching solution was titrated with Na_2EDTA at pH 9, maintained with an ammonia buffer mixture. Murexide served as indicator.

The content of nickel in the catalyst sample was 7.05% according to the results of complexometric ti-

tration, and 7.04% as indicated by X-ray fluorescence analysis.

Nickel was leached-out from the catalyst under static and dynamic conditions.

Nickel was leached-out under static conditions as follows. The reactor having the form of a cylindrical glass vessel (height 15–25 cm, diameter 3–8 cm, volume 200–1000 ml) with a discharge cock was charged with a weighed portion of a mixture of spent catalysts. Then a prescribed volume of a sulfuric acid solution was poured into the reactor. Every hour, the acid solution was discharged from the reactor, a sample for analysis was taken, and the solution was again poured into the reactor. The experiment was performed until a constant nickel concentration was reached in the leaching solution.

In the case of leaching under dynamic conditions, a weighed portion of a catalyst was placed in a conical vessel, poured over with a prescribed volume of a sulfuric acid solution, and agitated with a mechanical stirrer at a rate of 40–50 rpm. Samples for analysis were taken from the leaching solution at regular intervals of time. As a pH value of 2 was reached in the leaching solution, concentrated sulfuric acid was added to pH 0.7. The experiment was terminated as a constant nickel concentration was reached in the leaching solution at pH 2.

The sulfuric acid solutions were prepared by dilution of concentrated (91–92%) sulfuric acid. The concentration of sulfuric acid in the solutions prepared was determined by acid–base titration.

The influence exerted by the concentration of sulfuric acid on the rate and extent of nickel leaching-out from the catalyst under static conditions was studied. Irrespective of the acid concentration, complete recovery of nickel from the catalyst could not be achieved. Therefore, leaching was performed in several stages in order to obtain the maximum possible degree of nickel recovery. For this purpose, the leaching solution was discharged after a steady state was attained. After that the catalyst was poured over with the same volume of a fresh sulfuric acid and leaching was continued until a new steady state was attained. The results obtained are listed in Table 1.

Table 1. Ni recovery from catalysts with sulfuric acid solutions of various concentrations under static conditions (weight of catalyst sample 50 g)

Acid concentration, M	Acid volume, ml	Leaching time, h	Ni concentration in the leaching solution		Degree of recovery, %
			g l^{-1}	M	
First stage					
0.5	75	59	21.2	0.36	55
1.0	75	59	23.1	0.39	61
2.4	60	59	29.5	0.50	58
3.7	67	59	23.6	0.40	56
Second stage					
0.5	75	43	7.1	0.12	70*
1.0	75	43	7.7	0.13	77*
2.4	60	43	8.3	0.14	72*
3.7	67	43	7.4	0.13	69*
Third stage					
0.5	75	6.5	3.0	0.05	76**
1.0	75	6.5	3.0	0.05	83**
2.4	60	6.5	5.3	0.09	81**
3.7	67	6.5	5.3	0.09	79**

* Total degree of recovery in the first and second stages.

** Total degree of recovery in the first, second, and third stages.

The studies demonstrated that equilibrium is attained in the second and third stages of leaching at a lower nickel concentration in solution: about 0.13 M in the second stage, and 0.07 M in the third. In all cases, the concentration of sulfuric acid has no effect on the degree of nickel recovery (nickel concentration in leaching solutions). These facts indicate that the attainment of equilibrium by the leaching process is not related to formation of nickel-saturated leaching solutions in the reactor volume. The solubility of nickel sulfate in sulfuric acid solutions was evaluated. It was found that the solubility of nickel sulfate at 25°C is 59 g l^{-1} in a 30% sulfuric acid solution and 103 g l^{-1} in a 5% solution.

It was assumed that the equilibrium position is determined in this process mode by saturation with nickel of leaching solutions that fill pores in catalyst particles and by blocking of these pores by nickel sulfate precipitated from saturated solutions.

To confirm the blocking of pores in catalyst particles by nickel sulfate, an attempt was made to perform a microscopic study of the cross-section of catalyst samples before and after leaching. However, no reliable and unambiguous results confirming that crystalline nickel sulfate is present in the pores of catalyst particles could be obtained. Therefore, to verify the assumption made above and to examine the possibility of preventing the blocking of the pores in the

Table 2. Ni recovery from catalysts with a 1% sulfuric acid solution under static conditions, with the leaching solution strengthened at regular intervals of time (initial H_2SO_4 concentration in the leaching solution 0.1 M)

Weighed portion of a catalyst, g	Acid volume, ml	T, °C	Leaching time, h	Final Ni concentration in the leaching solution		pH of the leaching solution	Degree of recovery, %
				g l^{-1}	M		
250	500	25	384	23.16	0.40	0.75	82.3
5000	10000	15	233	28.47	0.49	1.65	81.3
100	150	20	233	20.65	0.36	1.13	88.4

Table 3. Ni recovery from catalysts with 1% sulfuric acid solutions under dynamic conditions (total leaching time 240 h, s : l = 1 : 2, temperature 23°C, pH of the leaching solution 1)

Catalyst sample	Ni concentration in the leaching solution		Degree of recovery, %	Catalyst sample	Ni concentration in the leaching solution		Degree of recovery, %
	g l^{-1}	M			g l^{-1}	M	
1	8.1	0.14	23	3	12.7	0.22	36
2	10.0	0.17	28	4	19.5	0.34	55

catalyst by particles of nickel sulfate, leaching under static conditions with a dilute (1%) sulfuric acid solution, strengthened at regular intervals of time, was studied.

The leaching solution was strengthened with a 20% sulfuric acid solution after the solution pH reached values of 2–3. The volume of the 20% sulfuric acid solution added to the leaching solution was chosen so as to restore the initial concentration of sulfuric acid in the leaching solution. The leaching-out of nickel in this mode was also performed until the leaching solution was saturated with nickel ions. The results obtained in these experiments are listed in Table 2. In all cases, leaching solutions with a high concentration of nickel sulfate and greater degree of nickel leaching-out from the catalyst were obtained. The results of these experiments confirmed the validity of the assumption that the catalyst pores are blocked by nickel sulfate when concentrated sulfuric acid solutions are used as a leaching agent.

A study of the leaching process under static conditions demonstrated that its rate is low. The possible reason may be the appearance of an outer-diffusion control over the leaching process. Therefore, leaching was studied under dynamic conditions, because the outer-diffusion limitations are lifted in this mode.

Nickel was leached from four catalyst samples differing in the outward appearance with a 1% sulfuric acid solution at 20–25°C, with permanent strengthening of the leaching solution. The results of these experiments are listed in Table 3. It can be seen that the degree of nickel recovery does rather strongly depend on the type of a sample, but does not exceed 55% at the very best.

As demonstrated by the results of the experiments, the concentration of the sulfuric acid solution has no effect on the extent of nickel leaching-out from catalyst particles. In leaching-out of nickel with both concentrated and dilute sulfuric acid solutions, the degree of nickel recovery is virtually the same (55–60%). The experimental study also revealed that, in leaching-out of nickel with a dilute (1%) sulfuric acid solution under dynamic conditions, the degree of nickel recovery from the catalysts is lower than that in leaching with the same solution under static conditions, with the leaching solution periodically discharged from the reactor and the same solution poured in.

It follows from the experimental results that the leaching-out of nickel from the catalyst is limited by its diffusion from catalyst pores into the bulk of the leaching solution. In those cases when the rate of nickel diffusion from the catalyst pores is lower than the nickel dissolution rate, nickel sulfate is deposited in the catalyst pores, pore mouths are completely blocked by solid products, and leaching terminates. Agitation of the leaching solution (dynamic mode) does not lift the inner-diffusion limitations.

The leaching rate can be markedly raised if the catalyst pores are periodically freed of the leaching solution.

CONCLUSIONS

(1) Nickel recovery from spent alumina–nickel catalysts for methane conversion mainly occurs in the inner-diffusion region and is controlled by the rate of nickel diffusion from catalyst pores into the bulk of the leaching solution.

(2) The maximum possible degree of nickel recovery from catalyst particles (85–90%) and the minimum expenditure of the reagents are achieved in leaching with a dilute (1%) sulfuric acid solution, with permanent strengthening of this solution in the course of leaching and catalyst pores periodically freed of the leaching solution.

REFERENCES

1. Akhmedov, M.M., Ibragimov, A.A., and Kasumova, N.M., *Zh. Prikl. Khim.*, 2000, vol. 73, no. 2, pp. 234–236.
2. Sukhanov, V.P., *Kataliticheskie protsessy v neftepererabotke* (Catalytic Processes in Oil Refining), Moscow: Khimiya, 1979.
3. Perel'man, F.M. and Zvorykin, A.Ya., *Kobal't i nikel'* (Cobalt and Nickel), Moscow: Nauka, 1975.
4. Dresvyannikov, A.F., Grigor'eva, I.O., Kolpakov, M.E., and Sopin, V.F., Abstracts of Papers, *Vserossiiskaya nauchno-tekhnicheskaya konferentsiya po tekhnologii neorganicheskikh veshchestv* (All-Russia Scientific and Technical Conf. on Technology of Inorganic Substances), Kazan–Mendeleevsk, June 19–22, 2001, pp. 85–86.
5. Demidov, A.I. and Krasovitskaya, O.A., *Zh. Prikl. Khim.*, 2001, vol. 74, no. 5, pp. 717–721.
6. Demidov, A.I. and Krasovitskaya, O.A., *Zh. Prikl. Khim.*, 2000, vol. 73, no. 10, pp. 1656–1660.
7. Australian Patent 728 941.
8. Rubisov, D.H., Krowinkel, J.M., and Rapahgelakis, V.G., *Hydrometallurgy*, 2000, no. 58, pp. 1–11.
9. Denisov, S.A. and Sorokin, M.V., *Vybor optimal'nogo vremeni pri izvlechenii soedinenii nikelya kislotnym vyshchelachivaniem* (Choice of the Optimal Time in Recovery of Nickel Compounds by Acid Leaching), Available from VINITI, 1998, Dzerzhinsk, no. 3798-V 98.
10. Denisov, S.A., *Vybor optimal'nogo ekstragenta pri kislotnom vyshchelachivanii soedinenii nikelya* (Choice of the Optimal Extracting Agent in Acid Leaching-out of Nickel Compounds), Available from VINITI, 1998, Dzerzhinsk, no. 3660-V 98.
11. Denisov, S.A. and Sorokin, M.V., *Vybor optimal'noi kontsentratsii kisloty pri kislotnom vyshchelachivanii soedinenii nikelya* (Choice of the Optimal Acid Concentration in Acid Leaching-out of Nickel Compounds), Available from VINITI, 1998, Dzerzhinsk, no. 3662-V 98.
12. Denisov, S.A., *Vybor optimal'noi temperatury pri kislotnom vyshchelachivanii soedinenii nikelya* (Choice of the Optimal Temperature in Acid Leaching-out of Nickel Compounds), Available from VINITI, 1998, Dzerzhinsk, no. 3663-V 98.
13. US Patent 6 261 526.

ISSN 1070-4272, Russian Journal of Applied Chemistry, 2006, Vol. 79, No. 4, pp. 544–548. © Pleiades Publishing, Inc., 2006.
Original Russian Text © V. N. Antsiferov, S. E. Porozova, V. I. Karmanov, E. N. Pogorelova, 2006, published in Zhurnal Prikladnoi Khimii, 2006, Vol. 79, No. 4, pp. 556–559.

INORGANIC SYNTHESIS AND INDUSTRIAL INORGANIC CHEMISTRY

Effect of Alkanotrophic Rhodococcus Strain on Mechanical and Structural Characteristics of Quartz Glass

V. N. Antsiferov, S. E. Porozova, V. I. Karmanov, and E. N. Pogorelova

Scientific Center of Powder Materials Technology, Ural Division, Russian Academy of Sciences, Perm, Russia
Institute of Technical Chemistry, Ural Division, Russian Academy of Sciences, Perm, Russia

Received September 8, 2005; in the final form, January 2006

Abstract—The effect of alkanotrophic Rhodococcus strain on mechanical and IR spectroscopic characteristics of highly porous quartz glass was studied.

DOI: 10.1134/S1070427206040070

Controllable modification of silica surface with stable nanostuctural units is an urgent problems of modern materials technology. This problem is commonly solved by colloidal-chemical technique. New uncommon approaches to modification of the silica surface were discussed in [1]. Taking into account that specific bacterial strains can excrete colloidal silica [2], one of promising approaches to solution of the above problem can be based on treatment of silica with bacteria. Silicon is one of the most abundant elements in the lithosphere. Its stable (quartz) and metastable (colloidal) forms are widely involved into environmental biogeochemical processes [3].

In this study we examined the effect of the bacterial suspension on the IR spectra and physicochemical characteristics of quartz glass both in the absence and in the presence of a carbon source.

EXPERIMENTAL

Samples of highly porous quartz glass were prepared by replication of a polymeric matrix (Fig. 1) [4]. The cells of network-cellular framework of these samples were, on average, 0.5 mm in diameter. The specific surface area determined by the BET technique was about 0.1 $m^2 g^{-1}$. No less than five samples were tested in each experimental series. The surface area of the tested samples (weight 1–2 g, volume 1–1.5 cm^3) was in the range 0.5–1.0 m^2.

The samples of porous quartz glass were treated with an aqueous suspension of alkanotrophic Rhodococcus strain cells *R. Ruber* IEGM 231 submitted by the Regional Profiled Collection of alkanotrophic microorganisms at the Institute of Genetics and Ecology of Microorganisms (IEGM), Ural Division, Russian Academy of Sciences [5]. The treatment of quartz glass with aqueous bacterial suspension was carried out in the laboratory of alkanotrophic microorganisms at IEGM. Before experiments, all the quartz glass samples were treated in an autoclave with superheated steam at 120°C. To ensure favorable conditions for vital activity of alkanotrophic microorganisms, all the experiments were carried out in aqueous potassium phosphate buffer recommended in [6]. In the reference experiments, quartz glass samples were placed into potassium phosphate buffer solution containing no microorganisms. The Rhodococcus strain content in the test systems was 4.0×10^9 cells per ml. The preliminary immobilization of the bacterial cells on

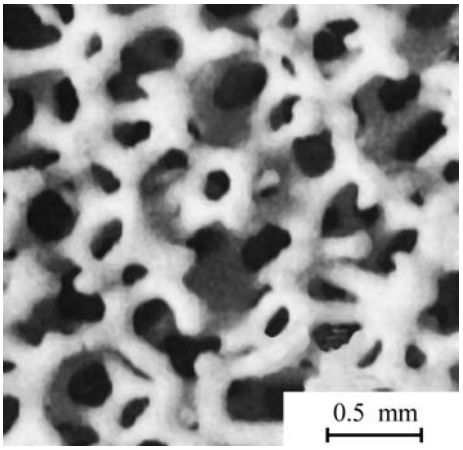


Fig. 1. Structure of highly porous permeable quartz glass.

Table 1. Effect of Rhodococcus strain on the IR spectra of quartz glass (ν and $A_{rel,\,i}$, %) {test system 1C [(R) reference system and (T) test system]}

ν, cm^{-1}	$A_{rel,\,i}$, %, after keeping for indicated time, day													
	PB*		1		3		7		14		30		90	
	R	T	R	T	R	T	R	T	R	T	R	T	R	T
1446–1426	4.6	3.1	5.2	3.7	4.4	4.0	4.0	2.9	4.3	5.0	4.3	4.1	4.1	4.7
1368–1347	7.3	7.3	6.6	7.0	8.6	10.3	8.3	8.3	6.3	6.9	5.3	7.4	6.3	6.7
1241–1222	9.8	9.4	10.1	9.0	12.1	10.0	10.9	7.8	11.2	9.6	10.2	12.3	12.8	10.8
1173–1158	12.3	13.8	13.4	12.7	12.7	11.0	15.1	17.8	12.5	14.6	13.7	11.4	12.0	10.0
1104–1091	20.5	22.0	22.9	23.9	20.0	18.5	16.1	21.7	19.7	22.4	27.4	27.6	21.3	23.1
1036–1029	17.7	18.2	13.9	14.4	14.4	11.1	20.2	17.4	21.9	17.6	14.4	14.8	19.1	16.0
991–956	2.8	2.5	4.5	5.4	4.1	6.2	1.5	2.7	1.7	2.6	3.5	1.2	2.5	2.2
924–908	2.2	2.2	2.5	3.4	2.5	3.5	2.2	1.7	1.9	1.7	2.1	2.1	1.9	2.5
803–799	3.9	3.8	4.2	3.9	4.4	4.8	4.1	3.3	3.6	3.4	3.4	3.4	3.5	4.1
683–673	0.5	0.4	0.5	0.3	0.5	0.4	0.5	0.3	0.5	0.5	0.4	0.3	0.4	0.4
588–581	0.5	0.4	0.6	0.6	0.5	0.9	0.5	0.5	0.5	0.3	0.4	3.7	0.6	0.4
543–525	0.6	0.8	1.4	1.0	1.4	3.3	0.5	1.1	1.0	0.7	1.1	1.2	0.9	0.8
468–465	14.1	15.0	12.3	11.9	11.9	12.5	15.5	13.6	14.1	13.1	12.5	12.9	13.9	15.0
422–416	1.1	1.0	2.1	2.8	2.5	3.5	0.8	0.9	1.0	1.6	1.3	0.9	0.7	1.6

* Immediately after immobilization in PB.

the quartz glass surface was carried out by two-week keeping of a quartz glass sample in peptone broth (PB). The effect of Rhodococcus strain on quartz glass was studied under following conditions: (1) after preliminary immobilization of microorganisms on the quartz glass surface from peptone broth, (2) without preliminary immobilization, (C) with addition of acrylamide (0.003%) as an accessible carbon source (CS), and (b) without it. The following combinations of these conditions were used in our experiments: 1C (preliminary immobilization + CS), 1b (preliminary immobilization, without CS), 2C (without preliminary immobilization + CS) and 2b (without preliminary immobilization, without CS).

After completion of the experiments, the quartz glass samples were washed, dried, and calcined, and their compression strength was measured on a 2054 R-5 tensile-testing mashine at a loading rate of 2 mm min^{-1}.

We failed to reliably determine the effect of Rhodococcus strain on the quartz glass structure by X-ray phase analysis.

The IR spectra of quartz glass (crushed in an agate mortar, mull in Vaseline oil), were recorded on an IFS-66 Fourier spectrometer (Bruker, Germany) (KBr windows, resolution 1 cm^{-1}, 100 scans). All the IR spectra were reduced to the zero baseline. The resolution of complicated absorption bands was carried out with an OPUS-3 computer program. Taking into account the heterogeneity of crushed quartz, the shape of separate absorption bands was approximated by Gaussian functions. The IR spectra were characterized by the wavenumber ν, half-width, and maximal (D_m) and integral (D_i) optical densities of the individual absorption bands.

Since, in recording the IR spectra, the absorption layer thickness and Vaseline oil amount were not standardized, the intensity of absorption bands of various samples noticeably differs. Therefore, in comparison of intensities of particular absorption bands of various samples, instead of their intensity we used the ratios

$$A_{rel,\,i} = D_i/\Sigma D_i,$$

where $A_{rel,\,i}$ is the relative intensity of ith absorption band; D_i, integral optical density of ith absorption band; and ΣD_i, sum of the integral optical densities of all the absorption bands of the stretching vibrations of the SiO_4 tetrahedra.

Table 1 shows the effect of immobilized Rhodococcus strain on the IR spectra of quartz glass in system 1C.

The characteristic vibration frequences of free and condensed SiO_4 tetrahedral groups are in the ranges 800–1050 and 1000–1250 cm^{-1}, respectively [7, 8]. The ratio A_2/A_1 of the total relative intensity of the absorption bands of condensed SiO_4 groups A_2 (1095–1250 cm^{-1}) to the total relative intensity of the absorp-

Table 2. Effect of treatment of quartz glass with Rhodococcus strain on quartz glass characteristics (weight loss, compression strength, and relative content of associated SiO_4 groups)

Treatment conditions			Δm, %	σ_c, MPa	A_2/A_1	Treatment conditions			Δm, %	σ_c, MPa	A_2/A_1
medium	time τ, days	system				medium	time τ, days	system			
No treatment	–	–	3.4 ± 0.5	–		1b	7	R	0.44 ± 0.39	2.7 ± 1.0	1.60
Autoclave	–	–	0.09 ± 0.07	3.9 ± 0.4	1.24			T	0.68 ± 0.14	3.8 ± 1.0	1.42
PB	7	R	0.30 ± 0.05	2.2 ± 0.4	1.68		14	R	–	3.0 ± 0.7	1.29
		T	0.43 ± 0.06	1.9 ± 0.1	1.67			T	0.64 ± 0.08	4.0 ± 0.6	1.08
1C	1	R	0.34 ± 0.07	2.8 ± 0.1	1.85	2C	1	R	0.33 ± 0.09	4.40 ± 0.06	2.18
		T	0.51 ± 0.09	2.3 ± 0.2	1.68			T	0.25 ± 0.07	3.25 ± 0.45	2.29
	3	R	0.33 ± 0.05	2.6 ± 0.4	1.76		3	R	0.40 ± 0.07	2.27 ± 0.61	2.29
		T	0.54 ± 0.13	2.7 ± 0.5	1.54			T	0.34 ± 0.07	2.32 ± 0.74	2.37
	7	R	0.37 ± 0.04	2.5 ± 0.2	1.51		5	R	0.61 ± 0.02	2.63 ± 0.25	1.99
		T	0.40 ± 0.06	2.5 ± 0.2	1.88			T	0.43 ± 0.11	2.17 ± 0.87	2.02
	14	R	0.18 ± 0.07	3.9 ± 0.9	1.49		14	R	0.61 ± 0.02	2.63 ± 0.25	2.52
		T	0.20 ± 0.07	3.4 ± 0.8	1.84			T	0.46 ± 0.12	3.36 ± 1.10	2.19
	30	R	0.30 ± 0.10	2.2 ± 0.9	2.19	2b	1	R	0.26 ± 0.10	2.72 ± 0.39	2.29
		T	0.18 ± 0.05	2.4 ± 0.6	2.39			T	0.24 ± 0.07	3.99 ± 0.93	1.58
	90	R	0.35 ± 0.06	1.8 ± 0.6	1.71		3	R	0.22 ± 0.07	3.42 ± 0.46	2.06
		T	0.22 ± 0.04	2.0 ± 0.8	1.77			T	0.21 ± 0.07	4.20 ± 0.99	1.96
1b	1	R	–	2.9 ± 0.9	1.76		5	R	0.28 ± 0.07	4.23 ± 1.36	2.17
		T	0.33 ± 0.14	1.4 ± 0.6	1.60			T	0.25 ± 0.04	4.98 ± 0.66	2.15
	3	R	0.29 ± 0.13	4.9 ± 0.6	1.20		14	R	0.34 ± 0.08	5.93 ± 0.71	2.02
		T	1.12 ± 0.49	1.6 ± 0.9	1.41			T	0.21 ± 0.07	6.65 ± 0.85	1.84

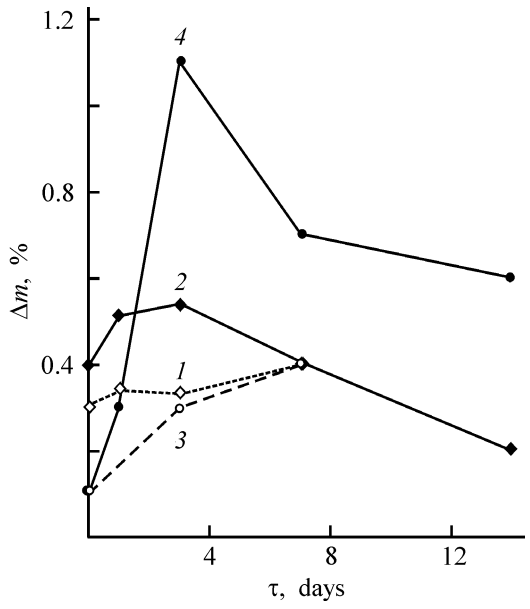


Fig. 2. Weight loss of quartz sample Δm vs. treatment time τ. (*1*, *3*) Reference systems and (*2*, *4*) test systems. Systems: (*1*, *2*) 1C and (*3*, *4*) 1b.

tion bands of free SiO_4 groups A_1 (800–1050 cm^{-1}) characterizes the relative content of condensed SiO_4 tetrahedra in the structure of quartz glass, i.e. the degree of crystallinity of quartz. Table 2 and Fig. 2 show the quartz glass characteristics (weight loss, Δm, %; compression strength, σ_c, MPa; and relative content of condensed SiO_4 groups, A_2/A_1) as influenced by treatment with Rhodococcus strain.

Figure 3 shows the dependence of the compression strength of quartz glass samples on their degree of crystallinity A_2/A_1 for reference (Fig. 3a) and test (Fig. 3b) systems, constructed from the data in Table 2. It should be noted that these plots are identical for systems containing a carbon source and without it.

It is seen that in the reference systems an increase in the degree of crystallinity of quartz glass is accompanied by a decrease in its strength. The similar effect was observed in gradual annealing of highly porous quartz glass and is caused by transformation of quartz into cristobalite [4]. In the test systems, we found no correlation between the degree of crystallinity of quartz glass and its strength.

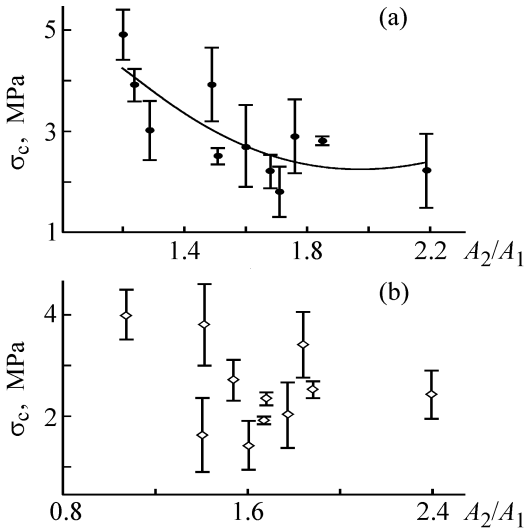


Fig. 3. Compression strength σ_c, vs. degree of crystallinity of quartz glass (A_2/A_1). (a) Reference systems and (b) test systems.

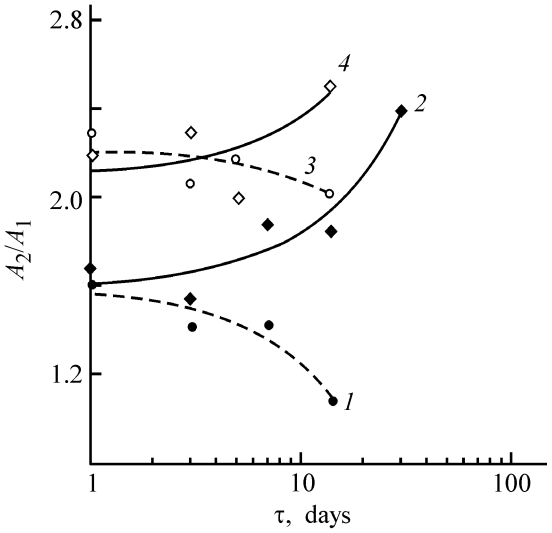


Fig. 4. Degree of crystallinity of quartz glass A_2/A_1 vs. treatment time τ in the systems containing a carbon source and without it. System: (*1*) 1b, (*2*) 1C, (*3*) 2b, and (*4*) 2C.

The time dependence of the effect of Rhodococcus on the degree of crystallinity of quartz glass in the presence and absence of a carbon source is shown in Fig. 4. It seen that in the systems containing no CS the crystallinity decreases with increasing treatment time, i.e., quartz glass becomes more amorphous. Even after 14-day incubation we observed no large-scale death of microorganisms. In the presence of carbon source, the crystallinity of quartz glass increased. After 90-day treatment, it started to decrease, apparently due to both the exhaustion of a carbon source and changes in the system composition. Figure 4 also shows that, irrespective of preliminary immobilization of Rhodococcus strain, the bacterial activity in the absence of CS causes amorphization of quartz glass (decrease in crystallinity), whereas, in the presence of CS, the structure-making effect prevails (increase in crystallinity).

Physicochemical characteristics of amorphous quartz significantly differ from those of crystalline quartz. In the series quartz, cristobalite, quartz glass the entropy of formation in the aqueous solution decreases in the order –41.84, –42.68 and –46.86 J mol^{-1} K^{-1} [9]. It is known that the structural ordering is accompanied by lowering of the entropy, whereas the structural disordering increases the entropy [10]. We believe that, in the absence of a carbon source, the methabolism of Rodhococcus strain is maintained by the energy released in amorphization of quartz glass. On the contrary, in the presence of a carbon source, the energy consumed by Rhodococcus cells from the carbon source can be partly used for increasing the crystallinity of quartz glass with accumulation of the energy for the future.

CONCLUSIONS

(1) In keeping porous quartz glass samples in aqueous potassium phosphate buffer containing no Rhodococcus strain (reference experiment), their crystallinity (relaive content of condensed SiO_4 groups) increases and the strength of quartz glass decreases, irrespective of the presence or absence of a carbon source.

(2) In keeping porous quartz samples in aqueous potassium phosphate buffer (without carbon source) populated with Rhodococcus strain, the crystallinity of quartz (relative content of condensed SiO_4 tetrahedra) decreases. In the presence of a carbon source, the crystallinity of quartz increases. In the reference systems these structural effects are absent.

REFERENCES

1. Lygin, V.I., *Ross. Khim. Zh.*, 2002, vol. 46, no. 3, pp. 12–18.
2. Iler, R.K., *The Chemistry of Silica*, New York: Wiley–Interscience, 1979.
3. Vernadsky, V.I., *Biosfera (Izbrannye trudy po biogeokhimii)* (Biosphere (Selected Works on Biogeochemistry)), Moscow: Mysl', 1967.
4. Antsiferova, V.N. and Porozova, S.E., *Vysokoporistye pronitsaemye materialy na osnove alyumosilikatov* (Highly Porous Permeable Materials Based on Aluminosilicates), Perm: Permsk. Gos. Tekh. Univ., 1996.

5. *Katalog shtammov Regional'noi profilirovannoi kollektsii alkanotrofnykh mikroorganizmov, Institut Ekologii i Genetiki Mikroorganizmov Ural'skogo Otdeleniya Rossiiskoi Akademii Nauk* (Catalog of Strains of Regional Profiled Collection of Alkanotrophic Microorganisms, Inst. of Ecology and Genetics of Microorganisms, Ural Division, Russian Acad. Sci.), Ivshina, I.B., Ed., Moscow: Nauka, 1994.
6. Malashenko, Yu.R., Romanovskaya, V.A., Bogachenko, V.N., et al., *Mikrobiologiya*, 1973, vol. 42, no. 3, pp. 403–408.
7. Plyusnina, I.I., *Infrakrasnye spektry mineralov* (Infrared Spectra of Minerals), Moscow: Mosk. Gos. Univ., 1976.
8. Plyusnina, I.I., *Metamorficheskie reaktsii nizkotemperaturnogo kremnezema v zemnoi kore* (Metamorphic Reactions of Low-Temperature Silica in the Earth Crust), Moscow: Mosk. Gos. Univ., 1983.
9. *Kratkii spravochnik fiziko-khimicheskikh velichin* (Concise Handbook of Physicochemical Quantities), Ravdel', A.A. and Ponomareva, A.M., Eds., Leningrad: Khimiya, 1983, 8th ed.
10. Aleskovskii, V.B., *Zh. Prikl. Khim.*, 2002, vol. 75, no. 5, pp. 706–713.

ISSN 1070-4272, Russian Journal of Applied Chemistry, 2006, Vol. 79, No. 4, pp. 549–554. © Pleiades Publishing, Inc., 2006.
Original Russian Text © L. V. Stepakova, M. Yu. Skripkin, L. V. Chernykh, 2006, published in Zhurnal Prikladnoi Khimii, 2006, Vol. 79, No. 4, pp. 560–564.

PHYSICOCHEMICAL STUDIES OF SYSTEMS AND PROCESSES

Comparative Analysis of Solubility in CuCl–MCl–H_2O Systems at 25°C (M^+ = Li^+, Cs^+, NH_4^+)

L. V. Stepakova, M. Yu. Skripkin, and L. V. Chernykh

St. Petersburg State University, St. Petersburg, Russia

Received February 24, 2005

Abstract—Solubility in the ternary system CuCl–NH_4Cl–H_2O at 25°C was determined by the method of isothermal lifting of oversaturation. A comparative analysis of solubility in this system and the previously studied systems CuCl–MCl–H_2O (M^+ = Li^+, Na^+, K^+, Cs^+) was made. The results obtained were interpreted in terms of competition between hydration, association, and complexation processes in water–salt systems.

DOI: 10.1134/S1070427206040082

We have been systematically studying the solubility in multicomponent halide water–salt systems for years. It has been shown that the solubility, as well as other physical and chemical macroscopic properties, should be considered as a result of the combination of all competitive interactions occurring in solutions: association of ions, their hydration, and complexation. In this study, such an approach was applied to analysis of solution–solid equilibria in ternary systems containing copper monochloride.

Multicomponent systems containing copper monohalides are of great interest from the practical point of view. For example, CuCl admixtures strongly affect the photochromic properties of silver halide glasses by sharply reducing the rate of relaxation of the photoinduced form into the initial form, which expands potentialities of practical use of these glasses [1]. The development of copper halide photochromic glasses in the 1970s initiated a study of chloride-containing sodium and potassium borosilicate glasses [2–4], whose optical characteristics are determined by the mutual solubility of the components. In the process, a pronounced analogy between the equilibrium diagrams of salt melts and those of the corresponding aqueous solutions was revealed [5]. Aqueous-alcoholic solutions containing copper monochloride and magnesium chloride or lithium chloride and hydrochloric acid are used to extract ethylene from cryogenically inseparable exhaust gases [6, 7] and also serve as sorbents for carbon monoxide [8].

The ability of copper(I) to form complexes with organic compounds predetermines its high catalytic activity in a number of organic reactions, such as decomposition of diazo compounds, double carbonylation, dimerization of acetylene, etc. [9–15]. The catalytic activity, in turn, can be strongly modified by introduction of halides of other elements, including alkali metals. Thus, the results obtained in studying copper(I) complexation in multicomponent water–salt systems can be used to optimize the existing processes and develop new ones.

We have studied previously the solubility in ternary systems constituted by copper(I) halide, alkali metal halide, and water (M^+ = Li^+, Cs^+) [16–18]. The phase equilibria in such a technologically important system as CuCl–NH_4Cl–H_2O (it is the main component of the industrial contact solution for dimerization of acetylene into vinylacetylene [11]) were studied in [19]. Unfortunately, the results obtained were only represented as a schematic diagram, with no numerical data given. The difference between the CuCl–NH_4Cl–H_2O system and its analogs, clearly seen even in such a schematic representation, and its practical importance stimulated a study of solution–solid equilibria in this system.

We studied the solubility by the method of isothermal lifting of oversaturation, because application of the method of isothermal saturation gives poorly reproducible results for systems containing copper monochloride. Heterogeneous samples were heated to

Table 1. Solubility in the system $CuCl–NH_4Cl–H_2O$ at 25°C

Liquid phase, concentration				Solid phase	Liquid phase, concentration				Solid phase
c, wt %		*m*, mol kg^{-1}			*c*, wt %		*m*, mol kg^{-1}		
CuCl	NH_4Cl	CuCl	NH_4Cl		CuCl	NH_4Cl	CuCl	NH_4Cl	
0.01	0.00	1.1×10^{-3}	0.00	CuCl	21.60	25.68	4.14	9.11	$NH_4Cu_2Cl_3$
1.29	4.67	0.138	0.93	The same	27.90	26.70	6.20	11.00	The same
1.58	6.40	0.17	1.30	"	30.78	26.76	7.32	11.79	"
5.50	9.10	0.65	1.99	"	31.70	27.02	7.76	12.24	"
8.60	12.00	1.08	2.82	"	34.30	28.16	9.23	14.03	$NH_4Cu_2Cl_3$
10.40	12.70	1.37	3.10	"	30.77	27.76	7.50	12.52	$(NH_4)_3Cu_2Cl_5$
10.50	13.80	1.40	3.42	"	28.54	27.78	6.60	11.90	The same
11.98	14.57	1.65	3.71	"	26.42	27.61	5.80	11.23	"
14.40	15.23	2.07	4.05	"	24.55	28.00	5.22	11.04	"
17.53	16.22	2.67	4.58	"	22.34	29.06	4.64	11.18	"
20.30	17.10	3.30	5.10	"	22.93	29.80	4.90	11.80	"
22.25	17.45	3.73	5.41	"	23.20	30.30	5.05	12.20	"
24.83	18.38	4.42	6.05	"	23.44	31.20	5.22	12.87	$(NH_4)_3Cu_2Cl_5$ + NH_4Cl
28.10	19.70	5.44	7.06	"					
33.51	22.00	7.61	9.25	CuCl	23.10	30.80	5.06	12.50	NH_4Cl
37.75	23.23	9.77	11.14	CuCl + $NH_4Cu_2Cl_3$	22.00	30.00	4.63	11.70	The same
					20.25	29.34	4.06	10.89	"
32.00	23.00	7.18	9.55	$NH_4Cu_2Cl_3$	15.98	25.84	3.43	10.23	"
28.54	21.97	5.82	8.30	The same	17.37	28.92	3.27	10.07	"
23.50	20.81	4.26	6.99	"	14.14	28.54	2.50	9.30	"
21.00	20.38	3.62	6.50	"	10.04	28.27	1.64	8.57	"
17.03	20.40	2.75	6.10	"	8.13	28.00	1.30	8.20	"
14.72	20.77	2.30	6.02	"	5.60	27.82	0.85	7.80	"
14.90	22.15	2.39	6.58	"	2.26	28.08	0.33	7.54	"
14.91	23.70	2.45	7.22	"	1.16	28.38	0.167	7.53	"
15.81	24.22	2.66	7.55	"	0.00	28.54	0.00	7.47	NH_4Cl
21.21	25.45	4.00	8.92	"					

complete dissolution of the solid phase, and then thermostated at 25 ± 0.1°C for three days with continuous stirring. To prevent the photoinitiated disproportionation of copper(I), the experiment was carried out in the dark. To reveal the possible oxidation of copper(I), we carried out, on completion of the experiment, an iodometric titration of copper(II): the content of copper(II) did not exceed 0.2% of the total copper (i.e., it was within the experimental error), which does not affect significantly the solubility.

The samples being analyzed were treated with nitric acid to oxidize copper(I) to copper(II) and then the copper(II) concentration was determined by EDTA titration, and that of chloride anions, by the mercurimetric titration. The accuracy of analysis was ±0.5%. The concentration of ammonium chloride was calculated from the difference. The composition of the solid phase was found by the Schreinemakers method of wet residues and additionally confirmed by X-ray phase analysis. The results obtained are listed in Table 1.

The data obtained enabled a comparative analysis of solubility in all the $CuCl–MCl–H_2O$ systems (M^+ = Li^+, Cs^+, NH_4^+) at 25°C. It was demonstrated the domination of the Cu(I) complexation ($\beta_2 = 3.47 \times 10^5$ [20]) predetermines the qualitative similarity of systems containing copper monohalides.

(1) The solubility of CuCl in ternary solutions, s_{eut}, is higher than the solubility s_0 in binary solutions:

MCl	LiCl	NaCl	KCl	CsCl	NH_4Cl
s_{eut}/s_0	6360	5020	4070	600	9770

(2) Salting-in of an alkali metal chloride is observed in all the systems (only in the system CuCl–LiCl–H_2O, the crystallization branch of $LiCl \cdot H_2O$ is a salting-out–salting-in branch).

Undoubtedly, both these effects are accounted for by strong complexation of copper(I), which is known to increase the solubility [21].

(3) Complex salts crystallize in all the systems except CuCl–NaCl–H_2O.

At the same time, there is a significant quantitative difference in solubility, depending on the nature of an alkali metal ion M^+, which, in our opinion, is determined by two main factors: action of M^+ ions on the structure of water and solutions and association of MCl.

As a quantitative measure of the effect of M^+ on the solubility we used the quantity dm_1/dm_2, which characterizes the intensity of salting-in (salting-out) of salt components. The variation of this parameter along the crystallization branches of copper monochloride and alkali metal chlorides is shown in Fig. 1.

The data obtained indicate that the intensity of CuCl salting-in at low MCl concentrations (approximately up to 0.5 *m*) grows in the order: LiCl < NaCl < KCl < CsCl < NH_4Cl, i.e., it changes in parallel with the structure-breaking effect of the M^+ cation. At high concentrations (>0.8 *m*) the order of variation of the salting-in intensities changes: LiCl < CsCl < NaCl < KCl < NH_4Cl.

The specific position of CsCl in the last series is caused by the ability of Cs(I) to form contact ion pairs, in contrast to the other ions, which form non-contact ion pairs. As a result, association of CsCl

$$Cs^+ + Cl^- \rightleftarrows Cs^+Cl^-$$

competes with the complexation Cu^+–Cl and, accordingly, shifts to the left the equilibrium

$$CuCl + xCl^- \rightleftarrows Cu^+Cl^{x-}_{x+1}$$

and this is the reason why the solubility decreases.

As for the intensity of MCl salting-in, the order of its variation remains the same within the entire range of concentrations. It is similar to the series of CuCl salting-in intensity at high concentrations: LiCl < NH_4Cl < NaCl < KC1, i.e., to the series of the structure-breaking effect of the M^+ cation (LiCl < NaCl < KCl).

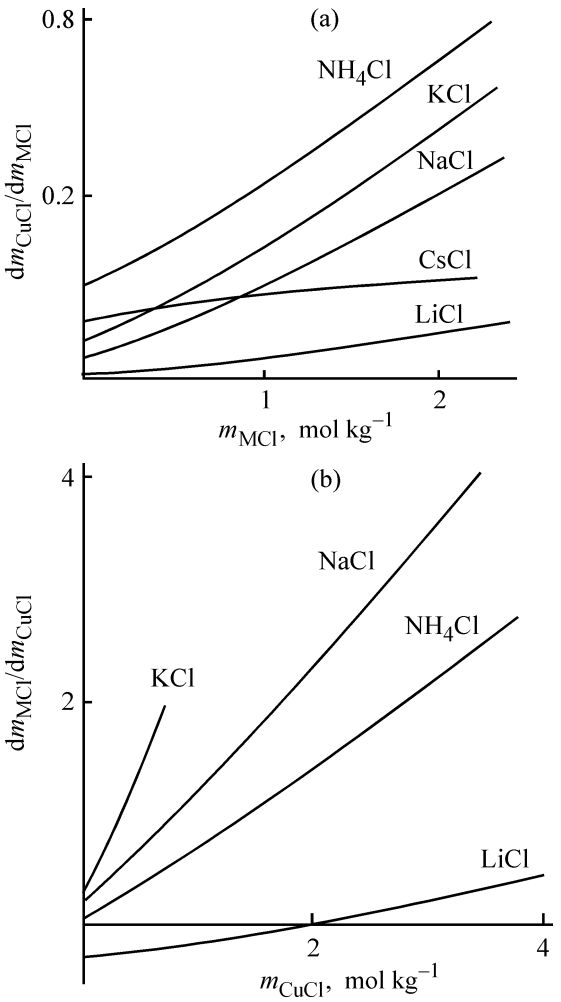


Fig. 1. Salting-in intensity of a salt, dm_1/dm_2, vs. the concentration *m* of a component being added for the crystallization branches of (a) CuCl and (b) MCl.

The acido complexation and association should also significantly affect the length of the branches of copper chloride crystallization. The necessity for structural rearrangements in solution before the onset of crystallization of complex compounds {transition from linear $CuCl_2$ anions to tetrahedral mono- and polynuclear acido-complexes $CuCl_3(H_2O)^{2-}$, $CuCl_4^{3-}$, $Cu_2Cl_5^{3-}$, and $Cu_2Cl_6^{4-}$ [22]} and the high stability of the zinc-blende-type CuCl lattice predetermine the considerable length of CuCl crystallization branches. The specificity of the alkali metal cation markedly affects in this case the competition for the chloride ion in formation of polynuclear acido complexes of copper and association of the alkali metal chloride. Noteworthy is the clearly pronounced correlation between the concentrations at which the crystallization of CuCl and MCl terminates, on the one hand, and the concentrations at which the ion–ion association

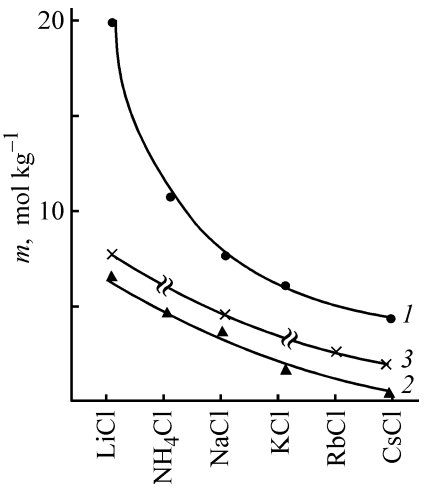


Fig. 2. Correlations between the positions of the eutonic points of (*1*) CuCl/complex compound and (*2*) MCl/complex compound, on the one hand, and (*3*) concentrations *m* of the onset of domination of associative processes in binary MCl solutions, on the other.

starts to dominate in binary MCl solutions [23], on the other (Fig. 2).

The correlation between the concentrations of completion of the crystallization of CuCl, $m^{eut}_{MCl}(CuCl)$, and MCl, $m^{eut}_{CuCl}(MCl)$ and the concentrations $m_a(MCl)$ of the onset of domination of association processes in binary MCl solutions is as follows:

Table 2. Bond length *r* and frequency ν of Cu–Cl stretching vibrations in copper(I) compounds

Compound	r_{M-Cl}, Å		r_{Cu-Cl}, Å	ν_{M-Cl}, cm^{-1}	Reference
	Compound	MCl			
CuCl			2.46	225, 246	
Li_2CuCl_3				220, 242	
$NH_4Cu_2Cl_3$	3.34	3.24	2.34	228, 246	[26]
$(NH_4)_3Cu_2Cl_5$				227, 247	
K_2CuCl_3	3.27	3.15	2.31	229, 249	[27]
$Cs_3Cu_2Cl_5$	3.69	3.56	2.28	243, 252	[28, 29]
$Cs_3CuCl_4 \cdot H_2O$				242, 251	

m, mol kg^{-1} H_2O:	LiCl	NH_4Cl	NaCl	KCl	CsCl
$m^{eut}_{MCl}(CuCl)$	22.01	11.14	8.4	6.35	4.08
$m^{eut}_{CuCl}(MCl)$	6.89	5.06	4.16	0.3	0.05
$m_a(MCl)$	7.4	4.5	2.3		

These data clearly demonstrate that MCl association strongly affects the length of branches of copper monochloride crystallization.

The system CuCl–NH_4Cl–H_2O also occupies a special position both in the salting-in intensity and in the length of branches of CuCl and MCl crystallization (Fig. 1). We calculated the distribution of complex species in this system, which indicated that the formation of copper(I) chloride ($K_{st} = 10^6$) and ammonia complexes ($K_{st} = 10^{14}$) occurs in parallel. Ammonia is formed in hydrolysis of ammonium ions, $NH_4^+ + H_2O = NH_3 \cdot H_2O + H^+$, with the complexation strongly shifting the hydrolytic equilibrium to the right. It is the joint action of both the parallel processes that determines the maximal intensity of CuCl salting-in in the system CuCl–NH_4Cl–H_2O. The values of $m^{eut}_{CuCl}(NH_4Cl)$ and $m^{eut}_{NH_4Cl}(CuCl)$ fall within the range between those for the least associated lithium and sodium, although, taking into account the hydration energy of ammonium ions and their action on the water structure, we could expect that the concentrations of completion of crystallization of binary components would be intermediate between the corresponding characteristics of the systems with sodium and potassium salts. The reason is that NH_4Cl is not associated up to very high concentrations. The "concentration-induced" formation of ion pairs is only observed when the amount of water in solution is insufficient for complete hydration of ions.

As mentioned above, the formation of copper(I) acido complexes is the predominant type of interaction in all the systems under consideration, which predetermines the similarity in form, composition, and structures between the crystallizing solid compounds. In this case, we can expect that the complex salts formed in this systems will be of the same type, i.e., products of the acido complex formation of chloride ions with Cu^+ cations. In salts of this kind, cations occupy voids in the forming structure [23]. As demonstrated previously [24, 25], elongation of M–Cl bonds and shortening of the bonds between the central atom and ligands, compared with the corresponding binary compounds, are characteristic of compounds of this type. The available published data on the structure of potassium, ammonium, and cesium chlorocuprates(I) support our assumption concerning the type of crystallizing compounds (Table 2). The formation of stronger copper–chlorine bonds, compared with

those in copper monochloride, is also confirmed by the shift of the frequency of stretching vibrations to higher frequencies.[1] In this case, the Cu–Cl bond in copper(I) compounds should be the stronger, the weaker the polarizing action of the outer-sphere cation M^+ ($Li^+ > NH_4^+ > K^+ > Cs^+$), and this is confirmed experimentally.

CONCLUSIONS

(1) A study of the systems CuCl–MCl–H_2O (M^+ = Li^+, Na^+, K^+, Cs^+, NH_4^+) revealed that the predominance of Cu(I) acido-complex formation predetermines the qualitative similarity of the systems under consideration.

(2) At low MCl concentrations, the intensity of salting-in of copper monochloride ($Cs^+ > K^+ > Na^+ > Li^+$) is determined by the action of a singly charged cation on the solution structure and varies in the opposite direction with the hydration energy of cations. The length of the crystallization branches of copper monochloride is determined by competitive processes of copper complexation and association of an alkali metal chloride. A stronger MCl association results in a decrease in the length of the crystallization branches of copper monochloride.

(3) The particular position of the system CuCl–NH_4Cl–H_2O is caused by specificity of the ammonium cation and by the fact that ammonia formed in its hydrolysis can form complexes with copper; the parallel occurrence of ammonia- and acido complex formation results in the highest salting-in intensity and the longest branches of CuCl and NH_4Cl crystallization.

(4) The predominance of copper acido complex formation in all the systems results in that the type of crystallizing solid compounds is the same. The different polarizing effects of alkali metal cations lead to only slight changes in the strength of Cu–Cl bonds.

ACKNOWLEDGMENTS

This study was supported by INTAS (program for support of young scientists, project no. 3830), Program "Development of the Scientific Potential of Higher School" of the Ministry of Education and Science of the Russian Federation (project no. 37 849), and Russian Foundation for Basic Research (project no. 05-03-32 099).

[1] Raman spectra of the complex compounds were measured on a Renishaw System 100 spectrometer equipped with a Leica DMLM microscope, 25 mW diode laser (emission wavelength 780 nm), and a Peltier-cooled CCD detector.

REFERENCES

1. Barachevskii, V.A., Lashkov, G.I., and Tsekhomskii, V.A., *Fotokhromizm i ego primenenie* (Photochromism and Its Application), Moscow: Khimiya, 1977, pp. 74–161.
2. Zimin, L.G., Gaponenko, S.V., Lebed, V.Ju., et al., *J. Modern Opt.*, 1990, vol. 37, no. 5, pp. 849–853.
3. Valov, P.M., Gracheva, L.V., and Leiman, V.I., *Fiz. Khim. Stekla*, 1997, vol. 23, no. 2, pp. 187–198.
4. Golubkov, V.V., Vasil'ev, M.I., Pshenitsyna, V.V., and Tsekhomskii, V.A., *Fiz. Khim. Stekla*, 2000, vol. 26, no. 1, pp. 48–54.
5. Chernykh, L.V., Tsekhomskii, V.A., and Skripkin, M.Yu., *Trudy I Mezhdunarodnoi konferentsii "Khimiya vysokoorganizovannykh veshchestv i nauchnye osnovy nanotekhnologii"* (Proc. I Int. Conf. "Chemistry of Highly Organized Substances and Scientific Foundations of Nanotechnology"), St. Petersburg, 1996, vol. 3, pp. 558–561.
6. Ksandrov, N.V., Nikandrov, I.S., and Bochkova, K.F., *Zh. Prikl. Khim.*, 1994, vol. 67, no. 6, pp. 982–986.
7. Ksandrov, N.V., Nikandrov, I.S., *Izv. Vyssh. Uchebn. Zaved., Khim. Khim. Tekhnol.*, 1995, vol. 38, no. 3, pp. 53–59.
8. Ksandrov, N.V., *Izv. Vyssh. Uchebn. Zaved., Khim. Khim. Tekhnol.*, 1999, vol. 42, no. 4, pp. 146–148.
9. Sladkov, A.M. and Gol'ding, I.R., *Usp. Khim.*, 1979, vol. 10, no. 9, pp. 1625–1679.
10. Temkin, O.N., Flid, R.M., Shestakov, G.K., et al., *Kinet. Katal.*, 1969, vol. 10, no. 6, pp. 1230–1238.
11. Han, X., Stoltz, V.M., and Corey, E.J., *J. Am. Chem. Soc.*, 1999, vol. 121, no. 33, pp. 7600–7605.
12. Shestakov, G.K., Tikhonov, G.F., Temkin, O.N., and Flid, R.M., *Kinet. Katal.*, 1970, vol. 11, no. 4, pp. 875–881.
13. Donkervoort, J.G., Vicario, J.L., Jastrzebski, J.T.B.H., et al., *J. Organomet. Chem.*, 1998, vol. 558, nos. 1–2, pp. 61–69.
14. Tanaka, H, Yamaguchi, Y., Sumida, S.-I., and Torii, S.H., *Chem. Commun.*, 1996, no. 24, pp. 2705–2706.
15. Tanaka, H, Yamaguchi, Y., Sumida, S.-I., and Torii, S.H., *J. Chem. Soc., Perkin Trans. 1*, 1999, no. 23, pp. 3463–3468.
16. Chernykh, L.V. and Skripkin, M.Yu., *Zh. Obshch. Khim.*, 1996, vol. 66, no. 1, pp. 26–30.
17. Stepakova, L.V. and Skripkin, M.Yu., *Zh. Neorg. Khim.*, 1999, vol. 44, no. 2, pp. 325–326.

18. Skripkin, M.Yu., Chernykh, L.V., Stepakova, L.V., and Samokhvalova, V.A., *Zh. Prikl. Khim.*, 2002, vol. 75, no. 7, pp. 1069–1071.
19. Morozova, I.S. and Ustavshchikova, G.V., *Izv. Akad. Nauk SSSR, Otd. Khim. Nauk*, 1943, no. 1, pp. 74–80.
20. Sillen, L.G. and Martell, A.E., *Stability Constants of Metal-Ion Complexes: Section 1. Inorganic Ligands*, London: Pergamon, 1971, pp. 163–168.
21. Kumok, V.N., Kuleshova, O.N., and Karabin, L.A., *Proizvedeniya rastvorimosti* (Solubility Products), Novosibirsk: Nauka, 1983.
22. *Solubility Data Series: vol. 46. Copper(I) Halides and Pseudohalides*, Fritz, J.J. and Koninsberger, A., Eds., Oxford: Pergamon, 1997.
23. Chernykh, L.V. and Skripkin, M.Yu., *Koord. Khim.*, 1996, vol. 22, no. 5, pp. 413–416
24. Grinberg, A.A., *Vvedenie v khimiyu kompleksnykh soedinenii* (Introduction to the Chemistry of Complex Compounds), Moscow: Khimiya, 1951, pp. 378–382.
25. Skripkin, M.Yu. and Chernykh, L.V., *Zh. Neorg. Khim.*, 1994, vol. 39, no. 7, pp. 1747–1751.
26. Brink, C., *Acta Cryst.*, 1949, vol. 2, pp. 158–163.
27. Brink, C. and van Arkel, A.E, *Acta Cryst.*, 1952, vol. 5, pp. 506–510.
28. Brink, C., Binnendijk, N.F., and van de Linde, J., *Acta Cryst.*, 1954, vol. 7, pp. 176–180.
29. Meyer, G., *Z. Anorg. Allg. Chem.*, 1984, vol. 515, pp. 127–132.

ISSN 1070-4272, Russian Journal of Applied Chemistry, 2006, Vol. 79, No. 4, pp. 555–558. © Pleiades Publishing, Inc., 2006.
Original Russian Text © N. V. Sych, N. T. Kartel', N. N. Tsyba, V. V. Strelko, A. D. Nikolaichuk, T. I. Mironyuk, 2006, published in Zhurnal Prikladnoi Khimii, 2006, Vol. 79, No. 4, pp. 565–569.

SORPTION AND ION-EXCHANGE PROCESSES

Porosity and Sorption Properties of Activated Carbons Prepared from Anthracite by Steam–Air Activation

N. V. Sych, N. T. Kartel', N. N. Tsyba, V. V. Strelko, A. D. Nikolaichuk, and T. I. Mironyuk

Institute of Sorption and Problems of Endoecology, National Academy of Sciences of the Ukraine, Kiev, Ukraine

Received August 9, 2005; in final form, December 2005

Abstract—Fundamental aspects of the steam–air activation of anthracite from Donets coal fields were studied. The effect of the flow rate of moistened air on the development of a porous structure and the sorption properties of the adsorbents obtained were examined.

DOI: 10.1134/S1070427206040094

The intense development of sorption technologies imposes increasingly stringent requirements to such properties of adsorbents as high sorption capacity determined by the pore structure, presence of surface functional groups, and service characteristics associated with purity, abrasion resistance, and cost.

Fossil coals used as one of the main raw materials for manufacturing carbon adsorbents for various purposes largely satisfy these requirements [1, 2].

Among these coals, anthracite is one of the most attractive raw materials owing to the high content of carbon and low ash content, as well as to the high mechanical strength of the final product, activated carbon.

At the same time, activation of anthracite to obtain an adsorbing material encounters the problem of its low reactivity in a high-temperature contact with the conventionally used activating gases. This is due to the high degree of metamorphism of this kind of fossil coals (a strong change in the texture, structure, and mineral composition under the action of temperature, pressure, and chemical activity of stratal solutions). It is for this reason that an adsorbent with a polymodal pore structure frequently cannot be produced by steam activation [3–5].

Of high importance in the technology of sorption purification of liquids to remove inorganic and organic contaminations, recovery of precious metals from solutions, and accumulation of process gases is the possibility of controlling the pore structure.

In manufacture of activated carbons, the pore structure and properties are controlled by selecting the activation method and the activating agent and by varying the process duration and conditions.

The porous structure is rather frequently developed by chemical activation [6–12], which consists in that coal is treated with carbonates, sulfates, hydroxides, sulfuric and phosphoric acids, and zinc chloride, which release an activating gas (e.g., CO_2, O_2) at high temperatures.

As a rule, chemical activation gives an adsorbent with a sufficiently developed surface and comparatively wide micropores. However, it is contaminated with inorganic admixtures. Moreover, such a catalytic activation impairs the mechanical strength of the final product. Thus, the chemical activation is a technologically unjustified procedure: it complicates the process of manufacture of activated coals because the process is corrosive and it is necessary to wash carbon.

The authors made an attempt, as an alternative procedure for production of activated coals with a developed porous structure, to use activation with a combined activating gas, humidified air.

The aim of the study was to examine kinetic aspects of the anthracite activation with a steam–air mixture, specific features of the process of formation

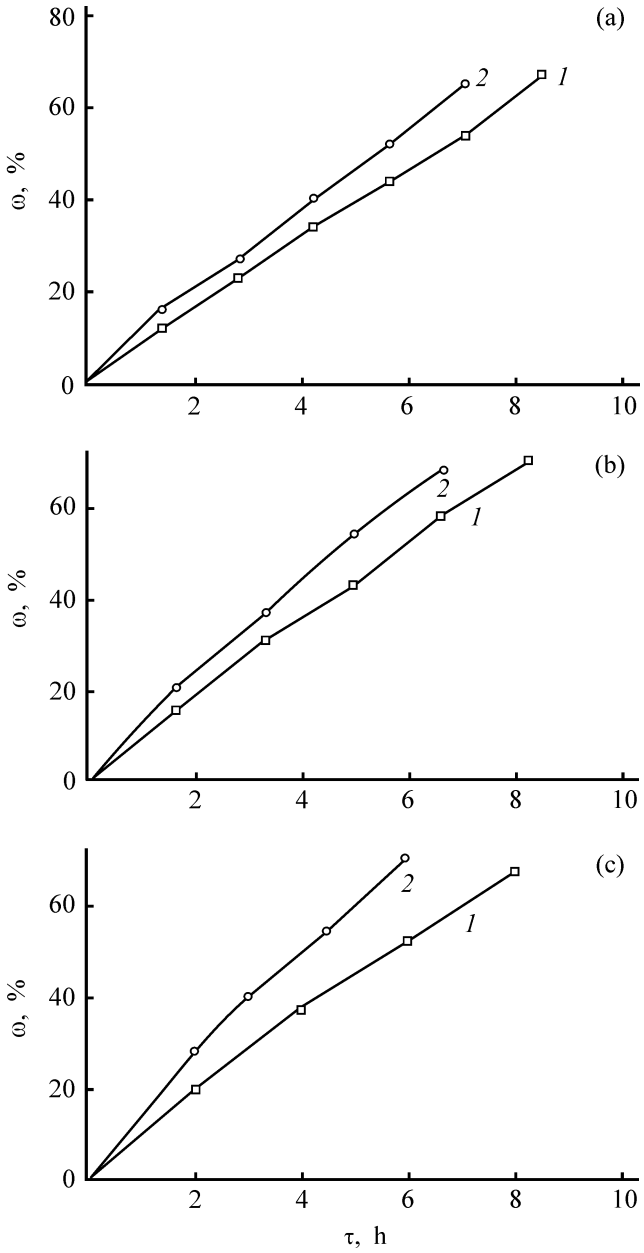


Fig. 1. Kinetics of anthracite activation with (*1*) steam and (*2*) steam–air activating mixture (air flow rate 100 ml min^{-1}) at different temperatures. Temperature (°C): (a) 800, (b) 850, and (c) 900. (ω) Combustion loss and (τ) time.

of a porous structure, and sorption parameters of the activated carbons obtained in various temperature modes.

EXPERIMENTAL

Anthracite of A brand from the Donets coal field (Sverdlovsk, Lugansk oblast, Ukraine) served as the starting material. The chemical composition of the main components of the raw material was as follows: A_c = 4–5%, V_{daf} = 6–7%, C_{daf} = 95%. Size of anthracite particles 0.5–2.0 mm, initial volume of sorption pores for benzene <0.01 $cm^3\ g^{-1}$, bulk density 0.94 $g\ cm^{-3}$.

The activation was performed in a SUOL-044/12-M2-U42 laboratory furnace [GOST (State Standard) 13474–79]. Anthracite samples were placed in a 500 × 45-mm cylindrical quartz reactor. The study was carried out in the static mode with intermittent rotation of the reactor in the furnace. The temperature was monitored with a built-in platinum–platinum-rhodium thermocouple and controlled with the control unit (GOST 9736–68) supplied with the SUOL furnace.

The activation process included supply of steam preliminarily mixed with a flow of air. The flow rate of steam was 0.28×10^{-7} $m^3\ s^{-1}$, and that of air passing across a layer of hot (boiling) water, 0.33×10^{-6} and 1.67×10^{-6} $m^3\ s^{-1}$.

To reveal the influence of atmospheric oxygen in steam–air activation, the initial sample was also directly activated with pure steam at the same temperature and flow rate of steam.

In all stages of the study, the samples were subjected to porometric analysis by measuring the sorption pore volume V_s for benzene [13]. In the course of activation, the sample yields by mass and volume (R_m and R_v) were recorded and the bulk density Δ and combustion loss ω were determined.

To evaluate the sorption properties of the activated carbons obtained, the sorption capacity for Methylene Blue and the sorption activity for iodine were determined.

Of particular importance for understanding of the fundamental aspects of steam–air activation of anthracite is a study of the process kinetics. Figures 1a–1c show the kinetics of the combustion loss of anthracite in various modes of activation with pure steam and steam with addition of atmospheric oxygen bubbled across a hot water layer. It follows from the data presented that use of steam mixed with atmospheric oxygen as an activating agent starts to take effect even at 800–850°C, which is manifested in a change in the activation rate (Figs. 1a and 1b). At 900°C, the acceleration of the process becomes more considerable (Fig. 1c). For example, the combustion losses of 40–60% are reached in 3 to 5 h in the first case, and in 4–6 h in activation with pure steam.

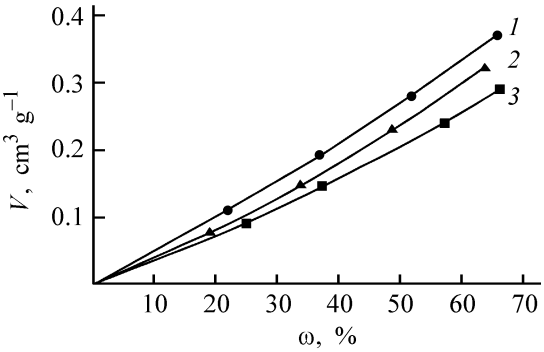


Fig. 2. Effect of the flow rate of humidified air on the development of the sorption pore volume V for benzene. (*1*) Activation with H_2O, (*2*) activation with H_2O + humidified air (flow rate 0.33×10^{-6} m^3 s^{-1}), and (*3*) activation with H_2O + humidified air (flow rate 1.67×10^{-6} m^3 s^{-1}). (ω) Combustion loss; the same for Fig. 3.

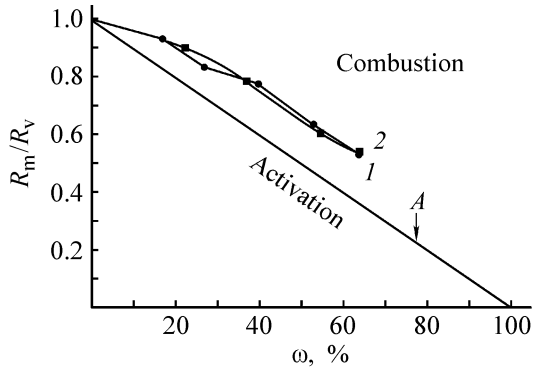


Fig. 3. Variation of the activation index in activation of anthracite with (*1*) steam and (*2*) steam–air mixture (air flow rate 1.67×10^{-6} m^3 s^{-1}) at 900°C.

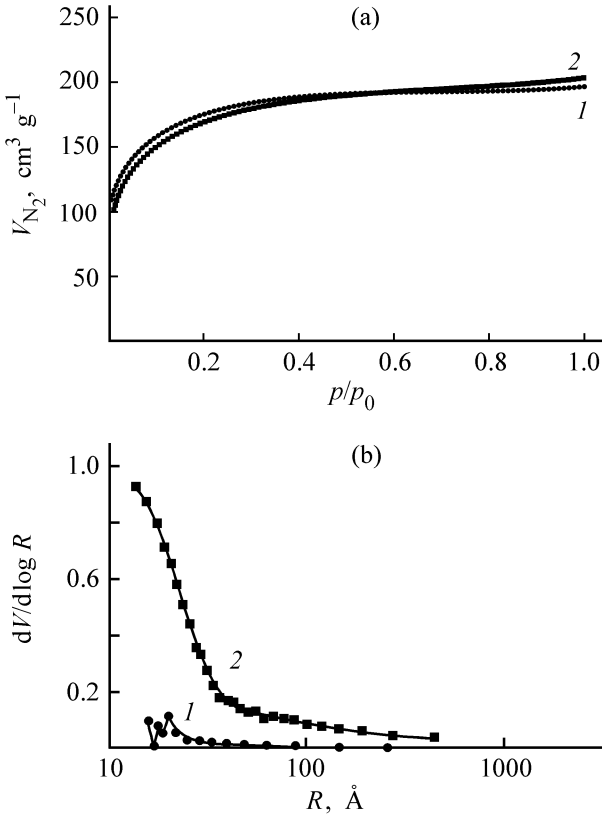


Fig. 4. (a) Isotherms of nitrogen adsorption for anthracite samples activated with (*1*) combined steam–air activating agent and (*2*) steam and (b) their differential curves of pore volume distribution with respect to pore radii. (V_{N_2}) Volume of absorbed nitrogen, (p/p_0) relative pressure, and (R) pore radius.

At the same time, the sorption pore volumes for benzene (Fig. 2) slightly decrease upon application of the combined activating agent, which may point to redistribution of pore sizes at the surface of the carbon matrix.

In this case, an increase in the concentration of oxygen in the air–steam flow also leads to a decrease in the sorption pore volume for benzene that can be obtained upon the activation.

The activation index, defined as the ratio of the product yield by mass to that by volume, characterizes the activation efficiency. Figure 3 shows that, in the case of both direct activation (curve *1*) and activation in the steam–air system (curve *2*), the activation index varies similarly and is close to that characteristic of pure pore formation (line *A*).

The virtually coincident runs of the curves in Fig. 3 verify the assumption that the change in the porometric characteristics is in all probability due to redistribution of the pore structure, rather than to the possible enhancement of combustion, accompanied by formation of the gaseous oxides CO and CO_2, for which carbon may be expended. Presumably, atmospheric oxygen introduced into the flow of the activating gas exerts a milder effect because of its humidification in bubbling across a water layer.

One more evidence in favor of modification of the pore structure is the difference between the specific surface areas for nitrogen of samples subjected to direct activation and activation with a steam–air mixture (900°C) to a combustion loss of 65% (Figs. 4a and 4b). The specific surface area is 800 m^2 g^{-1} in the first case, and 680 m^2 g^{-1} in the second (Fig. 4a), whereas the volume of nitrogen absorbed at $p/p_0 \approx 1.0$ is the same and equal to 200 cm^3 g^{-1} in both cases. The decrease in the specific surface area of samples activated to the same combustion loss is presumably due to an increase in the meso component of the pore structure.

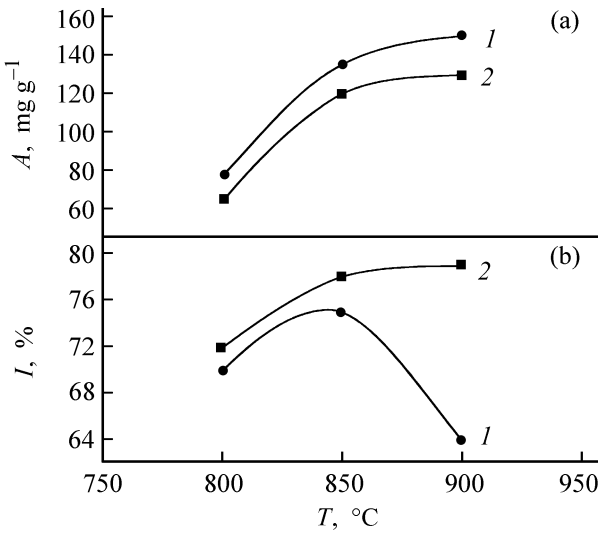


Fig. 5. Temperature dependences of (a) absorption capacity for MB and (b) sorption activity with respect to I_2 in activation of anthracite samples with (*1*) combined steam–air activating agent (air flow rate 1.67×10^{-6} $m^3 s^{-1}$) and (*2*) steam. (*A*) Absorption capacity for MB, (*I*) sorption activity with respect to I_2, and (*T*) temperature.

It is of interest that the differential curves of pore volume distribution with respect to pore radii (Fig. 4b) also show significant changes. The intensity of peaks corresponding to the effective pore radii dramatically falls when the combined steam–air activating agent is used, which points to a decrease in the microporosity of the samples studied.

Figures 5a and 5b show temperature dependences of the adsorption of Methylene Blue (MB) and iodine for anthracite samples activated with steam (curve *2*) and combined (curve *1*) activating agent. It can be seen that the sorption capacity for MB is higher upon steam–air activation, whereas the sorption activity with respect to iodine is markedly lower.

In this case, the activation temperature strongly affects the development of the surface porous structure in activation with both steam and combined activating agent. As temperature is raised, the sorption capacity of the activated carbons obtained for MB grows. This fact clearly confirms the change in the absorption capacity for MB for anthracite samples treated to a combustion loss of 65% at 800, 850, and 900°C (Fig. 5a).

The variation of the absorption capacity for I_2 indicates that the volume of micropores changes as the activation temperature is raised (Fig. 5b). In the case of steam–air activation, the sorption activity with respect to I_2 reaches a maximum at 850°C and then falls dramatically at 900°C, whereas in the case of steam activation, the maximum activity is observed at 850°C. This indicates that the number of micropores increases at high activation temperatures, whereas the number of mesopores increases, which confirms that the sorption capacity for MB grows.

CONCLUSIONS

(1) The results obtained in a study of the steam–air activation of anthracite from Donets coal fields demonstrate that it is possible to obtain highly porous activated carbons with a specific surface area for N_2 of up to 680 $m^2 g^{-1}$ and pore volume for benzene of up to 0.32 $cm^3 g^{-1}$ at a product yield of 35%.

(2) Activation with a steam–air mixture depends on temperature and flow rate of air in the flow of the activating gas.

(3) Comparison of the porometric and sorption characteristics of adsorbents produced by activation with steam and steam–air mixture indicates that the volumes of micro- and mesopores are redistributed in favor of the latter if humidified air is used as an activating gas.

REFERENCES

1. Parra, J.B., Pis, J.J., Sousa, J.C. de, et al., *Carbon*, 1996, vol. 34, pp. 783–787.
2. Parra, J.B., Sousa, J.C. de, Pis, J.J., et al., *Carbon*, 1995, vol. 33, no. 6, pp. 801–817.
3. Lebedev, V.V., Golovina, G.S., and Surinova, S.I., *Khim. Pererab. Topl.* (Moscow), 1974, vol. 30, no. 1, pp. 40–44
4. Bessant, G.A.R. and Walker, P.L., Jr., *Carbon*, 1994, vol. 32, no. 4, pp. 1171–1176.
5. Walker, P.L., Jr. and Almargo, A., *Carbon*, 1995, vol. 33, no. 2, pp. 239–241.
6. Strelko, V.V., Gerasimenko, N.V., and Kartel', N.T., *Zh. Prikl. Khim.*, 2001, vol. 74, no. 6, pp. 931–933.
7. Kartel', N.T., Gerasimenko, N.V., and Strelko, V.V., *Zh. Prikl. Khim.*, 2002, vol. 75, no. 9, pp. 1443–1447.
8. Sych, N.V., Improvement of the Technology for Production of Carbon Adsorbents from Anthracite from the Donets Coal Fields, *Doctoral Dissertation*, Kiev, 2005.
9. Illan-Gomez, M.J., Garcia-Garcia, A., Salinas-Martinez de Lecea, C., and Linares-Solano, A., *Energy Fuels*, 1996, vol. 10, no. 5, pp. 1108–1114.
10. Lozano-Castello, D., Lillo-Rodenas, M.A., Casorla-Amoros, D., and Linares-Solano, A., *Carbon*, 2001, vol. 39, no. 5, pp. 741–749.
11. Lillo-Rodenas, M.A., Lozano-Castello, D., Casorla-Amoros, D., and Linares-Solano, A., *Carbon*, 2001, vol. 39, no. 5, pp. 751–759.
12. Lillo-Rodenas, M.A., Casorla-Amoros, D., and Linares-Solano, A., *Carbon*, 2003, vol. 41, no. 5, pp. 267–275.
13. Kel'tsev, N.K., *Osnovy adsorbtsionnoi tekhniki* (Fundamentals of Adsorption Technology), Moscow: Khimiya, 1984.

ISSN 1070-4272, Russian Journal of Applied Chemistry, 2006, Vol. 79, No. 4, pp. 559–562. © Pleiades Publishing, Inc., 2006.
Original Russian Text © A. M. Akimbaeva, 2006, published in Zhurnal Prikladnoi Khimii, 2006, Vol. 79, No. 4, pp. 570–573.

SORPTION AND ION-EXCHANGE PROCESSES

Sorption of Palladium(II) Chloride Complexes by Nitrogen-containing Modified Shungites

A. M. Akimbaeva

Bekturov Institute of Chemical Sciences, Ministry of Education and Science of the Republic of Kazakhstan, Almaty, Kazakhstan

Received June 3, 2005; in final form, November 2005

Abstract—The sorption properties of anion exchangers based on modified shungites with respect to palladium(II) ions from chloride solutions were studied. The effect of sorbent nature, pH of a solution, and process duration on the degree of their recovery was considered.

DOI: 10.1134/S1070427206040100

Sorbents based on organic polymers, chemically modified silicas, and fibrous and carbon materials have been suggested for selective sorption and recovery of platinum metals from solutions [1–8]. Particular attention is paid in concentration of platinum metal ions to nitrogen-containing sorbents, which are the most effective [9] because of having the highest capacity for complexation with platinum-group metals. However, the complex ion exchangers recommended for selective recovery of platinum metals are difficultly accessible and rather expensive. A promising way to obtain such ion exchangers is to modify the surface of natural sorbents to improve their capacity and kinetic characteristics. Carbon-containing materials are insufficiently widely used as a matrix for production of modified sorbents. Of particular interest among carbon-containing materials is shungite rock, whose main components are carbon and silicon dioxide, which constitute a common composite system. Materials of this kind are particularly promising for recovery of platinum metals [10] and, in particular, palladium ions.

The aim of this study was to examine recovery of palladium(II) ions from chloride solutions with modified nitrogen-containing shungites.

EXPERIMENTAL

A shungite-based ion exchangers (Sh) was produced by chemical modification of a natural sample containing 20% carbon with polyethylen imine (PEI) with the subsequent cross-linking with glycidyl methacrylate (GMA) [11]. Shungite containing grafted groups of polymethylvinylpyridine (PMVP) was synthesized by polymerization of 2-methyl-5-vinylpyridine in grains of a shungite concentrate containing 80% carbon [12].

Sorption of palladium(II) ions was studied under static conditions at room temperature. The starting solution was prepared by dissolving the metal in a mixture of nitric and hydrochloric acids. The concentration of Pd(II) ions in the working solution was 11 mg l^{-1} at pH 1.3. To study the process kinetics, a 0.5-g portion of the sorbent was brought in contact with 50 ml of a Pd(II) solution ($c_{Pd^{2+}}$ = 11 mg l^{-1}) and agitated with a magnetic stirrer at the 400–500 rpm. The necessary pH values were adjusted with HCl and KOH solutions and monitored with an EV-74 pH-meter equipped with an ESL-43-07 glass electrode. The amount of sorbed Pd(II) ions was calculated from the difference of the Pd content in the solution before and after sorption. Atomic-absorption measurements were performed on a Carl Zeiss Jena AAS-1 spectrophotometer with an acetylene–air flame atomizer. The atomic absorption was recorded at 247.6 nm and monochromator slit width of 0.2 mm.

The capacity characteristics of sorbents depend on the content of functional groups, nature of an ion being recovered, and recovery conditions and may vary widely.

According to the results obtained in a study of the sorption of palladium(II) chloride complexes at a liquid-to-solid phase ratio (l : s) of 100–1000 [Pd(II) concentration 11 mg l^{-1}], the degree of recovery (R, %)

Table 1. Sorption of palladium(II) chloride complexes in relation to the phase ratio ($c_{Pd^{2+}}$ = 11 mg l^{-1}, 24 h)

Anion exchanger	l : s	*R*(Pd), %
Sh : PMVP	100	99
	200	61
	1000	26
Sh : PEI : GMA	100	70
	200	50
	1000	15

markedly decreases as the solution volume becomes larger (Table 1). For example, upon a tenfold increase in l : s, the sorption value decreases for anion exchangers based on Sh : PMVP and Sh : PEI : GMA by a factor of 3.8 and 4.6, respectively.

The pH value of the medium largely determines the relative amounts of various palladium(II) and makes it possible to vary the acid–base properties of the anion exchanger. Most of schemes used to determine palladium in geological and technological objects include decomposition of samples and use of chloride media, in which Pd(II) ions are present in the form of labile complex ($PdCl_4^{2-}$) and some polynuclear species. They readily interact both with various reagents in solution and with functional groups of sorbents, e.g., with nitrogen-containing groups. It has been noted [13] that stable complexes with a palladium(II)–nitrogen coordination bond are mostly formed in weakly acidic solutions. For the anion exchangers under study, the degree of recovery increases with decreasing acidity in the range pH 1–3 (Fig. 1). Presumably, this is due to Pd(II) sorption not only via anionic exchange, but also via complexation. As the pH value increases, amino groups in sorbents with ethylenediamine groups undergo deprotonation, and

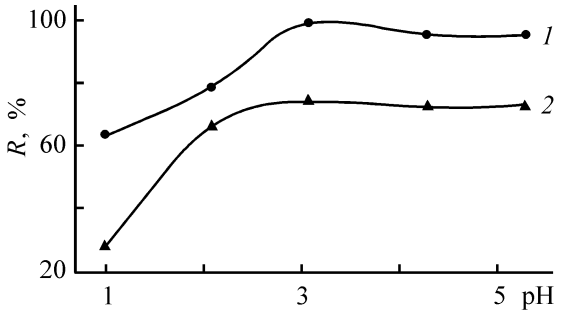
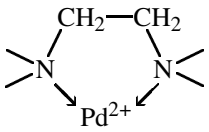


Fig. 1. Effect of the acidity of the aqueous phase on the degree of recovery of palladium(II) chloride complexes, *R*, with the anion exchangers. $c_{Pd^{2+}}$ = 11 mg l^{-1}, V_{el} = 10 ml, m_s = 0.1 g, 24 h, 0.5 M HCl, 20°C. Anion exchanger: (*1*) Sh : PMVP and (*2*) Sh : PEI : GMA; the same for Fig. 3.

the recovery will presumably occur mostly via coordination of the functional groups to metal ions. The anion exchangers mentioned above can absorb palladium(I) ions to give a chelate complex



With the anion exchanger based on Sh : PMVP, the sorption proceeds much better, which possibly due to formation of more stable surface complexes Pd–N_{Py}. The degree of recovery is as high as 74 and 95% (pH 3.1) for anion exchangers based on Sh : PEI : GMA and Sh : PMVP, respectively.

The sorption of palladium(II) ions in a weakly acid medium involves complex $PdCl_4^{2-}$ ions and aqua chloride $Pd(H_2O)Cl_3^-$ anions [14], which interact via anion exchange and coordination interaction with the deprotonated functional groups of the anion exchanger.

It may be assumed that, in a strongly acidic medium, protonated amino groups sorb complex anions on the shungite surface mostly by the ion-exchange mechanism, whereas the complexation predominates in a neutral medium. The presence of functional groups with donor atoms of nitrogen and oxygen in the modified shungites determines their chemical-analytical characteristics and ability to recover complex anions of palladium(II).

The pH value corresponding to 50% recovery of metal ions (pH_{50}) characterizes the selectivity of a sorbent. It may be assumed that pH_{50} lies within a rather narrow range for the anion exchangers under study and indicates that complex ions of palladium(II) are firmly fixed on the sorbents studied.

A quantitative measure of the applicability of a sorbent to concentration of an ion is the distribution coefficient *D* (ml g^{-1}) of this ion. Table 2 lists values of *D* and the sorption capacities of the anion exchangers for sets of experiments with different solution acidities. It can be seen that the sorbents suggested are rather efficient, with distribution coefficients reaching values of 10^3–10^5 ml g^{-1}.

The kinetic properties of sorbents are commonly characterized by determining the time in which the equilibrium is attained at a certain ratio of the volume of a solution being analyzed to the mass of a sorbent at constant temperature and concentration of the supporting electrolyte. It was found that the equilibrium in the distribution of metal ions between sorbents and solution is attained in 2 h for the anion exchanger based on Sh : PMVP, in 3 h for the commercial sor-

Table 2. Distribution coefficients D and sorption capacities SC of the anion exchangers ($c_{Pd^{2+}}$ = 11 mg l^{-1}, V_{el} = 10 ml, m_s = 0.1 g, 24 h)

pH	D, ml g^{-1}		SC, mg g^{-1}		
	Sh : PEI : GMA	Sh : PMVP	Sh : PEI : GMA	Sh : PMVP	Sh : AN-31
1 ± 0.08	60 ± 3.1	168 ± 3.2	0.40 ± 0.07	0.87 ± 0.07	5.19 ± 0.8
2.1 ± 0.07	200 ± 6.1	360 ± 12.1	0.93 ± 0.09	1.10 ± 0.8	2.99 ± 0.4
3.1 ± 0.08	280 ± 7.1	50000 ± 67	1.03 ± 0.1	1.39 ± 0.4	0.028 ± 0.01
4.3 ± 0.09	260 ± 5.2	205 ± 6.1	1.01 ± 0.1	1.33 ± 0.06	0.065 ± 0.02
5.3 ± 0.06	260 ± 4.8	195 ± 4.2	1.01 ± 0.09	1.32 ± 0.2	0.068 ± 0.03

Table 3. Sorption of palladium(II) ions on anion exchangers in the presence of transition metal ions* ($c_{Pd^{2+}}$ = 11 mg l^{-1}, V_{el} = 50 ml, m_s = 0.5 g, 24 h, pH 2)

Anion exchanger	c_M/c_{Pd}	R(Pd), %	Anion exchanger	c_M/c_{Pd}	R(Pd), %
Sh : MVP	10	86	Sh : PEI : GMA	10	70
	100	83		100	53

* c_M, total concentration of Cu^{2+}, Co^{2+}, and Ni^{2+}.

bent, and is not reached at all during the time of the experiment for the anion exchanger based on Sh : PEI : GMA. The degree of recovery of ion complex Pd(II) is high (>90%) for the sorbents under study and as low as 58% for the commercial anion exchanger AN-31. (Fig. 2). The results obtained indicate that the surface characteristics of the sorbents govern the kinetic parameters of the process. The amount of sorbed chloride complexes of palladium(II) decreases, under comparable conditions, in the order Sh : MVP > Sh : PEI : GMA > AN-31. The high affinity of the modified shungite containing pyridine nitrogen for Pd^{2+} ions predetermines the kinetic and sorption parameters of the process. Even though the anion exchanger based on Sh : PEI : GMA and the commercial AN-31 have the same ethylenediamine fragments, they markedly differ in sorption activity. This is probably due to the fact that metal ions may interact on the surface of chemically modified carbon sorbents both with functional groups of a grafted ligand and with residual groups on the surface of the material. The mechanism of sorption of platinum metal ions necessary involves their interaction with the π-conjugated electron system of the carbon matrix, and the process rate may be slow.

A necessary factor that determines the possibility of using a sorbent for concentration of palladium(II) complex ions in analysis of real objects is the selectivity of recovery in the presence of macrocomponents. In practice, it is frequently necessary to recover microscopic amounts of platinum metals from multicomponent systems containing considerable amounts of nonprecious metals. Because chlorides and sulfates of nonferrous metals are, as a rule, the main components of industrial solutions, the selectivity of new sorption materials with respect to Pd(II) chloride complexes on their background invites a special study. In this context, experiments on concentration of Pd(II) in model solutions containing cobalt chloride and sulfates of copper and nickel were carried out (Table 3). It was found that the highest selectivity is observed for the anion exchanger based on Sh : MVP, which sorbs 83–86% of palladium(II) ions at 10–100 times

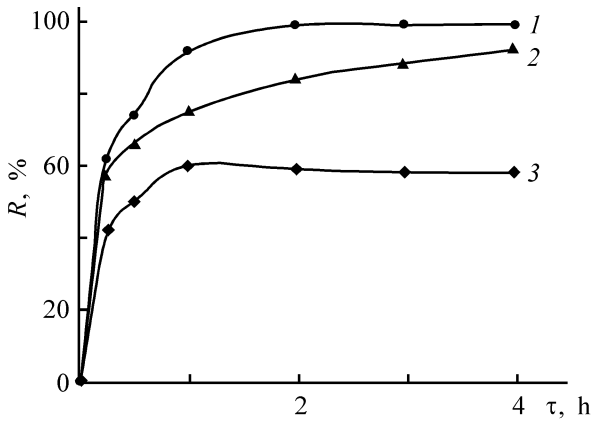


Fig. 2. Degree of recovery of palladium(II) chloride complexes, R, with anionites vs. the process duration τ. $c_{Pd^{2+}}$ = 11 mg l^{-1}, V_{el} = 50 ml, m_s = 0.5 g, 0.5 M HCl, 20°C. Anionite: (*1*) Sh : MVP, (*2*) Sh : PEI : GMA, and (*3*) AN-31.

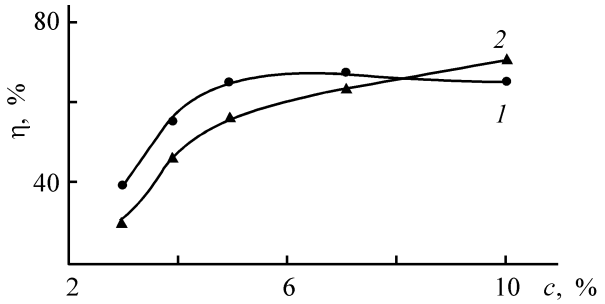


Fig. 3. Degree of desorption of Pd(II) ions, η, vs. the concentration c of thiourea. V_{el} = 50 ml, m_s = 0.15 g, 24 h, 20°C.

higher content of nonferrous metals in solution. Because platinum metal ions tend to coordinate donor nitrogen atoms and form more stable complexes as compared with ions of transition metals, the sorption will be quantitative in a more acidic medium, which creates prerequisites for separation of ions of platinum metals from other ions.

The desorption of palladium(II) ions with various eluents was studied under static conditions. It was found that a minor amount of Pd(II) ions (5%) is desorbed upon treatment with water, 10–20% is eluted with a 0.5–1.0 M HCl solution, and more than 50%, with a solution of thiourea in 1 M HCl. A similar type of desorption of palladium(II) ions has been observed in treatment of activated carbons and carbon fabrics [15], which is caused by the complexity of the mechanism of sorption of palladium(II) ions, their uptake by different active centers, and various other factors: physical sorption (part desorbed by water), anion exchange (displaced by HCl solutions), formation of strong donor–acceptor bonds with the carbon matrix or functional groups, and reduction to the metallic state. The degree of desorption is 65% for a shungite containing grafted groups of PMVP at a concentration of the eluting solution of 5 wt % and more (Fig. 3). For a polyfunctional anion exchanger based on Sh : PEI : GMA, the desorption is enhanced as the concentration of thiourea increases.

CONCLUSIONS

(1) The optimal conditions of recovery of palladium(II) chloride complexes on shungites with grafted ethylenediamine and pyridine groups were found.

(2) It was shown that the structure of functional groups of anion exchangers is the major factor affecting the process. The sorption activity of the anion exchangers studied substantially exceeds that of the commercial AN-31.

(3) The selectivity of a modified shungite containing pyridine nitrogen enables efficient recovery of palladium(II) ions in the presence of concomitant elements, whose content in solution exceeds by several orders of magnitude that of the target component.

REFERENCES

1. Rovira, M., Cortina, J.L., and Sastre, A.M., *Solvent Extr. Ion Exch.*, 1998, vol. 16, pp. 1279–1302.
2. Turanov, A.N., Karandashev, V.K., and Reznik, A.M., *Zh. Prikl. Khim.*, 2000, vol. 73, no. 5, pp. 744–750.
3. Rovira, M., Hurtado, L., Cortina, J.L., et al., *Solv. Extr. Ion Exch.*, 1998, vol. 16, pp. 545–564.
4. Losev, V.N., Kudrina, Yu.V., Maznyak, N.V., and Trofimchuk, A.K., *Zh. Anal. Khim.*, 2003, vol. 58, no. 2, pp. 146–150.
5. Skorokhodov, V.I., Goryaeva, O.Yu., Radionov, B.K., et al., *Izv. Vyssh. Uchebn. Zaved., Tsvet. Metall.*, 2004, no. 1, pp. 31–33.
6. Losev, V.N., Barash, A.N., Volkova, G.V., et al., *Izv. Vyssh. Uchebn. Zaved., Khim. Khim. Tekhnol.*, 1999, vol. 42, no. 2, pp. 41–44.
7. Tarkovskaya, I.A., Tikhonova, L.P., Rosokha, S.V., and Kulik, N.V., *Khim. Tekhnol. Vody*, 2001, vol. 23, no. 6, pp. 565–582.
8. Tikhonova, L.P., Goncharik, V.P., Kozhara, L.I., et al., *Ukr. Khim. Zh.*, 2003, vol. 69, no. 9, pp. 14–18.
9. Borbat, V.F., Adeeva, L.N., and Shindler, A.A., *Tsvet. Met.*, 2004, no. 3, pp. 30–33.
10. Akimbaeva, A.M., Ergozhin, E.E., and Sadvokasova, A.B., *Izv. Vyssh. Uchebn. Zaved., Khim. Khim. Tekhnol.*, 2004, vol. 47, no. 1, pp. 110–112.
11. Akimbaeva, A.M., *Plast. Massy*, 2004, no. 7, pp. 41–42.
12. Akimbaeva, A.M. and Ergozhin, E.E., *Zh. Prikl. Khim.*, 2004, vol. 77, no. 11, pp. 1772–1774.
13. Gordeeva, V.P., Kochelaeva, G.A., Tsizin, G.I., et al., *Zh. Anal. Khim.*, 2002, vol. 57, no. 8, pp. 820–826.
14. Kholmogorov, A.G., Kononova, O.N., Kachin, S.V., et al., *Zh. Fiz. Khim.*, 1998, vol. 72, no. 2, pp. 318–321.
15. Tarkovskaya, I.A., Tikhonova, L.P., Svarkovskaya, I.P., and Kuznetsova, I.R., *Khim. Tekhnol. Vody*, 1995, vol. 17, no. 2, pp. 174–180.

ISSN 1070-4272, Russian Journal of Applied Chemistry, 2006, Vol. 79, No. 4, pp. 563–567. © Pleiades Publishing, Inc., 2006.
Original Russian Text © N. V. Abovskaya, S. A. Simanova, E. S. Boichinova, M. K. Fedorov, 2006, published in Zhurnal Prikladnoi Khimii, 2006, Vol. 79, No. 4, pp. 574–577.

SORPTION AND ION-EXCHANGE PROCESSES

Sorption Recovery of Sulfate Complexes of Iridium on Hydrated Zirconium Dioxide

N. V. Abovskaya, S. A. Simanova, E. S. Boichinova, and M. K. Fedorov

St. Petersburg State Technological Institute (Technical University), St. Petersburg, Russia

Received March 1, 2006

Abstract—The sorption on a hydrated zirconium(IV) dioxide from solutions of trinuclear iridium(IV,IV,IV) and iridium(III,III,IV) oxosulfates was studied. The effect of temperature, sorbent grain size, concentration of sulfate complexes of iridium in solution, and acidity of the medium on the sorption recovery was considered.

DOI: 10.1134/S1070427206040112

In recent decades, an intense interest has been aroused in development of methods for concentration and separation of microscopic amounts of platinum metals (PM) with the use of oxohydrates of transition and main-group metals: iron, aluminum, zirconium, titanium, etc. [1, 2].

A particular place among sorbents of this kind is occupied by hydrated zirconium hydroxide (HZH), for which reproducible synthesis conditions yielding sorbents with stable ion-exchange properties have been well developed [3].

Previously, a set of studies has been carried out, concerned with sorption of PM chloro complexes on HZH [4–7], including iridium(III) and iridium(IV) chloro complexes from chloride and sulfate-chloride solutions [8, 9]. It has been shown that HZH selectively and irreversibly sorbs microscopic amounts of PM from acid solutions by the anion-exchange mechanism. In the course of time, ligand-exchange transformations occur in the HZH phase, which are accompanied by formation of PM aqua complexes [10]. Chloride, sulfate–chloride, and sulfate solutions are of particular interest for analysis and refining of noble metals [11].

In this study we examined the sorption properties of HZH with respect to sulfate complexes of iridium in sulfate acid solutions.

EXPERIMENTAL

Iridium may be present in sulfate acid solutions in widely diverse forms, depending on preparation conditions [12, 13]. As objects of study were chosen trinuclear oxosulfate complexes of iridium, the so-called blue iridium(IV,IV,IV) sulfates $\{K_{10}[Ir_3O_2(SO_4)_9]\cdot 2H_2O\}$ and green iridium(III,III,IV) sulfates $\{K_{10}[Ir_3O(SO_4)_9]\cdot 3H_2O\}$. The compounds were synthesized using the known procedures [14]. Hydrated zirconium dioxide was obtained from zirconium(IV) oxochloride by precipitation with a 1 M solution of sodium hydroxide by the method described in [15]. The grain size of the "working" fraction of the sorbent was 0.50–0.80 mm. When studying the effect of the sorbent grain size on the sorption, the grain diameter was varied from 0.125 to 0.800 mm. The static exchange capacity (SEC) was measured as the difference of the iridium concentrations in the starting solution and in that after contact with the sorbent. The content of iridium in solution was found spectrophotometrically by the method of "three acids" [16].

The sorption properties of HZH with respect to sulfate compounds of iridium(IV,IV,IV) and iridium(III,III,IV) were studied under static conditions (s : l = 1 : 50) in 0.01 M H_2SO_4 solutions under continuous agitation (in a Laboratory shakes type 358S shaking device at a rate of 200 cycles/min). The sorption kinetics of sulfate complexes of iridium (c_{Ir} = 1×10^{-4} M) was studied in freshly prepared sulfate acid solutions of blue iridium(IV,IV,IV) sulfate and green iridium(III,III,IV) sulfate at temperatures in the range from 20 to 90°C.

At room temperature, equilibrium in the distribution of blue and green iridium sulfates between the solutions and sorbent is attained in 20 h; the sorption

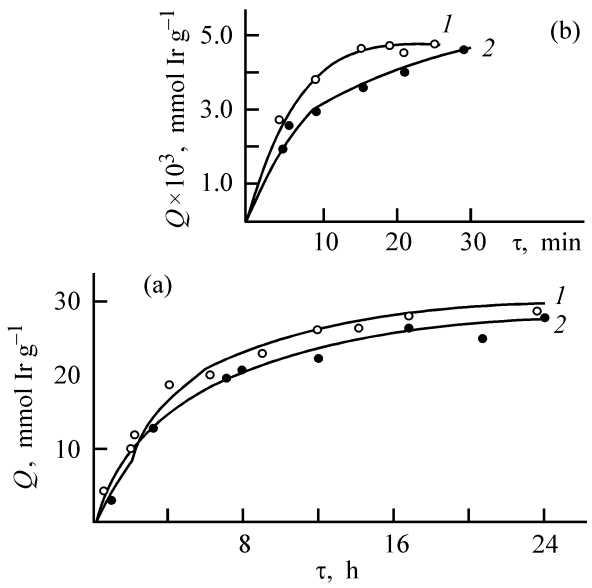


Fig. 1. Integral kinetic curves of iridium sorption on HZH from solutions. (Q) Sorption capacity and (τ) sorption time. (a) (*1*) Blue iridium(IV,IV,IV) sulfate and (*2*) green iridium(III,III,IV) sulfate; (b) (*1*) iridium(IV) chloro complex and (*2*) iridium(III) chloro complex.

half-times ($\tau_{1/2}$) are 3.6 and 4.2 h, respectively (Fig. 1, curves *1*, *2*). The recovery of blue iridium(IV,IV,IV) sulfate is about 60%, and that of green iridium(III,III,IV) sulfate, about 50%. These values do not exceed those in indium recovery from solutions of chloro complexes of the same concentration [8, 9]. It was of interest to compare the sorption capacities from solutions of chloro complexes and sulfate complexes of iridium. For example, approximately 90% of iridium(III) chloro complexes is sorbed from solutions of 1×10^{-4} M of $K_3[IrCl_6]$ in 0.01 M HCl, and about 100% of iridium(IV) is sorbed from a solution of $K_2[IrCl_6]$ in 0.01 M HCl under similar conditions (the sorption half-time is 6 and 4 min, respectively) [8, 9]. The dissimilar behavior of iridium complexes in sorption processes of its recovery from chloride and sulfate media with HZH is apparently due to different forms of its existence in these solutions and to different mechanisms of its sorption.

Effect of temperature on the sorption capacity and rate of iridium sorption from solutions for blue iridium(IV,IV,IV) sulfate and green iridium(III,III,IV) sulfate

T, °C	Time in which equilibrium is attained, h	$\tau_{1/2}$, h	SEC × 10^3, mmol g^{-1}
Blue iridium(IV,IV,IV) sulfate			
20	20	3.6	3.0
50	3	1.2	4.5
90	1	0.4	5.0
Green iridium(III,III,IV) sulfate			
20	20	4.2	2.5
50	3	0.8	3.1
90	2	0.8	5.0

Similarly to the case of iridium chloro complexes [8, 9], the rate of sorption recovery of blue and green iridium sulfates is also strongly affected by the sorbent grain diameter. As the radius of HZH particles increases, the sorption rate of sulfate complexes of iridium grows, which is characteristic of the diffusion control of sorption recovery. For example, as the radius of HZH particles decreases from 0.800 to 0.125 mm, the sorption time of sulfate complexes of iridium decreases from 20 to 8 h. The sorption half-time from a solution of blue iridium(IV,IV,IV) sulfate decreases from 3.6 to 2.4 h as the grain size of HZH decreases from 0.800 to 0.300 mm. The sorption half-time from a solution of green iridium(III, III,IV) sulfate decreases to a greater extent, from 4.2 to 1 h in the same range of sorbent grain sizes.

The temperature strongly affects the sorption process (see table). On heating the solutions, the rate of recovery of sulfate complexes of iridium with HZH grows. For example, as the temperature is raised from 20 to 90°C, the time in which equilibrium is attained in sorption from a solution of blue iridium sulfate falls from 20 to 1 h, and, accordingly, the sorption half-time decreases from 3.6 h to 25 min. In the case of green iridium sulfate, heating affects the recovery rate to a considerably lesser extent. In this case, the time in which the equilibrium is attained at 90°C is 2 h ($\tau_{1/2}$ = 47 min). The apparent activation energies are 13.7 and 18.2 kJ mol^{-1} for blue iridium(IV,IV,IV) sulfate and green iridium(III,III,IV) sulfate, respectively.

To determine the type of kinetics of sorption for solutions of blue and green iridium sulfates on HZH, we used the method of "sorption interruption" and the dependence of the degree of exchange, F, and examined $-\ln(1 - F)$ on the sorption time (Fig. 2).

The experimental data obtained in studying the interrupted sorption from iridium sulfate solutions were found to be less unambiguous. The time of contact between a solution of green iridium sulfate and HZH till interruption was 4 h. After the solution of green iridium sulfate is again brought in contact with the sorbent, there is virtually no increase in the sorption rate. This behavior is characteristic of a process controlled by outer diffusion and is probably due to a higher

stability of green iridium(III,III,IV) sulfate. A similar pattern is observed for trinuclear blue iridium(IV,IV,IV) oxosulfate only during the first 3 h of contact between its solution and HZH (if sorption is interrupted after 3 h of contact with a solution of blue iridium sulfate, the sorption rate does not increase). However, interruption of sorption after 4 h of contact with more labile complexes of blue iridium sulfate leads to a dramatic increase in the sorption rate on resuming the process. The whole set of data on the behavior of iridium sulfates in solutions gives no way of making an unambiguous choice between the inner- and outer-diffusion control. In all probability, the increase in the recovery rate after the sorption is interrupted in the case of blue iridium sulfate is due to a change of the state of the trinuclear iridium(IV,IV,IV) complex in solution in the course of time, rather than to changing type of kinetics [11, 12].

The linear dependence of F on $\sqrt{\tau}$ in the initial stage of sorption (Fig. 2a) and the linear dependence of $-\ln(1 - F)$ on τ (Fig. 2b) in sorption from solutions of blue and green iridium sulfates also confirm the diffusion type of the sorption kinetics.

The isotherms of sorption of sulfate complexes of iridium from a 0.01 M H_2SO_4 solution were obtained at equilibrium metal concentrations ranging from 1×10^{-4} to 1×10^{-3} M (Fig. 3). As the concentration in solution of both blue and green iridium sulfates increases, the amount of trinuclear iridium(IV,IV,IV) and iridium(III,III,IV) oxosulfates sorbed on HZH increases. The sorption isotherms are linear under the conditions studied. The same pattern was observed in sorption of chloro and sulfate complexes of other platinum metals [4–9]. The sorbent is not saturated by any of the complexes studied on raising the equilibrium concentration in solution not only by a factor of 10, but also by a factor of 100, as demonstrated by the example of sorption of palladium(II) chloro complexes [5].

Raising the concentration of H_2SO_4 in solutions of iridium(IV,IV,IV) and iridium(III,III,IV) sulfates from 0.01 to 2.0 M leads to a decrease in the amount of metal sorbed on HZH (Fig. 4, curves *3*, *4*). The sorption of green iridium sulfate is suppressed to a lesser extent by nitric and hydrochloric acid (Fig. 4, curves *1*, *2*). The competing action of sulfate ions can be attributed to a higher selectivity of HZH with respect to sulfate ions, compared with chloride and nitrate ions.

Recovery of green iridium(III,III,IV) sulfate from solutions in the presence of 0.5 M of HNO_3 and HCl is about 24%, and that in the presence of 0.5 M of

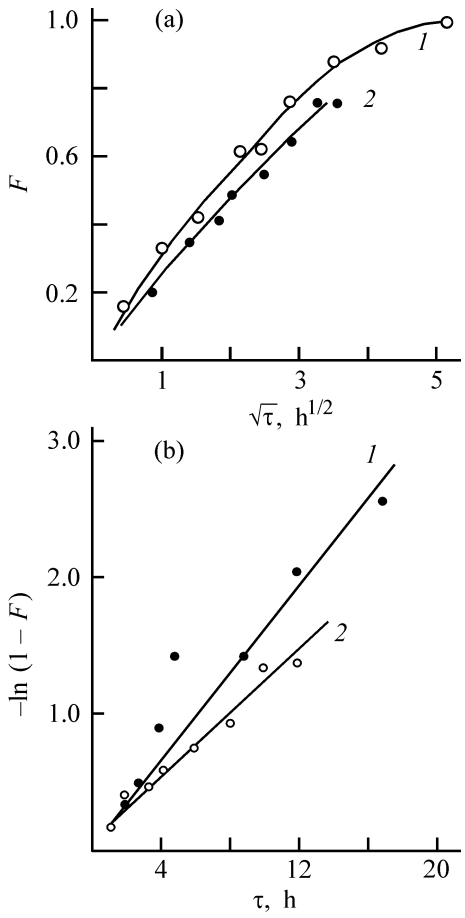


Fig. 2. (a) F–$\sqrt{\tau}$ and (b) $-\ln(1 - F)$–τ dependences for (*1*) blue and (*2*) green iridium sulfates. $F = Q_\tau/Q_\infty$, (Q_τ) sorption of ions from solution in time τ, and (Q_∞) equilibrium sorption.

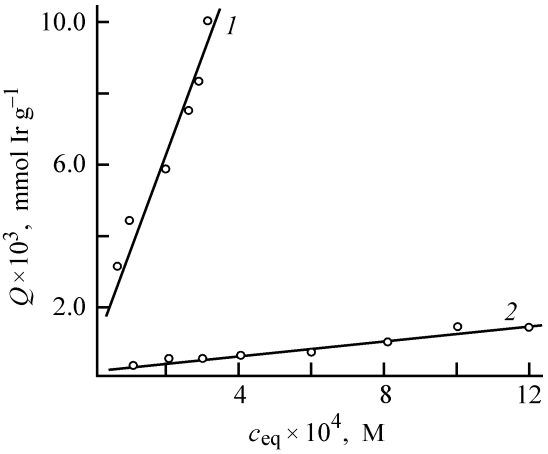


Fig. 3. Isotherms of sorption of (*1*) blue iridium(IV,IV,IV) sulfate and (*2*) green iridium(III,III,IV) sulfate from a 0.01 M H_2SO_4 solution. (Q) Static sorption capacity and (c_{eq}) equilibrium concentration.

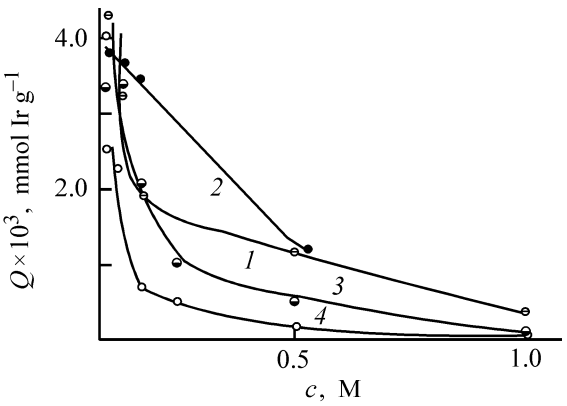


Fig. 4. Iridium sorption on HZH vs. the concentration in solution of (*1*) HNO_3, (*2*) HCl, and (*3*, *4*) H_2SO_4. (*Q*) Sorption capacity and (*c*) acid concentration. (*1*, *2*, *4*) Green iridium(III,III,IV) sulfate and (*3*) blue iridium(IV,IV,IV) sulfate.

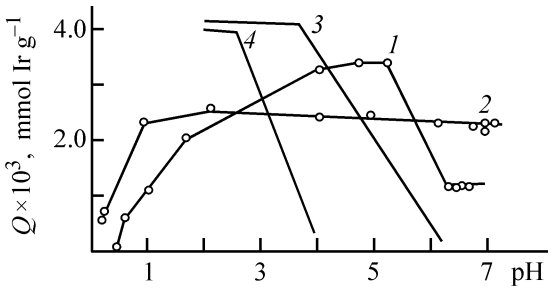


Fig. 5. Iridium sorptin on HZH vs. pH of the equilibrium solution. (*Q*) Static sorption capacity. (*1*) Blue iridium(IV,IV,IV) sulfate, (*2*) green iridium(III,III,IV) sulfate, (*3*) iridium(IV) chloro complex [8], and (*4*) iridium(III) chloro complex [9].

H_2SO_4, only 3%. It should be noted that mineral acids suppress sorption of iridium(IV) and iridium(III) from a solution of chloro complexes to a greater extent, compared with that of sulfate complexes. For example, the amount of iridium sorbed from a solution of iridium(III) chloro complex in the presence of 0.05 M HCl does not exceed 20% of its content in the solution [9]. As demonstrated in [8, 9], iridium chloro complexes are sorbed from weakly acidic solutions by the anion-exchange mechanism, and at higher concentrations of hydrochloric acid the competing action of chloride ions becomes more pronounced. The mechanism of recovery of sulfate complexes of iridium on HZH is more complicated than that operative in the case of iridium chloro complexes and is probably governed not only by ion-exchange processes.

The sorption capacity of HZH for sulfate complexes of iridium strongly depends on the pH of the solution. As can be seen in Fig. 5, the amount of Ir(IV) sorbed from a solution of blue iridium(IV, IV,IV) sulfate grows as the pH of the equilibrium solution increases from 0.5 to 3.5, remains virtually constant in the pH range from 4 to 5.5 (SEC = 3.32×10^{-3} mmol g^{-1}), and steeply falls as pH becomes even higher. At pH 6.5, the sorption capacity is 1.22×10^{-3} mmol g^{-1}. The pH range at which oxosulfate complexes of iridium are recovered to the greatest extent from a solution of a green sulfate is rather extended, from pH 2.0 to 7.0. The sorption capacity is constant (2.35×10^{-3} mmol g^{-1}) in this pH range. It should be noted that the amount of sorbed iridium chloro complexes decreases as the solution pH increases and becomes virtually zero at pH 4.2 (Fig. 5, curves *3*, *4*). The difference in the types of pH dependences of the sorption recovery of iridium from solutions of blue and green sulfates and chloro complexes of iridium is also due to different mechanisms of iridium recovery on HZH.

CONCLUSIONS

Sorption of microscopic amounts of trinuclear oxosulfate complexes of iridium(IV,IV,IV) and iridium(III,III,IV) from sulfate acid solutions on hydrated zirconium dioxide is distinguished by a slow sorption kinetics, compared with iridium(III) and iridium(IV) chloro complexes. The rate-determining stage of sorption from solutions of sulfate complexes of iridium is outer diffusion.

REFERENCES

1. Simanova, S.A. and Boichinova, E.S., in *Ionnyi obmen i ionometriya* (Ion Exchange and Ionometry), Leningrad: Leningr. Gos. Univ., 1988, no. 6, pp. 3–17.
2. Pechenyuk, S.I., *Sorbtsionno-gidroliticheskoe osazhdenie platinovykh metallov na poverkhnosti neorganicheskikh sorbentov* (Sorption-Hydrolytic Deposition of Platinum Metals onto the Surface of Inorganic Sorbents), Leningrad: Nauka, 1991.
3. Boichinova, E.S., in *Ionnyi obmen i ionometriya* (Ion Exchange and Ionometry), Leningrad: Leningr. Gos. Univ., 1984, no. 4, pp. 76–82.
4. Abovskaya, N.V., Boichinova, E.S., Simanova, S.A., et al., *Zh. Prikl. Khim.*, 1986, vol. 59, no. 2, pp. 278–283.
5. Boichinova, E.S., Abovskaya, N.V., Simanova, S.A., et al., *Zh. Prikl. Khim.*, 1984, vol. 57, no. 6, pp. 1217–1221.
6. Nikol'skaya, L.V., Boichinova, E.S., and Simanova, S.A., *Zh. Prikl. Khim.*, 1986, vol. 59, no. 5, pp. 979–983.

7. Nikol'skaya, L.V., Boichinova, E.S., and Simanova, S.A., *Zh. Prikl. Khim.*, 1985, vol. 58, no. 7, pp. 1448–1452.
8. Nikol'skaya, L.V., Boichinova, E.S., and Simanova, S.A., *Zh. Prikl. Khim.*, 1986, vol. 59, no. 5, pp. 983–987.
9. Nikol'skaya, L.V., Simanova, S.A., and Boichinova, E.S., *Zh. Prikl. Khim.*, 1987, vol. 69, no. 4, pp. 735–739
10. Simanova, S.A., Boichinova, E.S., Abovskaya, N.V., et al., *Problemy sovremennoi khimii koordinatsionnykh soedinenii* (Problems of Modern Chemistry of Coordination Compounds), Leningrad: Leningr. Gos. Univ., 1989, issue 9, pp. 81–98.
11. *Analiticheskaya khimiya metallov platinovoi gruppy* (Analytical Chemistry of Platinum-Group Metals), Zolotov, Yu.A., Varshal, G.M., and Ivanov, V.M., Eds., Moscow: EditornalURSS, 2003.
12. Kukushkin, Yu.N., Simanova, S.A., and Leonenko, E.P., *Izv. Sib. Otd. Akad. Nauk SSSR, Ser. Khim. Nauk*, 1970, issue 4, no. 9, p. 42.
13. Zhilyaev, A.N. and Fomina, T.A., *Koord. Khim.*, 1997, vol. 23, no. 8, pp. 563–582.
14. Ginzburg, S.I., Yuz'ko, M.I., and Sal'skaya, L.G., *Zh. Neorg. Khim.*, 1963, vol. 8, no. 4, p. 839.
15. Chernykh, O.A. and Boichinova, E.S., *Zh. Prikl. Khim.*, 1971, vol. 44, no. 12, pp. 2628–2632.
16. Ginzburg, S.I., Ezerskaya, N.A., Prokof'eva, I.V., et al., *Analiticheskaya khimiya elementov* (Analytical Chemistry of Elements), Moscow: Nauka, 1972.

ISSN 1070-4272, Russian Journal of Applied Chemistry, 2006, Vol. 79, No. 4, pp. 568–572. © Pleiades Publishing, Inc., 2006.
Original Russian Text © I. K. Khmel'nitskii, E. D. Makarov, L. A. Kartsova, 2006, published in Zhurnal Prikladnoi Khimii, 2006, Vol. 79, No. 4, pp. 578–582.

SORPTION AND ION-EXCHANGE PROCESSES

Comparative Study of Sorption Properties of Fullerene C_{60} and Dibenzo-24-crown-8 by Gas Chromatography and Solid-Phase Microextraction

I. K. Khmel'nitskii, E. D. Makarov, and L. A. Kartsova

St. Petersburg State University, St. Petersburg, Russia

Received February 16, 2006

Abstract—Flat concentrators for flow solid-phase microextrcation, packed with carbon materials (C_{60} and Carbochrom C), DB-24C-8 crown ether, and its composite with fullerene were prepared and tested. The possibility of using these units for concentrating organic compounds of different classes in the vapor–gas phase and aqueous solutions was studied.

DOI: 10.1134/S1070427206040124

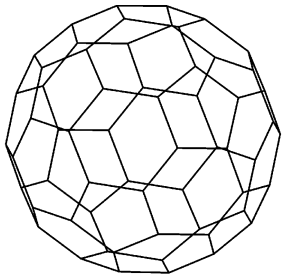
New selective thermally and chemically stable sorbents and stationary phases suitable for simultaneous analysis of hydrophilic and hydrophobic compounds are being extensively developed. Some of the new sorbents characterized by gas chromatography can be used for preconcentration of components of interest in real samples.

In this study we examined carbon materials (graphitized black and fullerene) and dibenzo-24-crown-8-ether (Fig. 1). Fullerenes are highly thermally stable and hydrophobic compounds resistant to oxidation and capable of donor–acceptor interactions. Graphitized thermal black (GTB) is a nonspecific sorbent with a small specific surface area (6–12 $m^2\ g^{-1}$), which is used for a long time in chromatography (Carbochroms and Carbopaks). The structure and physicochemical properties of fullerenes substantially differ from those of graphitized black [1–6]. A C_{60} molecule can be considered as an electron-deficient polyene with partially delocalized π electrons.

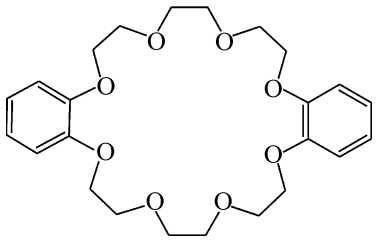
Previously we found [7] that C_{60}-containing stationary phase for gas chromatography strongly differs from graphitized black and has an increased affinity for aromatic compounds. A mixture of C_{60} with DB-24-crown-8 as a gas-chromatographic phase has an increased affinity for aromatic, amine, and hydroxy compounds and can be used for separating positional isomers [7].

In this study we examined these materials as sorbents for solid-phase microextraction (SPME) used for analysis of aromatic hydrocarbons, phenols, and nitriles. Many of these compounds are environmentally hazardous.

SPME is widely used for concentrating volatile and nonvolatile organic compounds from liquid and vapor phases [8–12]. It is an important step of sample preparation in practical analysis and has definite advantages over the conventional solid-phase extraction: shot time required, no organic solvents used, compact facility, combination of the sampling and sample preparation steps, and hence decreased detection limits.



Fullerene [60]



Dibenzo-24-crown-8

Fig. 1. Fullerene [60] and dibenzo-24-crown-8.

In this study we compared the sorption properties of fullerene black and DB-24-crown-8 by gas chromatography and solid-phase microextraction.

EXPERIMENTAL

Fullerenes C_{60}, C_{70}, C_{60} + C_{70} (75% + 25%, 85% + 15%), mixtures of fullerenes with more than 70 carbon atoms, and fullerene black were kindly supplied by Astrin Private Company (St. Petersburg).

The stationary phases for chromatography were prepared from fullerene C_{60} and dibenzo-24-crown-8 (Reaktiv-Servis Research and Production Complex Ltd.). Interton N-AW (0.2–0.25 mm), Interton N-AW (0.315–0.4 mm), and Interton N-AW (0.16–0.2 mm) (Chemapol, Prague) were used as supports for the stationary phases.

n-Alkanes (C_6–C_{20}), aromatic hydrocarbons (benzene, toluene, ethylbenzene, *p*-xylene), phenols (phenol, *o*-, *m*-, *p*-cresol, *m*-, *p*-chlorophenols), aromatic amines (aniline, *o*-, *m*-, *p*-toluidines), nitriles (acetonitrile, propionitrile, benzonitrile, phenylacetonitrile) were used to characterize the stationary phases. All the chemicals were of pure grade.

Distilled water, chloroform, dichloromethane, *o*-xylene, hexane (pure grade), and toluene (analytically pure grade) were used as solvents.

Gas chromatographic analysis was performed on Tsvet-500M and Tsvet-100 chromatographs equipped with flame ionization detectors. The chromatographic data were analyzed using the Multikhrom software. The flow rate of the carrier gas, nitrogen, in "analysis" and "desorption" operation modes was 22–25 and 10–30 ml min^{-1}, respectively. The flow rate of H_2 and air was 25 and 360 ml min^{-1}, respectively. A 3-m glass column with $d_{internal}$ = 4 mm was packed with 10 wt % Triton X-305 supported by Chromaton N-AW (0.25–0.315 mm). The temperature of the column and vaporizer was 70–150 and 275°C, respectively. The working scale of an electrometer was 10^{-9} A.

Nitrogen flows containing simple aromatic hydrocarbons in concentrations form 3.2 to 66.3 mg m^{-3} were produced with the aid of vapor phase sources of gas mixtures VPSGM (Monitoring Research and Production Association). This source produced a vapor containing (mg m^{-3}): benzene 7.7, toluene 7.1, ethylbenzene 3.2, and *o*-xylene 5.8. Extraction of vapor–gas mixtures was performed using the sorption unit (Fig. 2) and VPSGM.

Solid-phase extraction was performed on a flat microextractor packed with a solid sorbent or a stationary phase on a solid support (Fig. 2). We used C_{60} on Inerton N-AW, Carbochrom C, and DB-24-C-8 on Inerton N-AW as sorbents. The sorbent weigh ranged from 10 to 50 mg.

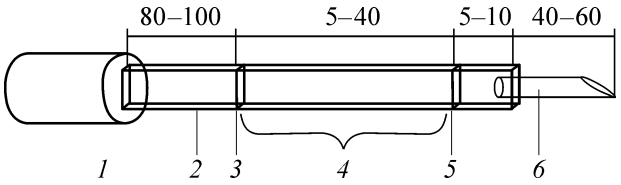


Fig. 2. Scheme of SPME unit: (*1*) threaded coupler, (*2*) flat rectangular column, (*3*, *5*) fiber glass seals restricting the sorbent bede, (*4*) sorbent bede, and (*6*) connecting needle.

The sorption unit was attached to the outlet connecting pipe of VPSGM, small internal excess pressure was produced, and the vapor phase was fed through a sorbing needle. The sorption time was measured with a stopwatch. The flow rate was determined with an IRG-10 electronic flow meter. For flow SPME, the vessel was filled with a model solution to be analyzed. The needle of the sorption unit was placed in the solution to be analyzed, which was fed with a 50-ml gas syringe. After a definite time, the sorption unit was removed from the vessel. To remove the residual water, the unit was purged with nitrogen until the last drop of the working aqueous solution was blown out but for no less than 30–45 s. Then the unit was attached to a working gas chromatograph.

To desorb the concentrated components from the sorption unit, a three-way gas cock was turned into the "desorption" position. The connecting needle (or needle concentrator as a whole) was fixed in the vaporizer of the gas chromatograph, the column with the sorbent was heated at 250°C with an external electric microfurnace, and the unit was continuously purged with the carrier gas. It should be noted that the sorption unit for TPME was located in the vaporizer chamber during the whole time of recording the chromatogram, which was no longer than 20 min. To study the composition of each model solution and vapor–gas mixture, 3–5 analytical cycles involving sorption, desorption, and recording of the detector signals were performed.

We studied aqueous-methanolic solutions containing 143 μg ml^{-1} of phenol and 139 μg ml^{-1} of *p*-cresol and aqueous solutions containing 100, 200, and 500 μg ml^{-1} and 1 and 2 mg ml^{-1} of acetonitrile. The solutions of the phenols and acetonitrile were analyzed using flat sorption units packed with C_{60}, dibenzo-24-crown-8 on Inerton N-AW (0.25–0.315 mm), and Carbochrom B. The model solutions of phenols

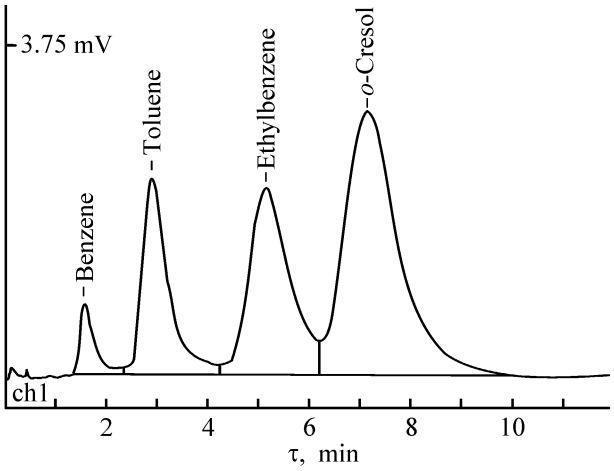


Fig. 3. Representative chromatogram of a hydrocarbon mixture concentrated from the gas–vapor phase with the aid of a flat concentrator packed with 10 wt % dibenzo-24-crown-8 on Inerton N-AW Column: 10 wt % Triton X-305 on Inerton N-AW. T_{column} = 90°C, $T_{vaporizer}$ = 250°C, $T_{furnace}$ = 200°C, flame ionization detector. (τ) Retention time; the same for Fig. 5.

and acetonitrile were prepared from the freshly prepared stock solutions.

The representative chromatogram of desorbed aromatic hydrocarbons is shown in Fig. 3.

To concentrate the analytes, a known amount of the sample (gas or liquid) was passed through the microreactor packed with the sorbent.

Sorption preconcentration for analytical purposes is performed in two different modes: complete sorption of the components and their equilibrium distribution between the sorbent and the sample. In some cases, the equilibrium preconcentration is preferable since it does not require a strict control of the time and flow rate of the examined gas thorough a sorption unit.

In the case of Carbochrom C, the peak area of *o*-xylene increases with increasing the gas volume passed through the column from 100 to 600 ml, which indicates complete sorption of the analytes (Fig. 4a). However, under these conditions, a rapid benzene breakthrough is observed.

The equilibrium concentration is attained on C_{60} supported by Inerton. As seen from Fig. 4b, a rapid breakthrough of benzene, toluene, and ethylbenzene through a column with C_{60} is observed. In the case of *o*-xylene, the sorption equilibrium is also attained, but within a time longer than that for the other aromatic hydrocarbons.

The equilibrium sorption of all the examined arenes in the sorption units packed with DB-24-crown-8

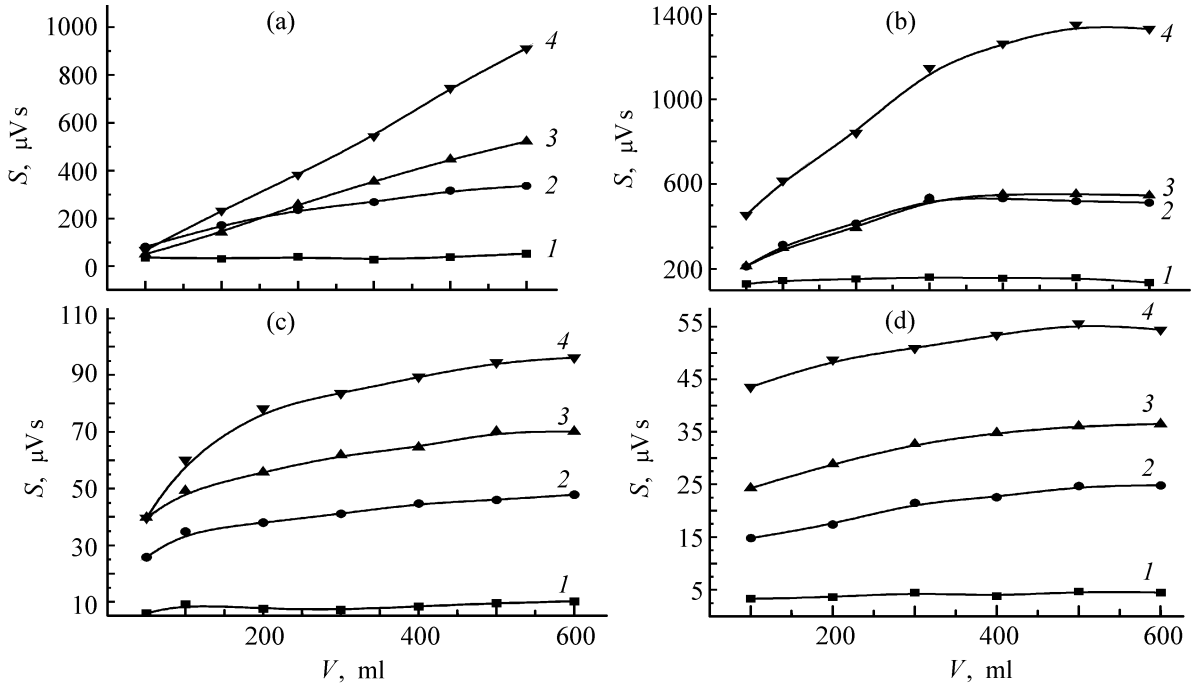


Fig. 4. Attainment of equilibrium sorption of a vapor–gas mixture containing (mg m^{-3}) benzene 7.7, toluene 7.1, ethylbenzene 3.2, and *o*-xylene 5.8 in a microreactor packed with (a) Carbochrom C, (b) 10% C60 on Inerton N-AW, (c) 10% DB-24-C-8 on Inerton N-AW, and (d) 10% DB-24-C-8 + 10% C_{60} on Inerton N-AW. Component: (*1*) benzene, (*2*) toluene, (*3*) ethylbenzene, and (*4*) *o*-xylene. (*S*) peak area and (*V*) volume passed through the column.

(Fig. 4c) and its mixture with C_{60} (Fig. 4d) is attained fairly rapidly. However, the peak areas of the desorption products are substantially smaller than those obtained with Carbochrom C carbon sorbents and fullerene. This is due to low sorption capacity of the crystalline crown ether caused by its small specific surface area.

Since dibenzo-24-crown-8 on Inerton and C_{60} on Inerton are characterized by increased retention of phenols and nitriles under the gas chromatographic conditions, we used the flat concentrators with these sorbents for analysis of aqueous solutions. We analyzed aqueous solutions of phenol–*p*-cresol mixtures. Preliminaryly, we determined the content of compounds of interest in aqueous solutions (in the case of phenols, in methanol) by the direct gas-chromatographic analysis.

We also used these sorbents for analyzing aqueous solutions with various acetonitrile concentrations. The dependence of the peak area of the desorbed products is linear (correlation coefficient 0.997) at the acetonitrile concentration ranging from 0.1 to 10 g l^{-1}. It should be noted the degree of concentration of acetonitrile (~10^4) on the flat concentrator packed with C_{60} on Inerton is higher than that obtained after direct injection of the sample into the chromatographic column.

Taking into account the results obtained with the model vapor–gas mixtures, we analyzed the thermolysis products of styrene–butadiene copolymer (Fig. 5).

The use of the concentrator allowed us to eliminate the sorption of high-boiling components on the wall of the gas syringe (cf. the chromatograms shown in Figs. 5a and 5b) and to increase the sample of the vapor–gas mixture and hence the sensitivity of the analysis.

We performed a large number of experiments to optimize the sorption conditions and elucidate the influence of the volume and flow rate of the vapor–gas mixture on the signal intensity of the flame ionization detector. We found that the main factor affecting the detection limit is the volume of the vapor–gas mixture. We determined the best conditions of preconcentration (flow rate 50 ml min^{-1}) and desorption (temperature of the external furnace ~200°C). The chromatographic peak areas of the model vapor–gas mixtures of aromatic hydrocarbons are reproduced well. The relative standard deviation does not exceed 0.12.

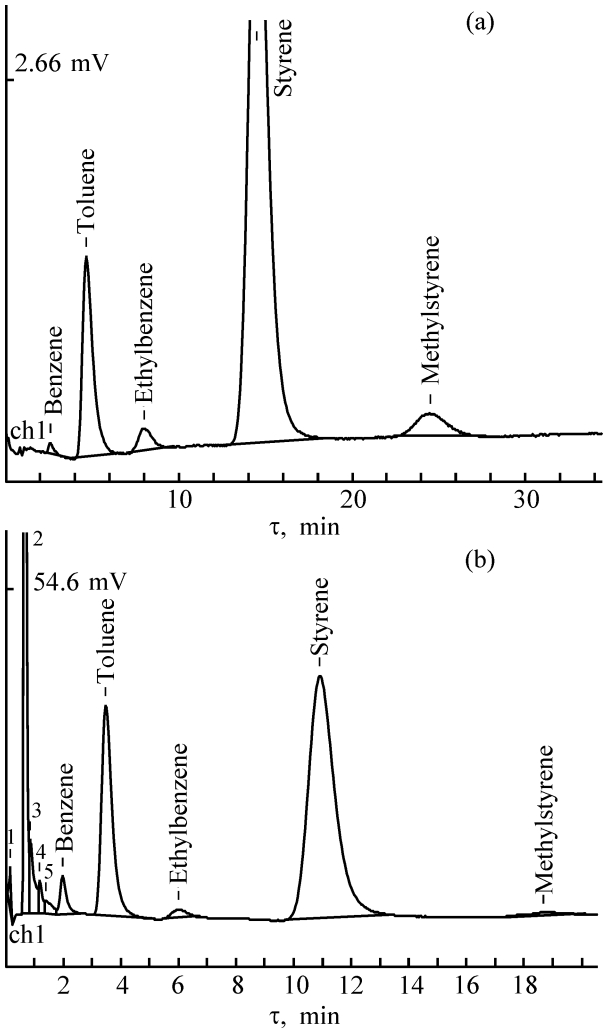


Fig. 5. Desorption chromatographic pattern of the thermolysis products of styrene–butadiene copolymer (a) concentrated on the flat concentrator with DB-24-crown-8 and (b) injected directly with a gas syringe. Tsvet 500 chromatograph; flame ionization detector; column packed with 10% Triton X-305 on Inerton N-AW. T_{column} = 70°C, $T_{vaporizer}$ = 250°C, $T_{furnace}$ = 200°C.

CONCLUSIONS

(1) Sorbents containing C_{60} and DB-24-crown-8 can be used for preconcentration and subsequent quantitative analysis of different classes of organic compounds in aqueous solutions and vapor–gas mixtures.

(2) The detection limit of benzene and its nearest homologs is ~0.01 mg m^{-3}. The polymer thermolysis products were analyzed and the residual concentration of acetonitrile was determined under the optimal conditions of SPME with the new sorbents.

REFERENCES

1. Golovnya, R.V., Terenina, M.B., Ruchkina, E.L., and Karnatsevich, V.L., *Mendeleev Commun.*, 1993, no. 6, pp. 231–233.
2. Davydov, V.Ya., Roshchina, T.M., Filatova, G.N., and Khrustaleva, N.M., *Shch. Fiz. Khim.*, 1996, vol. 70, no. 10, pp. 1857–1862.
3. Jinno, K., Tanabe, K., Saito, Y., and Nagashima, H., *Analyst*, 1997, vol. 122, no. 8, pp. 787–791.
4. Fang, P.F., Zeng, Z.R., Fan, J.H., and Chen, Y.Y., *J. Chromatogr. A*, 2000, vol. 867, nos. 1–2, pp. 177–185.
5. Ballesteros, E., Gallego, M., and Valcarcel, M., *J. Chromatogr. A*, 2000, vol. 869, nos. 1–2, pp. 101–110.
6. Chen, C., Chen, J., Wang, X., et al., *J. Chromatogr. A*, 2000, vol. 886, nos. 1–2, pp. 313–317.
7. Kartsova, L.A. and Makarov, A.A., *Zh. Prikl. Khim.*, 2002, vol. 75, no. 11, pp. 1830–1833.
8. De Fatima Alpendurada, M., *J. Chromatogr. A*, 2000, vol. 889, nos. 1–2, pp. 3–14.
9. Lord, H. and Pawliszyn, J., *J. Chromatogr. A*, 2000, vol. 885, nos. 1–2, pp. 153–193.
10. De Fatima Alpendurada, M., *J. Chromatogr. A*, 2000, vol. 889, nos. 1–2, pp. 3–14.
11. Yun, L. *Anal. Chim. Acta*, 2003, vol. 486, no. 1, pp. 63–72.
12. Xiao, C., Han, S., Wang, Z., et al., *J. Chromatogr. A.*, 2001, vol. 927, nos. 1–2, pp. 121–130.

ISSN 1070-4272, Russian Journal of Applied Chemistry, 2006, Vol. 79, No. 4, pp. 573–578. © Pleiades Publishing, Inc., 2006.
Original Russian Text © Yu. V. Sokolova, 2006, published in Zhurnal Prikladnoi Khimii, 2006, Vol. 79, No. 4, pp. 583–588.

SORPTION AND ION-EXCHANGE PROCESSES

Sorption of Sc(III) on Phosphorus-containing Cation Exchangers

Yu. V. Sokolova

Moscow State Institute of Steel and Alloys (Technological University), Moscow, Russia

Received October 4, 2005

Abstract—Kinetics of Sc(III) sorption from hydrochloric acid solutions on KRF-20t-60 cation exchanger is studied. The experimental data are analyzed in terms of the gel and film kinetic models. The Sc(III) diffusion coefficient in the resin phase is estimated. Static and dynamic sorption data are obtained on Sc(III) sorption from various process solutions on KRF-20t-60, PA-1, AFI-22 ion exchangers, and also on ion exchangers supported on polyacrylonitrile-based fibrous material. Desorption of Sc(III) from KRF-20t-60 is also studied.

DOI: 10.1134/S1070427206020136

It is advisable to use cation exchange resins for primary concentration of Sc(III) from solutions and pulps with low concentration of Sc (from several to tens mg l^{-1}), more so from saline solutions (at salt concentration from tens to hundreds g l^{-1}). In this case, ion exchangers should be highly selective with respect to Sc(III).

Thanks to high affinity of functional groups of phosphorus-containing ion exchangers for Sc(III), sorbents of this class demonstrate high selectivity with respect to Sc(III), and their use allows recovery of Sc(III) from acidic solutions (pH < 2.5) by the complexation mechanism, which makes it possible to perform separation of Sc from alkali and alkaline-earth elements, Al(III), and some other cations that do not form stable complexes under conditions when the dissociation of the functional groups of the resin is suppressed.

High selectivity of phosphorus-containing ion exchangers with respect to Sc(III) in its recovery from multicomponent saline solutions was found by several authors. Kazantsev et al. [1] demonstrated high performance of KFP resin in recovery of Sc(III) from the spent salt filter solution from production of titanium tetrachloride. AFI-21 and AFI-22 nitrogen–phosphorus-containing ion-exchange resins and SF-4 and SF-5 phosphonate resins were recommended for sorption recovery of Sc(III) from red mud from alumina production [2]. Phosphorylated cellulose was used for sorption concentration of Sc(III) from the filtrate obtained after separation of titanium(IV) hydroxide in production of titanium white [3]. Komissarova in her monograph [4] reviewed data on sorption concentration of scandium from various solutions on phosphorus-containing ion exchangers for analytical purposes as well as on Sc(III) speciation in hydrochloric and sulfuric acid solutions and the composition of adsorbed complexes.

In this study we examined static and dynamic sorption of Sc(III) from various process solutions on KRF-20t-60, PA-1, and AFI-22 ion exchangers.

EXPERIMENTAL

We studied the sorption recovery of Sc(III) from the following solutions. Solution no. 1: solution after filtration of zirconium basic sulfate (Verkhnedneprovsk Mining and Smelting Combine); solution no. 2: solution after sulfuric acid pressure leaching of silicate–carbonate ore (Zheltorechensk ore deposit); and solution no. 3: hydrochloric acid solution of spent salt filter from production of titanium tetrachloride (Ust'-Kamenogorsk Titanium and Magnesium Combine), obtained at a solid to liquid (3% HCl) phase ratio of 1 : 2.5. The compositions of these solutions are given in Table 1, and characteristics of the ion exchangers used, in Table 2. The resins were pretreated by the standard procedure [5]. The cation-exchange resins

Table 1. Compositions of process solutions (g l^{-1})

Component	Solution no.			Component	Solution no.		
	1	2	3		1	2	3
Sc(III)	0.001–0.002	0.025–0.035	0.07–0.08	Al(III)	0.5	0.3–2.3	4.1–4.3
Y(III)	0.010–0.013	0.15–0.20	0.19–0.54	Ca(II)	0.01–0.04	0.5–1.0	2.8–3.0
Zr(IV)	0.10–0.12	0.09–0.28	0.6–0.7	Mg(II)	0.01–0.04	12–13	34–40
Ti(IV)	–	0.08–0.19	0.8–0.9	K(I) + Na(I)	–	N.d.	100–120
U(VI)	–	0.08–0.55	–	Sum of REEs	0.15	0.015–0.020	0.13–0.14
V(IV) + V(V)	–	0.5–0.6	N.d.**	Free acid	HCl	H_2SO_4	HCl
Fe(II) + Fe(III)	0.4–0.6	0.5–11.0*	45–47		10–13	80–140	70–80

* Depending on the leaching conditions.

** Not determined.

Table 2. Characteristics of the investigated ion-exchange resins in the H form [determined according to GOST (State Standard) 1-8.98.1–74] [(TEC) total exchange capacity of an ion exchanger, determined using 0.1 N NaOH (mg-equiv g^{-1})]

Ion exchanger	Functionality of ion exchanger	TEC, mg-equiv g^{-1}	Grain size, mm
PA-1	$-CH_2NH(CH_2)_2NHCH_2PO(OH)_2$	3.6	0.5–1.0
KRF-20t-60*	$-PO(OH)_2$	6.5	0.5–1.0
AFI-22	$-N(CH_2CH_2OP(=N)OH)_2$	6.5	0.63–1.0

* $pK_1 = 3.5$; $pK_2 = 9.5$.

were converted into the H form, and the ampholytes, into the H and chloride forms (solution nos. 1 and 3) or H and sulfate forms (solution no. 2).

Static sorption was carried out at a fixed $V : m$, where V is the solution volume and m, resin weight. The system was equilibrated to constant concentration of Sc(III) in the solution.

The kinetics of Sc(III) sorption was studied at a fixed $V : m$ using the solution volume limitation method. The experimental error caused by a decrease in the solution volume due to sampling was within 2%.

The equilibrium sorption isotherms were obtained by varying $V : m$.

The Sc(III), Zr(IV), V(IV + V), and Y(III) concentrations in the solution were determined by ICP. The lower limit of determination was 10^{-5}%, and the error of determination was within 20%.

The Fe(III) and free acid concentrations were determined volumetrically. U(VI), Ti(IV), and Al(III) were determined photometrically with Arsenazo III, hydrogen peroxide, and aurintricarboxylic acid, respectively [6], on a KFK-3 instrument. Na, K, Ca, and Mg were determined by atomic absorption. The sum of REEs in the solution was determined as follows. The sesquioxides obtained by ammonia precipitation were dissolved in 4–5 N HCl, and Sc(III) was separated by extraction with 0.16 M di-(2-ethylhexyl) hydrogen phosphate in a hydrocarbon solvent. Finally, REEs were determined photometrically with Arsenazo III.

The recovery of Sc(III) from solution no. 1 was monitored using the ^{46}Sc, ^{59}Fe, ^{95}Zr, and ^{91}Y tracers. The activity was measured on an IN-96 γ-ray radiometer to within 1%. The sensitivity of the method was 10^{-6}%.

In addition to the high salinity, among specific features of the investigated solutions is a high concentration of multicharged cations such as Zr(IV), Ti(IV), V(V), and U(VI), which considerably exceeded that of Sc(III). Previously we demonstrated that, in sorption recovery of Sc(III) from these solutions, the best performance was shown by KRF-20t-60 cation exchanger and PA-1 polyampholyte [7–9]. In this study, to optimize the sorption parameters, for

the indicated ion exchangers we examined the static sorption, sorption kinetics, and desorption of Sc(III).

The sorption kinetics on the phosphorus-containing ion exchangers was studied with an example of a hydrochloric acid solution of scandium trichloride and also with solution nos. 1–3.

To find the rate-determining stage, we examined the sorption kinetics of Sc(III) from the hydrochloric acid solution of $ScCl_3$ (c_{Sc} = 3.2 mg l^{-1}; c_{HCl} = 10 g l^{-1}) on KRF-20t-60 (mean radius of a swollen grain 0.12 cm). The results showed (Fig. 1) that the equilibrium was attained only in ca. 6 h, i.e., the sorption rate is low.

The kinetic data were processed using the Boyd–Adamson–Myers equation for the diffusion from the limited volume of the solution [10]:

$$F = 1 - \frac{6}{\pi^2} \Sigma \frac{1}{n} \exp(-Btn^2), \quad (1)$$

where F is the degree of sorption defined as the ratio of the current sorption to the limiting sorption; $Bt = (Dp^2t)/r_0^2$; r_0, mean radius of the swollen grain of the ion exchanger (0.12 cm); D, diffusion coefficient of the ion in the grain of the resin ($cm^2\ s^{-1}$); and t, sorption time (s).

For each F we estimated B by dividing the known Bt values by the sorption time, and then, from B we estimated the Sc(III) diffusion coefficient in the resin grain. The effective diffusion coefficient of Sc(III) was calculated to be 1.38×10^{-7} $cm^2\ s^{-1}$. From D and r_0 we estimated Bt for a fixed t, and then, the degree of sorption F (Fig. 1, curve *1*).

The experimental data were analyzed in terms of the film kinetic model using Eq. (2).

$$F = 1 - \exp(-Kt), \quad (2)$$

where $K = 3D/(\delta r_0 \alpha)$, D is the diffusion coefficient of an ion in the solution, $cm^2\ s^{-1}$; δ, thickness of the diffusion layer, which was taken equal to 10^5 molecular layers, i.e., to 0.001 cm; r_0, mean radius of the swollen grain of the resin (0.12 cm); and α, distribution coefficient, ml g^{-1}. From the distribution coefficients, we computed F (Fig. 1, curve *2*).

As seen from Fig. 1, the experimental points are between the curves obtained by Eqs. (1) and (2), suggesting commensurable contributions of both external and internal diffusion mechanisms to the sorption kinetics.

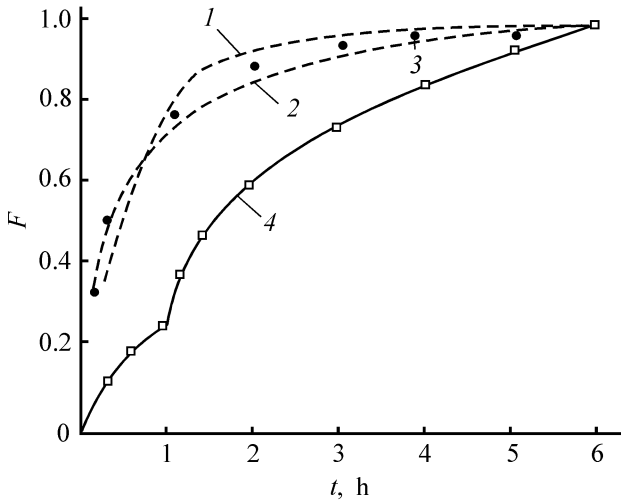


Fig. 1. Kinetic curves of Sc(III) sorption from the $ScCl_3$ solution (c_{Sc} = 3.2 mg l^{-1}; c_{HCl} = 10 g l^{-1}; $V:m$ = 100 ml g^{-1}) on KRF-20t-60: (*1*) calculation by Eq. (1), (*2*) calculation by Eq. (2), (*3*) experimental points, and (*4*) experiment with interrupted (for 30 min) contact of the phases. (F) Degree of sorption and (t) time.

In the experiment with interrupted phase contact, we can found a distinctly pronounced "diffusion memory" effect (Fig. 1, curve *4*): the sorption rate 1 h after interruption of the process for 30 min considerably increases again. It was demonstrated in studying the effect of stirring rate that, with increasing Reynolds number from 50 to 130, the process rate increased by a factor of 2.5 in 30 min, which gives an additional evidence in favor of the above conclusion.

Thus, to increase the Sc sorption rate on the selected cation exchanger, it is advisable to use fine fractions of the resin and to apply rigorous stirring.

A considerable increase in the process rate in the same system was obtained by using the sorbent prepared by inclusion of fine (112 μm and smaller) particles of the resin into a polyacrylonitrile matrix. The fibrous sorbents were synthesized at the Research Institute of Chemicals and Ultrapure Substances (Moscow) and Khimvolokno Research and Production Association (Tver) [11]. Kinetic data obtained with the fibrous sorbents showed that it takes only 20 min to establish the equilibrium in the same system, and that crushing of the resin to a grain size less than 52 μm had no effect on the process rate [12].

In recovery of Sc(III) from multicomponent solutions with the phosphorus-containing ion exchangers, the equilibrium was established in several days. However, the degree of sorption in 6 h was about 90% of the limiting value (Fig. 2), which makes it possible

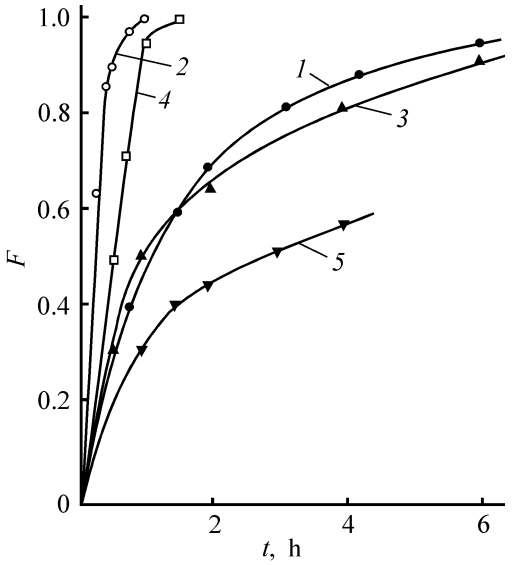


Fig. 2. Kinetic curves of Sc(III) sorption from (*1*, *2*, *5*) solution no. 1 ($V : m$ = 100 ml g^{-1}) and (*3*, *4*) solution no. 3 ($V : m$ = 20 ml g^{-1}) on (*1*, *3*, *5*) granulated PA-1 and (*2*, *4*) fibrous PA-1. Temperature (°C): (*1*–*4*) 22 and (*5*) 60. (*F*) Degree of sorption and (*t*) time.

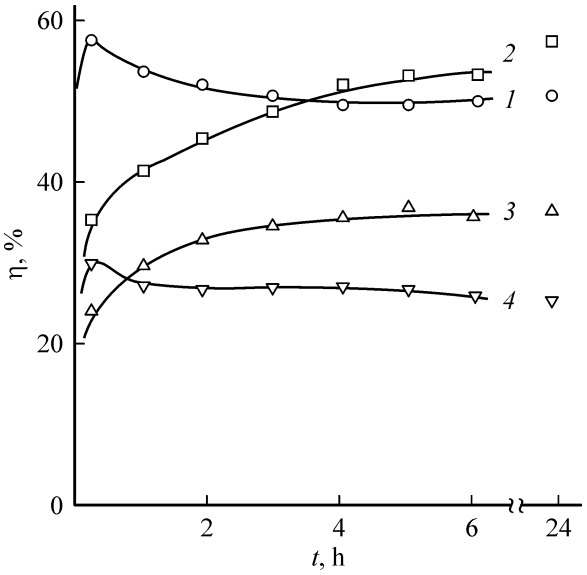


Fig. 3. Kinetic curves of sorption of the cations from solution no. 2 on AFI-22 ($V : m$ = 20 ml g^{-1}): (*1*) Sc(III), (*2*) Fe(III). (*3*) Ti(IV), and (*4*) Zr(IV). (η) Degree of sorption and (*t*) time.

to recommend these ion exchangers for practical application. With the fibrous sorbents, the equilibrium was established in 1–1.5 h (Fig. 2).

The kinetic data on the sorption of Sc(III) and concomitant elements from solution no. 3 with AFI-22 nitrogen–phosphorus-containing ion exchanger demonstrate that the degree of Sc sorption passes through a maximum at t = 20 min and then decreases (Fig. 3). The same trend was observed for Fe(III), while for Ti(IV) and Zr(IV), reversely, the degree of sorption increases on approaching the equilibrium (Fig. 3). These results suggest that, in multicomponent systems, ions penetrating to the resin grain are involved in multiple sorption–desorption equilibria, which are established in correspondence with the selectivity coefficients, thus decelerating the net process. Therefore, to recover Sc(III) efficiently, the sorption time should be limited to 20 min, since, at this time, the degree of sorption is maximal for Sc and minimal for hardly separable Ti(IV) and Zr(IV).

With increasing concentration of the multicharged interfering cations such as Fe(III) and, particularly, Zr(IV), the capacity of the phosphorus-containing ion exchangers for Sc(III) considerably decreased (Table 3).

We used the higher affinity of the phosphorus-containing ion exchangers for Zr(IV), as compared to Sc(III), for treatment of the hydrochloric acid solution of scandium trichloride to remove Zr(IV) by sorption on KRF-20t-60 in the H^+ and Sc^{3+} forms in the static and dynamic modes. The decontamination factor was about 50 [13].

The selectivity of this class of ion exchangers with respect to Sc(III) noticeably decreases in the case of sorption from multicomponent solutions at elevated temperature. For example, in sorption of Sc(III) from solution no. 1 at 60°C, the capacity of KRF-20t-60 for Zr(IV) considerably increased, and that for Sc(III) decreased as well as the sorption rate of Sc(III) (Fig. 2).

Table 3. Capacity E of KRF-20t-60 resin for Sc(III) in sorption from solution no. 1 ($V : m$ = 100 ml g^{-1}) at various Fe(III) and Zr(IV) concentrations in solution

[Fe(III)]	[Zr(IV)	E, mg l^{-1}
g l^{-1}		
0.5	0.05	512
2.0	0.05	484
4.1	0.05	400
8.1	0.05	282
8.4	0.05	284
0.5	0.1	545
0.5	0.6	374
0.5	0.9	280
0.5	1.0	21

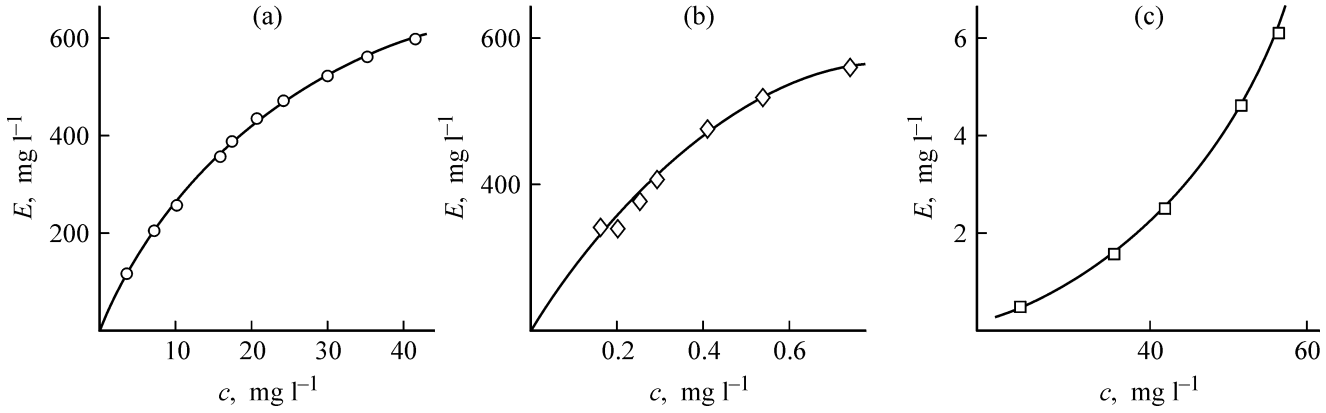


Fig. 4. Isotherms of Sc(III) sorption from solution nos. (a) 2, (b) 1, and (c) 3 on PA-1. (E) Capacity of the ion exchanger for Sc(III) and (c) equilibrium concentration of Sc(III) in solution.

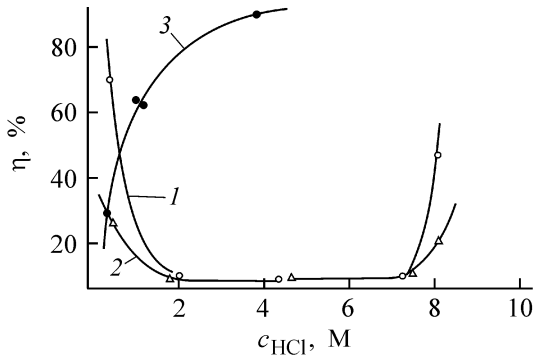


Fig. 5. Sorption of Y(III) on (*1*) KRF-20t-60, (*2*) PA-1, and (*3*) AFI-22 vs. the HCl concentration (c_{Sc} = 10 mg l^{-1}, c_Y = 14 mg l^{-1}; $V : m$ = 20 ml g^{-1}). (η) Degree of sorption and (c_{HCl}) HCl concentration in solution.

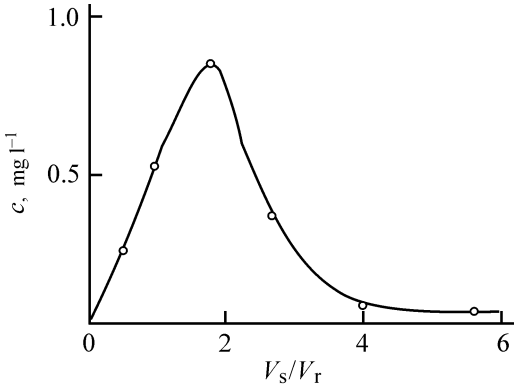


Fig. 6. Desorption of Sc(III) from KRF-20t-60 vs. the NH_4F specific volume. (c) Sc(III) concentration in solution of NH_4F and (V_s/V_r) solution to resin volume ratio.

The isotherms of Sc(III) sorption from solution nos. 1–3 on PA-1 polyampholyte are shown in Fig. 4. In the cases of solution nos. 1 and 2, the isotherms are convex, and the working exchange capacity of the ion exchanger for Sc(III) is about 600 mg l^{-1}. The necessary number of sorption steps, estimated by the method described in [9], is 2 and 4 for solution nos. 1 and 2, respectively. The Sc(III) sorption isotherm from solution no. 3 is concave, and the necessary number of sorption steps is 7–8. In this case, to obtain acceptable sorption parameters, it is necessary to correct the solution composition by, e.g., dilution.

One more specific feature of the phosphorus-containing ion exchangers (KRF-20t-60 and PA-1) is that the Y(III) and Ln(III) distribution coefficients are, generally, low. In this case, separation of, e.g., Y(III), can be realized over wide pH range (Fig. 5). Therefore, sorption concentration of Sc(III) on such ion exchangers considerably facilitates further processing of the resulting concentrates. On the contrary, AFI-22 demonstrates high affinity for Y(III).

It is known that sodium, potassium, and ammonium carbonates effectively desorb Sc(III) from phosphorus-containing ion exchangers [4]. However, it should be pointed out that it is inadvisable to use acidic and alkaline solutions in the same sorption cycle, since changing an acidic solution for alkaline one and back results in considerable osmotic stress, thus reducing the useful life of the resin. Furthermore, acidification produces CO_2, and the resin remains "fluidized" even after thorough washing with water to remove the acid prior to desorption, thus making the process design more complicated. Thus, a satisfactory result was obtained by the author only using additional treatment of the resin with a dilute ammonia solution before carbonate desorption of Sc(III).

It appeared advisable to use ammonium fluoride or bifluoride for Sc(III) desorption. The Sc(III) elution curve from KRF-20t-60 (after sorption from solution no. 2) with 4% NH_4F is shown in Fig. 6. The desorption efficiency was 92% at V_s/V_r = 4. The use of higher concentration of NH_4F resulted in precipita-

tion. At elevated temperature, no maximum was observed in the elution curve.

Scandium(III) can be separated from the eluate as a poorly soluble salt, e.g., Na_3ScF_6, and the NH_4F solution can be recycled after correction.

CONCLUSIONS

(1) Kinetics of Sc(III) sorption from the solution of $ScCl_3$ in HCl on KRF-20t-60 cation exchanger is controlled by the gel and film diffusion mechanisms. The Sc(III) effective diffusion coefficient in the resin grain is 1.38×10^{-7} $cm^2\ s^{-1}$.

(2) The static and dynamic sorption of Sc(III) from process solutions from production of zirconium basic sulfate [solution after filtration of zirconium basic sulfate (solution no. 1), solution after sulfuric acid pressure leaching of silicate–carbonate ore (solution no. 2), and hydrochloric acid spent salt filter solution from production of titanium tetrachloride (solution no. 3)] on KRF-20t-60 cation exchanger and PA-1 polyampholyte resin are studied. The working exchange capacity for Sc(III) of the indicated sorbents is about 600 $mg\ l^{-1}$ for solution nos. 1 and 2 and about 5 $g\ l^{-1}$ for solution no. 3. The sorption rate can be considerably increased by using polyacrylonitrile-supported fibrous sorbents.

(3) In sorption from a multicomponent salt solution on AFI-22 resin, the maximal capacity for Sc(III) was obtained far from the equilibrium. The capacity of the phosphorus-containing ion exchangers decreases with increasing temperature and concentration of multicharged cations in the solution.

(4) It was suggested to use 4% ammonium fluoride for desorption of Sc(III) from the phosphorus-containing ion exchangers.

REFERENCES

1. Kazantsev, E.A., Kazantsev, E.I., Bezvoritnyi, V.A., et al., *Zh. Prikl. Khim.*, 1975, vol. 48, no. 8, pp. 1670–1673.
2. Smirnov, D.I., Molchanova, T.V., and Vodolazov, L.I., *Tsvetn. Met.*, 1995, no. 10, pp. 44–46.
3. Granovskii, Yu.V., Komissarova, L.N., Krivenko, S.V., et al., *Zh. Prikl. Khim.*, 1974, vol. 47, no. 10, pp. 2261–2265.
4. Komissarova, L.N., *Neorganicheskaya khimiya skandiya* (Inorganic Chemistry of Scandium), Moscow: URSS, 2001.
5. Polyanskii, N.G., Gorbunov, G.N., and Polyanskaya, N.P., *Metody issledovaniya ionitov* (Methods for Studying Ion Exchangers), Moscow: Khimiya, 1976.
6. Korostelev, P.P., *Fotometricheskii i kompleksometricheskii analiz v metallurgii* (Photometric and Chelatometric Analyses in Metallurgy), Moscow: Metallurgiya, 1984.
7. Sokolova, Yu.V. and Koryakov, V.B., in Abstracts of Papers, *Pervyi Mezhdunarodnyi simpozium "Problemy kompleksnoi pererabotki rud"* (1st Int. Symp. "Problems of Integrated Ore Processing"), St. Petersburg, 1994, p. 258.
8. Sokolova, Yu.V., Abstracts of Papers, *Mezhdunarodnaya nauchno-prakticheskaya konferentsiya "Skandii i perspektivy ego ispol'zovaniaya"* (Int. Scientific and Practical Conf. "Scandium and Prospects for Its Application"), Moscow, 1994, p. 11.
9. Sokolova, Yu.V. and Koryakov, V.B., *Izv. Vyssh. Uchebn. Zaved., Tsvetn. Metall.*, 2004, no. 5, pp. 14–18.
10. Vol'dman, G.M., *Osnovy ekstraktsionnykh i ionoobmennykh protsessov gidrometallurgii* (Principles of Extraction and Ion-Exchange Processes for Hydrometallurgy), Moscow: Metallurgiya, 1982.
11. Mezhirov, M.S. and Chegolya, A.S., *Preprint of III Int. Symp. on Man-Made Fibers*, Kalinin (Russia), 1981, vol. 5, pp. 13–19.
12. Sokolova, Yu.V., Kurdyumov, G.M., Smirnov, A.V., and Mezhirov, M.S., *Zh. Prikl. Khim.*, 1991, vol. 64, no. 8, pp. 1766–1768.
13. Sokolova, Yu.V., *Zh. Prikl. Khim.*, 2001, vol. 74, no. 3, pp. 406–408.

ISSN 1070-4272, Russian Journal of Applied Chemistry, 2006, Vol. 79, No. 4, pp. 579–583. © Pleiades Publishing, Inc., 2006.
Original Russian Text © A. G. Kasikov, L. V. D'yakova, E. G. Bagrova, 2006, published in Zhurnal Prikladnoi Khimii, 2006, Vol. 79, No. 4, pp. 589–592.

SORPTION AND ION-EXCHANGE PROCESSES

Effect of the Nature and Concentration of Salting-out Agents on the Extraction of Cobalt(II) from Chloride Solutions with Trialkylamine

A. G. Kasikov, L. V. D'yakova, and E. G. Bagrova

Tananaev Institute of Chemistry and Technology of Rare Elements and Mineral Resources, Kola Scientific Center, Russian Academy of Sciences, Apatity, Murmansk oblast, Russia

Received January 18, 2006

Abstract—The effect of chlorides of Ca^{2+}, Ni^{2+}, Mg^{2+}, Al^{3+}, Li^{+}, Fe^{2+}, Cr^{3+}, Na^{+}, NH_4^{+}, La^{3+}, Nd^{3+} on the extraction recovery of cobalt from chloride solutions with mixtures based on trialkylamine was studied. The series of the salting-out activity of differently charged cations and the degree of their coextraction were determined.

DOI: 10.1134/S1070427206040148

Salts of various metals can strongly affect the extraction recovery of a target component from multicomponent solutions. This influence is primarily manifested in that well-extractable elements hinder the extraction of the target component. Occasionally, background salt components are not extracted themselves, but substantially affect the recovery of other elements. This influence is due to the fact that, depending on the nature and concentration of a salting-out agent, not only the activity of water changes, but also that of all other components of a solution. In this case, the distribution coefficients of an element may either increase (salting-out) or decrease (salting-in) [1].

Published data on extraction of cobalt(II) with tertiary amines in the presence of various salting-out agents are scarce [2–6]. There is no way of comparing the available published data for the salting-out agents used, because the extraction conditions and the compositions of the extraction mixtures were different. Moreover, there are no published data on extraction of metal chloro complexes in the presence of such elements as Cr(III) and lanthanides, which may be contained in secondary cobalt raw materials and can pass into solution in its hydrochloride processing. In this context, the influence exerted by the nature and concentration of a large number of metal chlorides on the extraction of cobalt(II) with organic mixtures based on tertiary amines was examined in this study.

EXPERIMENTAL

A 35 vol % solution of trialkylamine of the C_7–C_8 fraction (TAA) in an inert diluent (Escaid-100) with addition of 20 vol % modifying agent was used as an extracting agent. An alcohol (octanol) served as the modifying agent. It was introduced in order to preclude formation of a third phase, which could occur because of the low solubility of the amine salt in the inert diluent. Prior to extraction, TAA was converted to a chloride form by bringing it in contact with 4 M HCl at a 1 : 1 ratio of the organic and aqueous phases. The excess amount of the acid was removed by washing with water.

The salt background was created with metal chlorides of chemically pure and analytically pure grades. Weighed portions of these salts (taken with an accuracy of ±1 mg) were dissolved in distilled water to obtain the necessary concentration of cobalt ions and chloride anions.

The extraction and backwashing were performed in separation funnels with a mechanical shaker, with a single contact for 5 min at 20 ± 1°C.

The aqueous phases were analyzed for the content of cobalt and nonferrous elements by atomic-absorption spectrometry. The concentration of cobalt in the organic phase was found as the difference between its contents in the starting solution and in raffinates

Table 1. Effect of the nature of a salting-out agent on the recovery of cobalt(II) at o : a = 3 : 1 (initial concentration of Co^{2+} 6.5 g l^{-1})

Salting-out agent	Content of the chloride ion, M			
	6		8	
	D_{Co}	E, %	D_{Co}	E, %
LiCl	41.6	97.6	280.0	99.6
HCl	0.45	31.0	1.87	66.2
NaCl	0.45	31.0	1.84	64.8
NH_4Cl	0.40	28.4	1.34	57.2
$MgCl_2$	10.0	90.0	13.7	93.2
$CaCl_2$	6.3	86.3	10.1	90.9
$NiCl_2$	2.0	66.8	4.2	81.0
$FeCl_2$	0.48	32.4	1.90	66.4
$AlCl_3$	10.1	90.9	16.8	94.4
$CrCl_3$	2.0	66.8	4.1	80.3
$NdCl_3$	0.60	37.2	3.6	78.2
$LaCl_3$	0.52	34.2	3.6	78.2

or by analysis of solutions obtained after exhaustive backwashing of cobalt. The results obtained in studying the influence exerted by the nature of the salting-out agent on the distribution coefficient D_{Co} and degree E (%) of cobalt(II) recovery are listed in Table 1.

As can be seen in Table 1, an increase in the concentration of any of the salting-out agents makes higher the distribution coefficients of cobalt(II). The recovery of cobalt depends to an even greater extent on the nature of a salting-out agent. For example, the distribution coefficient of Co(II) in the presence of 8 M LiCl exceeds by a factor of more than 200 that in the presence of 8 M NH_4Cl. This large difference in the salting-out activity is in good agreement with the difference of the radii of the Li^+ and NH_4^+ cations.

Averaged radii of the cations of the salting-out agents used

Cation	Al^{3+}	Cr^{3+}	Li^+	Ni^{2+}	Fe^{2+}
Radius, Å	0.55	0.60	0.72	0.74	0.78

Cation	Mg^{2+}	Na^+	Ca^{2+}	Nd^{3+}	La^{3+}	NH_4^+
Radius, Å	0.69	0.96	1.02	1.04	1.14	1.51

It follows from the data presented that the ammonium cation has the largest radius among all the salting-out agents studied, whereas the Li^+ cation has an approximately 2.2 times smaller radius.

The effect of the cation radius and charge on the salting-out capacity is due to the fact that different cations bind in their hydrate shell different amounts of water, and, as a result, the fraction of water that can solvate the metal compound being extracted widely varies [8].

The salting-out action of the cations can be characterized as follows: the lower the degree of hydration of a salting-out agent, the higher the active concentration of the solute.

Thus, hydration of ions of the salting-out agent will lead to a decrease in the amount of free water and to an increase in the activity of $CoCl_2$. In other words, a decrease in the free concentration of water leads to an increase in the concentration of chloride ions, which favors formation of the anionic complex $CoCl_4^{2-}$.

Comparison of the salting-out capacities of the cations, judged from how their radii vary at the same charge, gives the following series: $Al^{3+} > Cr^{3+} > Nd^{3+} > La^{3+}$; $Mg^{2+} > Ni^{2+} > Fe^{2+} > Ca^{2+}$; $Li^+ > Na^+ > NH_4^+$.

Comparison of experimental data on the variation of the distribution coefficients of cobalt(II) with the nature of a salting-out agent gives similar dependences for single- and triple-charged cations. However, it should be noted that, despite that Cr^{3+} has a radius close to that of Al^{3+}, chromium(III) chloride is a considerably weaker salting-out agent. For double-charged cations, the experimental series does not coincide at all with the order in which the radii vary, because the degree of Co(II) recovery in the presence of $CaCl_2$ substantially exceeds that in the presence of $FeCl_2$.

The observed inconsistency of the experimental data can be attributed to the fact that, in addition to interaction with water, cations of the salting-out agents can also interact with Cl^- ions [9]. In particular, Cr^{3+} interacts with chloride ions to give chloro complexes by the scheme

$$[Cr(H_2O)]Cl_3 \rightleftarrows [Cr(H_2O)_5Cl]Cl_2 \rightleftarrows [Cr(H_2O)_4Cl_2]Cl.$$

This, first, leads to a decrease in the charge of a cation and, second, makes lower the concentration of free Cl^- ions.

Iron(II) can also form complexes with chloride ions to give neutral octahedral complexes of the composition $Fe(H_2O)_4Cl_2$. Alkali and alkaline-earth elements and NH_4^+ form no inner-sphere complexes with Cl^- and, therefore, their influence on the distribution coefficient of Co(II) is only manifested via the varying degree of hydration of a cation.

Table 2. Parameters of coextraction of some salting-out metals with TAA solutions in an inert diluent and in TBP ($c_{Co_{in}}$ = 0.1 M) from solutions containing 8 M of Cl^-

Salting-out metal	Content of metals				Distribution coefficient		Co/M separation coefficient β
	initial solution		extract		$D_M \times 10^{-2}$	D_{Co}	
	g l^{-1}	M	g l^{-1}	M			
Inert diluent							
Ca(II)	160.3	4.0	0.52	0.013	0.33	10.1	3107
Ni(II)	230.6	4.0	0.15	0.003	0.065	4.2	6461
Mg(II)	97.2	4.0	0.50	0.020	0.51	13.7	2686
Al(III)	69.3	2.7	0.36	0.014	0.53	16.8	3170
Li(I)	55.5	8.0	0.22	0.030	0.40	280	70000
Fe(II)	223.4	4.0	2.00	0.036	0.09	1.9	211
Cr(III)	138.7	2.7	1.24	0.020	0.89	4.5	506
Tributyl phosphate							
Ca(II)	160.3	4.0	1.28	0.032	0.81	12.7	1567
Ni(II)	230.6	4.0	0.96	0.017	0.42	12.2	2904
Mg(II)	97.2	4.0	0.62	0.025	0.64	12.4	1938
Al(III)	69.3	2.7	0.47	0.018	0.66	26.9	4076
Li(I)	55.5	8.0	0.34	0.049	0.62	333.8	53839
Fe(II)	223.4	4.0	2.60	0.040	1.13	2.2	195

Comparison of the salting-out capacities of all the chlorides studied gives the following series: $LiCl > AlCl_3 > MgCl_2 > CaCl_2 > NiCl_2 > CrCl_3 > LaCl_3 \geq NdCl_3 \gg FeCl_2 \geq NaCl > NH_4Cl$.

Despite that H^+ is also strongly hydrated in aqueous solutions, the degree of Co(II) recovery from HCl is considerably lower than that from most of salt solutions. This is due to the fact that chlorides of tertiary amines can provide an additional extraction of hydrochloric acid [10], and the acid suppresses the extraction of $CoCl_4^{2-}$.

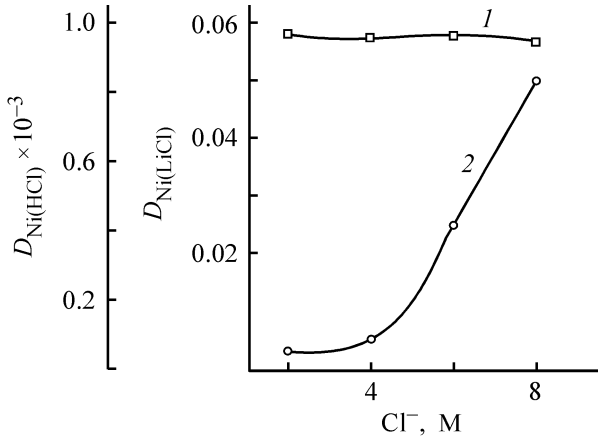
Thus, it follows from the series obtained that the extraction of Co(II) in the presence of most of salting-out metals proceeds better than that in the presence of HCl. The distribution coefficients are particularly high in the case of Co(II) extraction from LiCl and $AlCl_3$ solutions. A rather high degree of Co(II) recovery is achieved from 8 M Cl^- as salts of solutions containing Cr^{3+}, Ni^{2+}, and Nd^{3+}, which accompany cobalt in processing of secondary raw materials.

Commonly, the transfer of the salting-out metals used to the organic phase is neglected because of their exceedingly low extraction coefficients. However, very large amounts of a metal are to be introduced into a solution to create a 8 M chloride background. Therefore, it would be expected that noticeable amounts of metals pass into the organic phase even in the case of their insignificant coextraction. To determine the degree of coextraction of macrocomponents and the separation coefficients of Co and a salting-out metal, additional studies were performed.

As extracting agents were used 35 vol % solutions of TAA in an inert diluent (1) and tributyl phosphate (TBP) (2) [11]. The choice of the second mixture was due to the fact that TBP is also recommended as a modifier for tertiary amines, with this compound promoting, in contrast to alcohols, the recovery of cobalt (Table 2).

Table 2 shows that the degree of recovery of salting-out metals is indeed insignificant, because, for the most part, the distribution coefficient does not exceed 0.01. Accordingly, this circumstance provides a very high Co/M separation coefficient β; in particular, for Co/Li it is 70000 and 53389 for mixtures (1) and (2), respectively.

The separation coefficients for other salting-out metals are lower and decrease in the following order:



Distributions coefficients of nickel, D_{Ni}, vs. the concentration of chloride ion Cl^- in solutions of (*1*) HCl and (*2*) LiCl.

$Li^+ > Ni^{2+} > Al^{3+} > Ca^{2+} > Mg^{2+} > Cr^{3+} > Fe^{2+}$ for mixture (1) and $Li^+ > Al^{3+} > Ni^{2+} > Mg^{2+} > Ca^{2+} > Fe^{2+}$ for mixture (2).

Both the series were obtained by comparing the amounts of extracted elements (g l^{-1}). If all the salting-out elements are compared in their content in the extracts (M), the following series can be written: $Ni^{2+} < Ca^{2+} < Al^{3+} < Cr^{3+} < Ni^{2+} < Fe^{2+}$ for mixture (1) and $Ni^{2+} < Al^{3+} < Mg^{2+} < Ca^{2+} < Fe^{2+} < Li^+$ for mixture (2).

It can be seen that these series markedly differ from the sequences of variation of the separation coefficients. This is primarily due to a changed, because of the very low molecular weight, position in these series of the strongest salting-out agent, lithium.

To prevent contamination of cobalt extracts with impurities in processing of multicomponent solutions, the nature of the salting-out agent introduced into the system should be taken into account. For example, it is known that LiCl can markedly enhance the extraction of not only Co(II), but of many other elements as well [12].

To evaluate the extent of this influence on nickel(II), which commonly accompanies cobalt in processing of various kinds of raw materials [13, 14], the effect of a change in the concentration of LiCl and HCl on the distribution coefficient of Ni(II) was studied. It was found that an increase in the concentration of HCl has virtually no effect on D_{Ni}, whereas raising the concentration of LiCl results in that the distribution coefficient of nickel(II) grows to reach a value of 0.052, which is nearly two orders of magnitude higher than that in extraction from $NiCl_2$ solutions (see figure). Thus, it is necessary to take into account the influence exerted by a salting-out agent not only on the recovery of the target component, but on the coextraction of impurities as well.

CONCLUSIONS

(1) The series of the salting-out capacity of differently charged cations in extraction of Co(II) from chloride solutions with trialkylamine hydrochloride were experimentally obtained: $Li^+ > Al^{3+} > Mg^{2+} > Ca^{2+} > Ni^{2+} > Nd^{3+} > H^+ > La^{3+} > Cr^{3+} > Fe^{2+} > Co^{2+} > Na^+ > NH_4^+$.

(2) The separation coefficients of cobalt and salting-out agents were determined in extraction with mixtures based on trialkylamine with addition of various modifiers.

(3) It is recommended to use $NiCl_2$ as a salting-out agent in processing of nickel-containing cobalt solutions. Even though this compound has a comparatively low salting-out capacity, it does not lead to noticeable coextraction of other elements and does not require introduction of additional reagents into process solutions.

REFERENCES

1. Zolotov, Yu.A. and Golovanov, V.I., *Vzaimnoe vliyanie elementov pri ikh ekstraktsii iz khloridnykh rastvorov* (Mutual Influence of Elements in Their Extraction from Chloride Solutions), Moscow: GEOKhI, 1971.
2. Mezhov, E.A., *Ekstraktsiya aminami i chetvertichnymi ammonievymi osnovaniyami: Spravochnik* (Extraction with Amines and Quaternary Ammonium Bases: Reference Book), Moscow: Energoatomizdat, 1999.
3. Navtanovich, M.L. and Lutova, L.S., *Issledovaniya v oblasti tekhnologii proizvodstva nikelya i kobal'ta* (Studies in Manufacture Technology of Nickel and Cobalt), Leningrad: Gipronikel', 1986.
4. USSR Inventor's Certificate, no. 884324.
5. USSR Inventor's Certificate, no. 1627577.
6. D'yakova, L.V., Rtveladze, V.V., and Kosyakov, A.I., *Gidrometallurgiya i khimiya redkikh elementov* (Hydrometallurgy and Chemistry of Rare Elements), Apatity: Kol'sk. Nauchn. Tsentr Akad. Nauk SSSR, 1991, pp. 50–52.
7. Lur'e, Yu.Yu., *Spravochnik po analiticheskoi khimii* (Handbook of Analytical Chemistry), Moscow: Khimiya, 1971.
8. Grechishkina, A.Yu., Sokol'skii, V.E., Goncha-

ruk, V.V., et al., *Khim. Tekhnol. Vody*, 2004, vol. 26, no. 2, pp. 147–157.

9. Ripan, R. and Ceteanu, I., *Chemia metalelor*, Bucuresti: Editura Didactica si Pedagogica, 1968, vol. II. Translated under the title *Neorganicheskaya khimiya*, Moscow: Mir, 1972, vol. 2.
10. Shmidt, V.S., *Ekstraktsiya aminami* (Extraction with Amines), Moscow: Atomizdat, 1970.
11. Meretukov, M.A., *Protsessy zhidkostnoi ekstraktsii v tsvetnoi metallurgii* (Liquid Extraction in Nonferrous Metallurgy), Moscow: Metallurgiya, 1985.
12. Zolotov, Yu.A., Ioffe, B.Z., and Chuchalin, L.K., *Ekstraktsiya galogenidnykh kompleksov metallov* (Extraction of Metal Halide Complexes), Moscow: Nauka, 1973.
13. Reznik, I.D., Sobol', S.I., and Khudyakov, V.M., *Kobal't* (Cobalt), Moscow: Mashinostroenie, 1955, vol. 2.
14. Reznik, I.D., Ermakov, G.P., and Shneerson, Ya.M., *Nikel'* (Nickel), Moscow: Nauka i Tekhnologiya, 2003, vol. 3.

ISSN 1070-4272, Russian Journal of Applied Chemistry, 2006, Vol. 79, No. 4, pp. 584–589. © Pleiades Publishing, Inc., 2006.
Original Russian Text © V. N. Pavlyuchenko, N. A. Ushakov, S. A. Novikov, V. F. Danilichev, V. A. Reituzov, S. S. Ivanchev, 2006, published in Zhurnal Prikladnoi Khimii, 2006, Vol. 79, No. 4, pp. 593–598.

SORPTION AND ION-EXCHANGE PROCESSES

Polymer Hydrogels Based on 2-Hydroxyethyl Methacrylate: Modification, Sorption, and Desorption of Aminoglycosides

V. N. Pavlyuchenko, N. A. Ushakov, S. A. Novikov, V. F. Danilichev, V. A. Reituzov, and S. S. Ivanchev

Kirov Military Medicine Academy, St. Petersburg, Russia

St. Petersburg Branch, Boreskov Institute of Catalysis, Siberian Division, Russian Academy of Sciences, St. Petersburg, Russia

Received March 16, 2006

Abstract—Methods of modification of polymer hydrogels based on 2-hydroxyethyl methacrylate with the aim to improve their hydrophilic characteristics are described. The absorption of antibiotics such as aminoglycosides and the kinetics of their liberation from modified hydrogels are studied.

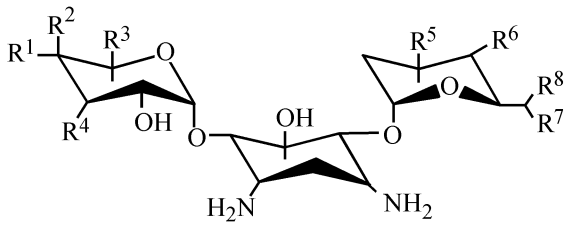
DOI: 10.1134/S107042720604015X

Polymer hydrogels are widely used as drug carriers. Binding of drug with a hydrogel provides not only its immobilization but also its controlled removal in prolonged use. It is important that binding of a drug with a hydrogel in some cases decreases the toxicity of the drug. For example, this was established for Gentamicin bonded with *N*-vinylpyrrolidone copolymer [1]. Soft contact lenses impregnated with drugs and used for treatment of ocular diseases are typical examples of medical hydrogels.

In this study we examined the absorption and liberation of such antibiotics as aminoglycosides with polymer hydrogels based on 2-hydroxyethyl methacrylate and used in production of soft contact lenses.

EXPERIMENTAL

As antibiotics we used aminoglycosides[1] (Kanamycin and Gentamicin) with the following structure:



Aminoglycoside	R^1	R^2	R^3	R^4
Kanamycin	OH	H	OH	NH_2
Gentamicin	CH_3	OH	H	CH_3NH

Aminoglycoside	R^5	R^6	R^7	R^8
Kanamycin	OH	OH	H	H
Gentamicin	H	H	CH_3	NH_2

Aminoglycosides are commercially available in the form of sulfates. We also used them in the base form. The bases were synthesized by passing aqueous solutions of sulfates through a column packed with an anion-exchange resin. This process can be presented by the scheme:

$$\text{Aminoglycoside}\begin{matrix}\diagup\ NH_3\\ \ \ +\\ \diagdown\ NH_3\end{matrix}\ SO_4^{2-}$$

$$\downarrow \text{Anion-exchange resin}$$

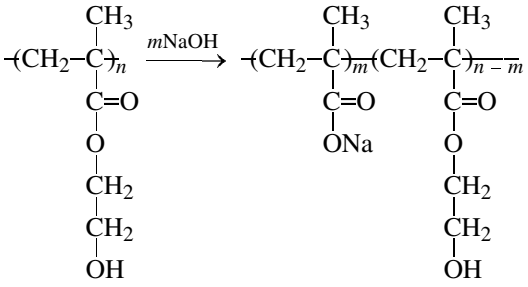
$$\text{Aminoglycoside}\begin{matrix}\diagup\ NH_3OH\\ \ \ +\\ \diagdown\ NH_3\bar{O}H\end{matrix}$$

Hydrogels presenting weakly cross-linked polymers of 2-hydroxyethyl methacryalte were used as soft contact lenses.[2] The equilibrium water content in hydrogels of this type is 38 wt %. To increase the sorption

[1] Aminoglyocsides were purchased from the Sintez Joint-Stock Company (Kurgan, Russian Federation).

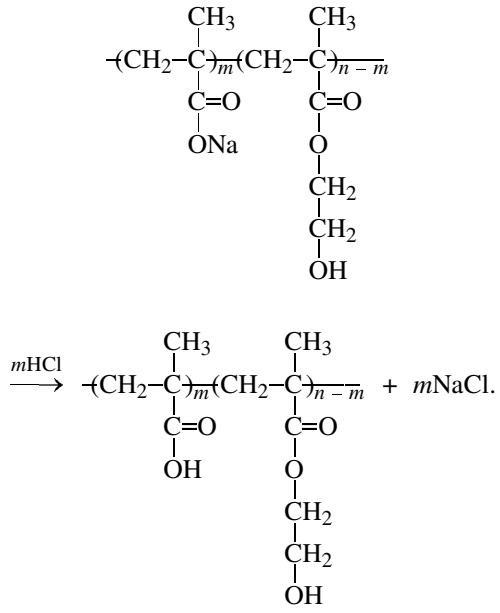
[2] Purchased from the Konkor Company (Vologda, Russian Federation).

activity with respect to aminoglycosides, the water content of hydrogels was increased by their partial conversion into the ionic form by treatment with 2% alkali at 95°C.



+ mHO–CH_2–CH_2–OH.

In some cases, hydrogels in the acidic form were used. For this purpose, after base hydrolysis, the hydrogels were treated with an acid (5% HCl) at room temperature:



After each treatment, the hydrogels were repeatedly washed with distilled water to remove excess reagents (NaOH and HCl) and by-products (ethylene glycol and NaCl).

The degree of hydrolysis of hydrogels was determined by titration. After converting the hydrogels to acid form we added to them 10 ml of 0.1 N NaOH to neutralize carboxy groups and then, 24 h latter, titrated excess NaOH with 0.1 N H_2SO_4. The degree of hydrolysis was estimated by formula (1) as the content of functional groups formed c_{COOH} (mol %) in the dried hydrogel:

$$c_{COOH} = 0.01(V_{NaOH} - V_{H_2SO_4})\,M/W, \qquad (1)$$

where V is the volume of 0.1 N NaOH solution (ml) added to the hydrogel; $V_{H_2SO_4}$, volume of 0.1 N H_2SO_4 solution (ml) spent for titration; M, molecular weight of 2-hydroxyethyl methacrylate (130); and W, weight of dry hydrogel (g).

The content of aminoglycosides sorbed with the hydrogel from concentrated solutions of antibiotics was determined gravimetrically. The hydrogel dried to constant weight was placed into an aminoglycoside solution. After a certain time, the hydrogels were removed from the solution, solution drops were removed from the surface with filter paper, and the hydrogels were dried to constant weight. The content of aminoglycoside (gram per gram of hydrogel) adsorbed with the hydrogel was evaluated by the formula

$$c_A = (m_2 - m_1)/m_1, \qquad (2)$$

where m_1 is the weight of the dry hydrogel and m_2 is the weight of the hydrogel with the absorbed aminoglycoside.

The hydrogels were kept in an antibiotic solution for 4 h. Further increase in time did not result in increasing amount of the antibiotic sorbed with the hydrogel.

Sorption of antibiotics from dilute solutions was studied spectrophotometrically. This procedure was used only for analysis of aminoglycosides in the form of sulfates, since this procedure is based on determination of sulfate ions.

In addition of a certain amount of $BaCl_2$ to an aminoglycoside sulfate solution, Ba^{2+} ions are bound in the form of water-insoluble $BaSO_4$. The consumption of Ba^{2+} ions in this reaction and, hence, the amount of sulfate ions in the solution are determined from the difference between the initial concentration of Ba^{2+} ions and their concentration found in the sample after a definite time. The Ba^{2+} ions were determined in the form of a colored complex with Chlorophosphonazo III [2].

In practice, the determination was performed as follows. The hydrogel containing aminoglycoside (approximately 0.1 g) was placed into 10 ml of saline, 2 ml of a 0.45 g l^{-1} $BaCl_2$ solution was added, and the solution was kept at room temperature for 24 h. Then, 5 ml of a 0.08 g l^{-1} solution of Chlorophosphonazo III in a standard buffer solution (pH 4.01)

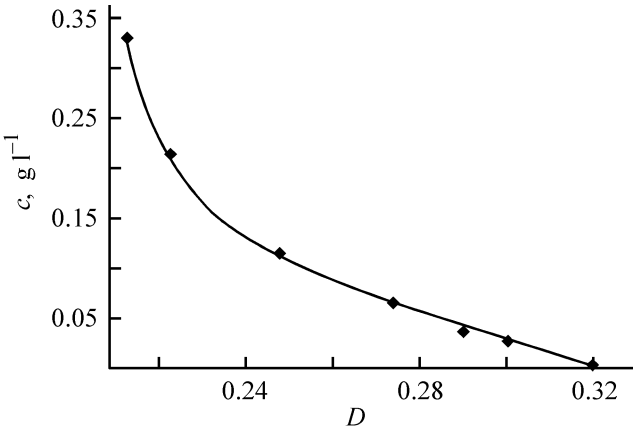


Fig. 1. Calibration plot for photometric determination of Gentamicin sulfate concentration in aqueous solution *c*. (*D*) Optical density.

was added, and the optical density of the solution was measured on a KFK-3 photocolorimeter at a wavelength of 670 nm after preliminary calibration. The calibration plot for Gentamicin sulfate is shown in Fig. 1 as an example.

In analysis of the solutions containing aminoglycoside in the base form, the concentration of aminoglycoside was determined by titration with 0.02 N HCl. Bromphenol blue was used as an indicator. The amount of aminoglycoside in the solution *A* was evaluated by the formula

$$A = V_{HCl} M_A \times 0.02/n, \quad (3)$$

where V_{HCl} is the amount of 0.02 N HCl (ml) spent for titration of the sample; M_A, molecular weight of aminoglycoside; and *n*, amount of amino groups in the aminoglycoside molecule.

Table 1. Physicochemical characteristics of hydrogels based on 2-hydroxyethyl methacrylate depending on the time of hydrolysis in 2% NaOH at 95°C

τ, min	Degree of hydrolysis, mol % of COONa groups	Water content of hydrogel, wt %, in the form		
		–COONa (water)	–COONa (saline)	–COOH (water)
0	0	38	37	38
30		49	40	34
60	1.30	55	41	34
90	2.16	62	43	33
120		70	50	31
180	3.12	78	57	30

In study of the desorption, th hydrogel (approximately 0.3 g) was saturated with the aminoglycoside, placed into 50 ml of saline at 20°C, and the antibiotic content in the solutions was determined at regular intervals. The amount of desorbed aminoglycoside was evaluated from the initial content of aminoglycoside in the hydrogel and the amount of the antibiotic that passed into the solution.

The water content in the hydrogels c_w (%) was determined gravimetrically at 20°C and evaluated by the formula

$$c_w = \frac{W_w - W_d}{W_w} \times 100, \quad (4)$$

where W_w is the weight of the moist hydrogel and W_d is weight of the hydrogel dried at 70°C to constant weight.

The mechanical characteristics of hydrogels were measured at equilibrium swelling on an RTM-1T universal tearing machine (Orientec, Japan).

The characteristics of hydrogels depending on the duration of their treatment with alkaline solution are presented in Table 1. It is seen that the hydrophilic characteristics of the modified hydrogels significantly increase, which is caused by appearance of ionic groups in the polymer structure and effects typical for polyelectrolytes along with osmotic phenomena. In total, this results in the fact that at the maximal degree of hydrolysis the amount of water adsorbed by 1 g of the polymer increases by a factor of approximately 6. It is of interest that such a significant effect is reached at very low degree of hydrolysis. As seen from Table 1, among 100 units of 2-hydroxyethyl methacrylate no more than three units transform into carboxylate anions. With increasing duration of alkaline treatment, the degree of hydrolysis increases; in this case, the water content can reach 90%. However, low mechanical strength (ultimate tensile strength 0.05 MPa) does not allow us to recommend this material for use. Hydrogels with a water content of up to 70% have quite acceptable strength characteristics (2.1 MPa). The characteristics of hydrogels based on ionic polymers essentially depend on the presence of electrolytes in water. For example, in the saline the water content in the hydrogel is significantly lower. This is due to the fact that excess Na^+ ions in the solution suppress dissociation of functional groups –COONa, which, in turn, decreases the hydration of polymer molecules. The effect of decreasing hydration is manifested to a larger extent in conversion of readily ionizable –COONa groups into acidic groups COOH.

In this case, the water content is even lower than that in the initial hydrogel, which is caused by associative interactions of carboxy groups resulting in pseudostructuring accompanied by some compaction of the hydrogel.

Figure 2 shows the dependences of the sorption of aminoglycosides on their concentration in aqueous solution for two hydrogels: ordinary hydrogel with c_w = 38 wt % and hydrogel subjected to alkaline treatment (c_w = 62 wt %). Figure 2 also shows the theoretical dependences plotted assuming that the concentration of the absorbed antibiotic in the aqueous part of the hydrogel is equal to that in the bulk of the solution. To plot the theoretical dependences, the aminoglycoside sorption c_A (gram of antibiotic per gram of dry hydrogel) for each concentration of the solution was evaluated by the formula

$$c_A = \frac{c_w A}{(100 - c_w) \times 100}, \quad (5)$$

where A is the aminoglycoside concentration in the solution (wt %).

It is seen that the experimental dependences practically coincide with the theoretical dependence for ordinary hydrogel. This means that in sorption of aminoglycoside with hydrogel there are no specific interactions of the antibiotic with the hydrogel. A different pattern is observed in sorption of aminoglycosides with hydrogel subjected to alkaline modification. First, c_A values are four times greater than those in sorption of antibiotics with nonmodified hydrogel. Second, the experimental and calculated dependences do not coincide. The increase in c_A is caused not only by increased water content of the modified hydrogels (from 38 to 62%), but also by specific ionic interactions of antibiotics with the partially ionized polymer.

Still higher values of sorption are observed in using aminoglycoside in the base form in comparison with the salt form. The c_A value for Kanamycin is 0.380 g per gram of the hydrogel. In this case, we also used the modified hydrogel with a water content of 62%. This result cannot be explained solely by ionic interactions, since hydroxides of primary and secondary amines (amino groups of both types are present in aminoglycosides) have fairly low ionization constants (of the order of 10^{-4} [3]), i.e., they are ionized to a significantly lesser extent than their salts. It is evident that in this case the specificity of interactions is largely caused by the fact that the major fraction of the glycoside in aqueous solution occurs in the amine rather than hydroxide form. The ability of

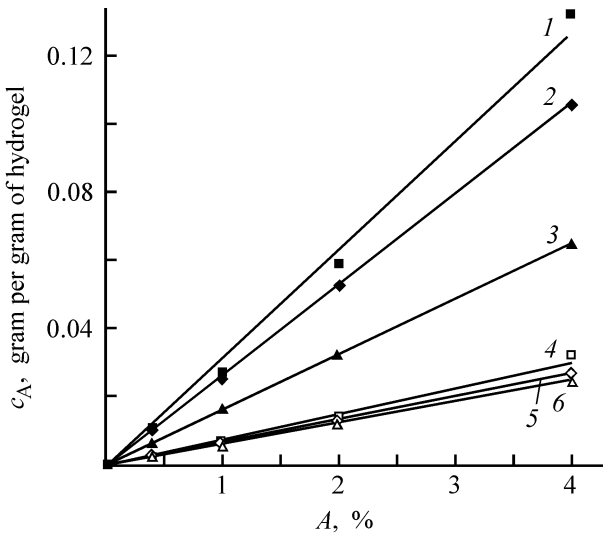


Fig. 2. Sorption c_A of (*2*, *5*) Kanamycin and (*1*, *4*) Gentamicin sulfates with (*1–3*) the initial hydrogel with c_w = 38 wt % and (*4–6*) alkali-modified hydrogel with c_w = 62 wt % vs. the antibiotic concentration in solution *A*. Dependences *3* and *6* were evaluated by Eq. (5).

amines to form hydrogen bonds, among them, with hydroxyl-containing compounds is well known. It is believed that combination of ionic interactions and hydrogen bonding results in high c_A values. A significant contribution of hydrogen bonds to sorption is suggested by the value of sorption of the aminoglycoside in the base form with the nonmodified hydrogel: 0.197 g per gram of hydrogel in sorption of Kanamycin from 4% solution. When the hydrogel after an alkaline treatment is converted into the acid form and the aminoglycoside is used in the base form, c_A reaches 0.52 g per gram of hydrogel. This high value of sorption is caused by the following factors: (1) direct acid–base interaction between carboxy groups of the hydrogel and amino groups of the aminoglycoside, resulting in binding of the aminoglycoside with the hydrogel due to salt formation; (2) formation of hydrogen bonds between hydroxy groups of the polymer and amino groups of the antibiotic; (3) conversion of the hydrogel from the weakly dissociated acidic form into the strongly dissociated state as a result of salt formation, which increases the water absorption of the hydrogel (from 33 to 64%) and the nonspecific sorption of the aminoglycoside.

Data on the sorption of Kanamycin (Table 2) show that successive modification of the hydrogel with alkali and then with acid and conversion of the aminoglycoside into the base form result in an increase in the sorption activity of the hydrogel by a factor of more than 20.

Table 2. Sorption of Kanamycin c_A from 4% aqueous solution with hydrogel based on 2-hydroxyethyl methacrylate (HEMA)

Hydrogel type	c_w, wt %	Kanamycin form	c_A, g per gram of hydrogel
PolyHEMA:			
initial	38	sulfate	0.025
		base	0.197
hydrolyzed with NaOH	62	sulfate	0.105
		base	0.380
after hydrolysis, treated with HCl	33	base	0.52

We used Kanamycin in the base form, since this form allows binding of the largest amount of the antibiotic with the hydrogel. After equilibrium saturation from a 4% solution of Kanamycin, the hydrogel was placed into the saline. We used the hydrogel subjected to alkaline treatment and also hydrogel converted then into acid form. The characteristics of these hydrogels are given in Table 2.

To describe the kinetics of the antibiotic desorption from the hydrogel, we used the relationship

$$c_{At} = kc_{A0}t^n, \quad (6)$$

where c_{At} is the amount of the aminoglycoside that passed from the hydrogel to the solution by the instant of time t (gram per gram of hydrogel); c_{A0}, initial content of aminoglycoside in the hydrogel (gram per gram of hydrogel); t, desorption time; k, constant characterizing the system hydrogel–solvent; and n, index characterizing desorption process.

The dependences were plotted using the log–log form of this relation (Fig. 3).

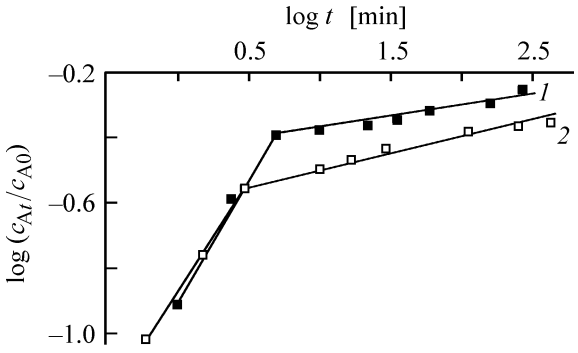


Fig. 3. Kinetic curves of desorption of Kanamycin in the base form from hydrogels into saline at 20°C. (t) Time. Hydrogel: (*1*) subjected to base hydrolysis and (*2*) converted into acid form after base hydrolysis. The characteristics of the hydrogels are presented in Table 2.

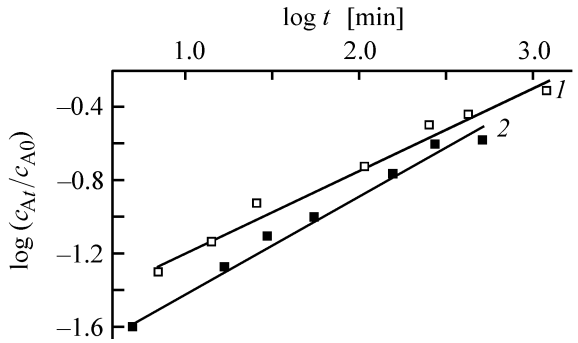


Fig. 4. Kinetic curves for slow stage of Kanamycin desorption from modified hydrogels. Hydrogel: (*1*) in salt form and (*2*) in acid form. c_{A0} (gram per gram of hydrogel): (*1*) 0.228 and (*2*) 0.406.

Figure 3 shows that in both cases the initial stage of the process is characterized by very fast desorption. In this stage, n is high: 0.69 for the hydrogel in the salt form (–COONa) and 0.75 for the hydrogel in the acid form (–COOH). This suggests anomalous character of aminoglycoside transfer into solution, caused not only by ordinary diffusion but also by other phenomena which can be related, e.g., to the difference in c_w of the hydrogels measured in water and in saline (Table 1).

It is known that similar phenomena are typical for ionic hydrogels, which are extremely sensitive to variation of pH and ionic strength of the solution. Thus, the hydrogel saturated with an antibiotic from an aqueous solution, when transferred into saline, gets somewhat collapsed, losing a part of water with the dissolved aminoglycoside. As a result, in the fast stage of the process 40% of Kanamycin is desorbed from the hydrogel in the salt form and 28%, from the hydrogel in the acid form.

After completion of the fast stage (within 3–5 min), the desorption rate abruptly decreases and the process continues in the prolonged mode for several hours. If the kinetic dependence of the desorption in the slow stage is interpreted considering the residual content of Kanamycin in the hydrogel after completion of the fast stage as its initial content, it takes absolutely normal form (Fig. 4) characterized by n close to 0.5

(0.53 for the hydrogel in the acid form and 0.5 for the salt form of the hydrogel), i.e., in this stage the process is governed by simple diffusion of Kanamycin from the hydrogel and is described by the Fick law. The above concept of the desorption mechanism is confirmed by the fact that in using antibiotic solution in saline the fast portion in the kinetic curves disappears.

A simple modification (base hydrolysis) of the hydrogels based on 2-hydroxyethyl methacrylate, characterized by low water content (38 wt %), allows significant increase in their swellability in water and, correspondingly, in the water content. This results in that the hydrogels gain the capability to sorb increased amounts of antibiotics (aminoglycosides) due to the natural increase in the hydrogel volume (nonspecific sorption) and to the specific sorption caused by ionic interactions and formation of hydrogen bonds. Desorption of aminoglycosides from modified hydrogels is a complex process. In the first stage, some amount of the aminoglycoside is rapidly liberated from the hydrogel due to its collapse in saline. This is followed by slow desorption lasting for several hours and controlled simply by diffusion. Considering specific therapeutic purposes, we can recommend different procedures for saturation of hydrogels with aminoglycosodes. When it is necessary to obtain a high concentration of an antibiotic in the therapeutic area for a short time, for saturation of hydrogels it is appropriate to use aqueous solutions with increased concentration of aminoglycosides. When a high local concentration of an antibiotic is undesirable, e.g., due to toxicity of some aminoglycosides, it is appropriate to perform sorption from solutions prepared in saline. In this case, the fast stage of desorption disappears and the antibiotic is liberated from the hydrogel in prolonged mode in the course of several hours.

CONCLUSIONS

(1) In base hydrolysis of polymer hydrogels based on 2-hydroxyethyl methacrylate, their swellability in water increases due to partially ionic character of the polymer in water. In parallel, the sorption activity of the modified hydrogel with respect to antibiotics such as aminoglycosides (Kanamycin, Gentamicin sulfates) increases due to an increase in the hydrogel volume and appearance of ionic interactions. Desorption of the aminoglycoside from the hydrogel into saline is a complex process. First, the fast stage of desorption is caused by some collapse of the hydrogel in the NaCl solution. Second, the slow stage of the antibiotic liberation from the hydrogel is described by a simple diffusion mechanism.

(2) Depending on therapeutic purposes, aminoglycosides can be sorbed with hydrogels either from aqueous solutions of the antibiotic or from solutions prepared in saline. In the first case, fast liberation of high concentrations of the aminoglycoside from the hydrogel is realized and in the second case, the antibiotic is desorbed in the prolonged mode in the course of several hours.

REFERENCES

1. Sokolovskii, M.V., Zaikina, N.A., Akulova, N.V., and Belokhvostova, A.T., *Antibiot. Khimioterap.*, 2000, vol. 45, no. 6, pp. 10–12.
2. Lukin, A.M., Smirnova, K.A., and Chernysheva, T.V., *Zh. Anal. Khim.*, 1966, vol. 21, no. 11, pp. 1300–1302.
3. Temnikova, T.I., *Kurs teoreticheskikh osnov organiheskoi khimii* (A Course of Theoretical Foundations of Organic Chemistry), Leningrad: Khimiya, 1968.
4. *Hydrogels in Medicine and Pharmacy*, Peppas, N.A., Ed., CRC, 1987, pp. 109–135.

ISSN 1070-4272, Russian Journal of Applied Chemistry, 2006, Vol. 79, No. 4, pp. 590–595. © Pleiades Publishing, Inc., 2006.
Original Russian Text © A. A. Gaile, V. E. Somov, G. D. Zalishchevskii, E. A. Kaifadzhyan, L. L. Koldobskaya, 2006, published in Zhurnal Prikladnoi Khimii, 2006, Vol. 79, No. 4, pp. 599–604.

SORPTION AND ION-EXCHANGE PROCESSES

Extractive Refining of Atmospheric Gas Oil with *N*-Methylpyrrolidone

A. A. Gaile, V. E. Somov, G. D. Zalishchevskii, E. A. Kaifadzhyan, and L. L. Koldobskaya

St. Petersburg State Technological Institute (Technical University), St. Petersburg, Russia

Kirishinefteorgsintez Production Association, Open Joint-Stock Company, Kirishi, Leningrad oblast, Russia

Received January 24, 2006

Abstract—A study was carried out of extractive refining of atmospheric gas oil with *N*-methylpyrrolidone in the presence of undecane to remove aromatic hydrocarbons and sulfur-containing compounds and thus obtain a summer diesel oil component.

DOI: 10.1134/S1070427206040161

Rapid growth of the number of diesel motor cars causes the consumption and production of diesel oils to increase. For example, in 1990–2006, the proportion of diesel cars increased worldwide from 14 to 40–50% [1]. Within 1999–2004, diesel oil production in Russia increased by 18.4%, from 46.8 to 55.4 mln tons [2]. By contrast to car gasolines consumed mostly inside Russia, diesel oils are mostly exported: In 2004, the domestic consumption and export were 25.8 and 29.6 mln tons, respectively [3]. This was paralleled by posing ever more stringent environmental requirements on the diesel oil quality [4]. These requirements can be met by using hydrogenation methods only if the end boiling point of the feed will be decreased, so that dialkylated dibenzothiophenes exhibiting low reactivity in hydrogenolysis will not enter the initial diesel fraction. However, this will decrease production of diesel oils. Lowering of the initial boiling point of the diesel fraction is also undesirable, as this would decrease production of jet fuel.

When light gas oils from secondary processes (catalytic and thermal cracking, coking), having an increased content of aromatic hydrocarbons, are involved in production of diesel and ship oils, this decreases the quality of the resulting oil products.

The above-mentioned contradiction, namely, the need in increasing both the production and quality of diesel oil, can be overcome by involving into processing atmospheric gas oil yielded in significant amounts on AVT (atmospheric-vacuum pipe still) installations. In extractive refining of atmospheric gas oil, dibenzothiophene derivatives and polycycloarenes, which are the most difficult to remove in hydrorefining, should be extracted most readily. Aromatic nitrogen-containing components (carbazole, indole, and quinoline homologs) poisoning hydrorefining catalysts are even more easily extracted with polar solvents [5].

Sulfur-containing compounds that partially remain in the raffinate from extractive refining of atmospheric gas oil are mostly saturated compounds such as dialkyl sulfides, thiacyclanes, and disulfides, which can be readily cleaved in hydrorefining. Thus, it seems possible to combine the resulting raffinate with lightened diesel fraction and obtain high grade diesel oil after hydrorefining of a combined flow under mild conditions.

Previously [6] we studied the extractive refining of atmospheric gas oil with 2-methoxyethanol (methyl Cellosolve) using methyl Cellosolve–water–pentane extraction system. We confirmed a high economic efficiency of the designed process for combined production of a diesel oil component from atmospheric gas oil by extraction with aqueous methyl Cellosolve in the presence of pentane, followed by hydrorefining of the raffinate [7].

A drawback of the method of extractive refining of atmospheric gas oil is that it requires fairly high aqueous methyl Cellosolve : feed and pentane : feed weight ratios of 5 : 1 and 1 : 1.5, respectively, which makes the process power-consuming.

In this study we developed a power-saving technology of extractive refining of atmospheric gas oil, suitable for highly selective extraction of polycycloarenes and organosulfur compounds that are difficult to remove by hydrorefining, at moderate extractant : feed ratios.

As selective solvent we chose *N*-methylpyrrolidone surpassing methyl Cellosolve in the selectivity and solvency with respect to arenes [8].

N-Methylpyrrolidone is widely used in oil refining and petrochemical industries as a selective solvent for recovery of benzene and its homologs from reformer naphthas, as well as of 1,3-butadiene, isoprene, acetylene; it is also used for selective refining of lubricating oils [9]. However, when installations for selective refining of lubricants at Russian refineries changed from phenol and furfural to more efficient *N*-methylpyrrolidone, this posed a serious problem. Namely, *N*-methylpyrrolidone can be oxidized at high temperatures to *N*-methylsuccinimide which is hydrolyzed into succinic acid exerting a corrosive impact on the equipment. All these reactions are especially accelerated at temperatures close to 300°C, which can be attained in regeneration of *N*-methylpyrrolidone.

We suggested previously [10, 11] to eliminate or mitigate these drawbacks of *N*-methylpyrrolidone in extractive refining of vacuum gas oils and fuel oil by using an *N*-methylpyrrolidone–undecane (or undecane fraction) extraction system. Undecane completely substitutes nonpolar solvent pentane, used for refining of the diesel fraction, namely, increases the refining selectivity, yield of the raffinate, the difference in the densities and settling rates of the equilibrium phases, and performance of the extractor. At the same time, undecane performs another two important functions essential for selective refining of atmospheric gas oil as well. First, undecane forms with *N*-methylpyrrolidone an azeotrope boiling at 179°C (which is 25°C lower than the boiling point of *N*-methylpyrrolidone). This decreases the probability of decomposition and corrosion of the equipment during regeneration of the reagent. Also, with undecane there are no *N*-methylpyrrolidone impurities in the raffinate, which is also essential: To be suitable as a diesel oil component, raffinate needs additional refining. As known, hydrorefining catalysts are poisoned even by weakly basic nitrogen-containing compounds, in particular, *N*-methylpyrrolidone.

Another drawback of *N*-methylpyrrolidone is its ability to form azeotropes with hydrocarbons boiling at temperatures lower than 280°C, which can be responsible for "oiling" of the extractant [12]. However, this holds only for systems comprised of *N*-methylpyrrolidone and saturated hydrocarbons with low mutual solubility, so that distillable azeotropic mixtures easily settle after condensation and cooling. *N*-Methylpyrrolidone does not form azeotropic mixtures with arenes occurring in atmospheric gas oil, which could really "oil" the extractant.

Table 1. Characteristics of atmospheric gas oil fractions from AVT-2 and AVT-6 installations

Characteristic	AVT-2, sample no.		AVT-6, sample no. 3
	1	2	
Boiling range, °C:			
initial boiling point	279	278	290
10%	298	311	320
30%	313.5	323	333
50%	326	341	352
70%	341	361	373
90%	366	384	397
Density at 20°C, g cm^{-3}	0.865	0.871	0.874
Refractive index at 20°C	1.4822	1.4885	1.4902
Cloud point, °C	4.0	+18	+19
Freezing point, °C	–1.0	+14	+14.5
Viscosity, mm^2 s^{-1}, at:			
20°C	12.5	19.62	20.0
50°C	5.0	8.03	8.15
Content, wt %, of compounds reactive in sulfonation	27.2	28.2	29.3
sulfur	1.13	1.15	1.17
Cetane index	49.3	50.3	51.0

Thus, we chose *N*-methylpyrrolidone–undecane (or undecane fraction) extraction system for refining of atmospheric gas oil. Decane and dodecane impurities in the undecane fraction do not deteriorate the above-mentioned characteristics, since both these alkanes, like undecane, form with *N*-methylpyrrolidone azeotropes with minimal boiling points.

EXPERIMENTAL

As feed we used three atmospheric gas oil samples from Kirishinefteorgsintez Production Association, Open Joint-Stock Company, taken from AVT-2 and AVT-6 installations (Table 1).

The total sulfur content in atmospheric gas oil and the resulting raffinates and extracts was determined by the lamp method according to GOST (State Standard) 19 121–73. The cetane index was calculated according to GOST 27 768–88:

$$CI = 454.74 - 1641.416\rho^{15} + 774.74(\rho^{15})^2 - 0.554t_{50} + 97.803(\log t_{50})^2.$$

The multistep extraction was carried out with a set of temperature-controlled funnels by the counterflow scheme simulating operation of a full-size extraction column [13]. Table 2 presents the conditions of experiments on extractive refining of sample nos. 1–3.

An azeotropic mixture of water, *N*-methylpyrrolidone, and saturated hydrocarbons was distilled off on a 15-TP fractionating column from the extract phase obtained by extractive refining of sample no. 1 with neat *N*-methylpyrrolidone (without undecane). The remaining *N*-methylpyrrolidone was vacuum-distilled, which yielded the extract in the bottoms. Partial removal of saturated hydrocarbons from the extract phase in the form of azeotropes decreases their content form 18.4 to 14.5 wt %. The saturated hydrocarbons isolated from azeotropic mixtures upon cooling to 0°C were combined with the raffinate.

The raffinate was recovered from the raffinate phase by back-extraction of *N*-methylpyrrolidone with water. Table 3 presents the characteristics of

Table 2. Conditions of experiments on extractive refining of atmospheric gas oil samples with *N*-methylpyrrolidone and methyl Cellosolve

Characteristic	Sample no. 1		Sample no. 2, N-MP	Sample no. 3, N-MP
	N-MP	methyl Cellosolve		
Number of theoretical steps of extraction	4	5	4	4
Process temperature, °C				
extractor top	40	30	40	40
extractor bottom	30	30	30	30
Water content in extractant, wt %	0.5	4	0.5	0.5
Extractant : feed weight ratio	2 : 1	3 : 1	2 : 1	2.5 : 1
Undecane : feed weight ratio	–	–	0.3 : 1	0.4 : 1

Table 3. Characteristics of the raffinates and extracts yielded by extractive refining of atmospheric gas oil sample no. 1

Characteristic	Refining with *N*-MP		Refining with methyl Cellosolve	
	raffinate	extract	raffinate	extract
Yield, wt %	75.1	24.9	80.5	19.5
Boiling range, °C:				
initial boiling point	267	–	265	–
10%	291	–	289	–
30%	307	–	308	–
50%	317	–	321	–
70%	332	–	334	–
90%	347	–	355	–
94%	350	–	366	–
Density at 20°C, g cm^{-3}	0.832	0.965	0.844	0.952
Refractive index at 20°C	1.4625	1.5450	1.4719	1.5420
Cloud point, °C	13.0	–	4.0	–
Freezing point, °C	3.0	–2.0	–1.5	–
Viscosity, $mm^2 s^{-1}$, at:				
20°C	10	–	10.3	–
50°C	4.41	–	4.5	–
Content, wt %, of				
compounds reactive in sulfonation	7.87	85.5	15.5	75.5
sulfur	0.40	3.40	0.74	2.72
Degree of extraction, wt %, of				
arenes	–	78.3	–	54.1
sulfur	–	75.0	–	47.0
Cetane index	60.3	–	56.3	–

the combination of the raffinate and extract yielded by extractive refining of atmospheric gas oil sample no. 1 with *N*-methylpyrrolidone (*N*-MP) and, for comparison, with methyl Cellosolve.

Despite the fact that *N*-methylpyrrolidone : feed ratio is by a factor of 1.5 lower than that in the case of methyl Cellosolve, the refining is more efficient. With *N*-methylpyrrolidone, undesirable components are removed more selectively and completely, as indicated by higher density, refractive index, and content of sulfur and compounds reactive in sulfonation in the extract, as well as by a higher degree of extraction of arenes and sulfur-containing compounds. Also, *N*-methylpyrrolidone provides a higher quality of the combined raffinate, namely, lower density, refractive index, and content of arenes and sulfur (by factors of 1.9 and 1.8, respectively) compared to methyl Cellosolve. When atmospheric gas oil is refined with *N*-methylpyrrolidone and methyl Cellosolve, the cetane index of the raffinate increases by 11 and 7 units, respectively.

Thus, extractive refining of atmospheric gas oil with *N*-methylpyrrolidone is more efficient than with methyl Cellosolve: At a lower reagent : feed ratio (2 : 1 against 3 : 1 by weight), the undesirable impurities are removed more selectively and completely, thus yielding a higher-quality raffinate.

Gas oil sample no. 2 and especially sample no. 3 are distinguished from sample no. 1 by the presence of higher-boiling fractions, as well as by fairly high cetane indices, despite enhanced content of arenes, which is due to the presence in them of *n*-alkanes C_{17^+} with cetane indices of over 100.

To increase the selectivity of refining of higher-boiling samples and to decrease the temperature of the extractant regeneration, we performed the extraction with *N*-methylpyrrolidone in the presence of undecane (Table 2).

The solvents from the extract phases were regenerated in three stages. First, a water–undecane–*N*-methylpyrrolidone azeotrope was distilled off on a 15-TP fractionating column. Then most of *N*-methylpyrrolidone was vacuum-distilled at the bottoms temperature of no higher than 250°C. The remaining small proportion of *N*-methylpyrrolidone (ca. 3 wt %) was vacuum-distilled as an azeotropic mixture with undecane, which was returned to the still in the desired amount.

From the raffinate phase, an undecane–*N*-methylpyrrolidone azeotropic mixture was distilled off; excess undecane was removed from the raffinate by vacuum fractionation.

Table 4. Characteristics of the raffinate and extract yielded by extractive refining of atmospheric gas oil sample no. 2 with *N*-methylpyrrolidone in the presence of undecane

Characteristic	Raffinate	Extract
Yield, wt %	77.6	22.4
Boiling range, °C:		
initial boiling point	267	–
10%	300	–
30%	312	–
50%	333	–
70%	345	–
90%	367	–
Density at 20°C, g cm^{-3}	0.840	0.978
Refractive index at 20°C	1.4665	1.5502
Cloud point, °C	22	–
Freezing point, °C	15	–
Viscosity, mm^2 s^{-1}, at:		
20°C	18.1	–
50°C	7.85	–
Content, wt %, of compounds reactive in sulfonation	9.81	89.8
sulfur	0.47	3.49
Degree of extraction, wt %, of		
arenes	–	71.1
sulfur	–	68.0
Cetane index	59.2	–

Table 4 shows that the raffinate yielded by refining of sample no. 2 contains <10 wt % arenes; their content decreases by a factor of 3.5, and the sulfur content decreases by a factor of 2.45. The cetane index of the raffinate increases by 9 units, the point of 90% distillation of the raffinate under standard distillation decreased by 17°C relative to the feed. This can be attributed to a virtually complete removal of the highest-boiling components, namely, homologs of tricycloarenes and dibenzothiophene. The density, refractive index, and viscosity of the raffinate decrease. The freezing point of the raffinate remains virtually identical to that of the feed, but the cloud point increases by 4°C. However, the cloud and freezing points abruptly decrease after mixing the raffinate with the hydrorefined diesel fraction. For example, for 20 wt % atmospheric gas oil raffinate in the combined product the cloud and freezing points decrease to –24 and –28°C, respectively (for hydrorefined diesel fraction they are equal to –32 and <–35°C, respectively).

Extractive refining of atmospheric gas oil from AVT-2 installation with *N*-methylpyrrolidone in

Table 5. Characteristics of the raffinate and extract yielded by extractive refining of atmospheric gas oil sample no. 3 with *N*-methylpyrrolidone in the presence of undecane

Characteristic	Atmospheric gas oil form AVT-6 installation		Characteristic	Atmospheric gas oil form AVT-6 installation	
	raffinate	extract		raffinate	extract
Boiling range, °C:			Freezing point, °C	+17	–
initial boiling point	279	–	Viscosity, $mm^2 s^{-1}$, at		
10%	305	–	20°C	18.0	–
30%	319	–	50°C	7.8	–
50%	339	–	Content, wt %, of		
70%	357	–	compounds reactive in sulfonation	9.5	88.7
90%	380	↓	sulfur	0.45	3.34
Yield, wt %	75.0	25.0	Degree of extraction, wt %, of		
Density at 20°C, $g\ cm^{-3}$	0.842	0.970	arenes	–	75.7
Refractive index at 20°C	1.4675	1.5495	sulfur	–	71.3
Cloud point, °C	+23	–	Cetane index	60.0	–

the presence of undecane is much more efficient compared to that with the methyl Cellosolve–pentane extraction system. The aqueous methyl Cellosolve : feed and pentane : feed weight ratios were much higher, namely, 5 : 1 and 1.5 : 1, respectively [6]. Nevertheless, the raffinate obtained with the *N*-methylpyrrolidone–undecane system has a much higher quality: The content of compounds reactive in sulfonation and sulfur is by 4.7 and 0.26 wt %, respectively, lower, and the cetane index is by 2.2 units higher.

Thus, the raffinate from extractive refining of atmospheric gas oil from the AVT-2 installation is suitable as a summer diesel oil component on the Russian domestic market. The sulfur content in the raffinate can be decreased by hydrorefining jointly with straight-run diesel fraction. In view of the fact that extractive refining of atmospheric gas oil removes benzothiophene and dibenzothiophene homologs, which are the least reactive in hydrogenolysis, it is unnecessary to perform the hydrorefining under more severe conditions.

Close results were obtained in extractive refining of the highest-boiling sample no. 3 from AVT-6 installation, but this required increased *N*-methylpyrrolidone : feed and undecane : feed weight ratios (Table 5).

CONCLUSIONS

(1) Extractive refining of atmospheric gas oil with *N*-methylpyrrolidone in the presence of undecane increases the selectivity of removal of undesirable arenes and organosulfur compounds and also decreases both the temperature of regeneration and probability of decomposition of the extractant because of formation of an undecane–*N*-methylpyrrolidone azeotropic mixture. Extractive refining of atmospheric gas oil gives raffinate in a yield of ca. 78% with the cetane index of 59 and <10 wt % content of arenes; the sulfur content is decreased by a factor of 2.5 compared to the feed.

(2) The raffinates obtained are promising as diesel oil components.

REFERENCES

1. Mitusova, T.N. and Kalinina, M.V., *Mir Nefteprod.*, 2005, no. 2, pp. 5–7.
2. Russia's Oil: Branch Review, *Neftegaz. Vertikal'*, 2005, nos. 8–9, pp. 62–69.
3. Levinbuk, M.I., *Mir Nefteprod.*, 2005, no. 5, p. 438.
4. Kaminskii, E.F. and Khavkin, V.A., *Glubokaya pererabotka nefti: tekhnologicheskie i ekologicheskie aspekty* (Deep Oil Processing: Technological and Environmental Aspects), Moscow: Tekhnika, 2001.
5. Gaile, A.A., Kostenko, A.V., Semenov, L.V., and Koldobskaya, L.L., *Zh. Prikl. Khim.*, 2005, vol. 78, no. 9, pp. 1428–1432.
6. Gaile, A.A., Zalishchevskii, G.D., Semenov, L.V., et al., *Neftepererab. Neftekhim.*, 2004, no. 5, pp. 29–32.
7. Zalishchevskii, G.D., Gaile, A.A., Yakovlev, A.A., et al., *Neftepererab. Neftekhim.*, 2004, no. 10, pp. 26–30.

8. Gaile, A.A., Semenov, L.V., Zalishchevskii, G.D., and Varshavskii, O.M., *Ekstraktsionnaya dearomatizatsiya neftyanykh fraktsii: Sbornik trudov OOO "KINEF"* (Extractive Dearomatization of Oil Fractions: Coll. of Works by KINEF Open Joint-Stock Company), Gaile, A.A. and Somov, V.E., Eds., St. Petersburg: Sankt-Peterb. Gos. Tekh. Univ., 2002, pp. 5–34, 164–285.
9. Gaile, A.A. and Zalishchevskii, G.D., *N-Metilpirrolidon: Poluchenie, svoistva i primenenie v kachestve selektivnogo rastvoritelya* (*N*-Methylpyrrolidone: Preparation, Properties, and Application as Selective Solvent), St. Petersburg: Khimizdat, 2005.
10. Gaile, A.A., Kaifadzhyan, E.A., Koldobskaya, L.L., et al., in *5-i Mezhdunarodnyi forum "TEK Rossii: regional'nye aspekty": Sbornik trudov* (Int. Forum "Fuel and Energy Complex of Russia: Regional Aspects": Coll. of Works), St. Petersburg, April 4–7, 2005, pp. 173—177.
11. Gaile, A.A., Kostenko, A.V., Zalishchevskii, G.D., et al., *Khim. Tekhol. Topl. Masel*, 2005, no. 4, pp. 3–9.
12. Shkol'nikov, V.M., Kolesnik, I.O., Oktyabr'skii, F.V., et al., *Neftepererab. Neftekhim.*, 1998, no. 12, pp. 11–14.
13. Alders, L., *Liquid–Liquid Exration. Theory and Laboratory Practice*, Amsterdam: Elsevier, 1959.

ISSN 1070-4272, Russian Journal of Applied Chemistry, 2006, Vol. 79, No. 4, pp. 596–601. © Pleiades Publishing, Inc., 2006.
Original Russian Text © G. Ya. Kolbasov, V. S. Vorobets, A. M. Korduban, A. P. Shpak, M. M. Medvedskii, I. G. Kolbasova, O. V. Linyucheva, 2006, published in Zhurnal Prikladnoi Khimii, 2006, Vol. 79, No. 4, pp. 605–610.

APPLIED ELECTROCHEMISTRY AND CORROSION PROTECTION OF METALS

Electrodes Based on Nanodispersed Titanium and Tungsten Oxides for a Sensor of Dissolved Oxygen

G. Ya. Kolbasov, V. S. Vorobets, A. M. Korduban, A. P. Shpak, M. M. Medvedskii, I. G. Kolbasova, and O. V. Linyucheva

Vernadsky Institute of General and Inorganic Chemistry, National Academy of Sciences of the Ukraine, Kiev, Ukraine
Kurdyumov Institute of Metal Physics, National Academy of Sciences of the Ukraine, Kiev, Ukraine
Kiev Polytechnic Institute National Technical University, Kiev, Ukraine

Received December 13, 2005

Abstract—It is suggested to use films of nanodispersed Ti and W oxides as electrodes in a sensor for dissolved oxygen. It is shown that films of this kind have stable characteristics in electroreduction of O_2 in saline.

DOI: 10.1134/S1070427206040173

Oxygen dissolved in biologically active liquids plays an important role in redox processes. Therefore, development of sensitive methods for determining its concentration is a topical problem. Oxygen sensors are now used to control biological processes in fermenters and at plants for treatment and processing of biological wastes, to monitor the content of dissolved oxygen in water used at thermal power stations, and to make various technological analyses. However, the most important is application of such sensors in medical practice.

For example, in oxygen-inhalation hypoxia therapy, it is necessary to monitor that part of oxygen in blood plasma, which is not bound to hemoglobin; a similar analysis is required in hyperbaric-oxygenation therapy of lungs, in hypoxytherapy of cardiac and gastroenteric illnesses, in determining the effect of fetal hemoglobin on the blood pathology in oncology, in therapy of pathological pregnancy, etc.

The concentration of dissolved oxygen should also be monitored in preparation and storage of physiological solutions, blood plasma, and other biologically active fluids.

Because of its high sensitivity the electrochemical method is promising for analyzing oxygen concentration in biologically active fluids [1–4]. The operation of a sensor is based on electroreduction of oxygen, whose total concentration is described, for a number of metals, by the equations [1, 3, 4]

$$O_2 + 4H^+ + 4e \rightarrow 2H_2O, \quad \text{(I)}$$

for an acid medium and

$$O_2 + 2H_2O + 4e \rightarrow 4OH^-, \quad \text{(II)}$$

for an alkaline medium.

In this case, the process goes via an intermediate stage of hydrogen peroxide formation. For a number of metallic electrodes, a two-electron overall process without formation of hydrogen peroxide is also possible [1, 3–5]:

$$O_2 \rightarrow 2O_{ads}, \quad \text{(III)}$$

$$O_{ads} + 2H^+ + 2e \rightarrow H_2O, \quad \text{(IV)}$$

$$O_{ads} + H_2O + 2e \rightarrow 2OH^-; \quad \text{(V)}$$

reaction (IV) proceeds in an acid medium, and reaction (V), in an alkaline medium.

The specificity of electrochemical reactions on semiconductor electrodes primarily consists, in contrast to reactions on metallic electrodes, in a potential redistribution between the ionic double layer and the space charge region near the semiconductor surface, which can affect the kinetics of these reactions [5, 6]. For example, it has been shown for mixed oxides SiO_2/Nb_2O_5 [7] that oxygen reduction involves

two electrons to form hydrogen peroxide. At the same time, for a TiO_2^- electrode fabricated by anodic oxidation of titanium, the total number of electrons involved in the reaction may vary from $n_s = 4$ to $n_s = 2$ in passing from alkaline to acid solutions [8]. It is noteworthy that n_s affects the limiting sensitivity of an oxygen sensor. Electrodes based on ultradispersed semiconducting materials and, in particular, on transition metal oxides, exhibit a high catalytic activity [9–11] and are being extensively studied now.

In this study, nanodispersed Ti and W oxides, which are stable in many biologically active liquids, on Ti and InP substrates were examined as semiconducting electrode materials for oxygen sensors. The oxygen reduction in a 0.9% isotonic physiological and 7.5% hypertonic NaCl solutions was analyzed.

EXPERIMENTAL

TiO_2 nanoparticles were obtained by the sol–gel method from $TiCl_4$. The procedure used included synthesis of a sol of amorphous titanium peroxide from titanium hydroxide and its subsequent heat treatment [12]. Titanium hydroxide was synthesized by hydrothermal decomposition of Ti(IV) chloride. To completely shift the equilibrium toward formation of the target product, an NH_4OH solution was introduced into the reaction mixture. After the neutralization was complete, the pH of the medium was adjusted to 6.5–6.8. The precipitate formed was washed with distilled water to remove chloride ions. A sol of amorphous titanium peroxide was obtained by adding a solution of hydrogen peroxide to a titanium hydroxide solution. The subsequent heating of the sol of amorphous titanium peroxide at 100°C yielded a TiO_2 sol, which was converted to TiO_2 (anatase) at 400–430°C. Titanium served as a substrate for deposition of TiO_2 nanoparticles. The size of the semiconducting TiO_2 nanoparticles (d = 2.9–4.0 nm) was determined from the band gap of the semiconductor [9–11], found by measuring spectra of the photoelectrochemical current [6], using the method described in [13, 14]. The average thickness of the TiO_2 films (500 to 1000 nm) was determined from the change in the substrate mass after their deposition. The TiO_2 films were modified with Pt nanoparticles from a solution of chloroplatinic acid by exposure of the semiconductor to light in the spectral range of fundamental absorption [15].

TiO_2 particles were obtained on an InP substrate by the method used in semiconductor industry to produce protective TiO_2 films on crystals with p–n junctions. The deposition was performed in a quartz tube containing a heated TiO_2 powder and InP single crystals at its opposite ends. An inert gas (purified Ar) was passed through the working chamber. The InP samples were placed in the temperature zone 400–480°C. The average size d of the TiO_2 particles on InP was determined with a scanning electron microscope (d = 100–300 nm).

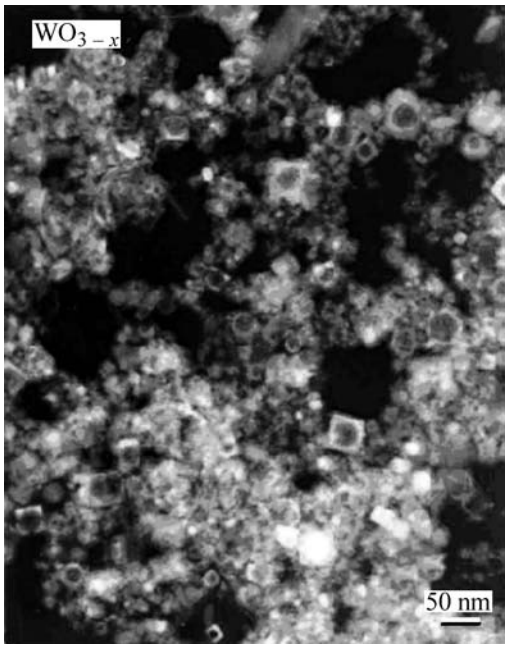


Fig. 1. TEM micrograph of WO_{3-x} nanoparticles.

Nanoparticles of a nonstoichiometric tungsten oxide WO_{3-x} were obtained by the method of electric explosion of conductors (EEC). The procedure included purification of a tungsten wire, formation of an oxygen-deficient atmosphere in the explosion chamber, and choice of the optimal energy range [16]. The average size of the nanoparticles, d, was determined by transmission electron microscopy (TEM). According to the TEM data, d varies within 5–50 nm, the nanoparticles are anisotropic, have the form of a sphere inscribed in a parallelepiped, and are not agglomerated (Fig. 1). The WO_{3-x} films were obtained by sedimentation from a sol of nanoparticles in water. Titanium served as a substrate onto which WO_{3-x} nanoparticles were deposited. The average thickness of the WO_{3-x} films (about 2000 nm) was determined from the change in the substrate mass after the deposition.

The electronic structure of the nanodispersed titanium and tungsten oxides was studied by X-ray photoelectron spectroscopy (XPS) on an ES-2402 spectrometer equipped with a PHOIBOS-100-SPECS en-

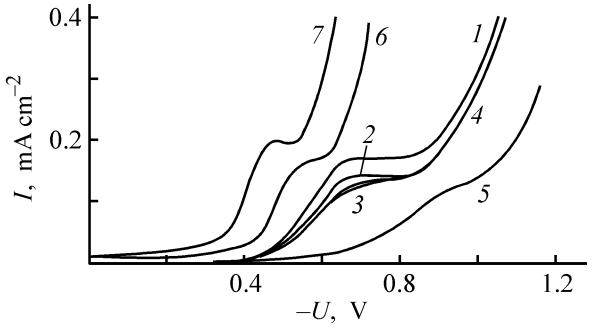


Fig. 2. *I–U* curves measured in oxygen reduction in a 0.9% NaCl solution at a potential sweep rate v = 10 mV s^{-1} in relation to a cycle number. Curves: (*1–5*) TiO_2/Ti electrodes; (*6*, *7*) TiO_2/Ti electrodes modified with Pt nanoparticles, (*6*) cycle 1, and (*7*) cycle 4. (*I*) Current density and (*U*) potential; the same for Fig. 3.

ergy analyzer. As the excitation source served an X-ray gun with a magnesium anode (E MgK_α = 1253.6 eV, P = 200 W). The absolute resolution, measured for the Au $4f_{7/2}$ peak of gold, was 0.9 eV, and the accuracy in determining the peak of the W $4f_{7/2}$ line, 0.05 eV. The procedure used to calibrate the spectrometer was described in [15]. The residual pressure in the vacuum chamber was 2×10^{-7} Pa. As substrates served 10 × 10-mm Al plates.

The W4*f* and Ti2*p* spectra were resolved into the interconnected component pairs, $4f_{7/2}/4f_{5/2}$ and $2p_{3/2}/2p_{1/2}$ (ΔE = 2.1 eV, I_1/I_2 = 0.77 and ΔE = 5.7 eV, I_1/I_2 = 0.5, respectively), to take into account the spin-orbit splitting. We employed the Gauss–Newton method for coupled parameters. The intensity of the components and their binding energies were varied. The width of the corresponding components and the relative contributions of the Gauss–Lorentz distributions in spectral resolution were fixed. The areas of the components were determined after the background was subtracted by the Shirley method [17]. The integral intensities of the components, obtained in this way, are proportional to the concentration of nonequivalent titanium and tungsten ions in the samples.

The current–voltage (*I–U*) dependences of the electrodes were measured in the potentiodynamic mode, using a special computerized electrochemical installation. The installation has the following characteristics: measurable currents in the range from 2×10^{-9} A to 10^{-1} A, potential sweep rate of 0.01–50 mV s^{-1}, and potential of the working electrode varying from 4 to –4 V. The electrochemical studies were performed in a cell with separated cathode and anode compartments. The electrode potential was measured relative to a silver chloride reference electrode. The oxygen concentration in solution was varied by adding a deaerated NaCl solution. For this purpose, argon was bubbled through the solution for 2–3 h. The solution was mixed in a certain proportion with the working NaCl solution containing dissolved oxygen. This was done in a box filled with Ar.

The polarization curves measured in oxygen reduction on the TiO_2 electrodes are shown in Fig. 2. As is known, the titanium foil used as a support for deposition of TiO_2 nanoparticles is covered with an oxide film under natural conditions and upon its annealing and anodizing. Oxygen is also reduced on this film, but its activity is lower as compared with the activity of films based on TiO_2 nanoparticles produced by the sol–gel method. This is also indicated by the *I–U* curves measured in oxygen reduction on films of TiO_2 nanoparticles (Fig. 2, curves *1–4*) and on TiO_2 films formed upon annealing of Ti (Fig. 2, curve *5*). As in the case of platinum metals, all the polarization curves show a single wave at potentials from –0.45 to –1.2 V, which may correspond to the overall process of oxygen reduction, (III)–(V), without formation of hydrogen peroxide. As can be seen from Fig. 2, the hydrogen evolution is clearly pronounced at U < –1.3 V.

The reduction of oxygen on TiO_2 films obtained upon annealing of Ti occurred at a potential shifted to the cathodic region by 0.23 V, compared with the electrodes based on TiO_2 nanoparticles, which points to a lower electrocatalytic activity of these films. The high overvoltage of oxygen reduction may cause difficulties in analysis for the oxygen content of, because in this case side reactions may proceed at the cathode in a number of biologically active solutions. To make the potential of oxygen reduction lower, the TiO_2 films were modified with Pt nanoparticles, because the potentials of O_2 reduction at the Pt electrode are more positive than those at the TiO_2 electrode [4]. However, the modification of the electrodes with Pt considerably deteriorated their stability, which was manifested in that their *I–U* characteristics were irreproducible in cycling (Fig. 2, curves *6*, *7*). In addition, the hydrogen evolution potential for such electrodes was markedly shifted to the anodic region. As a result, the region of potentials at which analysis for the content of oxygen in solution is possible became narrower. For TiO_2/InP electrodes, the reproducibility of the characteristics in cycling was better (Fig. 3, curves *1–3*). At the same time, the potentials of oxygen reduction at these electrodes were more positive than those at electrodes based on TiO_2 nanoparticles. The differences in current density between

TiO_2/Ti and TiO_2/InP electrodes based on nanoparticles are related both to a surface macroporosity and to nonuniformity of film deposition on the electrode surface, with these parameters affecting the current density in the opposite directions.

The most stable characteristics were exhibited by WO_{3-x}/Ti electrodes. Their *I–U* characteristics remained virtually unchanged already after the third cycle (Fig. 3, curves *4–7*).

Analysis of the structure of XPS spectra of the O1*s* level in these samples shows that, along with the signal related to the lattice oxygen (O^{2-}, E_b = 530.6 eV for tungsten oxide and E_b = 530.0 eV for titanium oxide), there are a strong signal due to the oxygen of OH groups (E_b = 531.0–531.8 eV) and a weaker signal associated with the oxygen from the H_2O molecule (533.0–533.8 eV). The results of resolution into components of normalized XPS spectra of the W4*f* and Ti2*p* levels of the samples studied are presented in Figs. 4a, 4b, and 4c and in the table. As can be seen from Fig 4a, the surface of nanoparticles from which the electrodes were fabricated is mainly formed by the W^{6+} states of tungsten ions with binding energies $E_b W4f_{7/2}$ = 36.1 eV and $E_b W4f_{7/2}$ = 35.7 eV and by W^{5+} states ($E_b W4f_{7/2}$ = 34.8 eV [17–18]. The components in the range E_b = 35.7 eV (W^{6+}) and E_b = 34.8 eV (W^{5+}) correspond to the main phase of protonated oxide $W_x^{5+}W_{1-x}^{6+}O_{3-x}\cdot(OH)_x$. The contributions from the W^{5+} and W^{6+} states (11.7 and 36.5%, respectively, see table) can be used to determine the nonstoichiometry coefficient (x = 0.243) and the composition of the main phase, $WO_{2.76}\cdot(OH)_{0.24}$. The signal at E_b = 36.1 eV can be attributed to formation on the surface of nanoparticles of a hydroxide phase, $WO_3\cdot nH_2O$, which was possibly formed from the main phase upon its contact with water.

The results obtained in resolution of the Ti2*p* spectra of the sample of titanium oxide nanoparticles are shown in Fig. 4. The components at $E_b Ti\,2p_{3/2}$ = 458.5 eV (Ti^{4+}, 69.7%, see table) and $E_b Ti\,2p_{3/2}$ = 457.5 eV (Ti^{3+}, 7.2%, see table) [18, 19] can be assigned to the phase of a protonated oxide $Ti_x^{3+}Ti_{1-x}^{4+}O_{2-x}\cdot(OH)_x$. The nonstoichiometry coefficient determined from the contributions of the Ti^{3+} and Ti^{4+} ions to the oxide phase (7.2% and 69.7%, respectively) can be used to find the nonstoichiometry coefficient (x = 0.093), which corresponds to a composition $TiO_{1.91}\cdot(OH)_{0.09}$. The component at $E_b Ti\,2p_{3/2}$ = 459.4 eV (Ti^{4+}, 23.1±0.7%, see table) can be attributed to formation of the phase $TiO_2\cdot nH_2O$ on the surface of nanoparticles.

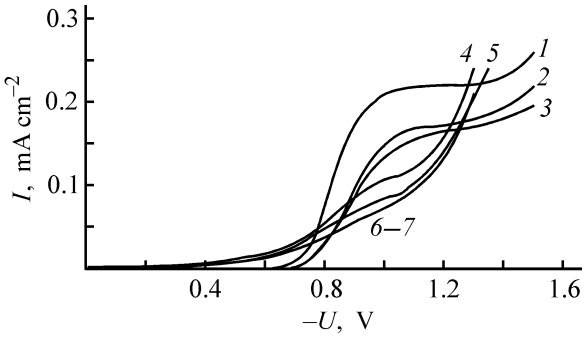


Fig. 3. *I–U* curves measured in oxygen reduction in a 7.5% NaCl solution at a potential sweep rate v = 10 mV s^{-1} in relation to a cycle number. Curves: (*1–3*) TiO_2/InP electrodes; (*4–7*) WO_{3-x}/Ti electrodes, (*4*) cycle 1, and (*5–7*) cycles 2–4.

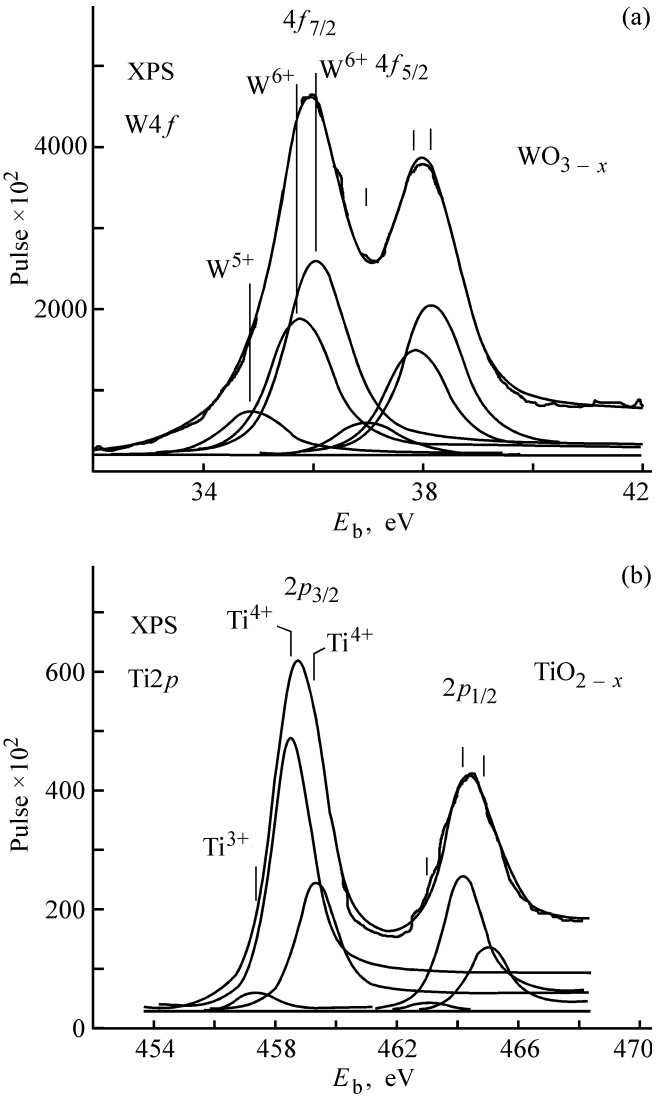


Fig. 4. Resolution of the XPS spectra of (a) W4*f* levels of WO_{3-x} and (b) Ti2*p* levels of TiO_{2-x} into components. (E_b) Binding energy.

Results* of decomposition of the Ti2*p* and W4*f* spectra into components for nanodispersed oxides WO_{3-x} and TiO_{2-x}

E_b, eV	*I*, %	
	WO_{3-x}	TiO_{2-x}
W^{3+}, 34.8	11.7 ± 0.7	–
W^{6+}, 35.7	36.5 ± 0.7	–
W^{6+}, 36.1	51.8 ± 0.7	–
Ti^{3+}, 457.5	–	7.2 ± 0.9
Ti^{4+}, 458.5	–	69.7 ± 0.7
Ti^{4+}, 459.3	–	23.1 ± 0.7

* E_b, binding energies of W4$f_{7/2}$, Ti2$p_{3/2}$ electrons; *I*, integral intensities of the components.

Thus, according to the XPS data, the electrode surface is composed of nonstoichiometric oxides of tungsten, $WO_{2.76}\cdot(OH)_{0.24}$, and titanium, $TiO_{1.91}\cdot(OH)_{0.09}$, and of their hydroxide phases. The high catalytic activity of the nanoparticles under study in oxygen reduction can be attributed to formation of catalytically active W^{5+} and Ti^{3+} centers and to presence of OH groups in the oxide matrix. The comparatively high stability of tungsten oxide electrodes in redox processes, compared with titanium oxide electrodes, may be due to an increase in the contribution of the valence *d* states to the W–W bond. For example, a subband absent in the spectrum of stoichiometric oxides [20] is formed in the XPS spectra of the valence band of nonstoichiometric tungsten and molybdenum oxides. The integral intensity of this subband grows as the number of the $M^{(n-1)+}$ states increases. The formation of this subband is mainly due to contributions from the W5*d* states involved in the formation of W–W bonds in the oxides $WO_{2\le x<3}$ [21].

The oxygen reduction at the electrodes studied is characterized by mixed kinetics. It was shown that the limiting current of oxygen reduction for the semiconductor electrodes under study is the limiting diffusion current. This assumption was verified by studying how the maximum limiting current varies with the potential sweep rate *v* at potentials in the region of limiting currents. It was found that the plot of this dependence in the coordinates $i_d = f(\sqrt{v})$ [22] is a straight line, which shows that the oxygen reduction in this region is controlled by diffusion. In the region of potentials corresponding to currents lower than the limiting current, the polarization curve of oxygen reduction was described by the Tafel equation $\eta_c = a_k + b_k \log i$ [23], where η is the overvoltage of the reaction; a_k, Tafel constant; $b_k = 0.059/\alpha n$ and α, transfer coefficient (α = 0.5 [23]). The relation $\alpha n = 0.5$ was obtained, i.e., the number of electrons involved in oxygen reduction at the discharge stage is $n = 1$. The value $n = 1$ has been reported for platinum and silver in an acid medium and $n = 2$ for alkaline solutions, and also $n = 1$ for a number of other metals [1, 3, 4]. In the given case, the behavior of the semiconductor electrodes studied is similar to that of metallic electrodes, in which the applied potential drops across the ionic double layer. Such a behavior of the semiconductor electrodes is due to the fact that oxygen reduction occurs at cathodic potentials in the region of a pronounced accumulation of electrons at the surface and the shielding of the surface charge by these electrons is important. In this case, as also in the case of metals, the potential mostly drops across the ionic double layer [5, 6].

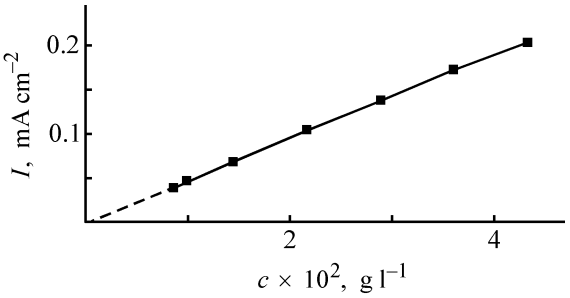


Fig. 5. Current *I* of oxygen reduction vs. oxygen concentration *c* for a TiO_2/InP electrode in a 0.9% NaCl solution. $v = 2$ mV s^{-1}.

We determined the dependence of the limiting current on the concentration of dissolved oxygen in a NaCl solution at potentials from –0.6 to 1.0 V, when the catalytic activity of the electrodes studied was at a maximum (Fig. 5). The current remained stable during several hours. From the results presented in Fig. 5, the total amount n_s of electrons involved in oxygen reduction was determined. For this purpose, we measured the dependence of the current of the working electrode on the time of the electrolysis in the potentiostatic mode at a potential in the range of diffusion currents of oxygen reduction and, using the data of Fig. 5, calculated the concentration of reduced oxygen. We found that $n_s = 2$ in NaCl solutions.

CONCLUSIONS

(1) The maximum sensitivity of electrodes based on nanodispersed Ti and W oxides to dissolved oxygen is reached at cathode potentials from –0.6 to –1.0 V (relative to a silver chloride reference electrode), at which the limiting diffusion current of oxygen reduction is observed.

(2) A single electron is involved at $\alpha = 0.5$ in the oxygen reduction at TiO_2 electrodes at the discharge stage. The total number of electrons involved in the oxygen reduction was found to be $n_s = 2$.

(3) The high catalytic activity of the electrodes based on nanodispersed tungsten and titanium oxides, WO_{3-x} and TiO_2, may be due to formation of W^{5+} and Ti^{3+} states and presence of OH groups in the oxide matrix.

(4) The stability of the TiO_{2-x} and WO_{3-x} electrodes in the course of oxygen reduction was studied. These electrodes have highly renewable characteristics in prolonged cycling, which makes them promising for manufacture of electrochemical sensors for dissolved oxygen. The higher stability of the electrodes based on WO_{3-x} nanoparticles in redox processes may be due to the increased strength of the W–W bond upon formation of W^{5+} states.

REFERENCES

1. Vetter, K.J., *Elektrochemische Kinetik*, Berlin: Springer, 1961.
2. Chviruk, V.P. and Linyucheva, O.V., *Elektrokhimiya*, 1996, vol. 32, no. 10, pp. 1212–1220.
3. *Modern Aspects of Electrochemistry*, Bockris, J.O'M. and Conway, B.E., Eds., New York: Plenum, 1969.
4. Delahay, P., *J. Electrochem. Soc.*, 1950, vol. 97, no. 6, pp. 198–212.
5. Damaskin, B.B. and Petrii, O.A., *Vvedenie v elektrokhimicheskuyu kinetiku* (Introduction to Electrochemical Kinetics), Moscow: Vysshaya Shkola, 1983.
6. Gurevich, Yu.Ya. and Pleskov, Yu.V., *Fotoelektrokhimiya poluprovodnikov* (Photoelectrochemistry of Semiconductors), Moscow: Nauka, 1983.
7. Francisco, M.S.P., Cardoso, W.S., and Gushikem, Y., *J. Electroanal. Chem.*, 2005, vol. 574, no. 2, pp. 291–297.
8. Mentus, S.V., *Electrochim. Acta*, 2004, vol. 62, no. 2–3, pp. 27–32.
9. Hagfeld, A. and Grötzel, M., *Chem. Rev.*, 1995, vol. 95, no. 1, pp. 49–68.
10. Hoffmann, M.R., Martin, S.T., and Choi, W., *Chem. Rev.*, 1995, vol. 95, no. 1, pp. 69–96.
11. Khairutdinov, R.F., *Usp. Khim.*, 1998, vol. 67, no. 2, pp. 125–139.
12. Seok, Sang Il, Kim, Mi Sun, and Suh, Tae Soo, *J. Am. Ceram. Soc.*, 2002, vol. 85, no. 7, pp. 1888–1890.
13. Kublanovsky, V.S., Kolbasov, G.Ya., and Litovchenko, K.I., *Polish J. Chem.*, 1996, vol. 70, no. 11, pp. 1453–1458.
14. Kolbasov, G.Ya., Krasnov, Yu.S., and Volkov, S.V., Abstracts of Papers, *55th ISE Annual Meet.*, Thessaloniki (Greece), September 19–24, 2004, p. 541.
15. Shpak, A.P., Korduban, A.M., Mel'nikova, V.A., and Medvedskii, M.M., *Metallofiz. Noveishie Tekhn.*, 2003, vol. 25, no. 11, pp. 1409–1415.
16. *Practical Surface Analysis by Auger and X-ray Photoelectron Spectroscopy*, Biggs, D. and Seah, M.P., Eds., Chichester: Wiley, 1983.
17. Nefedov, V.I., *Rentgenoelektronnaya spektroskopiya khimicheskikh soedinenii* (X-ray Photoelectron Spectroscopy of Chemical Compounds), Moscow: Khimya, 1984.
18. Wagner, C.D., Moulder, J.F., Davis, L.E., and Riggs, W.M., *Handbook of X-ray Photoelectron Spectroscopy*, New York: Perkin–Elmer, 1979.
19. Crist, B.V., *Handbook of Monochromatic XPS Spectra. The Elements of Native Oxides*, 2000.
20. Firment, E. and Ferretti, A., *Surface Sci.*, 1983, vol. 129, pp. 155–160.
21. Khizhun, O.Yu. and Solonin, Yu.M., *Nanosist., Nanomater., Nanotekhnol.*, 2004 vol. 2, no. 4, pp. 1177–1184.
22. Galus, Zb., *Teoretyczue podstawy elektroanalisy chemicznej*, Warsaw: Naukowe, 1971.
23. Antropov, L.I., *Teoreticheskaya elektrokhimiya* (Theoretical Electrochemistry), Moscow: Vysshaya Shkola, 1984.

ISSN 1070-4272, Russian Journal of Applied Chemistry, 2006, Vol. 79, No. 4, pp. 602–604. © Pleiades Publishing, Inc., 2006.
Original Russian Text © N. D. Ivanova, O. A. Stadnik, 2006, published in Zhurnal Prikladnoi Khimii, 2006, Vol. 79, No. 4, pp. 611–613.

APPLIED ELECTROCHEMISTRY AND CORROSION PROTECTION OF METALS

Kinetics of Electrooxidation of Co(II) Ions in a Fluorine-containing Electrolyte

N. D. Ivanova and O. A. Stadnik

Vernadsky Institute of General and Inorganic Chemistry, National Academy of Sciences of the Ukraine, Kiev, Ukraine

Received June 16, 2005; in final form, December 2005

Abstract—The electrochemical oxidation of Co(II) ions in fluorine-containing electrolytes on stationary and rotating disc electrodes was studied.

DOI: 10.1134/S1070427206040185

In recent years [1,2], thin-film chemical power sources (CPs) have been actively developed. CPs are rather widely used in various electronic circuits, miniature batteries with high specific electrical characteristics, displays, integrated circuits, high-quality amplifiers, etc. Thin-film cathodes are promising for development of rolled CPss, which have high specific capacity. There are great expectations for application of disordered nanostructure electrode materials [3]. The disordered structure ensures a high rate of introduction of cations (lithium, hydrogen, etc.) into the cathode mass.

Cobalt oxides find increasing use in batteries, for making higher their voltage, and in thin-film CPss [1], which poses the question of their manufacture. Pyrolytic and chemical methods are known, as well as the electrochemical technique involving oxidation of metallic cobalt at a constant anodic polarization [4]. A sufficiently simple method has been developed for synthesis of oxide compounds, including cobalt oxides, from fluorine-containing electrolytes via incomplete oxidation–reduction [5].

The aim of this study was to synthesize oxide compounds of cobalt by the electrochemical method and to determine the kinetics of this process.

EXPERIMENTAL

We used in the study solutions containing 10–30 g l^{-1} cobalt sulfate heptahydrate and 20–40 g l^{-1} ammonium fluoride. The current–voltage dependences were studied on a PI-50-1.1 potentiostat with an LKD-4 *XY*-recorder. The potential sweep rate was 2 to 20 mV s^{-1}. Platinum pressed into polyethylene served as a working electrode (0.13 cm^2) and a 4 cm^2 platinum plate, as a cathode.

The mass-transfer components were determined by the method of a rotating disc electrode (RDE). The same solutions as in the preceding case were used in the study, with and without a supporting electrolyte (1 M solution of sodium sulfate). The rate of disc rotation was varied within the range 200–600 rpm, which corresponds to $255 < Re < 766$ [6]. At the disc rotation rates chosen, convective diffusion can be disregarded. A saturated calomel electrode (SCE) served as reference in both cases. All the potentials in Figs. 1–4 are given relative to a standard hydrogen electrode.

To determine the diffusion coefficient, the viscosity of working solutions was evaluated using a capillary viscometer as the ratio of the times of gravity

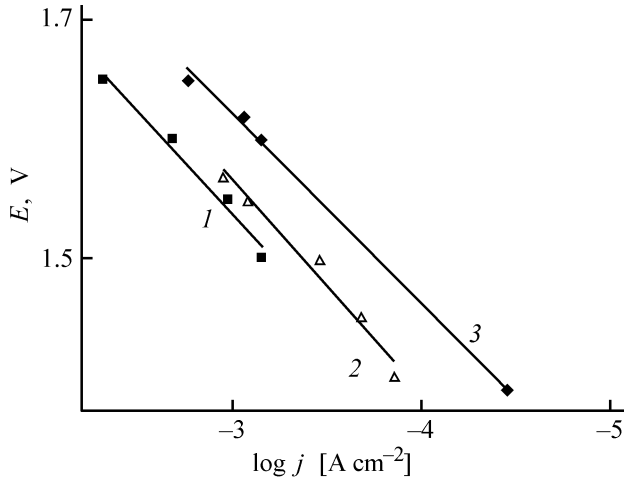


Fig. 1. *E*–log *j* dependences obtained for electrolytes of different compositions. (*j*) Current density. Curve numbers correspond to electrolyte numbers in Table 1; the same for Figs. 2 and 4.

out-flow of the working solution and water (equal volumes).

The polarization curves j–E plotted in the Tafel coordinates in Fig. 1 are linear. The electrochemical parameters of the Co(II) oxidation process are listed in Table 1, in which a and b are the Tafel coefficients, and β, the transfer coefficient of ions oxidized at the anode. At a constant concentration of metal ions in the electrolyte, the electrochemical parameters of the process depend on the concentration of a fluorine-containing additive.

The results obtained indicate that charge transfer is the slow stage at low polarizations. The number of electrons involved in the reaction is unity, because, as demonstrated by X-ray diffraction analysis, the compound obtained is close in composition to CoO(OH). According to the results of an atomic-absorption analysis and IR spectroscopy, the oxide–hydroxide compound of cobalt, formed at the anode, has a composition $Co_xO_y(OH)_z$, where $x = 0.65$–0.71, $y = 1.34$–1.79, and $z = 1.3$–1.52. The total concentration of cobalt is 47–53%. It should be noted that the content of the metal depends on the concentration of the ligand in the electrolyte. The particles of the compound are 80–120 nm in size.

The presence of OH^- groups and water in the samples studied is confirmed by their IR spectra containing the characteristic absorption bands at around 3400, 1620, and 1410 cm^{-1}, which correspond to stretching and bending vibrations of hydroxy groups, and by the results of a thermogravimetric analysis, according to which the total concentration of oxygen, including that in H_2O and OH^- groups, is 53–47%.

The cobalt oxide compound is formed at polarizations of 1.45–1.70 V. The limiting current is observed at potentials of 1.75–1.95 V, depending on the potential sweep rate. In this case, the oxide compound is formed with a lower current efficiency by the product under the diffusion control. This is indicated by the fact that the dependences of the current density on the potential sweep rate are linear (Fig. 2).

Raising the concentration of the metal and ligand ions in the electrolyte leads to an increase in the limiting currents (Fig. 2). As the potential increases further, the current again grows exponentially, which is due to a rise in hydrogen evolution rate.

The kinetics of Co(II) electrooxidation was studied in detail with a rotating disc electrode at different rotation rates.

In the general case, mass transfer in an electrolyte occurs via diffusion, migration, and convection, and,

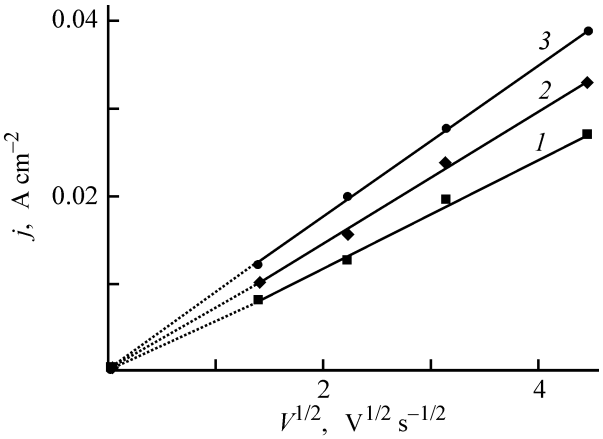


Fig. 2. Limiting current density j vs. the potential sweep rate V in electrolytes of different compositions.

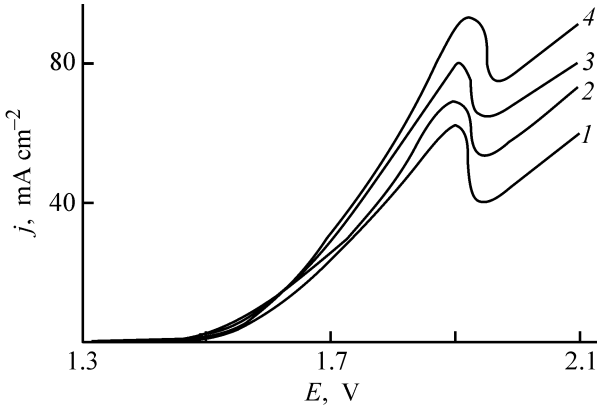


Fig. 3. Potentiodynamic curves measured on RDE in the electrolyte of the optimum composition at different rotation rates. (j) Current density and (E) potential. Rotation rate of RDE (rpm): (*1*) 200, (*2*) 400, (*3*) 500, and (*4*) 600.

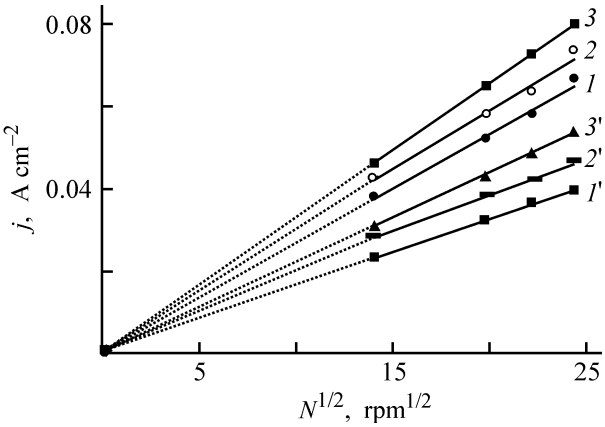


Fig. 4. Dependences of the limiting current density j on the rate of RDE rotation N, obtained in various electrolytes (*1–3*) without and (*1'–3'*) with supporting electrolyte.

Table 1. Electrochemical parameters of Co(II) electrooxidation on a stationary electrode

Sample no.	Electrolyte composition, g l^{-1}	a	b	β	$j_0 \times 10^5$, A cm^{-2}
1	$CoSO_4 \cdot 7H_2O$ 10, NH_4F 20	0.70	0.16	0.16	2.24
2	$CoSO_4 \cdot 7H_2O$ 10, NH_4F 25	0.87	0.20	0.13	3.98
3	$CoSO_4 \cdot 7H_2O$ 10, NH_4F 30	1.12	0.25	0.10	5.01

Table 2. Electrochemical parameters of electrooxidation of Co(II) ions in fluorine-containing electrolytes on RDE [electrolyte composition (g l^{-1}): $CoSO_4 \cdot 7H_2O$ 10 and NH_4F 25]

N, rpm	ω, rad s^{-1}	j_{lim}, A cm^{-2}	$D \times 10^5$, cm^2 s^{-1}	δ × 10^5, m
Without supporting electrolyte				
600	62	0.073077	–	4.4
500	52	0.063077	–	4.7
400	42	0.057692	–	5.3
200	21	0.042308	–	7.7
With supporting electrolyte				
600	62	0.053846	6.0	3.8
500	52	0.048462	5.9	4.1
400	42	0.042308	5.7	4.6
200	21	0.030769	5.9	6.5

consequently, the limiting current is determined by these three processes. The contributions of diffusion and migration can be evaluated by RDE measurements in solutions with and without a supporting electrolyte.

The general run of the polarization curves obtained on RDE is illustrated by Fig. 3. The limiting diffusion and migration currents, diffusion coefficients, and thickness of the diffusion layer were calculated (Table 2).

As the rotation rate becomes higher, the limiting current increases (Fig. 4). The linear behavior of the j–$n^{1/2}$ dependence is also retained when a supporting electrolyte is introduced, with the limiting currents decreasing.

The diffusion coefficient was determined in terms of the theory developed by V.G. Levich, using the equation for the limiting diffusion current:

$$j_d = 0.62nFD^{2/3}\omega^{1/2}\nu^{-1/6}c_0,$$

where j_d is the limiting diffusion current (A cm^{-2}); n, number of electrons involved in the electrode reaction; F, Faraday constant (A s mol^{-1}); D, diffusion coefficient of ions being oxidized (cm^2 s^{-1}); ν, kinematic viscosity coefficient (cm^2 s^{-1}); ω, rotation angle (rad s^{-1}); and c_0, concentration of ions being oxidized (mol cm^{-3}).

Hence

$$D = [j_d\nu^{1/6}/(0.62nF\omega^{1/2}c_0)]^{3/2}.$$

The calculated diffusion coefficients are close, $(5.7–6.04) \times 10^{-5}$ cm^2 s^{-1} (Table 2).

CONCLUSIONS

(1) Electrooxidation of Co(II) in fluorine-containing electrolytes is accompanied by formation of cobalt oxide–hydroxide compounds $Co_xO_y(OH)_z$, where x = 0.65–0.71, y = 1.34–1.79, and z = 1.3–1.52.

(2) The optimum conditions for product formation are: NH_4F concentration 25 g l^{-1}, j_a = 0.5 A dm^{-2}, and T = 20–25°C.

(3) Electrooxidation of Co(II) occurs at low polarizations under the kinetic control, and at high polarizations diffusion becomes notiseable.

(4) The kinetic parameters of the process were calculated. A considerable contribution to mass transfer in fluorine-contaning electrolytes is made by migration, which results in high limiting currents, and, consequently, in high working current densities in these electrolytes.

REFERENCES

1. Wakihara, M., *Mater. Sci. Eng.*, 2001, pp. 109–134.
2. *Khimicheskie istochniki toka. Spravochnik* (Chemical Power Sources. Reference Book), Korovin, N.V. and Skundin, A.M., Eds., Moscow: Mosk. Energ. Inst., 2003.
3. Zlomanov, V.P., *Soros. Obraz. Zh.*, 2001, no. 5, pp. 29–35.
4. Anderton, D.I. and Sole, F.R., *Power Metall.*, 1979, vol. 22, no. 1, pp. 14–16.
5. Ivanova, N.D. and Ivanov, S.V., *Usp. Khim.*, 1993, vol. 62, no. 10, pp. 963–974.
6. Pleskov, Yu.V. and Filinovskii, V.Yu., *Vrashchayushchiisya diskovyi elektrod* (Rotating Disc Electrode), Moscow: Nauka, 1972.

ISSN 1070-4272, Russian Journal of Applied Chemistry, 2006, Vol. 79, No. 4, pp. 605–609. © Pleiades Publishing, Inc., 2006.
Original Russian Text © N. A. Ogurtsov, G. S. Shapoval, 2006, published in Zhurnal Prikladnoi Khimii, 2006, Vol. 79, No. 4, pp. 614–618.

APPLIED ELECTROCHEMISTRY AND CORROSION PROTECTION OF METALS

Protective Properties of Electrochemical Polyaniline Coatings on Low-Carbon Steel

N. A. Ogurtsov and G. S. Shapoval

Institute of Bioorganic Chemistry and Petrochemistry, National Academy of Sciences of the Ukraine, Kiev, Ukraine

Received May 4, 2005

Abstract—Protective properties of polyaniline coatings electrochemically deposited in the galvanostatic mode from oxalic acid solutions onto the surface of low-carbon steel were studied by measuring polarization curves.

DOI: 10.1134/S1070427206040197

Electrically conducting polymers, such as, e.g., polyaniline, have been the object of intensive scientific studies during the last two decades. According to [1], they can reduce the rate of corrosion of low-carbon steel by a factor of 10^4. These materials can replace the widely used noxious pigments of the passivating type, based on chromates and lead compounds [2, 3]. Moreover, coatings based on these materials have already been developed and are employed in Germany for corrosion protection of carbon steel at wastewater treatment plants, sea ships, and port constructions [4]. This made it possible to replace, in a number of cases, stainless steel with carbon steel protected with a paint coating based on polyaniline [5].

The protective properties of polyaniline can be used not only as a component of paint coatings, but also in coatings that contain no additional polymeric binder. However, films of chemically synthesized polyaniline, and especially those in the doped form, show poor adhesion to the metal and, as a rule, cannot be used in practice. In contrast, electrochemically synthesized polyaniline can form sufficiently stable coatings on the metal surface. However, in this case, too, researchers encounter certain difficulties. The electrochemical synthesis of polyaniline is performed at anodic potentials in an acid medium, and, therefore, it is complicated by fast dissolution of the metal. Therefore, this process commonly cannot be performed on the surface of low-carbon steel. However, it has been found that in some solutions, e.g., in oxalic [6–10], *p*-toluenesulfonic [11], and phosphoric [10, 12, 13] acids, aniline can be polymerized.

Based on this circumstance, the Camalet et al. [6] suggested using electrosynthesis of polyaniline, instead of the environmentally hazardous phosphating and chromating, to produce an anticorrosive prime layer. At present, the protective properties of the above-mentioned coatings remain poorly understood. Separate experiments have been described in the literature, which employed methods for determining the amount of iron that passed into a 0.4 M NaCl + 0.1 M HCl solution [6, 7, 11] and the time dependence of the electrode potential in 0.1 M K_2SO_4 + H_2SO_4 solutions (pH 2 and 4.5) [9, 10, 13].

The aim of this study was to examine the influence exerted by the aniline polymerization conditions on the anticorrosive properties of the resulting coatings and the fundamental aspects of deposition of these coatings. In addition, the properties of polyaniline and conventional phosphate coatings were compared.

EXPERIMENTAL

Chemically pure grade NaCl and HCl and analytically pure grade oxalic acid were used in the study without additional purification; KCl of chemically pure grade was preliminarily twice recrystallized. Aniline of pure grade before use was purified by fractional distillation at reduced pressure in an argon flow and was stored under argon in a dark vessel with ground-glass stopper, placed in a refrigerator.

Polyaniline coatings were deposited and their properties studied on edges of cylindrical steel (St.3) electrodes (area 2.06 mm^2), whose lateral surfaces were insulated with epoxy resin. Preliminarily, the electrodes were polished with a fine emery paper (Carbimet, Grid 600, USA), after which their surface was degreased with soda, washed with distilled water, and

Table 1. Constants of Eq. (1) in solutions of various compositions

Concentration in solution, M		$n \pm \Delta_{0.95}$	$C \pm \Delta_{0.95}$, mA cm^{-2} s^n	Q,* mC cm^{-2}
$(COOH)_2$	$PhNH_2$			
0.2	–	0.98 ± 0.04	135 ± 4	142
0.3	–	0.98 ± 0.05	144 ± 3	153
0.4	–	0.99 ± 0.04	152 ± 5	155
0.5	–	0.99 ± 0.05	167 ± 3	170
0.6	–	0.99 ± 0.03	172 ± 2	177
0.2	0.1	0.71 ± 0.03	47 ± 2	78
0.3	0.1	0.71 ± 0.03	54 ± 3	94
0.4	0.1	0.70 ± 0.03	56 ± 2	100
0.5	0.1	0.72 ± 0.04	59 ± 3	103
0.6	0.1	0.71 ± 0.03	60 ± 2	109
0.3	0.125	0.57 ± 0.03	29 ± 2	49
0.3	0.15	0.46 ± 0.03	20 ± 2	30

* Quantity of electricity expended for passivation of a steel electrode at i = 14.3 mA cm^{-2}.

dried with filter paper. For comparison, we used plates of UP phosphated cold-rolled steel (18 kg m^{-2}, ACT Laboratories, USA).

Polyaniline was electrochemically synthesized from oxalic acid solutions [polyaniline(oxalic acid)] on steel electrodes in the galvanostatic mode in a three-electrode cell with separated cathode and anode spaces. In deposition of polyaniline films, the current density was varied in the range 4–40 mA cm^{-2}. In the process, 0.2–0.6 M oxalic acid solutions containing 0.1–0.5 M of aniline, prepared immediately before use, were used.

The electrochemical properties of the thus obtained coatings were studied by measuring polarization curves in a single-chamber three-electrode cell. A platinum electrode served as an auxiliary electrode, and a saturated Ag/AgCl electrode, as reference. All the potentials are given relative to this electrode. Potentiodynamic curves were measured at a potential sweep rate of 10 mV s^{-1}. The curves obtained were transformed into Tafel curves, and extrapolation of Tafel portions of the anodic and cathodic polarization curves to intersection yielded the corrosion potentials E_{cor} and currents i_{cor} from which the corrosion retardation coefficients γ were calculated. Aqueous solutions of 3.5% NaCl and 0.1 N HCl were used as corrosion-active media.

All the electrochemical measurements were made at room temperature with a PI-50-1.1 potentiostat with a PR-8 programming unit. Voltammograms were recorded with an LKD4-003 *XY*-recorder.

The simplest and the most reliable method for synthesis of polyaniline on steel is the galvanostatic technique. The resulting chronopotentiometric curves show two gently sloping portions. The first of these, lying at negative potentials (about –0.4 V), corresponds to dissolution of the metal to the instant of its passivation, and has a characteristic time t_{pas}. The electropolymerization of aniline occurs within the second portion at potentials in the range 1.6–1.9 V, depending on the current density at the working electrode.

The duration of the induction period, t_{pas}, decreases as the current density i increases. Under galvanostatic conditions, these parameters are related by

$$i t_{pas}^n = C, \quad (1)$$

where n and C are constants.

Such a relationship between the parameters is frequently observed in passivation of metals in the galvanostatic mode [6, 7, 11, 14].

Table 1 lists the constants of Eq. (1), obtained in passivation of a steel electrode in media of various compositions. As expected, the passivation time and constants n and C depend both on the acidity of the medium and on the aniline concentration in solution. As can be seen from Table 1, $n \approx 1$ in electrode passivation in oxalic acid solutions in the absence of aniline, in agreement with published data [6, 7]. In this case, the quantity of electricity expended for electrode passivation is independent of the current density in the range studied and increases with the acid concentration.

As aniline is added to the solution, the quantity of electricity expended for electrode passivation markedly decreases. It may be assumed that this is due to adsorption of anilinium cations on the steel surface at cathodic potentials. In contrast to the results obtained by Camalet and co-authors [6, 7], coefficient n decreases in this case from 0.71 to 0.46 as the aniline concentration increases from 0.1 to 0.15 M. As can be seen from Table 1, such an increase in the aniline concentration leads to a threefold decrease in Q at a current density of 14.3 mA cm^{-2}. As a result, it is advantageous to perform the process at the maximum possible current densities, because the current expenditure for metal passivation becomes lower in this case.

The passivation ends in formation of a mixed oxalate-oxide layer, whose semiconducting properties do not preclude polymerization of aniline at anodic potentials [7]. Despite that the formation of polyani-

line at potentials of 1.6–1.9 V leads to a strong excessive oxidation of the polymer and depresses its electroactivity, the forming polyaniline layer retains its protective properties.

The results obtained in testing the protective properties of polyaniline coatings deposited under various conditions are listed in Tables 2–4. It can be seen that the coatings exhibit a pronounced protective effect (γ = 1.6–7.1), which exceeds in some cases that of the standard phosphate layer (γ = 2.1–2.6). For comparison, the anticorrosive properties of an oxalate layer obtained in electrode polarization in aniline-free solutions were analyzed. The protective effect γ of the last coating was found to be significantly lower in both neutral and acid media (1.6 and 1.2, respectively) than that in the case of a polyaniline coating (2.8 and 1.9).

Analysis of the results presented in Tables 2 and 4 shows that electrochemical polyaniline coatings obtained at low current density have better protective properties. For example, polyaniline coatings synthesized at I = 26.7 mA cm^{-2} have γ = 1.9 in an acid medium (Table 2), whereas for coatings synthesized at i = 5 mA cm^{-2}, γ = 3.8 (Table 4). Presumably, this is due to the fact that raising the current density leads to an increase in the potential at which aniline polymerizes and, apparently, to enhancement of the excessive oxidation of the polymer being formed.

It can be seen from Table 3 that polyaniline films obtained at higher quantities of passed electricity show higher corrosion retardation coefficients. For example, in a neutral medium, γ is 1.8 at Q = 3.2 C cm^{-2} and 6.8 at Q = 24 C cm^{-2}. This would be expected because the coating becomes thicker in this case [7]. The increase in the thickness of the polyaniline film also leads to an anodic shift of the corrosion potential of St.3 in neutral and acid media by 22 and 30 mV, respectively.

Comparison of the protective properties of coatings obtained in solutions of various acidities (Table 4) indicates that the corrosion retardation coefficients for coatings formed on St.3 in more acid media are significantly higher. In addition, coatings deposited from solutions with a higher aniline concentration and, accordingly, lower concentration of free acid exhibit poorer protective properties. These effects are apparently due to aggravation of the conditions of polyaniline synthesis, which requires fairly low pH of the medium, necessary for protonation of such a weak base as aniline [15].

An important factor in analysis of the mechanism of protective action of coatings is, in addition to

Table 2. Parameters characterizing the corrosion behavior of low-carbon steel with various coatings in NaCl and HCl solutions (coatings deposited at Q = 8.5 C cm^{-2} in 0.2 M $H_2C_2O_4$ with and without addition of 0.1 N $C_6H_5NH_2$)

Steel	i, mA cm^{-2}	E_{cor}, V	i_{cor}, μA cm^{-2}	γ
St.3: starting		–0.615 –0.545	34.0 258	
with a polyaniline (oxalic acid) coating	14.6	–0.608 –0.537	11.4 139	3.0 1.9
	26.7	–0.612 –0.536	12.0 139	2.8 1.9
with a FeC_2O_4 coating	26.7	–0.630 –0.540	25.0 305	1.5 1.2
PU steel: starting		–0.483 –0.473	1.73 43.2	
with a phosphate coating		–0.423 –0.453	0.67 20.4	2.6 2.1

Note: E_{cor}, i_{cor}, γ: numerator, in 3% NaCl; denominator, in 0.1 M HCl.

Table 3. Parameters characterizing the corrosion behavior of St.3 steel with polyaniline coatings obtained at various quantities Q of passed electricity (coatings deposited at i = 26.7 mA cm^{-2}, [oxalic acid] 0.2 M)

Steel	Q, C cm^{-2}	E_{cor}, V	i_{cor}, μA cm^{-2}	γ
St.3: starting		–0.615 –0.545	34.0 258	
with a polyaniline (oxalic acid) coating	3.2	–0.615 –0.537	19.2 166	1.8 1.6
	16	–0.627 –0.530	11.6 71.0	2.9 3.7
	24	–0.593 –0.515	5.0 38.5	6.8 6.7

Note: E_{cor}, i_{cor}, γ: numerator, in 3% NaCl; denominator, in 0.1 M HCl.

Table 4. Parameters characterizing the corrosion behavior of St.3 steel with polyaniline coatings obtained in solutions of various compositions (coatings deposited at $i = 5$ mA cm^{-2}, $Q = 0.5$ C cm^{-2})

Steel	Concentration in solution, M		E_{cor}, V	i_{cor}, μA cm^{-2}	γ
	$(COOH)_2$	$PhNH_2$			
St.3: starting			–0.615 –0.545	34.0 258	
with a polyaniline (oxalic acid) coating	0.2	0.1	–0.595 –0.534	9.4 67.9	3.6 3.8
	0.3	0.1	–0.591 –0.514	7.7 36.3	4.4 7.1
	0.3	0.125	–0.587 –0.524	14.2 53.8	2.4 4.8
	0.3	0.15	–0.598 –0.526	14.2 58.6	2.4 4.4

Note: E_{cor}, i_{cor}, γ: numerator, in 3% NaCl; denominator, in 0.1 M HCl.

the corrosion retardation coefficients, the direction in which the corrosion potential of a metal with a coating is shifted. As can be seen in Tables 2–4, the corrosion potential of St.3 with oxalate coatings in a neutral medium is shifted in the negative direction. This indicates that the cathodic reaction, which occurs for iron under conditions of this kind via oxygen depolarization with preferential control by the oxygen diffusion [16], is retarded. In an acid medium, in which the cathodic process is limited by hydrogen depolarization, oxalate coatings are apparently a weak obstacle for hydroxonium cations. In this case, a minor shift of E_{cor} in the positive direction is observed. This fact, taken together with the observation of a small corrosion retardation coefficient, suggests that retardation of the anodic reaction predominates in the acid medium.

Polyaniline-containing coatings exhibit, in both neutral and acid media, a positive shift of the corrosion potential of St.3. This gives reason to conclude, with account of the corrosion retardation coefficients obtained, which were found to be comparable in both the corrosive media, that polyaniline hinders the anodic reaction. This result is in agreement with published data, according to which polyaniline coatings on steel favor formation of a denser protective oxide layer [1, 17–19].

CONCLUSIONS

(1) The influence exerted by the conditions under which polyaniline coatings are formed on the surface of low-carbon steel on their protective properties and fundamental aspects of the process of synthesis of these coatings in an oxalic acid medium were studied.

(2) It is shown that carrying out polymerization at the maximum possible current density, aniline concentration, and low acid concentration makes it possible to markedly reduce the expenditure of electricity for anodic dissolution of iron during the induction period. However, the protective properties of polyaniline coatings are deteriorated in this case. The protective properties of polyaniline coatings are markedly improved as the concentration of free acid becomes higher.

(3) The polyaniline coatings obtained at low current density exhibit higher corrosion retardation coefficients. This is apparently due to a decrease in the extent of excessive oxidation of polyaniline synthesized at lower potentials.

(4) Analysis of the results obtained shows that the mechanism of protective action of polyaniline is based on retardation of the anodic reaction. In some cases, electrochemical polyaniline coatings surpass in corrosion protection efficiency ($\gamma = 1.6–7.1$) the standard phosphate coating ($\gamma = 2.1–2.6$).

REFERENCES

1. Lu, W.-K., Elsenbaumer, R.L., and Wessling, B., *Synth. Met.*, 1995, vol. 71, p. 2163.
2. Sitaram, S.P., Stoffer, O.J., and Okeefe, T.J., *J. Coat. Technol.*, 1997, vol. 69, p. 65.
3. He, J., Gelling, V.J., Tallman, D.E., et al., *J. Electrochem. Soc.*, 2000, vol. 147, pp. 3667–3672.
4. Wessling, B., *Chem. Innovation*, 2001, vol. 31, p. 34.
5. Wessling, B., *Synth. Met.*, 1998, vol. 93, p. 143.
6. Camalet, J.L., Lacroix, J.C., Aeiyach, S., et al., *J. Electroanal. Chem.*, 1996, vol. 416, p. 179.
7. Camalet, J.L., Lacroix, J.C., Aeiyach, S., et al., *Synth. Met.*, 1998, vol. 93, p. 133.
8. Sazou, D. and Georgolios, C., *J. Electroanal. Chem.*, 1997, vol. 429, pp. 81–93.
9. Bernard, M.C., Goff, A.H.L., Joiret, S., et al., *J. Electroanal. Soc.*, 1999, vol. 146, pp. 995–998.
10. Bernard, M.C., Goff, A.H.L., and Joiret, S., *Synth. Met.*, 1999, vol. 102, p. 1383.

11. Camalet, J.L., Lacroix, J.C., Aeiyach, S., and Lacaze, P.C., *J. Electroanal. Chem.*, 1998, vol. 145, p. 117.
12. Bernard, M.C., Goff, A.H.L., Joiret, S., and Phong, P.V., *Synth. Met.*, 2001, vol. 119, p. 283.
13. Bernard, M.C., Goff, A.H.L., Joiret, S., and Phong, P.V., *J. Electrochem. Soc.*, 2001, vol. 148, pp. B12–B16.
14. Bagotskii, V.S., *Osnovy elektrokhimii* (Fundamentals of Electrochemistry), Moscow: Khimiya, 1988.
15. Okamoto, H. and Kotaka, T., *Polymer*, 1998, vol. 39, p. 4349.
16. Tomashov, N.D., *Teoriya korrozii i zashchity metallov* (Theory of Corrosion and Metal Protection), Moscow: Akad. Nauk SSSR, 1960.
17. Wessling, B., *Synth. Met.*, 1997, vol. 85, p. 1313.
18. Jasty, S. and Epstein, A.J., *Polym. Mat. Sci. Eng.*, 1995, vol. 72, p. 565.
19. Fahlman, M., Jasty, S., and Epstein, A.J., *Synth. Met.*, 1997, vol. 85, p. 1323.

ISSN 1070-4272, Russian Journal of Applied Chemistry, 2006, Vol. 79, No. 4, pp. 610–613. © Pleiades Publishing, Inc., 2006.
Original Russian Text © V. V. Ivanov, V. I. Balakai, A. V. Ivanov, A. V. Arzumanova, 2006, published in Zhurnal Prikladnoi Khimii, 2006, Vol. 79, No. 4, pp. 619–621.

APPLIED ELECTROCHEMISTRY AND CORROSION PROTECTION OF METALS

Synergism in Composite Electrolytic Nickel–Boron–Fluoroplastic Coatings

V. V. Ivanov, V. I. Balakai, A. V. Ivanov, and A. V. Arzumanova

Southern-Russian State Technical University (Novocherkassk Polytechnic Institute), Novocherkassk, Rostov oblast, Russia

Received December 2, 2005

Abstract—The possible synergism of manifestation of wear resistance and antifriction properties by composite electrolytic nickel–boron–fluoroplastic properties is analyzed. The results of calculation of the diagnostic properties of the coatings in terms of the "concentration wave" model are discussed in comparison with the relevant experimental data.

DOI: 10.1134/S1070427206040203

According to the "concentration wave" model [1], the basic properties of antifriction and wear-resistant composite coatings can be represented, in a two-component approximation [solid (s) + lubricating (lub)], as:

linear wear rate

$$I_l = \alpha\langle I_{l,lub}\rangle + (1 - \alpha)\langle I_{l,lub}\rangle + \Delta\alpha(\langle I_{l,s}\rangle - \langle I_{l,s}\rangle), \quad (1)$$

friction coefficient

$$f = \alpha\langle f_s\rangle + (1 - \alpha)\langle f_{lub}\rangle - \Delta\alpha(\langle f_s\rangle - \langle f_{lub}\rangle), \quad (2)$$

where $\alpha = \alpha_s$ and $(1 - \alpha) = \alpha_{lub}$ are the volume fractions of the solid and lubricating components of the composite coating, respectively; $\Delta\alpha = 4(1 - \alpha) \times \alpha^2[1 - k(1 - k_n)]$, relative magnitude of the synergistic effect; k, dimensional parameter that characterizes the dispersity of phases of the solid component and is equal to the ratio between the average size r_s of microparticles in the solid phases of the surface layer and the thickness Δx of this layer [$k = r_s/(\Delta x + r_s)$, $0.5 \le k < 1$]; and k_n, nanostructural parameter of the solid component of the composite layer, which characterizes the volume fraction of nanofragments of the solid phases in the surface layer Δx with a spherical or cylindrical shape ($r_s \approx \Delta x$ at $k \approx 0.5$; $0 \le k_n \le 1$).

To determine the volume fractions and averaged linear wear rates ($\langle I_{l,s}\rangle$ and $\langle I_{l,lub}\rangle$) and friction coefficients ($\langle f_s\rangle$ and $\langle f_{lub}\rangle$) for coating components, it is necessary to obtain data on the qualitative and quantitative phase composition of the composite coating. In this case, it is necessary to take into account not only the possible composition of the coating after its formation, but also the fact that the following processes may occur in friction at the surface of composite coatings: (a) chemical modification accompanied by formation of new phases; (b) dispersion of particles of the surface phases and their transition to the highly dispersed state, which hinders experimental phase analysis; and (c) redistribution of the chemical components of the system, which gives rise to local gradient fields of concentration of separate phases.

In this context, to obtain data necessary for prognostication of the properties of composite coatings in accordance with formulas (1) and (2), it is preferable to solve the phase problem analytically.

The phase composition of a composite coating not subjected to tribological treatment is determined by the technology of its preparation. Nickel–boron–fluoroplastic coatings were produced from an electrolyte of the following composition ($g\ l^{-1}$): nickel chloride hexahydrate 200–250, nickel sulfate heptahydrate 2.5–5.0, boric acid 25–35, chloramine B 0.5–1.5, salt of anionic polyhedral borate of general formula $M_zC_nB_mH_x$ (M is sodium, potassium, or ammonium; $z = 1, 2$; $n = 0, 2$; $m = 3, 9, 10, 12$; $x = 8, 10, 12$) 1.5–4.0; and F-4D-E fluoroplastic emulsion 10–20. Electrolysis modes: pH 1.0–5.5, temperature 18–30°C, cathode current density 0.5–10 $A\ dm^{-2}$ [2].

Table 1. Phase composition and concentration of components of composite coatings

Coating	Component of a composite coating	Phase composition	Mass fraction, %	Volume fraction, %	α
Ni–B	Solid	Ni, Ni_3B, Ni_2B, NiB	100	100	1.00
	Libricating	–	0	0	
Ni–B–fluoroplastic (1)	Solid	Ni, Ni_3B, Ni_2B, NiB	99.1	95.4	0.954
	Libricating	Fluoroplastic	0.9	4.6	
Ni–B–fluoroplastic (2)	Solid	Ni, Ni_3B, Ni_2B, NiB	97.9	89.8	0.898
	Libricating	Fluoroplastic	2.1	10.2	
Ni–B–fluoroplastic (3)	Solid	Ni, Ni_3B, Ni_2B, NiB	96.4	83.5	0.835
	Libricating	Fluoroplastic	3.6	16.5	

Table 2. Wear and antifriction properties of composite coatings

Coating	Δα, rel. units	Linear wear rate, μm h^{-1}		Friction coefficient	
		$\langle I_l \rangle^{calc}$	$\langle I_l \rangle^{exp}$	$\langle f \rangle^{calc}$	$\langle f \rangle^{exp}$
Ni–B	0	1.100	1.10	0.25	0.25
Ni–B–fluoroplastic (1)	0.098	0.767	0.74	0.218	0.21
Ni–B–fluoroplastic (2)	0.192	0.530	0.56	0.185	0.17
Ni–B–fluoroplastic (3)	0.269	0.434	0.42	0.155	0.15

After thermal treatment, the following phases of the solid component of composite coatings (Ni, Ni_3B, and Ni_2B) and an additionally introduced phase of the lubricating component (fluoroplastic) were found in the coatings [2]. After the steady state is attained under dry friction conditions at a specific load of 3 MPa (friction velocity $V = 0.048$ m s^{-1}), the NiB phase was found in the surface layers of all the composite coatings [2] (Table 1). The possible processes of chemical modification, which could yield the phases detected, are as follows:

$$Ni_3B \rightarrow Ni_2B + Ni \rightarrow NiB + 2Ni, \quad (3)$$

$$6Ni + 6B \rightarrow 2Ni_3B + 4B \rightarrow 3Ni_3B + 3B \rightarrow 6NiB. \quad (4)$$

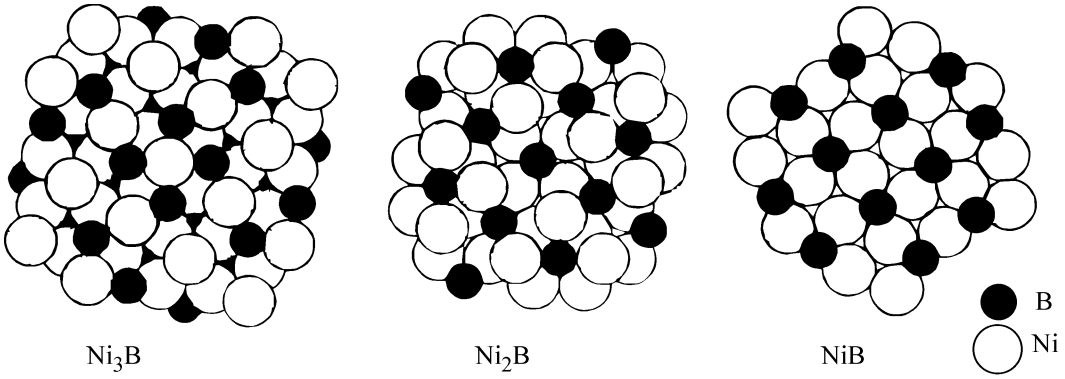
It is noteworthy that the chain of transformations (3) is accompanied by removal of a part of Ni atoms from the crystal lattice of Ni_3B (and then from that of Ni_2B) and by deformation rearrangement of Ni networks and B layers (in Ni_3B) or only B layers (in Ni_2B) [3].

With the composition of the working electrolyte solution for coating deposition, possible mechanism of deposition of nickel- and boron-containing particles, modes in which these particles capture fluoroplastic microparticles in deposition of composite coatings, and possible processes of chemical modification in friction taken into account, it became possible to roughly determine the probable qualitative and quantitative phase composition of the solid and lubricating components and the value of α (Table 1).

Prescribed values of the linear wear rates in the dry friction mode for the phases of the solid component: Ni, Ni_3B, and Ni_2B (~1.1 μm h^{-1}) and NiB (~1.0 μm h^{-1}), and of the phase of the lubricating component, fluoroplastic (~7.5 μm h^{-1}), were used to calculate by formula (1) values of I_l (at $k \approx 0.5$ and $k_n \approx 0.17$). The results of this calculation are in a satisfactory agreement with the corresponding experimental data [2] (Table 2).

Taking into account the averaged values of the friction coefficient, $\langle f \rangle$, in the dry friction mode for the phases of the solid component: Ni, Ni_2B, and Ni_3B (~0.25) and NiB (~0.30), and phases of the lubricating component, fluoroplastic (~0.03), made it possible to calculate by formula (2) values of f (also at $k \approx 0.5$ and $k_n = 0.17$). They are in satisfactory agreement with experimental data [2] (Table 2).

Thus, the concentration wave model with the parameters $k \approx 0.5$ and $k_n = 0.17$ provides a satisfactory interpretation of experimental data on linear wear rate



Two-layer fragments of nickel boride structures in the direction perpendicular to the 3^2434 network of nickel atoms.

I_1 and friction coefficient f of composite coatings. An increase in the dimensional factor k or a change in the parameter k_n leads to a significant discrepancy between the experimental and calculated data. In terms of the model employed, this means that the dispersity of microparticles of the phases of the solid component of composite coatings is high and spherical or cylindrical nanofragments, which enhance the action of the lubricating component, are present among these microparticles. Now, the possibility of their formation in composite coatings will be analyzed.

All the structures of the nickel borides listed in Table 1 are described by atomic network packing of the types 3^2434 and 4^4 [4]. In the structure of Ni_3B, atomic networks 3^2434 of nickel form a system of trigonal and tetragonal prisms. Boron atoms in the trigonal prisms and nickel atoms in the tetragonal prisms close to a hexahedron form two superposed in a plane and slightly distorted square networks 44. In the structure of Ni_2B, the closest nickel networks 3^2434 are shifted with respect to each other and form a system of tetragonal antiprisms and tetrahedra of two types. Boron atoms occupy central positions in the antiprisms and form a square network. In the structure of NiB, nickel atoms form a system of empty trigonal prisms and tetragonal prisms occupied by boron atoms.

The low-boron nickel phases are contained in the solid component of composite coatings and undergo dispersion in friction both under a mechanical action of the conjugated surface of the tribosystem and via a dynamic process of structural-phase disordering, accompanied by multiple reversible phase transformations of a symmetric phase into a dissymmetric phase. The possible structures of dissymmetric phases are $P2_12_12_1$ (4), $Pmc2_1$ (4), $Pna2_1$ (4), $Pmn2_1$ (4) for the rhombic phases Ni_3B and NiB [$Pbnm$ (z = 4)] and $I422$ (4), $I4cm$ (4), $I\bar{4}2m$ (4), $I\bar{4}c2$ (4), $I4/m$ (4), $Ibam$ (4), $Ima2$ (4), $Fmmm$ (8), $Fmm2$ (8) for the tetragonal phase Ni_2B [$I4/mcm$ (z = 4)]. In this case, nanoparticles can be probably formed in the form of multilayer packages composed of two-layer fragments, such as those shown in the figure.

It may be assumed that part of these nanoparticles will correspond in their characteristic size (1.2–2.5 nm) and shape (nearly spherical or cylindrical) to those theoretically taken into account in formulas (1) and (2) by the parameter k_n. It is noteworthy that formation of such nanoparticles is less probable for the NiB phase, in which the atomic density [$\psi = z(V_{Ni} + V_B)/V_{unit.cell} = 0.80$] is approximately 10% lower than that in the Ni_2B and Ni_3B phases (0.88 and 0.89, respectively).

CONCLUSION

The synergism in nickel–boron–fluoroplastic composite coatings was analyzed. This effect is manifested as an improvement of the wear resistance and antifriction properties of the coatings, compared with the magnitudes of the same properties calculated in terms of the additive model (positive synergism). The synergism of the soid and lubricating components of the composite coatings studied presumably consists in the "concentration" of the lubricating phases on the friction surface, which improves the antifriction properties and the wear resistance of the solid phases of the coating, and in the presence of spherical or cylindrical nanoparticles of some solid phases, which act as solid lubricants.

REFERENCES

1. Ivanov, V.V., Shcherbakov, I.N., Ivanov, A.V., and Bashkirov, O.M., *Izv. Vyssh. Uchebn. Zaved. Sev.-Kavk. Regiona, Tekh. Nauki*, 2005, no. 5, pp. 42–46.

2. Balakai, V.I., Kudryavtseva, I.D., and Shevchenko, V.V., *Materialy Mezhdunarodnoi nauchno-prakticheskoi konferentsii "Problemy sinergetiki v tribologii, triboelektrokhimii, materialovedenii i mekhanotronike", Novocherkassk, 8 noyabrya 2002 g*. (Proc. Int. Scientific and Practical Conf. "Problems of Synergetics in Tribology, Triboelectrochemistry, Materials Science, and Mechanotronics," Novocherkassk, November 8, 2002), in 3 parts, Southern-Russian State Technical University (NPI), Novocherkassk: OOO Research-and-Production Association TEMP, 2002, part 1, pp. 48–52.
3. Shcherbakov, I.N., Development of a Nickel–Phosphorus Composite Coating Modified with Boron Nitride and Polytetrafluoroethylene, *Cand. Sci. Dissertation*, Novocherkassk, 2003.
4. Wells, A.F., *Structural Inorganic Chemistry*, Oxford: Clarendon, 1984, 1st ed. Translated under the title *Strukturnaya neorganicheskaya khimiya*, Moscow: Mir, 1988, vol. 3.

ISSN 1070-4272, Russian Journal of Applied Chemistry, 2006, Vol. 79, No. 4, pp. 614–618. © Pleiades Publishing, Inc., 2006.
Original Russian Text © M. V. Sukhanov, M. M. Ermilova, N. V. Orekhova, V. I. Pet'kov, G. F. Tereshchenko, 2006, published in Zhurnal Prikladnoi Khimii, 2006, Vol. 79, No. 4, pp. 622–626.

CATALYSIS

Catalytic Properties of Zirconium Phosphate and Double Phosphates of Zirconium and Alkali Metals with a $NaZr_2(PO_4)_3$ Structure

M. V. Sukhanov, M. M. Ermilova, N. V. Orekhova, V. I. Pet'kov, and G. F. Tereshchenko

Lobachevskii State University, Nizhni Novgorod, Russia

Topchiev Institute of Petrochemical Synthesis, Russian Academy of Sciences, Moscow, Russia

Received March 7, 2006

Abstract—Zirconium orthophosphate $Zr_3(PO_4)_4$ and double phosphates of zirconium and alkali metals $AZr_2(PO_4)_3$ (A = Na, K, Rb, Cs) with a $NaZr_2(PO_4)_3$ structure were synthesized and characterized by X-ray diffraction and electron microprobe analyses and capillary condensation of nitrogen. The catalytic properties of the phosphates in the dehydration of methanol were studied.

DOI: 10.1134/S1070427206040215

The development of competitive, effective, and environmentally safe fuels is among the global trends of progress in chemistry. Dimethyl ether (DME) is one of the most promising types of diesel fuel [1, 2]. At present, DME is produced on the commercial scale by conversion of natural gas with dosed access of atmospheric oxygen to synthesis gas, subsequent formation of methanol in steam on copper–zinc–aluminum catalysts, and dehydration of methanol to give DME on mechanical mixtures of aluminum, silicon, and boron oxides or on molecular sieves [3–5]. It is still a topical task to develop new catalysts for these processes, which should be more active, selective, and less subject to coking.

Zirconium-containing phosphates with a structure of the $NaZr_2(PO_4)_3$ type (NZP) are of interest as catalysts for dehydration of alcohols because of the high stability of their structural skeleton, which ensures their resistance to action of water at high temperature and enables regeneration of a catalyst at elevated temperatures without any changes in its phase composition.

The structural family of NZP includes compounds and solid solutions described by the crystal-chemical formula $(M1)_{0\to1}(M2)_{0\to3}\{[L_2(TO_4)_3]^{p-}\}_{3\infty}$, where $\{[L_2(TO_4)_3]^{p-}\}_{3\infty}$ is the framework of the structure (p is the charge of the framework); $(M1)_{0\to1}$ and $(M2)_{0\to3}$ are types of out-of-framework cationic positions with a designation of the number of positions in each type [6]. The framework of the structure is formed by LO_6 octahedra and TO_4 tetrahedra with sharing common vertices; M1 and M2 voids of different sizes can accommodate a wide variety of cations compensating the framework charge. Most of members of the NZP family contain phosphorus as an anion-forming element T. The structure-forming cations L, with mainly covalent nature of the metal–oxygen bond, are in oxidation states from +5 to +1. These are, for example, Group IV *d*-transition metals. The out-of-framework positions M1 and M2 can include identical cations or a certain set of mainly low-charged cations in oxidation states from +1 to +4 or may remain vacant, depending on the oxidation state of the ions in positions L and T, so as the compound as a whole be electroneutral.

Owing to a wide isomorphism of cations of varied nature in all the crystallographic positions, phosphates of the NZP structure can exhibit acid, base, or redox properties and can be used in organic synthesis as multifunctional catalysts with controlled properties.

It is known that phosphates of an NZP-like structure, $CuZr_2(PO_4)_3$, $Cu_{0.5}L_2(PO_4)_3$ (L = Ti, Zr, Sn), $AgZr_2(PO_4)_3$, and $Na_{1+x}Fe_xZr_{2-x}(PO_4)_3$ are active catalysts for dehydration and dehydrogenation of butyl alcohols and isopropanol [7–10]. It should be noted that the catalytic properties of NZP phosphates in methanol transformations have not been studied.

The aim of this study was to examine the catalytic properties, such as activity and selectivity, of zirconium-containing phosphates $Zr_3(PO_4)_4$ [$\equiv Zr_{0.25}Zr_2(PO_4)_3$] and $AZr_2(PO_4)_3$ (A = Na, K, Rb, Cs) with a structure of the NZP type and kinetic parameters of dehydration of methanol on these compounds.

EXPERIMENTAL

The following reagents of chemically pure grade were used as starting substances in synthesis of the phosphates $Zr_3(PO_4)_4$ and $AZr_2(PO_4)_3$ (A = Na, K, Rb, Cs): zirconium oxychloride $ZrOCl_2 \cdot 8H_2O$, phosphoric acid H_3PO_4, and chlorides of alkali metals ACl (A = Na, K, Rb, Cs). Stoichiometric amounts of chlorides of alkali metals were added to a 1 M solution of zirconium oxychloride (to prevent hydrolysis, it was dissolved in distilled water acidified with hydrochloric acid). Then a 1 M solution of phosphoric acid, also taken in agreement with the stoichiometry of a phosphate, was added at room temperature with continuous stirring. The gel formed upon heating was dried at 353 K and thermally treated under conditions of free access of air at 873 and 1073 K for no less than 20 h in each stage. The final temperature of synthesis of $Zr_3(PO_4)_4$ was 1153 K. It is determined by the temperature of crystallization onset (1073 K) and the decomposition point of this compound (1173 K). The final temperature of synthesis of $CsZr_2(PO_4)_3$ was 1273 K. Pure crystalline cesium zirconium phosphate can be obtained at 1073 K; however, this requires prolonged crystallization, which can be made shorter by raising the synthesis temperature. The stage-by-stage heating of the samples was alternated with their dispersion to make the mixtures homogeneous.

The chemical composition and homogeneity of samples of the phosphates synthesized were monitored using a CamScan MV 2300 (VEGA TS 5130 MM) scanning electron microscope with YAG detectors of secondary and reflected electrons and a Link INCA ENERGY 200C energy-dispersive X-ray microanalyzer with a semiconductor Si(Li) detector. The PAP correction method was used to calculate the composition. The accuracy of determination of sample compositions was 2 at. %. The microprobe analysis of the phosphates demonstrated their homogeneity and correspondence to the theoretical composition.

The phase composition of the powders synthesized was determined by X-ray phase analysis on a DRON 3.0 diffractometer with Ni-filtered Cu K_α radiation in the range of 2θ angles 10°–50°. The recording rate was 2 deg min^{-1}. The X-ray data for the phosphates synthesized indicate that the positions and intensities of the diffraction peaks are close to published data [11, 12]. The calculated unit cell parameters are listed in Table 1.

Table 1. Unit cell parameters of the phosphates synthesized (space group $R\bar{3}c$, $Z = 6$)

Phosphate	a, Å	c, Å	V, Å^3
$Zr_{0.25}Zr_2(PO_4)_3$	8.802(3)	23.060(4)	1547(1)
$NaZr_2(PO_4)_3$	8.811(1)	22.750(7)	1530(1)
$KZr_2(PO_4)_3$	8.717(2)	24.00(1)	1579(1)
$RbZr_2(PO_4)_3$	8.661(2)	24.440(6)	1588(1)
$CsZr_2(PO_4)_3$	8.582(1)	24.920(5)	1590(1)

Table 2. Porosity-related parameters of the phosphates $NaZr_2(PO_4)_3$ and $CsZr_2(PO_4)_3$

Parameter	$NaZr_2(PO_4)_3$	$CsZr_2(PO_4)_3$
Specific surface area (BET), $m^2\ g^{-1}$	26.8	6.4
Surface area of pores* (BJH), $m^2\ g^{-1}$	66.8	10.7
Pore volume, $cm^3\ g^{-1}$	0.078	0.008
Pycnometric density, g cm^{-3}	3.20	3.75
Volume fraction of pores,* %	25	3
Average pore size, Å	98	86

* Pore diameter in the range from 0 to 300 Å.

The porosity parameters of the phosphates were calculated from adsorption–desorption isotherms measured on a Micromeritics ASAP 2020 installation by the method of capillary condensation of nitrogen at 77 K. The results of the calculations are listed in Table 2. To calculate the volume fraction of pores in the samples, their pycnometric density was measured (Table 2) using *n*-decane as a pycnometric liquid. The volume fraction of pores was calculated as the ratio of their volume in 1 g of a phosphate to the volume of 1 g of the phosphate. The specific surface area of sodium zirconium phosphate and the volume fraction of pores for this phosphate are 4 and 8 times, respectively, larger than the corresponding values for cesium zirconium phosphate at close average pore sizes for both samples (Table 2). Possibly, the higher temperature of synthesis of the cesium-containing phosphate reduces its porosity and specific surface area and makes its particles coarser.

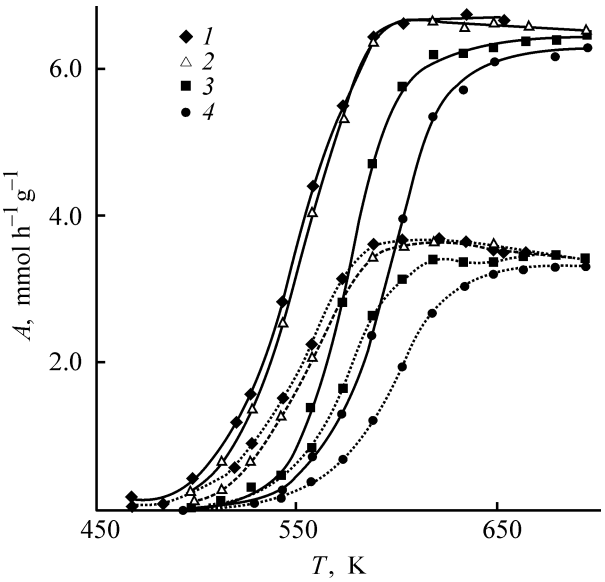


Fig. 1. Yield A of DME (*dashed lines*) and spent amount of methanol (*solid lines*) in its dehydration reaction on the phosphates: (*1*) $Zr_3(PO_4)_4$, (*2*) $NaZr_2(PO_4)_3$, (*3*) $KZr_2(PO_4)_3$, and (*4*) $CsZr_2(PO_4)_3$ vs. temperature T. Feed rate of methanol vapor 0.88 ml min^{-1}.

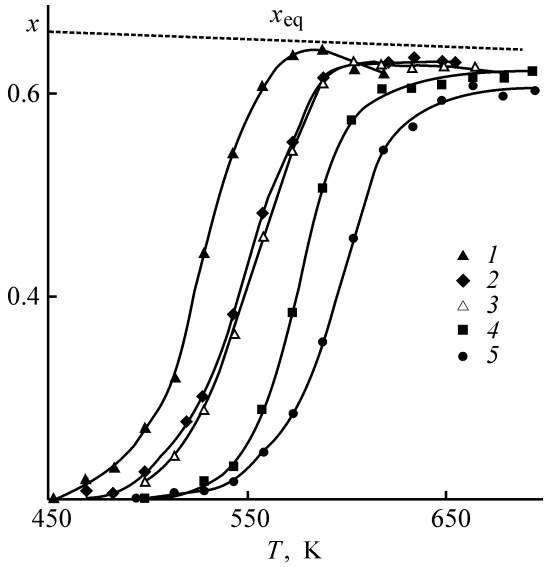


Fig. 2. Degree of methanol conversion, x, on the phosphates (*1*, *3*) $NaZr_2(PO_4)_3$, (*2*) $Zr_3(PO_4)_4$, (*4*) $KZr_2(PO_4)_3$, and (*5*) $CsZr_2(PO_4)_3$ vs. temperature T. Feed rate of methanol vapor (ml min^{-1}): (*1*) 0.20 and (*2*–*5*) 0.88.

We studied the catalytic properties of zirconium phosphate and double alkali metal zirconium phosphates in the conversion of methanol in a flow-through steel reactor in a flow of argon under atmospheric pressure in the temperature range 453–693 K. A 0.300-g weighed portion of a phosphate was mixed with quartz (average particle diameter 1 mm). The alcohol vapor from a temperature-controlled bubbler was fed into the reactor in an argon flow at a total rate of 1.2 l h^{-1}. The reaction products were analyzed on an LKhM-5 chromatograph with a thermal conductivity detector, columns packed with activated charcoal and Porapak T, and computer processing of chromatograms. From the results of the analysis, we calculated the conversion of the alcohol x (%), selectivity S (%), and the yield of target products A (mmol h^{-1} g^{-1} or mmol h^{-1} m^{-2}) by the formula

$$A = FxS/W.$$

Here F is feed rate of the alcohol vapor (mmol h^{-1}), and W, weighed portion of the catalyst (g) or its surface area (m^2).

All the phosphates under study exhibited a catalytic activity in the dehydration of methanol, which was reproducible in different sets of experiments. No products of dehydrogenation and decomposition of methanol were detected in the temperature range studied. The temperature dependences of the DME yield and of the spent amount of the alcohol for zirconium phosphate and sodium zirconium, potassium zirconium, and cesium zirconium phosphates as catalysts are shown in Fig. 1. The 2 : 1 : 1 molar ratio of the spent amount of alcohol to that of the products, DME and water, which is characteristic of the dehydration of methanol

$$2CH_3OH \rightleftarrows H_3COCH_3 + H_2O,$$

is reflected in the positions of the corresponding curves in Fig. 1 (the yield of water coincides with that of DME and is not shown in the figures). This is a criterion of validity of the calibrating factors we used and points to correctness of the experiments. The least active catalyst, as regards the yield of the products of alcohol dehydration, was rubidium zirconium phosphate (at the maximum temperature of 693 K, the methanol conversion was as low as 11%). The phosphates investigated can be ranked in order of decreasing catalytic activity as $Zr_3(PO_4)_4 \approx NaZr_2(PO_4)_3 > KZr_2(PO_4)_3 > CsZr_2(PO_4)_3 \gg RbZr_2(PO_4)_3$.

The temperature dependences of methanol conversion x on these phosphates are shown in Fig. 2. The equilibrium degree of methanol conversion was calculated using the temperature dependence of the equilibrium constant $K_{eq} = 2.145\exp(1239.8/T)$ [13]. The methanol conversion approaches the equilibrium value x_{eq} = 88–90% (dashed line in Fig. 2) at different temperatures for different catalysts.

To determine the reaction order of methanol dehydration for the phosphate $NaZr_2(PO_4)_3$, we varied

the flow rate of the alcohol vapor, V, from 0.20 to 1.27 ml min^{-1} at a constant reactor temperature of 543 K. The dependence of the degree of methanol conversion, x, on the reciprocal rate of feeding of its vapor into the reactor, $1/V$, is shown in Fig. 3. The rate of the heterogeneous-catalytic reaction in the flow-through reactor is given by the expression [14]

$$r = dx/d(1/V).$$

The linear portion of the $x = f(1/V)$ dependence corresponds to low conversions and points to the zero order of the dehydration reaction. For the zero-order reaction, the conversion rate is independent of reagent concentrations, i.e., $r = k$, where k is the reaction rate constant. This means that $x = k(1/V)$.

The experimental values of the methanol conversion at feed rates of the methanol vapor exceeding 0.61 ml min^{-1} (zero order of the dehydration reaction) are fitted by a straight line (Fig. 3) with a linear correlation coefficient of 0.999. We find from the equation of this straight line that the rate constant of methanol dehydration is $k = 0.013$ mmol min^{-1}.

We constructed the Arrhenius dependences $\ln x$–T^{-1}, for which the linear correlation coefficient was 0.98–0.99. The activation energies of the dehydration of methanol, E_a, and the logarithms of the preexponential factors, $\ln A_0$, are listed in Table 3. The activation energy and the preexponential factor, obtained for zirconium phosphate, are lower than the corresponding values for alkali metal zirconium phosphates; and for these latter, the two parameters increase with the atomic number of an alkali metal.

The activity of the phosphates under study in the dehydration of methanol can be accounted for by their acid properties, which are determined by coordination-unsaturated Zr^{4+} cations carrying a large charge and exhibiting a high polarizing effect. These ions are possible centers of alcohol adsorption [15, 16]. This is confirmed by the high activity of the phosphate $Zr_3(PO_4)_4$, which contains no alkali metals, in the conversion of methanol. The activity of this phosphate may also be due to its poorer crystallinity (and, as a consequence, to its high specific surface area and porosity), compared with alkali metal zirconium phosphates.

Comparison of the activities (Figs. 1 and 2) and specific surface areas of sodium zirconium phosphates, and of the volume fractions and surface areas of pores in these compounds (Table 2), shows that the catalytic properties depend on all of these factors. The greater these parameters, the higher the activity of the phosphate in the dehydration of methanol. It should be noted that the alkali metal introduced into the structure affects the activity of phosphates in the reaction under consideration not only owing to its electronic structure, but also indirectly, because of a rise in the final temperature of synthesis of the samples, observed as the size of alkali metal atoms increases. This leads to formation of a less defective crystal structure with a lower porosity.

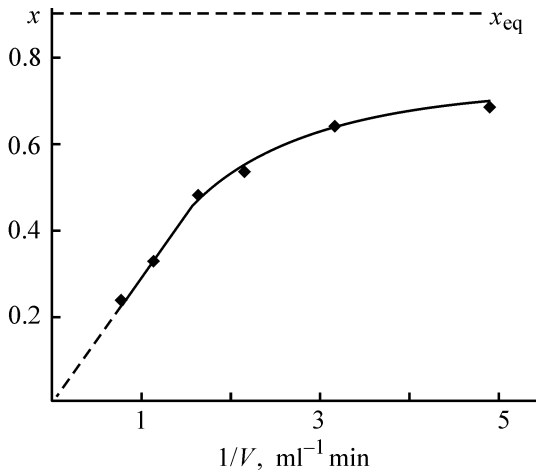


Fig. 3. Degree of methanol conversion, x, on the phosphate $NaZr_2(PO_4)_3$ in the dehydration vs. the reciprocal feed rate of methanol vapor, $1/V$.

The influence of the nature of an alkali metal in alkali metal zirconium phosphates is manifested in the difference in their activities calculated per unit surface area of a catalyst (Table 4). In the tem-

Table 3. Activation energy of the dehydration of methanol, E_a, and logarithm of the preexponential factor, $\ln A_0$, for the phosphates under study

Phosphates	E_a, kJ mol^{-1}	$\ln A_0$
$Zr_{0.25}Zr_2(PO_4)_3$	85	18
$NaZr_2(PO_4)_3$	105	22
$KZr_2(PO_4)_3$	126	25
$CsZr_2(PO_4)_3$	130	26

Table 4. Activity of the phosphates $NaZr_2(PO_4)_3$ and $CsZr_2(PO_4)_3$ in methanol conversion at various temperatures

Phosphate	A, mmol h^{-1} m^{-2}, at indicated temperature, K			
	513	528	543	558
$NaZr_2(PO_4)_3$	0.02	0.05	0.09	0.15
$CsZr_2(PO_4)_3$	0.01	0.02	0.04	0.11

perature range corresponding to the kinetic control of methanol conversion, the activity of the phosphate $NaZr_2(PO_4)_3$ is twice that of $CsZr_2(PO_4)_3$. This can be accounted for by the fact that cations of alkali metals affect the electron density on oxygen atoms bound to zirconium atoms, thereby changing their electropositive and, consequently, acid properties.

The catalysts under study can compete with industrial catalysts for methanol dehydration. For example, the dehydration of methanol in a flow-through reactor on synthetic aluminosilicates was studied in [17]. The authors of that study used for comparison a commercial catalyst DME-FCAT. Comparison of the catalytic activities and methanol conversions at the same temperature for the samples we studied, aluminosilicates examined in [17], and commercial catalysts DME-FCAT suggests that the phosphates $Zr_3(PO_4)_4$ and $NaZr_2(PO_4)_3$ possess a higher output capacity, because they can provide higher, nearly equilibrium degrees of conversion at a 2–10 times greater load on the catalyst.

CONCLUSIONS

(1) Zirconium phosphate $Zr_3(PO_4)_4$ and alkali metal zirconium phosphates $AZr_2(PO_4)_3$ (A = Na, K, Rb, Cs) with NZP-type structure were synthesized by the sol–gel method and characterized by X-ray diffraction analysis, electron microprobe analysis, and capillary condensation of nitrogen.

(2) A study of their catalytic properties in the dehydration of methanol demonstrated that they are active and selective catalysts and compare well with commercial catalysts for methanol dehydration.

(3) It was shown that the activity and the working temperature range of alkali metal zirconium phosphate catalysts depend on the conditions of their synthesis and their composition, porosity, and specific surface area, and also on load.

ACKNOWLEDGMENTS

The study was financially supported by the Russian Foundation for Basic Research (project nos. 05-03-32127 and 03-03-32538).

REFERENCES

1. Williams, R.H and Larson, E.D., *Energy Sustain. Develop.*, 2003, vol. 7, no. 4, pp. 103–129.
2. Ki-Won Jun, Hye-Soon Lee, Hyun-Seog Roh, and Sang-Eon Park, *Bull. Kor. Chem. Soc.*, 2002, vol. 23, pp. 803–806.
3. Bercic, G. and Levec, J., *Ind. Eng. Chem. Res.*, 1992, vol. 31, pp. 1035–1040.
4. Bandiera, J. and Naccache, C., *Appl. Catal.*, 1991, vol. 69, pp. 139–148.
5. Wang, A., Wiegel, S., and Muraro, G., Molecular Sieves as Catalyst for Methanol Dehydration, Topical Report, Air Products and Chemicals Inc., 2002.
6. Pet'kov, V.I. and Orlova, A.I., *Neorg. Mater.*, 2003, vol. 39, no. 10, pp. 1177–1188.
7. Serghini, A., Brochu, R., Ziyad, M., and Vedrine, J.C., *J. Alloys Comp.*, 1992, vol. 188, nos. 1–2, pp. 60–64.
8. Serghini, A., Brochu, R., Ziyad, M., and Vedrine, J.C., *J. Chem. Soc., Faraday Trans.*, 1991, vol. 87, no. 15, pp. 2487–2493.
9. Arsalane, S., Ziyad, M., Courdurier, G., and Vedrine, J.C., *J. Catal.*, 1996, vol. 159, no. 1, pp. 162–169.
10. Orlova, A.I., Pet'kov, V.I., Gul'yanova, S.G., et al., *Zh. Fiz. Khim.*, 1999, vol. 73, no. 11, pp. 1965–1967.
11. Alamo, J. and Roy, J., *J. Am. Ceram. Soc.*, 1984, vol. 67, p. 80.
12. Hong, H.Y.-P., *Mater. Res. Bull.*, 1976, vol. 11, no. 2, pp. 173–182.
13. Song, W., Venimadhayan, G., Manning, J.M., et al., *Ind. Eng. Chem. Res.*, 1998, vol. 37, pp. 1917–1928.
14. Kiperman, L.S., *Vvedenie v kinetiku geterogennykh kataliticheskikh reaktsii* (Introduction to Kinetics of Heterogeneous-Catalytic Reactions), Moscow: Nauka, 1964.
15. Ziyad, M., Rouimi, M., and Portefaix, J.-L., *Appl. Catal. A.*, 1999, vol. 183, pp. 93–105.
16. Ramos, F.S., Duarte de Farias, A.M., Borges, L.E.P., et al., *Catal. Today*, 2005, vol. 101, pp. 39–44.
17. Yaripour, F., Baghaei, F., Schmidt, I., and Perregaard, J., *Catal. Commun.*, 2005, vol. 6, pp. 147–152.

ISSN 1070-4272, Russian Journal of Applied Chemistry, 2006, Vol. 79, No. 4, pp. 619–623. © Pleiades Publishing, Inc., 2006.
Original Russian Text © V. N. Krasil'nikov, A. P. Shtin, V. I. Malkiman, 2006, published in Zhurnal Prikladnoi Khimii, 2006, Vol. 79, No. 4, pp. 627–631.

CATALYSIS

Loss of Activity by Vanadium Sulfuric Acid Catalysts under the Action of Arsenic(III) Oxide Vapor

V. N. Krasil'nikov, A. P. Shtin, and V. I. Malkiman

Institute of Solid State Chemistry, Ural Division, Russian Academy of Sciences, Yekaterinburg, Russia

UNIKhIM SOZ Federal State Unitary Enterprise, Yekaterinburg, Russia

Received September 2, 2005; in final form, December 2005

Abstract—Chemical processes leading to inactivation of vanadium sulfuric acid catalysts by arsenic(III) oxide vapor were studied. The interaction and solubility in the system $VO(H_2AsO_4)_2$–$VOAsO_4$–H_3AsO_4–H_2O and the composition of oxovanadium arsenate in a mixed oxidation state, used as a starting substance in synthesis of $(V^{IV}O)(V^{V}O)_2(As_2O_7)_2$, were examined.

DOI: 10.1134/S1070427206040227

Vanadium catalysts for conversion of sulfur dioxide are comparatively stable against As_2O_3 vapor. Nevertheless, the activity of the catalysts gradually decreases upon a prolonged contact with an insufficiently purified gaseous reaction mixture and may be completely lost if concentration of impurities is too high. By the term "catalyst poisoning" is commonly understood the considerable and abrupt loss of activity, caused by contact with trace amounts of a catalytic poison. There exist various concepts concerning the nature of the inactivating effect of arsenic(III) oxide on vanadium sulfuric acid catalysts. In Boreskov's opinion [1], As_2O_3 is oxidized in the course of sulfur dioxide conversion to As_2O_5, which further reacts with the active component to form a compound of composition $V_2O_5 \cdot As_2O_5$, which is volatile at $T > 550$°C. As a rule, there is no arsenic in the first catalyst bed of a reactor, in which temperature may be as high as 600–650°C. However, arsenic is deposited in the subsequent beds, and especially in the third and fourth, in which the temperature commonly does not exceed 450°C, in the maximum amounts, presumably in the form of the compound $V_2O_5 \cdot As_2O_5$. At temperatures lower than 600°C, the surface of catalyst grains can be blocked by arsenic(V) oxide. According to another interpretation, As_2O_5 reacts with molten potassium bisulfate to give potassium arsenates or sulfate–arsenates [2], in which case sulfur trioxide is released into the gas phase.

Interpretations of the mechanism by which arsenic(III) oxide is oxidized on vanadium catalysts are also ambiguous. According to [3], oxidation of SO_2 and As_2O_3 involves various activating centers. Van'kov and Perevozchikov [4] regard potassium bisulfate as the most probable oxidant of As_2O_3 and believe that the presence of arsenic in the active component favors transition of vanadium to the highest oxidation state, V(V). At the same time, Boreskov believes [1] that vanadium(V) is the agent that oxidizes arsenic(III) on the vanadium(V) catalyst.

The concentration of As_2O_3 vapor in the contact gas mixtures in manufacture of sulfuric acid depends on the degree of their purification. It is believed that, at plants of nonferrous metallurgy in the Ural region, the most arsenic-contaminated gas mixtures are used by Krasnoural'sk copper-smelting combine (KUMK), because the service life of vanadium catalysts for sulfur dioxide conversion at this plant is strongly limited [5]. To reveal the nature of the inactivating influence exerted by arsenic(III) oxide, we examined grains of SVD catalyst (vanadium sulfate catalyst on diatomite) that had worked for 1.5 years in a reactor for sulfur dioxide conversion under conditions of an increased concentration of As_2O_3 vapor and completely lost its catalytic activity for this reason.

EXPERIMENTAL

Samples of grains of an inactivated catalyst were taken at different points of catalyst beds II, III, and

Results obtained in a chemical analysis of grains of an SVD-type catalyst inactivated in operation in a sulfuric acid reactor at KUMK

Bed	As(V)	V(IV)	V(V)	V_{tot}
	wt %			
I	–	–	–	–
II	0.98	2.60	0.56	3.16
III	2.68	3.47	3.54	7.01
IV	3.05	3.44	3.86	7.30

IV of the reactor, in which the concentration of arsenic compounds was very high. The grains taken for study were stored under conditions that provided their total isolation from the environment. The phase analysis of the samples was made using a DRON-3 UM X-ray diffractometer with Cu K_α radiation and a POLAM S-112 polarization microscope with optical-immersion control. The chemical analysis of the samples for the content of potassium, vanadium(V) and (IV), sulfur, and arsenic was performed by the standard commonly accepted procedures. Particular attention was given to analysis of the chemical and phase composition and structure of the surface (0.1–0.2-mm-thick) layer of the grains. Individual chemical compounds necessary for the experiments and, in particular, $VOAsO_4 \cdot 3H_2O$ and $VO(H_2AsO_4)_2$ were synthesized by previously developed techniques [6–8] with reagents of, at least, chemically pure grade.

The table lists the results of a chemical analysis of grains taken from catalyst beds II, III, and IV of a reactor for sulfur dioxide conversion at KUMK. To the observed increase in the concentration of arsenic(V) on passing from bed II to bed IV corresponds the rise in the total concentration of vanadium, in agreement with the opinion that it is transferred together with arsenic in the form of a volatile compound $V_2O_5 \cdot As_2O_5$ [1, 9]. At the same time, the high concentration of vanadium(IV) in the grains (especially in their surface layer) gives reason to assume that arsenic(V) compounds containing reduced vanadium can be formed in the grains. In 0.1–0.2-mm-thick sections from the surface of grains, the concentration of As(V) was as high as 11.6–12.2 wt %.

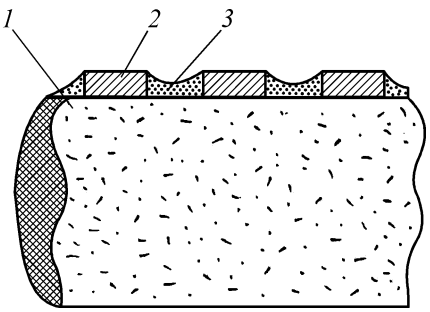


Fig. 1. Schematic cross-sectional view of a grain of inactivated SVD-type catalyst. (*1*) Cross-section of a grain, (*2*) deposited crystals of arsenic compounds, and (*3*) gray-blue glass.

Grains of a freshly prepared SVD catalyst are yellow and have a rough surface; the coloration of grains of an inactivated catalyst is light blue or gray-blue, and the grain surface is smooth and hard. An analysis of sections of the grain surface under a microscope demonstrated that the crust covering the grains is a gray-blue glass well soluble in water. According to the results of a chemical analysis, the content of vanadium(V) in this glass is virtually zero, that of vanadium(IV) is close to 7.5 wt %, and the content of arsenic(V), 21 wt %. After the glass is removed by dissolution in water, regularly arranged black cylindrical outgrowths composed of coarse well-formed lamellar crystals become visible on the grain surface (Fig. 1). A characteristic feature of these crystals is a clearly pronounced dichroism (their coloration varies from greenish brown, nearly black to light green with their rotation in polarized light under a microscope). This fact indicates the possible presence of vanadium in two oxidation states, (V) and (IV), in their structure. Optical properties of this kind are observed for crystals of a phase of composition $(V^{IV}O)(V^{V}O)_2(As_2O_7)_2$, synthesized by partial oxidation of $VO(AsO_3)_2$ with atmospheric oxygen upon heating [6] and by dehydration of $(V^{IV}O)(V^{V}O)_2(HAsO_4)_4 \cdot 5H_2O$ and $(V^{IV}O)(V^{V}O)_2(HAsO_4)_4$ in an inert medium at 450°C [7, 8].

The contents of vanadium(V), vanadium(IV), and arsenic(V) in aggregates of crystals detached from the surface of grains from catalyst bed IV of the reactor are 10.6, 4.9, and 30.2 wt %, respectively; the average concentration of potassium does not exceed 0.5 wt % (V^V/V^{IV}) ~2]. This indicates that potassium is not contained in the compound that forms outgrowths on the surface of catalyst grains. In the atmosphere of saturated water vapor, inactivated grains very rapidly disintegrate, with crystals in the surface outgrowths being decomposed into light yellow and blue phases, whose crystal-optical constants and interplanar spacings coincide with published values for $VOAsO_4 \cdot 3H_2O$ (light yellow coloration) [10] and $VO(H_2AsO_4)_2$ (blue) [11]. Consequently, the compound found in the outgrowths on the surface of inactivated catalyst grains is close in chemical nature and composition to the above-described oxovanadium

arsenates, i.e., it includes vanadium in two oxidation states, V(V) and V(IV).

The following transformations were observed in a saturated water vapor for $(V^{IV}O)(V^{V}O)_2(As_2O_7)_2$:

$$(V^{IV}O)(V^{V}O)_2(As_2O_7)_2 + 2H_2O = (V^{IV}O)(V^{V}O)_2(HAsO_4)_4, \quad (1)$$

$$(V^{IV}O)(V^{V}O)_2(As_2O_7)_2 + 7H_2O = (V^{IV}O)(V^{V}O)_2(HAsO_4)_4 \cdot 5H_2O. \quad (2)$$

Reaction (1) is an intermediate stage of reaction (2), and, therefore, the best way to synthesize hygroscopic $(V^{IV}O)(V^{V}O)_2(HAsO_4)_4$ is thermolysis of $(V^{IV}O)(V^{V}O)_2(HAsO_4)_4 \cdot 5H_2O$ with slow heating to 120–130°C. AS a result of contact with an excess amount of water at room temperature, $(V^{IV}O)(V^{V}O)_2(HAsO_4)_4 \cdot 5H_2O$ decomposes to give crystals of $VOAsO_4 \cdot 3H_2O$ and $VO(H_2AsO_4)_2$.

A comparison of the crystal-optical properties and X-ray diffraction patterns of $(V^{IV}O)(V^{V}O)_2(HAsO_4)_4 \cdot 5H_2O$, $(V^{IV}O)(V^{V}O)_2(HAsO_4)_4$, $(V^{IV}O)(V^{V}O)_2(As_2O_7)_2$, and crystals from the outgrowths on the surface of grains of an inactivated SVD catalyst demonstrated that each of these compounds may be present in the outgrowths. Apparently, an arsenate of composition $(V^{IV}O)(V^{V}O)_2(As_2O_7)_2$ is originally formed on the grain surface and then, in storage in air, it absorbs water vapor and transforms into $(V^{IV}O)(V^{V}O)_2(HAsO_4)_4$ or $(V^{IV}O)(V^{V}O)_2(HAsO_4)_4 \cdot 5H_2O$. A similar transformation may occur in washing grains with water to remove the glass and crystal aggregates from their surface. In addition to $(V^{IV}O)(V^{V}O)_2(As_2O_7)_2$, presence of oxovanadium(V) orthoarsenate of composition $VOAsO_4$ or $V_2O_5 \cdot As_2O_5$ was revealed [1], even though not indisputably, by X-ray phase analysis in out-growths on grains of an inactivated catalyst that worked in the middle part of catalyst bed IV.

Figure 2 compares X-ray diffraction patterns of $(V^{IV}O)(V^{V}O)_2(HAsO_4)_4 \cdot 5H_2O$ and a preparation composed of ground crystal aggregates scraped-off from grains of an inactivated SVD crystal, preliminarily washed in water to remove the glass. The X-ray diffraction pattern of the preparation of crystal aggregates differs from that for $(V^{IV}O)(V^{V}O)_2(HAsO_4)_4 \cdot 5H_2O$ only in the presence of a line (marked by arrow) coinciding in position with the strongest line in the X-ray diffraction pattern of $(V^{IV}O)(V^{V}O)_2(As_2O_7)_2$ [6, 7]. The X-ray diffraction pattern of the aggregates cut-off from the grains not washed with water contained only lines of $(V^{IV}O)(V^{V}O)_2(As_2O_7)_2$, whereas

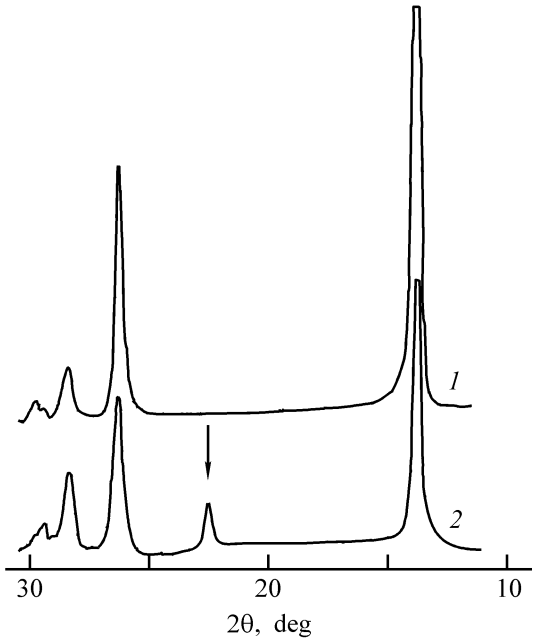


Fig. 2. X-ray diffraction patterns of (*1*) $(V^{IV}O)(V^{V}O)_2(AsO_4)_4 \cdot 5H_2O$ and (*2*) crystal aggregates removed from the surface of grains of the SVD catalyst. Arrow denotes the strongest line belonging to $(V^{IV}O)(V^{V}O)_2(As_2O_7)_2$.

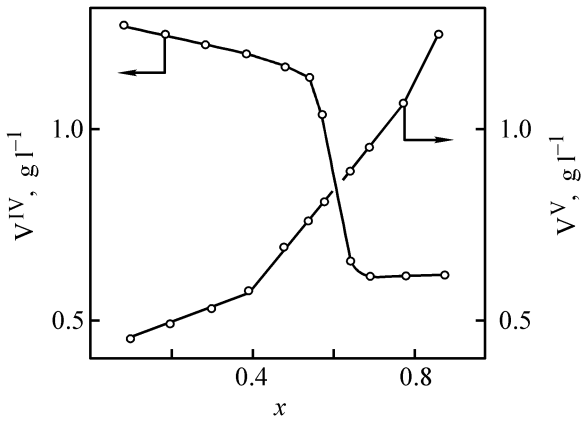


Fig. 3. Content of vanadium(V) and vanadium(IV) in the liquid phase of the system $VO(H_2AsO_4)_2$–$VOAsO_4$–H_3AsO_4–H_2O vs. x in the isomolar set of compositions of the section $(1 - x)VO(H_2AsO_4)_2 + xVOAsO_4 \cdot 3H_2O$.

after washing, lines of $(V^{IV}O)(V^{V}O)_2(HAsO_4)_4 \cdot 5H_2O$ and $(V^{IV}O)(V^{V}O)_2(HAsO_4)_4$ appeared in the pattern.

To reveal the possibility of formation of oxovanadium arsenates in a mixed oxidation state (IV, V), other than $(V^{IV}O)(V^{V}O)_2(HsO_4)_4 \cdot 5H_2O$, which serves as the main starting substance in synthesis of $(V^{IV}O)(V^{V}O)_2(As_2O_7)_2$, the interaction and solubility in the system $VO(H_2AsO_4)_2$–$VOAsO_4$–H_3AsO_4–H_2O

was studied at room temperature. The starting mixtures of solid oxovanadium(IV) and oxovanadium(V) arsenates comprised an isomolar set of compositions from the section $(1 - x)VO(H_2AsO_4)_2 + xVOAsO_4 \cdot 3H_2O$ at a total molar content of the arsenates equal to 0.01 M. The initial concentration of arsenic acid was constant (2 M).

Analysis of the solubility curves of vanadium for the system under study (Fig. 3) shows that, at $x \geq 0.6$, the concentration of vanadium(IV) in solution abruptly decreases and then remains constant at $x > 0.7$. The curve describing the dependence of the concentration of vanadium in solution on x shows two weak bends at $x = 0.4$ and 0.75. According to the results of a microscopic analysis, the bottom phase is constituted at $x = 0.1–0.5$ by blue crystals of $VO(H_2AsO_4)_2$ and by a new compound, whose formation is evidenced by the presence of black squared plates. At $x = 0.6–0.7$, the bottom phase has the form of black squared plates that well reflect light; at $x > 0.7$ yellow crystals of $VOAsO_4 \cdot 3H_2O$ are additionally present. The liquid phase acquires a dark green coloration, which is the most intense at $x = 0.6–0.7$. Microscopic, X-ray phase, and chemical analyses revealed that the new phase is identical to the previously obtained [7] compound of composition $(V^{IV}O)(V^{V}O)_2(HAsO_4)_4 \cdot 5H_2O$. The study performed demonstrated that no other oxovanadium arsenates in mixed oxidation state are formed in the given system.

The most probable agent that oxidizes As_2O_3 on vanadium catalysts is vanadium(V). This is confirmed by the results of a study of reaction of As_2O_3 with $K_4V_2O_3(SO_4)_4$ and $K_3VO(SO_4)_3$, compounds simulating the active component of vanadium catalysts [8], in sealed argon-filled quartz ampules at 300–450°C:

$$K_4V_2O_3(SO_4)_4 + As_2O_3 = \{4K_2VO(SO_4)_2 + As_2O_5\}, \quad (3)$$

$$K_3VO(SO_4)_3 + As_2O_3 = \{4K_2VO(SO_4)_2 + 2K_2S_2O_7 + As_2O_5\}. \quad (4)$$

Under the same conditions, vanadium(V) oxide reacts with arsenic(III) oxide [12]:

$$2V_2O_5 + As_2O_3 = V_4As_2O_{13} \quad (5)$$
$$[4V^{(V)} + 2As^{(III)} = 4V^{(IV)} + 2As^{(V)}].$$

Reactions (3) and (4) are written with account of the constant mass of the samples; the reaction products are enclosed in braces because they form blue glasses and were not isolated in the form of crystals. As the concentration of As_2O_3 is lowered, green hygroscopic glasses containing vanadium in two states, V(V) and V(IV), are formed in the reaction mixtures.

The interaction of sulfur dioxide with oxovanadium(V) orthoarsenate at 400–450°C occurs in accordance with the most probable reaction

$$2VOAsO_4 + SO_2 = (VO)_2As_2O_7 + SO_3\uparrow. \quad (6)$$

The composition of the X-ray amorphous phase $(VO)_2As_2O_7$ was determined from the results of chemical [quantitative analysis for the content of V(V), V(IV), and arsenic] and gravimetric analysis (evaluation of the sample mass in the course of the reaction). Thus, reactions (3)–(6) show that vanadium(V) in the active component of sulfuric acid catalysts is the only oxidizing agent both for SO_2 and for As_2O_3. Raising the reaction temperature leads only to elimination of sulfur trioxide (reversible process) in the first case, and to removal of vanadium from the active component and to volatilization of vanadium at high temperatures, presumably in the form of $VOAsO_4$ or $V_2O_5 \cdot As_2O_5$, and its transfer to reaction zones having lower temperatures [1]. Sulfur dioxide reduces vanadium even in the structure of $VOAsO_4$. Therefore, this compound, present on the surface of catalyst grains in catalyst beds III and IV, can react with sulfur dioxide to give compounds of vanadium(IV) or vanadium in a mixed oxidation state (IV, V) and, in particular, $(V^{IV}O)(V^{V}O)_2(As_2O_7)_2$. In any case, formation of oxovanadium arsenates leads to removal of vanadium from the active component and, consequently, adversely affects the performance of the catalysts.

CONCLUSIONS

(1) A study of grains of an SVD catalyst that lost its activity upon prolonged operation under conditions of insufficient purification of contact gases to remove arsenic(III) oxide vapor revealed aggregates of crystals composed of arsenates of oxovanadium in a mixed oxidation state, $(V^{IV}O)(V^{V}O)_2(As_2O_7)_2$ and a gray-blue glass with an exceedingly high content of vanadium(IV) and arsenic.

(2) In activation of sulfuric acid vanadium catalysts lose their activity upon a prolonged contact with As_2O_3 vapor is caused by blocking of the working surface of their grains by compounds of arsenic with vanadium(V) and (IV) and vanadium in a mixed oxidation state (V, IV). The formation of com-

pounds of arsenic and vanadium on the surface of catalyst grains leads to an irreversible change in the composition of the active component and, accordingly, to inactivation of the catalyst. As_2O_3 and SO_2 are oxidized at the same active vanadium centers.

REFERENCES

1. Boreskov, G.K., *Kataliz v proizvodstve sernoi kisloty* (Catalysis in Manufacture of Sulfuric Acid), Moscow: Goskhimizdat, 1954.
2. Kholostov, S.B., Ketov, L.N., and Bankovskaya, V.R., *Zh. Prikl. Khim.*, 1981, vol. 26, no. 7, pp. 1900–1904.
3. Adadurov, I.E., Pershin, P.P., and Novikova, T.N., *Zh. Prikl. Khim.*, 1934, vol. 7, no. 1–2, pp. 18–27.
4. Van'kov, B.P. and Perevozchikov, L.A., Available from ONIITEKhIM, 1985, Cherkassy, no. 66 khp–85 Dep.
5. Kopylov, N.I. and Kalinskii, Yu.D., *Khim. Inter. Ustoich. Razv.*, 1997, no. 5, pp. 221–258.
6. Krasil'nikov, V.N. and Shtin, A.P., *Zh. Prikl. Khim.*, 1991, vol. 64, no. 9, pp. 1818–1822.
7. Krasil'nikov, V.N. and Shtin, A.P., *Zh. Neorg. Khim.*, 1993, vol. 38, no. 7, pp. 1118–1120.
8. Krasil'nikov, V.N., Oxosulfovanadates and the Chemical Nature of the Active Component in Vanadium Sulfuric Acid Catalysts, *Doctoral Dissertation*, Yekaterinburg: Inst. of Solid State Chemistry, Ural Division, Russian Acad. Sci., 2003.
9. Petrovskaya, G.I., Gerke, L.S., and Novikova, T.N., *Khim. Prom–st.*, 1999, no. 2, pp. 12–15.
10. Chernorukov, N.G., Egorov, N.P., and Korshunov, I.A., *Zh. Neorg. Khim.*, 1978, vol. 23, no. 10, pp. 2672–2675.
11. Aranda, M.A.G., Attfield, J., Bruque, S., and Martinez-Lara, M., *J. Solid State Chem.*, 1991, vol. 91, no. 1, pp. 25–31.
12. Haddad, A., Jouini, T., and Piffard, Y., *J. Solid State Chem.*, 1992, vol. 54, no. 1, pp. 57–63.

ISSN 1070-4272, Russian Journal of Applied Chemistry, 2006, Vol. 79, No. 4, pp. 624–630. © Pleiades Publishing, Inc., 2006.
Original Russian Text © V. M. Chernyshev, V. A. Rakitov, A. V. Astakhov, A. N. Sokolov, N. D. Zemlyakov, V. A. Taranushich, 2006, published in Zhurnal Prikladnoi Khimii, 2006, Vol. 79, No. 4, pp. 632–638.

ORGANIC SYNTHESIS AND INDUSTRIAL ORGANIC CHEMISTRY

Regioselective Synthesis of Alkyl Derivatives of 3,5-Diamino-1,2,4-triazole

V. M. Chernyshev, V. A. Rakitov, A. V. Astakhov, A. N. Sokolov, N. D. Zemlyakov, and V. A. Taranushich

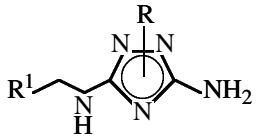
South-Russian State Technical University, Novocherkassk, Rostov oblast, Russia

Received December 21, 2005

Abstract—New procedures were suggested for regioselective synthesis of alkyl derivatives of 3,5-diamino-1,2,4-triazole.

DOI: 10.1134/S1070427206040239

Alkyl derivatives of 3,5-diamino-1,2,4-triazole of general formula **I** are used in medicine as blockators of histamine [1, 2] and neurokinin [3] receptors, inhibitors of peroxide oxidation of lipids [4], and agents for treating diabetes and other diseases [5, 6].



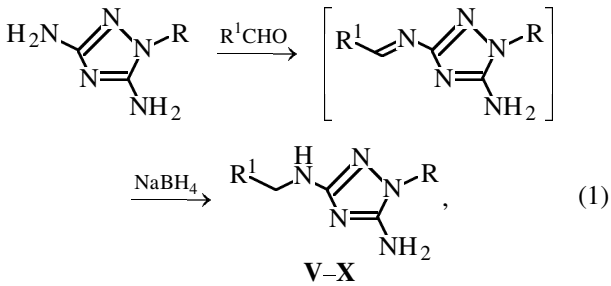
I

The most important synthetic routes to compounds **I** are based on condensation of hydrazines $RNHNH_2$ with *N*-alkyl-*N*'-cyano-*S*-methylisothioureas [2, 6, 7], 3-R^1-2-cyanoiminothiazolidines [4], or *N*-alkyl-*N*'-cyano-*O*-phenylisoureas [3, 8], or on base-catalyzed cyclization of 1-alkyl-3-isopropylidenaminoamidinothioureas [9] prepared by the reaction of isopropylidenaminoguanidine with alkyl isothiocyanates. The major drawbacks of methods [2, 4, 6–9] is the use of difficultly available expensive chemicals or low yield of the target products. Furthermore, the reactions of *N*-cyano compounds with substituted hydrazines ($R \neq H$) sometimes yield mixtures of regioisomers [8].

It seems more promising to prepare compounds **I** from readily accessible 3,5-diamino-1-R-1,2,4-triazoles (R = H, Alk, Ar). For example, by alkylation of 3,5-diamino-1-phenyl-1,2,4-triazole with 2-methoxybenzyl chloride under the conditions of deprotonation of the amino group (THF, *t*-BuOK), Dunstan et al. [3] prepared 3-amino-5-*o*-methoxybenzylamino-1-phenyl-1,2,4-triazole in 30% yield [3]. However, alkylation is not a versatile route to compounds **I**, because at R = H this reaction occurs at the 1-position of the triazole ring [7, 10].

The goal of this study was to develop new procedures for regioselective synthesis of alkyl derivatives of 3,5-diamino-1,2,4-triazole of general formula **I**. We found that an efficient route to 3-alkylamino-5-amino-1-R-1,2,4-triazoles (R = H, Bn, Ph) is hydrogenation of Schiff bases prepared by reactions of 3,5-diamino-1-R-1,2,4-triazoles **II**–**IV** with aldehydes.

Condensation of diamines **II** and **III** with aldehydes at eqimolar ratio of the reactants or at a small excess of diamine in ethanol occurs regioselectively at the 3-amino group [10]. Hydrogenation of Schiff bases with sodium borohydride was performed without their isolation from the reaction mixture [scheme (1)]; in the process, we obtained 5-amino-1-benzyl-3-benzylamino-1,2,4-triazole **V**, 5-amino-1-benzyl-3-*p*-methoxybenzylamino-1,2,4-triazole **VI**, 5-amino-3-*o*-methoxybenzylamino-1-phenyl-1,2,4-triazole **VII**, 5-amino-1-phenyl-3-(2-furylmethyl)amino-1,2,4-triazole **VIII**, 5-amino-3-(4-benzyloxybenzyl)amino-1-phenyl-1,2,4-triazole **IX**, and 5-amino-1-phenyl-3-(3-phenylpropyl)-amino-1,2,4-triazole **X**:



V–**X** (1)

where R = Bn (**II**, **V**, **VI**), Ph (**III**, **VII**–**X**), R^1 = Ph (**V**), *p*-$MeOC_6H_4$ (**VI**), *o*-$MeOC_6H_4$ (**VII**), 2-furyl (**VIII**), = *p*-$BnOC_6H_4$ (**IX**), $PhCH_2CH_2$ (**X**).

The yields and properties of **V**–**X** are given in the table.

To prepare 3-alkylamino-5-amino-1,2,4-triazoles (R = H), it is advisable to use instead of expensive 3,5-diamino-1,2,4-triazole **IV** its more available derivatives: nitrate **XI** [11, 12] or 1-acetyl-3,5-diamino-1,2,4-triazole **XII** [13]. To prepare alkyl derivatives from nitrate **XI**, it is necessary to add to the reaction

Yields and properties of the sompounds synthesized

Compound no.*	Yield, % (synthesis procedure)	mp, °C	Found, % / Calculated, %			Formula	^{1}H NMR spectrum, δ, ppm (*J*, Hz)
			C	H	N		
V	61	173–175	68.5 / 68.8	6.0 / 6.1	25.2 / 25.0	$C_{16}H_{17}N_5$	4.16 d (2H, CH_2, *J* = 6.5), 4.86 s (2H, CH_2), 5.85 t (1H, NH, *J* = 6.5), 6.04 s (2H, NH_2), 7.11–7.30 m (10H, 2Ph)
VI	65	169–170	66.1 / 66.0	6.3 / 6.2	22.4 / 22.6	$C_{17}H_{19}N_5O$	3.70 s (3H, OMe), 4.08 d (2H, CH_2, *J* = 6.5), 4.86 s (2H, CH_2), 5.73 t 1H, NH, *J* = 6.5), 6.03 s (2H, NH_2), 6.80 m (2H, arom.), 7.11–7.31 m (7H, arom.)
VII	72	171–172	65.3 / 65.1	5.7 / 5.8	23.5 / 23.7	$C_{16}H_{17}N_5O$	3.79 s (3H, OMe), 4.24 d (2H, CH_2, *J* = 6.4), 5.63 t (1H, NH, *J* = 6.4), 6.22 s (2H, NH_2), 6.84–6.96 m (2H, arom.), 7.15–7.21 m (2H, arom.), 7.28 m (1H, arom.), 7.37–7.47 m (4H, arom.)
VIII	66	136–137	61.2 / 61.2	5.0 / 5.1	27.7 / 27.4	$C_{13}H_{13}N_5O$	4.22 d (2H, CH_2, *J* = 6.3), 6.12 t (1H, H, *J* = 6.3), 6.21 m (1H, CH of furan), 6.24 s (2H, NH_2), 6.35 m (1H, CH of furan) 7.20 m (1H, CH of furan), 7.39–7.52 m (5H, Ph)
IX	60	167–168	71.4 / 71.1	5.6 / 5.7	19.0 / 18.9	$C_{22}H_{21}N_5O$	4.17 d (2H, CH_2, *J* = 6.2), 5.05 s (2H, CH_2), 6.13 t (1H, NH, *J* = 6.2), 6.21 s (2H, NH_2), 6.92 m (2H, arom.), 7.17–7.48 m (12H, arom.)
X	70	114–115	70.0 / 69.6	6.4 / 6.5	23.8 / 23.9	$C_{17}H_{19}N_5$	1.80 m (2H, CH_2), 2.62 t (2H, CH_2, *J* = 7.6), 3.05 m (2H, CH_2), 5.67 br.s (1H, NH), 6.18 s (2H, NH_2), 7.15–7.28 m (6H, arom.), 7.38–7.49 m (4H, arom.)
XIII	40 (A)	147–148 148–149 [9]	57.3 / 57.1	6.1 / 5.9	36.9 / 37.0	$C_9H_{11}N_5$	4.20 d (2H, CH_2, *J* = 6.2), 5.32 br.s (2H, NH_2), 6.09 br.s (1H, NH), 7.17–7.28 m (5H, Ph), 10.72 s (1H, NH)
XIV	60 (A) 76 (B)	194–196	54.7 / 54.8	6.0 / 6.0	32.0 / 31.9	$C_{10}H_{13}N_5O$	3.69 s (3H, OMe), 4.11 d (2H, CH_2, *J* = 6.5), 5.37 br.s (2H, NH_2), 5.85 br.s (1H, NH), 6.82 d (2H, arom., *J* = 8.6), 7.21 d (2H, arom.), 10.68 s 1H, NH)
XV	60 (A)	193–194	48.1 / 48.3	4.6 / 4.5	31.5 / 31.3	$C_9H_{10}N_5Cl$	4.18 d (2H, CH_2, *J* = 6.3), 5.50 br.s (2H, NH_2), 6.0 br.s (1H, NH), 7.26–7.35 m (4H, arom.), 10.7 br.s (1H, NH)
XVI	62 (B)	178–180	46.2 / 46.1	4.3 / 4.3	36.0 / 35.9	$C_9H_{10}N_6O_2$	4.31 d (2H, CH_2, *J* = 5.9), 5.65 br.s (2H, NH_2), 6.16 br.s (1H, NH), 7.57 m (1H, arom.), 7.76 m (1H, arom.), 8.04 m (1H, arom.), 8.17 s (1H, arom.), 10.71 s (1H, NH)

Table. (Contd.)

Compound no.*	Yield, % (sinthesis procedure)	mp, °C	Found, % / Calculated, %			Formula	^{1}H NMR spectrum, δ, ppm (*J*, Hz)
			C	H	N		
XVII	78 (B)	207–208	40.3 / 40.3	3.9 / 3.8	26.0 / 26.1	$C_9H_{10}N_5Br$	4.19 d (2H, CH_2, *J* = 6.4), 5.42 br.s (2H, NH_2), 6.15 br.s (1H, NH), 7.25 m (2H, arom.), 7.37 m (1H, arom.), 7.47 s (1H, arom.), 10.73 br.s (1H, NH)
XVIII	70 (B)	238–240	53.1 / 53.0	6.2 / 6.1	28.0 / 28.1	$C_{11}H_{15}N_5O_2$	3.69 s (3H, OMe), 3.70 s (3H, OMe), 4.11 d (2H, CH_2, *J* = 6.4), 5.50 br.s (3H, NH + NH_2), 6.82 m (2H, arom.), 6.92 s (1H, arom.), 10.70 br.s (1H, NH)
XIX	50 (B)	138–139	43.1 / 43.0	4.6 / 4.7	36.0 / 35.9	$C_7H_9N_5S$	4.35 d (2H, CH_2, *J* = 5.8), 5.63 br.s (2H, NH_2), 5.81 br.s (1H, NH), 6.91 m (2H, 2CH of thiophene), 7.30 m (1H, CH of thiophene), 10.7 s (1H, NH)
XX	40	123–124	61.0 / 60.8	7.1 / 7.0	31.9 / 32.2	$C_{11}H_{15}N_5$	1.74 m (2H, CH_2), 2.58 t (2H, CH_2, *J* = 7.7), 2.98 m (2H, CH_2), 4.81 br.s (1H, NH), 5.40 br.s (2H, NH_2), 7.11–7.28 m (5H, Ph), 10.66 s (1H, NH)
XXI	34	170–171	71.3 / 71.6	7.6 / 7.5	20.7 / 20.9	$C_{20}H_{25}N_5$	1.75 m (4H, $2CH_2$), 2.58 t (4H, $2CH_2$, *J* = 7.7), 2.99 m (4H, $2CH_2$), 5.72 br.s (2H, 2NH), 7.12–7.28 m (10H, 2Ph), 10.76 s (1H, NH)
XXIV	72	181–182	64.3 / 64.5	5.2 / 5.1	20.9 / 20.9	$C_{18}H_{17}N_5O_2$	2.07 s (3H, Me), 3.94 s (3H, OMe), 7.09 m (1H, arom.), 7.21 m (1H, arom.), 7.42 m (1H, arom.), 7.56–7.65 m (3H, arom.), 7.79 m (2H, arom.), 7.98 m (1H, arom.), 9.58 s (1H, CH=N), 10.60 s (1H, NH)
XXV	78	194–195	64.0 / 64.1	5.9 / 5.7	20.5 / 20.8	$C_{18}H_{19}N_5O_2$	1.95 s (3H, Me), 3.79 s (3H, OMe), 4.40 d (2H, CH_2, *J* = 5.6), 6.86–6.96 m (2H, arom.), 7.06 t (1H, NH, *J* = 5.6), 7.18–7.23 m (2H, arom.), 7.38 m (1H, arom.), 7.50–7.57 m (4H, arom.), 10.18 br.s (1H, NH)
XXVI	73	114–115	68.1 / 68.0	6.2 / 6.3	20.7 / 20.9	$C_{19}H_{21}N_5O$	1.90 s (3H, Me), 2.25 s (3H, Me), 4.36 d (2H, CH_2, *J* = 5.5), 5.08 s (2H, CH_2), 7.07–7.35 m (10H, arom. NH), 10.0 br.s (1H, NH)
XXVII	68	128–129	67.3 / 67.3	5.9 / 6.0	21.7 / 21.8	$C_{18}H_{19}N_5O$	1.98 s (3H, Me), 2.25 s (3H, Me), 4.37 d (2H, CH_2, *J* = 5.8), 7.08–7.51 m (10H, arom. + NH), 10.13 s (1H, NH)
XXVIII	78	186–187	58.2 / 57.9	4.5 / 4.6	24.1 / 23.9	$C_{17}H_{16}N_6O_3$	1.96 s (3H, Me), 4.54 d (2H, CH_2, *J* = 5.6), 7.36–7.64 m (7H, arom. + NH), 7.81 m (1H, arom.), 8.04–8.19 m (2H, arom.), 10.15 s (1H, NH)
XXIX	74	121–123	57.5 / 57.5	5.0 / 4.9	22.6 / 22.4	$C_{15}H_{15}N_5OS$	2.00 s (3H, Me), 4.58 d (2H, CH_2, *J* = 5.9), 6.92–7.00 m (2H, CH of thiophene + NH), 7.34–7.54 m (7H, Ph + CH of thiophene), 10.18 s (1H, NH)

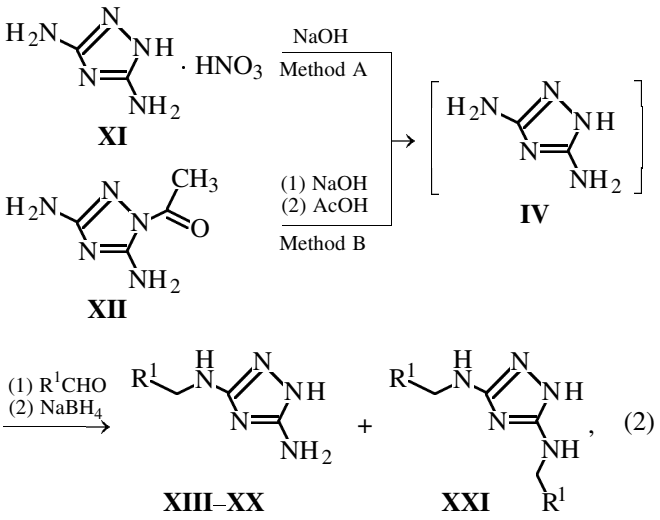
Table. (Contd.)

Compound no.*	Yield, % (sinthesis procedure)	mp, °C	Found, % / Calculated, %			Formula	^{1}H NMR spectrum, δ, ppm (*J*, Hz)
			C	H	N		
XXX	70	125–126	65.3 / 65.1	5.8 / 5.8	23.6 / 23.7	$C_{16}H_{17}N_5O$	3.79 s (3H, OMe), 4.38 d (2H, CH_2, *J* = 5.8), 5.19 s (2H, NH_2), 6.74 t (1H, NH, *J* = 5.8), 6.86–6.96 m (2H, arom.), 7.17–7.26 m (3H, arom.), 7.43–7.52 m (4H, arom.)
XXXI	86	131–132	69.4 / 69.6	6.6 / 6.5	23.7 / 23.9	$C_{17}H_{19}N_5$	2.25 s (3H, Me), 4.33 d (2H, CH_2, *J* = 5.9), 4.84 s (2H, NH_2), 4.89 s (2H, CH_2), 6.88 t (1H, NH, *J* = 5.9), 7.06–7.32 m (9H, arom.)
XXXII	85	121–122	68.6 / 68.8	6.2 / 6.1	25.2 / 25.1	$C_{16}H_{17}N_5$	2.25 s (3H, Me), 4.35 d (2H, CH_2, *J* = 5.7), 5.17 s (2H, NH_2), 6.90 (1H, NH, *J* = 5.7), 7.09 m (2H, arom.), 7.19–7.24 m (3H, arom.), 7.40–7.48 m (4H, arom.)
XXXIII	83	137–138	58.3 / 58.1	4.7 / 4.6	27.3 / 27.1	$C_{15}H_{14}N_6O_2$	4.51 d (2H, CH_2, *J* = 5.7), 5.19 s (2H, NH_2), 7.16 t (1H, NH, *J* = 5.7), 7.22–7.28 m (1H, arom.), 7.43–7.48 m (4H, arom.), 7.58–7.63 m (1H, arom.), 7.77–7.81 m (1H, arom.), 8.06–8.18 m (2H, arom.)
XXXIV	68	144–146	57.3 / 57.5	4.7 / 4.8	26.0 / 25.8	$C_{13}H_{13}N_5S$	4.55 d (2H, CH_2, *J* = 5.9), 5.23 s (2H, NH_2), 6.91–6.98 m (2H, CH of thiophene), 7.04 t (1H, NH, *J* = 5.9), 7.23–7.44 m (6H, Ph + CH of thiophene)

* Compounds **V**, **VI**, **VIII**, **IX**, **XIV**–**XVIII**, **XXI**, **XXIV**–**XIX**, **XXXII**, and **XXXIII** were srystallized from EtOH; **VII**, **X**, and **XXX**, from MeCN; and **XIII**, **XIX**, **XIX**, **XX**, and **XXXIV**, from H_2O.

mixture an equivalent amount of NaOH to adjust the required pH 7–9.

With acetyl derivative **XII** used as the starting compound, the first step is base hydrolysis to diamine **IV**; this is followed by the reaction with an aldehyde and hydrogenation of the resulting Schiff base [scheme (2)]:



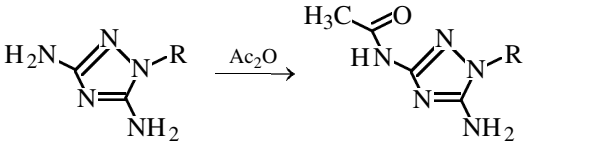
(2)

where R^1 = Ph (**XIII**), *p*-$MeOC_6H_4$ (**XIV**), *p*-ClC_6H_4 (**XV**), *m*-$NO_2C_6H_4$ (**XVI**), *m*-BrC_6H_4 (**XVII**), 3,4-$(MeO)_2C_6H_3$ (**XVIII**), 2-thienyl (**XIX**), $PhCH_2CH_2$ (**XX**, **XXI**).

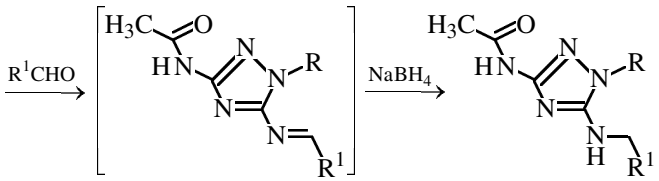
All the steps can be performed in the one-pot mode without isolation of the intermediates. By this scheme we prepared 5-amino-3-benzylamino-1,2,4-triazole **XIII**, 5-amino-3-*p*-methoxybenzylamino-1,2,4-triazole **XIV**, 5-amino-3-*p*-chlorobenzylamino-1,2,4-triazole **XV**, 5-amino-3-*m*-nitrobenzylamino-1,2,4-triazole **XVI**, 5-amino-3-*m*-bromobenzylamino-1,2,4-triazole **XVII**, 5-amino-3-(3,4-dimethoxybenzyl)amino-1,2,4-triazole **XVIII**, 5-amino-3-(2-thienylmethyl)amino-1,2,4-triazole **XIX**, and 5-amino-3-(3-phenylpropyl)-amino-1,2,4-triazole **XX**. It should be noted that in the synthesis of **XX** we obtained as the second product 3,5-bis(3-phenylpropyl)amino-1,2,4-triazole **XXI**. The yield of **XXI** decreased with a decrease in the temperature in the step of condensation of diamine **IV** with 3-phenylpropanal, with a simultaneous increase in the yield of **XX**. Thus, condensation of diamine **IV** with aliphatic aldehydes is less selective than the condensation with aromatic aldehydes.

The yields and properties of **XIII**–**XXI** are listed in the table.

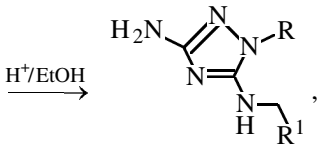
To prepare 5-alkylamino-3-imino-1-R-1,2,4-triazoles, we suggested a procedure based on the following reaction sequence:



II, **III** **XXII**, **XXIII**



XXV–**XXIX**



XXX–**XXXIV**

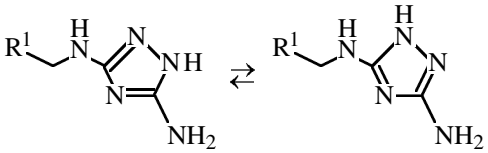
where R = Bn (**XXII**, **XXVI**, **XXXI**), Ph (**XXIII**, **XXV**, **XXVII**–**XXX**, **XXXII**–**XXXIV**); R^1 = *o*-$MeOC_6H_4$ (**XXV**, **XXX**), *p*-MeC_6H_4 (**XXVI**, **XXVII**, **XXXI**, **XXXII**), *m*-$NO_2C_6H_4$ (**XXVIII**, **XXXIII**), 2-thienyl (**XXIX**, **XXXIV**).

The synthesis of acetyl derivatives **XXII** and **XXIII** is described in [14]. The condensation of **XXII** and **XXIII** with aldehydes was performed in refluxing DMF, because under milder conditions the reaction is very slow. By so doing, we obtained 3-acetylamino-5-*o*-methoxybenzylidenamino-1-phenyl-1,2,4-triazole **XXIV** (see table) in 72% yield. To prepare the alkyl derivatives, the Schiff bases were hydrogenated without isolation; by so doing, we prepared 3-acetylamino-5-*o*-methoxybenzylamino-1-phenyl-1,2,4-triazole **XXV**, 3-acetylamino-1-benzyl-5-*p*-methylbenzylamino-1,2,4-triazole **XXVI**, 3-acetylamino-5-*p*-methylbenzylamino-1-phenyl-1,2,4-triazole **XXVII**, 3-acetylamino-5-*m*-nitrobenzylamino-1-phenyl-1,2,4-triazole **XXVIII**, and 3-acetylamino-5-(2-thienylmethyl)amino-1-phenyl-1,2,4-triazole **XXIX**. By hydrolysis of **XXV**–**XXIX**, we prepared 3-amino-5-*o*-methoxybenzylamino-1-phenyl-1,2,4-triazole **XXX**, 3-amino-1-benzyl-5-*p*-methylbenzylamino-1,2,4-triazole **XXXI**, 3-amino-5-*p*-methylbenzylamino-1-phenyl-1,2,4-triazole **XXXII**, 3-amino-5-*m*-nitrobenzylamino-1-phenyl-1,2,4-triazole **XXXIII**, and 3-amino-5-(2-thienylmethyl)amino-1-phenyl-1,2,4-triazole **XXXIV**. The yields and properties of **XXX**–**XXXIV** are given in the table.

The structures of the compounds were determined by elemental analysis and ^1H NMR spectroscopy, and their purity was confirmed by HPLC.

The position of the R^1CH_2 group in **V**–**X** and **XXX**–**XXXIV** was determined from the ^1H NMR spectra taking into account the facts [7, 14] that the chemical shift of the protons of the unsubstituted amino group in 3-alkylamino-5-amino-1-R-1,2,4-triazoles is about 6 ppm, and in 5-alkylamino-3-amino-1-R-1,2,4-triazoles, about 5 ppm. Isomeric triazoles **VII** and **XXX** were described previously [3], and their structure was determined by single crystal X-ray diffraction. The ^1H NMR spectra of **VII** and **XXX** are similar to those given in [3].

Alkyl derivatives **XIII**–**XX** can exist in the form of tautomers **A** and **B**:



A **B**

The prototropy can lead to strong broadening of the signals of the amino and imino groups. According to the ^1H NMR spectra, in DMSO tautomer **B** prevails (the signal of amino group protons is observed at 4.8–5.6 ppm, see table).

EXPERIMENTAL

The ^1H NMR spectra were taken on a Varian Unity-300 spectrometer (300 MHz, DMSO-d_6, internal reference TMS). HPLC analysis was performed on a Milikhrom-5 chromatograph equipped with a UV detector. An 80 × 2-mm column was packed with Separon C18; eluent methanol, elution rate 80 μl min^{-1}, detection at 210 nm. The starting compounds **II** and **III** were prepared by procedures described in [10, 15].

3-Alkylamino-5-amino-1-R-1,2,4-triazoles V–IX. A solution of 0.06 mol of diamine **II** or **III** and 0.06 mol of appropriate aldehyde in 100 ml of ethanol was refluxed for 1 h, after which 3.42 g (0.09 mol) of $NaBH_4$ was added in small portions at a rate providing uniform boiling of the reaction mixture. The mixture was refluxed for an additional 30 min, after which the solvent was distilled off, and 40 ml of water was added to the residue. The resulting solution was cooled, and the precipitate was filtered off, washed with water, and recrystallized.

5-Amino-1-phenyl-3-(3-phenylpropyl)amino-1,2,4-triazole X. A solution of 0.74 g (0.0055 mol) of 3-phenylpropanal in 5 ml of ethanol was added dropwise over a period of 10 min with vigorous stirring at 0–5°C to a solution of 1.05 g (0.006 mol) of **III** in 10 ml of ethanol. The mixture was stirred for 2 h, after which 0.34 g (0.009 mol) of $NaBH_4$ was added in portions at 20–30°C. The mixture was stirred for 30 min, heated to boil, and refluxed for 30 min. The solvent was distilled off, 10 ml of water was added to the residue, the oil that separated out was extracted with chloroform (3 × 5 ml), and the extract was filtered through a bed of alumina (4 cm in diameter, 3 cm high). The solvent was distilled off, and compound **X** was crystallized from acetonitrile.

3-Alkylamino-5-amino-1,2,4-triazoles XIII–XIX. *a*. A solution of 2.9 g (0.072 mol) of NaOH in 2 ml of water was added to a suspension of 10 g (0.063 mol) of nitrate **XI** in 20 ml of ethanol. The mixture was refluxed for 5 min, after which a solution of 0.057 mol of appropriate aldehyde in 10 ml of ethanol was added, the mixture was refluxed for 1 h, and 3.3 g (0.086 mol) of $NaBH_4$ was added in portions. The mixture was refluxed for an additional 30 min, the solvent was evaporated to a small volume, and 40 ml of water was added to the residue. The resulting solution was cooled, and the precipitate thus formed was filtered off, washed with water, and crystallized.

b. A solution of 4.8 g (0.12 mol) of NaOH in 10 ml of H_2O was added with stirring to a suspension of 14.1 g (0.1 mol) of acetyl derivative **XII** in 50 ml of ethanol. The mixture was refluxed until it became fully homogeneous (10–15 min), after which it was neutralized with acetic acid to pH 7–9, and 10.1 g (0.09 mol) of appropriate aldehyde was added dropwise with stirring. The mixture was refluxed for 20 min, after which 5.13 g (0.135 mol) of $NaBH_4$ was added in portions over a period of 10 min. The mixture was refluxed for an additional 20 min and evaporated to a small volume. The residue was diluted with 100 ml of water, and the resulting solution was evaporated by half and cooled. The precipitate thus formed was filtered off, washed with water, and crystallized.

5-Amino-3-(3-phenylpropyl)amino-1,2,4-triazole XX and 3,5-di(3-phenylpropyl)amino-1,2,4-triazole XXI. A solution of 12.06 g (0.09 mol) of 3-phenylpropanal in 10 ml of ethanol was added with vigorous stirring over a period of 10 min at 0–5°C to the reaction mixture obtained as described above by hydrolysis of 14.1 g (0.1 mol) of acetyl derivative **XII.** The mixture was stirred for 2 h, after which 5.7 g (0.15 mol) of $NaBH_4$ was added in small portions at 20–30°C. The mixture was stirred for 30 min, heated to boil, and refluxed for 30 min. The solvent was distilled off, 300 ml of water was added to the residue, and the precipitate (compound **XXI**) was filtered off, washed with water, dried, and crystallized.

The filtrate and wash waters were evaporated to a volume of 50 ml; the precipitate that formed on cooling (compound **XX**) was filtered off and crystallized.

3-Acetylamino-5-*o*-methoxybenzylidenamino-1-phenyl-1,2,4-triazole XXIV. A mixture of 1 g (0.0046 mol) of **XXIII**, 0.75 g (0.0055 mol) of 2-methoxybenzaldehyde, and 1 ml of DMF was refluxed for 1 h, diluted with 10 ml of water, and extracted with chloroform (3 × 10 ml). The extract was dried over $CaCl_2$ and filtered through a bed of alumina (4 cm in diameter, 3 cm high); the solvent was distilled off, and the residue was crystallized.

5-Alkylamino-3-acetylamino-1-R-1,2,4-triazoles XXV–XXIX. A mixture of 0.01 mol of **XXII** or **XXIII** and 0.012 mol of appropriate aldehyde in 2 ml of DMF was refluxed for 1 h and diluted with 20 ml of ethanol. To the resulting solution, 0.68 g (0.018 mol) of $NaBH_4$ was added in small portions at 50–60°C, after which the mixture was refluxed for 30 min. The solvent was evaporated to a small volume, and 40 ml of water was added to the residue. The precipitate thus formed was filtered off, washed with water, and crystallized.

5-Alkylamino-3-amino-1-R-1,2,4-triazoles XXX–XXXIV. A mixture of 0.005 mol of **XXV–XXIX**, 10 ml of ethanol, and 3 ml of concentrated HCl was refluxed for 2 h and then neutralized with a 10% aqueous solution of sodium acetate. The precipitate thus formed was filtered off, washed with water, and crystallized.

CONCLUSIONS

(1) Condensation of 3,5-diamino-1-R-1,2,4-triazoles (R = Alk, Ar) with aldehydes at an equimolar ratio of the reactants, followed by hydrogenation of the resulting Schiff bases, is a one-pot method for regioselective synthesis of 3-alkylamino-5-amino-1-R-1,2,4-triazoles.

(2) 3,5-Diamino-1,2,4-triazole (R = H) reacts selectively only with aldehydes in which the carbonyl group is conjugated with the aromatic ring. Condensation with aliphatic aldehydes followed by hydrogenation yields a mixture of 3-alkylamino-5-amino-1,2,4-triazoles and 3,5-dialkylamino-1,2,4-triazoles.

(3) Condensation of 5-amino-3-acetylamino-1-R-1,2,4-triazoles with aldehydes in dimethylformamide, followed by hydrogenation of the resulting Schiff bases (without their isolation) with sodium borohydride and by acid hydrolysis of the reduction products, 5-alkylamino-3-acetylamino-1-R-1,2,4-triazoles, is a convenient method for regioselective synthesis of 5-alkylamino-3-amino-1-R-1,2,4-triazoles (R = Alk, Ar).

REFERENCES

1. Granik, V.G. and Grigor'ev, N.B., *Oksid azota (NO): Novyi put' k poisku lekarstv* (Nitrogen Oxide (NO): A New Route in Searching for Drugs), Moscow: Vuzovskaya Kniga, 2004.
2. US Patent 4318913.
3. Dunstan, A.R., Weber, H.-P., Rihs, G., *et al., Tetrahedron Lett.*, 1998, vol. 39, no. 43, pp. 7983–7986.
4. US Patent 5028716.
5. WO Patent 01/09106.
6. Berecz, G., Reiter, J., Argay, G., and Kalman, A., *J. Heterocyclic Chem.*, 2002, vol. 39, no. 2, pp. 319–325.
7. Reiter, J., Pongo, L., Somorai, T., and Dvortsak, P., *J. Heterocyclic Chem.*, 1986, vol. 23, no. 2, pp. 401–408.
8. Garratt, P.G., Thorn, S.N., and Wrigglesworth, R., *Tetrahedron*, 1993, vol. 49, no. 1, pp. 165–176.
9. Blank, B., Nichols, D.M., and Vaidya, P.D., *J. Med. Chem.*, 1972, vol. 15, no. 6, pp. 694–696.
10. Fuentes, J.J. and Lenoir, J.A., *Can. J. Chem.*, 1976, vol. 54, no. 22, pp. 3620–3625.
11. Chernyshev, V.M., Zemlyakov, N.D., Taranushich, V.A., and Rakitov, E.A., *Zh. Prikl. Khim.*, 1999, vol. 72, no. 10, pp. 1688–1691.
12. Chernyshev, V.M., Zemlyakov, N.D., Il'in, V.B., and Taranushich, V.A., *Zh. Prikl. Khim.*, 2000, vol. 73, no. 5, pp. 791–793.
13. Chernyshev, V.M., Gaidukova, G.V., Zemlyakov, N.D., and Taranushich, V.A., *Zh. Prikl. Khim.*, 2005, vol. 78, no. 5, pp. 790–795.
14. Chernyshev, V.M., Rakitov, V.A., Taranushich, V.A., and Blinov, V.V., *Khim. Geterotsikl. Soedin.*, 2005, no. 9, pp. 1342–1350.
15. Steck, E.A., Brundage, R.P., and Fletcher, L.T., *J. Am. Chem. Soc.*, 1958, vol. 80, no. 15, pp. 3929–3931.

ISSN 1070-4272, Russian Journal of Applied Chemistry, 2006, Vol. 79, No. 4, pp. 631–633. © Pleiades Publishing, Inc., 2006.
Original Russian Text © I. P. Pogorelova, V. D. Orlov, A. D. Isak, 2006, published in Zhurnal Prikladnoi Khimii, 2006, Vol. 79, No. 4, pp. 639–641.

ORGANIC SYNTHESIS AND INDUSTRIAL ORGANIC CHEMISTRY

Synthesis of 6-Methyluracil-5-sulfonyl Chloride

I. P. Pogorelova, V. D. Orlov, and A. D. Isak

Rubezhnoe Branch, Dal' East-Ukrainian National University, Rubezhnoe, Lugansk oblast, Ukraine

Received November 25, 2005

Abstract—Sulfochlorination of 6-methyluracil with chlorosulfonic acid in the presence of thionyl chloride was studied. The lactam–lactim tautomerism of 6-methyluracil was considered. Ways to increase the yield of the sulfonyl chloride were suggested. The mechanism of the effect exerted by thionyl chloride additions was discussed.

DOI: 10.1134/S1070427206040240

Sulfochlorination reactions are widely used in organic (in particular, pharmaceutical) chemistry. Sulfonyl chlorides are intermediates in syntheses of active and dispersible dyes, herbicides, and fungicides [1]. Among six-membered heterocyclic compounds containing two nitrogen atoms, a prominent place is occupied by pyrimidine derivatives used as drugs (sulfamide drugs such as Sulfadimethoxine, Sulfamonomethoxine; antitumor agent Fluorouracil; antibiotic Amecytin, etc.) [2, 3].

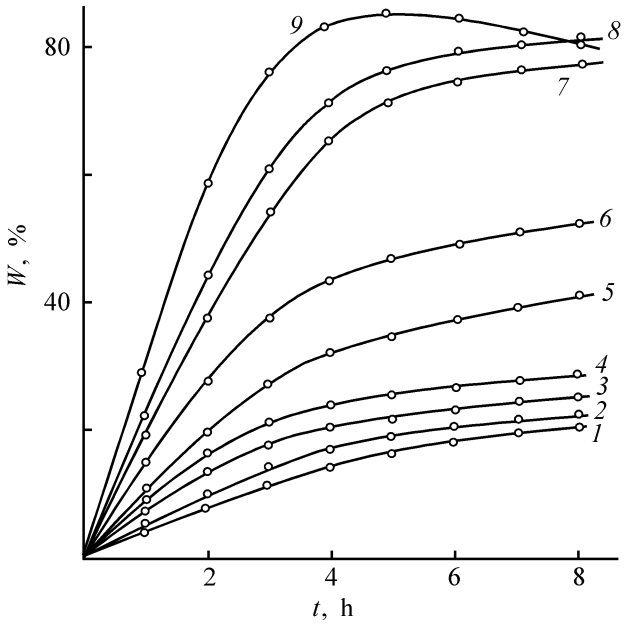
Of particular interest in this respect is readily available methyluracil, which is used in syntheses of sulfonamides, sulfonyldiureides, sulfonylhydrazides, and sulfonates; some of these compounds showed biological activity.

Data on sulfochlorination of 6-methyluracil are relatively few. As shown in [4–6], uracil and 6-methyluracil **1** react with a tenfold excess of chlorosulfonic acid to form uracil-6-sulfonyl chloride and 6-methyluracil-5-sulfonyl chloride **2** in a low yield (≤22%).

To develop a more efficient procedure for preparing 6-methyluracilsulfonyl chloride, we examined the effect of various factors on the sulfochlorination of **1** [7, 8].

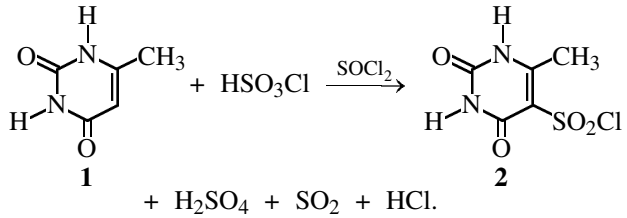
At 30°C, compound **1** does not noticeably react with chlorosulfonic acid; the reaction starts only at 35°C, and the yield of **2** under these conditions does not exceed 15%. With increasing temperature, the reaction rate and sulfonyl chloride yield increase, but even after the sulfochlorination for 7 h at 75°C the yield of **2** does not exceed 28% (see figure). When the reaction mixture is poured onto ice to isolate the product, a considerable part of **2** undergoes hydrolysis and transforms into 6-methyluracilsulfonic acid, which was isolated from the solution by salting-out with NaCl. Thus, the desired sulfonyl chloride is unstable and is readily hydrolyzed in aqueous solution. To suppress the hydrolysis, the reaction mixture was poured onto a 1 : 1 mixture of ice and acetic acid.

It was found in [9, 10] that the use of chlorosulfonic acid in combination with thionyl chloride (volume ratio 1.5 : 1) considerably increases the rate of formation and yield of **2** (see figure). In contrast to $SOCl_2$, addition of SO_2Cl_2 or $POCl_3$ does not noticeably af-



Yield of 6-methyluracilsulfonyl chloride W vs. time t (*1*–*4*) in the absence and (*5*–*9*) in the presence of thionyl chloride. T, °C: (*1*, *5*) 45, (*2*, *6*) 55, (*3*, *7*) 65, (*4*, *8*) 75, and (*9*) 85.

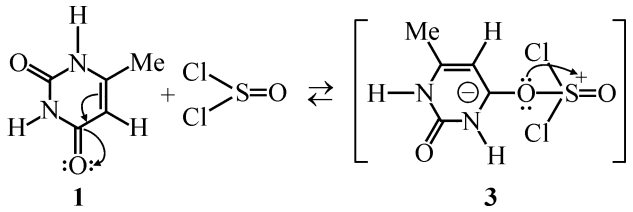
fect the sulfochlorination rate and yield of the target product. Sulfochlorination of 6-methyluracil follows the scheme



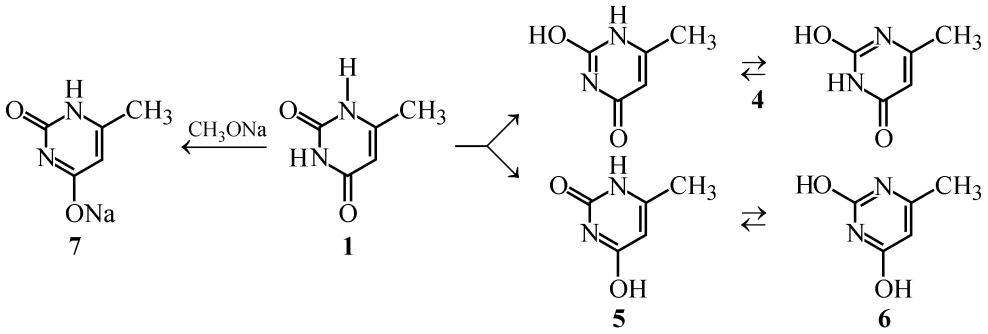
As seen from the figure, addition of $SOCl_2$ results in that the rate of formation of **2** increases by a factor of 3–4 even at 45°C, with the yield of **2** reaching 40%. Similar relationships are observed at higher temperatures.

The highest yield of **2** (82%) was obtained after heating at 85°C for 5 h. Further increase in the temperature decreases the yield of the target product because of formation of the sulfone (see figure, curve *9*).

The favorable effect of thionyl chloride on the rate of formation and yield of sulfonyl chlorides is apparently due to the presence of a lone electron pair at the S(IV) atom. The S atoms in SO_2Cl_2 and $SOCl_2$ differ in the electronic structure and affect the substrate differently. In contrast to the S atom in chlorosulfonic acid and sulfuryl chloride, in which all the valence electrons are fully involved in formation of six covalent bonds, in thionyl chloride a lone *p*-electron pair remains on the sulfur atom, and it may compensate the electron density deficiency on the O atom in the 4-position of methyluracil, facilitating electrophilic substitution of the H atom by the SO_2Cl group:

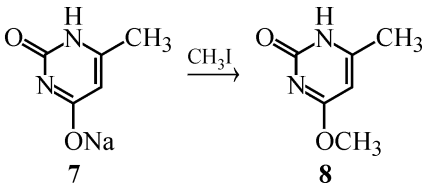


The ready incorporation of the SO_2Cl group in the 5-position of methyluracil is due to its lactam–lactim tautomerism. 6-Methyluracil can exist in the form of five tautomers, four of which contain one or two hydroxy groups. Nonaqueous titration shows that 1 mol of sodium methylate is spent per mole of methyluracil, suggesting the presence of only one OH group (structures **4**, **5**):



As shown by quantum-chemical calculations, ^1H NMR spectra, and certain chemical transformations, structure **5** is the most favorable energetically. In this structure, the 5-position will be the most reactive owing to the concerted effect of CH_3 and OH groups. Sulfochlorination occurs at a higher rate via intermediate **3** (see above).

Experiments showed that methyluracil reacts with sodium methylate to form monosodium derivative **7**, which reacts with methyl iodide CH_3I to form compound **8**:



The structures of **7** and **8** were confirmed by IR and NMR spectra and by elemental analysis.

EXPERIMENTAL

The ^1H NMR spectra were recorded in $CDCl_3$ on a Tesla BS-487c spectrometer operating at 80 MHz. The chemical shifts (δ, ppm) are given relative to TMS. The IR spectra were measured on a UR-20 spectrometer (KBr pellets).

6-Methyluracil-5-sulfonyl chloride 2. A four-necked flask equipped with a power-driven stirrer, a thermometer, a reflux condenser, and a dropping funnel was charged with 7.6 g (0.054 mol) of 6-methyluracil **1** dried in an oven at 110–115°C for 3–4 h. The flask was placed on a water bath, and 10 ml (16.5 g, 0.138 mol) of freshly distilled thionyl chlo-

ride was added with vigorous stirring. The contents were stirred for 20–30 min, after which 16 ml (28.6 g, 0.265 mol) of freshly distilled chlorosulfonic acid was added dropwise at such a rate that the reaction mixture temperature did not exceed 30–35°C. The reflux condenser was connected through a $CaCl_2$ tube with a beaker absorbing the released gases.

The mixture was heated to 60–65°C and kept at this temperature with vigorous stirring for 4.5–5 h, after which it was heated to 75–80°C and kept for an additional 5.5–6 h. The reaction progress was monitored chromatographically on Silufol UV-254 plates, eluent ethyl acetate. After the reaction completion, the mixture was cooled to 0–5°C and poured with vigorous stirring onto a mixture of 50 g of crushed ice and 35 ml of glacial acetic acid, keeping the temperature in the range from –5 to 0°C. 6-Methyluracil-5-sulfonyl chloride precipitated as a white crystalline substance; it was filtered off and washed several times with ice-cold water and acetic acid. Yield 9.95 g (82%). White needle-like crystals, mp 269–270°C (from glacial acetic acid).

Found, %: C 26.91, H 2.61, N 12.40, Cl 15.94, S 14.48.

$C_5H_5ClN_2O_4S$.

Calculated, %: C 26.74, H 2.69, N 12.47, Cl 15.78, S 14.27.

IR spectrum, cm^{-1}: 985, 1030 ($\omega_{C=C}$); 1305 (C=N–); 1675, 1730 ($\nu_{C=O,\ =N-C=O}$); 3275 (ν_{NH}); 1355, 1380 ($\nu_{S(CH_3)}$). ^1H NMR spectrum, δ, ppm ($CDCl_3$): 2.45 s (3H, C^6–CH_3); 11.68 d (1H, N^1–H), 5.85 s (1H, C^4–OH).

4-Methoxy-6-methyluracil. Sodium metal (1.25 g, 0.054 mol) was dissolved in 50 ml of absolute methanol, and 6.25 g (0.050 mol) of methyluracil was added. The mixture was heated at 65°C for 45 min with stirring. To the resulting colorless solution, 3.7 ml (0.060 mol) of methyl iodide was added, and the mixture was heated with weak refluxing for 4–5 h until the methyluracil spot disappeared from the chromatogram (Silufol UV-254, eluent ethyl acetate). On cooling, colorless needle-like crystals precipitated. The precipitate was filtered off, washed with water, and dried. Yield of 4-methoxy-6-methyluracil 6.31 g (89.9%), mp 192–193°C.

Found, %: C 51.63, H 5.71, N 19.86.

$C_6H_8N_2O_2$.

Calculated, %: C 51.42, H 5.75, N 19.99.

IR spectrum, cm^{-1}: 1020 ($\omega_{C=C}$); 1025 ($\nu_{S(=C-O-C)}$); 1245 ($\nu_{as(=C-O-C)}$); 1055–1275 (C=N–); 1685, 1745 ($\nu_{C=O,\ =N-C=O}$); 1380 ($\nu_{S(CH_3)}$); 2825 (OCH_3); 2850 ($\nu_{S(OCH_3)}$); 2870 ($\nu_{S(CH_3)}$); 2965 ($\nu_{as(CH_3)}$). ^1H NMR spectrum, δ, ppm ($CDCl_3$): 2.11 s (3H, C^6–CH_3), 4.92 d (1H, C^5–H), 4.01 s (3H, C^4–OCH_3), 11.92 s (1H, N^1–H).

CONCLUSIONS

(1) Sulfonation of 6-methyluracil with a mixture of chlorosulfonic acid and thionyl chloride allows the rate of formation and yield of 6-methyluracil-5-sulfonyl chloride to be appreciably increased, with the yield reaching 82%.

(2) In solution, 6-methyluracil mainly occurs in the lactim form (4-hydroxy-6-methyl-1,2-dihydropyrimidin-2-one).

(3) The favorable effect of thionyl chloride on the sulfochlorination rate and yield of sulfonyl chloride is due to the fact that the lone electron pair of the S atom of thionyl chloride eliminates the electron density deficiency on the oxygen atom, thus facilitating the electrophilic substitution of hydrogen by the SO_2Cl group.

REFERENCES

1. Vorozhtsov, N.N., *Osnovy sinteza promezhutochnykh produktov i krasitelei* (Fundamentals of the Synthesis of Intermediates and Dyes), Moscow: Goskhimizdat, 1955.
2. Makarov, V.A., Sedov, A.L., and Nemeryuk, M.P., *Khim.-Farm. Zh.*, 1993, no. 4, pp. 26–34.
3. Mashkovskii, M.D., *Lekarstvennye sredstva* (Drugs), Kharkov: Torsing, 1997.
4. Khromov-Borisov, M.V. and Karpinskaya, R.O., *Zh. Obshch. Khim.*, 1957, vol. 27, pp. 2577–2590.
5. Khromov-Borisov, M.V. and Karpinskaya, R.O., *Zh. Obshch. Khim.*, 1964, vol. 34, pp. 2212–2214.
6. Elderfield, R.E. and Prusad, R.N., *J. Org. Chem.*, 1961, vol. 26, no. 10, pp. 9863–9866.
7. Isak, A.D. and Pogorelova, I.P., in *Nitrogen-Containing Heterocycles and Alkaloids*, Moscow, 2001, vol. 1, pp. 282–285.
8. Isak, A.D., Pogorelova, I.P., Shemchuk, L.A., and Bibik, T.S., in *Nitrogen-Containing Heterocycles and Alkaloids*, Moscow, 2001, vol. 2, p. 105.
9. Pogorelova, I.P. and Isak, A.D., Abstracts of Papers, *Int. Conf. on Chemistry of Nitrogen-Containing Heterocycles (CNH-2003)*, Kharkov, 2003, p. 239.
10. Pogorelova, I.P., Isak, O.D., Esipova, G.P., and Shemchuk, L.A., *Visn. Farm.*, 2004, no. 1(37), pp. 20–23.

ISSN 1070-4272, Russian Journal of Applied Chemistry, 2006, Vol. 79, No. 4, pp. 634–636. © Pleiades Publishing, Inc., 2006.
Original Russian Text © N. A. Zhukovskaya, E. A. Dikusar, K. L. Moiseichuk, O. G. Vyglazov, 2006, published in Zhurnal Prikladnoi Khimii, 2006, Vol. 79, No. 4, pp. 642–644.

ORGANIC SYNTHESIS AND INDUSTRIAL ORGANIC CHEMISTRY

Preparative Synthesis of Menthone Oxime Esters

N. A. Zhukovskaya, E. A. Dikusar, K. L. Moiseichuk, and O. G. Vyglazov

Institute of Physical Organic Chemistry, Belarussian National Academy of Sciences, Minsk, Belarus

Received January 11, 2006

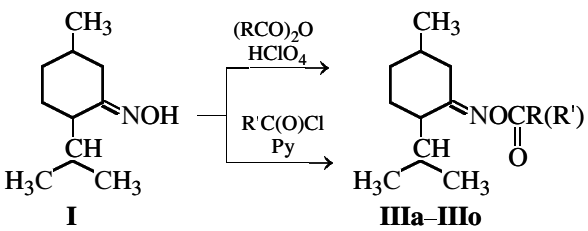
Abstract—Procedures are developed for the preparation of menthone oxime esters as accessible perfumes and fragrant additives synthesized from natural raw materials.

DOI: 10.1134/S1070427206040252

Oxime ethers and esters exhibit a wide range of biological activity and are accessible perfumes and fragrant additives [1, 2].

The goal of this study is development of procedures for preparing menthone oxime esters. Menthone is prepared from natural raw materials (*L*-menthone is prepared by vacuum distillation of *Mentha arvensis* essential oil after separation of *L*-menthol [3]); it exhibits fresh mint odor. Menthone oxime **I** is a valuable perfume with a black currant scent and is widely used for preparing fragrant additives and food aromatizers [3]. Interesting scents can also be expected from menthone oxime esters.

Menthone oxime esters were prepared by reactions of menthone oxime **I** with alkanoic acid anhydrides **IIa**–**IId** in absolute diethyl ether in the presence of catalytic amounts of 57% $HClO_4$ or with alkanoic, alkenoic, or arenecarboxylic acid chlorides **IIe**–**IIo** in the presence of pyridine. The syntheses were performed at 20–23°C for 24–36 h and involved simple mixing of the reactants; they did not require efficient cooling or prolonged stirring. Menthone oxime esters **IIIa**–**IIIo** were prepared in 76–90% yield.



I **IIIa**–**IIIo**

III, R = CH_3 (**a**), C_2H_5 (**b**), $(CH_2)_2CH_3$ (**c**), $CH(CH_3)_2$ (**d**); R' = $CH_2CH(CH_3)_2$ (**e**), $(CH_2)_4CH_3$ (**f**), $(CH_2)_5CH_3$ (**g**), $(CH_2)_6CH_3$ (**h**), $(CH_2)_8CH_3$ (**i**), $CH{=}CH_2$ (**j**), $C(CH_3){=}CH_2$ (**k**), C_6H_5 (**l**), CH_2Cl (**m**), C_6H_4Cl-4 (**n**), 1/2 $[(CH_2)_4]$ (**o**).

Menthone oxime esters **IIIa**–**IIIo** are colorless or weakly colored viscous liquids; their characteristics are listed in the table.

The IR, UV, and ^1H NMR spectra of menthone oxime esters **IIIa**–**IIIo** confirm their structure. The IR spectra of **IIIa**–**IIIo** contain absorption bands (cm^{-1}) of the groups CH_{Alk} (3000–2800), C=O (1743–1766), C=N (1632–1634), CH_2 (1455–1460), and C–O (1280–1000); the spectra of aromatic esters **IIIl** and **IIIn** also contain absorption bands (cm^{-1}) of the groups CHAr (3100–3000), Ar (1595–1600, 1485–1487, 1386–1400, 1310–1313), and CH_{Ar} (902–683), and the IR spectra of **IIIm** and **IIIn**, also C–Cl bands (592 amd 527 cm^{-1}, respectively). The UV spectra of oxime esters exhibit the following absorption maxima (nm): **IIIa**–**IIIi** and **IIIm**, 208 (ε = 8000); **IIIj** and **IIIk**, 209 (ε = 15000); **IIIl**, 207 (ε = 23000), 226 (ε = 14000), and 260 (ε = 11000); **IIIn**, 207 (ε = 28000), 220 (ε = 6000), and 252 (ε = 8000); and **IIIo**, 208 (ε = 15000). In the ^1H NMR spectra of menthone oxime esters **IIIa**–**IIIo**, the CH_3 proton signals appear at 0.75–1.10 ppm, and the CH and CH_2 proton signals, at 1.10–3.00 ppm. The CH_3CO group in **IIIa** gives a singlet at 2.12 ppm; the CH_3CH_2CO group in **IIIb**, a triplet at 1.22 ppm (CH_3) and a quartet at 2.42 ppm (CH_2); the $(CH_3)_2C$ group of **IIId**, a doublet at 1.21 ppm; the $CH{=}CH_2$ group in **IIIj**, a multiplet at 5.70–6.30 ppm; the $CH_3C{=}C$ group in **IIIk**, a singlet at 2.00 ppm; the $C{=}CH_2$ group in **IIIl** and **IIIn**, two broadened singlets at 5.62 and 6.16 ppm; the aromatic protons in **IIIl** and **IIIn**, multiplets at 7.30–8.30 ppm; and the CH_2Cl group in **IIIm**, a singlet at 4.23 ppm.

Properties of menthone oxime esters **IIIa**–**IIIo**

Compound no.	Yield, %	d_{20}^{20}	n_D^{20}	Found, %			Formula	Calculated, %			*M*	
				C	H	N		C	H	N	found	calc.
IIIa	76	0.7973	1.4752	68.04	10.24	6.72	$C_{12}H_{21}NO_2$	68.20	10.02	6.62	204.6	211.3
IIIb	80	1.1002	1.4748	69.14	10.56	6.08	$C_{13}H_{23}NO_2$	69.30	10.29	6.21	217.1	225.3
IIIc	79	0.9684	1.4734	69.93	10.58	6.17	$C_{14}H_{25}NO_2$	70.25	10.53	5.85	229.4	239.3
IIId	90	0.9758	1.4690	70.40	10.87	6.04	$C_{14}H_{25}NO_2$	70.25	10.53	5.85	231.9	239.3
IIIe	76	0.9314	1.4718	71.11	10.86	5.74	$C_{15}H_{27}NO_2$	71.10	10.74	5.53	241.8	253.4
IIIf	82	0.8800	1.4732	72.97	11.71	5.22	$C_{16}H_{29}NO_2$	71.87	10.97	5.24	258.3	267.4
IIIg	88	1.0673	1.4716	72.59	11.32	5.02	$C_{17}H_{31}NO_2$	72.55	11.10	4.97	273.2	281.4
IIIh	80	1.0079	1.4722	73.58	11.14	4.68	$C_{18}H_{33}NO_2$	73.17	11.26	4.74	284.7	295.5
IIIi	77	1.0963	1.4705	74.68	11.65	4.65	$C_{20}H_{37}NO_2$	74.25	11.53	4.33	315.6	323.5
IIIj	83	0.9490	1.4902	69.66	9.38	6.48	$C_{13}H_{21}NO_2$	69.92	9.48	6.27	214.7	223.3
IIIk	78	0.9692	1.4878	70.80	9.84	6.16	$C_{14}H_{23}NO_2$	70.85	9.79	5.90	230.0	237.3
IIIl	80	1.2857	1.5372	74.07	8.32	5.16	$C_{17}H_{23}NO_2$	74.7	8.48	5.12	260.8	273.4
IIIm*	79	1.0695	1.4925	59.43	8.94	5.86	$C_{12}H_{20}NClO_2$	58.65	8.20	5.70	237.2	245.8
IIIn*	81	1.0831	1.5375	66.92	7.60	4.70	$C_{17}H_{22}NClO_2$	66.33	7.20	4.55	294.4	307.8
IIIo	77	1.0105	1.4943	70.06	10.15	6.59	$C_{26}H_{44}N_2O_4$	69.61	9.88	6.24	430.1	448.6

* Cl, %, found, calculated: 14.31, 14.43 (**IIIm**); 11.10, 11.52 (**IIIn**).

It should be noted that esters **IIIb**–**IIIg** and **IIIo** have pronounced and interesting scents and show promise as components of grassy, fruit, and berry fragrances and of food aromatizers.

Odors of menthone oxime **I** and menthone oxime esters **IIIa**–**IIIo** (averaged results of organoleptic tests[1] of pure compounds)

Ia Grassy, with black currant tint
IIIa Anise-grassy, with spicy and mint tints
IIIb Oleoresin-grassy, with spicy tint
IIIc Berry–fruit, with pineapple tint
IIId Berry–fruit, with a tint of sea buckthorn berries
IIIe Berry, with a tint of guelder rose berries
IIIf Fruit-grassy, with valerian tint
IIIg Berry-grassy, with cranberry tint
IIIh Fruit-grassy, with aldehyde tint
IIIi Powder-grassy, with phenolic tint
IIIj Nut, with wood-grassy tint
IIIk Mint-grassy, with berry tint
IIIl Wood-grassy, with mint tint
IIIm Mint-grassy, with bitter tint
IIIn Fruit-grassy with vanilla–powder tint
IIIo Mint–anise, chilling

[1] Organoleptic evaluation of the odors of menthone oxime esters **IIIa**–**IIIo** was performed by the Tasting Council at the Accredited Chek-out and Analytical Laboratory of the Tereza-Inter Limited Liability Company (Moscow).

EXPERIMENTAL

The IR spectra of **IIIa**–**IIIo** were recorded on a Nicolet Protege-460 IR Fourier spectrometer (KBr). The UV spectra were measured on a Specord UV–Vis spectrometer from 1×10^{-3} M solutions of the compounds in methanol. The ^{1}H NMR spectra were taken on a Tesla BS-587A spectrometer (100 MHz) from 5% solutions in $CDCl_3$ using octamethylcyclotetrasiloxane as internal reference. The molecular weight *M* was determined cryoscopically in benzene. Menthone oxime **I** was prepared as described in [4, 5].

Menthone oxime esters IIIa–**IIId** (general procedure). Menthone oxime **I** (0.01 mol) and 0.02 mol of appropriate anhydride **IIa**–**IId** were dissolved in 10 ml of absolute ether, and 1–2 drops of 47% $HClO_4$ were added with cooling to 15°C. The components were mixed by shaking, and the mixture was allowed to stand at 20–23°C for 24–36 h. Then the mixture was diluted with water, and the product was extracted with hexane. The organic layer was separated, washed with water and 5% $NaHCO_3$, and dried over $CaCl_2$. The solvent was removed, and the product was vacuum-dried (2×10^{-2} mm Hg).

Menthone oxime esters IIIe–**IIIo** (general procedure). Menthone oxime **I** (0.01 mol) was dissolved in 0.011 mol of absolute pyridine, and 0.011 mol of appropriate acid chloride **IIe**–**IIn** was added with

gentle shaking while cooling to 15°C. To prepare **IIIo**, 0.02 mol of **I**, 0.022 mol of pyridine, and 0.01 mol of **IIo** were taken. The mixture was allowed to stand at 20–23°C for 24–36 h. Then the mixture was diluted with water, and the product was extracted with hexane. The organic layer was separated, washed with water and 5% $NaHCO_3$, and dried over $CaCl_2$. The solvent was removed, and the product was vacuum-dried (2×10^{-2} mm Hg).

Menthone oxime esters **IIIa**–**IIIo** were purified by column chromatography (neutral alumina, Brockmann grade II, eluent hexane).

CONCLUSIONS

(1) Menthone oxime reacts with carboxylic acid anhydrides and chlorides to form the corresponding esters.

(2) Menthone oxime esters are accessible perfumes and fragrant additives synthesized from natural renewable raw materials.

REFERENCES

1. Peshkova, V.M., Savostina, V.M., and Ivanova, E.K., *Oksimy* (Oximes), Moscow: Nauka, 1977.
2. Dikusar, E.A., Kozlov, N.G., Zhukovskaya, N.A., et al., *Khim. Prirodn. Soedin.*, 2004, no. 2, pp. 154–156.
3. Voitkevich, S.A., *865 dushistykh veshchestv dlya parfyumerii i bytovoi khimii* (865 Fragrant Substances for Perfumery and Domestic Chemistry), Moscow: Pishchevaya Prom–st., 1994.
4. Beckman, T., *Liebigs Ann. Chem.*, 1889, vol. 250, no. 1, pp. 330–338.
5. Grassi, G., *Gazz. Chim. Ital.*, 1908, vol. 38, no. 2, pp. 32–38.

ISSN 1070-4272, Russian Journal of Applied Chemistry, 2006, Vol. 79, No. 4, pp. 637–641. © Pleiades Publishing, Inc., 2006.
Original Russian Text © V. N. Serova, N. A. Zhukova, V. A. Mamedov, 2006, published in Zhurnal Prikladnoi Khimii, 2006, Vol. 79, No. 4, pp. 645–649.

ORGANIC SYNTHESIS AND INDUSTRIAL ORGANIC CHEMISTRY

Structure and Properties of Functionally Substituted Azothiazoles

V. N. Serova, N. A. Zhukova, and V. A. Mamedov

Kazan State Technological University, Kazan, Tatarstan, Russia
Arbuzov Institute of Organic and Physical Chemistry, Kazan Scientific Center, Russian Academy of Sciences, Kazan, Tatarstan, Russia

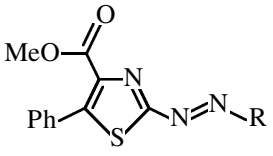
Received January 27, 2006

Abstract—Absorption and luminescence spectra of a series of functionally substituted azothiazoles in dimethylformamide and transparent polymeric matrix (bulk copolymer of methyl methacrylate and methacrylic acid) were studied. Kinetics of decolorization of liquid and solid solutions under the action of the integral light of a mercury lamp was measured to evaluate their lightfastness.

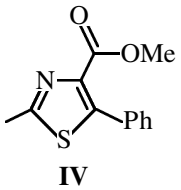
DOI: 10.1134/S1070427206040264

Azo derivatives form the most numerous group of organic dyes, covering the total color spectrum from yellow to black and differing in the lightfastness and resistance to hydrolysis and effect of various chemicals. Azo dyes are used in dyeing of plastics, fibers, and fabrics, and as color-forming components of photomaterials [1–4]. However, their color and service characteristics are determined by the nature of fragments bonded with the azo group and by the number, character, and location of electron-donor and electron-acceptor substituents [5]. In accordance with [6–9], the purposeful synthesis of new azo dyes can be of interest for laser engineering and other branches of high technology.

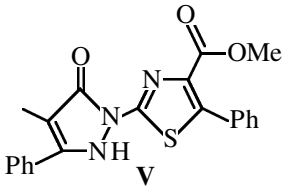
In this study, we examined optical properties and lightfastness of a series of functionally substituted azothiazoles (ATs) of the general formula



where R is Ph (**I**), *p*-HOC_6H_4 (**II**), and *p*-$Me_2NC_6H_4$ (**III**),



IV



V

Liquid and solid solutions of ATs in dimethylformamide (DMF) and transparent polymeric matrix (PM), a bulk copolymer of methyl methacrylate (MMA) and methacrylic acid (MAA), were considered. This PM is widely used today for preparation of laser dye active media (new class of solid-state materials in quantum electronics), resistive materials for microelectronics, and polygraphic printing plates [10–12]. The synthesis and properties of this copolymer doped with laser dyes were studied in [13–15].

EXPERIMENTAL

Compounds **I**–**III** [16] and compounds **IV** and **V** [17, 18] were synthesized by the methods described elsewhere.[1] All these compounds are highly dispersed powders colored from yellow to red and purple; mp, °C: **I**, 152–153; **II**, 105–106; **III**, 179–180; **IV**, 265–266; and **V**, 197–200.

We used DMF [GOST (State Standard) 20289–74], n_D^{20} = 1.4310, ρ = 945 kg m^{-3}, bp 152°C; MMA (GOST 20370–74), main substance content 99.99%, bp 100°C, n_D^{20} = 1.4130, ρ = 936 kg m^{-3}; MAA [TU (Technical Specification) 6-09-487–76], main substance content 99.50%, bp 163°C, n_D^{20} = 1.4314, ρ = 1015.3 kg m^{-3}; copolymerization initiator, azobis(isobutyronitrile) (AIBN) [MRTU (Interrepublican Technical Specification) 6-09-5749–68], mp 106°C.

[1] Azothiazoles were synthesized in the Arbuzov Institute of Organic and Physical Chemistry, Kazan Scientific Center, Russian Academy of Sciences, Kazan.

Comparative spectral characteristics of AT in DMF and PM* (concentration of **IV** in DMF 2.5×10^{-4} M, in PM 1.0×10^{-4} M; concentrations of the other ATs in DMF and PM 1.0×10^{-3} M)

AT	λ_a^{max}, nm		$\lambda_{0.5}$, nm		$\varepsilon \times 10^{-4}$, l mol^{-1} cm^{-1}		W_ε, rel. un. l mol^{-1}	
	DMF	PM	DMF	PM	DMF	PM	DMF	PM
I	380	–	66	–	1.87	–	1.9	–
II	415 (548)	405	85	100	1.90	0.71	2.0	1.0
III	511 (390)	500	110	120	0.52	0.56	0.5	–
IV	455	442	117	140	7.29	4.39	8.5	–
V	430	423	110	118	1.09	1.11	1.2	0.3

* DMF and MMA–MAA copolymer within the λ = 380–548 nm range have close values of transmittance, which within the 400–500 nm range vary within 88–91%.

Polymer samples as 0.5–0.6-mm-thick plates were prepared by bulk radical copolymerization of MMA and MAA in the presence of AT. The MMA : MAA ratio, 9 : 1 (by weight), was optimal to attain the required optical and service properties of the organic glass obtained [10]. The AIBN concentration in the monomer mixture was 0.1 wt %. The AT concentration in liquid and solid solutions was varied within the (0.1–2.3) $\times 10^{-3}$ M range. The reaction temperature was 45°C. Polymerization was performed for 3 h at 110°C.

The absorption spectra of ATs in DMF and PM were recorded on an SF-18 spectrophotometer. The solution layer thickness was 1.07 mm. The AT luminescence was excited by a He–Ne laser radiation with λ = 440 nm. The luminescence spectra were recorded on a GIPO device. The integral light of a DRG 230 mercury lamp was used to evaluate the lightfastness of the polymer samples.

The absorption spectra of ATs in DMF are shown in Fig. 1. The concentration of all the solutions was 1×10^{-3} M, except for the most strongly colored compound **IV**; its liquid and solid solutions had lower concentration by a factor of 4 and 10, respectively. The spectral characteristics of ATs are listed in the table.

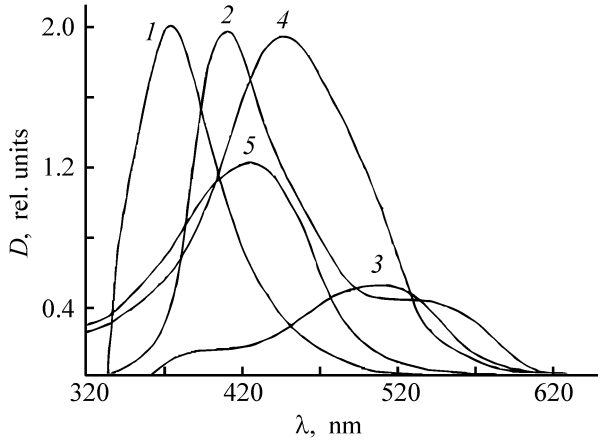


Fig. 1. Absorption spectra of ATs in DMF. (*D*) Optical density and (λ) wavelength. Concentration of **IV** 2.5×10^{-4}, concentration of the remaining ATs 1.0×10^{-3} M. Compound: (*1*) **I**, (*2*) **II**, (*3*) **III**, (*4*) **IV**, and (*5*) **V**.

As seen, the wavelength of the absorption maximum increases in the order **I** < **II** < **V** < **IV** < **III**, i.e., the color deepens from yellow to reddish-purple. The band half-width $\lambda_{0.5}$ decreases (increase in brightness and color purity) in the order **IV** > **V** ~ **III** > **II** > **I**. The molar extinction coefficient ε and hence the color intensity of AT in DMF increases in the order **III** < **V** < **I** ~ **II** < **IV**. For the solid matrix (PM) this order is violated as follows: ε for **V** becomes higher than for **II**. This may be explained by the effect of labile hydrogen atom of OH group of compound **II** on the kinetic parameters of the radical copolymerization of MMA with MAA.

To find correlation between the spectral characteristics and structure of AT molecule, we compared the following three groups of compounds: (1) **I**, **II**, and **III**, (2) **I** and **IV**, and (3) **IV** and **V**. The π-electron chromophore system of monoazo compounds **I**–**III** includes, on the one hand, a thiazole core with methoxycarbonyl and phenyl substituents, and, on the other hand, phenyl, phenolic, and *para*-dimethylaniline fragments. For compound **I** in DMF, λ_a^{max} is located on the boundary of the UV and visible spectral ranges, which determines its yellow color. The comparison of the spectra of **I**–**III** in the solution shows that the OH group introduced into the benzene ring shifts λ_a^{max} by 35 nm to longer wavelengths. Still larger bathochromic shift (by 131 nm) is observed when the OH group in the AT aromatic core is substituted by the stronger electron-donor group NMe_2.

The color deepening in the series **I**–**III** is accompanied by broadening of the absorption band (increase in $\lambda_{0.5}$), i.e., by a decrease in the brightness and purity

of the dye color. Introduction into the thiazole core of the *p*-dimethylaniline fragment gives a hypochromic effect, i.e., decrease in ε. Compounds **II** and **III** in DMF have complex absorption bands with additional shoulders in the region of longer and shorter wavelengths. Approximate location of their maxima in the spectrum is shown in the table in parentheses. The long-wave shoulder of the absorption band of compound **II** can originate from H bonding between its molecules through OH groups. Formation of such H bonds between azo dye molecules was found in [19]. The resulting red color of **II** in the solution can be caused by the sum of complementary colors: greenish-yellow and purple [1]. The absorption band of **III** in DMF has a short-wave inflection at λ ~ 390 nm, close to λ_a^{max} of compound **I**. In contrast to solutions, the absorption bands of **II** and **III** in PM have no shoulders.

We found that substitution of DMF by a less polar solvent, dioxane, does not change λ_a^{max} of compound **I** but shifts it for **III** to shorter wavelengths. Similar effect was observed for monoazo dyes in [6] and was attributed to solvation by the more polar solvent.

The chromophore system of compound **IV** combines two identically functionalized thiazole rings linked by the azo group. Substitution of the benzene ring in **I** by the thiazole ring causes color deepening from yellow to orange (bathochromic shift of λ_a^{max} 75 nm) and increase in the absorption intensity (ε increases by a factor of approximately 4). This effect may be caused by an increase in the delocalization of π electrons in the common chromophore system due to increased size of the conjugation system in **IV**. As mentioned above, compound **IV** exceeds in this parameter all the other ATs including **V**.

Disturbance of the symmetry of **IV** due to introduction of a pyrazole ring with carbonyl and phenyl substituents between identical N- and S-containing heterocycles (this corresponds to the structure of **V**) is accompanied by a hypsochromic shift (by 25 nm) and a considerable (by a factor of 6.5) decrease in ε.

The absorption bands in the spectra of ATs in the polymer matrix are broadened in comparison with solutions, especially for **II** and **IV** ($\lambda_{0.5}$ increases by 15 and 23 nm, respectively). In addition, their ε decreases (by a factor of 2.7 and 1.7, respectively). These effects may be caused by partial degradation of AT molecules under the action of initiator radicals and propagating radicals during copolymerization in the MMA–MAA mixture. At the same time, for **III** and **V**, the difference in $\lambda_{0.5}$ values in DMF and PM is substantially smaller (8 and 10 nm, respectively)

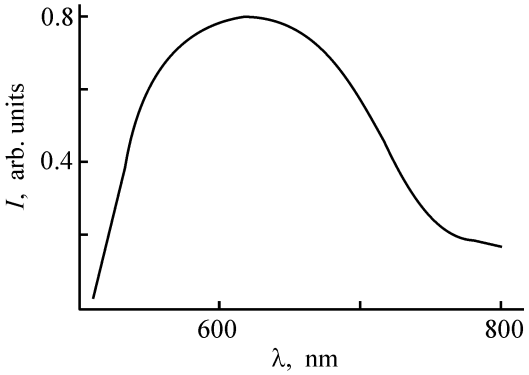


Fig. 2. Luminescence spectrum of compound **IV** in DMF. Solution concentration 1×10^{-4} M. (*I*) Intensity and (λ) wavelength.

and ε remains actually the same, which is indicative of high stability of their molecules during formation of PM.

In the first AT group, compound **III** is fairly resistant to degradation during copolymerization (the difference in ε in DMF and PM is small), whereas for **II** ε in PM is lower by a factor of 2.7. Thus, substitution of hydroxyl in the aromatic ring by the *p*-dimethylamino group increases the molecular stability of AT under conditions of radical polymerization. The comparison of **V** and **IV** shows enhanced stability of **V**, which differs from **IV** by the presence of the pyrazole ring.

With an increase in solution concentration, the intensity of AT absorption increases at different rates W_ε correlating with ε (see table). As seen, the W_ε values in PM are lower than in the solution by a factor of 2 and more. Compound **IV**, for which a luminescence spectrum in DMF was observed (Fig. 2), is characterized by the maximal value of W_ε.

To evaluate the lightfastness of ATs, we examined the kinetics of decolorization of their solutions and polymeric samples under the action of the integral light of a mercury lamp. The kinetic data in the D_t/D_0–t axes are shown in Figs. 3 and 4.

It follows from different shapes of the kinetic curves that the structure of AT affects its lightfastness. The solutions of **II** and **IV** were decolorized at a constant rate during the irradiation (Fig. 3, curves *3*, *5*). The rate of decolorization of **V** gradually decreases (Fig. 3, curve *4*). Solutions of **III** and **I** are decolorized only in the beginning of the irradiation (up to t = 0.5 h), whereupon the D_t/D_0 ratio becomes virtually constant (Fig. 3, curves *1* and *2*, respectively). The least-absorbing compound **III** exhibits the highest lightfastness in the solution. In this case, decoloriza-

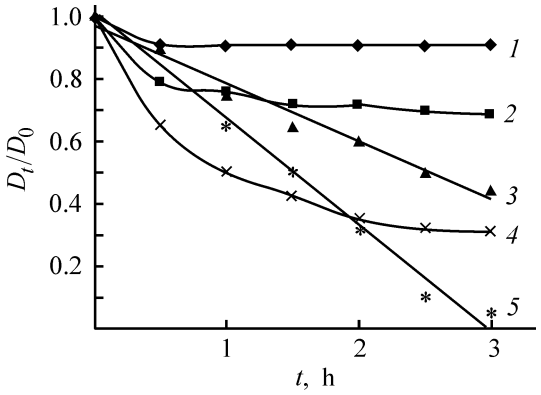


Fig. 3. Kinetic curves of photodecolorization of ATs in DMF. Concentration of **II**, **III**, and **V** 1×10^{-3} M and of **IV** 2.5×10^{-4} M. (D_0, D_t) Optical density at λ_a^{max} before and after irradiation, respectively (rel. units) and (t) irradiation time; the same for Fig. 4. Compound: (*1*) **III**, (*2*) **I**, (*3*) **III**, (*4*) **V**, and (*5*) **IV**.

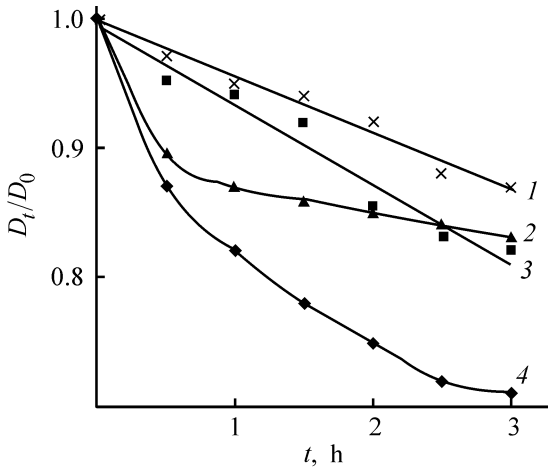


Fig. 4. Kinetic curves of photodecolorization of ATs in PM. Concentration of **II**, **III**, and **V** 1×10^{-3} M and of **IV** 1.0×10^{-4} M. Compound: (*1*) **V**, (*2*) **II**, (*3*) **III**, and (*4*) **IV**.

tion does not exceed 10% after 3 h of irradiation, which can be caused by quenching of the excited electronic states by solvent molecules [20].

Photodecolorization of ATs in PM is substantially lower than in the solution. For instance, after 2 h of irradiation the maximal decrease in the optical density of AT in PM does not exceed 25%, which is by a factor of almost 3 less than in DMF.

The comparison of Figs. 3 and 4 shows that the shapes of certain kinetic curves related to liquid and solid media are different. This fact can be explained by mutual influence of photochemical aging of PM and AT and the specific influence of AT on the kinetic parameters of the synthesis of the polymeric samples. The exception is compound **IV**, whose photochemical aging mechanism is apparently the same in DMF and PM. This compound demonstrates the lowest lightfastness in both liquid and solid media. Compound **V** has the maximal lightfastness in PM (Fig. 4) and, as noted above, shows enhanced stability under the conditions of the synthesis of polymeric samples. For compounds **II** and **III** in PM, the lightfastness and stability of AT also correlate: to the greater lightfastness of **III** corresponds the higher stability of its molecules during polymerization.

CONCLUSIONS

(1) The influence of the chemical composition on the absorption spectra of functionally substituted azothiazoles in dimethylformamide and transparent polymer matrix, for which λ_a^{max} varied within the 380–511 nm range, was examined. In the series of compounds **I**, **II**, and **III** with phenyl, phenol, and *p*-dimethylaniline substituents, respectively, bound to the azo group, the bathochromic shift and broadening of the absorption band take place. For compound **III**, the hypochromic effct was additionally observed.

(2) As a rule, the absorption bands of azothiazoles in solutions are narrower than in the polymeric matrix.

(3) The difference in the chemical composition substantially affects the character of the kinetic curves and degree of photodecolorization of azothiazoles, whose value in the polymeric matrix is by a factor of almost 3 smaller than in dimethylformamide.

ACKNOWLEDGMENTS

The authors are indebted to A.I. Lyubimov (State Institute of Applied Optics) for measurement of the luminescence spectra.

The study was financially supported by the Research and Development Foundation, Academy of Sciences of Tatarstan Republic (grant nos. 07-7.1-224/2004 and 07-7.5-224/2005).

REFERENCES

1. Stepanov, B.I., *Vvedenie v khimiyu i tekhnologiyu organicheskikh krasitelei* (Introduction to the Chemistry and Technology of Organic Dyes), Moscow: Khimiya, 1984.
2. Porai-Koshits, B.A., *Azokrasitely* (Azo Dyes), Leningrad: Khimiya, 1972.
3. Levkoev, I.I., *Organicheskie veshchestva v fotograficheskikh protsessakh* (Organic Substances in Photographic Processes) Moscow: Nauka, 1982.

4. Singh, R., Singh, S., and Taylor, J., *Dyes Pigm.*, 2002, vol. 54, no. 3, pp. 189–200.
5. Zollinger, H. *Chemie der Azofarbstoffe*, Basel: Birkhauser, 1958.
6. Kasali, A. Bello and Griffiths, J., *J. Chem Soc., Chem. Commun.*, 1986, no. 22, pp. 1639–1640.
7. Watanabe, T., Anmano, M., and Tomaru, S., *Jpn. J. Appl. Phys.*, 1994, vol. 33, p. 1683.
8. Branger, C., Leguan, M., Leguan, R, et al., *Chem. Phys. Lett.*, vol. 272, nos. 3–4, pp. 265–270.
9. Griffiths, J. and Lee, W., *Dyes Pigm.*, 2003, vol. 57, pp. 107–114.
10. Denisov, L.K., D'yachkov, A.I., Kristaleva, V.N., et al., *Plast. Massy*, 1987, no. 12, pp. 22–23.
11. Boiko, V.A., Vainer, A.Ya., Dyumaev, K.M., et al., *Zh. Tekh. Phys.*, 1982, vol. 52, no. 11, pp. 15–20.
12. Klimova, E.D., *Fotopolimerizuyushchiesya kompozitsii dlya pechatnykh i otdelochnykh protsessov* (Photopolymerizing Compositions for Printing and Finishing Processes), Moscow: Mosk. Gos. Univ. Polim., 2000.
13. Serova, V.N., Vasil'ev, A.A., Shmotova, L.N., et al., *Zh. Prikl. Khim.*, 1993, vol. 66, no. 10, pp. 2371–2375.
14. Serova, V.N., Shmotova, L.N., Chirkov, V.V., and Arkhireev, V.P., *Zh. Prikl. Khim.*, 1999, vol. 72, no. 8, pp. 1363–1368.
15. Serova, V.N., Cherkasova, O.A., Cherezova, E.N., et al., *Zh. Prikl. Khim.*, 1999, vol. 72, no. 11, pp. 1883–1888.
16. Nurkhametova, I.Z., Synthesis, Hetero-, and Carbocyclization of Functionally Substituted Thiazolidines, Thiazoles, and 1,3,4-Thiadiazines, *Cand. Sci. Dissertation*, Kazan, 2001.
17. Mamedov, V.A., Nurkhametova, I.Z., Gubaidullin, A.T., et al., *Khim. Geterotsikl. Soedin.*, 1999, no. 11, pp. 1554–1560.
18. Mamedov, V.A., Mustakimova, L.V., Gubaidullin, A.T., et al., *Zh. Org. Khim.*, 2005, vol. 41, no. 5, pp. 710–717.
19. Slark, A.T. and Hadgett, P.M., *Polym.*, 1999, vol. 40, pp. 1325–1332.
20. Barltrop, J.A. and Coyle, J.D., *Excited States in Organic Chemistry*, London: Wiley, 1975.

ISSN 1070-4272, Russian Journal of Applied Chemistry, 2006, Vol. 79, No. 4, pp. 642–646. © Pleiades Publishing, Inc., 2006.
Original Russian Text © I. Yu. Dmitriev, S. V. Gladchenko, V. K. Lavrent'ev, O. E. Praslova, G. K. El'yashevich, 2006, published in Zhurnal Prikladnoi Khimii, 2006, Vol. 79, No. 4, pp. 650–654.

MACROMOLECULAR CHEMISTRY AND POLYMERIC MATERIALS

Dependence of the Dielectric Constant on the Structure of Extruded Polyvinylidene Fluoride Films

I. Yu. Dmitriev, S. V. Gladchenko, V. K. Lavrent'ev, O. E. Praslova, and G. K. Elyashevich

Institute of Macromolecular Compounds, Russian Academy of Sciences, St. Petersburg, Russia

Received February 2, 2006

Abstract—The structure of extruded polyvinylidene fluoride films obtained at different die drawing ratios and melt temperatures was studied by X-ray scattering, differential scanning calorimetry, and gravimetry. Their dielectric constant and mechanical properties were examined. The influence exerted by the structure of the amorphous phase and by the molecular weight of the polymer on the dielectric constant of the samples was revealed.

DOI: 10.1134/S1070427206040276

Polyvinylidene fluoride (PVDF) occupies a particular place among other thermoplastic polymers owing to its dielectric properties, and primarily to high dielectric constant. The interest in PVDF was due to a pronounced pyro- and piezoelectric effect observed in this polymer [1]. At the same time, understanding of the nature of the dielectric properties of PVDF is complicated by a considerable heterogeneity of its structure, polymorphism and diverse morphologier of the crystalline phase, and inhomogeneity of amorphous zones [2].

It is known that crystalline regions of PVDF show at least four polymorphic modification (α, β, γ, and α_p), which differ in the conformational structure of chains and packing of macromolecules in the unit cell of crystallites [2], with the piezoelectric properties attributed to the presence of ferroelectric crystals of β-type. It is also known that the dielectric properties of PVDF are determined to a greater extent by the structure of the amorphous phase, rather than by that of the crystalline phase, and the former cannot be regarded as a structurally uniform medium. The dielectric properties of PVDF films can be optimized by modifying the chain packing density in the amorphous phase and initiating formation of microscopic defects and discontinuities [3, 4].

Extrusion of flexible-chain polymers from a melt makes it possible to form a structure constituted by parallel folded crystals (lamellas) whose surface is oriented perpendicular to the flow direction of the melt and which are connected with one another by a certain number of tie chains. Apparently, the oriented nature of extruded PVDF films affects their dielectric characteristics. It was shown in [5] that a material with increased content of strongly anisotropic crystallites of β-type, which also contains microscopic defects in the polymer bulk, can be obtained on the basis of extruded films. It is of interest in this context to carry out a detailed study of the structure and properties of extruded films, which will make it possible not only to characterize the film as a sample for further studies, but also to relate the dielectric properties of the samples to their oriented molecular organization.

It is noteworthy that PVDF films are for the most part industrially manufactured by extrusion, whereas research is carried in the overwhelming majority of cases on samples produced by casting from a solution, compaction, or cast molding. Thus, a study of properties of extruded films will enable a comparison of experimental data for samples obtained in laboratory and industrial films.

EXPERIMENTAL

Two industrially manufactured PVDF brands with M_w 1.9×10^5 and 4.5×10^5 were used. A melt was extruded through a planar-slit die. The degree of sample orientation was varied by changing the rotation rate of the receiving calendar and was characterized by the die drawing ratio λ equal to the ratio between the cross-sectional area of the film and that of the die.

Three temperature modes with different die temperatures T_d were used in film forming.

The supramolecular structure was studied by X-ray scattering at large (DRON-2.0 X-ray diffractometer) and small (Kratki camera with a VIP-2-50-60 high-voltage source) angles with CuK_α radiation.

The dielectric constant was measured with an E7-11 device at a frequency of 1 kHz and room temperature by the contact method without deposition of electrodes onto the film.

The enthalpy of melting and degree of crystallinity were determined from curves of differential scanning calorimetry (DSC). The sample density was found gravimetrically. Mechanical properties of the films were measured on an R-5 tensile-testing machine (Ivanovo, Russia).

The dielectric constant ε' was determined for samples formed from PVDF with $M_w = 1.9 \times 10^5$ at a forming temperature of 200°C. The measurements demonstrated that the highest values are observed for samples extruded at the lowest die drawing ratio (ε' = 8.4 was achieved at λ = 6.5). At higher λ, the dielectric properties steadily decrease as the degree of film orientation increases (Fig. 1, curves *1* and *2*). To explain this fact, changes in the sample structure upon an increase in λ were analyzed. It was found that the film density is virtually independent of λ (Fig. 2, curve *1*), whereas the degree of crystallinity markedly grows as the die drawing ratio increases (Fig. 2, curve *2*). This fact suggests that the density of the amorphous regions substantially decreases as the degree of orientation increases. To verify this assumption, we calculated the density of the amorphous phase of extruded samples.

The density of a partly crystalline polymer can be represented as [6]

$$\rho = \rho_a(1 - \chi_{vol}) + \rho_c\chi_{vol}, \quad (1)$$

where χ_{vol} is the volume degree of crystallinity; ρ_c, crystal density; and ρ_a, density of the amorphous phase.

The weight degree of crystallinity χ can be written as [6]

$$\chi = \chi_{vol}(\rho_c/\rho). \quad (2)$$

It follows from Eqs. (1) and (2) that

$$\rho_a = \frac{\rho_c\rho(1 - \chi)}{\rho_c - \chi\rho}. \quad (3)$$

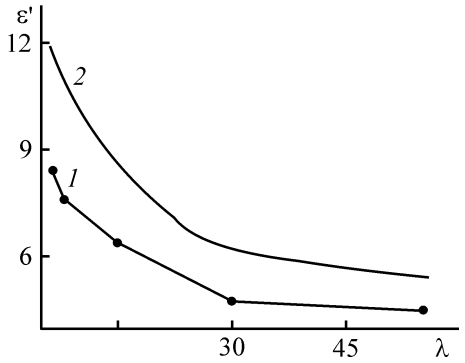


Fig. 1. (*1*) Dielectric constant ε' and (*2*) dielectric constant of the amorphous phase (calculation) of extruded PVDF films vs. the die drawing ratio λ. $M_w = 1.9 \times 10^5$, T_d = 200°C; the same for Figs. 2, 3, and 5.

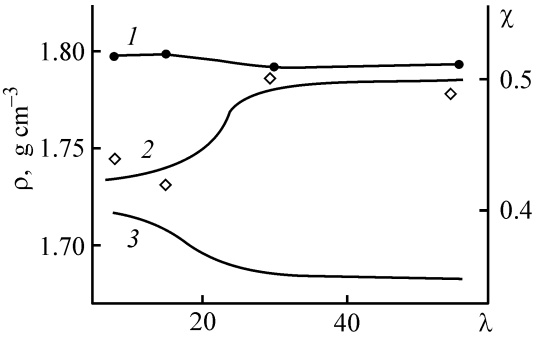


Fig. 2. (*1*) Density ρ (*2*) degree of crystallinity, χ, and (*3*) density of the amorphous phase (calculation) of extruded PVDF films vs. the die drawing ratio λ.

As shown by large-angle X-ray data, the crystalline phase of all the samples studied is completely composed of crystallites of β-modification. The density of a PVDF crystal of α-form is $\rho_c = 1.92$ g cm^{-3} [7]. The dependence of ρ_a on λ, calculated by Eq. (3) (Fig. 2, curve *3*), confirms the above assumption that the density of the amorphous region decreases as the die drawing ratio increases. This result is in agreement with the known evidence that, in contrast to orientation drawing of extruded samples, die drawing does not make larger the number of tie chains in the amorphous phase of the polymer. In addition, curve *2* in Fig. 2 shows that the potentialities of die drawing in raising the degree of crystallinity are also limited: die drawing is effective in this regard at λ < 25–30, whereas at higher die drawing ratios, the degree of crystallinity ceases to grow with λ because of the slipping of polymer chains as a result of an increase in the melt flow velocity and decrease in the influence exerted by orientation on the crystallization process. The fact that the difference in density between the crystalline and amorphous phases becomes more pronounced is also indicated by an increase

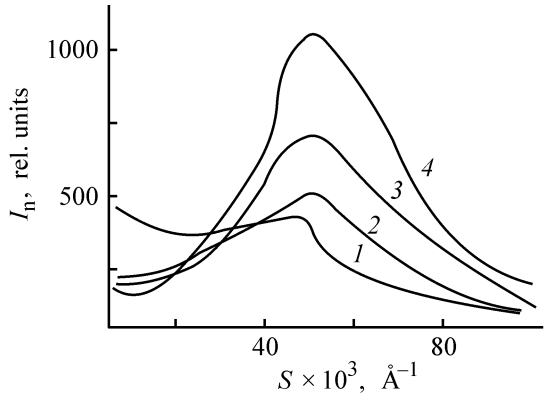


Fig. 3. Intensity I_n of the small-angle X-ray meridional reflection vs. the scattering angle S for films with die drawing factors of (*1*) 8, (*2*) 15, (*3*) 30, and (*4*) 55.

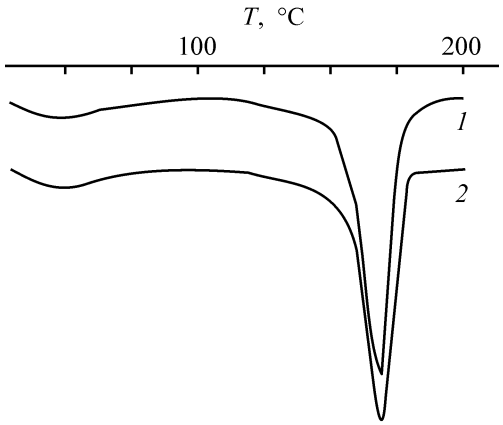


Fig. 4. DSC thermograms for PVDF films with M_w of (*1*) 1.9×10^5 and (*2*) 4.5×10^5, extruded at $\lambda = 15$. (T) Temperature.

in the intensity of small-angle X-ray scattering in the films at higher λ (Fig. 3).

The structure of an extruded film can be represented as a set of crystalline lamellas connected by amorphous interlayers and arranged in parallel to one another and perpendicular to the film surface. In terms of this model, the following relation for the dielectric constant of a two-phase system is valid for an electric field directed parallel to the interface between the constituent layers [9]:

$$\varepsilon' = \varepsilon'_a(1 - \chi_{vol}) + \varepsilon'_c\chi_{vol}, \quad (4)$$

where ε'_c is the dielectric constant of the crystal, and ε'_a, that of the amorphous phase.

With account of (2), an expression for ε' can be derived:

$$\varepsilon'_a = \frac{\varepsilon'\rho_c - \varepsilon'_c\chi\rho}{\rho_c - \chi\rho}. \quad (5)$$

Because all the samples used in the experiment in question are composed of crystallites of α-type and crystallized under the same temperature conditions, ε'_c was taken to be 3 for all the films [10]. The values of ε'_a, calculated by expression (5), were found to exceed the overall macroscopic ε' for the films obtained at all values of λ (Fig. 1, curve *3*). This fact, and also similar shape of the dependences of ε'_a and ε' on λ, indicate that the structure of the amorphous phase makes an important contribution to formation of the dielectric properties of PVDF films.

As can be seen in Figs. 1 and 2, ε'_a and ρ_a decrease as the degree of orientation becomes higher. The relationship between these parameters can be revealed by analyzing the mechanism of relaxation phenomena in PVDF.

It is known [6] that macromolecules may be present in intercrystallite spaces of amorphous-crystalline polymers in different states (as strained and unstrained tie chains, regular and irregular loops, free ends), which leads to splitting of the α-transition and gives rise to an additional glass transition point [11]. It is this fact that accounts for the appearance in PVDF, in addition to the main glass transition point at –40°C, of a "second glass transition point" at 50–80°C. This temperature is attributed by many authors to the α_c-transition [12–14] and indicates that strained tie chains (STC) are present in the amorphous phase. For the samples studied, this process is observed as a thermal transition in DSC thermograms in the temperature range 40–60°C (Fig. 4).

Thus, the noncrystalline phase of the polymer is not homogeneous and contains, in addition to the truly amorphous phases composed of unstrained tie chains, loops, and chain ends, also a zone intermediate between the crystalline and amorphous phases, which contains strained tie chains and is manifested in that a higher glass transition point appears. According to [15], it is in this intermediate region that the presence of crystallites restricts the dipole mobility of macromolecules. Thus, the decrease in ε'_a with increasing λ can be attributed to an enhanced orientation of tie chains and their transition to the strained state. This leads to a decrease in the concentration of mobile polar groups in the amorphous phase, which make the largest contribution to the overall ε'.

It is noteworthy that a *trans–trans* conformation, which has a higher dipole moment than the spiral *trans–gauche* conformation characteristic of the isotropic part of the amorphous phase, may be favorable

Properties of extruded PVDF films obtained at $\lambda = 15$*

M_w	T, °C	ΔH, J g^{-1}	χ, %	ε'	ε_a	ρ	ρ_a	E, MPa
						g cm^{-3}		
190 000	200	44	42	6.4	8.6	1.799	1.720	1920
	205–210	46	44	6.3	8.6	1.796	1.709	2200
	220–225	45	43	6.1	8.2	1.791	1.705	2470
450 000	205–210	46	44	4.0	4.7	1.813	1.737	2330

* Melting point was the same (169°C) for all the samples.

for STC. The present study disregards the possible conformational nonuniformity of the amorphous phase. At the same time, this factor can strongly affect both the dielectric properties and the mechanical behavior of the films.

The fraction of the intermediate amorphous-crystalline interlayer is determined by such parameters of supramolecular formations as orientation, size, and perfection of the crystallites. The small-angle X-ray diffraction patterns in Fig. 3 show for all the samples a peak indicative of the existence of a large period $L \approx 12.5$ nm. It may be concluded, with account of the increase in the degree of crystallinity of the films with λ (Fig. 2), that the crystallites also grow in size. The deformation behavior of extruded PVDF films obtained at different λ (Fig. 5) also points to significant differences in their structure, and, consequently, they may also differ in the percentage content of this interlayer.

The accuracy of the DSC experiment was insufficient for evaluating the fraction of STC; however, its increase with λ can be judged from the observed change in mechanical characteristics (Fig. 6). In addition to demonstrating that the modulus of elasticity grows with the degree of orientation λ, the stress–strain curves also show an increase in the breaking strength, which is directly related to a rise in the fraction of strained, i.e., loaded chains. Noteworthy is the fact that the elongation at break very weakly increases with λ at small λ, where the degree of crystallinity χ increases and ρ_a decreases. At the same time, the elongation at break is markedly different for samples that were obtained at λ of 30 and 55 and, correspondingly, have close values of χ and ρ_a (Fig. 2). It may be assumed that the forming process at large λ leads, because of the chain slipping at a high flow velocity of the melt, to strong differences in the extent to which chains are strained in the amorphous phase. This difference in the extent of strain leads, on loading a sample, to successive transfer of strain on rupture of more strained chains to those strained to a lesser extent, which leads to an increase in the elongation at break and to weakly pronounced yield point.

The table shows that varying the forming temperature in extrusion of films does not change the degree of crystallinity; however, ε', ρ, and ρ_a of the samples decrease as the melt temperature becomes higher. In the whole range of die drawing ratios, the elastic

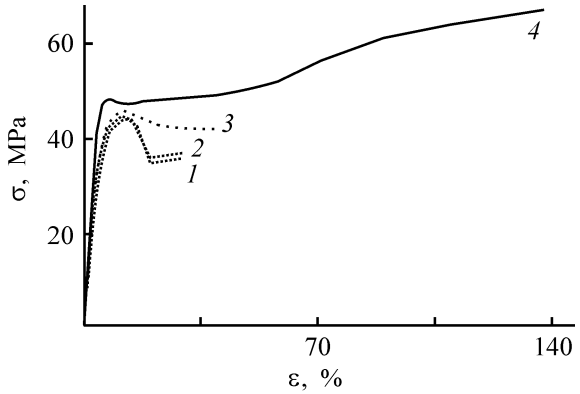


Fig. 5. Stress–strain (σ–ε) curves in the orientation direction for PVDF films extruded at die drawing ratios of (*1*) 8, (*2*) 15, (*3*) 30, and (*4*) 55.

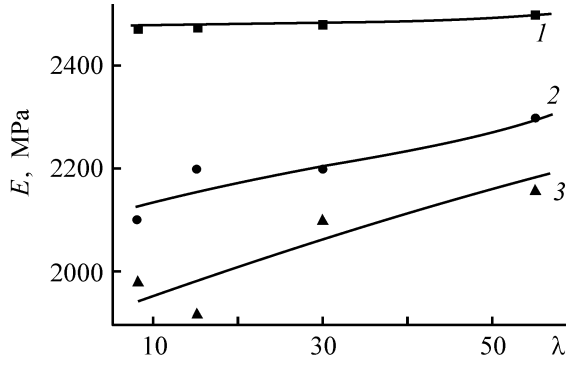


Fig. 6. Modulus of elasticity E vs. the die drawing ratio for PVDF films ($M_w = 1.9 \times 10^5$) extruded at T_d of (*1*) 220–225, (*2*) 205–210, and (*3*) 200°C.

modulus of films increases with the melt temperature (see table), which indicates that the degree of sample orientation grows. Thus, the increase in the degree of orientation with the forming temperature, which causes with a high probability a rise in the fraction of STC in the amorphous phase, impairs the dielectric properties and confirms the above conclusion about the adverse effect of orientation on ε' of extruded films.

The parameters of the crystalline phase of films with different M_w were the same; however, films with $M_w = 4.5 \times 10^5$ had a lower ε' than those prepared from a polymer with $M_w = 1.9 \times 10^5$ (see table). At the same time, samples with $M_w = 4.5 \times 10^5$ had higher values of ρ_a than films prepared from a lower-molecular-weight polymer. The densification of the amorphous phase, observed as the molecular weight increases, is a phenomenon that is typical of flexible-chain polymers and is associated with a high density of intermolecular contacts in the melt of a high-molecular-weight polymer and with hindrance to "disentangling" of its chains in the course of crystallization. The large values of ρ_a and modulus of elasticity of films with a higher M_w (see table) point to an increased content of STC in their amorphous phase. In the given case, the dense packing of tie chains may cause steric hindrance to motion of polar groups and be a reason for the decrease in ε' of the film.

Thus, our study revealed the influence exerted by forming conditions and molecular weight of the polymer on the structure and dielectric properties of extruded PVDF films. It was shown that raising the degree of orientation and densification of the amorphous phase restrict the dipole mobility of chains in amorphous interlayers and, as a result, lead to a decrease in the dielectric constant of the samples.

CONCLUSIONS

(1) The conditions of crystallization of polyvinylidene fluoride films in forming from a melt affect the density of the amorphous phase and the dielectric constant of the samples.

(2) Raising the melt temperature and the die drawing ratio leads to a decrease in the dielectric constant of extruded polyvinylidene fluoride films.

(3) The polyvinylidene fluoride films produced from a polymer with a higher M_w have a lower dielectric constant.

ACKNOWLEDGMENTS

The study was financially supported by the Russian Foundation for Basic Research (grant no. 04-03-32 229).

REFERENCES

1. *The Applications of Ferroelectric Polymers, Wang*, T.T., Herbert, J.M., and Glass, A.M., Eds., Glasgow: Blackie, 1988.
2. Kochervinskii, V.V., *Usp. Khim.*, 1996, vol. 65, no. 10, pp. 936–987.
3. Kochervinskii, V.V., *Neorg. Mater.*, 1995, vol. 31, no. 6, pp. 851–858.
4. McGrath, J.C., Holt, L., and Jones, D.M., *Ferroelectrics*, 1983, vol. 50, pp. 13–20.
5. Dmitriev, I.Yu., Lavrent'ev, V.K., and Elyashevich, G.K., *Vysokomol. Soedin., Ser. A*, 2006, vol. 48, no. 3, pp. 447–453.
6. Wunderlich, B., *Macromolecular Physics*, New York: Academic, 1973.
7. Humphrews, J., Ward, I.M., Nix, E.L., and McGrath, J.C., *J. Appl. Polym. Sci.*, 1985, vol. 30, pp. 4069–4079.
8. Zyabitskii, A., *Teoreticheskie osnovy formovaniya volokon* (Theoretical Foundations of Fiber Formation), Moscow: Khimiya, 1979.
9. Sazhin, B.I., Lobanov, A.M., Romanovskaya, O.S., et al., *Elektricheskie svoistva polimerov* (Electrical Properties of Polymers), Leningrad: Khimiya, 1986.
10. Broadhurst, M.G., Davis, G.T., and McKinney, J.E., *J. Appl. Phys.*, 1978, vol. 49, no. 10, pp. 4992–4999.
11. Boyer, R., *J. Macromol. Sci. Phys.*, 1973, vol. 8B, no. 3, pp. 503–537.
12. Sajkiewicz, P., Wasiak, A., and Goclowski, Z., *Eur. Polym. J.*, 1999, vol. 35, pp. 423–429.
13. Mano, J.F., Sencadas, V., Mello Costa, A., and Lanceros-Mendos, S., *Mater. Sci. Eng.*, 2004, vol. 370A, pp. 336–340.
14. Neagu, E.R., Hornsby, J.S., and Das-Gupta, D.K., *J. Phys. D, Appl. Phys.*, 2002, vol. 35, no. 11, pp. 1229–1235.
15. Gregorio, R. and Ueno, E.M., *J. Mater. Sci.*, 1999, vol. 34, pp. 4489–4500.

ISSN 1070-4272, Russian Journal of Applied Chemistry, 2006, Vol. 79, No. 4, pp. 647–653. © Pleiades Publishing, Inc., 2006.
Original Russian Text © L. V. Vinogradova, O. V. Ratnikova, E. A. Butorina, D. Kukling, H.-J. P. Adler, 2006, published in Zhurnal Prikladnoi Khimii, 2006, Vol. 79, No. 4, pp. 655–662.

MACROMOLECULAR CHEMISTRY AND POLYMERIC MATERIALS

Structural Features and Initiating Properties of the Hexaadduct of Polystyryllithium and Fullerene C_{60} in Tetrahydrofuran and Their Role in Synthesis of Heteroarm Star-Like Polymers

L. V. Vinogradova, O. V. Ratnikova, E. A. Butorina, D. Kukling, and H.-J. P. Adler

Institute of Macromolecular Compounds, Russian Academy of Sciences, St. Petersburg, Russia

Received January 17, 2006

Abstract—Structural transformations of the hexaadduct of polystyryllithium and fullerene C_{60} in the course of interaction with a proton donor or 1,1-diphenylethylene and at initiation of styrene polymerization were studied, and their role in the formation of heteroarm star-like polymers with C_{60} center of branching and arms of polystyrene and poly-2-vinylpyridine was elucidated.

DOI: 10.1134/S1070427206040288

Synthesis and study of star-like polymers are of particular importance because they can be used as viscosity-modifying agents, surfactants, oil additives, biologically compatible and biodegradable materials, micelle-forming agents [1, 2], nanocontainers [3], materials with nonlinear optical properties [4], liquid-crystal [5] and conducting polymers [6], highly ordered porous films [7, 8], Langmuir films [9], etc.

Among known types of star-like polymers, μ-star polymers containing arms of various chemical nature (polar–nonpolar) or block arms (nonpolar–*block*-polar) are of primary importance. Such starts exhibit the properties of "smart" polymers in solutions at formation of nanomicelles and at conversion into nanostructures [10]; on the support surface they form monolayers with changing morphology depending on the solution type [11, 12], act as nanoreactors [13] in synthesis of nanocomposite materials containing stable metal nanoparticles, and possess interesting optical and electrooptical properties [14].

These μ-star polymers can be prepared by various methods, and among them the procedures based on controlled anionic polymerizations are the most effective. Two main approaches are used: "arm first" and "core first." In the "arm first" method, "living" linear polymers (or diblock copolymers) are prepared first and are then combined using a divinyl derivative to form the core of macromolecule in the course of cross-linking and copolymerization. For example, star-like polymers with arms of diblock copolymers polystyrene (PS)–poly-2-vinylpyridine (P2VP) were prepared by this procedure [13]. In the "core first" method, a core is prepared first, which actually acts as polyfunctional initiating agent and new polymeric arms are grown on the active centers of this core. Using this procedure, the stars with arms of PS and P2VP $[(PS)_n(P2VP)_n]$ were prepared [15]. In both cases, the size of the macromolecule core formed from cross-linked diene agent is rather large, and large contribution of the core to the total molecular weight of the polymer (MW) not only hinders calculation of the number of branches, but also affects the polymer properties.

In this paper we suggested an alternative procedure for preparing heteroarm star-like polymers with alternating PS and P2VP arms and macromolecular branching center C_{60} whose small size allows us to consider it as a "point" center. Owing to combination in the star-like macromolecule of hydrophobic PS arms and pH-sensitive P2VP arms, these polymers should be able to form micelles and supramolecular aggregates in solutions, whose structure can be rearranged under the effect of external factors such as acidity and special additives, and to exhibit properties

of "smart" polymers. The "point" branching center does not hinder penetration of various agents to the "point" center, which suggests that these polymers can be used as nanocontainers and nanoreactors. Moreover, the star-like polymers allow preparation of nanocomposites and highly porous films.

In this paper we also analyzed the data on the properties of hexaadduct of polystyryllithium and fullerene C_{60} [$(PS)_6C_{60}Li_6$] as the initiating agent of polymerization of 2-vinylpyridine (2VP) and styrene in THF and studied structural changes in the hexaadduct in the course of its conversion into polyfunctional initiating agent.

EXPERIMENTAL

Materials. Tetrahydrofuran, benzene, toluene, and 1,1-diphenylethylene (DPE) (Aldrich) were purified in accordance with requirements to highly sensitive anionic systems [16]. Powdered lithium chloride was calcined in a vacuum (10^{-6} mm Hg). Fullerene (C_{60} content >99%) purchased from the Fullerenovye Tekhnologii Limited Liability Company was pretreated by the known method [17].

Monomers. Styrene was purified by the procedure given in [18] using prepolymerization in benzene in the presence of oligostyryllithium (OSL). 2-Vinylpyridine (Fluka) was treated with Al_2O_3 to remove the stabilizing agent and sublimed in a vacuum from CaH_2; 2VP was used as solution in THF. Traces of moisture were removed from the vacuum system with calcined CaH_2.

Polymerization and synthesis of polymers. The polymerization was performed in a special high-vacuum (10^{-6} mm Hg) all-soldered glass apparatus with break seals.

Oligostyryllithium (OSL) with an average degree of polymerization of 4 was prepared by the reaction of *sec*-butyllithium with styrene in benzene, and polystyryllithium (PSL) was obtained at room temperature in the presence of OSL [18].

The model adducts $(PS)_nC_{60}Li_n$ with the PSL : C_{60} ratio of 6.2 : 1, 5 : 1, and 4 : 1 were prepared in a benzene–toluene mixture at room temperature; the reaction time was 1 h.

The heteroarm polymers $(PS)_nC_{60}(P2VP)_n$ were synthesized in several steps. First, $(PS)_nC_{60}Li_n$ was prepared from PSL and C_{60} (at given reactant ratio) at room temperature in a benzene–toluene mixture. The solution samples were taken and deactivated. Then, the reaction of the adducts with DPE was carried out in the presence of LiCl (C_{60}–Li : DPE : LiCl = 1 : 2 : 2); THF was added to the reaction mixture by condensation in a vacuum. The mixture was kept at –30°C for 15 min and cooled to –78°C, and then 2VP was added. The mixture was polymerized for 1 h.

Polymerization of styrene in the presence of hexaadduct $(PS)_6C_{60}Li_6$ was carried out in the mixed solvent (50% THF) at –40°C [19].

The reaction mixtures were deactivated using a solution of butanol in toluene (1 : 3) without admitting air. The heteroarm polymers were precipitated from the reaction mixture with hexane; the styrene polymers were precipitated with methanol and dried in a vacuum.

The exclusion chromatography of polymers was performed on a chromatograph (Waters, the United States) equipped with 994 UV and 410 RI detectors at 30°C using the columns packed with linear Styrogel and Styrogels 10^4 and 10^3 Å; the eluent was chloroform containing 0.1% Et_3N. The chromatograph was calibrated with linear P2VP and PS references.

Hexaadduct of polystyryllithium and fullerene C_{60} [$(PS)_6C_{60}Li_6$] is a product of addition of maximally possible number of chains of the "living" polystyrene to a single C_{60} molecule [20–22]. The reaction of PSL and C_{60} (6 : 1 reactant ratio) yields a homogeneous product with a highly symmetrical regular structure. One fullerene center is linked with six PS arms of given molecular weight (from several to hundred thousands monomer units) [21] and six C_{60}–Li centers. In the active state, $(PS)_6C_{60}Li_6$ is a hexafunctional organolithium compound exhibiting various initiating properties in polymerization of vinyl monomers [19, 23, 24]. In polymerization of styrene in nonpolar solvents, only one C_{60}–Li center acts as initiating agent. As a result, only one additional (seventh) PS arm is grown on the six-arm molecule [19, 24]. In polar solvents (THF), styrene polymerization proceeds through the radical-anion mechanism by electron transfer from the hexaadduct to the monomer molecule [19]. Thus, in polymerization of nonpolar monomers, the hexaadduct does not behave as polyfunctional initiating agent.

The conditions of involving two active centers of $(PS)_6C_{60}Li_6$ in polymerization of methyl methacrylate (MMA) were found in [23], and the resulting hybrid macromolecule was described as $(PS)_6C_{60}(MMA)_2$. Hexaadduct $(PS)_6C_{60}Li_6$ was also used to initiate polymerization of *tert*-butyl methacrylate (TBMA) in THF after its preliminarily reaction with DPE [25]; the resulting data suggested formation of $(PS)_6C_{60}(PTBMA)_6$ macromolecule.

Statistical distribution of the products of PSL addition to fullerene C_{60}. Some disadvantages complicate the use of $(PS)_6C_{60}Li_6$ as initiating agent. Since attainment of precise PSL : C_{60} ratio of 6 : 1 is virtually impossible, the reaction mixture can contain free PSL, which can also initiate polymerization of vinyl monomers. Therefore, in our experiments the reactant ratio was taken maximally close to 6 : 1 or slightly lower; however, in this case (excess C_{60}) the question on the contribution of the other structures (penta-, tetra-, tri-, etc.) arises.

Amsharov [26] suggested the scheme of statistical distribution of the products of PSL reaction with fullerene C_{60} to form adducts with addition number from 1 to 6 at equal probability of all the addition events. In accordance with this scheme, at the PSL : C_{60} ratio varied within 5–6, the reaction should yield the star-like products with the number of arms n = 3–6. At PSL : $C_{60} \le 4$, the reaction product can contain up to 10% mono- and diadducts. To check this experimental approach, we performed a comparative chromatographic analysis of the model adducts of PSL with fullerene prepared at PSL : C_{60} ratios of 6.2 : 1, 5 : 1, and 4 : 1. Polystyrene (M_n 2.24×10^3, M_w/M_n 1.07) was used as PSL precursor. The PSL excess at the first ratio should provide formation of the hexaadduct only. In accordance with star-like regular structure, polymers with the number of arms from 3 to 6 (n = 3–6) should have similar hydrodynamic size. This is chromatographically confirmed by close "peak" molecular weights of the resulting adducts (M_p 10.01×10^3, 9.34×10^3, and 8.92×10^3) and narrow molecular-weight distribution M_w/M_n (1.19,[1] 1.12, and 1.16) (Fig. 1, refractometric detection) and 1.09, 1.11, and 1.16 (photometric detection at λ 330 nm, selective to fullerene-containing compounds), respectively. The contents of the adducts with various n prepared at PSL : C_{60} ratios of 6 : 1, 5 : 1, and 4 : 1, calculated in accordance with [26], are listed in Table 1. At a PSL : C_{60} ratio of 6 : 1, the reaction product contains the hexaadduct only, with an insignificant PLS impurity. At a PSL : C_{60} ratio of 5 : 1, various star-like structure are formed in the reaction mixture, and the content of the hexaadduct is only 30%. These results agree with the experimental data (Fig. 1, curves *2–4*). As seen, the peaks of adducts are narrow and symmetrical. At a PSL : C_{60} ratio of 4 : 1, the chromatographic peak becomes slightly broader (Fig. 1, curve *4*), which is probably due to the presence of mono- and diadducts (Table 1).

[1] Taking into account PSL precursor.

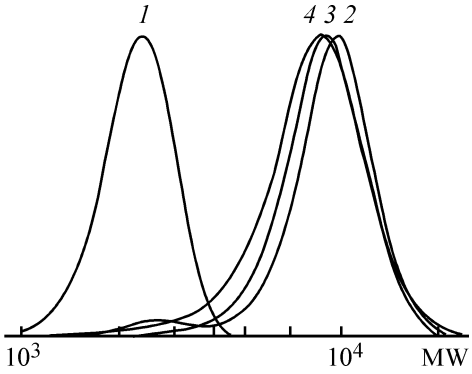


Fig. 1. Chromatographic curves (*1*) PS precursor; model adducts $(PS)_nC_{60}H_n$ at PSL : C_{60} ratio (*2*) 6.2 : 1, (*3*) 5 : 1, and (*4*) 4 : 1. (MW) Molecular weight, the same for Figs. 2–4.

Thus, using this statistical approach, we can determine the fractions of adducts with different number of arms formed in synthesis of star-like organolithium initiating agents based on polystyrene derivatives of fullerene.

Features of 2VP polymerization initiated by hexaadduct modified with DPE in the presence of THF. Heteroarm polymers $(PS)_nC_{60}(P2VP)_n$ with arms of PS and P2VP were prepared by polymerization of polar monomer (2VP) and adduct $(PS)_nC_{60}Li_n$ preliminarily modified with DPE in mixed solvent containing about 50% THF. The adducts were synthesized from PSL precursor with the following characteristics: M_n 6.35×10^3 and M_w/M_n 1.06 (Fig. 2, curve *1*). The chromatographic data[2] on the precursor adducts and heteroarm polymers are listed in Table 2. As seen, when synthesis is performed at PSL : C_{60} ratios of 6.2 : 1 and 6.0 : 1, the reaction mixture, along with the main fullerene-containing product ($M_p \approx 39 \times 10^3$), contains the fraction ($M_p \approx 20 \times 10^3$) containing no fullerene (photometric data, λ 330 nm) (Fig. 2, curves *3*, *4*).

Table 1. Statistical distribution of adducts $(PS)_nC_{60}H_n$ with various n

PSL : C_{60} ratio	Content of $(PS)_nC_{60}H_n$ adduct, %					
	hexa-	penta-	tetra-	tri-	di-	mono-
6 : 1	100	–	–	–	–	–
5 : 1	30	40	20	8	2	–
4 : 1	9	25	34	22	9	1

[2] Chromatographic values of M_p can be considered only as qualitative characteristics of star-like polymers.

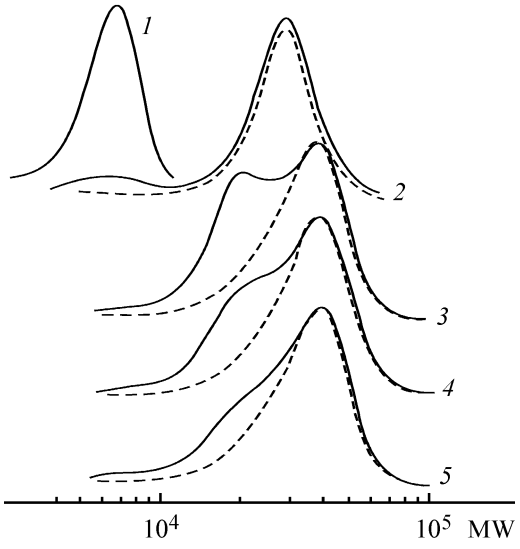


Fig. 2. GPC curves: (*1*) PS precursor, (*2*) $(PS)_nC_{60}Li_n$ macroinitiating agent; heteroarm polymers $(PS)_nC_{60}(P2VP)_n$ prepared in the presence of macroinitiating agents at PSL : C_{60} ratio of (*3*) 6.2 : 1, (*4*) 6.0 : 1, and (*5*) 5.0 : 1. *Solid curves*, refractometric detection; *dashed curves*, UV detection, λ 330 nm; the same for Fig. 3, 4.

Since the hexaadduct macroinitiating agent $(PS)_nC_{60}(P2VP)_n$ was first prepared with a slight excess of PSL (PSL : C_{60} ratio 6.2 : 1), the experimental results can be interpreted assuming simultaneous participation of two initiating agents (namely, hexaadduct and "free" PSL) in 2VP polymerization. The star-like hybrid polymer $(PS)_nC_{60}(P2VP)_n$ could be formed with the hexaadduct initiator, whereas "free" PSL provided formation of the linear diblock copolymer.

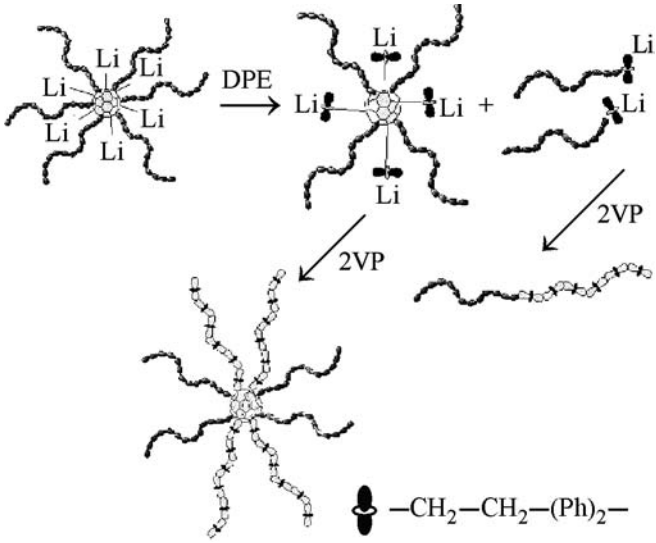
When the synthesis was performed at a PSL : C_{60} ratio of 6.0 : 1, the reaction mixture also involved the fullerene-free fraction, but in smaller amounts (Fig. 2, curve *4*). In this case, formation of this fraction can also be caused by excess PSL due to the possible error in reagent weighing. However, this conclusion contradicts the molecular weight of the resulting fraction ($M_p \approx 20 \times 10^3$) (Fig. 2, curve *4*), because the polymer with this molecular weight can be prepared only at a concentration of "free" PSL significantly higher than the experimental measurement error.

Table 2. Molecular properties of adducts $(PS)_nC_{60}H_n$ and heteroarm polymers $(PS)_nC_{60}(P2VP)_n$ [photometric detection (λ 330 nm)]

PSL : C_{60} ratio	Chromatographic characteristics			
	adduct $(PS)_nC_{60}H_n$		hybrid polymer	
	$M_p \times 10^{-3}$	M_w/M_n	$M_p \times 10^{-3}$	M_w/M_n
6.2 : 1	30.0	1.17	38.6	1.18
6.0 : 1	30.1	1.12	39.8	1.17
5.0 : 1	28.7	1.13	39.1	1.17

To find a more convincing explanation of our experimental results, we synthesized a hybrid polymer using $(PS)_nC_{60}Li_n$ macroinitiating agent prepared at PSL : C_{60} ratio of 5.0 : 1, because in this case no "free" PSL should remain in the reaction mixture. Although the narrow peak of the precursor adduct in the chromatographic pattern is similar to those registered at PSL : C_{60} ratios of 6.2 : 1 and 6.0 : 1 (Table 2), the reaction mixture prepared at a PSL : C_{60} ratio of 5.0 : 1 also contained the fullerene-free fraction (Fig. 2, curve *5*).

To explain this phenomenon, we put forward the following hypothesis. The hexaadduct prepared in nonpolar solvents undergoes certain transformations at addition of polar solvents. Lithium counterions are solvated by THF. The adduct structure with six nonsolvated anionic centers at the fullerene core become labile. In the reaction with DPE, the PSL arms are eliminated from the fullerene core; as a result, we obtained the tetraadduct and two PSL chains. In accordance with published data [20], the tetraadduct is stable in polar solvents. Hence, two types of initiating agents can be present simultaneously in the reaction system, namely, tetraadduct with four active centers and linear polystyryllithium. Thus, in the course of synthesis 2VP can polymerize on these initiating agents yielding either hybrid star-like polymer or diblock copolymer:



Elimination of PSL chains from hexaadduct $(PS)_6C_{60}Li_6$ in the presence of DPE or proton-donor agent in polar medium. To check the above hypothesis, we prepared the hexaadduct at PSL : C_{60} ratio of 6.1 : 1 in a nonpolar solvent (benzene–toluene). We too excess PSL, because it provides formation of the hexaadduct only, and, moreover, the PS precursor is a reliable chromatographic reference. After synthesis, one portion of the reaction mixture was sampled and deactivated with alcohol. The remainder was mixed with THF (up to 50% by volume), and DPE was added to the reaction mixture. The reaction of the hexaadduct with DPE was carried out at –30°C for 1 h, after which the mixture was deactivated in a vacuum.

After deactivation of the hexaadduct in the benzene–toluene mixture, the typical chromatographic pattern was observed (Fig. 3, curve *1*); it contained two peaks (hexaadduct and precursor polymer) with the height ratio h_1 (hexaadduct)/h_2 (PS precursor) of 6.6. After the reaction of the hexaadduct with DPE in THF and subsequent deactivation, the content of "free" PS sharply increased (Fig. 3, curve *2*); h_1/h_2 2.3.

These data confirm the elimination of PSL arms, but cannot explain whether elimination proceeds in reaction with DPE or by solvation with polar THF. To solve this problem, we carried out the following experiment. A solution of the hexaadduct in nonpolar solvent was mixed with THF (50%) and the mixture was deactivated with alcohol in a vacuum. The chromatographic pattern recorded after deactivation was similar to that recorded after the reaction of the hexaadduct with DPE and subsequent deactivation. The resulting peak ratio h_1/h_2 was 2.4.

At first glance, this result suggests that reorganization of the hexaadduct and cleavage of the PS chains are predominantly induced by the polar solvent (THF), whereas the effect of DPE is secondary. It only reacts with the active centers of both tetraadduct and linear PSL. However, this conclusion contradicts the radical-anion mechanism of styrene polymerization initiated with hexaadduct in the presence of THF [19]. If THF provides elimination of the PSL arm, then styrene polymerization should proceed under the effect of this "free" radical and not by the radical-anion mechanism as given in [19].

Structural changes in the hexaadduct $(PS)_6C_{60}Li_6$ in the course of styrene polymerization in the presence of THF. The experiment on polymerization of styrene in the presence of THF using $(PS)_6C_{60}Li_6$ initiating agent was carried out with the PSL precursor (M_n 4.2×10^3 and M_w/M_n 1.06).

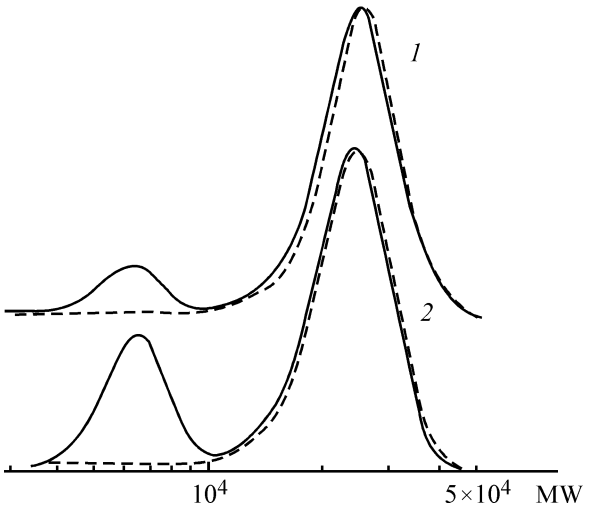
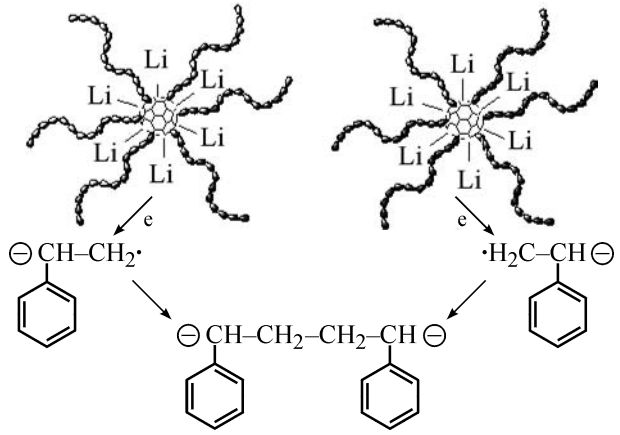


Fig. 3. GPC curves: (*1*) hexaadduct $(PS)_6C_{60}Li_6$ prepared in benzene–toluene mixture at PSL : C_{60} ratio of 6.1 : 1 and deactivated in nonpolar medium and (*2*) after reaction with DPE in THF and subsequent deactivation.

As seen from the experimental data, the reaction mixture contained the fullerene-free fraction and its molecular weight (M_p 40.6×10^3) was higher than the theoretical molecular weight per C_{60} core (M_{theor} 21.0×10^3) by a factor of approximately 2. If only one PS chain were eliminated from each hexaadduct molecule, the molecular weight of the resulting linear polystyrene would be close to the theoretical value, and if two chains were eliminated, it would be smaller than the theoretical value by a factor of 2. The experimental peak molecular weight (M_p 40.6×10^3) only suggests the radical-anion mechanism of polymerization. Each hexaadduct transmits one electron to the monomer (styrene) molecule to form radical anions, which then recombine into dianions. Styrene polymerizes under the action of the resulting bifunctional initiating agent:



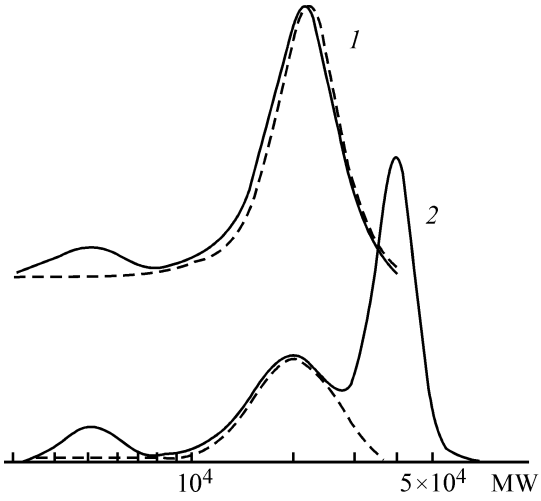


Fig. 4. GPC curves: (*1*) hexaadduct $(PS)_6C_{60}Li_6$ prepared in benzene–toluene mixture and (*2*) product of styrene polymerization in the presence of THF.

The only question concerns subsequent transformations of the hexaadduct after the loss of one electron, if styrene polymerization proceeds by the radical-anion mechanism. As seen, the chromatographic pattern of the hexaadduct precursor prepared and deactivated in the nonpolar medium contains two peaks, namely, hexaadduct and PS precursor (Fig. 4, curve *1*); the h_1/h_2 ratio is 8.9. The chromatographic pattern of the product of styrene polymerization shows three peaks corresponding to PS precursor, fullerene-containing product, and macromolecular fraction containing no fullerene (photometric data). After polymerization, the peak of the fullerene-containing product remained almost constant, whereas the ratio of the adduct and "free" PS sharply changed, h_1/h_2 = 3.1. This fact is attributable to elimination of PSL chains from the hexaadduct on treatment with a proton-donor agent (alcohol, water) in the stage of deactivation of the reaction mixture.

Hence, THF only promotes weakening of C_{60}–Li bonds due to solvation of counterions and destabilization of the hexaadduct structure. Additional agent (in the latter case, proton donor) causes elimination of the PSL bonds from the hexaadduct converting them into the tetraadduct. These results confirm not only the radical-anion initiation of styrene polymerization in the polar medium, but also elimination of PSL arms from the hexaadduct under the effect of the additional agent.

Synthesis of heteroarm polymers after modification of hexaadduct in nonpolar medium. To confirm the solvent effect on the reaction of the hexaadduct with DPE, we performed synthesis of polymers $(PS)_nC_{60}(P2VP)_n$ under various experimental conditions. The synthesis was performed at a PSL : C_{60} ratio of 6 : 1; the time of reaction of the hexaadduct $(PS^-)_6C_{60}(Li^+)_6$ with DPE in the nonpolar medium was increased to 1 h and reaction temperature was increased to –10°C, after which THF was added; the PSL precursor with $M_n \approx 6.91 \times 10^3$ and M_w/M_n 1.05 was used. The chromatographic data showed that the fraction of diblock copolymer ($M_p \approx 16 \times 10^3$) strongly decreased in comparison with the previous experiment (Fig. 1, curve *4*). Hence, the conditions of hexaadduct modification strongly affect the reaction of DPE with active C_{60}–Li groups. The reaction with DPE in nonpolar medium probably proceeds slowly and is far from completion by the time of adding THF. As a result, hexaadduct $(PS)_6C_{60}Li_6$ retains some amount of unmodified centers able to eliminate PS arms under the effect of DPE. In reaction in the nonpolar medium, the effect of elimination processes strongly decreases, which allows us to optimize the conditions of the synthesis of the heteroarm polymer $(PS)_nC_{60}(P2VP)_n$ with the structure close to desired one (n = 6).

CONCLUSIONS

(1) Heteroarm star-like polymers with "point" C_{60} center of branching and arms of polystyrene and poly-2-vinylpyridine were prepared from polyfunctional initiating agent, hexaadduct $(PS)_6C_{60}Li_6$ modified with 1,1-diphenylethylene.

(2) The dependences of the structure and initiating properties of the hexaadduct on polarity and nature of the modifying agent were elucidated. A proton donor or 1,1-diphenylethylene in THF causes elimination of up to two PSL chains from the hexaadduct, which affects the composition of the initiating system and structure of the products of synthesis of heteroarm polymers.

(3) The experimental data confirm the radical-anion mechanism of initiation of styrene polymerization in THF in the presence of $(PS)_6C_{60}Li_6$.

(4) The reaction of $(PS)_6C_{60}Li_6$ with 1,1-diphenylethylene in nonpolar medium causes more complete conversion of the active groups of the hexaadduct into the initiating groups, which promotes formation of hybrid macromolecules with a required structure.

ACKNOWLEDGMENTS

The study was financially supported by the Deutsche Forschungsgemeinschaft within the Sonderforschungsbereich 287 "Reactive Polymers."

REFERENCES

1. Heise, A., Hedric, J.L., Frank, C.W., and Miller, R.D., *J. Am. Chem. Soc.*, 1999, vol. 121, no. 37, pp. 8647–8648.
2. Tsitsilianis, C., Voulgaris, D., Stepanek, M., et al., *Langmuir*, 2000, vol. 16, no. 17, pp. 6868–6876.
3. Beil, J.B. and Zimmerman, S.C., *Macromolecules*, 2004, vol. 37, no. 3, pp. 778–787.
4. Ishizu, K., Ichimura, A., and Ono, T., *Polymer*, 1998, vol. 39, no. 12, pp. 2579–2582.
5. Tsitsilianis, C., Alexandridis, P., and Lindman, B., *Macromolecules*, 2001, vol. 34, no. 17, pp. 5979–5983.
6. Wang, F., Michael, S., Wilson, R., et al., *Macromolecules*, 2000, vol. 33, no. 6, pp. 2083–2091.
7. Voulgaris, D., Tsitsilianis, C., Esselink, F.J., and Hadziioanou, G., *Polymer*, 1998, vol. 39, no. 25, pp. 6429–6439.
8. François, B., Ederle, Y., and Mathis, C., *Synth. Met.*, 1999, vol. 103, pp. 2362–2363.
9. Xu, H., Erhardt, R., Abetz, V., et al., *Langmuir*, 2001, vol. 17, no. 22, pp. 6787–6793.
10. Xu, J. and Zubarev, E.R., *Angew. Chem., Int. Ed.*, 2004, vol. 43, pp. 5491–5496.
11. Kiriy, G., Gorodyska, G., Minko, S., et al., *Polym. Mater.: Sci. Eng.*, 2003, vol. 88, pp. 233–243.
12. Lipitskyy, R., Roiter, Y., Tsitsilianis, C., and Minko, S., *Langmuir*, 2005, vol. 21, no. 19, pp. 8591–8593.
13. Youk, J.H., Park, M.-K., Locklin, J., et al., *Langmuir*, 2002, vol. 18, no. 7, pp. 2455–2458.
14. Lee, T.-W., Park, O., Kim, J., and Kim, Y.Ch., *Chem. Mater.*, 2002, vol. 14, pp. 4281–4285.
15. Tsitsilianis, C. and Voulgaris, D., *Macromol. Chem. Phys.*, 1997, vol. 198, pp. 997–1007.
16. Vinogradova, L., Fedorova, L., Adler, H.-J.P., et al., *Macromol. Chem. Phys.*, 2005, vol. 206, pp. 1126–1133.
17. Zgonnik, V.N., Vinogradova, L.V., Melenevskaya, E.Yu., et al., *Zh. Prikl. Khim.*, 1995, vol. 68, no. 1, pp. 99–105.
18. Eremina, M.A., Erenburg, E.G., Zgonnik, V.N., et al., *Vysokomol. Soedin., Ser. A.*, 1985, vol. 27, no. 6, pp. 1308–1313.
19. Vinogradova, L.V., Amsharov, K.Yu., Kever, E.E., and Zgonnik, V.N., *Vysokomol. Soedin., Ser. A.*, 2003, vol. 45, no. 8, pp. 1282–1289.
20. Ederle, Y. and Mathis, C., *Macromolecules*, 1997, vol. 30, no. 9, pp. 2546–2555.
21. Veber, V., Duval, M., Ederle, Y., and Mathis, C., *Carbon*, 1998, vol. 36, nos. 5–6, pp. 839–842.
22. Lavrenko, P.N. and Vinogradova, L.V., *Vysokomol. Soedin., Ser. A*, 2000, vol. 42, no. 7, pp. 1117–1123.
23. Ederle, Y. and Mathis, C., *Macromolecules*, 1997, vol. 30, no. 15, pp. 4262–4267.
24. Ederle, Y. and Mathis, C., *Macromolecules*, 1999, vol. 32, no. 1, pp. 554–558.
25. Vinogradova, L.V., Lavrenko, P.N., Amsharov, K.Yu., and Zgonnik, V.N., *Vysokomol. Soedin., Ser. A*, 2002, vol. 44, no. 5, pp. 750–757.
26. Amsharov, K.Yu., New Star-Like Polymers with Fullerene Core, based on Styrene and Polar Monomers, *Cand. Sci. Dissertation*, St. Petersburg, 2005.

ISSN 1070-4272, Russian Journal of Applied Chemistry, 2006, Vol. 79, No. 4, pp. 654–659. © Pleiades Publishing, Inc., 2006.
Original Russian Text © A. D. Zorina, L. V. Balykina, O. V. Nazarova, A. A. Rebezov, 2006, published in Zhurnal Prikladnoi Khimii, 2006, Vol. 79, No. 4, pp. 663–668.

MACROMOLECULAR CHEMISTRY AND POLYMERIC MATERIALS

Polymeric Derivatives of Dipterocarpol, a Dammarane Triterpenoid

A. D. Zorina, L. V. Balykina, O. V. Nazarova, and A. A. Rebezov

St. Petersburg State University, St. Petersburg, Russia
Institute of Macromolecular Compounds, Russian Academy of Sciences, St. Petersburg, Russia

Received December 26, 2005

Abstract—Polymeric derivatives of dammarane triterpenoids with both labile and strong (covalent) polymer–triterpenoid bonds were prepared from *N*-vinylpyrrolidone copolymers.

DOI: 10.1134/S107042720604029X

Treatment of virus diseases requires development of effective nontoxic antiviral preparations. Synthesis of polymeric derivatives of low-molecular-weight biologically active substances (BASs) opens prospects for development of improved medicinals of reduced toxicity, enhanced efficiency, and prolonged effect.

Polymers based on *N*-vinylpyrrolidone (VP) are among the most widely used polymeric carriers [1, 2]. VP copolymers containing amino groups show promise as BAS carriers. Alkylation with various alkyl halides of VP copolymers with primary and tertiary amines allows preparation of polymers containing, along with the ionic ammonium group, alkyl substituents providing hydrophobic interaction in aqueous solutions [3]. Preparation of water-soluble derivatives (salts) of polyene antibiotics Levorin and Nystatin on the basis of such copolymers was reported in [4].

Previous studies revealed more pronounced antiviral properties of polymeric derivatives of certain triterpene acids compared to the nonmodified acids [5].

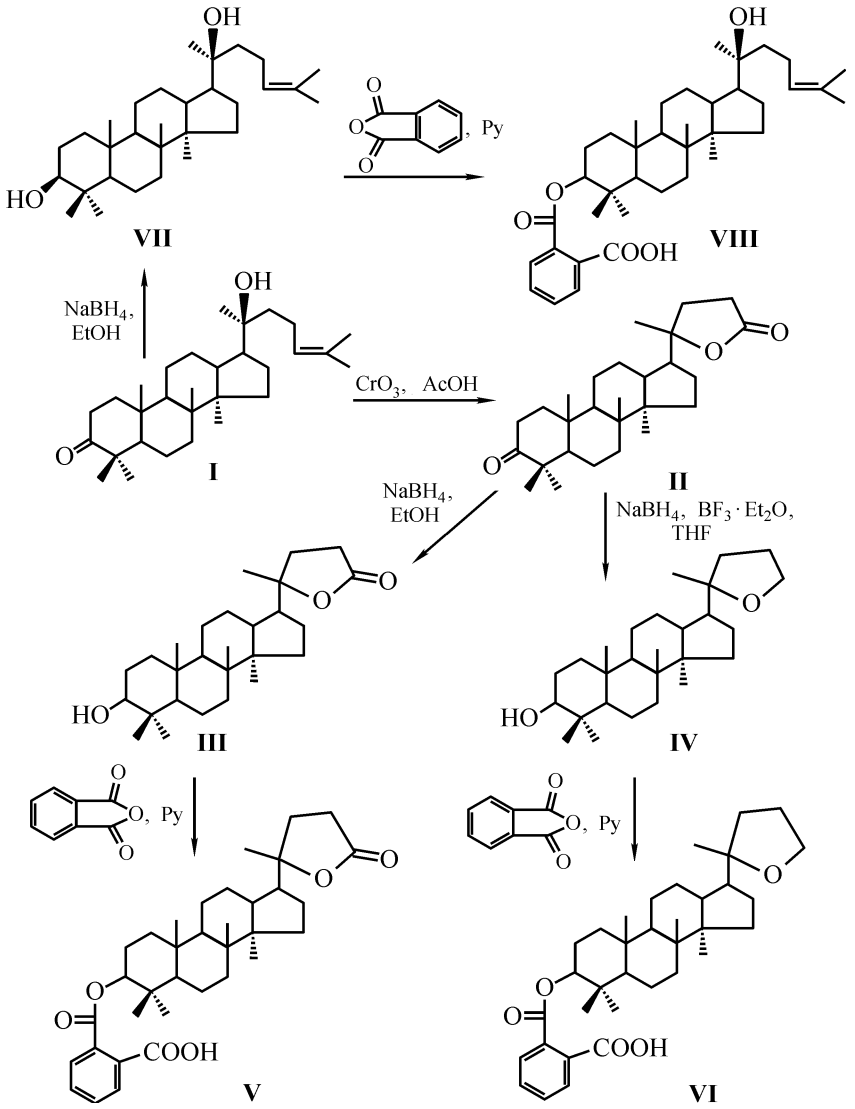
The goal of this study was to develop procedures for preparing from VP copolymers polymeric derivatives of triterpenoids of the dammarane series differing in the type and lability of the polymer–triterpenoid bond.

Among dammarane triterpenoids, the highest antiviral activity is exhibited by alnincanone, 24-methyl-20*S*,24*R*-epoxydammaran-3-one [6]; however, its content in plant sources is insufficient for more comprehensive biological studies. As a model compound we chose 20(*S*)-hydroxydammar-24-en-3-one (dipterocarpol) **I**. It can be prepared in amounts required for the studies from *Dipterocarpus alatus* latex [7].

We prepared dammarane derivatives containing at C-17 an open chain (**VII**), a γ-lactone ring (**III**), and a tetrahydrofuran ring (**IV**). Diol **VII** was prepared by reduction of dipterocarpol with sodium borohydride in ethanol. To prepare compounds **III** and **IV**, dipterocarpol was oxidized with chromic anhydride in acetic acid to lactone **II**. Reduction of **II** with sodium borohydride in ethanol yielded hydroxy lactone **III**, and reduction with sodium borohydride in the presence of $BF_3 \cdot OEt_2$ in THF yielded epoxydammaranol **IV**. From compounds **III**, **IV**, and **VII** (Scheme 1) containing the 3β-hydroxy group, we prepared by refluxing with phthalic anhydride phthalic acid monoesters **V**, **VI**, and **VIII**, respectively (Scheme 1). Through the free carboxy group, these compounds were bonded to an amino group of the polymer.

To prepare polymeric derivatives of triterpenoids of the dammarane series with a labile BAS–polymer bond (BAPs), we used a copolymer of VP with dimethylaminoethyl methacrylate (DMAEM) and with its derivative quaternized with dodecyl iodide ($DMAEM \cdot C_{12}H_{25}I$) [8]. Polymeric salts of phthalic acid monoesters were prepared by Scheme 2.

As solvent we used methanol in which all the reactants (triterpenoid hydrogen phthalates and the polymer) and products (polymeric salts) are soluble. After the synthesis completion, methanol was gradually replaced by water [4]. As a result, we obtained polymeric derivatives which, in contrast to the starting



Scheme 1.

triterpenoid hydrogen phthalates, are soluble in water. The UV spectra of all the derivatives contain absorption bands of the corresponding triterpenoid hydrogen phthalates **V**, **VI**, and **VIII** (λ_{max} = 274 nm), which allowed determination of the BAS content in the polymeric products. The results are given in Table 1.

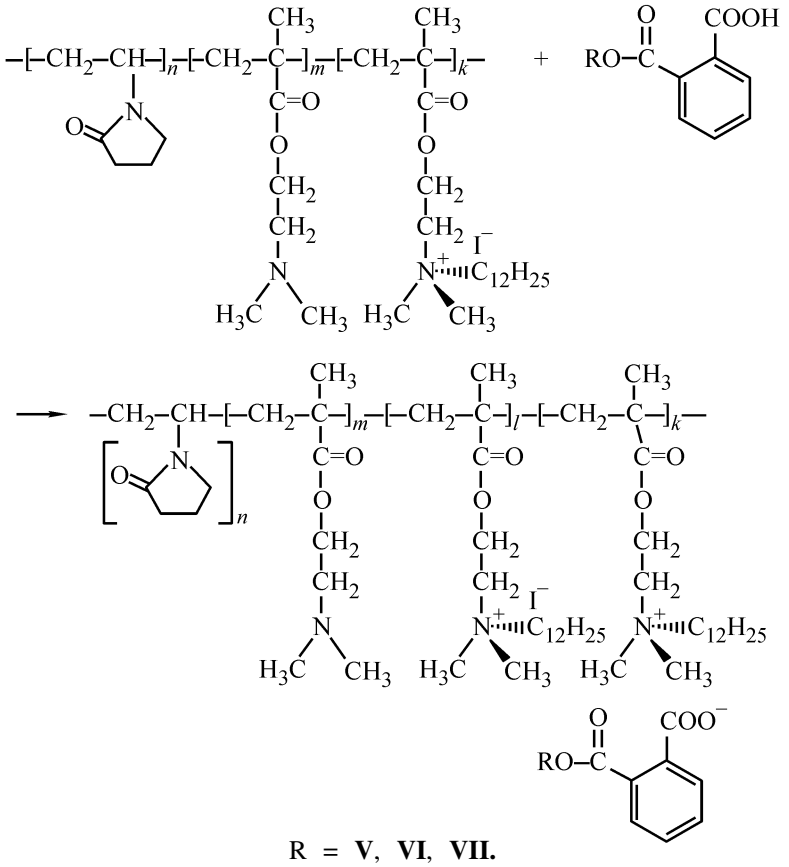
It is known that polyvinylpyrrolidone (PVP) forms complexes with many substances [1, 2]. We attempted to prepare PVP derivatives of triterpenoid hydrogen phthalates by the procedure similar to that used for preparing salts of VP–DMAEM–DMAEM · $C_{12}H_{25}I$ copolymer. We failed to obtain water-soluble products. Addition of water to a solution of the reactants in methanol resulted in precipitation of triterpenoid hydrogen phthalates. This fact confirms that, to obtain a water-soluble product, the starting copolymer should contain ionic groups.

The products were separated by gel permeation chromatography (GPC) on a column packed with Sephadex LH-20 gel (eluent ethanol). The absorption of the fractions taken was measured at 274 nm (the starting polymer is virtually transparent in this range). The chromatograms of all the polymeric salts obtained

Table 1. Polymeric salts of hydrogen phthalates of dipterocarpol derivatives*

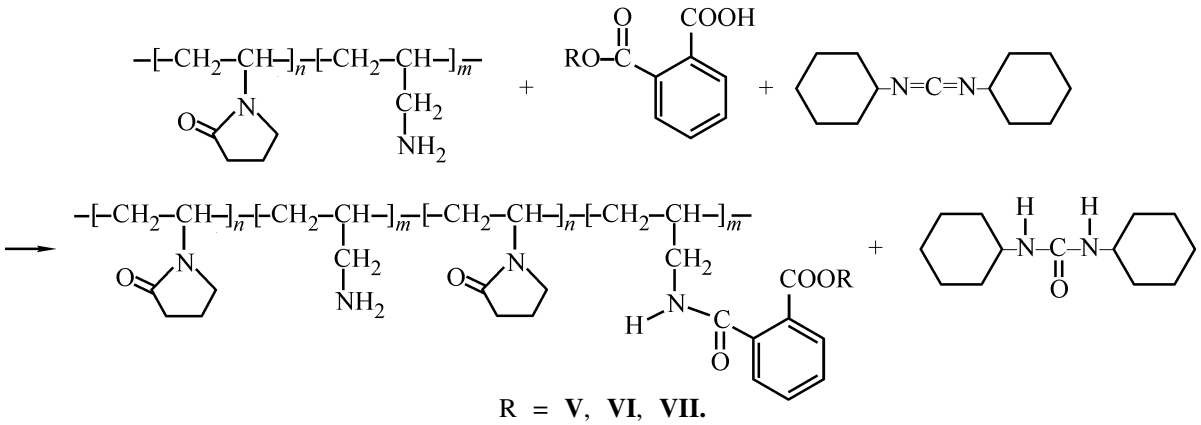
Run no.	Hydrogen phthalate	ε, l mol^{-1} cm^{-1}	[R–]	
			wt %	mol %
1	**VIII**	1600	10.2	2.3
2	**V**	1600	9.1	2.2
3	**VI**	1300	11.6	2.9

* The salts are water-soluble.



R = **V**, **VI**, **VII.**

Scheme 2.



R = **V**, **VI**, **VII.**

Scheme 3.

exhibit peak I in the same region as for the unmodified BAS (Fig. 1). There is also a weak peak II in the region of small retention volumes corresponding to polymer-containing fractions (for comparison, we show a chromatogram of a copolymer of VP with *N*-hydroxyphthalimide ester of acrylic acid). The UV spectra of fractions I and II are similar to the spectra of the low-molecular-weight BAS and starting polymer, respectively.

To prepare polymeric derivatives of hydrogen phthalates **V**, **VI**, and **VIII** in which the BAS is linked to the polymer by a strong covalent bond, we used a copolymer of VP with allylamine (AlAm) [9].

The reactions of triterpene hydrogen phthalates with this copolymer were performed in CH_2Cl_2 in the presence of *N,N'*-dicyclohexylcarbodiimide (DCC), as shown in Scheme 3.

The reaction should yield derivatives in which BAS is linked to the polymeric carrier by an amide bond. The characteristics of the reaction products are given in Table 2. Their composition, similarly to the polymeric salts, was determined by UV spectroscopy, as the absorption band at λ_{max} = 274 nm was observed in the spectra of all the products. As seen from Table 2, in all the cases, as in the case of the polymeric salts, the derivatives containing ≤12 wt % triterpenoid hydrogen phthalate are water-soluble (run nos. 5–7). At a high BAS content, as in the case of betulinic and betulonic acid derivatives [5], the solubility in water is lost (run no. 4).

The chromatograms of covalent derivatives of triterpenoid hydrogen phthalates (Fig. 2) differ from those of polymeric salts (Fig. 1). As seen from Fig. 2, for the covalent derivatives, with the same gel (LH-20) and eluent (ethanol), peak I is weak, and peak II, on the contrary, strong. The UV spectra of the fractions corresponding to peak II, as those of the initial BASs, contain a band with λ_{max} = 274 nm. Similar chromatograms are obtained with Sephadex G-75 gel and water as eluent. This fact confirms that, in contrast to the derivatives obtained in run nos. 1–3, in the products from run nos. 4–7 the BAS is strongly bound to the polymeric carrier, because its chromatographic behavior is similar to that of the carrier.

EXPERIMENTAL

20(*S*)-Hydroxydammar-24-en-3-one I. Dipterocarpol **I** was eluted with hexane–ethyl acetate (15 : 1) in the course of chromatographic separation (silica gel, 5/40 μm) of an ethyl acetate solution of *Dipterocarpus alatus* latex; mp 133–135°C [7]. IR spectrum, cm^{-1}: 3480, 1690. Yield 67%.

25,26,27-Trinordammaran-3-on-20(*S*),24-olide II. Dipterocarpol **I** (10 g) was dissolved in 50 ml of benzene and 30 ml of acetic acid; 4 g of CrO_3 and 3 ml of H_2O were added, The mixture was cooled with ice and allowed to stand for 12 h at room temperature, after which it was diluted with water. The precipitate was filtered off and washed with water, 5% sodium carbonate solution, and again water to neutral reaction. The dry precipitate was chromatographed on a column packed with silica gel.

Fractions containing dipterocarpol lactone **II** were combined, and the solvent was evaporated. The residue was crystallized from ethyl acetate. Yield of dipterocarpol lactone **II** (25,26,27-trinordammaran-3-on-20(*S*),24-olide) 7.9 g, mp 180–182°C (published data [7]: mp 184–186°C). IR spectrum, cm^{-1}: 1765 (C=O in γ-lactone), 1695 (C=O).

Table 2. Polymeric derivatives of hydrogen phthalates of dammarane triterpenoids with an amide bond BAS–polymer

Run no.	Hydrogen phthalate	[R–]		Degree of conversion, %	Solubility in water
		wt %	mol %		
4	**VIII**	19.6	4.1	75	Insoluble
5	**VIII**	8.6	1.7	62	Soluble
6	**VI**	11.6	2.6	91	Soluble
7	**V**	10.2	2.2	80	Soluble

25,26,27-Trinordammaran-3β-ol-20(*S*),24-olide III. Dipterocarpol lactone **II** (2 g) was refluxed with 250 mg of $NaBH_4$ in 85 ml of isopropyl alcohol for 24 h, after which the solution was diluted with water and acidified to pH < 2. The precipitate was filtered off, washed with water, dried, and recrystallized from ethyl acetate. Yield of reduced lactone **III** 1.5 g

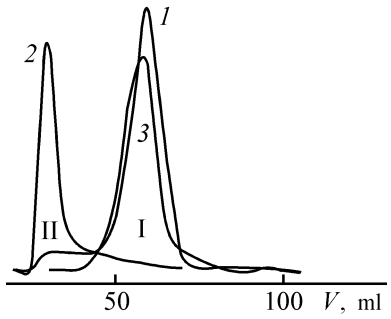


Fig. 1. Chromatograms (LH-20, eluent ethanol): (*1*) dammar-24-ene-3β,20(*S*)-diol hydrogen phthalate **VIII**, (*2*) copolymer of VP with *N*-hydroxyphthalimide ester of acrylic acid, and (*3*) polymeric salt of dammar-24-ene-3β,20(*S*)-diol hydrogen phthalate **VIII** and VP–DMAEM–DMAEM · $C_{12}H_{25}I$ copolymer (run no. 1).

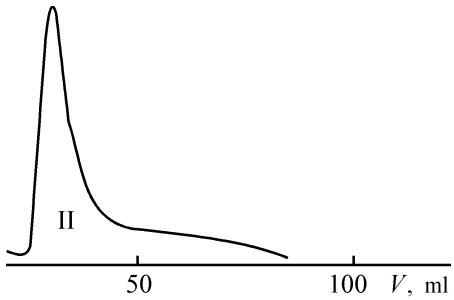


Fig. 2. Chromatogram (LH-20, eluent ethanol) of the derivative of dammar-24-ene-20(*S*),3β-diol hydrogen phthalate **VIII** and VP–AlAm copolymer (run no. 5).

(75%), mp 199–201°C (published data [7]: mp 203–204°C). IR spectrum, cm^{-1}: 3450 (OH), 1765 (C=O in γ-lactone).

Dammar-24-ene-20(*S*),3β-diol VII. Dipterocarpol **I** [20(*S*)-hydroxydammar-24-en-3-one] was reduced with $NaBH_4$ under the same conditions as compound **II**. Diol **VII** was obtained in 40% yield; mp 132–134°C (published data [10]: mp 131–133°C). ^{13}C NMR spectrum, δ, ppm: 78.4 (C-3β–OH).

25,26,27-Trinor-20(*S*),24-epoxydammaran-3β-ol IV. A solution of 5 g of dipterocarpol lactone **II** in 100 ml of THF and 10 ml of $BF_3 \cdot OEt_2$ were added over a period of 3 h at –15°C to 1.28 g of sodium borohydride in 50 ml of THF. The mixture was allowed to stand for 2 h at –15°C, after which it was refluxed on a water bath for 5 h. Then the mixture was cooled, diluted with a fivefold volume of water, and acidified with 2 N HCl to pH < 2. The precipitate was filtered off, washed with water, and dried. The residue (4.7 g) was chromatographed on a column packed with 150 g of silica gel (70/230 μm). Elution with hexane–5% ethyl acetate gave 2.9 g (65%) of **IV**, mp 182–183°C (published data [7]: mp 180–182°C). IR spectrum, cm^{-1}: 3450 (OH stretching vibrations) [7]. ^1H NMR spectrum, δ, ppm: CH_3 (0.79 s, 0.89 s, 1.05 s, 0.9 s, 0.69 s, 0.79 s); 3.09 t; 3.6 m.

Hydrogen phthalates of compounds **III**, **IV**, and **VII**. Hydroxy derivative **III**, **IV**, or **VII** (0.01 mol) and phthalic anhydride (0.02 mol) were refluxed in pyridine for 48 h, after which the mixture was diluted with a fourfold volume of water and acidified with 10% HCl to pH < 2. The white precipitate was filtered off, washed with water to neutral reaction, and dried; the residue was recrystallized from petroleum ether–ethyl acetate.

Dammar-24-ene-20(*S*),3β-diol hydrogen phthalate VIII: mp 208–210°C. ^1H NMR spectrum, δ, ppm: 4.8 (α-H at C-3) and 7.5–7.9 (4H).

25,26,27-Trinor-20(*S*),24-epoxydammaran-3β-ol hydrogen phthalate VI: mp 219–221°C. ^1H NMR spectrum, δ, ppm: 4.75 (α-H at C-3) and 7.6–7.9 (4H).

25,26,27-Trinordammaran-3β-ol-20(*S*),24-olide V: mp 258–260°C. ^1H NMR spectrum, δ, ppm: 4.75 (α-H at C-3) and 7.6–7.9 (4H).

Synthesis of polymeric derivatives of triterpenoids. Polymeric salts of triterpenoids were prepared from the VP (87.8 mol %)–DMAEM (9.2 mol %)–DMAEM · $C_{12}H_{25}I$ (3.0 mol %) copolymer, [η] at 25°C in 0.1 M CH_3COONa 0.13 dl g^{-1}, molecular weight M_η = 21 000, by the following procedures.

Example 1. VP–DMAEM–DMAEM · $C_{12}H_{25}I$ copolymer (0.35 g) was dissolved in 30 ml of methanol, and 0.044 g of dammar-24-ene-3β,20(*S*)-diol hydrogen phthalate **VIII** was added. The mixture was stirred for 24 h at room temperature. The polymeric salt was isolated by gradual replacement of methanol as solvent by water (stepwise addition of water with distillation of methanol) [4]. The polymer was isolated from the resulting aqueous solution by freeze drying. Yield 0.38 g (96%) (run no. 1).

Under similar conditions we prepared the polymeric salts of hydrogen phthalates **V** [yield 61% (0.24 g) (run no. 2)] and **VI** [yield 94% (0.37 g) (run no. 3)].

Polymeric derivatives of triterpenoids with a polymer–BAS covalent bond were prepared from the VP (94.5 mol %)–AlAm (5.5 mol %) copolymer, [η] at 25°C in 0.1 M CH_3COONa 0.12 dl g^{-1}, M_η = 18 000.

Example 2. A solution of 0.23 g of VP–AlAm copolymer, 0.075 g of **VIII**, and 0.025 g of DCC in 4.5 ml of CH_2Cl_2 was kept for 2 h at –18°C and then for 72 h at –5°C. The molar ratio of the reactants was 1 : 1 : 1. Then the polymer was precipitated into diethyl ether, and the precipitate was separated on a glass frit and vacuum-dried to constant weight. The low-molecular-weight impurities were separated by gel permeation chromatography on a column packed with Sephadex LH-20 gel (h = 44 cm, d = 1.5 cm), eluent ethanol. The high-molecular-weight fraction was collected, and ethanol was distilled off on a rotary evaporator.

Run no. 5: polymeric derivative of **VIII**, yield 89% (0.31 g); run no. 6: polymeric derivative of **VI**, yield 69% (0.24 g); run no. 7: polymeric derivative of **V**, yield 64% (0.22 g).

CONCLUSIONS

(1) Previously unknown 25,26,27-trinordammaran-3β-ol-20(*S*),24-olide hydrogen phthalate **V**, 25,26,27-trinor-20(*S*),24-epoxydammaran-3β-ol hydrogen phthalate **VI**, and dammar-24-ene-20(*S*),3β-diol hydrogen phthalate **VIII** were prepared.

(2) Procedures were developed for preparing polymeric water-soluble derivatives of **V**, **VI**, and **VIII** with *N*-vinylpyrrolidone copolymers, with both labile and strong covalent bonding of the polymer with the triterpenoid.

REFERENCES

1. Sidel'kovskaya, F.P., *Khimiya N-vinilpirrolidona i ego polimerov* (Chemistry of *N*-Vinylpyrrolidone and Its Polymers), Moscow: Nauka, 1970.
2. Kirsh, Yu.E., *Poli-N-vinilpirrolidon i drugie poli-N-vinilamidy* (Poly-*N*-vinylpyrrolidone and Other Poly-*N*-vinylamides), Moscow: Nauka, 1998.
3. Panarin, E.F., Gavrilova, N.I., and Gorbunova, O.P., in *Novye biologicheskie aktivnye polimery i immobilizovannye imi steroidy* (New Biologically Active Polymers and Steroids Immobilized by Them), Leningrad: Leningr. Pediatr. Med. Inst., 1988, pp. 17–25.
4. Redi, N.S. and Panarin, E.F., *Khim.-Farm. Zh.*, 1978, no. 5, pp. 96–100.
5. RF Patent 2253657.
6. Platonov, V.G., Zorina, A.D., Gordon, M.A., et al., *Khim.-Farm.* Zh., 1995, no. 2, pp. 42–46.
7. Crabbe, P., Ourisson, G., and Takahashi, T., *Tetrahedron*, 1958, vol. 3, pp. 279–302.
8. Panarin, E.F. and Gavrilova, I.I., *Vysokomol. Soedin., Ser. B*, 1977, vol. 19, no. 4, pp. 251–254.
9. Panarin, E.F., Tarasova, N.N., and Gorbunova, O.P., *Zh. Prikl. Khim.*, 1993, vol. 66, no. 11, pp. 2525–2530.
10. Mills, S. and Werner, A.E.A., *J. Chem. Soc.*, 1955, pp. 3132–3133.

ISSN 1070-4272, Russian Journal of Applied Chemistry, 2006, Vol. 79, No. 4, pp. 660–664. © Pleiades Publishing, Inc., 2006.
Original Russian Text © O. V. Shevchenko, I. S. Voloshanovskii, T. I. Berbat, 2006, published in Zhurnal Prikladnoi Khimii, 2006, Vol. 79, No. 4, pp. 669–673.

MACROMOLECULAR CHEMISTRY AND POLYMERIC MATERIALS

Radical Polymerization in the Presence of Vinyl-Substituted Transition Metal β-Diketonates

O. V. Shevchenko, I. S. Voloshanovskii, and T. I. Berbat

Mechnikov National University, Odessa, Ukraine

Received June 22, 2005; in final form, December 2005

Abstract—The influence of vinyl-substituted cobalt(II), copper(II), nickel(II), and iron(II) β-diketonates on radical polymerization of methyl methacrylate and styrene was studied.

DOI: 10.1134/S1070427206040306

Transition metal β-diketonates are used as a free radical source in initiation of radical polymerization [1, 2]. However, a few papers reported on deceleration of polymerization [1, 3] and formation of polymeric products with decreased molecular weight [4] in the presence of these compounds. The inhibiting properties of β-diketonates and their use in oxidation and stabilization of polymers were studied in greater detail [5]. Thus, the inhibiting effect of β-diketonates on polymerization, influencing the polymerization kinetics and molecular-weight properties of the products, was studied nonsystematically.

Previously [6, 7] we prepared a series of vinyl-containing β-diketonates and studied their copolymerization with vinyl monomers. We found that the polymerization rate v_p and MW of the products decreased and the polydispersity index (PI) increased with increasing amount of the monomeric β-diketonate in the initial mixture [8]. This can be due to complexation of the propagating radical with the quasiaromatic β-diketonate ring [9]. We also showed that vinyl-substituted cobalt(II) β-diketonates not only catalyze but also inhibit the polymerization at their concentrations higher than 10^{-2} M.

The aim of this study was to examine the decelerating and stopping effect of vinyl-substituted Co(II), Ni(II), Cu(II), and Fe(III) β-diketonates on polymerization.

EXPERIMENTAL

To initiate polymerization of styrene (St) and methyl methacrylate (MMA), we used cobalt(II) 7-octene-2,4-dionate (Co-OD), cobalt(II) 3-allylpentane-2,4-dionate (CoAPD), cobalt(II) 1-phenyl-6-heptene-1,3-dionate (Co-PHD), cobalt(II) 3-allyl-1,1,1-trifluoropentane-2,4-dionate (Co-ATPD), copper(II) 7-octene-2,4-dionate (Cu-OD), iron(III) 5-methyl-5-hexene-2,4-dionate (Fe-MHD), copper(II) 5-methyl-5-hexene-2,4-dionate (Cu-MHD), nickel(II) 2-allyl-1-phenylbutane-1,3-dionate (APBD-Ni), and nickel(II) 1-phenyl-6-heptene-1,3-dionate (PHD-Ni). Vinyl-substituted β-diketones were prepared by the procedure described in [6, 7], and their metal complexes, by the procedure described in [10]. Polymerization of St and MMA was performed in the bulk and in solvents [toluene (Tl), dimethylformamide (DMF), and methyl ethyl ketone (MEK)]. The monomer concentration was 3.54 M. The polymerization rate was determined dilatometrically and gravimetrically. The molecular weight of the polymers was estimated by gel permeation chromatography on a Waters-2000 chromatograph using monodisperse references (Waters).

We studied MMA polymerization initiated by vinyl-substituted Co(II), Ni(II), Cu(II), and Fe(III) β-diketonates. The initial polymerization rates v_p^0 were determined. The results are summarized in Table 1. As seen from Table 1, the initial polymerization rate does not increase with increasing Co-OD concentration over 10^{-2} M. The initial polymerization rate v_p^0 increases when the concentration of Co-APD and Co-PHD increases up to 0.5×10^{-2} and 10^{-2} M, respectively. When the initiator content is higher than this limiting concentration (LC), v_p^0 decreases, i.e., these compounds become inhibitors. The v_p^0 increases with decreasing the FeMHD concentration.

Table 1. Initial rate v_p^0 of MMA polymerization at 70°C and different concentrations c_c of vinyl-substituted cobalt(II), copper(II), and iron(III) β-diketonates

$c_c \times 10^2$, M	$v_p^0 \times 10^4$, mol l^{-1} s^{-1}						
	Co-OD	Co-APD	Co-PHD	Co-ATPD	Cu-MHD	Cu-OD	Fe-MHD
5.0	15.9	–	–	–	–	–	
3.0	–	10.8	–	–	0	0	0.3
2.5	–	–	2.4	–	–	–	–
1.0	15.2	13.7	14.3	16.7	0.5	1.2	2.0
0.5	10.7	16.7	8.6	10.7	0.5	0.7	2.7
0.25	6.3	10.3	7.4	8.5	0.5	0.6	3.6
0.10	–	–	5.8	5.0	–	–	–

Table 2. Reaction orders of St polymerization with respect to vinyl-substituted cobalt(II) and nickel(II) β-diketonates

Monomer	T, °C	Reaction order with respect to initiator				Monomer	T, °C	Reaction order with respect to initiator			
		Co-OD	Co-APD	Ni-APBD	Ni-PHD			Co-OD	Co-APD	Ni-APBD	Ni-PHD
St	70	0.4	0.4	0.3	0.3	MMA	60	–	–	0.4	0.4
	85	0.4	0.3	0.3	0.3		70	–	–	0.5	0.4

At the 3.0×10^{-2} M concentration of Cu-OD and Cu-MHD, even thermal polymerization is inhibited. When the concentration of these complexes is 10^{-2} M, the polymerization is very slow. Hence, LC for these compounds is $(1.0–2.0) \times 10^{-2}$ M. We failed to determine the LC for the Ni(II) chelates, since their solubility of in MMA is 10^{-2} M. The solubility of vinyl-substituted cobalt(II) and nickel(II) β-diketonates in St does not exceed 0.5×10^{-2} M, and hence it is also impossible to determine the LC for these complexes. The fact that the examined vinyl-substituted metal β-diketonates exhibit both the initiating and inhibiting properties affects the reaction order of polymerization with respect to the initiator. At low concentrations of these complexes, the $\log v_p^0$–$\log c_c$ dependence (c_c in the chelate concentration) is linear and can be used to determine the reaction order with respect to the initiator (Table 2). In all cases, the reaction order of the polymerization of St and MMA was 0.3 – 0.4 and 0.4 – 0.5, respectively. However, the reaction order with respect to peroxy and dinitrile initiators is 0.5.

The fact that the reaction orders with respect to the chelate are underestimated suggests the occurrence of a latent inhibition process up to reaching of LC. The fact that the reaction orders of St polymerization with respect to the initiator are lower than those for MMA polymerization can be due to higher reactivity of growing St radicals in their coordination to the metal atom of the chelate. This can be due to several reasons: first, St radicals are donors (the Alfrey–Price factor e for ST and MMA is +0.8 and – 0.4, respectively) and the metal atoms are always acceptors; second, coordination of the secondary St radical to the metal atom is more sterically favorable that that of tertiary MMA radicals; and third, the reactivity of tertiary MMA radicals is lower than that of secondary St radicals. Thus, the LC of initiation or small polymerization orders with respect to the initiator can be used as criteria of the inhibiting effect. Since the solubility of vinyl-substituted copper(II) and iron(III) β-diketonates in St is 3×10^{-2} M, the v_p^0 vs. c_c dependence for St polymerization in the presence of these complexes also passes through a maximum (Fig. 1). The LC for Cu-APD, Cu-OD, Cu-MHD, and

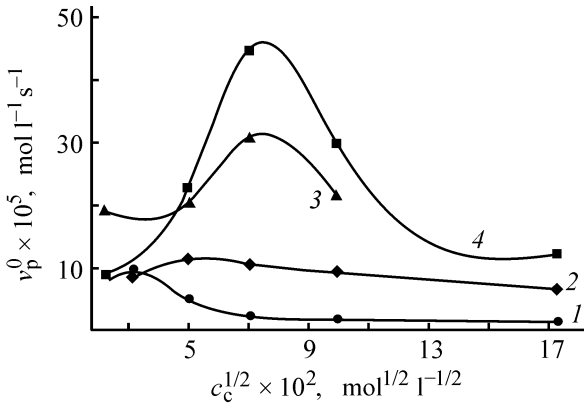


Fig. 1. Initial polymerization rate of St v_p^0 at 85°C vs. concentration c_c of (*1*) Cu-MHD, (*2*) Fe-MHD, (*3*) Cu-OD, and (*4*) Cu-APD.

Table 3. Kinetic parameters of MMA polymerization initiated by Co(II)-APD

$c_c \times 10^2$, M	60°C				70°C			
	$v_p^0 \times 10^5$	$v_p^{av} \times 10^5$	S_d	S_g	$v_p^0 \times 10^5$	$v_p^{av} \times 10^5$	S_d	S_g
	mol l^{-1} s^{-1}		%		mol l^{-1} s^{-1}		%	
2.0	0	0	–	–	0	0	–	–
1.0	17.4	10.5	10.8	7.9	34.5	11.8	10.0	9.4
0.5	22.4	19.7	10.4	9.8	61.3	25.1	10.0	10.0
0.25	29.9	19.9	10.4	8.7	39.9	24.1	10.0	9.5
0.10	15.7	9.0	13.1	12.3	28.1	20.0	10.3	10.3
TI*	1.1	1.1			2.6	2.6		

* TI is thermal initiation.

Table 4. Molecular-weight properties of poly(methyl methacrylates) prepared in the presence of Co-APD initiator*

T, °C	$c_c \times 10^3$, M	MW × 10^5		M_w/M_n	T, °C	$c_c \times 10^3$, M	MW × 10^5		M_w/M_n
		M_n	M_w				M_n	M_w	
50	25	1.95	4.30	2.20	70	25	3.48	8.81	2.53
	10	1.12	2.46	2.21		10	1.62	4.28	2.65
	5	2.64	3.95	1.49		5	1.92	4.01	2.08

* M_n and M_w are number-average and weight-average molecular weights; M_w/M_n is the polydispersity index.

Fe-MHD is 0.5×10^{-2}, 0.5×10^{-2}, 0.1×10^{-2}, and 0.25×10^{-2} M, respectively.

Since metal β-diketonates exhibit both initiating and inhibiting properties, the propogating polymer radicals can be involved in two reactions with different activation energy:

$$\sim R^{\cdot} + H_2C{=}\underset{\displaystyle X}{\underset{|}{CH}} \xrightarrow{E_P} \text{Polymer},$$

$$\sim R^{\cdot} + \text{chelate} \xrightarrow{E_i} \text{Low-reactive radicals or nonradical products},$$

where E_p is the activation energy of chain propagation and E_i is the activation energy of chain termination on the inhibitor.

It is known that the activation energy of chain propagation for styrene is 29.1 kJ mol^{-1} [11] and the activation energy of addition of radicals to common inhibitors is 4.2–8.3 kJ mol^{-1} [12]. The activation energy of formation of radical–β-diketonate adducts is unknown. If this energy is lower than E_p, the first step should be the most temperature-dependent. In this case the inhibiting properties of the β-diketonates will be weaker than the initiating properties, which can affect the LC of the initiator and MW of the polymer.

To determine the temperature dependence of the ratio of the initiation and inhibition reactions, we studied the kinetics of MMA polymerization initiated by Co-APD (Table 3) and determined the molecular-weight parameters of the resulting polymers (Table 4). As seen from Table 3, the LC at 60 and 70°C is 0.25×10^{-2} and 0.5×10^{-2} M, respectively, which confirms the above assumptions. In addition, comparison of the degree of polymerization determined dilatometrically (S_d) and gravimetrically (S_g) also confirms that the inhibiting effect of the chelate decreases with increasing temperature. The difference between S_d and S_g can be due to the fact that the inhibited reaction yields the low-molecular-weight fraction which is removed after reprecipitation from ethanol. Hence S_d is usually higher than S_g. However, at 70°C this difference is significantly smaller than at 60°C.

The molecular-weight parameteres of poly(methyl methacrylate) prepared at 50 and 70°C are presented in Table 4. The MW of the polymer prepared in the presence of benzoyl peroxide decreases by a factor

of approximately 1.5 when the reaction temperature increases by 20°C. As seen from Table 4, MW increases with temperature, thus confirming the weakening of the inhibiting effect under these conditions. However, the increase in the MW can be due to other reasons. Among them is copolymerization of the vinyl-substituted β-diketonate with MMA, which results in formation of reactive sites in the polymer and growth of the side chains [9].

There is another fundamental reason why the inhibiting effect of β-diketonates decreases in the course of polymerization. It is known that donor additives substantially enhance the initiating power of β-diketonates [1, 2]. To determine whether activation of radical generation affects the polymerization kinetics, we studied MMA polymerization initiated by Co-ADP in Tl, MEK, and DMF (Table 5). As seen from Table 5, the LC of the initiator in Tl is 10^{-2} M and is close to the LC in the bulk polymerization with this initiator (0.5×10^{-2}). The LC in MEK is also 10^{-2} M. The LC in DMF having the maximal donor power increases by a factor of 10 (10.0×10^{-2}). The difference in S_d and S_g (Table 5) also suggests the inhibition of the polymerization in the presence of these chelates. In Tl and MEK, S_g is substantially lower than S_d. In DMF this difference is smaller.

Thus, in donor solvents, the inhibition of the polymerization with the chelate decreases. Donor additive has probably a dual effect on the polymerization. On the one hand, formation of an adduct between the chelate and the additive favors generation of radicals and hence enhances the initiating power [1, 2]. On the other hand, a donor additive blocks the inner coordination sphere of the chelate, thus complicating its reaction with propagating radicals.

Polymerization of St and MMA initiated by the vinyl-substituted metal β-diketonates is characterized by two features which are untypical for polymerization

Table 5. Polymerization of MMA in the presence of Co-APD at 70°C (c_{MMA} = 3.54 M)

Solvent	$c_c \times 10^2$, M	$v_p^0 \times 10^5$	$v_p^{av} \times 10^5$	S_d	S_g
		mol l^{-1} s^{-1}		%	
Tl	25	0	0	–	–
	2.0	4.9	6.1	12.1	5.6
	1.0	27.1	21.4	11.7	9.1
	0.5	15.5	10.3	9.9	9.0
	0.25	9.1	8.4	10.1	10.0
DMF	50.0	14.8	8.1	11.1	10.2
	25	23.6	20.9	27.5	27.1
	10	22.4	14.8	11.4	9.3
	2.0	16.7	4.9	10.2	10.2
	1.0	9.1	3.0	9.0	7.8
	0.5	0.5	0.5	1.3	–
	0.25	0.25	0.3	1.4	–
MEK	25.0	4.18	4.2	14.0	8.5
	10.0	6.2	6.2	13.6	10.4
	2.0	74.3	41.8	13.1	10.4
	1.0	77.5	48.5	16.0	11.3
	0.5	76.5	40.3	24.1	20.0
	0.25	41.4	19.4	13.5	9.9

in the presence of peroxy initiators and are related to the inhibition. Polymerization of MMA in the presence of all the examined initiators is characterized by long induction periods (Fig. 2). The styrene polymerization has no induction period. This fact can be due to a change in the valence state of the metal in the chelate up to the polymerization start, which was shown previously [13]. However, in the case of styrene polymerization the metal valence also changes but the induction period is absent. In addition, the time dependence of the MMA conversion is linear, whereas in the case of styrene polymerization this dependence is nonlinear even at the monomer conversion of several percents (Fig. 3), which is manifested in strong dif-

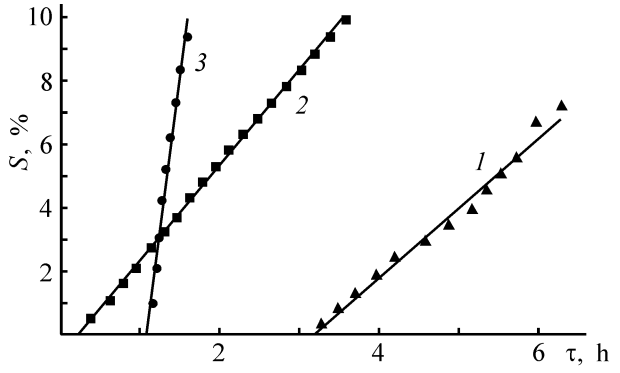


Fig. 2. Conversion of MMA S in the presence of (*1*) Cu-OD, (*2*) Cu-APD, and (*3*) Co-APD vs. time τ. $c_c = 5 \times 10^{-3}$ M and T = 70°C.

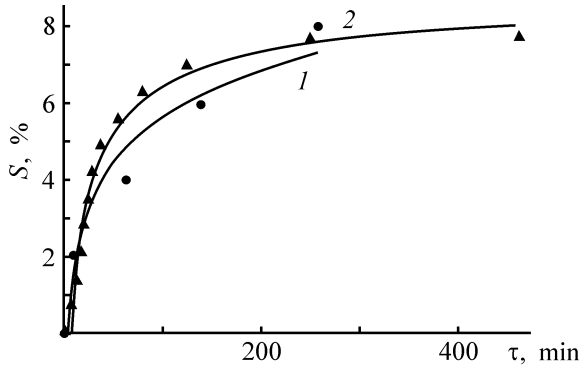


Fig. 3. Conversion of St in the presence of (*1*) Co-APD and (*2*) Cu-APD vs. time τ. $c_c = 5 \times 10^{-3}$ M and T = 85°C.

ference between the initial and average (v_p^{av}) polymerization rates. This fact can be explained as follows. It is known that the products of radical reactions involving β-diketonates can irreversibly form stable complexes with the chelate, which results in catalyst poisoning [14]. The carbonyl group of MMA can coordinate with the chelates to form stable complexes preventing catalyst poisoning with the reaction products.

Since the vinyl-substituted metal β-diketonates are polyfunctional components of radical polymerization (initiators, inhibitors, monomers), their inhibiting effect is masked. The processes initiated by vinyl-substituted β-diketonates substantially depend on the type of the monomer and the metal. The ligand structure affects only the quantitative parameters but does not affect the general course of the process. The inhibition of polymerization can be controlled to a definite extent by variation of the polymerization conditions (chelate concentration, temperature, use of donor solvents).

CONCLUSIONS

(1) Vinyl-substituted transition metal β-diketonates are both initiators and inhibitors of radical polymerization. The ratio of the initiating and inhibiting effects depends on the chelate concentration, the type of the metal atom in the chelate, and the polymerization conditions.

(2) The dependence of the polymerization rate on the chelate concentration is nonlinear. In addition, styrene polymerization is strongly decelerated even at small conversion of the monomer. The polymerization of methyl methacrylate is characterized by long induction periods.

(3) The inhibiting effect of the metal complexes decreases with increasing the polymerization temperature and when using donor solvents.

REFERENCES

1, Bamford, C.H., in *Reactivity, Mechanism and Structure in Polymer Chemistry*, Jenkins, A.D. and Ledwith, A., Eds., London: Wiley, 1974.

2. Nizel'skii, Yu.N., *Kataliticheskie svoistva β-diketonatov metallov* (Catalytic Properies of Metal β-Diketonates), Kiev: Naukova Dumka, 1983.

3. Paushkin, L.M., Vishnyakova, T.P., Korshak, Yu.V., et al., *Dokl. Akad Nauk Bel. SSR*, 1974, vol. 18, no. 1, pp. 42–45.

4. Nikolaev, A.F., Belgorodskaya, K.V., Shibalovich, V.G., and Starevskaya, G.P., *Vysokomol. Soedin., Ser. B*, 1971, vol. 13, no. 11, pp. 837–842.

5. Maletin, Yu.A., in *Teoreticheskaya i prikladnaya khimiya β-diketonatov metallov* (Theoretical and Applied Chemistry of Metal β-Diketonates), Moscow: Nauka, 1985, pp. 256–262.

6. Voloshanovskii, I.S., Butova, T.D., and Shevchenko, O.V., *Zh. Obshch. Khim.*, 1999, vol. 69, no. 9, pp. 1504–1507.

7. Voloshanovskii, I.S., Manaeva, T.I., Shevchenko, O.V., and Mamontov, V.P., *Zh. Prikl. Khim.*, 2000, vol. 73, no. 2, pp. 283–287.

8. Voloshanovskii, I.S., Shevchenko, O.V., Butova, T.D., and Manaeva, T.I., *Zh. Prikl. Khim.*, 2003, vol. 76, no. 2, pp. 279–283.

9. Shevchenko, O.V., Voloshanovskii, I.S., Berbat, T.I., and Zakhariya, A.I., *Vopr. Khim. Khim. Teknol.*, 2003, no. 6, pp. 111–115.

10. Voloshanovskii, I.S., Shevchenko, O.V., Berezhnitskaya, A.S., and Krasnova, E.A., *Ukr. Khim. Zh.*, 2001, vol. 67, no. 5, pp. 5–10.

11. Bagdasar'yan, Kh.S., *Teoriya radikal'noi polimerizatsii* (Theory of Radical Polymerization), Moscow: Nauka, 1966.

12. Tüdös, F., *Rassmotrenie kinetiki radikal'noi polimerizatsii na osnove gipotezy goryachikh radikalov* (Consideration of Radical Polymerization Kinetics on the Basis of Hot Radical Hypothesis), Moscow: Mir, 1966.

13. Voloshanovskii, I.S. and Shevchenko, O.V., *Kompoz. Polimer. Mater.*, 2000, vol. 22, no. 2, pp. 108–113.

14. Ivanov, S.K. and Karshalykow, C.S., *J. Catal.*, 1979, vol. 56, pp. 141–149.

ISSN 1070-4272, Russian Journal of Applied Chemistry, 2006, Vol. 79, No. 4, pp. 665–671. © Pleiades Publishing, Inc., 2006.
Original Russian Text © Yu. V. Savel'ev, V. Ya. Veselov, L. P. Robota, O. A. Savel'eva, G. V. Chumikova, 2006, published in Zhurnal Prikladnoi Khimii, 2006, Vol. 79, No. 4, pp. 674–680.

MACROMOLECULAR CHEMISTRY AND POLYMERIC MATERIALS

Utilization of Unsymmetrical Dimethylhydrazine in the Production of Polyurethanes: Synthesis, Structure, and Properties of New Products

Yu. V. Savel'ev, V. Ya. Veselov, L. P. Robota, O. A. Savel'eva, and G. V. Chumikova

Institute of Macromolecular Chemistry, National Academy of Sciences of Ukraine, Kiev, Ukraine

Received June 16, 2005

Abstract—Unsymmetrical dimethylhydrazine is used to design novel polyurethane-based film materials, film-forming aqueous dispersions, and closed-cell polyurethane foams.

DOI: 10.1134/S1070427206040318

Until recently unsymmetrical dimethylhydrazine (UDMH) was widely used as a rocket propellant [1]. However, as a result of reduction of strategic armaments, large amounts of UDMH have been accumulated worldwide, and, because of strong toxicity, its storage represents a danger to the environment [2]. The problem of UDMH utilization is still very topical, and only a few processes exist including direct breakdown through neutralization with an electrochemically activated solution of NaCl [3], introduction of UDMH as a high-energy additive into hydrocarbon fuel, and conversion into low-toxic compounds [4–6]. Presently, processes for utilization of UDMH through conversion into its low-toxic derivatives for various purposes are in progress. The resulting products can be used, e.g., as starting reagents (precursors) in various physicochemical processes [7–12].

Our thought is that utilization of UDMH through the use in production of macromolecular compounds, e.g., polyurethanes and ionomers, shows good prospects. Up to now, the efforts of utilizing UDMH in macromolecular chemistry were directed essentially to modification of polymers [4]. Note here that the high reactivity of the tertiary nitrogen atom of UDMH results in formation of hydrazinium derivatives, and only in the cases when the quaternization of this atom is sterically hindered, the amine hydrogen could be reactive. Thus, the applicability of UDMH in the synthesis of polyurethanes was regarded as doubtful until recently.

In this study we examined the possibility of using UDMH in synthesis of polyurethanes, and also the effects of the reagent ratio and process conditions on the synthesis and properties of various types of polyurethane elastomers.

Polyurethane elastomers. It is known that, in two-step synthesis of a polyurethane elastomer, violation of the stoichiometric ratio of reagents may result in formation of a cross-linked polymer. A different result was obtained when isocyanate prepolymer (PP), prepared from 4,4'-diphenylmethane diisocyanate (DPMDI) and poly(oxytetramethylene) glycol (PTMEG-1000), was reacted with UDMH [13, 14]. In this case, high-molecular-weight compounds soluble in DMF were formed with increasing mole fraction of the prerpolymer by a factor of 2, 5, and even 10. The polymeric films prepared from the resulting DMF solutions demonstrated mechanical characteristics well comparable with the traditional polyurethane elastomers (Table 1).

To estimate the number-average molecular weight of the polymers, we used the end-group analysis [15]. The amounts of the amide and attached hydrazide groups were determined by potentiometric titration in glacial acetic acid with an acetic acid solution of $HClO_4$ [16]. The number of nitrogen atoms in PU samples was determined by the Kjeldahl method, and MW (Table 2) of certain oligomers, ebullioscopically. Such a comprehensive approach to analysis allowed estimation of the number-average molecular weight of the elastomers obtained and some conclusions on their structure. As in our previous study [17], we noted the formation of two types of the structure. Only at prepolymer to UDMH ratios of 1 : (6–1) and 2 : 1

Table 1. Formulation and selected properties of UDMH-based polyurethane elastomers

Sample	PP : UDMH	Intrinsic viscosity [η], dl g^{-1}	Density ρ, g cm^{-3}	Tensile strength σ, MPa	Relative elongation ε, %
PU 1/1	1 : 1	0.34	–	–	–
PU 2/1	2 : 1	0.72	1.1235	24.5	630
PU 3/1	3 : 1	0.68	1.1227	24.1	650
PU 4/1	4 : 1	0.56	1.1157	23.7	700
PU 5/1	5 : 1	0.57	1.1126	23.3	725
PU 6/1	6 : 1	0.55	1.1124	23.1	765
PU 7/1	7 : 1	0.54	1.1119	22.8	775
PU 8/1	8 : 1	0.49	1.1115	22.5	780
PU 9/1	9 : 1	0.50	1.1112	22.4	790
PU 10/1	10 : 1	0.51	1.1111	22.2	800
PU 20/1	20 : 1	0.66	1.1017	26.1	960

Table 2. Composition of PU samples

Sample	MW_{exp}	Number of hydrazide groups	Number of amide groups	Number of nitrogen atoms	Inferred structure and number of units	MW_{theor}
PU 1/4	2640	2	–	9	$(A)_2$	2800
PU 1/1	3446	1	1	10	$(A)_3$	4200
PU 5/1	9808	1	5	24	$(B)_2$	9050
PU 10/1	23981	1	5	52	$(B)_5$	22400
PU 20/1	35834	2	17	96	$(B)_9$	40250

(catalyzed reaction), oligomers or linear low-molecular-weight polymers are formed, while in all other cases, weakly branched (comb-shaped) polymers (through intermediate biuret structures) [18]. The intrinsic viscosity [η] of the polymers changed antiparallel to the PP fraction (Table 1). Generally, a decrease in the viscosity (at the same or slightly different MW) is an indication of a branched structure, unless the length of the side chains is comparable with that of the backbone and the macromolecule has a star-like shape [19].

Analysis of the structure of the elastomers (PP : UDMH = 2 : 1) obtained at 60 and 80°C by the uncatalyzed reaction reveals the formation of branched polymers. Generally, such reactions, e.g., the formation of the allophanate and biuret structures, proceed at higher temperatures (120–140 and 100°C, respectively) [19]. The tendency of UDMH to form hydrazinium cations suggests that the synthesis of the UDMH-based elastomers proceeds via formation of ionic reactive centers like that in the Ritter reaction, in which *N*-substituted amides of carboxylic acids are synthesized through the intermediate stage of formation of the carbonium cation [20]. The suggested mechanism is supported by the following findings: (a) the highest activity in the catalytic processes was shown by $SnCl_2(acac)_2$, providing the formation of hydrazinium chloride and (b) introduction of HCl into the reaction system considerably accelerates the reaction.

The structure of the UDMH-based polyurethanes was confirmed by the IR spectra. The spectra show all the bands typical of polyurethanes: 2865 and 2950 cm^{-1} (CH_2), 1115 cm^{-1} (C–O–C of the glycolic fragment), 1650 and 1710 cm^{-1} (associated and free CO groups) (intensities of these bands increased considerably against those in the prepolymer), and 3320 cm^{-1} (NH). The band at 2270 cm^{-1} (NCO group) is lacking, i.e., all the NCO groups were converted.

Water-dispersible polyurethane ionomers. The routes to preparation of hydrophilic and water-soluble polyurethane elastomers based on UDMH, 1,6-hexamethylene diisocyanate (1,6-HMDI), and PTMEG-1000 can be found in [21]. The hydrophilicity of the resulting polymers could be increased by a factor of 5–10, depending on the concentration of ionic

Table 3. Composition and selected colloidal-chemical properties of aqueous polyurethane dispersions based on UDMH, PTMEG-1000, and 1,6-HMDI

Sample	UDMH, M	Quaternizing agent, 100%	Dry residue, wt %	pH	Particle size, nm
WDP-38	0.75	HCl	10.8	1.55	–
WDP-17	0.75	HCl	17.7	2.65	57
WDP-17/1	0.1	HCl	0.1	–	440
WDP-17/2	0.5	HCl	0.5	3.35	210
WDP-17/3	0.25	HCl	0.25	3.55	~550
WDP-17/4	0.75	HCl	22.7	2.8	–
WDP-17/5	0.75	H_2SO_4	31.2	1.55	–
WDP-17/6	0.75	H_2SO_4	30.4	2.3	–

groups and functionality of quaternizing agents. The products are obtained as organic or aqueous-organic solutions, and, occasionally, as thermoreversible gels.

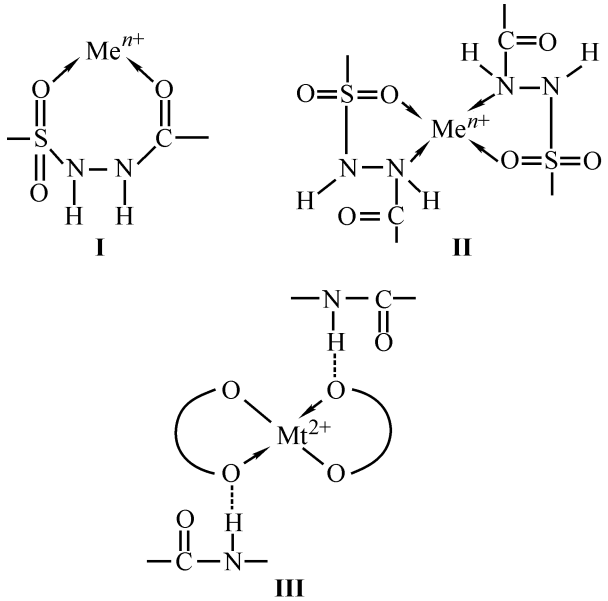
Polyurethane ionomers synthesized using pyromellitic dianhydride (PADA) are amphoteric. One fragment of their macrochain contains tertiary nitrogen atoms capable of quaternization, and the other fragment, carboxy groups, tending to salt formation. Depending on the ratio between these groups in the polymer, stable aqueous ionomer dispersions with various particle sizes from 185 to 520 nm (pH 3.15–3.95) were obtained. The films prepared from these dispersions demonstrate good mechanical properties (tensile stress 20 MPa and elongation at break up to 800%). Their hydrophilicity ranged from 20 to 150%.

The colloidal-chemical properties of the polyurethane dispersions strongly depend on the dilution: particle size abruptly increases from 57 to 550 nm (Table 3). This is a surprising finding in view of the same number of ionic sites.

Polyurethane foams. Thanks to their unique properties, polyurethane foams find a very broad spectrum of applications. Structural-chemical and physical modification of these polymers allows imparting novel performance characteristics to them. Unsymmetrical dimethylhydrazine was used as an initiator in synthesis of branched polyurethanes [22]. The resulting close-cell polyurethane elastomers demonstrated good performance: density 0.03 – 0.07 g cm^{-3} and water absorption 0.18 – 0.83 g cm^{-3}.

Resistance of polymers against biocorrosion. In the recent decades the problem of biocorrosion of structural materials, particularly, with micromycetes (mould fungi *Aspergillus*, *Penicillinum*, etc.) has become very topical [23, 24]. We examined the resistance of the branched polyurethane elastomers modified with inorganic additives against micromycete-induced biocorrosion.

Like other living bodies, mould fungi are sensitive to toxic metal ions, which react with functional groups of proteins, thus deteriorating their structural organization and function [25]. Linear and branched polymers modified with inorganic fungicidal additives such as $ZnCl_2$, $SnCl_2$, and $Zn(acac)_2$ can be involved in complexation with the semicarbazide and urethane fragments of macrochains by the inter- (**I**) and intramolecular (**II**, **III**) mechanisms [26]:



In designing biocorrosion-resistant polymers, the necessary condition is their safety for the human, i.e., lack of diffusion of metal-containing modifiers to the polymer surface, which can be realized through fixation of metal ions on the semicarbazide and urethane fragments of the polymer matrix [27].

Table 4. Biocorrosion of branched polyurethanes modified with inorganic additives

Sample code*	Initial polymer		Polymer after corrosion test				
	tensile strength σ, MPa	relative elongation, ε_{rel}, %	tensile strength σ, MPa	relative elongation, ε_{rel}, %	K_δ, %	K_ε, %	severity of corrosion [29] after 20/30-day tests
13/0	43.7	525.0	60.9	558.0	139.36	106.3	3/3
14	68.0	550.0	57.5	583.3	84.51	106.1	2/3
15	65.9	566.7	48.7	626.8	73.88	110.6	1/2
16	55.9	491.7	50.5	526.1	90.48	107.0	1/2

* PTMEG-1000, DPMDI, and UDMH; PP : ADMG = 20 : 1 [13].

To characterize the interaction in the system micromycete–bioactive compound, the value of the fungicidal activity is used, i.e., specific inhibiting effect of a given compound on mould fungi. In the case of polymers, such parameters are also used as resistance to fungal growth and biodeterioration (deterioration in the physicochemical characteristics of polymers under the action of microorganisms) [28].

Therefore, the resistance of polyurethanes to micromycete-induced biocorrosion can be characterized by the fungicidal (fungistatic) activity [29] and biodeterioration. The biodeterioration under the action of mould fungi was characterized by the relative change in the strength properties such as tensile stress σ and relative elongation ε:

$$K_\sigma = (\sigma/\sigma_0) \times 100\%,$$

$$K_\varepsilon = (\varepsilon/\varepsilon_0) \times 100\%.$$

As seen from Table 4, branched polymers PU 13/0–16 demonstrate biocorrosion resistance (i.e., fungistatic activity) and increase in the elasticity (K_ε > 100%).

In phase-segregated systems such as the investigated polymers, the rigid-block domains and transition regions are the most susceptible to any attack, which is controlled by the degree of association of the –NH– and –C=O groups. For all the samples studied, the perfection of the domain structure may be characterized by the intensity ratio of the IR bands at 1540 (δ, free NH groups), 3330 (ν, associated NH groups), and 1230 cm^{-1} (ν, associated C=O); ν = 1705 and 1730 cm^{-1} correspond to the C–O stretching vibrations in the self-associates of the rigid-block segments and in the carbonyl groups not involved in H bonding.

The disturbance of the system of physical bonds of polyurethanes under the action of organic acids and water, produced by micromycetes (for example, *Aspergillus niger* is a citric acid producer), resulted in a slight increase in the elasticity.

The susceptibility of the urethane and semicarbazide fragments to the action of micromycetes can be quantified by comparison of the intensities of the corresponding IR bands. As an internal reference one may take the band at 1600 cm^{-1} characteristic of the benzene ring. In the spectra of samples PU 13–PU 16, after the exposure to micromycetes we observed a slight redistribution in the band intensities: the intensity of the band at 1670 cm^{-1} (CO of the semicarbazide fragment) increased and that at 1730 cm^{-1} (carbonyl group of the urethane fragment) decreased, which can be attributed to the action of low-molecular-weight organic acids produced by micromycetes [30]. In all the samples the intensity of the band at 1540 cm^{-1} (δ, free NH groups), related to the band at 1600 cm^{-1} (benzene ring), remained unchanged after the exposure to the test cultures of micromycetes, suggesting that our samples are resistant to the action of these microorganisms. This is supported by the fact that the band at 1120 cm^{-1} sensitive to the action of micromycetes remained practically unchanged also.

Antitranspiration and antiphytotoxic activities of water-dispersible polyurethane ionomers. The UDMH-based water-dispersible polyurethanes (WDP) are capable of forming thin films on the surface of mesophile (plants), which are permeable for water vapor and CO_2. The films decelerate the transpiration, but to a lesser extent than the photosynthesis, thus providing more efficient utilization of water in plants (Table 5).

Single treatment of a plant with a WDP emulsion (water content in emulsions ranged from 90 to 98%)

Table 5. Effect of various aqueous dispersions of polyurethane ionomers on the yield and protein and gluten contents in Odesskaya-162 winter wheat grain in drought

Sample	Weight, g		Content in grain, %	
	grains in Wagner tank	1000 grains	protein	gluten
WDP-1	21.8 ± 0.6	38.5 ± 0.2	12.2 ± 0.3	26.2 ± 0.8
WDP-2	19.4 ± 0.9	36.2 ± 0.2	11.7 ± 0.5	25.0 ± 0.6
WDP-3	18.6 ± 0.9	35.7 ± 0.5	11.5 ± 0.7	24.6 ± 0.3
WDP-4	21.0 ± 0.7	37.8 ± 0.5	12.0 ± 0.1	25.8 ± 0.5
SPU-5	17.5 ± 0.8	34.6 ± 0.4	11.2 ± 0.3	24.0 ± 0.4
WDP-6	20.4 ± 0.4	37.0 ± 0.5	11.7 ± 0.5	24.8 ± 0.6
SPU-7	16.2 ± 0.6	33.4 ± 0.9	10.9 ± 0.5	23.8 ± 0.6
WDP-8	22.5 ± 0.5	39.2 ± 0.4	12.6 ± 0.4	28.4 ± 0.9

under drought conditions facilitated the water and gaseous metabolism, ear formation (this growth stage is the most sensitive to deficiency of water), and also induced some protective reaction on the surface of leaves, thus reducing the crop loss and the protein loss in the winter wheat grain in drought [31].

Based on the results obtained one may recommend the polyurethane dispersions (WDP-2, WDP-4, and WDP-6) for optimization of the water metabolism and production in drought.

EXPERIMENTAL

Commercial unsymmetrical dimethylhydrazine was distilled in flowing inert gas (nitrogen or argon) prior to use. Commercial poly(oxytetramethylene) glycol with MW 1000 (PTMEG-1000) was dried. Commercial 4,4'-diphenylmethane diisocyanate (DPMDI), toluene diisocyanate (mixture of 2,4- and 2,6-isomers) (TDI), and 1,6-hexamethylene diisocyanate (HMDI) were purified by vacuum distillation. Commercial pyromellitic dianhydride (PADA) was used without additional purification. DMF was purified by standard procedures.

Polyurethane elastomers. A two-stage synthesis was employed [14]. In the first stage, the prepolymer was synthesized by the reaction of PTMEG-1000 with a diisocyanate (1 : 2 molar ratio) at 80–85°C for 2 h with vigorous stirring. The reaction was considered as complete when the theoretical molecular weight was achieved, which corresponded to the 6.29% content of the NCO groups. The resulting prepolymer was cooled to 40–45°C, and the estimated amount of UDMH (PP : UDMH ratio varied from 10 : 1 to 1 : 1) was added dropwise with stirring [13]. The mixture was stirred for 1 h at 40–45°C, then the temperature was raised to 55°C, the estimated volume of DMF was added, and the reaction was continued for an additional 4 h. Finally, the DMF solution of polyurethane was degassed in a vacuum. To prepare films, the solution was cast onto glass or Teflon supports. The samples were initially dried at room temperature and then in an oven at 60°C for several hours.

At PP to UDMH ratios of 1 : (6–1), oligomers or linear low-molecular-weight film-forming polymers, and in all other cases, film-forming polymers soluble in organic solvents were formed.

Inorganic modifiers such as tin(II) and zinc(II) chlorides and zinc(II) acetylacetonate were introduced into the polymers at the synthesis stage in an amount from 0.1 to 5 wt %. Polymer 13/0 was prepared without modifying additive.

The molecular weights of the polymers were estimated from the amount of amide and attached hydrazide groups determined by nonaqueous potentiometric titration (end-group analysis), and from the amount of the nitrogen atoms (Kjeldahl method) [15].

Aqueous polyurethane dispersions. A weighed portion of PTMEG-1000 and estimated amount of HMDI were continuously stirred in a nitrogen or argon atmosphere for 2 at 90–95°C. To the resulting prepolymer, the solvent (acetone) was added to obtain a 30% solution, and the mixture was stirred for 15 min to attain homogeneity. Then the estimated amount of UDMH was added dropwise [21]. After the chain extension was completed, the solution was neutralized with an equimolar amount of HCl. The reaction mass was stirred again and diluted with distilled water. The resulting dispersion was gently stirred, and acetone was removed in a water-jet pump vacuum. Finally, the dispersion was cast onto a Teflon support,

Table 6. Composition of aqueous polyurethane dispersions based on WDP-38

Sample	Dry residue	Water	Acetone	Isopropanol
	%			
SPU-1	0.1	98.4	1.5	–
SPU-2	0.1	98.12	0.36	1.42
SPU-3	0.25	75.0	18.5	6.25
SPU-4	0.5	92.5	3.5	3.5
SPU-5	0.1	98.6	0.65	0.65
SPU-6	0.5	91.0	7.5	1.0
SPU-7	0.1	98.2	1.6	0.3
SPU-8	0.5	90.6	1.8	7.1

dried at room temperature to form a film, and then in an oven at 60°C to constant weight. Table 6 shows the compositions of the aqueous polyurethane dispersions used in this study for characterization of the antitranspiration and antiphytotoxic activity of water-dispersed ionomer polyurethanes.

Polyurethane foams. The foams were prepared from the compounds having at least two reactive hydrogen atoms: mixtures of polyesters (P-2200, PDA-800) and polyethers (POPG-2500, POPG-3003, POPG-3603-2P, POPG-5003) with MW from 800 to 5000, $HO–[CH_2CH(CH_3)O]_n–OH$ and $H–[O[(CH_2)_2O]_2–OC(CH_2)_4–COOCH_2CH(OH)–CH_2O]_m–H$; 2,4(2,6)-toluene diisocyanate $CH_3C_6H_3(NCO)_2$; catalysts, diazabicyclooctane and bis(2,4-pentanedionato)Sn(II) dichloride; water; organosilicon stabilizer for foams; and Nujol [32]. The blowing agent was CO_2 formed by the reaction of the isocyanate with water.

The IR spectra of the samples in KBr were recorded on an UR-20 spectrophotometer (Carl Zeiss, Jena, Germany) over the range 400–4000 cm^{-1}. Attenuated total internal reflection infrared spectra were recorded using a germanium ATR plate as an internal reflection element with an aperture angle of 45°; $N = 14$ (KRS-5 trapezium prism, $N = 21$, $\varphi = 450$).

Mechanical characteristics [tensile strength σ (MPa) and relative elongation ε (%)] of the polymer films were determined on an RM-30-1 tensile testing machine at an extension rate of 100 mm min^{-1}, using standard procedures.

The rheological properties of the polymers were studied by viscometry. The unit weight of the polyurethane films was determined by hydrostatic weighing in isooctane.

Determination of the fungicidal activity of the polyurethane samples, growth of test cultures of micromycetes, preparation of conidium suspensions, contamination of the samples, and testing were carried out according to GOST (State Standard) 9.049–91 [29].

Antitranspiration and antiphytotoxic activities of water-dispersible polyurethane ionomers.[1] The plants were cultivated in 8-kg Wagner tanks at a 60% total moisture capacity and daylight. Details of the experimental procedure were reported elsewhere [31].

CONCLUSIONS

(1) Novel polyurethane elastomers are synthesized using unsymmetrical dimethylhydrazine at various prepolymer to UDMH ratios; the reaction involved formation of ionic reactive centers. Only at prepolymer to UDMH ratios of 1 : (1–6) and 2 : 1 (catalyzed reaction), oligomers or linear low-molecular-weight film-forming polymers are formed, and in all other cases, weakly branched (comb-shaped) polymers are obtained.

(2) The structures of the polymers were confirmed by the IR spectra, by the amount of the amide and attached hydrazide groups detemined by nonaqueous potentiometric titration (end-group analysis), and also by the amount of the nitrogen atoms (Kjeldahl method).

(3) The resistance of the polymeric materials to micromycete-induced biocorrosion is studied. Generally, the biodegradability of polyurethanes is insignificant, and they demonstrate prolonged fungicidal effect. The nature of biodegradation of polyurethanes is controlled by their structure. The products of metabolism of micromycetes have a stronger effect on branched polyurethanes, and in the linear polymers, the degree of biodegradation is low.

(4) Novel polyurethane-based aqueous dispersions are prepared. They can be used as efficient regulators of water and gaseous metabolism in winter wheat in drought, to optimize the water metabolism and production.

(5) Novel polyurethane foams are prepared using unsymmetrical dimethylhydrazine and its derivatives. The possibility of controlling the mechanical characteristics of the polyurethane foams and the presence

[1] Study was performed in cooperation with the Institute of Plant Physiology and Genetics, National Academy of Sciences of Ukraine; Grishko Central Botanical Garden, National Academy of Sciences of Ukraine; and Uzhgorod National University.

of ionic centers in their structure allow their application as a polufunctional matrix in development of organo-organic and organo-inorganic hybrid materials.

ACKNOWLEDGMENT

The authors are grateful to V.K. Kharitonova, V.A. Khranovskii, E.Z. Koval', and I.A. Grigoryuk for assistance.

REFERENCES

1. Grekov, A.P. and Veselov, V.Ya., *Fizicheskaya khimiya gidrazina* (Physical Chemistry of Hydrazine), Kiev: Naukova Dumka, 1979.
2. Filippov, V.A., Filippova, O.I., Fedotov, D.D., et al., *Med. Truda Prom. Ekol. (Gigiena Truda Prof. Zabol.)*, 1997, no. 11, pp. 10–14.
3. RF Patent 2092205.
4. Lopyrev, V.A., Dolgushin, G.V., and Voronkov, M.G., *Zh. Prikl. Khim.*, 1998, vol. 71, no. 8, pp. 1233–1248.
5. Lekomtsev, A.I., Sakhina, G.L., Malysheva, G.E., et al., *Zh. Prikl. Khim.*, 1999, vol. 72, no. 12, pp. 1970–1983.
6. Drozdetskii, A.G., Drozdova, S.V., Koval'chuk, I.N., et al., *Zh. Prikl. Khim.*, 1999, vol. 72, no. 12, pp. 1983–1985.
7. Levkovskaya, G.G., Bozhenkov, G.V., Larina, L.I., and Mirskova, A.N., *Zh. Org. Khim.*, 2002, vol. 38, no. 10, pp. 1554–1559.
8. Elokhina, V.N., Larina, L.I., Nakhzmanovich, A.S., et al., *Zh. Obshch. Khim.*, 2000, vol. 70, no. 11, pp. 1860–1862.
9. Bozhenkov, G.V., Levkovskaya, G.G., Mirskova, A.N., et al., *Zh. Org. Khim.*, 2003, vol. 39, no. 5, pp. 1140–1146.
10. Rakhlin, V.I., Gostevskii, B.A., Fomina, A.I., et al., *Zh. Org. Khim.*, 2004, vol. 40, no. 1, pp. 136–137.
11. Kirillin, A.D., Dokuchaev, A.A., Sokova, N.B., et al., *Zh. Obshch. Khim.*, 2000, vol. 70, no. 1, pp. 51–60.
12. Juppo, M., Ritala, M., and Leskela, M., *J. Electrochem. Soc.*, 2000, vol. 147, no. 9, pp. 3377–3381.
13. Savel'ev, V.Yu., Akhranovich, E.R., Kharitonova, V.K., et al., *Dopov. Nats. Akad. Nauk Ukr.*, 2003, no. 8, pp. 138–143.
14. UA Patent 54533.
15. Rabek, J.F., *Experimental Methods in Polymer Chemistry. Physical Principles and Applications*, Chichester: Wiley, 1980.
16. Gyenes, I., *Titration in Non-aqueous Media*, Cohen, D., Ed., Budapest: Akademiai Kiado, 1967.
17. Savel'ev, Yu.V., Khranovskii, V.A., Veselov, V.Ya, et al., *Dopov. Nats. Akad. Nauk Ukr.*, 2005, no. 1, pp. 141–143.
18. Savel'ev, Yu.V., Robota, L.P., Rudenko, A.V., et al., *Dopov. Nats. Akad. Nauk Ukr.*, 2005, no. 1, pp. 144–146.
19. Saunders, J. H. and Frisch, K.C., *Polyurethanes: Chemistry and Technology*, New York: Interscience, 1964.
20. Lee, T.C.L. and Pearce, M.E., *J. Polym. Sci., Part A-1*, 1971, vol. 9, no. 2, pp. 557–561.
21. UA Patent 53729.
22. Savel'eva, O.A., Veselov, V.Ya., Markovskaya, L.A., et al., Abstracts of Papers, *XXIV Mezhdunarodnaya ezhegodnaya konferentsiya "Kompozitsionnye materially v promyshlennosti"* (XXIV Int. Annual Conf. "Composite Materials in Industry") (Slavpolikom), Yalta (Crimea), May 31–June 4, 2005.
23. Dong Gu, J.-D., *Int. Biodeter. Biodegr.*, 2003, vol. 52, no. 2, pp. 69–91.
24. Nielsen, K.F., Holm, G., Uttrup, L.P., et al., *Int. Biodeter. Biodegr.*, 2004, vol. 54, pp. 325–336.
25. Lugauskas, A., Levinskaite, L., and Peč̆iulyte, D., *Int. Biodeter. Biodegr.*, 2003, vol. 52, pp. 233–242.
26. Savel'ev, Yu.V., Grekov, A.P., Koval', E.Z., et al., *Ukr. Khim. Zh.*, 1997, vol. 63, nos. 5–6, pp. 70–73.
27. Savelyev, Yu., in *Handbook of Condensation Thermoplastic Elastomers*, Fakirov, S., Ed., New York: Wiley, 2005, pp. 355–380.
28. *Int. Standard ISO 846:1997 (E): Plastics—Evaluation of the Action of Microorganisms*, 1997–06–15, 2nd ed.
29. *GOST* (State Standard) *9.049–91: Polymeric Materials and Their Components: Methods for Laboratory Testing for Resistance Against Mould Fungi*, Moscow: Izd. Standartov, 1995.
30. Vatulev, V.N., Laptii, S.V., and Kercha, Yu.Yu., *Infrakrasnye spektry i struktura poliuretanov* (Infrared Spectra and Structure of Polyurethanes), Kiev: Naukova Dumka, 1987.
31. Grigoryuk, I.A., Savel'ev, Yu.V., Mashkovskaya, S.P., et al., *Nauk. Visn. Uzhgorod. Nats. Univ., Ser. Biol.*, 2003, no. 12, pp. 73–81.
32. *Metody eksperimental'noi mikologii: Spravochnik* (Methods for Experimental Mycology: A Handbook), Moscow: Nauka, 1989.

ISSN 1070-4272, Russian Journal of Applied Chemistry, 2006, Vol. 79, No. 4, pp. 672–673. © Pleiades Publishing, Inc., 2006.
Original Russian Text © E. M. Shvarts, R. G. Belousova, 2006, published in Zhurnal Prikladnoi Khimii, 2006, Vol. 79, No. 4, pp. 681–682.

BRIEF COMMUNICATIONS

Formation of Tricuprotetraborate $3CuO \cdot 2B_2O_3 \cdot 6H_2O$ in Aqueous Solutions

E. M. Shvarts and R. G. Belousova

Institute of Inorganic Chemistry, Riga Technical University, Salaspils, Latvia

Received December 27, 2005

Abstract—The reaction of copper sulfate, boric acid, and sodium hydroxide in an aqueous solution was studied in relation to the molar ratio and concentration of components, solution pH, temperature, and reaction duration. The conditions under which tricuprotetraborate hexahydrate $3CuO \cdot 2B_2O_3 \cdot 6H_2O$ is formed were determined.

DOI: 10.1134/S107042720604032X

Only few hydrated copper borates are known: amorphous $2CuO \cdot B_2O_3 \cdot 3H_2O$ and $3CuO \cdot 2B_2O_3 \cdot nH_2O$ (n=5, 4, 2, 1) [1, 2]. They are finely grained blue powders, which require a very long time to be formed (115 days to 2 years). The amorphous copper borates $3CuO \cdot 2B_2O_3 \cdot nH_2O$ (n = 5, 4, 2, 1) mentioned in [2] have not been isolated, either. Some minerals are known, which are crystalline copper(II) borates: bandylite $CuB(OH)_4Cl$ and henmilite $[Ca_2Cu(OH)_4B(OH)_4]_2$ [3]. In addition, the following synthetic borates have been described: $Na_6\{Cu_2[B_{16}O_{24}(OH)_{10}]\} \cdot 12H_2O$ [4], $K_5H\{Cu_4O[B_{20}O_{32}(OH)_8]\} \cdot 32H_2O$ [5], and $Cu(NH_3)_4B_4O_7 \cdot 6H_2O$ [1].

Most of synthetic copper borates are water-insoluble, they precipitate from solutions as very finely dispersed particles and readily adsorb various impurities. That is why it is very difficult to judge the real composition of borates.

Previously, we tried to obtain a product of the exchange reaction between copper(II) sulfate and borax and to use it for presowing treatment of sugar beet seeds. A dose of 5 g per 1 kg of seeds led to an increase in harvest of root crops and beet tops and in the percentage of beet sugar. The product, the so-called copper borate, was found to be a mixture of several copper borates with H_3BO_3 and was finely dispersed, which caused considerable difficulties in filtration.

The aim of this study was to obtain an individual copper(II) borate that would be sufficiently dispersed, but suitable for filtration. We varied the conditions of the reaction between copper(II) sulfate, orthoboric acid, and sodium hydroxide. The dependence of the composition of the resulting copper borate on the reaction conditions is illustrated by Table 1. Copper borate $3CuO \cdot 2B_2O_3 \cdot 6H_2O$ was obtained at pH 7.5–8.0,

Table 1. Composition of products and conditions of the reaction between $CuSO_4$, H_3BO_3, and NaOH at 80°C

Molar ratio of components $CuSO_4 : H_3BO_3 :$ NaOH	pH	Composition of the solid phase, %					Molar ratio $CuO : B_2O_3$ in the solid phase	Filtrate
		CuO	B_2O_3	H_2O	SO_4^{2-}	total impurities		
1 : 4 : 4	9.0	51.37	27.51	20.24	–	$Cu(OH)_2$	3.56 : 2	Borax precipitates on cooling
1 : 4 : 3.5	8.0	49.06	28.65	21.82	–	–	3.02 : 2	No precipitates
1 : 4 : 3.25	7.5	49.55	28.77	21.73	–	–	3.02 : 2	〃
1 : 4 : 3	7.0	46.17	26.98	21.35	0.97	5.50	2.99 : 2	〃
1 : 1.33 : 2*	6.0	52.62	15.16	25.86	–	6.36	3.04 : 2	〃
1 : 4 : 3.5	8.0	48.17	28.71	21.35	0.57	1.77**	2.94 : 2	〃
1 : 4 : 3.25	7.5	44.85	28.15	22.22	1.5	4.78**	–	〃
1 : 4 : 3.5	8.0	38.33	27.74	20.47	5.93	13.46***	–	〃
1 : 4 : 3.25	7.5	36.88	25.78	21.70	6.02	15.64***	–	〃

* Stoichiometric ratio of the components. ** Double amount of the reaction mixture. *** Fivefold amount of the reaction mixture.

a nonstoichiometric ratio $CuSO_4 : H_3BO_3 : NaOH$ = [1 : 4 : (3.25–3.5)], and high concentrations of the components. Strict observation of all the conditions is very important for the individual compound to be isolated.

The isolated product $3CuO \cdot 2B_2O_3 \cdot 6H_2O$ is a greenish finely dispersed powder insoluble in cold and hot water, but soluble with decomposition in mineral and organic acids and ammonia. Thermal-analysis curves show that $3CuO \cdot 2B_2O_3 \cdot 6H_2O$ is stable in air up to 40°C. When temperature is raised to 180°C, the mass loss is 14.15%, which corresponds to elimination of four moles of water. The two remaining water molecules are gradually lost on heating to 465°C. In the temperature range 465–878°C, there is no mass loss any more, but three exothermic peaks at 600, 630, and 758°C and a endothermic minimum at 888°C are observed in the DTA curve. The mass loss at 1000°C is 21.82%.

An analysis of the conditions of the reaction between $CuSO_4$, H_3BO_3, and NaOH (Table 1) shows that pure borate $3CuO \cdot 2B_2O_3 \cdot 6H_2O$ is obtained at high reagent concentrations and high temperature (80°C), at pH 7.5–8.0. The synthesis duration is 4 h; heating and stirring favor formation of particles suitable for filtration. Copper(II) borate contains $Cu(OH)_2$ as an admixture at a higher pH 9 and sodium sulfate admixtures at pH below 7.5. A twofold increase in the volume of the reaction mixture results in a higher content of admixtures in the products, and a fivefold increase in the volume, in a considerable decrease in the copper(II) content in the product. We could not identify the product, but believe that this may be a mixture of various borates. At a stoichiometric ratio of the reagents in accordance with the equation

$$3CuSO_4 + 4H_3BO_3 + 6NaOH \rightarrow 3CuO \cdot 2B_2O_3 \cdot 6H_2O + 3Na_2SO_4 + 3H_2O$$

the resulting solid phase contains a considerably greater amount of copper(II) oxide and a smaller amount of boron oxide, and it also can be a mixture of various products.

EXPERIMENTAL

Synthesis of $3CuO \cdot 2B_2O_3 \cdot 6H_2O$. A weighed portion of $CuSO_4 \cdot 5H_2O$ (7.45 g) was dissolved in 19 ml of distilled water at 50–60°C; 7.4 g of boric acid was dissolved in 50 ml of distilled water at 80°C. The solutions were combined, thoroughly mixed, and then cooled to 60°C. Solid NaOH (3.875–4.17 g) was dissolved in 6.5–7.0 ml of distilled water, the solution was cooled and added to the reaction mixture in small portions with stirring. Then the temperature was slowly raised in the course of 2 h to 80°C, and the heating and stirring were continued for additional 2 h. The precipitate was filtered off from the hot solution, washed with 50 ml of a warm 1% solution of orthoboric acid, and dried in air. The analitical data for the product are listed in Table 2.

Table 2. Composition of copper(II) borate $3CuO \cdot 2B_2O_3 \cdot 6H_2O$

Main component	Found, %		Calculated, %
	1	2	
CuO	45.55	49.06	49.11
B_2O_3	28.77	28.65	28.65
H_2O	21.73	21.82	22.23

The Cu(II) content was determined by titration, EDTA with PAN as an indicator [6]. The boron content in the substance was determined by alkalimetric titration in presence of *D*-mannitol, with the pH-metric determination of the equivalence point by the method of constant pH. The interfering copper(II) was masked by adding EDTA. The water content was determined from the mass loss on heating to 700°C. The content of Na_2SO_4 impurity was determined gravimetrically (by precipitation in the form of $BaSO_4$). Thermal analysis curves were recorded on a Q-1500 D derivatograph.

CONCLUSIONS

The conditions under which tricuprotetraborate hexahydrate $3CuO \cdot 2B_2O_3 \cdot 6H_2O$ is formed are as follows: $CuSO_4 : H_3BO_3 : NaOH = 1 : 4 : (3.25–3.5)$, pH 7.5–8.0, 80°C. The synthesis duration is 4 h. Under other conditions, amorphous finely dispersed tricuprotetraborate with a significant amount of admpurities [Na_2SO_4, $Cu(OH)_2$, etc.] is formed.

REFERENCES

1. Adams, R.M., *Boron, Metallo-Boron Compounds and Boranes*, New York: Wiley, 1964.
2. Boiko, B.F., in *Khimiya boratov* (Chemistry of Borates), Riga: Akad. Nauk Latv. SSR, 1953, pp. 105–115.
3. Nakai, J., Okada, H., and Masutomi, K., *Am. Mineral.*, 1986, vol. 71, nos. 9/10, pp. 1234–1238.
4. Behm, H., *Acta Crystallogr., Sect. C*, 1983, vol. 39, no. 1, pp. 20–22.
5. Heller, G., Z. *Naturforsch. (b)*, 1985, vol. 40, no. 4, pp. 462–466.
6. Schwarzenbach, G. und Flaschka, H., *Die komplexometrische Titration*, Stuttgart: Ferdinand Enke, 1965.

ISSN 1070-4272, Russian Journal of Applied Chemistry, 2006, Vol. 79, No. 4, pp. 674–676. © Pleiades Publishing, Inc., 2006.
Original Russian Text © E. I. Isaeva, T. B. Boitsova, V. V. Gorbunova, 2006, published in Zhurnal Prikladnoi Khimii, 2006, Vol. 79, No. 4, pp. 683–685.

BRIEF COMMUNICATIONS

Photochemical Synthesis of Gold Nanoparticles in Latexes

E. I. Isaeva, T. B. Boitsova, and V. V. Gorbunova

Herzen Russian State Pedagogic University, St. Petersburg, Russia

Received July 5, 2005; in final form, December 2005

Abstract—Gold nanoparticles in aqueous dispersions of 100-nm polystyrene microspheres were prepared by photochemical synthesis under exposure to monochromatic light with an excitation wavelength of 254 nm. The kinetic relationships in formation of gold nanoparticles were examined in relation to the $H[AuCl_4]$ and polymer concentration in the photolyte.

DOI: 10.1134/S1070427206040331

Nanoparticles of transition metals, especially gold, show much promise for the development of functional nanophase materials for medical, biochemical, and cytometric applications [1, 2]. Microspheres of polymers with grafted functional groups can be considered as model systems for deposition of metal nanparticles and development of specific labels in diagnostics of genetic and pathogenic diseases.

In this study we carried out photochemical synthesis of gold nanoparticles in aqueous polystyrene dispersions.

Gold nanoparticles were prepared from solutions of analytically pure grade $H[AuCl_4]$. All solutions were prepared in double-distilled water. We used polystyrene carboxylated with 4,4'-azobis(4-cyanoisovaleric acid) in the form of a latex consisting of 100-nm microspheres, stabilized with sodium dodecyl sulfate.

A preliminary study of the aggregation stability of the latex dispersions showed that introduction of $H[AuCl_4]$ in concentrations above 0.1 mM leads to destabilization of the systems, manifested in coagulation and precipitation of the latex particles. The gold nanoparticles were synthesized in the presence of the latex in $H[AuCl_4]$ solutions with concentrations from 2×10^{-4} to 2×10^{-2} M, which were mixed with latexes containing 5×10^{-3} and 5×10^{-2} wt % polystyrene. The resulting compositions were irradiated for 4 h with a monochromatic light at the excitation wavelength λ_{exc} = 254 nm and the light flux intensity of 4.8×10^{16} quanta cm^{-2} s^{-1}. Irradiation was carried out in quartz cells with the optical path length of 1 cm. Formation of nanostructures was monitored spectrophotometrically (an SF-2000 spectrophotometer) from the appearance of absorption within 200–700 nm. Figure 1 presents the absorption spectra of aqueous dispersions of 100-nm polystyrene microspheres, containing 2×10^{-4} M $H[AuCl_4]$. After 60-min UV ir-

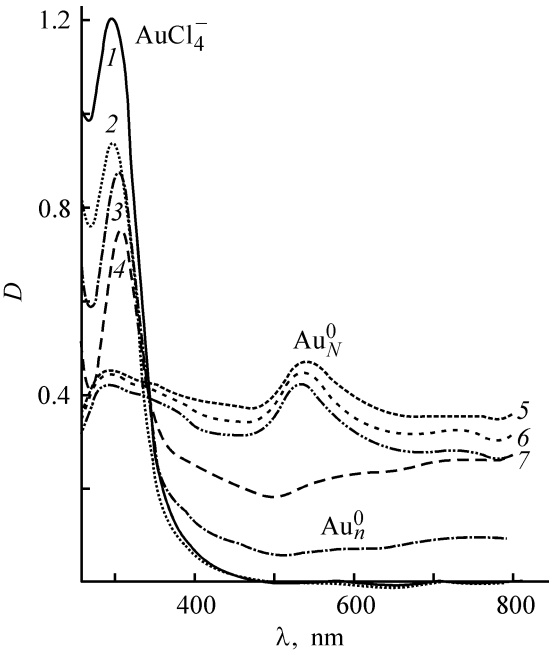


Fig. 1. Absorption spectra of an aqueous dispersion of 100-nm polystyrene microspheres, containing 2×10^{-4} M $H[AuCl_4]$, recorded during photolysis with monochromatic light (λ_{exc} = 254 nm). (*D*) Optical density and (λ) wavelength. Time, min: (*1*) 0, (*2*) 30, (*3*) 60, (*4*) 90, (*5*) 120, (*6*) 150, and (*7*) 180.

radiation of the dispersions, the absorption band at 300 nm, corresponding to $[AuCl_4]^-$ ions, tended to decrease in intensity due to partial photoreduction of Au(III) to Au(I). The initially yellow solution gets colorless. After 60-min irradiation, the absorption in the visible region builds up, and a structureless band with a minimum at 480 nm appears in the spectrum, which suggests the presence of small gold clusters up to 0.8–1.5 nm in size [3]. After 100-min irradiation, a broad band appears at 540 nm, corresponding to colloid polydisperse gold species, and the system acquires a pink color. This period is equal to the induction period in formation of metal particles, which, under identical conditions, exceeds that in formation of silver particles (70 min) [4].

A longer induction period in the case of gold can be due, first, to a three-quantum Au(III) → Au(0) transition, while Ag(I) → Ag(0) is a one-quantum transition, and second, to a strong oxidative power of Au(III) (the $[AuCl_4]^-/Au^0$ couple has a redox potential of +1.00 V [5]) with respect to the small gold clusters being formed. Irradiation of the photolyte initiates two simultaneous processes, formation of the colloid phase and dark reoxidation of intermediate small clusters with Au(III) ions and dissolved oxygen [6]. Hence, a stable growth of the number of gold particles is observed only after Au(III) is completely converted to Au(I) and Au(0). The optical densities thus attained do not exceed 0.5 rel. units. Irradiation of the systems for more than 120 min causes the optical density to decrease throughout the wavelength range studied. This is due to sedimentation of the system and is accompanied by formation of dark loose precipitates on the cell bottom. At the same time, we showed previously [4] that the systems based on silver particles are stable during 300-min irradiation.

This fact can be explained as follows. When silver ions are introduced into solution, they enter into an exchange reaction with carboxy groups of the polymer microspheres. Hence, clusters form and grow directly on the microsphere surface. In the case of gold, the initial gold complex is anionic, which does not favor formation of such bonds, and the rate of the three-quantum Au(III) → Au(0) transition exceeds that of diffusion of Au(I) ions to the microsphere surface. Gold particles are formed, most probably, in the photolyte volume rather than on the microsphere surface. Because of oxidation effect of Au(III) ions, the number of the nuclei is significantly smaller than that in silver-based systems. This leads to formation of polydisperse systems with larger particles, which subsequently settle down.

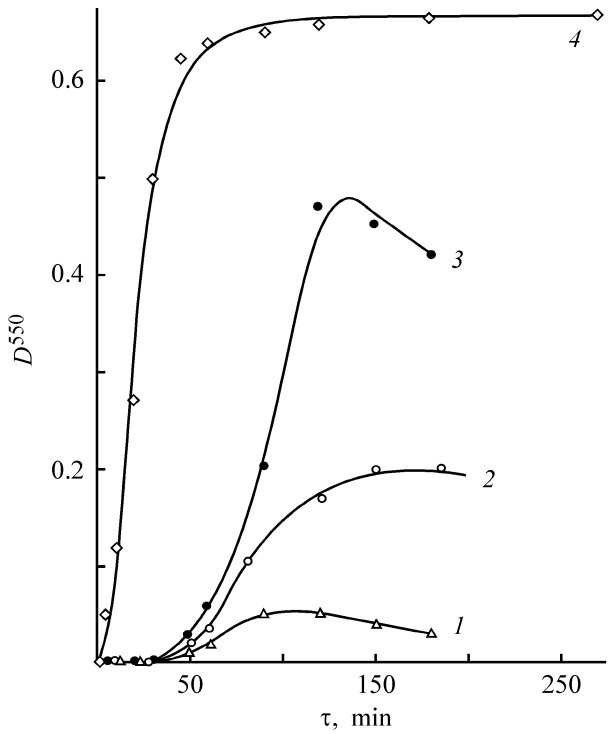


Fig. 2. Kinetic curves of formation of gold nanoparticles during photolysis of systems containing polystyrene and $H[AuCl_4]$. (D^{550}) Optical density and (τ) time. Polystyrene content, wt %: (*1–3*) 5×10^{-3} and (*4*) 5×10^{-2}. $H[AuCl_4]$, M: (*1*, *4*) 2×10^{-3}, (*2*) 1×10^{-4}, and (*3*) 2×10^{-4}.

We analyzed how the average size and degree of polydispersity of the nanoparticles are influenced by the concentration of the $H[AuCl_4]$ introduced into the polystyrene dispersion. As suggested by appearance in the spectra of broad absorption bands, the polydispersity of the systems increases with the $H[AuCl_4]$ concentration increasing from 2×10^{-4} to 2×10^{-3} M, other photolysis conditions being identical. Also, the average size of the gold particles tends to increase, as suggested by the position of the absorption maximum, namely, 550 (2×10^{-4} M)–700 nm (2×10^{-3} M) after irradiation for 100 min. This is due to an increase in the Au(III) oxidant concentration and the ensuing decrease in the number of the nuclei formed. As a result, the size of the gold particles being formed increases in proportion to the amount of $H[AuCl_4]$ introduced. Large particles efficiently settle down, as seen from decreases in the maximal optical densities. For example, an increase in the $H[AuCl_4]$ concentration by an order of magnitude (Fig. 2) causes the optical density D to decrease also by an order of magnitude. Introduction of $H[AuCl_4]$ in concentrations above 2×10^{-3} M causes only the growth of structureless bands corresponding to formation of

gold clusters, and during irradiation for up to 250 min no particles are formed.

An increase in the amount of the dry residue of the polymer in the system from 5×10^{-3} to 5×10^{-2} wt % favors more efficient formation of metal particles, as manifested in a decrease in the induction period to 5 min, in appearance in the spectrum of absorption bands with a maximum at 550 nm, characteristic for colloidal gold, and in an increase in the optical densities to 0.7 rel. unit during 60-min irradiation. Figure 2 (curve *4*) shows that further irradiation to 270 min does not cause any kinetic changes in the system. Probably, reduction of $[AuCl_4]^-$ ions can involve radicals generated by photolysis of 4,4'-azobis(4-cyanoisovaleric acid), sensitive to light with λ_{exc} = 254 nm [7].

CONCLUSION

A procedure was developed for photochemical synthesis of gold nanoparticles in aqueous polystyrene dispersions. The average size and polydispersity of the gold particles formed in these dispersions are governed by the amount of the dry residue of the polymer and the concentration of $H[AuCl_4]$ introduced.

ACKNOWLEDGMENT

This study was financially supported by the Federal Agency for Science and Innovations (project no. 2005-RI-19.0/002/110).

REFERENCES

1. Storhoff, J.J., Elghanian, R., Mucic, C.R., et al., *J. Am. Chem. Soc.*, 1998, vol. 120, no. 9, pp. 1959–1964.
2. Siiman, O. and Burshteyn, A., *J. Phys. Chem. B*, 2000, vol. 104, no. 42, pp. 9795–9810.
3. Bohren, C.F. and Huffman, D.R., *Absorption and Scattering of Light by Small Particles*, New York: Wiley, 1983.
4. Isaeva, E.I., Gorbunova, V.V., Boitsova, T.B., et al., *Zh. Obshch. Khim.*, 2005, vol. 75, no. 9, pp. 1412–1417.
5. *Spavochnik khimika* (Chemist's Handbook), Nikol'skii, B.P., Ed., Moscow: Khimiya, 1966, vol. 3, p. 743.
6. Boistova, T.B., Loginov, A.V., and Gorbunova V.V., *Izv. Ross. Akad. Nauk, Neorg. Mater.*, 1999, vol. 35, no. 12, pp. 1449–1454.
7. *Vvedenie v fotokhimiyu organicheskikh soedinenii* (Introduction to Photochemistry of Organic Compounds), Bekker, G.O., Ed., Leningrad: Khimiya, 1976.

ISSN 1070-4272, Russian Journal of Applied Chemistry, 2006, Vol. 79, No. 4, pp. 677–679. © Pleiades Publishing, Inc., 2006.
Original Russian Text © A. I. Demidov, M. S. Kokhatskaya, B. V. Chernovets, 2006, published in Zhurnal Prikladnoi Khimii, 2006, Vol. 79, No. 4, pp. 686–687.

BRIEF COMMUNICATIONS

Thermodynamics of Discharge of the Negative Electrode of a Nickel–Iron Battery

A. I. Demidov, M. S. Kokhatskaya, and B. V. Chernovets

St. Petersburg State Polytechnic University, St. Petersburg, Russia

Received March 14, 2006

Abstract—The standard Gibbs energies and standard potentials of reactions expected to occur in discharge of the negative electrode of a nickel–iron battery were calculated.

DOI: 10.1134/S1070427206040343

The following equation was suggested for describing the discharge and charging of an iron electrode in an alkaline electrolyte as far back as the beginning of the past century [1–3]:

$$Fe + 2OH^- = Fe(OH)_2 + 2e,\ E^0 = -0.876\ V. \quad (1)$$

In the general form, this equation adequately reflects the initial and final states of the active paste. However, Kabanov and Leikis [4, 5] believe that process (1) occurs in two stages: first, iron is oxidized to $HFeO_2^-$ ions and then a loose porous $Fe(OH)_2$, weakly bound to the metal, precipitates from solution:

$$Fe + 3OH^- \rightarrow HFeO_2^- + H_2O + 2e,\ E^0 = -0.748\ V, \quad (2)$$

$$HFeO_2^- + H_2O \rightarrow Fe(OH)_2 + OH^-,\ \Delta G^0_{298} = -24.7\ kJ. \quad (3)$$

A study of anodic films on iron in alkaline solutions by the ellipsometry and chronoamperometry [6–8] made it possible to suggest the following mechanism of growth of anodic films on iron. A denser anodic film adjacent to the metal is formed via deposition of a $Fe(OH)_2$ layer onto the electrode. Its growth in the course of time is limited by the velocity of migration of Fe^{2+} ions, formed in anodic polarization, under the action of the potential and concentration gradients toward the interface between the film and solution. $HFeO_2^-$ ions are possibly formed, together with $Fe(OH)_2$, in anodic polarization of iron [reaction (2)]. The near-electrode layer is supersaturated with $HFeO_2^-$ ions and, as a result of hydrolysis, they precipitate on the electrode in the form of $Fe(OH)_2$ [reaction (3)], capturing ions from the solution and forming an outer hydrated film. Further, the outer film degrades, loses water, and, giving up OH^- ions to the diffusing Fe^{2+} ions, becomes denser.

In the case of a strong anodic polarization of the iron electrode, the following processes may occur in a solution of the hydroxide of an alkali metal [9, 10]: first anodic process, reaction (1); and the second,

$$Fe(OH)_2 + OH^- \rightarrow \delta\text{-}FeOOH + H_2O + e, \quad (4)$$
$$E^0 = -0.634\ V.$$

Teplinskaya et al. [9, 10] believe that the compound Fe_3O_4 is formed by the reaction between iron hydroxides in different oxidation states:

$$Fe(OH)_2 + 2\delta\text{-}FeOOH \rightarrow Fe_3O_4 + 2H_2O, \quad (5)$$
$$\Delta G^0_{298} = -74.9\ kJ,$$

rather than by an electrochemical process.

An additional potential plateau, lying between the two known potential plateaus [reactions (1), (4)] was recorded in [11] when studying the anodic dissolution of an iron electrode at 35–55°C. An X-ray phase analysis of electrodes withdrawn from solutions after discharge at potentials of the additional plateau demonstrated that, in the electrodes, the amount of iron(II) hydroxide formed during the first anodic process decreases, and that of magnetite increases. Based on this fact, Novakovskii et al. [11] concluded that the conversion of $Fe(OH)_2$ into Fe_3O_4 is described by the reaction equation

$$3Fe(OH)_2 + 2OH^- \rightarrow Fe_3O_4 + 4H_2O + 2e, \quad (6)$$
$$E^0 = -1.022\ V.$$

Standard Gibbs energies of various substances and ions according to [12, 13]

Substance	ΔG^0_{298}, kJ mol^{-1}	Substance	ΔG^0_{298}, kJ mol^{-1}
Fe	0	δ-FeOOH	–465.0
Fe_3O_4	–1014.2	O_2	0
$Fe(OH)_2$	–483.7	H_2O	–237.2
$HFeO_2^-$	–379.1	OH^-	–157.3

In the case of anodic polarization of an iron electrode within the range of the first potential plateau at 55°C, a considerable amount of magnetite is formed together with the main discharge product, $Fe(OH)_2$. Novakovskii et al. [11] believe that there occurs direct electrochemical conversion of Fe into Fe_3O_4:

$$3Fe + 8OH^- \rightarrow Fe_3O_4 + 4H_2O + 8e, \quad (7)$$
$$E^0 = -0.913 \text{ V}.$$

At elevated temperatures, the surface of separators and battery vessels is covered with a black deposit of magnetite, which indicates that magnetite may be formed in solution. The formation of magnetite is hindered on passing from LiOH solutions to those of NaOH and KOH.

In view of the wide diversity of reactions that occur in discharge of the negative electrode of a nickel–iron battery and their different orders suggested by different authors, the standard Gibbs energies and standard potentials of the above-mentioned reactions were calculated and the order of processes occurring at the electrode was refined. The calculations were based on the published standard Gibbs energies of formation [12, 13] (see table).

The resulting values of the standard potentials suggest the following sequence of electrochemical reactions in discharge of the negative electrode. Reaction (1) occurs at a potential of –0.876 V; reaction (2) is possible at –0.748 V to give $HFeO_2^-$ ions hydrolyzed by reaction (3); reaction (4) occurs at –0.634 V; the reaction between iron hydrates in different oxidation states [reaction (5)] yields Fe_3O_4. It should be noted that the difference of the standard potentials of reactions (4) and (1), equal to 0.242 V, is in good agreement with the abrupt potential change (0.24 V) in the discharge curve measured on a smooth iron electrode in an aqueous solution of NaOH at a current density of 2.4×10^{-5} A cm^{-2} [4].

Because the standard potential of reaction (6) is –1.022 V and significantly differs from the experimental values obtained in [11], the additional potential plateau in discharge curves at elevated temperatures is possibly due to electrochemical reaction (3) whose potential lies between the potentials of reactions (1) and (4). Magnetite is possibly formed by the reactions

$$3HFeO_2^- + 1/2O_2 = Fe_3O_4 + 3OH^-, \quad (8)$$
$$\Delta G^0_{298} = -348.8 \text{ kJ},$$

$$3Fe(OH)_2 + 1/2O_2 = Fe_3O_4 + 3H_2O, \quad (9)$$
$$\Delta G^0_{298} = -275.0 \text{ kJ},$$

which involve oxygen dissolved in the electrolyte. Reaction (8) also proceeds in the electrolyte bulk, which results in that a black deposit of magnetite is formed on the surface of separators and battery vessels.

Reaction (7) has a more negative standard potential than reaction (1) and, presumably, does not occur in the discharge of the iron electrode. Because iron reacts with water in accordance with the equation

$$Fe + 2H_2O \rightarrow Fe(OH)_2 + H_2, \quad (10)$$
$$\Delta G^0_{298} = -9.3 \text{ kJ},$$

the discharge process and the subsequent charging occur across a film of iron hydroxide [reaction (1)].

The theoretical emf of the nickel–iron battery, calculated from the standard potentials of the reactions occurring at the positive [14] and negative electrodes, is 1.367 V. This value is in good agreement with the theoretical emf of 1.37 V, reported in the monograph [15].

REFERENCES

1. Foester, F., *Z. Elektrochem.*, 1907, vol. 13, no. 28, pp. 414–434.
2. Foester, F., *Z. Elektrochem.*, 1908, vol. 14, no. 21, pp. 285–292.
3. Foester, F., *Z. Elektrochem.*, 1910, vol. 16, no. 13, pp. 461–498.
4. Kabanov, B. and Leikis, D., *Zh. Fiz. Khim.*, 1946, vol. 20, no. 9, pp. 995–1003.
5. Kabanov, B. and Leikis, D., *Dokl. Akad. Nauk SSSR*, 1947, vol. 58, no. 8, pp. 1685–1688.
6. Stepina, T.G. and Iofa, Z.A., *Elektrokhimiya*, 1979, vol. 15, no. 1, pp. 151–154.

7. Stepina, T.G. and Iofa, Z.A., *Elektrokhimiya*, 1980, vol. 16, no. 6, pp. 888–891.
8. Stepina, T.G., Iofa, Z.A., Kasatkin, E.V., et al., *Elektrokhimiya*, 1980, vol. 16, no. 12, pp. 1884–1887.
9. Teplinskaya, T.K., Fedorova, N.N., and Rozentsveig, S.A., *Zh. Fiz. Khim.*, 1964, vol. 38, no. 9, pp. 2176–2180.
10. Teplinskaya, T.K., Shcherbakova, Z.V., and Rozentsveig, S.A., in *Sbornik rabot po khimicheskim istochnikam toka* (Coll. of Works on Chemical Power Cells), Leningrad: Energiya, 1966, pp. 5–11.
11. Novakovskii, A.M., Grushkina, S.A., Kozlova, G.M., and Kozlova, R.L., in *Sbornik rabot po khimicheskim istochnikam toka* (Coll. of Works on Chemical Power Cells), Leningrad: Energiya, 1976, issue 11, pp. 68–74.
12. Garrels, R.M. and Christ, Ch.L., *Solutions, Minerals, and Equilibria*, New York: Harper and Row, 1965.
13. Sukhotin, A.M., *Fizicheskaya khimiya passiviruyushchikh plenok na zheleze* (Physical Chemistry of Passivating Films on Iron), Leningrad: Khimiya, 1989.
14. Demidov, A.I., Kokhatskaya, M.S., and Chernovets, B.V., *Zh. Prikl. Khim.*, 2006, vol. 79, no. 3, pp. 506–507.
15. Bagotskii, V.S. and Skundin, A.M., *Khimicheskie istochniki toka* (Chemical Power Cells), Moscow: Energoizdat, 1981.

ISSN 1070-4272, Russian Journal of Applied Chemistry, 2006, Vol. 79, No. 4, pp. 680–682. © Pleiades Publishing, Inc., 2006.
Original Russian Text © V. R. Islamgulova, S. G. Akhmerova, V. G. Gil'mkhanova, A. P. Tomilov, 2006, published in Zhurnal Prikladnoi Khimii, 2006, Vol. 79, No. 4, pp. 688–690.

BRIEF COMMUNICATIONS

Electrochemical Methoxylation of Alkenyldichloroanisoles

V. R. Islamgulova, S. G. Akhmerova, V. G. Gil'mkhanova, and A. P. Tomilov

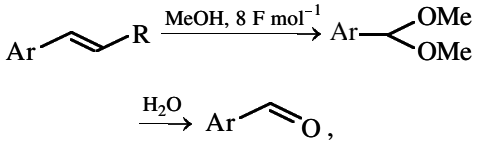
State Research Institute of Organic Chemistry and Technology, Moscow, Russia

Received December 8, 2005

Abstract—Electrochemical oxidation of chlorinated alkenylanisoles in anhydrous methanol was studied.

DOI: 10.1134/S1070427206040355

Electrochemical oxidation of alkenylarenes in methanol results in selective cleavage of the C=C bond of the alkenyl substituent and can be described in the general form by the equation [1]



where Ar = Ph, *o*-MeC_6H_4, *p*-$MeOC_6H_4$.

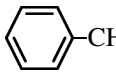
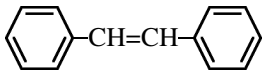
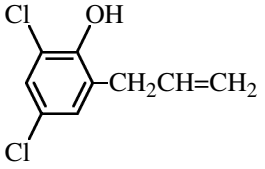
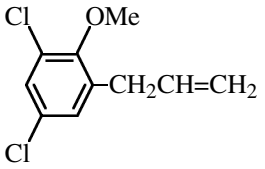
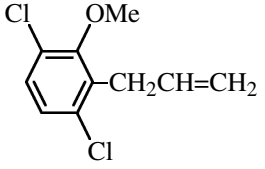
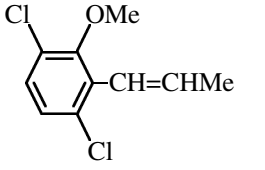
The cleavage of the C=C bond yields the corresponding acetals whose hydrolysis, in turn, yields aldehydes. Conditions ensuring high yield of acetals were reported [2–5].

To prepare acetals, it is advisable to use as supporting electrolyte either trifluoroacetic acid salts or *p*-toluenesulfonic acid [2] and to perform the process at as low concentration of the starting compound as possible (by adding it in small portions in the course of the electrolysis) to minimize formation of dimeric and polymeric by-products. This reaction is a simple route to aromatic aldehydes. Introduction of the methyl or methoxy group into the *p*-position does not noticeably affect the yields of the acetal and aldehyde.

We examined the possibility of using this reaction for preparing aromatic aldehydes containing Cl atoms in the benzene ring, in particular, 2,5-dichloro-6-methoxybenzaldehyde.

Since the yield of acetal can depend on the oxidation potential of the starting compound, we determined this quantity on a rotating platinum electrode for 2-allyl-4,6-dichloroanisole, 2-allyl-3,6-dichloroanisole, 2-(propen-1'-yl)-3,6-dichloroanisole, and 2-allyl-4,6-dichlorophenol. The results are listed in the table, together with the data for 1-methoxystyrene and (propen-1-yl)benzene given for comparison.

Oxidation half-wave potentials E_{ox} of alkenylarenes (anhydrous methanol, 0.5 M $LiClO_4$, Pt anode)

Compound	E_{ox}, V
	1.50
	1.15
	1.23
	2.05
	2.17
	2.26

The table shows that introduction of two Cl atoms shifts the oxidation potential of alkenylanisoles toward more positive values.

It is interesting that chlorinated alkenylphenol is oxidized considerably more readily, which is apparently due to the possible formation of a quinoid derivative (E_{ox} = 1.23 V) in the anodic region; this derivative is reduced to hydroquinone (E_{red} = –1.05 V) in the cathodic region. Oxidation of anisoles is irreversible, as indicated by the absence of cathodic peaks in the cyclic voltammogram at reverse potential scanning.

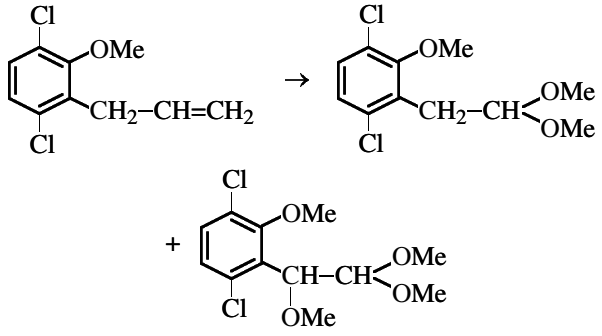
Preliminary experiments performed under the conditions favorable for the cleavage of the C=C bond (anhydrous methanol, *p*-toluenesulfonic acid supporting electrolyte [2, 3]) failed. Better results were obtained with NaF as supporting electrolyte. In this case, noticeable oxidation of methanol starts at an anode potential of +0.8 V, and hence the transformation of alkenyldichloroanisoles will occur by the mechanism of indirect electrochemical oxidation:

$$MeOH \xrightarrow[-e]{} MeO^{\cdot} + H^{+},$$

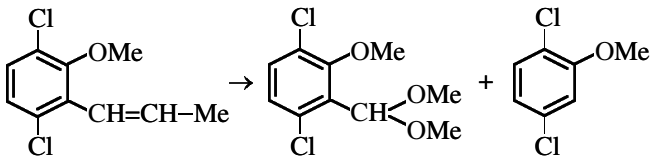
$$>C{=}C< + MeO^{\cdot} \rightarrow >\dot{C}-\underset{|}{C}-OMe,$$

$$>\dot{C}-\underset{|}{C}-OMe \xrightarrow{MeO^{\cdot}} \overset{MeO}{\underset{|}{-C}}-\underset{|}{C}-OMe \xrightarrow[-2e]{2MeOH} >C\begin{matrix}OMe\\OMe\end{matrix}$$

Preparative electrolyses showed that, at continuous supply of the substrate so as to maintain its minimal concentration in the solution, the methoxylation of 2-allyl-3,6-dichloroanisole occurs without formation of substituted benzaldehyde acetal, and two products are formed:



However, in the methoxylation of 2-(propen-1'-yl)-3,6-dichloroanisole under the same conditions, the C=C bond is cleaved, and 2,5-dichloro-6-methoxybenzaldehyde dimethyl acetal is formed in a yield of about 50% by the reaction



Trimethyl 2,5-dichloro-6-methoxyorthobenzoate was obtained as by-product in ~17% yield. We failed to increase the yield of the acetal by varying the electrolysis conditions.

EXPERIMENTAL

Voltammetric measurements were performed on a PI-50-1 potentiostat with a rotating platinum disk electrode. The supporting electrolyte was 0.5 M $LiClO_4$ in dry acetonitrile. The potential scanning rate was 50 mV s^{-1}, and the electrode rotation rate, 3000 rpm. The reference electrode was Ag/0.1 M $AgNO_3$.

The starting compounds were purified by vacuum distillation (2 mm Hg) before measurements.

Syntheses were performed in a diaphragmless cell equipped with a graphite anode (S = 26.6 cm^2), a platinum cathode, a thermometer, and a reflux condenser. The solution was stirred with a propeller stirrer.

The electrolyzer was charged with 30 ml of absolute methanol and 0.12 g of KF. The electrolysis was performed with a current of 2.65 A (current density 0.1 A cm^{-2}). Immediately after switching on the current, 10 mmol of a substrate [2-(propen-1'-yl)-3,6-dichloroanisole or 2-allyl-3,6-dichloroanisole] dissolved in 8 ml of methanol was added; its amount corresponded to 8 F of electricity per mole of the substrate. After the whole amount of the substrate was added, the electrolysis was continued for a certain period, so that the total amount of electricity was 10 F per mole of the substrate. The electrolysis was performed at 55–60°C.

After the electrolysis completion, methanol was removed on a rotary evaporator, the bottoms were extracted with benzene to separate the supporting electrolyte, and the extract was analyzed chromatographically.

CONCLUSIONS

(1) Introduction of chlorine atoms into alkenylanisole molecule appreciably shifts the oxidation potential toward positive values. An increase in the oxidation potential complicates cleavage of the C=C bond.

(2) In oxidation of 2-allyl-3,6-dichloroanisole, substituted benzaldehyde acetal is not formed, whereas from 2-(propen-1'-yl)-3,6-dichloroanisole 2,5-dichloro-6-methoxybenzaldehyde dimethyl acetal was obtained in a yield (based on the substrate) not exceeding 50%.

REFERENCES

1. Ogibin, Yu., Ilovaisky, A., and Nikishin, G., in *Novel Trends in Electroorganic Synthesis*, Tokyo: Springer, 1997, pp. 29–32.
2. Ogibin, Yu.N., Elinson, M.N., Sokolov, A.V., and Nikishin, G.I., *Izv. Akad. Nauk SSSR, Ser. Khim.*, 1990, no. 2, p. 424.
3. Ogibin, Yu.N., Sokolov, A.V., Ilovaiskii, A.I., et al., *Izv. Akad. Nauk SSSR, Ser. Khim.*, 1991, no. 3, pp. 644–649.
4. Ogibin, Yu.N., Ilovaiskii, A.I., and Nikishin, G.I., *Izv. Akad. Nauk SSSR, Ser. Khim.*, 1994, no. 9, pp. 1624–1627.
5. Ogibin, Yu., Ilovaisky, A., and Nikishin, G., *J. Org. Chem.*, 1996, pp. 3256–3258.

ISSN 1070-4272, Russian Journal of Applied Chemistry, 2006, Vol. 79, No. 4, pp. 683–684. © Pleiades Publishing, Inc., 2006.
Original Russian Text © B. F. Kukharev, V. K. Stankevich, V. A. Lopyrev, G. R. Klimenko, B. N. Gutsalyuk, V. A. Kukhareva, 2006, published in Zhurnal Prikladnoi Khimii, 2006, Vol. 79, No. 4, pp. 691–692.

BRIEF COMMUNICATIONS

1-Alkyl-1,1-Dimethylhydrazinium Chlorides as Modifiers of Oil Asphalts for Road Building Applications

B. F. Kukharev, V. K. Stankevich, V. A. Lopyrev, G. R. Klimenko, B. N. Gutsalyuk, and V. A. Kukhareva

Favorskii Irkutsk Institute of Chemistry, Siberian Division, Russian Academy of Sciences, Irkutsk, Russia

Received January 11, 2006

Abstract—Aklylation of 1,1-dimethylhydrazine with higher alkyl chlorides was studied. The resulting 1-alkyl-1,1-dimethylhydrazinium chlorides were tested as modifiers of oil asphalt for preparation of asphalt concrete.

DOI: 10.1134/S1070427206040367

Nitrogen-containing cationic additives such as Katamin, Katapin, BP-3 are widely applied in road building for oil asphalt modification. Alkyl ammonium (especially quaternary) salt additives increase adhesion of oil asphalt to mineral components of asphalt concrete mixtures, thus improving the performance characteristics of pavements [1, 2].

One of the simplest ways to solve the problem of utilization of highly toxic propellant component, 1,1-dimethylhydrazine, which arose at the end of XX century, is its quarternization with alkyl halides into quaternary salts to find further technical application [3–5].

In this study, we treated a mixture of technical-grade fatty primary alcohols C_{10}–C_{16} with thionyl chloride to obtain a mixture of the corresponding chloroalkanes to be used for quarternization of 1,1-dimethylhydrazine. The yield of quaternary hydrazinium salts (1-alkyl-1,1-dimethylhydrazinium chlorides) was 97%:

$$2R\text{–}OH + SOCl_2 \rightarrow 2R\text{–}Cl + H_2O + SO_2,$$

$$NH_2NMe_2 + R\text{–}Cl \rightarrow [NH_2NMe_2R]^+Cl^-,$$

where R = Alk(C_{10}–C_{16}).

As known, 1-alkyl-1,1-dimethylhydrazinium chlorides (alkyl C_{10}–C_{16}), when administered perorally, are moderately toxic hazard class III substances; when contacting skin, they exhibit no toxicity and, according to their skin-resorptive effect, are classed with hazard class IV substances [5, 6]. Thus, 1-alkyl-1,1-dimethylhydrazinium chlorides belong to the same toxicity classes as quaternary ammonium salts used for asphalt modification.

This fact, along with a high thermal stability, which allows 1-alkyl-1,1-dimethylhydrazinium chlorides to be introduced into molten asphalt, as well as close structures of ammonium and hydrazinium salts, suggest the possibility of using 1-alkyl-1,1-dimethylhydrazinium chlorides for modifying oil asphalt used for preparation of asphalt concrete.

We studied the properties of asphalt concrete mixtures as influenced by the amount of the quaternary hydrazinium salts introduced into asphalt and estimated the optimal amounts at 1.7–2.5% of the asphalt weight (0.1–0.15% of asphalt concrete weight). In this case, the compression strength of the asphalt concrete mixtures prepared from crushed carbonate rock, natural sand, and 6% of modified asphalt is 1.5–2 times that of mixtures prepared with unmodified asphalt. The water resistance coefficient of the asphalt concrete prepared from modified asphalt increases by 0.06–0.07 units relative to the asphalt concrete prepared from unmodified asphalt. The hydrazinium salts that we synthesized surpass in the modifying properties the analogous ammonium salts (see table).

EXPERIMENTAL

1,1-Dimethyl-1-alkyl(C_{10}–C_{16})hydrazinium chloride. The raw materials were technical-grade C_{10}–C_{16}

Properties of asphalt concrete prepared from asphalts of various modifications

Characteristic	GOST (State Standard) 9128–97 requirements	Percentage of modifier in asphalt concrete mixture					
		alkyldimethylhydrazinium chloride					alkylaryltrimethylammonium chloride, 0.1 [1]
		0	0.06	0.10	0.15	0.20	
Compression strength, MPa:							
at +20°C, no less than	2.2	2.5	3.1	3.4	4.25	4.08	2.6
at +50°C, no less than	0.9	1.06	1.27	1.43	1.00	1.95	–
Water resistance coefficient	No less than 0.9	0.91	0.96	0.96	0.97	0.97	0.95

primary fatty alcohols. These alcohols were treated with thionyl chloride [7] to obtain a mixture of the corresponding chloroalkanes in 95% yield. For the product synthesized, found, %: C 71.65, H 12.25, and Cl 16.10.

A flask equipped with a reflux condenser and a stirrer was charged with 45 g of C_{10}–C_{16} chloroalkanes with the chlorine content of 16.1% and 12 g (0.2 mol) of 1,1-dimethylhydrazine. The resulting mixture was refluxed for 8 h (the boiling point of the reaction mixture during the synthesis slowly increased from 67 to 84°C). After cooling, the reaction mixture crystallized; 50 ml of *p*-xylene was added, and the mixture was stirred and filtered. The residue on the filter was washed with two 20-ml portions of xylene, squeezed, and vacuum-dried at 50°C and a pressure of 10 mm Hg to constant weight. Yield of 1,1-dimethyl-1-alkylhydrazinium chloride 55.4 g (97%). Melting point of the product 62–70°C. Found, %: C 65.61, H 11.75, N 9.68, and Cl 12.96.

Asphalt concrete was prepared, and its physical properties were determined, by the techniques from [8]. Into 990 g of BND 90/130 oil asphalt heated to melting, 10 g of alkyldimethylhydrazinium chloride was introduced with stirring, which yielded 1000 g of modified asphalt containing 1% alkyldimethylhydrazinium chloride. This asphalt (600 g), 4000 g of crushed carbonate rock (5–20 mm fraction), and 5400 g of natural sand (0.071–5 mm fractions) yielded 10 kg of asphalt concrete mixture containing 0.06% alkyldimethylhydrazinium chloride, 5.94% asphalt, and 94% mineral filler. Asphalt concretes containing 0.1, 0.15, and 0.2% alkyldimethylhydrazinium chloride were obtained similarly.

CONCLUSIONS

(1) Asphalt concrete was prepared from oil asphalt modified with a mixture of alkyldimethylhydrazinium chlorides (0.1–0.15 wt% relative to asphalt concrete) synthesized from 1,1-dimethylhydrazine. Its compression strength is 1.5–2 times that of asphalt concrete obtained from unmodified asphalt, and the water resistance coefficient is by 0.06–0.07 units higher.

(2) The hydrazinium salts synthesized surpass in the modifying properties the analogous ammonium salts.

REFERENCES

1. USSR Inventor's Certificate no. 876817.
2. Portnyagin, V.D., *Kontrol' kachestva organicheskikh vyazhushchikh* (Quality Control of Organic Binders), Moscow: Minavtodor RSFSR, 1984.
3. Grib, A., *Voenno-Ekon. Zh.*, 1994, no. 4, pp. 20–22.
4. Lopyrev, V.A., Dolgushin, G.V., and Voronkov, M.G., *Zh. Prikl. Khim.*, 1998, vol. 71, no. 8, pp. 1233–1248.
5. Lopyrev, V.A., Dolgushin, G.V., and Laskin, B.M., *Ross. Khim. Zh.*, 2001, vol. 45, nos. 5–6, pp. 149–156.
6. Aleksandrova, G.A., Prokhorova, T.S., Lesnov, A.E., et al., *Khim.-Farm. Zh.*, 1995, vol. 29, no. 11, pp. 22–24.
7. Weigand–Hilgetag, *Organisch-Chemische Experimentierkunst*, Leipzig: Johann Ambrosius Barth, 1964, 3rd ed.
8. Grushko, I.M., Zolotarev, V.A., Glushchenko, N.F., et al., *Ispytanie dorozhno-stroitel'nykh materialov* (Testing Road-Building Materials), Moscow: Transport, 1985.

ISSN 1070-4272, Russian Journal of Applied Chemistry, 2006, Vol. 79, No. 4, p. 685. © Pleiades Publishing, Inc., 2006.
Original Russian Text © G. E. Zaikov, N. N. Madyuskin, 2006, published in Zhurnal Prikladnoi Khimii, 2006, Vol. 79, No. 4, pp. 693–694.

INFORMATION

RePlast International Conference

DOI: 10.1134/S1070427206040379

The Third RePlast Conference was held within the scope of the Interplastika-2005 Exhibition on December 14–15, 2005 at the Moscow Business Center. The main objective of the Conference was polymer recycling. The Conference was organized by the *Plastics: Plastics Processing Industry* journal and Messe Düsseldorf–Moscow Ltd.

The Conference participants were more than 100 researchers, technologists, and businessmen from 60 organizations of seven countries (Austria, Belarus Republic, Germany, Italy, Russia, Slovakia, and Ukraine).

The Conference Program included five plenary sessions. In the Opening Session there was outlined the topicality of the problem of plastics recycling. It was demonstrated that, counted in the volume units, the worldwide production of polymers exceeds that of steel, cast iron, rolled metal, and nonferrous metals combined, being about 400 millions cubic meters, i.e., the mankind lived, first, in the Stone Age, then in the Bronze and Iron Ages, and now it is living in the Polymer Age. It was important also to outline the dynamics of polymer production: the worldwide production of polymers outdistances that of metals by 15–29% annually. But the more polymers, the more wastes, which makes the problem of recycling very topical.

Session 1 included two lectures. R. Binder (Austria) reported on recent developments in recycling of polyethylene terephthalate (PET), and Ch. Fellner (Austria), on the problems of single-step reprocessing of various plastics.

Session 2 included five presentations. Advances in recovery of metallic inclusions from raw material to eliminate sudden interrupts and breakage of facilities in production of plastic goods were overviewed by A.A. Sandulyak (Russia). The problems of magnetic separation in recycling of plastics were analyzed by O.A. Dolgopolov (Russia).

The great interest has been expressed by the participants in the lecture presented by E. Condini and J. Martini (Italy) and devoted to modern processes of recycling of PET bottles, developed at the Amut Company. The last two lectures of this Session were devoted to production of binders from polystyrene foam wastes and their application in the foundry [O.I. Shinskii (Ukraine)] and also to manufacture of face slabs from polystyrene foam [A. Werner and E. Adler (Germany)].

Session 3 included four presentations. V.V. Devyatkin (Russia) reported on the major drawbacks of the legal control in management of wastes as secondary raw materials. He demonstrated the need in improvement of legislation in this area. Yu.M. Demidov (Russia) reported on novel extrusion facilities developed at the Ekokhimmash for polymer reprocessing. Scientific principles of polymer recycling were considered by G.E. Zaikov (Russia). Finally, the presentation entitled Recycling as a Special Column in the Plastics Catalogue-2006 was made by D.V. Ishchenko (Russia).

Session 4 included four presentations. I.A. Kirsh (Russia) considered new prospects for the technology of reprocessing of polymeric composites, developed at the Moscow State University of Applied Biotechnology.

The use of recycled PET in contact with foodstuffs was the topic of the lecture presented by P. Niedl (Austria). F. Matel and R. Jchocova (Slovak Republic) reported on industrial applications of sound insulating materials based on tire reprocessing products. The last lecture of this Session was devoted to the progress in crushing of polymer wastes on crushers from BSZ Atlant Private Company [Yu.P. Belyaev (Belarus Republic)].

Session 5 also included four presentation. S.S. Khachatryan (Russia) considered commercial application of wood–polymer composites, and P. Pecchiardi and Kralij (Italy) reported on new recycling processes.

The last two contributions were devoted to reprocessing of recycled PET without predrying and crystallization in twin-screw extruders [M. Berndt (Germany)] and to presentation of the Solid Domestic Wastes Bulletin [S.S. Emel'yanova (Russia)]. The discussions performed at the Conference showed that the problems of polymer recycling are very topical, being yet far from final solution.

G. E. Zaikov and N. N. Madyuskin

ISSN 1070-4272, Russian Journal of Applied Chemistry, 2006, Vol. 79, No. 4, pp. 686–691. © Pleiades Publishing, Inc., 2006.
Original Russian Text © A. G. Morachevskii, 2006, published in Zhurnal Prikladnoi Khimii, 2006, Vol. 79, No. 4, pp. 695–699.

Academician Dmitrii Petrovich Konovalov (To 150th Anniversary of His Birthday)

DOI: 10.1134/S1070427206040380

D.P. Konovalov, one of prominent Russian physical chemists of the late XIX and early XX centuries, made an outstanding contribution to the development of the theory of solutions, delivered lectures at a number of higher-school institutions in St. Petersburg, created the known school of physical chemistry, occupied a number of high administrative positions, and was elected president of the Russian Physicochemical Society (in 1923–1924 and 1927).

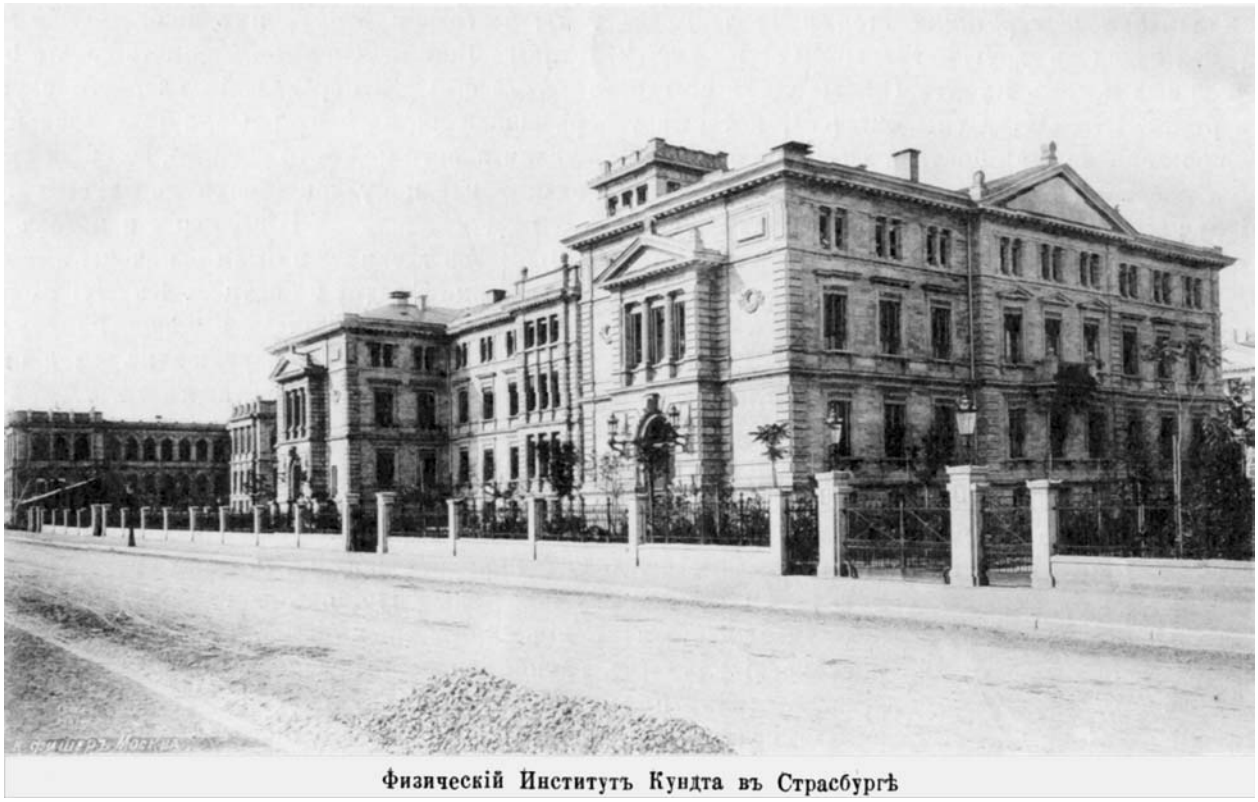
Dmitrii Petrovich Konovalov was born on March 10 (22), 1856, in Verkhedneprovsk uezd of Yekaterinoslav province (now Dnepropetrovsk oblast, Ukraine) into a wealthy nobleman's family. Having received primary education at home, he entered Yekaterinoslav classical gymnasium in 1866 and finished it with a gold medal in 1873. Konovalov expressed particular interest in physicomathematical and natural sciences. Immediately after finishing the gymnasium, he entered the metallurgical department of the Mining Institute in St. Petersburg. Founded by Empress Catherine II in 1773, this higher-school institution, one of the oldest in Russia, had an excellent pedagogical staff and was very popular with youths. Chemistry was taught by K.I. Lisenko, a prominent specialist in technical chemistry, lecturers of chemical-metallurgical disciplines included K.D. Sushin, V.V. Bek, and N.A. Iossa.

In 1878, Konovalov successfully finished the Mining Institute. He received the title of a first-class mining engineer and his name was put up on the marble board of honor in the conference hall of the Institute. However, Konovalov considered his knowledge in the field of chemistry and, in particular, organic chemistry insufficient and joined as an external student the physicomathematical faculty of St. Petersburg University, to spend there nearly two academic years. Konovalov performed his first experimental studies under supervision of A.M. Butlerov (1828–1886) in his laboratory. In addition, the young scientist had an opportunity to attend lectures on mineral technology by Butlerov, analytical and organic chemistry by N.A. Menshutkin, higher mathematics by P.L. Chebyshev and K.A. Posse, and physiology by I.M. Sechenov. In the autumn of 1879, D.I. Mendeleev (1834–1907) returned from a long-term business trip and



Konovalov had an opportunity to make acquaintance with him and attend his lectures.

In the beginning of 1879, Konovalov became a member of the Russian Physicochemical Society on Butlerov's recommendation. In 1880, the first Konovalov's scientific study was published in a number of periodic editions. The study, performed under Butlerov's supervision, was concerned with the action of sulfuric acid of isobutyl alcohol and that of nitric acid on butylenes derivatives. Konovalov was on very friendly terms with Butlerov and received an excellent experimental training in his laboratory. However, Konovalov's expectations of his future scientific activities were associated with physicochemical problems. To receive further education and obtain a scientific degree, Konovalov decided to go, at his own expense, to one of major research centers in France or Germany. On Mendeleev's advice, he chose the laboratory of a young German physicist, professor A. Kundt (1839–1894) at Strasbourg University (Germany) [1]. During his business trip abroad, Mendeleev made acquaintance with Kundt, who produced a very good impression on him. In May 1880, Konovalov came to Stras-



Kundt's Institute of Physics in Strasbourg.

bourg with a recommendation letter from Butlerov and was cordially welcomed there. After passing the physical practicum and accomplishing a minor task on Kundt's instructions, Konovalov obtained a working place and commenced studies of the saturated vapor pressure over liquid mixtures. During the preparatory period, Konovalov spent a certain time at the laboratory of physical chemistry, headed by professor R. Fittig (1835–1910). However, he soon realized that the scientific level of Butlerov's laboratory is higher in all respects and concentrated his whole attention on Kundt's laboratory. Already in August and October 1881, the German journal *Wiedemanns Annalen* published the results of Konovalov's studies of the vapor pressure. The material of the first of his publications was submitted as dissertation. After passing the required examination, Konovalov successfully defended in July 1881 the dissertation *Über die Dampfspannung der Flüssigkeitsgemische* (On Vapor Pressure of Liquid Mixtures) and received his Ph.D. and the degree of a master of natural science from Strasbourg University [2]. During his stay abroad, Konovalov visited scientific and industrial centers in France and Switzerland. In Paris, he made acquaintance with H. Le Chatelier (1850–1936), M. Berthelot (1827–1907), and other prominent French scientists. Konovalov particularly highly appreciated studies performed by H. Sainte-Claire Deville (1818–1881) and his classical works in the field of thermal dissociation of compounds. Konovalov also expressed a considerable interest in various chemical plants in Western Europe.

In the end of July 1881, Konovalov returned to Russia and, after summer vacations, continued studies of solutions at Butlerov's laboratory. However, a vacancy soon appeared and Konovalov was elected a laboratory assistant to the laboratory of analytical chemistry at St. Petersburg University, headed by professor N.A. Menshutkin (1842–1907). Laboratory assistant's duties included preparation of practical works for students, help in setting of demonstration experiments for lectures, and pedagogical work in laboratory practicum. Despite the wide range of duties, Konovalov passed master's examinations in 1882, with Mendeleev and Butlerov as the examiners in chemistry, and continued work on dissertation. He submitted in an extended form as master's dissertation the study "On Vapor Pressure of Solutions." The dissertation was successfully defended on March 11, 1884, with Mendeleev and Menshutkin as opponents. In conformity with the regulations of that time, the full text of

the dissertation was published beforehand [3]. Later, this study was twice republished in 1909 and 1928.

Having received his master's degree, Konovalov started to deliver as a privatdocent a facultative course of lectures in physical chemistry for third- and fourth-year students. Simultaneously, Menshutkin suggested to Konovalov to commence studies in chemical kinetics. The first results obtained in this field were published by Konovalov and Menshutkin already in May 1884. They observed catalytic effects in decomposition of ether vapor and Konovalov soon started to study them on his own. In 1885, he published in *Zhurnal Russkogo Fiziko-Khimicheskogo Obshchestva* (Journal of the Russian Physicochemical Society) and also as a separate edition [4] his study "Role of Contact Actions in Dissociation Phenomena," submitted as a doctoral (Chem. Sci.) dissertation. The dissertation was defended on November 4, 1885. In April 1886, at the age of only thirty, Konovalov was appointed extraordinary professor at the chair of analytical and technical chemistry of St. Petersburg University. When recommending Konovalov for this position, Menshutkin mentioned the "excellently passed master's examination and talent in formulation of independent tasks and setting his own work and experiments" [5]. In 1890, after Mendeleev left the University, Konovalov headed the chair of inorganic chemistry, with organic chemistry still taught by Menshutkin and lecturing in technical and analytical chemistry taken up by A.E. Favorskii (1860–1945, academician of the Academy of Sciences of the USSR since 1929) and V.E. Tishchenko (1861–1941, academician since 1935). Konovalov was the closest, among any of the known Russian chemists, to Mendeleev as a scientist, practical figure, and man. Mendeleev highly appreciated Konovalov's works; the relationship between the scientists was maintained after Mendeleev left the University.

One of the closest Konovalov's disciples, A.A. Baikov (1870–1946, academician of the Academy of Sciences of the USSR since 1932), wrote in his memoirs: "From the very first steps of his activities as a professor, Konovalov became an outstanding and brilliant lecturer. His lectures were distinguished by unusual simplicity, clarity, and logicality of presentation. This was the time of a rapid and vigorous development of physical chemistry, which made novel and significant changes in the basic chemical problems. Konovalov, closely involved in the activities of this scientific movement, delivered lectures in inorganic and general chemistry for first-year students of the physicomathematical faculty. In his presentation, this main subject of natural science acquired a fundamentally new character and produced a deep and indelible impression on listeners... The laws of a labile chemical equilibrium, theory of solutions, relationship between chemical and electrical phenomena and chemical dynamics were presented in the course of chemistry and enabled widest generalizations linking into a harmonious whole numerous, previously absolutely uncoordinated factors. The outstanding service of Konovalov as a professor consists in that he was the first to take this way and significantly changed the manner of presentation and teaching of inorganic and general chemistry" [6].

In 1893, Konovalov and Tishchenko were sent to a business trip to the United States to Chicago, to visit the World Exhibition timed with the 400th anniversary of the discovery of America. During six months, the scientists familiarized themselves not only with exhibits (Konovalov was one of supervisors of the group of experts of the largest department), but also visited a large number of industrial plants. As a result of this trip, a book *Promyshlennost' Soedinennykh Shtatov Severnoi Ameriki i sovremenye priemy khimicheskoi tekhnologii* (The Industry of the United States of North America and Modern Methods of Chemical Technology) (St. Petersburg, 1894) was published by Konovalov.

Soon after returning from the United States, Konovalov was appointed an ordinary professor of St. Petersburg University. In 1890–1894, the scientist paid a considerable attention to the construction of a new building for chemical laboratories of the University. The opening ceremony of the building was held on October 16, 1894. In 1895–1896, Konovalov was among those who organized and held the All-Russia Industrial and Art Exhibition in Nizhni Novgorod. Later, he became a member of the Organizing Committee of the Russian section at the World Exhibition in Paris. Here, it should be kept in mind that Konovalov taught in those years not only at St. Petersburg University, but also at the Institute for Railway Engineers and at the Mining Institute (beginning in 1900). He also continued his intensive scientific activities. N.P. Vrevskaya, the widow of the closest Konovalov's disciple M.S. Vrevskii (1871–1929, corresponding member of the Academy of Sciences of the USSR since 1929), wrote in her memoirs devoted to her husband and his colleagues: "The brilliant, talented, and full of creative force Dmitrii Petrovich Konovalov was then at the summit of his fame" [7].

This, in all respects fruitful period of Konovalov's life terminated in the end of 1903, when the scientist, remaining a professor at the University, became director of the Mining Institute. As noted in the mono-

graph [5], at the turn of the XX century, the Mining Institute was distinguished among the rest of the higher-school institutions by the comparatively free mode of students' life and existence of independent student organizations. The period of time from 1904 till 1906 was difficult for Russia in political regard. Having come in conflict with the student organizations of the Mining Institute, the new director took a position of principle, did not make a compromise, and resigned already on June 27, 1905. In continuation of the conflict, in the autumn of 1906, the honored professor, doctor of chemistry, and senior state councillor, Konovalov, also terminated teaching at St. Petersburg University. In the summer of 1907, the scientist fully devoted himself to administrative activities, he was appointed director of the Mining department of the Ministry of Trade and Industry, and in May 1908, was elevated to become deputy minister of trade and industry. He occupied this position during nearly eight years, till the end of 1916.

Only in March 1916, Konovalov returned to pedagogical activities: he was elected professor of Petrograd Technological Institute and was engaged in 1916/17 and 1917/18 academic years in the development of a new course of chemical technology. After nearly ten years' break, Konovalov also resumed his scientific activities. For the summer of 1918, Konovalov went with his family to his homeland, Yekaterinoslav province. Because of the civil war and famine in Petrograd, his stay at homeland was prolonged, and he could return to Petrograd only in the spring of 1922. In those years, Konovalov taught at higher-school institutions of Yekaterinoslav, University and Mining Institute, and was actively involved in the organization of the State chemical laboratory, which was later transformed into the Research Institute of Chemistry and Power Engineering.

Meanwhile, the life in the country gradually returned to the normal course. In December 1921, Konovalov was elected a corresponding member of the Russian Academy of Sciences on recommendation of prominent Russian scientists, academicians V.N. Ipat'ev (1867–1952), N.S. Kurnakov (1860–1941), P.P. Lazarev (1878–1942), and A.E. Fersman (1883–1945). At that same time, he received an offer to become president of the Principal Board of Weights and Measures in Petrograd. After he have his preliminary consent, Konovalov was elected to this position on February 25, 1922 and started to execute his duties in March of the same year. Simultaneously, he became head of the chair of mineral technology at the Technological Institute. On January 13, 1923, Konovalov was elected a full member of the Russian Academy of Sciences.

After returning to Petrograd, Konovalov continued research in the field of thermochemistry of organic compounds, wrote the textbook *Materialy i protsessy khimicheskoi tekhnologii* (Materials and Processes of Chemical Technology) (Petrograd; part 1, 1924; part 2, 1925), and supervised preparation of a posthumous publication of *Osnovy khimii* (Fundamentals of Chemistry) by Mendeleev. At the IV Mendeleev Congress, which was held in September 1925, Konovalov was chairman and presented a report "About Russia's Chemical Industry." On December 9, 1928, the Academy of Sciences celebrated the 50 years of Konovalov's scientific activities.

The central place in Konovalov's scientific legacy is occupied by his studies of solutions. Konovalov was one of the most convinced followers of Mendeleev's concept of the nature of solutions, based on the interaction between a solute with a solvent. A detailed analysis of Konovalov's works in the field of solutions can be found in monographs by Yu.I. Solov'ev [9–11] and A.Ya. Kipnis [12], as well as in quite a number of other publications [13–20]. In particular, B.P. Nikol'skii noted that Konovalov was one of the first scientists who understood the importance of the thermodynamic method in studies of solutions. Among Russian scientists who developed this approach later were G. Tamman (1861–1938) at Derpt (Yur'ev, now Tartu, Estonia) University, I.F. Shreder (1858–1918) at the Mining Institute in St. Petersburg, and, especially, Vrevskii at St. Petersburg University.

Konovalov's study "On Vapor Pressure of Solutions" was analyzed in close detail by A.V. Storonkin [18]. He believes that the principal result of this study is the establishment of general thermodynamic concepts, now named Konovalov's laws. The discovery of these laws is the most important result of the whole scientific activities of Konovalov. The basic works of Gibbs in thermodynamics of heterogeneous systems, published in 1875–1878, were not known to anybody as yet. Konovalov's laws, combined with the laws discovered by his disciple, Vrevskii [7], constitute the general thermodynamic theory of solutions. The thermodynamic concepts established by Konovalov are also valid for heterogeneous systems of other types. Therefore, Konovalov can be regarded, with good reason, as one of the founders of the thermodynamic theory of phase equilibria. When assessing the scientific importance of the classical Konovalov's study "On Vapor Pressure of Solutions," Storonkin concludes: "In this study, Konovalov laid foundation of the general thermodynamic theory of solutions and heterogeneous systems, theoretically substantiated one of the most important methods of substance separation, distilla-

tion, and made an outstanding theoretical and experimental contribution to the chemical theory of solutions" [18]. The importance of Konovalov's laws for modern science and chemical technology was considered in [17–19].

In addition to the materials of his master's dissertation "On Vapor Pressure of Solutions," Konovalov published several series of studies in other areas of physical chemistry. They are devoted to osmotic pressure of solutions, solubility issues, critical phenomena of phase separation of, electrical conductivity of solutions, catalysis, and thermochemistry. With the exception of measurements of the calorific power of carbon-containing compounds, all the studies were carried out during the period from 1885 till 1907. As noted by Nikol'skii [17], Konovalov was the first to give, as far back as 1890, a thermodynamic description of the osmotic pressure, which virtually coincides with the modern approaches. Konovalov's studies in electrochemistry of nonaqueous solutions were performed in 1891–1893. The scientist examined the electrical conductivity of binary systems composed of aromatic amines and aliphatic acids. In these systems, the maximum electrical conductivity corresponds to compositions with a certain stoichiometric ratio of components, whereas pure components show virtually no conductivity. Thus, Konovalov was the first to discover a class of electrolytes that were later named "solvoelectrolytes." The existence of electrolytes of this kind confirms the opinion of supporters of the "chemical" or "hydrate" theory of solutions, being an example of interaction between the solvent and the solute [5, 20]. Konovalov's works in the field of physicochemical foundations of the theory of catalysis were analyzed in detail by S.Z. Roginskii [21]. Konovalov, in particular, demonstrated that the catalytic action of a solid is determined not only by its nature, but also by the state of its surface. Taking into account the state and nature of the surface is a distinctive feature of modern theories of heterogeneous catalysis.

The high appraisal of Konovalov's scientific activities was made by the Russian Physicochemical Society in 1914, which awarded him a major Mendeleev Prize for "the whole set of his outstanding studies in the field of solutions and scientific-pedagogical activities which gave rise to the original school of Russian physical chemists [22, 23]. In addition to the already mentioned Baikov and Vrevskii, the best-known representatives of Konovalov's school include professors E.V. Biron (1874–1919), I.I. Zhukov (1880–1949, corresponding member of the Academy of Sciences of the USSR since 1946), V.Ya. Kurbatov (1878–1957), and N.N. Tuturin (1866–1912). Among those who worked under Konovalov's supervision in Yekaterinoslav were A.I. Brodskii (1895–1969, corresponding member of the Academy of Sciences of the USSR since 1943) and S.Z. Roginskii (1900–1970, corresponding member of the Academy of Sciences of the USSR since 1939).

Konovalov's contribution to the development of physical chemistry was also highly appraised by the world community: he was elected honorary member of the London Chemical Society (in 1914), honorary member of the Swiss Society of Natural Science, corresponding member of the Göttingen Scientific Society (1923), honorary member of the French Chemical Society (1926), and member of the International Committee of Weights and Measures (1926).

To Konovalov's life have been devoted monograph by Solov'ev and Kipnis [5], articles by Baikov [6], Storonkin [18], V.V. Mikhailov [23], and other materials [14, 24–27].

Dmitrii Petrovich Konovalov died of pneumonia on January 6, 1929, at the age of 72. At a meeting of the Department of Applied Chemistry of the Russian Physicochemical Society, devoted to Konovalov's memory, Tishchenko voiced the opinion of Russian chemists: "In Dmitrii Petrovich's person, we lost an exceedingly gifted man with astute mind, high spirit, strong will, and strength of the sense of duty and love for work" [5]. The main thing in Konovalov's live was work, he had worked much and hard during his whole life till his very last days.

REFERENCES

1. Konovalov, D.P., *A.M. Butlerov, 1828–1928*, Leningrad: Akad. Nauk SSSR, 1929, pp. 55–72.
2. *Biograficheskii slovar' professorov i prepodavatelei Sankt-Peterburgskogo universiteta* (Biographic Dictionary of Professors and Teachers of St. Petersburg University), St. Petersburg, 1896, vol. 1, pp. 340–341.
3. Konovalov, D.P., *Ob uprugosti para rastvorov* (On Vapor Pressure of Solutions), St. Petersburg, 1884.
4. Konovalov, D.P., *Rol' kontaktnykh deistvii v yavleniyakh dissotsiatsii* (Role of Contact Actions in Dissociation Phenomena), St. Petersburg, 1885.
5. Solov'ev, Yu.I. and Kipnis, A.Ya., *Dmitrii Petrovich Konovalov, 1856–1929*, Moscow: Nauka, 1964.
6. Baikov, A.A., *Sobranie trudov*, (Coll. of Works), vol. 1: *Stat'i, vystupleniya, rechi* (Articles, Reports, and Speeches), Moscow: Akad. Nauk SSSR, 1952.
7. Vrevskii, M.S., *Raboty po teorii rastvorov* (Works on

on Theory of Solutions), with Biographic Essay by Vrevskaya, N.P., Moscow: Akad. Nauk SSSR, 1958.

8. Atroshchenko, V.I., Berezhnoi, A.S., Boyarskaya, L.A., et al., *Razvitie neorganicheskoi khimii na Ukraine* (Development of Inorganic Chemistry in the Ukraine), Gorodyskii, A.V. Ed., Kiev: Naukova Dumka, 1987.
9. Solov'ev, Yu.I., *Istoriya ucheniya o rastvorakh* (History of the Theory of Solutions), Moscow: Akad. Nauk SSSR, 1959.
10. Solov'ev, Yu.I., *Ocherki po istorii fizicheskoi khimii* (Essays on the History of Physical Chemistry), Moscow: Nauka, 1964.
11. Solov'ev, Yu.I., *Istoriya khimii v Rossii* (History of Chemistry in Russia), Moscow: Nauka, 1985.
12. Kipnis, A.Ya., *Razvitie khimicheskoi termodinamiki v Rossii* (Development of Chemical Thermodynamics in Russia), Moscow: Nauka, 1964.
13. Usanovich, M.I., *Materialy po istorii otechestvennoi khimii* (Materials on the History of Domestic Chemistry), Moscow: Akad. Nauk SSSR, 1950, pp. 63–66.
14. Usanovich, M.I., *Iz istorii khimii. Ocherki iz zhizni i deyatel'nosti vydayushchikhsya uchenykh* (Excerpts from the History of Chemistry, Essays about Life and Activities of Outstanding Scientists), Almaty: Kaz. Nats. Univ., 2004.
15. Nikol'skii, B.P., *Vestn. Leningr. Gos. Univ.*, 1946, no. 1, pp. 67–80.
16. Nikol'skii, B.P., *Vestn. Leningr. Gos. Univ.*, 1960, no. 22, issue 4, pp. 11–25.
17. Nikol'skii, B.P., *Zh. Obshch. Khim.*, 1982, vol. 52, no. 10, pp. 2382–2392.
18. Storonkin, A.V., *Vestn. Leningr. Gos. Univ.*, 1954, vol. 20, no. 5, pp. 167–176.
19. Stabnikov, V.N. and Fertman, G.I., *Usp. Khim.*, 1951, vol. 20, no. 6, pp. 776–783.
20. Pospekhov, L.A., *Zh. Obshch. Khim.*, 1952, vol. 22, no. 1, pp. 48–51.
21. Roginskii, S.Z., *Materialy po istorii otechestvennoi khimii* (Materials on the History of Domestic Chemistry), Moscow: Akad. Nauk SSSR, 1950, pp. 37–51.
22. Makarenya, A.A. and Solov'ev, Yu.I., *Vestn. Leningr. Gos. Univ.*, 1960, no. 22, issue 4, pp. 82–88.
23. Mikhailov, V.V., *Usp. Khim.*, 1954, vol. 23, no. 4, pp. 510–523.
24. Balezin, S.A. and Beskov, S.L., *Vydayushchiesya russkie uchenye-khimiki* (Outstanding Russian Chemists), Moscow: Prosveshchenie, 1972.
25. Musabekov, Yu.S. and Chernyak, A.Ya., *Vydayushchiesya khimiki mira. Bibliograficheskii ukazatel'* (Outstanding Chemists of the World: Bibliographic Index), Moscow: Kniga, 1971.
26. Pozin, M.E. and Kopylev, B.A., *Zh. Prikl. Khim.*, 1954, vol. 27, no. 4, pp. 353–355.
27. Soloviev, Y.I., *Dictionary of Scientific Biography*, Gillispie, Ch.C., Ed., New York: Charles Scribner's Sons, 1981, vol. 7, pp. 461–462.

A. G. Morachevskii

ISSN 1070-4272, Russian Journal of Applied Chemistry, 2006, Vol. 79, No. 4, pp. 692–693. © Pleiades Publishing, Inc., 2006.
Original Russian Text © A. G. Morachevskii, 2006, published in Zhurnal Prikladnoi Khimii, 2006, Vol. 79, No. 4, pp. 701–702.

BOOK REVIEWS

Martem'yanova, Z.S. and Esina, N.O., *Struktura elektroliticheskikh pokrytii. Atlas* (Structure of Electrodeposited Coatings: Atlas)

Yekaterinburg: Ural'sk. Otd. Ross. Akad. Nauk, 2005, 192 pp.

DOI: 10.1134/S1070427206040392

About forty years ago, systematic studies of the fundamental aspects of electrocrystallization of a number of refractory metals, as well as germanium and silicon, from molten electrolytes of various compositions were commenced at the Institute of High-Temperature Electrochemistry, Ural Division, Russian Academy of Sciences on the initiative and under supervision of A.N. Baraboshkin (1925–1995), an academician of the Russian Academy of Sciences. By now, staff members of the laboratory of electrocrystallization at the Institute of High-Temperature Electrochemistry have accumulated a vast and largely unique body of data on electrocrystallization from molten electrolytes, revealed fundamental aspects of structure formation and growth of electrolytic deposits, developed methods for deposition of solid layers of refractory metals with a thickness of several millimeters. Electrolytic deposits and their structure and growth have been studied using a set of modern physical, physicochemical, and electrochemical techniques. The main content of the book by Z.S. Martem'yanova and N.O. Esina is presented in the form of micrographs of very high quality.

The atlas comprises two parts: the first of these (pp. 4–132), including nine chapters, considers deposition of polycrystalline coatings and the second (pp. 133–187), including two chapters, discusses oriented electrodeposition. Each part has its own list of references.

Continuous deposits are complex structures. In deposition on a foreign substrate, their development occurs in three stages: nucleation of separate crystals on a substrate, growth of separate crystals till their merging into a continuous layer, and collective growth of crystals in the continuous deposit. The main parameters that affect the structure of continuous cathodic deposits in electrolysis of molten salts as the following: melt composition, concentration of discharging ions, cathode current density, material and structure of the substrate, anode current density, and oxidation state of ions of the metal being deposited in the melt. All these factors were taken into account in the experimental study of the processes that occur in deposition of continuous layers.

The first three chapters of the first part of the book are devoted to preparation of continuous deposits of molybdenum from a chloride–molybdate and a number of molybdenum-containing chloride melts of various cation compositions. Chapter 4 considers the structure of continuous electrodeposited layers of molybdenum alloys with tungsten, nickel, rhenium, and niobium. Chapter 5 discusses the results obtained in a study of continuous tungsten coatings deposited on various substrates by electrolysis of oxide and oxide–chloride molten electrolytes. Chapter 6 is devoted to the structure of rhenium coatings, and chapter 7 describes the results obtained in studies of electrodeposition of chromium, titanium, and hafnium. Chapter 8 presents data on the structure of silicon deposits produced by electrolysis of a chloride–fluoride melt on polycrystalline and single-crystal substrates made of various materials. The temperature dependence of the structure of silicon deposits on graphite, glassy carbon, and singlecrystal silicon was clearly revealed. Also presented are data on the structure of silicon coatings deposited from a LiF–KF–K_2SiF_6 fluoride melt. Germanium coatings were deposited onto a tungsten substrate from a Na_2WO_4–Na_2GeO_3 melt. The small chapter 9 presents the structural characteristics of uranium dioxide deposits produced by electrolysis of a 3LiCl–KCl–UO_2Cl_2 chloride melt at various current densities and temperatures. The bibliographic list in the first part of the atlas contains references to 39 studies performed at the Institute of High-Temperature Electrochemistry, Ural Division, Russian Academy of Sciences.

In the brief introduction to the second part of the atlas, the authors note that oriented metal layers find steadily increasing use in various fields of technology and allow deeper elucidation of the mechanism of electrooxidation processes. Chapter 1 of the second part presents results of an experimental study of single-crystal layers of molybdenum and tungsten, produced by electrolysis of molten salts. Molybdenum

layers of thickness 100 μm were deposited onto single-crystal molybdenum substrates with various orientations. At 800°C, the current densities were in the range 0.01–1.0 A cm^{-2}. Chloride solutions containing $MoCl_3$ were subjected to electrolysis. Tungsten was deposited onto single-crystal tungsten substrates with various orientations from a Na_2WO_4–K_2WO_4–WO_3 melt. Chapter 2 is devoted to electrodeposition of rhenium from molten electrolytes onto oriented rhenium and tungsten substrates. The bibliographic list in the second part of the atlas includes references to 12 studies by staff members of the Institute of High-Temperature Electrochemistry.

The Institute of High-Temperature Electrochemistry, Ural Division, Russian Academy of Sciences was organized with participation of professors M.V. Smirnov, S.V. Karpachev, and A.N. Baraboshkin. The Institute is the only specialized scientific institution in the world which studies the electrochemistry of ionic melts and solid electrolytes. The book-atlas by Martem'yanova and Baraboshkin, which has no analogs in the world literature, makes a kind of final review of the research in one of the areas of Institute's activities. The processes of electrocrystallization of refractory metals have exceedingly wide prospects for application in various fields of technology. The book is very well published and is, undoubtedly, of interest for specialists in the electrochemistry of ionic melts.

A. G. Morachevskii

ISSN 1070-4272. Russian Journal of Applied Chemistry, 2006, Vol. 79, No. 5, pp. 695–706. © Pleiades Publishing, Inc., 2006.
Original Russian Text © B.M. Ginzburg, D.G. Tochil'nikov, V.E. Bakhareva, A.V. Anisimov, O.F. Kireenko, 2006, published in Zhurnal Prikladnoi Khimii, 2006, Vol. 79, No. 5, pp. 705–716.

REVIEWS

Polymeric Materials for Water-Lubricated Plain Bearings

B. M. Ginzburg, D. G. Tochil'nikov, V. E. Bakhareva, A. V. Anisimov, and O. F. Kireenko

Institute of Problems in Machine Science, Russian Academy of Sciences, St. Petersburg, Russia
Prometei Central Research Institute of Structural Materials, St. Petersburg, Russia

Received February 6, 2006

Abstract—Results of tribological studies of modern polymeric materials (thermoplastics, thermosetting materials, composites) used to fabricate water-lubricated bearings are considered. Particular attention is given to carbon-fiber-reinforced plastics modified with powdered metals, fullerene-containing additives, and carbon nanotubes.

DOI: 10.1134/S1070427206050016

INTRODUCTION

The machine-building industry has conventionally used in friction units such metallic antifriction materials as babbit alloys, bronzes, and aluminum alloys, which can only work with oil lubricants. In recent years, an increasingly close attention has been given to the environmental safety of the friction units of modern ships, hydraulic turbines, pumps, shipping locks, and oil-extracting and oil-processing equipment operating in water. This problem can be mostly solved if oil lubrication of friction units is eliminated by using such natural lubricant as water. The problem of elimination of oil lubrication of friction units is also important for heavy and chemical machine building, road-building and mining machines, hoisting machinery, and food, textile, perfumery, and other industries.

This review considers the main types of modern polymeric materials used in water-lubricated bearings.

1. WATER AS A LUBRICANT

To have a general notion of lubrication with water in sliding friction, it is of use to consider the Hersey diagram (Fig. 1) [1]. The diagram is the plot of dependence of the friction coefficient on the Hersey parameter $\eta N/P_N$, where η is dynamic viscosity; N, rotation rate or sliding velocity of counterbodies; and P_N, contact pressure. Zones of (*1*) boundary and (*2*) mixed friction exist to the left of the minimum value of the friction coefficient, and (*3*) region of liquid friction, to the right.

The viscosity of water is more than 100 times lower than that of oils (Fig. 2). This means that, in most cases of lubrication with water, bearings operate during a considerable part of their service life under conditions of boundary and mixed friction. The characteristics of boundary and mixed friction are primarily determined by the materials of the contacting surfaces, and, therefore, their choice is exceedingly important. However, the practical choice is governed not only by the properties of materials, but also by their price, simplicity of production and processing, and design parameters of a friction unit. The concept

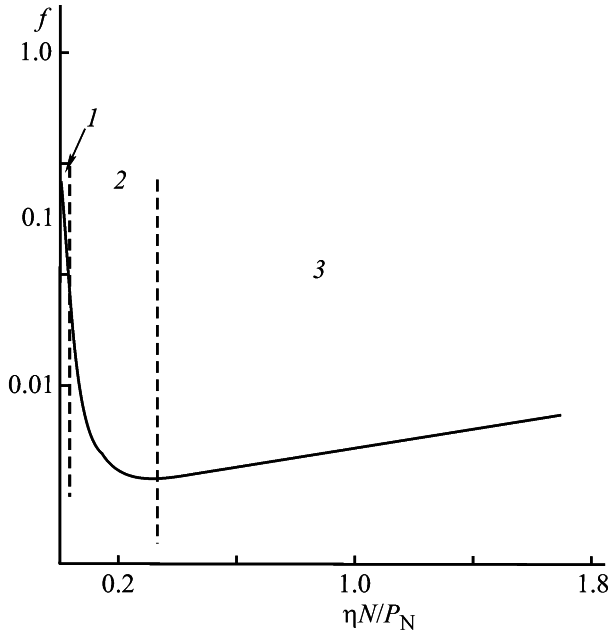


Fig. 1. Friction coefficient f vs. the Hersey number (Hersey diagram) [1]. (η) Dynamic viscosity (Pa s), (N) shaft rotation rate (rpm), and (P_N) normal contact pressure (MPa). Friction region: (*1*) boundary, (*2*) mixed, and (*3*) liquid.

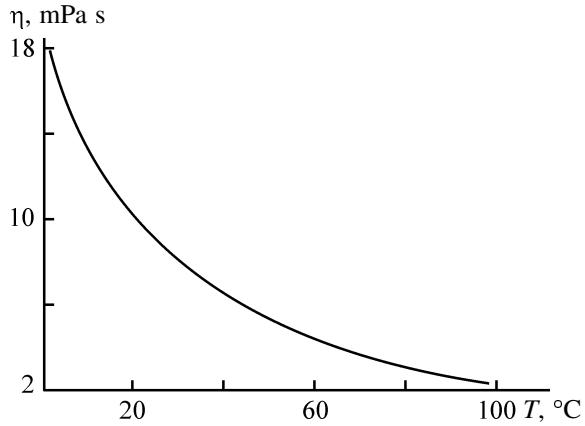


Fig. 2. Viscosity η of water vs. temperature T [1].

of how materials should be chosen with account of design and service parameters was formulated in [1]. In this review, we only consider the problem in terms of the materials science, with the specific conditions of operation in water only briefly mentioned.

2. EFFECT OF CORROSION

Naturally, attention should be given in the case of water lubrication to such a factor as corrosion of friction surfaces. Use of insulators as a material of one of the two surfaces or as a protective coating must diminish the effect of corrosion [2–4].

3. EFFECT OF CONTAMINANTS

In the case of contaminated water, preliminary filters or other devices are commonly used to remove the contaminants. However, these measures frequently fail to prevent ingress of soil, sand, clay, or other impurities into the clearance between the counterbodies. Therefore, the abrasion nature of wear should be taken into account in choosing the materials for counterbodies. The extent of this wear largely depends on the place of the operation mode in the Hersey diagram [1].

Table 1. List of selected tribological parameters of materials and friction units

Parameter	Designation	Illustrating figure
Friction coefficient	f	
Linear wear intensity	I_h	
Energy-related wear intensity	I_w	
Range of working pressures	P_C–P_{SS}	3a
Load-carrying capacity	P_C	3a
Alignment time	τ_R	
Lifetime of a friction unit after emergency failure of lubricant supply	τ_L	3b
Volume wear rate	ν_w	
Critical pressures for change of wear mechanism	P'_C, P''_C...	3c
Optimization parameter of alignment of mating friction surfaces	Q	3d

As contaminants find their way into the clearance, the nature and extent of the subsequent damage will be determined by the properties of the friction surfaces. If the contaminants are softer than these surfaces, the damage will be insignificant. If, however, the contaminant particles are harder than the friction surfaces, the softer surface will suffer scuffing.

4. TRIBOLOGICAL STUDIES OF POLYMERIC MATERIALS FOR WATER-LUBRICATED BEARINGS

Table 1 and Fig. 3 summarize the most important, in our opinion, parameters of the tribotechnical properties of materials and friction units [5].

The choice of materials to be lubricated with water cannot be based on the behavior of a material in the case of a dry sliding friction, with only the increased heat removal by water additionally taken into account. The wear and other parameters of dry sliding friction can be grossly misleading if extended to water-lubricated sliding friction. In particular, such an approach ignores chemical aspects of the interaction between water and counterbodies.

Many friction units operating in the boundary region of lubrication with water are characterized by low sliding velocities, frequent service interruptions, wide range of loads, and comparatively short sliding way during the service life. As examples of friction units of this type can serve rudder bearings of ships of various classes and purposes, guide units of hydraulic turbines, bearings of valves, etc. Friction units of other types, for which comparatively high sliding velocities and loads are typical, are bearings of propeller shafts in ships, shafts of hydraulic turbines and pumps, etc.

The main materials used in the case of water lubrication are ceramics and carbon and polymeric materials. The review will only consider modern polymeric materials or composites on their base, with the exception of wood or rubbers, which have long been used in water-lubricated bearings and are considered in detail in the literature [6–11].

4.1. Polymeric Antifriction Thermoplastics

The following materials have found the widest application among water-lubricated antifriction thermoplastics: (i) polytetrafluoroethylene (PTFE) and its copolymers of various technical names and commercial brands: Ftorlon-4 and Ftoroplast-4 (Russia); Teflon (the United States); Polyflon (Japan); Algoflon (Italy), Hostaflon (Germany), Fluon (the United Kingdom); (ii) various flexible-chain polyamides (PA): Kapron, Kaprolon, Fenilon (Russia); Nylon, Kaprolan, Nylon-11 (the United States); Rilsan (France); (iii) polyformaldehydes: SFD and STD (Russia); Delrin (the United States); Hostaform (Germany); (iv) polycarbonates: Diflon (RF); Makrolon (Germany); Lexan, Murloc (the United States); Penlite, Upiloc (Japan); (v) polyphenylene oxide: Ariloks (Russia) and Noryl (the United States); and (vi) polyurethanes: Thordon XL, Thordon (Canada), etc.

Polytetrafluoroethylene and its copolymers occupy a particular place among the known antifriction thermoplastics. The low values of its friction coefficient (0.2 to 0.002, depending on the load), high softening point, and the highest water and chemical resistance among all the polymers favored its wide use in friction units. At the same time, PTFE most clearly demonstrates the disadvantages characteristic of antifriction thermoplastics: poor strength and low heat conductivity, tendency toward cold flow, dependence of the friction coefficient on the sliding velocity, high coefficient of linear thermal expansion. Therefore, pure PTFE is comparatively rarely used in bearings, with the exception of cases of contact with corrosive media.

Various brands of filled materials containing PTFE as a matrix, modifier, or filler are manufactured. For example, filled fluoroplastics of KV, 80 FG, 7V2A, and F40G40 brands are used in ship and machine building [12–16].

Polyamides are inferior to fluoroplastics in antifriction properties and heat, water, and chemical resistance, but markedly surpass them in strength, elastic modulus, and feasibility of processing. The main disadvantage of PA, compared with fluoroplastics, is the instability of linear dimensions of bearings in their prolonged operation in water. This instability gives no way of fabricating precision bearings with clearances characteristic of metallic bearings [17–19]. The swelling in water is also typical of materials manufactured by Thordon Co. (Canada), which are used to fabricate bearings for ships and hydraulic turbines [20–23].

Comparison tests of polymers of various classes

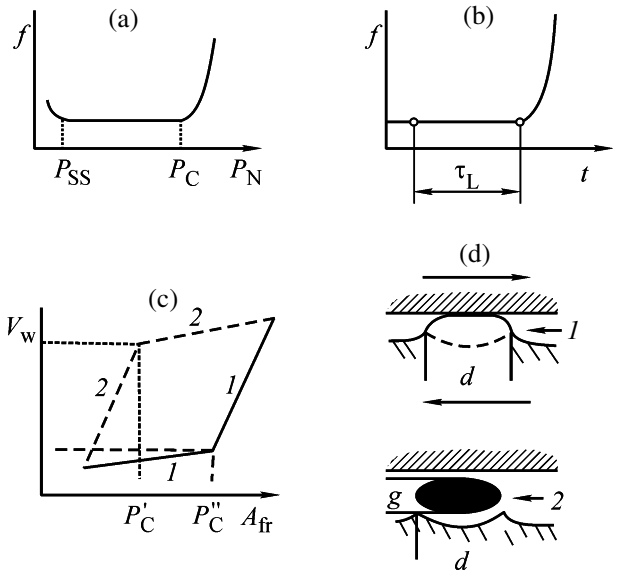


Fig. 3. Some important parameters characterizing the tribological properties of a friction unit and its components [5]. (a) Schematic dependence of the friction coefficient f on the normal contact pressure P_N; the interval of working pressures (from P_{SS} to P_C) throughout which the friction coefficient is permanently low is shown. (P_C) Load-carrying capacity of the friction unit. (b) Schematic dependence of the friction coefficient f on time t in the case of an emergency failure of lubricant supply. (τ_L) Lifetime of a friction unit from the time of termination of lubricant supply till the onset of scuffing, judged from the sharp rise in the friction coefficient. (c) Schematic dependences of the volume wear V_w of a counterbody being tested on the work A_{fr} of the friction force for two modes of variation of this work: (*1*) via an increase in the normal contact force F_N at an invariable friction path L = const and (*2*) via an increase in L at F_N = const. (P'_C, P''_C) Critical pressures corresponding to a change of the friction and wear mechanism. (d) Illustration of the physical meaning of the parameter $Q = I_h H_B/3P_N(d/g)$, the probability that the contact spot *1* will transform into a wear particle 2 upon a relative shift of the counterbodies by a distance equal to the contact spot diameter d. (H_B) Brinell hardness and (g) height of the wear particle.

demonstrate [1, 24–39] that, as a rule, presence of water in a tribocontact reduces the friction coefficient, compared with the case of dry friction, owing to the lubricating action of a water film. For certain polymers (e.g., polyphenylene oxide), the plasticizing effect of water is enhanced in the case of friction, compared with exposure to water without friction, and changes the strength and deformation properties of the surface layers, with the friction coefficient also affected [26]. For polyethylene (PE), the friction coefficient in a sulfuric acid vapor is lower than that in water, because the chemical modification of the PE surface raises the free energy of the polymer by mak-

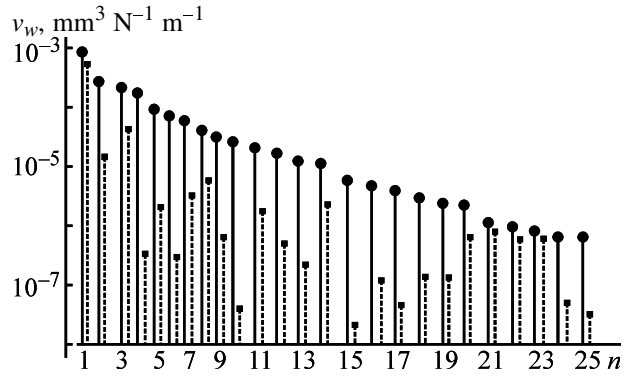


Fig. 4. Wear rate v_W for different materials in the case of lubrication with distilled water (solid lines) and in dry friction (dashed lines) [28]. Counterface, S80 stainless steel; temperature 25°C; friction unit constituted by a finger (truncated cone) moving on a disc (sample). (*n*) Sample number. (1) Polyester-17 449, (2) LY558 epoxy resin, (3) polyphenylene oxide, (4) PTFE + 25% carbon fibers of type I (CFI), (5) PTFE + 25% glass, (6) polyester + 25% CFI + 10% Pb, (7) polyimide + MoS_2, (8) PTFE + 25% mica, (9) polyester + 60% carbon fibers of type II (CFII), (10) polyphenylene oxide + 25% CFI, (11) polyimide, (12) polyacetal, (13) PTFE + bronze + graphite, (14) PTFE + 25% asbestos, (15) epoxy resin + 60% CFI, (16) epoxy resin + 60% CFII, (17) phenol–formaldehyde resin + cotton + PTFE, (18) polyimide + graphite, (19) polyphenylene + 60% CFII, (20) PTFE + 25% coke, (21) polyacetal + 25% glass, (22) PTFE + 25% CFII, (23) polyacetal + 45% CFII, (24) polyphenylene oxide + 25% CFII, and (25) PTFE + CFII + 20% Cu.

ing larger the relative content of the polar component and reduces the surface tension of the fluid [32].

The friction coefficient frequently decreases in the presence of water, compared with the case of dry friction [40, 41]. However, the wear rate of a polymer subjected to friction in water most frequently substantially increases, compared with the case of dry friction [1, 26, 28, 33]. For example, Lancaster [28] demonstrated that this is the case for 29 different polymers and polymeric composites, including composites based on epoxy resins, polyacetals, PTFE, polyesters, polyphenylenes, polyimides, and polyphenylene oxides (Fig. 4). However, this property depends on the type of a filler; at least, PTFE with different fillers may exhibit both a decrease and an increase in the wear resistance [40, 41].

On passing from pure water to seawater and dilute solutions of some salts, all the three cases are possible: the wear rate may decrease, remain unchanged, or increase [27, 28].

A comparative study of the tribotechnical characteristics of a number of polymeric materials (polyvinyl butyral, phenol–formaldehyde resin of the resol type, polyethylene terephthalate, PA 6, high-density PE, and some copolymers) in their friction with steel in water has been carried out [35]. It revealed substantial differences in the dependences of the friction coefficient and wear on load in the range 0.25–2 MPa for different polymers and the fact that the results obtained cannot be described by common dependences. The differences are accounted for by the different adsorption interactions of water with the surface of the polymers and steel.

Presence of ether and hydroxy groups in polymer molecules favors formation of wear-resistant structures, which has been confirmed by a study of wear products [36]. It is noted that the adsorption of water by the surface of PA (in friction) is enhanced as the density of amide groups grows in the order PA-12, PA-5, and PA-46 [37].

The extremely high wear rates of various polymers in water can be hardly understood in terms of a common mechanism, because manifestations of the interaction of water with a friction surface are widely diverse (absorption, adsorption, diffusion, plasticization, chemical reactions) and depend on time, temperature, applied stress, sliding velocity, surface topography of a counterbody, etc. [1, 26, 28]. It has been shown experimentally that, in the case when the tribological properties in dry friction are improved because of the formation of a polymeric transfer film on the counterbody, the wear in friction in water is enhanced because water precludes formation of films of this kind [24, 26, 28, 38, 39]. This is accounted for by the high surface tension of water, which, being adsorbed on the surface of a material, hinders formation of transfer films. Frequently, it is also very difficult to remove water layers from surfaces because of the formation of hydrogen bonds with the atoms of the surface [42]. Water differently interacts with polar and nonpolar surfaces [43], by changing the microhydrodynamics of the fluid in the contact zone.

In the case of friction of steel against polyetheretherketone (PEEK), a semicrystalline thermoplastic with high strength and good mechanical properties, in water, diffusion of water into the surface layer of the polymer enhances wear by making lower the hardness of the surface, although wetting of the polymer in the absence of friction has no effect on the hardness [44]. The friction against polyphenylene sulfide (PPS) under the same conditions leads (because of the formation of FeS and improvement of adhesion) to tribotransfer of a polymeric film onto the surface of steel. If carbon fibers are added to PEEK, and carbon

and glass fibers, to PPS, this improves the wear resistance of the polymer, especially at high contact pressures [45]. In the case of friction against edges of reinforcing fibers, the wear is smaller than that in friction along the fibers. Thus, the result obtained with reinforced polymers depends both on the topography of a friction surface and on parameters of the counterbody [28, 31]. The wear rate of the composite material in water substantially decreases if, e.g., a small amount of an abrasive (0.1% Al_2O_3 particles 3 μm in diameter) is introduced into the material of the surface layer, which can be attributed to the polishing effect [28], although other explanations are also possible. In [39], a positive effect of addition of 10% polyurethane to polyoxymethylene (POM) under conditions of water-drop lubrication was mentioned.

In [46], the influence exerted by the mode of sliding on the wear of cross-linked PE in friction against the same material was noted: in the case of a reciprocating sliding of a finger over a plate, the wear in water is 10 times that in dry friction, whereas in a reciprocating-rotational sliding, the excess is insignificant. In the case of a plane-against-plane friction, the wear also decreases.

In principle, the processes that occur in the friction zone with polymers involved are rather complex and may lead to formation of at all unknown compounds. This has been demonstrated for the example of friction of a number of polymers (PTFE, PA-6, PMMA) against steel in a study of the friction surface of the counterbody and particles formed in wear of the polymers [47]. Therefore, it is exceedingly difficult to fully characterize the effect of water on tribochemical processes in the friction zone.

The aforesaid leads to a rather general conclusion that presence of water in the zone of a tribological contact involving polymeric materials may affect in totally different ways the friction coefficient and wear, compared with the case of dry friction: these parameters may decrease, increase, or remain unchanged, depending on the applied load [48].

Sufficiently strong and stable polymers of the PEEK type, reinforced with carbon fibers [45], or PE with ultrahigh molecular weight [49] can be used for operation in water.

In some cases, application under conditions of water lubrication of composite materials based on polymers widely used in tribology (PTFE) requires a special study of their behavior in an aqueous medium because of the unpredictable effect of water on the components used. For example, it has been found that use of a metallic grid made of stainless steel, combined with powdered graphite, for reinforcement of PTFE reduces the wear by a factor of 300 in the case of dry friction [50], but it is difficult to predict the behavior of a material of this kind in a medium in which water promotes oxidation of the metal, penetrates into the material along phase boundaries thereby changing its properties, and is involved in tribochemical reactions.

In [51], we determined how additions of fullerene black affect the load-carrying capacity of F-4 fluoroplastic in the case of sliding friction with water lubrication. The fullerene black (C–C_{60}) remaining after most of fullerenes were extracted with toluene, i.e., a waste product formed in manufacture of fullerenes, was used in the study. However, this black still contains up to 12% higher fullerenes [52]. Introduction of only 1% black (C–C_{60}) into F-4 fluoroplastic raises its load-carrying capacity by 30%. There are indications that introduction of C_{60} fullerene into Kapron improves its antifriction and antiwear properties in the case of water lubrication [53].

Materials based on F-4 with addition of 1–10% fullerene black were suggested in [54]. In this case, the antifriction and antiwear properties of the materials are improved both in dry friction and in the case of water lubrication.

4.2. Polymeric Antifriction Thermosetting Materials

The strength and rigidity of antifriction materials become several times higher on passing to thermosetting composites reinforced with fabrics, textolites [55].

Phenol–formaldehyde resins have been long used as matrices [1], and cotton cloth or synthetic fabric, as the reinforcing material [56]. Textolites are used to fabricate plain bearings for various machines, e.g., bearings of rolling mills. However, cotton and synthetic fibers strongly swell in water, and, therefore, precision plain bearings fabricated from such textolites are unsuitable for prolonged operation in water because of the dimension instability.

At the same time, the machine-building industry uses a group of large plain bearings, for which elimination of oil lubrication is exceedingly important. These are bearings of propeller shafts and rudders in ships of various classes, floating cranes and drilling rigs, shafts and guide units of hydraulic turbines, unique pumps, etc. The working conditions of the bearings in these devices widely vary. The bearings of ship rudders and units of hydraulic turbines are slow-running (sliding velocities of 0.005 to 0.5 m s^{-1}) and

operate in the unfavorable mode of boundary (or "semidry") friction at high contact pressures of up to 50 MPa (it will be recalled that the contact pressures in most of standard bearings do not exceed 0.25–0.5 MPa). The journal bearings of ship propeller shafts (including those of the stern-shaft type), bearings of turbine shafts, and end seals of turbines and pumps are high-speed (sliding velocities of 12–15 m s^{-1} and up to 40 m s^{-1} for some pumps) and operate in the hydrodynamic friction mode, with the contact pressures being considerable in some cases. For example, the edge contact pressures are 15–20 MPa for stern-shaft bearings. The materials to be used in plain bearings of both groups should satisfy the requirements of a high dimension stability (absence of swelling), shock resistance, and workability.

A group of materials suitable for highly reliable precision plain bearings operating with water lubrication is constituted by carbon-reinforced plastics with a thermosetting matrix.

4.3. Carbon-Reinforced Plastics Based on Thermosetting Matrices

4.3.1. General information. In contrast to all the known fillers of antifriction polymers, carbon fabrics have high strength, elastic modulus, and heat conductivity, do not change their dimensions in water (zero swelling), and the products of dispersion of carbon fabrics, formed in the process of friction, possess properties of a solid lubricant (graphite).

The industry manufactures a wide variety of structural carbon-reinforced plastics on the basis of various binders and reinforcing materials. The dependence of the mechanical and thermal properties of high-strength and high-modulus carbon-reinforced plastics on their chemical composition and reinforcement scheme has been studied [57–62]. However, the structural carbon-reinforced plastics have not been used as antifriction materials and, therefore, their tribotechnical properties have not been analyzed in detail. It was shown in [6, 63–73] that the tribotechnical properties of various classes of carbon-reinforced plastics in friction in water differ by one or two orders of magnitude and the friction coefficient and wear resistance of these materials strongly depend on the structure of the carbon fiber, chemical composition, structure of the polymeric matrix, modifiers, and processing parameters.

In the course of these studies, a relationship between the molecular, topological, and supramolecular structures of the polymeric matrix, on the one hand, and the physicochemical properties of the matrix and the polymeric composite material (PCM), on the other, was established. The results of the studies were used to formulate the criteria to be used in choosing the starting components of the polymeric matrix of PCM [74].

It was found for the first time that the wear resistance of polymers in friction in water depends to the greatest extent on the chemical nature of thermosetting oligomers and curing agents. The highest wear resistance in boundary friction in water is observed for dense-network epoxy polymers containing a strictly specified amount of active "doping" elements: chlorine, nitrogen, phosphorus, and nickel. Contrariwise, presence of titanium leads to a dramatic increase in the extent of wear.

It was shown in a study of friction of a number of epoxy compounds with various counterbodies that the best result in friction in water is obtained in the case of filling with carbon fibers and an Al_2O_3 ceramics as a counterbody [75].

The relationship between the structure of the carbon fiber, direction of reinforcing fibers in fabrics, and properties of PCM was determined. It was shown that the highest wear resistance [linear wear intensity of $(0.3–0.5)\times10^{-9}$ at a boundary friction and contact pressure of 50 MPa] is observed for epoxy carbon-reinforced plastics based on low-modulus carbonized fibers whose structure is constituted by fine disoriented crystallites and a considerable amount of the amorphous phase, which serves as a soft component in friction. An X-ray diffraction analysis of the supramolecular structure of carbon fibers obtained at different temperatures (700–2800°C) and of structural changes in the course of friction revealed a strong dependence of the wear resistance of the carbon-reinforced plastic on the preparation conditions of carbon fibers.

Optical and electron microscopy, X-ray diffraction, and chemical analysis were used to study the processes occurring on the contact surfaces of friction units constituted by a carbon-reinforced plastic and stainless steel, titanium alloy, or bronze. The high wear resistance of carbon-reinforced plastics is due to the successive occurrence of tribohydrolysis, secondary tribopolymerization of the polymeric matrix to give a separating antifriction tribopolymeric layer, chemical modification of the counterbody surface, and changes in the structure of the reinforcing carbon fiber [74].

A set of studies revealed a relationship between the structure and basic properties of carbon-reinforced

plastics based on thermosetting matrices and made it possible to formulate the criteria to be used when choosing the starting components.

(1) The molecular, topological, and supramolecular structure of the thermosetting polymer (matrix) should provide occurrence on the contact surface of tribohydrolysis and secondary tribopolymerization to give a separating antifriction layer (film of a friction polymer), which results in that the rule of a positive gradient of shear resistances along the normal to the contact surface is observed.

(2) Active elements (e.g., chlorine and nitrogen) should be present in the composition of the epoxy oligomer and the curing agent. These elements promote a favorable modification of the counterbody surface, which improves its antiwear properties. Surfactants, e.g., oleic acid should be additionally introduced into the phenol oligomers.

(3) The supramolecular structure of the thermosetting matrix should be microheterogeneous and should contain a molecular-dispersed phase, which can act as a soft structural component in friction.

(4) The glass-transition point of the polymeric matrix should exceed the temperature in the friction contact zone. A polyfunctional epoxy matrix (glass-transition point 180°C) is recommended for heavily loaded slow-running bearings (sliding velocities not exceeding 1.0 m s^{-1}) operating with water lubrication. A modified phenol–formaldehyde matrix is recommended for high-speed bearings (sliding velocities of 1.0 to 40 m s^{-1}).

(5) The reinforcing material should have a high heat conductivity to provide efficient heat removal from the friction zone.

(6) The products of dispersion of the reinforcing material, formed in the process of friction, should have properties of a solid lubricant or acquire these properties in the course of the contact interaction.

(7) The specific surface area of carbon-fiber reinforcing materials should exceed 100–150 $m^2 g^{-1}$ (to facilitate dispersion in the course of friction interaction), and the limiting volume of the sorption space (for water vapor) should be larger than 0.2 $cm^3 g^{-1}$, with a pore radius of gyration less than 0.5–2 nm.

(8) To facilitate orientation of turbostratic crystals in a friction interaction, the crystallite dimensions should be smaller than 3–5 nm and the angle of misorientation of crystallites should not exceed 15–20°.

(9) The binder content in a carbon-reinforced plastic should be no less than 40%.

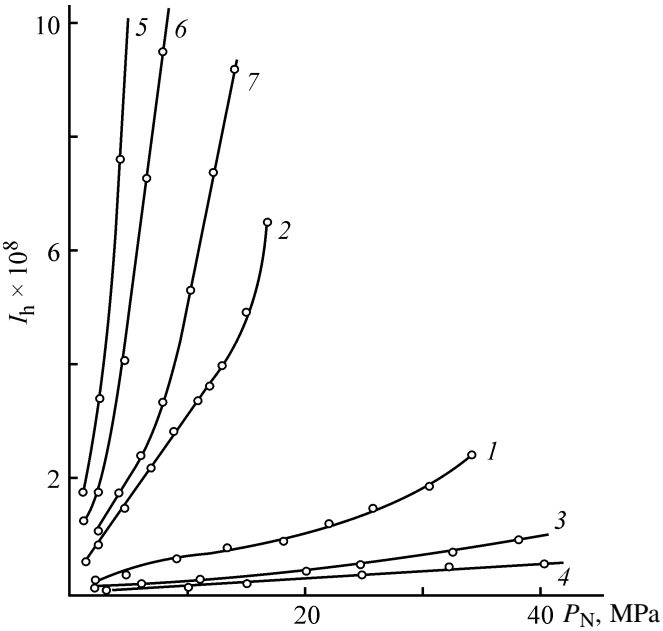


Fig. 5. Linear wear intensity I_h (friction against 18Kh2N4MA hard steel) vs. the contact pressure P_N for various polymer-based materials. Water lubrication, sliding velocity 1 m s^{-1}; the same for Figs. 6 and 8. (*1*) Kaprolon, (*2*) Thordon XL, (*3*) FUT (along direction X), (*4*) UGET (along direction X), (*5*) F-4, (*6*) F-4K20, and (*7*) F-4K20 modified with 1% fullerene black (C–C_{60}).

4.3.2. Tribological properties of carbon-reinforced plastics with phenol–formaldehyde and epoxy matrices. Carbon-reinforced plastics of the UGET and FUT brands [TU (Technical Specifications) 5.966-11704–99] with an epoxy and phenol–formaldehyde matrices, respectively, show a good performance as materials for water-lubricated plain bearings in a wide range of contact pressures [67, 73, 74]. Carbon-fiber fabrics are used as a reinforcing material in these carbon-reinforced plastics. A binder based on a chlorine-containing tetrafunctional oligomer has been used in manufacture of UGET materials [76]. The UGET materials, intended for heavily loaded slow-running plain bearings, are used in friction units of ship rudders, hoisting machines, valves, guide units of hydraulic turbines, etc.

Materials of the FUT type have been produced with an LBS resol phenol–formaldehyde lacquer [77]. The FUT materials are intended for fast-running friction units (1–40 m s^{-1}): journal bearings of ship propeller shafts, end and slit seals in hydraulic turbines, bearings and seals in pumps, etc.

Figures 5 and 6 show the results obtained in tests of carbon-reinforced plastics and, for comparison, data for a number of thermoplastics in friction against steel

Table 2. Selected physical and tribological properties of antifriction polymeric materials used in water-lubricated bearings

Material	Physical properties				Tribological properties			
	ρ, kg m^{-3}	σ_t, MPa	E, GPa	ε, %	P_m, MPa	$I_h \times 10^8$	$I_w \times 10^6$, mm J^{-1}	χ
UGET	1450	250	15	0	60	0.4	1.5	0.11
FUT	1450	150	15	0	35	0.6	5	0.06
Kaprolon B	1150	65	2	5	30	2	29	0.02
Thordon XL	1200	35	0.5	1.3	15	6	210	0.02
F-4	2000	10	0.5	0	7	10	410	0.03
F-4K20	2100	12.5	0.85	0	12	9	140	0.08

Note: (ρ) Density, (σ_t) tensile strength, (E) modulus of elasticity, (ε) change in linear dimensions on keeping in water for a year, (P_m) maximum admissible contact pressure (load-carrying capacity), ($I_h \times 10^8$) linear wear intensity, ($I_w \times 10^6$) energy-related wear intensity, and (χ) friction coefficient for friction against 18Kh2N4MA steel at P_m, water lubrication, and sliding velocity of 1 m s^{-1}.

[78]. Table 2 lists selected parameters characterizing the mechanical properties of the materials and the tribological properties at the maximum admissible pressure at the tribocontact. It can be seen that the strength and elastic properties of the carbon-reinforced plastics severalfold exceed the corresponding parameters of thermoplastics; in addition, carbon-reinforced plastics exhibit dimension stability, no swelling in water, and a coefficient of linear thermal expansion typical of metals. The main advantage of antifriction carbon-reinforced plastics is their high wear resistance at substantial contact pressures. The carbon-reinforced plastics are inferior to thermoplastics in antifriction properties, but many times surpass them in wear resistance.

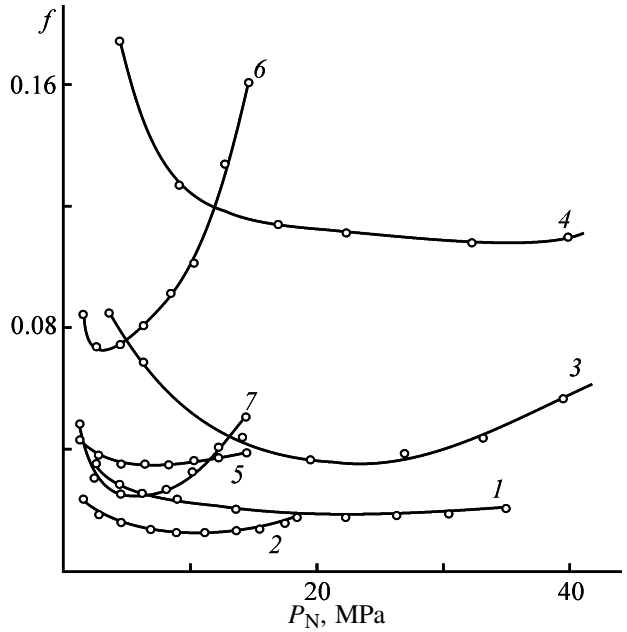


Fig. 6. Friction coefficient f (friction against 18Kh2N4MA hard steel) vs. the contact pressure P_N for various polymer-based materials. (*1*) Kaprolon, (*2*) Thordon XL, (*3*) FUT (along direction *X*), (*4*) UGET (along direction *X*), (*5*) F-4, (*6*) F-4K20, and (*7*) F-4K20 modified with 1% fullerene black (C–C_{60}).

4.3.3. Anisotropy of the physical and tribological properties of antifriction carbon-reinforced plastics. Because of their layered structure (Fig. 7), carbon-reinforced plastics show anisotropy of properties; in addition, the anisotropy is due to the fact that the ratio between the amounts of fibers in the warp and weft of the fabric used is 10 : 8. It is noteworthy that the tensile strength in the transverse direction Z is approximately 20 times lower than that along the fabric layers. The behavior of carbon-reinforced plastics in compression markedly differs from that in tension. In this case, the strength in direction Z exceeds by approximately a factor of 1.5 that in directions X and Y. This fact is rather important, because a material mostly experiences compressive loads in bearings.

The heat conductivity coefficient in directions X and Y exceeds by a factor of approximately 50 that in direction Z, which is accounted for by the pronounced difference in heat conductivity between the matrix and carbon fibers [6]. A similar anisotropy should be observed for other physical properties of carbon-reinforced plastics: thermal diffusivity, electrical conductivity, etc. It was shown in [79] that the linear dimensions of articles made of carbon-reinforced plastics remain virtually unchanged in prolonged operation in water (for 5 years) and their strength and elasticity parameters decrease by no more than 8–10%.

In [80], the anisotropy of the tribological properties of carbon-reinforced plastics was studied for varied composition and nature of binder modifiers and different brands of steel used as a counterbody. The

counterbody was slid along direction *X*, i.e., along fibers of the warp of fabric layers, and along *Z* axis, perpendicularly to these fibers. The tests demonstrated that the anisotropy of the friction coefficient was comparatively low: the coefficient along *Z* axis was only 10–20% higher. The orientation of the sliding direction affects to a greater extent the wear intensity, which decreases by a factor of 1.4–1.6 in friction along *Z* axis (Fig. 8). Apparently, this is due to the following. In wear particle formation and friction along *Z* axis, it is necessary to destroy fibers by shear deformation across the fiber axis (i.e., to rupture intramolecular covalent bonds), whereas in wear along *X* axis, it is necessary either to destroy the considerably less strong matrix or to cleave fibers along their axis (i.e., to rupture intermolecular van der Waals bonds).

4.3.4. Effect of materials of counterbodies on the tribological properties of carbon-reinforced plastics in lubrication with water. When carbon-reinforced plastics are used in water-lubricated friction units, various metals serve as counterbodies. The effect of these metals on the tribological properties of friction units was studied in [81, 82]. The type of a metal affects the friction coefficient comparatively slightly (within 10–25%). However, the load-carrying capacity of a friction pair and the wear intensity of the carbon-reinforced plastic change very noticeably. The best are the friction pairs constituted by FUT and BrO10Ts2 bronze and by UGET and BrO10Ts2. However, bronze is a comparatively expensive metal and is inferior to steels in strength, and, therefore, shafts are commonly made of steel with a bronze facing. The hard alloyed steel 18Kh2N4MA sufficiently well works with both the carbon-reinforced plastics, but this steel is also comparatively expensive and has insufficient workability. The most workable and corrosion-resistant steel is the 08Kh18N10T low-hardness stainless steel, but it satisfactorily works only with the UGET carbon-reinforced plastic. In operation with this steel, the wear intensity of FUT is 2.5–3 times that in operation with the 18Kh2N4MA steel and 8–10 times that in operation with a bronze. The load-carrying capacity of the FUT–08Kh18N10T pair is also lower (<10 MPa).

Seemingly, the pair constituted by UGET and low-hardness stainless steel could be chosen, but this can be done only for friction units with low sliding velocities because of the properties of the carbon-reinforced plastic itself. Thus, an important applied problem arises: a material satisfactorily working in pair with a comparatively inexpensive kind of steel, the most frequently used in water-lubricated friction units, is to be sought for. A possible way to solve this problem is

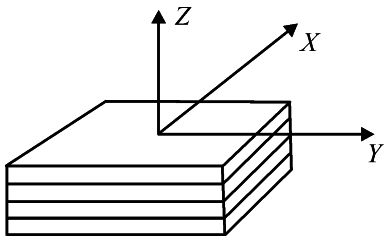


Fig. 7. Schematic structure of a carbon-reinforced plastic. *X*, direction along fibers of the warp of the reinforcing fiber; *Y*, that along fibers of the weft; and *Z*, that perpendicular to the plane of the reinforcing fabric.

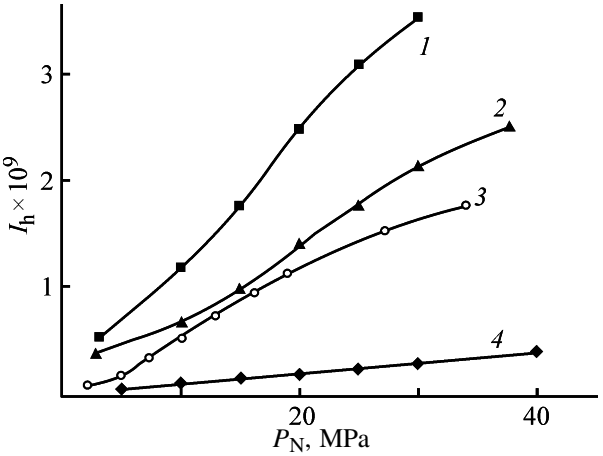


Fig. 8. Linear wear intensity I_h vs. the contact pressure P_N for carbon-reinforced plastics variously oriented with respect to the direction of sliding friction against 18Kh2N4MA steel. (*1*) FUT, along *X* axis; (*2*) FUT, along *Z* axis; (*3*) UGET, along *X* axis; and (*4*) UGET, along *Z* axis.

to modify carbon-reinforced plastics. Another way is to change fundamentally the nature of components of the plastics, both binders and fillers.

4.3.5. Modification of carbon-reinforced plastics with Ftoroplast-4. Ftoroplast-4 (F-4, Russian analog of Teflon) was studied as one of the first antifriction modifiers in the form of a highly dispersed powder. The URAL-T15R carbon fiber used as filler was treated with powders with a particle size of 0.1 μm. The study demonstrated that modified carbon-reinforced plastics have virtually the same strength as the untreated ones. The load-carrying capacity increased by a factor of 2, the linear wear intensity decreased by 20–30%, and the friction coefficient became 15–20% lower [41] in lubrication with water and friction against the 18Kh2N4MA hard steel.

4.3.6. Modification of carbon-reinforced plastics with powdered metals. Introduction of powders of various metals into composites is a widely used procedure. The choice of metals is commonly limited to

their small number, in accordance with the existing concepts of their antifriction and antiwear properties, and is largely governed by the intuition of researchers. In [83] were reported the results obtained in a study of the influence exerted by powdered-metal modifiers (introduced into carbon-reinforced plastics) on the tribological properties of the friction pair constituted by FUT and 08Kh18N10T steel in lubrication with water. The influence exerted by addition of powders of copper (5%), mixture of aluminum and tin (3.5%), nickel (5%), and B-83 babbit was studied. The best results were obtained upon introduction of B-83 babbit into a carbon-reinforced plastic: the load-carrying capacity increased by 15% and the linear wear intensity and friction coefficient decreased by factors of 2–2.5 and 1.2–1.4, respectively. Also noteworthy are the results obtained upon introduction of a nickel powder: at a comparatively small increase in the friction coefficient (by 10–20%), the load-carrying capacity increased by a factor of 1.7 and the linear wear intensity decreased by a factor of 5–7.

Also, the influence exerted by modifiers having the form of a mixture of F-4 and powdered metals was studied. However, the positive effects observed in this case were less significant than those achieved upon introduction of B-83 babbit and nickel.

4.3.7. Modification of carbon-reinforced plastics with fullerene blacks and carbon nanotubes. In [84], we studied how additions of fullerene black or a mixture of various carbon nanotubes to the epoxy binder of carbon-reinforced plastics of the UGET type affect the alignment of mating surfaces and tribological properties of the plastics in sliding friction against 18Kh2N4MA steel and lubrication with water. The antiwear properties are improved to the greatest extent upon introduction into the binder of a minor amount (5%) of carbon nanotubes: The load-carrying capacity of the carbon-reinforced plastic increased (by a factor of 1.4), and the volume wear and linear wear intensity substantially decreased (by a factor of 2–7) at an insignificant decrease in the friction coefficients (by no more than 10%). The introduction of 5% fullerene black into the binder improved the antiwear properties, which consisted in that the range of contact pressures at which a stable low friction coefficient is observed was extended. However, wide use of fullerene black and, especially, nanotubes is hindered by their comparatively high production cost.

CONCLUSIONS

In our opinion, the polymeric materials presently used to fabricate water-lubricated bearings can be conditionally divided into three groups. The first group of materials, intended for lightly loaded bearings (with pressures of up to 10 MPa), is constituted by PTFE-based composites. It is noteworthy that, retaining the low friction coefficients typical of pure F-4, composites based on F-4 and modified with 1% fullerene black acquire a wear resistance characteristic of F-4K20 composite. It should be noted that fullerene black is present in the F-4 matrix as a separate phase, and conglomerates of black particles contain crystallites of C_{60} fullerene and graphite, i.e., the black is dispersed on the supramolecular, rather than molecular level. It may be assumed that the wear resistance of composites formed by F-4 and fullerene black is improved because, in the course of their propagation, microcracks appearing in the course of tests are closed (healed) at fullerene molecules owing to their high electron-acceptor properties, and do not go around fullerene-containing particles as ordinary inclusions. The free chain radicals generated in mechanical degradation of F-4 are covalently bound to fullerene molecules.

The second group of materials, intended for bearings working at medium pressures (up to 20–25 MPa), is constituted by thermoplastics (mainly polyamides, polyurethanes, polyesters, polyformaldehydes, etc.) or composites on their base.

Finally, the third group of materials, intended for heavily loaded bearings working in a wide range of contact pressures (up to 40–45 MPa), is constituted by plastics based on thermosetting matrices and, primarily, carbon-reinforced plastics.

In our opinion, further substantial progress in the improvement of strength parameters of plastics (by a factor of several tens) can be provided by manufacture of fibers (and then fabrics) with high filling with carbon and other nanotubes, with simultaneous reinforcement of matrices with nanoparticles, acceptors of free radicals.

ACKNOWLEDGMENTS

The study was performed in the framework of the scientific program no. 14 (coordinator I.G. Goryacheva) of basic research of the Department of Power Engineering, Machine Building, Mechanics, and Control Processes, Russian Academy of Sciences (Institute of Problems in Machine Science, Russian Academy of Sciences) and scientific program "National Technological Resources," section "Technologies of New Materials" (Prometei Central Research Institute of Structural Materials).

REFERENCES

1. Smith, W.V., *Wear*, 1973, vol. 25, no. 1, pp. 139–153.
2. Smith, W.V. and Schneider, L.G., *Naval Eng. J.*, 1963, vol. 75, no. 4, pp. 841–854.
3. Serre, I., Celati, N., and Pradeilles-Duval, R.M., *Wear*, 2002, vol. 252, no. 9–10, pp. 711–718.
4. Lizandier, M.F., Lanza, E., Sebaoum, A., et al., *Wear*, 1992, vol. 153, no. 2, pp. 387–397.
5. Ginzburg, B.M., Kireenko, O.F., Shepelevskii, A.A., et al., *J. Macromol. Sci., Physics*, 2005, vol. 44B, no. 1, pp. 93–115.
6. Rubin, M.B. and Bakhareva, V.E., *Podshipniki v sudovoi tekhnike: Spravochnik* (Bearings in Ship Technology: Reference Book), Moscow: Sudostroenie, 1987.
7. Sokov, E.V., *Sudostroenie*, 1997, no. 1, pp. 47–50.
8. Davydov, A.P., *Rezinovye podshipniki v mashinostroenii* (Rubber Bearings in Machine Building), Leningrad: Mashinostroenie. 1976.
9. Burenin, V.V., *Khim. Neftegaz. Mashinostr.*, 2000, no. 3, pp. 52–54.
10. Orndorf, Jr. and Roy, L., *Naval Eng. J.*, 1985, vol. 97, no. 7, pp. 39–52.
11. Zhang, S.W., Liu, H., and He, R., *Wear*, 2004, vol. 256, nos. 3–4, pp. 226–232.
12. Sagalaev, G.V. and Shtembel', I.A., *Trenie Iznos*, 1982, vol. 3, no. 4, pp. 626–632.
13. Zamyatina, T.F., Mashkov, Yu.K., Surikov, V.I., et al., *Plast. Massy*, 1985, no. 8, pp. 56–57.
14. Gertsyk, M.A., Nikitin, V.A., Petrov, V.M., et al., *Vopr. Materialoved.*, 2001, no. 2(26), pp. 148–156.
15. Vorontsov, P.A. and Semenov, A.P., *Vestn. Mashinostr.*, 1996, no. 10, pp. 9–11.
16. *Spravochnik po kompozitsionnym materialam* (Reference Book of Composite Materials), Lyubin, J., Ed., Moscow: Mashinostroenie, 1988, vol. 2.
17. Sokov, E.V. and Lysenkov, P.M., *Sudostroenie*, 1995, nos. 2–3, pp. 42–45.
18. Lubenko, V.N., Improving the Reliability of Kaprolon Stern-Shaft Bearings for Fishing Ships, *Doctoral Dissertation*, St. Petersburg, 1996.
19. Kudryashov, Yu.A., *Vopr. Materialoved.*, 2001, no. 2(26), pp. 116–118.
20. *Ekologicheski chistaya podshipnikovaya sistema dlya deidvudnykh ustroistv: Tekhnicheskoe rukovodstvo* (Environmentally Clean System of Bearings for Stern-Shaft Devices: Technical Manual), Barlington: Thordon, 1998, issue 3.0.
21. Advertising Information: Thordon Bearings for Polar Sea, *Can. Ship. Marine Eng.*, 1986, vol. 57, no. 5, pp. 19.
22. Lhymn, C., *Wear*, 1988, vol. 122, no. 1, pp. 13–15.
23. Derzhavin, Yu.A., Nikitin, V.A., Petrov, V.M., et al., *Problemy mashinovedeniya v mashinostroenii: Mezhvuzovskii sbornik* (Materials Science Problems in Machine Building; Intercollegiate Coll. of Works), St. Petersburg: Sev.-Zap. Zaochn. Politekh. Inst., 2000, issue 21, pp. 79–87.
24. Cohen, S.C. and Tabor, D., *Proc. Roy. Soc.*, 1966, vol. 291A, no. 1425, pp. 186–207.
25. Smith, W.V., *J. Test. Polym.*, 1967, vol. 3, pp. 231–244.
26. Evans, D.C., *The Wear of Nonmetallic Materials, Proc. Symp. Tribology, Mech. Eng. Publ.*, 1978, pp. 47–55.
27. Craig, W.D., *Lubric. Eng.*, 1964, vol. 20, no. 12, pp. 456–462.
28. Lancaster, J.K., *Wear*, 1972, vol. 20, no. 3, pp. 315–333.
29. Tsukamoto, N., Mariyama, H., and Mimura, H., *JSME Int. J., Ser. C*, 1993, vol. 36, no. 4, pp. 499–506.
30. Lancaster, J.K., *J. Phys. D, Ser. 2*, 1968, vol. 1, no. 5, pp. 549–559.
31. Lancaster, J.K., *Tribol. Int.*, 1990, vol. 23, pp. 380–390.
32. Senior, J.M. and West, G.H., *Wear*, 1971, vol. 18, no. 4, pp. 311–323.
33. Tanaka, K., *Trans. ASME, J. Lubric. Technol.*, 1980, vol. 102, no. 4, pp. 526–533.
34. Mens, J.W.M. and Gee, A.W. de, *Wear*, 1991, vol. 149, nos. 1–2, pp. 255–268.
35. Kirilenko, V.P. and Zaitsev, A.L., *Trenie Iznos*, 2003, vol. 24, no. 3, pp. 289–294.
36. Zaitsev, A.L. and Kirilenko, V.P., *Trenie Iznos*, 2003, vol. 24, no. 2, pp. 210–215.
37. Kurokawa, M., Uchiyama, Y., Iwai, T., and Nagai, S., *Wear*, 2003, vol. 254, nos. 1–2, pp. 468–473.
38. McNicol, A., Dowson, D., and Davies, M., *Wear*, 1995, vols. 181–183, part 2, pp. 603–612.
39. Hu Xianguo, *Polym.-Plast. Technol. Eng.*, 2000, vol. 39, no. 1, pp. 137–150.
40. Abozin, I.Yu., Bakhareva, V.E., Ginzburg, B.M., et al., *Vopr. Materialoved.*, 2002, no. 3(31), pp. 58–67.
41. Abozin, I.Yu., Bakhareva, V.E., Ginzburg, B.M., and Tochil'nikov, D.G., *Vopr. Materialoved.*, 2002, no. 3(31), pp. 68–72.
42. Scherge, M., Li, X., and Schaefer, J.A., *Tribol. Lett.*, 1999, vol. 6, no. 2, pp. 215–220.
43. Hild, W., Opitz, A., Schaefer, J.A., and Scherge, M., *Wear*, 2003, vol. 254, no. 9, pp. 871–875.
44. Yamamoto, Y. and Takashima, T., *Wear*, 2002, vol. 253, nos. 7–8, pp. 820–827.
45. Yamamoto, Y. and Hashimoto, M., *Wear*, 2004, vol. 257, nos. 1–2, pp. 181–189.

46. Joyce, T.J., Vandelli, C., Cartwright, T., and Unsworth, A., *Wear*, 2001, vol. 250, nos. 1–12, pp. 206–211.
47. Gao, J., Mao, S., Liu, J., and Feng, D., *Wear,* 1997, vol. 212, no. 2, pp. 238–243.
48. Silva, C.N. da, Tanaka, D.K., and Sinatora, A., *Wear*, 1999, vols. 225–229, part 1, pp. 339–342.
49. Marcus, K. and Allen, C., *Wear*, 1994, vol. 178, no. 1, pp. 17–28.
50. Gong, D., Xue, Q., and Wang, H., *Wear*, 1989, vol. 134, no. 2, pp. 283–295.
51. Ginzburg, B.M. and Tochil'nikov, D.G., *Zh. Tekh. Fiz.*, 2001, vol. 71, no. 2, pp. 120–124.
52. Beer, F., Ggel, A., Martin, K., et al., *J. Mater. Chem.*, 1997, vol. 7, no. 8, pp. 1327–1330.
53. Potalitsyn, M.G., Alekhin, O.S., Khisamutdinov, R.S., et al., Modification of Kaprolon with Fulleroid Materials, *Programma 3-i Mezhdunarodnoi nauchno-tekhnicheskoi konferentsii "Polimernye kompozity v tribotekhnike. Problemy sozdaniya i primeneniya. Opyt ekspluatatsii"* (Program of 3rd Int. Scientific and Technical Conf. "Polymeric Composites in Tribotechnology. Problems of Development and Use. Working Experience"), St. Petersburg: Prometei, April 26–28, 2005.
54. RF Patent 2216553.
55. Klestov, M.I. and Sokov, E.V., *Sudostroenie*, 1998, no. 3, pp. 36–39.
56. Chou, T.W., Textile Structural Composites, Their Processing and Properties, *Polymeric Composites—Expanding the Limits: 18th Riso Int. Symp. on Materials Science*, Sept. 1–5, 1997, pp. 15–24.
57. Konkin, A.A., *Uglerodnye i drugie zharostoikie voloknistye materially* (Carbon-Type and Other Refractory Fibrous Materials), Moscow: Khimiya, 1974.
58. *Uglerodnye volokna i uglekompozity* (Carbon Fibers and Their Composites), Fitzer, E.M., Ed., Moscow: Mir, 1988.
59. Difendorf, R.I. and Takarsky, E., *Polym. Eng. Sci.*, 1975, vol. 15, no. 3, pp. 150–159.
60. Bennet, S.C. and Johnson, D.I., *Carbon*, 1979, vol. 17, pp. 25–39.
61. Bezruk, A.I. and Khoreva, G.B., *Mekh. Kompoz. Mater.*, 1982, no. 3, pp. 15–18.
62. Fridman, L.I., Perlin, V.A. and Tarasova, V.V., *Uglevoloknistye sorbenty: Obzornaya informatsiya, Promyshlennost' khimicheskikh volokon* (Carbon-Fiber Sorbents: Review Inf., Chemical Fiber Indistry), Leningrad: NIITEKhIM, 1987.
63. Giltrow, I.P. and Lancaster, J.K., *Nature*, 1967, vol. 214, no. 5093, pp. 1106–1107.
64. Carbon Fibre Reinforced Plastics Tribo/Comp. TDF for Bearings, *Flight Int.*, 1987, no. 7, pp. 16–20.
65. Bakhareva, V.E., Kuz'min, V.N., Nikolaev, G.I., and Kholupko, E.P., *Sudostr. Prom-st., Materialoved.: Polim. Kompoz. Mater.*, 1991, issue 17, pp. 94–98.
66. Kryzhanovskii, V.K., *Iznosostoikie reaktoplasty* (Wear-Resistant Thermosetting Plastics), Leningrad: Khimiya, 1984.
67. Bakhareva, V.E, Nikolaev, G.I., and Panfilov, N.A., *Vopr. Materialoved.*, 1999, no. 3(20), pp. 261–276.
68. Nikolaev, G.I. and Panfilov, N.A., *Sudostroenie*, 1999, no. 4, pp. 59–61.
69. US Patent 5662993.
70. German Patent 4430130.
71. Trukizoe, T. and Ohmae, N., *Fibre Sci. Technol.*, 1983, vol. 18, no. 4, pp. 742–746.
72. Bakhareva, V.E., Utkina, V.F., and Abozin, I.Yu., *Sudostr. Prom-st., Materialoved.: Polim. Kompoz. Mater.*, 1991, issue 17, pp. 12–19.
73. RF Patent 2153107.
74. Bakhareva, V.E., Abozin, I.Yu., and Rybin, V.V., *Vopr. Materialoved.*, 2001, no. 2(26), pp. 9–21.
75. Jacobs, O., Jaskulka, R., Yang, F., and Wu, W., *Wear*, 2004, vol. 256, no. 1–2, pp. 9–15.
76. Nikolaev, G.I., Abozin, I.Yu., Bakhareva, V.E., et al., *Vopr. Materialoved.*, 2001, no. 2(26), pp. 30–38.
77. Abozin, I.Yu., Bakhareva, V.E., Lobyntseva, I.V., et al., *Vopr. Materialoved.*, 2001, no. 2(26), pp. 38–44.
78. Abozin, I.Yu., Bakhareva, V.E., Ginzburg, B.M., et al., *Vopr. Materialoved.*, 2002, no. 3(31), pp. 49–58.
79. Abozin, I.Yu., Bakhareva, V.E., Blyshko, I.V. and Nikolaev, G.I., *Vopr. Materialoved.*, 2001, no. 2(26), pp. 54–61.
80. Abozin, I.Yu., Anisimov, A.V., Bakhareva, V.E., et al., *Vopr. Materialoved.*, 2003, no. 3(35), pp. 7–15.
81. Tochil'nikov, D.G. and Ginzburg, B.M., *Vopr. Materialoved.*, 2002, no. 3(31), pp. 39–48.
82. Anisimov, A.V., Bakhareva, V.E., Panfilov, N.A., et al., *Vopr. Materialoved.*, 2002, no. 3(31), pp. 73–77.
83. Anisimov A.V., Bakhareva V.E., Blyshko I.V., et al., Anisotropy and Effect of Modification of Carbon-Reinforced Plastics on Their Tribotechnical Properties, *Programma 3-i Mezhdunarodnoi nauchno-tekhnicheskoi konferentsii "Polimernye kompozity v tribotekhnike. Problemy sozdaniya i primeneniya. Opyt ekspluatatsii"* (Program of 3rd Int. Scientific and Technical Conf. "Polymeric Composites in Tribotechnology. Problems of Development and Use. Working Experience"), St. Petersburg: Prometei, April 26–28, 2005.
84. Ginzburg, B.M., Tochil'nikov, D.G., Bakhareva, V.E., and Rybin, V.V., *Probl. Mashinostr. Nadezhn. Mashin*, 2003, no. 4, pp. 46–52.

ISSN 1070-4272. Russian Journal of Applied Chemistry, 2006, Vol. 79, No. 5, pp. 707–710. © Pleiades Publishing, Inc., 2006.
Original Russian Text © I.I. Obraztsova, G.Yu. Simenyuk, N.K. Eremenko, 2006, published in Zhurnal Prikladnoi Khimii, 2006, Vol. 79, No. 5, pp. 717–720.

INORGANIC SYNTHESIS AND INDUSTRIAL INORGANIC CHEMISTRY

Preparation of Ultradisperse Copper Powders by Reduction of Copper Salts with *L*-Ascorbic Acid and Electrically Conducting Formulations Based on These Powders

I. I. Obraztsova, G. Yu. Simenyuk, and N. K. Eremenko

Kemerovo Branch, Institute of Solid-State Chemistry and Mechanochemistry, Siberian Division, Russian Academy of Sciences, Kemerovo, Russia

Received January 27, 2006

Abstract—Production of ultradisperse copper powders by reduction of various copper salts with *L*-ascorbic acid was studied.

DOI: 10.1134/S1070427206050028

Synthesis and studies of ultradisperse powders (UDPs) of copper and development of electrically conducting formulations based on them is a topical area in modern science and technology. These composite materials find wide application in electronics as components of electrically conducting glues and pastes used in low-temperature soldering of parts of instruments, assembly of integrated circuits and flexible printed-circuit boards.

Previously, methods for production of copper UDP by reduction of copper sulfide with glycerol have been developed and patented [1, 2]. It was shown in [3] that chemical modification of copper UDPs makes it possible to obtain on their basis formulations with enhanced stability (epoxy formulations, more than 10 years; novolac formulations, >6 years) and low electrical resistivity (10^{-6}–10^{-7} Ω m).

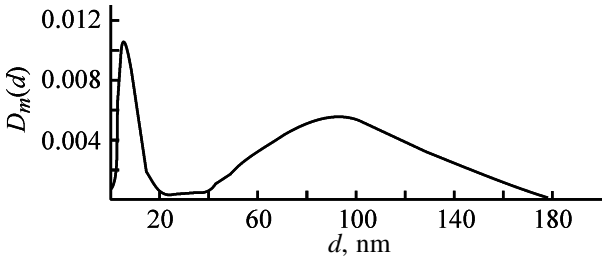
It has been shown [4] that reduction of various copper salts with sodium hypophosphite and hypophosphorous acid is performed under milder conditions (reaction temperature <95°C, reaction time 2–35 min), compared to the reduction with glycerol (130–200°C, 15–240 min), and formulations based on the resulting powders show sufficient stability and electrical conductivity. The UDPs obtained under these conditions have particle size of 8–100 nm, with about 45 wt % of particles being less than 30 nm in size. It was shown that, upon introduction of 1-naphthol and glycerol, copper-UDP-based formulations prepared by the hypophosphite method become comparable in stability and electrical conductivity with copper ultradisperse powders prepared by the reduction with glycerol.

It was noted that it is preferable to reduce copper(II) compounds with hypophosphite ions in the water–hexanol system, rather than in an aqueous medium, because hexyl alcohol adsorbed on the surface of UDPs enhances their stability and electrical conductivity via blocking of the surface of copper particles to preclude their oxidation by atmospheric oxygen. It was also shown that additional treatment of copper UDPs with formic acid makes them more stable and electrically conducting.

In this study, we examined the reduction of various copper salts with *L*-ascorbic acid. The choice of *L*-ascorbic acid is based on the fact that the reduction occurs at a low temperature of 25–60°C and does not require any intricate equipment.

The synthesis procedure is based on the reduction of copper sulfate with *L*-ascorbic acid (or with its optical isomer, *D*-erythorbic acid) in an aqueous or aqueous-ammonia medium [5]. The reaction yields an ultradisperse powder of copper and dehydroascorbic acid. The difference was in that aminoacetic acid was used as a complexing agent, in addition to ammonia, and various copper salts were reduced: formate, acetate, nitrate, and basic carbonate.

The resulting ultradisperse powders of copper were washed with water and treated with a 1% solution of hydroquinone in ethanol and stored under a layer of a 0.05% solution of stearic acid in ethanol, as mentioned in [1]. The copper UDPs obtained were used to prepare formulations with SF-010 phenol–formaldehyde novolac resin, with the content of the metallic phase equal to 80 wt %. The effect of various factors



Particle size distribution function for an ultradisperse copper powder prepared by reduction of copper sulfate with *L*-ascorbic acid. [$D_m(d)$] Weight function of particle size distribution and (d) particle size.

on the stability and electrical conductivity of the formulations was analyzed.

EXPERIMENTAL

Copper salts were reduced with *L*-ascorbic acid as follows: An aqueous solution of a copper salt was prepared in one vessel, and an aqueous solution of *L*-ascorbic acid, in another; the latter was neutralized to pH 5.5–6.5 by adding a minor amount of an alkali (NaOH or KOH) and heated to 30–35°C. Then the solution of the reducing agent was added dropwise to the solution of the copper salt under thorough continuous stirring. As a result, a UDP was formed in 3–20 min, depending on the copper salt taken. The UDP was washed with water to neutral reaction of the washing water, treated with solutions of hydroquinone and stearic acid in ethanol, and stored under a layer of a solution of stearic acid in ethanol, as described above. The yield of the metallic phase was 75–90%, depending on conditions.

According to X-ray phase analysis, the UDP obtained contained no impurities of oxides, and the average particle size was 50–55 nm. The figure shows the weight function of particle size distribution for the copper powder produced by reduction of copper sulfate with *L*-ascorbic acid. The distribution was calculated from small-angle X-ray scattering curves. It can be seen that the distribution shows two peaks at 10 and 100 nm. The weight-average size of particles, calculated from the particle size distribution function, is about 52 nm, in agreement with the results of X-ray phase analysis.

To improve the oxidation resistance, all the UDPs were treated with a solution of hydroquinone and stearic acid in ethanol.

The formulations with SF-010 phenol–formaldehyde resin, prepared on the basis of copper UDP, were kept at 140–145°C for 4 h. The stability and electrical conductivity of the copper powders were evaluated by changes in the electrical resistivity ρ of the formulations on their base during tests. The resistance of the formulations was measured in the dc mode (12 V, 2.5 mA) at room temperature (20–25°C).

Owing to their increased dispersity, the copper UDPs obtained were rather active and were easily oxidized in air; therefore, the formulations produced on their base had a rather high resistivity and were unstable in the course of time.

To eliminate these disadvantages, we examined the effect of complexing agents on the reduction of copper sulfate with *L*-ascorbic acid and on the properties of the copper powders obtained. The results obtained are listed in Table 1. As complexing agents served ammonia (sample no. 3) and aminoacetic acid (sample nos. 4, 5). A 1 M solution of ammonia or an aminoacetate buffer solution with pH 9 was introduced into a solution of *L*-ascorbic acid to pH 7. Then the solution of the reducing agent was gradually, under continuous stirring, added to a solution of copper sulfate.

It is known from the literature [6] that introduction of complexing agents shifts the redox potential of the Cu^{2+}/Cu couple to a more negative region. If the difference between the redox potentials of the reducing agent and the metal being reduced is large, a highly dispersed powder may be formed fast, occasionally even instantaneously. If the difference is small, the metal is obtained in the form of a solid layer, which mostly leads to formation of metallic films and coatings. Thus, the properties of the powders obtained can be modified by varying the concentration of the complexing agent. It was noted that, if ammonia is introduced in the amount suggested in [5], a mirror is formed on the vessel walls, which results in that the yield of the copper powder decreases dramatically. In this study, the amount of the complexing agent was chosen so as to preclude formation of a mirror. The optimal amount of the ammonia solution added was that providing pH 6–7. A smaller amount of the complexing agent failed to noticeably improve the stability and the electrical conductivity of the powders. At a higher ammonia concentration, a mirror was formed. The amount of aminoacetic acid was chosen in a similar way.

Table 1 shows that the complexing agents (ammonia and aminoacetic acid) favor a decrease in the specific surface area of the powders and make higher their stability and electrical conductivity, and treat-

Table 1. Reduction of copper sulfate with *L*-ascorbic acid in the presence of complexing agents. SF-010 novolac resin : copper UDP = 25 : 100

Sample no.	Complexing agent	τ_r, min	T_r, °C	S_{sp}, $m^2 g^{-1}$	$\rho \times 10^6$, Ω m, at indicated testing time, years		
					1 day	0.5	1
1	–	8	30–40	2.82	45.6	62.4	81.3
2*	–	8	30–40	2.82	6.5	7.6	8.5
3	Ammonia	10	30–40	1.45	3.5	3.8	4.0
4	Aminoacetic acid	10	25–30	0.33	3.5	3.7	3.8
5*	Aminoacetic acid	10	25–30	0.33	1.1	1.2	1.2

Notes: (τ_r, T_r) Time and temperature of reduction of copper salts with *L*-ascorbic acid; (S_{sp}) specific surface area of ultradisperse copper powders.
* Copper UDPs were additionally treated with formic acid.

Table 2. Reduction of various copper salts with *L*-ascorbic acid. SF-010 novolac resin : copper UDP = 25 : 100

Sample no.	Copper salt	τ_r, min	T_r, °C	$\rho \times 10^6$, Ω m, at indicated testing time, years		
				1 day	0.5	1
1	$CuSO_4 \cdot 5H_2O$	10	30–40	3.5	3.8	4.0
2	$Cu(CH_3COO)_2 \cdot 2H_2O$	20	50–60	3.2	3.5	3.7
3	$Cu(HCOO)_2$	3	25–30	3.0	3.1	3.2
4	$CuCO_3 \cdot Cu(OH)_2$	5	25–30	4.6	5.4	6.5
5	$Cu_2(C_6H_5O_7) \cdot 2.5H_2O$	15	50–60	4.8	5.5	6.8

Note: (τ_r, T_r) Time and temperature of reduction of copper salts with *L*-ascorbic acid.

ment of the powders with formic acid (sample nos. 2, 5) leads to a considerable increase in their stability and electrical conductivity, compared with the initial samples (nos. 1, 4). This agrees with the results of earlier studies [4].

Apparently, the best parameters are observed for the formulation based on the copper UDP prepared by the reduction of copper sulfate with a solution of aminoacetic acid and additionally treated with formic acid (sample no. 5).

The reduction of various organic (formate, acetate, citrate) and inorganic (sulfate, basic carbonate) salts of copper with *L*-ascorbic acid in an ammonia medium is illustrated in Table 2.

It can be seen that copper formate (sample no. 3) and basic copper carbonate (sample no. 4) are reduced at 25–30°C; copper sulfate (sample no. 1), at 30–40°C; and copper acetate and citrate (sample nos. 2, 5), at 50–60°C. All the formulations have virtually the same electrical resistivity. The most stable formulations were those based on copper sulfate, acetate, and formate (sample nos. 1–3). Therefore, the best results are obtained, as also in the case of reduction with other reducing agents, with copper formate and sulfate.

Thus, use of *L*-ascorbic acid as a copper-reducing agent makes it possible to obtain ultradisperse powders of copper and formulations on their base under milder conditions at low temperatures. These formulations are comparable in their parameters with those produced by reduction with glycerol [1–3] and sodium hypophosphite [4] and can compete with similar materials based on silver [7–9].

CONCLUSIONS

(1) Ultradisperse copper powders were prepared by reduction of various copper salts with *L*-ascorbic acid.

(2) Ultradisperse copper powders obtained in the presence of ammonia and aminoacetic acid as complexing agents possess increased stability and electrical conductivity.

REFERENCES

1. RF Patent 2 031 759.
2. RF Patent 2 115 516.
3. Obraztsova, I.I., Simenyuk, G.Yu., and Eremenko, N.K., *Zh. Prikl. Khim.*, 2002, vol. 75, no. 11, pp. 1772–1775.
4. Obraztsova, I.I., Simenyuk, G.Yu., and Eremenko, N.K., *Zh. Prikl. Khim.*, 2004, vol. 77, no. 4, pp. 386–390.
5. US Patent 4 863 510.
6. *Khimicheskoe osazhdenie metallov iz vodnykh rastvorov* (Electroless Deposition of Metals from Aqueous Solutions), Sviridov, V.V., Ed., Minsk: Universitetskoe, 1987.
7. US Patent 5 891 367.
8. US Patent 5 929 141.
9. EPV Patent 1 291 390.

ISSN 1070-4272. Russian Journal of Applied Chemistry, 2006, Vol. 79, No. 5, pp. 711–714. © Pleiades Publishing, Inc., 2006.
Original Russian Text © A.A. Kabanov, 2006, published in Zhurnal Prikladnoi Khimii, 2006, Vol. 79, No. 5, pp. 721–724.

INORGANIC SYNTHESIS AND INDUSTRIAL INORGANIC CHEMISTRY

Thermal Stability of Limestone with a Low Iron Content

A. A. Kabanov

Astaf'ev Krasnoyarsk State Pedagogical University, Krasnoyarsk, Russia

Received December 21, 2005

Abstract—The thermal stability of reagent-grade calcite and limestone samples with high and low content of iron compounds was compared. The causes of the revealed differences were discussed.

DOI: 10.1134/S107042720605003X

The properties and thermal stability of limestone with a high content (0.81 wt %) of iron(II, III) as compared to analytically pure grade $CaCO_3 \cdot 0.17H_2O$ have been considered in [1–3]. It was of interest to ascertain how they will change on passing to low iron(II, III) concentrations.

We used limestone from the Slyudyankinskoe deposit (Irkutsk oblast). Its 0.08-nm fraction was sieved after dispersion and kept over P_2O_5 for 10 days. Then the preparation was degassed at 200°C for 6 h and stabilized again by keeping over P_2O_5 for no less than 10 days. The limestone sample thus pretreated was taken as the starting sample.

The quantitative analysis of the samples was carried out according to GOSTs (State Standards) 4530–76 and 5382–91. The X-ray analysis was performed on a DRON-3 diffractometer. The mass spectra were obtained on an MI-1305 ionization spectrometer. Thermal measurements were performed in air on a Q-1500D derivatograph. The Mössbauer spectra were recorded on an electrodynamic spectrometer based on an AI-5006-3M-V100 analyzer in the constant acceleration mode. The spectra were processed on an ES-1022 computer. The ^{57}Co isotope with an activity of 0.5 GBq in a chromium matrix was the γ-radiation source. The kinetic curves of the limestone decomposition were taken at 825 ± 0.5°C with 0.100-g samples using the volumetric analysis. All the methods have been considered in more detail in [1–4].

According to the chemical analysis, limestone contains (wt %): main substance $CaCO_3$ 78.67, Ca (species other than $CaCO_3$) 8.14, Fe 0.02, K + Na 0.13, Si 2.21, Al 0.24, Mg 0.96, S 1.60, and other impurities 8.03. The X-ray phase analysis (Fig. 1) shows that the starting limestone contains $CaCO_3$ in the form of calcite, dolomite $CaMg(CO_3)_2$, calcium oxide, and gypsum $CaSO_4 \cdot 2H_2O$. The concentrations of other crystalline phases, if present, are less than 0.50%. The calculations based on the data of chemical analysis (with due regard to the data of Fig. 1) give the following mineralogical composition of the starting limestone (wt %): calcite $CaCO_3$ 78.67 (probably, with H_2O), CaO (probably, with H_2O) 3.94, gypsum $CaSO_4 \cdot 2H_2O$ 3.83, dolomite $CaMg(CO_3)_2$ 8.60, and the remaining phases 4.96.

The data on the iron minerals were obtained from the Mössbauer spectra of the samples heat-treated at 825°C for 6 days (Fig. 2). It follows from the spectrum that the isomer chemical shift is δE = 0.2 mm s^{-1}. The sensitivity in determining iron by this method is 20–30-fold higher than that of the X-ray phase analysis; to determine the effect of iron(II, III) impurities on the limestone decomposition, it is necessary to take into account the products of decomposition of its compounds at a base temperature of 825°C. The shape and parameters of the spectrum show [5] that the doublet peak in the center belongs to wüstite FeO and diffuse peaks of weak intensity at its edges, to magnetite Fe_3O_4. As a whole, the Mössbauer spectrum (Fig. 2) confirms the low concentration of iron(II, III) in the limestone.

The limestone derivatogram shows that the weight loss in air becomes noticeable starting from 360°C (Fig. 3). The maximal rate of its decomposition is at 868 ± 1°C, and the sample weight gets stabilized at about 889°C. According to the mass-spectrometric data (Fig. 4), the maximal decomposition rate of the limestone in a vacuum of 10^{-6} mm Hg is at 620 ± 1°C. A significant difference between the maximal decomposition rates (at 248°C) in air and in a vacuum is typical for calcite [6].

Three experimental maxima of limestone dehydration rate (Fig. 4) are indicative of the presence of at

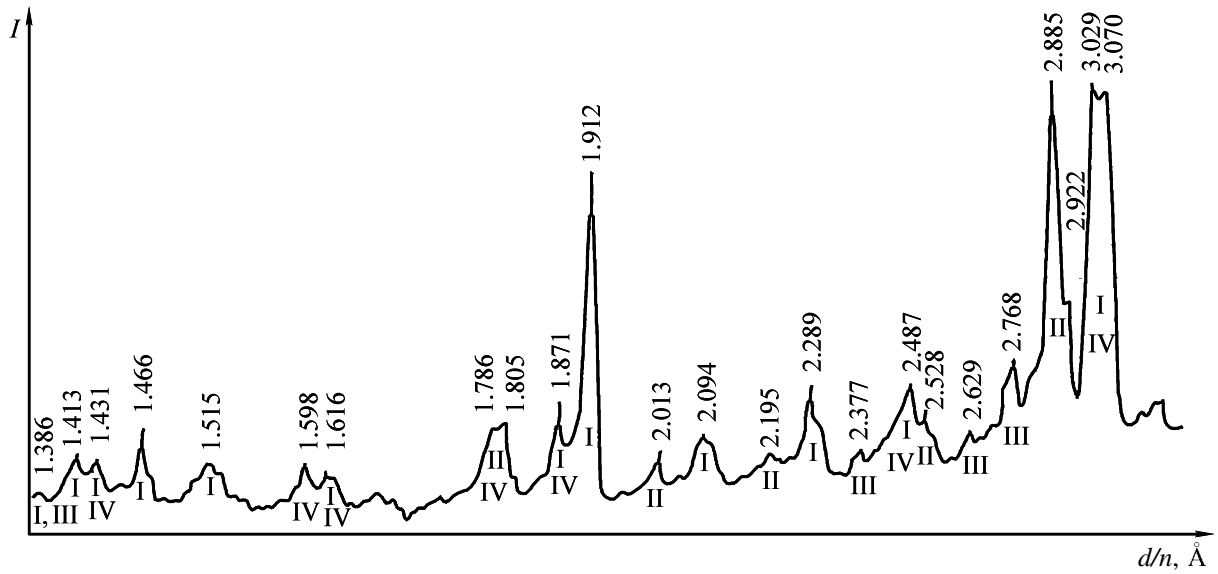


Fig. 1. X-ray diffraction pattern of the starting limestone. (*I*) Absorption intensity and (*d*/*n*) interplanar spacing. (I) $CaCO_3 \cdot 0.03H_2O$, (II) dolomite $CaMg(CO_3)_2$, (III) hydrated oxide $CaO \cdot H_2O$, and (IV) gypsum $CaSO_4 \cdot 2H_2O$.

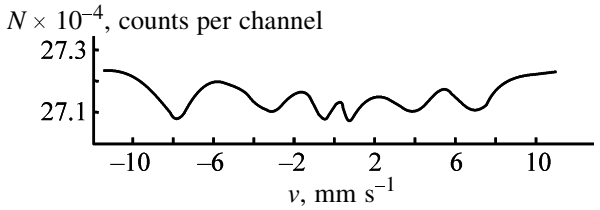


Fig. 2. Mössbauer spectrum of the limestone heated at 825 ± 1°C for 6 h. (*N*) Intensity and (*v*) velocity of the γ-ray source.

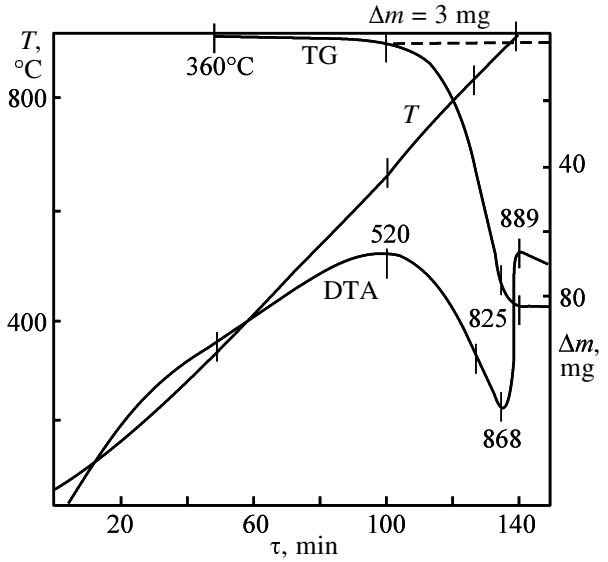


Fig. 3. Diffraction pattern of the starting limestone. m = 0.2 g, $dT/d\tau$ = 6 K min^{-1}. (*T*) Temperature, (τ) time, and (Δ*m*) weight loss.

least three centers of water localization in limestone. The total concentration of water in the limestone and its fractions in these centers can be calculated from the integral peak intensities (Fig. 4). However, first it was necessary to calibrate these areas with respect to the amount of the released water. For this purpose, we used the thermogravimetric curve (Fig. 3). The range 360–520°C in this curve shows that the limestone weight is lost solely due to H_2O release. At the same time, Fig. 4 shows that the release of water from the limestone occurs starting from 50°C (curve *1*). This

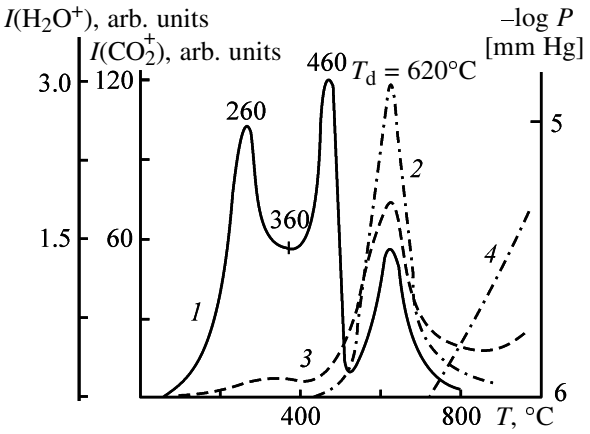


Fig. 4. Mass-spectrometric monitoring of thermal decomposition of the starting limestone. m = 0.01 g, $dT/d\tau$ = 18.0 K min^{-1}, 10^{-6} mm Hg. (*I*) Intensity and (*T*) temperature. (*1*) H_2O, (*2*) CO_2, (*3*) pressure P in the reactor, and (*4*) H_2O signal from the vessel glass.

process is not detected gravimetrically because of lower sensitivity of this method compared to mass spectrometry.

It was taken into account in the calibration that the starting limestone samples lose 3×10^{-3} g of H_2O before 520°C (Fig. 3). This region in Fig. 4 corresponds to the integral of curve *1* taken up to T = 520°C. The part of curve *1* (Fig. 4) from 50 to 360°C corresponds [7–9] to complete dehydration of gypsum $CaSO_4 \cdot 2H_2O$. The X-ray analysis (Fig. 1) and the calculation based on the data of the chemical analysis and mass spectrometry (Fig. 4) confirm this result and lead to a formula of calcium sulfate dihydrate. The 360–550°C portion of curve *1* (Fig. 4) corresponds to the temperature range of the dehydration of $Ca(OH)_2$ [10]. The X-ray diffraction pattern (Fig. 1) and the calculation based on the results of chemical analysis and mass-spectrometric data (Fig. 4) show that $CaO \cdot H_2O$, indeed, is dehydrated in this temperature range. And, finally, the third maximum at 620°C (Fig. 4, curve *1*) corresponds to the dehydration of calcite [1–4, 6]. The calculation leads to the formula $CaCO_3 \cdot 0.03H_2O$. The starting limestone loses this water only in a vacuum of 10^{-6} mm Hg at 800°C, when the decomposition of calcite itself is also complete. As a whole, the gravimetric analysis and mass spectrometry revealed 1.96 wt % H_2O in the starting limestone samples.

The kinetic curves of the analytically pure grade reagent $CaCO_3 \cdot 0.17H_2O$ (curve *1*) and of the limestone samples from the Slyudyankinskoe (curve *2*) and Solomenskoe (curve *3*) deposits are presented in Fig. 5 for comparison. All samples were prepared for the experiment [2–4] by the similar method. The kinetic curve of the limestone from the Slyudyankinskoe deposit (curve *2*) is more similar to that of reagent-grade $CaCO_3 \cdot 0.17H_2O$ than to that of the limestone from the Solomenskoe deposit (curve *3*). The similarity is manifested in the decomposition rate (as seen from the slope of the curves), in the rate of attaining the "intermediate" equilibrium, and, which is the most important, in the diffusion control of the process. This follows from the linearity of the kinetic curve after the first equilibrium is attained and reflects the independence of the decomposition rate from the sample amount.

The fact that the decomposition of the limestone from the Slyudyankinskoe deposit (85%) is complete in a shorter time can be accounted for by the presence in the starting limestone of free CaO and by high concentration of inert impurities (21.37%). They facilitate

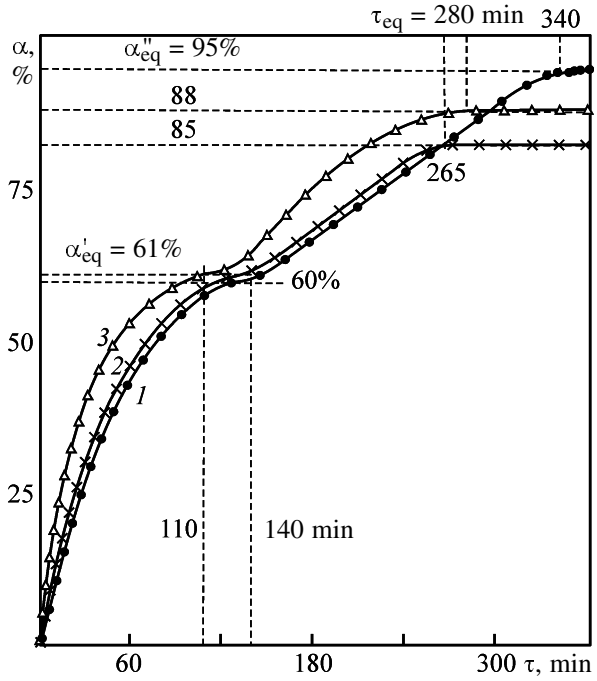


Fig. 5. Kinetic curves of the limestone decomposition at 825 ± 0.5°C. (α) Degree of the sample decomposition, (τ) time, (α'_{eq}, α''_{eq}) degree of decomposition by the moment of reaching the first and the second equilibrium, respectively, and (τ_{eq}) time of attaining the second equilibrium. Sample: (*1*) $CaCO_3 \cdot 0.17H_2O$, (*2*) limestone from the Slyudyankinskoe deposit, and (*3*) limestone from the Solomenskoe deposit.

the formation of a thick protective layer on the calcite particles that have not yet decomposed, or sorb CO_2 released from the calcite. To compare the effects exerted by the impurities of iron compounds and water on the calcite thermal stability, we present the main data on the thermal stability of different calcite samples (see table).

By comparing the data of the table, we can conclude that water bound to calcium carbonate is present not only in reagent-grade $CaCO_3$ but also in natural limestones. It is removed only after the decomposition of all the calcite modifications at 800°C in a vacuum of 10^{-6} mm Hg is complete. The fact that the maximal decomposition rates in a vacuum and in air differ by 245–250°C (see table) is typical for calcium carbonate and limestones. This conclusion was made previously in studying the thermal stability of $CaCO_3$ [6]. Without H_2O bound to $CaCO_3$, the crystalline calcite phase seems to be formed neither in laboratory conditions nor in the nature. This water plays the role of a structure-forming factor. Therefore, the effect exerted by this water on the limestone thermal stability is difficult to evaluate quantitatively. At the same

Comparative data on the thermal stability for reagent-grade calcium carbonate [GOST (State Standard) 4530–76] and limestones*

Sample	Content, wt %			T_{min}	T_{max}	H_2O (in $CaCO_3$), mole fraction	τ'_{eq}, min	References
	$CaCO_3$	Fe	H_2O	°C				
Analytically pure grade reagent	99.00	0.005	3.19	870 ± 3	620 ± 2	0.13	140	[1, 2, 6]
Limestone from Slyudyankinskoe deposit	78.67	0.020	1.96	868 ± 1	620 ± 1	0.03	130	–
Limestone from Solomenskoe deposit	95.08	0.810	7.52	825 ± 2	580 ± 2	0.06	110	[1, 2]

* Fe denotes total content of iron(II, III); H_2O denotes H_2O concentration after the treatment for 6 h at 200°C in air; T_{min}, temperature corresponding to the endothermic peak in the DTA curve; T_{max}, temperature corresponding to the maximal rate of CO_2 evolution in a vacuum of 10^{-6} mm Hg (mass-spectrometric data); H_2O (in $CaCO_3$), fraction of water directly bound to calcite; τ'_{eq}, time of attaining the first equilibrium at 825 ± 0.5°C.

time, it may be already considered that the higher the concentration of this water, the more stable the limestone. The table shows that iron(II, III) in the form of various compounds is a major impurity decreasing the thermal stability of limestone. This is consistent with the effect exerted by the additions of iron compounds on the thermal stability of reagent-grade $CaCO_3 \cdot 0.17H_2O$ [11].

CONCLUSIONS

(1) The limestone from the Slyudyankinskoe deposit (Irkutsk oblast) contains 21.33 wt % impurities, including 1.96% water, which is not removed by drying of dispersed limestone in air at 200°C for 6 h.

(2) The real composition of the limestone is as follows (wt %): $CaCO_3 \cdot 0.03H_2O$ 79.10, dolomite $CaMg(CO_3)_2$ 8.60, gypsum $CaSO_4 \cdot 2H_2O$ 3.83, hydrated calcium oxide $CaO \cdot H_2O$ 5.20, and other impurities 3.27.

(3) In the thermal stability and thermal decomposition kinetics at 825°C, the limestone from the Slyudyankinskoe deposit is closer to analytically pure grade calcite than to the limestone from the Solomenskoe deposit in which the iron(II, III) concentration is higher by a factor of 40.

(4) The fact that the limestone from the Slyudyankinskoe deposit shows slightly lower thermal stability than reagent-grade $CaCO_3$ can be accounted for by lower (by a factor of 4) content of water bound to $CaCO_3$ and by higher (by a factor of 4) iron(II, III) concentration.

REFERENCES

1. Kabanov, A.A., *Zh. Prikl. Khim.*, 2003, vol. 76, no. 7, pp. 1077–1079.
2. Kabanov, A.A., *Zh. Fiz. Khim.*, 2003, vol. 77, no. 11, pp. 1961–1965.
3. Kabanov, A.A., *Zh. Prikl. Khim.*, 2004, vol. 77, no. 9, pp. 1435–1437.
4. Kabanov, A.A., *Zh. Fiz. Khim.*, 2002, vol. 76, no. 2, pp. 227–232.
5. Kündig, W., Lindquist, R., and Constabaris, G., *Magnetic Resonance and Relaxation*, Amsterdam: North-Holland, 1967.
6. Kabanov, A.A., *Zh. Fiz. Khim.*, 2001, vol. 75, no. 4, pp. 746–748.
7. Voznesenskii, A.A., *Teplovye ustanovki v proizvodstve stroimaterialov* (Thermal Installations in Production of Building Materials), Moscow: Stroiizdat, 1964.
8. Eyrayd, C., Murat, M., and Barriac, P., *Bull. Soc. Chim. Fr.*, 1967, no. 10, pp. 3730–3735.
9. Kazimir, I., *Chem. Zvesti*, 1976, vol. 30, no. 2, pp. 167–170.
10. Bensted, I., *Cemento*, 1980, vol. 77, no. 3, pp. 169–182.
11. Kabanov, A.A., *Zh. Fiz. Khim.*, 2002, vol. 76, no. 9, pp. 1719–1721.

ISSN 1070-4272. Russian Journal of Applied Chemistry, 2006, Vol. 79, No. 5, pp. 715–721. © Pleiades Publishing, Inc., 2006.
Original Russian Text © N.G. Rachkova, I.I. Shuktomova, A.I. Taskaev, 2006, published in Zhurnal Prikladnoi Khimii, 2006, Vol. 79, No. 5, pp. 725–731.

SORPTION AND ION-EXCHANGE PROCESSES

Sorption of Uranium, Radium, and Thorium from Saline Solutions on Hydrolyzed Wood Lignin

N. G. Rachkova, I. I. Shuktomova, and A. I. Taskaev

Institute of Biology, Komi Scientific Center, Ural Division, Russian Academy of Sciences, Syktyvkar, Komi Republic, Russia

Received July 22, 2005; in final form, January 2006

Abstract—Sorption of U, Ra, and Th from multicomponent aqueous salt solutions on hydrolyzed wood lignin is studied. The mechanism of radionuclide sorption from saline solutions is suggested on the basis of the results of sequential extraction.

DOI: 10.1134/S1070427206050041

Making decision on a sorbent for deactivation of natural waters is a difficult task. Such a sorbent should meet a series of requirements; the major among them is its ability to tightly fix radionuclides. Because of a great diversity of radionuclide speciation in natural waters, it appears advisable to use polyfunctional sorbents, e.g., hydrolyzed wood lignin. We demonstrated previously [1, 2] that it tightly absorbs Th, U, and Ra from aqueous solutions of various acidities. In this case, Ra and Th are effectively sorbed at pH 3–9, and U, at pH 6–9. Our results showed that the sorption of radionuclides on lignin may proceed by several mechanisms including surface absorption of colloids and pseudocolloids, ion exchange, complexation with ionic species of radionuclides, and formation of strong sorption complexes with organic-bound species. An IR study of the U-loaded sorbent showed for the first time that the interaction of the carboxy and phenolic groups of lignin with uranium occurs as ion exchange between the hydrogen ion and uranyl and its hydrolyzed species, and also by the coordination mechanism with the formation of oxonium complexes.

In this study we examined the capacity of hydrolyzed wood lignin to sorb radionuclides from multicomponent aqueous salt solutions.

EXPERIMENTAL

Working solutions were prepared by adding potassium, calcium, and ammonium nitrates, ammonium dihydrogen phosphate, and magnesium and ammonium sulfates to a solution of dioxouranium nitrate [$UO_2(NO_3)_2$]. The elements were taken in amounts typical of soil solutions in loam podzolic soils [3]. The salinity of the resulting solution amounted to 3.3 mg-equiv l^{-1} (Table 1). The radionuclidic composition corresponded to the natural mixture of isotopes [4]. The initial concentrations of the radionuclides were as follows: Th 1.0 and 10.0 mg l^{-1}, U 1.0 and 10 mg l^{-1}, and Ra 1.19 and 11.90 ng l^{-1}, which is higher by 1–3 orders of magnitude than the maximal permissible concentrations of ^{232}Th, ^{238}U, and ^{226}Ra in potable water [5]. The initial (before sorption) pH of the liquid phase was 6. The sorption experiments were carried out in the static mode at room temperature. Each experiment was replicated three times. In all the experiments, the sorption time was 24 h. The particle size of hydrolyzed lignin was 0.25–0.5 mm. The Komarov's lignin fraction in the sorbent was 82 wt % at the ash content of 6%. Prior to use, weighed portions of hydrolyzed lignin were kept in distilled water for 1 day, to increase its specific surface area. After the sorption, the phases were separated by filtration. The degree of recovery and distribution coefficient were estimated from the metal concentration loss in the liquid phase. The concentrations of Th, U, and Ra were determined by the photometric, luminescence, and emanation methods, respectively [6–8]. The tightness of fixation of the radionuclides on the sorbent was studied by sequential extraction with distilled water and 1 M solutions of CH_3COONH_4 and HCl. The residual radionuclides in the sorbent phase constitute the so-called tightly fixed fraction. The statistical data treatment was carried out by the standard methods [9].

Table 1. Mineral composition of simulated solutions

Solution no.	K^+	NH_4^+	Mg^{2+}	Ca^{2+}	$H_2PO_4^-$	SO_4^{2-}	NO_3^-
	mg-equiv l^{-1}						
1	0	0	0	0	0	0	0
2	0.012	0.10	0.028	0.024	0.024	0.066	0.075
3	0.06	0.50	0.14	0.12	0.12	0.33	0.37
4	0.12	1.00	0.28	0.24	0.24	0.66	0.75

It is well known that the salinity of the liquid phase considerably influences the sorption efficiency [10–12]. Analysis of the published data shows that, in saline solutions, sorption on lignin is a resultant of several processes, whose contribution depends directly on the sorbent and sorbate properties. According the the theoretical concepts [10–12], the suppression of the sorption may be caused by the competition for the active sites on the background of a manyfold excess of alkaline-earth metal and other cations and also by the formation of poorly sorbable species, among them complex ions of the sorbate. Very likely, a decrease in the sorption originates from the salt effect, i.e., an increase in the solubility of precipitates in the presence of electrolytes not containing the same ions [15]. At the same time, in the presence of sufficiently high concentrations of the precipitating ions, in multicomponent systems, some additional precipitation and coprecipitation reactions can occur, as well as coagulation of radio- and pseudocolloids, thus favoring the recovery of radionuclides from the liquid phase. Furthermore, addition of electrolytes into sorption systems containing humus substances increases the association of humic acids and surface tension on the sorbents, thus promoting the physisorption of radionuclides on them [16, 17].

Our results show that the sorption of Th on hydrolyzed lignin is controlled primarily by reactions promoting its absorption (Table 2; Figs. 1a, 1b). The high degree of radionuclide recovery is observed in both the radioactive saline solutions and the solutions without addition of inorganic salts. Depending on the experimental conditions, from 95.2 to 98.9% of Th was sorbed on lignin. Increasing salinity only slightly influenced the sorption tightness (Figs. 1a, 1b). Thus, with and without addition of the mineral salts, the water-soluble and exchangeable fractions of Th in the sorbent phase were small (their total content was within 8.5%). The water-soluble fraction, which is less tightly bound to the sorbent, ranged from 2.3 to 8.4%. With increasing initial radionuclide concentration, the content of this fraction significantly ($p < 0.05$) increases. The exchangeable fraction of Th was smaller by a factor of 10 and more as compared to the water-soluble fraction, and at an initial Th concentration of 1.0 mg l^{-1}, its content was lower than the detection limit. Generally, from 91.5 to 97.0% of Th sorbed from the saline solutions was tightly bound to the sorbent. With increasing salinity, the degree of Th recovery significantly ($p < 0.01$) increased. In this case, from 28 to 41% of the adsorbed Th was very tightly fixed on the sorbent, i.e., was not eluted with reagents commonly used for such a characterization. Comparative analysis of the sorption characteristics shows that introduction of calcium, potassium, ammonium, and magnesium salts into the solution increased the selectivity of Th sorption on lignin in five cases of six. In four cases, the Th distribution coefficient significantly ($p < 0.001$ and 0.05) exceeded the values obtained without addition of the mineral salts. Particularly, at an initial Th concentration of 10.0 mg l^{-1} it increased from 127.5 to 320 ml g^{-1}. Thus, in most cases, with increasing salinity, the Th sorption selectivity significantly increases as well as the tightly fixed fraction, whereas the less tightly bound fractions (soluble in water and ammonium acetate solution) decrease. The sorption from less concentrated Th solutions is characterized by higher distribution coefficients and desorption parameters, all other conditions being equal. It follows from the corresponding chemical equilibrium equations and solubility products that, in our sorption system, highly selective precipitation of Th as a phosphate should occur [SP $Th_3(PO_4)_4 = 2.6 \times 10^{-79}$] [18]. Our estimates show that the initial phosphate concentration in the solution was at least 1.9×10^{-11} M. In our experiments, the Th concentration was 4.3 and 43.0 μM, i.e., the liquid phase contained Th and phosphate in concentrations sufficient for the precipitation of thorium phosphate. However, visually we observed no formation of a precipitate. Most likely, the precipitation is suppressed through stabilization and masking of the Th cations and its hydrolyzed species with some organic com-

Table 2. Sorption efficiency of radionuclides from saline solutions on hydrolyzed wood lignin [initial Th, U, and Ra concentrations in the liquid phase are 1.0, 1.0, and 1.19×10^{-6} (upper row) and 10.0, 10.0, and 11.9×10^{-6} mg l^{-1} (lower row), respectively]

Solution no.	Radionuclide	Concentration in liquid phase after sorption, mg l^{-1}	Distribution coefficient, ml g^{-1}	Degree of recovery, %
1 (reference)	Th	0.03 ± 0.01	340.0 ± 10.0	98.27 ± 0.07
		0.75 ± 0.00	127.5 ± 0.4	95.47 ± 0.03
	U	0.09 ± 0.02	107.0 ± 9.0	94.60 ± 0.40
		5.20 ± 0.08	13.2 ± 0.4	69.00 ± 7.00
	Ra	$(0.11 \pm 0.02) \times 10^{-6}$	73.0 ± 7.0	92.30 ± 0.60
		$(3.51 \pm 0.27) \times 10^{-6}$	23.0 ± 2.0	79.00 ± 2.00
2	Th	0.027 ± 0.001	380.0 ± 10.0	98.47 ± 0.07
		0.80 ± 0.01	119.0 ± 2.0*	95.20 ± 0.10*
	U	0.03 ± 0.00**	300.0 ± 40.0**	97.90 ± 0.30**
		13.66 ± 0.73	17.0 ± 3.0	73.00 ± 5.00
	Ra	$(0.14 \pm 0.08) \times 10^{-6}$	150.0 ± 70.0	92.00 ± 5.00
		$(1.62 \pm 0.54) \times 10^{-6}$*	70.0 ± 20.0	90.00 ± 4.00
3	Th	0.025 ± 0.001	390.0 ± 10.0*	98.50 ± 0.06
		0.55 ± 0.02***	177.0 ± 5.0***	96.70 ± 0.10***
	U	0.08 ± 0.01	120.0 ± 10.0**	94.50 ± 0.60
		5.37 ± 0.41	17.0 ± 2.0	68.00 ± 3.00
	Ra	$(0.14 \pm 0.05) \times 10^{-6}$	90.0 ± 30.0	92.00 ± 5.00
		$(2.02 \pm 0.02) \times 10^{-6}$*	43.4 ± 0.6	90.00 ± 4.00
4	Th	0.019 ± 0.000	520.0 ± 10.0***	98.87 ± 0.03**
		032 ± 0.05***	320.0 ± 40.0***	98.10 ± 0.20***
	U	0.03 ± 0.00***	380.0 ± 20.0***	98.43 ± 0.07***
		5.77 ± 0.41	12.0 ± 1.0	66.00 ± 2.00
	Ra	$(0.27 \pm 0.03) \times 10^{-6}$**	22.8 ± 0.0**	82.80 ± 0.00***
		$(2.42 \pm 0.02) \times 10^{-6}$*	35.3 ± 0.3**	85.50 ± 0.10*

Note: The differences from the reference are significant at the following levels: * $p < 0.01$, ** $p < 0.01$, and *** $p < 0.001$.

pounds [12, 19–21]. Note that the presence of organics is inevitable in weakly acidic solutions in equilibrium with lignin. Our results show that Th is sorbed by the same mechanism from both saline solutions and solutions with no addition of mineral salts. As the dominating mechanisms we suggest the coordination of hydrolyzed Th species to the electron-donor groups of the sorbent and also the adsorption of Th complexes with humus acids, including colloid and pseudocolloid complexes. It may be suggested also that, in saline solutions, these processes are promoted by the solubilization of humus acids associated with the lignin matrix, followed by their coagulation. Less tightly fixed Th species are, presumably, those physisorbed or absorbed through incorporation of Th in the associates formed by the low-molecular-weight fraction of humus matter. In weakly saline solutions (solution no. 2), the increase in the fraction of less tightly bound Th species in the sorbent phase is accompanied by the statistically significant ($p < 0.05$) decrease in the sorption efficiency and selectivity. Most likely, this is due to changes in the surface properties of lignin and also due to the salt effect. In this case, the indicated suppressing effects surpass the contribution of the factors promoting the sorption. In more concentrated saline solutions, the major factor controlling the sorption is thought to be the coagulation.

The sorption of uranium is characterized by small contribution of the ion-exchange mechanism and relatively equal distribution of U between other fractions obtained by sequential extraction (Figs. 1c, 1d). The efficiency and selectivity of U sorption depend on its initial concentration to a larger extent than on the salinity of the liquid phase. The tenfold increase in the U concentration resulted in a statistically significant ($p < 0.001$) decrease in the distribution coefficient from several hundreds to 12–17 ml g^{-1}, which was accompanied by the decrease in the sorption efficiency from 94.5–98.4 to 66–73%. In this case, we observed a change in the fraction distribution of U. The acid-

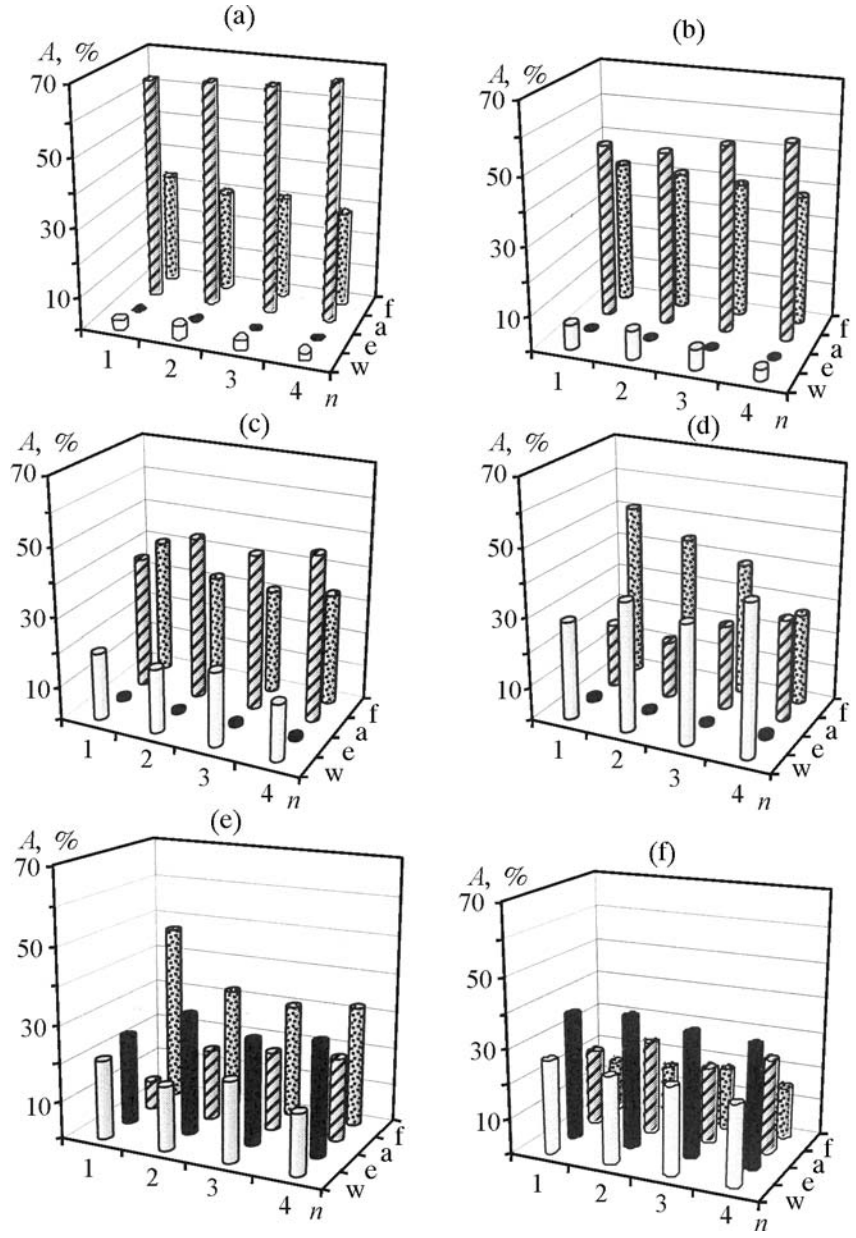


Fig. 1. Fraction distribution of radionuclides in hydrolyzed lignin at various initial radionuclide concentrations. (*A*) Sorption and (*n*) solution number. Fractions: (w) water-soluble, (e) exchangeable, (a) acid-soluble, and (f) tightly fixed. Radionuclide concentration in the liquid phase, mg l^{-1}: Th: (a) 1.0 and (b) 10.0, U: (c) 1.0 and (d) 10.0, Ra (ng l^{-1}): (e) 1.19 and (f) 11.9.

soluble fraction decreased from 39–49 to 17–30%, while the water-soluble fraction increased from 16.8–22 to 29–44%. At the same time, an increase in the salinity of the liquid phase had practically no effect on the sorption, all other conditions being equal. At higher initial concentration of U in the liquid phase, the salt effect was more clearly pronounced. In this case, with increasing salinity, the fixed fraction significantly decreased ($p < 0.05$). These results suggest that the contributions of different sorption mechanisms depend primarily on the initial U speciation in the liquid phase, and only in the second place, on the functionality and other characteristics of lignin. Strong fixation of U is suggested to occur through coordination of its hydrolyzed species to the active electron-donor sites of the sorbent, adsorption of U complexes with humus acids, and precipitation of poorly soluble uranyl phosphates on the lignin surface. A significant contribution of the latter mechanism is supported by both our and published data. For example, in the case

of solution no. 4 (Table 1), after addition of ammonium dihydrogen phosphate, the equilibrium concentrations of the dihydrogen phosphate, hydrogen phosphate, and phosphate ions are estimated to be 0.24×10^{-3}, 1.5×10^{-5}, and 1.9×10^{-11} M, respectively ($K_{disII} = 6.34 \times 10^{-8}$, $K_{disIII} = 1.26 \times 10^{-12}$). It was demonstrated [22] that, in weakly acidic and neutral natural waters with a phosphate concentration above 1 μM, U occurs predominantly in the form of uranyl phosphate complexes. Therefore, in the liquid phase of our sorption system, various uranyl phosphate complexes should be formed, which, competing with the hydrolysis and complexation with humus acids and thus changing the initial U speciation, could significantly alter the sorption mechanisms and parameters. At a U concentration of 10.0 mg l^{-1} (42.0 μM), the solubility products of several phosphate complexes are attained at once (SP $UO_2HPO_4 = 2.11 \times 10^{-11}$, SP $NH_4UO_2PO_4 = 4.36 \times 10^{-27}$, and SP $KUO_2PO_4 = 7.76 \times 10^{-24}$) [11, 18]. We monitored their formation by changes in the color and clarity of the initial uranyl nitrate solutions and also in the U sorption efficiency. With increasing salinity of the uranyl nitrate solution, the water- and acid-soluble fractions of U in the sorbent phase increased. The increase in the former fraction can be attributed to the facilitated physisorption of soluble organic and uranyl phosphate complex ions and compounds. Most likely, the most part of the acid-soluble fraction is composed by the above-mentioned poorly soluble phosphates.

In the solutions with a uranium concentration of 1.0 mg l^{-1}, the salinity level only slightly influenced the sorption capacity of lignin. In this case, not the salt concentration, but the fact itself of the increased salinity of the initial solutions is of the critical importance for the change in the sorption characteristics. The reason could be in some specific reactions not affected drectly by the ionic composition of the liquid phase, but indirectly subjected to its modifying effect. The processes promoting strong fixation of U on lignin are coordination of hydrolyzed uranyl ions to the active electron-donor sites and adsorption of complexes with humus acids. In solutions of higher salinity, these processes are promoted by the coagulation, as demonstrated by a strong tendency of lignin to absorb hydolyzed radionuclide species [11] and also by the clearly pronounced dependence of the U sorption on its initial concentration in the liquid phase.

The sorption on lignin reduced the Ra concentration in the saline solutions by a factor of 3.5–11 (Table 2). The degree of Ra recovery ranged from 79 to 92%, from 37 to 54% of the adsorbed element being tightly fixed on the sorbent. The Ra sorption selectivity increased in the saline solutions, but remained rather low (distribution coefficient ranged from 23 to 150 ml g^{-1}). Generally, the selectivity increased with increased salinity, as demonstrated by five experiments. Statistically significant difference of the selectivity from the reference solution (no addition of mineral salts) was observed in two experiments ($p < 0.05$). In this case, on the one hand, the presence of competing ions stimulated an increase in the selectivity, but on the other hand, the same effect was observed with decreasing salinity level within the experimental range (0.3–3.3 mg-equiv l^{-1}). In the solutions of higher salinity (solution no. 4) with a lower initial radionuclide concentration, we observed significant changes in the fraction composition of the adsorbed species (Fig. 1e, 1f).

The desorption of radium is characterized by relatively uniform distribution of Ra between the fractions obtained by sequential extraction (Figs. 1c, 1d). A considerable amount of Ra was found in the solution obtained after treatment with 1 M ammonium acetate, which is consistent with the alkaline-earth nature of the sorbate, suggesting a significant contribution of sorption by the ion-exchange mechanism. At the same initial Ra concentration, the salinity level only slightly influenced the amounts of the water-soluble and exchangeable fractions in the sorbent phase, demonstrating strong fixation of Ra. At the same time, with increasing Ra concentration, we observed a statistically significant decrease of the tightly fixed fraction from 30–32 to 15–18% ($p < 0.05$). At a Ra concentration of 1.19 ng l^{-1}, with increasing salinity level, the amount of the acid-soluble fraction increased from 7.7 to 19–22% and the tightly fixed fraction decreased from 47 to 30–32%.

Our results show that the selectivity and efficiency of sorption on hydrolyzed wood lignin increase with increasing salinity and decreasing starting radionuclide concentration in the liquid phase. Furthermore, the sorption characteristics could be strongly affected by the mobilization of the native ions from the sorbent into the solution. Previously Khmelinin [23] reported that addition of salts into the liquid phase promotes solubilization of the potassium, sodium, calcium, and magnesium ions from lignin. It is known also that, when the calcium ions and organic substances are simultaneously present in the solution, the degree of Ra recovery with natural sorbents generally increases [24]. In this regard we suggested that the increased efficiency and selectivity of radionuclide sorption from saline solutions is caused by its ion-exchange

reactions stimulated by the solubilization of the native elements from lignin, and also by the occlusion of the radionuclide with formation of colloidal aggregates of humus acid compounds with components of the liquid phase. The observed statistically significant decrease in the degree of recovery ($p < 0.001$) and distribution coefficient ($p < 0.01$) in solution no. 4 with a total salinity of 3.3 mg-equiv l^{-1} and a Ra concentration of 1.19 ng l^{-1} can be attributed to partial degradation of these colloidal structures by virtue of the salt effect.

CONCLUSIONS

(1) In aqueous solutions with a salinity from 0.3 to 3.3 mg-equiv l^{-1}, containing potassium, calcium, and ammonium nitrates, ammonium dihydrogen phosphate, and magnesium and ammonium sulfates, hydrolyzed lignin keeps its sorption capacity with respect to uranium, radium, and thorium. Several mechanisms controlling the sorption characteristics of radionuclides in saline solutions act simultaneously. The sorption of Th is characterized by small amount of water-soluble and exchangeable Th species in the lignin phase, while the sorption of U, by a small amount of the element in the exchangeable fraction and nearly equal distribition between the other fractions. In the case of Ra, the element is practically equally distributed among the fractions different in the tightness of fixation on lignin.

(2) The increase in the salinity level and decrease in the initial Th and Ra concentrations result in increasing degree of recovery and sorption selectivity of the elements, as demonstrated by the increase in their distribution coefficients and in the fraction of tightly fixed radionuclide species. The coagulation of colloid compounds can play a significant role in absorption of Th from saline solutions. The increased Ra sorption efficiency from saline solutions is caused, most likely, by ion-exchange reactions stimulated by the solubilization of the native elements from lignin, and also by the occlusion of the radionuclide with formation of colloidal aggregates of humus acid compounds with components of the liquid phase.

(3) At a fixed U concentration, increasing salinity has no effect on its absorption or results in statistically insignificant changes. With increasing U concentration from 1.0 to 10.0 mg l^{-1}, the distribution coefficient as well as the fraction of tightly fixed U species significantly decrease. Strong fixation of U is suggested to proceed through coordination of its hydrolyzed species to the active electron-donor sites of the sorbent, adsorption of U complexes with humus acids, and precipitation of poorly soluble uranyl phosphates on the lignin surface.

REFERENCES

1. Rachkova, N.G., Shuktomova, I.I., and Taskaev, A.I., *Zh. Prikl. Khim.*, 2004, vol. 77, no. 3, pp. 474–477.
2. Rachkova, N.G., Shuktomova, I.I., Karmanov, A.P., and Kocheva, L.S., *Tr. Komi Nauchn. Tsentra Ural. Otd. Ross. Akad. Nauk*, 2003, no. 172, pp. 67–80.
3. Archegova, I.B., *Pochvovedenie*, 1976, no. 5, pp. 66–75.
4. Titaeva, N.A., *Yadernaya geokhimiya* (Nuclear Geochemistry), Moscow: Mosk. Gos. Univ., 1992.
5. *Normy radiatsionnoi bezopasnosti (NRB-99): Gigienicheskie normativy* (Radiation Safety Regulations (NRB-99): Hygienic Standards), Moscow: Tsentr Sanitarno-Epidemiologicheskogo Normirovaniya, Gigienicheskoi Sertifikatsii i Ekspertizy Minzdrava Rossii, 1999.
6. Kuznetsov, V.I. and Savvin, B.N., *Radiokhimiya*, 1961, vol. 3, no. 1, pp. 79–86.
7. Dobrolyubskaya, T.S., *Analiticheskaya khimiya urana* (Analytical Chemistry of Uranium), Moscow: Nauka, 1962.
8. Starik, I.E., *Osnovy radiokhimii* (Principles of Radiochemistry), Leningrad: Nauka, 1969.
9. Lakin, G.F., *Biometriya* (Biometry), Moscow: Vysshaya Shkola, 1990.
10. Rozhkova, E.V., Razumnaya, E.G., Serebryakova, M.B., and Shcherbak, O.V., in *Proc. 2nd Geneva Conf.*, Geneva, 1956, vol. 3.
11. *Osnovnye cherty geokhimii urana* (Major Features of Uranium Geochemistry), Vinogradov, A.P., Ed., Moscow: Akad. Nauk SSSR, 1963.
12. Kuznetsov, Yu.V., Shchebetkovskii, V.N., and Trusov, A.G., *Osnovy ochistki vody ot radioaktivnykh zagryaznenii* (Principles of Water Treatment To Remove Radionuclides), Moscow: Atomizdat, 1974.
13. Dent, A.J., Ramsay. J.D.F., and Swanton, S.W., *J. Colloid Interface Sci.*, 1992, vol. 150, no. 1, pp. 45–60.
14. Tsunashima, A., Brindley, G.W., and Bastovanov, M., *Clays Clay Miner.*, 1981, vol. 29, no. 1, pp. 10–16.
15. Zolotov, Yu.A., Dorokhova, E.N., Fadeeva, V.I., et al., *Osnovy analiticheskoi khimii* (Principles of Analytical Chemistry), Moscow: Vysshaya Shkola, 1996.
16. Koganovskii, A.M. and Rovinskaya, T.M., *Kolloidn. Zh.*, 1955, vol. 17, no. 2, pp. 81–89.

17. Flaig, W. and Beutelspacher, H., in *Isotopes and Radiation. Soil Organic Matter Studies*, Vienna, 1968, pp. 23–30.
18. Lur'e, Yu.Yu., *Spravochnik po analiticheskoi khimii* (Handbook of Analytical Chemistry), Moscow: Khimiya, 1989.
19. Dement'ev, V.S. and Syromyatnikov, N.G., *Geokhimiya*, 1965, no. 2, pp. 211–216.
20. Choppin, G.R., *Trans. Am. Nucl. Soc*., 1979, vol. 32, pp. 166–167.
21. Znang, Y.J., Bryan, N.D., Livens, F.R., and Jones, M.N., *Environ. Pollution*, 1997, vol. 96, no. 3, pp. 361–367.
22. *Transuranic Elements in the Environment*, Hanson, W.C., Ed., Technical Information Center, US Department of Energy, 1980.
23. Khmelinin, N.G., *Pogloshchenie biofil'nykh elementov ligninom i koroi* (Absorption of Biophilic Elements by Lignin and Bark), Syktyvkar, 1994.
24. Gil', T.V., in *Radiologicheskoe issledovanie pochv, rastenii i zhivotnykh biogeotsenozov Severa* (Radiological Study of Soils, Plants, and Animals of Northern Biogeocenoses), Syktyvkar, 1983, pp. 84–88.

ISSN 1070-4272. Russian Journal of Applied Chemistry, 2006, Vol. 79, No. 5, pp. 722–726. © Pleiades Publishing, Inc., 2006.
Original Russian Text © N.V. Sych, N.T. Kartel', A.D. Nikolaichuk, V.V. Strelko, N.N. Tsyba, V.A. Denisovich, 2006, published in Zhurnal Prikladnoi Khimii, 2006, Vol. 79, No. 5, pp. 732–736.

SORPTION AND ION-EXCHANGE PROCESSES

Integrated Processing of Anthracite into Sorption Materials

N. V. Sych, N. T. Kartel', A. D. Nikolaichuk, V. V. Strelko, N. N. Tsyba, and V. A. Denisovich

Institute of Sorption and Problems of Endoecology, National Academy of Sciences of Ukraine, Kiev, Ukraine

Received January 16, 2006

Abstract—The possibility of using anthracite to produce activated carbon in the form of microporous and mesoporous anthracite, a cation exchanger, and composite sorption materials was analyzed and the porometric properties of a variety of sorption materials based on anthracite from the Donets coal basin were studied. A flowsheet for integrated processing of anthracite to give a set of four products was composed.

DOI: 10.1134/S1070427206050053

The intensive development of sorption techniques imposes increasingly stringent requirements to such properties of adsorbents as the sorption capacity determined by their porous structure, content of surface functional groups, and service characteristics associated with purity, abrasion resistance, and cost [1].

A promising application field of carbon adsorbents is storage of gaseous and liquid substances and accumulation of gases, which makes it possible to raise the sorption capacity of a cylinder with an adsorbent and enables its use at lower pressures (≤35 atm) without any decrease in volume [2].

Fossil coals used as one of the main raw materials for production of various carbon adsorbents satisfy these requirements to a considerable extent [3–6].

Among a wide variety of precursors for production of activated carbons, anthracite is one of the best suitable raw materials [7–11].

An important prerequisite for production of adsorbents from anthracite is that the fine fraction produced in coal mining is virtually a waste. Moreover, such grainy starting material does not require any additional grinding; only a necessary fraction is to be selected. All these factors make anthracite fines an inexpensive, readily accessibly, and plentiful raw material for manufacture of high-quality highly porous sorption materials.

The attractiveness of this kind of raw materials is also due to the high content of carbon and low ash content, as well as to the high mechanical strength of the final product, activated carbon.

All the above-mentioned application fields of adsorbents predetermine the necessity for integrated processing of anthracite, which extends the assortment of inexpensive adsorbents, including composite sorption materials [12], which compare well in quality and service characteristics with industrially manufactured activated carbons.

This study is devoted to a search for ways of integrated use of highly metamorphized anthracite in manufacture of sorption materials. Previous publications describe production of a single type of activated carbon in anthracite processing [8–10, 13]. Here we made an attempt to process anthracite to obtain an assortment of adsorbents differing in the pore structure and, consequently, used in different sorption processes. Conversion of anthracite fines into activated carbons is a topical task, because this would allow manufacture of inexpensive mechanically strong adsorbents suitable for a wide variety of applications.

The integrated processing of anthracite into various-purpose carbon adsorbents consists in that technological procedures are carried out successively and in parallel with the aim of the most complete utilization of anthracite.

Integrated use of such a raw material is intimately associated with the most advanced and economical form of organization of the chemical process, combined production [14]. A characteristic example of combining is, in this case, utilization of wastes formed in the main process to organize additional processing of anthracite into disperse powders to be used in manufacture of composite sorption materials [15].

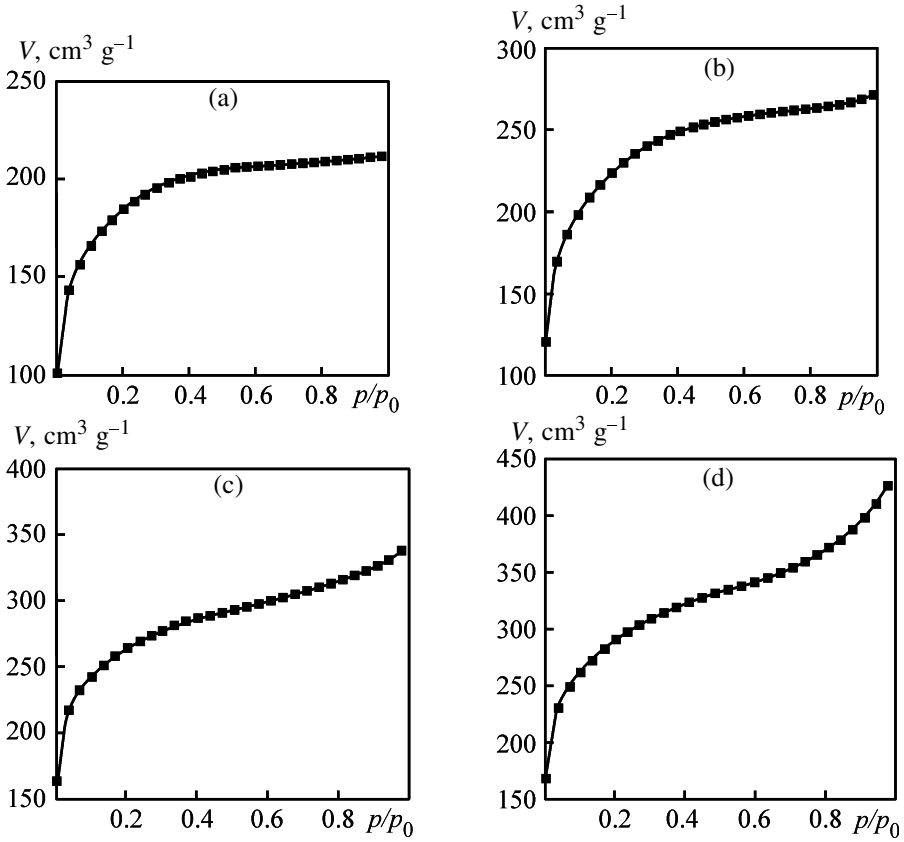


Fig. 1. Adsorption isotherms of sorption materials produced from anthracite. Adsorbent: (a) microporous, (b) cation exchanger, (c) mesoporous, and (d) composite sorbing material. (V) Volume of sorption pores and (p/p_0) relative pressure.

The basic principles to which the authors adhered in designing a scheme for integrated processing of anthracite consist in that the technology developed should be low-waste and power-saving.

Anthracite of brand A from the Donets coal basin (Sverdlovsk, Lugansk oblast, Ukraine) served as the starting material. The content of the main components in the raw material was as follows (%): A^c = 4–5, V^{daf} = 6–7, C^{daf} = 95. The anthracite particle size was 0.5–2.0 mm; initial volume of sorption pores for benzene, less than 0.01 $cm^3\ g^{-1}$; and bulk density, 0.94 $g\ cm^{-3}$.

The starting raw material was subjected to the following kinds of processing:

(i) physical activation with steam to give a microporous adsorbent;

(ii) chemical activation with $NaNO_3$ as a catalytic additive to give a mesoporous adsorbent;

(iii) physical activation with steam, with the subsequent oxidation with air, to give a cation exchanger;

(iv) formation of composite sorbing materials with a novolac resin as a binder.

An important characteristic of sorption materials is their pore structure. Therefore, the study is mainly focused on porosity characteristics of anthracite samples obtained in processing.

The pore structure of the sorption materials obtained was analyzed on the basis of the isotherms of low-temperature adsorption of nitrogen, measured with a Quantachrom Nova 2200 device. The data obtained were used to calculate the BET specific surface area and other porometric characteristics.

The adsorption isotherms of the sorption materials produced from anthracite and studied here are shown in Figs. 1a–1d.

The adsorbent produced by physical activation has a rather developed porous structure with predominance of micropores. The pore structure parameters are given in the table.

Chemical activation with a catalytic additive changes the porous structure of anthracite (Fig. 1b). The adsorption isotherm clearly shows an increase in the fraction of mesopores. This indicates that the pore

Variation of porometric parameters of activated carbons produced from anthracite

Sorbent	Combustion loss ω, %	V_S for C_6H_6, $cm^3\ g^{-1}$	S_{sp} by BET, $m^2\ g^{-1}$	V_{micro}, $cm^3\ g^{-1}$	ΣV, $cm^3\ g^{-1}$	V_{micro}/V_{tot}
Microporous adsorbent	65–70	0.35–0.42	593	0.25	0.33	0.76
Carbon cation exchanger	68–70	0.39–0.40	731	0.27	0.42	0.65
Mesoporous adsorbent	82–85	0.60	831	0.30	0.52	0.58
Composite sorbing materials	45–50	0.54–0.67	936	0.35	0.66	0.53

structure can be varied by selecting the type of activation.

Oxidation of preliminarily activated anthracite with atmospheric oxygen makes it possible to change the pore structure, which is manifested in that the volume of nitrogen absorbed at –196°C increases. Figure 1c shows an absorption isotherm of oxidized anthracite, cation exchanger.

Compounding of activated anthracite with a novolac phenol–formaldehyde resin as a binder yields a sorption material with a highly developed porous structure, with predominance of the mesoporous component (Fig. 1d).

The calculated pore structure parameters are listed in the table.

A set of experiments made it possible to compose a flowsheet for integrated processing of anthracite, which yields an assortment of carbon adsorbents of four brands. A versatile flowsheet is suggested (Fig. 2), according to which one or another type of carbon sorbents can be produced from anthracite, depending on production needs determined by the market demand and availability of raw materials.

The production of an assortment of adsorbents from anthracite fines is described below.

Production of a microporous adsorbent. Ground coal from bunker *1* is fed by mechanical transporter *2* into furnace *3* and is activated in a fluidized bed. Solid particles are separated from the steam-and-gas phase in cyclone *4*. Gaseous reaction products are removed by ventilator to sanitary treatment. The activated carbon produced is discharged from the reaction chamber at 850–875°C into a tubular water-cooled bunker *6*, where it is cooled to 50°C in a continuously moving bed. The resulting activated anthracite is delivered by a transporter *7* to vibrosieve *8* for sieving into fraction. The fine fraction is delivered into receiver *9*, and the coarse fraction, into bunker *11*.

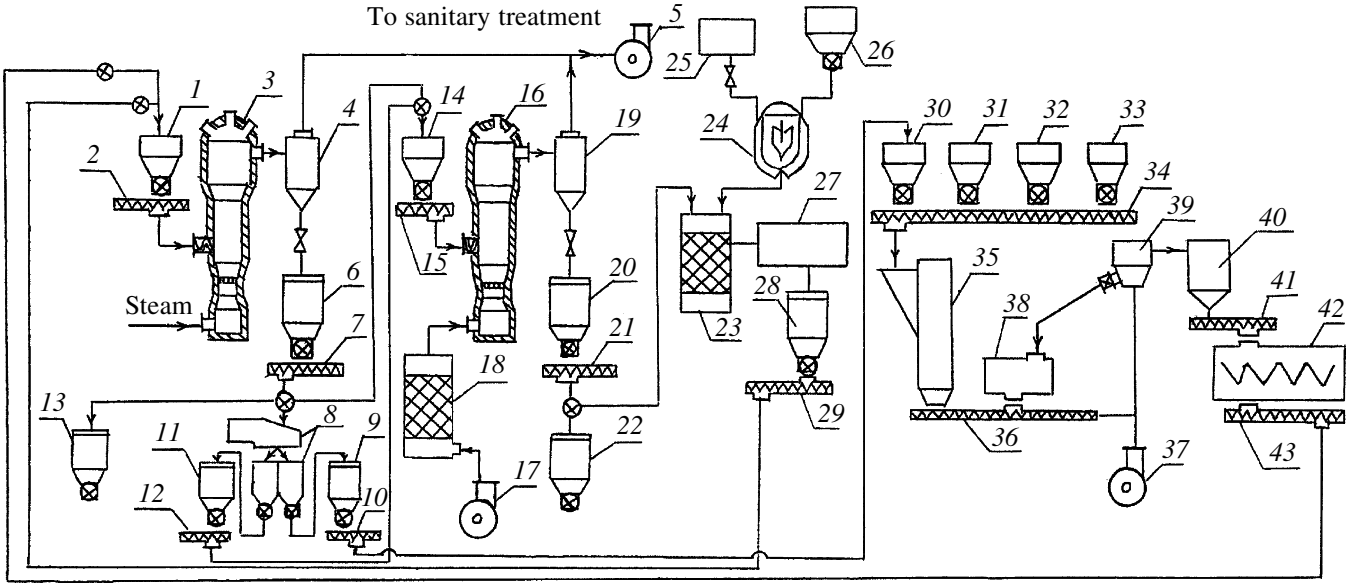


Fig. 2. Flowsheet of integrated processing of anthracite. For comments, see text.

Production of a carbon cation exchanger. After fractionation, a part of the coarse fraction from the final-product receiver *11* (particle size 0.5–2 mm) is delivered by transporter *12* into bunker *14* and then fed by transporter *15* into furnace *16*, where the carbon material is oxidized by humidified air produced by bubbling the air delivered by ventilator *17* through spray column *18*. The oxidation is performed at 350–400°C. Particles carried away from the furnace are caught in the cyclone. The oxidized product, which is a carbon cation exchanger, is discharged from the reaction chamber in a water-cooled tubular bunker *20*, where it is cooled in a moving layer, and then delivered by transporter *21* into finished-product receiver *22*.

Production of mesoporous anthracite. To perform chemical activation, the process is carried out as follows. Anthracite from bunker *1* is charged by transporter *2* into furnace *3* and activated in a fluidized bed to a combustion loss of 30%. The partly activated carbon is discharged from the reaction chamber at 850–875°C into a water-cooled tubular bunker *6* and then delivered by transporter *7* into bunker *14*, after which it is fed by transporter *15* into furnace *16*, where it is subjected to an oxidative treatment at 350–400°C by the procedure described above.

The oxidized anthracite is discharged into bunker *20* and delivered by transporter *21* into impregnating column *23*, into which is poured a sodium nitrate solution prepared in mixer *24* from water delivered from tank *25* and $NaNO_3$ supplied from bunker *26*. The oxidized anthracite is impregnated for 3 h. The chemically modified anthracite is delivered into a drum drier *27* for drying. Then it arrives to a receiver *28* for modified anthracite and is transported by screw conveyer *29* into activating furnace *3* and activated with steam at 850°C. This procedure yields a mesoporous anthracite. The finished product is delivered to vibrosieve *8* to be sieved into fractions. After fractionation, particles less than 0.5 mm in size are fed into bunker *9* for further use in manufacture of composite sorbing materials by the procedure described below.

Production of composite sorbing materials. The fine fraction of activated anthracite (particle size less than 0.5 mm) is delivered from bunker *9* by a pneumatic transporter to the section for manufacture of composite sorbing materials, into bunker *30*. In bunkers *31*, *32*, and *33*, mounted in parallel, are contained, respectively, carbon black, activated fiber, and binder (novolac resin) used for producing composites. To obtain disperse powders of a certain composition, the components are delivered by screw conveyor *34* into mixer *35*, in which the starting components are mixed and particles are preliminarily ground. The ground product is supplied by screw conveyor *36* and an air flow forced by ventilator *37* into a system for an air-flow separation and further into classifier *39*, where the product is separated into two fractions. One of these, with a particle size of less than 100 μm, is returned into vibration mill for grinding. After being ground in the vibration mill, the product is again delivered to the system for air-flow separation, etc. The finely dispersed mixture from cyclone *40* is delivered by screw conveyor *41* to compaction into extruder *42*. The resulting formed material is supplied by transporter *43* into bunker *1*, and then by transporter *2*, into furnace *3*. After activation, the finished product is discharged into cooling bunker *6*, and then by transporter *7*, into bunker *13* for the finished product.

The process presented makes it possible to produce an assortment of four sorption materials in a process with zero waste of raw materials.

CONCLUSIONS

(1) An assortment of sorption materials was produced from anthracite: microporous and mesoporous anthracite, a cation exchanger, and composite sorption materials.

(2) A study of the porometric characteristics of the adsorbents obtained revealed that the resulting activated carbons possess high specific parameters of porosity. The porous structure of the final product can be varied by changing the method used for processing of the starting raw material.

(3) A scheme of the suggested integrated technique for anthracite processing was composed. The scheme makes it possible to obtain an assortment of activated carbons (four brands).

REFERENCES

1. Derbyshire, F., Jagtoyen, M., Andrews, R., et al., *Carbon Materials in Environmental Applications*, vol. 27 of Chemistry and Physics of Carbon, New York: Dekker, 2001, pp. 1–66.
2. Kuznetsov, B.N., *Soros. Obrazov. Zh.*, 1999, no. 12, pp. 29–34.
3. Wilson, J., *Fuel*, 1981, vol. 60, no. 9, pp. 823–831.
4. Butuzova, L.F., *Adsorbenty na osnove prirodnykh uglei. Sbornik nauchnykh trudov* (Adsorbents Based

on Natural Carbon: Coll. of Scientific Works), Kiev: Naukova Dumka, 1989, pp. 37–49.

5. Lillo-Rydenas, M.A., Lozano-Castelly, D., Cazorla-Amoros, D., and Linares-Solano, A., *Carbon*, 2001, vol. 39, no. 5, pp. 751–759.
6. Parra, J.B., Pis, J.J., and Sousa, J.C. de, *Carbon*, 1996, vol. 34, no. 6, pp. 783–787.
7. Strelko, V.V., Gerasimenko, N.V., and Kartel', N.T., *Teor. Eksp. Khim.*, 2001, vol. 37, no. 1, pp. 48–52.
8. Kononova, O.N., Kholmogorov, A.G., and Danilenko, N.V., *Carbon*, 2005, vol. 43, no. 1, pp. 17–22.
9. Strelko, V.V., Gerasimenko, N.V., and Kartel', N.T., *Zh. Prikl. Khim.*, 2001, vol. 74, no. 6, pp. 931–933.
10. Kartel', N.T., Gerasimenko, N.V., and Strelko, V.V., *Zh. Prikl. Khim.*, 2002, vol. 75, no. 9, pp. 1443–1447.
11. Strelko, V.V., Gerasimenko, N.V., Kartel', N.T., et al., *Khim. Tverd. Topl.*, 2003, no. 1, pp. 77–82.
12. Fedorov, N.F., Ivakhnyuk, G.K., and Babkin, O.E., *Zh. Prikl. Khim.*, 1990, vol. 63, no. 4, pp. 787–791.
13. Sych, N.V., Kartel', N.T., and Strelko, V.V., *Dopov. Akad. Nauk Ukr.*, 2003, no. 7, pp. 53–57.
14. *Osnovy khimicheskoi tekhnologii* (Fundamentals of Chemical Technology), Mukhlenov, I.P., Ed., Moscow: Vysshaya Shkola, 1991.
15. Sych, N.V., Kartel', N.T., Strelko, V.V., et al., *Zh. Prikl. Khim.*, 2004, vol. 77, no. 2, pp. 210–213.

ISSN 1070-4272. Russian Journal of Applied Chemistry, 2006, Vol. 79, No. 5, pp. 727–732. © Pleiades Publishing, Inc., 2006.
Original Russian Text © L.P. Tikhonova, S.B. Lyubchik, Yu.A. Tarasenko, V.P. Goncharik, O.L. Galushko, I. Fonseca, 2006, published in Zhurnal Prikladnoi Khimii, 2006, Vol. 79, No. 5, pp. 737–743.

SORPTION AND ION-EXCHANGE PROCESSES

Modified Anthracites as Selective Sorbents for Platinum Metals

L. P. Tikhonova, S. B. Lyubchik, Yu. A. Tarasenko, V. P. Goncharik, O. L. Galushko, and I. Fonseca

Institute of Sorption and Problems of Endoecology, National Academy of Sciences of Ukraine, Kiev, Ukraine
Litvinenko Institute of Physicoal Organic Chemistry and Coal Chemistry, National Academy of Sciences of Ukraine, Donetsk, Ukraine
Faculty of Science and Technology, New University, Lisbon, Portugal

Received December 12, 2005

Abstract—Methods of preliminary modification were used to obtain activated carbons with low ash content (0.2%), developed π-conjugated electronic system, large surface area, and wide pore size distribution, from exclusively microporous carbons to those of mesoporous type. The adsorption of compounds of platinum-group metals on activated anthracite from single-component (as regards the platinum metal: Pd, Pt, or Rh) and multicomponent (Pd, Pt) solutions containing compounds of concomitant metals was studied.

DOI: 10.1134/S1070427206050065

The capacity of natural coals and other carbon materials for selective sorption concentration of microscopic amounts of platinum-group metals (PGMs) from highly mineralized acid solutions has been established previously [1, 2]. Such a selective recovery of PGMs on activated carbons is primarily due to the interaction of complex ions of platinum metals with the π-conjugated electronic system of the carbon matrix, namely, to formation of a metal–carbon bond, which is considerably less characteristic of ions of concomitant base metals [4, 5], and to spontaneous partial or complete reduction of their ions, caused by the electron-donor properties of activated carbons. This is confirmed by high sorption capacity for PGMs of carbon materials with a minimum content of oxygen-containing surface functional groups, whose presence commonly markedly diminishes the amount of reactive carbon atoms on the surface of activated carbon, weakens their reducing capacity, and hinders access of sorbates to the carbon matrix. In addition, it is known that an increase in the specific surface area of activated carbons also enhances the sorption of PGMs.

The aim of this study was to obtain from available natural carbon raw materials new highly efficient adsorbents with high capacity and selectivity for PGM ions. Anthracite, which has a comparatively low ash content and developed π-electron polyconjugation system owing to specific features of metamorphism [6–8], was chosen for this purpose. To disadvantages of anthracite belong the difficult accessibility of its natural microporosity to gases in the course of activation and the low reactivity of its external surface.

A new combined method of coal preparation has been developed [9–11]. This method is based on preliminary demineralization of the starting coals, oxidative treatment of anthracite, and its subsequent activation. This approach is fairly versatile: variation of the chemical modification conditions makes it possible to control the subsequent activation process and thereby to process anthracite into an activated carbon whose surface and structural characteristics could be varied in a wide range. Particular attention was given to revealing the relationship between the preparation conditions of activated anthracites and their selectivity in sorption recovery and concentration of PGMs from multicomponent salt solutions.

EXPERIMENTAL

Anthracites from Ukraine (Progress mine, Torezantratsit Production Association) and France (La Mure deposit) were chosen for study. The coals were demineralized with a mixture of hydrochloric and hydrofluoric acids, with the result that the ash content of the samples decreased from 4.2 and 5.3% to 0.46 and 0.47% for the Ukrainian and French anthracites, respectively. The chemical modification was performed with perchloric acid or magnesium perchlorate [9–11];

Table 1. Anthracites under study

Anthracite	Deposit	Designation
Activated	Progress	AU-1
$HClO_4$-modified, nonactivated	Progress	AU-2
$HClO_4$-modified, activated	Progress	AU-3
Nonactivated	La Mure	AF-1
Activated	La Mure	AF-2
$HClO_4$-modified, nonactivated	La Mure	AF-3
$HClO_4$-modified, activated	La Mure	AF-4
$Mg(ClO_4)_2$-modified, nonactivated	La Mure	AF-5
$Mg(ClO_4)_2$-modified, activated	La Mure	AF-6
Pyrolyzed, nonactivated	La Mure	AF-7
Pyrolyzed, activated	La Mure	AF-8
Pyrolyzed and $HClO_4$-modified, nonactivated	La Mure	AF-9
Pyrolyzed and $HClO_4$-modified, activated	La Mure	AF-10

Table 2. Elemental composition of the initial, demineralized, and chemically modified anthracites after activation

Coal	C	O	H/C	O/C
	wt %			
AU-1	92.1	4.2	0.038	0.045
AU-3	91.9	6.7	0.011	0.073
AF-2	90.6	3.1	0.067	0.034
AF-4	86.3	5.8	0.075	0.067
AF-6	87.6	4.4	0.087	0.050
AF-8	97.6	0.3	0.021	0.003
AF-10	96.7	1.3	0.020	0.013

in so doing, the ash content of the samples decreased to 0.14%. In some of the experiments, coals were thermally treated at 100°C for 10 h in an inert atmosphere for the development of the porosity and activation.

The anthracites were thermally activated by short-time (10-min) heating of the samples to 850°C ("thermal shock") in a flow of CO_2 and then heated for varied time (5 to 72 h) in order to obtain coals with different combustion loss (10 to 70%).

The composition and physicochemical properties (specific surface area, pore volume, presence and nature of functional groups) of the adsorbents obtained were studied by elemental and X-ray diffraction (XRD) analysis, nitrogen adsorption at 77 K (BET), and X-ray photoelectron spectroscopy (XPS).

The coals studied and their designations are listed in Table 1. The elemental compositions of the starting, demineralized, chemically modified, and graphitized carbon samples are listed in Table 2.

Model solutions of PGM chlorides were produced from the commercial chemicals, distilled water, and hydrochloric acid, with the concentrations of Pd(II), Pt(IV), and Rh(III) in the working solutions varied within the range 0.01–0.5 g l^{-1}. The adsorption of PGMs from multicomponent solutions was studied using the initial solutions with fixed concentrations of Pd(I) and Pt(IV), to which excess amounts of chlorides of typical concomitant metals, Fe(II), Co(II), Ni(II), Cu(II), and Cr(III), were added to obtain various Pd(Pt)/M(II) ratios.

The adsorption of Pd(II), Pt(IV), and Rh(III) complexes from aqueous hydrochloric acid solutions on activated carbons was studied by the method of separate weighed portions under standard conditions at the same s : l ratio (m = 0.1 g, V = 10 ml) at 25 ± 1°C. After a virtually constant distribution of metals between the liquid and solid phases was attained (the time in which the equilibrium was established was determined separately and found to be, in most of experiments, 24 h), the coal was separated from the solution.

The concentration of metals in solutions was determined as follows: Pd(II), by the reaction with the thiocyanate ion; Pt(IV) and Rh(III), by the reaction with tin(II) chloride; microscopic amounts of metal compounds in solutions and on carbons after the sorption were found by the atomic-absorption technique and previously developed catalytic methods [12].

The adsorption equilibrium in the systems studied was quantitatively characterized by the sorption capacity A (mg g^{-1}) of a coal and by the degree of PGM recovery (%).

As follows from the data obtained, preliminary chemical modification of anthracite strongly alters the coal structure. For example, treatment of anthracites with perchloric acid or magnesium perchlorate leads not only to a considerable oxidation of the coal surface (Table 3), but also to intercalation of perchlorate ions into the interlayer space. According to XPS data, ClO_4^- ions are presumably located in the interlayer space of coal in the form of perchloric acid or are directly bound to the matrix. In the case of activation of modified samples in a flow of CO_2, ClO_4^- ions are partly removed from anthracite, which promotes additional development of the microporous structure of activated carbons.

Table 3. Composition of functional surface groups for Progress anthracite modified with perchloric acid before and after its activation

Coal	Positions (eV) and intensities (at. %, in parentheses) of C, O, and Cl signals and their assignment to surface functional groups containing carbon, oxygen, and chlorine										
	C1*s*						O1*s*			Cl2*p*	
	C–C, sp^2	C–C, sp^3	C–OH, C–O–C	C=O, O–C–O, C–Cl	COOH, COOC, OCOO	OCOO	C=O	C–O–C, C–O–H	H_2O	C–Cl	$HClO_4$
AU-2	284.4 (20.7)	285 (50.3)	286.5 (10.6)	287.9 (4.5)	289.3 (3.2)	290.7 (3.4)	531.3 (1.9)	533.3 (3.1)	536.7 (0.5)	–	–
AU-3	284.4 (9.8)	285 (66.0)	286.5 (8.7)	287.9 (2.9)	289.3 (2.6)	290.8 (1.9)	532.2 (3.6)	533.4 (2.6)	535.9 (0.4)	200.6 (0.17)	207.2 (0.05)

The influence exerted by oxidation of coal and its intercalation with $HClO_4$ or $Mg(ClO_4)_2$ on the development of porosity is determined by the nature of anthracite, oxidizing agent, modification conditions (temperature and time of treatment, type and concentration of an oxidizing agent) (Tables 2, 3). The highest degrees of surface oxidation and intercalation of ClO_4^- ions into the interlayer space of anthracites were obtained upon their modification with perchloric acid, whereas treatment of the coal surface with magnesium perchlorate leads to a significant (up to 20–25%) combustion loss because of the "explosive" nature of the reaction between a coal and the oxidizing agent. Treatment of activated carbons with perchloric acid results in that predominantly carboxy and, in lesser amounts, carbonyl and phenol groups appear on its surface (Table 3).

The subsequent activation of modified samples changes the surface "chemistry": the total amount of oxygen-containing groups decreases, the fraction of aromatic carbon increases, and the remaining oxygen passes from a more reactive (in hydroxy groups of aliphatic chains) to a less reactive bound state in aromatic ether bridges (compare the intensity of C1*s* and O1*s* signals in Table 3). Also, the weight fraction of carbon increases because of the partial loss of hydrogen and oxygen, which is due both to a decrease in the number of surface functional groups and to further crystallization of the carbon matrix (Tables 3, 4). Thus, a combination of oxidative chemical modification and subsequent activation does not lead to any noticeable accumulation of surface functional groups.

One more factor of importance in modification of anthracites is that the surface area of the sorbents obtained increases. As can be seen in Table 5, activation of modified starting anthracites makes it possible

Table 4. XRD parameters for samples of the Progress anthracite

XRD parameters	Sample	Parameter
Interplanar spacing d_{002}, nm	AU-1	0.326
	AU-2	0.327
	AU-3	0.338
Average diameter of crystalline stacks, B_{av}, nm	AU-1	7.297
	AU-2	7.010
	AU-3	7.831
Height of crystalline stacks, *h*, nm	AU-1	3.543
	AU-2	3.703
	AU-3	2.712
Number of layers in stack, *N*	AU-1	11.9
	AU-2	12.3
	AU-3	9.0

Table 5. Specific surface area and pore volume of activated samples (activation for 24 h)

Sample	S_{sp}, $m^2\ g^{-1}$	Combustion loss, %	V_{tot}	V_{micro}	V_{meso}
			$cm^3\ g^{-1}$		
Progress					
AU-1	277	11	0.11	0.08	0.03
AU-3	425	28	0.16	0.12	0.04
La Mure					
AF-2	865	52	0.65	0.54	0.11
AF-4	1430	72	0.87	0.71	0.16
AF-6	785	55	0.41	0.25	0.16
AF-8	300	43	0.13	0.06	0.07
AF-10	642	47	0.45	0.35	0.10

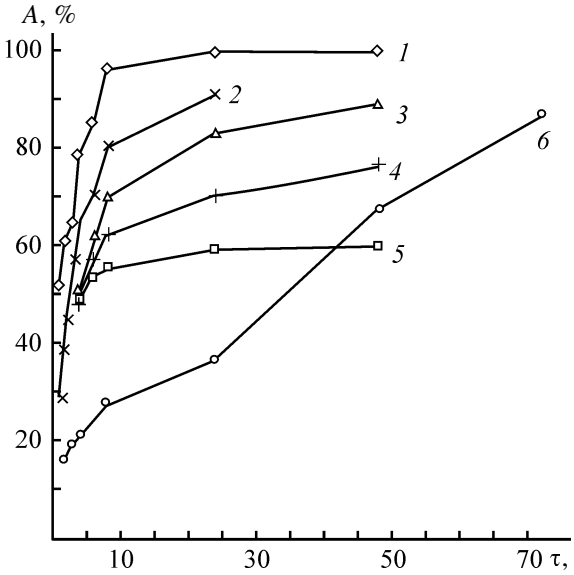


Fig. 1. Kinetics of palladium adsorption on (*1–5*) AU-3 and (*6*) AU-2 anthracites Adsorption conditions: weighed portion of a sorbent, m = 0.1 g; solution volume V = 10 ml, 1 M HCl. Content of Pd(II) in solution, mg ml^{-1}: (*1, 6*) 0.01, (*2*) 0.1, (*3*) 0.2, (*4*) 0.3, and (*5*) 0.5. (*A*) Adsorption and (τ) time.

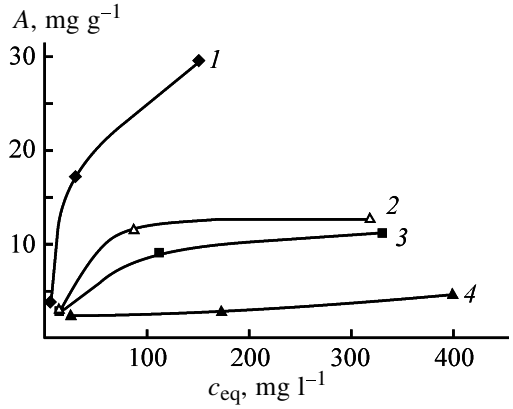


Fig. 2. Isotherms of palladium adsorption on various samples of activated La Mure anthracite (activation time 6 h). Adsorption conditions: 1 M HCl and 0.01 mg ml^{-1} Pd(II); sorvent weighed portion m = 0.1 g; solution volume V = 10 ml; adsorption time 24 h; the same for Figs. 3, 4. (c_{eq}) Equilibrium concentration of Pd(II). (*A*) Adsorption. Anthracite: (*1*) AF-4, (*2*) AF-6, (*3*) AF-10, and (*4*) AF-8; the same for Fig. 3.

to raise, by a factor of at least 1.5 (from 860 to 1430 m^2 g^{-1} for La Mure anthracite), their specific surface area, compared to activated starting anthracites. In pyrolysis of activated carbons, graphitized samples are activated to a considerably lesser extent because of the rearrangement and ordering of the anthracite structure: the surface is developed in 24 h only to 300 m^2 g^{-1}, but in this case, too, treatment

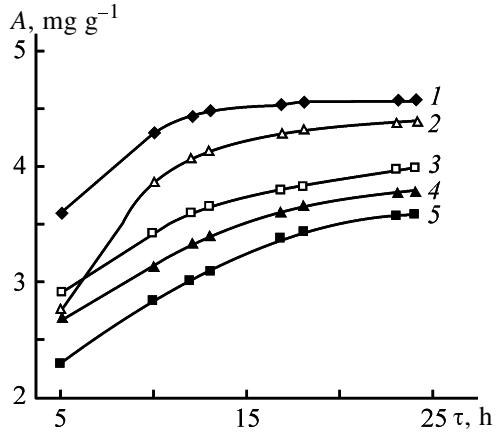


Fig. 3. Effect of the duration of activation of La Mure anthracites τ on the adsorption A of palladium.

with perchloric acid also enhances the reactivity of pyrolyzed samples in the course of activation via oxidation of their surface (Table 5). However, the effect of chemical modification on the activation process is considerably weaker than that in the case of starting anthracites.

The data obtained, combined with the results of previous studies [1–3], suggest that the increase in the specific surface area and total volume of micro- and mesopores in activated carbons as a result of their chemical modification must significantly improve the sorption properties of activated anthracite in recovery of PGMs from aqueous solutions. These suggestions were verified in a study of Pd(II) adsorption on coal samples subjected to various kinds of preliminary treatment and activation for different times.

A study of the kinetics of palladium adsorption on AU-3 (Fig. 1) showed that the kinetic curves tend to level-off in 10–20 h, with more than 90% of microgram amounts of palladium adsorbed on coal. On a modified, but not activated anthracite sample AU-2, virtually complete adsorption of minor amounts of palladium is not reached even in 3 days. This can be attributed to a lesser accessibility of the carbon matrix partly shielded by oxygen-containing SFGs and to a less developed porosity.

Figures 2 and 3 show that the highest sorption capacity of activated carbons for palladium is observed for modified and activated anthracites. The changes in the adsorption of palladium on pyrolyzed anthracite samples also correspond to changes of their surface. For example, comparison of the influence exerted by the surface properties on the sorption capacity of the sorbents obtained (preliminarily modified or graphitized samples) (Fig. 4) shows that, vir-

tually irrespective of the pretreatment conditions (modification with chemical agents or graphitization), the specific surface area is the dominating factor: the larger the surface area, the higher the sorption capacity of activated carbon.

The second factor determining the sorption capacity is the developed π-conjugated electronic system of the coal matrix. Analysis of the data obtained (XPS, XRD) confirms that the most graphitized samples, activated pyrolyzed anthracite not subjected to chemical modification (97.6% C), exhibits the sorption capacity for PGMs comparable with that of less graphitized anthracite modified with magnesium perchlorate and activated (87.6% C) (compare data for a fixed specific surface area in Fig. 4).

Thus, combination of two factors, the developed π-polyconjugated electronic system of the coal matrix and the large surface area of activated carbons, determines the sorption capacity of these materials for PGMs.

In choosing anthracite-based sorbents for practical use, account should be taken of the efficiency of the process of coal preparation as a whole. For example, Figs. 2–4 clearly show that preliminary chemical modification makes markedly shorter the time of activation in production of sorbents with a sufficiently developed surface, and, consequently, with a comparatively high sorption capacity for PGMs: the largest surface area of anthracite modified with perchloric acid can be obtained after 5–7 h of activation, to which also corresponds the highest sorption capacity for palladium. For pyrolyzed anthracite, close values of the sorption capacity for palladium can be obtained upon activation under identical conditions for 24 h.

The following important conclusion can be made on the basis of these results: the adsorption capacity of activated carbon for palladium increases from 10 mg g^{-1} for unmodified activated anthracite to 28–30 mg g^{-1} for coals treated with perchloric acid (Fig. 5).

A comparison of the adsorption behavior of chloride complexes of platinum(IV), palladium(II), and rhodium(III) on AU-3 anthracite samples modified with perchloric acid (Fig. 5) confirmed the previously revealed decrease in the sorption capacity in the order Pd > Pt > Rh [1–3].

Also, we checked the possibility of using the anthracites studied for selective adsorption of microscopic amounts of PGM from multicomponent solutions. The results obtained confirmed that modified anthracites, as well as other carbon sorbents, recover

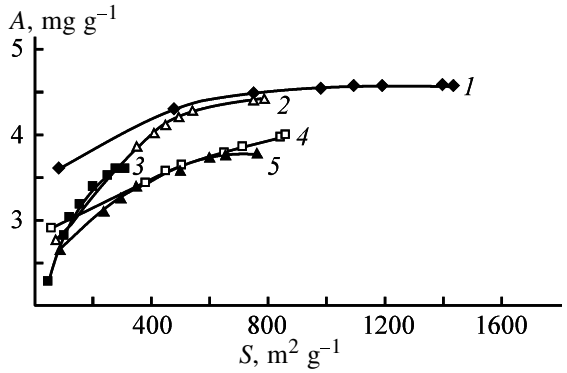


Fig. 4. Adsorption A of palladium vs. the specific surface area S of various samples of activated modified La Mure anthracites. Anthracite: (*1*) AF-4, (*2*) AF-6, (*3*) AF-7, (*4*) AF-2, and (*5*) AF-10.

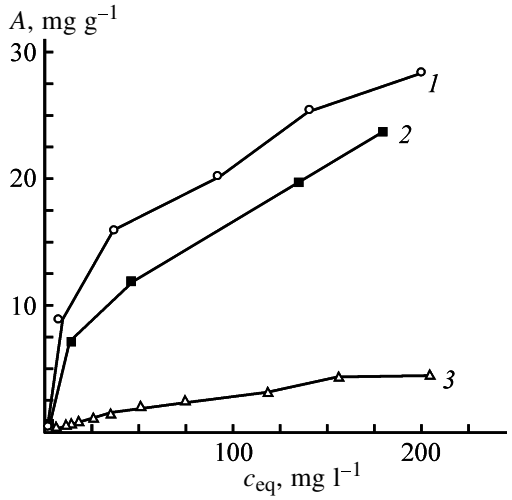


Fig. 5. Isotherms of adsorption of (*1*) palladium, (*2*) platinum, and (*3*) rhodium on Progress anthracite AU-3 activated after modification with perchloric acid. Weighed portion of the sorbent $m = 0.1$ g; solution volume $V = 10$ ml; adsorption time 24 h. (c_{eq}) Equilibrium concentration of PGM. HCl concentration, M: (*1, 2*) 1.0 and (*3*) 0.01.

more than 80–95% of PGMs from solutions containing compounds of other common concomitant metals, as demonstrated for the example of recovery of platinum and palladium (Table 6). The amount of metals adsorbed on coal from solutions containing Pd(II) in the presence of base metals was determined. It was found (Table 7) that the concomitant metals are recovered to a considerably lesser extent than palladium: at the initial Pd : M ratio of 1 : 50, the same ratio on the sorbent does not exceed 1 : 4. The results obtained suggest that the activated carbons under study can be used for concentration of palladium from multicomponent solutions and selective separation of palladium from an excess amount of chromium, nickel, and cobalt.

Table 6. Recovery of Pt(IV) and Pd(II) from multicomponent hydrochloric acid solutions: AU-3; m = 0.1 g; V = 10 ml, 1 M HCl; Pt(IV) 100 μg, Pd(II) 91 μg, sum of chlorides MCl_x of Cu(II), Ni(II), Co(III), Fe(II), Cr(III)

Metal being recovered	Recovered Pt(Pd), %, at indicated Pt(Pd) : MCl_x ratio*			
	1 : 1	1 : 10	1 : 50	1 : 1000
Platinum	92.8	90.6	95.6	85.0
Palladium	85.5	90.5	86.5	77.9

* The Pt(Pd) : MCl_x ratio is the ratio of Pt(Pd) to each metal ion in the mixture of chlorides of the metals indicated.

Table 7. Content of palladium and concomitant metals on activated carbon after sorption of palladium(II) from a multicomponent solution. Adsorbent AU-3, m = 0.1 g; V = 10 ml, 1 M HCl, initial amounts: 200 μg of Pd and 10 mg of each of the concomitant elements

Mixture in solution	Found on coal after sorption		
	μg	% of introduced amount	Pd : M
Pd(II)	142.5 (188*)	71.2 (94*)	
Fe(II)	482	4.82	1 : 3.39
Ni(II)	<18.75	<0.1875	>1 : 0.13
Cu(II)	432.75	4.32	1 : 3.04
Cr(II)	<22.5	<0.225	>1 : 1.58
Co(II)	<10	<0.1	>1 : 0.07

* Burning of activated carbon after sorption can give organometallic compounds of palladium of the type of undeterminable volatile carbonyls; the sorption of palladium, defined as the difference of its amounts in the starting solution and in the filtrate after separation of the adsorbent, is given in parentheses.

CONCLUSIONS

(1) Activated carbons with a developed π-conjugated electronic system, specific surface area of up to 1500 $m^2 g^{-1}$, low ash content (>0.2%), and controlled pore size distribution (from exclusively microporous to mesoporous) were produced by varying the conditions of modification and activation of anthracites. Preliminary chemical modification of anthracites allows a substantial shortening of the time of their activation to give carbon materials with the best adsorption properties with respect to PGMs.

(2) Activated natural anthracites completely recover platinum, palladium, and rhodium in the micro- and milligram range of concentrations from acid aqueous solutions, and platinum and palladium, from solutions with an excess content of concomitant base metals. It was shown for the example of palladium recovery that the main part (>90%) of compounds of concomitant metals remain in the solution after sorption.

(3) It was confirmed that the main factors determining the sorption capacity of carbon materials for PGMs are the developed π-conjugated electronic system of the carbon matrix and the specific surface area. The maximum sorption capacity for palladium may reach values close to 30 mg g^{-1} for anthracites preliminarily treated with perchloric acid.

(4) It was demonstrated that the approach to modification and activation of anthracite, developed in the study, provides synthesis of efficient selective PGM adsorbents from available natural materials.

ACKNOWLEDGMENTS

The study was financially supported by the NATO program in the framework of the SfP 977984 project and by the SFRH/BPD/7150/2001 program (Portugal).

REFERENCES

1. Tikhonova, L.P., Tarkovskaya, I.A., Rosokha, S.V., et al., *Zh. Prikl. Khim.*, 1998, vol. 71, no. 10, p. 1632.
2. Tarkovskaya, I.A., Kulik, N.V., Rosokha, S.V., et al., *Teor. Eksp. Khim.*, 1999, vol. 35, no. 4, p. 240.
3. Tarkovskaya, I.A., Tikhonova, L.P., Stavitskaya, S.S., and Strelko, V.V., *Zh. Fiz. Khim.*, 2002, vol. 76, no. 2, pp. 334–340.
4. Tarasenko, Yu.A., Antonov, S.P., Bagreev, A.A., et al., *Ukr. Khim. Zh.*, 1991, vol. 57, no. 4, p. 385.
5. Tarasenko, Yu.A., Bagreev, A.A., and Yatsenko, V.V., *Zh. Fiz. Khim.*, 1993, vol. 67, no. 11, p. 2328.
6. Walker, P.L., Jr. and Almargo, A., *Carbon*, 1995, vol. 33, p. 239.
7. Bessant, G.A.R. and Walker, P.L., Jr., *Carbon*, 1994, vol. 32, p. 1171.
8. Parra, J.B., Pis, J.J., Sousa, J.C. de, et al., *Carbon*, 1996, vol. 34, p. 783.
9. Lyubchik, S.B., Benaddi, H., Shapranov, V.V., and Beguin, F., *Carbon*, 1997, vol. 35, p. 162.
10. Daulan, C., Lyubchik, S.B., Rouzaud, J.-N., and Beguin, F., *Fuel*, 1998, vol. 77, no. 6, p. 495.
11. Lyubchik, S.B., Benoit, R., and Beguin, F., *Carbon*, 2002, vol. 40, p. 1287.
12. *Analiticheskaya khimiya platinovykh metallov* (Analytical Chemistry of Platinum Metals), Zolotov, Yu.A., Varshal, G.M., and Ivanov, V.M., Compilers and Eds., Moscow: URSS, 2003.

ISSN 1070-4272. Russian Journal of Applied Chemistry, 2006, Vol. 79, No. 5, pp. 733–735. © Pleiades Publishing, Inc., 2006.
Original Russian Text © E.E. Ergozhin, K.I. Imanbekov, 2006, published in Zhurnal Prikladnoi Khimii, 2006, Vol. 79, No. 5, pp. 744–746.

SORPTION AND ION-EXCHANGE PROCESSES

Ion Exchangers Based on Homo- and Copolymers of Vinyloxyethylamine and Glycidyl Methacrylate

E. E. Ergozhin and K. I. Imanbekov

Bekturov Institute for Chemical Science, Ministry of Education and Science of Kazakhstan Republic, Almaty, Kazakhstan

Received October 4, 2005; in final form, February 2006

Abstract—An efficient method is developed for synthesis of highly permeable ion-exchange resins through the reaction of glycidyl methacrylate with polyvinyloxyethylamine and its copolymers with nitrogen-containing monomers with preservation of the nitrogen functional groups in the latter monomers. The synthesis conditions are optimized, and physicochemical and sorption properties of the resulting polymers are examined.

DOI: 10.1134/S1070427206050077

Polyvinyloxyethylamine (PVOEA, monoethanolamine polyvinyl ether) and its copolymers with 2-methyl-5-vinylpyridine (2M5VP), 4-vinylpyridine (4VP), and *N*-vinylpyrrolidone (NVP), containing reactive and complexing functional groups, represent a particular class of water- and organo-soluble polymers [1, 2]. The presence of the VOEA units with primary amino groups in the structure of such homo- and copolymers provides high reactivity in polycondensation with epoxy compounds (no need in additional hardeners like di- and polyamines), thus allowing maintenance of the complexing capacity of the tertiary nitrogen atom of the pyridine and lactam rings.

In this study we synthesized the polyfunctional ion-exchange resins by the reaction of glycidyl methacrylate (GMA) with VOEA homo- and copolymers containing the pyridine and lactam rings and characterized their properties.

EXPERIMENTAL

Glycidyl methacrylate, VOEA polymers, and its copolymers with *N*-vinylpyrrolidone and vinylpyridines (VOEA–NVP, VOEA–4VP, and VOEA–2M5VP; VOEA : vinylpyridine = 25 : 75 mol/mol) were synthesized by the standard procedures [1–4].

Polycondensation of GMA with homo- and copolymers of VOEA was carried out in DMF in a three-necked flask equipped with a mechanical stirrer, a thermometer, and a dropping funnel. The mixture was stirred with heating to the onset of gelation. Then the gel was transferred into a porcelain bottle and cured at 60–120°C under argon. The subsequent processing of the polymers and their physicochemical characterization were performed by the standard methods [5, 6].

The static sorption of the copper ions was studied by the separate portion method. Potentiometric titration was carried out on an OR-265 digital pH-meter at 25°C. The stock solution was prepared from copper sulfate (analytically pure grade). The ionic strength of the solution (μ) was varied by adding Na_2SO_4. The IR spectra of the as-prepared polymers and metal-containing samples were recorded on UR-20 and Specord spectrophotometers using the KBr technique [7]. The potentiometric titration was performed using the separate portion method [8].

To optimize the synthetic route, we studied the effects of the component ratios and curing temperature and time.

We found that the characteristics of the final products are influenced to a greater extent by the starting reagent concentrations and the nature of VOEA polymers (Table 1). In all cases, the static exchange capacity (SEC) and nitrogen content in the resins increased with increasing concentration of VOEA or its copolymer in the initial mixture. The SEC of the anion exchangers is largely controlled by the nature of the VOEA polymer. The exchange capacity of the polyelectrolytes based on homo- and copolymers of VOEA increased in the order PVOEA < VOEA–4VP < VOEA–2M5VP, which can be attributed to the fact that, among the indicated polyamines, the aliphatic one is the most reactive, allowing protection of the pyridine groups against quaternization in the course of

Table 1. Influence of nature and ratio of starting components on SEC of resulting GMA–polyamine anion exchangers (curing temperature 100°C; 3 h)

VOEA-based polymer	Epoxy : NH_2 initial molar ratio	c_{N_2}, wt %	SEC_{HCl} (0.1 N HCl), mg-equiv g^{-1}
PVOEA	1.0 : 1.0	6.50	4.59
	1.0 : 2.0	9.30	6.58
	1.0 : 3.0	10.75	7.70
	1.0 : 4.0	11.74	8.36
VOEA–4VP	1.0 : 1.0	7.34	5.20
	1.0 : 2.0	8.80	6.20
	1.0 : 3.0	9.50	7.00
VOEA–2M5VP	1.0 : 1.0	6.80	4.80
	1.0 : 2.0	8.00	5.70
	1.0 : 3.0	8.80	6.20
VOEA–NVP	1.0 : 1.0	7.05	2.50
	1.0 : 2.0	8.32	2.95
	1.0 : 3.0	9.18	3.23

Table 2. SEC and nitrogen content in anion-exchange resins obtained at various temperatures (epoxy : NH_2 initial molar ratio 1.0 : 2.0; curing time 3 h)

VOEA-based polymer	T, °C	c_{N_2}, wt %	SEC_{HCl} (0.1 N HCl), mg-equiv g^{-1}
PVOEA	60	8.42	6.00
	80	9.27	6.53
	100	9.30	6.58
VOEA–4VP	60	6.45	4.60
	80	7.60	5.41
	100	8.80	6.20
	120	8.81	6.24
VOEA–2M5VP	60	6.10	4.35
	80	7.40	5.24
	100	8.00	5.70
VOEA–NVP	60	6.65	2.35
	80	7.50	2.60
	100	8.32	2.95

curing. This is demonstrated by the retention of the band of the low-basic pyridine ring at 1554 cm^{-1} and also by the lack of the band of the quaternized heterocycle at 1532 cm^{-1}. In the IR spectra of the polymers, the intensity of the bands of bending (1570 cm^{-1}) and asymmetric (3360 cm^{-1}) and symmetric (3290 cm^{-1}) stretching vibrations of the N–H bond decreases, which is consistent with the reference IR data for the initial linear polymer of VOEA and its copolymers with 4VP and NVP [1, 2], polyvinylpyridines [7], and strongly basic commercial anion-exchange resins VP-1Ap and VP-100 [9].

At the optimal ratio of the starting components, we studied the effect of the curing temperature on the characteristics of the resulting resins. Table 2 shows that, with increasing temperature, SEC increases. The maximal SEC of the resins based on VOEA homopolymer was observed at 80°C, and that of the resins based on VOEA–4VP, VOEA–2M5VP, and VOEA–NVP copolymers, at 100°C. Increase in the curing time at the optimal temperature also improves SEC of the resins (Table 3).

As a measure for the chemical resistance of the resins we used the SEC loss after their treatment with 5 N solutions of sulfuric acid or NaOH for 30 min at 100°C, or with 10% H_2O_2 at 25°C for 24 h (Table 4).

The network polyelectrolytes based on GMA and VOEA homopolymers and copolymers with 4VP and 2M5VP were found to be stable in the indicated aggressive media.

The acid–base and sorption characteristics of the resins were studied by potentiometric titration in the absence (Fig. 1, curves *1, 3*) and in the presence of Cu ions (curves *2, 4*). The titration curves suggest the polyfunctional structure of the resins based on PVOEA and its nitrogen-containing copolymers. The pK_a values estimated by the Henderson–Hasselbach equation are 8.65 and 8.90 for the resins based on PVOEA and VOEA–NVP, respectively. In the presence of Cu ions, the potentiometric titration curves shift toward lower pH values.

Table 3. SEC and nitrogen content in anion-exchange resins at various curing times τ (epoxy : NH_2 initial molar ratio 1.0 : 2.0; GMA : VOEA–VP = 1.0 : 1.0; curing temperature 100°C)

VOEA-based polymer	τ, h	c_{N_2}, wt %	SEC_{HCl} (0.1 N HCl), mg-equiv g^{-1}
PVOEA	1.0	6.22	4.41
	2.0	9.21	6.55
	3.0	9.30	6.58
	4.0	9.30	6.58
VOEA–4VP	1.0	6.05	4.20
	2.0	8.40	6.00
	3.0	8.80	6.20
	4.0	8.81	6.24
VOEA–NVP	1.0	5.56	1.91
	2.0	6.74	2.38
	3.0	8.32	2.95
	4.0	8.51	3.00

Table 4. Chemical resistance of anion-exchange resins (epoxy : NH_2 initial molar ratio 1.0 : 2.0; GMA : VOEA–VP = 1.0 : 1.0; curing temperature 100°C; 3 h)

VOEA-based polymer	SEC_{HCl} (0.1 N HCl), mg-equiv g^{-1}	Swellability, ml g^{-1}	Chemical resistance with respect to indicated agent, %		
			5 N H_2SO_4	5 N NaOH	10% H_2O_2
PVOEA	9.30	4.50	95	96	91
VOEA–4VP	8.80	4.25	98	97	93
VOEA–2M5VP	8.00	4.20	98	97	94

The IR spectrum of the complex of the PVOEA-based resin with copper shows a low-frequency shift by 60 cm^{-1} of the N–H stretching vibration band at 3300 cm^{-1} and a decrease in the intensity of the C–O–C stretching vibration (1100 cm^{-1}). In the case of the resin based on VOEA–2M5VP, containing Cu ions, the band at 1490 cm^{-1} (pyridine ring) is broadened. Furthermore, all the complexes with Cu(II) demonstrate a decrease in the intensity and a low-frequency shift by 30 cm^{-1} of the stretching vibration band of the carbonyl groups of the GMA polymer and lactam ring.

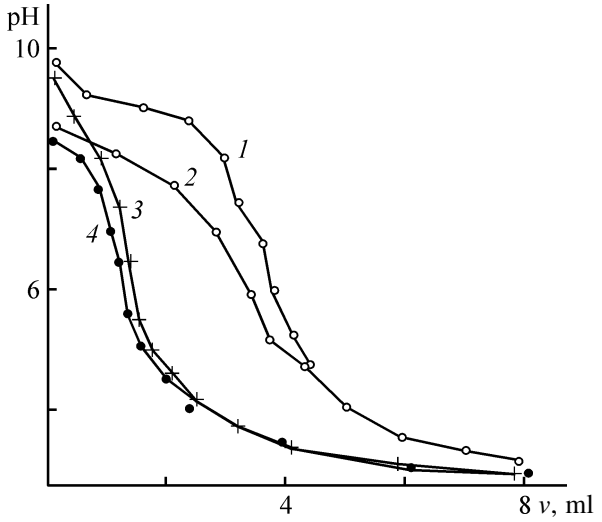
To conclude, the polycondensation of GMA with homo- and copolymers of VOEA yields novel chelating medium-basic network polymers, which could be used for recovering transition and noble metals.

CONCLUSIONS

(1) The chemical resistance of anion-exchange resins synthesized from glycidyl methacrylate and homo- and copolymers of vinyloxyethylamine in 5 N solutions of sulfuric acid and NaOH is 95–98%, and that in such a strong oxidizing agent as 10% H_2O_2, 91–94%.

(2) The IR spectra of the resins based on the copolymers of vinyloxyethylamine with 2-methyl-5-vinylpyridine and 4-vinylpyridine confirm preservation of the complexing pyridine groups after the reaction with glycidyl methacrylate.

(3) The pK_a values of the resins based on glycidyl methacrylate and the homopolymer of vinyloxyethylamine or vinyloxyethylamine–*N*-vinylpyrrolidone copolymer, estimated by the Henderson–Hasselbach equation, suggest the formation of medium-basic anion exchangers.



Potentiometric titration curves of anion-exchange resins at various concentrations of Cu ions (μ = 1.0): (*1, 2*) PVOEA/GMA and (*3, 4*) VOEA–NVP/GMA. (*v*) Volume of 0.1 N HCl consumed for titration.

REFERENCES

1. Nurkeeva, Z.S., Shaikhutdinov, E.M., Seitov, A.Z., et al., *Vysokomol. Soedin., Ser. A*, 1987, vol. 29, no. 5, pp. 932–937.
2. Nurkeeva, Z.S., Baimagambekov, K.B., Sigitov, V.B., and Ergozhin, E.E., *Vysokomol. Soedin., Ser. A*, 1992, vol. 34, no. 4, pp. 84–88.
3. JPN Patent 58-49552.
4. Ergozhin, E.E., Bektenov, N.A., and Akimbaeva, A.M., *Polielektrolity na osnove glitsidilmetakrilata i ego sopolimerov* (Polyelectrolytes Based on Glycidyl Methacrylate and Its Copolymers), Almaty, 2004.
5. *GOST* (State Standard) *10898–84, 10898–2.74, 10898–5.84: Ion-Exchange Resins: Physicochemical Testing Methods.*
6. Polyanskii, I.P., *Metody issledovaniya ionitov* (Methods for Studying Ion Exchangers), Moscow: Khimiya, 1976.
7. Bellamy, L.J., *The Infrared Spectra of Complex Molecules*, New York: Wiley, 1957.
8. Ergozhin, E.E., Chalov, T.K., Kovrigina, T.V., and Iskakova, R.A., *Zh. Prikl. Khim.*, 2005, vol. 78, no. 1, pp. 146–150.
9. Stupin, N.P., Dmitrochenkova, T.S., Zhukova, N.G., et al., *Plast. Massy*, 1983, no. 7, p. 59.

ISSN 1070-4272. Russian Journal of Applied Chemistry, 2006, Vol. 79, No. 5, pp. 736–740. © Pleiades Publishing, Inc., 2006.
Original Russian Text © S.I. Lazarev, A.S. Gorbachev, V.A. Shaposhnik, V.M. Stamov, 2006, published in Zhurnal Prikladnoi Khimii, 2006, Vol. 79, No. 5, pp. 747–751.

SORPTION AND ION-EXCHANGE PROCESSES

Kinetics of Reverse Osmosis Desalination of Aqueous Sodium Sulfanilate

S. I. Lazarev, A. S. Gorbachev, V. A. Shaposhnik, and V. M. Stamov

Tambov State Technical University, Tambov, Russia

Received November 10, 2005; in final form, March 2006

Abstract—Kinetics of reverse osmosis desalination of aqueous sodium sulfanilate is studied on a laboratory pressure filter unit, in relation to the solution concentration, temperature, and pressure in the intermembrane channel.

DOI: 10.1134/S1070427206050089

The goal of this work was to study the membrane methods in desalination of aqueous solutions of low-molecular-weight organic compounds, as applied to intermediate products of organic synthesis and also to wastewaters from chemical and related branches of industry. As a model we used aqueous sodium sulfanilate, since it is a component of many process solutions and wastewaters from production of bleaching agents [1].

The major kinetic characteristics of reverse osmosis separations are the retention factor and transmembrane flux [2–6].

In this study we examined the influence of the process parameters on the kinetics and other performance characteristics of the reverse osmosis. The experiments were carried out in a unit with loop circulation of the solution and a two-compartment pressure filter cell using MGA90T [Vladipor, Vladimir (Russia)] and ESPA (Hydronautic) composite membranes. The flow speed in the intermembrane channel was 0.4 m s^{-1}. The simulated solution was prepared by dissolving dry sodium sulfanilate (98.7%; analytically pure grade) in distilled water. The experimental procedure was described in detail in [7].

Data on the retention factor for MGA-90T and ESPA as influenced by the sodium sulfanilate concentration and temperature are given in Figs. 1 and 2.

The results show that the retention factor is a linear function of the process parameters. It increases with increasing concentration of the organic compound in the solution. The observed high retention factors can be explained taking into account the interrelation between the solubility of the compound and the sorption capacity of the membranes [8]. Since sodium sulfanilate is infinitely soluble in water, water is preferentially sorbed in the pores and on the surface of the membrane, which is confirmed by low distribution coefficient and diffusion-controlled permeability of the membranes.

At the same process parameters, the retention factor is slightly higher for ESPA membrane, which can be attributed to the differences in the structural characteristics and the sign of the charge of the membranes [5, 7, 9].

We found that K decreases with increasing temperature, suggesting the temperature effect on the crystal lattice of the active layer of the membrane.

Analysis of the experimental data reveals that K is strongly influenced by such parameters as the nature and concentration of the solute, pressure in the system, and temperature. Therefore, in this study we made efforts to employ one of the known theoretical models for prediction of the retention factor.

As a basic equation we used that derived in [10] in terms of the convective diffusion model:

$$K = 1 - \{1 + (\gamma - 1)[1 - \exp(\nu h/D_m)]\exp(-\nu\delta/D_0)\}^{-1}, \quad (1)$$

where D_0 and D_m are the diffusion coefficient in the bulk and membrane phase, respectively, which are the functions of the solute concentration and temperature; $k = 1/\gamma$ is the distribution coefficient, which is determined from the sorption data for reverse-osmosis membranes; h, thickness of the membrane; ν, filtration rate; δ, thickness of the laminar sublayer at the mem-

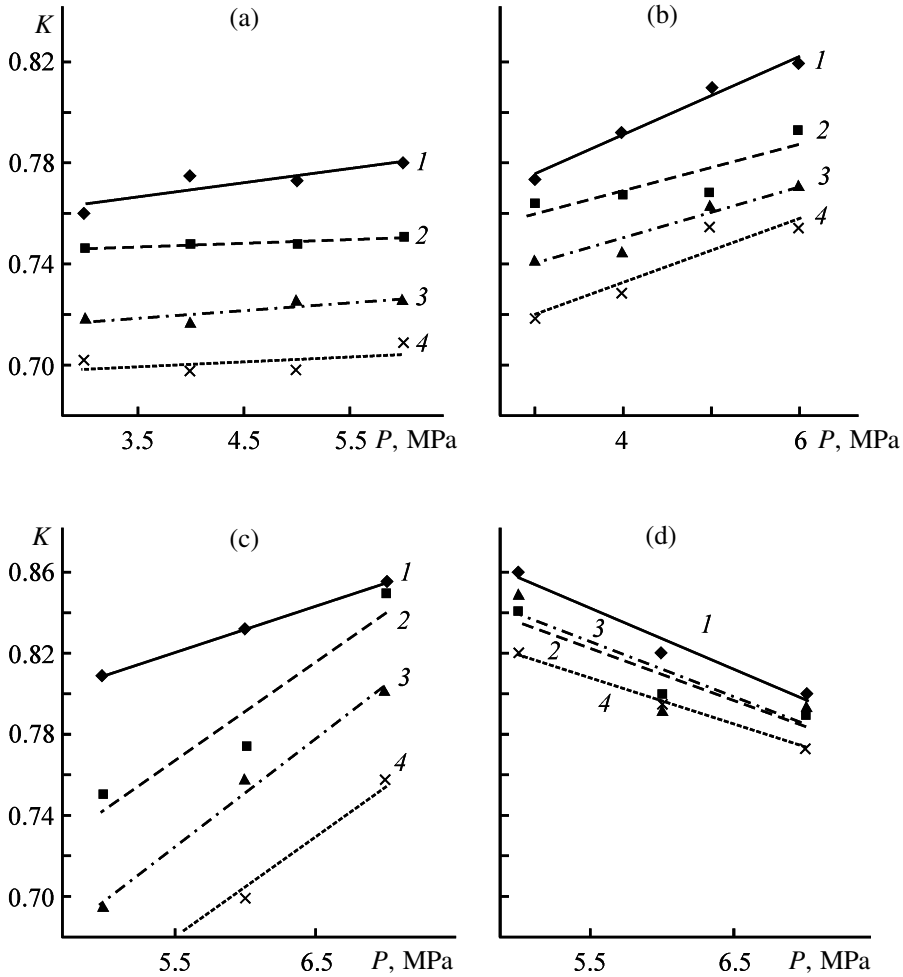


Fig. 1. Retention factor K of sodium sulfanilate on MGA-90T membrane as a function of the pressure P. Initial sodium sulfanilate concentration (g l^{-1}): (a) 10, (b) 50, (c) 200, and (d) 300; the same for Figs. 2–4. Temperature (K): (*1*) 293, (*2*) 303, (*3*) 313, and (4) 323; the same for Figs. 2–4.

brane surface; and γ, parameter characterizing the sorption on the membrane.

After rearrangement, for the investigated system, Eq. (1) takes the form of Eq. (2):

$$K = 1 + \{1 + (1/kk_1 - 1)[1 - \exp(Ghkk_2/P_d)] \times \exp(-G \times 0.00021k_3/D_0w^{1/2})\}^{-1}, \quad (2)$$

where k_1, k_2, and k_3 are the membrane- and solution-specific coefficients; k is the distribution coefficient; P_d, diffusion-controlled permeability coefficient defined as $P_d = D_m k$; G, permeate flux; and w, solution flow speed in the intermembrane channel.

After fitting the experimental data by Eq. (2), we obtained k_1, k_2, and k_3 for the investigated membranes and solutions (Table 1).

The transmembrane flux of the solvent is one of the most important characteristics of reverse osmosis. It characterizes the process efficiency and depends on such system parameters as the kinds of membranes and solutions, solute concentration, temperature, pressure, and hydrodynamic regime of the separating unit.

Let us consider the influence of the solute concentration on the transmembrane flux. The experimental data obtained at various transmembrane pressures are presented in Figs. 3 and 4.

Our results showed that, with increasing sodium sulfanilate concentration, the permeate flux decreases for both types of membranes. This is due to the increase in the osmotic pressure (in accordance with the van't Hoff theory) and the formation of a boundary diffusion (gel) layer (sodium sulfanilate is a low-molecular-weight organic compound with a fairly low mass transfer coefficient), which increases the resistance to the solvent flux. It should be noted also that

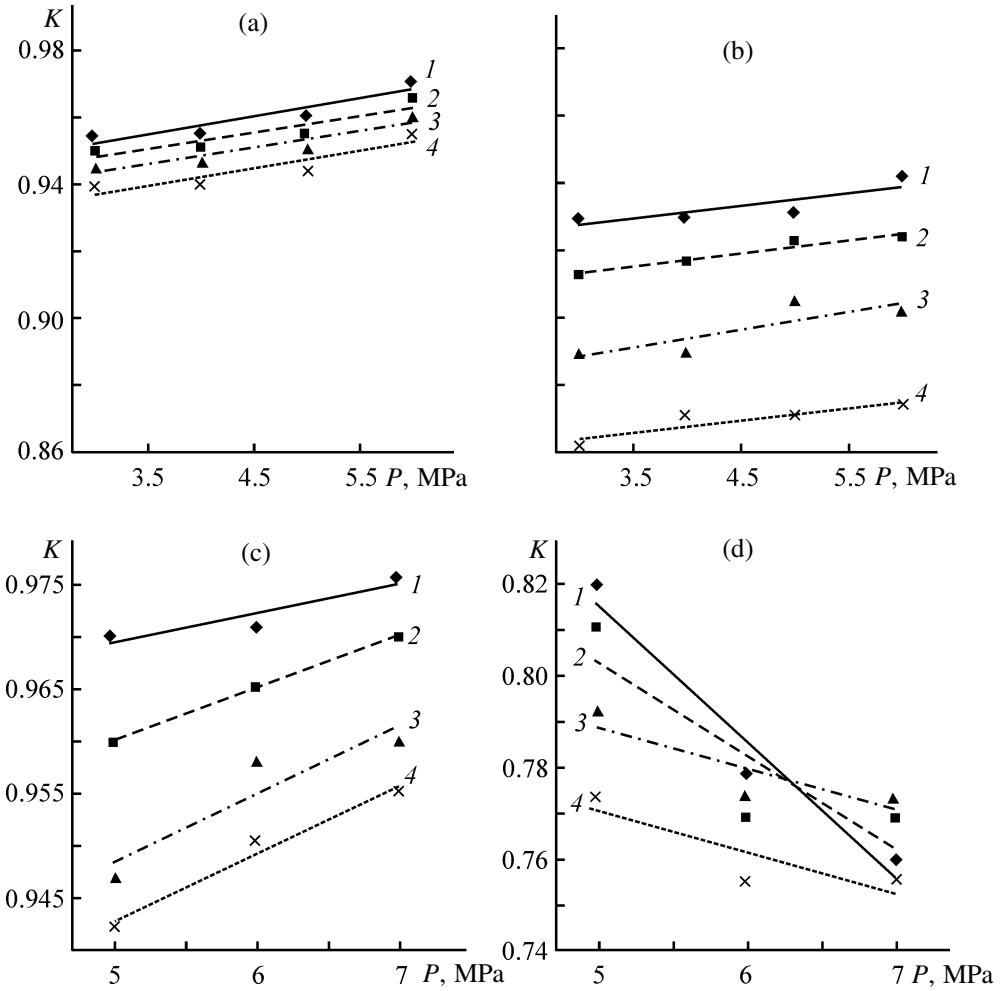


Fig. 2. Retention factor K of sodium sulfanilate on ESPA membrane as a function of the pressure P.

the osmotic pressure increases with increasing solute concentration, thus weakening the driving force of the separation process.

Analysis of the dependence of the water permeability on the transmembrane pressure suggests that the pressure drop on the membrane is the major driving force of the process (parameters increase with increasing pressure).

We found also that the transmembrane flux increases with increasing temperature, suggesting the temperature effect on the crystal structure of the active layer of the membrane. Our results show that the flux depends also on the type of membrane. Thus, the flux across ESPA membrane is slightly higher than that across MGA-90T, all other conditions being equal. This is probably due to the differences in the structure of the active layer [8, 11, 12] and in the nature of interaction of the membrane with the solute and solvent.

Finally, the major factors influencing the transmembrane flux are the working pressure in the system, solution temperature, and solute concentration.

Table 1. Coefficients of Eq. (2) for estimating the retention factor

Membrane	k_1	k_2	k_3
MGA-90T	–3.32485	–3.59228	1.280075
ESPA	–0.18511	–0.03646	0.011113

On the basis of the experimental dependences of the water permeability on the pressure, concentration, and temperature, we derived the following equation for the transmembrane flux:

$$G = k(P - \Delta\pi)c^n (T/T_0)^m, \quad (3)$$

where k, n, and m are the empirical coefficients; T_0 and T, reference (293 K) and working temperature of

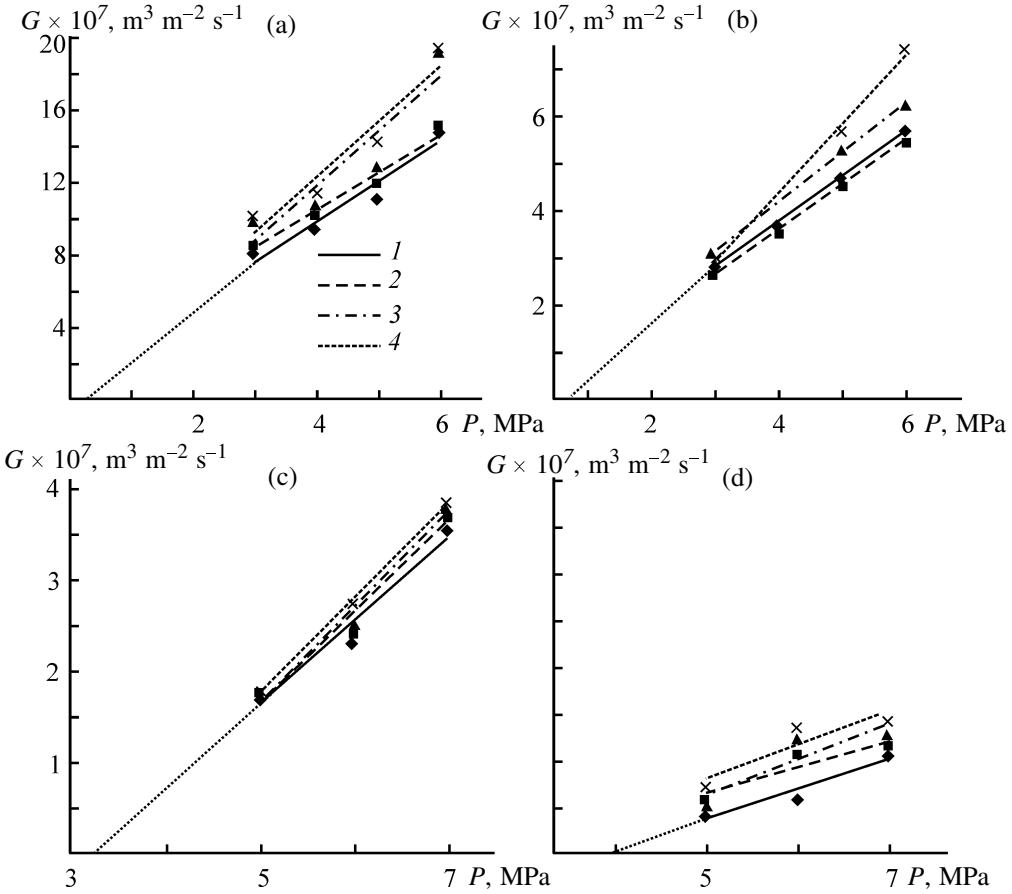


Fig. 3. Transmembrane flux G across MGA-90T membrane as a function of the pressure P.

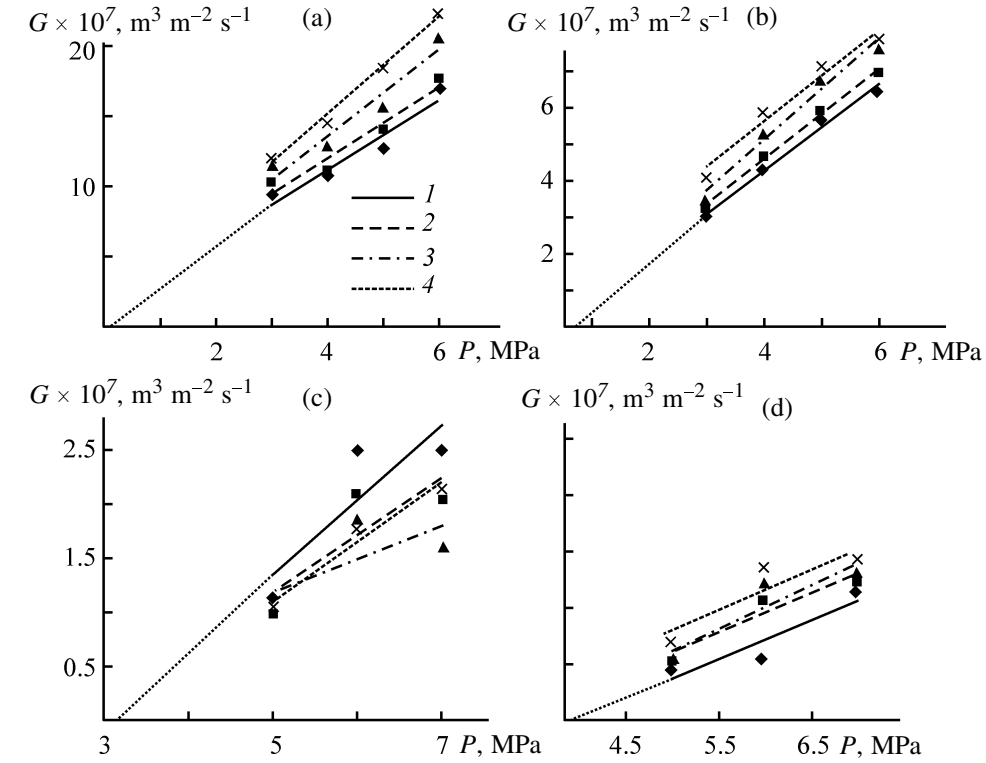


Fig. 4. Transmembrane flux G across ESPA membrane as a function of the pressure P.

Table 2. Coefficients of Eq. (3) for estimating the fluxes

Membrane	$k \times 10^7$	n	m
MGA-90T	5.745294	–0.39065	2.894219
ESPA	8.615161	–40.48844	3.17998

the solution to be separated; and c is the initial solution concentration.

The empirical coefficients are given in Table 2. The experimental and theoretical retention factors and fluxes are consistent to within 15%.

CONCLUSIONS

(1) The effects of the sodium sulfanilate concentration, transmembrane pressure, and solution temperature on the retention factor of MGA-90T and ESPA membranes are studied. The retention factor linearly increases with increasing solute concentration up to 250 g l^{-1} and decreases with increasing temperature. The retention factor is slightly higher for ESPA membrane as compared to MGA-90T.

(2) The transmembrane flux increases with increasing pressure and temperature, which is consistent with the common views, and decreases with increasing solute concentration, as a result of the increase in the osmotic pressure. The flux across ESPA membrane is slightly higher than that across MGA-90T.

REFERENCES

1. Lazarev, S.I., Korobov, V.B., Kliot, M.B., and Pirogov, P.A., *Izv. Vyssh. Uchebn. Zaved., Khim. Khim. Tekhnol*., 1993, no. 6, pp. 79–80.
2. Dytnerskii, Yu.I., *Baromembrannye protsessy: Teoriya i raschet* (Baromembrane Processes: Theory and Calculations), Moscow: Khimiya, 1986.
3. Hwang, S.-T. and Kammermeyer, K., *Membanes in Separations*, New York: Wiley, 1975.
4. Karelin, F.N., *Obessolivanie vody obratnym osmosom* (Water Desalination by Reverse Osmosis), Moscow: Stroiizdat, 1988.
5. Bryk, M.T. and Tsapyuk, E.A., *Ul'trafil'tratsiya* (Ultrafiltration), Kiev: Naukova Dumka, 1989.
6. Deryagin, B.V., Churaev, N.V., Martynov, G.A., et al., *Khim. Tekhnol. Vody*, 1981, vol. 3, no. 2, pp. 99–104.
7. Sourirajan, S., *Pure Appl. Chem*., 1978, vol. 50, pp. 593–615.
8. Koganovskii, A.M., Levchenko, T.M., Kirichenko, V.A., et al., *Adsorbtsiya rastvorennykh veshchestv* (Adsorption of Solutes), Kiev: Naukova Dumka, 1977.
9. Tone, S., Shinokhara, K., Igorashi, Y., and Otake, T., *J. Membrane Sci*., 1984, vol. 19, pp. 195–208.
10. Deryagin, B.V., Churaev, N.V., and Muller, V.M., *Poverkhnostnye sily* (Surface Forces), Moscow: Nauka, 1985.
11. Reid, R.F., *Properties and Reactions of Bonds in Organic Molecules*, London: Longmans, 1968.
12. Churaev, N.V., *Fizikokhimiya protsessov massoperenosa v kapillyarno-poristykh telakh* (Physical Chemistry of Mass Transfer in Capillary-Porous Bodies), Moscow: Khimiya, 1990.

ISSN 1070-4272. Russian Journal of Applied Chemistry, 2006, Vol. 79, No. 5, pp. 741–745. © Pleiades Publishing, Inc., 2006.
Original Russian Text © M.Yu. Berezkin, I.N. Chernykh, E.G. Polyakov, A.P. Tomilov, 2006, published in Zhurnal Prikladnoi Khimii, 2006, Vol. 79, No. 5, pp. 752–756.

APPLIED ELECTROCHEMISTRY AND CORROSION PROTECTION OF METALS

Electrochemical Synthesis of Niobium(V) Ethylate

M. Yu. Berezkin, I. N. Chernykh, E. G. Polyakov, and A. P. Tomilov

State Research Institute of Organic Chemistry and Technology, Federal State Unitary Enterprise, Moscow, Russia
St. Petersburg State Polytechnic University, St. Petersburg, Russia

Received January 27, 2006

Abstract—The effect exerted by the supporting electrolyte and cathode material on the anodic dissolution of niobium in ethanol solutions was studied.

DOI: 10.1134/S1070427206050090

The goal of this study was to develop an electrochemical method for preparing Nb(V) alkoxide. The latter can serve as the starting material for preparation of ultrapure Nb(V) and Nb(V) oxide, which are widely used in various areas of industry.

The anodic dissolution of a metal in the corresponding alcohol in the presence of a supporting electrolyte is one of promising but insufficiently studied methods of preparing transition metal alkoxides. At the same time, in an extensive monograph [1] reviewing in detail the properties and methods of preparation of all the presently available metal alkoxides, the electrochemical method is given the least attention. Alkoxides prepared by the electrochemical method are listed in a review [2], demonstrating the potential of the method.

As a rule, it is recommended to perform the synthesis in a diaphragmless electrolyzer from electrolytes chosen empirically, with as high electrical conduction as possible. The influence of electrolysis conditions on the yield of alkoxides virtually was not studied. The existing views on the mechanism of the alkoxide formation are controversial. According to Lemkuhl et al. [3], who synthesized iron, cobalt, and nickel alkoxides using alkali metal halides as electrolytes, the initial anodic process is the discharge of halide ions. Then, the atomic halogen reacts with a metal of the anode to form the corresponding halide, which is reduced to the alkoxide on the cathode, i.e., the reaction pattern is as follows:

Anode:

$$Hal^- \rightarrow Hal^\bullet + e,\ M + 2Hal^\bullet \rightarrow MHal_2;$$

Cathode:

$$MHal_2 \xrightarrow{+e} [MHal_2]^- \xrightarrow{+e} [MHal_2]^{2-} \xrightarrow{+2HOR} H_2 + 2Hal^- + M(OR)_2. \quad (1)$$

Based on the general views on the possible mechanism of the formation of transition metal alkoxides by the anodic dissolution in alcohol electrolyte solutions, Shreider et al. [4] suggested the following reactions as the most probable:

Anode:

$$M - e \xrightarrow{Hal^- + OR^-} M(OR)_nHal_m\ [+M(OR)_pHal_q\downarrow],$$

Cathode:

$$M(OR)_nHal_m + e \rightarrow M(OR)_nHal_m^{-\bullet} \xrightarrow{-Hal^-} M(OR)_nHal^\bullet_{m-1} \xrightarrow{+ROH,\ -1/2H_2} M(OR)_{n+1}Hal^\bullet_{m-1} \xrightarrow{+e} \ldots \xrightarrow{+ROH,\ -1/2H_2,\ -Hal^-} M(OR)_{n+m}. \quad (2)$$

Contrary to Shreider et al. [4], who ruled out the alcohol dissociation with the formation of RO^- and a proton with its subsequent reduction on the cathode, Bukhtiarov et al. [5] detected by cyclic voltammetry intense hydrogen evolution during the electrolysis of alcohol solutions in aprotic solvents on the cathode made of transition metals. Based on these observations, Bukhtiarov et al. [5] suggested an alternative mechanism of the alkoxide formation, involving ionization of a metal with the formation of the corresponding cations on the anode and decomposition of an al-

cohol molecule accompanied by evolution of hydrogen and formation of the RO^- anion on the cathode. In the bulk of a solution, alkoxide anions react with the metal cations to form alkoxide. The reaction pattern can be presented as follows:

$$\text{Anode: } M^0 \rightarrow M^{2+} + 2e,$$

$$\text{Cathode: } ROH + e \rightarrow OR^- + 1/2H_2,$$

$$\text{In solution bulk: } M^{2+} + 2RO \rightarrow M(OR)_2. \quad (3)$$

Thus, with rather scarce and controversial data available on the electrochemical formation of transition metal alkoxides, we started a systematic study of this process with niobium ethylate as example. Shreider [4] obtained for the first time niobium ethylate by the electrochemical method involving electrolysis of an ethanol solution of triethylamine hydrobromide with a platinum cathode and a niobium anode. Niobium pentaethoxide was isolated and identified, but the Shreider's experiment is the only example of niobium alkoxide electrosynthesis described in detail in the literature.

This study is the first step of the investigation of the electrochemical synthesis of niobium alkoxide; we examined the anodic dissolution of niobium in an ethanol solution of various electrolytes.

EXPERIMENTAL

According to the published data, alkoxide synthesis is a moisture-sensitive process. Therefore, particular attention was given to the ethanol drying. After performing a number of the experiments, we used in the study the following method.

Water was preliminarily separated from ethanol by distillation of a ternary azeotrope with benzene [6]. Then the solution was treated with sodium metal and diethyl oxalate. After distillation, the ethanol fraction (boiling point point 78.2–78.3°C) contained 0.03–0.05 wt % H_2O. The content of water in the alcohol was determined by Fischer titration.

As supporting electrolytes were used chemically pure grade salts. Tetraethylammonium acetate was prepared by mixing an aqueous solution of tetraethylammonium hydroxide with an excess amount of dilute acetic acid. After that, the solution was evaporated to dryness and the residue was dried at 100–120°C/5 mm Hg.

The experiments were performed in a diaphragmless electrolyzer in the form of a 90 cm^3 glass cylinder equipped with a temperature-control jacket and a magnetic stirrer. The electrolyzer was hermetically closed with a lid, in which a thermometer, an outlet pipe with a calcium chloride tube, and electrode current leads were inserted. A flat niobium anode was arranged between the two cathodes.

The niobium anode (working area 8 cm^2) was made of an Nb-1 niobium sheet [GOST (State Standard) 16099–80], and the cathodes (working area 18 cm^2), of a 1-mm platinum wire. Prior to the electrolysis, the electrodes were weighed after trimming and degreasing with Vienna lime. After the experiment was complete, the solution was removed for further treatment. The weight of the dissolved metal was determined from the weight loss of the anode.

The product was isolated by fractional distillation. First alcohol was distilled off, and then niobium pentaethoxide, a light-yellow liquid, was distilled in a vacuum (boiling point 165°C/1.5 mm Hg).

The current–voltage dependences were measured on an IPC-2000 electronic potentiostat and processed on a computer. For the measurements we used a 45 cm^3 diaphragmless cell equipped with a temperature-control jacket. The electrodes and an outlet rube were inserted into the cell lid. The electrode system consisted of a stationary working electrode made of the corresponding metal (working area 0.5 cm^2), a platinum auxiliary electrode, and a silver chloride reference electrode.

To measure the anodic curve, the cell was charged with an electrolyte solution of the required concentration and was purged with dry argon through the outlet tube for 0.5 h. Then, the trimmed electrode was set into the cell preheated to the required temperature and was polarized by the prescribed program.

To record the cathodic curves in the presence of niobium ethoxide, the electrodes were withdrawn and trimmed prior to each measurement, and niobium ethoxide was added to the electrolyte just before the measurement. The current–voltage curves were processed on a computer.

Niobium forms penta-, tetra-, and trialkoxy compounds [1], i.e., it may exist in the penta-, tetra-, or trivalent state. With lithium chloride, lithium *p*-toluenesulfonate, triethylamine hydrohalides, or tetraethylammonium quaternary salts in ethanol as electrolytes, the niobium anode dissolves with the formation of a Nb(V) compound. This is confirmed by calculation of the current efficiency and by the lack of solution coloration typical for Nb(III) and Nb(IV) alkoxides [1]. At the same time, it was shown experimentally [1] that, at a cathodic current density from 0.01 to

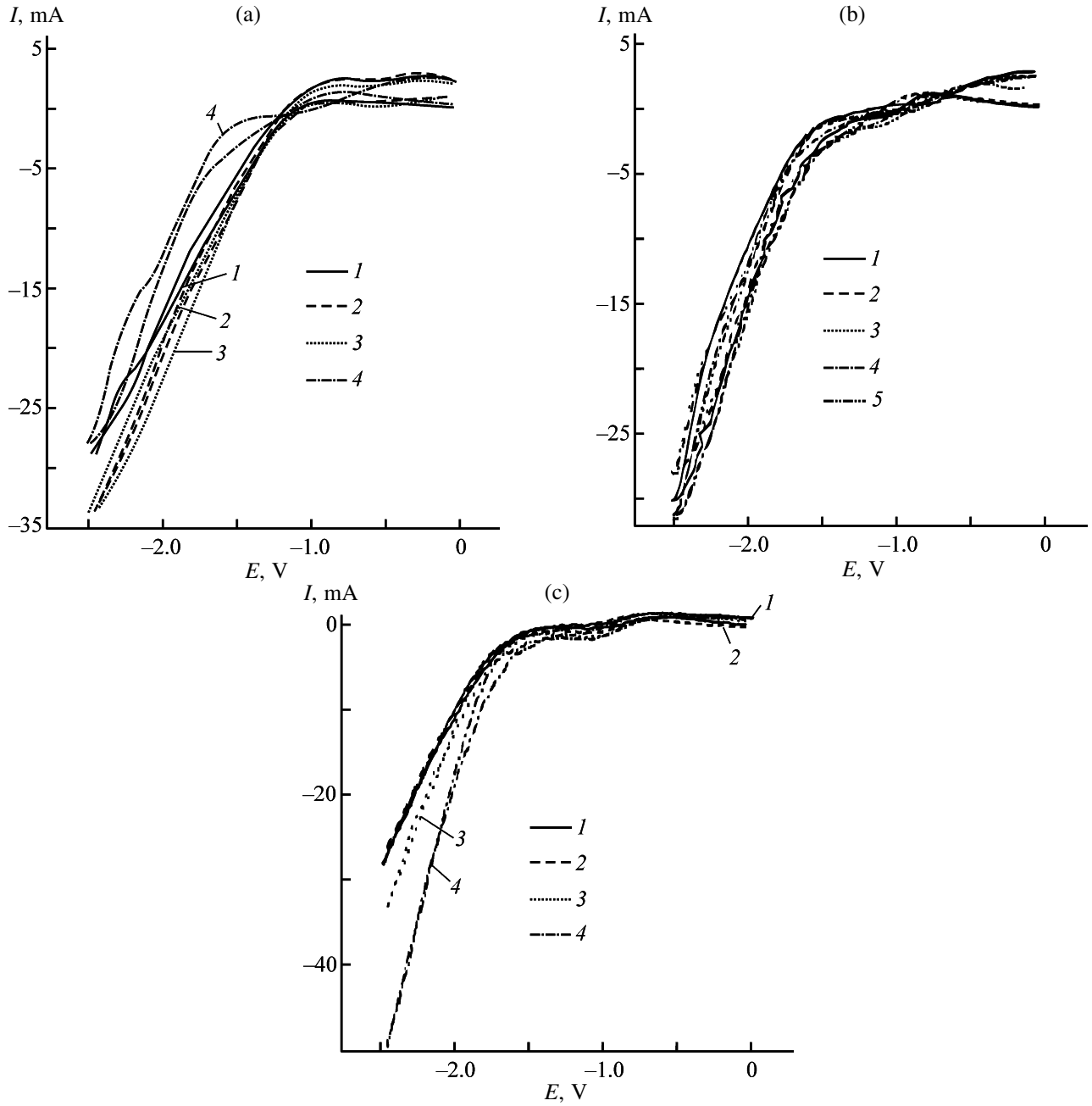


Fig. 1. Current–voltage curves measured in a 0.5 N solution of LiCl in ethanol (0.027% water) in the presence of $Nb(OEt)_5$ additions. T = 25°C, V = 0.2 V s^{-1}; the same for Fig. 2. (*I*) Current strength and (*E*) potential (vs. silver chloride electrode); the same for Fig. 2. Cathode: (a) Pt, (b) Ni, and (c) stainless steel. $Nb(OEt)_5$ concentration (M): (*1*) 0, (*2*) 0.001, (*3*) 0.01, (*4*) 0.02, and (*5*) 0.04.

0.0025 A cm^{-2}, niobium pentaalkoxide can be reduced to the tetraalkoxide on the cathode, with a colorless solution becoming brown in the course of the electrolysis. After testing a number of cathodic materials (lead, niobium, titanium, stainless steel, molybdenum, nickel, and platinum), we chose metals with the lowest hydrogen overvoltage, platinum and nickel, as the working materials.

The cathodic reduction was also examined voltammetrically. The reduction of niobium pentaethoxide on the cathodes made of different materials was determined by measuring the voltammograms on platinum, nickel, and stainless steel at the cathodic polarization in a 0.5 N solution of lithium chloride supporting electrolyte at different concentrations of niobium pentaethoxide (Figs. 1a–1c). The curves obtained

Table 1. Comparison of total currents and currents spent for reduction of niobium pentaethoxide at its different concentrations in solution and at different potentials

Addition, M	Current, mA		Current spent for reduction, %
	background	total	
Potential –2.0 V			
0.001	10	10	0
0.01	10	12	16.7
0.02	10	17	41.2
Potential –2.5 V			
0.001	27	27	0
0.01	27	33	15.2
0.02	27	48	43.8

Table 2. Effect of the anion on the dissolution of a niobium anode (S_{work} = 8 cm^2) at an anodic current density of 0.03 A cm^{-2} from a 0.1 M electrolyte with a Pt cathode (S_{work} = 18 cm^2) at 35°C

Electrolyte	Current efficiency by Nb(V), %	$Nb(OEt)_5$ yield based on Nb(V)
Et_4NCl	99.16	42.9
Et_4NAc	99.92	1.71
Et_4NBF_4	97.72	20.9
Et_4NBr	95.79	0
LiCl	99.46	65.4
$Li(CH_3C_6H_4SO_3)$	95.70	23.1

Table 3. Effect of the cation on the current efficiency by Nb(V) in electrolysis with Nb anode (S_{work} = 8 cm^2) and Pt cathode (S_{work} = 18 cm^2) in a 0.1 M electrolyte at an anodic current density of 0.03 A cm^{-2} and 35°C

Electrolyte	Current efficiency by Nb(V)
LiCl	99.46
Et_4NCl	99.16
$Et_3N \cdot HCl$	100.37
Et_4NBr	95.79
$Et_3N \cdot HBr$	78.69
Bu_4NBr	90.09

show that niobium pentaethoxide is reduced only on the steel electrode (Fig. 1c). The parameters characterizing this process are listed in Table 1.

Table 1 shows that the current spent for the reduction of niobium pentaethoxide depends on the concentration of the substance in a solution and does not noticeably depend on the cathodic current density in the examined range. Thus, the current–voltage curves obtained are in agreement with the results of the preparative electrolyses.

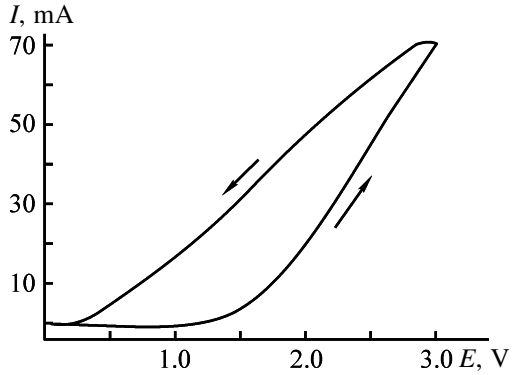


Fig. 2. Current–voltage curve obtained on Nb in a 0.5 N solution of Et_4NCl in ethanol (0.027% water).

The effect of the electrolyte on the efficiency of the anodic dissolution of Nb was studied in two series of experiments. The fact that the solution remains colorless indicates that the dissolution occurs to Nb(V). In the first series of the experiments (Table 2) we studied the effect of the anion, with tetraethylammonium as cation. As seen from Table 2, niobium dissolves at a current efficiency exceeding 95% [as calculated for Nb(V)]. Hence, the anion only slightly affects the anodic dissolution of niobium. The effect of the cation is also weak, at least in the case when niobium is dissolved in chloride solutions (Table 3). The further study showed that, whereas the supporting electrolyte affects the dissolution of a niobium anode only slightly, its influence on the formation of niobium alkoxide is decisive. Table 2 shows that niobium ethylate is best formed in chloride solutions, whereas in bromide solutions it is not formed at all. Although with tetraborate and acetate anions the alkoxide is formed, its yield (based on Nb) is considerably lower than in chloride solutions. We do not have sufficient data yet to account for this trend, and the study in this area is being continued.

To study the anodic process in more detail, we measured the current–voltage curves. One of typical cyclic voltammograms obtained at anodic polarization of a niobium electrode in an ethanol solution of tetraethylammonium is shown in Fig. 2. The voltammogram has a clear hysteresis. At forward potential scanning, the dissolution is not observed up to 1.2 V, whereas at the reverse scanning the electrode dissolution continues down to 0.25 V. Presumably, the anodic polarization breaks the passivation film on the elec-

Table 4. Potentials of the niobium transition from the active to the passive state in solutions of various compositions.* Solvent: ethanol containing 0.027% water

Electrolyte	E_a	E_p	ΔE
	V		
LiCl	0.65	0.30	0.35
Et_4NCl	1.20	0.25	0.95
$Et_4NOOCCH_3$	1.60	0.40	1.20

* $\Delta E = E_a - E_p$.

trode surface, making the electrode active. The potential of the onset of the niobium dissolution at forward scanning can be designated as the potential of transition to the active state, and the potential of the passivation at reverse scanning, as the passivation potential E_p. The similar effect was also observed for solutions of lithium chloride and tetraethylammonium acetate (Table 4). As can be seen, the supporting electrolyte significantly affects the potential of transition to the active state, but does not noticeably affect the passivation potential. From the viewpoint of easiness of niobium anode activation, it is preferable to use lithium chloride as electrolyte.

The experiments performed showed that the current efficiency in dissolution of a niobium anode depends only slightly on the supporting electrolyte and is close to 100% [as calculated for Nb(V)] in all the media studied. This result and the closeness of the passivation potentials for different electrolytes show that, contrary to Lemkuhl's suggestion, niobium ionization rather than oxidation of the anion takes place in the course of the anodic process. Another important observation consists in that the yield of niobium ethylate based on Nb significantly depends on the supporting electrolyte anion. Probably, the anion is involved in the synthesis reaction. Presumably, the intermediate formation of alkoxy halides, suggested in [4], plays a certain role in the alkoxide synthesis.

CONCLUSIONS

(1) The anodic dissolution of niobium is accompanied by transition of niobium into the pentavalent state. The supporting electrolyte affects only slightly the current efficiency of the metal dissolution.

(2) The supporting electrolyte strongly affects the yield of niobium alkoxide. The highest yield is observed in chloride electrolytes.

(3) To avoid the reduction of Nb(V) to Nb(IV), it is advisable to use cathode materials with the lowest hydrogen overvoltage.

REFERENCES

1. Turova, N.Ya., Turevskaya, E.R., Kessler, V.G., and Yanovskaya, M.I., *The Chemistry of Metal Alkoxides*, Boston: Kluwer, 2002.
2. Tomilov, A.P., *Elektrokhimiya*, 2000, vol. 36, no. 2, pp. 115–132.
3. Lemkuhl, H., and Eisenbach Liebigs, W., *Ann. Chem.*, 1975, no. 4, pp. 672–691.
4. Shreider, V.A., Turevskaya, E.P., Kozlova, N.I., and Turova, N.Ya., *Izv. Akad. Nauk SSSR, Ser. Khim.*, 1981, no. 8, pp. 1687–1693.
5. Bukhtiarov, A.V., Golyshin, V.N., Kuzmin, O.V., et al., *Zh. Obshch. Khim.*, 1986, vol. 56, no. 6, pp. 1356–1360.
6. Weissberger, A. and Proskauer, E.S., *Organic Solvents. Physical Properties and Methods of Purification*, Riddick, J.A. and Toops, E.E., Eds., New York: Interscience, 1955.

ISSN 1070-4272. Russian Journal of Applied Chemistry, 2006, Vol. 79, No. 5, pp. 746–751. © Pleiades Publishing, Inc., 2006.
Original Russian Text © G.A. Kolyagin, V.L. Kornienko, 2006, published in Zhurnal Prikladnoi Khimii, 2006, Vol. 79, No. 5, pp. 757–761.

APPLIED ELECTROCHEMISTRY AND CORROSION PROTECTION OF METALS

Effect of Trialkylammonium Salts and Current Density on the Electrosynthesis of Hydrogen Peroxide from Oxygen in a Gas-Diffusion Electrode in Acid Solutions

G. A. Kolyagin and V. L. Kornienko

Institute of Chemistry and Chemical Technology, Siberian Division, Russian Academy of Sciences, Krasnoyarsk, Russia

Received June 21, 2004

Abstract—The influence exerted by the nature of cation of a supporting electrolyte and by the current density on the electroreduction of oxygen to hydrogen peroxide in acid K_2SO_4 solutions (pH 0.9–1.4) in gas-diffusion hydrophobized carbon black electrodes with varied electrolyte porosity was studied.

DOI: 10.1134/S1070427206050107

It is known that the rate of electrochemical processes is strongly affected by the supporting electrolyte and various additives [1]. For example, addition of tetraalkylammonium salts affects the electroreduction of CO and CO_2 [2], acetophenone [3], 1,1,2-trifluorotrichloroethane [4, 5], and trichlorofluoromethane [6], electrodeposition of gold [7] and copper [8], and electroreduction of oxygen to H_2O [9–11] and of H_2O_2 to water [12]. Changes in the reduction kinetics of oxygen and H_2O_2 in the presence of tetraalkylammonium cations are due to their adsorption on the electrode and to changes in parameters of the electrical double layer [1, 9].

In [9], a 0.26 M solution of H_2O_2 was prepared on a hydrophilic porous glassy-carbon electrode from oxygen dissolved in a 0.1 M H_2SO_4 solution under atmospheric pressure with addition of trioctylmethylammonium chloride ($[CH_3(CH_2)_7]_3CH_3NCl$) with a current efficiency of up to 55% at a geometric current density of 30 mA cm^{-2}. In [10, 11], a three-phase system constituted by an acid aqueous electrolyte, organic phase, and oxygen gas with 2-ethyl-9,10-anthraquinone as electron-transfer catalyst and addition of tetrabutylammonium perchlorate and trioctylmethylammonium chloride was used to accelerate the electrosynthesis of H_2O_2 on electrodes of this type.

It is known that porous gas-diffusion hydrophobized electrodes are widely used for intensifying electrosynthesis with gas reagents poorly soluble in water [13].

It has been shown that the electroreduction of oxygen to hydrogen peroxide in an acid medium on porous hydrophobized carbon black electrodes strongly depends on the extent to which an electrolyte penetrates into the pore space [14, 15]. An increase in pH makes lower the rate of further reduction of H_2O_2 to water. Addition of a salt with a common anion into an acid solution diminishes the diffusion- and migration-related hindrance in proton transfer deep into the electrode, which leads to an increase in the pH of the catholyte and in the current efficiency. Raising the rate of agitation of a solution makes higher the content of protons in the near-electrode layer and, consequently, leads to an increase in the rate of reduction of hydrogen peroxide to water. The rate of oxygen reduction is also strongly affected by the cathode current density [16].

In this context, it is of scientific and practical interest to study the influence exerted by the nature of electrolyte cations and current density on the electrosynthesis of H_2O_2 on porous hydrophobized electrodes of varied structure. Also, mention should be made of the close attention to electrosynthesis of acid solutions of H_2O_2, associated with their use for *in situ* oxidation of various organic compounds both for synthesis and for mineralization of wastewater [17, 18].

In this study we examined the influence exerted by addition of tetraalkylammonium salts to electrolytes on the kinetics of accumulation of hydrogen peroxide in acid aqueous solutions in electroreduction of oxygen on gas-diffusion hydrophobized carbon black electrodes with varied electrolyte porosity.

EXPERIMENTAL

The experimental conditions and the electrolyzer design were similar to those described in [13–15, 19]. The preparative electrolysis was performed in the galvanostatic mode at a geometric current density of 50–100 mA cm^{-2} at 20°C in the course of 6–7 h in an electrolyte of composition 0.2 M K_2SO_4 + 0.087 M H_2SO_4 (pH 1.4) with and without addition of tetrabutylammonium bromide (0.01 M). The current density was calculated per unit apparent frontal surface area (5 cm^2). The catholyte volume was 0.023 l. Oxygen was delivered into the electrode from its backside under atmospheric pressure. The catholyte was agitated by bubbling argon via a tube 1.5 in diameter permanently at a rate of 10 ml min^{-1} (agitation mode no. 1) or hourly for 1 min at a rate of 38 ml min^{-1} before sampling the solution for analysis for H_2O_2 (agitation mode no. 2). The catholyte and anolyte were separated by an MF-4SK-100 cation-exchange membrane. The electrodes were fabricated from an electrode paste containing an A-437E acetylene black and 8 or 60 wt % 4D fluoroplastic (Teflon). The electrode paste was preliminarily heated to 300°C, and electrodes were sintered in air at 360°C in the course of 10 min. To eliminate hindrance to oxygen supply into the electrode, the electrodes were fabricated with a high porosity of 65 vol %. The electrolyte porosity was measured by hydrostatic weighing [20]. It was, on the average, 7.6 and 1.3 vol % for electrodes with 8 and 60 wt % fluoroplastic, respectively. The fraction γ of current expended for the synthesis of hydrogen peroxide was determined by gasometry [19]. The electrode potential was measured relative to a silver chloride reference electrode (EVL-1M1). Polarization curves were measured at a potential sweep rate of 4 mV s^{-1} under continuous agitation of the electrolyte. A solution of 0.025 M K_2SO_4 + 0.12 M H_2SO_4 (pH 0.9) served as the main electrolyte, to which the following salts were added: tetrabutylammonim bromide (TBAB), tetrabutylammonim iodide (TBAI), diethyldibenzylammonium bromide (DEDBAB), tetraethylammonium chloride (TEAC), and allyltrimethylammonium bromide (ATMAB). Also, in some experiments K_2SO_4 was replaced with LiCl or $CsNO_3$.

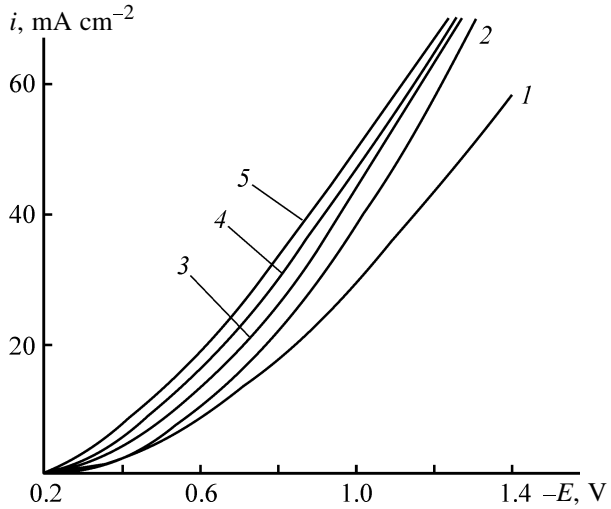


Fig. 1. Polarization curves for electroreduction of oxygen on a gas-diffusion carbon black electrode containing 60 wt % fluoroplastic in solutions of various compositions. (*i*) Current density and (*E*) electrode potential; the same for Fig. 2. Solution composition: (*1*) 0.11 M H_2SO_4, (*2*) 0.025 M K_2SO_4 + 0.12 M H_2SO_4, (*3*) 2 + 0.05 M TEAC, (*4*) 2 + 0.01 M DEDBAB, and (*5*) 2 + 0.01 M TBAB.

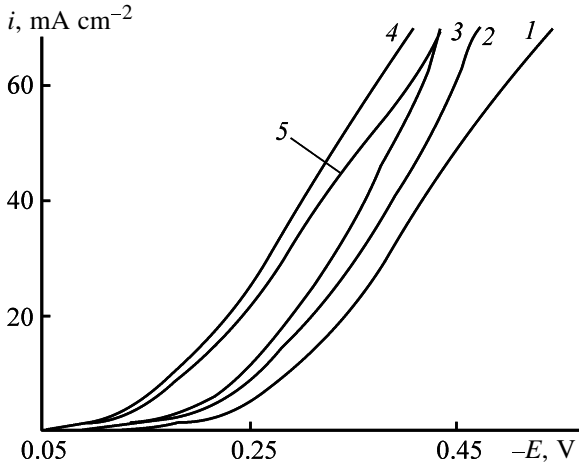


Fig. 2. Polarization curves for electroreduction of oxygen on a gas-diffusion carbon black electrode containing 8 wt % fluoroplastic in (*1*) 0.1 M H_2SO_4 solution, (*2*) solution of 0.025 M K_2SO_4 + 0.12 M H_2SO_4, and (*3*–*5*) that with TBAB added in various concentrations. TBAB concentration (M): (*3*) 0,001, (*4*) 0.01, and (*5*) 0.1.

The polarization curves obtained are shown in Figs. 1 and 2. It should be noted that the fraction γ of the current expended for the synthesis of H_2O_2 in all of the electrolytes studied, except for acid solutions without additives, is high. This indicates that the curves refer virtually only to the oxygen reduction to H_2O_2. The influence exerted on the reduction of oxygen by the kinds of anions of the salts used or of alkali metal cations was insignificant. The values of γ and the polarization curves for electroreduction of O_2, obtained in solutions of 0.025 K_2SO_4 + 0.12 M H_2SO_4, 0.05 M LiCl + 0.12 M H_2SO_4, and 0.05 M $CsNO_3$ + 0.12 M H_2SO_4 are identical. The reduction of oxygen begins in these solutions at +0.05 V. Simi-

Results of a preparative electrosynthesis of hydrogen peroxide and electrolysis parameters* (electrolysis time 6 h)

Run no.	Teflon content, wt %	i, mA cm^{-2}	$-E$, V		$c_{H_2O_2}$, M	γ	η	Equation	
			initial	final		fraction units at $c_{H_2O_2}$ = 0.9 M		$\gamma = b - ac_{H_2O_2}$	$\eta = b_1 - a_1c_{H_2O_2}$
1	8	50	0.31	0.44	0.87	0.81	0.75	$0.95-0.16c_{H_2O_2}$	$0.95-0.22c_{H_2O_2}$
2		100	0.38	0.47	1.82	0.90	0.89	$0.94-0.042c_{H_2O_2}$	$0.94-0.058c_{H_2O_2}$
3**		100	0.40	0.51	1.91	0.95	0.92	const = 0.95	$0.95-0.034c_{H_2O_2}$
4	60	50	0.74	0.90	0.87	0.66	0.73	$0.99-0.37c_{H_2O_2}$	$0.94-0.23c_{H_2O_2}$
5		100	1.20	1.37	1.11	0.49	0.56	$0.89-0.43c_{H_2O_2}$	$0.89-0.37c_{H_2O_2}$
6**		100	1.32	1.39	1.43	0.73	0.73	$0.88-0.16c_{H_2O_2}$	$0.86-0.15c_{H_2O_2}$

* i, E, and η are the current density, electrode potential, and integral current efficiency by H_2O_2, respectively.
** Electrolysis with addition of 0.01 M TBAB to the electrolyte.

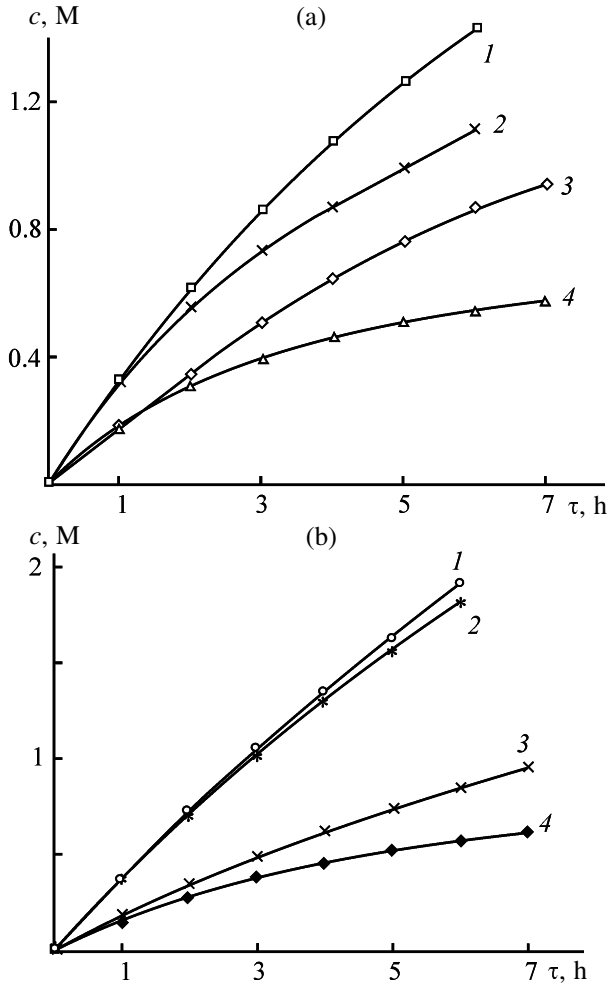


Fig. 3. H_2O_2 accumulation curves obtained on a gas-diffusion carbon black electrode containing (a) 60 and (b) 8 wt % fluoroplastic under varied conditions. (c) H_2O_2 concentration and (τ) time. Current density (mA cm^{-2}): (*1, 2*) 100 and (*3, 4*) 50. Electrolyte: (*2–4*) 0.2 M K_2SO_4 + 0.087 H_2SO_4 and (*1*) the same with addition of 0.01 M TBAB. Agitation mode: (*1–3*) no. 2 and (*4*) no. 1.

lar results were obtained in solutions of 1.0 M $CsNO_3$, 1.0 M LiCl, and 0.5 M K_2SO_4.

The enhancement of the electrode polarization at a higher Teflon content (60 wt %) (see table, Fig. 1) is due to a decrease in the volume of electrolyte-filled pores at a higher content of fluoroplastic, which makes thinner the zone of the oxygen electroreduction. The true working surface area of the electrode decreases and the true current density increases, which enhances the electrode polarization.

The polarization curves obtained in solutions with TBAI and ATMAB additives are not shown in Fig. 1 because they coincided with the curves measured in solutions with TBAB and TEAC, respectively. Figure 1 shows for comparison the curve obtained in 0.1 M H_2SO_4 (pH 0.9). Figures 1 and 2 show that addition of tetraalkylammonium salts accelerates the oxygen reduction; this effect is also observed upon addition of these salts to 0.1 M solutions of H_2SO_4 and HCl. Addition of TBAB has the strongest effect, and that of TEAC, the weakest. No specific effect of the unsaturated bond present in the tetraalkylammonium cation (ATMAB) or of the benzene ring in DEDBAB on the oxygen reduction was observed. The presence of tetraalkylammonium salts in an alkaline electrolyte (0.5 M NaOH) has no effect on the polarization characteristics of the oxygen reduction. The influence exerted by the salt concentration on the electrode polarization is illustrated for TBAB as example (Fig. 2, curves *3–5*). Raising the TBAB concentration from 10^{-4} to 10^{-2} M accelerates the process, but further increase in this concentration to 0.1 M leads to a decrease in the rate of oxygen reduction, which is commonly the case in practice of electrosynthesis, e.g., in dehalogenation of 1,1,2-trifluorotrichloroethane [4]. As the current density is raised, the effect of tetraalkylammonium cations on the electrode polariza-

tion tends to decrease. This is particularly noticeable when performing a preparative electrolysis. The results obtained in the preparative electrolysis are shown in Figs. 3 and 4 and listed in the table. The data in the table correspond to the conditions in which curves *1–3* in Fig. 3 were measured.

An increase in the current density makes higher the rate of accumulation and the concentration of hydrogen peroxide, but, in this case, the change in γ and, consequently, in the current efficiency depends on the electrolyte porosity of the electrode. For example, upon an increase in i from 50 to 100 mA cm^{-2}, the slope of the dependence $\gamma = f(c_{H_2O_2})$ decreases by a factor of 3.8 on electrodes containing 8 wt % fluoroplastic and increases by a factor of approximately 1.2 on electrodes with 60% fluoroplastic (see table). As the current density increases in the case of electrodes containing 8 wt % Teflon, the H_2O_2 concentration, γ, and current efficiency become higher. Raising the Teflon content to 60 wt % leads to a decrease in the extent to which the H_2O_2 concentration grows, with a decrease in γ and current efficiency observed. This is accounted for by the fact that, as the fluoroplastic content decreases, the volume of electrolyte-filled pores increases and the reaction zone extends deeper into the electrode, away from its frontal surface. As a result, the hindrance to proton transport into the electrode is enhanced and thereby the rate of further reduction of H_2O_2 is lowered. To illustrate the effect of mass transfer of protons, Fig. 3 shows curves of H_2O_2 accumulation in different catholyte agitation modes. In an excess of water in neutral and alkaline solutions, synthesis of H_2O_2 involves water and, therefore, the effects observed above are not revealed [15].

The table shows that the addition of TBAB and an increase in the current density have no effect on the run of the dependence of γ and current efficiency on the H_2O_2 concentration [14, 15]. The accumulation curves obtained in the presence of TBAB (Fig. 3) have the common shape [9, 14, 18] and are described by the equation [14, 15]

$$c = \frac{AI|b|V^{-1}\{\exp[(-AI|a|V^{-1} - k)\tau] - 1\}}{-AI|b|V^{-1} - k},$$

where c is the concentration of H_2O_2 in the catholyte (M); A, electrochemical equivalent of H_2O_2 (mol A^{-1} h^{-1}); I, current (A); a and b, coefficients of the equation $\gamma = f(c_{H_2O_2})$ (see table); V, catholyte volume (l); τ, electrolysis time (h); and k, rate constant of H_2O_2 decomposition (h^{-1}).

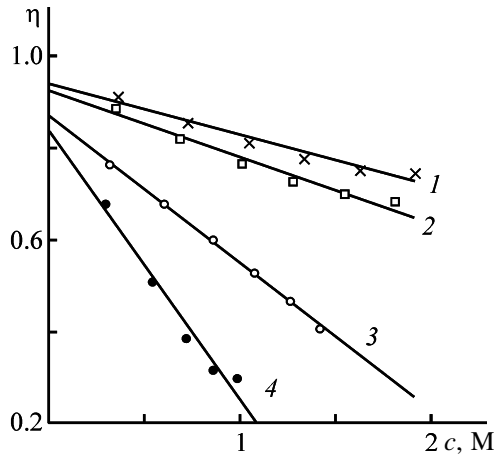


Fig. 4. Differential current efficiency η vs. the concentration c of H_2O_2 in an electrolyte (*2, 4*) without and (*1, 3*) with TBAB added. Teflon content, wt %: (*1, 2*) 8 and (*3, 4*) 60.

The rate of hydrogen peroxide decomposition in the presence of TBAB, as well as that in other acid solutions, is described by a first-order equation. A certain decrease in the rate of H_2O_2 decomposition in the presence of TBA sulfate, reported in [12], was not observed in this study.

The increase in γ upon addition of TBAB to the electrolyte may be due to an increase in the rate of oxygen reduction to H_2O_2 and to a decrease in the rate of further reduction of H_2O_2 to water. The decrease in the rate of H_2O_2 reduction is due to a decrease in the surface activity of protons in the presence of tetraalkylammonium ions. For example, it was shown in [12] that, being adsorbed on the electrode, tetrabutylammonium sulfate markedly diminishes the rate of H_2O_2 reduction to water. The calculations made in [9] for an acid solution containing trioctylmethylammonium chloride (TOMAC) show that tetraalkylammonium cations adsorbed on the electrode can raise the pH of the diffuse part of the electrical double layer from 0.9 to 9.4. Under these conditions, oxygen is reduced on the electrode, with water molecules involved, to give the peroxide ion (HO_2^-) and OH^-, and the H_2O_2 molecule is only formed after HO_2^- is removed from the electrode surface and interacts with a proton in the catholyte bulk. The rate constant of oxygen reduction to H_2O_2 increases in the presence of tetraalkylammonium cations. For example, the rate constant in 0.1 M H_2SO_4 increases from 5.1×10^{-13} to 9.9×10^{-10} m s^{-1} in the presence of 0.017 M TOMAC. The TOMAC layer formed on the electrode surface favors an increase in the content of oxygen in

the catholyte and makes lower its diffusion coefficient [9]. The decrease in the diffusion coefficient of oxygen, observed when a certain concentration of TBAB is reached, makes lower the rate of O_2 reduction (Fig. 2).

The effect of TBAB on the H_2O_2 accumulation depends on the electrode structure. For example, in 6 h of electrolysis on electrodes containing 60 wt % fluoroplastic in the presence of TBAB, the concentration of H_2O_2 increased by 0.32 M and the slope of the $\gamma = f(c_{H_2O_2})$ dependence decreased by a factor of 2.5, whereas on electrodes containing 8 wt % fluoroplastic, the concentration of H_2O_2 and the value of γ increased only slightly (see table). As demonstrated above, the higher the electrolyte porosity of the electrode, the stronger the hindrance to transport of protons into the electrode, and, hence, the weaker the effect of TBAB and the change in the rate of H_2O_2 reduction to water. A study in a 0.5 M NaOH solution demonstrated that, under the given conditions, addition of TBAB to an alkaline electrolyte has no effect on the H_2O_2 accumulation. The attainment of constant γ may be due to the fact that pH is higher than 7 within the electrode and reduction of H_2O_2 to water virtually does not occur in alkaline solutions on carbon black [13].

The table lists the integral current efficiencies, but an important quantity for determining the output capacity of the process at a given instant of time is the differential current efficiency. Figure 4 shows how addition of TBAB affects this parameter (see table, run nos. 2, 3, 5, 6). The differential current efficiency was calculated using the formula reported in [21] by differentiating the accumulation curve. Figure 4 shows that the differential current efficiency linearly depends on the concentration of H_2O_2, but the slope of this dependence somewhat exceeds that for the integral current efficiency. In this case, the effect of TBAB in electrolysis on electrodes with 60 wt % Teflon is stronger than that on electrodes with 8 wt % Teflon.

CONCLUSIONS

(1) Addition of tetraalkylammonium salts to an acid electrolyte accelerates the oxygen electroreduction to H_2O_2. The strongest influence is exerted by tetrabutylammonium chloride. Replacement of K_2SO_4 with $CsNO_3$ or LiCl has no effect on the polarization characteristics of the electrode.

(2) An increase in the current density and addition of tetrabutylammonium bromide to an acid electrolyte make higher the concentration of H_2O_2. In this case, the change in the fraction of the current expended for oxygen reduction to H_2O_2 and in the current efficiency depend on the electrolyte porosity of the electrode. An appropriate combination of the electrolyte porosity, composition of the electrolyte, and mode of its agitation can provide that the current efficiency will increase with the current density. The effect of the above-mentioned factors is based on a change in the parameters of the electrical double layer and in the pH in the pore space of the electrode and in the near-electrode layer.

REFERENCES

1. Mairanovskii, S.G., in *Elektrosintez i bioelektrokhimiya: Progress elektrokhimii organicheskikh soedinenii* (Electrosynthesis and Bioelectrochemistry: Advances in Electrochemistry of Organic Compounds), Moscow: Nauka, 1975, pp. 252–281.
2. Muraya Akira and Hori Yoshio, *Bull. Chem. Soc. Jpn.*, 1991, vol. 64, no. 1, pp. 123–127.
3. Yorimitsu Kodama, Mitsutaka Imoto, Nobuaki Ohta, et al., *J. Electroanal. Chem.*, 2001, vol. 507, no. 1, pp. 103–109.
4. Kolyagin, G.A. and Kornienko, V.L., *Elektrokhimiya*, 1996, vol. 32, no. 2, pp. 302–304.
5. Kolyagin, G.A. and Kornienko, V.L., *Zh. Prikl. Khim.*, 1990, vol. 63, no. 7, pp. 1550–1554.
6. Fotadis, T., Kyriacou, G., Lambrou, C., and Hadjispyrou, S., *J. Electroanal. Chem.*, 2000, vol. 480, nos. 1–2, pp. 249–254.
7. Fanigliulo, A. and Bozzini, B., *J. Electroanal. Chem.*, 2002, vol. 530, no. 1, pp. 53–62.
8. Vicenzo, A. and Cavallotti, P.L., *J. Appl. Electrochem.*, 2002, vol. 32, no. 7, pp. 743–753.
9. Gyenge, E.L. and Oloman, C.W., *J. Appl. Electrochem.*, 2001, vol. 31, no. 2, pp. 233–243.
10. Gyenge, E.L. and Oloman, C.W., *J. Appl. Electrochem.*, 2003, vol. 33, no. 8, pp. 655–663.
11. Gyenge, E.L. and Oloman, C.W., *J. Appl. Electrochem.*, 2003, vol. 33, no. 8, pp. 665–674.
12. Anurova, A.I., Chernova, L.A., and Rotinyan, A.L., in *Sbornik rabot po khimicheskim istochnikam toka* (Coll. of Works on Chemical Power Cells), Leningrad: Energiya, 1973, issue 8, pp. 191–197.
13. Kornienko, V.L., Kolyagin, G.A., and Saltykov, Yu.V., *Zh. Prikl. Khim.*, 1999, vol. 72, no. 3, pp. 353–361.
14. Kolyagin, G.A. and Kornienko, V.L., *Khim. Inter. Ustoich. Razv.*, 2000, vol. 8, no. 6, pp. 803–807.

15. Kolyagin, G.A. and Kornienko, V.L., *Zh. Prikl. Khim.*, 2003, vol. 76, no. 7, pp. 1103–1108.
16. Kublanovskii, V.S., Gorodyskii, A.V., Belinskii, V.N., and Glushchak, T.S., *Kontsentratsionnye izmeneniya v prielektrodnykh sloyakh v protsesse elektroliza* (Concentration Changes in Near-Electrode Layers in the Course of Electrolysis), Kiev: Naukova Dumka, 1978.
17. Kornienko, V.L. and Kolyagin, G.A., *Elektrokhimiya*, 2003, vol. 39, no. 12, pp. 1462–1470.
18. Brillas, E., Casado, J., and Caple, J.C., *Water Res.*, 2000, vol. 34, no. 8, pp. 2253–2263.
19. Kolyagin, G.A. and Kornienko, V.L., *Zh. Prikl. Khim.*, 1997, vol. 70, no. 3, pp. 500–502.
20. Baranov, A.P., Shteinberg, G.V., and Bagotskii, V.S., *Elektrokhimiya*, 1971, vol. 7, no. 3, pp. 387–390.
21. Kenova, T.A., Abolin, O.E., and Kornienko, V.L., *Zh. Prikl. Khim.*, 1991, vol. 64, no. 3, pp. 670–673.

ISSN 1070-4272. Russian Journal of Applied Chemistry, 2006, Vol. 79, No. 5, pp. 752–760. © Pleiades Publishing, Inc., 2006.
Original Russian Text © A.F. Dresvyannikov, I.O. Grigor'eva, 2006, published in Zhurnal Prikladnoi Khimii, 2006, Vol. 79, No. 5, pp. 762–769.

APPLIED ELECTROCHEMISTRY AND CORROSION PROTECTION OF METALS

Contact Reduction of Copper(II) on Aluminum in Ammonia Solutions

A. F. Dresvyannikov and I. O. Grigor'eva

Kazan State Technological Uiversity, Kazan, Tatarstan, Russia

Received December 27, 2005

Abstract—A procedure for obtaining copper in the form of finely dispersed metal from alkaline ammonia solutions with a low copper concentration was developed.

DOI: 10.1134/S1070427206050119

Finely dispersed copper powder is used in production of cables and conducting parts of electric installations, as the base component of bronzes and brasses and copper–nickel alloys, for deposition of corrosion-resistant coatings, and as component of certain compositions in powder metallurgy. It is usually produced by traditional processes: electrolysis of aqueous solutions of copper compounds, reduction of Cu_2O and CuO with hydrogen, or from aqueous solutions of Cu(II) salts [1]. These methods are frequently inapplicable for obtaining copper or its compositions from such sources as liquid and solid technogenic media accumulated in various plants: in machine-building (electroplating), metallurgy, production of batteries, etc. Such wastes constitute a serious environmental hazard, as copper compounds are toxic [2]. Copper can be recovered from technogenic media as a metal by electrolysis. However, its efficiency is not always high [3, 4], which makes indispensable the development of combined methods of waste treatment.

It should be noted that hydrometallurgical methods of copper recovery are based on selective dissolution of copper-containing minerals in dilute acids or ammonia. As a rule, copper is recovered from these solutions in the elemental state by reduction with hydrogen in autoclaves [1], by electrolytic precipitation [5, 6], or by electrolysis [7, 8]. To increase the electrolysis efficiency, bulk electrode materials with a developed surface (graphite) are used [9]. The current efficiency in the electrolysis of copper etching solutions containing ammonium salts and ammonia reaches 94% [10]. In certain cases, elemental aluminum is used as a reducing agent. Compositions for the contact deposition of copper from ammonia electrolytes with operating pH range 11.9–13.5 are known [11]. However, data on the contact deposition of copper on aluminum from dilute ammonia solutions are virtually lacking. Therefore, in this study we examined the deposition of copper on both compact and dispersed aluminum from dilute (10^{-2}–10^{-4}) solutions in aqueous ammonia.

EXPERIMENTAL

Polarization measurements were carried out by the potentiometric method with a PI 50-1 potentiostat and a YaSE-2 electrochemical cell. Cathodic polarization curves were recorded in model solutions under study on a copper electrode (a cylinder 0.5 cm in diameter pressed in fluoroplastic). Anodic polarization curves were recorded on an aluminum (A999 grade) electrode in supporting Na_2SO_4 solutions. The potential sweep rate was 2 mV s^{-1}; an EVL-1M silver chloride electrode was used as a reference electrode, and a platinum electrode, as an auxiliary electrode. In addition, chronopotentiometric curves of an aluminum electrode were taken in solutions under study. In this case, potentials were also measured relative to silver chloride electrode.

Dispersed aluminum (DA) of ASD-4 grade was also used in the study. The aluminum activity was checked by gas-volumetric monitoring of its dissolution in 2 M aqueous NaOH. The content of the metal phase was determined to be $96.21 \pm 0.47\%$.

The compositions of the model solutions containing copper(II) ions, hereinafter referred to under the corresponding numbers, are given in Table 1.

The reaction of Cu(II) with DA was carried out in a temperature-controlled glass vessel at room temperature with stirring at a constant rate of 250 rpm. Pre-

liminary experiments were carried out with an inert gas bubbled through solutions and under the conditions of natural aeration. These experiments showed that the presence of atmospheric oxygen had no noticeable effect on the rate of the reduction Cu(II) powder by DA powder; therefore; further studies were carried out at natural aeration. The reaction course was monitored by the solution color changing from deep violet to colorless and by the appearance of particles with the color characteristic of copper.

Samples of the reaction mixture were taken at certain time intervals and titrated by a standard Na_2EDTA solution [12]. The Cu(II) content in the reaction mixture was also monitored at regular intervals by atomic absorption spectrometry (an AAS-1N spectrometer, Carl Zeiss).

The precipitate was separated from the solution by decanting, washed with a 3.0 M NaOH solution to remove excess aluminum and with distilled water to neutral reaction, and treated with a 0.4% naphthenate soap solution for the stabilization. Then the resulting powder was dried to constant weight in a vacuum.

The contents of the main component and impurities in the precipitate were determined by X-ray fluorescence analysis (a VRA-20L Carl Zeiss installation) and by X-ray diffraction (a DRON-3M installation). To decrease the background from scattering of the primary X-ray beam in air, we used long-wave FeK_α radiation with a β-filter. The recording mode was as follows: U_a = 30 kV, I_a = 15 mA, range of recording 2θ angles from 20° to 140°.

The samples were identified by comparison of their X-ray patterns with reference data (ASTM). The fractional composition of powders was determined by the sedimentation method (Figurovskii's balance) [13]. The size, shape, and morphology of particles were estimated by scanning electron microscopy (an REMMA-202 microscope-analyzer).

Numerous studies, e.g., [14, 15], show that the reactivity of aluminum in alkaline media is higher than that in acid media. According to the published data [14], the rate of aluminum dissolution reaches a maximum (150–170 g m^{-2} h^{-1}) in 5–7 M alkali. In this case, the potential ranges from –1.4 to –1.8 V. The difference of the aluminum and copper standard potentials in alkaline solutions is very large (more than 2 V [16]); therefore, an intense contact exchange in the Al–Cu(II) system is thermodynamically possible.

Specific features of contact deposition of copper on aluminum in ammonia solutions are well illustrated by corrosion diagrams and cyclic voltammograms.

Table 1. Chemical composition of model solutions

Solution no.	Solution composition (M)		
	$CuSO_4$	NH_4OH	NaOH
1	0.095	0.9038	
2	0.095	0.5874	0.1391
3	0.095	0.5874	0.1545
4	0.095	0.9038	0.0927
5	0.0095	0.9038	0.0927
6	0.00095	0.9038	0.0927
7	0.095	0.9038	0.0773
8	0.0095	0.9038	0.0773
9	0.00095	0.9038	0.0773
10	0.000095	0.9038	0.0773
11	0.095	0.9038	0.0989
12	0.095	0.9038	0.0618
13	0.0095	0.9038	0.0618
14	0.00095	0.9038	0.0618
15	0.095	1.3556	0.0618
16	0.0095	1.3556	0.0618
17	0.00095	1.3556	0.0618
18	0.095	1.3556	0.0773
19	0.0095	1.3556	0.0773
20	0.00095	1.3556	0.0773

The cathodic polarization curves on a copper electrode (Fig. 1) have a typical shape for a multistep (in particular, two-step) process of copper(II) deposition from dilute electrolytes containing complex ions. This process is associated with the conjugate course of the reduction of copper(II) ions and proton donors. The cathodic curve ascends and then the limiting diffusion current of copper(II) reduction is observed. The subsequent current growth is caused by hydrogen evolution.

A different pattern is observed in more dilute solutions: first a long interval (up to 1.5 V) of low current is observed, as the copper deposition is characterized by a fairly high overvoltage. A small peak in this region is most likely of the diffusion nature.

We found that an increase in the copper(II) and ammonia concentrations shifts the cathodic curve to more electronegative values (Figs. 1b, 1c), whereas variation of the alkali concentration in solutions does not noticeably affect the shape and position of the cathodic curves.

The anodic polarization curves taken on the aluminum electrode have a simpler shape: the region of active dissolution gradually transforms into the region of diffusion limitations. An increase in the concentration of copper(II) ions in solutions with a relatively low

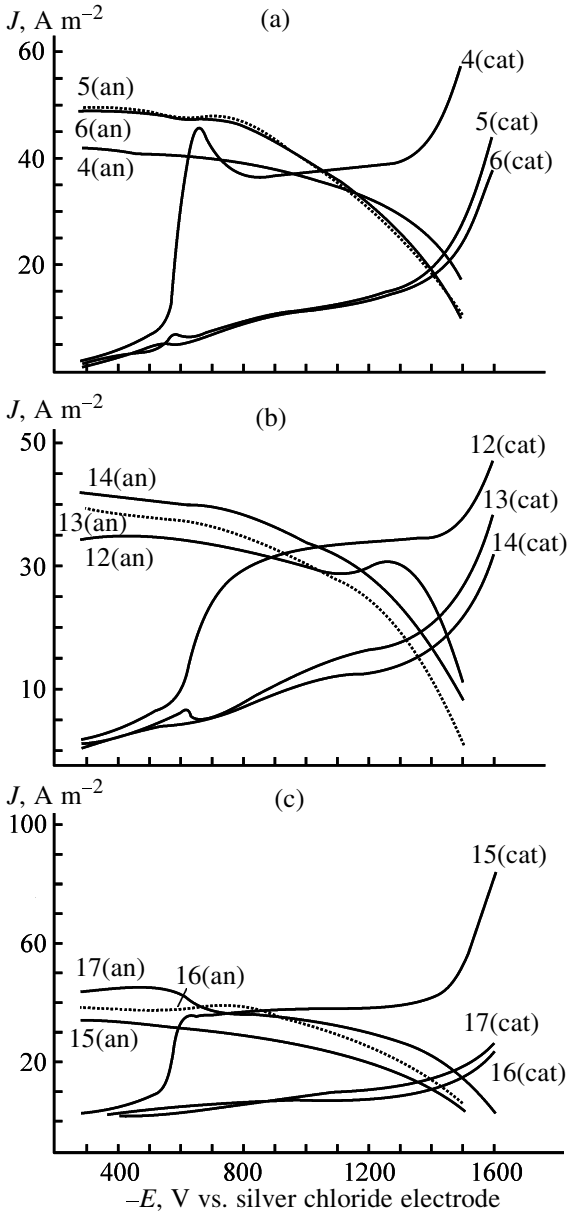


Fig. 1. Anodic (an) and cathodic (cat) polarization curves of copper deposition on aluminum at various concentrations of copper(II) ions in solution. Solution nos.: (a) 4–6, (b) 12–14, and (c) 15–17. (*J*) Current density and (*E*) potential. Figures at curves correspond to the numbers of solutions in Table 1; the same for Figs. 3 and 4.

ammonia concentration (0.9038 M NH_4OH) increases the anodic current (Figs. 1a, 1b). We emphasize that increasing concentration of OH^- ions facilitates the anodic dissolution of aluminum (Figs. 1a, 1b). The activating effect of OH^- ions is also manifested as a shift of the corrosion potential to more negative values. An increase in the ammonia concentration results in the growth of the aluminum dissolution current. As the concentrations of copper(II) ions and ammonia increase, the compromise potential becomes more electropositive.

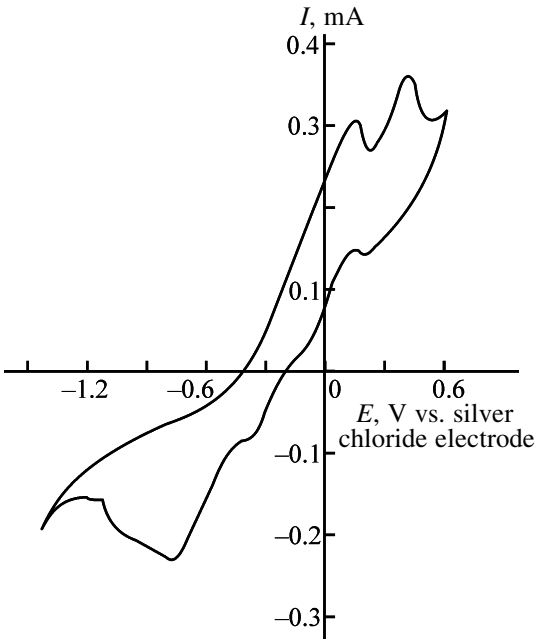


Fig. 2. Cyclic voltammogram of a copper electrode. (*I*) Current and (*E*) potential; the same for Fig. 3.

To obtain more complete information on the behavior of copper and aluminum electrodes under contact exchange conditions, we carried out electrochemical measurements in the mode of cyclic potential variation. To elucidate the influence of solution components on the copper contact deposition, we took cyclic voltammetric (CVA) characteristics on a platinum electrode.

A typical voltammogram on a copper electrode is shown in Fig. 2. It is evident that the copper reduction (and oxidation) passes in steps: $Cu^{2+} \rightarrow Cu^{1+} \rightarrow Cu^0$. This is manifestsed as two maxima in the voltammogram. However, it is necessary to take into account that copper(I) accumulated on the electrode surface is not completely reduced to the metal state and a part of it, most likely, passes into solution.

The voltammetric characteristics for the solutions on a platinum electrode are given in Fig. 3. The measurements were carried out over the potential range from –1.5 to 0.8 V.

In all the experiments, the region of oxygen evolution was observed at high potentials.

The cathodic branch of the cyclic voltammogram begins from 0.7 V and is characterized by a high current of water oxidation, and then at a potential of –0.2 V a cathodic current appears. Initially this cur-

rent is caused by the oxygen desorption, and then, by the copper(II) reduction, which occurs in steps. At the same time, the measurements with variation of the scanning range have shown that copper is deposited even near the first maximum. A potential noticeably higher than the equilibrium potential in any of solutions under study corresponds to this process. This fact suggests that, in these electrolytes, a prephase reduction of copper ions occurs, i.e., a layer of adsorbed atoms is formed on the platinum surface. In connection with the possibility of stepwise copper reduction, it is interesting to consider the problem of the formation of a layer of adsorbed atoms at potentials exceeding the equilibrium potential in these conditions. It is likely that this process also occurs in steps, in spite of the fact that it is limited to the adsorption and no new phase is formed.

The second peak in the cathodic region is also clearly seen. It is followed by exponential growth of the cathodic current, which corresponds to the hydrogen evolution. As the polarization direction is changed, the cathodic current is retained up to a potential of about –1 V, after which the current appears in the anodic direction. In the case of low copper(II) concentrations in solution, a current peak is observed at a potential of about –0.9 V, which corresponds to the oxidation of hydrogen accumulated on the electrode in the previous steps of the process. The ascent of the anodic part of the curve at a potential of –0.2 V, most likely, is due to the adsorption of oxygen, which passes into the stage of its release as a separate phase at 0.6 V.

As the concentration of copper ions in solution is increased, current peaks in the cathodic region become more pronounced. The contribution of the copper reduction current to the total cathodic current increases, and the hydrogen component of the current decreases. The region of the limiting current, which has the diffusion nature, also becomes better defined. At high copper concentrations, a clear extended step of the limiting current of copper reduction is observed in the range from –0.1 to 0.6 V.

The potential corresponding to the current sign change in the anodic region also changes. In the anodic region, as the concentration of copper increases, the current peak of the dissolution of the metal accumulated on the platinum electrode when the potential changes from –0.3 up to –1.3 and then from –1.3 up to –0.6 V increases.

The quantity of electricity determined by the area limited by the curve in the specified range of potentials is equal to the quantity of electricity which is

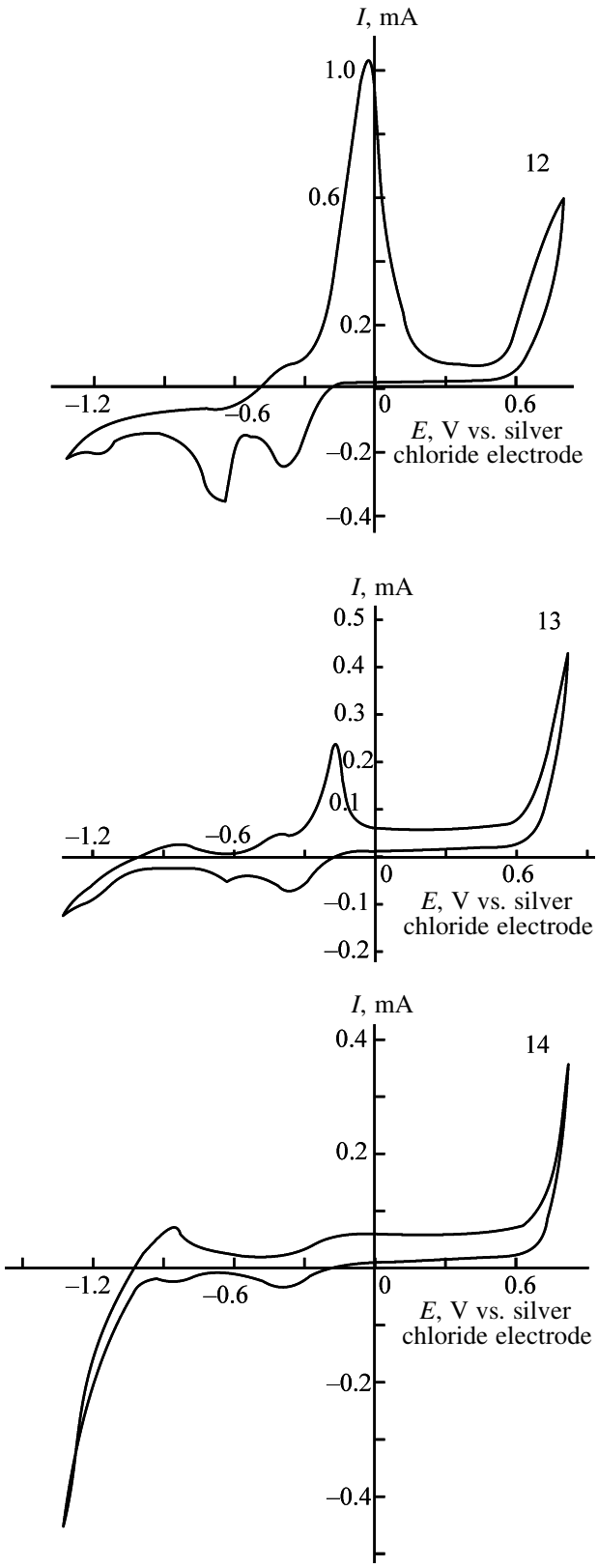


Fig. 3. Cyclic voltammograms of a platinum electrode.

Table 2. CVA characteristics of solutions

Solution no.	Reduction of copper on platinum electrode				Reduction of copper on copper electrode				H_2 evolution on platinum electrode		O_2 evolution on copper electrode	
	$Cu^{2+} \rightarrow Cu^{1+}$		$Cu^{1+} \rightarrow Cu^0$		$Cu^{2+} \rightarrow Cu^{1+}$		$Cu^{1+} \rightarrow Cu^0$		–*E*, mV	–*I*, mA	–*E*, mV	–*I*, mA
	–*E*, mV	–*I*, mA	–*E*, mV	–*I*, mA	–*E*, mV	–*I*, mA	–*E*, mV	–*I*, mA				
12	0.42	0.35	0.75	0.52	–	–	–	–	0.4	–	0.17	
13	0.35	0.075	0.63	0.045	0.4	1.5	0.9	0.55	0.53		0.25	10^{-6}
14	0.4	0.025	0.83	0.02	0.38	0.075	0.76	0.225	0.64	10^{-4}	0.02	10^{-4}

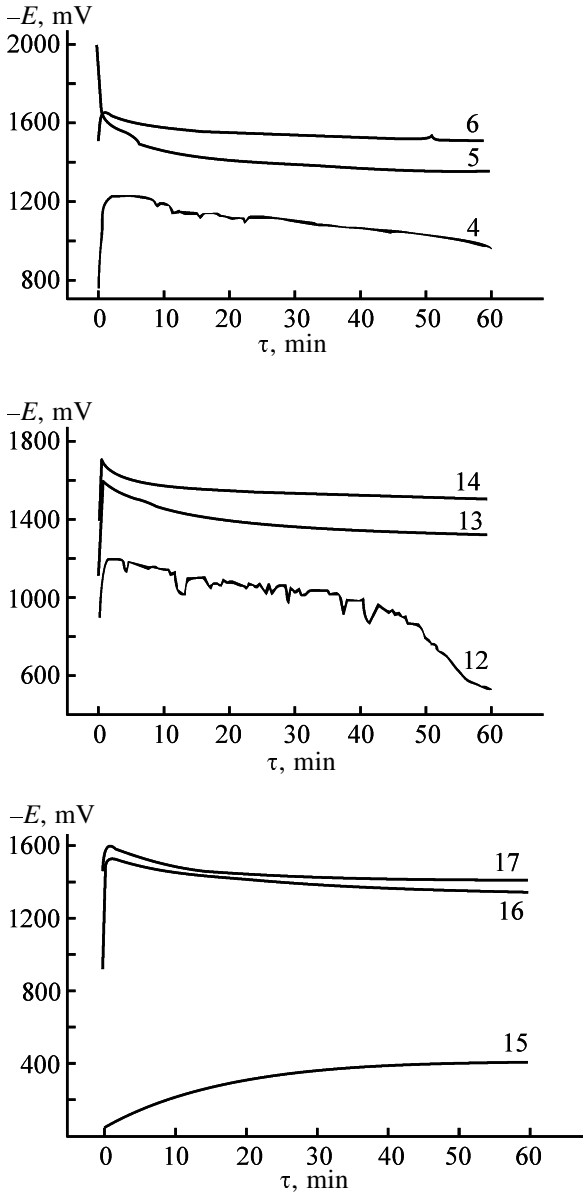


Fig. 4. Chronopotentiograms of A999 aluminum in solutions with various copper(II) concentrations. (*E*) Potential vs. to silver chloride electrode) and (τ) time.

expended for copper dissolution on sweeping the potential to the anodic region from –0.5 to 0.3 V.

The CVA curves plotted in the Tafel coordinates show that the quasiequilibrium potential in the positive region corresponds to the oxygen adsorption–desorption, and the quasiequilibrium potential in the cathodic region, to the equilibrium potential of the copper electrode in this solution. The exchange current can be calculated from the linear portions of the polarization curves, which allows quantitative estimation of the reaction kinetics in this range of potentials. Certain characteristic parameters found from the voltammograms are given in Table 2.

To gain a notion of the dynamics of the copper–aluminum contact exchange, we took chronopotentiograms in working solutions in the absence of external current (Fig. 4). The reproducibility of these curves is insufficient; nevertheless, it can be noted that the contact exchange potential is close to the aluminum corrosion potential and generally tends to grow. Variations of the potential in the chronopotentiograms taken in solutions with a relatively low ammonia concentration are caused, most likely, by the fact that the copper reduction occurs in two steps, [Cu(II) → Cu(I) → Cu(0)]. The peaks observed in the chronopotentiograms correlate with the intermittently occurring exfoliation of copper from the support. The range of potentials where the contact deposition of copper takes place corresponds to its cathodic deposition and, therefore, this step is limiting.

An increase in the copper(II) concentration shifts the aluminum electrode potential to more positive values and results in the formation of a less porous layer of the deposit. A simulations increase in the concentration of alkali and ammonia results in a potential shift to more positive values by 0.5–1.0 V.

The electrochemical and gravimetric measurements have shown that the contact deposition of copper is accompanied by a considerable conjugate hydrogen

Table 3. Results of studying copper–aluminum contact exchange

Solution no.	E_{max}, mV	$-E_{min}$, mV	$-E_c$, mV	j_{Al}, A m^{-2}	j_{Cu}, A m^{-2}	j_H, A m^{-2}	Current efficiency by Cu, %	Current efficiency by H, %
1	1000	455	472	26.46	9.611	16.84	36.33	63.67
2	1570	900	1320	4.276	2.304	1.972	53.88	46.12
3	1540	800	1460	27.85	10.494	17.36	37.68	62.32
4	1220	750	950	52.87	38.021	14.85	71.91	28.09
5	2000	1340	1340	66.96	5.04	61.92	7.53	92.47
6	3270	1550	3265	52.49	2.148	50.34	4.09	95.91
7	1230	800	885	50.38	21.097	29.28	41.88	58.12
8	1750	1190	1360	45.34	16.92	28.42	37.32	62.68
9	1820	1520	1520	48.7	0.895	47.81	1.84	98.16
11	1450	800	1140	40.13	18.51	11.62	71.04	28.96
12	1200	525	525	50.05	45.454	4.6	90.8	9.2
13	1620	1320	7.44	26.08	6.55	19.54	25.1	74.9
14	1780	1500	1500	71.27	9.105	62.17	12.78	87.22
15	400	40	400	32.5	12.488	20.01	38.43	61.57
16	1540	1342	1342	24.37	5.09	19.28	20.89	79.11
17	1605	1405	1405	7.27	0.73	6.54	10	90
18	400	60	392	28.65	10.42	18.22	36.39	63.6
19	572	50	572	26.08	6.669	19.42	25.57	74.43
20	570	40	570	26.94	0.242	26.7	0.9	99.1

evolution (Table 3). It mainly occurs on the copper surface, as the overvoltage of hydrogen evolution on it is lower than on aluminum. At a relatively high concentration of copper ions, a dense precipitate is formed. It covers the aluminum surface and correspondingly reduces the anodic and total currents of the process. The contribution of the cathodic evolution of hydrogen in the course of the exchange is less than in more dilute copper solutiuons. An increase in the concentration of copper ions results in an increase in the current efficiency by copper. In more concentrated copper(II) solutions (~0.1 M), an increase in the ammonia concentration increases the yield of hydrogen and correspondingly decreases the yield of copper by a factor of 3–6. Thus, the growth of the ammonia concentration inhibits the contact deposition of copper.

The reported results (Table 3) show that the rate of aluminum dissolution j_a(Al) in dilute copper(II) solutions somewhat increases. As this rate is much higher in this case than the rate of copper(II) reduction j_c (Cu), we can conclude that the process of hydrogen evolution prevails:

$$j_a(\mathrm{Al}) = j_c(\mathrm{Cu}) + j_c(\mathrm{H}), \quad (1)$$

$$j_c(\mathrm{H}) = j_a(\mathrm{Al}) - j_c(\mathrm{Cu}). \quad (2)$$

According to Eq. (1), the rate of aluminum anodic dissolution is equal to the total rate of the conjugate reactions of cathodic hydrogen evolution and copper deposition. It seems reasonable that, at a sufficient duration of the contact exchange process (for example, more than 100 s), both cathodic reactions practically completely occur on the surface of copper that has been deposited on the aluminum support. In this case, the fraction of cathodic areas of the electrode surface is close to unity. The cathodic electrochemical behavior of such a sample can be considered, to a rough approximation, as the cathodic behavior of the copper electrode. Therefore, to a first approximation, we can take the current of aluminum dissolution to be equal to the current in the cathodic polarization curve at this potential, which, in turn, was found from the chronopotentiogram for this instant of time.

The evolution of hydrogen reduces the current efficiency of the copper cathodic reduction in dilute solutions at a sufficiently high current density of aluminum dissolution. In such case, the compromise electrode potential is frequently close to the aluminum corrosion potential in a supporting electrolyte solution. This fact indicates that the reduction of proton donors, occurring simultaneously with the reduction of copper complexes on the surface of freshly precipitated copper, exerts a principal influence on the contact exchange.

Thus, the behavior of the aluminum electrode in alkaline copper-containing solutions depends on the

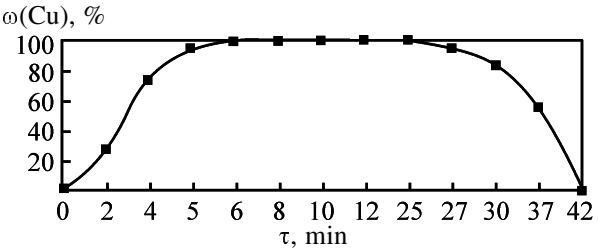


Fig. 5. Kinetic curve of copper contact deposition on dispersed aluminum. $C(Cu^{2+})$ = 0.0954 M, $C(NH_3 \cdot H_2O)$ = 0.5 M, m(Al) = 0.0430 g. [ω(Cu)] Amount of deposited copper and (τ) time.

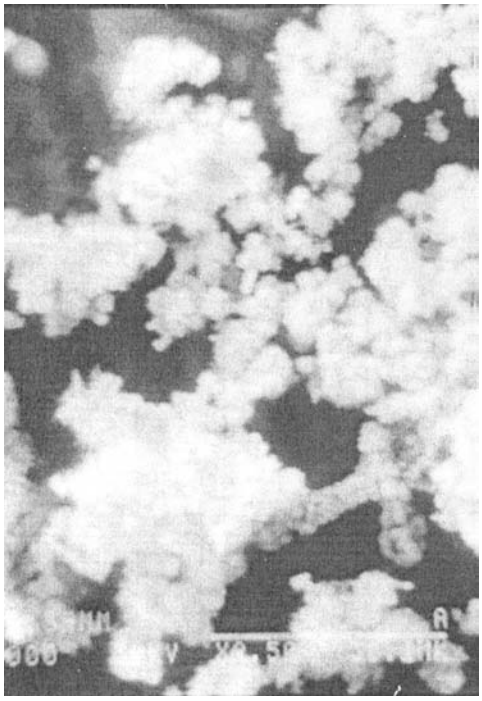


Fig. 6. Photomicrograph of a dispersed copper deposit.

occurrence of the following complex of reactions: aluminum ionization on anodic areas of the surface, cathodic reduction of copper(II), and cathodic evolution of hydrogen on aluminum and copper. The overall process rate is determined by the dissolution of aluminum and depends on the potential of the electrode at a given time instant and also on the state of its surface. However, it is rather difficult to judge the rate of the aluminum anodic dissolution by recording anodic polarization curves of the aluminum electrode in supporting electrolyte solutions, as at these potentials the conjugate reaction of hydrogen cathodic evolution occurs.

Taking into account the fact that the deposition of elemental copper can be intensified by increasing the area of contact between the solid and liquid phases, we also carried out experiments with dispersed aluminum.

We reduced copper(II) in an ammonia solution both with addition of an alkali and without it. We found that the reduction of copper(II) with metallic aluminum occurs directly in an ammonia medium. A typical kinetic dependence of the copper(II) deposition on dispersed aluminum (DA) is shown in Fig. 5. It is seen from this dependence that the complete deposition (99.9%) of elemental copper is attained within 6–7 min. It is interesting that the amount of the deposited elemental copper decreases on the further contact of the highly dispersed precipitate with the solution, which is caused by the oxidation of copper with atmospheric oxygen entering into the solution during stirring. The oxidized copper passes into the ammonia solution as complex ions $[Cu(NH_3)_n]^{2+}$, n = 2–4.

Examination of the influence of the ammonia concentration on the copper(II) reduction has shown that the complete reduction is reached at an ammonia concentration of no less than 0.5 M or at its concentration exceeding the copper(II) concentration in the solution by a factor of 5.5 and more.

Taking into account the possibility of intensifying the process by aluminum activation in an alkaline medium, we also carried out experiments involving the pretreatment of DA with an alkali. The experiments have shown that virtually complete deposition of copper metal is reached at a 2.4-fold weight excess of aluminum when it is introduced simultaneously without preliminary activation with an alkali, and at a 1.6-fold excess of aluminum when it is introduced in portions in the activated form. This difference results from the increased aluminum activity in the second case because of removal of the oxide layer by concentrated alkali. We found that a 1.3-fold weight excess of aluminum is the minimum required to reach the highest degree of copper deposition.

A microscopic examination showed that the copper deposit consists of particles of different size (according to a sedimetric analysis, particles of size 30–50 μm dominate) and predominantly spherical shape (Fig. 6). The shape factors calculated by Hausner's method [13] correspond to these qualitative characteristics. The factor of prolateness and the factor of voluminosity are x = 1.2 and y = 0.75, respectively, which allows the particles to be assigned to group I (smooth) or II (plaited sphere) in accordance with Hausner's classification. The surface factor z = 0.997 indicates that the precipitated particles are sufficiently smooth, opaque, and have a developed porosity. A large number of subindividuals of size 0.1–1 μm are observed on their surface. Furthermore, a large

Table 4. Data of X-ray phase analysis of a copper deposit on an aluminum foil and of a deposit obtained using dispersed aluminum (DA)

hkl	Interplanar spacing, Å		Coherent scattering region, Å		Microstress	
	DA	foil	DA	foil	DA	foil
111	2.0866	2.0872	808.3518	630.9424	1.1146	0.0011
200	1.8071	1.8076	398.3527	347.8750	0.0018	0.0031
220	1.2778	1.2781	705.8520	560.1756	9.0835	0.0018
311	1.0897	1.0900	591.4928	481.2208	0.0013	0.0024
222	1.0433	1.0436	808.3518	630.9424	1.1146	0.0011

number of individual submicroparticles are observed, which seem to be formed by the disintegration of large aggregates as a result of gaseous hydrogen evolution.

We can point out that the precipitates are rather homogeneous in the chemical composition. The X-ray patterns of the precipitates obtained on an aluminum foil and dispersed aluminum indicate that the precipitates contain no oxo and hydroxo compounds of aluminum and copper. Furthermore, we found that the precipitate of elemental copper on a foil has smaller coherent scattering regions and microstresses than the copper powder obtained with dispersed aluminum (Table 4). The content of elemental copper in both cases reaches 98.5–98.7%, the remainder being aluminum.

CONCLUSIONS

(1) Contact deposition of copper on compact and dispersed aluminum was studied. An increase in the concentrations of an alkali and copper(II) in solutions increases the rate of a contact exchange, whereas an increase in the ammonia concentration decreases it.

(2) According to electrochemical measurements, the rate of hydrogen evolution substantially increases in dilute solutions, becoming several times higher than the rate of copper reduction: $j_a(\mathrm{Al}) = j_c(\mathrm{Cu}) + j_c(\mathrm{H})$.

(3) Quantitative deposition of copper(0) occurs under optimal conditions within 6–10 min, and after 20–25 min copper dissolves due to oxidation with atmospheric oxygen, and copper(II) ammonia complexes are formed.

(4) The use of dispersed aluminum in alkaline ammonia solutions makes it possible to obtain technical-grade (98.5–98.7% purity) powders of elemental copper consisting of particles with preset size, shape, and morphology.

REFERENCES

1. *Poroshkovaya metallurgiya: materialy, tekhnologiya, svoistva, oblasti primeneniya: Spravochnik* (Powder Metallurgy: Materials, Technology, Properties, Fields of Application: Handbook), Fedorochenko, I.M., Ed., Kiev: Naukova Dumka, 1985.
2. Grushko, Ya.M., *Vrednye neorganicheskie soedineniya v promyshlennykh stochnykh vodakh* (Harmful Inorganic Compounds in Industrial Wastewaters), Leningrad: Khimiya, 1979.
3. Kolesnikov, V.A. and Din, S.V., *Ekol. Prom. Proizv.*, 1993, no. 1, pp. 37–41.
4. Sankaranarayana, M., Murugan, K., Bacha, C.A., et al., *Bull. Electrochem.*, 1991, vol. 7, no. 2, pp. 75–77.
5. Alkatsev, M.I., *Protsessy tsementatsii v tsvetnoi metallurgii* (Electrolytic Precipitation Processes in Nonferrous Metallurgy), Moscow: Metallurgiya, 1981.
6. Hsu, Y.J., Kim, M.J., and Tran, T., *Electrochim. Acta*, 1999, vol. 44, pp. 1617–1625.
7. Bykov, E.D., D'yakov, V.S., Litvinenko, B.G., and Kirichenko, T.G., *Khim. Prom-st.*, 1995, no. 7, pp. 49–51.
8. Kolosnitsyn, V.S. and Yapryntseva, O.A., *Zh. Prikl. Khim.*, 2004, vol. 77, no. 1, pp. 60–64.
9. Erusalimskaya, E.M., in *Tekhnologiya fiziko-khimicheskoi ochistki stochnykh vod, analiticheskii kontrol' i regulirovanie protsessov ochistki: Sbornik trudov instituta VODGEO* (Technology of Physicochemical Treatment of Wastewaters, Analytical Monitoring and Control of Treatment Processes: Coll. of Papers of the All-Union Research Inst. of Water Supply, Sewage, Hydrotechnical Facilities, amd Engineering Geology), Moscow: VNIIVODGEO, 1985, pp. 24–27.
10. Terskaya, I.N. and Budanov, V.V., *Zh. Neorg. Khim.*, 2002, vol. 47, no. 7, pp. 1180–1183.

11. Naboichenko, S.S. and Smirnov, V.I., *Gidrometallurgiya medi* (Hydrometallurgy of Copper), Moscow: Metallurgy, 1983.
12. Schwarzenbach, G. und Flaschka, H., *Die komplexometrische Titration*, Stuttgart: Ferdinand Enke, 1965.
13. Bulanov, V.Ya., Kvater, L.I., Dolgal', T.V., et al., *Diagnostika metallicheskikh poroshkov* (Diagnostics of Metallic Powders), Moscow: Nauka, 1983.
14. Gorotilova, V.G., Berkman E.A., Sysoeva, V.V., and Artyugina, E.D., *Zh. Prikl. Khim*., 1985, vol. 58, no. 4, pp. 921–924.
15. Lukomskii, Yu.Ya., Priyatkin, G.M., Mulina, T.V., et al., *Usp. Khim*., 1991, vol. 60, no. 5, pp. 1077–1085.
16. *Spravochnik po elektrokhimii* (Handbook of Electrochemistry), Sukhotin, A.M., Ed., Leningrad: Khimiya, 1981.
17. Zhilinskii, V.V., Lokenbakh, A.K., and Lepin', L.K., *Izv. Akad. Nauk Latv. SSR, Khim. Nauki*, 1986, no. 2, pp. 157–161.

ISSN 1070-4272. Russian Journal of Applied Chemistry, 2006, Vol. 79, No. 5, pp. 761–768. © Pleiades Publishing, Inc., 2006.
Original Russian Text © V.I. Vigdorovich, S.E. Sinyutina, L.E. Tsygankova, V.I. Kichigin, 2006, published in Zhurnal Prikladnoi Khimii, 2006, Vol. 79, No. 5, pp. 770–777.

APPLIED ELECTROCHEMISTRY AND CORROSION PROTECTION OF METALS

Inhibition of Corrosion and Hydrogenation of Carbon Steel in Media Containing Hydrogen Sulfide and Carbon Dioxide with Low Concentrations of Salts of Oxyethylated Amines

V. I. Vigdorovich, S. E. Sinyutina, L. E. Tsygankova, and V. I. Kichigin

Derzhavin State University, Tambov, Russia
Institute of Natural Science, Perm, Russia

Received December 2, 2005; in final form, April 2006

Abstract—Impedance spectroscopy was used to study the protective action of salts of higher aliphatic oxyethylated amines as universal inhibitors of the hydrogen sulfide and carbon dioxide corrosion and hydrogenation of carbon steel.

DOI: 10.1134/S1070427206050120

The hydrogen sulfide and carbon dioxide corrosion of the metal is one of the most important reasons for corrosive failure of steel equipment at oil and gas fields. A grave danger in the case of exposure to such media consists in the enhancement of hydrogenation, which leads to embrittlement of the metal and to its corrosive cracking. Despite the existing wide choice of inhibitors, it is necessary to develop new efficient inhibitors and, primarily, those exerting an integrated influence (simultaneous inhibition of the hydrogen sulfide and carbon dioxide corrosion, prevention of a local damage and hydrogenation of the metal) by studying the mechanism of their protective action. In addition, one of modern requirements to inhibitors is their high performance even at low concentrations [1], which lowers the cost of the corrosion protection and diminishes the environmental impact.

In this study, we examined the performance of salts of higher aliphatic oxyethylated amines as universal inhibitors of hydrogen sulfide and carbon dioxide corrosion and hydrogenation of carbon steel. We used impedance spectroscopy to refine, if possible, the mechanism of the inhibiting action and specific features of the influence exerted by an inhibitor on the anodic and cathodic processes and adsorption in the pores of a film.

EXPERIMENTAL

We performed corrosion tests with St.3 steel by the gravimetric method in solutions of NaCl (50 g l^{-1}) and HCl (0.005–0.05 M) with and without H_2S and CO_2. The necessary concentration of hydrogen sulfide (200 mg l^{-1}) was created by introducing a calculated amount of sodium sulfide and generating H_2S by the reaction with HCl. Some solutions were saturated with carbon dioxide (1.6 g l^{-1}, deoxygenated medium). An excess pressure of CO_2 (1 atm) was created as described in [2], in plastic vessels equipped with nipple valves. Carbon dioxide was pumped from a cylinder with manometric pressure monitoring, further continued during the whole experiment (24 h). As inhibitors served homological mixtures of salts of higher oxyethylated amines (OEAs) and acetic and ethylhexanoic acids of the general formula

$$R\text{–}NH^{+}Ac^{-}\begin{matrix}(CH_2CH_2O)_xH\\(CH_2CH_2O)_yH,\end{matrix}$$

where R = C_{10}–C_{14}, C_{16}–C_{18}; $x + y = n = 3$; and Ac, the corresponding acyl, both as an active species and in 20% solutions in a mixed organic solvent.

The concentration of the inhibitors was in the range 25–100 mg l^{-1}. We calculated the protective effect Z (%) by the formula

$$Z = [(K_0 - K_{inh})/K_0] \times 100,$$

where K_0 and K_{inh} are the corrosion rates in the media under study in the absence and presence of an inhibitor, respectively.

Electrochemical measurements were made by the potentiometric method (P-5827M potentiostat) in a

Table 1. Protective effect Z of OEA salts in NaCl solutions containing CO_2 and H_2S at an excess CO_2 pressure P_{CO_2} = 1 atm. Test duration 24 h, room temperature, c_{NaCl} = 50 g l^{-1}, c_{H_2S} = 200 mg l^{-1}, c_{CO_2} = 1.6 g l^{-1}

Inhibitor	c_{inh}, mg l^{-1}	Z, %, in the presence of			
		H_2S	CO_2	$H_2S + CO_2$	
				c_{SO_2} = 1.6 g l^{-1}	P_{CO_2} = 1 atm
C_{10}–C_{14} OEA acetate	25	64	61	87	79
	50	68	70	89	80
Salt of ethylhexanoic acid and C_{16}–C_{18} OEA	25	69	63	78	78
	50	75	65	81	81

three-electrode cell with separated anode and cathode spaces. A silver chloride electrode served as reference, and Pt, as an auxiliary electrode. The potentials are given relative to a standard hydrogen electrode.

We studied the hydrogen permeability in a two-chamber cell separated by a vertical steel membrane (St. 3, 300 μm) at the corrosion potential [3]. The duration of the tests was 3 h. The suppression coefficient of the hydrogen diffusion, γ, was found by the formula $\gamma = i_H^0/i_H$, where i_H and i_H^0 are the fluxes of solid-phase diffusion in the system with and without an inhibitor, respectively. All the experiments were performed at room temperature.

We studied the electrochemical impedance of steel electrodes in the frequency range from 60 kHz to 10 MHz at an ac voltage amplitude of 10 mV with a potentiostat and a Solartron 1250 spectrum analyzer (the United Kingdom). The working (S_{el} = 0.785 cm^2) and auxiliary platinum (S_{Pt} = 54 cm^2) electrodes were arranged coaxially. The working electrode was polished, degreased, and subjected to cathodic activation (ΔE = –0.2 V) for 15 min to remove the air-oxide film, after which is was kept in solution for a quasistationary potential to be attained (15 min), and the impedance was measured at E_{cor}. A quantitative analysis of the experimental data obtained was made with software developed for IBM PC, which enables calculations for arbitrary equivalent circuits with a number of elements of up to 12 [4]. The calculational part of the program is based on a simplex search method for finding an extremum of a function of several variables. The criterion used for circuit assessment is the root-mean-square deviation s; a circuit is considered satisfactory at $s \leq 5\%$.

Table 2. Protective effect Z of OEA salts (25 mg l^{-1}) in HCl solutions containing CO_2 and H_2S. Test duration 24 h, room temperature, c_{H_2S} = 200 mg l^{-1}, c_{CO_2} = 1.6 g l^{-1}

Inhibitor	c_{HCl}, M	Z, %, in the presence of			
		–	CO_2	H_2S	$H_2S + CO_2$
C_{10}–C_{14} OEA acetate	0.005	66	80	79	82
	0.01	73	84	88	90
	0.05	86	89	93	92
C_{16}–C_{18} OEA acetate	0.005	77	80	81	83
	0.01	77	81	88	88
	0.05	82	91	92	91
Salt of ethylhexanoic acid and C_{10}–C_{14} OEA	0.005	79	84	79	81
	0.01	81	84	86	89
	0.05	88	89	90	91
Salt of ethylhexanoic acid and C_{16}–C_{18} OEA	0.005	65	83	81	85
	0.01	77	87	89	88
	0.05	81	88	90	89

In NaCl solutions containing hydrogen sulfide and carbon dioxide, OEA salts exhibit a protective effect of 65–75%, which increases by approximately 10–15% in the simultaneous presence of H_2S and CO_2 and with increasing c_{inh} (Table 1).

Making lower the pH value and the degree of mineralization of the medium enhances the protective effect of inhibitors (Table 2). In hydrogen sulfide and hydrogen sulfide–carbon dioxide media, Z of ~90% can be obtained even at c_{inh} = 25 mg l^{-1}. The length of the hydrocarbon substituent of OEA and the anion of an organic acid affect the performance of additives only slightly.

OEA salts shift E_{cor} to the positive region (Fig. 1), especially in the presence of H_2S, and strongly decelerate the anodic reaction. Depending on the composition of the corrosion medium, the cathodic process is hindered or, by contrast, facilitated (hydrogen sulfide media).

Introduction of OEA acetates with a concentration

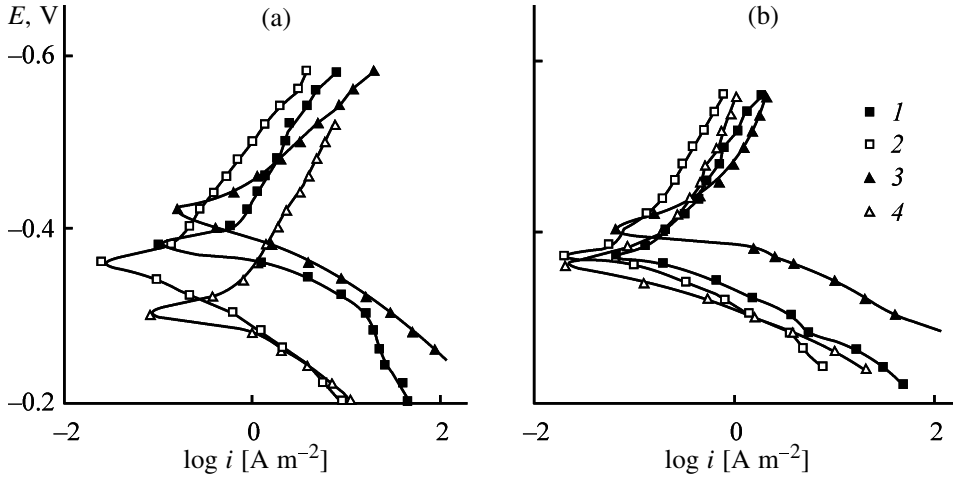


Fig. 1. Potentiostatic polarization curves obtained on St. 3 steel in (a) NaCl and (b) HCl solutions containing H_2S and CO_2 (*1, 3*) in the absence and (*2, 4*) in the presence of C_{10}–C_{14} OEA acetate. Room temperature, immobile electrode, c_{NaCl} = 50 g l^{-1} (pH 6), c_{HCl} = 0.005 M, c_{H_2S} = 200 mg l^{-1}, c_{CO_2} = 1.6 g l^{-1}, c_{inh} = 100 mg l^{-1}. (*E*) Potential and (*i*) current density. (a) (*1*) NaCl, (*2*) *1* + inhibitor, and (*3*) *1* + H_2S. (b) (*1*) HCl + CO_2, (*2*) *1* + inhibitor, (*3*) *1* + H_2S, and (*4*) *3* + inhibitor.

of 25 mg l^{-1} into 0.005 M HCl solutions makes lower the hydrogen permeability of the steel membrane (Table 3, $\gamma > 1$). Under these conditions, salts of OEA and ethylhexanoic acid enhance the hydrogenation of steel.

In the presence of H_2S or CO_2, all the products studied suppress the diffusion flow of hydrogen into the steel, i_H. The salt of ethylhexanoic acid and C_{10}–C_{14} OEA is the most effective: γ increases to 2.5–2.7. In hydrogen sulfide–carbon dioxide media, the hydrogenation-inhibiting effect of OEA salts is virtually independent of their nature.

The impedance has on a complex plane (Fig. 2) up to three overlapping semicircles, and, therefore, no less than three time constants are generally necessary for describing the experimental data. The impedance data were analyzed using equivalent electric circuits, simplified models that, nevertheless, yield a qualitative and, in some cases, semiquantitative information about the behavior of the metal in a corrosion medium [5].

When choosing an equivalent circuit, we took into account the fact that films of varied nature exist on the electrode surface. An X-ray diffraction analysis revealed on the electrode surface Fe_3O_4 with trace amounts of Fe_2O_3 in HCl solutions at an excess CO_2 pressure of 1×10^5 Pa; iron oxides and $FeCl_3$ in a CO_2-saturated solution, Fe_3O_4 and $FeCO_3$ in neutral salt media; and FeS and FeS_2 in the presence of H_2S. Taking into account the experimental conditions (15-min preliminary keeping at E_{cor} and approximately 30-min measurement of the impedance), we assumed that an oxide or sulfide–carbonate film, or a film of even more complex composition, with a thickness of at least several monolayers, can be formed on the electrode surface during the experiment. In hydrogen sulfide media, the film is visually observed on the electrode. Undoubtedly, the forming films are defective, because otherwise the corrosion process would be dramatically decelerated, which is not the case in the experiment.

The electrical properties of iron oxides and sulfides strongly depend on the stoichiometry of the compounds. The oxides Fe_3O_4 and Fe_2O_3, which exist

Table 3. Coefficients of suppression of hydrogen diffusion across the membrane, γ, in the presence of inhibitors in 0.005 M HCl containing H_2S and CO_2. Test duration 2 h, room temperature, c_{H_2S} = 200 mg l^{-1}, c_{CO_2} = 1.6 g l^{-1}, c_{inh} = 25 mg l^{-1}

Inhibitor	γ in the presence of indicated additives			
	–	CO_2	H_2S	H_2S + CO_2
C_{10}–C_{14} OEA acetate	2.2	1.2	1.0	2.0
C_{16}–C_{18} OEA acetate	1.1	1.3	1.4	1.9
Salt of ethylhexanoic acid and C_{10}–C_{14} OEA	0.8	2.7	2.5	1.8
Salt of ethylhexanoic acid and C_{16}–C_{18} OEA	0.8	1.6	1.4	2.0

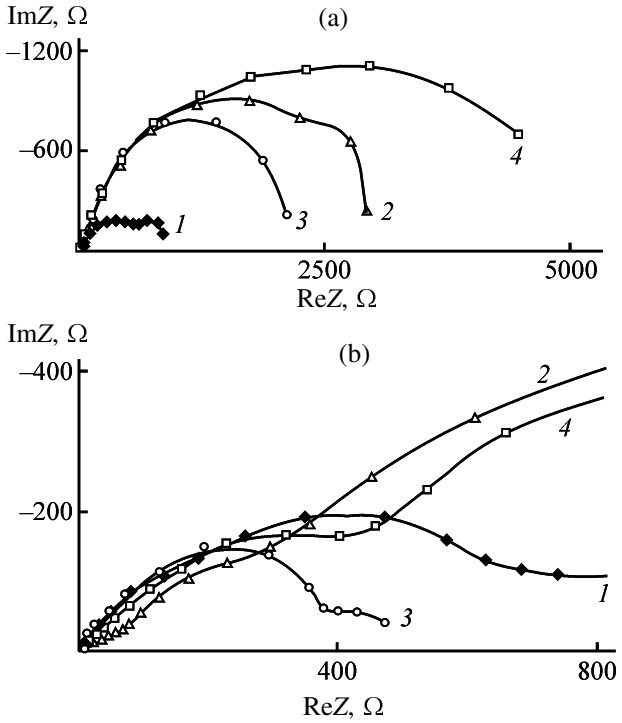


Fig. 2. Impedance loci for St. 3 steel in a NaCl solution containing CO_2 and H_2S (*1, 3*) in the absence and (*2, 4*) in the presence of the inhibitor at (a) pH 6 and (b) pH 2. (ReZ, ImZ) Real and imaginary parts of the impedance; the same for Fig. 5. c_{NaCl} = 50 g l^{-1}, c_{H_2S} = 200 mg l^{-1}, c_{CO_2} = 1.6 g l^{-1}, c_{inh} = 100 mg l^{-1}. (*1*) NaCl + CO_2, (*2*) *1* + inhibitor, (*3*) *1* + H_2S, and (*4*) *3* + inhibitor.

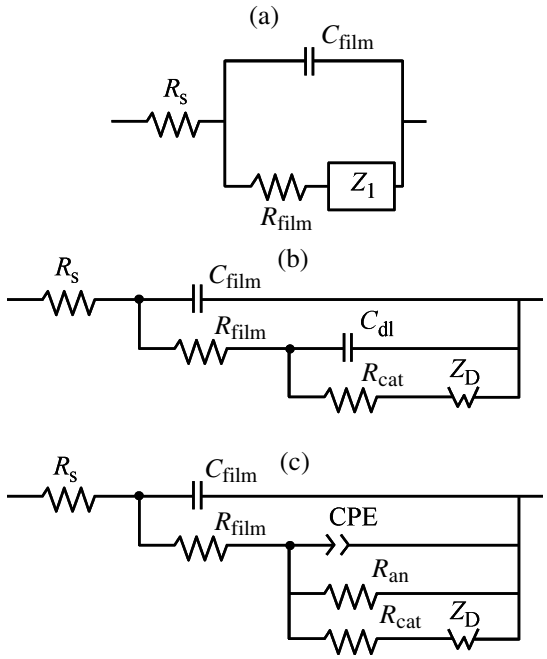


Fig. 3. (a) General equivalent circuit [10], (b) Mansfeld's equivalent circuit, and (c) its modification.

at the potentials of active dissolution of iron, have a minor deficiency of oxygen and are *n*-type semiconductors [6, 7]. The iron(II, III) oxides formed at $E \approx -0.4$ V (s.h.e.) in a sodium sulfate solution are nondefective equimolar compositions [6]. In the case in question, the corrosion potential of the steel electrode in various solutions ranges from –0.26 to –0.49 V, i.e., the deviations of the oxide composition from the stoichiometry must be insignificant (including those in the presence of Cl^- ions) and, accordingly, the electrical conductivity of the oxide must be close to the minimum value. Nonstoichiometric iron sulfides, Fe_xS_y, are semiconductors [8, 9], whereas FeS and FeS_2 have a rather high conductivity [7, 9]. There is certain evidence that iron carbonate belongs to semiconductors with widely varying conductivity, and it is an insulator according to [10]. Dielectric films can be formed via polymolecular adsorption of the organic corrosion inhibitor.

A general equivalent circuit (Fig. 3a) was suggested in [11] for an electrode with a porous dielectric film. In this circuit, R_s is the resistance of a solution outside the surface film; C_{film} and R_{film}, the capacitance of the film proper and resistance of the solution within its pores; and Z_1, impedance of the metal–electrolyte interface at the bottom of the pores. The particular form of Z_1 depends on the nature of the reactions occurring at the electrode. If, e.g., the process includes stages of charge diffusion and transfer, Z_1 is described by the Ehrschler–Randles scheme and the total impedance can be represented by the equivalent circuit in Fig. 3b [11]. By contrast, the equivalent circuit in Fig. 3a, in which Z_1 is represented by a parallel RC circuit, was used for a low-carbon steel electrode in a solution of HCl with addition of higher amines (decylamine, dodecylamine) [12]. In this circuit, we interpreted the resistance and capacitance in the interface impedance, not included in Z_1, as the resistance of the solution within the pores of the inhibitor film and capacitance of the film itself.

If measurements are made at the corrosion potential, the Faraday impedance contains contribution from the cathodic and anodic reactions. In this case, the equivalent circuit suggested in [13] (Fig. 4a) can be used to simulate processes at the metal–electrolyte interface, and the full impedance of the electrode with a porous surface film can be represented by the equivalent circuit in Fig. 3c. In this circuit, R_{an} and R_{cat} are the charge-transfer resistances in the anodic and cathodic reactions, respectively. To refine the model, we used, instead of the final diffusion im-

Table 4. Values of the parameters of the equivalent circuit in Fig. 3c in H_2S-containing NaCl solutions in the presence of C_{10}–C_{14} OEA acetate. c_{NaCl} = 50 g l^{-1}, c_{H_2S} = 200 mg l^{-1}, c_{inh} = 100 mg l^{-1}

Solution	pH	R_{an}, Ω	R_{cat}, Ω	R_D, Ω	τ, s	p	CPE-T, μF	CPE-P	C_{film}, μF	R_{film}, Ω
NaCl	6	2400* 9145	215 650	9100 16 100	2.3 9.1	0.72 0.53	50 0.6	0.88 0.73	37 0.6	5 240
	4	1310 6445	200 1550	5960 1603	15.2 12.8	0.65 0.61	51 8.4	0.85 0.46	13 0.6	4 90
	2	650 3300	160 1455	1970 5320	12.0 3.5	0.55 0.56	65 9.3	0.58 0.46	3.4 1.4	5 28
NaCl + H_2S	6	1125 2310	125 1485	5470 11 240	6.2 5.3	0.76 0.68	35 22	0.94 0.73	19 1.3	9 11
	4	1100 3090	130 310	1190 7490	4.2 13.0	0.70 0.67	45 40	0.92 0.70	15 1.4	7 6
	2	640 2270	120 1080	1520 5810	1.8 19.5	0.61 0.61	56 53	0.77 0.70	9.1 1.3	4 30

* In the numerator is the value of a parameter in the absence of inhibitor, and in the denominator, that in the presence of an inhibitor; the same for Tables 5 and 6.

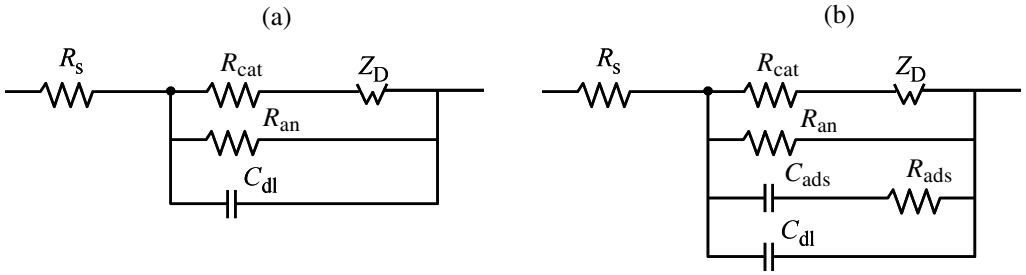


Fig. 4. (a) Keddam's equivalent circuit and (b) its modification.

pedance, the generalized final diffusion impedance

$$Z_D = R_D \tanh (j\omega\tau)^p/(j\omega\tau)^p,$$

where R_D is the diffusion resistance; τ, characteristic time of diffusion; $0 \le p < 1$; C_{dl} is replaced with a constant-phase element CPE [14], which models the distributed capacitance: $Z_{CPE} = K(j\omega)^{-n}$ {$j = (-1)^{1/2}$; ω, angular frequency; K, proportionality factor; and n, exponent characterizing the phase deviation [15]}.

The electric circuit in Fig. 3c is satisfactory according to the criterion of rms deviation ($s \le 5\%$) (Fig. 5). The value of C_{film} in solutions with addition of C_{10}–C_{14} OEA acetate is 0.6–1.4 μF cm^{-2} (Table 4), whereas that in uninhibited media is as high as 37 μF cm^{-2}. If the dielectric constant is taken to be $\varepsilon \approx 2$ for the inhibitors studied in accordance with the data of [12], the thickness of the inhibitor film at C_{film} = 0.6–1.4 μF cm^{-2} will be 3.5–6 nm, which corresponds to tens of monolayers. However, the values of certain impedance parameters, obtained in minimization of s for the equivalent circuit in Fig. 3c, have unclear physical meaning. For example, the exponent n in the expression for the CPE frequently has too low values (~0.6, and occasionally <0.5). The value of K is, in some cases, higher in a solution with

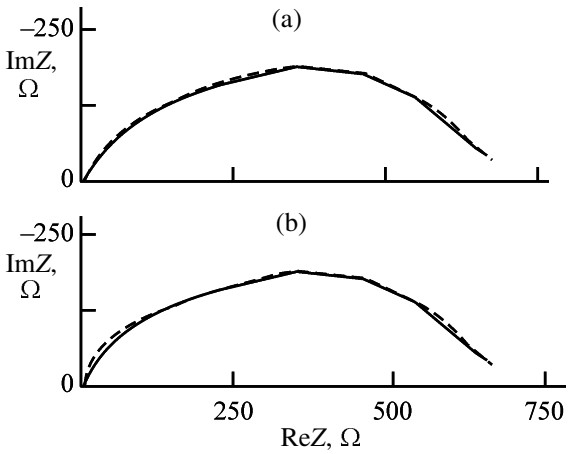


Fig. 5. Nyquist diagrams for St. 3 steel in a NaCl solution. c_{NaCl} = 50 g l^{-1}, pH 2. Solid line, experimental data; dashed line, calculation for circuits in (a) Fig. 3c and (b) Fig. 4b.

Table 5. Values of the parameters of the equivalent circuit in Fig. 4b in H_2S-containing NaCl solutions in the presence of C_{10}–C_{14} OEA acetate. c_{NaCl} = 50 g l^{-1}, c_{HCl} = 0.01 M, c_{H_2S} = 200 mg l^{-1}, c_{CO_2} = 1.6 g l^{-1}, c_{inh} = 100 mg l^{-1}

Solution	R_{an}, Ω	R_{cat}, Ω	R_D, Ω	τ, s	p	C_{ads}, μF	R_{ads}, Ω	C_{dl}, μF
NaCl	1800 / 2930	38 / 214	9160 / 7335	6.4 / 10.8	0.70 / 0.50	26 / 0.2	18 / 81	40 / 0.5
NaCl + H_2S	1200 / 1695	24 / 12	4190 / 10 195	1.3 / 4.5	0.72 / 0.69	43 / 1.2	14 / 22	11 / 1.0
NaCl + CO_2	1020 / 2620	25 / 40	8035 / 13 260	5.7 / 8.1	0.68 / 0.54	15 / 15	56 / 220	29 / 0.9
NaCl + H_2S + CO_2	1480 / 4135	40 / 30	6300 / 35 770	6.4 / 7.6	0.72 / 0.66	7.2 / 2.4	52 / 110	55 / 1.5
HCl	1090 / 2390	62 / 69	3355 / 6140	0.7 / 4.7	0.60 / 0.49	11 / 0.2	75 / 84	12 / 1.3
HCl + H_2S	1210 / 3970	8 / 92	7730 / 8950	6.1 / 9.1	0.67 / 0.37	14 / 0.2	93 / 138	16 / 0.5

Table 6. Values of the parameters of the equivalent circuit in Fig. 4b in H_2S-containing NaCl solutions in the presence of C_{10}–C_{14} OEA acetate at various pH values. c_{NaCl} = 50 g l^{-1}, c_{H_2S} = 200 mg l^{-1}, c_{inh} = 100 mg l^{-1}

Solution	pH	R_{an}, Ω	R_{cat}, Ω	R_D, Ω	τ, s	p	C_{ads}, μF	R_{ads}, Ω	C_{dl}, μF
NaCl	6	1800 / 2930	38 / 214	9160 / 7335	6.4 / 10.8	0.70 / 0.50	26 / 0.2	18 / 81	40 / 0.5
	4	1020 / 1460	32 / 105	3060 / 2425	1.2 / 4.2	0.68 / 0.44	8.6 / 0.3	25 / 160	11 / 0.6
	2	930 / 1670	29 / 40	1920 / 4695	0.6 / 5.1	0.51 / 0.44	5.0 / 0.3	22 / 86	4.7 / 1.2
NaCl + H_2S	6	1200 / 1695	24 / 50	4190 / 10 195	1.3 / 4.5	0.72 / 0.69	43 / 1.2	14 / 22	11 / 1.0
	4	1090 / 2905	22 / 62	4050 / 11 090	13.6 / 33.4	0.69 / 0.56	36 / 10	16 / 170	10 / 1.0
	2	650 / 1120	9 / 12	1720 / 4130	0.5 / 18.1	0.52 / 0.39	23 / 18	37 / 417	9.1 / 1.0

an inhibiting additive than in the inhibitor-free solution. That is why the model presented in Fig. 3c is, in our opinion, not quite adequate to the processes under study. This is probably due to the fact that this equivalent circuit presumes that only a film whose substance is an insulator is present on the electrode surface. Taking into account the presence on the electrode of also porous conducting [16, 17] and semiconducting [18] films results in a rather complex equivalent circuit whose impedance contains more than 12 parameters. Practical use of so complex equivalent circuits is extremely difficult.

In this context, let us consider, as in [19], the equivalent circuit presented in Fig. 4b. This circuit is constructed on the basis of the equivalent circuit in Fig. 4a, suggested in [12] for an electrode corroding in a neutral solution. In the equivalent circuit in Fig. 4b, R_{ads} and C_{ads} are elements defined by adsorption of intermediates formed in the anodic reaction; the meaning of the rest of the elements of the circuit was explained above. However, this circuit takes into account the presence of films of the inhibitor and corrosion products only indirectly, via a certain change in the values of the elements of the electrical model. Presumably, this equivalent circuit can also model the corrosion behavior of a steel electrode in carbon dioxide media, in which several depolarizers can be simultaneously involved in the cathodic reaction (H_2CO_3, H_3O^+, O_2) and processes may occur with both diffusion and kinetic control [20].

The values of the elements of the equivalent circuit in Fig. 4b are listed in Tables 5 and 6. In all the

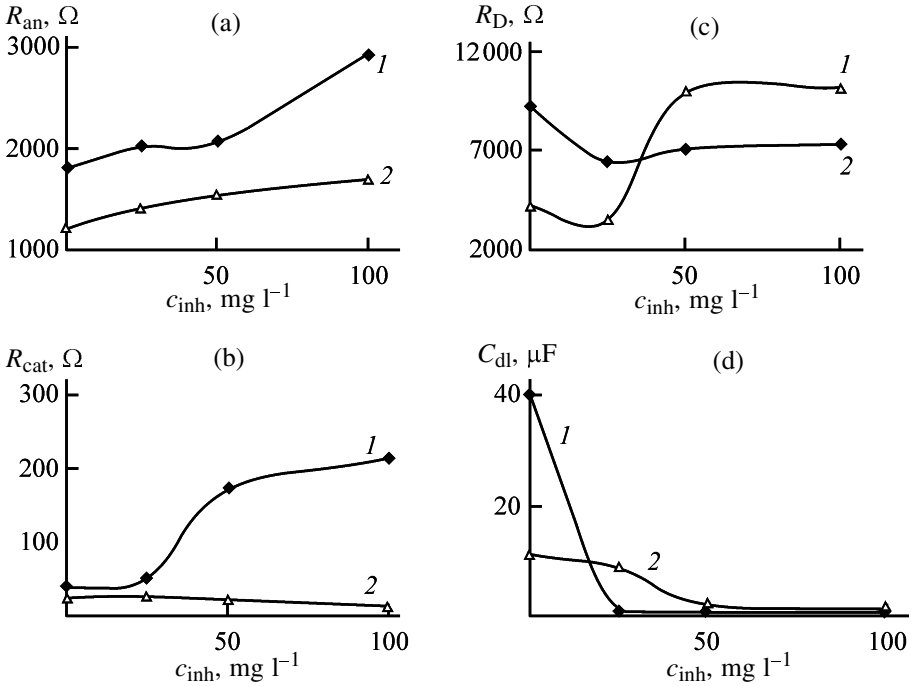


Fig. 6. Charge-transfer resistance in (a) anodic (R_{an}) and (b) cathodic (R_{cat}) reactions, (c) diffusion resistance R_D, and (d) capacitance C_{dl} of the electrical double layer vs. the concentration c_{inh} of the C_{10}–C_{14} OEA acetate in (*1*) NaCl and (*2*) NaCl + H_2S solutions. c_{NaCl} = 50 g l^{-1} (pH 6), c_{H_2S} = 200 mg l^{-1}.

media, adsorption of the inhibitor leads to an increase in R_{cat} (except in NaCl + H_2S and NaCl + H_2S + CO_2 solutions), R_D, τ, R_{ads}, and R_{an} and to a decrease in C_{ads} (except in carbon dioxide solutions), p, and C_{dl}. As the inhibitor concentration increases, these changes become, as a rule, more pronounced (Fig. 6). Thus, the results of the impedance measurements demonstrate that adsorption of an inhibitor hinders both the anodic (increase in R_{an}) and cathodic (increase in R_{cat}, R_D, τ) reactions. In a hydrogen sulfide medium, the cathodic polarization becomes less pronounced upon introduction of an inhibitor (Fig. 1). However, the presence of H_2S shifts the corrosion potential by 0.16–0.21 V in the positive direction. Therefore, the impedance measurements made at E_{cor} show a lower rate of the cathodic reaction in the inhibited solution, compared with that containing no inhibitor. In hydrogen sulfide media, the deceleration of the cathodic process is due only to an increase in R_D and τ, whereas the charge-transfer resistance R_{cat} decreases. In other media, introduction of C_{10}–C_{14} OEA acetate makes lower the rates of both stages of the cathodic process, charge transfer and diffusion. In the presence of an inhibitor, the double-layer capacitance C_{dl} reaches values of 0.5–1.5 μF cm^{-2}, which is due to the formation of very thin inhibitor films on the electrode surface.

CONCLUSIONS

(1) In the presence of H_2S and CO_2, salts of hydroxyethylated amines are combined inhibitors of general corrosion and hydrogenation of steel even at low concentrations. Their protective effect increases with the acidity of the medium to reach a value of 90%.

(2) In hydrogen sulfide–carbon dioxide media, salts of hydroxyethylated amines decrease the flux of hydrogen diffusion into steel by a factor of 2–2.7.

(3) According to impedance measurements, the additive effectively decelerates the anodic (increase in R_{an}) and cathodic (increase in R_{cat}, R_D, τ) processes.

(4) The decrease in the capacitance of the electrical double layer to 0.5–1.5 μF upon introduction of C_{10}–C_{14} OEA acetate indicates that thin inhibitor films are formed on the electrode surface. A polylayer adsorption occurs to virtually a full extent on the porous deposit of oxide, sulfides, or carbonates.

ACKNOWLEDGMENTS

The authors are grateful to Yu.I. Kuznetsov for the opportunity to perform impedance measurements and to D.B. Vershok and S.V. Oleinik (Institute of Phys-

ical Chemistry, Russian Academy of Sciences) for help in measurements.

REFERENCES

1. Moiseeva, L.S., Gurov, S.A., and Voloshin, A.I., *Korroz.: Mater., Zashch.*, 2005, no. 4, pp. 35–41.
2. Kuznetsov, Yu.I. and Vagapov, R.K., *Zashch. Met.*, 2000, vol. 36, no. 5, pp. 520–526.
3. Kardash, N.V. and Batrakov, V.V., *Zashch. Met.*, 1995, vol. 31, pp. 441–444.
4. Oleinik, S.V., Kuznetsov, Yu.I., Veselyi, S.S., et al., *Elektrokhimiya*, 1992, vol. 28, no. 6, pp. 856–863.
5. Safonov, V.A., *Elektrokhimiya*, 1993, vol. 29, no. 1, pp. 152–159.
6. Oshe, E.K. and Rozenfel'd, I.L., *Itogi Nauki Tekh., Ser.: Korroz. Zashch. Korroz.*, 1978, vol. 7, pp. 111–158.
7. Wilhelm, S.M., *Galvanic Corrosion*, Hack, H.P., Ed., Philadelphia: ASTM, 1988, pp. 23–34.
8. Herzog, E., *Les méthodés d'essai de corrosion des métaux et alliages*, Paris: Hermann, 1936. Translated under the title *Korroziya metallov (v zhidkikh i gazoobraznykh sredakh)*, Moscow: Metallurgiya, 1964, pp. 315–339.
9. Gonik, A.A., *Serovodorodnaya korroziya i mery ee preduprezhdeniya* (Hydrogen Sulfide Corrosion and Measures for Its Prevention), Moscow: Nedra, 1976.
10. Moiseeva, L.S. and Kuksina, O.V., *Zashch. Met.*, 2003, vol. 39, no. 5, pp. 542–551.
11. Mansfeld, F. and Kendig, M.W., *Mater. Sci. Forum*, 1986, vol. 8, pp. 337–350.
12. De Damborenea, J. and Vazquez, A.J., *Rev. Met. CENIM*, 1986, vol. 22, no. 5, pp. 283–287.
13. Bonnel, A., Dabosi, F., Deslouis, C., et al., *J. Electrochem. Soc.*, 1989, vol. 130, no. 4, pp. 753–761.
14. Brug, G.J., Eeden, A.L.G. van den, Sluyters-Rehbach, M., and Sluyters, J.H., *J. Electroanal. Chem.*, 1984, vol. 176, nos. 1–2, pp. 275–295.
15. Stoinov, Z.B., Grafov, B.M., Savavo-Stoinova, B., and Elkin, V.V., *Elektrokhimicheskii impedans* (Electrochemical Impedance), Moscow: Nauka, 1991.
16. Memet, J.B., Girault, P., Sabot, R., et al., *Electrochim. Acta*, 2002, vol. 47, pp. 1043–1053.
17. Mac-Donald, D.D., in *Corrosion'87*, Houston: NACE, 1987, paper no. 479.
18. Alves, V.A. and Brett, C.M.A., *Electrochim. Acta*, 2002, vol. 47, pp. 2081–2091.
19. Kim, Ya.R., Tsygankova, L.E., and Kichigin, V.I., *Korroz.: Mater., Zashch.*, 2005, no. 8, pp. 30–37.
20. Moiseeva, L.S., *Zashch. Met.*, 2005, vol. 41, no. 1, pp. 82–90.

ISSN 1070-4272. Russian Journal of Applied Chemistry, 2006, Vol. 79, No. 5, pp. 769–773. © Pleiades Publishing, Inc., 2006.
Original Russian Text © Yu.S. Dzyaz'ko, V.N. Belyakov, N.V. Stefanyak, S.L. Vasilyuk, 2006, published in Zhurnal Prikladnoi Khimii, 2006, Vol. 79, No. 5, pp. 778–782.

APPLIED ELECTROCHEMISTRY AND CORROSION PROTECTION OF METALS

Anion-Exchange Properties of Composite Ceramic Membranes Containing Hydrated Zirconium Dioxide

Yu. S. Dzyaz'ko, V. N. Belyakov, N. V. Stefanyak, and S. L. Vasilyuk

Vernadsky Institute of General and Inorganic Chemistry, National Academy of Sciences of Ukraine, Kiev, Ukraine

Received November 16, 2005

Abstract—Composite membranes consisting of an inert ceramic matrix based on aluminum and zirconium oxides and of an ion-exchange component, hydrated zirconium dioxide, were prepared. The selectivity of these membranes to Cl^- ions was studied.

DOI: 10.1134/S1070427206050132

Process cycles of many industrial enterprises involve the formation of highly toxic wastes, including soluble inorganic compounds. A promising method of removing such impurities from solutions is electrodialysis, as it allows continuous recovery of both cations and anions and their simultaneous concentration [1–4]. This method involves the use of both cation- and anion-exchange membranes made of organic polymers. The presence of oxidizing anions in solutions results in irreversible deterioration of mechanical and ion-selective properties of anion-exchange membranes. In this connection, an urgent problem is obtaining anion-exchange membranes with increased resistance to oxidants.

Hydrated oxides of multiply charged metals are highly stable in corrosive media [5]. At the same time, in acid media these compounds show anion-exchange properties. For example, the anion exchange with hydrated zirconium(IV) dioxide (HZD) proceeds according to scheme (1) [6, 7]:

$$ZrO_m(OH)_{p-1}(OH_2)^+ + An^- \rightleftarrows ZrO_m(OH)_{p-1}(OH_2)^+An^-, \quad (1)$$

where m and p are integers.

This fact suggests that hydrated zirconium oxide $ZrO_m(OH)_p$ can be used for production of chemically stable anion-exchange membranes.

The aim of this study was to develop such membranes and to examine their anion-exchange properties. For comparison we also studied a dispersed HZD ion exchanger obtained by similar methods.

EXPERIMENTAL

We used inert ceramic membranes based on Zr and Al oxides as starting materials. They had the following characteristics: molar ratio $Al_2O_3 : ZrO_2 = 7 : 3$, pore diameter 0.19 μm, specific surface area 4.5–5.0 $m^2 g^{-1}$. The membranes had the shape of tubes (internal diameter 10 mm, wall thickness 1 mm, length 20 cm).

Series I of samples of the anion-exchange membranes was prepared as follows. An inert membrane was filled with HZD in stages by a direct precipitation of particles of the ion-exchange component in the matrix volume. Each cycle of the preparation procedure included the following stages.

(1) Preparation of a $ZrO_m(OH)_p$ sol by gradual addition of 1 M NH_4OH solution to 1 M $ZrOCl_2$ with vigorous stirring. The volume ratio of the solutions was approximately 1 : 1. The temperature of the reaction mixture was maintained at a level of 330 K. The sol was left to stand for 48 days at 298 K.

(2) Impregnation of the membrane by the sol for 24 h.

(3) Treatment of the membrane with 1 M NH_4OH.

(4) Washing with deionized water to neutral reaction.

(5) Drying at 298 K to constant weight.

For more complete filling of matrix pores, operations 1–5 were multiply repeated. Membranes with various degrees of filling were prepared by this procedure.

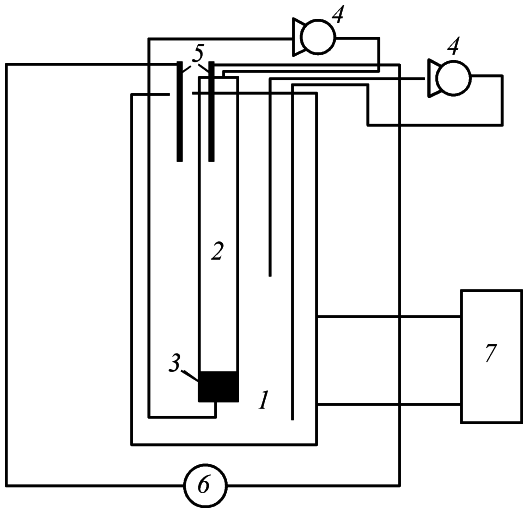


Fig. 1. Scheme of an installation for measuring the membrane potential: (*1*) vessel, (*2*) tubular membrane, (*3*) stopper, (*4*) pumps, (*5*) silver chloride electrodes, (*6*) voltmeter, and (*7*) thermostat.

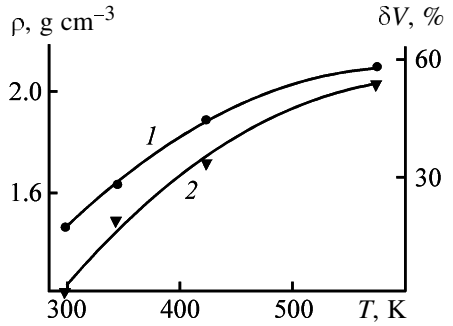


Fig. 2. Temperature dependences of the (*1*) bulk density ρ and (*2*) relative volume change δV of dispersed HZD.

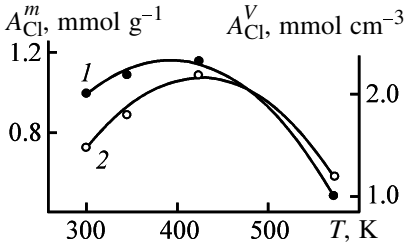


Fig. 3. Total anion-exchange capacity (*1*) A^m_{Cl} and (*2*) A^V_{Cl} of dispersed HZD as a function of the drying temperature T.

Series II of membrane samples was prepared similarly. In this case, the drying temperature in stage 5 was 343 K. Samples of series III were dried at 423 (cycles 1–8 of the ion-exchange component introduction), 573 (cycle 9), and 423 K (the subsequent cycles).

We also prepared samples of dispersed HZD. The procedure was as follows: (1) preparation of a $ZrO_m \cdot (OH)_p$ sol as described above; (2) precipitation of a $ZrO_m(OH)_p$ gel with a 1 M NH_4OH solution; (3) washing with deionized water to neutral reaction; (4) drying at 298 (HZD-I), 343 (HZD-II), 423 (HZD-III), and 573 K (HZD-IV) to constant weight.

The effective sizes of membrane pores were determined by mercury porosimetry using a Promoter 2000 porosimeter. To remove capillary-condensed water from membrane pores, samples were preliminarily dried to constant weight at 423 K.

To determine the total anion-exchange capacity for Cl^- ions per unit weight A^m_{Cl}, we kept a weighed sample (0.1 g) in 0.1 M HCl (100 cm^3) for 24 h. The membranes were washed with deionized water to neutral reaction and treated with 50 cm^3 of 0.1 M NaOH. The eluate was acidified with a 0.1 M HNO_3 solution, the Cl^- content was determined by potentiometric titration with an $AgNO_3$ solution [8], and A_{Cl} was calculated.

The selectivity of membranes to anions was estimated by measuring the membrane potential E_m [7]. A membrane under study, filled with an HCl solution (0.07–0.10 M), was placed into a vessel containing 0.01 M HCl (Fig. 1). One of the membrane openings was insulated. The internal and external solutions circulated in two independent contours under the action of a Zalimp PP 2-15 peristaltic pump. The circulation rate was 1.67×10^{-6} $m^3\ s^{-1}$. Silver chloride reference electrodes were placed inside and outside the membrane. The membrane potential was measured with a V7-34A high-resistance voltmeter.

The bulk density ρ of dispersed HZD samples was determined volumetrically [9]. In this case, A^m_{Cl} was determined by the technique given above. From the results obtained, we calculated the total anion-exchange capacity of an ion exchanger per unit volume A^V_{Cl}.

Sorption experiments and measurements of the membrane potentials were carried out at 298 K. This temperature was maintained with a UTU-2/77 fluid thermostat.

The dependences of the bulk density and relative volume change δV for dispersed HZD samples are shown in Fig. 2. Here $\delta V = (V_0 - V)/V_0$, where V_0 and V are the apparent volumes of an ion exchanger dried at 298 K and at higher temperatures, respectively. It is seen that, as T increases, δV and, correspondingly, ρ increase. Figure 3 illustrates the dependences of the total anion-exchange capacities per unit volume

and unit weight of the ion exchanger on the drying temperature. In the range 298–423 K, A_{Cl}^{V} and A_{Cl}^{m} increase as the drying temperature increases. Further increase in the drying temperature results in deterioration of the anion-exchange properties of the material. Thus, the decrease in δV and ρ of the ion exchanger after drying at 298–423 K is apparently associated with the removal of physically bound and capillary-condensed water. The decrease in the ion exchanger volume is naturally accompanied by an increase in the volume exchange capacity.

The deterioration of the ion-exchange properties of HZD-IV ion exchanger is apparently caused by the condensation of ion-exchange groups:

$$\equiv Zr\text{–}OH + HO\text{–}Zr \equiv \longrightarrow \equiv Zr\text{–}O\text{–}Zr\equiv + H_2O. \quad (2)$$

The dependences of the total anion-exchange capacity per unit weight for membranes of series I–III on the number n of cycles of filling the matrix with an ion-exchange component are shown in Fig. 4. It is seen that A_{Cl}^{m} increases as the number of filling cycles is increased up to 4. Further introduction of the ion exchanger into the membrane volume does not appreciably increase its anion-exchange capacity. It should also be noted that the drying temperature does not noticeably affect the anion-exchange capacity of the membranes of series I and II. In series III, a pronounced minimum corresponding to n = 9 in the A_{Cl}^{m}–n dependence is observed. Thus, the increase in the drying temperature from 423 to 573 K results in the deterioration of the anion-exchange properties of the membranes.

The dependences of the effective pore diameter d of the membranes of series III on the number of cycles of HZD introduction are shown in Fig. 5 (because of the necessity of thermal pretreatment, the use of mercury porosimetry for samples of other series was not appropriate). It is seen that d decreases in the range of n 0–8, sharply increases at n = 9, and decreases again as n increases further. Thus, the modification of ceramic membranes consists in successive filling of their pores with the ion-exchange component. The pore structure and the anion-exchange properties are determined by the number of cycles of HZD introduction, on the one hand, and by the drying temperature, on the other.

As should be expected, the stage-by-stage introduction of the ion-exchange component in the membrane matrix affects the charge-selective properties of this latter. In all the cases, we recorded emf arising in

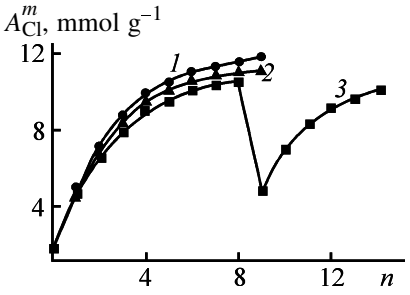


Fig. 4. Total anion-exchange capacity A_{Cl}^{m} as a function of the number n of cycles of filling the matrix for membrane samples of series (*1*) I, (*2*) II, and (*3*) III.

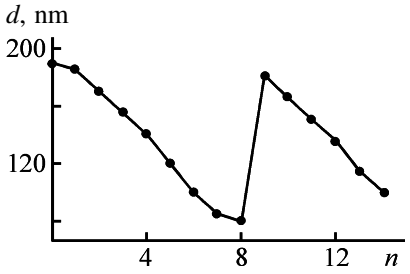


Fig. 5. Effective pore diameter d as a function of the number n of cycles of filling a matrix for membrane samples of series III.

the following circuit.

Ag	AgCl, KCl	Internal solution	Membrane	External solution	KCl, AgCl	Ag

(3)

In the case of membranes modified with HZD, the emf was stabilized within a certain period of 0.5–6 h. The stabilization period became shorter as the number of HZD layers was increased and the thermal treatment temperature was decreased.

Thus, the membranes containing an ion-exchange component represent a barrier virtually impermeable to negatively or positively charged ions. In this connection, the leveling of concentrations by diffusion becomes impossible.

The results obtained suggest that in this case the examined membranes exhibit charge-selective properties and the recorded emf corresponds to the membrane potential E_m.

The dependences of the membrane potential on the number of successive cycles of HZD introduction into an inert ceramic membrane are shown in Fig. 6. For samples of series I and II, the membrane potential shifts to more negative values with increasing n and tends to certain constant values, which nevertheless

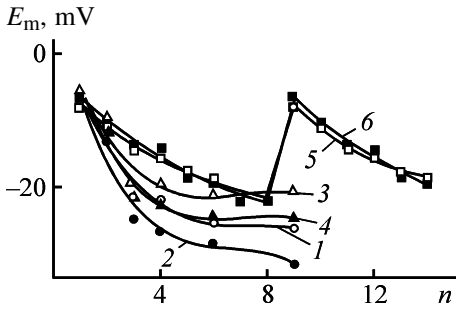


Fig. 6. Membrane potential E_m as a function of n for membranes of series (*1, 2*) I, (*3, 4*) II, and (*5, 6*) III. Internal solution 0.01 M HCl; external solution (*1, 3, 5*) 0.07 M HCl and (*2, 4, 6*) 0.1 M HCl.

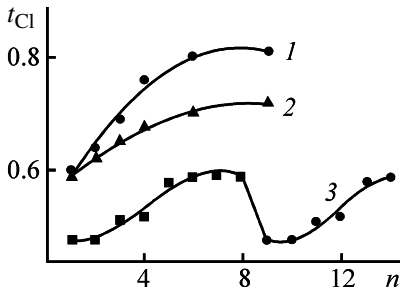


Fig. 7. Transport number t_{Cl} of Cl^- ions as a function of n for membrane samples of series (*1*) I, (*2*) II, and (*3*) III.

are higher than the theoretically calculated values (–50 and –59 mV at the internal solution concentrations of 0.07 and 0.1 M, respectively). In the case of series III samples, E_m decreases with increasing n from 1 to 8, approaching a certain constant value, sharply increases at $n = 9$, and again decreases as n increases further. A comparison of the E_m–n curves for various samples shows that the decrease in the drying temperature results in a decrease in the membrane potential.

The results obtained allow us to make some quantitative estimations.

At a high concentration of the 1,1-electrolyte (HCl), at variation of its content in the more concentrated solution, the equation relating the membrane potential to the potentiometric transport number t_{Cl} of potential-determining ions has the form [7]

$$E_m = \frac{RT}{F}\left[\ln(c_{Cl,1}/c_{Cl,2}) + 2\int_1^2 (1 - t_{Cl})\,d\ln c_{Cl,2}\right], \quad (4)$$

where R is the universal gas constant; F, Faraday constant; T, temperature; and $c_{Cl,1}$ and $c_{Cl,2}$, concentrations of potential-determining ions in less and more concentrated solutions, respectively.

The integration is performed within the limits of concentrations from $c_{Cl,3}$ (external solution) to $c_{Cl,2}$ (internal solution). From Eq. (4) we obtain

$$t_{Cl} = 1 - \frac{F}{2RT}\frac{d[E_m - RTF^{-1}\ln(c_{Cl,1}/c_{Cl,2})]}{d\ln a_{Cl,2}}, \quad (5)$$

where a_{Cl} is the activity of Cl^- ions.

As in all the cases the deviations of the membrane potentials from the theoretically calculated values $[E_m - RTF^{-1}\ln(c_{Cl,1}/c_{Cl,2})]$ do not change when the internal solution concentration increases from 0.07 to 0.1 M, we can state that the differentials in Eq. (5) are constant in this concentration range and, hence, the transport numbers of Cl^- ions can be calculated by formula (6):

$$t_{Cl} = 1 - \frac{F\{(E''_m - E'_m) - RTF^{-1}[\ln(c_{Cl,1}/c''_{Cl,2}) - \ln(c_{Cl,1}/c'_{Cl,2})]\}}{2RT(\ln c''_{Cl,2} - \ln c'_{Cl,2})}, \quad (6)$$

where primed and double-primed quantitites correspond to the concentrated internal solution of lower (0.07 M) and higher (0.1 M) concentration, respectively.

The dependences of potentiometric transport numbers of Cl^- on the number of layers of the ion-exchange component, calculated on the basis of the data of Fig. 6, are presented in Fig. 7. It is seen that the transport numbers increase as the amount of HZD in the membrane increases. It should also be noted that the decrease in the drying temperature in the final stage of the process results in a significant improvement of the anion-selective properties of the membranes.

For samples of series I and II, the t_{Cl} values approach a certain constant value as the number of successive introductions of the ion-exchange component into the ceramic membrane increases. The t_{Cl}–n dependence can be approximated by the sigmoidal function

$$E_m = a_1 + a_2[1 + e^{(n - a_3)/a_4}]^{-1}, \quad (7)$$

where a_1–a_4 are empirical coefficients.

It follows from Eq. (7) that, at $n \to \infty$, t_{Cl} approaches $a_1 + a_2$. Taking into account that a_1 and a_2 are, respectively, 0.58 and 0.23 (series I), 0.48 and 0.28 (series II), we obtain t_{Cl} 0.81 (series I) and 0.76

(series II). For samples of series III, a similar trend in the range of n 1–8 is observed. In this case, the coefficients a_1 and a_2 are 0.47 and 0.12, respectively; hence, the transport numbers approach 0.59 at $n \to \infty$.

Thus, the introduction of HZD into pores of a ceramic membrane imparts anion-selective properties to it, which is associated with a decrease in the pore size, on the one hand, and with an increase in the surface charge density, on the other. An increase in the drying temperature from 298 to 423 K does not result in the deterioration of the anion-exchange properties of membranes. Nevertheless, the increase in temperature, apparently, results in an increase in the pore size owing to the HZD "shrinkage". The disappearance of anion-selective properties after drying at 578 K is probably due not only to an increase in the pore size of an HZD-containing membrane, but also to a decrease in the anion-exchange capacity of a sorption-active component.

It should be noted that the method used for the introduction of the ion-exchange component does not make it possible to obtain a membrane ideally selective to anions, which is probably caused by charge limitations. At low pH values of solution, colloidal HZD particles are charged positively. The surface of the membrane containing the ion-exchange component also has a positive charge. Thus, the penetration of particles of the $ZrO_m(OH)_{p-1}(OH_2)^+$ sol into pores of a membrane filled with HZD is hampered. The pore size and the surface charge density seem to be among factors restricting such a penetration. When the temperature increases from 298 to 423 K, the role of the second factor apparently increases. At a drying temperature of 573 K, the pore size of the membrane filled with HZD increases, and the anion-exchange capacity appreciably decreases, which facilitates the penetration of positively charged sol particles into pores.

CONCLUSIONS

(1) Composite membranes consisting of aluminum and zirconium oxides as the base of an inert ceramic matrix and hydrated zirconium dioxide as an ion-exchange component were prepared. The procedure consisted in the precipitation of a gel of hydrated zirconium dioxide in pores of the membranes followed by drying at various temperatures.

(2) The anion-exchange capacity of the composite membranes and the effective pore size are determined by the drying temperature in the final stage of the preparation process.

(3) The selectivity of the membranes prepared to Cl^- ions was studied by the electrochemical method. The potentiometric transport numbers of Cl^- were found to increase as the matrix is filled with the ion-exchange component and reach 0.59–0.81 depending on the drying temperature. These values are comparable with those for heterogeneous membranes based on organic polymers. As the upper temperature limit for electrodialysis processes is 323 K, it should be expected that the exploitation of composite membranes will not lead to a significant deterioration of their anion-selective properties.

REFERENCES

1. Katz, P., *Ultrapure Water*, 1999, vol. 16, no. 4, pp. 52–57.
2. Grebenyuk, V., *Elektrodializ* (Electrodialysis), Kiev: Tekhnika, 1976.
3. Walsh, F., *A First Course in Electrochemical Engineering*, London: Alresford, 1993.
4. Koruta, J., *Ions, Electrodes and Membranes*, Chichester (UK): Wiley, 1991.
5. Amphlett, C. B., *Inorganic Ion Exchangers*, Amsterdam: Elsevier, 1964.
6. Sukharev, Yu.I., *Sintez i primenenie spetsificheskikh oksigidratnykh sorbentov* (Synthesis and Application of Specific Oxyhydrate Sorbents), Moscow: Energoatomizdat, 1987.
7. Helfferich, F., *Ionenaustauscher*, Weinheim: Chemie, 1959, vol. 1.
8. Charlot, G., *Les methods de la chimie analytique. Analyse quantitative minerale*, Paris: Masson, 1961, 4th ed.
9. Marhol, M., *Ion Exchangers in Analytical Chemistry. Their Properties and Use in Inorganic Chemistry*, Prague: Academia, 1982.

ISSN 1070-4272. Russian Journal of Applied Chemistry, 2006, Vol. 79, No. 5, pp. 774–777. © Pleiades Publishing, Inc., 2006.
Original Russian Text © Yu.G. Chesnokov, A.V. Bauman, O.M. Flisyuk, 2006, published in Zhurnal Prikladnoi Khimii, 2006, Vol. 79, No. 5, pp. 783–786.

PROCESSES AND EQUIPMENT OF CHEMICAL INDUSTRY

Calculation of the Velocity Field of a Fluid in a Hydrocyclone

Yu. G. Chesnokov, A. V. Bauman, and O. M. Flisyuk

St. Petersburg State Technological Institute, St. Petersburg, Russia

Received February 22, 2005; in final form, November 2005

Abstract—Influence exerted by parameters dependent on the design dimensions of a hydrocyclone and by the flow rate on the distribution of the fluid velocity in a hydrocyclone was studied.

DOI: 10.1134/S1070427206050144

Calculating the components of a fluid velocity in a hydrocyclone is important because a theoretically substantiated method for calculation of the process of suspension separation in a hydrocyclone cannot be developed without accomplishing this task. A calculation of this kind involves integration of equations describing the motion of solid particles in a hydrocyclone at a prescribed particle size. These equations include the fluid velocity, which should be found beforehand. As shown in [1], determination of the velocity profile of a fluid in the main flow core, which exerts the strongest influence on separation processes, can be reduced under certain conditions to integration of a certain ordinary differential equation, which can be done in a comparatively simple way by numerical methods.

It is assumed that the intensity of turbulent pulsations in the main flow core is comparatively low and the fluid can be considered ideal. The flow is assumed to be steady and axially symmetric. In this case, it is convenient to use the cylindrical coordinate system (r, θ, z) whose z axis coincides with the symmetry axis. Nondimensional variables will be used in calculations. When passing to dimensionless variables, we use as length, velocity, and pressure scales the quantities R_0, $u_0 = Q/(2\pi R_0^2)$, and $p_0 = \rho u_0^2$, respectively, where R_0 is the radius of the cylindrical part of the hydrocyclone; Q, flow rate of the fluid; and ρ, its density. The axial, radial, and tangential velocity components of the fluid are designated as u, v, and w, respectively. The stream function ψ for the meridian motion of the fluid can be sought for as $\psi = z^m F(s)$, where m is a certain number and $s = r/z$. With the assumptions made in [1], we obtain the following ordinary differential equation for the function $F(s)$:

$$(1 + s^2)\frac{d^2F}{ds^2} - [s^{-1} + 2(m - 1)s]\frac{dF}{ds} + (m - 1)mF = -as^2F^{(m-4)/m} - bF^{(m-2)/m}, \quad (1)$$

where a and b are constants.

The boundary conditions for Eq. (1) have the form

$$F(0) = F(s_0) = 0, \quad (2)$$

where $s_0 = \tan\alpha$ and α is the half opening angle of the cone formed by the surface of the conical section of the hydrocyclone.

Let us denote by r_1 and z_1 the coordinates of the lower edge of the discharge pipe in some meridian section of the hydrocyclone. The flow rate of the fluid (in dimensionless variables) through this pipe is expressed in terms of the stream function as $\psi(r_1, z_1)$. Therefore, one of the parameters (a or b) in Eq. (1) can be found from the condition

$$\psi(r_1, z_1) = 1. \quad (3)$$

The expressions for the axial, radial, and tangential velocity components in terms of the stream function have the form

$$u = z^{m-2}F's^{-1}, \quad (4)$$

$$v = z^{m-2}(F' - mFs^{-1}), \quad (5)$$

$$w = w_0 r_0 r^{-1}\{1 + bmz^{2(m-1)}F^{2(m-1)/m}[r_0^2 w_0^2(m - 1)]^{-1}\}^{1/2}. \quad (6)$$

In relation (6), w_0 is a constant (independent of the coordinate z) value of the tangential velocity component at the wall of the conical section of the hydrocyclone. More precisely, this quantity is to be understood as the value of the tangential velocity component at the outer boundary of a thin hydrodynamic boundary

layer formed near the wall. This velocity is proportional to the average velocity of the fluid at the apparatus inlet, and the proportionality factor (so-called velocity drop coefficient at the apparatus inlet) can be calculated by empirical formulas presented in the monograph [2]. It primarily depends on the ratio between the diameter of the inlet pipe and that of the hydrocyclone.

Formulas (4) and (5) show that the axial and tangential velocity components take at $m = 2$ a constant (independent of z) value at conical surfaces $s = \text{const}$. As shown in [1], the function $F(s)$ can be found at this value of m analytically. According to formula (4), the axial velocity component changes its sign at the surface $s_2 = \text{const}$, where the value of s_2 is found from the equation

$$dF(s_2)/ds = 0, \quad (7)$$

This is the so-called shell with zero vertical velocity.

The streamline $\psi = 1$ delimits the region of closed circulation of the fluid, which appears in the hydrocyclone. It is impossible to calculate the fluid flow in this region in terms of the theory under consideration. The possible approaches to description of the fluid motion in the circulation region were discussed in the monograph by Gol'dshtik [3]. This circulation region has a comparatively weak effect on processes of suspension separation in the hydrocyclone. In the case when $b = 0$ ($\Gamma = w r = \text{const}$), we can eliminate parameter a from the differential equation (1) by making the substitution $F = a^{m/4}F_1$. The numerical value of this parameter is found from condition (3):

$$a = z_1^{-4} F_1(s_1)^{-4u/m}.$$

Then the formulas for calculating the axial and radial velocity components have the form

$$u = \frac{z^{m-2}F'_1}{z_1^m F_1(s_1)s},$$

$$v = \frac{z^{m-2}(F'_1 - mF_1 s^{-1})}{z_1^m F_1(s_1)}.$$

If $b \neq 0$, parameter b is eliminated from Eq. (1) by substitution $F = b^{m/2}F_2$. In this case, parameter b is found from condition (3):

$$b = z_1^{-2} F R_2(s_1)^{-2/m},$$

and the formulas for calculating the axial, radial, and tangential velocity components of the fluid are written as

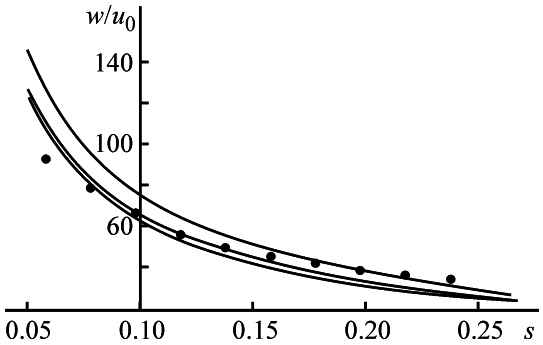


Fig. 1. Tangential velocity component w/u_0 vs. the coordinate s at varied parameter m. For comments, see text.

$$u = \frac{z^{m-2}F'_2}{z_1^m F_1(s_1)s},$$

$$v = \frac{z^{m-2}(F'_2 - mF_2 s^{-1})}{z_1^m F_2(s_1)},$$

$$w = w_0 r_0 r^{-1}\left[1 + \frac{mz^{2(m-1)}F_2^{2(m-1)/m}}{r_0^2 w_0^2 (m-1) z_1^{2m} F_2(s_1)^2}\right]^{1/2}.$$

At $b = 0$, the tangential velocity component is calculated by the formula [Eq. (6)]

$$w = w_0/r. \quad (8)$$

This dependence and the dependences obtained at $a = 0$, $b \neq 0$, and varied parameter m are shown in Fig. 1. Naturally, the theory becomes inapplicable near the apparatus axis. A comparatively thin air column is formed in this zone, and the fluid rotates in a certain vicinity of this column as a solid body. The curves were plotted at the following values of the parameters s_0, w_0, and z: $s_0 = 0.268$, $w_0 = 16.5$, $z = 1/(2s_0)$, $z_1 = 4.27$, and $s_1 = 0.0563$. The curve describing the dependence (8) is the closest to the abscissa. The two other curves were plotted for $m = 1.2$ and 2.1. The points in Fig. 1 represent the experimental data from [4]. The agreement with the experimental data is good. The most pronounced deviations are observed at small values of s, which correspond to radial coordinates comparable with the radius of the discharge pipe.

The larger the value of parameter m, the lower the run of the corresponding curve. Figure 1 shows that parameter m exerts a comparatively weak influence on the dependence of the tangential velocity component

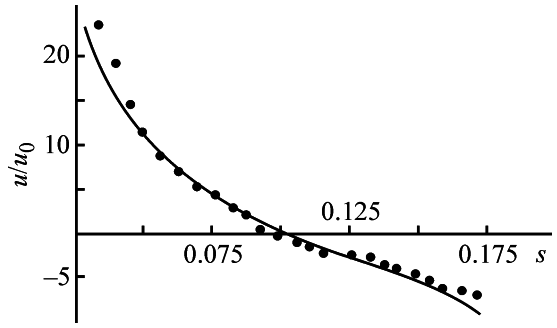


Fig. 2. Dependence of the axial velocity component u/u_0 on the coordinate s, compared with experimental data.

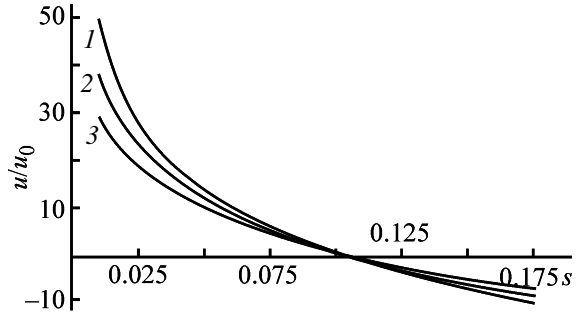


Fig. 3. Dependence of the axial velocity component u/u_0 on the coordinate s at $a = 0$ and $m = 1.8$ (*1*), 2.0 (*2*), and 2.2 (*3*).

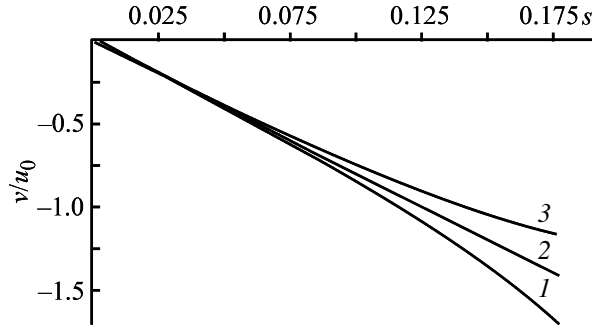


Fig. 4. Dependence of the radial velocity component v/u_0 vs. the coordinate s at $a = 0$ and $m = 1.8$ (*1*), 2.0 (*2*), and 2.2 (*3*).

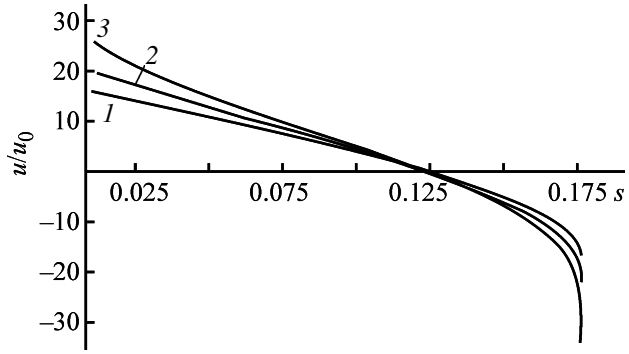


Fig. 5. Dependence of the axial velocity component u/u_0 on the coordinate s at $b = 0$ and $m = 2.6$ (*1*), 2.4 (*2*), and 2.2 (*3*).

on the distance from the apparatus axis. Also weak is the dependence of this quantity on coordinate z at a fixed value of s. The tangential velocity component differs the most strongly from the value calculated by formula (8) at such a value of s at which the second term in the radicand in the right-hand part of formula (6) reaches a maximum, i.e., at the shell of zero vertical velocity.

Parameter m exerts the strongest influence on the dependence of the axial and radial velocity components on coordinate z. The radial velocity component of the fluid in the hydrocyclone is small in magnitude. Therefore, reliable experimental data concerning the dependence of the radial component on the axial and radial coordinates are lacking. The experimental dependences of the axial velocity component on the radial coordinate at various axial coordinates have been obtained by Monderon with a laser Doppler anemometer [5]. These data make it possible to find parameter m for the hydrocyclone analyzed here. Figure 2 compares the experimental data with the calculated dependence. The following values of the parameters were taken in plotting the curves: $s_0 = 0.1763$, $z_1 = 6.338$, $s_1 = 0.05259$, $z = 4.471$, and $m = 1.2$. It is noteworthy that Monderon's experimental data confirm the self-modeling dependence of the velocity on coordinates, adopted in this study.

The dependences of the axial and radial velocity on coordinate s, plotted for the case $a = 0$ and $b \neq 0$ at varied parameter m, are shown in Figs. 3 and 4, respectively. These dependences were plotted for the following values of the parameters: $s_0 = 0.176$ ($\alpha = 10°$), $z_1 = 8.74$, $s_1 = 0.0305$, and $z = 1/s_0$. The larger the value of parameter m, the closer to the abscissa the run of the curve for the radial velocity component. As parameter m increases, the zero-vertical-velocity shell shifts toward the apparatus wall. The dependence of coordinate s_2 at which the axial velocity becomes zero on parameter m is weak. For example, $s_2/s_0 = 0.5962$ at $s_0 = 0.268$ and $m = 1.5$, $s_2/s_0 = 0.6051$ at $m = 2.0$, and $s_2/s_0 = 0.6113$ at $m = 2.5$. According to the experimental data presented in Bradley's monograph [6], s_2/s_0 is approximately 0.61, in good agreement with the values mentioned above.

The plots of the axial velocity component against coordinate s, constructed for the case $a \neq 0$ and $b = 0$ and varied parameter m, are shown in Fig. 5. The values of parameters s_0, z_1, s_1, and z were taken to be the same as those in plotting Figs. 3, 4. As m becomes higher, the magnitude of the velocity decreases. The most pronounced difference from the case $a = 0$ is in that the zero-vertical-velocity shell is situated

closer to the apparatus wall. The calculations performed at $a \neq 0$ and $b \neq 0$ show that, at a constant m and varied a/b^2, the zero-vertical-velocity shell shifts toward the hydrocyclone wall as the a/b^2 ratio increases.

Thus, parameter m exerts the strongest influence on the behavior of the axial and radial velocity components with coordinate z [formulas (4), (5)] and on the maximum value of the axial velocity component. The relation between parameters a and b has the most pronounced effect on the position of the zero-vertical-velocity shell. These conclusions can be used in determining the numerical values of these parameters from experimental data. The values of the parameters ($a = 0$, $m = 2$) accepted by Bloor and Ingham [7] correspond to the following conditions at the hydrocyclone inlet. The fluid flow arriving at the hydrocyclone at $z = z_1$ and $r_i < r < 1$ has a constant pressure p, zero radial velocity component ($v = 0$), and constant axial and tangential velocity components ($u = -u_i = \text{const}$, $w = w_i = \text{const}$). Here, the value of coordinate r_i is not known beforehand.

With the exception of two particular cases ($a = 0$, $m = 2$ and $b = 0$, $m = 4$), no analytical solution to Eq. (1) can be constructed and we are forced to use the results of a numerical solution of this equation for calculating the fluid velocity components. In calculating the process of suspension separation in a hydrocyclone, it would be convenient to have approximate analytical expressions for the fluid velocity components. To construct these expressions, we could make an attempt to use asymptotic expansions of the solution at small values of parameter s, similar to those considered in [1]. Each expansion of this kind contains an uncertain parameter that cannot be found when constructing an asymptotic expansion. We could make an attempt to retain a certain finite number of terms in the asymptotic expansion and define the uncertain constant in the resulting approximate expression so that the condition $F(s_0)$ should be satisfied. It is in this way that the approximate expression for the stream function is constructed in [8], with only the first two terms retained in this expression. However, comparison with the exact solution shows that this method fails to produce good results. The point is that the asymptotic expansion becomes inapplicable at $s = s_0$ because of the existence of the nonlinear right-hand part of the equation. We can use two expansions at s close to zero and s close to s_0. The uncertain constants in these expansions can be found from the matching condition for these expansions at intermediate values of s. However, the expressions obtained in this case are rather cumbersome and it is simpler to directly use the numerical solution.

CONCLUSION

Relations that can be used to calculate the fluid velocity components in a hydrocyclone were derived. It was shown that the results obtained are in good agreement with the experimental data. These results are necessary for developing a procedure for calculating processes of suspension separation in hydrocyclones.

REFERENCES

1. Chesnokov, Yu.G., Bauman, A.V., and Flisyuk, O.M., in *MMTT-16: Sbornik trudov XVI mezhdunarodnoi konferentsii* (Proc. XVI Int. Conf. MMTT-16), St. Petersburg, 2003, vol. 10, section 11, pp. 107–108.
2. Ternovskii, I.G. and Kutepov, A.M., *Gidrotsiklonirovanie* (Hydrocyclonation), Moscow: Nauka, 1994.
3. Gol'dshtik, M.A., *Vikhrevye potoki* (Vortex Flows), Novosibirsk: Nauka, 1981.
4. Kuznetsov, A.A., Kutepov, A.M., and Ternovskii, I.G., *Zh. Prikl. Khim.*, 1980, vol. 23, no. 11, pp. 1442–1445.
5. Monderon, T.C., Hsieh, K.T., and Rajamant, R.K., *Int. J. Miner.*, 1992, vol. 35, nos. 1–2, pp. 65–83.
6. Bradley, D., *The Hydrocyclone*, Oxford: Pergamon, 1965.
7. Bloor, M.I.G. and Ingham, D.B., *J. Fluid Mech.*, 1987, vol. 178, pp. 507–519.
8. Bloor, M.I.G. and Ingham, D.B., *Trans. Inst. Chem. Eng.*, 1973, vol. 51, no. 1, pp. 36–41.

ISSN 1070-4272. Russian Journal of Applied Chemistry, 2006, Vol. 79, No. 5, pp. 778–782. © Pleiades Publishing, Inc., 2006.
Original Russian Text © E.V. Fomina, Yu.A. Kurskii, L.N. Beloded, G.N. Chervyakova, 2006, published in Zhurnal Prikladnoi Khimii, 2006, Vol. 79, No. 5, pp. 787–791.

ORGANIC SYNTHESIS AND INDUSTRIAL ORGANIC CHEMISTRY

Synthesis and Properties of Aliphatic Oligoamides Containing Methionine Fragment

E. V. Fomina, Yu. A. Kurskii, L. N. Beloded, and G. N. Chervyakova

Kargin Research Institute of Polymers, Federal State Unitary Enterprise, Dzerzhinsk, Nizhni Novgorod oblast, Russia

Received January 11, 2006

Abstract—Oligoamides were prepared from dimerized fatty acid, hexamethylenediamine, and an amino acid (methionine). The effect of methionine on the course of polycondensation and properties of the reaction products was examined. New thermoplastic adhesive compounds based on these products were developed.

DOI: 10.1134/S1070427206050156

Oligoamide products derived from dimerized fatty acid (DFA) and aliphatic diamines are widely used as base components of thermoplastic (hot-melt) adhesives [1–3].

The specific structural features and composition of the DFA used allow preparation of oligoamides exhibiting high adhesion to various materials, high shock resistance, flexibility, and resistance to water and oils [4, 5].

Introduction of various modifying agents (e.g., carbonyl compounds and dicarboxylic acids) into these oligoamides strongly affects the structure and properties of the products and, as a consequence, the characteristics of hot-melt adhesives based on them [6, 7].

Of particular interest in this respect is the modifying effect of methionine (α-amino-γ-methylthiobutyric acid), due to several reasons. First, a fairly bulky substituent, $CH_3SCH_2CH_2$, in the α-position of methionine should affect the physicochemical properties of the products [8–10]. At the same time, methionine plays an important role in biosynthesis processes, and introduction of its fragment into an oligoamide macromolecule may be a route to promising biodegradable materials, which would allow solution of environmental problems associated with the utilization of spent oligo- and polyamides [11, 12].

In this study we prepared a series of oligoamides differing in the content of methionine fragments and examined the specific features of polycondensation and the structure and properties of the products.

EXPERIMENTAL

As starting reagents we used methionine (Met) [GOST (State Standard) 23423–89], DFA of the PRIPOL 1017 brand (the Netherlands, CAS no. 61788-89-4), hexamethylenediamine (HMDA) [TU (Technical Specifications) 6-09-36–73), and wollastonite filler (NordKalk, Finland) FW-70, FW-325, and WIC-10 (mean particle diameter ≤90, ≤13, and ≤4.5 μm, respectively).

The procedure for preparing oligo- and polyamides derived from DFA and aliphatic diamines is described in detail in [1, 2] and involves the polycondensation in a nitrogen atmosphere at 160–240°C for 5–6 h without solvents and catalysts.

The synthesis of oligoamides modified with methionine is characterized by certain specific features associated with the fact that at 200–240°C *D*-methionine melts with decomposition; also, the tendency of α-amino acids to cyclize on heating with the formation of 2,5-diketopiperazines [13, 14] should be taken into account.

Therefore, the joint polycondensation of DFA, HMDA, and methionine was performed under milder conditions, which allowed us to minimize the formation of diketopiperazines and avoid thermal decomposition of the amino acid molecules into low-molecular-weight products.

A reactor was charged with the required amounts of DFA and HMDA. The mixture was heated to 80–100°C with stirring until a homogeneous mass was obtained. Then methionine was added, and the mix-

ture was slowly (over a period of 40 min) heated with vigorous stirring to 160–165°C, after which the water release started. Then the mixture was gradually (over a period of 7–8 h) heated to 195–200°C. The final step was performed under the conditions ensuring efficient removal of water (133.32–666.60 Pa, 1–1.5 h, 140–190°C). The product yield was 97.5–98.3%.

The modification of oligoamides with methionine can be represented by the scheme

$$(n+1)H_2N\text{–}R\text{–}NH_2 + nHOOC\text{–}R'\text{–}COOH + nHOOC\text{–}\underset{\displaystyle NH_2}{\underset{|}{CH}}\text{–}(CH_2)_2SCH_3 \longrightarrow H_2N[RNHC(O)R'C(O)NH\underset{\displaystyle (CH_2)_2SCH_3}{\underset{|}{CHC}}(O)NH]_nRNH_2 + 3nH_2O,$$

where R = $(CH_2)_6$, R' = $C_{34}H_{62}$, n = 3–5.

The structure of the compounds prepared was studied by IR and NMR spectroscopy. The IR spectra were recorded on a Specord M80 spectrometer in the range 4000–700 cm^{-1}. The NMR spectra were measured on a Bruker DPX-200 spectrometer (operating frequency 200 MHz for ^1H and 50 MHz for ^{13}C; solvent $CDCl_3$; reference tetramethylsilane).

The molecular-weight characteristics of the reaction products were studied by gel permeation chromatography (GPC) using a set of five Styrogel columns with pore diameters of 10^5, 3×10^4, 10^4, 10^3, and 250 Å (Waters). An R-403 differential refractometer (Waters) was used as detector; an LCD 2563 photometer (λ 254 nm) was additionally used; the eluent was tetrahydrofuran (THF). The chromatograph was calibrated with polystyrene references (polydispersity coefficient $\overline{M}_w/\overline{M}_n \le 1.1$, molecular weight M in the range 2000–100 000).

The amine numbers (AmN), acid numbers (AcN), and molecular weights (M) of the oligoamides were determined chemically from the amounts of terminal functional groups following the standard protocols [15]; the softening point T_s was determined by the ring-and-ball method (GOST 11506–73), and the shear strength of glue joints, according to GOST 14759–69.

The kinetics of the reaction of DFA, HMDA, and methionine was studied by measuring the amount of water distilled off during the reaction.

The kinetic curves (Fig. 1) show that the polycondensation of DFA with HMDA occurs more actively

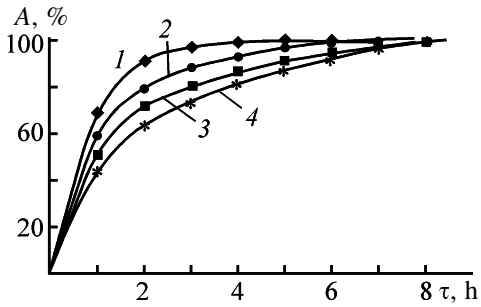


Fig. 1. Amount A of water released in the polycondensation as a function of the reaction time τ. DFA : HMDA : Met ratio: (*1*) 0.40 : 0.50 : 0, (*2*) 0.40 : 0.50 : 0.10, (*3*) 0.40 : 0.50 : 0.25, and (*4*) 0.40 : 0.50 : 0.50.

in the absence of methionine: 70% of the theoretical amount of water is released during the first hour of the reaction; ~90%, within 2 h; and ~96%, within 3 h. Then, as the concentration of the functional groups of the starting compounds decreases, the reaction decelerates; it is complete in 6 h. In the reaction of DFA with HMDA and methionine, the rate of formation of the final product noticeably decreases with an increase in the methionine content. Addition of 0.1 molar equivalent of metionine causes the amount of water released during the first hour of the reaction to decrease to 60% of the theoretical amount; with 0.25 molar equivalent of methionine, this quantity decreases to 53%, and with 0.5 molar equivalent of methionine, to 45%. The total reaction time in the presence of methionine increases to 7–8 h.

Presumably, the mutual influence of the amino and carboxy groups in the methionine molecule and the presence of a bulky substituent, $CH_3SCH_2CH_2$, in the α-position relative to these groups lead to a certain deceleration of the polycondensation in the system DFA–HMDA–Met, compared to the Met-free system.

The polycondensation products are golden-yellow solids with a weak methionine odor; their properties are given in Table 1.

With an increase in the amount of Met added, the molecular weight of the polycondensation product gradually decreases. As compared to the product prepared from DFA and HMDA without methionine, M of the oligoamides containing methionine fragments is lower by a factor of 1.2–2.3. This fact may be due to structural features of methionine and to its capability to terminate the propagating oligomer chain. Correspondingly, the softening point decreases with increasing methionine content. Apparently, incorporation of methionine makes the oligoamide structure irregular, causing an increase in the distance between

Table 1. Properties of modified oligoamides prepared at different reactant ratios

Sample no.	Equivalent ratio of reactants			AmN	AcN	M	T_s, °C
	DFA	HMDA	Met	mg KOH/g oligoamide			
1	0.40	0.50	–	20.5	1.5	5100	85
2	0.40	0.50	0.05	23.5	2.0	4400	80
3	0.40	0.50	0.10	30.3	2.3	3500	75
4	0.40	0.50	0.20	33.8	2.5	3100	68
5	0.40	0.50	0.25	40.8	3.9	2500	62
6	0.40	0.50	0.50	45.4	4.6	2200	56

the adjacent macromolecules and hence in the number of hydrogen bonds between the adjacent oligoamide chains; as a result, the softening point decreases [16].

To confirm the incorporation of methionine into the oligomer and determine how methionine is bonded with the oligomer, we examined the chemical structure of polycondensation products formed in the system DFA–HMDA–methionine by IR and NMR spectroscopy. The expected amide structure was confirmed by the characteristic amide vibrations [1]. However, we revealed no specific shift of the absorption bands under the influence of intra- and intermolecular interactions caused by the introduction of the amino acid containing a heteroatomic substituent in the α-position. Furthermore, assignment of S–C bands is complicated by their weak intensity, and identification of this fragment by IR spectroscopy is impossible.

The NMR spectra furnish more information. They convincingly confirm the incorporation of the amino acid into the oligoamide; the methionine fragments were detected in different parts of the oligomer chain:

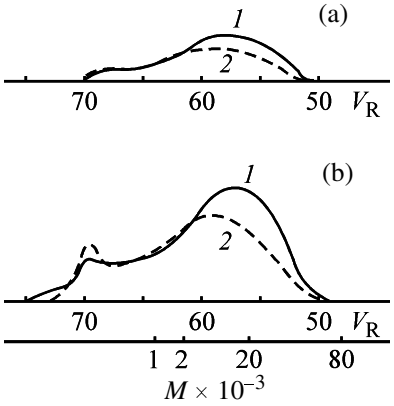
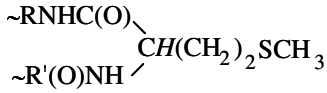
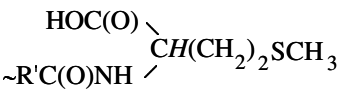


Fig. 2. Gel chromatograms [(a) refractometric and (b) UV detector] of oligoamide samples. DFA : HMDA : Met ratio in the reaction system: (*1*) 0.40 : 0.50 : 0.25 and (*2*) 0.40 : 0.50 : 0.50. (V_R) Relative retention volume and (M) molecular weight (polystyrene references).

both in the middle and on the ends. In the ^{1}H NMR spectrum, along with strong signals belonging to amide groups [1], we additionally detected signals of CH_3S protons at about 2.1 ppm, signals of the methine protons of the fragment



at 4.2 ppm, and signals at 4.6 ppm assignable to the methine protons of the fragment



.

At the same time, we detected no expected signals of the methine protons of the fragment ~RNHC(O)·$CH(NH_2)CH_2CH_2SCH_3$ at 3.1 ppm. These signals, however, may be obscured by strong signals of the $–CH_2C(O)NH–$ protons.

Examination of the molecular-weight distribution (MWD) of the compounds obtained involved certain problems due to low solubility in THF of higher-molecular-weight samples containing from 0.05 to 0.2 molar equivalent of methionine. It is known that oligo- and polyamides are resistant to the majority of solvents used and dissolve only in substances containing strongly polar groups [17]. Therefore, we determined the molecular-weight parameters only for products containing 0.25 (Table 1, sample no. 5) and 0.50 (sample no. 6) molar equivalent of methionine, which had lower molecular weight (Table 1) and higher solubility in THF. This fact confirms the previous data [17] that the solubility of oligo- and polyamides in common solvents can be increased by performing the synthesis in the presence of components containing a sulfur heteroatom.

The gel chromatograms of the reaction products obtained from DFA, HMDA, and methionine are shown in Fig. 2. It should be noted that calculation of the molecular weights from the polystyrene calibration

Table 2. Molecular parameters of sample nos. 5 and 6

Sample no.	Chemical method, M_n	GPC (refractometric detector)		
		$\overline{M}_n$	$\overline{M}_w$	$\overline{M}_w/\overline{M}_n$
5	2500	2000	7800	3.9
6	2200	1500	5400	3.6

does not give true molecular weights but allows adequate comparison of the MWDs of different samples of similar nature [18].

The chromatographic patterns show that the fractional composition of the samples obtained is nonuniform, with the prevalence of low-molecular-weight and oligomeric fractions; the MWD curves are essentially bimodal. The mean molecular weights M are $600 < M < 40\,000$ for sample no. 5 and $600 < M < 32\,000$ for sample no. 6.

The MWD data for methionine-containing oligoamides are given in Table 2.

A comparative analysis of the molecular weights of methionine-containing oligoamides shows that the number-average molecular weights obtained using various methods are in reasonable agreement. The GPC examination confirmes a decrease in M of the oligomer with an increase in the methionine content.

Methionine-modified oligoamides were used for the development of new thermoplastic adhesive formulations. Along with single-component hot-melt adhesives consisting of the base thermoplastic only, we tested a series of filled adhesives. Here we report the results obtained with wollastonite, one of the most promising fillers. Table 3 shows that introduction of wollastonite considerably expands the working temperature range of adhesive formulations, shortens the curing time, enhances the shear strength of the glue joint, and decreases the cost of the adhesive.

It should be noted that such an effect of wollastonite on the properties of adhesive formulations is determined by a characteristic needle-like shape of its crystals and by the specific chemical composition. Owing to the active surface of the particles, this filler is capable of hydrogen bonding with oligoamide molecules; an important factor is the dispersity of the wollastonite [19, 20]. Our results show that the best physicomechanical and processing characteristics are exhibited by filled hot-melt adhesives containing 20 or 50 wt % wollastonite; the strongest effect is attained with 50 wt % wollastonite WIC-10.

CONCLUSIONS

(1) Addition of methionine to the reaction mixture in the synthesis of oligoamides from dimerized fatty acid and hexamethylenediamine decelerates by a factor of 1.5, on the average, the polycondensation and formation of the final product.

(2) With an increase in the relative amount of methionine, the molecular weight of the product decreases by a factor of 1.2–2.3, and the softening point, by 5–29°C.

Table 3. Composition and properties of hot-melt adhesives based on methionine-modified oligoamide (DFA : HMDA : Met = 0.40 : 0.50 : 0.25)

Component, wt %		T_s	T_{appl}	Curing time, s	Shear strength (Al–Al), MPa
oligoamide	wollastonite	°C			
100	–	62	110–115	4	5.0
	FW-70:				
90	10	66	110–120	3	5.4
80	20	75	120–130	3	6.0
50	50	89	130–140	2	7.3
	FW-325:				
90	10	65	110–120	3	5.3
80	20	74	120–130	3	5.8
50	50	85	130–140	2	6.5
	WIC-10:				
90	10	69	115–120	3	5.6
80	20	78	125–135	3	7.2
50	50	89	140–145	2	8.0

(3) A series of wollastonite-filled thermoplastic adhesive formulations based on methionine-containing oligoamides were developed.

REFERENCES

1. Fomina, E.V., Chervyakova, G.N., Kurskii, Yu.A., and Sineokov, A.P., *Zh. Prikl. Khim.*, 2005, vol. 78, no. 7, pp. 1142–1145.
2. RF Patent 2 237 697.
3. FRG Patent Application 10 031 992.
4. *Condensation Monomers*, Stille, J.K. and Campbell, T.W., Eds., New York: Wiley–Interscience, 1972.
5. FRG Patent Application 4 408 276.
6. Fomina, E.V. and Batueva, L.I., Abstracts of Papers, *II Mezhdunarodnaya nauchno-tekhnicheskaya konferentsiya "Polimernye kompozitsionnye materialy i pokrytiya"* (II Int. Scientific and Technical Conf. "Polymeric Composite Materials and Coatings"), Yaroslavl, May 17–19, 2005, p. 38.
7. Fomina, E.V., Beloded, L.N., Kurskii, Yu.A., and Sineokov, A.P., Abstracts of Papers, *IX Mezhdunarodnaya konferentsiya po khimii i fizikokhimii oligomerov "Oligomery-2005"* (IX Int. Conf. on Chemistry and Physical Chemistry of Oligomers "Oligomers-2005"), Odessa, September 13–16, 2005, p. 78.
8. Ol'khovskaya, N.V., Maslova, I.P., Zvegintseva, G.B., et al., *Svoistva i primenenie metionina: Obzor* (Properties and Use of Methionine: Review), Moscow: NIITEKhIM, 1973. 27 s.
9. Besshaposhnikova, V.I., *Izv. Vyssh. Uchebn. Zaved., Khim. Khim. Tekhnol.*, 2005, vol. 48, no. 2, pp. 61–64.
10. Kovarskaya, B.M., Blyumenfel'd, A.B., and Levantovskaya, I.I., *Termicheskaya stabil'nost' geterotsepnykh polimerov* (Heat Resistance of Heterochain Polymers), Moscow: Khimiya, 1977.
11. JPN Patent 7 157 557.
12. WO Patent 97/40 116.
13. Neniţescu, C.D., *Chemie Organica*, Bucharest: Tehnica, 1960, vol. 2.
14. *Khimiya biologicheski aktivnykh prirodnykh soedinenii* (Chemistry of Biologically Active Natural Compounds), Moscow: Khimiya, 1970.
15. Toroptseva, A.M., Belogorodskaya, K.V., and Bondarenko, V.M., *Laboratornyi praktikum po khimii i tekhnologii vysokomolekulyarnykh soedinenii* (Laboratory Manual on Chemistry and Technology of Macromolecular Compounds), Leningrad: Khimiya, 1972.
16. Floyd, D.E., Poliamide Resins, *Reinhold Plastics Applications Ser.*, New York: Reinhold, 1958.
17. Hopff, H., Müller A.M., and Wenger, F., *Die Polyamide*, Berlin: Springer, 1954.
18. Styskin, E.L., Itsikson, L.B., and Braude, E.V., *Prakticheskaya vysokoeffektivnaya zhidkostnaya khromatografiya* (Practical High-Performance Liquid Chromatography), Moscow: Khimiya, 1986.
19. Fomina, E.V., Perevaryukha, M.A., and Safonova, N.N., *Klei. Germet. Tekhnol.*, 2006, no. 1, pp. 17–19.
20. Vakhtinskaya, T.N., Gurinovich, L.N., and Andreeva, T.I., *Plast. Massy*, 2004, no. 1, pp. 31–32.

ISSN 1070-4272. Russian Journal of Applied Chemistry, 2006, Vol. 79, No. 5, pp. 783–786. © Pleiades Publishing, Inc., 2006.
Original Russian Text © V.M. Chernyshev, A.V. Chernysheva, V.A. Taranushich, 2006, published in Zhurnal Prikladnoi Khimii, 2006, Vol. 79, No. 5, pp. 792–795.

ORGANIC SYNTHESIS AND INDUSTRIAL ORGANIC CHEMISTRY

Synthesis of Esters and Amides of 5-Amino-1,2,4-triazole-3-carboxylic and 5-Amino-1,2,4-triazol-3-ylacetic Acids

V. M. Chernyshev, A. V. Chernysheva, and V. A. Taranushich

South-Russian State Technical University, Novocherkassk, Rostov oblast, Russia

Received October 4, 2005

Abstract—Various synthetic routes to esters and amides of 5-amino-1,2,4-triazole-3-carboxylic and 5-amino-1,2,4-triazol-3-ylacetic acids were examined.

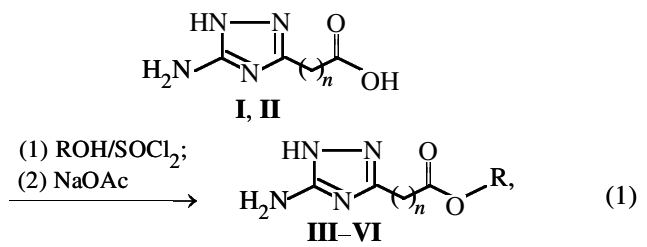
DOI: 10.1134/S1070427206050168

5-Amino-1,2,4-triazole-3-carboxylic (**I**) and 5-amino-1,2,4-triazol-3-ylacetic (**II**) acids and their esters and amides are valuable chemicals for the synthesis of drugs, herbicides [1–5], dyes [6–8], and high-energy-capacity compounds [9].

The goal of this study was the development of improved procedures for preparing esters and amides of acid **I** and **II**.

The above esters are most frequently prepared by esterification of acids **I** and **II** with alcohols in the presence of dry HCl [2, 4, 10, 11]. The reaction is reversible; therefore, its products are formed in moderate yields, and a large excess of anhydrous alcohol is required; to be reused, the alcohol should be dehydrated. The recently suggested [1] procedure for esterification of acid **I** with methanol in the presence of $SOCl_2$ (total yield of ester **III** 67%) eliminates this drawback; however, the reaction takes much time (24 h) and is performed at low temperature.

We found that methyl and ethyl esters **III**–**VI** can be prepared in good yields by esterification of acids **I** and **II** with alcohols in the presence of $SOCl_2$ with refluxing [reaction (1), see table]; in so doing, the synthesis time is as short as 4 h, and the spent alcohol can be repeatedly reused without preliminary dehydraion.

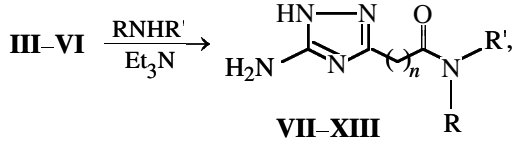


(1)

where n = 0 (**I**, **III**, **V**), 1 (**II**, **IV**, **VI**); R = Me (**III**, **IV**), Et (**V**, **VI**).

One of the simplest routes to amides of acids **I** and **II** might be the reaction of chlorides of these acids with amines. However, we failed to prepare the required acid chlorides. Refluxing of acids **I** and **II** with $SOCl_2$ or their heating with PCl_5 yielded an unseparable mixture of products, apparently because of side reactions such as self-acylation of amino group and nitrogen atoms of the triazole ring with the COCl group. Attempts to prepare the desired amides by the reaction of acids **I** and **II** with thionyl chloride and amines in pyridine at 0–100°C also failed.

The synthesis of amide of acid **I** by heating of ester **III** with aqueous ammonia was reported in [12]. However, we failed to prepare other amides by this procedure. The reactions of **III**–**VI** with amines in THF, performed by the procedure suggested previously [5] for preparing amides of 5-amino-4-alkyl-1,2,4-triazole-3-carboxylic acids, were very slow, probably because of the low solubility of the esters in THF. The best results were obtained when esters **III**–**VI** were heated with aliphatic amines in the presence of triethylamine at 85–90°C [reaction (2), see table]:



(2)

where n = 0 (**VII**, **IX**, **XI**, **XIII**), 1 (**VIII**, **X**, **XII**); NRR' = morpholine (**VII**, **VIII**), pyrrolidine (**IX**, **X**); R = Bn, R' = H (**XI**, **XII**; R = *i*-Pr, R' = H (**XIII**).

With less nucleophilic anilines containing various

Synthesis conditions, yields, and properties of **III–XVIII**

Compound no.	Yield, % (method)	mp, °C*	^{1}H NMR spectrum, δ, ppm	Found, %			Formula	Calculated, %		
				C	H	N		C	H	N
III	69	217–218**	4.00 s (3H, OCH_3), 6.00 s (2H, NH_2), 12.35 s (1H, NH)	33.7	4.2	39.4	$C_4H_6N_4O_2$	33.8	4.3	39.4
IV	55	164–165	3.40 s (2H, CH_2), 3.62 s (3H, OCH_3), 5.65 s (2H, NH_2), 11.58 s (1H, NH)	38.2	5.16	35.8	$C_5H_8N_4O_2$	38.5	5.16	35.9
V	70	242–243**	1.35 t (3H, CH_3), 4.23 q (2H, OCH_2), 6.00 s (2H, NH_2), 12.38 s (1H, NH)	38.6	5.2	36.0	$C_5H_8N_4O_2$	38.5	5.2	35.9
VI	68	156–158**	1.25 t (3H, CH_3), 3.40 s (2H, CH_2), 4.20 q (2H, OCH_2), 5.60 s (2H, NH_2), 11.56 s (1H, NH)	42.2	6.1	40.1	$C_6H_{10}N_4O_2$	42.4	5.9	39.9
VII	74 (a)	222–224	3.55 m (8H, $4CH_2$), 5.62 s (2H, NH_2), 11.52 s (1H, NH)	43.0	5.6	35.4	$C_7H_{11}N_5O_2$	42.6	5.6	35.5
VIII	54 (a)	240–242	3.58 m (10H, $5CH_2$), 5.62 s (2H, NH_2), 11.58 s (1H, NH)	45.8	6.1	33.4	$C_8H_{13}N_5O_2$	45.5	6.2	33.2
IX	84 (a)	284–286	1.90 m (4H, $2CH_2$), 3.47 m (2H, NCH_2), 3.82 m (2H, NCH_2), 5.80 s (2H, NH_2), 12.05 s (1H, NH)	46.4	6.2	38.4	$C_7H_{11}N_5O$	46.4	6.1	38.7
X	54 (a)	266–268	1.80 m (4H, $2CH_2$), 3.22 t (2H, NCH_2), 3.38 s (2H, CH_2), 3.49 t (2H, NCH_2), 5.83 s (2H, NH_2), 11.67 s (1H, NH)	49.0	6.8	36.0	$C_8H_{13}N_5O$	49.2	6.7	35.9
XI	78 (a)	236–238	4.42 d (2H, NCH_2), 5.89 s (2H, NH_2), 7.21 m (5H, arom.), 8.27 s (1H, NH), 12.33 s (1H, NH)	55.4	5.2	32.0	$C_{10}H_{11}N_5O$	55.3	5.1	32.2
XII	76 (a)	172–175	3.31 s (2H, CH_2), 4.26 d (2H, NCH_2), 5.87 s (2H, NH_2), 7.23 m (5H, arom.), 8.43 s (1H, NH), 11.58 s (1H, NH)	56.9	5.7	30.6	$C_{11}H_{13}N_5O$	57.1	5.7	30.3
XIII	61 (a)	247–250	1.16 m (6H, $2CH_3$), 4.03 m (1H, NCH), 5.71 s (2H, NH_2), 7.33 m (1H, NH), 12.31 s (1H, NH)	42.4	6.4	41.7	$C_6H_{11}N_5O$	42.6	6.6	41.4
XIV	58 (b)	235–237	6.01 s (2H, NH_2), 7.01 m (1H, arom.), 7.24 m (2H, arom.), 7.77 m (2H, arom.), 9.60 s (1H, NH), 12.41 s (1H, NH)	53.0	4.6	34.4	$C_9H_9N_5O$	53.2	4.5	34.5
XV	46 (b)	209–210	3.45 s (2H, CH_2), 5.83 s (2H, NH_2), 7.01 m (1H, arom.), 7.26 m (2H, arom.), 7.56 m (2H, arom.) 10.23 s (1H, NH), 11.72 s (1H, NH)	55.5	5.2	32.2	$C_{10}H_{11}N_5O$	55.3	5.1	32.2
XVI	74 (b)	280–282	6.00 s (2H, NH_2), 7.24 m (2H, arom.), 7.82 m (2H, arom.), 9.84 s (1H, NH), 12.41 s (1H, NH)	45.8	3.2	29.4	$C_9H_8N_5ClO$	45.5	3.4	29.5
XVII	51 (b)	221–223	3.45 s (2H, CH_2), 5.84 s (2H, NH_2), 7.33 m (2H, arom.), 7.60 m (2H, arom.), 10.26 s (1H, NH), 11.74 s (1H, NH)	47.7	4.1	28.1	$C_{10}H_{10}N_5ClO$	47.7	4.0	27.8

Table (Contd.)

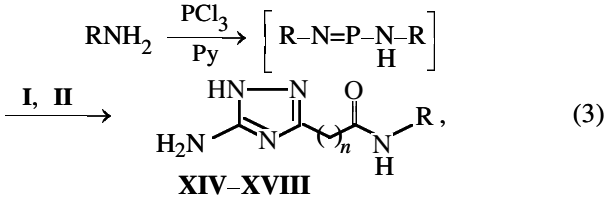
Compound no.	Yield, %	mp, °C*	^{1}H NMR spectrum, δ, ppm	Found, %			Formula	Calculated, %		
				C	H	N		C	H	N
XVIII	64 (b)	276–278	3.75 s (3H, OMe), 5.97 s (2H, NH_2), 6.81 m (2H, arom.), 7.66 m (2H, arom.), 9.48 s (1H, NH), 12.36 s (1H, NH)	51.2	4.7	29.7	$C_{10}H_{11}N_5O_2$	51.5	4.8	30.0

* Compounds **III** and **V** were recrystallized from H_2O; **IV**, **VI**–**X**, **XII**, **XIII**, and **XV**–**XVII**, from EtOH; and **XI**, **XIV**, and **XVIII**, from DMF.

** Published data, mp, °C: **III**, 220 [10]; **V**, 247 [11]; **VI**, 156–158 [3].

substituents in the benzene ring, the desired amides were not formed under the above conditions, and under more severe conditions (heating to 150°C without solvent or refluxing in DMF) an unseparable mixture of products was obtained.

We managed to prepare the anilides by treatment of anilines with PCl_3 followed by the reaction of the resulting organophosphorus compound, without its isolation, with acids **I** and **II**. By this procedure we prepared compounds **XIV**–**XVIII** [reaction (3), see table]:



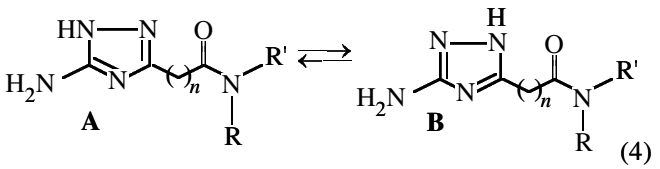
(3)

XIV–**XVIII**

where n = 0 (**XIV**, **XVI**, **XVIII**), 1 (**XV**, **XVII**); R = Ph (**XIV**, **XV**), *p*-ClC_6H_4 (**XVI**, **XVII**), *p*-$MeOC_6H_4$ (**XVIII**).

The compositions and structures of the compounds prepared were determined by elemental analysis, ^{1}H NMR spectroscopy, and mass spectrometry; their purity was confirmed by HPLC.

The compounds obtained exhibit prototropy and can exist in the form of tautomers **A** and **B** [equilibrium (4)]. According to ^{1}H NMR spectra, in DMSO tautomer **A** prevails [δ(NH_2) 5.6–6.0 ppm, see table]. Minor amounts of tautomer **B** were detected in the spectra of amides **VII**, **IX**, **X**, **XIV**, and **XVIII** (additional broadened singlet ot the amino group at 4.8–5.1 ppm). The chemical shifts of amino group protons in tautomers **A** and **B** are consistent with published data for other 3(5)-amino-1,2,4-triazoles [13].



(4)

The mass spectra of all the compounds prepared contain a strong peak of molecular ion.

EXPERIMENTAL

The ^{1}H NMR spectra were recorded on a Varian Unity 300 spectrometer (300 MHz, DMSO-d_6, internal reference TMS). The mass spectra were taken on a Finnigan MAT-Incos 50 device with direct sample inlet (electron impact, 70 eV). The melting points were determined with a PTP device. The HPLC analysis was performed with a Milikhrom-5 chromatograph equipped with a UV detector and an 80 × 2-mm column packed with Separon C_{18}; the mobile phase was methanol (flow rate 80 μl min^{-1}). The detection was performed at λ 210 nm.

Acids **I** and **II** were predried in a vacuum at 105–110°C for 24 h.

Esters of 5-amino-1,2,4-triazole-3-carboxylic (III, V) and 5-amino-1,2,4-triazol-3-ylacetic (IV, VI) acids. A 0.047-mol portion of $SOCl_2$ was added dropwise with stirring to a mixture of 0.047 mol of acid **I** or **II** and 0.4 mol of anhydrous methanol or ethanol. The mixture was heated to boil and refluxed for 1 h, after which an additional 0.047 mol of $SOCl_2$ was added, and the refluxing was continued for 3 h more. Excess alcohol was distilled off in a water-jet-pump vacuum, and a saturated solution of sodium acetate was added with cooling to the residue to pH 5–6. The precipitate thus obtained was filtered off, washed with water, and recrystallized.

Amides of 5-amino-1,2,4-triazole-3-carboxylic (VII, IX, XI, XIII, XIV, XVI, XVIII) and 5-amino-1,2,4-triazol-3-ylacetic (VIII, X, XII, XV, XVII) acids. (a) A mixture of 0.1 mol of ester **III**–**VI**, 0.02 mol of triethylamine, and 0.012 mol of aliphatic amine was heated at 85–90°C for 3 h (synthesis of **XIII** was performed in a sealed ampule), after which triethylamine and excess aliphatic amine were distilled

off in a vacuum, 2–3 ml of water was added to the residue, and the precipitate was filtered off and recrystallized.

(b) A 0.006-mol portion of PCl_3 was added with stirring and cooling to a mixture of 0.012 mol of appropriate aniline and 4 ml of pyridine. The mixture was stirred for 10 min at room temperature, after which 0.01 mol of acid **I** or **II** was added, the mixture was stirred for an additional 10 min at room temperature, heated to 110–120°C, kept at this temperature for 45 min, and diluted with 10 ml of H_2O. The precipitate thus formed was filtered off and recrystallized.

CONCLUSIONS

(1) It is advisable to prepare methyl and ethyl esters of 5-amino-1,2,4-triazole-3-carboxylic and 5-amino-1,2,4-triazol-3-ylacetic acids by esterification of the corresponding acids with alcohols in the presence of $SOCl_2$ with refluxing (yield 55–70%).

(2) It is advisable to prepare amides of 5-amino-1,2,4-triazole-3-carboxylic and 5-amino-1,2,4-triazol-3-ylacetic acids by the reactions of aliphatic amines with methyl or ethyl esters of the corresponding acids at 85–90°C in the presence of triethylamine (yield 54–84%) or by successive treatment of aromatic amines with PCl_3 and the corresponding acids in pyridine (the second step, at 110–120°C); yield 46–74%.

REFERENCES

1. Dżygiel, A., Rzeszotarska, B., Masiukiewicz, E., et al., *Chem. Pharm. Bull.*, 2004, vol. 52, no. 2, pp. 192–198.
2. Kofman, T.P., Uvarova, T.A., and Kartseva, G.Yu., *Zh. Org. Khim.*, 1995, vol. 31, no. 2, pp. 271–275.
3. Kiseleva, V.V., Gakh, A.A., and Fainzil'berg, A.A., *Izv. Akad. Nauk SSSR, Ser. Khim.*, 1990, no. 9, pp. 2075–2084.
4. Bos, B.G., Koopmans, M.J., and Huisman, H.O., *Recl. Trav. Chim. Pays-Bas*, 1960, vol. 79, no. 8, pp. 807–822.
5. US Patent 5021081.
6. US Patent 5541299.
7. US Patent 4051117.
8. US Patent 4039539.
9. Pevzner, M.S., *Ross. Khim. Zh.*, 1997, vol. 41, no. 2, pp. 73–83.
10. Chipen, G.I. and Grinshtein, V.Ya., *Izv. Akad. Nauk Latv. SSSR, Ser. Khim.*, 1965, no. 2, pp. 204–208.
11. Thiele, J. and Manchot, W., *Lieb. Ann.*, 1898, vol. 303, pp. 33–56.
12. USSR Inventor's Certificate no. 320497.
13. Reiter, J., Pongó, L., Somorai, T., and Dvortsák, P., *J. Heterocyclic Chem.*, 1986, vol. 23, no. 2, pp. 401–408.

ISSN 1070-4272. Russian Journal of Applied Chemistry, 2006, Vol. 79, No. 5, pp. 787–790. © Pleiades Publishing, Inc., 2006.
Original Russian Text © A.M. Magerramov, M.M. Kurbanova, R.T. Abdinbekova, I.A. Rzaeva, V.M. Farzaliev, M.A. Allakhverdiev, 2006, published in Zhurnal Prikladnoi Khimii, 2006, Vol. 79, No. 5, pp. 796–800.

ORGANIC SYNTHESIS AND INDUSTRIAL ORGANIC CHEMISTRY

Synthesis and Antioxidative Properties of Some 3,4-Dihydropyrimidin-2(1*H*)ones (-thiones)

A. M. Magerramov, M. M. Kurbanova, R. T. Abdinbekova, I. A. Rzaeva, V. M. Farzaliev, and M. A. Allakhverdiev

Baku State University, Baku, Azerbaijan

Received October 12, 2005; in final form, March 2006

Abstract—3,4-Dihydropyrimidinones (-thiones) were prepared by ternary condensation of various aromatic aldehydes with ethyl acetoacetate and urea (thiourea) in the presence of trichloroacetic acid in ethanol.

DOI: 10.1134/S107042720605017X

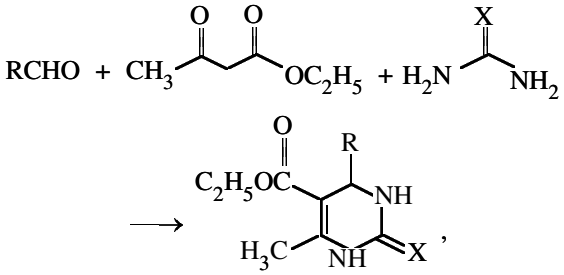
Dihydropyrimidinones attract growing interest due to their therapeutical and pharmacological activity [1]. Some functional derivatives of dihydropyrimidinones exhibit a broad spectrum of biological activity, including antiviral, antitumor, and antibacterial activity. Furthermore, 4-aryldihydropyrimidinones are powerful blockators of calcium channels and antihypertonic, α-adrenergic, and neuropeptide antagonists [2].

The simplest and direct route to dihydropyrimidinones, suggested for the first time by Biginelli and involving ternary condensation of an aldehyde, a β-keto ester, and urea, often gives the desired product in a low yield, especially with aliphatic aldehydes [3]. Higher yields can be obtained by performing the reaction in several steps, but in this case the process is not so simple as the one-step Biginelli reaction. Therefore, the Biginelli reaction continues to attract the attention of researchers looking for facile and efficient procedures for preparing dihydropyrimidinones.

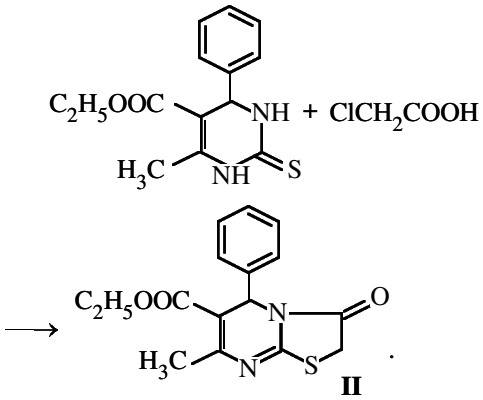
Somewhat improved procedures for preparing dihydropyrimidinones were reported in [4–6]. However, despite their potential significance, these methods are characterized by long reaction time, low selectivity, and problems with isolation of the products from the reaction mixture.

Thus, it is important to develop alternative one-pot procedures for preparing 3,4-dihydropyrimidin-2(1*H*)-ones.

Here we report on a new procedure for preparing 3,4-dihydropyrimidin-2(1*H*)-ones (-thiones) in the presence of trichloroacetic acid. We obtained 3,4-dihydropyrimidinones (-thiones) in high yield by the reaction of various aldehydes with ethyl acetoacetate and urea (thiourea) in the presence of CCl_3COOH as catalyst. The reaction required refluxing in ethanol for 2–4 h.



where X = O, R = CH_3 (**I**), 2-HO-5-BrC_6H_3 (**IV**), 1-naphthyl (**V**); X = S, R = 2-HOC_6H_4 (**III**);



II

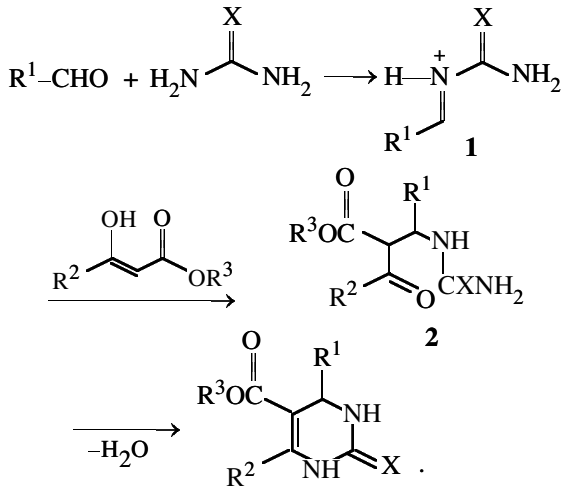
The reaction progress was monitored by TLC on Silufol UV-254 plates.

The suggested procedure ensures higher product yields (60–80%). The product can be readily isolated from the reaction mixture by filtration and washing with ethanol and water; recrystallization or chromatographic purification is not required.

Table 1. Physicochemical characteristics and spectral data for the compounds prepared

Compound no.	Yield, %	R_f	mp, °C	Found, %/Calculated, %				Empirical formula	IR spectrum, ν, cm^{-1}	^1H NMR spectrum, δ, ppm
				C	H	N	S			
I	65	0.72	194–196	54.50/54.54	7.02/7.07	14.22/14.14	–/–	$C_9H_{14}N_2O_3$	NH (3200) C=O (1648)	1.09 d (3H, CH_3), 1.28 t (3H, CH_3), 2.15 s (3H, CH_3), 3.86 d (2H, CH_2O), 4.06 s (1H, CH), 7.19 s (1H, NH), 8.97 s (1H, NH)
II	60	0.36	192–193	60.80/69.75	5.15/5.06	8.92/8.86	10.10/10.12	$C_{16}H_{16}N_2SO_3$	C=O (1630)	1.17 t (3H, CH_3), 2.35 s (3H, CH_3), 3.90 s (2H, CH_2S), 4.30 d (2H, CH_2O), 5.35 s (1H, CH), 7.50–7.70 s (5H, Ar)
III	80	0.54	215–216	57.65/57.53	5.51/5.47	9.62/9.58	10.87/10.95	$C_{14}H_{16}N_2O_3S$	NH (3225) C=O (1700)	1.30 t (3H, CH_3), 2.35 s (3H, CH_3), 4.36 d (2H, CH_2O), 4.90 s (1H, CH), 7.10–7.60 m (4H, Ar), 9.40 s (1H, NH), 9.75 s (1H, OH)
IV	75	0.27	190–191	49.59/49.55	4.50/4.42	8.27/8.25	–/–	$C_{14}H_5N_2O_4Br$	NH (3175) C=O (1635)	1.30 t (3H, CH_3), 2.57 s (3H, CH_3), 4.25 d (2H, CH_2O), 5.70 s (1H, CH), 7.00–7.70 m (4H, Ar), 8.00 s (1H, NH), 9.41 s (1H, NH), 10.4 s (1H, OH)
V	7	0.21	210–212	66.31	5.47	8.63	–	$C_{18}H_{18}N_2O_3$	NH (3250) C=O (1640)	1.21 t (3H, CH_3), 2.60 s (3H, CH_3), 4.42 d (2H, CH_2O), 5.60 (1H, CH), 8.10–9.75 m (7H, $C_{10}H_7$), 8.05 s (1H, NH), 9.91 s (1H, NH)

The mechanism of formation of dihydropyrimidinones (-thiones) was studied for a long time; the majority of researchers today agree with the following transformation sequence suggested by Kappe [7]:



First, protonated imine **1** is formed; it subsequently reacts with the enol form of the keto ester to give ureide **2**. This is followed by cyclization with the release of a water molecule.

The structures of the compounds were confirmed by IR, ^1H, and ^{13}C NMR spectroscopy.

The physicochemical characteristics and spectral properties of the compounds are given in Table 1.

To evaluate the antioxidative power of **I**–**V** in elementary steps of cumene oxidation, we studied the reactions of **I**–**V** with cumylperoxy radicals (CPRs) and cumyl hydroperoxide (CHP).

The capability of **I**–**V** to terminate oxidation chains by the reaction with CPRs was evaluated using as example the cumene oxidation at 60°C, initiated with azobis(isobutyronitrile) in a concentration of 2×10^{-2} M. We found that compounds **I**–**V** actively terminate oxidation chains by reacting with CPRs (Fig. 1).

From the duration of the induction period τ_{ind}, we calculated the stoichiometric coefficient of inhibition f, equal to the number of oxidation chains terminated on one inhibitor molecule and its transforma-

tion products:

$$f = \tau_{ind} W_i / [In]_0,$$

where W_i is the initiation rate and $[In]_0$ is the initial concentration of the inhibitor In.

From the kinetics of the oxygen uptake, we calculated the rate constants of the reactions of **I**–**V** with CPR, k_7 [8, 9]. To this end, the kinetic curves of the oxygen uptake $[O_2]$–τ were linearized in the coordinates $[O_2]^{-1}$–τ^{-1}, and k_7 was calculated from the line slope: $\tan\alpha = fk_7[In]_0/(k_2[RH]W_i)$ [9, 10], hence, $k_7 = (\tan\alpha)k_2[RH]W_1/(f[In]_0)$, where k_2 is the chain initiation rate [8, 9], equal to 1.51 l mol^{-1} s^{-1}, [RH] = 7.17 M.

The high antioxidative activity and the kinetic parameters of the reactions involving **I**–**V** were also confirmed in experiments on autooxidation of cumene at 110°C (Fig. 2).

Table 2 shows that the parameter f for **I**–**V** varies from 0.5 to 4.22, and the rate constants k_7 of the reactions of the inhibitors with CPR vary from 2.01×10^4 to 2.92×10^4 l mol^{-1} s^{-1}. The transformation products of **I**–**V** formed in the reactions with CPR also exhibit certain inhibiting effect; the oxidation rate after the induction period is somewhat lower than in the uninhibited oxidation (Fig. 1).

The reactions of **I**–**V** with CHP were performed in chlorobenzene in a nitrogen atmosphere at 110°C. All these compounds decompose CHP. The kinetic curves of CHP decomposition under the action of **I**–**V** (the curve obtained with **I** is shown as example in Fig. 3) are S-shaped, which is characteristic of an autocatalytic process. The reaction has a certain induction period in which the CHP consumption is insignificant; this is followed by its catalytic decomposition, and then, as the CHP is consumed, the reaction rate decreases.

Apparently, the inhibitor first reacts with CHP, and the resulting transformation product catalytically decomposes CHP. To determine the reaction stoichiometry, CHP was taken in excess.

The catalytic factor ν is the number of CHP molecules decomposed by one inhibitor molecule; it was calculated as $\nu = ([ROOH]_0 - [ROOH]_\infty)/[In]_0$, where $[ROOH]_0$ and $[ROOH]_\infty$ are, respectively, the initial and final concentrations of CHP, and $[In]_0$ is the initial inhibitor concentration.

Our experiments showed that one molecule of **I**–**V** can decompose up to several ten thousands of CHP molecules. Presumably, compounds **I**–**V** exert a combined inhibiting effect, terminating the oxidation chains in the reaction with CHP and catalytically decomposing CHP.

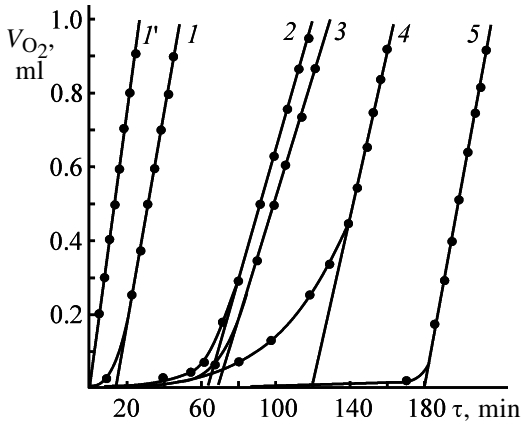


Fig. 1. Kinetic curves of initiated oxidation of cumene in the presence of **I**–**V** (curves *1*–*5*, respectively). 60°C; [AIBN] = 2×10^{-2} M. (V_{O_2}) Oxygen volume and (τ) time; the same for Fig. 2. [InH], M: (*1*') 0 and (*1*–*5*) 5×10^{-5}; the same for Fig. 2.

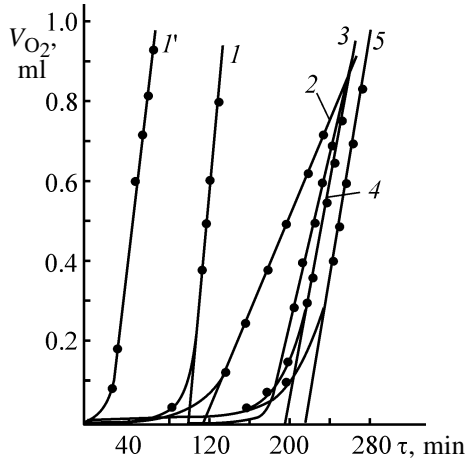


Fig. 2. Kinetic curves of cumene autooxidation in the presence of **I**–**V** (curves *1*–*5*, respectively) at 110°C.

EXPERIMENTAL

The ^{1}H and ^{13}C NMR spectra were recorded on a Bruker-300 NMR spectrometer (300 MHz for ^{1}H), and the IR spectra, on a Specord 75-R spectrometer (mulls in mineral oil). To check the purity of the compounds prepared and monitor the reaction progress, we used TLC on Silufol UV-254 plates (eluent isopropyl alcohol–hexane, 1 : 1).

3,4-Dihydropyrimidin-2(1*H*)-ones (-thiones). A round-bottomed flask equipped with a reflux condenser and a power-driven stirrer was charged with appropriate aldehyde (1.25 mol), ethyl acetoacetate (1.90 mol), urea or thiourea (1.25 mol), CCl_3COOH

Table 2. Kinetic parameters of the reactions of **I**–**V** with cumylperoxy radicals (k_7, f, 60°C, [AIBN] = 2×10^{-2} M) and of the decomposition of cumyl hydroperoxide (k, ν, 110°C)

Compound	T = 60°C		T = 110°C			
	f	$k_7 \times 10^{-4}$, l mol^{-1} s^{-1}	k, l mol^{-1} s^{-1}	ν	$[In]_0$, M	τ, min
I	0.5	2.01	11	20000	5×10^{-5}	100
II	1.54	2.3	33	27000	5×10^{-5}	120
III	1.68	2.92	18.5	22000	5×10^{-5}	180
IV	2.88	2.4	20.8	25000	5×10^{-5}	200
V	4.32	2.85	16.6	30000	5×10^{-5}	220

(25 mg), and 95% ethanol (10 ml). The mixture was stirred for 2–4 h. The reaction progress was monitored by TLC. After the reaction completion, the mixture was cooled to room temperature, and the crystalline product was filtered off, washed with ethanol, dried, and recrystallized from aqueous ethanol (1 : 3).

Cumyl hydroperoxide was purified [10] and then distilled.

Chlorobenzene and cumene were purified by a common procedure based on sulfonation of impurities with concentrated sulfuric acid [11, 12]. The CHP concentration was determined by iodometric titration [10] of samples taken at regular intervals.

Experiments on CHP decomposition were performed in chlorobenzene at 110°C in a glass bubbler in an inert gas atmosphere; the CHP concentration was varied in the range 0.16–0.64 M, and the concentrations of **I**–**V**, in the range $(1–5) \times 10^{-4}$ M.

Experiments on the initiated oxidation of cumene were performed on a manometric unit [12]. As initiator we used AIBN (initiation rate 1×10^{-5} l mol^{-1} s^{-1} at 60°C [13]; initiator concentration 2×10^{-2} M in all the experiments). The concentrations of **I**–**V** were $(1–5) \times 10^{-4}$ M.

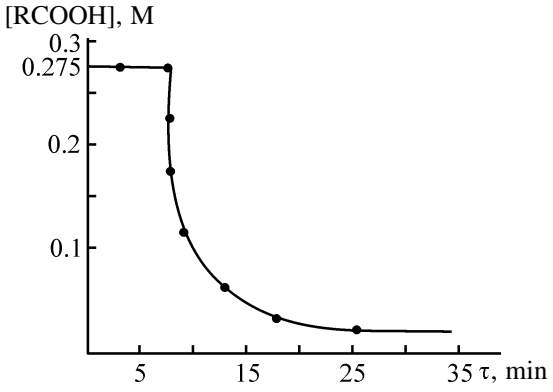


Fig. 3. Kinetic curve of CHP decomposition in the presence of **I**. 110°C; $[In]_0 = 1 \times 10^{-4}$ and $[CHP]_0 = 0.275$ M. (τ) Time.

CONCLUSION

3,4-Dihydropyrimidinones (-thiones) exhibiting high antioxidative power were prepared by ternary condensation.

REFERENCES

1. Kappe, C.O., *Tetrahedron*, 1993, vol. 49, pp. 6937–6963.
2. Rovnyak, G.C., Atwal, K.S., Hedberg, A., et al., *J. Med. Chem.*, 1992, vol. 35, pp. 3254–3263.
3. Wipf, P. and Cunningham, A., *Tetrahedron Lett.*, 1995, vol. 36, pp. 7819–7822.
4. Big, F., Carloni, S., Frullanti, B., et al., *Tetrahedron Lett.*, 1999, vol. 40, pp. 3465–3473.
5. Lu, J. and Ma, H., *Synlett.*, 2000, pp. 63–64.
6. Yadav, J.S., Subba Reddy, B.V., Jagan Reddy, E., and Ramalingam, T.J., *Chem. Res.*, 2000, pp. 354–359.
7. Kappe, C.O., *J. Org. Chem.*, 1997, vol. 62, pp. 7201–7204.
8. Emanuel', N.M., Denisov, E.T., and Maizus, Z.K., *Tsepnye reaktsii okisleniya uglevodorodov v zhidkoi faze* (Chain Reactions of Liquid-Phase Oxidation of Hydrocarbons), Moscow: Nauka, 1965.
9. Emanuel', N.M. and Denisov, E.T., *Neftekhimiya*, 1976, vol. 16, no. 313, pp. 366–368.
10. Karnojitzki, V., *Les peroxides organiques*, Paris: Hermann, 1958.
11. *Organic Solvents. Physical Properties and Methods of Purification*, Weissberger, A., Proskauer, E.S., Riddick, J.A., and Toops, E.E., Eds., New York: Interscience, 1955.
12. Emanuel', N.M., Gladyshev, G.P., and Denisov, E.T., Regulations on Testing Chemical Compounds as Stabilizers of Polymeric Materials, *Preprint of the Inst. of Chemical Physics, USSR Acad. Sci.*, Chernogolovka, 1976.
13. Denisov, E.T., *Konstanty skorosti gomoliticheskikh zhidkofaznykh reaktsii* (Rate Constants of Homolytic Liquid-Phase Reactions), Moscow: Nauka, 1971.

ISSN 1070-4272. Russian Journal of Applied Chemistry, 2006, Vol. 79, No. 5, pp. 791–798. © Pleiades Publishing, Inc., 2006.
Original Russian Text © O.N. Zabelina, V.E. Kirichenko, M.G. Pervova, Yu.G. Yaltuk, V.I. Saloutin, 2006, published in Zhurnal Prikladnoi Khimii, 2006, Vol. 79, No. 5, pp. 801–808.

ORGANIC SYNTHESIS AND INDUSTRIAL ORGANIC CHEMISTRY

Products of the Reaction of Polychlorinated Biphenyls with Ethanol and Potassium Hydroxide in Dimethyl Sulfoxide

O. N. Zabelina, V. E. Kirichenko, M. G. Pervova, Yu. G. Yaltuk, and V. I. Saloutin

Institute of Organic Synthesis, Ural Division, Russian Academy of Sciences, Yekaterinburg, Russia

Received October 29, 2005

Abstract—The reaction of a technical mixture of polychlorinated biphenyls with ethanol and potassium hydroxide in dimethyl sulfoxide was studied. The composition of the products formed in the process was determined by gas chromatography and gas chromatography–mass spectrometry.

DOI: 10.1134/S1070427206050181

Polychlorinated biphenyls (PCBs) are persistent global environmental pollutants [1, 2]. The search for methods of their safe destruction or conservation is under way now worldwide. Also, PCBs can be processed into useful materials [2, 3]. We showed previously [4, 5] that PCBs readily react with sodium alkoxides in polar solvents, forming a mixture of products whose composition depends on the structure of the alcohol and the reaction conditions. A possible way of utilization of PCBs is to convert them to hydroxy and alkoxy derivatives to be further introduced into polymer compounds.

In this study we examined reactions of congeners of PCBs from the Sovol technical mixture with ethanol and potassium hydroxide in a polar solvent and sought for conditions ensuring the deepest conversion. Of primary importance is identification of the reaction products, which can be done by gas chromatography–mass spectrometry (GC–MS) only. This study is also of scientific importance, since nucleophilic substitution reactions in the PCB series are virtually not studied.

EXPERIMENTAL

The reaction mixtures were analyzed on a Shimadzu GC-17A gas chromatograph with a flame-ionization detector (FID), an MDN quartz capillary column (an analog of HP-5; length 30 m, inner diameter 0.25 mm, stationary phase film thickness 0.25 μm). Carrier gas nitrogen, flow split ratio 1 : 30. Column temperature: initial 100°C (1 min isotherm), programmed heating at a rate of 10 deg min^{-1} to 200°C and further at a rate of 2 deg min^{-1} to 300°C. Vaporizer temperature 250°C; detector temperature 280°C.

The mass-spectrometric analysis was carried out on a Fisons MD 800 instrument at the electron energy of 70 eV, scanning rate of 1 spectrum per second, recording of the total ion current in the range of m/z 30–400. We used an HP-5 quartz capillary column (length 25 m, inner diameter 0.25 mm, stationary phase film thickness 0.25 μm). Carrier gas helium, flow split ratio 1:20. Column temperature: initial 60°C (3 min isotherm), programmed heating at a rate of 10 deg min^{-1} to 200°C and further at a rate of 2 deg min^{-1} to 280°C. Vaporizer temperature 250°C.

We used a Sovol technical mixture comprising ca. 20% tetrachlorobiphenyls, over 50% pentachlorobiphenyls, ca. 20% hexachlorobiphenyls, and also minor amounts of trichloro- and heptachlorobiphenyls. Previously [6], we identified the major congeners of PCBs in the mixture, which were numbered in accordance with IUPAC recommendations.

The reaction of the PCB mixture with ethanol and KOH in dimethyl sulfoxide (DMSO) was carried out as follows. A round-bottomed flask equipped with a stirrer and a thermometer was charged with a solution of 5.6 g of KOH (0.1 M) in 11.5 ml (0.2 M) of ethanol, 23 ml of DMSO, and 0.05 g of biphenyl as internal reference. The resulting mixture was heated to 130°C until the components dissolved. Then a solution of 8.2 g (0.025 M) of the PCB mixture in 13 ml in DMSO was added into the mixture. The temperature was raised to 150°C and kept constant for a certain period, whereupon the mixture was cooled. Then 50 ml of water, 2 ml of HCl(conc.), and 20 ml of

chloroform were added. The mixture was shaken and transferred into a separatory funnel. The organic layer was separated and dried over anhydrous Na_2SO_4; chloroform was distilled off. We prepared a solution of the reaction product with a concentration of 10 mg ml^{-1} in toluene with tridecane as internal reference in a concentration of 1 mg ml^{-1}, and analyzed the resulting solution by GC with FID (GC–FID).

The reaction progress was monitored in time. The samples were taken just after the PCB mixture was introduced into DMSO at 130°C, after heating to 140°C (15 min), and then every 20 min during 2 h at 150°C. The samples were treated by the following procedure: A 10-ml volumetric flask was charged with 0.5 ml of the reaction mixture, after which 1 ml of water and 5 ml of toluene with the internal reference (tridecane in a concentration of 1 mg ml^{-1}) were added. The resulting mixture was acidified with 0.1 ml of HCl(conc.) and shaken, which was followed by GC–FID analysis of the organic layer after the phase separation.

Then 1 ml of the organic layer was taken, additionally treated with 5 ml of a 1% NaOH solution, and analyzed. Upon this treatment, the hydroxy derivatives of PCBs pass into the alkaline solution, whereas the ethoxy derivatives of PCBs and the initial unchanged PCBs remain in the organic phase.

Formation of hydroxy derivatives of PCBs was additionally confirmed by acylation of the toluene solution with trifluoroacetic anhydride. To this end, 1 ml of the solution was placed into a 10-ml volumetric test tube, 0.02 ml of trifluoroacetic anhydride and 0.005 ml of pyridine were added, and the resulting mixture was kept for 20 min. Then 5 ml of saturated $NaHCO_3$ solution was added, and the mixture was shaken. After the phase separation, the organic layer was analyzed by GC–FID.

The amounts and relative contents of the reaction mixture components were determined relative to the internal reference, biphenyl, and the accuracy of preparation of the solutions analyzed and the stability of operation of the GC system were checked with tridecane as reference.

We showed previously [5] that treatment of the Sovol PCB mixture with sodium ethoxide in the presence of ethanol with DMSO yields monoethoxy derivatives of tri- and tetrachlorobiphenyls, mono- and diethoxy derivatives of pentachlorobiphenyls, and di- and triethoxy derivatives of hexachlorobiphenyls.

In this study, we used a mixture of KOH and ethanol in DMSO as reagent in order to examine the possibility of formation of ethoxy and hydroxy derivatives of PCBs. We carried out a series of experiments with varying the reactant ratio, temperature, and treatment time. The reaction products were analyzed by GC–FID. By so doing, we determined the conditions providing the maximal conversion of the initial PCBs. The molar ratio of the reactants, PCBs : KOH : ethanol, was 1 : 4 : 8; the reaction temperature, 150°C; and the treatment time, up to 120 min.

The reaction products contained certain amounts of unchanged tri- and tetrachlorobiphenyls and no penta- and hexachlorobiphenyls. The chromatographic pattern is much more complex than in the case of ethoxylation [5]. After treating the solution of the reaction products with a NaOH solution, the chromatogram gets simpler; some peaks disappear, and the chromatogram resembles that of ethoxy derivatives. Acylation also causes the chromatographic pattern to change; some peaks are shifted in time. All these facts suggest that the resulting derivatives are ethoxy and hydroxy derivatives of PCBs.

Our study followed the procedure described in Experimental, with sampling. The substitution of the chlorine atoms by ethoxy groups occurs already when the PCB mixture is introduced into a solution of ethanol and KOH in DMSO at 130°C. The chromatogram of the sample taken just after mixing the reactants substantially differs from the initial chromatogram of the PCB mixture. Peaks of tri- and tetrachlorobiphenyls are recorded; their total relative area decreased by 20% compared to that of the initial mixture. The total area of the peaks of pentachlorobiphenyls decreased by 80%, and the peaks of hexachlorobiphenyls fully disappeared.

The GC–MS data showed that, at this moment, the reaction mixture contained the following derivatives: monoethoxytrichlorobiphenyls **2**, monoethoxytetrachlorobiphenyls **4**, diethoxytrichlorobiphenyls **5**, and diethoxytetrachlorobiphenyls **8** (see table). The major transformation products that can be chromatographically detected at this moment are derivatives **4**, products of substitution of one chlorine atom in pentachlorobiphenyls. We never detected monoethoxypentachlorobiphenyls **7**. After treating the extract with a NaOH solution, the chromatographic pattern remained unchanged, all the peaks were recorded; the content of the components remained unchanged. Thus, the first stage of the reaction yields ethoxy derivatives of PCBs only.

After heating the mixture for 15 min (140°C), we obtained a different chromatogram. There were peaks of tri- (PCBs 28, 33, 22) and tetrachlorobiphenyls

Estimation of the relative content of the reaction products of PCBs with ethanol and KOH in DMSO from the base peak areas

Compound	Formula	Molecular ion	Base peaks	Content of indicated derivative	Total content of derivatives
				%	
PCB-3	$C_{12}H_7Cl_3$	256–260	256	0.3	1.2
PCB-4	$C_{12}H_6Cl_4$	290–294	220	0.9	
1	$C_{12}H_7Cl_2OC_2H_5$	266–270	238, 168	1.8	1.8
2	$C_{12}H_6Cl_3OC_2H_5$	300–304	272, 202	12.4	24.7
2-1	$C_{12}H_6Cl_3OH$	272–276	272, 202	4.4	
3	$C_{12}H_6Cl_2(OC_2H_5)_2$	310–314	254, 218	7.9	
4	$C_{12}H_5Cl_4OC_2H_5$	334–338	308, 236	1.8	61.2
4-1	$C_{12}H_5Cl_4OH$	306–310	308, 236	25.8	
5	$C_{12}H_5Cl_3(OC_2H_5)_2$	344–348	316, 288	9.2	
5-1	$C_{12}H_5Cl_3(OC_2H_5)OH$	316–320	316, 288	15.0	
6	$C_{12}H_5Cl_2(OC_2H_5)_3$	354–358	270, 234	7.1	
6-1	$C_{12}H_5Cl_2(OC_2H_5)_2OH$	326–328	270, 234	2.3	
8	$C_{12}H_4Cl_4(OC_2H_5)_2$	378–382	324	1.2	10.8
8-1	$C_{12}H_4Cl_4(OC_2H_5)OH$	350–354	324	6.7	
8-2	$C_{12}H_4Cl_4(OH)_2$	322–326	324	0.9	
9	$C_{12}H_4Cl_3(OC_2H_5)_3$	388–392	304	0.9	
9-1	$C_{12}H_4Cl_3(OC_2H_5)_2OH$	360–364	304	1.1	

(PCBs 52, 49, 44) only; the content of these PCBs in the reaction mixture decreased twofold. The relative area of the PCB peaks was 6%. There were no peaks corresponding to other initial PCBs.

The reaction mixture contained derivatives of tetrachlorobiphenyls (monoethoxytrichlorobiphenyls **2** and diethoxydichlorobiphenyls **3**, with **2** dominating), pentachlorobiphenyls [monoethoxytetrachlorobiphenyls **4**, diethoxytrichlorobiphenyls **5** (dominated, 25% of the total mass), and triethoxydichlorobiphenyls **6**], and hexachlorobiphenyls (diethoxytetrachlorobiphenyls **8**, triethoxytrichlorobiphenyls **9**). Hydroxy derivatives of PCBs were manifested both as individual, fairly intense, peaks, and in the peaks of coeluted compounds. This is suggested by the results obtained after treating the reaction mixture with a NaOH solution. In the GC–FID pattern of the toluene extract, some peaks disappear, and some of them decrease in intensity. The relative decrease in intensity of the sum of the PCBs and derivatives was estimated at 25%.

The chromatogram recorded 35 min after the beginning of the reaction (150°C) also substantially differs from that of the previous one. There are peaks that can be assigned to monoethoxydichlorobiphenyls **1**, derivatives of trichlorobiphenyls. Peaks **2**, which are preserved until the end of the experiment, increased in intensity, as well as a number of peaks of compounds **5** and **8** and peaks of monohydroxytetrachlorobiphenyls **4-1**. Thus, the chromatographic pattern suggests that transformations of less reactive tri- and tetrachlorobiphenyls are still under way and the initially formed derivatives undergo further transformations (both alcoholysis and elimination of the ethyl cation).

The chromatogram of the reaction mixture recorded 55 min after the beginning of the reaction also differs from those observed for the previous samples, but many peaks with identical retention times are preserved. The chromatogram is very complex; there is a large number of overlapping weak peaks. It should be noted that, since this moment, the general chromatographic pattern of the reaction mixture samples remains unchanged until the end of the experiment, with only the relative intensity of the peaks changing.

We gave special attention to studying the composition of the reaction mixture at the end of the process (125 min after the beginning of the reaction). A GC–FID analysis revealed the presence of <2% trichlorobiphenyls and tetrachlorobiphenyls in total. Treatment of the mixture with a NaOH solution showed that the content of the hydroxy derivatives exceeded that of the ethoxy derivatives in the mixture. In this case, we determined the composition of the reaction mixture by GC–MS. It should be noted that the chromatograms obtained on different instruments were not identical, with a better peak resolution characteristic of the GC–FID method. However, processing of the chro-

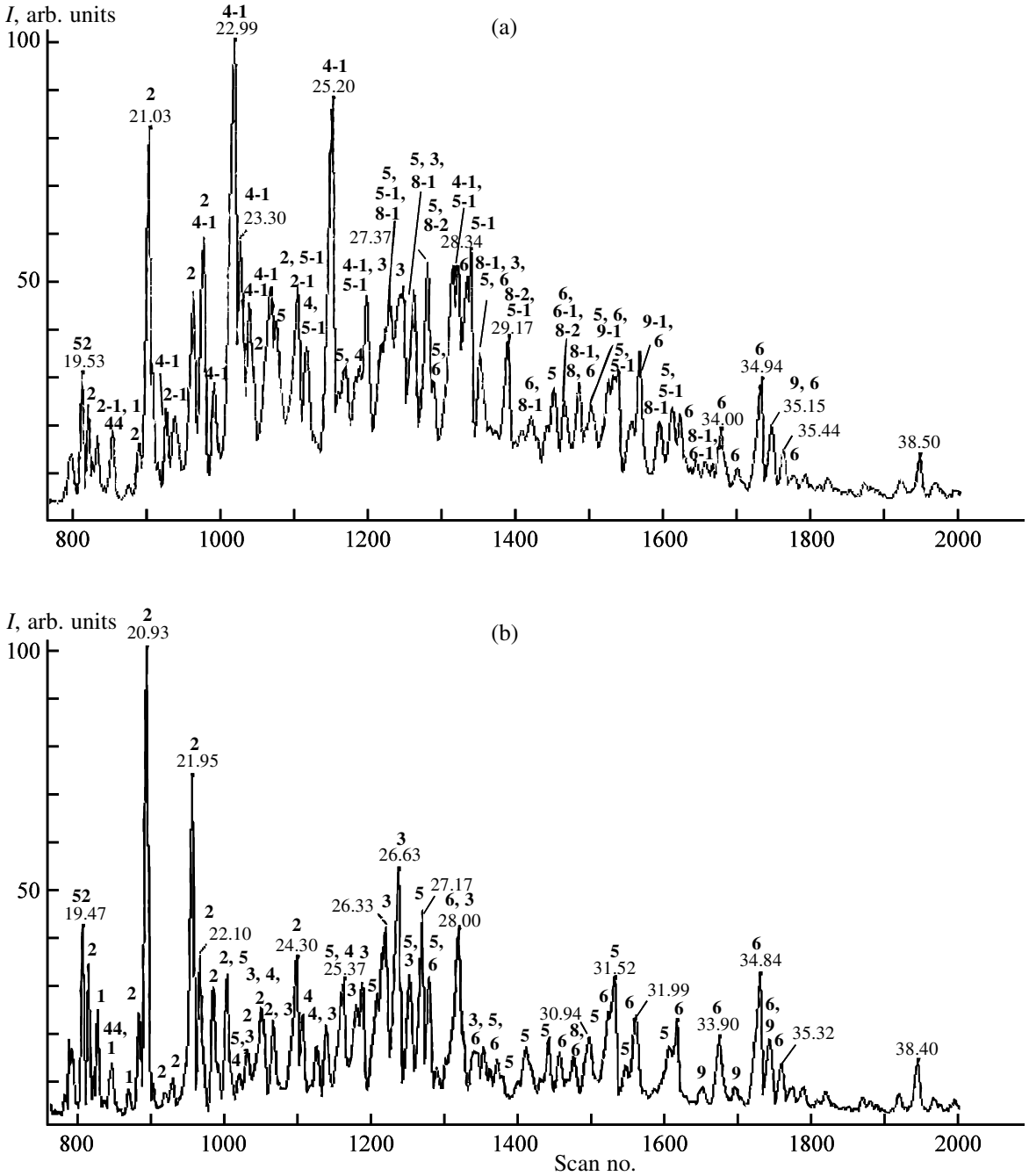


Fig. 1. GC–MS patterns of the products of alcoholysis of the PCB mixture with alcoholic alkali in DMSO. Reaction product (a) untreated and (b) treated with a NaOH solution.

matograms obtained by GC–MS involved reconstruction based on selective ions corresponding to certain types of derivatives, which enabled identification of individual compounds in coelution. We studied the compositions of the reaction mixture extract and the extract after treatment with a NaOH solution. Figures 1a and 1b show the chromatograms of the PCB reaction products. In the latter case, the chromatograms become somewhat simpler; only peaks of the initial PCBs and ethoxy derivatives of PCBs are recorded.

We identified five monoethoxydichlorobiphenyls **1**, whose relative content slowly grew throughout the keeping time.

We identified 14 monoethoxytrichlorobiphenyls **2**; two peaks have a high intensity and individual composition. They are prominent even in the first sample

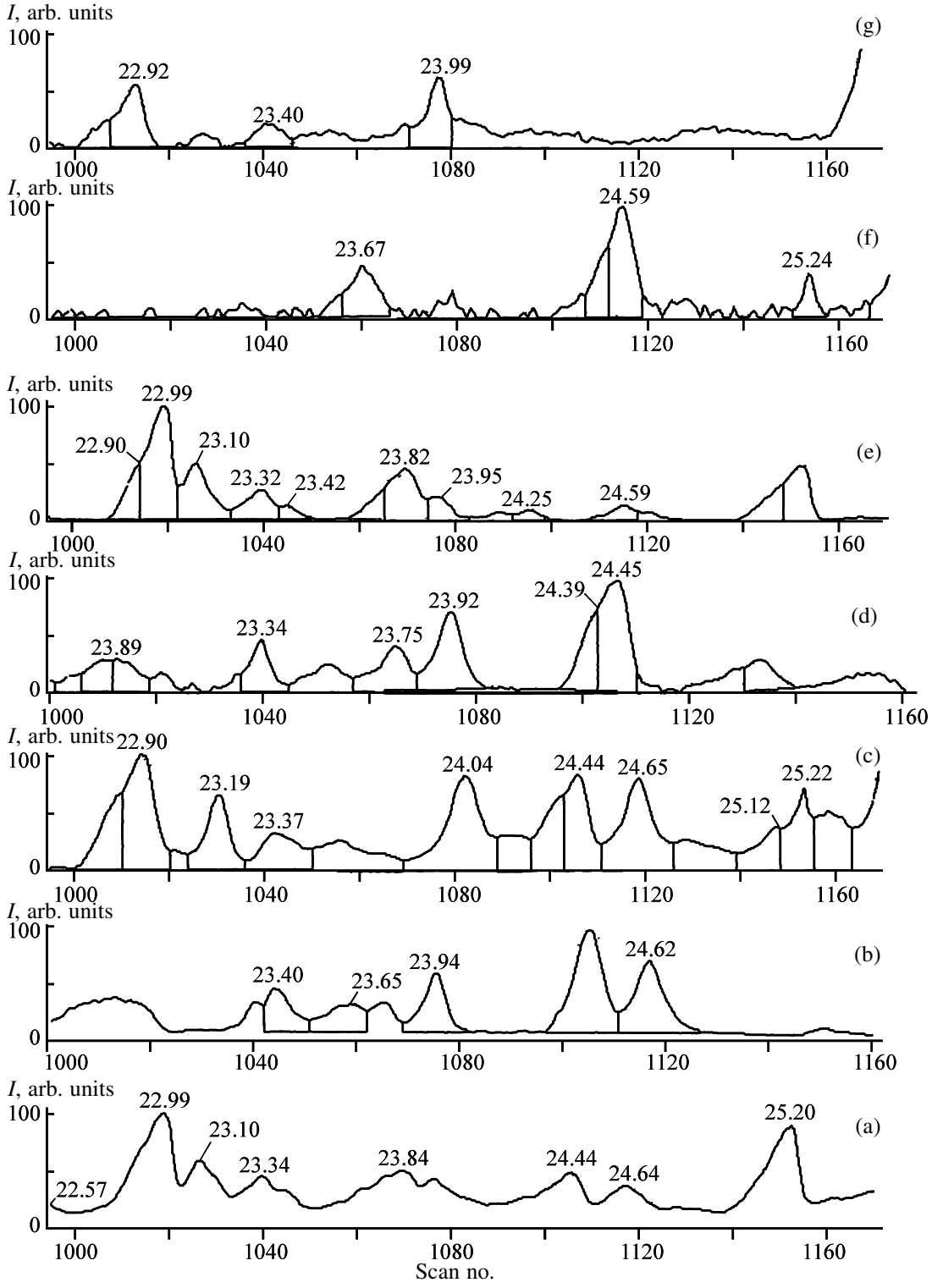


Fig. 2. Processing of the chromatogram of the reaction products: (a) total ion current; *m*/*z*: (b) 202 (**2, 2-1**), (c) 288 (**5, 5-1**), (d) 300 (**2**), (e) 308 (**4, 4-1**), (f) 336 (**4**), and (g) 344 (**5**).

and grow in intensity as the reaction goes; seven medium-intensity peaks are clearly recorded, of which four are individual peaks. We identified 16 diethoxydichlorobiphenyls **3**; six peaks among those corresponding to these compounds are attributed to individual compounds. Comparison of the total areas of the peaks belonging to molecular or base ions of mono- and diethoxy derivatives obtained from tetrachlorobi-

phenyls suggests that the amount of diethoxydichlorobiphenyls **3** is approximately half that of monoethoxytrichlorobiphenyls **2**. In the GC–MS pattern of the reaction mixture extract, many peaks are obscured by intense peaks of hydroxy derivatives of PCBs.

The mixture contains only trace amounts of ethoxytetrachlorobiphenyls **4** (no more than five compounds), and only one peak corresponds to an individual derivative. As already mentioned, these products were recorded just after mixing the reactants, whereupon they rapidly underwent further transformations.

Diethoxytrichlorobiphenyls **5** and triethoxydichlorobiphenyls **6** are present in the mixture in almost identical amounts. The chromatogram contains 17 and 13 low- and medium-intensity peaks belonging to such derivatives, respectively. About one-third of the peaks belong to individual compounds, and the remaining peaks, to mixtures. The relative content of the ethoxy derivatives of pentachlorobiphenyls is slightly lower than that of the derivatives of tetrachlorobiphenyls. More reactive diethoxytrichlorobiphenyls **5** underwent further transformations.

In the reaction mixture analyzed we detected only minimal amounts of diethoxytetrachloro- (**8**, six compounds) and triethoxytrichlorobiphenyls (**9**, three compounds) derivatives of hexachlorobiphenyls.

As already mentioned, the chromatogram of the reaction mixture extract is much more complex, with most peaks belonging to mixtures of products (Fig. 1a). We considered the mass spectrum of each peak, and the chromatograms were reconstructed using molecular ions and ions characteristic for a certain type of products. The relative content was estimated from the areas of the peaks of the base ions. For each compound we took only one base ion. Figure 2 shows as example the processing of a part of the chromatogram. Table presents the structures of the compounds considered, the characteristic ions, and the results of the calculations.

We identified at least seven peaks (three with a noticeable intensity) whose spectra corresponded to hydroxytrichlorobiphenyls **2-1**; their content was 30% of that of compounds **2**.

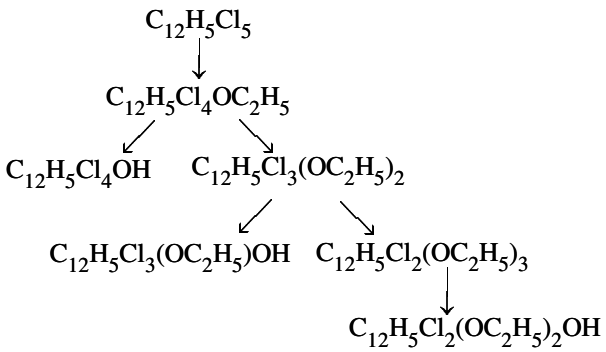
Derivatives **3** are stable under the reaction conditions; we recorded no compounds with the structure $C_{12}H_6Cl_2(OC_2H_5)OH$.

The products were the most abundant in the case of the reaction of pentachlorobiphenyls; they initially gave very rapidly ethoxytetrachlorobiphenyls **4**, which further transformed into hydroxy derivatives. Hydroxytetrachlorobiphenyls **4-1** (a total of 16 compounds) had the maximal content in the reaction mixture.

In this study, we observed for the first time formation of hydroxyethoxytrichlorobiphenyls **5-1** (15 compounds) and hydroxydiethoxydichlorobiphenyls **6-1** (4 compounds). As suggested by redistribution of the peak intensities, derivatives **5-1** are formed from diethoxytrichlorobiphenyls, and derivatives **6-1**, from triethoxydichlorobiphenyls. It should be noted that the content of compounds **5-1** exceeds that of **5**, and the content of compounds **6-1** was estimated at ca. 30% of that of **6**. Thus, the three chlorine atoms in the molecule of **5** favor substitution, and two chlorine atoms are insufficient for such a reaction. Moreover, ethoxy groups themselves exhibit an electron-donating power.

As to derivatives of hexachlorobiphenyls, the content of individual components in the reaction mixture is fairly low. We detected only three peaks corresponding to derivative **8-1** as the main component. Reconstruction of the mass chromatograms based on the characteristic ions revealed a total of 14 peaks corresponding to the structure of **8-1** and three peaks corresponding to the structure of **8-2** at trace level. Also, we identified six compounds with the structure of **9-1** in low concentrations.

Our data suggest the occurrence of a series of successive reactions proceeding at different rates and yielding different sets of final products, depending on the structure of the initial PCB congener. The first stage of the reaction consists in substitution of a chlorine atom by an ethoxy group, and hydroxy derivatives are formed specifically from ethoxy derivatives of PCBs. Given below is an example of transformations for pentachlorobiphenyls:



These conclusions are consistent with the results obtained by Shein and Ignatov [7, 8] in studies of the reaction of 1,2,4,5-tetrachlorobenzene with sodium methylate in anhydrous or aqueous methanol. A kinetic study showed that 2,4,5-trichloroanisole is initially formed; it further reacts with sodium methylate or NaOH to form 2,4,5-trichlorophenol.

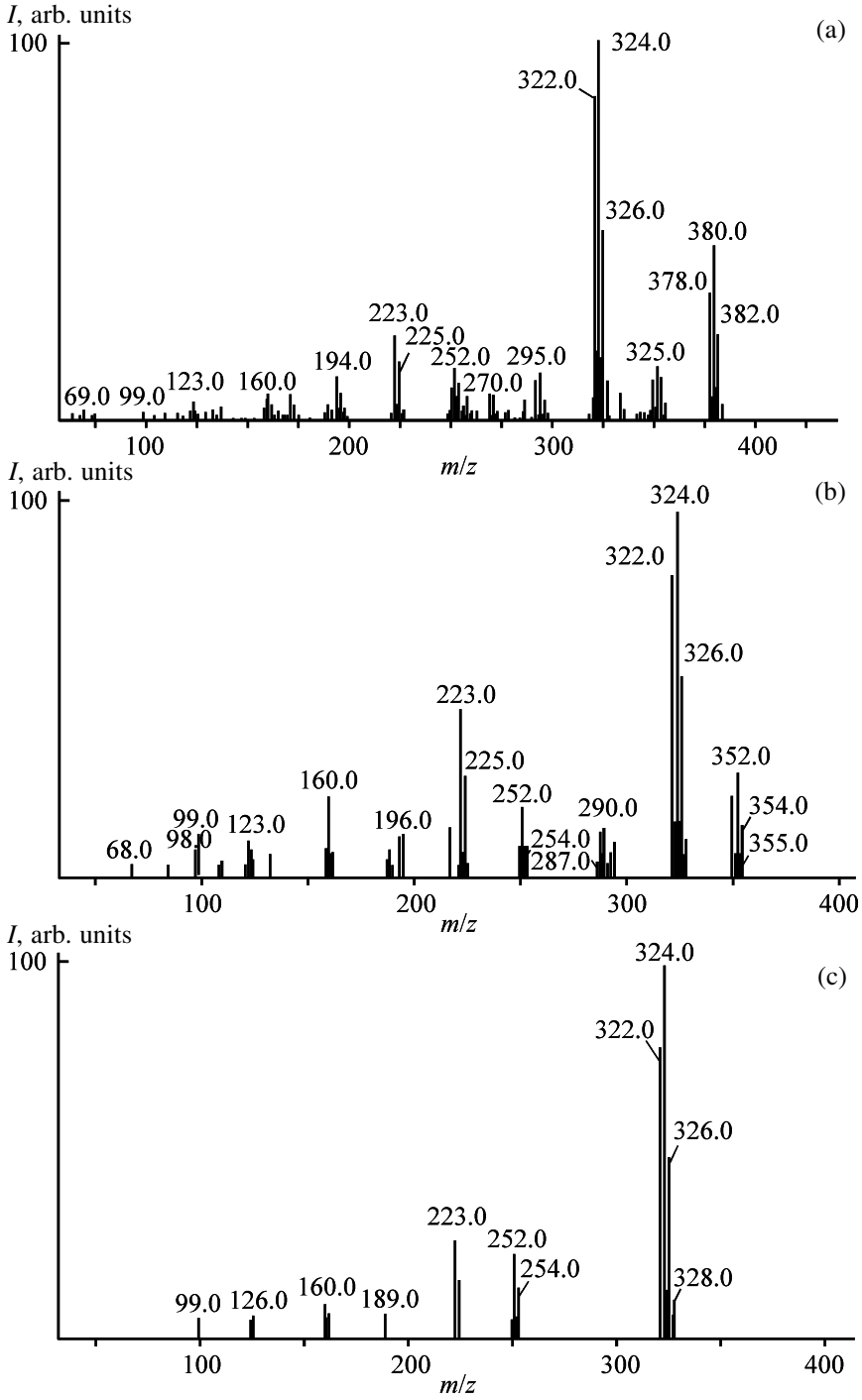


Fig. 3. The mass spectra of compounds **8** (a), **8-1** (b), and **8-2** (c).

We studied the composition of the products of the reaction of the PCB mixture with ethanol and KOH in sulfolane under identical conditions. In this case, only ethoxy derivatives of PCBs are formed, whose composition is similar to that of the ethoxy derivatives formed in DMSO. Alcoholysis is slower; the final mixture contains ca. 10% partially reacted tri- and tetrachlorobiphenyls, as well as pentachlorobiphenyls (PCBs 66, 95, 110).

We studied in detail the mass spectra of the PCB derivatives containing an ethoxy group and a hydroxy group. Previously [5] we discussed the mass spectra of the ethoxy derivatives of PCBs. We showed that all the mass spectra contain peaks corresponding to suc-

cessive loss of ethylene molecules. In most cases, specifically the peak of the radical ion corresponding to the hydroxypolychlorobiphenyl thus formed is the most intense.

The mass spectra of derivatives **5-1** contain molecular ions that are not the base ions. Initially, an ethylene molecule is lost, and the mass spectrum contains a base peak of the $[C_{12}H_5Cl_3(OH)]^+$ ion with *m*/*z* 288. Then Cl or HCl is lost, with the formation of characteristic ions with *m*/*z* 253 (252). After the loss of the second chlorine atom, the ion with *m*/*z* 218 is formed, which is the most intense for the majority of the mass spectra. The next step involves successive loss of two CHO groups, and the mass spectra contain characteristic peaks of the $[C_{11}H_5ClOH]^+$ ion at *m*/*z* 189 and the $[C_{10}H_5Cl]^+$ ion at *m*/*z* 160. Eventually, the remaining chlorine atom is lost with the formation of the $[C_{10}H_5]^+$ ion.

The mass spectra of derivatives **6-1** containing two ethoxy and one hydroxy groups exhibit medium-intensity peaks of molecular ions. Similar to fragmentation of diethoxytrichlorobiphenyls, ethylene molecules are successively lost; the peak at *m*/*z* 270 ($M - 2C_2H_4$) has the highest intensity. The characteristic peaks are those at *m*/*z* 234, corresponding to the subsequent loss of HCl, and at *m*/*z* 200 ($M - 2C_2H_4 - 2Cl$); both peaks have medium intensities. A CHO group is lost from the $[C_{12}H_4Cl(OH)_3]^+$ ion, with the formation of an ion with *m*/*z* 205. Further fragmentation corresponds to the successive loss of two CHO groups.

We have not observed the patterns assignable to ethoxy- (**7**) and hydroxypentachlorobiphenyls (**7-1**).

The mass spectra of ethoxyhydroxytetrachlorobiphenyls **8-1** contain peaks corresponding to molecular ions. The base ion is that formed by the loss of an ethylene molecule from M^+. Then two chlorine atoms are successively lost. The characteristic ion is that with *m*/*z* 223 ($M - C_2H_4 - 2Cl - CHO$). This is followed by the loss of a second CHO group and successive loss of the remaining chlorine atoms.

It is difficult to follow the fragmentation pattern of derivatives **9-1**, since we have not obtained the individual mass spectra. The mass spectra contain peaks of a molecular ion which successively loses ethylene molecules, yielding the characteristic ion with *m*/*z* 304. Then Cl or HCl is lost.

Comparison of the mass spectra that we recorded with those of the related ethoxy derivatives of PCBs [5] suggests that the fragmentation patterns of the PCB derivatives containing ethoxy and hydroxy groups are, on the whole, similar. Figure 3 compares the mass spectra of compounds **8**, **8-1**, and **8-2**.

Thus, a GC–MS study of the reaction mixture suggests the presence of over 150 derivatives of polychlorinated biphenyls belonging to 15 types of compounds. The total content of hydroxy and hydroxyethoxy derivatives of PCBs among the products was estimated at ca. 56%, and that of ethoxy derivatives of PCBs, at 42%.

CONCLUSIONS

(1) Reaction of a mixture of polychlorinated biphenyls with ethanol and potassium hydroxide in dimethyl sulfoxide yields a complex mixture of products; its components were identified.

(2) The reaction proceeds in two steps: Initially, ethoxy derivatives of polychlorinated biphenyls are formed, which are converted to hydroxy derivatives in the course of the process.

(3) Under the optimal conditions, trichlorobiphenyls form only ethoxydichlorobiphenyls, and tetrachlorobiphenyls form ethoxytrichloro-, diethoxydichloro-, and hydroxytrichlorobiphenyls. The reaction products formed from pentachlorobiphenyls are mono-, di-, and triethoxy derivatives and monohydroxy, hydroxyethoxy, and hydroxydiethoxy derivatives. The reaction products formed from hexachlorobiphenyls are predominantly hydroxyethoxy, diethoxy, and hydroxydiethoxy derivatives. Tri- and tetrachlorobiphenyls are not completely converted to the reaction products.

(4) The mass spectra of the obtained derivatives of polychlorinated biphenyls suggest similar fragmentation patterns of the ethoxy and hydroxy derivatives.

REFERENCES

1. Lang, V., *J. Chromatogr.*, 1992, vol. 595, pp. 1–43.
2. *Polikhlorirovannye bifenily: Supertoksikanty XXI veka* (Polychlorinated Biphenils: Supertoxicants of the XXI Century), Arskii, Yu.M., Ed., Moscow: VINITI, 2000, p. 189.
3. Zanaveskin, L.N. and Aver'yanov, V.A., *Usp. Khim.*, 1998, vol. 67, no. 8, pp. 789–800.
4. Zabelina, O.N., Gorbunova, T.I., Kirichenko, V.E., et al., *Zh. Prikl. Khim.*, 2004, vol. 77, no. 9, pp. 1533–1538.
5. Zabelina, O.N., Yatluk, Yu.G., Kirichenko, V.E., et al., *Mass-Spektrometriya*, 2005, vol. 2, no. 3, pp. 139–144.
6. Piterskikh, I.A., Kirichenko, V.E., Pervova, M.G., et al., *Zavod. Lab.*, 2001, vol. 67, no. 8, pp. 63–66.
7. Shein, S.M. and Ignatov, V.A., *Zh. Obshch. Khim.*, 1962, vol. 32, no. 10, pp. 3220–3222.
8. Shein, S.M. and Ignatov, V.A., *Zh. Obshch. Khim.*, 1962, vol. 32, no. 10, pp. 3223–3227.

ISSN 1070-4272. Russian Journal of Applied Chemistry, 2006, Vol. 79, No. 5, pp. 799–801. © Pleiades Publishing, Inc., 2006.
Original Russian Text © N.B. Sokolova, I.V. Bezova, O.I. Nastoyashchaya, 2006, published in Zhurnal Prikladnoi Khimii, 2006, Vol. 79, No. 5, pp. 809–811.

ORGANIC SYNTHESIS AND INDUSTRIAL ORGANIC CHEMISTRY

Lightfast Filter Dyes Derived from Five-Membered Heterocycles

N. B. Sokolova, I. V. Bezova, and O. I. Nastoyashchaya

St. Petersburg State Technological Institute, St. Petersburg, Russia

Received November 7, 2005

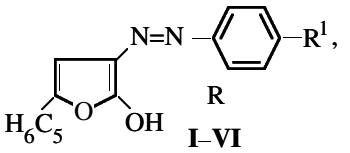
Abstract—The lightfastness of new potential filter dyes derived from furan and pyrazole in three polymer matrices, cellulose acetobutyrate, poly(methyl methacrylate), and styrene–acrylonitrile copolymer, was studied.

DOI: 10.1134/S1070427206050193

Development and improvement of polymeric optical filters is impossible without development of new dyes with specific spectral characteristics, extending the possibilities of available dyes. The technical class of dyes used in the development of color filters is determined by the structure of the polymer used. For example, with cellulose esters such dyes can be used as fat-, alcohol-, and acetone-soluble and dispersible dyes produced in Russia, and also Sudans, Cellitons, Zapons, and other dyes produced in the world. However, not all hydrophobic dyes are suitable as filter dyes. Along with the solubility in organic solvents, they should exhibit a set of properties: high saturation limit both in the solvent and in the polymer, chemical inertness toward the polymer, thermal stability, and lightfastness.

New filter dyes were searched for previously among azo dyes derived from five-membered heterorings such as furan, thiophene, and pyrazole [1, 2]. These dyes have yellow-orange color with narrow absorption bands in the electronic spectra. Thanks to the fact that the absorption ranges of these dyes vary in succession (pyrazole dyes, 380–420 nm; furan dyes, 410–450 nm; thiophene dyes, 460–480 nm), it becomes possible to cover a large wavelength range depending on specific task. Our studies showed that, by varying substituents in the dye molecule, it is possible to obtain dyes that have with similar absorption maxima but differ in the solubility and lightfastness. Furthermore, the lightfastness largely depends on particular polymer matrix [1, 2].

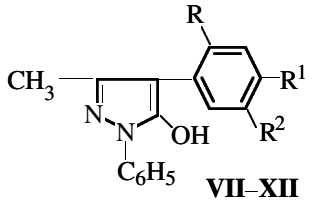
To choose the most lightfast dyes, we prepared and studied new azo dyes derived from 2-phenyl-5-furanone and 1-phenyl-3-methyl-5-pyrazolone. Furan dyes were described previously [3], but their properties were not studied. By the procedure described in [3] we prepared six dyes of the general formula



I–VI

where R = CH_3, R^1 = H (**I**); R = H, R^1 = CH_3 (**II**); R = H, R^1 = OC_2H_5 (**III**); R = Cl, R^1 = H (**IV**); R = OCH_3, R^1 = H (**V**); R = H, R^1 = OCH_3 (**VI**).

Six pyrazolone dyes **VII**–**XII** of the general formula



VII–XII

were prepared by the standard procedure [1]; their properties are given in Table 1.

With dyes **I**–**XII**, we prepared 36 colored polymer films from cellulose acetobutyrate (CAB), poly(methyl methacrylate) (PMMA), and styrene–acrylonitrile copolymer (SAN-25). In all the cases, the spectral characteristic of the dye in the polymer coincided with that in chloroform, i.e., there was no specific interaction of dyes with the polymer. The lightfastness of the dyes in the polymer matrix was studied on a Xenon Long Life Fade Meter XFL-1 accelerated aging installation by the procedure described previously [4, 5]. Under similar conditions we irradiated colorless films of the corresponding polymers containing no dyes; these samples were used as references when measuring the electronic absorption spectra of the insolated

Table 1. Physicochemical properties of pyrazolone dyes **VII–XII**

Dye	R	R^1	R^2	Yield, %	mp, °C	Solvent	Found, %/Calculated, %			Empirical formula
							C	H	N	
VII	COOH	H	H	70	298	Toluene	63.42/63.35	4.50/4.34	17.49/17.39	$C_{17}H_{14}N_4O_3$
VIII	Cl	H	H	69	224	Ethanol	6161/61.44	4.14/4.16	17.77/17.92	$C_{16}H_{13}N_4OCl$
IX	OCH_3	H	H	68	200	Toluene	66.32/66.20	5.23/5.19	18.39/18.18	$C_{17}H_{16}N_4O_2$
X	NO_2	H	H	72	202	Toluene	59.64/59.41	3.98/4.02	21.78/21.67	$C_{17}H_{13}N_5O_3$
XI	H	H	NO_2	70	173	Toluene	59.54/59.41	4.10/4.02	21.68/21.67	$C_{17}H_{13}N_5O_3$
XII	H	NO_2	H	71	214	Ethanol	59.50/59.41	3.96/4.02	21.75/21.67	$C_{17}H_{13}N_5O_3$

Table 2. Degree of photochemical degradation Φ_d of dyes **I–XII** in polymer matrices

Dye	λ_{max}, nm	Φ_d, %, in indicated insolation time, h								
		1	10	20	1	10	20	1	10	20
		CAB			PMMA			SAN-25		
I	420	75.0	100	–	32.0	79.0	–	2.4	54.0	–
II	440	56.5	100	–	13.3	74.0	–	19.6	64.9	–
III	415	67.7	100	–	29.1	96.2	–	10.8	65.0	–
IV	415	30.1	87.0	–	10.0	67.2	–	5.3	49.0	–
V	395	52.5	100	–	10.2	73.0	–	15.1	60.2	–
VI	410	42.9	100	–	24.1	91.2	–	27.8	69.9	–
VII	400	0	3.9	6.3	0	0	0	0	0	0
VIII	390	0	2.0	4.1	0	0	0	0	0	1.8
IX	410	2.5	15.3	25.4	0	4.2	8.4	0.7	9.3	13.9
X	410	0	0	0	0	0	1.0	0	0	0
XI	380	0	0	2.7	12.2	53.8	65.3	0	0	2.2
XII	400	0	0	0	0	0	0	0	0	0

irradiated films. As analytical wavelength we chose λ_{max} of the dyes. The degree of photochemical degradation Φ_d (%) was calculated by the formula

$$\Phi_d = (\Phi_0 - \Phi_i/\Phi_0) \times 100.$$

The time of accelerated photochemical aging of the films was usually 10 h, which corresponds to the service time of filters under usual conditions; however, the insolation of pyrazolone dyes in the chosen polymer matrices for 10 h did not lead to any photochemical degradation in most cases. That is, pyrazolone dyes exhibit extremely high lighthfastness; however, the effect of substituents in the phenyl moiety on the lightfastness cannot be revealed. Therefore, we performed longer insolation (20 h) of films with pyrazolone dyes; however, even under these, more severe, conditions some of the dyes showed no degradation. The results are listed in Table 2.

These data show that pyrazolone dyes surpass the majority of the known dyes in the lightfastness but absorb the light only in the near-UV range and at the violet edge of the visible range (380–410 nm). The most resistant to photochemical degradation are *o*- and *p*-nitro-substituted dyes, and specifically these dyes can be recommended as filter dyes providing the absorption at 400–410 nm.

The lightfast dye with λ_{max} = 390 nm was described previously [1]. This is fat-soluble Yellow 3Zh dye containing no substituents in the phenyl moiety. *o*-COOH-substituted dye **VIII** prepared in this study is not inferior to Yellow 3Zh in the lightfastness. A pyrazolone dye with λ_{max} = 380 nm, *o*-OCH_3-substituted dye **IX**, was prepared in this study. This dye is the least stable among the pyrazolone dyes; nevertheless, it is considerably more stable than furan and thiophene dyes: The degree of its photochemical degradation in 20 h in the CAB matrix, in which it is the least stable, is 25.4%.

Furan dyes are appreciably less lightfast than pyrazolone dyes, but they are unique in that they absorb at λ_{max} = 415–450 nm with very steep wings of the absorption curve.

Dyes absorbing at λ_{max} = 415–420 nm were not studied previously. Such dyes are **I**, **III**, and **IV**. In the CAB matrix, the most lightfast among them is dye **IV** containing *o*-Cl substituent; dyes **I** (*o*-CH_3) and **III** (*p*-OC_2H_5) are considerably more lightfast in SAN-25, approaching in this characteristic the pyrazolone dyes.

In this study we failed to obtain furan dyes with λ_{max} = 430 nm, but two dyes with such absorption were studied previously [1]: the dye unsubstituted in the phenyl moiety and the dye with the *p*-Cl substituent. Among them, the unsubstituted dye is more lightfast, and it is recommended as filter dye.

Finally, dyes with λ_{max} = 440 nm (**II**, *p*-CH_3) and 450 nm (*p*-NO_2 [1]) show satisfactory lightfastness only in SAN-25. With the other polymers, special photostabilization of these dyes is required.

EXPERIMENTAL

Dyes **I**–**VI** were prepared by the procedure described in [3]. They were purified by column chromatography on silica gel (eluent $CHCl_3$) followed by recrystallization from appropriate solvent until the melting points agreeing with the published data [3] were obtained.

Dyes **VII**–**XII** were prepared as described in [1] and purified by the same procedure as dyes **I**–**VI**. The characteristics of the dyes are given in Table 1.

The colored films were prepared in the laboratory by casting of a solution of a dyed polymer formulation onto polished glass with a bounding frame of a definite size, followed by drying according to the prescribed schedule [4, 5].

The films were insolated on a Suga Standard Xenon Long Life Fade Meter, model XFL-1, equipped with a 1-kW xenon lamp. The insolation was performed in the automatic mode at 30°C and 65% air humidity, in 15-min periods until the 1-h exposure was accumulated and then in 1-h periods to a total exposure of 20 h. After the completion of each irradiation cycle, the films were kept in the dark for 24 h at room temperature, after which the electronic absorption spectra were recorded on an SF-16 spectrophotometer.

CONCLUSIONS

(1) The furan and pyrazolone dyes synthesized can be used as filter dyes.

(2) Azo dyes derived from 1-phenyl-3-methyl-5-pyrazolones surpass in the lightfastness all the heterocyclic azo dyes studied.

(3) Dyes derived from 2-phenyl-5-furanone exhibit high lightfastness only in SAN-25; in the other polymers, these dyes can be used only in the presence of photostabilizers.

REFERENCES

1. Kovzhina, L.P., Sokolova, N.B., Dmitrieva, N.M., and Pesenko, E.V., *Zh. Prikl. Khim.*, 1996, vol. 69, no. 3, pp. 477–482.
2. Kovzhina, L.P., Sokolova, N.B., and Dmitrieva, N.M., *Zh. Prikl. Khim.*, 1998, vol. 71, no. 3, pp. 453–458.
3. Khattab, S.A., Shawali, S.A., and Faray, A.M., *J. Chem. Eng. Data*, 1977, vol. 22, no. 1, pp. 104–110.
4. Kovzhina, L.P., Sokolova, N.B., Dmitrieva, N.M., and Popova, T.N., *Zh. Prikl. Khim.*, 1998, vol. 71, no. 12, pp. 2024–2028.
5. Kovzhina, L.P., Sokolova, N.B., Dmitrieva, N.M., and Vins, T.Yu., *Zh. Prikl. Khim.*, 1999, vol. 72, no. 9, pp. 1507–1509.

ISSN 1070-4272. Russian Journal of Applied Chemistry, 2006, Vol. 79, No. 5, pp. 802–805. © Pleiades Publishing, Inc., 2006.
Original Russian Text © G.U. Ostrovidova, E.V. Zamyslov, 2006, published in Zhurnal Prikladnoi Khimii, 2006, Vol. 79, No. 5, pp. 812–815.

MACROMOLECULAR CHEMISTRY AND POLYMERIC MATERIALS

Sorption of Trypsin on the Polysiloxane Rubber Surface

G. U. Ostrovidova and E. V. Zamyslov

St. Petersburg State Technological Institute, St. Petersburg, Russia

Received February 1, 2006

Abstract—The sorption kinetics of trypsin on medical polysiloxane rubber and polysiloxane rubber modified with graphite was studied. The effect of the nonuniformity and hydrophilicity of the rubber surface on the trypsin immobilization rate was analyzed.

DOI: 10.1134/S107042720605020X

In contact of protein-containing biological solutions with foreign solids, the process occurring first is the sorption of protein. This process is mainly responsible for biocompatibility of medical materials [1]. In this study we examined the interaction of proteolytic enzyme trypsin with the polysiloxane rubber surface. The positive effect of trypsin on the hemocompatibility of medical materials was reported in [2, 3].

EXPERIMENTAL

The initial polysiloxane rubber of medical purity grade $SKTV_{med}$ (M = 60 000) and polysiloxane rubber modified in the bulk with graphite [20–50 wt % relative to rubber, $SKTV_{med}$ composite material (CM)] [4] were used as sorbents. Trypsin (proteolytic enzyme) was purchased from Spofa (Czechia). Other chemicals were of ultrapure, analytically pure, and chemically pure grade.

The surface trypsin concentration was determined spectrophotometrically (λ = 280 nm) [5]. The proteolytic activity was determined with casein as a substrate. The contact angles were measured with a horizontal microscope. The free surface energy was calculated by the equation [6]

$$\sigma = \sigma_1(1 + \cos\theta)^2/4,$$

where σ_1 = 72.5 mJ m^{-2} is the water surface tension.

The X-ray photoelectron spectra of trypsin immobilized on both the initial and modified polysiloxane rubber were recorded on a PH1 5400 spectrophotometer (Perkin–Elmer, the United States) using MgK_α radiation (1253.6 eV) at a pressure in the spectrophotometer chamber of 1.3×10^{-6} Pa. The binding energy was measured with an accuracy of ±0.1 eV. The trypsin determination error was 10 rel. %. The spectrophotometer was calibrated relative to the C1s line of residual hydrocarbons (electron binding energy 285.0 eV) taking into account the sample charging. The X-ray photoelectron spectra were processed with the Perkin–Elmer program.

Figure 1 shows the kinetic curves of trypsin sorption on the initial polysiloxane rubber and composite material with varied graphite content. It is seen that, for all the materials tested, the sorption saturation is attained within 30–60 min. At high graphite content in the modified rubber, its surface becomes mosaic and acquires a negative charge. Owing to the presence of graphite, the modified rubber surface contains specific sorbing groups influencing the trypsin immobilization. The shape of the kinetic curves (Fig. 1) shows that the sorption of trypsin on the initial rubber

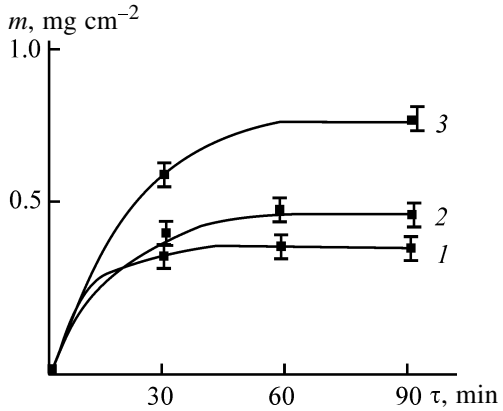


Fig. 1. Kinetic curves of trypsin sorption on polysiloxane rubber. (m) Trypsin surface concentration and (τ) time. (*1*) Initial polysiloxane rubber ($SKTV_{med}$); graphite content in composite material, wt % relative to rubber: (*2*) 20 and (*3*) 50.

Table 1. Physicochemical and sorption characteristics of the initial and modified polysiloxane rubber

Support	Contact angle, deg	Surface energy, mJ m^{-2}	Sorbed trypsin fraction, %	Trypsin enzymatic activity, % of native
$SKTV_{med}$	90–107	18.2–20	11	52
CM, 50 wt % graphite	72	31.2	25	76

reaches saturation in a shorter time than on the modified rubber. For the initial rubber $SKTV_{med}$, the saturation in the trypsin sorption is attained within 30–40 min. However, this does not mean that within this time the true sorption equilibrium is reached. Actually, only a steady state is attained within 20–120 min and even in longer time [7]. Thus, the short-time sorption experiments reflect the nonequilibrium protein immobilization depending on particular experimental conditions [7].

The increased sorption capacity of the modified rubber for trypsin is caused by enhanced hydrophilicity of this material, which is manifested as a decrease in the contact angle (Table 1). It is believed that the free surface energy of solid medical materials (in the range 20–50 mJ m^{-2}) correlates with their biocompatibility [9]. The surface defects of medical materials sharply increase their surface energy and, as a result, increase a risk for thrombosis. To evaluate the suitability of any material for medical use, its roughness is monitored profilographically, and the roughness height is determined [8]. The modified medical rubber under consideration had roughness height of about 2.66 μm, which is too small to promote thrombosis.

With increasing the graphite content in the modified rubber, its surface electrical charge increases and the electrostatic attraction between trypsin and rubber surface is strengthened. As a result, the sorption of trypsin increases. In spite of stronger binding to modified rubber surface, immobilized trypsin exhibits high enzymatic activity. Figure 2 shows that the trypsin sorption increases with increasing surface energy of the modified rubber. The trypsin sorbability correlates also with the wettability of the modified rubber. In going from the initial rubber to the composite material containing 50 wt % graphite relative to the rubber, the contact angle decreases from 90°–107° to 72°. It should be noted that the surface energy of medical rubber under consideration was within 20–50 mJ m^{-2}; this range is typical of materials preventing thrombosis [6, 9].

The X-ray photoelectron spectra of all the rubber samples under consideration show that the new N1*s* and S2*p* bands appear after sorption of trypsin. In addition, the carbon band becomes broadened from the high-binding-energy side suggesting the appearance of organic carbon. The complicated N1*s* band of immobilized trypsin can be resolved into two separate bands. One of them (E = 399.7 eV) belongs to nitrogen atoms of the NH_2 groups bound by hydrogen bonds and other (E = 401.6 eV), to the NH_2 groups free of hydrogen bonds. Based on trypsin molecular structure, the high-energy band (E = 401.6 eV) can be assigned to nitrogen atoms of the side functional groups:



The low-energy band (E = 399.7 eV) belongs to the nitrogen atoms of the main polypeptide chain of the trypsin molecule.

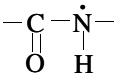


Table 2 shows that the ratio of the areas of nitrogen bands of trypsin immobilized on the modified rubber (401.6 and 399.7 eV) depends on the incidence angle

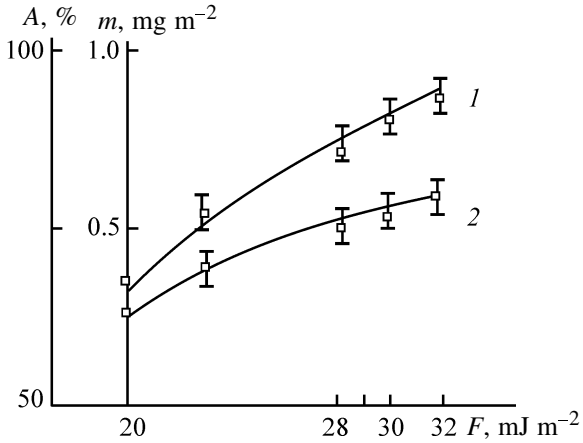


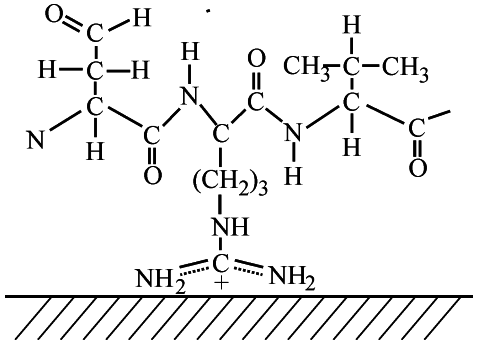
Fig. 2. (*1*) Surface concentration m and (*2*) enzymatic activity A of trypsin vs. free surface energy F of rubber. Initial polysiloxane rubber $SKTV_{med}$, F = 20 mJ m^{-2}; composite material [graphite content (wt %), surface energy (mJ m^{-2})]: 40, F = 28 mJ m^{-2}; 50, F = 32 mJ m^{-2}.

Table 2. Dependence of the intensity of the photoelectron bands of trypsin immobilized on modified rubber (50 wt % graphite) on incidence angle of X-ray radiation relative to the rubber surface

Sample no.	Incidence angle, deg	E_b N1*s*, eV	Peak area, %
no. 1	15	403.77	25.17
		401.6	64.82
		399.7	10.01
no. 2	60	403.77	39.26
		401.6	46.94
		399.7	13.8

of X-ray radiation relative to the rubber surface. The tertiary protein structure is mainly formed by hydrophobic interactions between side functional groups of polypeptide chains. The intermolecular hydrogen bonding between side functional groups and intramolecular hydrogen bonding between the NH and CO groups of polypeptide chain also contribute to this process. For trypsin sorbed on the modified rubber, the ratio of the 401.6- and 399.7-eV peak areas shows that this enzyme is predominantly fixed on the rubber surface with the side NH_2 groups. We believe that trypsin is immobilized due to electrostatic attraction between the positively charged $NH_2 \cdots C^+ \cdots NH_2$ groups and negatively charged graphite-containing sites of the composite material (see scheme).

Scheme of trypsin immobilization on composite material



In going to the initial (unmodified) polysiloxane rubber whose surface has lower surface energy and contains no specifically sorbing functional groups, the sorption of trypsin decreases. In this case, the intermolecular interactions between trypsin molecules prevail and their denaturation occurs. Table 1 shows that, under these conditions, the trypsin proteolytic activity decreases [11]. The maximal surface concentration of trypsin is reached within 60 min (Fig. 1).

It is known that the enzyme–support interactions affect the enzymatic activity. It is believed that, in enzyme immobilization by sorption on a solid support or by any other method, the first stage is the protein concentration at the surface. This "primary adsorption" is accompanied by formation of a small number of bonds between trypsin and specific surface sorbing sites. With increasing surface concentration of protein, weak nonspecific contacts appear along with these specific bonds [11]. In the case of mosaic surface structure containing, for example, polysiloxane and graphite sites, the protein immobilization occurs through its binding with different surface sites. Owing to this multimode sorption, immobilized trypsin preserves its enzymatic activity (see scheme).

CONCLUSIONS

(1) The kinetics of sorption of trypsin on polysiloxane rubber, initial and modified in the bulk with graphite, was studied.

(2) The surface of modified polysiloxane rubber is more nonuniform and hydrophilic than that of the initial rubber. The modified polysiloxane rubber sorbs 2.5 times larger amount of trypsin than does the initial polymer.

(3) Trypsin molecules are immobilized on the modified rubber surface by attraction of their positively charged NH_2-containing side groups to negatively charged sorbing sites.

REFERENCES

1. *Polimery meditsinskogo naznacheniya* (Polymers for Medical Purposes), Manabu, S., Ed., Moscow: Meditsina, 1981.
2. Bueva, O.A., Zamyslov, E.V., and Ostrovidova, G.U., *Patofiziologiya mikrotsirkulyatsii i gemostaza* (Pathophysiology of Microcirculation and Hemostasis), Petrishcheva, N.N., Ed., St. Petersburg: Sankt-Peterb. Gos. Med. Univ. im. I.P. Pavlova, 1998, pp. 447–453.
3. Ostrovidova, G.U., Makeev, A.V., and Shamtaian, M.M., *J. Mater. Sci. Eng.*, 2003, vol. 23, pp. 545–550.
4. Zamyslov, E.V., Klochkov, V.I., and Ostrovidova, G.U., *Zh. Prikl. Khim.*, 1997, vol. 70, no. 7, pp. 1212–1214.
5. Aleinikova, T.L. and Rubtsova, G.V., *Rukovodstvo k prakticheskim zanyatiyam po biologicheskoi khimii*

(Guide on Practical Training on Biological Chemistry), Moscow: Vysshaya Shkola, 1988.

6. Lyman, L.J., Muir, W.H. Lee, I.J., et al., *Trans. Am. Soc. Artif. Int. Organs*, 1965, vol. 11, pp. 301–305.
7. Sinitsyn, A.P., Rainina, E.I., Lozinskii, V.I., and Spasov, S.D., *Immobilizovannye kletki mikroorganizmov* (Immobilized Microorganism Cells), Moscow: Mosk. Gos. Univ., 1994.
8. Vitenberg, Yu.P., *Sherokhovatost' poverkhnosti i metody ee otsenki* (Surface Roughness and Techniques for Its Estimation), Moscow: Sudostroenie, 1971.
9. Zisman, W.A., *Adv. Chem. Ser.*, Washington, DC: Am. Chem. Soc., 1964, no. 43.
10. Nefedov, V.I., *Rentgenoelektronnaya spektroskopiya khimicheskikh soedinenii: Spravochnik* (X-ray Photoelectron Spectroscopy of Chemical Compounds: Handbook), Moscow: Khimiya, 1984.
11. Ishihara, K., *Trends Polym. Sci.*, 1997, vol. 5, no. 12, pp. 401–406.

ISSN 1070-4272. Russian Journal of Applied Chemistry, 2006, Vol. 79, No. 5, pp. 806–810. © Pleiades Publishing, Inc., 2006.
Original Russian Text © E.S. Sashina, A.V. Vnuchkin, N.P. Novoselov, 2006, published in Zhurnal Prikladnoi Khimii, 2006, Vol. 79, No. 5, pp. 816–820.

MACROMOLECULAR CHEMISTRY AND POLYMERIC MATERIALS

Properties of Films Prepared from Solutions of Fibroin–Cellulose Blends in *N*-Methylmorpholine *N*-Oxide

E. S. Sashina, A. V. Vnuchkin, and N. P. Novoselov

St. Petersburg State University of Technology and Design, St. Petersburg, Russia

Received January 17, 2006

Abstract—The physicomechanical properties and thermal stability of films prepared from solutions of fibroin–cellulose blends in *N*-methylmorpholine *N*-oxide were studied.

DOI: 10.1134/S1070427206050211

The unique physicomechanical properties of fibroin, a natural polymer, are well known [1]. This polypeptide is the main component of silk threads and cobweb and consists to more than 80% of the simplest amino acids (glycine, alanine, serine). The content of crystalline fraction of the polymer can be as high as 70%. In this fraction, the macromolecules form antiparallel β-folded structure and α-spiral secondary structure.

The possibility of using fibroin in the form of powders, gels, and films for biotechnological and biomedical purposes was studied in [2–4]. Fibroin membranes can be used to separate aqueous alcoholic solutions and to immobilize enzymes. Fibroin is a biocompatible compound suitable for preparing contact lenses.

The main disadvantage of films prepared from fibroin solutions is their high brittleness. Dry films are virtually unsuitable for practical purposes. Fibroin in natural silk threads is plasticized with natural sericin, which imparts strength and elasticity to silk. Therefore, we studied blends of fibroin with other polymers [5, 6] with the aim to improve the film properties. Taking into account the possible applications of the films, we used natural and biodegradable polymers as the second component.

In this study we examined properties of films prepared from solutions of fibroin–cellulose blends. *N*-Methylmorpholine *N*-oxide (NMMO) readily dissolving cellulose [7] and fibroin [8] was used as the solvent.

EXPERIMENTAL

We used the following polymers: fibroin of *Bombyx mori* silk (washed to remove fat, wax, and mineral compounds) and wood sulfite pulp with the degree of polymerization of 495. The polymers were dissolved in NMMO at 95°C for 2–5 h. The resulting solutions with the polymer concentration of 4% were mixed to obtain solutions with the fibroin/cellulose ratios of 90/10, 50/50, 30/70, and 10/90. The films were prepared by application of these solutions to glass plates with subsequent coagulation with aqueous alcohol. After coagulation, the films were washed with distilled water to completely remove the solvent and were dried in air. The film thickness was 10–30 μm.

The physicomechanical properties of the films were studied on an Instron tensile-testing machine in accordance with DIN EN ISO 527-3. The IR spectra were recorded on a IFS25 IR spectrometer. Thermal gravimetric analysis was performed in air on a MOM Q-1500D derivatograph (Hungary) in the temperature range 23–500°C. The heating rate was 2.5 deg min^{-1}.

The IR spectra of recovered fibroin, cellulose, and their blends with different ratios of the components are shown in Fig. 1. The band assignment is given in Table 1. According to the published IR data, the crystalline fraction with the β-structure has particular spectrum, whereas the IR spectra of the α-spiral crystal structure are similar to those of the amorphous random globules [9–13]. Therefore, we could not distinguish the α-structure and the amorphous fraction by IR spectroscopy. The bands at 1624 (Amide I), 1521 (Amide II), and 671 cm^{-1} (Amide V) in the spectrum of fibroin (curve *6*) can be assigned to the crystalline β-structure. The band at 1230 cm^{-1} (Amide III) in the spectrum of pure fibroin suggests that a part of the macrololecues has the α-spiral or random globule conformation. The cellulose spectrum (curve *1*) is typical of cellulose II [14].

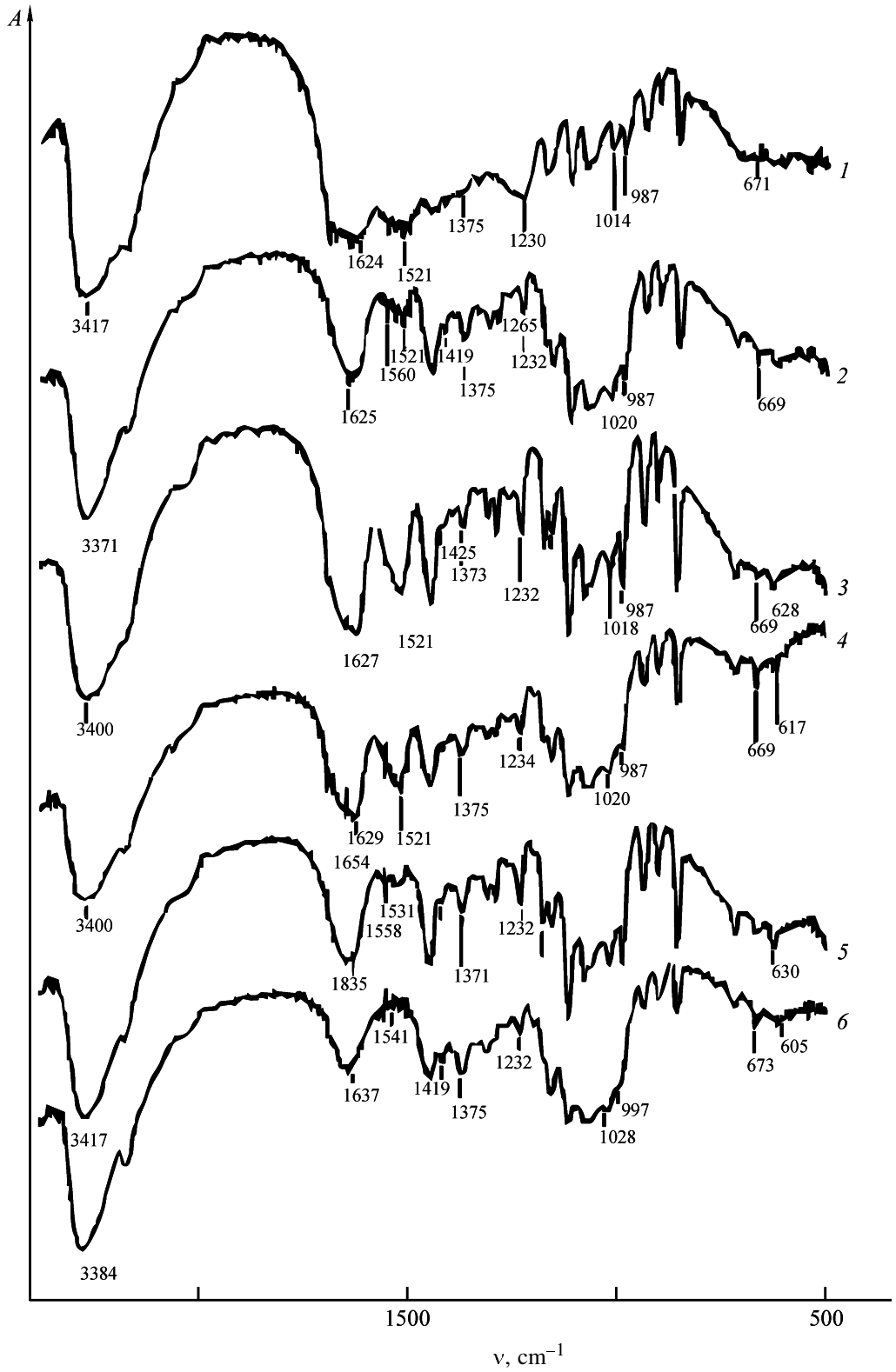


Fig. 1. IR spectra of the films of (*1*) 100% cellulose, fibroin–cellulose [component ratio: (*2*) 10/90, (*3*) 30/70, (*4*) 50/50, (*5*) 90/10], and (*6*) 100% fibroin; the same for Fig. 2. (*A*) absorption and (ν) wavenumber. The same for Fig. 2.

Table 1. Assignment of the absorption bands in the IR spectra of the films of fibroin–cellulose blends to various fibroin conformations

Absorption band	Frequency, cm^{-1}					
	100% fibroin	90 : 10	50 : 50	30 : 70	10 : 90	100% cellulose
Characteristic fibroin bands						
Amid I (C=O)	1624 (β)	*1652* (α)	1627 (β)	*1654* (α), 1629 (β)	1635 (β)	1637
Amid II (N–H bound, C–N)	1521 (β)	*1560* (α), 1521 (β)	1521 (β)	1521 (β)	*1558* (α), 1531 (β)	1541
Amid III (C–N, N–H bound)	1230 (α)	*1265* (β), 1232 (α)	1232 (α)	1234 (α)	1232	1232
Amid V	671 (β)	669 (β)	669 (β), *628* (α)	669 (β), *617* (α)	667 (β), *630* (α)	673, 605
Gly–Gly	1014	1020	1018	1020	1020	1028
Gly–Ala	987	987	987	987	987	997
Characteristic cellulose bands						
O···H	3417	3371	3400	3400	3417	3384
OH	–	1419	1425	1423	1423	1419
CH_2	1375	1375	1373	1375	1371	1375
OH	671	669	669	669	667	673

The IR spectra of the films of fibroin–cellulose blends (curves *2*–*5*) contain the typical bands of the components and new bands assigned to the spiral and random conformations of fibroin macromolecules (printed italic in Table 1). The spectrum in the range 1250–800 cm^{-1} characterizing the primary polypeptide structure changes. The bands of the Gly–Gly units at 1014 cm^{-1} change to the greatest extent. The frequency and the intensity of the bands of H-bonded hydroxy groups of cellulose at 3384, 1419, and 673 cm^{-1} change in the spectra of the films of the blends.

These data suggest that the hydroxy groups of cellulose macromolecules form intermolecular hydrogen bonds with the amide groups of fibroin and prevent β-folding of the polypeptide macromolecules.

Table 2. Physicomechanical properties of films of fibroin–cellulose blends

Fibroin content in the blend, %	Tensile strength, N mm^{-2}	Elongation at break, %
100	31.1	2.9
90	31.2	3.1
50	35.0	9.5
30	47.5	10.4
10	45.3	10.3
–	50.1	10.4

The TG curves of the films are shown in Fig. 2. The samples undergo stepwise thermal oxidative degradation accompanied by weight loss. The weight loss of the fibroin in air at 130°C (curve *6*) is due to vaporization of adsorbed water. On further heating, gradual weight loss owing to transformations of the amorphous fractions is observed. The thermolysis rate increases at 250°C and reaches a maximum at 278°C. At this temperature, the H bonds of nonoriented β-crystalline fractions of the polymer start to rupture [15–18]. The weight loss at 500°C is 77%.

The TG curve of the cellulose film (curve *1*) contains a step at 105°C with a weight loss of 11.2%, caused by vaporization of adsorbed water. The thermolysis sharply accelerates on heating above 157°C. The maximal rate of the weight loss is observed at 190°C. The total weight loss at this temperature is 43%. On further heating, the thermolysis rate decreases and then increases again, reaching a maximum at 349°C (weight loss 73.5%). This can be due to dehydroxylation of cellulose units mainly in the amorphous fractions and then, at higher temperatures, to depolymerization of the crystalline fraction of the polymer [19, 20]. The weight loss at 500°C is 96%, owing to liberation of volatile thermolysis products.

The temperature of the intense weight loss of the cellulose film containing 10% fibroin (curve *2*) is 10°C higher than that of the pure cellulose film. With increasing fibroin concentration, this temperature in-

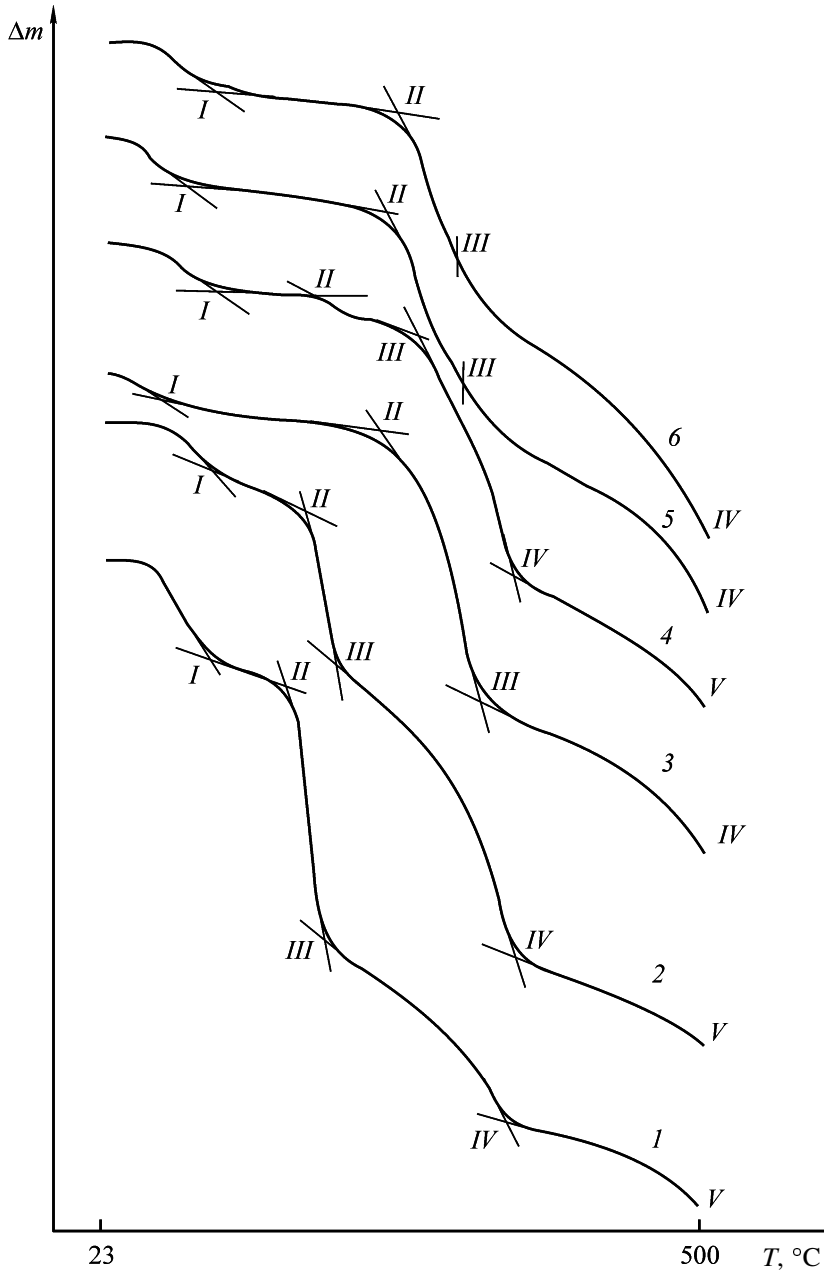


Fig. 2. TG curves of the films (Δ*m*) Weight loss and (*T*) heating temperature. Heating temperature (°C), weight loss (%): (*1*) (*I*) 105, 11.2; (*II*) 157, 17; (*III*) 197.5, 47.5; (*IV*) 349, 73.5; (*V*) 500, 96; (*2*) (*I*) 120, 6; (*II*) 167, 12; (*III*) 192, 28.5; (*IV*) 347, 71; (*V*) 500, 95; (*3*) (*I*) 81, 3; (*II*) 252, 9; (*III*) 345, 22.5; (*IV*) 500, 67.5; (*4*) (*I*) 105, 4.8; (*II*) 180, 6; (*III*) 254, 11; (*IV*) 350, 40; (*V*) 500, 74.2; (*5*) (*I*) 100, 6, 245, 12; (*III*) 280, 26; (*IV*) 500, 70; (*6*) (*I*) 130, 6; (*II*) 250, 11; (*III*) 278, 26; (*IV*) 500, 77.

creases, approaching the thermolysis temperature of fibroin (curves *3–5*). The weight loss of these samples at 500°C decreases to 70–74%. The film with a fibroin–cellulose ratio of 30/70 is the most stable at temperatures of up to 500°C. Thus, addition of fibroin increases the heat resistance of cellulose. Nishioka et al. [21] showed that the heat resistance of cellulose in blends with synthetic polymers decreases or remains virtually the same depending on the type of the synthetic polymer.

The tensile strength and elongation at break of the films with different component ratios are presented in Table 2. As seen from Table 2, the sample containing 30% fibroin and 70% cellulose has the best combination of the tensile strength and elongation.

CONCLUSIONS

(1) An IR study of the films of fibroin–cellulose blends revealed intermolecular interaction between the components.

(2) The fibroin–cellulose films are characterized by good physicomechanical properties and high heat resistance.

REFERENCES

1. *Silk Polymers: Material Science and Biotechnology*, Kaplan, D., Ed., Washington: Am. Chem. Soc., 1994.
2. Asakura, T., Kitaguchi, M., Demura, M., et al., *J. Appl. Polym. Sci*., 1992, vol. 46, no. 1, pp. 49–53.
3. Minoura, N., Tsukada, M., and Nagura, M., *Biomaterials*, 1990, vol. 11, no. 3, pp. 430–435.
4. Minoura, N., Tsukada, M. and Magura, M., *Polymer*, 1990, vol. 31, no. 3, pp. 265–269.
5. Sashina, E.S. and Novoselov, N.P., *Zh. Prikl. Khim*., 2005, vol. 78, no. 3, pp. 493–498.
6. Sashina, E.S., Novoselov, N.P., and Heinemann, K., *Zh. Prikl. Khim*., 2005, vol. 78, no. 1, pp. 155–160.
7. Philipp, B., *Polym. News*, 1990, vol. 15, no. 6, pp. 170–175.
8. RF Patent 2002107622.
9. Miyazawa, T., Shimanouchi, T., and Mizuchima, S., *J. Chem. Phys*., 1958, vol. 29, no. 3, pp. 611–616.
10. Asai, M., Tsuboi, M., Shimanouchi, T., and Mizushima, S., *J. Phys. Chem*., 1955, vol. 59, no. 3, pp. 322–325.
11. Venyaminov, S.Yu. and Kalnin, N.N., *Biopolymers*, 1990, vol. 30, no. 6, pp. 1259–1271.
12. Magoshi, J., Mizuide, M., and Magoshi, Y., *J. Polym. Sci., Polym. Phys. Ed*., 1979, vol. 17, no. 3, pp. 515–520.
13. Freddi, G., Pessina, G., and Tsukada, M., *Int. J. Biol. Macromol*., 1999, vol. 24, no. 2, pp. 251–263.
14. Asai, M., Tsuboi, M., and Shimanouchi, T., *J. Phys. Chem*., 1955, vol. 59, no. 3, pp. 322–326.
15. Kweon, H., Woo, S.O., and Park, Y.H., *J. Appl. Polym. Sci*., 2001, vol. 81, no. 13, pp. 2271–2276.
16. Nam, J. and Park, Y.H., *J. Appl. Polym. Sci*., 2001, vol. 81, no. 15, pp. 3008–3021.
17. Motta, A., Fambri, L., and Migliaresi, C., *Macromol. Chem. Phys*., 2002, vol. 203, no. 9, pp. 1658–1665.
18. Kweon, H. and Park, Y.H., *J. Appl. Polym. Sci*., 2001, vol. 82, no. 5, pp. 750–758.
19. Milosavljevic, I. and Snuberg, E.M., *Ind. Eng. Chem. Res*., 1995, vol. 34, no. 4, pp. 1081–1091.
20. Rubtsov, Yu.I., Kazakov, A.I., Andrienko, L.P., and Manelis, G.B., *Fiz. Goren. Vzryva*, 1993, vol. 29, no. 6, pp. 49–53.
21. Nishioka, N., Hamabe, S., et al., *J. Appl. Polym. Sci*., 1998, vol. 69, no. 11, pp. 2133–2137.

ISSN 1070-4272. Russian Journal of Applied Chemistry, 2006, Vol. 79, No. 5, pp. 811–813. © Pleiades Publishing, Inc., 2006.
Original Russian Text © I.N. Bakirova, L.A. Zenitova, N.A. Rozental', 2006, published in Zhurnal Prikladnoi Khimii, 2006, Vol. 79, No. 5, pp. 821–824.

MACROMOLECULAR CHEMISTRY AND POLYMERIC MATERIALS

Effect of Acetylacetone on the Reaction of Polyethylene Glycol Adipate with Diisocyanate in the Presence of Phenolic Mannich Bases and Properties of Castable Polyurethanes

I. N. Bakirova, L. A. Zenitova, and N. A. Rozental'

Kazan State Technological Institute, Kazan, Tatarstan, Russia

Received May 31, 2005; in final form, February 2006

Abstract—The effect of acetylacetone on the reaction of polyethylene glycol adipate with diisocyanate in the presence of catalytic amounts of Mannich bases was examined.

DOI: 10.1134/S1070427206050223

Polyestes (PEs) stabilized with acetylacetone (AcA) are used as raw material in synthesis of castable monolythic polyurethanes (PUs) via prepolymers [1]. Addition of AcA to a PE allows preparation on its basis of linear prepolymers with terminal isocyanate groups. The role of AcA consists in conversion of metal impurities in PEs into acetylacetonate complexes. These complexes accelerate exclusively the formation of urethanes and prevent the formation of allophanates and triisocyanurates causing branching of the prepolymer [1, 2].

In the synthesis of PUs of the SKU-OM type [3], formed by the reactions of PEs with diisocyanate in the presence of catalytic amounts of (dimethylaminomethyl)phenol derivatives (phenolic Mannich bases, MBs), it was noted that the use of stabilized PEs requires increased catalyst dosage. Otherwise the PUs are not hardened. In this connection, it was interesting to examine the effect of AcA on the reaction of a PE with diisocyanate in the presence of catalytic amounts of MBs and on the properties of PUs of the SKU-OM type.

EXPERIMENTAL

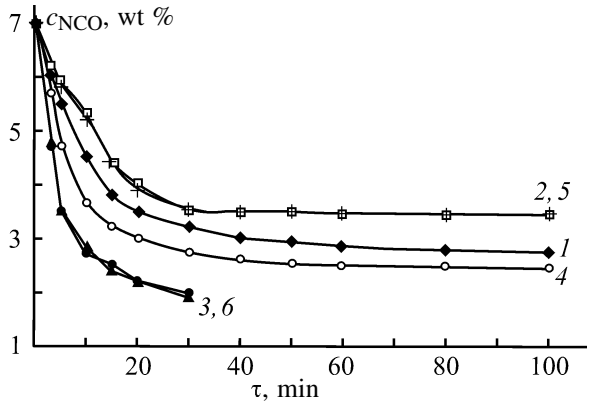
For the kinetic study of the reaction of diisocyanate with PE, we chose 2,4-toluene diisocyanate (TDI) and nonstabilized polyethylene glycol adipate (PEGA) with the number-average molecular weight of 2040, into which we introduced in advance AcA, 2,4,6-tris-(dimethylaminomethyl)phenol (MB), or their mixture. The AcA dosage in PEGA corresponded to its content commonly used in the commercial production of stabilized PEs. The reaction was performed at an NCO : OH molar ratio of 2 : 1 and 80°C. The content of free NCO groups was determined chemically. The apparent reaction rate was evaluated from the content of free NCO groups after heating at 80°C for 30 min, $c_{NCO,\,30}$. The rates of the reaction of PEGA with TDI in the presence of the above additives were compared using as criterion the difference Δc_{NCO} between the "ideal" content of free NCO groups $c_{NCO,\,id}$ (3.52 wt % if the only reaction pathway is the urethane formation) and $c_{NCO,\,30}$.

The SKU-OM was prepared from TDI and PEGA containing various amounts of AcA and MB, at NCO : OH = 2 : 1. The physicomechanical tests of PUs were performed according to GOSTs (State Standards) 270–75, 6950–73, and 263–75.

Table 1 and the figure show that the shapes of the

Table 1. Effect of AcA, MB, and their mixture on the content of NCO groups in the reaction of PEGA with TDI. Molar ratio NCO : OH = 2 : 1, 80°C, 30 min

System no.	Reaction system, mol	$c_{NCO,\,30}$	Δc_{NCO}
		wt %	
1	PEGA + 2TDI	3.21	0.31
2	PEGA + 2TDI + 0.008AcA	3.52	0
3	PEGA + 2TDI + 0.008MB	1.90	1.62
4	PEGA + 2TDI + 0.008AcA + 0.008MB	2.75	0.77
5	PEGA + 2TDI + 0.016AcA + 0.008MB	3.52	0
6	PEGA + 2TDI + 0.008AcA + 0.016MB	1.95	1.57



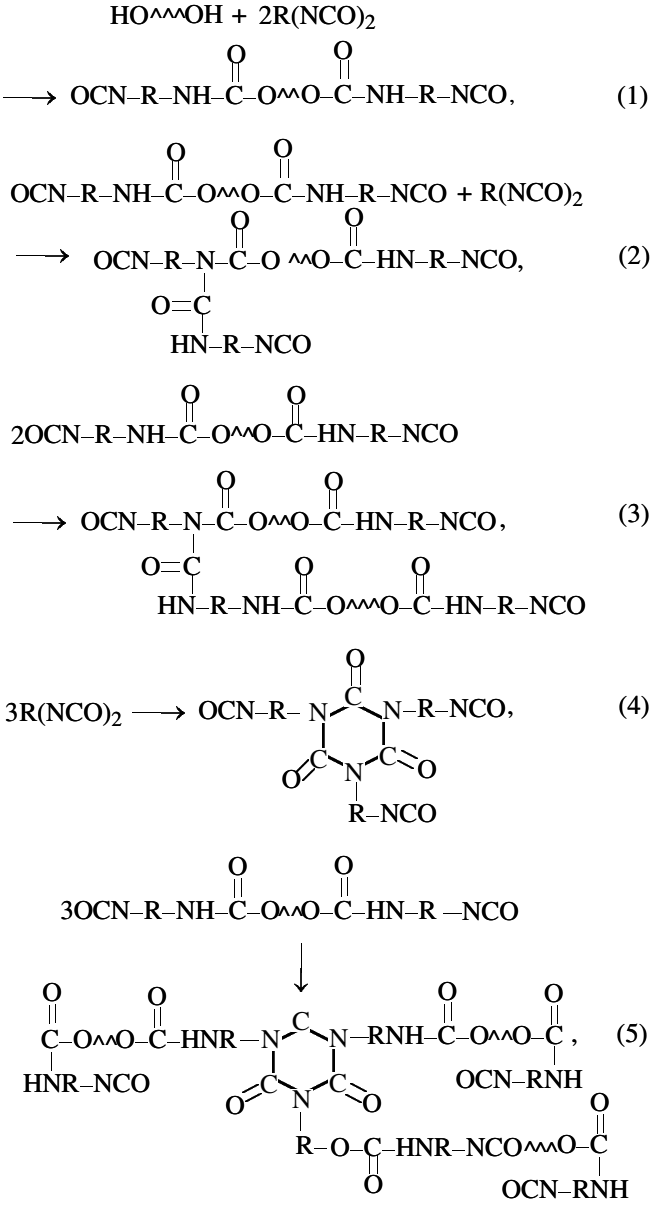
Kinetic curves of consumption of NCO groups in the course of the reaction of PEGA with TDI at 80°C in the presence of AcA, MB, or their mixture. (c_{NCO}) Content of NCO groups and (τ) time. Curve numbers are system numbers in Table 1.

kinetic curves and the rates of the reaction of PEGA with TDI are different in the absence and in the presence of the above additives.

Kinetic curve *1* (see figure), indicating that the concentration of the isocyanate groups monotonically decreases during a long period, and the numerical value of $c_{NCO, 30}$, which is lower than $c_{NCO, id}$, show that the starting PEGA is a relatively active PE. A sharp decrease in c_{NCO} within the first ~30 min is mainly due to the formation of urethanes [reaction (1)] and insignificant amount of allophanates [by the reaction of unchanged TDI with a urethane group of the prepolymer, reaction (2)]. The further decrease in the content of the isocyanate groups in the system is mainly due to the continuing formation of allophanate structures from the NCO groups of both TDI and the prepolymer [reactions (2), (3)]. The presence of allophanates in the prepolymers prepared from active batches of PEGA was proved in [2], where it was suggested that the allophanate formation is promoted by complexes of crown ethers with metal compounds (salts, oxides, hydroxides, etc.), present as impurities in the starting PE.

Addition of AcA to PEGA decreases the rate of the reaction of the PE with TDI (see figure, curve *3*) to the value corresponding to the "ideal" content of NCO groups ($c_{NCO, 30} = c_{NCO, id} = 3.52$ wt %, $\Delta c_{NCO} = 0$), after which this parameter varies insignificantly. This fact is due to the reaction of AcA with metal compounds, including unstable complexes of crown ethers with metal complexes, yielding metal acetylacetonates [4], which catalyze only the urethane formation [reaction (1)] and do not promote secondary reactions [5].

In the presence of MBs, the reaction of PEGA with TDI is considerably accelerated (see figure, curve *2*) and is virtually complete in 40 min. Such a rapid reaction is due not only to the catalysis of urethane formation, but also to the formation of allophanate and triisocyanurate structures [reactions (1)–(5)] whose presence was proved previously [6]:



where HO^^OH is a polyester and $R(NCO)_2$ is a diisocyanate.

When equimolar amounts of MB and AcA are added simultaneously, the rate of the reaction of PEGA with TDI (Table 1, system no. 4) differs insignificantly from that without additives (Table 1, system no. 1). However, the reaction is considerably slower than that of PEGA with TDI catalyzed by MB (Table 1, system no. 3). Apparently, AcA not only

Table 2. Physicomechanical parameters of SKU-OM derived from PEGA and TDI at the molar ratio NCO : OH = 2 : 1 in relation to the concentration of AcA, MB, or their mixture*

Formulation no.	SKU-OM formulation, mol	f_{100}	f_{300}	f_t	ε	Δε	E	H_{TM-2}, arb. units
		MPa			%			
1	PEGA + 2TDI + 0.024MB	3.4	7.4	26.6	360	0	34	62
2	PEGA + 2TDI + 0.024MB + 0.024AcA	3.0	–	12.4	280	0	32	60
3	PEGA + 2TDI + 0.024MB + 0.048AcA	No curing						
4	PEGA + 2TDI + 0.048MB + 0.024AcA	3.4	7.1	25.9	380	0	35	61

* (f_{100}, f_{300}) Nominal strain at 100 and 300% elongation, respectively; (f_t) nominal tensile strength; (ε) relative break elongation; (Δε) relative elongation set; (E) rebound elasticity; and (H_{TM-2}) hardness evaluated with TM-2 device.

reacts with metal impurities in PE but also forms a complex with MB, thus decreasing the concentration of free MB in the system and hence its catalytic effect.

At a higher AcA content, when its amount is sufficient not only for the formation of metal acetylacetonates but also for complete suppression of the catalytic effect of MB, the shape of the kinetic curve of the reaction of PEGA with TDI (see figure, curve *5*) is identical to that obtained for the reaction of PE with diisocyanate in the presence of AcA only (see figure, curve *2*). Therefore, $\Delta c_{NCO} = 0$, and only reaction (1) occurs in the system. On the contrary, when the MB content is higher compared to AcA and is sufficient not only for suppressing the negative effect of AcA but also for catalyzing the reactions of PEGA with TDI [reactions (1)–(5)], variation of the concentration of the NCO groups is virtually similar to variation of c_{NCO} in the reaction of PEGA with TDI in the presence of the MB only (see figure, curve *3*).

The influence of the AcA concentration on the physicomechanical characteristics of SKU-OM is illustrated by Table 2. It should be noted that, for the faster curing of PU, the amount of MB and, correspondingly, that of AcA were increased relative to their amounts in the kinetic experiments, with their molar ratio being preserved. Table 2 shows that AcA (formulation no. 2) decreases the strength of the elastomer, and at a large excess of AcA the polymer is not cured at all (formulation no. 3). This fact is caused by the fact that the catalytic formation of allophanate and triisocyanurate groups, acting as cross-links in the network PU structure, does not occur in the system. An increase in the content of MB relative to AcA eliminates the negative effects of AcA and allows preparation of the polymer whose properties are similar to those of the SKU-OM derived from the nonstabilized PE (formulation no. 4).

Similar trends were observed upon introduction of AcA into other PEs differing in the structure and activity in the reaction with the diisocyanate, and also with various commercial stabilized PEs.

CONCLUSIONS

(1) Acetylacetone inhibits the reaction of polyethylene glycol adipate with diisocyanate in the presence of catalytic amounts of phenolic Mannich bases, which is due to a decrease in the catalyst concentration in the system as a result of its consumption for the formation of the acetylacetonate complex.

(2) Synthesis of castable polyurethanes of the SKU-OM brand from stabilized polyesters should be performed at increased dosage of the Mannich base, eliminating the negative effect of acetylacetone.

REFERENCES

1. USSR Inventor's Certificate no. 1 121 974.
2. Davidenko, V.T., Stepanova, T.V., Teteruk, T.S., and Apukhtina, N.P., in *Sintez i svoistva poliefiruretanovykh elastomerov: Sbornik nauchnykh trudov* (Synthesis and Properties of Polyetherurethane Elastomers: Coll. of Scientific Papers), Moscow: TsNIITEneftekhim, 1987, pp. 29–41.
3. RF Patent 914 574.
4. Korneev, N.N., Popov, A.F., Korneev, B.A., and Krentsel', B.A., *Kompleksnye metalloorganicheskie kataliza-tory* (Complex Organometallic Catalysts), Leningrad: Khimiya, 1969.
5. Fisher, J.R., *Tetrahedron*, 1963, no. 19, pp. 97–101.
6. Kirpichnikov, P.A., Bakirova, I.N., Valuev, V.I., and Zenitova, L.A., in *Materialy yubileinoi nauchno-metodicheskoi konferentsii "III Kirpichnikovskie chteniya"* (Proc. Jubilee Scientific and Methodical Conf. "III Kirpichnikov Readings"), Kazan, 2003, pp. 41–45.

ISSN 1070-4272. Russian Journal of Applied Chemistry, 2006, Vol. 79, No. 5, pp. 814–818. © Pleiades Publishing, Inc., 2006.
Original Russian Text © S.S. Galibeev, A.M. Gafarov, A.M. Kochnev, V.P. Arkhireev, A.I. Rakhmatullin, 2006, published in Zhurnal Prikladnoi Khimii, 2006, Vol. 79, No. 5, pp. 825–829.

MACROMOLECULAR CHEMISTRY AND POLYMERIC MATERIALS

Chemical Transformations in the Course of Modification of Crystalline Polyolefins with Mixtures Based on 2,4-Toluene Diisocyanate and ε-Caprolactone

S. S. Galibeev, A. M. Gafarov, A. M. Kochnev, V. P. Arkhireev, and A. I. Rakhmatullin

Kazan State Technological University, Kazan, Tatarstan, Russia

Received August 17, 2005; in final form, March 2006

Abstract—Chemical modification of polyolefins (polypropylene, high-density polyethylene) with mixtures of isocyanates and ε-caprolactone was studied. Chemical transformations occurring in the course of modification of polyolefins with a binary modifying system containing 2,4-toluene diisocyanate and ε-caprolactone in the presence of sodium caprolactamate catalyst were studied using model systems based on α-olefins.

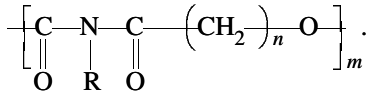
DOI: 10.1134/S1070427206050235

Modification with various reactive compounds is widely used for improving properties of commercial polyolefins (POs). One of the promising procedures for preparing polymeric materials with a required set of properties is their modification with binary mixtures of chemically active compounds able to react under the conditions of PO processing to form copolymer products. It was found [1–3] that binary mixtures of isocyanates (ICs) with a series of heterocyclic compounds (in particular, epoxides and lactames) exert a synergistic effect on the thermal stability and physicochemical properties, which is due to the formation of copolyamide and copoly(amide–ester) fragments grafted to PO unsaturated bonds.

As shown in [1], IC and epoxides added simultaneously in concentrations of up to 3 wt % in the presence of catalytic amounts (with respect to the components of the modifying system) of tertiary amines exert a synergistic effect on the thermal stability and physicochemical properties. This is due to chemical reactions of the additives with each other and with residual unsaturated bonds of polyolefins, which act as potential active centers of degradation.

The mixtures based on 2,4-toluene diisocyanate (TDI) and lactames (LCs) of various structure are also characterized by significant modifying affect in a wide concentration range (1–12 wt %) [2, 3]. These effects are due to decreasing defectiveness of the supramolecular aggregates [4] and to copolymerization of the modifying agents under the conditions of anionic initiation, in particular, in the presence of alkali metal caprolactamates [5, 6]. For example [2], two local optima with respect to relative elongation were determined in the course of PO modification at simultaneous addition of TDI and ω-dodecalactam (ω-DL). In this case, at low concentrations (up to 3 wt %), the optimum is due to deactivation of unsaturated PO bonds and formation of the grafted copolyamide fragments, whereas at high concentrations certain increase in the relative elongation is due to phase segregation of the resulting composites as the products of LC and IC copolymerization form a separate phase [2].

Similar results are obtained with the system based on TDI and ε-caprolactone (cyclic ester, ε-CLN). It was found [7] that, at temperatures close to those of PO processing, in the presence of sodium caprolactamate (Na-LC) catalyst, ICs and CLNs can form copoly(amide–esters) (CPAEs) of the following structure:



Macro- and supramolecular properties and processing and service characteristics of the resulting copolymer products can vary within wide ranges depending on the ratio of the initial monomers.

In this study we examined modification of crystalline POs [polypropylene (PP), high-density polyethylene (HDPE)] with binary mixtures based on TDI and ε-CLN in the presence of Na-CL catalyst; chemical transformations occurring in the course of the modi-

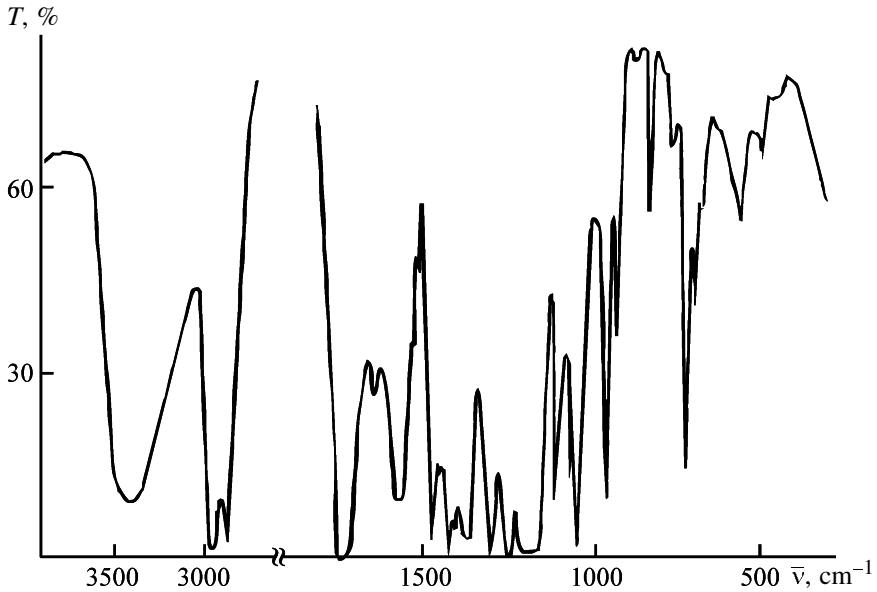


Fig. 1. IR spectra of the product of reaction of heptene and ε-CLN (molar ratio of the initial components 1 : 3). (*T*) Transmission and ($\bar{\nu}$) wavenumber; the same for Fig. 2.

fication were analyzed using real and model systems containing α-olefins.

EXPERIMENTAL

The chemical reaction of α-olefins (hexene, octene, and decene) with ε-CLN and TDI was carried out in a three-necked flask equipped with a reflux condenser and a magnetic stirrer under an inert gas (argon) flow. The required amounts of the monomers and catalyst (Na-CL) were melted at 100°C and then the temperature was increased stepwise to 180°C. The reaction was performed to the formation of the viscous product, and then the reaction mixture was depolymerized in 120 min.

The unchanged reagents were separated from the products of the model reactions by refluxing with acetone in a Soxhlet apparatus for 8 h. The IR spectra of the products of the model reactions were recorded on a PC-16 Perkin–Elmer Fourier IR spectrometer. The IR spectra were analyzed using an internal reference [8].

In our study we used a Balen brand polypropylene (Polipropilen Private Company, Ufa, Russia) and 273–77 brand high-density polyethylene (Kazan'orgsintez Joint-Stock Company, Kazan, Tatarstan, Russia). PO modification was performed in a melt on the rolls at 185 and 165°C for PP and HDPE, respectively. The rolling time was 5 min; the components of the modifying system were added simultaneously with the catalyst.

The samples were cut out from the plates prepared by the direct pressing in accordance with GOST (State Standard) 12019–66 at 210 and 185°C for PP and HDPE, respectively. The specific pressure of the pressing was 7–10 MPa, the heating time was 10 min, the pressing time was 5 min per 1 mm thickness, and the cooling time was 4 min. The thickness of the samples used to determine physicomechanical properties was 0.1 ± 0.01 and 0.2 ± 0.02 cm for PP and HDPE, respectively. We studied the samples with smooth surface without swellings, cracks, and other defects.

The physicomechanical properties (ultimate tensile stress σ_t and relative elongation ε) were determined on an RM 500-T relaxometer in accordance with GOST (State Standard) 11262–80; the velocity of the shifting clamp was 100 mm min^{-1}. The samples were tested for no less than 24 h after the preparation and were preliminarily stored at the test temperature for 4 h.

The melt flow index (MFI) was determined using an IIRT-type capillary viscometer with a capillary diameter of 0.095 ± 0.005 cm. The test temperature and load were 300°C and 5 kg, and 190°C and 2.16 kg for PP and HDPE, respectively. The search for efficient mixtures of the modifying agents was optimized by the simplex–grid method of the experiment design using the Scheffe model of the third and fourth order as a polynomial approximant [9].

To understand the origin of chemical transformations probably occurring at PO modification with

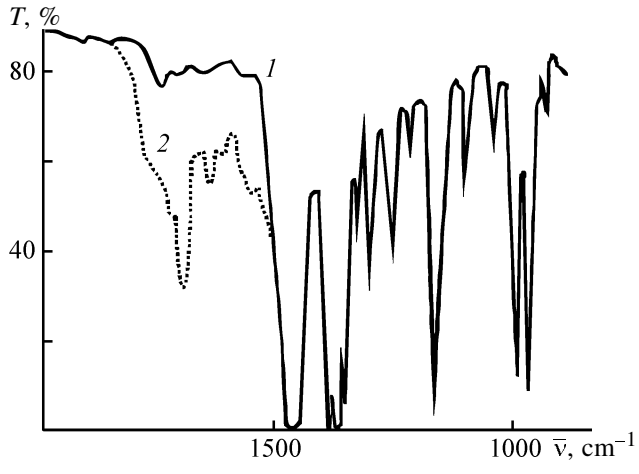


Fig. 2. IR spectra of the (*1*) initial PP and (*2*) PP modified with the ε-CLN + TDI system; weight ratio of the modifying agents 1 : 1, concentration 12 wt %.

the binary system based on TDI and ε-CLN, we should take into account the possibilities of their reaction both with each other and with terminal unsaturated groups of the modified monomers. Therefore, we studied the reactions occurring in binary (ε-CLN + α-olefin) and ternary (ε-CLN + TDI + α-olefin) systems under the conditions of anionic initiation. In the presence of Na-CL the reaction of α-olefins with ε-CLN yield only the ε-CLN homopolymer, and no copolymerization with unsaturated compound was observed. The IR spectrum of the product after removal of the unchanged components (Fig. 1) contains the bands at 2920 (stretching vibrations of the C–H bond in the methylene group), 1730 (vibrations of the carbonyl ester groups), 1472 (bending vibrations of the C–H bond in the methylene group), and 1172 cm^{-1} (stretching vibrations of the C–O bond).

Table 1. Variation in the content of vinylidene bonds in PP modified with the TDI + ε-CLN system

System composition, wt %			$\log(I_{888}/I_{1380})$
PP	TDI	ε-CLN	
100	–	–	0.92
94	–	6	0.91
94	6	–	0.79
88	6	6	0.84

Note: I_{888} and I_{1380} are the intensities of the absorption bands at 888 and 1380 cm^{-1}, belonging to out-of-plane bending vibrations of the terminal vinylidene groups and symmetrical bending vibrations of the methylene groups, respectively.

Formation of the ε-CLN copolymer as the only product was confirmed by the ^1H NMR spectra, which contained signals at 4.1–3.9 and 2.3–2.1 ppm belonging to the protons of the CH_2–O and CH_2–C(O) groups in poly-ε-CLN, respectively. No signals of the methylene and methine groups were found, which suggests the absence of the olefin component.

Previous studies of chemical transformations in the reaction of TDI with α-olefins in the presence of Na-CL showed that their copolymerization proceeded at a high rate and the yield of the final product was as high as 97% [2]. An IR study of the chemical structure of TDI copolymers with various α-olefins showed that the isocyanate reacted with unsaturated bond of the α-olefin through opening of the N=C=O group.

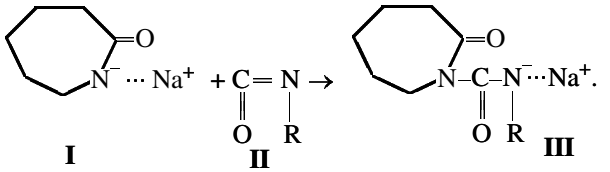
Based on the above facts, we assumed that only the isocyanate component of the TDI + ε-CLN system is chemically active with respect to PO macromolecule; however, formation of more complex copolymers is also possible.

The data on chemical transformations in the ternary α-olefin + ε-CLN + TDI systems showed that, under the given experimental conditions, isocyanate copolymerizes with both CLN and olefin. The resulting products are transparent yellowish solids soluble in strongly polar solvents (such as DMSO, DMF) at elevated temperatures. The yield of the products of reaction of TDI and ε-CLN with various α-olefins depends on both the monomer ratio and the chemical nature of the unsaturated compound and varies from 24 to 89%. These results are confirmed by the IR spectra of PP modified with ε-CLN + TDI. For example, the IR spectrum (Fig. 2) contains the bands at 1720 and 1710 cm^{-1} belonging to the stretching vibrations of the carbonyl group in esters and tertiary amides, respectively.

The decreased intensity of the band at 888 cm^{-1} confirms the reaction of isocyanate with terminal unsaturated bonds in PP (Table 1).

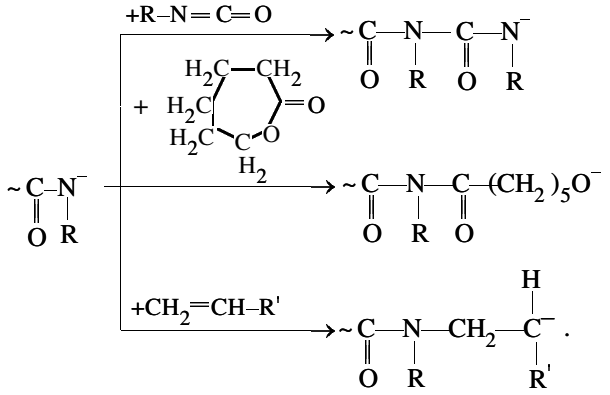
Thus, the data on the model reactions and on the chemical structure of the PO compositions suggest that both copolymerization of the system components and reaction of isocyanates with unsaturated terminal groups of PO occur in the course of modification of PO with TDI + ε-CLN systems under the conditions of anionic initiation. In this case, the ester fragments can be grafted to the PO macromolecule owing to high chemical activity of the isocyanate anion. The main chemical transformations in the tertiary α-olefin + TDI + ε-CLN systems are probably as follows. In the first stage, the catalyst dissociates to form the lactam

anion and alkali metal cation, and this anion reacts with unsaturated N=C bond:



I **II** **III**

In the second stage, anion **III** arising in the α-olefin + TDI + ε-CLN system reacts with the corresponding monomers:



The resulting chain is terminated by the reaction of the anion of the propagating chain with compounds containing labile hydrogen atoms to form terminal hydroxy and amino groups. The data on copolymerization of ε-CLN with diisocyanates [7] showed that either branched or cross-linked structures are formed depending on the content of the initial components.

Similar processes occur in the systems studied. For example, the solubility of the products strongly decreases with increasing concentration of isocyanate component in the monomer system. The data on the service and processing properties of the modified POs showed that the relative elongation ε of the HDPE formulations strongly increases with addition of both individual ε-CLN and its mixtures with the other modifying agents in concentrations of up to 3 wt % (Fig. 3a). Similar results are observed with PP (Fig. 3b). It should be noted that in this case the σ_t values remain virtually constant (Table 2). In the case of the mixtures, the viscosity of the molten PO formulations decreases (Fig. 3c). Such simultaneous changes in the viscosity and elasticity characteristics are probably due to both plasticizing effect of the copoly(amide–ester) formed in the PO matrix and deactivation of the terminal unsaturated bonds.

No effect on the relative elongation ε of PO of the second concentration optimum was observed in modification of polyolefins with systems based on TDI and

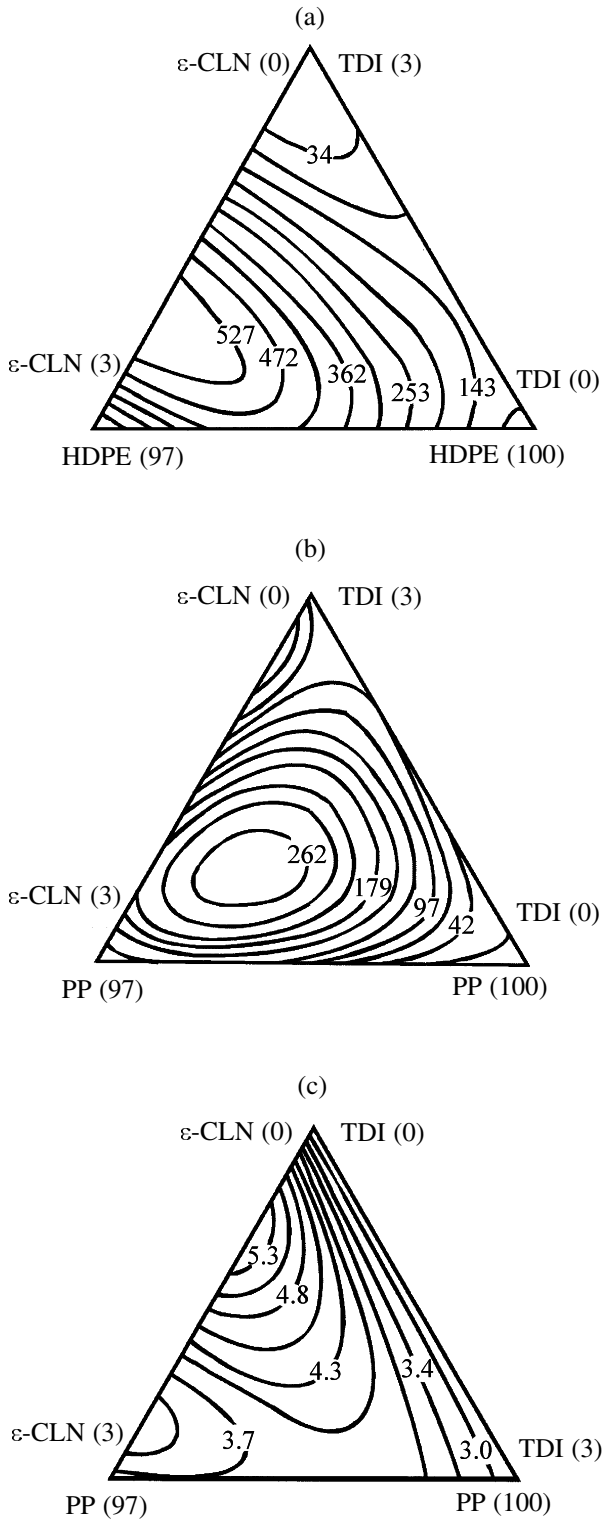


Fig. 3. Diagrams of the relative elongation of the (a) HDPE + TDI + ε-CLN and (b) PP + TDI + ε-CLN, and (c) PP + TDI + ε-CLN systems; figures in parentheses indicate the content of corresponding compound (wt %); the same for Fig. 4.

Table 2. Ultimate tensile stress σ_t of PP and HDPE modified with ε-CLN and TDI

System composition, wt %			σ_t, MPa	
PO	TDI	ε-CLN	HDPE	PP
100	–	–	30.3	34.3
98	2	–	34.7	34.5
98	–	2	32.0	37.4
98	1	1	30.4	34.2
97	1	2	29.2	33.7

ω-DL. This is obviously due to the fact that in the case of 13-membered LC the separate phase appears only at concentration of the modifying system of more than 6%, whereas with mixtures based on CLN it is formed at concentrations as low as 2–3%. This is confirmed by increasing optical density of PP in this concentration range (Fig. 4). These results can be probably explained as follows: opening of the ε-CLN ring yields an aliphatic radical of smaller length (as compared to ω-DL) and, as a result, the copolymer products formed in the course of modification are characterized by lower compatibility with PO.

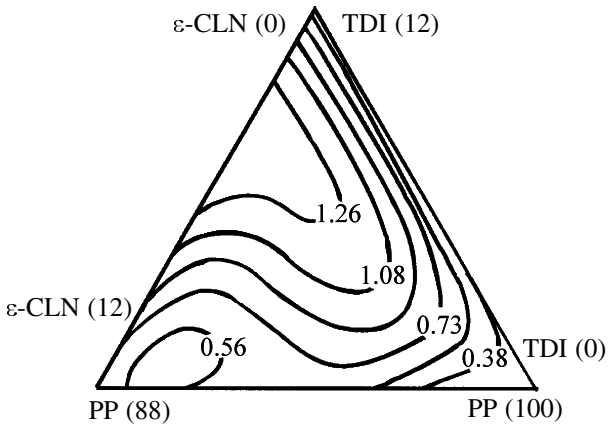


Fig. 4. Diagram of the optical density of the PP + TDI + ε-CLN system (λ 1000 nm).

CONCLUSIONS

(1) Modification of polyolefins with a binary system consisting of 2,4-toluene diisocyanate and ε-caprolactone improves the physicomechanical characteristics of the resulting composites by up to 8–10%.

(2) Isocyanate groups react with the terminal vinyl groups of polyolefins, providing grafting of the polymer matrix with copoly(amide–ester) fragments.

REFERENCES

1. Spiridonova, R.R., Galibeev, S.S., Kochnev, A.M., and Arkhireev, V.P., *Zh. Prikl. Khim.*, 2003, vol. 76, no. 2, pp. 298–303.
2. Gafarov, A.M., Chemical Modification of Polyolefins with Mixtures of Diisocyanates and Unsubstituted Lactams, *Cand. Sci. Dissertation*, Kazan, 2005.
3. Gafarov, A.M., Galibeev, S.S., Kochnev, A.M., et al., *Zh. Prikl. Khim.*, 2004, vol. 77, no. 4, pp. 622–625.
4. Gafarov, A.M., Galibeev, S.S., Kochnev, A.M., et al., *Zh. Prikl. Spektrosk.*, 2004, vol. 71, no. 4, pp. 456–459.
5. Galibeev, S.S., Arkhireev, V.P., Barnyagina, O.V., et al., *Izv. Vyssh. Uchebn. Zaved., Khim. Khim. Tekhnol.*, 2003, vol. 46, no. 4, pp. 88–90.
6. Galibeev, S.S., Barnyagina, O.V., Kochnev, A.M., and Ivanova, A.V., *Vysokomol. Soedin., Ser. B*, 2005, vol. 47, no. 9, pp. 1745–1749.
7. Mukhametzyanova, E.A., Galibeev, S.S., Yakimov, R.V., and Kochnev, A.M., *Vysokomol. Soedin., Ser. B*, 2005, vol. 47, no. 9, pp. 1750–1754.
8. *Praktikum po khimii i fizike polimerov* (Practical Works on Chemistry and Physics of Polymers), Kurenkov, V.F., Ed., Moscow: Khimiya, 1995.
9. Zergenidze, I.G., *Planirovanie eksperimenta dlya issledovaniya mnogokomponentnykh system* (Experimental Design in Studying Multicomponent Systems), Moscow: Nauka, 1976.

ISSN 1070-4272. Russian Journal of Applied Chemistry, 2006, Vol. 79, No. 5, pp. 819–822. © Pleiades Publishing, Inc., 2006.
Original Russian Text © V.I. Grachek, A.N. Lukashik, 2006, published in Zhurnal Prikladnoi Khimii, 2006, Vol. 79, No. 5, pp. 830–834.

MACROMOLECULAR CHEMISTRY AND POLYMERIC MATERIALS

Boric Acid Esters as Thermal Stabilizers and Fungicidal Additives for Elastomers from Natural Rubber

V. I. Grachek and A. N. Lukashik

Institute of Physical Organic Chemistry, National Academy of Sciences of Belarus, Minsk, Belarus

Received November 14, 2005

Abstract—New and previously synthesized boric acid esters were studied as thermal stabilizing and fungicidal additives to elastomers based on natural rubbers.

DOI: 10.1134/S1070427206050247

The world's consumption of natural rubber, mainly used in tire and car industry, steadily increases. Natural rubber, having a unique set of characteristics and being a standard of general-purpose rubber, also has a number of drawbacks hampering its processing and application, such as low fungus resistance [1] and susceptibility to heat aging. The fungus and heat resistance of a material can be enhanced by modification of the rubber, i.e., by purposeful variation of its characteristics using appropriate additives. Proceeding with studies on modification of elastomers [2], we attempted to improve the fungus and heat resistance of natural rubber by introduction of boric acid esters.

The use of organoboron compounds as additives improving the quality of polymer materials is well known [3–5]. With the aim to synthesize promising thermal stabilizing and fungicidal additives for natural rubber, we studied new boric acid esters and those described previously [2].

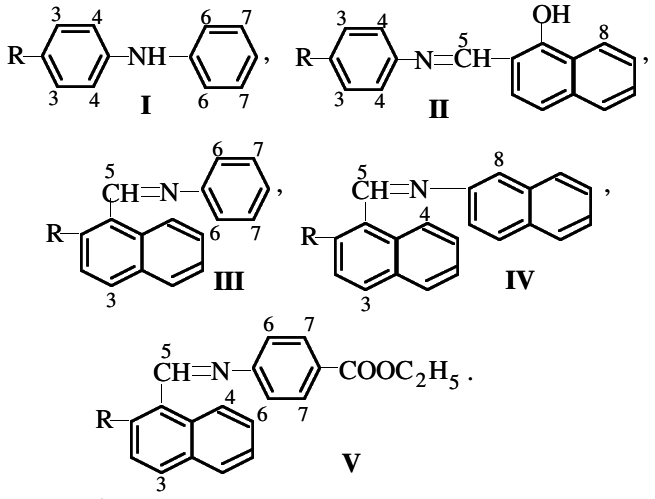
EXPERIMENTAL

The ^{1}H NMR spectra of solutions in $CDCl_3$ were recorded on a Tesla BS-567 spectrometer (100 MHz), hexamethyldisiloxane was used as internal reference. The IR spectra were recorded on a UR-20 spectrophotometer in KBr pellets. The melting points of the compounds were determined on a Köfler unit.

Borates were prepared by heating of a mixture of boric acid with pyrocatechol and hydroxo compounds at 70–100°C in toluene or benzene with simultaneous removal of the released water as a heteroazeotrope. The structure of the resulting compounds was proved by IR spectroscopy, ^{1}H NMR, mass spectrometry, and elemental analysis.

The absorption bands in the ranges 1350 ± 10 and 1040 ± 10 cm^{-1} are assigned to the symmetric and asymmetric vibrations of the B–O group, and those in the ranges 1240 ± 5 and 1090 ± 10 cm^{-1}, to the symmetric and asymmetric vibrations of the C–O group. The bands at 1640 ± 5 cm^{-1} are assigned to vibrations of the CH=N group. The absorption at 1754 ± 10 cm^{-1} corresponds to the stretching mode of the ester group.

The ^{1}H NMR spectra of previously unknown compounds **I**–**V** are presented in Table 1:



The ^{1}H NMR spectra of **VI**–**IX** were described in [2]:

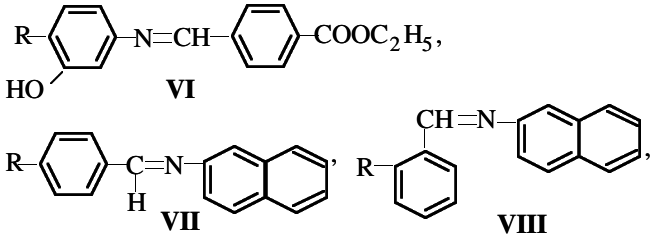


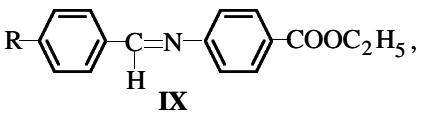
Table 1. ^{1}H NMR spectra of **I–V**

Compound	δ, ppm								Mass spectrum, M^+ (*I*, %)
	CH^1	CH^2	CH^3, s	CH^4	CH^5	CH^6	CH^7	CH^8	
I	6.18	5.60	5.67	5.48		5.69	5.83		303 (30)
II	6.20	5.61	5.70	5.49	8.12			6.72	381 (32)
III	6.22	5.62	7.02	6.81	8.18	5.70	5.96		365 (34)
IV	6.24	5.62	7.01	6.84	8.14			6.78	415 (38)
V	6.23	5.63	7.03	6.80	8.17	5.71	5.98		437 (36)

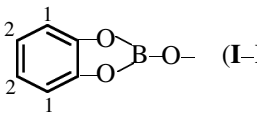
Table 2. Yields, melting points, and elemental analyses of **I–V***

Compound	Yield, %	*T*, °C	Found, %/Calculated, %				Formula
			C	H	N	B	
I	55	149–150	71.38/71.35	4.68/4.62	4.71/4.62	3.60/3.56	$C_{18}H_{14}BNO_3$
II	60	156–157	72.44/72.50	4.27/4.20	3.62/3.67	2.81/2.83	$C_{23}H_{16}BNO_4$
III	83	137–138	75.52/75.67	4.31/4.38	3.88/3.84	3.01/2.96	$C_{23}H_{16}BNO_3$
IV	86	264–265	78.16/78.12	4.38/4.34	3.39/3.37	2.58/2.60	$C_{27}H_{18}BNO_3$
V	68	219–220	71.39/71.45	4.59/4.57	3.19/3.20	2.51/2.47	$C_{26}H_{20}BNO_5$

* Compounds **VI–IX** were described in [2].



IX

where R =  (**I–IX**).

As seen from Table 1, protons of the pyrocatechol ring give signals at 6.18 ± 0.06 and 5.60 ± 0.03 ppm. The proton of the azomethine group gives a signal at 8.12 ± 0.05 ppm. The chemical shifts of substituent proton signals in the spectra of **I–V** are given in Table 1.

The mass spectra of boric acid esters contain weak peaks of molecular ions (Table 1). The molecular peaks have approximately the same intensity for all the compounds. Hence, the degree and features of electron delocalization in the substituents, affecting the resistance to electron impact, the yield of molecular ions, and formation of stable radicals, are similar.

The physicochemical characteristics of the newly synthesized compounds are given in Table 2.

Boric acid esters were incorporated into formulations based on natural rubber. The rubber stocks were prepared on 320/320 laboratory rolls. We used the following formulas (wt proportion): plasticized natural rubber, thick "light crepe," sort 1, 100; stearin, 0.5; Captax, 0.7; zinc oxide, 5.0; sulfur, 3.0; and boric acid ester, 0.5 or 1.0 (a total of 160 samples). The temperature of rolls was 55–60°C; clearance, 0.4 mm; and mixing duration, 3 min. Standard plates 2 mm thick were vulcanized on a 300 × 400 hydraulic press at 140°C for the time corresponding to the optimum of vulcanization determined from the physicomechanical characteristics of rubber and equal to 22–25 min.

Thermal oxidative aging of vulcanized rubbers was examined using samples in the form of blades in a thermostat with air circulation at 100°C for 37 h.

The fungicidal resistance of vulcanized rubbers was evaluated according to requirements of GOST (State Standard) 9048–75. The degree of fungus development on the samples of vulcanized rubber was evaluated on the six-point scale.

Aging of elastomers is one of the main causes of decreasing working capacity and service life of items made of them. The resistance of rubbers to thermal action is appreciably governed by the rubber structure. The unique characteristics of natural rubber are due to strict and fine adjustment of the composition, structure, and length of macromolecules, realized in biosynthesis in plant cells [6]; therefore, not all additives

Table 3. Thermal aging of vulcanized rubbers in the presence of boric acid esters*

Compound	Amount added, wt proportion	Ultimate tensile strength, P		Relative elongation, L		Elongation set, l	
		P_0, MPa	K_P	L_0, %	K_L	l_0, %	K_l
I	0.5	12.11	0.11	760	0.35	12	0.34
II	0.5	10.05	0.20	758	0.42	10	0.45
	1.0	9.57	0.23	780	0.46	12	0.47
III	0.5	10.92	0.14	800	0.40	14	0.39
IV	0.5	12.19	0.16	762	0.40	16	0.40
V	0.5	11.58	0.23	764	0.43	11	0.45
	1.0	10.93	0.24	752	0.47	12	0.48
VI	0.5	10.87	0.24	768	0.43	11	0.47
	1.0	10.73	0.28	771	0.48	14	0.50
VII	0.5	13.53	0.19	772	0.39	16	0.44
VIII	0.5	10.57	0.19	760	0.38	14	0.43
IX	0.5	10.44	0.22	771	0.44	13	0.45
Neozon D	0.5	8.78	0.15	748	0.41	12	0.39
	1.0	10.52	0.20	795	0.42	16	0.38
No additive	–	12.00	0.10	758	0.33	13	0.31

* $K_P = P/P_0$, $K_L = L/L_0$, $K_l = l/l_0$.

are compatible with natural rubber. In aging, the bonds are ruptured and rearranged, which can also initiate thermal oxidative degradation of the chains. Boric acid esters containing an electron-seeking boron atom able to accept electrons on the vacant orbitals can block the radicals formed in aging of elastomers. In addition, borates contain a nitrogen atom able to terminate the chains.

The thermal stability of rubbers with borates added was compared to that of the rubber without additives and with the rubber containing a commercial stabilizing agent, Neozon D (Table 3). Organoboron compounds are uniformly distributed in the natural rubber, do not affect vulcanization of the rubbers, do not deteriorate the initial physicochemical characteristics, and do not color the rubber items. In thermal aging (100°C, 37 h), the rubbers containing boric acid esters have higher physicochemical characteristics than the rubbers without additives, i.e., all the compounds studied thermally stabilize vulcanized rubbers. Compound **I** containing no azomethine group is less efficient as stabilizing agent. All boric acid esters contain a common phenylene borate group bonded by a bridging oxygen atom with an aromatic radical. In this case, the presence of substituents in the *o*- or *p*-position of the aromatic radical does not noticeably affect the thermal stabilizing characteristics of borates. For example, compounds **VII** and **VIII** differing only in the substituent position have the same stabilizing activity. Borates containing, along with azomethine group, hydroxy or ester group (**II, V, IX**) have a high thermal stabilizing effect. A comparison with Neozon D shows that the boric acid esters containing azomethine group have approximately the same thermal stabilizing activity as Neozon, but, contrary to Neozon, do not color rubber items. Compound **VI** in an amount of 1.0 wt % relative to rubber is the most efficient thermal stabilizing agent for natural rubber and is somewhat more active than Neozon D. The strength of vulcanized rubber containing this compound varies in aging by a factor of 2.5, and the elasticity of this rubber is 15% lower than that of the rubber without an additive. The high thermal stabilizing effect of this borate is caused by the presence of a boron atom, an azomethine group, and also, contrary to the other esters, an ester group in a combination with hydroxy group.

Natural rubber is not fungus-resistant and is very easily overgrown with fungi at high relative humidity (approximately 85%), elevated temperature (20–30°C), and in stagnant air, which accelerates degradation of the material. Various compounds, among them polyalkyleneguanidine salts, are used as disinfectants for natural rubber [7]. Since organoboron compounds have a fungicidal effect on polymer materials [8, 9], we studied the effect of boric acid esters on biofouling of vulcanized rubbers with fungi. The results are listed in Table 4.

Table 4 shows that biofouling of rubbers with fungi is significantly weaker in the presence of borates than without additives. The results obtained show

Table 4. Estimation of fungus development on vulcanized rubbers according to six-point scale

Compound	Amount added, wt %	Estimation of fungus development, points, in indicated period, days			
		28	56	84	120
I	0.5	2	3	3–4	4
II	0.5	0–1	0–1	1–2	2
	1.0	0	0	0–1	1–2
III	0.5	2	3	3	3–4
IV	0.5	1–2	2	2–3	3–4
V	0.5	0	1–2	2–3	3
	1.0	0	0–1	1–2	2–3
VI	0.5	0	0–1	1	1–2
	1.0	0	0	0–1	0–1
VII	0.5	0–1	0–1	1–2	2
VIII	0.5	1–2	2	2–3	3–4
IX	0.5	0	1–2	1–2	2
No additive	–	4	4–5	5	5

that esters of different structures differently affect the resistance of rubbers to biofouling with fungi. The most efficient additives are the compounds containing a *p*-substituted phenylene group bonded to the boron atom through the oxygen bridge. In particular, compounds **VII** and **VIII** have similar thermal stabilizing activity, but the fungicidal effect of **VII** is stronger. Addition of the substituted azomethine group to phenyl ring in the *p*-position makes the borate molecule more mobile, and this molecule more readily diffuses in the material bulk to the surface; to suppress development of microorganisms at the surface, the fungicide concentration at the surface should be sufficiently high [10]. Therefore, compounds **III**–**V** and **VIII** containing bulky substituents in the *o*-position of the phenyl ring or in the α-position of the naphthalene ring show lower fungicidal activity than **VII**.

Compound **VI** has the highest fungicidal activity with respect to vulcanized natural rubber, and, as we showed, this compound is the most efficient thermal stabilizing agent. The compounds synthesized meet the requirements imposed on fungicidal additives: they have a high toxicity for fungi but are virtually nontoxic for humans (LD_{50} = 580–670 mg kg^{-1}), are well compatible with natural rubber, and do not prevent vulcanization.

The studies showed that boric acid esters are multitarget process additives whose introduction enhances the resistance of rubbers to thermal aging and fungi.

CONCLUSIONS

(1) Boric acid esters were synthesized. They are thermal stabilizing agents for vulcanized rubbers and protect them from biofouling with fungi.

(2) Boric acid ester containing azomethine, hydroxy, and ester groups exhibit the strongest thermal stabilizing and fungicidal effects.

REFERENCES

1. Borisova, N.N., Rebizova, V.G., and Kosenkova, A.S., *Vliyanie faktorov tropicheskogo klimata na svoistva kauchukov i rezin* (Influence of Tropical Climate Factors on Characteristics of Rubbers), Moscow: TsNIITeneftekhim, 1976.
2. Grachek, V.I., Bukanova, N.N., Smolyakov, A.V., et al., *Zh. Prikl. Khim.*, 2001, vol. 74, no. 1, pp. 147–150.
3. US Patent 6 111 000.
4. Meilakhs, L.A., Gorelik, R.A., and Dorokhov, V.A., *Kauchuk Rezina*, 1986, no. 2, pp. 42–43.
5. Grachek, V.I., Naumova, S.F., Motol'ko, G.R., et al., *Dokl. Akad. Nauk Bel. SSR*, 1985, vol. 29, no. 6, pp. 536–539.
6. Archer, B.L., *Biochem. J.*, 1960, vol. 75, no. 2, pp. 236–239.
7. RF Patent 2 190 640.
8. Fedortsova, E.V., Idlis, G.S., Shvarts, E.M., et al., *Zh. Obshch. Khim.*, 1994, vol. 64, no. 1, pp. 139–141.
9. JPN Patent Appl. 59-30 807.
10. Gumargalieva, K.Z., Zaikov, G.E., Semenov, S.A., et al., *Vysokomol. Soedin., Ser. A–B*, 1998, vol. 40, no. 10, pp. 1551–1553.

ISSN 1070-4272. Russian Journal of Applied Chemistry, 2006, Vol. 79, No. 5, pp. 823–826. © Pleiades Publishing, Inc., 2006.
Original Russian Text © I.A. Opeida, Yu.I. Skichko, O.V. Kush, 2006, published in Zhurnal Prikladnoi Khimii, 2006, Vol. 79, No. 5, pp. 835–838.

MACROMOLECULAR CHEMISTRY AND POLYMERIC MATERIALS

Initiation of Radical-Chain Processes with Mixtures of Benzoyl Peroxide and Azobis(isobutyronitrile)

I. A. Opeida, Yu. I. Skichko, and O. V. Kush

Litvinenko Institute of Physical Organic Chemistry and Coal Chemistry, National Academy of Sciences of Ukraine, Donetsk, Ukraine
Donetsk National University, Donetsk, Ukraine

Received August 11, 2005

Abstract—The initiating power of binary mixture of initiators, benzoyl peroxide and azobis(isobutyronitrile), in polymerization of methyl methacrylate and in liquid-phase oxidation of cumene in acetonitrile at 339 K was studied.

DOI: 10.1134/S1070427206030259

Initiation of radical-chain polymerization reactions with mixtures of initiators attracts steady researchers' attention [1–4]. These studies are aimed to choose the optimal conditions for preparing polymers with desired physicochemical characteristics. When the reaction mixture contains initiators or catalysts promoting low-temperature homolytic decomposition of the arising hydroperoxides, the liquid-phase radical-chain oxidation proceeds in the mixed initiation mode [5].

Mixtures of initiators of different chemical natures are of particular interest. Among these initiators are benzoyl peroxide and azobis(isobutyronitrile), which are widely used in polymerization reactions, in particular, as components of binary mixtures when it is necessary to provide a high efficiency of initiation with variation of the process temperature [1, 6]. Azobis(isobutyronitrile) is also used for acceleration of radical-chain oxidation of alkylaromatic hydrocarbons at a temperature below 360 K. The initiating power of each of these initiators was studied, and the kinetic parameters of their decomposition and the initiation efficiencies are well known [5].

In this study we examined the combined action of benzoyl peroxide and azobis(isobutyronitrile) in the radical-chain reactions of cumene oxidation and methyl methacrylate polymerization.

EXPERIMENTAL

Cumene (Cum), acetonitrile used as a solvent, benzoyl peroxide (BPO), and azobis(isobutyronitrile) (AIBN) were purified by standard procedures [7, 8]. Commercial methyl methacrylate (MMA) was washed 2–3 times with 10–15% aqueous alkali to remove completely the inhibitor. Then, MMA was washed 2–3 times with distilled water, dried over anhydrous calcium chloride, and distilled in a nitrogen atmosphere at reduced pressure; the fraction boiling at 22 ± 0.2°C/25 mm Hg was collected. Freshly distilled MMA was used. The kinetics of MMA polymerization was studied dilatometrically to a monomer conversion of 10%. The monomer content in the reaction mixture was 25 vol %. Polymerization of MMA in the presence of BPO and AIBN was performed in acetonitrile at 339 K. The concentrations of peroxide and azobis(isobutyronitrile) in the initiation systems were 1×10^{-2} and 5×10^{-3} M, respectively.

The oxidation rate W was determined volumetrically from the amount of oxygen taken up at a constant oxygen pressure; the reaction mixture was stirred sufficiently intensely to provide the kinetic control of the reaction.

Polymerization initiated by benzoyl peroxide can be described by the following scheme:

$$\mathrm{BPO} \longrightarrow \mathrm{R}^{\bullet},$$

$$\mathrm{R}^{\bullet} + \mathrm{M} \longrightarrow \mathrm{M}^{\bullet},$$

$$\mathrm{M}^{\bullet} + \mathrm{M} \longrightarrow \mathrm{M}_n^{\bullet},$$

$$2\mathrm{M}^{\bullet} \longrightarrow \text{Products}.$$

In the case of the polymerization initiation with a mixture of benzoyl peroxide and azobis(isobutyro-

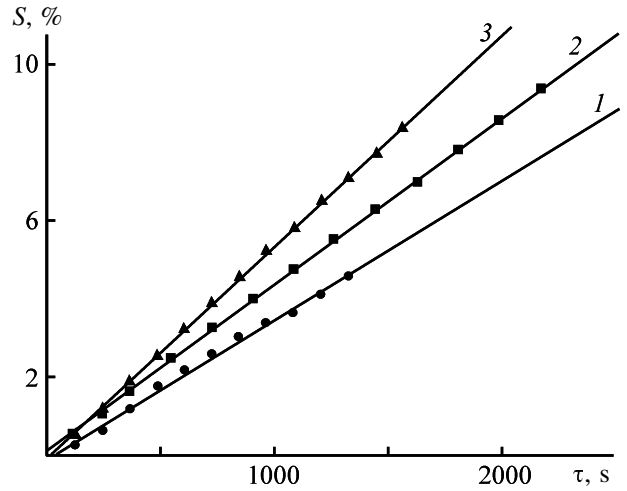


Fig. 1. Kinetic curves of polymerization S of methyl methacrylate ($[MMA]_0$ = 25 vol %) in acetonitrile in the presence of benzoyl peroxide and azobis(isobutyronitrile) at 339 K. (τ) Time. Initial concentration, M: (*1*) $[BPO]_0$ = 0.01, (*2*) $[AIBN]_0$ = 0.005, and (*3*) $[BPO]_0$ = 0.01 and $[AIBN]_0$ = 0.005.

nitrile), the above scheme is supplemented with the following reactions:

$$AIBN \longrightarrow r^{\bullet},$$

$$r^{\bullet} + M \longrightarrow M^{\bullet}.$$

For the initial steady-state stage of the polymerization, the polymerization rate is described by the equation [9]

$$W_{pol} = k_p(2k_t)^{-1/2}[M]W_i^{1/2}, \quad (1)$$

where k_p and k_t are the rate constants for chain propagation and termination, respectively; [M] is the monomer concentration; and W_i is the initiation rate.

In the absence of induced decomposition of the initiator, the initiation rate can be presented as follows:

$$W_i = 2fk_d[I][M]^m, \quad (2)$$

Rates of initiated polymerization of methyl methacrylate W_{pol} at 339 K. $[MMA]_0$ = 25 vol %, solvent acetonitrile

$[BPO]_0$	$[AIBN]_0$	$W_{pol} \times 10^5$, mol l^{-1} s^{-1}
M		
–	0.005	9.83 ± 0.05
0.01	–	8.14 ± 0.18
0.01	0.005	12.29 ± 0.05
0.04	–	14.58 ± 0.50
0.04	0.005	18.17 ± 0.11

where the coefficient 2 is the number of radicals formed by the initiator decomposition; f, initiation efficiency; k_d, rate constant of the initiator decomposition; and [I], initiator concentration.

It is well known [9] that the initiation rate of MMA polymerization at a monomer concentration above 2 M is independent of the monomer concentration. Under the experimental conditions, the MMA concentration was 2.24 M, i.e., the experiment was performed under conditions when the monomer concentration did not affect the polymerization rate. Thus, the rate of initiated MMA polymerization is

$$W_{pol} = a(fk_d[I])^{1/2}, \quad (3)$$

where $a = k_p(2k_t)^{-1/2}[M]$.

The total polymerization rate is

$$W_{pol\Sigma} = a(f_{BPO}k_{dBPO}[BPO] + f_{AIBN}k_{dAIBN}[AIBN])^{1/2} = (W_{polBPO}^2 + W_{polAIBN}^2)^{1/2}. \quad (4)$$

The amount of the polymerized monomer as a function of the duration of methyl methacrylate polymerization initiated by the system BPO–AIBN at 339 K is plotted in Fig. 1. The polymerization rates were determined from the slopes of the straight lines.

The kinetic parameters of methyl methacrylate polymerization in the presence of benzoyl peroxide and azobis(isobutyronitrile) separately and in a mixture are presented in the table.

As seen from the table, the calculated polymerization rate with the combined action of the initiators is $(12.7 \pm 0.19) \times 10^{-5}$ mol l^{-1} s^{-1}, and the experimental value is $W_{pol\Sigma} = (12.29 \pm 0.05) \times 10^{-5}$ mol l^{-1} s^{-1}. Thus, the effect of a mixture of initiators is additive, i.e., the initiators do not affect the initiating power of each other.

It can be assumed that the rate equation for the liquid-phase oxidation of cumene in the presence of binary mixture BPO–AIBN, which proceeds by the same nonbranched radical-chain mechanism, will be similar to the rate equation for the polymerization of methyl methacrylate in the presence of BPO and AIBN. The kinetic scheme of oxidation of hydrocarbons is well known [5]. The initiation and oxidation rates can be presented by the equations

$$W_{iBPO} = k_i[I], \quad (5)$$

$$W_{oBPO} = a(k_i[I])^{1/2}. \quad (6)$$

The total rate of oxidation in the presence of two

initiators is

$$W_{o\Sigma} = a(k_{iBPO}[BPO] + k_{iAIBN}[AIBN])^{1/2} = (W_{oBPO}^2 + W_{oAIBN}^2)^{1/2}. \quad (7)$$

However, the experimental oxidation rates in initiation with individual initiators and their mixtures do not confirm this assumption.

The examples of the kinetic curves of oxygen uptake in cumene oxidation are presented in Fig. 2. They show that the reaction rate remains practically constant during the experiments. It follows from Fig. 2 that at a fixed concentration of benzoyl peroxide addition of AIBN into the reaction mixture increases the oxidation rate.

If we substitute the rate of cumene oxidation in the presence of only AIBN (1.71×10^{-5} mol l^{-1} s^{-1}) or BPO (0.74×10^{-5} mol l^{-1} s^{-1}) in Eq. (7), the calculated oxidation rate at the combined action of the initiators should be equal to 1.86×10^{-5} mol l^{-1} s^{-1}, whereas the experimental value is $W_{o\Sigma} = 1.23 \times 10^{-5}$ mol l^{-1} s^{-1}.

To check whether the initiation efficiency varies in this case, we used the method of inhibitors. The experiments were performed as follows: cumene was oxidized in the presence of BPO and AIBN individually and in a mixture at the ratio cumene : acetonitrile = 1 : 1 at 339 K with addition of 3×10^{-4} M Ionol as an inhibitor.

The equation for the induction period τ in the case of a single initiator is in the form

$$\tau_I = [In]/(k_i[I]). \quad (8)$$

For a mixture of the initiators, the total induction period is

$$\tau_\Sigma = [In]/(k_{iBPO}[BPO] + k_{iAIBN}[AIBN]). \quad (9)$$

If Eq. (8) is substituted in Eq. (9), we obtain the total induction period:

$$\tau_\Sigma = [In]/([In]/\tau_{BPO} + [In]/\tau_{AIBN}) = 1/(1/\tau_{BPO} + 1/\tau_{AIBN}) = \tau_{BPO}\tau_{AIBN}/(\tau_{BPO} + \tau_{AIBN}). \quad (10)$$

If we substitute the induction period in the presence of only AIBN (540 s) or BPO (480 s) in Eq. (10), the calculated total induction period is 254 s, whereas the experimental value is τ_Σ = 360 s.

Thus, the effective initiation rate is significantly lower than the additive value, i.e., the two-component initiating mixture BPO–AIBN exhibits lower initiating power in comparison with the individual effect of

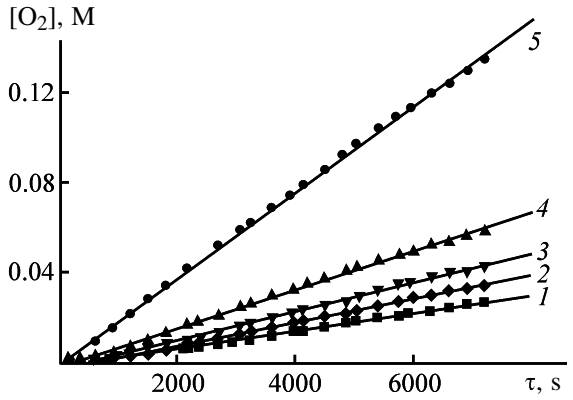


Fig. 2. Kinetic curves of cumene oxidation ([Cum]$_0$ = 3.58 M) in acetonitrile in the presence of benzoyl peroxide and azobis(isobutyronitrile) at 339 K. [BPO]$_0$ = 0.15 M. ([O_2]) Oxygen uptake and (τ) time. [AIBN]$_0$, M: (*1*) 0, (*2*) 0.005, (*3*) 0.01, (*4*) 0.02, and (*5*) 0.06.

AIBN in low-temperature oxidation of cumene. The decrease in the total rate of oxidation can be explained by the reactions of initiator molecules or radicals formed by the decomposition of BPO and AIBN, e.g., by the reaction of 2-cyano-2-propyl radical formed by AIBN decomposition with a BPO molecule:

$$r^\bullet + BPO \longrightarrow r_1^\bullet + P. \quad (11)$$

The reactions of peroxy radicals with peroxide molecule or benzoate radical

$$rO_2^\bullet + BPO \longrightarrow R^\bullet + P_1, \quad (12)$$

$$rO_2^\bullet + R^\bullet \longrightarrow P_2. \quad (13)$$

are also possible.

However, a study of the thermal decomposition of benzoyl peroxide ([BPO]$_0$ = 0.06 M) taken alone and in a mixture with azobis(isobutyronitrile) ([AIBN] = 0.06 M) in ethylbenzene and acetonitrile (1 : 1) does not confirm the occurrence of reaction (11). The experiments were performed as follows. Ampules filled with the reaction mixture were purged with argon for 3 min and heated at 339 K for 12 h. The concentration of benzoyl peroxide was monitored by iodometric titration. In both cases, approximately 17% of the benzoyl peroxide decomposed in 12 h ([BPO] is concentration of benzoyl peroxide after thermal decomposition for 12 h; solvent acetonitrile):

[AIBN]$_0 \times 10^2$, M	[BPO]$_0 \times 10^2$, M	[BPO] $\times 10^2$ M
–	5.97	4.93
6.00	5.85	5.05

The above data show that the presence of AIBN, which decomposes under these conditions with the formation of C-centered radicals, does not accelerate thermal decomposition of benzoyl peroxide. Therefore, reactions (12) and (13) decreasing the total oxidation rate in the presence of a mixture of initiators BPO and AIBN should be included in the scheme of cumene oxidation.

CONCLUSIONS

Initiation of methyl methacrylate polymerization with a mixture of initiators, peroxide and azo compound, occurs by the additive scheme without a reaction between the initiator radicals. In the liquid-phase oxidation of cumene with the same initiators and in the same temperature range, a significant antagonistic effect is observed.

REFERENCES

1. Pan, Z.R., Shan, G.R., Weng, Z.X., and Huang, Z.M., *Chin. J. Chem. Eng*., 2001, vol. 9, no. 1, pp. 1–4.
2. Pinto, J.M. and Gludict, R., *Chem. Eng. Sci*., 2001, vol. 56, no. 3, pp. 1021–1028.
3. Xia, W.Z. and Cook, W.D., *Polymer*, 2003, vol. 44, no. 1, pp. 79–88.
4. Kiparissides, C., Baltsas, A., Papadopoulos, S., et al., *Ind. Eng. Chem. Res*., 2005, vol. 44, p. 2592–2605.
5. Denisov, E.T., *Konstanty skorosti gomoliticheskikh zhidkofaznykh reaktsii* (Rate Constants of Homolytic Liquid-Phase Reactions), Moscow: Nauka, 1971.
6. Wilson, Z.X. and Wayne, D.C., *Polymer*, 2003, vol. 44, no. 1, pp. 79–88.
7. Gordon, A.J. and Ford, R.A., *The Chemist's Companion. A Handbook of Practical Data, Techniques, and References*, New York: Wiley, 1972.
8. Toroptseva, A.M., Belogorodskaya, K.V., and Bondarenko, V.M., *Laboratornyi praktikum po khimii i tekhnologii* (Laboratory Guide to Chemistry and Technology), Leningrad: Khimiya, 1972.
9. Bagdasar'yan, Kh.S., *Teoriya radikal'noi polimerizatsii* (Theory of Radical Polymerization), Moscow: Nauka, 1966.

ISSN 1070-4272. Russian Journal of Applied Chemistry, 2006, Vol. 79, No. 5, pp. 827–832. © Pleiades Publishing, Inc., 2006.
Original Russian Text © I.Yu. Bakunina, O.I. Nedashkovskaya, T.N. Zvyagintseva, Yu.A. Shchipunov, 2006, published in Zhurnal Prikladnoi Khimii, 2006, Vol. 79, No. 5, pp. 839–844.

MACROMOLECULAR CHEMISTRY AND POLYMERIC MATERIALS

Immobilization of α-Galactosidase inside Hybrid Silica Nanocomposites Containing Polysaccharides

I. Yu. Bakunina, O. I. Nedashkovskaya, T. N. Zvyagintseva, and Yu. A. Shchipunov

Pacific Ocean Institute of Bioorganic Chemistry, Vladivostok, Russia
Institute of Chemistry, Far-East Division, Russian Academy of Sciences, Vladivostok, Russia

Received July 12, 2005

Abstract—α-Galactosidase was encapsulated into sol–gel derived hybrid polysaccharide–silica nanocomposites. The main properties of the immobilized enzyme were studied.

DOI: 10.1134/S1070427206030260

Immobilization has long been successfully used for storage and prolongation of action of enzymes, as well as for development of artificial biocatalysts [1, 2]. Encapsulation into a matrix or immobilization on a support allows repeated use of enzymes and facilitates isolation of products of enzymatic reaction, which is essential for development of biotechnological processes. An important advantage of immobilization is the stabilization effect, i.e., significant prolongation of the lifetime and enhancement of the stability of enzymes. Therefore, new efficient supports and matrices for encapsulation of enzymes are constantly sought for.

α-Galactosidase (α-*D*-galactoside galactohydrolase, EC 3.2.1.22) is a promising biochemical tool for studying the antigene structure of various biological objects, in particular, blood cells. Immobilization of α-galactosidase was repeatedly attempted. For example, enzyme from coffee beans was covalently bound to dextran activated with cyanogen bromide [3].

α-Galactosidase from *Pycnoporus cinnabarinus* was immobilized on chitin dispersions with glutaric dialdehyde [4]. Enzyme from *Aspergillus oryzae* was immobilized on Eupergit C containing epoxy groups, which provided covalent bonding of the protein by amino, SH, and carboxy groups [5]. α-Galactosidase from the same source was placed into calcium alginate gel, in which it was additionally immobilized with glutaric dialdehyde [6]. Also, this enzyme was immobilized with polyacrylamide gel [7].

It should be noted that, in the cited studies, the enzyme was encapsulated via cross-linking. Immobilization inside a matrix or on a support by covalent bonding can adversely affect the enzyme through disturbing the conformation of the protein macromolecule. In some cases this is the main reason for partial or complete denaturation of not very stable enzymes [8, 9]. In the case of sol–gel technology, immobilization involves no cross-linking agents. The protein macromolecules are encapsulated into the inorganic matrix formed in situ by polycondensation reactions. The macromolecules undergo minimal structural changes, and the enzymes can preserve their activity [1–3]. α-Galactosidase from *Pseudoalteromonas sp*. KMM 701 sea bacterium can eliminate α-1,3-bound galactose residues from the nonreducing end of glucoconjugates, blood group substances, and antigene determinants for erythrocytes in B(III) blood group via suppressing their serologic activity [10]. α-Galactosidase is a thermally labile enzyme. In concentrated solutions at 20°C α-galactosidase remained active for 1 week, and at 30°C lost 50% activity within 10 min [10]. Dilution of concentrated solutions of the enzyme accelerated its inactivation. A low thermal stability and short lifetime of α-galactosidase in solution hinder its biotechnological application.

Our preliminary studies showed that encapsulation of α-galactosidase into polysaccharide–silica matrices obtained by the method we suggested previously [11, 12] significantly prolonged the lifetime of the enzyme. In this study we examined in more detail the conditions for α-galactosidase immobilization inside new hybrid nanocomposites and the properties of immobilized α-galactosidase in order to select candidate nanocomposites for development of biocatalysts suitable for biotechnological and biosensing applications.

EXPERIMENTAL

Tetrakis(2-hydroxyethyl) orthosilicate (THEOS) was synthesized from tetraethoxysilane (ABCR, Germany) as described in [13]. Polysaccharides xanthan and galactomannan (locust bean gum, from here on, LBG) (Fluka) was used without additional purification. Laminaran (β-1,3-glucan) was isolated from *Laminaria cichorioides* brown alga [14], and α-galactosidase, from biomass of *Pseudoalteromonas sp.* KMM 701 sea bacterium, cultivated at the Laboratory of Microbiology, Pacific Ocean Institute of Bioorganic Chemistry, Far-East Division, Russian Academy of Sciences, by the procedure from [10].

α-Galoactosidase was encapsulated into hybrid polysaccharide–silica nanocomposites by the procedure described in our previous paper [12]. First, 1.9 ml of solution containing 10 or 30 wt % precursor, different concentrations (0.25, 0.35, 0.75, and 1.5 wt %) of one of the three polysaccharides, and 0.1 M sodium phosphate buffer solution (to adjust pH) was prepared. It was kept for some time, determined in previous experiments and required for its conversion into a pregel state by partial polymerization of silicic acids formed from hydrolysis of THEOS. Then, 0.1 ml of the enzyme solution with an activity of 10 units ml^{-1} was added. All the solutions were precooled to 3–5°C in a refrigerator. After mixing and thorough stirring, they once again were placed into the refrigerator in order to minimize denaturation of the enzyme during immobilization.

The activity of immobilized α-galactosidase was determined with *p*-nitrophenyl-α-*D*-galactopyranoside (Sigma) as substrate. The reaction mixture was prepared by mixing 0.35 ml of a 3.3×10^{-3} M solution of substrate in the buffer solution (10^{-1} M sodium phosphate, pH 7.2) and 0.05 ml of solution of free α-galactosidase, or 0.05 g of the gel with the enzyme immobilized, and incubated at 20°C. The reaction was terminated by adding 0.6 ml of an aqueous solution of 1 M sodium carbonate, whereupon the gel was separated by centrifugation. The amount of *p*-nitrophenol yielded by the enzymatic reaction was determined spectrophotometrically at 400 nm (ε = 18 300 l mol^{-1} cm^{-1}). The enzyme activity unit *U* was taken equal to the amount of the enzyme in 1 ml of solution (free enzyme) or 1 g of gel (immobilized enzyme) with which 10^{-6} mol of *p*-nitrophenol was formed per minute. The control was a solution of the enzyme (free enzyme) prepared by 20-fold dilution of the initial solution of α-galactosidase with 0.1 M sodium phosphate buffer solution (pH 7.2). It was free from additions of the precursor and polysaccharide used for immobilization.

α-Galactosidase from *Pseudoalteromonas sp.* KMM 701 sea bacterium was immobilized inside hybrid polysaccharide–silica nanocomposites synthesized using a new precursor, THEOS. It is distinguished by complete solubility in water and compatibility with biopolymers. Polysaccharides were used because they catalyze sol–gel processes [15, 16]. In their presence gelation proceeds at any pH, as well as at low temperatures, which is essential for thermolabile enzymes. In particular, to minimize denaturation of α-galactosidase exhibiting a low thermal stability during encapsulation into silica matrix, immobilization was carried out at a temperature close to 0°C and pH 7.2. Commonly used precursors, such as tetramethoxy- and tetraethoxysilanes, do not form gels under such conditions [8, 9, 17, 18].

To elucidate how the structure of the polysaccharide and its charge affect the catalytic properties of α-galactosidase, we tested negatively charged xanthan and neutral LBG and laminaran. Previously we studied the possibility of immobilization of endo-1 → 3-β-*D*-glucanase L_{IV} from *Spisula sacchalinensis* and α-galactosidase in hybrid polysaccharide–silica nanocomposites [12]. The immobilized proteins remained functionally active for 165 days. The activity of the proteins varied with the formulation of the nanocomposite and structure of the polysaccharide, but these aspects were not studied in detail.

Table 1 lists the activities of α-galactosidase immobilized inside hybrid polysaccharide–silica nanocomposites with various formulations, synthesized in this study. It was tested for 16 months after matrix immobilization of the enzyme. It is seen that the enzyme remained active by the end of the test in selected cases only. To elucidate how the catalytic properties of α-galactosidase are influenced by the structure and concentration of the polysaccharide, as well as by the silica concentration in the matrix, we will consider the activities determined just after gel formation.

Table 1 shows that the highest activity was exhibited by sample no. 5 prepared by mixing 0.25 wt % solution of xanthan and 10 wt% solution of THEOS. It was nearly two times that of the free enzyme. Also, it exceeded the activity of galactosidase in a matrix with identical formulation that we examined previously [12], but in that study the content of the enzyme was by an order of magnitude lower.

The enzymatic activity of sample nos. 2 and 3, containing 0.25 and 0.75 wt % LBG, respectively,

Table 1. Activity of α-galactosidase in relation to the immobilization conditions and storage time

Sample no.	SiO_2, wt %	Polysaccharide, wt %	$U \times 10^3$, g^{-1}, at indicated storage time, days						
			0	6	19	30	43	165	417
1	0	Free enzyme*	33.6	21.8	16.5	N.d.**	18.7	0	0
2	10	LBG: 0.25	34.6	50.9	76.8	N.d.	54.1	N.d.	28.9
3	10	0.75	32.8	56.7	81.8	N.d.	63.5	N.d.	N.d.
4	10	1.5	9.2	10.9	12.0	N.d.	8.4	N.d.	9.6
5	10	Xanthan: 0.25	63.9	N.d.	N.d.	21.7	N.d.	N.d.	N.d.
6	30	0.25	14.1	N.d.	N.d.	0.1	N.d.	N.d.	N.d.
7	10	Laminaran, 0.35	20.0	N.d.	N.d.	0	N.d.	N.d.	N.d.

* U, ml^{-1}
** Not determined.

just after immobilization was comparable to that of the enzyme in solution. With increasing amount of LBG in the silica matrix to 1.5 wt % (sample no. 4), the activity decreased almost threefold. This suggests that the activity depends on the concentration of the polysaccharide in the hybrid nanocomposite. As shown in [15, 16], this can be due to the fact that the network structure of the nanocomponent becomes thicker, which can hinder diffusion of the substrate and the enzymatic reaction products.

Most probably, a similar factor also operates when the content of silica in the nanocomposite is increased. Comparison of the data for sample nos. 4 and 5 (Table 1), containing identical amounts of xanthan and different amounts of THEOS (10 and 30 wt %, respectively), shows that the activities of the enzyme immobilized differed for them by a factor of nearly 5. Among the polysaccharides that we studied only laminaran in the gel did not exert a stabilizing effect on the immobilized α-galactosidase. This follows from the fact that the enzymatic activity of control sample no. 1 was 1.5 times that of sample no. 7 (see Table 1).

A 16-month testing of the samples showed that, by the end of this time, α-galactosidase lost its enzymatic activity in most cases (Table 1). The situation with the free enzyme was similar. The activity was preserved by sample nos. 2–4 only: By the end of the test period it was virtually identical to that in the beginning of the experiment. However, the activity of the biocatalysts varied during the tests. For sample nos. 2 and 3 it increased more than twofold within the first 19 days and then tended to decrease. The activity of sample no. 4 significantly varied in the beginning of the experiment, whereupon it remained virtually unchanged throughout the test period.

Tests of xanthan- (nos. 5 and 6) and laminaran-containing (no. 7) samples showed that the activity of the immobilized enzyme decreased with time. Also, the lifetime of α-galactosidase in matrices containing these polysaccharides was shorter than that in the previously discussed samples with LBG.

The retention of the immobilized enzymes in(on) the support is of practical importance. To estimate the strength of immobilization of α-galactosidase in the polysaccharide–silica matrices, we tested sample nos. 2–4 in which the enzyme was best preserved. To 0.1 g of gels, 0.4 ml of 10^{-1} M buffer sodium phosphate solution (pH 7.2) was added. After 2-day keeping in a refrigerator at 4°C with intermittent stirring, the samples were centrifuged at 10000 rpm. The activity was determined in both supernatants and gels by the above-described procedure.

The solutions in which the biocatalysts were kept and separated by centrifugation virtually lack enzymatic activity (Table. 2). This suggests a fairly strong immobilization of the enzyme macromolecules in the gel matrix, when only insignificant number, if any, of them can liberate. However, the activity in gel nos. 2 and 3 proper proved to be significantly lower than the initial activity (Table 2). Probably, centrifugation was responsible for compaction of gels, which do not exhibit high mechanical strength, and

Table 2. Retention of α-galactosidase in the silica nanocomposite (10 wt %) containing different amounts of LBG

Sample no.	LBG, wt %	$U \times 10^3$, g^{-1}	$U \times 10^3$	
			in 1 ml of supernatant	in 1 g of gel
2	0.25	34.6	0.076	3.7
3	0.75	32.8	0.018	12.5
4	1.50	9.2	0.009	12.6

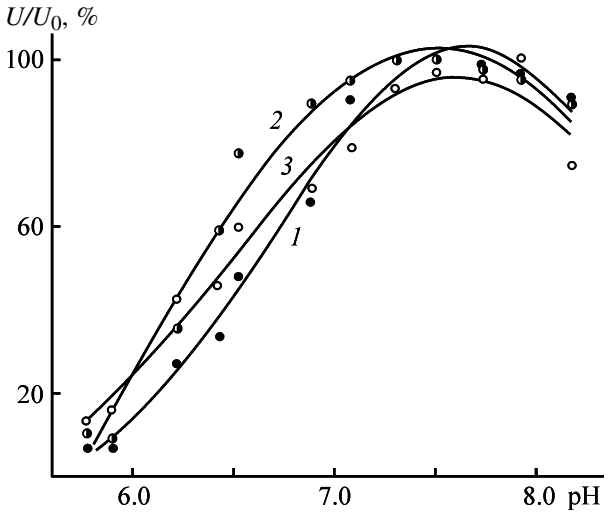


Fig. 1. pH dependence of the residual activity U of (*1*) free and (*2, 3*) immobilized α-galactosidase in gel nos. 4 (*2*) and (*3*) 5. 0.1 M sodium phosphate buffer solution.

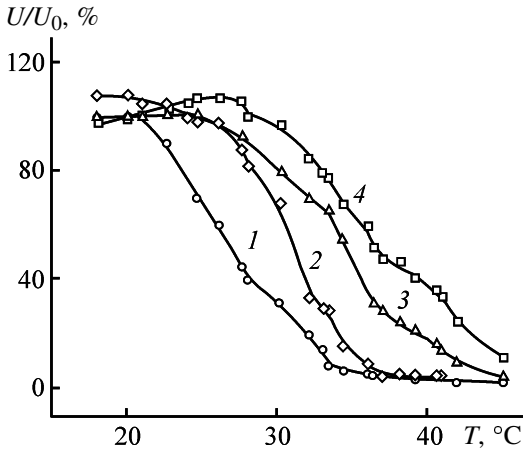


Fig. 2. Temperature dependence of the residual activity U of (*1, 2*) free and (*3, 4*) immobilized α-galactosidase in sample nos. (*3*) 4 and (*4*) 5. 0.1 M sodium phosphate buffer solution, pH 7.3. Time of keeping at the required temperature, min: (*1, 3*) 30 and (*2, 4*) 10.

this either hindered the accessibility of the enzyme for the substrate, or inactivated the enzyme immobilized. When the LBG concentration in the gel (sample no. 4) was increased, the mechanical exposure affected the enzyme activity to a significantly lesser extent.

We determined the pH corresponding to the optimal activity of immobilized α-galactosidase. To 0.05 ml of free enzyme preparation, or 0.05 g of gel, 0.25 ml of 0.1 M sodium phosphate buffer solution with pH under study and 0.1 ml of 10^{-2} M aqueous solution of the substrate were added. The activity of the enzyme was determined by the above-described procedure. The residual activity was calculated as the ratio, %, of the activity U at various pH values to that of the enzyme at optimal pH values, U_0. Figure 1 presents the pH dependences of the residual activity of the enzyme for free (curve *1*) and immobilized α-galactosidase in gels with LBG (sample no. 2) and xanthan (sample no. 3) (curves *2* and *3*, respectively). It is seen that encapsulation into a silica matrix caused the pH range to broaden to a certain extent, but left the pH corresponding to the optimal activity of the enzyme virtually unaffected.

As shown by analysis of published data, immobilization by cross-linking noticeably shifted the pH corresponding to the highest activity of α-galactosidases. For example, for enzyme isolated from *A. oryzae*, immobilized inside an alginate matrix with glutaric dialdehyde, this pH shifted to the acid region by 0.3 pH unit [6], and for α-galactosidases from *Gibberella fujikuroi* in polyacrylamide gel and from green coffee beans in dextran, by 0.4 pH unit [3, 7]. In the case of sepharose-immobilized enzyme isolated from fig, the pH corresponding to the best activity shifted by 1 pH unit [19]. These published data suggest that the properties of α-galactosidase changed more substantially in the case of immobilization by cross-linking than in the case of the sol–gel technology that we applied here.

Another problem addressed by this study is the thermal stability of α-galactosidase. Gel (0.05 g) with the enzyme immobilized was placed into a thermostat, kept at the required temperature for 10 or 30 min, and cooled to room temperature, whereupon the residual activity was estimated as described above. The control sample was subjected to analogous manipulations.

Figure 2 shows the temperature dependences of the residual activity for free (curves *1* and *2*) and immobilized α-galactosidase in gels with LBG (sample no. 3) and xanthan (sample no. 5) (curves *3* and *4*, respectively). The keeping time was 10 min (curves *2* and *4*) and 30 min (curves *1* and *3*). Analysis of these dependences showed that, after 10-min keeping, free α-galactosidase lost its activity at 37°C (curve *2*), and after 30-min keeping, at 32°C (curve *1*). Under identical conditions, the immobilized enzyme preserved from 50 to 70% of its activity (curves *3* and *4*). Major shift of curves *3* and *4* to higher temperatures relative to curves *1* and *2* suggests that encapsulation into the polysaccharide–silica gel causes the thermal stability of α-galactosidase to increase. This can be due to a stabilizing effect of the inorganic matrix, hindering temperature-induced conformational transitions of the protein molecule. This effect was observed, for example, in the case of proteins immobilized inside

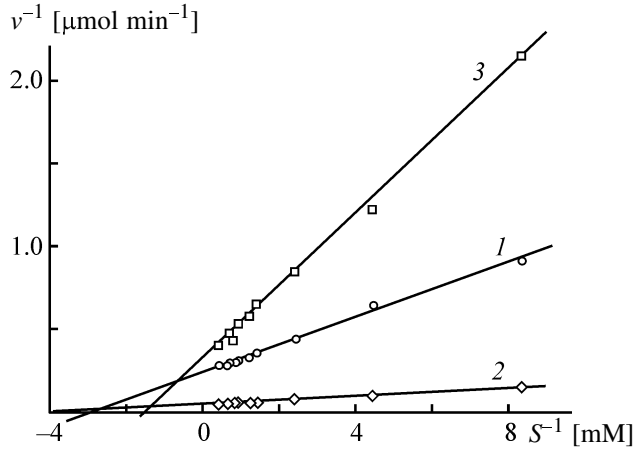


Fig. 3. Reciprocal rate of accumulation of *p*-nitrophenol v^{-1} vs. the reciprocal concentration of *p*-nitrophenyl galactoside S^{-1} for α-galactosidase (*1*) in solution and (*2*, *3*) in immobilized state in sample nos. (*2*) 2 and (*3*) 5.

silica hydrogel [20–23]. Immobilization typically increases the thermal stability of enzymes. In the majority of studies with α-galactosidase it increased by several degrees [3, 5–7, 19]. At the same time, Mitsutomi [4] reported that the thermal stability of α-galactosidase from *P. cinnabarinus*, immobilized in chitin, did not change relative to free α-galactosidase [4].

To compare the catalytic properties of free and gel-immobilized α-galactosidase, we determined the corresponding Michaelis constants K_m. We tested gels containing 0.75 wt % LBG (sample no. 2) and 0.25 wt % xanthan (sample no. 5) at 20°C in 0.1 M sodium phosphate buffer solution, pH 7.7, at a time when the free and immobilized gels still exhibited the maximal activity. The concentration of the substrate, *p*-nitrophenyl galactopyranoside, was varied from 0.12×10^{-3} to 2.49×10^{-3} M. To 0.05 ml of dilute enzyme, or to 0.05 g of gel, 0.350 ml of the buffer solution of the substrate was added. The reaction was terminated by introducing 0.6 ml of aqueous solution of 1 M sodium carbonate. The samples with the gels immobilized were centrifuged at 10000 rpm, whereupon the concentration of *p*-nitrophenol in the supernatant was determined by the above-described procedure. The K_m constant was calculated by the standard Lineweaver–Berk method.

Figure 3 presents the plots of the reciprocal enzymatic reaction rate vs. the reciprocal substrate concentration for α-galactosidase in solution (curve *1*) and in the immobilized state in gel nos. 2 (curve *2*) and 5 (curve *3*), containing LBG and xanthan, respectively. It is seen that immobilization did not substantially affect the catalytic properties of the enzyme. A minor and a twofold increase in K_m, respectively, for the enzyme in gel nos. 2 (0.42×10^{-3} M) and 5 (0.72×10^{-3} M) compared to that for free α-galactosidase (0.36×10^{-3}) can be due to hindered diffusion of the substrate and reaction products in the silica matrix pores. A similar increase in K_m was observed, e.g., for α- and β-galactosidases immobilized in polyacrylamide and alginate gels using cross-linking agents [5, 6, 15].

CONCLUSIONS

(1) α-Galactosidase was immobilized inside sol–gel derived hybrid polysaccharide–silica nanocomposites with different formulations.

(2) The catalytic activity of α-galactosidase varies with the formulation of the silica–polysaccharide matrix. The enzymatic activity tends to decrease with increasing content of the inorganic component. The activity and stability of the enzyme are also influenced by the structure of the polysaccharide and its concentration in the matrix.

(3) α-Galactosidase immobilized inside a tetrakis-(2-hydroxyethyl) orthosilicate (10 wt %) matrix containing galactomannan (0.25 and 0.75%) preserved the catalytic activity for a long time; its thermal stability increased by 10°C. The immobilized α-galactosidase exhibited the maximal activity at the same pH values as the free enzyme; the Michaelis constant K_m did not substantially change.

REFERENCES

1. Hoffman, A.S., *Biomaterials Science*, Ratner, B.D., Hoffman, A.S., Schoen, F.J., and Lemons, J.E., Eds., 1996, Boston: Academic, pp. 124–130.
2. Sinitsin, A.P., Rainina, B.I., Lozinskii, V.I., and Spasov, S.D., *Immobilizovannye kletki mikroorganizmov* (Immobilized Cells of Microorganisms), Moscow: Mosk. Gos. Univ., 1994.
3. Kuo, J.-Y. and Goldstein, J., *Enzyme Microb. Technol.*, 1983, vol. 5, no. 4, pp. 285–290.
4. Mitsutomi, M., Uchida, Y., and Ohtakara, A., *J. Ferment. Technol.*, 1985, vol. 63, no. 4, pp. 325–329.
5. Hernaiz, M.J. and Crout, D.H.G., *Enzyme Microb. Technol.*, 2000, vol. 27, nos. 1–2, pp. 26–32.
6. Prashanth, S.J., and Mulimani, V.H., *Process Biochem.*, 2005, vol. 40, nos. 3–4, pp. 1199–1205.
7. Tippeswamy, S. and Mulimani, V.H., *Process Biochem.*, 2003, vol. 38, no. 5, pp. 635–640.

8. Dave, B.C., Dunn, B., Valentine, J.S., and Zink, J.I., *Anal. Chem*., 1994, vol. 66, no. 22, pp. 1120A–1127A.
9. Gill, I. and Ballesteros, A., *Trends Biotechnol*., 2000, vol. 18, no. 11, pp. 282–296.
10. Bakunina, I.Yu., Sova, V.V., Nedashkovskaya, O.I., et al., *Biokhimiya*, 1998, vol. 63, no. 10, pp. 1420–1427.
11. Shchipunov, Yu.A. and Karpenko, T.Yu., Abstracts of Papers, *The 2nd Int. Rhodia Conf. "Physical Chemistry of Polymeric Systems,"* Bristol: Bristol Univ., 2002, p. 72.
12. Shchipunov, Yu.A., Karpenko, T.Yu., Bakunina, I.Yu., et al., *J. Biochem. Biophys. Meth*., 2004, vol. 58, no. 1, pp. 25–38.
13. Mehrotra, R.C. and Narain, R.P., *Ind. J. Chem*., 1967, vol. 5, no. 12, pp. 32–39.
14. Zvyagintseva, T.N., Schevchenko, N.M., Popivnich, I.B., et al., *Carbohydr. Res*., 1999, vol. 322, no. 2, pp. 32–39.
15. Shchipunov, Yu.A., *J. Colloid Interf. Sci*., 2003, vol. 268, no. 1, pp. 68–76.
16. Shchipunov, Yu.A. and Karpenko, T.Yu., *Langmuir*, 2004, vol. 20, no. 10, pp. 3882–3887.
17. Livage, J., Coradin, T., and Roux, C., *J. Phys.: Condens. Matter*, 2001, vol. 13, no. 33, pp. R673–R691.
18. Lu, Z.-L, Lindner, E., and Mayer, H.A., *Chem. Rev*., 2002, vol. 102, no. 10, pp. 3543–3577.
19. Schram, A.W., Hamers, M.N., Oldenbroek-Haverkamp, E., et al., *Biochim. Biophys. Acta*, 1978, vol. 527, no. 2, pp. 456–464.
20. Eggers, D.K. and Valentine, J.S., *J. Mol. Biol*., 2001, vol. 314, no. 4, pp. 911–922.
21. Eggers, D.K. and Valentine, J.S., *Protein Sci*., 2001, vol. 10, no. 2, pp. 250–261.
22. Ellis, R.J., *Trends Biochem. Sci*., 2001, vol. 26, no. 10, pp. 597–604.
23. Bodalo, A., Gomez, E., Gomez, J.L., et al., *Process Biochem*., 1991, vol. 26, no. 6, pp. 349–353.

ISSN 1070-4272. Russian Journal of Applied Chemistry, 2006, Vol. 79, No. 5, pp. 833–840. © Pleiades Publishing, Inc., 2006.
Original Russian Text © V.P. Nekhoroshev, Yu.P. Turov, A.V. Nekhorosheva, V.D. Ogorodnikov, K.N. Gaevoi, 2006, published in Zhurnal Prikladnoi Khimii, 2006, Vol. 79, No. 5, pp. 845–852.

MACROMOLECULAR CHEMISTRY AND POLYMERIC MATERIALS

Composition and Structure of Low-Molecular-Weight Products of Thermal Oxidative Degradation of Atactic Polypropylene

V. P. Nekhoroshev, Yu. P. Turov, A. V. Nekhorosheva, V. D. Ogorodnikov, and K. N. Gaevoi

Surgut State University, Surgut, Khanty–Mansi avtonomnyi okrug, Russia

Received December 9, 2005; in final form, February 2006

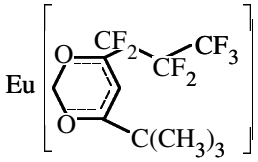
Abstract—The composition and structure of low-molecular-weight products of thermal oxidative degradation of atactic polypropylene were studied.

DOI: 10.1134/S1070427205030272

In this study we examine the composition and structure of low-molecular-weight products of thermal oxidative degradation (TOD) of atactic polypropylene (APP) and discuss the most probable pathways of formation of oxidized atactic polypropylene (OAPP) and low-molecular-weight by-products of TOD.

EXPERIMENTAL

The mixture of low-molecular-weight organic compounds formed by oxidation of APP melt at 180°C was separated on a silica gel column (eluents hexane and chloroform); the solvent was distilled off in a vacuum. The yield of the hexane fraction of the concentrate of low-molecular-weight compounds was 63.8, and that of the chloroform fraction, 34.4 wt %. The ^{1}H NMR spectra were recorded at 27°C on a Tesla BS 497 spectrometer (100 MHz; solvent CCl_4; reference HMDS). A shift reagent, tris(6,6,7,7,8,8,8-heptafluoro-2,2-dimethyloctane-4,6-dionato)europium(III), was used:



The measurement error did not exceed 3%.

The GC–MS analysis was performed on a Nermag R10-10C device (France). The mixture was separated on a quartz capillary column (length 30 m, internal diameter 0.32 mm) under the following conditions: stationary phase SE-54, carrier gas He, inlet carrier gas pressure 0.45 atm, vaporizer and interface temperature 250°C; column temperature schedule: 65°C, 2 min; heating to 280°C at a rate of 5 deg min^{-1}; 280°C, 60 min; sample inlet with a flow splitting ratio of 1 : 40; sample volume 1 μl; mass-selective quadrupole detector; electron impact, 70 eV; scanning range 33–330 amu; scan time 0.4 s; Wiley138 library of mass spectra; software: Technivent-1 for data collection and HP Chemstation for data processing. The relative measurement error did not exceed 5%.

The compositions and structures of low-molecular-weight condensable compounds formed by TOD of APP at 180°C furnish information on the radical mechanism of degradation and on the structure of OAPP. The IR spectrum of the low-molecular-weight compounds (Fig. 1) shows that they contain hydrocarbons and ketones with various degrees of unsaturation. In the range 3400–3200 cm^{-1}, there is a characteristic broad absorption band of stretching vibrations of hydrogen-bonded hydroxy groups (probably those of the enol form of unsaturated ketones); this is confirmed by the presence of the ⩾C–O–H band at 1125–1030 cm^{-1}. The medium-intensity band at 1720 cm^{-1} is characteristic of carbonyl stretching vibrations. It has a complex shape suggesting the presence of ketones of different structures; in particular, the shoulder at 1774 cm^{-1} may be assigned to the stretching vibrations of the carbonyl group in cyclic ketones, and the shoulder at 1700 cm^{-1} is characteristic of a >C=O group conjugated with a C=C bond. The presence of large amounts of aliphatic compounds is confirmed

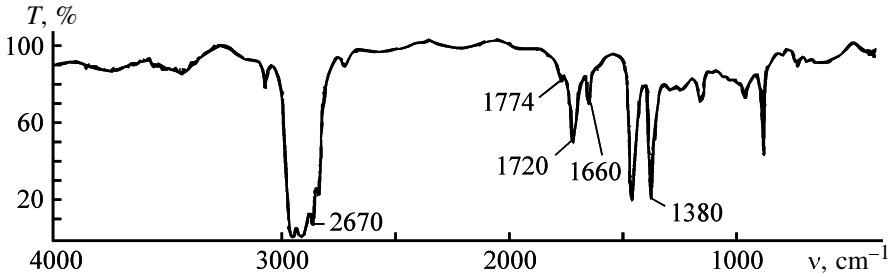


Fig. 1. IR spectrum of the low-molecular-weight products of TOD of APP. (*T*) Transmission and (ν) wave number; the same for Fig. 2.

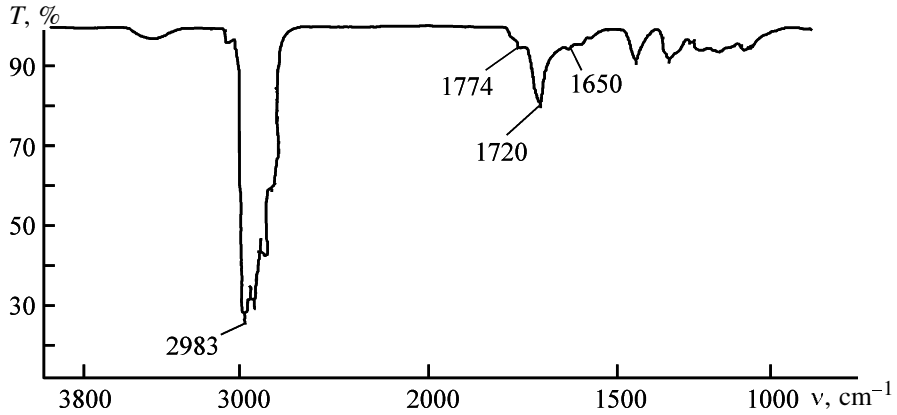


Fig. 2. IR spectrum of the chloroform fraction of the low-molecular-weight products of TOD of APP.

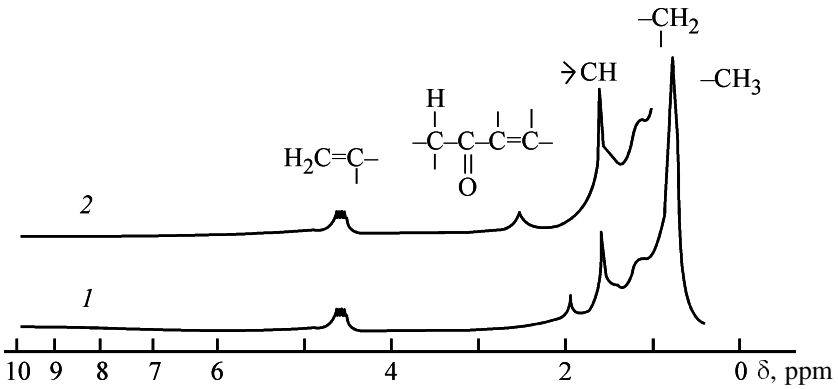


Fig. 3. ^{1}H NMR spectrum of the chloroform fraction of the low-molecular-weight products of TOD of APP. (δ) Chemical shift. (*1*) Initial spectrum and (*2*) spectrum recorded in the presence of $Eu(FOD)_3$ shift reagent.

by strong bands of C–H stretching vibrations in $>CH_2$ and CH_3 groups (2900–2800 cm^{-1}), 1415–1465, 1380, and 720–723 cm^{-1}. The absorption bands at 1660–1580 cm^{-1} can be assigned to vibrations of the >C=C< bonds, possibly conjugated with the carbonyl group [1, 2]. For more detailed analysis we took the chloroform and hexane fractions obtained by separation of the starting mixture of low-molecular-weight compounds by column chromatography. The IR spectrum of the chloroform fraction containing polar compounds (Fig. 2) was indicative of the following structural features. The absorption at 3400–3200 and 1125–1030 cm^{-1} confirms the presence of the hydroxy group in the enol form of unsaturated ketones; these bands are also present in the spectra of other α,β-unsaturated ketones, e.g., of mesityl oxide. At 1720, 1660–1580, and 980–950 cm^{-1}, there are characteristic absorption bands of the carbonyl group and >C=C< bond [1, 2].

The ^{1}H NMR spectrum of the chloroform fraction (Fig. 3) contains signals from vinyl and alkyl protons. The ratio of their integral intensities is as follows: alkyl protons : protons at the α-C atom relative to carbonyl group : vinyl protons = 20 : 1 : 2. The empirical formula of the ketone is $C_{13}H_{22}O$.

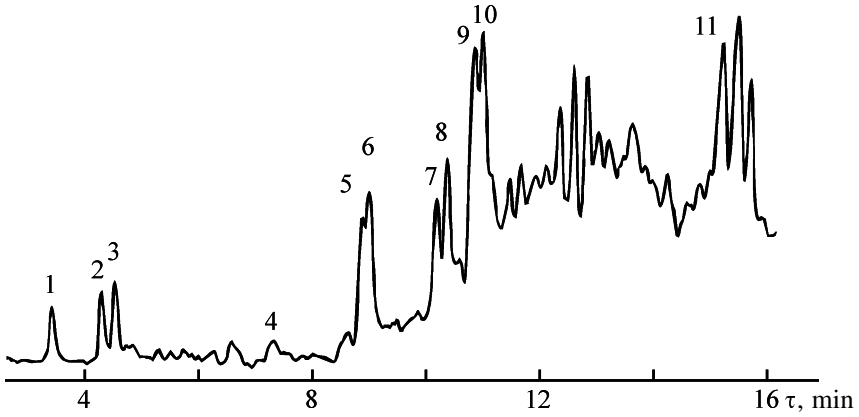
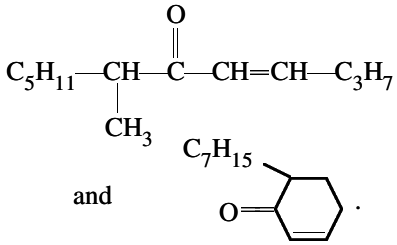


Fig. 4. Fragment of the chromatogram of the chloroform fraction of ketones. (τ) Time; the same for Fig. 5. The peak assignment is given in the text (parent compounds in the corresponding reactions); the same for Fig. 5.

The relatively high content of vinyl protons suggests the presence of C=C bonds, possibly conjugated with a carbonyl group, e.g.,



The IR spectrum of the hexane fraction differs from that of the chloroform fraction by the absence of absorption bands of oxygen-containing groups. The absorption bands at 2900–2800 cm^{-1} belong to the stretching vibrations of the C–H bonds in $–CH_2–$ and $–CH_3$ groups; the presence of a large amount of aliphatic structures is confirmed by strong absorption at 1465–1415 and 1380 cm^{-1}; the absorption bands at 723–720 cm^{-1} are assigned to the rocking vibrations of the CH_2 groups in polymethylene chains; the bands at 1070–650 cm^{-1} are characteristic of bending vibrations of C–H and C–C bonds; the bands at 980–950, 1640, and 1660 cm^{-1} are indicative of the presence of unsaturated structures.

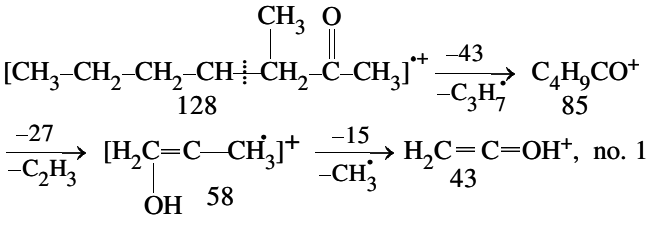
The fractions obtained were subjected to GC–MS analysis. A fragment of the chromatogram of the chloroform fraction is shown in Fig. 4. The group identification by characteristic ions showed that the chloroform fraction contained a large set of ketones, both saturated and unsaturated. The mass spectra were interpreted only for the peaks numbered in the initial part of the chromatogram, because the stability of molecular ions drastically decreases with an increase in the molecular weight and with branching. The mass spectra of the other homologous compounds in the chloroform fraction contain no molecular ion peaks, which does not allow complete elucidation of their structures. The fragment peaks confirm the presence of saturated and unsaturated ketones and of alkylcyclohexenones.

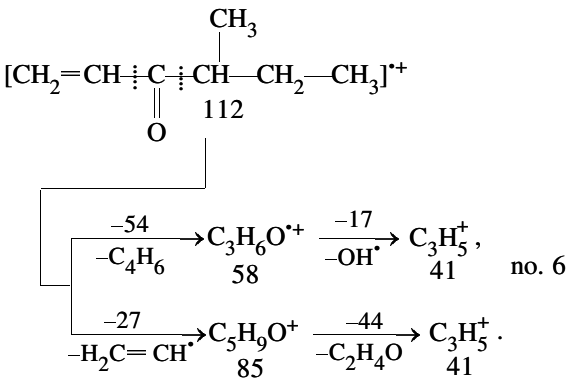
The most characteristic fragmentation pattern of molecular radical cations of ketones under electron impact involves formation of acyl ions and their subsequent decarbonylation to alkyl cations. Other fragmentation pathways of ketones involve the McLafferty rearrangement which occurs if at least one of the alkyl groups contains no less than three carbon atoms and a γ-H atom [3].

For α,β-unsaturated ketones, there are two characteristic fragmentation pathways. One of them involves the loss of the ketene molecule formed from the carbonyl group and adjacent saturated carbon atom. The formation of $R–CH_2CO^+$ ions is particularly facilitated in ketones containing alkyl substituents in the γ-position relative to the CO group. The other fragmentation pathway noted for 2-cyclohexenones involves the retro-diene cleavage competing with the previous pathway [4]. In the chloroform fraction, we identified by GC–MS the following compounds: 4-methyl-2-heptanone, 3,5-dimethyl-1-hepten-4-one, 4,6-dimethyl-4-hepten-2-one, 3,5-dimethyl-2-cyclohexen-1-one, 1-hepten-3-one, 4-methyl-1-hexen-3-one, 1-hepten-3-one, 4-methyl-1-hexen-3-one, 2,4-dimethyl-1-hexen-3-one, 2,5-dimethyl-1-hexen-3-one, 3,4,5-trimethyl-2-cyclopenten-1-one, 6-methyl-3,5-heptadien-2-one, and 2,4,6-trimethyl-2-cyclohexen-1-one.

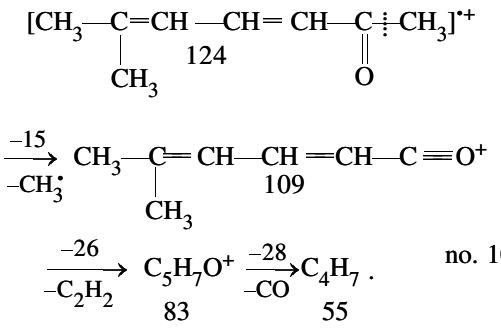
The mass spectra of the majority of these compounds well coincide with those of the same compounds from the library. The fragmentation patterns of other isomers differ from those described above, but the main genetic evidences are preserved. For

example, the presence of a strong peak with *m/z* 58, corresponding to the rearranged radical cation $[CH_2=C(OH)–CH_3]^+$, suggests the occurrence of the McLafferty rearrangement characteristic of some aliphatic and α,β-unsaturated ketones:

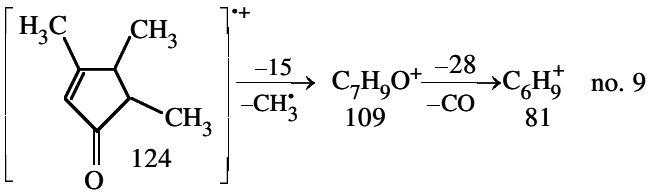


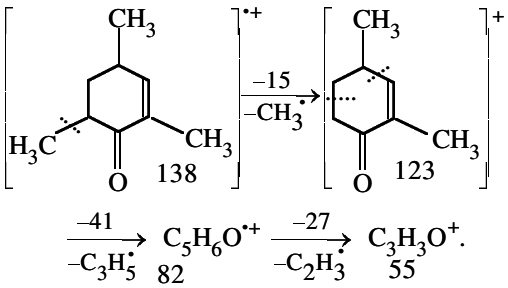


Ketones that contain less than three C atoms in the carbon chain or do not contain a γ-H atom do not undergo the McLafferty rearrangement:



The mass spectra of cyclic unsaturated ketones differ from those of all the other ketones by the considerably smaller number of peaks, which is due to limited number of possible fragmentation pathways of the molecular ion:





The GC–MS study of the hexane fraction of the low-molecular-weight products of TOD of APP showed that this fraction contained a mixture of hydrocarbons differing from each other in the number and position of C=C bonds and in the extent of branching of the carbon skeleton.

The group identification based on the characteristic ions suggests that the compounds formed are homologs differing in the amount and position of multiple bonds and in the extent of branching of the carbon skeleton.

Thus, the hexane fraction consists of isoparaffins (with regularly repeating structural fragments) and hydrocarbons with one, two, or three double bonds. The presence of cyclic structures with double bonds in the ring (of the alkylcyclohexene type) is not improbable, but these compounds are difficult to identify reliably because of the similarity of their mass spectra to those of open-chain dienes. All the four groups of hydrocarbons (alkanes, alkenes, dienes, trienes) present in the hexane fraction of low-molecular-weight products of APP oxidation are characterized by the branched structure and high molecular weights, which severely complicates their identification. In the mass spectra of components of the hexane fraction, only one alkene with MW = 126 (2,4-dimethyl-1-heptene) contains a fairly strong peak of molecular ion (Fig. 5, peak *1*); in the mass spectra of the other hydrocarbons, the peak of the molecular ion is lacking because of its low stability. The group composition of the identified low-molecular-weight compounds is given in the table.

The structure of low-molecular-weight TOD products explains the kinetic features of the accumulation of oxygen-containing groups in TOD of APP and confirms the OAPP structure. Unsaturated ketones present among low-molecular-weight products may be of practical interest, e.g., as metal extractants. Up to now, these compounds and their properties remained poorly studied, because their purposeful synthesis was difficult. Possible pathways of reactions yielding low-molecular-weight products are of scientific interest, because they are associated with the mechanism of

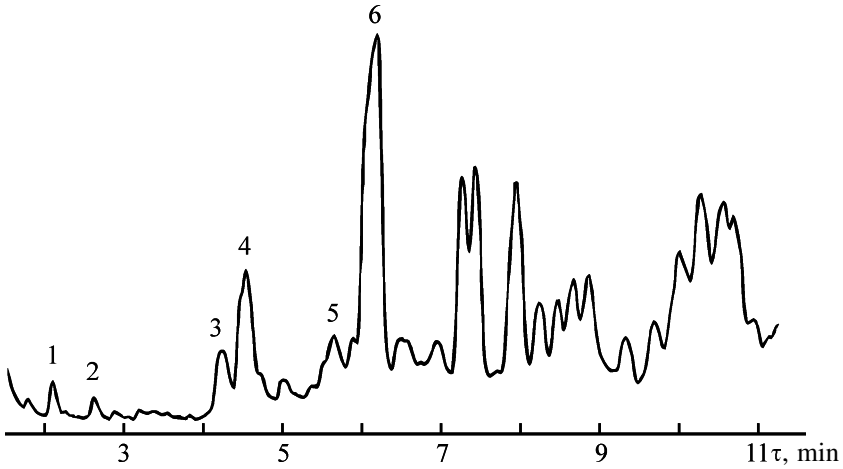


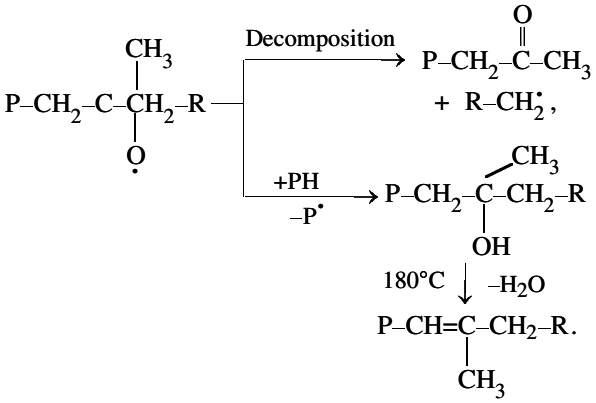
Fig. 5. Fragment of the chromatogram of the hexane fraction of low-molecular-weight APP TOD products.

TOD of APP at temperatures above 150°C:

$$PH + O_2 \xrightarrow[-{}^{\bullet}OOH]{} P^{\bullet} \xrightarrow{+O_2} POO^{\bullet} \xrightarrow[-P^{\bullet}]{+PH} POOH \rightarrow PO^{\bullet} + {}^{\bullet}OH,$$

where $P^{\bullet}$ is the radical of heterotactic polypropylene.

Tertiary alkoxyl radicals tend to decompose with the formation of primary alkyl radicals $R–CH_2^{\bullet}$ exhibiting low regioselectivity in hydrogen abstraction [5]:



$$R–\dot{C}H_2 + P–CH_2–\underset{\displaystyle CH_3}{\underset{|}{CH}}–P \xrightarrow[-R–CH_3]{} P–\dot{C}H–\underset{\displaystyle CH_3}{\underset{|}{CH}}–P$$

$$\xrightarrow[-\dot{O}H,\ -P^{\bullet}]{+O_2,\ +PH} P–\underset{\displaystyle OH}{\underset{|}{CH}}–\underset{\displaystyle CH_3}{\underset{|}{CH}}–P \xrightarrow[-H_2O_2]{+O_2} P–\underset{\displaystyle O}{\underset{\|}{C}}–\underset{\displaystyle CH_3}{\underset{|}{CH}}–P.$$

Secondary alkoxyl radicals are apparently oxidized to keto groups by the reaction with alkyl radicals $R^{\bullet}$:

$$P–\underset{\displaystyle O^{\bullet}}{\underset{|}{CH}}–P + R^{\bullet} \xrightarrow[-RH]{} P–\underset{\displaystyle O}{\underset{\|}{C}}–P.$$

The APP chain is ruptured randomly, which accounts for the formation of homologous series of all the four types of hydrocarbons. The formation of alkenes, dienes, and trienes is characterized by the following features.

(1) The thermal oxidative degradation is controlled by the diffusion of the oxygen molecule to the reactive center; therefore, because of the low kinetic mobility of the polymeric chains, the unstable tertiary alkyl radicals can decompose:

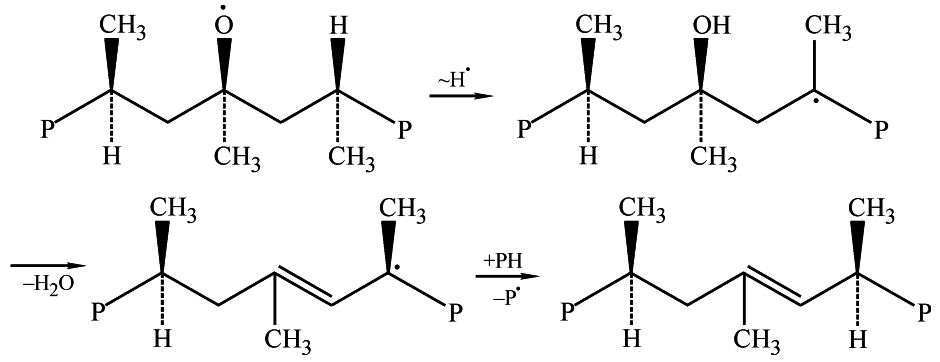
$$P–CH_2–\underset{\displaystyle CH_3}{\underset{|}{\dot{C}}}–CH_2–\vdots–P_1 \longrightarrow P–CH_2–\underset{\displaystyle CH_3}{\underset{|}{C}}=CH_2 + P_1^{\bullet},$$

where the MW of P is higher than that of P_1.

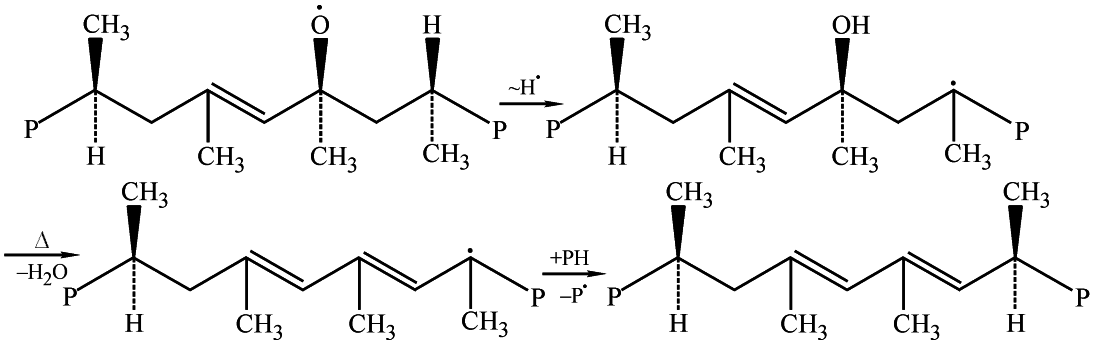
(2) The presence of dienes and trienes in the low-molecular-weight APP oxidation products suggests formation of several hydroperoxy groups in the polymer macromolecule and prevailing intramolecular abstraction of the hydrogen atom by the alkoxy radical:

Composition of the organic phase of the condensate, according to GC–MS analysis

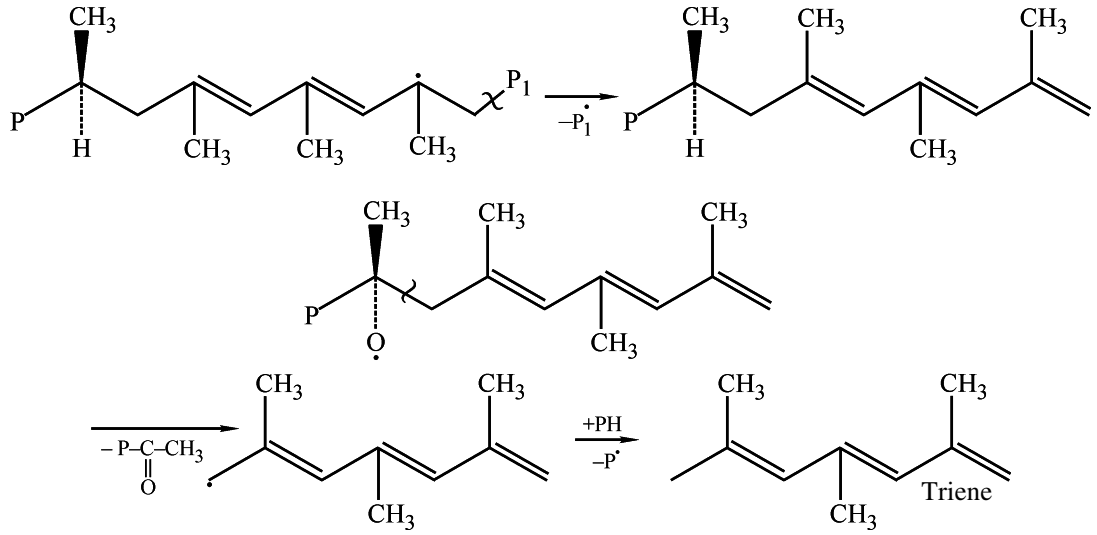
Parameter	Fraction	
	hexane	chloroform
Yield, wt %	63.75	34.40
MW range	126–238	128–286
Relative content, %:		
saturated hydrocarbons	<5.0	0.0
unsaturated hydrocarbons	88.7	13.0
unsaturated ketones of various structures	0.0	71.6
unidentified compounds	6.3	15.4



In this case, the carbon atoms undergo rehybridization, and the most stable tertiary allyl-type radical is formed; this radical can react with the oxygen molecule, with propagation of the oxidation chain [6]:



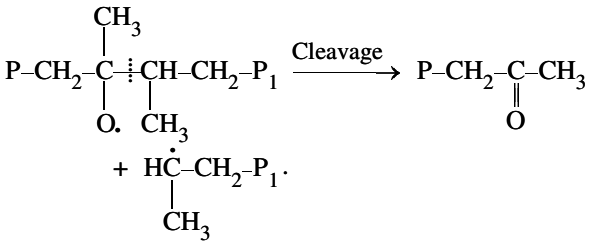
(3) Conjugated trienes are formed by the similar reaction. Low-molecular-weight alkenes and trienes are eliminated upon cleavage of tertiary alkyl and alkoxyl radicals, e.g., by the scheme



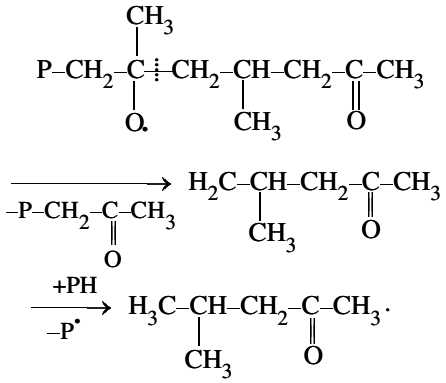
At intermolecular hydrogen abstraction by the alkoxyl radical, the forming alkyldienes and trienes should contain nonconjugated double bonds. Alkyltetraenes were not detected in the examined hexane

fraction of the low-molecular-weight products of APP oxidation.

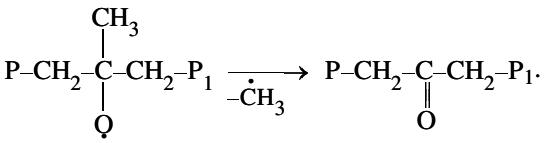
The formation and decomposition of tertiary alkoxyl radicals do not follow any regular trends, i.e., occur at the sites of an APP macromolecule that are the most accessible to reagents (hydroxy, methyl, alkyl radicals). As a result, homologous saturated ketones with different structures of alkyl chains are formed [5]. The structure of alkyl chains in ketones undoubtedly depends on the presence in APP macromolecule of units originating from anomalous tail-to-tail addition and of backbone branchings. Such sections of the macromolecular chain are particularly reactive in oxidation and degradation, e.g.,



Low-molecular-weight saturated ketones are formed by successive formation and degradation of tertiary alkoxyl radicals:

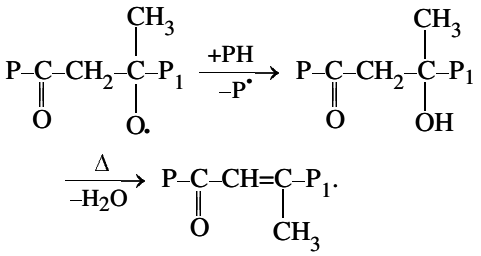


In the process, alkoxyl radicals can decompose with the elimination of the methyl group, which appreciably affects the structure of the forming ketone, e.g.,

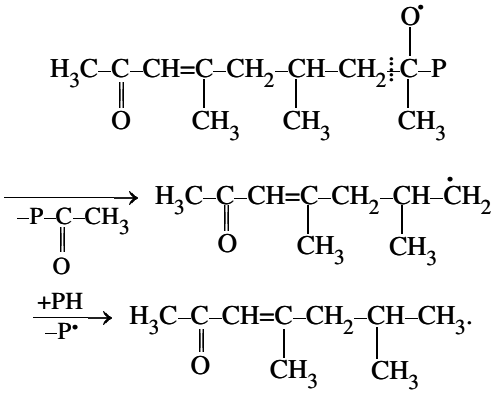


Unsaturated ketones of various structures are the major components in the mixture of condensable low-molecular-weight APP oxidation products. The majority of them are conjugated α,β-unsaturated ketones with an impurity of nonconjugated unsaturated ketones and of ketones containing two double bonds.

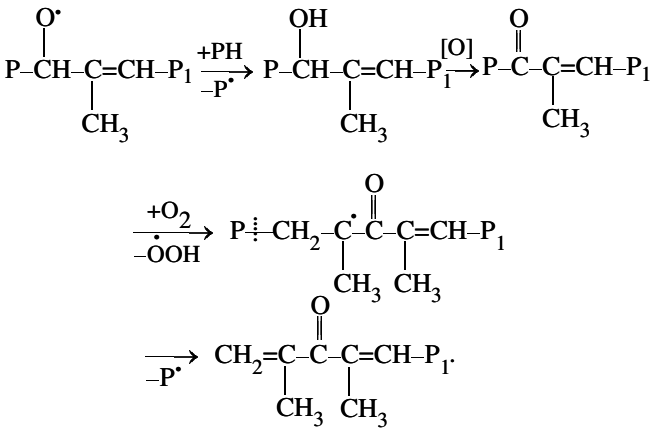
In the course of the APP oxidation, several reactions yielding low-molecular-weight unsaturated ketones occur simultaneously, e.g., dehydration and oxidation of hydroxy groups in the polymer and decomposition of polymeric alkoxyl radicals:



The subsequent oxidation of the polymer occurs via formation of intermediate alkoxyl radicals, which results in the elimination of unsaturated ketones:



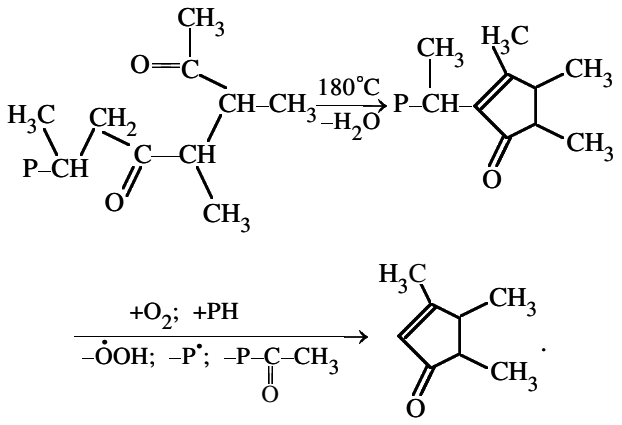
Allyl-type radicals exhibit increased stability, which enhances the reactivity of the α-C atom adjacent to the double bond:



The identification of cyclic six- and five-membered conjugated unsaturated ketones in the mixture of low-molecular-weight APP oxidation products is rather unexpected and difficult to explain. Possible pathways of their formation involve aldol and crotonic condensation, diene synthesis, and intramolecular cyclization

of biradical products formed in the course of the oxidation. Owing to the minimal distortions of the bond angles and minimal ring strain, five- and six-membered rings and the transition states preceding their formation are energetically the most favorable among cyclic systems. Rings of this size are formed almost spontaneously if this is possible, and competing reactions are excluded in this case.

The diene synthesis can be a route to cyclic ketones only if ketene or its derivatives R–CH=C=O are used as dienophiles. Ketene and its derivatives were not detected in a mixture of low-molecular-weight ketones; their formation as reaction intermediates is also improbable, because their generation methods are rather specific. Therefore, the occurrence of the diene synthesis in the course of the APP oxidation is improbable. The intramolecular cyclization by the radical mechanism is possible in the case of formation of biradical intermediates, with simultaneous abstraction of hydrogen atoms from tertiary carbon atoms. The intramolecular cyclocondensation should involve units originating from anomalous tail-to-tail addition, which apparently affects the most energetically favorable cyclic conformation of carbon chains in oxidized APP [7]:



Six-membered alkyl-substituted cyclohexenones are formed similarly.

CONCLUSIONS

(1) Examination of the structure of low-molecular-weight by-products of thermal oxidative degradation of atactic polypropylene at 180°C showed that these products consist of unsaturated hydrocarbons and ketones of various structures.

(2) Reaction schemes describing the formation of oxidized atactic polypropylene and low-molecular-weight thermal oxidative degradation products were suggested.

REFERENCES

1. Smith, A.L., *Applied Infrared Spectroscopy: Fundamentals, Techniques, and Analytical Problem-Solving*, New York: Wiley, 1979.
2. Kazitsyna, L.A. and Kupletskaya, N.B., *Primenenie UF-, IK- i YaMR-spektroskopii v organicheskoi khimii* (Application of UV, IR, and NMR Spectroscopy to Organic Chemistry), Moscow: Vysshaya Shkola, 1971.
3. Vul'fson, N.S., Zaikin, V.G., and Mikaya, A.I., *Mass-spektroskopiya organicheskikh soedinenii* (Mass Spectroscopy of Organic Compounds), Moscow: Khimiya, 1986.
4. Zenkevich, I.G. and Ioffe, B.V., *Interpretatsiya mass-spektrov organicheskikh soedinenii* (Interpretation of the Mass Spectra of Organic Compounds), Leningrad: Khimiya, 1986.
5. Denisov, E.T., *Okislenie i destruktsiya karbotsepnykh polimerov* (Oxidation and Degradation of Carbon-Chain Polymers), Leningrad: Khimiya, 1990.
6. Kuz'minskii, A.S. and Sedov, V.V., *Khimicheskie prevrashcheniya elastomerov* (Chemical Transformations of Elastomers), Moscow: Khimiya, 1984.
7. Aladyshev, A.M., Polymerization of Propylene in the Presence of Highly Active Microspherical $TiCl_3$ in the Medium of the Liquefied Monomer, *Cand. Sci. Dissertation*, Moscow, 1987.

ISSN 1070-4272. Russian Journal of Applied Chemistry, 2006, Vol. 79, No. 5, pp. 841–844. © Pleiades Publishing, Inc., 2006.
Original Russian Text © V.I. Chursin, 2006, published in Zhurnal Prikladnoi Khimii, 2006, Vol. 79, No. 5, pp. 853–856.

MACROMOLECULAR CHEMISTRY AND POLYMERIC MATERIALS

Effect of Mixture Components on the Rheological Characteristics of the Composite

V. I. Chursin

Central Research Institute of Leather-Shoe Industry, Joint-Stock Company, Moscow, Russia

Received January 24, 2006

Abstract—Rheological characteristics and properties of composites prepared from tanning industry wastes were studied in relation to the ratio and composition of components in the mixture.

DOI: 10.1134/S1070427206050284

Any production involves formation of wastes whose certain fraction is recycled, whereas the other fraction is dumped, polluting the environment. Therefore, utilization of collagen-containing wastes (chrome leather chips, hide crops, etc.) formed in significant amounts in the course of the rawstock treatment is an urgent problem from both commercial and environmental viewpoints.

An alternative solution of the problem of utilizing collagen-containing wastes can be based on modern procedures developed for processing of polymeric and biopolymeric systems [1, 2]. New polymeric materials with a wide range of service properties can be prepared from compounds of various chemical nature, including wastes from the tanning industry. These materials can be most efficiently used in production of insole and support materials, especially for sports, childhood, and orthopedic footwear.

Elucidation of the relationship between the composition and structural and mechanical properties of the composites is one of the main problems in production of composite materials with required characteristics [3]. However, data on the rheological properties of mixtures for preparing composites based on the protein–polymer matrix and collagen-containing filler are scarce.

In this study we examined the elastoplastic and heat-protecting properties of composites prepared from disperse systems containing latexes, products of collagen dissolution (PCD), products of collagen hydrolysis (PCH), and polyethylene glycol oleate (PEGO) plasticizer. The following latexes were used: Lenteks A5 (acrylate–styrene), Lenteks AN7 (terpolymer of acrylate with styrene and acrylonitrile), BS-50 (butadiene–styrene), and BN3 (copolymer of acrylate with acrylonitrile). As a filler, we used chrome leather chips, wastes from shaving of the chroming half-finished product, preliminarily ground to 1.0–1.5 mm size, with water and chromium oxide contents of ≥30 and ≥3.8–4.3%, respectively. The dry residues of PCD and PCH were 2.81 and 8.57%, respectively.

The rheological properties of the mixtures were determined on a DV-II Brookfield viscometer at a shear rate of 30 s^{-1}. First, we studied the rheological properties of mixtures of the initial components. The viscosity of the protein-containing solutions is plotted in Fig. 1 vs. the content of chrome leather chips. As seen, with increasing content of the chips in the mixture its viscosity increases. The strongest increase in the viscosity of the PCH- and PCD-containing systems is observed at the chip content of 20–25 and 10–20 wt %, respectively. Probably, at these compositions fine chips are saturated with macromolecules of hydrolyzate and PCD, whereas further linear increase in the viscosity is due to the system thickening. At the viscosity of the chrome leather chips–PCD system higher than 8000 mPa s, casting of the resulting mixture to prepare the composite material is complicated by its poor distribution in the mold.

Changes in the viscosity of the chrome leather chips– PCD system also depend on the content of PCD (Fig. 2).

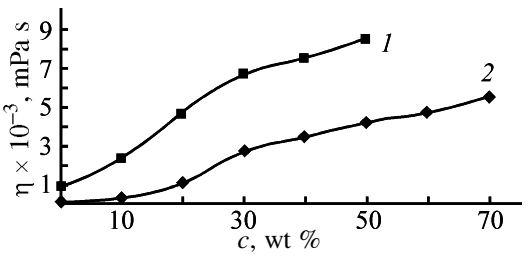


Fig. 1. Viscosity η of (*1*) PCD and (*2*) PCH systems as a function of the chip content *c*.

Table 1. Properties of composites in relation to the ratio of the initial components

Sample no.	Chips : PCD : AN7 latex ratio	Volume, cm^3	Thickness, cm	Weight, g	Specific density, g cm^{-3}	Heat conductivity, W m^{-1} deg^{-1}
1	1 : 1 : 0.1	16.06	0.3	6.8	0.42	0.059
2	1 : 1 : 0.5	23.59	0.4	11.4	0.48	0.047
3	1 : 1 : 1.3	46.07	1.0	23.2	0.50	0.168
4	1 : 0.5 : 0.1	18.28	0.3	6.4	0.35	0.079
5	1 : 0.5 : 0.2	20.90	0.4	8.2	0.39	0.086
6	1 : 0.5 : 0.5	26.12	0.4	12.0	0.42	0.104
7	1 : 0.5 : 1	37.21	0.7	16.6	0.45	0.138

For example, the viscosity strongly decreases with adding AN7 latex at a small content of PCD. This suggests that, under the given experimental conditions, the system viscosity decreases due to the plasticization of the chrome leather chips with the polymer. With increasing PCD content in the system, the dependence becomes more complex, probably due to the interaction between PCD and latex (solutions of protein and acrylonitrile polymer), and this interaction determines the viscosity of the system. First, the polymeric complexes exhibiting no plasticizing effect are formed, and, as a result, the viscosity increases. Then, due to the affinity for the chromic collagen, certain fraction of the hydrolyzate is adsorbed on the chip surface, plasticizing the system and decreasing its viscosity. The system stabilizes at a PCD : latex ratio of 1 : 1, and its viscosity decreases with further addition of the polymer. In excess PCD, the maximal viscosity is observed at the polymer content of 5 wt %.

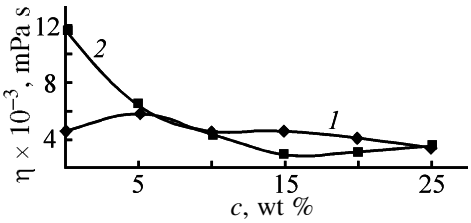


Fig. 2. Viscosity η of the system as a function of the AN7 latex content *c*. PCD content, wt %: (*1*) 12.8 and (*2*) 6.4.

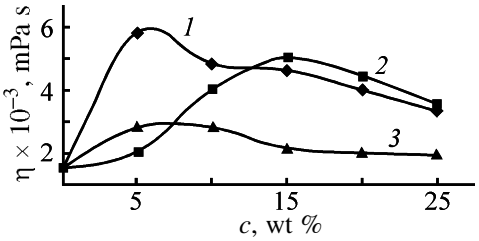


Fig. 3. Viscosity η of the system as a function of the latex content *c*. Latex: (*1*) AN7, (*2*) BN3, and (*3*) BS-50.

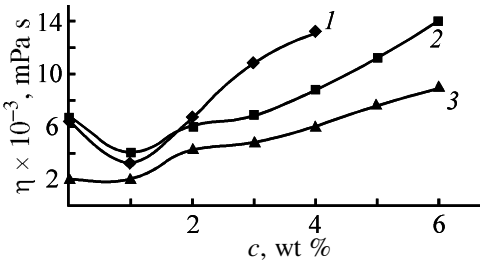


Fig. 4. Viscosity η of the system as a function of the plasticizer content *c*. PCD content, wt %: (*1*) 3.2, (*2*) 6.4, and (*3*) 12.8.

The effect of various latexes on the rheological properties of the system is illustrated in Fig. 3. In all the systems, the viscosity passes through a maximum, though at different polymer concentrations. The best structuring effect is observed for AN7 latex exhibiting the maximal viscosity of 6000 mPa s at its content in the system of 5 wt %. Slightly lower viscosities are typical of the mixtures with BN3 latex at its content of 15 wt %. BS-50 latex is efficient in the concentration range 5–10%, but the system viscosity does not exceed 3000 mPa s, i.e., it is lower by a factor of 2 as compared to the system with AN7 latex. These data suggest intermolecular interactions between the protein functional groups and polar groups of the latexes in the systems studied.

Study of the rheological characteristics of the system in the presence of PEGO (Fig. 4) showed that the viscosity of the system first decreases and then increases upon addition of the plasticizer, and the system becomes thickened. Since the viscosity range is limited, 2 wt % plasticizer content was suggested.

As seen from Table 1, sample nos. 4 and 5 have the smallest density, and sample nos. 1 and 2, the lowest heat conductivity. The use of these materials as insoles would provide the comfortable conditions of shoe wearing [4].

The elastoplastic characteristics of the resulting composites were studied on a Relaks apparatus [5]. It is known that comparison of the deformation and

Table 2. Elastoplastic properties of the composites

Sample no.	Modulus of Hookean elasticity E_1	Modulus of hyperelasticity E_2	Viscosity coefficient N_1	Viscosity coefficient N_2	Viscoplasticity coefficient N_3
	MPa		MPa s		
1	55.3	159	2.74	354	15192
2	52.4	120	14.6	366	7203
3	229	513	151	1809	13428
4	24.9	55.1	3.51	154	2858
5	11.1	23.1	5.41	55.9	1073
6	11.0	25.9	10.2	89.5	666
7	73.6	169	77.25	656	4261

strength properties of the composites allows evaluation of the contribution of one or another component to formation of the structure and properties of the materials. The relaxation spectra of the composites prepared using AN7 latex with various ratios of the initial components are shown in Fig. 5. The elastoplastic characteristics of the composites are listed in Table 2. Figure 5 shows a strong effect of the latex content on the composite properties. At a small latex content, the relaxation spectra have two maxima characterizing various structural levels, which indicates that the composite structure in this case most strongly resembles natural leather. These relaxation maxima suggest formation of the developed inner surface of the composite and high porosity, which is confirmed by the data on air permeability (maximal value 36000 ml cm^{-2} h^{-1}) and density of the samples (minimal value, Table 1).

Comparison of these results with the rheological characteristics of the mixtures suggests that, to prepare composites with high molding properties, low heat conductivities, and small densities, the composition viscosity should vary within the 3000–4500 mPa s range.

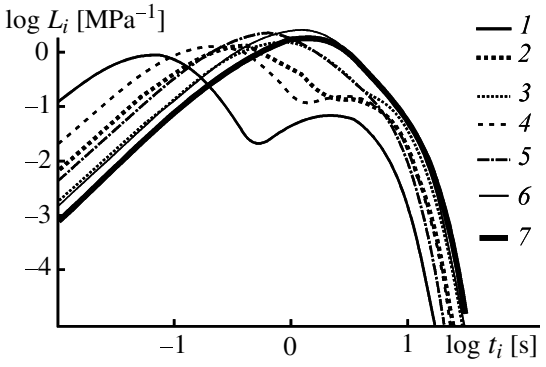


Fig. 5. Relaxation spectra of the composite samples in $\log t_i$–$\log L_i$ coordinates. (t_i) Relaxation time and (L_i) ductility. Numbers at the curves correspond to the sample nos. in Table 1.

As seen, with increasing content of AN7 latex (sample nos. 1–3), the viscosity coefficient of the rapid relaxation processes N_1 increases, and at a latex content of 25 wt %, N_1 increases by an order of magnitude. The elasticity characteristics also sharply increase. In the systems with smaller content of PCD (sample nos. 4–7), with increasing content of the latex from 6 to 25 wt %, the moduli of Hookean elasticity and hyperelasticity first decrease and then increase. As shown previously, these trends are due to the interaction of the protein and acrylonitrile polymer in solutions. The moduli of Hookean elasticity and hyperelasticity are the most informative in evaluation of the effect of the polymer content on the composite properties.

Using the rheological characteristics of the systems studied, we determined the optimal ratios of the initial components to prepare the mixtures with high moldability. Variation of the chrome leather chips : PCD : latex ratio allows control of the properties of the composite materials. The composites prepared from the tanning industry wastes show promise for the development of the modern footwear design and production of building and decorative panels with high heat-protection properties.

CONCLUSIONS

(1) Viscosity of the mixtures is determined by both the ratio of the initial components and their chemical nature. Styrene and acrylate latexes exhibit different structuring effect. The optimal viscosity of the system studied varies within 3000–4500 mPa s.

(2) The heat conductivity of the composite increases with increasing latex content in the mixture.

(3) Moduli of Hookean elasticity and hyperelasticity strongly increase and the heat-protection properties decrease with increasing latex content in the mixture over 25 wt %.

REFERENCES

1. RF Patent 2018540.
2. RF Patent 2198225.
3. Gol'dman, A.Ya., *Prognozirovanie deformatsionno-prochnostnykh svoistv polimernykh i kompozitsionnykh materialov* (Prediction of the Deformation and Strength Properties of Polymeric and Composite Materials), Leningrad: Khimiya, 1988.
4. Vershinin, L.V., Repina, N.S., and Burtseva, I.V., *Kozh.-Obuv. Prom-st.*, 2002, no. 4, pp. 19–20.
5. Burmistrov, A.G., Chursin, V.I., and Manukyan, A.N., *Kozh.-Obuv. Prom-st.*, 2000, no. 4, pp. 21–30.

ISSN 1070-4272. Russian Journal of Applied Chemistry, 2006, Vol. 79, No. 5, pp. 845–849. © Pleiades Publishing, Inc., 2006.
Original Russian Text © E.N. Fedoseeva, L.A. Smirnova, M.A. Sorokina, M.O. Pastukhov, 2006, published in Zhurnal Prikladnoi Khimii, 2006, Vol. 79, No. 5, pp. 857–861.

MACROMOLECULAR CHEMISTRY AND POLYMERIC MATERIALS

Radical Degradation of Chitosan under the Action of a Redox System

E. N. Fedoseeva, L. A. Smirnova, M. A. Sorokina, and M. O. Pastukhov

Lobachevsky Nizhni Novgorod State University, Nizhni Novgorod, Russia

Received August 1, 2005

Abstract—Degradation of chitosan in solution under the action of redox radical initiators was studied with the aim to prepare chemically oligomers of natural polysaccharides. The influence of temperature on the rate and extent of the process was examined. The optimal ratios of the substrate to initiator and of the reductant to oxidant in the initiating system were determined.

DOI: 10.1134/S1070427206050296

Chitosan (β-1,4-bonded 2-deoxy-2-amino-*D*-glucopyranose) is the deacetylation product of chitin, a natural polysaccharide. Chitosan is a structural analog of cellulose; it has unique properties. In contrast to cellulose, chitosan is soluble in dilute aqueous solutions of some mineral and organic acids. Chitosan is widely used today in biology, cosmetics, paper production, and treatment of wastewater containing heavy metals [1]. The application fields of chitosan and its derivatives will expand because, firstly, chitin, which is the natural source of chitosan, is a renewable raw material. Chitin is present in crustacean processing wastes; it can also be recovered from insects (dead bees, mulberry silkworm, etc.), mushrooms, segmented worms, and mollusks [2, 3]. Secondly, chitosan is biodegradable, i.e., it can be utilized without environmental pollution. The molecular weight of chitosan recovered from various natural sources is usually in the range 10^5–10^6. A decrease in the molecular weight of chitosan to values typical of oligomers would expand its application field, because chitosan oligomers exhibit certain specific properties untypical of high-molecular-weight products [4]. Chitosan oligomers dissolve in water at neutral pH values.

To obtain a low-molecular-weight product, the starting chitosan is subjected either to chemical hydrolysis or to enzymatic degradation [5–8]. However, the enzymatic degradation requires thorough purification of the raw material to remove impurities that diminish the activity of enzymes (in particular, calcium) and of the final product to remove the enzymes. Chemical hydrolysis is most frequently performed with aqueous solutions of hydrogen peroxide of various concentrations. Other reagents such as potassium persulfate [8] or ozone [5] are also used; however, in this case the purification of the oligochitosan obtained may be labor-consuming. Hydrogen peroxide seems to be preferable as degradation agent, because products of its decomposition are nontoxic and excess reagent can be readily removed from the reaction medium. However, low-molecular-weight chitosan and its oligomers are prepared with these reagents, as a rule, at elevated temperatures (50–70°C). Under these conditions, the chemical composition of the polysaccharide may change. In particular, Galiaskarova [5] observed deamination of chitosan and oxidation of hydroxy groups to carboxy groups. At lower temperatures and reagent concentrations, water-soluble chitosan is not formed.

Hsu et al. [8] proved the radical mechanism of the chemical degradation of chitosan chains under the action of reagents capable of radical generation under various conditions. The radical mechanism of the degradation in the presence of free radical initiators suggests the suitability of redox initiators. Such initiators allow the reactions to be performed at lower temperatures; the probability of undesirable transformations of chitosan functional groups can be thus decreased. It is known [9] that the hydrogen peroxide–ascorbic acid redox system efficiently initiates reactions performed at room or even lower temperature.

The goal of this study was the preparation of chitosan oligomers at low temperatures by the degradation of chitosan under the action of the hydrogen peroxide–ascorbic acid redox system. The choice of ascorbic

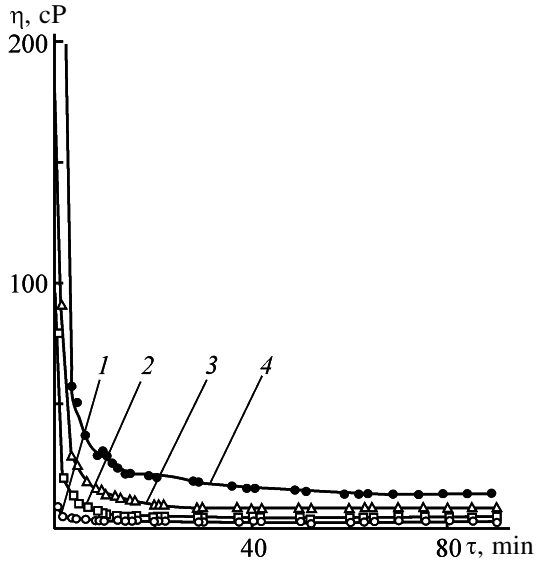


Fig. 1. Viscosity η of chitosan solutions of various concentrations as a function of the degradation time τ in 3 wt % acetic acid solution. Molar ratios: chitosan : H_2O_2 20 and H_2O_2 : ascorbic acid 1; 21°C. Chitosan concentration, wt %: (*1*) 2, (*2*) 3, (*3*) 4, and (*4*) 6.

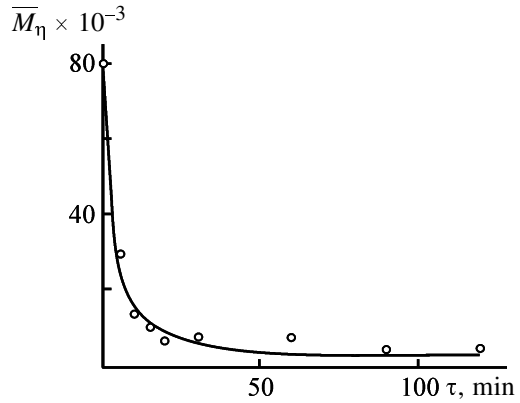


Fig. 2. Molecular weight of chitosan $\overline{M}_\eta$ as a function of the degradation time τ. Concentrations, wt %: chitosan 3 and acetic acid 1.5; molar ratios: chitosan : H_2O_2 10 and H_2O_2 : ascorbic acid 1; 21°C.

acid is governed by its efficiency as reductant [9] and by the nontoxicity of ascorbic acid and its oxidation products [10].

EXPERIMENTAL

Chitosan samples with M 8.0×10^4 and 9.6×10^4 (Sonat, Moscow) were used without additional purification (degree of deacetylation 82%, weight fraction of insoluble substances 0.25%, weight fraction of dry residue after calcination 0.3%). Ascorbic acid was of chemically pure grade, and hydrogen peroxide (30% aqueous solution), of analytically pure grade; 0.1 N HCl solution was prepared from the titrimetric standard. The solvent was prepared using chemically pure grade glacial acetic acid.

The molecular weight of samples of chitosan and its oligomers was determined viscometrically with an Ubbelohde viscometer at 21°C in an aqueous solution containing 0.33 M acetic acid and 0.3 M NaCl. The viscosity-average molecular weight was calculated by the Mark–Houwink equation $[\eta] = k\overline{M}_\eta^\alpha$, $k = 3.41 \times 10^{-5}$, $\alpha = 1.01$ [11].

The degree of deacetylation of chitosan was determined by potentiometric titration of its solutions in 0.1 N HCl with a 0.1 N solution of KOH, using an EV-74 pH meter.

The initial concentration of the hydrogen peroxide solution was determined by volumetric titration with a potassium permanganate solution in the presence of sulfuric acid [12].

To perform the chitosan degradation under the action of the redox system, we added the required weighed portion of ascorbic acid to a chitosan solution of the required concentration. After the acid dissolved, the required amount of a hydrogen peroxide solution in distilled water was added. The reaction progress was monitored by measuring the viscosity of chitosan solutions with an Ubbelohde (for dilute solutions) or Hoeppler (for moderately concentrated solutions) viscometer. The total extent of degradation was evaluated from the change in the molecular weight of chitosan after performing the reaction for 24 h.

The chemical composition of chitosan was determined by Fourier IR spectroscopy, potentiometric titration, and analysis for nitrogen (Kjeldahl method).

In this study we examined the performance of redox systems in the degradation of the chitosan backbone in solutions with pH 4.5–5.5 and the influence of the temperature and component ratio on the rate and extent of the process.

Figure 1 shows how the viscosity of chitosan solutions of different concentrations varies with time in the presence of the hydrogen peroxide–ascorbic acid redox system. The relative and dynamic viscosities of solutions (Fig. 1) and the molecular weight of chitosan (Fig. 2) sharply decrease in the first 10 min; within 15–20 min, the curves flatten out. Thus, the chosen redox system efficiently breaks the chitosan chains. Measurements of the molecular weight of chitosan as a function of the reaction time (a typical curve is shown in Fig. 2) demonstrate that the kinetic curves for the viscosity and molecular weight fully correlate

with each other, i.e., a decrease in the solution viscosity is due to a decrease in the molecular weight of the starting chitosan.

The nitrogen content in the initial and final products, determined by the Kjeldahl method, is the same (8%), which shows that the reaction does not involve chitosan amino groups. This conclusion is also confirmed by the titration results. The degree of deacetylation was 82% for all the samples.

The Fourier IR spectra of chitosan before and after the reaction are somewhat different. A new band at 1667 cm^{-1}, assigned to the stretching vibrations of the ketone carbonyl group, appears in the absorption spectrum of the low-molecular-weight product.

To determine how the extent of the decrease in the molecular weight of chitosan depends on the ratio of the redox system components, we varied the amount of ascorbic acid relative to hydrogen peroxide at a fixed ratio of the other components. Figure 2 shows that it is most appropriate to take the redox system components in an equimolar ratio. Excess ascorbic acid relative to hydrogen peroxide does not cause further changes in the molecular weight of chitosan relative to the equimolar ratio. Thus, in our further experiments we chose the equimolar ratio of H_2O_2 to ascorbic acid as the optimum.

There is also a certain limiting ratio between the substrate and initiating system (with equimolar ratio of the components) (Fig. 4). It could be expected that the degree of polymerization of chitosan would gradually decrease with an increase in the amount of hydrogen peroxide per chitosan molecule in solution; however, this is not the case. Figure 4 shows that there is a saturation plateau whose onset corresponds to approximately 0.1 mol of hydrogen peroxide per mole of the glucosamine units. Further addition of hydrogen peroxide (and, correspondingly, ascorbic acid) is virtually inefficient. Theoretically, this amount of H_2O_2 should lead to the formation of an oligomer with the degree of polymerization of 10–11. The calculated curve (Fig. 4, curve *2*) shows that actually the efficiency of utilization of hydrogen peroxide as a source of radicals breaking the chitosan backbones is appreciably less than unity (about 50%), i.e., H_2O_2 is also consumed in side reactions.

The decreased efficiency of radical initiation was also observed by Hsu et al. [8], who performed radical degradation of chitosan under the action of potassium persulfate. They considered as one of the possible reasons the deactivation of the generated free radicals in their reaction with the carbonyl groups of the arising terminal units of the oligomer. Hsu et al. believe that this reaction is responsible for the rapid reaction completion (within 1 h), compared to the half-life of the initiator at the reaction temperature (20.9 h).

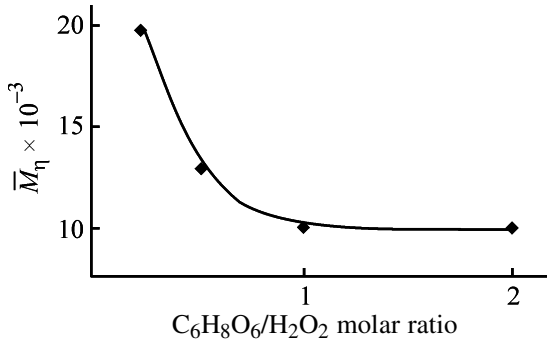


Fig. 3. Molecular weight of chitosan $\overline{M}_\eta$ measured 24 h after adding the redox system as a function of the molar ratio of ascorbic acid to hydrogen peroxide. Concentrations, wt %: chitosan 3 and acetic acid 2; molar ratio chitosan : H_2O_2 10; 21°C.

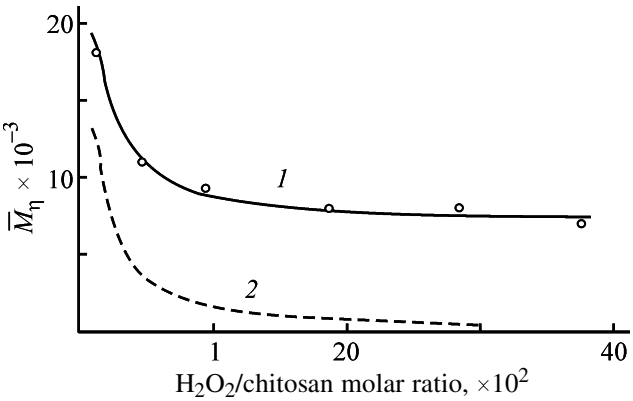


Fig. 4. Molecular weight of chitosan $\overline{M}_\eta$ measured 24 h after adding the redox system as a function of the molar ratio of hydrogen peroxide to chitosan. Concentrations, wt %: chitosan 3 and acetic acid 2; molar ratio H_2O_2 : ascorbic acid 1; 21°C. (*1*) Experimental curve and (*2*) theoretical dependence.

Presumably, under the conditions of radical degradation in the presence of redox system, the degradation reactions yielding low-molecular-weight chitosan compete with other reactions involving free radicals. In particular, radicals can decay in the reactions with ascorbic acid [9]. In this case, an increase in the ascorbic acid concentration at a constant substrate concentration may increase the relative rate of reactions leading to the decay of radicals. Furthermore, low-molecular-weight chains also participate in the decay of radicals. We suggest the following reaction scheme.

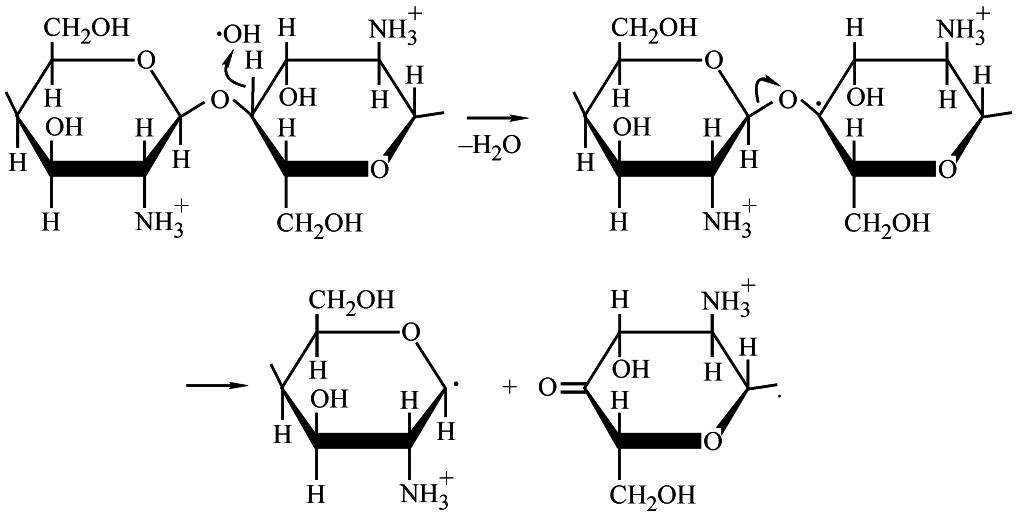
Generation of radicals by the reaction of hydrogen

peroxide with ascorbic acid (AAH_2 is ascorbic acid and AA, dehydroascorbic acid):

$$AAH_2 \rightleftarrows AAH^{\bullet} + H_2O + OH^{\bullet},$$

$$AAH^{\bullet} + H_2O_2 \rightarrow AA + H_2O + OH^{\bullet}.$$

Cleavage of the chitosan backbone with the formation of low-molecular-weight products:



Deactivation of radicals:

$$AA^{-} + OH^{\bullet} \rightarrow AA + OH^{-},$$

$$AAH^{\bullet} + OH^{\bullet} \rightarrow AA + H_2O,$$

$$OH^{\bullet} + AAH^{-} \rightarrow AAH^{\bullet} + OH^{-},$$

$$OH^{\bullet} + AAH_2 \rightarrow AAH^{\bullet} + H_2O,$$

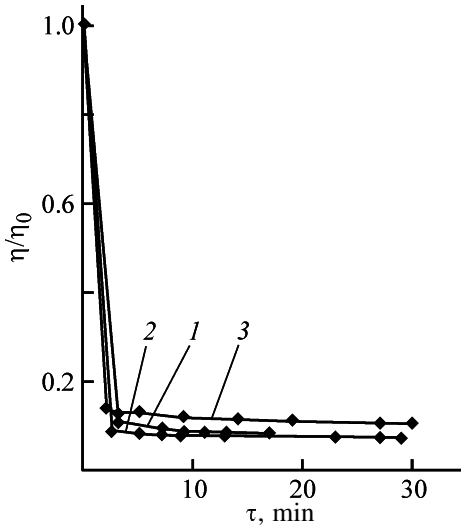
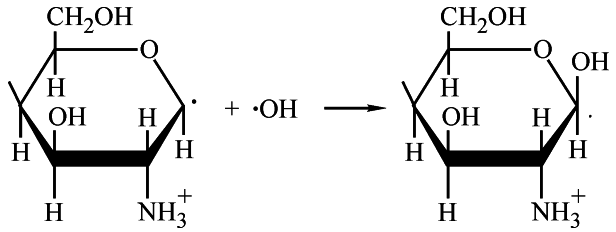


Fig. 5. Variation of the viscosity η/η_0 of chitosan solutions with time τ at (*1*) 24, (*2*) 40, and (*3*) 60°C. Concentrations in solution, wt %: chitosan 2 and acetic acid 1.5; molar ratios: chitosan : H_2O_2 40 and H_2O_2 : ascorbic acid 2.



The rate of the latter reaction should sharply increase as the low-molecular-weight chitosan is accumulated in the reaction mixture with an increase in the concentration of the initiating system.

The influence of temperature on the degradation of chitosan chains was examined by comparing the initial reaction rates and molecular weights of products in the range 0–60°C. We found that raising the temperature only slightly affects the rate at which the viscosity of chitosan solutions decreases (Fig. 5). Such a behavior is consistent with the general concept that processes occurring by the redox mechanism have a low activation energy. The activation energy calculated from data in Fig. 5 is 5 kJ.

The molecular weight of chitosan after the degradation at 0°C was 8.5×10^3, against 9.5×10^3 at 21°C and equal other conditions.

CONCLUSIONS

(1) Chitosan with a degree of polymerization of 10–40 can be prepared by low-temperature chemical

degradation of high-molecular-weight natural chitosan using the hydrogen peroxide–ascorbic acid redox system.

(2) It is the most appropriate to perform the process at molar ratios H_2O_2 : substrate 0.1 and H_2O_2 : ascorbic acid 1 : 1.

(3) The chitosan degradation rate weakly depends on temperature (activation energy 5 kJ).

REFERENCES

1. Skorikova, E.E., Kolyuzhnaya, R.I., and Vikhoreva, R.A., *Vysokomol. Soedin.*, 1996, vol. 38, no. 1, pp. 61–65.
2. Shepherd, R., Reader, S., and Falshaw, A., *Glycoconjugate J.*, 1997, no. 14, pp. 535–542.
3. Bykova, V.M. and Nemtsev, S.V., *Khimiya khitina i khitozana* (Chemistry of Chitin and Chitosan), Moscow: Nauka, 2002, pp. 6–22.
4. Mi Zhang and Tianwei Tan, *J. Bioact. Compat. Polym.*, 2003, vol. 18, September, pp. 391–400.
5. Galiaskarova, G.G., Regular Trends in Chitosan Degradation under the Action of Hydrogen Peroxide and Ozone, *Cand. Sci. Dissertation*, Ufa, 1997.
6. RF Patent 2 001 115 860/04 RU.
7. Murinov, K.Yu., Voloshin, A.I., Krasnogorskaya, I.N., and Sokov, Yu.F., *Izv. Ross. Akad. Nauk, Ser. Khim.*, 2002, no. 1, pp. 52–55.
8. Shih-Chang Hsu, Trong-Ming Don, and Wen-Yen Chiu, *Polym. Degrad. Stab.*, 2002, vol. 75, pp. 73–83.
9. Grinstead, R.R., *J. Am. Chem. Soc.*, 1960, vol. 82, pp. 3464–3471.
10. Berezovskii, V.M., *Khimiya vitaminov* (Chemistry of Vitamins), Moscow: Pishchevaya Prom-st., 1973.
11. Pogodina, N.V., Pavlov, G.M., Mel'nikov, A.V., et al., *Vysokomol. Soedin., Ser. A*, 1982, vol. 28, no. 2, pp. 232–239.
12. Melent'eva, G.A. and Antonova, L.A., *Farmatsevticheskaya khimiya* (Pharmaceutical Chemistry), Moscow: Meditsina, 1985.

ISSN 1070-4272. Russian Journal of Applied Chemistry, 2006, Vol. 79, No. 5, pp. 850–852. © Pleiades Publishing, Inc., 2006.
Original Russian Text © L.D. Kurbatova, D.I. Kurbatov, 2006, published in Zhurnal Prikladnoi Khimii, 2006, Vol. 79, No. 5, pp. 862–864.

BRIEF COMMUNICATIONS

Extraction Recovery of Vanadium(V) from Sulfuric Acid Solutions

L. D. Kurbatova and D. I. Kurbatov

Institute of Solid State Chemistry, Ural Division, Russian Academy of Sciences, Yekaterinburg, Russia

Received December 21, 2005

Abstract—The IR and electronic absorption spectra of di-2-ethylhexyl hydrogen phosphate (HDEHP) extracts of vanadium(V) and sulfuric acid and of vanadium(V) solutions in sulfuric acid were studied. The composition of the extractable complex was determined, and the equation of vanadium(V) extraction with HDEHP was suggested. The equilibrium constant of vanadium(V) extraction from concentrated sulfuric acid solutions was found.

DOI: 10.1134/S1070427206050302

Vanadium is a polyvalent element forming a variety of ionic species; it is susceptible to hydrolysis, polymerization, and reduction. Therefore, search for new efficient methods of its recovery is an urgent problem. This particularly concerns vanadium extraction recovery from sulfuric acid solutions, which are widely used in vanadium analytical chemistry and technology, because in sulfuric acid solutions vanadium(V) is not reduced and HDEHP does not noticeably extract sulfuric acid [1].

We showed previously [2] that HDEHP can effectively recover vanadium(V) from weakly acidic solutions. In this study we examined vanadium(V) extraction from concentrated sulfuric acid solutions.

EXPERIMENTAL

Vanadium(V) extraction and spectroscopic measurements were performed at 25 ± 0.5°C. HDEHP was preliminarily purified to remove an impurity of 2-ethylhexyl dihydrogen phosphate. Vanadium(V) was extracted with neat HDEHP at the ratio of the organic to aqueous phases $V_o : V_{aq} = 1$ and repeated phase contact (~4 min). Vanadium(V) solutions were prepared from chemically pure grade sodium metavanadate. Vanadium(V) concentration in aqueous solutions was determined by atomic absorption spectroscopy and titration [3]. The vanadium content in the organic phase was calculated as the difference of the concentrations in the aqueous phase before and after extraction. The IR spectra were recorded on a Specord 75IR spectrometer within the 400–4000 cm^{-1} range. KRS-6 optical windows were used.

In the IR spectra of the vanadium(V) extracts with HDEHP, the ν(P–OH) band, observed in the spectrum of the HDEHP extract of sulfuric acid at 1680 cm^{-1}, shifts to 1630 cm^{-1}. The components at 2260 and 2660 cm^{-1} of the ν(P–OH) band are absent. This pattern shows that deprotonated P–OH groups coordinate to V(V) [4]. Probably, protons of the extractant are substituted by vanadium(V) cations existing in the concentrated sulfuric acid solutions [5]. In addition, the spectra of the vanadium(V) extracts with HDEHP from concentrated sulfuric acid solutions contain the bands at 1070 and 1170 cm^{-1} assigned to ν_s(POO) and ν_{as}(POO), respectively [4]. The shift of the ν_{as}(POO) band to lower frequencies in the spectrum of the V(V) extract relative to the sulfuric acid extract shows that POO groups participate in coordination to vanadium(V). In accordance with published data [6], the extractable vanadium(V) complex with HDEHP is characterized by γ coordination, because $\Delta = \nu_{as}(POO) - \nu_s(POO) = 1170 - 1070 = 100$ cm^{-1}.

The other types of coordination, α, β, and γ', are characterized by higher ν_s(POO) 1085–1100 cm^{-1}, and δ coordination, by large Δ and lower ν_s(POO), <1070 cm^{-1} [6].

The comparison of the IR spectra of the vanadium(V) extract with HDEHP and vanadium(V) solution in 12 M sulfuric acid allowed identification of the vanadium(V) extractable complex. It was shown in [5] that in concentrated sulfuric acid solutions vanadium(V) exists as a dimeric oxovanadium(V) cation. Compensation of sulfuric acid absorption reveals bands at 988 and 750 cm^{-1} (shoulder) in the IR spec-

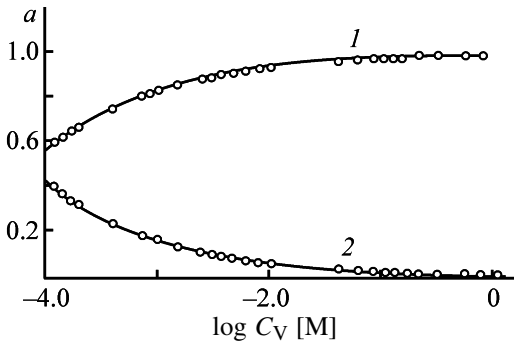
trum of vanadium(V) in sulfuric acid (12 M). In the spectrum of the HDEHP extract, we found a 970, 990 cm^{-1} doublet, which transforms into a strong band at 985 cm^{-1} after compensation of the HDEHP absorption. By the analogy with [7], we assigned this band to ν_1 of the dimeric oxovanadium(V) cation. The band at 750 cm^{-1} was not revealed, since it is probably obscured by the strong HDEHP band. All these facts show that HDEHP recovers vanadium(V) from sulfuric acid solutions as a complex of dimeric vanadium(V) oxocation. To determine the composition of the extractable complex, we studied the reaction of vanadium(V) with HDEHP by the molar ratio method, which showed that the stoichiometry of the vanadium(V) reaction with HDEHP, $V_{aq} : R_o$, is 1 : 2. In the spectrum of the complex formed, the band of sulfate anion splits into two bands at 570 and 600 cm^{-1} (shoulder), suggesting sulfate coordination to vanadium(V) [8]. The presence of the band at 3450 cm^{-1} in the IR spectrum of the extract shows that the vanadium extractable complex contains water molecules [8]. All these facts suggest the following composition of the extractable complex: $V_2O_3(H_2O)_{6-n}(HSO_4)_n \cdot (HR_2)_2$. Formation of the mixed-ligand complex of dimeric oxovanadium(V) with anions of sulfuric acid and HDEHP is confirmed by the electronic spectrum of the vanadium(V) extract, in which the band at 29000 cm^{-1} is shifted to lower frequencies [5]. Thus, vanadium(V) extraction with HDEHP can be described by the following equation:

$$V_2O_3(H_2O)_{8-n}(HSO_4)_n^{(4-n)+} + 2H_2R_2 \rightleftarrows V_2O_3(H_2O)_{6-n}(HSO_4)_n(HR_2)_2^{(2-n)+} + H_3O^+. \quad (1)$$

The equilibrium constant of this reaction was determined with regard to the composition of the extractable complex and vanadium(V) ionic state in 12 M H_2SO_4. Preliminarily, we found the optimal conditions of the extraction and the lower limit of the vanadium(V) concentration at which the extraction with HDEHP is still detectable. For this purpose, we studied the formation of the complex of the dimeric vanadium(V) oxocation in 12 M H_2SO_4 by electronic absorption spectroscopy. We found previously that at $C_{H_2SO_4} \geq 9.0$ M vanadium(V) transforms into a complex of dimeric oxovanadium in accordance with the equation

$$2VO_2(H_2O)_4^+ + 3H_3O^+ \rightleftarrows V_2O_3(H_2O)_8^{4+} + 3H_2O. \quad (2)$$

The following equilibrium constant of vanadium(V) dimerization in 12 M H_2SO_4 was found at three wavenumbers, 30000, 26000, and 23000 cm^{-1}:



Relative content α of vanadium(V) complexes in 12 M sulfuric acid. (C_V) Vanadium concentration. (*1*) $V_2O_3(H_2O)_8^{4+}$ and (*2*) $VO_2(H_2O)_4^+$.

$K = (1.57 \pm 0.01) \times 10^4$ l mol^{-1}. The optical densities of vanadium(V) solutions in sulfuric acid, calculated with this K, reasonably agree with the experimental values.

The figure shows the fractions of the monomeric and dimeric vanadium(V) species in 12 M H_2SO_4 as functions of the vanadium concentration. As seen, the higher the vanadium(V) concentration, the higher is the concentration of the dimer. At vanadium(V) concentration of 1×10^{-4} M, ~60% of vanadium is bound in a dimer, whereas at $C_V \geq 1 \times 10^{-3}$ M, the dimer fraction exceeds 80%.

To determine the equilibrium constant of extraction reaction (1) at $C_{H_2SO_4}$ 12 M, we used a series of vanadium(V) solutions with concentrations from 1×10^{-3} to 5×10^{-3} M. We determined the equilibrium concentration of the complex of dimeric oxovanadium(V) $V_2O_3(H_2O)_{8-n}(HSO_4)_n^{(2-n)+}$ using the above equilibrium constant of vanadium(V) dimerization in 12 M H_2SO_4.

The extraction constant calculated assuming $\alpha = 0.95$ is independent of the V concentration in the examined range and equal to $(2.51 \pm 0.03) \times 10^{-1}$, which confirms the adequacy of the suggested scheme of vanadium(V) extraction with HDEHP from concentrated sulfuric acid.

The constant obtained is consistent with the constants of vanadium(IV) extraction with HDEHP from perchloric and sulfuric acid solutions [9, 10], which also occurs by the cation-exchange mechanism.

CONCLUSION

A study of the IR and electronic spectra of vanadium(V) extracts showed that extraction of vanadium(V) with HDEHP from concentrated sulfuric acid

solutions (12 M) occurs by the cation-exchange mechanism. The composition of the extractable complex was determined, and an equation of the extraction reaction was suggested. The equilibrium constant of vanadium(V) extraction was determined.

REFERENCES

1. Kurbatova, L.D., Yaltuk, Yu.G., Kurbatov, D.I., and Sinitsyna, T.A., *Zh. Prikl. Khim.*, 2002, vol. 75, no. 1, pp. 171–173.
2. Kurbatova, L.D., Medvedeva, N.I., and Kodess, M.I., *Zh. Neorg. Khim.*, 1997, vol. 42, no. 11, pp. 1927–1929.
3. Ul'yanov, V.S. and Sviridova, R.A., *Radiokhimiya*, 1963, vol. 5, no. 4, pp. 419–421.
4. Stoyanov, E.S., Popov, V.M., and Mikhailov, V.A., *Zh. Prikl. Spektrosk.*, 1984, vol. 40, no. 1, pp. 77–81.
5. Kurbatova, L.D., Kurbatov, D.I., and Medvedeva, N.I., *Zh. Prikl. Khim.*, 2004, vol. 77, no. 4, pp. 680–682.
6. Stoyanov, E.S., *Zh. Strukt. Khim.*, 1994, vol. 35, no. 6, pp. 60–65.
7. Madic, C., Begun, G.M., Hahn, R.L., et al., *Inorg. Chem.*, 1984, vol. 23, no. 4, pp. 469–476.
8. Nakamoto, K., *Infrared and Raman Spectra of Inorganic and Coordination Compounds*, New York: Wiley, 1986.
9. Khyarsing, I.V. and Filippov, A.P., *Zh. Neorg. Khim.*, 1988, vol. 33, no. 4, pp. 900–904.
10. Hughes, M.A. and Biswas, R.K., *Hydrometallurgy*, 1991, vol. 26, no. 3, pp. 281–297.

ISSN 1070-4272. Russian Journal of Applied Chemistry, 2006, Vol. 79, No. 5, pp. 853–855. © Pleiades Publishing, Inc., 2006.
Original Russian Text © M.V. Bazunova, S.V. Kolesov, A.V. Korsakov, 2006, published in Zhurnal Prikladnoi Khimii, 2006, Vol. 79, No. 5, pp. 865–867.

BRIEF COMMUNICATIONS

Preparation of Ion-Exchange Fiber from Polypropylene Waste with Grafted Polyacrylic Acid

M. V. Bazunova, S. V. Kolesov, and A. V. Korsakov

Bashkir State University, Ufa, Bashkortostan, Russia
Building Materials and Technologies Research and Production Association, Limited Liability Company, Ufa, Bashkortostan, Russia

Received January 16, 2006

Abstract—A procedure was developed for preparing weakly acidic cation exchanger from polypropylene fiber wastes by grafting of acrylic acid to the preoxidized surface of the fiber in an aqueous solution.

DOI: 10.1134/S1070427206050314

Polypropylene (PP) articles find wide application owing to their good consumer properties, low cost of the monomer, and minimal consumption of the polymer per unit of the product. Approximately 30% of the produced PP is processed into the fiber. The annual demand of the Russian market for woven polypropylene fiber bags is 1.5 billion pieces [1]. Therefore, utilization of PP waste becomes an urgent problem. PP fiber can be used for preparing ion-exchange fibrous materials [2, 3]. One of the procedures for preparing fibrous polyolefin ion exchangers is grafting of macromolecular electrolytes (e.g., polyacrylic acid) to the fiber surface. This process is performed, as a rule, in organic solvent in the presence of radical initiators [3]. It involves expensive and power- and labor-consuming step of solvent regeneration and results in pollution of the environment with vapors of organic solvents. Therefore, development of a procedure for preparing weakly acidic anion exchanger by oxidation of PP fiber waste and grafting of acrylic acid to the oxidized surface in aqueous solution is an urgent problem.

EXPERIMENTAL

In this study we used PP fiber waste. To graft acrylic acid to the fiber surface, reactive surface centers capable of initiating growth of grafted macromolecules should be produced [4]. The surface of PP fiber was preactivated by initiated oxidation to form hydroperoxy (HP) groups. Thermolysis of these groups yields surface free radicals which initiate growth of the grafted macromolecules.

Novoselova [5] studied oxidation of PP fiber with atmospheric oxygen in toluene in the presence and in the absence of radical initiators at 120°C for 0.5–180 h. A procedure was developed for oxidizing PP wastes with atmospheric oxygen in aqueous solutions in the presence of H_2O_2/Fe^{2+} initiating system.

The IR spectra of oxidized PP waste contain the C–O stretching band at 1160 and the OH stretching bands at 3300–3500 cm^{-1}. Thus, the IR data and the results of iodometric titration confirm the presence of HP groups in the macromolecules.

As seen from Table 1, the material with the maximal content of the HP groups [3.3×10^{-4} mol (0.1 g of PP)$^{-1}$] was prepared by oxidation at 80–85°C for 13 h in the presence of 2.7 M H_2O_2.

The content of the HP groups does not increase in the course of longer oxidation. The hydroxyperoxy groups of oxidized PP are fairly stable. When the material is stored at room temperature or in the cold for 7 days, the concentration of HP groups decreases by 30 and 10%, respectively.

The degradation rate of a polymerization initiator at the reaction temperature is characterized by its half-life [6]. The half-life of HP groups determined from the kinetic curve of their thermolysis at 80°C (see figure) is $\tau_{1/2}$ 102 min. The half-life of HP in oxidized PP is comparable with that of the well-known radical initiator (at indicated temperature).

The ionic monomer grafted to the surface was acrylic acid (AA). The acid was grafted to oxidized PP fiber with the HP content of 2.70×10^{-4} mol (0.1 g of PP)$^{-1}$. The grafting was performed in an aqueous

Table 1. Oxidation conditions of PP

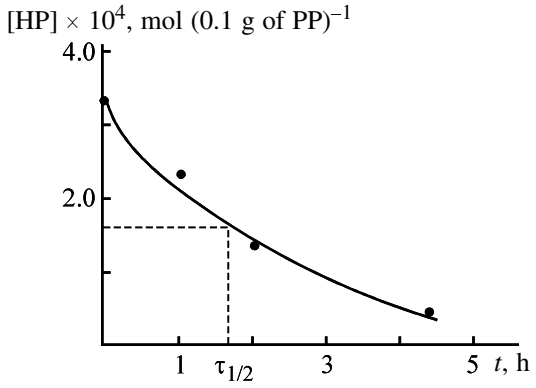
t, h	*T*, °C	Content		Amount of HP groups in 0.1 g of PP, mol
		$[H_2O_2]$, M	$[FeSO_4 \cdot 7H_2O]$, mg l^{-1}	
7.0	80	1.05	5.8×10^2	5.20×10^{-5}
7.5	85	2.00	1.1×10^3	7.53×10^{-5}
6.0	80	2.50	7.0×10^2	2.70×10^{-4}
7.0	80–85	2.70	1.5×10^3	2.51×10^{-4}
13.0	80–85	2.70	7.0×10^2	3.32×10^{-4}
14.0	80–85	2.70	7.0×10^2	3.30×10^{-4}
15.5	80–85	2.70	7.0×10^2	1.74×10^{-4}
19.0	80–85	2.70	7.0×10^2	1.48×10^{-4}

Table 2. Conditions of grafting of AA to oxidized PP fiber and exchange capacity of the resulting samples*

T, °C	AA concentration, %	*t*, h	Concentration, M		SEC, mg-equiv g^{-1}
			$[FeSO_4 \cdot 7H_2O]$	$[H_2O_2]$	
80	20	5.5	–	–	1.6
80	20	5.0	1.0×10^{-4}	6.7×10^{-2}	3.4
85–87	20	7.0	1.0×10^{-4}	2.2×10^{-3}	1.7
85–95	20	6.0	1.0×10^{-4}	1.7×10^{-2}	3.1
80–85	20	13.5	1.0×10^{-4}	–	2.9
75–80	20	7.0	9.0×10^{-4}	9.0×10^{-3}	2.3
70–75	20	12.0	2.7×10^{-4}	–	1.3

* For comparison: the SEC of commercial weakly acidic ion-exchange fiber KN-2 is 4.5–6.0 mg-equiv g^{-1}.

solution under inert atmosphere both in the absence and in the presence of a water-soluble initiator, hydrogen peroxide. An iron(II) salt was added to prevent formation of homopolymer of polyacrylic acid (PAA) [4]. The resulting material was thoroughly washed with distilled water to remove the homopolymer and dried. To recover PAA homopolymer, the wash waters were evaporated.



Concentration of HP groups in oxidized PP at 353 K as a function of time *t*.

The content of grafted PAA was determined by the weight gain ΔP of the grafted fiber

$$\Delta P = \frac{m_1 - m_0}{m_0} \times 100,$$

where m_0 and m_1 are the sample weight before and after grafting. The grafting degree ΔP of the samples ranged from 10 to 45%.

The presence of carboxy groups in PP samples with grafted PAA was confirmed by IR spectroscopy. The IR spectra of the samples contain the band of carboxy group at 1700 cm^{-1} and broad bands of OH groups in the range 3000–3400 cm^{-1}. The static exchange capacity (SEC) of the samples was determined in accordance with GOST (State Standard) 20255.1–89.

The conditions of grafting of AA to oxidized PP fiber and the exchange capacity of the resulting samples are summarized in Table 2. As seen from Table 2, SEC of the ion-exchange fibers prepared by grafting of AA to the surface of oxidized PP fiber is not higher

than 2.9 mg-equiv g^{-1}. The samples prepared in the presence of hydrogen peroxide initiator have the highest exchange capacity (3.4 mg-equiv g^{-1}). Probably, in this case the grafting becomes more efficient: the monomer is grafted owing to both degradation of HP and the chain-transfer reactions.

CONCLUSIONS

(1) Weakly acidic cation exchanger was prepared by grafting of acrylic acid in an aqueous solution in the presence of H_2O_2/Fe^{2+} initiating system to the surface of PP fiber waste preoxidized with atmospheric oxygen.

(2) This procedure has the following advantages: It allows utilization of polypropylene waste, thus decreasing the environment pollution with solid organic waste; hazardous, toxic, and expensive organic solvents and radical initiators are not used; the resulting material has the fibrous structure.

(3) The suggested process is virtually waste-free.

REFERENCES

1. Filonov, A.N., Maksimova, N.V., Knyr', I.N., and Maier, E.A., *Plast. Massy*, 2004, no. 5, pp. 30–34.
2. Shunkevich, A.A., Popova, O.P., Belotserkovskaya, T.N., and Soldatov, V.S., *Zh. Prikl. Khim.*, 1986, vol. 59, no. 3, pp. 2708–2711.
3. Novoselova, L.Yu. and Bordunov, V.V., *Plast. Massy*, 2002, no. 8, pp. 6–8.
4. Filimoshkin, A.G. and Voronin, N.I., *Khimicheskie reaktsii polimerov propilena i etilena* (Chemical Reactions of Propylene and Ethylene Polymers), Tomsk: Tomsk. Univ., 1990.
5. Novoselova, L.Yu., *Plast. Massy*, 2002, no. 11, pp. 42–44.
6. Semchikov, Yu.D., *Vysokomolekulyarnye soedineniya* (Macromolecular Compounds), Moscow: Academa, 2003.

ISSN 1070-4272. Russian Journal of Applied Chemistry, 2006, Vol. 79, No. 5, pp. 856–857. © Pleiades Publishing, Inc., 2006.
Original Russian Text © I.P. Kalinina, 2006, published in Zhurnal Prikladnoi Khimii, 2006, Vol. 79, No. 5, pp. 868–869.

BRIEF COMMUNICATIONS

Melting Diagram of the Ternary System Cyclohexane–*n*-Hexadecane–*n*-Docosane

I. P. Kalinina

Samara State Technical University, Samara, Russia

Received February 9, 2005; in final form, December 2005

Abstract—The ternary system cyclohexane–*n*-hexadecane–*n*-docosane was studied by low-temperature differential thermal analysis.

DOI: 10.1134/S1070427206050326

Systems based on paraffin hydrocarbons are of interest for petroleum chemistry and oil refining. These hydrocarbons are characterized by chemical inertness, high stability, and high heats of phase transitions. However, their studies involve certain problems. First, the temperature interval of interest is inconvenient for studies. Second, the phase diagrams in this case are extremely complex, despite the fact that the substances constituting the systems do not react chemically with each other, because in some cases the systems involve all the existing types of nonchemical phase equilibria: eutectics, peritectics, and formation of solid solutions with and without extrema. Interpretation of the diagrams in the course of construction is very sophisticated and requires high skill.

In this study we examined the ternary system cyclohexane–*n*-hexadecane–*n*-docosane by low-temperature differential thermal analysis (LTDTA) [1–3]. This method allows determination of the melting points for compositions of the system studied and enables construction of its melting diagram.

The cyclohexane–*n*-hexadecane–*n*-docosane (C_6H_{12}–*n*-$C_{16}H_{34}$–*n*-$C_{22}H_{46}$) system forms three binary subsystems (cyclohexane–*n*-hexadecane, cyclohexane–*n*-decosane, and *n*-hexadecane–*n*-docosane). The characteristics of these subsystems are given in Table 1.

The available data on the binary systems suggest that the ternary system C_6H_{12}–*n*-$C_{16}H_{34}$–*n*-$C_{22}H_{46}$ is eutectic; this assumption was confirmed experimentally.

The polythermal section e_2–e_3 in the crystallization field of *n*-$C_{22}H_{46}$ was chosen in the phase diagram of the ternary system (see figure). The phase diagram of this section was constructed from the LTDTA data and was used for determining the ratio of C_6H_{12} to *n*-$C_{16}H_{34}$ in the ternary eutectic *E*. The eutectic composition of the ternary system determined from the *n*-$C_{22}H_{46}$–$\bar{E}\rightarrow E$ section (see figure) is as follows (wt %): C_6H_{12} 79.9, *n*-$C_{16}H_{34}$ 19.1, and *n*-$C_{22}H_{46}$ 1.0. The phase diagram of the ternary system cyclohexane–*n*-hexadecane–*n*-docosane is characterized in Table 2.

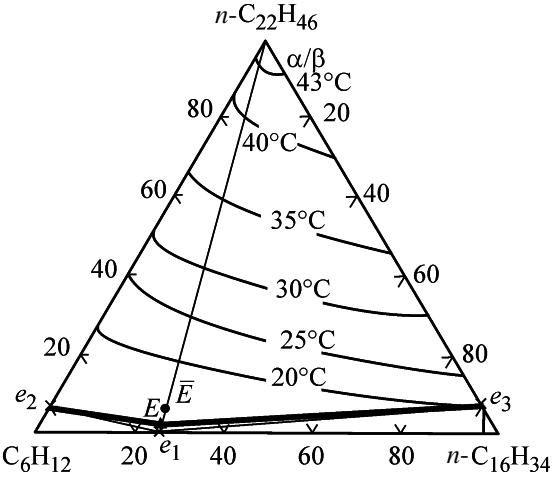
The specific enthalpy of melting for the eutectic composition of the ternary system (80 J g^{-1}) was determined by quantitative low-temperature differential thermal analysis.

Table 1. Characteristics of binary subsystems of eutectic type

System	T_m, °C	Content in eutectic, wt %		
		cyclohexane	*n*-hexadecane	*n*-docosane
Cyclohexane–hexadecane [4]	12.7	80.77	19.23	–
Cyclohexane–docosane [4]	4.6	83.8	–	16.2
n-Hexadecane–docosane [5]	16.2	–	94.3	5.7

Table 2. Characterization of the phase diagram of the ternary system C_6H_{12}–*n*-$C_{16}H_{34}$–*n*-$C_{22}H_{46}$

Element of phase diagram	Equilibrium	
	nonvariant	monovariant
Eutectic E; T_m = –17.9°C	l $\rightleftarrows$ C_6H_{12}–*n*-$C_{16}H_{34}$–β-*n*-$C_{22}H_{46}$	
e_1E		l $\rightleftarrows$ C_6H_{12}–β-*n*-$C_{22}H_{46}$
e_2E		l $\rightleftarrows$ *n*-$C_{16}H_{34}$–β-*n*-$C_{22}H_{46}$
e_3E		l $\rightleftarrows$ C_6H_{12}–*n*-$C_{16}H_{34}$



Projection of the phase diagram of the C_6H_{12}–*n*-$C_{16}H_{34}$–*n*-$C_{22}H_{46}$ system (wt %). (e_1, e_2, e_3) Binary and (E) ternary eutectics.

CONCLUSIONS

The ternary system cyclohexane–*n*-hexadecane–*n*-docosane is eutectic, the melting point of the eutectic is –17.9°C, and the specific enthalpy of melting is 80 J g^{-1}. The eutectic composition is as follows (wt %): C_6H_{12} 79.9, *n*-$C_{16}H_{34}$ 19.1, and *n*-$C_{22}H_{46}$ 1.0.

REFERENCES

1. Kopnina, A.Yu., Agafonov, I.A., and Garkushin, I.K., in *Trudy respublikanskoi nauchno-tekhnicheskoi konferentsii molodykh uchenykh "Khimicheskie nauki. Khimicheskie tekhnologii"* (Proc. Regional Scientific and Technical Conf. of Young Scientists "Chemical Sciences. Chemical Technologies"), Samara, 1999, pp. 14–16.
2. Kopnina, A.Yu., Agafonov, I.A., and Garkushin, I.K., *Izv. Vyssh. Uchebn. Zaved., Khim. Khim. Tekhnol.*, 2001, vol. 44, no. 5, pp. 84–87.
3. Kopnina, A.Yu., Agafonov, I.A., and Garkushin, I.K., *Zh. Obshch. Khim.*, 2001, vol. 71, no. 11, pp. 1921–1922.
4. Kopnina, A.Yu., Phase Equilibria in the Series of Binary Systems Consisting of Cyclic Aromatic Hydrocarbons and *n*-Alkanes, *Cand. Sci. Dissertation*, Samara, 2003.
5. Agafonov, I.A., Interactions in Some Binary Systems Involving *n*-Alkanes, *Cand. Sci. Dissertation*, Samara, 1997.

ISSN 1070-4272. Russian Journal of Applied Chemistry, 2006, Vol. 79, No. 5, pp. 858–860. © Pleiades Publishing, Inc., 2006.
Original Russian Text © M.V. Uspenskaya, N.V. Sirotinkin, V.A. Gorskii, Yu.G. Goloshchapov, 2006, published in Zhurnal Prikladnoi Khimii, 2006, Vol. 79, No. 5, pp. 870–872.

BRIEF COMMUNICATIONS

Composites of Acrylate Copolymers and Fullerene

M. V. Uspenskaya, N. V. Sirotinkin, V. A. Gorskii, and Yu. G. Goloshchapov

St. Petersburg State University of Information Technologies, Mechanics, and Optics, St. Petersburg, Russia
St. Petersburg State Technological Institute, St. Petersburg, Russia

Received April 22, 2005

Abstract—Preparation conditions of composites of vinylmethyltetrazole–acrylate copolymers with fullerene were studied. The sorption properties of the composites were studied in relation to the C_{60} content.

DOI: 10.1134/S1070427206050338

Fullerene-containing polymers and composites are promising materials for medicine, biology, building, and optics [1–3]. Materials with required particular properties can be prepared by modification of the initial polymer matrix with fillers. Introduction of fullerenes (F) into atactic PMMA affects the thermal oxidative degradation of the polymer matrix [4].

Previously we showed that introduction of fullerene into acrylate formulations slightly decreases the tensile strength of the films but substantially increases their relative elongation (ε ~1100%). Data on the preparation and properties of composites of vinylmethyltetrazole–acrylate copolymers with fullerene are scarce. The aim of this study was to prepare fullerene-containing acrylate composites and to examine their sorption properties.

EXPERIMENTAL

Films of composites of vinylmethyltetrazole–acrylate copolymers with fullerene were prepared by radical polymerization in aqueous solutions at 10–60°C in the presence of the ammonium persulfate (APS)–tetramethylethylenediamine initiating system. *N,N'*-Methylenebisacrylamide (MBAA) was used as the cross-linking agent. The degree of neutralization of acrylic acid α ranged from 0.1 to 0.9. The polymerization was performed at the initial monomer concentration of 10–57%, the concentration of 2-methyl-5-vinyltetrazole (MVT) of 0–65 wt % of the weight of acrylic acid (AA), and the concentration of the cross-linking agent of 0–0.9 wt % of the total monomer weight. The properties and purification procedures of other chemicals and the procedures for preparing composites and studying their sorption properties were reported previously [6]. The composites were prepared in aqueous solutions in 8–15 h.

Solid fullerene (C_{60}) was introduced with stirring in the first polymerization step. Since the composite is heterogeneous, the fraction of the unchanged modifier was determined gravimetrically after swelling of the composite in distilled water for 5–7 days.

The preparation conditions and some properties of composites of new vinylmethyltetrazole–acrylate copolymer with fullerene are presented in the table. It is seen that the copolymer yield decreases and the gelation onset time increases with increasing the fullerene concentration in the reaction mixture. This fact suggests that fullerene inhibits the initiation of the free-radical copolymerization [7]. It should be noted that the copolymer yield increases with increasing the AA concentration in the initial monomer mixture.

The kinetic curves of swelling of composites of vinylmethyltetrazole–acrylate copolymers with fullerene, prepared at different concentration of the cross-linking agent, are shown in Fig. 1a. The equilibrium swelling of these composites with different fullerene content is attained within 5–10 h, which is significantly faster than the time required for equilibrium swelling of vinylmethyltetrazole–acrylate hydrogels without the modifier.

As seen from Fig. 1a, the equilibrium swelling of the absorbing composites decreases with increasing the concentration of the cross-linking agent. This is due to shortening of the polymer segment between the cross-links of the polymeric network.

The kinetic curves of swelling of the fullerene-containing acrylate composites with different modifier content are shown in Fig. 1b. As seen from Fig. 1b,

Preparation conditions and properties of the composites of acrylate copolymers (solvent water)

Sample no.	Copolymerization conditions							Gelation onset time, h	Copolymer yield, %
	AA : MVT weight ratio	α	bath ratio	[MMBA]	[APS]	[F]	*T*, °C		
				wt %					
1	100 : 0	0.4	57	0.2	0.6	0.1	60	0.5	70
2	100 : 0	0.4	50	0.2	1	0.0	50	1	85
3	100 : 0	0.4	50	0.2	0.6	0.0	50	1.2	80
4	100 : 0	0.4	50	0.1	0.6	0.1	50	1.5	80
5	100 : 0	0.4	50	0.15	0.6	0.1	50	1.4	82
6	100 : 0	0.3	35	0.15	1	0.0	30	2	64
7	100 : 0	0.3	35	0.15	1	0.1	30	2.5	65
8	100 : 0	0.3	35	0.15	1	0.0	30	2.5	72
9	100 : 0	0.3	30	0.15	1	–	30	1	93
10	100 : 0	0.6	30	0.1	1	0.0	30	1.5	76
11	50 : 50	0.6	50	0.2	0.6	0.1	50	0.25	67
12	35 : 65	0.9	50	0.2	0.6	0.1	50	0.5	60
13	65 : 35	0.5	50	0.2	0.6	0.1	50	1	73
14	100 : 0	0.4	57	0.2	0.6	–	50	1	92
15	100 : 0	0.1	50	0.1	0.6	2.3	11	10	56
16	35 : 65	0.9	50	0.1	0.6	0.1	50	5	76
17	35 : 65	0.3	50	0.1	0.6	0.7	11	12	48

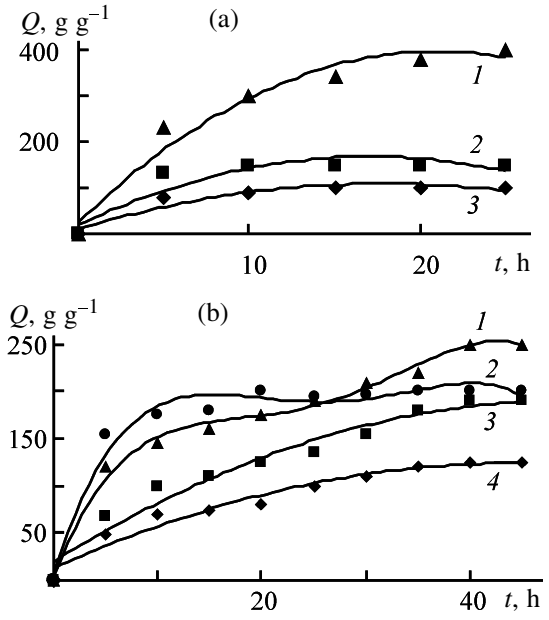


Fig. 1. Equilibrium degree of swelling *Q* of (a) vinylmethyltetrazole–acrylate copolymer and (b) fullerene-containing polymer composites in distilled water at 15°C as a function of time *t*. (a) Concentrations of fullerene and APS 0.1 and 0.6 wt %, respectively; α = 0.4. MBAA concentration, wt %: (*1*) 0.1, (*2*) 0.15, and (*3*) 0.2. (b) Concentrations of APS and MMBA 1 and 0.15 wt %, respectively; α = 0.3. Fullerene concentration, wt %: (*1*) 0.03, (*2*) 0.1, (*3*) 0.01, and (*4*) 0.

the initial swelling is accelerated as the fullerene content in the composite increases. The dependence of the equilibrium swelling passes through a maximum at the fullerene C_{60} concentration of 0.03 wt %. Ginzburg et al. showed [4] that aggregation of C_{60} molecules at their definite concentrations decreases the effect of the fullerene on the properties of PMMA films.

Fullerene C_{60} is insoluble in water but is a component of partially water-soluble material. The fullerene can be removed from the condensed phase during dissolution of the polymer. This is the case in prolonged swelling of the composites with the fullerene content higher than 0.7 wt %.

It should also be noted that the equilibrium degree of swelling of the vinylmethyltetrazole–acrylate copolymer prepared under the similar conditions but without the modifier is smaller that that of the copolymer modified with C_{60}. This can be due to fullerene–copolymer intermolecular interactions affecting the absorption properties of the acrylate composites. Stabilization of monomolecular layers of C_{60} by aqua aggregation was demonstrated in [8].

The fact that swollen fullerene-containing composite holds its shape allows preparation of articles with required geometrical parameters.

CONCLUSIONS

(1) Absorbing composites of vinylmethyltetrazole–acrylate copolymer with fullerene were prepared.

(2) The influence of the modifier on the absorption properties of the composites was demonstrated. The dependence of the equilibrium degree of swelling of the composites on the fullerene content passes through a maximum. These dependences allow prediction of the properties of composites with different modifier content.

(3) The rate of the swelling of the composites in distilled water depends on the fullerene content in the sample.

REFERENCES

1. Karpacheva, G.P., *Vysokomol. Soedin*., 2000, vol. 42, no. 11, pp. 1974–1999.
2. Vinogradova, L.V., Melenevskaya, E.Yu., Khachaturov, A.S., et al., *Vysokomol. Soedin., Ser. A*, 1998, vol. 40, no. 11, pp. 1854–1862.
3. Zgonnik, V.N., Vinogradova, L.V., Melenevskaya, E.Yu., et al., *Zh. Prikl. Khim*., 1995, vol. 68, no. 1, pp. 99–105.
4. Ginzburg, B.M., Melenevskaya, E.Yu., Novoselova, A.V., et al., *Vysokomol. Soedin., Ser. A*, 2004, vol. 46, no. 2, pp. 295–303.
5. Uspenskaya, M.V., Sirotkin, N.V., and Ostrovskii, V.A., in *Materialy V Vserossiiskoi konferentsii "Keramika i kompozitsionnye materialy"* (Proc. V All-Russian Conf. "Ceramics and Composites"), Syktyvkar, June 20–27, 2004, pp. 207–208.
6. Igrunova, A.V., Sirotinkin, N.V., and Uspenskaya, M.V., *Zh. Prikl. Khim*., 2001, vol. 74, no. 5, pp. 793–797.
7. Zgonnik, V.N., Vinogradova, L.V., Melenevskaya, E.Yu., et al., *Zh. Prikl. Khim*., 1997, vol. 70, no. 9, pp. 1538–1542.
8. Glibin, A.S., in *Materialy I Vserossiiskoi shkoly-konferentsii "Molodye uchenye novoi Rossii. Fundamental'nye issledovaniya v oblasti khimii i innovatsionnaya deyatel'nost"* (Proc. I All-Russian School Conf. "Young Scientists of New Russia. Basic Research in Chemistry and Innovation Activity"), Ivanovo, September 26–29, 2005, pp. 62–63.

ISSN 1070-4272. Russian Journal of Applied Chemistry, 2006, Vol. 79, No. 5, pp. 861–864. © Pleiades Publishing, Inc., 2006.
Original Russian Text © E.V. Gavryushin, T.I. Gorbunova, A.Ya. Zapevalov, V.I. Saloutin, 2006, published in Zhurnal Prikladnoi Khimii, 2006, Vol. 79, No. 5, pp. 873–876.

MACROMOLECULAR CHEMISTRY AND POLYMERIC MATERIALS

Hydrophobicity and Thermal Stability of Fluorinated Pentaerythritol Esters

E. V. Gavryushin, T. I. Gorbunova, A. Ya. Zapevalov, and V. I. Saloutin

Postovskii Institute of Organic Synthesis, Ural Division, Russian Academy of Science, Yekaterinburg, Russia

Received August 17, 2005

Abstract—Wetting angles and limits of thermal stability of esters derived from pentaerythritol and perfluoro-, ω-chloropolyfluoro-, and perfluoropolyethercarboxylic acids were studied.

DOI: 10.1134/S107042720605034X

Esters derived from polyhydric alcohols and carboxylic acids occupy leading positions on the market of lubricants thanks to their high resistance to heat and oxidation, good lubricating characteristics, and favorable viscosity–temperature parameters [1]. Depending on the demands, these esters are used as working bodies or as additives to other commercial oils. The field of application of lubricants based on esters derived from polyhydric alcohols and carboxylic acids ranges from the production of consumer goods to operation of jet and high-temperature gas turbines.

A particular place among such lubricants is occupied by pentaerythritol (PE) esters. An advantage of PE esters is the presence of a quaternary carbon atom in the β-position to the ester group [2], which enhances their thermal stability.

Much attention is given to synthesis procedures and physicochemical properties of esters derived from PE and alkylcarboxylic acids. Halogenated PE esters have been studied insufficiently.

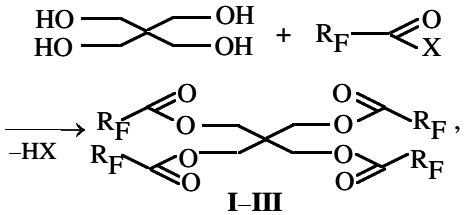
Synthetic lubricating oils derived from alcohols and perfluoro acids exhibit chemical inertness, high stability, and inflammation resistance [2].

In this study we examined the hydrophobicity and thermal stability of new fluorinated PE tetraesters. Among the most studied analogs of fluorinated PE esters are perfluoro polyesters prepared by reactions of PE with perfluoropolyetheracids [3]. These compounds were recommended as lubricants and hydraulic fluids.

Commercial procedures for preparing carboxylic acid esters involve direct esterification of alcohols with fatty acids or ester interchange of esters (e.g., methyl esters) with appropriate alcohol in a solvent in the presence of a catalyst.

Application of these methods to the synthesis of esters from PE and perfluorocarboxylic acids does not ensure high yields of the target products. Since PE contains four OH groups, esterification by the classical procedure in the presence of a catalyst (H_2SO_4, KU-2 cation-exchange resin, etc.) yields a mixture of four compounds (from mono- to tetraesters).

Therefore, we attempted to use as acylating agents halides of fluorocarboxylic acids:



I–III

(41–53%)

where $R_F = C_6H_{13}$, X = F (**I**); $R_F = Cl(CF_2)_8$, X = Cl (**II**); $R_F = C_3F_7OCF(CF_3)CF_2OCF(CF_3)$, X = F (**III**).

The process occurs without catalyst. The reaction medium is excess acyl halide; after the reaction completion, it is removed from the reaction mixture.

Compounds **I**–**III** are insoluble in common solvents but readily soluble in fluorinated liquids (hexafluorobenzene, Freons, etc.).

The structures of **I**–**III** were determined by elemental analysis and IR spectroscopy, and also from the saponification numbers [4] (see Experimental).

Different structures of acid residues in **I**–**III** suggest their different physicochemical properties; in-

Results of the derivatographic thermal gravimetric analysis of **I**–**III**

Compound no.	Weight loss, %/*T*, °C								
I	1/100	1.5/150	2.8/200	15/250	91/300	100/350	–	–	–
II	0/100	0/150	0.8/200	1.5/250	6/300	40/350	97/400	98.5/450	100/500
III	0/100	1/150	4/200	23.5/250	98/300	100/350	–	–	–

Compound no.	Temperature *T*, °C, of weight loss indicated in denominator, %						Interval of intense weight loss, *T*, °C
I	50/0.5	100/1	220/5	240/10	280/50	305/100	220–305
II	190/0.5	210/1	290/5	315/10	355/10	475/100	270–370
III	130/0.5	150/1	212/5	230/1	275/10	305/100	212–305

deed, these compounds differ in the hydrophobicity and thermal stability.

Introduction of fluorinated acid residues into PE by esterification should enhance the hydrophobicity as compared to esters of PE with common carboxylic acids, because of weakness of the intermolecular interaction on the water–organofluorine compound phase boundary [5].

The hydrophobic properties of tetraesters **I**–**III** were evaluated by measuring the wetting angle by the stagnant drop method [6]. To obtain surface layers of **I**–**III**, we used their 2 and 4% solutions in hexafluorobenzene; aluminum foil was used as support. The conditions for determining the wetting angle are given in the Experimental.

As reference compounds for studying the hydrophobicity of **I**–**III** we used commercially available PE tetrabutyrate and PE tetrabenzoate.

The wetting angles we obtained show that compound **I** containing four perfluoroalkyl groups is the most hydrophobic. Tetraester **II** with four ω-chloroperfluoroalkyl groups is less hydrophobic, and compound **III** is the least hydrophobic, which agrees with the data from [5].

Parallel determination of the wetting angle with the reference compounds showed that PE tetrabutyrate and tetrabenzoate are wetted well, which is due to their low hydrophobicity.

Fluorinated esters are used as synthetic lubricating oils and as additives to commercial lubricating materials [2]. The thermal stability of synthetic ester oils and additives is largely determined by the steric structure of the acid or alcohol residues. However, the service temperatures of esters derived from PE and alkylcarboxylic acids do not exceed 175–200°C.

To evalulate the thermal stability of the new tetraesters and the possibility of using them as additives, we studied both neat compounds **I**–**III** and their 0.2% solutions (prepared by ultrasonic dispersion) in I-12A industrial oil [GOST (State Standard) 20799–88] by derivatographic thermal gravimetric analysis (see table). Our results show that ester **II** considerably surpasses in the thermal stability compounds **I** and **III**, which is apparently associated with the structure of fluoroalkyl radicals.

Similar trends are observed when studying the thermal stability of I-12A industrial oil with additions of **I**–**III**. The most thermostable is a solution of **II** in I-12A; esters **I** and **III** enhance the thermal stability of I-12A to a lesser extent, giving similar results.

EXPERIMENTAL

The IR spectra were recorded on a Spectrum One Perkin–Elmer Fourier spectrophotometer. Compounds **I** and **III** were taken as thin layers, and for **II** the diffuse reflection mode (DRA) was used. Derivatographic thermogravimetric analysis was performed with a Ditector-MOM device with programmed heating at a rate of 5 deg min^{-1}; the sample weight was 100 mg. Elemental analysis was performed with an EA1108 CHN analyzer (Carlo Erba, Italy).

Ester of PE and perfluoroenanthic acid (I). To 0.1 mol of PE, 0.6 mol of perfluoroenanthic acid fluoride was added dropwise at a rate allowing the reaction mixture temperature to be maintained within 55°C. After adding the whole amount of the acid fluoride, the mixture was heated at 140°C for 30 h. Excess acid fluoride was distilled off, and the residue was distilled in an oil-pump vacuum. Yield of ester **I** 76 g (50%), bp 280–282°C (60 mm Hg). IR spectrum

(ν, cm^{-1}): 1797 (–O–C=O).

Found, %: C 26.10, H 0.46, F 65.05.
$C_{33}H_8F_{52}O_8$.
Calculated, %: C 26.07, H 0.53, F 64.98.

Saponification number, found: 155.

Ester **II** of PE and ω-chloroperfluoropelargonic acid was prepared similarly; yield 41%, mp 92°C. IR spectrum, ν, cm^{-1}: 1789 (–O–C=O).

Found, %: C 25.01, H 0.38, F 61.77.
$C_{41}H_8Cl_4F_{64}O_8$.
Calculated, %: C 24.79, H 0.41, F 61.22.

Saponification number, found: 117.

Ester **III** of PE and perfluoro-3,6-dioxa-2,5-dimethylnonanoic acid was prepared similarly; yield 53 %, bp 225–228°C (60 mm Hg). IR spectrum (ν, cm^{-1}): 1795 (–O–C=O).

Found, %: C 24.28, H 0.48, F 62.70.
$C_{41}H_8F_{68}O_{16}$.
Calculated, %: C 24.04, H 0.39, F 63.07.

Saponification number, found: 116.

Determination of the wetting angle. Two stands were arranged on an antivibration table. The stands were equipped with levels with which the stands were aligned relative to the table surface. A Nikon Coolpix 5200 digital camera was arranged on one of the stands. A thin rigid plate acting as a microscopic stage was arranged on the other stand. On this plate we arranged on aluminum foil treated with solutions of tetraesters **I**–**III** in hexafluorobenzene as described in [6]. The Macro mode of the camera was set. A 50-μl water drop was applied with a pipet to the foil surface treated with solutions of **I**–**III**, the camera lens was focused on the drop surface, and the image was taken. The images were treated with a computer using ACDSee 6.0 program and various program filters. The inital image of a water drop (before using filters) is shown in Fig. 1a. Figure 1b shows the same water drop after application of the program filters. The borders of the water drop, required for the mathematical calculation of the wetting angle (line width 1 pix) are clearly seen in Fig. 1b.

The mathematical treatment of the images was performed using data of [7], according to which the wetting angle is calculated from the length of the drop base ($d = 2r$) and the drop height (h). For wetting angles $\theta > 90°$, when the surface is hydrophobic, the following expressions are valid:

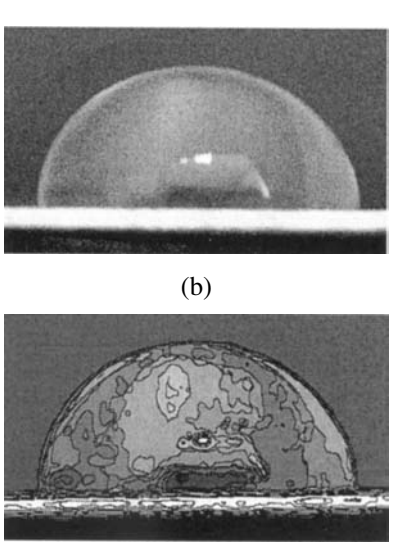


Fig. 1. Photograph of a water drop on films of **I**–**III**: (a) before and (b) after computer treatment of the image.

$$\tan\alpha = (2hr - h^3)^{1/2}(r - h)^{-1}, \qquad \alpha = \pi - \theta.$$

The angle α was found from tables [8]. For wetting angles $\theta < 90°$, the use of this expression is unnecessary.

The witting angles on films of **I**–**III** (deg) are as follows. Films prepared from 2% solutions: **I**, 100; **II**, 91; **III**, 67. Films prepared from 4% solutions: **I**, 103; **II**, 93; **III**, 71.

CONCLUSION

The synthesized esters of pentaerythritol and fluorinated acids show high hydrophobicity and thermal stability.

ACKNOWLEDGMENTS

The study was financially supported by the Russian Foundation for Basic Research (project no. 04-03-96 109).

REFERENCES

1. Klamann, D., *Lubricants and Related Products: Synthesis, Properties, Applicatoins, International Standards*, Weinheim: Chemie, 1984.

2. Mamed'yarov, M.A., *Khimiya sinteticheskikh masel* (Chemistry of Synthetic Oils), Leningrad: Khimiya, 1989.
3. US Patent 3 646 112.
4. Houben–Weyl, *Methoden der organischen Chemie*, vol. 2: *Analytische Methoden*, Stuttgart: Thieme, 1953.
5. *Fluoropolymers*, Wall, L.A., Ed., New York: Wiley–Interscience, 1972.
6. *Praktikum po kolloidnoi khimii* (Practical Course of Colloid Chemistry), Neiman, R.E., Ed., Moscow: Vysshaya Shkola, 1971.
7. *Laboratornye raboty i zadachi po kolloidnoi khimii* (Laboratory Works and Problems on Colloid Chemistry), Frolov, Yu.G., Ed., Moscow: Khimiya, 1986.
8. Bradis, V.M., *Chetyrekhznachnye matematicheskie tablitsy* (Four-Digit Mathematical Tables), Moscow: Drofa, 2000.

ISSN 1070-4272. Russian Journal of Applied Chemistry, 2006, Vol. 79, No. 5, p. 865. © Pleiades Publishing, Inc., 2006.
Original Russian Text © A.G. Morachevskii, 2006, published in Zhurnal Prikladnoi Khimii, 2006, Vol. 79, No. 5, p. 877.

BOOK REVIEWS

Meretukov, M.A., Tsepin, M.A., Vorob'ev, S.A., and Syrkov, A.G., *Klastery, struktury i materially nanorazmera: innovatsionnye i tekhnicheskie perspektivy* (Nanosize Clusters, Structures, and Materials: Innovational and Technological Prospects),

Moscow: Ruda i Metally, 2005, 128 pp.

DOI: 10.1134/S1070427206050351

A strong interest in nanostructures composed of various substances has been expressed in recent 15–20 years, and quite a number of domestic and translated monographs of varied scientific level on nanotechnologies and nanochemistry have been published. On passing to the nanometer range (to objects of size less than 10 nm), quite a number of the most important parameters of substances change fundamentally. The small-volume book by M.A. Meretukov and coauthors presents in form understandable for a wide audience of readers modern concepts of high nanometer technologies, nanoobjects, and areas of their application. The principal feature of the book, which distinguishes it from other publication devoted to similar topics, is that gold is chosen as the object metal illustrating the advances in nanotechnology and new properties of gold are clearly shown for the example of its nanoparticles.

The book comprises an introduction and eight chapters, with each section provided with its own list of references and recommended literature. The introduction (pp. 6–17) gives a general notion of nanostructured materials and the extent to which nanotechnologies are developed and applied in a number of countries, including Russia, and discusses prognoses of development of nanotechnologies and their potentialities that can be implemented in the nearest five years and in 50–60 years. The concluding part of the introduction considers the potentialities of nanotechnologies as applied to some metallurgical processes.

Chapter 1 (pp. 18–29) presents the general concepts concerning the nature of nanostructures, by which are understood formations with at least one dimension of several nanometers. The authors give notion of the tunneling effect and scanning probe microscopy. Chapter 2 (pp. 30–43) gives notion of physical and chemical methods for production of nanostructured metals. Chapter 3 (pp. 44–53) presents the concepts of clusters and the cluster state of metals. Chapter 4 (pp. 54–69) presents evidence about fullerenes, their structure, properties, synthesis, and possible application areas. Chapter 5 (pp. 70–87) continues with this subject and presents various data on carbon nanotubes.

As already noted, the book is made original by Chapters 6 (pp. 88–98), 7 (pp. 99–111), and 8 (pp. 112–125) considering gold-based nanomaterials. Chapter 6 notes that nanosize particles of gold are used as biosensors and in chemical catalysis, with an important role assigned to these nanoparticles in the development of new generations of nanosize optical and electronic devices. Gold clusters, specific features of their structure, geometrical dimensions, and synthesis methods are described in detail. Of interest is the evidence presented in the book (Chapter 7) about natural nanosize particles of gold. The development of analytical methods using various kinds of microprobes in the last 20 years has revealed in ores invisible gold localized on the surface and in the bulk of sulfide and other minerals. The final Chapter 8 is devoted to synthesis and application of gold nanostructures. The authors, in particular, note that of special interest is the possibility of obtaining ordered (regular) structures that can be deposited in the form of films on specialized substrates, mostly those composed of metal oxides. Use of gold nanomaterials in electronics, as catalysts in chemical industry, and in solution of certain environmental problems is considered.

Owing to the well-understandable manner of presentation, the book by Meretukov and co-authors is of interest not only to specialists in nanotechnology, but also to the widest audience of students and teachers at higher-school and secondary educational institutions. The book is very well published and contains a large number of illustrative schemes and figures, which improves its cognitive value.

A. G. Morachevskii

ISSN 1070-4272. Russian Journal of Applied Chemistry, 2006, Vol. 79, No. 5, pp. 866–867. © Pleiades Publishing, Inc., 2006.
Original Russian Text © A.G. Morachevskii, 2006, published in Zhurnal Prikladnoi Khimii, 2006, Vol. 79, No. 5, p. 878.

BOOK REVIEWS

Kazantsev, G.F., Barbin, N.M., Brodova, I.G., Vatolin, N.A., Moiseev, G.K., and Bashlykov, D.V., *Pererabotka loma i otkhodov tsvetnykh metallov v ionnykh rasplavakh* (Processing of Scrap and Waste Nonferrous Metals in Ionic Melts),

Yekaterinburg: Ural'sk. Otd. Ross. Akad. Nauk, 2005, 210 pp.

DOI: 10.1134/S1070427206050363

The monograph devoted to a rather topical subject was prepared by a group of specialists from institutes affiliated with the Ural Division of the Russian Academy of Sciences: Institute of Metallurgy, Institute of High-Temperature Electrochemistry, and Institute of Metal Physics. The authors summarized the results of mostly their own studies in the field of theoretical foundations and technology of processing of nonferrous-metal secondary raw materials.

The book comprises an introduction, seven chapters, and reference lists for each chapter separately. The brief introduction (pp. 3, 4) notes that the many years' studies carried out at the institutes of the Ural Division demonstrated the possibility and advisability of processing of secondary raw materials (scrap aluminum and aluminum alloys, copper, zinc, and tin) in ionic melts and, in particular, in molten halides of alkali and alkaline-earth metals. The authors considered it appropriate to include into the monograph evidence concerning use of light metals and their alloys in various fields of technology and to present data on selected physicochemical properties of nonferrous metals.

Chapter 1 (pp. 5–43) is mostly devoted to application of aluminum alloys. Also presented is evidence concerning the composition of certain aluminum alloys, both cast and wrought. There is no escape from mentioning that a considerable part of the material presented in Chapter 1 bears no direct relation to the problem under discussion. Chapter 2 (pp. 44–81) considers the equipment used in processing of various kinds of secondary raw materials containing nonferrous metals. Unfortunately, the companies manufacturing such equipment in Russia or CIS countries are not named by the authors.

Chapter 3 (pp. 82–103) briefly discusses the properties of molten electerolytes and presents a number of tables with data on the physicochemical properties of individual molten compounds and mixtures of these. Among issues related to refinable metals, only melting of scrap aluminum under a layer of molten salts is very briefly considered. Chapter 4 (pp. 104–150) mainly includes results obtained when studying the remelting of aluminum alloy shavings under a layer of flux composed of molten salts. Chapter 5 (pp. 151–167) considers remelting, under a layer of halide fluxes, of a complex scrap constituted by various cables, bimetals, and oxidized secondary aluminum. The brief Chapter 6 (pp. 168–184) describes application of fluxes composed of molten salts in modification of certain aluminum alloys. The final Chapter 7 (pp. 185–199) discusses remelting of wastes containing copper, zinc, tin, and titanium.

On the whole, the book by G.F. Kazantsev and co-authors contains useful recommendations concerning use of molten salts as fluxes in processing of secondary raw materials containing, primarily, aluminum and, to a lesser extent, other nonferrous metals. Despite the positive assessment of the monograph written by the group of authors, there is no escape from mentioning the certain incoherence of the structure of the book, its narrowly applied nature, and its overloading with reference data and other materials that bear no direct relation to the technologies discussed. Probably, the authors should have more clearly formulated the subject of the monograph in the introductory part. In fact, the book is only devoted to remelting of secondary raw materials containing nonferrous metals and, primarily, aluminum. Separation or reduction processes occur in remelting only in some cases. The term "processing of scrap and wastes" presumes, in its modern understanding, a deeper processing of the starting secondary raw ma-

terials, with not only remelting, but also the subsequent separation of components. It seems that, in compiling the reference tables, primarily for individual metals and salts, the authors did not always select the best source of these data.

The monograph by Kazantsev and co-authors is of interest for engineers and technicians working in the field of utilization of secondary aluminum-containing raw materials and is also of use for specialists in processing of various secondary raw materials in nonferrous metallurgy.

A. G. Morachevskii

ISSN 1070-4272, Russian Journal of Applied Chemistry, 2006, Vol. 79, No. 6, pp. 869–876. © Pleiades Publishing, Inc., 2006.
Original Russian Text © E.S. Sashina, A.M. Bochek, N.P. Novoselov, D.A. Kirichenko, 2006, published in Zhurnal Prikladnoi Khimii, 2006, Vol. 79, No. 6, pp. 881–888.

REVIEWS

Structure and Solubility of Natural Silk Fibroin

E. S. Sashina, A. M. Bochek, N. P. Novoselov, and D. A. Kirichenko

St. Petersburg State University of Technology and Design, St. Petersburg, Russia
Institute of Macromolecular Compounds, Russian Academy of Sciences, St. Petersburg, Russia

Received March 7, 2006

Abstract—The solubility of silk fibroin in aqueous-salt, aqueous-organic, and organic media is analyzed. Factors affecting the formation of the secondary structural organization of fibroin in solutions and in the solid state after the recovery from solutions are analyzed.

DOI: 10.1134/S1070427206060012

Of particular importance among natural polymers widely used in various spheres of human activity are polysaccharides (cellulose, chitin, their derivatives, starch, etc.) and proteins (primarily silk fibroin).

Articles made of silk fibers exhibit high wear resistance and physicomechanical properties making their wearing comfortable: good capability of silk fibers for moisture absorption, air permeability, and low electrifiableness. Processing of fibers produced by cultivated *Bombyx mori* mulberry silkworm involves formation of large amounts of wastes (fibers that are difficult to take out from cocoons), which are potentially valuable and can be processed into films, artificial fibers, or nonwoven materials by dissolution of silk fibroin, followed by its recovery. The silk fibroin dissolution is affected by the nonuniformity of fibroin in the chemical composition, by the system of hydrogen bonds existing in the polymer, by its supramolecular structure, and by the morphological features of natural fibers. The solubility of silk and web thread fibroin in aqueous and organic salt-containing systems and in certain salt-free organic solvents has been studied in recent years. It seems appropriate to summarize papers that deal with the factors affecting the solubility of silk fibroin in aqueous and nonaqueous solvent systems, with the properties of the solutions obtained, and with conformational changes of silk fibroin macromolecules in the course of recovery of the polymer from solutions.

1. STRUCTURE OF NATURAL SILK FIBROIN

Silk fibroin, like creatine and collagen, belongs to fibrillar proteins [1]. The elements of the supramolecular structure of silk fibers are macrofibrils with a width of up to 6.5×10^5 nm, which, in turn, consist of helically packed nanofibrils 90–170 nm in diameter [2, 3]. Nanofibrils may play an important role in imparting enhanced strength to silks. The molecular weight of natural silk fibroin reaches 370000 Da; fibroin macrochain length, 150 nm; and macrochain diameter, 0.45 nm [4, 5].

Silk fibers produced by cultivated *Bombyx mori* mulberry silkworm mainly consist of two proteins, sericin and fibroin; they also contain minor amounts of residues of other amino acids and various impurities: fats, waxes, dyes, and mineral salts. Depending on the cocoon strain, the fibroin content is 66.5–73.5, and the sericin content, 26.5–33.5 wt % [6].

As for the chemical composition, *Bombyx mori* fibers consist of residues of no less than 16 amino acids whose ratio varies between different areas of the supramolecular structure of fibroin (Table 1). "Heavy" areas of the polymer, with a mean molecular weight of up

Table 1. Amino acid composition of *Bombyx mori* fibroin [7]

Amino acid	Composition, mol %		
	total	heavy areas	light areas
Glycine	42.9	49.4	10.0
Alanine	30.0	29.8	16.9
Serine	12.2	11.3	7.9
Tyrosine	4.8	4.6	3.4
Valine	2.5	2.0	7.4
Aspartic acid	1.9	0.65	15.4
Glutamic acid	1.4	0.70	8.4
Threonine	0.92	0.45	2.8
Phenylalanine	0.67	0.39	2.7
Methionine	0.37	–	0.37
Isoleucine	0.64	0.14	7.3
Leucine	0.55	0.09	7.2
Proline	0.45	0.31	3.0
Arginine	0.51	0.18	3.8
Histidine	0.19	0.09	1.6
Lysine	0.38	0.06	1.5

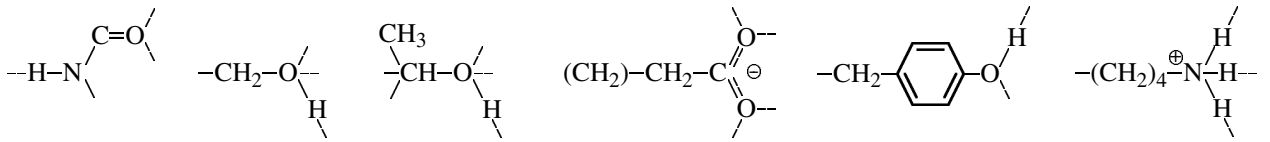
to 350000–370000, mainly consist of highly ordered hydrophobic macromolecules, and in looser "light" areas with a mean molecular weight of about 25000 the major components are polar amino acid residues [7].

The mole fraction of glycine, alanine, serine, and tyrosine residues combined is 90%; their sequence is represented by the general formula [8, 9]

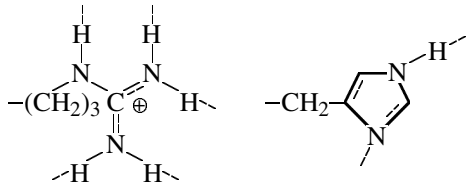
$$-Gly-Ala-Gly-Ala-Gly-Ser-Gly-Ala-Ala-Gly-[-Ser-Gly-(Ala-Gly)_n-]_8-Tyr-$$

The pendant fragments of fibroin macromolecules are nonpolar hydrophobic aliphatic hydrocarbon (alanine, leucine, isoleucine, valine, proline) and aromatic (phenylalanine) substituents, polar hydrophilic hydroxyl-containing residues of serine, threonine, and tyrosine, carboxy groups of aspartic and glutamic acids, amino groups of lysine, and guanidine groups of arginine.

The secondary structure of fibroin is stabilized by various kinds of interactions. Hydrogen bonds arise between functional groups of peptide macrochains and between side fragments of macromolecules [10]:



Peptide Ser Thr Gly, Asp Tyr Lys



Arg His

The polar carboxy and amino groups in fibroin can also be involved in dipole interactions, and in the case of proton transfer, also in electrostatic interactions [11]. As the content of acid and base groups in fibroin is low, the electrostatic factor is not decisive in the formation of the secondary structure; it, however, may become decisive in the fibroin dissolution.

Since fibroin consists to 3/4 of nonpolar hydrophobic amino acids, it is necessary to take into account also hydrophobic (dispersion) interactions making fibroin resistant to the majority of solvents.

Three main kinds of secondary structures of natural silk fibroin are distinguished today: in crystalline areas, α-helical and β-folded structures (silk I and silk II, respectively), and in amorphous areas, disordered conformation of random globules. Liquid silk synthesized by the silkworm gland is a 26.0 vol % aqueous solution of fibroin in which the macromolecules have the conformation of globule or α-helix. Fibroin of natural *Bombyx mori* fibers contains 56 ± 5% macromolecules in the β-folded form and 13 ± 5% macromolecules in the α-helical form [12]. Thus, the fraction of highly ordered (crystalline) areas of the polymer reaches 60–70%.

Figures 1 and 2 show the projections of macrmolecule segments forming the α-helical and β-folded structures. The α-helical structure is formed by intramolecular hydrogen bonds, with the hydrophobic fragments displaced to the periphery [13]. In the β-folded structure, the macromolecules are arranged in the parallel or antiparallel mode, forming a folded sheet or layer (β-sheet). Antiparallel β-sheets of silk fibroin are packed in the face-to-face, back-to-back mode: double layer of glycine residues (interplanar spacing 3.5 Å)–double layer of alanine/serine residues (interplanar spacing 5.7 Å)–double layer of glycine residues, etc. [1]. For the hydrophobic fragments of macromolecules, this structure is the most favorable energetically [14, 15].

Okuyama et al. [17] reported the interatomic distances and bond angles for various conformations of

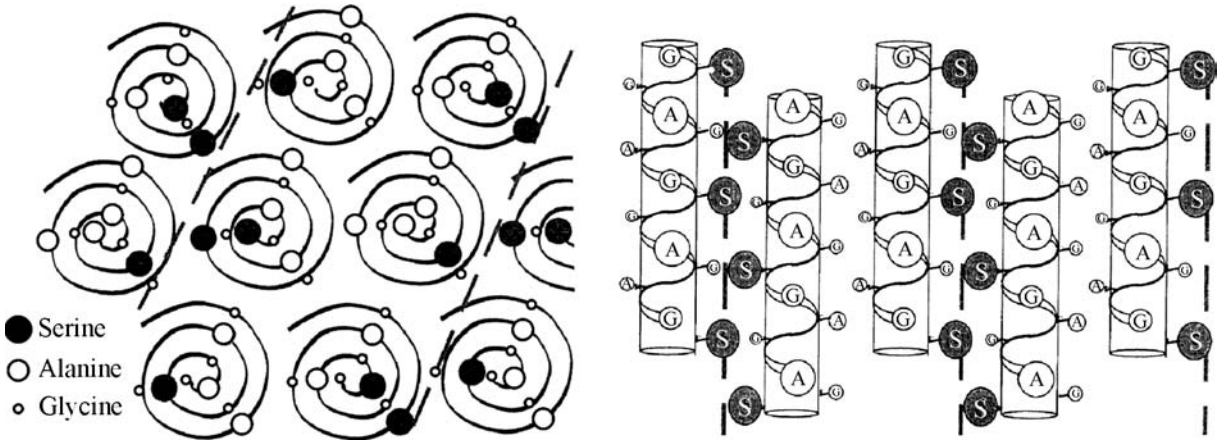


Fig. 1. α-Helical structure of fibroin macromolecules in two projections [9].

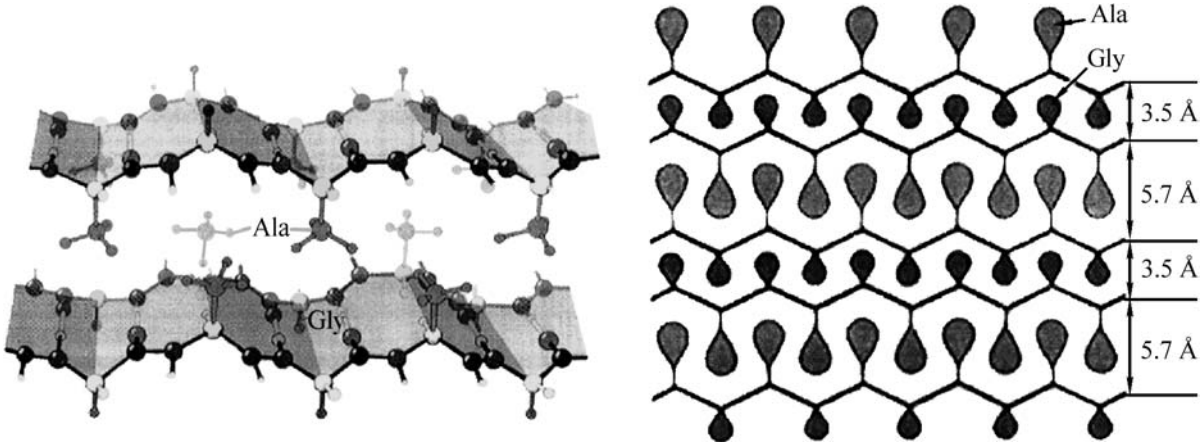


Fig. 2. β-Folded structure of fibroin [16].

protein chains, calculated from the X-ray scattering data. The most energetically favorable model was that with the antiparallel arrangement of the macrochains, in which the alanine–glycine diads (Ala–Gly) form two intramolecular and one intermolecular hydrogen bonds, and the $(Ala–Gly)_2$–Ser–Gly fragments form three intra- and one intermolecular hydrogen bonds (Table 2).

Table 2. Interatomic distances and angles in hydrogen bonds in the most stable models of crystalline areas of fibroin [17]

Fibroin structure model	Intermolecular hydrogen bonds			Intramolecular hydrogen bonds		
	bond	interatomic distance, Å	angle, deg	bond	interatomic distance, Å	angle, deg
Ala–Gly	N(Ala)...O(Gly)	2.87	77.7	N(Gly)...O(Ala)	3.02	123.7
				N(Ala)...O(Ala)	2.84	83.6
$(Ala–Gly)_2$–Ser–Gly	N(Ala)...O(Gly)	2.98	76.9	N(Gly)...O(Ala)	3.13	125.6
				N(Ala)...O(Ala)	2.88	86.4
				O(Ser)...O(Ala)	2.65	88.5

2. SOLUTIONS OF SILK FIBROIN IN SALT-CONTAINING AQUEOUS AND NONAQUEOUS SOLVENT SYSTEMS

Natural silk fibers dissolve only in a limited number of solvents, compared to globular proteins, because of the presence in fibroin of a large amount of intra- and intermolecular hydrogen bonds and its high crystallinity and specific physicochemical properties (wetting angle of silk fibroin 69° ±3° [18]). Sadov et al. [19] estimate the Kuhn segment of fibroin macromolecules at 40 Å, and the solubility parameter δ, at 24.3 $(mJ\ m^{-3})^{0.5}$. Fibroin does not dissolve in water and in the majority of organic solvents, but only swells to 30.0–40.0%; 2/3 of the absorbed solvent is retained by the amorphous fraction of the polymer [20]. The isoelectric point of fibroin varies in the range pH 3.6–5.2, depending on the conditions of solution preparation [21, 22].

Fibroin dissolves in concentrated aqueous solutions of acids (phosphoric, formic, sulfuric, hydrochloric) and in concentrated aqueous, organic, and aqueous-organic solutions of salts [LiCNS, LiBr, $CaCl_2$, $Ca(CNS)_2$, $ZnCl_2$, NH_4CNS, $CuSO_4$ + NH_4OH, $Ca(NO_3)_2$]. The main disadvantages of salt-containing aqueous, aqueous-organic, and organic solutions of fibroin are the long preparation time (aqueous solutions of fibroin should be dialyzed for several days) and large power consumption for the regeneration of the solvents for their reuse. It should be noted that the concentrations of salts in such solutions reach the saturation limit.

The solvency of aqueous salt systems depends on the salt concentration and increases in the following order: for anions, sulfate < citrate < tartrate < acetate < chloride < nitrite < bromide < iodide < thiocyanate < dichloroacetate; for cations, $Ca^{2+} < Sr^{2+} < Ba^{2+} < Li^+ < Zn^{2+}$ [1, 8, 20]. In some one-component organic solvents (hexafluoroisopropanol [23], hexafluoroacetone [24]), fibroin can be dissolved only after its preliminary activation. The fibroin activation consists in the preliminary dissolution of the protein in an aqueous salt solution followed by dialysis of the solution and recovery of the polymer as a film from aqueous solution by dry forming.

High solvency is exhibited by solutions of lithium halides in organic solvents: dimethylacetamide (DMAA) and dimethylformamide (DMF). For example, a 10.0% solution of fibroin can be obtained at 50°C in a 2–3 M solution of LiBr in DMAA or DMF and in 9.5–10 M solution of LiBr in water [25]. Thus, an important characteristic of a complex solvent is the nucleophilicity of the anion, which attacks the electrophilic centers (hydroxy, amide, amino groups) of fibroin macromolecules. In aprotic solvents, anions are not solvated; therefore, their nucleophilicity can be even higher than in aqueous solutions [26]. Indeed, the solvency of organic salt solutions decreases, depending on an anion, in the following order: $Cl^- > Br^- > SCN^-$, correlating with decrease in the nucleophilicity of the anion. In aqueous solutions, the trend is opposite, because water molecules compete with the electrophilic centers of fibroin, and more nucleophilic anions interact with water more strongly than with the polymer. Solutions of thiocyanates in organic solvents proved to be inefficient, despite that an aqueous solution of LiSCN readily dissolves the polymer. As for the activity of cations, the aqueous and organic systems also differ in this respect. Aqueous solutions of $ZnCl_2$ are the most effective solvents, whereas in solutions of $ZnCl_2$ in DMAA, DMF, and *N*-methyl-2-pyrrolidone, fibroin dissolves only at 155°C to form relatively dilute solutions (1.0–2.0 wt %).

The specific features of fibroin dissolution in various systems are associated with its molecular structure. In concentrated solutions of acids, the fibroin macromolecules are solvated owing to strong ion–ion interaction, which becomes possible upon protonation of the amino and amide groups of the polymer. Dissolution in salt systems is due to interaction of solvent ions with functional groups of the fibroin macromolecules. By analogy with dissolution of cellulose in the DMAA–LiCl system, it can be assumed that the intra- and intermolecular hydrogen bonds in the fibroin structure are ruptured as a result of the nucleophilic attack by the anion [27]. The solvent ions interact with polar and charged groups of pendant chains of fibroin, breaking the hydrogen bonds between the macromolecules.

In the course of dissolution, fibroin from the amorphous areas characterized by a high content of amino acid residues with bulky and polar groups dissolves first. The amino acid composition of fibroin precipitated from various solutions differs from that of the initial fibers. Tsukada et al. [28, 29] reported how the amino acid composition of *Bombyx mori* fibroin changed after its recovery from aqueous LiBr and LiSCN solutions. They found that, irrespective of the dissolution temperature, the relative content of glycine and alanine residues characteristic of the hydrophobic areas increased and the content of amino acid residues forming the amorphous areas decreased after the precipitation of the polymer. In organic salt solutions (LiCl in DMAA), the amorphous fraction also dissolves first [25].

Table 3. Molecular characteristics of fibroin in solutions [34]

Characteristic	Aqueous solution of fibroin after dialysis	Fibroin in methanol–water system (20 : 80)
Molecular weight, Da	188000	302000
Hydrodynamic length L_H, Å	8563	13800
Rotation radius R, Å	81.5	121.2
Cross section rotation radius R_c, Å	43.0	45.4
Persistent length a^*, Å	37.3	32.7
Volume $V \times 10^{-6}$, Å^3	2.30	4.85
Cross section area A, Å^2	7.9	9.6

As the dissolution temperature is raised over 70°C, the macromolecules undergo degradation [25]. As shown in [20, 28, 30], the molecular weight of natural silk fibroin is 370000, and that of the fibroin dissolved in aqueous LiBr, 30000 to 200000.

The fibroin macromolecules strongly differ in size in aqueous and organic solvents, as indicated by the intrinsic viscosity [η] of fibroin in 7.7 M aqueous NaCNS and a 2.5 M solution of LiCl in DMF (0.46 and 1.30 dl g^{-1}, respectively) [31]. In a salt-containing aprotic organic solvent, the polymer macromolecules exist in a more unrolled conformation as compared to the aqueous salt solution, because, under equal other conditions, [η] is proportional to the cube of the rms radius of particles [32].

Mathur et al. [33] showed that, in solutions of fibroin in the $Ca(NO_3)_2$–methanol system (salt concentration 60–75 wt %), [η] is a nonlinear function of temperature (8.71, 10.41, and 8.94 at 25, 30, and 40°C, respectively). The activation energy of viscous flow of a 0.1% fibroin solution in this solvent increases by 30.0%, compared to the straight solvent (9.03 and 7.01 kcal mol^{-1}, respectively).

Canetti et al. [34] studied by the methods of circular dichroism and small-angle X-ray scattering how addition of organic solvents to an aqueous solution of fibroin (dissolution in aqueous LiBr, followed by dialysis) affects the secondary (supramolecular) structure of the protein. They showed that, after the dialysis, the dilute aqueous solution of silk fibroin contains associates of two and more solvated macrochains, mainly rolled up in globules. Addition of methanol or dioxane increases the degree of association, and a β-folded structure is formed. On adding trifluoroethanol, a labile equilibrium is observed between the disordered globule and β-folded structures. Proceeding from the length of the monomeric unit of 6.95 Å (two amino acid residues), they calculated the geometric characteristics of macromolecules in aqueous and mixed aqueous–organic solvent systems (Table 3).

Aqueous and aqueous-organic solutions of LiCl, LiBr, NaSCN, and KSCN dissolve up to 20 wt % fibroin; the solvency of mixtures increases with a decrease in the relative content of water in the solvent [35]. The intrinsic viscosity of solutions [η] is inversely proportional to the water content of the mixtures and amounts to 0.3–0.7 dl g^{-1} at 30°C. The Huggins constant k_H is 0.5–1.0, with a minimum observed at 10% water content. An increase in the LiBr concentration, at equal other conditions, affects k_H insignificantly; the salt effect consists in unrolling of fibroin macromolecules. By contrast, in the NaSCN–water–isopropanol system, the effective viscosity and surface tension of the fibroin solution decrease as the isopropanol content is raised from 2 to 20% [36]. Thus, due to differences in the solvation of ions in aqueous and nonaqueous solutions, the properties of fibroin solutions vary with the water : organic solvent ratio differently, depending on a particular salt.

The interaction with the solvent necessarily leads to a change in the conformation of fibroin macromolecules and their secondary structure. Addition of polar solvents (alcohols, acetone, acetic acid) to water-soluble silk I initiates formation of the β-folded conformation of the macromolecules in solution [37]. The same trend is observed in treatment of fibroin films. Apparently, nonpolar solvents solvate hydrophobic fragments of fibroin; as a result, the amide, hydroxy, and other polar groups interact with each other through H bonds and thus fix the α-helix structure. In polar solvents, the existing H bonds are broken, which promotes transition to the β-structure; in the process, the macromolecules are arranged in the same plane, the hydrophobic groups of adjacent macromolecules interact with each other within the planes, and the polar groups outside the macromolecule plane form intra- and intermolecular H bonds.

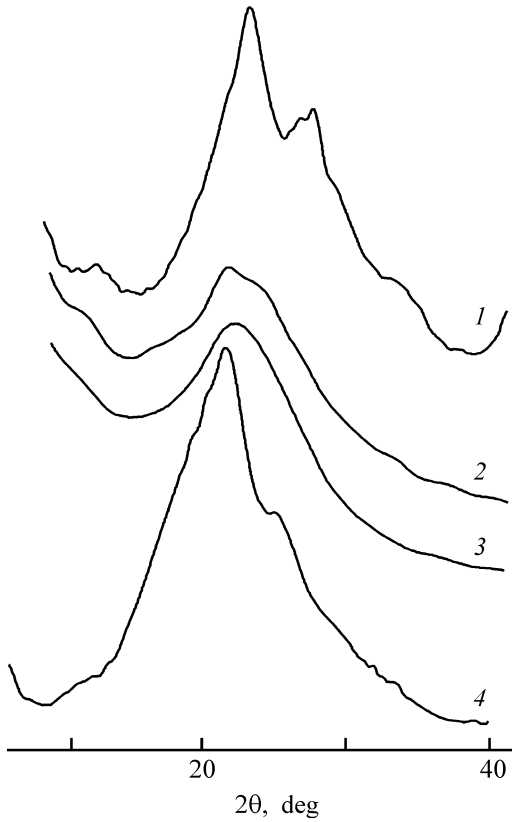


Fig. 3. X-ray diffraction pattern of (*1*) natural fibroin and of fibroin films recovered from solutions in (*2*) aqueous LiBr after dialysis, (*3*) hexafluoroisopropanol, and (*4*) NMMO [41]. (2θ) Bragg angle.

The fibroin recovered from dialyzed solutions in LiBr–H_2O has a disordered structure [34, 38–40], whereas the silk fibroin in a film cast from a solution in LiBr–ethanol has a lamellar β-sheet secondary structure. Thus, by choosing a solvent system, it is possible to control the formation of the secondary structure in solutions and, correspondingly, in the precipitated polymer [40].

3. SOLUTIONS OF FIBROIN IN ORGANIC SOLVENTS

Fibroin dissolves in hexafluoroisopropanol [23] and hexafluoroacetone [24], but this only occurs after its preliminary activation by dissolution in aqueous-salt systems followed by the recovery. In hexafluoroisopropanol, fibroin has mainly the α-helical structure with a small content of the β-folded structure [41, 42]. These data are well consistent with the data of Kimura et al. [43], who showed that macromolecules of proteins consisting of alanine residues form predominantly α-helical structures in hexafluoroisopropanol.

A procedure for fibroin dissolution without preliminary activation was suggested in [44, 45], and solutions containing more than 10 wt % fibroin in *N*-methylmorpholine *N*-oxide (NMMO) were obtained. The dissolution occurs in the hydrated form of the amine oxide at a water content of no more than 0.8 mol per mole of NMMO. NMMO monohydrate melts at 78°C, and, with a decrease in the water content, the melting point increases to 100°C and over. To lower the melting point of the hydrated amine oxide, it was suggested to add organic diluentes; DMSO appeared to be the most effective [46]. The addition of DMSO in an amount of 2–3 mol per mole of NMMO does not deteriorate the system solvency.

As expected, with an increase in the temperature, the intrinsic viscosity of the solutions decreases and the Huggins constant increases. The intrinsic viscosity of fibroin solutions in NMMO–H_2O–DMSO (molar ratio 1 : 0.3 : 1.8) at 95 and 115°C is 0.86 and 0.60 dl g^{-1}, and the Huggins constant, 0.41 and 0.71, respectively [47].

The structural organization of fibroin after its recovery from an aqueous-salt solution (LiBr–water) and salt-free organic solvents (hexafluoroisopropanol, NMMO) was studied by X-ray diffraction, IR spectroscopy, and DSC [41]. Figure 3 shows the X-ray diffraction patterns of natural fibroin (*Bombyx mori* silk) and fibroin recovered as films from solutions in LiBr–water, hexafluoroisopropanol, and NMMO. The diffraction pattern of natural fibroin (curve *1*) contains a pronounced peak at 2θ = 20.6° and well-defined reflections at 2θ 9.5°, 24.6°, and 25.3°, indicative of the β-folded structure of fibroin [48–53]. The fibroin recovered as a film from an aqueous-salt solution shows a diffuse halo with a maximum at 2θ = 20.5°, characteristic of amorphous or disordered fibroin (curve *2*). The presence of a small amount of fibroin forming an α-helical or β-folded structure is indicated by weak reflections at 2θ 9.50° and 22.0°. The diffraction pattern of the fibroin sample obtained from hexafluoroisopropanol (curve *3*) is virtually identical to that of the sample obtained from the aqueous-salt solution.

The fibroin recovered from the solution in NMMO (curve *4*) has the most ordered structure, approaching natural fibroin in the degree of ordering. This is indicated by peaks at 2θ 20.5° and 24.7°, characteristic of the β-folded ordered structure.

CONCLUSIONS

(1) The conformational state of fibroin macromolecules in solutions depends on the solvent. Fibroin

macromolecules in solution undergo association to an extent that increases in going from aqueous to organic solvents. In aqueous salt systems, the macromolecules mainly exist in the form of random globules, and a disordered secondary structure is observed. In organic and mixed aqueous-organic salt systems, the α-helical and β-folded structures are formed. The prevalence of one or another structure of fibroin depends on a particular organic solvent.

(2) Fibers and films with the prescribed supramolecular organization can be prepared by properly choosing the solvent systems and conditions of the fibroin recovery from the solution.

(3) *N*-Methylmorpholine *N*-oxide is the most promising for development of a technology for fibroin processing into fibers and films, because the step of salt removal, required with salt-containing aqueous, aqueous-organic, and organic solvents, is thus eliminated.

REFERENCES

1. Finkel'shtein, A.V. and Ptitsyn, O.B., *Fizika belka* (Physics of Protein), Moscow: Universitet, 2002.
2. Putthanarat, S., Stribeck, N., Fossey, S.A., et al., *Polymer*, 2000, vol. 41, no. 38, pp. 7735–7747.
3. Altman, G.H., Diaz, F., Jakuba, C., et al., *Biomaterials*, 2003, vol. 24, no. 3, pp. 401–416.
4. Tsukada, M., Gotoh, Y., and Minoura, N., *J. Seric. Sci. Jpn.*, 1990, vol. 59, no. 2, pp. 325–330.
5. Gotoh, Y., Niimi, S., Hayakawa, T., and Miyashita, T., *Biomaterials*, 2004, vol. 25, no. 5, pp. 1131–1140.
6. Yunusov, L., *Fiziko-khimicheskie svoistva natural'nogo shelka v protsesse pererabotki kokonov* (Physicochemical Properties of Natural Silk in Cocoon Processing), Tashkent: Fan, 1978.
7. Shimura, K., Kikuchi, A., Katagata, Y., and Ohotomo, K., *J. Seric. Sci. Jpn.*, 1982, vol. 51, no. 1, pp. 20–26.
8. *Silk Polymers: Material Science and Biothechnology*, Kaplan, D., Ed., Washington: Am. Chem. Soc., 1994.
9. Valluzzi, R. and Gido, S.P., *Biopolymers*, 1997, vol. 42, no. 4, pp. 705–717.
10. Baker, E.N. and Hubbard, R.E., *Prog. Biophys. Molec. Biol.*, 1984, vol. 44, no. 1, pp. 97–179.
11. Dill, K.A., *Biochemistry*, 1990, vol. 29, no. 31, pp. 7133–7156.
12. Trabbic, K.A. and Yager, P., *Macromolecules*, 1998, vol. 31, no. 3, pp. 462–471.
13. Takanashi, Y., Gehoh, M., and Yuzuriha, K., *J. Polym. Sci.*, Polym. Phys. Ed., 1991, vol. 29, no. 5, pp. 889–891.
14. Lazo, N.D. and Downing, D.T., *Macromolecules*, 1999, vol. 32, no. 24, pp. 4700–4705.
15. Dwyer, D.S., *Biopolymers*, 1999, vol. 49, no. 7, pp. 635–645.
16. Voet, B., *Biochemistry*, New York: Wiley, 1990.
17. Okuyama, K., Somashekar, Y., Noguchi, K., and Ichimura, S., *Biopolymers*, 2001, vol. 59, no. 2, pp. 310–319.
18. Cai, K., Yao, K., Lin, S., et al., *Biomaterials*, 2002, vol. 23, no. 6, pp. 1153–1160.
19. Sadov, F.I., Korchagin, M.V., and Matetskii, A.I., *Khimicheskaya tekhnologiya voloknistykh materialov* (Chemical Technology of Fibrous Materials), Moscow: Legkaya Industriya, 1968.
20. Rubinov, E.B., *Shelkosyr'e i kokonomotanie: Spravochnik* (Silk Raw Materials and Cocoon Reeling: Handbook), Moscow: Legprombytizdat, 1986.
21. Iizuka, E., *Biorheology*, 1966, vol. 3, no. 1, pp. 141–152.
22. Freddi, G., Pessina, G., and Tsukada, M., *Int. J. Biol. Macromol.*, 1999, vol. 24, no. 3, pp. 251–263.
23. WO Patent 93/15 244.
24. Ohgo, K., Zhao, C., Kobayashi, M., and Asakura, T., *Polymer*, 2003, vol. 44, no. 5, pp. 841–846.
25. Furuhata, K.-I., Okada, A., Chen, Y., et al., *J. Seric. Sci. Jpn.*, 1994, vol. 63, no. 4, pp. 315–322.
26. Parker, A.J., *Chem. Rev.*, 1969, vol. 69, no. 1, pp. 1–32.
27. Dawsey, T.R. and McCormick, C.L., *Macromol. Chem. Phys.*, 1990, vol. 30, no. 3, pp. 405–440.
28. Tsukada, M., Goto, Y., and Minoura, S., *J. Seric. Sci. Jpn.*, 1990, vol. 59, no. 4, pp. 325–330.
29. Goto, Y., Tsukada, M., and Minoura, S., *J. Seric. Sci. Jpn.*, 1990, vol. 59, no. 5, pp. 402–409.
30. Pauling, L., *The Nature of the Chemical Bond*, Ithaca: Cornell Univ., 1960.
31. Kholmuminov, A.A., Sattorov, Kh.A., and Urinov, E.U., *Vysokomol. Soedin., Ser. B*, 1994, vol. 36, no. 5, pp. 878–880.
32. Tsvetkov, V.N., Eskin, V.E., and Frenkel', S.Ya., *Struktura makromolekul v rastvorakh* (Structure of Macromolecules in Solutions), Moscow: Nauka, 1964.
33. Mathur, A.B., Tonelli, A., Rathke, T., and Hudson, S., *Biopolymers*, 1997, vol. 42, no. 1, pp. 61–74.
34. Canetti, M., Seves, A., Secundo, F., and Vecchio, G., *Biopolymers*, 1989, vol. 28, no. 9, pp. 1613–1624.
35. Matsumoto, K. and Uejima, H., *J. Polym. Sci., Polym. Chem. Ed.*, 1997, vol. 35, no. 10, pp. 1949–1954.
36. Babadzhanov, Kh., Geller, B.E., and Kamilova, S.D., *Khim. Volokna*, 1986, no. 3, pp. 23–24.
37. Magoshi, J., Magoshi, Y., and Nakamura, S., *J. Appl. Polym. Sci., Appl. Polym. Symp.*, 1985, vol. 41, no. 2, pp. 187–204.
38. Magoshi, J., Mizuida, M., Magoshi, Y., et al., *J. Polym. Sci.*, Polym. Phys. Ed., 1979, vol. 17, no. 3, pp. 515–520.

39. Matsumoto, K., Uejima, H., Iwasaki, T., et al., *J. Appl. Polym. Sci.*, 1996, vol. 60, no. 3, pp. 503–511.
40. Chen, X., Knight, D.P., Shao, Z., and Vollrath, F., *Polymer*, 2001, vol. 42, no. 48, pp. 9969–9974.
41. Sashina, E.S., Novoselov, N.P., Vorbach, D., and Meister, F., *Vysokomol. Soedin., Ser. A*, 2005, vol. 47, no. 10, pp. 1832–1840.
42. Livak, O., Blye, A., Shah, N., and Jelinski, L.W.A., *Macromolecules*, 1998, vol. 31, no. 15, pp. 2947–2951.
43. Kimura, S., Naito, A., Tuzi, S., and Saito, H., *Biopolymers*, 2001, vol. 58, no. 1, pp. 78–88.
44. RF Patent 2 002 107 622.
45. Sashina, E.S., Novoselov, N.P., and Heinemann, K., *Zh. Prikl. Khim.*, 2003, vol. 76, no. 1, pp. 133–137.
46. Sashina, E.S. and Novoselov, N.P., *Zh. Fiz. Khim.*, 2006, vol. 80, no. 1, pp. 1–4.
47. Novoselov, N.P. and Sashina, E.S., *Zh. Fiz. Khim.*, 2003, vol. 77, no. 5, pp. 852–855.
48. Magoshi, J., Magoshi, Y., and Nakamura, S., *J. Appl. Polym. Sci., Appl. Polym. Symp.*, 1985, vol. 41, no. 2, pp. 187–204.
49. Noishiki, Y., Nishiyama, Y., Wada, M., et al., *J. Appl. Polym. Sci.*, 2002, vol. 86, no. 18, pp. 3425–3429.
50. Freddi, G., Monti, P., Nagura, M., et al., *J. Appl. Polym. Sci.*, 1996, vol. 59, no. 3, pp. 841–847.
51. Tsukada, M., *J. Seric. Sci. Jpn.*, 1986, vol. 55, no. 2, pp. 126–130.
52. Nam, J. and Park, Y.H., *J. Appl. Polym. Sci.*, 2001, vol. 81, no. 16, pp. 3008–3021.
53. Park, S.J., Lee, K.Y., Ha, W.S., and Park, S.Y., *J. Appl. Polym. Sci.*, 1999, vol. 74, no. 13, pp. 2571–2575.

ISSN 1070-4272, Russian Journal of Applied Chemistry, 2006, Vol. 79, No. 6, pp. 877–883. © Pleiades Publishing, Inc., 2006.
Original Russian Text © V.I. Samoilov, 2006, published in Zhurnal Prikladnoi Khimii, 2006, Vol. 79, No. 6, pp. 889–895.

INORGANIC SYNTHESIS AND INDUSTRIAL INORGANIC CHEMISTRY

Development of a Technology for Sulfuric Acid Breakdown of a Bertrandite–Phenacite–Fluorite Flotation Concentrate

V. I. Samoilov

Ulba Metal Works AO, Ust Kamenogorsk, East-Kazakhstan oblast, Kazakhstan

Received March 14, 2006

Abstract—The possibility of direct sulfuric acid breakdown of the bertrandite–phenacite–fluorite concentrate from the Ermakovskoe deposit was studied experimentally using samples taken from 23 different batches of the concentrate over the period from 1997 to 2004.

DOI: 10.1134/S1070427206060024

The bertrandite–phenacite–fluorite concentrate manufactured by the Zabaikal'skii mining and ore-dressing plant, which contains 4 wt % beryllium, is a rather new promising type of raw materials for beryllium chemical-metallurgical plants [1]. The industrial use of this concentrate was commenced at the end of the XX century at Ulba Metal Works joint-stock company. The existing technology for processing of the concentrate [2] involves a large number of stages and requires an expensive activating preparation of raw materials for sulfuric acid breakdown, including high-temperature smelting of a mixture of a high-grade bertrandite–phenacite–fluorite concentrate and a low-grade beryl concentrate (containing 2 wt % beryllium) with soda ash and limestone in an ore-smelting furnace (the temperature and duration of the smelting are approximately 1500°C and 4 h). The fusion cake obtained by smelting of the above-mentioned stock in this furnace is granulated in cold water and then is subjected to wet crushing and classification. The thus prepared water pulp of the crushed granulate is condensed and treated with 93% H_2SO_4 (sulfation of the granulate at a temperature of about 100°C in the course of 2 min). After the sulfation, the granulate is leached in water to obtain a beryllium sulfate solution and a poorly soluble silica- and gypsum-containing waste cake. The sulfate solution is neutralized with ammonium hydroxide, which results in the precipitation of the poorly soluble $Be(OH)_2$. The process is characterized by large volumes of ecologically harmful unutilizable beryllium-, silica-, and gypsum-containing cake formed in the stage of sulfuric acid breakdown of granulated fusion cake, by significant loss of beryllium with the cake, and by the formation of a waste mother liquor in the stage of $Be(OH)_2$ precipitation [1–3]. The considerable loss of beryllium with the cake (about 2.5 wt %) is due to use of limestone in the smelting of the concentrates, which leads to formation of gypsum in the sulfation stage and leads to a significant increase in the mass of the waste cake. The considerable loss of beryllium with the mother liquor (approximately 2.5 wt %) is caused by the high content of fluorine in the bertrandite–phenacite–fluorite concentrate (and, as a consequence, in the stock mixture). Further, the main part of fluorine passes into a beryllium sulfate solution and then binds beryllium into stable water-soluble complexes in the stage of $Be(OH)_2$ precipitation. For comparison, less than 1 wt % of beryllium is lost with the mother liquor when a preliminarily defluorinated concentrate (washed with an aluminum nitrate solution to remove fluorite) is used [2]. However, this washing procedure is ineffective because it leads to a considerable loss of beryllium with the nitric acid solution.

A study of the mineralogical composition of the concentrate demonstrated (Table 1) that the content of fluorite, bertrandite, and phenacite varies. A study of the granulometric composition of nine samples of the concentrate (Table 1) showed that the concentrate is composed only of particles with size of 0.12 mm and less (most of particles belong to the –0.064-mm fraction). These particles form unstable conglomerates approximately 1–4 mm in size (about 50 wt % of the concentrate is represented by

Table 1. Mineralogical and granulometric composition of the Ermakovskoe concentrate

Sample no.	Content of minerals, wt % (fraction, mm)			
	bertrandite	phenacite	fluorite	quartz, calcite, micas, feldspars
1	6.5 (–0.04)	12.0 (–0.104)	22.2	59.3
2	8.0 (–0.04)	9.5 (–0.104)	19.2	63.3
3	3.5 (–0.04)	15.0 (–0.104)	19.5	62.0
4	14.0 (0.10–0.12)	4.8 (0.04–0.06)	–	–
5	4.8 (0.06–0.08)	12.3 (0.06–0.08)	–	–
6	8.0 (–0.08)	17.0 (–0.05)	20.0 (0.02–0.10)	55.0 (0.02–0.07)
7	16.0 (–0.10)	8.0 (–0.05)	26.0 (0.01–0.06)	50.0 (0.01–0.06)
8	10.0 (–0.05)	12.0 (–0.064)	24.0 (0.01–0.07)	54.0 (0.01–0.06)
9	15.0 (–0.07)	8.0 (–0.04)	30.0 (0.01–0.07)	47.0 (0.01–0.06)
Average	9.5	11.0	23.0	–

Table 2. Chemical composition of the Ermakovskoe concentrate

Sample no. in Table 1	Content in the concentrate, wt %							
	Be	F	Al	Ca	Si	Fe	Mn	Cr
1	3.97	10.80	–	17.40	13.80	–	–	–
2	4.12	9.35	–	10.89	10.51	3.00	0.48	0.0029
3	3.97	9.49	–	11.42	11.87	2.96	0.50	0.0030
4	3.67	12.00	2.55	22.80	11.99	5.40	0.49	0.0036
5	4.13	14.12	1.89	24.15	8.80	3.33	0.23	<0.0010
6	3.77	9.37	3.14	19.05	14.08	4.55	0.44	<0.0010
7	3.88	13.75	2.55	21.90	12.52	4.93	0.39	0.0061
8	3.82	12.87	2.52	19.24	11.78	4.85	0.44	0.0077
9	3.35	14.00	2.77	23.00	10.10	4.35	0.27	0.0110
7*	3.12	12.00	1.58	22.30	10.05	4.24	1.30	0.0054
12*	3.78	10.75	2.52	19.85	12.67	5.13	0.74	0.0085
35*	4.04	10.00	2.00	24.60	10.71	4.13	0.46	0.0059
55*	4.55	12.40	1.76	22.50	10.80	3.85	0.74	0.0049
173*	3.03	–	–	–	–	3.13	0.43	–
197*	3.49	5.20	1.83	13.60	15.48	5.78	1.63	0.0077
201*	3.84	9.30	1.78	19.90	12.60	4.56	1.04	0.0060
212*	4.22	10.50	2.04	19.51	12.51	4.75	0.72	0.0056
214*	3.65	10.75	2.52	20.90	12.37	4.45	1.00	0.0080
217*	3.99	9.65	2.41	20.90	12.65	4.65	0.73	0.0078
Average	3.81	10.91	2.27	19.64	12.00	4.13	0.67	0.0050

* Numbers of warehouse lots; the same for Table 4.

the conglomerates). Data on the chemical composition of 19 batches of the concentrate are listed in Table 2.

Research experiments on direct sulfation of 12 batches of the Ermakovskoe concentrate were carried out using a 2.5-l glassy graphite cup covered with a fluoroplastic lid. The concentrate (–0.045 mm fraction or no preliminary sieving into fractions) was mixed with a prescribed amount of 93% H_2SO_4 in the glassy graphite cup placed on an electric heater (the reaction mixture was a jelly-like product). The reaction mass was kept at a prescribed temperature for a prescribed sulfation time. The reaction mixture was periodically agitated with a putty knife. After the sulfation was complete, the sulfated concentrate, which had the form of a semidry mass with lumps, was treated with water (leaching-out of soluble sulfates), the leaching pulp was neutralized with ammonium

Table 3. Results of research experiments on direct sulfuric acid breakdown of the Ermakovskoe concentrate with 93% H_2SO_4; sulfation: 100-g portion of the concentrate; leaching: s : l = 1 : (4–6) (in terms of the starting concentrate), τ = 20 min, T = 95°C, V = const; pulp neutralization to pH 3.0–3.5 (with a 8–10% NH_3 solution); first cake washing with 5% $(NH_4)_2SO_4$ solution acidified with H_2SO_4 to pH 3.0–3.5: s : l = 1 : 7 (in terms of the initial concentrate), τ = 15 min, T = 95°C, V = const; second washing of the cake with 5% $(NH_4)_2SO_4$ solution acidified with H_2SO_4 to pH 3.0–3.5: (see first washing)

Run no.	Sulfation			Leaching, neutralization, filtration					Drying of washed cake				Recovered, %	
	H_2SO_4 consumption, ml g^{-1} of the concentrate	T, °C	t, h	H_2SO_4 content in the stock solution before neutralization, g l^{-1}	volume of filtered stock solution after neutralization, ml	content in the stock solution after neutralization, g l^{-1}		F extracted into the stock solution after neutralization, %	mass of the dry cake, g	content in the dry cake, %		F recovered into the dry cake, %	Be into the sulfate solution (in terms of the cake)	F into the gas phase (in terms of the stock solution and cake)
						Be	F			Be	F			
Starting concentrate (batch number in accordance with Tables 1, 2) without sieving-off the –0.045 mm fraction														
1	0.8	225 ± 25	1	103.9	520	2.36	0.4	1.9	84.76	2.3	0.78	6.1	50.9	92.0
2	0.8	225 ± 25	2	51.9	520	2.67	0.56	2.7	89.6	2.12	1.15	9.5	52.2	87.8
3	0.8	225 ± 25	3	57.82	400	2.43	–	–	75.7	2.28	0.87	6.1	56.5	–
4	1.6	225 ± 25	1	85.3	560	–	–	–	67.61	1.05	–	–	82.1	–
5	1.6	225 ± 25	8	–	390	7.63	0.02	0.1	79.0	0.49	0.36	2.6	90.2	97.3
6	1.6	225 ± 25	11	–	410	7.18	0.23	0.9	62.0	0.64	0.57	3.2	90.0	95.9
7	1.6	250	14	–	730	3.93	0.37	2.8	66.4	0.51	0.76	4.7	91.5	92.5
8	2.5	250	1	–	–	–	0.36	–	78.47	0.91	0.60	4.1	82.0	–
9	2.5	250	3	–	480	4.19	0.26	1.6	80.8	0.78	–	–	84.1	–
10	2.5	250	11	–	–	–	0.11	–	71.3	0.3	0.32	2.1	94.6	–
11	2.5	325 ± 25	4	–	480	5.60	1.20	0.9	89.46	0.56	–	–	87.4	–
12	2.5	325 ± 25	7	pH 2–3	500	5.62	0.10	0.5	78.2	0.46	0.21	1.5	90.9	98.0
13	2.5	325 ± 25	10	pH 2–3	500	6.66	–	–	75.0	0.37	–	–	93.0	–
Fraction of the concentrate (batch no. 1 in Tables 1 and 2) –0.045 mm														
14	1.6	275 ± 25	1	–	950	2.46	0.38	3.7	80.7	0.40	0.63	4.7	91.9	91.6
15	1.6	275 ± 25	6	–	400	6.26	0.33	0.9	77.8	0.35	0.38	2.7	93.1	96.4

hydroxide and filtered, and the silicon-sulfate cake was washed with water to remove the water-soluble beryllium in the standard mode (Table 3).

It follows from the research experiments on direct sulfuric acid breakdown of the Ermakovskoe concentrate (Tables 3 and 4) that the technology tested provides a statistical-average recovery of beryllium from the concentrate into a sulfate solution equal to about 92.4%.

The completeness of beryllium precipitation from the thus prepared sulfate solutions approaches 100%, because an industrially acceptable defluorination of the concentrate (94.8% on the average) is achieved in our experiments (Table 4). Nevertheless, the recovery of beryllium from the raw material into beryllium hydroxide is insufficiently high (about 92%), although a significant reduction in the number of expensive technological operations for recovery of $Be(OH)_2$ from mineral raw materials is achieved.

The reaction of bertrandite and phenacite with H_2SO_4 at the optimal process temperature presumably occurs in accordance with the reaction equations (1) and (2).

$$4BeO \cdot 2SiO_2 \cdot H_2O + 4H_2SO_4 \xrightarrow{550–300°C} 4BeSO_4 + 2SiO_2 + 5H_2O\uparrow, \quad (1)$$

$$2BeO \cdot SiO_2 + 2H_2SO_4 \xrightarrow{250–300°C} 2BeSO_4 + SiO_2 + 2H_2O\uparrow. \quad (2)$$

The mechanism of defluorination of the Ermakovskoe concentrate is based on the reaction of sulfation of its fluorite component:

$$CaF_2 + H_2SO_4 \xrightarrow{250–300°C} CaSO_4 + 2HF\uparrow. \quad (3)$$

Table 4. Results of experiments on direct sulfuric acid breakdown of various batches of the Ermakovskoe concentrate with 93% H_2SO_4 (initial weighed portion of the concentrate 50 g; other technological parameters of the experiment are listed in Table 3)

Run no.	Charged with the concentrate for sulfation, g		Sulfation			Volume of the sulfate solution (stock solution + washing water 1), ml	Content in the sulfate solution (stock solution + washing water 1), g l^{-1}		Content in the dry cake, g		Recovered, %	
	Be	F	H_2SO_4 expenditure, ml g^{-1} of concentrate	T, °C	τ, h		Be	F	Be	F	Be into the sulfate solution (in terms of the cake)	F into the gas phase (in term of stock solution, washing water 1, and cake), %
Concentrate batch no. 7 in Tables 1 and 2												
1	1.56	6.00	1.6	275±25	1	800	1.62	0.1	0.06	0.06	96.1	91.2
2	1.56	6.00	1.6	275±25	1	–	–	–	0.09	–	94.2	–
3	1.56	–	1.6	275±25	–	–	–	–	0.09	–	94.2	–
4	1.56	–	1.6	275±25	1	–	–	–	0.07	–	95.5	–
5	1.56	–	1.6	275±25	1	–	–	–	0.13	–	91.7	–
6	1.56	–	1.6	275±25	1	–	–	–	0.12	–	92.3	–
7	1.56	–	1.6	275±25	1	–	–	–	0.10	–	93.6	–
8	1.56	–	1.6	275±25	1	–	–	–	0.07	–	95.5	–
9	1.56	–	1.6	275±25	1	–	–	–	0.06	–	96.2	–
10	1.56	–	1.6	275±25	1	–	–	–	0.07	–	95.5	–
11	1.56	–	1.6	275±25	–	–	–	–	0.09	–	94.2	–
									Average		94.5	–
Concentrate batch no. 12 in Tables 1 and 2												
12	1.89	5.37	1.6	275±25	1	670	2.19	0.27	0.12	0.18	93.7	93.3
13	1.89	5.37	1.6	275±25	1	620	2.43	–	0.24	–	87.3	–
14	1.89	5.37	1.6	275±25	1	770	1.75	0.20	–	–	89.4	–
15	1.89	5.37	1.6	275±25	1	640	2.22	–	0.25	–	86.8	–
									Average		89.3	–
Concentrate batch no. 20 in Tables 1 and 2												
16	3.54	11.73	1.6	275±25	1	–	1.95	–	0.14	–	96.0	–
17	3.54	11.73	1.6	275±25	1	–	1.84	–	0.12	–	96.6	–
18	3.54	11.73	1.6	275±25	1	–	1.93	–	0.13	–	96.3	–
19	3.54	11.73	1.6	275±25	1	–	2.35	–	0.03	–	99.1	–
20	3.54	11.73	1.6	275±25	1	–	1.97	–	0.27	–	92.4	–
									Average		96.1	–
Concentrate batch no. 35 in Tables 1 and 2												
21	2.02	5.00	1.6	275±25	1	650	2.17	–	0.10	–	95.1	–
22	2.02	5.00	1.6	275±25	1	780	–	–	0.18	–	91.1	–
23	2.02	5.00	1.6	275±25	1	580	2.47	0.14	0.30	0.12	85.1	96.0
24	2.02	5.00	1.6	275±25	1	630	2.14	0.08	0.24	–	88.1	97.0
25	2.02	5.00	1.6	275±25	1	630	2.14	–	0.24	–	88.1	96.5
									Average		89.7	–
Concentrate batch no. 55 in Tables 1 and 2												
26	2.27	6.20	1.6	275±25	1	800	2.19	0.10	0.15	0.10	93.4	97.1
27	2.27	6.20	1.6	275±25	1	–	–	–	0.15	–	93.4	–
									Average		93.4	–

Table 4. (Contd.)

Run no.	Charged with the concentrate for sulfation, g		Sulfation			Volume of the sulfate solution (stock solution + washing water 1), ml	Content in the sulfate solution (stock solution + washing water 1), g l^{-1}		Content in the dry cake, g		Recovered, %	
			H_2SO_4 expenditure, ml g^{-1} of concentrate	T, °C	τ, h						Be into the sulfate solution (in terms of the cake)	F into the gas phase (in term of stock solution, washing water 1, and cake), %
	Be	F					Be	F	Be	F		
Concentrate batch no. 173 in Tables 1 and 2												
28	1.51	–	1.6	275±25	1	–	–	–	0.02	–	98.3	–
29	1.51	–	1.6	275±25	1	–	–	–	–	–	95.4	–
30	1.51	–	1.6	275±25	1	–	–	–	0.06	–	96.0	–
									Average		96.6	–
Concentrate batch no. 201 in Tables 1 and 2												
31	1.92	4,65	1.6	275±25	1	785	2.02	0.14	0.12	0.13	93.8	94.8
32	1.92	4.65	1.6	275±25	1	–	–	–	0.14	–	92.7	–
									Average		93.3	–
Concentrate batch no. 212 in Tables 1 and 2												
33	2.11	5.25	1.6	275±25	1	690	–	–	0.19	–	91.0	–
34	2.11	5.25	1.6	275±25	1	700	–	–	0.15	–	92.9	–
									Average		92.0	–
Concentrate batch no. 214 in Tables 1 and 2												
35	1.82	5.37	1.6	275±25	1	610	2.41	0.16	0.11	0.14	94.0	95.6
36	1.82	5.37	1.6	275±25	1	675	–	–	0.17	–	90.7	–
									Average		92.4	–
Concentrate batch no. 217 in Tables 1 and 2												
37	1.99	4.82	1.6	275±25	1	645	–	–	0.14	–	93.0	–
38	1.99	4.82	1.6	275±25	1	730	1.99	–	0.35	–	83.9	–
39	1.99	4.82	1.6	275±25	1	680	2.18	–	0.34	–	82.9	–
									Average		86.6	–
						Average over experiment nos. 1–39					92.4	94.8

The evolving gaseous hydrogen fluoride intensifies the breakdown of the phenacite–bertrandite component of the concentrate, presumably by reactions (4)–(6).

$$4BeO \cdot 2SiO_2 \cdot H_2O + 16HF \xrightarrow{250–300°C} 4BeF_2 + 2SiF_4\uparrow + 9H_2O\uparrow, \quad (4)$$

$$2BeO \cdot SiO_2 + 8HF \xrightarrow{250–300°C} 2BeF_2 + SiF_4\uparrow + 4H_2O\uparrow, \quad (5)$$

$$BeF_2 + H_2SO_4 \xrightarrow{250–300°C} BeSO_4 + 2HF\uparrow. \quad (6)$$

Thus it may be assumed that the presence of fluorite in the concentrate tested in this study positively affects the recovery of beryllium from the concentrate into a water-soluble sulfate.

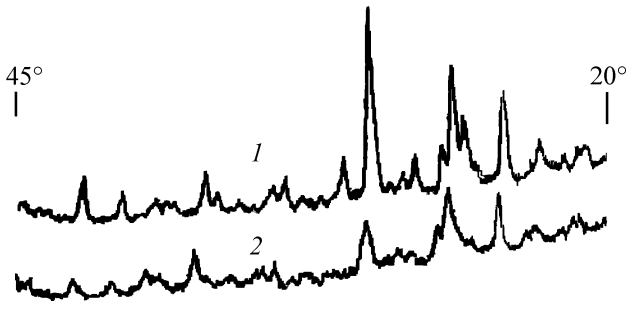
To additionally raise the recovery of beryllium from the concentrate, the influence exerted by mechanical activation of this type of beryllium raw materials on the completeness of its breakdown by

Table 5. Results of experiments on direct sulfuric acid breakdown of a crushed Ermakovskoe concentrate; crushing of the concentrate into the –0.045-mm fraction; sulfation: initial weighed portion of the concentrate 100 g; expenditure of 93% H_2SO_4 1.6 ml g^{-1} of concentrate, T = 250–30°C, τ = 5 h; leaching s : l = 1 : (4–6) (in terms of the starting concentrate), T = 80°C; neutralization of pulp to pH 3.0–3.5 (with a 8–10% NH_3 solution); first washing of the cake with a 5% $(NH_4)_2SO_4$ solution acidified with H_2SO_4 to pH 3.0–3.5: s : l = 1 : 7 (in terms of the starting concentrate), τ = 15 min, T = 80°C; second washing of the cake with a 5% $(NH_4)_2SO_4$ solution acidified with H_2SO_4 to pH 3.0–3.5: (see 1st washing)

	Number of the initial concentrate sample (as in Tables 1 and 2)	Stock solution				Dry cake				Recovered, %	
		V, ml	concentration, g l^{-1}		F recovery into the stock solution,* %	cake mass, g	content in the cake, wt %		F recovery into the cake, %	Be into the solution (in terms of the cake)	F into the gas phase (in terms of the stock solution and cake)
			Be	F			Be	F			
1	1	720	5.25	0.19	1.3	82.3	0.23	0.19	1.4	95.2	97.3
2		–	10.37	0.39	–	73.5	0.18	0.49	3.3	96.7	–
3		350	9.25	0.15	0.5	88.0	0.18	0.16	1.3	96.0	98.2
4		580	7.34	0.70	3.7	81.0	0.30	0.46	3.4	93.9	93.6
5	2	535	5.96	0.68	3.9	80.5	0.25	0.30	2.6	95.1	93.5
6		550	6.35	0.20	1.2	73.3	0.14	0.27	2.1	97.5	96.7
7		580	5.64	0.14	0.9	80.5	0.13	0.38	3.3	97.5	95.8
8		–	–	–	–	77.9	0.10	0.36	3.0	98.1	–
9	3	570	5.43	0.22	1.3	67.6	0.15	0.44	3.1	97.4	95.6
10		500	6.45	0.20	1.1	65.7	0.13	0.50	3.5	97.8	95.4
11		650	5.21	0.22	1.5	65.5	0.14	–	–	97.7	–
12		–	–	–	–	67.7	0.167	0.58	4.1	97.2	–

* The content of F in combined washing waters 1 and 2 did not exceed hundredths of a gram per liter; recovery of F from the concentrate into combined washing waters 1 and 2 did not exceed 1%.

sulfuric acid was studied. Experiments on crushing of the Ermakovskoe bertrandite–phenacite–fluorite flotation concentrate in the beaker of a laboratory vibrating grinder to –45 μm with the subsequent sulfation of the activated material were carried out (see figure and Table 5).



Results of X-ray structural analysis of the starting and crushed concentrate at reflection angles of 20° to 45°. (*1*) Starting concentrate; (*2*) concentrate (100 g) crushed on a vibrating grinder (τ_{cr} = 40 min).

An X-ray structural analysis of the concentrate demonstrated (see figure) that crushing of the concentrate on a vibrating grinder leads to partial destruction of the crystal lattices of the minerals contained in the concentrate.

As follows from Table 5, crushing of the Ermakovskoe concentrate on a vibrating grinder provides a high recovery of beryllium into a sulfate solution (at a level of 96.7%) with a simultaneous (~96%) defluorination of the concentrate, which results in that beryllium is almost completely (99.9 % [2]) recovered from the sulfate solution into $Be(OH)_2$ in the following stage. The recovery of beryllium from the raw material into beryllium hydroxide is 96.6%.

Comparative analysis of the data in Tables 4 and 5 shows that preliminary crushing of the Ermakovskoe concentrate makes it possible to raise the completeness of its breakdown with sulfuric acid from 92.4% (completeness of breakdown of a nonactivated concen-

trate) to 96.7%. Dry-grinding ball mills can be recommended for the industrial implementation of the process for crushing of the Ermakovskoe concentrate. The experience of the Brash Wellman plant, which employs dry crushing of thermally activated beryl in ball mills prior to sulfation [2, 3], can be used in this case.

CONCLUSIONS

(1) Application of a mechanical activation of the bertrandite–phenacite–fluorite concentrate makes it possible to reduce the number of preparatory operations before its sulfation from six to one and to rule out use of expensive fluxes, stock smelting, and granulate crushing.

(2) The presented technology of sulfation of a mechanically activated concentrate makes it possible to raise the recovery of beryllium from raw materials into $Be(OH)_2$ approximately from 95 to 96.5% and to reduce the volumes of both the ecologically harmful waste cake and the mother liquor.

REFERENCES

1. Samoilov, V.I., Borsuk, A.N., Zadorin, V.S., et al., Sbornik dokladov Mezhdunarodnoi nauchno-practicheskoi konferentsii "Mineral'no-syr'evye resursy tantala, niobiya, zirkoniya i ftora: geologiya, ekonomica, tekhnologiya" (Proc. Int. Sci.-Pract. Conf. "Mineral Resources of Tantalum, Niobium, Zirconium and Fluorine: Geology, Economy, Technology"), Ust'-Kamenogorsk: Ust-Kam. Metall. Zavod AO, 2003, pp. 210–216.
2. Samoilov, V.I. and Borsuk, A.N., *Metody sovmestnoi pererabotki bertrandita, fenakita and berila v gidrometallurgii berilliya* (Methods of Joint Processing of Bertrandite, Phenacite and Beryl in Hydrometallurgy of Beryllium), Ust Kamenogorsk: Media-Al'yans, 2005.
3. Silina, G.F., Zarembo, J.I., and Bertina, L.E., *Berillii, khimmicheskaya tekhnologiya i metallurgiya* (Beryllium, Chemical Technology and Metallurgy), Moscow: Atomizdat, 1960.

ISSN 1070-4272, Russian Journal of Applied Chemistry, 2006, Vol. 79, No. 6, pp. 884–889. © Pleiades Publishing, Inc., 2006.
Original Russian Text © V.I. Samoilov, A.N. Borsuk, A.A. Kishlyanova, 2006, published in Zhurnal Prikladnoi Khimii, 2006, Vol. 79, No. 6, pp. 896–901.

INORGANIC SYNTHESIS AND INDUSTRIAL INORGANIC CHEMISTRY

Improvement of the Technology for Processing of Sulfate Solutions Produced in the Stage of Sulfuric Acid Breakdown of Beryllium Ore Concentrates

V. I. Samoilov, A. N. Borsuk, and A. A. Kishlyanova

Ulba Metal Works AO, Ust Kamenogorsk, East-Kazakhstan oblast, Kazakhstan

Received March 14, 2006

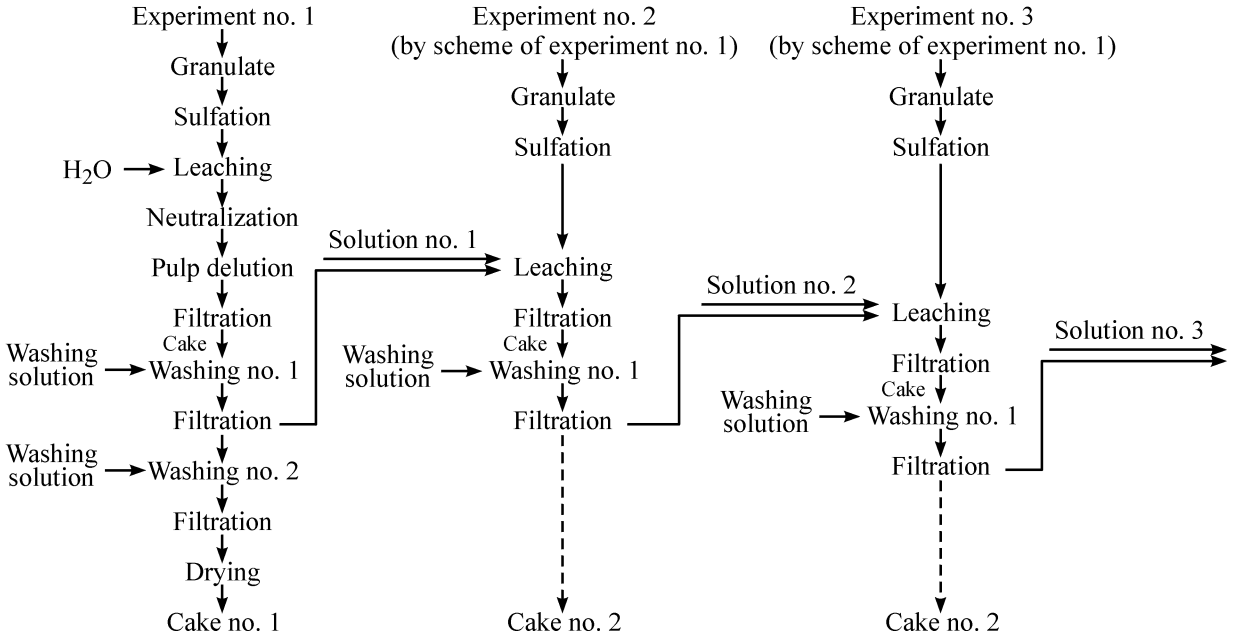
Abstract—The possibility of purifying a sulfate solution to remove silicon and calcium by concentrating beryllium in this solution was studied.

DOI: 10.1134/S1070427206060036

The classical sulfuric acid technology of beryllium recovery from low-grade ores has essential drawbacks. These are the low beryllium content in the sulfate solution formed in the stage of sulfuric acid breakdown of granulated fusion cakes produced from the stock composed of beryllium ore concentrates, soda ash, and limestone (approximately 1–2 g l^{-1}), and the high content of silicon and calcium in this solution (about several tens of percent relative to beryllium) [1–4].

In this study, we tested three procedures for concentration of beryllium in a sulfate solution. According to the first procedure, the granulate from the Ulba Metal Works joint-stock company was decomposed by the scheme presented below. (The shop granulate, obtained by fusion of beryl and bertrandite–phenacite–fluorite concentrates with soda and limestone, contained (wt %): Be 2.21, Al 6.99, Fe 2.28, Ca 10.48, Si 19.03, Mn 0.40, and Cr 0.015.)

In the breakdown of the shop granulate, it was sulfated by mixing a weighed portion of the granulate (25 g) with water at a rate of 0.8 ml per 1 g of the granulate (see scheme). The thus obtained water-granulate pulp was treated with 93% sulfuric acid (0.8 ml per 1 g of the granulate). In the first run,



Technological scheme of beryllium concentration in sulfate solutions.

Table 1. Results of experiments on concentration of beryllium in a sulfate solution

Run no.	Content* in the stock sulfate solution, g l^{-1}			Be content in the cake, wt %	Be extraction into solution (in terms of the cake), %	Content in the sulfate solution, percent relative to Be	
	Be	Ca	Si			Ca	Si
				Series 1			
1	2.29	0.72	0.48	0.120	95.8	31.44	20.96
2	–	0.84	0.17	–	–	–	–
3	3.44	0.77	0.38	–	–	–	–
4	4.59	0.90	0.10	0.024	99.2	19.60	2.10
				Series 2			
1	1.79	0.76	1.76	0.059	98.1	42.50	98.30
2	2.68	0.97	0.92	0.081	97.5	–	–
3	3.05	0.93	0.36	0.055	98.5	–	–
4	4.14	0.80	0.61	0.105	96.1	–	–
5	4.83	0.57	0.25	0.084	97.1	11.80	5.20
				Series 3			
1	2.39	1.05	0.64	0.033	99.1	43.90	26.80
2	3.07	0.87	0.77	0.060	98.1	–	–
3	3.27	0.94	0.72	0.120	96.6	–	–
4	4.41	1.14	0.47	<0.010	99.7	–	–
5	4.57	1.49	0.94	–	–	32.60	20.60
				Series 4			
1	2.53	1.32	0.30	0.059	97.9	52.20	11.90
2	3.52	1.49	0.13	0.086	96.9	–	–
3	3.80	1.65	0.08	0.086	96.9	–	–
4	4.29	1.49	0.14	0.150	94.3	34.70	3.30
				Average values in run nos. 1			
	2.25					42.51	39.49
				Average values in run nos. 4, 5			
	4.57					26.68	7.80

* Content of H_2SO_4 in a sulfate solution at the instant of termination of leaching of sulfates was 29.4–37.2 g l^{-1} (run nos. 1–4, series 4).

the sulfates obtained by sulfation of the granulate were leached with water for 20 min at 80–95°C and s : l = 1 : 5 (in terms of the granulate) with stirring. In the following runs, the leaching was done with stock sulfate solutions (with addition of the first washing water in required amounts) obtained in the preceding run. In this case, water-soluble beryllium, aluminum, and iron sulfates and other admixtures pass into solution. The insoluble residue mostly consists of gel-like silicic acid $SiO_2 \cdot nH_2O$ and hydrated gypsum $CaSO_4 \cdot 2H_2O$. The resulting pulp was neutralized with 8–10% ammonium hydroxide to pH 3.0–3.5 and diluted with hot water to s : l = 1 : 10 (in terms of the granulate) (see scheme).

Then the pulp was delivered to filtration to be separated into a liquid phase (stock solution of sulfates) and cake. The filtered sulfate solution was analyzed for the content of beryllium and limited impurities and delivered to the following stage of leaching-out of sulfates (see scheme). The filtered-off cake was washed to remove water-soluble beryllium with an ammonium sulfate solution (concentration 50 g l^{-1}) acidified with sulfuric acid to pH 3.0–3.5 for 15 min at s : l = 1 : 7 (in terms of the granulate) and temperature of 80–95°C. Then the resulting pulp was filtered, and the filtered-off cake was again washed to remove water-soluble beryllium. In this case, the filtrate from the stage of the first cake washing was used to compensate for the deficiency of the main solution to be used for leaching a next portion of a sulfated granulate (see scheme). The mode of repeated cake washing is similar to that of its first washing. The cake filtered-off after the repeated washing was dried to constant weight and analyzed for the content of beryllium.

The results of experiments on concentration of beryllium and impurities in a sulfate solution are listed in Table 1.

Table 2. Results of experiments on concentration of beryllium in a sulfate solution*

Run no.	Content* in the stock sulfate solution, g l^{-1}			Be content in the cake, wt %	Be extraction into solution (in terms of the cake), %	Content in the sulfate solution, percent relative to Be	
	Be	Ca	Si			Ca	Si
				Series 5			
1	3.96	0.99	1.49	0.044	98.3	25.00	37.60
2	5.17	0.88	0.55	0.096	96.2	–	–
3	6.05	0.80	0.14	0.073	97.4	–	–
4	7.32	0.66	0.04	0.039	98.6	9.00	0.55
				Series 6			
1	2.68	1.22	1.17	0.130	95.8	45.54	43.51
2	–	–	–	0.046	98.3	–	–
3	–	–	–	0.075	97.4	–	–
4	–	–	–	0.072	97.4	–	–
5	8.58	0.72	0.11	0.034	98.7	8.39	1.28
				Series 7			
1	2.09	1.0	0.84	0.068	97.8	47.80	40.22
2	–	–	–	0.057	97.9	–	–
3	–	–	–	0.063	97.8	–	–
4	–	–	–	0.87	96.8	–	–
5	8.75	0.61	0.14	0.052	98.2	7.00	1.60
				Series 8			
1	3.02	1.19	1.21	0.066	97.8	39.54	40.10
2	–	–	–	0.075	97.4	–	–
3	–	–	–	0.094	96.6	–	–
4	–	–	–	0.067	97.5	–	–
5	6.88	0.61	0.23	0.077	97.1	–	–
6	10.29	0.66	0.05	0.066	97.6	6.40	0.49
				Average values in run nos. 1			
	2.94					39.47	40.36
				Average values in run nos. 4–6			
	8.74					7.70	0.98

* Content of H_2SO_4 in solution at the instant of termination of leaching of sulfates was 24.5–36.8 g l^{-1} in run nos. 1 of series 5–8 and 63.7–90.7 g l^{-1} in final runs of series 5–8.

It is seen from Table 1 that three to four turnovers of the stock sulfate solution, with its recycling to the "head" of the process, resulted in that the beryllium content increased, on average, from 2.25 (run nos. 1, series 1–4) to 4.57 g l^{-1} (run no. 4, series 1; run no. 5, series 2 and 3; run no. 4, series 4). In this case, the beryllium content in the cake did not exceed the admissible value of 0.15 wt %. Further increase in the number of solution turnovers in series 1–4 does not raise the beryllium content in them, presumably, because of the supersaturation of the solutions with sulfates of ammonium, aluminum, iron, etc. After five to six cycles of series 1–4, the solutions became viscous and the rate of their filtration decreased. A large amount of ammonium alum crystallized from the thus obtained solutions upon their cooling.

The degrees of purification of the sulfate solution to remove impurities are listed in Table 1. It can be seen 1 that the concentration of beryllium in the sulfate solution resulted in its deep purification to remove silicon (whose content decreased by a factor of 5) and noticeable purification to remove calcium (by approximately a factor of 1.6).

The second technological scheme of beryllium concentration in sulfate solutions was studied on an enlarged laboratory scale. Similarly to the preceding runs (see scheme and Table 1), the breakdown of a 25-g portion of a shop granulate (the same granulate as that in the first scheme) was performed by its sulfation. In the first run, the sulfates obtained in the sulfation of the granulate were leached with water for 20 min at s : l = 1 : 5 (in terms of the granulate) and 80–95 °C with stirring. In the subsequent runs, this was done using stock sulfate solutions (mixed with the first washing water in the case of their deficiency) obtained in the preceding run. Unlike the first scheme, the resulting pulp was delivered to filtration without neutralization and dilution to be separated into a liquid phase (stock solution of sulfates) and a cake. The filtered sulfate solution was analyzed for the content of beryllium and limited impurities and delivered to the following stage of leaching of sulfates. The filtered-off cake was washed to remove water-soluble beryllium with an acidified solution of ammonium sulfate. The filtrate from the stage of the first cake washing was used to compensate for the deficiency of the stock solution for leaching of the next portion of a sulfated granulate (see scheme).

The results of the experiments on concentration of beryllium in a sulfate solution are listed in Table 2. It can be seen that the content of beryllium in solution after 3–5 turnovers of the stock sulfate solution increased, on average, from 2.94 (run nos. 1, series 5–8) to 8.74 g l^{-1} (run no. 4, series 5; run no. 5, series 6 and 7; run no. 6, series 8). In this case, the content of beryllium in the cake did not exceed the admissible value of 0.15 wt %. It follows from the data in Table 2 that further increase in the number of turnovers does not provide an additional rise in the beryllium content in the stock solution because of the formation of solutions saturated with sulfuric acid and sulfates of aluminum, iron, beryllium, etc. In the course of the experiment, we estimated the completeness of purification of the sulfate solution to remove impurities (Table 2). It follows from Table 2 that a deep purification of this solution to remove silicon (by approximately a factor of 41) and calcium (by approximately a factor of 5) was achieved in the course of concentration of beryllium in the sulfate solution.

According to the third technological scheme, the breakdown of the shop granulate and concentration of beryllium in a sulfate solution were carried out as follows [shop granulate contained (wt %): Be 2.34, Al 2.65, Fe 2.28, Ca 10.10, Si 19.09, Mn 0.49, and Cr 0.034; the granulate was produced by fusion of beryl and bertrandite–phenacite–fluorite concentrates with soda and limestone]. As in the preceding series of experiments, the breakdown of 25-g weighed portions of the shop granulate was performed by its sulfation in the standard mode. In the first run, sulfates obtained by the sulfation of the granulate were leached with water, and in the following runs, this was done with stock sulfate solutions mixed with the first washing water obtained in the preceding run. The pulp obtained in leaching was delivered to filtering without neutralization and dilution. The filtered sulfate solution was analyzed for the content of beryllium and the main impurities and delivered to the following stage of leaching of the sulfates. In the first run, the filtered-off cake was washed to remove water-soluble beryllium with a solution of ammonium sulfate at pH 3.0–3.5. In the following runs, the cake was washed with the first washing water obtained in the preceding run via filtration of the pulp after the first washing of the cake. If the amount of the first washing water was insufficient, it was mixed with the second washing water. Then the resulting pulp was filtered and the filtered-off cake was repeatedly washed to remove watersoluble beryllium. The mode of the repeated washing of the cake was similar to that of the first washing: in the first run, an ammonium sulfate solution with pH 3.0–3.5 was used, and in the following runs, the second washing water from the preceding run, whose deficiency was compensated for by adding a fresh washing solution. The cake filtered-off after the repeated washing was dried to constant weight and analyzed for the beryllium content.

The results of the experiments on concentration of beryllium in a sulfate solution by the third technological scheme are listed in Table 3. It can be seen that the technological variant we tested provides, after five to six turnovers of the stock sulfate solution, an average increase in the beryllium content from 3.78 (run nos. 1 of series 9–11) to 13.30 g l^{-1} (run no. 6 of series 9; run no. 6 of series 10; run no. 7 of series 11). In this case, the content of beryllium in the cake did not exceed the admissible value of 0.15 wt %. Further increase in the number of turnovers of the solutions (Table 3) does not provide any additional rise in the beryllium content in the sulfate solution because of the formation of solutions saturated with sulfuric acid and sulfates of aluminum, iron, beryllium, etc.

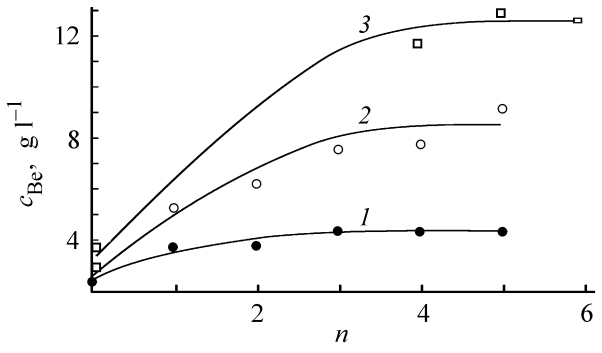
In the course of the experiment, we estimated the completeness of purification of the stock sulfate solution to remove impurities (Table 3). It follows

Table 3. Results of experiments on concentration of beryllium in a sulfate solution*

Run no.	Content* in the stock sulfate solution, g l^{-1}			Be content in the cake, wt %	Be extraction into solution (in terms of the cake), %	Content in the sulfate solution, percent relative to Be	
	Be	Ca	Si			Ca	Si
				Series 9			
1	3.58	1.01	4.12	0.017	99.5	28.21	115.08
2	–	–	–	0.080	97.2	–	–
3	–	–	–	0.10	96.6	–	–
4	–	–	–	0.110	96.2	–	–
5	10.73	0.51	0.030	0.150	94.9	–	–
6	12.65	0.66	<0.055	0.130	95.6	5.22	0.43
				Series 10			
1	3.63	0.99	3.63	0.043	98.8	27.27	100.00
2	–	–	–	0.055	98.1	–	–
3	–	–	–	0.087	97.1	–	–
4	–	–	–	0.110	96.3	–	–
5	11.77	0.72	<0.055	0.120	95.8	–	–
6	13.86	0.61	<0.055	0.10	96.6	4.40	0.40
				Series 11			
1	4.13	1.05	4.510	0.015	99.6	25.42	109.20
2	–	–	–	0.068	97.5	–	–
3	–	–	–	0.086	97.1	–	–
4	–	–	–	0.110	96.0	–	–
5	10.29	0.54	<0.055	0.088	97.0	–	–
6	12.21	–	0.099	0.142	94.9	–	–
7	13.37	0.53	0.007	0.145	94.7	3.96	0.05
				Average values in run nos. 1			
	3.78					26.97	108.09
				Average values in run nos. 6, 7			
	13.30					4.53	0.29

* Content of H_2SO_4 in solution at the instant of termination of leaching of sulfates was 39.2–44.1 g l^{-1} in run nos. 1 of series 9–11 and 124.0–128.9 g l^{-1} in the final runs of series 9–11.

from the data in Table 3 that a deep purification of the sulfate solution to remove silicon (by approximately a factor of 372) and calcium (by approximately a factor of 6) is achieved in the process of beryllium concentration.



Dependence of the beryllium contents c_{Be} in a sulfate solution on the number of its recyclings to the "head" of the process. Technological scheme: (*1*) first (Table 1), (*2*) second (Table 2), and (*3*) third (Table 3).

Comparison of the three variants of the technological scheme we tested shows that the last of these is the most efficient in concentration of beryllium in a sulfate solution (see figure) and in purification of this solution to remove calcium and silicon impurities (Tables 1–3).

As follows from the figure (curve *3*), the process we developed can significantly raise the content of beryllium in a sulfate solution. This can, accordingly, diminish the energy consumption in the production process and the volumes of ecologically harmful unutilizable mother liquor formed in the stage of $Be(OH)_2$ precipitation from the sulfate solution with ammonia [4]. As for removal of silicon and calcium from the sulfate solution, the process we developed (Table 3) makes it possible to reduce the content of

these impurities in solution by approximately factors of 372 and 6, respectively.

CONCLUSIONS

(1) The technological process developed for processing of a beryllium sulfate solution formed in the stage of sulfuric acid breakdown of mineral raw materials makes it possible to raise many-fold the content of beryllium and drastically reduce the content of silicon and calcium in this solution.

(2) The technology developed provides a significant increase in the economic efficiency of the beryllium chemical-metallurgical process and in its ecological safety.

REFERENCES

1. *The Metal Beryllium*, White, D.W., Jr. and Burke, J.E., Eds., Cleveland: American Society for Metals, 1955.
2. Darwin, G.E. and Buddery, J.H., *Beryllium*, New York: Academic, 1960.
3. Silina, G.F., Zarembo, J.I., and Bertina, L.E., *Berillii, khimicheskaya tekhnologiya i metallurgiya* (Beryllium, Chemical Technology and Metallurgy), Moscow: Atomizdat, 1960.
4. Samoilov, V.I. and Borsuk, A.N., *Metody sovmestnoi pererabotki bertrandita, fenakita i berila v gidrometallurgii berilliya* (Methods for Joint Processing of Bertrandite, Phenacite, and Beryl in Hydrometallurgy of Beryllium), Ust Kamenogorsk: Media-Al'yans, 2005.

ISSN 1070-4272, Russian Journal of Applied Chemistry, 2006, Vol. 79, No. 6, pp. 890–892. © Pleiades Publishing, Inc., 2006.
Original Russian Text © Yu.V. Sokolova, R.N. Cherepanin, 2006, published in Zhurnal Prikladnoi Khimii, 2006, Vol. 79, No. 6, pp. 902–904.

INORGANIC SYNTHESIS AND INDUSTRIAL INORGANIC CHEMISTRY

Leaching-out of Scandium(III) in Processing of a Fluoride Concentrate

Yu. V. Sokolova and R. N. Cherepanin

Moscow Institute of Steel and Alloys, Moscow, Russia

Received February 17, 2005; in final form, January 2006

Abstract—Leaching-out of scandium(III) from a fluoride concentrate with a solution of ammonium hydrofluoride is analyzed. Results of a kinetic experiment on leaching-out of scandium(III) at various temperatures and reagent concentrations are presented. The basic characteristics of the process are calculated: activation energy, reaction order with respect to the reagent, and rate constant. Specific features of the process of leaching-out of scandium(III) from a fluoride concentrate are demonstrated.

DOI: 10.1134/S1070427206060048

Recovery of scandium(III) in processing of a uranium ore, zircon, ilmenite [1], and silicate-carbonate ore [2] yields fluoride concentrates with varied content of scandium(III). The conventional methods for decomposition of fluoride concentrates are leaching with a 15–20% NaOH solution at 75–90°C (or fusion with the alkali) and dissolution in concentrated sulfuric acid at the boiling point of the solution [1, 3]. In [1], in processing of thortveitite, a mixture of metal compounds was isolated from the resulting fluoride concentrate of scandium(III); further, this mixture was dissolved in hydrochloric acid and impurities were separated.

This study is concerned with the kinetics of leaching-out of scandium(III) with an ammonium hydrofluoride solution from a fluoride concentrate produced in utilization of wastes that are formed in manufacture of Al + 2% Sc alloy by aluminothermy and contain 1.5–1.7% Sc.

EXPERIMENTAL

The leaching was performed in a thermostated fluoroplastic reactor equipped with a stirrer at solution volume to concentrate mass ratio of 10. The insoluble residue was separated by filtration through a "wide-band" filter.

For analytical purposes, a weighed portion of the fluoride concentrate was fused with potassium hydroxide at a temperature of 500°C in the course of 15 min, and the fusion cake was dissolved in hydrochloric acid. The concentration of Sc(III) in solution was determined by emission spectroscopy with inductively coupled plasma on a Labtam V-310 Plasma Spectrometer and Perkin Elmer Model 300 AA Spectrometer. The lower determination limit of Sc(III) was 10^{-6}%.

The phase composition of the concentrate was studied by means of X-ray phase analysis on a DRON-1 instrument with Fe_{K_α} radiation. The determination accuracy of interplanar spacings was 5×10^{-3} Å, the lower determination limit of phases in multiple-phase and discrete systems was 1%.

The degree of leaching-out, α, was calculated as the ratio of the Sc(III) mass in solution to that in the concentrate. All the procedures involving fluoride salts were performed in fluoroplastic or polyethylene vessels. Nickel crucibles were used in fusion.

The fluoride concentrate of scandium(III), used in the study, was produced by grinding and water-leaching of a salt flux formed in manufacture of the Al + 2% Sc alloy. According to the results of a microscopic study, particles of the concentrate have the shape of prisms of size 10 to 200 μm (predominantly 10–60 μm), i.e., the concentrate is a polydisperse material composed of isometric particles.

According to X-ray phase analysis, the fluoride concentrate of scandium(III) (FC) contains hexafluoroaluminate of potassium and sodium, K_2NaAlF_6, as the main substance. Scandium is represented by several phases: scandium(III) oxide; mixed oxide of scandium and aluminum, $(Al, Sc)_2O_3$; and a minor amount of an intermetallic compound Al_3Sc and a complex salt Na_3ScF_6 [4]. Therefore, it should be

kept in mind when discussing the kinetics of Sc(III) leaching-out from FC that the process includes several concurrent reactions, the main of which can be expressed by the equations

$$Sc_2O_{3(cake)} + 6NH_4HF_{2(sol)} \rightarrow 2(NH_4)_3ScF_{6(sol)} + 3H_2O_{(l)}, \quad (1)$$

$$(Al, Sc)_2O_{3(cake)} + 6NH_4HF_{2(sol)} \rightarrow (NH_4)_3AlF_{6(sol)} + (NH_4)_3ScF_{6(sol)} + 3H_2O_{(l)}. \quad (2)$$

The kinetics of scandium(III) leaching-out from FC was studied at NH_4HF_2 concentrations in the range 0.8–2.8 M at 20–90°C. According to the results obtained, the process rate is independent of the agitation intensity in a wide range of variation of the rotation speed of the stirrer. As specific features of the process should be mentioned the small change in the NH_4HF_2 concentration under conditions of a manyfold excess of the reagent and the insignificant loss of mass (7–8%).

The kinetic curves of leaching-out of scandium(III) at various NH_4HF_2 concentrations are shown in Fig. 1. The degree of leaching-out of scandium(III) markedly increases on passing from a 4% to a 10% solution of the reagent, but grows only slightly as the NH_4HF_2 concentration is raised further. The rate of the process substantially increases with the NH_4HF_2 concentration and decreases in the course of leaching. In this case, the Van't Hoff method [5] can be used to determine the process order with respect to the reagent. Figure 2 shows the data in the $\log v$–$\log c$ coordinates, where the reaction rate v is calculated as the ratio $\Delta\alpha/\Delta\tau$ (τ is time) for a degree of leaching equal to 0.6. The linear run of the dependence makes it possible to determine the process order with respect to the reagent as the slope of the straight line in the chosen coordinates. In the case in question, the reaction order is 0.54 ± 0.01.

The data obtained enable calculation of the rate constant at T = 90°C as the intercept on the abscissa axis for a reagent concentration of 1 M. The rate constant is $(10.2 \pm 0.2) \times 10^{-3}$ mol s^{-1}. The equation for calculating the rate of scandium(III) leaching-out of from FC for a temperature of 90°C has the form

$$\log v = -10.2 \times 10^{-3} - 0.54 \log c, \quad (3)$$

where c is the NH_4HF_2 concentration (M).

The kinetic curves of scandium(III) leaching-out of from FC with a 15% solution of NH_4HF_2 at 20–90°C are shown in Fig. 3. The data obtained point to a strong dependence of the degree of leaching and process rate on temperature. The highest values of α were obtained at 90°C, with the equilibrium attained in 2 h.

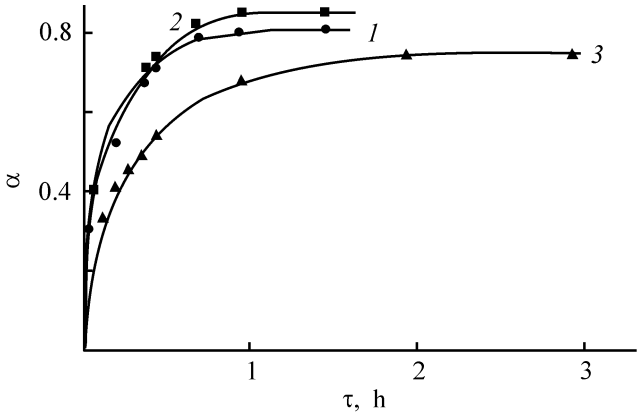


Fig. 1. Kinetics of leaching-out of scandium(III) from FC with an NH_4HF_2 solution at 90°C. (α) Degree of leaching-out of scandium and (τ) time; the same for Fig. 3. $c_{NH_4HF_2}$ (wt %): (*1*) 15, (*2*) 10, and (*3*) 4.

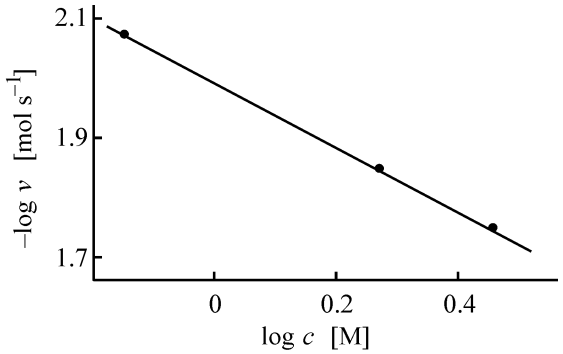


Fig. 2. Rate v of leaching-out of scandium(III) from FC vs. the NH_4HF_2 concentration c (T = 90°C).

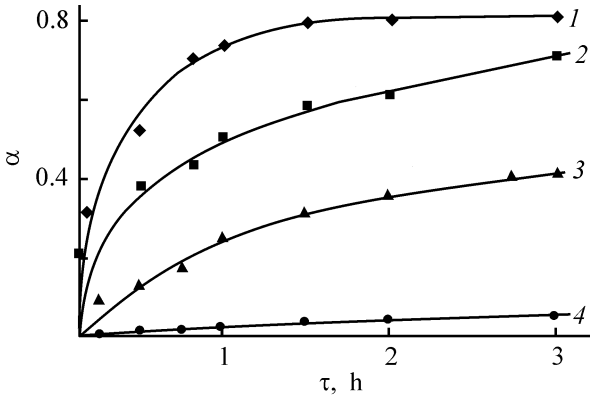


Fig. 3. Kinetics of leaching-out of scandium(III) from FC with a 15% NH_4HF_2 solution. Temperature (°C): (*1*) 90, (*2*) 70, (*3*) 50, and (*4*) 20.

In order to determine the activation energy of the process, the experimental data are plotted in

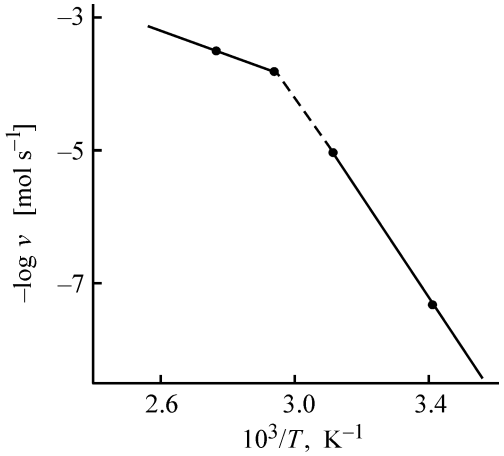


Fig. 4. Rate v of leaching-out of scandium(III) vs. temperature T.

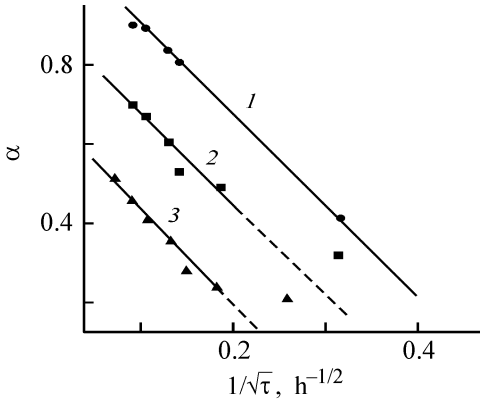


Fig. 5. Degree α of leaching-out of scandium(III) from FC with a 15% NH_4HF_2 solution vs. time τ. Temperature (°C): (*1*) 90, (*2*) 70, and (*3*) 50.

Fig. 4 in the $\ln v$–$1/T$ coordinates. The absence of a linear dependence in this case may be due to simultaneous occurrence of two reactions with different activation energies [6] or to a change of the rate-determining stage of the process with increasing temperature. In the temperature range 20–50°C, the apparent activation energy is 64.7 ± 1.5 kJ mol^{-1}, which indicates that the process occurs in the kinetic mode. In the range 70–90°C, the apparent activation energy is 19.4 ± 0.5 kJ mol^{-1}, which is a characteristic indication that the process occurs in the inner-diffusion region. As the temperature and the degree of leaching increase, the thickness of a layer of waste (leached) rock grows, i.e., the diffusion path for the reagent or leaching product becomes longer and, therefore the diffusion resistance grows. In this case, the amount of diffused substance (and, in the case of diffusion hindrance, the degree of leaching, as well) is proportional to $\sqrt{\tau}$ (τ is time), provided that the reagent concentration and the surface area of the material change only slightly [6]. Figure 5 shows the dependence of the degree of leaching on $1/\sqrt{\tau}$ for the temperature range under study. The dependence is linear only at 90°C, which is evidence that the rate-determining stage changes on passing to the diffusion mode. Therefore, the existence of a break in the given case suggests that the rate-determining stage of the process changes: the process occurs in the kinetic region at temperatures below 70°C, and inner diffusion is the rate-determining stage at above 70°C.

The data obtained make it possible to optimize the conditions of leaching-out of scandium(III) from FC and to suggest ways to intensify the process under study.

CONCLUSIONS

(1) The kinetics of leaching-out of scandium(III) from a fluoride concentrate with a solution of ammonium hydrofluoride was studied. It was shown that the process rate increases with temperature and reagent concentration.

(2) It was found that the process order with respect to the reagent is 0.54 ± 0.01. At temperatures below 70°C, the process occurs in the kinetic mode (apparent activation energy $E_a = 64.7 \pm 1.5$ kJ mol^{-1}), and at temperature of 70°C and more, in the diffusion mode ($E_a = 19.4 \pm 0.5$ kJ mol^{-1}).

(3) It was shown that the dependence of the rate of leaching-out of scandium(III) on the reagent concentration at a temperature of 90°C is described by Eq. (3).

REFERENCES

1. Komissarova, L.N., *Neorganicheskaya i analiticheskaya khimiya skandiya* (Inorganic and Analytical Chemistry of Scandium), Moscow: Editorial URSS, 2001.
2. Sokolova, Yu.V., Koryakov, V.B., and Per'kov, P.G., *Izv. Vyssh. Uchebn. Zaved., Tsvetn. Metall.*, 2004, no. 4, pp. 30–36.
3. Korshunov, B.G., Reznik, A.M., and Semenov, S.A., *Skandii* (Scandium), Moscow: Metallurgiya, 1987.
4. Cherepanin, R.N., Sokolova, Yu.V., and Sagalova, T.B., Abstracts of Papers, *Mezhdunarodnaya nauchno-prakticheskaya konferentsiya "Metallurgiya legkikh metallov. Problemy i perspektivy"* (Int. Sci.-Pract. Conf. "Metallurgy of Light Metals: Problems and Prospects"), Moscow: Mosk. Inst. Stali Splavov, 2004, pp. 226–227.
5. Denisov, E.T., Sarkisov, O.M., and Likhtenshtein, G.I., *Khimicheskaya kinetika* (Chemical Kinetics), Moscow: Khimiya, 2000.
6. Zhukhovitskii, A.A. and Shvartsman, L.A., *Fizicheskaya khimiya* (Physical Chemistry), Moscow: Gos. Nauch.-Tekhn. Izd. Lit. Chern. Tsvetn. Metall., 1963.

ISSN 1070-4272, Russian Journal of Applied Chemistry, 2006, Vol. 79, No. 6, pp. 893–895. © Pleiades Publishing, Inc., 2006.
Original Russian Text © E.M. Shvarts, R.G. Belousova, 2006, published in Zhurnal Prikladnoi Khimii, 2006, Vol. 79, No. 6, pp. 905–907.

INORGANIC SYNTHESIS AND INDUSTRIAL INORGANIC CHEMISTRY

Synthesis of Zinc and Copper Borates in a Single Technological Cycle

E. M. Shvarts and R. G. Belousova

Institute of Inorganic Chemistry, Riga Technical University, Salaspils, Latvia

Received December 21, 2005

Abstract—A zero-waste technology was developed for obtaining in a single technological cycle four valuable products: combustion retarder $Zn_3B_{10}O_{18} \cdot 14H_2O$, microfertilizer $2ZnO \cdot 3B_2O_3 \cdot 7H_2O$, copper borate $3CuO \cdot 2B_2O_3 \cdot nH_2O \cdot mNa_2SO_4$, and wood antiseptic "Mebor."

DOI: 10.1134/S107042720606005X

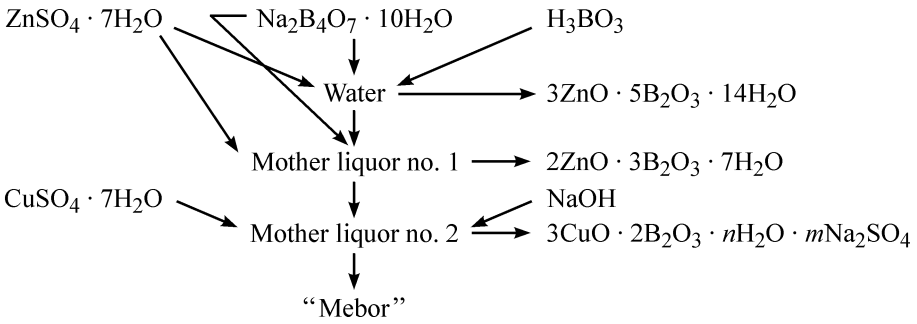
Many zinc borates are known. Among them are various hydrates $2ZnO \cdot 3B_2O_3 \cdot nH_2O$ (n 7.5, 7, 5, 4, 3.2–3.7) [1]. Most of them are obtained from zinc sulfate, sodium tetraborate, zinc carbonate, zinc oxide or hydroxide, and boric acid under various conditions. The hydrate containing 3.2–3.7 molecules of crystallization water, obtained from zinc chloride, sodium tetraborate, and sodium hydroxide on heating [2], is the most important. Zinc borate $2ZnO \cdot 3B_2O_3 \cdot (3.2–3.7)H_2O$ is widely used under the brand name "Firebrake" as a synergetic additive to halogen-containing antipyrenes and antimony oxides to protect polyvinyl chloride, polyesters, polyolefines, and rigid polyurethanes against fire.

In 1993, zinc borates, $4ZnO \cdot B_2O_3 \cdot H_2O$ and $4ZnO \cdot B_2O_3$, were obtained by the reaction of zinc oxide or its corresponding salt with boric acid or with its salts in water at high temperature. It was also suggested to use these borates as fire retarding and smoke suppressing additives to organic polymers [3]. Also, a borate $Zn_3 \cdot B_{10}O_{18} \cdot 14H_2O$ (3-5-14) is known. It was first synthesized by Putnin' and Jevin'sh [4] but failed to find application in industry because of the low yield. The authors of [5] developed a method for synthesizing zinc borate $Zn_3 \cdot B_{10}O_{18} \cdot 14H_2O$ in a 80–94% yield.

As for copper borates, their amorphous {$2CuO \cdot B_2O_3 \cdot H_2O$ and $3CuO \cdot 2B_2O_3 \cdot nH_2O$ (n 1, 2, 4, 5) [6]}, crystalline {bandylite $CuB(OH)_4Cl$ [7] and henmilite $[Ca_2Cu(OH)_4B(OH)_4]_2$ [8]} minerals, and synthetic borates {$Na_6Cu_2[B_{16}O_{24}(OH)_{10}] \cdot 12H_2O$ [9], $K_5HCu_4O[B_{20}O_{32}(OH)_8] \cdot 32H_2O$ [10], and $Cu(NH_3)_4B_4O_7 \cdot 6H_2O$ [11]} are known.

Synthesis of $Zn_3 \cdot B_{10}O_{18} \cdot 14H_2O$ yields a mother liquor containing (g l^{-1}): B(III) ~10 and Zn(II) 4.22.

The goal of our study was to develop methods that involve utilization of the forming wastewater. We achieved this by developing a zero-waste cycle that simultaneously yielded four valuable products: $Zn_3 \cdot B_{10}O_{18} \cdot 14H_2O$ ("Pyroteran"), dizinc hexaborate heptahydrate $2ZnO \cdot 3B_2O_3 \cdot 7H_2O$ (2-3-7) (BZn), copper borate $3CuO \cdot 2B_2O_3 \cdot nH_2O \cdot mNa_2SO_4$ (BCu), and wood antiseptic "Mebor." An example of a zero-waste cycle for joint synthesis of 3-5-14, 2-3-7 zinc borates and copper borate is presented in the scheme.



Scheme for synthesis of zinc and copper borates in a single cycle.

Results of analyses of zinc and copper borates

Borate	Main components	Composition, wt %		X-ray diffraction patterns	
		found	calculated	D, Å	Intensity, %
$3ZnO \cdot 5B_2O_3 \cdot 14H_2O$	ZnO	29.30	29.91	9.591	100
	B_2O_3	40.82	41.21	6.689	100
	H_2O	30.58	29.88	2.935	80
$2ZnO \cdot 3B_2O_3 \cdot 7H_2O$	ZnO	32.66	32.70	6.79	100
	B_2O_3	41.60	41.98	3.36	80
	H_2O	25.65	25.35	3.02	80
$3CuO \cdot 2B_2O_3 \cdot nH_2O \cdot mNa_2SO_4$	CuO	39.90			
	B_2O_3	26.60			
	Na_2SO_4	10.30			
	H_2O	21.30			
	ZnO	2.50			

The 3-5-14 zinc borate was obtained by reacting zinc sulfate solutions and a solution containing borax and boric acid under heating, with stirring of the reaction mixture and isolation of a crystalline 3-5-14 zinc borate from mother liquor no. 1 by filtration. Mother liquor no. 1 was used to obtain a 2-3-7 zinc borate. To mother liquor no. 1 we added calculated amounts of borax and zinc sulfate (both dry). After the reaction mixture was heated and stirred, crystalline zinc borate was filtered off. The remaining mother liquor no. 2 was used to synthesize copper borate.

Copper borate was obtained by addition of calculated amounts of copper sulfate and sodium hydroxide. Mother liquor no. 3, obtained upon separation of copper borate, corresponds in composition to the known wood preservative "Mebor."

The 3-5-14 zinc borate can be used as nontoxic fire-retarding additive to lacquers, paints, and polymer materials, and as a constituent of fireproofing formulations for impregnation of wood. It is effective even in the absence of antimony halides and oxides [12]. The 2-3-7 zinc borate and copper borate can be used as microfertilizers for a presowing seed treatment of vegetables, flax, sugar beet, and other cultures [13].

EXPERIMENTAL

Trizinc decaborate tetradecahydrate $Zn_3 \cdot B_{10}O_{18} \cdot 14H_2O$. Borax $Na_2B_4O_7 \cdot 10H_2O$ (38.1 g) and boric acid (61.8 g) were dissolved in 800 ml of distilled water, and zinc sulfate $ZnSO_4 \cdot 7H_2O$ (28.8 g), in 200 ml. Both solutions were poured into a 2-l flask and heated to 30–40°C under mechanical agitation to complete crystallization of amorphous precipitate (~6 h).

The crystalline precipitate was filtered off, washed with 100 ml of warm water, and dried in air to give 26.5 g of 3-5-14 zinc borate (in 94% yield), identified by X-ray analysis. This is a white crystalline substance in the form of very fine needles. The results of the analysis are listed in the table.

Dizinc hexaborate heptahydrate $Zn_2 \cdot B_6O_{11} \cdot 7H_2O$. After separation of 3-5-14 zinc borate, mother liquor no. 1 contains 4.22 g l^{-1} Zn(II) and 10.03 g l^{-1} B(III). The mother liquor was heated in a 2-l round-bottomed flask to 50–60°C, and then 39.45 g zinc sulfate was dissolved in it. After that, 78.48 g of borax was added and agitation was continued until an amorphous precipitate was formed. The precipitate crystallized in 4 h under heating and stirring. The crystals were filtered off, washed with warm water (50 ml), and dried in air. The 2-3-7 zinc borate (49.28 g) was obtained in 96% yield, identified by chemical analysis (see table).

Copper borate. Mother liquor no. 2, containing Zn(II) (2.27 g l^{-1}) and B(III) (11.62 g l^{-1}), was used to obtain copper borate. Copper sulfate $CuSO_4 \cdot 5H_2O$ (88.73 g) was dissolved in 140 ml of distilled water under heating, and 42 g of NaOH was dissolved in 72 ml of distilled water. A copper sulfate solution was added to mother liquor no. 2, placed in a 2-l round-bottomed flask and agitated with a mechanical stirrer. A NaOH solution was added in small portions under agitation, the temperature was raised to 80°C, and the solution was stirred for 4 h. The resulting

blue precipitate was filtered off from a hot solution, washed with 100 ml of warm 1% boric acid, and dried in air to give the product (75.6 g) in 96.5% yield. The composition of the product is listed in the table.

Copper borate is a blue finely dispersed amorphous powder with admixture of sodium sulfate, whose content depends on its concentration in mother liquor no. 2. The product has the formula $3CuO \cdot 2B_2O_3 \cdot nH_2O \cdot mNa_2SO_4$. In this case, the ZnO content can be disregarded. The product is insoluble in water.

Precipitation of zinc and copper borates in a common process yields mother liquor no. 3. It contains (wt %): 0.002 CuO, 1.77 B_2O_3, and 5.75 Na_2SO_4 and can be used as a preservative for plywood and lumber.

CONCLUSIONS

(1) Zinc and copper borates, $3ZnO \cdot 5B_2O_3 \cdot 14H_2O$, $2ZnO \cdot 3B_2O_3 \cdot 7H_2O$, and $3CuO \cdot 2B_2O_3 \cdot nH_2O \cdot mNa_2SO_4$, were obtained by the reaction of the corresponding sulfates and borax in the presence of boric acid or sodium hydroxide in a single technological cycle.

(2) The mother liquors obtained, which are saturated solutions of boric acid, are used for further synthesis of zinc borates.

(3) The borates obtained can be used as a fire-retarding and smoke-suppressing additives and a microfertilizers for presowing seed treatment of vegetable cultures and flax.

REFERENCES

1. *Supplement to Mellor's Comprehensive Treatise on Inorganic and Theoretical Chemistry*, New York: Longman, 1980, vol. 5, part A, pp. 577–578.
2. US Patent 100526.
3. PCT Int. Appl. WIPO Pat. 9310045.
4. Putnin', Ya.K. and Ievin'sh, A.F., *Nauch. Trudy Len. Gos. Univ.*, 1958, Ser. 22, *Khim. Facul't., VI*, pp. 69–71.
5. LV Patent 10101.
6. Boiko, B.F., *Khimiya boratov* (Borate Chemistry), Riga: Akad. Nauk Latv. SSR, 1953, pp. 105–115.
7. Palache, Ch. and Fostag, W.T., *Am. Mineral.*, 1938, vol. 23, no. 2, pp. 85–90.
8. Nokai, J., Okada, H., and Masutomi, K., *Am. Mineral.*, 1986, vol. 11, nos. 9/10, pp. 1234–1238.
9. Behm, H., *Acta Crystallogr.*, 1983, vol. 39, no. 1, pp. 20–22.
10. Heller, G., Z. *Naturforsch.*, 1985, vol. 406, no. 4, pp. 462–466.
11. Adams, R.M., *Boron, Metallo-Boron Compounds and Borates*, New York: Wiley, 1964.
12. Shvarts, E.M. and Belousova, R.G., *Latv. Kimijas Zurnals*, 2002, no. 3, pp. 271–275.
13. Stramkale, V., Kondratovics, U., Vikmane, M., et al., *Proc. in Agronomy*, 2000, no. 2, pp. 61–65.

ISSN 1070-4272, Russian Journal of Applied Chemistry, 2006, Vol. 79, No. 6, pp. 896–902. © Pleiades Publishing, Inc., 2006.
Original Russian Text © V.I. D'yachkov, 2006, published in Zhurnal Prikladnoi Khimii, 2006, Vol. 79, No. 6, pp. 908–913.

INORGANIC SYNTHESIS AND INDUSTRIAL INORGANIC CHEMISTRY

High-Temperature Oxidation of Titanium, Zirconium, and Hafniyum in Steam

V. I. D'yachkov

St. Petersburg State University, St. Petersburg, Russia

Received February 1, 2006

Abstract—The influence exerted by the nature of titanium, zirconium, and hafnium on the kinetic parameters of oxidation and on the diffusion mechanism of scale formation in steam at 973–1473 K is analyzed. The results obtained are compared with the data for the air medium.

DOI: 10.1134/S1070427206060061

In the preceding paper [1], the results obtained in systematic studies of the influence exerted by the physical and chemical properties of Ti, Zr, and Hf on their behavior in oxidation in air at 973–1473 K were reported. The present study was undertaken with a similar purpose to examine a technologically important medium of steam in the same temperature interval. The main goal was to reveal how specific features of the nature of these elements and their dioxides affect the oxidation rate and the type of the oxidation law, the temperature dependence of the rate constants and activation energy of this process, diffusion mechanism of scale formation, and properties of scale.

The tests were performed in a dynamic medium of steam at a pressure of 101.3 kPa and flow velocity of 0.06 m s^{-1}. The procedure used to prepare samples of refined Ti, Zr, and Hf of high purity (99.93 Ti, 99.80 Zr, 99.70 Hf) remelted in an electromagnetic crucible in the atmosphere of purified argon and the experimental procedures employed were described in [1–5]. In particular, metals were analyzed for the content of hydrogen by the spectral-isotopic method with an accuracy of ±(5–7)% [5].

According to [1–4, 6–9] and to the summary in Table 1, the oxidation rate of Ti in steam at 973–1473 K markedly exceeds that of Zr and, especially, Hf. In contrast to Ti, for which replacement of air with steam leads to a dramatic increase in the overall oxidation rate, the opposite is observed for Zr and Hf, which was previously found for Zr in [10]. This means that the mechanism responsible for the increase in the oxidation rate of Ti in the case when hydrogen from steam is involved [6, 7] is not operative for Zr and Hf.

A processing of the oxidation curves revealed the applicability of the Evans equation [11]:

$$K_{lin}q^2 + K_p q = K_{lin}K_p\tau + C, \quad (1)$$

Table 1. Effect of temperature on the mass gain Δq upon 3-h oxidation of Ti, Zr, and Hf in steam and air

Medium	Metal	Values of Δq, mg cm^{-2}, at indicated temperatures, K						
		973	1073	1173	1273	1323	1373	1473
Steam	Ti	3.40	9.1	18.0	196	211	295	361
	Zr	1.10	2.1	3.9	9.8	21.4	28.8	51.9
	Hf	0.37	0.6	1.3	2.8	3.9	5.0	8.3
Air	Ti	0.40	1.5	7.9	21.5	34.4	31.7	35.7
	Zr	2.00	3.1	13.2	31.1	54.5	43.1	82.9
	Hf	0.40	1.5	2.2	9.3	8.0	10.3	19.2

Table 2. Effect of temperature and duration τ of oxidation of Ti, Zr, and Hf on the type of the kinetic behavior

Oxidation law and the temperature range and duration of its action		
Ti	Zr	Hf
1) Eq. (1): (973–1423, $\tau \geq 3$ h); (1473, in. st.,* $\tau \leq 2$ h) 2) Eq. (4): (1473, after in. st.,** $\tau > 2$ h, $n > 2$)	1) Eq. (1): (973–1473, in. st., $\tau \leq 0.7$ h) 2) Eqs. (2), (4): (1123–1473, after in. st., 0.7 h $\leq \tau \leq 2$ h, $2.0 \leq n \leq 2.4$) 3) Eqs. (3), (4): (973–1373, after in. st., $\tau > 2$ h, $2.6 \leq n \leq 3.4$)	1) Eq. (1): (1073–1473, in. st., $\tau \leq 0.2$ h) 2) Eq. (2), (4): (973–1473, after in. st., 0.2 h $\leq \tau \leq 1.0$ h, $2.0 \leq \tau \leq 2.4$) 3) Eqs. (3), (4): (973–1473, after in. st., $\tau > 1$ h, $2.6 \leq n \leq 3.4$)

* In. st., initial stage. ** After in. st., after initial stage.

and parabolic

$$q^2 = K_p\tau + C, \quad (2)$$

and cubic laws

$$q^3 = K_c\tau + C. \quad (3)$$

Here, q is mass; τ, time; C, constant; and K_{lin}, K_p, and K_c oxidation rate constants by the linear, parabolic, and cubic laws, respectively.

In contrast to the air medium [1], no linear oxidation law was revealed in the case of steam, whereas it is obeyed in the initial stage of Ti oxidation at 923–1123 K and then gives way to the parabolic behavior. In the case of strong deviations of the oxidation rate in steam from the laws (2), (3), which are observed more frequently as compared with air, the results can be formally represented by the expression

$$q^n = K\tau + C \quad (4)$$

at different values of the exponent n.

The results concerning the type of the kinetic laws of oxidation of Ti, Zr, and Hf are summarized in Table 2, in which the temperature range and duration of their action are given in parentheses, together with the value of n in expression (4). It can be seen that, at least during 3 h at 973–1423 K and 2 h at 1473 K, the oxidation rate of Ti is totally governed by the Evans equation (Fig. 1). This indicates that the oxida-

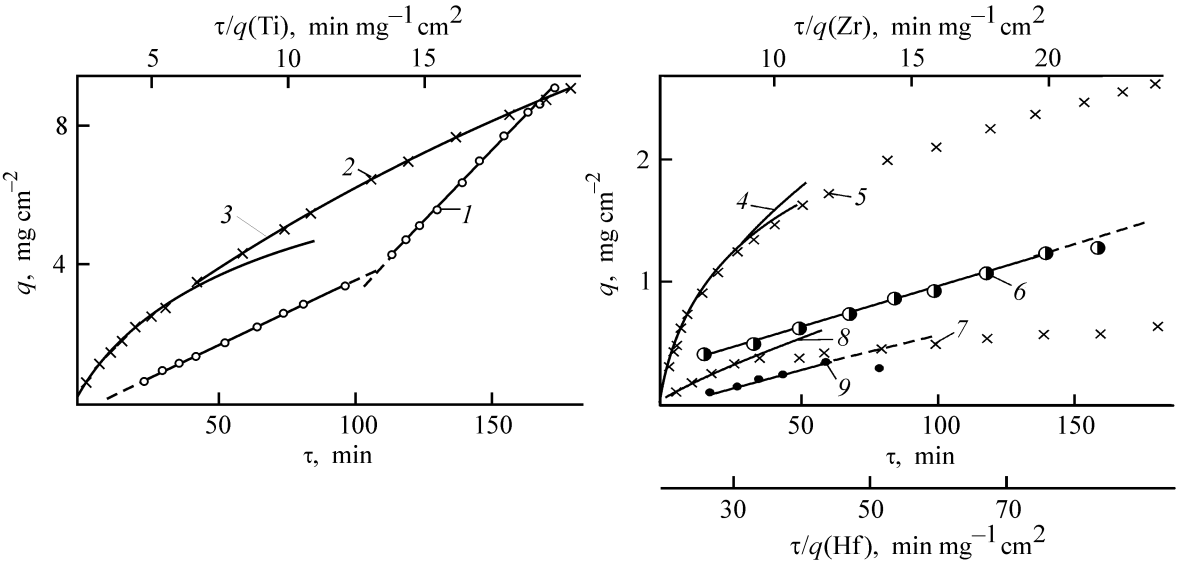


Fig. 1. (*1*, *6*, *9*) Data on oxidation of (*1–3*) titanium, (*4–6*) zirconium, and (*7–9*) hafnium in steam, plotted in the coordinates of the Evans equation, and (*2*, *5*, *7*) positions of the experimental points with respect to (*3*, *4*, *8*) curves described by the Evans equation, plotted with the use of the K_{lin} and K_p values obtained. (*q*) Mass and (τ) time. Temperature (K): (*1–3*, *7–9*) 1073 and (*4–6*) 1023; the same for Figs. 2, 3.

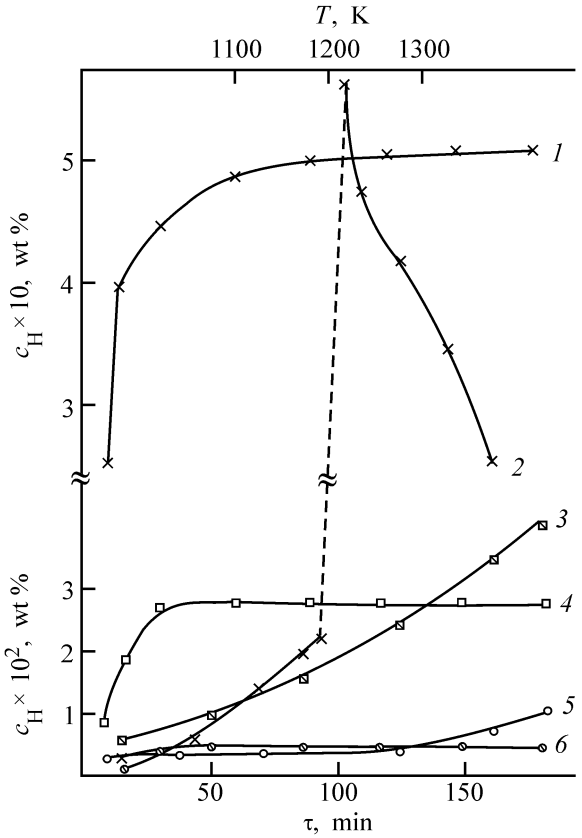


Fig. 2. Content of hydrogen in a metal vs. (*2*, *3*, *5*) temperature T and (*1*, *4*, *6*) duration of oxidation at 1273 K of (*1*, *2*) titanium, (*3*, *4*) zirconium, and (*5*, *6*) hafnium. (c_H) Content of hydrogen and (τ) time.

tion is nonstationary and, consequently, it is governed to comparable extents by diffusion and interphase processes [11, 13]. By contrast, the Evans equation is obeyed in the case of Zr and Hf only at the very beginning of tests, during $\tau \leq 40$ and $\tau \leq 15$ min, respectively (Fig. 1), and later gives way to laws close to the parabolic (2) and then cubic (3) types of behavior, which largely determine the overall rate of the process (3 h).

It can be concluded, with account of the data of [1], that replacement of air with steam leads to a certain stabilization of the Evans equation (1) in oxidation of Ti and, in part, Zr, and to a dramatic shortening of the duration of its action in the case of Hf.

The absorption of hydrogen by titanium at $T \leq (1218 \pm 5)$ K also obeys the Evans law [6, 7]. As, however, the temperature increases to (1273 ± 5) K, the absorption isotherms take a shape of an asymptote when a curve levels-off to become a nearly horizontal straight line after 20–30 min of oxidation for Zr and Hf and 120 min for Ti (Fig. 2). In this case, the rate of hydrogen absorption by titanium is many times that for Zr and Hf.

As can be seen in Fig. 2, the concentration of hydrogen in Zr and Hf steadily increases with temperature, whereas for Ti, it shows a steep rise on going from (1218 ± 5) to (1233 ± 5) K and a nearly equally steep fall at $T > (1233 \pm 5)$ K. This curve reflects the change with temperature of the degree and mechanism of involvement of hydrogen in the Ti oxidation process [6, 7]. Because, according to these reports, the oxidation kinetics is mostly controlled by the cubic law below 810 K, no accelerating effect of hydrogen on this process is observed. Above 810 K and up to (1218 ± 5) K, the noticeable increase in the rate of hydrogen absorption leads to a higher, compared with oxygen and air, oxidation intensity (Table 1), to a more important role of the cation diffusion in scale formation, and to a larger degree of deviation of its composition from stoichiometry. This is mainly due to a rise in the concentration of cation defects in the lattice of rutile upon its partial reduction by hydrogen, e.g., by the following reaction (in the Kroger–Vink notation [14])

$$4Ti_{Ti} + O_O + H_2 = 3Ti^{\bullet}_{Ti} + Ti^{\bullet\bullet\bullet\bullet}_{Ti} + H_2O.$$

On passing to temperatures exceeding $(1218–1233) \pm 5$ K, there occurs a dramatic increase in the overall oxidation rate of titanium (Table 1) and in the porosity of scale, with the mechanism of its formation changing and the decree of nonstoichiometry of rutile decreasing. This is, in particular, due to an increase in the volume of the metal upon its fast saturation with hydrogen. Such a behavior is also favored by accumulation of molecular hydrogen at the metal–scale interface via the reaction of OH^- with Ti:

$$Ti + 2OH^{\bullet}_O = Ti_{Ti} + xO^{(Ti)} + (2 - x)O_O + 2V^{\bullet\bullet}_O + yH^{(Ti)} + [(2 - y)/2]H_2 + 2e,$$

where $xO^{(Ti)}$ and $yH^{(Ti)}$ are oxygen and hydrogen absorbed by the metal, respectively. In this case, the OH^- ($OH^{\bullet}_O$) ions at anion sites of the rutile lattice are generated at the outer surface of the oxide film by the reaction

$$H_2O_{chem.bound} + VO^{\bullet\bullet}_O + e = OH^{\bullet}_O + 1/2H_2$$

and diffuse toward the metal–scale interface because of the smaller radius of OH^- ions (r = 95 pm), compared with O^{2-} (r = 136 pm). As the temperature is elevated, the considerable increase in the rate of oxy-

Table 3. Effect of the composition of the gas phase, temperature, and duration τ of oxidation of Ti and Hf on the content q and fraction z of oxygen in DLO

Metal	Medium	Parameter	T, K						
			1073	1173	1273			1373	1473
Ti	Steam	τ, min	180	180	15	60	180	180	180
		q, mg cm^{-2}	1.5	2.4	1.7	4.5	6.8	7.5	10.1
		z, %	16	13	11	6.2	3.4	3.8	2.8
	Air	q, mg cm^{-2}	0.3	1.3	1.0	2.0	3.4	8.2	10.4
		z, %	24	16	24	16	13	26	29
Hf	Steam	q, mg cm^{-2}	0.2	0.5	0.4	0.8	1.3	2.8	5.4
		z %	28	36	43	44	47	55	65
	Air	q, mg cm^{-2}	–	1.5	1.0	2.6	5.4	2.7	3.6
		z, %	–	69	71	61	60	24	18

gen dissolution in the metal leads to a decrease in the intensity of hydrogen absorption, which diminishes its destructive action on scale. In addition, the density of scale also grows because of an increase in its plasticity and sinterability. By contrast, only minor changes in the color of scale and, consequently, in the degree of its nonstoichiometry are observed for Zr and Hf as temperature increases.

According to the data in Table 3, the growth rate of the diffusion layer of oxygen (DLO) in steam at 1073–1473 K on Ti strongly exceeds that on Hf. At the same time, as the temperature and duration of oxidation (at 1273 K) become higher, the fraction of oxygen in the DLO on Ti decreases, whereas that on Hf, contrastingly, increases, which is due to differences in the law governing the growth of DLO (quadratic parabola) and scale for Ti (Evans equation) and Hf (cubic parabola).

The composition of the gas phase also affects the growth rate of DLO. For example, replacement of air with steam in the case of Ti leads to an increase in the growth rate of DLO up to 1273 K, but causes its decrease at 1373–1473 K. At the same time, the opposite behavior is observed in oxidation of Hf.

It can be seen in Fig. 3, in which $K_{lin}^{(1)}$ and $K_p^{(1)}$ characterize the nonstationary stage of oxidation (in accordance with the Evans equation), and $K_p^{(2)}$, that by the parabolic law (2), that, as a rule, the temperature dependences of these constants for Ti, Zr, and Hf show inflections and a certain difference between the slopes and lengths of the corresponding linear portions. The possible reasons for the occurrence of these inflections were described in the preceding paper [1].

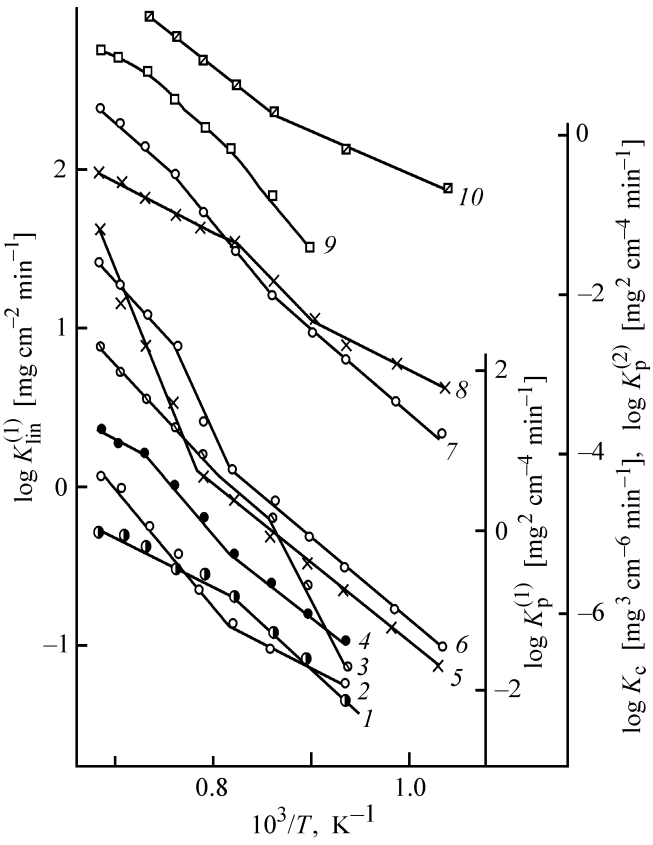


Fig. 3. Oxidation rate constants (*2*, *3*, *5*) $K_{lin}^{(1)}$, (*1*, *4*, *6*) $K_p^{(1)}$, (*8*, *9*) $K_p^{(2)}$, and (*7*, *10*) K_c in oxidation of (*5*, *6*) titanium, (*3*, *4*, *9*, *10*) zirconium, and (*1*, *2*, *7*, *8*) hafnium vs. temperature T.

Table 4. Apparent activation energies E of oxidation of Ti, Zr, and Hf in steam by the linear [$E_{lin}^{(1)}$], parabolic [$E_p^{(1)}$, $E_p^{(2)}$], and cubic (E_c) laws

Metal	$E_{lin}^{(1)}$	$E_p^{(1)}$	$E_p^{(2)}$	E_c
	kJ mol^{-1}, at indicated temperature, K			
Ti	92 973–1273	200 973–1218	–	–
	290 1273–1473	490 1218–1323	–	–
	–	280 1323–1473	–	–
Zr	200 973–1173	210 973–1173	310 1023–1223	190 973–1173
	130 1173–1473	240 1173–1373	200 1223–1373	390 1173–1373
	–	180 1373–1473	120 1373–1473	–
Hf	75 1973–1223	220 1073–1223	110 973–1123	200 973–1173
	125 1223–1473	140 1223–1373	250 1123–1223	280 1173–1373
	–	70 1373–1473	125 1373–1473	70 1373–1473

Table 5. Effect of the nature of a metal, temperature, and composition of the gas phase on the $K_{lin}^{(1)}/K_p^{(1)}$ ratio at the initial stage of oxidation

Medium	Metal	Values of $K_{lin}^{(1)}/K_p^{(1)}$, mg cm^{-2}, at indicated temperature, K						
		1073	1123	1173	1223	1273	1373	1423
Steam	Ti	0.7	0.4	0.3	0.2	0.04	0.02	0.02
	Zr	3.4	2.9	2.6	2.0	1.40	0.40	0.50
	Hf	6.8	5.0	3.4	1.1	0.80	1.70	1.40
Air	Ti	3.1	1.7	0.2	0.05	0.07	0.10	0.14
	Hf	5.7	2.2	2.0	2.0	0.40	0.20	0.21

The values of the apparent activation energies E of oxidation by the corresponding laws (Table 4) are, for the most part, determined with an error of ± (3–5)%. The temperature ranges of their action are given in parentheses. It can be seen that, in the case of nonstationary oxidation, the energy of the diffusion processes ($E_p^{(1)}$) increases on passing from Ti to Zr and Hf in the temperature range 973–1218 K, and, contrariwise, noticeably decreases in the same direction at higher temperatures. The values of $E_{lin}^{(1)}$ for Ti and its analogues also noticeably differ, as also do $E_p^{(2)}$ and E_c for Zr and Hf.

The data of Table 5 suggest that the $K_{lin}^{(1)}/K_p^{(1)}$ ratio markedly increases on going from Ti to Zr and Hf and its variation is to a certain extent nonmonotonic in the range 1223–1273 K. This indicates that the role of diffusion in the control over the rate of nonstationary oxidation grows in the same order. As, however, the temperature increases to 1323 K for Ti and 1273 K for Hf, the $K_{lin}^{(1)}/K_p^{(1)}$ ratio decreases, with this decrease particularly pronounced in oxidation of Ti. For Zr, such a behavior is observed in the entire interval 1073–1423 K. This result demonstrates that the role of interphase processes in determining the overall oxidation rate becomes more important, in agreement with the existing concepts concerning this issue [15]. The increase in $K_{lin}^{(1)}/K_p^{(1)}$ at $T > 1323(1373)$ K for Hf and Ti is presumably due, as in the case of the air medium [1], to specific features of the temperature dependence of $K_{lin}^{(1)}$ and $K_p^{(1)}$ (Fig. 3) and to a change of the mechanism of nonstationary oxidation. With account of the data for air, it can also be concluded that its replacement with steam in tests with Ti leads (except at 1173, 1223 K) to a decrease in $K_{lin}^{(1)}/K_p^{(1)}$ and, consequently, makes more important the role of interphase reactions in the control over the oxidation rate. By contrast, an increase in $K_{lin}^{(1)}/K_p^{(1)}$ on passing from air to steam is observed for Hf, and the control over the oxidation rate goes to diffusion processes.

In tests of Ti, Zr, and Hf in steam, the parts played by the cation and anion diffusion in scale formation

also strongly differ. Indeed, in oxidation of Zr and Hf at temperatures of up to 1473 K, the scale thickness grows, as it also does in air, via the anion diffusion. In the case of Ti, however, the role of the cation diffusion in this process markedly grows as the temperature increases to (1218 ± 5) K. According to the data furnished by the method of "inert" tracers, it governs at this temperature the growth of no less than 80% of the whole amount of scale [6]. At the same time, the role of cation diffusion falls dramatically at $T > (1218 \pm 5)$ K and the growth of the oxide film is mostly governed by the diffusion of oxygen.

The scale formed in tests in steam is composed, mostly for Ti and completely for Zr and Hf, of their nonstoichiometric oxides if $T \leq 1218$, $T < 1223$, and $T \leq 1473$ K, respectively. As the temperature increases, the degree of nonstoichiometry of the scale composition markedly decreases, and this decrease is the most pronounced for Ti. In contrast to the case of an air medium, not only rutile, but also Ti_3O_5 and, occasionally, also Ti_4O_7 are found in scale upon oxidation of Ti in steam. TiO is found at the interface between the scale and the metal (T = 1373 K), and Ti_2O, in the surface layer of scale.

A porous, but denser than that produced in air, oxide film is formed in oxidation of the metals under consideration in steam [at $T \leq (1218 \pm 5)$ K for Ti]. This film shows no microlamination and high adhesion to the matrix surface, which increases on passing from Ti to Zr and Hf. In addition, the thickness of scale formed at sample edges in tests of Ti in steam markedly exceeds that at the matrix faces, in contrast to tests in air. In the case of Zr and Hf, replacement of air with steam does not lead to any noticeable changes in scale morphology, both in this zone and in the whole volume. This indicates that, in contrast to the case of Ti, the mechanisms of scale formation on Zr and Hf in both media are similar.

The revealed differences in the behavior of Ti, Zr, and Hf in oxidation in steam are undoubtedly associated with specific features of their physical and chemical properties, reported in [1]. Here, mention should be primarily made of the decreasing influence of the unfilled state of the outer *d*-shells on the properties of these elements in passing from Ti to Zr and Hf, which is due to the screening of the 4*d* and 5*d* shells of Zr and Hf from the nucleus by the filled, in contrast to Ti, 3*d* shell. This results in that their electronegativity decreases in the same direction, as also, accordingly, do the acceptor capacity and oxygen solubility in the metal lattice. Therefore, a decrease in the growth rate of DLO should be observed on going from Ti to Zr and Hf, which is confirmed experimentally (Table 3). In addition, the metallic chemical bonding in the suboxides Ti_6O and Ti_3O becomes mostly covalent for Zr_6O and Zr_3O. In this case, the oxidation rate decreases as the concentration of oxygen in the metal becomes higher for Ti, but increases for Zr [16, 17]. The departure from this behavior in the case of tests in steam (Table 1) is due to specific features of the mechanism and degree of involvement of hydrogen in the oxidation of Ti and its analogues. The differences in the diffusion mechanisms of scale formation on Ti, Zr, and Hf are mostly due to specific features of the defective structure of their dioxides [14]: $V_O^{\cdot\cdot}$ vacancies are dominant in Zr and Hf dioxides, whereas rutile additionally contains interstitial cations $Ti_{Ti}^{\cdot\cdot\cdot\cdot}$.

Analysis of the results obtained, with account of the phenomenological scheme of oxidation of the metals in the nonstationary (transition) region [13], suggests that the reason why this process is nonstationary in the case of steam is, mostly, the lower, compared with that in equilibrium, activity of oxygen in scale at its interface with the gas medium (steam). At the same time, in tests of Ti in oxygen or air, the nonequilibrium oxidation conditions are mostly confined to the scale–metal interface [18]. However, a more precise solution of these questions in the case of oxidation of the metals under consideration in a steam-and-water medium, and for Hf also in air, requires a special study.

CONCLUSIONS

(1) On passing from Ti to its chemical analogues (Zr, Hf), the overall oxidation rate and the role of interphase processes in the control over this rate markedly decrease, the period of nonstationary oxidation (Hf) becomes shorter, the type of the rate-determining oxidation law is altered, the position and extent of separate zones in the temperature dependence of the rate constants and the activation energy of oxidation change, the growth rate of DLO and rate of hydrogen absorption by a metal decrease at an increasing fraction of oxygen in it, and the contribution of anion diffusion to scale formation becomes more important.

(2) The closeness of many properties of Zr and Hf and of their dioxides predetermines the similarity in the kinetics of their oxidation, diffusion mechanism of scale formation, and scale morphology. As regards the duration of the nonstationary stage of oxidation, Zr is more similar to Ti, than Hf.

(3) The considerable changes in the oxidation rate and, for Ti, in contrast to Zr and Hf, also in the diffusion mechanism of scale formation upon replacement of air with steam are due to the involvement of hydrogen in this process, with the mechanism of this involvement determined by the temperature and duration of tests. The difference between the behavior of Ti and that of Zr and Hf in oxidation with steam is more substantial than that in the air medium.

REFERENCES

1. D'yachkov, V.I., *Zh. Prikl. Khim.*, 2004, vol. 77, no. 9, pp. 1409–1415.
2. Tikhomirov, V.I. and D'yachkov, V.I., *Zh. Prikl. Khim.*, 1967, vol. 40, no. 11, pp. 2405–2413.
3. D'yachkov, V.I. and Tikhomirov, V.I., *Zh. Prikl. Khim.*, 1977, vol. 50, no. 12, pp. 2648–2652.
4. D'yachkov, V.I., *Zh. Prikl. Khim.*, 1990, vol. 63, no. 4, pp. 758–762.
5. Petrov, A.A., *Spektral'no-izotopnyi metod issledovaniya materialov* (Spectral-Isotopic Method for Examination of Materials), Leningrad: Len. Gos. Univ., 1974, pp. 205–230.
6. Dyachkov, V.I., *J. Chim. Phys.*, 1991, vol. 88, no. 2, pp. 233–248.
7. D'yachkov, V.I., *Zh. Prikl. Khim.*, 2000, vol. 73, no. 8, pp. 1241–1246.
8. D'yachkov, V.I., *Zh. Prikl. Khim.*, 1991, vol. 64, no. 10, pp. 2029–2037.
9. D'yachkov, V.I., *Zh. Prikl. Khim.*, 1991, vol. 64, no. 12, pp. 2561–2567.
10. Westerman, R.E., *J. Electrochem. Soc.*, 1964, vol. 111, no. 2, pp. 140–149.
11. Evans, U.R., *Trans. Electrochem. Soc.*, 1924, vol. 46, no. 1, pp. 247–274.
12. Wouters, Y., Galerie, A., and Petit, J.-P., *Solid State Ionics*, 1997, vol. 104, pp. 89–96.
13. Tikhomirov, V.I. and D'yachkov, V.I., *Fiz. Met. Metalloved.*, 1969, vol. 27, no. 3, pp. 459–465.
14. Kofstad, P., *Otklonenie ot stekhiometrii, diffuziya i elektroprovodnost' v prostykh okislakh metallov* (Deviations from Stoichiometry, Diffusion and Electrical Conductivity in Simple Metal Oxides), Moscow: Mir, 1973.
15. Khauffe K. *Reaktsii v tverdykh telakh i na ikh poverkhnosti* (Reactions in Soids and on Their Surfaces), Moscow: Izd. Inostr. Lit., 1963, vol. 2.
16. Kornilov, I.I., *Titan* (Titanium), Moscow: Nauka, 1975.
17. Kornilov, I.I. and Glazova, V.V., *Vzaimodeistvie tugoplavkikh metallov perekhodnykh grupp s kislorodom* (Interaction of Refractory Transition Metals with Oxygen), Moscow: Nauka, 1967.
18. D'yachkov, V.I. and Tikhomirov, V.I., *Fiz. Met. Metalloved.*, 1969, vol. 27, no. 4, pp. 655–662.

ISSN 1070-4272, Russian Journal of Applied Chemistry, 2006, Vol. 79, No. 6, pp. 903–908. © Pleiades Publishing, Inc., 2006.
Original Russian Text © I.I. Gnativ, Z.F. Tomashik, V.N. Tomashik, I.B. Stratiichuk, 2006, published in Zhurnal Prikladnoi Khimii, 2006, Vol. 79, No. 6, pp. 914–919.

INORGANIC SYNTHESIS AND INDUSTRIAL INORGANIC CHEMISTRY

Chemical Etching of $Cd_xHg_{1-x}Te$ Single Crystals in Bromine-releasing Aqueous H_2O_2–HBr–Solvent Solutions

I. I. Gnativ, Z. F. Tomashik, V. N. Tomashik, and I. B. Stratiichuk

Lashkarev Institute of Semiconductor Physics, National Academy of Sciences of Ukraine, Kiev, Ukraine

Received February 13, 2006

Abstract—The nature and mechanism of dissolution of single crystals of a $Cd_{0.21}Hg_{0.79}Te$ solid solution in H_2O_2–HBr–solvent bromine-releasing aqueous solutions were determined, with water, ethylene glycol, and tartaric, citric, and lactic acids used as solvents. Projections of the surfaces of equal etching rates were constructed and the concentration limits were found for solutions that can be used for chemical-dynamical polishing of the surface of $Cd_{0.21}Hg_{0.79}Te$ single crystals.

DOI: 10.1134/S1070427206060073

$Cd_xHg_{1-x}Te$ solid solutions are the main material for fabrication of IR photodetectors, including multiple-element linear and matrix arrays. Despite the wide practical use of this semiconducting material, there exist severe difficulties associated with the technology of its processing, which includes chemical etching as one of stages.

Most frequently, Br_2–CH_3OH etchants are used for chemical treatment of the surface of $Cd_xHg_{1-x}Te$ single crystals [1]. A study of the process of chemical etching of $Cd_{0.21}Hg_{0.79}Te$ in bromine-releasing etching formulations of the system HBr–HNO_3–H_2O was reported in [2]. In [3], the possibility that etchants containing hydrogen peroxide as an oxidizing agent can be used for chemical treatment of $Cd_xHg_{1-x}Te$ single crystals was mentioned. The kinetics and mechanism of dissolution in aqueous solutions containing H_2O_2 and a mineral acid (nitric, sulfuric, phosphoric, and hydrochloric) were analyzed. The experimental results obtained demonstrated that regions of polishing solutions exist in virtually all of the systems studied.

The authors of [4] examined the nature of chemical dissolution of CdTe and $Cd_xHg_{1-x}Te$ in aqueous solutions of H_2O_2–HI. The dependence of the dissolution rate of these materials on the concentration of the starting etching formulations and on the composition of the solid solutions. The concentration limits of solutions that can be used for chemical-dynamical polishing (CDP) of CdTe and $Cd_xHg_{1-x}Te$ were determined.

The ellipsometric method has been applied to analyze the composition of films formed on the surface of $Cd_{0.21}Hg_{0.79}Te$ treated with H_2O_2-containing solutions [5].

No evidence concerning application of bromine-releasing solutions based on the H_2O_2–HBr system for CDP of the surface of single-crystal wafers of $Cd_xHg_{1-x}Te$ solid solutions could be found in the literature, despite that preliminary experiments revealed their real promise.

The aim of this study was (i) to analyze the nature of the physicochemical interaction between single crystals of $Cd_xHg_{1-x}Te$ solid solutions and H_2O_2–HBr–solvent etching formulations containing water, ethylene glycol, and tartaric, citric, and lactic acids as solvents; (ii) construct the corresponding diagrams of etchant composition versus etching rate; (iii) establish concentration boundaries for the solutions with respect to the type of action of these solutions on the surface; (iv) reveal the rate-determining stages of the dissolution process; and (v) optimize the compositions of polishing etching mixtures and the processing modes of the materials.

EXPERIMENTAL

The chemical dissolution of single-crystal wafers was performed on an installation for CDP, with the rotating-disc method employed. $Cd_{0.21}Hg_{0.79}Te$ single crystals *n*-type, grown by the Bridgman technique, were used. The samples under study had a surface area

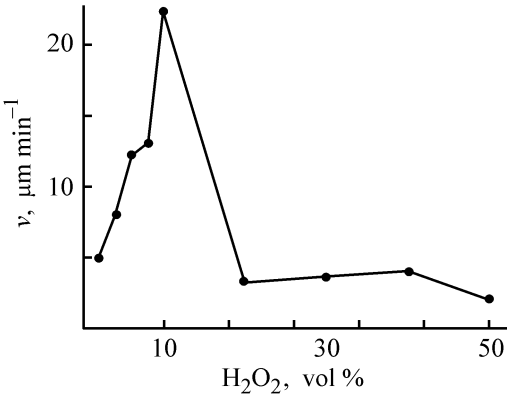


Fig. 1. Concentration dependence of the etching rate ν of $Cd_{0.21}Hg_{0.79}Te$ in aqueous solutions of H_2O_2–HBr. T = 291 K, γ = 86 rpm. (H_2O_2) Content.

of approximately 0.5 cm^2 and thickness of 1.5–2 mm. Prior to being etched, they were mechanically ground with abrasive dusts of M5 and M1 brands, polished with diamond pastes, and degreased with acetone and ethanol. After that, a 50–100-μm-thick layer distorted by the preceding treatments was removed from the sample surface by an etchant of the composition that was used in further measurements. Then, the samples were glued with picein, with nonworking surface down, onto glass substrates and placed in a holder that enabled dissolution in the rotating-disc mode (with the rate of rotation varied in the range 36–120 rpm).

The dissolution rate of the samples was determined from the decrease in their thickness, measured with an ICh-1 watch indicator to within ±0.5 μm. Two or three samples were dissolved simultaneously, with the scatter of the thickness measured not exceeding 5%. The microstructure of the surfaces obtained upon etching was studied with a Zeiss Jenatech Inspection versatile control microscope equipped with a digital camera, at magnifications of 25 to 1600. The microprofile and structure of the etched wafer surfaces were studied using the mechanical-contact method intended for determining the surface roughness. The measurements were done with a Dectac 3030 Auto II profilograph, which can precisely determine vertical deviations from the mean line: microirregularities with heights of 50 Å to 100 μm.

The etching mixtures were prepared using 40% hydrobromic acid of special-purity grade, 35% aqueous solution of chemically pure H_2O_2, 80% aqueous solution of lactic acid ($C_3H_6O_3$) of analytically pure grade, 27% aqueous solution of tartaric acid ($C_4H_6O_6$), and 20% aqueous solution of citric acid ($C_6H_8O_7$) (the last two of chemically pure grade). These components were mixed in amounts corresponding to their volume ratio in the etching formulation (i.e., the composition of the etchant was expressed in volume percent). The etchant components were mixed in a vessel placed in water with ice for cooling in order to preclude overheating of the mixture. The solutions studied were prepared immediately before etching and kept for 2 h for equilibrium to be attained by the chemical reaction that occurs in aqueous solutions between the starting components of the etchant:

$$H_2O_2 + 2HBr = Br_2 + 2H_2O. \quad (1)$$

Depending on the $[H_2O_2]$: [HBr] ratio, the forming bromine can either dissolve in the excess amount of HBr to give etching mixtures similar in properties and composition to Br_2–HBr solutions or be in the free state together with an excess amount of H_2O_2. At a H_2O_2 content in the mixture equal to 22.6 vol %, reaction (1) between the starting components proceeds virtually to completion. After the end of the etching process, the samples were first washed in a 0.01 M solution of sodium thiosulfate for complete removal of the remaining etchant and then rinsed several times with plentiful of distilled water and dried in air.

The concentration dependence of the rate of $Cd_{0.21}Hg_{0.79}Te$ dissolution in aqueous solutions of H_2O_2–HBr is shown in Fig. 1. The study was performed at a H_2O_2 content in the mixture in the range 2–50 vol %, disc rotation rate of 86 rpm, and temperatures of 291–293 K. It can be seen that this dependence shows a maximum at 10 vol % H_2O_2 in the mixture. At this point the molar ratio of the reacting components of the etchant is $[H_2O_2]$: [HBr] = 1 : 5. Possibly, the maximum occurs because the largest amount of bromine, which can dissolve in the excess amount of hydrobromic acid, is released at this ratio of the starting components.

Raising the H_2O_2 content in the mixture from 2 to 10 vol % leads to a gradual increase in the dissolution rate from 5.3 to 22.3 μm min^{-1}, and treatment of samples in solutions of this kind favors formation of a lustrous surface. Further increase in the H_2O_2 content in the etching mixture from 10 to 50 vol % leads to a decrease in the etching rate to 6 μm min^{-1}, with a deteriorated quality of the surface being treated. After treatment in etching mixtures belonging to this range, $Cd_{0.21}Hg_{0.79}Te$ samples are covered with a film and yellow, green, or gray spots appear, depending on the H_2O_2 content. Possibly, at H_2O_2 content in the etchant exceeding 10 vol %, bromine starts to be removed from solution, which depletes the solutions of the active components and impairs the quality of a surface being treated.

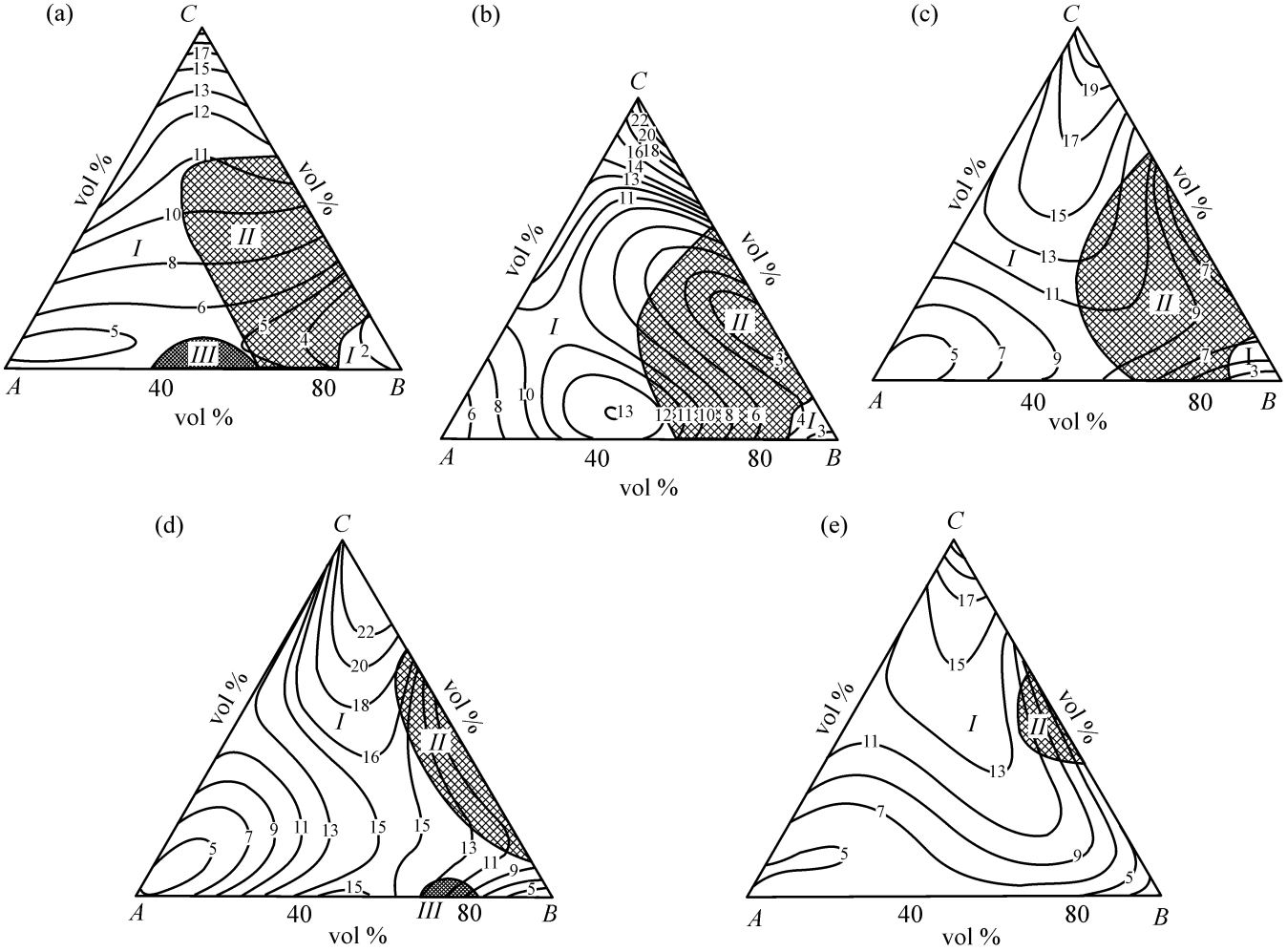


Fig. 2. Concentration dependences of the etching rate ν of $Cd_{0.21}Hg_{0.79}Te$ in aqueous H_2O_2–HBr–solvent solutions at a volume ratio H_2O_2 : HBr : solvent at vertices *A*, *B*, and *C* (vol %): *A*, 2 : 98 : 0; *B*, 10 : 10 : 80; and *C*, 10 : 90 : 0. Region of solutions: (*I*) polishing, (*II*) nonpolishing, and (*III*) selective. Solvent: (a) ethylene glycol, (b) water, (c) tartaric acid, (d) citric acid, and (e) lactic acid.

The results obtained suggest that a third component is to be used to improve the quality of the etching formulations with H_2O_2–HBr. This component could partly control the interaction between H_2O_2 and HBr, favor dissolution of the forming bromine, and convert interaction products into the soluble form. To study the dissolution of single-crystal $Cd_{0.21}Hg_{0.79}Te$ samples in solutions of the system H_2O_2-HBr–solvent, the interval delimited by the triangle ABS was chosen. At vertices *A*, *B*, and *C* of this triangle, the volume ratio H_2O_2 : HBr : solvent was (vol %) 2 : 98 : 0, 10 : 10 : 80, and 10 : 90 : 0, respectively. This approach makes it possible to exclude from consideration passivation regions and regions of strong fluctuations of the etching rate. This is necessary because addition of a minor amount of one component to another may drastically change the mechanism of the heterogeneous chemical reaction occurring in etching.

The experimental results obtained were used to construct, with mathematical simplex design of the experiment [8] for 291 K and disc rotation rate γ = 86 rpm, projections of the surfaces of equal dissolution rates (Gibbs diagrams) for $Cd_{0.21}Hg_{0.79}Te$ in solutions of the system H_2O_2–HBr–solvent, in which water, ethylene glycol, and tartaric, citric, and lactic acids served as solvents.

As can be seen in Fig. 2a, the etching rate of $Cd_{0.21}Hg_{0.79}Te$ samples in aqueous solutions composed of H_2O_2, HBr, and ethylene glycol is comparatively low and falls within the range 1.5–22.3 μm min^{-1}. It is at a maximum in solutions enriched in HBr and has the minimum value in solutions containing the

largest amount of ethylene glycol. Polishing etching formulations are constituted by solutions in two concentration ranges. The first of these, with the minimum content of ethylene glycol, falls within the limits (vol %) (2–10) H_2O_2, (55–98) HBr, and (0–38) ethylene glycol, and the second, with the maximum content of ethylene glycol, within the limits (8–10) H_2O_2, (10–21) HBr, and (69–80) ethylene glycol. The CDP rates in these ranges are 5.3–22.3 and 1.5–3.0 μm min^{-1}, respectively. The region of selective etchants (range *III*) falls within the interval (5–7) H_2O_2 : (44–65) HBr : (30–50) ethylene glycol and occupies about 5% of the whole concentration range studied.

Comparison of the concentration dependences of the etching rates of $Cd_{0.21}Hg_{0.79}Te$ in H_2O_2–HBr–H_2O and H_2O_2–HBr–$C_4H_6O_6$ etching mixtures shows their similarity. This suggests that the mechanisms of dissolution of these materials in the etchants under study are of the same type (Figs. 2b, 2c). Polishing etching formulations are formed in these systems by solutions containing the minimum and maximum amounts of the solvent and are virtually similar in the size and position of the corresponding regions in the concentration triangle. The etching rates of $Cd_{0.21}Hg_{0.79}Te$ samples in etchants of these systems are comparatively low and fall within the ranges 2.1–22.3 and 0.5–22.3 μm min^{-1}, respectively. Their maximum values are observed in solutions enriched in HBr, and the minimum values, in those containing the largest amount of water or tartaric acid. As can be seen in Fig. 2, the regions of polishing etchants are virtually the same and are delimited by the contents (vol %): (2–10) H_2O_2 : (49–98) HBr : (0–65) water, $C_4H_6O_6$ and (9–10) H_2O_2 : (10–16) HBr : (74–80) water, $C_4H_6O_6$.

In the case when citric acid is used as a solvent (H_2O_2–HBr–$C_6H_8O_7$), the etching rate of $Cd_{0.21}Hg_{0.79}Te$ samples is, as in the preceding systems, within the range 2.4–22.3 μm min^{-1}, but the boundaries of the polishing region change significantly (Fig. 2d). The maximum etching rate is observed in solutions enriched in HBr, and the minimum etching rate in those containing the largest amount of citric acid. The larger part of the concentration range of the solutions under study is occupied by the region of polishing compositions (Fig. 2d, region *I*). This region covers about 80% of the whole concentration range studied and is limited to (vol %): (2–10) H_2O_2, (10–98) HBr, and (0–80) $C_6H_8O_7$. The region of selective etchants (region *III*) is limited to (vol %) H_2O_2 : (27–37) HBr : (55–65) $C_6H_8O_7$ and occupies about 5% of the entire concentration range.

With lactic acid ($C_3H_6O_3$) used as a solvent, the etching rate of $Cd_{0.21}Hg_{0.79}Te$ samples somewhat decreases, from 0.8 to 22.3 μm min^{-1} (Fig. 2e). The minimum dissolution rate is observed for all the samples in mixtures with the highest content of lactic acid at a volume ratio H_2O_2 : HBr : $C_3H_6O_3$ = 10 : 10 : 80, and the minimum rate, in mixtures enriched in hydrobromic acid at a ratio H_2O_2 : HBr : $C_3H_6O_3$ = 10 : 90 : 0. Nearly the entire concentration range of the solutions under study is occupied by the region of polishing compositions (Fig. 2e, region *I*). This region, limited to (vol %): (2–10) H_2O_2 : (10–98) HBr : (0–80) $C_3H_6O_3$, is the largest among those for all of the solutions studied and occupies about 95% of the entire concentration range studied.

To study the nature of processes occurring in dissolution of $Cd_{0.21}Hg_{0.79}Te$, kinetic experiments were carried out and dependences of the dissolution rate ν of these materials on the disc rotation rate γ and temperature were constructed. Dependences of this kind make it possible to determine which stage, diffusion-related or kinetic, is rate-determining and to exclude from consideration the influence exerted by some side effects occurring in dissolution of a semiconductor on the chemical etching rate [9]. If the diffusion stage of the dissolution process is rate-determining, dependences of this kind can be extrapolated to the origin of coordinates. If, however, the importance of the surface (chemical) reaction in the overall dissolution process increases and it becomes rate-determining, then the corresponding straight line runs parallel to the abscissa axis. In the case of dissolution of the semiconductor by a mixed mechanism, the straight line or its extension intersects the ordinate axis and the length of the intercept can be used to calculate the rate constant of the overall chemical reaction.

The study was performed in the temperature range 285–310 K at a disc rotation rate of 36–120 rpm, with the dependences of the etching rate on the disc rotation rate plotted in the coordinates ν–$\gamma^{-1/2}$, and the temperature dependences of the etching rate, in the coordinates $\ln \nu$–$10^3/T$.

Figure 3a shows the dependences of the dissolution rate of $Cd_{0.21}Hg_{0.79}Te$ on the disc rotation rate for several aqueous H_2O_2–HBr–solvent solutions. It can be seen that these dependences can be extrapolated to the origin of coordinates for all the etching

mixtures studied. The data obtained indicate that the dissolution of $Cd_{0.21}Hg_{0.79}Te$ samples is limited by the diffusion stage in all of the solutions mentioned above. Analysis of the temperature dependences in Fig. 3b confirms the conclusion that the dissolution process is limited by the diffusion stages, because the apparent activation energies E_a, found from the temperature dependences in the range 285–310 K, do not exceed 35 kJ mol^{-1}, which is characteristic of diffusion processes.

Thus, the experimental study revealed the main specific features of the dissolution of $Cd_{0.21}Hg_{0.79}Te$ in bromine-releasing etching formulations H_2O_2–HBr–solvent. It was shown that, in the solution concentration ranges studied, a difference both in the rates of chemical etching and in the size of the concentration ranges corresponding to polishing solutions is observed upon replacement of one solvent with another. On changing the solvent in the H_2O_2–HBr–solvent system, the region of polishing solution increases in size in the order ethylene glycol → water, tartaric acid → citric acid → lactic acid.

The experimental data obtained made it possible to develop and optimize, for the first time, a set of bromine-releasing etching formulations, which were found to be promising for various technological treatments of single crystals of $Cd_{0.21}Hg_{0.79}Te$ solid solutions. The etchant compositions were optimized with respect to the etching rate, surface roughness, and contamination of the surface with etchant components, using data derived from the concentration dependences of the dissolution rate and results of metallographic and profilographic analyses. The technological modes of CDP and other kinds of treatment (wafer thinning, selective etching) were optimized for the etching mixtures selected with the use of the data on the dissolution kinetics of the semiconductors specified in relation to temperature, velocity at which the etchant flows around wafers, etc. A sequence of procedures for chemical treatment of the surface was developed. This sequence includes cleaning of the wafers with organic solvents, etching, and finishing washing in solutions of reagents that well dissolve both the remaining etching formulations and some products formed in the chemical interaction. It was shown that, to obtain a polished surface by the CDP method, it is necessary to use etchants from the polishing regions in the diagrams (region *I*) and to perform the CDP process at 295–298 K at a disc rotation rate of 86 rpm, with the subsequent washing of the samples with a 0.01 M solution of sodium thiosulfate and with distilled water.

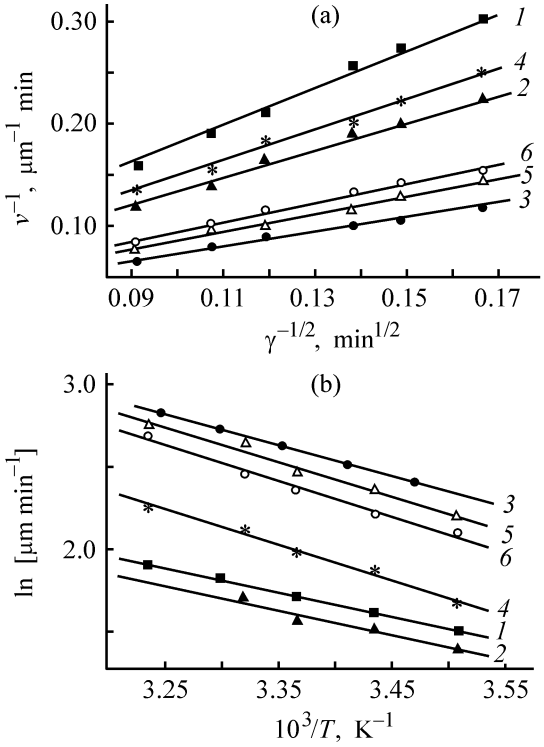


Fig. 3. Dissolution rate ν of $Cd_{0.21}Hg_{0.79}Te$ vs. (a) disc rotation rate γ and (b) temperature *T*. (a) *T* = 291 K and (b) γ = 86 rpm. Solution (vol %): (*1*) $2H_2O_2$ + 98HBr, (*2*–*4*) $4H_2O_2$ + 76HBr + 20 [(*2*) ethylene glycol, (*3*) H_2O, and (*4*) tartaric acid], and (*5*–*6*) $6H_2O_2$ + 74HBr + 20 [(*5*) citric acid and (*6*) lactic acid].

CONCLUSIONS

(1) A study of the physicochemical interaction of single crystals of $Cd_{0.21}Hg_{0.79}Te$ solid solutions with H_2O_2–HBr–solvent etching formulations, with ethylene glycol, water, and tartaric, citric, and lactic acids used as solvents, made it possible to construct surfaces of equal etching rates and determine the boundaries of the existence regions of polishing, nonpolishing, and etching-pit-forming solutions. It was shown that introduction of the above-mentioned solvents into the etching mixtures based on H_2O_2–HBr–solvent affects the nature of the dissolution process, rate of chemical etching of $Cd_{0.21}Hg_{0.79}Te$, and concentration limits of polishing solutions, with the dissolution in polishing solutions of the system H_2O_2–HBr–solvent system limited by diffusion stages.

(2) It was suggested to use, for chemical treatment of $Cd_{0.21}Hg_{0.79}Te$, bromine-releasing formulations based on an aqueous solution of H_2O_2 and hydrobromic acid. With these formulations, the etching rates are low (1–23 μm min^{-1}) and the amount of

bromine released can be to a certain extent controlled by introduction of a solvent. A set of etching formulations for various technological treatments (chemical-dynamical polishing, selective etching) was suggested. The etchant compositions and the technological modes of chemical treatment of the material were optimized.

REFERENCES

1. Artamonov, V.V., Valakh, M.Ya., Strel'chuk, V.V., et al., *Zh. Prikl. Spektrosk.*, 1988, vol. 48, no. 6, pp. 990–994.
2. Tomashik, V.N. and Sava, A.A., *Neorg. Mater.*, 1992, vol. 26, no. 2, pp. 324–328.
3. Tomashik, Z.F., Lukiyanchuk, E.M., and Tomashik, V.N., *Optoelektron. Poluprovodn. Tekh.*, 2003, no. 38, pp. 204–209.
4. Gumenyuk, O.R., Tomashik, V.N., and Tomashik, Z.F., *Optoelektron. Poluprovodn. Tekh.*, 2002, no. 37, pp. 147–149.
5. Shcherbak, L.P., Nikonyuk, E.S., and Panchuk, O.E., *Izv. Akad. Nauk SSSR, Neorg. Mater.*, 1977, vol. 13, no. 3, pp. 415–418.
6. Izidinov, S.O. and Blokhina, A.P., *Zh. Prikl. Khim.*, 1978, vol. 51, no. 12, pp. 2645–2648.
7. Izidinov, S.O., Petrin, A.N., and Blokhina, A.P., *Zh. Prikl. Khim.*, 1984, vol. 57, no. 2, pp. 275–280.
8. Tomashik, V.N. and Sava, A.A., *Zavod. Lab.*, 1987, vol. 53, no. 7, pp. 65.
9. Perevoshchikov, V.A., *Vysokochist. Veshchestva*, 1995, no. 2, pp. 5–29.

ISSN 1070-4272, Russian Journal of Applied Chemistry, 2006, Vol. 79, No. 6, pp. 909–913. © Pleiades Publishing, Inc., 2006.
Original Russian Text © V.F. Travkin, A.V. Antonov, V.L. Kubasov, A.A. Ishchenko, Yu.M. Glubokov, 2006, published in Zhurnal Prikladnoi Khimii, 2006, Vol. 79, No. 6, pp. 920–924.

INORGANIC SYNTHESIS AND INDUSTRIAL INORGANIC CHEMISTRY

Extraction of Rhenium(VII) and Molybdenum(VI) with Hexabutyltriamide of Phosphoric Acid from Acid Media

V. F. Travkin, A. V. Antonov, V. L. Kubasov, A. A. Ishchenko, and Yu. M. Glubokov

Lomonosov State Academy of Fine Chemical Technology, Moscow, Russia

Gintsvetmet Institute, Federal State Unitary Enterprise, State Scientific Center of the Russian Federation, Moscow, Russia

Received March 21, 2005; in final form, March 2006

Abstract—Extraction of rhenium(VII) and molybdenum(VI) from sulfuric, hydrochloric, and nitric acid solutions with hexabutyltriamide of phosphoric acid was studied. The influence exerted on the extraction of Re(VII) and Mo(VI) by the nature and concentration of an acid in the aqueous phase, temperature, time of contact between phases, and concentration of the extracting agent in the organic phase was analyzed. Isotherms of extraction of rhenium(VII) and molybdenum(VI) with solutions of hexabutyltriamide phosphoric acid in kerosene were obtained, the composition of the complexes being extracted was determined, the enthalpies and entropies were evaluated, and the concentration constants of extraction of the metals were found.

DOI: 10.1134/S1070427206060085

A promising way to effectively solve the problem of separation of rhenium(VII) and molybdenum(VI) is application of sorption and extraction methods. At present, the extraction recovery of rhenium(VII) and molybdenum(VI) from solutions of complex salt composition is the most widely used in technological practice [1–4].

Rhenium(VII) is, as a rule, present in real technological solutions containing a rather high concentration of sulfuric acid in the form of the perrhenate ion ReO_4^-. Rhenium(VII) is recovered from solutions of this kind with anion-exchange extracting agents (aliphatic amines and their salts) or neutral reagents [5, 6]. The most effective among the latter are neutral organophosphorus extracting agents and especially trialkylphosphine oxides [7, 8].

Molybdenum(VI) is known to be a frequent accessory of rhenium(VII). Compounds of molybdenum(VI) are strongly different in neutral, weakly acidic, and strongly acidic solutions. For example, molybdenum(VI) is present in solutions with pH ~2–3 as paramolybdate ($Mo_7O_{24}^{6-}$) and metamolybdate ($Mo_8O_{26}^{4-}$) ions. In strongly acidic solutions, molybdenum(VI) forms oxycations MoO_2^{2+}, which tend to polymerize to give polynuclear ($Mo_xO_{x-1}^{2+}$) ions [9]. Apparently, these polyions will markedly differ, when being extracted with anion-exchange and neutral extracting agents, from the monomeric perrhenate ion. This enables extractive separation of rhenium(VII) and molybdenum(VI).

It is of interest to study the possibility of extraction of simultaneously present rhenium(VII) and molybdenum(VI) with organic reagents close in their properties to trialkylphosphine oxide and possessing electron-donor substituents in the form of alkyl-substituted amino groups at the phosphoryl group.

This communication presents data on extraction of rhenium(VII) and molybdenum(VI) from acid solutions with hexabutyltriamide of phosphoric acid, $[(C_4H_9)_2N]_3PO$ (HBTA).

EXPERIMENTAL

The starting aqueous solution was prepared by dissolving a known amount of metal salts, potassium perrhenate ($KReO_4$) and sodium molybdate deca-

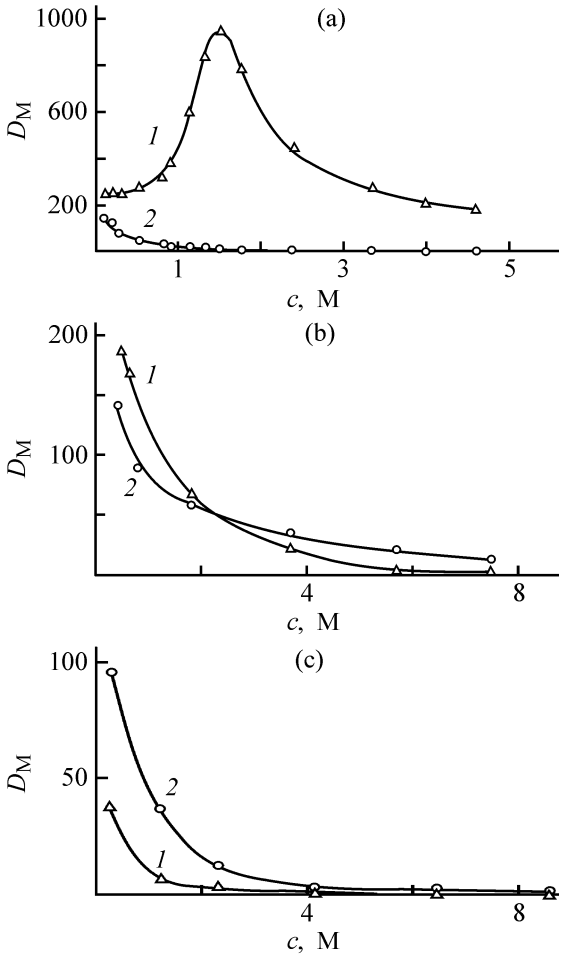


Fig. 1. Effect of the concentration c of (a) sulfuric, (b) hydrochloric, and (c) nitric acids on the extraction of (*1*) rhenium(VII) and (*2*) molybdenum(VI). Initial concentration (M): Re(VII) 5.4×10^{-3} and Mo(VI) 20.8×10^{-3}. Time of contact τ = 5 min, $V_{org} : V_{aq}$ = 1 : 1, 0.3 M solution of HBTA in kerosene; the same for Figs. 2–4. (D_M) Distribution coefficient; the same for Fig. 4.

hydrate ($Na_2MoO_4 \cdot 10H_2O$), both of analytically pure grade, in distilled water. The concentrations of the metals in the solutions did not exceed 5.4×10^{-3} for Re(VII) and 20.8×10^{-3} for Mo(VI). The necessary concentrations of sulfuric, nitric, and hydrochloric acids in the solution prepared were created with the corresponding concentrated acid of analytically pure grade.

Organic solutions of the extracting agent were prepared by diluting concentrated HBTA containing no less than 96–98 wt % main substance with kerosene with a flash point of more than 60°C. All the experiments were performed at 20–25°C with the use of separation funnels.

The number of HBTA molecules contained in the compounds being extracted was found from the logarithmic dependence of the distribution coefficient D_M on $[HBTA]_0$, processed using the least-squares method. In a similar way were found the extraction constants, enthalpies, and entropies. The equilibrium concentrations of the metals were determined by atomic-emission spectroscopy with inductively coupled plasma. The equilibrium concentrations of the acids were found by titration with a standard KOH solution. IR spectra of organic extracts were measured in a KBr cuvette (d = 0.1 mm) at 4000 – 400 cm^{-1} with an Infralyum FT-02 Fourier spectrometer with a resolution of 1 cm^{-1}, manufactured by Lyumeks NPF AP.

This study was concerned with the influence exerted by the concentration of sulfuric, nitric, and hydrochloric acids in the aqueous phase on the extraction of rhenium(VII) and molybdenum(VI) with HBTA (Figs. 1a–1c). Noteworthy are the different ways in which the extractability of rhenium(VII) and molybdenum(VI) vary with the nature and concentration of the acids. The difference observed is presumably due to the dissimilar states of Re(VII) and Mo(VI) in the equilibrium phases and to the extraction of mineral acids at their various concentrations. The extremal distribution of rhenium(VII) and molybdenum(VI) is typically observed in extraction from aqueous solutions of sulfuric, hydrochloric, and nitric acids. The distribution coefficient D for rhenium(VII) at a maximum in the case of extraction from a sulfuric acid solution at its concentration of about 1.5 M. For molybdenum(VI), the maximum value is shifted to the existence region of its anionic forms, i.e., into the region of low acidity. The maximum values of the distribution coefficients for Re(VII) and Mo(VI) in extraction from hydrochloric acid solutions are obtained if the concentration of the acid is less than 1 M. The maximum extent of Re(VII) and Mo(VI) recovery from nitric acid solutions is achieved for even less acid solution than in the case of hydrochloric acid. The observed positions of the maximum extents of recovery of rhenium(VII) and molybdenum(VI) are in a rather good agreement with the series of extrastability of HBTA and mineral acids used to create the acidity of the medium. Because the difference in the extrastability of rhenium(VII) and molybdenum(VI) with HBTA is most completely manifested in extraction from sulfuric acid solutions, it is appropriate to separate these metals in solutions of this acid.

The effect of other parameters on the extraction of rhenium(VII) and molybdenum(VI) was studied under the conditions providing the maximum recovery of rhenium(VII), i.e., at a sulfuric acid concentration of 1.5 M.

Effect of the time of contact between the phases on the extraction of rhenium(VII) and molybdenum(VI) [concentration (M): H_2SO_4 1.5, Re(VII) 5.4×10^{-3}, Mo(VI) 20.8×10^{-3}; $V_{org} : V_{aq} = 1 : 1$; 0.3 M solution of HBTA in kerosene]

Time, min	Metal content $c \times 10^{-3}$, M				D		E, %	
	aqueous phase		organic phase					
	Mo	Re	Mo	Re	Mo	Re	Mo	Re
1	2.10	0.046	19.35	5.87	9	128	90.2	99.2
3	1.40	0.038	20.06	5.88	14	154	93.5	99.4
5	1.36	0.038	20.10	5.88	15	156	93.7	99.4
10	1.57	0.038	19.89	5.88	13	154	92.7	99.4
30	1.59	0.038	19.87	5.88	13	155	92.6	99.4

The rate of extraction is one of the most important parameters. The experimental data (see table) demonstrate that the process of extraction of rhenium(VII) and molybdenum(VI) from solutions of sulfuric acid with HBTA solutions in kerosene has a rather slow kinetics. To attain an extraction equilibrium for Re(VII) and Mo(VI), the phases should be in contact for no less than 5 min. In this case, the recovery E of Mo(VI) and Re(VII) is 93–94 and 99.4%, respectively. Consequently, it is advisable to perform extraction in nearly equilibrium conditions to achieve the maximum recovery and separation of rhenium(VII).

The effect of temperature on the recovery of rhenium(VII) and molybdenum(VI) into the organic phase was considered. It was found that, as the temperature of extraction increases, the extent of recovery of rhenium(VII) and molybdenum(VI) decreases. The temperature dependence $\log D_M - 1/T$ was used to evaluate the enthalpy and entropy of extraction of the metals (Fig. 2). The processing of the results by the least-squares method yielded dependences described by the following equations:

$\log D_{Re(VII)} = 2112/T + 4.98$, correlation coefficient 0.96;

$\log D_{Mo(VI)} = 555.6/T + 0.734$, correlation coefficient 0.99.

For rhenium(VII), $\Delta H^{org} = 40.44 \pm 3.97$ kJ and $\Delta S^{org} = 11.47 \pm 1.12$ J mol^{-1} K^{-1}; for molybdenum(VI), $\Delta H^{org} = -10.64 \pm 1.01$ kJ and $\Delta S^{org} = 1.69 \pm 0.11$ J mol^{-1} K^{-1}. These heat effects of extraction of rhenium(VII) and molybdenum(VI) are in an agreement with the dependence of the heat effects on the distribution constants in extraction of acids, which decrease in the order hydrochloric > rhenic > nitric > sulfuric > molybdenic [10].

Isotherms of rhenium(VII) and molybdenum(VI) extraction with HBTA from aqueous sulfuric acid solutions were measured (Fig. 3). Their run indicates that rhenium(VII) and molybdenum(VI) can be concentrated in the organic phase.

The experimental data on the distribution of rhenium(VII) and molybdenum(VI) were processed by

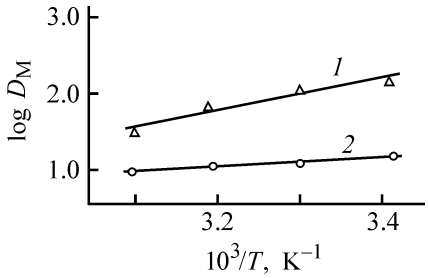


Fig. 2. Distribution coefficient D_M for (*1*) rhenium(VII) and (*2*) molybdenum(VI) vs. temperature T. H_2SO_4 concentration 1.5 M; the same for Figs. 3, 4.

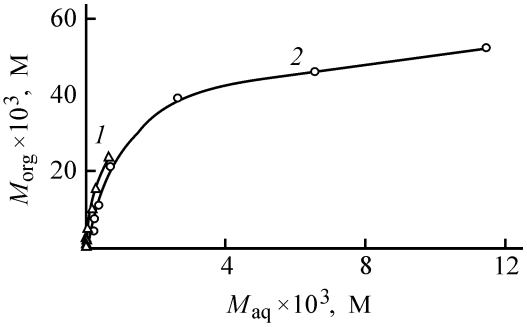


Fig. 3. Isotherms of extraction of (*1*) rhenium(VII) and (*2*) molybdenum(VI). (M_{org}, M_{aq}) Concentrations of Re(VII) and Mo(VI) in the organic and aqueous phases, respectively.

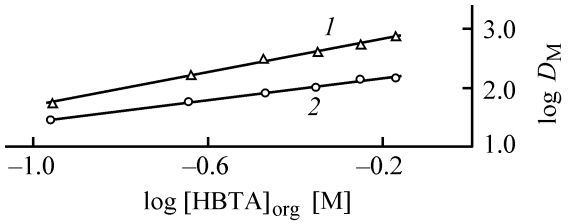


Fig. 4. Effect of the HBTA concentration on the extraction of (*1*) rhenium(VII) and (*2*) molybdenum(VI).

the least-squares method. This yielded the following equations for the extraction isotherms:

$$[Re]_{org} = (156 \pm 14)[Re]_{aq},$$

$$[Mo]_{org} = (29 \pm 2)[Mo]_{aq}.$$

Thus, the concentration constant for the extraction with HBTA is 156 ± 14 for rhenium(VII) and 29 ± 2 for molybdenum(VI).

The composition of the compounds of rhenium(VII) and molybdenum(VI) with HBTA, extracted in the experiments, was determined by the method of the equilibrium shift. The dependence of the distribution coefficients for rhenium(VII) and molybdenum(VI) on the HBTA concentration in extraction from 1–2 M sulfuric acid solutions (Fig. 4) was processed by the least-squares method to give the following equations:

$$\log D_{Re} = (1.41 \pm 0.13)\log[HBTA]_{org} + (3.12 \pm 0.05),$$

$$\log D_{Mo} = (0.93 \pm 0.08)\log[HBTA]_{org} + (2.35 \pm 0.03),$$

where $[HBTA]_{org} = [HBTA]_{in} - q[HReO_4]_{org} - [H_2MoO_2(SO_4)_2]_{org} - [H_2SO_4]_{org}$.

The correlation coefficients for both the equations are 0.99. It follows from the equations that the solvation number is 1.41 ± 0.13 for rhenium(VII) and 0.93 ± 0.08 for molybdenum(VI). These values indicate that rhenium(VII) is presumably extracted as a mixture of a monosolvate and disolvate, and molybdenum(VI), as a monosolvate. It should be kept in mind that, as the concentration of the extracting agent in the organic phase increases, the phase stratification starts to take a noticeably longer time. This somewhat restricts the possibility of using concentrated HBTA solutions for extraction.

Certain conclusions concerning the interactions that occur in the course of extraction can be made on the basis of the whole set of changes in the IR absorption spectra in the range from 4000 to 400 cm^{-1}, in which the characteristic vibrations of metal anions and bonds in the molecule of the extraction agent occur. Therefore, to identify the spectra of the solvates, a comparative analysis of the vibration spectra of solutions of the extracting agents used and of the spectra of extracts containing compounds of rhenium(VII) and molybdenum(VI) with HBTA was made. The samples were studied in a thin layer.

IR spectra of a 0.3 M solution of HBTA in carbon tetrachloride and those of extracts saturated with rhenium(VII) or molybdenum(VI) were analyzed. The extracts were obtained by recovery of the corresponding metal compound from an aqueous solution containing 3 M of hydrochloric acid and 0.08 M of rhenium(VII) or 0.21 M of molybdenum(VI).

The IR spectra of the 0.3 M solutions of HBTA in carbon tetrachloride contain the absorption band ν(P=O) at 1150–1180 cm^{-1}. In the IR spectra of the HBTA extracts saturated with rhenium(VII), this band is shifted to longer wavelengths, 1100–1150 cm^{-1}. A strong absorption band at 905 cm^{-1}, associated with triply degenerated antisymmetric vibrations of the perrhenate ion ReO_4^- having a tetrahedral structure, appears in the IR spectra of the HBTA extracts saturated with rhenium(VII). The fact that this band is not split points to the predominantly ionic nature of bonding between the cationic and anionic parts of the complex being extracted. The IR spectra of the HBTA extracts saturated with molybdenum(VI) contain absorption bands at 930 and 900 cm^{-1}, which correspond to antisymmetric and symmetric stretching vibrations of the Mo=O bond. In addition, the IR spectra of the HBTA extracts with rhenium(VII) and molybdenum(VI) contain bands at 3550–3200 cm^{-1} (antisymmetric and symmetric stretching vibrations of O–H) and 1630–1600 cm^{-1} (deformation vibrations of H–O–H), which belong to water molecules contained in the complexes being extracted. This confirms the assumption that the extraction of rhenium(VII) and molybdenum(VI) occurs by the hydration-solvation mechanism.

The whole body of the data obtained, combined with published evidence [11–13], makes it possible to represent the extraction of rhenium(VII) and molybdenum(VI) with HBTA by the following equations:

$$nS_{org} + H_3O^+ + ReO_4^- + mH_2O \rightleftarrows [H_3O \cdot mH_2O \cdot nS]^+(ReO_4)^-_{org},$$

$$nS_{org} + H_3O^+ + A^{n-} + MoO_2^{2+} + mH_2O \rightleftarrows [H_3O \cdot mH_2O \cdot nS]^+\{MoO_2^{2+}(A^{n-})\}^{(n-2)-}_{org},$$

where S denotes the molecule of the extracting agent, and A^{n-}, the anion of a mineral acid (i.e., SO_4^{2-}, NO_3^-, Cl^-).

CONCLUSIONS

(1) Hexabutyltriamide of phosphoric acid is an effective extracting agent for recovery of rhenium(VII) and molybdenum(VI) from sulfuric acid, hydrochloric acid, and nitric acid solutions.

(2) Solutions of hexabutyltriamide of phosphoric acid in kerosene can be used for extractive separation of rhenium(VII) and molybdenum(VI) from solutions with a high content of sulfuric acid.

REFERENCES

1. Borisova, L.V. and Ermakov, A.N., *Analiticheskaya khimiya elementov. Renii* (Analytical Chemistry of Elements. Rhenium), Moscow: Nauka, 1974.
2. Busev, A.I., *Analiticheskaya khimiya elementov. Molibden* (Analytical Chemistry of Elements. Molybdenum), Moscow: Nauka, 1962.
3. Korovin, S.S., Bukin, V.I., Fedorov, P.I., and Reznik, A.M., *Redkie i rasseyannye elementy: Khimiya i tekhnologiya* (Rare and Scattered Elements: Chemistry and Technology), Moscow: Mosk. Inst. Stali Splavov, 2003, book 3.
4. Ritcey, G.M. and Ashbrook, A.W., *Ekstraktsiya: principy i primenenie v metallurgii* (Solvent Extraction Principles and Application to Process Metallurgy), Moscow: Metllurgiya, 1983.
5. Zelikman, A.N. and Dregan, L., *Zh. Neorg. Khim.*, 1967, vol. 12, no. 1, pp. 261–264.
6. Travkin, V.F., Sinitsyn, N.M., and Merkin, E.N., *Tsv. Metall.*, 1967, no. 24, pp. 21–22.
7. Travkin, V.F., Borisov, V.V., Bol'shakov, K.A., and Sinitsyn, N.M., *Zh. Neorg. Khim.*, 1975, vol. 20, no. 9, pp. 2541–2545.
8. Rozen, A.M., Skotnikov, A.S., and Andrutskii, L.G., *Zh. Neorg. Khim.*, 1982, vol. 27, pp. 732–738.
9. Palant, A.A., Iatsenko, N.A., and Petrova, V.A., *Hydrometallurgy*, 1998, vol. 48, pp. 83–90.
10. Vinetskaya, T.N., Thermochemistry of Extraction of Acids with Amines, *Cand. Sci. Dissertation*, Moscow, 1973.
11. Adamova, A.Zh. and Ponomareva, E.I., *Kompleksn. Ispol'z. Miner. Syr'ya*, 1980, no. 6, pp. 75–77.
12. Vol'dman, G.M. and Zelikman, A.N., *Zh. Neorg. Khim.*, 1993, vol. 38, no. 7, pp. 1234–1246.
13. Keshavarz Alamdari, E. and Sadrnezhaad, S.K., *Hydrometallurgy*, 2000, vol. 55, pp. 327–341.

ISSN 1070-4272, Russian Journal of Applied Chemistry, 2006, Vol. 79, No. 6, pp. 914–919. © Pleiades Publishing, Inc., 2006.
Original Russian Text © A.G. Kasikov, A.M. Petrova, 2006, published in Zhurnal Prikladnoi Khimii, 2006, Vol. 79, No. 6, pp. 925–929.

INORGANIC SYNTHESIS AND INDUSTRIAL INORGANIC CHEMISTRY

Recovery of Rhenium(VII) with Triisooctylamine from Sulfuric Acid Solutions

A. G. Kasikov and A. M. Petrova

Tananaev Institute of Chemistry and Technology of Rare Elements and Mineral Resources, Kola Scientific Center, Russian Academy of Sciences, Apatity, Murmansk oblast, Russia

Received March 23, 2006

Abstract—Extraction recovery of rhenium(VII) with triisooctylamine from model sulfuric acid solutions was studied. The effect of the composition of the organic and aqueous phases on the recovery of rhenium(VII) was analyzed, and the composition of rhenium(VII) complexes in the organic phase was determined. The possibility of effective re-extraction of rhenium(VII) from triisooctylamine with ammonia solutions was demonstrated.

DOI: 10.1134/S1070427206060097

Rhenium is one of the most needed rare elements; the demand for rhenium has markedly increased recently because of its larger-scale consumption in manufacture of refractory alloys [1, 2]. The main sources of rhenium are solutions of washing sulfuric acid, in which rhenium concentrated is in catching of roaster gases formed in pyrometallurgical processing of molybdenum, copper, and copper-nickel ores [2–5].

The method of liquid extraction is widely used in practice for recovery of rhenium(VII) from industrial washing sulfuric acid solutions, with mixtures containing trialkylamine used as extracting agents in most cases [2–8]. The extraction of rhenium(VII) with tertiary amines of normal structure was also studied in [9–14].

Data on application of tertiary amines of branched structure, which are industrial extracting agents [15], for recovery of rhenium(VII) are exceedingly scarce [5, 16].

In view of the fact that the extracting capacity of branched amines may markedly differ from that of similar compounds of normal structure [17–19] and sulfuric acid solutions are frequently used in practice, the present study was aimed to examine the extraction of rhenium(VII) from H_2SO_4 solutions with mixtures containing triisooctylamine.

EXPERIMENTAL

As extracting agent served solutions containing 5–30 vol % industrial triisooctylamine (TIOA) of Hostarex A 324 brand (no less than 95% main substance and up to 5% primary and secondary amines) in a Escaid 100 diluent with addition of 20–70 vol % isomeric aliphatic alcohols (1-octanol or 2-ethyl-hexanol-1 of pure grade).

The extracting agent was preliminarily converted into the salt form via contact with a H_2SO_4 solution of the same concentration as a solution of rhenium, from which the extraction was performed.

Model rhenium-containing solutions were prepared by dissolution of ammonium perrhenate in distilled water, with addition of a necessary amount of chemically pure sulfuric acid. The concentration of rhenium(VII) was varied from 0.001 to 0.036 M, and that of sulfuric acid, from 0.1 to 9 M.

The extraction was performed in separatory funnels at a volume ratio of the organic to aqueous phase equal to 1 : 25 at room temperature in the course of 5 min, which provided that equilibrium was attained by the system.

The content of rhenium(VII) in the aqueous phase was determined spectrophotometrically from the coloration intensity of the thiourea complex of rhenium(IV), formed in the presence of Sn(II) as reducing agent. The light absorption was measured with a KFK-3 photoelectric colorimeter at a wavelength λ = 390 nm [20] or by the atomic-emission method on a Plazma 400 spectrometer. The content of rhenium in the organic phase was calculated as the difference of its contents in the aqueous phase before and after extraction.

Industrial extracting agents based on tertiary amines are solutions of amine in a nonpolar organic solvent (commonly, kerosene), with addition of a modifier that precludes formation of a third phase. Changing the relative amounts of components in organic mixtures of this kind strongly affects their extraction capacity, and, therefore, the effect of the composition of the organic phase on the recovery of rhenium(VII) was studied in the first place.

Apparently, the extraction capacity of a mixture is most affected by the content of the active component in it. For example, it is known that, if tributylphthalate (TBP) is diluted, its extraction capacity for rhenium(VII) considerably decreases [10]. For extracting agents belonging to the class of tertiary amines, published data are contradictory [7, 9–11]. The present study demonstrated that, as the content of TIOA in the extracting mixture is raised from 5 to 30%, the distribution coefficient D_{Re} of rhenium(VII) steadily increases (Fig. 1). Consequently, more effective recovery of rhenium(VII) requires mixtures with higher amine concentration. However, concentrated solutions of the sulfate salt of TIOA are highly viscous and, therefore, organic mixtures with TIOA content not exceeding 35% can be recommended for practical application, whereas the extracting agents presently used to recover rhenium(VII) from industrial solutions commonly contain no more than 10% tertiary amine [7, 8].

The type and content of a modifier in the extracting mixture also largely determine its properties. As a rule, polar organic solvents (higher alcohols, ketones, TBP, etc.) are used as modifiers. In this study, isomers of octyl alcohol served for this purpose.

High-molecular-weight aliphatic alcohols, as a rule, suppress extraction of metals [21], which is due to solvation of a part of amine salt anions with alcohol molecules. At the same time, just this process diminishes the association of the amine salt, thereby raising its solubility and precluding formation of a third phase in the extracting agent [22]. In addition, aliphatic alcohols can themselves recover rhenium(VII) from sulfuric acid solutions with a rather high distribution coefficient [23, 24]. As shown experimentally, the volume ratio amine : octyl alcohol in the extracting mixture based on TIOA should be no less than 2 : 1. The structure of an alcohol affects the extraction capacity of TIOA for rhenium(VII) as follows: 1-octanol suppresses the extraction of rhenium(VII) to a greater extent than does 2-ethyl-1-hexanol (Fig. 1). This is probably due to the fact that, being a more electrophilic reagent, 1-octanol, an alcohol of linear structure, more strongly solvates anions of TIOA sulfate [22] as compared with octyl alcohol with a hydrocarbon radical of branched structure. On the whole, an increase in the concentration of an alcohol in the extracting mixture only slightly diminishes the distribution coefficient for rhenium(VII) via solvation of amine molecules (Fig. 2).

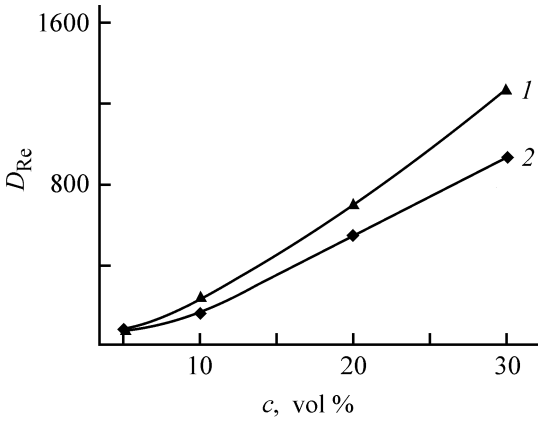


Fig. 1. Effect of the TIOA content in the organic phase on the distribution coefficient of rhenium(VII). (D_{Re}) Distribution coefficient of Re(VII) and (c) content of TIOA. Starting aqueous phase: Re(VII) 200 mg l^{-1}, H_2SO_4 4 M. Composition of the extracting agent (vol %): 5–30 TIOA and (*1*) 20 2-ethyl-1-hexanol or (*2*) 20 1-octanol.

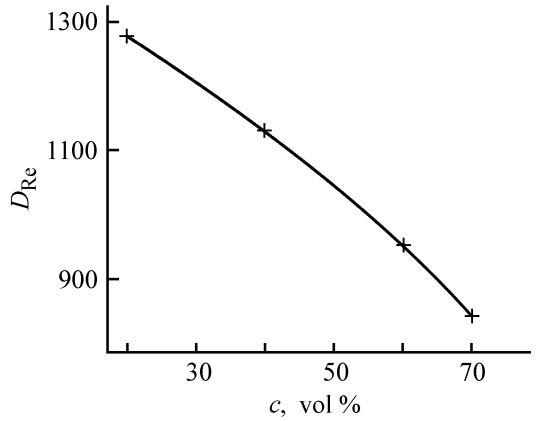


Fig. 2. Effect of the content c of 2-ethyl-1-hexanol in the organic phase on the distribution coefficient D_{Re} of rhenium(VII). Composition of the extracting agent (vol %): 30 TIOA and 20–70 2-ethyl-1-hexanol.

In addition, it was found that the concentration of a modifier in the extracting agent affects the composition of rhenium(VII) solvates formed in the organic phase in extraction with TIOA. The solvation numbers determined by the method of the equilibrium shift [10] from the slope of the straight lines corresponding to

Table 1. Solvation numbers of rhenium(VII) in the organic phase in recovery with extracting mixtures of various compositions, containing 5–30 vol % TIOA

Composition of the extracting agent	Solvation number n	Composition of the extracting agent	Solvation number n
TIOA + 20 vol % 1-octanol in Escaid 100	1.45	TIOA in 1-octanol	1.25
TIOA + 20 vol % 2-ethyl-1-hexanol in Escaid 100	1.68	TIOA in 2-ethyl-1-hexanol	1.37

the dependence $\log c_{TIOA}$–$\log D_{Re}$ (Fig. 3) for organic complexes of rhenium(VII) in extraction with mixtures containing different amounts of alcohols are listed in Table 1. As the content of octyl alcohol in the mixtures increases, the ratio TIOA : Re in the solvate decreases from ~1.5 to ~1.3. Consequently, the degree of polymerization of the TIOA salt in the extracting agent decreases as the content of the modifier becomes lower.

It should be noted that similar values of the solvation numbers were obtained in another way, by the saturation method, for extracting mixtures containing 30% TIOA and 20 or 70% 1-octanol (~1 and ~1.4, respectively).

In addition to the composition of the extracting agent, the factors that strongly affect the equilibrium of the extraction process include its conditions and the composition of the aqueous phase.

One of the most important technological parameters of the extraction process is the ration between the volumes of the organic and aqueous phases. It is known that the phase volume ratio affects the efficiency of extraction of rare-earth elements with TBP [25]. No published data of this kind are available for extracting agents belonging to the class of tertiary amines. Therefore, a set of experiments were performed, which demonstrated that the distribution coefficient of rhenium(VII) varies with the Org : Aq ratio in extraction of the metal with a mixture of TIOA and 1-octanol. As, in particular, the volume ratio of the organic and aqueous phases is changed from 1 : 1 to 1 : 100 for a 30% solution of TIOA in octyl alcohol, D_{Re} decreases by approximately a factor of 5 (Fig. 4), which corresponds to a decrease in the recovery of ReO_4^- into the organic phase from 99.8 to 51.2%. However, the value of D_{Re} remains large (about 100) even at Org : Aq = 1 : 100, which enables practical use of TIOA in a wide range of Org : Aq ratios, with extracts with high concentration of rhenium obtained.

The parameters of rhenium(VII) extraction with solutions of tertiary amines are noticeably affected by the composition of the aqueous phase [7, 9–11, 16]. The largest contribution to this process is made by the acidity of the starting aqueous phase [2, 7, 9–11, 22]. This can be probably attributed to the ability of extracting agents of this kind to extract the acid from solutions, in addition to rhenium(VII) [24, 26]. How-

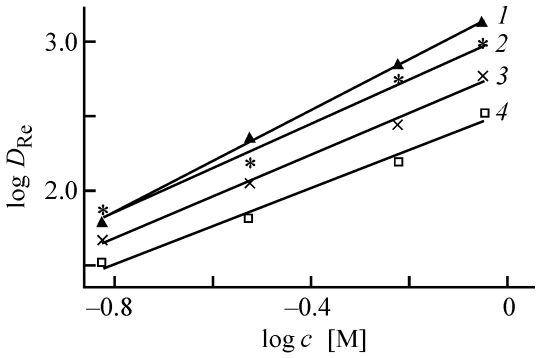


Fig. 3. Distribution coefficient D_{Re} of rhenium(VII) vs. concentration c of TIOA in the organic phase, plotted in the log–log coordinates for extracting agents of various compositions. Composition of the extracting agent (vol %): 5–30 TIOA and (*1*) 20 2-ethyl-1-hexanol or (*2*) 10 1-octanol in (*3*) 2-ethyl-1-hexanol or (*4*) 1-octanol.

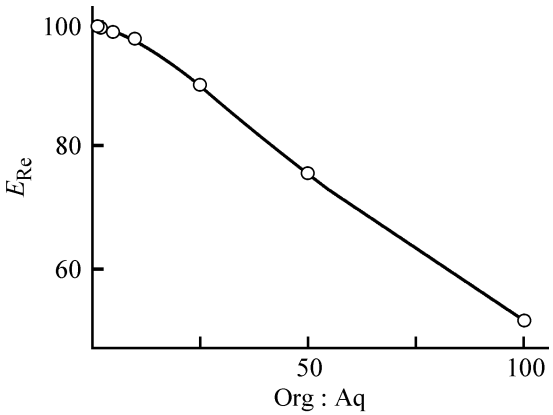


Fig. 4. Effect of the Org : Aq ratio on the recovery E of rhenium(VII) in extraction with 30 vol % TIOA in 1-octanol. Starting aqueous phase: Re(VII) 1.3 g l^{-1} and H_2SO_4 4 M. Composition of the extracting agent: 30 vol % TIOA in 1-octanol.

Table 2. Effect of the phase ratio and concentration of NH_4OH on the recovery E of rhenium(VII) from a 30% solution of TIOA in 2-ethyl-1-hexanol, washed with water to remove H_2SO_4 [$c(Re)_{org}$ = 2.85 g l^{-1}, $c(Re)_{re\text{-}extr}$ is the concentration of Re in the re-extract]

Org : Aq	3 N NH_4OH			6 N NH_4OH		
	E, %	$c(Re)_{re\text{-}extr}$, g l^{-1}	pH of the re-extract	E, %	$c(Re)_{re\text{-}extr}$, g l^{-1}	pH of the re-extract
1 : 5	95.9	0.55	10.7	97.61	0.56	11.1
1 : 1	90.6	2.58	9.9	92.28	2.63	10.5
2 : 1	88.4	5.03	9.1	89.68	5.10	10.1
5 : 1	0.08	0.024	7.52	0.92	0.13	8.06

ever, the relevant published data are contradictory, with authors reporting incomparable dependences of D_{Re} on the concentration of sulfuric acid in extraction with tertiary amines [7, 9–11, 16, 22].

The present study demonstrated that, as the H_2SO_4 concentration in the starting solution increases from 0.1 to 9 M in extraction with 30% TIOA, the distribution coefficient of rhenium(VII) decreases, with this decrease being the most pronounced at 0.1–1 M H_2SO_4 (Fig. 5). Similar results were obtained in [7, 27] in the case of Re(VII) extraction with tri-*n*-octylamine (TOA).

The decrease in D_{Re} on passing from weakly acidic to more concentrated solutions is probably due to a change in the state of the TIOA salt in the organic phase under conditions of an increasing concentration of H_2SO_4 in the aqueous phase. For example, it has been reported [26] that three forms of TOA sulfate exist at the equilibrium concentration of the acid in the aqueous phase equal to 0.1–0.5 M, and virtually the whole amount of TOA is converted into the hydrosulfate form at a sulfuric acid content of 2–3 M. The strongest decrease in D_{Re} can be attributed to differences in the extraction capacities of different sulfate forms of the amine for rhenium(VII). As for the gradual decrease in the distribution coefficient of Re(VII) with further increase in the concentration of sulfuric acid, it can be readily accounted for by the competing extraction of the acid by the amine, which hinders the extraction of rhenium(VII).

D_{Re} is affected not only by the acidity of the aqueous phase, but also by the concentration of ReO_4^- in the starting solution. It was found that raising the concentration of rhenium(VII) in the starting solution from 200 mg l^{-1} to 7 g l^{-1} in extraction with 30% TIOA leads to a more than fivefold decrease in the distribution coefficient. Accordingly, the degree of recovery falls from 93 to 23% (Fig. 6). Probably, such a dependence is due to a limited capacity of the extracting agent for rhenium(VII).

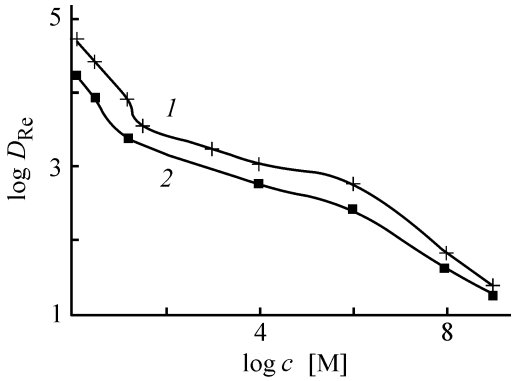


Fig. 5. Effect of the concentration c of sulfuric acid in the starting aqueous phase on the distribution coefficient D_{Re} of rhenium(VII). Starting aqueous phase: Re(VII) 200 mg l^{-1} and H_2SO_4 0.1–0.9 M. Composition of the extracting agent (vol %): (*1*) 30 TIOA + 20 2-ethyl-1-hexanol and (*2*) 2-ethyl-1-hexanol.

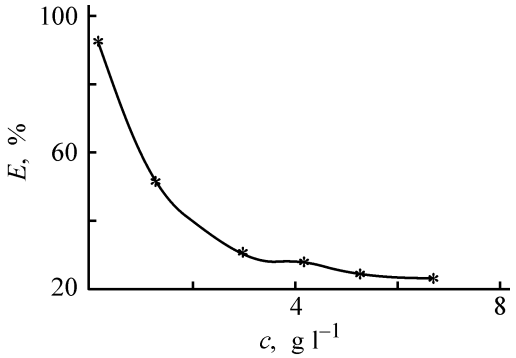


Fig. 6. Effect of the concentration of rhenium(VII), c_{Re}, in the starting aqueous phase on its recovery E from acid sulfate solutions. Starting aqueous phase: Re(VII) 0.2–6.7 g l^{-1} and H_2SO_4 4 M. Composition of the reagent: 30 vol % TIOA in 1-octanol.

An additional important characteristic of an extracting agent is its regeneration capacity. Rhenium(VII) is commonly re-extracted from tertiary amines of normal structure with ammonia solutions [20]. It was found that efficient re-extraction of rhenium(VII) from TIOA with ammonia solutions occurs, after its washing to remove sulfuric acid, under conditions providing a pH of no less than 9 in the re-extracts. It can be seen in Table 2 that, depending on the process conditions, a degree of re-extraction of up to 97.6% can be reached in a single stage to give solutions containing up to 5 g l^{-1} of rhenium.

Apparently, the concentration of rhenium(VII) can be additionally raised in the case of a counterflow re-extraction, and the solutions obtained can be further used to obtain ammonium perrhenate.

CONCLUSIONS

(1) Organic mixtures based on TIOA are effective extracting agents of rhenium(VII) from a sulfuric acid medium in a wide range of concentrations of both the organic and aqueous phases. ReO_4^- is best recovered from weakly acid solutions of rhenium(VII) with extracting mixtures that contain the maximum amount of TIOA (30–35 vol %) and the minimum amount of a modifier (15–20 vol % octyl alcohol).

(2) The distribution coefficient of rhenium(VII) in extraction with TIOA grows as the concentration of rhenium(VII) in solution decreases and the ratio between the organic and aqueous phases increases.

(3) The composition of the complex being extracted depends on the type and concentration of octyl alcohol. The complex contains 1.2–1.7 TIOA molecules per each perrhenate ion, and the solvation number decreases as the alcohol concentration becomes higher.

(4) Deep ammonia re-extraction of rhenium(VII) from TIOA can be performed to give concentrated solutions of ammonium perrhenate.

ACKNOWLEDGMENTS

The study was financially supported by the Program "Leading Scientific Schools" (project. no. NSh-4383.2006.3).

REFERENCES

1. Kablov, E.N., *Vestn. Mos. Gos. Univ., Ser. Khim.*, 2005, vol. 46, no. 3, pp. 155–157.
2. Korovin, S.S., Bunin, V.I., Fedorov, P.I., and Reznik, A.M., in *Khimiya i tekhnologiya* (Chemistry and Technology), 2003, book 3.
3. Reznichenko, V.A., Palant, A.A., and Solov'ev, V.I., *Kompleksnoe ispol'zovanie syr'ya v tekhnologii tugoplavkikh metallov* (Integrated Use of Raw Materials in the Technology of Refractory Metals), Moscow: Nauka, 1988.
4. Troshkina, I.D., Recovery of Rhenium from Raw Materials with Low Content of the Metal, *Doctoral Dissertation*, Moscow, 2003.
5. Kasikov, A.G., Areshina, N.S., Kudryakov, M.V., and Khomchenko, O.A., *Khim. Tekhnol.*, 2004, no. 6, pp. 25–31.
6. Stepanov, A.V., Palant, A.A., Reznichenko, V.A., et al., *Tsvetn. Met.*, 1979, no. 19, pp. 42–44.
7. Gladyshev, V.P., Andreeva, N.N., Kovaleva, S.V., et al., *Zh. Prikl. Khim.*, 1985, no. 7, pp. 1462–1466.
8. Abisheva, Z.S. and Zagorodnyava, H.N., *Hydrometallurgy*, 2002, vol. 63, pp. 55–63.
9. Zaitsev, A.A., Lebedev, I.A., Pirozhkov, S.V., and Yakovlev, G.N., *Zh. Prikl. Khim.*, 1963, vol. 8, no. 9, pp. 2184–2186.
10. Zelikman, A.N. and Dregan, L., *Zh. Prikl. Khim.*, 1967, vol. 12, no. 1, pp. 261–268.
11. Brodskaya, G.A., Gureev, E.S., and Gapurova, O.I., *Radiokhimiya*, 1988, vol. 30, no. 6, pp. 709–774.
12. Volk, V.I. and Vakhrushin, A.Yu., *Tsvetn. Met.*, 1988, nos. 11–12, pp. 18–21.
13. Abisheva, Z.S., Bodnar', N.M., Bukurov, T.N., et al., *Tsvetn. Met.*, 1994, no. 9, pp. 33–35.
14. Kasikov, A.G., Areshina, N.S., and Gromov, P.B., *Tsvetn. Met.*, 2000, no. 10, pp. 19–22.
15. Mezhov, E.A., *Ekstraktsiya aminami i chetvertichnymi ammonievymi osnovaniyami: Spravochnik* (Extraction with Amines and Quaternary Ammonium Bases: Reference Book), Moscow: Energoatomizdat, 1999.
16. Kertes, A.S. and Beck, A., *J. Chem. Soc.*, 1961, no. 5, pp. 1921–1930.
17. Shmidt, V.S. and Mezhov, E.A., *Usp. Khim.*, 1965, vol. 34, no. 8, pp. 1988–1415.
18. Vol'dman, G.M. and Zelikman, A.N., *Teoriya gidrometallurgicheskikh protsessov* (Theory of Hydrometallurgical Processes), Moscow: Ingermet Inzhiniring, 2003.
19. Akimova, I.D., Nikonov, V.I., Sokal'skaya, L.I., et al., Abstracts of Papers, *XIII Rossiiskaya konferentsiya po ekstraktsii* (XIII Russian Conf. on Extraction), Moscow, part 1, pp. 105–106.
20. Borisova, L.V. and Ermakov, A.N., *Analiticheskaya khimiya reniya* (Analytical Chemistry of Rhenium), Moscow: Nauka, 1974.
21. Medkov, M.A. and Steblevskaya, I.I., *Vliyanie modifikatorov na ekstraktsiyu metallov* (Effect of Modifiers on Extraction of Metals), Available from Inst. Khim.

Dal'nevost. Otd. Ross Akad. Nauk, 1995, Vladivostok, no. 1827, B 95.

22. Shmidt, V.S., *Ekstraktsiya aminami* (Extraction with Amines), Moscow: Atomizdat, 1970.
23. Travkin, V.F., Kubasov, V.L., Ishchenko, A.A., et al., *Tsvetn. Met.*, 2005, no. 1, pp. 5–10.
24. Kasikov, A.G. and Petrova, A.M., *Materialy mezhdunarodnoi naucho-tekhnicheskoi konferentsii "Nauka i obrazovanie – 2005", Murmansk, 6–14 aprelya 2005 g., Chast' V* (Proc. Int. Sci.-Pract. Conf. "Science and Education 2005," Murmansk, April 6–14, 2005), Murmansk: Murm. Gos. Tekhn. Univ., 2005, part V, pp. 166–169.
25. Reznik, A.M. and Semenov, S.A., *Trudy Mos. Khim.-Tekhnol. Inst. im. D.I. Mendeleeva "Khimiya i tekhnologiya redkikh metallov"* (Trans. Mendeleev Inst. Chem. Eng., Moscow, "Chemistry and Technology of Rare Metals"), 1986, issue 143, pp. 54–56.
26. Shmidt, V.S. and Shesterikov, V.N., *Radiokhimiya*, 1968, vol. 10, no. 3, pp. 314–319.
27. Malek, Z., Ianovich, E., and Zaitseva, N.G., *Radiokhimiya*, 1968, vol. 10, no. 3, pp. 359–362.

ISSN 1070-4272, Russian Journal of Applied Chemistry, 2006, Vol. 79, No. 6, pp. 920–923. © Pleiades Publishing, Inc., 2006.
Original Russian Text © A.D. Budaeva, E.V. Zoltoev, V.D. Tikhova, N.V. Bodoev, 2006, published in Zhurnal Prikladnoi Khimii, 2006, Vol. 79, No. 6, pp. 930–933.

SORPTION AND ION-EXCHANGE PROCESSES

Interaction of Heavy Metal Ions with Ammonium Humates

A. D. Budaeva, E. V. Zoltoev, V. D. Tikhova, and N. V. Bodoev

Baikal Institute of Nature Management, Siberian Division, Russian Academy of Sciences, Ulan-Ude, Buryatiya, Russia

Institute of Organic Chemistry, Siberian Division, Russian Academy of Sciences, Novosibirsk, Russia

Received February 10, 2006

Abstract—Sorption properties of ammonium humates with respect to Fe(III), Cu(II), Al(III), Ni(II), Pb(II), and Zn(II) are studied. The effect of the metal ion concentration on the ammonium humate consumption is examined and the corresponding dependences are analyzed using regression equations. The IR spectra of brown coal humic acids, ammonium humates, as well as Fe, Cu, Ni, Zn, Pb, and Al humates are presented.

DOI: 10.1134/S1070427206060103

Humic acids (HAs) are polyfunctional high-molecular-weight compounds with fairly high reactivity caused by the presence of the carboxy, hydroxy, amino, carbonyl, and other groups in their structure. These compounds can form stable complexes with heavy metal ions and, therefore, can be used for recovery of heavy metals from galvanic and metallurgic wastewaters.

In this study, we examined the interaction of ammonium humates with Fe(III), Cu(II), Al(III), Ni(II), Pb(II), and Zn(II), using IR spectroscopy and chemical analysis.

EXPERIMENTAL

The starting material for preparation of ammonium humates was oxidized brown coal from the Gusinoozersk deposit. The HA content in this coal ranges from 70 to 90%. Humic acids were extracted with 1% aqueous NH_4OH (s : l = 1 : 20).

To study the interaction of ammonium humates with metal ions, we used solutions prepared from $FeCl_3 \cdot 6H_2O$, $CuSO_4 \cdot 5H_2O$, $Ni(NO_3)_2 \cdot 6H_2O$, $Zn(CH_3COO)_2 \cdot 2H_2O$, $Pb(NO_3)_2$, and $KAl(SO_4)_2 \cdot 12H_2O$ [concentration 100–1000 mg l^{-1} (in terms of the metal)] and aqueous ammonium humate (20 g l^{-1}). Sorption was carried out in the static mode with stirring for 15 min at 20°C. A precipitate of ammonium humate was separated by filtration trough a paper filter and washed with a small amount of distilled water. The volume of the filtrate was adjusted to a fixed value (resulting filtrate was a transparent yellowish solution). The metal ion concentration in the mother liquor was determined photocolorimetrically [1]. The weak coloration of the mother liquor virtually did not interfere with the photometric determinations.

The degree of recovery of the metals, X (%), was estimated from the difference between the initial and equilibrium concentrations:

$$X = (c_0 - c_{eq})/c_0,$$

where c_0 and c_{eq} are the initial and equilibrium concentrations of the metal ions, respectively (mg l^{-1}).

In this study, we examined the dependence of the optimal consumption of the humate on the metal ion Fe(III), Cu(II), Al(III), Ni(II), Pb(II), and Zn(III), concentrations at pH 1–2. As the optimal consumption P we regarded the minimum amount of the sorbent required to recover metal ions to the maximum extent under given conditions. The results are summarized in the table.

Sorbent consumption at various concentrations of Fe(III), Cu(II), Al(III), Ni(II), Zn(II), and Pb(II)

Concentration, mg l^{-1}	Sorbent consumption, g l^{-1}	Degree of recovery, %	Concentration, mg l^{-1}	Sorbent consumption, g l^{-1}	Degree of recovery, %
Fe^{3+}:			Ni^{2+}:		
100	2.4	95.98	100	2.1	41.85
300	7.0	97.44	300	6.4	63.33
500	14.0	99.05	500	11.0	69.52
700	18.0	99.22	700	15.0	73.76
1000	25.0	98.70	1000	22.0	78.98
Cu^{2+}:			Zn^{2+}:		
100	2.4	21.49	100	2.0	35.64
300	7.0	39.86	300	6.5	59.48
500	13.0	38.65	500	11	68.63
700	16.0	54.02	700	15.5	74.96
1000	24.0	69.91	1000	22.0	75.35
Al^{3+}:			Pb^{2+}:		
100	4.0	61.82	100	0.8	25.47
300	14.0	86.78	300	2.5	53.36
500	24.0	98.06	500	4.1	76.95
700	32.0	97.31	700	5.8	83.55
1000	48.0	96.35	1000	8	87.10

The experimental data obtained in these experiments were processed by the least-squares method [2]. Over the metal concentration range 100–1000 mg l^{-1}, the experimental dependences are linear with a 99.0% probability (Fig. 1).

The sorption capacity of ammonium humate with respect to metal ions is as follows: Fe(III) 58 mg g^{-1} (3.1 mg-equiv g^{-1}), Cu(II) 31 mg g^{-1} (0.97 mg-equiv g^{-1}), Ni(II) 35 mg g^{-1} (1.2 mg-equiv g^{-1}), Zn(II) 36 mg g^{-1} (1.1 mg-equiv g^{-1}), Pb(II) 119 mg g^{-1} (1.15 mg-equiv g^{-1}), and Al(III) 24 mg g^{-1} (2.7 mg-equiv g^{-1}). Note that adsorption of the metal ions is accompanied by neutralization of the acidic solutions.

The humate provides a high degree of recovery (96–99%) of Al(III) and Fe(III) from water. The recovery of lead is 87%, while that of copper, nickel, and zinc is slightly lesser (70–78%). Thus, the recovery of the metal ions decreases in the order Fe(III) > Al(III) > Pb(II) > Ni(II) > Zn(II) > Cu(II). In the case of an iron-containing solution, water was completely clarified with the humate, whereas in the presence of other cations, some coloration remained, caused by the formation of water-soluble metal humates through chelation with electron-donor groups of the humate. The FTIR spectra of the humic acids and metal humates (Fig. 2) confirm the formation of metal humate complexes.

The spectra of brown coal humic acids and humates of ammonium and heavy metals show the ab-

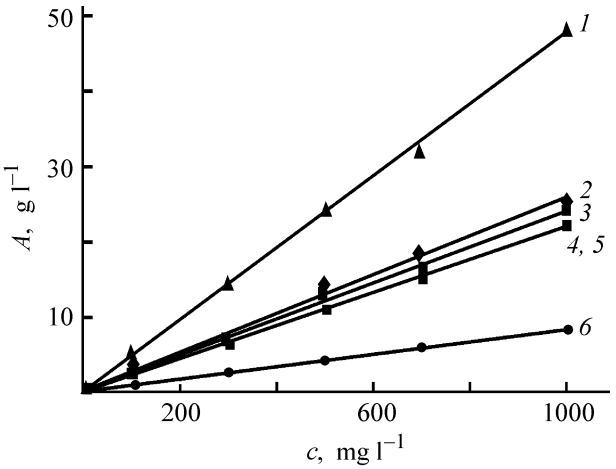


Fig. 1. Optimal consumption of ammonium humate A vs. the metal concentration in the initial solution c: (*1*) Al(III), (*2*) Fe(III), (*3*) Cu(II), (*4*, *5*) Zn(II) and Ni(II), and (*6*) Pb(II). Coefficients b of the regression equations ($P = bc_{Me}$) for estimating the optimal consumption of the sorbent: Al(III) 0.0473, Fe(III) 0.0255, Cu(II) 0.0239, Zn(II) 0.022, Ni(II) 0.022, and Pb(II) 0.0081.

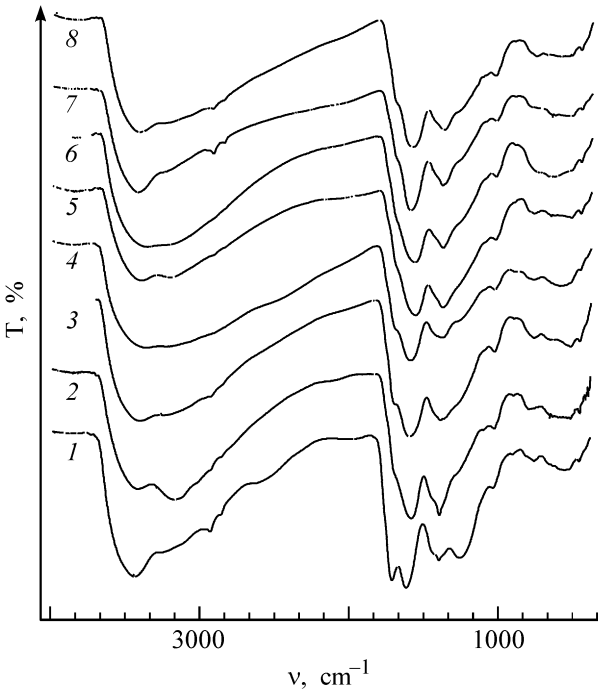


Fig. 2. IR spectra of (*1*) humic acids from the Kholbol'dzhinskoe deposit and humates of (*2*) ammonium, (*3*) iron, (*4*) aluminum, (*5*) lead, (*6*) nickel, (*7*) zinc, and (*8*) copper. (T) Transmittance and (ν) wavenumber.

sorption band at 3450–3300 cm^{-1} (H-bonded hydroxy groups) (Fig. 2). In the range 690–400 cm^{-1}, the samples of the humic compounds show weak absorption bands, presumably associated with the mineral fraction, but not organic structures [3]. The signature of aromatic structures is observed as the bands near 1600 (C=C skeleton vibrations) and at 773 (C–H out-plane bending vibrations). The bands at 1050–910 cm^{-1} are assigned to ether clay minerals or some phenoxy structures (aromatic CCH moieties in ordinary or condensed rings, or substituted phenolic and hydrocarbon structures). Asymmetric and symmetric stretching vibrations of the $-CH_2$ groups are observed at 2925–2935 and 2855 cm^{-1}. As a shoulder, these bands are found in the spectra of iron, ammonium, and lead humates. In the spectra of nickel and aluminum humates, these bands are unnoticeable or concealed by the broad absorption band of the hydroxy groups.

In the spectra of humic acids, the characteristic bands at 1720–1700 (vibrations of the carbonyl groups) and 1250–1270 cm^{-1} (C–O stretching vibrations or OH bending vibrations) are assigned to the carboxy groups.

Treatment of humic acid with ammonium hydroxide resulted in predictable changes in the IR spectra, caused by the conversion of free carboxy groups into the carboxylate form. The IR spectrum of ammonium humate shows a new strong band at 3174 cm^{-1} as well as a band at 1400 cm^{-1} whose intensity is higher than in the spectrum of humic acid. These bands are assigned to the N–H vibrations of ammonium. The bands of the carboxy groups (1714 and 1267 cm^{-1}) disappear, which is generally due to their transformation into the carboxylate groups. In this case, new bands of carboxylate appear at 1610–1550 and 1420–1300 cm^{-1}, which are not resolved because of the superposition with other bands. Additionally, the band at 1616 cm^{-1} shifts to 1589 cm^{-1} (C=C skeleton vibrations in arenes), which can be attributed to the superposition with a new band of carboxylate. The expected band of carboxylate at 1400 cm^{-1} is not resolved because of the superposition with the strong band due to N–H vibrations in the ammonium cation.

The spectra of the heavy metal humates show a low-frequency shift and decrease in the intensity of the band at 1400 cm^{-1} (symmetric stretching vibrations of COO^-). The band at 1589 cm^{-1} (asymmetrical stretching vibrations of COO^-) shifts also, suggesting the substitution of the ammonium ions by heavy metal ions in the carboxylate. The slight splitting of the bands at 1379–1398 cm^{-1} in Fe, Zn, and Cu humates, and of the band at 1569–1570 cm^{-1} in the Pb salt can be assigned to vibrations in the metal carboxylate COOMe (Me is a heavy metal) and carbonyl group, weakened by the resonance between the C–O–M and C=O...M structures [4]. It is quite possible that the metal humate structures contain β-diketone fragments ($-CO-CH_2-CO-$) whose carbonyl groups are coordinated to the metal cations. The appearance of the band near 3200 cm^{-1} in the spectra of Fe, Pb, and Al humates can be attributed to the formation of coordination polymers. These metal ions tightly cross-link the humate macromolecules to give poorly soluble metal humates, providing efficient water treatment. In the spectra of Cu, Ni, and Zn humates, this band appears as a shoulder. Evidently, the resulting polymeric associates are less stable than those of Fe, Al, and Pb.

CONCLUSIONS

(1) In treating water to remove Fe(III), Cu(II), Al(III), Ni(II), Pb(II), and Zn(II), the consumption of ammonium humate linearly increases with increasing metal ion concentration.

(2) The maximum decontamination efficiency with humates is 96–99% for Fe(III) and Al(III), 87% for Pb(II), and 70–78% for Cu(II), Zn(II), and Ni(II). The recovery of the metal ions decreases in the order Fe(III) > Al(III) > Pb(II) > Ni(II) > Zn(II) > Cu(II).

(3) The IR spectra of the metal humates show that Fe, Al, and Pb form more stable polymeric associates as compared to Zn, Cu, and Ni, providing an explanation for the observed higher efficiency of decontamination to remove Fe(III), Al(III), and Pb(II).

REFERENCES

1. Charlot, G., *Les Methods de la Chemie Analytique. Analyse quantitative Minerale, Quatrieme Edition*, Paris: Masson, 1961.
2. Lupeiko, T.G., Gorbunova, M.O., and Bayan, E.M., *Zh. Prikl. Khim.*, 2004, vol. 77, no. 1, pp. 83–86.
3. *Applied Infrared Spectroscopy*, Kendall, D.N., Ed., New York: Reinhold, 1966.
4. Bellamy, L.J., *The Infra-red Spectra of Complex Molecules*, New York: Wiley, 1957.

ISSN 1070-4272, Russian Journal of Applied Chemistry, 2006, Vol. 79, No. 6, pp. 924–929. © Pleiades Publishing, Inc., 2006.
Original Russian Text © A.P. Suponina, L.G. Kolzunova, M.A. Karpenko, 2006, published in Zhurnal Prikladnoi Khimii, 2006, Vol. 79, No. 6, pp. 934 – 939.

APPLIED ELECTROCHEMISTRY AND CORROSION PROTECTION OF METALS

Effect of Electrochemically Synthesized Polymethylolamide Coatings on the Corrosion Resistance of Steel in Seawater

A. P. Suponina, L. G. Kolzunova, and M. A. Karpenko

Institute of Chemistry, Far-Eastern Division, Russian Academy of Sciences, Vladivostok, Russia

Received August 5, 2005

Abstract—The effect of coatings based on a copolymer of acrylamide, *N*,*N*'-methylenebisaxcrylamide and formaldehyde deposited by electrochemical polymerization on the corrosion resistance of 08Kh18N10T stainless steel (field studies at sea) and low-carbon steel (laboratory experiments) was examined.

DOI: 10.1134/S1070427206060115

The problem of protection of metals from biogrowth and corrosion in seawater is a matter of acute current interest, because corrosion processes lead to a large-tonnage loss of metals and failure of ships, devices, and equipment working in marine conditions and in coastal regions. Solution of this problem would prolong the service life of high-cost objects and save metals and alloys. However, no versatile methods that could forever close the issue of article protection from biogrowth and corrosion have been developed so far. Therefore, the necessity for continuation of investigations in this area is quite apparent.

Commonly, various metallic coatings or polymer and paint-and-varnish layers, or combinations of these, are used as protective materials. In recent years, increasingly close attention has been given to polymer coatings. Apparently, the advances in application of polymer materials are determined both by the level of understanding of their physicochemical and biochemical properties and by the development of new materials and progressive technologies for deposition of polymer coatings on metal surfaces. A particular place among technologies of this kind is occupied by the electrochemical polymerization method [1]. This method makes it possible to control the properties of polymers deposited on metallic substrates both by varying the composition of the starting monomeric formulations and by immobilization of fillers of varied nature, which impart new special properties to the coatings, into the polymer matrix directly in the course of electrolysis. In addition, the electrochemical polymerization method can control the quality and thickness of coatings by varying the electrolysis modes. Control over the electrolysis potential also makes it possible to vary the polymerization mechanism and obtain (co)polymers of prescribed composition. The simplicity of the technique, combined with the high rate of formation of polymer layers and the valuable properties of (co)polymers, make apparent the advisability of a study of the protective properties of electrically synthesized polymer coatings.

The evidence concerning the method and mechanism of electrochemical polymerization of acryl monomers and formaldehyde and possible application areas of the polymethylolamine coatings obtained was the most completely represented in [2]. It has been shown that formaldehyde contained in the starting monomeric formulation is incorporated, in the course of electrochemical polymerization, into the macromolecular chain of a polymer (methylolamide groups) [3]. In addition, it is well sorbed in pores and on the surface of a polymer film. Being the main toxic component of the starting solution and of the material being formed, formaldehyde imparts bactericidal properties to the polymer film [4]. The presence in the polymer of such a highly toxic compound, whose threshold content is only 1×10^{-4}%, should exert a sterilizing influence on microorganisms, including those corrosion-hazardous. As a result coatings of this kind can protect equipment used in natural water from biogrowth and corrosion. However, no

investigations of this kind have been performed until now.

The aim of this study was to examine the influence exerted by poly(acrylamide-*N*,*N*-methylenebisacrylamide–formaldehyde) coatings electrochemically deposited on metals on the corrosion activity of the marine environment with respect to St.3 low-carbon steel and on the corrosion resistance and formation of micro- and macroovergrowths on the surface of special steels that are stable against general corrosion in seawater, but are damaged by biogrowth.

EXPERIMENTAL

Acrylamide (AA) and *N*,*N*'-methylenebisacrylamide (MBAA) of Reanal brand (without additional purification), formaldehyde (F) in the form of a 29.3% aqueous solution, and zinc chloride of chemically pure grade were used in the study. The concentrations of these reagents in the aqueous electrolysis bath were as follows (M): AA 3, MBAA 0.1, F 7, and $ZnCl_2$ 0.1.

Prior to experiments, in accordance with the procedure described in [5], steel plates were marked, their edges were trimmed, and the plates were ground, degreased with ethanol, and weighed on a VLR-200-M analytical balance.

Polymer coatings were formed on $80 \times 40 \times 2$ mm samples of 08Kh18N10T high-alloyed steel and $40 \times 20 \times 1$ mm samples of St.3 steel (cathodes) in quarts glass cells in the potentiostatic electrolysis mode. Aluminum foil was used as anodes. An EVL-1M3 silver chloride electrode equipped with a Luggin capillary filled with a working solution served as reference. Solution temperature 20–25°C, electrochemical polymerization potential E = –1.16 V, electrolysis duration 5 min. The metallic electrodes were treated before experiments by techniques commonly accepted in electropating [6]. Part of the plates were electroplated with zinc under conditions similar to those used in electrochemical polymerization (c_{ZnCl_2} = 0.1 M, τ = 5 min).

Some of the samples with a polymer coating were twice washed, after electrolysis, with 100 ml of distilled water for 30 min, whereas the rest were used without washing.

Seawater was used in the laboratory experiments.[1] The temperature of water in nature was 7–8°C. Freshly taken water was used in all the experiments, with its temperature gradually, in the course of several hours, elevated to room temperature (20–23°C).

The laboratory experiments included two sets. In the first set, glass vessels were filled with 0.5 l of pretreated seawater and three coated samples were suspended on Kapron threads in each vessel. In the second set, samples without coatings were exposed, with addition of a certain amount of a formamide solution to the test corrosive media. The duration of the tests was seven days.

The study included the following tests: (1) seawater + steel samples (control); (2) seawater + F (M): 1×10^{-3} (trace concentration), 1×10^{-2} (concentration of fixation of bacteria), and 1×10^{-1} (excess of formaldehyde), coated steel samples; (3) seawater + steel samples modified with a polymer film (a) without treatment with water and (b) washed with water; and (4) seawater + steel samples coated with zinc metal.

After the completion of experiments in the test and control media with natural seawater, the biological response to a changed state of the medium was studied by measuring the abundance of four physiological groups of bacteria: saprophytes (S), iron bacteria (IB), sulfate-reducing bacteria (SRB), and putrefactive anaerobes (PA) [8]. In parallel, the pH value of the medium and the concentration of dissolved oxygen were determined [9]. Steel samples were removed from exposure and weighed, the loss of mass was evaluated, and the corrosion rate was calculated by the equation

$$K = (P_1 - P_2)/S\tau,$$

where K is the corrosion rate (g m^{-2} h^{-1}); P_1, initial sample mass (g); P_2, sample mass after tests (g); S, sample area (m^2); and τ, test duration (h).

In tests under natural conditions, steel samples-plates (control and coated) were submerged in seawater in the near-shore part of the Golden Horn Bay (Vladivostok port) at a depth of 2.5–3 m. The tests were commenced during the period (last days of June) of mass settling of larvae of Balanus barnacles (BB) and continued for 120 days without interruptions.

After the samples were taken away from testing, the biological film formed during the whole time of exposure was subjected to microbiological analysis. Samples of the film were taken with a sterile spatula from different parts of the surface: (I) from under barnacles, no corrosion; and (II) the same, but with

[1] The water was taken at the Rynda Bay (Japan Sea, water area of the Amur Bay), whose water corresponds in the main hydrochemical parameters to that in the open Japan Sea [7]. Water was taken at a distance of 10–15 from the shoreline at a depth of 1 m.

Table 1. Abundance A of physiological groups of bacteria in test media

Coating on St.3	Abundance, thousand cells per milliliter, of indicated bacteria			
	S	IB	SRB	PA
Control	30.4	11.81	0.002	0.004
Poly-AA–MBAA–F:				
without washing	Not determined	Not determined	Not determined	Not determined
washing with distilled water	"	"	"	"
Electrochemical deposit of zinc	22.1	3.32	0.001	0.002
Without coating, addition of formaldehyde, M:				
1×10^{-3}	0.86	1.2	0.001	0.0015
1×10^{-2}	Not determined	Not determined	Not determined	Not determined
1×10^{-1}	"	"	"	"

corrosion. A bacterial suspension was formed and seeded onto nutrient media. The abundance of S was counted on fish-peptone agar; IB, on Kalinenko medium; PA, on Morris medium; and SRB, on Van Delden medium [8]. The species composition of the community of microscopic overgrowers and their raw biomass were studied. The intensity of steel disintegration under BB was expressed as the ratio between the number of BB with recorded corrosion sites under them and the total number of settled BB. The mass loss by a sample was determined.

Potentiostatic electrolysis in AA–F–MBAA–$ZnCl_2$ solutions at $E = -1.1\ldots-1.3$ V enables formation of two-layer Zn/polymer coatings on the cathode surface [2]. The results obtained in determining in laboratory conditions the biocide effect of coatings of this kind, without pretreatment with distilled water and with double washing, on the bacteriocenosis in the test media are listed in Table 1. The analysis performed demonstrated that metallic zinc, which belongs to toxic heavy metals, gradually dissolves during the exposure of the samples under study. As can be seen from Table 1, exposure of St.3/Zn samples in the test media results in that the abundance of the physiological groups of bacteria decreases by a factor of 1.5–3.5 as compared with the control media. A similar suppressive bacteriostatic effect was observed in test media with formaldehyde added in amounts recommended for fixation of bacteria (0.1–1.0 M of a 40% solution [10]). As shown by the experiments, even trace amounts of formaldehyde strongly suppress the development of bacteria (Table 1), and this suppression is the most pronounced for saprophytes. Their abundance decreases by a factor of 35, whereas that of IB, SRB, and PA, by factors of 10, 2, and 2.6, respectively. An increase in the formaldehyde concentration to 1×10^{-2} M completely eliminates any vital activity of bacteria and microorganisms present in seawater.

Exposure of steel samples with a Zn/polymer coating in test media gives results similar to those obtained in the presence of 1×10^{-2}–1×10^{-1} M of formaldehyde. Irrespective of whether untreated or water-washed samples are used, their inhibiting action is manifested in full measure, which terminates the vital activity of microorganisms. This result is a consequence of a joint toxic effect of Zn and formaldehyde incorporated into the polymer matrix.

Thus, the biological response of the natural marine medium is totally suppressed in laboratory experiments owing to the complex effect of two-layer composite Zn/polymer layers deposited on test metallic substrates.

Further studies were aimed to examine the corrosion resistance of metals coated with polymethylolamide films and to analyze factors that govern the corrosion processes. Table 2 lists the pH values and oxygen contents in the control and test media. The data obtained indicate that there is, on the whole, only a little change in these parameters in the course of the process. The insignificant decrease in the pH value both in test media with fixed steel plates and in solutions with addition of formaldehyde can hardly serve as in important corrosion factor, especially if the fact that the accuracy of pH measurements is an order of magnitude poorer than that in determining the oxygen concentration [9] is taken into account. It is known that the rate of oxygen supply to a corroding surface governs the corrosion rate of the majority of metals. The observed minor increase, with respect to the control values, in the oxygen concentration in the test

Table 2. Concentration of dissolved oxygen, corrosion loss by St.3, and pH value in the test media

Coating on St.3	O_2, mg l^{-1}	pH	m, g	K, g m^{-2} h^{-1}
Control (no coating)	3.22	8.02	0.01430	0.053
Poly-AA–MBAA–F:				
without washing	3.5	7.75	0.01093	0.041
washing with distilled water	3.67	8.0	0.0123	0.045
Electrochemical deposit of zinc	3.69	7.98	0.00845	0.031
Without coating, addition of formaldehyde, M:				
1×10^{-3}	2.38	7.76	0.0104	0.039
1×10^{-2}	3.32	8.04	0.0114	0.042
1×10^{-1}	3.37	7.96	0.0111	0.041

media may be due to absence of, or decrease in, the consumption of O_2 for respiration by microorganisms because of their death or suppression of their vital activity. Therefore, it may be assumed that the corrosion loss by steel samples will also depend on the biological activity of a medium.

At the same time, there exist a number of reasons why corrosion processes are hindered and, consequently, the corrosion rate decreases. One of these is the method of electrochemical deposition of one metal onto another, exceedingly widely used in modern technology [11]. This technique provides cathodic protection of the base metal from disintegration. Just this result was obtained in the present study: the corrosion rate of zinc-plated St.3 samples decreases by 40% (Table 2).

The results obtained demonstrate that the mass loss by the test samples also considerably decreases (by 25–30%) after certain amounts of formaldehyde, the known adsorbing organic inhibitor [12], are introduced into seawater. A similar result was observed after polymer coatings were deposited onto steel by electrochemical polymerization of AA, *N*,*N*'-MBAA, and F, in which case the corrosion processes are hindered by combination of several factors: antiseptic properties of the films, inhibiting action of residual formaldehyde, and cathodic protection by zinc.

Because attainment of a passive state is virtually impossible for iron, cast iron, and medium-alloyed steels in seawater [13], the corrosion of these materials occurs at a permanently high rate. A visual inspection of the surface of the steel samples during their exposure in test media demonstrated that the corrosion of the control sample starts virtually immediately after the beginning of an experiment. In media with formaldehyde, changes on the steel surface were observed after 1–1.5 h. The most stable were samples with polymer and Zn coatings, on which no corrosion products could be seen during several hours. Further, the corrosion pattern was the same for all the samples, with a continuous bulky loose mass formed on their surface. It should, however, be mentioned that polymer films in a swollen state shielded the sample surface during the entire experiment.

Thus, it was found that, without any treatment in water after electrochemical synthesis or being twice washed with distilled water, copolymers of acrylamide, *N*,*N*'-methylolbisacrylamide, and formaldehyde exhibit biocide properties, with the microflora of the test media totally eliminated, and effectively reduce the corrosion loss.

The influence exerted by electrochemically synthesized (AA–*N*,*N*'-MBAA–F) copolymers on the formation of micro- and macrogrowths and the corrosion resistance of steel was further studied in summer–autumn (July–October) in the field conditions of the Golden Horn Bay, which is a typical port harbor with anthropogenic contaminations of both organic and inorganic origin. As practice shows, this permanently acting ecological factor predetermines the specific type of formation of the bacteriocenosis and community of overgrowers, with their transformation toward development of certain physiological groups of organisms stimulated [14, 15].

In performing field tests, it is necessary to take into account that, in the case of open water, when samples exposed are permanently washed with fresh water, the concentration of formaldehyde will rapidly decrease and this will diminish its overall biocide effect. In this case, the corrosion resistance of samples will depend to a greater extent on formation of micro- and macrogrowths on the surface of high-alloyed steel, which is known to be damaged under biogrowth.

Table 3. Abundance *B* of microorganisms on different areas on the surface of 08Kh18N10T high-alloyed steel (exposure duration 120 days)

Steel sample	Surface area	*B*, thousand cells per square centimeter, for indicated microorganisms			
		S*	IB*	SRB**	PA**
Control	I	104.0	106.2	0.8	35.6
	II	143.0	136.6	2.5	17.1
Samples with polymer coating	I	250.8	249.0	1.47	3.1
	II	269.5	164.0	1.45	7.6

* Areobes.

** Anaerobes.

Table 4. Parameters of biogrowth and local damage to 08Kh18N10T steel under barnacles (sample exposure duration 120 days)

Type of the steel surface	Raw mass of biogrowth, kg m^{-2}	Total abundance of barnacles, sp m^{-2}	Number of corrosion sites under barnacles per square meter	Corrosion intensity, %	Corrosion rate, g m^{-2} h^{-1}
Control	13.85	10516	1875	17.85	0.017
Polymer films	16.21	10781	1106	10.99	0.023
Deposit of metallic zinc		11953	703	5.88	0.0105

Table 3 lists the results obtained in counting the abundance of all the groups of bacteria under study on the surface of test and control samples under bases of barnacle shells. It can be seen from Table 3, that the number of saprophytes and iron bacteria on plates with polymer coatings exceeds by a factor of 2–2.5 the number of microorganisms of these physiological groups on the control. The abundance of SRB also tends to increase. However, the abundance of putrefactive anaerobes decreases by an order of magnitude. The decrease in the number of putrefactive anaerobes on plates with polymer coatings may be due to sensitivity of the microorganisms of this group to the biocide action of formaldehyde and polymethylolamide or to other factors, which require a more detailed study.

According to [16], the vital activity of bacteria on a metallic surface coated with a layer of adsorbed organic substances is markedly enhanced. Therefore, the presence on the metal surface of an additional organic source of nutrients in the form of the polymer matrix with removed toxic component activates to an even greater extent the reproductive capacity of the bacteria, which is manifested in the noticeable difference in their abundance on the experimental and control samples.

The sharply increasing number of bacteria colonizing the substrate surface predetermines the large volume of the biological film, which, in turn, attracts larvae of micro-overgrowers. This relationship can be considered confirmed both by the results of this study and by previous investigations [17]. The experiments demonstrated that the macro-overgrowth of the test plates is exceedingly abundant, multilayer, and continuous, and is predominantly represented by *Balanus improvisus* and *Balanus crenatus* barnacles, sludge worms, bivalves (mussels) *Mytilus trossilus*, hydroids *Obelia longissima*, and by single specimens of sea squirts *Ascidia de.sp* and amphipods. No differences in the species composition and climax phase of the overgrowers' community on the control and test samples are observed. However, the raw mass of overgrowers per sample on steel surfaces exceed in quantitative regard that on the control samples (Table 4). The present communication gives averaged data on biogrowth on samples with polymer coatings.

After removal of the biogrowth, the local damage to the surface of steel samples was observed under barnacle shells and, occasionally, between these shells at places of their mass accumulation. No corrosion damage was found under other types of overgrowers.

The maximum number of barnacles was observed on samples with a zinc deposit. However, the intensity of steel disintegration and the corrosion rate are the lowest on these samples.

On samples with polymer coatings, the total abundance of barnacles is close to that on the control. Nevertheless, the absolute number of damages sites on these surfaces is nearly twice lower than that on the control, with the result that the corrosion intensity decreases by a factor of 1.5–2, as in the case of the zinc coating. At the same time, it was found that the corrosion rate of the control sample is 1.5 times lower than that on polymer-coated samples. This is possibly due to the weaker biogrowth on the control samples, whereas on the samples with polymethylolamide films deposited by electrochemical polymerization, the abundant mass of biogrowth and the denser settlement of barnacles restrict the supply of oxygen to the surface and hinder formation of a passivating film on steel, with the result that the corrosion rate of these samples increases.

CONCLUSIONS

(1) A study of the influence exerted by electrochemically synthesized copolymer coatings based on acrylamide and formaldehyde on the corrosion resistance of St.3 steel and 08Kh18N10T stainless steel in natural seawater revealed that corrosion in a limited volume of a corrosive medium is hindered by the biocide action of the polymer, its components, and zinc sublayer. As a result, the loss of mass by St.3 steel is reduced by 25–30%.

(2) An increase in the corrosion rate of modified stainless steel samples was observed in field tests at sea. It was demonstrated that the corrosion disintegration of steel in open water is controlled by the biological factor of the medium. This may occur because the polymer layer on the metal surface can serve as an additional organic source of nutrients for microorganisms.

REFERENCES

1. Bezuglyi, V.D. and Karpinets, A.P., *Elektrokhimicheskaya polimerizatsiya. Itogi nauki i tekhniki* (Electrochemical Polymerization. Advances of Science and Technology), VINITI, Elektrokhimiya (Electrochemistry), 1993, vol. 39, pp. 65–94.
2. Kolzunova, L.G., *Vestn. Dal'neVost. Otd. Ross. Akad. Nauk*, 2002, no. 4, pp. 49–61.
3. Kolzunova, L.G. and Kovarskii, N.Ya., *Vysokomol. Soedin. Ser. A*, 1983, vol. 25, no. 8, pp. 1702–1707.
4. Kolzunova, L.G. and Suponina, A.P., Abstracts of Papers, *XVII Mendeleevskii s"ezd, 21–26 sentyabrya 2003 g., Kazan'* (XII Mendeleev Congress, September 21–26, 2003, Kazan), 2003, vol. 3, p. 205.
5. Gerasimenko, A.A. and Matyusha, G.V., *Zashch. Met.*, 1999, vol. 35, no. 4, pp. 386–395.
6. Kudryavtsev, N.T., *Elektroliticheskie pokrytiya metallov* (Electroplated Coatings on Metals), Moscow: Khimiya, 1979.
7. Koryakova, M.D., *Voprosy okeanografii dal'nevostochnykh morei* (Problems of Oceanography of Far-Eastern Seas), Leningrad: Gidrometeoizdat, 1987, pp. 59–66.
8. Kuznetsov, S.I. and Romanenko, V.I., *Mikrobiologicheskoe izuchenie vnutrennikh vodoemov (laboratornoe rukovodstvo)* [Microbiological Study of Inland Water Basins (Laboratory Manual)], Moscow: Akad. Nauk SSSR, 1963.
9. *Metody gidrokhimicheskikh issledovanii okeana* (Methods for Hydrchemical Study of the Ocean), Bordovskii, O.K., Ed., Moscow: Nauka, 1978.
10. Egorov, N.S., *Praktikum po mikrobiologii* (Practicum of Microbiology), Moscow: Mos. Gos. Univ., 1976.
11. Zhuk, N.P., *Kurs teorii korrozii i zashchity metallov* (Theory of Corrosion and Metal Protection), Moscow: Metallurgiya, 1976.
12. Walker, J.F., *Formal'degid* (Formaldehyde), Moscow: Gos. Nauchn.-Tekh. Izd. Khim. Lit., 1957.
13. Alekin, O.A. and Lyakhin, Yu.I., *Khimiya okeana* (Chemistry of the Ocean), Leningrad: Gidrometeoizdat, 1984.
14. Videla, H.A., De Mele, M.F.L., and Brankevich, G., *Corrosion–87*, San Francisco, California, March 9–13, 1987. Paper no. 365.
15. Koryakova, M.D., Nikitin, V.M., Suponina, A.P., et al., *Zashch. Met.*, 2002, vol. 38, no. 5, pp. 544–548.
16. Ulanovskii, I.B., Rozenberg, L.A., and Ledenev, A.V., *Mikrobiologicheskaya korroziya metallov v morskoi vode* (Microbiological Corrosion of Metals In Seawater), Moscow: Nauka, 1983, pp. 11–16.
17. Koryakova, M.D., Nikitin, V.M., Speshneva, N.V., and Suponina, A.P., *Zashch. Met.*, 2001, vol. 37, pp. 279–283.

ISSN 1070-4272, Russian Journal of Applied Chemistry, 2006, Vol. 79, No. 6, pp. 930–933. © Pleiades Publishing, Inc., 2006.
Original Russian Text © V.Ya. Kustovskii, I.A. Starostina, O.V. Stoyanov, 2006, published in Zhurnal Prikladnoi Khimii, 2006, Vol. 79, No. 6, pp. 940 – 943.

APPLIED ELECTROCHEMISTRY AND CORROSION PROTECTION OF METALS

Acid–Base Interactions and Adhesion Capacity in the System Constituted by an Epoxy Coating and a Metal

V. Ya. Kustovskii, I. A. Starostina, and O. V. Stoyanov

Kazan State Technological University, Kazan, Tatarstan, Russia

Received February 1, 2005; in final form, December 2005

Abstract—Free surface energy and acidity parameter of solid surfaces of polyepoxides used as anticorrosive coatings were measured. Formulations of epoxy resins with various curing agents were studied. The adhesion capacity of epoxy films to various metallic surfaces was evaluated.

DOI: 10.1134/S1070427206060127

The presently widely used three-layer (epoxy primer, polyolefin-based thermoplastic melt-adhesive, and polyethylene) anticorrosive coatings (ACC) for steel pipes combine high adhesion properties of polyepoxides with good mechanical properties and high chemical resistance of polyolefins. As, however, the temperature is elevated and working time made longer, the adhesion capacity of ACC decreases. The performance of these coatings can be markedly improved by varying the composition of an epoxy formulation and the set of design elements of a three-layer ACC. This type of anticorrosive coatings is an interesting object of study and matter for further development, because a high adhesion between the constituent layers is to be achieved.

As is known, the phenomenon of adhesion consists in various kinds of interaction between molecules of the contacting phases. For an adhesion interaction to occur, it is necessary that bonds between molecules of the adhesive and active centers on the substrate surface should be formed. The existing thermodynamic approaches are based on the results obtained in studying the energy of interphase tension, wetting angles at the substrate–adhesive interface, and adhesive spreading angles at phase boundaries, with account of various contributions of intermolecular forces [1].

Recently, the approach according to which an important role in bonding between the contacting phases is played by acid–base interactions has gained wide acceptance [2]. In this context, the best properties should be observed for an adhesion joint in which one side shows acidic (by Lewis) properties, and the other, basic properties. In view of the aforesaid, a study of surface characteristics of all components of a coating is a matter of strong current interest. Further purposeful modification of the layers, aimed to enhance their acid–base interaction, could improve the properties and extend the service life of ACC.

The surface characteristics that allow prognostication of the capacity of a material for adhesion interaction include, in the first place, the surface energy with two components, dispersion and acid–base (previously named polar), and the acidity parameter [3], or reduced acidity parameter [4], which is the difference of the acidity parameters of the adhesive and substrate. The acidity parameter gives information about the acid–base properties of a surface under study and, consequently, about its capacity for an acid–base interaction in an adhesion joint.

The aim of our study was to reveal and assess the relationship between the above-mentioned characteristics and the adhesion capacity in the system constituted by an epoxy coating and a metal, which is highly important for a multilayer coating and ensures its adhesion to the metal and resistance to cathode flaking.

EXPERIMENTAL

We used in the study ED-20 epoxydiane resin and PEF-3A low-molecular weight epoxyurethane

caoutchouc. The formulation was cured with diethylenetriamine (DETA), polyethylenepolyamine (PEPA), AF-2M aminophenol, and DTB-2 curing agent, which is formed in the reaction of diethylenetriamine and butylmethacrylate in the presenece of a catalyst, a solution of boron trifluoride in diethylene glycol. The curing agent was taken in the stoichiometric amount with respect to the epoxy resin.

Copper, titanium, brass, steels (St. 10, St. 20, EP696, and Ya1T brands), and duralumin alloys (D16T, D16ATV, and D16AM brands) served as metallic substrates.

To evaluate the surface properties, film samples of epoxy formulation were formed on glass substrates and cured in air at room temperature (cold method) and in an oven at 80°C for 2 h (hot method).

We evaluated the components of the free surface energy (FSE) by measuring the wetting angles for test fluids on the sample surface with a KM-6 cathetometer and calculated them graphically, with processing by the least-squares method with the use of Microsoft Excel software.

As test fluids served water, aniline, phenol, formamide, glycerol, dimethylformamide, dimethyl sulfoxide, saturated aqueous solution of K_2CO_3, methylene iodide, and α-bromonaphthalene. Their parameters are listed in Table 1 [1, 3].

We calculated the acidity parameter by the Berger method [3], which consists in the following. If we use the known Owens–Wendt equation [5]

$$\gamma_{lv}(1 + \cos\Theta)/2 = (\gamma^d_{lv}\gamma^d_s)^{1/2} + (\gamma^p_s\gamma^p_{lv})^{1/2},$$

which can be brought to the form

$$W_a/2(\gamma^d_{lv})^{1/2} = (\gamma^d_s)^{1/2} + (\gamma^p_s\gamma^p_{lv})^{1/2}/(\gamma^d_{lv})^{1/2}$$

(γ^{ab}_1 and γ^d_1 are the acid–base and dispersion components of the FSE of the test fluids; W_a, thermodynamic work of adhesion of a fluid on the surface under study; γ^d_s and γ^{ab}_s, dispersion and acid–base components of the FSE of the surface under study) and plot, using a linear approximation, a curve in the coordinates $(\gamma^{ab}_1/\gamma^d_1)^{1/2}$–$W_a/2(\gamma^d_1)^{1/2}$, then the coordinate of the intersection point of the curve and the ordinate axis will be $(\gamma^d_s)^{1/2}$ and the slope of the straight line, $(\gamma^{ab}_s)^{1/2}$. The sum of the values of γ^d_s and γ^{ab}_s, graphically found in this way, is the geometric-mean approximation of the free surface energy of the material.

Table 1. Free surface energy γ_1 of model fluids and its acid–base (γ^{ab}_1) and dispersion (γ^d_1) components

Model fluid	γ_1^d	γ_1^{ab}	γ_1
	mJ m^{-2}		
Water	22	50.2	72.2
Dimethylformamide	32.4	4.9	37.3
Glycerol	33.9	29.8	63.7
Formamide	31.8	25.7	57.5
Aniline	41.2	2.0	43.2
Phenol	37.8	2.6	40.4
Dimethyl sulfoxide	34.9	8.7	43.6
Saturated aqueous solution of K_2CO_3	34	70.9	104.9
α-Bromonaphthalene	44.6	0	44.6
Methylene Iodide	49.8	2.4	52.2

Figure 1 shows as an example a plot in the coordinates $(\gamma^{ab}_1/\gamma^d_1)^{1/2}$–$W_a/2(\gamma^d_1)^{1/2}$ for one of the surfaces studied, that of a film based on the PEF-3A + PEPA formulation. Figure 1 demonstrates the strong deviations from linear behavior are observed for some of the fluids. This refers to all of the surfaces studied and indicates that values of γ^{ab}_s depend on the nature of a test fluid. These deviations furnish information about the acid–base interaction.

In the method used, we calculated values of γ^{ab}_s for the surfaces we studied from their individual interaction with each of two test Lewis acids and two test bases. The test acids and bases used have

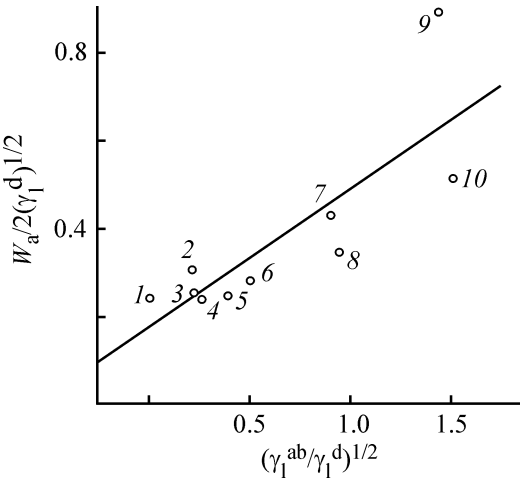


Fig. 1. Determination of the geometric-mean approximation of the FSE of a PEF-3A film cured with PEPA. Test fluid: (*1*) α-bromonaphthalene, (*2*) methylene iodide, (*3*) aniline, (*4*) phenol, (*5*) dimethylformamide, (*6*) dimethyl sulfoxide, (*7*) formamide, (*8*) glycerol, (*9*) saturated aqueous solution of K_2CO_3, and (*10*) water. For explanations see text.

Table 2. Characteristics of epoxy primers with various curing agents (cold curing)

Resin	Curing agent	γ_s^d	γ_s^{ab}	γ_s	D, $(mJ\ m^{-2})^{1/2}$
		mJ m^{-2}			
ED-20	DETA	36.1	6.8	42.9	6.8
	DTB-2	31.2	6.9	38.1	2.0
	AF-2M	31.4	16.2	47.6	3.0
	PEPA	31.7	16.5	48.2	5.1
PEF-3A	DETA	34.4	7.9	42.3	4.0
	PEPA	34.0	8.2	42.2	3.8
	AF-2M	32.8	8.0	40.8	1.1

Table 3. Surface characteristics of metallic surfaces

Metal	γ_s^d	γ_s^{ab}	γ_s	D, $(mJ\ m^{-2})^{1/2}$
	mJ m^{-2}			
Titanium	25.1	15.4	40.5	0.9
Ya 1T	24.2	11.3	35.5	2.9
Copper	24.8	7.2	32	3.3
Bronze	23.1	13.3	36.4	4.0
St. 20	22.0	19.3	39.3	5.5
St. 10	26.3	8.3	34.6	8.1
D 16T	25.5	21.1	46.6	4.2
D 16AM	21.0	24.1	45.1	3.2
D 16ATV	25.2	19.1	44.3	2.7
EP 696	22.2	19.2	41.4	1.3

rather close, in pairs, values of γ_1^{ab} and γ_1^d (these are phenol and aniline, and glycerol and formamide). The differences in surface energy between the members of the above pairs are insignificant (Table 1). The aniline base has a somewhat higher FSE than the phenol acid, and the formamide base, a somewhat lower FSE than the acidic glycerol. The base having a lower FSE (formamide) in one pair should compensate for the influence of the acid with a lower FSE (phenol) in the other. If there were no acid–base interaction, these pairs would have approximately equal wetting angles on the surface under study and virtually coinciding points in the plot mentioned above. The values of γ_s^{ab} would be same for aniline and phenol, and glycerol and formamide. However, this is not the case. The occurrence of an acid–base interaction leads to the deviations of the points from the straight lines, mentioned above. In Fig. 1, the values of γ_s^{ab} for phenol and glycerol lie below the straight line. This means that the acids interact with the surface under consideration to a substantially lesser extent than it follows from the geometric mean and that preference is given to interactions with bases. Consequently, the surface has acid properties. In other words, if both bases wet the surface under study better than the acids do, it can be considered acidic.

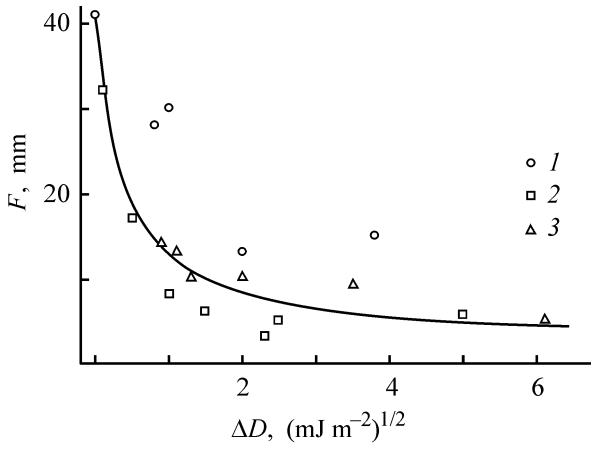


Fig. 2. Resistance to cathode flaking, F, vs. reduced acidity parameter ΔD for adhesion pairs constituted by a metal and an epoxy ACC. (*1*) ED-20 + PEPA, (*2*) ED-20 + AF-2M, and (*3*) ED-20 + DTB-2.

The difference between the values of γ_s^{ab} for acids and bases, calculated by the formula

$$D = 2\{[\gamma_s^{ab}(\text{aniline})]^{1/2} + [\gamma_s^{ab}(\text{formamide})]^{1/2}\} - 2\{[\gamma_s^{ab}(\text{phenol})]^{1/2} + [\gamma_s^{ab}(\text{glycerol})]^{1/2}\},$$

gives the measure of the acidity of the surface. And just this is the physical meaning of the acidity parameter.

The adhesion capacity of an epoxy coating to a metal was judged from the diameter of a defect produced in cathode flaking in a 0.1 N solution of sodium chloride at room temperature and voltage of 6 V during 8 h from the "seed" defect 3 mm in diameter.

According to the approach under consideration, a most important role in the interphase adhesion interaction is played by acid–base binding of the interacting surfaces. In three-layer ACC, particular attention is given to enhancement of the interaction at the interface between a metal and an epoxy primer.

Data on surface characteristics of a cured epoxy primer are listed in Table 2. As follows from the results obtained, the surface properties of films based both on the epoxydiane resin and on epoxyurethane caoutchouc strongly depend on the nature of a curing agent. For both primers, the acid properties increase in the order DTB-2 < AF-2M < PEPA < DETA. The full free surface energy of cured ED-20 is about 40 mJ m^{-2}, with the main contribution to this energy coming from the dispersion component of FSE, γ_s^d. The acid–base component is small ($\leq$10 mJ m^{-2}). The acidity par-

ameter D is positive, which points to the acid nature of the surfaces, and reaches the highest values for ED-20 + DETA and ED-20 + PEPA produced by cold curing.

We made a comparative estimate of the surface parameters of a primer cooled by the cold and hot methods. It was found that curing at elevated temperatures leads to a decrease in the acidity parameter for all the samples. This is presumably due to a slow rate of the curing reaction at low temperatures, so that amine reacts with atmospheric moisture and carbon dioxide to give an ammonium salt that is a Lewis acid.

To obtain coatings with the optimal adhesion properties, it is necessary to possess information about the surface (and, primarily, acid–base) properties of a metal. Therefore, we studied these parameters for various metallic surfaces. The experimental data obtained are listed in Table 3.

According to the acid–base approach, the best adhesion capacity should be observed between surfaces with the largest reduced acidity parameter ΔD. To confirm this suggestion, we evaluated the adhesion interaction of epoxy ACC with various metals by the method of cathode flaking (Fig. 2). Each of the dependences presented in the figure demonstrates that the intensity of interaction between these surfaces increases with the difference of their functionalities, and this is manifested in that the defect diameter decreases.

Previously, a dependence of this kind has been observed for ACC of modified low-pressure polyethylene, deposited on various metallic surfaces [4].

Thus, the analysis we made suggests that the films based on epoxy resins, we studied, exhibit acid properties, which are enhanced in the case of cold curing. The surface properties of the metals used in the study rather widely vary as regards the acidity (from nearly neutral for titanium to high for St. 10 steel). The best adhesion capacity, evaluated by the resistance to cathode flaking, is observed for the following adhesion joints: (ED-20 + PEPA)–titanium (ΔD = 4.6), (ED-20 + AF-2M)–St. 10 steel (ΔD = 5.1), and (ED-20 + DTB-2)–St. 10 steel (ΔD = 6.1).

CONCLUSIONS

(1) A relationship was revealed between the adhesion capacity of epoxy films to various metallic surfaces and the reduced acidity parameter for the elements of the adhesion joint, involved in the interaction.

(2) It was shown that application of the acid–base approach to the problem of improvement of the adhesion interaction between contacting phases and can be used in design of particular coating systems based on polyepoxides.

REFERENCES

1. Kinloch, A.J., *Adgeziya i adgezivy: Nauka i tekhnologiya* (Adhesion and Adhesives: Science and Technology), Moscow: Mir, 1991.
2. Fowkes, F.M., *J. Adhes. Sci. Technol.*, 1990, vol. 4, no. 8, pp. 669–684.
3. Berger, E.J., *J. Adhes. Sci. Technol.*, 1990, vol. 4, no. 5, pp. 373–391.
4. Starostina, I.A., Khasbiullin, R.R., Stoyanov, O.V., and Chalykh, A.E., *Zh. Prikl. Khim.*, 2001, vol. 74, no. 11, pp. 1859–1862.
5. Owens, D.K. and Wendt, R.C., *J. Appl. Polym. Sci.*, 1969, vol. 13, pp. 1740–1755.

ISSN 1070-4272, Russian Journal of Applied Chemistry, 2006, Vol. 79, No. 6, pp. 934–940. © Pleiades Publishing, Inc., 2006.
Original Russian Text © A.G. Bubnov, V.I. Grinevich, O.N. Maslova, 2006, published in Zhurnal Prikladnoi Khimii, 2006, Vol. 79, No. 6, pp. 944–950.

ENVIRONMENTAL PROBLEMS OF CHEMISTRY AND TECHNOLOGY

Barrier-Discharge Plasma Treatment of Surface Water to Remove Organic Compounds

A. G. Bubnov, V. I. Grinevich, and O. N. Maslova

Ivanovo State University of Chemical Engineering, State Educational Establishment of Higher Professional Education, Moscow oblast, Russia

Received July, 6, 2005; in final form, February 2006

Abstract—Barrier-discharge plasma treatment of real surface water to remove organic pollutants was studied. Plasma treatment decreases the potential toxicity of snowmelt and rainfall runoff containing ammonium and chloride ions, oil products, phenols, and carboxylic acids (as recalculated for CH_3COOH).

DOI: 10.1134/S1070427206060139

Recent trends toward increasing contamination of natural surface and ground water make urgent water treatment to satisfy the potable water quality standards and to remove persistent organic pollutants, among which phenols are typically classified as criterial pollutants as well [1]. Along with adsorption and electrochemical methods, plasmochemical methods and, in particular, those using low-temperature barrier-discharge plasma (BDP) [2], rank among the most promising for water treatment to remove organic compounds. However, plasmochemical methods do not have widespread application now, probably, because the processes involved in treatment of real water need to be adequately understood, and the implementation of these methods, to be developed in more detail.

This study was aimed to elucidate the physicochemical relationships in the BDP treatment of wastewater to remove phenol, as well as to identify the most effective process parameters, based on the yield of the least toxic final products of oxidation of the pollutant.

EXPERIMENTAL

The experiments were carried out on the setup we described in [3]. The volumetric flow rate of the water to be treated was varied from 0.02 to 0.56 $cm^3\ s^{-1}$. Technical-grade oxygen (99.8 vol % pure, main impurities N_2 and Ar) at a flow rate $\leq 3.2\ cm^3\ s^{-1}$ served as the plasma-forming gas.

A barrier discharge was excited from a high-voltage transformer (current frequency 50 Hz); the interelectrode gap was 2 mm.

The voltage applied to the electrodes, measured with a V7-47 high-voltage voltmeter, was constant in all the experiments, 16 kV, which corresponded to the specific power input to the discharge, $W = 0.8\ W\ cm^{-3}$. The current in the secondary circuit was monitored oscillographically (C 1-55) from the voltage drop across the resistor (the discharge current was constant, 1.7 μA).

The time of contact of the solution with the plasma zone, τ_c, s, was calculated by the formula

$$\tau_c = \frac{S_{flow} h \tau_{tr}}{V_{tr} \times 1000}, \quad (1)$$

where S_{flow} is the area of the ring of the liquid layer in which the treatment is performed (in a layer of a hydrophilic material), cm^2; h, size of the discharge zone, cm; V_{tr}, volume of the solution being treated, ml; and τ_{tr}, time required for treatment of the given volume of the solution, s.

Our experiments were performed with prefiltered samples of real surface water (rainfall and snowmelt runoff) taken in the central, most urbanized, part of the city of Ivanovo; the runoff composition is presented in Table 1. Also, we carried out experiments with model solutions, namely, aqueous solutions of phenol and potassium chloride: model solution no. 1 (M1), $c_{phenol} = 4.2\ mg\ l^{-1}$ (or 268.1 μM the content of atomic carbon in the C_6H_5OH molecule); $c_{KCl} = 33.6\ mg\ l^{-1}$ (451 μM in terms of the content of atomic chlorine in the KCl molecule); model solution no. 2 (M2), $c_{phenol} = 3.97\ mg\ l^{-1}$ (253.4 μM in terms of the content of atomic car-

Table 1. Change in the concentration of the pollutants and the potential toxicity, PT, of the surface runoff after BDP treatment ($\tau_c \approx 300$ s)

Indicator	MPC_{fish}	Storm runoff				Snowmelt runoff			
		before treatment		after treatment		before treatment		after treatment	
		c_i, mg l^{-1}	PT	c_i, mg l^{-1}	PT	c_i, mg l^{-1}	PT	c_i, mg l^{-1}	PT
pH	–	6.95	–	6.12	–	6.98	–	5.15	–
COD, mg O_2 l^{-1}	15	420	28	112	7.47	852	56.8	469	31.22
$O_{2,dis}$, mg l^{-1}	–	1.42	–	27.2	–	1.65	–	18.02	–
BOD_5, mg O_2 l^{-1}	2	0.73	0.37	0.20	0.10	5.63	2.82	1.48	0.74
NH_4^+, mg l^{-1} (for N)	0.35	0.48	1.37	1.18	3.37	6.07	17.34	3.09	8.83
Chlorides, mg l^{-1}	300	2.38	0.01	2.26	0.01	35.67	0.11	27.13	0.09
Active chlorine, mg l^{-1}	–	0	–	0.24	–	0	–	17.62	–
Oil products, mg l^{-1}	0.05	18.5	370	0.96	19.2	1.10	22	0.10	2
Phenols, mg l^{-1}	0.001	1.05	1050	0.73	730	0.50	500	0.27	27
Carboxylic acids (recalculated for CH_3COOH), mg l^{-1}	0.01	8.94	894	9.33	933	49.79	4979	37.98	3798
Σ PT_i			2343		1693		5578		3868

* The potential toxicity of the surface runoff was estimated from the $PT = c_i/MPC_{fish.i}$ ratio, where c_i is the concentration of the pollutant, mg l^{-1}, and $MPC_{fish.i}$, the maximum permissible concentration of the pollutant in a water basin used for fishing purposes, mg l^{-1}.

bon in the C_6H_5OH molecule), $c_{KCl} = 2.52$ mg l^{-1} (33.8 μM in terms of the content of atomic chlorine in the KCl molecule), this solution contained 123.74 μM of dissolved CO_2 (in terms of the content of atomic carbon in the CO_2 molecule); and model solution no. 3 (M3), $c_{phenol} = 10.0$ mg l^{-1} (or 638 μM in terms of the content of atomic carbon in the C_6H_5OH molecule).

The qualitative indicators (including pH) characterizing the composition of the initial and treated water (Table 1) were determined by standard techniques used for analysis of surface water and wastewater [4, 5].

Table 1 shows that the total efficiency of plasmochemical treatment of the surface runoff tends to decrease with increasing initial concentration of the water components that are monitored in the experiments. For example, treatment of storm and snowmelt runoff decreases the content of difficultly biochemically oxidizable organic compounds (COD) by factors of 3.8 and 1.8, respectively, the content of easily oxidizable organic compounds (BOD), by factors of 2.7 and 3.8, respectively, the content of oil hydrocarbons, by factors of 19 and 11, respectively, the content of volatile phenols, by factors of 1.4 and 1.8, respectively, and the content of carboxylic acids, by a factor of 1.3 in the snowmelt runoff only.

It should be noted that, despite the high initial concentrations (relative to MPC_{fish}) of organic compounds, the efficiency of decomposition for most of them remains sufficiently high, namely, 91–95 for oil products, 45–73 and 73–74 for reduction of COD and BOD, respectively, 30–46 for phenols, and up to 24 wt % for carboxylic acids.

These figures suggest that, during the BDP treatment of real snowmelt and rainfall runoff, phenols and carboxylic acids are formed once again, now as intermediates in decomposition of more complex organic compounds and, in particular, oil hydrocarbons.

We carried out a chromatomass-spectrometric analysis of the surface runoff (an extract in hexane) and interpreted the chromatograms using the library of mass spectra. We found that, along with typical compounds classified as oil products (ethylbenzene, *p*-xylene, 1,2-dimethylbenzene, propylbenzene, isopropylbenzene, 1-methyl-3-ethylbenzene, 1-methyl-2-ethylbenzene, 1,2,3-trimethylbenzene, propylbenzene, ethyldimethylbenzene, *o*-isopropenyltoluene, tetramethylbenzene, dimethylstyrene), the water also contained

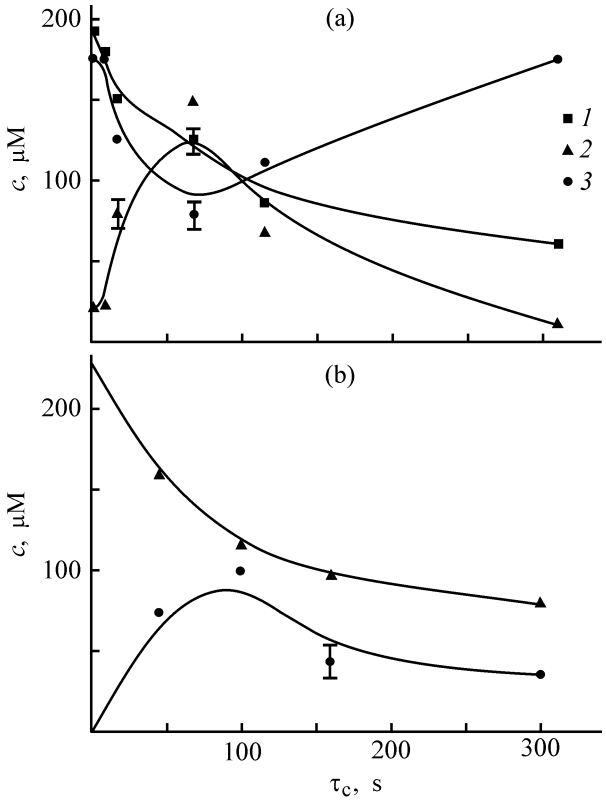


Fig. 1. Variation of the concentration of organic compounds, c (in terms of the content of atomic carbon in the molecule), in plasmochemical treatment of (a) the surface snowmelt runoff and (b) solution M1, with the contact time τ_c. (*1*) Oil products, (*2*) phenols, and (*3*) carboxylic acids (*points*, experiment; *lines*, calculation).

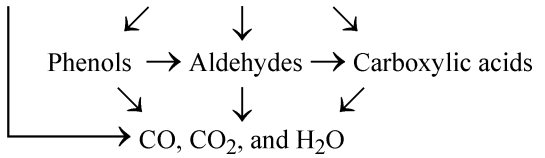
complex [4-(2-methyl-1,3-dioxalane-2-yl)benzonitrile, 1-methyl-2,8,9-trioxa-5-aza-1-silabicyclo[3,3,3]undecane] and, in particular, polycyclic (naphthalene, benzocycloheptatriene) and halogenated (1,2,3-trimethylbromobenzene) compounds, as well as triethanolamine, 1-phenylisoquinoline, dibutyl phthalate, and bis(2-ethylhexyl) phthalate. Probably, decomposition of these organic compounds can be an additional source of low-molecular-weight oxidation products occurring in the BDP-treated water.

Assessment of the potential toxicity of the initial and BDP-treated waters shows that, after plasma treatment, the PT decreases by a factor of 1.4 on the average, irrespective of the initial content of the organic compounds in water (Table 1). Thus, even taking into account the residual content of pollutants of various nature in the water treated, BDP seems promising for treatment of at least rainfall and snowmelt runoff.

The formation and decomposition of intermediate and final oxidation products of complex organic compounds in an oxygen medium can be represented by the following simplified schemes:

Complex derivatives of aromatic compounds → benzene → phenols → aldehydes → carboxylic acids → carbon and hydrogen oxides

Oil products (including aromatic hydrocarbons)



Our experiments showed that the rate of decomposition of phenols is, evidently, much lower than that of their accumulation as intermediates, as suggested by the peak in the kinetic curve describing variation of the phenol concentration (Fig. 1). Probably, specifically the efficiency of decomposition of the initial organic impurities makes the deciding contribution to the total efficiency (to reduction of the content of organic compounds) of the wastewater treatment.

In plasmochemical treatment, one of the main decomposition pathways for molecules of organic compounds (which is usually considered under the model experiment conditions) is their oxidation in reactions involving active species of the oxygen plasma (in particular, electronically excited O_2 molecules and oxygen atoms in the ground state), including those yielded by O_3 [6]. Ozone can react with diverse organic, organomelement, and inorganic compounds, and, thermodynamically, these reactions can go to completion [7]. A limiting factor is the low rate of the reactions in the final stages of decomposition. It should be noted that O_3 is a strong, but selective oxidant. For example, it is known that ozone very rapidly oxidizes phenols and unsaturated organic compounds, and fairly slowly, saturated acids and ketones (acetone) [7].

The specific features of the reactions of O_3 with various organic compounds account for, in part, the observed relationships in transformation of organic compounds whose content was monitored during our experiments. However, the results of our measurements suggest the necessity for taking into account the action of an additional oxidizer (Table 1), active chlorine (e.g., in the form of HClO or ClO^-) which can be yielded in natural waters by inorganic salts, e.g., potassium chloride. For example, an increase in the time of contact of water with the plasma zone is accompanied by conversion of chloride ions to an ac-

tive form (Fig. 2); the kinetic relationships in the formation of active chlorine from chloride anions, observed in the experiments with model solutions, were independent of the initial KCl concentration and identical for the M1 and M2 solutions.

Unlike ozone, radicals formed in the discharge by the scheme

$$HClO + ClO^- \rightarrow ClO^\bullet + Cl^- + OH^\bullet,$$

can effectively react with all the substances in solution that are capable of oxidation.

Radicals $ClO^\bullet$ can be involved participate in formation of atomic oxygen and $OH^\bullet$ [8]:

$$ClO^\bullet + ClO^- + OH^- \rightarrow 2Cl^- + OH^\bullet + 2O.$$

The appearance of strong oxidizers in the system is also indirectly confirmed by the change in pH of the solution from 7.23 to 6.65 during the experiments.

Chloride ions are formed in water, above all, via dissociation of inorganic salts, e.g., potassium chloride, which is widely used for elimination of the ice cover on roads and, probably, occurrs in the surface snowmelt runoff in city territories. Also, we cannot rule out possible occurrence in the water we studied of other, both inorganic and organic, chlorinated compounds, whose decomposition can yield chlorine in the form of ions and radicals capable, in turn, of reacting not only with the impurities occurring in water but also with one another.

We estimated the apparent rate constants of decomposition of the organic compounds occurring in the real runoff and in the model solution, based on the data in Fig. 1 by solving the problem of parametric and structural identification of the models of the kinetics of complex chemical reactions. To this end, we utilized the approach taken in [9]; we obtained the most likely estimates of parameters by the Gauss–Newton method and represented the step-by-step schemes of the processes of transformation of the organic compounds in the systems examined as follows:

for model solution

$$C_6H_6O\ (F) \xrightarrow{k_1} CH_3COOH\ (A) \xrightarrow{k_2} CO_2 + H_2O,$$

for surface runoff

$$\text{Oil products} \xrightarrow{k_3} C_6H_6O \xrightarrow{k_1} CH_3COOH$$
$$\searrow^{k_4} \qquad\qquad \swarrow_{k_2}$$
$$CO_2 + H_2O$$

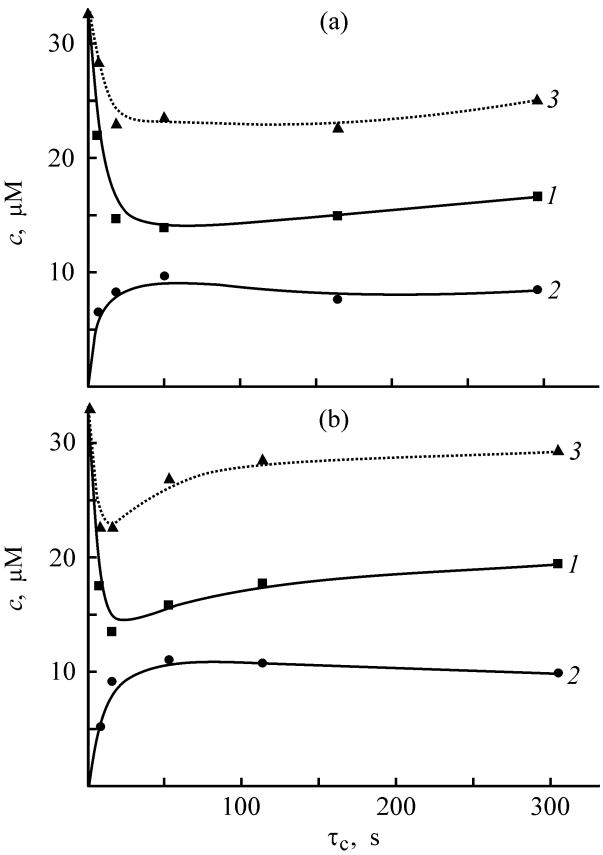


Fig. 2. Variation of the concentration of the chloride ions and active chlorine, c, in (a) M2 solution and (b) snowmelt runoff with the contact time τ_c. (*1*) Chloride ions, (*2*) active chlorine, and (*3*) total chlorine (*points*, experiment; *lines*, calculation).

The results of calculation in terms of these models are graphically represented in Fig. 1, and the calculated apparent rate constants of the reactions are listed in Table 2. The tabulated data suggest that the apparent rate constant of oxidation of phenol, k_1, is weakly dependent on its initial concentration and on the composition of the solution being treated.

Table 2 confirms the validity of the previous assumption that the rate of decomposition of phenol, k_1, though being comparatively high, is nevertheless lower than that of its accumulation in oxidation of more

Table 2. Apparent rate constants of the reactions of decomposition of organic compounds

Constant	Model solution M1	Storm runoff
$k_i \times 10^{-3}$, s^{-1}:		
k_1	2.43 ± 0.01	2.92 ± 0.06
k_2	3.93 ± 0.01	1.98 ± 0.03
k_3	–	3.33 ± 0.04
k_{3+4}	–	1.57 ± 0.02

Table 3. Characteristic lifetime of phenol molecules, τ^*, during BDP treatment

τ	Model solution M1	Snowmelt runoff	Storm runoff
τ^*, s:			
τ_c	0–310	0–310	0–310
τ_d		325–1299	
τ_p	412	350	556

Table 4. Concentration of phenol, intermediates in its decomposition, chlorides, and active chlorine, μM, after the BDP treatment of the model solutions and the surface snowmelt runoff

Compound	$\tau_c \approx 50$ s			$\tau_c \approx 300$ s		
	runoff	solution M2	solution M3	runoff	solution M2	solution M3
C_6H_5OH	30	3.8	9.6	8.3	<0.8	1.9
HCOH	72.0	10.7	10.8	74.4	3.2	0.7
CH_3COOH	26.9	32.4	80.9	28.5	32.9	67.8
CO_2 (in the liquid phase)	151	159	389.1	160	180	450.5
CO_2 (in the gas phase)	1.7	21.9	67.4	2.4	37.1	84.2
Σc^*_{pr}	281.6	227.8	557.8	273.6	253.2	605.1
$\pm\Delta c$:						
μM	154.0	149.3	80.5	162.0	123.9	33.2
mol %	35.4	39.6	12.6	37.2	32.9	5.2
Cl^-	15.77	13.80		19.44	16.62	
Cl_{act}	10.99	9.58		9.86	8.45	
$\pm\Delta$Cl:						
μM	7.04	10.42		4.50	8.73	
mol %	20.8	30.8		13.3	25.8	

* Σc_{pr} is the total content of atomic carbon in the molecules of phenol and monitored products of its decomposition after BDP treatment; $\pm\Delta c$, disagreement in the balance of the content of atomic carbon in the molecules of the compounds analyzed [in the surface runoff examined, the total content of atomic carbon in the molecules of the compounds analyzed is 435.55 μM (of which 253.4 μM is accounted for by phenol)]; and $\pm\Delta$Cl, disagreement in the balance of the content of chlorine (Cl^-) in the molecule of chlorides (in terms of KCl) and active chlorine (Cl_{act}) in the form of HClO or ClO^-.

complex organic compounds, k_3, during BDP treatment of real systems.

Under BDP exposure of the model solutions, the rate of accumulation of carboxylic acids is lower than that of their decomposition, whereas in treatment of real waters the situation is the reverse. This can be accounted for by the fact that, in the case of the BDP treatment of real waters, there are additional pathways for formation of alkyl radicals (decomposition products of alkoxy radicals) which, eventually, yield a significant proportion of low-molecular-weight products, such as aldehydes, ketones, acids [10].

To identify the limiting step of the plasmochemical processes, we analyze the characteristic lifetime τ^* of the molecules of the substances occurring in the solution, with phenol as an example (Table 3): (1) the time of contact of the liquid with the electrodes, τ_c; (2) diffusion time of movement of the molecules toward the electrode in the liquid phase, $\tau_d \sim h^2/D$, where h is the thickness of the liquid layer ($h \approx 0.05$–0.1 cm), D is the diffusion coefficient in the liquid phase, $cm^2\ s^{-1}$ (e.g., $D = 0.77 \times 10^{-5}$ $cm^2\ s^{-1}$ for resorcinol [11]), $\tau \approx 325$–1299 s; and (3) lifetime τ_p based on the oxidation rate (the rate constants are taken equal to those calculated by numerical modeling), $\tau_p = 1/k_1$.

Thus, if the real thickness of the liquid layer is 1 mm, the diffusion lifetime of the phenol molecules is the largest among all the parameters considered. Evidently, specifically this step of the processes of interest can be regarded as the limiting in this case. If the thickness of the liquid layer is smaller (which is closer to reality), we can consider directly the chemical reaction in solution as the limiting step of the process. This is more probable in view of the behavior of the water film in strong electric fields.

Table 4 presents the change in the contents of the main products of decomposition of organic com-

pounds in the model solutions and the real surface runoff. Also presented is the estimated balance for the carbon atoms; it is satisfied accurately to within 5–13 mol % in the case of treatment of an aqueous solution of phenol. The disagreement in the carbon balance for the phenol solution lies within the accuracy of measurement for the compounds listed in Table 4. This suggests that all the main products of decomposition of phenol are measured and any other compounds and, in particular, those more toxic than phenol, are unlikely to be formed. This assumption is confirmed by the fact that the disagreement in the carbon balance is the smaller, the larger the time of contact of the solution with the plasma zone. When potassium chloride was added to the phenol solution, the disagreement in the carbon balance increased (33–41 mol %) and went beyond the accuracy of measurements for the compounds of interest. Hence, any other compounds that are not monitored in our experiments can be formed along with those monitored.

Similar conclusions are suggested by the results we obtained for a real surface runoff (the disagreement in the carbon balance was 35–37 mol %, and that for chlorine compounds, 13–21 mol %). The appearance of additional decomposition products both in the model solution and in the real runoff, when exposed to BDP, is, probably, due to formation of an additional amount of active species (in particular, active chlorine), which can be responsible for a change in the decomposition mechanism for the organic compounds on the whole.

Despite certain advantages offered by the plasmochemical treatment of wastewater, there is residual, unchanged, ozone at the reactor output in the gas phase [12]. Its amount was 9.4–42.3 g m^{-3}, which substantially exceeded the maximum permissible one-time concentration for atmospheric air (0.16 mg m^{-3}). Our experiments showed that, when a cartridge with a commercial catalyst, such as GTT,[1] was placed at the reactor output, ozone was not detected within the sensitivity of the method of measurement, i.e., its concentration at the output was under 0.1 g m^{-3} (the efficiency of removal of O_3 was not lower than 98.9–99.8 wt %). Thus, with a catalyst like GTT the ozone emission can be reduced to the permissible level.

[1] Manganese-nickel-copper, developed at the Novomoskovsk Institute of Nitrogen Industry, Chemical Faculty, Lomonosov Moscow State University, and Timis Scientific and Promotion Firm.

CONCLUSIONS

(1) Barrier-discharge plasma treatment in the gas-liquid system is suitable for removing organic compounds from surface rainfall and snowmelt runoff.

(2) The degrees of decomposition of phenol in plasma treatment of its model solutions (99 wt %) and real surface waters (95 wt%) are comparable, like the corresponding apparent rate constants of decomposition of phenol (2.43×10^{-3} and 2.92×10^{-3} s^{-1} for the model solution and real runoff, respectively).

(3) Plasma treatment of the model solutions of phenol and real surface waters leads to formation of carboxylic acids as basic products of plasmochemical oxidation, as well as of CO_2 and HCO_3^-; the yield of these latter is 81 mol % for the model phenol solutions and 64 vol % for the real surface waters.

(4) In plasma treatment of the model phenol solutions and surface waters to remove organic compounds, the limiting step of the process is the reaction of the active species of plasma, predominnantly O_3, with the molecules of organic compound (phenol), as well as formation of the final decomposition products.

(5) Plasma treatment reduces the potential toxicity of wastewater by a factor of no less than 1.4.

ACKNOWLEDGMENT

This study was supported by the Russian Foundation for Basic Research (project no. 03-03-96441).

REFERENCES

1. Danilov-Danil'yan, V.I. and Edmin, E.Yu., in *6 Mezhdunarodnyi congress "Voda: ekologiya i tekhnologiya EKVATEK 2004": Sbornik dokladov* (6 Int. Congr. "Water: Ecology and Technology EKVATEK, 2004": Coll. of Papers), Moscow: 2004, p. 32.
2. Kutepov, A.M., Zakharov, A.G., Maksimov, A.I., and Titov, V.A., *Khim. Vys. Energ.*, 2003, vol. 37, no. 5, pp. 362–366.
3. Bubnov, A.G., Grinevich, V.I., Kuvykin, N.A., and Maslova, O.N., *Inzh. Ekol.*, 2002, no. 4, pp. 27–32.
4. Lur'e, Yu.Yu. and Rybnikova, A.I., *Khimicheskii analiz proizvodstvennykh stochnykh vod* (Chemical Analysis of Industrial Wastewater), Moscow: Khimiya, 1974.
5. *Metody issledovaniya kachestva vody vodoemov* (Methods of Investigation of the Water Quality of Water Basins), Shitskova, A.P., Ed., Moscow: Meditsina, 1990.

6. Kutepov, A.M., Zakharov, A.G., and Maksimov, A.I., *Vakuumno-plazmennoe i plazmenno-rastvornoe modifitsirovanie polimernykh materialov* (Vacuum-Plasma and Plasma-Dissolution Modification of Polymeric Materials), Moscow: Nauka, 2004.
7. Lunin, V.V., Popovich, M.P., and Tkachenko, S.N., *Fizicheskaya khimiya ozona* (Physical Chemistry of Ozone), Moscow: Mosk. Gos. Univ., 1998.
8. Krasnoborod'ko, I.G., *Destruktivnaya ochistka stochnykh vod ot krasitelei* (Destructive Treatment of Wastewater to Remove Dyes), Leningrad: Khimiya, 1988.
9. Bubnov, A.G., Grinevich, V.I., Kuvykin, N.A., and Maslova, O.N., *Khim. Vys. Energ.*, 2004, vol. 38, no. 1, pp. 44–49.
10. Kuzubova, L.I. and Korbrina, V.N., *Khimicheskie metody podgotovki vody (khlorirovanie, ozonirovanie, ftorirovanie): Ekologiya* [Chemical Methods of Water Treatment (Chlorination, Ozonation, Fluorination: Ecology], Novosibirsk: Sib. Otd. Ross. Akad. Nauk, Gos. Publ. Nauch.-Techn. Bibl., Vorozhtsov Novosibirsk Inst. Org. Khim., 1996, issue 38.
11. *Fizicheskie velichiny: spravochnik* (Physical Quantities: Reference Book), Grigor'ev, I.S and Meilikhov, E.Z., Eds., Moscow: Energoatomizdat, 1991.
12. *Khimiya plazmy: Sbornik nauchnykh statei* (Chemistry of Plasma: Coll. of Scientific Articles), Smirnov, B.M., Ed., Moscow: Energoatomizdat, 1990, issue 16.

ISSN 1070-4272, Russian Journal of Applied Chemistry, 2006, Vol. 79, No. 6, pp. 941–944. © Pleiades Publishing, Inc., 2006.
Original Russian Text © G.G. Shelopin, D.S. Pashkevich, D.A. Mukhortov, V.B. Petrov, Yu.I. Alekseev, 2006, published in Zhurnal Prikladnoi Khimii, 2006, Vol. 79, No. 6, pp. 951–954.

PROCESSES AND EQUIPMENT OF CHEMICAL INDUSTRY

Synthesis of Perfluoroalkanes by Fluorination of Graphite with Elementary Fluorine in a Vertical Ascending Gas-Dust Flow

G. G. Shelopin, D. S. Pashkevich, D. A. Mukhortov, V. B. Petrov, and Yu. I. Alekseev

Prikladnaya Khimiya Russian Scientific Center, Federal State Unitary Enterprise, St. Petersburg, Russia

Received September 12, 2005; in final form, February 2006

Abstract—Synthesis of lower pefluoroalkanes, tetrafluoromethane, hexafluoroethane, octafluoropropane, and decafluorobutane, in a high-temperature reaction of graphite with fluorine in a reactor with a vertical ascending gas-dust flow was studied.

DOI: 10.1134/S1070427206060140

Tetrafluoromethane (TFM), hexafluoroethane (HFE), octafluoropropane (OFP), and decafluorobutane (DFB) are large-tonnage products used in processing (etching) of silicon in the semiconductor industry [1].

Tetrafluoromethane is produced in a high-temperature reaction of an immobile (fixed) bed of graphite with fluorine [2]. The rest of the above-listed perfluorocarbons are industrially manufactured by various methods, mainly with the use of ozone-hazardous chlorine-containing raw materials [1]. At the same time, TFM, HFE, OFP, and DFB can be synthesized from graphite and fluorine [3].

The primary goal of this study, which continues earlier investigations [3], is to search for conditions of carbon fluorination in which a mixture of perfluoroalkanes, containing HFE, OFP, and DFB in commercial amounts, is formed.

A study of the process of fluorination of graphite with a mixture of fluorine and nitrogen (or argon) in a fluidized bed [3] at various concentrations of fluorine in the gas phase enabled a conclusion that synthesis of CF_4, C_2F_6, C_3F_8, and C_4F_{10} at a temperature of about 600°C occurs in accordance with the two-stage scheme in which synthesis of a solid carbon polyfluoride $(CF_x)_n$ is followed by its thermal decomposition. The composition of the products formed in thermal decomposition of carbon polyfluoride depends on presence of gaseous fluorine in the decomposition zone. An increase in its amount makes smaller the fraction of fluorocarbons with a longer carbon chain. Therefore, spatial separation of the synthesis zone from the zone of thermal decomposition of carbon fluoride can lead to an increase in the fraction of hydrocarbons with the number of carbon atoms exceeding unity in the gaseous reaction products.

It was impossible to achieve a stable separation of the zone of $(CF_x)_n$ synthesis and decomposition in a reactor with a fluidized bed. Therefore, it was suggested to study synthesis of perfluoroalkanes from graphite and fluorine in a reactor in which $(CF_x)_n$ is synthesized in a vertical ascending gas-dust flow and decomposed in a fixed bed of a powder at a higher temperature.

To study the fluorination of graphite in a gas-dust flow, a laboratory installation schematically shown in Fig. 1 was created. The installation comprises an ejector *1*, uptake pipe *2* (inner diameter 9 mm, length 1.2 m), separator *3*, and down pipe *4* of diameter 20 mm. Filter *5* and solid-phase-expenditure meter *6* are installed in the separator of the reactor. Pipes *2* and *4* are equipped with electric heaters and with immersion-type and wall thermocouples.

The basic part of the installation is ejector unit *1*, which forms a gas-dust flow of a prescribed composition from nitrogen and graphite. The working principle of this unit is based on mixing of, and energy exchange between, two flows with different pressures to give a mixed flow with an intermediate pressure.

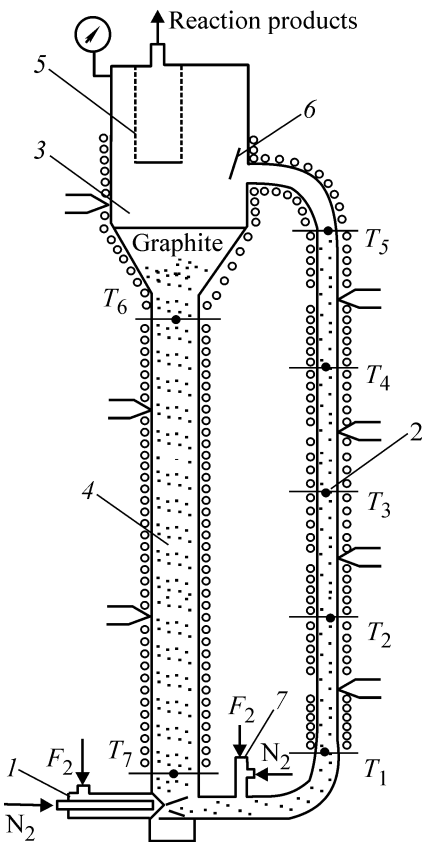


Fig. 1. Schematic of the laboratory reactor for fluorination of graphite in a vertical ascending gas-dust flow: (*1*) ejector, (*2*) uptake pipe, (*3*) separator, (*4*) down pipe, (*5*) filter, (*6*) expenditure meter, and (*7*) nozzle. T_1–T_7, thermocouples.

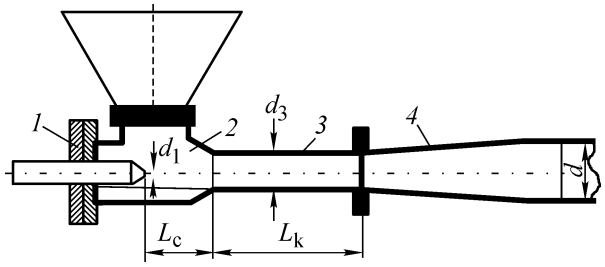


Fig. 2. Schematic of the unit for graphite ejection: (*1*) working nozzle, (*2*) receiving chamber, (*3*) mixing chamber, and (*4*) diffuser. d_1 = 1.5, d_2 = 8, and d = 9 mm.

The design of unit *1* is shown in Fig. 2. The main elements of the apparatus are the working nozzle, receiving chamber, mixing chamber, and diffuser. Their parameters were chosen on recommendations given in [4].

Nitrogen is fed into ejector unit *1*, and a gas-dust flow is formed in it.

A loose graphite powder is delivered to receiving chamber *2*. The gas jet outflowing at a high linear velocity from the working nozzle *1* carries away the graphite powder and imparts to it a part of its kinetic energy. The mixture of the gas and graphite is delivered to chamber *3*, where the velocity field of the moving flow becomes uniform and pressure partly increases. Then, this mixture is fed into diffuser *4*, where the pressure of the moving flow increases further. Leaving the diffuser, the flow is delivered to the uptake pipe under a certain excess pressure.

Fluorine is introduced by nozzle *7* into the gas-dust flow moving upwards in a heated vertical pipe *2* (uptake pipe). In this unit, carbon polyfluoride is formed, with complete consumption of fluorine.

In separator *3*, the gas and powder are separated. Filter *5* serves to remove fine particles from the gas. Expenditure meter *6*, which is an electrostatic capacitor with a movable plate, is installed in the separator opposite the inlet of the uptake pipe. Under the action of the flow, the plate deviates, with the electric capacitance of the capacitor changed, which is recorded with a digital meter. The extent to which the plate deviates and, consequently, the capacitance of the capacitor depend on whether or not the solid phase is present in the flow.

The powder separated from the gas is directed into down pipe *4*, in which it moves downwards in a constricted state under the action of the gravity force. Pipe *4* is equipped with an electric heater, which makes it possible to set a temperature necessary for decomposition of carbon polyfluoride.

Thus, the graphite powder circulates in the installation, being delivered successively into the zone of synthesis of carbon polyfluoride (pipe *2*) and that of its decomposition (pipe *4*).

Gaseous perfluorocarbons are discharged from the separator together with the flow of nitrogen, with the excess pressure in the reactor not exceeding 0.5 atm.

In the first stage of the study, the physicomechanical characteristics of the installation were analyzed: conditions for stable formation of a gas-dust flow (gas flow rate and the corresponding expenditure of the powder), residence time of the powder in uptake pipe *2* and down pipe *4*, and coefficient of heat transfer from the gas-dust flow to the wall of the uptake pipe. A graphite fraction with a particle size less than 1 mm was used.

A conclusion that a stable mode of powder circulation is attained was made using readings of the capacitive transducer *6*: the signal from the transducer subjected to the action of a gas flow is 8–10 times smaller that that in the case of a gas-dust flow.

Table 1. Expenditure of the solid phase (W_C) and the residence time of the powder in pipe *2* (t_2) and pipe *4* (t_4) in relation to the gas flow rate

Nitrogen flow rate, $cm^3 s^{-1}$, T_f = 500°C	Expenditure of graphite, $g s^{-1}$	Residence time, s		Powder circulation mode
		in uptake pipe	in down pipe	
32	–	–	–	No circulation
47	6.7	0.6	43	
52	5.7	0.6	50	Unstable
52	4.0	0.6	71	Stable
54	3.8	0.5	75	
55	5.0	0.5	57	
60	4.2	0.5	68	
62	4.7	0.5	61	
81	4.0	0.4	71	
90	4.0	0.3	71	
95	4.2	0.3	68	
118	4.0	0.3	71	
118	4.3	0.3	66	

The expenditure of the powder was determined in two ways: (i) by direct sampling of the powder, with removed upper cover of separator *3* and interrupted circulation, and (ii) from change in the temperature of the powder upon its heating in pipe *2*, with the cover and circulation circuit closed.

Table 1 lists the results obtained in measuring the expenditure of the solid phase and the residence time of the powder in pipe *2* and pipe *4* in relation to the gas flow rate. It follows from these data that no ejection of the graphite powder occurs at a nitrogen flow rate less than 60 $cm^3 s^{-1}$. At a higher flow rate of the gas, a stable gas-dust flow is formed and the expenditure of the solid phase is virtually independent of the gas flow rate.

At a nitrogen flow rate of 60 $cm^3 s^{-1}$, the residence time of the powder in pipe 2 is 0.5 s at the reactor temperature of 500°C, which is sufficient, according to [3], for complete binding of fluorine with carbon at a temperature exceeding 500°C.

The coefficient α of heat transfer from the gas-dust flow to the wall of pipe *2* was found from the rise in the temperature of the gas-dust flow in the region between the 1st and 5th thermocouples (T_5–T_1) at different wall temperatures of the uptake pipe. The heat-transfer coefficient was 120–180 $W m^{-2} K^{-1}$ in the working range of flow rates.

In the second stage of the study, the composition of the gaseous products formed in the reaction between fluorine and graphite in the reactor was examined (Fig. 1).

The reaction of fluorine with graphite to give $(CF_x)_n$ leads to heat release, with the heat effect of the reaction equal to 198 kJ mol^{-1} [5]. Table 2 lists the results of calculation of the adiabatic warming-up of the gas-dust flow in relation to the flow rate of fluorine.

In order that the temperature of the gas-dust flow from pipe *2* should not exceed 600–650°C at the initial temperature of 500–600°C, the flow rate of fluorine was maintained in the experiments within the range 4–8 $cm^3 s^{-1}$.

In the experiments performed, fluorine was delivered via injector *7*, and the flow rate of nitrogen was set to be about 60 $cm^3 s^{-1}$. The temperature of the powder in pipes *2* and *4* was varied.

Table 2. Parameters of the reaction between fluorine and graphite to give $(CF_x)_n$: adiabatic warming-up of the gas-dust flow (ΔT), heat release (ΔQ), ratio of the flow rate of fluorine to expenditure of carbon ($G_F G_C^{-1}$), and concentration of fluorine in the mixture with nitrogen (c_F) in relation to the flow rates of fluorine (G_F) and nitrogen (G_N) and expenditure of graphite (G_C)

C_F, $cm^3 s^{-1}$	G_N, $cm^3 s^{-1}$	G_c, $g s^{-1}$	c_F, vol %	$G_F G_C^{-1}$, %	ΔQ, $J s^{-1}$	ΔT, °C
15	60	2	20	1.2	250	160
8	60	2	12	0.6	130	90
4	60	2	6	0.3	65	45
2	60	2	3	0.1	33	23

Table 3. Composition of the gaseous products formed in the reaction between fluorine and graphite at different temperatures in the zones of synthesis and decomposition of carbon polyfluoride

T_5	T_6	CF_4	C_2F_6	C_2F_4	C_3F_8	C_3F_6	C_4F_{10}
°C		vol %					
580	600	57.6	20.6	1.5	10.4	3.5	6.5
570	600	52.3	24.8	1.8	10.6	2.4	8.1
550	570	53.2	25.8	–	10.5	1.7	8.8
530	580	53.0	27.8	–	10.6	–	8.7

In all the experiments, there was no breakthrough of fluorine across the zone of $(CF_x)_n$ synthesis.

Table 3 lists, in relation to the temperature at the outlet of pipe *2* (T_5) and to that in pipe *4* (T_6), the composition of the gaseous products formed in fluorination of graphite by the procedure described above.

According to the data in Table 3, the content of TFM is 50–55 vol %, which is approximately 15–20% lower than that in experiments on fluorination of graphite in a fluidized bed [3]. C_2F_4 and C_3F_6, absent in the case of fluorination in a fluidized bed, were found in the gaseous reaction products.

These facts suggest that carbon polyfluoride decomposes in the absence of fluorine in the gas phase. Thus, the use of the procedure for fluorination of carbon by the two-stage scheme in the installation shown in Fig. 1 made it possible to spatially separate the zone of synthesis of $(CF_x)_n$ and that of its thermal decomposition and to raise the yield of perfluoroalkanes with more than one atom of carbon.

It should be noted that the technological processing of the gas produced in fluorination of graphite is to include the stage of fluorination of unsaturated compounds with, e.g., cobalt trifluoride. This is necessary in order to rule out appearance of trace amounts of perfluoroisobutylene, which is extremely toxic [1], in the products formed. In doing so, tetrafluoroethylene and hexafluoropropylene will be fluorinated to give HFE and OFP, which will raise the yield of the last two products.

CONCLUSIONS

(1) It was shown that use of the ejection principle provides a stable formation of the nitrogen–fluorine–graphite gas-dust flow.

(2) The composition of the gaseous products formed in fluorination of graphite by the scheme including synthesis of $(CF_x)_n$ in a gas-dust flow and thermal decomposition of $(CF_x)_n$ in a fixed bed was determined (wt %): tetrafluoromethane 35–40, hexafluoroethane 25–30, octafluoropropane 15–20, and decafluorobutane 15–20.

(3) It was found that, in synthesis of the above-listed perfluoroalkanes from graphite and fluorine in a reactor with spatial separation of stages, the achievable yield of tetrafluoromethane is 15–20% lower than that of the reaction performed in a reactor in which both the stages occur within the same space.

(4) It was shown that the products formed in fluorination of graphite in a reactor with spatially separated stages contain tetrafluoroethylene and hexafluoropropylene, in contrast to the case of a reactor with spatially combined stages.

REFERENCES

1. Maksimov, B.N., Barabanov, V.G., Serushkin, I.L., et al., *Promyshlennye ftororganicheskie produkty: Spravocnoe izdanie* (Industrial Organofluorine Products: Reference Book), St. Petersburg: Khimiya, 1996.
2. RF Patent 2117652.
3. Pashkevich, D.S., Shelopin, G.G., Mukhortov, D.A., et al., *Zh. Prikl. Khim.*, 2004, vol. 77, no. 11, pp. 1865–1871.
4. Sokolov, E.Ya. and Zinger, N.M., *Struinye apparaty* (Jet Apparatus), Moscow: Energiya, 1970, 2nd ed.
5. Wood, J.L., Badachape, R.B., Lagow, R.J., and Margrave, J.L., *J. Phys. Chem.*, 1963, vol. 78, pp. 3139–3142.

ISSN 1070-4272, Russian Journal of Applied Chemistry, 2006, Vol. 79, No. 6, pp. 945–948. © Pleiades Publishing, Inc., 2006.
Original Russian Text © V.V. Tarasov, N.E. Kruchinina, S.A. Shilin, N.I. Shchedrova, 2006, published in Zhurnal Prikladnoi Khimii, 2006, Vol. 79, No. 6, pp. 955–958.

PROCESSES AND EQUIPMENT OF CHEMICAL INDUSTRY

Kinetics of Heterogeneous Hydrodynamic Coagulation of Microscopic Drops

V. V. Tarasov, N. E. Kruchinina, S. A. Shilin, and N. I. Shchedrova

Mendeleev Russian University of Chemical Technology, Moscow, Russia

Received October 5, 2005; in final form, January 2006

Abstract—A prototype reactor for heterogeneous hydrodynamic coagulation of emulsions was developed and tested. The efficiency of coagulation of water emulsions of some organic liquids was studied in relation to process conditions.

DOI: 10.1134/S1070427206060152

Development of new methods for separation of emulsions into constituent phases is a topical task. Stable emulsions are the main reason for considerable loss in oil production and for contamination of the environment with oils, fats, and oil products. Separation of dilute emulsions of the "oil-in-water" type, i.e., raffinates produced in extraction of nonferrous, precious, rare, and radioactive elements, is also a complicated problem. This is so because emulsions with particles of submicrometer and micrometer size ("medusas"), formed in radiochemical industry, show high sedimentation and aggregative stability. Their separation requires application of special methods [1]. Separation of the dispersed phase from the dispersion medium occurs via coagulation (aggregation) of drops with their subsequent coalescence.

The method of heterogeneous hydrodynamic coagulation (HHC), we suggest here, is implemented in a batch installation (Fig. 1) [2, 3]. The stainless steel reactor *1* of volume 500 cm^3 and inner diameter of 80 mm, mounted on support *2*, was charged with 450 cm^3 of emulsion via opening *3* in cover *4*. An electric motor set in motion shaft *5* with plastic discs *6* attached to it. The rotation frequency of the discs was maintained constant in each set of experiments. To preclude formation of a whirlpool, four cylindrical reflector partitions *7* of diameter 4 mm were installed in the reactor. Samples were taken at certain intervals of time via opening *3*. Upon completion of an experiment, the contents of the reactor were discharged via bottom pipe *8*. The experiments were performed with 5 or 10 plastic discs of diameter 57 mm with smooth and corrugated surface, with the distance between the discs equal to 10 and 5 mm, respectively. All the experiments were carried out at 25°C. The apparatus in Fig. 1 is shown without a thermostating jacket. The unit maintaining the stable rotation of the discs was of the PE-8310 type. The discs were rotated by an electric motor at a strictly constant to within 10% prescribed speed in the range 200–3500 rpm.

The coagulation and coalescence in the reactor we developed necessarily involve immobile solid bodies (reflector partitions and reactor walls) [2, 3]. Because the emulsion is composed of at least two fluids, the process suggested here is to be regarded as occurring in a fluid–fluid–solid system (i.e., heterogeneous coagulation is meant). Moreover, the method being described is performed in a system of moving fluids,

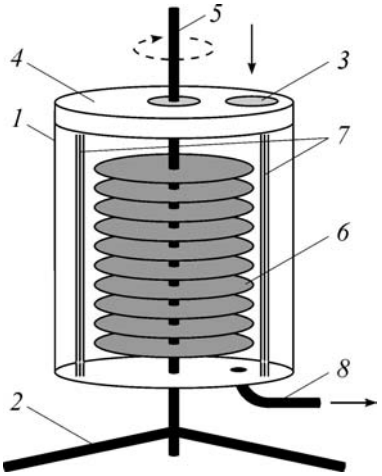


Fig. 1. Schematic of the installation for hydrodynamic heterogeneous coagulation. For explanations see text.

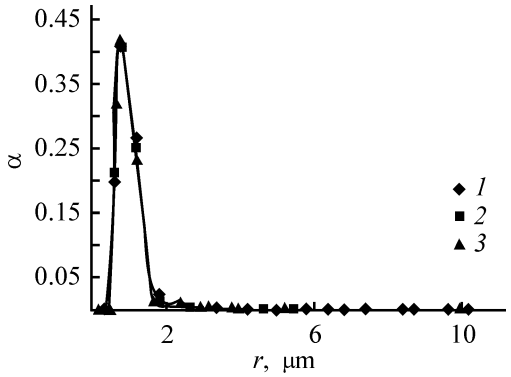


Fig. 2. Normalized size distribution of the counted number of drops in an emulsion of I-40 oil at disperser rotation speed of (*1*) 8000, (*2*) 9500, and (*3*) 13 500 rpm. (α) Fraction of drops of a certain size and (r) drop radius.

whence follows the term "hydrodynamic heterocoagulation."

Because moving fluids may have a considerable velocity relative to immobile bodies (e.g., walls) and high gradients of numerous properties are created near these bodies, a considerable acceleration of coagulation and coalescence would be expected in this case.

Thus, the aim of our study was to reveal how motion of fluids affects the kinetics of separation of comparatively stable emulsions in the presence of walls and other immobile bodies.

EXPERIMENTAL

The experiment comprised the following stages: (1) preparation of stable emulsions; (2) heterogeneous hydrodynamic coagulation, coalescence; and (3) analysis of the dispersion composition of the emulsions and determination of the efficiency of their separation.

We mean by stable emulsions those changing their optical transparence by 10–15% in 24 h.

To prepare an emulsion of this kind, we placed 200 ml of distilled water and 2–3 ml of a substance being dispersed ("oil") in the vessel of an MPW-303 homogenizer and vigorously agitated the mixture with an impeller at a rate of up to 8000 rpm. Also, an IKA DI 25 disperser equipped with an S 25 N-18G spraying unit having a rotor rotation speed of up to 25 000 rpm and fluid pulsation frequency of 4000 Hz. The emulsions formed under these conditions had well-reproducible light-absorption characteristics and possessed a strictly specified dispersion composition.

The vessel of the disperser was cooled from its outer surface with flowing water to preclude heating of its contents. After the agitation was terminated, the resulting emulsion was placed in a separation funnel and subjected to prolonged settling for 10 h to remove "coarsely dispersed" oil drops. In this way we prepared comparatively concentrated emulsions, which were further diluted with water containing 0.8–1.5 g l^{-1} of sodium chloride. These emulsions acquired more unchangeable properties, including light absorption. The oil particle size was 1–5 μm after a preliminary settling of the emulsion. This diminished to a minimum the probability of collisions between drops and their coagulation in the bulk of the fluid.

We were interested in such properties of the emulsions prepared as light absorption and particle distribution over size and volume. The absorption of light was measured in the spectral range 460–590 nm on a photoelectrocolorimeter. At a content of the dispersed phase of 0.8–1.5%, the Bouger–Lambert–Beer law was obeyed; the direct proportionality between the light absorption by an emulsion and the percentage content of the dispersed phase in it made it possible to measure the concentration of the dispersed phase.

To study the particle distribution over size, area, and volume, we developed a computer complex intended to obtain micrographs of emulsions and their processing. The number of drops on a single photograph was from several units to several hundred. Tens of photographs had to be taken for strongly diluted emulsions. The minimum recordable drop size was 0.6 μm.

Figure 2 shows as an example a normalized size distribution of counted drops of I-40 oil. At rotations rate of the disperser rotor in the range 8000–13 500 rpm, the distributions virtually completely coincide. Figure 2 can be used to determine the averaged drop radius ($r \approx 1$ μm); the curve in Fig. 2 is the closet to a logarithmically normal distribution.

To study the HHC process, we chose the method of rotating disks. The material of the inner surface of the apparatus walls was exceedingly important, as also that of the reflector partitions. In the experiments described in this communication, we used only stainless steel (reactor) and plastic discs and reflector partitions. The choice of discs as agitating devices was due to the fact that they create no excess turbulence in the emulsion and do not favor drop disintegration. At the same time, they form emulsion flows perpendicularly directed toward the reactor walls, where drops collide and the velocity vectors of the flows strongly change.

We used as fluids being dispersed Midel 7131 transformer oil, I-40 machine oil, olive oil, and decane. Midel 7131 has a density of 0.97 g cm^{-3}, which is extremely close to that of water. It is very important to keep this feature in mind when discussing the role of centrifugal forces. In addition it is necessary to take into account the not-too-high coefficient of kinematic viscosity (μ = 56 mm^2 s^{-1}) and rather considerable polarity (~12) of Midel 7131. The I-40 oil is a viscous mixture ($\mu \approx 80$ mm^2 s^{-1}, density 0.89 g cm^{-3}) of saturated hydrocarbons frequently used in practice as lubricants. The olive oil ($\mu \approx$ 60 mm^2 s^{-1}, density 0.87 g cm^{-3}) contains unsaturated fatty acids of medium polarity, which are widely used in food industry. Decane is an analogue of diesel fuel, a typical contaminant contained in wastewater from oil refineries and gas-filling stations, which has a viscosity close to that of water and density of 0.73 g cm^{-3}.

As a criterion characterizing the degree of recovery of an organic fluid from emulsions serves the quantity E (%) defined by the formula

$$E = 100(1 - A_\tau/A_0),$$

where A_0 and A_τ are the light absorptions by the initial emulsion and that at instant of time τ, respectively.

The Deryagin–Landau–Verwey–Overbeek (DLVO) theory [4] serves as a basis for the concepts of HHC. The kinetic energy of the flows created by rotating discs can be used by drops to overcome the potential barriers that appear in the DLVO curve when drops approach one another. The agitation of the emulsion by the discs has the following specific feature: it gives rise to flows perpendicular to the cylindrical wall and guarantees collision of these flows. The volume of the fluid between the discs is poorly agitated, and drops formed at and on the wall move upwards and then are removed from the process in the form of separate coarse drops and clusters of these. The organic phase is accumulated in the upper (immobile) part of the reactor (Fig. 1) and is virtually not subjected to repeated disintegration if the rotation rate of the discs is not too high. Nevertheless, repeated dispersion occurs and its extent is the more noticeable, the higher the degree of purification.

The agitation of the "oil-in-water" emulsion by the discs in the HHC installation leads to formation of transparent phases. This indicates that the coagulation, which is the rate-determining stage, culminates in coalescence. Calculations show that the separation of the emulsion into phases occurs at a rate exceeding that of natural sedimentation by a factor of 100–200. Indeed, several days are necessary in the latter case to reach the same separation as that we readily observe in the prototype reactor.

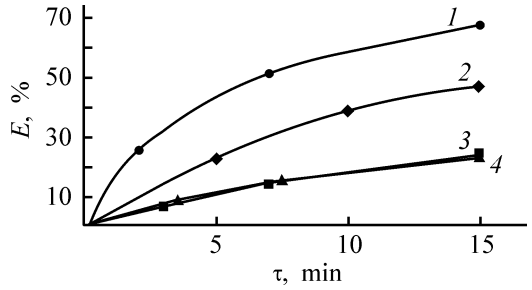


Fig. 3. Degree of clarification, E, of an emulsion vs. the process duration τ at a disc rotation rate n = 700 rpm. Emulsion composition: (*1*) decane, (*2*) Midel 7131, (*3*) I-40 oil, and (*4*) olive oil.

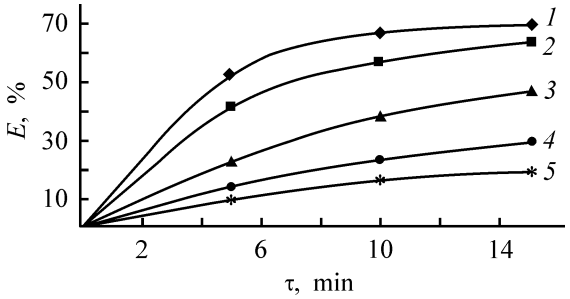


Fig. 4. Degree of clarification, E, of the emulsion with Midel 7131 vs. the process duration τ at different disc rotation rates n. n (rpm): (*1*) 2200, (*2*) 1100, (*3*) 700, (*4*) 500, and (*5*) 400.

Figure 3 shows kinetic curves of HHC separation of emulsions of various organic fluids at a disc rotation rate of 700 rpm. The highest coagulation rate is observed in the case of processing of the decane emulsion. The coagulation rate of organic fluids decreases in the order decane > Midel 7131 > I-40 oil > olive oil; however, there is no strong correlation of the HHC rate with such quantities as viscosity, interphase tension, and density of the dispersed phase. Although the difference between the fluid densities in the system with Midel 7131 is record-breaking small (only 0.03 g cm^{-3}), the coagulation in this system is two times faster than that in systems with olive oil and I-40 oil. This indicates that centrifugal forces do not play any noticeable role. I-40 oil and olive oil exhibited virtually the same coagulation rates despite that they have different densities and viscosities. Apparently, the kinetics of the process is governed by a set of factors, among which physicochemical surface-related quantities, such as wetting angles and dynamics of drop spreading, are important.

Figure 4 shows how the agitation intensity affects the transparence of the emulsion with I-40 oil at its in-

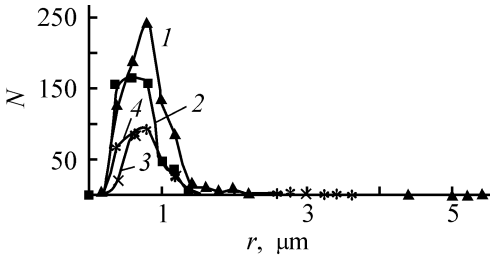


Fig. 5. Evolution of the drop size distribution for the emulsion with I-40 oil. (*N*) Counted number of drops and (*r*) drop radius. Process duration (min): (*1*) 0, (*2*) 10, (*3*) 30, and (*4*) 45.

variable dispersion composition, expressed as the number of drops of a given size related to the total number of drops.

The necessity for simulation and optimization of the HHC process is apparent. The simulation is all the more important because we observed a noticeable influence exerted by the number of discs and their design on the rate of purification of the aqueous phase to remove microscopic drops. For example, reducing the number of discs to five even led to a certain increase in the degree of purification. Replacement of smooth discs with corrugated ones also improved the phase separation.

Let us call attention to the "saturation" of the coagulation process, which is especially clearly manifested at high disc rotation rates and high degrees of purification. This phenomenon can be attributed to reversibility of the HHC process. The fact that it is impossible to reach high degrees of I-40 removal (>70%) means that repeated disintegration of drops becomes the key process. To obtain higher degrees of purification, it would be necessary to remove part of the upper fluid or perform continuous counterflow coagulation, rather than carrying out the batch HHC. In general, the dependence of the degree of clarification of an emulsion on the agitation intensity passes through a maximum at high degrees of purification, which also indicates that simulation and optimization of the process are necessary. The apparent reason for the existence of the maximum is the secondary disintegration of drops.

Another reason why the dependence of the rate of phase separation on the disc rotation rate levels-off and even passes through a maximum is caused by exhaustion of drops that can coagulate [5], rather than being due to reversibility. The aforesaid is confirmed by the type of evolution of the drop size distribution with the time of emulsion processing by the HHC method (Fig. 5). The last fractions of drops, seemingly having a similar distribution, are not "removed" on making the process longer.

Thus, we can suggest the following model of HHC: transport of oil drops to the surface of an immobile solid body (reactor walls); formation of guiding centers in interaction between drops of the organic phase and the reactor surface; surface coagulation of fine drops with the guiding centers and, possibly, coalescence; detachment of coarsened drops or their clusters from the surface of a solid body under the action of the incident vortices and pulsations; rise of coarse drops (clusters) and their removal from the agitation zone.

The results we obtained indicate that HHC may become an efficient method for purification of emulsions to remove drops of the dispersed phase. This technique may prove especially efficient in the case of moderately diluted emulsions and suspensions, and also very "fine" dispersed systems stable against sedimentation. The method requires no reagents or heating.

CONCLUSIONS

(1) An installation for performing the process of heterogeneous hydrodynamic coagulation simultaneously with coalescence was designed and tested.

(2) It was shown that the heterogeneous hydrodynamic coagulation leads to purification of the aqueous phase to remove microscopic drops, with the rate of this process exceeding that of gravitational sedimentation by a factor of 100–200.

REFERENCES

1. *Coagulation and Flocculation: Theory and Application* Dobias, B., Ed., New York: Dekker, 1993.
2. Dudko, K.V., Ogunmoela, T.O., and Tarasov, V.V., *Usp. Khim. Khim. Tekhnol.*, 2003, vol. 17, no. 12 (37), pp. 36–46.
3. Tarasov, V.V., Dudko, K.V., and Dobrokhlop, K.A., *Nauchnaya sessiya MIFI–2004: 3-e nauchno-innovatsionnoe sotrudnichestvo: Sbornik nauchnykh trudov* (Scientific Session of Moscow Institute of Engineering Physics in 2004: 3rd Scientific-Innovational Cooperation: Coll. of Sci. Works), Moscow, 2004, part 1, pp. 69–70.
4. Deryagin, V.V., *Teoriya ustoichivosti kolloidov i tonkikh plenok* (Stability Theory of Colloids and Thin Films), Moscow: Nauka, 1986.
5. Dobrokhlop, K.A. and Tarasov, V.V., *Usp. Khim. Khim. Tekhnol.*, 2003, vol. 17, no. 12 (37), pp. 17–24.

ISSN 1070-4272, Russian Journal of Applied Chemistry, 2006, Vol. 79, No. 6, pp. 949–956. © Pleiades Publishing, Inc., 2006.
Original Russian Text © O.A. Sadygov, Kh.M. Alimardanov, Ch.A. Chalabiev, 2006, published in Zhurnal Prikladnoi Khimii, 2006, Vol. 79, No. 6, pp. 959–965.

ORGANIC SYNTHESIS AND INDUSTRIAL ORGANIC CHEMISTRY

Induced Bromination of Aromatic Hydrocarbons with Alkali Metal Bromides in the Presence of Oxidants

O. A. Sadygov, Kh. M. Alimardanov, and Ch. A. Chalabiev

Mamedaliev Institute of Petrochemical Processes, National Academy of Sciences of Azerbaijan, Baku, Azerbaijan

Institute of Polymeric Materials, National Academy of Sciences of Azerbaijan, Sumgait, Azerbaijan

Received April 20, 2005; in final form, March 2006

Abstract—The features of induced bromination of aromatic hydrocarbons in the NaBr(KBr)–HX–H_2O_2(NaOCl) system were studied.

DOI: 10.1134/S1070427206060164

Halogen derivatives of arenes are widely used for preparing drugs, dyes, fire-resistant composites, etc. At present, chloro- and bromoaromatic compounds are produced on the industrial scale by substitution halogenation of benzene derivatives with appropriate halogens [1, 2]. However, the selectivity of this process with respect to monohalo derivatives is low, and a certain fraction of halogens is lost in the formation of hydrogen halides, which require additional efforts for their utilization. Higher yields of monobromo derivatives of aromatic hydrocarbons are attained with alkali metal bromides and various oxidants, and almost all bromide anions are consumed in the course of the process.

Some data on oxidation of HCl and HBr with H_2O_2 were presented in [3], and the use of HCl + H_2O_2 and HBr + H_2O_2 oxidation system for preparing aliphatic halohydrins [4–6] and haloaromatic hydrocarbons [7–12] was studied. It was found [13, 14] that the bromide anion is incorporated into the substrate upon oxidation of aromatic hydrocarbons in the presence of Co(III) and Mn(III) bromide catalysts. At the same time, bromination of arenes, especially that of toluene and isomeric xylenes, predominantly occurs in the side chain. Benzyl bromide and its derivatives are formed either by ligand transfer of bromine atoms in the intermediate benzyl radicals or through steps of electron transfer [13]. Analogous data on oxidation of 2,4-dichlorotoluene were given in [14]. In [15], accumulation of bromoarene in the oxidate in the presence of cobalt(II) salts and bromine was analyzed assuming that an intermediate is formed by the following reaction:

$$[Co^{2+}\cdots L\cdots BrH]\cdot RH + 2O_2 \rightarrow [Co^{2+}\cdots L] + RBr + 2HO_2^{\cdot}.$$

It was found that, in the case of oxidation systems consisting of equimolar amounts of alkali metal bromides and hydrogen peroxide, the reaction direction shifts toward substitution bromination of alkylaromaic hydrocarbons via substitution of hydrogen atoms in the benzene ring [16–20]. In this case, bromination involves hypobromous acid and molecular bromine, whose formation was noted previously in oxidation of *p*-xylene and toluene in the presence of cobalt(II) bromide [21, 22]. Taking into account that, in contrast to polyvalent metal bromides, alkali metal bromides are not involved in the formation of intermediate complexes, ligand transfer of bromine atom in bromination of the initial hydrocarbons in their presence should be excluded. However, nascent bromine can participate in the process initiation. In [22], the oxidation of *p*-xylene, pseudocumene, and durene with $CoAc\cdot 4H_2O$–NaBr–*N*-bromosuccinimide system was interpreted assuming the following reaction scheme with the participation of bromine radical:

$$>NBr \rightarrow >N^{\cdot} + Br^{\cdot},$$

$$Br^{\cdot} + RH \rightarrow R^{\cdot} + HBr,$$

$$HBr + >NBr \rightarrow >NH + Br_2,$$

$$Br_2 + R^{\cdot} \rightarrow RBr + Br^{\cdot},$$

$$R^{\cdot} + O_2 \rightarrow RO_2^{\cdot} \text{ etc.}$$

In this case, only hydrogen atoms in the side chains are substituted. In the above papers, the formation of bromoarenes in the presence of polyvalent metal bromide catalysts and various oxidants was studied under the conditions in which aromatic acids are produced, and this reaction direction is strongly different from that of the induced bromination of arenes.

In this study, we examined the features of substitution bromination of alkylarenes in the presence of alkali metal bromides.

EXPERIMENTAL

The experiments were carried out in a standard glass reactor equipped with a reflux condenser, a system for reagent supply, and a magnetic stirrer. The reactor was placed in a thermostat with automatic temperature control. The required amounts of an aromatic hydrocarbon and of an aqueous solution of NaBr (or KBr) were placed in the reactor, and then the required amounts of H_2SO_4 (or HCl) and 28–30% aqueous hydrogen peroxide or 18.5–26% aqueous solution of sodium hypochlorite (110–115 g-ion l^{-1} content of available chlorine) were added dropwise.

After the experiment was complete, the organic layer was separated, neutralized with a solution of sodium bicarbonate, washed with water, dried with $CaCl_2$, and distilled. The reactions of induced bromination of aromatic hydrocarbons were monitored by gas-liquid chromatographic analysis for the amounts of unchanged arene and the isomeric composition of the resulting bromo derivatives, using an LKhM-7 chromatograph. The products of bromination of benzene, toluene, and xylenes were analyzed on a column (300 × 0.3 cm) packed with Silichrom-2 impregnated with 10 wt % $CoCl_2$ at (150°C column temperature); and of ethyl-, isopropyl-, and ethoxybenzene, on a column (300 × 0.3 cm) packed with Chromaton N-AW-DMCS impregnated with 5 wt % XE-60 at a column temperature of 150°C and a flow rate of helium carrier gas of 40 ml min^{-1}. In some cases, the individual bromo derivatives of aromatic compounds were prepared by the Sandmeyer reaction [23]. The consumption of hydrogen peroxide was monitored by permanganate titration [3], and the content of Br_2 and NaOCl in the reaction mixture was determined by iodometric titration [24]. The ^1H NMR spectra were recorded in CCl_4 on a Tesla BS-484B spectrometer (80 MHz) with hexamethyldisiloxane as internal reference. The IR spectra of liquid bromoarenes were recorded on a Specord-80 spectrometer in the 4000–400 cm^{-1} range (thin layer between KBr windows). The initial reaction rates were calculated by a differential procedure, using the kinetic curves of accumulation of the desired products at various temperatures [25].

The induced bromination of benzene and its alkyl and alkoxy derivatives was performed in a heterophase system, because arenes are insoluble in aqueous solutions of NaBr (or KBr) and H_2O_2 (or NaOCl). The main reaction products are the corresponding monobromo derivatives formed by the following reactions:

$$MBr \xrightarrow{HX} A \underset{-H_2O\ (NaCl)}{\overset{H_2O_2 \text{ or NaOCl}}{\rightleftarrows}} B \underset{-A}{\overset{C}{\rightarrow}} D, \qquad (1)$$

where M = Na or K; A = [HBr]; B = [HOBr] or [Br_2]; C = $R_1R_2ArH_m$, R_1 = R_2 = H; m = 4, 5; R_1 = H, R_2 = Me, Et, *i*-Pr, EtO; R_1 = R_2 = Me; D = $R_1R_2ArH_{m-1}Br$; X = Cl^-, SO_4^{2-}, RSO_3^- (R = Me/C_6H_4).

Since the formation of HOBr and Br_2 and the induced bromination of arenes proceed in aqueous and organic phases, respectively, stirring of the reaction mixture is one of the decisive factors affecting the yield of the reaction products. Without stirring of the reaction mixture, the yield of bromoarenes is as low as 15–20%. Stirring facilitates the transfer of HOBr and Br_2 from aqueous into the organic phase, and at a stirring rate of 600–700 rpm, the yield of bromo derivatives reaches 63–96%. It was found that, as the stirring rate is raised from 100 to 800 rpm, the initial rate w of formation of monobromotoluenes (at 293 K) increases from 1.45×10^{-3} to 9.14×10^{-3} mol l^{-1} s^{-1} (Fig. 1a). Further increase in the stirring rate does not significantly affect the reaction rate, and thus the stirring rate of 600–700 rpm ensures the kinetic control of the reaction.

Special experiments showed that, when the initial reagents are charged into the reactor simultaneously, the formation of bromine by the above scheme proceeds faster than in the induced bromination of arenes. The yield of the products of induced bromination of hydrocarbons can be controlled by the rate of the oxidant supply. In particular, at simultaneous charging of toluene and aqueous solutions of alkali metal bro-

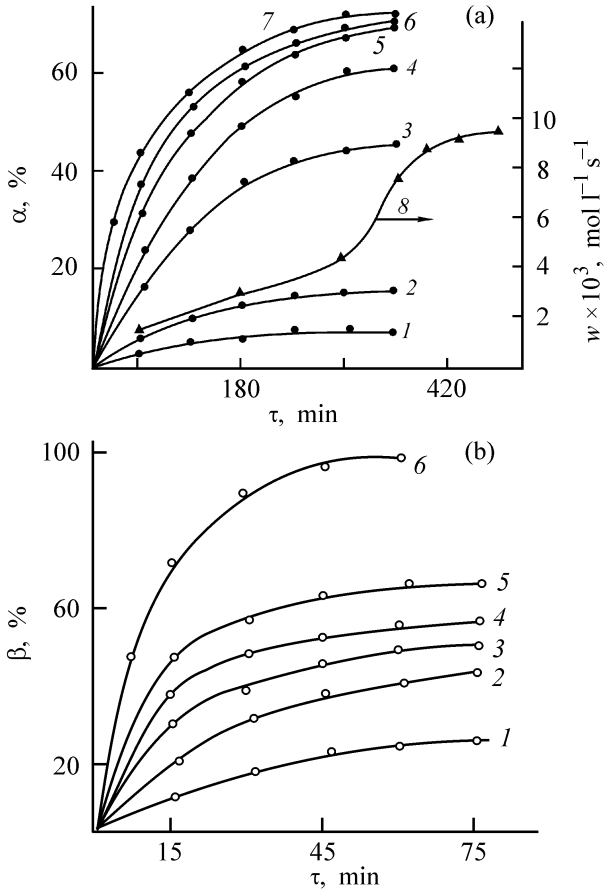


Fig. 1. (a) (*1–7*) Yields of bromotoluenes, α, and (*8*) rate of induced bromination, *w*, and (b) yield of Br_2, β, vs. the reaction time τ at 293 K. (a) Stirring rate (rpm): (*1*) 0, (*2*) 100, (*3*) 300, (*4*) 500, (*5*) 600, (*6*) 700, and (*7*) 800. (b) NaBr concentration (M): (*1*) 0.65, (*2*) 1.25, (*3*) 1.84, (*4*) 2.45 (*5*) 3.69, and (*6*) 5.26.

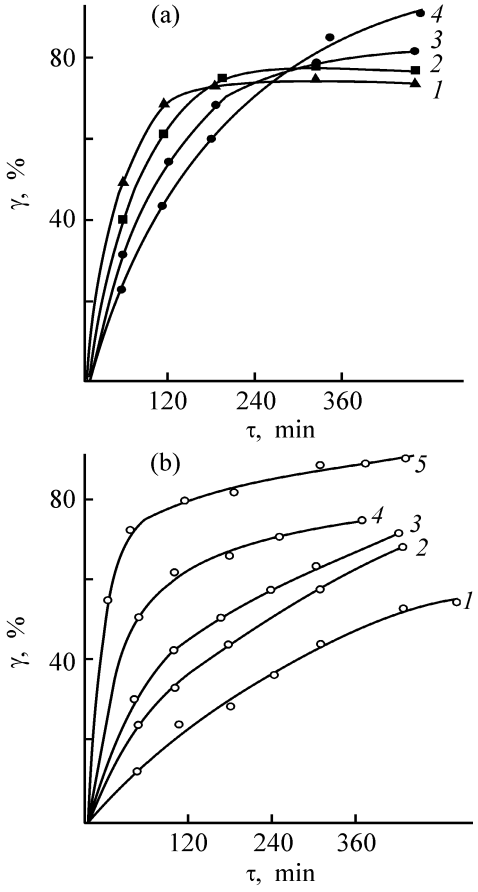


Fig. 2. Yield of a mixture of isomeric bromotoluenes, γ, at 293 K vs. time τ at (a) various times of H_2O_2 supply and (b) various initial concentrations of NaBr solutions. (a) (*1*) Simultaneous supply, (*2*) 60 min, (*3*) 120 min, and (*4*) 180 min. (b) $[NaBr]_0$, wt %: (*1*) 15, (*2*) 20, (*3*) 25, and (*4*) 30, and (*5*) 43.

mides and oxidants (Fig. 2a), monobromotoluenes are formed at 303 K at the initial rate of 1.25×10^{-2} (H_2O_2 oxidant) and 9.53×10^{-3} mol l^{-1} s^{-1} (NaOCl oxidant), and the yield of the desired product is 68%. Such a low yield of bromoarenes in the case of a simultaneous addition of H_2O_2 or NaOCl and the other reagents is apparently due to consumption of H_2O_2 and NaOCl in side reactions in the presence of HOBr and Br_2:

$$2MBr + 2HX + H_2O_2 \rightarrow Br_2 + 2MX + 2H_2O, \quad (2)$$

$$Br_2 + ArH \rightarrow ArBr \rightarrow HBr, \quad (3)$$

$$2HBr + H_2O_2 \rightarrow Br_2 + 2H_2O, \quad (4)$$

$$HBr + H_2O_2 \rightarrow HOBr + H_2O, \quad (5)$$

$$HOBr + ArH \rightarrow ArBr + H_2O, \quad (6)$$

$$H_2O_2 + Br_2 \rightarrow 2HBr + O_2, \quad (7)$$

$$HOBr + H_2O_2 \rightarrow H_2O + HBr + O_2. \quad (8)$$

Introduction of arenes into the reaction mixture and further gradual supply of the oxidant prevent nonproductive consumption of H_2O_2 and NaOCl by reactions (7) and (8) and thus provide a high yield of monobromoarenes.

To gain further insight into this process, we studied the oxidation of NaBr and HBr of various concentrations with H_2O_2 and NaOCl in the absence of arene. We found that no free bromine was formed in the presence of catalytic amounts (0.22 M) of HBr and NaBr. However, bromine was formed as the concentration of NaBr or HBr was raised from 0.65 to 5.26 M (Fig. 1b).

As can be seen from Fig. 1b, that raising the NaBr or HBr concentration in the above range makes higher the rate of their oxidation; the initial rate of bromine formation increases to 1.25×10^{1} mol l^{-1} s^{-1}, i.e, by more than an order of magnitude.

It should be noted that H_2O_2 and NaOCl decompose not only by reactions (7) and (8), but also through formation of hypobromous acid, which is less stable than NaOCl and H_2O_2 [3]:

$$\left.\begin{array}{l} H_2O_2 + HBr \\ NaOCl + HBr \end{array}\right\} \xrightarrow[-NaCl]{-H_2O} HOBr \rightarrow HBr + \frac{1}{2}O_2. \quad (9)$$

As can be seen from reaction (1), formation of intermediate HOBr and Br_2 is a reversible process, whereas the reactions of bromine or BrO^- anion with arenes are irreversible. No induced bromination occurs in the absence of H_2O_2 and NaOCl, because NaBr (KBr) or HBr are not involved in the electrophilic substitution in the aromatic ring. Thus, the induction in the above system only provides in situ formation of more reactive intermediates, which then effectively participate in the arene bromination.

Accumulation of the intermediate electrophilic reagent in the system probably occurs by the following scheme:

$$H_2O_2 + HBr \rightleftarrows H{-}\underset{\vdots}{O}{-}O{-}H \underset{-H_2O}{\rightleftarrows} HOBr, \quad \begin{matrix} \\ \vdots \\ HBr \end{matrix} \quad (10)$$

$$NaOCl + HBr \rightleftarrows Na{-}\underset{\vdots}{O}{-}Cl \underset{-NaCl}{\rightleftarrows} HOBr. \quad \begin{matrix} \\ \vdots \\ HBr \end{matrix}$$

With increasing concentrations of MBr or HBr, the rate of bromine formation grows [4]:

$$HOBr + HBr \rightleftarrows H_2O + Br_2. \quad (11)$$

In contrast to the formation of Br_2 and HOBr, bromination of arenes proceeds by the ionic mechanism [reactions (3) and (6)].

Both the yield of monobromoarenes and the rate of their formation increase with the content of NaBr (or KBr) in the system, which is due to increasing concentration of intermediate bromine and hypobromous acid. For example, at a NaBr concentration of 0.65 M, the yield of bromine in the first 15 min from the reaction start is 10% (Fig. 1b), and it increases to 72 wt % with the NaBr concentration increasing to 5.26 M. Hence, at a high concentration of MBr or HBr at beginning of the process, the bromination is predominantly effected by bromine formed in situ, and in further stages, by the BrO^- anion. The concentrations of MBr or HBr affect only the rate of induced bromination, whereas the process selectivity with respect to monobromoarenes is independent of this factor. With the NaBr concentration increasing from 15 to 43 wt %, the initial rate of monobromotoluene formation grows from 4.87×10^{-3} to 3.25×10^{-2} mol l^{-1} s^{-1} (Fig. 2b).

This rise in the bromination rate of arenes with increasing concentration of the above compounds is due not only to the easier formation of the intermediate brominating agent, but also to involvement of H_2O_2 and HBr molecules in the step of Br_2 and HOBr activation and to better solvation of the transition state:

$$Br^+{-}Br^- \cdots H{-}Br, \quad Br^+{-}Br^- \cdots H{-}O{-}H, \quad H{-}\underset{\vdots}{O}{-}Br^+. \quad \begin{matrix} \\ \\ HBr \end{matrix}$$

Various reaction parameters were studied in order to select the optimal reaction conditions. The yield of monobromoarenes and the process selectivity strongly depend on the ArH : NaBr : H_2O_2(NaOCl) molar ratio. The presence of electron-donor substituents in the benzene ring facilitates induced bromination. With the NaBr : H_2O_2(NaOCl) : arene molar ratio increasing from 1 : 1 : 1 to 4 : 1 : 1, the yield of bromoaromatic compounds grows from 38 to 64% (C_6H_5Br), from 82 to 98% ($CH_3C_6H_4Br$), from 64 to 94 ($C_2H_5C_6H_4Br$), from 52 to 69 (*iso*-$C_3H_7C_6H_4Br$), from 83 to 97 [1,2-$(CH_3)_2C_6H_3Br$), from 89 to 98 [1,3-$(CH_3)_2C_6H_3Br$), and from 89 to 98 [1,4-$(CH_3)_2C_6H_3Br$). Further increase in this ratio does not noticeably affect the yield of the desired product. With the molar ratio of benzene or its alkyl derivatives to the oxidant increasing from 1 to 4, the yield of the corresponding monobromoarenes grows from 5 to 15% per mole of converted hydrocarbon. However, in the case of ethyl- and isopropylbenzenes, we observed partial substitution of alkyl fragments with bromine (i.e., dealkylation and further bromination), with the formation of bromobenzene. In this case, the yield of bromobenzene increases from 1 to 23 and from 2 to 22% in the case of ethylbenzene and isopropylbenzene, respectively (Figs. 3a and 3b).

In this case, no dibromo derivatives are formed. The data of gas-liquid chromatography and IR and NMR spectroscopy showed that the content of a particular compound in the reaction products changes with temperature and nature of substituents in the aromatic

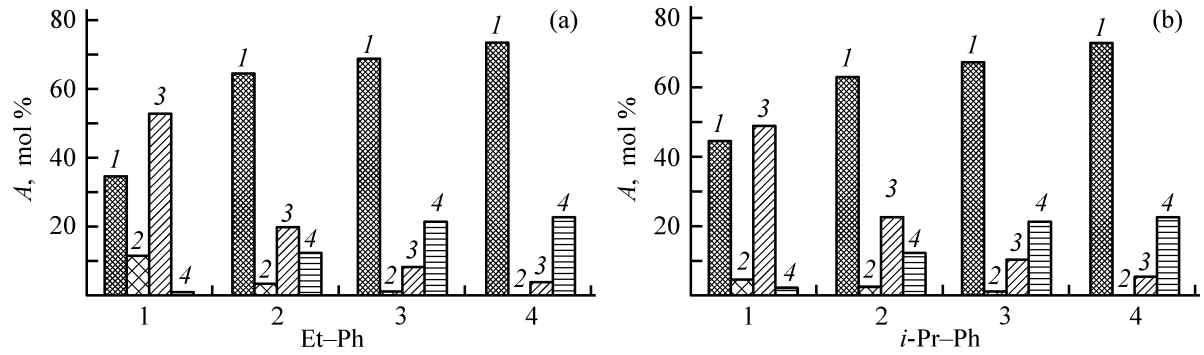


Fig. 3. Dependence of the catalyzate composition *A* on the on the molar ratio of (a) ethylbenzene and (b) isopropylbenzene to the oxidant. (a): (*1*) Et–Ph, (*2*) 2-Br–C_6H_4, (*3*) 4-Br–Et–C_6H_4, and (*4*) Br–Ph. (b): (*1*) *i*-Pr–Ph, (*2*) 2-Br–*i*-Pr–C_6H_4, (*3*) 4-Br–*i*-Pr–C_6H_4, and (*4*) Br–Ph.

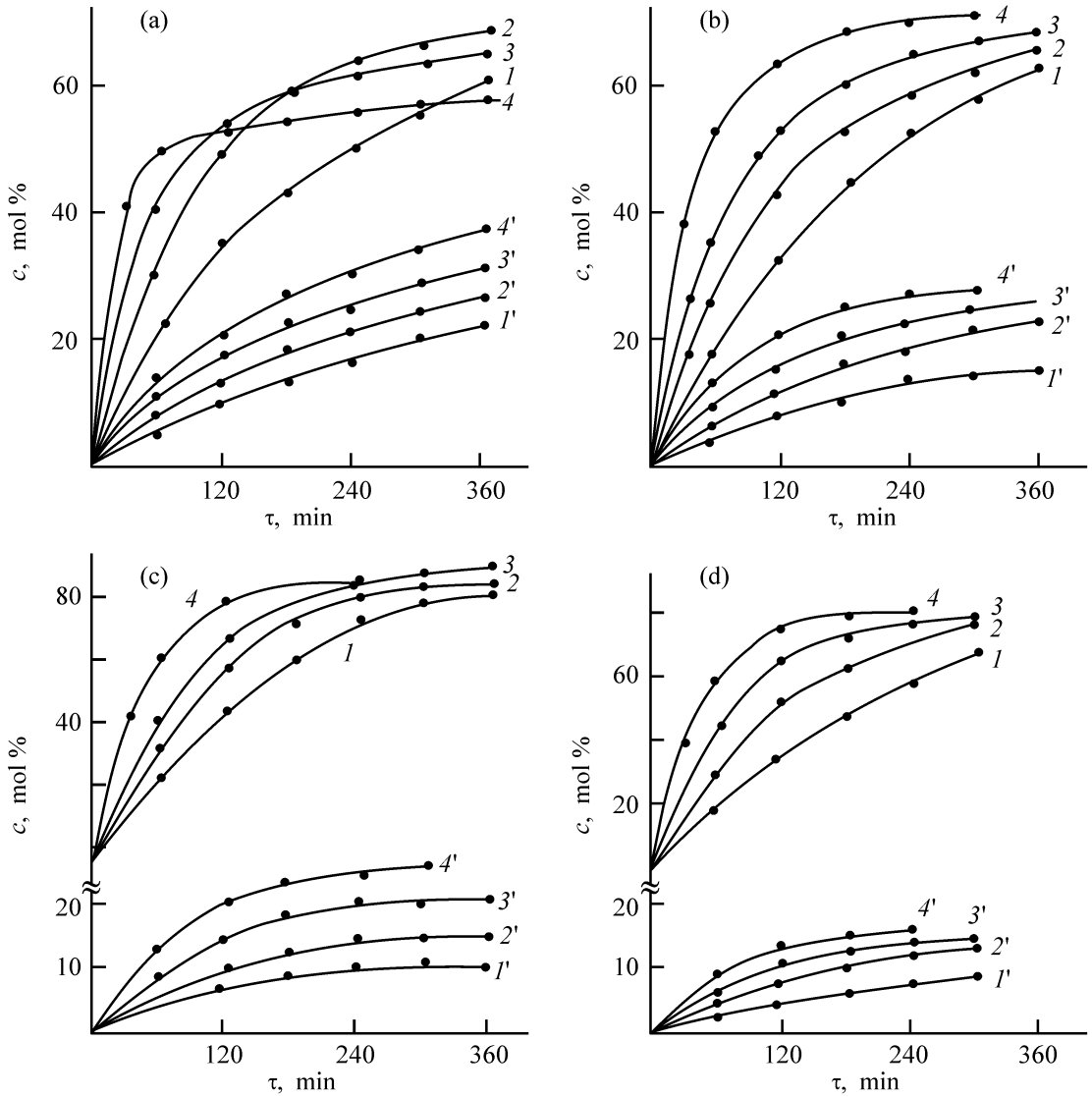


Fig. 4. Kinetics of accumulation *c* of isomeric bromoarenes (a) Br–Me–Ph, (b) Br–Et–Ph, (c) Br–*i*-Pr–Ph, and (d) Br–EtO–Ph. (τ) Time. (*1*–*4*) 4-Br and (*1*'–*4*') 2-Br derivatives. *T*, K: (*1*, *1*') 293, (*2*, *2*') 303, (*3*, *3*') 313, and (*4*, *4*') 323.

Table 1. Initial rate w, activation energy E, and entropy ΔS of induced bromination of aromatic compounds in the presence of various oxidants (293 K)

ArBr	Isomer	Oxidant					
		NaOCl			H_2O_2		
		$w \times 10^3$, mol l^{-1} min^{-1}	E_a, kJ mol^{-1}	$-\Delta S^{\neq}$, J mol^{-1} deg^{-1}	$w \times 10^3$, mol l^{-1} min^{-1}	E_a, kJ mol^{-1}	$-\Delta S^{\neq}$, J mol^{-1} deg^{-1}
Ph–Br		2.685	43.9	82.3	1.213	41.4	77.2
Me–Ph–Br	2-	0.93	34.6	73.4	2.142	46.9	86.9
	4-	3.75	38.3	77.4	2.524	55.6	91.2
Et–Ph–Br	2-	0.709	29.5	69.0	1.495	30.2	71.3
	4-	3.075	40.6	75.4	4.538	40.8	85.1
i-Pr–Ph–Br	2-	0.496	25.1	64.4	0.318	27.6	63.2
	4-	3.60	30.8	65.2	2.512	35.2	72.4
1,2-$(Me)_2$Ph–Br	3-	0.925	33.9	73.9	1.845	25.1	61.5
	4-	3.158	37.7	77.6	9.092	37.6	75.8
1,3-$(Me)_2$Ph–Br	4-	3.337	50.3	85.4	7.625	48.4	85.7
1,4-$(Me)_2$Ph–Br	2-	4.31	39.6	75.2	7.0	37.1	76.0
EtO–Ph–Br	2-	0.44	40.8	69.9	0.678	40.2	69.5
	4-	3.302	39.6	76.1	4.189	40.8	75.8

ring. For example, with the temperature increasing from 293 to 323 K, the yield of monobromobenzene grows from 54 to 75%. Under similar experimental conditions, the yields of monobromo derivatives of toluene, ethylbenzene, and isopropylbenzene grow from 91, 90, and 95 to 96, 97, and 97%, respectively. The same trend is observed in induced bromination of individual isomeric xylenes. In particular, 1,2-dimethylbenzene yields two isomers: 3-bromo- and 4-bromo-1,2-dimethylbenzene and, with the temperature increasing from 293 to 323 K, their total yield grows from 91 to 99%. Under similar conditions, 1,3- and 1,4-dimethylbenzene give only one isomer, and its yield increases from 94 and 88 to 98 and 94%, respectively.

Hence, we observed in the course of induced bromination of alkylbenzenes only substitution of the proton in the aromatic ring, whereas hydrogen atoms of the alkyl radical are not involved in the reaction.

To obtain comparable data on the reactivity of aromatic compounds in induced bromination, we performed special experiments with each hydrocarbon, with simultaneous charging of the starting reactants under similar conditions. From the data given in Figs. 4a, 4b, 4c, and 4d, we calculated the initial rates of formation of bromoarenes. These data show that the rate of substitution of hydrogen atoms in the aromatic ring of methyl-, ethyl-, and isopropylbenzenes in the *ortho* position is lower than that in the *para* position. With increasing size of the alkyl group, the difference between these rates becomes more pronounced (Table 1). For example, the rates of formation of 2-bromotoluene and 2-bromoethyl- and 2-bromoisopropylbenzenes in the presence of NaOCl are smaller than those of formation of 4-bromomethyl-, 4-bromoethyl-, and 4-bromoisopropylbenzenes by factors of 3.7, 5.2, and 10.2, respectively, and in the case of H_2O_2 oxidant, these rates differ by a factor of 1.2, 3.7, and 10.1, respectively. The activation energies are independent of the oxidant and decrease with increasing size of substituents (e.g., on passing from toluene and isopropylbenzene). However, due to a decrease in the activation entropy in the above series of aromatic compounds, the rate of formation of the *ortho* isomer decreases. A similar dependence was observed for catalytic chlorination of arenes in the liquid phase, which is due to the fact that formation of the σ complex with the *ortho* orientation of the aromatic ring becomes more hindered with increasing size of substituents [27]. Based on the isomer composition and using the equations given in [28], we calculated the partial rate factors and the selectivity [29] of induced bromination in the *ortho*

Table 2. Composition of isomers, partial rate factors *f*, and the selectivity S_f of induced bromination of aromatic compounds (293 K)

ArBr	Isomer	Isomer content, wt %	f_2	f_4	S_f
Me–Ph–Br	2-	10.2	0.54	10.0	2.73
	4-	80.5			
Et–Ph–Br	2-	24.2	0.895	14.7	3.1
	4-	65.3			
i-Pr–Ph–Br	2-	4.2	0.023	11.2	3.4
	4-	90.4			
1,2-$(Me)_2$Ph–Br	3-	40.5	1.85*	22.8	1.1
	4-	50.6			
EtO–Ph–Br	2-	8.5	0.143	10.7	2.18
	4-	78.6			

* Value corresponding to f_3.

and *para* positions for Me–Ph, Et–Ph, and *i*-Pr–Ph and in the *meta* and *para* positions for 1,2-$(Me)2C_6H_4$ (Table 2). It can be seen that the partial rate factor of induced bromination of methyl-, ethyl-, isopropyl-, and ethoxybenzenes is 0.54, 0.895, 0.023, and 0.143 for the *ortho* (f_2) isomers and 10, 14.7, 11.2, and 10.7 for the *para* (f_4) isomers. In the case of 1,2-dimethylbenzene, the following results were obtained: 1.85 for the *meta* (f_3) and 22.8 for *para* (f_4) isomers. These partial rate factors show that, in comparison with benzene, the *para* positions of the above compounds are activated to a greater extent than the ortho and *meta* positions. For monosubstituted derivatives, the reaction selectivity increases in the following order EtO–Ph < Me–Ph < Et–Ph < *i*-Pr–Ph. Using the known Brown–Nelson equation [29], we determined the relationship between the intra- and intermolecular selectivities of aromatic compounds studied and found that this system is characterized by an extremely low intramolecular selectivity but a very high intermolecular selectivity, i.e., it exhibits a high selectivity with respect to the *para* position of the aromatic ring.

CONCLUSIONS

(1) Induced bromination of arenes with metal bromides in the presence of H_2O_2 and HOCl proceeds by the radical-ion mechanism that involved in situ formed bromine and hypobromous acid, through substitution of a hydrogen atom in the benzene ring exclusively.

(2) Bromination is highly selective with respect to monobromo derivatives in the *para* position of the aromatic ring. With increasing molar content of ethyl- and isopropylbenzenes, formed by the yield of bromobenzene increases to 23% due to partial substitution of the alkyl groups with bromine atoms.

REFERENCES

1. Yukel'son, I.I., *Tekhnologiya osnovnogo organicheskogo sinteza* (Technology of Basic Organic Synthesis), Moscow: Khimiya, 1968.
2. Lebedev, N.N., *Khimiya i tekhnologiya osnovnogo i neftekhimicheskogo sinteza* (Chemistry and Technology of Basic and Petrochemical Syntheses), Moscow: Khimiya, 1975.
3. Shamb, W., Setterfield, C., and Wentworth, L., *Perekis' vodoroda* (Hydrogen Peroxide) Moscow: Izd. Inostr. Lit., 1958.
4. Muganlinskii, F.F. and Guseinov, M.M., *Zh. Vses. Khim. O–va im. D.I. Mendeleeva*, 1985, vol. 30, no. 3, pp. 340–345.
5. Salakhov, M.S., Guseinov, M.M., Mamedov, Ya.N., et al., *Zh. Prikl. Khim.*, 1978, vol. 41, no. 6, pp. 1428–1430.
6. USSR Inventor's Certificate, no. 776033.
7. Sadykhzade, S.I., Aliev, A.B., Mustafaev, R.I., and Kuliev, L.G., *Azerb. Khim. Zh.*, 1977, no. 5, pp. 42–47.
8. Salakhov, M.S., Guseinov, M.M., Chalabiev, Ch.A., and Abdullaev, D.K., *Neftekhimiya*, 1974, vol. 14, no. 3, pp. 471–475.
9. Salakhov, M.S., Guseinov, M.M., Chalabiev, Ch.A., and Abdullaev, D.K., *Neftekhimiya*, 1975, vol. 15, no. 4, pp. 601–603.
10. Salakhov, M.S., Guseinov, M.M., Chalabiev, Ch.A., and Abdullaev, D.K., *Azerb. Neft. Khoz.*, 1975, no. 2, pp. 61–62.
11. Salakhov, M.S., Guseinov, M.M., Chalabiev, Ch.A., and Mamedova, O.M., *Zh. Prikl. Khim.*, 1980, vol. 53, no. 5, pp. 1122–1125.
12. Salakhov, M.S., Guseinov, M.M., Chalabiev, Ch.A., and Mamedova, O.M., *Azerb. Khim. Zh.*, 1984, vol. 53, no. 5, pp. 69–72.
13. Samadumov, A. and Ostanina, V.A., *Izv. Vyssh. Uchebn. Zaved., Khim. Khim. Tekhnol.*, 1980, vol. 23, no. 9, pp. 1079–1084.
14. Fedorishcheva, M.N., Ariko, N.G., and Mistkevich, N.M., *Neftekhimiya*, 1987, vol. 27, no. 6, pp. 787–790.
15. Tmenov, D.I., Lysukho, T.V., and Shcherbina, F.F., *Neftekhimiya*, 1977, vol. 17, no. 1, pp. 120–123.
16. USSR Inventor's Certificate, no. 1468896.
17. USSR Inventor's Certificate, no. 1768574.
18. Sadygov, O.A., Gurbanov, M.Sh., and Chalabiev, Ch.A., *Neftekhim.*, 1990, vol. 30, no. 1, pp. 109–112.

19. Sadygov, O.A., Gurbanov, M.Sh., and Chalabiev, Ch.A., *Khim. Prom–st.*, 1991, no. 12, pp. 717–719.
20. Sadygov, O.A., Gurbanov, M.Sh., and Chalabiev, Ch.A., *Vysokomol. Soedin.*, 1992, vol. 33, no. 6, pp. 58–63.
21. Redutko, N.V. and Kashieva, A.I., *Dokl. Akad. Nauk SSSR*, 1975, vol. 220, no. 4, pp. 884–887.
22. Ivanov, S. and Khinkova, M., *Neftekhimiya*, 1997, vol. 37, no. 1, pp. 124–128.
23. Vatsuro, K.V. and Mishchenko, G.L., *Imennye reaktsii v organicheskou khimii* (Named Reactions in Organic Chemistry), Moscow: Khimiya, 1976.
24. Babko, A.K. and Pyatnitskii, I.V., *Kolichestvennyi analiz* (Quantitative Analysis), Moscow: Mir, 1962.
25. Emanuel', N.M. and Knorre, D.G., *Kurs khimicheskoi kinetiki* (Course of Chemical Kinetics), Moscow: Vysshaya Shkola, 1984.
26. Schmid, R. and Sapunov, V.N., *Non-Formal Kinetics*, Weinheim: Chemie, 1982.
27. Chalabiev, Ch.A. and Abdullaev, D.K., *Azerb. Khim. Zh.*, 2003, no. 3, pp. 62–66.
28. Yankovskaya, L.A., *Sovremennye teoreticheskie osnovy organicheskoi khimii* (Modern Theoretical Bases of Organic Chemistry), Moscow: Khimiya, 1978.
29. Brown, H.C. and Nelson, K.L.R., *J. Am. Chem. Soc.*, 1953, vol. 75, no. 23, pp. 6292–6299.

ISSN 1070-4272, Russian Journal of Applied Chemistry, 2006, Vol. 79, No. 6, pp. 957–966. © Pleiades Publishing, Inc., 2006.
Original Russian Text © A.A. Kotomin, A.S. Kozlov, 2006, published in Zhurnal Prikladnoi Khimii, 2006, Vol. 79, No. 6, pp. 966–977.

ORGANIC SYNTHESIS AND INDUSTRIAL ORGANIC CHEMISTRY

Calculation of Densities of Organic Compounds from Contributions of Molecular Fragments

A. A. Kotomin and A. S. Kozlov

St. Petersburg State Technological Institute, St. Petersburg, Russia

Received October 28, 2005

Abstract—A method for calculating the densities of organic compounds from the contributions of molecular fragments was suggested. A correlation between the densities of solid and liquid substances at 20°C was examined.

DOI: 10.1134/S1070427206060176

Density is one of the main characteristics of substances. It is connected with the fundamental physicochemical properties of substances and performance of materials produced from them. Along with performing a molecular design, it is necessary to forecast the properties of organic compounds to be synthesized, including density, which is required to design the production process. Therefore, the development of the most general and precise methods of density calculations is an topical problem, especially for high-energy-capacity substances whose density largely determines the efficiency, detonation power, sensitivity, and tendency for passing from combustion to detonation. Density is used in calculations of the detonation rate, explosion energy, burning rate, detonation critical diameter, and parameters of the impact of the explosion on the environment [1–8].

All the known methods of density calculation can be divided into three groups.

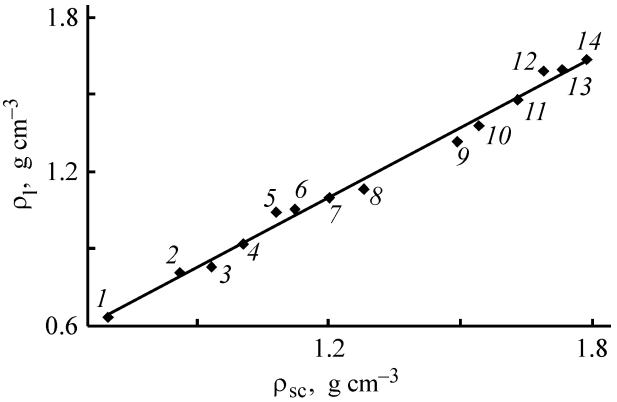
Theoretical methods. Molecular mechanics methods of Stine and Keddy allow calculation of the density of a substance from the basic physical characteristics of the molecules, such as van der Waals atomic radius, interatomic distances and angles, etc. In so doing, principles of simulation of the molecular structure of solids and molecular crystal packing for various steric configurations are used [9–12].

Empirical methods. The Smirnov, Tarver, Immirizi, and Perini methods are additive and allow calculation of the molar volume and substance density using atomic or group contributions, and also correction and other factors calculated directly from the measured densities of various types of organic compounds [13, 14].

Semiempirical methods. Piacenza, Jacob, Graindorge, Blaive, and Gallo methods include both physical characteristics of molecules and empirical coefficients [10].

The majority of methods estimating the density through the atomic and group contributions operate with a limited set of these and hence are insufficiently general or have poor accuracy. For solid substances, the theoretical, semiempirical, and empirical methods give average relative calculation errors of 5.0–6.0, 3.0–3.5, and 2.0–3.0%, respectively. Therefore, studies of correlations between the density and chemical structure of the compounds and the development of modern calculation methods are of interest.

We suggested a calculation method based on contributions of molecular fragments. A complex system of contributions to the molar volume was developed for solid substances: aliphatic, alicyclic, aromatic, and heteroaromatic compounds, including annelated and skeleton compounds, and for combined structures consisting of alicyclic and aromatic (heteroaromatic) rings. The corrections for fragment interaction, structure type, and bonding between rings, allowing finer consideration of the structural features, were found. The contributions and corrections were derived from the experimental densities and, correspondingly, from the molar volumes of more than 6000 organic substances [15–34]. The molar volume of each fragment was calculated for 15–25 compounds containing this fragment.



Correlation between the densities of aliphatic compounds in the solid (ρ_{sc}) and liquid (ρ_l) states. (*1*) *N*,*N*,*N*-Trimethylnitramine, (*2*) butanol, (*3*) diethyl acetal, (*4*) 2,2-difluoropropane, (*5*) 1-nitroethane, (*6*) *N*,*N*-diethylnitramine, (*7*) ethyl nitrate, (*8*) 3-nitrobutanol, (*9*) triethylene glycol dinitrate, (*10*) diethylene glycol dinitrate, (*11*) ethylene glycol dinitrate, (*12*) bis-(fluorodinitroethyl) formal, (*13*) glycerol trinitrate, and (14) nitroisobutylglycerol trinitrate.

In this method, the structural components are molecular fragments whose contributions take into account the interaction of the elements within the fragments and with the nearest atoms. Such fragments are functional groups and, for certain structures, atoms. Division of molecules into fragments is performed step by step from larger to smaller fragments. Initially, the molecule is divided into larger fragments, and then, the residual part of the molecule is divided into smaller fragments, and the probable residue, into atoms. The sum of the molecular weights of the fragments is equal to the molecular weight of the compound.

The molar volumes and molecular weights of the molecular fragments of solid organic compounds and the above corrections are listed in Tables 1–9. The structural fragments into which molecule of various classes should be divided are shown in Tables 1, 3, and 6.

Interaction of electronegative groups, H bonding, and steric factors were considered both in the fragment contributions dependent on the surrounding and in various corrections. Special attention was paid to high-energy-capacity substances. The densities of salts, coordination compounds, and crystal hydrates can also be calculated. Such compounds can contain C, H, N, O, S, F, Cl, Br, I, Na, K, Fe, and Co atoms.

Using mathematical methods of analysis [35], we found linear correlations between the densities of organic compounds of various classes in the solid and liquid states at 20°C, which allow prediction of the densities of liquid organic substances. For example, such a correlation for aliphatic compounds is shown in the figure: along the abscissa are the densities of solid compounds calculated by our method, and along the ordinate, the experimental densities for the liquid state. The correlation coefficient is 0.99.

The method developed allows calculation of densities at the standard temperature of 20°C with the average relative error of 1.5% for solid substances and 2.5% for liquids. The maximal error does not exceed 3.5%. The method can be used in scientific research and for express estimation of the densities of new high-energy-capacity and other organic compounds in the step of synthesis planning. The density of a solid organic compound is determined as

$$\rho_{sc} = M/V,$$

where $M = \Sigma M_i$; $V = \Sigma V_i + \Sigma \delta_i$; ρ_{sc}, density of a single crystal of an organic substance; M, molecular weight of the compound; M_i, molecular weight of the fragment; V, molar volume of the compound; V_i, molar volume of the fragment; and $\Sigma \delta_i$, sum of corrections for fragment interactions, structure type, and bonding between rings.

The density of a liquid organic substance is given by

$$\rho_l = k\rho_{sc},$$

where ρ_l is the density of a liquid substance and k, coefficient (k = 0.92 for aliphatic and alicyclic compounds; k = 0.88 for aromatic and heteroaromatic compounds, and k = 0.90 for combined structures including alicyclic and aromatic or heteroaromatic rings).

The calculated density of a liquid substance at 20°C can be recalculated to another temperature by the methods described in [36, 37].

Three examples of calculations of the density of various organic compounds are presented below.

(1) Aliphatic compound: glycerol trinitrate (nitroglycerol), $C_3H_5O_9N_3$, M = 227.09, liquid substance, mp 13.5°C:

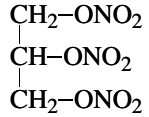


Table 1. Fragment contributions for calculation of the molar volume of aliphatic compounds

Fragment	V_i	M_i
Fragments containing: C, CH, CH_2, CH_3		
$-CH_3$ (for *ortho* esters, formals, acetals)	28.52 24.69	15.03
$-CH_2-$	14.77	14.03
$-\underset{\vert}{CH}-$	1.76	13.02
$\rangle C\langle$	–8.92	12.01
$=CH_2$	25.93	14.03
$=CH-$	13.05	13.02
$\rangle C=$	–2.85	12.01
$=C=$	6.32	12.01
$\equiv CH$	23.02	13.02
$\equiv C-$	7.92	12.01
Fragments containing: OH, O, CO, COO		
$-OH$	11.77	17.01
$-O-$	4.19	16.00
$(N)\rightarrow O$	5.87	16.00
$-C(=O)-O-$	21.83	44.00
$-C(=O)-H$	22.47	29.02
$-C(=O)-OH$	23.35	45.01
$(C)_2C=O$	9.71	28.01
$(C,O)(N,O)C=O$	12.83	28.01
$(N)_2C=O$	14.89	28.01
$=C=O$	22.95	28.01
$H_2C(O-)_2$	38.35	46.02
$-HC(O-)_2$	23.03	45.01
$HC(O-)_3$	34.61	61.00
$-C(O-)_3$	18.74	59.99
$-O-C(O-)_2-O-$	37.27	76.00
$O=C(O-)_2$	24.38	59.99
$F_2C(O-)_2$	46.45	82.00
$(NF_2)_2C(O-)_2$	82.61	148.01
Fragments containing: N, NH, NH_2, N_3, CN, CNH, NOH		
$-NH_2$ (in position 1,2 with $-NO_2$, $-COOH$)	15.52 11.96	16.03
$-NH-$	6.03	15.01
$\rangle N-$	–2.25	14.01
$-N=$	7.03	14.01
$(N)_2C=NH$	15.75	27.03
$(C)_2C=N-$	3.64	26.02
$(N)_2C=N-$	9.62	26.02
$-N=C=N-$	17.63	40.03
$-C\equiv N$	21.00	26.02
$-N_3$	29.87	42.02
$=NOH$	15.28	31.02
Fragments containing: NO_2, ONO_2, NO		
$-CH_2NO_2$	40.47	60.02
$\rangle CHNO_2$	24.72	59.01
$=CHNO_2$	36.05	59.01
$\rangle CNO_2$	18.64	58.01
$-CH(NO_2)_2$	53.28	105.01
$\rangle C(NO_2)_2$	41.69	104.00
$=C(NO_2)_2$	50.17	104.00
$-C(NO_2)_3$	75.40	150.00
$-CH_2ONO_2$	46.77	76.02
$\rangle CNONO_2$	39.24	75.01
$\rangle C(CH_2ONO_2)_2$	104.80	164.13
$-C(CH_2ONO_2)_3$	145.64	240.19
$-ONO$	22.57	46.01
$-C(NO_2)_2F$	63.85	123.00
$F_2C(-NO_2)_2$	59.71	69.00
$-OC(NO_2)_2F$	72.02	138.99
Fragments containing: NNO_2, $NHNO_2$		
$-NHNO_2$	30.44	61.01
$\rangle NNO_2$	17.69	60.00
$-N(NO_2)_2$	50.58	106.00
$(N)_2C=NNO_2$	36.24	72.01

Table 1. (Contd.)

Fragment	V_i	M_i
Fragments containing: F, Cl, Br, S		
$-CF_3$	46.37	69.01
$-CHF_2$	37.22	51.02
$-CF_2-$	21.75	50.01
$-OCF_3$	52.81	85.00
$-NF_2$	30.02	52.00
$-F$	15.49	19.00
$-Cl$	21.14	35.45
$-CCl_3$	67.01	118.36
$-C(=O)Cl$	36.59	63.46
$-Br$	25.02	79.90
$-S-$	12.99	32.06
$-SH$	24.46	33.07
$=S$	17.21	32.06
$(C)_2C=S$	13.82	44.07
$(N)_2C=S$	19.80	44.07
$>S(=O)_2$	27.52	64.06
$-O-S(=O)-O-$	33.64	80.06
$-O-S(=O)_2-O-$	36.09	96.06
Ionic fragments		
$^+NH_4$	17.45	18.04
$^+N_2H_5$	30.36	33.07
$N(CH_3)_4^+$	81.64	74.15
$-\overset{+}{N}H_3$	23.59	17.03
Na^+	8.84	22.99
K^+	16.71	39.10
Fe^{2+}	4.38	55.85
Co^{2+}, Co^{3+}	4.49	58.93
^-OH	10.40	17.01
$^-NO_3$	29.02	61.99
$^-NO_2$	21.76	46.00
$^-N_3$	27.59	42.02
$^-N(NO_2)_2$	45.30	106.00
$^-C(NO_2)_3$	67.18	150.00
$-\bar{N}NO_2$	17.83	60.00
$-\bar{C}(NO_2)_2$	40.21	104.00
^-CN	22.14	26.02
F^-	9.20	19.00
Cl^-	17.68	35.45
ClO_3^-	35.58	83.45
ClO_4^-	41.83	99.45
Br^-	22.97	79.90
HCO_3^-	30.97	61.02
CO_3^{2-}	22.21	60.01
SO_3^{2-}	30.19	80.06
HSO_4^-	47.22	97.07
SO_4^{2-}	36.53	96.06
For coordination compounds and crystal hydrates		
NH_3	15.91	17.03
H_2O	15.90	18.02

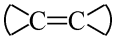
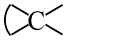
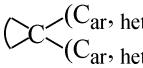
Table 2. Corrections for fragment interaction (for each) in aliphatic compounds

Fragments	δ_i	Fragment	δ_i	Fragments	δ_i	Fragment	δ_i
$-OH\ldots-OH$ (position 1,2; vic)	+1.56	$>NNO_2\ldots>C=O$ $-NO_2\ldots>C=O$ α-nitro(nitramino)carbonyl	+3.88	$>NNO_2\ldots-N_3$ (position 1,1; gem)	+1.78	$=NNO_2\ldots>NNO_2$ (position 1,1; gem)	+11.06
$-NO_2\ldots NO_2$ $-NO_2\ldots ONO_2$ $-ONO_2\ldots ONO_2$ (position 1,2; vic)	+0.42	$-NHNO_2\ldots-NHNO_2$ $-NHNO_2\ldots>NNO_2$ $>NNO_2\ldots>NNO_2$ $=NNO_2\ldots-NHNO_2$ (position 1,1; gem)	+1.24	$-NF_2\ldots-NO_2$ (position 1,1; gem)	+1.38	$-Cl\ldots-Cl$ $-Cl\ldots-NO_2$ (position 1,1; gem)	+2.23
				$-OH\ldots-C(=O)OH$ (position 1,2; vic)	+4.42	$>C=O\ldots>C=O$ (position 1,2; vic)	+4.50

Notes: (1) For aliphatic compounds, the molar volume includes the sum of fragment contributions (Table 1) and corrections for their interaction listed in Table 2.

(2) Atom indicated in parentheses is not included into the molar volume of the fragment. When a fragment is not connected with an atom in parentheses, it is connected with any atom.

Table 3. Fragment contributions for calculating the molar volume of alicyclic compounds

Fragment	V_i	M_i
Fragments containing: C, CH, CH_2		
$(C_c)-CH_2-(C_c)$	16.60	14.03
$(C_c)-CH_2-(N_c)$	17.00	14.03
$(N_c)-CH_2-(N_c)$	19.92	14.03
$(O_c)-CH_2-(C_c)$	17.30	14.03
$(O_c)-CH_2-(N_c)$	17.77	14.03
$(O_c)-CH_2-(O_c)$	19.09	14.03
$(C_c)_2CH-(C_c)$	5.47*	13.02
$(N_c)_2CH-(C_c)$	14.34*	13.02
$(N_c)_2CH-(N_c)$	17.06*	13.02
$(O_c)_2CH-(C_c)$	10.28*	13.02
$(C_c)_2CH-(N_c, C_c)$	10.01*	13.02
$(O_c)(C_c)CH-(N_c)$	12.76*	13.02
$(A_c)_2CH-$	5.38	13.02
$(C_c)_2(A_c)C-$	–5.63	12.01
$(A_c)-CH=CH-(A_c)$	27.89	26.04
$(A_c)-CH=C(C, A_c)(A_c)$	13.98	25.03
$(C_c)_2C=$	–2.92	24.02
$(A_c)-C(C, A_c)=C(C, A_c)-(A_c)$	–1.75	24.02
	26.50	24.02
	–8.90	12.01
	–5.52	12.01
	26.61	12.01
Fragments containing: NO_2, ONO_2, NO		
$(C_c)_2CHNO_2$	28.40	59.02
$(C_c)-NO_2$	25.64	46.01
$(C_c)_3(C_c)-CNO_2$	23.25*	58.01
$(C_c)_2C(NO_2)_2$	44.47	104.00
$(C_c)_2CHONO_2$	38.27	75.01
$(C_c)_3(C_c)-CNO$	11.57*	42.01
Fragments containing: NNO_2, $NHNO_2$, NNO		
$(C_c)_2NNO_2$	21.22	60.00
$(C_c)-NHNO_2$	31.05	61.01
$(C_c)_2NNO$	15.30	44.01
$(N_c)_2C=NNO_2$	40.18	72.01
Fragments containing: N, NH, CH, NOH		
$(C_c)-NH-(C_c, N_c)$	7.26	15.02
$(C_c)_2N-(C_c)$	–3.92*	14.01
$(C_c)_2N-$	–2.61	14.01
$(A_c)-CH=N-(A_c)$	20.48	27.03
$(C, A_c)(A_c)C=N-(A_c)$	10.54	26.02
$(C_c)-N=N-(C_c)$	24.82	28.01
$(C_c)_2C=NOH$	18.37	43.02
Fragments containing: O, CO		
$(C_c)-O-(C_c)$	5.05	15.99
$(C_c)-O-(O_c)$	6.52	15.99
$(C_c)(A_c)C=O$	12.41	28.01
$(O_c)_2C=O$	16.69	28.01
$(N_c)_2C=O$	13.34	28.01
Fragments containing: F, S		
$(C_c)_2C(NF_2)_2$	62.13	116.03
$(A_c)_2SO_2$	25.36	64.05

Note: * For nodal atoms of annelated and framework structures.

Table 4. Corrections for fragment interaction (for each) in alicyclic compounds

Fragments	δ_i
$(C_c)_2C(NO_2)_2 \cdots (C_c)_2C(NO_2)_2$ (position 2,4 in framework structures)	+8.18
$(N_c)_2C{=}O \cdots (C_c)(C_c,N_c)NH$ (vicinal position)	–2.35
$(N_c)_2C{=}O \cdots (C_c)_2NNO_2$ (vicinal position)	+2.29

Table 5. Corrections for structure type of alicyclic compounds

Structure type	δ_i
3-membered	+11.55
4-membered	+7.13
5-membered	+3.54
6-membered	0.00
7-membered	–4.63
8-membered	–8.79
9-membered	–12.54
10-membered	–15.12
11-membered	–15.86
12-membered	–16.34
16-membered	–10.30
Adamantane	+3.50
Cubane	+38.24

Notes: (1) For alicyclic compounds, the molar volume includes the sum of contributions of the ring (Table 3), corrections for their interaction (Table 4), and correction for structure type (Table 5). For side chains and fragments between rings, the contributions for aliphatic compounds (Table 1) are used. For polycyclic and framework structures, the molar volume includes the sum of corrections for structure type for all the rings in the compound.

(2) Atom in parentheses is not included in the fragment molar volume (A_c denotes any atom of the ring). When the fragment is not connected with an atom in parentheses, it is connected with any atom of the side chain or any other ring.

The molar volume of nitroglycerol includes fragment contributions (Table 1) and corrections for fragment interaction (Table 2).

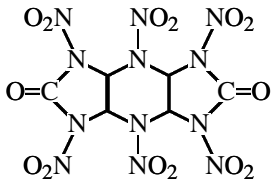
The molar volume is calculated as the sum of the fragment contributions and corrections:

$$V = \Sigma V_i + \Sigma \delta_i = 46.77 \times 2 + 39.24 + 0.42 \times 2$$

$$= 133.62 \text{ cm}^3 \text{ mol}^{-1}.$$

Density of solid nitroglycerol $\rho_{sc} = M/V = 227.09/133.62 = 1.70$ g cm^{-3} (experimental value: 1.73 g cm^{-3}). Density of liquid nitroglycerol: $\rho_l = k\rho_{sc} = 0.92 \times 1.70 = 1.57$ g cm^{-3} (experimental value: 1.60 g cm^{-3}).

(2) Condensed alicyclic compound: 2,6-dioxo-1,3,4,5,7,8-hexanitrodecahydro-1*H*,5*H*-diimidazopyrazine (Hexanitroglycoluryl), $C_6H_4O_{14}N_{12}$, $M = 468.18$, solid compound:



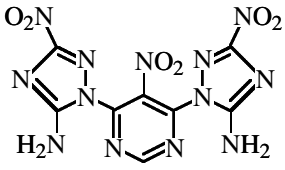
The molar volume of Hexanitroglycoluryl includes fragment contributions (Table 3), corrections for fragment interaction (Table 4), and corrections for structure type (Table 5).

$$V = \Sigma V_i + \Sigma \delta_i = 14.34 \times 4 + 21.22 \times 6 + 13.34 \times 2$$

$$+ 2.29 \times 4 + 3.54 \times 2 = 227.60 \text{ cm}^3 \text{ mol}^{-1}.$$

The density of Hexanitroglycoluryl $\rho_{sc} = M/V = 468.18/227.60 = 2.06$ g cm^{-3} (experimental value: 2.07 g cm^{-3}).

(3) Polycyclic heteroaromatic compound: bis-2,4-(3-nitro-5-aminotriazol-1-yl)-3-nitropyrimidine (DANTNP), $C_8H_5O_6H_{13}$, $M = 379.22$, solid substance:



The molar volume of DANTNP includes fragment contributions (Table 6) and corrections for the bond between rings (Table 7).

$$V = \Sigma V_i + \Sigma \delta_i = 34.80 + 28.68 \times 2 + 25.78 \times 3$$

$$+ 11.74 \times 2 + 7.96 + 1.16 \times 2 = 203.26 \text{ cm}^3 \text{ mol}^{-1}.$$

Table 6. Fragment contributions for calculation of the molar volume of aromatic and heteroaromatic compounds

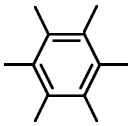
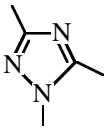
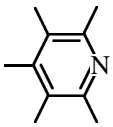
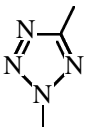
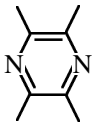
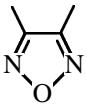
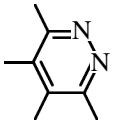
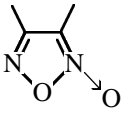
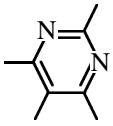
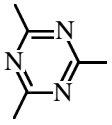
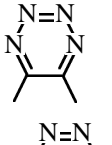
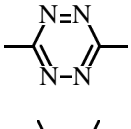
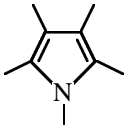
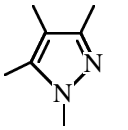
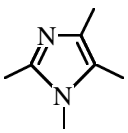
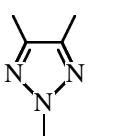
Fragment	V_i	M_i	Fragment	V_i	M_i
Rings			Rings		
	23.52	72.06		28.68	66.04
	28.06	74.06		32.29	68.04
	32.39	76.06		33.94	68.03
	33.68	76.06		39.78	84.02
	34.80	76.06	Fragments containing: H, CH, CH_2, CH_3		
	35.30	78.05	$(C_{ar,het})$–H	7.96	1.01
	37.81	80.05	(N_{het})–H	5.63	1.01
	36.94	80.05	$(C_{ar,het}, N_{het})$–CH_3	22.04	15.03
	21.97	62.06	$(C_{ar,het})$–CH_2	10.19	14.03
	22.79	64.05	(N_{het})–CH_2	16.72	14.03
	25.79	64.05	$(C_{ar,het})$–CH_2–$(C_{ar,het}, A_c)$	16.20	14.03
	28.31	66.04	$(C_{ar,het})$–CH– |	–0.70	13.02
			$(C_{ar,het})$–C– |	–16.03	12.01
			$(C_{ar,het}, N_{het})$–CH=	12.60	13.02
			$(C_{ar,het})$–C= |	–6.56	12.01
			Fragments containing: N, NH, NH_2, N_3, NF_2		
			$(C_{ar,het}, N_{het})$–NH_2 (in the presence of NH_2 substituent in the ring)	14.96 11.74	16.02
			$(C_{ar,het})$–NH–	3.83	15.01
			$(C_{ar,het})$–$NHNH_2$	24.50	13.04
			$(C_{ar,het})$–C(=NH)–$(C_{ar,het})$	20.47	13.02
			$(C_{ar,het})$–N_3	30.78	42.02
			$(C_{ar,het})$–N(C, N)(C)	–7.73	14.01

Table 6. (Contd.)

Fragment	V_i	M_i
Fragments containing: N, NH, NH_2, N_3, NF_2		
$(C_{ar,\,het})-N<^{(C,\,C_{ar,\,het})}_{(C_{ar,\,het})}$	2.14	14.01
$(C_{ar,\,het})-NF_2$	29.64	52.00
$(C_{ar,\,het})-CH(NF_2)_2$	65.40	117.03
$(C_{ar,\,het})-NH-(C_{ar,\,het})$	16.74	15.01
$(C_{ar,\,het})-NHNH-(C_{ar,\,het})$	28.49	30.03
$(C_{ar,\,het})-N=N-(C_{ar,\,het})$		
for coplanar system	13.87	28.01
for noncoplanar system	23.01	
$(N_{het})-N=N-(N_{het})$	28.71	28.01
$(C_{ar,\,het})=N-(C_{ar,\,het})$	8.67	14.01
$(C_{ar,\,het})-N(\rightarrow O)-(C_{ar,\,het})$	27.13	44.01
$(C_{ar,\,het})-C\equiv N$	25.27	26.02
Fragments containing: NO_2, ONO_2, NO		
$(C_{ar,\,het},\ N_{het})-NO_2$	25.78	45.99
$(C_{ar,\,het})-NO$	10.96	30.00
$(C_{ar,\,het},\ N_{het})-CH(NO_2)_2$	56.72	105.01
$(C_{ar,\,het},\ N_{het})-C(NO_2)_3$	80.17	150.00
$(C_{ar,\,het},\ N_{het})-C(NO_2)_2$	45.56	104.00
$(C_{ar,\,het},\ N_{het})-C(NO_2)_2F$	62.55	123.00
$(C_{ar,\,het})-C(NO_2)_2Cl$	71.33	139.46
$(N_{het})-C(NO_2)_2NF_2$	83.04	156.00
$(C_{het})-CH_2ONO_2$	48.11	76.02
$(N_{het})-CH_2ONO_2$	43.39	76.02
Fragments containing: NNO_2, $NHNO_2$		
$(C_{ar,\,het})-NHNO_2$	27.69	61.01
$(C_{ar})-N<^{}_{NO_2}$	19.62	60.00
$(C_{het})-N<^{NO_2}_{}$	27.67	60.00
$(C_{ar,\,het})-N(\rightarrow O)-NO_2$	49.27	90.00

Fragment	V_i	M_i
Fragments containing: OH, O, CO, COO		
$(C_{ar,\,het})-OH$	12.49	17.00
$(C_{ar,\,het})-O-$	4.82	15.99
$(C_{ar,\,het})-OCH_3$	26.99	31.03
$(C_{ar,\,het})-C(=O)-$	11.08	28.01
$(C_{ar,\,het})-C(=O)OH$	25.80	45.00
$(C_{ar,\,het})-C(=O)-O-$	15.74	44.00
$(C_{ar,\,het})-C(=O)H$	21.31	29.01
$(N_{het})\rightarrow O$	5.41	15.99
$(C_{ar,\,het})-O-(C_{ar,\,het})$	8.46	15.99
$(C_{ar,\,het})-C(=O)-(C_{ar,\,het})$	32.24	28.01
Fragments containing: F, Cl, Br, S		
$(C_{ar,\,het})-F$	13.13	19.00
$(N_{het})-F$	9.99	19.00
$(C_{ar,\,het})-Cl$	22.12	35.45
$(N_{het})-Cl$	19.93	35.45
$(C_{ar,\,het})-Br$	26.53	79.90
$(C_{ar,\,het})-I$	28.17	126.90
$(C_{ar,\,het})-CF_3$	38.00	69.01
$(C_{ar,\,het})-S-(C_{ar,\,het})$	31.72	32.06
Ionic fragments		
$(C_{ar,\,het})-\bar{O}$	9.06	15.99
$(C_{het})-\bar{C}(NO_2)_2$	35.99	104.00
$(N_{het})-\bar{C}(NO_2)_2$	41.33	104.00
$(N_{het})-\bar{N}NO_2$	22.61	60.00

Table 7. Corrections for the bonds between aromatic (heteroaromatic) rings

Bond	δ_i	Bond	δ_i
(C_{ar})–(C_{ar})	+5.39	(C_{ar})–(N_{het})	+2.28
$(C_{ar,het})$–(C_{het})	+1.97	(C_{het})–(N_{het})	+1.16

Table 8. Atomic contributions for calculating the molar volume of aromatic (heteroaromatic) monocycles

Atom	V_i	Atom	V_i
$C_{ar,het}$	3.92	>C=O	14.10
=N–	7.89	(C_{het})–O–(C_{het}, N_{het})	9.24
–N–	5.27	(N_{het})–O–(N_{het})	10.54
|		–S–	21.30

Table 9. Atomic contributions for calculating the molar volume of annelated aromatic (heteroaromatic) rings

Atom	V_i	Atom	V_i
$C_{ar,het}$	4.00	(C_{het},N_{het})–N–(N_{het})	6.42
$C_{ar,het}$(as)	6.86	|	
N_{het}(as)	5.38	(C_{het})–O–(C_{het}, N_{het})	10.00
(C_{het},O_{het})–N=(C_{het})	6.40	(N_{het})–O–(N_{het})	11.50
(C_{het})–N=(N_{het})	7.64	>C=O	13.83
(N_{het})–N=(N_{het})	9.89	–S–	15.96
(C_{het})–N–(C_{het})	1.24	$>S\overset{O}{\underset{O}{=}}$	27.22
|			

Notes: (1) For aromatic and heteroaromatic compounds, the molar volume includes the contributions of rings and substituents (Table 6) and correction for bonding between rings (Table 7). For side chains, including ions, the contributions for aliphatic compounds are used (Table 1). When ring contributions in Table 6 are lacking, they can be estimated through the atom contributions (Table 8). The heterocycle contribution is taken as independent of the presence and sign of the charge.

(2) Atom in parentheses is not included in the fragment molar volume (A_c denotes any atom of the ring). When the fragment is not connected with an atom in parenthenes, it is connected with any atom.

(3) For annelated aromatic (heteroaromatic) compounds, the molar volumes of rings are calculated through atomic contributions (Table 9); $C_{(as)}$ and $N_{(as)}$ are common atoms belonging to neighboring rings.

(4) For polycyclic compounds of the combined type consisting of aromatic (heteroaromatic) and alicyclic rings, the molar volume includes the contributions for aromatic structures from Tables 6, 8 (for annelated compounds, Table 9); contributions of fragments for alicyclic structures (Table 3) excluding atoms composing aromatic structure (for annelated compounds); and sum of corrections for structure type for all alicycles in the compound (Table 5).

The density of DANTNP single crystal $\rho_{sc} = M/V = 379.22/203.26 = 1.87$ g cm^{-3} (experimental value: 1.86 g cm^{-3}).

CONCLUSIONS

(1) A method for calculating densities of organic compounds (including high-energy-capacity substances) from the contributions of molecular fragments was suggested. The complex system of contributions of molecular fragments to the molar volume for aliphatic, alicyclic, aromatic, and heteroaromatic compounds (including annelated and skeleton compounds) and combined structures consisting of alicyclic and aromatic (heterearomatic) rings was developed. Corrections for fragment interaction, structure type, and bonds between rings, allowing more precise consideration of the structural features, were found.

(2) A correlation between the densities of the organic compounds of various classes in the solid and liquid states at 20°C was found.

REFERENCES

1. Loskutova, L.A. and Egorov, A.P., *Khimicheskaya fizika vzvryvchatykh sistem* (Chemical Physics of Explosive Systems), St.Petersburg: Sankt-Peterb. Gos. Tekhnol. Inst. (Tekh. Univ.), 2001.
2. *Fizika vzryva* (Explosion Physics), Orlenko, L.P., Ed., Moscow: Fizmatlit, 2002, vol. 1.
3. Andreev, K.K. and Belyaev, A.F., *Teoriya vzryvchatykh veshchestv* (Theory of Explosives), Moscow: Oborongiz, 1960.
4. Dubnov, L.V., Bakharevich, N.S., and Romanov, A.I., *Promyshlennye vzryvchatye veshchestva* (Industrial Explosives), Moscow: Nedra, 1988.
5. Dremin, A.N., Savrov, S.D., Trofimov, V.S., and Shvedov, K.K., *Detonatsionnyr volny v kondensirovannykh sredakh* (Detonation Waves in Condensed Media), Moscow: Nauka, 1970.
6. Cook, M.A., *The Science of Industrial Explosives, IRECO Chemicals*, Salt Lake City, Utah, USA, 1974.
7. Chelyshev, V.P., Shekhter, B.I., and Shushko, L.A., *Teoriya goreniya i vzryva* (Theory of Burning and Explosion), Moscow: Min. Oborony SSSR, 1970.
8. Johansson, C.H. and Person, P.A., *Detonics of High Explosives*, London: Academic, 1970.
9. Stine, J.R., *J. Energetic Mater.*, 1990, vol. 8, pp. 41–49.
10. Piacenza, G., Jacob, G., Graindorge, H., et al., *30th Int. Ann. Conf. on Energetic Materials, Karlsruhe (FRG), June 29–July 2, 1999*, Karlsruhe, 2000, pp. 123/1–123/14.
11. Holden, J.R., *J. Comp. Chem.*, 1993, vol. 14, pp. 422–430.
12. Kitaigorodskii, A.I., *Stroenie organicheskikh i elementoorganicheskikh molekul* (Structure of Organic and Organoelemental Molecules), Moscow: Nauka, 1984.
13. Tarver, C.M., *J. Chem. Eng. Data*, 1979, vol. 24, no. 2, pp. 136–145.
14. Immirizi, A. and Perini, B., *Acta Crystallogr.*, 1977, vol. 33, pp. 216–218.
15. Goronovskii, I.T., *Kratkii spravochnik po khimii* (Concise Handbook of Chemistry), Kiev: Naukova Dumka, 1974.
16. *Osnovnye svoistva neorganicheskikh, organicheskikh i elementoorganicheskikh soedinenii: Novyi spravochnik khimika-tekhnologa* (Basic Properties of Inorganic, Organic, and Organoelemental Compounds: New Handbook of Chemical Engineer), Skvortsova, N.K., Ed., St. Petersburg: Mir i Sem'ya, 2002.
17. *Fiziko-khimicheskie svoistvaindividual'nykh uglevodorodov* (Physicochemical Properties of Individual Hydrocarbons), Tatevskii, V.M., Ed., Moscow: Gostekhizdat, 1960.
18. *Dictionary of organic compounds*, Heilbron, I. and Bunbury, H.M., Eds., London: Eyre and Spottiswoode, 1946, vol. 1–3.
19. *Khimicheskii entsiklopedicheskii slovar'* (Chemical Encyclopedia), Prokhorov, A.M., Ed., Moscow: Sovetskaya Entsiklopediya, 1983.
20. Fieser, L.F. and Fieser, *M., Reagents for Organic Synthesis*, New York: Wiley-Interscience, 1968–1972.
21. Bagrii, E.I., *Adamantany. Poluchenie, svoistva, primenenie* (Adamantanes. Synthesis, Properties, and Application), Moscow: Nauka, 1989.
22. Orlova, E.Yu., *Khimiya i tekhnologiya brizantnykh vzryvchatykh veshchestv* (Chemistry and Technology of Brisant Explosives), Leningrad: Khimiya, 1968.
23. Tselinskii, I.V., *Khimiya i tekhnologiya vzryvchatykh veshchestv. Klassifikatsiya alifaticheskikh i alitsiklicheskikh nitrosoedinenii* (Chemistry and Technology of Explosives. Classification of Aliphatic and Alicyclic Nitrocompounds), St. Petersburg: Sankt-Peterb. Gos. Tekhnol. Inst. (Tekh. Univ.), 2002.
24. Khmel'nitskii, L.I., *Spravochnik po vzryvchatym veshchestvam* (Handbook of Explosives), Moscow: VIA im. F.E.Dzerzhinskogo, 1961.
25. *Energeticheskie kondensirovannye sistemy: Kratkii entsiklopedicheskii slovar'* (Energetic Condensed Systems: Short Encyclopedia), Zhukov, B.P., Ed., Moscow: Yanus-K, 2000.
26. Dudek, K., Marecek, P., and Jalovy, Z., *4th Int. Seminar "New Trends in Research of Energetic Materials," Pardubice (Czechia), April 11–12, 2001*, Pardubice, 2002, pp. 75–80.
27. Suceska, M., Zeman, S., Rajir, M., and Jalovy, Z., *4th Int. Seminar "New Trends in Research of Energetic Materials," Pardubice (Czech. Rep.), April 11–12, 2001*, Pardubice, 2002, pp. 308–318.
28. Pagoria, P.F., Lee, G.S., Mitchell, A.R., and Schmidt, R.D., *Thermochim. Acta*, 2002, vol. 384, pp. 187–204.
29. Jalovy, Z. and Matias, R., *5th Int. Seminar "New Trends in Research of Energetic Materials," Pardubice (Czech. Rep.), April 24–25, 2002*, Pardubice, 2003, pp. 92–98.
30. Doherty, R.M. and Simpson, R.L., *28th Int. Ann. Conf. on Energetic Materials, Karlsruhe (FRG), June 24–27, 1997*, Karlsruhe, 1998, pp. 32/1–32/23.
31. Klapotke, M., *J. Eng. Data*, 2001, vol. 26, pp. 221–224.
32. Sikder, A.K., Maddala, G., Agrawal, J.P., and Singh, H., *J. Hazardous Mater.*, 2001, vol. A84, pp. 1–26.
33. Agrawal, J.P., *Prog. Energy Combust. Sci.*, 1988, vol. 24, pp. 1–30.
34. Lempert, D.B., Nechiporenko, G.N., and Soglasnova, S.I., *Khim. Fiz.*, 2004, vol. 23, no. 5, pp. 75–81.
35. Azizov, A.M., Kuritsyn, A.G., and Nikitenko, V.G., *Osnovy prikladnoi matematiki* (Foundations of Applied Mathematics), St. Petersburg: Khimiya, 1994.
36. Stolyarov, E.A. and Orlova, N.G., *Raschet fiziko-khimicheskikh svoistv zhidkostei: Spravochnik* (Calculation of Physicochemical Properties of Liquids: Handbook), Leningrad: Khimiya, 1976.
37. Morachevskii, A.G. and Sladkov, I.B., *Fiziko-khimicheskie svoistva molekulyarnykh neorganicheskikh soedinenii* (Experimental'nye dannye i metody rascheta): *Spravochnik* [Physicochemical Properties of Molecular Inorganic Compounds (Experimental Data and Calculation Methods): Handbook], St. Petersburg: Khimiya, 1996.

ISSN 1070-4272, Russian Journal of Applied Chemistry, 2006, Vol. 79, No. 6, pp. 967–974. © Pleiades Publishing, Inc., 2006.
Original Russian Text © Yu.E. Zevatskii, S.S. Lysova, 2006, published in Zhurnal Prikladnoi Khimii, 2006, Vol. 79, No. 6, pp. 978–985.

ORGANIC SYNTHESIS AND INDUSTRIAL ORGANIC CHEMISTRY

Relationship between the Molar Volume and Enthalpy of Formation, Polarizability, and Ionization Potential of CHNO-containing Organic Substances

Yu. E. Zevatskii and S. S. Lysova

St. Petersburg State Technological Institute, St. Petersburg, Russia

Received March 1, 2006

Abstract—A new approach to revealing a relationship between various physicochemical properties of organic compounds is suggested. The basic principle of this approach consists in that deviations of experimental values of various molecular parameters from linear dependences for the constituent elements are due to intramolecular forces of the same nature.

DOI: 10.1134/S1070427206060188

The precision achieved in calculation of physicochemical parameters of substances still remains a key issue in chemistry and physics. Despite the existence of a wide variety of additive methods, which make it possible to calculate with a small error the properties of molecules with various structures, their number continues to grow. The general principle of the known calculation procedures is that the value of a property (enthalpy of formation, polarizability, volume of a molecule, etc.) is regarded, in accordance with the additivity rule, as a sum of partial properties of separate fragments of the molecule. Atoms, chemical bonds, functional groups, etc. can be chosen as fragments of this kind.

In calculating the density of substances, the molar volume is determined on the basis of the molecular elements suggested by Stine [1], by the Cady method [2] with the use of Van der Waals radii; in addition, procedures with certain refinements and corrections were reported in [3–6].

The additive methods for calculation of the enthalpy of formation of substances can be divided into three groups [7]. The first of these is based on the additivity principle for bond energies, developed by Pauling, Tatevskii, Leidler, and others. The second group employs dependences of the thermochemical properties of substances on other thermodynamic parameters (methods of Karas and Handrick). To the third group belong methods based on the principle of additivity of the thermochemical properties of various structural groups contained in a molecule (reports by Esterman and Raikova).

Modern methods for calculation of the polarizability of molecules were described in [8, 9]. The review [9] is devoted to a critical analysis of experimental and calculated data on the static polarizability of more than 650 molecules of various classes of substances. In [10], the previously suggested [11] empirical method for calculation of the molecular polarizability from parameters of "atomic hybrids" was further developed. The results obtained in calculation of the mean polarizability, anisotropy, and principal components of the polarizability were compared with calculations based on the polarizability of bonds [12] and groups [13], and the possibility of passing from the "hybrid parameters" suggested by the authors to other empirical parameters was demonstrated.

The methods for calculation of the ionization potentials of molecules are based on the generalized Koopmans' theorem in the form of certain approximations [14]. The effect of substituents is taken into account using the principle of linearity of free energies, with a distinction made between the inductive, resonance, and polarization effects linearly appearing in the expression for the ionization potentials [15, 16]. Dependences of the ionization potentials on linear dimensions have been obtained only for atoms, with attempts to establish a relationship of this kind for nonpolar molecules undertaken only recently [18].

Some of the methods mentioned above have a number of advantages and disadvantages, compared with other techniques, but all of them give deviations from experimental values. The discrepancies are not large, but they can in no way be attributed to errors in measurement of the relevant parameters, even if the statistical nature of the measurement process is taken into account.

We assume in this study that the deviations of physicochemical parameters calculated by empirical additive methods from the corresponding experimental values are inevitable. Taken by themselves, the deviations have a certain physical meaning and are due to intramolecular forces of the same nature. A consequence of this concept is that the above deviations for different molecular constant should be linearly interrelated.

A fact supporting our hypothesis was first reported in [19]. It was found that there is a linear relationship between the enthalpy of atomization and the experimentally determined molecular polarizability minus the polarizabilities of the atoms constituting the molecule within the same homological series of organic substances. The method suggested is a generalization of this approach and it can be extended to calculation of other molecular parameters.

The enthalpy of formation, molecular polarizability, and molar volume of substances were chosen for demonstration of the practical applicability of the method for the following reasons. The enthalpy of formation belongs to the main thermodynamic potentials of substances. The polarizability is a parameter of a substance subjected to a strong perturbing action. The ionization potential is a parameter of a substance that is measured for a strongly perturbed molecule. The molar volume is a quantity that can be readily obtained with high reliability by a chemist experimenter from the density and structural formula of a substance under study. In addition, published data on the densities of substances are well consistent.

Calculation procedure. We determined the molar volume of substances by the formula

$$V = M/\rho, \tag{1}$$

where M is the molecular weight of a substance, and ρ, its density in the condensed state, determined at atmospheric pressure and constant temperature, further taken to be 20°C [20]. Then, depending on whether the substance is in the liquid or solid state under the conditions specified, we used indices l or s. We define the molecular-volume defect ΔV as the difference of the molecular volume and atomic volumes of atoms constituting the molecule of the substance:

$$\Delta V = \frac{V}{N_A} - \frac{4}{3}\pi \Sigma g_i r_i^3, \tag{2}$$

where r_i is the covalent radius of ith atom, found using the data of [21]; g_i, number of ith atoms in the molecule; and N_A, Avogadro number. We use the value of the molecular polarizability as a coefficient η relating the polarization P of the molecule of a substance in a uniform external electrostatic field to the field strength E:

$$P = \eta \varepsilon_0 E, \tag{3}$$

where ε_0 is the permittivity of free space. We define the molecular-polarizability defect similarly to (2):

$$\Delta\eta = \eta - \Sigma g_i \eta_i, \tag{4}$$

where η_i is the polarizability of ith atom [22]. We used the notion of the enthalpy of atomization of a substance, as in [19], on the per-molecule basis:

$$\delta H = (\Delta_f H^0 - \Sigma g_i \Delta_f H_i^0) N_A^{-1}, \tag{5}$$

where $\Delta_f H^0$ is the standard enthalpy of formation of the substance, and $\Delta_f H_i^0$, standard enthalpy of formation of ith atom [23]. We defined the ionization-potential defect of a substance for the first ionization potentials of the molecule, U, and of its constituent atoms, U_i, as

$$\Delta U = U - \Sigma g_i U_i. \tag{6}$$

We calculated the molecular-volume defect by Eq. (2) for 72 substances, molecular-polarizability defect by Eq. (4) for 49 substances, enthalpy of atomization by Eq. (5) for 66 substances, and ionization-potential defect By Eq. (6) for 67 molecules. It should be emphasized that the enthalpy of atomization was measured in units of 1 eV per molecule. The ionization potentials were taken from [24]. The results of our calculations are listed in Table 1.

It was found that the molecular-volume, molecular-polarizability, and ionization-potential defects and the enthalpies of atomization, calculated by Eqs. (2), (4)–(6) linearly depend on one another:

$$\Delta\eta = \alpha_\eta \Delta V + \Delta\eta_0, \tag{7}$$

$$\delta H = \alpha_H \Delta V + \delta H_0, \tag{8}$$

$$\Delta U = \alpha_U \Delta V + \Delta U_0, \tag{9}$$

Table 1. Experimental (M, ρ_4^{20}, $\Delta_f H^0$, η, U) and calculated (ΔV, δH, $\Delta\eta$, ΔU) values

Sample no.	Molecule	M, g mol^{-1}	ρ_4^{20}, g cm^{-3}	$\Delta_f H^0$, kJ mol^{-1}	η, Å^3 [22]	U, eV [24]	ΔV, Å^3	δH, eV	$\Delta\eta$, Å^3	ΔU, eV
1	C_5H_{12} *n*-pentane	72.15	0.6262(l)	–146.8	9.99	10.37	176.87	–65.77	–6.81	–209.1
2	C_6H_{14} *n*-hexane	86.18	0.6603(l)	–167.2	11.9	10.29	199.55	–77.93	–8.00	–247.6
3	C_7H_{16} *n*-heptane	100.20	0.6838(l)	–187.8	13.7	10.15	223.42	–90.09	–9.29	–286.2
4	C_8H_{18} *n*-octane	114.23	0.7025(l)	–208.4	15.9	10.01	247.38	–102.3	–10.2	–324.8
5	C_9H_{20} *n*-nonane	128.29	0.7176(l)	–201.1	17.4	9.87	271.50	–114.1	–11.8	–363.4
6	$C_{10}H_{22}$ *n*-decane	142.29	0.7300(l)	–249.7	19.10	9.73	295.58	–126.6	–13.17	–402.0
7	$C_{11}H_{24}$ *n*-undecane	156.31	0.7402(l)	–270.3	21.0	9.59	319.85	–138.7	–14.4	–440.6
8	C_5H_{10} pentene-1	70.13	0.6405(l)	–21.16	9.65	9.50	168.18	–59.95	–5.82	–182.8
9	C_6H_{12} hexene-1	84.16	0.6732(l)	–42.09	11.7	9.46	191.23	–72.12	–6.86	–221.2
10	C_7H_{14} heptene-1	98.19	0.6970(l)	–62.30	13.5	9.38	214.84	–84.27	–8.16	–259.8
11	C_8H_{16} octane-1	112.22	0.7149(l)	–82.93		9.43	238.84	–96.43		–298.2
12	C_5H_8 pentyne-1	68.12	0.6901(l)	+144.3	9.12	10.10	151.09	–53.72	–5.02	–154.9
13	C_6H_{10} hexyne-1	82.15	0.7155(l)	+122.3	10.9	10.07	175.11	–65.89	–6.33	–193.2
14	C_7H_{12} heptyne-1	96.17	0.7328(l)	+103.8	12.8	10.04	199.65	–78.03	–7.52	–231.9
15	C_8H_{14} octyne-1	110.20	0.7461(l)	+80.7		9.95	224.26	–90.22		–270.5
16	CH_3–OH methanol	32.04	0.7914(l)	–201.0	3.32	10.85	62.48	–21.13	–1.91	–68.41
17	C_2H_5–OH ethanol	46.07	0.7893(l)	–235.3	5.41	10.47	89.45	–33.43	–2.91	–107.2
18	C_3H_7–OH *n*-propanol	60.09	0.8035(l)	–255.6	7.34	10.22	113.98	–45.59	–4.08	–145.9
19	$(CH_3)_2CH$–OH isopropanol	60.09	0.7855(l)	–272.3	6.97	10.12	116.83	–45.76	–4.45	–146.0
20	C_4H_9–OH *n*-butanol	74.12	0.8099(l)	–275.3	9.52	10.04	139.04	–57.74	–4.99	–184.6
21	Me_2CHCH_2OH isobutanol	74.12	0.8020(l)	–283.8	8.92	10.02	140.54	–57.83	–5.59	–184.6
22	C_5H_{11}–OH *n*-pentanol	88.15	0.8144(l)	–295.6		10.00	164.08	–69.90		–223.1
23	$(CH_3)_2CH(CH_2)_2OH$ isopentanol	88.15	0.8120(l)	–301.3			164.61	–69.96		
24	C_6H_{13}–OH *n*-hexanol	102.20	0.8136(l)	–314.7		9.89	190.20	–82.04		–261.6
25	C_7H_{15}–OH *n*-heptanol	116.23	0.8219(l)	–339.7		9.84	213.72	–94.25		–300.1

Table 1. (Contd.)

Sample no.	Molecule	M, g mol^{-1}	ρ_4^{20}, g cm^{-3}	$\Delta_f H^0$, kJ mol^{-1}	η, Å^3 [22]	U, eV [24]	ΔV, Å^3	δH, eV	Δη, Å^3	ΔU, eV
26	C_8H_{17}–OH *n*-octanol	130.26	0.8270(l)	–356.9	17.55		237.71	–106.4	–9.34	
27	C_9H_{19}–OH *n*-nonanol	144.29	0.8273(l)	–375.6			263.05	–118.5		
28	$C_{10}H_{21}$–OH *n*-decanol	158.32	0.8297(l)	–395.2			287.57	–130.7		
29	$(CH_3)_2CO$ acetone	58.08	0.7910(l)	–218.5	6.39	9.69	112.54	–40.69	–3.69	–119.3
30	CH_3–CO–C_2H_5 butan-2-one	72.11	0.8054(l)	–238.6	8.13	9.54	136.56	–52.84	–5.05	–157.9
31	CH_3–CO–C_3H_7 pentan-2-one	86.13	0.8089(l)	–259.1	9.93	9.39	161.97	–65.00	–6.34	–196.5
32	C_2H_5–O–C_2H_5 diethylether	74.12	0.7138(l)	–252.2	8.73	9.55	159.50	–57.50	–5.78	–185.1
33	C_3H_7–O–C_3H_7 dipropylether	102.18	0.7360(l)	–293.0	12.8	9.32	212.15	–81.82	–7.90	–262.2
34	C_4H_9–O–C_4H_9 dibuthylether	130.23	0.7704(l)	–334.0	17.2	9.28	256.86	–106.1	–9.69	–339.1
35	C_2H_4O ethanal	44.05	0.7780(l)	–170.7	4.59	10.22	87.36	–28.25	–2.40	–80.30
36	C_3H_6O propanal	58.08	0.8058(l)	–188.7	6.50	9.98	110.30	–40.38	–3.58	–119.0
37	C_4H_{8O} butanal	72.11	0.8040(l)	–211.8	8.20	9.86	136.82	–52.56	–4.98	–157.6
38	$C_7H_{14}O$ heptanal	114.19	0.8495(l)	–264.0		9.65	202.91	–88.95		–273.1
39	$C_8H_{16}O$ octanal	128.21	0.8211(l)	–291.9			236.26	–101.2		
40	CH_3COOH acetic acid	60.05	1.0492(l)		5.1	10.37	87.18		–2.7	–93.77
41	C_2H_5COOH propionic acid	74.08	0.9942(l)		6.9	10.24	113.14		–4.0	–132.4
42	C_3H_7COOH butyric acid	88.11	0.9583(l)		8.38	10.16	139.36		–5.60	–170.9
43	C_4H_9COOH pentanic acid	102.13	0.9394(l)				164.49			
44	C_5H_{10} cyclopentane	70.13	0.7454(l)	–76.40	9.21	9.83	142.59	–60.53	–36.26	–182.4
45	C_6H_{12} cyclohexane	84.16	0.7786(l)	–123.1	11.00	9.80	163.13	–72.96	–7.56	–220.9
46	$C_{10}H_{18}$ naphthalene	138.25	0.8967(l)	–169.2	17.34	9.43	229.56	–116.7	–12.27	–347.9
47	C_6H_6 benzene	78.11	0.879(l)	+82.93	10.32	9.24	133.64	–57.26	–4.24	–139.9
48	C_7H_8 toluene	92.14	0.8669(l)	+50.00	12.26	8.83	159.85	–69.55	–5.39	–178.8
49	C_8H_{10} *o*-xylene	106.17	0.8802(l)	+19.0	14.25	8.56	180.92	–81.82	–6.50	–217.5
50	C_8H_{10} *m*-xylene	106.17	0.8642(l)	+17.2	14.20	8.56	184.63	–81.84	–6.55	–217.5
51	C_8H_{10} *p*-xylene	106.17	0.8611(l)	+17.9	13.7	8.52	185.37	–81.83	–7.05	–217.5

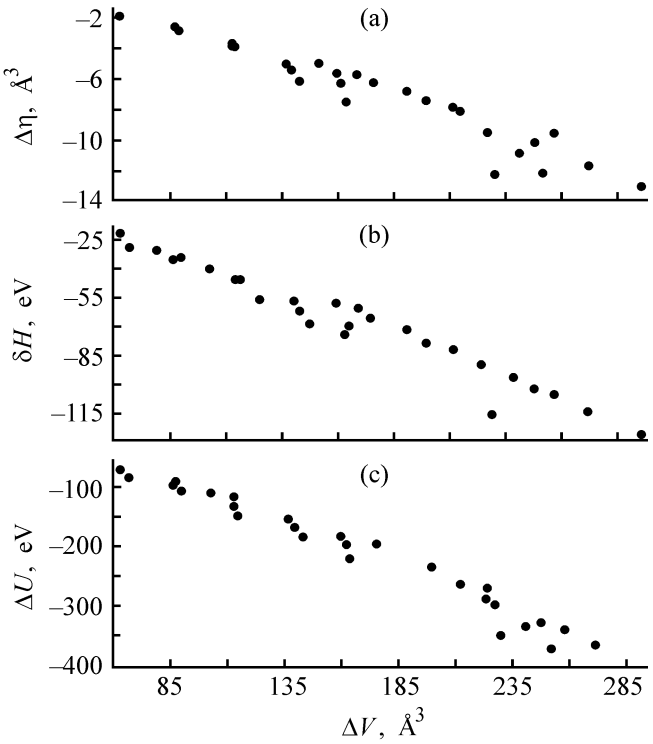
Table 1. (Contd.)

Sample no.	Molecule	M, g mol^{-1}	ρ_4^{20}, g cm^{-3}	$\Delta_f H^0$, kJ mol^{-1}	η, Å^3 [22]	U, eV [24]	ΔV, Å^3	δH, eV	$\Delta\eta$, Å^3	ΔU, eV
52	C_9H_{12} 1,3,5-trimethylbenzene	120.19	0.8652(l)		16.14	8.41	208.58		–7.70	–256.1
53	C_9H_{12} 1,2,3-trimethylbenzene	120.19	0.894(l)	–9.6		8.42	201.15	–94.06		–256.1
54	C_9H_{12} 1,2,4-trimethylbenzene	120.19	0.876(l)	–13.9		8.27	205.73	–94.11		–256.2
55	$C_{10}H_{14}$ 1,2,3,4-tetramethylbenzene	134.22	0.9053(l)	–36.0		8.14	221.37	–106.3		–294.8
56	$C_{10}H_{14}$ 1,2,3,5-tetramethylbenzene	134.22	0.8903(l)	–43.2		8.47	230.82	–106.4		–294.5
57	$C_{10}H_{14}$ 1,2,4,5-tetramethylbenzene	134.22	0.8875(s)	–47.1	17.3	8.07	226.31	–106.4	–9.64	–294.9
58	$C_{11}H_{16}$ pentamethylbenzene	148.24	0.917(s)	–67.2	19.1	7.92	240.89	–118.6	–10.9	–333.5
59	$C_{12}H_{18}$ hexamethylbenzene	162.27	0.956(s)	–77.4	20.9	7.85	251.58	–130.6	–12.2	–372.0
60	C_5H_5N pyridine	79.10	0.9835(l)	+140.2	9.5	9.30	120.26	–51.88	–3.74	–129.5
61	$C_4H_4N_2$ 1,2-diazine	80.09	1.1054(l)	+278.4	9.27	8.90	107.64	–45.66	–2.64	–119.6
62	$C_4H_4N_2$ 1,3-diazine	80.09	1.0517(s)	+195.8	8.53	9.35	113.78	–46.52	–3.38	–119.1
63	$C_3H_3N_3$ 1,3,5-triazine	81.08	1.370(s)	+225.87		9.98	86.22	–41.42		–108.2
64	$C_2H_2N_4$ 1,2,4,5-tetrazine	82.06	1.552(s)			9.14	76.37			–98.70
65	C_4H_5N pyrrol	67.09	0.9698(l)	+108.3	7.94	8.02	103.49	–44.79	–3.54	–119.5
66	$C_3H_4N_2$ pyrazol	68.08	1.002(s)	+179.4	7.23	9.38	102.06	–39.26	–2.92	–107.9
67	$C_2H_3N_3$ 1,2,3(1,2,4)-triazol	69.07	1.1861(s)	+192.7		9.80	86.56	–34.33		–97.10
68	CH_2N_4 tetrazol	70.05	1.527(s)	+320.0		10.95	66.66	–28.23		–85.63
69	C_2H_5N aziridine	43.07	0.832(l)	+126.5		9.31	78.402	–29.74		–95.72
70	C_4H_9N pyrrolidine	71.12	0.8586(l)	–3.4		8.41	124.53	–54.98		–173.5
71	$C_5H_{11}N$ piperidine	85.14	0.8698(l)	–47.15		8.7	146.80	–67.38		–211.7
72	$C_6H_{13}N$ hexahydroazepine	99.18	0.8643(l)	–45.0		8.5	172.07	–79.30		–250.3

Table 2. Linear and free coefficients and the correlation coefficients k for dependences (7)–(9) for some classes of organic substances

Substance (number of compounds)	α_H, eV/Å^3	δH_0, eV	$\lvert k \rvert$	α_η	$\Delta\eta_0$, Å^3	$\lvert k \rvert$	α_U, eV/Å^3	ΔU_0, eV	$\lvert k \rvert$
Alkanes (7)	–0.508	23.74	0.9999	–0.053	2.63	0.9987	–1.615	75.19	0.9999
Alkenes (4)	–0.516	26.71	0.9999	–0.050	2.66	0.9984	–1.633	91.49	0.9999
Alkynes (4)	–0.498	21.50	0.9999	–0.051	2.73	0.9994	–1.578	83.38	0.9999
n-Alcohols (10)	–0.488	10.03	0.9999	–0.043	0.83	0.9996	–1.522	27.59	0.9998
Isoalcohols (3)	–0.506	13.39	0.9999	–0.048	1.17	0.9999			
Ethers (3)	–0.498	22.61	0.9989	–0.040	0.62	0.9999	–1.579	68.69	0.9989
Ketones (3)	–0.492	14.53	0.9999	–0.054	2.32	0.9995	–1.561	56.07	0.9999
Aldehydes (5)	–0.500	15.05	0.9986	–0.052	2.16	0.9999	–1.666	66.28	0.9994
Carboxylic acids				–0.056	2.22	0.9983	–1.478	34.99	0.9999
Alicycles (3)	–0.649	32.39	0.9999	–0.069	3.71	0.9998	–1.905	89.49	0.9999
Aromatic compounds:									
(10) (l)	–0.536	15.58	0.9940	–0.048	2.14	0.9898	–1.675	87.34	0.9930
(3) (s)	–0.951	109.27	0.9963	–0.101	13.3	0.9961	–3.028	392.08	0.9961
Azines:									
(2) (l)	–0.493	7.39	–	–0.087	6.74	–	–0.786	–34.98	–
(3) (s)	–0.185	–25.46	–				–0.514	–61.30	0.9749
Azoles (3) (s)	–0.311	–7.45	0.9999				–0.625	–43.65	0.9986
Alicyclic imines (4)	–0.533	11.69	0.9995				–1.659	33.62	0.9998

with the coefficients α_η, α_H, α_U, $\Delta\eta_0$, δH_0, and ΔU_0 being constant within certain broad classes of CHNO-containing organic substances. The dependences (7)–(9) are graphically shown in the figure for substances from the classes chosen. The classes of organic substances with the above-mentioned coefficients and correlation coefficients are listed in Table 2. If no correlation coefficients are given, this means that we reconstructed the dependence from two points.



Polarizability defect $\Delta\eta$, enthalpy of atomization δH, and ionization-potential defect ΔU vs. the volume defect ΔV.

Analysis of the data obtained shows an insignificant, compared with the difference in free terms ($\Delta\eta_0$, δH_0, ΔU_0), scatter of the linear coefficients α for virtually all of the substance classes considered. Noteworthy is the fact that the correlation coefficients obtained in statistical processing of the dependences (7)–(9) are close to unity: the coefficients are no less than 0.9940 for enthalpies, 0.9898 for polarizabilities, and 0.9749 for ionization potentials. The best correlation achieved for the dependence of the enthalpy of atomization on the volume defect is, in all probability, accounted for by the fact that more advanced and precise methods are used to determine the enthalpy.

Thus, we can determine, with high reliability, the polarizability, enthalpy of formation, and first ionization potential of a substance from its known structure and density:

$$\eta = \Sigma g_i\eta_i + \alpha_\eta\left(\frac{M}{\rho N_A} - \frac{4}{3}\pi\Sigma g_i r_i^3\right) + \Delta\eta_0, \quad (10)$$

$$\Delta_f H^0 = \Sigma g_i \Delta_f H_i^0 + \alpha_H\left(\frac{M}{\rho} - \frac{4}{3}\pi N_A \Sigma g_i r_i^3\right)e + N_A e\,\delta H_0, \quad (11)$$

Table 3. Experimental and calculated ionization potentials for the series of unsubstituted and mono- and dimethyl-substituted tetrazoles*

Substance	CAS no.	$\Delta_f H^0$, kJ mol^{-1}	U	δH	ΔU	Coefficients in the dependence $\Delta U = a\delta H + b$, $a = 3.28$, $b = 7.21$ eV
			eV			
1*H*-tetrazole	288-94-8	320.0	10.95	–28.23	–85.63	
2-methyl-2*H*-tetrazole	16681-78-0	328.4	10.0	–40.14	–125.1	
1-methyl-1*H*-tetrazole	16681-77-9	322.9	10.3	–40.20	–124.8	
5-methyl-1*H*-tetrazole	4076-36-2	280.7	(9.0)	–40.64	–126.1	
2,5-dimethyl-2*H*-tetrazole	4135-93-7	251.2	(7.2)	–52.90	–166.3	
1,5-dimethyl-1*H*-tetrazole	5144-11-6	273.2	(8.0)	–52.67	–165.5	

* The list of certain tetrazoles of practical importance was kindly placed at our disposal by Prof. G.I. Koldobskii.

$$U = \Sigma g_i U_i + \alpha_U\left(\frac{M}{\rho N_A} - \frac{4}{3}\pi\Sigma g_i r_i^3\right) + \Delta U_0, \quad (12)$$

where e is the elementary charge. The resulting dimensionalities for the quantities in the left-hand parts of formulas (10)–(12) are cubic angstroms, joules per mole, and electronvolts, respectively.

Table 3 lists the results obtained in calculation by formulas (6), (8), and (9) for a number of heterocyclic compounds. The experimental values were taken from [23]; the calculated ionization potentials are given in Table 3 in parentheses. The choice of these compounds for prognostication of their physicochemical properties is due to the fact that, despite the strong scientific interest and large number of publications, data on the enthalpy of formation and ionization potentials in the authoritative reference literature [25] are rather scarce. Closing this gap may be of practical importance for assessing the ability of substances to enter electrophilic and nucleophilic reactions.

A natural continuation of the study of the method we suggested is verification of its applicability to calculation of other physicochemical properties, e.g., protonation energy, chemical potential, specific heat, electron affinity, dipole moment, transfer coefficients, etc. Of particular interest is elucidation of the physical meaning of the linear coefficients: dimensionless α_η and also α_H and α_U with dimensionality of electronvolts per cubic angstroms. In addition, certain useful results can be furnished by analysis of hypothetical values of the volume, polarizability, and ionization-potential defects obtained in the limit of zero enthalpy of atomization for various classes of substances.

CONCLUSIONS

Linear relationships between the molar volume, enthalpy of formation, polarizability, and ionization potential were revealed within various classes of CHNO-containing organic substances. High correlation coefficients were obtained. The method developed was used to calculate the first ionization potentials from the enthalpies of formation for several heterocyclic compounds.

REFERENCES

1. Stine, J.R., *J. Energetic Mater.*, 1990, vol. 8, pp. 41–49.
2. Piacenza, G., et al., *30th Int. Ann. Conf. Energ. Mater., Carlsruhe, FRG, 29 June–2 July 1999*, Carlsruhe, 2000, pp. 123/1–123/14.
3. Tarver, C.M., *J. Chem. Eng. Data*, 1979, vol. 24, no. 2, pp. 136–145.
4. Immirizi, A. and Perini, B., *Acta Cryst.*, 1977, vol. 33, pp. 216–218.
5. Sikder, A.K., Maddala, G., et al., *J. Hazardous Mater.*, 2001, vol. A84, pp. 1–26.
6. Kotomin, A.A. and Kozlov, A.S., *Metod rascheta plotnosti organicheskikh soedinenii po vkladam fragmentov molekul: Uchebnoe posobie* (Method for Calculation of the Density of Organic Compounds from the Contributions of Molecular Fragments: Manual), St. Petersburg: SPb. Gos. Tekhnol. Inst. (Tekhnol. Univ.), 2005.
7. Egorova, L.F. and Gidaspov, A.A., *Eksperimental'nyi i raschetnye metody opredeleniya ental'pii obrazovaniya vzryvchatykh veshchestv* (Experimental and Calculational Methods for Determining the Enthalpy of Formation of Explosives), Kuibyshev: Kuibysh. Politekhn. Inst., 1984.

8. Potapov, A.A., *Deformatsionnaya polyarizatsiya* (Deformation-induced Polarization), Novosibirsk: Nauka, 2004.
9. Gussoni, M., Rui, M., and Gerbi, G., *J. Mol. Struct.*, 1998, vol. 447, pp. 163–215.
10. Miller, K.J., *J. Am. Chem. Soc.*, 1990, vol. 112, pp. 8533–8543.
11. Miller, K.J. and Savchik, J.A., *J. Am. Chem. Soc.*, 1979, vol. 101, no. 24, pp. 7206–7213.
12. Denbigh, K.G., *Trans. Faraday Soc.*, 1940, vol. 36, pp. 936–948.
13. Vogel, A., *J. Chem. Soc.*, 1948, pp. 1833–1855.
14. Luzanov, A.V., *Zh. Strukt. Khim.*, 2003, vol. 44, no. 4, pp. 743–747.
15. Egorochkin, A.N., Voronkov, M.G., Zderenova, O.V., and Skobeleva, S.E., *Izv. Akad. Nauk, Ser. Khim.*, 2001, no. 1, pp. 41–47.
16. Egorochkin, A.N., Voronkov, M.G., Skobeleva, S.E., and Zderenova, O.V., *Izv. Akad. Nauk, Ser. Khim.*, 2001, no. 1, pp. 34–40.
17. Politzer, P., Jin, P., and Murray, J.S., *J. Chem. Phys.*, 2002, vol. 117 (18), pp. 8197–8202.
18. Zevatskii, Yu.E., *Zh. Prikl. Khim.*, 2005, vol. 78, no. 3, pp. 466–470.
19. Sam P. de Visser, *Phys. Chem. Chem. Phys.*, 1999, vol. 1, pp. 749–753.
20. *Novyi spravochnik khimika i tekhnologa* (New Reference Book for Chemists and Technologists), Skvortsov, N.K., Ed., St. Petersburg: NPO Mir i Sem'ya, 2002.
21. *Khimicheskaya entsiklopediya* (Chemical Encyclopedia), Knunyants, I.L., Ed., Moscow: Sovetskaya Entsiklopediya, 1988, vols. 1, 2.
22. *CRC Handbook of Chemistry and Physics*, Lide, D.R., Ed., Boca Raton, Florida, 2002, Section 10, pp. 162–173.
23. *NIST Chemistry WebBook. NIST Standart Reference Database*, June 2005, no. 69.
24. *Energii razryva khimicheskikh svyazei: Potentsialy ionizatsii i srodstvo k elektronu: Spravochnik* (Rupture Energies of Chemical Bonds: Ionization Potentials and Electron Affinity), Kondrat'ev, V.N., Ed., Moscow: Nauka, 1974.
25. *Comprehensive Heterocyclic Chemistry: Review of Literature 1982–1995: the Structure, Reactions, Synthesis, and Uses of Heterocyclic Compounds*, Katritzky, A.K., Ed., Oxford, 1996, vol. 3.

ISSN 1070-4272, Russian Journal of Applied Chemistry, 2006, Vol. 79, No. 6, pp. 975–980. © Pleiades Publishing, Inc., 2006.
Original Russian Text © I.V. Zinchenko, V.A. Ivanov, V.M. Potekhin, 2006, published in Zhurnal Prikladnoi Khimii, 2006, Vol. 79, No. 6, pp. 986–991.

ORGANIC SYNTHESIS AND INDUSTRIAL ORGANIC CHEMISTRY

Oxidation of Soap Chips and Antioxidative Stabilization with Phenolic Inhibitors

I. V. Zinchenko, V. A. Ivanov, and V. M. Potekhin

St. Petersburg State Technological Institute, St. Petersburg, Russia

Received November 17, 2005

Abstract—The initiation of free radicals and oxidizability of soap chips were studied by the methods of inhibited and initiated oxidation. A scheme accounting for the effect of phenolic inhibitors (with Ionol and 2-ethylhexyl gallate as examples) was suggested. The kinetic parameters of the main reactions determining the inhibiting activity of these additives were found.

DOI: 10.1134/S107042720606019X

Recently there has been an increased interest in the oxidation and stabilization of detergents and, in particular, of toilet soaps. This is caused by the fact that requirements to consumer properties of soaps (preservation of the external appearance and odor provided by fragrant additives) become more and more stringent. The requirements to stabilizers added to cosmetics and soaps also increased [1]. Toilet soap is produced from soap chips with appropriate additives. The main components of soap chips are sodium salts of C_8–C_{20} fatty acids; the content of unsaturated acids can reach 28–42%. During the production and storage, toilet soap undergoes oxidation on coming in contact with atmospheric oxygen to form labile oxygen-containing intermediates, peroxides. Peroxides decompose into free radicals and more stable products: alcohols, carbonyl compounds, etc. [2–4].

Free radicals accelerate the oxidation, and some of the forming oxygen-containing compounds impair the consumer properties of soap, imparting to it an unpleasant odor and altering its color and structure.

Ample data have been accumulated on the liquid- and solid-phase oxidation of organic materials and on their stabilization under the conditions of artificial aging [5, 6]. However, as applied to detergents, the available data on their oxidation and stabilization are scarce.

The lack of kinetic data on the oxidation and stabilization of detergents and on the mechanism of action of various antioxidants gives no way of predicting the shelf life of commercial products and making a substantiated choice of the most promising stabilizers for detergents and toilet soap.

This paper deals with the kinetics of oxidation of soap chips and their stabilization with phenolic antioxidants.

We examined three samples of soap chips (Nevskaya Kosmetika Private Company) without additives; the fatty acid composition of the samples is given in Table 1.

The soap chips were oxidized in a gasometric installation at 130–160°C at an oxygen pressure of

Table 1. Fatty acid composition of soap chip samples

Fatty acid	Content, wt %, in indicated sample		
	no. 1	no. 2	no. 3
Caprylic $C_8H_{18}O_2$	0.69	0.22	–
Capric $C_{10}H_{20}O_2$	1.00	0.76	0.26
Lauric $C_{12}H_{24}O_2$	8.01	8.05	13.80
Myristic $C_{14}H_{24}O_2$	5.52	5.98	5.48
Myristooleic $C_{14}H_{22}O_2$	0.28	0.26	0.15
Pentadecanoic $C_{15}H_{30}O_2$	0.83	0.76	0.30
Palmitic $C_{16}H_{32}O_2$	29.34	29.09	27.98
Palmitooleic $C_{16}H_{30}O_2$	2.00	2.09	1.76
Margaric $C_{17}H_{36}O_2$	1.39	0.89	1.60
Stearic $C_{18}H_{38}O_2$	18.34	17.81	15.59
Oleic $C_{18}H_{36}O_2$	28.90	27.66	30.79
Linoleic $C_{18}H_{34}O_2$	2.62	2.08	2.02
Linolenic $C_{18}H_{32}O_2$	0.53	1.22	–
Eicosanoic $C_{20}H_{42}O_2$	0.19	0.22	–
Eicosenoic $C_{20}H_{40}O_2$	0.36	0.49	0.27
Eicosadienoic $C_{20}H_{38}O_2$	–	0.20	–
Other	–	2.22	–

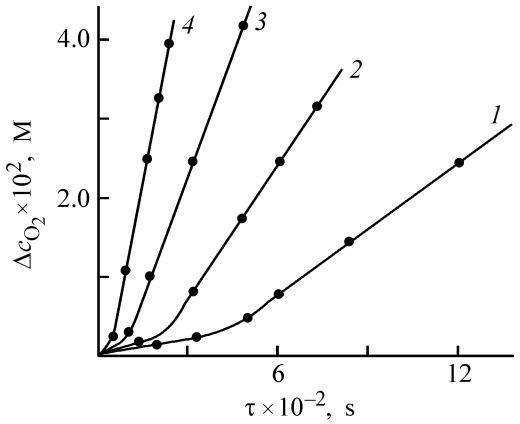


Fig. 1. Oxidation of soap chip sample no. 1 at various temperatures. (Δc_{O_2}) Oxygen uptake and (τ) time. Temperature, °C: (*1*) 130, (*2*) 140, (*3*) 150, and (*4*) 160.

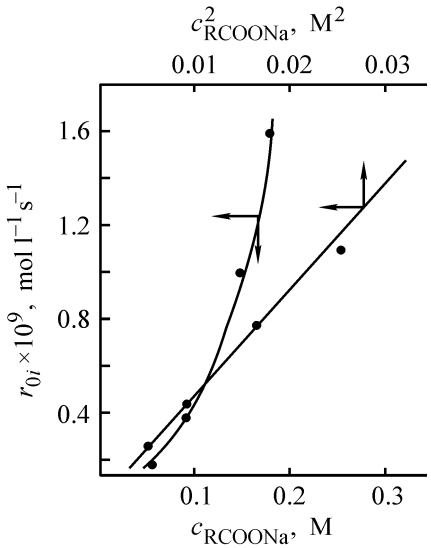


Fig. 2. Chain initiation rate r_{0i} vs. the soap concentration c_{RCOONa} in solution (sample no. 1). 160°C; solvent *o*-dichlorobenzene.

0.1 MPa in *o*-dichlorobenzene at a 0.36-M concentration of sodium salts of fatty acids, c_{RCOONa}.

The oxidation course was monitored by the oxygen uptake.

Table 2. Kinetic parameters of chain initiation in oxidation of various soap chip samples

Soap chip sample no.	$k_{0i} \times 10^6$, l mol^{-1} s^{-1}		E_{0i}, kJ mol^{-1}	
	T = 155°C	T = 145°C	T > 150°C	T < 150°C
1	1.10 ± 0.06	0.51 ± 0.06	49 ± 8	105 ± 8
2	1.26 ± 0.06	0.73 ± 0.06	50 ± 8	94 ± 8
3	0.50 ± 0.06	0.22 ± 0.06	74 ± 8	116 ± 8

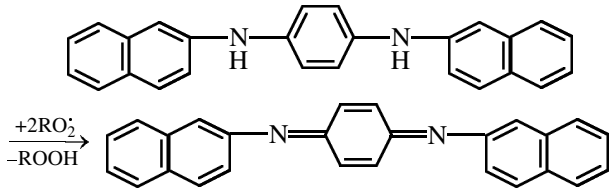
The results are shown in Fig. 1.

It can be seen from Fig. 1 that the oxidation of soap chips occurs autocatalytically. An inflection in kinetic curves *1–4* is due to accumulation of peroxy compounds, which are sources of free radicals. The inflection point is followed by the section corresponding to the steady-state process, when the rate of generation of free radicals (species leading the chain process) from peroxides is constant.

Thus, the oxidation of soap chips is a typical autooxidation process; it can be characterized by the rate constants of chain initiation (k_{0i}), chain propagation (k_p), chain termination (k_t), and degenerate chain branching (k_i), and also by the oxidizability $k_p/k_t^{0.5}$.

To determine the rate constants of chain initiation and degenerate branching, we used the method of inhibitors [5, 7].

When determining the rate constant of chain initiation, we used as peroxy radical scavenger *N*,*N*'-di-β-naphthyl-*p*-phenylenediamine (DNPD), which is highly reactive toward peroxy radicals:



The chain initiation rate was determined from the amount of the reaction product, quinone diimine (determined spectrophotometrically, λ = 490 nm, ε = 1.03×10^4 l mol^{-1} cm^{-1}). We found that the chain initiation in the oxidation of soap chips in the temperature range 130–160°C is a second-order reaction with respect to the substrate (Fig. 2).

The trimolecular reaction of chain initiation can be represented by the following equation:

$$2C_nH_{2n-1}COOM + O_2 \xrightarrow{r_{0i}} 2^{\bullet}C_{4n}H_{2n-2}COOM + H_2O_2.$$

Trimolecular reactions of chain initiation are characteristic of the oxidation of unsaturated compounds with weak C–H bonds (D_{R-H} = 330–340 kJ mol^{-1}) [5]. Apparently, salts of unsaturated acids play an important role in the chain initiation in oxidation of soap chips. Taking into account the amount of oxygen dissolved in the reaction mixture, we calculated the rate constants and kinetic parameters of chain initiation for various chip samples (Table 2).

The chain initiation rate is the highest in the oxidation of sample no. 2, which contains salts of not only monoenoic, but also di- and trienoic fatty acids.

The determination of the apparent activation energy gave interesting results. Figure 3 shows that the dependence of the logarithm of the chain initiation rate on reciprocal temperature is nonlinear, with a break at about 150°C. It is difficult to account for this fact; it may be due to variation of the viscosity and structural characteristics of the soap solution with temperature.

Thus, our results suggest that unsaturated monocarboxylic acid salts are the most reactive components of soap chips in the step of chain initiation.

The apparent activation energies and rate constants of chain initiation can be used for predicting the shelf life of the soap and for determining the optimal concentration of an antioxidant introduced into soap chips.

With the progress of soap oxidation, peroxides, as already noted, become an additional source of free radicals. We found that, at the concentration of peroxides in the soap chip oxidate (sample no. 1) of 5×10^{-3} M and lower, their decomposition at 75–85°C follows the first-order law with an apparent activation energy of 94 ± 8 kJ mol^{-1}. The results are listed in Table 3 and Fig. 4.

As already noted, an important kinetic parameter is the oxidizability, i.e., the ratio of the rate constants of the chain propagation and termination $[k_p/(2k_t)^{0.5}]$, which depends on the structures of the compounds being oxidized and radicals leading the chain process. The oxidizability of soap chips was evaluated by the method of initiated oxidation in *o*-dichlorobenzene at 70–90°C and atmospheric pressure in the presence of an initiator, azobis(isobutyronitrile) (AIBN).

Our experiments showed that, in the AIBN concentration range 1.0×10^{-2}–1.0×10^{-1} M and soap concentrations below 0.6 M, the dependence of r_{O_2}/r_i on $1/r_i^{0.5}$ (Fig. 5) follows the rate equation

$$r_{O_2}/r_i = A + k_p c_{RCOONa}/[(2k_i)^{0.5} r_i^{0.5}],$$

where r_{O_2} is the soap oxidation rate (mol l^{-1} s^{-1}); r_i, rate of initiated oxidation (mol l^{-1} s^{-1}); and A, coefficient taking into account the oxygen consumption in the steps of chain initiation and termination.

The linearization of the kinetic curves in the coordinates r_{O_2}/r_i–$1/r_i^{0.5}$ is a kinetic indication that peroxy radicals are involved in square-law chain termination.

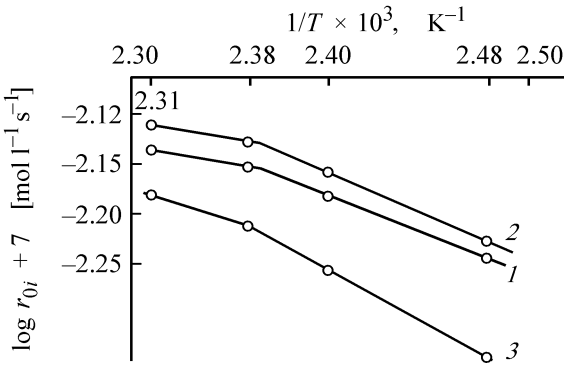


Fig. 3. Logarithm of the chain initiation rate, $\log r_{0i}$, vs. reciprocal temperature T. Sample no.: (*1*) 1, (*2*) 2, and (*3*) 3.

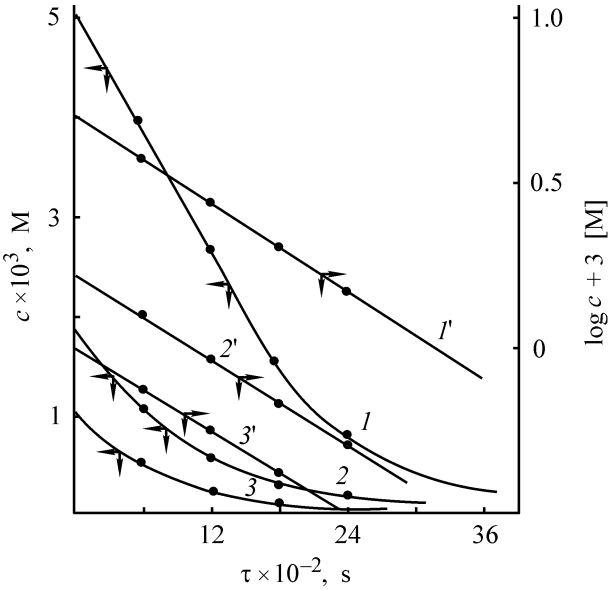


Fig. 4. Kinetic curves of peroxide decomposition in soap chip oxidate (sample no. 1) at 80°C. Initial peroxide concentration, M: (*1*, *1'*) 5×10^{-3}, (*2*, *2'*) 1.7×10^{-3}, and (*3*, *3'*) 1.0×10^{-3}. (*c*) Peroxide concentration and (τ) time.

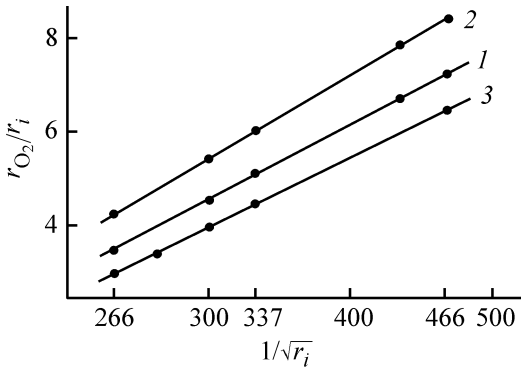


Fig. 5. Linearization of the kinetic curves at 80°C for sample nos. (*1*) 1, (*2*) 2, and (*3*) 3.

Table 3. Kinetic parameters of the peroxide decomposition in the oxidate of soap chip sample no. 1

T, °C	Rate constant of peroxide decomposition $k_{dec} \times 10^4$, s^{-1}	Apparent activation energy E_{dec}, kJ mol^{-1}
75	5.5 ± 0.1	94 ± 8
80	9.1 ± 0.1	
85	13.0 ± 0.1	

Table 4. Kinetic parameters of the initiated oxidation of soap chip samples (AIBN initiator; 80°C; $r_i = 2.1 \times 10^{-6}$ mol l^{-1} s^{-1})

Soap chip sample no.	Chain length ν	$k_p/(2k_t)^{0.5} \times 10^2$, $(l\ mol^{-1}\ s^{-1})^{0.5}$	$E_p - 0.5E_t$, kJ mol^{-1}
1	6	2.5 ± 0.5	36 ± 4
2	5	3.3 ± 0.5	30 ± 4
3	6	2.2 ± 0.5	40 ± 4

The oxidizabilities of the three soap chip samples are listed in Table 4. They differ insignificantly, which is quite natural if we take into account similar composition of the samples.

The oxidizability of soap chips is close to that of individual unsaturated monocarboxylic acids [8]. The oxidizability of saturated fatty acids is approximately two orders of magnitude lower than that of unsaturated carboxylic acids. Thus, it can be concluded that the oxidizability of soap chips is determined by the presence of unsaturated carboxylic acid salts.

The antioxidants commercially used for stabilization of detergents and toilet soap are phenol derivatives and aromatic and aliphatic amines.

In this study, we used phenolic antioxidants: Ionol and 2-ethylhexyl gallate. Experiments on inhibited oxidation of soap chips were performed on a gasometric unit in *o*-dichlorobenzene at 75–90°C in the presence of AIBN initiator. Oxidation of soap chips in the presence of the initiator in the mode of a radical-chain reaction at low initiator conversion occurs at a constant rate, r_i = const.

Addition of an inhibitor, Ionol or 2-ethylhexyl gallate, leads to deceleration of the initiated oxidation of soap chips (Fig. 6).

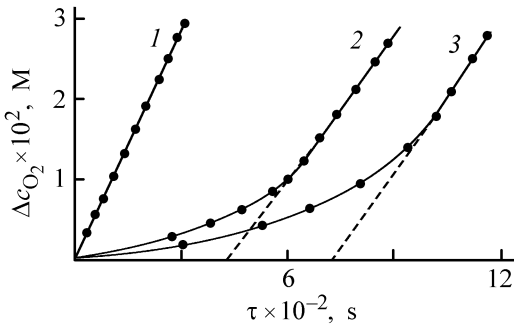


Fig. 6. Oxygen uptake Δc_{O_2} in oxidation of soap chips in the initiated mode. (τ) Time. $r_i = 2.1 \times 10^{-6}$ mol l^{-1} s^{-1} at 80°C, $c_{RCOONa} = 0.6$, $c_{InH} = 3 \times 10^{-3}$ M. Additive: (*1*) none, (*2*) ionol, and (*3*) 2-ethylhexyl gallate.

We found that the antiradical capacity of 2-ethylhexyl gallate is higher than that of Ionol, which is attibutable to the involvement of three hydroxy groups of 2-ethylhexyl gallate in the reaction with peroxy radicals; as a result, the induction period increases as compared to Ionol. The antioxidative effect of the inhibitor depends on the rate of key reactions involving it [4, 5], e.g.,

$$RO_2^{\bullet} + InH \xrightarrow{k_{InH}} ROOH + In^{\bullet},$$
$$RO_2^{\bullet} + In \xrightarrow{k_{In}} ROOIn,$$
$$RH + In^{\bullet} \xrightarrow{k_{RH}} R^{\bullet} + InH.$$

This inhibition scheme in the initiated oxidation of a substrate (RH) is described by the rate equation

$$r_{O_2} = r_\infty + k_p[RH]^{0.5}\sqrt{\frac{k_{RH}r_i}{f k_{InH}k_{In}[InH]}},$$

where r_∞ is the oxidation rate at $[InH] \to \infty$, equal to $(k_{RH}/k_{In})[RH](r_i)^{1/2}$ (mol l^{-1} s^{-1}); r_i, initiation rate (mol l^{-1} s^{-1}); [RH] and [InH], substrate and inhibitor concentrations, respectively (M); f, stoichiometric coefficient of inhibition.

Figure 7 shows the dependence of the oxidation rate of soap chips on the inhibitor concentration to

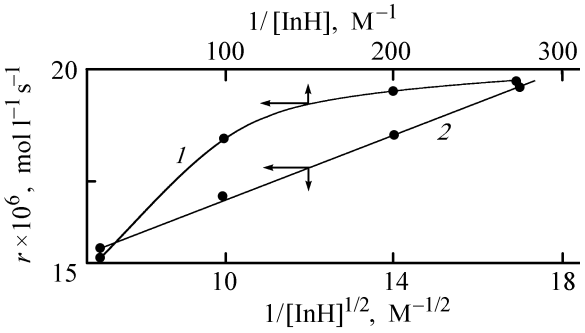


Fig. 7. Oxidation rate r (mol l^{-1} s^{-1}) of soap chips (sample no. 2) at 80°C vs. the inhibitor concentration to the power (*1*) –1 and (*2*) –1/2. $r_i = 2.1 \times 10^{-6}$ mol l^{-1} s^{-1}; c_{RCOONa} = 0.6 M.

the powers –1 (curve *1*) and –1/2 (curve *2*) at a constant initiation rate.

The linear dependence of the oxidation rate on the inhibitor concentration to the power –1/2 indicates that there is no linear chain termination at inhibitor molecules. Radicals generated from the inhibitor are involved in the chain termination and propagation in accordance with to the above scheme; the intercept on the ordinate axis ([InH] $\to \infty$) indicates that oxyphenyl radicals are involved in the chain propagation; these radicals, apparently, react with the allyl C–H bonds in acid molecules.

The involvement of phenols in the chain propagation is uncommon for inhibited oxidation. Apparently, the relatively high viscosity of soap solutions and possible occurrence of the substrate in the colloidal state decrease the mobility of phenoxyl radicals; as a result, the probability of their involvement in the chain propagation increases.

A graphic solution of Eq. (1), carried out with account of published data on k_{RH} and k_{In} [9], allowed us to estimate the $k_p/(fk_{InH})$ ratio characterizing the performance of the inhibitors (Table 5).

Table 5 shows that the phenolic inhibitors Ionol and 2-ethylhexyl gallate show approximately the same performance in stabilization of soap chips.

EXPERIMENTAL

Oxidation of soap chips in *o*-dichlorobenzene was performed on a manometric unit and was monitored by measuring the volume of oxygen taken up, with the pressure in the system maintained constant [10]. In experiments on initiated oxidation, we used azobis(isobutyronitrile) (AIBN) recrystallized from CH_3OH (mp 102–103°C) as a source of free radicals.

The fatty acid composition of soap chip samples was analyzed according to GOSTs (State Standards) 790 and 25219.

2-Ethylhexyl gallate was prepared by esterification of gallic acid with 2-ethylhexanol in *p*-xylene in the presence of *p*-toluenesulfonic acid as catalyst and was purified by recrystallization from diethyl ether.

o-Dichlorobenzene was purified before use by treatment with sulfuric acid, followed by distillation.

Table 5. Parameters of the initiated oxidation of soap chips (sample no. 2) in the presence of inhibitors (80°C; $r_i = 2.1 \times 10^{-6}$ mol l^{-1} s^{-1})

Inhibitor	$k_p/fk_{InH} \times 10^3$, mol l^{-1} s^{-1}	$E_p - 0.5E_{InH}$
Ionol	2.90 ± 0.03	32 ± 5
2-Ethylhexyl gallate	2.17 ± 0.03	25 ± 5

CONCLUSIONS

(1) Oxidation of soap chips consisting of sodium salts of saturated and unsaturated C_8–C_{20} aliphatic monocarboxylic acids occurs autocatalytically. Initially, the chains are initiated by a trimolecular reaction, and in the developed oxidation process, labile peroxides become an additional source of free radicals.

(2) The oxidizability, characterized by the ratio of the rate constant of chain propagation to the square root of the rate constant of chain termination, is largely determined by the presence of unsaturated acid salts in soap chips.

(3) Phenolic inhibitors, Ionol and 2-ethylhexyl gallate, inhibit the oxidation. The inhibitor effect is due not only to its involvement in the chain termination reactions by the nonlinear mechanism, but also to chain propagation by the reaction of oxyphenyl radicals with molecules of sodium salts of fatty acids.

REFERENCES

1. Yasnitskii, B.G. and Korobeinikova, I.E., *Antioksidanty v farmatsevticheskoi i pishchevoi promyshlennosti: Obzornaya informatsiya* (Antioxidants in Pharmaceutical and Food Industry: Review), Moscow: VNIISUEINTIMedprom, 1990, issue 8.
2. Hawkins, E.G.E., *Organic Peroxides. Their Formation and Reactions*, London: F.F. Spon, 1961.
3. Emanuel', N.M., Denisov, E.T., and Maizus, Z.K., *Tsepnye reaktsii okisleniya uglevodorodov v zhidkoi faze* (Chain Reactions of Liquid-Phase Oxidation of Hydrocarbons), Moscow: Nauka, 1965.
4. Nonhebel, D.C. and Walton, J.C., *Free-Radical Chemistry. Structure and Mechanism*, Cambridge: Univ., 1974.
5. Denisov, E.T. and Kovalev, G.I., *Okislenie i stabili-*

zatsiya reaktivnykh topliv (Oxidation and Stabilization of Jet Fuels), Moscow: Khimiya, 1983.

6. Denisov, E.T., *Okislenie i destruktsiya karbotsepnykh polimerov* (Oxidation and Degradation of Carbon-Chain Polymers), Leningrad: Khimiya, 1990.
7. Denisov, E.T., *Konstanty skorosti gomoliticheskikh zhidkofaznykh reaktsii* (Rate Constants of Homolytic Liquid-Phase Reactions), Moscow: Nauka, 1971.
8. Denisov, E.T., Mitskevich, V.E., and Agabekov, V.E., *Mekhanizm zhidkofaznogo okisleniya kislorodsoderzhashchikh soedinenii* (Mechanism of Liquid-Phase Oxidation of Oxygen-Containing Compounds), Minsk: Nauka i Tekhnika, 1975.
9. Roginskii, V.A., *Fenol'nye antioksidanty: Reaktsionnaya sposobnost' i effektivnost'* (Phenolic Antioxidants: Reactivity and Performance), Moscow: Nauka, 1988.
10. Golubeva, M.V., Ivanov, V.A., Potekhin, V.M., and Mikhailovskii, A.V., *Zh. Prikl. Khim.*, 1987, vol. 60, no. 8, pp. 1841–1846.

ISSN 1070-4272, Russian Journal of Applied Chemistry, 2006, Vol. 79, No. 6, pp. 981–986. © Pleiades Publishing, Inc., 2006.
Original Russian Text © I.V. Mel'nik, N.V. Stolyarchuk, Yu.L. Zub, A. Dabrowski, 2006, published in Zhurnal Prikladnoi Khimii, 2006, Vol. 79, No. 6, pp. 992–997.

ORGANIC SYNTHESIS AND INDUSTRIAL ORGANIC CHEMISTRY

Polysiloxane Xerogels Containing Arch-fixed Urea Groups

I. V. Mel'nik, N. V. Stolyarchuk, Yu. L. Zub, and A. Dabrowski

Institute of Surface Chemistry, National Academy of Sciences of Ukraine, Kiev, Ukraine
Maria Curie-Sklodowska University, Lublin, Poland

Received February 21, 2006

Abstract—A sol–gel procedure was suggested for preparing polysiloxane xerogels containing arch-fixed urea groups. The presence of these groups was confirmed by IR spectroscopy. The surface layer of the xerogels prepared exhibits enhanced hydrolytic stability in nonoxidizing acids.

DOI: 10.1134/S1070427206060206

Functional materials based on silica are well known and are widely used in many areas, including chromatography, heterogeneous catalysis, and sorption processes [1–4]. A frequently used method of their preparation involves modification of a surface with chloro or alkoxy derivatives of silicon, which allows formation of a surface layer with required properties. However, this method does not allow preparation of materials with a high and controllable content of functional groups. Furthermore, the hydrolytic and thermal stability of functional surface layers prepared by this method is, as a rule, relatively low. The low stability may be caused by the fact that, with traditional modifiers (e.g., trifunctional silanes), a large amount of structural units of type $-Si(OR)_2R'$ (T^1) is formed (R = H or alkyl; R' is a functional group being introduced) [5]. In this case, the functional group is linked to the matrix surface by a single siloxane bond, $\equiv Si-O-Si(OR)_2R'$, and the silicon atom bearing the functional group also contains alkoxy and/or silanol groups.

An alternative pathway is based on the sol–gel method; it allows one-step preparation of functionalized polysiloxane xerogels [6, 7] containing mainly structural units of types $=Si(OR)R'$ (T^2) and $\equiv SiR'$ (T^3) on the surface. In addition, an increase in the number of spacers (hydrocarbon chains) linking the functional group with the surface of the polysiloxane framework and leading to formation of arch structures should also enhance the hydrolytic and thermal stability of the surface layer.

The goal of this study was to develop sol–gel procedures for preparing xerogels containing arch-fixed functional groups in the surface layer. As functional groups we chose urea groups, which are efficient in recovery and separation of rare-earth metal ions [8] and in preparation of membranes [9] and wear-resistant protective coatings on the surface of lenses made of organic polymers [10].

EXPERIMENTAL

As starting compounds we used diethylenetriamine $H_2N(CH_2)_2NH(CH_2)_2NH_2$ (DETA, Aldrich, 99%); 1,4,10-trioxa-7,13-diazacyclopentadecane (TDCPD, Aldrich, 99%); tetraethoxysilane $Si(OC_2H_5)_4$ (TEOS, Aldrich, 98%); bis[3-(trimethoxysilyl)propyl]amine $[(CH_3O)_3Si(CH_2)_3]_2NH$ (BTMPA, Fluka, ≥97%); 3-isocyanatopropyltriethoxysilane $(C_2H_5O)_3Si(CH_2)_3 \cdot NCO$ (IPTES, Aldrich, 95%); NH_4F (Fluka, 98%). Nonaqueous solvents (>99% pure) were dehydrated by the standard procedures. All the manipulations preceding the sol–gel syntheses were performed in a dry nitrogen flow, using the standard Schlenk technique.

The elemental analysis was performed with a Carlo Erba EA 1108 analyzer. The IR spectra of the alkoxysilanes were recorded on a Nicolet Nexus FTIR spectrometer in the transmission mode (NaCl windows), and those of the xerogels, on a Thermo Nicolet Nexus FTIR spectrometer in the reflection mode (4000–400 cm^{-1}); for this purpose, samples were ground with preliminarily calcined KBr in a 1 : 20 ratio. The ^1H NMR spectra were measured on a Bruker AC-300 spectrometer, using tetramethylsilane as reference. The mass spectra were taken on a Finnigan SSQ 710 mass spectrometer. The thermal analysis was performed with a Q-1500D in an air flow (temperature

range 20–800°C, heating rate 5 deg min^{-1}). The thermobalance sensitivity was ±0.1 mg. Electron micrographs of samples in the scanning mode (SEM) were obtained with a Tesla BS301 device. To eliminate the electrostatic effect, samples were coated with a thin gold or platinum film using a Polaron SC 7640 device. Electron micrographs in the transmission mode (TEM) were obtained with a Tesla BS 540 device. Platinum–carbon replicas were preliminarily obtained for the samples studied. Low-temperature nitrogen adsorption isotherms were measured with an ASAP-2405N device (Micromeritics). Samples were preliminarily degassed in a vacuum at 150°C for 2 h.

Trifunctional silane $(C_2H_5O)_3Si(CH_2)_3NHC(O)N\cdot[(CH_2)_3Si(OCH_3)_3]_2$ (1). A 0.025-mol portion of IPTES was added dropwise with continuous stirring to a solution of 0.025 mol of BTMPA in 10 ml of methanol. An exothermic reaction occurred. After stirring for 1 h, the solution was allowed to stand for 18 h at room temperature, after which the solvent was removed under isothermal conditions. The residue (virtually colorless oil) was kept for several hours in a vacuum. ^{1}H NMR spectrum ($CDCl_3$), δ, ppm: 0.49 m ($SiCH_2$), 1.09 t (CH_3CH_2O), 1.51 m ($SiCH_2CH_2$), 3.01–3.10 m (CH_2N), 3.43 s (CH_3O), 3.69 q (CH_2O), 4.83 t (NH). MS, *m*/*z* (%): 160 (18), 192 (28), 202 (12), 340 (38), 439 (15), 543 (62), 557 (100), 559 (28), 588 (82), 600 (52), 618 (16). IR spectrum, cm^{-1}: 3365 (ν_{NH}); 2974, 2942, 2882, 2842 (ν_{CH}); 1631 (ν_{CO}); 1533 (ν_{CNH}).

Xerogel A. Silane **1** (0.025 mol) was dissolved in 20 ml of ethanol; the solution was cooled on an ice bath. To this solution, a solution of 0.75 mmol of ammonium fluoride in 0.2125 mol of water was added with vigorous stirring. After the mixture became fully transparent, 0.05 mol of TEOS precooled on an ice bath was added. After 3 min, the stirring was stopped, and 2 min later a transparent gel started to form. After standing for 24 h, the gel was crushed and dried in a vacuum at 70/80/90°C (2 h at each temperature). Then the xerogel was washed with 500 ml of water and again dried in a vacuum at 90°C for 6 h. Yield 14.0 g; white product.

Trifunctional silane $[(C_2H_5O)_3Si(CH_2)_3NHC(O)\cdot NH(CH_2)_2]_2NC(O)NH(CH_2)_3Si(OC_2H_5)_3$ (2). A solution of 0.0167 mol of DETA in 10 ml of ethanol was added dropwise with vigorous stirring to a solution of 0.05 mol of IPTES in 20 ml of *n*-hexane. After stirring for 2 h at room temperature, the solvents were removed under isothermal conditions. The residue (highly viscous oil) was kept in a vacuum for several hours with intermittent heating to 40–50°C. ^{1}H NMR spectrum ($CDCl_3$), δ, ppm: 0.60 m ($SiCH_2$); 1.17 t (CH_3CH_2O); 1.55 m ($SiCH_2CH_2$); 3.10 m [$Si(CH_2)_2\cdot CH_2N$]; 3.20, 3.27 m [$N(CH_2)_2N$]; 3.77 q (CH_2O); 5.29 m [$NH(CH_2)_2N$]; 5.85 m [$NH(CH_2)_3$]; 6.36 m [NHC(O)N]. MS, *m*/*z* (%): 202 (100), 218 (14), 246 (28), 320 (10), 333 (16), 423 (10), 555 (30), 625 (10), 799 (12), 846 (16). IR spectrum, cm^{-1}: 3358, 3320 sh (ν_{NH}); 2975, 2928, 2886 (ν_{CH}); 1644 sh, 1618 (ν_{CO}); 1569 (ν_{CNH}).

Xerogel B. Silane **2** (0.0167 mol) was dissolved in 40 ml of ethanol; the solution was cooled on an ice bath, and a solution of 0.75 mmol of ammonium fluoride in 0.2088 mol of water was added with vigorous stirring. After the mixture became fully transparent, 0.0668 mol of TEOS precooled on an ice bath was added. The mixture was stirred for several minutes, after which the stirring was stopped, and the transparent solution was allowed to stand at room temperature. A slight opalescence appeared, and a gel formed in 3 h. After standing for 24 h, the elastic gel was crushed and dried in a vacuum at 60/70/80°C for 2 h at each temperature. Then the xerogel was washed with 1000 ml of water and again dried in a vacuum at 80/90/105°C (2 h at each temperature). Yield 13.0 g; white product.

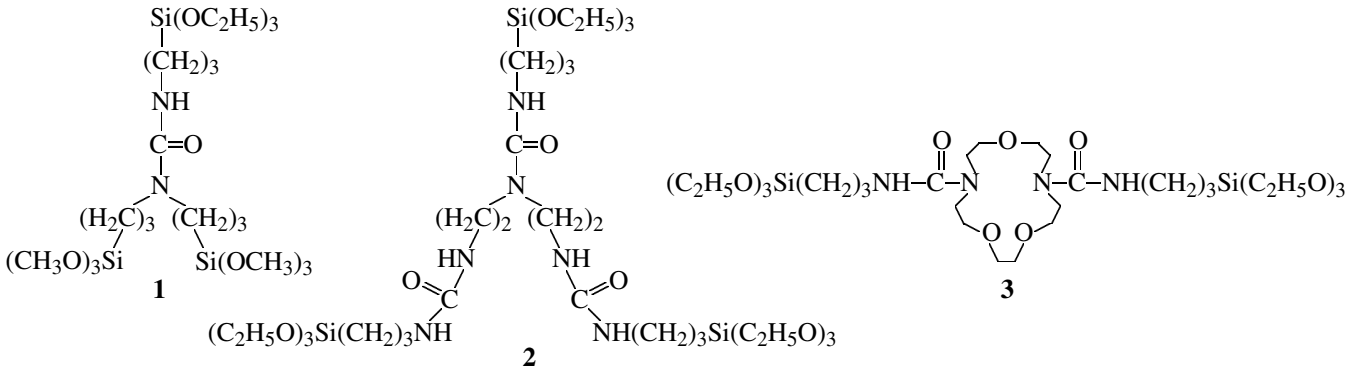
Trifunctional silane $[(C_2H_5O)_3Si(CH_2)_3NHC(O)\cdot N]_2C_{10}H_{22}O_3$ (3). The starting TDCPD (0.005 mol) was dissolved in 25 ml of ethanol, and a solution of 0.01 mol of IPTES in 5 ml of ethanol was added dropwise with vigorous stirring. An exothermic reaction occurred. After stirring for 3 h at room temperature, the solvent was removed under isothermal conditions. The residue (pale yellow oil) was kept for 48 h in a vacuum. ^{1}H NMR spectrum ($CDCl_3$), δ, ppm: 0.61 m ($SiCH_2$), 1.20 t (CH_3CH_2O), 1.56 m ($SiCH_2\cdot CH_2$), 3.13 m (CH_2N), 3.13 m [$O(CH_2)_2O$], 3.57 m (OCH_2CH_2N), 3.69 t (OCH_2CH_2N), 3.78 q (CH_2O), 5.76 m (NH). MS, *m*/*z* (%): 202 (18), 219 (12), 466 (25), 667 (100), 668 (45), 713 (22), 742 (8). IR spectrum, cm^{-1}: 3364 (ν_{NH}); 2975, 2927, 2885 (ν_{CH}); 1640 (ν_{CO}); 1538 (δ_{CNH}).

Xerogel C. Silane **3** (0.005 mol) was dissolved in 10 ml of ethanol, and a solution of 0.15 mmol of ammonium fluoride in 0.035 mol of water was added with vigorous stirring. The resulting solution was cooled on an ice bath, and 0.01 mol of TEOS was added with stirring. The stirring was continued for 10 min, after which the transparent solution was allowed to stand at room temperature. After standing for 48 h, the elastic gel was crushed and dried in a vacuum at 50/60/70°C for 2 h at each temperature. Then the xerogel was washed with 100 ml of water and

50 ml of ethanol and again dried in a vacuum for 2 h at 70°C and 4 h at 80°C. Yield 2.85 g; white product.

RESULTS AND DISCUSSION

To prepare the starting trifunctional silanes **1**–**3** containing a urea functional group >N–C(O)–N<, we used the well-known reaction of primary or secondary amines with isocyanates. As a rule, this reaction readily occurs even at room temperature, often with a quantitative yield. Since we used IPTES containing a triethoxysilyl group as the starting isocyanate, the new trifunctional silanes contained two or three such groups:



In the synthesis of **3**, we used as the starting amine a macrocycle containing two secondary amino groups. Thus, the pathway we suggest can be an alternative to the synthesis of alkoxysilyl-substituted macrocycles reported in [11].

All the trifunctional silanes prepared are oils. A particularly viscous oil is obtained in the case of alkoxysilane **2**; therefore, in [9], this compound was obtained and subsequently used as a 70% solution in 2-propanol. The alkoxysilanes obtained were identified by mass spectrometry and by IR and ^{1}H NMR spectroscopy. Since the purity of alkoxysilanes **1**–**3** was no less than 95%, according to the IR and NMR data, they were brought into the subsequent reaction without additional purification. The possibly present traces of the residual solvent do not prevent the hydrolytic polycondensation to give xerogels (the more so as the solvent used in this step was the same, ethanol). As the condensation catalyst we used ammonium fluoride (F^-/Si ratio from 1/130 to 1/150). We chose this catalyst because an acid catalyst could react with the functional group, and use of alkaline media frequently leads to formation of xerogels with a low specific surface area, especially when the trifunctional silanes contain bulky functional groups [7].

To prepare gels, we used a two-component system; along with alkoxysilanes containing urea functional groups we used tetraethoxysilane as cross-linking agent. The TEOS : trifunctional silane ratio was 2 : 1 (in the case of xerogel **B**, 4 : 1). The amount of water added was half that required for complete hydrolysis of all the ethoxy groups. Further treatment of the gels to prepare xerogels was performed similarly to [7]. The xerogels prepared are white substances readily forming aerosols. The analytical data and the content of functional groups, calculated from these data, are listed in Table 1. The calculated content of functional groups is fairly high, 1.2–1.6 mmol g^{-1}.

Table 1. Analytical data and content of functional groups in the xerogels prepared

Sample	C	N	H	C : N : H	$c_{f.\,gr}$,* mmol g^{-1}	Total loss of organics, wt %
	wt %					
A	30.5	4.4	6.2	8.2 : 1 : 20	1.6	41.1** (38.4)***
B	22.6	9.4	5.0	2.8 : 1 : 7.5	1.2	37.0 (35.4)
C	32.4	7.9	6.4	4.8 : 1 : 11.4	1.5	46.7 (47.4)

* Calculated from the nitrogen content.

** Calculated from analytical data.

*** Calculated from data of thermal analysis.

Table 2. Main absorption bands in the IR spectra of the xerogels synthesized and their assignment

Sample	ν(NH)+ν(OH)	ν(CH)	ν(CO)	δ(CNH)	ν(SiO)
	cm^{-1}				
A	3630, 3513, 3439, 3291	2973, 2939, 2886	1630	1539	1143, 1056
B	3630, 3517, 3330	2978, 2939, 2882	1656	1560	1195, 1082
C	3626, 3504, 3330	2939, 2869	1630	1543	1200, 1082

The modification of the silica surface does not allow a high content of functional groups to be reached, even when performed in the liquid phase [12]. It should be noted also that xerogel **B** contains three urea groups per unit. Thus, the actual amount of ligand centers in this case is three times larger: 3.7 mmol g^{-1}. The analytical data (Table 1) also show that the content of C and H is somewhat higher than that calculated assuming complete hydrolysis of all the ethoxy groups in the starting alkoxysilanes. This is not unexpected for hydrogen, because the samples may contain silanol groups and certain amount of water; as for carbon, its increased content suggests the presence of a small amount of unchanged alkoxy groups.

The presence of urea functional groups in the xerogels prepared is also confirmed by IR spectroscopy, namely, by the presence of characteristic absorption bands in the ranges ~3380–3400 and 1530–1640 cm^{-1} (Fig. 1). A strong broadened band in the first range is due to the stretching vibrations ν(NH) of the –NH–C(O)–NH– or –NH–C(O)–N= (in the case of secondary amine) fragment. This band apparently overlaps with the ν(OH) band. In the second range, there are two strong and sharp, but somewhat broadened bands assigned to ν(CO) and δ(CNH) [13, 14] (also termed amide I and amide II bands, Table 2). The strongest band in the IR spectra of all the xerogels is observed at 1050–1130 cm^{-1}; it has a shoulder (or shoulders) on the high-frequency side (Table 2). This band is indicative of the formation of a siloxane framework [15].

All the xerogels prepared were studied by thermal analysis; the curves obtained for xerogel **A** are shown as an example in Fig. 2. It is seen that all the samples exhibit a high thermal stability. In the range 100–150°C, there is an endothermic effect accompanied by a small weight loss: 5.5, 3.8, and 2.7% for xerogels **A**, **B**, and **C**, respectively. This effect can be attributed to the removal of water and residual solvent. At higher temperatures, there are exothermic effects caused by thermal oxidative degradation of the organic functional groups. The first exothermic effect is observed for all the matrices at 380–430°C; it can be assigned to

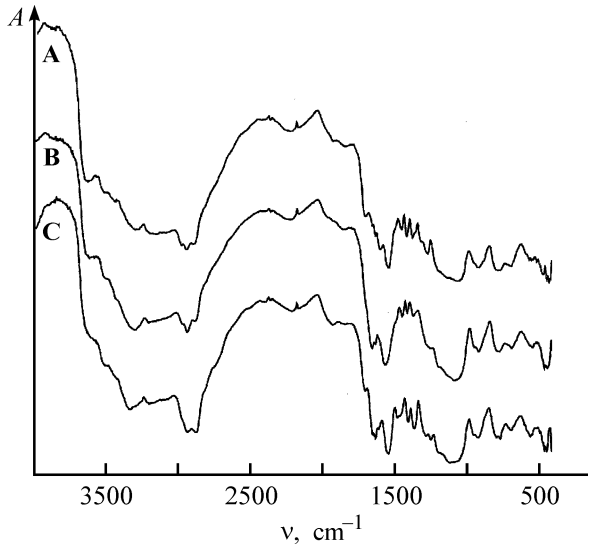


Fig. 1. IR spectra of xerogels: (*A*) reflection and (ν) wavenumber.

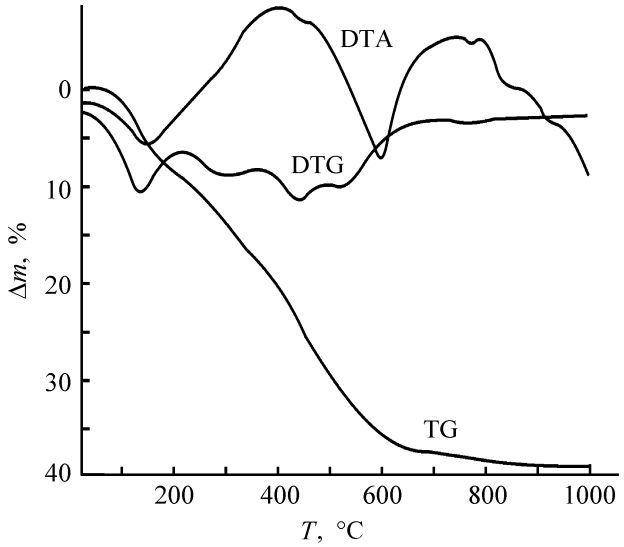


Fig. 2. Thermal analysis curves of xerogel **A**: (Δ*m*) weight loss and (*T*) temperature.

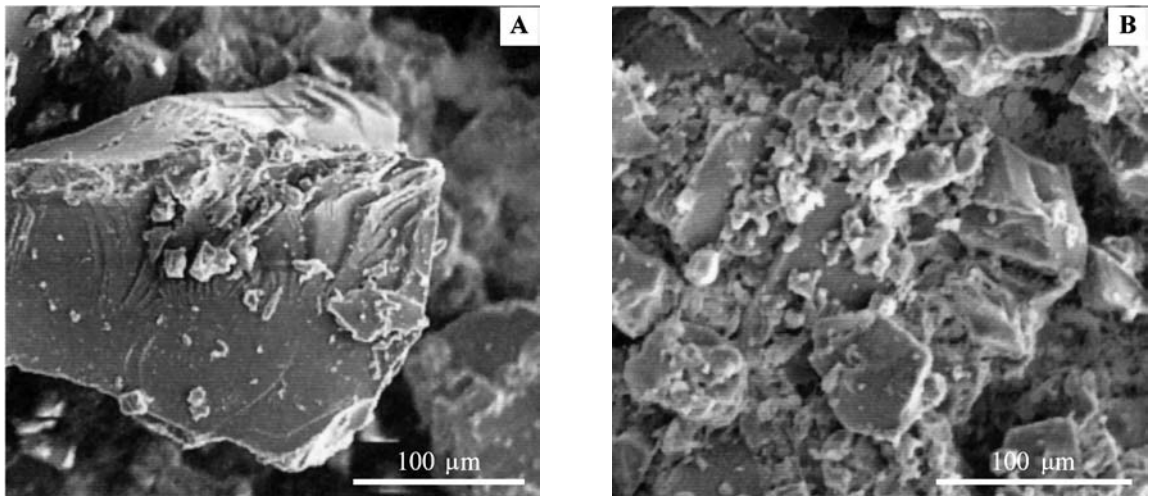


FIg. 3. SEM images of xerogels **A** and **B**.

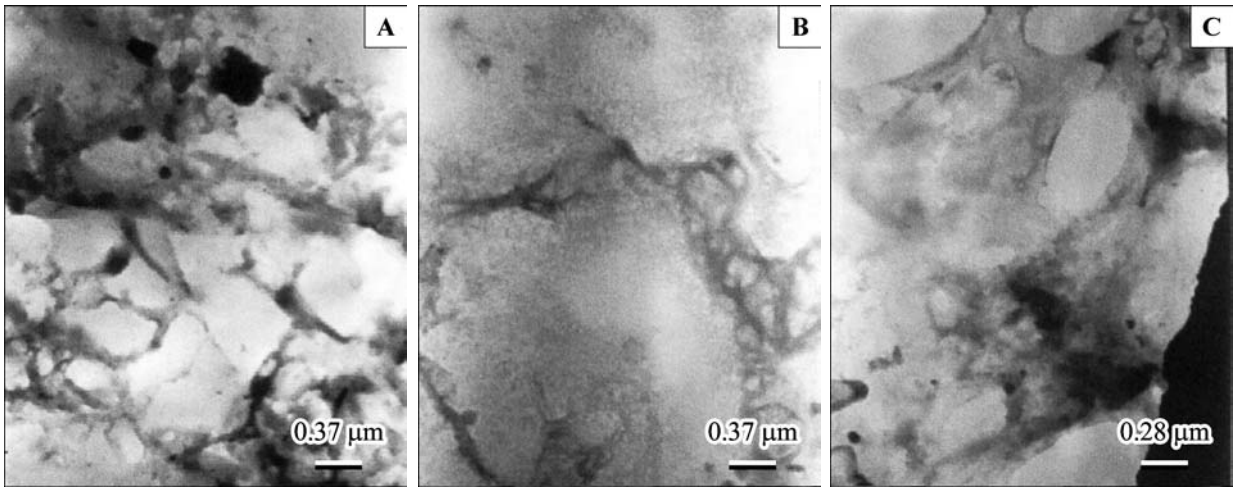


Fig. 4. TEM images of xerogels **A**, **B**, and **C**.

decomposition of structurally similar fragments. We believe that these are the >N–C(O)–N< fragments. The second effect is observed at different temperatures decreasing in the order **A** (750°C) > **B** (720°C) > **C** (620°C), i.e., with an increase in the structural strain. The total weight loss for all the samples is consistent with the analytical data (Table 1).

The hydrolytic stability of the surface layer of the xerogels obtained was evaluated by stirring 1 g of a sample in 25 ml of 0.1 N HCl for 4 h. After that, the sample was filtered off and dried at 120°C for 6 h. The IR spectra of the thus treated xerogels are identical to those recorded before the acid treatment, i.e., the surface layer is hydrolytically stable under these conditions. Furthermore, the weight loss estimated by the evaporation of the filtrate was less than 0.5 wt %.

The specific surface area of the xerogels, determined by low-temperature adsorption of nitrogen, is less than 2–3 $m^2 g^{-1}$, i.e., they are nonporous, which is typical of xerogels containing bulky functional groups [7].

Figure 3 shows the SEM images of the xerogels. They are typical of such materials and indicate that the xerogels consist of particles of irregular shapes and different sizes. The TEM images (Fig. 4) suggest that the xerogels prepared do not have a globular structure and are similar to organic polymers. Therefore, their pore structure parameters are low.

CONCLUSIONS

(1) Alkoxysilanes containing urea functional groups were prepared by the reactions of primary and

secondary amines with 3-isocyanatopropyltriethoxysilane.

(2) Xerogels containing 1.2–1.6 mmol g^{-1} functional groups were prepared by hydrolytic polycondensation catalyzed by fluoride ions.

(3) It was demonstrated that the synthesized xerogels with arch-fixed urea functional groups exhibit fairly high thermal and hydrolytic stability.

REFERENCES

1. Lisichkin, G.V., Fadeev, A.Yu., Serdan, A.A., et al., *Khimiya privitykh poverkhnostnykh soedinenii* (Chemistry of Grafted Surface Compounds), Moscow: Fizmat, 2003.
2. Tertykh, V.A. and Belyakova, L.A., *Khimicheskie reaktsii s uchastiem poverkhnosti kremnezema* (Chemical Reactions Involving Silica Surface), Kiev: Naukova Dumka, 1991.
3. Zaitsev, V.N., *Kompleksoobrazuyushchie kremnezemy: sintez, stroenie privitogo sloya i khimiya poverkhnosti* (Complexing Silicas: Synthesis, Structure of the Grafted Layer, and Surface Chemistry), Kharkov: Folio, 1997.
4. *Khimiya poverkhnosti kremnezema* (Silica Surface Chemistry), Chuiko, A.A., Ed., Kiev: Inst. Khimii Poverkhnosti, Nats. Akad. Nauk Ukr., 2001, vol. 1, parts 1, 2.
5. Vansant, E.F., Van Der Voort, P., and Vrancken, K.C., *Characterization and Chemical Modification of the Silica Surface*, Amsterdam: Elsevier, 1995.
6. Zub, Yu.L. and Parish, R.V., *Stud. Surf. Sci. Catal.*, 1996, vol. 99, pp. 285–299.
7. Zub, Yu.L. and Chuiko, A.A., *Colloidal Silica: Fundamentals and Applications*, Bergna, H.E., Ed., Washington, DC: Dekker, 2005, pp. 397–424.
8. Voronkov, M.G., Vlasova, N.N., and Pozhidaev, Yu.N., *Appl. Organomet. Chem.*, 2000, vol. 14, pp. 287–303.
9. Li, C., Glass, T., and Wilkes, G.L., *J. Inorg. Organomet. Polym.*, 1999, vol. 9, pp. 79–106.
10. Guizaro, C. and Lacan, P., *New J. Chem.*, 1994, vol. 18, pp. 1097–1107.
11. Dubois, G., Coriu, R.J.P., Reye, C., et al., *Chem. Commun.*, 1999, pp. 2283–2284.
12. Voroshilova, O.I., Kiselev, A.V., and Nikitin, Yu.S., *Kolloidn. Zh.*, 1980, vol. 42, no. 2, pp. 223–229.
13. Lin-Vien, D., Colthup, N.B., Fateley, W.G., and Grasselly, J.G., *The Handbook of Infrared and Raman Characteristic Frequencies of Organic Molecules*, San Diego, CA: Academic, 1991.
14. Bellamy, L.J., *The Infra-Red Spectra of Complex Molecules*, New York: Wiley, 1957.
15. Finn, L.P. and Slinyakova, I.B., *Kolloidn. Zh.*, 1975, vol. 37, no. 4, pp. 723–729.

ISSN 1070-4272, Russian Journal of Applied Chemistry, 2006, Vol. 79, No. 6, pp. 987–990. © Pleiades Publishing, Inc., 2006.
Original Russian Text © E.A. Vlasova, I.Yu. Vashurina, Yu.A. Kalinnikov, 2006, published in Zhurnal Prikladnoi Khimii, 2006, Vol. 79, No. 6, pp. 998–1001.

ORGANIC SYNTHESIS AND INDUSTRIAL ORGANIC CHEMISTRY

Effect of Peat Humic Acids on the Kinetics of Reduction of Anthraquinone Dye with Sulfur-containing Reducing Agents

E. A. Vlasova, I. Yu. Vashurina, and Yu. A. Kalinnikov

Institute of Chemistry of Solutions, Russian Academy of Sciences, Ivanovo, Russia

Received January 11, 2006

Abstract—The influence of peat humic acids on the aerobic reduction of Chrome Green Anthraquinone dye with sodium hydroxymethanesulfinate and thiourea dioxide in alkaline solutions was studied.

DOI: 10.1134/S1070427206060218

Textile dyeing with water-insoluble vat dyes necessarily involves the stage of temporary reductive transfer of the dye into solution, followed by its back oxidation on a fiber. The reduction of vat dyes is based on reversible quinone/hydroquinone reaction [1], which requires that not only strong reductants such as hydroxymethanesulfinate (HMS) or thiourea dioxide (TUDO), but also a catalyst should be used. The most widely employed catalysts for this purpose are synthetic anthraquinones [2], which are generally components of commercial vat dyes. In some cases, the catalysts are directly introduced into the printing dye. In these cases, the most commonly used catalysts are cobalt dioximates [3–5]. Naturally, some part of the indicated compounds, along with the unfixed dye, is rejected to wastewater of textile mills.

It has been demonstrated that absolutely nontoxic and environmentally friendly humic acid (HAs) can be used as a full-value alternative to the synthetic reduction catalysts. These acids can be readily extracted from peat [4].

Since the reduction of vat dyes is caused by only the presence of the quinoid groups in them, it becomes possible to study this process with model compounds readily soluble in water. Such model compounds can be anthraquinone dyes.

In this study, we examined the influence of peat humic acids on the kinetics of reduction of Chrome Green Anthraquinone (CGA) (CI Acid Green 27) with two sulfur-containing reducing agents, HMS and TUDO.

EXPERIMENTAL

In the experiments, we used an aqueous solution of HA salt obtained by alkaline extraction from peat, using the standard procedure [4]. HMS was purified by recrystallization of the commercial product. TUDO was synthesized as in [5]. CGA dye was purified to constant extinction coefficient [6].

The rate of CGA reduction by an excess amount of the reductant was determined by measuring the optical density at the absorption peak of the oxidized dye (λ_{max} = 612 nm, ε = 10 870 l mol^{-1} cm^{-1}). It was demonstrated in the preliminary experiments that this peak is well resolved from the absorption peak of the reduced dye.

The rate of dithionite formation by decomposition of TUDO under aerobic conditions was also determined spectrophotometrically at 315 nm (ε = 8043 l mol^{-1} cm^{-1} [7]) on a Specord M-40 instrument. The kinetic curves of reduction of CGA with HMS and TUDO are shown in Fig. 1.

The CGA reduction is described by a first-order kinetic equation [8], which suggests that the initial CGA molecule is involved in the reaction, i.e., that the reaction is kinetically controlled by the dye concentration [9]:

$$\mathrm{Dye(CO)_2} + \mathrm{HOCH_2SO_2^-} \rightleftarrows \mathrm{DyeCOCOH^-} + \mathrm{SO_2} + \mathrm{CH_2O}. \quad (1)$$

The reaction of the dye with sulfoxylate ions (active reducing species formed in decomposition

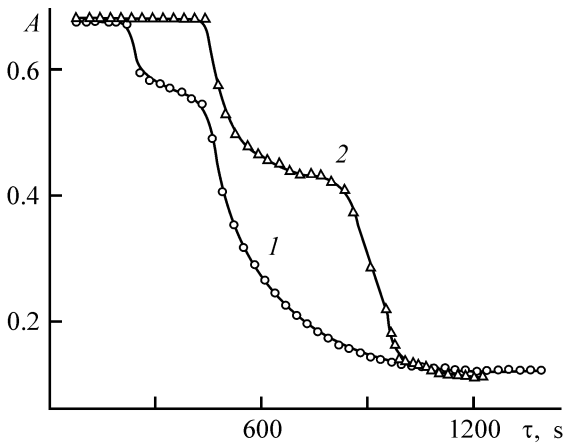


Fig. 1. Kinetic curves of CGA reduction with (*1*) HMS at 65°C and (*2*) TUDO at 20°C. Reagent concentrations (M): CGA 5.98×10^{-5}, HMS 2.37×10^{-2}, TUDO 1×10^{-3}, and NaOH 0.1; the same for Fig. 2. (*A*) Optical density of the CGA solution and (τ) time; the same for Fig. 2.

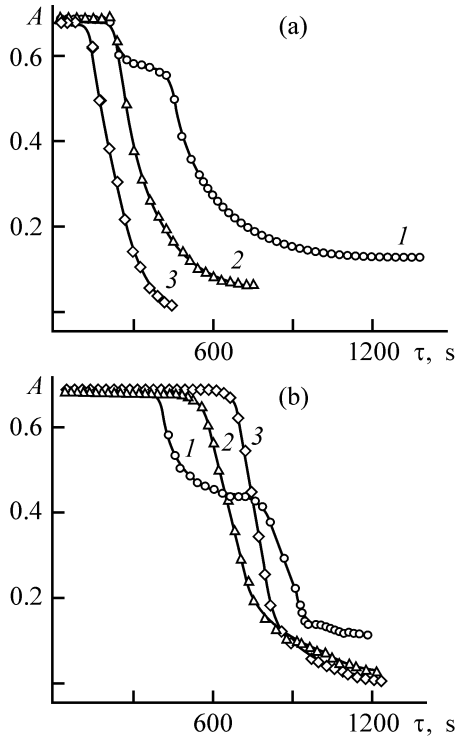


Fig. 2. Influence of HAs on the kinetics of CGA reduction with (a) HMS at 65°C and (b) TUDO at 20°C. Rate constants (s^{-1}): (a) $k_1 = 0.009$, $k_2 = 0.010$, and $k_3 = 0.092$ and (b) $k_1 = 0.0018$, $k_2 = 0.0021$, and $k_3 = 0.0025$.

of HMS [9]) also contributes significantly to the overall process:

$$HOCH_2SO_2^- + OH^- \rightleftarrows SO_2^{2-} + CH_2O + H_2O, \quad (2)$$

$$Dye(CO)_2 + SO_2^{2-} \rightleftarrows Dye(CO)_2^{2-} + SO_2. \quad (3)$$

This conclusion is based on the fact that the curve of CGA reduction with HMS shows an induction period, which, as is well known, is typical of only aerobic reactions, and is caused by the reaction of sulfoxylate with oxygen occurring in the solution [9, 10]:

$$SO_2^{2-} + O_2 \rightarrow SO_2^- + O_2^-, \quad (4)$$

$$SO_2^- + O_2 \rightarrow SO_2 + O_2^-. \quad (5)$$

Thus, the CGA reduction with HMS involves both the initial reductant molecule and the sulfoxylate ion, a reactive product of its decomposition [reactions (1) and (3)].

The kinetics of CGA reduction with TUDO, unlike that with HMS, is independent of the dye concentration, being described by a zero-order equation [8]. The reaction is kinetically controlled by the generation of the SO_2^{2-} ion as a reactive reducing species [11]:

$$(NH_2)_2CSO_2 + 2OH^- \rightarrow SO_2^{2-} + (NH_2)_2CO + H_2O. \quad (6)$$

This is demonstrated by the occurrence of an induction period in the initial reduction stage, which is considerably longer in the case of TUDO (Fig. 1, curve *2*) as compared to HMS (Fig. 1, curve *1*). The reasons are the lower reaction temperature and the lack of any reduction pathways other than the reaction with sulfoxylate.

It has been demonstrated in special experiments that the second induction period in the kinetic curves of dye reduction with both reductants is caused by the accumulation of oxygen reduction products, such as superoxide (O_2^-) formed by reaction (4) [12].

The influence of humic acids on the kinetics of CGA reduction with both reductants is shown in Fig. 2.

In the case of HMS (Fig. 2a), addition of HAs resulted in the following changes in the kinetic features: (i) the second induction period is completely vanishes (with account of the aforementioned reasons for its appearance [12], this suggests that, in the presence of HAs, the oxygen reduction products are either not accumulated or transformed); (ii) the yield of CGA reduction increases by about 20%; (iii) the reduction rate increases (the rate constant increases by more than an order of magnitude with the HA concentration increasing from 0 to 0.1 $g\,l^{-1}$); (iv) the slope of the kinetic curves decreases, suggesting a decrease in the contribution of reaction (1) and increase in the contribution of (3) to the overall process; and (v) the first induction period becomes shorter.

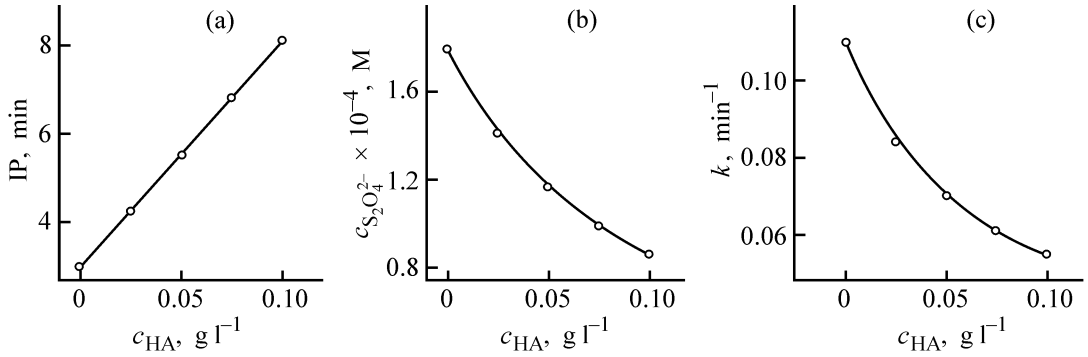


Fig. 3. Kinetic parameters of TUDO decomposition with the formation of $S_2O_4^{2-}$ ions as influenced by the HA concentration c_{HA}. $c_{TUDO} = 1.0 \times 10^{-3}$ M and $c_{NaOH} = 0.5$ M; $T = 20$°C. (a) (IP) Induction period, (b) $c_{S_2O_4^{2-}}$ concentration of $S_2O_4^{2-}$ ions, and (c) (k) rate constant of dithionite accumulation.

In CGA reduction with TUDO (Fig. 2b), the first three effects are the same (the second induction period vanished, the reaction yield increased by 20%, and the rate constant, by a factor of 2). The differences were that, firstly, HAs do not alter the reduction mechanism (kinetic curves are linear both in the presence and in the absence of HAs). Secondly (and most importantly), the first induction period is not only reduced, as with HMS, but even becomes considerably longer.

To analyze the last of the two indicated features, we examined in separate experiments the influence of HAs on the kinetics of anaerobic decomposition of TODO [reaction (6)]. The appearance of sulfoxylate ions in the system was judged from the absorption spectra of dithionite ions ($S_2O_4^{2-}$) formed from the sulfoxylate ions by reaction (7) and having a well-resolved peak in the near UV region [11]:

$$2SO_2^- \rightleftarrows S_2O_4^{2-}. \quad (7)$$

The influence of the HA concentration on the kinetics of accumulation of the dithionite ions is shown in Fig. 3. It is seen that the duration of the induction period linearly increases with the HA concentration (Fig. 3a) and with the content of dissolved oxygen [11]. Therefore, as in the case of oxygen, HAs entirely react with sulfoxylate ions. Among the diverse functional groups present in the HA molecules, only carbonyl groups can be reduced under mild conditions, the reaction being reversible [13–15]:

$$HA(C{=}O)_n + nS_2O_4^{2-} \rightleftarrows HA(C{-}O)_n^- + 2nSO_2. \quad (8)$$

Other groups (amide, imine, anhydride, and ester) are reduced at high temperature and pressure [16]. In addition to the carbonyl groups, the reduction of transition metal ions, primarily Fe(III), in the HA structure is also quite probable:

$$HA(Fe^{3+})_n + nS_2O_4^{2-} \rightleftarrows HA(Fe^{2+})_n + 2nSO_2. \quad (9)$$

The reversible redox reaction of iron (without rupture of its bonds with the organic fraction of the HA molecule) is comprehensively considered in the literature [17].

The interaction of HAs with sulfoxylate ions by reactions (8) and (9) results in a decrease in the equilibrium concentration of $S_2O_4^{2-}$ (Fig. 3b) and the process rate constant (Fig. 3c). However, as mentioned above, the rate and completeness of CGA reduction increase in this case. Therefore, the reduction of the dye involves not only sulfoxylate ions [reaction (3)], but also HAs reversibly reduced by sulfoxylate:

$$2HA(C{-}O)_n^- + n\text{Dye}(CO)_2 \rightleftarrows 2HA(C{=}O)_n + n\text{Dye}(CO)_2^{2-}, \quad (10)$$

$$2HA(Fe^{2+})_n + n\text{Dye}(CO)_2 \rightleftarrows 2HA(Fe^{3+})_n + n\text{Dye}(CO)_2^{2-}. \quad (11)$$

This mechanism is operative in reduction of CGA with TUDO. In the case of HMS, as demonstrated above, the process involves not only sulfoxylate ions, but also the molecular form of the reductant. Undoubtedly, the latter also can reduce HAs, since the redox potential of HAs under the experimental conditions is as low as 70–120 mV:

$$HA(C{=}O)_n + nHOCH_2SO_2^- \rightleftarrows HA(C{-}O)_n^- + nSO_2 + nCH_2O, \quad (12)$$

$$HA(Fe^{2+})_n + nHOCH_2SO_2^- \rightleftarrows HA(Fe^{3+})_n + nSO_2 + nCH_2O. \quad (13)$$

Evidently, it is these reactions that are responsible for the observed considerably more effective accelerating effect of HAs on the CGA reduction with HMS (Fig. 2a) as compared to TUDO (Fig. 2b).

The high catalytic activity of peat HAs in reduction of the quinone groups of the dyes, observed with an example of the model water-soluble dye, was verified in the laboratory and industrial tests in printing textiles with water-insoluble vat dyes [18]. Introduction of small amounts of HAs into the vat dyes for printing cotton fabrics reduces by half of the time of water-steam treatment and allows a simultaneous increase the adsorption of the dye on the fibers by 2–9%. In this case, the color fastness, as well as the color purity, are not deteriorated, which is virtually impossible with the common synthetic catalysts.

CONCLUSIONS

(1) Small additions of peat humic acids have a considerable catalytic effect on the reduction of Chrome Green Anthraquinone dye with sodium hydroxymethanesulfinate in alkaline solutions.

(2) Comparison of the effect of peat humic acids on the kinetics of reduction of the anthraquinone dye with two sulfur-containing reductants (sodium hydroxymethanesulfinate and thiourea dioxide) and also on the kinetics of accumulation of the dithionate ions in aerobic decomposition of thiourea dioxide in solutions reveals that the catalytic action of humic acids occurs by the mechanism of redox catalysis.

(3) Humic-acid catalysis of the reduction of the carbonyl groups in the molecules of organic dyes, observed for the example of the water-soluble acid dye, also virtually impossible under conditions of printing textiles with water-insoluble vat dyes. In industry, this can save material resources and energy supply.

REFERENCES

1. Totskaya, N.V., Dolmat, M.I., and Romanova, M.G., *Tekstil'n. Prom–st.*, 1986, no. 3, pp. 43–44.
2. Yakimchuk, R.P., Mishchenko, A.V., and Bulusheva, N.E., *Primenenie kubovykh krasitelei* (Application of Vat Dyes), Moscow: Legprombytizdat, 1985.
3. Proskina, N.N., Egorova, Z.N., Bulusheva, N.E., et al., *Tekstil'n. Prom–st.*, 1982, no. 9, pp. 56–57.
4. Ponomareva, V.V. and Plotnikova, T.A., *Gumus i pochvoobrazovanie* (Humus and Soil Formation), Leningrad: Nauka, 1980.
5. Makarov, S.V., *Usp. Khim.*, 2001, vol. 70, no. 10, pp. 995–1006.
6. Vashurina, I.Yu., Association of Active Dyes and Development of Efficient Technology of Dyeing and Crease Resist Processing of Cotton Fabric, *Cand. Sci. Dissertation*, Ivanovo, 1988.
7. McKenna, C.E., Gutheil, V.G., and Song, W., *Biochim. Biophys. Acta*, 1991, vol. 1075, pp. 109–117.
8. Panchenkov, G.M. and Lebedev, V.P., *Khimicheskaya kinetika i kataliz* (Chemical Kinetics and Catalysis), Moscow: Khimiya, 1985.
9. Budanov, V.V. and Makarov, S.V., *Khimiya serosoderzhashchikh vosstanovitelei (rongalit, ditionit, dioksid tiomocheviny)* [Chemistry of Sulfur-Containing Reducing Agents (Rongalite, Ditionite, Thiourea Dioxide)], Moscow: Khimiya, 1994.
10. Polenov, Yu.V., Physicochemical Features of Homogeneous and Heterogeneous Redox Reactions with Participation of Sulfinic Acid Derivatives, *Cand. Sci. Dissertation*, Ivanovo, 2003.
11. Svarovsky, S.A., Simoyi, R.H., and Makarov, S.V., *J. Chem. Soc.*, Dalton Trans., 2000, no. 4, pp. 511–514.
12. Vashurina, I.Yu., Makarov, S.V., Kalinnikov, Yu.A., and Vlasova, E.A., *Zh. Prikl. Khim.*, 2006, vol. 79, no. 2, pp. 275–278.
13. Landgraf, M.D., da Silva, S.C., and de O. Rezende M.O., *Anal. Chim. Acta*, 1998, vol. 368, pp. 155–164.
14. Lindqvist, I., *Swed. J. Agr. Res.*, 1983, vol. 13, no. 2, pp. 69–73.
15. Goodman, B.A. and Cheshire, M.V., *Nature*, 1982, vol. 299, no. 5884, pp. 618–620.
16. Struyk, Z. and Sposite, G., *Geoderma*, 2001, vol. 102, pp. 329–346.
17. Morrison, R.T. and Boyd, R.N., *Organic Chemistry*, Boston: Allyn and Bacon, 1970.
18. Stevenson, F.J., *Humic Chemistry: Genesis, Composition, Reaction*, vol. 1, New York: Wiley, 1982.
19. Pogorelova, A.S., Development of Theoretical Principles of Application of Humic Acids to Dyeing and Printing of Textiles with Vat Dyes, *Cand. Sci. Dissertation*, Ivanovo, 2002.

ISSN 1070-4272, Russian Journal of Applied Chemistry, 2006, Vol. 79, No. 6, pp. 991–996. © Pleiades Publishing, Inc., 2006.
Original Russian Text © V.F. Kurenkov, E.S. Shchelkonogova, A.V. Kurenkov, H.-G. Hartan, F.I. Lobanov, 2006, published in Zhurnal Prikladnoi Khimii, 2006, Vol. 79, No. 6, pp. 1002–1006.

MACROMOLECULAR CHEMISTRY AND POLYMERIC MATERIALS

Copolymerization of Acrylamide and Sodium 2-Acrylamido-2-Methylpropanesulfonate in Water–Ethanol Mixtures

V. F. Kurenkov, E. S. Shchelkonogova, A. V. Kurenkov, H.-G. Hartan, and F. I. Lobanov

Kazan State Technological University, Kazan, Tatarstan, Russia
Stockhausen, GmbH Krefeld, Germany
Degussa Euraziya Limited Liability Company, Moscow, Russia

Received February 1, 2006

Abstract—Homogeneous copolymerization of acrylamide and sodium 2-acrylamido-2-methylpropanesulfonate was carried out in water–ethanol mixtures at pH 9 in the presence of potassium peroxosulfate as promoter in the temperature range 40–70°C. The copolymerization kinetics and molecular characteristics of the copolymers formed were studied in relation to the composition of water–ethanol mixtures, reagent concentrations, temperature, and degree of monomer conversion.

DOI: 10.1134/S107042720606022X

Owing to numerous useful properties, water-soluble polymers are widely applied in various fields of modern industry. Synthesis and use of these polymers involve no toxic, inflammable, and dangerously explosive solvents, and no risk of pollution. Water-soluble copolymers of acrylamide (AA) and sodium 2-acrylamido-2-methylpropanesul-fonate (Na-AMS) deserve a special attention because of their wide application as thickeners, stabilizers, and flocculants in petroleum production, well-boring, and water treatment [1–3].

It is known [4] that the radical copolymerization of water-soluble monomers significantly depends on the kind of solvent. Therefore, the use of binary solvents of variable composition allows efficient control over copolymerization. Copolymerization of AA and Na-AMS in aqueous salt solutions [5], and in water–dimethyl sulfoxide [6] and water–dimethylformamide [7] mixtures has been studied peviously. In this study, we examined the kinetics of homogeneous radical copolymerization of AA and AMS monomers in water–ethanol mixtures in the presence of potassium peroxosulfate as initiator at 40–70°C.

EXPERIMENTAL

2-Acrylamido-2-methylpropanesulfonic acid (HAMS), mp 185°C, was purchased from the Lubrizol (England). Na-AMS was prepared by potentiometric titration of aqueous HAMS with aqueous NaOH to pH 9. Acrylamide, mp 84.5°C, was purchased from Mitsubishi Chem Ind. Ltd. (Japan). Potassium peroxosulfate (PP), chemically pure grade, was twice recrystallized from water. The main substance content in potassium persulfate, determined by redox titration, was 97.8%. All other chemicals were of chemically pure grade.

The copolymerization of AA and Na-AMS was carried out to small degrees of conversion ($x < 2.5\%$) in a 8.4-cm^3 glass dilatometer and to higher degrees of conversion in 50-cm^3 weighing bottles. The copolymerization experiments were performed as follows. The aqueous HAMS monomer or its solution in the water–ethanol mixture was neutralized under cooling with aqueous alkali to pH 9, and then aqueous PP and AA solutions were added. The resulting mixture was transferred with a long-needle syringe into a dilatometer or a weighing bottle and kept in a thermostat (45–70°C) at a temperature control accuracy of ±0.05°C. The copolymerization kinetics was studied by dilatometry. In these experiments, both the copolymerization conditions and the dilatometric technique were identical to those reported in [8]. The initial rate of copolymerization, v_0, at low degree of conversion (<2.5%) was determined from the slope of the initial linear portion of the kinetic curve.

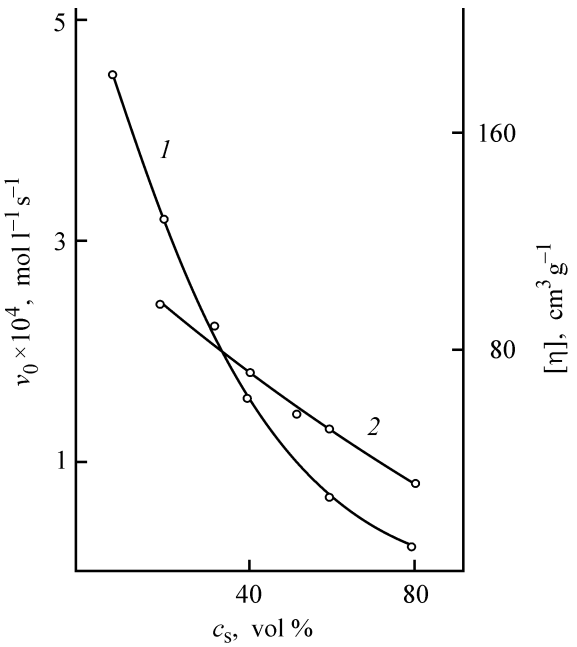


Fig. 1. Dependence of (*1*) initial rate of copolymerization of AA and Na-AMS, v_0, in the water–ethanol mixture ($H_2O : C_2H_5OH$ = 3 : 1) and (*2*) intrinsic viscosity of the copolymer, [η], on the ethanol content in the reaction mixture, c_s. $[M_1] + [M_2]$ = 20%; $[M_1]/[M_2]$ = 1.

After the copolymerization completion, the resulting copolymer was precipitated from the reaction mixture by adding a large excess of acetone. This procedure allowed separation of the target copolymer from the unchanged monomers. The isolated copolymer was washed with acetone and dried in a vacuum to constant weight. Its yield was determined gravimetrically. The sulfur content of the copolymer was determined by the method described in [9].

The molecular weight of the AA–Na-AMS copolymer was estimated from its intrinsic viscosity [η] determined from the concentration dependence of the reduced viscosity (η_{sp}/c) of the copolymer solution in 0.5 M aqueous NaCl at 30°C:

$$[\eta] = \lim(\eta_{sp}) \text{ at } c \to 0.$$

The viscosity was measured with a VPZh-3 capillary viscometer (d_c = 0.56 mm).

The pH was measured using a pH-121 pH-millivoltmeter equipped with an ESL-63-07 glass electrode and an EVL-1M3 silver chloride reference electrode.

The copolymerization of AA and Na-AMS was carried out in aqueous solution or water–ethanol mixtures at ethanol-to-water volume ratios of 4 : 1, 3 : 1, 1.5 : 1, 1 : 1, 1 : 1.5, and 1 : 4 in the presence of PP (3×10^{-4} M) at 60°C. The AA and Na-AMS content of all the reaction mixtures was 20%. To ensure homogeneity of the reaction mixture in the course of the copolymerization, the ethanol content of the water–ethanol mixtures did not exceed 80%. At higher ethanol concentrations, the reaction mixture gave a precipitate. To stabilize the activating effect of PP [10] at the ionic strength of the reaction mixture varying with the initial Na-AMS monomer concentration and Na-AMS consumption in the course of polymerization, pH 9 of the reaction mixture was maintained [11]. Under these conditions, both the imidization of the Na-AMS amido groups [12] and hydrolysis of this salt [3] were suppressed. We found that AA and Na-AMS copolymerize only in the presence of an initiator (PP).

Figure 1 shows the rate of copolymerization of AA and Na-AMS in relation to the composition of water–ethanol mixtures. It is seen that, with increasing water content, both the copolymerization rate v_0 and the intrinsic viscosity [η] of the copolymer increase. These effects are due to the fact that the mobile protons and the hydroxy groups of water molecules prevent chain transfer to ethanol molecules. Our results are consistent with the data on copolymerization of AA and Na-AMS in aqueous-organic media, reported in [13], which showed that the number of hydrogen bonds between H_2O molecules and the CO groups in the AA and Na-AMS monomers increases with the water content of the water–ethanol mixture. As a result, the electron density on the double bonds of both monomers decreases and their reactivity increases. Therefore, an increase in the water content in the reaction mixture leads to a rise in both the copolymerizaion rate v_0 and the yield of the copolymer (Table 1). Table 1 also shows that the AA–Na-AMS copolymers are formed in high yield.

Table 1. Yield of AA–Na-AMS copolymer in copolymerization of AA and Na-AMS in water–ethanol mixtures of varied composition ($[M_1] + [M_2]$ = 20%; $[M_1]/[M_2]$ = 1)

Water–ethanol ratio, vol %	Yield in 1 h, %
25 : 75	78
40 : 60	81
50 : 50	81
60 : 40	83
80 : 20	84

Figure 2 shows how the Na-AMS content of the water–ethanol mixture ($H_2O : C_2H_5OH = 3 : 1$) affects the copolymerization rate, and the intrinsic viscosity [η] and yield of the copolymer, other factors being the same. It is seen that, with increasing relative content of Na-AMS in the reaction mixture, both v_0 and [η] decrease in parallel. Thus, on enrichment of the reaction mixture with AA, the copolymerization is accelerated. These data indicate that AA is more reactive in copolymerization than Na-AMS.

Figure 3 shows the correlation between the Na-AMS concentration in the initial reaction mixture and content of Na-AMS units in the AA–Na-AMS copolymers obtained at low degrees of conversion ($x < 2.5\%$). Curve *2* refers to copolymerization in water, and curve *1* to that in the water–ethanol mixture ($H_2O : C_2H_5OH = 3 : 1$). S-shaped curve *2* has an azeotropic point at the Na-AMS mole fraction 0.35, whereas the AA–Na-AMS copolymers obtained in water within the entire Na-AMS concentration range, are enriched in AA units. The relative reactivity of AA and AMS monomers toward like and different macroradicals [ratio of the probability of formation of AA–AA (11), AA–Na-AMS (12), and Na-AMS–Na-AMS (22) fragments in a copolymeric chain in the course of AA and Na-AMS copolymerization] is characterized by the ratio of the corresponding rate constants: $r_1 = k_{11}/k_{12}$ and $r_2 = k_{22}/k_{21}$. The r_1 and r_2 parameters were calculated from the relation $m_2 = f(M_2)$ by the Mayo–Lewis, Fineman–Ross, and Kelen–Tudos methods. All these methods gave close r_1 and r_2 values which are as follows: water, $r_1 = 1.31 \pm 0.09$ and $r_2 = 0.11 \pm 0.01$ [6]; and water–ethanol mixture ($H_2O : C_2H_5 = 3 : 1$), $r_1 = 0.78 \pm 0.12$ and $r_2 = 0.31 \pm 0.01$. These results show that, for AA and Na-AMS copolymerization in water, $r_1 > r_2$, i.e., AA is more reactive than Na-AMS. In copolymerization of AA and Na-AMS in the water–ethanol mixture, $r_1 < 1$ and $r_2 < 1$, i.e., formation of the AA–Na-AMS fragments is preferential.

Comparison of curves *1* and *2* at $m_2 = \text{const}$ (Fig. 3) shows that, with increasing water content, the copolymers become enriched in the AA units because of an increase in r_1 and a decrease in r_2.

Figure 4 shows the plots of the reduced viscosity η_{sp} of solutions prepared from identical AA–Na-AMS copolymer samples in water (curve *1*) and water–ethanol mixtures of varied composition (curves *2–4*) against the copolymer concentration. These plots are typical of polyelectrolyte solutions whose rheological

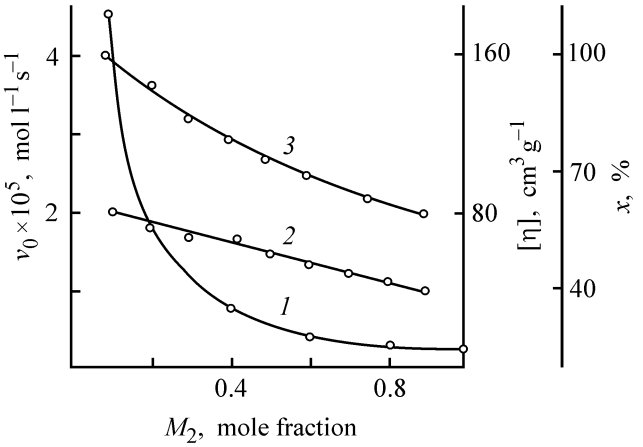


Fig. 2. Dependence of the (*1*) initial rate of copolymerization of AA and Na-AMS v_0, (*2*) intrinsic viscosity of the copolymer [η], and (*3*) yield of the copolymer x on mole fraction M_2 of the Na-AMS monomer in the initial water–ethanol mixture ($H_2O : C_2H_5OH = 3 : 1$).

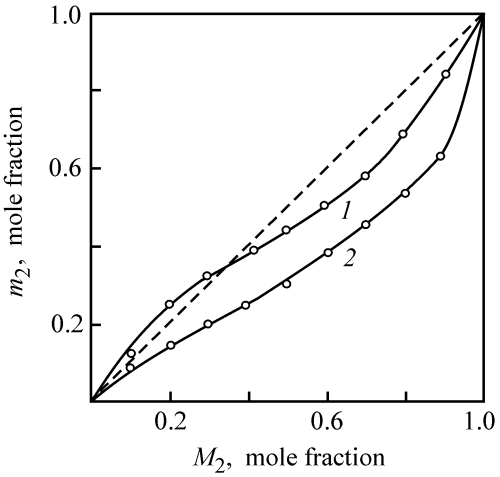


Fig. 3. Dependence of the content of Na-AMS units in AA–Na-AMS copolymers m_2 prepared at low degrees of conversion ($x < 2.5\%$) on the mole fraction of Na-AMS monomer M_2 in (*2*) water and (*1*) water–ethanol mixture ($H_2O : C_2H_5OH = 3 : 1$).

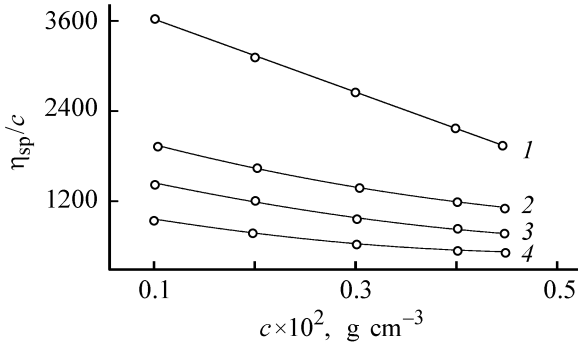


Fig. 4. Dependence of the reduced viscosity of solution of AA–Na-AMS copolymer ([η] = 96 cm^3 g^{-1}, content of Na-AMS units 24 mol %) on its concentration in (*1*) water and (*2–4*) water–ethanol mixtures with water : ethanol ratios of (*2*) 3 : 1, (*3*) 1 : 1, and (*4*) 1 : 3 at 30°C.

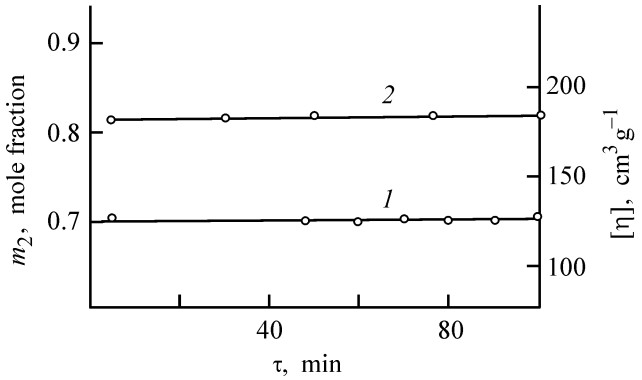


Fig. 5. Dependence of (*1*) [η] and (*2*) content of Na-AMS units in the copolymer (m_2) on the copolymerization time τ in water–ethanol mixture (water : ethanol = 3 : 1). M_2 = 0.9.

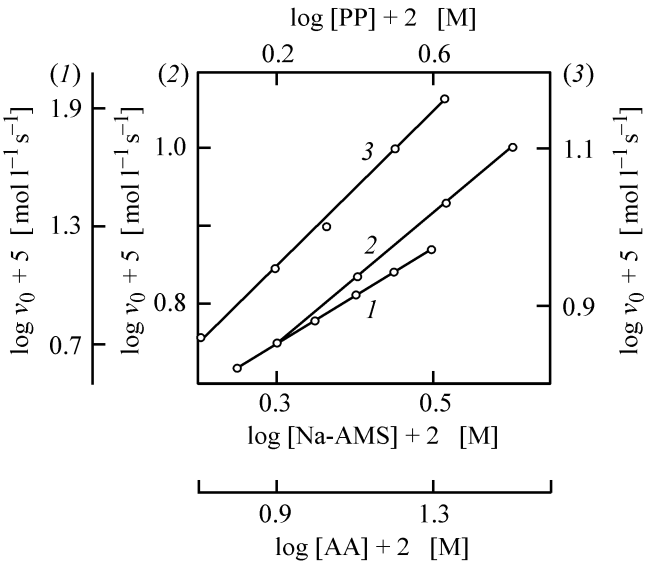


Fig. 6. Logarithmic plot of the initial rate of AA and Na-AMS copolymerization v_0 in the water–ethanol mixture (water : ethanol = 3 : 1) vs. (*1*) AA, (*2*) Na-AMS, and (*3*) PP concentrations. (*1*) [Na-AMS = 0.66 M, [PP] = 3.2×10^{-3} M; (*2*) [AA] = 0.66 M, [PP] = 3.2×10^{-3} M; and (*3*) [Na-AMS] = [AA] = 0.66 M.

behavior is controlled by the electrostatic effects. On adding water to AA–Na-AMS copolymer in ethanol, both the polarity of the medium and the degree of ionization of Na-AMS ionic groups increase. The increase in the polarity enhances repulsion between like-charged sulfonate anions situated along the polymeric chain. Therefore, in going from the reaction mixture with the lowest water content (curve *4*) to water (curve *1*) at c = const, the macromolecular globules of copolymers become bulkier and the viscosity of the solutions increases. With increasing water content in the reaction mixture, the electrostatic repulsion between the like-charged Na-AMS units and macroradicals with terminal Na-AMS units also becomes stronger. This repulsion decreases the rate constant k_{22} and, as it is seen from comparison of curves *1* and *2* (Fig. 3), the copolymer becomes depleted of Na-AMS units. On adding water to ethanol, the charge of copolymer chains increases. This factor makes lower the local concentration of Na-AMS monomer in the vicinity of the Na-AMS reaction centers, which causes depletion of the copolymer in Na-AMS units.

Figure 5 shows how the intrinsic viscosity [η] of AA–Na-AMS copolymers in the water–ethanol mixture ($H_2O : C_2H_5OH$ = 3 : 1) and the Na-AMS unit content of the copolymer depend on the conversion. It is seen that both [η] and the Na-AMS content remain constant in the course of copolymerization. Similar results have been obtained preliminarily for homopolymerization of AA and N-vinylpyrrolidone [14, 15] and copolymerization of AA and Na-AMS in water [16]. These results can be attributed to micelle formation. The bulkier Na-AMS monomers penetrate into micelles to the propagating macroradical more difficultly than smaller AA monomers do. Therefore, the ratio of Na-AMS and AA monomers within micelles remains constant in the course of copolymerization. Under these conditions, the copolymer composition is virtually independent of the degree of conversion.

The copolymerization kinetics of AA and Na-AMS monomers in the water–ethanol mixture ($H_2O : C_2H_5$ = 3 : 1) was studied in relation to the concentrations of the monomers and PP, all other factors being the same (Fig. 6). It is seen that, with increasing concentration of the monomers and PP, v_0 grows. The order of the copolymerization reaction with respect to both the monomer and initiator was determined from the slopes of the corresponding plots in Fig. 6. Based on these data, the following empirical equation for the rate of AA and AMS copolymerization in the presence of PP was derived

$$V = k_c[\text{AA}]^{1.4}[\text{Na-AMS}]^{0.8}[\text{PP}]^{0.5},$$

where k_c is the rate constant of AA and Na-AMS copolymerization.

In this equation, the reaction order with respect to the initiator is 0.5, which indicates a bimolecular mechanism of termination of propagating polymeric chains.

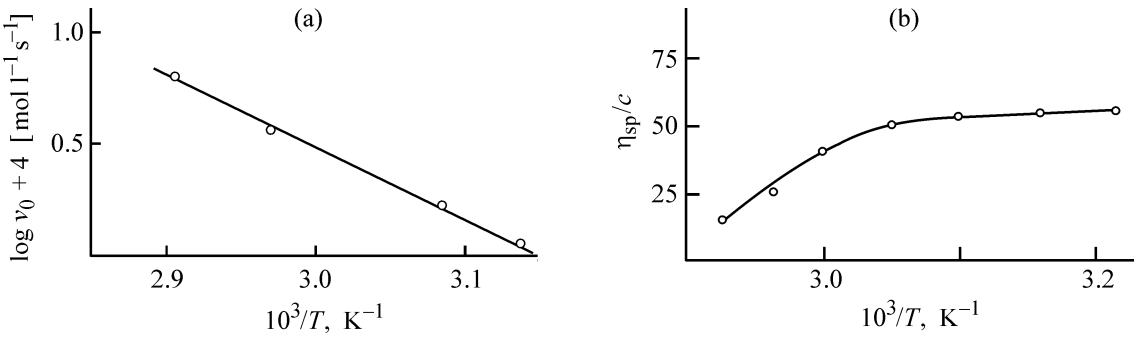


Fig. 7. Dependence of (a) initial copolymerization rate v_0 in the water–ethanol mixture ($H_2O : C_2H_5OH$ = 1 : 3) and (b) reduced viscosity η_{sp} of the copolymer solution ([η] = 182 cm^3 g^{-1}, Na-AMS unit content 8.4 mol %) on the reciprocal temperature. (b) Solvent : water–ethanol mixture (3 : 1), c = 0.5%.

Table 2 shows that AA–Na-AMS copolymers are formed in a the water–ethanol mixture in high yield. With increasing comonomer concentrations, the intrinsic viscosity [η] of the copolymers and their yield grow.

The influence of temperature on the copolymerization was studied within the temperature range 40–70°C. The plot of log v_0 vs. reciprocal temperature (Fig. 7) shows that, with increasing temperature, v_0 grows. The apparent overall activation energy of the copolymerization is 30 kJ mol^{-}1. We believe that a decrease in η_{sp}/c with temperature (Fig. 7b) is caused by contraction of the macromolecular globules. The reason for this contraction is a decrease in the degree of Na-AMS ionization with increasing temperature. This factor weakens the electrostatic repulsion between like-charged Na-AMS units situated along the copolymeric chain. This decrease in the electrical charge is also accompanied by an increase in the local concentration of Na-AMS monomer in the vicinity of Na-AMS reactive centers of propagating macromolecular chains. As a result, the copolymerization accelerates with temperature.

Table 2. Dependence of the intrinsic viscosity [η] of the reaction mixture and the yield of AA–Na-AMS copolymers on the comonomer concentration in the water–ethanol mixture ($H_2O : C_2H_5OH$ = 3 : 1)

Monomer	c, M	Yield in 1 h, %	[η], cm^3 g^{-1}
AA	0.60	39	187
	0.63	51	253
	1.20	62	300
Na-AMS	1.60	70	349
	0.90	22	98
	1.20	28	101
	1.40	36	125
	1.70	48	180

CONCLUSIONS

(1) In radical copolymerization of AA and Na-AMS monomers in the water–ethanol mixture, high-molecular-weight copolymers of varied molecular structure are formed.

(2) With increasing water content of the reaction mixture, the initial copolymerization rate v_0, intrinsic viscosity [η], and content of AA units in the copolymer become higher due to increasing r_1 and decreasing r_2. Neither [η] nor the copolymer composition change with the conversion.

(3) Both [η] and the yield of copolymers increase with the total comonomer concentration in the reaction mixture. At $[M_1] + [M_2]$ = const, v_0 and [η] increase with the AA content in the reaction mixture. The copolymerization of AA and Na-AMS is accelerated with increasing initiator concentration and temperature.

REFERENCES

1. Lisovtsev, V.V., Rostokin, G.A., and Kulikova, A.N., in *Khimicheskaya promyshlennost': akrilaty i polivinilkhlorid* (Chemical Industry: Acrylates and Polyvinyl Chloride), Moscow: NIIITEKHIM, 1984, pp. 1–20.
2. McCormick, C.L., *Macromol. Sci. Chem., part A*, 1985, vol. 22, nos. 5–7, pp. 955–982.
3. *2-Acrylamido-2-Methylpropane Sulfonic Acid Monomer. Wickliffe*, Ohio (USA): Lubrizol, 1994, pp. 1–18.
4. Kabanov, V.A., Zubov, V.P., and Semchikov, Yu.D., *Kompleksno-radikal'naya polimerizatsiya* (Complex-Radical Polymerization), Moscow: Khimiya, 1987.
5. Kurenkov, V.F., Antonovich, O.A., and Khusaino-

va, A.F., *Zh. Prikl. Khim.*, 2002, vol. 75, no. 10, pp. 1707–1711.

6. Kurenkov, V.F., Antonovich, O.A., Demina, T.A., and Selezneva, O.Yu., *Vysokomol. Soedin., Ser. A*, 2003, vol. 45, no. 8, pp. 1246–1252.
7. Kurenkov, V.F., Antonovich, O.A., Zigulyaeva, T.V., and Lobanov, F.I., *Khim. Tekhnol.*, 2005, no. 7, pp. 14–19.
8. Kurenkov, V.F., Khairullin, M.R., and Utkeeva, A.R., *Zh. Prikl. Khim.*, 1999, vol. 72, no. 7, pp. 1177–1182.
9. Charlot, G., *Les Methods de la Chemie Analytique. Analyse Quantitative Minerale, Quatrieme Edition*, Paris: Masson, 1961.
10. Kholodkova, L.V., Pavlyuchenko, V.N., Alekseeva, Z.M., and Andreeva, A.I., *Kataliticheskie i initsiiruyushchie systemy dlya sinteza i modifikatsii polimerov* (Catalytic and Initiating Systems for Synthesis and Modification of Polymers), Leningrad: Plastpolimer, 1984, pp. 90–104.
11. Kolthoff, I.M., and Miller, I.K., *J. Am. Chem. Soc.*, 1951, vol. 73, no. 7, pp. 3055–3059.
12. USSR Inventor's Certificate, no. 235997.
13. Gromov, V.F., Bune, E.V., and Teleshov, E.N., *Usp. Khim.*, 1994, vol. 63, no. 6, pp. 530–541.
14. Barabanova, A.I., Gromov, V.F., Bune, E.V., et al., *Vysokomol. Soedin., Ser. A*, 1994, vol. 36, no. 6, pp. 901–907.
15. Gromov, V.F., Bune, E.V., Barabanova, A.I., et al., *Vysokomol. Soedin., Ser. A*, 1995, vol. 37, no. 11, pp. 1818–1822.
16. Kurenkov, V.F., Zhelonkina, T.A., Meshcheryakov, A.N., and Lobanov, F.I., *Zh. Prikl. Khim.*, 2005, vol. 78, no. 10, pp. 1697–1702.

ISSN 1070-4272, Russian Journal of Applied Chemistry, 2006, Vol. 79, No. 6, pp. 997–1000. © Pleiades Publishing, Inc., 2006.
Original Russian Text © A.I. Vorob'eva, M.N. Gorbunova, S.V. Kolesov, Yu.B. Monakov, 2006, published in Zhurnal Prikladnoi Khimii, 2006, Vol. 79, No. 6, pp. 1007–1010.

MACROMOLECULAR CHEMISTRY AND POLYMERIC MATERIALS

Copolymerization of *N*-Vinylpyrrolidone with 3-Methacryloyloxytetrahydrothiophene 1,1'-Dioxide

A. I. Vorob'eva, M. N. Gorbunova, S. V. Kolesov, and Yu. B. Monakov

Institute of Organic Chemistry, Ufa Scientific Center, Russian Academy of Sciences, Ufa, Bashkorkostan, Perm, Russia
Institute of Technical Chemistry, Ural Division, Russian Academy of Sciences, Russia

Received December 13, 2005; in final form, February 2006

Abstract—Radical copolymerization of *N*-vinylpyrrolidone with 3-methacryloyloxytetrahydrothiophene 1,1'-dioxide in the bulk and in dimethyl sulfoxide in the range of low conversions was studied. The kinetic features of copolymerization were examined. The relative activities of monomers and the structure and some characteristics of the copolymers were determined.

DOI: 10.1134/S1070427206060231

Poly-*N*-vinylpyrrolidone (PVP) is of prime importance among other macromolecular compounds. A combination of practically valuable characteristics of PVP: solubility in water and in most of organic solvents, absence of toxicity, biological compatibility, immune inactivity, and also clearly pronounced capability for complex formation with a wide variety of inorganic and organic compounds and biological systems, allows use of this compound as a disintoxication agent and prolongation agent for drugs [1, 2]. Copolymers of *N*-vinylpyrrolidone (VP) have a still wider set of valuable characteristics. The copolymerization reactions allow modification of PVP characteristics and therefore acquire growing practical importance. Copolymers based on VP are components of a great number of drugs, act as carriers of biologically active substances, and are the base of membranes, sorbents, coagulants, flocculants, etc. [3–7]. Copolymers of VP with 3-methacryloyloxytetrahydrothiophene 1,1'-oxide (MAHTO) can be of some interest for medical purposes. MAHTO is nontoxic, has clearly pronounced antimicrobial, antiphlogistic, and wound-healing effects, and enters into the composition of the medicinal glue widely used in surgery for gluing of soft tissues of a living body [8, 9]. It is well known that MAHTO is highly active in radical homo- and copolymerization with vinyl monomers, methyl methacrylate, methacrylic acid, and styrene [10, 11]. There are no published data on copolymerization of MAHTO with VP; at the same time, it is our opinion that copolymerization of VP with MAHTO could widen the set of valuable characteristics and the range of application of copolymers based on VP in medicine and biotechnology.

Our aims were to study the copolymerization of VP with MAHTO, namely, to determine the activities of monomers and to examine the kinetic features of the reaction and some characteristics of the resulting copolymers.

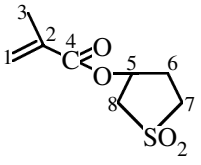
EXPERIMENTAL

N-Vinylpyrrolidone of chemically pure grade was dried with potassium hydroxide and distilled in a vacuum. For polymerization we used the fraction with bp 65°C at a pressure of 200 Pa, n_D^{20} 1.5117.

3-Methacryloyloxytetrahydrothiophene 1,1'-oxide was synthesized by the procedure described in [12]. The purity was monitored by the elemental analysis, determination of the content of double bonds, and ^{13}C NMR.

Found (%): C 47.25, H 6.11, S 15.41, C=C 11.80.
Calculated (%): C 47.06, H 5.88, S 15.69, C=C 11.76.

Chemical shifts δ (ppm) and multiplicity of signals for the indicated atoms are presented below.



C_1	C_2	C_3	C_4
109.5	153.0	20.4	164.5
t	s	q	s
C_5	C_6	C_7	C_8
70.3	28.3	48.5	55.8
d	t	t	t

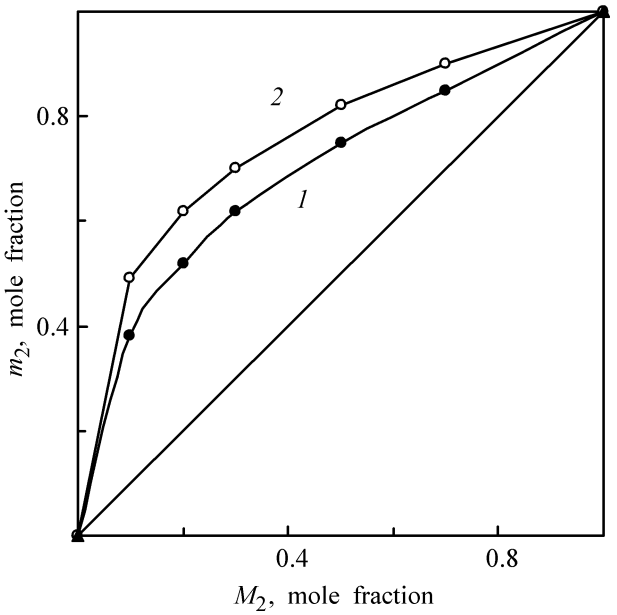


Fig. 1. Composition of copolymers of VP with MAHTO vs. the composition of the initial monomer mixture. [AIBN] = 3.05×10^{-2} M, T = 55°C; the same for Fig. 2. (M_2) MAHTO content in the initial mixture, and (m_2) MAHTO content in the copolymer. (*1*) In the bulk and (*2*) in DMSO, $[M_1 + M_2]$ = 3.2 M; the same for Fig. 2.

Azobis(isobutyronitrile) (AIBN) of chemically pure grade was thrice recrystallized from methanol and dried in a vacuum at room temperature to constant weight, mp 103°C with decomposition.

Dimethyl sulfoxide (DMSO) and acetone after purification by standard procedures corresponded in their characteristics to published data.

Copolymerization of VP with MAHTO was performed in a vacuum to low conversions in the bulk and in a DMSO solution in the presence of AIBN initiator at 55°C. The process kinetics was monitored dilatometrically. The initial rate was evaluated from the initial portions of the kinetic curves (at ≤7% conversions). When the required degree of conversion was reached, the polymerization was terminated by cooling and subsequent precipitation of the copolymer. The copolymers were purified by twofold reprecipitation from DMSO solutions in acetone. The purified polymers were dried in a vacuum at 50°C to constant weight.

Table 1. Effective constants of copolymerization of VP (M_1) with MAHTO (M_2) AIBN, 55°C

Medium	r_1	r_2
In bulk	0.05 ± 0.01	1.20 ± 0.30
DMSO	0.01 ± 0.005	2.72 ± 0.32

The composition of the copolymers was determined from the results of elemental analysis. The effective copolymerization constants were evaluated by the Mayo–Lewis [13] and Kelen–Tudos [14] methods.

The ^{13}C NMR spectra were recorded on a Bruker AM-300 spectrometer operating at 75.46 MHz. DMSO-d_6 was used as a solvent, and tetramethylsilane, as an internal reference.

The intrinsic viscosity of the copolymers was measured on an Ubbelohde viscometer (DMSO, 25°C).

The parameters of acute toxicity of copolymers of VP with MAHTO were determined on outbred white mice of both sexes with a weight of 18–22 g, by the procedure described in [15]. The bactericidal activity was studied on three samples of conditionally pathogenic strains (*Staphylococcus aureus*, strain 906; *Staphylococcus saprophiticus*, strain 15305; *Micrococcus luteus*, strain 4698) by two-fold dilution method [16]. DMSO was used as a solvent for the copolymer in screening.

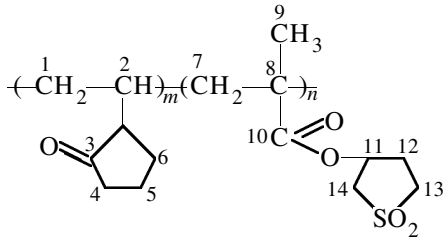
A thermomechanical testing was performed on powder-like samples compacted in pellets (pressure 185 MPa, pressing duration 5 min). The measurements were performed by permanent loading of the samples with linear heating at a rate of 2.5 deg min^{-1}.

Thermal gravimetric measurements were performed in air on a MOM Q 1000 derivatograph at a heating rate of 5.0 deg min^{-1}.

The studies showed that, irrespective of the reaction conditions (in the bulk or in solution), copolymerization of VP with MAHTO yields copolymers with a random distribution of monomeric units in the macrochain. The dependence of the copolymer composition on the composition of the initial mixtures (Fig. 1) and the effective copolymerization constants (Table 1) suggest that MAHTO (r_2) has a significantly higher activity in comparison with VP ($r_2 >> r_1$) and, irrespective of the reaction conditions, the copolymers are significantly enriched in MAHTO units throughout the entire range of the copolymer ratios in the initial mixture.

Table 1 shows that the relative activity of VP in the reaction in DMSO is significantly lower than that in copolymerization in the bulk, which is apparently caused by associative interactions of the components in the polar system: electron-donor DMSO, being associated with a propagating radical having a MAHTO

Table 2. Chemical shifts and multiplicity of signals in the ^{13}C NMR spectra of VP–MAHTO copolymer



C_1	C_2	C_3	C_4	C_5	C_6	C_7	C_8	C_9	C_{10}	C_{11}	C_{12}	C_{13}	C_{14}
30.99 t	43.29 d	174.55 s	30.96 t	17.58 t	43.94 t	40.96 t	43.70 s	19.20 q	174.56 s	70.26 d	28.24 t	48.96 t	55.73 t

terminal unit, displaces VP from the solvation layers of the propagating chains.

A study of kinetic features of the reaction at low conversions showed that an increase in the MAHTO fraction in the initial monomer mixture results in acceleration of the reaction both in the bulk and in DMSO (Fig. 2). The reaction rate in the bulk is significantly higher than that in DMSO.

In copolymerization in DMSO, the reaction orders with respect to the sum of the monomers (at their equimolar ratio) and initiator are 1 and 0.5, respectively, which suggests that the common relationships of radical polymerization with biomolecular mechanism of the termination of the propagating chains are obeyed.

The structure of copolymers was found by ^{13}C NMR (Table 2).

Copolymers of VP with MAHTO are white powders. The solubility of the copolymers depends on the ratio of the comonomer units in the polymer chain. At any ratio of the monomers, the copolymers are soluble in DMSO and DMF, and at the content of MAHTO units in the copolymer less than 10 mol %, they are soluble in water and methanol. The copolymers show film-forming properties; flexible transparent films can be prepared by casting from solutions. The intrinsic viscosity of VP–MAHTO copolymer of the equimolar composition is 1.4 dl g^{-1} (DMSO, 25°C), which suggests a high molecular weight of the copolymer.

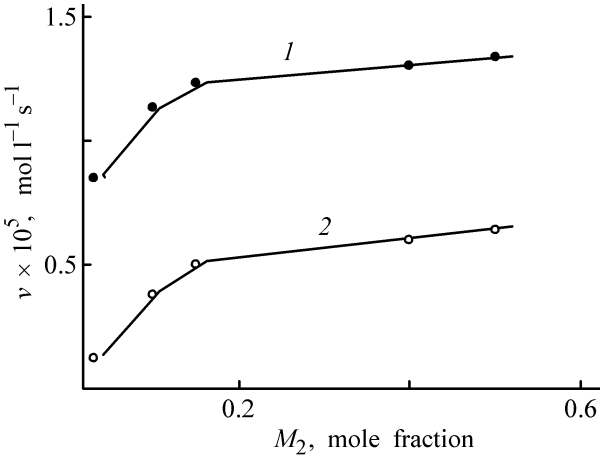


Fig. 2. Initial rate of copolymerization of VP with MAHTO v vs. the composition of the initial monomer mixture, M_2.

The toxicity tests on mice showed that VP–MAHTO copolymers belong to hazard class 4 (in stomach administration LD_{50} >> 3000 mg per 1 kg) and can be used for medical purposes.

The studies of the bactericidal activity showed that VP–MAHTO copolymer of the equimolar composition exhibits pronounced bactericidal effect with respect to *Staphylococcus aureus* and *Staphylococcus saprophiticus* in a concentration of 62.5 μg ml^{-1} and to *Micrococcus luteus* in a concentration of 32.2 μg ml^{-1}.

The glass transition point of the copolymer (at the equimolar ratio of VP units and MAHTO) is 68, flow point 170, and onset point of intense decomposition 264°C.

CONCLUSIONS

(1) Radical copolymerization of *N*-vinylpyrrolidone with 3-methacryloyloxytetrahydrothiophene 1,1'-dioxide was studied. The optimum reaction conditions are the reaction in the bulk at 55°C in the presence of $(3.0–3.1) \times 10^{-2}$ M azobis(isobutyronitrile).

(2) The resulting copolymers are nontoxic, belong to hazard class 4, have pronounced antimicrobial ac-

tivity with respect to gram(+)-microflora, and can be used in production of drugs and in biotechnology.

ACKNOWLEDGMENT

This work was financially supported by the Foundation for Support of Leading Scientific Schools (grant no. NSh-728.2003.3).

REFERENCES

1. Plate, N.A. and Vasil'ev, A.E., *Fiziologicheski aktivnye polymery* (Physiologically Active Polymers), Moscow: Khimiya, 1986.
2. Kirsh, Yu.E. and Sokolova, L.V., *Khim.-Farm. Zh.*, 1983, vol. 17, no. 6, pp. 711–721.
3. Gallardo, A., Fernandez, F., Bermejo, P., et al., *Biomaterials*, 2000, vol. 21, pp. 915–921.
4. Solovskii, M.V., Nazarova, O.V., and Panarin, E.F., *Zh. Prikl. Khim.*, 1992, vol. 65, no. 9, pp. 2103–2107.
5. RF Patent 2015993.
6. Panarin, E.F., Tarasova, N.N., and Gorbunova, O.P., *Zh. Prikl. Khim.*, 1993, vol. 66, no. 11, pp. 2525–2529.
7. RF Patent 2152958.
8. Savel'ev, V.S., Visaitov, B.A., Stupin, I.V., and Sapelkina, I.M., *Khirurgiya*, 1982, no. 10, pp. 89–93.
9. USSR Inventors' Certificate, no. 1005455.
10. Vorob'eva, A.I., Ablyakimov, E.I., Leplyanin, G.V., et al., *Vysokomol. Soedin., Ser. A*, 1974, vol. 16, pp. 765–768.
11. Vorob'eva, A.I., Leplyanin, G.V., Dovlichin, T.Kh., et al., *Vysokomol. Soedin., Ser. B*, 1974, vol. 16, no. 5, pp. 443–446.
12. USSR Inventors' Certificate, no. 412773.
13. Mayo, F.R. and Lewis, F.J., *J. Am. Chem. Soc.*, 1944, vol. 66, pp. 1594–1601.
14. Kelen, T. and Tudos, F., *J. Macromol. Sci. Chem.*, 1975, vol. 9, no. 1, pp. 1–27.
15. Prozorovskii, V.B., Prozorovskaya, M.P., and Demchenko, V.M., *Farmakol. Toksikol.*, 1978, no. 4, pp. 497–502.
16. Pershin, G.N., *Metody eksperimental'noi khimioterapii: Prakticheskoe rukovodstvo* (Methods of Experimental Chemotherapy: A Practical Guide), Moscow: Meditsina, 1971.

ISSN 1070-4272, Russian Journal of Applied Chemistry, 2006, Vol. 79, No. 6, pp. 1001–1004. © Pleiades Publishing, Inc., 2006.
Original Russian Text © I.F. Gun'kin, V.N. Tseluikin, N.Yu. Loginova, 2006, published in Zhurnal Prikladnoi Khimii, 2006, Vol. 79, No. 6, pp. 1011–1013.

MACROMOLECULAR CHEMISTRY AND POLYMERIC MATERIALS

Synthesis and Properties of Water-Soluble Derivatives of Fullerene C_{60}

I. F. Gun'kin, V. N. Tseluikin, and N. Yu. Loginova

Saratov State Technical University, Saratov, Russia

Received September 19, 2006

Abstract—Procedures for synthesized of water-soluble forms of fullerene C_{60} and its derivatives were developed.

DOI: 10.1134/S1070427206060243

Development of methods for synthesis of functionalized derivatives of fullerene C_{60} is imported for preparation of new materials and biologically active compounds. Compounds intended for biological application should be water-soluble. However, C_{60} is hydrophobic. Its solubility in water is as low as 1.3×10^{-11} mg ml^{-1} [1].

A search for ways to raise the water-solubility of C_{60} and its derivatives is a topical task. A study of reactions of fullerenes in water is also of separate interest for applied chemistry. In principle, there are several procedures for raising the solubility of fullerene C_{60} and its derivatives in water.

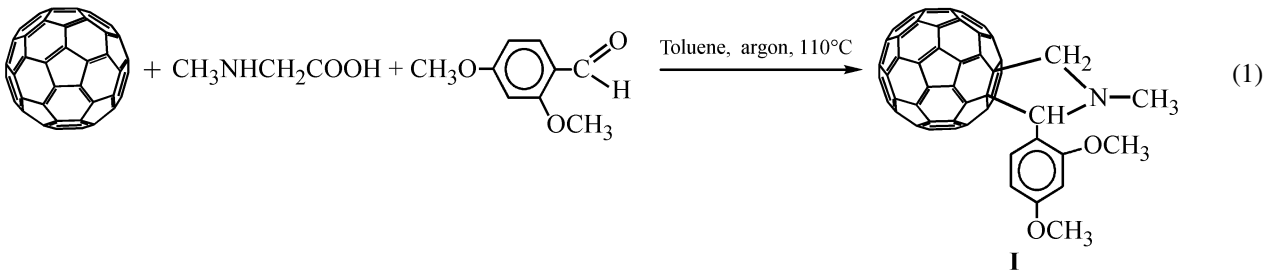
The first is modification of the C_{60} sphere. It is known [2] that the 6–6 bonds of a fullerene molecule are unsaturated and dienophilic. Hence, dienes and nucleophilic agents containing various hydrophilic substituents can be attached to these bonds to form adducts whose solubility in water is higher that that of the initial fullerene C_{60}. Physiologically active fullerenes can be prepared by grafting of pharmacophore groups.

To raise the solubility of fullerene C_{60}, its complexes with various water-soluble polymers, e.g., with polyvinylpyrrolidone (PVP) can be prepared [3–7]. The polymer partially envelops fullerene molecules, which leads to partial solubilization and to increase in its solubility in water.

The third procedure is to prepare colloidal C_{60}. It is known that surfactants can convert water-insoluble organic compounds into colloids or solubilize them. For example, colloid solutions of C_{60} in water are formed in the presence of sodium dodecyl sulfate.

Using these methods, we prepared water-soluble derivatives of fullerene C_{60}.

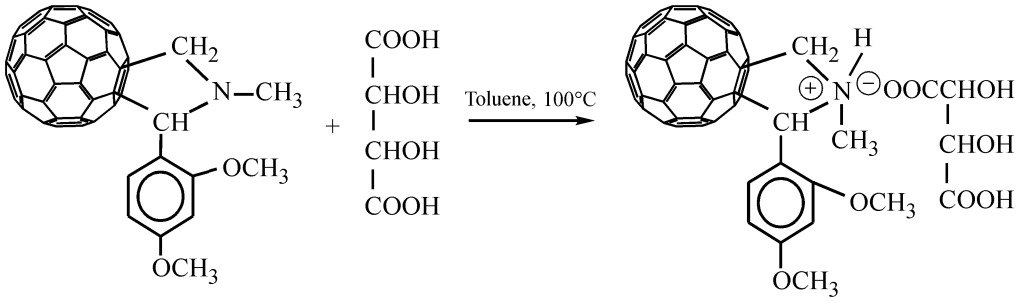
The fullerene sphere was modified by the Plato procedure [8]. The reaction of fullerene C_{60} with *N*-methylglycine (sarcosine) and 2,4-dimethoxybenzaldehyde in refluxing toluene under Ar atmosphere yields *N*-methyl-1-[2,4-dimethoxyphenyl]fullereno-C_{60}[1,9*c*]pyrrolidine (**I**) [reaction (1)]:



(1)

I

To raise the solubility of compound **I** in water, the pyrrolidine ring should be substituted with additional hydrophilic groups. For this purpose, we performed reaction of compound **I** with mesotartaric acid to form the corresponding pyrolidinium tartrate (**II**) [reaction (2)].



I **II**

(2)

Unlike fullerene C_{60}, tartrate **II** is soluble in a water–DMSO mixture (3 : 1).

To obtain water-soluble derivatives of fullerene C_{60}, we prepared its complexes with PVP. These complexes were reported in [3–7]. However, it should be noted that we failed to prepare PVP solutions with high concentrations of fullerene C_{60} by the procedure described in [3]. This is due to the following reasons. When pure toluene is used, problems caused by its low polarity arise, whereas the solubility of fullerene C_{60} in more polar solvents (a chloroform–toluene mixture) is insufficient. An analysis of previous studies [3–7] showed that water-soluble PVP–C_{60} complexes with a high fullerene concentration should be prepared in a single-component polar solvent which readily dissolves both C_{60} and PVP. We suggested that chlorobenzene is a suitable solvent. The dielectric constant of chlorobenzene is $\varepsilon = 5.6$, i.e., it is more polar than chloroform ($\varepsilon = 4.8$). The solubility of fullerene C_{60} in chlorobenzene (5.7 mg ml^{-1} [1]) is an order of magnitude higher than that in a toluene–chloroform mixture. PVP is also readily soluble in chlorobenzene. The use of chlorobenzene allowed us to significantly improve the procedure for preparing complex **III** and to raise the fullerene content in the complex. Complex **III** is water-soluble. The C_{60} content in the complex reaches 1.6%, i.e., it is a factor of 2 higher that than obtained in [3]. The UV spectrum of an aqueous solution of complex **III** contains two bands at 255 and 330 nm. The complex is fairly stable at room temperature but gradually decomposes in an aqueous solution. At 80°C, the complex gradually decomposes in an aqueous solution to form fullerene C_{60}. Decomposition of complex **III** is complete within 70 h. The solubility of complex **III** and the fullerene content were determined both gravimetrically and from the absorption at 255 and 330 nm.

Our third procedure developed for raising the solubility of fullerene C_{60} in water was to prepare a C_{60} colloid, using sodium dodecyl sulfate as a stabilizer. A colloid solution of C_{60} in water was prepared by evaporation of organic solvents from a toluene–acetone–water mixture in the presence of sodium dodecyl sulfate. In the course of evaporation, a dispersion of fullerene C_{60} in water stabilized with sodium dodecyl sulfate is formed. The average size of colloid particles in water, determined from a turbidity spectrum, was 24 nm. The C_{60} content in the dispersion ranged from 0.01 to 0.5 g l^{-1}. The color of these dispersions changed from yellow to dark brown as the fullerene concentration increased.

The stabilizing effect of sodium dodecyl sulfate is caused by adsorption of its molecules on the surface of the fullerene sphere by the hydrocarbon radicals, so that the polar groups form an external layer preventing coagulation. In an aqueous solution, the polar groups partially dissociate to form colloidal C_{60} particles whose structure can be described by the formula

$$\{n[C_{60}]mC_{12}H_{25}SO_4(m - x)Na^+\}xNa^+.$$

Thus, water-soluble derivatives of fullerene C_{60} were prepared by different methods that can be used in chemical industry.

EXPERIMENTAL

The IR spectra of fullerene C_{60} and compounds **I** and **III** (Nujol of hexachlorobutadiene mulls, or KBr

pellets) were recorded on a Specord-80 spectrophotometer. The UV spectra of these compounds in $CHCl_3$ and water were recorded on an SF-26 spectrophotometer.

The TLC analysis was performed on Silufol UV-254 plates, using hexane–toluene (1 : 1) mixture as the eluent. The chromatograms were developed with an iodine vapor.

Fullerene C_{60} (99.5% main compound) was purchased from Merck and used as received, R_f 0.9. UV spectrum ($CHCl_3$), λ_{max}, nm (ε): 258 (86 000), 328 (11 000), 401 (13 000), shoulder 490–500. IR spectrum, ν, cm^{-1}: 528, 576, 1180, 1428.

Sarcosine and 2,4-dimethoxybenzaldehyde were recrystallized prior to use. The physicochemical properties of these compounds were consistent with the published data.

***N*-Methyl-1-[2,4-dimethoxyphenyl]fullereno-C_{60}-[1,9*c*]pyrrolidine (I)**. To a solution of fullerene C_{60} (0.072 g) in toluene (100 ml), sarcosine (0.0267 g) and 2,4-dimethoxybenzaldehyde (0.0332 g) (molar ratio of the reactants 1 : 3 : 2, respectively) were added. The reaction mixture was refluxed under Ar for 8 h, cooled, and washed with several portions of water. The reaction mixture was evaporated to a volume of ~4 ml in a vacuum under Ar. The residue was placed in a column packed with SiO_2. The column was eluted with hexane to remove the unchanged fullerene C_{60}. Compound **I** was eluted with a hexane : toluene (1 : 1) mixture. The eluent was removed. The yield of compound **I** was 15%. R_f 0.1. IR spectrum, ν, cm^{-1}: 528, 550, shoulder 560–580, 670, 725, 770, 850, 915, shoulder 930–950, 970, 1150, 1170, 1210, 1360, 1370, 1450, 1460, 1500–1600, shoulder 1650–1670. 1680, 1700–1750, 2856, 2924, 2960. UV spectrum ($CHCl_3$), λ_{max}, nm (ε): 260 (36 058), 350 (2163), 425 (721), 475–485 shoulder, 525–535 shoulder.

***N*-Methyl-1-[2,4-dimethoxyphenyl]fullereno-C_{60}-[1,9*c*]pyrrolidinium mesotartrate (II)**. To a solution of compound **I** (4 mg) in toluene (10 ml), a solution of mesotartaric acid (0.9 mg) in ethanol (reactant molar ratio 1 : 1) was added. The reaction mixture was refluxed under argon for 1.5 h. The solvent was removed in a vacuum in an argon atmosphere. The yield of compound **II** was 4.9 mg. A single spot was observed at the start on the TLC pattern of this compound. Unlike the initial fullerenopyrrolidine **I**, compound **II** is soluble in aqueous DMSO at ~30–40°C.

Complex PVP–C_{60} (III). The synthesis was performed in anhydrous chlorobenzene. PVP (Enterodez pharmaceutical trademark, molecular weight 12 600 ± 2700) was dried in a vacuum at 80°C for 50 h. To PVP (0.7529) in chlorobenzene (20 ml), C_{60} (0.0231 g) in chlorobenzene (10 ml) was added. The reaction mixture was stirred, heated at 60°C for 5 h, cooled to room temperature and then to 0°C, and kept at room temperature for 50 h. Chlorobenzene was removed in a vacuum at 60°C. The residue was dried in a vacuum, powdered to completely remove the residual chlorobenzene, and dried to constant weight at 60°C in a vacuum. Analysis showed the absence of chlorobenzene in the product. Complex **III** is soluble in water. Its UV spectrum contains bands at 255 and 330 nm. IR spectrum, ν, cm^{-1}: 578, 844, 894, 933, 1077, 1227, 1266, 1375, 1490, 1630, 1687, 1703, 2127, 2395, 2575, 2922, 3329, 3493, 3800, 3943.

Aqueous dispersions of fullerene C_{60}. Fullerene C_{60} was dissolved in toluene to give a 1 mg ml^{-1} solution. A 5–20 mM solution of stabilizer (sodium dodecyl sulfate) in an acetone-water mixture (1 : 3) was prepared. The toluene solution of fullerene C_{60} was added dropwise to the solution of the stabilizer, with vigorous stirring on a magnetic stirrer. The resulting yellow homogeneous solution was distilled under atmospheric pressure with vigorous stirring. The first fraction was acetone, and the second, a toluene–water azeotrope. In the course of azeotrope distillation, an aqueous fullerene dispersion stabilized with sodium dodecyl sulfate was gradually formed. After complete evaporation of the organic solvent from the reaction mixture, only the water fraction with a refractive index n_D^{20} 1.3330 was distilled off. The thus obtained solution was a colloid solution of fullerene C_{60} with a particle size of 24 nm.

CONCLUSIONS

(1) Fullerenopyrrolidine was prepared by functionalization of fullerene C_{60}. Fullerenopyrrolidinium tartrate soluble in a water–DMSO mixture (3 : 1) was prepared by the reaction of this compound with mesotartaric acid.

(2) Procedures for preparing water-soluble derivatives of fullerene C_{60} were developed. These derivatives can be used for preparing composite electrochemical coatings and can exhibit biological activity.

REFERENCES

1. Bezmel'nitsyn, V.N., Eletskii, A.V., and Okun', M.B., *Usp. Fiz. Nauk*, 1998, vol. 168, no. 11, pp. 1195–1220.
2. Yurovskaya, M.A. and Trushkov, I.V., *Izv. Ross. Akad. Nauk, Ser. Khim.*, 2002, no. 3, pp. 343–413.
3. Yamakoshi, Y.N., Yamagami, T., and Fukuhara, K., *J. Chem. Soc., Chem. Commun.*, 1994, pp. 517–518.
4. Evlampieva, N.P., Lavrenko, P.N., Zaitseva, I.I., et al., *Vysokomol. Soedin., Ser. A*, 2002, vol. 44, no. 9, pp. 1564–1570.
5. Ratnikova, O.V., Tarasova, E.V., Melenevskaya, E.Yu., et al., *Vysokomol. Soedin., Ser. A*, 2004, vol. 46, no. 7, pp. 1211–1216.
6. Vinogradova, L.V., Melenevskaya, E.Yu., Khachaturov, A.S., et al., *Vysokomol. Soedin., Ser. A*, 1998, vol. 40, no. 11, pp. 1854–1862.
7. Ratnikova, O.V., Melenevskaya, E.Yu., Mokeev, V.M., et al., *Zh. Prikl. Khim.*, 2003, vol. 76, no. 10, pp. 1663–1668.
8. Plato, M. and Maggini, M., *Acc. Chem. Res.*, 1998, vol. 31, no. 9, pp. 519–526.

ISSN 1070-4272, Russian Journal of Applied Chemistry, 2006, Vol. 79, No. 6, pp. 1005–1008. © Pleiades Publishing, Inc., 2006.
Original Russian Text © P.M. Pakhomov, M.N. Malanin, A.Yu. Kuznetsov, S.D. Khizhnyak, T.A. Anan'eva, 2006, published in Zhurnal Prikladnoi Khimii, 2006, Vol. 79, No. 6, pp. 1014–1017.

MACROMOLECULAR CHEMISTRY AND POLYMERIC MATERIALS

IR Spectroscopic Study of Filled Polymeric Films

P. M. Pakhomov, M. N. Malanin, A. Yu. Kuznetsov, S. D. Khizhnyak, and T. A. Anan'eva

Tver State University, Tver, Russia

St. Petersburg State University of Technology and Design, St. Petersburg, Russia

Received January 24, 2006

Abstract—Distribution of scattering centers (filler particles and pores) in films of an ultra-high-molecular-weight polyethylene xerogel was studied by IR spectroscopy and optical microscopy.

DOI: 10.1134/S1070427206060255

Preparing new polymeric composites, studying their structure and properties, and searching for their new application areas are important problems of modern science and technology. Polymeric composites can be prepared by various processes and, among them, the gel-casting process shows much promise. In this process, the polymeric matrix is filled with both organic and inorganic fillers in the initial stage of the solution preparation before its conversion into the gel and then into the xerogel (solvent-free gel). Since solutions used in the gel preparation are often relatively dilute, a very high degree of filling can be attained upon substitution of the solvent with an appropriate filler. IR spectroscopy is a powerful tool for studying porous structure of xerogel films, because it allows determination of the total porosity of a sample [1] and the average diameter of pores on the micrometer scale [2, 3]. Also, IR spectra furnish information about how the filler affects the xerogel porous structure [4, 5].

In this study, we developed an IR spectroscopic procedure for studying the size distribution of pores and filler particles in a filled polymeric composite.

EXPERIMENTAL

In the tests, we used films of xerogels of ultra-high-molecular-weight polyethylene (UHMWP) with an average molecular weight of 4.0×10^6, filled with particles of micrometer size and various shapes (sphere, tetrahedron, fiber, and flat flake) of vermiculite, strontium ferrite, zeolite, talc, Kopan (modified Nitron fiber), and montmorillonite.

The filled films of 60-μm thickness were prepared by the procedure given in [4, 5]. The degree of filling was varied in the 0–90% range. The IR spectra were recorded on an Equinox 55 Fourier IR spectrometer.

The total porosity of the xerogel films was determined from the absorption coefficient ε_ν of the most intense band in the IR spectra [1, 3]. For polyethylene, we used the absorption band at 730 cm^{-1}, which belongs to rocking vibrations of CH_2 groups in the crystalline phase.

Analysis of scattering and its effect on the IR spectra of a sample allows evaluation of such parameters as the average pore diameter and pore size distribution [3]. As a rule, the bending point in the IR spectrum of a porous material corresponds to the average pore diameter. To evaluate the size distribution function of the scattering centers (pores or filler particles), we recorded IR spectra of a monolithic film of high-density polyethylene with an average molecular weight of 1.5×10^5, prepared from the melt, and of a filled film of the same thickness, prepared from solution by gel-casting (Fig. 1a, curves *1*, *2*). Then, by subtracting the spectra of the porous film from those of the monolithic sample, we obtained the difference spectrum characterizing the dependence of the scattering *S* on the wavenumber (Fig. 1b), which is represented by an S-shape dependence with a characteristic bending point. Then, by assuming that the strongest scattering is observed in the case of coincidence of the scattering particle size and the wavenumber of incident light (so-called diffraction scattering), by passing from wavenumber to the wavelength, and by differentiating this

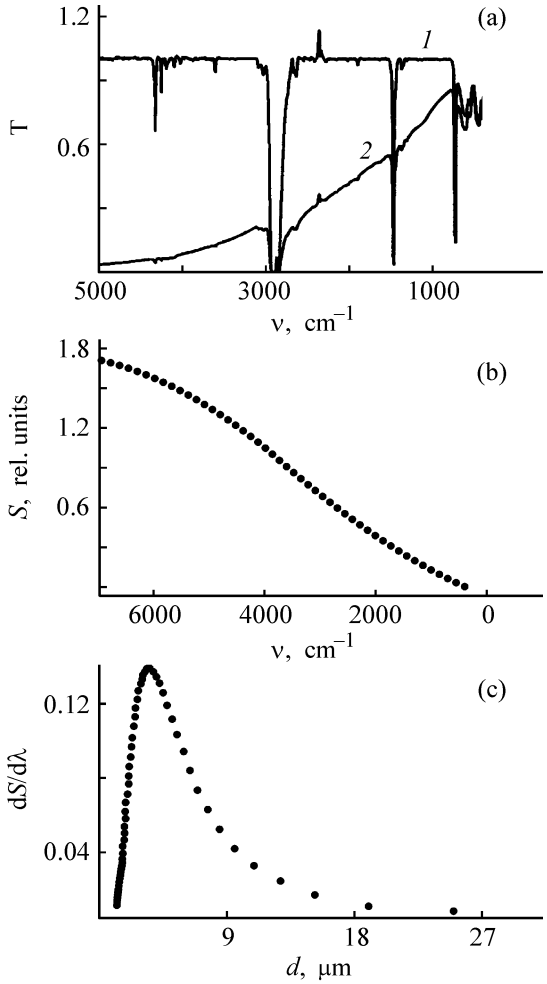


Fig. 1. (a) IR spectra of (*1*) a monolithic film of high-density polyethylene and (*2*) a UHMWP film containing 10 wt % strontium ferrite; (b) difference and (c) differential IR spectra of the above films. (T) Transmission, (*S*) scattering, (ν) wavenumber, and (d) average pore diameter.

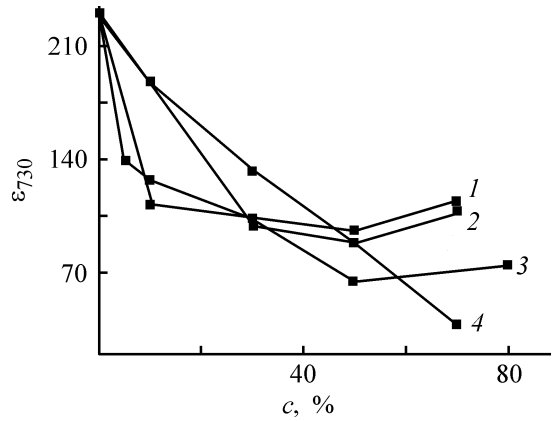


Fig. 2. Absorption coefficient ε_{730} vs. the degree of filling *c* for UHMWP xerogel films with various fillers. (*1*) Montmorillonite, (*2*) strontium ferrite, (*3*) vermiculite, and (*4*) zeolite.

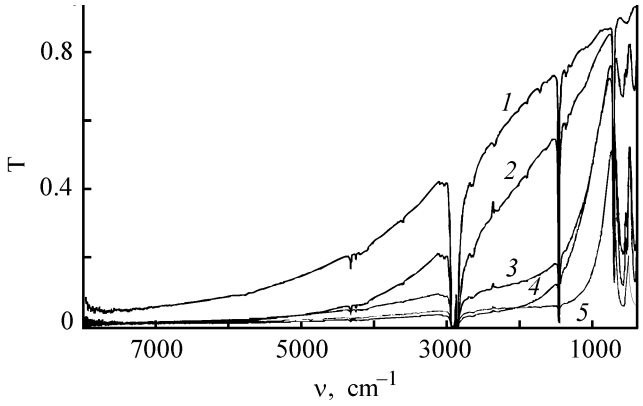


Fig. 3. IR transmission spectra of the UHMWP xerogel films with the degree of filling with strontium ferrite of (*1*) 0, (*2*) 10, (*3*) 30, (*4*) 50, and (*5*) 70%. (T) Transmission and (ν) wavenumber.

diffraction curve, we obtained the size distribution curve of the scattering centers (for pores and filler particles combined) (Fig. 1c) [6].

The composite structure was studied independently by optical microscopy. Photomicrographs of the filled films were recorded on an Neophot 30 optical microscope equipped with a digital camera. The size distribution of the filler particles in the sample was evaluated with the Image Pro program, and the diameters of the filler particles were calculated from the areas of their cross sections on the surface photomicrographs.

It was found [4, 5] that, with the filler concentration increasing to 50%, the total porosity of the sample increases, whereas in some cases, at higher degrees of filling, the sample porosity decreases. The dependences of the absorption coefficient ε_{730} of the UHMWP xerogel films on the degree of filling with various fillers are shown in Fig. 2. Actually, the total porosity increases with the degree of filling for all the fillers studied, and the strongest changes are observed in the initial stage (up to 20%). Since the slope of the curve at the initial point varies with the filler, we can control the dynamics of growth of the total porosity of a polymeric composite and, thus, its properties by using appropriate filler. A certain increase in the absorption coefficient ε_{730} at high degrees of filling (more than 50%) is in some cases indicative of an insignificant decrease in the sample porosity at high degrees of filling, which well agrees with the data reported in [4, 5].

The IR transmission spectra of UHMWP xerogel films with various degrees of filling with strontium ferrite are shown in Fig. 3. It can be seen that, with

increasing degree of filling, the characteristic bending point is shifted toward larger wavenumbers due to scattering of IR light on pores and filler particles. By subtracting the IR spectra of the porous film from the IR spectra of the monolithic film and differentiating the difference spectra with respect to wavelength (Fig. 1) [6], we obtained the size distribution curves of the scattering centers (pores and filler particles) (Fig. 4). It can be seen that, with increasing degree of filling, the average diameter of the scattering centers increases and the size distribution curve of the pores and filler particles becomes significantly broader. Actually, the electron microscopic data on these polymeric films showed that, with increasing degree of filling with strontium ferrite particles, coarser aggregates are formed.

The dependences of the average diameter of the scattering centers (pores and filler particles) on the filler content are shown in Fig. 5. The average diameters of the scattering centers were calculated from the peaks the size distribution curves, similar to those given in Fig. 4. As can be seen from Fig. 5, the most pronounced increase in the average diameter of the scattering is observed with strontium ferrite, and the least pronounced, with Kopan. This indicates that the filler type directly affects the pore diameter and ability to form filler aggregates in the polymeric composite. Obviously, ferromagnetic strontium ferrite should show the strongest tendency to form aggregates. Hence, by adding various fillers in a polymeric composite, we can significantly change its morphology and the mechanical, sorption, and other properties.

In accordance with the Babinet principle [7], the scattering of electromagnetic radiation on holes (pores) is identical to that on the solid particles. Thus, it is rather difficult to distinguish the contributions of pores and filler particles to the overall pattern of light scattering with a porous composite using the IR data only. For this purpose we used an independent method, optical microscopy, which allows evaluation of the size distribution function of only particles that occur on the sample surface. The size distribution curves of the scattering centers (pores and filler particles) in the UHMWP xerogel films filled with strontium ferrite, evaluated by two above methods, are shown in Figs. 6a and 6b. Curve *1* illustrates the size distribution of the filler particles obtained by optical microscopy, and curve *2* (IR data), the size distribution of both pores and filler particles. As seen, at a 10% degree of filling the size distribution curves of the scattering centers are similar (Figs. 6a and 6b) and are only slightly shifted with respect to each other. This fact suggests that, at a small content of the strontium ferrite filler (≤10%), the size distri-

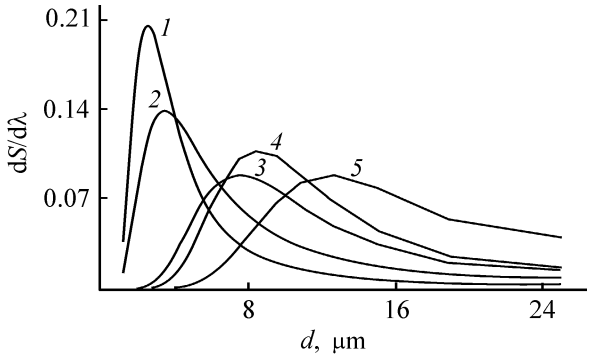


Fig. 4. Size distribution of the scattering centers (pores and filler particles) of the UHMWP xerogel films with degree of filling with strontium ferrite of (*1*) 0, (*2*) 10, (*3*) 30, (*4*) 50, and (*5*) 70%. (*d*) Average pore diameter; the same for Fig. 6.

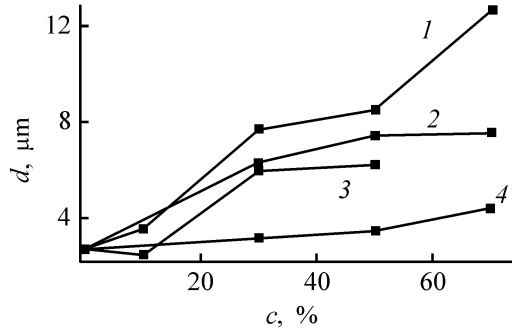


Fig. 5. Average size *d* of pores and filler particles vs. the filler content in the composite based on UHMWP. (*1*) Strontium ferrite, (*2*) zeolite, (*3*) talc, and (*4*) kopan.

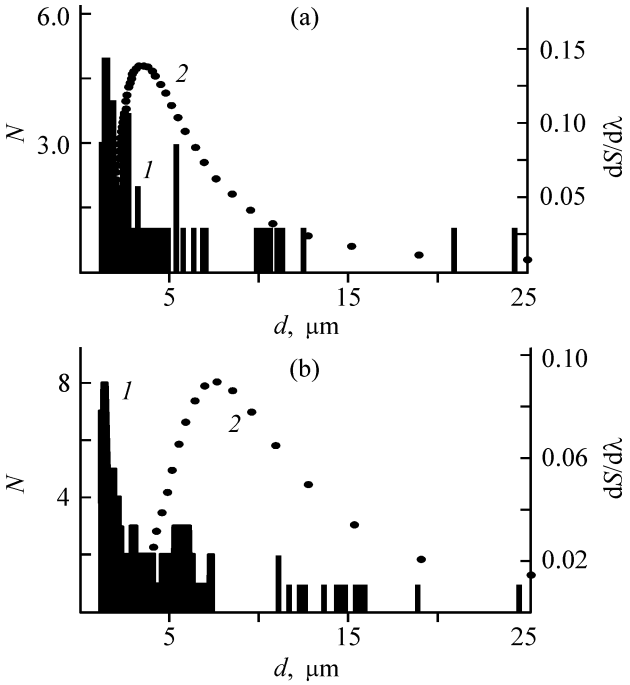


Fig. 6. Size distribution of the scattering centers in UHMWP xerogel films with the degree of filling with strontium ferrite of (a) 10 and (b) 30%. (*1*) Optical microscopy and (*2*) IR spectroscopy.

bution functions of the filler particles and pores in the xerogel film are similar. With increasing filler content (Fig. 6b), the contribution of scattering on pores grows, and the difference in the size distribution curves obtained by optical microscopy and IR spectroscopy becomes more pronounced; simultaneously, the shift between these curves also increases. This shift is due to the increasing porosity of the film; it is related to the growth of the pore size rather than to that of the pore concentration. This increase in the film porosity with increasing filler content well agrees with the results presented in [4, 5] and can be attributed to changes in the crystallization conditions at formation of the xerogel film. Thus, combined use of optical microscopy and IR spectroscopy furnishes rich information on the aggregation of the filler particles and formation of the porous structure of UHMWP xerogel films.

CONCLUSUIONS

(1) The dependences of the total porosity and average diameter of the scattering particles of ultra-high-molecular-weight polyethylene on the content and type of filler were evaluated by IR spectroscopy; the filler type strongly affects the porosity and aggregation of the filler particles.

(2) A study of the dependences of the size distribution functions on the degree of filling of ultra-high-molecular-weight polyethylene with strontium ferrite filler demonstrated that, at high degrees of filling, the effect of the pore scattering on the distribution function is decisive.

REFERENCES

1. Pakhomov, P.M., Kruglov, E.V., and Khizhnyak, S.D., *Vysokomol. Soedin., Ser. B*, 2000, vol. 42, no. 6, pp. 1081–1088.
2. Pakhomov, P.M., Malanin, M.N., Kruglova, E.V., and Khizhnyak, S.D., *Vysokomol. Soedin., Ser. B*, 2001, vol. 43, no. 4, pp. 764–768.
3. Pakhomov, P.M., Khizhnyak, S.D., Malanin, M.N., and Mikhailova, Yu.N., *Zavod. Lab. Diagnost. Mater.*, 2002, vol. 68, no. 5, pp. 31–33.
4. Mikhailova, Yu.N., Nazarova, E.V., Khizhnyak, S.D., et al., *Zh. Prikl. Khim.*, 2002, vol. 75, no. 1, pp. 107–112.
5. Pakhomov, P.M., Nazarova, E.V., Anan'eva, T.A., et al., *Zh. Prikl. Khim.*, 2003, vol. 76, no. 3, pp. 479–482.
6. Pakhomov, P.M., Malanin, M.N., and Khizhnyak, S.D., *Vysokomol. Soedin., Ser. B*, 2005, vol. 47, no. 6, pp. 1066–1072.
7. Born, M. and Wolf, E., *Osnovy optiki* (Principles of Optics), Moskow: Nauka, 1973.

ISSN 1070-4272, Russian Journal of Applied Chemistry, 2006, Vol. 79, No. 6, pp. 1009–1015. © Pleiades Publishing, Inc., 2006.
Original Russian Text © B.I. Lirova, E.A. Lyutikova, A.P. Safronov, T.V. Terziyan, B.A. Berkuta, S.I. Degtyarev, M.I. Prusskii, 2006, published in Zhurnal Prikladnoi Khimii, 2006, Vol. 79, No. 6, pp. 1018–1024.

ORGANIC SYNTHESIS AND INDUSTRIAL ORGANIC CHEMISTRY

Migration of Plasticizers from Plasticized Polyvinyl Chloride Films

B. I. Lirova, E. A. Lyutikova, A. P. Safronov, T. V. Terziyan, B. A. Berkuta, S. I. Degtyarev, and M. I. Prusskii

Gor'kii Ural State University, Yekaterinburg, Russia

Stroiplastpolimer Open Joint-Stock Company, Yekaterinburg, Russia

Received February 14, 2006

Abstract—The migration of plasticizers [EDOS, di(2-ethyl hexyl) *o*-phthalate, di-*n*-butyl *o*-phthalate] from unfilled and chalk-filled polyvinyl chloride films plasticized with individual and binary plasticizers was studied by gravimetric analysis and IR spectroscopy. The intermolecular interaction of components in model systems was studied by IR spectroscopy and isothermal calorimetry.

DOI: 10.1134/S1070427206060267

EDOS plasticizer attracts attention of researchers and producers of polymer materials as a substance allowing partial or complete replacement of expensive phthalate plasticizers [1–4]. EDOS is prepared from large-volume isoprene production waste and is a mixture of dioxane alcohols and their high-boiling derivatives [5].

The properties of polyvinyl chloride (PVC) materials plasticized with EDOS were compared in [1, 2] with the properties of the same materials plasticized with commercially used di(2-ethylhexyl) *o*-phthalate (DOP) and di-*n*-butyl phthalate (DBP). It was shown that complete (with DOP) or partial (with DBP) replacement of phthalate plasticizers with EDOS is appropriate. However, the high volatility of EDOS can lead to its substantial loss in the course of processing of PVC formulations.

It is also known [6–9] that the release from PVC materials of such plasticizers as DOP, DBP, dibutoxyethyl adipate, or dibutyl sebacate can be controlled both by the volatility of the plasticizers themselves and by their diffusion in a polymer matrix, depending on the temperature, chemical structure of the plasticizer, its initial content in the sample, and other factors. In this connection, various procedures can be considered for decreasing the migration of plasticizers from polymeric materials with the aim to ensure their environmental safety and stability of service parameters. Data on the mechanism of EDOS migration from polymer formulations are lacking; therefore, it is interesting to study its migration from PVC compounds in comparison with the formulations plasticized with DOP and DBP.

EXPERIMENTAL

Experiments were performed with PVC films simulating linoleum prepared by rolling and calendering; both filled and unfilled films were tested. The formulations were prepared from the following commercial components: S-70 suspension PVC; EDOS, DOP, and DBP plasticizers; and MTD-2 chalk (filler). All the formulations were stabilized with calcium stearate and urea. Samples for gravimetric experiments had the following composition (weight proportion): PVC 100, plasticizer 64, chalk 0 or 245, Ca stearate 0.9, and urea 0.45. Samples were prepared as films by rolling on laboratory rolls at 140°C for 10 min. The film thickness was about 1 mm. Experiments were started approximately 1 month after the sample preparation.

Samples for studying the thermodynamics of component interaction in PVC formulations containing up to 50% plasticizer were rolled as films. Formulations containing more than 50% plasticizer were prepared by adding strictly the required amount of the same plasticizer to samples containing 50% plasticizer, followed by heating at 50°C in sealed glass calorimetric ampules to complete homogenization.

Model polymer-containing systems for studying intermolecular interaction by IR spectroscopy were prepared as films from 3% solutions in tetrahydrofuran (THF) on a glass support. Tetrahydrofuran was evaporated at room temperature, and the films were kept for 9 h at 70°C to remove the residual solvent; the process was monitored spectroscopically.

The weight loss of the samples in air at atmospheric pressure under isothermal conditions at room temperature and 90°C was monitored gravimetrically.

The qualitative composition of substances released from the films to air and the kinetics of their release at 90°C in a dynamic vacuum (residual pressure about 30 Pa) were studied by the previously developed procedure [9, 10] based on IR spectroscopy, using a thermovacuum chamber (TVC).

The intermolecular interactions of components in the films were evaluated from changes in the absorption bands of functional groups in the IR spectra of model systems plasticizer–polymer, plasticizer–filler, and plasticizer–plasticizer. The IR spectra were recorded on a Specord 75-IR spectrometer.

The thermodynamics of the interactions in PVC formulations was studied by isothermal calorimetry. The enthalpies of mixing of the plasticizers, PVC, and PVC formulations with a solvent (THF) at 25°C were measured with a Calvet calorimeter (cell sensitivity 0.22 V W^{-1}). The enthalpy of wetting of chalk with EDOS plasticizer was also determined. The error of the calorimetric measurements did not exceed 5%.

The enthalpy of mixing of a polymer with an individual or mixed plasticizer was calculated in accordance with the Hess law:

$$\Delta H^m = \omega_1 \Delta H_1 + \omega_2 H_2 - \Delta H_3, \quad (1)$$

where ω_1 and ω_2 are the weight fractions of the plasticizer and polymer in the formulation; ΔH^m, enthalpy of mixing of the polymer with an individual or mixed plasticizer per gram of PVC formulation; ΔH_1, ΔH_2, and ΔH_3, enthalpies of solution of the plasticizer, polymer, and formulations in excess solvent.

When analyzing the enthalpies of mixing of PVC with plasticizers, it should be taken into account that at room temperature PVC is in the glassy state; therefore, the measured enthalpies of solution of the formulations and individual polymer are integral quantities and involve two contributions: that from intermolecular interaction of the components and that from the breakdown of the glassy structure of the polymer [11, 12]:

$$\Delta H^m = \Delta H_{int} + \Delta H_g. \quad (2)$$

The contribution from the component interaction is calculated in accordance with the Flory–Huggins theory as follows:

$$\Delta H_{int} = \chi RT \varphi_1 \varphi_2, \quad (3)$$

where φ_2 is the volume fraction of the polymer in the formulation; φ_1, volume fraction of the plasticizer in the formulation; and χ, Flory–Huggins interaction parameter. The contribution associated with the glassy state of the polymer is determined in accordance with the semiempirical model of polymer solution suggested in [12] as

$$\Delta H_g = \varphi_v^0 \varphi_2 \varepsilon_{22} (1 - \varphi_2^{[(1/\varphi_v^0) - 2)]}), \quad (4)$$

where φ_v^0 is the fraction of metastable vacancies in the initial polymer sample and ε_{22} is the cohesion energy density of the polymer chain units.

By interpolation of the experimental data on the enthalpies of solution, using Eqs. (1)–(4), we calculated the enthalpies of the interaction and glassy structure for the PVC–DOP and PVC–EDOS systems for the entire concentration ranges. For EDOS, the mean molecular weight and mean van der Waals volume of the plasticizer were calculated taking into account the structures and amounts of its components.

To calculate the enthalpies of mixing of components of the DOP–EDOS plasticizing mixture, we also used the thermochemical cycle and Eq. (1). In this case, ω_1 and ω_2 are the weight fractions of the plasticizer in the mixture; ΔH_1 and ΔH_2, enthalpies of solution of the individual plasticizers in THF; and ΔH_3, enthalpy of solution of the mixed plasticizer of a definite composition in excess solvent.

The weight loss of the unfilled and chalk-filled PVC films containing the individual plasticizers at room temperature (T_r) and 90°C under atmospheric pressure is shown in Fig. 1 (curves *1–3*). It is seen that the weight loss of the EDOS-containing films is larger than that of the DOP- and DBP-containing films, except the weight loss of the filled films at 90°C; in the latter case, with DBP the weight loss is larger than with EDOS. In the substances released from the samples, we detected by IR spectroscopy only the plasticizers present in the films. Since the samples contain stabilizers, release of HCl at 90°C (and, the more so, at T_r) does not occur, and the weight loss is exclusively due to the plasticizer migration and not to the PVC degradation. The weight loss data were

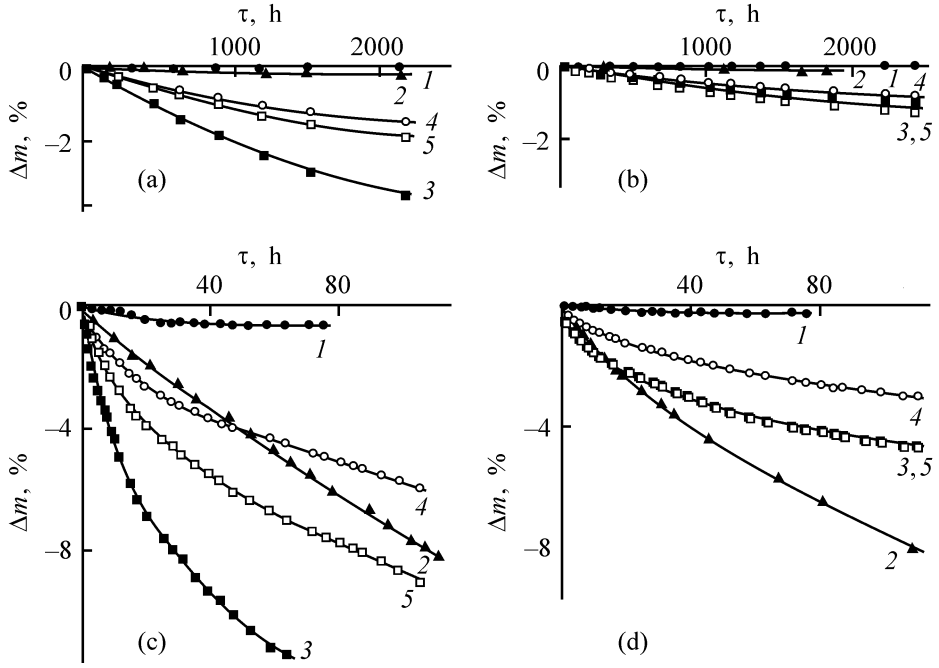


Fig. 1. Weight loss Δm vs. time τ. Temperature: (a, b) T_r and (c, d) 90°C. PVC films: (a, c) unfilled and (b, d) filled with chalk. Plasticizer: (*1*) DOP, (*2*) DBP, (*3*) EDOS, and (*4*, *5*) DOP + EDOS. Weight proportions of DOP and EDOS (PVC = 100): (*4*) 35 and 35, and (*5*) 20 and 50, respectively.

plotted in the coordinates $M_\tau/M_\infty = f(\tau^{1/2})$ [9], where M_τ is the amount of the plasticizer released by the moment τ, assumed to be equal to the sample weight loss, and M_∞ is the initial content of the plasticizer in the sample. The initial linear portions in the plots obtained suggest that in these periods the release of the plasticizers to the atmosphere is controlled by their diffusion in the sample. This fact allows calculation of the diffusion coefficients (Table 1), which are apparent quantities (especially for EDOS) characterizing the migration rate.

The weight loss of some samples containing DOP and DBP (Table 1) during the experiment is small, which does not allow any reliable conclusions about the shape of the $M_\tau/M_\infty = f(\tau^{1/2})$ dependences. However, according to [6, 8], at room temperature the release of DOP and DBP from PVC formulations is limited by the volatility of the plasticizers, whereas the release of DOP at 90°C is limited by the diffusion of the plasticizer in the polymer matrix.

For the EDOS-containing samples at room temperature, during the first 15 days after the sample preparation, the $M_\tau/M_\infty = f(\tau^{1/2})$ dependence is nonlinear, suggesting that the release of the plasticizer is controlled by its volatility. In the subsequent period, the dependence becomes linear, which indicates that the plasticizer diffusion becomes the limiting step. The D values calculated from this dependence are listed in Table 1. At 90°C and atmospheric pressure, the release of EDOS, like that of DOP, is controlled by the plasticizer diffusion (in both unfilled and filled PVC films), even in the initial steps of the desorption. The results obtained with DOP are consistent with

Table 1. Diffusion coefficients D of plasticizers in PVC films containing DOP, DBP, and EDOS, and volatility v of plasticizers

Plasticizer	Filler	$D \times 10^{14}$, $m^2\ s^{-1}$		$D \times 10^{12}$, $m^2\ s^{-1}$	$v^* \times 10^8$, $g\ cm^{-2}\ s^{-1}$
		atmospheric pressure		vacuum	atmospheric pressure
		T_r	90°C	90°C	90°C
DOP	–	DOP + DBP**	0.02	0.7	2.0
	+	〃	DOP + DBP	0.9	
DBP	–	〃	–	1.5	3.4
	+	〃	14.7	2.8	
EDOS	–	0.01	5.7	1.0	6.4
	+	0.02	7.3	1.3	

* The volatility of plasticizers was evaluated from the time dependences of the weight loss of individual plasticizers (measurement time 10 h).

** Samples contain DOP and DBP.

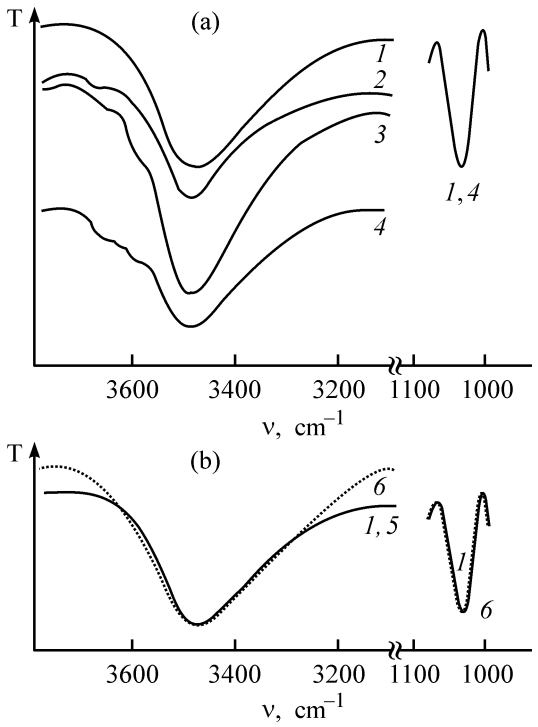


Fig. 2. IR spectra of (a, b) (*1*) EDOS, (a) (*2–4*) PVC–EDOS films, and (b) (*5*, *6*) chalk–EDOS mixtures in the range of the EDOS absorption bands ν_{OH} and ~1030 cm^{-1}. (T) Transmission and (ν) wavenumber. Weight ratio of components in the films and mixtures: (*1*) 0 : 100, (*2*) 100 : 100, (*3*) 100 : 60, (*4*) 100 : 25, (*5*) 10 : 100, and (*6*) 40 : 100.

the data of [6, 9]. For unfilled films containing DBP, the dependence was nonlinear throughout the experiment, i.e., the DBP release is controlled by its volatility. However, in the filled films with DBP plasticizer, its diffusion in the film becomes the limiting step. The results obtained with DBP are consistent with the data of [8, 10]. In particular, Dedov and Nazarov [8] indicate that the limiting step of the DBP release from PVC films depends on the initial content of DBP in the sample. The diffusion control in the release of DBP and EDOS from the filled compounds under the examined conditions also follows from a comparison of the weight loss curves for the filled samples containing DBP and EDOS ($\Delta m_{DBP} > \Delta m_{EDOS}$, Fig. 1d), volatility of these plasticizers ($v_{DBP} < v_{EDOS}$, Table 1), and their diffusion coefficients ($D_{DPB} > D_{EDOS}$, Table 1).

The migration of the plasticizers from the samples was also studied at 90°C under the conditions of forced removal of the plasticizers from the surface. To this end, we performed experiments in a dynamic vacuum (TVC). The IR spectra of the released products confirm that the released substances are the plasticizers initially present in PVC films. The kinetic data on the release of the plasticizers were plotted in the coordinates $A_\tau/A_\infty = f(\tau^{1/2})$ [10], where A_τ is the optical density of the chosen absorption band in the IR spectra of the released substances by the instant of time τ (~1720 cm^{-1} for DOP and DBP; ~1030 cm^{-1} for EDOS), and A_∞ is the optical density of this absorption band corresponding to the initial plasticizer content. The band at ~1720 cm^{-1} is the stretching vibration band of the carbonyl groups in DOP and DBP [13]. The band at ~1030 cm^{-1} for EDOS is common for all the EDOS components. It can be assigned to bending vibrations ($\delta_{C–OH}$) of the OH groups of primary alcohols and to stretching vibrations ($\nu_{C–O}$) of the C–O groups of primary alcohols and ethers [13, 14].

After the establishment of the temperature in the TVC, the initial portions of the desorption curves for all the samples are linear, suggesting that the release of the plasticizers is controlled by their diffusion in the samples. The *D* values calculated from the linear portions of the dependences are listed in Table 1. It is seen that in the unfilled and filled films *D* increases in the order DOP < EDOS < DBP. Introduction of chalk as a filler leads to an increase in *D*, which is consistent with the data of [10] for the phthalate plasticizers (DOP, DBP). The difference in the diffusion coefficients of the plasticizers may be caused, along with the steric factors, also by the difference in their interaction with the polymer macromolecules and filler particles [9, 10, 15, 16]. We showed previously by IR spectroscopy [9, 10] that DOP and DBP interact with the polymer, forming H bonds with the CHCl groups of PVC via the C=O groups [17]. In addition, a donor–acceptor interaction may arise between the π electrons of the benzene ring of the plasticizers and the vacant 3*d* orbitals of the Cl atoms of PVC macromolecules [18]. Safronov and Somova [19] indicate that the contribution of dispersion interactions in the systems PVC–phthalate plasticizer should also be taken into account. The total enthalpy of interaction of PVC with DOP is higher than with DBP [19], which is consistent with the lower diffusion coefficient of DOP, compared to DBP, as we determined in this study.

Figure 2a shows the IR spectra of the EDOS plasticizer and PVC–EDOS films in the range of OH stretching vibrations (ν_{OH}) of the hydroxyl-containing EDOS component [5, 13] and the ~1030 cm^{-1} band of EDOS at varied concentration of the polymer in the film. The position of the ν_{OH} maximum in the spectrum of pure EDOS (~3480 cm^{-1}) and the half-width of this band ($\Delta\nu_{1/2}$ ~290 cm^{-1}) (Fig. 2a, curve *1*) are

indicative of the association of EDOS molecules through OH···C–O and OH···OH hydrogen bonds [20, 21]. In going to the plasticized PVC film (curves *2–4*), the band intensities are redistributed in favor of the higher-frequency components, suggesting the decomposition of EDOS associates. However, the H bonding between the EDOS C–O groups and CHCl groups of PVC (of the type C–O···CHCl) is quite possible, taking into account high electron-donor power of dioxane (DN_{SbCl_5} = 28.2 [22]). These two processes exert opposite (and hence mutually compensating) effects: the decomposition of the associates should increase ν_{C-O} and decrease δ_{C-OH}, whereas the H bonding should decrease ν_{C-O} and increase δ_{C-OH} [20]; as a result, the EDOS band at ~1030 cm^{-1} undergoes no appreciable changes.

The interaction of PVC with EDOS and DOP also follows from the thermodynamic data. The experimentally measured enthalpies of solution of PVC, plasticizers, and plasticized PVC formulations in THF are given in Table 2.

From the experimental data, we calculated by Eq. (1) the enthalpies of mixing of PVC with the plasticizers. These quantities are negative throughout the composition range. The calculated contributions of intermolecular interactions to the enthalpies of mixing of PVC with the EDOS and DOP in the whole composition range are plotted in Fig. 3. Figure 3 shows that EDOS interacts with PVC more weakly than does DOP, which correlates with its higher diffusion coefficient compared to DOP (Table 1).

In the filled systems, the filler can interact with the plasticizer. It is known that chalk does not interact with PVC and does not noticeably interact with phthalate plasticizers [10, 18, 23]. Data on the interaction of chalk with EDOS are lacking. We determined the heat of wetting of chalk with EDOS: –2.3 J g^{-1}. This value differs from the heats of wetting of chalk with DOP and DBP, which are close to zero [18]. The wetting of chalk with EDOS is consistent with the fact that both EDOS (its components, in contrast to DOP and DBP, appreciably dissolve in water [4]) and carbonates (carbonates are wetted with water better than with nonpolar hydrocarbons [24]) are hydrophilic. Figure 2b shows the IR spectra of EDOS with additions of chalk. Introduction of chalk (40 wt % relative to EDOS) leads to a slight broadening of the plasticizer bands ν_{OH} and ~1300 cm^{-1}, suggesting certain interaction between the components. Presumably, the interaction of the filler with EDOS may lead to a nonmonotonic dependence of *D* on the filler content in PVC films, in contrast to the phthalate plasticizers [10].

Table 2. Enthalpies of solution in THF of PVC–plasticizer formulations and of PVC and plasticizers taken separately

ω_{PVC}	ΔH_s, J g^{-1}	
	PVC–EDOS	PVC–DOP
1.00	–41.3	–41.3
0.90	–33.6	–31.9
0.80	–17.0	–18.2
0.70	–13.3	–13.5
0.60	–11.2	–10.2
0.50	–7.6	–8.4
0.41	–8.0	–
0.23	–4.9	–
0.25	–	–4.5
0.17	–	–4.0
0.13	–	–3.0
0.08	–	–2.8
0	–3.0	–2.2

We also studied the PVC films containing mixed plasticizers (DOP + EDOS), because it is known [1] that partial replacement of DOP with EDOS improves the service characteristics of PVC finishing materials (the use of DBP–EDOS mixtures is not appropriate because of possible ester interchange of dibutyl phthalate with dioxane alcohols in the course of storage of PVC materials [1]). Figure 1 (curves *4*, *5*) shows data on the mass transfer in unfilled (Figs. 1a, 1c) and chalk-filled (Figs. 1b, 1d) PVC films plasticized with DOP–EDOS mixtures, measured at room temperature or 90°C and atmospheric pressure. The formulations containing the mixed plasticizers occupy an intermediate position between the formulations with the individual plasticizers. The IR spectra of the released substances are attributable to the plasticizers initially present in the formulations. Data on the release of the plasticizers under the conditions of forced removal of the plasticizers from the film surface (90°C, TVC) allowed us to calculate *D* of the plasticizer mixtures

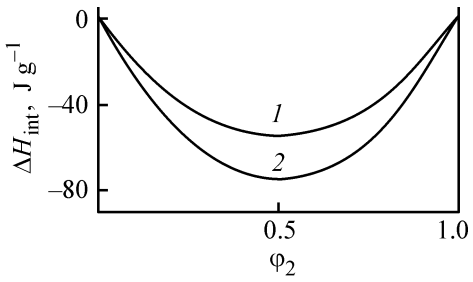


Fig. 3. Concentration dependence of the contribution from the component interaction ΔH_{int} to the enthalpy of mixing of PVC with (*1*) EDOS and (*2*) DOP. (φ_2) Volume fraction of the polymer at 25°C.

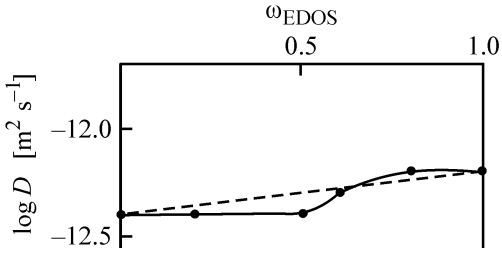


Fig. 4. Diffusion coefficient D of the DOP–EDOS mixed plasticizer in unfilled PVC films at 90°C in a vacuum vs. the EDOS weight fraction in the mixed platicizer. PVC : plasticizer weight ratio 100 : 50.

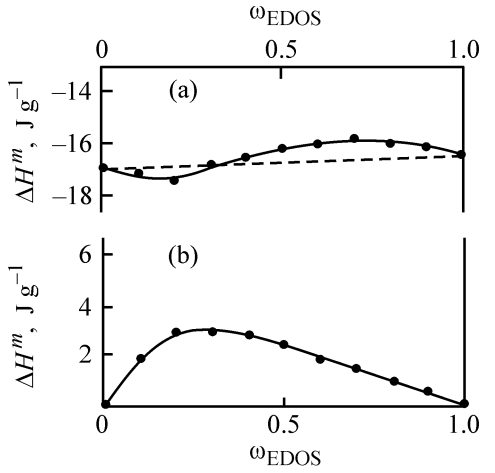


Fig. 5. Enthalpy of mixing ΔH^m (a) of PVC with DOP–EDOS mixed plasticizer and (b) of DOP with EDOS vs. of the EDOS weight fraction ω_{EDOS} in the DOP–EDOS mixture. (a) PVC : plasticizer weight ratio 100 : 50.

in the initial steps of the desorption. The values of D for the DOP–EDOS mixtures were evaluated using the absorption band at ~1030 cm^{-1}, which is common for EDOS and DOP (a weak band at ~1030 cm^{-1} is present in the spectrum of DOP [25]), and the DOP band at ~1720 cm^{-1}. Previous experiments showed that the calculations of D from data of the same experiment but using different absorption bands gave similar results.

Figure 4 shows the dependence of D on the composition of the DOP–EDOS plasticizing mixture. It is seen that D grows with an increase in the EDOS content in the plasticizing mixture and that the dependence of D on the mixture composition shows no strong deviations from the additivity. In Fig. 5a the enthalpy of mixing of PVC with the DOP–EDOS mixed plasticizer (50 wt % relative to PVC) is plotted vs. the ratio of the plasticizer components. This dependence well correlates with the dependence of the diffusion coefficient on the composition of the mixed plasticizer. At a low EDOS content, ΔH^m is more negative and D is lower than the additive value, whereas at a high EDOS content ΔH^m becomes less negative and D exceeds the additive value. On the whole, however, the deviations from the additivity are small; this fact can be accounted for by the absence of specific interactions between the components of the mixed plasticizer [26].

Figure 5b shows the dependence of the enthalpy of mixing of DOP with EDOS on the component ratio. In the entire composition range, the mixing is endothermic, i.e., the energy of the interaction of the different molecules is lower than that of the interaction of the like molecules. This fact is also confirmed by IR spectroscopy. On adding DOP to EDOS, the ν_{OH} maximum shifts toward higher frequencies, i.e., the decomposition of EDOS associates prevails:

ω_{EDOS}	1.0	0.8	0.6	0.5	0.4	0.2	0
ω_{OH}, cm^{-1}	3482	3490	3496	3500	3507	3529	–

Monitoring at ~1030 (EDOS) and 1720 cm^{-1} (DOP) is complicated by overlap of the absorption bands of the plasticizers.

The absence of preferential interaction of EDOS with DOP in the plasticizer mixture is apparently responsible for the fact that the diffusion coefficient of the mixed plasticizer and the enthalpy of mixing of PVC with the mixed plasticizer are approximately linear functions of the plasticizing mixture composition.

CONCLUSIONS

(1) The release of EDOS from plasticized polyvinyl chloride films of the examined composition into air at room temperature and at 90°C is mainly controlled by the EDOS diffusion in the polymer matrix, rather than by its volatility.

(2) Replacement of di(2-ethylhexyl) *o*-phthalate and di-*n*-butyl phthalate with EDOS in unfilled films is not appropriate because of the large loss of the plasticizer in air, especially on heating.

(3) Filling of polyvinyl chloride films with chalk can reduce the weight loss. For the filled films, complete replacement of di-*n*-butyl phthalate or partial replacement of di(2-ethylhexyl) phthalate with EDOS is appropriate, provided that the other service characteristics will be preserved.

(4) The characteristics of migration of the plasticizers from polyvinyl chloride formulations correlate with the thermodynamics of interaction of the components.

REFERENCES

1. Sokolova, A.G., Polyvinyl Chloride and Polyvinyl Acetate Materials Plasticized with EDOS, *Cand. Sci. Dissertation*, Penza, 1999.
2. Glazyrin, A.B., Kalganov, V.A., Abdullin, M.I., and Chuklina, N.S., *Plast. Massy*, 2001, no. 9, pp. 18–19.
3. Akhmerov, A., Gotlib, E.M., Safina, N.P., and Leksin, V., *Izv. Vyssh. Uchebn. Zaved., Khim. Khim. Tekhnol.*, 2001, vol. 44, no. 1, pp. 70–72.
4. Gotlib, E.M., Koltun, E.E., and Averko-Antonovich, I.Yu., *Kauchuk Rezina*, 1999, no. 5, pp. 5–8.
5. *TU* (Technical Specifications) *2493-003-13 004 749–93: EDOS Plasticizer. Technical Specifications*.
6. Nazarov, V.G., Dedov, A.V., and Semenov, A.A., *Vysokomol. Soedin., Ser. B*, 1991, vol. 33, no. 12, pp. 927–933.
7. Dedov, A.V. and Nazarov, V.G., *Vysokomol. Soedin., Ser. B*, 2001, vol. 43, no. 9, pp. 1574–1577.
8. Dedov, A.V. and Nazarov, V.G., *Vysokomol. Soedin., Ser. B*, 2002, vol. 44, no. 4, pp. 729–732.
9. Lirova, B.I., Lyutikova, E.A., Degtyareva, A.N., et al., *Zh. Prikl. Khim.*, 2004, vol. 77, no. 10, pp. 1707–1713.
10. Lirova, B.I., Lyutikova, E.A., Mel'nik, A.I., and Pyzh'yanova, L.G., *Vysokomol. Soedin., Ser. B*, 2002, vol. 44, no. 2, pp. 363–368.
11. Safronov, A.P. and Adamova, L.V., *Polymer*, 2000, vol. 43, pp. 2653–2662.
12. Safronov, A.P., Thermodynamics of Mixing of Regular Solutions of Polymers, *Doctoral Dissertation*, Yekaterinburg, 2000.
13. Bellamy, L.J., *The Infra-Red Spectra of Complex Molecules*, New York: Wiley, 1957.
14. *Fiziko-khimicheskie svoistva produktov proizvodstva izoprena* (Physicochemical Properties of Products from Isoprene Production), Ogorodnikov, S.K., Ed., Moscow: TsNIITEneftekhim, 1974.
15. Shtarkman, B.P., *Plastifikatsiya polivinilkhlorida* (Plasticization of Polyvinyl Chloride), Moscow: Khimiya, 1975.
16. Chalykh, A.E., *Diffuziya v polimernykh sistemakh* (Diffusion in Polymer Systems), Moscow: Khimiya, 1987.
17. Ganaik Baijayatimala and Sivaram Swaminathan, *Macromolecules*, 1996, vol. 29, no. 1, pp. 185–190.
18. Yushkova, S.M., Tager, A.A., Bessonov, Yu.S., et al., *Vysokomol. Soedin., Ser. A*, 1982, vol. 24, no. 7, pp. 1373–1377.
19. Safronov, A.P. and Somova, T.V., *Vysokomol. Soedin., Ser. A*, 2002, vol. 44, no. 11, pp. 2014–2022.
20. Pimentel, G.C., *The Hydrogen Bond*, McClellan, A.L. and Pauling, L., Eds., San Francisco: Freeman, 1960.
21. Gotlib, E.M., Verizhnikov, M.L., Leksin, V.V., and Zverev, A.V., *Izv. Vyssh. Uchebn. Zaved., Khimi. Khim. Tekhnol.*, 2000, vol. 43, no. 4, pp. 82–85.
22. Gutmann, V., *Coordination Chemistry in Non-Aqueous Solutions*, Vienna: Springer, 1968.
23. Bessonov, Yu.S., Tager, A.A., Yushkova, S.M., et al., *Vysokomol. Soedin., Ser. A*, 1978, vol. 20, no. 1, pp. 99–105.
24. Voyutskii, S.S., *Kurs kolloidnoi khimii* (Course of Colloid Chemistry), Moscow: Khimiya, 1964.
25. Haslam, J. and Wills, H.A., *Identification and Analysis of Plastics*, London: Iliffe, 1965.
26. Barashkov, O.K. and Barshtein, R.S., *Vysokomol. Soedin., Ser. A*, 1985, vol. 27, no. 12, pp. 2538–2542.

ISSN 1070-4272, Russian Journal of Applied Chemistry, 2006, Vol. 79, No. 6, pp. 1016–1020. © Pleiades Publishing, Inc., 2006.
Original Russian Text © Yu.S. Krainova, T.V. Bashkatova, A.D. Khusainov, E.N. Cherezova, Ya.D. Samuilov, 2006, published in Zhurnal Prikladnoi Khimii, 2006, Vol. 79, No. 6, pp. 1025–1029.

MACROMOLECULAR CHEMISTRY AND POLYMERIC MATERIALS

Polyfunctional Complex Sulfur-containing Additives to SKI-3 Rubber and Vulcanizates Thereof

Yu. S. Krainova, T. V. Bashkatova, A. D. Khusainov, E. N. Cherezova, and Ya. D. Samuilov

Kazan State Technological University, Kazan, Tatarstan, Russia

Received November 8, 2004; in final form, April 2006

Abstract—The performance of new polyfunctional additives containing bis(2,6-di-*tert*-butyl-4-hydroxyphenyl) polysulfide and dicyclopentadiene–sulfur copolymer was studied with respect to SKI-3 and vulcanizates thereof. These additives act not only as stabilizers but also as vulcanizing agents improving a number of physicomechanical characteristics of the vulcanizates.

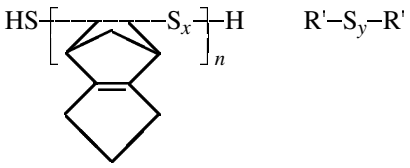
DOI: 10.1134/S1070427206060279

Polyisoprene rubber SKI-3 is widely used in the polymer industry. This is a highly unsaturated and, thus, easily oxidizable compound [1], which makes urgent its stabilization during storage, processing, and exploitation.

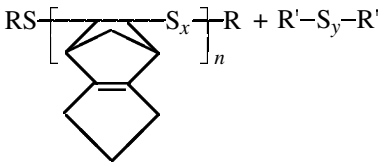
Today, aging of SKI-3 is prevented by antioxidants (AOs) from among aromatic amines and substituted phenols [2]. Despite a wide diversity of the available AOs, active studies aimed at finding new and more rationally using the existing AOs are still under way [3]. Of much significance in the future will be polyfunctional AOs and mixed compositions of stabilizers exhibiting a synergistic antioxidative effect [4–6].

Of no less importance for the polymer industry is development of an effective system for vulcanization of rubbers based on SKI-3 [7]. Elemental sulfur is typically used as vulcanizing agent [1, 8]. Polysulfide oligomers, Thiokols, are used for these purposes less frequently [9], though sulfuring-up on the vulcanized rubber surface occurs with them to a much lesser extent than with sulfur.

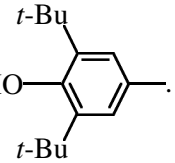
Previously, we have developed a method for synthesis of dicyclopentadiene–sulfur cooligomers (DCPD-S_x) with controlled sulfidity and bis(2,6-di-*tert*-butyl-4-hydroxyphenyl) polysulfide (SHP-S_y) [10, 11], as well as a one-step method for preparation of complex additives with various sulfidities (DCPD-S_x : SHP-S_y) [12].



DCPD-S_x SPH-S_y



DCPD-S_x : SPH-S_y

where R = H, R'; R' = 

.

The structure of the ingredients of the (DCPD-S_x : SHP-S_y) complex additives make them suitable as AOs for rubbers owing to the presence of a compound with sterically hindered phenol moiety and a vulcanizing agent. The function of the latter can be performed by a polysulfide oligomeric component.

This study examines the performance of the (DCPD-S_x : SHP-S_y) additives synthesized as stabilizers for SKI-3 rubber, as well as their influence on the rheological and physicomechanical characteristics of SKI-3-based vulcanized rubbers.

Table 1. Designations and main physicochemical characteristics of the additives

Designation	Average number of sulfur atoms in the polysulfide fragment		Total sulfur content, wt %	Content of –SH groups, wt %	Upper MWD limit
	x	y			
DCPD-S_4 : SHP-S_y	4	2–4	46.0	0.08	6000
DCPD-S_2 : SHP-S_y	2	2–4	33.20	0.12	10000
DCPD-S_4	4	–	49.28	0.90	6000
DCPD-S_2	2	–	32.20	0.65	10000
SHP-S_y	–	2–4	20.95	–	–

Table 2. Induction periods τ in thermal oxidation of the samples of SKI-3 rubber stabilized by the additives synthesized (p_{O_2} = 250 mm Hg, T = 140°C)

Composition of the polymer introduced	Amount of the stabilizer relative to rubber		τ, min	Composition of the polymer introduced	Amount of the stabilizer relative to rubber		τ, min
	wt %	$C\times 10^3$, mol			wt %	$C\times 10^3$, mol	
No additive	–	–	10	$DCPDS_4$	2.0	8.4	85
Diaphene PP	0.3	1	80	DCPD-S_4 : SHP-S_y	2.0	32	165
$DCPDS_2$	2.0	10	75	SHP-S_y	0.3	1	55
DCPD-S_2 : SHP-S_y	2.0	64	150				

EXPERIMENTAL

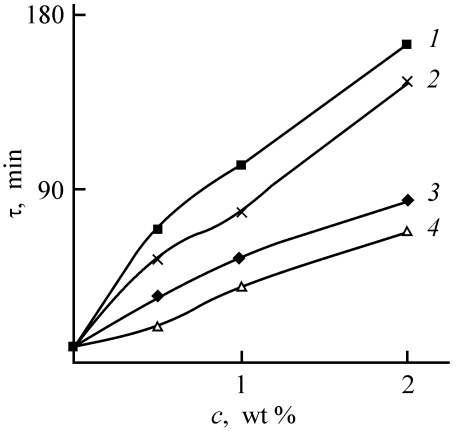
The procedure for preparation of DCPD-S_x : SHP-S_y allows the content of the SHP groups, as well as the sulfidity of the oligomer, to be widely varied. In this study, we used the $DCPDS_x$: SHP-S_y products containing 10 wt % SHP-S_y ingredient with the sulfidities x = 2 and 4.

To elucidate the role and performance of the components of the DCPD-S_x : SHP-S_y complex additive, we separately prepared (DCPD–S) cooligomers with different sulfidities and bis(2,6-di-*tert*-butyl-4-hydroxyphenyl) polysulfide (SHP-S_y) by the techniques described in [10, 11].

Table 1 lists the main physicochemical characteristics of the additives synthesized.

In the first stage of the study, the antioxidative performance of the additives synthesized was estimated from the induction period of oxidation of SKI-3 rubber at 135–140°C in an oxygen atmosphere [13]. Testing consisted in determining by the manometric method the period before the polymer begins to take up oxygen. SKI-3 was preliminarily thrice reprecipitated (with toluene as solvent and acetone as precipitating agent) to remove low-molecular-weight products [14]. Our experiments showed that, with a complex stabilizer DCPD-S_x : SHP-S_y, the induction period τ in oxidation of SKI-3 can be significantly prolonged relative to the DCPD-S_x additives without SHP-S_y. This can be evidently attributed to the synergistic antioxidative effect. Table 2 shows that the induction period in oxidation of SKI-3 in the presence of DCPD-S_x : SHP-S_y exceeds that of the rubber containing a commercial antioxidant like Diaphene PP (*N*,*N*'1-diphenyl-1,4-phenylenediamine).

When the oligomeric additives, both with and without SHP-S_y, are introduced in concentrations within 0.5–2.0 wt %, the induction periods in oxidation of SKI-3 tend to linearly increase (see figure).



Induction period τ in oxidation of SKI-3 rubber vs. the concentration c relative to rubber, of the additive introduced at p_{O_2} = 250 mm Hg, T = 140°C. (*1*) DCPD-S_4 : SHP-S_y, (*2*) DCPD-S_2 : SHP-S_y, (*3*) DCPD-S_4, and (*4*) DCPD-S_2.

Table 3. Composition of the rubber stock for coating of the brass-plated metal cord for shaping of radial tire elements (breakers, squeegees) (T = 70°C)

Ingredients	Weight proportion	Time of beginning of the introduction, min	Ingredients	Weight proportion	Time of beginning of the introduction, min
Stage 1 (rotor rotation rate 60 rpm)			Stage 2 (rotor rotation rate 30 rpm)		
SKI-3	100	0	Mother stock kept		0
TU P 245 (2/3)	58	0.5	for 1 day at room		
PN-6Sh (1/2) oil	6	0.5	temperature		
Zinc white	8	1	Santogard PVI	0.2	0.5
Pine rosin	2	1	PU modifier	1.0	0.5
Stearic acid	1	1	Sulfur (varied part)	0–3.5	0.5
KS modifier	1	1	Additive examined	0–7.0	0.5
Diaphene PP	1	1	(varied part)		
TU P 245 (1/3)	58	2	Discharge		2
PN-6Sh (1/2) oil	6	2			
Discharge		5			

Table 4. Stock number and composition of the varied part in the vulcanizates

Stock no.	Sulfur	Copolymer	Stock no.	Sulfur	Copolymer
	wt %, relative to rubber			wt %, relative to rubber	
	DCPD-S_4 : SHP-S_y			DCPD-S_2 : SHP-S_y	
1	3.5	–	11	3.0	0.5
2	3.0	0.5	12	2.5	1.0
3	2.5	1.0	13	2.0	1.5
4	2.0	1.5	14	1.5	2.0
5	1.5	2.0	15	1.0	2.5
6	1.0	2.5	16	0.5	3.0
7	0.5	3.0	17	0	3.5
8	0	3.5	18	0	5.0
9	0	5.0	19	0	7.0
10	0	7.0			

In the next stage, the additives synthesized were introduced into the rubber stocks based on SKI-3. The rubber stocks were prepared on a laboratory mixer of the Brabender plasticorder (see Table 3 for the formulation and mixing mode).

In preparation of the rubber stock, a part of the vulcanizing agent, sulfur, was replaced with DCPD-S_x : SHP-S_y with a step of 0.5 wt % (Table 4).

The influence of DCPD-S_x : SHP-S_y on the vulcanization kinetics of the rubber stocks was studied on a Monsanto Reometr-100S rheometer. From the resulting rheograms, we derived the rheological and vulcanization characteristics of the stocks: the minimal ($M_{min)}$ and maximal ($M_{max)}$ torques, the torque level in vulcanization ΔM, the torque at the optimal vulcanization point M_{90}, the time of attainment of the vulcanization optimum T_{90}, and the vulcanization rate V_C. Table 5 lists the results of analysis of the rheometric curves.

Table 5 shows that the replacement (partial or complete) of sulfur with DCPD-S_x : SHP-S_y in the rubber stock decreases the viscosity of the stock, characterized by $M_{min.}$ This suggests an increase in the plasticity of the resulting rubber stocks. This holds for the copolymer with both disulfide and tetrasulfide bridges. At the same time, replacement of sulfur with

Table 5. Rheometric characteristics of the rubber stocks (T_{vulc} = 150°C)

Stock no.	Rheometric characteristics						
	M_{min}	M_{max}	ΔM	T_s, min	M_{90}, N m	T_{90}, min	V_c, % min^{-1}
	N m						
1	37.00	76.00	39.00	1.75	72.10	10.75	11.11
2	28.00	40.00	12.00	2.50	38.80	22.00	5.12
3	33.00	42.00	9.00	4.25	41.10	17.00	12.50
4	28.00	39.00	11.00	3.75	37.90	23.50	5.06
5	34.00	48.00	14.00	3.00	46.60	23.75	4.82
6	33.00	51.00	18.00	5.00	49.20	10.00	20.00
11	31.00	50.00	19.00	6.00	48.10	11.25	19.05
12	28.00	41.00	13.00	4.75	39.70	9.50	21.05

Table 6. Physicomechanical characteristics of the vulcanizates containing the DCPD–sulfur copolymer with tetrasulfide bridges (DCPD-S_4 : SHP-S_y)

Characteristic	Stock no.									
	1 (reference)	2	3	4	5	6	7	8	9	10
Relative elongation at break, %	647	667	723	847	777	683	707	633	597	360
Nominal strength, MPa	10.7	3.6	6.5	6.6	6.4	11.6	11.9	5.4	6.5	5.8
True strength, MPa	79.5	27.6	53.8	62.3	56.3	91.2	96.6	39.8	45.2	26.9
Relative elongation set, %	72	63	47	53	52	9	25	13	8	8
Tear strength, N m^{-1}	22.9	18.8	20.1	34.3	35.3	18.8	34.6	9.8	26.5	16.6

Table 7. Physicomechanical characteristics of the vulcanizates containing the DCPD–sulfur copolymer with disufide bridges (DCPD-S_2 : SHP-S_y)

Characteristic	Stock no.					
	1 (reference)	11	12	13	14	15
Relative elongation at break, %	647	707	903	867	833	710
Nominal strength, MPa	10.7	9.1	6.3	9.9	16.9	14.9
True strength, MPa	79.5	74.0	63.7	96.4	158.6	120.5
Relative elongation set, %	72	9	8	7	12	7
Tear strength, N m^{-1}	22.9	19.3	12.8	32.5	32.3	24.2

the DCPD-S_x : SHP-S_y copolymer in the vulcanizing system leads to decrease in the maximal torque M_{max}. On the whole, the torque level in vulcanization of the polymer (ΔM) is slightly lower than that of the reference sample. Polysulfide additives DCPD-S_x : SHP-S_y do not cause scorching of the rubber stocks based on SKI-3, but with increasing content of DCPD-S_x : SHP-S_y the time of attainment of the vulcanization optimum tends to increase. Deceleration of the vulcanization of the rubber stock occurring by the radical mechanism can be attributed to the ability of the SHP-S_y component to react with radicals [15] with chain termination.

We studied the physicomechanical characteristics of the vulcanized rubbers, taking into account the time of attainment of the vulcanization optimum equal to 25 min at 150°C. Tables 6 and 7 present the results.

A study of the strength properties of the vulcanizates [16] showed that the nominal tensile strength of the samples containing 0.5–2.5 wt % DCPD-S_x : SHP-S_y increases insignificantly. Introduction of 3.0 wt % DCPD-S_x : SHP-S_y sharply raises the nominal strength. This is probably due to the synergistic effect of DCPD-S_x : SHP-S_y and elemental sulfur introduced simultaneously. With a further increase in the amount of DCPD-S_x : SHP-S_y introduced, the nominal strength of the vulcanizates decreases; this also holds for the true strength. The increase in the relative elongation of the vulcanized rubber at break and in the relative elongation set at break is, evidently, due to the change in the structure of the vulcanization network.

CONCLUSIONS

(1) Introduction of DCPD-S_x : SHP-S_y increases the oxidation period of SKI-3 rubber. The induction period linearly grows with the amount of the additive introduced in the range 0.5–2.0 wt %.

(2) DCPD-S_x : SHP-S_y blends decrease the viscosity and rigidity of the rubber stocks, i.e., they exhibit plasticizing properties.

(3) The time of attainment of the vulcanization optimum increases relative to the reference sample.

(4) When introduced in amounts of up to 3.0 wt %, DCPD-S_x : SHP-S_y enhances the physicomechanical parameters. Further increase in the content of the additive is unreasonable because of the deterioration of the physicomechanical properties.

REFERENCES

1. Dogadkin, B.A., *Khimiya elastomerov* (Chemistry of Elastomers), Moscow: Khimiya, 1972.
2. Grassie, N. and Scott, G., *Polimer Degradation and Stabilisation*, Cambridge: Cambridge Univ., 1985.
3. Denisov, E.T. and Azatyan, V.V., *Ingibirovanie tsepnykh reaktsii* (Inhibition of Chain Reactions), Chernogolovka: Ross. Akad. Nauk, 1977.
4. Kavun, S.M., *Kauchuk Rezina*, 1994, no. 5, pp. 32–34.
5. Bol'shakova, S.I. and Kuz'minskii, A.S., *Vysokomol. Soedin., Ser. B*, 1982, vol. 24, no. 5, pp. 347–353.
6. Tokareva, M.Yu., Sidorova, L.A., Matveev, A.V., and Lykin, A.S., *Kauchuk Rezina*, 1990, no. 5, pp. 14–17.
7. JPN Patent 1-197542.
8. JPN Patent 1-135843.
9. Averko-Antonovich, L.A. and Averko-Antonovich, I.Yu., *Polimery i sopolimery sery v kachestve modifikatorov i vulkanizuyushhcikh agentov dlya kauchukov* (Sulfur Polymers and Copolymers as Modifiers and Vulcanizing Agents for Rubbers), Moscow: TsNIITEneftekhim, 1994.
10. Rylova, M.V., DCPD–Elemenal Sulfur Copolymers with Reduced Sulfidity: Formation Mechanism, Structure, and Possible Applications, *Cand. Sci. Dissertation*, Kazan, 2004.
11. Bashkatova, T.V., Abstracts of Papers, *XXXVIII Nauchnaya studencheskaya konferentsiya v Chuvashskom gosudarstvennom universitete imeni I.N. Ul'yanova* (XXXVIII Scientific. Students' Conf. at Ul'yanov Chuvash State University), Cheboksary, 2004, pp. 78–79.
12. Krainova, Yu.S., Bashkatova, T.V., Rylova, M.V., et al., Abstracts of Papers, *Mezhdunarodnaya nauchnaya konferentsiya "Molodezh' i khimiya"* (Int. Scientific Conf. "Young People and Chemistry"), Krasnoyarsk, 2004, pp. 137–138.
13. Piotrovskii, K.B. and Tarasova, Z.N., *Starenie i stabilizatsiya sinteticheskikh kauchukov i vulkanizatorov* (Aging and Stabilization of Synthetic Rubbers and Vulcanizing Agents), Moscow: Khimiya, 1980.
14. Lazarev, S.Ya., Reisfel'd, V.O., and Erkova, L.N., *Laboratornyi praktikum po sinteticheskim kauchukam* (Laboratory Manual on Synthetic Rubbers), Leningrad: Khimiya, 1986.
15. Sigeru Oae, *Khimiya organicheskikh soedinenii sery* (Chewmistry of Organic Compounds of Sulfur), Moscow: Khimiya, 1975.
16. Averko-Antonovich, Yu.O., *Laboratornyi praktikum po khimii i fizike vysokomolekulyarnykh soedinenii* (Laboratory Manual on Chemistry and Physics of Macromolecular Compounds), Kazan: Kazan. Gos. Tekhnol. Univ., 2001.

ISSN 1070-4272, Russian Journal of Applied Chemistry, 2006, Vol. 79, No. 6, pp. 1021–1024. © Pleiades Publishing, Inc., 2006.
Original Russian Text © O.V. Luksha, O.N. Opanasenko, N.P. Krut'ko, Yu.V. Loboda, 2006, published in Zhurnal Prikladnoi Khimii, 2006, Vol. 79, No. 6, pp. 1030–1034.

MACROMOLECULAR CHEMISTRY AND POLYMERIC MATERIALS

Modification of Oxidized Bitumen with Styrene–Butadiene–Styrene Copolymers of Various Structures

O. V. Luksha, O. N. Opanasenko, N. P. Krut'ko, and Yu. V. Loboda

Institute of General and Inorganic Chemistry, National Academy of Sciences of Belarus, Minsk, Belarus

Received November 2, 2005; in final form, January 2006

Abstract—Mechanical and structural-rheological properties of oxidized bitumen modified with styrene–butadiene–styrene copolymers side vinyl groups in their butadiene fragment were studied. A comparative analysis of the modified and unmodified bitumen composites was performed.

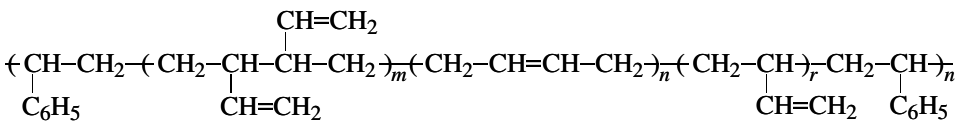
DOI: 10.1134/S1070427206060280

The problem of modification of oxidized bitumen with polymers of varied chemical nature, to improve its structural and rheological characteristics, was overviewed in our previous publications [1–3]. Among the existing variety of polymers recommended for modification of bitumen, only two kinds have found wide use, namely, thermoplastic elastomers based on styrene–butadiene–styrene (SBS) block copolymers and thermoplastics based on ethylene–vinyl acetate copolymers (EVA) [4]. However, research is being conducted primarily on modification of residual bitumen, whose group composition differs considerably from that of the oxidized bitumen used in both Belarus and Russia. Characterization of bitumens is performed by the methods included into the quality standards for bitumens. Numerous studies and wide experience of practical applications of bitumens characterized using standard parameters often reveal some inconsistency between these values and the behavior of bitumens in road pavements. Standard parameters do not characterize the structure of bitumens, can be considered only as some arbitrary values for comparison of bitumens under given testing conditions [5]. Structural changes are adequately characterized by the rheological parameters (softening and melting points), which are governed by the structure of the bitumen composite [6, 7].

A novel class of block copolymers, SBS, has been developed, which differs in the structure of the polymer chain from the previously existed ones. In this study, we examined the effect of SBS copolymers with modified butadiene block on the structural and rheological properties of oxidized bitumens.

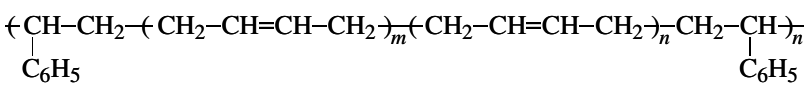
EXPERIMENTAL

In the experiments, we used BND 90/130 paving bitumen from Novopolotsk Oil Refinery with the following characteristics: ring and ball softening temperature 43°C, penetration at 25°C (0.1 mm) 98; and a linear block copolymer with modified central block [Kraton D-1192 (**1**)]. Unlike the SBS copolymer described previously [Kraton D-1101 (**2**)], the polymer chain of **1** is characterized by the presence of side vinyl groups in the polybutadiene fragment and also by the lower number of double C=C bonds in the macromolecular chain.



Kraton D-1192

1



Kraton D-1101

2

Two brands of Kraton D-1192 copolymer were used: Kraton D-1192 ES represents porous granules dustcoated with amorphous SiO_2, and Kraton D-1192 EM, a powder treated with amorphous SiO_2.

Bitumen formulations with 3% polymer content were prepared by mixing components in a cylindrical reactor equipped with an anchor stirrer (250 rpm) and a heating jacket providing a homogeneous heating throughout the reactor volume. After attaining temperature of 150°C, Kraton was added in small portions with stirring. Kraton D-1192 EM powder is readily (in 1.5–2 h) dissolved at 160°C, while dissolution of the granulated product takes 5–6 h at about 180°C. The completeness of dissolution was controlled by the homogeneity of the bitumen-polymer film using a Rheotest-2 rotary viscometer.

We determined the mechanical characteristics of the bitumen–polymer formulations (BPFs), such as the softening and Fraas (brittle) points, needle penetration depth (penetration), impact resistance, adhesion to mineral matrix, elasticity, and extensibility using standardized procedures (STB 1220–2000). The aging of samples was performed by heating at 163°C for 300 min in accordance to the GOST (State Standard) 18 180–72 [ST SEV (COMECON Standard) 4543–84].

The viscosity was measured on a Rheotest-2 rotary viscometer using a cone–plate working unit over the shear rate range 11.1–4860 s^{-1}. The measurements were carried out at 70 and 130°C, to model conditions of preparation and laying of the road concrete mix.

Table 1 summarized data on mechanical characteristics for the initial bitumen and BPFs before and after aging.

The results show that SBS copolymers taken at a concentration of 3%, regardless of the structure of their polymer chain, form a 3*D* network in the bitumen dispersion medium. When sorbing the oil components of bitumen, the polymer network, formed by the styrene domains, increases in volume, but preserves its continuity, thus imparting elasticity to bitumen and decreasing the brittleness at low temperatures. It should be pointed out that, despite different structures of the polymer chain, the elasticities and extensibility of the investigated copolymers are practically the same.

High content of the vinyl fragments (40 wt %) decreases the total chain length, thus decreasing the viscosity of BPFs, as demonstrated by data on the needle penetration depth. It should be pointed out that BPFs obtained with Kraton D-1192 are aging-resistant. Their

Table 1. Mechanical characteristics

Parameter	Formulation			
	bitumen	bitumen + Kraton D-1101	bitumen + Kraton D-1192 ES	bitumen + Kraton D-1192 EM
Needle penetration depth at 25°C (mm^{-1})	98 (71)*	58.8	67 (49)	73 (55)
T_s (ring and ball), °C	43 (45)	58.5	53 (54.2)	51 (54.1)
Extensibility at 0°C, mm	55	156	120 (142)	155 (144)
Elasticity, %, at 13°C	–	60	59 (65.5)	55 (63)
Fraas point, °C	–20.5	–24	–22	–23
Adhesion to mineral material, %	25 (25)	25	30 (30)	30 (30)
Impact resistance, %, at –20°C	–		74 (72)	86 (76)

* Characteristics after heat treatment at 163°C for 300 min.

Table 2. Structural and rheological characteristics of BPFs at 70 and 130°C

Sample	P_{k1}, 10^{-1} Pa	P_m, 10^{-1} Pa	P_{k2}, 10^{-1} Pa	P_m/P_{k1}
Temperature 70°C				
Bitumen	2178	13072	6000	6.00
Bitumen + Kraton D-1192 EM	4357	26144	11000	6.00
Bitumen + Kraton D-1192 ES	4357	17429	4000	4.00
Bitumen + Kraton D-1101 S	16650	172200	83000	10.34
Temperature 130°C				
Bitumen	907	8714	2500	
Bitumen + Kraton D-1192 EM	1000	13072	6000	
Bitumen + Kraton D-1192 ES	1000	8714	3000	
Bitumen + Kraton D-1101 S	1200	36900	5000	

Table 3. Viscosity of BPFs at 70 and 130°C

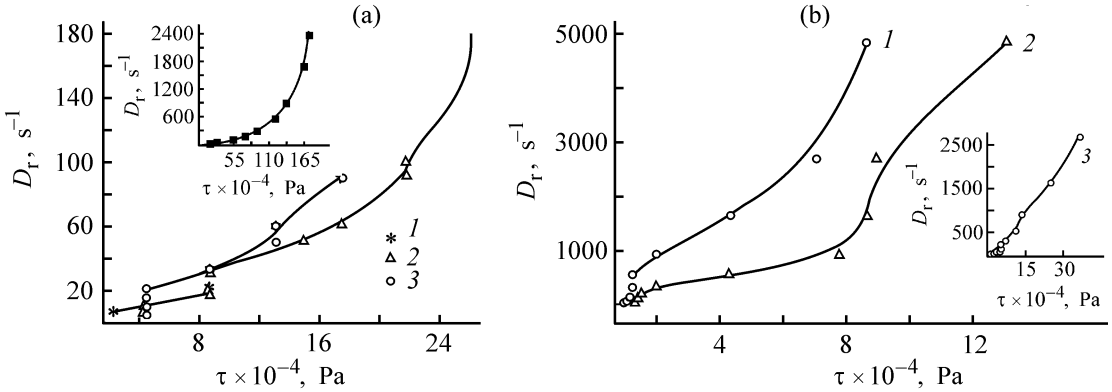
Sample	Viscosity, mPa s		
	maximal (practically unbroken structure), η_0	minimal (maximally broken structure), η_{min}	Effective, η^*
Temperature 70°C			
Bitumen	39172	21787	35000
Bitumen + Kraton D-1192 EM	78370	14524	45000
Bitumen + Kraton D-1192 ES	78370	19365	40000
Bitumen + Kraton D-1101 S	160000	7000	56000
Temperature 130°C			
Bitumen	8180	179	3000
Bitumen + Kraton D-1192 EM	9000	268	6000
Bitumen + Kraton D-1192 ES	9000	268	6000
Bitumen + Kraton D-1101	11000	1500	7000

mechanical characteristics only slightly changed after heat treatment, remaining meeting the requirements of STB 1220–2000. Such a resistance to thermooxidative degradation can be attributed to the fact that oxidation of the vinyl bond in the side fragment only slightly changes the molecular structure, since the backbone of the molecule remains intact, keeping on playing the role of a constituent of the 3*D* network. If a double bond is in the backbone, as in the case of BPFs based on Kraton D-1101, the oxidation results in its breakdown, thus distorting the 3*D* network and deteriorating mechanical properties.

It follows from Table 1 that, the standard tests of the investigated bitumen–polymer formulations, obtained by modification of bitumen with SBS copolymers with different structure of the polymer chain, revealed no significant differences in their mechanical characteristics.

Tables 2 and 3 and Fig. 1a represent data on the structural and rheological characteristics of BPFs with Kraton D-1192 and Kraton D-1101, measured at 70 and 130°C.

The results show that the structural viscosity of the samples with Kraton D-1101 is twice that of BPFs



Flow curves for SBS-modified bitumens at (a) 70 and (b) 130°C. (τ) Shear stress and (D_r) shear rate. (a): (*1*) Bitumen, (*2*) bitumen + Kraton D-1192 EM, (*3*) bitumen + Kraton D-1192 ES, and (*4*) bitumen + Kraton D-1101 (3%); and (b): (*1*) bitumen + Kraton D-1192 ES, (*2*) bitumen + Kraton D-1192 EM, and (*3*) bitumen + Kraton D-1101 (3%).

with Kraton D-1192. For the formulations with Kraton D-1101, the conditional static elastic limit P_{k1}, characterizing the resistance to deformation, is higher by a factor of 4 than that for BPFs with Kraton D-1192. The rheological characteristics of the samples with Kraton D-1192, unlike BPFs with Kraton D-1101, only slightly differ from those of the initial bitumen. Modification with Kraton D-1192 copolymer does not considerably change the viscosity, which is an important factor in preparation of a road concrete mix and emulsified polymer–bitumen formulations. Estimation of P_{k2} characterizing the elastoplastic properties of bituminous materials allowed characterization of the efficiency of the modifying action of the copolymers studied. The polymer-bitumen composites prepared with Kraton D-1101 are characterized by higher P_{k2} as compared to those with Kraton D-1182 (by a factor of 8 and 20 for Kraton D-1192 EM and Kraton D-1192 ES, respectively), although the standard tests revealed practically no differences in their elasticity and extensibility. The increase in the elastoplastic characteristics in the formulations with Kraton D-1101 can be attributed to the fact that molecules of this polymer contain a polybutadiene chain formed through anionic polymerization of *cis*-1,3-butadiene and contain about 90% of double bonds. These bonds impart elastoplastic properties, typical of polybutadiene (glass-transition temperature –95°C), to the polymer. Because of lower content of double bonds in the polymer chain of Kraton D-1192, the elastoplastic characteristics of BPFs with this copolymer are worse. The estimated P_m/P_{k1}, characterizing the structural strength, do not virtually change for Kraton D-1192, suggesting that the size of structural elements in the dispersion medium remains unchanged in the bitumens modified with Kraton D-1192, while in the case of Kraton D-1101, this parameter increases by a factor of 1.7. Therefore, the increase in the viscosity of BPFs modified with Kraton D-1101 can be attributed to both formation of a strong 3*D* structure and increase in the size of the structural units.

Tables 2 and 3 and Fig. 1b also include data obtained at 130°C. At this temperature, bitumen and the modified samples have practically the same static elastic limit. Differences from the initial bitumen are found with increasing shear rate, which is reflected in increase in P_m and P_{k2}. It should be pointed out that the structural viscosity in BPFs based on the polymers with the modified polybutadiene block falls in the same range as that in the initial bitumen. This opens the door for application of such BPFs to preparation of bitumen emulsions using the modes accepted for the unmodified bitumens.

CONCLUSIONS

(1) Introduction of the modified polybutadiene block into the polymer molecule changes both mechanical and structural and rheological characteristics of bitumen, like that in the case of the use of the unmodified styrene–butadiene–styrene copolymer. The polymer formulation based on Kraton D-1192 demonstrate high aging resistance. However, standard mechanical tests of the investigated bitumen–polymer formulations revealed no significant differences.

(2) In modification of bitumen with styrene–butadiene–styrene copolymer containing side vinyl groups, the size of structural units of the dispersion medium remains unchanged, and no considerable increase in the viscosity is observed, compared to the unmodified polymer, thus improving the performance characteristics of the bitumen–polymer formulation based on Kraton D-1192.

(3) Characterization of bitumen–polymer formulations using science-based rheological parameters opens the door for their application in various road construction technologies.

REFERENCES

1. Luksha, O.V., in *Collection of Works of Young Scientists from National Academy of Sciences of Belarus*, Minsk, 2004, vol. 4, pp. 29–32.
2. Krutko, N.P., Opanasenko, O.N., Ovseyenko, L.V., et al., *Proc. 3rd Int. Congress "Euroasphalt and Eurobitume"*, vol. 2, Vienna (Austria), 2004, pp. 1685–1694.
3. Luksha, O.V., Krutko, N.P., Opanasenko, O.N., and Ovseyenko, L.V., *Vestsy Nats. Akad. Navuk Belarus., Ser. Khim. Navuk*, 2005, no. 3, pp. 12–18.
4. Champion, L., Gerard, J.F., Planche, J.P., and Martin, D., *Eurobitume Workshop'99 on Performance Related Properties for Bituminous Binders*, Luxemburg, 1999, p. N049.
5. Gorshenina, G.I. and Mikhailov, N.V., *Polimerbitumnye isolyatsionnye materially* (Polymer–Bitumen Insulating Materials), Moscow: Nedra, 1967.
6. Filippova, A.G., Kirillova, L.G., Okhotina, N.A., et al., *Kolloidn. Zh.*, 2000, vol. 62, no. 6, pp. 832–836.
7. Belokon', N.Yu. and Inozemtsev, K.I., *Khim. Topliv Masel*, 2002, issue 7, no. 3, pp. 38–40.

ISSN 1070-4272, Russian Journal of Applied Chemistry, 2006, Vol. 79, No. 6, pp. 1025–1027. © Pleiades Publishing, Inc., 2006.
Original Russian Text © A.I. Demidov, M.S. Kokhatskaya, 2006, published in Zhurnal Prikladnoi Khimii, 2006, Vol. 79, No. 6, pp. 1035–1037.

BRIEF COMMUNICATIONS

Kinetics of the Reaction between the Active Paste from the Positive Electrode of a Dead Nickel–Iron Battery and Sulfuric Acid

A. I. Demidov and M. S. Kokhatskaya

St. Petersburg State Polytechnic University, St. Petersburg, Russia

Received May 24, 2006

Abstract—The kinetics of dissolution of a powdered active paste from the positive electrode of a worked-out nickel–iron battery in 0.1 N sulfuric acid at 25, 50, and 75°C was studied by measuring the electrolyte resistance.

DOI: 10.1134/S1070427206060292

In continuation of previous publications [1, 2], we present the results obtained in studying the reaction between a powdered active paste from the positive electrode of a worked-out nickel–iron (NI) battery and sulfuric acid in the temperature range 25–75°C. The active paste was taken from worked-out NI battery of the TNZh-250-U2 type, the particle size of the powder did not exceed 200 μm.

The overall reaction that occurs in charging and discharge of a NI battery can be represented by the equation:

$$2NiOOH + Fe + 2H_2O = 2Ni(OH)_2 + Fe(OH)_2, \quad (1)$$

It follows from this equation that the worked-out active paste from the positive electrode should contain $Ni(OH)_2$ and NiOOH. An X-ray diffraction analysis revealed graphite and dispersed nickel hydroxide $Ni(OH)_2$ in the active paste. An X-ray diffraction pattern of the powdered active paste from a worked-out NI battery is shown in Fig. 1.

In hydrometallurgical processing of worked-out electrodes, it is necessary to know the content of sodium or potassium carbonate and hydrocarbonate remaining in pores of the active paste, because their amount affects the expenditure of sulfuric acid for processing of worked-out positive electrodes contain-

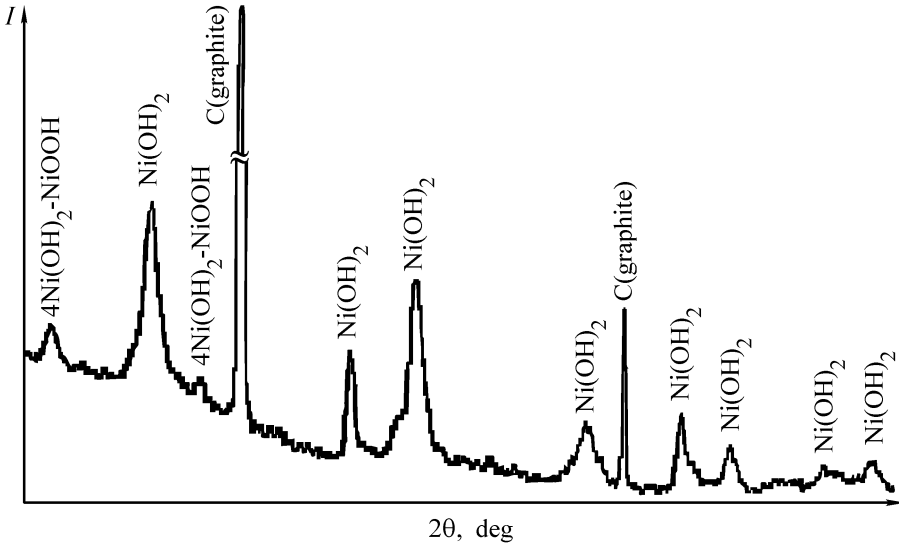


Fig. 1. X-ray diffraction pattern of the powdered active paste from the positive electrode of a worked-out TNZh-250-U2 nickel–iron battery. (*I*) Intensity and (2θ) Bragg angle.

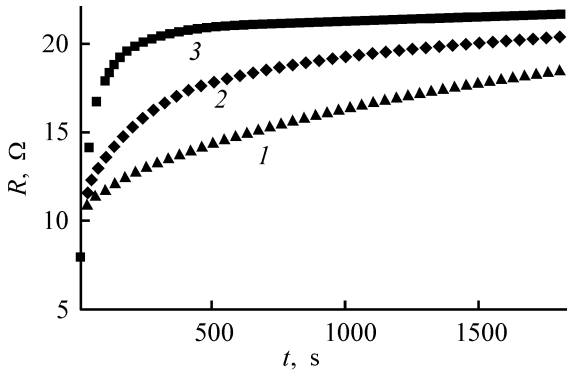


Fig. 2. Variation of the resistance R with time t in dissolution of the powdered active paste from the positive electrode of a worked-out NI battery in 0.1 N sulfuric acid at different temperatures. Temperature (°C): (*1*) 25, (*2*) 50, and (*3*) 75; the same for Fig. 3.

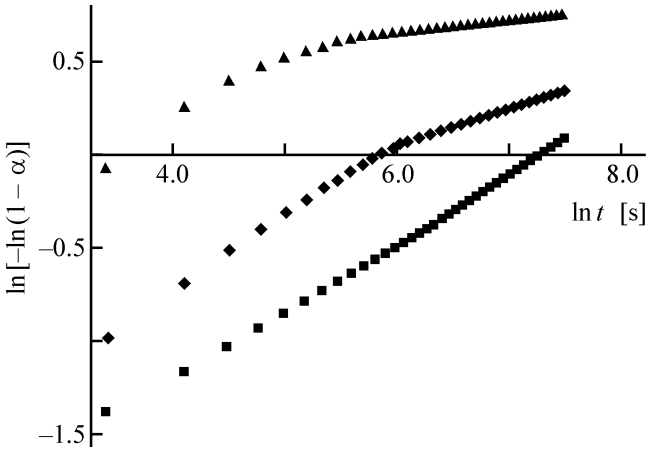


Fig. 3. Dependence of $\ln[-\ln(1-\alpha)]$ on $\ln t$ in dissolution of the powdered active paste from a worked-out NI battery in 0.1 N sulfuric acid at different temperatures.

ing nickel hydroxide. A conductometric titration showed that, after its prolonged storage in air, the worked-out active paste contains sodium carbonate and hydrocarbonate whose content varies with time. Sodium carbonate is converted into hydrocarbonate, with the result that the content of carbonates in the active paste decreases, and that of hydrocarbonates increases [2].

The kinetics of the reaction of the active paste with sulfuric acid was studied in a thermostated conductometric cell, with vigorous agitation of a solution with magnetic stirrer. Changes in the resistance were measured with an E7-15 immitance meter, with the use of graphite electrodes, during 30 min at intervals of 30 s. The variation of the resistance with time in the course of the dissolution of the powdered active paste from the positive electrode in a 0.1 N sulfuric acid at 25, 50, and 75°C is shown in Fig. 2.

Two portions can be distinguished in the curve describing the variation of the resistance in dissolution of the active paste from the positive electrode in sulfuric acid. In the first of these, sodium carbonate and hydrocarbonate remaining in the pores of the active paste after its prolonged storage in air are neutralized, and in the second, nickel hydroxide contained in the worked-out active paste reacts with sulfuric acid. The reaction of nickel(II) hydroxide with sulfuric acid results in that the type of charge carriers changes. The rather mobile hydrogen ions are replaced with less mobile nickel ions. As a result, the electrical conductivity of the solution changes in the course of the process [1].

The data obtained were processed using the Erofeev–Kholmogorov equation

$$\alpha = 1 - \exp(-kt^n), \qquad (2)$$

where α is the fraction of the reacted substance; k, rate constant; t, time; and n, exponent that accounts for a change in the surface area in the dissolution of the powdered active paste.

The applicability of Eq. (2) can be verified by the existence of a linear dependence $\ln[-\ln(1-\alpha)] = f(\ln t)$ obtained by twice taking the logarithm of the initial equation. The fact that the curves plotted (Fig. 3) using experimental data are linear shows that the Erofeev–Kholmogorov equation can be used to describe the dissolution kinetics of the powdered active paste from the positive electrode of a worked-out NI battery in sulfuric acid.

Further, the straight lines obtained were processed by the least-squares method to give the value of $\ln k$, from which the rate constant was found by taking the antilogarithm and the activation energy of the process was calculated. The calculation was done using the formula:

$$\Delta E = \frac{RT_1T_2 \ln \dfrac{k_2}{k_1}}{T_2 - T_1}, \qquad (3)$$

where R is the universal gas constant (8.314 J mol^{-1} K^{-1}) and k_1, k_2 are the rate constants at temperatures T_1 = 298.15 and T_2 = 348.15 K, respectively.

It was found that the neutralization of sodium carbonate and hydrocarbonate occurs in the temperature range 25–75°C in the mixed region (ΔE = 23.9 kJ mol^{-1}), and the dissolution of nickel hydrox-

ide in sulfuric acid, in the kinetic region (ΔE = 52.7 kJ mol^{-1}).

To determine the degree of nickel recovery from the active paste, a sample was taken after completion of each test, and the content of nickel that passed into solution was determined by titration with Trilon B, as described in [3]. The degree of nickel recovery in dissolution of the powdered active paste from the positive electrode in 0.1 N sulfuric acid at 25, 50, and 75°C was 66, 75 and 88%, respectively.

CONCLUSION

The dissolution of a powdered worked-out active paste from the positive electrode in sulfuric acid occurs as follows. First, sodium carbonate and hydrocarbonate, and then, nickel hydroxide react with sulfuric acid. The neutralization of sodium carbonate and hydrocarbonate in the range 25–75°C occurs in the mixed region, and the dissolution of nickel hydroxide, in the kinetic region.

REFERENCES

1. Demidov, A.I. and Kokhatskaya, M.S., *Zh. Prikl. Khim.*, 2003, vol. 76, no. 9, pp. 1490–1493.
2. Demidov, A.I., Kokhatskaya, M.S., and Sun Lyu Bin, *Zh. Prikl. Khim.*, 2005, vol. 78, no. 8, pp. 1303–1305.
3. Schwarzenbach, G. and Flaschka, H., *Die Komplexometrische Titration*, Stuttgart: Ferdinand Enke, 1965.

ISSN 1070-4272, Russian Journal of Applied Chemistry, 2006, Vol. 79, No. 6, pp. 1028–1030. © Pleiades Publishing, Inc., 2006.
Original Russian Text © S.I. Lazarev, V.L. Golovashin, V.V. Mamontov, S.V. Kovalev, 2006, published in Zhurnal Prikladnoi Khimii, 2006, Vol. 79, No. 6, pp. 1038–1039.

BRIEF COMMUNICATIONS

A Study of the Diffusion Permeability Coefficient of a Tubular Membrane Unit in an Aqueous Solution of Sodium Sulfate

S. I. Lazarev, V. L. Golovashin, V. V. Mamontov, and S. V. Kovalev

Tambov State Technical University, Tambov, Russia

Received December 8, 2005

Abstract—Experimental data on the diffusion permeability coefficient of sodium sulfate in a fluoroplastic membrane were obtained and analyzed.

DOI: 10.1134/S1070427206060309

Mathematical simulations of the operation of a membrane apparatus are commonly based on the self-diffusion coefficient of water and diffusion coefficient of a substance in the membrane [1]. However, it is difficult to determine these parameters experimentally, and, therefore, the coefficients of diffusion and osmotic permeability are used in calculations. With a knowledge of the diffusion permeability coefficient, we can evaluate the contribution of the diffusion flux to the mass transfer. The coefficients of diffusion and osmotic permeability can be determined experimentally. This is done in membrane cells of various types. The simplest cell is the flat-chamber cell [2]. A disadvantage of this cell is that it does not reflect the hydrodynamics of real apparatus, e.g., of tubular type. This disadvantage is not characteristic of the installation schematically shown in Fig. 1.

The installation comprises a membrane unit *1*, thermostated vessels with pumps for a solution under study (*2*) and distilled water (*3*), and a set of valves *4*. The temperature of the solutions in tubes and intertubular space is monitored with Chromel–Copel thermocouples *5* connected to potentiometers *6*, *7*.

This installation is intended for studies of the diffusion and osmotic permeability of polymeric membranes for two-, three-, and multiple-component solutions. It can also be used for experiments aimed to examine the influence exerted by various kinds of turbulators on the hydrodynamics of the annular channel and the effect of externally applied magnetic and temperature fields on a solution being separated. The membrane unit used in the process is shown in Fig. 2. It comprises the following elements: cylindrical case *1* with flanges *2*; porous tube *3* with mem-

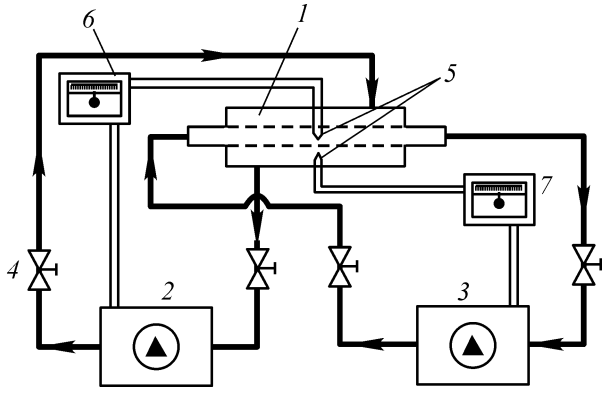


Fig. 1. Schematic of a tubular flow-through installation. For explanations see text; the same for Fig. 2.

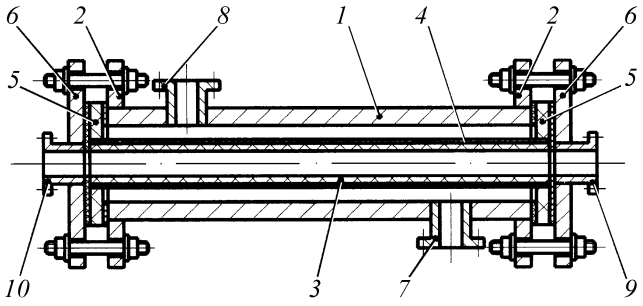


Fig. 2. Schematic of the tubular membrane unit.

brane *4* on its outer surface, supported by tube sheets *5* fixed between flanges *2* and *6*; and inlet and outlet pipes for the starting solution (*7*, *8*) and distilled water (*9*, *10*).

The diffusion permeability coefficient was calculated by the formula [2]:

$$P_d = c_2 V_2 \delta / [(c_1 - c_2) S_\tau], \quad (1)$$

where P_d is the diffusion permeability coefficient ($m^2\ s^{-1}$); c_1, concentration of the solute in the initial solution ($kg\ m^{-3}$); c_2, concentration of the solute that passed across the membrane ($kg\ m^{-3}$); V_2, volume of the solution under study (m^3); δ, membrane thickness (m); S, working area of the membrane (m^2); and τ, duration of an experiment (s).

The experiments aimed to determine the coefficients of diffusion permeability P_d were performed on a fluoroplastic membrane for an aqueous solution of Na_2SO_4 with initial concentrations of the salt in solution equal to 0.5, 1.0, 2.0, and 5.0 $kg\ m^{-3}$, at temperatures of 22, 25, 32, and 45°C. The experimental data obtained are presented in Fig. 3.

When analyzing the concentration dependence of the diffusion permeability coefficient (Fig. 3), we should keep in mind the fact that the solute can diffuse within the membrane both via the pore space filled with the solution and via amorphous regions of membrane swelling. As the concentration of the sodium sulfate solution increases, the pores in the membrane are first constricted and then clogged because of the sorption, which leads to a decrease in the diffusion permeability coefficient [3]. Apparently, the sodium sulfate solution does not plasticize the membrane, or does so only slightly, and, therefore, the diffusion permeability coefficient decreases over the entire range of concentrations of this solution.

It was found that, as the temperature of the sodium sulfate solution increases, the diffusion permeability coefficient becomes larger. This conforms to the generally accepted concept of the effect of temperature on the diffusion permeability coefficient in polymers [2, 4].

Because the dependences of the diffusion permeability on the solution concentration and temperature are gradual, it seems appropriate to consider an approximating dependence of the type

$$P_d = A \exp(Bc)(T/T_0)^m, \quad (2)$$

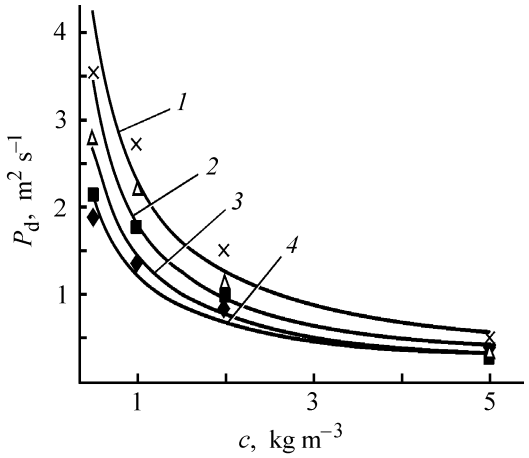


Fig. 3. Diffusion permeability coefficient P_d vs. the initial concentration c of the salt in the solution. Temperature (°C): (*1*) 22, (*2*) 25, (*3*) 32, and (*4*) 45.

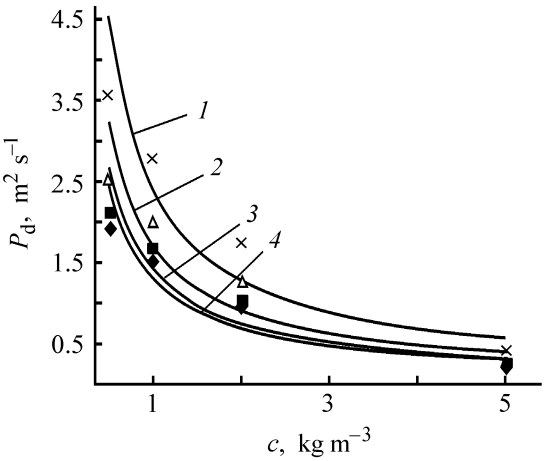


Fig. 4. Approximating dependence of the diffusion permeability coefficient P_d vs. the initial concentration c of the salt in the solution. Temperature (K): (*1*) 295, (*2*) 298, (*3*) 305, and (*4*) 318.

where P_d is the diffusion permeability coefficient ($m^2\ s^{-1}$); c, concentration of the solute in the initial solution ($kg\ m^{-3}$); T, working temperature (K); T_0, initial temperature (K); and A, B, and m, empirical coefficients obtained by calculation.

The approximating dependences are shown in Fig. 4.

A comparison of the experimental and calculated values of the diffusion permeability of a sodium sulfate solution, shown in Figs. 3 and 4, demonstrated that the calculation error is within admissible limits (±15%).

CONCLUSIONS

It was found that the diffusion permeability coefficient decreases as the initial concentration of sodium sulfate in a solution becomes higher and increases as the solution temperature is elevated.

REFERENCES

1. Lazarev, S.I., Korobov, V.B., and Konovalov, V.I., *Issledovanie diffuzionnoi i osmoticheskoi pronitsaemosti polimernykh membrane* (A Study of the Diffusion and Osmotic Permeability of Polymeric Membranes), Available from ONIITEKhIM, 1989, Tambov, no. 807-khp 89.
2. Nikolaev, N.I., *Diffuziya v membranakh* (Diffusion in Membranes), Moscow: Khimiya, 1980.
3. Hwang, S.-T. and Kammermeyer, K., *Membrane in Separations*, New York: Wiley, 1975.
4. Reitlinger, S.A., *Pronitsaemost' polimernykh materialov* (Permeability of Polymer Materials), Moscow: Khimiya, 1974.

ISSN 1070-4272, Russian Journal of Applied Chemistry, 2006, Vol. 79, No. 6, pp. 1031–1034. © Pleiades Publishing, Inc., 2006.
Original Russian Text © G.G. Shelopin, D.S. Pashkevich, Yu.I. Alekseev, D.A. Mukhortov, V.B. Petrov, V.S. Asovich, 2006, published in Zhurnal Prikladnoi Khimii, 2006, Vol. 79, No. 6, pp. 1040–1042.

BRIEF COMMUNICATIONS

Synthesis of Perfluoroalkanes in High-Temperature Fluorination of Graphite with Fluorine in a Reactor with a Free-Falling Graphite Bed

G. G. Shelopin, D. S. Pashkevich, Yu. I. Alekseev, D. A. Mukhortov, V. B. Petrov, and V. S. Asovich

Prikladnaya Khimiya Russian Scientific Center, Federal State Unitary Enterprise, St. Petersburg, Russia

Received November 9, 2005; in final form, February 2006

Abstract—Reaction between fluorine and graphite in a reactor with a free-falling bed of graphite was studied in relation to the temperature in the reaction zone, ratio of the feeding rates of fluorine and graphite, and dilution of fluorine with an inert gas.

DOI: 10.1134/S1070427206060310

Tetrafluoromethane, hexafluoromethane, octafluoromethane, and decafluoromethane are large-tonnage products used in etching of silicon in semiconductor industry [1].

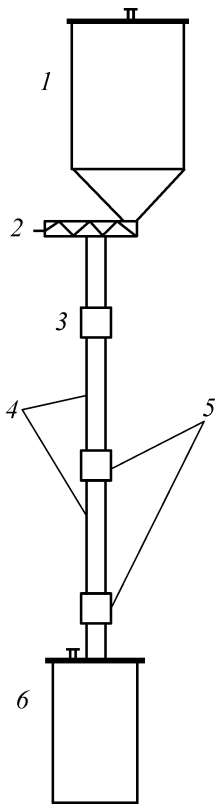
The present paper reports on a continuation of previous studies [2, 3], whose main goal was to search for conditions of carbon fluorination in which a mixture perfluoroalkanes is produced and this mixture contains hexafluoroethane, octafluoropropane, and decafluorobutane in commercial amounts.

A study of graphite fluorination with a mixture of fluorine and nitrogen (or argon) in a fluidized bed and in an ascending gas-dust flow [2, 3] led to a conclusion that synthesis of CF_4, C_2F_6, C_3F_8, and C_4F_{10} at a temperature of about 600°C occurs by a two-stage scheme: synthesis of a solid carbon polyfluoride $(CF_x)_n$ and thermal decomposition of $(CF_x)_n$. The composition of the products formed in thermal decomposition of carbon polyfluoride depends on whether or not gaseous fluorine is present in the decomposition zone. An increase in the amount of gaseous fluorine in the decomposition zone makes smaller the fraction of fluorocarbons with a longer carbon chain. Therefore, spatial separation of the zone in which fluorine reacts with graphite to give carbon polyfluoride and the zone in which carbon fluoride undergoes thermal decomposition leads to an increase in the fraction of fluorocarbons with the number of carbon atoms greater than unity in the gaseous reaction products.

In performing the fluorination of graphite in a fluidized bed, it is impossible to spatially separate the zones of synthesis and thermal decomposition of carbon polyfluoride [2]. The reactor with an ascending gas-dust flow also has a number of disadvantages: it is necessary to use an inert gas (approximately nine volumes per volume of fluorine) to create as gas-dust flow; it is virtually impossible to vary the feed rate of graphite; there occur uncontrollable disruptions of powder ejection in the device forming the gas-dust flow.

Therefore, it was suggested to examine the possibility of using a reactor with a free-falling powder bed to obtain perfluoroalkanes by fluorination of carbon, as it has been done in synthesis of sulfur tetrafluoride from elements [4]. In this reactor, powdered graphite is delivered by a screw conveyor into the upper part of a hollow vertical tube, within which graphite particles move in the free-fall mode. Fluorine is also fed into the upper part of the tube. The reaction between fluorine and graphite (which is present in a large excess) yields carbon polyfluoride at a complete conversion of fluorine. Thermal decomposition of carbon polyfluoride is performed in the fixed powder bed in the lower part of the reactor.

The process in a reactor with a free-falling bed has a number of advantages over that in reactor with a fluidized bed or a gas-dust flow. The most important distinctive features of the reactor with a free-falling bed are as follows: reagents are delivered separately and in controlled way by a screw conveyor [5], which should provide stable formation of the gas-dust flow (falling bed) of prescribed composition; the zones in



Schematic of a free-fall reactor: (*1*) feeding bunker, (*2*) screw conveyor, (*3*) fluorine input unit, (*4*) reaction tube, (*5*) control unit, and (*6*) receiving bunker.

which fluorine is absorbed and carbon polyfluoride decomposes are separated; application of a screw may diminish (or make unnecessary) the use of an inert gas; and the technology of isolation of target products is simplified.

Table 1. Adiabatic warming-up ΔT of a falling graphite bed and heat release ΔQ in the reaction of fluorine with graphite to give $(CF_x)_n$ in relation to flow rate W_{F_2} of fluorine and feed rates of fluorine and graphite (G_{F_2} and G_C), and molar ratio M of the feed rates of fluorine and graphite

W_{F_2}, ml s^{-1}	G_{F_2}	G_C	M	$G_{F_2}G_C^{-1}$, fraction units	ΔQ, J	ΔT, °C
	g s^{-1}					
25	0.040	1.00	0.025	0.040	400	580
10	0.016	1.00	0.010	0.016	160	200
5	0.008	1.00	0.005	0.008	80	100
10	0.016	0.75	0.013	0.021	160	300
5	0.008	0.75	0.007	0.011	80	150

EXPERIMENTAL

Fluorination in the reactor with a free-falling graphite bed occurs in the vertical tube to give carbon polyfluoride, under the conditions of a free fall of a graphite particle at a temperature lower than 600°C in a large excess of graphite, with fluorine completely bound. $(CF_x)_n$ is decomposed in the receiving bunker at a temperature exceeding 600°C.

The laboratory reactor (see figure) comprises the following elements: feeding bunker *1* with graphite (diameter 120 mm, volume 2100 ml); screw conveyor *2*; fluorine input unit *3*; reaction tubes *4* (diameter 12 mm, length 300 mm); control units *5* for monitoring the temperature and presence of fluorine in the reaction zone; and receiving bunker *6* (diameter 120 mm, volume 2400 ml. The required temperature of the feeding bunker *1*, reaction tubes *4*, and receiving bunker *6* is maintained by electric heaters. To enable variation of the time of contact between fluorine and the carbon material, the reaction tube is fabricated in the form of interchangeable parts connected by the control units. Bunker *6* is equipped with a filter for gas cleaning to remove fine particles and with a sampling line serving to take samples for chromatographic analysis.

The screw conveyor *2*, fabricated on the basis of the recommendations given in [5], has the form of a rigid spiral screw with a pitch of 8 mm, placed in a cylindrical channel 12 mm in diameter and 8 mm long. The screw is rotated by an electric motor with variable rotation rate, which enables variation of the graphite feed.

The reactor is used in experiments as follows. Powdered graphite is charged into heated bunker *1* and the temperature of the carbon material is brought to 450–500°C by electric heaters. Then, screw *2* delivers heated graphite into the reaction tube, in whose upper part unit *3* for input of gaseous fluorine is situated. Under the action of the gravity force, graphite moves downwards along the reaction tube in the free-fall mode. The gaseous fluorine fed into the reactor reacts with particles of free-falling graphite to give $(CF_x)_n$. In the course of $(CF_x)_n$ synthesis, the powder warms-up to a temperature of about 550–600°C, and arrives to receiving bunker *6*, in which $(CF_x)_n$ decomposes to give perfluoroalkanes.

To choose the feed rate of graphite and fluorine, the dependence of the heat release and adiabatic warming-up of falling graphite particles on the feed rates of the components delivered into the reactor was calculated on the condition that $(CF_x)_n$ is formed, using the data of [6] (Table 1).

Table 2. Composition of the gaseous products formed in the reaction between fluorine and graphite in the reactor with a free-falling graphite bed

Fluorine content, vol %	CF_4	C_2F_6	C_2F_4	C_3F_8	C_3F_6	C_4F_{10}
	vol %					
100	85	8	0.05	5	0.2	1
50	60	20	0.3	10	2	5

For perfluoroalkanes to be synthesized by the scheme comprising synthesis of $(CF_x)_n$, followed by thermal decomposition of $(CF_x)_n$, the temperature of graphite should be 450–550°C at the inlet of the fluorination reactor, and the temperature of the powder at the reactor outlet, about 550–600°C. At the feed rate of graphite fixed at about 1 g s^{-1}, the interval of possible variation of the flow rate of fluorine will be 5–10 cm^3 s^{-1}. Thus, the duration of a single experiment will be, at a completely filled feed bunker *1* (see figure) and the chosen feed rate of graphite, 30–35 min.

Experiments on fluorination of powdered graphite were performed on the laboratory setup with a reactor with a free-falling graphite bed. The fluorination was performed at a temperature of 400–500°C in the zone of reaction between fluorine and graphite and 550–600°C in the zone of decomposition of carbon polyfluoride. The temperature of 550–600°C is sufficient for complete thermal decomposition of carbon polyfluoride [2, 3] in several seconds to tens of seconds.

The 0.2–1-mm fraction of the graphite powder was isolated for use in the study. The feed rate of graphite in the experiments performed was 1 g s^{-1}. The fluorination was done using a fluorine–argon mixture with fluorine content of 50 vol % or gaseous fluorine with dilution with an inert gas.

The flow rate of the fluorine–argon mixture was 8–10 cm^3 s^{-1}, and that of undiluted fluorine, 5–6 cm^3 s^{-1}. The theoretical heat release under adiabatic conditions in the reaction between fluorine and graphite at a given ratio of the feed rates will lead to a rise in the powder temperature by 100°C. The true rise in the temperature of the falling flow of graphite particles, caused by the heat of the reaction, is 50–60°C. Table 2 presents the averaged composition of the gaseous reaction products.

An analysis of values of the parameter $\Sigma S_{CF}/S_N$, whose physical meaning was described in detail in [2, 3], led to a conclusion that carbon polyfluoride formed in the reaction of fluorine and graphite completely decomposes.

Experiments with various inert gases, fluorine diluents, were carried out on the laboratory setup with a reactor with free-falling graphite bed. As inert gases served argon and tetrafluoromethane. The compositions of gaseous perfluorocarbons obtained in fluorination of graphite with mixtures containing 50 and 80 vol % fluorine were studied. In the case of a fluorinating mixture composed of 50 vol % CF_4 and 50 vol % fluorine, the composition of the gaseous reaction products was the following (with tetrafluoromethane coming into the gas mixture together with fluorine disregarded) (wt %): tetrafluoromethane, about 38–40; hexafluoroethane, 24–26; octafluoropropane, 19–21; and decafluorobutane, 10–12.

CONCLUSIONS

(1) It was shown that, in synthesis of perfluoroalkanes from graphite and fluorine under laboratory conditions in a reactor with a free-falling graphite bed by the scheme comprising synthesis of carbon polyfluoride and its thermal decomposition, the reaction products of the following composition can be obtained (wt %): tetrafluoromethane, about 38–40; hexafluoroethane, 24–26; octafluoropropane, 19–21; and decafluorobutane, 10–12.

(2) It was demonstrated, on a laboratory model of a reactor with free-falling powder bed, that a screw conveyor provides a stable formation of a gas-dust flow of fluorine and graphite in a wide range of feed rates of the components. In turn, the stable delivery of the components provides and maintains those temperature conditions of synthesis and thermal decomposition of carbon polyfluoride which are close to the optimal, as regards the composition of the gaseous reaction products, conditions.

(3) It was shown that use of a reactor with a free-falling graphite bed makes it possible to reduce the concentration of an inert gas in its mixture with fluo-

rine, compared with reactors with a fluidized bed and ascending gas-dust flow.

REFERENCES

1. Maksimov, B.N., Barabanov, V.G., Serushkin, I.L., et al, *Promyshlennye ftororganicheskie produkty: Spravocnoe izdanie* (Industrial Organofluorine Products: Reference Book), St. Petersburg: Khimiya, 1996.
2. Pashkevich, D.S., Shelopin, G.G., Mukhortov, D.A., et al., *Zh. Prikl. Khim.*, 2004, vol. 77, pp. 1865–1871.
3. Shelopin, G.G., Pashkevich, D.S., Mukhortov, D.A., et al., *Zh. Prikl. Khim.*, 2006, vol. 79, no. 6, pp. 951–954.
4. Alekseev, Yu.I. and Pashkevich, D.S., Abstracts of Papers, *16-ya Vserossiiskaya konferentsiya po khimicheskim reaktoram (s mezhdunarodnym uchastiem) "Khimreaktor-16"* [16th All-Russia Conf. on Chemical Reactions (with foreign participants) "Khimreaktor-16"], Kazan, 2003, p. 201.
5. Herrmann, H., *Schneckenmaschinen in der Verfahrenstechnik*, Berlin: Springer, 1972. Translated under the title *Shnekovye mashiny v tekhnologii*, Leningrad: Khimiya, 1975.
6. Wood, J.L., Badachape, R.B., Lagow, R.J., and Margrave, J.L., *J. Phys. Chem.*, 1963, vol. 78, pp. 3139–3142.

ISSN 1070-4272, Russian Journal of Applied Chemistry, 2006, Vol. 79, No. 6, pp. 1035–1037. © Pleiades Publishing, Inc., 2006.
Original Russian Text © E.A. Dikusar, 2006, published in Zhurnal Prikladnoi Khimii, 2006, Vol. 79, No. 6, pp. 1043–1045.

BRIEF COMMUNICATIONS

New Esters of Vanillin and Vanillal with Some Alkane- and Arenecarboxylic Acids

E. A. Dikusar

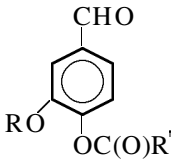
Institute of Physicoorganic Chemistry, National Academy of Sciences of Belarus, Minsk, Belarus

Received February 13, 2006

Abstract—Previously unknown esters were synthesized by the reaction of vanillin and vanillal with carboxylic acid chlorides.

DOI: 10.1134/S1070427206060322

Natural plant aldehydophenols, vanillin and vanillal (**Ia**, **Ib**), are available precursors for preparing fragrance compounds and food aromatizers [1–3], medical products, and biologically active compounds [4–8]:



IIa–**IIh**, **IIIa**–**IIIv**

where **II**, R is Me, R' is (**a**) $(CH_2)_7Me$, (**b**) $(CH_2)_{14}Me$, (**c**) cyclo-C_6H_{11}, (**d**) $(CH_2)_2C_6H_5$, (**e**) $CBrCCl{=}CCl_2$, (**f**) $(CH_2)_2C(O)OMe$, (**g**) $C(CN){=}CHC_6H_5$, and (**h**) 3,5-$C_6H_3(NO_2)_2$; **III**, R is Et, R' is (**a**) $(CH_2)_4Me$, (**b**) $(CH_2)_5Me$, (**c**) $(CH_2)_6Me$, (**d**) $(CH_2)_7Me$, (**e**) $(CH_2)_8Me$, (**f**) $(CH_2)_{11}Me$, (**g**) $(CH_2)_{14}Me$, (**h**) $(CH_2)_{16}Me$, (**i**) cyclo-C_6H_{11}, (**j**) $CH_2C_6H_5$, (**k**) $(CH_2)_2C_6H_5$, (**l**) $CH_2CHMeC_6H_5$, (**m**) *trans*-$CH{=}CHC_6H_5$, (**n**) $CBrCCl{=}CCl_2$, (**o**) $CHBrCHBrC_6H_5$, (**p**) $(CH_2)_2C(O)OMe$, (**q**) $C(CN){=}CHC_6H_5$, (**r**) 2,4-$C_6H_3C_{12}$, (**s**) 2,4-$CH_2OC_6H_3C_{12}$, (**t**) 3-$C_6H_5NO_2$, (**u**) 4-$C_6H_5NO_2$, and (**v**) 3,5-$C_6H_3(NO_2)_2$.

Here we describe a convenient procedure for preparing new esters of vanillin and vanillal with a number of alkane- and arenecarboxylic acids (**IIa**–**IIh** and **IIIa**–**IIIv**).

Esters **IIa**–**IIh** and **IIIa**–**IIIv** were prepared by simpler, more convenient, and more practically feasible procedure in comparison with that described previously for similar compounds [1–3].

Esters **IIa**–**IIh** and **IIIa**–**IIIv** were synthesized by the reaction of vanillin and vanillal (**Ia**, **Ib**) with chlorides of the corresponding alkane- and arenecarboxylic acids in anhydrous benzene in the presence of pyridine. We used the stoichiometric ratio of the reactants, 1 : 1 : 1. As a result of this reaction, the initial aldehydophenols **Ia** and **Ib** were converted to the corresponding esters **IIa**–**IIh** and **IIIa**–**IIIv** with a yield of 90–96%.

Vanillin and vanillal esters **IIa**–**IIh** and **IIIa**–**IIIv** are colorless viscous liquids or crystalline substances (crystallized from a mixture of benzene and hexane) (see table). The esters do not require additional purification, distillation, or recrystallization.

The structure and composition of vanillin and vanillal esters **IIa**–**IIh** and **IIIa**–**IIIv** were confirmed by elemental analysis, cryoscopic determination of the molecular weight (see table), and ^{1}H NMR, IR, and UV spectra. According to the ^{1}H NMR data, the purity of the resulting compounds was $98 \pm 1\%$.

In the IR spectra of vanillin and vanillal esters **IIa**–**IIh** and **IIIa**–**IIIv**, there are the following characteristic absorptions bands, ν, cm^{-1}: 3100–3000 (CHAr), 2990–2795 (CHAlk), 2740 ± 5 (CH of CHO group), 1720–1770 (C=O of ester group), 1695–1705 (C=O of CHO group), 1600–1350 (vibrations of aromatic system), 1300–1000 (C–O vibrations), and 800–600 (CHAr) [1, 3].

In the UV spectra of vanillin and vanillal esters **IIa**–**IIh** and **IIIa**–**IIIw**, there are the following absorption peaks, λ_{max}, nm (ε): 206 (9000), 224 (15 000), 260 (8000), and 310 (3000), caused by the presence of the 4-alkanoyloxy-3-alkoxybenzaldehyde fragment

Characteristics of vanillin and vanillal esters **IIa**–**IIh** and **IIIa**–**IIIv**

Ester	Yield, %	mp, °C	Found, %		Formula	Calculated, %		*M*	
			C	H		C	H	found	calculated
IIa*	90	–	70.02	8.34	$C_{17}H_{24}O_4$	69.84	8.27	281.9	292.4
IIb	92	37–38	74.05	9.93	$C_{24}H_{38}O_4$	73.81	9.81	372.3	390.6
IIc	90	73–74	68.90	7.11	$C_{15}H_{18}O_4$	68.69	6.92	252.7	262.3
IId	93	46–47	71.94	5.75	$C_{17}H_{16}O_4$	71.82	5.67	275.5	284.3
IIe**	93	103–104	36.08	2.12	$C_{12}H_8BrCl_3O_4$	35.81	2.00	393.4	402.5
IIf	90	72–73	58.91	5.42	$C_{13}H_{14}O_6$	58.65	5.30	254.4	266.3
IIg**	94	165–166	70.58	4.35	$C_{18}H_{13}NO_4$	70.35	4.26	300.2	307.3
IIh**	96	163–164	52.17	3.10	$C_{15}H_{10}N_2O_8$	52.03	2.91	328.3	346.3
IIIa*	90	–	68.37	7.65	$C_{15}H_{20}O_4$	68.16	7.63	258.6	264.3
IIIb*	93	–	69.18	8.01	$C_{16}H_{22}O_4$	69.04	7.91	270.1	278.3
IIIc*	92	–	70.02	8.29	$C_{17}H_{24}O_4$	69.84	8.27	286.6	292.4
IIId*	92	–	70.64	8.60	$C_{18}H_{26}O_4$	70.56	8.55	299.2	306.4
IIIe*	93	–	71.45	8.95	$C_{19}H_{28}O_4$	71.22	8.81	313.0	320.4
IIIf	91	42–43	73.08	9.49	$C_{22}H_{34}O_4$	72.89	9.45	354.7	362.5
IIIg	90	35–36	74.30	10.00	$C_{25}H_{40}O_4$	74.22	9.96	395.6	404.6
IIIh	96	47–48	75.14	10.31	$C_{27}H_{44}O_4$	74.96	10.25	426.8	432.6
IIIi	92	61–62	69.75	7.42	$C_{16}H_{20}O_4$	69.55	7.29	270.0	276.3
IIIj*	91	–	71.98	5.77	$C_{17}H_{16}O_4$	71.82	5.67	277.1	284.3
IIIk	93	73–74	72.74	6.19	$C_{18}H_{18}O_4$	72.47	6.08	290.3	298.3
IIIl*	94	–	73.32	6.58	$C_{19}H_{20}O_4$	73.06	6.45	300.5	312.4
IIIm	93	107–108	73.21	5.60	$C_{18}H_{16}O_4$	72.96	5.44	288.7	296.3
IIIn**	94	84–85	37.66	2.47	$C_{13}H_{10}BrCl_3O_4$	37.49	2.42	402.9	416.5
IIIo**	94	110–111	47.50	3.59	$C_{18}H_{16}Br_2O_4$	47.40	3.54	442.3	456.1
IIIp*	92	–	60.27	5.85	$C_{14}H_{16}O_6$	60.00	5.75	271.7	280.3
IIIq**	93	127–128	71.54	4.76	$C_{19}H_{15}NO_4$	71.33	4.70	314.6	321.3
IIIr**	90	117–118	56.92	3.70	$C_{16}H_{12}Cl_2O_4$	56.66	3.57	329.8	339.2
IIIs**	91	107–108	55.68	3.95	$C_{17}H_{14}Cl_2O_5$	55.31	3.82	354.2	369.2
IIIt**	91	133–134	61.20	4.25	$C_{16}H_{13}NO_6$	60.95	4.16	303.4	315.3
IIIu**	90	155–156	61.15	4.20	$C_{16}H_{13}NO_6$	60.95	4.16	308.0	315.3
IIIv**	90	137–138	53.60	3.38	$C_{16}H_{12}N_2O_8$	53.34	3.36	348.9	360.3

* d_{20}^{20}, n_D^{20}: 0.9908, 1.5090 (**IIa**); 0.9169, 1.5090 (**IIIa**); 0.9679, 1.5070 (**IIIb**); 0.9358, 1.5065 (**IIIc**); 0.9103, 1.5060 (**IIId**); 0.9213, 1.5030 (**IIIe**); 1.2079, 1.5700 (**IIIj**); 1.0866, 1.5580 (**IIIl**); 1.1222, 1.5234 (**IIIp**).

** Br + Cl, %: found 46.10, calculated 46.28 (**IIe**); N, %: found 4.30, calculated 4.56 (**IIg**); N, %: found 7.90, calculated 8.09 (**IIh**); Br + Cl, %: found 44.45, calculated 44.72 (**IIIn**); Br, %: found 34.88, calculated 35.04 (**IIIo**); N, %: found 4.03, calculated 4.36 (**IIIq**); Cl, %: found 20.70, calculated 20.91 (**IIIr**); Cl, %: found 18.93, calculated 19.21 (**IIIs**); N, %: found 4.37, calculated 4.44 (**IIIt**); N, %: found 4.30, calculated 4.44 (**IIIu**); N, %: found 7.51, calculated 7.78 (**IIIv**).

[1]. In addition, the UV spectra of esters of functionality substituted and aromatic carboxylic acids (**IId**, **IIe**, **IIg**, **IIh**, **IIIj**–**IIIo**, and **IIIq**–**IIIv**) contain absorption bands typical of the corresponding fragments of these acids [3].

In the ^{1}H NMR spectra of vanillin derivatives **IIa**–**IIh**, the MeO group gives a singlet in the range 3.90–3.96 ppm, and in the ^{1}H NMR spectra of vanillal derivatives **IIIa**–**IIIv** the EtO group gives a triplet at 1.40–1.45 ppm (Me) and a quartet at 4.08–4.18 ppm (CH_2). The aromatic protons of esters **IIa**–**IIh** and **IIIa**–**IIIv** (C_6H_3) give a multiplet in the range 7.10–7.60 ppm, and the aldehyde proton of the CHO group gives a singlet in the range 9.95–10.0 ppm. The ^{1}H NMR spectra of compounds **IIa**–**IIh** and **IIIa**–**IIIv** contain characteristic signals of ester fragments [1, 3].

EXPERIMENTAL

The IR spectra were recorded on a Protege-460 Nicolet Fourier spectrophotometer in thin layer or

in KBr. The UV spectra of 1×10^{-4} M solutions in methanol were recorded on a Specord UV-Vis spectrophotometer. The ^{1}H NMR spectra were recorded on a Tesla BS-587A spectrometer operating at 100 MHz (5% solutions in $CDCl_3$, TMS internal reference). The molecular weights were determined cryoscopically in benzene.

Carboxylic acid chlorides were synthesized by refluxing the corresponding carboxylic acids with a 1.5-fold excess of $SOCl_2$ in benzene. Freshly distilled carboxylic acid chlorides and anhydrous benzene and pyridine were used.

Vanillin and vanillal alkanoates IIa–IIh and IIIa–IIIv. To a solution of 0.02 M of vanillin or vanillal (**Ia**, **Ib**) and 0.02 mol of alkene- or arenecarboxylic acid chlorides in 50 ml of benzene, a solution of 0.02 mol of pyridine in 10 ml of benzene was added with shaking. The vessel with the reaction mixture was hermetically sealed and the mixture allowed to stay for 10–12 h at 20–23°C with intermitted careful shaking. Then it was placed in a separating funnel, thoroughly washed with water and 20% NaCl for suppression of emulsion formation, and washed 2–3 times with 5% $NaHCO_3$. The organic layer was separated and filtered through a paper filter. Benzene was removed in a vacuum, with heating of the residue above 30°C avoided. Compounds **IIb**–**IIh**, **IIIf**–**IIIi**, **IIIk**, **IIIm**–**IIIo**, and **IIIq**–**IIIv** were crystallized from a mixture of benzene and hexane.

CONCLUSIONS

(1) An improved procedure was developed for preparing vanillin and vanillal esters with a yield of 90–96%.

(2) Some of the resulting compounds may be of interest as components for perfume and food industry and can serve as accessible precursors in synthesis of biologically active substances and medicinals.

REFERENCES

1. Dikusar, E.A., Vyglazov, O.G., Moiseichuk, K.L., et al., *Zh. Prikl. Khim.*, 2005, vol. 78, no. 1, pp. 122–126.
2. Dikusar, E.A. and Kozlov, N.G., *Khim. Prirodn. Soedin.*, 2005, no. 1, pp. 74–75.
3. Dikusar, E.A. and Kozlov, N.G., *Zh. Org. Khim.*, 2005, vol. 41, no. 7, pp. 1015–1019.
4. Kozlov, N.G., Basalaeva, L.I., and Dikusar, E.A., *Khim. Prirodn. Soedin.*, 2004, no. 1, pp. 70–73.
5. Dikusar, E.A., Kozlov, N.G., Zhukovskaya, N.A., and Moiseichuk, K.L., *Khim. Prirodn. Soedin.*, 2004, no. 2, pp. 154–156.
6. Dikusar, E.A., Kozlov, N.G., Potkin, V.I., et al., *Khim. Prirodn. Soedin.*, 2005, no. 2, pp. 164–169.
7. Dikusar, E.A., Kozlov, N.G., and Potkin, V.I., *Vestsi Nats. Akad. Navuk Bel., Ser. Khim.*, 2005, no. 4, pp. 39–46.
8. Kozlov, N.G., Basalaeva, L.I., and Dikusar, E.A., *Zh. Org. Khim.*, 2005, vol. 41, no. 11, pp. 1671–1680.

ISSN 1070-4272, Russian Journal of Applied Chemistry, 2006, Vol. 79, No. 6, pp. 1038–1039. © Pleiades Publishing, Inc., 2006.
Original Russian Text © B.F. Kukharev, V.K. Stankevich, N.A. Belogorlova, G.R. Klimenko, 2006, published in Zhurnal Prikladnoi Khimii, 2006, Vol. 79, No. 6, pp. 1046–1047.

BRIEF COMMUNICATIONS

Butyl Vinyl Ether–1-Amino-3-[2-(vinyloxy)ethoxy]-2-propanol Cooligomer as a Stabilizer of Mazut–Coal Blended Fuel

B. F. Kukharev, V. K. Stankevich, N. A. Belogorlova, and G. R. Klimenko

Favorskii Institute of Chemistry, Siberian Division, Russian Academy of Sciences, Irkutsk, Russia

Received January 11, 2006

Abstract—Butyl vinyl ether–1-amino-3-[2-(vinyloxy)ethoxy]-2-propanol cooligomer was prepared and studied as a stabilizer of mazut–coal blended fuel.

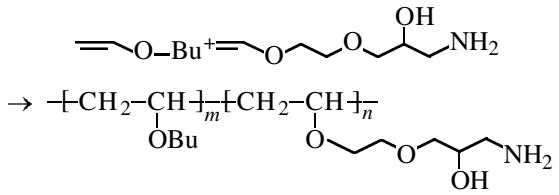
DOI: 10.1134/S1070427206060334

Vinyl polymers (copolymers of *N*-vinylpyrrolidone with ethylene glycol vinyl-OCH_2CH_2O-glycidyl ether and butyl vinyl ether of various molar compositions, and homopolymers of these monomers) can be used as stabilizers of a promising fuel, mazut–coal blends [1].

In this study, we prepared butyl vinyl ether–1-amino-3-[2-(vinyloxy)ethoxy]-2-propanol cooligomer and studied this compound as a stabilizer of a mazut–coal blended fuel.

Cooligomerization of butylvinyl ether with 1-amino-3-[2-(vinyloxy)ethoxy]-2-propanol was performed by heating an equimolar mixture of these monomers in the presence of azobisisobutyric acid dinitrile [2]. The cooligomer was isolated by precipitation from an ethanol solution with diethyl ether; it was a light yellow viscous resin soluble in organic solvents and water.

The absence of the bands of vinyloxy group (820, 1320, 1645, 1625, 3120 cm^{-1}) and the presence of the bands of methyl group of butyl vinyl ether (1380, 1460, 2960 cm^{-1}) and amino and hydroxy groups (3310, 3446 cm^{-1}) in the IR spectrum of the oligomer confirm oligomerization via opening of the double bond and the presence of both monomeric units in the oligomer. The molar ratio of the monomeric units in the oligomer is 32 : 68 (mol %). The intrinsic viscosity in water is 0.12 dl g^{-1}. The weight-average molecular weight is 1100.



where m = 32, n = 68 mol %.

The stabilizing effect of the oligomer was studied by the known procedure [1, 3].

The stability and viscosity of the suspension at different concentrations of the stabilizer are listed in the table.

Among the known copolymers of *N*-vinylpyrrolidone with ethylene glycol vinyl glycidyl ether and butyl vinyl ether of various molar compositions and the homopolymers of these monomers, the best results were obtained with *N*-vinylpyrrolidone-butyl vinyl ether copolymer. The stability of the mazut–coal blend containing 20% coal and 0.3–0.5% stabilizer at 70°C was 96–100 in 24 h and 75.7–80.2% in 1 month, respectively, depending on the copolymer composition [1]. As can be seen from the table, the stabilizing effect of the copolymer is noticeably stronger than that

Stability and viscosity of a mazut–coal blend at 70°C

Cooligomer content in mazut–coal blend, %	Viscosity, Pa s^{-1}	Stability, %	
		in 24 h	in 1 month
0	0.585	11.2	0
0.02	1.492	74.6	22.7
0.03	1.651	80.1	37.4
0.04	2.432	88.2	49.8
0.08	2.826	98.2	88.9
0.10	3.117	100.0	98.2
0.15	3.994	100.0	99.1
0.20	4.252	100.0	100.0
0.30	7.107	100.0	100.0

of known stabilizers. The stability of a mazut–50% coal blend containing 0.1% copolymer in 24 h and 1 month at 70°C was 100 and 98.2%, respectively.

EXPERIMENTAL

Butyl vinyl ether–1-amino-3-[2-(vinyloxy)ethoxy]-2-propanol cooligomer. A mixture of butyl vinyl ether (100.2 g, 1 mol), 1-amino-3-[2-(vinyloxy)ethoxy]-2-propanol (161.2 g, 1 mol), and azobisisobutyric acid dinitrile (2 g) was heated at 80°C for 60 h. To remove unchanged monomers, the cooligomer was precipitated from an aqueous solution with diethyl ether and then dried in a vacuum (5 mm Hg). The cooligomer yield was 72.4 g. The butyl vinyl ether : 1-amino-3-[2-(vinyloxy)ethoxy]-2-propanol molar ratio determined by GLC analysis of a solution of the reprecipitated product is 68 : 32, i.e., the ratio of the monomer units is 32 : 68%.

Found (%): C 57.01, H 10.09, N 6.73.

$(C_6H_{12}O)_{0.32}(C_7H_{15}NO_3)_{0.68}$.

Calculated (%): C 56.63, H 9.99, N 6.72.

The mazut–coal blend was prepared from coal with the particle size smaller than 70 μm, 6.9% ash content and the water content of about 6% and M-100 mazut with viscosity of 70 cP at 70°C and the water content of 4.0%. The suspension was prepared in a DS-106 disintegrator (the linear collision speed of particles with the rotor fingers is 120 m s^{-1}). The coal content in all blends used in this study was 50 wt %. The stabilizer concentration ranged from 0.02 to 0.30 wt %.

The viscosity of the mazut–coal blend was measured on a Hoeppler viscometer using a 10.0172-g ball 13.5 mm in diameter. To determine the stability of the mazut–coal blend, its was controlled thermostatically at 70°C in sedimentation cylinders [3] for 24 h and 30 days. The stability of the suspension was determined gravimetrically from the carbon content in the upper layer. A sample (1/3 of the whole volume) of the upper part of the suspension was taken, and washed with toluene. The coal was separated by centrifugation and dried. The stability (Y, %) was calculated by the equation

$$Y = m_c \times 100/(m_s c),$$

where m_s is the weight of the suspension sample (g); m_c, weight of coal recovered from the suspension sample (g); and c, weight fraction of coal in the initial suspension.

CONCLUSIONS

(1) Butyl vinyl ether–1-amino-3-[2-(vinyloxy)ethoxy]-2-propanol cooligomer with molar ratio of the monomeric units of 32 : 68 (mol %) was prepared.

(2) The stability of a mazut–coal blend containing the cooligomer in an amount of 0.1% and more, evaluated upon heating at 70°C for 24 h and 1 month, is 100 and 98.2–100%, respectively. The stabilizing effect of the cooligomer is substantially stronger than that of the known stabilizers derived from vinyl monomers.

REFERENCES

1. Minakova, T.T., Livanova, E.P., Polubentsev, A.V., and Belogorlova, N.A., *Khim. Tekhnol. Top. Masel*, 1990, no. 4, pp. 6–7.
2. Minakova, T.T., Morozova, L.V., and Trofimov, B.G., *Zh. Prikl. Khim.*, 1984, vol. 57, no. 7, pp. 1667–1668.
3. Kustov, V.F., *Toplivnye suspenzii* (Fuel Suspensions), Moscow: Akad. Nauk SSSR, 1942, p. 55.

ISSN 1070-4272, Russian Journal of Applied Chemistry, 2006, Vol. 79, No. 6, pp. 1040–1041. © Pleiades Publishing, Inc., 2006.
Original Russian Text © Editorial Board, 2006, published in Zhurnal Prikladnoi Khimii, 2006, Vol. 79, No. 6, pp. 1048–1049.

OBITUARY

Valentin Borisovich Aleskovskii (1912–2006)

DOI: 10.1134/S1070427206060346

On January 29, 2006, passed away, at the age of 93 after short illness, Valentin Borisovich Aleskovskii, a known scientist-chemist, one of the patriarchs of domestic solid-state chemistry, Honored scientist of the Russian Federation, participant of the Great Patriotic War, corresponding member of the Russian Academy of Sciences, doctor of chemical science, and professor of the chair of chemistry at the chemical faculty of St. Petersburg State University.

V.B. Aleskovskii was born on July 3, 1912, in the town of Mary in Turkmenia.

Having graduated from Leningrad Technological Institute in 1937, Aleskovskii became a post-graduate student at the chair of sorption technology and defended his candidate dissertation in 1940.

In June 1941, Valentin Borisovich volunteered to the frontline. He was wounded in action near Pulkovo at the end of 1943.

After returning from the front to the Institute, Aleskovskii defended his doctoral dissertation in 1952. He was appointed rector of Leningrad Technological Institute in 1965. In 1967, he founded the first chair of solid-state chemistry in the country and headed this chair. In 1972, Aleskovskii was elected a corresponding member of the Academy of Sciences of the USSR.

Aleskovskii's pedagogical, scientific, and organizational activities had been associated with Leningrad State University since 1975, when he was appointed rector of the University. Occupying this position, Aleskovskii modernized the structure of the University and transformed it into an educational-scientific center comprising two complexes, on the Vasil'evskii Island in St. Petersburg and at Petrodvorets at the outskirts of the city, which include faculties of the University and the corresponding scientific institutes.

Aleskovskii was among those who gave birth to solid-state chemistry in our country. In 1977, he organized at the chemical faculty of Leningrad University the chair of solid-state chemistry, headed by him till 1986, and later held the position of a professor of



this chair. The main area of Aleskovskii's scientific interests was study of the nature and chemical transformations of solids and development of a technology of new inorganic materials. He was the author of more than 450 scientific publications, including 12 monographs and textbooks, and made more than 150 inventions.

Most widely known are Aleskovskii's works of the 1960s, in which he created (by a certain analogy with DNA replication) methods for chemical assembly and, in particular, for synthesis of solid compounds of reproducible composition by the molecular layering technique. Abroad, this technique (known as atomic layer epitaxy) was developed 20 years later. At present, molecular layering is one of the most promising methods for synthesis of nanomaterials for electronics and other areas of solid-phase materials science.

Aleskovskii developed the concept of chemistry of supramolecular compounds (early 1990s) and later reconsidered it with account of the results of his own theoretical and experimental studies and published data in the field of supramolecular chemistry (J.-M. Lehn, 1989). This allowed him to suggest

the concept of chemistry of highly organized substances (1993).

Numerous results of studies and inventions by Aleskovskii and his pupils have been implemented in practice, a new effective and economically efficient material Anod for electrochemical power cells has been put into production, an electrochemical generator autonomously working in seawater has been developed on the basis of a novel material Mikrovors, and the new sorbing materials created in the 1980s by the molecular layering technique have been successfully used in instrument engineering for more than 20 years, with the quality and reliability of aircraft improved.

Aleskovskii was a talented pedagogue. He trained a pleiad of specialists in solid-state chemistry, who are working in our country and abroad, and created a highly productive scientific school "Chemistry of highly organized substances." There are several tens of doctors of science and more than 100 candidates of science among his pupils.

He was a member of the Supreme Soviet of the Russian SFSR (Soviet Federative Socialist Republic) and made an important contribution to the development of higher school in Russia by heading not only the leading higher-school institutions of the country, but also the Commission for education of the Supreme Soviet of the Russian SFSR.

During a number of years, Aleskovskii was a member of the Editorial board of *Zhurnal Prikladnoi Khimii* (Russian Journal of Applied Chemistry) published by the Russian Academy of Sciences.

The following conferences are regularly held in the framework of activities of the scientific school: International Conference "Chemistry of Highly Organized Substances and Scientific Foundations of Nanotechnology" (at St. Petersburg State University: 1st in 1996, 2nd in 1998, 3rd in 2001, and 4th in 2004); All-Russia Conference with foreign participation "Surface Chemistry and Nanotechnology" (at St. Petersburg State Technological Institute: 1st in 1999, 2nd in 2002, and 3rd to be held on September 2006).

For his scientific and educational-pedagogic activities, Aleskovskii was decorated with honorary titles and government awards.

The illness untimely terminated the vigorous scientific activities of the scientist, who remained faithful to his scientific interests till the end of his days and was agitated by problems associated with the development of highly organized substances, of the chair he organized, and of the chemical faculty of St. Petersburg University. To proceed with his deeds is the duty of his pupils and the best way to preserve his memory.

St. Petersburg State University

St. Petersburg State Technological Institute

Pupils and colleagues, and the Editorial Board and editorial staff of Zhurnal Prikladnoi Khimii

ISSN 1070-4272, Russian Journal of Applied Chemistry, 2006, Vol. 79, No. 6, pp. 1042–1043. © Pleiades Publishing, Inc., 2006.
Original Russian Text © A.G. Morachevskii, 2006, published in Zhurnal Prikladnoi Khimii, 2006, Vol. 79, No. 6, pp. 1050–1051.

BOOK REVIEWS

L. D. Khegai, *Svintsovye akkumulyatory. Sostoyanie, problemy, resheniya* (Lead Batteries: State of Affairs, Problems, Solutions), Vladivostok: Dal'nauka, 2005, 256 pp.

DOI: 10.1134/S1070427206060358

Despite that lead batteries appeared about 150 years ago, no real alternative to their use in various vehicles has been found so far. The steady increase in the number of automobiles, especially characteristic of some regions of Russia, requires that the production of lead batteries should be raised, with their quality simultaneously improved. At present, 70 to 80% of the world's output of lead is consumed by battery industry. The geopolitical changes at the end of the XX century resulted in that the battery plants of the former Soviet Union, mostly concentrated on the territory of Russia, virtually lost their resources of raw materials. By 1990, Russia produced no more than 10% of the whole amount of lead manufactured in the USSR, whereas the leading position was occupied by Kazakh SSR.

The service life of the majority of lead batteries is, in the case when all exploitation requirements are satisfied, 3–5 years (starter batteries), after which they should be obligatorily utilized. At present, no less than 55% of the world's production of lead is based on processing of secondary raw materials, and scrap lead batteries in the first place. Measures are undertaken all over the world to organize an efficient system for collection of batteries and to improve the technology of their utilization. These problems are of not only economical, but also ecological importance, because lead and its compounds are highly toxic for living organisms.

The book by L.D. Khegai comprises an introduction, two parts (each dived into chapters), conclusion, and reference lists for the first and second parts separately (18 and 142 reference to various publications, respectively). In the brief introduction of most general nature (p. 3), some figures given without any reference seem to be questionable. In particular, the author states that "the present-day yearly output of lead batteries is 12 million batteries and will increase by 5 million in the near future." These data seem to be strongly overestimated and too optimistic.

The first part of the book (pp. 4–77) contains general evidence concerning lead batteries, description of the electrochemical behavior of the positive and negative electrodes (chs. 1–3), data on the electrolyte and separators (chs. 4, 5), information about design features and basic parameters of various-purpose lead batteries (ch. 6), brief description of the technology of their production (ch. 7), working conditions of lead batteries (chs. 8, 9), and prospects for further development of this kind of secondary power sources (ch. 10). The possibility of improving the performance of batteries is related by the author to application of new lighter materials for fabrication of their separate parts. Such a way to improve batteries as doping of lead-antimony alloys with various elements is only briefly mentioned when discussing the possible impurities in the metallic fraction of lead battery scrap.

The second part of the book (pp. 78–242), which also comprises ten chapters, is devoted to problems of integrated utilization of worked-out lead batteries. The author discusses a wide variety of problems: composition of the battery scrap, its fractionation and reparation for pyrometallurgical processing (chs. 1, 2); utilization of the electrolyte (ch. 3); remelting of the metallic fraction of battery scrap (ch. 4); pyrometallurgical, electrochemical, and hydrometallurgical methods for production of secondary lead (chs. 5–7); refining of raw lead (ch. 8); separation of lead-antimony alloys into components (ch. 9), and methods for production of various salts of lead, red lead, and oxidized lead powder from wastes formed in battery production (ch. 10). A number of critical remarks concerning the second part of the book should be made.

Until recently, a substantial part of studies in processing of lead battery scrap have been performed at Gintsvetmet Institute under general supervision of A.V. Tarasov and A.D. Besser. They suggested and implemented at the Ryaztsvetmet plant (Ryazan) a technological scheme for processing of battery scrap, which is based on soda-free electrosmelting. This technological procedure has been described in quite a number of publications and in the monograph *Metalurgicheskaya pererabotka vtorichnogo svibntso-*

vogo syr'ya (Metallurgical Processing of Secondary Lead-containing Raw Materials) (Tarasov, A.V., Besser, A.D., Mal'tsev, V.I., and Sorokina, V.S., Tarasov, A.V., Ed., Moscow: Gintsvetmet, 2003). Unfortunately, these domestic achievements found no reflection in Khegai's book. There are rather numerous annoying inaccuracies in description of quite a number of technological operations. For examples, discharged electrolyte (sulfuric acid) should in no way be delivered to the apparatus in which desulfation (desulfurization) of the oxide-sulfate fraction of lead battery scrap is carried out with the use of sodium hydroxide or carbonate (Fig. 2.6, p. 101). It is hardly appropriate to describe, in a serious book, the calculation of the amount of soda ash necessary for neutralization of sulfuric acid (p. 107). The description of the express method for determining the content of antimony in alloys with lead is unsatisfactory (p. 129). Figure 2.14 can only illustrate crystallization of a pure component or eutectic mixture. The electrochemical behavior of lead in ionic melts was considered in detail in the monograph *Elektrokhimiya svintsa v ionnykh rasplavakh* (Electrochemistry of Lead in Ionic Melts) (Morachevskii, A.G., Vaisgant, Z.I., and Demidov, A.I., St. Petersburg: Khimya, 1994). Unfortunately, this book failed to draw attention of the author of the book being refereed. Table 2.29 (p. 190) is extremely poorly compiled: all values in it should have been negative. Table 2.32 (p. 193) requires comments. It is unclear what is understood by the degree of interaction.

The author erroneously considers that the method for separation of lead and antimony by introduction of aluminum is new. More than 40 years ago, this method was described in ample detail in the book *Proizvodstvo vtorichnykh tsvetnykh metallov i splavov* (Manufacture of Secondary Nonferrous Metals and Alloys) (Tsyganov, A.S., Moscow: Metallurgizdat, 1961). It should be noted that the method based on interaction of aluminum with antimony dissolved in lead was not considered new in those years, either.

The presence of conclusions (pp. 243–246) in a book that is an industrial-technological publication is hardly at all appropriate. It would be more correct to only make a conclusion containing necessary recommendations. The author pays a considerable attention to description of various apparatus and technological equipment. Not quite successful are those parts of the book in which Khegai employs notions of electrochemistry or chemical thermodynamics. A large body of reference data contained in the book should be used with caution. For example, the melting point of lead(II) chloride is given as 1091°C (p. 86), 495°C (p. 215), and 508 ± 5°C (p. 217). The same thermodynamic function should not be differently named within the same book: isobaric-isothermal potential, free energy, Gibbs energy. Numerous critical remarks can be made concerning the reference list, especially that for the second part of the book, in which there are numerous departures from the commonly accepted rules for reference lists.

The manuscript of the book should have been refereed with closer attention and subjected to better-qualified scientific editing. Khedai's book, and especially its second part, is devoted to a problem that is topical for Russia, but the ways to tackle with this issue, suggested by the author, are rather questionable. Most part of domestic publications of recent years remained out of author's sight. Separate industrial-technological sections of the book may be of interest to engineers and technicians working in manufacture of lead batteries and processing of secondary lead raw materials.

A. G. Morachevskii

ISSN 1070-4272, Russian Journal of Applied Chemistry, 2006, Vol. 79, No. 6, pp. 1044–1045. © Pleiades Publishing, Inc., 2006.
Original Russian Text © A.G. Morachevskii, 2006, published in Zhurnal Prikladnoi Khimii, 2006, Vol. 79, No. 6, pp. 1052–1053.

BOOK REVIEWS

K. K. Kalnin'sh, and L. I. Pavlova, *Voda – rodnik zhizni. Monographiya* (Water, A Spring of Life: Monograph),

St. Petersburg: Inst. Vysokomol. Soedin. Ross. Akad. Nauk, 2005, 293 pp.

DOI: 10.1134/S107042720606036X

The central place in the fascinating monograph written by known scientists, K.K. Kalnin'sh and L.P. Pavlova, is occupied by studies of the fundamental role of water in vital processes. The authors for the first time consider water as a catalyst of biochemical reactions, which can serve to explain, from purely scientific standpoint, many properties of water and to subject to critical analysis various pseudoscientific hypotheses.

The book comprises authors' address to readers, introduction, seven chapters, afterword, and supplement. Each chapter, afterword, and supplement are provided with reference lists. The address to readers notes that such a unique property of water as catalytic activity has been discovered, and a method for its measurement has been developed by one of the authors of the book, Kalnin'sh, during his many-years investigations at the Institute of Macromolecular Compounds, Russian Academy of Sciences, in St. Petersburg. The co-author of the book, Pavlova, studies the catalytic properties of water and performs biological investigations at St. Petersburg State University.

In the introduction (pp. 9–12), the authors describe in a rather condensed form the contents and specific features of the monograph, emphasize that the book presents a new interpretation of both the very notion of chemical catalysis and the catalysis in water as applied to biological enzymatic processes, and note the important role of the electron-proton effect in analysis of catalytic processes. This previously unknown physical phenomenon[1] exceedingly strongly lowers energy barriers and thereby facilitates a complex train of biochemical reactions.

In the small first chapter (pp. 13–23), the authors discuss the exceedingly important role of water in various processes in Earth's biosphere on the basis of works of Academician V.I. Vernadskii (1863–1945). The second chapter (pp. 24–55), devoted to analysis of the relationship between water and living organisms, also pays a considerable attention to works by Vernadskii [*Zhivoe veshchestvo* (Living Substance) (Moscow: Nauka, 1978)], Academician A.I. Oparin (1894–1980) [*Materiya. Zhisn', Intellect* (Matter, Life, Intelligence) (Moscow: Nauka, 1977)], and a number of other scientists (E.S. Bauer, B.P. Tokin). Particular attention is given by the authors to analysis of studies that considered to any extent the involvement of electronically excited states in biological processes.

The third chapter (pp. 56–79) substantiates the novel concept suggested by the authors. According to this concept, water is an active participant and catalyst of biochemical processes, with the catalytic function of water being of a fundamental nature and making possible to asses, from a new standpoint, the role of water in the formation of the biogeosphere of our planet at all stages of its development. The fourth chapter (pp. 80–104) presents the evidence, obtained by the authors by calculation, that water molecules are directly actively involved in the principal bioenergetic process, splitting of the molecule of adenosine triphosphoric acid (ATP).

In the fifth chapter (pp. 105–133), the authors introduce and discuss in detail the notion "activity of water." According to the concepts developed in the monograph, the degree of activity of water is determined by its ability to accelerate or decelerate chemical reactions whose elementary stage involves transfer of an electron and a proton. To reactions of this kind belongs majority of biochemical processes and numerous chemical reactions involving organic substances. In the authors' opinion, the new parameter they suggested for evaluation of the quality of water, activity, is an important characteristic of water of any origin and purpose.

In the sixth chapter (pp. 134–186), Kalnin'sh and Pavlova subject to constructive criticism the concepts of the "information" role played by the struc-

[1] Kalnin'sh is the author of the monograph *Elektronnoe vozbuzhdenie v khimii* (Electronic Excitation in Chemistry) (St. Petersburg, 1998).

ture of water and "memory" of water, and discuss the widely accepted concepts of "alive" and "dead" water. The fluid water having a labile instantaneously rearranging structure cannot serve for writing, storage, and transmission of information. The problem of the "memory" of water and effect on water of various external treatments is considered. In the final part of the chapter, the authors emphasize that water possesses a unique dissolving ability. Dissolved molecules of various chemical compounds affect the shortlived instantaneous structure of water.

The seventh chapter (pp. 187–239) considers facts and hypotheses associated with the medicinal and some other properties attributed to water from various sources or to that subjected to certain treatments. In particular, the medicinal properties and the probable mechanism of action of "silica" and "shungite" water, "alive" and "dead" water produced by electrolysis, and "silver" water are discussed. Special attention is given to properties of thaw water and water subjected to magnetic treatment ("magnetized water"). The authors make an attempt to explain the observed effects in scientific terms, primarily taking into account the concept of catalytic properties of water.

The afterword to the book is entitled "From Myths to Reality," which is rather symbolic. The authors realize that the issue of water is a matter of acute current interest and gives rise to active discussions on pages of popular-science publications and mass media. Frequently, this occurs in the form of incorrect statements and pseudoscientific hypotheses. The desire to distinguish between the myths and reality and to scientifically substantiate the real, verified facts is a notable achievement of the authors.

The supplement to the monograph (pp. 248–292) describes the essence of the electron-proton effect and its role in various physical and chemical processes. It is particularly important for catalysis.

In the book, a vast material is collected and analyzed and rather valuable evidence of practical nature is contained. The monograph is very well written, and a considerable part of the material is presented in a form understandable for a wide audience of readers. Unfortunately, only 600 copies of the book have been printed, and, what is more, the existing system of distribution of the scientific literature is far from being perfect.

A. G. Morachevskii

ISSN 1070-4272, Russian Journal of Applied Chemistry, 2006, Vol. 79, No. 7, pp. 1047–1056. © Pleiades Publishing, Inc., 2006.
Original Russian Text © T. Bauer, M. Schubert, R. Lange, R.Sh. Abiev, 2006, published in Zhurnal Prikladnoi Khimii, 2006, Vol. 79, No. 7, pp. 1057–1066.

REVIEWS

Intensification of Heterogeneous Catalytic Gas–Fluid Interactions in Reactors with a Multichannel Monolithic Catalyst

T. Bauer, M. Schubert, R. Lange, and R. Sh. Abiev

Technical University of Dresden, Dresden, Germany
St. Petersburg State Technological Institute (Technical University), St. Petersburg, Russia

Received January 25, 2006

Abstract—The review discusses the present-day state of research, industrial experience, and prospects for application of reactors with a multichannel catalyst for gas–fluid catalytic reactions.

DOI: 10.1134/S107042720607019

INTRODUCTION

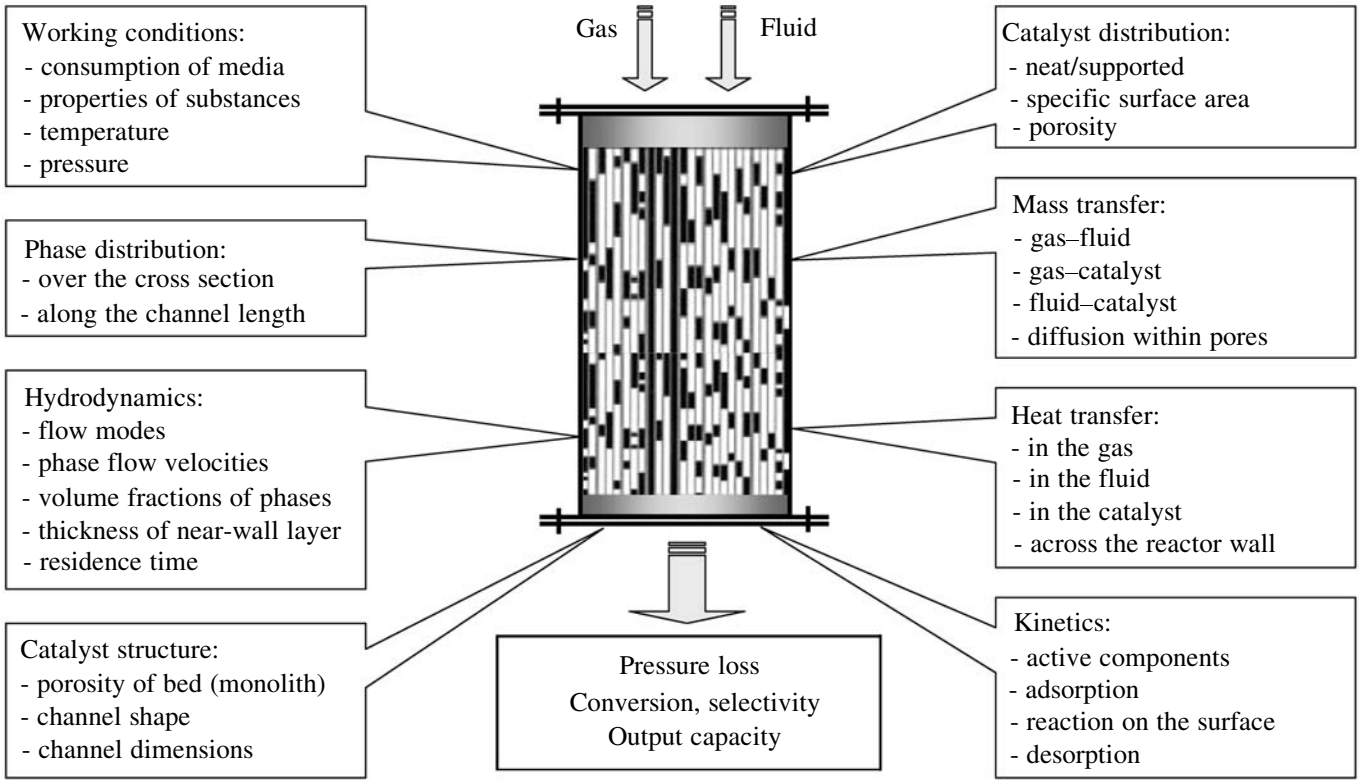
Optimization of the existing chemical processes is one of key requirements put forward by modern industry with the aim to achieve technological efficiency and environmental safety [1, 2]. This problem can be successfully solved by developing new apparatus and processes of chemical industry that would fundamentally improve the efficiency of the processes and save energy. In the technology of multiphase reactions, application of the so-called structured reactors with a "monolithic" (multichannel[1]) catalyst (Monolith reactors) instead of the conventional apparatus, such as reactors with a suspended catalyst or a fixed catalyst bed arranged in a disordered way, is a very promising alternative.

New designs and methods are being developed with the claimed goal of process intensification. Stankiewicz and Moulijn [3] defined this notion as fundamental improvement of an apparatus or a process as regards their scale, energy consumption, and environmental impact. A significant decrease in the dimensions of an installation can lead to additional improvement of the process safety (for example, miniature heat exchangers with a volume of 1 cm^3 and heat-transfer capacity of up to 20 kW and reactors of similar dimensions have already been developed at the Research Center in Karlsruhe, Germany).

Heterogeneous catalytic gas–fluid reactions are performed in numerous petrochemical installations, in manufacture of many materials and substances, in fine chemical technology, in pharmaceutical industry, and in biotechnology. Reactors with impellers, bubbling reactors (including those of airlift type) [4], and reactors with a chaotically arranged (disordered) fixed catalyst bed [5] have found the widest application in hydrogenation, oxidation, and (since recently) biological reactions. The most important requirement in design and operation of these reactors is that a large phase contact area should be provided in order to achieve highly intense mass transfer. An inhomogeneous phase distribution or nonuniform wetting of the catalyst leads to a nonuniform mass transfer, which adversely affects the overall reaction rate and the selectivity of the reaction process. The result is known: loss of product quality, lower output capacity of the reactor, and its poorer safety. Similar phenomena have been observed in an apparatus with a similar hydrodynamic situation, ion-exchange apparatus with a fixed resin bed [6]. The temperature distribution in exothermic reactions could be made more uniform by using a catalyst based on a nickel–aluminum support reinforced with a stainless steel grid [7]. The conventional reactors for the gas–fluid–solid systems are also very difficultly scaled because the flow fields of the fluid and gas, parameters of bubbles, and properties of phases, including the catalyst, are not proportional to the reactor dimensions [8].

In [9], steam conversion of methane with a catalyst of regular structure in the form of a plane-parallel packing was studied. It was shown that, for the given process, the working volume of the apparatus is approximately three times smaller than that of reaction tubes in a Kellogg methane-reforming furnace, which are filled with a granulated catalyst, and two orders

[1] Both the terms, monolithic and multichannel, will be used in this review.



Scheme 1.

of magnitude smaller than the total volume of the furnace.

The review [10] noted the advantages of catalysts with irregularly shaped grains (stars, tubes, tri- and quarterfoils, multichannel tubes, etc.): increased accessible grain surface area, a certain rise in the porosity of the bulk bed, lower hydraulic resistance, higher degree of utilization, and longer service life of a grain. Investigations aimed to develop new catalysts with irregularly shaped grains are being conducted at Yarsintez Research Institute Open Joint-Stock Company.

The processes that occur when carrying out multiphase reactions can be intensified by improving the contact in the gas–fluid–solid system in such a way that the diffusion length becomes shorter (i.e., the fluid film on the catalyst surface becomes thinner) and the agitated volume of the fluid in the reactor decreases. The studies performed in recent years have shown that directed introduction of the fluid phase into catalyst channels having a certain shape can be a successful way to achieve a highly intense and uniform mass transfer. A parallel connection of channels of this kind results in an ordered and structured multichannel (monolithic) catalyst [11]. This catalyst with active components on the channel surface is fixed within the reaction volume. Owing to the regular arrangement of the channels and their identical sizes, a rather simple scaling is possible, because an increase in the flow section and in the active surface area of the catalyst means in the given case that only the number of parallel channels becomes larger. However, an engineering task of developing a reliable device for distribution of the gas and fluid among all the channels remains topical in designing and scaling of apparatus [12].

Having better characteristics of energy consumption, smaller dimensions, and improved safety at an, at a minimum, equal output capacity, reactors with a multichannel catalyst can oust the conventional three-phase reactors [13]. However, the elementary processes occurring in reactors with a multichannel catalyst (Scheme 1) affect one another in a complicated way and have not been completely accounted for as yet. Here we discuss the current state of research and the experience of industrial use of reactors with a multichannel catalyst for gas–fluid catalytic reactions.

1. COMPARISON WITH CONVENTIONAL MULTIPHASE REACTORS

Catalytic gas–fluid reactions are performed in reactors with impellers, whose design has not changed

significantly until now. The hydrodynamic and agitation processes in these reactors are exceedingly complex and, despite the considerable efforts made by researchers, are still difficult to describe. Neither rigid inserts in the form of reflecting partitions, nor the improved design of impellers can completely eliminate the problem of the quality of agitation. Noninvasive (i.e., not affecting a system under study) studies of the hydrodynamics of apparatus with impellers, performed using radioactive tracers (Computer-Automated Radioactive Particle Tracking, CARPT), revealed a great difference in velocities within each phase, inhomogeneous distribution of the gas and fluid phases, strongly limited nature of circulation zones, and presence of stagnant zones [14]. As the reactor volume increases, these agitation-related problems become more severe.

Many chemical processes employ bubble columns. Their significant advantage over apparatus with impellers is the possibility of working at a high content of the solid phase, commonly up to 30 vol %. However, similar problems associated with the phase distribution and with achieving a large specific area of contact between phases arise in bubble columns. Density measurements by computer tomography with γ-radiation revealed that the gas content decreases in the direction from the reactor axis toward its walls [15].

Despite the use of the most recent measurement techniques and modern software for flow simulation by the method of finite elements (Computational Fluid Dynamics, CFD), complex processes of mixing in reactors with a suspended catalyst have not been fully described so far.

A possible alternative to apparatus of the above kind are reactors with disordered packing with the catalyst: trickle-bed reactors with upflowing gas and downflowing fluid (Rieselbettreaktoren) and upflow packed-bed reactors (Sumpfphasenreaktoren). The reactors with disordered packing with a catalyst are mostly used in petrochemistry to perform reactions that involve hydrogen. The reactors with a fixed catalyst bed are not sufficiently versatile as regards a change of a catalyst or product, but show a comparatively low production expenditure. Because of the incomplete wetting of the catalyst surface, difficulties associated with the optimal utilization of the catalyst and heat removal in the case of exothermic reactions may be encountered in reactors with disordered packing, which is indicated by tomographic studies [16, 17].

Reactors with a multichannel (monolithic) catalyst have a number of decisive fundamental advantages over the conventional multiphase reactors. Compared with reactors with a fixed bed, they have a very low hydraulic resistance, large specific surface area, and virtually full wetting of the catalyst surface. Compared with reactors with a suspended catalyst, reactors with a monolithic catalyst show high mechanical strength of the catalyst and rule out any possibility of crushing and carry-over of the expensive catalyst. The studies performed by the time of publication of this review revealed advantages of reactors with a multichannel catalyst in mass-transfer, selectivity, and output capacity [18–21]. The rise in output capacity is primarily due to a closer contact between the gas, fluid, and solid phases within the ordered monolithic multichannel structure and to a shorter diffusion length across the thin phase boundary [22].

It should be noted that no direct experimental comparison of the output capacities of the reactors with an appropriate comparison criterion has been carried out so far. An integral characteristic of the output capacity at the appropriate working parameters typical of each kind of apparatus could serve as a criterion of this kind. Analysis of the economical efficiency with account of energy expenditure and installation cost could supplement such a comparison and thereby reveal the reasonable fields of application of new catalysts.

2. FUNDAMENTAL ASPECTS OF REACTORS WITH A MULTICHANNEL (MONOLITHIC) CATALYST

2.1. Manufacture and materials. The monolithic catalysts have a cellular structure constituted by a large number of parallel, regularly arranged, and separated channels. The most important characteristics of the multichannel catalysts are cell density (number of channels per unit area of the apparatus cross section), hydraulic diameter of a channel, porosity of the cross section (fraction of a free cross section), and partition strength [23].

The catalyst support is prepared by extrusion of a forming paste with the subsequent drying and sintering or by rolling over corrugated metallic sheets. The monolith may be wholly composed of the active component, or this component is deposited onto a ceramic forming paste. Both methods yield a solid catalyst with a very high degree of saturation with the active component.

The most frequently used method is coating of a ceramic skeleton with a supporting substance making

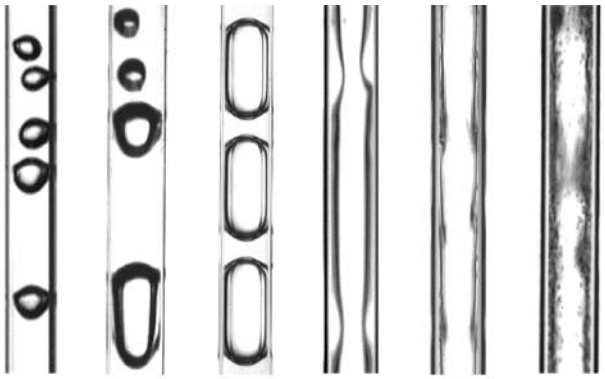


Fig. 1. Flow modes in a square-cross-section capillary with a hydraulic diameter of 1.0 mm [26]. Flow: (a) bubble mode, (b) transition from bubble to slug mode, (c) slug mode, (d) transition from slug to film mode, (e) film mode, and (f) "explosive" emulsion mode.

larger the specific surface area (washcoat). Typical supporting materials are aluminum oxide, aluminum silicate, silicic acids, and carbon. A supporting material can be deposited by introducing it into the porous structure of the ceramic skeleton or by creating a thin coating layer on the ceramic skeleton. The active components (Pt, Pd, etc.) can be introduced into the fine structure by impregnation, ion exchange, or precipitation [24].

The general requirement to a method for coating deposition is that it should yield a large and uniform specific surface area, strong binding of all the components, and homogeneous distribution of the catalytically active components within the monolith or on its surface. In view of the large longitudinal dimensions and the structure of the monolithic bodies, their coating with the active components is a more complicated task than that in the case of the conventional forms of the catalyst.

Use of catalyst-coated supports is recommended for reactions that occur at a high rate with a comparatively slow mass transfer (i.e., diffusion-controlled reactions). The integral characteristic of the output capacity of a catalyst, the overall performance, depends in this case on the specific surface area and, to a lesser extent, on the amount of the catalyst. At a comparatively low reaction rate (i.e., for kinetically controlled reactions), a neat monolithic catalyst [e.g., activated carbon or iron(III) oxide] should be used. The catalyst may be wholly composed of the active component, or this component is homogeneously distributed in the ceramic skeleton.

2.2. Hydrodynamics. The hydrodynamics strongly affects the mass and heat transfer in multiphase processes and thereby largely determines the output capacity of reaction apparatus. Of particular importance is the intense contact of the phases with one another and with the solid catalyst. As regards the reaction technology, preference should be given to large phase contact areas and to as thin as possible boundary layers. In multiphase systems, these parameters are directly or indirectly related to hydrodynamic parameters of the flow mode, fraction of phases, film thickness, quality of catalyst wetting, residence time, dispersion, and pressure loss. A detailed knowledge of these parameters is necessary for deep understanding of the working principles of these reactors and their putting into industrial practice [25].

The hydrodynamics of reactors with a multichannel catalyst is governed by the flow mode of the gas–fluid medium in separate channels. The flow modes of the gas–fluid medium in narrow channels depend on the flow section, catalyst material, and channel properties (Fig. 1). Until now, of particular interest for the reaction technology have been the slug and film flow modes in multichannel catalysts. The slug flow is characterized by sequence of elongated gas bubbles and fluid drops along the channel. In this flow mode, the ratio of flow rates of the gas and fluid varies from 0.2 to 2.0. As regards the reactor technology, the advantages of the slug mode are the very small thickness of a fluid film between the cylindrical part of gas bubbles and the porous catalyst wall and the uniform agitation within each fluid drop (the later is determined by the Taylor diffusion).

At very low fluid flow velocities (<0.01 m s^{-1}), a transition to a film flow may occur in the case of a downflow in narrow channels. In this mode, the gas phase flows in the same direction as the fluid or is oppositely directed. The film flow mode is of particular interest if a large conversion (related to the fluid flow rate) should be achieved or the process requires a counterflow of the phases, as, e.g., in reactive evaporation in stripping columns.

An important criterion of reliable and adequate description and calculation of reactors is the homogeneous distribution of the fluid and gas, because approximately the same conditions and stable flow modes occur in all the channels. However, such optimal working conditions are difficult to achieve in practice. A study of the gas and fluid distribution along the flow direction by NMR tomography [27] demonstrated that there is a clearly pronounced difference in gas distribution between the channels. Also, the bubble sizes within separate channels are strongly different, so that a nonuniform bubble distribution can

be inferred. Similar results characterizing an inhomogeneous phase distribution have been obtained in studies of the fluid and gas distribution over the cross section of a monolithic catalyst by capacitance tomography [28] and γ-ray computer tomography [29]. It was stated in these publications that, depending on the distribution of the fluid and gas and on the phase flow rate, various contents of the phases both over the cross section and along the reactor axis can be obtained. This suggests that each of the distributing systems can operate in the optimal mode only at certain phase flow rates.

The following distributing devices have demonstrated good performance in experimental practice: spraying nozzles [30] and ejectors [31] for the downflow of gas–fluid systems and static mixers [32] for the upflow.

For better understanding of the fundamental aspects of flow within monolithic reactors, studies in glass capillaries of round and square cross sections, in which any influence of the uniformity of phase distribution is excluded, have been carried out. Examples of the flows formed in this case and the transition regions were obtained by photographing and video recording and then analyzed as regards the type of flow, distribution and flow velocity of phases, phase boundaries, etc. [33, 34]. These experimental data are used for precise determination of the corresponding model parameters, which should be taken into account in the mathematical model of the reactor (mostly in mass and energy balance equations).

It should be noted that most part of the studies have been performed in the water–air system under atmospheric conditions in glass capillaries of round cross section. It seems hardly probable that the data obtained and correlation equations can describe with sufficient accuracy the predominant industrial conditions. That is why two-phase flows in the so-called mini channels (with a hydraulic diameter of about 1 mm) are being intensively studied at the Institute of Process Engineering and Environmental Technology, Technical University of Dresden (Institut für Verfahrenstechnik und Umwelttechnik der TU Dresden) with account of the real industrial conditions and material systems.

2.3. Mass transfer. A distinctive feature of monolithic reactors is that they exhibit improved mass-transfer characteristics, compared to those having an irregular filling with a fixed catalyst. An advantageous mode in this case is the so-called slug (piston) flow constituted by a sequence of gas bubbles and fluid drops. As shown in Fig. 2, the flow mode characteristically involves three stages of mass transfer: (i) at the gas–fluid interface, from the semispherical nose of a bubble and from its end part into the fluid; (ii) at the gas–solid interface, from the cylindrical part of a bubble across a thin fluid film to the catalyst; and (iii) from the fluid itself and from the gas dissolved in the fluid to the catalyst at the fluid–solid interface. In addition, the reagents should also diffuse into the catalyst pores to the active centers. Particularly high rates of mass transfer are achieved in the case of the piston flow owing to the circulation currents within fluid drops and to the small thickness of the fluid film between the gas bubble and the catalyst. In this case, the mass transfer is a very complex process largely determined by the gas and fluid flow velocities, bubble length, and fluid film thickness.

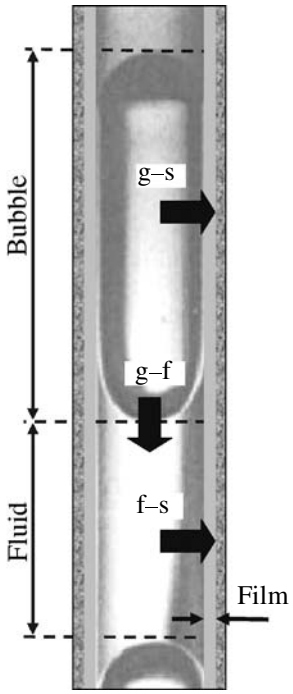


Fig. 2. Stages of mass transfer in unit cells: gas–catalyst (g–s), gas–fluid (g–f), and fluid–catalyst (f–s). Characteristic hydrodynamic dimensions: fluid drop length, bubble length, and fluid film thickness.

At very low fluid flow rates and a hydraulic channel diameter exceeding 2.0 mm, a film-type flow occurs. In this mode, an exceedingly long residence time of liquid reagents in the reactor and a high ratio of gas and fluid flow rates can be achieved.

Theoretical analysis demonstrated that mass transfer is improved as the fluid flow velocity decreases. The effect of the fluid flow velocity is more pronounced in the piston mode, compared to the film

flow. The reason is that the film thickness decreases, which leads to a significant improvement of the mass transfer. Another advantage of low fluid flow velocities is that, in this case, the pressure loss is small.

To exclude any influence of the nonuniformity of distribution among the catalyst channels and to set the necessary hydrodynamic parameters, mass transfer is frequently studied in glass capillaries of round or square cross section [35, 36]. However, the adequacy and applicability of the results obtained in this case seem to be questionable for the following two reasons. First, the occurrence of a certain flow mode is strongly affected by the system of gas and fluid distribution, so that different experimental capillary setups give markedly dissimilar results. Second, in monolithic (multichannel) structures there exist, as described in the section devoted to hydrodynamics, such distributions of gas bubbles and fluid drops which can hardly be reproduced in experiments performed in capillaries. The existing correlations on mass transfer are not dimensionless and require that the bubble and drop lengths should be known. Hence follows that evaluation of mass-transfer characteristics in monolithic reactors is a very complicated task, and experimental and theoretical studies should be performed to resolve this issue.

The mathematical models of two-phase flows can be further improved using the results obtained in [37–39]. It seems appropriate to develop mathematical models that would describe phase distribution among monolith channels and formation of bubbles and drops in capillaries.

2.4. Application fields. Monolithic catalysts were originally developed for use in reactions in gas–solid systems to treat automobile exhaust fumes. These catalysts have also been successfully used in processing of industrial gases (e.g., in power engineering), in selective catalytic reduction of NO_x, and in catalytic combustion systems. The widely diverse application fields of monolithic catalysts in the reaction technology of gas–solid systems have been reviewed by Heck et al. [40].

In the 1980s, studies of the applicability of monolithic catalysts in heterogeneous catalytic processes in the gas–solid system were commenced. The first of these were carried out at the Chalmers Technical University (Sweden). The hydrogenation of nitroaromatic compounds [41, 42], 2-ethylhexenal [43], anthraquinone [44], acetylene, thiophene, and dibenzothiophene [45] was examined.

Based on these data, Eka Chemicals Company developed the so-called anthraquinone process for manufacture of hydrogen peroxide using monolithic catalysts. At present, Akzo Nobel Company successfully employs numerous large-scale installations of this kind all over the world [46].

In recent years, extensive studies, both fundamental and those oriented toward industrial application of monolithic catalysts in multiphase reactions, have been carried out at the Delft University of Technology (the Netherlands). The hydrogenation of styrene [47], α-methylstyrene [48], benzaldehyde [49], and 3-methyl-1-pentyn-3-ol [50] has been studied on a pilot installation. In addition, cyclohexanone has been oxidized in a monolithic reactor [51]. It has been shown, when examining the Fischer–Tropsch synthesis, that monolithic reactors may become a good alternative to the conventional types of multiphase reactors, with the requirements of a high selectivity, low pressure loss, and good heat removal, etc., satisfied [52].

At the University of Tulsa (the United States), "wet" oxidation of acetic acid [53] and glucose and cellulose [54] has been performed in an upflow monolithic reactor, and various substances have been manufactured from cellulose and biomass [55].

A research group from the University of Birmingham (the United Kingdom) studied the hydrogenation of 2-butene-1,4-diol in a downflow monolithic reactor [56].

Recently, Air Products and Chemicals Inc. developed, together with a catalyst manufacturer Johnson Matthey Company, a technique for manufacture of monolithic catalysts for fine chemical technology. In this connection, Air Products and Chemicals Inc. designed a pilot monolithic reactor. The same company has successfully tested hydrogenation of nitroaromatic compounds [57] and sorbitol [58].

Corning Inc. has tested hydrogenation of vegetable oil in a monolithic reactor [59] and hydrogenation of alkenes in a monolithic channel with various configurations [60, 61].

The number of studies devoted to the potentialities of monolithic reactors in biological conversion of substances is growing. Airlift reactors have been used to study the biological decomposition of 2,4-dichlorophenol with immobilized cells of *Achromobacter sp.* [62] and that of quinoline with *Burkholderia pickttii* bacteria [63]. Recently, the formation of a biological film in monoliths has been studied experimentally and theoretically [64].

Selected applications of monolithic reactors

Reaction	Active component, support	Direction of flows	References
Hydrogenation of anthraquinone	Silica gel	Downwards	[44]
Hydrogenation of α-methylstyrene	1.8 wt % Pd, γ-Al_2O_3	Downwards	[48]
Oxidation of cyclohexanone	Carbon	Downwards	[51]
Oxidation of glucose and cellulose	0.26 wt % Pt, Al_2O_3	Upwards	[54]
Hydrogenation of 2-butene-1,4-diol	1.0 wt % Pd, α-Al_2O_3	Downwards	[56]
Hydrogenation of nitroaromatic compounds	Co–Mo, γ-Al_2O_3	Downwards	[57]
Hydrogenation of vegetable oils	2.0 wt % Pd	Downwards	[59]
Biological decomposition of quinoline	*Burkholderia pickttii*	Upwards	[63]

Monoliths have been tested in numerous application fields of reactors (see table). As follows from the data presented, monolithic reactors find use in fast reactions, e.g., in hydrogenation and oxidation. Together with having high output capacity and selectivity, reactors of this kind possess one more advantage of being compatible with other basic processes. For example, monoliths can be used for the reaction process of pressure flotation (Strippen) [65] and reactive distillation [66, 67]. One more application opportunity of interest is combination of a chemical reaction with agitation in a monolithic reactor [68], in which the conventional mixer is replaced with a monolith. The advantage of such a mixer is that the catalyst is fixed within the reaction shell, which saves the catalyst by preventing its carry-over.

Another interesting way to intensify chemical processes with monolithic reactors is the so-called built-in monolithic reactor [69]. In this reactor design, delivering reagents via pipes to other apparatus of the process scheme can be combined with performing a chemical reaction. A simulation of the reactor, carried out by DSM Research Company, demonstrated that use of this reactor can lead to a significant decrease in the installation dimensions. Irrespective of the reactor configuration, the possibility of application of the new types of reactors has been so far studied only at moderate loads. To extend the applicability range, the Institute of Process Engineering and Environmental Technology, Technical University of Dresden (Germany) has developed, in cooperation with Sigmar Mothes Hochdrucktechnik Company, an installation for study of multiphase reactions in reactors with a fixed bed at pressures of up to 100 bar.

3. PRACTICAL CONCLUSIONS

The possibility of independent variation of the dimensions and shape of channels and of the wall thickness in order to satisfy requirements imposed by various multiphase processes is an important advantage in performing the optimal design of monolithic reactors. The conventional monolithic reactors, such as, e.g., trickled-bed reactors (Rieselbettreaktoren) and upflow packed-bed reactors (Sumpfphasenreaktoren), have a lesser number of degrees of freedom.

In monolithic reactors, the efficiency of interaction in the gas–fluid–solid system and the concentration of reagents in the fluid film are directly determined by the structure of the monolith (square, triangular, rounded, etc.). In this case, the shape of the channel predetermines the uniformity of fluid distribution over the catalyst surface. It has been shown that no stagnant zones are formed in rounded channels and a high rate of mass transfer is achieved because of the small thickness of the film on the catalyst surface [60]. Development of new techniques for coating of predominantly square monolith channels to make them rounded would be an important stage in further improvement of their efficiency.

Gas–fluid flows in separate mini channels can be regarded as approximately independent of the flow direction. At comparatively high phase flow velocities, the hydrodynamic situation in monolithic reactors is also the same throughout a reactor. At low phase flow velocities, the distribution of the gas and fluid over the cross section of a bed in an upward flow occurs with certain difficulties and, in the case of a nonuniform distribution, may adversely affect the output capacity of a reactor. It should be added here that studies of reactions revealed a higher output capacity in the upflow [61].

Monolithic reactors can find use in industrial practice in the following way: (1) by replacing the fixed grained bed in the existing reactors with a monolithic catalyst, (2) by supplementing the design of the existing reactors with an additional monolithic reactor, and (3) by creating separate monolithic reactors. Presum-

ably, the first way can only be followed with strong limitations. The main obstacle is that the loads by the gas and fluid are different. The slug flow with intense mass transfer requires that the fluid flow velocity should be comparatively high (no less than 0.1 m s^{-1}), whereas trickle-bed reactors operate at a velocity of about 0.01 m s^{-1}. In the case of hydrogenation reactions requiring an excess of hydrogen, the slug flow mode can hardly be used, since an insufficient amount of hydrogen may be present in the mixture because of the small gas/fluid flow rate ratio. This flow mode is advantageous if the component being hydrogenated has a low concentration and a high process selectivity should be achieved.

Another interesting application opportunity furnished by the good mass-transfer characteristics of the monolithic reactor is associated with catalytic reactions in fluid–fluid and gas–fluid–fluid systems with two mutually insoluble fluids. Operation of the reactor in the film mode, which is similar to the trickle mode in a reactor with a fixed grained bed, could be its additional possible application. However, the problems of film flow have been studied by only few researchers. Moreover, a uniform distribution of the gas and fluid over the cross section of the monolith is much more difficult to be achieved in this mode [30]. Replacement of the grained catalyst with a monolithic one requires a new organization of the process.

Monolithic reactors may become an efficient supplement to reactors with a suspended catalyst, whose life in the industrial practice was short. Thus, a monolithic catalyst can replace the suspended one. The necessary additional equipment may have the form of a reactor with a fixed bed (monolith) or an impeller with monoliths fixed on it, or a reactor with a differential circulation contour (reactor with a fixed catalyst bed and recycled liquid components) [70]. An additional advantage in this case is that a catalyst can be rapidly replaced, which is particularly important at a short operation cycle characteristic of, e.g., pharmaceutical industry. This concept allows a simple reconstruction of the existing reactors with a suspended catalyst, which leads to an economically efficient increase in the output capacity of the existing production facilities and to a predictable financial risk: replacement of a suspended catalyst in a reactor with an external monolith can diminish the reconstruction expenditure even at a preserved output capacity.

4. CONCLUSION

The results of studies published before August 2005 suggest that monolithic reactors can find wide application. However, numerous fine processes mentioned in the review are rather complex and insufficiently understood, which hinders optimization of this kind of reactors. It was also demonstrated that, as regards processes intensification, the monolithic reactor is rather promising because it has a high output capacity, high selectivity, low pressure loss, and a number of design advantages over the conventional types of multiphase reactors. It should be admitted that, at present, there is deficiency of data obtained on semicommercial installations, which could open up new application fields. This is mostly due to the excess output capacity of the existing large installations and insufficient preparedness of industrial managers to take a certain risk. It can be predicted with confidence that monolithic reactors can very soon be successfully used in manufacture of expensive products in fine chemical technology and pharmaceutics, where the production process is small-tonnage and can be readily reconstructed. Long-term planning should be oriented to use of these reactors also in the Fischer–Tropsch synthesis for manufacture of synthetic fuels from natural gas, as well as in the presently evolving biotechnology, in which new methods of deep substance conversion will be developed.

ACKNOWLEDGMENTS

The authors thank the Rossendorf Research Center (Forschungszentrum Rossendorf) for the support of videographic studies of the two-phase flow in capillaries, Corning Inc. for provision of monoliths in connection with an interesting technical discussion, and Prof. Dr. Muthanna Al-Dahhan and Dr. Shaibal Roy from Washington University in St. Louis for helpful discussion in the course of preparation of this review.

REFERENCES

1. Kuhling, S., Laue, S., Grunert, W., et al., *Nachr. Chem*., 2003, vol. 51, no. 3, pp. 352–357.
2. Kardashev, G.A., *Fizicheskie metody intensifikatsii protsessov khimicheskoi tekhnologii* (Physical Methods for Intensification of Processes of Chemical Technology), Moscow: Khimiya, 1990.
3. Stankiewicz, A.I. and Moulijn, J.A., *Chem. Eng. Prog*., 2000, vol. 96, no. 1, p. 22.
4. Sokolov, V.N. and Domanskii, I.V., *Gazozhidkostnye reaktory* (Gas–Fluid Reactors), Leningrad: Mashinostroenie, 1976.
5. Ioffe, I.I. and Pis'men, L.M., *Inzhenernaya khimiya geterogennogo kataliza* (Engineering Chemistry of Heterogeneous Catalysis), Leningrad: Khimiya, 1972.

6. Ostrovskii, G.M. and Brisovskii, I., *Teor. Osn. Khim. Tekhnol.*, 1999, vol. 33, no. 3, pp. 247–251.
7. Danilova, M.M., Kuzin, N.A., Kirillov, V.A., et al., *Zh. Prikl. Khim.*, 2002, vol. 43, no. 6, pp. 893–901.
8. Stitt, E.H., *Chem. Eng. J.*, 2002, vol. 90, nos. 1–2, pp. 47–60.
9. Voskresenskii, N.M., Bel'nov, V.K., Serdyukov, S.I., and Safonov, M.S., *Teor. Osn. Khim. Tekhnol.*, 2002, vol. 36, no. 2, pp. 189–194.
10. Kotel'nikov, G.R. and Kachalov, D.V., *Kinet. Katal.*, 2001, vol. 42, no. 5, pp. 790–798.
11. Roy, S., Bauer, T., Al-Dahhan, M., et al., *Am. Inst. Chem. Eng. J.*, 2004, vol. 50, no. 11, p. 2918.
12. Bauer, T., Roy, S., Al-Dahhan, M., and Lange, R., *Chem.-Ing.-Tech.*, 2004, vol. 76, no. 9, p. 1296.
13. Kapteijn, F., Nijhuis, T.A., Heiszwolf, J.J., and Moulijn, J.A., *Catal. Today*, 2001, vol. 66, nos. 2–4, p. 133.
14. Rammohan, A.R., Kemoun, A., Al-Dahhan, M., and Dudukovic, M.R., *Chem. Eng. Res. Des.*, 2001, vol. 79, no. A8, pp. 831–844.
15. Chen, J., Gupta, P., Degaleesan, S., et al., *Flow Meas. Instr.*, 1998, vol. 9, no. 2, pp. 91–101.
16. Pokusaev, B.G., Karlov, S.P., and Shreiber, I., *Teor. Osn. Khim. Tekhnol.*, 2004, vol. 38, no. 1, pp. 3–8.
17. Pokusaev, B.G., Kazenin, D.A., and Karlov, S.P., *Teor. Osn. Khim. Tekhnol.*, 2004, vol. 38, no. 6, pp. 595–603.
18. Edvinsson, R.K. and Cybulski, A., *Catal. Today*, 1995, vol. 24, nos. 1–2, p. 173.
19. Cybulski, A., Stankiewicz, A., Albers, R.K.E., and Moulijn, J.A., *Chem. Eng. Sci.*, 1999, vol. 54, nos. 13–14, p. 2351.
20. Nijhuis, T.A., Dautzenberg, F.M., and Moulijn, J.A., *Chem. Eng. Sci.*, 2003, vol. 58, no. 7, p. 1113.
21. Bauer, T., Guettel, R., Roy, S., et al., *Chem. Eng. Res. Des.*, 2005, vol. 83, no. A7, p. 811.
22. Liu, W., *Am. Inst. Chem. Eng. J.*, 2002, vol. 48, no. 7, p. 1519.
23. Cybulski, A. and Moulijn, J.A., *Structured Catalysts and Reactors*, New York: Marcel Dekker, 1998.
24. Nijhuis, T.A., Beers, A.E.W., Vergunst, T., et al., *Catal. Rev. Sci. Eng.*, 2001, vol. 43, no. 4, p. 345–380.
25. Dudukovic, M.P., Larachi, F., and Mills, P.L., *Catal. Rev. Sci. Eng.*, 2002, vol. 44, no. 1, pp. 123–246.
26. Bauer, T., Hillert, S., and Lange, R., *XXXVII. Jahrestreffen Dt. Katalytiker*, Weimar, März 2004, poster.
27. Mantle, M.D., Sederman, A.J., Gladden, L.F., et al., *J. Am. Inst. Chem. Eng.*, 2002, vol. 48, no. 4, pp. 909–912.
28. Mewes, D., Loser, T., and Millies, M., *Chem. Eng. Sci.*, 1999, vol. 54, no. 21, pp. 4729–4747.
29. Bauer, T., Roy, S., Lange, R., and Al-Dahhan, M., *Chem. Eng. Sci.*, 2005, vol. 60, no. 11, pp. 3101–3106.
30. Heibel, A.K., Vergeldf, F.J., As, H. van, et al., *Am. Inst. Chem. Eng. J.*, 2003, vol. 49, no. 12, pp. 3007–3017.
31. Broekhuis, R.R., Machado, R.M., and Nordquist, A.F., *Catal. Today*, 2001, vol. 69, nos. 1–4, pp. 87–93.
32. US Patent Appl. 2003049185.
33. Reinecke, N. and Mewes, D., *Int. J. Multiphase Flow*, 1999, vol. 25, nos. 6–7, pp. 1373–1393.
34. Triplett, K.A., Ghiaasiaan, S.M., Abdel-Khalik, S.I., and Sadowski, D.L., *Int. J. Multiphase Flow*, 1999, vol. 25, no. 3, pp. 377–394.
35. Bercic, G. and Pintar, A., *Chem. Eng. Sci.*, 1997, vol. 52, no. 2122, pp. 3709–3719.
36. Vandu, C.O., Liu, H., and Krishna, R., *Chem. Eng. Sci.*, 2005, vol. 60, no. 22, pp. 6430–6437.
37. Okhotskii, V.B., *Teor. Osn. Khim. Tekhnol.*, 2001, vol. 35, no. 5, pp. 540–542.
38. Pokusaev, B.G., Zaitsev, A.A., and Zaitsev, V.A., *Teor. Osn. Khim. Tekhnol.*, 1999, vol. 33, no. 6, pp. 595–607.
39. Nakoryakov, V.E., Pokusaev, B.G., Petukhov, A.V., and Fominykh, A.V., *Inzh.-Fiz. Zh.*, 1985, vol. 48, no. 4, pp. 533–538.
40. Heck, R.M., Gulati, S., and Farrauto, R.J., *Chem. Eng. J.*, 2001, vol. 82, nos. 1–3, pp. 149–156.
41. Hatziantoniou, V. and Andersson, B., *Ind. Eng. Chem. Fundam.*, 1984, vol. 23, no. 1, pp. 82–88.
42. Hatziantoniou, V., Andersson, B., Larsson, T., et al., *Ind. Eng. Chem. Process Des. Dev.*, 1986, vol. 25, no. 4, pp. 964–970.
43. Irandoust, S. and Andersson, B., *Chem. Eng. Sci.*, 1988, vol. 43, no. 8, pp. 1983–1988.
44. Irandoust, S., Andersson, B., Bengtsson, E., and Siverstroem, M., *Ind. Eng. Chem. Res.*, 1989, vol. 28, no. 10, pp. 1489–1493.
45. Edvinsson, R. and Irandoust, S., *Ind. Eng. Chem. Res.*, 1993, vol. 32, no. 2, pp. 391–395.
46. Albers, R.E., Nystrom, M., Siverstrom, M., et al., *Catal. Today*, 2001, vol. 69, nos. 1–4, pp. 247–254.
47. Smits, H.A., Stankiewicz, A., Glasz, W.Z., et al., *Chem. Eng. Sci.*, 1996, vol. 51, no. 11, pp. 3019–3025.
48. Kreutzer, M.T., Du, P., Heiszwolf, J.J., et al., *Chem. Eng. Sci.*, 2001, vol. 56, nos. 21–22, pp. 6015–6023.
49. Nijhuis, T.A., Kreutzer, M.T., and Romijn, A.C.J., *Catal. Today*, 2001, vol. 66, nos. 2–4, pp. 157–165.

50. Nijhuis, T.A., Koten, G. van, and Moulijn, J.A., *Appl. Catal. A*, 2003, vol. 238, no. 2, pp. 259–271.
51. Crezee, E., Barendregt, A., Kapteijn, F., and Moulijn, J.A., *Catal. Today*, 2001, vol. 69, nos. 1–4, pp. 283–290.
52. Deugd, R.M. de, Kapteijn, F., and Moulijn, J.A., *Catal. Today*, 2003, nos. 79–80, pp. 495–501.
53. Klinghoffer, A.A., Cerro, R.L., and Abraham, M.A., *Catal. Today*, 1998, vol. 40, no. 1, pp. 59–71.
54. Pattrick, T.A. and Abraham, M.A., *Environ. Sci. Techol.*, 2000, no. 34, p. 3480.
55. Schutt, B.D., Serrano, B., Cerro, R.L., and Abraham, M.A., *Biomass Bioenergy*, 2002, vol. 22, no. 5, pp. 365–375.
56. Winterbottom, J.M., Marwan, H., Stitt, E.H., and Natividad, R., *Catal. Today*, 2003, vols. 79–80, p. 391.
57. US Patent 6 005 143.
58. Broekhuis, R.R., Budhlall, B.M., and Nordquist, A.F., *Ind. Eng. Chem. Res.*, 2004, vol. 43, no. 17, p. 5146.
59. Boger, T., Zieverink, M.M.P., Kreutzer, M.T., et al., *Ind. Eng. Chem. Res.*, 2004, vol. 43, no. 10, pp. 2337–2344.
60. Liu, W. and Roy, S., *Chem. Eng. Sci.*, 2004, vol. 59, nos. 22–23, pp. 4927–939.
61. Liu, W., Roy, S., and Fu, X., *Am. Inst. Chem. Eng. J.*, 2005, vol. 51, no. 8, pp. 2285–2297.
62. Quan, X., Shi, H., Zhang, Y., et al., *Process Biochem.*, 2003, vol. 38, no. 11, pp. 1545–1551.
63. Zhang, Y., Han, L., Wang, J., et al., *Biochem. Eng. J.*, 2002, vol. 11, nos. 2–3, pp. 149–157.
64. Ebrahimi, S., Picioreanu, C., and Xavier, J.B., *Catal. Today*, 2005, vol. 105, pp. 448–454.
65. Schildhauer, T.J., Kapteijn, F., and Moulijn, J.A., *Chem. Eng. Process*, 2005, vol. 44, no. 6, pp. 695–699.
66. US Patent 5 235 102.
67. US Patent Appl. 2 003 012 711.
68. Hoek, I., Nijhuis, T.A., Stankiewicz, A.I., and Moulijn, J.A., *Chem. Eng. Sci.*, 2004, vol. 59, nos. 22–23, pp. 4975–4981.
69. Stankiewicz, A., *Chem. Eng. Sci.*, 2001, vol. 56, no. 2, pp. 359–364.
70. Boger, T., Heibel, A.K., and Sorensen, C.M., *Ind. Eng. Chem. Res.*, 2004, vol. 43, no. 16, pp. 4602–4611.

ISSN 1070-4272, Russian Journal of Applied Chemistry, 2006, Vol. 79, No. 7, pp. 1057–1061. © Pleiades Publishing, Inc., 2006.
Original Russian Text © L.V. Morozova, A.E. Lapshin, I.A. Drozdova, 2006, published in Zhurnal Prikladnoi Khimii, 2006, Vol. 79, No. 7, pp. 1067–1071.

INORGANIC SYNTHESIS AND INDUSTRIAL INORGANIC CHEMISTRY

Effect of Mechanochemical Activation on the Synthesis and Sintering of Solid Solutions Based on ZrO_2

L. V. Morozova, A. E. Lapshin, and I. A. Drozdova

Grebenshchikov Institute of Silicate Chemistry, Russian Academy of Sciences, St. Petersburg, Russia

Received December 19, 2005; in final form, April 2006

Abstract—The effect of mechanochemical activation on the synthesis of tetragonal solid solutions in the systems ZrO_2–Y_2O_3 and ZrO_2–Y_2O_3–CeO_2 and also the possibility of preparing the substances in amorphous and nanocrystalline states were studied.

DOI: 10.1134/S1070427206070020

Achievements of the last decade in the field of ceramics processing and sintering theory clearly show that the possibilities for the development of new ceramic materials based on oxides and their compounds are far from being exhausted. Presently there is an increased interest in ultradispersed powders (particle size up to 150 nm) in the processing of structural ceramics, caused by their high activity allowing compact products to be obtained at relativelly low sintering temperatures (1400°C).

Structural ceramics based on partially stabilized zirconium dioxide belongs to new advanced kinds of ceramics with a unique combination of properties: high melting point, reagent and corrosion resistance, high hardness and strength, resistance to thermal shock, and low thermal conductivity [1].

To obtain ultradispersed powders, precursors of stabilized zirconium dioxide, chemical methods of synthesis (coprecipitation [2–5], decomposition of solutions by evaporation [6, 7], and the sol–gel method [8–10]) are widely used.

The sol–gel method and chemical precipitation make it possible to synthesize nanopowders (3–5 nm) of stabilized ZrO_2; however, these methods are rather labor- and time-consuming; they and also require special research and a choice of optimal conditions for each particular system. Such powders tend to form many-particle agglomerates negatively affecting the densification in the course of compaction and sintering of ceramic materials.

At present the method of mechanochemical activation (MA) is used to accelerate syntheses of solid solutions and compounds in oxide systems, and also to prepare ultradispersed powders. This method is highly competitive with liquid-phase synthetic methods and allows chemical processes to be performed at relatively low temperatures when the formation of a perfect crystal structure is complicated. This opens up a way to the synthesis of substances in nanocrystalline and amorphous states. The MA method is characterized by simplicity and low cost; thus, it can be considered as an alternative to modern chemical synthetic methods.

Its essence consists in carrying out solid-phase reactions in grinding devices (mills and disintegrators). A joint mechanical treatment leads to crushing and plastic deformation of substances, acceleration of mass transfer, and efficient mixing of the components. The mean particle size of ceramic materials obtained by MA is as small as 30–150 nm at a contamination of no more than 0.05 wt %; the advantages of the solid-phase synthesis in this case are preserved [11].

The aim of this work was to study the effect the mechanochemical activation on the synthesis and sintering of the tetragonal solid solutions $(ZrO_2)_{0.97} \cdot (Y_2O_3)_{0.03}$ and $(ZrO_2)_{0.92}(Y_2O_3)_{0.03}(CeO_2)_{0.05}$ and to prepare compact ceramic materials based on them.

EXPERIMENTAL

Zirconium, yttrium, and cerium nitrates: $ZrO \cdot (NO_3)_2 \cdot nH_2O$ (analytically pure grade), $Y(NO_3)_3 \cdot 6H_2O$ (chemically pure grade), and $Ce(NO_3)_3 \cdot 5H_2O$ (analytically pure grade) were chosen as starting reagents for the study.

The use of hydrated nitrates is caused by the fact that their hardness is several times lower than that of the anhydrous compounds, which allows us to reduce

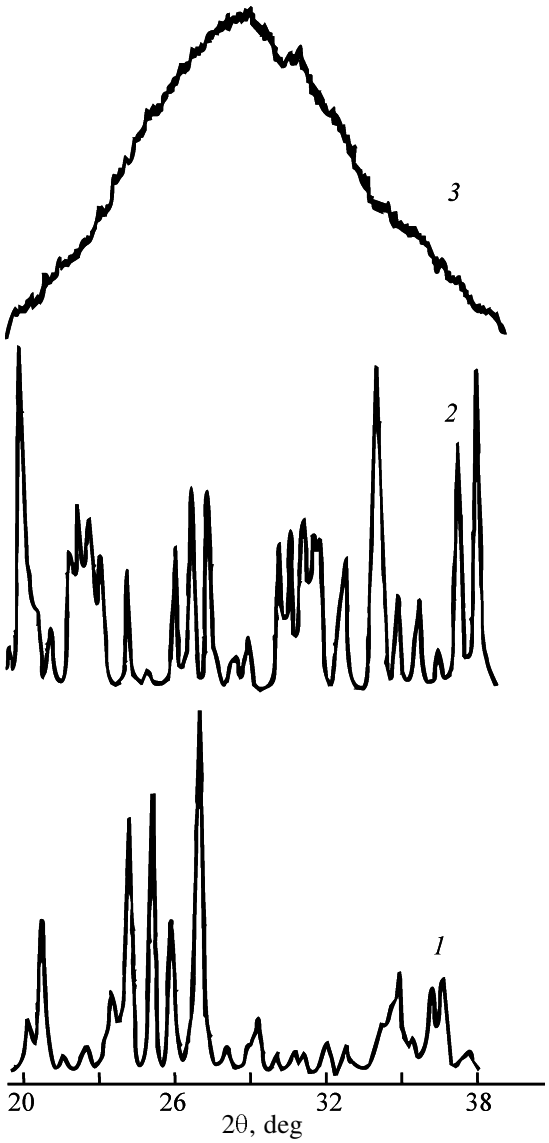


Fig. 1. X-ray patterns of the starting reagents (*1*) $ZrO(NO_3)_2 \cdot nH_2O$, (*2*) $Y(NO_3)_3 \cdot 6H_2O$, and (*3*) MA powder with the stoichiometric composition $ZrO_2 : Y_2O_3 = 97 : 3$ (the pattern for the ZrO_2–Y_2O_3–CeO_2 system is similar). (2θ) Bragg angle; the same for Figs. 2, 4, and 5.

the mechanical load and to avoid the contamination of the resulting products by the material of milling balls.

The mechanochemical activation of powder mixtures with specified stoichiometric contents of oxides in the systems ZrO_2–Y_2O_3 and ZrO_2–Y_2O_3–CeO_2 was carried out on a Fritsch planetary mill in electrocorundum beakers (with Al_2O_3 balls as a milling material) in air. It should be noted that all the starting reagents were preliminarily heat-treated at 100°C to remove water adsorbed on the surface of crystal hydrates (as shown by the gravimetric analysis, the water loss is approximately 10–12%) and to avoid sticking of activated salts on the beaker walls and milling balls. The duration of the mechanical treatment was 1, 2, and 4 h.

During MA, particles of salts were exposed to impacts and frictional forces; the dose of the absorbed energy varied from 5 to 20 kJ mol^{-1}.

Powder X-ray phase analysis of samples was carried out on a Siemens D-500/HS diffractometer in the range of angles 2θ 15°–65° at room temperature in air using CuK_α radiation and a nickel filter. The scanning rate was 1 deg min^{-1}.

The average size of crystallites of the forming phases was calculated from the X-ray diffraction data. The X-ray patterns obtained in the digital form were processed with a WINFIT 1.2.1. program [12] using the Fourier transform of peak profiles. For the calculation we chose the diffraction peak (111) of the ZrO_2 phase, whose profile was preliminarily corrected for instrumental distortion and approximated by Voigt's pseudo-function [13].

The differential thermal analysis (DTA) was carried out on a Q-1000 derivatograph (MOM, Hungary) in air in the range 20–800°C.

The heat treatment of samples under study was carried out in a Silit furnace with silicon carbide (SiC) heaters in the range 400–1500°C. Depending on the sintering temperature, the heating rate varied from 350 to 450 deg h^{-1}.

The ceramic samples were examined by electron microscopy using the method of cellulose–coal replicas. The replicas were taken from the surface of fresh chips of the samples. Morphological studies were carried out on an EM-125 transmission electron microscope at an accelerating voltage of U = 75 kV.

The apparent density and open porosity were determined in accordance with GOST (State Standard) 473.4–81 [14]. The relative density of samples ρ (%) was calculated by the formula $\rho = \rho_a/\rho_0$, where ρ_a is the apparent density (g cm^{-3}) and ρ_0 is the theoretical density calculated from the X-ray data. The Vickers microhardness H_V was determined with a PMT-3 microhardness meter [15]. The procedure of the determination of the critical coefficient of stress intensity, crack resistance K_{IC}, of the samples has been described in [16].

Structural transformations resulting from MA in a mixture of nitrates were monitored by X-ray phase analysis. We found that, as the mechanical treatment duration increases (from 1 to 4 h), starting components are gradually destroyed and X-ray amorphous phases are formed in the systems (Fig. 1).

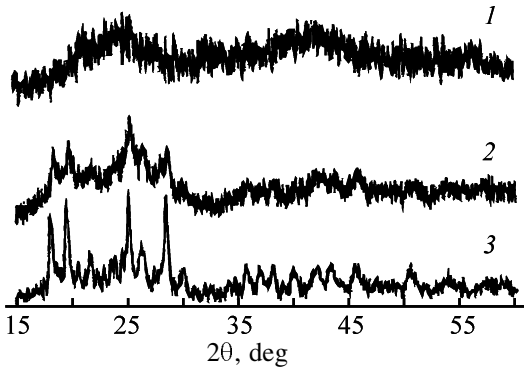


Fig. 2. Effect of air (20°C) on the structure of fresh MA powder. Contact duration (h): (*1*) 0, (*2*) 1, (*3*) 2, and (*4*) 4.

A study of the behavior of fresh mechanically activated powders in certain oxide systems by IR and ESR spectroscopy [11, 17, 18] revealed the appearance of vibrationally and electronically excited states of interatomic bonds, formation of radical ions, and ionization of particles. The authors have concluded that the valence-unsaturated bonds arising during the mechanochemical activation enhance the reactivity of MA powders.

An X-ray phase analysis we made in this study revealed structural changes in the ZrO_2–Y_2O_3 and ZrO_2–Y_2O_3–CeO_2 systems on contact of fresh MA powders with air. Apparently, valence-unsaturated bonds arising upon the mechanical activation initiate the uptake of oxygen, carbon oxides, and H_2O vapor from air, which results in the disappearance of the X-ray amorphous phase and formation of new crystalline phases (Fig. 2). Therefore, it is necessary to make the time interval between the MA process and the use of activated powders as short as possible.

The thermal decomposition of the MA powders in the range 20–500°C was studied by differential thermal analysis. The DTA curves for MA powders in the ZrO_2–Y_2O_3–CeO_2 system before the activation and after the mechanical treatment for 1, 2, and 4 h are shown as an example in Fig. 3.

In each of the DTA curves two characteristic effects are detected: an endothermic dehydration effect and an exothermic effect caused by transformation of the MA powder from the X-ray amorphous to crystalline state.

The DTA data show that both the MA process proper and its duration affect the thermal decomposition of MA powders. The shift of the endothermic peaks to lower temperatures is attributable to the fact that the increase in the duration of the mechanical treatment weakens the bonds between the molecules of nitrates and water of crystallization, which, in turn,

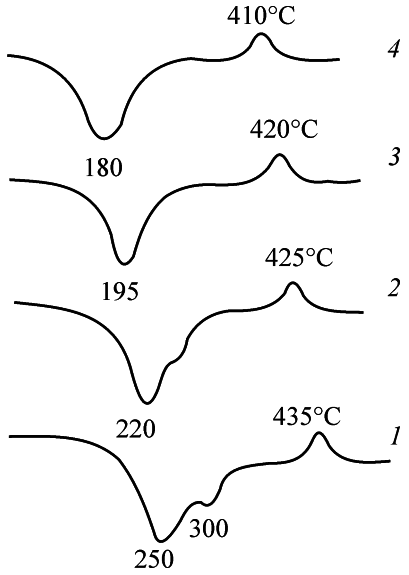


Fig. 3. DTA curves of MA powder of the stoichiometric composition $ZrO_2 : Y_2O_3 : CeO_2 = 92 : 3 : 5$ in the range 20–500°C. Mechanical treatment duration (h): (*1*) 0, (*2*) 1, (*3*) 2, and (*4*) 4.

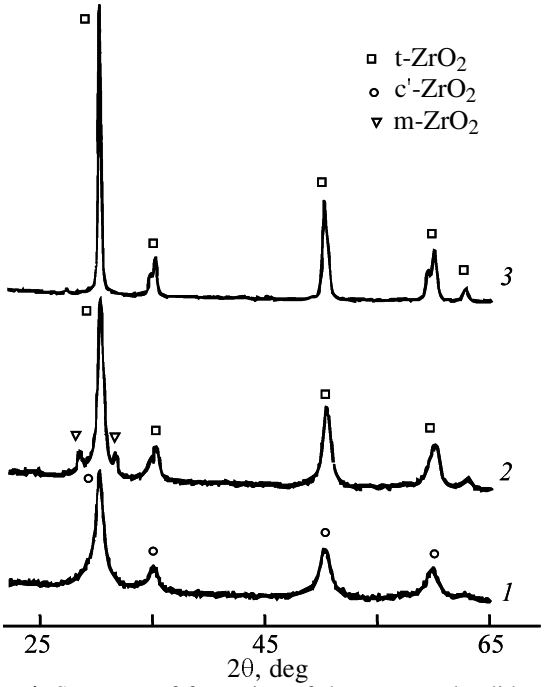


Fig. 4. Sequence of formation of the tetragonal solid solution based on ZrO_2 for the ZrO_2–Y_2O_3 and ZrO_2–Y_2O_3–CeO_2 systems. Calcination temperature, °C: (*1*) 400, (*2*) 800, and (*3*) 1300.

facilitates the dehydration of MA powders. It was found by X-ray phase analysis that the exothermic effects in the DTA curves in the range 400–430°C correspond to the crystallization of solid solutions based on ZrO_2 in the cubic metastable modification (c'-ZrO_2) (Fig. 4). As the duration of the mechanical

Average size of crystallites d, relative density ρ_a/ρ_0, open porosity P, microhardness H_V, and crack resistance K_{IC} of the solid solutions $(ZrO_2)_{0.97}(Y_2O_3)_{0.03}$ and $(ZrO_2)_{0.92}(Y_2O_3)_{0.03}(CeO_2)_{0.05}$ in the range 1200–1500°C

Sample	T, °C	d, nm	ρ_a/ρ_0, %	P, %	H_V, GPa	K_{IC}
$(ZrO_2)_{0.97}(Y_2O_3)_{0.03}$	1200*	81	97	3	10	5
	1300	95	98.5	<1	12	6
	1400	110	97.5	3	10	–
$(ZrO_2)_{0.92}(Y_2O_3)_{0.03}(CeO_2)_{0.05}$	1300*	98	95	5.5	–	–
	1400	115	99	1	11	14
	1500	133	98	1.5	10	13

* Temperature of the formation of t-ZrO_2 single-phase solid solutions.

treatment increases, the temperature at which the phase of the stabilized ZrO_2 solid solution is formed decreases by 25°C, owing to increased reactivity of MA powders [11]. The average size of the crystallites of this phase is 8–10 nm (calculated by the Fourier transform method).

According to the X-ray data, at temperatures above 500°C the c'-ZrO_2 solid solution transforms into the tetragonal modification (t-ZrO_2), as indicated by splitting of the diffraction maxima in the range 2θ = 34°–36° (Fig. 5).

The average size of t-ZrO_2 crystallites at 600°C is 15 nm for the $(ZrO_2)_{0.97}(Y_2O_3)_{0.03}$ solid solution and 20 nm for the $(ZrO_2)_{0.92}(Y_2O_3)_{0.03}(CeO_2)_{0.05}$ solid solution.

Figure 4 shows the sequence of formation of the tetragonal solid solutions $(ZrO_2)_{0.97}(Y_2O_3)_{0.03}$ and $(ZrO_2)_{0.92}(Y_2O_3)_{0.03}(CeO_2)_{0.05}$. When MA powders are heat-treated at temperatures above 600°C, a small amount (~9–10%) of the monoclinic phase (m-ZrO_2) is detected in the X-ray patterns. This phase coexists with the t-ZrO_2 phase in a wide temperature range, up to 1000–1100°C. At 1200°C and higher temperatures, single-phase solid solutions based on t-ZrO_2 are formed. The half-width of diffraction maxima corresponding to the t-ZrO_2 phase decreases in the range 600–1200°C, which indicates that the average size of crystallites of this phase increases (from 15 to 85 nm).

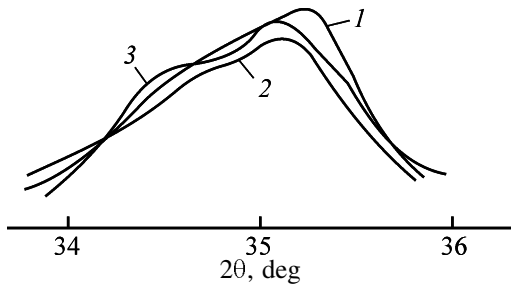


Fig. 5. Fragments of the X-ray pattern of a solid solution based on ZrO_2, sintered at (*1*) 500, (*2*) 550, and (*3*) 600°C.

We studied sintering of tetragonal solid solutions in the ZrO_2–Y_2O_3 and ZrO_2–Y_2O_3–CeO_2 systems using samples in the form of pellets (d = 12 mm and h = 4 mm) prepared by semidry pressing at 150 MPa of MA powders preliminarily heat-treated at 450°C. A 10% aqueous solution of polyvinyl alcohol was used as a binding agent. The calcination was carried out in the range 1200–1500°C; the duration of isothermal heating at each temperature was 2 h. Characteristics of the tetragonal solid solutions in the ZrO_2–Y_2O_3 and ZrO_2–Y_2O_3–CeO_2 systems are presented in the table.

The table shows that the densest samples of the $(ZrO_2)_{0.97}(Y_2O_3)_{0.03}$ and $(ZrO_2)_{0.92}(Y_2O_3)_{0.03}\cdot(CeO_2)_{0.05}$ solid solutions were obtained at 1300 and 1400°C, respectively.

We have studied the microstructure of sintered samples by transmission electron microscopy. We found that the microstructure of the ceramic sample of $(ZrO_2)_{0.97}(Y_2O_3)_{0.03}$ (T = 1300°C) is characterized by close packing of well developed crystalline grains with a smooth surface (Fig. 6a). As the temperature is increased to 1400°C, small cracks appear on intercrystallite boundaries (Fig. 6b). An electron-microscopic examination shows that 1300°C is the optimal temperature for sintering of dense ceramic materials based on the $(ZrO_2)_{0.97}(Y_2O_3)_{0.03}$ solid solution. Properties of the ceramics sintered at this temperature are better compared to 1400°C (see table).

The microstructure of samples of the $(ZrO_2)_{0.92}\cdot(Y_2O_3)_{0.03}(CeO_2)_{0.05}$ solid solution was studied similarly. We found that these ceramic materials reach a high degree of sintering at 1400°C, whereas at 1500°C cracks are formed, affecting the porosity of samples, their microhardness, and crack resistance (see table).

To sum up, we can conclude that the mechanochemical activation provides efficient mixing of the

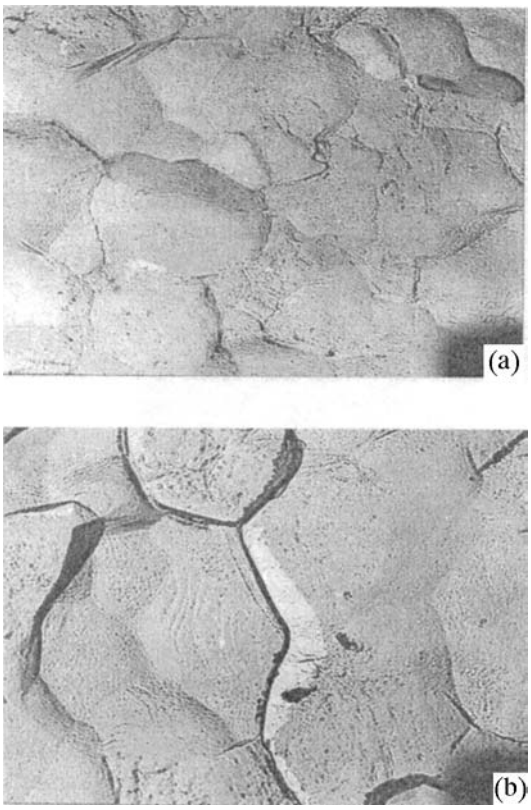


Fig. 6. Microstructure of a sample of the $(ZrO_2)_{0.97} \cdot (Y_2O_3)_{0.03}$ solid solution sintered at (a) 1300 and (b) 1400°C. Magnification 40000.

reactants in the ZrO_2–Y_2O_3 and ZrO_2–Y_2O_3–CeO_2 systems and enhances their reactivity; it allows preparation of precursor powders based on zirconium dioxide in the nanocrystalline state (particle size as small as 10 nm); it intensifies sintering of solid solutions based on ZrO_2, increases their phase stability, and allows preparation at 1200–1400°C of dense ceramic materials based on the tetragonal solid solution of zirconium dioxide.

CONCLUSIONS

(1) Mechanochemical activation extends the potential of the standard ceramic method and makes it possible to synthesize ceramic materials with specified properties under milder conditions.

(2) The particle size of the resulting ceramic materials varies from 10 to 130 nm in the range 400–1500°C.

(3) Studies in the field of the mechanochemical synthesis of oxide materials allow us to develop and improve the mechanonochemical ceramic technology, which can be incorporated in complex processes when necessary.

REFERENCES

1. Lukin, E.S., *Ogneupory Tekh. Keram.*, 1996, no. 1, pp. 5–14.
2. Durun, P., Villegas, M., Capel F., et al., *J. Eur. Ceram. Soc.*, 1996, vol. 16, no. 9, pp. 945–952.
3. Lawson, S. and Gill, S., *J. Mater. Sci.*, 1995, vol. 30, no. 12, pp. 3057–3060.
4. Abraham, I. and Gritzner, G., *J. Eur. Ceram. Soc.*, 1996, vol. 16, no. 1, pp. 71–77.
5. Podzorova, L.I., Il'icheva, A.A., Mikhailina, N.A., et al., *Ogneupory Tekh. Keram.*, 1995, no. 6, pp. 2–5.
6. Taha, M., Poletto, J., Jorond, Y., et al., *J. Eur. Ceram. Soc.*, 1995, vol. 15, no. 10, pp. 759–768.
7. Savchenko, N.L., Sablina, T.Yu., Poletika, T.M., et al., *Poroshk. Metall.*, 1993, nos. 9–10, pp. 96–100.
8. Il'icheva, A.A., Olenin, A.Yu., Podzorova, L.I., et al., *Neorg. Mater.*, 1996, vol. 32, no. 7, pp. 833–837.
9. Panova, T.I., Malysheva, S.I., Drozdova, I.A., and Glushkova, V.B., *Zh. Prikl. Khim.*, 1995, vol. 68, no. 8, pp. 1385–1387.
10. Goplan, R., Cang, C.-H., and Lin, Y.S., *J. Mater. Sci.*, 1995, vol. 30, no. 12, pp. 3075–3081.
11. Avvakumov, E.G., *Mekhanicheskie metody aktivatsii khimicheskikh protsessov* (Mechanical Methods of Activation of Chemical Processes), Novosibirsk: Nauka, 1986.
12. Site of the Program http//www.geol.uni-erlangen.de.
13. Warren, B.E. and Averbach, B.L., *J. Appl. Phys.*, 1950, vol. 21, p. 595.
14. *GOST* (State Standard) *473.4–81*, Moscow: Izd. Standartov, 1981.
15. Lebedeva, S.I., *Opredelenie mikrotverdosti mineralov* (Determination of Microhardness of Minerals), Moscow: Akad. Nauk SSSR, 1963.
16. Barinov, S.M. and Shevchenko, V.Ya., *Prochnost' tekhnicheskoi keramiki* (Strength of Technical Ceramics), Moscow: Nauka, 1996.
17. Butyagin, P.Yu., *Usp. Khim.*, 1994, vol. 6, no. 12, pp. 1031–1043.
18. Pavlova, S.N., Sadykov, V.A., Zabolotnaya, G.V., et al., *Dokl. Ross. Akad. Nauk*, 1999, vol. 364, no. 2, pp. 210–212.

ISSN 1070-4272, Russian Journal of Applied Chemistry, 2006, Vol. 79, No. 7, pp. 1062–1066. © Pleiades Publishing, Inc., 2006.
Original Russian Text © D.E. Chirkst, T.E. Litvinova, V.S. Starshinova, V.I. Kuchina, 2006, published in Zhurnal Prikladnoi Khimii, 2006, Vol. 79, No. 7, pp. 1072–1076.

INORGANIC SYNTHESIS AND INDUSTRIAL INORGANIC CHEMISTRY

Extraction of Ce(III) with Naphthenic Acid from Nitrate Solutions

D. E. Chirkst, T. E. Litvinova, V. S. Starshinova, and V. I. Kuchina

St. Petersburg State Mining Institute, St. Petersburg, Russia

Received November 2, 2005; in final form, February 2006

Abstract—Extraction of Ce(III) with naphthenic acid from nitrate solutions was studied. The composition of solvation complexes, extraction constants, and Gibbs energies of extraction were found from the dependences of the distribution coefficients on pH and compositions of the aqueous and organic phases.

DOI: 10.1134/S1070427206070032

Tri-*n*-butyl phosphate (TBP) is a traditional extractant for recovery of rare-earth metals (REM) from nitrate media. However, leaching with sulfuric [1] and hydrochloric acids [2] is usually used for processing of lean and technogenic raw materials. In these media, REM mainly exist in the form of charged complexes $[M(An)_z]^{3-zx}$, where An is an acid residue and x, its charge (x = 1 or 2) [3]. In this case, TBP is inefficient for REM recovery and separation [4], and ion-exchange extractants, e.g., carboxylic acids (in particular, oleic) are widely used [5].

Previously, we studied extraction of Ce(III) with naphthenic acid [6]. The goal of this study is detailed examination of the extraction within the pH 3–5 range and more precise elucidation of the extraction equation. At pH > 5, the system represents a difficultly settling emulsion.

Cerium(III) extraction was studied using model aqueous solutions with a Ce(III) content of 0.01 mol kg^{-1}, which corresponds to the concentration of hydrometallurgical solutions of REM extractive recovery from lean or technogenic raw materials. The solution of naphthenic acid in dodecane was used as extractant. The average molar weight of the naphthenic acid fraction studied was 226 g mol^{-1}, and the acid dissociation constant pK_d = 5.1 [7].

The cerium(III) concentration in the equilibrium aqueous phase and in the initial solution was determined photometrically with Arsenazo III [8].

The Ce(III) content in the organic phase was determined as the difference between the concentrations in the initial and equilibrium aqueous phases with regard to the difference in the phase volumes (or weights):

$$c_{org} = [(c_0 - c_{aq})m_{aq}]/m_{org}, \quad (1)$$

where c_{org} and c_{aq} are the equilibrium concentrations of the metal ions in the organic and aqueous phases, respectively (mol kg^{-1}); c_0, initial REM content in the aqueous phase (mol kg^{-1}); m_{aq}/m_{org}, weight ratio of the aqueous and organic phases, which was 40 : 2.6 at the organic phase density of 0.86 ± 0.01 g cm^{-3}.

The distribution coefficient was calculated by the formula

$$D = c_{org}/c_{aq}. \quad (2)$$

Within the framework of our goals, we measured the dependences of the Ce(III) distribution coefficient on pH of the aqueous phase at a constant concentration of naphthenic acid, 0.5 M (Table 1), and on

Table 1. Cerium(III) distribution coefficient D_{Ce} at various pH. Initial Ce(III) concentration 0.014 mol kg^{-1}

pH	$c_{aq} \times 10^3$	$c_{org} \times 10^2$	D_{Ce}
	mol kg^{-1}		
4.1	9.10	2.02	2.2
4.3	7.72	4.16	5.4
4.5	5.52	7.57	13.7
4.7	3.72	10.36	27.8
4.9	3.04	11.42	37.6
5.1	2.83	11.74	41.5
5.6	2.53	12.20	48.2

Table 2. Cerium(III) distribution coefficient D_{Ce} at various concentrations of naphthenic acid c_{HR}. pH 4.95, initial Ce(III) concentration 0.014 mol kg^{-1}

c_{HR}, M	$c_{aq} \times 10^3$	$c_{org} \times 10^2$	D_{Ce}
	mol kg^{-1}		
0.1	3.25	0.94	2.89
0.125	2.91	1.31	4.49
0.167	2.57	1.92	7.46
0.2	2.17	2.55	11.55
0.25	1.83	3.45	18.85
0.5	2.86	11.69	40.9

the naphthenic acid concentration at a constant pH (Table 2).

In separate experiments, we showed that nitrate ions are not incorporated in the extractable solvate. Therefore, the extraction reaction is as follows:

$$M^{3+}_{aq} + zH_2O + (3 - z)R^-_{org} \rightleftarrows M(OH)_zR_{(3-z)org} + zH^+_{aq}, \quad (3)$$

where R^- is naphthenate ion.

The equilibrium constant is

$$K = \frac{a_{Ce^{3+}_{org}} a^z_{H^+_{aq}}}{a_{Ce^{3+}_{org}} a^{3-z}_{R^-_{org}}} = \frac{\gamma_{\pm org} c_{Ce^{3+}_{org}} a^z_{H^+_{aq}}}{\gamma_{\pm aq} c_{Ce^{3+}_{org}} \gamma^{3-z}_{\pm org} [R^-]^{3-z}_{org}}$$
$$= \frac{c_{org} a^z_{H^+_{aq}}}{c_{aq}\gamma_{\pm aq}[R^-]^{3-z}_{org}} = \frac{D a^z_{H^+_{aq}}}{\gamma_{\pm aq}[R^-]^{3-z}_{org}}, \quad (4)$$

where $\gamma_{\pm aq}$ is the mean ionic activity coefficient of Ce^{3+} in the equilibrium aqueous phase.

The equilibrium concentration of cerium(III) nitrate in the aqueous phase was 0.0030 ± 0.0016 mol kg^{-1}, and the ionic strength, 0.018 ± 0.010 mol kg^{-1}. The activity coefficient was taken equal to that for lanthanum chloride at an ionic strength of 0.70 ± 0.05 [9]. Then, $\log \gamma_{\pm aq} = -0.16 \pm 0.03$. The mean ionic activity coefficient of the component in the organic phase was taken equal to unity because of the use of a nonpolar solvent (dodecane). The concentration of naphthenic acid anions $[R^-]^{3-z}_{org}$ depends on pH:

$$[R^-]^{3-z}_{org} = [HR]K_d/a_{H^+}, \quad (5)$$

where K_d is the dissociation constant of naphthenic acid.

The concentration of the nondissociated acid species is

$$[HR] = c_{extr} - (3 - z)c_{org} - [R^-]^{3-z}_{org}, \quad (6)$$

where c_{extr} is the total concentration of the extractant in the organic phase and c_{org}, REM concentration in the organic phase.

Dissociation of naphthenic acid can be considered as a heterogeneous process described by the equation

$$HR_{org} \rightleftarrows H^+_{aq} + R^-_{org}, \quad (7)$$

because H^+ cations are hydrated and completely pass into the aqueous phase, whereas the hydrophobic molecules of nondissociated acid and acid anions remain in the organic phase. Nominally, this process can be considered as a sum of the following equilibria:

$$HR_{org} \rightleftarrows HR_{aq}, \quad (8)$$

whose equilibrium constant is $k_8 = [HR]_{aq}/[HR]_{org}$, i.e., is inversely proportional to the distribution coefficient of naphthenic acid between dodecane and aqueous phase, D^{-1}_{HR}.

$$HR_{aq} \rightleftarrows H^+_{aq} + R^-_{aq}. \quad (9)$$

The equilibrium constant of this process is the dissociation constant of naphthenic acid in the aqueous phase.

$$R^-_{aq} \rightleftarrows R^-_{org}. \quad (10)$$

The equilibrium constant of process (10) is the distribution coefficient of naphthenate anion D_{R^-}.

Thus, the equilibrium constant of heterogeneous process (7) is

$$K = (K_d D_{R^-})/D_{HR} \cong K_d. \quad (11)$$

The distribution coefficients of naphthenic acid and naphthenate anion can be considered to be approximately equal, because, in accordance with Duclot–Traube rule, the hydrophobicity is determined by the organic radical.

The concentration of naphthenic acid anions depends on pH as follows:

$$[R^-]_{org} = [HR]_{org}K_d/a_{H^+_{aq}}, \quad (12)$$

where K_d is the dissociation constant of naphthenic acid, and the concentration of nondissociated naphthenic acid in the organic phase is

$$[HR]_{org} = c_{extr} - (3 - z)c_{org} - [R^-]_{org}, \quad (13)$$

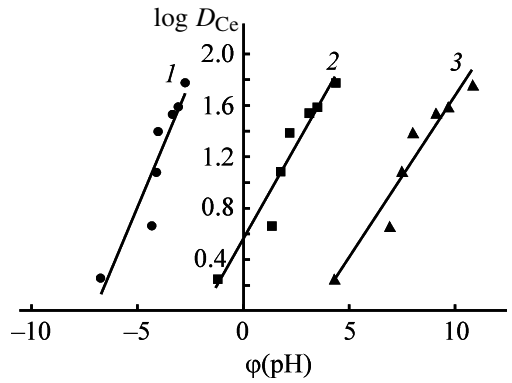


Fig. 1. Logarithm of Ce(III) distribution coefficient $\log D_{Ce}$ vs. the function of pH. Solvation number z: (*1*) 0, (*2*) 1, and (*3*) 2.

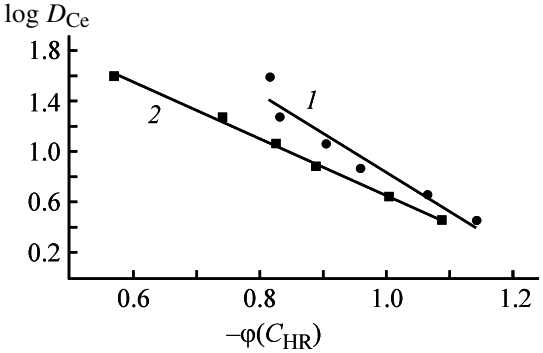


Fig. 2. Logarithm of Ce(III) distribution coefficient $\log D_{Ce}$ vs. the function of extractant concentration $\varphi(c_{HR})$ at z (*1*) 0 and (*2*) 1.

where c_{extr} is the total concentration of the extractant in the organic phase, and c_{org}, REM concentration in the organic phase.

Thus, naphthenate bound into the solvate complex was considered. The equilibrium concentration of free naphthenate anion in the organic phase was determined by combined solution of Eqs. (12) and (13):

$$[R^-]_{org} = [c_{extr} - (3 - z)c_{org}](1 + a_{H^+_{aq}}/K_d)^{-1}. \quad (14)$$

After substitution in Eq. (4), we obtain

$$K = \frac{D a^z_{H^+_{aq}} (1 + a_{H^+_{aq}}/K_d)^{3-z}}{\gamma_\pm [c_{extr} - (3 - z)c_{org}]^{3-z}}. \quad (15)$$

The logarithm of the distribution coefficient is

$$\log D = \log K + z\text{pH} - (3 - z)\log(1 + a_{H^+_{aq}}/K_d)^{3-z} + (3 - z)\log[c_{extr} - (3 - z)c_{org}] + \log\gamma_\pm. \quad (16)$$

The dependences of $\log D$ on the argument

$$\varphi(\text{pH}) = z\text{pH} + (3 - z)\log[c_{extr} - (3 - z)c_{org}] - (3 - z)\log(1 + a_{H^+_{aq}}/K_d) \quad (17)$$

for various probable values of the solvation number z were plotted using data of Table 1 (Fig. 1).

For cerium(III) these dependences are linear at z 0–2 and in accordance with Eq. (16) are described by the equations

$$\log D = 0.4\varphi(\text{pH}) + 2.75 \quad (z = 0), \quad (18)$$

$$\log D = 0.3\varphi(\text{pH}) + 0.56 \quad (z = 1), \quad (19)$$

$$\log D = 0.25\varphi(\text{pH}) - 0.83 \quad (z = 2), \quad (20)$$

with the correlation coefficient $R^2 = 0.93$.

The constants of the extraction equilibrium and Gibbs energies were calculated using the absolute term of Eqs. (18)–(20) with regard to Eq. (16):

$$\log K = 2.75 \ (z = 0), \ \Delta_r G = -15.7 \text{ kJ mol}^{-1};$$

$$\log K = 0.56 \ (z = 1), \ \Delta_r G = -3.2 \text{ kJ mol}^{-1};$$

$$\log K = -0.83 \ (z = 2), \ \Delta_r G = 4.7 \text{ kJ mol}^{-1}.$$

For $z = 2$, the constant of the extraction equilibrium and Gibbs energy contradict the experimental data (fairly high distribution coefficient), so this model is inadequate.

Cerium can be extracted in the form of both Ce^{3+} cations and $CeOH^{2+}$ hydroxo complexes. In this case, the slope of the logarithmic dependence of the Ce(III) distribution coefficient on the function of the extractant equilibrium concentration $\varphi(c_{HR}) = \log[c_{extr} - (3 - z)c_{org}]$ should be equal to 3 (for $z = 0$) or 2 (for $z = 1$). These dependences are shown in Fig. 2 for z 0 and 1.

As seen, linear dependences are observed for both cases and are described by the equations

$$\log D = 3.9\varphi(c_{HR}) + 3.1 \text{ at } zG = 0, \quad (21)$$

$$\log D = 2.2\varphi(c_{HR}) + 2.9 \text{ at } zG = 1, \quad (22)$$

with $R^2 = 0.95$.

For $z = 0$, the slope does not correspond to the model taken. For $z = 1$, the slope corresponds to the model; however, the logarithm of the equilibrium constant [calculated from the absolute term of the dependence in accordance with Eq. (16)] and Gibbs energy $\log K = -13$ ($z = 1$) and $\Delta_r G = 7.4$ kJ mol^{-1}

contradict experimental data (fairly high distribution coefficient).

Therefore, we suggested that both Ce(III) species participate in the extraction in proportion with their content in the equilibrium aqueous phase:

$$[CeOH]^{2+}_{aq} + H_2O + 2R^-_{org} = CeOHR_{2org} + H^+_{aq}, \quad (23)$$

$$Ce^{3+}_{aq} + 3R^-_{org} = CeR_{3org}. \quad (24)$$

The IR spectra of Ce(III) extracts (Table 3) confirmed the existence of $CeOHR_2$ species in the organic phase (bands at 1400–1500 cm^{-1} are observed, which, in accordance with [10–12], belong to OH groups in the metal complex; they are absent in the spectrum of naphthenic acid).

Mathematical simulation with various z within the range 0–1 gave the best results for $z = 0.67$ (Figs. 3 and 4).

The dependences shown in Figs. 3 and 4 are described by the following equations, for which the logarithms of the equilibrium constants and the Gibbs energies were calculated from the absolute terms:

$$\log D = 0.35\varphi(pH) + 1.31, \ \log K = 1.31,$$

$$\Delta_r G = -7.47 \text{ kJ mol}^{-1}; \quad (25)$$

$$\log D = 2.43\varphi(pH) + 3.14, \ \log K = 1.04,$$

$$\Delta_r G = -5.93 \text{ kJ mol}^{-1}. \quad (26)$$

Thus, the thermodynamic parameters of Ce(III) extraction with naphthenic acid obtained by two independent methods are satisfactorily consistent with each other. The average values of the extraction constant and Gibbs energies are $K_{extr} = 1.18$ and $\Delta_{extr}G = -6.7$ kJ mol^{-1}, respectively.

The overall equation of Ce(III) extraction with naphthenic acid can be represented as follows:

$$Ce^{3+}_{aq} + 0.67H_2O + 2.33R^-_{org} \rightleftarrows CeOH_{0.67}R_{2.33org} + 0.67H^+_{aq}. \quad (27)$$

With regard to the thermodynamic characteristics of Ce(III) hydrolysis, for which the Gibbs energy $\Delta_h G$ calculated from reference data [13] is 53.98 kJ mol^{-1}, the Gibbs energy of solvation can be calculated as the difference between the Gibbs energies of extraction and hydrolysis with regard to the slope of the dependence $\log D = \varphi(pH)$: $\Delta_{solv}G = \Delta_{extr}G - 0.67\Delta_h G = -36.2 \pm 1.7$ kJ mol^{-1}.

Table 3. IR spectra of naphthenic acid and cerium naphthenate

Naphthenic acid		Cerium naphthenate	
ν, cm^{-1}	optical density	ν, cm^{-1}	optical density
1080	0.1	1076	0.2
1200	0.09	1263.7	0.36
1300	0.22	1310.1	0.47
1410	0.1	1373.4	0.91
1700	0.88	1424.1	1.64
2370	0.1	1470.5	0.78
2660	0.2	1546.4	1.7
2850	2.13	1685.6	0.42
2870	2.1	1732.1	0.11
2900	2.05	2680	0.19
2950	1.75	2732.1	0.23
		2852.3	0.46

The results obtained are compared in Table 4 with the data on cerium(III) nitrate extraction with a 20% solution of tributyl phosphate (TBP) in *o*-xylene, a 0.5 M solution of trialkylbenzylammonium nitrate

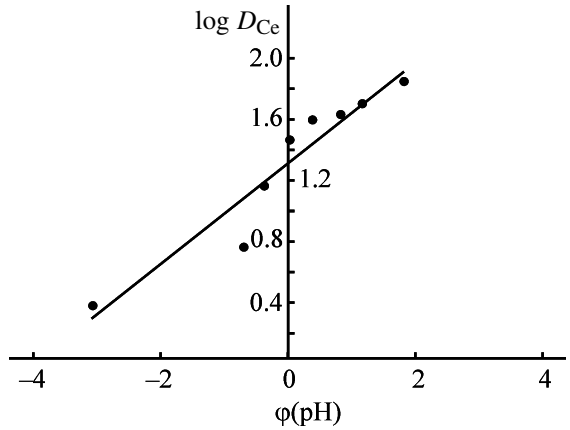


Fig. 3. Logarithm of Ce(III) distribution coefficient $\log D_{Ce}$ vs. the function of pH at $z = 0.67$.

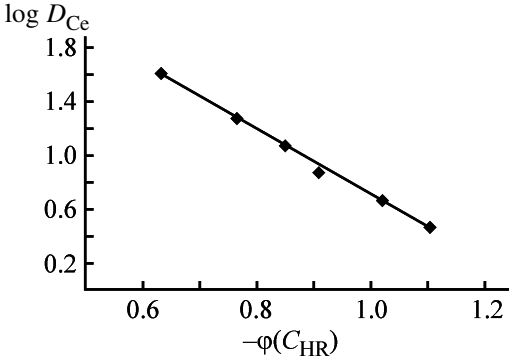


Fig. 4. Logarithm of Ce(III) distribution coefficient $\log D_{Ce}$ vs. the a function of extractant concentration $\varphi(c_{HR})$ at $z = 0.67$.

Table 4. Comparison of parameters of Ce(III) extraction with various extractants

Extractant	pH	D	$-\Delta_r G^0_{298}$, kJ mol^{-1}
TBP [4]	5	9.0 ± 0.4	5.92 ± 0.03
TABAN [3]	3	35 ± 4	8.9 ± 0.3
Oleic acid	5	100 ± 3	58.6 ± 1.7
Naphthenic acid	5	39 ± 0.5	36.2 ± 1.3

(TABAN), and a 0.5 M solution of oleic acid in dodecane.

As seen, the Ce(III) extraction from nitrate solutions at pH 5 is the most efficient when oleic or naphthenic acid is used as extractant. This fact confirms the existence of Ce(III) at such pH as positively charged hydroxo complexes. In the more acidic media (pH 3), Ce(III) exists in the form of negatively charged anionic complexes, which ensures its preferred extraction with salts of quaternary ammonium bases.

CONCLUSIONS

(1) Extraction of cerium(III) with carboxylic acids from nitrate solutions is the most efficient at pH of formation of metal hydroxo complexes.

(2) The extraction involves transfer of Ce^{3+} and $[Ce(OH)]^{2+}$ cations into the organic phase in the 1 : 2 molar ratio.

(3) The equilibrium constant and Gibbs energy of solvation of these species were determined.

REFERENCES

1. Dibrov, I.A., Chirkst, D.T., and Litvinova, T.E., *Zh. Prikl. Khim.*, 1996, vol. 69, no. 5, pp. 727–730.
2. Zakharov, V.I., Voskoboinikov, N.B., Skiba, G.S., et al., *Zap. Gorn. Inst.*, vol. 165, pp. 102–105.
3. Dibrov, I.A., Chirkst, D.T., and Litvinova, T.E., *Zh. Prikl. Khim.*, 2002, vol. 75, no. 2, pp. 197–201.
4. Dibrov, I.A., Chirkst, D.T., and Litvinova, T.E., *Tsvetn. Met.*, 2003, no. 3, pp. 112–115.
5. Voropanova, L.A. and Yakovleva, V.N., *Zap. Gorn. Inst.*, vol. 165, pp. 63–65.
6. Chirkst, D.T., Litvinova, T.E., Devyatkin, P.N., and Zhadovskii, I.T., *Zh. Prikl. Khim.*, 2004, vol. 77, no. 10, pp. 1630–1633.
7. Khan, I.V. and Gabrielova, Yu.A., *Khimiya flotatsionnykh reagentov* (Chemistry of Flotation Agents), Moscow: Nauka, 1981.
8. Savvin, S.B., *Arsenazo III*, Moscow: Atomizdat, 1966.
9. *Kratkii spravochnik fiziko-khimicheskikh velichin* (Concise Handbook of Physicochemical Quantities), Ravdel', A.A., Ed., Moscow: Vysshaya Shkola, 2001.
10. Illyuvieva, G.V., *Zap. Leningr. Gorn. Inst. im. G.V. Plekhanova*, 1966, vol. 46, no. 3, pp. 96–109.
11. Nakamoto, K., *Infrared and Raman Spectra of Inorganic and Coordination Compounds*, New York: Wiley, 1986.
12. Ioffe, B.V., Kostikov, R.R., and Razin, V.V., *Fizicheskie metody opredeleniya stroeniya organicheskikh molekul* (Physical Methods of Determination of the Composition of Organic Molecules), Leningrad: Leningr. Gos. Univ., 1976.
13. *Termicheskie konstanty veshchestv: Spravochnik* (Thermal Constants of Substances: Handbook), Glushko, V.P., Ed., Moscow: Akad. Nauk SSSR, 1978, vol. 8.

ISSN 1070-4272, Russian Journal of Applied Chemistry, 2006, Vol. 79, No. 7, pp. 1067–1071. © Pleiades Publishing, Inc., 2006.
Original Russian Text © A.P. Yaroshenko, M.V. Savos'kin, A.N. Magazinskii, S.V. Khripunov, L.A. Prokof'eva, V.V. Burkhovetskii, 2006, published in Zhurnal Prikladnoi Khimii, 2006, Vol. 79, No. 7, pp. 1077–1081.

INORGANIC SYNTHESIS AND INDUSTRIAL INORGANIC CHEMISTRY

Specific Features of Preparing Residual Graphite Hydrosulfate

A. P. Yaroshenko, M. V. Savos'kin, A. N. Magazinskii, S. V. Khripunov, L. A. Prokof'eva, and V. V. Burkhovetskii

Litvinenko Institute of Physical Organic Chemistry and Coal Fuel Chemistry, National Academy of Sciences of Ukraine, Donetsk, Ukraine

Received February 13, 2006

Abstract—The hydrolysis of graphite hydrosulfate prepared in the system aqueous solution of sodium dichromate–sulfuric acid was studied, and the composition of gases evolving from the solid phase during the hydrolysis was determined. The effects of the duration of the graphite hydrosulfate hydrolysis on the expansion factor and also on the morphology and particle size of the final product, residual graphite hydrosulfate, was studied.

DOI: 10.1134/S1070427206070044

A highly efficient procedure for preparing residual graphite hydrosulfate (RGH) has been developed previously [1]. This procedure involves successive treatment of natural flaky graphite with a saturated aqueous solution of sodium dichromate and concentrated sulfuric acid, hydrolysis of the resulting graphite hydrosulfate (GH), washing of the final product with water, and drying at 100–110°C. This procedure allows preparation of high-quality RGH at the total consumption of reagents in the stage of graphite oxidation of about 60–80 wt % relative to graphite. The resulting product effectively expands at a relatively low temperature (400–500°C), it is characterized by low values of the sulfur content (1.5–1.0 wt %) and pH of the aqueous extract (2.5–3.5). In previous studies the main attention was paid to the influence of conditions of graphite oxidation on the thermal properties of the final product, though it was noted that conditions of the oxidized graphite hydrolysis also exert a substantial effect.

In this study we examined changes in the morphology of GH particles as a result of their treatment with water and the influence of hydrolysis conditions on the properties of the final product (RGH).

We used in the experiments GSM-1 grade natural flaky graphite (Zaval'e, Ukraine) with ash content of about 0.1 wt % with the average particle size of 0.200–0.315 mm, a 67.7 wt % aqueous solution of sodium dichromate, and concentrated chemically pure grade sulfuric acid (concentration 95.8 wt %).

The synthesis of RGH was carried out at room temperature in a glass reactor by the following technique. An aqueous solution of sodium dichromate (1.5 cm^3) was added with stirring to 10 g of the starting graphite. After 10 min, 4.4 cm^3 of sulfuric acid was added, and the reaction mixture was stirred for an additional 10 min. The resulting mixture was stirred in the reactor with 200 cm^3 of distilled water for 1–2 min and then washed with water either directly after the synthesis (direct washing) or with an intermediate keeping of the suspension for the hydrolysis to occur. The oxidized graphite was washed with distilled water on a paper filter until the wash water became colorless. To carry out the hydrolysis, the aqueous suspension of the oxidized graphite was transferred into a mixture of water with ice and left without stirring for graphite hydrosulfate to be hydrolyzed. The hydrolysis duration was varied from 0.5 to 18 h. In all the cases, the final products were dried at 100–110°C to constant weight.

The granulometric composition of the final product (RGH) was determined using a standard set of sieves and a Fritsch Analisette 3 Pro laboratory vibrating screen.

The thermal expansion factor K_V ($cm^3\,g^{-1}$) of the products obtained was determined at 500 and 900°C by two methods: in cold (K_V^{cool}) and heated (K_V^{hot}) cells. The swelling was carried out in a 100-g cylindrical cell made of stainless steel.

The expansion in a heated cell was carried out as

Effect of the GH hydrolysis duration on the RGH expansion factor at 500 and 900°C in cold and heated cells

Hydrolysis duration, h	Expansoin factor K_v, $cm^3\ g^{-1}$, at indicated temperature, °C			
	cold cell		heated cell	
	500	900	500	900
0*	69	130	140	263
0.5	85	189	216	337
1	89	199	219	348
2	108	253	261	390
4	114	280	282	404
6	122	266	271	384
8	128	268	284	405
12	122	270	274	385
18	124	272	281	389

* Direct washing of GH with water without its keeping in water.

follows. The cell was placed in a muffle and kept there for 10 min. Then an RGH weighed portion of m = 0.20–0.25 g was placed quickly in the cell and kept there until the expansion was complete. The duration of heating in the muffle was 120 s at 500 and 60 s at 900°C.

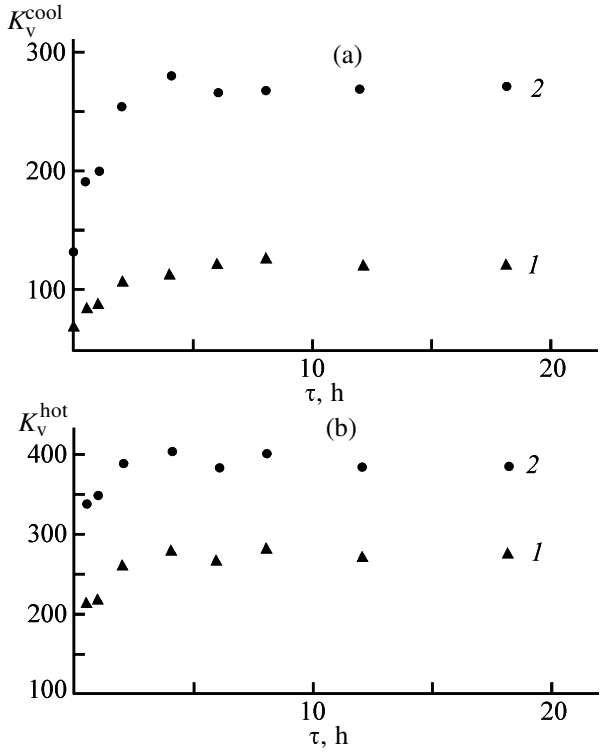


Fig. 1. Effect of duration of graphite hydrosulfate hydrolysis τ on the expansion factor K_v of residual graphite hydrosulfate in (a) cold and (b) heated cells. Temperature, °C: (*1*) 500 and (*2*) 900.

In the case of expansion in a cold cell, a weighed portion of m = 0.40–0.42 g was introduced in a cell at room temperature, then the cell with the sample was placed in a preheated muffle. The cell with the sample was kept in the muffle for 300 s at 500°C and for 120 s at 900°C.

The cell with expanded graphite was taken from the muffle, the expanded graphite was carefully transferred in a graduated glass cylinder, and the volume of expanded graphite V (cm^3) was measured. The expansion factor was determined from the relationship $K_v = V/m$ as an arithmetic mean of three replicate measurements. The relative error did not exceed 5%.

The morphology of RGH particles was studied by scanning electron microscopy (SEM) using a JEOL JSM-T300 scanning electron microscope.

The qualitative composition of gaseous products evolved from the reaction mass in various steps of the RGH synthesis was studied by gas chromatography, using an LKhM-8M chromatograph with a thermal conductivity detector and a stainless-steel column of length 2 m packed with AG-3 activated carbon (fraction 0.2–0.315 mm). The temperature of the columns was 60°C; the carrier gas was helium. Components of the gas mixtures were identified by comparison of their retention times with those of the pure gases.

It was noted previously that gases intensively escape from a layer of oxidized graphite when a suspension of oxidized graphite in water is kept without stirring. It was assumed that these gases are carbon oxides formed in the GH interlayer space as a result of oxidation-hydrolytic processes involving a carbon matrix, an intercalating compound, and intercalated particles. In this study we proved experimentally that the liberated gases contain CO and CO_2. We found that the evolution of carbon oxides is absent if the graphite powder is wetted with a solution of sodium dichromate and it begins in the stage of treating the reaction mass with concentrated sulfuric acid. The gas evolution continues throughout the time of the GH contact with water and stops only after drying the final product (RGH) at 100–110°C.

The effect of the GH hydrolysis duration on the final product expansion factor at 500 and 900°C in cold and heated cells is shown in the table. The same data in the graphic form are presented in Figs. 1a and 1b.

These data show that the expansion factors for all the studied RGH samples in a heated cell are higher by a factor of 1.5–2.5 than in a cold cell. The expan-

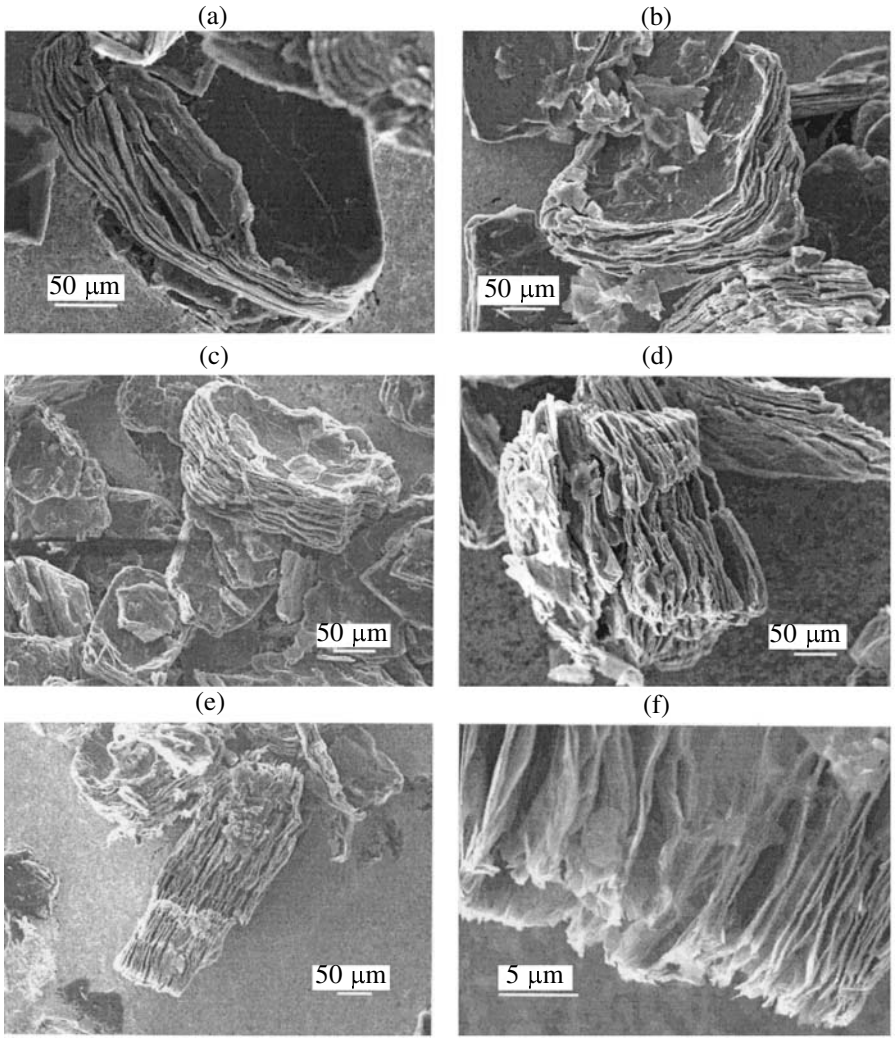


Fig. 2. Variation of the shape of residual graphite hydrosulfate particles with the hydrolysis time. (a) Direct washing; hydrolysis duration, h: (b) 0.5, (c) 1, (d) 4, and (e, f) 24.

sion factors are the lowest for the sample obtained by direct washing of GH with water, i.e., without the hydrolysis stage. As the duration of the hydrolysis stage increases, the expansion factor of the final product increases and flattens out at the hydrolysis duration of 4–5 h.

The data on the granulometric composition of RGH obtained from GSM-1 graphite with a particle size of 0.200–0.315 mm at the duration of the hydrolysis stage of 18 h are given below:

Size of mesh aperture, mm	Fraction content, wt %
–0.630+0.400	1.5
–0.400+0.315	31.3
–0.315+0.200	49.1
–0.200+0.160	10.0
–0.160+0.100	6.8
–0.100+0.063	0.3

The final product contains about 17% of particles smaller than 0.200 mm. It appeared unexpectedly that the product contains not only smaller particles, but also about 30% of particles larger than 0.315 mm, and only about 50% of particles have sizes in the range 0.200–0.315 mm. The possibility of breakdown of graphite particles during oxidizing intercalation is rather obvious, but the formation of a significant amount of larger particles seems unusual. This result stimulated us to study the effect of the hydrolysis on the morphology of particles in more detail.

The SEM photomicrographs showing the variation of the morphology of RGH particles in the course of the hydrolysis are given in Figs. 2a–2f. They show that the hydrolysis causes expansion of RGH flakes along the *c* axis, their bursting, stratification, and fragmentation with the formation of particles with

smaller diameters and thicknesses. The appearance of particles larger than the starting particles seems to be due both to their expansion along the *c* axis and to the increase in their diameter along the *a* axis owing to the formation of radial cracks and incomplete fragmentation of the flakes.

We have found that, as in the case with graphite compounds with chromium sesquioxide Cr_2O_3 [2], the hydrolysis of thus obtained oxidized graphite is accompanied by so-called ashtray effect, which is manifested as swelling of a flat flake of an intercalation compound with the formation of a flake in the form of an ashtray with deformed peripheral region. The end surface of such particles has a structure reminiscent of the honeycombed structure of thermally expanded graphite. During the further hydrolysis, the swelling front gradually moves to the center of the flake, which leads to the disappearance of the ashtray shape and to the formation of an evenly swollen particle in the final process stages. At the hydrolysis time of 4–5 h, the flakes already have approximately equal thickness both on edges and in centers, being similar in the outwards appearance to the particles of thermally expanded graphite at a low degree of expansion.

The data obtained allow us to assume the following mechanism of the RGH formation. Most likely, when concentrated sulfuric acid is added to the reaction mass containing graphite particles and concentrated aqueous solution of sodium dichromate distributed over their surface, an intercalating solution is formed. It contains hydrosulfate anions solvated by sulfuric acid molecules, sulfuric and chromic acids, and also chromosulfuric acid, H_2CrSO_7, and its anions $HCrSO_7^-$. Chromic acid plays a role of an oxidant of the graphite matrix and provides the formation of graphene macrocations. As positive charges appear on the graphene planes of a graphite matrix, anionic species present in the intercalating solution start to penetrate into the interlayer space. Simultaneously anionic species of two types, HSO_4^- and $HCrSO_7^-$, solvated by sulfuric acid intercalate in the interlayer space to form compounds of bi- and(or) cointercalation containing hydrosulfate and hydrochromosulfate anions. The possibility for the formation of chromosulfuric acid in mixtures of concentrated sulfuric and chromic acids has been shown in [3–5], and the formation of similar compounds was detected experimentally during the electrochemical oxidation of a graphite intercalation compound with chromic anhydride in concentrated sulfuric acid [6].

When the graphite compound obtained is brought in contact with water, its molecules penetrate into peripheral regions of the carbon matrix interlayer space and enter into oxidation-hydrolytic reactions with the graphite matrix and intercalated species. Gases liberated in this process give rise to a slight initial expansion of the compound. Water molecules gradually diffuse further and further into the central part of the interlayer space, and the swelling front also gradually moves from a flake periphery to its center. In the course of the further hydrolysis, the central part of a graphite flake swells, which results in the disappearance of the ashtray shape and in the formation of evenly swollen particles within 4–5 h.

Most likely, oxygen-containing functional groups of the graphite oxide type [7] are formed simultaneously with moving of the front of oxidation-hydrolytic processes from the periphery of the interlayer space to its central part. Extremely reactive $OH^{\bullet}$ radicals formed by the oxidation of water with chromic or chromosulfuric acid [8, 9] can be responsible for the process. Apparently, it is the formation of such oxygen-containing functional groups that ensures high thermal expansion factors K_v and a low temperature of the onset of final product expansion (about 220°C). Possibly, the formation of such functional groups in the interlayer space of the graphite matrix is almost finished at the duration of the starting GH hydrolysis of 4–5 h.

CONCLUSIONS

(1) The liberation of carbon oxides (CO and CO_2) begins in the stage of treatment of the reaction mass with concentrated sulfuric acid. The evolution of gases continues throughout the time of graphite hydrosulfate hydrolysis and ceases only after drying of the final product.

(2) As the hydrolysis duration increases, the expansion factor of the final product increases and flattens out within 4–5 h.

(3) A significant amount of both larger and smaller particles, as compared to the starting graphite particles, appear in the product.

(4) A probable mechanism of the formation of residual graphite hydrosulfate has been suggested. Its key step is the formation of a compound of bi- and(or) cointercalation of graphite with sulfuric and chromosulfuric acids.

REFERENCES

1. Yaroshenko, A.P., Savos'kin, M.V., Magazinskii, A.N., et al., *Zh. Prikl. Khim.*, 2003, vol. 76, no. 8, pp. 1269–1272.

2. Skowronski, J.M., *Synth. Met*., 1998, vol. 95, no. 2, pp. 135–142.
3. Yatsimirskii, K.B. and Vasil'eva, V.N., *Zh. Neorg. Khim*., 1956, vol. 1, no. 9, pp. 1983–1990.
4. Lee, D.G. and Stewart, R., *J. Am. Chem. Soc*., 1964, vol. 86, no. 15, pp. 3051–3056.
5. Mishra, H.C. and Symons, M.C.R., *J. Chem. Soc*., 1962, no. 11, pp. 4411–4417.
6. Skowronski, J.M. and Shioyama, H., *Carbon*, 1995, vol. 33, no. 10, pp. 1473–1478.
7. Besenhard, J.O., Minderer, P., and Bindl, M., *Synth. Met*., 1989, vol. 34, nos. 1–3, pp. 133–138.
8. Pezzin, S.H., Rivera, J.F.L., Collins, C.H., and Collins, K.E., *J. Braz. Chem. Soc*., 2004, vol. 15, no. 1, pp. 58–65.
9. Atkinson, T.D., Fjellvag, H., and Kjekshus, A., *J. Solid State Chem*., 2004, vol. 177, no. 11, pp. 4351–4358.

ISSN 1070-4272, Russian Journal of Applied Chemistry, 2006, Vol. 79, No. 7, pp. 1072–1075. © Pleiades Publishing, Inc., 2006.
Original Russian Text © B.K. Kasenov, Zh.K. Tukhmetova, A.V. Boldashevskii, A. Nukhuly, Sh.B. Kasenova, S.M. Adekenov, A.M. Gazaliev, S.D. Fazylov, 2006, published in Zhurnal Prikladnoi Khimii, 2006, Vol. 79, No. 7, pp. 1082–1085.

PHYSICOCHEMICAL STUDIES OF SYSTEMS AND PROCESSES

Thermodynamic Properties of Cytisine Dithiocarbamate Derivatives

B. K. Kasenov, Zh. K. Tukhmetova, A. V. Boldashevskii, A. Nukhuly, Sh. B. Kasenova, S. M. Adekenov, A. M. Gazaliev, and S. D. Fazylov

Institute of Phytochemistry, Ministry of Education and Science of the Kazakhstan Republic, Karaganda, Kazakhstan
Pavlodar University, Pavlodar, Kazakhstan
Institute of Organic Synthesis and Coal Chemistry, Karaganda, Kazakhstan

Received January 11, 2006

Abstract—The heat of solution in water and the heat capacity in the range 173 K–T_m of triethylammonium, sodium, and potassium dithiocarbamates derived from cytisine were studied by calorimetry. The heats of combustion and melting and the standard enthalpies of formation of the compounds were calculated.

DOI: 10.1134/S1070427206070056

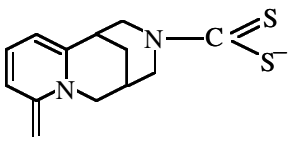
The researcher's interest in natural compounds considerably increased recently in the context of the modification and preparation on their basis of highly effective drugs.

Cytisine alkaloid is very interesting in this respect, because it enters into various chemical reactions and in the form of a 0.15% solution is used in medical practice under the brand Cytiton [1]. More than 200 cytisine derivatives of various structures are known. The scientists from the Institute of Organic Synthesis and Coal Chemistry (Karaganda) showed that a number of phosphorus-containing cytisine derivatives [Cytaphat, Cybunat] exhibit hepatoprotective properties. Cytisine dithiocarbamates are characterized by a broad spectrum of biological action and by low toxicity, which gives grounds to recommend them as drugs, preservatives, pesticides, etc. [2–5].

To estimate the reactivity with respect to molecules of different nature, it is of theoretical and practical significance to study the thermodynamic characteristics of these compounds. Therefore, the heat capacity in the range 173K–T_m and the enthalpy of solution in water of triethylammonium, sodium, and potassium dithiocarbamates derived from cytisine were studied by the dynamic and isothermal calorimetry. The standard enthalpy of formation and the heats of combustion and melting of the compounds were also determined.

EXPERIMENTAL

Cytisine-derived dithiocarbamates of triethylammonium $C_{18}H_{29}N_3OS_2$ (**I**), sodium $C_{12}H_{13}N_2OS_2Na$ (**II**), and potassium $C_{12}H_{13}N_2OS_2K$ (**III**) were synthesized, purified to the level of analytical purity, and studied calorimetrically.[1] The compounds under study have the following structural formulas:



X^+,

where X^+ is $HN(C_2H_5)_3$ (**I**), Na^+ (**II**), and K^+ (**III**).

The enthalpies of solution of the compounds in water was measured at dilutions (here and hereinafter, salt : water molar ratios) of 1 : 18000, 1 : 36000, and 1 : 72000 on a DAK-1-1A isothermal differential automated calorimeter. The calorimeter measures the integral heat flow passed from the ampule with substances through differentially connected thermal batteries and a massive central block of the microcalorimeter. The heats of solution were determined in the automated heat compensation mode. The thermal effects were recorded with a KSP-4 recording potentiometer and an IP-4 precision integrator. The

[1] The samples were synthesized by staffmembers of the Institute of Organic Synthesis and Coal Chemistry (Karaganda).

sample was placed into a thermostat preheated to a prescribed temperature and kept there for 2 h. Prior to testing, the device was calibrated by the Joule heat. To do this, a reference voltage was applied to a built-in heater, and the liberated power was measured. The calibration was checked by measuring the heat of solution of triply recrystallized potassium chloride at dilutions of 1 : 1600, 1 : 2400, and 1 : 3200. Five replicate measurements were made at each dilution, and the results were averaged. The average heat of solution of KCl in water at 298.15 K and the above dilutions (17.780 ± 2.62 kJ mol^{-1}) is in good agreement with the recommended reference value [6] (17.577 ± 0.340 kJ mol^{-1}) and with the reference data of [7] on the enthalpy of KCl solution at the indicated dilutions.

The experimental errors and the uniformity of their variance were treated by mathematical statistics using the Student and Bartlett criteria [8].

The results of the calorimetric measurements of the heats of solution of triethylammonium, sodium, and potassium dithiocarbamates derived from cytisine at various dilutions, where ΔH_s^m is the enthalpy of solution of a compound at a definite dilution, taking into account the molar weight of the solute, are presented in Table 1.

The heat capacities of the compounds were measured on an IT-s-400 calorimeter. Liquid nitrogen was used as a coolant. The specific heat capacity was measured at a step of 25 K, according to the technical characteristics. The time of the measurement, including the treatment of the experimental data, did not exceed 2.5 h. The standard admissible deviation of the device was ±10% according to the certificate.

The samples under study were placed into a metallic ampule of the measuring cell. Then they were continuously heated by a heat flow through the heat meter. The delay of the ampule temperature with respect to the temperature of the base was measured at 25 K intervals.

First, the heat meter was calibrated by the thermal conductivity K_t [9]. To do this, five replicate experiments, both with and without the copper sample in the ampule, were performed. As in the calibration, five replicate experiments were made at each tempertuare (25 K step) for each compound under study, with the results obtained averaged and treated by mathematical statistics [8].

At each measured temperature, the root-mean-square deviation $\bar{\delta}$ was calculated for the average value of the specific heat capacity and the random error $\mathring{\Delta}$, for the molar heat capacities.

Table 1. Enthalpies of solution of triethylammonium ($C_{18}H_{29}N_3OS_2$), sodium ($C_{12}H_{13}N_2OS_2Na$), and potassium ($C_{12}H_{13}N_2OS_2K$) dithiocarbamates derived from cytisine in water at various dilutions

Compound	Dilution	ΔH_{dis}^m, kJ mol^{-1}
$C_{18}H_{29}N_3OS_2$	1 : 18000	12.63 ± 0.18
	1 : 36000	14.89 ± 0.13
	1 : 72000	18.22 ± 0.21
$C_{12}H_{13}N_2OS_2Na$	1 : 18000	18.47 ± 0.33
	1 : 36000	19.88 ± 0.34
	1 : 72000	21.74 ± 0.33
$C_{12}H_{13}N_2OS_2K$	1 : 18000	15.72 ± 0.11
	1 : 36000	17.73 ± 0.33
	1 : 72000	19.30 ± 0.27

The work of the device was checked by measuring the heat capacity of α-Al_2O_3: the measured C_p^0 value of α-Al_2O_3 (298.15 K), equal to 76.0 J mol^{-1} K^{-1}, is in satisfactory agreement with the recommended value of 79.0 J mol^{-1} K^{-1} [10].

The experimental specific and molar heat capacities of the compounds are presented in Table 2.

To calculate the standard enthalpy of formation of the compounds, we determined their standard heats of combustion at 298.15 K by the Karash and Frost methods [11]. The heat of melting ΔH_m of cytisine dithiocarbamates was estimated from the empirical equation [12].

The experimentally determined enthalpies of solution of $C_{18}H_{29}N_3OS_2$, $C_{12}H_{13}N_2OS_2Na$, and $C_{12}H_{13}N_2OS_2K$ at various dilutions were then used for calculating ΔH^0 at infinite (standard) dilution. The mathematical treatment of the experimental data showed that, as in [13], the dependences of the enthalpy of solution ΔH_s^m (kJ mol^{-1}) on the molal concentration $m^{1/2}$ are described by the following equations:

$$\Delta H_s^m(C_{18}H_{29}N_3OS_2) = 23.30 - 198.22m^{1/2}, \quad (1)$$

$$\Delta H_s^m(C_{12}H_{13}N_2OS_2Na) = 24.76 - 116.26m^{1/2}, \quad (2)$$

$$\Delta H_s^m(C_{12}H_{13}N_2OS_2K) = 22.87 - 129.30m^{1/2}, \quad (3)$$

The standard enthalpies of solution of $C_{18}H_{29}N_3 \cdot OS_2$, $C_{12}H_{13}N_2OS_2Na$, and $C_{12}H_{13}N_2OS_2K$ in water at standard (infinite) dilution, obtained from these equations, are 23.3 ± 0.27, 24.76 ± 0.41, and 22.87 ± 0.30 kJ mol^{-1}, respectively.

Table 2. Experimental heat capacities of (**I**) triethylammonium, (**II**) sodium, and (**III**) potassium dithiocarbamates derived from cytisine

T, K	$C_p \pm \bar{\delta}$, J g^{-1} K^{-1}	$C_p^0 \pm \AA$, J mol^{-1} K^{-1}	$C_p \pm \bar{\delta}$, J g^{-1} K^{-1}	$C_p^0 \pm \AA$, J mol^{-1} K^{-1}	$C_p \pm \bar{\delta}$, J g^{-1} K^{-1}	$C_p^0 \pm \AA$, J mol^{-1} K^{-1}
	I (T_m = 163°C)		**II** (T_m = 215°C)		**III** (T_m = 235°C)	
173	0.5383 ± 0.0136	198 ± 14	0.2668 ± 0.0089	77 ± 7	0.3125 ± 0.0095	95 ± 8
198	0.5937 ± 0.0289	218 ± 19	0.3315 ± 0.0067	95 ± 5	0.4437 ± 0.0143	135 ± 12
223	0.7040 ± 0.0171	258 ± 17	0.3893 ± 0.0125	112 ± 10	0.5752 ± 0.0134	175 ± 11
248	0.7957 ± 0.0161	292 ± 16	0.4944 ± 0.0149	142 ± 12	0.7952 ± 0.0250	242 ± 21
273	0.9131 ± 0.0324	335 ± 33	0.5387 ± 0.0167	155 ± 13	0.9221 ± 0.0112	280 ± 9
298.15	1.0082 ± 0.0210	370 ± 21	0.6037 ± 0.0194	174 ± 16	1.1394 ± 0.0206	346 ± 17
323	1.1071 ± 0.0245	406 ± 25	0.6403 ± 0.0226	184 ± 18	1.3294 ± 0.0241	404 ± 20
348	1.2452 ± 0.0277	457 ± 28	0.7554 ± 0.0091	218 ± 7	1.4994 ± 0.0347	456 ± 29
373	1.3011 ± 0.0420	478 ± 43	0.7863 ± 0.0194	226 ± 16	–	–
398	–	–	0.8464 ± 0.0246	244 ± 20	–	–
423	–	–	0.9049 ± 0.0133	261 ± 11	–	–
448	–	–	0.9867 ± 0.0183	284 ± 15	–	–
473	–	–	1.0230 ± 0.0307	295 ± 25	–	–

Table 3. Calculated values of thermal chemical characteristics of compounds

Compound	$-\Delta H_{comb}^0$	ΔH_m	$-\Delta_f H^0(298.15)$, kJ mol^{-1}	
	kJ mol^{-1}		liquid	solid
$C_{18}H_{29}N_3OS_2$	10694 ± 313	320.2	1135	1455
$C_{12}H_{13}N_2OS_2Na$	6335 ± 314	177.6	1053	1231
$C_{12}H_{13}N_2OS_2K$	6335 ± 314	200.1	1025	1225

The experimental heat capacities were used to obtain the equations for the temperature dependences of the heat capacity of the compounds (J^{-1} mol^{-1} K^{-1}):

$$C_p^0(C_{18}H_{29}N_3OS_2) = -(68.52 \pm 4.93) + (1455.5 \pm 104.8) \times 10^{-3}T + (4.26 \pm 0.31) \times 10^5 T^{-2}, \quad (4)$$

$$C_p^0(C_{12}H_{13}N_2OS_2Na) = (34.25 \pm 2.51) + (566.06 \pm 41.55) \times 10^{-3}T - (16.6 \pm 1.22) \times 10^5 T^{-2}, \quad (5)$$

$$C_p^0(C_{12}H_{13}N_2OS_2K) = -(475.05 \pm 31.16) + (2586.4 \pm 169.7) \times 10^{-3}T + (36.69 \pm 2.41) \times 10^5 T^{-2}. \quad (6)$$

The Karash and Frost methods [12], which are the most suitable to take into account the contribution of different groups, were used to calculate the heat of combustion of the compounds. The average values of the enthalpy of combustion of the compounds in the liquid and solid states are given in Table 3.

Using the equations

$$2C_{18}H_{29}N_3OS_{2(l)} + 53.5O_{2(g)} = 36CO_{2(g)} + 29H_2O_{(l)} + 3N_{2(g)} + 4SO_{2(g)} - \Delta H_{comb}^0, \quad (7)$$

$$2C_{12}H_{13}N_2OS_2Na_{(l)} + 22O_{2(g)} = 24CO_{2(g)} + + 13H_2O_{(l)} + 2N_{2(g)} + 4SO_{2(g)} + Na_2O_{(s)} - \Delta H_{comb}^0, \quad (8)$$

$$C_{12}H_{13}N_2OS_2K_{(l)} + 22O_{2(g)} = 24CO_{2(g)} + 13H_2O_{(l)} + 2N_{2(g)} + 4SO_{2(g)} + K_2O_{(s)} - \Delta H_{comb}^0, \quad (9)$$

we calculated $\Delta_f H_{298.15}^0$ of the compounds in the liquid states (Table 3). The required values of $\Delta_f H_{298.15}^0$ $CO_{2(g)}$, $H_2O_{(l)}$, $N_{2(g)}$, $SO_{2(g)}$, $Na_2O_{(s)}$, and $K_2O_{(s)}$ were taken from [14].

Because at the standard temperature (298.15 K) the compounds considered are crystalline, we calculated $\Delta_f H_{298.15}^0$ for their solid state. To do this, we esti-

mated ΔH_m of the compounds from the empirical equation [12]

$$\Delta H_m/T_m = 20.72 \times 10^{0.00324M}. \quad (10)$$

The ΔH_m values calculated by Eq. (10) are presented in Table 3. Then, we calculated, using the equations

$$\Delta_f H^0(C_{18}H_{29}N_3OS_{2(s)}, 298.15) = \Delta_f H^0(C_{18}H_{29}N_3OS_{2(l)}, 298.15) - \Delta H_m, \quad (11)$$

$$\Delta_f H^0(C_{12}H_{13}N_2OS_2Na_{(s)}, 298.15) = \Delta_f H^0(C_{12}H_{13}N_2OS_2Na_{(l)}, 298.15) - \Delta H_m, \quad (12)$$

$$\Delta_f H^0(C_{12}H_{13}N_2OS_2K_{(s)}, 298.15) = \Delta_f H^0(C_{12}H_{13}N_2OS_2K_{(l)}, 298.15) - \Delta H_m, \quad (13)$$

the standard enthalpies of formation of crystalline triethylammonium, sodium, and potassium dithiocarbamates derived from cytisine (Table 3).

CONCLUSIONS

The standard enthalpies of solution in water, enthalpies of combustion and melting, and standard heats of formation in liquid and solid states were determined for triethylammonium, sodium, and potassium dithiocarbamates derived from cytisine. The equations describing the temperature dependence of the heat capacity in the range studied were derived for each compound.

REFERENCES

1. Mashkovskii, M.D., *Lekarstvennye sredstva* (Drugs), Moscow: Meditsina, 1977, vol. 1.
2. Terent'ev, A.P., Rukhadze, E.G., Dunina, V.V., and Drobyshevskaya, E.V., *Zh. Obshch. Khim.*, 1968, vol. 38, no. 4, pp. 715–720.
3. Dinzhumanova, R.T., Synthesis of Some Piperidine, Tetrahydro-, and 1,4-Dihydropyridine Derivatives as Novel Compounds with a Potential Biological Activity, *Cand. Sci. Dissertation*, Almaty, 1997.
4. Nazarov, I.N., *Izbrannye trudy* (Selected Works), Moscow: Akad Nauk SSSR, 1961, pp. 593–600.
5. Boldyrev, B.G. et al., in *Biopovrezhdenie v promyshlennosti: Mezhvuzovskii sbornik* (Biodamage in Industry: Intercollegiate Coll.), Gor'kii, 1983, pp. 44–51.
6. Mishchenko, K.P., and Poltoratskii, G.M., *Termodinamika i stroenie vodnykh i nevodnykh rastvorov elektrolitov* (Thermodynamics and Structure of Aqueous and Nonaqueous Solutions of Electrolytes), Leningrad: Khimiya, 1977.
7. *Termicheskie konstanty veshchestv: Spravochnik* (Thermal Constants of Substances: Reference Book), Glushko, V.P., Ed., Moscow: Nauka, 1982, issue 10, part 2.
8. Spiridonov, V.P., and Lopatkin, A.A., *Matematicheskaya obrabotka eksperimental'nykh dannykh* (Mathematical Treatment of Experimental Data), Moscow: Mosk. Gos. Univ., 1970.
9. Platunov, E.S., *Teplofizicheskie izmereniya v rezhime* (Thermal Measurements in the Various Modes), Moscow: Energiya, 1973.
10. Robie, R.A., Hewingway, B.S., and Fisher, J.K., *Thermodynamic Properties of Minerals and Related Substances at 298.15 K and 1 bar Pressure and at Higher Temperatures*, Washington: US Government 1978.
11. Kazanskaya, A.S., and Skoblo, V.A., *Raschety khimicheskikh ravnovesii* (Calculation of Chemical Equilibria), Moscow: Vysshaya Shkola, 1974.
12. Viktorov, V.V., *Metody vychisleniya fiziko-khimicheskikh velichin i prikladnye raschety* (Methods for Calculating Physicochemical Parameters and Applied Calculations), Moscow: Khimiya, 1977.
13. Krestov, G.A., *Termodinamika ionnykh protsessov v rastvorakh* (Thermodynamics of Ionic Processes in Solutions), Leningrad: Khimiya, 1984.
14. Ryabin, V.A., Ostroumov, M.A., and Svit, T.F., *Termodinamicheskie svoistva veshchestv: Spravochnik* (Thermodynamic Properties of Substances: Reference Book), Leningrad: Khimiya, 1977.

ISSN 1070-4272, Russian Journal of Applied Chemistry, 2006, Vol. 79, No. 7, pp. 1076–1082. © Pleiades Publishing, Inc., 2006.
Original Russian Text © E.P. Myul'khi, M.S. Khristenko, M.V. Andryukhova, 2006, published in Zhurnal Prikladnoi Khimii, 2006, Vol. 79, No. 7, pp. 1086–1092.

PHYSICOCHEMICAL STUDIES OF SYSTEMS AND PROCESSES

Choice of an Extractive Separating Agent for the 1-Pentanol–Cyclohexanone Binary Mixture

E. P. Myul'khi, M. S. Khristenko, and M. V. Andryukhova

Polzunov Altai State Technical University, Barnaul, Russia

Received July 11, 2005; in final form, January 2006

Abstract—Phase equilibria in binary and ternary systems formed by the components to be separated (1-pentanol, cyclohexanone) with extractive separating agents (methyl Cellosolve, butyl Cellosolve, aniline, acetophenone, ethylene glycol) were studied.

DOI: 10.1134/S1070427206070068

Catalytic synthesis of ε-caprolactam involves formation of a waste which is a multicomponent mixture containing solvents [1-butanol, cyclopentanone, 3-methyl-1-butanol, 1-pentanol (PL)] and target components of the main process [cyclohexanone (CON) and cyclohexanol]. Phase equilibria in binary [1] and ternary [2] subsystems of this mixture were studied previously. Fractional distillation [3] allows recovery of an alcoholic PL–CON fraction from this mixture. The phase equilibria in this system were studied in [4]; this system showed tangential zeotropy [5], which was confirmed by the shape of the *K* lines (*K* is the distribution ratio) and data on the azeotropy at different pressures. Such mixtures cannot be separated into components by common fractional distillation, because the required number of separation steps and reflux ratio are so large that the process becomes unfeasible. Therefore, we examined a specific separation method, extractive distillation.

The goal of this study was to choose an efficient separating agent (SA) for the PL–CON mixture. This task involves construction of a new system of higher dimension than the base system, with a definite type of the phase diagram, in which the relative fugacity of components of the base mixture would increase. The following strategy of choosing the best separating agent seems to be appropriate [5, 6]: (1) choice of a group of potential separating agents, (2) comparison of their selectivity by instrumental methods (prompt analysis [7, 8] and classical methods for studying liquid–vapor equilibria), and (3) experimental check and choice of the most efficient separating agent.

Components of the base mixture belong to different classes of organic compounds: 1-pentanol is an alcohol and cyclohexanone is a cyclic ketone. These compounds can be involved in various kinds of intermolecular interactions. When choosing an SA for such systems, it is advisable [5, 6] to use high-boiling homologs of the less volatile component. As possible agents for separating alcohol–ketone mixtures it is suggested [5] to use esters and glycols.

Taking into account these recommendations and the physicochemical properties and molecular structure of the components, we tested the following SAs for the PL–CON system: methyl Cellosolve (2-methoxyethanol, ethylene glycol monomethyl ether), butyl Cellosolve (2-butoxyethanol, ethylene glycol monobutyl ether), ethylene glycol (1,2-ethanediol), acetophenone (methyl phenyl ketone), and aniline. These polar solvents belong to different classes of organic compounds: glycols, ethylene glycol ethers, aromatic amines, and aromatic ketones. Their choice was governed by the fact that ethylene glycol and its monoethers are capable of forming three-dimensional networks of strong hydrogen bonds; primary amines (aniline) contain an active H atom and a donor –N atom; ketones (acetophenone) contain no active H atoms but are capable of hydrogen bonding via donor –O atoms.

EXPERIMENTAL

To assess the efficiency of the separaing agents chosen, we studied experimentally the liquid–vapor phase equilibria in binary and ternary systems formed by the components (PL, CON) with the suggested SAs. Experiments were performed at atmospheric pressure following the known procedures and using

Table 1. Parameters of the Antoine equation for the separating agents

Component	T_b, °C	A	B	C
Methyl Cellosolve (MC)	124.3	8.2655	1543.735	162.03
Butyl Cellosolve (BC)	170.6	7.6194	1639.863	175.00
Aniline (AN)	184.5	7.2500	1677.180	200.00
Ethylene glycol (EG)	197.0	8.7945	2615.394	244.75
Acetophenone (AC)	202.3	7.0600	1643.940	192.00

a Gillespie device [5, 9] for homogeneous mixtures and a modified Smirnova–Morachevskii device [10] for mixtures with phase separation. The boiling point was measured with a mercury thermometer (accuracy 0.1°C), with the correction for the protruding mercury column [11].

The compositions of the vapor and liquid phases were determined with an LKhM-80 chromatograph equilled with a flame ionization detector. We used metal columns 3 m long and 3 mm in diameter; as a stationary phase we used polyethylene glycol 1000, 30 wt % on Tsvetokhrom support. Measurement conditions: detector temperature 150°C, column temperature 120–140°C, flow rates: H_2 500, O_2 250, and N_2 (carrier gas) 10–50 ml min^{-1}. The mixture compositions were determined using internal normalization with calibration coefficients.

The mathematical description of the experimental data in the binary systems was made using the Wilson equation [12], by minizing the $(T_{calc} - T_{exp})^2$ functional by Barker's method with the program developed at NIIneftekhim (Ufa). The compositions of the equilibrium phases were calculated assuming ideal behavior of the components in the vapor phase. The temperature dependence of the vapor pressure was described by the Antoine equation

$$\log P = A - B(T + C),$$

where P is the vapor pressure (mm Hg); T, temperature (°C); and A, B, and C, constants of the Antoine equation.

The Antoine's constants for the SAs and their boiling points are given in Table 1; for PL and CON, these quantities are given in [1]. The temperature range to which these constants are applicable corresponds to the vapor pressure range 10–1500 mm Hg, i.e., it corresponds to the vapor pressure range used in industrial distillation processes.

Data on the phase equilibria in the binary systems are given in Table 2.

The results of the mathematical description of the experimental data on the binary systems are given in Table 3 in the form of the Wilson equation parameters λ_{12} and λ_{21} and the average and maximal deviations of the temperature. The binary interaction parameters ("large parameters") obtained are dimensionless.

From data on the phase equilibria in the binary systems, we can calculate the selectivity of the separating agents, $S = \alpha_{SA}/\alpha$, where α_{SA} and α are the relative fugacity coefficients of the PL–CON system averaged over the whole range of their concentrations, measured in the presence and in the absence of the separating agent, respectively [5]. The high selectivity is one of major requirements to an agent for extractive distillation. There are indications [13, 14] that of practical value are SAs that increase α from 1.0–1.1 to 1.5 and more, i.e., agents whose selectivity is higher than 1.5. The selectivity was calculated using the mixing functions Φ_{1S} and Φ_{2S} by the formulas [5]

$$\log S = (\Phi_{1S} - \Phi_{2S})/(1 - X_{SA}),$$

$$\Phi_{1S} = X_1 \log \gamma_1 + (1 - X_1) \log \gamma_{SA},$$

$$\Phi_{2S} = X_1 \log \gamma_2 + (1 - X_2) \log \gamma_{SA},$$

where X_1, X_2, X_{SA}, γ_1, γ_2, and γ_{SA} are, respectively, the mole fractions and activity coefficients of PL, CON, and separating agent.

The values of S, α, and α_{SA} at X_{SA} = 90 mol % are listed in Table 4.

The binary interaction parameters obtained allow simulation of the phase equilibria in multicomponent systems. When choosing the investigation objects, we took into account the fact that only two agents, acetophenone and ethylene glycol, exerted the positive effect, increasing the relative fugacity of the base components, $\alpha_{SA} > \alpha$. Therefore, we studied experimentally the phase equilibria in two systems: PL–CON–EG and PL–CON–AC. The X–Y–T dependences (X, liquid phase composition; Y, vapor phase compo-

Table 2. Data on equilibria in the binary systems at P = 760 mm Hg

System	Content of component 1, mol %		T_b, °C		Activity coefficient	
	in liquid, s_1	in vapor, y_1	T_{exp}	T_{calc}	γ_1	γ_2
MC (1)–PL (2)	8.39	12.95	136.5	136.2	0.9565	0.9995
	11.29	17.17	132.9	135.7	0.9597	0.9992
	17.60	25.80	135.8	134.6	0.9660	0.9981
	30.24	41.37	134.8	132.7	0.9768	0.9946
	45.18	57.30	130.8	130.6	0.9865	0.9887
	58.79	69.91	128.9	128.9	0.9927	0.9820
	67.46	77.15	127.9	127.9	0.9956	0.9772
	80.09	86.76	126.1	126.6	0.9984	0.9694
	88.34	92.51	125.0	125.7	0.9995	0.9640
MC (1)–CON (2)	10.08	34.98	143.2	143.2	1.6318	1.0091
	20.00	49.19	137.8	137.8	1.4286	1.0329
	31.00	58.96	134.1	134.2	1.2760	1.0733
	40.50	65.40	132.0	132.0	1.1845	1.1185
	50.00	71.03	130.3	130.3	1.1187	1.1724
	57.00	74.94	129.2	129.2	1.0826	1.2175
	64.00	78.78	127.4	128.3	1.0548	1.2670
	80.00	87.70	126.7	126.4	1.0151	1.3968
	90.00	93.63	125.6	125.5	1.0036	1.4900
PL (1)–BC (2)	8.90	10.07	170.4	170.8	0.9419	0.9960
	16.00	19.14	170.4	170.3	0.9426	0.9863
	31.20	41.06	168.1	168.1	0.9458	0.9801
	47.10	64.86	163.5	163.7	0.9586	0.9730
	56.70	77.45	159.6	159.7	0.9092	0.9643
	66.00	87.09	154.9	155.0	0.9781	0.9546
	77.50	94.93	148.7	148.6	0.9827	0.9495
	88.70	98.72	142.7	142.5	0.9972	0.9452
CON (1)–BC (2)	6.75	15.51	167.7	167.7	1.6966	1.0092
	8.80	18.70	167.0	167.0	1.5949	1.0144
	14.30	25.79	165.6	165.6	1.4011	1.0315
	16.92	28.71	165.1	165.1	1.3362	1.0406
	31.45	42.74	162.7	162.7	1.1346	1.0940
	51.70	60.45	160.3	160.3	1.0375	1.1621
	66.45	72.98	158.8	158.8	1.0126	1.2025
	80.70	84.77	157.5	157.4	1.0030	1.2340
PL (1)–AN (2)	5.80	40.65	167.1	166.7	2.9587	1.0061
	10.00	52.07	160.6	160.6	2.6010	1.0172
	15.00	59.84	155.8	156.0	2.2725	1.0369
	17.40	62.45	154.1	154.4	2.1431	1.0488
	31.20	71.56	148.3	148.5	1.6278	1.1445
	55.50	80.42	143.6	143.4	1.2032	1.4370
	64.50	83.43	142.3	142.0	1.1218	1.5961
	78.40	88.64	140.4	140.1	1.0423	1.9174
CON (1)–AN (2)	9.58	45.32	165.6	165.5	3.6070	1.0192
	19.00	57.24	159.4	159.4	2.6849	1.0702
	29.60	63.32	156.3	156.4	2.0686	1.1632
	40.00	66.85	154.7	154.8	1.6888	1.2958
	50.70	69.60	153.7	153.9	1.4290	1.4882
	60.00	71.89	153.1	153.2	1.2713	1.7204
	72.00	73.39	152.6	152.3	1.1311	2.1595
	82.00	79.72	152.6	152.7	1.0177	3.4083
PL (1)–EG (2)	9.99	72.51	160.4	161.0	3.6106	1.0390
	20.00	78.84	156.7	155.1	2.3204	1.1211

Table 2. (Contd.)

System	Content of component 1, mol %		T_b, °C		Activity coefficient	
	in liquid, s_1	in vapor, y_1	T_{exp}	T_{calc}	γ_1	γ_2
	30.00	81.88	152.5	152.1	1.7539	1.2293
	40.00	84.25	149.1	149.8	1.4488	1.3615
	50.05	86.49	147.3	147.7	1.2654	1.5202
	60.00	88.77	144.7	145.8	1.1508	1.7066
	69.98	91.19	143.1	143.8	1.0773	1.9283
	80.00	93.84	141.9	141.8	1.0318	2.1930
	90.00	96.75	140.1	139.8	1.0075	2.5088
CON (1)–EG (2)	9.52	34.97	186.6	186.6	1.7424	1.0142
	19.60	51.20	180.4	180.4	1.4250	1.0488
	29.71	61.59	176.1	176.2	1.2515	1.0937
	39.95	69.69	172.4	172.4	1.1481	1.1448
	51.66	77.39	168.7	168.7	1.0780	1.2067
	70.03	87.42	163.4	163.5	1.0228	1.3068
	79.03	91.64	160.9	161.0	1.0100	1.3559
	91.04	96.66	157.9	157.9	1.0016	1.4205
PL (1)–AC (2)	10.00	49.16	180.2	180.1	1.4773	1.0014
	20.03	68.67	166.8	167.3	1.4355	1.0066
	29.96	78.63	158.8	158.8	1.3899	1.0176
	40.00	84.67	153.7	152.6	1.3394	1.0382
	49.90	88.59	147.3	148.1	1.2853	1.0741
	60.00	91.40	144.8	144.7	1.2258	1.1388
	69.98	93.47	142.2	142.1	1.1634	1.2566
	80.00	95.14	139.9	140.3	1.0987	1.4972
	90.00	96.75	139.0	138.9	1.0371	2.1045
CON (1)–AC (2)	7.80	23.97	194.0	194.2	1.2346	1.0000
	15.30	40.93	188.2	187.8	1.2345	1.0000
	24.00	55.47	182.1	181.4	1.2315	1.0006
	30.24	63.45	176.9	177.4	1.2273	1.0019
	39.90	72.96	170.2	171.9	1.2166	1.0068
	43.40	75.74	169.1	170.2	1.2113	1.0099
	53.44	82.25	165.3	165.8	1.1913	1.0261
	65.59	87.14	163.3	162.1	1.1628	1.0626
	71.60	90.16	160.2	159.7	1.1332	1.1221

Table 3. Results of describing the equilibria by the Wilson equation

System	λ_{12}	λ_{21}	ΔT_{av}	ΔT_{max}
			°C	
MC (1)–PL (2)	0.7749	1.3101	0.31	0.74
MC (1)–CON (2)	0.4937	1.0417	0.12	0.97
PL (1)–BC (2)	3.3146	0.7246	0.28	0.69
CON (1)–BC (2)	0.2127	1.7361	0.31	0.92
PL (1)–AN (2)	0.3730	0.6952	0.24	0.38
CON (1)–AN (2)	0.3407	0.4030	0.50	1.02
PL (1)–EG (2)	0.1475	0.8121	0.65	1.01
CON (1)–EG (2)	0.2869	1.3899	0.47	0.85
PL (1)–AC (2)	1.6014	0.1137	0.36	1.07
CON (1)–AC (2)	2.0460	0.0746	0.51	0.78

sition; T, boiling point) were obtained for selected compositions of the ternary systenms (Table 5).

The reliability of the previously obtained binary interaction parameters (Table 3) was checked by comparing the results of simulation of the phase equi-

Table 4. Comparative evaluation of the efficiency of the separating agents

Parameter	MC	BC	AN	AC	EG
S	0.7	0.6	0.9	1.7	2.8
α	1.4	1.4	1.4	1.4	1.4
α_{SA}	1.0	0.9	1.2	2.4	4.0

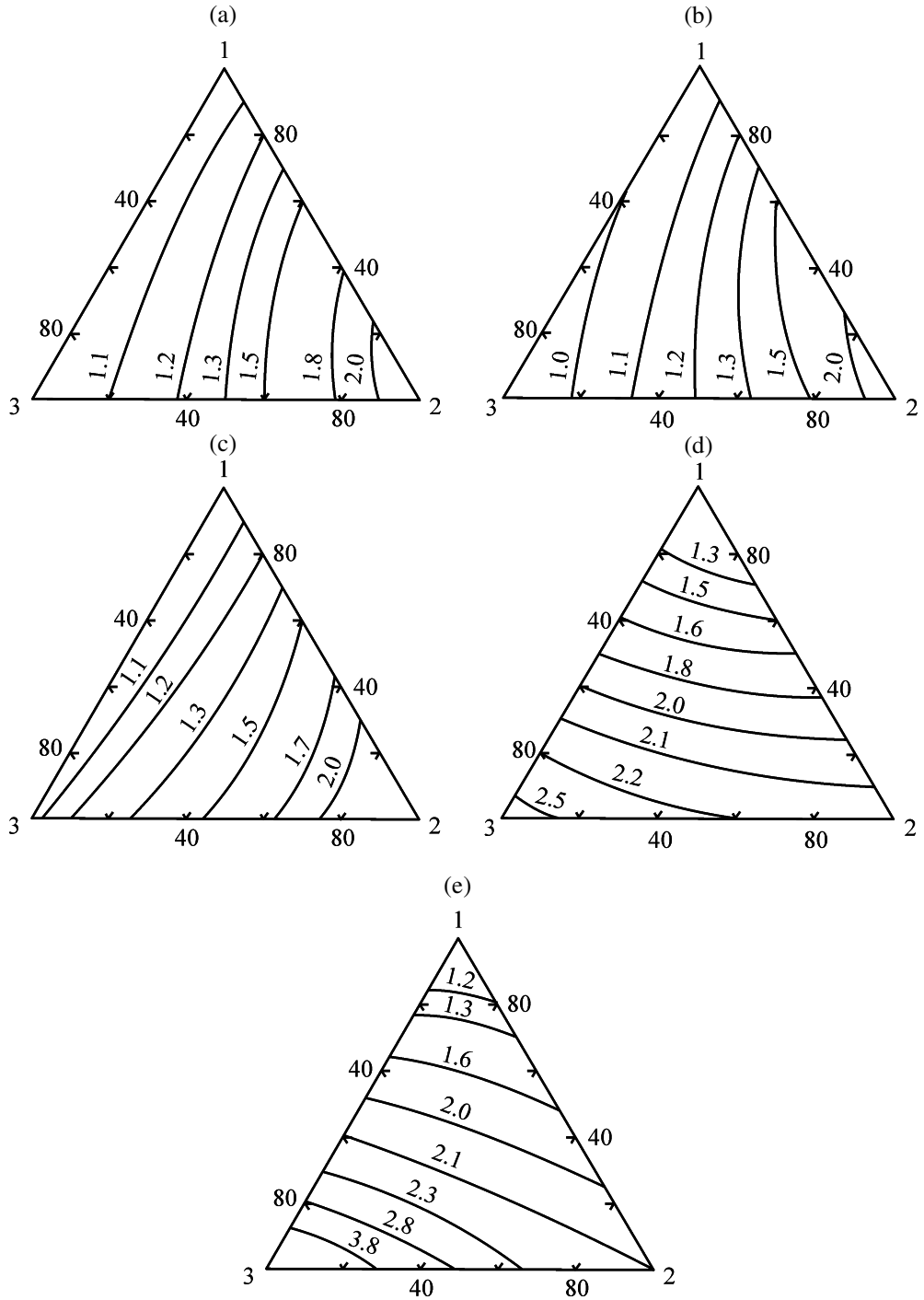


Fig. 1. Structures of iso-α-line diagrams of the ternary systems: (a) PL (1)–CON (2)–MC (3), (b) PL (1)–CON (2)–BC (3), (c) PL (1)–CON (2)–AN (3), (d) PL (1)–CON (2)–AC (3), and (e) PL (1)–CON (2)–EG (3).

libria in the ternary systems with the experimental data. The deviations of the calculated boiling points and vapor phase compositions for the ternary systems from the experimental data are given in Table 6; they show that the Wilson equation adequately describes these systems.

The efficiency of the separating agents can be assessed most comprehensively using the isolines of the relative fugacity. The iso-α-lines in the systems PL (1)–CON (2)–SA (3) (Fig. 1) were plotted with a computer [12] using the Wilson equation parameters given in Table 3.

Table 5. Liquid–vapor equilibrium in ternary systems at P = 760 mm Hg

Liquid phase composition, mol %		Vapor phase composition, mol %		T, °C
x_1	x_2	y_1	y_2	
PL (1)–CON (2)–EG (3)				
64.50	17.00	80.00	13.05	143.0
48.21	32.00	69.20	24.00	144.3
33.00	47.58	55.94	40.17	148.6
15.43	63.76	34.56	58.30	152.0
46.85	12.57	78.00	10.04	147.0
36.71	25.00	67.97	22.01	150.1
24.00	37.34	55.10	33.35	152.4
10.96	48.76	36.12	51.03	157.0
32.06	8.10	76.46	7.97	151.1
24.76	15.32	66.81	15.60	153.0
16.10	23.45	54.31	27.29	157.5
8.77	30.98	35.45	41.72	160.6
16.09	4.00	72.46	5.55	157.9
12.51	7.87	63.52	12.10	160.5
8.00	12.07	51.34	20.47	162.7
3.59	16.00	32.80	32.45	170.8
PL (1)–CON (2)–AC (3)				
63.59	16.00	82.14	13.25	141.4
47.06	33.13	68.87	26.59	143.4
32.12	47.97	53.59	41.65	146.3
15.87	64.08	33.12	61.39	151.1
48.41	12.07	79.98	11.29	146.9
35.75	26.00	67.28	24.74	148.0
24.67	35.68	52.01	38.14	150.7
12.53	48.11	31.40	57.17	156.6
33.15	8.00	74.25	9.47	154.9
24.52	16.13	62.16	20.27	155.1
16.74	24.03	47.27	33.21	160.0
7.86	32.00	27.75	49.94	164.7
16.05	4.59	59.47	7.00	167.0
11.71	8.13	48.76	15.01	171.6
8.83	12.15	35.80	25.41	173.7
4.00	16.71	20.01	35.76	178.5

Table 6. Results of simulation of the ternary systems using the Wilson equation

System	ΔT_{av}, °C	ΔT_{max}, °C	ΔY_{av}, mol %
PL (1)–CON (2)–AC (3)	0.97	1.56	2.87
PL (1)–CON (2)–EG (3)	1.07	1.13	2.02

Figures 1a and 1b and Table 2 show that methyl Cellosolve and butyl Cellosolve exhibit negative deviations from the ideality ($\gamma < 1$) in the interaction with 1-pentanol, which is due to association of the components with each other. In the interaction with cyclohexanone, there are weak positive deviations; as a result, the relative fugacity of 1-pentanol in the presence of methyl Cellosolve and butyl Cellosolve decreases, and that of cyclohexanone increases.

Aniline (Fig. 1c) is also inefficient and shows a similar pattern; according to experimental data, cyclohexanone and aniline form a minimal heteroazeotrope with a boiling point of 152.6°C.

Acetophenone and ethylene glycol (Figs. 1d, 1e), in contrast to the separating agents mentioned above, increase the fugacity of 1-pentanol, providing positive changes in the relative fugacity; ethylene glycol is apparently more efficient.

Thus, our results lay the foundation for further quantitative studies aimed to elucidate the relationships of the extractive distillation and determine the optimal process parameters of the separation.

CONCLUSIONS

(1) Acetophenone and ethylene glycol are efficient as extractive separating agents for the 1-pentanol–cyclohexanone mixture.

(2) Nine binary mixtures formed by 1-pentanol and cyclohexanone with separating agents are zeotropic.

(3) In the cyclohexanne–aniline system, a minimal heteroazeotrope with a boiling point of 152.6°C was revealed.

(4) The Wilson equation adequately reproduces the features of the liquid–vapor equilibria in the binary and ternary systems under consideration.

REFERENCES

1. Katunina, E.P., Marchenko, I.M., Chervova, O.V., et al., *Zh. Prikl. Khim.*, 1992, vol. 65, no. 9, pp. 2028–2033.
2. Katunina, E.P., Marchenko, I.M., Polyakova, L.V., et al., *Zh. Prikl. Khim.*, 1992, vol. 65, no. 11, pp. 2485–2489.
3. Katunina, E.P., Development of a Process for the Regeneration of Solvents from the Alcoholic Fraction from ε-Caprolactam Production Using Extractive Distillation in the Batch Mode, *Cand. Sci. Disserta-*

tion, Angarsk, 1995.

4. Marchenko, I.M., Oleneva, O.V., Polyakova, L.V., et al., *Zh. Prikl. Khim.*, 1989, vol. 62, no. 12, pp. 2759–2764.
5. Kogan, V.B., *Azeotropnaya i ekstraktivnaya rektifikatsiya* (Azeotropic and Extractive Distillation), Leningrad: Khimiya, 1971.
6. Halland, C.D., Gallum, S.E., and Lockett, M.Y., in *Encyclopedia of Chemical Processes and Design*, New York, 1982, vol. 16, pp. 96–133.
7. Marchenko, I.M., Polyakova, L.V., Shaganova, S.B., et al., *Zh. Prikl. Khim.*, 1991, vol. 64, no. 11, pp. 2664–2668.
8. Khristenko, M.S., Polyakova, L.V., and Garber, Yu.N., *Zh. Prikl. Khim.*, 1990, vol. 63, no. 8, pp. 2010–2016.
9. Kogan, V.B., Fridman, V.M., and Kafarov, V.V., *Ravnovesie mezhdu zhidkost'yu i parom* (Liquid–Vapor Equilibrium), Moscow: Nauka, 1966, vol. 1.
10. Smirnova, N.A. and Morachevskii, A.G., *Vestn. Leningr. Gos. Univ.*, 1959, issue 2, no. 10, pp. 106–108.
11. Weissberger, A. and Proskauer, E.S., *Organic Solvents. Physical Properties and Methods of Purification*, Riddick, J.A., and Toops, E.E., Eds., New York: Interscience, 1955.
12. Reid, R.G., Prausnitz, J.M., and Sherwood, T.K., *The Properties of Gases and Liquids*, New York: McGraw-Hill, 1977.
13. Barnicki, S.D. and Fair, J.R., *Ind. Eng. Chem. Res.*, 1990, vol. 29, no. 3, pp. 421–432.
14. Inyutin, S.M., Computer-Aided Choice of Separating Agents in Azeotropic and Extractive Distillation, *Cand. Sci. Dissertation*, Barnaul, 1983.

ISSN 1070-4272, Russian Journal of Applied Chemistry, 2006, Vol. 79, No. 7, pp. 1083–1086. © Pleiades Publishing, Inc., 2006.
Original Russian Text © Yu.Yu. Eroshina, N.N. Nikitina, A.V. Kostochko, 2006, published in Zhurnal Prikladnoi Khimii, 2006, Vol. 79, No. 7, pp. 1093–1096.

PHYSICOCHEMICAL STUDIES OF SYSTEMS AND PROCESSES

Study of Compatibility in Polymeric System Cellulose Nitrate–Cellulose Acetate by Reversed-Phase Gas Chromatography

Yu. Yu. Eroshina, N. N. Nikitina, and A. V. Kostochko

Kazan State Technological University, Kazan, Tatarstan, Russia

Received July 7, 2005; in final form, February 2006

Abstract—Thermodynamic compatibility in the polymeric system cellulose nitrate–cellulose acetate is studied by reversed-phase gas chromatography. The excess enthalpy ΔH_{ji}^E, entropy ΔS_{ji}^E, and Gibbs energy ΔG_{ji}^E of mixing of the components, and also the Flory–Huggins interaction parameter χ_{ji} are estimated.

DOI: 10.1134/S107042720607007X

Mixing of two or more polymers of different chemical nature shows promise as a way to design composite materials surpassing the individual polymers in performance characteristics. Study of cellulose nitrate–cellulose acetate (CN–CA) blends is of interest from the standpoint of improving performance and extending application area of such practically important products as technical films, paint-and-varnish materials, and slow-burning powder composites.

Prediction of properties of such products is based on the thermodynamic data characterizing the interaction between components of the blend. Thermodynamic characteristics of polymer blends can be derived from experimental data obtained by reversed-phase gas chromatography (RGC) [1, 2]. The theory of the method has been developed for the case of ideal gas chromatography, i.e., it is valid for an infinitely dilute solution of a sorbate in the stationary phase on the condition of the establishment of the sorption–desorption equilibrium. Such equilibrium is observed in the case of a sufficiently fast diffusion of the solvent molecules to the polymer, which is realized, e.g., in polymers in the hyperelastic state at a temperature 50° above the glass-transition point. Our test subject, CN, cannot be brought to the hyperelastic state by heating, and the experimental temperature range is bound by thermal degradation of the polymer. Nevertheless, despite all the factors distorting the experimental results, RGC was successively used to study polymers in the glassy state [3, 4]. Yampol'skii and Durgar'yan [3] observed an exothermic effect in mixing glassy polyvinyltrimethylsilane with low-molecular-weight organic compounds (sorbates), as well as a strong dependence of the excess functions of mixing on the molar volume of the sorbate. Based on these and published data, the authors concluded that the observed trends are general in the sorption on glassy polymers. Data of [4] reveal that the retained volume, the basic parameter to be determined in the experiment, is influenced by the thickness of the polymeric film and the amount of the sorbate introduced into the chromatographic column. Results obtained in this study were also obtained after optimization of the experimental conditions (film thickness, volume of the sorbate sample, and carrier gas flow rate) for the CN–CA system.

EXPERIMENTAL

In the study we used commercial CN (nitrogen content 12%; viscosity-average molecular weight in ethyl acetate M = 72 500) and laboratory CA samples obtained by homogeneous acetylation (acetate group content 51.0%; viscosity-average molecular weight in acetone M = 57 000).

The thermodynamics of interaction of the components in the CN–CA system was studied by RGC on a Khrom-4 chromatograph with a thermal conductivity detector. Helium was used as a carrier gas. We used Teflon columns 0.6 m long and 5 mm in diameter. As an inert support we used diatomite with a particle size of 0.2–0.4 mm. Samples of the individual polymers and polymer blends were deposited onto the support by evaporation from 5% solution in

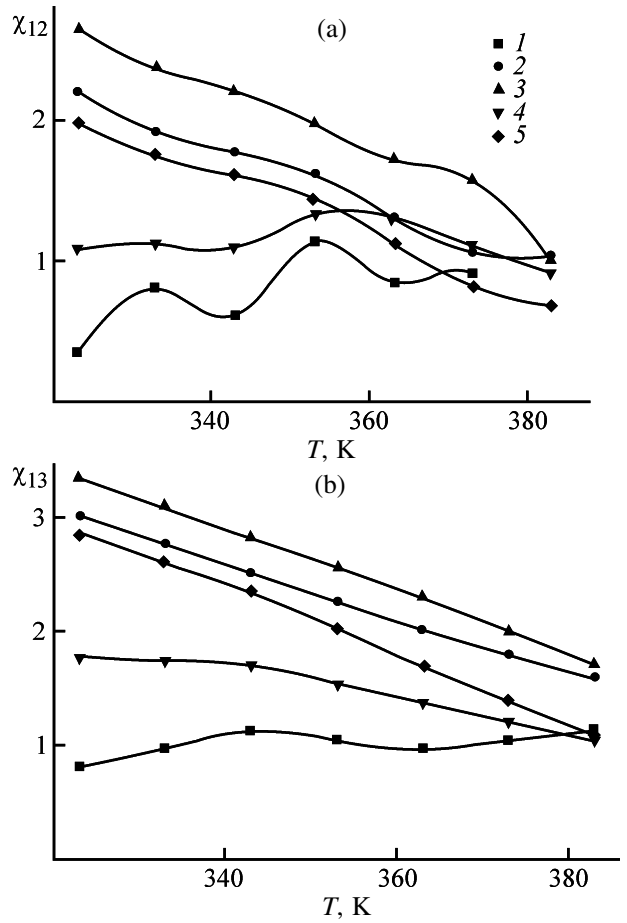


Fig. 1. Flory–Huggins interaction parameters χ_{ij} of the sorbates with (a) CN and (b) CA. (*T*) Temperature. (*1*) Methanol, (*2*) chloroform, (*3*) CCl_4, (*4*) ethanol, and (*5*) hexane.

acetone [1]. In all cases, the content of the polymer phase was 10% relative to the inert support weight. Such a content provided full coverage of the support surface with a polymer film, allowing establishment of the sorption–desorption equilibrium by virtue of the accessibility of the functional groups of the polymer for the sorbate. The measurements were carried out at 323–383 K. The CA content in the blends was 3–97%.

As sorbates we selected a series of low-molecular-weight organic solvents including hexane, methanol, ethanol, benzene, toluene, ethyl acetate, chloroform, and carbon tetrachloride with close boiling points near 60–80°C.

The sorbates (0.1 μl) were introduced into the column using a microsyringe. It was demonstrated in the preliminary experiments that the sorbate concentration in the experiments corresponded to infinite dilution, i.e., to the initial part of the sorption isotherm.

From the retained volume of the sorbates on the individual polymers and their blends we estimated the activity coefficients γ_1^∞ and Flory–Huggins parameters χ_{1k} over the entire temperature range using the equations suggested in [1]. The excess thermodynamic functions (enthalpy ΔH_{1k}^E, entropy ΔS_{1k}^E, and Gibbs energy ΔG_{1k}^E) of mixing of the individual polymers and their blends with the sorbates were estimated by Eqs. (1)–(3):

$$\Delta G_{1k}^E = RT\ln\gamma_1^\infty, \quad (1)$$

$$\Delta H_{1k}^E = R[\partial\ln\gamma_1^\infty/\partial(1/T)], \quad (2)$$

$$\Delta S_{1k}^E = (\Delta H_{1k}^E - \Delta G_{1k}^E)/T, \quad (3)$$

where the index k refers to the polymer phase.

Then we estimated the excess molar thermodynamic functions of mixing of two polymers ΔG_{23}^E, ΔG_{23}^E, ΔG_{23}^E, and χ_{23}, as the differences between the parameters of retention of the sorbate on the individual polymers and their blends [2].

Reversed-phase gas chromatography is among the methods allowing quantitative characterization of the thermodynamic compatibility of polymers in binary composites. Generally, the compatibility is characterized by the sign and value of ΔG_{23}^E and χ_{23} [1, 2, 5].

The interaction parameter is influenced by a variety of factors, the major of which are the natures of the polymers and sorbates [6, 7]. The problem of selection of the sorbate was discussed in [4, 6, 7]. Most often, the authors recommend taking an ideal solvent demonstrating equal affinity for both polymers, to eliminate the effect of the sorbate on the thermodynamics of the interaction in the system. However, it is practically impossible to find such a solvent for a giver pair of solvents. Therefore, the decision on the sorbate is restricted to low-molecular-weight solvents, which, equally interacting with both polymers, have a minimal effect on the experimental results.

The interaction of the polymers with the sorbates was characterized by the Flory–Huggins interaction parameters χ_{12} (CN–sorbate) and χ_{13} (CA–sorbate) (Fig. 1). In this case, we focused primarily on the closeness of χ_{12} and χ_{13}. The condition $(\chi_{12} - \chi_{13}) \approx 0$, suggesting the same interaction of the sorbate with both polymers, is met to the maximal extent for hexane and carbon tetrachloride over the entire temperature range. Additionally, we analyzed the temperature dependences of the interaction parameters. The temperature dependences of χ_{12} and χ_{13} are linear with the correlation coefficients of 0.99 and 0.96

for CCl_4 and hexane, respectively. However, the molar volume is higher for hexane (136 against 100 cm^3 mol^{-1} for CCl_4), which negatively affects its ability to penetrate the structure of the cellulose esters. Therefore, carbon tetrachloride could be recommended as the optimal sorbate for the system in hand.

The concentration dependences of ΔG_{23}^E and χ_{23} in the CN–CA system, determined from the experimental data on the retention of CCl_4, are given in Figs. 2 and 3.

Figure 2 shows that the concentration dependences of the Gibbs energy of mixing are in the region of negative values over the entire temperature range studied, suggesting that CN and CA are thermodynamically compatible. The dependences are convex-concave in shape, which is typical of systems with phase separation. The second derivative of the Gibbs energy with respect to the composition $\partial^2 \Delta G_{23}^E / \partial w_3^2$ (w_3 is the mass fraction of CA in the system) more than once changes its sign as the CA concentration in the system increases, suggesting that the stability of the system with respect to diffusion is strongly influenced by the composition [8].

Our analysis shows that the negative Gibbs energy of mixing in the CN–CA system is provided by the entropy factor. The increase in the absolute value of ΔG_{23}^E with the temperature and the fulfillment of the inequalities $(\partial^2 \Delta H_{23}^E / \partial w_3^2)_T < 0$ and $(\partial^2 \Delta S_{23}^E / \partial w_3^2)_T < 0$ allows classification of the investigated system with polymer blends with upper critical point of mixing [8], for which the thermodynamic compatibility increases with the temperature.

One of the criteria of thermodynamic compatibility of polymers in blends is a negative or nearly zero value of χ_{23} [9]. Figure 3 shows that this condition is not met for the blend with c_{CA} = 50% over the entire temperature range and for the blends with c_{CA} = 60 and 80% at 373 K.

The lowest χ_{23} values, i.e., the maximal compatibility of the components, are obtained for the blends with the CA concentration of 3, 7, 93, and 97%. At c_{CA} from 10 to 90%, χ_{23} is close to zero, being only slightly dependent on the temperature and composition.

In addition to experimental determination, we estimated the thermodynamic functions of mixing using the Flory–Huggins theory [2]. According to this theory, at the total volume of the mixture V, the Gibbs energy of mixing can be determined by Eq. (4)

$$\Delta G_{23}^E = (RTV/v_r)[(\varphi_2/r_2)\ln\varphi_2 + (\varphi_3/r_3)\ln\varphi_2 + \chi_{23}\varphi_2\varphi_3], \quad (4)$$

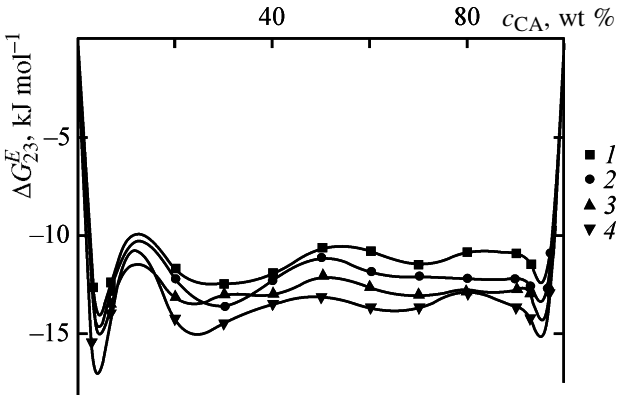


Fig. 2. Gibbs energy of mixing ΔG_{23}^E as a function of the component concentration c_{CA} in the CN–CA system over the temperature range 323–383 K, as determined by RGC. Temperature (K): (*1*) 323, (*2*) 343, (*3*) 363, and (*4*) 383; the same for Figs. 3, and 4.

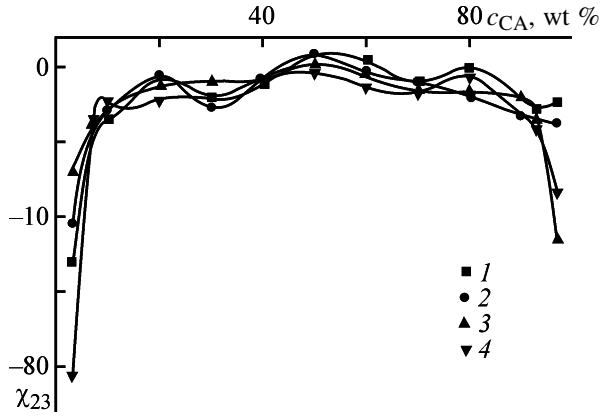


Fig. 3. Interaction parameter χ_{23} as a function of the component concentration c_{CA} in the CN–CA system over the temperature range 323–383 K.

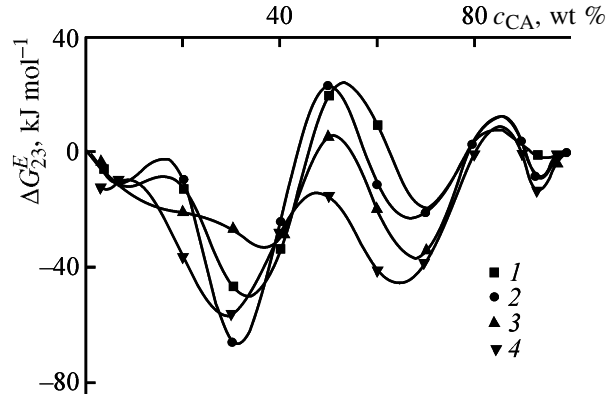


Fig. 4. Gibbs energy of mixing ΔG_{23}^E as a function of the component concentration c_{CA} in the CN–CA system, as estimated by the Flory–Huggins theory.

where v_r is the segment volume equal to the volume of the repeated unit of the chain (this parameter is taken the same for both polymers); r_2 and r_3 are the numbers of segments in polymer nos. 2 and 3; and

φ_2 and φ_3, volume fractions of the polymers in the blend.

Comparison of the Gibbs energies of mixing obtained from the experimental retention volume of the sorbate (Fig. 2) and by Eq. (4) with the experimental χ_{23} (Fig. 4) shows that the Flory–Huggins theory can be used as only a qualitative model of the interaction between the components in the CN–CA system.

CONCLUSIONS

(1) Carbon tetrachloride is the optimal sorbate for studying cellulose nitrate–cellulose acetate blends.

(2) The components of the cellulose nitrate–cellulose acetate system are thermodynamically compatible at 323–383 K. The system is unstable with respect to the diffusion, the entropy factor being responsible for the negative Gibbs energies of mixing.

(3) The compatibility in the cellulose nitrate–cellulose acetate system increases with increasing temperature and with decreasing fraction of one of the component to below 10%.

REFERENCES

1. Nesterov, A.E. and Lipatov, Yu.S., *Obrashchennaya gazovaya khromatografiya v termodinamike polimerov* (Reversed-Phase Gas Chromatography in Studying the Thermodynamics of Polymers), Kiev: Naukova Dumka, 1976.
2. Nesterov, A.E. and Lipatov, Yu.S., *Termodinamika rastvorov i smesei polimerov* (Thermodynamics of Polymer Solutions and Blends), Kiev: Naukova Dumka, 1984.
3. Yampol'skii, Yu.P. and Durgar'yan, S.G., in *Thermodynamics of Sorption in Glassy Polymers: Chromatography and Thermodynamics*, Stryek, R., Ed., Warsaw, 1986, pp. 35–42.
4. Tyukova, I.S., Tager, A.A., Morozov, E.V., and Lavrikova, Yu.G., *Vysokomol. Soedin., Ser. A*, 1990, vol. 32, no. 9, pp. 2002–2005.
5. Barashkov, O.K. and Barshtein, R.S., *Vysokomol. Soedin., Ser. A*, 1988, vol. 30, no. 4, pp. 686–699.
6. Tager, A.A., Blinov, V.S., and Kirillova, T.I., *Kompoz. Polim. Mater.*, 1987, issue 32, pp. 20–23.
7. Blokhina, S.V., Alekseeva, O.V., and Prusov, A.N., *Vysokomol. Soedin., Ser. B*, 1998, vol. 40, no. 12, pp. 2099–2104.
8. Tager, A.A., *Osnovy ucheniya o rastvorakh neelektrolitov: Uchebnoe posobie* (Principles of the Theory of Nonelectrolyte Solutions: A Handbook), Yekaterinburg: Ural. Univ., 1993.
9. Askadskii, A.A., *Usp. Khim.*, 1999, vol. 68, no. 4, pp. 349–364.

ISSN 1070-4272, Russian Journal of Applied Chemistry, 2006, Vol. 79, No. 7, pp. 1087–1090. © Pleiades Publishing, Inc., 2006.
Original Russian Text © K.A. Gavronskaya, A.A. Petushkov, S.M. Shilov, V.N. Pak, 2006, published in Zhurnal Prikladnoi Khimii, 2006, Vol. 79, No. 7, pp. 1097–1100.

SORPTION AND ION-EXCHANGE PROCESSES

Adsorption and Luminescence Properties of Tb^{3+}-Modified Perfluorosulfonic Acid Membrane

K. A. Gavronskaya, A. A. Petushkov, S. M. Shilov, and V. N. Pak

Herzen Russian State Pedagogical University, St. Petersburg, Russia

Received March 1, 2006

Abstract—After treatment of perfluorosulfonic acid membrane MF-4SK with an aqueous solution of $TbCl_3$, the protons in sulfo groups are completely replaced by the hydrated terbium cations. Specific features of the water adsorption and its influence on the luminescence of the modified membrane were examined.

DOI: 10.1134/S1070427206070081

High chemical stability of the fluorocarbon skeleton, combined with developed pore structure, high transparency, and pronounced cation-exchanging power, make Nafion perfluorosulfonic acid membranes (PFSMs) suitable as carriers for preparation of a broad spectrum of polyfunctional composite materials [1–8]. Possible applications of modified PFSMs include development of fuel cells [1, 2], catalysts [3, 4], optically active media, in particular, intercalation compounds of aromatic substances [5], fluorescent dyes [6], and compounds of transition metals [7, 8]. At the same time, the prospects for preparation of film luminophores incorporating compounds of rare-earth elements from PFSMs still remain to be elucidated. In this connection, we carried out in this study modification of a polyfluorosulfonic acid membrane with terbium(III) and examined the adsorption and luminescence properties of the resulting material.

EXPERIMENTAL

Our study was concerned with 0.25-mm-thick perfluorosulfonic acid membranes MF-4SK produced in Russia. They were purified by boiling in concentrated nitric acid for 2–3 h and thoroughly washing with distilled water to negative reaction for NO_3^- anions. The quality of purification of the membranes was judged from the transparency in the visible and near UV ranges, as well as from the lack of luminescence excited with nitrogen laser. The content of the accessible sulfo groups was determined by the following procedure. The membranes with the known weight were immersed in an aqueous solution of NaOH for 1 day so that all the protons in the sulfo groups be replaced by sodium cations. Next, the alkali was titrated with hydrochloric acid and, from the difference in the solution concentrations before and after contacting the PFSM, the content of the sulfo groups [$–SO_3H$] was determined. The membranes were modified by keeping in 0.003–0.01 M aqueous solutions of terbium(III) chloride. The establishment of equilibrium and the content of the cations fixed in the membrane were judged from the decrease in the optical density of the impregnating solution (Fig. 1) in the maximum λ_{max} = 219 nm of the narrow absorption band corresponding to the $4f^8 \rightarrow 4f^7 5d$ transition of terbium(III) [9], for which the extinction coefficient was preliminarily determined to be ε = 326.6 l mol^{-1} cm^{-1}. The amount of the sulfo groups [$–SO_3H$]* spent in the reaction was estimated from the change in pH of the impregnating solution. The modified membranes were washed with distilled water to complete removal of the excess impregnating solution and hydrochloric acid from the pore space. Given below are the results of the analytical and adsorption measurements for the modified membranes:

[$–SO_3H$], mmol g^{-1}	0.840
[$–SO_3H$]*, mmol g^{-1}	0.828
[Tb^{3+}], mmol g^{-1}	0.276
[$–SO_3H$]*/[Tb]	3
V_p, cm^3 g^{-1}	0.200
V_p^*, cm^3 g^{-1}	0.145
ΔV_p/[Tb^{3+}], nm^3 atom^{-1}	0.332
r^*, nm	0.43

Water adsorption by the initial and modified membranes was examined gravimetrically at the relative

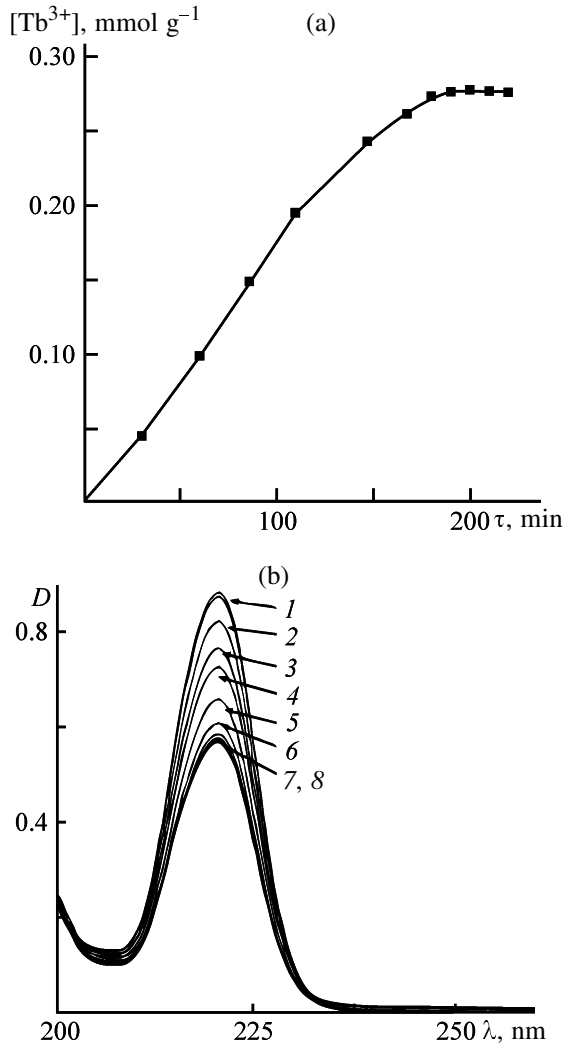


Fig. 1. Plots of (a) sorption of terbium(III) and (b) optical density D in the absorption band of the 0.003 M aqueous solution of $TbCl_3$ during its contact with the PFS membrane with a weight of 0.068 g. ([Tb^{3+}]) Terbium(III) content in the membrane and (λ) wavelength. (τ) Contact time, min: (*1*) 0, (*2*) 30, (*3*) 60, (*4*) 90, (*5*) 120, (*6*) 150, (*7*) 180, and (*8*) 210.

humidity $p/p_0 = 0.1–0.95$ set in desiccators with sulfuric acid solutions. The samples were preliminarily dehydrated by keeping over phosphorus(V) oxide to constant weight, since the heat treatment of the membranes even at temperature near 100°C is accompanied by decreases in the pore volume and the number of the accessible sulfo groups [10].

The luminescence in the visible range and the lifetime of the excited state of the membranes before and after water adsorption was recorded in air-tight quartz cells at room temperature on a setup assembled on the basis of a KSVU-1 universal spectral-computing complex [11]. As the excitation source served an

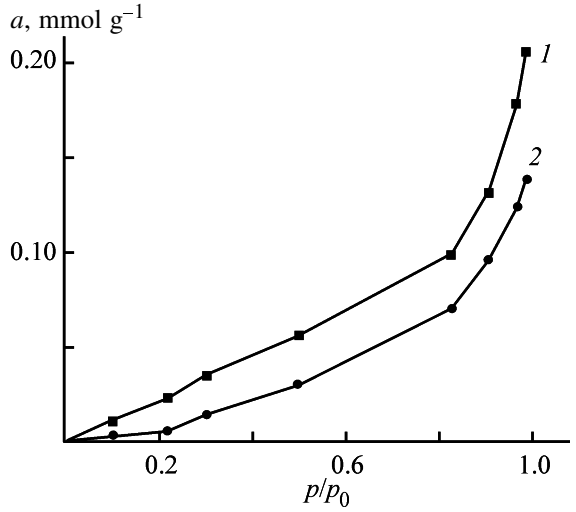


Fig. 2. Isotherms of water adsorption a by the (*1*) initial and (*2*) modified membranes. (p/p_0) Relative humidity.

LGI-21 pulsed nitrogen laser (λ = 337 nm, τ = 10 ns); the luminescence was recorded at an angle of 90° with respect to the laser beam.

Our analytical and adsorption data suggest that terbium sorption in the PFS membrane involves virtually all the accessible sulfo groups and follows the mechanism providing a definite stoichiometry: The experimentally determined molar ratio of the reacted sulfo groups to fixed terbium(III) [$–SO_3H$]* : [Tb^{3+}] was close to 3 in all the experiments. The predominant occurrence of the reaction by the scheme

$$3(–SO_3H) + TbCl_3 \cdot nH_2O \rightarrow (–SO_3–)_3Tb(H_2O)_n + 3HCl$$

with complete compensation of the charge of the Tb^{3+} cations, as we revealed, is determined, most likely, not only by the uniform distribution but also by certain mobility of the exchange centers in the PFSM: Flexible fluorocarbon chains connecting the sulfo groups with the polymeric σ skeleton [1–8] are able of additional orientation in the pore space of the membrane. The fact that the sorption kinetics is close to linear (Fig. 1) suggests that the process is controlled by diffusion of $TbCl_3$ in the pore space of the membranes. Rapid chemical stage and strong fixation of the cations, confirmed by their invariable content in the membrane after prolonged contact with water, suggest formation of a surface species of terbium(III) sulfonate with a low solubility, like its polycrystalline "analog" $Tb_2(SO_4)_3$ [9].

Replacement of the protons in the sulfo groups by terbium(III) cations significantly suppresses the water adsorption throughout the humidity range examined (Fig. 2). It should be noted that the bound water can-

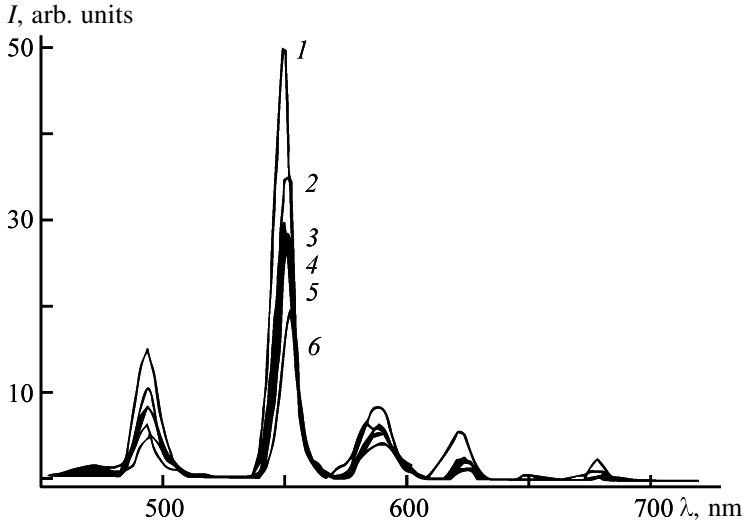


Fig. 3. Luminescence spectra of the modified membrane (*1*) before and (*2–6*) after water adsorption. (*I*) Luminescence intensity and (λ) wavelength. Relative humidity p/p_0: (*2*) 0.1, (*3*) 0.2, (*4*) 0.5, (*5*) 0.8, and (*6*) 0.95.

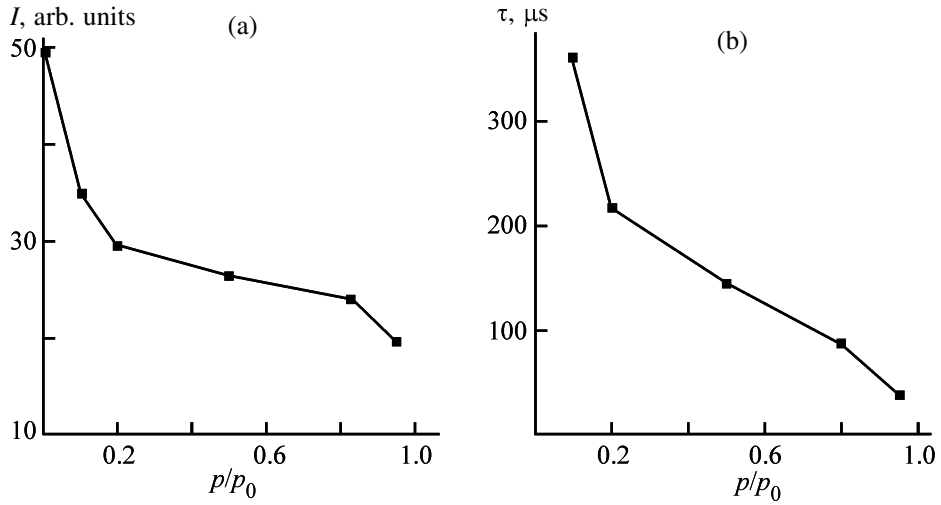


Fig. 4. (a) Intensity I of the band of the main transition $^5D_4 \rightarrow {}^7F_5$ in the luminescence spectrum of Tb^{3+} in the membrane and (b) lifetime of the excited state τ as a function of the relative humidity p/p_0.

not be completely removed by preliminary dehydration of the membranes under mild conditions. Most of the molecules that are strongly fixed in the coordination sphere of terbium(III) are preserved and serve as adsorption centers that are appreciably less reactive than the sulfo groups of the initial membranes. Notably, the sorption space of the PFSM after modification is strongly contracted (Fig. 2). The ratio of the parameter $\Delta V_p = (V_p - V_p^*) = 0.055$ cm^3 g^{-1}, estimated from the end points of the isotherms, to the terbium(III) content in the membrane gives the apparent volume $\Delta V_p/[Tb^{3+}]$ occupied by the hydrated cation, which, in the spherical model approximation, yields a reasonable value of its radius $r^* = 0.43$ nm.

The luminescence spectrum of the modified membrane dried over P_2O_5 (Fig. 3) exhibits five out of seven bands due to radiative transitions from the excited $^5D_4$ to the ground ^7F_j (j = 6, 5, 4, 3, 0) state of terbium(III) [9]. Good resolution of the spectrum suggests a high symmetry of the coordination surrounding of the central atom; the band with a maximum at 546 nm, having the maximal intensity, corresponds to the hypersensitive $^5D_4 \rightarrow {}^7F_5$ transition. It is well known that the water molecules coordinated to the rare-earth metal cations cause nonradiative degradation of the excitation energy via its transfer to high-frequency vibrations ν_{O-H} [9]. Nevertheless, despite low content of bound terbium(III) and the

presence of water in its coordination sphere, the modified membranes dried over P_2O_5 exhibit a visually observed bright green luminescence excited with a nitrogen laser. However, subsequent water adsorption significantly decreases the luminescence intensity (Fig. 3). Sharp simultaneous decreases in the intensity of the hypersensitive band and the lifetime of the excited state of terbium were recorded in a narrow range of the humidities $p/p_0 \leq 0.2$ (Figs. 3, 4). It should be noted in this connection that the ratio of the adsorption at $p/p_0 = 0.2$ to the content of terbium(III) in the membrane corresponds exactly to one water molecule per cation. This suggests that, in the initial stage of adsorption, formation of the nearest water surrounding is complete for most of the terbium(III) cations. Further monotonic quenching of the luminescence is due, most likely, to the gradual, sterically hindered hydration of the cations localized in difficultly accessible sites of the pore space of the membrane.

CONCLUSION

Attaining stable brightness parameters of luminescence of terbium(III)-modified perfluorosulfonic acid membranes requires protecting the luminescence centers against water adsorption. At the same time, the sensor properties of the resulting film luminophore with respect to water can be used in the luminescence control of systems and working items requiring dry atmosphere.

REFERENCES

1. Broka, K. and Ekdunge, P., *J. Appl. Electrochem.*, 1997, vol. 27, no. 2, pp. 117–123.
2. Yen, T.J., Fang, N., Zhang, X., et al., *Appl. Phys. Lett.*, 2003, vol. 83, no. 19, pp. 4056–4058.
3. Pillai, K.C., Kumar, A.S., Zen, J.-M., *J. Mol. Catal. A*, 2000, vol. 160, no. 2, pp. 277–285.
4. Byun, H. and Lee, T., *Desalination*, 2002, vol. 144, no. 3, pp. 419–424.
5. Blatt, E., Launikonis, A., and Mau, A., *Aust. J. Chem.*, 1987, vol. 40, no. 1, pp. 1–12.
6. Karasz, M.A. and Wnek, G.E., *Electrochim. Acta*, 1998, vol. 42, no. 10–11, pp. 1623–1628.
7. Finlayson, M.F., Park, K.H., Kakuta, N., et al., *J. Luminescence*, 1988, vol. 39, no. 4, pp. 205–214.
8. Wang, Y. and Mahler, W., *Opt. Commun.*, 1987, vol. 61, no. 3, pp. 233–236.
9. Poluektov, N.S., Kononenko, L.I., Efryushina, N.P., and Bel'tyukova, S.V., *Spektrofotometricheskie i lyuminestsentnye metody opredeleniya lantanoidov* (Spectrophotometric and Luminescence Methods of Determination of Lanthanides), Kiev: Naukova Dumka, 1989.
10. Petushkov, A.A., Shilov, S.M., and Pak, V.N., *J. Luminescence*, 2006, vol. 116, nos. 1–2, pp. 127–131.
11. Andreeva, D.A. and Puzyk, M.V., *Opt. Spektrosk.*, 2003, vol. 95, no. 5, pp. 764–765.

ISSN 1070-4272, Russian Journal of Applied Chemistry, 2006, Vol. 79, No. 7, pp. 1091–1095. © Pleiades Publishing, Inc., 2006.
Original Russian Text © D.E. Chikrst, O.V. Cheremisina, M.V. Ivanov, A.A. Chistyakov, I.T. Zhadovskii, 2006, published in Zhurnal Prikladnoi Khimii, 2006, Vol. 79, No. 7, pp. 1101–1105.

SORPTION AND ION-EXCHANGE PROCESSES

Isotherm of Exchange of Nickel and Sodium Cations on Iron–Manganese Nodules

D. E. Chikrst, O. V. Cheremisina, M. V. Ivanov, A. A. Chistyakov, and I. T. Zhadovskii

St. Petersburg State Mining Institute, St. Petersburg, Russia

Received October 26, 2005; in final form, February 2006

Abstract—The isotherm of ion exchange of Ni^{2+} and Na^{+} cations on iron–manganese nodules was studied. The ion exchange was described by an equation similar to the Langmuir isotherm. The limiting sorption and the apparent ion-exchange constant were calculated.

DOI: 10.1134/S1070427206070093

Wastewater and spent process solutions containing nonferrous metal cations in amounts exceeding the maximum permissible concentration are presently treated by the reagent method. This method yields a large amount of precipitates with a rather high content of valuable metals, which are virtually irrevocably lost [1]. Other waste treatment techniques: electrocoagulation, electrodialysis, reverse osmosis, and ultrafiltration, are used only locally. Therefore, a particular importance is acquired by sorption and ion exchange, which allow effective recovery of nonferrous metals from waste solutions of various salt compositions [1].

It was shown in [2, 3] that iron–manganese nodules (IMNs) are a promising natural sorbent for treatment of natural and deep-well water used for drinking purposes and of wastewater and spent process solutions.

Deposits of iron–manganese nodules widely occur on the bottom of the Gulf of Finland in the Baltic Sea, being mostly found on the bottom surface [4].

Two types of deposits are found in the Gulf of Finland. Those of the first type lie at a depth of 60 m and more in the southern and northern parts of the gulf. Nodules in these deposits are spherical formations with grain size of 1–2 to 30 mm (predominant diameter 1–16 mm), strength of 100 kPa (1 kg cm^{-2}), and density of 1.6 g cm^{-3}. Tentative estimates of the nodule resources in this region yield 25–30 million tons, which corresponds to a mainland deposit of medium profitableness [5].

Another deposit lies at smaller depths of 25–30 m in the Kopor'e bay. The predominant nodule diameter is 3–5 mm, and less frequently up to 15–30 mm. In the summer of 2005, the first 2500 tons of a nodule-containing material was recovered from this deposit from depths of up to 30 m [5].

The technology of IMN recovery has been developed by Dobretsov and co-workers [5]. The possibility of utilization of spent nodules by the pyrometallurgical method at metallurgical plants by a technology involving the recovery of nonferrous metals (manganese, copper, cobalt, nickel) has been studied [6, 7].

An analysis of the substance composition of IMNs demonstrated [8] that the main part of the ore component is represented by iron and manganese hydroxides and nonferrous metals are in an isomorphic association with minerals of manganese and iron. A characteristic feature of IMNs is their hygroscopicity caused by the developed surface of the material (58% porosity). The environmentally safe IMN material has the form of ready-for-use rounded grains with a granulometric composition suitable for use in poured filters.

Table 1 lists the chemical composition (the most important components) of nodules from the Kopor'e bay, determined by X-ray fluorescence analysis, in comparison with that reported in [3]. Because the specific surface area of the nodules is 43.81 $m^2 g^{-1}$ [9], the content of MnO_2 in these nodules exceeds that in imported pyrolusite sorbents of the Aquamandix brand. The sorption capacity of IMNs for iron(II) is 46.34 to 123.56 g kg^{-1}, against 3.25 g kg^{-1} for the imported analog [9]. Granulation of IMNs with bentonite clays makes the capacity of the modified

Table 1. Chemical composition of nodules from the Kopor'e bay

Component	Content, wt %, determined by X-ray fluorescence analysis	Average content, wt %, found in [3]
Total Mn in terms of MnO_2	35.87	33.80
Fe_2O_3	36.23	20.19
Sr	0.263	0.0027
Cu	0.339	0.0034
Pb	0.449	0.0034
Zn	0.074	0.0057
SiO_2	–	17.87
Al_2O_3	–	4.49
P_2O_5	–	2.70

nodules 2–3 times higher, which is due to an increase in the specific surface area in the course of grinding and granulation with the binder.

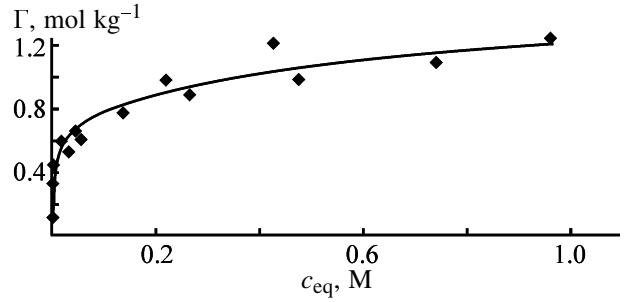
The large resources of IMNs, their comparatively large specific surface area and high sorption capacity, and the possibility of their utilization make application of IMNs in purification techniques economically efficient.

This study is concerned with the isotherm of exchange of sodium and nickel ions on the IMN surface.

Natural samples of iron–manganese nodules contain various exchange cations, and, therefore, the IMNs were converted prior to experiments into the sodium form, because sodium ions are displaced with any cations [8].

An air-dry IMN sample with a grain size of –0.25+0.10 mm was soaked in a NaOH solution (5 wt %) for 5 days with intermittent stirring. The alkali solution was daily replaced with a fresh one. The IMN conversion into the sodium form was considered complete when the activity of Na^+ cations after treatment of IMNs with an alkaline solution reached a constant value. The activity of Na^+ ions in alkaline solutions diluted upon contact with IMNs to concentrations of 0.001–0.01 mol kg^{-1} using a volumetric flask was measured with an ion-selective electrode and an Anion ion meter. After that, IMNs were washed many times with distilled water to pH 7 in a water extract and dried to an air-dry state. The ion exchange was studied on model aqueous $NiSO_4$ solutions with a Ni(II) concentration of 0.0107–1.0846 M at 298 K. The sorption value, Γ (mol kg^{-1}), of nickel cations was determined under static conditions at a ratio between the volume of the liquid phase and the weight of the solid phase V/m = 10 ml g^{-1} and a 5-g portion of IMNs from the difference of the concentrations of the starting (c_0) and equilibrium (c_{eq}) solutions by the formula

$$\Gamma = (c_0 - c_{eq})V/m. \quad (1)$$



Isotherm of sorption Γ of nickel(II) ions on the IMN surface. (c_{eq}) Equilibrium concentration of nickel(II) ions.

The nickel sulfate solution with a weighed portion of IMNs was agitated with a magnetic stirrer at a rate of 400 rpm to the equilibrium state. The equilibrium corresponding to a constant solution concentration was attained within 5–6 h; in the experiments, the time of phase contact was set to be no less than 10 h.

After an experiment, the solution was filtered through a blue-band filter, and the equilibrium concentration of sodium ions was measured with an ion-selective electrode and an Anion ion meter, and that of nickel(II) ions, by the photometric method [10]. This method is based on the formation of a colored nickel(II) complex with dimethylglyoxime (Chugaev reagent), occurring in an alkaline medium in the presence of an oxidizing agent.

Solution aliquots with volumes of 2 to 10 ml, depending on the content of nickel ions, were transferred into a 50-ml vessel. Then, 5 ml of an aqueous $Na_2S_2O_8$ solution (5 wt %), 5 ml of a solution of the Rochelle salt ($C_4H_4O_6KNa \cdot H_2O$) (20 wt %), and 5 ml of a solution of dimethylglyoxime in a sodium hydroxide solution (5 wt %) were added, and the mixture was brought to the mark with water. The content of nickel(II) in the solution under study was determined from the intensity of the absorption band associated with the nickel complex with dimethylglyoxime at a wavelength of 540 nm. This technique makes it possible to determine the content of nickel(II) in the range 2–20 μg in 25 ml of a solution. The determination is hindered by substances that have their own coloration and cations that form hydroxide precipitates in an alkaline medium (Fe^{2+}, Fe^{3+}, Al^{3+}, Mg^{2+}, Cu^{2+}, Mn^{2+}).

The figure shows the isotherm of sorption of nickel(II) cations on the IMN surface, plotted using the

Table 2. Results of experiments on ion exchange of Na^+ for Ni^{2+}

c_0	c_{eq}	Γ, mol kg^{-1}	$1/\Gamma$, mol^{-1} kg	$\gamma_\pm$		c_{Na^+}, M
M				Na_2SO_4	$NiSO_4$	
0.0107	0.0000	0.1071	9.3350	0.681	0.536	0.0214
0.0330	0.0006	0.3238	3.0885	0.564	0.301	0.0648
0.0451	0.0013	0.4375	2.2860	0.532	0.256	0.0875
0.0777	0.0175	0.6021	1.6609	0.469	0.187	0.1204
0.0847	0.0321	0.5264	1.8998	0.455	0.175	0.1053
0.1110	0.0453	0.6569	1.5223	0.427	0.152	0.1314
0.1157	0.0554	0.6033	1.6575	0.420	0.147	0.1207
0.2142	0.1373	0.7695	1.2996	0.352	0.105	0.1539
0.3200	0.2216	0.9843	1.0159	0.309	0.085	0.1969
0.3539	0.2645	0.8935	1.1192	0.297	0.080	0.1787
0.5546	0.4328	1.2179	0.8211	0.250	0.063	0.2436
0.5768	0.4786	0.9820	1.0184	0.245	0.061	0.1964
0.8523	0.7435	1.0884	0.9188	0.203	0.050	0.2177
1.0846	0.9606	1.2400	0.8065	0.178	0.044	0.2480

data of Table 2: initial and equilibrium concentrations of nickel ions, c_0 and c_{eq}; sorption value of nickel ions, Γ; reciprocal sorption value of nickel ions, $1/\Gamma$; equilibrium concentrations of sodium ions, c_{Na^+}; and mean ionic activity coefficients $\gamma_\pm$ of Na_2SO_4 and $NiSO_4$ [11]. Measurements of the equilibrium concentration of sodium ions with an ion-selective electrode confirmed the equivalence of exchange of sodium ions for those of nickel. The isotherm presented in the figure is described by the Freundlich equation $\Gamma = 1.218\,c_{eq}^{0.195}$ with an approximation confidence $R^2 = 0.96$.

The ion exchange of nickel and sodium ions was thermodynamically described on the assumption that the solid phase is ideal, i.e., with the activity coefficients of ions in the sorbed state disregarded. The previously suggested [12] method of linearization of an analog of the Langmuir equation was used. The equation describing the mass action law for the ion-exchange reaction

$$2Na_s^+ + Ni_{aq}^{2+} \rightleftarrows 2Na_{aq}^+ + Ni_s^{2+}$$

has the form

$$K = \frac{\Gamma_{Ni^{2+}} a_{Na^+}^2}{\Gamma_{Na^+}^2 a_{Ni^{2+}}}, \quad (2)$$

where K is the apparent exchange constant; $\Gamma_{Ni^{2+}}$ and Γ_{Na^+}, sorption values of nickel and sodium ions (mol kg^{-1}); and a_{Na^+} and $a_{Ni^{2+}}$, activities of the ions in solution (mol kg^{-1}).

The limiting sorption capacity for the ions (Γ_∞, equiv kg^{-1}) is given by

$$\Gamma_\infty = \Gamma_{Na^+} + 2\Gamma_{Ni^{2+}},$$

where the sorption values of the ions are expressed in moles per kilogram.

Equation (1) can be brought to the form

$$K = \frac{\Gamma_{Ni^{2+}}[Na^+]^2\gamma_{\pm(Na_2SO_4)}^2}{\Gamma_{Na^+}^2[Ni^{2+}]\gamma_{\pm(NiSO_4)}} = \frac{\Gamma_{Ni^{2+}} c_{Na^+}^2 \gamma_{\pm(Na_2SO_4)}^2}{(\Gamma_\infty - 2\Gamma_{Ni^{2+}})^2 c_{eq}\gamma_{\pm(NiSO_4)}}. \quad (3)$$

Equation (2) was transformed to formula (4), which is similar to the equation of the Langmuir isotherm (3):

$$\Gamma = \Gamma_\infty Ka(1 + Ka)^{-1}, \quad (4)$$

$$\Gamma_{Ni^{2+}}^{1/2} = \Gamma_\infty(Kc_{eq})^{1/2}[c_{Na^+}(\gamma_{\pm(Na_2SO_4)}^2/\gamma_{\pm(NiSO_4)})^{1/2} + 2(\Gamma_{Ni^{2+}}Kc_{eq})^{1/2}]^{-1}. \quad (5)$$

The linear form of the equation has the following appearance:

$$1/\Gamma_{Ni^{2+}} = 2/\Gamma_\infty + c_{Na^+}(\gamma_{\pm(Na_2SO_4)}^2/\gamma_{\pm(NiSO_4)})^{1/2} \times [\Gamma_\infty(K\Gamma_{Ni^{2+}}c_{eq})^{1/2}]^{-1}. \quad (6)$$

which is similar to the linear Langmuir equation:

$$1/\Gamma = 1/\Gamma_\infty + 1/(\Gamma_\infty Ka).$$

The dependence of the reciprocal sorption value of nickel ions, $1/\Gamma_{Ni^{2+}}$, on the argument

$$f(c) = c_{Na^+}(\gamma^2_{\pm(Na_2SO_4)}/\gamma_{\pm(NiSO_4)})^{1/2}(\Gamma_{Ni^{2+}}c_{eq})^{-1/2}$$

is approximated by the linear equation

$$1/\Gamma_{Ni^{2+}} = 1.190 + 0.403f(c),$$

with an approximation confidence $R^2 = 0.99$. This equation was used to calculate the limiting sorption capacity for the ions, $\Gamma_\infty = 1.68$ equiv kg^{-1}, the apparent ion-exchange constant $K_{Na^+/Ni^{2+}} = 2.18$, and the Gibbs energy of exchange of nickel ions for those of sodium on the IMN surface, $\Delta G^0_{298} = -1.932$ kJ mol^{-1}.

The limiting sorption capacity for strontium ions on the IMN surface $\Gamma_\infty = 0.97$ equiv kg^{-1} [13], which exceeds by a factor of 1.73 that for nickel ions, $\Gamma_\infty = 1.68$ equiv kg^{-1}. Apparently, this is due to the fact that the landing site for Ni^{2+} ions is smaller. The specific surface area of IMNs, $S_{sp} = 43.1$ m^2 g^{-1} [9] and the limiting sorption capacity for nickel ions of 0.84 mol kg^{-1} were used to estimate the landing site area for Ni^{2+} ions (m^2):

$$S_M = \frac{S_{sp}}{\Gamma_\infty N_A} = \frac{43.81 \times 10^3}{0.84 \times 6.02 \times 10^{23}} = 8.66 \times 10^{-20},$$

where N_A is the Avogadro number.

Hence follows that the radius of a sorbed Ni^{2+} ion is 166 pm. This value exceeds the crystallographic radius of Ni^{2+} by Bokii (74 pm) [11]. The experimentally determined radius of the nickel ion is to be regarded as the mean effective radius of hydrated Ni^{2+} ions.

The resulting value of the radius of Ni^{2+}_{aq} on the IMN surface is smaller than the radius of the Sr^{2+}_{aq} cation sorbed on IMNs (219 pm) [13] and smaller than the radius of hydrated Fe^{3+} ions on clay (348 pm) [12].

The radius of strontium ions sorbed on clay (302 pm) [14] coincides with the Stokes radius of hydrated ion (309 pm) [11]. Consequently, the strontium ion is sorbed in the totally hydrated form on clay and is partly dehydrated on IMNs. The hydrated radius of the nickel(II) ion should by larger than that of strontium because of the stronger polarizing action resulting from the smaller crystallographic radius of the nickel ion at the same ion charges ($r_{Sr} = 120$ pm and $r_{Ni} = 74$ pm [11]). This assumption is also confirmed by the lower equivalent electrical conductivity of the strontium ion ($\lambda_{0,Ni^{2+}} = 1.080 \times 10^{-2}$ and $\lambda_{0,Sr^{2+}} = 1.188 \times 10^{-2}$ S m^2 equiv^{-1} [11]). Because the radius of the hydrated Ni^{2+} ion, equal to 166 pm, is smaller than that of the Sr^{2+} ion (219 pm), the nickel(II) ion is more strongly dehydrated on IMNs and is more firmly bound to IMNs than the strontium ion.

The cations under study are arranged, as regards the Gibbs energies of ion exchange, in the following order of displacement powers, which correlates with the increase in the ionic potential z/r of the cations, where z is the charge and r the crystallographic radius of the cations by Bokii [11] ($r_{Na} = 97$, $r_{Sr} = 120$, $r_{Ni} = 74$, $r_{Fe} = 80$ pm):

	Na^+	$< Sr^{2+}$	$< Ni^{2+}$	$< Fe^{3+}$
ΔG^0_{298}, kJ mol^{-1}		–0.78	–1.93	–8.85
$(z/r) \times 10^3$, pm^{-1}	10.31	17.86	28.99	42.25

The ionic potential of the Ni^{2+} ion is higher and, consequently, nickel(II) ions will displace Na^+ and Sr^{2+} ions from the IMN surface.

CONCLUSIONS

(1) The isotherm of ion exchange of Na^+ and Ni^{2+} ions on iron–manganese nodules was described by an equation similar to the Langmuir equation and can be represented in the linear form with an approximation confidence $R^2 = 0.99$.

(2) The apparent ion-exchange constant $K = 2.18$ and the Gibbs energy of exchange of nickel ions for those of sodium on the surface of iron–manganese nodules, $\Delta G^0_{298} = -1.932$ kJ mol^{-1}, were determined. The area of the landing site for nickel ions was estimated to be 8.66×10^{-20} m^2. The radius of the sorbed ion, equal to 166 pm, indicates that its binding to the iron–manganese nodule is stronger.

REFERENCES

1. Romankova, P.G. and Nikol'skii, B.P., *Ionity v khimicheskoi tekhnologii* (Ion Exchangers in Chemical Technology), Leningrad: Khimiya, 1982.
2. Chelishchev, N.F., Gribanova, N.K., and Novikov, G.V., *Obogashch. Rud*, 1988, no. 3, pp. 32–34.
3. Zaritskii, V.P., in *Konkretsii i konkretsionnyi analiz: Sbornik statei* (Nodules and Nodule Analysis: Coll. of Articles), Moscow: Nauka, 1977, pp. 79–84.
4. Rogalev, V.A., Dobretsov, V.B., and Evdokimenko, V.S., in *Sbornik nauchnykh dokladov VI Mezhdu-*

narodnoi konferentsii "Ekologiya i razvitie Severo-Zapada Rossii" (Coll. of Scientific Reports at VI Int. Conf. "Ecology and the Development of Northwestern Russia"), St. Petersburg, July 11–16, 2001, St. Petersburg: MANEB, 2001, pp. 116–122.

5. Dobretsov, V.B., Chirkst, D.E., Kuleshov, A.A., and Glazov, A.N., *Gorn. Zh.*, 2002, no. 8, pp. 636–650.
6. Telyakov, N.M. and Fedorov, I.A., in *Gornoe oborudovanie, pererabotka mineral'nogo syr'ya, novye tekhnologii, ekologiya: Tezisy dokladov V Mezhdunarodnogo gorno-geologicheskogo foruma "Mineral'no-syr'evye resursy stran SNG"* (Mining Equipment, Processing of Mineral Raw Materials, New Technologies, Ecology: Abstracts of Papers, V Int. Mining-Geological Forum "Mineral Resources of CIS Countries"), October 7–10, 1997, St. Petersburg: Sankt-Peterb. Gos. Gornyi Inst., 1997, pp. 27–28.
7. Telyakov, N.M., *Teoriya i praktika izvlecheniya blagorodnykh metallov pri kompleksnoi pererabotke rud s primeneniem agregatsionnogo i sul'fatiziruyushchego obzhigov* (Theory and Practice of Recovery of Noble Metals in Integrated Processing of Ores with the Use of Aggregation and Sulfatizing Calcination), St. Petersburg: Sankt-Peterb. Gos. Gornyi Inst., 2000.
8. Chelishchev, N.F., *Sorbtsionnye svoistva okeanicheskikh zhelezomargantsevykh konkretsii i korok* (Sorption Properties of Oceanic Iron–Manganese Nodules and Crusts), Moscow: Nedra, 1992.
9. Chirkst, D.E., Cheremisina, O.V., Ivanov, M.I., and Chistyakov, A.A., *Zh. Prikl. Khim.*, 2005, vol. 78, no. 4, pp. 599–605.
10. Lur'e, Yu.Yu., *Unifitsirovannye metody analiza vod* (Unified Methods for Water Analysis), Moscow: Khimiya, 1971.
11. *Kratkii spravochnik fiziko-khimicheskikh velichin* (Consise Handbook of Physicochemical Quantities), Ravdel', A.A. and Ponomareva, A.M., Eds., Leningrad: Khimiya, 2002.
12. Chirkst, D.E., Litvinova, T.E., Cheremisina, O.V., and Ivanov, M.V., *Zh. Prikl. Khim.*, 2004, vol. 77, no. 5, pp. 580–582.
13. Chirkst, D.E., Cheremisina, O.V., Ivanov, M.V., et al., *Zh. Prikl. Khim.*, 2006, vol. 79, no. 3, pp. 374–377.
14. Chirkst, D.E., Litvinova, T.E., Cheremisina, O.V., et al., *Zh. Prikl. Khim.*, 2003, vol. 76, no. 5, pp. 755–758.

ISSN 1070-4272, Russian Journal of Applied Chemistry, 2006, Vol. 79, No. 7, pp. 1096–1099. © Pleiades Publishing, Inc., 2006.
Original Russian Text © D.V. Bryk, R.G. Makitra, E.Ya. Pal'chikova, 2006, published in Zhurnal Prikladnoi Khimii, 2006, Vol. 79, No. 7, pp. 1106–1109.

SORPTION AND ION-EXCHANGE PROCESSES

Extraction of Carpathian Menilite Shales with Organic Solvents

D. V. Bryk, R. G. Makitra, and E. Ya. Pal'chikova

Institute of Geology and Geochemistry of Fossil Fuels, National Academy of Sciences of Ukraine, Lviv, Ukraine

Received March 24, 2006

Abstract—Extraction of Carpathian menilite shales with 18 solvents at 20°C was examined.

DOI: 10.1134/S107042720607010X

Oil shales are used as power-plant fuel to only a small extent but are regarded as potential power resources for the future. This concerns especially shales with a fairly high content of organic substances, such as Estonian, Australian, some Chinese shales, and shales from the Green River deposit in the United States. At the same time, a number of applications were suggested for resins obtained from shales by pyrolysis or extraction with organic solvents: transformation into motor fuel [1], coke [2], adhesives, surfactants, etc. It should be specially mentioned that the resin of Estonian shales contains alkylresorcinols used in a number of industries, for example, in preparation of epoxy resins or synthetic tanning agents that are difficult to obtain synthetically [3]. Therefore, a number of studies [4, 5] were devoted to the properties and possible applications of oil shales.

Pyrolysis to obtain resins makes sense only if shales contain no less than 20% organic substance, which yields up to 10% liquid fractions and also certain amount of fuel gases [6]. At a lower content of organic components, the power consumed in pyrolysis is too large, which makes more reasonable extraction of the shale with organic solvents at room or elevated temperature, followed by blowing off the residual solvents from the shale. For example, heating the shale containing 12.8% carbon with a tetralin–water mixture to 374°C at a pressure of 6.8 MPa allows 85% recovery of organic components of the mineral [7].

The Carpathian menilite shales from the Sinevidne deposit typically contain less than 10% organic components and, hence, the yield of the resin in pyrolysis is several per cents of their weight only. Therefore, it is more reasonable to recover resins by extraction with organic solvents. However, this requires choosing solvents with the best extraction properties.

Previously [8] we studied extraction of these shales with a number of organic solvents. The content of carbon in the sample examined was 12.0%, and the calcination loss, 26%. Such experiments on extraction are typically carried out in a Soxhlet apparatus. Since our study was aimed at comparing the performances of the extracting agents under identical conditions, extraction was carried out at room temperature by keeping the shale sample in excess solvent for 24 h with intermittent stirring. This eliminates both the interference of the temperature factor in extraction and possible partial tarring of high-boiling extracting agents. Such a procedure does not ensure complete extraction of the organic component, but more than 90% of soluble substances passes into solution even in the first extraction run, as shown by Kröger [9] in a study of extraction of coals.

Since the shale extract contains phenols and carboxylic acids [10], it could be expected that the amount of the extract Q will depend on the basicity of the extracting agent. However, there exists no definite relationship between Q and the Gutmann donor number DN of the solvents (Fig. 1), although these parameters show similar trends in variation. Also, there exists no correlation between Q and the Hildebrand solubility parameter δ. All these facts suggest a complex interaction of the solvents with the substance being extracted. We attempted previously [8] to describe the relationship between the physicochemical characteristics of the solvents and the apparent equilibrium constant of dissolution P (i.e., the ratio of the amount of the extract to that of the residue) in terms of the linear free energy relationship. To this end, we used a multiparameter equation which takes into account the capability of the extracting agent for specific and nonspecific interactions. However, those results

Amount Q and W of the extractable substances recovered from shales by 1 mol of the solvent with the donor number DN

Solvent no.	Solvent	DN	Q, %	$\log W_{exp}$	$\log W_{calc}$	$\Delta \log W$
1	Methanol	19.1	0.27	–1.2620	–1.1490	0.1131
2	Diethyl ether	19.2	0.30	–0.7932	–0.7839	0.0093
3	Ethyl acetate	17.1	0.30	–0.8327	–0.8386	–0.0059
4	Dichloroethane	2.7	0.33	–0.8794	–0.7619	0.1175
5	Benzene	0.1	0.32	–0.8477	–0.8353	0.0124
6	Chloroform	0.4	0.46	–0.7305	–0.9283	–0.1978
7	*n*-Butanol	19.5	0.58	–0.5768	–0.5506	0.0262
8	Bromobenzene	0.8	0.60	–0.4260	–0.2828	0.1431
9	Diethylamine	56.1	0.86	–0.3072	–0.1690	0.1382
10	Acetic acid*	12.7	1.08	–0.5000	–1.1254	–0.6153
11	Dimethyl sulfoxide	29.8	1.27	–0.3089	–0.1394	0.1695
12	Dimethylformamide	26.6	1.39	–0.2692	–0.3865	–0.1173
13	Nitrobenzene	4.4	1.64	–0.0894	–0.1091	–0.0197
14	Triethylamine	61.0	1.94	0.1351	0.0250	–0.1101
15	Quinoline*	39.6	2.01	0.0748	0.7228	0.6480
16	Formamide	22.8	2.03	–0.3925	–0.5677	–0.1752
17	*N*-Methylpyrrolidone	27.3	2.30	0.0434	–0.0597	–0.1031
18	Acetone*	17.0	0.48	–0.4401	–0.8681	–0.4280

* The data for these solvents were eliminated from the total calculation.

cannot be considered as satisfactory: For 18 solvents the multiple correlation coefficient R was as low as 0.800.

When treating extraction as an equilibrium physicochemical process governed by interaction of the dissolved substance with the solvent, it is more reasonable to assume that the free energy of the process ΔG will be proportional to the logarithm of the constant of the equilibrium between the solvated and nonsolvated substrate species, $\log K$. The molecular weight of the extracted (dissolved) resins is typically unknown, but in more recent studies on extraction of coals [11] we found that, with sufficient accuracy, $\log K$ can be replaced by the logarithm of the weight W of the substrate fraction dissolved in 1 mol of the extracting agent. Therefore, in this study we recalculated the data from [8] in this context. The table presents the amounts (in per cent Q and grams per mole of the extracting agent W) of the substance recovered with various solvents. Similar to [11], these data were correlated using a six-parameter equation

$$\log W = a_0 + a_1 f(n^2) + a_2 f(\varepsilon) + a_3 B + a_4 E_T + a_5 \delta^2 + a_6 V_M, \quad (1)$$

where n and ε are the light refractive index and dielectric permittivity of the solvents, respectively, i.e., the parameters related to the polarizability and polarity of the solvents, responsible for nonspecific solvation of the extract; B and E_T, Palm basicity and Reichardt acidity, respectively, determining the capability of the extracting agents for specific solvation [12]; δ^2, squared Hildebrand solubility parameter proportional to the cohesion energy of the solvents; and V_M, molar volume of the solvents.

The characteristics of the solvents were taken from [13], and the calculational procedure, from IUPAC recommendations [14].

For all the 18 solvents the parameter R was unsatisfactorily low, 0.880, though higher than that given in [8]. As shown in [14], successive exclusion of data for several most outlying extracting agents yields equations with higher R parameters: After elimination of

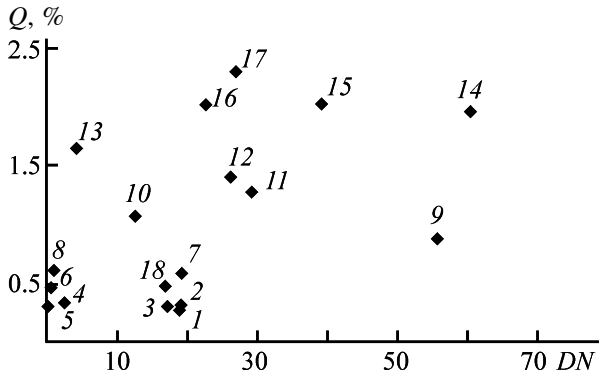


Fig. 1. Yield of the extract Q vs. the donor number DN of the extracting agents. Figures at points correspond to solvent nos. in the table; the same for Fig. 2.

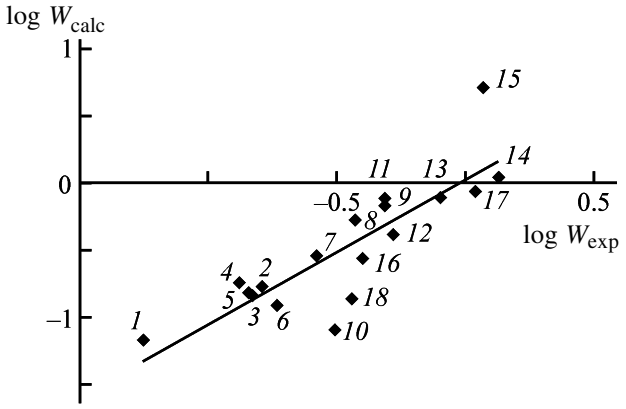


Fig. 2. Relationship between the experimentally determined and calculated [Eq. (3)] amounts of the extractable substances W, recovered with 1 mol of the extracting agent.

the data for acetic acid, quinoline, and acetone, R increased to 0.915, 0.935, and 0.960, respectively, which is acceptable according to the recommendations from [14]. Thus, we obtained with an acceptable accuracy Eq. (2) relating the yield of the extract to the physicochemical characteristics of the extracting agents:

$$\log W = -4.230 + (7.42 \pm 1.01) f(n^2) + (1.84 \pm 0.64) f(\varepsilon) + (1.42 \pm 0.18) \times 10^{-3} B + (0.73 \pm 1.06) \times 10^{-2} E_T - (0.42 \pm 0.25) \times 10^{-3} \delta^2 + (6.60 \pm 2.47) \times 10^{-3} V_M, \quad (2)$$

$N = 15$, $R = 0.960$, rms deviation $S = \pm 0.109$.

The pair correlation coefficients between $\log W$ and individual parameters r, which were estimated at 0.432, 0.059, 0.527, 0.225, 0.235, and 0.501, respectively, suggest the lack of unambiguous quantitative correlation between $\log W$ and any of the parameters used, taken alone. Evidently, extraction is governed by a combination of several factors, among which the most significant will be, probably, the basicity and the molar volume of the extracting agents, as judged from the r values. Therefore, we elucidated in more detail the significance/insignificance of individual terms of the equation: Following the recommendations from [14], these terms were successively excluded and the parameter R was determined for every resulting equation with a smaller number of the terms. If R decreases insignificantly, the eliminated term will be of little significance. In this way, we established insignificance of the electrophilic solvation parameter E (R decreased to 0.959 only) and relatively little significance of the δ^2 term. The dependence of the yield of the extract on the properties of the extracting agent can be adequately described by a four-parameter equation

$$\log W = -4.020 + (7.43 \pm 1.11) f(n^2) + (1.68 \pm 0.48) f(\varepsilon) + (1.45 \pm 0.20) \times 10^{-3} B + (6.19 \pm 1.81) \times 10^{-3} V_M, \quad (3)$$

$$R = 0.951, \; S = \pm 0.120.$$

The parameters $\log W$ calculated by Eq. (3) and their deviations from the experimental data $\Delta \log W = \log W_{calc} - \log W_{exp}$ are also presented in the table. It is seen that these deviations are less or only insignificantly larger (formamide, DMSO, chloroform) than the rms deviation $S = \pm 0.120$. More substantial deviations are observed only for the solvents excluded from consideration. Figure 2 shows the relationship between $\log W_{calc}$ and $\log W_{exp}$.

Further exclusion of any term of Eq. (3) yields expressions with unacceptably low parameters R [without $f(\varepsilon)$ or V_M, R decreases to 0.917], or completely breaks the correlation: Without $f(n^2)$ or B terms, the parameter R becomes equal to 0.77 or 0.73, respectively.

Equation (3) shows that the yield of the extractable substances from Carpathian menilite shale is governed by the solvation power of the solvents, which is above all connected to the polarizability and basicity of the solvents. This is easily understood in view of the presence of acid groups and aromatic moieties in the organic substance of the shales. The two other factors, polarity and molar volume of the extracting agents, affect the yield of the extract less significantly.

Thus, solvents with high basicities (amines, amides) and, desirably, enhanced polarizabilities will be the best extracting agents. This is generally consistent with our experimental data (see table), though the sequence of the performance of the extracting agents represented in mass fractions of the extractable substances will naturally differ from that of the solubilities in 1 mol of the solvent. Technologically, it is also necessary to take into account some other properties such as thermal stability, boiling point which should desirably be low, etc. Among the extracting agents examined, the best performance will be exhibited by formamide, *N*-methylpyrrolidone, and triethylamine.

CONCLUSIONS

(1) Experimental yields of the extractable substances from menilite shales, represented as the amounts of the substance recovered by 1 mol of the

extracting agent, can be adequately correlated with the physicochemical characteristics of the organic solvents.

(2) The extracting power of the solvents is determined, above all, by their basicity and polarity.

REFERENCES

1. Sikonia, J.G., Manudhane, A.R., Hilfman, L., and Board, P.G., in *Proc. Pan-Pacific Synthetic Fuels Conf.*, Tokyo, 1982, vol. 2, pp. 666–683.
2. Glezin, I.L., Lastovkin, G.A., Rudin, M.G., and Timofeev, G.A., *Problemy i perspektivy proizvodstva koksa iz slantsevoi smoly: tematicheskii obzor* (Production of Coke from Shale Resin: Problems and Prospects: Topical Review), Moscow: TsNIITEneftekhim, 1984.
3. Lille, Yu.Z., Bitter, L.A., Purre, T.A., et al., *Alkilrezorstiny: metody polucheniya, svoistva i primenneie: tematicheskii obzor* (Alkylresorcinols: Methods of Preparation, Properties, and Applications: Topical Review), Moscow: TsNIITEneftekhim, 1971.
4. Yen, T.F. and Chilingaryan, D.V., *Goryuchie slantsy* (Oil Shales), Leningrad: Nedra, 1980.
5. *Razrabotka i ispol'zovanie zapasov goryuchikh slantsev* (Development and Use of Reserves of Oil Shales), Petukhov, E.F., Ed., Tallinn: Valgus, 1970.
6. Taupitz, K.C., *Hydrocarbon Proc.*, 1977, vol. 56, no. 9, pp. 219–225.
7. US Patent 4158638.
8. Makitra, R.G., Fil'ts, D.I., Pirig, Ya.I., and Zhukovskii, V.Ya., *Khim. Tverd. Topl.*, 1984, no. 4, pp. 66–72.
9. Kröger, C., *Erdöl Kohle*, 1956, vol. 9, no. 7, pp. 441–445.
10. Selucky, M., Chu Yingli, Ruo Tomoki, and Strauss, O., *Fuel*, 1977, vol. 56, no. 4, pp. 369–381.
11. Bryk, D.V., Makitra, R.G., and Pal'chikova, O.Ya., *Khim. Tverd. Topl.*, 2005, no. 2, pp. 39–45.
12. Koppel, I.A. and Palm, V.A., *Advances in Linear Free Energy Relationships*, Chapman, N.B. and Shorter, J., Eds.: London: Plenum, 1972, pp. 203–280.
13. Makitra, R.G., Pirig, Ya.N., and Kivelyuk, R.B., *Vazhneishie kharakteristiki rastvoritelei, primenyaemykh v uravneniyakh LSE* (Major Characteristics of Solvents Used in LFE Equations), available from VINITI, December 29, 1985, no. 626-V 86.
14. Recommendations for Reporting the Results of Correlation Analysis in Chemistry Using Regression Analysis, *Quant. Struct. Act. Relat.*, 1985, vol. 4, no. 1, p. 29.

ISSN 1070-4272, Russian Journal of Applied Chemistry, 2006, Vol. 79, No. 7, pp. 1100–1104. © Pleiades Publishing, Inc., 2006.
Original Russian Text © R.I. Yurchenko, I.S. Pogrebova, T.N. Pilipenko, T.E. Shubina, 2006, published in Zhurnal Prikladnoi Khimii, 2006, Vol. 79, No. 7, pp. 1110–1114.

APPLIED ELECTROCHEMISTRY AND CORROSION PROTECTION OF METALS

Anticorrosive Properties of *N*-Acetylmethylpyridinium Bromides

R. I. Yurchenko, I. S. Pogrebova, T. N. Pilipenko, and T. E. Shubina

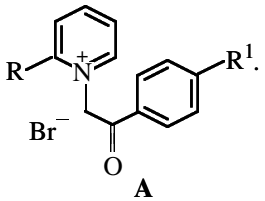
Kiev Polytechnic Institute, National Technical University of Ukraine, Kiev, Ukraine

Received October 25, 2005; in final form, February 2006

Abstract—The inhibiting action of *N*-acetylmethylpyridinium bromides on the corrosion of low-carbon steel in a 3 M sulfuric acid solution at 20, 40, 60, and 80°C was studied. The mechanism of their protective action was examined using electrochemical methods. Compounds exhibiting high anticorrosive properties at elevated temperatures were found.

DOI: 10.1134/S1070427206070111

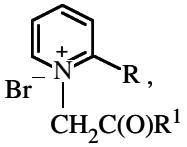
It has been shown previously [1] that *N*-phenacylmethylpyridinium bromides (**A**) are effective inhibitors of the acid corrosion of steel and their protective properties depend on the nature of the substituents R and R^1:



A

It was found, by varying R and R^1, that the coefficients γ of steel corrosion hindrance for these compounds at 20 and 40°C correlate with the σ_c^0 constants characterizing the combined action of the mesomeric and π-induction effects of the substituents R and with the induction σ_I constants of R^1 groups. As temperature increases, their anticorrosive action is significantly enhanced, but, in this case, the correlation between the corrosion hindrance factors and the electronic characteristics of the substituents is broken.

This study is concerned with the anticorrosive properties of pyridinium bromides containing a CH_3 or NH_2 group in position 2 and methylacyl groups with CH_3, *t*-Bu, 1-Ad, and 2-thienyl substituents at the nitrogen atom (compounds **Ia**–**Id**, **IIa**–**IId**):



where R = CH_3 (**I**), NH_2 (**II**); R^1 = CH_3 (**a**), *t*-Bu (**b**), 1-Ad (**c**), 2-thienyl (**d**).

The pyridinium bromides necessary for the study were synthesized by the standard procedure involving the reaction of 2-methyl- or 2-aminopyridine with the corresponding bromomethyl ketones.

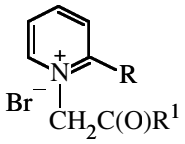
EXPERIMENTAL

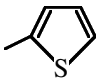
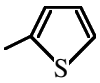
The anticorrosive properties of the compounds studied were evaluated at inhibitor concentrations of 1×10^{-2} M by the corrosion hindrance factors γ and degrees *Z* of corrosion protection of 08KP steel in a 3 M sulfuric acid solution at 20, 40, 60, and 80°C. The corrosion tests were carried out using the conventional gravimetric method [1]. Voltammetric measurements were performed in the potentiodynamic mode, after a free corrosion potential E_c of steel is attained, at a potential sweep rate of 2 mV s^{-1}.

The results obtained in the corrosion tests demonstrated that compounds **Ia**–**Id** and **IIa**–**IId** exhibit a stronger inhibiting effect than their phenacyl analogs **Ie** and **IIe** (Table 1). For compounds **Ie** and **IIe** at 20°C, the steel corrosion hindrance factors are 15.50 and 23.70, respectively [1]; and for compounds **Ia**–**Id** and **IIa**–**IId**, 19.60–39.60. As temperature increases, the anticorrosive effect of the compounds studied is enhanced, and at 60°C the hindrance factors are approximately 200–560 and 200–860 for compounds **Ia**–**Id** and **IIa**–**IId**; for their phenacyl analogs, the hindrance factors do not exceed 200 units.

It is known that, owing to the methylene group separating the pyridinium and phenacyl moieties, the compounds under study exhibit a conformational lability, which allows them to occupy, depending on conditions, a position on the steel surface that is the

Table 1. Hindrance factors γ and degree *Z* of corrosion protection of 08KP steel in a 3 M H_2SO_4 solution in the presence of *N*-acetylmethylpyridinium bromides



Compound	R	R^1	20°C		40°C		60°C		80°C	
			γ	*Z*, %	γ	*Z*, %	γ	*Z*, %	γ	*Z*, %
Ia	CH_3	CH_3	19.60	94.90	22.00	95.45	216.23	99.54	59.8	98.33
Ib	CH_3	$C(CH_3)_3$	22.50	95.56	–	–	297.31	99.66	–	–
Ic	CH3	1-Ad	23.70	95.58	36.40	97.25	317.13	99.68	157.00	99.36
Id	CH_3		19.10	94.76	31.90	96.86	559.60	99.82	369.86	99.73
Ie	CH_3	C_6H_5	15.50	93.54	18.70	94.65	209.10	99.52	150.40	99.34
IIa	NH_2	CH_3	32.00	96.88	40.50	97.53	218.70	99.54	68.00	98.53
IIb	NH_2	$C(CH_3)_3$	34.62	97.11	39.10	97.44	339.79	99.71	–	–
IIc	NH_2	1-Ad	39.60	97.47	43.00	97.67	413.70	99.76	273.70	99.63
IId	NH_2		24.30	95.88	35.40	97.18	864.90	99.88	651.66	99.85
IIe	NH_2	C_6H_5	23.70	95.78	29.00	96.55	200.30	99.50	144.60	99.31

most favorable for adsorption. As also in pyridinium bromides **Ie, IIe** [1], the most probable reaction center responsible for adsorption of the compounds under study at room temperature is the pyridinium moiety of the molecule, which gives rise to a positive adsorption-related step of the potential and hinders corrosion by the energy mechanism of inhibition. At the same time, the carbonyl group contained in these compounds is responsible for chemisorption of the compounds, which becomes more pronounced as the solution temperature increases [2].

It was found that compounds **Ia**–**Ic**, **Ie**, **IIa**–**IIc**, and **IIe** at 20°C show linear relationships between $\log\gamma$ and the induction σ* constants of the substituents R^1:

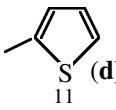
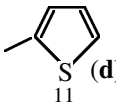
$$\log\gamma = 1.30 - 0.174\sigma^*R^1, \quad r = 0.999, \qquad (1)$$

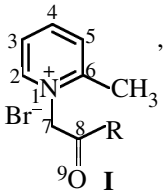
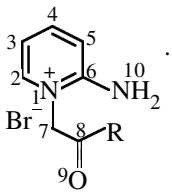
$$\log\gamma = 3.45 - 0.455\sigma^*R^1, \quad r = 0.991. \qquad (2)$$

The coefficients (0.174 and 0.455) in Eqs. (1) and (2) point to different sensitivities of the adsorption centers in compounds **Ia**–**Ic**, **Ie** and **IIa**–**IIc**, **IId** to the induction effect of the substituents R^1. This may be due to difference in the induction and mesomeric effects of the methyl and amino groups on the polarizability of the compounds and, consequently, on their adsorbability on the steel surface. It should also be noted that compounds **Id** and **IId** are not described by the dependences obtained and their inhibiting effect is considerably stronger than that expected with account of only the strength and type of the induction effect of the 2-thienyl radical. Such a behavior of inhibitors **Id** and **IId** can be attributed on the assumption that not only the main adsorption centers, but also the thiophene ring directly interact with the steel surface, as previously observed in [3]. As temperature increases, the linear relations $\log\gamma$–σ^*R^1 cease to be valid, which may occur for various reasons: transition from physical sorption to chemisorption; change of the mechanism of the protective action of the inhibitors; high rate of steel dissolution, which hinders their adsorption on the metal; and some other factors. In this case, the correlation coefficients decrease to 0.939, 0.936 at 40°C and 0.877, 0.886 at 60°C.

Quantum-chemical calculations of the charge distribution within the molecule were carried out for compounds **Ia**–**Ie** and **IIa**–**IIe** (Table 2). The molecular configurations were optimized by the B3LYP method [4] with the standard 6-31G basis set, using the GAUSSIAN software package [5]. All the stationary points were characterized via a complete analysis

Table 2. Charges q in compounds **Ia–Id** and **IIa–IId**

Compound*	q										
	N^1	C^2	C^3	C^4	C^5	C^6	C^8	O^9	N^{10}	S^{10}	S^{11}
I:											
R = CH_3 (**a**)	–0.295	0.078	–0.244	–0.126	–0.233	0.296	0.597	–0.516	–	–	–
R = *t*-Bu (**b**)	–0.296	0.075	–0.243	–0.126	–0.233	0.295	0.607	–0.526	–	–	–
R = 1-Ad (**c**)	–0.295	0.074	–0.244	–0.127	–0.233	0.294	0.610	–0.530	–	–	–
R =  (**d**)	–0.296	0.077	–0.244	–0.125	–0.234	0.300	0.518	–0.545	–	0.477	–
R = Ph (**e**)	–0.295	0.078	–0.244	–0.126	–0.233	0.296	0.552	–0.541	–	–	–
II:											
R = CH_3 (**a**)	–0.348	0.060	–0.269	–0.129	–0.278	0.466	0.599	–0.541	–0.806	–	–
R = *t*-Bu (**b**)	–0.347	0.060	–0.272	–0.131	–0.278	0.465	0.619	–0.551	–0.803	–	–
R = 1-Ad (**c**	–0.346	0.061	–0.273	–0.132	–0.279	0.465	0.629	–0.556	–0.804	–	–
R =  (**d**)	–0.351	0.059	–0.275	–0.134	–0.280	0.466	0.524	–0.572	0.800	–	0.488
R = Ph (**e**)	–0.351	0.059	–0.274	–0.133	–0.279	0.465	0.563	–0.573	–0.802	–	–

*  ,  .

of the normal modes of harmonic vibrations, in which NIMAG = 0 corresponds to minima on the potential energy surface for all of the optimized structures. The calculations demonstrated that, as the substituents R^1 in the compounds studied are varied, the effective charges on the respective atoms within each series remain virtually the same and change only slightly on passing from **Ia–Id** to **IIa–IId**. The only exception are charges on α-carbon atoms of the pyridine ring (C^6), which strongly differ between the series **I** and **II**. This is due to the different electronegativities of the carbon and nitrogen atoms in the CH_3 and NH_2 groups.

The results obtained (Table 1) suggest that an important role in the inhibiting action of acylmethylpyridinium bromides is played by steric factors. In the series of compounds **Ia–Ic** and **IIa–IIc** with CH_3, *t*-Bu, and 1-Ad groups, for which the steric constants E_s^c are, respectively, 0.00, –2.40 [6], and –2.68 [7], a correlation between the corrosion hindrance factors and the steric effect exerted by these substituents is observed.

The plots of the dependences $\log K_m$–$1/T$ (K_m is the gravimetric corrosion index, and T, absolute temperature) in Fig. 1 indicate that *N*-acylmethylpyridinium bromides affect the effective activation energy of corrosion. In the temperature range 20–40°C, the effective activation energies W_c increase in the presence of compounds **Ia–Ie** and **IIa–IIe** from 81.69 kJ mol^{-1} (no inhibitor) to 86.16–102.44 kJ mol^{-1}, which points to the activation mechanism of the inhibiting effect. At higher temperatures, a deviation from the linear dependences $\log K_m$–$1/T$ is observed and inflections appear, which are probably due to transition from the physical (specific) adsorption of the compounds to chemisorption. The effective activation energy of corrosion decreases to 58.88–26.33 kJ mol^{-1} in the presence of compounds **Ia–Ic**, **Ie** and to 19.15 and 9.57 kJ mol^{-1} for compounds **Id** and **IId**, respectively. This indicates that the inhibition mechanism changes as the temperature increases and the diffusion limitations appearing when reacting particles penetrate across the adsorbed film of an inhibitor play an important role. For these compounds, a noticeable aftereffect is observed, which consists in that their protec-

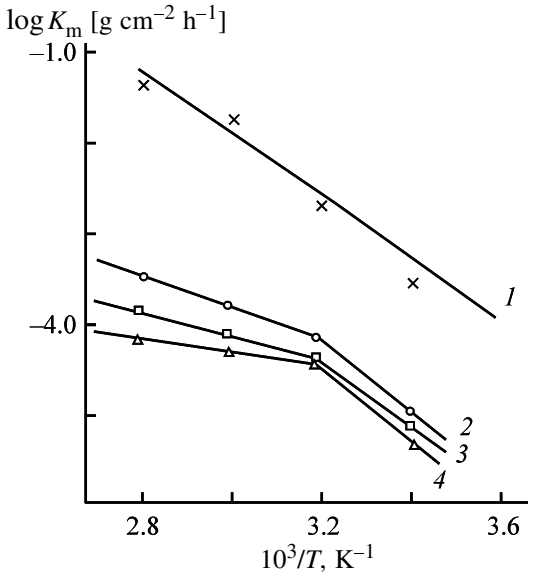


Fig. 1. Temperature dependence of the corrosion rate of 08KP steel in a 3 M H_2SO_4 solution in the presence of 1×10^{-2} M *N*-acylmethylpyridinium bromides. (K_m) Gravimetric corrosion index and (*T*) absolute temperature. Inhibitor: (*1*) none, (*2*) **Ie**, (*3*) **Id**, and (*4*) **IId**.

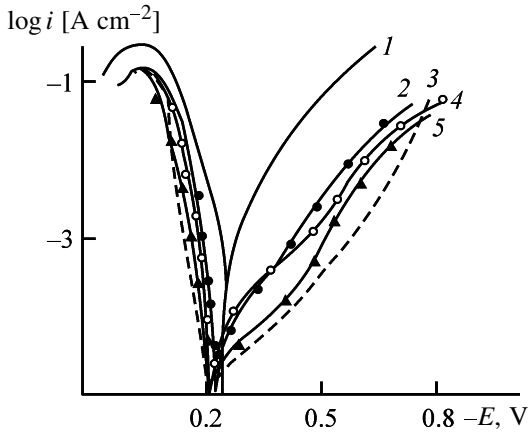


Fig. 2. Anodic and cathodic polarization curves measured on 08KP steel in a 3 M H_2SO_4 solution at 20°C in the presence of 1×10^{-2} M of the compounds under study. (*i*) Current density and (*E*) potential (vs. SHE); the same for Fig. 3. Inhibitor: (*1*) none, (*2*) **Ic**, (*3*) **IIc**, (*4*) **Id**, and (*5*) **IIb**.

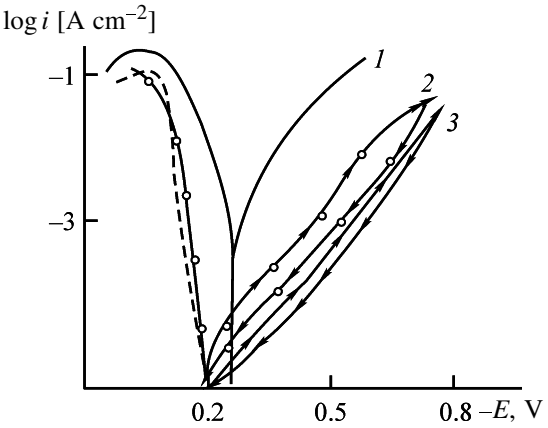


Fig. 3. Anodic and cathodic (forward and back runs) polarization curves measured on 08KP steel in a 3 M H_2SO_4 solution in the presence of 1×10^{-2} M of compounds **Id**, **IIc**. Inhibitor: (*1*) none, (*2*) **Id**, and (*3*) **IIc**.

tive action is preserved after metal samples are removed from the inhibiting medium. For example, the corrosion of steel in a 3 M H_2SO_4 solution at 60°C in the presence of 1×10^{-2} M **Ic** and **Id** is hindered by factors of 317 and 560, respectively, and that after their being kept in the same solutions for 1 h, washed with distilled water, and submerged in the acid solution without inhibitor at the same temperature, by factors of 30 and 38, respectively.

Voltammetric measurements demonstrated that both the cathodic reaction of hydrogen evolution and the anodic reaction of iron ionization are hindered in the presence of compounds **Ic**, **Id**, **IIb**, and **IId** (Fig. 2). The presence of these compounds in 3 M H_2SO_4 solutions affects only slightly the slopes of the cathodic and anodic polarization curves, i.e., has virtually no effect on the mechanism of partial reactions involved in corrosion. Only at weak cathodic polarizations of steel the curves show poorly pronounced regions of limiting current, which are possibly due to the occurrence of concurrent reactions of oxygen ionization or partial reduction of the compounds under study. A stronger change in the slope of the cathodic curve is observed in the presence of compound **Id**, which possibly indicates that the sulfur atom of the thiophene ring is involved in adsorption. The appearance, in its presence, of a narrow hysteresis loop (Fig. 3) is probably due to hindered desorption from the steel surface of inhibitor molecules or of products formed in partial chemical transformations of the inhibitor on the electrode. However, the hindrance factors calculated from the polarization curves satisfactorily coincide for all the compounds with the hindrance factors found in more prolonged gravimetric tests. This indicates that no noticeable chemical transformations of the inhibitors occur at the steel surface at 20°C.

The results of the calculations in Table 3 demonstrated that the corrosion of steel at 20°C in the presence of compounds **Ia**, **Ic**, **Id** and **IIa**, **IIc**, **IId** is hindered by the energy-related and blocking inhibition mechanisms with the predominant contribution of the energy effect. However, the effect of blocking of the metal surface dominates at 60°C, which is indicated by the fact that γ_{exp} markedly exceeds $\gamma_{\Delta\psi 1}$ calculated assuming an energy-related inhibition mechanism.

Table 3. Experimentally found (γ_{exp}) and calculated ($\gamma_{\Delta\psi 1}$) corrosion hindrance factors of 08KP steel in a 3 M H_2SO_4 solution for *N*-acylmethylpyridinium bromides **Ia**, **Ic**, **Id**, **IIa**, **IIc**, and **IId**

Compound, M	*T*, °C	ΔE_c, mV	γ_{exp}	$\gamma_{\Delta\psi 1}$	γ_θ
Ia:					
1×10^{-2}	20	46	19.60	14.96	1.38
4×10^{-3}	20	45	18.37	13.33	1.37
1.6×10^{-3}	20	15	3.17	2.37	1.34
6.4×10^{-4}	20	6	1.81	1.41	1.28
2.56×10^{-4}	20	2	1.20	1.12	1.07
Ic:					
1×10^{-2}	20	49	23.70	16.78	1.41
4×10^{-3}	20	44	17.31	12.59	1.37
1.6×10^{-3}	20	39	13.04	9.44	1.38
6.4×10^{-4}	20	13	2.34	2.11	1.10
2.56×10^{-4}	20	3	1.18	1.18	1.00
Id, 1×10^{-2}	20	46	19.10	14.12	1.35
Id, 1×10^{-2}	60	30	559.60	7.14	78.37
IIa:					
1×10^{-2}	20	54	32.00	22.38	1.43
4×10^{-3}	20	48	21.95	15.85	1.38
1.6×10^{-3}	20	29	5.40	5.31	1.02
6.4×10^{-4}	20	14	2.30	2.24	1.03
2.56×10^{-4}	20	8	1.66	1.58	1.05
IIc:					
1×10^{-2}	20	58	39.60	28.18	1.40
4×10^{-3}	20	53	28.13	21.13	1.33
1.6×10^{-3}	20	45	16.91	13.33	1.27
6.4×10^{-4}	20	22	4.45	3.54	1.25
2.56×10^{-4}	20	4	1.28	1.26	1.02
IId, 1×10^{-2}	20	50	24.30	17.78	1.37
Ic, 1×10^{-2}	60	10	317.13	1.93	164.31

Note: It was taken in the calculations [8] that $\gamma_{exp} = \gamma_{\Delta\psi 1}\gamma_\theta$, where $\gamma_{\Delta\psi 1}$ and $\gamma_{\Delta\psi 1}$ are, respectively, the energy-related and blocking hindrance factors; $\gamma_{\Delta\psi 1} = 10^{K\Delta\psi 1}$; $K = b_c/b_0(b_a + b_c)$, $\Delta\psi 1 = \Delta E_c/[1 - b_c b_a/b_0(b_a + b_c)]$; ΔE_c, shift of the free corrosion potential, caused by the inhibitor; b_c and b_a, Tafel slopes of the cathodic and anodic polarization curves in a 3 M H_2SO_4 solution; and $b_0 = 2.3RT/F$.

It is also not improbable that the steel corrosion is hindered by the compounds studied by a more complex mechanism, e.g., with a possible reduction of the carbonyl group they contain and subsequent formation of chemisorbed protective films on the metal surface [9].

CONCLUSIONS

(1) The *N*-acylmethylpyridinium bromides studied are highly effective inhibitors of acid corrosion of steel, especially at elevated temperatures.

(2) The presence in the acyl moiety of the molecule of groups that can be directly involved in an interaction with the steel surface or have a considerable volume markedly enhances the anticorrosive effect of the compounds studied. The hindrance factors at 60°C are as large as 414–865 units in separate cases, and the degree of corrosion protection of steel exceeds 99.5% for all of the compounds studied.

REFERENCES

1. Yurchenko, R.I., Pogrebova, I.S., Pilipenko, T.N., and Kras'ko, E.M., *Zh. Prikl. Khim.*, 2003, vol. 76, no. 11, pp. 1814–1818.
2. Ivanov, E.S., *Ingibitory korrozii metallov v kislykh sredakh: Spravochnik* (Inhibitors of Metal Corrosion in Acid Media: Reference Book), Moscow: Metallurgiya, 1986.
3. Yurchenko, R.I., Pogrebova, I.S., Pilipenko, T.N., and Shubina, T.E., *Zh. Prikl. Khim.*, 2004, vol. 77, no. 7, pp. 1132–1135.
4. Becke, A.D., *J. Chem. Phys.*, 1993, vol. 98, p. 5648.
5. Frisch, M.J., Trucks, G.W., Schlegel, H.B., et al., *GAUSSIAN*, Pittsburgh PA: Gaussian, 1999.
6. Kozlov, E.S. and Gaidamaka, S.N., *Zh. Obshch. Khim.*, 1975, vol. 45, no. 9, pp. 1939–1943.
7. Yurchenko, R.I., *Doctoral Dissertation*, Kiev, 1994.
8. Antropov, L.I. and Pogrebova, I.S., *Itogi Nauki, Ser.: Korroz. Zashch. Korroz.*, 1973, vol. 2, pp. 27–112.
9. Antropov, L.I., *Teoretichna elektrokhimiya* (Theoretical Electrochemistry), Kiev: Libid', 1993.

ISSN 1070-4272, Russian Journal of Applied Chemistry, 2006, Vol. 79, No. 7, pp. 1105–1109. © Pleiades Publishing, Inc., 2006.
Original Russian Text © Zh.I. Bespalova, Yu.A. Lovpache, M.S. Lipkin, L.G. Miroshnichenko, I.A. Pyaterko, Yu.D. Kudryavtsev, 2006, published in Zhurnal Prikladnoi Khimii, 2006, Vol. 79, No. 7, pp. 1115–1119.

APPLIED ELECTROCHEMISTRY AND CORROSION PROTECTION OF METALS

Composite Coatings Based on Copper Oxides Electrodeposited from Solutions and on Polymers

Zh. I. Bespalova, Yu. A. Lovpache, M. S. Lipkin, L. G. Miroshnichenko, I. A. Pyaterko, and Yu. D. Kudryavtsev

South-Russian State Technical University (Novocherkassk Polytechnic Institute), Novocherkassk, Rostov oblast, Russia

Received August 4, 2005; in final form, January 2006

Abstract—The possibility of obtaining composite coatings consisting of metal oxides deposited from solutions with an asymmetric ac current and of a polymer was studied. Protective properties of the composite coatings were examined.

DOI: 10.1134/S1070427206070123

Of particular interest among composite coatings are metal–polymer coatings (MPCs) in which fluoropolymers are used as the polymer component [1–3]. Incorporation of fluoropolymer particles in the metallic matrix imparts to an MPC antistatic, antiadhesive, and anticorrosive properties, but it retains metallic properties (high thermal and electrical conductivity and wear resistance) and has a good adhesion to the substrate.

Much promise is shown by composite MPCs in which oxides obtained using an asymmetric ac current serve as the matrix. Application of a nonstationary method of electrodeposition of metals opens up wide opportunities in control over the structure and, accordingly, properties of deposited metallic films [4].

The goal of the study was to obtain composite MPCs on the surface of St.3 steel and to examine the protective properties of these coatings. A composite MPC had the form of a porous matrix composed of copper oxide formed by deposition from solution with an asymmetric ac current, rather than by oxidation of the base metal in the course of electrolysis, and was filled with fluoroplastic.

Copper oxides were deposited from solutions containing copper(II) sulfate, chromium(VI) oxide, boric acid, and 1,4-butanediol under polarization with an asymmetric ac current of mains frequency in the form of two half-sinusoids with different amplitudes. A device [5] that comprised two diodes connected in parallel and conducting current in different directions via adjustable resistors served as a current source. As the cell served a glass vessel in which the St.3 steel working electrode with a surface area of 12 cm^2 was placed together with lead (or copper) counter electrodes in sheaths, thermometer, and magnetic rabble. The electrode surface was prepared using the standard stirrer [6]. However, a contact exchange may occur when samples are submerged in the sulfuric acid electrolyte, determined by the relative values of the potentials of these metals (0.34 V for copper and –0.44 V for steel). To suppress the contact exchange in surface treatment, a passivation stage was introduced.

The structure and phase composition of MPCs were determined by transmission electron microscopy (TEM) on a JEOL LEM-100cx electron microscope (Japan) at an accelerating voltage of 100 kV, by X-ray phase analysis (XPA) on a DRON-2 X-ray diffractometer (filtered CuK_α radiation), and by cathodic chronopotentiometry in a 1.0 M solution of $LiBF_4$ in dimethylformamide [7–9]. In the cathodic chronopotentiometry, a sample was polarized with dc current, with the time dependence of the potential recorded.

A preliminary XPA study of the samples demonstrated that the MPC on the samples has a mixed amorphous-crystalline structure, and, therefore, to perform XPA, the samples were calcined in an inert gas (helium).

The adhesion of the MPC was determined by the method of a grid cut. The electrical resistance of samples with MPC was measured with a V7-16A versatile voltmeter by pressing a graphite electrode against the surface of a sample under study with a constant force of 100 g. The resistance was found

Table 1. Conditions of the experiment, experimental results, and design matrix*

Design characteristic	X_1	X_2	X_3	X_4	X_5	Y_1	Y_2	$\overline{Y}_{exp}$	$\hat{Y}_c$
Zero level	18	38	100	5	25				
Variation range	5	5	30	2	5				
Upper level	23	43	130	7	30				
Lower level	13	33	70	3	20				
1	–	–	–	–	–	2.8	3.0	2.9	1.80
2	+	+	–	–	–	0.9	0.5	0.7	1.80
3	–	–	+	+	–	32.0	22.4	27.2	22.74
4	+	–	+	–	+	0.5	0.7	0.6	1.66
5	–	+	+	–	+	3.8	1.7	2.7	1.66
6	+	–	–	+	+	5.1	11.2	8.15	7.24
7	–	+	–	+	+	7.8	5.1	6.45	7.24
8	+	+	+	+	–	13.3	23.3	18.3	22.74

* $\overline{Y}_{exp}$, average experimental value of the resistance; $\hat{Y}_c$, calculated value.

at ten different points and the average value was taken. The porosity was studied by the chemical method [10]; accelerated corrosion tests were made in conformity with GOST (State Standard) 9.313–89. The optimal conditions for obtaining copper oxide on the surface of St.3 steel were determined using the method of mathematical experiment design using first-order designs and a fractional factorial experiment (FFE) [11].

Because pure copper has a high electrical conductivity (59.1 MS m^{-1}) and a very low resistance (1.5×10^{-6} Ω), the resistance of MPC should increase upon formation of copper oxides on the steel surface. Therefore, the electrical resistance of MPC (Y) was taken as the optimization parameter. As independent variables were chosen the average anode current J_a (mA) (X_1), average cathode current J_c (mA) (X_2), and the concentrations of the electrolyte components (g l^{-1}): copper(II) sulfate $CuSO_4 \cdot 5H_2O$ (X_3), chromium(VI) oxide (X_4), and 1,4-butanediol (X_5). The temperature, content of boric acid, and quantity of passed anodic electricity were maintained constant.

The coefficients of the linear regression equation

$$\hat{Y} = b_0 + b_1x_1 + b_2x_2 + b_3x_3 + b_4x_4 + b_5x_5$$

were found using quarter-replicates of a 2^5 FFE with the following generating relations: $X_4 = X_1X_2X_3$, $X_5 = -X_1X_2$. The experimental conditions and results and the design matrix are presented in Table 1.

According to the calculations, the regression equation has the form

$$Y = 8.36 + 3.84X_3 + 6.63X_4 - 3.91X_5. \quad (1)$$

The adequacy of Eq. (1) to the experiment was checked using the Fisher test F:

$$F = S^2_{ad}/S^2_{rep} = 11.42/15.08 = 0.75$$

The tabulated value $F_{tab} = 5.3$ and $F < F_{tab}$, and, therefore, the regression equation is adequate to the experiment. Thus, a rise in the MPC resistance is favored by an increase in the content of copper(II) sulfate and chromium(VI) oxide in the electrolyte and by a decrease in that of 1,4-butanediol. The insignificance of the rest of the coefficients in the regression equation means that the values of the variable factors are chosen near the optimum point.

As a result of generalization of the data on the influence exerted by the significant coefficients in Eq. (1) on the electrochemical deposition of copper oxide from solution, a steep ascension was performed. This made it possible to determine the optimal conditions of copper oxide deposition onto the surface of St.3 steel by nonstationary electrolysis.

The results of analyses of the phase composition and structure of MPC confirmed that copper oxide is deposited onto the steel surface in the case of polarization with an asymmetric ac current. The XPA data for the coatings obtained demonstrate that the main phases in MPC are CuO, compounds of the spinel type ($CuFe_2O_4$), and trace amounts of Cu_2O and Cu (Fig. 1).

A suggestion can be made on the basis of Fig. 1 that the MPC substance has poor crystallinity and high dispersity.

A study of the composition of oxide MPCs by cathodic chronopotentiometry is based on cathodic

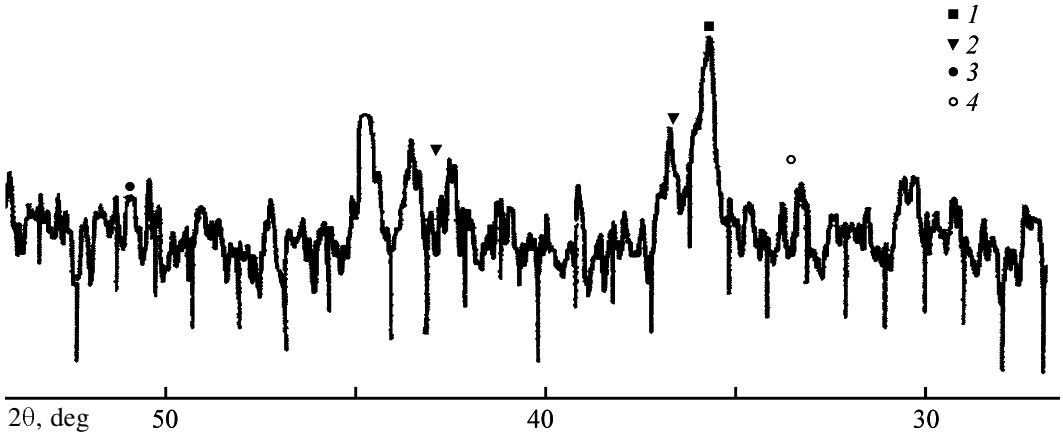


Fig. 1. X-ray diffraction pattern of the surface of oxidized samples. (2θ) Bragg angle. (*1*) $CuFe_2O_4$, (*2*) CuO, (*3*) Cu, and (*4*) Cu_2O.

intercalation of lithium ions from aprotic organic electrolytes

$$Cu_xO_y + zLi^+ + ze \rightarrow Li_2Cu_xO_y.$$

The process ends in the formation of lithium intercalation compounds of variable composition. The fundamental aspects of this process are determined by structural features of the phases under study, degree of oxidation of the metal, and number of point structural vacancies via which ions of intercalated lithium diffuse.

Figure 2 shows that the potentials of the horizontal portions of the chronopotentiograms widely differ between the samples. Comparison of the chronopotentiograms of MPCs with that of pure CuO shows that this phase is characteristic of sample nos. 2 and 5. The rest of the samples have lower potentials in the range 2.2–2.4 V. This can be interpreted as intercalation of Li^+ ions into a phase with a lower degree of copper oxidation, i.e., Cu_2O. The conditions of MPC deposition onto the samples were the same except that they differed in the duration of passivation in the course of surface pretreatment (Fig. 2). Thus, passivation furnishes an additional opportunity of control over the coating properties.

Electron microscopy made it possible to determine not only the qualitative, but also quantitative composition of the MPC substance. The results of calculation of electron diffraction patterns of MPC particles from sample nos. 2 and 5 (Table 2) confirmed the results of XPA and chronopotentiometry.

Table 2 shows that the electron diffraction pattern simultaneously contains lines of pure copper and copper oxide. No electron diffraction patterns of only pure copper or only pure copper oxide were observed.

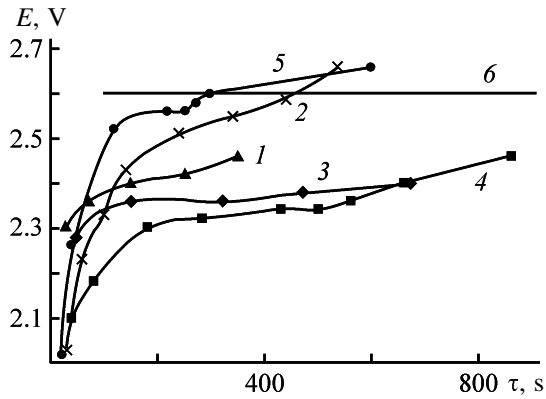


Fig. 2. Chronopotentiograms of oxidized sample nos. 1–6 in a 1.0 M solution of $LiBF_4$ in dimethylformamide at different passivation durations. Current density 0.25 mA cm^{-2}, potentials given vs. lithium electrode. (*E*) Potential and (τ) time. Sample passivation duration (min): (*1, 4*) 5, (*2, 5*) 10, and (*3*) 15; (*6*) CuO.

Table 2. Results of calculation of an electron diffraction pattern from coating particles

Sample no.	Ring diameter *D*, mm	Interplanar spacing *d*, Å			
		experiment	tabulated data		
			Cu	CuO	Cu_2O
1	12.2	3.000			3.000
2	14.6	2.510		2.510	
3	17.6	2.080	2.080		
4	20.3	1.800	1.798		
5	24.4	1.500		1.500	
6	25.7	1.270	1.270		
7	31.6	1.158		1.159	
8	33.8	1.083	1.083	1.086	
9	35.3	1.037	1.038		



Fig. 3. Cross-sectional electron micrographs of MPC at a magnification of 6000. (*1*) Upper layered part of MPC, (*2*) lower part of MPC, and (*3*) MPC–metal interface.

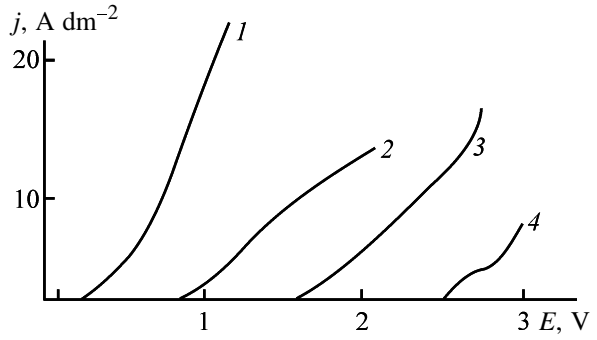


Fig. 4. Anodic polarization curves of samples in 3% NaCl. (*j*) Current density and (*E*) potential. Sample: (*1*) St.3, (*2*) copper oxide, (*3*) copper oxide and polyurethane latex, and (*4*) copper oxide combined with a fluoroplastic-containing formulation.

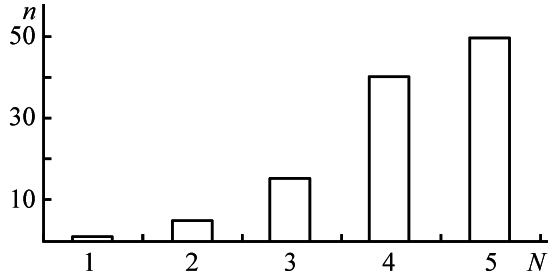


Fig. 5. Comparison of the protective capacities of the samples. (*n*) Number of cycles and (*N*) sample number. Sample: (*1*) St.3; copper oxide: (*2*) with lead counter electrodes, (*3*) with copper counter electrodes, (*4*) combined with a fluoroplastic formulation, and (*5*) with F32LN fluoroplastic and in combination with polyurethane latex.

This means that all coating particles are copper particles enveloped by copper oxide. An exceedingly weak reflection with an interplanar spacing $d = 3.00$ Å was also observed in the electron diffraction pattern. This reflection corresponds to copper(I) oxide. The phase composition determined by analysis of the data obtained is as follows (wt %): copper 50.0, copper(II) oxide 35.0–45.0, and copper(I) oxide ≤5.

The coating has nonuniform thickness and structure (Fig. 3) The thickness varies from 4 to 12 μm. Two regions, upper and lower, of a coating vary in thickness. The lower region, adjacent to the metallic substrate, has a thickness of 7–8 μm and is composed of discrete particles. The upper surface also shows separate layered islands. The high adhesion of the MPC to the substrate is provided by the intermediate sublayer composed of the $CuFe_2O_4$ spinel. This sublayer is formed in the course of cycling, but the MPC is porous in this case. The pores are formed during the cathodic period via discharge of hydrogen ions.

A fluoroplastic-containing formulation and polyurethane latex were deposited onto an oxidized surface of St.3 steel by heteroadagulation, and an F32LN fluoroplastic, by rubbing. The protective properties of the resulting composite coatings after their polymerization drying were assessed by measuring polarization curves in a 3% NaCl solution (Fig. 4). An analysis of these curves demonstrated that copper oxide formed on the steel surface markedly improves the corrosion resistance of steel, and modification of the surface with fluoroplastic substantially hinders the corrosion of the substrate.

The results of express corrosion tests (Fig. 5) are in full agreement with the conclusions made upon analysis of the polarization curves. The express corrosion tests of the composite MPC were terminated after 50 cycles because it still was a long way before the beginning of corrosion owing to the virtually total nonwettability of the coating.

The composite MPC exhibits a good adhesion because of the anchor fixation of the polymer within pores of the metallic matrix in polymerization drying.

CONCLUSIONS

(1) The possibility of obtaining copper oxides on the surface of St.3 steel by their deposition from solution under polarization with an asymmetric ac current was demonstrated.

(2) The optimal conditions of deposition of copper oxide from a copper(II) sulfate solution were found.

(3) The phase composition and structure of the coating substance were determined, and the presence of copper oxide in the coating was thereby confirmed.

(4) The conditions of substrate passivation and the nature of a counter electrode affect the phase composition and structure of a coating.

(5) The substrate corrosion is substantially diminished by copper oxide.

(6) Modification of a coating with fluoroplastic makes it hydrophobic and thereby strongly hinders the substrate corrosion.

REFERENCES

1. Dvornichenko, G.L., Nizhnik, Yu.V., Slavikovskii, T.V., and Nikolaichuk, L.V., *Kolloidn. Zh.*, 1993, vol. 55, no. 1, pp. 45–48.
2. Saifullin, R.S., *Zh. Vses. Khim. O–va. im. D.I. Mendeleeva*, 1980, vol. 25, no. 2, pp. 169–175.
3. Saifullin, R.S., *Kompozitsionnye pokrytiya i materialy* (Composite Coatings and Materials), Moscow: Khimiya, 1977.
4. Polish Patent 145465.
5. Zarokhovich, A.E., Bel'skii, V.P., and Eigel', F.I., *Ustroistvo zaryada i razryada akkumulyatornykh batarei* (Device for Battery Charging and Discharge), Moscow: Energiya, 1975.
6. Grikhiles, S.Ya., *Oksidnye i fosfatnye pokrytiya metallov* (Oxide and Phosphate Coatings on Metals), Leningrad: Mashinostroenie, 1985.
7. Gorbacheva, T.B., *Rentgenografiya tverdykh splavov* (X-ray Diffraction Analysis of Hard Alloys), Moscow: Metallurgiya, 1985.
8. Brainina, Kh.Z., *Inversionnye elektroanaliticheskie metody* (Stripping Electroanalytical Techniques), Moscow: Khimiya, 1988.
9. Manokhina, N.A., Lipkin, M.S., Lipkina, T.V., and Kopin, A.V., in *Novye khimicheskie tekhnologii: proizvodstvo i primenenie: Sbornik statei* (New Chemical Techniques: Production and Application), Penza: Privolzhskii Dom Znanii, 2003, pp. 86–88.
10. Bagazhkov, S.G. and Sukhanova, N.A., *Praktikum po tekhnologii lakokrasochnykh pokrytii* (Practical Course of Paint-and-Varnish Coatings), Moscow: Khimiya, 1982.
11. Akhnazarova, S.L. and Kafarov, V.V., *Metody optimizatsii eksperimenta v khimicheskoi tekhnologii* (Methods of Experiment Optimization in Chemical Technology), Moscow: Khimiya, 1985.

ISSN 1070-4272, Russian Journal of Applied Chemistry, 2006, Vol. 79, No. 7, pp. 1110–1114. © Pleiades Publishing, Inc., 2006.
Original Russian Text © L.A. Kartsova, O.V. Ganzha, 2006, published in Zhurnal Prikladnoi Khimii, 2006, Vol. 79, No. 7, pp. 1120–1124.

APPLIED ELECTROCHEMISTRY AND CORROSION PROTECTION OF METALS

Electrophoretic Separation of Tea Flavanoids in the Modes of Capillary (Zone) Electrophoresis and Micellar Electrokinetic Chromatography

L. A. Kartsova and O. V. Ganzha

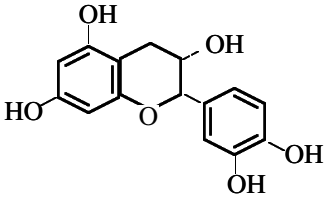
St. Petersburg State University, St. Petersburg, Russia
Analytical Spectrometry Multiple Users Center, St. Petersburg, Russia

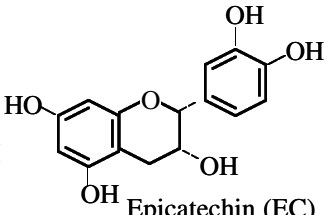
Received February 16, 2006

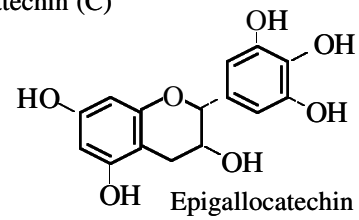
Abstract—Conditions for electrophoretic separation of tea phenolic enantiomers, (+)-catechin and (–)-epicatechin, by capillary (zone) electrophoresis using β-cyclodextrin as a component of the working electrolyte are developed. Optimization is made of the conditions for separating a multicomponent mixture of ionic and neutral polyphenols from various tea samples in the mode of micellar electrophoretic chromatography using sodium dodecyl sulfate as a micelle-forming agent and urea as an additive to the phosphate buffer.

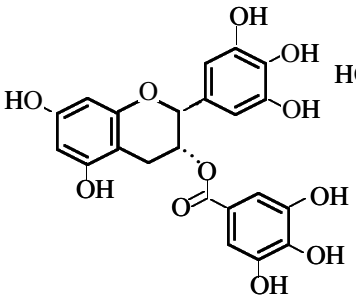
DOI: 10.1134/S1070427206070135

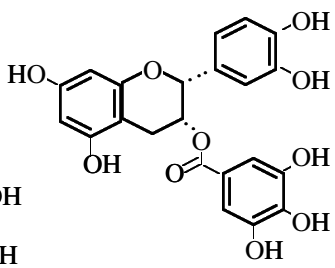
Tea flavanols are classed with the group of compounds known as catechins. These are water-soluble colorless compounds, which are readily oxidized (especially in alkaline solutions) and react with a variety of other compounds [1]:

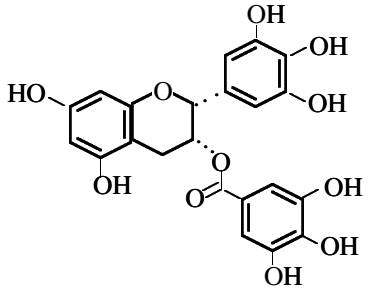

Catechin (C)


Epicatechin (EC)


Epigallocatechin (EGC)


Gallocatechin gallate (GCG)


Epicatechin gallate (ECG)


Epigallocatechin gallate (EGCG)

The characteristic chemical feature of tea flesh is high content of polyphenols.

Tea polyphenols demonstrate a strong antioxidant activity, scavenging free radicals in biological fluids of human body [2]. It was demonstrated experimentally that catechins have the anticarcinogenic, antisclerotic, and antiviral effects, and that tea caffeine acts as a stimulant [1–4].

The common methods for determination of organic compounds, primarily catechins, in tea are gas and liquid chromatography, spectrophotometric and chemiluminescence methods, and NMR [5]. However, in recent years, such methods as reversed-phase HPLC and capillary electrophoresis, namely, capillary (zone) electrophoresis (CE) and micellar electrokinetic chromatography (MEKC) with UV detection, are more and more often used for quantitative and qualitative analysis of tea [1, 4, 5–8].

In this study we tested MEKC as a method for simultaneous determination of tea polyphenols and caffeine. Among the advantages of this method is a small time required for analysis and the possibility of simultaneous determination of both ionic and neutral analytes.

Here we examined the effects of the surfactant [sodium dodecyl sulfate (DDS)] and organic additives (urea, acetonitrile, and methanol) on the resolution factor and selectivity of separation of bioflavanoids.

EXPERIMENTAL

The electrophoretic determinations were carried out on a Kapel' 105R capillary electrophoresis system with a spectrophotometric detector, equipped with a quartz capillary [75 μm i.d.; effective length 50 cm (total length 60 cm)] with a polyimide external coating. The operating temperature was 20°C. The detector operated at a wavelength of 200 nm.

(+)-Catechin, (–)-epicatechin, (–)-epicatechin gallate, (–)-epigallocatechin, (–)-gallocatechin gallate, (–)-epigallocatechin gallate, and gallic acid were purchased from Fluka and Sigma.

The stock buffer electrolyte solutions were prepared from standard reagents $Na_2B_2O_4 \cdot 10H_2O$ (chemically pure grade), $Na_2HPO_4 \cdot H_2O$ and $NaH_2PO_4 \cdot 12H_2O$ (REATEK), HCl (chemically pure grade), NaOH (chemically pure grade), β-cyclodextrin (Sigma), DMSO (chemically pure grade), DDS (chemically pure grade), urea (chemically pure grade), acetonitrile (ultrapure grade), and methanol (Merck).

In the determinations of tea polyphenols we used the working electrolyte containing 25 mM phosphate buffer (pH 7.0), 50 mM DDS, and 5 wt % acetone. Samples were injected hydrodynamically at 600 mbar s^{-1}. Electrophoretic separations were performed at +25 kV. Before use, the quartz capillary was washed with 1 M HCl and distilled water for 10 min and then conditioned with 0.5 M NaOH and distilled water for 10 min. Between the analyses, it was washed with the working electrolyte for 3 min.

The electrophoretic mobility of the analytes μ_{total}, resolution factor R_s, capacity factor, and separation selectivity and efficiency were estimated by Eqs. (1) and (2):

$$\mu_{tot} = (L_{eff} L_{tot})/U t_{migr}, \quad (1)$$

$$R_s = 1.77(t_2 - t_1)/(w_1^{0.5} - w_2^{0.5}), \quad (2)$$

where L_{eff} and L_{tot} are the effective and total length of the capillary (cm); U is the voltage (25 kV); t_{migr}, analyte migration time (min); t_1 and t_2 are the migration times of the first and second components; and $w_1^{0.5}$ and $w_2^{0.5}$, widths of the peaks at half-height (min).

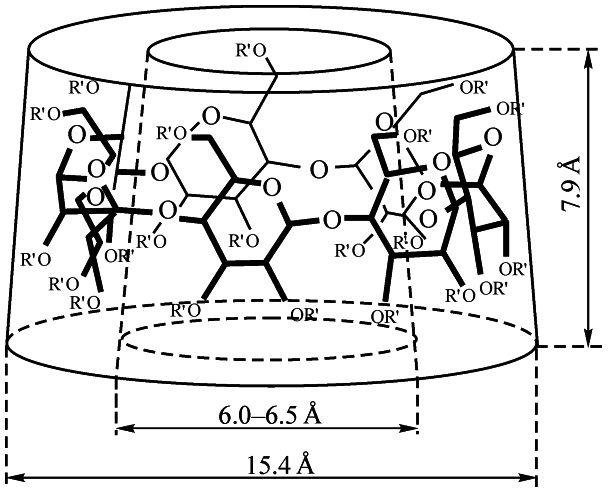


Fig. 1. Structure of cyclodextrin.

It is known that catechins are polyphenols which can be negatively charged at pH > 8 by virtue of the phenolic hydroxy groups in the analyte molecules, so that they can be separated as anions in the CE mode.

When optimizing the electrophoretic separation conditions, we varied the compositions and concentrations of the buffer electrolyte and complexing agent (β-cyclodextrin).

For CE determinations of the catechins, we selected the borate buffer (pH 9.0) containing 4 mM β-cyclodextrin and 10 mM NaOH.

The structure and hydrophobic inner cavity of cyclodextrins allow them to form inclusion complexes with a variety of organic and inorganic compounds via penetration of bulky hydrophobic fragments of analytes to the cavity and interaction of the secondary hydroxy groups of the macrocycle with polar groups of the guest molecule (Fig. 1).

Since β-cyclodextrin is a chiral selector, its introduction into the buffer electrolyte increased the selectivity of separation of the stereoisomers [(+)-catechin and (–)-epicatechin] by virtue of formation of different diastereomeric complexes between the chiral additive and analytes (Fig. 2).

However, even the introduction of the complexing agent, influencing the resolution factor, into the buffer electrolyte did not provide complete separation of the mixture of six most significant polyphenols

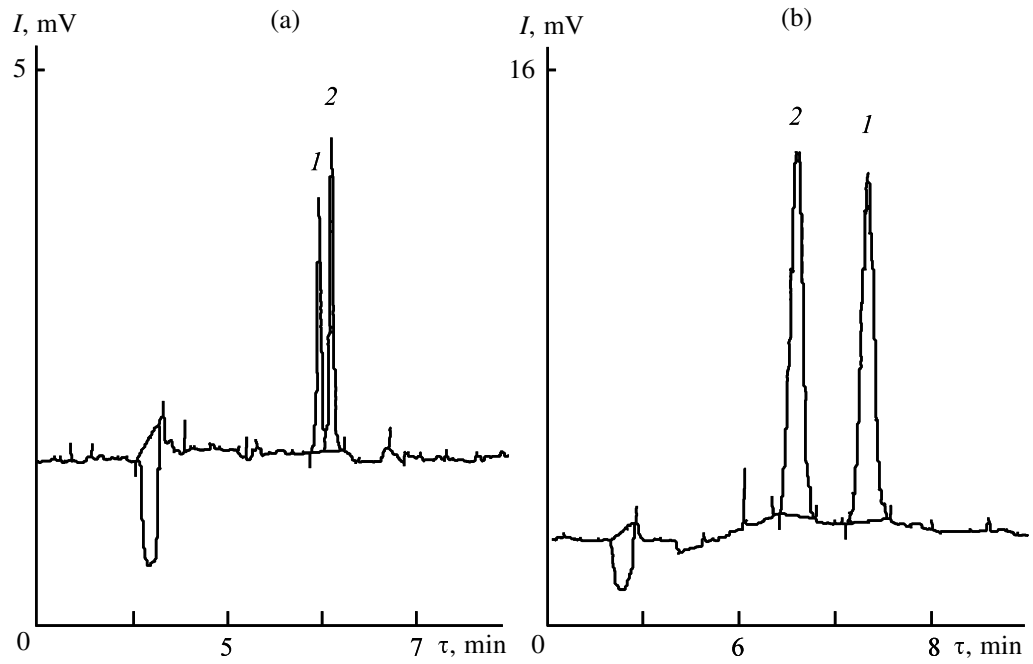


Fig. 2. Electrophoregram of a model mixture of (*1*) catechin and (*2*) epicatechin, obtained in the CE mode. Separation conditions: Kapel' 105R system (UV detection at 200 nm); capillary: 75 μm i.d., L_{eff} = 50 cm, and L_{tot} = 60 cm; injection: 30 mbar, 10 s, 20 kV. Working electrolyte: (a) 5 mM sodium tetraborate (pH 9.0) and (b) 5 mM sodium tetraborate (pH 9.0) + 4 mM β-cyclodextrin + 10 mM NaOH. (*I*) Intensity and (τ) time; the same for Figs. 3 and 5.

[(+)-catechin, (–)-epicatechin, (–)-epicatechin gallate, (–)-epigallocatechin, (–)-epigallocatechin gallate, and (+)-gallocatechin gallate] in the CE mode.

To increase the separation selectivity, we selected the MEKC mode. Additional argument in favor of using this method was that it allows simultaneous determination of catechins and caffeine, which is practically impossible by CE.

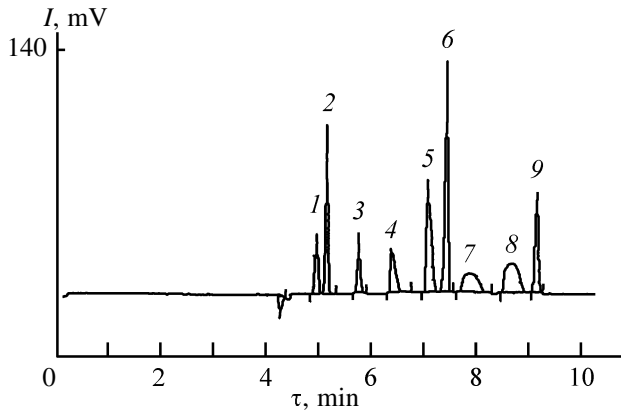


Fig. 3. Electrophoregram of a model mixture containing (*1*) caffeine, (*2*) catechin, (*3*) epigallocatechin, (*4*) epigallocatechin gallate, (*5*) epicatechin, (*6*) gallic acid, (*7*) gallocatechin gallate, (*8*) epicatechin gallate, and (*9*) benzoic acid. Working electrolyte: 25 mM phosphate buffer (pH 7.0) + 20 mM DDS + 10 mM urea; the same for Fig. 5.

Sodium dodecyl sulfate (DDS) is the most widely used anionic surfactant [4]. Above CMC (8 mM), DDS forms micelles representing a pseudostationary phase, thus increasing the separation selectivity as compared to the CE mode by virtue of analyte distribution between the micelles and buffer electrolyte.

Based on the results of preliminary experiments, for the determination of polyphenols we selected 25-mM phosphate buffer (pH 7.0) containing 15 mM DDS. To study the possibility of quantitative determination of tea polyphenols, we introduced benzoic acid as an internal reference. This made it necessary to change the initial separation conditions: we increased the surfactant concentration and additionally introduced urea in a concentration of up to 50 mM. The competitive interaction of urea with the micelles with formation of hydrogen bonds increased the separation selectivity (Fig. 3).

It was demonstrated that the resolution factors and electrophoretic mobilities of the analytes depend on the DDS and urea concentrations in the working electrolyte.

With increasing DDS concentration, the electrophoretic mobilities of the gallate and benzoate anions only slightly change as compared to the neutral analytes migrating to the detector in the form of micellar

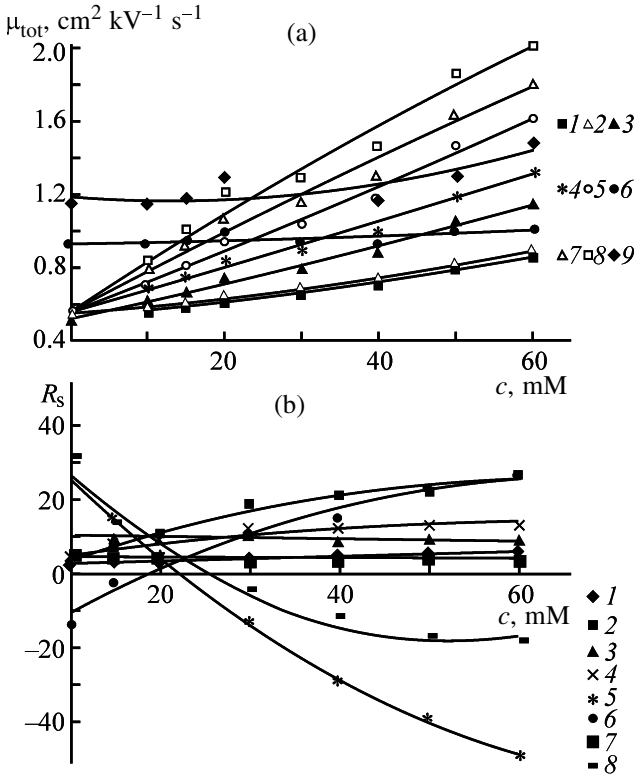


Fig. 4. Effects of the DDS concentration c in the working electrolyte on (a) electrophoretic mobility μ_{tot} of analytes and (b) resolution factors R_s: (a) (*1*) caffeine, (*2*) catechin, (*3*) EGC, (*4*) EGCG, (*5*) EC, (*6*) gallic acid, (*7*) GCG, (*8*) ECG, and (*9*) benzoic acid; (b) (*1*) caffeine/catechin, (*2*) catechin/EGC, (*3*) EGC/EGCG, (*4*) EGCG/EC, (*5*) EC/gallic acid, (*6*) gallic acid/GCG, (*7*) GCG/ECG, and (*8*) ECG/benzoic acid.

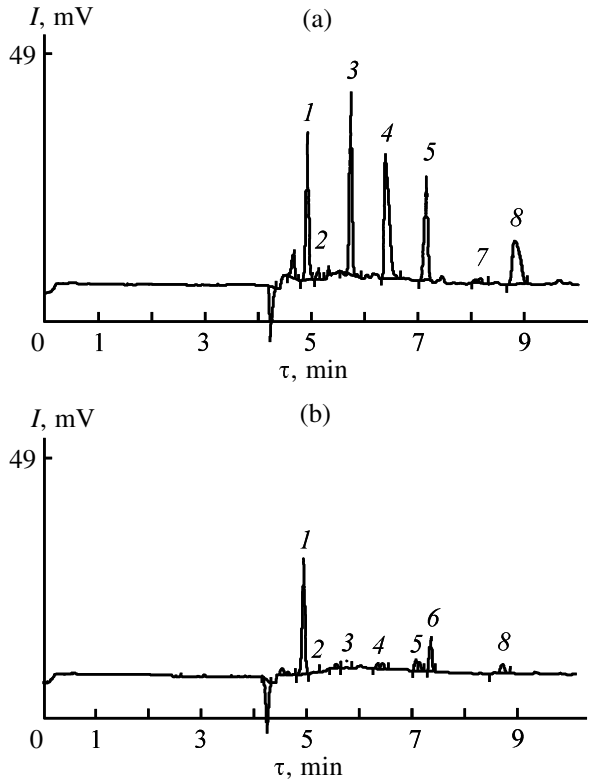


Fig. 5. Electrophoregram of actual aqueous extracts from (a) green and (b) black tea samples: (*1*) caffeine, (*2*) catechin, (*3*) EGC, (*4*) EGCG, (*5*) EC, (*6*) gallic acid, (*7*) GCG, and (*8*) ECG.

complexes (Fig. 4a). In this case, the resolution factors R_s of the pairs EC/gallic acid and ECG/benzoic acid considerably decrease. The R_s values increase for the pairs gallic acid/GCG and C/EGC, which can be attributed to the structural features of their molecules (Fig. 4b).

We also studied the effect of urea on the electrophoretic mobilities of the analytes and resolution factors. The electrophoretic mobilities of all the analytes decrease with increasing urea concentration. However, the resolution factors for the pairs EC/gallic acid and ECG/benzoic acid increase, which is probably due to the effect of urea on the distribution of EC and ECG between the micelles and buffer electrolyte.

Under the optimal conditions determined with the model mixtures, we performed MEKC analysis of the aqueous extracts from green (Fig. 5a) and black tea (Fig. 5b) samples (200-mg tea sample was treated with 20 ml of hot water). Our results showed that the polyphenol content is considerably higher in green tea.

CONCLUSIONS

(1) Conditions of chiral electrophoretic separation of tea polyphenols, (+)-catechin and (–)-epicatechin, in the capillary (zone) electrophoresis mode using β-cyclodextrin as a component of the buffer electrolyte are optimized.

(2) Optimization is made of electrophoretic separation of the multicomponent mixture of catechins in the mode of micellar electrokinetic chromatography. The electrophoretic mobility and resolution factors of the analytes are influenced by the concentrations of a micelle-forming agent (sodium dodecyl sulfate) and organic modifier (urea).

ACKNOWLEDGMENTS

The study was financially supported by the Nevskie Porogi Limited Liability Company and Orimi-Trade.

REFERENCES

1. Larger, P.J., Jones, A.D., and Dacombe, C., *J. Chromatogr. A*, 1998, vol. 799, pp. 309–320.
2. Lill, G., Voit, S., Schror, K., and Weber, A.-A., *FEBS Lett*., 2003, vol. 546, pp. 265–270.
3. Vaher, M. and Koel, M., *J. Chromatogr. A*, 2003, vol. 990, pp. 225–230.
4. Dalluge, J.J. and Nelson, B.C., *J. Chromatogr. A*, 2000, vol. 881, pp. 411–424.
5. Luypaert, J., Zhang, M.H., and Massart, D.L., *Anal. Chim. Acta*, 2003, vol. 478, pp. 303–312.
6. Kotani, A., Miyashita, N., and Kusu, F., *J. Chromatogr. A*, 2003, vol. 788, pp. 269–275.
7. Bronner, W.E. and Beecher, G.R., *J. Chromatogr. A*, 1998, vol. 805, pp. 137–142.
8. Stach, D. and Schmitz, O.J., *J. Chromatogr. A*, 2001, vol. 924, pp. 519–522.

ISSN 1070-4272, Russian Journal of Applied Chemistry, 2006, Vol. 79, No. 7, pp. 1115–1121. © Pleiades Publishing, Inc., 2006.
Original Russian Text © R.V. Prikhod'ko, I.M. Astrelin, M.V. Sychev, E.J.M. Hensen, 2006, published in Zhurnal Prikladnoi Khimii, 2006, Vol. 79, No. 7, pp. 1125–1131.

CATALYSIS

Influence of Preparation Procedure on the Surface Chemistry and Catalytic Characteristics of FeZSM-5 Zeolite in Selective Oxidation of Benzene to Phenol

R. V. Prikhod'ko, I. M. Astrelin, M. V. Sychev, and E. J. M. Hensen

Dumansky Institute of Colloid Chemistry and Water Chemistry, National Academy of Science of Ukraine, Kiev, Ukraine
Kiev Polytechnic Institute, National Technical University of Ukraine, Kiev, Ukraine
Technical University of Eindhoven, Eindhoven, Netherlands

Received January 24, 2006

Abstract—The influence of preparation procedure on the nature of active centers, surface chemistry, and catalytic characteristics of FeZSM-5 zeolite in selective oxidation of benzene to phenol using N_2O as an oxidizing agent was studied.

DOI: 10.1134/S1070427206070147

Phenol is produced on the industrial scale by the multistage cumene process [1]. Its main drawbacks are significant environmental hazard, high power consumption, and low selectivity [1, 2]. Therefore, substitution of this process by single-stage selective catalytic oxidation of benzene with N_2O as an oxidizing agent opens an opportunity for the development of economically beneficial procedure of phenol production [1]. The most efficient catalyst for this reaction is ZSM-5 zeolite (structural type MFI) containing Fe^{3+} ions in the structure and steam-treated at 773–973 K (steaming) [1, 3]. The need in such a treatment makes the single-stage synthesis of phenol considerably less attractive, which stimulates the search for alternative solutions. In addition, the activity and selectivity of the catalysts of this type can significantly depend on the procedure of their preparation [4, 5]. However, despite a great deal of publications in this field, this problem is not adequately studied.

These facts stimulated us to perform a detailed study of the relation between the procedure of preparation of catalysts based on ZSM-5 zeolite and their catalytic characteristics in selective oxidation of benzene.

EXPERIMENTAL

The FeZSM-5 samples were prepared by incorporation of Fe^{3+} ions into the crystal lattice during the synthesis [6] and also by ion exchange in the medium of Fe^{3+} ions generated *in situ* [7, 8], by common procedure [9] or solid-phase ion exchange [10]. The catalyst containing structural Fe^{3+} ions (Si/Fe = 130) was synthesized by the procedure described in [6, 11] using the reaction mixture TEOS : TPAOH : Fe_2O_3 : $H_2C_2O_4$ = 1.0 : 0.312 : 0.00385 : 0.0254. First 10.24 g of tetraethyl orthosilicate (TEOS) was added to 15.0 g of structuring agent (tetrapropylammonium hydroxide, TPAOH, 20% aqueous solution), and the mixture was stirred for 20 h. Then, 5.0 ml of an aqueous solution containing 0.147 g of $Fe(NO_3)_3 \cdot 9H_2O$ and 0.152 g of $H_2C_2O_4 \cdot 2H_2O$ was added dropwise to this solution with stirring. The resulting gel was placed into a steel autoclave with a Teflon insert and kept for 5 days at 443 K. The crystalline phase was washed with water and dried at 383 K. TPAOH sorbed in zeolite pores was removed by calcination in an N_2 flow for 8 h at 823 K and a heating rate of 1.0 K min^{-1} and then in a flow of dry air for 4 h at the same temperature. The catalyst thus prepared is denoted as FeZSM-5(FW). The [Fe, Al]ZSM-5(FW) sample containing iron and aluminum ions in the structure (Si/Fe = 130, Si/Al = 40) was synthesized similarly using the following reaction mixture (g): 10.24 TEOS, 15 TPAOH, 0.147 $Fe(NO_3)_3 \cdot 9H_2O$, 0.444 $Al(NO_3)_3 \cdot 9H_2O$, and 0.644 $H_2C_2O_4 \cdot 2H_2O$. A part of the FeZSM-5(FW) and [Fe, Al]ZSM-5(FW) samples was steamed at 973 K, 10% H_2O/90% Ar for 3 h.

For the ion exchange in the medium of Fe^{3+} ions generated *in situ* [7, 8], 2.0 g of NH_4ZSM-5 zeolite (atomic ratio Si/Al 20, 40; Akzo-Nobel) was sus-

Table 1. Chemical composition, specific surface area $S_{Langmuir}$, and micropore volume V_m of the catalysts studied

Catalyst	Si/Al	Fe, wt %	Fe/Al	$S_{Langmuir}$, $m^2\ g^{-1}$	V_m, $cm^3\ g^{-1}$
FeZSM-5(FW)	–	0.55	–	445	0.157
FeZSM-5(FW) after steaming	–	0.55		470	0.165
[Fe, Al]ZSM-5(FW)	40	0.51	0.263	450	0.145
[Fe, Al]ZSM-5(FW) after steaming	40	0.51	0.263	465	0.160
NH_4ZSM-5	40	–	–	442	0.168
FeZSM-5(IE)	40	0.53	0.273	438	0.140
FeZSM-5(IE)	40	0.07	0.036	440	0.155
FeZSM-5(CE)	40	0.50	0.263	430	0.132
FeZSM-5(SE)	40	0.50	0.263	390	0.120

pended at 298 K in 200 ml of a 0.06 M HCl solution containing 0.10 or 0.73 g of metallic iron powder (Fluka). This suspension was kept without stirring for 72–80 h at 298 K in an argon flow (20 $cm^3\ min^{-1}$), after which the solid phase was filtered, washed with ethanol, and dried in a vacuum at 373 K. The prepared catalysts are denoted with the IE index.

For the ordinary ion exchange [9], NH_4ZSM-5 (Si/Al = 40) was treated three times with a 1.0 M $Fe(NO_3)_3 \cdot 9H_2O$ solution (solid : liquid = 1 : 50) for 6 h at 333 K, then washed with distilled water to negative reaction for NO_3^- ions, separated by filtration, and dried at 383 K for 16 h. This catalyst is denoted as CE. The solid-phase ion exchange ($FeCl_2$ + NH_4ZSM-5 $\rightarrow$ FeZSN-5 + NH_4Cl [10]), FeZSM-5(SE) sample, was performed by the procedure described in [10] by impregnation of NH_4ZSM-5 (Si/Al = 40) with a $FeCl_2/C_2H_5OH$ solution with a concentration corresponding to the ratio Fe/Al = 0.26.

The content of iron ions in the catalysts studied was determined by the ICP-AES method (Perkin–Elmer Optima, DV-3300, ICP-AES Instrument). The X-ray analysis was performed with a Rigaku RINT-2000 diffractometer (CuK_α radiation, λ = 1.54178 Å) in the range of Bragg angles 2θ = 5°–50°. The electronic diffuse reflection (EDR) spectra (190–800 nm) were recorded on a Shimadzu UV 2401 spectrophotometer, reference $BaSO_4$. The IR spectra were recorded on a Nicolet Avatar 360 FT-IR spectrophotometer; the samples were pelletized with thoroughly dried KBr (ratio 1 : 60). The ^{27}Al NMR MAS spectra were recorded on a Bruker Avance 500 spectrometer at 130 MHz and MAS rate of 12.5 KHz with a saturated $Al(NO_3)_3$ solution used as a reference. The curves of temperature-programmed reduction of the catalysts with hydrogen (TPH) were obtained using a flow reactor connected with a heat conductivity detector. For reduction we used a hydrogen–argon mixture (66% H_2) fed at a rate of 20 $cm^3\ min^{-1}$. The temperature range was 298–1073 K, and the heating rate, 5 deg min^{-1}. The isotherms of nitrogen adsorption–desorption at 77 K (Micromeritics ASAP 2010 installation) were obtained on preliminarily evacuated samples (5 h, 673 K, 10 Pa). The isotherms were analyzed using Langmuir equation, BET theory, and Dubinin–Astakhov method [3].

The catalytic tests were performed in a flow-type reactor at 623 K, $C_6H_6 : N_2O$ = 1 : 4 vol % in a helium flow, flow rate of 100 ml min^{-1}, and space velocity of 30000 h^{-1}. The composition of the reaction mixture was determined with a Hewlett–Packard GC-5890 gas chromatograph (OV1 column, flame ionization detector) and a Balzers TPG-420 mass spectrometer. In so doing, the conversion of benzene and N_2O, selectivity with respect to N_2O (amount of oxygen atoms generated from N_2O and entering into composition of phenol), selectivity with respect to benzene (C_6H_6 fraction converted into benzene), and productivity with respect to phenol were determined. The matter balance with respect to carbon and nitrogen was 98 and 99%, respectively. Before the reaction, the catalysts were heated in a helium flow (100 ml min^{-1}) at 823 K for 3 h.

The X-ray powder patterns of the samples isomorphically substituted with Fe^{3+} and Al^{3+} cations contain all basal reflections typical for ZSM-5 (structural type MFI) [12]. In this case, the content of Fe^{3+} and Al^{3+} practically coincides with that in the reaction mixture used for their synthesis (Table 1). The Fe^{3+} ions are localized predominantly in the crystal lattice of the zeolite, which is suggested by the presence of an absorption band in their IR spectra at approximately 650 cm^{-1}, assigned to the stretching vibrations in the structural fragments ≡Si–O–Fe= [6]. This band practically completely disappears after steaming due to decomposition of these fragments and subsequent

migration of Fe^{3+} ions to the outer surface of zeolite pores [13]. In this case, the crystal structure does not significantly change, since there are no noticeable differences in the X-ray patterns of the initial and steamed samples. In addition, ion exchange does not appreciably affect the zeolite structure, irrespective of its procedure. Nevertheless, in the case of FeZSM-5(IE) catalysts prepared by the ion exchange in strongly acidic medium, the coordination state is altered and the surrounding of a part of Al^{3+} ions is distorted. This follows from a comparative analysis of the ^{27}Al NMR spectra of the NH_4ZSM-5 and FeZSM-5(IE) samples (Fig. 1). In the latter case, there is an insignificant shift of the NMR signal of tetrahedrally coordinated Al^{3+} skeleton ions (approximately 54 ppm) [14] and also weak signals of octahedrally coordinated out-of-framework Al^{3+} cations (approximately 8.0 and 0.3 ppm) appear [14]. The amount of these ions is in direct proportion to the content of aluminum(III) in the zeolite, as seen from a comparison of the intensities of these signals for the samples with different atomic ratio Si/Al (Fig. 1). The steamed sample [Fe, Al]ZSM-5(FW) also contains a significant amount of out-of-framework Al^{3+} ions, which is suggested by its ^{27}Al NMR spectrum. In the spectra of catalysts prepared by ordinary or solid-phase ion exchange, no signals characteristic of such Al^{3+} ions are observed.

As known, the electronic diffuse reflection (EDR) spectroscopy furnishes data on the coordination, oxidation, and aggregative states of iron ions or iron oxides [15]. In the EDR spectra of the FeZSM-5(FW) and [Fe, Al]ZSM-5(FW) samples (Fig. 2), there is a band in the region of 250 nm, reflecting the ligand-to-metal charge transfer [15, 16]. Since this band characterizes the coordination state of Fe^{3+} ions as tetrahedral [15, 16], it can be suggested that at least a part of these ions is localized in the zeolite structure. A similar conclusion can be made from the analysis of the spectra in the range of *d–d* transitions (300–500 nm). However, in the [Fe, Al]ZSM-5(FW) sample the content of these cations is lower, as seen from a comparison of the intensities of the bands at approximately 350 and 415 nm (Fig. 2). This can be explained by a competition between aluminum and iron ions in formation of the crystal structure of zeolite [17], resulting in that a noticeable part of Fe^{3+} ions occupies out-of-framework positions. Steaming of these samples results in a noticeable decrease in the intensity of the bands at 350 and 415 nm (isolated Fe^{3+} ions [18]) due to rupture of the Si–O–Fe bond. Simultaneous shift of the band at approximately 250 nm to longer wavelengths suggests alteration of the coordination state of iron ions from tetrahedral to octahedral and formation of oxide clusters Fe_xO_y [15]. In this case, the aggregated Fe_2O_3 phase is not formed since in the spectra of these samples there is no typical absorption in the range $\lambda > 400$ nm [18]. These results allows a conclusion that steamed samples contain iron mainly in the form of individual finely dispersed clusters Fe_xO_y localized outside zeolite skeleton.

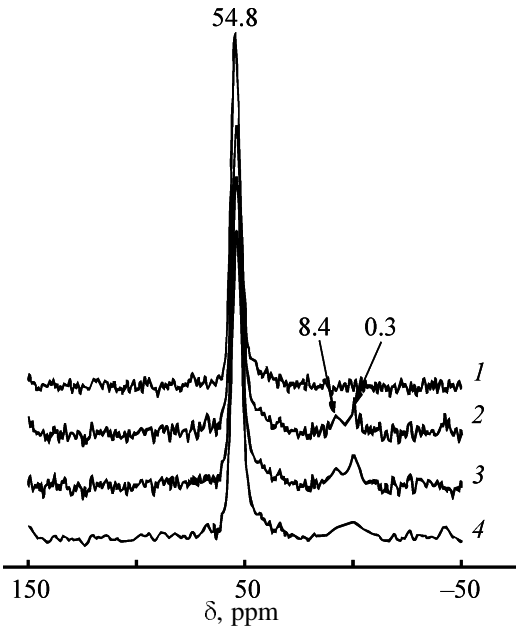


Fig. 1. ^{27}Al NMR spectra of the samples. (δ) Chemical shift. (*1*) NH_4ZSM-5; (*2*) FeZSM-5(IE), Si/Al = 40; (*3*) FeZSM-5(IE), Si/Al = 20; and (*4*) [Fe,Al]ZSM-5(FW) after steaming.

In the catalysts prepared by the ion exchange in the medium of iron ions generated in situ, formation of aggregated Fe_xO_y particles is not observed either, which follows from the absence of characteristic bands in the EDR spectra of FeZSM-5(IE) (Fig. 3). In this case, iron occurs predominantly in the double-charged state, since in the corresponding spectra the absorption bands of Fe^{3+} ions, namely at 224, 278, 350, and 485 nm [8, 15], are absent. For catalysts prepared by the ordinary procedure or solid-phase ion exchange, the pattern is cardinally different. In their EDR spectra (Fig. 3), there are bands with maxima at 230 and 238 nm, a peak or shoulder at 353 nm, and a broad absorption band in the range $\lambda > 400$ nm. This pattern is typical for tetra- and octahedrally coordinated Fe^{3+} ions forming aggregated oligomeric oxide clusters $(Fe_xO_y)_n$ [8], most of which is localized at the outer surface of zeolite crystals [15, 18].

Temperature-programmed reduction in hydrogen medium (H_2 TPR) furnishes data on the composition

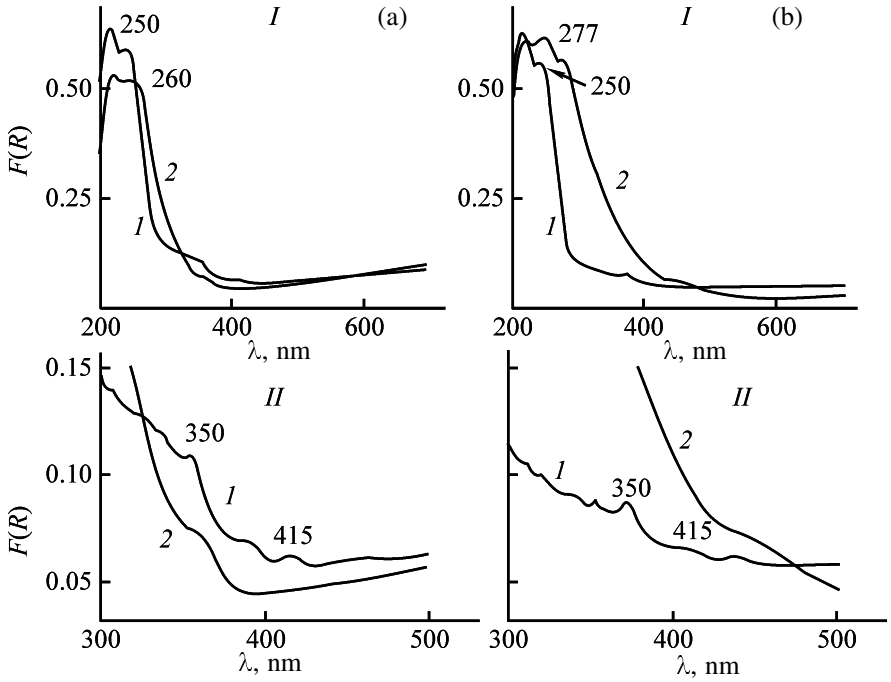


Fig. 2. EDR spectra of (a) FeZSM-5(FW) and (b) [Fe, Al]ZSM-5(FW) samples. [F(R)] Kubelka–Munk function and (λ) wavelength; the same for Fig. 3. (*I*) Entire range and (*II*) range of *d*–*d* transitions. Sample: (*1*) initial and (*2*) after steaming.

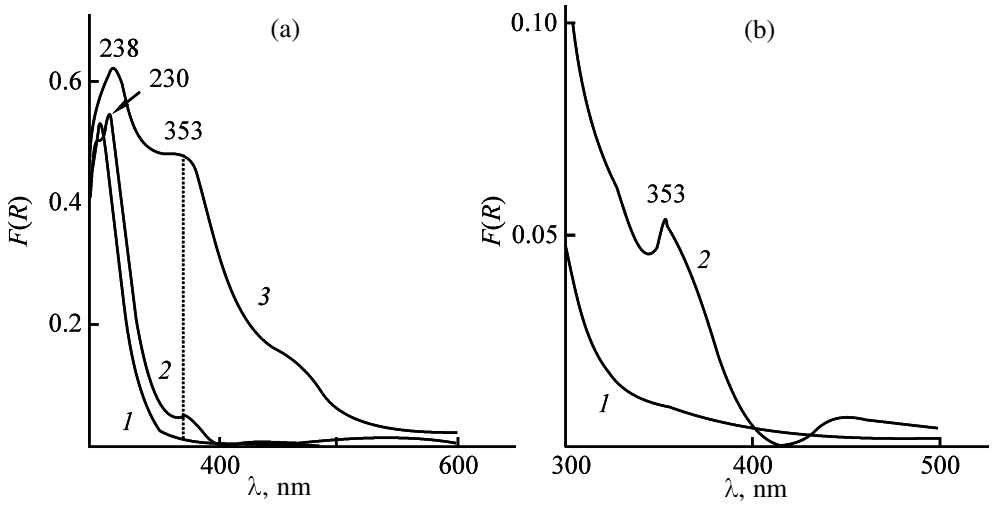


Fig. 3. EDR spectra of the FeZSM-5 samples. (a) Entire range and (b) range of *d*–*d* transitions. (*1*) FeZSM-5(IE) (0.53 wt % Fe^{n+}), (*2*) FeZSM-5(CE), and (*3*) FeZSM-5(SE).

of the metal oxide phase and also, indirectly, on the strength of its interaction with the catalyst surface [19]. The H_2 TPR curves of the samples isomorphically substituted with iron ions contain a broad peak of hydrogen uptake with a maximum at approximately 720 K corresponding to the reduction of Fe^{3+} apparently localized in the zeolite structure to Fe^{2+} (Fig. 4). This is supported by the shift of the temperature maximum and also by narrowing of this peak for the steamed sample (Fig. 4). As shown above, these materials contain iron in the form of highly dispersed Fe_xO_y clusters localized outside the zeolite skeleton. For the FeZSM-5(IE) catalysts, there is one broad peak of hydrogen uptake; however, the temperature of the onset of reduction is significantly higher (approximately 840 K) than that for the other materials (Fig. 4). The maximum of this peak is observed at 1020 K; it corresponds to the reduction of Fe^{2+} to Fe^0 [19], which additionally proves the presence of iron ions predominantly in the double-charged state.

The H_2 TPR curves of the samples prepared by the ordinary ion exchange or exchange in the solid phase

contain a strong peak of hydrogen uptake with a maximum at 675 and a shoulder at approximately 735 K (Fig. 4). This shape of the H_2 TPR spectrum is most probably caused by the differences in localization and dispersity of oxide clusters formed by the Fe^{3+} ions [20]. The hydrogen uptake in the range of higher temperatures (approximately 735 K) can reflect reduction of clusters located in the zeolite pores and separated clusters. In both cases, reduction occurs at a higher temperature in comparison with the oxide phase or oxide clusters localized at the outer surface of zeolite crystals. The H_2 TPR curve of the FeZSM-5(CE) sample contains also a weak peak at approximately 1027 K (Fig. 4), which is typical for the reduction $Fe^{2+} \rightarrow Fe^0$ [21]. It should be noted that, for all the catalysts prepared by ion exchange, the temperature of the maximum of the H_2 uptake is lower in comparison with their isomorphically substituted analogs. Since reduction of iron(III) bound in the structural fragments Fe–O–Si requires higher temperature than that of cations, this fact also proves that at least a part of Fe^{3+} ions is fixed in the crystal lattice of the catalysts.

Additional data on localization of iron compounds in the structure of the catalysts in hand were obtained using nitrogen adsorption [20]. For all the samples, the experimental adsorption isotherms can be classed with type I according to the IUPAC classification [22], which suggests their microporous structure typical for zeolites of the MFI type [23]. The BET method based on the polylayer model of N_2 adsorption inadequately describes adsorption processes occurring in zeolite channels because of the small size of their entrances (<0.7 nm). This follows from the negative value of the coefficient C in the BET equation, obtained for all the samples studied. Therefore, the isotherms were analyzed using the Langmuir and Dubinin–Astakhov equations. Owing to the similar synthesis conditions, the parameters of pore structure of the samples isomorphically substituted with Fe^{3+} ions differ insignificantly (Table 1). Steaming of these materials results in noticeable increase in the specific surface area and micropore volume (Table 1) as a result of an increase in their size. The most probable cause of this fact is migration of iron and aluminum ions from the structural positions to the outer surface. Lower values of the specific surface area and micropore volume of the FeZSM-5(IE) samples in comparison with the initial NH_4ZSM-5 (Table 1) suggest localization of iron ions and iron oxide clusters within zeolite pores. The decrease in these parameters for FeZSM-5(CE) and FeZSM-5(SE) can be explained by blocking of a part of their micropores with coarser

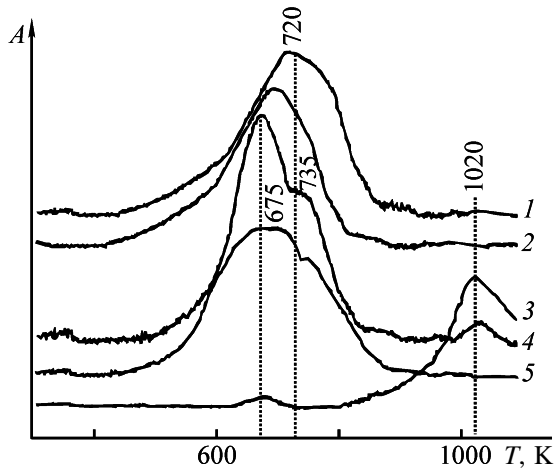


Fig. 4. Curves of temperature-programmed reduction of the catalysts studied: (*A*) H_2 uptake and (*T*) temperature. (*1*) FeZSM-5(FW), (*2*) FeZSM-5(FW) after steaming, (*3*) FeZSM-5(IE), (*4*) FeZSM-5(CE), and (*5*) FeZSM-5(SE).

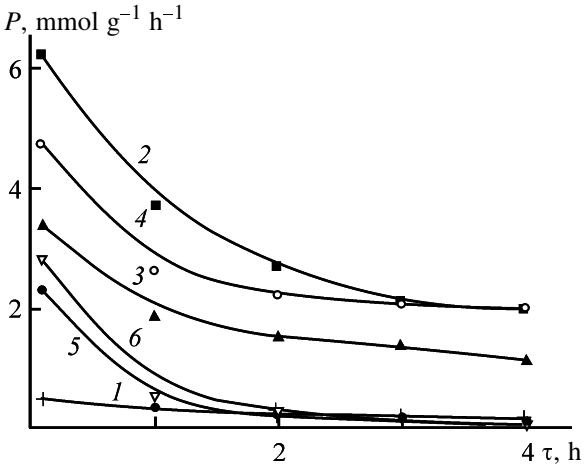


Fig. 5. Productive capacity with respect to phenol *P* of the FeZSM-5 catalysts as a function of duration of benzene oxidation τ: (*1*) FeZSM-5(FW), (*2*) [Fe, Al]ZSM-5(FW) after steaming, (*3*) FeZSM-5(IE) (0.53 wt % Fe^{n+}), (*4*) FeZSM-5(IE) (0.07 wt % Fe^{n+}), (*5*) FeZSM-5(CE), and (*6*) FeZSM-5(SE).

oligomeric oxide clusters $(Fe_xO_y)_n$ whose presence was shown by EDR spectroscopy.

The FeZSM-5(FW) sample prepared by incorporation of Fe^{3+} ions into the crystal lattice during synthesis was practically inactive in selective oxidation of benzene (Fig. 5). As a result of steaming its activity increases only insignificantly. At the same time, this treatment results in significant increase in the activity of the [Fe,Al]ZSM-5(FW) catalyst. These results are in good agreement with the concept that the Fe–O–Al clusters formed in steaming are active centers of the selective oxidation of benzene [3, 13, 24].

Table 2. Conversion X and selectivity S of the benzene oxidation to phenol

Catalyst	Benzene, %		N_2O, %		Benzene, %		N_2O, %	
	X	S	X	S	X	S	X	S
	5 min				240 min			
FeZSM-5(FW) after steaming	9	12	1	35	4	5	1	2
[Fe,Al]ZSM-5(FW) after steaming	36	67	16	42	6	98	3	55
FeZSM-5(IE) (0.53 wt % Fe^{n+})	18	71	8	41	5	82	3	49
FeZSM-5(IE) (0.07 wt % Fe^{n+})	23	77	4	100	6	100	1	100
FeZSM-5(CE)	15	58	2	100	0.5	38	3	2
FeZSM-5(SE)	22	48	5	50	0.2	6	1	0.4

In the course of the reaction, this catalyst is significantly deactivated, and the activity flattens out within approximately 3 h after the beginning of its operation. In the initial period (5 min), the selectivity of benzene conversion into phenol is approximately 70% (Table 2), which suggests partial conversion of C_6H_6 into other products. These are not only macromolecular compounds ("coke") adsorbed at the catalyst surface but also carbon dioxide and water. During further process, the selectivity of benzene conversion significantly increases (95–99%); however, this is accompanied by an abrupt decrease in its conversion (to 7%). In this case, the selectivity with respect to nitrous oxide is significantly lower, which can be explained by participation of N_2O in coke oxidation at the catalyst surface. The similar pattern is observed in the case of the FeZSM-5(IE) sample with a similar iron content (0.53 wt %, Fe/Al = 0.26) (Fig. 5). At the same time, an increase in the amount of Fe^{2+} ions to 0.07 wt % results in a significant increase in the activity and selectivity of the FeZSM-5(IE) catalyst, especially with respect to N_2O conversion (Table 2). This result can be explained as follows. The latter materials contain mainly double-charged iron ions, which pass into triple-charged state, being oxidized with nitrous oxide. In this case, the amount of Fe^{n+} ions plays a decisive role in formation of macromolecular by-products (coke). At increased concentration of these ions, the rate of side reactions increases, which is manifested as decreased selectivity of benzene conversion, observed for the samples containing 0.53 wt % Fe^{n+}. Since N_2O is also expended for coke oxidation, with an increase in its content a larger amount of nitrous oxide will participate in this process, which will result in decreasing selectivity of conversion along the main reaction pathway.

The steady-state activities of the FeZSM-5(IE) and steamed [Fe, Al]ZSM-5(FW) samples are the same (Fig. 5). This suggests the similar nature of active centers of these catalysts. As shown above by NMR spectroscopy, the samples prepared by ion exchange in the medium of Fe^{2+} ions generated in situ contain out-of-framework aluminum(III). In the steamed [Fe, Al]ZSM-5(FW) sample, there are also out-of-framework Al^{3+} ions. In both cases, they can occupy positions neighboring with Fe^{n+} ions and, hence, can participate in formation of Fe–O–Al clusters acting as active centers of the selective oxidation of benzene [3, 24]. The initial and steady-state activity of the catalysts prepared by ordinary and solid-phase ion exchange is significantly higher than that of the FeZSM-5(IE) samples (Fig. 5). The rate of deactivation of these catalysts, especially of the material prepared by solid-phase ion exchange is significantly higher than that of the FW and IE samples. This distinction in the behavior of the catalysts containing iron cations in exchange positions can be explained by the influence of various factors. First of all, these materials contain iron in the form of aggregated oligomeric oxide clusters of the $(Fe_xO_y)_n$ type, formed by tetra- and octahedrally coordinated Fe^{3+} cations, most of which are localized on the outer surface of the ZSM-5 crystals. Because of low dispersity of these centers, their specific activity will be significantly lower compared to the FeZSM-5(IE) catalysts containing iron mainly in the form of separated ions and highly dispersed oxide clusters. In addition, as shown by NMR, the catalysts prepared by the ordinary or solid-phase ion exchange do not contain out-of-framework Al^{3+} ions. This fact significantly decreases the probability of formation of Fe–O–Al clusters, i.e., active centers of the reaction in hand. Hence, the increased dispersity of the active centers formed predominantly by double-charged iron ions is responsible for a high activity of the catalysts prepared by the ion exchange in the medium of iron ions generated in situ.

CONCLUSION

The whole set of the results obtained suggests that the preparation procedure significantly affects the nature of active centers and chemical characteristics of the surface of Fe-containing ZSM-5 zeolite. Ion exchange in the medium of Fe^{2+} ions generated in situ allows preparation of active and selective catalysts for benzene oxidation to phenol using N_2O as an oxidizing agent. These catalysts can be used in this process without pretreatment at a high temperature, which makes the process significantly more feasible.

ACKNOWLEDGMENTS

M.V. Sychev is grateful to the Scientific Foundation of the Netherlands (NWO) for the guest grant.

This study was financially supported by the Ministry of Education and Science of Ukraine (grant no. 0104U000999).

REFERENCES

1. Panov, G.I., *CatTech*., 2000, vol. 4, no. 1, pp. 18–31.
2. Uriarte, A.K., Rodkin, M.A., Gross, M.J., et al., *Stud. Surf. Sci. Catal*., 1997, vol. 110, pp. 857–865.
3. Tatlier, M. and Kiwi-Minskler, L., *Catal. Commun*., 2005, vol. 6, no. 11, pp. 731–736.
4. Hall, W.K., Feng, X., Dumesic, J., and Watwe, R., *Catal. Lett*., 1998, vol. 52, nos. 1–2, pp. 13–19.
5. Fejes, P., Kiricsi, I., Lazar, K., Marsi, I., et al., *Appl. Catal., Ser. A: General*, 2003, vol. 242, no. 2, pp. 247–266.
6. Szostak, R., Nair, V., and Thomas, T.L., *J. Chem. Soc., Faraday Trans. 1*, 1987, vol. 83, pp. 487–494.
7. Long, R.Q. and Yang, R.T., *Catal. Lett*., 2001, vol. 74, nos. 3–4, pp. 201–205.
8. Schwidder, M., Santhosh Kumar, M., Bruckner, A., et al., *Chem. Commun*., 2005, pp. 805–807.
9. Perathoner, S., Pino, F., Centi, G., et al., *Top. Catal*., 2003, vol. 23, nos. 1–4, pp. 125–136.
10. Lazar, K., Micheaud, N., Mihalyj, R.M., et al., *React. Kinet. Catal. Lett*., 2001, vol. 74, no. 2, pp. 289–298.
11. Ratnasamy, P. and Kumar, R., *Catal. Today*, 1991, vol. 9, no. 4, pp. 329–416.
12. Treacy, M.M.J., Higgins, J.B., and Ballmoos, R. von, *Zeolites*, 1996, vol. 16, nos. 5–6, pp. 522–525.
13. Hensen, E.J.M., Zhu, Q., and Santen, R.A. van, *J. Catal*., 2003, vol. 220, no. 2, pp. 260–265.
14. Yan, Z., Ma, D., Zhuang, J., Liu, X., et al., *J. Mol. Catal., Ser. A: Chem*., 2003, vol. 194, nos. 1–2, pp. 153–167.
15. Murtarano, P., Drozdova, L., Kogelbauer, A., et al., *Stud. Surf. Sci. Catal*., 2001, vol. 135, pp. 143–151.
16. Ferretti, A.M., Oliva, C., Forni, L., et al., *J. Catal*., 2002, vol. 208, no. 1, pp. 83–88.
17. Centi, G., Fazzini, F., Fierro, J.L.C., et al., *Stud. Surf. Sci. Catal*., 1998, vol. 118, pp. 577–585.
18. Canizares, P., Valverde, J.L., Sun Kou, M.R., et al., *Micropor. Mesopor. Mater*., 1999, vol. 29, no. 3, pp. 267–281.
19. El-Malki, E.-M., Santen, R.A. van, and Sachtler, W.M.H., *J. Phys. Chem., Ser. B*, 1999, vol. 103, no. 22, pp. 4611–4622.
20. Hensen, E.J.M., Zhu, Q., Hendrix, M.M.R.M., et al., *J. Catal*., 2004, vol. 221, no. 2, pp. 560–574.
21. Lobree, L.J., Hwang, I.-C., Reimer, J.A., et al., *J. Catal*., 1999, vol. 186, no. 2, pp. 242–253.
22. Webb, P.A. and Orr, C., in *Analytical Methods in Fine Particles Technology*, Norcross: Micrometrics Instrument, 1997, pp. 59–73.
23. Cundy, C.S. and Cox, P.A., *Micropor. Mesopor. Mater*., 2005, vol. 82, nos. 1–2, pp. 1–78.
24. Zhu, Q., Teeffelen, R.M. van, Santen, R.A. van, et al., *J. Catal*., 2004, vol. 221, no. 2, pp. 575–583.

ISSN 1070-4272, Russian Journal of Applied Chemistry, 2006, Vol. 79, No. 7, pp. 1122–1126. © Pleiades Publishing, Inc., 2006.
Original Russian Text © E.V. Ivanov, 2006, published in Zhurnal Prikladnoi Khimii, 2006, Vol. 79, No. 7, pp. 1132–1136.

PROCESSES AND EQUIPMENT OF CHEMICAL INDUSTRY

Energy Approach to the Extraction Kinetics

E. V. Ivanov

St. Petersburg Academy of Chemistry and Pharmacology, St. Petersburg, Russia

Received December 7, 2005

Abstract—A method for description of the process kinetics is suggested on the basis of processing of a vast body of experimental data on the kinetics of extraction of target components from vegetable raw materials in apparatus with an intensive hydrodynamic mode. The method takes into account the input energy and type of hydrodynamic action on porous particles.

DOI: 10.1134/S1070427206070159

Hydromechanical methods for intensification of extraction of target components (TCs) from porous particles are aimed at partial replacement of the diffusion mass transfer with that of the convective type. An extracting agent moves within coarse pores when the process is performed under conditions of low-frequency pressure pulsations, under the action of pressure pulses near the surface of particles, or as a result of their mechanical deformation. In fine pores, mass transfer occurs exclusively as a result of molecular diffusion of the extracting agent and TCs, so that, on the whole, the extraction mechanism in apparatus with intensive hydrodynamic mode (in apparatus with a fast stirrer, in those of pulsatory and vibrational types, and in apparatus with vacuum-boiling, "explosive" boiling, and suspension subjected to ultrasonic treatment, electric discharges, etc.) can be regarded as that of diffusion-convective type. The theory of diffusion extraction has been developed in sufficient detail [1, 2], whereas for that of diffusion-convective extraction this is still to be done and the related publications are few in number [3–8].

Apparently, the rate of convective mass transfer in porous particles and the completeness of TC extraction depend on the intensity and duration of hydrodynamic treatment of particles and, in the end, on the amount of input energy and method of action on the particles.

The aim of this study was to develop a method for description of the extraction kinetics in apparatus with intensive hydrodynamic mode that would take into account the energy expenditure and the technique used for hydrodynamic action on the porous particles.

Processing of a vast body of experimental data on the kinetics of extraction from vegetable raw materials in apparatus with intensive hydrodynamic mode [9–13] demonstrated that, beginning with a certain instant of time, they are well approximated by the relations [5, 6]

$$\mu = a \ln E_{sp} + b, \quad (1)$$

where μ is the yield of TC in the extraction process (%); a and b, empirical coefficients dependent on the type of a raw material, method and mode of energy supply to a suspension being processed, apparatus type, and average concentration of TC in the bulk of the extracting agent (%); $E_{sp} = N_{br}\tau/V$ or $E_{sp} = N_{br}\tau/V\rho_l$, specific (related to the volume or mass of the suspension) input energy (J m^{-3} or J kg^{-1}); N_{br}, consumed power (W); τ, time (s); V, suspension volume (m^3); and ρ_l, density of the suspension being processed (kg m^{-3}).

Relation (1) can only be used within the interval $0 \le \mu \le 100$. A specific feature of this approximation consists in that, in the same hydrodynamic modes, but at different levels N_{br} of consumed power, the kinetic curves $\mu = f_1(\tau)$ are described by the same dependence $\mu = f_2(E_{sp})$. The results obtained can be explained as follows. The extraction rate, $d\mu/d\tau$, increases in the diffusion-convective mode with the intensity of the hydrodynamic impact on porous particles, and the hydrodynamic impact, in turn, becomes stronger as the specific power $N_{sp} = N_{br}/V$ delivered to the suspension being processed is raised. At the same time, the process rate decreases in an approximately inverse proportion to the extraction duration $\tau = E_{sp}/N_{br}$, because the surface layers of particles get depleted of TC. Hence follows

$$d\mu/d\tau \sim N_{sp}\tau, \quad d\mu \sim (N_{sp}\,d\tau)/\tau, \quad d\mu \sim (N_{sp}\,dE_{sp})/E_{sp},$$

$$\mu \sim N_{sp}\int (dE_{sp}/E_{sp}),\ \mu = a\ln E_{sp} + b.$$

The parameter N_{br} is implicitly included in the empirical coefficients a and b, which makes them dependent on the method of hydromechanical treatment of particles. Because E_{sp} is a dimensional quantity, it is more correct to use the relation

$$\mu = a\ln(E_{sp}/E_{0sp}), \quad (2)$$

where $E_{0sp} = \exp(b/a)$ is the specific input energy corresponding to $\mu = 0$ (J m^{-3} or J kg^{-1}).

An approximation of type (2) cannot describe the kinetics of the process in its initial stage and is only applicable when $E_{sp} > E_{0sp}$, and, naturally, kinetic curves based on (2) do not pass through the point $\tau = 0$, $\mu = 0$ ($\mu = 0$ at $\tau = \tau_0 > 0$). However, the experimental data on the extraction kinetics in this stage of the process are not found in the literature, which is due to difficulties is taking representative samples of the extract or raw material for analysis for the content of TC at time intervals of less than 2–5 min. After an extracting agent is mixed with the raw material, the extracting agent starts to penetrate into particles and to dissolve TC. Apparently, the rate of TC extraction is insignificant during a certain time ($0 \le \tau \le \tau_0$), and, therefore, the kinetic curves formally emerge from the point $\tau = \tau_0$, $\mu = 0$.

The consumed power is commonly a power function of one or several variables $N_{br} = cx_1^k x_2^l x_3^m$, where c is a coefficient; x_1, x_2, x_3, ..., variables on which the consumed power depends; and k, l, m, ..., exponents. Therefore, processing of experimental data can give approximations other than (1) and (2):

$$\mu = a\ln(g x_1^s x_2^i x_3^j), \quad (3)$$

where g is an empirical coefficient, and s, i, and j, empirical exponents.

Using (2) and (3), relations describing the change in the TC yield ($\Delta\mu$) caused by a change, all other conditions being the same, in the specific input energy from E_{1sp} to E_{2sp} (or in the power from N_{1sp} to N_{2sp} and in the variables from $x_{1,1}$, $x_{2,1}$, $x_{3,1}$, to $x_{1,2}$, $x_{2,2}$, $x_{3,2}$,...) during the same time:

$$\Delta\mu = a\ln(E_{2sp}/E_{1sp}) = a\ln(N_{2sp}/N_{1sp}), \quad (4)$$

$$\Delta\mu = a\ln[(x_{1,2}/x_{1,1})^s (x_{2,2}/x_{2,1})^i (x_{3,2}/x_{3,1})^j ...]. \quad (5)$$

It follows from expressions (4) and (5) that the extraction process is only intensified in its initial stage, and further (when samples are commonly taken for analysis), the kinetic curves run at approximately the same distance, equal to $\Delta\mu$, from one another. Apparently, the diffusion-convective mechanism of extraction is operative in the first stage of the process, and the inner-diffusion mechanism, in the second stage. Large energy expenditure is only effective in the first stage. In the second stage of extraction, it can (and should) be diminished by, e.g., lowering the frequency of pressure oscillations in pulsatory apparatus, temperature head in vacuum-boiling apparatus, stirrer rotation speed, etc. This has nearly no effect on the TC yield, but makes it possible to lower the energy expenditure for the process.

Let us illustrate the aforesaid with examples of processing of experimental data on the extraction kinetics for vegetable raw materials of varied anatomical structure in apparatus with intensive hydrodynamic mode. Semagina et al. [13] reported on the extraction kinetics of biologically active substances from pine needles with 25 and 40% aqueous solutions of ethanol under the action of an ultrasound with a frequency of 20–22 kHz and specific power N_{sp} = 2–3 MW m^{-3}. The intensity of the process was evaluated by a change in the TC content c (%) of the extracts. Values of c are related to those of μ by a constant proportionality factor, which could not be determined using the data of [13]. Processing of the experimental data demonstrated that they are satisfactorily described by the expression $c = 0.64\ln(3.6 \times 10^{-8} E_{sp})$.

The monograph by Balabudkin [12] presented the results obtained in extraction of tannin from galls in a rotary-pulsatory apparatus. The author reported neither the technical parameters of the apparatus used, nor any evidence concerning the volume of a suspension being processed. The consumed power was proportional to the rotor rotation speed n_{rot} raised to a certain power γ [12], and, therefore, the experimental data were approximated with the expression $\mu = a\ln(g n_{rot}^{\gamma}\tau)$.

At rotor rotation frequencies of 720, 940, and 1460 rpm, the experimental points (Fig. 1, dependence *1*) rather well fall on a straight line

$$\mu = 11.8\ln(6.71 \times 10^{-3} n_{rot}\tau), \quad (6)$$

where n_{rot} is the rotor rotation speed (rpm), and τ is time (min).

At the same time, the experimental points at a rotor rotation speed n_{rot} = 2960 rpm are grouped around the straight line $\mu = 8.1\ln(491.5\tau)$ (Fig. 1, dependence *2*), which indicates that the hydrodynamic impact on porous particles differs in this case from that at rotation speeds of 720–1460 rpm.

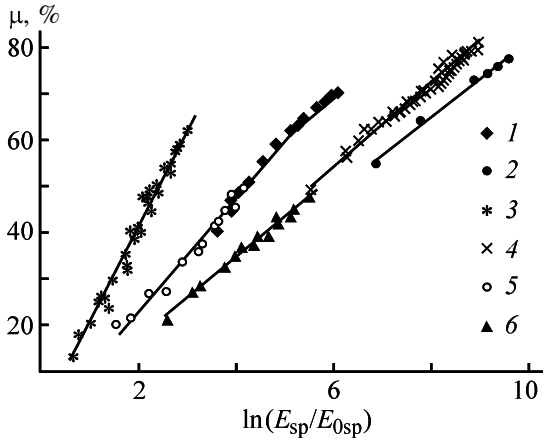


Fig. 1. Degree μ of TC extraction vs. $\ln(E_{sp}/E_{0sp})$ in the course of extraction. (E_{sp}) Specific input energy (J m^{-3}) and (E_{0sp}) specific input energy at μ = 0 (J m^{-3}). (*1, 2*) Tannin from gals in a rotary-pulsatory apparatus at rotor rotation frequencies of 72–1460 and 2960 rpm, (*3*) flavonoid compounds from hawthorn fruits in an oscillating vacuum-boiling mode, (*4*) flavonoid compounds from everlasting flowers in a vacuum-boiling mode at various temperature heads, and (*5, 6*) mushroom proteins in a pulsatory apparatus and that with a fast stirrer, respectively.

The extraction in the oscillating vacuum-boiling mode occurs under adiabatic conditions, in which the heat expended for boiling-up of the liquid is returned into the suspension being processed. For this purpose, the volume of the temperature-controlled system, constituted by the suspension being processed and vapor of the extracting agent, is periodically changed. As the volume of the system is raised, the pressure in it becomes lower, which causes intense boiling-up of the extracting agent and leads to formation of steam bubbles in the system. As the volume of the system decreases, the pressure increases, the bubbles collapse, and the heat of vaporization (condensation) is returned into the system. If the period of variation of the system volume is shorter than the time in which the bubbles rise to the surface, their collapse generates shock waves and thereby initiates filtration mass transfer in porous particles.

The useful consumed power is unknown because the process is complex and poorly understood. Apparently, it is proportional to the total power expended for agitation (transfer) of the suspension:

$$N_{sp} \sim \Delta P W,$$

where ΔP is the pressure difference (Pa), and W is the flow rate (m^3 s^{-1}).

Because the process is fast, ΔP could not be found experimentally. Calculations based on the thermal energy scheme of growth of a steam bubble in an overheated liquid [14] and on experimental data on the kinetics of bubble growth in the oscillating vacuum mode demonstrated that at boiling-up frequencies of 1–7.5 s^{-1} the pressure difference is insignificant, 310 kPa. As the boiling-up frequency ν increases, ΔP decreases following a nearly power-law dependence. Because the suspension flow rate is proportional to the amplitude A of suspension oscillations in the extractor, multiplied by the frequency ν, experimental data on the extraction kinetics were processed using the relation

$$\mu = a \ln(g A^{\alpha} \nu^{\beta} \tau), \quad (7)$$

where A is the amplitude of liquid oscillations in the extractor (m); ν, frequency of boiling-up (oscillations) of the liquid (s^{-1}); and α and β, empirical coefficients.

The experimental data on the extraction kinetics of flavonoid compounds (in terms of rutin) from noncrushed hawthorn fruits with a 40% aqueous solution of ethanol at 70°C and $0.035 \le A \le 1.75$ grouped around the straight line $\mu = 20.5 \ln[9.38 \times 10^{-3} (A\nu\tau)^{1/2}]$ (Fig. 1, dependence *3*).

The method of extraction in the vacuum-boiling mode was first suggested by Lysyanskii [15]. Since then, this technique has been repeatedly used and studied on laboratory and semicommercial installations [1, 9, 11, 16]. The experimental results obtained demonstrated that boiling under a vacuum markedly accelerates the extraction process. Lysyanskii believes that steam bubbles create, when moving across the layer of a material, identical conditions at all points of the layer, favor energetic mutual motion of particles and liquid, and thereby accelerate the external mass exchange. However, this is not the only intensifying factor. In the case of spontaneous growth of bubbles in the common boiling mode, the pressure gradient at local points exceeds 50 MPa m^{-1}, and the rate gradient in a direction perpendicular to that of the microflow, 10^{-5} s^{-1} [17, 18]. The forming shock waves exert dynamic influence on particles of the raw material with the result that molecular diffusion within these particles partly gives way to convective (filtration) mass transfer.

Despite the large number of publications devoted to this method, there is no published evidence about how the extraction rate is affected by the intensity of suspension agitation. This intensity can be defined as the flow rate of steam across unit area of the free surface of the liquid [19], or, if the heating surfaces are distributed within the apparatus volume, as a flow rate

of steam through unit volume of the suspension being processed:

$$I_V = q_h F / r_{st} \rho_{st} V_{st}.$$

where I_V is the agitation intensity ($m^3\ s^{-1}\ m^{-3}$); q_h, specific heat flux ($W\ m^{-2}$); F, heating surface area (m^2); r_{st}, heat of steam formation ($J\ kg^{-1}$); ρ_{st}, steam density ($kg\ m^{-3}$); and V, liquid (suspension) volume (m^3).

The specific power expenditure for agitation in a vacuum-boiling apparatus is given by

$$N_{sp} = q_h F / V.$$

The specific heat flux is proportional to the temperature head: $q_h \sim (\Delta t)^{\varphi}$ [14], where $\Delta t = t_s - t_l$ is the temperature head; t_s, temperature of the heating surface; t_l, temperature of the liquid; and φ, exponent ($\varphi = 3$ for water under atmospheric pressure). Therefore, in the same apparatus at the same filling with the liquid and at the same temperature,

$$I_V \sim (\Delta t)^{\varphi} \text{ and } N_{sp} \sim (\Delta t)^{\varphi}.$$

The temperature head of boiling onset, Δt_{0h}, is affected by a wide variety of factors: pressure, properties of the liquid, roughness and material of the heating surface, etc. Water starts to boil at a pressure P = 100 kPa at $\Delta t_{0h} \sim 5$–6°C and specific heat flux $q_{0h} \sim 6 \times 10^3\ W\ m^{-3}$ [14]. For ethanol at P = 100 kPa, the temperature head of boiling onset is Δt_{0h} = 15°C [20].

Processing of the experimental data on extraction of flavonoid compounds (in terms of rutin) from everlasting flowers with a 40% aqueous solution of ethanol at a boiling temperature of the extracting agent of about 70°C (t_1 = 68.4–72.5°C), pressure of 62 kPa, and temperature heads Δt = 6.5, 13.4, and 25.2°C demonstrated that the process kinetics is sufficiently precisely described by the expression $\mu = 9 \ln(2.09 \Delta t \tau)$ (Fig. 1, dependence *4*).

The power expenditure for the process in a pulsatory apparatus is largely determined, as in the apparatus of oscillating vacuum boiling, by the energy expenditure for suspension transfer. Therefore, a formula similar to (7) was used to process experimental data at the same pressure differences. Dependence *5* in Fig. 1 illustrates the fundamental kinetic aspects of protein extraction with a 0.11 M buffer solution with pH 9.0 from finely divided (particle size 1–5 mm) fruit bodies of a *Lactarius rufus Fr.* mushroom at pressure oscillation frequencies ν = 3–6 s^{-1}. The straight line is described by the expression $\mu = 11.5 \ln[2.95 \times 10^{-3} (\nu\tau)^{1/2}]$.

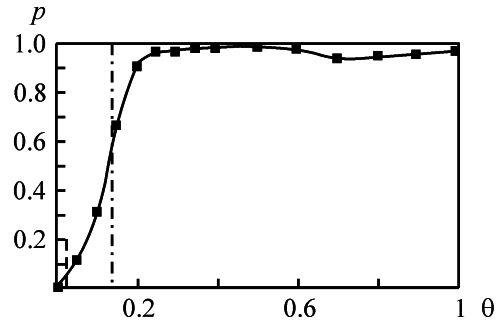


Fig. 2. Frequency p of satisfactory approximations vs. dimensionless extraction time θ.

Stirred vessels are the most frequently used reactors for extraction processes. In this case, the power expended for suspension agitation is $N_{sp} \sim n_{mix}^3$, where n_{mix} is the stirrer rotation speed (rpm). The experimental data on the kinetics of protein extraction from finely divided fruit bodies of a *Lactarius rufus Fr.* mushroom in a vessel with a fast stirrer (n_{mix} = 1500–3500 rpm) are well approximated by the expression $\mu = 8.67 \ln(5.94 \times 10^{-4} n_{mix} \tau)$ (Fig. 1, dependence *6*).

It is noteworthy that the exponent in the approximating dependence obtained for the extraction kinetics of tannin from galls is $\gamma = 1$. If the process were affected by the whole amount of energy expended by a rotary-pulsatory apparatus, the exponent would be $\gamma \approx 3$ [12]. The same can be said about the formula for the extraction kinetics of flavonoids from everlasting flowers in a vacuum-boiling apparatus. In this case, $\varphi = 1$ instead of $\varphi \approx 3$ [14]. Presumably, the parameter E_{sp} in relations (1) and (2) corresponds only to the "useful" part of the input energy, expended for initiation of the diffusion-convective mass-transfer mechanism, rather than to its whole amount. There is an apparent analogy with the dependence of the mass-transfer coefficient β on the specific energy dissipation ε, e.g., in dissolution of solid particles of size exceeding 60–100 μm in a stirred vessel, $\beta \sim \varepsilon^{0.25}$ [21, 22], and in dissolution of pellets in a vibration apparatus, $\beta \sim \varepsilon^{0.37}$ [23].

Figure 2 shows frequencies at which relations (1) and (2) satisfactorily (with an rms error less than 2.5%) approximate 90 kinetic curves of TC extraction from vegetable raw materials with various anatomical structures in apparatus with intensive hydrodynamic modes. As dimensionless time θ was taken the ratio between the running time and the time in which an "apparent" equilibrium is attained, when the process of TC extraction from the raw material still continues, but at an exceedingly low rate. The area under the curve, equal to 0.8, characterizes that part of the ex-

perimental data (with respect to the number of kinetic curves and the extraction time), which are satisfactorily described by formulas (1) and (2). Because there are no experimental data to the left of the curve (no samples were taken for technical reasons), the actual fraction of satisfactory approximations is 0.96. The average dimensionless time corresponding to $\mu = 0$ in the approximating relations (1) and (2) is $\theta_0 = 2.2 \times 10^{-2}$; this time is shown in Fig. 2 by a vertical dashed line. The average dimensionless time of first sampling, $\theta_1 = 0.14$, is denoted in Fig. 2 by a vertical dot-and-dash line. The average value of the ratio θ_0/θ_1 is 0.19. The approximation precision is somewhat deteriorated as the "apparent" equilibrium is approached, at dimensionless extraction times longer than 0.6.

CONCLUSION

The method suggested for processing of experimental data make it possible to describe with a sufficient precision the kinetics of TC extraction from porous particles in apparatus with an intensive hydrodynamic mode, reveal specific features and existence limits of hydrodynamic modes, analyze the utilization efficiency of the input energy, and find ways to diminish the energy expenditure for the process.

REFERENCES

1. Aksel'rud, G.A. and Lysyanskii, V.M., *Ekstragirovanie (sistema tverdoe telo–zhidkost')* (Extraction (Solid–Liquid System)), Leningrad: Khimiya, 1974.
2. Aksel'rud, G.A. and Al'tshuler, M.A., *Vvedenie v kapillyarno-khimicheskuyu tekhnologiyu* (Introduction to the Capillary-Chemical Technology), Moscow: Khimiya, 1983.
3. Abiev, R.Sh. and Ostrovskii, G.M., *Teor. Osn. Khim. Tekhnol.*, 2001, vol. 35, no. 3, pp. 270–275.
4. Abiev, R.Sh., *Zh. Prikl. Khim.*, 2001, vol. 74, no. 5, pp. 754–761.
5. Ivanov, E.V., *Sostoyanie i perspektivy podgotovki spetsialistov dlya farmatsevticheskoi otrasli: Materialy nauchno-metodicheskoi konferentsii* (State and Prospects for Training of Specialsts for Pharmaceutical Industry: Proc. Scientific and Methodological Conf.), St. Petersburg: Sankt-Peterb. Khim.-Farm. Akad., February 20, 2004, pp. 65–68.
6. Ivanov, E.V., Myasnikov, V.Yu., and Shvyrev, M.V., *Khim. Prom–st.*, 2004, vol. 81, no. 7, pp. 358–363.
7. Ivanov, E.V., Shvyrev, M.V., and Artemova, M.A., *Zh. Prikl. Khim.*, 2004, vol. 77, no. 10, pp. 1676–1680.
8. Ivanov, E.V. and Babenko, Yu.I., *Zh. Prikl. Khim.*, 2005, vol. 78, no. 9, pp. 1487–1497.
9. Molchanov, G.I., *Intensivnaya obrabotka rastitel'nogo syr'ya* (Intensive Treatment of Vegetable Raw Materials), Moscow: Meditsina, 1981.
10. Lysyanskii, V.M., *Protsess ekstraktsii sakhara iz svekly: Teoriya i raschet* (Extraction of Sugar from Beet: Theory and Calculation), Moscow: Pishchevaya Prom–st., 1973.
11. Lysyanskii, V.M. and Grebenyuk, S.M., *Ekstragirovanie v pishchevoi promyshlennosti* (Extraction in Food Industry), Moscow: Agropromizdat, 1987.
12. Balabudkin, M.A., *Rotorno-pul'satsionnye apparaty v khimiko-farmatsevticheskoi promyshlennosti* (Rotary-Pulsatory Apparatus in Chemical-Pharmaceutical Industry), Moscow: Meditsina, 1983.
13. Semagina, N.V., Sul'man, M.G., Sul'man, E.M., et al., *Khim.-Farm. Zh.*, 2000, vol. 34, no. 2, pp. 26–29.
14. Ametistov, E.V., Grigor'ev, V.A., Emtsev, B.T., et al., *Teplo- i massoobmen: Teplotekhnicheskii eksperiment: Spravochik* (Heat- and Mass-Transfer: Power-Engineering Experiment: Handbook), Grigor'ev, V.A. and Zorin, V.M., Eds., Moscow: Energoizdat, 1982.
15. USSR Inventor's Certificate no. 97418.
16. Ponomarev, V.D., *Ekstragirovanie lekarstvennogo syr'ya* (Extraction from Medicinal Raw Materials), Moscow: Meditsina, 1976.
17. Dolinskii, A.A., *Inzh.-Fiz. Zh.*, 1996, vol. 69, no. 6, pp. 35–43.
18. Dolinskii, A.A. and Basok, B.I., *Prom. Teplotekh.*, 1998, vol. 20, no. 6, pp. 7–10.
19. Gumnitskii, Ya.M. and Maistruk, I.N., *Teor. Osn. Khim. Tekhnol.*, 2002, vol. 36, no. 2, pp. 156–160.
20. Labuntsov, D.A., Yagov, V.V., and Gorodov, A.K., *Kipenie i kondensatsiya* (Boiling and Condensation), Riga, 1977, issue 1, pp. 16–23.
21. Nikolaishvili, E.K., Barabash, V.M., Braginskii, L.N., et al., *Teor. Osn. Khim. Tekhnol.* 1980, vol. 14, no. 3, pp. 349–357.
22. Barabash, V.M., Braginskii, L.N., and Vishnevetskaya, O.E., *Teor. Osn. Khim. Tekhnol.*, 1984, vol. 18, no. 6, pp. 744–748.
23. Abiev, R.Sh., Resonance Apparatus for Processes in Liquid-Phase Systems, *Doctoral Dissertation*, St. Petersburg, 2000.

ISSN 1070-4272, Russian Journal of Applied Chemistry, 2006, Vol. 79, No. 7, pp. 1127–1133. © Pleiades Publishing, Inc., 2006.
Original Russian Text © N.A. Samoilov, N.V. Zaichenko, 2006, published in Zhurnal Prikladnoi Khimii, 2006, Vol. 79, No. 7, pp. 1137–1143.

PROCESSES AND EQUIPMENT OF CHEMICAL INDUSTRY

Dynamics of Adsorption by Zeolites from the Liquid Phase, Simulated Using Data on Adsorption Statics

N. A. Samoilov and N. V. Zaichenko

Ufa State Technical University of Oil, Ufa, Bashkortostan, Russia

Received May 12, 2005; in final form, November 2005

Abstract—A mathematical model for calculation of the dynamics of liquid-phase adsorption in a fixed sorbent bed is constructed on the basis of material balance equations solved by numerical integration on the assumption of a constant mass-transfer coefficient and a limiting inner-diffusion resistance.

DOI: 10.1134/S1070427206070160

Adsorption separation of mixtures is one of the most efficient mass-exchange processes.

The primary goal of mathematical simulation of the operation of an adsorption column is the opportunity to calculate the adsorption dynamics, i.e., to plot the curve of variation of the concentration of an impurity being adsorbed in the purified flow (raffinate) leaving the column: the breakthrough curve or adsorption isoplane. This makes it possible to calculate the most important working characteristics of the column: dynamic activity of the adsorbent with respect to the impurity being extracted till its conditional (admissible) breakthrough into the raffinate, length of the mass-exchange zone, duration of column operation till conditional breakthrough of the impurity into the raffinate, etc.

An analysis of the adsorbate sorption, based on an integral or differential approach to solution of the problem, underlies the numerous existing methods for calculation of the adsorption dynamics. In the case of the integral approach, the dynamics equations have the form of algebraic equations with coefficients that characterize the adsorbate mass transfer in the adsorbent–adsorbate system [1]. The authors of numerous publications devoted to the adsorption dynamics assign to these coefficients different meanings (kinetic coefficient [2–4], partial mass-transfer coefficient in the liquid [5] and solid [6] phases, mass-transfer coefficient, etc.). The coefficients in question are not constants and commonly strongly depend on the nature of a component being sorbed and sorbent, concentration of a substance being sorbed in the feed, and flow rate of the feed in the column and markedly differ in processing of the results of the same experiment by different methods for calculation of the adsorption dynamics [7]. The equations of the adsorption dynamics in the differential form require that numerical calculation methods should be used and contain a number of numerical parameters: diffusion and thermodiffusion coefficients, barrier resistance, etc. [8, 9]. Finding the coefficients that appear in the adsorption dynamics equations requires special labor-consuming and prolonged experiments under dynamic conditions, with the subsequent construction of additional dependences of the kinetic coefficients on the flow rate and on the concentration of the impurity being adsorbed in the flow. Because the dimensions of research adsorption columns and their process modes markedly differ from those in the industrial conditions, extrapolation of experimental dependences beyond the investigation range leads to a gross error in simulations. Moreover, calculations of the adsorption dynamics require information about the potential activity of the sorbent in the form of an adsorption isotherm, which is also found experimentally. The necessity for a large number of results of laboratory and pilot experiments leads to a search for less labor-consuming ways to solve this problem.

The present study makes an attempt to directly calculate the adsorption dynamics in a column with a fixed zeolite bed from liquid-phase flows on the basis of data on the adsorption kinetics with account of the specificity of this process. The basic assumption of the model developed is that the limiting diffusion resistance in impurity adsorption from the flow of a liquid-phase feed is concentrated within micropores of the zeolite sorbent and the diameter of inlet windows through which molecules being adsorbed pen-

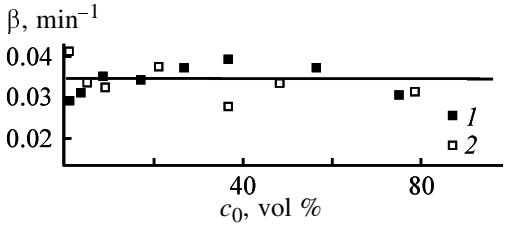


Fig. 1. Overall volume mass-transfer coefficient β vs. the content c_0 of the component being extracted in the feed in sorption of (*1*) benzene and (*2*) toluene with NaX zeolites from a solution in *n*-heptane.

etrate into voids of the crystal structure only slightly exceeds the critical size of the molecules. Such a behavior is typically observed, in particular, in separation of hydrocarbons with zeolites. Motion of molecules within the wide transport pores of the adsorbent and, the more so, in the space between adsorbent grains with linear dimensions of pores hundreds and thousands of times larger than the size of the molecules is provided at a significantly lower diffusion resistance, so that the outer-sphere diffusion can be neglected in this case. As a result, information obtained in studies of the adsorption kinetics can be used in developing a model of adsorption dynamics.

The easily performed basic experiment consists in that a set of kinetic curves of adsorption of an impurity is measured under static conditions. For this purpose, a number of weighed portions of the sorbent are brought in contact with portions of the feed with different concentrations of an impurity being extracted, the systems constituted by the adsorbent and the feed are kept for a necessary time, and then the samples are analyzed and the excess (Gibbs) adsorption of the impurity by the adsorbent is determined. The kinetic curves are used to plot the Gibbs adsorption isotherm.

The experience of kinetic studies of the sorption of various hydrocarbons shows that, to form the necessary minimum data file on the adsorption statics, it suffices to plot kinetic curves at two contents c_0 of the component being adsorbed, low (c_{0l}, 1–4%) and high (c_{0h}, 50–80%), with the corresponding equilibrium of adsorption values, a_l and a_h, determined. Processing of these data makes it possible to calculate the maximum adsorption value, a_{max}, at c_0 = 100%, with account of the adsorption gradient da/dc_0, and the coefficients A and B in the equation of Langmuir (full) adsorption isotherm

$$a_L = ABc_0(1 + Bc_0), \quad (1)$$

which characterizes the equilibrium adsorption of the impurity by the adsorbent. The relationship between the excess (Gibbs) adsorption a_G and full (Langmuir) adsorption is taken into account by the equation of the Gibbs adsorption isotherm in the form

$$a_G = a_L - (da/dc_0)c_0 = ABc_0/(1 + Bc_0) - (a_{max}/100)c_0. \quad (2)$$

A study of the kinetics of liquid-phase adsorption of aromatic hydrocarbons by NaX zeolites demonstrated [11] that the classical equation of adsorption kinetics [12]

$$da/d\tau = \beta(a_\infty - a). \quad (3)$$

where a_∞ is the equilibrium activity of the adsorbent; β, mass-transfer coefficient; and a, running value of the adsorbent activity after a time τ from the beginning of sorption, can be interpreted as the equation for the function of the response of a hydrodynamic model of the adsorption cell to a pulsed perturbation in the form of introduction of a portion of the feed into the cell. In this situation, the numerical value of β can be calculated as a reciprocal of the first static moment of the kinetic curve by the equation

$$\beta = 1/\int_0^\tau \tau(1 - a/a_\infty)d\tau. \quad (4)$$

In this case, β can be regarded in the conditions of liquid-phase sorption as the overall effective volume mass-transfer coefficient taking into account the diffusion resistance in macro- and micropores of the adsorbent.

Processing of kinetic curves of adsorption of certain aromatic hydrocarbons from solutions in *n*-heptane demonstrated that the thus determined value of β depends only on the physicochemical properties of the adsorbent and adsorbate, with the concentration of the component being adsorbed in the feed having virtually no effect on β (Fig. 1). This made it possible to calculate, with a minimum amount of input information, the Langmuir coefficients A and B (Table 1) and the Gibbs adsorption isotherm (Fig. 2) for the aromatic hydrocarbons studied.

To evaluate the diffusion resistance in the course of adsorption, the effective diffusion coefficient D of aromatic hydrocarbons within pores of the zeolite grains was calculated by the equation of diffusion in a finely crystalline adsorbent [14]

$$D_e = (\pi\gamma^2/4\tau)(V/S)^2. \quad (5)$$

where V and S are the volume of a zeolite grain (cm^3)

Table 1. Characteristic parameters of the adsorption kinetics

Adsorbate	Maximum activity, g g^{-1}		β, min^{-1}	Diffusion coefficient $D \times 10^8$, cm^2 s^{-1}			Constants of the Langmuir equation	
	by Gibbs	total		effective within pores		in solution		
				D_{max}	D_{min}		A, wt %	B, vol %
Benzene	0.14	0.17	0.031	281.5	31.9	4196.3	17.5	0.364
Toluene	0.25	0.285	0.029	228.9	31.9	3460.1	30.0	0.196
p-Xylene	0.196	0.225	0.025	224.5	28.4	2731.8	24.0	0.150
Isopropylbenzene	0.125	0.162	0.028	217.6	31.9	2228.9	27.0	0.586
Naphthalene	0.12	0.13	0.025	193.1	31.9	2714.5	13.2	0.774

and its outer surface area (cm^2); γ, relative adsorption found from the kinetic curve at instant of time τ (min). The diffusion coefficient D_s of aromatic hydrocarbons in a solution in *n*-heptane was calculated by the Wilke–Chang equation modified by Scheibel [15]

$$D_s = 8.2 \times 10^{-8}[1 + (3V_2/V_1)^{2/3}]T/(\mu_2 V_1^{1/3}), \quad (6)$$

where μ is the viscosity of *n*-heptane (cP): T, adsorption temperature (K); and V, molar volume of a diffusing aromatic hydrocarbon (cm^3 mol^{-1}).

The results of a calculation of the diffusion coefficients demonstrated that the dependence of the effective diffusion coefficient of aromatic hydrocarbons in zeolite grains on the adsorption time passes through a maximum in a wide range of concentrations of the aromatic hydrocarbons in the feed and durations of the adsorption process. Lower values of the diffusion coefficient D_e and, accordingly, a higher diffusion resistance in grains are reached in the final stage of the sorption process (Fig. 3). For example, the diffusion coefficient of benzene in a solution in *n*-heptane, D_s, is 42×10^{-6} cm^2 s^{-1}, i.e., is 14 times the maximum observed value of D_e, equal to 3×10^{-6} cm^2 s^{-1}, and 140 times the asymptotic values of D_e, equal to about 0.3×10^{-6} cm^2 s^{-1}. This makes it possible to consider quite correct the previous assumption that the limiting diffusion resistance is concentrated in the microporous space of sorbent grains, rather than in the flow of the feed between the grains, and to disregard diffusion phenomena in the intergrain space of the sorbent bed when developing the model of sorption dynamics.

The information basis considered enables simulation of the adsorption dynamics in a fixed sorbent bed with the use of material balance equations solved by numerical integration.

The sorption dynamics in separation of a binary mixture of, e.g., hydrocarbons with zeolites in a sorption column of height h (cm) and diameter D (cm) with an adsorbent charge G (g) at flow rate V (cm^3 min^{-1}) of the feed containing c_0 (vol %) of the adsorpate was

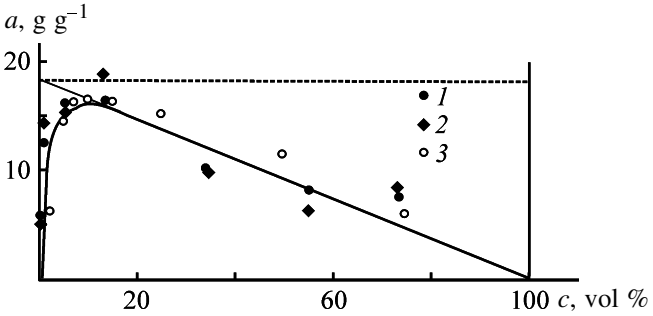


Fig. 2. Gibbs isotherm of benzene adsorption on NaX zeolites from a solution in *n*-heptane. (*a*) Zeolite activity with respect to benzene and (*c*) benzene content of the feed. Curve, calculation by Eq. (2); points: (*1, 2*) experimental data and (*3*) data of [13].

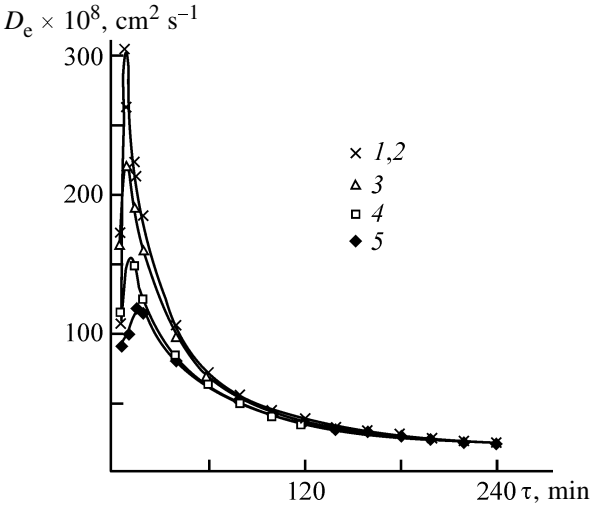


Fig. 3. Effective diffusion coefficient D_e of benzene in zeolite grains vs. the sorption time τ at different contents of benzene in a solution with *n*-heptane. Benzene content (vol %): (*1*) 26.9, (*2*) 58.6, (*3*) 8.0, (*4*) 4.0, and (*5*) 1.4.

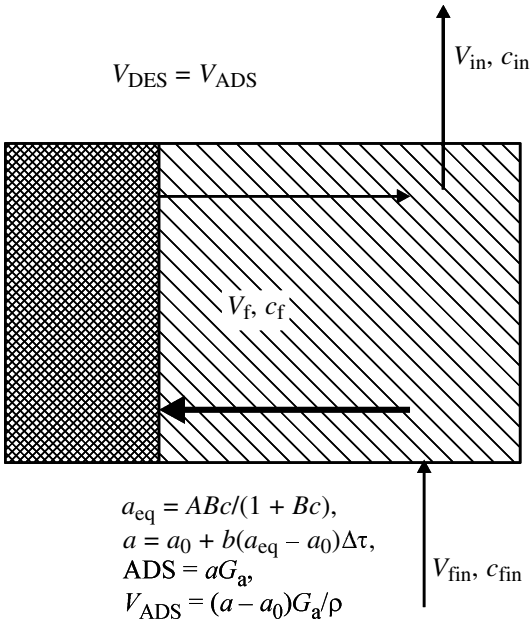


Fig. 4. Model of the adsorption cell.

calculated. As input data for the calculation served the following parameters: coefficients A (wt %) and B (vol %) of the Langmuir equation, mass-transfer coefficient β (min^{-1}), fraction of the free space in the sorbent bed with account of its porosity and specific volume of transport pores and micropores in the grains, and flow velocity w (cm min^{-1}) per total cross-section area of the column.

At the beginning of a calculation, the sorbent bed is divided along its height into N elementary cells of thickness Δh (Fig. 4). For each cell, the work of the corresponding part of the bed during a prescribed duration τ (min) of the sorption process is calculated in short intervals of time $\Delta\tau = \Delta h/w$. In view of the discrete nature of the calculation, Δh is 1 cm (several sorbent grain diameters). Commonly, the corresponding $\Delta\tau$ is in this case 0.5–2 min, which constitutes 0.2–0.5% of the time interval under study and provides that no less than 200–500 integration steps are made in calculation of each adsorption cell. The motion of the flow being purified along the column as a whole occurs in the ideal displacement mode, and that within a single cell, in the ideal mixing mode.

In the course of calculation of the adsorption process in ith cell during a time $\Delta\tau$, the following quantities are determined: (1) amount V_j of the feed that passed across the cell,

$$V_j = V_{in,j}\Delta\tau + V_f; \quad (7)$$

(2) content c_{feed} of the impurity in the feed, with account of the liquid present in the cell space free of the adsorbent, at the beginning of an adsorption event

$$c_{feed} = (V_{in,j}c_{in,j}\Delta\tau + V_f c_f)/V_j, \quad (8)$$

(3) equilibrium content a_{eq} of the adsorbed impurity in the adsorbent (equilibrium activity) by the Langmuir equation, and the running content a of the adsorbed impurity in the adsorbent (running activity), which enable calculation of the driving force of adsorption,

$$a_{eq} = ABc_0/(1 + Bc_0), \quad (9)$$

$$a = a_0 + \beta(a_{eq} - a_0)\Delta\tau, \quad (10)$$

[a_0, running content of the adsorbed impurity in the adsorbent (running activity) in the cell (wt %) at the preceding time step $\Delta\tau$ of the calculation], with the integral amount ADS of the adsorbed substance and its differential volume V_{ADS} calculated as

$$ADS = aG_a, \quad (11)$$

$$V_{ADS} = (a - a_0)G_a/\rho, \quad (12)$$

[G_a, mass of the adsorbent in the cell (g); ρ, adsorbate density (g cm^{-3})] and the gain in the sorbent activity in the cell during a time $\Delta\tau$ via transition of a part of the adsorbate from the bulk of the feed to the adsorbed state, equal to $a - a_0$; (4) content of the impurity in the feed with account of the liquid present in the cell space free of the adsorbent at the end of a sorption event

$$c_{fin,j} = (V_{in,j}c_{in,j}\Delta\tau + V_f c_f - 100V_{ADS})/V_j, \quad (13)$$

[$V_{in,j}$, $c_{in,j}$, the flow rate of the feed (cm^3 min^{-1}) and the content of the impurity in the feed (vol %) at the inlet into the cell being calculated; V_f, c_f, volume of the liquid filling the cell (cm^3) and content of the impurity in the liquid (vol %), $c_f = c_{fin,j}$ obtained in the preceding stage of cell calculation]; and (5) amount of liquid leaving the cell during the time $\Delta\tau$.

The calculation of the ith sorption cell during the whole time τ of the sorption process yields an array of the final amounts of the liquid and the contents of the impurity in the liquid at the cell outlet at small intervals of time, $\Delta\tau$. The subsequent readdress of the array of the final values of the parameters of the ith cell (flow rate of the liquid and the content of the component being adsorbed in the liquid) to the array of initial values of the corresponding parameters of $(i + 1)$st cell, which are distributed over the process duration τ, enables a calculation by the above al-

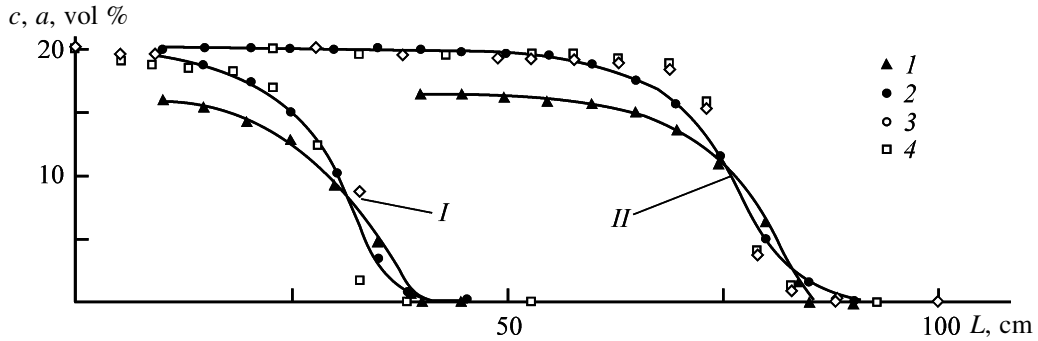


Fig. 5. Variation of the benzene content c of the flow and of the adsorbent activity a along the height L of the NaX zeolite bed, with the adsorption front recorded at (*I*) 61 and (*II*) 164 min in separation of a mixture of benzene and *n*-heptane. Linear flow velocity 0.572 cm min^{-1}, activation temperature 380°C. (*1*) Calculated activity, (*2*) calculated content, and (*3, 4*) experimental content in parallel measurements [19].

gorithm for the $(i + 1)$st cell. Calculations for all the cells of the adsorption column are performed similarly.

In the calculation of the sorption dynamics, three problems are successively solved for each cell in the course of the contact between the feed and the adsorbent, in addition to the calculation of the sorption: (1) filling of a cell with the feed (in the middle and end parts of the bed, cells are filled with the product purified to remove the impurity in the preceding cells); (2) exit of the first portion of the product being purified from a completely filled cell; and (3) steady flow out of the cell of the product being purified, considered on the assumption that the volume of the impurity adsorbed during time $\Delta\tau$ is equal to that of the purified product desorbed from the adsorbent, which is displaced from the adsorbent in an adsorption event and previously filled vacant places at adsorbate-free active centers of the zeolite.

The model developed forms the breakthrough curve of the adsorption process, adsorption isoplane, which is used to calculate the dynamic activity of the adsorbent to a conditional breakthrough into the raffinate of the impurity being extracted and the total dynamic activity of the adsorbent. The model also gives the concentration profile of the impurity being extracted and the curve of variation of the adsorbent activity across the adsorbent bed (along its height) for any process duration.

The obtained information about the concentration profile of the impurity being recovered along the height of the adsorbent bed makes it also possible to calculate the height of the working bed of the adsorbent (length of the mass-transfer zone) in processes with a moving adsorbent bed.

Owing to the simplicity of the model of adsorption dynamics, developed in this study, the problem can be solved with a computer to a full extent in only 2–3 min, despite the large number of the adsorption cells studied.

Thus, the model developed enables calculation of all the necessary characteristics of the adsorption dynamics.

In the experimental part of the study, dynamic characteristics of the liquid-phase adsorption of benzene with NaX zeolites from solutions in *n*-heptane were obtained in addition to the experiments on adsorption kinetics, considered above, and then the experimental data were compared with the results of calculations of the adsorption dynamics in terms of the model.

The adsorption of benzene under dynamic conditions was studied on a laboratory column of diameter 28 mm and zeolite bed height of 1010 mm (adsorbent charge ~420 g), in which it was possible, in addition to raffinate discharge from the upper level of the zeolite bed, to sample the liquid along the adsorbent bed height. This made it possible to determine, from the results obtained in analysis of the samples, how the content of benzene varies along the height of the adsorbent bed and find experimentally the length of the mass-transfer zone. The sampling system comprised 19 syringes mounted at intervals of 4–5 cm along the zeolite bed height and made it possible to take (virtually simultaneously, in the course of 15–20 s) 1 cm^3 samples from the axial zone of the column. The calculated length L_0 of the mass-transfer zone was found using the equation [16]

$$L_0 = L\frac{a_E - a_B}{a_E - (1 - f)a_B}, \qquad (14)$$

where a_E and a_B are, respectively, the total dynamic activity of the adsorbent and the dynamic activity of the adsorbent till conditional breakthrough of benzene

Table 2. Calculated and experimental parameters of the adsorption dynamics of benzene from a solution in *n*-heptane with NaX zeolites

Feed flow rate, $cm^3\ min^{-1}$	Activation temperature, °C	Results of calculation in terms of the model			Experimental data			
		activity, wt %		L_0, cm [Eq. (14)]	activity, wt %		L_0, cm [Eq. (14)]	L_0 (measured), cm*
		till breakthrough	till saturation		till breakthrough	till saturation		
4	380	13.75	16.75	39.27	13.85	16.82	38.1	40.5/35.0
4	380	13.75	16.75	39.27	13.17	16.85	40.3	38.0/41.0
20	300	3.36	16.22	91.92	–	–	–	–/–
15	300	5.73	16.42	84.91	–	–	–	–/–
10	300	9.00	16.44	70.9	10.30	16.50	62.5	65.5/>61.5
6	300	11.97	16.41	52.7	10.55	16.10	55.2	54.5/60.0
4	300	13.16	16.37	41.11	11.61	15.81	44.6	39.5/37.0
2	300	14.64	16.30	24.46	14.70	16.45	34.9	35.5/40.5
1	300	15.24	16.23	14.90	–	–	–	–/–
0.5	300	15.50	16.19	11.78	–	–	–	–/–

* Numerator, first measurement, denominator, second measurement.

into the raffinate (wt %); L, length of the adsorbent bed (cm); and f, symmetry factor of the breakthrough curve (adsorption isoplane).

The mass-transfer coefficient β and the constants A and B of the Langmuir equation, which are necessary for simulation of the process, were obtained in a study of the adsorption kinetics with ~2-g weighed portions of the zeolite, which were brought in contact with 10 cm^3 of the feed for 2–240 min (Table 1).

The results obtained in simulation of the adsorption of benzene from a solution in *n*-heptane demonstrated that the method for calculation of the sorption dynamics, developed in this study, makes it possibly to satisfactorily determine, both qualitatively and quantitatively, the position of the adsorption front in the adsorbent bed (Fig. 5) and the breakthrough curve (Fig. 6), as well as the basic characteristics of the adsorption process: activity of the adsorbent till conditional breakthrough of benzene into the raffinate, total dynamic activity of the adsorbent, and the length of the mass-transfer zone (Table 2). The inevitable minor discrepancies between the calculated and experimental data are due, in the case in question, to the neglect of the effect of the discrete sample volumes on the overall characteristics of the process, perturbation of the operation mode in the regeneration and adsorption stages of the process, errors of analysis, and a number of other factors.

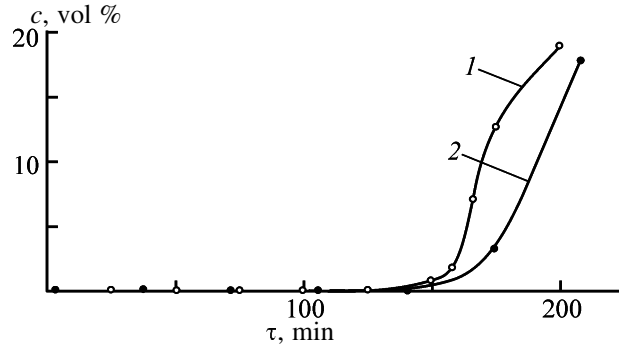


Fig. 6. Benzene content c of the raffinate vs. the elution duration τ at a feed flow velocity of 0.286 cm min^{-1} in separation of the benzene–*n*-heptane mixture with NaX zeolites. Zeolite activation temperature 300°C, zeolite bed height 1010 mm. (*1*) Experiment [19] and (*2*) calculation in terms of the model.

The adequacy of solution of the problem in hand in terms of the model developed was objectively assessed using the Fisher test [17]

$$F = S_{res}^2/S_r^2 = \frac{[\sum_M (y_{exp} - y_{calc})^2]/M}{[\sum_N (y_{exp} - y_{av})^2]/(N - 1)}, \qquad (15)$$

where S_{res}^2 and S_r^2 are, respectively the residual variance and variance of reproducibility; M and N, the number of parallel and independent experiments, respectively; and y_{exp}, y_{av}, and y_{calc}, the values of the parameters tested for adequacy: experimental, average over a set of parallel experiments, and calculated in terms of the model.

As follows from the results of adequacy assessment, calculation by the suggested mathematical

model of the adsorbent activity a_B till conditional breakthrough of benzene into the raffinate, total dynamic activity a_E of the adsorbent, and length L_0 of the mass-transfer zone is adequate with the probability of erroneously taking the hypothesis that the model is adequate equal to 0.05. The tabulated value of the Fisher test, equal to 234 [18], markedly exceeds the calculated values of the test for the parameters a_E, a_B, and L_0, which are 4.67, 166.6, and 13.8, respectively.

CONCLUSIONS

(1) A method for calculation of the dynamics of adsorption of hydrocarbons from solutions with zeolites was developed on the basis of a minimum amount of experimental data on the adsorption kinetics.

(2) An algorithm of simulation of the adsorption dynamics in a fixed sorbent bed was implemented on the basis of material balance equations solved by numerical integration.

(3) The model developed forms the output curve of the adsorption process, adsorption isoplane, which makes it possible to calculate the dynamic activity of the adsorbent till conditional breakthrough into the raffinate of the impurity being extracted, total dynamic activity of the adsorbent, and length of the mass-transfer zone.

(4) The adequacy of the results of calculations in terms of the model developed to the data obtained in control experiments on the dynamics of liquid-phase adsorption was confirmed.

(5) The method suggested for calculation of the adsorption dynamics is acceptable for rough prediction of the parameters of sorption dynamics.

REFERENCES

1. Kel'tsev, N.V., *Osnovy adsorbtsionnoi tekhniki* (Fundamentals of Adsorption Technology), Moscow: Khimiya, 1984.
2. Serpionova, E.N., *Promyshlennaya adsorbtsiya gazov i parov* (Industrial Adsorption of Gases and Vapors), Moscow: Vysshaya Shkola, 1965.
3. Kipling, J.J., *Adsorption from Solutions of Non-Electrolytes*, London: Academia, 1965.
4. Fenelonov, V.B., Fenelonova, V.E., Salyukov, A.N., et al., in *Tseolity, ikh sintez, svoistva i primenenie* (Zeolites, Their Synthesis, Properties, and Use), Moscow: Nauka, 1965, pp. 345–349.
5. Nutter, J.I. and Burnet, J.R., *Ind. Eng. Chem. Process Des. Develop.*, 1966, vol. 5, no. 1, pp. 76–83.
6. Eagliton, L.C. and Bluss, H., *Chem. Eng. Prog.*, 1953, vol. 49, no. 10, pp. 543–551.
7. Samoilov, N.A. and Fominykh, L.F., in *Tekhnologiya nefti i gaza: Voprosy fraktsionirovaniya* (Technology of Oil and Natural Gas: Fractionation Issues), Ufa: Bashkirskoe Knizhnoe, 1971, issue 2, pp. 325–333.
8. Zolotarev, P.P., A Study of the Kinetics and Dynamics of Physical Adsorption, *Doctoral Dissertation*, Moscow, 1974.
9. Zolotarev, P.P., *Adsorbtsiya v mikroporakh* (Adsorption in Micropores), Moscow: Nauka, 1983, pp. 124–128, 153–156, 170.
10. Serin, M.E., Lavrukhin, D.S., and Kulemina, L.B., in *Tseolity, ikh sintez, svoistva i primenenie* (Zeolites, Their Synthesis, Properties, and Use), Moscow: Nauka, 1965, pp. 304–306.
11. Samoilov, N.A., *Zh. Fiz. Khim.*, 1976, vol. 50, no. 10, pp. 2640–2641.
12. Glueckauf, E., *Trans. Faraday Soc.*, 1955, vol. 51, no. 11, pp. 1540–1541.
13. Samoilov, N.A., in *Tekhologiya nefti i gaza: Voprosy fraktsionirovaniya* (Technology of Oil and Natural Gas: Fractionation Issues), Ufa: Bashkirskoe Knizhnoe, 1975, issue 264, pp. 192–197.
14. Timofeev, D.P., *Kinetika adsorbtsii* (Adsorption Kinetics), Moscow: Akad. Nauk SSSR, 1962.
15. Reid, R.C. and Sherwood, T.K., *The Properties of Gases and Liquids*, New York: McGraw-Hill, 1966.
16. Fominykh, L.F. and Samoilov, N.A., in *Massoobmennye protsessy khimicheskoi tekhnologii* (Mass-Exchange Processes in Chemical Technology), Leningrad: Khimiya, 1969, pp. 121–123.
17. Kafarov, V.V., *Metody kibernetiki v khimii i khimicheskoi tekhnologii* (Methods of Cybernetics in Chemistry and Chemical Technology), Moscow: Khimiya, 1971.
18. Batuner, L.M. and Pozin, M.E., *Matematicheskie metody v khimicheskoi tekhnike* (Mathematical Methods in Chemical Technology), Leningrad: Khimiya, 1971.
19. Samoilov, N.A. and Fominykh, L.F., in *Doklady neftekhimicheskoi sektsii* (Reports of the Petrochemical Section), Ufa: Bashk. Resp. Pravlenie Vses. Khim. O–va. im. D.I. Mendeleeva, 1971, issue 6, pp. 174–178.

ISSN 1070-4272, Russian Journal of Applied Chemistry, 2006, Vol. 79, No. 7, pp. 1134–1137. © Pleiades Publishing, Inc., 2006.
Original Russian Text © V.M. Chernyshev, A.N. Sokolov, V.A. Taranushich, 2006, published in Zhurnal Prikladnoi Khimii, 2006, Vol. 79, No. 7, pp. 1144–1147.

ORGANIC SYNTHESIS AND INDUSTRIAL ORGANIC CHEMISTRY

Improved Synthesis of 2-Amino-1,2,4-triazolo[1,5-*a*]pyrimidines

V. M. Chernyshev, A. N. Sokolov, and V. A. Taranushich

South-Russian State Technical University, Novocherkassk, Rostov oblast, Russia

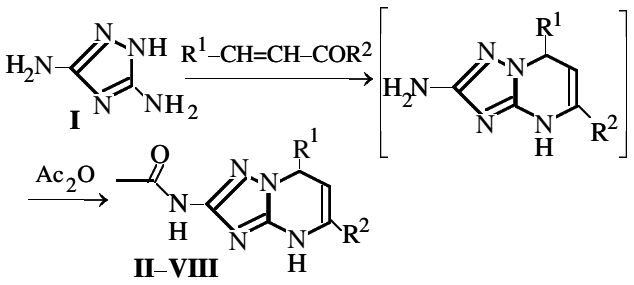
Received May 4, 2006

Abstract—An improved procedure is suggested for preparing 2-amino-1,2,4-triazolo[1,5-*a*]pyrimidines from 3,5-diamino-1,2,4-triazole and unsaturated aromatic ketones, with acetyl protection of the amino group in the step of oxidation of 2-amino-4,7-dihydro-1,2,4-triazolo[1,5-*a*]pyrimidines.

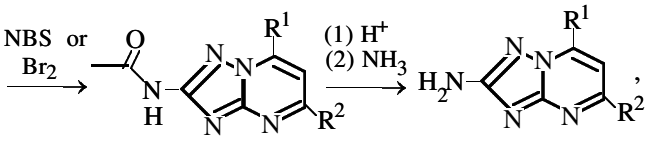
DOI: 10.1134/S1070427206070172

2-Amino-1,2,4-triazolo[1,5-*a*]pyrimidines exhibit a broad spectrum of biological activity and can be used as analgetics [1], blood pressure regulators [2], antibacterial agents [3], and herbicides [4, 5]. The presence of a reactive amino group makes these compounds valuable building blocks in syntheses of biologically active compounds [6, 7].

One of the most convenient routes to 2-amino-1,2,4-triazolo[1,5-*a*]pyrimidines is the cyclocondensation of 3,5-diamino-1,2,4-triazole **I** with α,β-unsaturated ketones [1, 7–11] followed by heteroaromatization of the resulting 2-amino-4,7-dihydro-1,2,4-triazolo[1,5-*a*]pyrimidines with bromine or *N*-bromosuccinimide (NBS) [11, 12]. An advantage of this route, compared to other methods for forming triazolopyrimidine core, is high regioselectivity and availability of the starting compounds [8, 9]. However, an experimental check showed that the oxidation of the dihydro derivatives is accompanied by formation of a large amount of impurities (presumably azo derivatives), probably because of side oxidation of the amino group. Separation of these impurities involves major loss of the desired 2-amino-1,2,4-triazolo[1,5-*a*]pyrimidines, so that their yield does not exceed 25–30%. We believe that this procedure can be improved by acetyl protection of the amino group in the oxidation step. This possibility was examined in the present study with a series of 2-amino-1,2,4-triazolo[1,5-*a*]-pyrimidines:



I **II–VIII**



IX–XV **XVI–XXII**

where R^1 = Ph, R^2 = Me (**II**, **IX**, **XVI**); R^1 = *p*-Cl·C_6H_4, R^2 = Ph (**III**, **X**, **XVII**); R^1 = Ph, R^2 = *p*-Cl·C_6H_4 (**IV**, **XI**, **XVIII**); R^1 = *p*-MeC_6H_4, R^2 = Ph (**V**, **XII**, **XIX**); R^1 = Ph, R^2 = *p*-MeC_6H_4 (**VI**, **XIII**, **XX**); R^1 = *p*-$MeOC_6H_4$, R^2 = Ph (**VII**, **XIV**, **XXI**); R^1 = R^2 = *p*-MeC_6H_4 (**VIII**, **XV**, **XXII**).

The first step of the suggested scheme involves the condensation of diamine **I** with unsaturated ketones to obtain 2-amino-4,7-dihydro-1,2,4-triazolo[1,5-*a*]-pyrimidines. Since it was difficult to isolate and purify the majority of the dihydro derivatives because of their high solubility, acetyl derivatives **II**–**VIII** were prepared by adding acetic anhydride to the reaction mixture after the condensation completion. The yield of **II**–**VIII** in the one-pot process was 52–90% (see table). These compounds were not described previously and were identified by elemental analysis, ^{1}H NMR spectroscopy, and mass spectrometry.

2-Acetylamino-1,2,4-triazolo[1,5-*a*]pyrimidines **IX**–**XV** were obtained in 84–95% yields (see table) by oxidation of **II**–**VIII** with *N*-bromosuccinimide in ethanol at 50–60°C or with bromine in acetic acid at 15–20°C. In this step, it is very important to maintain the required temperature and reactant ratio. Performing the oxidation at higher temperatures or with excess oxidant results in formation of difficult-to-separate impurities identified by mass spectrometry as brominated derivatives of **IX**–**XV**. Acid hydrolysis of acetyl derivatives **IX**–**XV** gave the desired 2-amino-1,2,4-triazolo[1,5-*a*]pyrimidines **XVI**–**XXII** in almost quan-

Yields and properties of **II**–**XXII**

Compound	Yield, %	mp, °C	Formula*	^{1}H NMR spectrum, δ, ppm (*J*, Hz)
II	86	244–245	$C_{14}H_{15}N_5O$	1.91 s (3H, CH_3), 2.00 s (3H, CH_3), 4.46 d (1H, CH, *J* = 3.2), 5.59 d (1H, CH, *J* = 3.2), 7.18–7.38 m (5H, arom.), 9.50 s (1H, NH), 9.91 s (1H, NH)
III	55	296–298	$C_{19}H_{16}N_5ClO$	2.00 s (3H, CH_3), 5.07 d (1H, CH, *J* = 3.3), 6.12 d (1H, CH, *J* = 3.3), 7.21–7.64 m (9H, arom.), 10.00 s (1H, NH), 10.10 s (1H, NH)
IV	76	257–259	$C_{19}H_{16}N_5ClO$	1.94 s (3H, CH_3), 5.24 d (1H, CH, *J* = 3.5), 6.10 d (1H, CH, *J* = 3.5), 7.21–7.38 m (5H, Ph), 7.46 d (2H, arom., *J* = 8.5), 7.61 d (2H, arom., *J* = 8.5), 10.05 s (1H, NH), 10.12 s (1H, NH)
V	90	264–266	$C_{20}H_{19}N_5O$	1.95 s (3H, CH_3), 2.26 s (3H, CH_3), 5.16 d (1H, CH, *J* = 3.5), 6.04 d (1H, CH, *J* = 3.5), 7.16 m (4H, arom.), 7.40 m (3H, arom.), 7.59 m (2H, arom.), 9.98 s (1H, NH), 10.12 s (1H, NH)
VI	61	228–230	$C_{20}H_{19}N_5O$	1.94 s (3H, CH_3), 2.30 s (3H, CH_3), 5.15 d (1H, CH, *J* = 3.5), 6.08 d (1H, CH, *J* = 3.5), 7.19–7.49 m (9H, arom.), 9.98 s (1H, NH), 10.17 s (1H, NH)
VII	52	259–261	$C_{20}H_{19}N_5O_2$	1.95 s (3H, CH_3), 3.71 s (3H, CH_3O), 5.15 d (1H, CH, *J* = 3.5), 6.04 d (1H, CH, *J* = 3.5), 6.91 d (2H, arom., *J* = 8.5), 7.20 d (2H, arom., *J* = 8.5), 7.39–7.58 m (5H, arom.), 9.97 s (1H, NH), 10.12 s (1H, NH)
VIII	81	273–274	$C_{21}H_{21}N_5O$	1.96 s (3H, CH_3), 2.26 s (3H, CH_3), 2.31 s (3H, CH_3), 5.12 d (1H, CH, *J* = 3.7), 6.03 d (1H, CH, *J* = 3.7), 7.12–7.22 m (6H, arom.), 7.47 d (2H, arom., *J* = 8.2), 9.94 s (1H, NH), 10.11 s (1H, NH)
IX	95 (b)	236–237	$C_{14}H_{13}N_5O$	2.14 s (3H, CH_3), 2.63 s (3H, CH_3), 7.45 s (1H, CH), 7.60 m (3H, arom.), 8.17 m (2H, arom.), 10.86 s (1H, NH)
X	92 (a)	314–315	$C_{19}H_{14}N_5ClO$	2.20 s (3H, CH_3), 7.44–7.70 m (5H, arom.), 8.00 s (1H, CH), 8.32–8.44 m (4H, arom.), 10.86 s (1H, NH)
XI	90 (a), 88 (b)	272–274	$C_{19}H_{14}N_5ClO$	2.18 s (3H, CH_3), 7.58–7.71 m (5H, arom), 8.06 s (1H, CH), 8.32–8.42 m (4H, arom.), 10.92 s (1H, NH)
XII	88 (a)	302–304	$C_{20}H_{17}N_5O$	2.18 s (3H, CH_3), 2.43 s (3H, CH_3), 7.44 d (2H, arom., *J* = 8.0), 7.57–7.59 m (3H, arom.), 8.04 s (1H, CH), 8.24–8.36 m (4H, arom.), 10.94 s (1H, NH)
XIII	91 (a), 90 (b)	276–277	$C_{20}H_{17}N_5O$	2.18 s (3H, CH_3), 2.39 s (3H, CH_3), 7.38 d (2H, arom., *J* = 8.0), 7.57– 7.69 m (3H, arom.), 8.02 s (1H, CH), 8.25–8.28 m (4H, arom.), 10.93 s (1H, NH)
XIV	84 (a)	278–280	$C_{20}H_{17}N_5O_2$	2.18 s (3H, CH_3), 3.88 s (3H, CH_3O), 7.19 d (2H, arom., *J* = 8.9), 7.59 m (3H, arom.), 8.04 s (1H, CH), 8.35–8.42 m (4H, arom.), 10.94 s (1H, NH)
XV	90 (a), 87 (b)	305–306	$C_{21}H_{19}N_5O$	2.18 s (3H, CH_3), 2.40 s (3H, CH_3), 2.43 s (3H, CH_3), 7.36–7.45 m (4H, arom.), 8.00 s (1H, CH), 8.22–8.27 m (4H, arom.), 10.92 s (1H, NH)
XVI	94	249–250**	$C_{12}H_{11}N_5$	2.53 s (3H, CH_3), 6.34 s (2H, NH_2), 7.16 s (1H, CH), 7.58 m (3H, arom.), 8.12 m (2H, arom.)
XVII	90	207–209	$C_{17}H_{12}N_5Cl$	6.52 s (2H, NH_2), 7.54 m (3H, arom.), 7.69 d (2H, arom., *J* = 8.1), 7.84 s (1H, CH), 8.30–8.33 m (4H, arom.)
XVIII	89	220–221***	$C_{17}H_{12}N_5Cl$	6.52 s (2H, NH_2), 7.59–7.62 m (5H, arom.), 7.83 s (1H, CH), 8.24–8.27 m (2H, arom.), 8.24 d (2H, arom., *J* = 8.6)
XIX	93	244–245	$C_{18}H_{15}N_5$	2.42 s (3H, CH_3), 6.47 s (2H, NH_2), 7.43 d (2H, arom., *J* = 8.1), 7.53 m (3H, arom.), 7.78 s (1H, CH), 8.21 d (2H, arom., *J* = 8.1), 8.28 m (2H, arom.)
XX	95	217–219****	$C_{18}H_{15}N_5$	2.38 s (3H, CH_3), 6.45 s (2H, NH_2), 7.35 d (2H, arom., *J* = 8.0), 7.59 m (3H, arom.), 7.76 s (1H, CH), 8.18–8.24 m (4H, arom.)

Table. (Contd.)

Compound	Yield, %	mp, °C	Formula*	^{1}H NMR spectrum, δ, ppm (*J*, Hz)
XXI	91	238–240	$C_{18}H_{15}N_5O$	3.87 s (3H, CH_3O), 6.46 s (2H, NH_2), 7.15 d (2H, arom., *J* = 8.9), 7.55 m (3H, arom.), 7.77 s (1H, CH), 8.27–8.35 m (4H, arom.)
XXII	92	187–188	$C_{19}H_{17}N_5O$	2.38 s (3H, CH_3), 2.42 s (3H, CH_3), 6.51 s (2H, NH_2), 7.35 d (2H, arom., *J* = 8.1), 7.41 d (2H, arom., *J* = 8.1), 7.74 s (1H, CH), 8.18 d (2H, arom., *J* = 8.1), 8.19 d (2H, arom., *J* = 8.1)

* The results of the C, H, N analysis were consistent with the calculated composition within ±0.32%; the mass spectra of all the compounds contain a strong $[M + H]^+$ peak.
** mp 245–250°C [4].
*** mp 210–211°C [11].
**** mp 220–222°C [11].

titative yield (see table). The overall yield of **XVI**–**XXII** based on **I** was 40–70%. Compounds **IX**–**XXII** were identified by elemental analysis, ^{1}H NMR spectroscopy, and mass spectrometry (see table).

EXPERIMENTAL

The ^{1}H NMR spectra were recorded on a Varian Unity-300 spectrometer (300 MHz, DMSO-d_6, internal reference TMS). The mass spectra were taken on a Finnigan LCQ Deca XP MAX device in the electrospray mode with positive polarization at direct inlet of 0.5 mg ml^{-1} solutions of the compounds in acetonitrile. Elemental analysis was performed with a Perkin–Elmer 2400 analyzer. The melting points were determined by the capillary method with a PTP device.

2-Acetylamino-4,7-dihydro-1,2,4-triazolo[1,5-*a*]-pyrimidines II–VIII. A mixture of 1 g (0.01 mol) of **I**, 0.01 mol of appropriate unsaturated ketone, and 4 ml of anhydrous DMF was refluxed for 20 min, after which 1.39 g (0.0136 mol) of Ac_2O was added, and the mixture was refluxed for an additional 3 min. Then the mixture was cooled, 4 ml of acetonitrile was added, and the precipitate of the target product was filtered off and washed with 20 ml of acetone. Compounds **II**–**VIII** were purified by twofold refluxing with 5 ml of acetonitrile.

2-Acetylamino-1,2,4-triazolo[1,5-*a*]pyrimidines IX–XV. (a) To a stirred mixture of 0.003 mol of acetyl derivative **III**–**VIII** and 0.27 g (0.0044 mol) of sodium acetate in 20 ml of ethanol, 0.52 g (0.003 mol) of *N*-bromosuccinimide was added in 0.1-g portions over a period of 10 min at 50–60°C. Then the mixture was refluxed for 15 min and diluted with 15–20 ml of water; the precipitate was filtered off, washed with 20 ml of water, and crystallized from DMF–ethanol (1 : 3).

(b) To a solution of 0.003 mol of **II**, **IV**, **VII**, or **VIII** and 0.27 g (0.0044 mol) of sodium acetate in 10–15 ml of acetic acid, 0.48 g (0.003 mol) of Br_2 was added dropwise over a period of 5 min at 15–20°C. The solution was stirred for 30 min and diluted with 15–20 ml of water. The precipitate was filtered off, washed with water (20 ml), and crystallized from DMF–ethanol (1 : 3).

2-Amino-1,2,4-triazolo[1,5-*a*]pyrimidines XVI–XXII. Concentrated HCl (1 ml) was added to a suspension of 0.0014 mol of **IX**–**XV** in 10 ml of ethanol; the mixture was refluxed for 40 min, the solvent was distilled off, and the residue was neutralized with aqueous NH_3 to pH 6–8. The precipitate was filtered off and crystallized from DMF–ethanol, 1 : 3.

CONCLUSIONS

(1) Successive reactions of 3,5-diamino-1.2.4-triazole with α,β-unsaturated aromatic ketones and acetic anhydride allow one-pot synthesis of 2-acetylamino-4,7-dihydro-1,2,4-triazolo[1,5-*a*]pyrimidines in 52–90% yield.

(2) The acetyl protection of the amino group in 2-amino-4,7-dihydro-1,2,4-triazolo[1,5-*a*]pyrimidines in the step of their oxidation with *N*-bromosuccinimide or bromine prevents oxidation of the amino group and allows the overall yield of 2-amino-1,2,4-triazolo[1,5-*a*]pyrimidines to be increased to 40–70% based on 3,5-diamino-1,2,4-triazole.

REFERENCES

1. Desenko, S.M., Orlov, V.D., Lipson, V.V., et al., *Khim.-Farm. Zh.*, 1994, vol. 28, no. 3, pp. 19–21.
2. Rusinov, V.L., Petrov, A.Yu., Pilicheva, T.L., et al., *Khim.-Farm. Zh.*, 1986, vol. 20, no. 2, pp. 178–182.

3. Rusinov, V.L., Myasnikov, A.V., Pilicheva, T.L., et al., *Khim.-Farm. Zh.*, 1990, vol. 24, no. 1, pp. 39–42.
4. US Patent 5 127 936.
5. US Patent 4 822 404.
6. Berecz, G., Reiter, J., Argay, G., and Kálmán, A., *J. Heterocyclic Chem.*, 2002, vol. 39, no. 2, pp. 319–325.
7. Lipson, V.V., Desenko, S.M., Borodina, V.V., et al., *Zh. Org. Khim.*, 2005, no. 1, pp. 115–120.
8. Desenko, S.M. and Orlov, V.D., *Azageterotsikly na osnove aromaticheskikh nepredel'nykh ketonov* (Aza Heterocycles Derived from Aromatic Unsaturated Ketones), Kharkov: Folio, 1998.
9. Desenko, S.M., *Khim. Geterotsikl. Soedin.*, 1995, no. 2, pp. 147–159.
10. Lipson, V.V., Desenko, S.M., Orlov, V.D., et al., *Khim. Geterotsikl. Soedin.*, 2000, no. 1, pp. 1542–1549.
11. Desenko, S.M., Kolos, N.N., Tueni, M., and Orlov, V.D., *Khim. Geterotsikl. Soedin.*, 1990, no. 7, pp. 938–941.
12. Desenko, S.M., Orlov, V.D., and Lipson, V.V., *Khim. Geterotsikl. Soedin.*, 1990, no. 12, pp. 1638–1642.

ISSN 1070-4272, Russian Journal of Applied Chemistry, 2006, Vol. 79, No. 7, pp. 1138–1142. © Pleiades Publishing, Inc., 2006.
Original Russian Text © T.K. Dzhumadilov, I.S. Saparbekova, B.M. Butin, E.A. Bekturov, 2006, published in Zhurnal Prikladnoi Khimii, 2006, Vol. 79, No. 7, pp. 1148–1152.

MACROMOLECULAR CHEMISTRY AND POLYMERIC MATERIALS

Influence of the Molecular Weight of a Polymer on the Phase Diagram of the System Polyethylene Glycol–Sodium Tetraphenylborate

T. K. Dzhumadilov, I. S. Saparbekova, B. M. Butin, and E. A. Bekturov

Kazakhstan State Woman's Pedagogical Institute, Ministry of Education and Science of Kazakhstan Republic, Almaty, Kazakhstan

Bekturov Institute of Chemical Sciences, Ministry of Education and Science of Kazakhstan Republic, Almaty, Kazakhstan

Received November 18, 2005

Abstract—The melting points of the polyethylene glycol–$NaBPh_4$ system synthesized in ethanol were determined by optical microscopy. The influence of the molecular weight of polyethylene glycol on the phase formation in the system was studied.

DOI: 10.1134/S1070427206070184

Molecular complexes of alkali and alkaline-earth metal salts with nonionic polymers containing heteroatoms are known to be ion-conducting materials [1, 2].

A wide variety of problems concerning the influence of various factors, such as flexibility of macromolecules, nature of heteroatoms in polymers, and type of cations and ions constituting the low-molecular-weight salts, on the ionic conductivity and structure of the complexes was considered previously [3]. At the same time, the effect exerted by the nature of the medium on the composition, morphology, and structure of complexes is as yet insufficiently studied.

In the previous studies, the possibility of formation of various complexes was demonstrated for the system polyethylene glycol (PEG)–sodium tetraphenylborate in organic solvents. The composition and structure of solid complexes formed in the solvent and their change upon solvent removal remain unclear.

At the same time, a study of the composition and structure of solid complexes and the features of their formation in organic solvents of different nature is of great significance for the development of processes for preparation of individual complexes or their mixtures.

In this connection, the features of formation of polyethylene glycol complexes in protonic solvents of linear and branched structure were studied previously by optical microscopy and X-ray diffraction analysis. The results obtained confirmed the formation of several complexes in the above media [4, 5]. It was established in these studies that the number of the formed complexes decreases as the structure of alcohol becomes more complex, i.e., in going from linear to branched alcohols. However, the effect exerted by the molecular weight of the polymer on the structure of complexes composed of polyethylene glycol and sodium tetraphenylborate was not considered.

In this study we examined how the length of the PEG macromolecule chain affects the composition and structure of the PEG–sodium teraphenylborate complexes formed in ethanol. Taking the PEG–$NaBPh_4$ system as example, we studied the features of the interaction of alkali metal salts with the polyether of a varied molecular weight (MW).

EXPERIMENTAL

Sodium tetraphenylborate $NaB(C_6H_5)_4$ (analytically pure grade) was used in the study after additional drying. Polyehtylene glycols with molecular weights (MWs) of 2000, 4000, 15000, 40000, and 100000 (Schuchardt, Germany) were used after drying in a rough vacuum. Ethanol was purified by the method described in [6].

The complexes were synthesized by mixing solutions of individual components under the standard conditions. The solvent was evaporated in a vacuum

at room temperature. Then, samples were kept in a vacuum at 30–35°C for several days to remove the residual solvent (to constant weight).

The melting points of the starting components and their molecular complexes were determined on a Boëtius optical microscope (Rapido, Germany) at ×16 magnification.

It was found previously that complexes constituted by PEG and alkali metal salt, synthesized in different media, have essentially different properties [4]. To ascertain the influence of the molecular weight of polyethylene glycol on the morphology and structure of the solid complexes, we continued a study of the PEG–salt system.

In this study we considered the phase state of the products formed by the interaction of PEG (MW 2000, 4000, 15000, 40000, and 100000) with $NaB(C_6H_5)_4$.

The phase diagram constructed from data on the melting points of the PEG (MW = 2000)–$NaBPh_4$ complexes is shown in Fig. 1. The melting points, T_m, of the formed molecular complexes strongly differ from those of the starting components, which confirms formation of new complex compounds. The constructed phase diagram has three distectic points at ratios of 6 : 1 (T_m = 513 K), 3 : 1 (T_m = 473 K), and 1 : 3 (T_m = 423 K) and two peritectic points at ratios of 15 : 1 (T_m = 323 K) and 8 : 1 (T_m = 396 K). The eutectic points are identified at ratios of 30 : 1 (T_m = 318 K), 4 : 1 (T_m = 423 K), 1 : 2 (T_m = 418 K), and 1 : 5 (T_m = 403 K). The liquidus curves and the solidus lines divide the phase diagram into 14 regions. The melting point of PEG is 326 K.

The first eutectic E_1 with a melting point of 318 K was observed in the PEG–$NaBPh_4$ system at a ratio of 30 : 1, i.e., in the region of high polymer : salt ratios. Region *1* above the liquidus curve corresponds to a liquid phase, i.e., a melt. The melting point of the solid complexes increases from the point E_1 to the peritectic point P_1, at which the complex of composition 15 : 1 melts incongruently. At a ratio of 10 : 1, the melting point increases along the liquidus curve, and the second peritectic point P_2 with T_m = 396 K is identified at a ratio of 8 : 1. Crystals of the molecular complex of the composition 15 : 1 are separated from P_1 to P_2. At ratios of 7 : 1 to 1 : 1, a part of the product in the PEG–$NaBPh_4$ system melts, whereas another its part starts melting at a higher temperature. In this case, two distectic points are observed: M_1 is observed at a ratio of 6 : 1 (T_m = 513 K) and M_2, at 3 : 1 (T_m = 473 K). The points below the main liquidus curve correspond to the melting point of a molecular complex

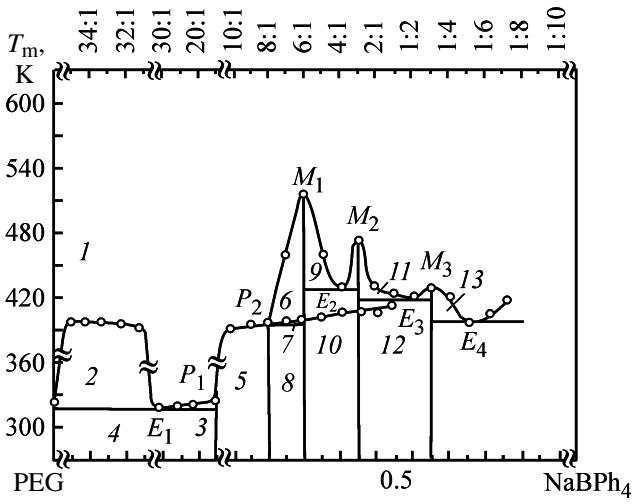


Fig. 1. Phase diagram of the system PEG (MW 2000)–$NaBPh_4$ prepared in ethanol. (T_m) Melting point; the same for Figs. 2–5. Points: (M_1, M_2, M_3) distectic, (P_1, P_2) peritectic, and (E_1, E_2, E_3, E_4) eutectic. The component ratio is indicated along the upper abscissa. Italic figures denote regions of the phase diagram; the same for Figs. 2–5.

of the composition 8 : 1. In this region (*4*), the liquid coexists with crystals of the molecular complex MC_1. The second melting points are observed above the indicated melting points. This confirms two morphologies of one newly formed complex. In region *6* below the $P_2M_1E_2$ curve, the liquid phase coexists with MC_1 crystals.

The crystals of MC_1 are separated along the M_1E_2 curve at the point E_2 at which three phases, liquid + crystals of MC_1 complex + crystals of MC_2 complex, coexist. At point M_2, the complex MC_2 melts. Region *12* below the solidus line constructed through the point E_3 includes two solid phases, which are crystals of MC_2 and MC_3 complexes.

At the 1 : 3 composition (T_m = 423 K), the third distectic point is identified. The liquid phase coexists with the crystalline phase of the MC_3 complex below the M_3E_4 curve. The obtained distectic points show that three stable complexes are formed in the PEG (MW 2000)–$NaBPh_4$ system: MC_1 complex with the 6 : 1 composition (T_m = 513 K), MC_2 complex with the 3 : 1 composition (T_m = 473 K), and MC_3 complex with the 1 : 3 composition (T_m = 423 K). Starting with the 1 : 8 composition, the interaction product does not transform into the liquid state, i.e., it does not melt. At higher temperatures, the complexes obtained become dark. This means that the molecular complexes formed in this region are carbonized. The high melting points of the solid complexes belong to the continuous highly ordered double-helix regions,

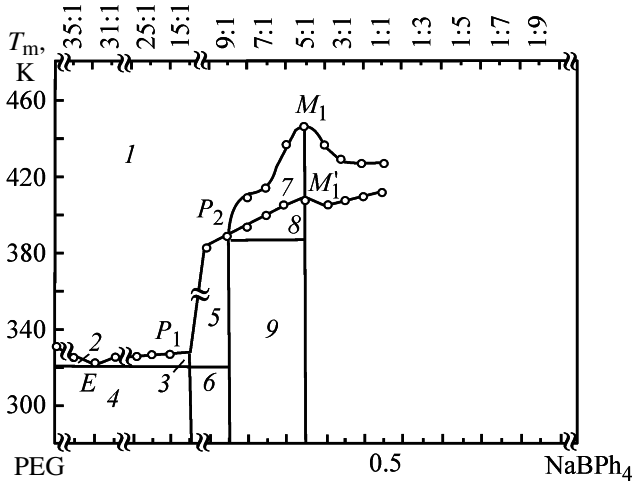


Fig. 2. Phase diagram of the PEG (MW 4000)–$NaBPh_4$ system. Points: (M_1, M_2) distectic, (P_1, P_2) peritectic, and (E) eutectic.

whereas their low values, to a defective disordered structure [3].

The results of this study show that the 6 : 1, 3 : 1, and 1 : 3 complexes are formed in the PEG (MW 2000)–$NaBPh_4$ system in ethanol.

For further studies we synthesized solid complexes in the PEG (MW 4000)–$NaBPh_4$ system. The phase diagram has one eutectic point, two peritectic points, and two distectic points (Fig. 2). The peritectic point P_1 (T_m = 328 K) is observed at a component ratio of 15 : 1 and the peritectic point P_2 (T_m = 388 K), at 9 : 1. The distectic points M_1 (T_m = 443 K) and M'_1 (T_m = 408 K) are identified at a ratio of 5 : 1. At a ratio of 33 : 1, the eutectic point E (T_m = 323 K) is observed.

The complexes formed by PEG with MW = 15000 have 2 : 1 and 7 : 1 compositions (Fig. 3). The phase diagram has two distectic points, M_1 (T_m = 533 K) and M'_1 (T_m = 473 K), at the same molar ratio of 2 : 1, two peritectic points at ratios of 15 : 1 (T_m = 323 K) and 7 : 1 (T_m = 413 K), and two eutectic points at ratios of 20 : 1 (T_m = 318 K) and 1 : 10 (T_m = 508 K).

In the phase diagram of the PEG (MW 40000)–$NaBPh_4$ system prepared in ethanol, the complexes of compositions 9 : 1, 8 : 1, and 2 : 1 were identified (Fig. 4). The peritectic points exist at component ratios of 9 : 1 (T_m = 368 K) and 8 : 1 (T_m = 453 K), the distectic points, at 2 : 1 (T_m = 468 and 558 K), and the eutectic points, at 30 : 1 (T_m = 321 K) and 1 : 2 (T_m = 543 K).

The existence of the distectic points M_1 and M'_1 at the same initial molar ratios (Figs. 2–4) shows that structures formed in these systems are polymorphous, i.e., they have the different morphologies at the same initial ratios of the interacting components.

According to the phase diagram (Fig. 5), the molecular complexes formed in the systems composed of polyethylene glycol with MW 100000 have 8 : 1 and 2 : 1 compositions.

The eutectic points are observed at ratios of 35 : 1 (T_m = 318 K) and 7 : 1 (T_m = 473 K); the distectic points, at 2 : 1 (T_m = 498 K) and 8 : 1 (T_m = 493 K), and the peritectic point, at 15 : 1 (T_m = 383 K).

The complexation involving PEG with MW 100000 differs from that involving polyethers of other

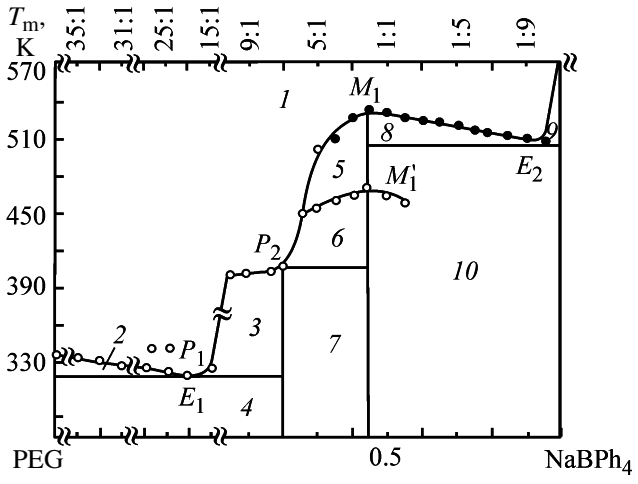


Fig. 3. Phase diagram of the PEG (MW 15000)–$NaBPh_4$ system. Points: (M_1, M_2) distectic, (P) peritectic, and (E_1, E_2) eutectic.

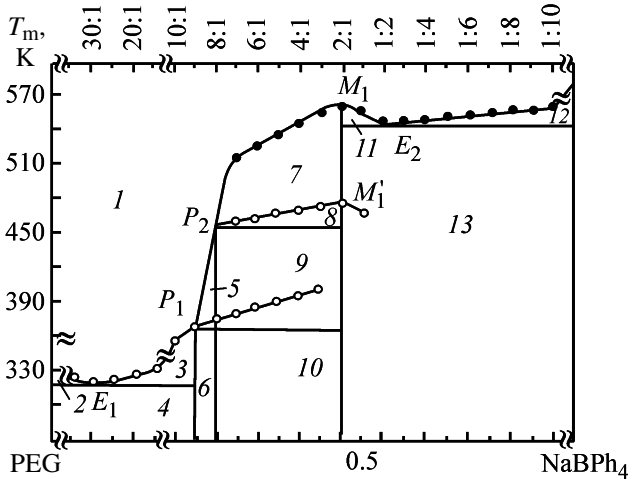


Fig. 4. Phase diagram of the PEG (MW 40000)–$NaBPh_4$ system. Points: (M_1, M'_1) distectic, (P_1, P_2) peritectic, and (E_1, E_2) eutectic.

Eutectic E, peritectic P, and distectic M points for PEG–$NaBPh_4$ complexes differing in the molecular weight of PEG

Points E, P, M	MW = 2000		MW = 4000		MW = 15000		MW = 40000		MW = 100000	
	composition	T_m, K	composition	T_m, K	composition	T_m, K	composition	T_m, K	composition	T_m, K
E_1	30 : 1	318	33 : 1	323	20 : 1	318	30 : 1	320	35 : 1	318
E_2	4 : 1	423	–	–	1 : 10	508	1 : 2	543	7 : 1	473
E_3	1 : 2	418	–	–	–	–	–	–	–	–
E_4	1 : 5	403	–	–	–	–	–	–	–	–
P_1	15 : 1	323	15 : 1	328	15 : 1	323	9 : 1	368	15 : 1	383
P_2	8 : 1	396	9 : 1	388	7 : 1	413	8 : 1	453	–	–
M_1	6 : 1	513	5 : 1	443	2 : 1	533	2 : 1	558	8 : 1	493
M'_1	–	–	5 : 1	408	2 : 1	473	2 : 1	468	–	–
M_2	3 : 1	473	–	–	–	–	–	–	2 : 1	498
M_3	1 : 3	423	–	–	–	–	–	–	–	–

MWs in that no polymorphism is observed.

The eutectic, peritectic, and distectic points for complexes involving polyethylene glycol of varied molecular weight and sodium tetraphenylborate are given in the table.

The eutectic points E_1 are identified from 318 to 323 K, and points E_2 are identified at various compositions with T_m from 423 to 508 K. At the same time, for complexes with MW 4000 this eutectic point was not revealed. The points E_3 and E_4 were determined for the complex with MW 2000 at T_m 418 and 403 K, respectively, whereas in the other cases these points do not exist.

For complexes composed of PEG with MW 2000, 4000, 15000, and 100000, the peritectic points P_1 are identified at a ratio of 15 : 1, and for those composed of PEG with MW 40000, at 9 : 1. The melting points of the complexes lie from 323 to 383 K, with the melting point of the PEG (MW 100000) complex being the highest (T_m = 383 K).

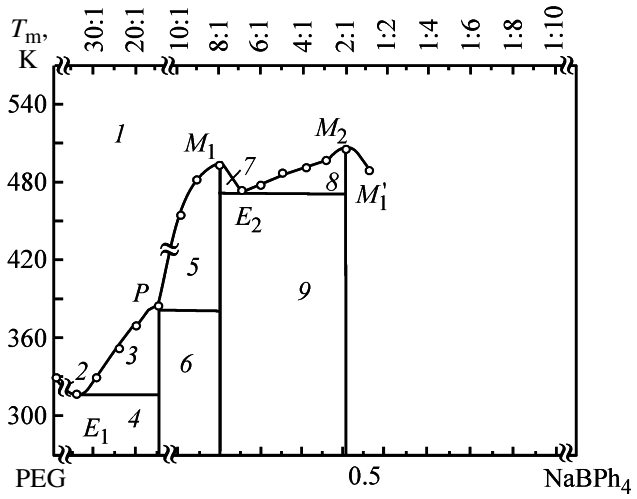


Fig. 5. Phase diagram of the PEG (MW 100000)–$NaBPh_4$ system. Points: (M_1, M_2) distectic, (P) peritectic, and (E_1, E_2) eutectic.

For complexes with MW 2000, 4000, 15000, and 40000, the peritectic points P_2 are identified at T_m 396, 388, 413, and 453 K, respectively, whereas for complexes with MW 100000 the point P_2 was not identified.

The distectic points M_1 for PEG complexes differing in the MW are observed at T_m from 443 to 513 K. The points M'_1 are found for the PEG systems (MW 4000, 15000, and 40000) at T_m 408, 473, and 468 K, respectively. For complexes with MW 2000 and 100000, the points M_2 were determined at T_m 473 and 498 K. The point M_3 is identified only for complexes with MW 2000 at T_m = 423 K. In the remaining cases, it is not identified. This shows that, as the MW of the polymer decreases, the number of molecular complexes increases. Probably, the different compositions and melting points of the complexes are due to the change in the polymer molecular weight and transformation of the structure of the complex.

CONCLUSIONS

(1) The phase diagrams of the systems consisting of polyethylene glycol of varied molecular weight and sodium tetraphenylborate, prepared in ethyl alcohol, differ considerably in eutectic, peritectic, and distectic points.

(2) Results obtained in studying the polyethylene glycol–$NaBPh_4$ complexes synthesized using polyethylene glycol with a varied length of macromole-

cules show that the molecular weight of the polymer affects the formation of new complex compounds significantly differing in the structure, composition, and morphology.

REFERENCES

1. Cray, F. M., *Solid Polymer Electrolytes*, New York: VCH, 1991.
2. *Polymer Electrolytes*, London: Elsevier, 1987.
3. Dzhumadilov, T.K., Bekturov, E.A., Bekturganova, G.K., et al., *Ion-dipol'nye kompleksy neionnykh polimerov* (Ion–Dipole Complexes of Nonionic Polymers), Almaty, 2002.
4. Sadykova, G.T., Dzhumadilov, T.K., and Asaubekov, M.A., *Izv. Min. Obraz. Nauki Resp. Kaz., Nats. Akad. Nauk Resp. Kaz., Ser. Khim.*, 2002, no. 3, p. 384.
5. Khakimova, G.T., *Trudy respublikanskoi nauchnoi konferentsii molodykh uchenykh, posvyashchennoi dnyu khimika* (Proc. Republican Conf. of Young Scientists Dedicated to the Chemist's Day), Almaty, 1998, p. 73A.
6. Weissberger, A., Proskauer, E.S., Riddick, J.A., and Toops, E.E., *Organic Solvents*, New York: Interscience, 1955.

ISSN 1070-4272, Russian Journal of Applied Chemistry, 2006, Vol. 79, No. 7, pp. 1143–1145. © Pleiades Publishing, Inc., 2006.
Original Russian Text © M.V. Solovskii, 2006, published in Zhurnal Prikladnoi Khimii, 2006, Vol. 79, No. 7, pp. 1153–1155.

MACROMOLECULAR CHEMISTRY AND POLYMERIC MATERIALS

Synthesis of Modified *N*-Vinylpyrrolidone–Crotonic Acid–*p*-Nitrophenyl Crotonate Terpolymer

M. V. Solovskii

Institute of Macromolecular Compounds, Russian Academy of Sciences, St. Petersburg, Russia

Received March 2, 2006

Abstract—Aminolysis of *N*-vinylpyrrolidone–crotonic acid–*p*-nitrophenyl crotonate terpolymers with 2-hydroxyethylamine and 3-hydroxypropylamine in dimethyl sulfoxide at 25°C was studied by UV spectroscopy. The factors affecting the aminolysis kinetics were determined. Preparative synthesis of the aminolysis products in dimethyl sulfoxide was performed and the composition of the aminolysis products was determined.

DOI: 10.1134/S1070427206070196

Previously [1], we prepared by reactions in the polymeric chains a reactive terpolymer of *N*-vinylpyrrolidone VP, an unsaturated carboxylic acid (acrylic, methacrylic, crotonic), and its *N*-nitrophenyl ester. The kinetics of aminolysis of these terpolymers with *n*-butylamine and *tert*-butylamine was studied. It was found that these terpolymers react with organic compounds containing sterically unhindered primary aliphatic amino group.

Proceeding with these studies, I examined aminolysis of VP–crotonic acid (CA)–*p*-nitrophenyl crotonate (NPC) terpolymers (**I**) with 2-hydroxyethylamine (HEA) and 3-hydroxypropylamine (HPA) with the aim to prepare VP copolymers containing reactive carboxy and primary hydroxy groups. These copolymers can be used to modify some biologically active compounds (BACs) and to prepare hydrophilic polymers with polyfunctional biological activity.

The choice of copolymers **I** is caused by the fact that they are prepared from water-soluble nontoxic *N*-vinylpyrrolidone–crotonic acid copolymers which have low molecular weight and narrow MWD and do not contain blocks of the reactive units [2]. These physicochemical and biological properties are required for a hydrophilic synthetic bionondegradable polymer to be used as a BAC carrier.

Copolymers **Ia**–**Ie** were prepared by condensation of BP–CA copolymers with pnitrophenol (NP) in DMF in the presence of *N,N'*-dicyclohexylcarbodiimide as a dehydrating agent. The composition of copolymers **I** was determined by UV spectroscopy in DMSO using the absorption band of bound *p*-NP at 274 nm (ε = 9500 l mol^{-1}, calibrated against *p*-nitrophenyl acetate). The UV spectra were recorded on an SF-46 spectrometer in a 1-cm cell. The IR spectra of the target terpolymers **II** were recorded in KBr pellets on a Bruker JFS spectrometer.

The kinetics of aminolysis of terpolymers **I** with amino alcohols in DMSO was studied by UV spectroscopy in 0.2-cm cells temperature-controlled at 25°C. The time dependence of the relative decrease in the intensity of the absorption band at 274 nm was determined [3]. The initial concentration of the *p*-nitrophenoxy groups (ONP) in the solution was constant (9.2×10^{-4} M) in all the experimnets. The ($-NH_2$) : (–ONP) molar ratio *n* was varied in a wide range. After reaction completion, concentrated ammonium hydroxide solution (20 μl) was added into the cell and the optical density corresponding to 100% aminolysis was measured in 24 h. The average half-conversion time $\tau_{1/2}$ in the examined reaction was determined from the results of 2–3 experiments. The determination error of $\tau_{1/2}$ was no higher than 5%.

Preparative synthesis of copolymers **II** was performed in DMSO at room temperature, initial concentration of terpolymer **I** of 0.85 M, and *n* = 20 or 40 for 6 h. Terpolymers **II** were isolated by precipitation with diethyl ether and purified by dialysis against water. In the course of dialysis, the unchanged –ONP groups of terpolymers **I** were hydrolyzed to carboxylate groups. To convert the carboxylate groups of copolymers **II** into the carboxy groups, aqueous solutions of terpolymers **II** were passed through a column packed with KU-2 cation exchnager in the H^+ form. The composition of terpolymers **II** was calculated from the content of their OH groups, determined by

Aminolysis of VP–CA–NPC terpolymers

Terpolymer	m_2	m_3	$\overline{M}_w$*	$\overline{M}_w/\overline{M}_n$	Amino alcohol	n	Product	Yield, %	m'_1	m'_2	m'_3	Q,** %
	mol %								mol %			
Ia	8.3	13.5	28 000	1.8	2-HEA	20	**IIa**	80.5	78.4	9.4	12.2	91.8
Ib	17.7	14.5	21 000	1.7	2-HEA	20	**IIb**	78.6	67.7	18.9	13.4	92.4
Ic	27.2	22.8	8000	1.8	2-HEA	50	**IIc**	88.3	50.0	28.5	21.5	94.3
Id	27.2	22.8	8000	1.8	2-HEA	20	**IId**	84.2	50.0	29.0	21.0	92.1
Ie	23.3	14.9	15 000	1.9	3-HPA	20	**IIe**	82.8	61.4	25.1	13.5	90.6

* Determined for the initial VP–CA coplymer by GPC on styrogels [2].
** Q is the degree of substitution of –ONP groups of terpolymers **I** by –NH–$(CH_2)_x$–OH groups.

acetylation [4]. The amino alcohols were purified by vacuum distillation, and DMF and DMSO, by the standard procedures [5].

The respesentative curves of aminolysis of terpolymers **I** with amino alcohols are shown in Fig. 1. As seen from Fig. 1, aminolysis of VP–CA–NPC terpolymer at n = 50 and 25°C is fast. The aminolysis rate estimated from the half-conversion time $\tau_{1/2}$ appreciably increases in going from 2-HEA ($\tau_{1/2}$ = 6.2± 0.2 min) to more nucleophilic 3-HPA ($\tau_{1/2}$ = 3.3± 0.1 min). As the molar ratio of the reacting groups increases, the half-conversion time in the examined reaction decreases (the aminolysis rate increases) in proportion to n (Fig. 2). Based on the kinetic data, we suggest that the examined reaction can be described by the following scheme:

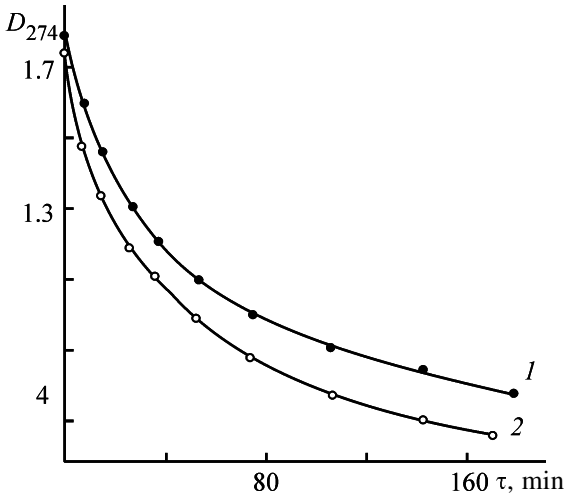


Fig. 1. Aminolysis of VP–CA–NPC terpolymer **Ic** with (*1*) 3-hydroxypropylamine and (*2*) 2-hydroxyethylamine in DMSO at 25°C and n = 50. (D_{274}) Optical density of the terpolymer solution at 274 nm and (τ) reaction time.

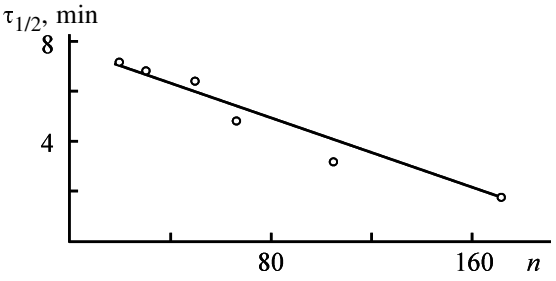
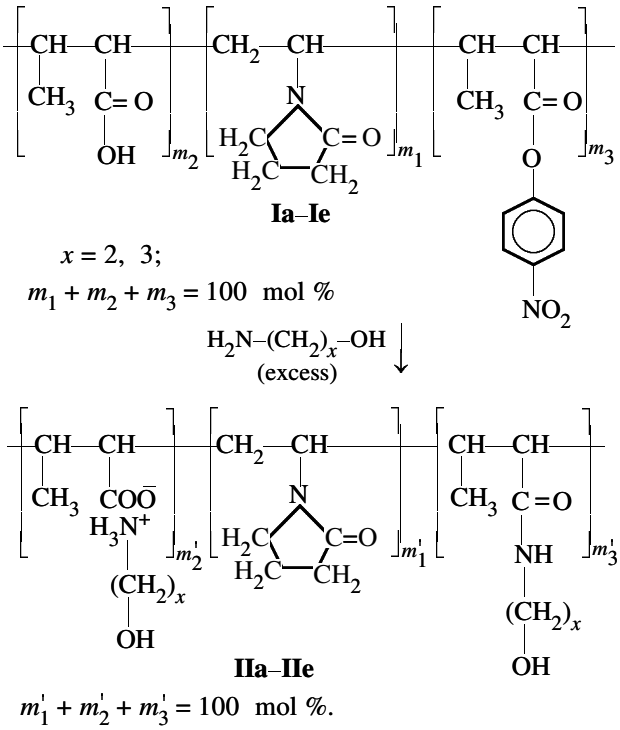


Fig. 2. Half-conversion time $\tau_{1/2}$ in aminolysis of terpolymer **Ic** with 2-hydroxyethylamine as a function of the molar ratio of the reacting groups n.



The results of the preparative synthesis of terpolymers **Ia**–**Ie** are presented in the table. As seen from the table, the degree of substitution Q of recative –ONP groups of terpolymers **I** with –NH–$(CH_2)_x$–OH groups under the examined conditions is as high as 90.6–94.3%. The content of hydroxy and carboxy

groups in the resulting water-soluble terpolymers **II** is up to 21.5 and 29.0 mol %. The IR spectra of terpolymers **II** contain the bands of stretching vibrations of the hydroxy group at 3430 cm^{-1}, which is absent in the IR spectra of the initial copolymers **I**. The strong band of bound *p*-NP at 274 nm, present in the UV spectra of terpolymers **I**, is absent in the UV spectra of the aminolysis products **II** in DMSO.

CONCLUSIONS

(1) The rate of aminolysis of *N*-vinylpyrrolidone–crotonic acid–*p*-nitrophenyl crotonate terpolymers in dimethyl sulfoxide depends on the chemical nature of the amino alcohol (the rate for 3-hydroxypropylamine is higher than that for 2-hydroxyethylamine) and increases with increasing the $[-NH_2] : [-ONP]$ molar ratio in the solution.

(2) The conditions of preparative synthesis of low-molecular-weight *N*-vinylpyrrolidone terpolymers containing 12.2–21.5 mol % hydroxy and 9.4–29.0 mol % carboxy groups were determined. These terpolymers can be used as supports for some biologically active compounds.

ACKNOWLEDGMENTS

This study was financially supported by the Research School Foundation (project NSh-1823.2003.3).

REFERENCES

1. Solovskii, M.V. and Petukhova, N.A., *Vysokomol. Soedin., Ser. B*, 1992, vol. 34, pp. 30–34.
2. Solovskij, M.V., Denisov, V.M., Panarin, E.F., et al., *Macromol. Chem. Phys*., 1996, vol. 197, pp. 2035–2046.
3. Solovskij, M.V., Ulbrich, K., and Kopeček, J., *Biomaterials*, 1983, no. 4, pp. 44–48.
4. Toroptseva, A.M., Belogorodskaya, K.V., and Bondarenko, V.M., *Laboratornyi praktikum po khimii i tekhnologii vysokomolekulyarnykh soedinenii* (Laboratory Course of Chemistry and Technology of Macromolecular Compounds), Leningrad: Khimiya, 1972.

ISSN 1070-4272, Russian Journal of Applied Chemistry, 2006, Vol. 79, No. 7, pp. 1146–1152. © Pleiades Publishing, Inc., 2006.
Original Russian Text © V.E. Proskurina, M.N. Akopyan, V.A. Myagchenkov, 2006, published in Zhurnal Prikladnoi Khimii, 2006, Vol. 79, No. 7, pp. 1156–1162.

MACROMOLECULAR CHEMISTRY AND POLYMERIC MATERIALS

Kinetics of Flocculation and Thickening of Precipitates of Bentonitic Clay Suspension in the Presence of Acrylamide Copolymers in Aqueous Salt Solutions

V. E. Proskurina, M. N. Akopyan, and V. A. Myagchenkov

Kazan State Technological University, Kazan, Tatarstan, Russia

Received February 1, 2006

Abstract—The kinetics of hindered sedimentation and thickening of the sediments of a real disperse system (bentonitic clay suspension) was studied. The flocculation parameters of acrylamide copolymers in aqueous and aqueous salt solutions were evaluated in relation to the chemical nature and concentration of flocculants and electrolytes.

DOI: 10.1134/S1070427206070202

The question of how to enhance efficiency of polymeric flocculants was analyzed in many studies dealing with the flocculation mechanism or with application of flocculants to solution of various technological problems such as intensification of sedimentation, filtration, and dehydration of sludge in coal-preparation and ore-dressing, selective separation of mineral components, treatment of natural and waste waters to remove dispersed pollutants, and concentration and recovery of biomass [1]. Domestic industry produces rather broad assortment of water-soluble polymeric flocculants, among which polyacrylamide flocculants (PAAFs) occupy the key position as regards both the application area and production volume. It should be noted that the flocculation power of PAAFs depends on various factors: chemical nature of alternating units and composition of copolymer macromolecules, flocculant concentration, and combination of chemical, physicochemical, and physical properties of the disperse phase particles (such as specific surface area, concentration of localized adsorption centers, lyophilic properties of the surface) and dispersion medium (pH, nature and concentration of electrolytes, surfactants, etc.). Main theoretical concepts and technological principles of flocculation for predominantly model disperse systems (DSs) are summarized in reviews [1–4].

Proceeding with systematic studies aimed to enhance the effectiveness of water-soluble ionic and nonionic PAAFs, we quantitatively evaluated the effect of the ionic strength and nature of three inorganic electrolytes on the sedimentation kinetics and flocculation parameters of acrylamide copolymers in the mode of hindered sedimentation and thickening of the precipitates of a real DS (bentonitic clay suspension). It should be noted that the kinetic data on the relationship between flocculation and thickening of the precipitates are scarce.

EXPERIMENTAL

We used a multicomponent real DS (Bentokam bentonitic clay suspension [TU (Technical Specifications) 39-0147001-105–93]) with an average particle radius $\bar{R} = 7.28 \times 10^{-6}$ m and density $\rho = 2.63 \times 10^3$ kg m^{-3}. As water-soluble PAAFs we used samples of nonionic polyacrylamide (N) and anionic (A1, A2) and cationic (C) acrylamide copolymers with various content of the ionic groups α. For comparison, polyoxyethylene (POE) and sodium salt of carboxymethyl cellulose (Na-CMC) were also studied. The main properties of the above polymers are listed in Table 1. Our preliminary experiments showed that the most reliable data on the sedimentation kinetics of bentonitic clay suspension in the mode of hindered sedimentation are obtained at the content of the dispersed phase (DP) $c_d = 4\%$. Below this optimal concentration, the phase boundary becomes very diffuse, whereas above it the working clarified area of the cylinder decreases. The kinetics of flocculation and thickening of the bentonitic clay suspension was studied in 100- and 2000-ml cylinders by the shift of the boundary between the clarified and unclarified

fractions of the suspension. For more correct determination of the phase boundary, the bottom part of the 2000-ml cylinder was equipped with an additional vertical (millimeter) scale.

To obtain the quantitative characteristics of the flocculation kinetics, we calculated the flocculation effect D [1]:

$$D = v/v_0 - 1 = t_0/t_i - 1, \quad (1)$$

where v and v_0, and t_i and t_0 are the rates and times of sedimentation of the bentonitic clay suspension to the degree of clarification $Q = 0.3$ in the presence of polymeric flocculant with concentration c_i and without it, respectively.

The flocculation activity, characterizing the relative change in the sedimentation rate due to the unit dose of the polymeric additive, was evaluated from the kinetic curves using the following equation:

$$\lambda = (v/v_0 - 1)/c_i. \quad (2)$$

The viscosities of the PAAF and POE solutions were measured on an Ostwald viscometer with a capillary diameter of 0.54×10^{-3} m. The correction for the kinetic energy of the liquid flow was smaller than 1.5% and was not taken into account in the calculations of the specific viscosity:

$$\eta_{sp} = (\tau - \tau_0)/\tau_0, \quad (3)$$

where τ and τ_0 are the times of outflow of the aqueous solutions of copolymers and solvent (water).

The electrokinetic potential ζ of the bentonitic clay suspension in aqueous and aqueous salt solutions was determined by macroelectrophoresis [5], by measuring the shift of the phase boundary between the clay suspension (DS) and electrolyte (0.003 M KCl) in the electrical field (potential $E = 127$ V, distance between the electrodes $I = 42.5$ cm). The shift of the phase boundary was controlled simultaneously in two elbows of the electrophoretic cell. The electrokinetic potential of the DP particles was calculated from the Smoluchowski equation [6].

$$\zeta = \frac{4\pi\eta u \times 300^2}{\varepsilon E l^{-1}}, \quad (4)$$

The electrophoretic rate u was calculated as the difference between the rates of movement of the DP particles in two cell elbows [5]. The factor 300^2 converts the electrokinetic potential ζ values to common volts; η and ε are the viscosity and dielectric permittivity of the bentonitic clay suspension, respectively. The viscosity η of the bentonitic clay suspension was calculated using the Einstein expression:

$$\eta = \eta_0(1 + 2.5\varphi) = \eta_0(1 + 2.5c/\rho), \quad (5)$$

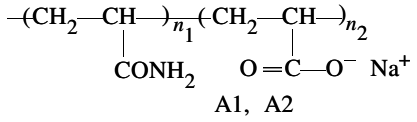
where ψ and c are the volume and weight fraction of the DP particles in the suspension, and $\eta_0 = 0.01$ P is the viscosity of the dispersion medium (water).

First we studied the flocculation kinetics of the bentonitic clay suspension in aqueous solutions of the polymeric flocculants given in Table 1. The effect

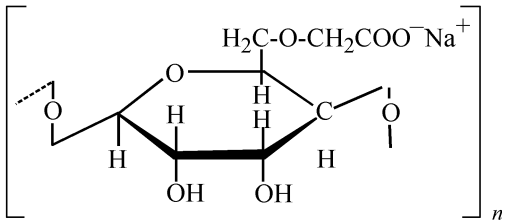
Table 1. Main characteristics of the polymeric flocculants studied

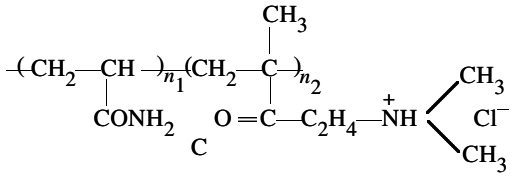
Polymer*	M	α, mol %	Name
A1	6.7×10^6	17.5	Copolymer of acrylamide and sodium acrylate
A2	5.08×10^6	4.5	
Na-CMC	1.4×10^5	100	Sodium carboxymethyl cellulose
C	2.3×10^6	16.3	Copolymer of acrylamide and dimethylaminoethyl methacrylate hydrochloride
N	8.7×10^6	0	Polyacrylamide
POE	2.2×10^6	0	Polyoxyethylene

*

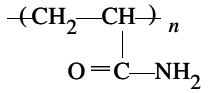


A1, A2

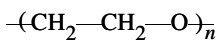




C



N



POE

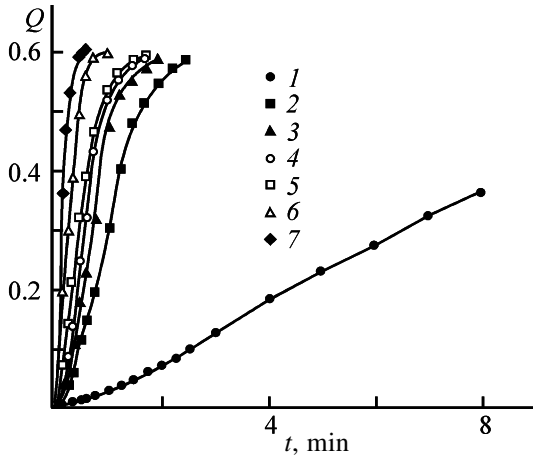


Fig. 1. Sedimentation kinetic curves of the bentonitic clay suspension in the presence of flocculant A1. (Q) Degree of clarification and (t) time. Concentration of A1, $c \times 10^4$, wt %: (*1*) 0, (*2*) 0.005, (*3*) 0.1, (*4*) 0.2, (*5*) 0.5, (*6*) 1.0, and (*7*) 2.0.

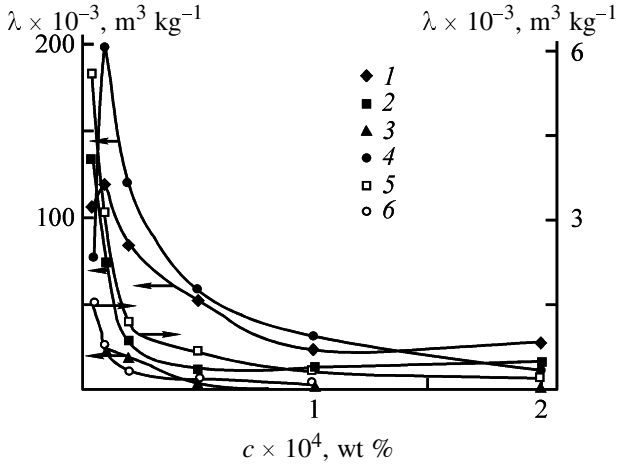


Fig. 2. Flocculation activity λ as a function of the polymer flocculant concentration c. Flocculant: (*1*) A1, (*2*) A2, (*3*) C, (*4*) N, (*5*) POE, and (*6*) Na-CMC.

of the copolymer concentration is illustrated by the flocculation kinetic curves obtained at various concentration of copolymer A1 (Fig. 1) and generalized data for all the six copolymer samples (Table 2). As seen from Fig. 1, even small flocculant additions ($c = 5 \times 10^{-6}$ wt %) strongly accelerate sedimentation of the bentonitic clay suspension, and with increasing polymer concentration this effect regularly increases. To compare the flocculation parameters of the copolymer samples in question, it is advisable to use the dependences of the flocculation activity on the flocculant concentration, i.e., $\lambda = f(c)$ (Fig. 2). As seen, the parameter λ decreases with increasing flocculant concentration for all the six copolymers studied. This phenomenon can be explained by the fact that the probability of formation of the bridging bond (γ_b) by a given macromolecule, providing formation of the floccules and their further growth, decreases with increasing flocculant concentration. With decreasing γ_b, the probability of formation of the anchor bond (γ_a) by a given macromolecule, when the macromolecule

Table 2. Flocculation parameters of water-soluble copolymers at sedimentation of the bentonitic clay suspension in the mode of hindered sedimentation

Polymer	$c \times 10^4$, wt %	D	$\lambda \times 10^{-3}$, $m^3\ kg^{-1}$	ρ_s, $kg\ m^{-3}$
A1	0	0	–	–
	0.05	5.23	105	–
	0.1	11.8	118	–
	0.2	16.8	84.0	–
	0.5	25.8	51.6	–
	1.0	22.8	22.8	–
	2.0	53.5	26.8	1.090
A2	0	0	–	–
	0.05	13.2	132	–
	0.1	14.6	73.0	–
	0.2	13.9	27.8	–
	0.5	12.1	12.1	–
	1.0	26.3	13.2	–
	2.0	53.5	15.3	1.077
Na–CMC	0	0	–	–
	0.05	–	–	–
	0.1	0.143	1.43	–
	0.2	0.146	0.73	–
	0.5	0.154	0.31	–
	1.0	0.190	0.19	–
	2.0	0.194	0.09	1.138
C1	0	0	–	–
	0.05			
	0.1	2.40	24.0	–
	0.2	3.70	19.0	–
	0.5	1.90	3.80	–
	1.0	1.20	1.20	–
	2.0	1.30	0.65	1.071
N	0	0	–	–
	0.05	3.86	77.2	–
	0.1	19.8	198	–
	0.2	23.0	119	–
	0.5	28.9	57.8	–
	1.0	30.2	30.2	–
	2.0	23.1	11.6	1.088
POE	0	0	–	–
	0.05	0.56	5.60	–
	0.1	0.58	2.90	–
	0.2	0.57	1.10	–
	0.5	0.63	0.63	–
	1.0	0.61	0.31	–
	2.0	0.62	0.18	1.121

is either adsorbed on the DP particle or on the globule, obviously increases. The reason is that in the case of adsorption of a given macromolecule $\gamma_b + \gamma_a = 1$, and hence $\gamma_a = 1 - \gamma_b$. Certain increase in λ with increasing c at small flocculant concentrations is probably due to the formation of superfloccules in the disperse system [7]. As seen from Table 2 and Fig. 2, anionic (A1, A2) and nonionic (N) PAAFs are the most efficient water-soluble flocculants studied, which is confirmed by their maximal parameters D and λ. For cationic PAAF (C) , POE, and Na-CMC, these parameters are somewhat smaller. The flocculation activities of various polymeric flocculants were compared at fixed copolymer concentrations c.

The flocculation characteristics of the water-soluble polymers studied are affected by certain active parameters determining the interaction of adsorbed copolymer macromolecules with localized or nonlocalized adsorption centers on the surface of the DP particles. These active parameters include the presence of defective elements (such as hollows, irregularities, crystal edges, foreign inclusions, etc.) in the near-surface layer of the DP particles, nature and concentration of the localized (formed predominantly by ions and charged functional groups) and nonlocalized adsorption centers on the DP particle surface, effective size and flexibility of the macromolecule globules, and actual ratio of the probabilities of formation of the bridging γ_b and anchor γ_a bonds between the PAAF macromolecules and DP particles [1, 7–9].

Before the analysis of the adsorption of separate ionic and nonionic (acrylamide) fragments of the copolymer macromolecules A1, A2, and C on the charged and neutral sections of the phase boundary surface, we should distinguish the "effective" macromolecules participating in bridging between two and more DP particles and the macromolecules that, being adsorbed through the anchor bond on the surface of a single DP particle, do not participate in the formation of floccules [1, 7]. To explain a sharp difference in the flocculation parameters of copolymers A1, A2, and C, we should take into account that γ_b(A1 or A2) $\gg \gamma_b$(C) and γ_a(A1 or A2) $\ll \gamma_a$(C). These ratios show that, for anionic copolymers A1 and A2, the fraction of the bridging contacts is significantly greater than that for copolymer C. To explain the above ratios, we should take into account the charges of the ionic acrylamide copolymer macromolecules and DP particles (namely, negative for anions A1 and A2 and for DP particles and positive for cation C). This difference in the charges of the ionic PAAFs promotes formation of predominantly bridging contacts between the DP particles and anions A1 and A2 and of predominantly anchor bonds (through the neutralization mechanism) for cation C, i.e., γ_b(A1 or A2) $\gg \gamma_b$(C). Moreover, the sediment density ρ_s (Table 2) and, thus, its permeability strongly depend on the polymeric additive. This fact should be taken into account in processing and utilization of the precipitates [10].

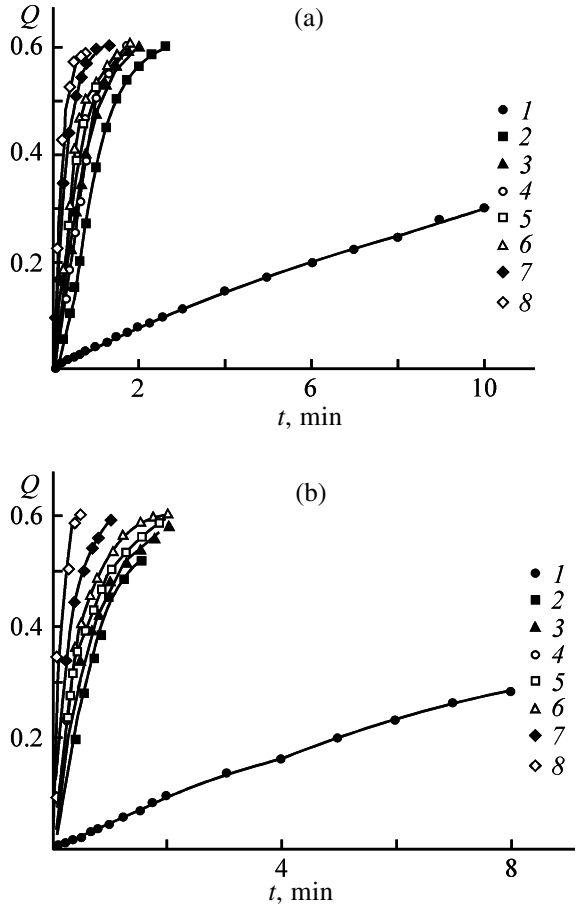


Fig. 3. Sedimentation kinetic curves of the bentonitic clay suspension in aqueous salt solution ($I = 1.8 \times 10^{-2}$ N) in the presence of ionic PAAF (A1) and (a) NaCl and (b) $FeCl_3$ electrolytes. Concentration of A1, $c \times 10^4$, wt %: (*1*) 0, (*2*) 0.5, (*3*) 1, (*4*) 2, (*5*) 5, (*6*) 10, (*7*) 20, and (*8*) 35.

Since in the oil production a bentonitic clay suspension is added to multicomponent aqueous solutions containing various salt additives, it was advisable to evaluate the effect of the ionic strength of solutions on the sedimentation kinetics of real DCs. The flocculation kinetic curves of the bentonitic clay suspension in the aqueous salt solution ($I = 1.8 \times 10^{-2}$ N) in the presence of anionic (A1) PAAF and NaCl and $FeCl_3$ coagulants are show in Fig. 3. As seen, with increasing PAAF concentration in the aqueous salt solution, the sedimentation rate of the

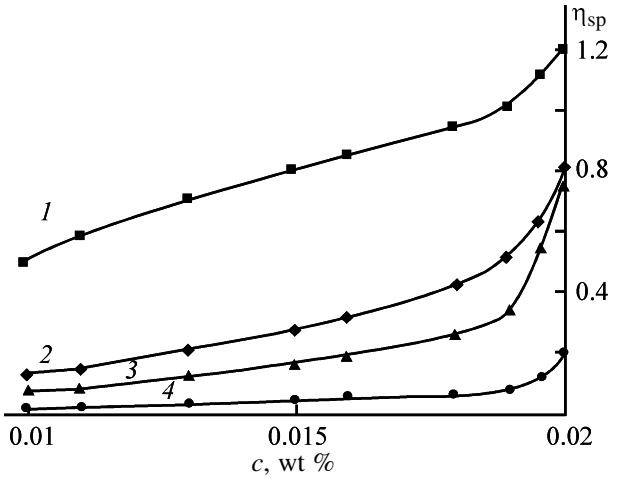


Fig. 4. Specific viscosity of the bentonitic clay suspension η_{sp} as a function of the A1 copolymer concentration c in solutions with I = 0.2 N upon addition of electrolytes. Electrolyte: (*1*) none (I = 0), (*2*) $K_4[Fe(CN)_6]$, (*3*) NaCl, and (*4*) $FeCl_3$.

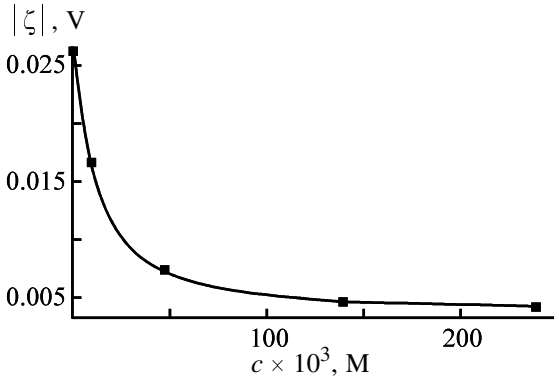


Fig. 5. Electrokinetic potential ζ as a function of the electrolyte (NaCl) concentration c.

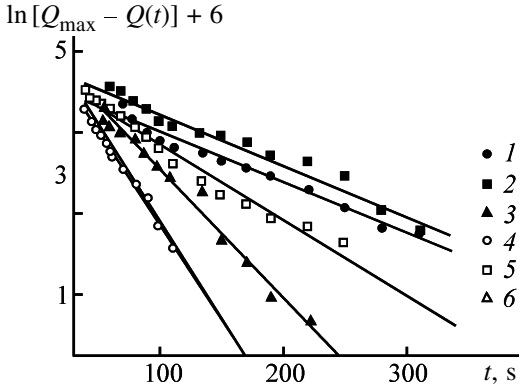


Fig. 6. Kinetic curves of thickening of the bentonitic clay suspension in the presence of copolymer A1 (1×10^{-4} wt %) and electrolyte NaCl ($I = 1.8 \times 10^{-2}$ N) in the $\log[Q_{max} - Q(t)] + 6 = f(t)$ coordinates: (*1*) without A1 and NaCl, (*2*) with NaCl only, and (*3*) with A1 only; the mode of adding A1 and NaCl: (*4*) first, (*5*) second, and (*6*) third.

bentonitic clay suspension also regularly increases, and the flocculation effect D changes simultaneously. It should be noted that addition of electrolytes to the bentonitic clay suspension primarily affects (1) the conformation state of macromolecules of the flocculant and especially ionic PAAFs and (2) the parameters of the electrical double layer of the DP particle, and hence the aggregation and sedimentation stability of the disperse system.

The first effect of the electrolyte is illustrated by Fig. 4. As seen, on adding NaCl, $FeCl_3$, and $K_4[Fe(CN)_6]$ electrolytes, the specific viscosity η_{sp} of the aqueous solution of copolymer A1 gradually decreases. The most pronounced decrease in η_{sp}, which corresponds to changes in the effective size of macromolecules [11], is observed with $FeCl_3$ (Fig. 4, curve *4*).

As for the second effect, with increasing electrolyte concentration the electrical double layer contracts [6, 12], which should be accompanied by a decrease in the electrokinetic potential ζ of the bentonitic clay suspension. This is confirmed by direct experiments on the macroelectrophoresis of the bentonitic clay suspension in aqueous salt (NaCl) solutions (Fig. 5). With increasing NaCl concentration, the ζ potential decreases, i.e., the aggregation (and sedimentation) stability of the DP particles decreases also. It is obvious that the electrolyte ions, along with the two above-mentioned factors, affect the physicochemical parameters of the localized and nonlocalized adsorption centers and, thus, the intensity of electrostatic interactions of PAAF ions with localized charges on the DP particle surface [9], and also the hydrophilic–hydrophobic balance at the phase boundary.

Studies on the flocculation in model dispersion systems [9, 13] revealed the dependence of the sedimentation stability on the process factors, in particular, on the mode of addition of the active flocculants into the system. At the same time, the effects of the process factors on the precipitate thickening are still poorly understood. In the second stage of our study, we analyzed the kinetics of flocculation and precipitate thickening at three modes of addition of the active components: (1) flocculant is added after electrolyte, (2) electrolyte is added after flocculant, and (3) aqueous solution containing both electrolyte and flocculant is added to the bentonitic clay suspension. It should be noted that in all three cases the overall compositions of the suspensions containing flocculant A1 and electrolytes were similar.

Figure 6 shows how the order of addition of the active components affects the precipitate thickening,

Table 3. Flocculation and thickening of the sediment of the bentonitic clay suspension in aqueous salt solutions at three addition modes of the active components (A1 and NaCl). Concentration: 1×10^{-4} wt % A1 and 1.8×10^{-2} M NaCl

System	$\lambda \times 10^{-3}$, $m^3\ kg^{-1}$	Q_{max}	$\rho_s \times 10^{-3}$, $kg\ m^{-3}$	$\gamma \times 10^4$, s^{-1}
BCS* ($I = 0$)	–	0.828	1.144	1.36
BCS + A1 ($I = 0$)	16.2	0.807	1.128	5.40
BCS + NaCl ($I = 1.8 \times 10^{-2}$ N)	4.16	0.827	1.143	1.37
First mode, BCS + (NaCl + A1) ($I = 1.8 \times 10^{-2}$ N)	8.00	0.803	1.126	3.60
Second mode, BCS + (A1 + NaCl) ($I = 1.8 \times 10^{-2}$ N)	3.00	0.803	1.126	2.06
Third mode, BCS + (NaCl + A1)	4.90	0.813	1.132	5.45

* BCS is 4% bentonitic clay suspension.

with a combination of copolymer A1 and NaCl ($I = 1.8 \times 10^{-2}$ N) as example. The kinetics of the precipitate thickening was studied at high degrees of clarification ($Q > 0.6$, 2000-ml cylinders). At the exposure time ≥800 min, all the kinetic curves recorded (in the presence of PAAF and without it) reach the constant degrees of clarification $Q = Q_{max} = \text{const}$. The experimental data (Fig. 6) were treated in the $\log[Q_{max} - Q(t)] = f(t)$ coordinates, which allowed us to calculate the constants of precipitate thickening θ from the curve slopes using the following expression [14]:

$$\ln[Q_{max} - Q(t)] = -\gamma t. \quad (6)$$

This procedure of evaluation of the precipitate thickening kinetics allows additional determination of two important characteristics for highly concentrated bentonitic clay suspension: minimal sediment volume V_s and sediment density ρ_s:

$$V_s = (1 - Q_{max})V_0, \quad (7)$$

$$\rho_s = m + (V_s - m/\rho)\rho_0 V_s^{-1}, \quad (8)$$

where V_0 is the volume of the bentonitic clay suspension in the cylinder, ρ and ρ_0 are the densities of the bentonitic clay ($\rho = 2.63 \times 10^3\ kg\ m^{-3}$) and water ($\rho_0 = 1.0 \times 10^3\ kg\ m^{-3}$), respectively, and m is the weight of the bentonitic clay sample ($m = 80$ g).

Data on the flocculation of the bentonitic clay suspension and sediment thickening in aqueous salt (NaCl) solutions ($I = 1.8 \times 10^{-2}$ N) in the presence of anionic PAAF (A1) at all the three addition modes of the active components are summarized in Table 3. The effect of the addition mode can be explained by the fact that, in the three-component system of the bentonitic clay suspension (BCS + electrolyte + A1), preliminarily addition of the salt provides formation of primary aggregates of the DP particles, which are suitable precursors to form secondary structural elements involving, along with DP particles and electrolyte, the PAAF macromolecules (A1), i.e. floccules. At the second addition mode (BCS + A1 + electrolyte), formation of the floccules is affected, in particular, by irreversible adsorption of macromolecules on the DP surface [7, 8]. At the third addition mode, changes in the flocculation of the bentonitic clay suspension and sediment thickening and in the structure of the resulting floccules are due to strong changes in the size of macromolecule floccules on preliminarily addition of the electrolyte to A1 solution.

As seen from Table 3, the mode of the active component addition strongly affects important macroscopic parameters of the dispersion system such as λ, ρ_s, and γ. The highest ρ_s and minimal γ are observed for the dispersion systems in the absence of PAAF (A1) (Fig. 6, curves *1, 2*). Significant differences in ρ_s and γ (Table 3) suggest certain differences in the sediment structure, i.e., the loosest sediment is formed in the bentonitic clay suspension with the systems containing both NaCl electrolyte and anionic PAAF (A1), i.e., when voluminous floccules in which the DP particles are packed more randomly are formed (including the $Q \sim Q_{max}$ areas). It should be noted that the above dependences of the flocculation and thickening of the bentonitic clay suspension on the addition modes become of particular importance in the development of promising processes for the control of the aggregation and sedimentation stability of real disperse systems at combined use of flocculants and electrolytes.

CONCLUSIONS

(1) The kinetics of flocculation and thickening of the sediment of a real disperse system (bentonitic clay suspension) in the mode of hindered sedimentation in the presence of water-soluble copolymers of various

nature in aqueous salt (NaCl, $FeCl_3$, $K_4[Fe(CN)_6]$) solutions with varied ionic strength was studied. The highest flocculation parameters are observed with nonionic and anionic acrylamide copolymers.

(2) The kinetic analysis reveals a strong dependence of the sedimentation stability of the bentonitic clay suspension on the chemical nature, concentration, and addition mode of the active components (flocculant and electrolyte) in the disperse system. The correlation between the flocculation characteristics and parameters of the sediment thickening (thickening constants and sediment density) of the bentonitic clay suspension in aqueous salt solutions was determined.

REFERENCES

1. Myagchenkov, V.A., Baran, A.A., Bekturov, V.A., and Bulidorova, G.V., *Poliakrilamidnye flokulyanty* (Polyacrylamide Flocculants), Kazan: Kazan. Tekhnol. Univ., 1998.
2. *Poliakrilamid* (Polyacrylamide), Kurenkov, V.F., Ed., Moscow: Khimiya, 1992.
3. Baran, A.A. and Teslenko, A.Ya., *Flokylyanty v biotekhnologii* (Flocculants in Biotechnology), Leningrad: Khimiya, 1990.
4. Myagchenkov, V.A., Proskurina, V.E., Bulidorova, G.V., et al., *Khim. Tekhnol. Vody*, 2001, vol. 23, no. 3, pp. 285–296.
5. Myagchenkov, V.A. and Bulidorova, G.V., *Zavod. Lab.*, 1995, no. 3, pp. 28–30.
6. Dukhin, S.S. and Deryagin, B.V., *Elektroforez* (Electrophoresis), Moscow: Nauka, 1986.
7. Baran, A.A., *Polimersoderzhashchie dispersnye sistemy* (Polymer-Containing Disperse Systems), Kiev: Naukova Dumka, 1986.
8. Lipatov, Yu.S. and Sergeeva, L.M., *Adsorbtsiya polimerov* (Adsorption of Polymers), Kiev: Naukova Dumka, 1972.
9. Bulidorova, G.V. and Myagchenkov, V.A., *Kolloidn. Zh.*, 1995, vol. 57, no. 6, pp. 778–782.
10. Lyubarskii, V.M., *Osadki prirodnykh vod i metody ikh obrabotki* (Sediments of Natural Waters and Procedures for Their Treatment), Moscow: Stroiizdat, 1980.
11. Tsvetkov, V.N., Eskin, V.E., and Frenkel', S.Ya., *Struktura makromolekul v rastvorakh* (Structure of Macromolecules in Solutions), Moscow: Nauka, 1964.
12. *Fizicheskaya khimiya* (Physical Chemistry), Stromberg, A.G., Ed., Moscow: Vysshaya Shkola, 2001, 4th ed.
13. Kurenkov, V.F., Nurutdinova, F.S., Churikov, F.I., and Myagchenkov, V.A., *Khim. Tekhnol. Vody*, 1991, vol. 13, no. 4, pp. 309–312.
14. Proskurina, V.E. and Myagchenkov, V.A., *Zh. Prikl. Khim.*, 2001, vol. 74, no. 3, pp. 499–504.

ISSN 1070-4272, Russian Journal of Applied Chemistry, 2006, Vol. 79, No. 7, pp. 1153–1157. © Pleiades Publishing, Inc., 2006.
Original Russian Text © M.F. Galikhanov, T.A. Luchikhina, 2006, published in Zhurnal Prikladnoi Khimii, 2006, Vol. 79, No. 7, pp. 1163–1167.

MACROMOLECULAR CHEMISTRY AND POLYMERIC MATERIALS

Electret Properties of Blends of High-Density Polyethylene and Polystyrene

M. F. Galikhanov and T. A. Luchikhina

Kazan State Technological University, Kazan, Tatarstan, Russia

Received February 13, 2006

Abstract—Corona-electrets based on heterogeneous blends of high-density polyethylene and polystyrene were studied. The observed double-maximum composition dependence of the electret properties of polymer blends was explained in terms of the concept of their colloid structure and electrical conductivity.

DOI: 10.1134/S1070427206070214

On the background of the increasing amount of studies in the field of electret materials science, the area associated with analysis of composite polymer electrets stands out [1]. As a basis for development of electrets serve polymer formulation composed of a polymer binder and dispersed fillers, plasticizers, and other additives, as well as gas-filled polymers and polymer blends [2–15]. A distinctive feature of the electret state of heterogeneous systems is the important role of the Maxwell–Wagner polarization caused by the difference in the electrical conductivities of the coexisting phases. In the overwhelming majority of composite materials studied, the electrical conductivities of their components differ rather strongly. A question arises concerning the polarization in composites with approximately the same electrical properties. This condition is satisfied by blends of nonpolar polymers. However, the reports that consider the charge state of formulations of this kind are few in number [10–15].

In [10, 11], a mixture of low-density polyethylene (LDPE) with 10 wt % ethylene–propylene copolymer (EPC) was considered. It was noted that the polymer blend possesses increased activation energy of charge traps, compared to polyethylene. The data of [13] demonstrated that, for blends of LDPE and EPC, the composition dependence of the electret properties has two maxima, with enhanced electret properties characteristic of blends with predominant content of one of the polymers.

Improved electret properties, compared to polypropylene (PP), have been observed for its blends with a cycloolefin copolymer (COC) [12]. A blend of COC with 10% PP has higher charge stability than blends with 25 and 40% polypropylene. Of interest are the data obtained in [15], whence follows that a blend of PP with a terpolymer of ethylene, propylene, and butadiene (EPBT) has good electret properties, whereas that of PP with polytetrafluoroethylene (PTFE) may, by contrast, be an antistatic at certain polymer ratios.

It was found in [14] that the dependence of the surface density and lifetime of electret charges in blends of PP and high-density polyethylene (HDPE) on the content of polyethylene shows a maximum.

In view of the incompleteness of data obtained in studies of the electret effect in blends of nonpolar polymers, it is of interest to examine the electret properties of blends of this kind in the entire range of ratios of their polymer components.

EXPERIMENTAL

We chose as objects of study HDPE of 276–73 brand [GOST (State Standard) 16338–85] (density 0.96 g cm^{-3}, weight-average molecular weight 27×10^4, volume resistivity 1.7×10^{14} Ω m) and polystyrene (PS) of PSM 115 brand (GOST 20282–86E) (density 1.06 g cm^{-3}, viscosity-average molecular weight 3×10^5, volume resistivity 9×10^{13} Ω m).

The polymers were mixed with laboratory microrolls at 175 ± 5°C and mixing time of 3 min. Plates of thickness 1.1–1.2 mm were produced by pressing in accordance with GOST 12019–66 at 180 ± 5°C and time of keeping under pressure equal to 5 min. The polymer plates were polarized in the field of a corona discharge with an electrode comprising 196 pointed

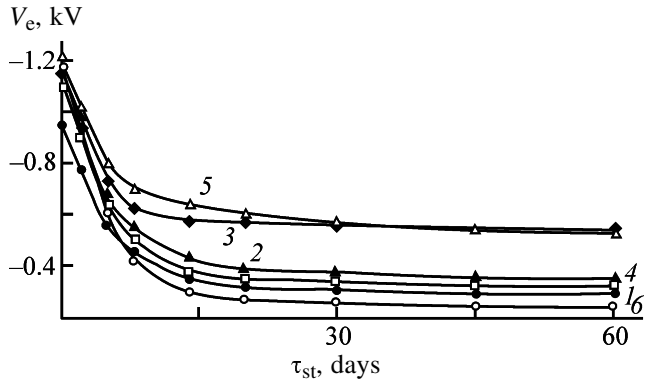


Fig. 1. Surface potential V_e of corona-electrets based on (*1*) polyethylene, (*6*) polystyrene, and blends of these in ratios of (*2*) 80 : 20, (*3*) 70 : 30, (*4*) 50 : 50, and (*5*) 20 : 80 vs. storage time τ_{st}.

needles uniformly distributed over a square of area 49 cm^2. The distance between the plates and the electrode was 20 mm, the polarization voltage was 35 kV, and the polarization time, 60 s. Before being polarized, the plates were kept in an oven at 90°C for 10 min.

We measured the electret potential difference U_{EPD} every 24 h during 150 days by the method of a vibrating electrode (noncontact induction method) in accordance with GOST 25209–82 (measurement error 0.15%). The time elapsed from the polarization of a plate till the first measurement of its surface potential was 1 h. The electrets were stored in an unshorted state in paper envelopes. The surface charge density σ_{eff} was calculated by the formula

$$\sigma_{eff} = U_c \varepsilon\varepsilon_0/\delta,$$

where U_c is the compensating voltage (U_{EPD}) (V); ε, dielectric constant of a formulation; ε_0, permittivity of free space, equal to 8.854×10^{-12} F m^{-1}; and δ, electret thickness (m) [16].

We measured the electric field strength *E* and surface potential V_e daily with an IPEP-1 meter whose operation principle is based on the method of periodic screening of the pick-up electrode situated at a certain distance from the electret surface. The measurement error of the electret characteristics did not exceed 3%.

To determine the phase structure of the polymer blend, we placed 15 × 15 mm plates in dimethylformamide (at a formulation : solvent ratio of 1 : 20) and kept them there with intermittent shaking for 21 days. The undissolved part of the formulations was dried in a vacuum oven and weighed.

We determined the volume resistivity of the polymer blend in accordance with GOST 6433.2–71 with an E6-13 teraohmmeter on samples having the form of 60 × 60 mm plates.

Of the several existing methods for fabrication of electrets based on polymeric materials, wide acceptance has been gained by the method of polarization in a corona discharge, whose advantages are the simplicity of the apparatus use and rather high speed. In charging of this kind, charge carriers (electrons, ions) are injected into the polymer and captured by energy traps of varied nature to give a homocharge.

Corona-electrets based on polymer insulators are described by the curve of charge relaxation in the course of time. One of parameters characterizing the electret state is the surface potential. The curve describing the dependence of the surface potential of the polyethylene-based corona-electret on the storage time consists of two portions (Fig. 1, curve *1*). The initial, steeper, portion is associated with release of injected charge carriers from shallow surface energy traps, whose role is played by chemically active impurities, specific surface defects produced by oxidation processes, adsorbed molecules, and disruptions in the short-range order of molecule arrangement on the surface and in the bulk. This process occurs during the first 24 h of storage of corona-electrets. The second portion is associated with release of charge carriers from deep traps, whose role is played by impurity ions, free volume of the polymer, defects of monomer units, chain irregularities and crystal imperfections, phase boundaries, etc. It is this portion that determines the stability of a corona-electret: a more gradually sloping curve corresponds to a high stability of an electret and, consequently, to a longer lifetime. A similar appearance is characteristic of the dependence of the surface potential of a polystyrene-based corona-electret on the storage time (Fig. 1, curve *6*). Other characteristics of polymer electrets (e.g., effective surface charge density) vary in storage in a similar way.

A study of the polarization of heterogeneous mixtures of polyethylene with a copolymer of ethylene and propylene of various compositions in the field of a corona discharge yielded the following data (see table; Figs. 1, 2).

It can be seen that, for mixtures of HDPE and PS stored for 45 days, the composition dependence of the surface potential has an unusual appearance: the curve has two peaks exceeding in intensity the additive values (theoretically calculated from the properties of individual polymers of the blend) (Fig. 2). In

Electret properties of polyethylene–polystyrene blends by 45th day of storage

Blend composition, vol %		V_e, kV	E, kV m^{-1}	$\lvert U_{EPD} \rvert$, kV	$\lvert \sigma_{eff} \rvert$, μC m^{-2}
HDPE	PS				
100	0	–0.30	–23.3	0.74	13.34
90	10	–0.29	–31.8	0.93	16.77
80	20	–0.36	–34.3	0.98	17.67
70	30	–0.55	–33.1	0.71	13.29
60	40	–0.43	–32.5	0.64	11.98
50	50	–0.33	–23.2	0.52	9.94
40	60	–0.36	–24.1	0.36	6.83
30	70	–0.51	–29.3	0.56	10.52
20	80	–0.55	–39.5	0.68	12.31
10	90	–0.50	–35.3	0.54	9.97
0	100	–0.25	–22.7	0.53	9.38

this case, enhanced electret properties are characteristic of polyethylene–polystyrene blends with predominant content of one of the polymers. The rest of the electret properties of the polymer blend (field strength, electret potential difference, and effective surface charge density) vary in a similar way (see table).

Taking into account that polyethylene and polystyrene have comparable electret characteristics, we can suggest that the key role in the manner in which the electret properties of their blends vary is played by the phase boundary. In this case, the stronger the structural heterogeneity of the blend [and this heterogeneity gives rise to polarization at the interface between the polymer phases (Maxwell–Wagner effect)], the higher should be the values of V_e, E, U_{EPD}, and σ_{eff} of corona-electrets. If this assumption were correct, the optimal polymer blend for preparing an electret would be that with a 1 : 1 volume ratio of the components. It can be seen, however, that, contrariwise, the electret properties of an HDPE–PS blend of this composition exhibit a clearly pronounced minimum (see table, Fig. 2).

Another factor determining the electret characteristics of polymer blends may be discontinuity of the phase boundary. In other words, the colloid structure of a polymer blend can exert key influence on its polarizability. A blend with a predominant content of polyethylene should be a common dispersion in which polystyrene is the dispersed phase, and polyethylene, dispersion medium. In the case of a predominant content of PS in a polymer blend, HDPE forms the dispersed phase. In the middle of the composition range, the blend has two continuous phases and forms a matrix structure. The discontinuity of the phase boundary in one case and its continuity in another may affect the electret properties exhibited by the blends.

We studied the colloid structure of the blend by the selective dissolution technique. Samples of formulations with various ratios of the polymer components were placed in dimethylformamide, in which polystyrene dissolves completely, and polyethylene swells to a limited extent (to 1–2 wt %). Then the undissolved part of the formulation was dried and weighed. The results obtained in extraction of polystyrene were used to judge the colloid structure of the polymer blend (Fig. 3, curve *1*). It should be noted that plates of formulations containing up to 30 vol % polystyrene remained virtually intact after the dissolution, those with 30–80 vol % PS became a continuous porous film, and those with 90 vol % polystyrene disintegrated into particles of a highly dispersed powder and formed a precipitate in the solvent. This means that HDPE–PS blends with component ratios in the range from 60 : 40 to 20 : 80 have

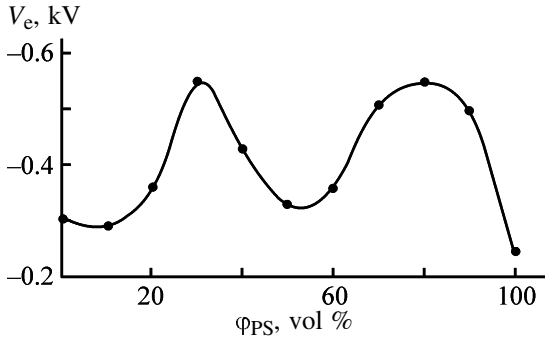


Fig. 2. Surface potential V_e of corona-electrets based on polyethylene–polystyrene blends vs. the volume content of polystyrene φ_{PS}. Electret storage time 45 days.

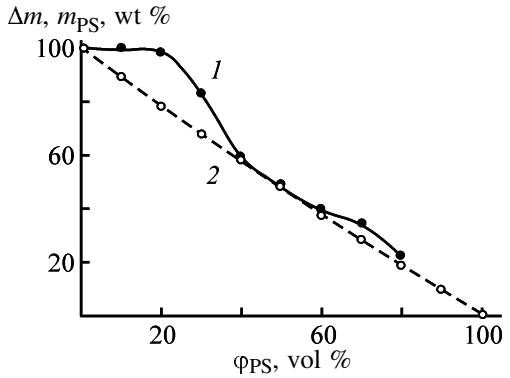


Fig. 3. (*1*) Change in the weight, Δm, of polyethylene–polystyrene blends after the extraction of polystyrene with dimethylformamide and (*2*) calculated weight fraction of polyethylene, m_{PS}, in polymer blends with varied volume fraction of polystyrene, φ_{PS}.

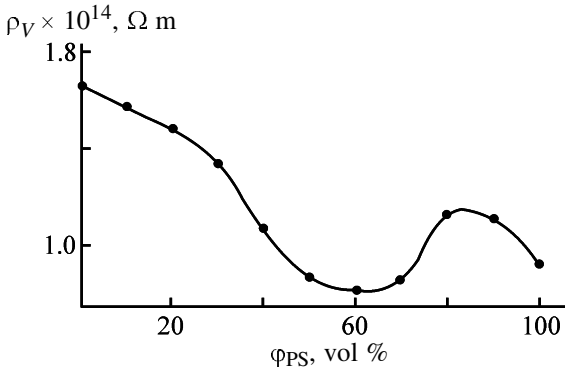


Fig. 4. Volume electrical resistivity ρ_V of a corona-electret based on polyethylene–polystyrene blends vs. the volume content of polystyrene, φ_{PS}.

a matrix structure, and the others are common dispersions. The shift of the phase inversion regions (transition from one colloid structure to another) toward predominance of polystyrene is due to the difference in viscosity between polyethylene and polystyrene.

Comparison of the data obtained in a study of the colloid structure of HDPE–PS blends with their electret characteristics suggests that, while one of polymers forms a continuous phase, values of V_e, E, U_{EPD}, and σ_{eff} increase with the content of the dispersed phase. This is due to an increase in the area of the phase boundary serving as the main source of traps for injected carriers in heterogeneous composite materials. However, as soon as the phase boundary becomes continuous, the electret properties of the blends are strongly impaired. This can be understood as resulting from the existence of the phase boundary as an interphase region with its own structure and properties, which governs the electret properties of the blend as a whole. It was noted in [17] that the interphase region in polymer blends is loose, i.e., it can have an increased electrical conductivity because of the higher mobility of macromolecules in it. A study of the volume electrical resistivity confirmed this assumption (Fig. 4). Consequently, charge carriers localized in polarization in a corona discharge at the phase boundary are released from traps in the course of time and "move" in the process of recapture within the interphase region with a higher conductivity, rather than within the phases of the polymeric blend components.

Using the results of this study, we can generalize the available published experimental data for electrets based on blends of various nonpolar polymers [10–16]. Addition to polyethylene of 10 wt % ethylene–propylene copolymer gives rise to a new type of traps at the polymer phase boundary, which is confirmed by the increased activation energies of charge traps in the blend, compared to polyethylene. This results in that the electret properties of LDPE are improved upon addition of EPC [10, 11]. The same phenomenon was observed in a study of a blend of polypropylene and terpolymer of ethylene, propylene, and butadiene [15].

The existence of a phase boundary can also be responsible for the improved electret properties of blends of a cycloolefin copolymer with propylene, compared to individual PP (unfortunately, the electret properties of COC were not reported) [12]. We can attribute the poorer stability of charge in blends with the PP content increased from 10 to 25 and 40% to a transition of the colloid structure from the dispersed to the matrix state, which is accompanied by formation of a continuous phase boundary with its own electrical conductivity. In the same way, we can explain the extremal behavior of the dependence of the surface density and lifetime of electret charges in blends of polypropylene and high-density polyethylene on the HDPE content [14].

We can suggest with high confidence that the electrical conductivity of the phase boundary between polypropylene and polytetrafluoroethylene exceeds the electrical conductivities of the individual components to such a great extent that blends of PP and PTFE with approximately equal contents of the polymers are not electrified [15].

CONCLUSIONS

(1) The composition dependence of the electret parameters of blends of high-density polyethylene and polystyrene has two maxima, with enhanced electret properties characteristic of blends with predominant content of one of the polymers.

(2) The polarizability of a polymer blend is governed by its colloid structure and, as a consequence, by the discontinuity of the phase boundary. While one of the polymers forms a continuous phase, the electret parameters increase with the content of the dispersed phase. This is due to an increase in the area of the phase boundary, which serves as the main source of traps for injected carriers in heterogeneous composite materials. If, however, the colloid structure of a blended formulation is of the matrix type and the phase boundary is continuous, the electret properties of the polymer blend are unsatisfactory. This is due to the fact that the phase boundary is an interphase region with increased electrical conductivity and the carrier transport to the surface of the electret and its depolarization both occur in this region.

REFERENCES

1. *Proc. 12th Int. Symp. on Electrets*, Salvador, Bahia (Brazil), 2005.
2. Sviridenok, A.I., Kovalevskaya, T.I., Kravtsov, A.G., et al., *Dokl. Akad. Nauk Bel.*, 2000, vol. 44, no. 5, pp. 119–122.
3. Motyl, E. and Lisowski, M., *Proc. 11th Int. Symp. on Electrets*, Melbourne (Australia), 2002, pp. 310–313.
4. Galikhanov, M.F., Eremeev, D.A., and Deberdeev, R.Ya., *Zh. Prikl. Khim.*, 2003, vol. 76, no. 10, pp. 1696–1700.
5. Galikhanov, M.F., Gol'dade, V.A., and Deberdeev, R.Ya., *Vysokomol. Soedin., Ser. A*, 2005, vol. 47, no. 2, pp. 264–269.
6. Pinchuk, L.S. and Gol'dade, V.A., *Elektretnye materialy v mashinostroenii* (Electret Materials in Machine-Building), Gomel: Infotribo, 1998.
7. Xia, Z., Buchtemann, A., Danz, R., et al., *Proc. 11th Int. Symp. on Electrets*, Melbourne (Australia), 2002, pp. 203–206.
8. Gromyko, Yu.V. and Klimovich, A.F., *Dokl. Akad. Nauk Bel. SSR*, 1989, vol. 33, no. 6, pp. 531–534.
9. Datt, S.C., Singh, R., Keller, J.M., et al., *Proc. 7th Int. Symp. on Electrets*, Berlin, 1991, pp. 606–611.
10. Mizutani, T., Zhang, C., and Ishioka, M., *Proc. 11th Int. Symp. on Electrets*, Melbourne (Australia), 2002, pp. 147–150.
11. Zhang, C., Mizutani, T., Kaneko, K., et al., *J. Phys. D: Appl. Phys.*, 2002, vol. 35, pp. 1875–1879.
12. Yang, G.M., Sessler, G.M., and Hatke, W., *Proc. 10th Int. Symp. on Electrets*, Delphi (Greece), 1999, pp. 317–320.
13. Galikhanov, M.F. and Deberdeev, R.Ya., *Vestn. Kazan. Tekhnol. Univ.*, 2005, no. 1, pp. 318–322.
14. Ramazanov, M.A., Abasov, S.A., and Ramazanova, S.Dzh., Abstracts of Papers, *XV Simpozium "Sovremennaya khimicheskaya fizika"* (XV Symp. "Modern Chemical Physics"), Tuapse, 2003, pp. 231–232.
15. Magerramov, A.M., Safarov, N.J., and Sharifov, Z.Z., *Turk. J. Phys.*, 1996, vol. 20, no. 12, pp. 1250–1255.
16. Lushcheikin, G.A., *Polimernye elektrety* (Polymeric Electrets), Moscow: Khimiya, 1984.
17. Lipatov, Yu.S., *Vysokomol. Soedin., Ser. A*, 1978, vol. 20, no. 1, pp. 14–16.

ISSN 1070-4272, Russian Journal of Applied Chemistry, 2006, Vol. 79, No. 7, pp. 1158–1161. © Pleiades Publishing, Inc., 2006.
Original Russian Text © V.N. Verezhnikov, I.N. Pshenichnaya, 2006, published in Zhurnal Prikladnoi Khimii, 2006, Vol. 79, No. 7, pp. 1168–1171.

MACROMOLECULAR CHEMISTRY AND POLYMERIC MATERIALS

Heterocoagulation of Anionic and Cationic Latexes with Particles Bearing Intrinsic Charge

V. N. Verezhnikov and I. N. Pshenichnaya

Voronezh State University, Voronezh, Russia

Received January 16, 2006

Abstract—Kinetics of coagulation of dilute latexes of styrene copolymers with methacrylic acid and *N*-dimethylaminoethyl methacrylate is studied turbidimetrically. The pH dependence of the limiting turbidity of the coagulating dispersion, characterizing the heterocoagulation efficiency, is examined.

DOI: 10.1134/S1070427206070226

Heterocoagulation represents the most common case of interparticle interaction in both the nature and technology. The use of polymer dispersions (latexes) is practically always accompanied by interaction of polymer globules with foreign particles or macroscopic surfaces (heteroadagulation), e.g., in impregnation and sizing of dispersed and fibrous materials, in combination of latexes with mineral fillers and binders, in production of nonwoven fabrics, in coating processes, etc. [1]. Of great interest are the cases of interaction of latex particles with oppositely charges substrates, e.g., in modification of cellulose fibers of pulp [2, 3] or natural and synthetic fibers [4, 5] with cationic latexes. It is known from the technological practice that anionic and cationic latexes are incompatible because of mutual coagulation of particles stabilized by the adsorption layers of, respectively, anionic and cationic surfactants. In this case, the specific character of heterocoagulation is lost to a considerable extent, since the mechanism of destabilization of a mixture of such latexes is restricted to only chemical interaction of anionic and cationic emulsifiers with formation of insoluble ion–salt complexes, which deprives the particles of the protective adsorption shell. Additionally, of a considerable interest is the interaction between anionic and cationic latexes stabilized by only their own charges, which could be imparted to them in the course of synthesis through the use of the respective ionic surface-active comonomers. In addition to purely theoretical interest, mutual coagulation of such latexes is worth noting as a possible route to preparation of polymeric composites free from inorganic salts, which is impracticable in the case of ordinary electrolyte-induced coagulation.

In this study we examined the interaction between two latexes obtained by copolymerization of the ionic monomers, *N*-dimethylaminoethyl methacrylate (DMAEM) and methacrylic acid (MAA), with styrene, which are composed by, respectively, positively and negatively charged particles. Our goal was to elucidate the pH effect on the heterocoagulation efficiency of the latexes (taking into account considerable difference in the acid–base characteristics of the charge-forming functional groups of the comonomers) and also the effects of the nature and concentration of inorganic salts.

EXPERIMENTAL

In synthesis of latexes we used freshly distilled styrene (n_D^{20} = 1.545) and methacrylic acid (n_D^{20} = 1.430), and DMAEM from Aldrich (n_D^{20} = 1.440). *N*-Dodecylpyridinium bromide (DDPB) and azobis(isobutyronitrile) (AIBN) were recrystallized twice from alcohol, and potassium persulfate (PPS), from water. The anionic emulsifiers, alkyl sulfonate (commercial product used in synthetic rubber production) and bis(2-ethylhexyl) sulfosuccinate sodium salt (SUS-875), were used without additional purification. The formulations used in synthesis of the latexes are given in Table 1.

In synthesis of the cationic latex, the aqueous phase (solution of sulfuric acid and the emulsifier) was heated to 50°C, and styrene was added. Ten minutes after, a solution of the initiator in a small volume of styrene was added stepwise. After 2 h, the reaction mixture was heated to 60°C. Two hours prior completion of the polymerization, the cationic monomer

(DMAEM) was added. The total process time was 7 h. The anionic latex was obtained as follows. The aqueous phase (solution of the sulfonate and succinate) was heated to 60°C, and styrene and partly MAA (0.5 wt % relative to styrene) were added. After 10 min, a solution of the initiator (PPS) in a small volume of the aqueous phase was added dropwise. The mixture was heated to 80°C. After 1 h, the rest amount of MAA (1.5 wt % relative to styrene) was added, and the polymerization was carried out for 2 h.

The resulting latexes were dialyzed for two weeks through a collodion membrane and then electrodialyzed with surface tension monitoring. Concentrations of the anionic and cationic functional groups in the dialyzed latexes were determined by conductometric back-titration [6] and coagulation titration (with sodium tetradecyl sulfate) [7], respectively.

The surface tension was measured by the ring detachment (Du Nouy) method [6]; the turbidity, on an NMF nephelometer calibrated by the standard sample; pH, on an EV-74 ion meter; and conductivity, on an N5701 conductometer (Poland).

Characteristics of the initial and dialyzed latexes are summarized in Table 2.

Table 2 shows that, as a result of dialysis, the polymer content in the latexes and conductivity decreased, and the surface tension σ considerably increased (to the values close to the surface tension of water) by virtue of removal of the emulsifiers. From the surface tension isotherms obtained for the emulsifiers used we found that the σ values of the dialyzed latexes correspond to the surfactant concentration below 10^{-4} M, i.e., the emulsifiers were virtually fully removed from the latexes. The mean particle size r remained practically unchanged, suggesting sufficiently high aggregative stability of the latexes, which can be attributed to the intrinsic charge of the particles. This charge is controlled by the pH-dependent degree of ionization of the functional groups (–COOH and –N=C) in the polymers. Therefore, it may be expected that pH has a considerable effect on the heterocoagulation.

The elucidate the pH effect, we performed a turbidimetric study of the kinetics of heterocoagulation of dilute latexes at various pHs [6]. An estimated volume of the cationic latex (m = 2.9 wt %) was introduced into a volumetric flask, and the volume was brought to the mark with a solution of H_2SO_4 or KOH. Then the anionic latex (m = 1.1 wt %) was added. The final concentration of the disperse phase was 1.8×10^{-3} wt %. The turbidity τ was measured as a function of the coagulation time t. Typical τ–t curves are given in Fig. 1. In all cases, regardless of pH, we observed an abrupt increase in τ in the first 1–1.5 min, followed by saturation at a level corresponding to the limiting turbidity τ_{lim}. Thus, the heterocoagulation

Table 1. Latex formulations

Component	Amount, wt proportion	
	anionic latex	cationic latex
Styrene	100.0	100.0
MAA	2.0	–
DMAEM	–	5.0
Alkyl sulfonate	4.0	–
SUS-875	0.5	–
DDPB	–	6.0
H_2SO_4	0.4	–
H_2O	150.0	200.0

Table 2. Characteristics of latexes

Parameter	Latex	
	anionic	cationic
Fraction of polymer m, wt %	30.4/2.9*	39.5/1.1
Surface tension σ, mN m^{-1}	36.0/71.4	40.5/70.8
Conductivity æ, mS m	350/5	240/22
pH	5.7/9.3	2.0/3.3
Functional group content in polymer, mol g^{-1}	$-/1.4 \times 10^{-4}$	$-/1.3 \times 10^{-4}$
Mean particle radius r, nm	40.5/41.3	31.2/32.0
Particle concentration $\nu \times 10^{19}$, cm^{-3}	–/9.8	–/8.0

* Before/after dialysis.

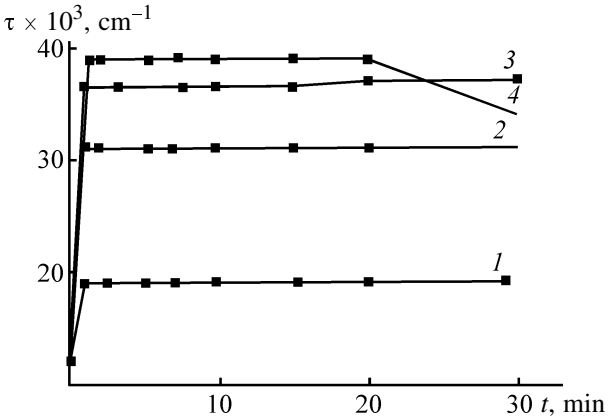


Fig. 1. Turbidimetric curves obtained during heterocoagulation of dilute latexes. Total concentration of the dispersed phase 1.8×10^{-3} wt %; cationic to anionic latex ratio 5 : 1; the same for Figs. 2 and 3. (τ) Turbidity and (t) time. pH: (*1*) 3.0, (*2*) 8.9, (*3*) 10.1, and (*4*) 11.0.

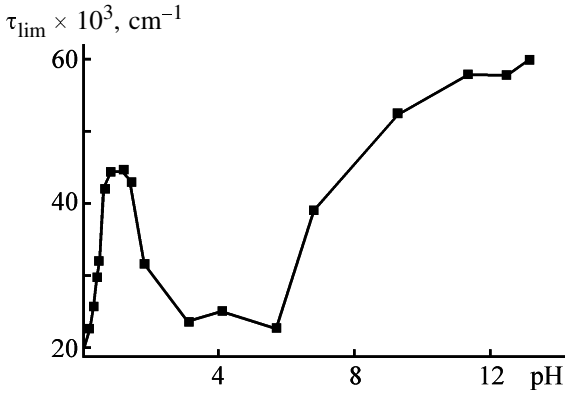


Fig. 2. Limiting turbidity τ_{lim} as a function of pH.

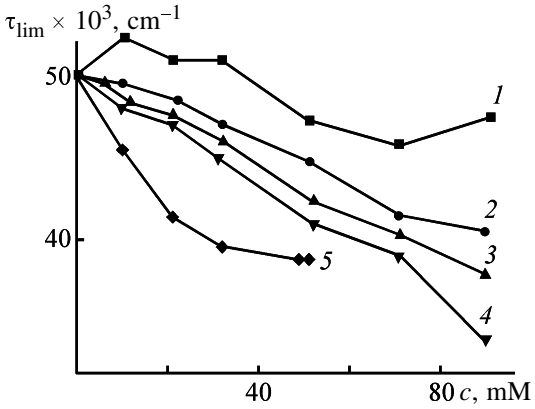


Fig. 3. Limiting turbidity τ_{lim} as a function of the electrolyte concentration c: (*1*) KF, (*2*) KCl, (*3*) KBr, (*4*) KI, and (*5*) K_2SO_4.

kinetics of cationically and anionically charged latexes differs considerably from the case of coagulation of latexes (stabilized with ionic emulsifiers) under the action of electrolytes [8]. In the latter case, as known, the duration of the initial agglomeration stage regularly depends on such factors as the electrolyte nature and concentration, degree of adsorption saturation of the particle surface with an emulsifier, etc., including pH [9]. Interpretation of this difference requires a special study.

Figure 1 shows that τ_{lim} characterizing the mean size of the aggregates formed strongly depends on pH. Therefore, τ_{lim} was chosen as a measure of the heterocoagulation efficiency. In the subsequent experiments, this parameter was determined as the turbidity at t = 5 min.

The pH dependence of τ_{lim} over a wide pH range is given in Fig. 2. The curve was obtained by subtracting the turbidity of the initial mixture of two latexes from the measured current turbidity. As seen, the τ_{lim}–pH curve is very complex in shape. In moderately acidic media (pH ~3–6), the heterocoagulation is insignificant. At pH < 3, τ_{lim} passes through a maximum, and in the alkaline range, it regularly increases with increasing pH. To interpret this result, let us consider the interparticle interaction as a sequence of two events: approach under the effect of electrostatic attraction force between the diffuse clouds of the counterions and fixation through chemical interaction between functional groups of the polymer chains on the particle surface. This interaction is essentially a process similar to ionic reactions between macromolecules of oppositely charged polyelectrolytes [10]. Evidently, at pH 3–6, the latex particles are weakly ionized, so that the mutual electrostatic attraction between them is only slightly pronounced, and the presence of the solvate shells blocks the coagulation. On passing to the strongly acidic range, the protonation of the nitrogen atom of the surface amino groups become more pronounced, promoting their interaction with anionic species. As a result, τ_{lim} increases with decreasing pH. The possibility of such interaction between the ionized amino groups (=NH^+–) and the carboxy groups at low pH is probably caused by the cooperative nature of the reactions between macromolecules of anionic and cationic polyelectrolytes, which are characterized by a significant shift of the equilibrium to the right, as compared to similar reactions between low-molecular-weight analogs. In this case, a weak polymeric acid may effectively replace a strong one from its salt with a polymeric base [10]. At pH < 1, as a result of increasing ionic strength, the screening of the particle charge by the counterions increases, thus suppressing the coagulation.

On the contrary, in the alkaline range, with increasing pH, the ionization of the carboxy groups of the anionic latex increases, thus enhancing the heterocoagulation efficiency.

To characterize the effect of the nature and charge of the coagulating ions on heterocoagulation, we studied the electrolyte effect on τ_{lim}. As electrolytes we used potassium halides, to eliminate the neutralization factor, which could be pronounced in the presence of multivalent cations, as a result of their interaction with the carboxy groups. A fixed volume of the anionic latex ($m = 1.1 \times 10^{-2}$ wt %) was introduced into a volumetric flask, and the volume was adjusted to the mark with a KOH solution containing the desired amount of the salt. Then the cationic latex ($m = 2.9 \times 10^{-2}$ wt %) was added, and τ_{lim} was measured. The solution pH was 8.1–8.2. The results are shown in Fig. 3.

In all cases, τ_{lim} decreased with increasing electrolyte concentration, i.e., the heterocoagulation effici-

ency decreased, which can be attributed to weakening electrostatic attraction as a result of compaction of the oppositely charged diffuse clouds of the counterions. The significant role of this factor is supported by the observed effect of the nature (size) of the halide ion: the effect of decreasing τ_{lim} increases with an increase in the ionic radius and, therefore, in the adsorbability in the series $F^- < Cl^- < Br^- < I^-$, i.e., on passing from fluoride to iodide, the suppression of the heterocoagulation becomes more pronounced (naturally, these considerations refer to the cationic component of the latex mixture, for which counterions are anions). The stronger the ability of the counterions to compact the diffuse part of the electrical double layer, the more efficiently they block the aggregation, which can be considered as the inversion of the Schulze–Hardy rule. Previously this effect was observed in studying the heterocoagulation in mixtures of certain inorganic colloids with oppositely charged species, such as aqueous sols of gold and iron(III) hydroxides [11], sols and suspensions of silica and Fe_2O_3 [12], and also in the AgI–$Pb(OH)_2$ system [13].

The inversion of the Schulze–Hardy rule is supported also by comparison of the effects of singly and doubly charged counterions (Fig. 3): In the presence of K_2SO_4, the decrease in τ_{lim} is considerably more pronounced as compared to the halides, as a result of stronger capacity of the sulfate for compaction of the electrical double layer.

CONCLUSIONS

(1) Heterocoagulation of anionic and cationic latexes with particles bearing intrinsic charge (due to acidic or basic functional groups) is strongly pH-dependent.

(2) The heterocoagulation efficiency is maximal in strongly acidic and strongly alkaline media.

(3) Introduction of electrolytes suppresses the heterocoagulation, the effect being more pronounced with increasing size and charge of the coagulating ions, i.e., inversion of the Schulze–Hardy rule is observed.

REFERENCES

1. Erkova, L.N. and Chechik, O.S., *Lateksy* (Latexes), Leningrad: Khimiya, 1983.
2. Inoue, M., Alince, B., Shao, Y., and Van de Ven, T., *Int. Paper Coating Chem. Symp*., Ottawa, June 11–13, 1996, Montreal, 1996, pp. 119–124.
3. Alince, B., Arnoldova, P., and Frolik, R., *J. Appl. Polym. Sci*., 2000, vol. 76, no. 11, pp. 1677–1682.
4. Hisachi, T., *J. Colloid Interface Sci*., 1982, vol. 88, no. 2, pp. 372–378.
5. Danyushin, G.V. and Volkov, V.A., Abstracts of Papers, *VIII Vsesoyuznaya nauchno-tekhnicheskaya konferentsiya "Sinteticheskie lateksy, ikh primenenie i modifitsirovanie"* (VIII All-Union Scientific and Technical Conf. "Synthetic Latexes: Application and Modification"), Voronezh, June 17–21, 1991, Moscow, 1991, p. 130.
6. Neiman, R.E., Kiseleva, O.G., Egorov, A.K., et al., *Kolloidnaya khimiya sinteticheskikh lateksov* (Colloid Chemistry of Synthetic Latexes), Voronezh: Voronezh. Gos. Univ., 1984.
7. Verezhnikov, V.N., Poyarkova, T.N., Vostrikova, G.Yu., and Rassokhin, A.V., *Vestn. Voronezh. Gos. Univ., Probl. Khim. Biol*., 2002, vol. 1, no. 1, pp. 12–14.
8. Neiman, R.E., *Ocherki kolloidnoi khimii sinteticheskikh lateksov* (Essays on Colloid Chemistry of Synthetic Latexes), Voronezh: Voronezh. Gos. Univ., 1980.
9. Neiman, R.E. and Verezhnikov, V.N., *Kolloidn. Zh*., 1962, vol. 24, no. 5, pp. 593–598.
10. *Praktikum po vysokomolekulyarnym soedineniyam* (Practical Course of Macromolecular Compounds), Kabanov, V.A., Ed., Moscow: Khimiya, 1985.
11. Chernoberezhskii, Yu.M. and Golikova, E.V., *Elektropoverkhnostnye yavleniya v dispersnykh sistemakh* (Electrosurface Phenomena in Disperse Systems), Grigorov, O.N. and Fridrikhsberg, D.A., Eds., Moscow: Nauka, 1972, pp. 170–173.
12. Chernoberezhskii, Yu.M., Golikova, E.V., and Girfanova, T.F., *Poverkhnostnye sily v tonkikh plenkakh i ustoichivost' kolloidov* (Surface Forces in Thin Films and Colloid Stability), Deryagin, B.V., Ed., Moscow: Nauka, 1974, pp. 256–261.
13. Chernoberezhskii, Yu.M., Bykova, N.I., Yanklovich, A.I., and Il'ina, V.S., *Kolloidn. Zh*., 1982, vol. 44, no. 5, pp. 942–946.

ISSN 1070-4272, Russian Journal of Applied Chemistry, 2006, Vol. 79, No. 7, pp. 1162–1166. © Pleiades Publishing, Inc., 2006.
Original Russian Text © E.N. Chebotok, V.Yu. Novikov, I.N. Konovalova, 2006, published in Zhurnal Prikladnoi Khimii, 2006, Vol. 79, No. 7, pp. 1172–1176.

MACROMOLECULAR CHEMISTRY AND POLYMERIC MATERIALS

Depolymerization of Chitin and Chitosan in the Course of Base Deacetylation

E. N. Chebotok, V. Yu. Novikov, and I. N. Konovalova

Murmansk State Technical University, Murmansk, Russia
Knipovich Polar Research Institute of Marine Fishery and Oceanography, Murmansk, Russia

Received February 2, 2006

Abstract—Depolymerization of chitin and chitosan in the course of deacetylation in an alkaline medium was studied, and the influence exerted on the process by the nature and concentration of the alkali (NaOH, KOH) and salts (NaCl, NaI, KI) was examined.

DOI: 10.1134/S1070427206070238

Base hydrolysis of chitin (CTN) and chitosan (CTS) is one of the main chemical methods for modification of these natural polysaccharides; it mainly involves cleavage of the acetamide bonds resulting in deacetylation [1, 2].

Depolymerization of the macromolecules in alkaline solution is considerably slower than the deacetylation and, as believed by many researchers, is due to oxidative degradation of glycoside units rather than to hydrolysis of glycoside bonds [3, 4].

This study was aimed to refine the factors affecting the depolymerization of chitin and chitosan in the course of their base deacetylation.

EXPERIMENTAL

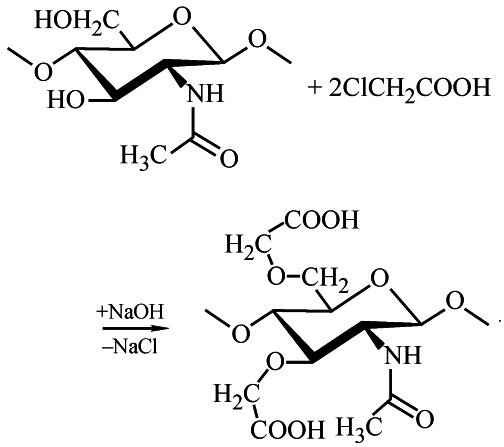
Chitin was recovered from Kamchatka crab shells by the standard procedure [5, 6]. Chitosan was prepared by deacetylation of chitin with 50% aqueous NaOH.

The extent of saturation of the examined solutions with oxygen or nitrogen was recorded with an Anion 4151 ion meter (Infraspak-Analit, Russia) equipped with an ammetric sensor of the oxygen partial pressure.

It is known that solutions of chitosans with the degree of deacetylation exceeding 85% are virtually transparent in the UV and visible range. At a degree of deacetylation less than 55%, chitosan and chitin are insoluble in weakly acidic aqueous solutions; therefore, chromatographic analysis of such samples requires special choice of suitable solvents and eluents. The conditions of chromatographic analysis of chitin and chitosan were close to those used for solutions of chitosan in HCl.

For this purpose, we modified the procedure for preparing carboxymethylated derivatives of chitins (CMCTN) [7] with the aim to use them for determining the molecular weight and molecular-weight distribution by exclusion chromatography.

Samples of chitins and chitosans with various degrees of deacetylation were acetylated with a 20% solution of acetic anhydride in ethanol at 4°C for 24 h. Similar procedure for pretreatment of chitooligosaccharide samples was used, e.g., in mass spectrometry of chitin hydrolyzates [3, 8]. The products of exhaustive acetylation were treated with monochloroacetic acid in alkaline solution [7] to obtain CMCTN:



Carboxymethylation was performed in isopropyl alcohol at 4°C for 3 days. After the reaction comple-

tion, the samples were washed with two portions of ethanol and one portion of acetone and dried at 60°C. The resulting chitin derivatives are readily soluble in water and have high extinction coefficients in the UV range (205–210 nm) due to acetyl groups. The monomeric units in these samples have virtually the same composition, which allows comparison of their chromatograms.

For chromatographic measurements, we prepared 0.1% solutions of carboxymethyl chitin in the eluent, 0.3 M NaCl, at pH 6.5–7.5. The chromatography of chitin samples with a high degree of deacetylation was performed in the eluent containing 0.3 M NaCl at pH 3.0. Chromatographic experiments were performed with an LC-10A_{VP} HPLC system (Shimadzu, Japan). Exclusion chromatography was performed with TSK-gel Alpha-4000 columns (30 × 0.78 cm) and a TSK-guardcolumn Alpha precolumn (6 × 0.4 cm) (TOSOH, Japan). The eluted fractions were monitored by the optical absorption of hydrolysis products using a SPD-10A_{VP} UV spectrophotometric detector or an SPD-M10A_{VL} diode matrix at wavelengths of 205 and 210 nm.

The column was calibrated using chitosan samples of known viscosity-average molecular weights (MW) determined from the intrinsic viscosity by the Mark–Kuhn–Houwink equation

$$[\eta] = K(\mathrm{MW})^{\alpha},$$

where $[\eta]$ is the intrinsic viscosity of chitosan in the system containing 0.334 M CH_3COOH and 0.3 M NaCl (dl g^{-1}); the coefficients K and α (based on data from [9]) are 3.41×10^{-3} and 1.02, respectively.

The viscometric method allows calculation of the viscosity-average molecular weight, which is close to the weight-average molecular weight [10, 11].

Calculation of MW from HPLC data was made using the calibration curve (Fig. 1) constructed from data for chitosan samples of known viscosity-average molecular weight:

$$\log \mathrm{MW} = -0.275V + 6.856,$$

where MW is the mean molecular weight (Da); V, eluent volume corresponding to the maximum of the chromatographic peak of the polymer (ml).

It is known that heterogeneous deacetylation of chitin in an alkaline medium is accompanied by depolymerization of the macromolecules; as a result, the molecular weight of chitosan and the viscosity of its solutions decrease [12].

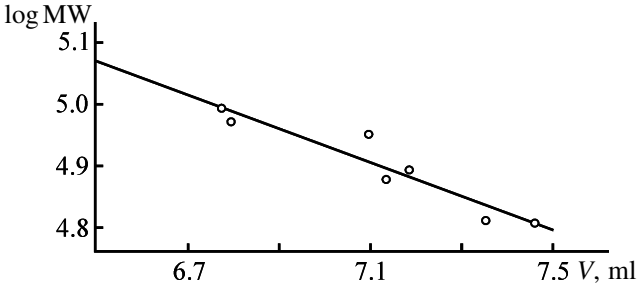


Fig. 1. Plot of log MW vs, eluent volume V corresponding to the maximum of the chromatographic peak of chitosan.

Although it was stated that the molecular weight of chitin and chitosan decreases in the course of base deacetylation, the mechanism of the cleavage of the glycoside bond leading to the depolymerization was not discussed.

The depolymerization of the polysaccharides under consideration in alkaline media, though being less pronounced than upon acid treatment, depends on the deacetylation conditions. The extent of the depolymerization increases with temperature and time [6, 13]. Nud'ga et al. [4, 14] observed degradation of chitin macromolecules in the presence of atmospheric oxygen when the deacetylation was performed under nitrogen at 140°C. They concluded that a combination of a low temperature with an oxygen-free atmosphere is required to prepare high-viscosity (high-molecular-weight) chitosans.

As for the effect of base hydrolysis conditions (concentration and nature of alkali, mutual arrangement of acetylated and deacetylated groups, presence of oxidants), there are different opinions in the literature.

Most attention was given to the dependence of the degree of deacetylation on the alkali concentration [15]. Virtually no attention was given to the effect exerted on the depolymerization of the polysaccharides by the nature of the alkali and its concentration.

It should be expected that an increase in the alkali concentration should promote the depolymerization. However, it was reported in some papers that the alkali concentration has no effect on MW of chitosans, in particular, of those prepared from β-chitin [16].

Smidsrod et al. [17, 18] showed that the mutual arrangement of the acetylated and deacetylated units exerts no effect on the redox and enzymatic cleavage of glycoside bonds in chitosan macromolecules.

It is believed [19, 20] that one of possible causes of the depolymerization of chitin and chitosan in alkaline solutions is oxidative degradation of glycoside bonds under the action of atmospheric oxygen. The deacetylation in that studies was performed in an inert atmos-

Table 1. Characteristics of chitosan samples prepared by deacetylation of chitin in 50% NaOH solution at 145–150°C

Sample no.	Atmosphere	τ, min	Total N, wt %	DD,* %	η,** cP	$M_\eta \times 10^{-6}$, Da
1	Nitrogen	5	7.74	53.0	5110	1.54
2		15	7.88	60.8	311	1.036
3	Air	5	7.86	59.7	460	1.317
4		15	7.97	65.6	117	0.768

* The degree of deacetylation, DD, was calculated from the weight fraction of total nitrogen.
** 1% chitosan solution in 2% solution of acetic acid.

Table 2. Molecular weights of carboxymethyl chitins prepared from chitin and chitosan samples

Sample no.	Treatment conditions	Molecular weight of carboxymethyl derivatives	
		MW, kDa	MW/MW_0,* %
1	Initial CTN	471.6	100.0
2	CTN + 0.5 M HCl	97.0	20.6
3	CTS from sample no. 2	96.5	20.5
4	CTN + 5.0 M HCl	78.6	16.7
5	CTS from sample no. 4	79.4	16.8

* MW_0 is the molecular weight of the carboxymethylated derivative of the initial chitin.

phere or in a vacuum. To suppress oxidative degradation of the polymeric chain, Domard and Rinaudo [19] used thiophenol as antioxidant.

We believe that the oxidative degradation exerts an ambiguous effect on the depolymerization. Bough et al. [12] studied the effect of oxygen on the molecular weight of the polymers evaluated from their intrinsic viscosities. They concluded that the dynamic viscosity of chitosan solutions and hence its molecular weight drastically decrease in the presence of atmospheric oxygen. The characteristics of chitosan samples prepared in [12] are given in Table 1.

From the data given in Table 1, we calculated the degree of deacetylation (DD) and plotted MW vs. DD (Fig. 2). It is seen that the points corresponding to the experimental data on the deacetylation in the presence

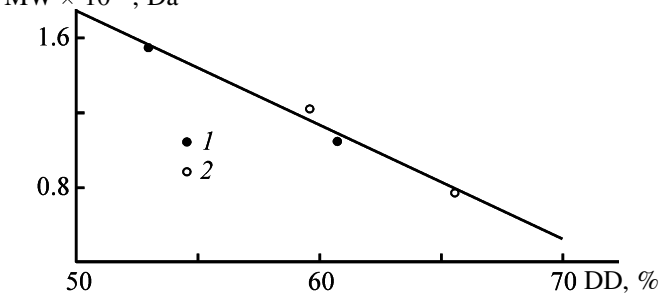


Fig. 2. Molecular weight MW of chitosan vs. degree of deacetylation DD (calculated using data from [12]). Deacetylation: (*1*) under nitrogen and (*2*) in air.

and in the absence of atmospheric oxygen fall on the same straight line. Thus, a decrease in MW is apparently associated with the variation of DD. With an increase in DD, the solubility of chitosan increased and hence the viscosity of its solutions decreased. In this case, MW correlates with DD, because MW is calculated from the solution viscosities.

The effect of oxygen on the decrease in the MW was noted by Focher et al. [21] who performed the deacetylation of chitosans at 140–150°C in a vacuum and obtained the same intrinsic viscosities as in common deacetylation in air at 80–100°C. They believe that this fact confirms the participation of oxygen in the degradation of chitosan in alkaline solutions.

However, experiments on base deacetylation made by Tolaimate et al. [20] showed that the use of the nitrogen atmosphere does not affect the molecular weight of the product. This fact is consistent with the assumption that cleavage of glycoside bonds in base hydrolysis is not an oxidative process.

In this study we made an attempt to estimate the contribution of oxidative and base-induced thermal depolymerization to the degradation of chitin and chitosan macromolecules.

The absence of noticeable depolymerization of chitin in the course of base deacetylation was confirmed by the example of samples that were preliminarily subjected to degradation in HCl (Table 2, sample nos.

Table 3. Influence of the conditions of chitin treatment on the relative MW of carboxymethyl chitins prepared from it

Sample no.	Chitin treatment at 98°C	MW/MW_0				
		air	oxygen		nitrogen	
		96 h	48 h	72 h	48 h	72 h
6	H_2O		21.1	18.9	21.6	18.4
7	25% NaCl		21.1	20.9	22.0	20.3
8	50% NaOH		22.2	21.2	22.1	21.3
9	50% NaOH	21.5				
10	50% NaI	20.9				
11	50% KOH	21.8				
12	50% KI	21.6				

2–5). Chitin samples were treated with HCl (0.5 and 5.0 M) at 50°C for 30 min. Then chitin sample nos. 2 and 4 and chitosan sample nos. 3 and 5 were exhaustively acetylated and converted to carboxymethyl chitins by the procedure described above. As seen from Table 2, the mean molecular weights of CMCTN samples prepared from the same chitin samples (sample nos. 2 and 3, 4 and 5) coincide and are appreciably lower than the molecular weight of CMCTN prepared from the initial chitin (sample no. 1). The molecular weights of CMCTN were determined by HPLC.

CMCTN sample nos. 2 and 3, and also 4 and 5 have the same molecular weight, and this fact confirms the absence of depolymerization in the course of base deacetylation.

It is known that hemiacetal bonds (including glycoside bonds) are hydrolyzed in the presence of dilute mineral acids. In alkaline and neutral solutions, these bonds are stable [22, 23].

By the analogy with the hydrolysis of an ether bond, the hydrolysis of a glycoside bond starts with an electrophilic attack (protonation) of the oxygen atom with the formation of an oxonium ion, followed by a nucleophilic attack of the C atom adjacent to oxygen, with the cleavage of the C–O bond.

To elucidate the role of nucleophilic agents in the cleavage of the glycoside bond, we examined the effect of alkalis (NaOH, KOH of different concentrations) and salts (NaCl, NaI, KI).

Depending on the substitution mechanism, the effect of the nature of the nucleophile can be the following.

If the S_N2 mechanism, in which the limiting step is the attack by the nucleophilic agent, is realized, an increase in the nucleophilicity of the attacking agent should facilitate the cleavage of the C–O bond.

In the case of the S_N1 mechanism, the rate is independent of the nature of the nucleophile, because it is not involved in the limiting step [24].

Table 3 shows how the conditions of chitin treatment affect the mean molecular weight of the resulting CMCTN samples. The initial chitin was treated for 2 and 3 days at 95°C with water, 25% NaCl solution, and 50% solutions of NaOH, KOH, NaI, and KI in air, under O_2, and under N_2.

Table 3 shows that the nucleophiles (OH^-, Cl^-, I^-) exert virtually no effect on the rate of cleavage of glycoside bonds. Oxidative degradation does not occur either, because the MW/MW_0 ratio for the samples prepared in air, under N_2, and under O_2 is essentially the same.

Since in all the experiments the deacetylation was performed in aqueous solutions (concentrations of salt and alkali solutions 25 and 50%), the cleavage of glycoside bonds could be effected by water. The hydrogen ion formed by the ionization of water could act as an electrophile. This assumption is apparently confirmed by the MW/MW_0 values for sample nos. 6–8: with an increase in the water content in the system, MW/MW_0 decreases.

Presumably, the glycoside bond in alkaline solution is cleaved by the same mechanism as in acidic solutions (S_N1). Apparently, even trace concentrations of H^+ ions in alkaline solutions lead to the formation of a carbenium ion. This reaction is fast, and it occurs even at low concentrations of hydrogen ions. Virtually equal rate of the reaction in water and in 50% NaOH confirms the possibility of occurrence of the reaction by the S_N1 mechanism.

CONCLUSIONS

(1) In base hydrolysis of chitin and chitosan, oxygen and hydroxide ions do not initiate cleavage of the glycoside bond. Apparently, this role is played by water, which is present in excess in all the examined systems.

(2) Trends in variation of the molecular weight of chitin in the course of its hydrolysis in solutions of NaOH, KOH, NaCl, NaI, and KI, and also in air, under O_2, and under N_2 are essentially similar.

REFERENCES

1. Horowitz, S.T., Roseman, S., and Blumental, H.J., *J. Am. Chem. Soc.*, 1957, vol. 79, no. 18, pp. 5046–5049.
2. Kurita, K., *Prog. Polym. Sci.*, 2001, vol. 26, no. 9, pp. 1921–1971.
3. Capon, B. and Foster, R.L., *J. Chem. Soc. C*, 1970, no. 12, pp. 1654–1655.
4. Nud'ga, L.A., Plisko, E.A., Danilov, S.N., *Zh. Obshch. Khim.*, 1971, vol. 41, no. 11, pp. 2555–2559.
5. *Chitin Handbook,* Muzzarelli, R.A.A. and Peter, M.G., Eds., Grottamare (Italy): Atec, 1997, pp. 195–198.
6. Chang, K.L.B., Lee, J., and Fu, W.-R., *J. Food Drug Anal.*, 2000, vol. 8, no. 2, pp. 75–83.
7. Chen, X.-G. and Park, H.-J., *Carbohydr. Polym.*, 2003, vol. 53, no. 4, pp. 355–359.
8. Lopatin, S.A., Ilyin, M.M., Pustobaev, V.N., et al., *Anal. Biochem.*, 1995, vol. 227, no. 2, pp. 285–288.
9. Pavlov, G.M. and Selyunin, S.G., *Vysokomol. Soedin., Ser. A*, 1986, vol. 28, no. 8, pp. 1727–1731.
10. Kuleznev, V.N. and Shershnev, V.A., *Khimiya i fizika polimerov: Uchebnik dlya khimiko-tekhnologicheskikh vuzov* (Chemistry and Physics of Polymers: Textbook for Higher Schools of Chemistry and Technology), Moscow: Vysshaya Shkola, 1988.
11. Belen'kii, B.G. and Vilenchik, L.Z., *Khromatografiya polimerov* (Chromatography of Polymers), Moscow: Khimiya, 1978.
12. Bough, W.A., Salter, W.L., Wu, A.C.M., and Perkins, B.E., *Biotechnol. Bioeng.*, 1978, vol. 20, no. 12, pp. 1931–1943.
13. Tsaih, M.L. and Chen, R.H., *J. Appl. Polym. Sci.*, 2003, vol. 88, no. 13, pp. 2917–2923.
14. Nud'ga, L.A., Preparation of Chitosan and Its Derivatives and Study of Their Properties, *Cand. Sci. Dissertation*, Leningrad, 1979.
15. Chang, K.L.B., Tsai, G., Lee, J., and Fu, W.R., *Carbohydr. Res.*, 1997, vol. 303, no. 3, pp. 327–332.
16. Methacanon, P., Prasitsilp, M., Pothsree, T., and Pattaraarchachai, J., *Carbohydr. Polym.*, 2003, vol. 52, no. 2, pp. 119–123.
17. Strand, S.P., Smidsrod, O., and Varum, K.M., *Advances in Chitin Science*, vol. 6: *Proc. 5th Int. Conf. of the European Chitin Society (EUCHIS'02)*, Trondheim (Norway), June 26–28, 2002, Varum, K.M. Domard, A. and Smidsrod, O., Eds., Trondheim: NTNU, 2003, pp. 27–34.
18. Nordtvein, R.J., Varum, K.M., and Smidsrod, O., *Carbohydr. Polym.*, 1994, vol. 23, no. 4, pp. 253–260.
19. Domard, A. and Rinaudo, M., *Int. J. Biol. Macromol.*, 1983, vol. 5, no. 1, pp. 49–52.
20. Tolaimate, A., Desbrieres, J., Rhazi, M., et al., *Polymer*, 2000, vol. 41, no. 7, pp. 2463–2469.
21. Focher, B., Beltrame, P.L., Naggi, A., and Torri, G., *Carbohydr. Polym.*, 1990, vol. 12, no. 4, pp. 405–418.
22. Shabarov, Yu.S., *Organicheskaya khimiya: Uchebnik dlya vuzov* (Organic Chemistry: Textbook for Higher Schools), part 1: *Netsiklicheskie soedineniya* (Acyclic Compounds), Moscow: Khimiya, 1994.
23. Petrov, A.A., *Organicheskaya khimiya: Uchebnik dlya vuzov* (Organic Chemistry: Textbook for Higher Schools), St. Petersburg: Ivan Fedorov, 2002.
24. March, J., *Advanced Organic Chemistry. Reactions, Mechanisms, and Structure*, New York: Wiley–Interscience, 1987, vol. 2.

ISSN 1070-4272, Russian Journal of Applied Chemistry, 2006, Vol. 79, No. 7, pp. 1167–1173. © Pleiades Publishing, Inc., 2006.
Original Russian Text © V.N. Kizhnyaev, A.F. Pokatilov, L.I. Vereshchagin, L.V. Adamova, A.P. Safronov, A.I. Smirnov, 2006, published in Zhurnal Prikladnoi Khimii, 2006, Vol. 79, No. 7, pp. 1177–1184.

MACROMOLECULAR CHEMISTRY AND POLYMERIC MATERIALS

Synthesis and Properties of Carbon-Chain Polymers with Pendant 1,3,4-Oxadiazole Rings

V. N. Kizhnyaev, A. F. Pokatilov, L. I. Vereshchagin, L. V. Adamova, A. P. Safronov, and A. I. Smirnov

Irkutsk State University, Irkutsk, Russia
Ural State University, Yekaterinburg, Russia

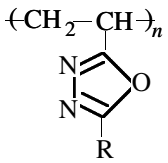
Received March 10, 2006

Abstract—Carbon-chain polymers with 1,3,4-oxadiazole rings were prepared by radical polymerization and polymer-analogous transformations. The kinetic relationships of the polymerization of vinyl-1,3,4-oxadiazole monomers and some properties of the resulting polymers were studied. The thermodynamics of interaction of poly-2-vinyl-5-methyl-1,3,4-oxadiazole, a nonionic water-soluble polymer, with water was examined.

DOI: 10.1134/S107042720607024X

Macromolecular compounds containing 1,3,4-oxadiazole rings in the backbone are widely used as chemically stable and heat-resistant, semiconducting, fiber-forming, and gas-separating materials [1, 2]. The main routes to these polymers, including commercial procedures, involve polycondensation of bifunctional heterocyclic compounds or formation of the 1,3,4-oxadiazole ring in a macromolecule of a polymeric precursor. At the same time, available data on vinyl derivatives of oxadiazoles, on their polymerization, and on the properties of carbon-chain polymers with pendant 1,3,4-oxadiazole rings are scarce and concern the synthesis of vinyl-1,3,4- and vinyl-1,2,4-oxadiazoles, and also the use of polyvinyl-1,2,4-oxadiazoles for preparing heat-resistant fibers [1, 3–5]. Recently we studied the polymerization of vinyl monomers with 1,3,4-oxadiazole rings [6].

This paper deals with the synthesis of poly-2-vinyl-5-R-1,3,4-oxadiazoles



[R = CH_3 (**I**), Ph (**II**), CF_3 (**III**), C_9H_{19} (**IV**)] by radical polymerization of the corresponding vinyl monomers and by polymer-analogous transformations of the macromolecular precursor, poly-5-vinyltetrazole (PVT), and with the properties of the resulting carbon-chain polymers containing pendant 1,3,4-oxadiazole rings.

EXPERIMENTAL

2-Vinyl-5-methyl-1,3,4-oxadiazole was prepared in one step from 5-vinyltetrazole as described in [4]; yield ~80%. 2-Vinyl-5-phenyl-1,3,4-oxadiazole was prepared in two steps. First 5-vinyltetrazole was acylated with benzoyl chloride in the water–toluene system at room temperature in the presence of a phase-transfer catalyst. Then the organic phase was separated and heated to 368–373 K to decompose the benzoyl derivative of vinyltetrazole. After the gas evolution ceased, the solvent was removed and the residue was subjected to fractional distillation. Yield of the target product ~70%. 2-Vinyl-5-trifluoromethyl-1,3,4-oxadiazole was prepared by mixing equimolar amounts of 5-vinyltetrazole and trifluoroacetic anhydride in methylene chloride at room temperature. After the reaction completion, the solvent was removed and the product was isolated by vacuum distillation (yield ~95%). The constants of the synthesized vinyl monomers purified by column chromatography on alumina are given in Table 1. The purity of the compounds was checked by NMR, IR, and UV spectroscopy. The kinetic relationships of the polymerization of the vinyl monomers were studied by the procedure described in [6].

The synthesis of poly-2-vinyl-5-R-1,3,4-oxadiazoles **I**–**IV** by polymer-analogous transformations

Table 1. Characteristics of 2-vinyl-5-R-1,3,4-oxadiazoles

R	bp, K (*P*, kPa)	n_D^{20}	*d*, g cm^{-3}
CH_3	314 (1.33)	1.4905	1.12
CF_3	313 (20.0)	1.3945	1.32
Ph	395 (1.33)	1.5885	1.17

involved the reaction of PVT with acetic anhydride, trifluoroacetic anhydride, benzoyl chloride, and decanoyl chloride, respectively, in pyridine or dimethylformamide (DMF) on heating. As in the case of the monomers, the reaction completion was judged from the cessation of evolution of gaseous nitrogen from the reaction mixture. The resulting polyvinyloxadiazoles were precipitated with diethyl ether, washed with the precipitant, and vacuum-dried to constant weight. The degree of conversion of the tetrazole fragments into oxadiazole fragments was calculated from elemental analysis data (Table 2).

The reaction of polyvinyloxadiazole **I** with formamide was performed by heating a solution of the polymer in excess formamide at 348 K in an argon flow for 5 h with continuous stirring. The resulting poly-3-vinyl-5-methyl-1,2,4-triazole was precipitated by pouring the reaction mixture into a mixture of acetone and diethyl ether, washed with the precipitant, and vacuum-dried to constant weight. The degree of conversion of the oxadiazole fragments into triazole fragments was about 97% according to ^{13}C NMR and elemental analysis of the resulting polymer.

The reaction of **I** with aniline was performed in polyphosphoric acid at 358–363 K in an argon flow for 7–8 h with continuous stirring. The resulting poly-3-vinyl-4-phenyl-5-methyl-1,2,4-triazole was precipitated by pouring the reaction mixture into water, reprecipitated from DMF into diethyl ether, and vacuum-dried to constant weight. The degree of conversion of oxadiazole fragments into triazole fragments was 95% according to ^{13}C NMR and elemental analysis of the resulting polymer.

Complexes of polyvinyloxadiazole **I** with metal salts were prepared by combining the solutions of the polymer and salt in appropriate solvent at room temperature with stirring. The precipitates of the metal complexes were washed with water, filtered off, and vacuum-dried to constant weight. The compositions of the products were determined by elemental analysis.

For thermodynamic studies of the interaction with water, we used nonfractionated, thoroughly dried in a vacuum, samples of polymer **I** prepared both by radical polymerization ($M = 6 \times 10^5$) and by polymer-analogous transformations ($M = 1.7 \times 10^5$). The isothermal sorption of water vapor with the polymer samples at 298 K was studied gravimetrically using highly sensitive quartz spirals [7]. The sorption isotherms were expressed in the coordinates $x/m = f(p/p_s)$, where x is the amount of water vapor absorbed by the polymer sample of weight m, and p/p_s is the relative water pressure. The Gibbs energies of mixing Δg_m were calculated from the sorption isotherms of water vapor [8]. The integral heat of solution of the polymers in water and the integral heat of dilution of polymer solutions of given concentration in a large amount of the solvent were determined with a DAK-1-1-A microcalorimeter. The mean specific enthalpies of mixing Δh_m and the mean entropies of mixing Δs_m were calculated by the procedure suggested in [9].

The ^{1}H and ^{13}C NMR spectra were recorded on a Varian VXR-500 spectrometer, and the IR spectra, on a Specord M80 spectrometer. The molecular weights of the polymer samples were determined by small-angle light scattering with an FSR laser photometer (Russia). The thermograms of the polymers were recorded on an MOM derivatograph (Hungary) in the dynamic mode at a heating rate of 5 deg min^{-1}. The

Table 2. Conditions and results of the synthesis of poly-2-vinyl-5-R-1,3,4-oxadiazoles **I**–**IV** by the modification of poly-5-vinyltetrazole (PVT). Molar ratio PVT : acylating agent = 1 : 5

Polyvinyl-oxadiazole	Acylating agent	Solvent	τ, h	*T*, K	Nitrogen content in reaction product, %		Conversion, %
					calculated	found	
I	$(CH_3CO)_2O$	Pyridine	2	373	28.07	25.45	91
II	PhC(O)Cl	〃	2	393	17.01	16.28	97
III	$C_9H_{19}C(O)Cl$	〃	1	373	13.42	12.61	96
IV	$(CF_3CO)_2O$*	DMF	0.5	318	18.81	17.07	93

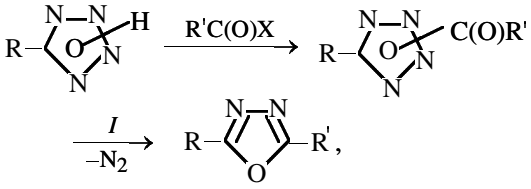
* Molar ratio PVT : acylating agent = 1 : 1.5.

Table 3. Kinetic parameters of the polymerization of 1-vinyl-5-R-1,3,4-oxadiazoles (acetonitrile, AIBN, 333 K)

R	E_{app}	$E_p - 0.5E_0$	$k_{app} \times 10^5$, $l^{0.5}$ mol$^{-0.5}$ s^{-1}	$K_i \times 10^5$, s^{-1}	$k_p/k_0^{0.5} \times 10^2$, $l^{0.5}$ mol$^{-0.5}$ s$^{-0.5}$
	kJ mol^{-1}				
CH_3	95.1	29.7	25.4	1.4	0.068
CF_3	88.5	21.0	76.5	1.3	0.21
Ph	109.3	35.2	1.8	1.1	0.0055

viscosities of polymer solutions were measured with an Ubbelohde viscometer at 273 K.

The synthesis of the monomeric and polymeric compounds containing 1,3,4-oxadiazole rings is based on the recyclization at elevated temperatures of unstable acylated derivatives of tetrazole into the oxadiazole ring with the release of gaseous nitrogen:



where R = CH_2=CH–, –(CH_2–CH–)$_n$–; X = Cl, O(O)CR'.

The starting compound can be 5-vinyltetrazole or its polymer. In the first case, the reaction yields monomeric vinyl derivatives of substituted 1,3,4-oxadiazoles, and in the second case, carbon-chain polymers with pendant 1,3,4-oxadiazole rings. A distinctive feature of the reaction with trifluoroacetic anhydride as acylating agent is that the transformation of the tetrazole ring into the 1,3,4-oxadiazole ring occurs virtually quantitatively at room temperature in the case of the synthesis of the vinyl monomer and at 313–318 K in the case of the modification of the polymeric precursor. In all the other cases, the similar transformation of the azole ring requires heating to 373–393 K.

As shown in [6], vinyl derivatives of 1,3,4-oxadiazole are very active in radical polymerization and form polymeric products of high molecular weights in high yields. The kinetic relationships of the radical polymerization of 2-vinyl-5-methyl-, 2-vinyl-5-phenyl-, and 2-vinyl-5-trifluoromethyl-1,3,4-oxadiazoles do not differ from those found previously for vinyl derivatives of azoles containing only nitrogen heteroatoms in the ring [10–13]. In the polymerization of all the three monomers in acetonitrile under the action of AIBN, the reaction order with respect to the initiator concentration is 0.5, and with respect to the monomer concentration, 1.0. As expected, the highest activity in the radical polymerization is exhibited by the monomer containing in the 1,3,4-oxadiazole ring an acceptor trifluoromethyl group. For 2-vinyl-5-trifluoromethyl-1,3,4-oxadiazole, the parameter $k_p/k_0^{0.5}$ used as a criterion of the monomer activity in radical polymerization is by a factor of 3 higher than for 2-vinyl-5-methyl-1,3,4-oxadiazole (Table 3). In turn, the latter monomer is by an order of magnitude more active than the vinyloxadiazole with the phenyl substituent in the ring. The energy consumption in the chain propagation step (the quantity $E_p - 0.5E_0$) regularly increases with a decrease in the monomer activity parameter. The fact that 2-vinyl-5-trifluoromethyl-1,3,4-oxadiazole is the most active in the polymerization among the compounds studied is well consistent with the typical trend noted previously for vinylazoles [14]: an increase in the activity of monomers in radical polymerization with an increease in the electron-withdrawing power of the heterocyclic substituent at the vinyl group.

The lower reactivity in polymerization of phenyl-substituted vinyloxadiazole compared to the methyl-substituted monomer is attributable to the steric effect of the bulky phenyl substituent or to the lower reactivity of the radical center due to additional delocalization of the unpaired electron. Comparison of the kinetic parameters of the polymerization of vinyl 1,3,4-oxadiazole derivatives (Table 3) with those reported for another *C*-vinylazole, 2-methyl-5-vinyltetrazole ($k_p/k_0^{0.5}$ = 0.31 $l^{0.5}$ mol$^{-0.5}$ s$^{-0.5}$ [14]), shows that the oxadiazole monomers are less reactive in the polymerization, which is consistent with the stronger electron-withdrawing power of the tetrazolyl substituent compared to the oxadiazolyl substituent. 2-Vinyl-5-methyl-1,3,4-oxadiazole is a water-soluble monomer, and water exerts a strong accelerating effect on its polymerization. In aqueous solution, the activity parameter of the monomer increases by a factor of 18 ($k_p/k_0^{0.5}$ = 1.24 $l^{0.5}$ mol$^{-0.5}$ s$^{-0.5}$ [6]) compared to the polymerization in acetonitrile (Table 3), and the

Table 4. Solubiity and decomposition points of polyvinyloxadiazoles

Polymer	Solvent	Softening point, K	Decomposition onset point, K
I	DMF, DMSO, acetone, acetonitrile, ethanol, acetic acid, 1,2-dichloroethane, water	478	622
II	DMF, DMSO, CH_2Cl_2	483	603
III	DMF, DMSO, acetonitrile, acetic acid	460	585
IV	1,2-Dichloroethane, benzene, dioxane	–	579

molecular weights of the resulting polymers increase. Whereas the molecular weight of samples of polyvinyloxadiazole **I** prepared in acetonitrile is within $(1–7) \times 10^5$, in an aqueous solution it is possible to prepare polymer samples with M as high as 4×10^6.

Spectroscopic studies of the polymers show that the polymer backbone is formed exclusively by opening of the vinyl double bonds, without involvement of the heterocyclic fragments. Polyvinyloxadiazoles **I**–**V** prepared by the polymer-analogous transformation from PVT have a similar structure. The absorption bands of the 1,3,4-oxadiazole ring at 1250, 1350, 1530, and 1580 cm^{-1} remain unchanged in the spectrum of the polymers prepared by various procedures. A minor distinctive feature of the spectra of the polymers prepared by the modification to a conversion less than 95% is the presence of a broad absorption band at 2250–3700 cm^{-1} corresponding to the vibrations of the residual N–H groups in the unsubstituted tetrazole rings [15]. The ^1H NMR spectra of polyvinyloxadiazoles **I** and **II** prepared by various procedures are similar in the shape and position of signals of the methyl (δ 2.4 ppm) and phenyl (δ 7.2–7.6 ppm) groups. Protons of the nonyl substituent in the spectra of **IV** give four signals at δ 0.9 (CH_3), 1.32, 2.02, and 3.25 ppm (CH_2). The CF_3 groups in the ^{13}C NMR spectra of samples of **III** prepared by different procedures give a quartet at 113.0–119.5 ppm.

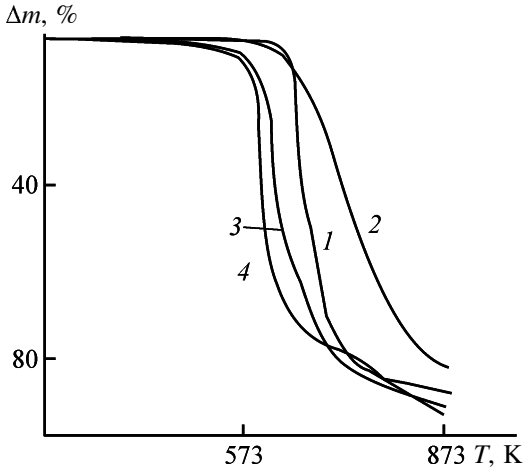


Fig. 1. Dynamic thermogravimetric analysis of polyvinyloxadiazoles (*1*) **I**, (*2*) **II**, (*3*) **III**, and (*4*) **IV**. (Δ*m*) Weight loss and (*T*) temperature.

Polyvinyloxadiazoles **I**–**III**, irrespective of the synthesis procedure, are amorphous colorless powders (polymer **IV** is rubber-like) with the softening and decomposition points depending on the substituent in the heteroring (Table 4, Fig. 1). On the whole, carbon-chain polyvinyloxadiazoles can be regarded as relatively heat-resistant polymers, despite the fact that they are inferior to the known heterochain oxadiazole-containing polymers by approximately 100°C [2].

The solubility of polyvinyloxadiazoles is characterized by the same trends as the solubility of vinylazole polymers containing only the nitrogen heteroatoms in the heterorings [16]. Polyvinyloxadiazole **I** whose heterocyclic fragments contain a small alkyl substituent, CH_3 group (Table 4), dissolve in the widest set of solvents. An increase in the size of the alkyl group (passing to nonyl-substituted polyvinyloxadiazole **IV**) results in the loss of the solubility in polar solvents, but makes the polymer more readily soluble in low-polarity liquids such as benzene and dioxane. Polyvinyloxadiazoles are not polyelectrolytes; therefore, solutions of polymers prepared by polymerization show a linear concentration dependence of the reduced viscosity (Fig. 2). However, the polymers prepared by the modification and containing residual N–H-unsubstituted tetrazole fragments (>5 mol %) behave in solutions as typical polyelectrolytes: Their reduced viscosity increases with the dilution.

In contrast to hydrophobized polyvinyloxadiazoles with phenyl, nonyl, and trifluoromethyl substituents, polymer **I**, similarly to polymers with the 1,2,4-triazole ring, is a nonionic water-soluble macromolecular compound. Comparison of 1,2,4-oxadiazole- and 1,2,4-triazole-containing polymers is interesting from the viewpoint of the effect of the ring-forming heteroatoms (at their equal number) on the compatibility with water. However, it was noted previously [16] that polyvinylazoles containing sequences of two and

more nitrogen atoms in the ring are insoluble in water (e.g., poly-1-vinyl-1,2,3-triazole, poly-1-vinyl-1,3,4-triazole, poly-1-vinyltetrazole). Polyvinylazoles containing an isolated "pyridine" nirogen atom in the heteroring are water-soluble (poly-1-vinylimidazole, poly-1-vinyl-1,2,4-triazole). In the structure of the 1,3,4-oxadiazole ring, there are two vicinal "pyridine" nitrogen atoms which, by analogy with poly-1-vinyl-1,3,4-triazole, is unfavorable for the affinity of the polymer for water, and an isolated oxygen atom of the furan ring. Apparently, this oxygen atom is responsible for the solubility of **I** in water.

The thermodynamic parameters of the interaction with water of polymer **I** prepared by polymerization and modification were estimated from the sorption and calorimetric data. For both samples of **I**, the isotherms of water vapor sorption asymptotically increase at $p/p_s \to 1$ (Fig. 3), which is typical of polymers infinitely miscible with water. The concentration dependences of the Gibbs energy of mixing (Δg_m) of the polymers with water, calculated from the sorption isotherms, are negative, and the second derivative $\partial^2 \Delta g_m / \partial W_2^2 > 0$, i.e., the systems are thermodynamically stable in the entire composition range. Polyvinyloxadiazole **I** prepared by the modification exhibits somewhat lower affinity for water because of the presence of residual tetrazole fragments. Comparison with the Δg_m values obtained for mixing of poly-1-vinyl-1,2,4-triazole with water shows that the oxadiazolyl substituent is substantially less hydrophilic than the triazolyl substituent. This fact cannot be attributed to the presence of the methyl substituent in the heteroring of **I**, since the previous studies showed that electron-donor methyl substituents in azolyl fragments of polyvinylazoles, as a rule, enhance the affinity of the polymer for water [16].

The weaker, compared to the 1,2,4-triazole-containing polymer, interaction of polyvinyloxadiazole **I** with water also follows from the substantially smaller negative enthalpies of mixing (Δh_m) of **I** with water (Fig. 4b). The stronger exothermic effect of the donor–acceptor interaction with water and the shape of the dependence $\Delta h_m = f(W_2)$ for the sample of **I** prepared by the polymer-analogous transformation are attributable to the presence of the residual monomeric units with N–H-unsubstituted tetrazole rings [17].

The difference in the water affinity of oxadiazole- and triazole-containing polymers is also manifested in variation of the entropy parameters at formation of the aqueous systems. Dissolution of oxadiazole polymers is characterized by substantially smaller negative entropies of mixing $T\Delta s$ (Fig. 4c), which indicates that these polymers show a weaker tendency to form joint ordered polymer–water structures, compared to the triazole-containing polymer. Thus, the difference between the triazole and oxadiazole derivatives in the kind of one of the three heteroatoms does not result in the loss of the capability of the polymer with the 1,3,4-oxadiazole pendant group to dissolve in water but appreciably decreases its thermodynamic affinity for water.

As noted above, poly-2-vinyl-1,3,4-oxadiazoles can be prepared by modification of PVT. In turn, oxadiazole polymers can act as precursors for preparing

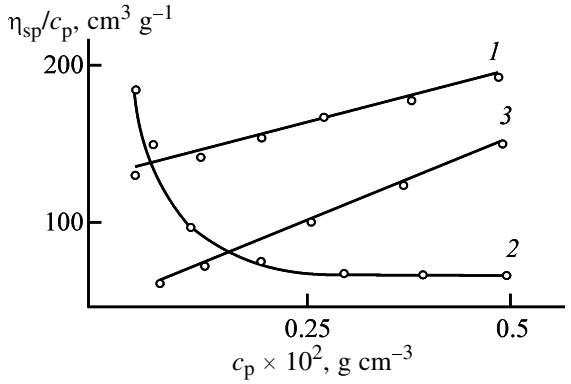


Fig. 2. Reduced viscosity η_{sp}/c_p of aqueous solutions as a function of polymer concentration c_p: polyvinyloxadiazole **I** prepared by (*1*) polymerization and (*2*) polymer-analogous transformation; (*3*) poly-3-vinyl-5-methyl-1,2,4-triazole.

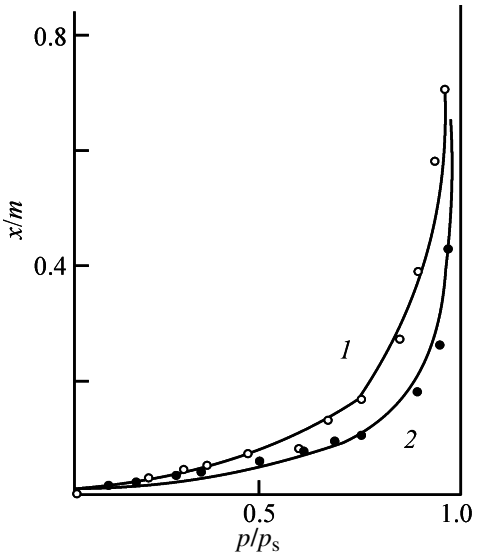


Fig. 3. Isotherms of water vapor sorption at 298 K for polyvinyloxadiazole **I** prepared by (*1*) polymerization and (*2*) polymer-analogous transformation. (x/m) Weight ratio of water and the polymer; (p/p_s) relative vapor pressure.

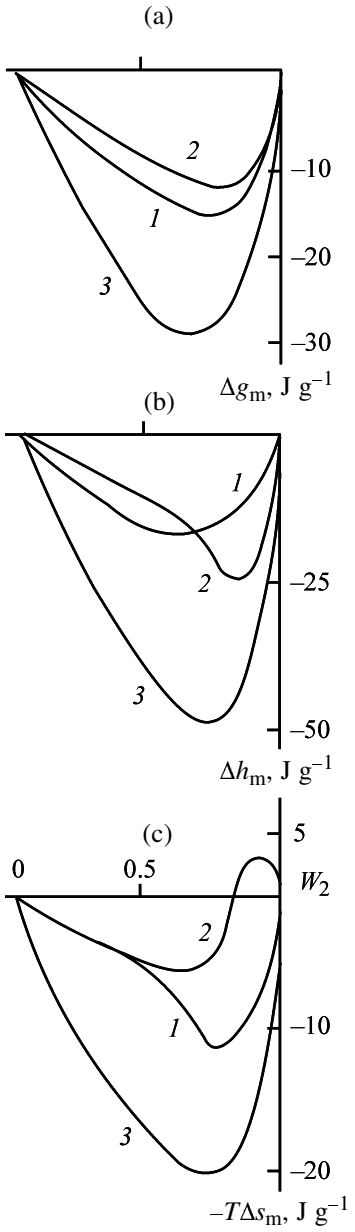
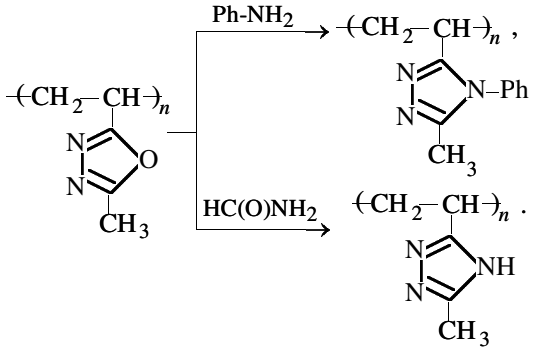


Fig. 4. Mean specific thermodynamic quantities of mixing with water at 298 K of polymer **I** prepared by (*1*) polymerization and (*2*) polymer-analogous transformation, and (*3*) of poly-1-vinyl-1,2,4-triazole [9]: (a) Gibbs energy Δg_m, (b) enthalpy Δh_m, and (c) $T\Delta s$. (W_2) Weight fraction of the polymer.

macromolecular compounds with other heterocyclic fragments. Similarly to the known transformations of heterochain polymers containing the 1,3,4-oxadiazole ring into those containing the 1,2,4-triazole ring [2], polyviyloxadiazole **I** reacts with formamide or aniline to form the corresponding poly-*C*-vinyl-1,2,4-triazoles, which are extremely difficult to prepare by polymerization:



The reaction with formamide gave poly-3-vinyl-5-methyl-1,2,4-triazole with a high conversion (up to 97%); this was confirmed by the ^{13}C NMR spectrum of the final product. The ^{13}C NMR spectrum of the starting polymer **I** consists of the following signals (ppm): 11.7 (–CH_3), 32.3–39.5 (–CH–CH_2– of polymer chain), 167.5 (C^2 of ring), and 169.5 (C^5 of ring). The chemical shifts in the spectrum of the triazole-containing polymer are somewhat different (ppm): 12.9 (–CH_3), 35.4–44.7 (–CH–CH_2– of polymer chain), 158.2 (C^3 of ring), and 172.7 (C^5 of ring). Assignment of the latter two signals to the triazole ring was based on the NMR data for model 3,5-disubstituted 1,2,4-triazoles. In contrast to the starting polyvinyloxadiazole, the triazole-containing polymer is insoluble in organic solvents but remains soluble in water. Because of weak acid properties of the 1,2,4-triazole ring, poly-3-vinyl-5-methyl-1,2,4-triazole in aqueous solutions exhibits no polyelectrolyte properties (linear concentration dependence of the reduced viscosity, Table 2), in contrast to tetrazole-containing polymeric NH acids [17].

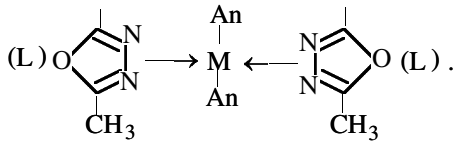
The reaction of polyvinyloxadiazole **I** with aniline in polyphosphoric acid yields poly-3-vinyl-4-phenyl-5-methyl-1,2,4-triazole with a high degree of conversion (up to 95%). The ^{13}C NMR data confirm that the final product contains the phenyl fragment (a set of signals in the range 126.1–130.8 ppm). The resulting triazole-containing polymer is soluble in DMF and DMSO but, in contrast to the starting polymer, insoluble in water.

Similarly to other known polyvinylazoles [18], polyvinyloxazole **I** forms complexes with metal ions. Complexes with Cu^{2+}, Ni^{2+}, Pd^{2+}, and Ag^+ salts are formed just when solutions of the polymer and salt are mixed at room temperature. The resulting complexes of the composition $L : MAn_n = 2 : 1$ (Table 5) are soluble neither in organic solvents nor in water and separate out from the reaction mixtures as finely dispersed precipitates. In the IR spectra of the reaction products, the absorption bands of the bending vibra-

Table 5. Complexation of poly-2-vinyl-5-methyl-1,3,4-oxadiazole with metal salts MAn_n. L : MA_n = 2 : 1 (base mole : g-equiv)

MAn_n	Solvent	Yield, %	Found, %		
			C	N	Cl
$CuCl_2$	Ethanol	80	32.6	14.5	15.9
$NiCl_2$	"	73	27.5	11.8	16.0
$AgNO_3$	H_2O	91	34.4	9.8	
$Pd(CH_3COO)_2$	DMF	55	27.4	11.4	

tions of the heteroring are shifted toward higher frequencies by approximately 10–20 cm^{-1}. In accordance with the generally accepted views on the structure of metal azole complexes, it can be suggested that the complexation with polyvinyloxadiazole is due to the donor–acceptor interaction of the ring nitrogen atoms with the metal ion:



Participation of the oxygen atom in the coordination is not confirmed.

CONCLUSION

Previously unknown carbon-chain polymers with pendant 1,3,4-oxadiazole fragments can be successfully prepared from low- and high-molecular-weight precursors. The synthesized vinyl-1,3,4-oxadiazole monomers are somewhat less active in radical polymerization than vinylazoles containing only nitrogen heteroatoms in the ring. Polyvinyl-1,3,4-oxadiazoles are nonionic, relatively heat-resistant polymers and can act as starting compounds for further chemical modification.

REFERENCES

1. *Khimicheskaya entsiklopediya* (Chemical Encyclopedia), Moscow: Bol'shaya Ross. Entsiklopediya, 1992, vol. 3, p. 673.
2. Buhler, K.-U., *Spezialplaste*, Berlin: Akademie, 1978.
3. Matsuda, K. and Morin, L., *J. Org. Chem.*, 1961, vol. 26, no. 9, pp. 3783–3787.
4. Arnold, C. and Thatcher, D., *J. Org. Chem.*, 1969, vol. 37, no. 4, pp. 1141–1143.
5. Macor, J., Ordway, T., Smith, R., et al., *J. Org. Chem.*, 1996, vol. 61, no. 10, pp. 3228–3229.
6. Kizhnyaev, V.N., Pokatilov, F.A., Kotikov, P.V., and Smirnov, A.I., *Vysokomol. Soedin., Ser. B*, 2005, vol. 47, no. 6, pp. 1054–1057.
7. Tager, A.A., Adamova, L.V., Kryakunov, A.A., et al., *Vysokomol. Soedin., Ser. B*, 1985, vol. 27, no. 8, pp. 593–596.
8. Tager, A.A., *Fizikokhimiya polimerov* (Physical Chemisatry of Polymers), Moscow: Khimiya, 1978, 3rd ed.
9. Tager, A.A., Safronov, A.P., Lopyrev, V.A., et al., *Vysokomol. Soedin., Ser. A*, 1987, vol. 29, no. 11, pp. 2421–2425.
10. Skushnikova, A.I., Domnina, E.S., and Skvortsova, G.G., *Vysokomol. Soedin., Ser. B*, 1977, vol. 19, no. 5, pp. 372–374.
11. Skushnikova, A.I., Domnina, E.S., and Skvortsova, G.G., *Vysokomol. Soedin., Ser. B*, 1985, vol. 27, no. 9, pp. 705–707.
12. Tsypina, N.A., Kizhnyaev, V.N., Pokatilov, F.A., and Smirnov, A.I., *Vysokomol. Soedin., Ser. B*, 2003, vol. 45, no. 2, pp. 358–362.
13. Kizhnyaev, V.N. and Vereshchagin, L.I., *Usp. Khim.*, 2003, vol. 72, no. 2, pp. 159–182.
14. Kizhnyaev, V.N., Ratovskii, G.V., Bazhenov, D.N., and Pokatilov, F.A., *Vysokomol. Soedin., Ser. A*, 2005, vol. 47, no. 10, pp. 802–1811.
15. Kruglova, V.A., Kizhnyaev, V.N., Ivanova, N.A., et al., *Vysokomol. Soedin., Ser. B*, 1987, vol. 29, no. 6, pp. 416–420.
16. Tsypina, N.A., Kizhnyaev, V.N., and Adamova, L.V., *Vysokomol. Soedin., Ser. A*, 2003, vol. 45, no. 10, pp. 1718–1723.
17. Kizhnyaev, V.N., Gorkovenko, O.P., Safronov, A.P., and Adamova, L.V., *Vysokomol. Soedin., Ser. A*, 1997, vol. 39, no. 3, pp. 527–532.
18. Pomogailo, A.D. and Savost'yanov, V.S., *Metallsoderzhashchie monomery i polimery na ikh osnove* (Metal-Containing Monomers and Polymers Derived from Them), Moscow: Khimiya, 1988.

ISSN 1070-4272, Russian Journal of Applied Chemistry, 2006, Vol. 79, No. 7, pp. 1174–1177. © Pleiades Publishing, Inc., 2006.
Original Russian Text © V.A. Petrov, A.I. Petrov, A.V. Kostochko, I.Kh. Garaev, 2006, published in Zhurnal Prikladnoi Khimii, 2006, Vol. 79, No. 7, pp. 1185–1189.

MACROMOLECULAR CHEMISTRY AND POLYMERIC MATERIALS

Degradation of Cellulose Nitrates in Low-Water Media

V. A. Petrov, A. I. Petrov, A. V. Kostochko, and I. Kh. Garaev

Kazan State Technological University, Kazan, Tatarstan, Russia

Received April, 13, 2006

Abstract—The kinetics of degradation of cellulose nitrates in low-water organic solvents in the presence of various catalysts was examined.

DOI: 10.1134/S1070427206070251

Low-viscosity colloxylins, a commercial brand of cellulose nitrates (CNs), which are used for production of a broad spectrum of paint and varnish materials, are in a high consumers' demand. The molecular weight of CNs (typically characterized by the viscosity of their solutions in acetone) is the limiting indicator of the duration of the stabilization phase and of the process of production of commercial low-viscosity cellulose nitrates as a whole, which is eventually responsible for the performance of the product.

In practice, to decrease the viscosity of CNs, they are subjected to degradation in an aqueous medium at a pressure of 0.5–0.7 MPa and temperature of about 140°C. Long time of the operation and high power consumption in high-temperature treatment of a CN suspension necessitate the search for alternative ways of controlling the molecular weight of CNs. This is especially urgent in preparation of low-viscosity lacquer colloxylins, when the use of batch autoclaves gives rise to certain process problems.

All these facts necessitate the search for methods to change to "milder" temperature regimes of treatment compared to those currently used, as well as to ambient-pressure reduction of viscosity so as to produce CNs with a higher quality at considerably lower costs. The relationships in hydrolysis of CNs in aqueous media were described in sufficient detail [1–3], whereas there are only limited data on degradation of CNs in low-water organic solvents [4].

In this study we examined the relationships in controlling the molecular weight of CNs by catalytic degradation in organic solvents in the presence of various catalysts.

EXPERIMENTAL

As the initial substance served CNs with the nitrogen content of 11.9–12.5% and intrinsic viscosity in acetone at 25°C $[\eta] = (1.23–3.00) \times 10^2$ cm^3 g^{-1}. Degradation was carried out in a three-necked flask equipped with a jacket for heating, a mechanical stirrer with a hydroseal, a thermometer, and a reflux condenser. The required temperature was maintained with a temperature-control device using a water thermostat. The CN : solvent ratio was 1 g : 10 cm^3. After the catalyst was introduced, samples were taken at regular intervals, precipitated into water, thoroughly washed with distilled water to neutral pH of the wash water, crushed, and dried. The change of the viscosity was estimated by determining the intrinsic viscosity of a series of acetone solutions of CNs at 25°C [5, 6].

In the initial stage, the catalytic performance of compounds of different nature (H_2O_2, NH_4OH, H_2SO_4, H_3PO_4, $HClO_4$, and HNO_3) was estimated in hydrolysis of CNs in a homogeneous medium. Table 1 presents the conditions and experimental degrees of hydrolytic degradation of cellulose nitrates.

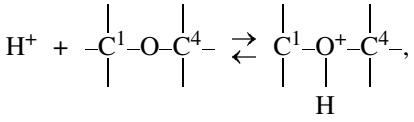
Table 1 shows that dissolution of CNs decreases the intensity of intermolecular interaction and the role of the diffusion component of the process, thereby substantially accelerating hydrolytic degradation of CNs. In a homogeneous medium, both hydrolysis of CNs (1) at the C^1–O–C^4 glycoside bond and hydrolysis of the –C–O–NO_2 moieties (2) (denitration of CNs) are accelerated. This is consistent with the conventional views on faster hydrolysis of cellulose and its derivatives in homogeneous media:

$$HA \rightleftarrows H^+ + A^-,$$

Table 1. Catalytic degradation of CNs in solution. Weighed portion of CNs 5 g

Reaction medium (solvent), ml	Catalyst, % of the CN weight	T, °C	Hydrolysis time, h	Nitrogen content, %	Time of outflow of 2% CN solution through viscometer capillary, s
		Colloxylin VV			
–	–	–	–	–	48.0
Ethyl acetate, 30	$HClO_4$, (55%),* 1	70	1	–	6.2
	$HClO_4$ 1	60	1	–	8.1
		Colloxylin NKh			
–	–	–	–	11.66	81.9
Ethyl acetate, 30	$HClO_4$, 1	70	2	–	7.1
	H_2SO_4, 1	70	2	–	49.2
	H_3PO_4 (65%), 1	70	2	–	30.0
	HNO_3 (70%), 1	70	1	9.34	37.7
	H_2O_2 (33%), 1	70	7	10.93	41.4
	H_2O_2, 5	70	7	10.04	30.8
	H_2O_2, 10	70	7	9.48	18.8
	NH_4OH (24%), 10	70	4	6.14	32.7

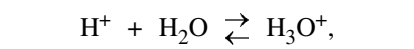
* Aqueous solution.



(1)



(2)



(3)



(4)



(5)

The nature of the catalyst strongly affects the degree of degradation and the rates of the constituent reactions. Hydrogen peroxide is the least active in the series of the substances examined; however, it significantly decreases the contribution of CN saponification. The catalytic activity of acids decreases in the series mentioned and qualitatively correlates with their dissociation constants, pK_a [$HClO_4$ ~–8.00, HNO_3 ~–1.64, H_3PO_4 (1) ~2.12]. The hydrolytic degradation of CNs is substantially accelerated with increasing content of the catalyst in the system. For example, an increase in the content of perchloric acid from 1 to 2% of the weight of CNs causes the viscosity to decrease almost by half, all other factors being the same. Rising the reaction temperature also promotes the hydrolysis. For example, rising the temperature from 60 to 70°C decreases the viscosity of CNs by a factor of 1.5–2.0, and that from 50 to 60°C, by a factor of almost 8.

As known [3], cleavage of the glycoside bond at C^1 under excess of water is described by a first-order equation; in the initial stages of the process, when the degrees of polymerization are high,

$$1/p_t - 1/p_0 \approx k_1 t, \quad (6)$$

holds, where p_0 is the number-average degree of polymerization of the initial sample; p_t, degree of polymerization after the hydrolysis time t; and k_1, rate constant of the reaction.

Taking into account the known constants $k = 5 \times 10^{-1}$ cm^3 g^{-1} and $\alpha = 1.0$ in the Mark–Houwink equation $[\eta] = kp^{\alpha}$ for the CN solutions in acetone [3], the relationship (1) can be represented as

$$1/[\eta] - 1/[\eta_0] \approx k_{app} t, \quad (7)$$

where k_{app} is the apparent constant taking into account k_1 and the degree of polydispersity of the CN sample.

Table 2 presents the conditions and experimental data for the hydrolytic degradation of CNs dissolved in ethyl acetate and, for comparison, the data on hydrolysis of CNs in an aqueous medium.

Data in Table 2 were used for calculating the $1/[\eta] - 1/[\eta_0]$ parameters and plotting their depen-

Table 2. Conditions and results of the hydrolytic degradation of CNs in various media at 70°C

Run no	Medium	H_2O content, M	Catalyst, M	Intrinsic viscosity of CNs $[\eta] \times 10^{-2}$, $cm^3\ g^{-1}$, at indicated hydrolysis time, h				$K_{app} \times 10$, $g\ cm^{-3}\ h^{-1}$
				1.0	2.0	3.0	4.0	
1	H_2O	55.580	$HClO_4$, 0.005	1.19	1.11	–	1.05	0.35
2	Ethyl acetate	–	CH_3COOH, 0.017	0.90	0.77	0.68	0.61	2.06
3		1.110	$HClO_4$, 0.005	0.86	0.72	0.67	0.54	2.60
4		0.025	$HClO_4$, 0.005	0.56	0.32	0.27	0.19	11.12

Table 3. Conditions and results of the hydrolytic degradation of CNs in a nondissolving medium at 40°C

Medium	H_2O content, M	Catalyst, M	Intrinsic viscosity of CNs $[\eta] \times 10^{-2}$, $cm^3\ g^{-1}$, at indicated hydrolysis time, h				$K_{app} \times 10$, $g\ cm^{-3}\ h^{-1}$
			1.0	2.0	3.0	4.0	
Benzene	0.025	$HClO_4$, 0.005	0.61	0.39	0.33	0.27	7.23
Toluene	0.025	$HClO_4$, 0.005	0.71	0.56	0.49	0.40	4.22
	0.033	HNO_3, 0.006	1.05	0.75	0.64	0.51	2.87
	0.041	HCl, 0.007	0.62	0.53	0.46	0.41	4.07

dences on the hydrolysis time. Figure 1a shows that, irrespective of the reaction conditions, the experimental data are adequately described by relationship (7).

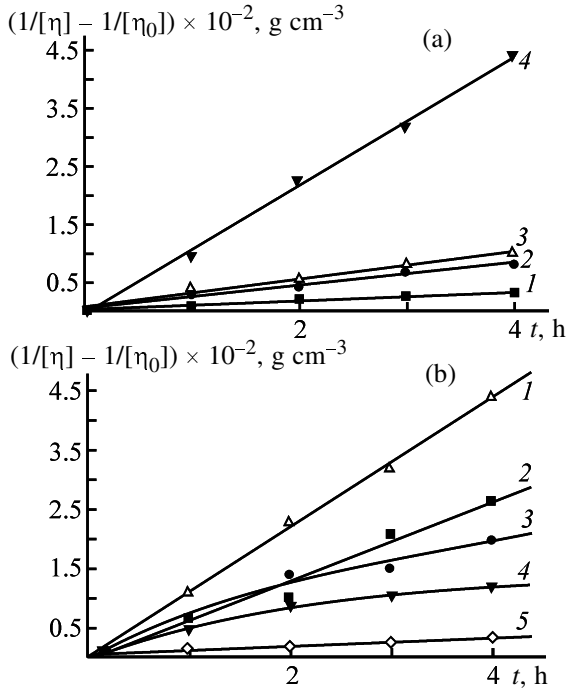


Fig. 1. Variation of $1/[\eta] - 1/[\eta_0]$ with the hydrolysis time t in various media (a) Figures at straight lines correspond to run nos. in Table 2; (b) (*1*) ethyl acetate, (*2*) toluene, (*3*) benzene, (*4*) methylene chloride, and (*5*) water.

Catalytic degradation is the most intense in ethyl acetate in the presence of $HClO_4$ as the catalyst, and in an aqueous medium the viscosity decreases most slowly. This agrees well with the published data on acceleration of saponification and hydrolysis in the presence of substances that cause swelling and dissolution of CNs [6, 7]. It should be noted that the reaction is accelerated with decreasing water content in the system. This is most likely due to increased role of the competing reaction of the acid with water, yielding hydroxonium cation (3), and the ensuing decrease in the concentration of the intermediate oxonium ion [reaction (1)].

It is also seen that the nature of the acid strongly affects the hydrolysis rate. For example, acetic acid with a lower catalytic power causes the viscosity of CNs to decrease in hydrolytic degradation to a lesser extent than does perchloric acid.

Table 3 presents the kinetic data on hydrolysis of CNs under heterogeneous conditions in nondissolving media.

Despite the heterogeneity of the process and fairly mild reaction conditions, in all the experiments the viscosity of CNs significantly decreases with increasing hydrolysis time, most rapidly in benzene. Thus, hydrochloric acid is close to perchloric acid in the catalytic power, and nitric acid has the lowest catalytic power.

Table 4. Conditions and selected results of hydrolysis of VNV colloxylin in various media at 70°C*

Medium	H_2O content, M	Intrinsic viscosity of CNs $[\eta] \times 10^{-2}$, $cm^3\ g^{-1}$, at indicated hydrolysis time, h				
		0.0	1.0	2.0	3.5	5.0
H_2O	55.578	3.00	2.77	2.33	2.23	1.97
Methanol**	–	3.00	1.91	1.71	1.56	1.36
Ethanol	2.244	3.00	1.87	1.70	1.70	1.44
Isopropanol	–	3.00	2.13	1.92	1.79	1.54
Butanol	0.028	3.00	2.76	2.00	2.00	1.66

* Content of the catalyst $HClO_4$ in the system 0.006 M (1 wt % of CNs).
** Hydrolysis was carried out at 60°C.

It should be noted that, in a homogeneous process, the kinetic plots are linear (in our case, this concerns the hydrolysis in ethyl acetate, i.e., the relationships in the reaction correspond to those in first-order reactions). In the case of heterogeneous hydrolysis, linear sections are observed in the initial stage only (1–2 h). At longer hydrolysis, the linearity is violated, due probably to enhanced role of the diffusion processes.

Our data show that, despite milder temperature conditions of hydrolysis in a heterogeneous medium, the reaction rate remains fairly high. As a result, the viscosity can be reduced to the level corresponding to that of the NV brand of lacquer CNs, $[\eta] = 0.66 \times 10^2\ cm^3\ g^{-1}$.

Table 4 shows how the intrinsic viscosity of the sample of preliminarily stabilized commercial CNs of VNV brand decreases upon hydrolysis in various alcohols and, for comparison, in water.

We found that, in all the experiments, the viscosity tends to decrease with increasing hydrolysis time.

The hydrolysis is the most intensive in methanol, and the least intensive, in an aqueous medium; it is naturally decelerated with increasing molecular weight of the alcohol. In the case of methanol and ethanol, the viscosity sharply decreases in the first 2 h, and in the case of isopropanol and butanol, it uniformly decreases throughout the hydrolysis time.

It is seen that, at the hydrolysis time of 5 h, the rates of hydrolysis of CNs in different alcohols become close, but the viscosities are lower than those of commercial samples of lacquer CNs. Minor changes in the rate of the catalytic degradation in alcohols compared to an aqueous medium are probably due to enhancement of the role of the competing reaction of the acid with the alcohol, yielding alkoxonium cation (5), and to the ensuing decreases in the concentration of the intermediate oxonium ion [reaction (1)] and in the rate of the main reaction of cleavage of the 1,4-β-glycoside bond.

CONCLUSIONS

(1) The catalytic degradation of cellulose nitrates in low-water organic solvents, catalyzed by $HClO_4$, goes at a high rate both in homogeneous (dissolving) and heterogeneous (nondissolving) media, and it is governed by the balance of the acid-base interaction of all the components of the system.

(2) The inhibiting action of water and alcohols can be due to the competing reactions yielding hydroxonium and alkoxonium cations, respectively.

(3) These relationships are used in the development of a power-saving process for production of paint and varnish materials based on low-viscosity cellulose nitrates.

REFERENCES

1. Mal'chevskiI, V.A. and Lur'e, B.A., *Vysokomol. Soedin.*, 2000, vol. 42, no. 7, pp. 1183–1191.
2. Lur'e, B.A., Namestnikov, V.V., Makhotkin, A.F., et al., *Vysokomol. Soedin., Ser. A*, 1991, vol. 33, no. 8, pp. 1683–1690.
3. *Cellulose and Cellulose Derivatives*, Bikales, N.M. and Segal, L., Eds., New York: Wiley–Interscience, 1971, part IV.
4. JPN Patent 54-83 528.
5. Toroptseva, A.N., *Laboratornyi praktikum po khimii i tekhnologii vysokomolekulyarnykh soedinenii* (Laboratory Practical Guide on Chemistry and Technology of Macromolecular Compounds), Leningrad: Khimiya, 1972.
6. Galitskaya, I.M., Dubina, V.P., and Shidyakov, S.I., *Metody polucheniya, analiza i ispytanii nitratov tsellyulozy* (Methods of Preparation, Analysis, and Testing of Cellulose Nitrates), Moscow: Khimiya, 1990.
7. Rogovin, Z.A., *Khimiya tsellyulozy* (Chemistry of Cellulose), Moscow: Khimiya, 1972.

ISSN 1070-4272, Russian Journal of Applied Chemistry, 2006, Vol. 79, No. 7, pp. 1178–1180. © Pleiades Publishing, Inc., 2006.
Original Russian Text © I.P. Dobrovol'skaya, M.K. Mokeev, Yu.N. Sazanov, A.V. Gribanov, T.E. Sukhanova, 2006, published in Zhurnal Prikladnoi Khimii, 2006, Vol. 79, No. 7, pp. 1190–1192.

MACROMOLECULAR CHEMISTRY AND POLYMERIC MATERIALS

Changes in the Supramolecular Structure of Heat-Resistant Polyimide Fibers in the Course of Thermal Treatment

I. P. Dobrovol'skaya, M. K. Mokeev, Yu. N. Sazanov, A. V. Gribanov, and T. E. Sukhanova

Institute of Macromolecular Compounds, Russian Academy of Sciences, St. Petersburg, Russia

Received April 4, 2006

Abstract—Changes in the supramolecular structure of heat-resistant fibers based on polyimide PM were studied by X-ray diffraction analysis and NMR spectroscopy.

DOI: 10.1134/S1070427206070263

It is well known that carbon fibers can be prepared from various macromolecular compounds whose properties determine the conditions of the preparation of these polymeric fibers and their subsequent carbonization. As seen from published data, heat-resistant fibers based on polyimides are widely used for this purpose, which is due to the absence of toxic gaseous carbonization products, thermal stability and high coke residue, and possibility of low-temperature carbonization without cracking and pore formation [1]. It should be noted that the majority of studies dealing with the behavior of polyimides under heat treatment with the aim to prepare carbon fibers predominantly concerned the role of the chemical structure of polyimides [2–4]. The studies of carbonization of polyamides [5] revealed the effect of the unit structure and macromolecule flexibility on the course of the polyimide pyrolysis. It was found that the three-dimensional cross-linked structure of polyimide affects the fiber carbonization and that polyimide and its derivatives can be used to initiate carbonization of the entire class of polyheteroarylenes (especially nitrogen-containing analogs).

Although pyrolysis and carbonization of polyheteroarylenes and, in particular, polyimides was concerned in numerous papers, there are virtually no data on changes in the supramolecular structure of these oriented polymers in the course of pyrolysis and on how these changes affect the formation of the turbostratic structure of carbon.

In this study we examined changes in the supramolecular structure of the fibers in the course of thermal treatment using one of the most stable aromatic polyimides, PI PM, prepared from pyromellitic dianhydride and diaminodiphenyl oxide.

EXPERIMENTAL

The arimide fibers were prepared from solutions of PM polyamido acid (PAA) in a coagulating bath: 20–25% DMA, 45% water, and 30–35% sodium thiocyanate.

The X-ray diffraction (XRD) patterns were recorded on DRON-1.5 and KRM-1 devices (Kratky collimation, CuK_α radiation). The high-resolution solid-state (HRSS) ^{13}C NMR spectra at room temperature were recorded on a CXP-100 (Bruker) spectrometer using the procedures of magic angle spinning (MAS) and cross-polarization (CP).

Changes in the polyimide structure at its thermal treatment were studied using a combination of the large- and small-angle XRD and HRSS ^{13}C NMR spectroscopy. The pyrolysis and carbonization of the fibers were carried out in a laboratory unit in a nitrogen flow (under the condition of unhindered shrinkage) at a heating rate of 20 deg min^{-1} (dynamic heating mode).

The XRD patterns (equatorial and meridional scattering) of the initial samples and those treated in the dynamic mode at 500–800°C are shown in Fig. 1. As seen, the XRD patterns of the fibers pyrolyzed at 500–575°C are virtually identical. Certain changes in the XRD patterns (namely, strong decrease in the peak intensity at $2\theta = 5.5°$ and disappearance of higher-order reflections) are observed in the samples pyro-

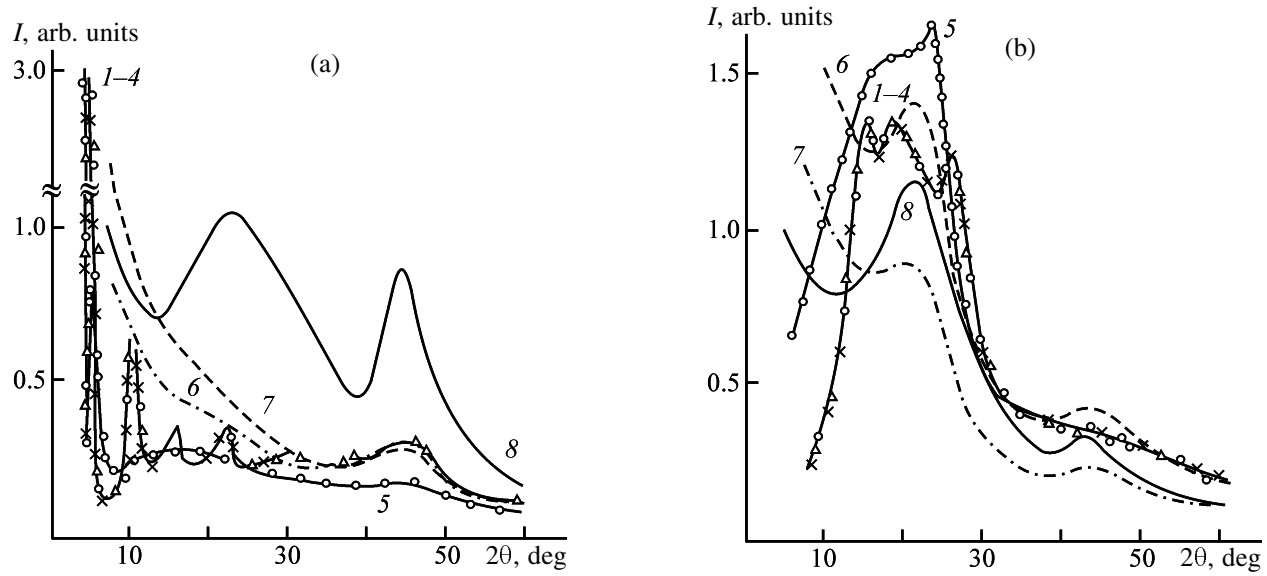


Fig. 1. Large-angle XRD patterns of the (*1*) initial polyimide fiber and fibers pyrolyzed at (*2*) 500, (*3*) 550, (*4*) 575, (*5*) 600, (*6*) 700, (*7*) 800, and (*8*) 900°C. (*I*) Intensity and (2θ) Bragg angle; the same for Fig. 2. (a) Meridional and (b) equatorial scattering.

lyzed at 600°C. However, the peak typical for the PI PM structure is retained up to 600°C, which suggests extremely high heat resistance of the PI PM crystallites. The HRSS ^{13}C NMR spectra showed that the typical peaks corresponding to the polymer chain only slightly change up to 600°C, which indicates that the polymer chain structure is preserved. Appearance of the carbon reflection (002) in the XRD patterns of the fibers pyrolyzed at 600°C suggests formation of turbostratic carbon (Fig. 1). With increasing temperature to 700–800°C, the reflections of the initial polyimide disappear and the intensity of reflections (002) and (110) belonging to carbon increases, which confirms intense carbonization of the fiber. In the NMR spectra, the half-width of the peak at 125 ppm corresponding to the polyaromatic structure increases.

Carbonization of the PI PM fibers at 900°C (Fig. 1, curve *8*) increases the reflections (110) and (002) belonging to carbon, which suggests formation of stacks of turbostratic carbon. The differences in the meridional and equatorial scattering, in particular, higher intensity of reflection (002) at equatorial scattering and its smaller intensity at meridional scattering, indicate that planes (002) are arranged in parallel to the fiber axes.

The small-angle XRD patterns (Fig. 2) showed that in the course of pyrolysis the density heterogeneity of the PI PM structure remains almost constant up to 550°C. This is confirmed by similar intensities of the reflections recorded at both equatorial and meridional scattering. On pyrolysis of the fibers at 575°C, the intensity of small-angle reflections increases. Exactly at this temperature the reflection (002) appears in the large-angle patterns (Fig. 1), indicating formation of turbostratic carbon. Further pyrolysis and carbonization at 700–800°C increases the heterogeneity of the carbon structure; as a result, the intensity of the small-angle scattering also increases. This structure contains the areas of turbostratic carbon, less ordered areas of amorphous carbon, and significant number of pores and cracks of various size and shape.

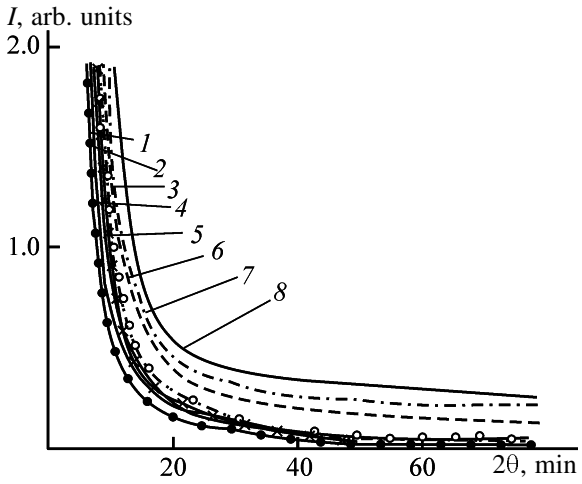


Fig. 2. Small-angle XRD patterns of the (*1*) initial polyimide fiber and fibers pyrolyzed at (*2*) 500, (*3*) 550, (*4*) 575, (*5*) 600, (*6*) 700, (*7*) 800, and (*8*) 900°C; meridional scattering.

Formation of the stacks of turbostratic carbons begins at 490–500°C in the less ordered regions of the polymer, where the pyrolysis proceeds at a higher rate. Degradation of polyimide crystallites occurs at temperatures significantly higher than 575°C, which would affect the kinetics of chemical degradation of the polymers and cause a local decrease in the coke residue. The deficit of carbon atoms should lead to the formation of a less ordered amorphous structure and appearance of pores.

This conclusion is confirmed by the fact that the carbon fibers formed from polyimide PM at 900°C exhibit low strength (σ = 560 MPa) and low elastic modulus (E = 34 GPa).

CONCLUSIONS

(1) Thermal degradation of polyimide PM and formation of the turbostratic carbon structure occur virtually simultaneously.

(2) The crystalline structure of the polyimide PM fibers exhibits high thermal stability, and its elements are retained up to 600°C.

(3) Low strength and elastic characteristics of carbon fibers prepared by carbonization of polyimide PM fibers at 900°C are associated with the high thermal stability of the crystallites.

REFERNCES

1. Gribanov, A.V., Sazanov, Yu.N., Beloborodova, E.V., and Fedorova, G.N., *Zh. Prikl. Khim.*, 1999, vol. 72, no. 3, pp. 467–473.
2. Bessonov, M.I., Koton, M.M., Kudryavtsev, V.V., and Laius, L.A., *Poliimidy – klass termostoikikh polimerov* (Polyimides: A Class of Heat-Resistant Polymers), Leningrad: Khimiya, 1983.
3. Gribanov, A.V. and Sazanov, *Zh. Prikl. Khim.*, 1997, vol. 70, no. 6, pp. 881–902.
4. Sazanov, *Zh. Prikl. Khim.*, 2001, vol. 74, no. 8, pp. 1217–1234.
5. Gribanov, A.V., Carbonization of Polyheteroarylenes. Structure of Intermediates and Final Products, *Doctoral Dissertation*, St. Petersburg, 2001.

ISSN 1070-4272, Russian Journal of Applied Chemistry, 2006, Vol. 79, No. 7, pp. 1181–1185. © Pleiades Publishing, Inc., 2006.
Original Russian Text © E.A. Sergeeva, T.P. Safiullina, O.P. Shmakova, I.N. Bakirova, L.A. Zenitova, 2006, published in Zhurnal Prikladnoi Khimii, 2006, Vol. 79, No. 7, pp. 1193–1197.

MACROMOLECULAR CHEMISTRY AND POLYMERIC MATERIALS

Structure of Castable Polyurethanes Filled with Aluminum Oxide

E. A. Sergeeva, T. P. Safiullina, O. P. Shmakova, I. N. Bakirova, and L. A. Zenitova

Kazan State Technological University, Kazan, Tatarstan, Russia
Nizhnekamsk Chemical Engineering Institute, Nizhnekamsk, Tatarstan, Russia

Received March 24, 2006

Abstract—The structure and properties of castable polyurethanes with different content of the aluminum oxide filler were studied by X-ray diffraction, electron microscopy, and determination of the apparent cross-link density.

DOI: 10.1134/S1070427206070275

Previously [1] we developed SKU-OM castable polyurethanes (PUs) with high content of aluminum oxide (AO), filler which is a waste from petrochemical industry. The relative elongation and elasticity of PUs do not decrease, and their elastic modulus and especially hardness increase after introduction of AO, unlike the use of conventional fillers. The increase in the hardness with preservation of the strength suggests that AO is a reinforcing filler for PUs.

To determine the mechanism of this influence of AO filler on PUs, we studied the structure of PUs filled with AO by X-ray diffraction and electron microscopy and determined the apparent cross-link density of PUs in a wide temperature range.

EXPERIMNETAL

We studied monolithic SKU-OM castable PUs prepared from oligoethylene glycol adipate (OEA) with $M \sim 2 \times 10^3$ and a mixture of 2,4- and 2,6-toluene diisocyanate (TDI) taken in an 80 : 20 molar ratio (OEA : TDI molar ratio 1.0 : 1.6) [2]. Active AO with the particle size of 5–20 μm (substandard desiccant) was used as the filler.

X-ray diffraction analysis of PUs was performed on a DRON-2.0 automated diffractometer (CuK_α radiation with λ = 1.54178 Å) in the Bragg–Brentano symmetrical recording mode [3].

The morphology of the initial and filled PUs was studied by high-resolution transmission electron microscopy using self-shadow-cast replicas. To determine the structural relief, the samples were etched in a high-frequency electrodeless discharge plasma [4, 5].

The apparent cross-link density was determined by the Clough–Gladding procedure on an axial compression relaxometer [6]. 5 × 6-mm cylindrical samples were tested in the range 25–170°C. The apparent cross-link density ν_a/V (mol m^{-3}) was calculated by the equation

$$\nu_a/V = A/RTS,$$

where A is the slope of the linear portion of the F vs. $(h/h_0)^2 - (h_0/h)^2$ dependence; F is the loading (N); h_0 is the initial sample height (m); h is the equilibrium height of the deformed sample after a 15-s exposure (m); R is the universal gas constant (8.314 J mol^{-1} K^{-1}); T is the temperature (K); and S is the initial cross-section area of the sample (m^2).

The X-ray pattern of PU is typical for an amorphous polymer (Fig. 1, curve *1*).

The interplanar spacing of the amorphous sample (4.371 Å) is not a characteristic value but lies in the range typical for amorphous rubbers [7]. In addition, as we showed previously [2], PUs prepared at NCO : OH ≥ 1.6 do not crystallize.

As determined by X-ray analysis, two AO samples differ not only in the water content but also in the crystal structure (Fig. 2). This unexpected result is caused by preparation of these desiccants and is

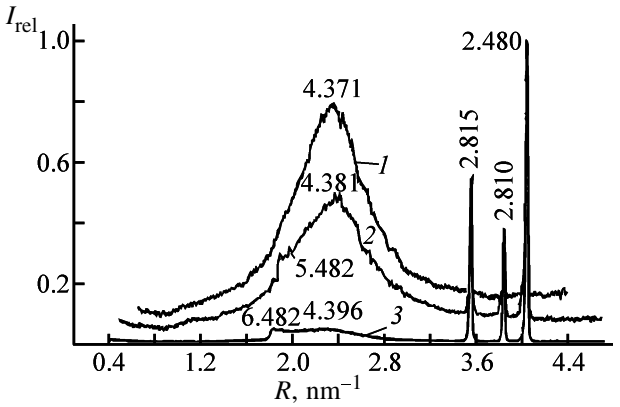


Fig. 1. X-ray pattern of PU containing (*1*) 0, (*2*) 5, (*3*) 50 wt % AO. (I_{rel}) relative intensity I/I_0 and (R) reciprocal interplanar spacing; the same for Fig. 2.

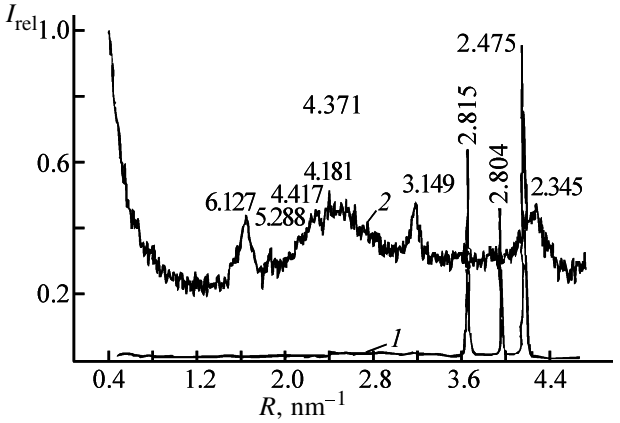


Fig. 2. X-ray pattern of AO containing (*1*) 1 and (*2*) 14 wt % water.

studied in detail in [8]. It is known that active aluminum oxide widely used as a sorbent in many processes of organic synthesis and oil refining is prepared from aluminum hydroxide having the undeveloped surface. Aluminum oxide with the required pore diameter is prepared by hydrothermal or thermal treatment.

The first step of hydrothermal treatment involves rehydration of active AO to form metahydroxide with the pseudoboehmite structure. Then the methahydroxide is converted into boehmite (Fig. 2, curve *2*) with coarse pores. After calcination at 550°C for 2 h, boehmite is converted into AO with the same pore structure (Fig. 2, curve *1*). The pore diameter of this product is 150–170 Å [9].

The reflections corresponding to interplanar spacings of 6.127, 3.149, and 2.345 Å (Fig. 2, curve *2*) are assigned to boehmite (γ-AlOOH) [7]. The other reflections are due to the presence of residual hydroxides.

The X-ray pattern of boehmite sharply ascends at small angles (Fig. 2, curve *2*). Since the X-ray pattern was recorded in the wide-angle range, the small-angle range was recorded incompletely. However, this shape of the X-ray pattern suggests that a second amorphous (disordered) phase with different density is present in the system [10]. In our case, this can be only due to the porous structure with a random pore arrangement. In the subsequent experiments, we used as a filler AO containing 1 wt % water.

No chemical reactions were observed after introduction of the filler into PU. The phase compositions of the polymer and filler also do not change, and the system is described by the additivity rule [3]. The X-ray pattern of the filled sample is a superposition of those of amorphous PU and crystalline AO. The fraction of the amorphous phase regularly decreases and that of the crystalline phase increases with increasing the filler content. However, an additional reflection with d 5.482 Å appears in the pattern of the PU phase (Fig. 1, curve *2*) after introduction of the filler. This suggests appearance of new phases.

These data agree well with the morphology of these samples studied by electron microscopy. The appearance of an additional reflection in the X-ray pattern is most likely due to formation of a dense physical network by the porous filler in the polymer matrix.

As seen from the electron micrograph (Fig. 3a), the globular structures are uniformly distributed in the initial PU. Rhombic-parallelepiped structures combined in chains are formed after introduction of the filler (Fig. 3b). Probably, these structures are AO particles coated with the adsorbed polymer. Apparently, in the course of PU synthesis, OEA molecules are adsorbed as a monolayer on the surface of AO particles, thus becoming more accessible for the reaction with TDI. This uniform distribution of the polyester and the filler favors formation of a regular polymer structure, which, in turn, affects the physicomechanical properties of PU (see table).

At an AO concentration of 30 wt % and more, the chain structures form a continuous phase in the area of the solid phase of the polymer (Fig. 3c). At a 50% filler content (Fig. 3d), a uniform network structure is formed. The composite consists of filler particles reinforcing the PU matrix. A polymer layer is adsorbed on the highly developed surface of these particles. This type of the three-dimensional network of a polymer is typical for composites with reinforcing fillers. The chain structures of the filler bind separate aggregates of rigid PU blocks and fill the whole volume. In addition, areas with globular structure of PU uniformly distributed between the chain structures formed by the filler are observed in the

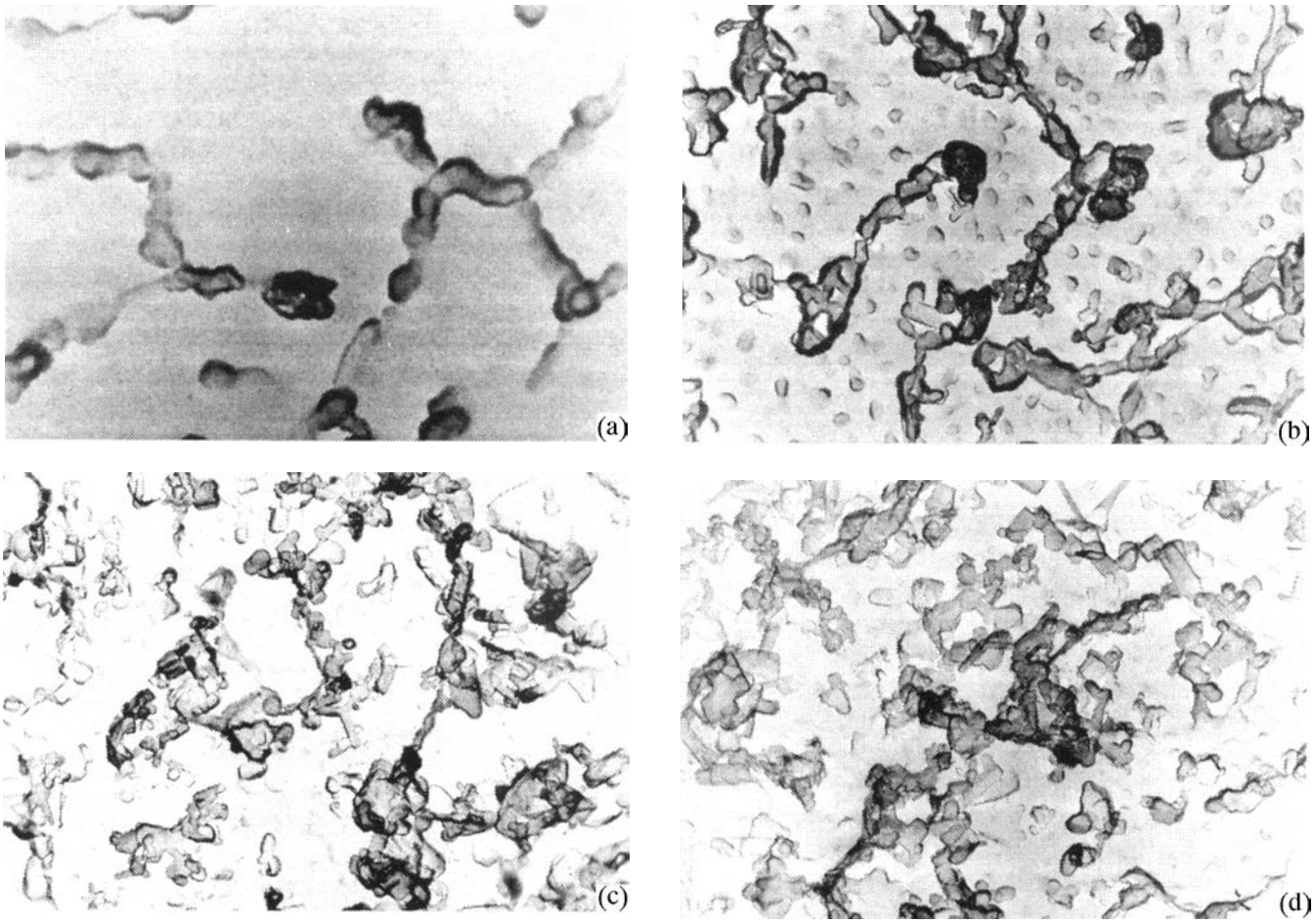


Fig. 3. Electron micrographs of (a) unfilled PU 10 and PU containing (b) 10, (c) 30, and (d) 50% AO. Magnification: (a) 14000 and (b–d) 10000.

electron micrographs. This structural arrangement enhances the physicomechanical properties of PU.

Hence, two reflections (d = 4.4 and 5.5 Å) in the X-ray patterns are assigned to the areas with globular PU structure observed in the micrographs. These structures are randomly distributed between the chain structures formed by the active filler.

A study of the apparent cross-link density of filled

Physicomechanical properties of PUs with different AO content

Property	AO content, wt %									
	0	1	3	5	7	10	20	30	40	50
Nominal stress, MPa at elongation, %:										
100	2.3	2.1	2.4	2.6	2.4	2.3	2.7	2.7	3.7	2.9
300	5.2	4.6	5.5	6.1	4.9	5.9	6.0	5.9	7.8	7.8
Nominal tensile strength, MPa	210.4	22.6	28.0	26.7	27.7	19.6	18.8	21.3	20.2	19.5
Relative elongation, %	360	410	400	430	390	400	360	390	370	360
Relative elongation set, %	0	0	0	0	0	0	0	2	2	4
Rebound elasticity, %	50	48	47	48	46	47	46	47	46	46
TIR-1 hardness, arb. units	60	60	60	63	63	62	63	64	69	71
Abradability, $pm^3\ J^{-1}$	9.3	8.9	8.6	7.5	6.8	6.3	5.4	5.0	3.8	3.2

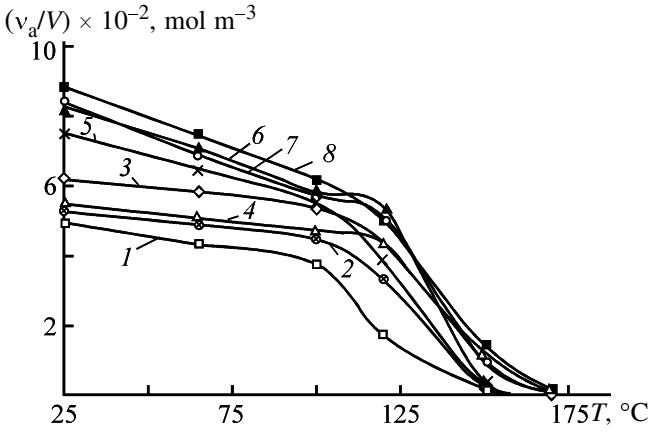


Fig. 4. Apparent cross-link density ν_a/V of PU containing (*1*) 0, (*2*) 3, (*3*) 5, (*4*) 10, (*5*) 20, (*6*) 30, (*7*) 40, and (*8*) 50 wt % AO as a function of temperature T.

PUs revealed the presence of a physical network produced by AO (Fig. 4.). Three temperature ranges 25–100, 100–150, and >150°C can be distinguished in these dependences. We suggest that the physical polymeric network degrades in the first temperature range. The second range is characterized by rupture of relatively weak chemical bonds. Heat-resistant bonds are ruptured on heating above 150°C.

The decrease in the cross-link density of the unfilled polymer in the first range is due to rupture of physical bonds. The decrease in the density in the second temperature range can be assigned to degradation of allophanic groups. In the third range, the urethane groups start do degrade. The isocyanurate units remain unchanged [11].

The shape of the temperature dependence of the cross-link density of PUs filled with AO is determined by the filler content. Generally, the higher the filler content, the higher is ν_a/V at a definite temperature (Fig. 4). The run of the initial portion of the curve becomes steeper with increasing filler content. In the range from 100–110 to 140–150°C, the curves sharply drop and flatten out above 150°C. The cross-link density in all cases is as low as 10–20 mol m^{-3}.

The features of the temperature dependence of the apparent cross-link density are caused by the presence of an additional physical network in the polymers filled with AO. The higher the filler content, the higher ν_a/V. The physical network formed by the filler degrades in the second temperature range. Since the contribution of the physical interactions to the total apparent cross-link density increases with increasing filler content, the descent of the temperature dependence of ν_a/V becomes steeper.

It should be noted that the temperature dependence of the apparent cross-link density of the composites containing more than 30 wt % filler flatten out in the range 100–120°C. As shown by electron microscopy and X-ray diffraction (Fig. 4, curves *6*–*8*), this is due to formation of a continuous phase of the filler in the polymeric matrix, which is stable under the experimental conditions.

However, at 140–150°C, all physical and weak chemical (allophanate and partially urethane) bonds are cleaved and the ν_a/V value reflects the presence of sufficiently heat-resistant triisocyanurate units in PU [11].

The high apparent cross-link density (870 mol m^{-3}) of the examined PU composites is due to a large number of physical interactions of AO. At the same time, PUs filled with AO remain highly elastic, whereas their hardness increases (see table).

CONCLUSION

The structural study of the filled polyurethanes showed that the presence of aluminum oxides with highly developed sorption surface in the system results in redistribution of intra- and intermolecular interactions, which favors formation of additional physical network in the polymer, preservation of high mechanical properties, and an increase in the elastic modulus and hardness.

REFERENCES

1. Safiullina, T.P., Sergeeva, E.A., Sopin, V.F., and Zenitova, L.A., Abstracts of Papers, *4-ya Respublikanskaya konferentsiya "Aktual'nye ekologicheskie problemy respubliki Tatarstan"* (4-th Republican Research Conf. "Urgent Environmental Problems of Tatarstan Republic"), Kazan, October 20–24, 2000, p. 146.
2. Bakirova, I.N., Zenitova, L.A., and Kirpichnikov, P.A., *Kauchuk Rezina*, 1985, no. 7, pp. 22–25.
3. Lipatov, Yu.S., Shilov, V.V., Gomza, Yu.P., et al., *Rentgenograficheskie metody izucheniya polimernykh sistem* (X-ray Diffraction Methods for Studying Polymeric Systems), Kiev: Naukova Dumka, 1982.
4. Luk'yanovich, V.M., *Elektronnaya mikroskopiya v fiziko-khimicheskikh issledovaniyakh* (Electron Microscopy in Physicochemical Studies), Moscow: Akad. Nauk SSSR, 1960.
5. Lipatov, Yu.S., Rosovitskii, V.F., and Babich, V.F., in *Novye metody issledovaniya polimerov* (New Methods for Studying Polymers), Kiev: Naukova Dumka, 1975, p. 106.
6. Kimel'blat, V.I., Study of the Properties of Poly-

urethane Composites Containing Polyethers and Polyesters, *Cand. Sci. Dissertation*, Kazan, 1973.

7. Kitaigorodskii, A.P., *Rentgenostrukturnyi analiz kristallicheskikh i amorphnykh tel* (X-ray Structural Analysis of Crystalline and Amorphous Solids), Moscow: Nauka, 1952.
8. Lamberov, A.A., Romanova, R.G., and Shustov, V.A., *Zavod. Lab.: Diagnost. Mater.*, 2000, vol. 66, no. 3, pp. 3–6.
9. Lamberov, A.A., Romanova, R.G., Gubaidullin, I.Kh., and Shustov, I.G., *Zh. Prikl. Khim.*, 2000, vol. 73, no. 11, pp. 1850–1855.
10. Gubaidullin, A.T., Disperse and Phase Structure of Segmented Polyether–Urethanes, Determined by Small-Angle X-ray Scattering), *Cand. Sci. Dissertation*, Kazan, 1993.
11. Bakirova, I.N., Sidorovich, E.A., Kirpichnikov, P.A., and Zenitova, L.A., *Kauchuk Rezina*, 1987, no. 11, pp. 23–27.

ISSN 1070-4272, Russian Journal of Applied Chemistry, 2006, Vol. 79, No. 7, pp. 1186–1190. © Pleiades Publishing, Inc., 2006.
Original Russian Text © V.A. Rozentsvet, V.G. Kozlov, A.S. Khachaturov, 2006, published in Zhurnal Prikladnoi Khimii, 2006, Vol. 79, No. 7, pp. 1198–1201.

MACROMOLECULAR CHEMISTRY AND POLYMERIC MATERIALS

Control of the Molecular Characteristics of Cationic Oligopiperylene Using Isomeric Methylbutenes

V. A. Rozentsvet, V. G. Kozlov, and A. S. Khachaturov

Institute of Ecology of Volga Basin, Russian Academy of Sciences, Togliatti, Samara oblast, Russia

Received January 24, 2006

Abstract—Additions of 2-methyl-1-butene or 2-methyl-2-butene to a monomer mixture with piperylene were tested as means for controlling the molecular parameters of cationic oligopiperylene prepared with the $TiCl_4$–H_2O catalytic system.

DOI: 10.1134/S1070427206070287

The process for commercial production of SKOP rubber (synthetic oligopiperylene rubber) is based on the cationic oligomerization of piperylene (1,3-pentadiene) in the presence of the $TiCl_4$–H_2O catalytic system [1]. It was found previously that the resulting cationic oligopiperylene can have either mono- or bimodal molecular-weight distribution depending on the oligomerization conditions [2, 3]. In the course of the oligomerization, the high-molecular-weight fraction of bimodal oligopiperylene can be cross-linked to form an insoluble gel fraction, which substantially impairs the consumer properties of the finished product [3, 4].

It is known that addition of certain olefins to the reaction mixture of cationic polymerization of dienes allows efficient control of the molecular weight of the resulting polymer [5].

In this study we examined how additions of isomeric methylbutenes (2-methyl-1-butene, 2M1B; 2-methyl-2-butene, 2M2B; 3-methyl-1-butene, 3M1B) affect the cationic oligomerization of piperylene on the $TiCl_4$–H_2O catalytic system and the molecular parameters of the resulting oligomer. From the practical viewpoint, search for an efficient agent for controlling the molecular weight is necessary for preparing cationic oligopiperylene containing no insoluble gel fraction.

EXPERIMENTAL

Piperylene was purchased from Sterlitamak Synthetic Rubber Joint-Stock Company; it contained (wt %) *trans*-piperylene 61.9, *cis*-piperylene 34.5, cyclopentene 1.6, isoprene 0.3, 2M2B 0.3, cyclopentadiene 0.1, and saturated hydrocarbons 1.3.

2-Methyl-2-butene (99 wt %, Aldrich), 2-methyl-1-butene (98 wt %, Fluka), and 3-methyl-1-butene (96 wt %, Aldrich) were used without additional purification.

Oligomerization was performed in heat-treated glass ampules in an atmosphere of purified Ar. The experimental details and procedures for purifying the solvent and catalyst components are described elsewhere [1–4]. The content of the gel fraction (GF) in the oligomer was determined by extraction with toluene in a Soxhlet apparatus for 24 h. The soluble (sol) fraction was separated from GF on a centrifuge from a solution of the oligomer in hexane.

The molecular paameters of the sol fraction were determined with a Waters-Alliance GPCV-2000 liquid chromatograph equipped with three Styrogel columns HR-2, HR-4, and HR-6. Eluent toluene; elution rate 1 ml min^{-1}.

The microstructure of the oligomers was analyzed by high-resolution ^{13}C NMR spectroscopy with a Bruker AM-500 spectrometer (operating frequency for ^{13}C 125 MHz). The spectra were recorded at room temperature with accumulation of 4000–6000 scans in the DEPT-135° mode, with the subsequent Fourier transform.

Figure 1 shows the dependence of the total yield of the oligomer on the concentration of methylbutenes in the starting mixture with piperylene. With 2M1B and

Table 1. Influence of th 2M2B concentration in the monomer mixture on the molecular parameters of the resulting oligomer. Oligomerization conditions: 50°C; 120 min; toluene; $[C_5H_8]$ = 9.0, $[TiCl_4] = 3.5 \times 10^{-2}$, $[H_2O] = 1 \times 10^{-2}$ M

2M2B content in monomer, mol %	GF content in oligomer, wt %	LMWF/HMWF ratio in sol fraction	LMWF parameters		HMWF parameters	
			$M_w \times 10^{-3}$	$M_n \times 10^{-3}$	$M_w \times 10^{-3}$	$M_n \times 10^{-3}$
0.3	18.2	85/15	9.5	3.7	201.0	154.0
5.0	3.0	87/13	6.8	2.4	187.0	151.0
12.0	1.0	90/10	6.2	2.0	143.0	115.0
22.0	0	95/5	3.9	1.1	82.0	71.0
26.0	0	100/0	3.2	0.7	–	–
40.0	0	100/0	2.2	0.5	–	–
50.0	0	100/0	1.0	0.2	–	–

2M2B, these dependences pass through a maximum at a methylbutene content in the starting monomer of 12–15 mol % (Fig. 1, curves *1*, *2*). In this point, the total yield of the oligomer increases from 66 (without methylbutenes added) to 80–83%. In contrast to 2M1B and 2M2B, addition of 3M1B to piperylene leads to a gradual decrease in the yield throughout the examined concentration range (Fig. 1, curve *3*).

Addition of methylbutenes to the piperylene significantly affects the molecular parameters of the oligomers formed. Figure 2 shows the molecular-weight distribution (MWD) curves for the sol fraction of the oligomers prepared at various contents of 2M2B in a mixture with piperylene. If no 2M2B was added to piperylene, the MWD curve showed two distinct maxima (Fig. 2, curve *1*). The left maximum describes the MWD of the high-molecular-weight fraction (HMWF), and the right maximum, the MWD of the low-molecular-weight fraction (LMWF) of the oligomer. As the 2M2B content in the monomer is increased to 12 mol %, the HMWF content in the oligomer decreases (Fig. 2, curve *2*), and at a 2M2B content of 26 mol % the HMWF fully disappears, and the MWD of the oligomer becomes unimodal (Fig. 2, curve *3*).

Table 1 shows the molecular-weight parameters of the oligomers in relation to the 2M2B content in the monomer mixture. With an increase in the 2M2B content, the number-average (M_n) and weight-average (M_w) molecular weights of both LMWF and HMWF of the oligomer decrease, apparently due to the transfer of the propagating chain to the olefin [5].

Additions of 2M1B exert a similar effect on the molecular parameters (Table 2). Addition of 15 mol % 2M1B fully suppresses the formation of the insoluble GF, and addition of 20 mol % 2M1B suppresses the formation of HMWF. As in the case with 2M2B, with an increase in the 2M1B content in the monomer mixture the molecular weights of the LMWF of the oligomer decrease and the polydispersity M_w/M_n increases.

3M1B is considerably less effective as an agent

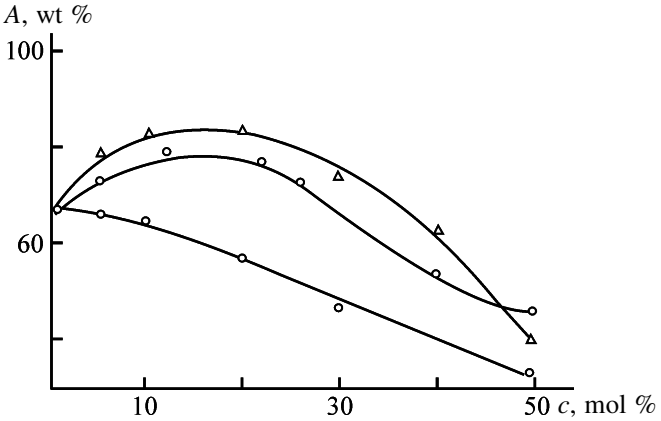


Fig. 1. Total yield of the oligomer *A* as a function of the concentration *c* of (*1*) 2M2B, (*2*) 2M1B, and (*3*) 3M1B in the mixture with piperylene. Oligomerization conditions: 50°C; 120 min; toluene; $[C_5H_8]$ = 9.0, $[TiCl_4] = 3.5 \times 10^{-2}$, $[H_2O] = 1 \times 10^{-2}$ M; the same for Fig. 3.

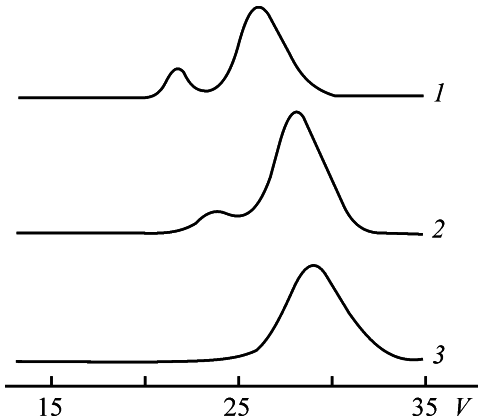


Fig. 2. Molecular-weight distribution curves for the oligomers prepared from a mixture of piperylene and 2M2B at 2M2B concentrations of (*1*) 0.3, (*2*) 12, and (*3*) 26 mol %.

Table 2. Influence of the 2M1B and 3M1B concentrations in the monomer mixture on the molecular parameters of the resulting oligomer

2M2B content in monomer, mol %	GF content in oligomer, wt %	LMWF/HMWF ratio in sol fraction	LMWF parameters		
			$M_w \times 10^{-3}$	$M_n \times 10^{-3}$	$M_w/M_n \times 10^{-3}$
2M1B:					
5.0	6.7	88/12	9.5	3.5	2.7
9.0	2.0	92/8	9.4	3.4	2.8
15.0	0.5	94/6	8.2	2.1	3.9
20.0	0	100/0	7.7	1.6	4.8
30.0	0	100/0	3.9	0.9	4.3
50.0	0	100/0	1.8	0.3	6.0
3M1B:					
5.0	17.5	86/14	9.4	3.5	2.7
10.0	14.2	85/15	8.7	3.6	2.4
20.0	7.4	90/10	8.2	3.2	2.6
30.0	5.0	89/11	7.3	2.9	2.5
50.0	1.0	90/10	6.1	2.4	2.5

controlling the molecular parameters of the oligomer (Table 2, Fig. 3). Addition of 30 mol % 3M1B to the monomer mixture does not fully suppress the formation of the insoluble GF; its content in the oligomer remains as high as 5.0 wt %. The LMWF/HMWF ratio changes insignificantly even on adding 50 mol % 3M1B to the monomer. The weight-average molecular weight of the LMWF of the oligomer prepared at both 50 and 100°C somewhat decreases on adding 3M1B (Fig. 3, curves *1*, *2*). For comparison, Fig. 3 shows how the weight-average molecular weight of the LMWF of the oligomer decreases in the presence of 2M2B, at the same polymerization temperatures (curves *3*, *4*).

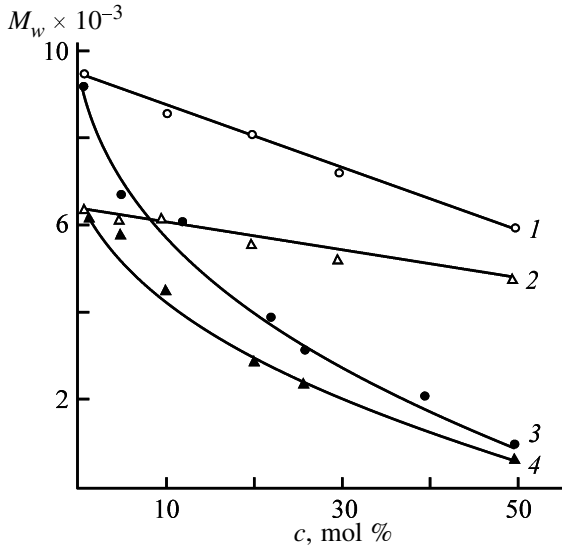


Fig. 3. Weight-average molecular weight M_w of the LMWF of the oligomer as a function of the concentration c of (*1*, *2*) 3M1B and (*3*, *4*) 2M2B in the mixture with piperylene. Oligomerization temperature, °C: (*1*, *3*) 50 and (*2*, *4*) 100.

A GLC analysis of the monomer mixtures before and after the oligomerization showed that during the process a part of 2M1B isomerizes into 2M2B (Table 3). In particular, upon oligomerization of a mixture of 50 mol % 2M1B + 50 mol % piperylene, the 2M2B concentration in the unchanged monomer increases by more than an order of magnitude relative to its initial content (from 0.24 to 2.81 mol %). For comparison, Table 3 shows changes in the concentrations of saturated hydrocarbons (2-methylbutane, *n*-pentane), which may play the role of "internal reference" in analysis of the monomer mixtures. At other contents of 2M1B in its mixture with piperylene, the 2M2B concentration also increases by more than an order of magnitude.

Table 3. Results of analysis of the monomer mixture before and after oligomerization

Components of monomer mixture	Content, mol %	
	before reaction	after reaction
trans-Piperylene	30.95	22.15
cis-Piperylene	17.25	15.13
2-Methyl-1-butene	49.05	56.60
2-Methyl-2-butene	0.24	2.81
2-Methylbutane	0.10	0.15
n-Pentane	0.10	0.14

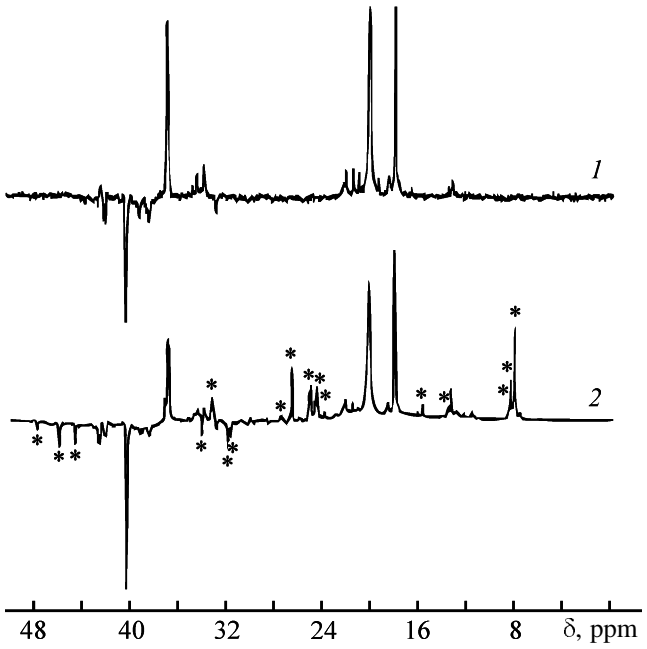


Fig. 4. ^{13}C NMR spectra of oligomers prepared from (*1*) 100 mol % piperylene and (*2*) 80 mol % piperylene + 20 mol % 3M1B. (δ) Chemical shift; the same for Fig. 5.

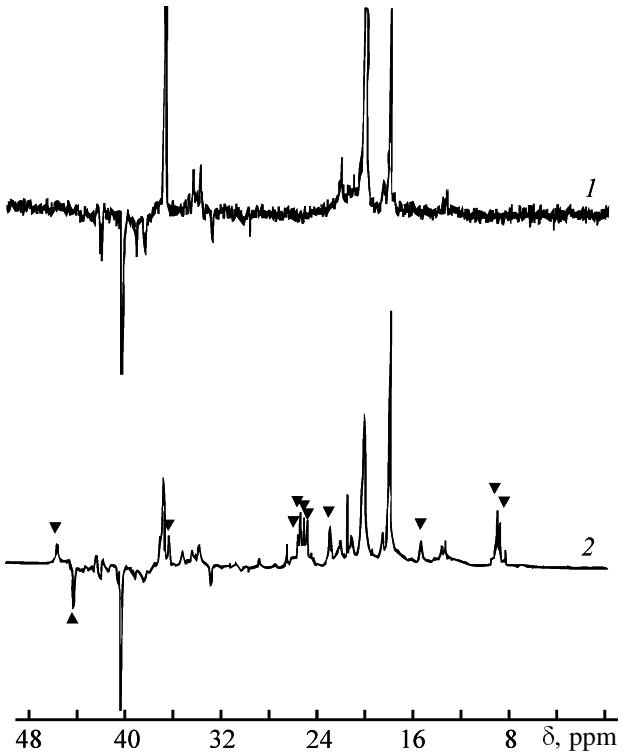


Fig. 5. ^{13}C NMR spectra of oligomers prepared from 80 mol % piperylene + 20 mol % methylbutene [(*1*) 3M1B and (*2*) 2M2B].

Therefore, we suggested that, under the conditions of the cationic oligomerization, 2M1B first fully or partially isomerizes into 2M2B and then cooligomerizes with piperylene.

To check this assumption, we studied the structures of the cooligomers of piperylene with methylbutenes by high-resolution ^{13}C NMR.

Figures 4 and 5 show the aliphatic portions of the ^{13}C NMR spectra of the piperylene homooligomer and its cooligomers with 2M1B, 2M2B, and 3M1B. The cooligomers of 2M1B and 2M2B with piperylene exhibit new well-defined signals corresponding to the olefinic structures in the oligopiperylene chain (asterisks and triangles, respectively, in Fig. 4, spectrum *2* and Fig. 5, spectrum *2*). The new signals in the spectrum of the piperylene–2M1B cooligomer (8.01, 8.33, 8.47, 13.46, 15.60, 23.75, 24.40, 24.88, 26.47, 27.43, 31.50, 31.92, 33.19, 34.02, 44.71, 45.92, 47.85 ppm) do not coincide in the position with those in the spectrum of the piperylene–2M2B cooligomer (8.83, 9.06, 15.26, 22.85, 24.77, 25.06, 25.34, 25.54, 36.39, 44.40, 45.74 ppm).

The observed difference in the structure of the cooligomers indicates that, although partial isomerization of 2M1B into 2M2B does occur in the course of the cooligomerization of 2M1B with piperylene, this process is not prevalent.

The ^{13}C NMR spectrum of the oligomer prepared by cooligomerization of piperylene wth 3M1B (Fig. 5, spectrum *1*) is essentially similar to the spectrum of the piperylene homooligomer (Fig. 4, spectrum *1*), which is indicative of a weak reactivity of 3M1B in the cationic cooligomerization with piperylene.

CONCLUSIONS

(1) Additions of 2-methyl-1-butene and 2-methyl-2-butene to piperylene allow efficient control of the molecular parameters of the cationic piperylene oligomer prepared on the $TiCl_4$–H_2O catalytic system: 12–15 mol % additions of 2-methyl-1-butene or 2-methyl-2-butene to the monomer fully suppress the formation of the insoluble gel fraction, and 20–25 mol % additions suppress the formation of the high-molecular-weight fraction in the resulting oligomer.

(2) 3-Methyl-1-butene added to the monomer is inefficient as an agent controlling the molecular parameters of cationic oligopiperylene.

(3) Recommendations on optimization of the composition of the piperylene fraction fed to the cationic

oligomerization unit were formulated and industrially implemented, which allowed preparation of SKOP rubber containing no high-molecular-weight and insoluble gel fractions and thus improvement of the product quality.

REFERENCES

1. Egoricheva, S.A., Rozentsvet, V.A., Pantukh, B.I., and Livshits, R.M., *Prom–st. Sint. Kauchuka, Shin Rezino-Tekh. Izdel.*, 1985, no. 11, pp. 7–12.
2. Kozlov, V.G., Rozentsvet, V.A., Shamaeva, Z.G., et al., *Dokl. Akad. Nauk SSSR*, 1989, vol. 307, no. 6, pp. 1402–1406.
3. Rozentsvet, V.A. and Kozlov, V.G., *J. Appl. Polym. Sci.: Appl. Polym. Symp.*, 1992, vol. 51, pp. 183–193.
4. Egoricheva, S.A., Rozentsvet, V.A., Pantukh, B.I., et al., *Lakokras. Mater. Ikh Primen.*, 1985, no. 1, pp. 12–13.
5. Kennedy, J.P. and Marechal, E., *Carbocationic Polymerization*, New York: Wiley, 1982.

ISSN 1070-4272, Russian Journal of Applied Chemistry, 2006, Vol. 79, No. 7, pp. 1191–1195. © Pleiades Publishing, Inc., 2006.
Original Russian Text © S.V. Nekhoroshev, Yu.P. Turov, V.P. Nekhoroshev, A.K. Golovko, 2006, published in Zhurnal Prikladnoi Khimii, 2006, Vol. 79, No. 7, pp. 1202–1206.

CHEMISTRY OF FOSSIL FUEL

Revealing the Common Sources of Commercial Explosive-Containing Articles

S. V. Nekhoroshev, Yu. P. Turov, V. P. Nekhoroshev, and A. K. Golovko

Surgut State University, Surgut, Khanty–Mansi autonomous okrug, Tyumen oblast, Russia

Received December 9, 2005

Abstract—A method for identification of explosive-containing commercial articles is suggested. The method is based on chromatographic analysis of petroleum products present in the articles as process admixtures and structural components.

DOI: 10.1134/S1070427206070299

Articles containing explosives (TNT blasting cartridges of various types, ammonite cartridges, cumulative perforating charges with retarded hexogen and octogen) have industrial marking with information about manufacturer, production batch, etc. In the case of illegal use of explosives, however, the industrial marking is eliminated and special expertise is necessary for identifying the supply sources of explosive articles.

As objects of expertise can serve both the main material of an article (explosives proper) and microscopic process impurities contained in it, as well as other structural elements of the article, package materials, waterproofing coatings, etc. At present, comparative studies of high explosives are performed by analyzing the composition of impurities contained in explosives by a set of chromatographic methods (gas and liquid chromatography combined with various detecting systems). This makes it possible to reveal specific features of the production process and to obtain indirect information about the manufacturer and production and storage condition of an explosive. For example, in the case of TNT, it is possible not only to identify the manufacturer, but also to reveal the source of raw material (toluene) and methods used to obtain (nitration) and purify the product [1, 2]. However, obtaining so detailed data requires, in addition to appropriate analytical equipment, samples for comparison and access to information about the technology employed by the manufacturer of an explosive. This approach is justified in the case of identification of explosive themselves, but seems to be inefficient for comparative studies of explosives in the form of charges and commercial articles.

Thus, analysis of the composition of an explosive proper is, in most cases, poorly informative for expertise purposes because the number of manufactures of explosives is limited and the basic composition of explosives of the same type and even that of process microimpurities they contain varies very narrowly. As a result, it is highly probable that studies of finished articles would reveal, in articles of different types (e.g., in 200- and 400-g TNT blasting cartridges) or in those of the same type, but produced by different manufacturers, explosives (e.g., technical-grade TNT) that are produced at the same plant or even belong to the same production batch.

A more detailed and reliable, as regards identification purposes, information about finished articles can be obtained by analysis of specific features that appear in final stages of article fabrication from raw materials.

Products of oil refining constitute a material that is the most widely used in final stages of fabrication of commercial articles and can contain identifying information. For example, blasting cartridges have waterproofing coatings composed of paraffin, petrolatum, and mixtures of these. Octogen and hexogen are virtually not used at all in pure form, and explosives based on these compounds are products of their retardation with paraffin-like materials. A similar situation takes place for blended explosives based on ammonium nitrate. In addition, ammonite cartridges have a multilayer sheath of waxed paper. Thus, virtually all explosive-containing commercial articles include heavy petroleum products or mixtures of these.

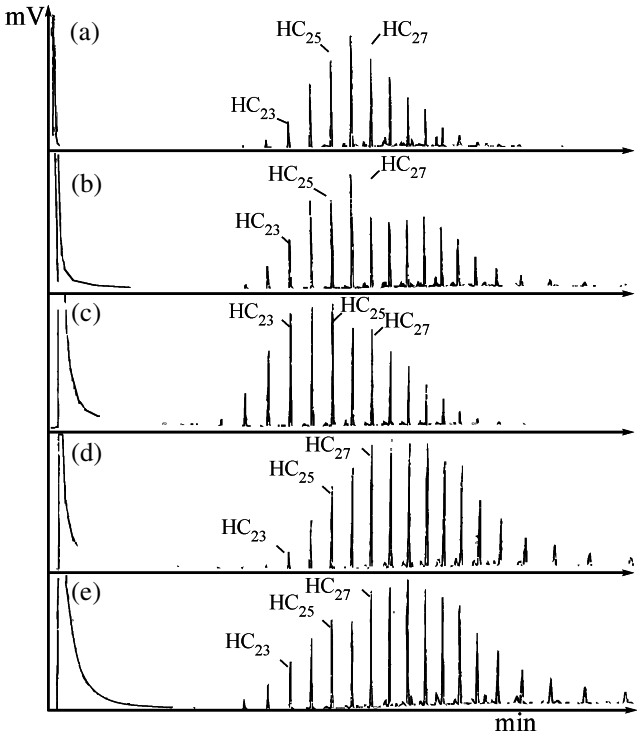


Fig. 1. Typical chromatograms of hydrocarbons extracted from structural elements of explosive-containing articles. Sample: (a) hexane solution of the waterproofing coating of a 200-g TNT blasting cartridge, (b) hexane solution of the waterproofing coating of a 400-g TNT blasting cartridge, (c) hexane extract of N 6ZhV ammonite, (d) hexane extract of retarded hexogen from a cumulative perforating charge of the ZPRK42S type, and (e) hexane extract of retarded octogen from a cumulative perforating charge of the ZPK105S type.

The petroleum products used in this case are multicomponent mixtures of individual hydrocarbons, and these mixtures are artificially produced from mixtures of natural origin, i.e., from oil. In the case of high-purity paraffin, the number of individual hydrocarbons in its composition rarely exceeds 25–30, whereas for petrolatum this number is several times larger. Hence follows that the quantitative and, to a certain extent, qualitative hydrocarbon composition of the starting petroleum products, and the more so that of the finished mixtures on their base, is accidental and may vary rather widely from one production batch to another (and even more so, from one manufacturer to another). For example, the compositions of waterproofing coatings of TNT blasting charges, prepared from different petroleum components or from starting components from the same batches, but taken in different ratios, will differ from one another in the quantitative composition of individual hydrocarbons in the mixtures and in the distribution of their relative contents. Because waterproofing coating of TNT blasting cartridges is the final stage of the production process, the composition of the waterproofing layer should provide information about a production batch in a narrower range, compared with the composition of process impurities in the technical-grade TNT.

It seems that the most efficient method for a comparative study of the qualitative and quantitative composition of petroleum products used in commercial high explosives and as structural elements of explosive-containing articles is gas–liquid chromatography.

EXPERIMENTAL

A FISONS-GC 8000 laboratory gas chromatograph was used in the study. The conditions of chromatographic analysis were as follows: flame-ionization detector; HP-Ultra-1 capillary column of length 12.5 and diameter 0.2 mm, with a thickness of the fixed phase of 0.33 μm; carrier gas helium; injector with a 1 : 20 flow division; flow velocity of carrier gas 1 ml min^{-1}; sample volume 1 μl; injector temperature 280°C; detector temperature 310°C; temperature schedule of the thermostat, 1-min isotherm at 100°C, heating at a rate of 10 deg min^{-1} to 300°C, and isothermal keeping at this temperature for 15 min.

Figure 1 shows typical chromatograms of petroleum products used in commercial high explosives and contained in structural elements of explosive-containing articles. Homologs of normal saturated hydrocarbons with 20 to 38 carbon atoms are readily identified in the chromatograms, and the chromatograms themselves differ in the quantitative ratios between the peaks of individual substances and in their relative distributions.

The results obtained demonstrated that the following general approach can be used for identification of various explosives and articles on their base: revealing the structural elements and comparing their quantitative hydrocarbon composition by gas chromatography. The modern level of development of the computing technology makes it possible to substantially facilitate comparison of quantitative characteristics and to create special databases for automated identification of a manufacturer and a production batch of articles.

To demonstrate the potential of the method for identification of explosives and articles on their base, we made a comparative study of the waterproofing coating of blasting cartridges of the TP-200G-K type

from five different batches manufactured in 1998–1999.

Waterproofed compacted TNT blasting charges of the TP-200GK type are commercially manufactured and intended to be used as explosives in seismic prospecting on the ground surface in all climatic zones of CIS countries at temperatures of –50 to +50°C. The TP-200G-K blasting charges comprise compacted TNT and a paper sheath and have a cylindrical shape with a pocket for a blasting cap or electric detonator. The weight of a blasting cartridge was 200 g. The surface of the blasting cartridges (except that of the pocket) is covered with a continuous thin waterproofing layer of a paraffin–petrolatum mixture [3].

The paraffin–petrolatum mixture used in waterproofing coatings of blasting cartridges is prepared by mixing petrolatum and paraffin in a melt to obtain a homogeneous mixture with a prescribed dropping point.

Now, the starting components of the waterproofing mixture will be analyzed in more detail. As is known, paraffin is a mixture of normal hydrocarbons of the methane series (*n*-paraffins) with 18–40 carbon atoms in a molecule. In addition, paraffin contains a certain amount of hydrocarbons with an aromatic or naphthene ring in the molecule. Technical-grade paraffin is a white crystalline substance with a melting point of 50–55°C and average molecular weight of 300–450. Paraffins are industrially produced in dewaxing of oil distillates [4].

Petrolatum is a light brown substance with a dropping point not lower than 55°C. It is a mixture of paraffin, ceresin, and oil, produced in dewaxing of oils obtained by sulfuric acid or selective purification [4].

In this study, ten blasting cartridges were randomly selected from each batch, and three 10-mg samples of the waterproofing coating were taken from different parts of the surface of each blasting cartridge. Each of the samples was dissolved in 1 ml of hexane and studied by gas–liquid chromatography under the conditions described above.

Examples of chromatograms of the waterproofing coatings of TNT blasting cartridges from five different production batches are shown in Fig. 2.

For a more detailed comparison of the quantitative hydrocarbon compositions of the coatings, it is suggested to use both the relative contents of *n*-paraffins and those (both total and individual) of the hydrocarbons eluted in chromatographic analysis between the

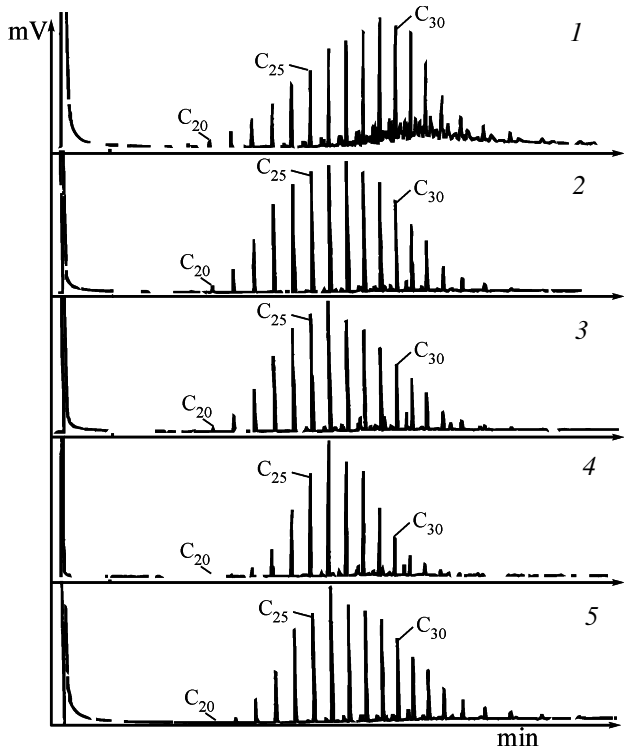


Fig. 2. Chromatograms of hydrocarbons from waterproofing coatings of TP-200G-K TNT blasting charges from five different production batches. Digits *1–5* denote batch numbers; the same for Figs. 3 and 4.

peaks of *n*-paraffins. These relative contents were found by the following normalization procedure:

$$X_i = \frac{100S_i}{\sum_{i=1}^{i=n} S_i},$$

where X_i is the relative content of *i*th component (%); S_i, area of the peak (group of peaks) of *i*th component (arb. units); $\sum_{i=1}^{i=n} S_i$, sum of areas of the component peaks (arb. units); and *n*, number of the components.

The results of parallel analyses were used to determine the average values of the quantities obtained and calculate the confidence intervals, after which the results obtained were compared. The relative contents of the normal saturated hydrocarbons and of the sum of hydrocarbon eluted between the peaks of the normal saturated hydrocarbons in samples of the objects being compared were considered the same if the confidence intervals of the average values of the

Total content of *n*-paraffins and other hydrocarbons of the article batches studied

Sample no.	Total content, %	
	n-paraffins	other hydrocarbons
1	54.8	45.2
2	89.6	10.4
3	79.8	20.2
4	80.6	19.4
5	85.0	15.0

corresponding quantities overlapped. In addition, we compared the relative contents of individual hydrocarbons in groups eluted between the peaks of normal saturated hydrocarbons.

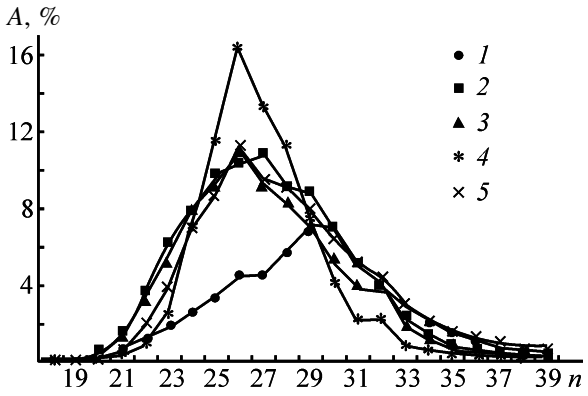


Fig. 3. Relative content *A* of *n*-paraffins in the waterproofing coatings of TNT blasting cartridges of the TP-200G-K type from five different production batches. (*n*) Number of carbon atoms in the molecule of a hydrocarbon.

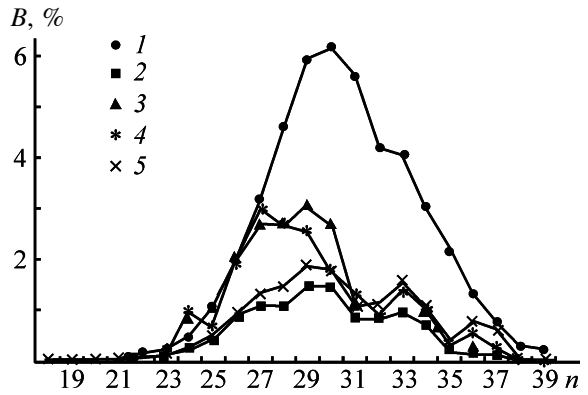


Fig. 4. Relative content *B* of sums of hydrocarbons eluted between the peaks of *n*-paraffins in waterproofing coatings of TNT blasting cartridges of the TP-200G-K type from five different production batches. (*n*) Number of carbon atoms in the molecule of a hydrocarbon after which this group is eluted.

The group contents of the normal saturated hydrocarbons and sums of hydrocarbons eluted between the peaks of *n*-paraffins are listed in the table.

As follows from the table, even the total contents of *n*-paraffins and other hydrocarbons can be used to differentiate most of the samples. However, the integral characteristics coincide within the determination error for sample nos. 3 and 4.

In this case, it is necessary to use data on the content of individual hydrocarbons to differentiate between samples with close integral characteristics. To ensure better clarity and easier perception, these data are presented in the graphic form in Figs. 3 and 4. For this purpose, the average relative percentage content was plotted against the number of carbon atoms in the molecule of the given *n*-paraffin (for *n*-paraffins) or of the *n*-paraffin whose peak precedes the peaks of the given hydrocarbons (for the sum of hydrocarbons).

The set of the chromatographic analyses performed revealed that the quantitative hydrocarbon composition of the waterproofing coatings of TNT blasting cartridges is the same within a production batch stored for a year in a dry reinforced-concrete warehouse without heating.

Clearly pronounced differences were revealed between blasting cartridges from different production batches both in the relative contents of *n*-paraffins (Fig. 3) and in total contents of hydrocarbons eluted between the peaks of normal saturated hydrocarbons (Fig. 4). The differences in the composition of waterproofing coatings in different batches are well identified even by the peaks of *n*-paraffins, and comparison of the contents of hydrocarbons eluted between the chromatographic peaks of normal hydrocarbons can be regarded as additional evidence confirming these differences.

CONCLUSIONS

The possibility of identifying classification of various commercial explosive-containing articles by the quantitative hydrocarbon content of admixtures of petroleum products in their structural elements was demonstrated. The identification features obtained in chromatographic analyses make it possible to differentiate articles of the same type but belonging to different production batches. The composition of hydrocarbons in the structural elements of the articles, by which they are classified, remains unchanged during a year of storage under warehouse conditions.

REFERENCES

1. Tuzkov, Yu.B., Makarov, S.Ya., and Semenov, A.Yu., *Kriminalisticheskoe issledovanie brizantnykh vzryvchatykh veshchestv: Metodologicheskie rekomendatsii* (Forensic Studies of High Explosives: Methodological Recommendations), Moscow: Ekspertno-Kriminalist. Tsentr Min. Vnutr. Del Ross. Feder., 1977.
2. Zbarskii, V.L. and Zhilin, V.F., *Toluol i ego nitroproizvodnye* (Toluene and Its Nitro Derivatives), Moscow: URSS, 2000.
3. *TU* (Technical Specifications) *84-08 628 424 706-398: TP-200G-K and TGFP-200G-K Waterproofed Compacted Blasting Cartridges*, Kristall, 1998.
4. *Tovarnye nefteprodukty, svoistva i primenenie: Spravochnoe izdanie* (Commercial Petroleum Products, Properties and Application: Handbook), Shkol'nikov, V.M., Ed., Moscow: Khimiya, 1978, 2nd ed.

ISSN 1070-4272, Russian Journal of Applied Chemistry, 2006, Vol. 79, No. 7, pp. 1196–1199. © Pleiades Publishing, Inc., 2006.
Original Russian Text © V.G. Maiorov, A.I. Nikolaev, 2006, published in Zhurnal Prikladnoi Khimii, 2006, Vol. 79, No. 7, pp. 1207–1209.

BRIEF COMMUNICATIONS

Extraction of Th(IV) with Tributyl Phosphate from Aqueous HCl Solutions Containing Sodium, Calcium, or Aluminum Chloride

V. G. Maiorov and A. I. Nikolaev

Tananaev Institute of Chemistry and Technology of Rare Elements and Mineral Raw Materials, Kola Scientific Center, Russian Academy of Sciences, Apatity, Murmansk oblast, Russia

Received March 1, 2006

Abstract—Extraction of thorium(IV) from 0.1–3 M aqueous hydrochloric acid solutions containing NaCl, $CaCl_2$, or $AlCl_3$ was studied. The experimental results are discussed.

DOI: 10.1134/S1070427206070305

Published data on the extraction of thorium(IV) from aqueous chloride solutions are scarce and contradictory [1–3]. The diversity of thorium(IV) speciation in aqueous chloride solutions is caused by its strong tendency to hydrolysis and complexation depending on the acidity and kind of anions. These factors affect also the chemical composition of Th-containing extractable complexes. It was reported [2, 4] that neutral organic solvents predominantly extract Th(IV) from moderately acidic solutions in the form of $ThCl_4$, and, to a lesser extent, of $ThOHCl_3$. In extraction from concentrated aqueous HCl, Th(IV) passes to the organic phase in the form of a complex acid $HThCl_5$. Currently the hydrochloric acid processing of rare-metal raw materials is being actively developed [5–7]. Therefore, the study of extraction of Th from hydrochloric acid solutions, especially from those containing large amount of metal salts, is an urgent problem.

In this study we examined the influence of sodium, calcium, and aluminum chlorides on the extraction of thorium from aqueous HCl solutions. It is known that these impurity metals significantly affect the distribution of thorium. The Na(I) and Ca(II) cations are common impurities in rare-earth titanoniobates loparite and perovskite. Al(III) was chosen as a typical trivalent element. Tributyl phosphate (TBP) was used as the most available and widely applied extractant. Aqueous solutions intended for extraction were prepared by mixing concentrated aqueous Th(IV), Ca(II), and Al(III) chlorides with aqueous HCl. The resulting solutions were kept before use for no less than 5 days. TBP and other chemicals were of pure grade. The extraction was carried out at the organic to aqueous phase volume ratio $V_o : V_{aq} = 1 : 1$ at room temperature (18 ± 2°C). The contact time was 15 min. To determine the Th(IV) content in the organic extract, it was backwashed with water. The backwash was acidified with HCl and Th was determined photometrically. The procedure was described in detail in [7].

Figure 1 shows how the degree of extraction of Th with TBP from 1 M aqueous HCl depends on the concentration of $CaCl_2$ or $AlCl_3$. On replacement of $CaCl_2$ or $AlCl_3$ by NaCl (up to 4 M), the degree of recovery of Th(IV) becomes less than 0.5%. It is known [2] that, on the addition of nonextractable electrolytes to the extraction system containing HCl in

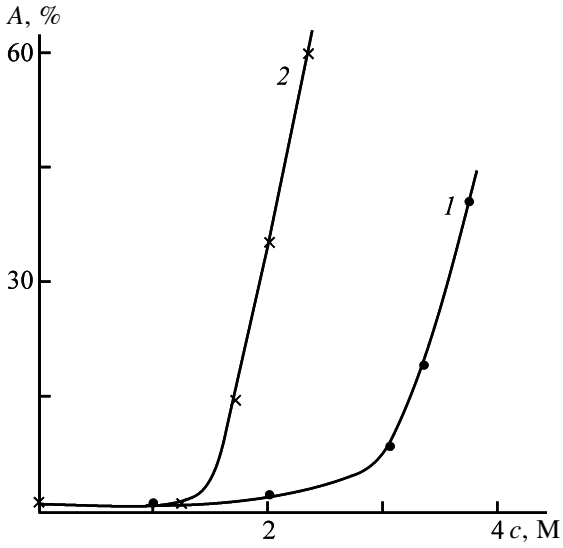


Fig. 1. Extraction of Th(IV) from 1 M HCl containing (*1*) $CaCl_2$ and (*2*) $AlCl_3$. (*A*) Degree of recovery of Th; (*c*) $CaCl_2$ or $AlCl_3$ concentration. Initial Th concentration (recalculated to ThO_2) 0.72 g l^{-1}.

the aqueous phase, the activity of water decreases and, as a result, the transfer of the extractable metal to the organic phase increases. This salting-out effect increases in the order $NH_4Cl < NaCl < CaCl_2 < MgCl_2 < AlCl_3$, i.e., with an increase in the cationic charge and a decrease in the cationic radius. In our study we observed the similar order of influence of foreign electrolytes on the extraction of Th ($NaCl < CaCl_2 < AlCl_3$). The plot of the degree of the Th extraction vs. $CaCl_2$ or $AlCl_3$ concentration shows that these salts do not affect the extraction of Th(IV) at their content less than 2 and 1.3 M, respectively, but with a further increase in their concentration, the extraction of Th(IV) sharply increases. It should be noted that, if the results are plotted as the degree of Th extraction vs. concentraiton of chloride anion supplied into the solution with $CaCl_2$ or $AlCl_3$, both extraction curves approach each other, and a sharp increase in the extraction of Th starts at a chloride content of about 4 M. These changes apparently show that the salting-out effect of the impurity metal chlorides under consideration includes both the cationic [Ca(II), Al(III)] and anionic (Cl^-) contributions.

The similar relationships were observed in the extraction of Mn(II) and Co(II) with TBP in the presence of $CaCl_2$ [8]. It was found that these nonferrous metals are poorly extracted at [$CaCl_2$] below 2–3 M, but their extraction sharply increases at higher $CaCl_2$ concentration. For example, at [$CaCl_2$] 4.9–5.8 M the distribution ratios were as follows: Ca 0.2, Mn(II) 20, and Co(II) 140. Jezowska-Trzebiatowska et al. believe [8] that this effect is specific for the extraction with TBP only. In the extraction of the above-mentioned nonferrous metals with alcohols, their distribution ratios are only about 0.1–0.5 at [$CaCl_2$] ~4.5 M. To elucidate how Th(IV) is extracted from concentrated solutions of chlorides of calcium and other metals, further studies are required.

Our results show that extraction of thorium and its separation from concomitant metals are strongly influenced by the salt content in the aqueous phase. Taking into account the divesity of thorium-containing raw materials, numerous extraction experiments should be carried out to comprehensively elucidate the influence of foreign metals on the extraction of Th(IV). It should be noted that the technologically acceptable efficiency of extraction of Th(IV) with TBP is reached only in the presence of large amounts of $CaCl_2$ (4 M) or $AlCl_3$ (2 M) in the aqueous phase. Under these conditions, at $V_o : V_{aq} = 1 : 1$, the degree of extraction of Th(IV) in one extraction step exceeds 50%, and Th can be quantitatively recovered from the aqueous phase by multistep countercurrent extraction with TBP.

Influence of the HCl concentration on the extraction of Th(IV) from its solution in HCl containing 2 M NaCl, $CaCl_2$, or $AlCl_3$

HCl, M	Recovery of Th(IV), %		
	NaCl	$CaCl_2$	$AlCl_3$
0.1	–	~1	17
1	<0.5	~2	36
3	~0.5	~3	59

We found that the extraction of Th(IV) increases not only with increasing salting-out agent concentration, but also, although to a smaller extent, with increasing HCl concentration. Whereas at metal chloride concentrations below 1 M the increase in the HCl concentration from 1 to 3 M insignificantly affects the degree of recovery of Th(IV), the similar change in the HCl content in a 2 M solution of the metal chlorides leads to a severalfold increase in the Th recovery (see table). This table also shows once again that the salting-out efficiency with respect to Th significantly increases in the order $NaCl < CaCl_2 < AlCl_3$.

Figure 2 shows the log–log plot of D vs. [Cl^-] at constant [H^+] = [HCl], where [Cl^-] is the total chloride amount introduced into solution with both HCl and $CaCl_2$ (or $AlCl_3$). Figure 3 shows the log–log plot of D vs. [H^+] at constant [Cl^-]. It is known [2] that

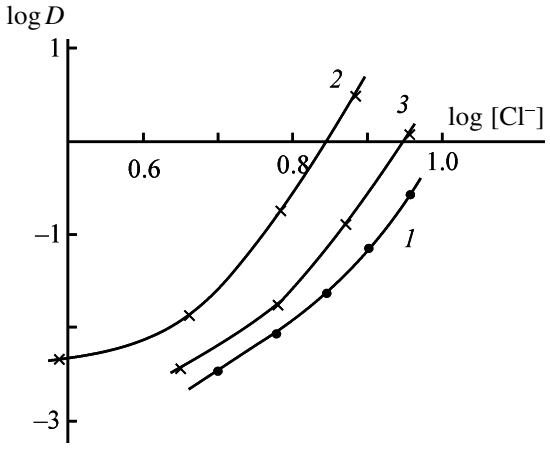


Fig. 2. Distribution ratio of Th(IV) vs. chloride ion concentration [Cl^-] in the aqueous phase in the extraction of Th(IV) from aqueous HCl solutions containing (*1*) $CaCl_2$ and (*2, 3*) $AlCl_3$ at constant [H^+] = [HCl], equal to (*2*) 0.1 and (*1, 3*) 3 M. (*D*) Distribution ratio of Th(IV); the same for Fig. 3. Initial Th concentration in the aqueous phase (recalculated to ThO_2) 0.72 g l^{-1}.

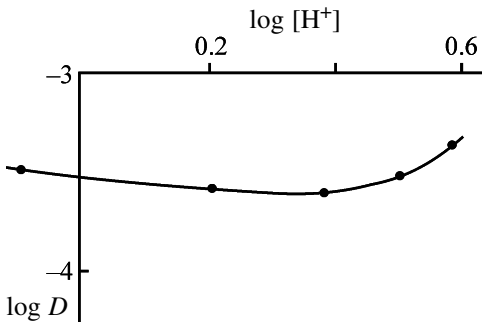


Fig. 3. Distribution ratio of Th(IV) vs. $[H^+]$ in the extraction of Th(IV) from HCl solutions containing NaCl. Initial Th concentration (recalculated to ThO_2) 10 g l^{-1}, $[Cl^-]$ 3.84 M.

the slope of these log–log plots is equal to the amount of Cl^- (Fig. 2) or H^+ (Fig. 3) entering the composition of the extractable complex. This technique for the determination of the composition of the extractable complex has several drawbacks. In particular, this method does not take into account the variations in the activity coefficients. Therefore, with this technique only approximate stoichiometry of the extractable complex can be obtained.

Figure 2 shows how the chloride anion concentration affects the distribution of Th. The nonlinearity of the distribution curves does not allow the determination of the number of chloride anions coordinated with thorium in the extractable complex. However, since these curves have a similar shape, we can suggest that the extraction of Th(IV) from all the solutions occurs by a similar mechanism. As seen from Fig. 2, the extraction of Th in the presence of $AlCl_3$ decreases with increasing HCl concentration. At first glance, these results contradict those listed in the table. However, this contradiction is only apparent, because the increase in the HCl concentration in a solution of $AlCl_3$ in HCl at constant $[Cl^-]$ means that the actual $AlCl_3$ content decreases and, as a result, its salting-out effect with respect to Th(IV) becomes weaker.

Figure 3 shows how the acidity of the aqueous phase $[H^+]$ affects the extraction of Th(IV) from an HCl solution containing NaCl at a constant chloride concentration $[Cl^-]$ 3.84 M. The use of NaCl as salting-out agent was found to be the most suitable for studying the dependence of the distribution ratio of Th(IV) on the acidity [2]. As seen from Fig. 3, the acidity virtually does not affect the Th(IV) recovery within the entire $[H^+]$ concentration range. This means that H^+ does not enter the composition of the extractable complex and Th(IV) is mainly extracted as $ThCl_4$. A small minimum present in this extraction curve is apparently caused by a decrease in the NaCl salting-out effect at partial replacement of NaCl with HCl. Further increase in $[H^+]$ is accompanied by an increase in the extraction of Th(IV) due to formation of an extractable complex acid $HThCl_5$. Taking into account that the extraction of Th(IV) is virtually independent of $[H^+]$ within the thorium concentration range studied, we can suggest that an increase in the extraction of thorium with increasing HCl concentration in the presence of $AlCl_3$ (see table) is caused by an increase in the total chloride concentration $[Cl^-]$ in the aqueous phase rather than an increase in the acidity.

CONCLUSIONS

(1) Thorium(IV) is not extracted with TBP from aqueous hydrochloric acid solutions containing $CaCl_2$ or $AlCl_3$ in the amount below 2 and 1.3 M, respectively. At higher concentration of these salts, the extraction of thorium strongly increases and the degree of its recovery exceeds 50% at $CaCl_2$ and $AlCl_3$ concentration exceeding 4 and 2 M, respectively. On replacement of $CaCl_2$ or $AlCl_3$ by NaCl, the degree of thorium(IV) recovery is smaller than 0.5% up to the NaCl concentration of 4 M.

(2) The plot of $\log D$ vs. $\log[H^+]$ shows that, in extraction of thorium(IV) with TBP from aqueous HCl containing $CaCl_2$ or $AlCl_3$, the extractable complex contains no protons. Under these conditions, thorium is apparently extracted in the form of $ThCl_4$ solvate with TBP.

ACKNOWLEDGMENTS

The study was financially supported by the Leading Scientific Schools grant (no. NSh-4383-2006.3).

REFERENCES

1. Ryabchikov, D.I. and Gol'braikh, E.K., *Analiticheskaya khimiya toriya* (Thorium Analytical Chemistry), Moscow: Akad. Nauk SSSR, 1996.
2. Zolotov, Yu.A., Iofa, B.Z., and Chuchalin, L.K., *Ekstraktsiya galogenidnykh kompleksov metallov* (Extraction of Metal Halide Complexes), Moscow: Nauka, 1973.
3. Zemtsova, L.I., Stepanova, N.A., Zheleznova, E.I., et al., *Opredelenie redkikh i radioaktivnykh elementov v mineral'nom syr'e* (Determination of Rare and Radio-

active Elements in Mineral Raw Materials), Moscow: Nedra, 1983.

4. Watanabe, K., *J. Nucl. Sci. Technol.*, 1964, vol. 1, no. 5, pp. 155–162.
5. Skiba, G.S., Voskoboinikov, N.B., Solov'ev, A.V., et al., *Zh. Prikl. Khim.*, 2003, vol. 76, no. 10, pp. 1738–1739.
6. Nikolaev, A.I., Gerasimova, L.G., Maiorov, V.G., et al., Abstracts of Papers, *XVII Mendeleevskii s''ezd po obshchei i prikladnoi khimii* (XVII Mendeleev Congr. on General and Applied Chemistry), vol. 3: *Materialy i nanotekhnologii* (Materials and Nanotechnologies), Kazan, September 21–26, 2003, p. 313.
7. Maiorov, V.G., Nikolaev, A.I., Kopkov, V.G., et al., *Zh. Prikl. Khim.*, 2004, vol. 77, no. 5, pp. 715–719.
8. Jezowska-Trzebiatowska, B. and Kopacz, S., *Radiokhimiya*, 1966, vol. 8, no. 2, pp. 145–153.

ISSN 1070-4272, Russian Journal of Applied Chemistry, 2006, Vol. 79, No. 7, pp. 1200–1201. © Pleiades Publishing, Inc., 2006.
Original Russian Text © Yu.P. Perelygin, S.Yu. Kireev, A.Yu. Kireev, 2006, published in Zhurnal Prikladnoi Khimii, 2006, Vol. 79, No. 7, pp. 1210–1211.

BRIEF COMMUNICATIONS

Electrodeposition of Bismuth from Acid Lactate Electrolyte

Yu. P. Perelygin, S. Yu. Kireev, and A. Yu. Kireev

Penza State University, Penza, Russia

Received February 2, 2006

Abstract—Electrodeposition of bismuth from acid lactate electrolyte was studied.

DOI: 10.1134/S1070427206070317

Bismuth and its alloys are widely used in industry as antifriction and corrosion-resisting coatings, as electrical contacts to semiconductors, including rectifying and ohmic contacts formed by them on silicon and germanium, and as coatings for soldering [1].

Presently, perchlorate, fluoroborate, phenolsulfonic, fluosilicate, sulfate, EDTA, pyrophosphate, and other electrolytes are used for the electrodeposition of bismuth and bismuth-containing alloys [1].

Though ensuring deposition of high-quality coatings at high cathodic current efficiency and possessing a high throwing power, the above electrolytes contain, apart from bismuth ions, toxic anions, which makes them more environmentally hazardous.

Much attention is given today to replacement of toxic anions in electroplating solutions by less toxic anions [2]. Lactic acid is abundant in nature and is an intermediate product of metabolism in biological tissues. The acid is readily biodegradable and, therefore, environmentally safe. In this respect, the development of a lactate bismuth-plating electrolyte is of certain theoretical and practical significance.

The effect of the electrolysis mode and electrolyte composition was studied at 20°C and a cathodic current density of 0.3 A dm^{-2} in the solution containing 80% lactic acid [GOST (State Standard) 490–79] 100 ml l^{-1}, bismuth nitrate (in terms of metal) 10 g l^{-1}, sodium sulfate 20 g l^{-1}, and 65% nitric acid (GOST 4461–77) 50 ml l^{-1}.

With an increase in the concentration of bismuth ions in the electrolyte from 10 to 20 g l^{-1}, the cathodic current efficiency decreases from 97.5 to 91.7%, with the coating quality improved. Raising the bismuth concentration further results in a drastic deterioration of the coating quality and a decrease in the cathodic current efficiency.

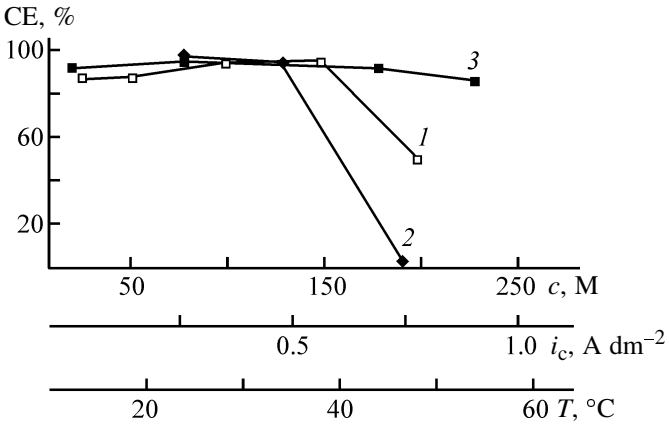


Fig. 1. Cathodic current efficiency (CE) by bismuth vs. (*1*) concentration of lactic acid *c* in the electrolyte, (*2*) cathodic current density i_c and (*3*) solution temperature.

As the concentration of lactic acid in the electrolyte is increased from 25 to 150 ml l^{-1}, the cathodic current efficiency by bismuth increases from 90.4 to 98.7%. In this case, light gray, good-quality coatings are deposited. Raising the concentration of lactic acid to 200 ml l^{-1} leads to a decrease in the cathodic current efficiency by bismuth to 55.1%, with the coating quality deteriorated (Fig. 1, curve *1*).

The further study was carried out in the electrolyte containing lactic acid 150 ml l^{-1}, bismuth nitrate (in terms of metal) 10 g l^{-1}, sodium sulfate 20 g l^{-1}, and 65% nitric acid (GOST 4461–77) 50 ml l^{-1}.

Increasing the cathodic current density within 0.3–0.75 A dm^{-2} leads to deterioration of the coating quality and a sharp decrease in the cathodic current efficiency by bismuth from 97 to 4.87%, which is due to intensification of hydrogen evolution (Fig. 1, curve *2*).

With an increase in temperature from 12 to 24°C, the cathodic current efficiency by bismuth increases

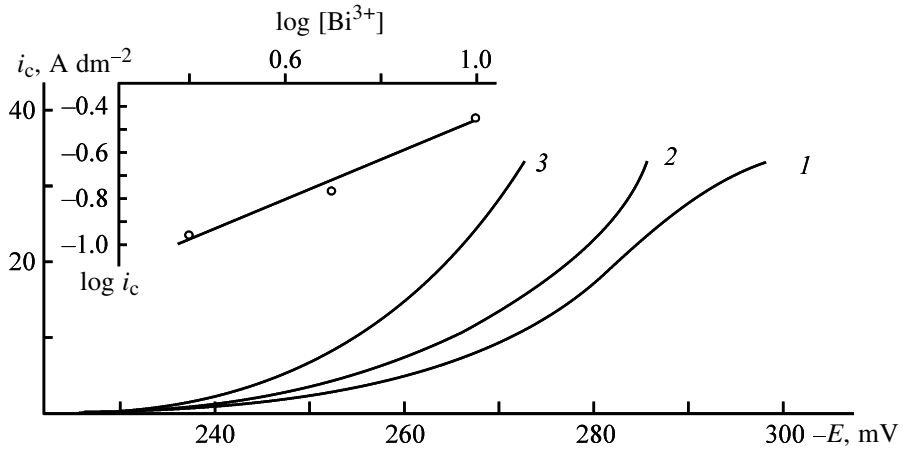


Fig. 2. Cathodic potentiodynamic curves taken in the course of bismuth deposition at different concentrations of bismuth ions in the solution. (*E*) Potential and (i_c) current density. Bi^{3+} concentration, g l^{-1}: (*1*) 2.5, (*2*) 5, and (*3*) 10. Insert: $\log i_c$ vs. $\log [Bi^{3+}]$ dependence at a cathode potential of –260 mV.

from 93 to 97%. At higher temperatures, the cathodic current efficiency by bismuth decreases to 88%, which may be accounted for by acceleration of chemical dissolution of the coating or by intensification of hydrogen evolution (Fig. 1, curve *3*).

Stirring of the solution results in drastic deterioration of the coating quality and a decrease in the cathodic current efficiency by bismuth.

The potentiodynamic curves taken at a potential sweep rate of 4 mV s^{-1} (Fig. 2) show that, with decreasing bismuth concentration, the polarization curves shift toward more negative potentials. For example, at the cathodic current density of 0.3 A dm^{-2} the cathode potentials (relative to SHE) in the solution containing 10, 5, and 2.5 g l^{-1} bismuth ions are 262, 274, and 278 mV, respectively (Fig. 2).

The log–log dependence of the cathodic current density on the bismuth concentration in the electrolyte is linear (Fig. 2, insert at the top). The slope of this straight line is 1.3, which shows that the discharge of bismuth ions occurs in steps [3].

The study of the processes occurring at the anode showed that, as the anodic current density increases from 0.1 to 0.5 A dm^{-2}, the anodic current efficiency by bismuth (in terms of Bi^{3+}) decreases from 141 to 102%. This high value of the current efficiency is likely due to the fact that the electrochemical dissolution is accompanied by the chemical dissolution of the anodes.

CONCLUSIONS

A process for the electrodeposition of high-quality bismuth coatings was developed, and a less toxic electrolyte containing 80% lactic acid (GOST 490–79) 150 ml l^{-1}, bismuth nitrate (in terms of metal) 10 g l^{-1}, sodium sulfate 20 g l^{-1}, and 65% nitric acid (GOST 4461–77) 50 ml l^{-1} was suggested. At a cathodic current density of 0.3 A dm^{-2} and 20–25°C, the cathodic current efficiency is 95–98%. The deposition rate of the bismuth coatings at these electrolysis conditions is 7.6 μm h^{-1}.

REFERENCES

1. Azhogin, F.F., Belen'kii, M.A., Gal', I.E., et al., *Gal'vanotekhnika: Spravochnik* (Electroplating: Reference Book), Moscow: Metallurgiya, 1987.
2. Vinogradov, S.S., *Ekologicheski bezopasnye gal'vanicheskie proizvodstva* (Environmentally Safe Electroplating Plants), Moscow: Globus, 2002.
3. Vetter, K.J., *Elektrochemische Kinetik*, Berlin: Springer, 1961.

ISSN 1070-4272, Russian Journal of Applied Chemistry, 2006, Vol. 79, No. 7, pp. 1202–1203. © Pleiades Publishing, Inc., 2006.
Original Russian Text © B.M. Ginzburg, V.L. Ugolkov, G.N. Fedorova, E.Yu. Melenevskaya, L.A. Shibaev, Sh. Tuichiev, 2006, published in Zhurnal Prikladnoi Khimii, 2006, Vol. 79, No. 7, pp. 1212–1213.

BRIEF COMMUNICATIONS

Influence of Fullerene C_{60} on the Kinetics of Toluene Evaporation

B. M. Ginzburg, V. L. Ugolkov, G. N. Fedorova, E. Yu. Melenevskaya, L. A. Shibaev, and Sh. Tuichiev

Institute of Problems of Machine Science, Russian Academy of Sciences, St. Petersburg, Russia
Institute of Macromolecular Compounds, Russian Academy of Sciences, St. Petersburg, Russia
Tadjik State National University, Dushanbe, Tadjikistan

Received March 28, 2006

Abstract—The kinetic dependences of the relative weight loss of the solvent from dilute solutions of fullerene C_{60} in toluene under ambient conditions were determined. Evaporation of the pure solvent is slower than that of the same solvent from dilute solutions (≤0.01%).

DOI: 10.1134/S1070427206070329

Previously the supramolecular structure of fullerene C_{60} solutions in aromatic solvents, *p*-xylene and toluene, was studied by the small-angle X-ray diffraction [1–3] and densitometry [4]. From the data obtained, it was concluded that addition of fullerene to the above solvents results in nonmonotonic variations in the structure. Formation of solvophobic shells with decreased solvent density around fullerene molecules predominates at low concentrations of fullerene (≤0.01%), and structuring and ordering of the solvent accompanied by an increase in its density and the overall solution density prevail at higher concentrations. The observed increase in the density is in good agreement with the heat release in dissolution of fullerene in toluene [5]. It is evident that the features of variation of the supramolecular structure of fullerene C_{60} solutions, formation of solvophobic shells and structuring of the solvent, should affect various characteristics of solutions. This study deals with the kinetics of solvent evaporation from solutions of fullerene C_{60} in toluene.

To prepare the solutions, we used 99.7% pure fullerene C_{60} synthesized by the Huffman–Krätschmer procedure [6] and toluene of chemically pure grade after its twofold distillation.

The solution of fullerene C_{60} in toluene (0.01%) was prepared by weight using an analytical balance. To accelerate dissolution, the suspension of fullerene in toluene was treated with ultrasound for 10 min (an UZV-1/100-TN device, power 95 W, frequency 22–44 KHz). The solutions with concentrations of 0.005 and 0.001% were prepared by dilution of the 0.01% solution.

For measurements we used two types of equipment and, correspondingly two approaches. First, we used a C derivatograph equipped with a microprocessor (MOM, Hungary). Heating in the device was switched off, and for solutions with various initial concentrations the weight loss due to free evaporation of the solvent from an open corundum crucible with the solution (initial weighed portion 100 mg) was measured over the course of 100 min (Fig. 1). It should be noted that even at the lowest concentrations of fullerene the rate of solvent evaporation from the solution

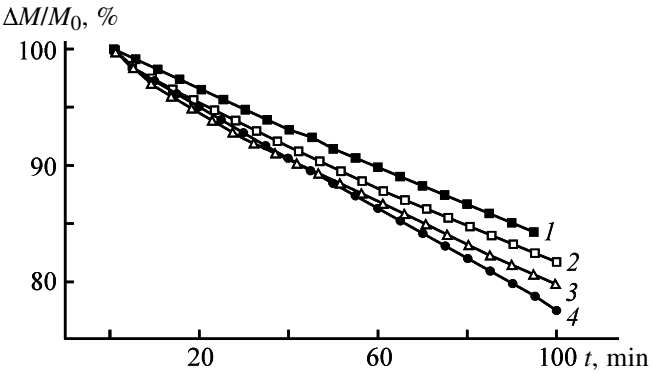


Fig. 1. Relative weight loss of fullerene C_{60} solutions $\Delta M/M_0$ as a function of time t at 25°C. Initial concentration, wt %: (*1*) 0 (pure solvent), (*2*) 0.005, (*3*) 0.01, and (*4*) 0.1.

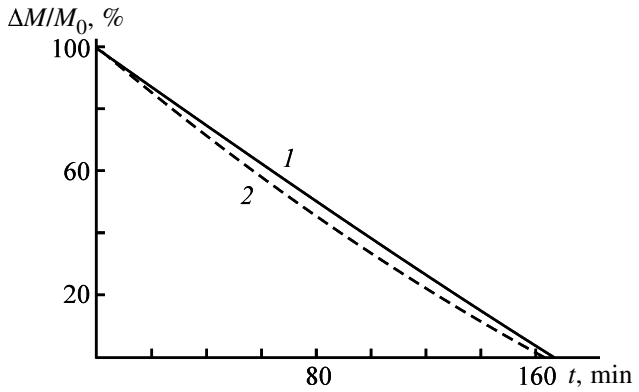


Fig. 2. Relative weight loss of fullerene C_{60} solutions $\Delta M/M_0$ as a function of time t at 30°C. Netzsch thermal analyzer, argon flow rate 50 ml min^{-1}. Initial concentration, wt %: (*1*) 0 (pure solvent) and (*2*) 0.01.

is higher than that from the pure solvent. This fact can be explained by formation of solvophobic shells of the solvent (with decreased density) around fullerene molecules. The higher the initial concentration of fullerene C_{60}, the higher the rate of weight variation and, correspondingly, the larger the total weight loss. Within 100 min, the weight loss reaches 22–23%.

The other series of the measurements was performed on a Netzsch thermal analyzer (Germany) at a constant temperature of 30°C. A solution sample (weighed portion 16–17 mg) was placed into a crucible. When the crucible was open, evaporation was so fast that at a high sensitivity of the device it was impossible to fix the initial concentration of the solution from which the experiment started. Therefore, the crucible filled with the solution was covered with a lid with a small orifice limiting the evaporation. The air space upon the crucible was purged with a weak argon flow (50 ml min^{-1}). The measurements were performed until complete evaporation of the solvent.

The results of measurements for the pure solvent (curve *1*) and 0.01% C_{60} solution (curve *2*) are presented in Fig. 2. Since the solution concentration increases as the solvent is evaporated, the evaporation rate is scanned along the run of curve *2*: the slope of curve *2* in each point characterizes the evaporation rate at the corresponding concentration. The run of curve *2* shows that initially (in the first 50 min) the evaporation rate is higher than that of the pure solvent, and then it decreases and becomes lower than the evaporation rate of the pure solvent. This transition occurs approximately 80 min after the beginning of the evaporation, when approximately 50% of the solvent is evaporated, i.e., the solution concentration reaches approximately 0.02%. This is in good agreement with the densitometry data [4] and data of small-angle X-ray diffraction [1–3] according to which in the above concentration range the run of the concentration dependences of the solution density and intensity of small-angle X-ray scattering becomes opposite. Thus, the increased rate of solvent evaporation from the solution is in good agreement with formation of solvophobic shells and the decreased rate, with structuring of the solvent.

ACKNOWLEDGMENTS

This work was financially supported by the Interdisciplinary project of the St. Petersburg Scientific Center, ISTC project no. T-1145, the Program of Basic Research of the Department of Power Engineering, Mechanical Engineering, Mechanics, and Management Processes, Russian Academy of Sciences, the Program "Fullerenes and Atomic Clusters," and the Russian Foundation for Basic Research (grant no. 03-03-32633).

REFERENCES

1. Ginzburg, B.M., Tuichiev, Sh., Tabarov, S.Kh., and Shepelevskii, A.A., *Kristallografiya*, 2005, vol. 50, no. 4, pp. 597–600.
2. Ginzburg, B.M., Tuichiev, Sh., Tabarov, S.Kh., et al., *Zh. Prikl. Khim.*, 2005, vol. 78, no. 6, pp. 1047–1049.
3. Ginzburg, B.M. and Tuichiev, Sh., *J. Macromol. Sci., Ser. B:, Physics*, 2005, vol. 44, no. 4, pp. 517–530.
4. Mekalova, N.V., *Fullereny v rastvorakh* (Fullerenes in Solutions), Ufa: Ufim. Gos. Neft. Tekh. Univ., 2001.
5. Herbst, M.H., Dias, G.H.M., Magalhaes, J.G., et al., *J. Mol. Liq.*, 2005, vol. 118, nos. 1–3, pp. 9–13.
6. Krätschmer, W. and Huffman, D.R., *Phil. Trans. Roy. Soc. London, Ser. A*, 1993, vol. 1667, no. 343, pp. 33–38.

ISSN 1070-4272, Russian Journal of Applied Chemistry, 2006, Vol. 79, No. 7, pp. 1204–1206. © Pleiades Publishing, Inc., 2006.
Original Russian Text © O.P. Korotkikh, N.N. Kochurova, 2006, published in Zhurnal Prikladnoi Khimii, 2006, Vol. 79, No. 7, pp. 1214–1216.

BRIEF COMMUNICATIONS

Micelle Formation in Aqueous Dodecylpyridinium Chloride

O. P. Korotkikh and N. N. Kochurova

Research Institute of Chemistry, St. Petersburg State University, St. Petersburg, Russia

Received December 12, 2005; in final form, April 2006

Abstract—Micelle formation in aqueous dodecylpyridinium chloride is studied at 20, 25, 30, 35, and 40°C using the surface tension and conductivity methods.

DOI: 10.1134/S1070427206070330

Physicochemical studies of surfactants are important in view of great importance of these substances for private life, agriculture, medicine, and a variety of industrial processes [1].

In this study we examined micelle formation in aqueous solutions of a cationic surfactant, dodecylpyridinium chloride ($C_{12}H_{25}NC_5H_5Cl$) (DPC), using the surface tension and conductivity methods.

The quality of DPC used was confirmed by the lack of a minimum in the surface tension isotherm near the critical micelle concentration (CMC), and also by the spectroscopic and HPLC tests. Aqueous DPC solutions were prepared using double-distilled water.

The surface tension was measured by the ring detachment method [2] on a digital instrument (Markada, St. Petersburg) [3].

The instrument was calibrated by measuring the surface tension of hexane, isopropanol, benzene, ethylene glycol, and double-distilled water. The calibration curve was linear, allowing easy recalculation of the readings to the surface tension. The error of determination was within 0.5 mN m^{-1}.

The measurements were carried out at 20°C. The DPC concentration was varied from 5.5×10^{-4} to 3.1×10^{-2} M. Figure 1 show that the surface tension decreases with increasing DPC concentration, which is typical of the surfactant solutions [1, 4]. The CMC was determined to be 1.78×10^{-2} M by crossing two straight lines obtained using the least-squares method (Fig. 1).

The conductometric measurements were carried out on a V3-60 ac bridge at 2500 Hz, to eliminate polarization. The cell was calibrated with 0.01 N KCl. The temperature was maintained constant to within 0.05°C. The error of the conductivity determination was within 2%.

The conductivity was measured after establishment of the temperature and concentration equilibria. Solution preparation and all the measurements were carried out in a temperature-controlled glass cell taking into account the recommendations made in [5–7].

Figures 2a–2e shows the concentration dependences of the equivalent conductivity $\lambda = f(c^{1/2})$ for aqueous DPC of solutions at 20, 25, 35, and 40°C and concentrations $(1–4) \times 10^{-2}$ M. The curves follow the general trend, i.e., the equivalent conductivity decreases with increasing concentration [7, 8]. There are maxima and minima in the curves, like those reported in [7]. The first maximum corresponds to CMC_1 determined from the dependence of the specific conductivity æ on the DPC concentration, as the

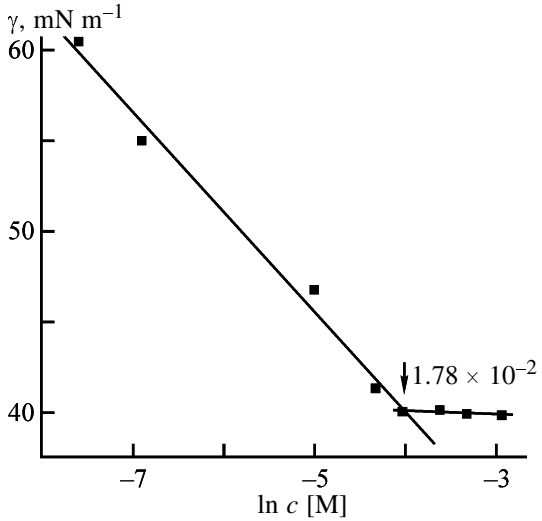


Fig. 1. Surface tension of DPC γ at 20°C as a function of ln *c*. (*c*) DPC concentration; the same for Fig. 2.

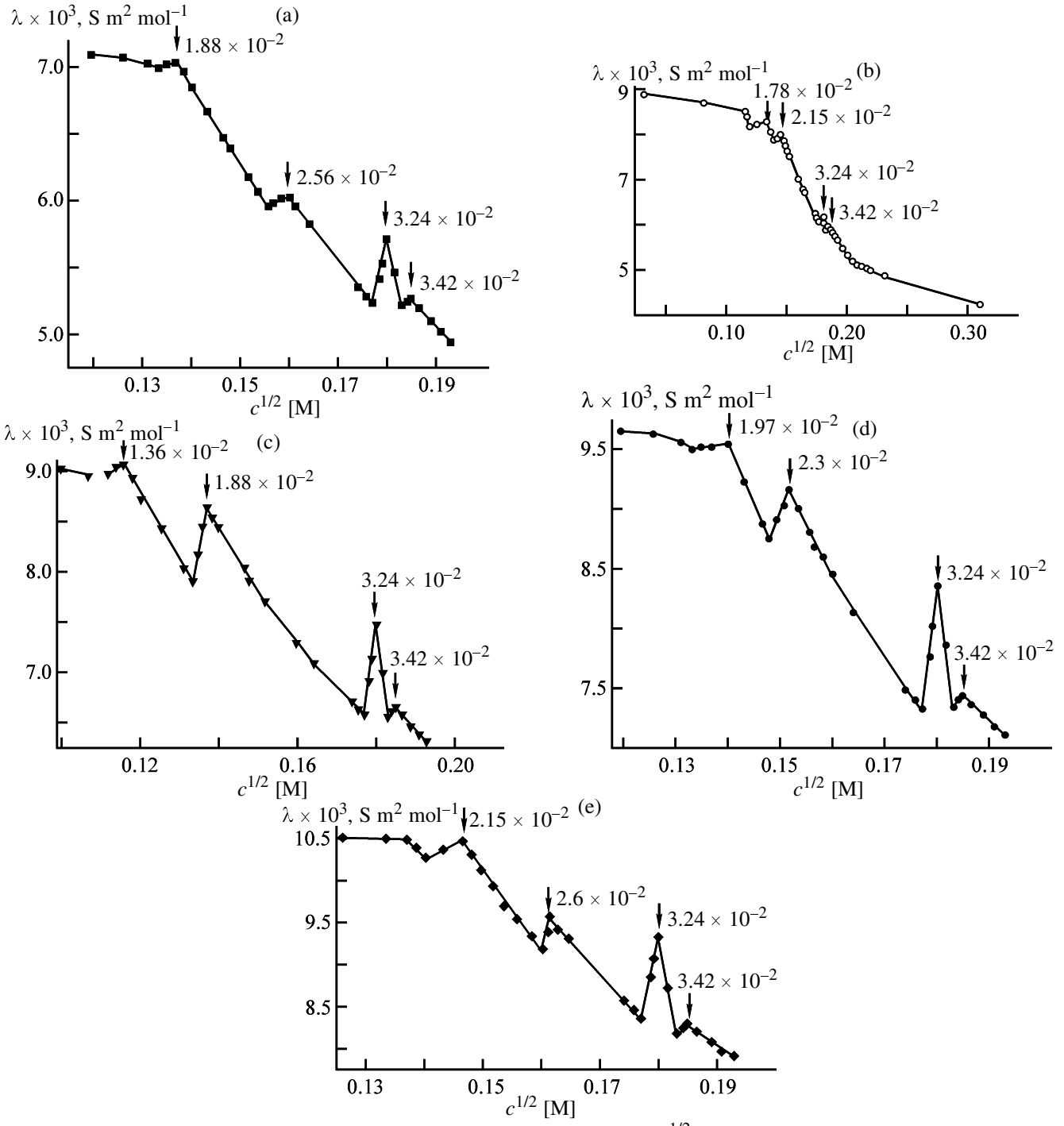


Fig. 2. Equivalent conductivity λ in aqueous DPC solutions as a function of $c^{1/2}$. Temperature (°C): (a) 20, (b) 25, (c) 30, (d) 35, and (e) 40.

intersection of two straight lines drawn using the least-squares method.

The table summarizes data on CMC_1 from various sources [4, 9] for the investigated surfactant at various temperatures. As seen, CMC_1 corresponding to the maximum in the curve $\lambda = f(c^{1/2})$ is in satisfactory agreement with the values determined by other methods.

There are three more features in the λ–$c^{1/2}$ curve above CMC_1 for which, as for CMC_1, each maximum follows a minimum [10], i.e., the conductivity abruptly changes in extremely narrow concentration ranges.

CMC_1 from various sources*

T, °C	$CMC_1 \times 10^2$, M		
	this work	[9], calorimetry	[4]
6		1.93	
20	1.88	1.75	
	1.78 (ST)		
25	1.78		1.4 (ST)
30	1.36	1.24	1.74 (EC)
35	1.97		
40	2.15		
45		2.0	
60		2.41	

* (ST) Surface tension and (EC) conductivity.

In this case, the maxima in the λ–$c^{1/2}$ curve correspond to the breaks in the æ–c curve at the respective concentration. Analyzing the behavior of the equivalent conductivity in micellar solutions, Rusanov has demonstrated [10] that the changes in the aggregation numbers, degree of aggregation, and degree of association with counterions in the course of micelle formation can be responsible for the appearance of extrema in the λ–$c^{1/2}$ curve.

In the range near 30°C, we found two maxima corresponding to CMC_1 and CMC_2. Similar temperature dependences of CMC were also observed for other surfactants [4, 11]. Such a behavior can be attributed to the structural transformations in water and to the change in the mode of hydration of the surface-active ions near 30°C [12].

At this temperature, the interaction mode of the cation with water changes. At lower temperatures, addition of ions decreases the activation energy of translational motion of the water molecules adjacent to the ion (negative hydration by Samoilov [13]), loosening the structure of water. Above 30°C, addition of ions increases the activation energy (positive hydration), thus structuring water. Therefore, there is a temperature (near 30°C) corresponding to the minimal CMC. At higher and lower temperatures, a higher surfactant concentration is required to form micelles.

No distinct temperature dependences were found for CMC_3 and CMC_4 (they are practically temperature-independent).

CONCLUSION

The experimental surface tension and conductance data show that the investigated surfactant is characterized by a series of CMC values (CMC_1–CMC_4). CMC_1 is consistent with the value obtained from the surface tension and calorimetric data. CMC_1 and CMC_2 are temperature-dependent, passing through a minimum at about 30°C, which is probably due to changing structure of water and hydration mode of the surfactant at this temperature. CMC_3 and CMC_4 are temperature-independent.

The study was performed under the Grants of the President of the Russian Federation for Support of Scientific Schools nos. NSh-789.2003.3 and NSh-4241.2006.3.

REFERENCES

1. Rusanov, A.I., *Mitselloobrazovanie v rastvorakh poverkhnostno-aktivnykh veshchestv* (Micelle Formation in Surfactant Solutions), St. Petersburg: Khimiya, 1992.
2. Rusanov, A.I. and Prokhorov, V.N., *Mezhfaznaya tenziometriya* (Interfacial Tensiometry), St. Petersburg: Khimiya, 1994.
3. Abdulin, N.G., Kochurova, N.N., and Rusanov, A.I., *Kolloidn. Zh.*, 1997, vol. 59, no. 6, pp. 725–728.
4. Abramzon, A.A., *Poverkhnostno-aktivnye veshchestva: Spravochnik* (Surfactants: A Handbook), Leningrad: Khimiya, 1979.
5. Robinson, R.A. and Stokes, R.H., *Electrolyte Solutions. The Measurement and Interpretation of Conductance, Chemical Potential, and Diffusion in Solutions of Simple Electrolytes*, London: Butterworths, 1959, 2nd ed.
6. Daggett, H.M., Bair, E.J., and Kraus, C.A., *Contribution from the Metcalf Research Laboratory of Brown University*, February 1951, pp. 799–803.
7. Markina, Z.N., Panicheva, L.P., and Zadymova, N.M., *Kolloidn. Zh.*, 1997, vol. 59, no. 3, pp. 341–349.
8. Kuhn, D.W. and Kraus, C.A., *Contribution from the Metcalf Research Laboratory of Brown University*, February 1950, vol. 72, pp. 3676–3678.
9. Mehrian, T., Keizer, A. de, Kortewegand, A.J., and Lyklema, J., *J. Colloids Surf. A: Physicochem. Eng. Aspects*, 1993, vol. 71, pp. 255–267.
10. Rusanov, A.I., *Kolloidn. Zh.*, 1998, vol. 60, no. 6, pp. 808–814.
11. Kochurova, N.N., Korotkikh, O.P., and Dmitrovskaya, M.V., *Zh. Prikl. Khim.*, 2004, vol. 77, no. 5, pp. 853–855.
12. Smirnov, T.L. and Kochurova, N.N., *Kolloidn. Zh.*, 2001, vol. 63, no. 1, pp. 123–126.
13. Samoilov, O.Ya., *Struktura vodnykh rastvorov elektrolitov i gidratatsiya ionov* (Structure of Aqueous Electrolyte Solutions and Ion Hydration), Moscow: Akad. Nauk SSSR, 1957.

ISSN 1070-4272, Russian Journal of Applied Chemistry, 2006, Vol. 79, No. 7, pp. 1207–1209. © Pleiades Publishing, Inc., 2006.
Original Russian Text © A.A. Rogachev, A.V. Rogachev, M.A. Yarmolenko, A.I. Egorov, 2006, published in Zhurnal Prikladnoi Khimii, 2006, Vol. 79, No. 7, pp. 1217–1219.

BRIEF COMMUNICATIONS

Morphology of Polytetrafluoroethylene Coatings Formed from the Active Gas Phase and Its Thermal Modification

A. A. Rogachev, A. V. Rogachev, M. A. Yarmolenko, and A. I. Egorov

Belarussian Sate University of Transport, Gomel, Belarus
Skorina State University, Gomel, Belarus

Received December 27, 2005; in final form, March 2006

Abstract—Changes in the morphology and surface energy of polytetrafluoroethylene coatings in the course of their growth and after annealing were determined.

DOI: 10.1134/S1070427206070342

Physicochemical processes occurring in the course of adsorption and nucleation of particles and in the initial steps of thin polymeric film growth from the active gas phase affect the structure of the resulting coatings and their properties [1, 2]. Previously we showed that the first deposition steps of polymer coatings from volatile products of electron-beam dispersion of the initial polymer, unlike adsorption and nucleation of, e.g., metallic phase, are obviously nonequilibrium [3, 4]. The parameters of the surface distribution of the polymer particles and the kinetics of the change in their density in the course of the deposition depend on the support and the degree of its activation [4]. We also found [5] that the volatile products of electron-beam dispersion are highly reactive and can react with the support during their adsorption. This feature, the long-range influence of the support surface, and selective desorption from the surface determine the physicochemical properties of the coatings and the structural nonuniformity of the boundary layers [6].

In the course of formation of thin polymer coatings from volatile dispersion products, the growth of the macromolecular chains and the films as a whole, as well as their structure and properties are determined by the mobility of the kinetic elements and by the intermolecular interactions [2]. Therefore, all external actions (heat treatment, irradiation, surface and bulk modification, etc.) affecting the synthesis and conformations of the macromolecules can be used to effectively control the deposition with the aim to change the structure and properties of the coatings.

In this study we examined the kinetic features of the first steps of deposition of polytetrafluoroethylene (PTFE) coatings and the influence of heat treatment on their morphology and surface properties.

EXPERIMENTAL

The coatings were prepared by electron-beam dispersion of PTFE by the procedure described in [3]. The coatings with the required properties were deposited using a special device with a controlled damper. The growth rate and the effective thickness of the coatings were measured with a quartz thickness gage (QTG). Polished silicon single-crystal wafers pretreated with R-646 organic solvent were used as the supports.

We studied the morphological changes and the adsorption properties of PTFE coatings in the course of their growth and vacuum annealing. The coatings were annealed in a vacuum at 455 K for 20 min with the aid of a resistive heater and then were cooled at a rate of 8–12 K min^{-1}. The morphology of the as-grown or annealed coatings was studied by atomic force microscopy (AFM) using a NANOTOP-2003 measuring setup. The scanning was performed in the tapping mode. To analyze the cluster formation, additional mathematical treatment was performed. The surface cluster distribution was constructed by the horizontal cross-section procedure with marking of the clusters. The cross sections with the minimal cluster content were analyzed [7]. The minimal considered surface area of the cluster (0.03 μm^2) did not exceed the microscope resolution. The maximal considered surface area of the cluster was 0.42 μm^2.

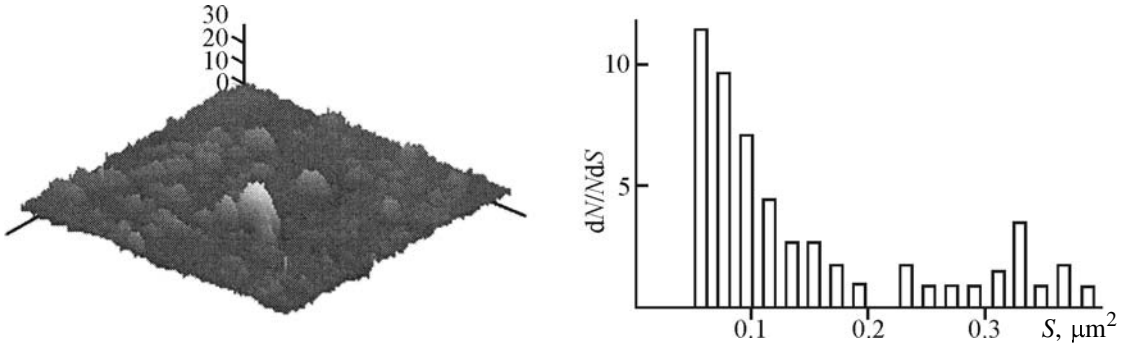


Fig. 1. AFM image of PTFE coating with the effective thickness of 9.1 nm and the particle distribution d*N*/*N*d*S* with respect to the surface area of their base *S*. Scanning area 13.5 × 13.5 μm.

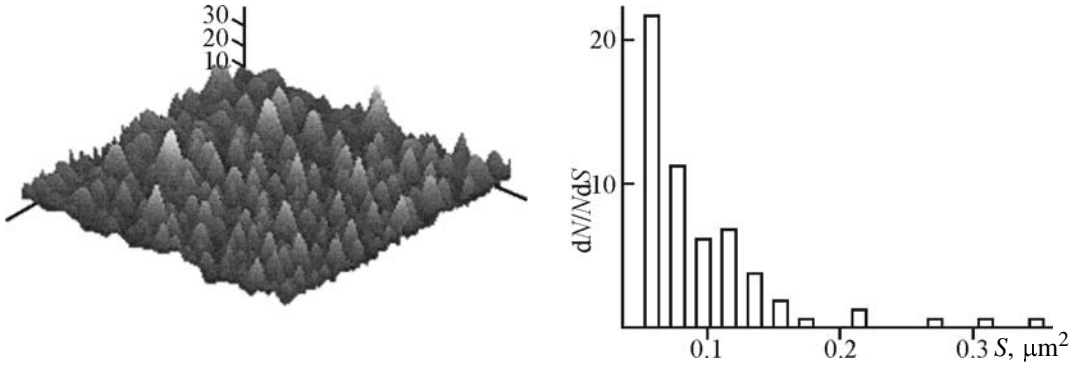


Fig. 2. AFM image of annealed PTFE coating with the effective thickness of 4.5 nm and the corresponding particle distribution d*N*/*N*d*S* with respect to the surface are of their base *S*. Scanning area 7.4 × 7.4 μm.

To study the surface properties of the coatings, the limiting wetting angles of their surface with distilled water and glycerol were measured. The polar and dispersion components of the surface energy were determined by the Fowkes procedure [8].

The shape of PTFE microparticles and their distribution over the surfcae of a silicon crystal in the initial deposition steps are determined by high adsorption nonuniformity of the support. The polymer microparticles grow on the active sites of the support, whose density is relatively low. This is consistent with our previous results [4]. The particle distribution with respect to the surface area of their base is complex (Fig. 1) and can be considered a superposition of the exponential distribution (in the range of low particle areas) and distribution with a maximum which is shifted to the larger particle size with increasing film thickness.

The density and height of polymer microparticles increase and the average surface area of their base decreases after annealing of the dispersed polymeric coating. The cluster density increases by a factor of 3.5, the weighted-average area decreases by a factor of 1.8, and the average cluster height increases form 7.6 to 12.2 nm after heat treatment of a PTFE coating with the effective thickness of 4.5 nm. When thicker coatings (e.g., with the effective thickness of 9.1 nm) are heated, the average height of their microparticles increases from 11.4 to 27.1 nm. To understand this experimental result, it should be taken into account that the adsorption layer of dispersed particles involved in polymerization is formed on the support surface in the first deposition steps [3, 4]. On heating of the coating above the glass-transition point, the macromolecules become more mobile and hence their agglomeration intensifies. The temperature effect on the density of polymeric particles sorbed from solutions is similar [9]. The parameters of particle distribution in annealed coatings of different thickness were determined. We expected that, as in the case of the unannealed samples, larger polymer microparticles are formed with increasing coating thickness. However, our experimental results showed that in the annealed samples the weighted-average particle surface area (0.12 μm^2) did not noticeably change and the particle density decreased from 2.28×10^{12} to 1.12×10^{12} m^{-2}. The distribution of the microiparticles with respect to the surface area of their base is close to exponential (Fig. 2). This is probably due to the fact that the adsorption phase of the 4–10-nm coatings is

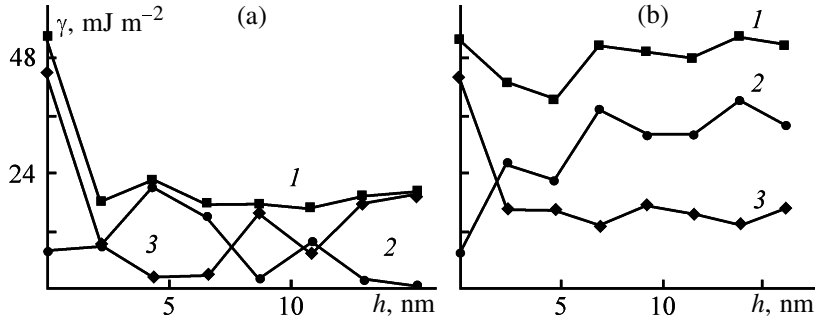


Fig. 3. (*1*) Total surface energy γ of PTFE coating and its (*2*) dispersion and (*3*) polar constituents as functions of the thickness *h*. (a) Before and (b) after annealing.

sufficiently continuous (the monolayer thickness is from 1 to 2 nm [10]) and the adlayer containing mobile particles is structured on heating. The increase in the average height of microparticles in the annealed samples can be due, on the one hand, to thermal desorption of low-molecular-weight fragments (decrease in the effective thickness of continuous adlayer) and, on the other hand, to thermal activation of structuring processes in the bulk.

It was found that the dependence of the surface properties of annealed and unannealed samples on the effective thickness of a polymer layer is complex. The surface energy of the coating increases by a factor of almost 2 after the heat treatment (Fig. 3).

As we expected, in both cases, the polar constituent of the surface energy substantially decreases in the course of monolayer deposition. This is caused by the features of adsorption interaction and appearance of more active sites of the macromolecules at the interface. The change in the dispersion and polar constituents of the surface energy is caused by this structuring.

The variation of the dispersion constituent of the surface energy correlates with that of the polar constituent. It should be noted that the run of the kinetic curves of the surface energy is similar to that of the fractal dimension determined in our previous study [4]. In both cases, the examined parameters are determined by the number of deposited monolayers, a change in the deposition conditions, and the transformation of the two-dimensional growth of the associates into the three-dimensional growth.

CONCLUSIONS

(1) The particle density and particle height of the polymer coatings increase and the average surface area of the particle base decreases after annealing of the coating.

(2) The surface energy of the annealed coating increases *S* by a factor of almost 2. The change in the dispersion constituent correlates with that of the polar constituent.

REFERENCES

1. Tkachuk, B.V. and Kolotyrkin, V.M., *Poluchenie tonkikh polimernykh plenok is gazovoi fazy* (Deposition of Thin Polymer Films from the Gas Phase), Moscow: Khimiya, 1977.
2. Bruk, M.A. and Pavlov, S.A., *Polimerizatsiya na poverkhnosti tverdykh tel* (Polymerization on the Solid Surfaces), Moscow: Khimiya, 1990.
3. Egorov, A.I., Kazachenko, V.P., Rogachev, A.V., and Yablokov, M.Yu., *Zh. Fiz. Khim.*, 2002, vol. 76, no. 11, pp. 2085–2089.
4. Rogachev, A.A., *Zh. Prikl. Khim.*, 2004, vol. 77, no. 2, pp. 285–288.
5. Kazachenko, V.P. and Rogachev, A.V., *Khim. Vys. Energ.*, 1999, vol. 33, no. 4, pp. 270–273.
6. Rogachev, A.V., Luchnikov, A.P., Rogachev, A.A., et al., in *Tonkie plenki i sloistye struktury: Materialy Mezhdunarodnoi nauchno-tekhicheskoi konferentsii* (Thin Films and Layered Structures: Proc. Int. Scientific and Technical Conf.), Moscow: MGIREA, 2002, p. 45.
7. Rogachev, A.A., Sarkisov, O.A., and Kazachenko, V.P., in *6-i Belorusskii seminar po skaniruyushchei zondovoi mikroskopii: Sbornik dokladov* (Sixth Belarussian Seminar on Scanning Probe Microscopy: Coll. of Papers), Minsk: Inst. Teplo- i Massoobmena im A.V. Lykova, 2004.
8. Pugachevich, P.P., Beglyarov, E.M., and Lavygin, I.A., *Poverkhnostnye yavleniya v polimerakh* (Surface Phenomena in Polymers), Moscow: Khimiya, 1982.
9. Lipatov, Yu.S., *Fiziko-khimicheskie osnovy napolneniya polimerov* (Physicochemical Foundations of Polymer Filling), Moscow: Khimiya, 1991.
10. Savenkov, G.N., Baidarovtsev, Yu.P., Yanchivenko, K.N., and Ponomarev, A.N., *Khim. Vys. Energ.*, 1996, vol. 30, no. 1, pp. 65–67.

ISSN 1070-4272, Russian Journal of Applied Chemistry, 2006, Vol. 79, No. 7, pp. 1210–1212. © Pleiades Publishing, Inc., 2006.
Original Russian Text © R.Kh. Mudarisova, E.I. Kulish, R.M. Zinatullin, N.E. Tamindarova, S.V. Kolesov, S.N. Khunafin, Yu.B. Monakova, 2006, published in Zhurnal Prikladnoi Khimii, 2006, Vol. 79, No. 7, pp. 1220–1222.

BRIEF COMMUNICATIONS

Interaction of Chitosan with Cefotaxime

R. Kh. Mudarisova, E. I. Kulish, R. M. Zinatullin, N. E. Tamindarova, S. V. Kolesov, S. N. Khunafin, and Yu. B. Monakova

Institute of Organic Chemistry, Ufa Scientific Center, Russian Academy of Sciences, Ufa, Bashkortostan, Russia
Bashkir State University, Ufa, Bashkortostan, Russia
Bashkir State Medical University, Ufa, Bashkortostan, Russia

Received April 12, 2006

Abstract—Features of complexation of chitosan with Cefotaxime antibiotic were examined. Optimal conditions for preparing the complexes were found, and their chemical composition and physicochemical properties were studied.

DOI: 10.1134/S1070427206070354

Recent studies show that chitosan (CTS) is promising as a carrier of pharmacological molecules and ions for biologically active preparations of prolonged effect [1–4]. For this application, such properties of the polysaccharide are important as its capability for fiber and film formation, ion exchange, and complexation. Complexation of CTS with metal ions was examined in numerous studies [5–7], but interactions of the polysaccharide with low-molecular-weight drugs are less understood [8–10].

In this study we examined the interaction of chitosan with an antimicrobial drug, Cefotaxime (CFT) [11].

EXPERIMENTAL

CTS was recovered from Far-Eastern crab shells and had the following characteristics: initial number-average degree of polymerization P_n = 860, degree of deacetylation 70–75%, and moisture content 4.5%. CFT (pharmaceutical preparation) was used without additional purification.

The IR spectra were recorded on a Specord M-80 spectrophotometer (KBr pellets or thin films). The ^{1}H NMR spectra were taken on a Bruker AM 300 spectrometer from samples dissolved in a solution of HCl in D_2O. The UV spectra of all the samples in 1% acetic acid were recorded on a Specord M-40 spectrophotometer in 1-cm quartz cells relative to water. The pH values of solutions were measured with an Anion 4100 pH meter. The specific rotation was measured with a Perkin–Elmer (model 141) polarimeter.

The complexes prepared were separated from unchanged CFT by double reprecipitation, which was performed by adding a solution of the complex into isopropyl alcohol (volume ratio of the reaction mixture and isopropyl alcohol 1 : 5); in so doing, the free antibiotic remained in the solution. The precipitate formed was washed with isopropyl alcohol and vacuum-dried to constant weight.

Cefotaxime is a β-lactam compound based on 7-aminocephalosporic acid. The presence of the carboxy group in CFT makes possible its complexation with amino groups of CTS. The electronic absorption spectrum of CFT at its concentration in 1% aqueous acetic acid (pH 4.2) of 1×10^{-5} M has a single maximum at 261 nm. On adding increasing amounts of chitosan, the intensity of the CFT absorption band increases, and the absorption maximum shifts toward shorter wavelengths by 22 nm. Chitosan has no absorption in this range. The spectral changes are indicative of a strong effect exerted by chitosan on the electronic system of CFT and of the formation of a complex. The band shift may be caused not only by complexation, but also by changes in the solution pH. However, variation of pH in the range 2–6 only slightly affects the intensity of the CFT absorption band and has no effect on its position. By the method of isomolar series [12] we showed that the stoichiometry of the CTS–CFT complex is 1 : 1 (Fig. 1). The complexation constants were calculated by the method of molar ratios [12]. At a constant concentration of CFT,

in the presence of a variable excess of chitosan, the spectral changes in CTS solutions are described by the equation [12]

$$[CTS]_0/(A - A_0) = 1/(\varepsilon - \varepsilon_0) + 1/\{(\varepsilon - \varepsilon_0)K[CFT]\},$$

where A and A_0 are the optical densities of the solutions in the presence and in the absence of CTS, respectively; [CTS], initial CTS concentration; ε and ε_0, molar extinction coefficients of the 1 : 1 complex and CFT, respectively; K, stability constant (β_c); and [CFT], CFT concentration.

From the slope of the plot of $[CTS]_0(A - A_0)$ vs. 1/[CFT] (Fig. 2), we determined by the least-squares method the stability constant of the complex, $\beta_c = (2.2 \pm 0.7) \times 10^5$ l mol^{-1}.

Complexes of CTS with CFT were isolated, purified, and characterized by IR, UV, and ^{1}H NMR spectroscopy and by elemental analysis (Table 1).

The electronic absorption spectra of the complexes are characterized by a hypsochromic shift of the absorption maximum of the modified chitosan molecule (λ_{max} = 253–258 nm; for free CFT, λ_{max} = 261 nm). Chitosan shows no absorption in this range. A new band at 1752 cm^{-1}, characteristic of the stretching vibrations of the carbonyl group in CFT, appears in the IR spectra of the complexes. In addition, the absorption maxima of the OH (3350–3250 cm^{-1}) and C–O (1200–1000 cm^{-1}) groups of the glycoside in the IR spectra of the complexes are shifted to lower frequencies by 30–50 and 10–15 cm^{-1}, respectively, suggesting formation of intermolecular hydrogen bonds between the CFT and CTS molecules. Comparison of the ^{1}H NMR spectra of CTS, CFT, and their complex shows that the proton signals of the complex (δ_H 3.20 ppm) are shifted downfield relative to free CTS (3.01 ppm). The electron density redistribution due to the complexation causes a downfield shift of the H^2 signal. As in the case of the complexation of dextrins with low-molecular-weight organic compounds [15], analysis of the chemical shifts in the ^{1}H NMR spectra of the CTS–CFT complex shows that the interaction of CTS with CFT is appreciable. The physicochemical properties of the CTS–CFT complex are given in Table 1.

Elemental analysis shows that approximately every fifth chitosan unit, on the average, participates in the complexation with CFT. Apparently, in a 2% CTS solution not all the polysaccharide units are accessible for the interaction with CFT. This is indicated by data on the influence exerted by the CTS : CFT ratio at

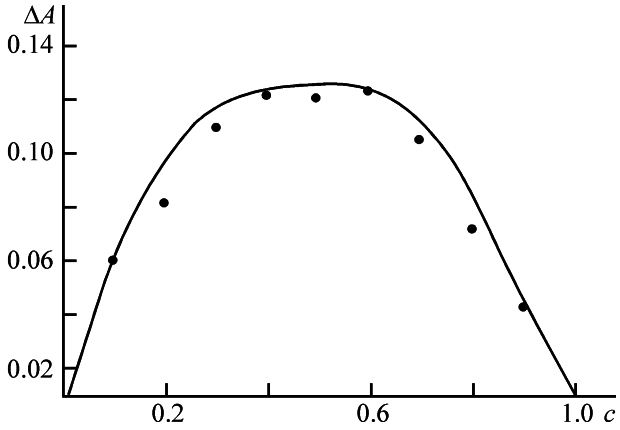


Fig. 1. Isomolar diagram. [CTS] + [CFT] = 5 × 10^{-4} M; pH 4.2; l 1 cm. (A) Optical density and (c) concentration ratio $c_{CFT}/(c_{CFT} + c_{CTS})$.

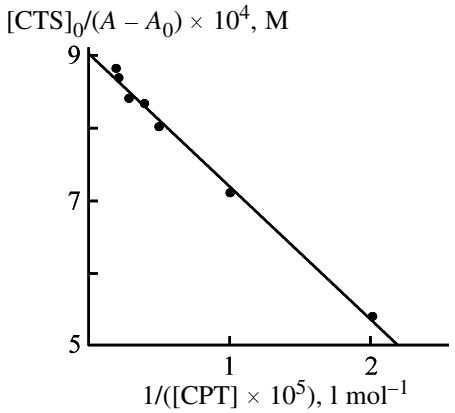


Fig. 2. Plot of $[CTS]_0/(A - A_0)$ vs. 1/[CFT] for the complex of chitosan with Cefotaxime.

[CTS] = 2 wt % on the CFT content in the complex (Table 2).

As the molar ratio of the components is changed from 1 : 0.25 to 1 : 3, the CFT content in the reaction product increases; the temperature and time of the

Table 1. Comparison of the physicochemical properties of CTS and CTS–CFT complex

Compound	D_{25}	Calculated, %/Found, %			
		C	H	N	S
Chitosan	+23	46.8 / 46.3	5.1 / 6.8	8.6 / 8.9	– / –
Cefotaxime	+54	42.2 / 41.4	3.7 / 3.9	15.4 / 14.7	14.1 / 13.5
CTS–CFT complex	–	43.2 / 42.0	4.9 / 5.3	11.0 / 11.3	8.2 / 2.5

Table 2. Influence of the complexation conditions on the drug content in the reaction products

CTS : CFT molar ratio	τ, h	*T*, °C	CH_3COOH concentration, %	CFT content in complex, %
1 : 1	0.25	25	1	14.1
1 : 1	0.5	25	1	22.5
1 : 1	1	25	1	21.3
1 : 1	6	25	1	20.3
1 : 1	24	25	1	21.4
1 : 0.25	1	25	1	8.9
1 : 0.5	1	25	1	11.3
1 : 1.5	1	25	1	25.2
1 : 2	1	25	1	33.5
1 : 3	1	25	1	33.4
1 : 1	1	40	1	20.9
1 : 1	1	60	1	22.3
1.5 : 1	1	25	1	23.4
0.25 : 1	1	25	1	13.4
0.25 : 1	1	25	10	3.8
0.25 : 1	1	25	50	4.0
0.25 : 1	1	25	70	3.4

complexation reaction do not appreciably affect the drug content.

Examination of the influence exerted by the chitosan concentration on the CFT content in the complex leads to interesting conclusions. Table 2 shows that the CFT content in the complex prepared from more concentrated solutions is higher than in the complex prepared from the dilute chitosan solution. Also, an increase in the concentration of acetic acid in solution, i.e., a decrease in pH of the medium, is accompanied by a considerable decrease in the CFT content in the reaction product (Table 2). These facts can be explained only taking into account the degree of protonation of chitosan amino groups. The lower the CTS concentration in solution and the higher the solution acidity, the higher the degree of protonation of the amino grops. Therefore, under these conditions the incorporation of CFT in the complex is insignificant. The lower the degree of protonation, the higher the probability of the complexation. Thus, by varying the reaction conditions, it is possible to prepare complexes based on chitosan with a CFT content from 3.4 to 33.5%.

CONCLUSIONS

(1) Examination of the complexation of chitosan with Cefotaxime revealed the formation of the stoichiometric complexes.

(2) Optimal conditions for preparing the complexes were found. Complexes containing from 3.4 to 33.5% drug were prepared depending on the complexation conditions.

ACKNOWLEDGMENTS

The study was financially supported in part by the Foundation for Support of Leading Scientific Schools (grant NSh 728.2003.3.), by project UR.05.01.008 within the framework of the scientific program of the Federal Education Agency "Development of the Scientific Potential of Higher School," and by the State Scientific and Technical Program of the Bashkortostan Republic for the years 2005–2007 (contract 419-Kh).

REFERENCES

1. Suzuki, K., Mikami, T., and Okawa, Y., *Carbohydr. Res.*, 1986, vol. 151, pp. 403–408.
2. Dubinskaya, A.M. and Dobrotvorskaya, A.E., *Khim.-Farm. Zh.*, 1989, no. 5, pp. 623–628.
3. Galiaskarova, G.G., Mullagaliev, I.R., and Monakov, Yu.B., *Bashk. Khim. Zh.*, 1996, vol. 3, nos. 5–6, pp. 3–12.
4. *Chitin and Chitosan: Sources, Chemistry, Biochemistry, Phisical Properties and Application*, Anthonsen, T., Ed., London: Elsevier, 1990.
5. Nieto, J.M., Peniche-Covas, C., and Del, B.J., *J. Carbohydr. Polym.*, 1992, vol. 18, no. 3, pp. 221–224.
6. Wang, X., Huang, H., and Jiang, Y., *Macromol. Chem. Macromol. Symp.*, 1992, vol. 59, pp. 113–121.
7. Kurita, K., Sannan, T., and Iwakura, I., *J. Appl. Polym. Sci.*, 1979, vol. 23, no. 2, pp. 510–515.
8. Giunchedi, P., Genta, I., and Muzzarelli, R.A., *Biomaterials*, 1998, vol. 19, nos. 1–3, pp. 157–161.
9. Kawashima, Y. and Kasai, A., *Chem. Pharm. Bull.*, 1985, vol. 33, no. 5, pp. 2107–2113.
10. Tan Tian, R., Ynjue, K., Mashida, Y., et al., *J. Pharm. Sci. Technol.*, 1988, vol. 48, no. 4, pp. 318–321.
11. Mashkovskii, M.D., *Lekarstvennye sredstva* (Drugs), Kharkov: Torsing, 1997, vol. 2.
12. Bulatov, I.P. and Kalinkin, M.I., *Prakticheskoe rukovodstvo po fotometricheskim metodam analiza* (Practical Guide on Photometric Methods of Analysis), Leningrad: Khimiya, 1986.
13. Kulikov, O.V., Terekhova, I.V., Kumeev, R.S., and Al'per, G.A., *Zh. Fiz. Khim.*, 2004, vol. 78, no. 9, pp. 1694–1699.

ISSN 1070-4272, Russian Journal of Applied Chemistry, 2006, Vol. 79, No. 7, pp. 1213–1214. © Pleiades Publishing, Inc., 2006.
Original Russian Text © A.G. Morachevskii, I.N. Beloglazov, 2006, published in Zhurnal Prikladnoi Khimii, 2006, Vol. 79, No. 7, pp. 1223–1224.

BOOK REVIEWS

Poole, C.P., Jr. and Owens, F.J., *Introduction to Nanotechnology*

New York: Wiley–Interscience, 2003

Translated under the title *Nanotekhnologiya*

Moscow: Tekhnosfera, 2004, 328 pp.

DOI: 10.1134/S1070427206070366

Among quite a number of monographs, textbooks, and popular-science editions published in recent years and devoted to nanomaterials and nanotechnologies, the book by C.P. Poole and F.J. Owens is one of the best in its scientific level, manner of presentation, and number of materials covered. The book is recommended by the Institute of Chemical Physics, Russian Academy of Sciences, as a textbook for students specializing in nanotechnology.

The book includes the authors' preface and that by the editor of the Russian translation (Prof. Yu.I. Golovin), thirteen chapters, two appendices, and a supplement. A brief list of the recommended literature is given at the end of each chapter.

The authors' preface (pp. 12, 13) notes that the interest in nanotechnologies originated in the United States in 1996–1998, when a government commission, aided by the World Technology Evaluation Center (WTEC) and financed by the National Science Foundation and other federal agencies, started to analyze the world's R&D experience in nanotechnology in order to assess its technological innovation potentialities. In the years that followed, a very large amount of funds was assigned to the development of nanoscience and nanotechnologies and interdisciplinary research covered a wide area at the frontline of physics, chemistry, biology, and technical sciences.

The preface of the editor of the Russian translation (pp. 14–16) discusses the advantages and certain disadvantages of the book by Poole and Owens and presents a list of domestic and foreign books on nanomaterials and nanotechnologies, published in 2001–2004. Chapter 1 (pp. 17–22) serves as introduction. The authors give a general historical notion of nanoparticles and specially emphasize at the conclusion of the introduction the interdisciplinary nature of work in the field of nanomaterials and nanotechnologies and the related difficulties and specific circumstances, which, in particular, affected the structure of the book. The authors admit that the field of nanotechnology is too wide, involves a too large number of disciplines, and too rapidly develops for an exhaustive book on the subject to be written. Chapter 2 (pp. 23–46) presents several concepts of solid state physics, which bear direct relation to understanding of nanostructures (atomic structure, energy band structure, localized particles, and quasi-particles).

The considerable recent progress in the development of nanotechnologies is, in particular, associated with improvement of the already existing instrumental means for determining the parameters of nanostructures and appearance of new ones. The operation principles of some of the devices and research techniques are considered and their opportunities are assessed in Chapter 3 (pp. 47–78). Chapter 4 (pp. 79–102) describes the properties of individual nanoparticles. It discusses metallic nanoclusters, semiconducting nanoparticles, clusters of inert gases, molecular clusters, and various methods for synthesis of nanoparticles. The authors demonstrate with a large number of specific examples that the physical, chemical, and electronic properties of nanoparticles strongly depend on the number and type of the constituent atoms. The authors emphasize that nanosize materials can serve as a basis for a whole new class of atomically engineered materials.

Chapter 5 of the book (pp. 103–126) is exclusively devoted to analysis of a wide variety of carbon nanostructures, and carbon nanotubes in the first place, methods of their fabrication, structure, various properties, and application fields. Chapter 6 (pp. 126–152) describes bulk nanostructured materials: disordered solid-state structures and nanostructured crystals.

Chapter 7 (pp. 153–174) contains evidence concerning ferromagnetism in nanostructures. It presents the basic concepts of ferromagnetism, effect of nanostructuring of a bulk material on its magnetic properties, deposition of films composed of nanosize mag-

netic particles, and development of materials by filling of pores with magnetic nanoparticles. The chapter also discusses nanocarbon ferromagnetic materials and ferromagnetic fluids.

Various kinds of spectroscopy are among the main methods used to study nanoparticles. Chapter 8 (pp. 175–198) discusses, together with optical spectroscopy in the visible and UV ranges, methods for analysis of nanomaterials by IR and Raman spectroscopy. Special attention is given to methods for obtaining additional information about nanostructures, such as photoluminescence, fluorescence, and thermoluminescence.

As the size of sample decreases from macroscopic to very small, its properties first remain unchanged and then start to be gradually modified, with fundamental changes observed at a size less than 100 nm. If a sample has size in the nanometer range in one dimension and is large in the other two, such a structure is named a quantum well. If a sample is small in two dimensions and is large in the third, such an object is named a quantum wire. The limiting case, when the sizes in three dimensions lie in the lower part of the nanometer range, is that of a quantum dot. The epithet "quantum" used for these three types of structures is due to the quantum-mechanical change in properties. The specific type of behavior of samples with one, two, or three dimensions lying in the nanometer range are the subject of Chapter 9 of the book (pp. 199–224).

Chapter 10 (pp. 225–244) is named "Self-Assembly and Catalysis." By self-assembly is understood spontaneous organization of small molecules into large, strictly defined, stable molecular complexes or aggregates and deposition of atoms or molecules onto a substrate with subsequent self-ordering into nanostructures suitable for various applications. The catalysis in nanoscience can play two basic roles. On the one hand, catalysts can be used in various methods for synthesis of quantum dots, nanotubes, and many other nanostructures. On the other, certain nanostructures can themselves serve as catalysts for particular chemical reactions.

Chapter 11 (pp. 245–270) is devoted to nanoparticles of organic origin. These nanoparticles can be obtained from large organic molecules of various types and from polymers composed of organic building blocks. Chapter 12 (pp. 271–290) is devoted to nanostructures in biology. The final Chapter 13 (pp. 291–310) describes nanomachines and nanodevices: micro- and nanoelectromechanical systems, molecular and supramolecular switches. Appendix *A* (pp. 311, 312) contains a number of mathematical expressions related to delocalization or partial localization of conduction electrons in nanostructures. Appendix *B* (pp. 313–318) includes evidence concerning the crystallographic, thermodynamic, and some other properties of III–V and II–VI semiconducting compounds in the bulk state.

The supplement to the Russian edition (pp. 319–327) is devoted to the technology of micromodification of composites with fulleroid nanomaterials.

The book by Poole and Owens is very well written and intended for a wide audience of specialists with moderate physicochemical background. The large number of clear illustrations favors better understanding of the material.

A. G. Morachevskii and I. N. Beloglazov

ISSN 1070-4272, Russian Journal of Applied Chemistry, 2006, Vol. 79, No. 8, pp. 1215–1219. © Pleiades Publishing, Inc., 2006.
Original Russian Text © V.M. Orlov, M.N. Miroshnichenko, V.V. Sukhorukov, 2006, published in Zhurnal Prikladnoi Khimii, 2006, Vol. 79, No. 8, pp. 1233–1237.

INORGANIC SYNTHESIS AND INDUSTRIAL INORGANIC CHEMISTRY

Heterogeneous Reduction of Potassium Heptafluorotantalate

V. M. Orlov, M. N. Miroshnichenko, and V. V. Sukhorukov

Tananaev Institute of Chemistry and Technology of Rare Elements and Mineral Raw Materials, Kola Scientific Center, Russian Academy of Sciences, Apatity, Murmansk oblast, Russia

Received October 25, 2005; in final form, April 2006

Abstract—The results obtained in the study of the influence of heterogeneous reduction conditions on the characteristics of the tantalum powder obtained are presented. A new technique for heterogeneous reduction of potassium heptafluorotantalate with sodium is described. The technique allows production of powders with characteristics corresponding to those obtained in a large-scale experiment, with small amounts of reactants.

DOI: 10.1134/S1070427206080015

The main method for production of metallic tantalum is its reduction with sodium from potassium heptafluorotantalate (PFT) by reaction (1) to give a tantalum powder.

$$K_2TaF_7 + 5Na = Ta + 2KF + 5NaF. \quad (1)$$

The reaction involves a significant heat release and proceeds spontaneously in a mixture of the reagents upon local heating to 450–500°C [1]. The resulting powder has a highly developed surface of particles. Up to 60% of the world's output of tantalum is used for fabrication of anodes of volume-porous tantalum capacitors. Therefore, the specific surface area of the powder is of great importance, because it predetermines the possibility of raising the specific charge of the capacitors and their miniaturization.

In practice, the reduction process is used in several variations. These may be reduction of PFT in a melt of salts, with liquid sodium delivered to the melt surface ("liquid-phase reduction") [2]. In another variant, the reaction is initiated in a mixture of solid PFT and sodium by heating the stock to the reaction onset temperature. This temperature is higher than the melting point of sodium and considerably lower than the melting point of PFT, and the reaction zone moves in the bulk as the heat front propagates. Therefore, the process should be considered "heterogeneous," because substances in different states (liquid and solid phases) enter into the reaction.

The aim of this study was to examine specific features of the reaction of potassium heptafluorotantalate with sodium, using both a premixed homogeneous stock and reagents loaded in layers, and also to analyze characteristics of the resulting tantalum powders.

EXPERIMENTAL

The reduction process is accompanied by heat release into the environment, whose share depends on the weight (volume) of the reactants. Preliminary studies demonstrated that, in experiments carried out with a small mass of reagents by the conventional technique in a steel retort heated by a resistance furnace, most part of the tantalum powder obtained significantly differs in granulometric characteristics from that formed in a large-scale experiment because of the considerable temperature differences in the volume of the stock. To obtain sufficiently reliable data in laboratory conditions, we developed a procedure that could eliminate this disadvantage to a considerable extent.

The reactor (Fig. 1) has the form of a quartz ampule *1* with an airtight cover *2* equipped with pipes *3* for evacuation and delivery of an inert gas, admission openings for the stirrer *4*, thermoelectric couple *5*, and holder *6* of a steel vessel *7* with a diameter of 6 cm and 8 cm high, filled with the stock. Ampule *8* with a weighed portion of an alkali metal was suspended

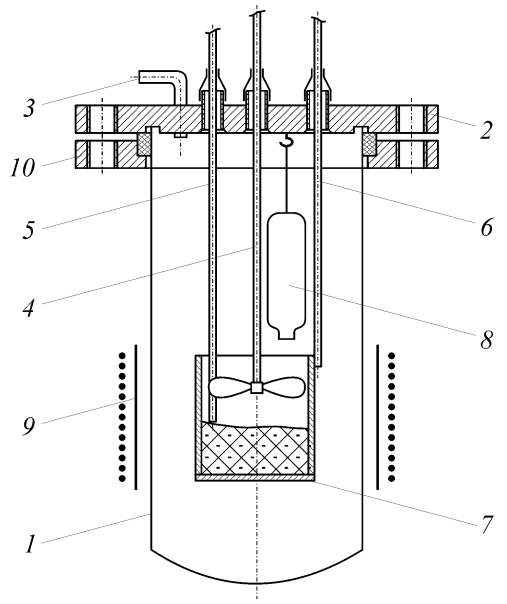


Fig. 1. Schematic of the reactor: (*1*) Quartz ampule, (*2*) airtight cover, (*3*) pipe for evacuation and delivery of an inert gas, (*4*) stirrer, (*5*) thermocouple, (*6*) holder of the steel vessel, (*7*) steel vessel, (*8*) ampule with a reducing metal, (*9*) resistance furnace, (*10*) flange.

from a hook on the inner side of the cover. The heating prior to an experiment was carried out with a resistance furnace *9*. To compensate for the pressure buildup in the course of reaction, a rubber tube (not shown in Fig. 1) was connected to the retort.

We used in the study high-purity potassium heptafluorotantalate with various granulometric compositions: original, with particle size of 5 to 50 μm; recrystallized, with particle size exceeding 250 μm; and recrystallized and thermally treated. The content of metallic impurities in the reagent did not exceed 0.001% for each impurity. The heat treatment of K_2TaF_7 consisted in twofold heating in a vacuum to 250°C with an intermediate cooling to 100°C. In the process, the size of crystals decreased to 300 μm and less (main fraction 40–140 μm) as a result of the polymorphic transformation at 203°C [3]. Chemically pure KCl, NaCl, KF, and NaF, used as fluxing additives, were preliminarily calcined at 650°C.

To obtain a homogeneous stock, a mixture of K_2TaF_7 (65 g) and a necessary amount of a flux were charged into the steel vessel and placed in the reactor, and an opened ampule with sodium (20 g) was suspended from the reactor cover. The reactor was evacuated, and the vessel with the salts was heated at 150°C for 1 h for additional dehydration. Then the furnace was shifted to the zone with the ampule, and sodium was melted and discharged. The reactor was filled with argon, and the stock was cooled to 100°C and thoroughly agitated to a homogeneous state. Then the reactor was cooled to room temperature, placed in an inductor of a VCHI-10/0.44 high-frequency generator, and the vessel was heated with a high-frequency current to initiate a reaction. This heating technique allowed high-rate heating, with the wall temperature of the reaction vessel maintained close to that of the reaction mass, which largely compensated the loss of heat into the environment. Owing to the low temperature of walls, the quartz retort was not destroyed by the sodium vapor and could be repeatedly used. The transparency of its walls allowed us to visually inspect the quality of mixing of the reactants and monitor the reaction course. The temperature was recorded with a measuring-computing complex comprising an analog-to-digital converter and a computer, with chromel–alumel thermocouples used as sensors.

In another variant, a mixture of the salts and sodium was charged layer by layer into the reaction vessel. The stock was covered with a NaCl layer serving as a heat shield, which, in addition, diminished the evaporation loss of the reducing agent. The vessel was placed in the reactor, which was evacuated and filled with argon. The reaction was also initiated by high-frequency heating.

After the process was complete and the reactor was cooled, it was opened, the remaining sodium was eliminated, reaction products were withdrawn, and the powder was washed to remove the salts [4]. After the powder was dried, its granulometric characteristics were determined: bulk weight γ, in conformity with GOST (State Standard) 19440 in a cell of volume 5.5 cm^3; and the specific surface area *S*, by the method of gas permeability in a vacuum with a UGP-2 instrument. The anodes were fabricated, and their characteristics, measured, using the standard technique [5].

Our study demonstrated that halides of alkali metals introduced into the stock are necessary not only as a thermal ballast controlling the maximum temperature reached in the reaction, but also as a condition for obtaining a homogeneous stock. Because PFT is not wetted by sodium at 100°C, preparation of a homogeneous mass without flux additives was virtually impossible. The introduction of KCl and KF into the stock considerably simplified the mixing. The mixture looked like a shining homogeneous paste. We may assume that the substitution reaction

$$KCl\,(KF) + Na = K + NaCl\,(NaF) \qquad (2)$$

yields a certain amount of metallic potassium, which improves the wetting. The occurrence of reaction (2) was indicated by the presence of a liquid alkali metal on the stock surface in a number of experiments at temperatures below the melting point of potassium. This could only be a low-melting alloy of sodium with potassium. However, the use of KF as a flux led to severe difficulties because the reaction frequently started spontaneously when mixing the stock. It is probable that sodium reacted with water, whose certain amount could be present despite all the precautions because of the high hygroscopicity of the salt. As a result, there occurred a local heating sufficient for the reaction to be initiated. With NaCl and NaF used as a flux, the stock had, after mixing with sodium, the form of a loose homogeneous black mass. The wetting of these salts by sodium favored formation of a homogeneous stock in this case.

The temperature variation during the reduction was monitored at two points: on the inner wall of the reaction vessel and in the central part of the stock. A typical temperature variation with time is shown in Fig. 2. The bend in curve *2* (point *a*) at 130°C corresponds to the onset temperature T_{on} of the reduction reaction. It varies rather widely, in the range 120–250°C. Noteworthy is the fact that the reaction begins at a temperature considerably lower than that (450–500°C) reported in [1]. It is seen from Fig. 2 (curve *2*) that the temperature first slowly increases to the inflection point, owing to the propagation of the heat front, and then a sharp rise in temperature is observed, which points to the onset of the reaction. Although the reaction itself occurs at a high rate, its propagation is limited by the motion rate of the temperature front. Measurements carried out with a high-frequency heating of the mixture of the flux with sodium demonstrated that the rate of the temperature front propagation is about 2 deg s^{-1} at a temperature of the mixture lower than the melting point of sodium, and 8 deg s^{-1} at a temperature higher than the melting point of sodium. Despite the excess pressure of argon, a significant amount of sodium vapor was observed at the instant when the reaction occurred. This suggests that the local temperature at the points of interaction of the reactants is higher than the average temperature of the stock, measured with a thermocouple, and exceeds the boiling point of sodium (883°C). No ejection of the stock, caused by pressure buildup, occurred. As can be seen from the plots, the temperature in the central part of the reaction mass is higher than the wall temperature of the reaction vessel, but this difference is insignificant. The temperature of the outer wall is maintained constant by the high-frequency heating, which minimizes the loss into the environment.

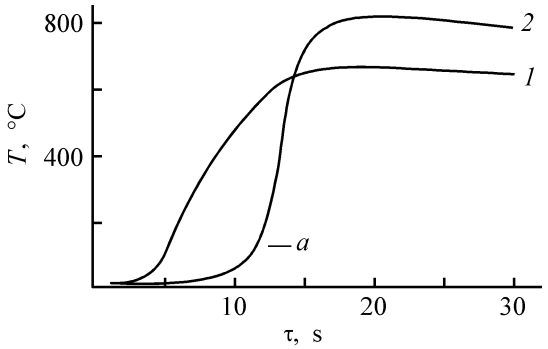


Fig. 2. Typical temperature variation in the course of the reaction. (*T*) Temperature and (τ) time. (*1*) Inner wall of the reaction vessel, (*2*) central part of the reaction mass.

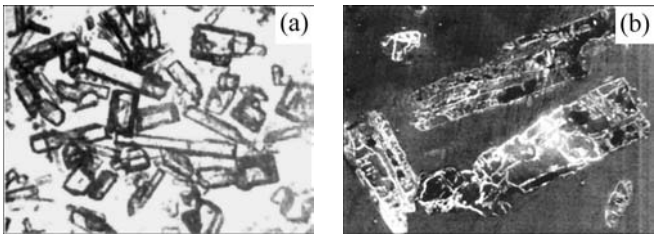


Fig. 3. Microstructure of (a) K_2TaF_7 crystals and (b) tantalum powder particles.

We can distinguish three regions in the reaction mass formed. In some cases, a loose layer composed of a mixture of salts and an alkali metal was observed on the surface. The probable reason is that the temperature in this zone is low because the heat released in reaction (1) is absorbed by the excess sodium displaced from pores onto the surface of the stock. This layer was removed by scraping. The main part of the reaction products was a light poorly sintered mass. The powder obtained from this part was composed of platelet particles with a metallic luster. The thin layer adjacent to the walls of the reaction vessel had the form of a black fusion cake of salts. The powder was finer, dark, and its coarse particles readily disintegrated under a mechanical action. The weight of this layer did not exceed 10%, whereas in the case of reduction of the same amount of the stock in a retort heated by a resistance furnace, its amount was no less than 60% of the total mass.

A microscopic study demonstrated that many particles, both light and dark, reproduce the shape of fluorotantalate particles (Fig. 3). We can assume that, at a close contact between K_2TaF_7 particles and a reducing agent, the heat released upon the reaction onset

Table 1. Parameters of the powder at various contents of a fluxing additive in the stock (temperature of anode sintering 1550°C)

Flux	K_2TaF_7 : flux (mole ratio)	T_{max}, °C	γ, g cm^{-3}	S, cm^2 g^{-1}	Q, μC l^{-1}
NaCl	2.0	960	1.0	5700	18 300
	1.0	935	1.0	7200	18 900
	0.3	825	0.7	9200	19 700
KCl	2.0	840	0.9	5700	17 700
	1.0	835	0.8	7100	17 900
	0.3	730	0.5	11 400	18 500
NaF	2.0	920	1.1	3200	14 400
	1.0	940	0.7	7500	21 400
	0.3	880	0.7	8400	22 600

is sufficient for melting of the remaining part of a salt particle, and the reaction further occurs between liquid heptafluorotantalate and liquid or even vaporous sodium. As a result, a metallic cocoon reproducing the shape of a K_2TaF_7 crystal is formed. Further growth of the particle occurs due to the reaction of the reducing agent penetrating through fractures with the remaining part of the PFT melt. The thickness of the metallic particle formed correlates with the size of a salt crystal. This model is confirmed by the dependence of the granulometric composition of the resulting powder on that of the starting heptafluorotantalate. In reduction of PFT with crystal sizes less than 300 μm, the amount of the fraction with a crystal size less than 44 μm in the tantalum powder was up to 35%. If a recrystallized salt with crystals larger than 250 μm was used, the amount of particles smaller than 44 μm in the powder did not exceed 15%.

The experiments showed that another factor affecting granulometric characteristics of the powder is the amount of a neutral salt in the stock. As the content of a fluxing additive decreases (Table 1), the maximum temperature reached in the bulk of the stock, the surface area of the powder and, accordingly, the specific charge of the anodes increase. The low bulk weight of the powders is accounted for by the specific features of their morphology [6]. Unfortunately, it is technically hardly possible to obtain powders with a larger surface area in such a process because of the decrease in sizes of K_2TaF_7 particles. When primary PFT with particle size less than 50 μm was used, its high reactivity resulted in that a spontaneous reaction, as a rule, commenced even under stirring at temperatures not higher than 100°C.

The use of finely dispersed PFT as a raw material for the heterogeneous reduction did not cause any complications in the case of the layer-by-layer charging of reagents. However, powders had in this process mode a smaller specific surface area and a considerably greater bulk weight (Table 2). The reduction itself started at a higher temperature (480–560°C). The addition of a flux (NaCl) to the stock had virtually no effect on the onset temperature of the process, but noticeably lowered the maximum temperature, which affected the parameters of the powder and anodes. A similar dependence of the onset temperature of the reduction on the state of the stock was also observed in the case of a sodium-reduction of zirconium from K_2ZrF_6 [7].

We can explain this phenomenon as follows: in the case of a layer-by-layer loading of the reactants, they are separated by the oxide layer present on the surface of the reducing agent and the reaction

Table 2. Comparative parameters of powders obtained in reduction of a homogeneous stock and that loaded in layers (mole ratio K_2TaF_7 : flux = 2)

Stock	K_2TaF_7	Flux	T_{on}, °C	T_{max}, °C	γ, g cm^{-3}	S, cm^2 g^{-1}	$\Delta d/d$, %	Q, μC l^{-1}
Homogeneous	Primary	NaCl	140	835	0.7	6300	8.5	21 600
	Heat-treated	NaCl	140	960	1.0	5700	6.4	18 300
		KCl	125	840	0.9	5700	4.8	17 700
		NaF	120	920	1.1	3200	2.7	14 400
Layered	Primary	No	485	890	1.8	3400	4.1	14 100
		NaCl	510	770	1.4	4400	5.8	15 000
	Heat-treated	No	530	960	1.7	3200	3.7	14 500
		NaCl	510	770	1.4	3800	4.4	15 100

begins only after this layer disintegrates, which occurs at a sufficiently high temperature. In the case of a homogeneous stock obtained by mixing of the reactants, there is no oxide film at the place of contact, and the main part of salt crystals are in a direct contact with the reducing agent, owing to which the reaction begins at a lower temperature. Varying the reduction conditions strongly affected the morphology of the powders. In the case of a layered stock, most part of the powder is represented by equiaxial particles with a developed surface, and only an insignificant amount of the particles have a shape corresponding to that of K_2TaF_7 crystals. The reason is that, initially, the main part of the salt has no direct contact with the reducing agent. The majority of particles of the tantalum powder are formed either as a result of the reaction of sodium vapor with K_2TaF_7 crystallites that had not enough time to melt, or as a result of coagulation and caking of finer primary powder particles.

The characteristics of the anodes sintered from powders of both types at 1550°C are listed in Table 2. Noteworthy is the fact that, at a large difference in surface area between the powders obtained by reduction of homogeneous and layered stocks, the specific charges of anodes made from these powders differ to a lesser extent. This means that a significant part of the surface of planar particles is constituted by microscopic irregularities smoothed-out in sintering of the anodes and in growth of the anodic oxide, making no contribution to the actual surface area of the powder.

CONCLUSIONS

(1) The conditions of heterogeneous reduction affect the characteristics of the tantalum powder obtained. In the case of reduction in a homogeneous mixture of K_2TaF_7 and sodium, a powder with platelet particles corresponding in size to K_2TaF_7 particles is formed. In the case of a layer-by-layer loading of the reactants, equiaxial particles with a developed surface constitute the main part of the powder.

(2) The onset temperature of the reduction reaction in a homogeneous mixture is 200–400°C lower than that for the layerwise loading of the reactants. Mechanisms responsible for the dependences of the parameters of K_2TaF_7 reduction by sodium and the characteristics of the resulting powder on the mode of the heterogeneous process were suggested.

(3) The onset temperature of the reduction reaction and the morphology of the powder are determined by the extent of contact between potassium heptafluorotantalate and sodium.

(4) The technique developed for studying the heterogeneous sodium-reduction makes it possible to obtain reliable results with small amounts of reactants.

ACKNOWLEDGMENTS

The study was financially supported by the Program "Leading Scientific Schools" (grant no. NSh 1616. 2003.03).

REFERENCES

1. Zelikman, A.N. and Meerson, G.A., *Metallurgiya redkikh metallov* (Metallurgy of Rare Metals), Moscow: Metallurgiya, 1973.
2. Belyaev, K.Yu., Orlov, V.M., Prokhorova, T.Yu., and Miroshnichenko M.N., *Rasplavy*, 1998, no. 5, pp. 67–72.
3. Agulyanskii, A.I., Bessonova, V.A., Kuznetsov, V.Ya., and Sklokina, N.F., *Zh. Neorg. Khim.*, 1982, vol. 27, no. 3, pp. 679–682.
4. Belyaev, K.Yu., Orlov, V.M., Prokhorova, T.Yu., and Savotkina, M.N., *Tekhnologiya mineral'nogo syr'ya i svoistva soedinenii redkikh elementov* (Technology of Mineral Raw Materials and Properties of Compounds of Rare Elements), Apatity: KNTs RAN (Kola Scientific Center of Russian Academy of Sciences), 1997, pp. 24–33.
5. Orlov, V.M., Prokhorova, T.Yu., Kolosov, V.N., and Belyaevskii, A.T., *Rasplavy*, 2003, no. 2, pp. 57–60.
6. Orlov, V.M., Belyaev, K.J., Prokhorova, T.Yu., et al., *Perspectivn. Mater.*, 2002, no. 3, pp. 74–78.
7. Orlov, V.M. and Fedorova, L.A., *Khim. Tekhnol.*, 2004, no. 7, pp. 26–29.

ISSN 1070-4272, Russian Journal of Applied Chemistry, 2006, Vol. 79, No. 8, pp. 1220–1224. © Pleiades Publishing, Inc., 2006.
Original Russian Text © E.P. Lokshin, T.A. Sedneva, 2006, published in Zhurnal Prikladnoi Khimii, 2006, Vol. 79, No. 8, pp. 1238–1241.

INORGANIC SYNTHESIS AND INDUSTRIAL INORGANIC CHEMISTRY

On Stabilization of Anatase with the Fluoride Ion

E. P. Lokshin and T. A. Sedneva

Tananaev Institute of Chemistry and Technology of Rare Elements and Mineral Resources, Kola Scientific Center, Russian Academy of Sciences, Apatity, Murmansk oblast, Russia

Received December 23, 2005; in final form, March 2006

Abstract—Introduction of fluoride ions into titanium oxo hydroxide causes calcination to result in the anatase modification of titanium dioxide, which is stable up to temperature of no less than 900°C and retains a high specific free surface area on heating.

DOI: 10.1134/S1070427206080027

For destruction of organic contaminants present in aqueous solutions, methods for their photocatalytic decomposition with anatase nanoparticles as a photocatalyst are being intensively studied [1–3]. These processes are especially promising for purification of wastewater containing nonbiodecomposable contaminants [3]. Methods based on hydrolysis of organometallic titanium compounds have been for the most part developed for synthesis of anatase nanopowders [4–6].

Moreover, a highly dispersed anatase retaining a high specific surface area on heating to a temperature of no less than 500°C is required as catalyst and catalyst support for a number of processes of organic synthesis [7]. The thermal stability is necessary for regeneration of the catalyst by high-temperature burning-out of tarry products accumulated in the catalyst in the course of its operation [7].

It has been suggested to obtain materials of this kind by hydrolysis of organic compounds of titanium (ethylate, propylate, butylate, and methyl cellosolvate) in the presence of stabilizers (hydrochloric or nitric acid) with subsequent drying at 120°C to constant mass and calcination at 500°C (calcination time not reported). In some cases (not specified in the study), samples with a specific surface area of up to 105 $m^2 g^{-1}$ have been obtained [7].

Titanium alkoxides are expensive and chemically active, which requires that special intricate equipment should be developed to enable their use in large-scale production. In addition, the formation of Ti^{3+} upon calcination of a xerogel has been revealed by EPR [8]. Therefore, it was of interest to obtain thermally stable anatase nanopowders from inorganic precursors. The most interesting among them are sulfate, chloride, and nitrate compounds of titanium, which can be obtained by various methods from mineral raw materials.

Titanium dioxide nanopowders obtained by plasmochemical synthesis initiated by a pulsed electron beam are a mixture of anatase and rutile. Their ratio in a mixture could be controlled by varying the synthesis conditions [9].

Data on the structure of phases formed in hydrolysis of sulfate, chloride, and nitrate solutions of titanium are contradictory [10]. It has been shown, however, that the crystal structure of the phases formed and its subsequent change upon heating depend on the composition of a starting titanium compound and of the impurities contained in solution. Metatitanic acid produced by thermal hydrolysis from sulfuric acid solutions contains about 7 wt % SO_4^{2-}. Its heating to about 850°C gives anatase, which is transformed into rutile only at 850–950°C [11]. At higher calcination temperatures, micrometer-size powders of titanium dioxide are formed.

Metatitanic acid produced by thermal hydrolysis from nitrate or chloride solutions is transformed into rutile below 500°C [10].

The phase composition and coarseness of titanium dioxide particles depend on the temperature (150–250°C interval was studied) and time (10 min–6 h) of the hydrothermal treatment [12]. Nanocrystalline anatase powders (crystallite size 10–30 nm) were obtained by hydrothermal treatment of the sulfate $TiOSO_4$,

nitrate $TiO(NO_3)_2$, a complex acid $H_2TiO(C_2O_4)_2$, and amorphous titanium hydroxide gel $TiO_2 \cdot nH_2O$, which was synthesized by precipitation from a H_2TiCl_6 solution with an excess amount of aqueous ammonia. Extending the time of hydrothermal treatment to 6 h revealed significant differences in the behavior of the systems studied. In the case of oxo titanium sulfate solutions and an amorphous titanium hydroxide gel, the nanocrystalline anatase was retained, whereas for other solutions, anatase was recrystallized into the rutile, with the crystallites coarsened to 50–100 nm [12]. These were oxo titanium nitrate solutions, a 0.07 M $H_2TiO(C_2O_4)_2$ solution (incomplete recrystallization at 150°C, and complete at 250°C), and 0.28 M $H_2TiO(C_2O_4)_2$ solution (complete recrystallization at 150°C).

Rutile nanopowders have been obtained by thermal hydrolysis of a $TiCl_4$ aqueous solution [13]. At the same time, it has been reported that nanocrystalline anatase with a minor content of brookite was precipitated in the presence of a $TiCl_4$ precursor [14]. As the pH of hydrolytic precipitation increased, the crystal lattice constants of the anatase became larger. The content of brookite in the mixture decreased with the pH value. As the volume fraction of brookite increased, the temperatures of the beginning and end of the anatase–rutile transformation decreased.

Thus, methods for synthesis from inorganic precursors of a highly dispersed anatase, which retains a high specific surface area upon being heated to 500°C or more, have not been developed so far.

It has been found that the insoluble titanium–silica residue formed in nitric [15] and sulfuric acid leaching-out of calcium from sphene concentrate contains a mixture of anatase and rutile and the relative fraction of rutile increases as the process temperature is elevated. When fluorinecontaining compounds (HF or H_2SiF_6) are introduced in an amount of 0.25–0.3 mol F^-/mol TiO_2 into nitric or hydrochloric acid, the whole amount of titanium dioxide is present in the titanium–silica residue in the form of anatase.

The goal of this study was to examine the effect of fluoride ions on the synthesis of anatase from inorganic precursors and on its thermal stability.

EXPERIMENTAL

Anatase doped with fluoride ions was synthesized by sintering a weighed portion of a pure-grade titanium dioxide of the rutile modification with ammonium hydrofluoride at 160 °C for 3 h. Ammonium hexafluorotitanate(IV) obtained by the reaction

$$TiO_2 + 3NH_4F \cdot HF \rightarrow (NH_4)_2TiF_6 + NH_3 + 2H_2O \quad (1)$$

was treated with ammonia water (or ammonium hydroxide) to obtain titanium hydroxide:

$$(NH_4)_2TiF_6 + (4 - x)NH_4OH \rightarrow TiO(OH)_{2-x}F_x + (6 - x)NH_4F + H_2O. \quad (2)$$

In an excess of ammonia, the following reaction proceeds [16]:

$$TiO(OH)_{2-x}F_x + (2 - x)NH_4OH \rightarrow TiO(ONH_4)_{2-x}F_x + (2 - x)H_2O. \quad (3)$$

The precipitate separated from the solution by filtration was washed by repulpation in water at a $V_1 : S$ ratio of 10 or 20.

In this case, the following reactions may occur in washing, depending on the equilibrium pH value [17]:

$$TiO(ONH_4)_{2-x}F_x + H_2O \rightarrow TiO(OH)(ONH_4)_{1-x}F_x + NH_4OH, \quad (4)$$

$$TiO(OH)(ONH_4)_{1-x}F_x + (1 - x)H_2O \rightarrow TiO(OH)_{2-x}F_x + (1 - x)NH_4OH. \quad (5)$$

Partial transfer of fluoride ions into solution also seems to be probable. In this case, the processes that occur in washing can be described by the reaction:

$$TiO(ONH_4)_{2-x}F_x + (2 - x)H_2O \rightarrow TiO(OH)_{2-y}F_y + (x - y)NH_4F + (2 - 2x + y)NH_4OH. \quad (6)$$

Raising the $V_1 : S$ ratio favors an increase in the extent of hydrolysis of ammonium titanates.

The precipitates obtained were thermally treated at 100–900°C, with the calcination loss determined for selected samples. The structure of the heat-treated powders was identified by X-ray phase analysis (DRON-3 diffractometer, Cu_{K_α}-radiation) and their specific surface area was found from the low-temperature adsorption of nitrogen (BET method, FlowSorb II 2300 apparatus). The powders were also ana-

Phase composition, specific surface area S_{sp}, fluorine content c, F/Ti atomic ratio α, and calcination loss for the product obtained from titanium hydroxide doped with fluoride ions in relation to washing conditions ($V_l : S$) and thermal treatment temperature T (thermal treatment time 2 h)

Phase composition (XPA)	$V_l : S$	T, °C	c, wt %	α	S_{sp}, g m^{-2}	Calcination loss, wt %
Amorphous	0	100	2.26	N.d.*	63	N.d.
	10	100	2.62	"	224.9	"
	20	100	1.56	"	227.2	"
	20	250	3.0	"	N.d.	"
	20	300	N.d.	"	177.9	9.1
Anatase + amorphous phase	20	350	"	"	N.d.	10.5
	10	400	2.51	0.11	117.0	28.5
	20	400	0.93	0.043	129.5	11.4
	10	500	0.79	0.034	70.9	33.7
	20	500	0.51	0.022	84.0	14.4
	10	700	0.40	0.017	57.2	38.0
	20	700	0.25	0.011	69.3	14.8
	10	900	0.19	0.008	54.2	36.4
	20	900	0.13	0.0055	68.1	15.1
Anatase + rutile	20	1000	0.049	0.0021	28.6	15.2
Rutile + anatase	20	1100	0.042	0.0018	3.1	15.2
Rutile	20	1200	0.036	0.0015	2.8	15.2

* Not determined.

lyzed for the content of TiO_2 and F. The results obtained are listed in the table.

As can be seen from the data in the table, the samples obtained by washing with water at $V_l : S = 10$ have a higher content of bound fluorine and a larger calcination loss than samples washed with water at $V_l : S = 20$. This is probably due to the higher content of ammonium ions in titanium hydroxide.

The powders obtained at treatment temperatures below 300°C were amorphous. They contained no less than 6 wt % water (as determined by comparison with the calcination loss of the sample obtained at $V_l : S = 20$ and calcined at 900°C). Heating in this temperature interval mostly leads to evaporation of water, with the bound fluorine remaining in the product.

The anatase structure starts to be formed at higher temperatures, and, according to XPA, the oxide treated even at 350°C contains the anatase TiO_2 phase, along with the amorphous phase, with the calcination loss increasing. The precipitates treated within the range 400–900°C, contain only the anatase modification of TiO_2.

As the calcination temperature is raised, the content of fluorine in the products and their specific surface areas decrease. For example, the specific surface area of the products treated at 100°C, which contain up to 3 wt % F, is as large as 227 m^2 g^{-1}. As the calcination temperature is elevated, the content of bound fluorine gradually decreases, to reach a value of 0.13–0.19 wt % at 900°C. In the process, the specific surface area of the powders decreases to 54–68 m^2 g^{-1}, but remains rather high. On elevating the heat treatment temperature to $T \geq 1000$°C, the content of fluorine and the specific surface area further decreased, with rutile appearing in the product. Rutile was predominant in the product calcined at 1100°C, and no anatase was found in that obtained at 1200°C.

It should be noted that powders obtained from more thoroughly washed precipitates ($V_l : S = 20$) have a more developed surface. This contradicts the tendency common to the experimental results obtained: direct relationship between the content of bound fluorine and the specific surface area of the precipitate, which invites an additional study.

Three crystalline modifications: anatase, brookite, and rutile, are known for titanium dioxide. Rutile and anatase belong to the tetragonal crystal system and are, in structural regard, alternative forms with a 6 : 3 coordination. In their structure, each titanium atom is surrounded by six oxygen atoms, and each oxygen atom, by three titanium atoms [17].

However, the anatase density (3.84 g cm^{-3}) is 9% lower than the rutile density (4.26 g cm^{-3}), i.e., atoms in the anatase lattice are less densely packed, compared with rutile.

It was assumed that formation of the thermodynamically most stable rutile modification in synthesis and the subsequent high-temperature treatment can be, in particular, hindered by anionic impurities forming chemically stable complexes with titanium. In the course of heat treatment, these impurities come to dislocation growth steps and block the recrystallization of anatase, thereby precluding formation of the rutile crystal lattice of titanium dioxide. In this case, anatase should be regarded as a solid solution that is based on titanium dioxide and contains microimpurities (in particular, OH^-, SO_4^{2-}, F^-, etc.), rather than a stoichiometric titanium dioxide.

It is known that the capacity of Ti(IV) for complexation increases in the order $NO_3^- < Cl^- < SO_4^{2-} < F^-$. This predetermines the higher content of SO_4^{2-} and F^- ions upon hydrolysis of the corresponding titanium compounds. It may be suggested that it is the high content of SO_4^{2-} ions (about 7 wt % [10, 11]), which cannot be washed out with water, that hinders direct crystallization of anatase or rutile in thermal hydrolytic precipitation of titanium from sulfate solutions.

Formation of anatase in thermal treatment of metatitanic acid precipitated from titanium-containing sulfate solutions is also hindered by the high concentration in the acid of difficultly removable sulfate ions and proceeds at a temperature of about 850°C, at which sulfur oxides start to be removed to a noticeable extent. However, there simultaneously occurs intense sintering of particles of the forming anatase, which results in that powders with a small specific surface area are formed.

Fluoride ions, which form rather strong complexes with titanium, must hinder rutile formation. The presence of minor concentrations of fluoride ions in the hydrolysis products should lead not only to formation of the thermally stable anatase modification of titanium dioxide, but also to the related preservation of its large specific surface area. Indeed, the bonding energy of titanium with fluorine is considerably higher than that with chlorine or oxygen, and the ionic radii of fluorine and oxygen are rather close (1.40 and 1.36 Å, respectively) [16].

Consequently, F^- can replace, for stereometric and thermodynamic reasons, oxygen in titanium–oxygen octahedra, which are structural elements of the crystal lattices of both rutile and anatase, but the charge of the titanium cation is not completely neutralized upon this substitution. It is this fact that probably leads to the formation of a less dense anatase structure.

The bound fluorine remains in a sufficient amount even upon heating to 900°C, and this is a probable reason why the anatase structure and rather large free specific surface area are retained at elevated temperatures. With the heat-treatment temperature raised further, the content of F^- decreases to 0.0021 wt % and less, the rutile phase appears, and the specific surface area rapidly decreases.

In conclusion, we note that anatase obtained by calcination at 850°C of metatitanic acid precipitated by thermal hydrolysis from sulfate solutions contained 0.15 wt % SO_4^{2-}, which corresponds to the S/Ti = 0.001 atomic ratio. In anatase calcined at 900°C, the F/Ti atomic ratio was found to be 0.0055–0.008. The higher relative concentration of fluoride ions is the probable reason for the enhanced thermal stability of anatase.

ACKNOWLEDGMENTS

The study was financially supported by the Leading Research Schools Program (project no. NSh-1616-2003.03).

REFERENCES

1. Huang Xing-Jiu, Ye Gang, Wang Lian-Chao, et al., *Chem. J. Chin. Univ.*, 2003, vol. 24, no. 8, pp. 1459–1463.
2. Hu Jifan, Lu Hongliang, Sui Zhengui, et al., *Rare Metal Mater. Eng.*, 2003, vol. 32, no. 4, pp. 280–282.
3. Stuhldreher, H. and Meisterjahn, P., *Chem. Ing. Techn.*, 2003, vol. 75, no. 8, pp. 1136.
4. Uekawa, N., Kajiwara, J., Kakegawa, K., and Sasaki, Y., *J. Colloid Interface Sci.*, 2003, vol. 250, no. 2, pp. 285–290.
5. Huang Biao, *J. Chem. Ind. Eng. (China)*, 2003, vol. 54, no. 9, pp. 1315–1318.
6. Huang Wei, Wu Yue, Gu Yu-hui, Gu Hong-chen, J.E., *China Univ. Sci. a. Technol.*, 2003, vol. 29, no. 2, pp. 198–201.
7. Pavlova-Verevkina, O.B., Kul'kova, N.V., Politova, E.D., et al., *Kolloid. Zh.*, 2003, vol. 65, no. 2, pp. 252–255.
8. Munoz, E., Boldu, J.L., Andrade, E., et al., *J. Am. Ceram. Soc.*, 2001, vol. 84, no. 2, pp. 392.
9. Pushkarev, A.I., Remnev, G.E., and Ponomarev, D.V., *Proceedings, Mezhdunarodnaya konferentsiya "Novye perspektivnye materialy i tekhnologii ikh polucheniya*

NPM–2004" (Int. Conf. "New Promising Materials and Relevant Technologies NPM – 2004"), Volgograd, 2004, vol. 1, pp. 126–128.

10. Goroshchenko, Ya.G., *Khimiya titana* (Chemistry of Titanium), Kiev: Naukova Dumka, 1970.
11. Khazin, L.G., *Dvuokis' titana* (Titanium Dioxide), Leningrad: Khimiya, 1970.
12. Kolen'ko, Yu.V., Burukhin, A.A., Churagulov, B.R., and Oleinikov, N.N., *Neorg. Mater.*, 2004, vol. 40, no. 8, pp. 942–949.
13. Sun Jing, Gao Lian, and Zhang Qinghong, *J. Am. Ceram. Soc.*, 2003, vol. 86, no. 10, pp. 1677–1682.
14. Hu Y., Tsai H.-L., and Huang C.-L., *J. Eur. Ceram. Soc.*, 2003, vol. 23, no. 5, pp. 691–696.
15. Lokshin, E.P., Sedneva, T.A., and Tikhomirova, I.A., *Zh. Prikl. Khim.*, 2004, vol. 77, no. 7, pp. 1057–1065.
16. Kalinnikov, V.T., Lokshin, E.P., Ivanenko, V.I., and Gromov, O.G., *Formirovanie osnov sovremennoi strategii prirodoispol'zovaniya v Evro-Arkticheskom regione* (Development of Foundations of Modern Strategy for Use of Natural Resources in the European-Arctic Region), Apatity: Kola Nauchn. Tsentr Ross. Akad. Nauk, 2005.
17. Bragg, W.L., Claringbull, G.F., and Taylor, W.H., *The Crystal Structures of Minerals*, London: Bell, 1965.

ISSN 1070-4272, Russian Journal of Applied Chemistry, 2006, Vol. 79, No. 8, pp. 1225–1229. © Pleiades Publishing, Inc., 2006.
Original Russian Text © S.M. Sergazina, B.K. Kasenov, E.S. Mustafin, Sh.B. Kasenova, Zh.I. Sagintaeva, R.Sh. Erkasov, 2006, published in Zhurnal Prikladnoi Khimii, 2006, Vol. 79, No. 8, pp. 1242–1246.

PHYSICOCHEMICAL STUDIES OF SYSTEMS AND PROCESSES

Thermodynamic Properties of Ferrites of Composition $GdM^{II}Fe_2O_{5.5}$ (M^{II} = Mg, Ca, Sr)

S. M. Sergazina, B. K. Kasenov, E. S. Mustafin, Sh. B. Kasenova, Zh. I. Sagintaeva, and R. Sh. Erkasov

Institute of Phytochemistry, Ministry of Education and Science of the Republic of Kazakhstan, Karaganda, Kazakhstan

Gumilev Eurasian National University, Astana, Kazakhstan

Received February 2, 2006

Abstract—Ferrites with the composition $GdM^{II}Fe_2O_{5.5}$ (M^{II} = Mg, Ca, Sr) were synthesized from the corresponding oxides by the solid-phase method. The temperature dependence of the specific heat was studied by dynamic calorimetry in the temperature range 298.15–673 K. Equations describing this temperature dependence were derived. The temperature dependences of the thermodynamic functions were calculated.

DOI: 10.1134/S1070427206080039

Ferrites are compounds of iron(III) oxide with oxides of other metals, which show a unique combination of magnetic, electrical, and other properties. They are interesting objects for study of the internal energy by methods of true specific heat. In many ferrites, processes of magnetic ordering are combined with polymorphic transformations and ion ordering.

In recent years, the creation of the magnetic bioceramic as an effective means of control over bone tissue cancer has been deserving particular attention. A glassy ceramic of this kind is formed via filling of an Al_2O_3–SiO_2–P_2O_5 glassy matrix with microscopic magnetic particles of lithium ferrite $LiFe_5O_8$ or hematite α-Fe_2O_3 [1].

The aim of the present study was to examine the thermodynamic properties of ferrites $GdM^{II}Fe_2O_{5.5}$ (M^{II} = Mg, Ca, Sr). The isobaric specific heat of the ferrites was studied on an IT-S-400 calorimeter under monotonic, nearly linear heating of a sample at an average rate of about 0.1 deg s^{-1} at temperature differences of 3–30 K. The temperature dependence of the parameter under study was measured in a single run. The measuring circuit of the instrument provided determination of the temperature at fixed points in the lower and upper parts of the working cell at intervals of 25 K with a built-in dc potentiometer and a switch. The working mode (temperature differences on a sample and nonlinearity of heating) was chosen in such a way that corrections for changes in the thermal properties and for the heating rate did not exceed 1–2% under normal conditions and could be neglected in calculations. The time in which measurements were performed in the whole temperature range, and the experimental data obtained were processed, did not exceed 2.5 h. The rated measurement error of the IT-S-400 instrument is ±10% [2].

At each temperature, chosen at 25-K intervals, five parallel runs were made and the data on the delay time of the heat meter were averaged and processed using method of mathematical statistics. Root-mean-square deviations $\bar{\delta}$ were calculated for the average values of specific heats at each temperature, and the random component of the error, $\mathring{\Delta}$, for the averaged values of the molar specific heat [3]. The random component of the error, $\mathring{\Delta}$, is expressed in J mol^{-1} K^{-1}, and the root-mean-square deviation $\bar{\delta}$, in J g^{-1} K^{-1}.

The operation of the instrument was tested by determining the specific heat of α-Al_2O_3. The resulting value of C_p^0 (298.15) for Al_2O_3 (76.0 J mol^{-1} K^{-1}) is in a satisfactory agreement with reference data (79.0 J mol^{-1} K^{-1}) [4].

Figure 1 and Table 1 present the results of a calorimetric determination of the specific heats of the ferrites under study.

Table 1. Experimental values of the specific heat of $GdM^{II}Fe_2O_{5.5}$ (M^{II} = Mg, Ca, Sr)

T, K	$C_p \pm \bar{\delta}$, J g^{-1} K^{-1}	$C_p^0 \pm \AA$, J mol^{-1} K^{-1}	T, K	$C_p \pm \bar{\delta}$, J g^{-1} K^{-1}	$C_p^0 \pm \AA$, J mol^{-1} K^{-1}
		$GdMgFe_2O_{5.5}$			
298.15	0.5266 ± 0.0155	177 ± 14	498	1.2495 ± 0.0217	420 ± 20
323	0.6571 ± 0.0192	221 ± 18	523	1.3305 ± 0.0165	448 ± 15
348	0.7790 ± 0.0180	262 ± 17	548	1.3806 ± 0.0311	464 ± 29
373	0.8694 ± 0.0185	292 ± 17	573	1.1860 ± 0.0230	399 ± 22
398	0.9312 ± 0.0141	313 ± 13	598	0.9658 ± 0.0293	325 ± 27
423	1.0316 ± 0.0217	347 ± 20	623	0.8344 ± 0.0257	281 ± 24
448	1.2235 ± 0.0186	412 ± 17	648	0.8517 ± 0.0195	287 ± 18
473	1.2413 ± 0.0241	418 ± 23	673	0.8565 ± 0.0236	288 ± 22
		$GdCaFe_2O_{5.5}$			
298.15	0.5241 ± 0.0148	208 ± 16	498	0.7169 ± 0.0150	285 ± 17
323	0.5413 ± 0.0057	215 ± 6	523	0.6180 ± 0.0081	245 ± 9
348	0.5767 ± 0.0101	229 ± 11	548	0.5955 ± 0.0099	236 ± 11
373	0.6252 ± 0.0125	248 ± 14	573	0.5905 ± 0.0118	234 ± 13
398	0.5876 ± 0.0133	233 ± 15	598	0.5808 ± 0.0120	231 ± 13
423	0.5684 ± 0.0146	226 ± 16	623	0.5722 ± 0.0073	227 ± 8
448	0.6434 ± 0.0140	255 ± 15	648	0.5531 ± 0.0101	220 ± 11
473	0.6578 ± 0.0124	261 ± 14	673	0.6205 ± 0.0096	246 ± 11
		$GdSrFe_2O_{5.5}$			
298.15	0.4857 ± 0.0110	216 ± 14	498	0.6075 ± 0.0085	270 ± 11
323	0.5146 ± 0.0060	229 ± 7	523	0.5601 ± 0.0054	249 ± 7
348	0.5541 ± 0.0083	246 ± 10	548	0.5504 ± 0.0124	245 ± 15
373	0.5641 ± 0.0067	251 ± 8	573	0.5358 ± 0.0132	238 ± 16
398	0.5090 ± 0.0109	226 ± 13	598	0.4713 ± 0.0130	210 ± 16
423	0.5430 ± 0.0089	241 ± 11	623	0.4991 ± 0.0115	222 ± 14
448	0.5742 ± 0.0114	255 ± 14	648	0.5146 ± 0.0083	229 ± 10
473	0.5869 ± 0.0076	261 ± 9	673	0.5420 ± 0.0148	241 ± 18

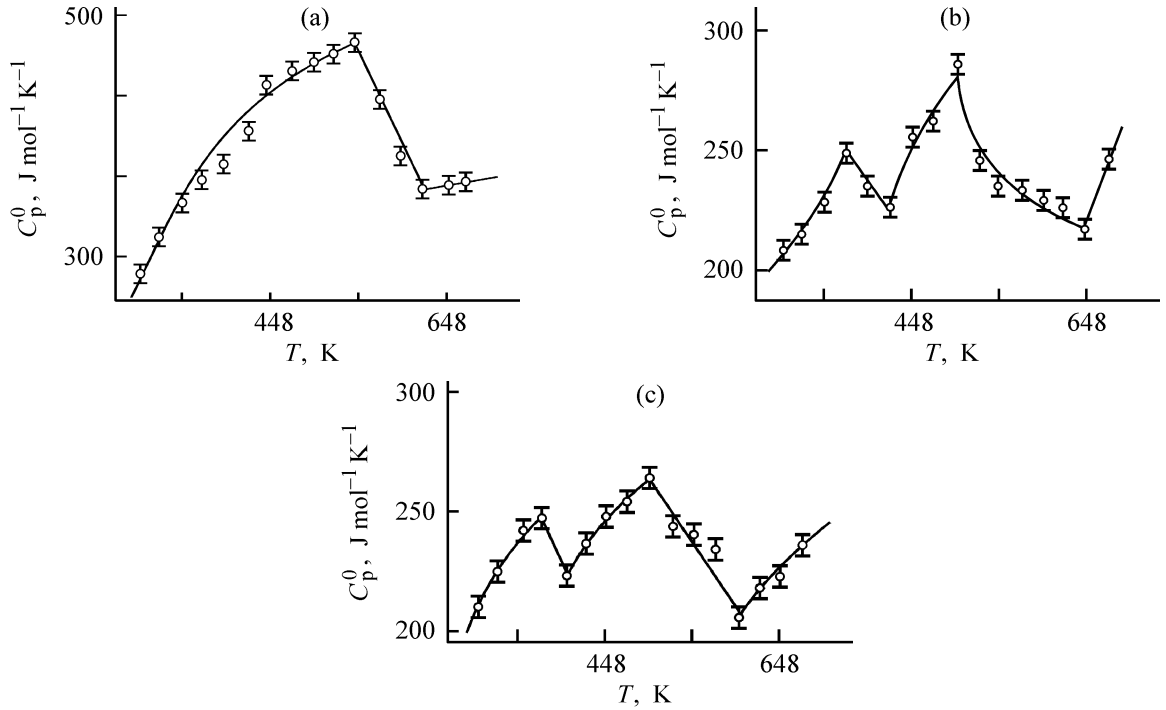


Fig. 1. Specific heat C_p^0 of the ferrites $GdM^{II}Fe_2O_{5.5}$ (M^{II} = Mg, Ca, Sr) vs. temperature T. (a) $GdMgFe_2O_{5.5}$, (b) $GdCaFe_2O_{5.5}$, and (c) $GdSrFe_2O_{5.5}$.

The experimental data were used to derive equations for the temperature dependence of the specific heats of the ferrites (Table 2).

As can be seen from Table 2 and Figs. 1a–1c, the ferrites under study show in the $C_p^0(T)$ curves a lambda-shaped behavior characteristic of second-order phase transitions: $GdMgFe_2O_{5.5}$ at 548 K, $GdCaFe_2O_{5.5}$ at 373 and 498 K, and $GdSrFe_2O_{5.5}$ at 373 and 498 K. These phase transitions are due to electronic transitions or Schottky effects. It should be noted that similar effects have been observed in studies of the specific heat of many oxides of 4*f*-elements. The reason for the splitting of the electron levels of paramagnetic rare-earth ions is the effect of the field of ligands-anions surrounding a cation [5].

Because the technical parameters of the IT-S-400 calorimeter give no way of calculating the entropy from experimental data, the standard entropies of the compounds were evaluated using the system of ionic entropy increments [6]. The temperature dependences of the functions $C_p^0(T)$, $S^0(T)$, $H^0(T) - H^0(298.15)$, and $\Phi^{**}(T)$ of the ferrites were calculated using the known relations in the temperature range 298.15–673 K (see Table 3) from the experimen-

Table 2. Equations for the temperature dependence of the specific heat of the ferrites

Ferrite	Coefficients of the equation $C_p^0 = a + bT + cT^{-2}$, J mol^{-1} K^{-1}			ΔT, K
	a	$b \times 10^{-3}$	$-c \times 10^5$	
$GdMgFe_2O_{5.5}$	191 ± 12	604 ± 37	172 ± 11	298–548
	1832 ± 114	–2495 ± 155	–	548–623
	188 ± 12	149 ± 9	–	623–673
$GdCaFe_2O_{5.5}$	–502 ± 26	1626 ± 86	200 ± 11	298–373
	416 ± 22	–451 ± 24	–	373–423
	1557 ± 82	–1617 ± 85	–1158 ± 61	423–498
	–542 ± 29	773 ± 41	1096 ± 58	498–648
	–475 ± 25	1071 ± 56	–	648–673
$GdSrFe_2O_{5.5}$	169 ± 9	283 ± 15	–33 ± 2	298–373
	616 ± 32	–979 ± 50	–	373–398
	657 ± 34	–459 ± 24	–392 ± 20	398–498
	572 ± 29	–605 ± 31	–	498–598
	552 ± 28	–202 ± 10	–792 ± 41	598–673

Table 3. Thermodynamic functions of the ferrites

T, K	$C_p^0(T)$, J mol^{-1} K^{-1}	$S^0(T)$, J mol^{-1} K^{-1}	$H^0(T) - H^0(298.15)$, J mol^{-1}	$\Phi^{**}(T)$, J mol^{-1} K^{-1}
		$GdMgFe_2O_{5.5}$		
298.15	177 ± 11	189 ± 6	–	189 ± 17
300	181 ± 11	190 ± 17	360 ± 20	189 ± 17
325	224 ± 14	206 ± 19	5440 ± 340	189 ± 17
350	262 ± 16	224 ± 21	11520 ± 710	191 ± 18
375	295 ± 18	243 ± 22	18490 ± 1150	194 ± 18
400	325 ± 20	263 ± 24	26240 ± 1630	198 ± 18
425	352 ± 22	284 ± 26	34710 ± 2150	202 ± 19
450	378 ± 23	305 ± 28	43840 ± 2720	207 ± 19
475	401 ± 25	326 ± 30	53580 ± 3320	213 ± 20
500	424 ± 26	347 ± 32	63900 ± 3960	219 ± 20
525	445 ± 28	368 ± 34	74770 ± 4640	226 ± 21
550	466 ± 29	389 ± 36	86160 ± 5340	233 ± 21
575	397 ± 25	408 ± 37	96870 ± 6010	240 ± 22
600	335 ± 21	424 ± 39	106020 ± 6570	247 ± 23
625	272 ± 17	436 ± 40	113600 ± 7040	255 ± 23
650	285 ± 18	447 ± 41	120670 ± 7480	262 ± 24
675	288 ± 18	458 ± 42	127840 ± 7930	269 ± 25

Table 3. (Contd.)

T, K	$C_p^0(T)$, J mol^{-1} K^{-1}	$S^0(T)$, J mol^{-1} K^{-1}	$H^0(T) - H^0(298.15)$, J mol^{-1}	$\Phi^{**}(T)$, J mol^{-1} K^{-1}
		$GdCaFe_2O_{5.5}$		
298.15	208 ± 11	204 ± 6	–	204 ± 17
300	208 ± 11	205 ± 17	420 ± 20	204 ± 17
325	216 ± 11	222 ± 18	5700 ± 300	205 ± 17
350	230 ± 12	239 ± 20	11260 ± 590	207 ± 17
375	250 ± 13	255 ± 21	17260 ± 910	209 ± 17
400	236 ± 12	271 ± 22	23300 ± 1230	213 ± 18
425	225 ± 12	285 ± 24	29060 ± 1530	217 ± 18
450	257 ± 14	299 ± 25	35160 ± 1850	221 ± 18
475	276 ± 15	313 ± 26	41840 ± 2200	225 ± 19
500	283 ± 15	328 ± 27	48860 ± 2570	230 ± 19
525	262 ± 14	341 ± 28	55650 ± 2930	235 ± 19
550	245 ± 13	353 ± 29	61960 ± 3270	240 ± 20
575	233 ± 12	363 ± 30	67940 ± 3580	245 ± 20
600	226 ± 12	373 ± 31	73680 ± 3880	250 ± 21
625	221 ± 12	382 ± 32	79260 ± 4180	255 ± 21
650	220 ± 12	391 ± 32	84770 ± 4470	260 ± 22
675	249 ± 13	400 ± 33	90650 ± 4780	265 ± 22
		$GdSrFe_2O_{5.5}$		
298.15	216 ± 11	215 ± 6	–	215 ± 18
300	217 ± 11	216 ± 18	430 ± 20	215 ± 18
325	230 ± 12	234 ± 19	6020 ± 310	216 ± 18
350	241 ± 12	252 ± 21	11900 ± 610	218 ± 18
375	252 ± 13	269 ± 22	18060 ± 930	221 ± 18
400	224 ± 12	284 ± 23	23980 ± 1230	224 ± 18
425	244 ± 13	298 ± 24	29890 ± 1540	228 ± 19
450	256 ± 13	313 ± 26	36160 ± 1860	232 ± 19
475	265 ± 14	327 ± 27	42680 ± 2200	237 ± 19
500	270 ± 14	341 ± 28	49370 ± 2540	242 ± 20
525	254 ± 13	353 ± 29	55900 ± 2880	247 ± 20
550	239 ± 12	365 ± 30	62050 ± 3200	252 ± 21
575	223 ± 11	375 ± 31	67830 ± 3490	257 ± 21
600	208 ± 11	384 ± 31	73230 ± 3770	262 ± 21
625	223 ± 11	393 ± 32	78650 ± 4050	267 ± 22
650	233 ± 12	402 ± 33	84350 ± 4340	272 ± 22
675	242 ± 12	411 ± 33	90280 ± 4650	277 ± 23

tal dependence $C_p^0(T)$ and calculated values of $S^0(298.15)$.

The inaccuracy of the temperature dependences of the thermodynamic functions was calculated with account of the average errors in determining the specific heat and calculating the entropy (3.0%).

CONCLUSIONS

(1) The isobaric specific heats of the ferrites $GdMgFe_2O_{5.5}$, $GdCaFe_2O_{5.5}$, and $GdSrFe_2O_{5.5}$ were studied for the first time in the temperature range 298.15–673 K, and equations describing the dependence $C_p^0(T)$ were derived.

(2) The standard entropies of the ferrites were calculated by the method of ionic increments, and the functions $H^0(T) - H^0(298.15)$ and $\Phi^{**}(T)$ were found from the experimental data on $C_p^0(T)$ and calculated values of $S^0(T)$.

(3) Lambda-shaped peaks associated with second-order phase transitions were found in the dependences

$C_p^0(T)$ for all of the ferrites studied ($GdMgFe_2O_{5.5}$ at 548 K, $GdCaFe_2O_{5.5}$ at 373 and 498 K, and $GdSrFe_2O_{5.5}$ at 373 and 498 K).

REFERENCES

1. Tret'yakov, Yu.D. and Brylev, O.A., *Zh. Ross. Khim. O–va im. D.I. Mendeleeva*, 2000, vol. 45, no. 4, pp. 10–16.
2. Platunov, E.S., *Teplofizicheskie izmereniya v monotonnom rezhime* (Thermal Measurements in the Monotonic Mode), Moscow: Energiya, 1973.
3. Spiridonov, V.P. and Lopatkin, L.V., *Matematicheskaya obrabotka eksperimental'nykh dannykh* (Mathematical Processing of Experimental Data), Moscow: Mos. Gos. Univ., 1970.
4. Robie, R.A., Hemingway, B.S., and Fisher, J.R., *Thermodynamic Properties of Minerals and Related Substances at 298.15 K and 1 Bar (10^5 Paskals) Pressure and at Higher Temperatures*, Washington: U.S. Gov. Print. Off., 1978.
5. Reznitskii, L.A., *Kalorimetriya tverdogo tela* (Calorimetry of Solids), Moscow: Mos. Gos. Univ., 1981.
6. Kumok, V.N., *Pryamye i obratnye zadachi khimicheskoi termodinamiki* (Direct and Inverse Problems of Chemical Thermodynamics), Novosibirsk: Nauka, 1987, pp. 108–123.

ISSN 1070-4272, Russian Journal of Applied Chemistry, 2006, Vol. 79, No. 8, pp. 1230–1237. © Pleiades Publishing, Inc., 2006.
Original Russian Text © I.G. Martinson, 2006, published in Zhurnal Prikladnoi Khimii, 2006, Vol. 79, No. 8, pp. 1247–1253.

PHYSICOCHEMICAL STUDIES OF SYSTEMS AND PROCESSES

Evaporation of Substances under Kinetic or Diffusion Control in Sublimation in a Vacuum

I. G. Martinson

Mendeleev Institute of Metrology, St. Petersburg, Russia

Received December 16, 2004; in final form, April 2006

Abstract—A diffusion–kinetic model of sublimation of substances in a vacuum is presented. The model defines two regions of the evaporation process depending on temperature: evaporation in the kinetic and diffusion control. The model was verified in experiments with benzoic acid and naphthalene by calculation of the sublimation rate of Zn, Co, V, and W, and by the known values of α.

DOI: 10.1134/S1070427206080040

Previously, an equation for the sublimation rate has been derived in terms of the diffusion model [1–3]. The sublimation rate of benzoic acid and naphthalene has been measured experimentally. The strongest disagreement between the experiment and calculation was about 10%. Substances purified by zone melting and by growth of single crystals from the melt were used in the experiments [4, 5]. A sublimation rate of the same order of magnitude was obtained in sublimation purification of diphenyl and benzophenone (~10^{-3} mol m^{-2} s^{-1}).

Kinetic sublimation model. The kinetic and diffusion modes are distinguished in the kinetics of physicochemical processes. The kinetic sublimation rate, i.e., the rate of transfer of molecules from the solid phase into a vapor, commonly is calculated by the Hertz–Knudsen equation

$$I = \alpha \frac{p}{(1\pi MRT)^{1/2}}, \quad (1)$$

where I is the sublimation rate (mol m^{-2} s^{-1}; p, saturated vapor pressure (N m^{-2}); M, molecular weight (kg mol^{-1}); R = 8.3144 (J mol^{-1} K^{-1}); T, temperature (K); and α, evaporation coefficient.

The Hertz–Knudsen equation was derived in [6, 7]. In the reference book [8], data obtained during the period of time from 1910 to 1968 were generalized: α = 1 for refractory metals (Ti, V, Cr, Co, Ir, etc.); α = 1 for salts (LiF_3, PrF_3, ZnSe, CdSe, etc.); α < 1 for certain metals and organic substances (camphor 0.18, thymol 0.14, benzoic acid 0.1, Sb_2S_3 0.1–0.4, α increases as temperature is lowered); α = 1 for some organic substances (naphthalene at –22…+15°C, anthracene at 49°C, etc.). More recent data were published in the review [9]. The values of the evaporation coefficient were found using different methods. Apparently, this is the reason for the diversity of the results. A value α = 1 was obtained for chromium in three studies, and α = 1.5–2.0, in one study under the same conditions. The coefficient α was defined in [8] by the equation

$$\alpha = I_{exp}/I_G,$$

where

$$I_G = p/(2\pi MRT)^{1/2}, \quad (2)$$

is the original Hertz equation.

In [10], the evaporation coefficient was defined as the ratio of the evaporation rate in the effusion Knudsen method to that in the Langmuir method, which is determined from the loss of mass by a pellet of the substance evaporating in a vacuum, and it was shown that the Hertz equation gives the maximum possible evaporation rate. It is commonly believed that α ≈ 1 in the Langmuir method and α < 1 in the Knudsen method because of the resistance of the effusion opening to the outflow of the saturated vapor. At the same time, it has been found experimentally that, at the same membrane thickness, the rates of evaporation through openings with d 0.832 and 0.258 mm differ by only several percent [11, 12]. In the monograph [13], the Hertz–Knudsen equation is represented as

$$dG/d\tau = F^+(M/2\pi RT)^{1/2}p, \quad (3)$$

where G is the mass of the substance (kg); F^+, evaporation area occupied by active molecules (m^2); and τ, time (s).

In this case, the evaporation coefficient

$$\alpha = F^+/F,$$

where F is the total surface area of the solid phase (m^2).

The coefficient α was also regarded in [13] as a function of the activation energy; in [14], this function was represented as the fraction of molecules having a velocity (kinetic energy) exceeding a certain required value.

When studying the evaporation, Knudsen obtained evaporation rates lower than that given by the Hertz equation, attributed this fact to surface contamination of substances, and supplemented the Hertz equation with a coefficient $\alpha < 1$ [15].

Thus, the evaporation coefficient in the kinetic Hertz–Knudsen equation (1) is regarded as the rate coefficient of the interphase reaction.

Diffusion sublimation model. In sublimation into air or an inert gas, the process rate is determined by the diffusion rate of the substance molecules in the medium. In the case of a forced convection of the medium, the diffusion equation can be used in the following form [7]

$$I = D\frac{\Delta c}{\delta}, \tag{4}$$

where D is the diffusion coefficient ($m^2\ s^{-1}$); Δc, difference of the concentrations in the diffusion layer (mol m^{-3}); and δ, thickness of the boundary diffusion layer (m) [16].

Because calculation of the diffusion sublimation rate in a medium gives coincidence with the experiment, the diffusion sublimation rate in the absence of a medium, in a vacuum, was considered [2].

The diffusion model of the sublimation process comprises the diffusion equation for the substance being evaporated, heat conduction equation, and gas-state equation. The equations contain the diffusion coefficient [17, 18] and the heat conductivity coefficient, which was taken to be constant. A solution of the system of these equations gave an equation for the substance evaporation rate (mol $m^{-2}\ s^{-1}$)

$$I_v = D_v\frac{c_v}{2L}\frac{T_v - T_c}{(T_v^{1/2} - T_c^{1/2})T_v^{1/2}}\log\frac{c_v}{c_c} \tag{5}$$

and that for the condensation rate

$$I_c = D_c\frac{c_c}{2L}\frac{T_v - T_c}{(T_v^{1/2} - T_c^{1/2})T_v^{1/2}}\log\frac{c_v}{c_c}, \tag{6}$$

where c_v and c_c are the concentrations of molecules in the saturated vapor near the evaporation and condensation surfaces (mol m^{-3}); T_v and T_c, temperatures of these surfaces (K); and L, distance between the surfaces (m).

The variation of the substance concentration in the vapor along the distance from the evaporation surface to the condensation surface is described by

$$\log c = \log c_v + \frac{[T_v - (T_v - T_c)x/L]^{1/2} - T_v^{1/2}}{T_v^{1/2} - T_c^{1/2}}\log\frac{c_v}{c_c}, \tag{7}$$

and the corresponding variation of temperature, by

$$T = T_v - (T_v - T_c)\frac{x}{L}, \tag{8}$$

where $x = 0$ at the evaporation surface and $x = L$ at the condensation surface.

Equations (7), (8) and the gas-state equation make it possible to determine how the pressure varies from $x = 0$ to $x = L$.

Thus, the sublimation process may occur under kinetic or diffusion control. Let us denote the kinetic sublimation rate by I_G (Hertz rate) and the diffusion rate by I_D. At high temperatures the process occurs in the diffusion region and the evaporation coefficient is given by

$$\alpha = I_D/I_G. \tag{9}$$

As the temperature of the evaporation surface is lowered, these rates become equal at a certain T_α and the evaporation coefficient $\alpha = 1$. As the evaporation temperature is lowered further, $I_G < I_D$, and the process occurs under kinetic control, in which the evaporation coefficient remains constant and equal to unity, because the evaporation rate is equal the Hertz rate. This is the general scheme of evaporation in a vacuum.

Equations (5), (6) contain the diffusion coefficient calculated as follows. Under atmospheric pressure at 273 K in the SI system

$$D_0 = \frac{0.02662\times10^{-20}}{\sigma^2\Omega p_0}\left(\frac{T_0^3}{M}\right)^{1/2}, \tag{10}$$

where σ is the gas-dynamic diameter of molecules, (m) and Ω, a tabulated function [17].

Table 1. Data for calculation of the sublimation rate of naphthalene

T, K	$p(1)$, Pa	$c(1) \times 10^3$ mol m^{-3}	$p(2)$, Pa	$c(2) \times 10^3$ mol m^{-3}	$D(1) \times 10^4$	$D(2) \times 10^4$
					m^2 s^{-1}	
283	2.523	1.072	2.987	1.271	519	439
331	223.2	81.11	173.8	63.16	6.349	8.153
335	306.0	109.7	231.4	83.08	4.657	6.158
339	416.4	147.7	305.9	108.5	3.444	4.688
343	562.6	197.3	401.9	140.9	2.563	3.588
348	811.6	280.5	560.1	193.6	1.791	2.594

Table 2. Sublimation rate of naphthalene, calculated by Eqs. (5), (6)

T, K	$I_v(1) \times 10^3$	$I_c(1) \times 10^3$	$I_v(2) \times 10^3$	$I_c(2) \times 10^3$
	mol m^{-2} s^{-1}			
331	4.290	5.013	3.877	4.537
335	4.539	5.378	4.107	4.869
339	4.794	5.740	4.329	5.192
343	5.026	6.087	4.537	5.509
348	5.323	6.541	4.808	5.919

The diffusion coefficient at the temperature of the experiments was calculated by the equation

$$D = D_0 \frac{p_0}{p}\left(\frac{T}{T_0}\right)^{1/2}. \quad (11)$$

For naphthalene, two equations describing the temperature dependence of the saturated vapor pressure were reported in [11]

$$\log p = 11.70 - 3798/T, \quad (12)$$

$$\log p = 10.52 - 3444/T. \quad (13)$$

We use designations $I_v(1)$ and $I_c(1)$ when applying Eq. (12), and $I_v(2)$ and $I_c(2)$ for Eq. (13). For naphthalene, we have from Eqs. (10), (11)

$$D_0 = \frac{0.02662 \times 10^{-20}}{34.669 \times 10^{-20} \times 2.377 \times 10\,1325}\left(\frac{273^3}{128.18}\right)^{1/2} = 1.270 \times 10^{-6}.$$

The input data for calculating the sublimation rate of naphthalene are listed in Table 1, and the results of calculation of the sublimation rate by Eqs. (12) and (13), in Table 2.

It was taken in the calculations that λ = const. The kinetic theory of gases [17–19] gives for the ideal gas the following heat conduction equation:

$$\lambda = \frac{1}{3}\rho C_Y v l = \rho C_V D = aT^{1/2}, \quad (14)$$

where ρ is the gas density; C_V, specific heat at constant volume; v, mean motion velocity of molecules; l, mean free path of molecules; and a, constant.

Using the dependence $\lambda = aT^{1/2}$ in the initial system of equations gives the following equations for the evaporation and condensation rates:

$$I_v = D_v \frac{2c_v}{3L}\frac{T_v^{3/2} - T_c^{3/2}}{(T_v - T_c)T^{1/2}} \log\frac{c_v}{c_c}, \quad (15)$$

$$I_c = D_c \frac{2c_v}{3L}\frac{T_v^{3/2} - T_c^{3/2}}{(T_v - T_c)T^{1/2}} \log\frac{c_v}{c_c}. \quad (16)$$

Calculation of I_v and I_c by these equations and Eqs. (5), (6) gives coinciding values of the sublimation rate, with a discrepancy of less than 1%.

It follows from Eq. (14) in accordance with Eq. (10) that

$$D = a\frac{1}{\Omega p}T^{1/2},$$

where a is a constant, and p, saturated vapor pressure. Then

$$\lambda = \frac{a}{\Omega T^{1/2}}.$$

The tabulated function can be approximated at its values in the range 1.88–2.66 by the dependence

$$\Omega = 4.837(T^*)^{-0.496} = 4.837(T^*)^{-1/2},$$

where $T^* = T/1.39 \times T_b$.

We obtain that the heat conductivity of the gas

$$\lambda = 0.287aT_b = \text{const}$$

is independent of pressure and temperature if the heat conductivity can be taken constant.

One more phenomenon is observed: pressure and temperature drops arise across phase boundaries in the course of sublimation and condensation, and these drops can be calculated [20, 21]. In sublimation of naphthalene at 348 K,

$$\Delta p = I_v(2\pi MRT)^{1/2} = 5.231 \times 10^{-3} \times 48.261 = 0.253 \text{ Pa},$$

$$\Delta T = 0.35 \text{ K}.$$

When testing the model of the process, with a calculation error of up to 10%, the pressure and temperature drops were disregarded.

EXPERIMENTAL

The substance fluxes in sublimation of naphthalene were measured on a modification of the installation used in [1]. A glass tube (sublimator proper) was placed in a hermetical steel container, which could be evacuated to a residual pressure of 0.1 Pa. A steel condenser was mounted in the upper part of this tube, and an evaporator, in its lower part. The surface area of the condenser was equal to that of the evaporator, i.e., the surface of naphthalene being sublimed in a steel vessel with an inner diameter of 24 mm and height of 16 mm. The condenser was in the form of a hollow flat cylinder cooled with water to 10°C. The glass with the substance was in thermal contact with the evaporator whose temperature was maintained constant by a temperature control unit. Five measurements were made at each temperature, with the successively longer durations of the experiments. The vessel was filled with molten naphthalene and weighed on a VLR-200 analytical balance. Prior to an experiment, the container was evacuated and kept in this state for 30–40 min. The instants when the heater was switched on and off were taken as the beginning and end of a run. The amount of sublimed naphthalene was found from the decrease in the weight of the vessel with the substance. Each run was performed with a new sample.

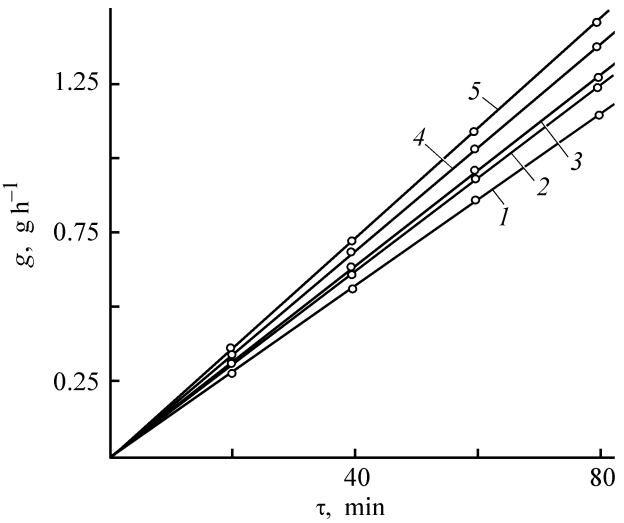


Fig. 1. Amount g of sublimed naphthalene vs. time τ. Temperature (K): (*1*) 331, (*2*) 335, (*3*) 339, (*4*) 343, and (*5*) 348.

The dependence of the amount g (g h^{-1}) of sublimed naphthalene on the experiment duration is shown in Fig. 1. All the dependences are plotted as straight lines, and, consequently, the saturated vapor pressure is attained near the evaporation surface considerably faster than substance is transferred from the evaporator to the condenser. Table 3 lists the results of the experiments.

The sublimation of naphthalene has been previously studied to give $\alpha = 0.85–0.95$ at –19…+5°C and $\alpha = 1$ at –22…+15°C. Because α increases for all substances as the temperature is lowered, the sublimation rate of naphthalene was calculated by Eqs. (2), (5). In doing so, the condenser temperature was taken to be $T_c = 250$ K; the evaporation temperature was 260, 270, 283, and 300 K; and $2L = 0.1$ m. The re-

Table 3. Sublimation rate of naphthalene

T_v, K	g, g h^{-1}	$I_v \times 10^3$, mol m^{-2} s^{-1}		Evaporation coefficient $\alpha \times 10^4$
		experiment	calculation by the Hertz equation	
331	0.8653	4.145	4.744	8.73
335	0.9405	4.505	6.463	6.97
339	0.9621	4.608	8.742	5.27
343	1.0351	4.958	11.743	4.22
348	1.0926	5.234	16.817	3.11

Table 4. Vapor pressure p at different temperatures of solid substances

Substance	T_m, °C	p, mm Hg = $f(T, K)$	Reference
Zn	419.5	$\log p = 9664 - 7198/T$	[24]
Co	1494	$\log p\,[\text{gPa}] = 12.68 - 24126/T - 0.114\log T + 0.874 \times 10^{-3}T$	[25]
V	1920	$\log p = 10.815 - 26650/T - 0.112 \times 10^{-3}T$	[26, 27]
W	3380	$\log p = 9.84 - 42000/T + 0.146\log T - 0.164 \times 10^{-3}T$	[26, 28]

Table 5. Conditions and rate of tungsten sublimation ($\lambda = 1$) (conditions on the condensation surface: T = 2200°C, $p = 1.003 \times 10^{-7}$ Pa, $c_c = 5.483 \times 10^{-12}$, $D_c = 9.787 \times 10^{-7}$ m^2 s^{-1})

T, K	p, Pa	c_v, mol m^3	D_v, m^2 s^{-1}	$I_v \times 10$	$I_c \times 10$	I_G
				mol m^{-2} s^{-1}		
3000	9.562×10^{-7}	3.834×10^{-7}	1.199×10^{3}	0.9519	1.297	5.634×10^{-5}
3272	1.285×10^{-1}	4.722×10^{-6}	9.317×10^{1}	1.094	1.627	7.248×10^{-4}
3400	3.715×10^{-1}	1.314×10^{-5}	3.285×10^{1}	1.144	1.768	2.056×10^{-3}
3500	8.095×10^{-1}	2.782×10^{-5}	1.530×10^{1}	1.178	1.873	4.416×10^{-3}
3653	2.446	8.053×10^{-5}	5.171	1.221	2.026	1.306×10^{-2}

sulting temperature dependences of the sublimation rate are shown in Fig. 2. It can be seen from the dependences for I_G and I_D that the kinetic sublimation rate is lower than the diffusion sublimation rate below 285.5 K, and, consequently, the former is the process-rate-determining factor, $\alpha = 1$. At $T > 288.5$ K the kinetic rate by Hertz rapidly increases and starts to exceed the diffusion rate of the naphthalene vapor, so that the latter becomes the rate-determining factor,

$$\alpha = \frac{I_D}{I_G} < 1,$$

and decreases as temperature grows.

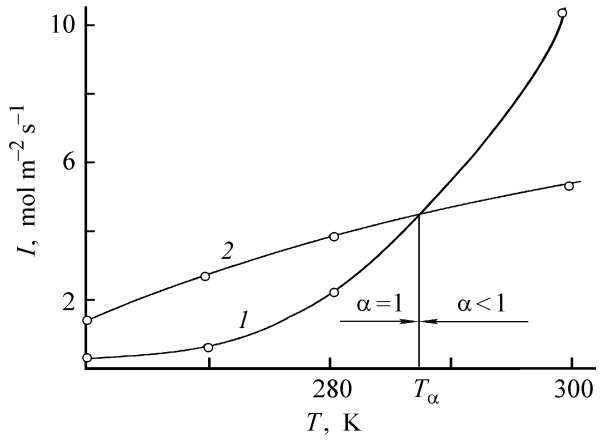


Fig. 2. Sublimation rate I of naphthalene at low temperatures T; T_c = 250 K, $2L$ = 0.1 m. (*1*) Kinetic rate by Hertz and (*2*) rate of vapor diffusion; the same for Fig. 3.

It should be noted that the transition from the kinetic to diffusion control occurs at 288.5 K under the experimental conditions we used, and this temperature will be different in some other conditions.

It was of interest to verify the diffusion-kinetic model of the sublimation process on substances having higher melting points. In monograph [22], the evaporation coefficient was considered in relation to crystal defects and association of atoms in vapor molecules, relevant publications were reviewed, and the following conclusion was made: "As regards the evaporation kinetics of magnetic substances and metallic alloys, the theory is in the initial stage of its development." In [23], a decrease in the evaporation coefficient (I_{exp}/I_G) from 0.48 to 0.13 was observed in the temperature range 1870–2200 K and the temperature dependence was represented as

$$\log\alpha = -3.71 + 0.63 \times 10^{-4}/T,$$

i.e., the evaporation coefficient grows as the evaporation temperature is lowered.

The diffusion sublimation rate of metals (Zn, Co, V, W) was calculated using the known temperature dependences of the saturated vapor pressure (Table 4) and Eqs. (1), (2), (5), (6), and (10). The temperature dependences of the sublimation rate for Zn, Co, and V are presented in Fig. 3, and that for W, in Table 5. As

standard experimental conditions were taken those for naphthalene, T_v and T_c were taken in accordance with the melting points of the metals.

In sublimation of zinc, the kinetic sublimation rate is lower than the diffusion sublimation rate nearly up to the melting point of zinc. At temperatures of up to 418.5°C, sublimation occurs in the kinetic mode, with $\alpha = 1$. At temperatures above 418.5°C, the process passes to the diffusion mode and α decreases as temperature becomes higher, which is also valid in the case of evaporation of the melt.

In sublimation of cobalt, $\alpha = 1$ up to 1387°C (kinetic control of the evaporation process). At higher temperatures (diffusion control), $\alpha < 1$ up to the melting point of cobalt (1494°C) and further, over the melt.

In sublimation of vanadium over solid vanadium, $\alpha = 1$ up to the melting point of 1920°C (kinetic control); as temperature is raised further, molten vanadium also evaporates under kinetic control up to approximately 2000°C, after which the process becomes diffusion controlled, with $\alpha < 1$.

In sublimation of tungsten, the diffusion sublimation rate substantially exceeds the kinetic rate in the temperature range from 2727°C to the melting point of 3380°C and above: the process occurs in the kinetic control, with $\alpha = 1$. The values of the process rates, obtained in the study, are listed in Table 5.

The diffusion-kinetic model of the sublimation process, represented by the scheme in Fig. 1, was confirmed by the available published data and verified by experiments with benzoic acid and naphthalene and by calculations of the evaporation rate of metals with high melting points. The sublimation process is commonly performed at temperatures close to the melting points of the substances involved, in order to raise the process rate. The following conclusions can be made on the basis of the results obtained.

(1) Sublimation of substances with melting points of up to approximately 200°C occurs under diffusion control; the sublimation rate of such substances is the rate of diffusion of the saturated vapor from the evaporation surface to the condensation surface. Sublimation of high-melting substances with melting points of about 1800°C and higher occurs under kinetic control; the sublimation rate of such substances, which is the kinetic rate of the phase transition of a substance from the solid phase to a vapor, is given by the Hertz equation.

For substances with melting points in the range 200–1800°C, the kinetic region lies at low tempera-

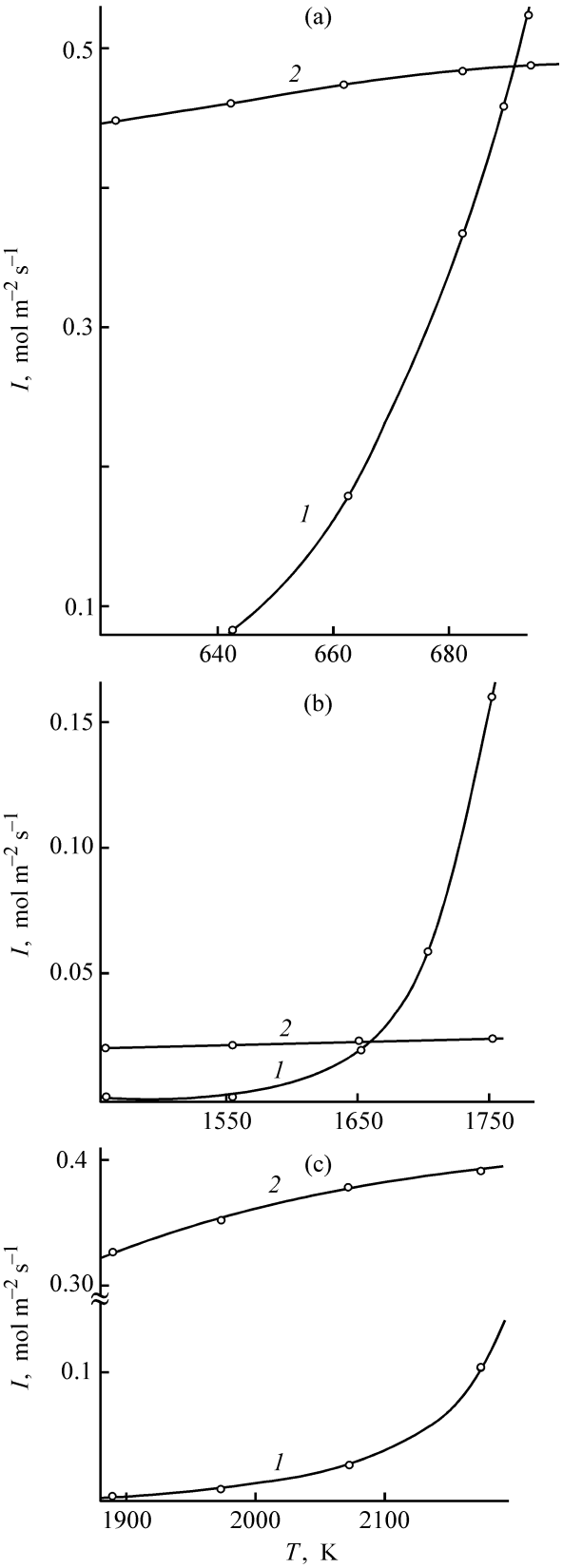


Fig. 3. Sublimation rate I of (a) zinc, (b) cobalt, and (c) vanadium vs. temperature T.

tures, and the diffusion region, at high temperatures. Depending on the objective to be achieved, the process can be performed in an appropriate region.

(2) The conditions of the adopted standard of the process, Eqs. (5) and (6) at $2L = 0.1$ m, as well as the ratios of T_v to T_c and c_v to c_c, will be different in other experiments (studies). If, for example, the sublimation of zinc is carried out in the evaporator–condenser system at $2L > 0.1$ m, the temperature dependence of the diffusion sublimation rate will be shifted downwards, the temperature range of the kinetic control will be shifted to low temperatures. In the experimental conditions corresponding to $2L < 0.1$ m, the temperature dependence of the diffusion sublimation rate will be shifted upwards and the region of the kinetic control over sublimation will extend to molten zinc. The rate of the diffusion process can also be raised by lowering the temperature of the condenser.

(3) It was found in experiments with benzoic acid and naphthalene that the evaporation rate is equal to the condensation rate. A calculation yielded that the latter somewhat exceeds the former. This circumstance can be attributed to inaccuracy of the equations describing the dependence of the saturated vapor pressure on temperature and that of the diffusion coefficient on temperature and pressure. Therefore, it is better to take the evaporation rate I_v as the process rate. It also follows that the evaporator–condenser method can be used to refine the equation $\log p = A - B/T$.

(4) A large number of substances with high melting points have an evaporation coefficient $\alpha = 1$ and there are no kinetic hindrances in evaporation of substances of this kind. However, it is not improbable that such hindrances may exist in condensation, when only part of molecules reaching the crystalline phase, rather than all of them, are involved in the crystallization process. In this case, the pressure and temperature drops Δp and ΔT at phase boundaries are related to the activation energy ΔG.

CONCLUSIONS

(1) The diffusion-kinetic model of sublimation, considered in the study, establishes two modes of the evaporation process: (i) with kinetic control at low temperatures, in which the evaporation rate is equal to the Hertz rate and the evaporation coefficient $\alpha = 1$ up to a temperature T_α, and (ii) with diffusion control at high temperatures, in which the evaporation rate is given by the diffusion equation and α rapidly decreases from unity to very small values.

(2) The model makes it possible to define the evaporation coefficient in the case of the diffusion control as a ratio of the diffusion rate of the process to the kinetic rate by Hertz and to calculate the evaporation rate with an error of up to 10% in the case of the diffusion control and, probably, with a very small error in that of the kinetic control.

(3) The model explains why small (down to 10^{-10}) values of the evaporation coefficient α are obtained for low-melting substances and $\alpha = 1$ for substances with high melting points.

REFERENCES

1. Martinson, I.G. and Cherepkova, I.A., *Zh. Prikl. Khim.*, 1996, vol. 69, no. 3, pp. 386–388.
2. Martinson, I.G. and Cherepkova, I.A., *Zh. Prikl. Khim.*, 1996, vol. 69, no. 9, pp. 1446–1449.
3. Martinson, I.G., *Zh. Prikl. Khim.*, 1998, vol. 71, no. 2, pp. 209–212.
4. Martinson, I.G., *Zh. Fiz. Khim.*, 1998, vol. 72, no. 9, pp. 1698–1703.
5. Martinson, I.G., *Zh. Fiz. Khim.*, 1996, vol. 70, no. 2, pp. 269–274.
6. Nesmeyanov, A.N., *Davlenie para khimicheskikh elementov* (Vapor Pressures of Chemical Elements), Moscow: Akad. Nauk SSSR, 1961.
7. Repinskii, S.M., *Vvedenie v khimicheskuyu fiziku poverkhnosti tverdykh tel* (Introduction to Chemical Physics of Soid Surfaces), Novosibirsk: Nauka, 1993, ch. 5.
8. Landolt, H. and Bornstein, R., *Zahlenwerte und Funktionen aus Physik, Chemie, Astronomie, Geophysik und Technik*, 6 Aufl., Band 2, Teil 5, Berlin: Springer-Verlag, 1968, pp. 238–246, Erganzung pp. 395–396.
9. Chickos, James S. and Acree, William E., Jr., *J. Phys. Chem. Ref. Data*, 2002, no. 31(2), pp. 537–698.
10. Lebedev, Yu.A. and Miroshnichenko, E.A., *Termokhimiya paroobrazovaniya organicheskikh veshchestv: Teploty ispareniya, sublimatsii i davlenie nasyshchennogo para* (Thermochemistry of Vaporization of Organic Substances: Heats of Evaporation and Sublimation and the Saturated Vapor Pressure), Moscow: Nauka, 1981.
11. Radchenko, L.G. and Kitaigorodskii, A.I., *Zh. Fiz. Khim.*, 1974, no. 11, pp. 2702–2704.
12. Krasulin, A.P., Kozyro, A.A., and Kabo, G.Ya., *Zh. Prikl. Khim.*, 1987, vol. 54, no. 1, pp. 104–107.
13. Lebedev, D.P. and Perel'man, T.L., *Teplo- i massoobmen v protsessakh sublimatsii v vakuume* (Heat-and-Mass Exchange in Sublimation in a Vacuum), Moscow: Energiya, 1973.
14. Moelwyn-Hughes, E.A., *Physical Chemistry*, London: Pergamon, 1961.
15. *Crystal Growth. Theory and Techniques*, Goodman, C.H.L., Ed., London: Plenum, 1974, vol. 1.

16. Schlichting, H., *Grenzschicht Theorie*, Karlsruhe: Verlag, 1965.
17. Bretsznajder, S., *Wlasnosci gazow i cieczy* (Properties of Gases and Liquids), Warszawa: Naukowo-Techniczne, 1962.
18. Viktorov, M.M., *Metody vychisleniya fiziko-khimicheskikh velichin i prikladnye raschety* (Methods for Calculation of Physicochemical Quantities and Applied Calculations), Leningrad: Khimiya, 1977.
19. Reid, R.C., Prausnitz, J.M., and Sherwood, T.K., The Properties of Gases and Liquids, New York: McGraw-Hill, 1977.
20. Kucherov, R.Ya. and Rikenglaz, L.E., *Zh. Eksp. Teor. Fiz.*, 1959, vol. 37, no. 1, pp. 125.
21. Kafarov, V.V. and Gorelik, A.M., *Protsessy sublimatsii i desublimatsii v khimicheskoi tekhnologii: Obzornaya informatsiya* (Sublimation and Desublimation Processes in Chemical Technology: A Review), Moscow: Khimiya, 1985.
22. Bogolyubov, N.A. and Masharov, S.I., *Isparenie atomno- i magnitouporyadochennykh kristallov s defektami* (Evaporation of Atomically and Magnetically Ordered Crystals with Defects), Novosibirsk: Nauka, 1989.
23. Andrievskii, R.A., Bairatashvili, I.A., and Soloev, Yu.I., *Davlenie para i koeffitsient ispareniya bora* (Vapor Pressure and Evaporation Coefficient of Boron), 1982, vol. 20, no. 5, pp. 862–865.
24. *Spravochnik khimika* (Chemist's Handbook), Nikol'skii, B.P., Ed., Moscow: Goskhimizdat, 1962, vol. 1.
25. *Khimicheskaya entsiklopediya* (Chemical Encyclopedia), Knunyants, I.L., Ed., Moscow: Sov. Entsiklopediya, 1990, vol. 2.
26. *Khimicheskaya entsiklopediya* (Chemical Encyclopedia), Knunyants, I.L., Ed., Moscow: Sov. Entsiklopediya, 1988, vol. 1.
27. Gmelin *Handbuch, 8 Aufl., Vanadium, Teil A – Lieferung 2*, 1968, p. 437.
28. *Gmelin Handbuch of Inorganic Chemistry with Supplement*, 1989, vol. A3, p. 146.

ISSN 1070-4272, Russian Journal of Applied Chemistry, 2006, Vol. 79, No. 8, pp. 1238–1243. © Pleiades Publishing, Inc., 2006.
Original Russian Text © Sh.B. Kasenova, A.Zh. Abil'daeva, S.A. Ivasenko, G.A. Atazhanova, S.M. Adekenov, Zh.K. Tukhmetova, B.K. Kasenov, 2006, published in Zhurnal Prikladnoi Khimii, 2006, Vol. 79, No. 8, pp. 1254–1258.

PHYSICOCHEMICAL STUDIES OF SYSTEMS AND PROCESSES

Calorimetric Study of the Enthalpies of Solution of Methyl Iodides of Dimethylamino Grosshemin and Diethylamino Grosshemin in Water and Evaluation of the Thermodynamic Properties of Their Analogues

Sh. B. Kasenova, A. Zh. Abil'daeva, S. A. Ivasenko, G. A. Atazhanova, S. M. Adekenov, Zh. K. Tukhmetova, and B. K. Kasenov

Institute of Phytochemistry, Ministry of Education and Science of the Republic of Kazakhstan, Karaganda, Kazakhstan

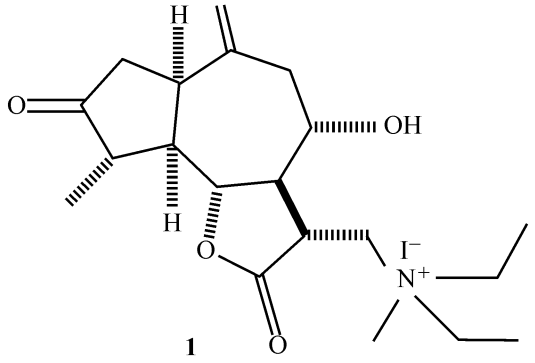
Received April 16, 2005; in final form, April 2006

Abstract—The method of isothermal calorimetry at dilutions (moles salt/moles water) of 1 : 9000, 1 : 18 000, and 1 : 36000 was applied to study the heats of solution of methyl iodides of dimethyl- and diethylamino grosshemin. The data obtained were used to calculate the standard enthalpies of solution of $C_{18}H_{28}O_4NI$ and $C_{20}H_{32}O_4NI$ in an infinitely diluted (standard) aqueous solution. The heats of combustion and melting of $C_{18}H_{28}O_4NI$ and $C_{20}H_{32}O_4NI$ were estimated. The experimental and calculational techniques were combined to calculate the standard heats of formation of methyl iodides of dimethyl- and diethylamino grosshemin and their 66 analogues.

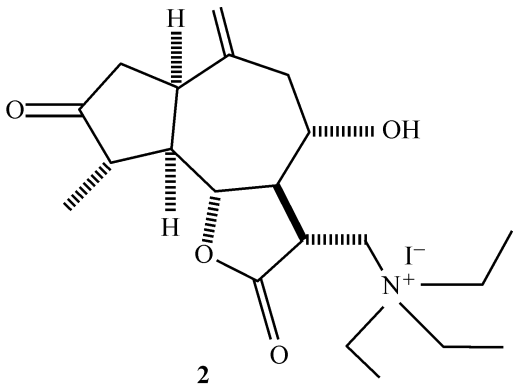
DOI: 10.1134/S1070427206080052

A study of thermochemical and thermodynamic properties of natural compounds and their derivatives is of certain theoretical and practical interest for directed synthesis and standardization of samples of medicinal substances based on these compounds [1, 2]. To biologically active compounds of this kind belongs a sesquiterpene lactone grosshemin, extracted from vegetable raw materials [3].

It should be noted that the thermochemical and thermodynamic properties of this theoretically and practically important sesquiterpene lactone and its derivatives have not been studied so far. Therefore, an experimental study of the thermochemical properties of methyl iodides of dimethyl- and diethylamino grosshemin was carried out and the data obtained were used to find by a combination of calculational techniques the standard enthalpies of formation of $C_{18}H_{28}O_4NI$ (**1**), $C_{20}H_{32}O_4NI$ (**2**), and their analogues:



1



2

EXPERIMENTAL

The calorimetric study of the enthalpy of solution of methyl iodides of dimethyl- and diethylamino grosshemin was performed on a DAK-I-IA calorimeter under isothermal conditions at different dilutions of 1 : 9000, 1 : 18000, and 1 : 36000 (moles salt/moles water). The theory of the calorimetric study and the procedure used were described in detail in [4–7]. The operation principle of the calorimeter is based on measurements of the integral heat flux from the calorimetric cartridge, with a substance being dissolved, through the differentially connected thermopiles and bulky central unit of the microcalorimeter. The rated determination accuracy of heat effects by the calorimeter is ±2.0%.

Five parallel runs were carried out for the compounds under study at each dilution. The results obtained were averaged and processed using methods of mathematical statistics [8]. The root-mean-square deviation $S(y_i)$ was calculated for the averaged values of the enthalpy of solution at each dilution and the random error ε_{rand} was determined using the Student coefficient $t_{1-\alpha}(n-1)$ [8]. The value $\alpha = 0.95$ was chosen as the optimal confidence probability.

The uniformity of variance $s^2(y_i)$ of the quantities $y_i = \log \Delta H_i^m$ was evaluated using the Cochran criterion [8] because the number of measurements of ordinates y_i for different x_i is the same ($n_1 = n_2 = n_3 = n_4 = n_5 = n$). The hypothesis of uniformity of the variances of reproducibility of the ordinates $y_i = \log \Delta H_i^m$ was taken with a 5% significance level.

Parameters of the regression line were determined: $a_0(\mathrm{I}) = 1.495$, $a_0(\mathrm{II}) = 1.073$, $b_0(\mathrm{I}) = -25.41$, $b_0(\mathrm{II}) = -63.54$, $a(\mathrm{I}) = 1.584$, $a(\mathrm{II}) = 1.298$. These parameters were used to derive the sought-for regression equation for models (I) and (II):

$$Y(\mathrm{I}) = 1.584 - 25.41x, \quad (1)$$

$$Y(\mathrm{II}) = 1.298 - 63.54x. \quad (2)$$

The linearity hypothesis is satisfied by the inequalities $F_{exp} = 36.67 < 243.9$ for model (I) and $F_{exp} = 2.552 < 243.9$ for model (II). Hence follows that the linearity hypothesis should be taken with a 5% significance level.

The enthalpies of combustion of methyl iodides of dimethyl- and diethylamino grosshemin were calculated by the Karas and Frost methods [9], and the enthalpies of melting, by the empirical equation recommended in [10].

A calculation of $\Delta_f H^0(298.15)$ for analogues of $C_{18}H_{28}O_4NI$ and $C_{20}H_{32}O_4NI$ was performed using the system of enthalpy increments of anions [11, 12].

The grosshemin derivatives, methyl iodide of dimethylamino grosshemin $C_{18}H_{28}O_4NI$ (**1**) and methyl iodide of diethylamino grosshemin $C_{20}H_{32}O_4NI$ (**2**) were obtained in high yields by reacting amino derivatives of grosshemin with methyl iodide.[1] The structure of the substances was determined by with the use of IR, UV, and ^{1}H NMR spectroscopies and X-ray diffraction analysis. The purity of the substances was better than 99.0%. The melting points of $C_{18}H_{28}O_4NI$ and $C_{20}H_{32}O_4NI$ are 217–218 and 107–108°C, respectively [13].

The calorimetric determination of the enthalpy of solution of the compounds under study in water was carried out in the mode of automatic heat compensation. The heat effects were recorded with a KSP-4 self-recorder and, in parallel, by an IP-4 precision integrator. A substance was placed in a metallic ampule, which was inserted into a metallic cartridge with the solvent. The time of preliminary thermostating of the solvent and substance was 2 h. The zero drift of the integrator did not exceed three units of the last digit in 100 s. The substance studied dissolved as the ampule was immersed in the solvent.

The operation of the instrument was tested by measuring the heat of solution of a thrice recrystallized KCl at dilutions of 1 : 1600, 1 : 2400, and 1 : 3200 (moles salt/moles water). The resulting average value of the heat of KCl solution in water at 25°C, equal to 17860 ± 283 J mol^{-1}, is in a satisfactory agreement with the reference values of 17577 ± 34 J mol^{-1} [14] and 17489 ± 371 J mol^{-1} [15] at the same temperature with an accuracy of 1.6 and 2.0%.

Table 1 lists the enthalpies of solution of methyl iodides of dimethyl- and diethylamino grosshemin at various dilutions.

The calorimetrically obtained enthalpies of solution of $C_{18}H_{28}O_4NI$ and $C_{20}H_{32}O_4NI$ at various dilu-

[1] Methyl iodides were obtained at the laboratory of chemistry of terpenoids, Institute of Phytochemistry, Ministry of Education and Science of the Republic of Kazakhstan.

Table 1. Enthalpies of solution of methyl iodides of dimethyl- and diethylamino grosshemin in water at various dilutions (moles salt/moles water)

Mass of $C_{18}H_{28}O_4NI$, g	ΔH_{sol}, J	ΔH^m_{sol}, kJ mol^{-1}	Mass of $C_{20}H_{32}O_4NI$, g	ΔH_{sol}, J	ΔH^m_{sol}, kJ mol^{-1}
Dilution 1 : 9000					
0.0136	0.836	27.59	0.0146	0.251	8.20
0.0135	0.815	27.10	0.0147	0.254	8.24
0.0135	0.803	26.70	0.0147	0.249	8.08
0.0135	0.815	27.10	0.0144	0.243	8.05
0.0136	0.824	27.20	0.0145	0.243	7.99
Average		27.14 ± 0.39	Average		8.11 ± 0.13
Dilution 1 : 18 000					
0.0066	0.462	31.42	0.0070	0.187	12.74
0.0067	0.462	30.95	0.0070	0.192	13.08
0.0066	0.467	31.76	0.0071	0.191	12.83
0.0066	0.465	31.63	0.0074	0.200	12.89
0.0067	0.476	31.89	0.0073	0.198	12.93
Average		31.53 ± 0.46	Average		12.89 ± 0.16
Dilution 1 : 36 000					
0.0034	0.271	35.78	0.0036	0.118	15.63
0.0033	0.261	35.50	0.0033	0.111	16.04
0.0034	0.268	35.38	0.0037	0.122	15.72
0.0033	0.263	35.77	0.0038	0.127	15.94
0.0032	0.257	36.05	0.0037	0.124	15.98
Average		35.70 ± 0.33	Average		15.86 ± 0.22

tions were used to calculate their ΔH^0 of solution at the infinite (standard) dilution. The dependences of the enthalpy of solution of the compounds, ΔH^m_{sol} (kJ mol^{-1}), on the molal concentration ($\sqrt{m}$) are described by the equations [16]

$$\Delta H^m_{sol}(C_{18}H_{28}O_4NI) = (44.1 \pm 0.6) - (218.4 \pm 3.0)\sqrt{m}, \quad (3)$$

$$\Delta H^m_{sol}(C_{20}H_{32}O_4NI) = (23.8 \pm 0.3) - (198.8 \pm 2.5)\sqrt{m}. \quad (4)$$

Equations (3) and (4) were used to calculate the standard enthalpies of solution of the methyl iodides in the infinitely diluted aqueous solution, equal to 44.1 ± 0.6 and 23.8 ± 0.3 kJ mol^{-1}, respectively. These values were further used to calculate the standard heats of formation of various derivatives of grosshemin.

The standard heats of combustion, $\Delta_f H^0(298.15)$, of $C_{18}H_{28}O_4NI$ and $C_{20}H_{32}O_4NI$ were evaluated by the Karas and Frost methods [9], which are the best suitable for taking into account the contributions of various groups to the heat of combustion. The averaged values of the heats of combustion of $C_{18}H_{28}O_4NI$ and $C_{20}H_{32}O_4NI$ are 10 697 ± 257 and 12 005 ± 257 kJ mol^{-1}, respectively. The reaction equations

$$2C_{18}H_{28}O_4NI_{(l)} + 46O_{2(g)} = 36CO_{2(g)} + 28H_2O_{(l)} + N_{2(g)} + I_{2(g)} - \Delta H^0_{comb}, \quad (5)$$

$$2C_{20}H_{32}O_4NI_{(l)} + 52O_{2(g)} = 40CO_{2(g)} + 32H_2O_{(l)} + N_{2(g)} + I_{2(g)} - \Delta H^0_{comb} \quad (6)$$

were used to calculate the standard enthalpies of formation of liquid $C_{18}H_{28}O_4NI$ and $C_{20}H_{32}O_4NI$, equal to –395.5 and –447.2 kJ mol^{-1}, respectively. With the exception of ΔH^0 of combustion, the data necessary for calculation of $\Delta_f H^0(298.15)_{(l)}$ by schemes (5) and (6) were taken from the reference book [17].

Because the given grosshemin derivatives are in the crystalline state at 298.15 K, their $\Delta_f H^0(298.15)$ in the solid state were determined. For this purpose, ΔH_{melt} of $C_{18}H_{28}O_4NI$ and $C_{20}H_{32}O_4NI$ was evaluated in accordance with the empirical equation [10]

$$\Delta H_{melt} = 44.4T_{melt} - 4400, \quad (7)$$

commonly used for strongly polar halide compounds. The values of ΔH_{melt}, found for $C_{18}H_{28}O_4NI$ and $C_{20}H_{32}O_4NI$ by Eq. (7), are 17.4 and 12.5 kJ mol^{-1}, respectively. The equations

$$\Delta_f H^0(C_{18}H_{28}O_4NI_{(s)}, 298.15) = \Delta_f H^0(C_{18}H_{28}O_4NI_{(l)}, 298.15) - \Delta H_{melt}, \quad (8)$$

$$\Delta_f H^0(C_{20}H_{32}O_4NI_{(s)}, 298.15) = \Delta_f H^0(C_{20}H_{32}O_4NI_{(l)}, 298.15) - \Delta H_{melt} \quad (9)$$

were used to calculate the standard enthalpies of formation of methyl iodides of dimethyl- and diethylamino grosshemin in the crystalline state, equal to –412.9 and –459.7 kJ mol^{-1}.

The values of ΔH^0 of solution of $C_{18}H_{28}O_4NI$ and $C_{20}H_{32}O_4NI$ at the infinite dilutions, were used to calculate by the equations

$$\Delta_f H^0(298.15)\,C_{18}H_{28}O_4NI\,(solution, H_2O, st. state) = \Delta_f H^0(298.15)\,C_{18}H_{28}O_4NI_{(s)} + \Delta H^0_{(solution)}, \quad (10)$$

$$\Delta_f H^0(298.15)\,C_{20}H_{32}O_4NI\,(solution, H_2O, st. state) = \Delta_f H^0(298.15)\,C_{20}H_{32}O_4NI_{(s)} + \Delta H^0_{(solution)} \quad (11)$$

$\Delta_f H^0(298.15)$ for $C_{18}H_{28}O_4NI$ and $C_{20}H_{32}O_4NI$ in the standard aqueous solution (–368.8 and –435.9 kJ mol^{-1}). The relations

$$[\Delta_f H^0(298.15)\,C_{18}H_{28}O_4N^+(solution, H_2O, st. state)] = [\Delta_f H^0(298.15)\,C_{18}H_{28}O_4NI\,(solution, H_2O, st. state)] - [\Delta_f H^0(298.15)I^-(solution, H_2O, st. state)], \quad (12)$$

$$[\Delta_f H^0(298.15)\,C_{20}H_{32}O_4N^+(solution, H_2O, st. state)] = [\Delta_f H^0(298.15)\,C_{20}H_{32}O_4NI\,(solution, H_2O, st. state)] - [\Delta_f H^0(298.15)I^-(solution, H_2O, st. state)] \quad (13)$$

served to calculate, using the data obtained and the reference value $[\Delta_f H^0(298.15)I^-$ (solution, H_2O, st. state)], $\Delta_f H^0(298.15)$ of formation of $C_{18}H_{28}O_4N^+$ and $C_{20}H_{32}O_4N_+$ ions in the standard aqueous solution, equal to –313.5 and –380.6 kJ mol^{-1}, respectively.

Further, the standard enthalpies of formation of $C_{18}H_{28}O_4N^+$ and $C_{20}H_{32}O_4N^+$ ions in the standard aqueous solution were used to calculate $\Delta_f H^0(298.15)$ for other grosshemin derivatives. In [11, 12], a system of thermochemical enthalpy increments was developed for calculating the standard enthalpies of formation of compounds in the crystalline state by the equation

$$\Delta_f H^0(298.15)Me_m(X_\alpha O_\beta)_n = [m\,\Delta_f H^0(298.15, Me^{n+}, solution, H_2O, st. state)]K + n\,\Delta_f H^j(298.15)X_\alpha O_\beta^{m-}, \quad (14)$$

where $\Delta_f H^j(298.15)$ is the enthalpy increment of the anion, and K, proportionality factor.

To calculate $\Delta_f H^0(298.15)$ of compounds by Eq. (14), it suffices to know $\Delta_f H^0(298.15$, solution, H_2O, st. state) of the cation, whereas the coefficients K and values of $\Delta_f H^i(298.15)$ of anions are tabulated [11, 12]; the accuracy of this calculation is ±5.0%. For two grosshemin derivatives ($C_{18}H_{28}O_4NI$ and $C_{20}H_{32}O_4NI$), Eq. (14) can be represented as

$$\Delta_f H^0(C_{18}H_{28}O_4NI_{(s)}, 298.15) = \Delta_f H^0(C_{18}H_{28}O_4N^+, solution, H_2O, st. state, 298.15)K + \Delta_f H^i(I^-, 298.15), \quad (15)$$

$$\Delta_f H^0(C_{20}H_{32}O_4NI_{(s)}, 298.15) = \Delta_f H^0(C_{20}H_{32}O_4N^+, solution, H_2O, st. state, 298.15)K + \Delta_f H^i(I^-, 298.15). \quad (16)$$

Table 2 lists the values of $\Delta_f H^0(298.15)$ for 66 derivatives of these compounds, calculated by Eqs. (15), (16).

Table 2. Standard heats of formation of derivatives of $C_{18}H_{28}O_4NI$ and $C_{20}H_{32}O_4NI$

No.	Compound	$-\Delta_f H^0(298.15)$, kJ mol^{-1}	No.	Compound	$-\Delta_f H^0(298.15)$, kJ mol^{-1}
1	$C_{18}H_{28}O_4NF$	633 ± 32	34	$C_{20}H_{32}O_4NF$	699 ± 35
2	$C_{18}H_{28}O_4NBr$	431 ± 21	35	$C_{20}H_{32}O_4NBr$	498 ± 25
3	$C_{18}H_{28}O_4NCl$	469 ± 23	36	$C_{20}H_{32}O_4NCl$	534 ± 27
4	$C_{18}H_{28}O_4NClO_3$	436 ± 22	37	$C_{20}H_{32}O_4NClO_3$	507 ± 25
5	$C_{18}H_{28}O_4NClO_4$	452 ± 23	38	$C_{20}H_{32}O_4NClO_4$	521 ± 26
6	$C_{18}H_{28}O_4NBrO_3$	423 ± 21	39	$C_{20}H_{32}O_4NBrO_3$	494 ± 25
7	$C_{18}H_{28}O_4NIO_3$	577 ± 29	40	$C_{20}H_{32}O_4NIO_3$	647 ± 32
8	$[C_{18}H_{28}O_4N]_2SO_4$	1526 ± 76	41	$[C_{20}H_{32}O_4N]_2SO_4$	1659 ± 83
9	$[C_{18}H_{28}O_4N]_2SO_3$	1241 ± 62	42	$[C_{20}H_{32}O_4N]_2SO_3$	1372 ± 69
10	$[C_{18}H_{28}O_4N]_2SeO_4$	1204 ± 60	43	$[C_{20}H_{32}O_4N]_2SeO_4$	1335 ± 67
11	$[C_{18}H_{28}O_4N]_2TeO_4$	1405 ± 70	44	$[C_{20}H_{32}O_4N]_2TeO_4$	1545 ± 77
12	$[C_{18}H_{28}O_4N]_2S_2O_3$	1298 ± 65	45	$[C_{20}H_{32}O_4N]_2S_2O_3$	1433 ± 72
13	$[C_{18}H_{28}O_4N]_2SeO_3$	1097 ± 55	46	$[C_{20}H_{32}O_4N]_2SeO_3$	1227 ± 61
14	$[C_{18}H_{28}O_4N]_2TeO_3$	1129 ± 56	47	$[C_{20}H_{32}O_4N]_2TeO_3$	1260 ± 63
15	$[C_{18}H_{28}O_4N]_2S$	550 ± 27	48	$[C_{20}H_{32}O_4N]_2S$	662 ± 33
16	$[C_{18}H_{28}O_4N]_2Se$	595 ± 30	49	$[C_{20}H_{32}O_4N]_2Se$	709 ± 35
17	$[C_{18}H_{28}O_4N]NO_3$	529 ± 26	50	$[C_{20}H_{32}O_4N]NO_3$	597 ± 30
18	$[C_{18}H_{28}O_4N]NO_2$	423 ± 21	51	$[C_{20}H_{32}O_4N]NO_2$	490 ± 24
19	$[C_{18}H_{28}O_4N]_3PO_4$	2167 ± 108	52	$[C_{20}H_{32}O_4N]_3PO_4$	2365 ± 118
20	$[C_{18}H_{28}O_4N]_4P_2O_7$	3437 ± 172	53	$[C_{20}H_{32}O_4N]_4P_2O_7$	3738 ± 187
21	$[C_{18}H_{28}O_4N]_2CO_3$	1281 ± 64	54	$[C_{20}H_{32}O_4N]_2CO_3$	1413 ± 71
22	$[C_{18}H_{28}O_4N]_2C_2O_4$	1448 ± 72	55	$[C_{20}H_{32}O_4N]_2C_2O_4$	1582 ± 79
23	$C_{18}H_{28}O_4NAlO_2$	1214 ± 61	56	$C_{20}H_{32}O_4NAlO_2$	1278 ± 64
24	$C_{18}H_{28}O_4NBO_2$	1041 ± 52	57	$C_{20}H_{32}O_4NBO_2$	1106 ± 55
25	$C_{18}H_{28}O_4NReO_4$	1160 ± 58	58	$C_{20}H_{32}O_4NReO_4$	1229 ± 61
26	$C_{18}H_{28}O_4NMnO_4$	898 ± 45	59	$C_{20}H_{32}O_4NMnO_4$	969 ± 48
27	$[C_{18}H_{28}O_4N]_2Cr_2O_7$	2175 ± 109	60	$[C_{20}H_{32}O_4N]_2Cr_2O_7$	2312 ± 116
28	$[C_{18}H_{28}O_4N]_2CrO_4$	1513 ± 76	61	$[C_{20}H_{32}O_4N]_2CrO_4$	1649 ± 82
29	$[C_{18}H_{28}O_4N]_2WO_4$	1712 ± 86	62	$[C_{20}H_{32}O_4N]_2WO_4$	1847 ± 92
30	$[C_{18}H_{28}O_4N]_2MoO_4$	1534 ± 77	63	$[C_{20}H_{32}O_4N]_2MoO_4$	1667 ± 83
31	$C_{18}H_{28}O_4NVO_3$	1224 ± 61	64	$C_{20}H_{32}O_4NVO_3$	1292 ± 65
32	$C_{18}H_{28}O_4NNbO_3$	1402 ± 70	65	$C_{20}H_{32}O_4NNbO_3$	1470 ± 73
33	$[C_{18}H_{28}O_4N]_3AsO_4$	1797 ± 90	66	$[C_{20}H_{32}O_4N]_3AsO_4$	1995 ± 100

CONCLUSIONS

(1) The enthalpies of solution of methyl iodides of dimethyl- and diethylamino grosshemin in water were determined for the first time by isothermal calorimetry.

(2) The enthalpies of combustion and melting of these compounds were calculated, a combination of calculated data and experimental values of the enthalpy of solution of the methyl iodides in a standard aqueous solution was used to find the standard heats of formation of $C_{18}H_{28}O_4N^+$ and $C_{20}H_{32}O_4N^+$ ions in the aqueous solution.

(3) The method of enthalpy increments was employed to calculate the standard heats of formation of $C_{18}H_{28}O_4NI$ and $C_{20}H_{32}O_4NI$ and their 66 analogues.

(4) The results of the study are of certain interest for thermochemistry of aqueous solutions of biologically active substances and for directed synthesis of derivatives of natural compounds. These results can serve as input data arrays to be loaded into fundamental databases and included in reference books with thermodynamic constants.

REFERENCES

1. Abrosimov, V.K., Agafonov, A.V., Chumakova, R.V., et al.,. *Biologicheski aktivnye veshchestva v rastvorakh: Struktura, termodinamika, reaktsionnaya sposobnost'*

(Biologically Active Substances in Solutions: Structure, Thermodynamics, Reactivity), Moscow: Nauka, 2001.

2. Arzamastsev, A.P. and Senov, P.L., *Standartnye obraztsy lekarstvennykh veshchestv* (Standard Samples of Medicinal Substances), Moscow: Meditsina, 1978.
3. Kagarlitskii, A.D., Adekenov, S.M., and Kupriyanov, A.N., *Seskviterpenovye laktony rastenii Tsentral'nogo Kazakhstana* (Sesquiterpene Lactones in Plants of Central Kazakhstan), Alma-Ata: Nauka, 1987.
4. Skuratov, S.M., Kolesov, V.P., and Vorob'ev, A.F., *Termokhimiya* (Thermochemistry), Moscow: Mosk. Gos. Univ., 1964.
5. Calvet, E. and Prat, H., *Microcalorimetrie. Applications Physico-Chemiques et Biologiques*, Paris: Masson, 1956.
6. Topor, N.D. and Suponitskii, Yu.L., *Usp. Khim.*, 1984, vol. 53, no. 9, pp. 1425–1462.
7. Calve, E., *Zh. Fiz. Khim.*, 1959, vol. 33, no. 6, pp. 1161–1175.
8. Spiridonov, V.P. and Lopatkin, A.A., *Matematicheskaya obrabotka fiziko-khimicheskikh dannykh* (Mathematical Processing of Physicochemical Data), Moscow: Mosk. Gos. Univ., 1970.
9. Kazanskaya, A.S. and Skoblo, V.A., *Raschety khimicheskikh ravnovesii* (Calculation of Chemical Equilibria), Moscow: Vysshaya Shkola, 1974.
10. Morachevskii, A.G. and Sladkov, I.B., *Termodinamicheskie raschety v metallurgii* (Thermodynamic Calculations in Metallurgy), Moscow: Metallurgiya, 1985.
11. Kasenov, B.K., Abishev, D.N., and Bukharitsyn, V.O., *Termokhimiya arsenatov shchelochnykh metallov* (Thermochemistry of Arsenates of Alkali Metals), Alma-Ata: Nauka, 1988.
12. Kasenov, B.K., Aldabergenov, M.K., and Pashinkin, A.S., *Termodinamicheskie metody v khimii i metallurgii* (Thermochemical Methods in Chemistry and Metallurgy), Almaty: Rauan, 1994.
13. Ivasenko, S.A., Kulijasov, A.T., and Adekenov, S.M., *V Int. Symp. on Chemistry of Natural Compounds*, Tashkent, 2003, p. 226.
14. Mishchenko, K.P. and Poltoratskii, G.M., *Termodinamika i stroenie vodnykh i nevodnykh rastvorov elektrolitov* (Thermodynamics and Structure of Aqueous and Nonaqueous Solutions of Electrolytes), Leningrad: Khimiya, 1976.
15. *Termicheskie konstanty veshchestv: Spravochnik* (Thermal Constants of Substances), Glushko, V.P., Ed., Moscow: Nauka, 1982, issue 10, ch. 2.
16. Krestov, G.A., *Termodinamika ionnykh protsessov v rastvorakh* (Thermodynamics of Ionic Processes in Solutions), Leningrad: Khimiya, 1984.
17. Ryabin, V.A., Ostroumov, M.A., and Svit, T.F., *Termodinamicheskie svoistva veshchestv: Spravochnik* (Thermodynamic Properties of Substances: Reference Book), Leningrad: Khimiya, 1977.

ISSN 1070-4272, Russian Journal of Applied Chemistry, 2006, Vol. 79, No. 8, pp. 1244–1250. © Pleiades Publishing, Inc., 2006.
Original Russian Text © Yu.G. Dobryakov, A.G. Vitenberg, 2006, published in Zhurnal Prikladnoi Khimii, 2006, Vol. 79, No. 8, pp. 1259–1264.

PHYSICOCHEMICAL STUDIES OF SYSTEMS AND PROCESSES

Determination of Distribution Coefficients of Volatile Sulfur-containing Compounds among Aqueous Solutions and Gas Phase by Continuous Gas Extraction

Yu. G. Dobryakov and A. G. Vitenberg

St. Petersburg State University, St. Petersburg, Russia

Received March 1, 2006

Abstract—The method of continuous gas extraction at 10–40°C was used to measure the distribution coefficients of hydrogen sulfide, methyl mercaptan, ethyl mercaptan, dimethyl sulfide, and dimethyl disulfide between the gas phase and buffer aqueous solutions with a constant pH value.

DOI: 10.1134/S1070427206080064

The problem of determining trace and microscopic concentrations of volatile sulfur-containing substances: hydrogen sulfide, alkyl mercaptans, sulfides, and disulfides, in air, aqueous, and hydrocarbon media remains topical because the existing methods, including those officially accepted, fail to satisfy in the overwhelming majority of cases the modern requirements to sensitivity, selectivity, and accuracy of analysis. A rather promising way to solve numerous problems encountered in the development of techniques for monitoring of volatile sulfur-containing impurities in particular liquid or gaseous objects consists in use, improvement, and development of the existing methods and procedures of gas-chromatographic vapor-phase analysis (VPA) [1, 2]. This technique is based on principles of gas extraction [3], i.e., on the distribution of a substance in the liquid–gas system. Therefore, a key parameter determining the reliability of data obtained in measurements of microscopic concentrations of volatile sulfur-containing substances is the distribution coefficient, which is the ratio of the equilibrium mass concentrations of a substance in the liquid (c_L) and gas (c_G) phases

$$K = c_L/c_G. \quad (1)$$

A group of the most important objects in which the content of volatile sulfur-containing substance is to be measured is constituted by aqueous solutions. Microscopic concentrations of hydrogen sulfide, volatile mercaptans, sulfides, and disulfides are to be monitored not only in wastewater and natural water, industrial discharges, and in the air of the working zone at pulp-and-paper and petrochemical plants, but also in various natural objects.

Data on the numerical values of the distribution coefficients of hydrogen sulfide, methyl mercaptans (MM), ethyl mercaptans (EM), dimethyl sulfide (DMS), and dimethyl disulfide (DMDS) among water or aqueous solutions of mineral substances and the gas phase can be found in two reports [3, 4], which, however, show strong discrepancies, as large as several tens of percent for some components. These discrepancies presumably result from use of different variants of static VPA to measure K. The fundamental difference between these variants consists in that different gas extraction procedures are employed. In [3], double extraction was used and the phase distribution constant was calculated from relative areas under peaks in chromatograms. In the later publication [4], a single-stage gas extraction was used and K was calculated from the absolute values of the substance concentrations in the liquid and gas phases.

The aim of this study was to refine the available published data and obtain reliable information about phase distribution constants among water or aqueous solutions and the gas phase for volatile sulfur-containing substances of priority importance in sanitary-chemical and ecological regards.

To improve the accuracy and eliminate the possible systematic errors inherent in the static VPA (especially in analysis of the unstable mercaptans), the numer-

ical values of K were measured by the dynamic VPA method based on continuous gas extraction (CGE). As a gas flow is passed through a solution that contains volatile components, the solutes are gradually recovered (extracted) from the liquid into the gas phase in accordance with the distribution law (1). The method requires a comparatively simple apparatus and can be used to measure distribution coefficients in a wide range, from small ($K < 10$) to large ($K > 10^3$). A very important advantage of the technique is that, when necessary, the CGE process can be performed in the absence of even trace amounts of oxygen, which is particularly important for the readily oxidized and unstable hydrogen sulfide and mercaptans. In addition, numerical values of K are calculated in the case of CGE from relative areas under the peaks of target components in chromatograms. This technique rules out any errors associated with calibration of chromatographic detectors for measurement of the absolute concentrations of substances in each of the two phases of a heterogeneous system.

The dynamic VPA diminishes the sorption effects in the gas circuit of the installation, which introduce significant errors into the results of analysis. Previously, this method has been used to measure large $K > 10^3$. The calculation of the numerical value was based on the approximate equation [1]:

$$c_L = c_L^0 \exp\left(-\frac{V_g}{KV_L}\right), \quad (2)$$

which describes how the concentration of the target substance in a solution of a virtually nonvolatile solvent varies from the initial value c_L^0 to the running value c_L corresponding to the volume V_g of the extracting gas passed through a solution volume V_L. However, Eq. (2) disregards the spreading of the substance concentration in the gas volume V_G of the extraction vessel, which has virtually no effect on the result in measurement of large K.

In this study, the dynamic VPA is applied for the first time to systems with small $K < 20$. In systems of this kind, the gas volume V_G can strongly affect the absolute concentrations of the substance in the gas phase, and this influence is accounted for by the equation suggested by Novak [5]:

$$c_G = c_G^0 \exp\left(-\frac{V_g}{KV_L + V_G}\right). \quad (3)$$

Equation (3) describes the CGE of volatile substances from a solution in a vessel with gas volume V_G and relates the initial concentration c_G^0 of the substance in the gas phase over the solution at $V_g = 0$ to its running value c_g in the gas flow at the outlet from the extraction vessel, which corresponds to the volume V_g of the gas passed.

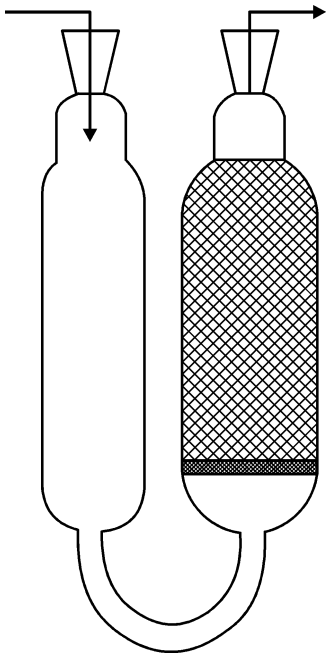


Fig. 1. Saturator for continuous gas extraction.

EXPERIMENTAL

The measurements were made on a Tsvet-500 chromatograph with a Khromdet-1020 photoionization detector. The use of the photoionization detector was due to its high sensitivity and selectivity toward sulfur-containing substances and low sensitivity to water. The recording and processing of chromatograms were done with a MultiKhrom computer complex (v. 1.5). The chromatographic separation and analysis of components were carried out on a 50 m × 0.53 mm quartz capillary column with an SE-30 immobile phase of thickness 3 μm. Gaseous samples were introduced into the column with a six-way two-position gas cock with a 0.5-cm^3 batching loop from the BDG-178 standard pneumatic unit of the Tsvet-500 chromatograph, supplemented with an electronic timer for automated batching. The CGE cell (Fig. 1), the saturator, comprises two cylindrical glass vessels of different diameters (40 and 30 mm), connected by a U-shaped tube. The larger vessel has a sealed-in disc of finely porous glass (porosity 3) and is used for bubbling of the extracting gas through the liquid. The smaller vessel acts as receiver for the gas. The saturator was placed in a U-10 liquid thermostat, which maintained a prescribed temperature with an accuracy not worse than ±0.1°C. The gas flow rate through the saturator

was set and monitored with an IRG-100 gas flow controller (Tsvet OAO). The flow rate of the extracting gas was maintained in the range 15–25 ml min^{-1} with an accuracy not worse than 0.05 ml min^{-1}. The volume of the aqueous buffer solutions was 100 ± 0.5 ml at a height of the liquid layer of 100 mm. The saturator was connected directly to the gas cock via a heated capillary, whose temperature was maintained constant at about 50°C.

Prior to an experiment, the buffer solution was thermostated and saturated with the vapors of the substance under study. As sources of hydrogen sulfide, methyl mercaptan, and ethyl mercaptan served cylinders with reference gas mixtures, purchased from Monitoring OOO. The gas mixture of three components, each with a concentration of 200 ppm, in nitrogen was bubbled through an aqueous solution till its saturation, and then the saturator was connected to IRG-100 to begin the gas extraction. In this way, the distribution coefficients were simultaneously measured for hydrogen sulfide, MM, and EM. Diffusion microflow sources (Monitoring OOO) served to supply the vapor of DMS. Dimethyl sulfide (Acros, USA) was metered directly as a liquid in amounts of 0.5 μl, using a microsyringe.

The aqueous buffer solutions were prepared from a mixture of acid salts KH_2PO_4 and Na_2HPO_4, pH 4.8 [6]; also, a 7% solution of sodium hydrosulfate $KHSO_4$, pH 0.9, was produced.

For sufficiently diluted solutions, the ratio of the concentrations of the volatile substance in the gas phase, c_G and c_G^0, can be replaced, within the linearity range of the chromatographic detector and in accordance with a value of the distribution coefficient (1), with the corresponding ratio of peak areas in the chromatograms, A_G and A_G^0. Then, the results of a chromatographic analysis of the flow of the extracting gas passed through a solution under study can be used to calculate, in accordance with Eq. (3), the numerical value of the distribution coefficient by the equation

$$K = \frac{V_g/V_L}{\ln(A_G^0/A_G)} - \frac{V_G}{V_L}. \quad (4)$$

The specificity of application of CGE for measuring the distribution coefficients consists in that the accuracy of the results obtained strongly depends on the ratio between the volumes of the solution and the extracting gas passed through it, or, in other words, on the fraction δ_g of the component being determined, recovered from the solution:

$$\delta_g = 1 - \exp\left(-\frac{V_g}{KV_L + V_G}\right) = 1 - \frac{A_G}{A_G^0}. \quad (5)$$

The error in measuring the volumes V_G and V_L is negligible as compared with the error in measuring the concentrations c_G and c_G^0 as the areas under the peaks in the chromatogram, A_G and A_G^0. In such cases, the relative error in determining the distribution coefficient ($\Delta K/K$) is related to the CGE conditions and to the fraction of the substance recovered from solution by the expressions

$$\frac{\Delta K}{K} = \left(\frac{\Delta A_G^0}{A_G^0} + \frac{\Delta A_G}{A_G}\right)\left[\ln\left(\frac{1}{1-\delta_g}\right)\right]^{-1}$$
$$= \left(\frac{\Delta A_G^0}{A_G^0} + \frac{\Delta A_G}{A_G}\right)\left[\ln\left(\frac{A_G^0}{A_G}\right)\right]^{-1}, \quad (6)$$

derived from Eq. (3). It is quite clear that the relative error in measurement of K by the CGE method decreases as the volume of the extracting gas passed through the solution increases, and it will not exceed the total error in measuring the peak areas in the chromatogram if the fraction of the substance recovered into the gas phase is no less than 63% and the ratio $(A_G^0/A_G) \geq e$ (e is the base of the natural logarithm).

The values of K were calculated in the CGE method in two ways. In the first of these, the calculation was done by EQ. (4) for two peak areas measured in the chromatogram: initial A_G^0 at $V_g = 0$ and A_G corresponding to a volume V_g of gas passed through a solution of volume V_L. Successive measurement of peak areas for different volumes of passed gas makes it possible to calculate K for the whole range of substance concentrations measured in the system. The error of the thus calculated distribution coefficient is found as the deviation from the average value of K.

Another, graphical, technique makes it possible to calculate the distribution coefficient from a set of values of the chromatographic signal A_G, which exponentially decrease with time [7]. At a constant flow rate w_g of the extracting gas, the volume V_g of the gas passed through the solution is proportional to the time t elapsed from the beginning of extraction till sampling ($V_g = w_g t$). In accordance with the procedure used, samples were periodically taken in the automatic mode at strictly equal intervals of time from the flow of a gas that was in equilibrium with the solution under study. Therefore, the time τ of appearance of a given component in the chromatogram was used as

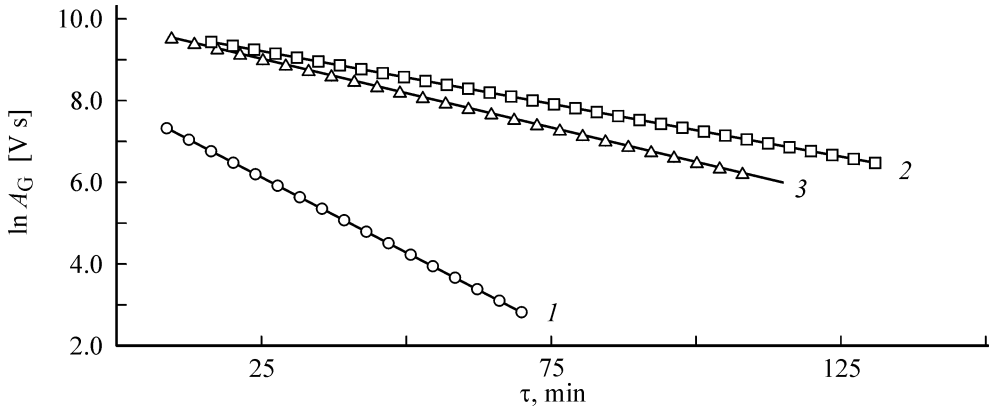


Fig. 2. Graphical method for determining the distribution coefficients. (*1*) Hydrogen sulfide, (*2*) methyl mercaptan, and (*3*) ethyl mercaptan. R^2: (*1, 2*) 0.9996 and (*3*) 0.9989. ($\ln A_G$) Logarithm of the peak area and (τ) time.

independent variable. To calculate K, the dependence $\ln A_G = f(\tau)$ was plotted (see for hydrogen sulfide, MM, and EM in Fig. 2). As a rule, this is a linear dependence (correlation factor $R^2 \geq 0.999$) and the slope α of the straight line is given by

$$\alpha = -w_g/(KV_L + V_G).$$

If the flow rate w_g of the carrier gas and the volume of the coexisting liquid and gas phases are known, the distribution coefficient can be easily calculated. In this method of processing of the measurement results, the experimental error was determined by the measurement accuracy of the volumes ΔV_L and ΔV_g of the liquid and the extracting gas passed through the liquid. For all of the systems studied, the error in measuring the distribution coefficients did not exceed 4%. The calculations of the distribution coefficients of DMDS for the phosphate buffer solution (pH 4.8) at 15°C by the two methods described above give close results (Table 1). The differences are in this case considerably smaller than the measurement error of K.

For components that dissociate in water, the solution acidity may affect the content (fraction) of their molecular form in the aqueous medium. In the case in question, these are hydrogen sulfide and mercaptans. The partial pressure of vapors of these substances over a solution and, consequently, their concentrations in the gas phase are proportional to the undissociated part of the substance in the system. As a result, the numerical values of the distribution coefficients of hydrogen sulfide and mercaptans strongly depend on the degree of their dissociation in solution. The pH value at which the dissociation equilibrium is virtually completely shifted to the left should satisfy the inequality [1, 8] pH $\leq$ pK_a – 2. At 25°C, hydrogen sulfide has $pK_a^{H_2S} = 7.2$, and methyl and ethyl mercaptans, $pK_A^{MM} = 10.33$ and $pK_a^{EM} = 10.61$ [9], and, therefore, the solution acidity has no effect on the distribution coefficients at pH $\leq$ 5 for hydrogen sulfide and at pH $\leq$ 8 for mercaptans. Therefore, an aqueous buffer solution wit pH 4.8 was chosen as

Table 1. Distribution coefficients of dimethyl sulfide among the phosphate buffer solution at 15°C and the gas phase, calculated by Eq. (4) (K_I) and graphically (K_{II})

Peak no.	τ, min	Area A_G, V s	K_I	K_{II}
1	0	20852	–	–
2	32.17	14503	21.85	21.15
3	36.82	13754	21.82	21.20
4	41.60	12970	21.60	21.07
5	46.35	12192	21.29	20.82
6	51.16	11744	21.98	21.52
7	55.95	11139	22.01	21.59
8	60.58	10605	22.10	21.71
9	65.24	10001	21.90	21.54
10	70.00	9427	21.74	21.42
11	74.79	8904	21.67	21.37
12	79.59	8482	21.82	21.53
13	84.28	7930	21.49	21.23
14	88.87	7593	21.69	21.44
15	93.61	7121	21.48	21.24
16	98.46	6720	21.44	21.21
17	102.99	6451	21.65	21.43
18	107.69	6041	21.43	21.22
19	112.28	5683	21.29	21.10
20	116.78	5405	21.32	21.13
21	121.19	5147	21.36	21.17
22	125.78	4792	21.08	20.91
23	130.45	4534	21.07	20.91
24	135.01	4208	20.79	20.63
25	139.58	4002	20.84	20.69
K_{av}			21.53	21.22
$\pm\Delta K$			0.36	0.28
$\pm\Delta K_{av}/K$, %			1.7	1.3

Table 2. Distribution coefficients of sulfur-containing substances among the gas phase and buffer solutions with pH 4.8 (KH_2PO_4–Na_2HPO_4) and 0.9 (7% $KHSO_4$ solution) at different temperatures

Substance	pH	*K* at indicated temperature, °C						
		10	15	20	25	30	35	40
H_2S	4.8	3.1	–	2.1	–	1.8	–	1.4
MM		9.3	–	5.8	–	4.9	–	3.5
EM		7.5	–	4.4	–	3.5	–	2.4
DMS		24.7	15.2	–	7.2	–	4.9	–
DMDS		31.2	21.1	–	11.7	–	6.5	–
H_2S	0.9	3.5	–	2.8	–	1.8	–	1.5
MM		10.2	–	6.2	–	4.8	–	3.5
EM		7.9	–	4.7	–	3.2	–	2.3
DMS		17.9	–	11.0	–	7.2	–	4.9
DMDS		27.7	–	14.2	–	8.8	–	6.0

Table 3. Distribution coefficients of hydrogen sulfide, methyl and ethyl mercaptans in the liquid–gas system for buffer solutions and distilled water at 20°C

Substance	Buffer solution		Distilled water
	hydrosulfate, pH 0.9	phosphate, pH 4.8	
H_2S	2.8	2.1	8.0
MM	6.2	5.8	7.9
EM	4.7	4.4	6.1

the liquid phase for measuring the distribution coefficients (temperature variations of the pH value in the phosphate buffer solutions used were disregarded because of being insignificant, several percent [10]). The data obtained (Table 2) confirm the conclusion that, at pH < 5 and 10–40°C, the solution acidity has virtually no effect on the numerical values of the distribution coefficients for all of the volatile sulfur-containing substances studied, including hydrogen sulfide and mercaptans. As the acidity of a solution decreases to the point of its becoming neutral, the distribution coefficients increase manyfold for hydrogen sulfide and change only slightly for mercaptans. In distilled water (Table 3), a significant part of hydrogen sulfide molecules are in the hydrated, bound state, with the fraction of molecular forms markedly decreasing. For mercaptans, the neutral medium is still sufficiently acidic for the numerical values of the distribution coefficients to be affected. Certain discrepancies between the experimental data for mercaptans in distilled water and in buffer solutions are, in all probability, due to the salt background of the buffer solutions.

Presence of mineral substances in a solution causes a "salting-out" effect, which affects the substance distribution among the aqueous and gas phases and the numerical values of the distribution coefficients. Presence of inorganic salts in the liquid phase, as a rule, leads to a decrease in *K*. The extent of this influence depends on the ionic strength of a solution, i.e., on the type, size, and charge of the ions present, as well as on the salt concentrations. For example, data on the distribution coefficients of certain mercaptans and organic sulfides at 25, 35, 45, and 75°C, obtained for distilled water with an ionic strength $I = 0$ and seawater ($I \approx 0.7$), and also for aqueous sodium sulfate solutions with varied salt concentration and ionic strength ($I = 1$–4), were reported in [14]. In this series, a clearly pronounced decrease in *K* is observed as the ionic strength of the solution increases. For example, the distribution coefficient of DMS at 25°C decreases from 13.42 in distilled water to 4.45 ($I = 4$), and that of DMDS, from 24.66 to 8.83. In this case, the data obtained for seawater somewhat "drop out" from the general pattern, which, in all probability, means that seawater has a more

complex composition than aqueous sodium sulfate solutions with about the same ionic strength.

The temperature dependence of the distribution coefficients characterizes the thermodynamic properties of the system and enables calculation of certain important parameters of diluted solutions, such as the limiting activity coefficients [11, 12], Henry constant, excess Gibbs energy and enthalpy [13], and the solvation energy of solutes [14]. A comprehensive study of these thermodynamic quantities makes it possible not only to obtain parameters for mathematical models that can predict the properties of systems of this kind in a wide range of temperatures and pressures, but also to elucidate the nature of intermolecular interactions in solution and assess the influence and role of hydrogen bonds.

The temperature at which the phase equilibrium is attained in the liquid–gas system is of interest for analytical purposes as regards its stability for providing an acceptable accuracy of analysis and the extent to which the distribution coefficient decreases as temperature is raised, for improving the sensitivity of VPA.

Commonly, a linear dependence on inverse temperature is observed in the range 20–30°C at temperatures close to room temperature. In the case in question, such dependences are observed at 10–40°C (Fig. 3). The sufficiently simple behavior of the dependence of the distribution coefficient on inverse temperature can be used to assess the temperature dependence in a certain range of extrapolation of the experimental data.

The results obtained when measuring the distribution coefficients of volatile sulfur-containing substances among aqueous solutions and the gas phase are in a rather good agreement with published values of K [2], measured by the static method. As can be seen in Fig. 4, the same behavior of the temperature dependence of the distribution coefficients is observed in both cases. The discrepancies are systematic, fall within the range 10–50% for different components, and are presumably associated with the chemical composition of the buffer solutions used.

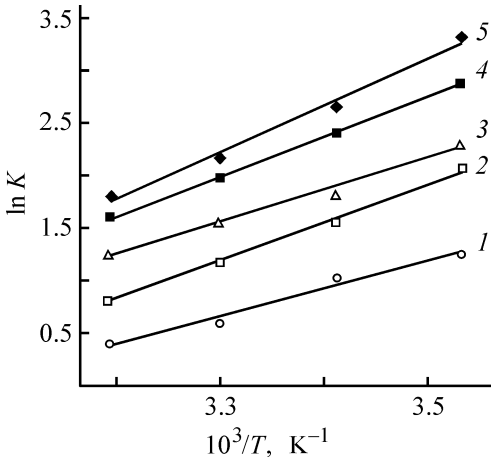


Fig. 3. Distribution coefficients K vs. temperature T. (*1*) Hydrogen sulfide, (*2*) methyl mercaptan, (*3*) ethyl mercaptan, (*4*) dimethyl sulfide, and (*5*) dimethyl disulfide.

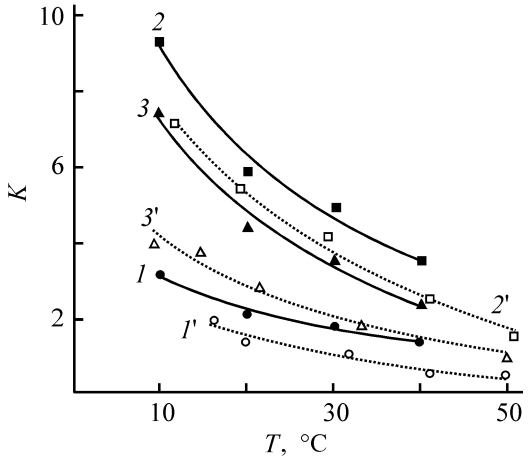


Fig. 4. Comparison of (*1–3*) experimental values of the distribution coefficients K with (*1'–3'*) published data [2]. (*1*, *1'*) Hydrogen sulfide, (*2*, *2'*) methyl mercaptan, and (*3*, *3'*) ethyl mercaptan. (*T*) Temperature.

CONCLUSIONS

(1) The method of continuous gas extraction was used to measure the distribution coefficients of hydrogen sulfide, methyl and ethyl mercaptans, dimethyl sulfide, and dimethyl disulfide among aqueous buffer solutions and the gas phase at different solution temperatures and acidities.

(2) It was shown that the phase behavior of easily volatile sulfur-containing substances in aqueous salt solutions is rather complicated and depends on factors that govern the ionic strength of the solutions, which should be taken into account in studies of natural objects without a prior knowledge of the composition and concentrations of solutes. Use of buffer solutions makes it possible to level the effect of the medium (supporting electrolyte) of the object being analyzed, and the numerical values of the distribution coefficients for buffer solutions of this kind can be used for analytical purposes in a quantitative analysis of solutes by the vapor-phase method.

REFERENCES

1. Vitenberg, A.G. and Ioffe, B.V., *Gazovaya ekstraktsiya v khromatograficheskom analize* (Gas Extraction in Chromatographic Analysis), Leningrad: Khimiya, 1982.
2. Butaeva, I.L., Development of a Method for Gas-Chromatographic Determination of Microscopic Impurities of Sulfur-containing Substances in Wastewater from Sulfate-Cellulose Industries by "Analysis of the Equilibrium Vapor," *Cand. Sci. Dissertation*, Leningrad, 1978.
3. Vitenberg, A.G., Kuznetsova, L.M., Butaeva, I.L., and Inshakov, M.D., *Anal. Chem.*, 1977, vol. 49, no. 1, pp. 128–133.
4. Przyjazny, A., Janicki, W., Chrzanowski, W., and Staszewski, R., *J. Chromatogr.*, 1983, vol. 280, pp. 249–260.
5. Novak, J., *Quantitative Analysis by Gas Chromatography*, New York: Dekker, 1975.
6. Goronovskii, I.T., Nazarenko, Yu.P., and Nekryach, E.F., *Kratkii spravochnik po khimii* (Concise Handbook of Chemistry), Kiev: Naukova Dumka, 1987.
7. Gruber, D., Krummen, M., and Gmehling, J., *Chem. Eng. Technol.*, 1999, vol. 22, pp. 827–831.
8. Vitenberg, A.G., *Ross. Khim. Zh.*, 2003, vol. 47, no. 1, pp. 7–22.
9. Serjeant, E.P. and Dempsey, B., *Ionisation Constants of Organic Acids in Aqueous Solution, IUPAC Chem. Data Ser.*, New York: Pergamon, 1979, no. 23, p. 989.
10. *Spravochnik khimika* (Chemist's Handbook), Nikol'skii, B.P., Ed., Moscow: Khimiya, 1964, vol. 3.
11. Leroi, J.-C., Masson, J.-C., Renon, H., et al., *Ind. Eng. Chem., Process Des. Dev.*, 1977, vol. 16, no. 1, pp. 139–144.
12. Duhem, P. and Vidal, J., *Fluid Phase Equil.*, 1978, vol. 2, pp. 231–235.
13. Morachevskii, A.G., Smirnova, N.A., Balashova, I.M., and Pukinskii, I.B., *Termodinamika razbavlennykh rastvorov neelektrolitov* (Thermodynamics of Diluted Solutions of Nonelectrolytes), Leningrad: Khimiya, 1982.
14. Dobryakova, I.E. and Dobryakov, Yu.G., *Zh. Prikl. Khim.*, 2005, vol. 78, no. 2, pp. 214–218.

ISSN 1070-4272, Russian Journal of Applied Chemistry, 2006, Vol. 79, No. 8, pp. 1251–1259. © Pleiades Publishing, Inc., 2006.
Original Russian Text © K.K. Konstantinova, S.V. Kurbatova, 2006, published in Zhurnal Prikladnoi Khimii, 2006, Vol. 79, No. 8, pp. 1265–1274.

SORPTION AND ION-EXCHANGE PROCESSES

Sorption Properties of Adamantane Derivatives

K. K. Konstantinova and S. V. Kurbatova

Samara State University, Samara, Russia

Received February 6, 2006

Abstract—The chromatographic behavior of adamantane derivatives as sorbates and sorbents was studied. The retention characteristics of adamantane derivatives and some organic compounds on an adamantylsilicone stationary phase were determined. The effect of various substituents on the chromatographic behavior of the compounds was examined. Correlations between the sorption and structural characteristics of adamantane derivatives were found.

DOI: 10.1134/S1070427206080076

Framework hydrocarbons have been attracting steady researchers' interest for many decades owing to the structural diversity of these compounds, their specific physicochemical properties, and biological activity. Various adamantane derivatives or compounds containing an adamantane core have been isolated from natural sources or synthesized, and the number of these compounds steadily grows [1]. Today more than 20000 structures belonging to the so-called diamondoid type are known, including derivatives of adamantane, diamantane, triamantane ($C_{18}H_{24}$), and even tetramantane ($C_{22}H_{28}$); pentamantanes ($C_{26}H_{32}$) and hexamantanes ($C_{30}H_{36}$) occur in the nature [2–4].

Other adamantane homologues have also been prepared. As far back as 1957, P. Schleyer prepared congressane, a hydrocarbon consisting of two fused adamantane molecules. Very numerous are heteroadamantanes containing in the framework the O, N, P, or S atoms, e.g., derivatives of 1,3,5,7-tetrasilaadamantane, 1,3,5,7-tetraazaadamantane (hexamethylenetetramine), 2,4,6,8,9,10-hexamethyl-2,4,6,8,10-hexaboraadamantane, etc. [5–7].

Diamondoids are classed with organic nanostructures; therefore, adamantane derivatives have become particularly popular with the development of nanotechnologies. The applications of adamantane derivatives are diverse: from antiviral drugs to nanorobots and molecular machines [8–10]. Crown ethers derived from adamantane and capable of complexation with metal ions and of their extraction have been studied [2]. Adamantane-containing films exhibiting specific properties and capable of acting as building blocks in the development of various nanomaterials have been prepared [9].

The structure and physicochemical properties of new adamantane derivatives have been studied by various methods. In particular, RHF calculations revealed the possibility of the overlap of the C^1–C^3–C^5–C^7 hybrid atomic orbitals in adamantane derivatives, giving rise to certain electron density inside the framework; the hybridization of carbon atoms that are not bonded to H atoms approaches sp^2 [11]. The thermochemical parameters (enthalpy of formation, bond dissociation energies, enthalpy of vaporization, etc.) have been determined by precision calorimetry for oxygen-containing, nitro, and nitrato derivatives of adamantane [8]. The structures of crystalline adamantane, diamantane [4], and 1,3-diphenyladamantane [12] have been studied by laser Raman spectroscopy; the luminescence of pyrene adamantane derivatives has been examined [10].

Particular attention is given to the chromatographic behavior of adamantane derivatives, because various chromatographic methods allow not only separation of multicomponent mixtures of isomers and structurally related framework hydrocarbons and their derivatives, but also qualitative and quantitative analysis of these mixtures [12]. For example, the relationships in the gas-chromatographic retention of hydrocarbons, ketones, and halo derivatives of the adamantane series on packed columns with stationary phases of different polarity have been revealed. It was shown that the retention of adamantane derivatives is determined by their electronic and steric structure; the major contribution to the retention is made by the bulky adamantyl fragment [13, 14].

We believe that the unusual structure of the adamantane core should also be manifested in the properties of stationary phases or sorbents derived from adamantane. There are indications in the literature that introduction of an adamantane fragment into the structure of the stationary phase should enhance its selectivity, at least toward polynuclear aromatic hydrocarbonds [15]. In this context, our goal was to study the sorption properties of adamantane derivatives as sorbates and sorbents, and also to examine the relationship between the physicochemical properties and chromatographic behavior of adamantanes.

EXPERIMENTAL

Experiments were performed on an M-3700 gas chromatograph equipped with a flame ionization detector in the mode of capillary chromatography with flow splitting. A 22000 × 0.22-mm column with grafted adamantylsilicone was used (film thickness d_f = 0.2 μm). As carrier gas we used helium. Solid substances were introduced into the chromatograph as solutions in acetone or hexane (sample volume 1 μl).

In the determination of the retention indices (RIs), the measurements were performed at a column temperature of 200°C and a vaporizer temperature of 230°C. The retention indices were calculated by the Kovats formula [16]. Their reproducibility was 1–2 units. The contributions of substituents and functional groups (δI_R) were determined from the experimental values of the retention indices of the substituted (I_{AdR}) and unsubstituted (I_{Ad}) compounds:

$$\delta I_R = I_{AdR} - I_{Ad}.$$

The differential molar free energy of sorption ΔG was calculated by the formula [17]

$$\Delta G = -RT \ln k\beta,$$

where k is the retention factor, $k = (t_x - t_m)/t_m$, t_x is the retention time of the substance being tested, and t_m is the retention time of a nonsorbable component (dead time).

The phase ratio β was calculated from the geometric parameters of the chromatographic column using the model of two coaxial cylinders [17]:

$$\beta = (d_c - 2d_f)^2/4(d_c d_f - d_f^2),$$

where d_c is the inside diameter of the capillary column and d_f is the thickness of the stationary phase film on the column walls.

Let us assign subscripts 0 and s to the gas and liquid, respectively. Then

$$V_0 = 1/4\pi L(d_c - 2d_f)^2,$$

$$V_s = V - V_0,$$

where $V = 1/4\pi L d_c^2$ is the volume of the empty capillary at a column length L.

The experimental values of the indices, averaged over 7–10 determinations, and the ΔG values are listed in Table 1.

The specific retention volumes V_v^T and V_s^T were calculated by the formulas

$$V_v^T = \frac{V_R' j_3^2}{V_s},$$

$$V_s^T = \frac{V_R' j_3^2}{A_s},$$

$$j_3^2 = \frac{3}{2}\frac{(P_i/P_0)^2 - 1}{(P_i/P_0)^3 - 1},$$

where V_s is the stationary phase volume; A_s, adsorbent surface area; and j_3^2, James–Martin coefficient [18].

Quantum-chemical calculations were performed with QSAR HyperChem software package (version 7.0) by the AM1 semiempirical method with full optimization of the molecular geometry. The calculated van der Waals volumes (V_{vdW}), molecular refractions (MR), distribution ratios in the *n*-octanol–water system (log P), polarizabilities α, and dipole moments μ of the compounds are listed in Table 2. The van der Waals volumes of the molecules were also calculated by the Bondi method [19] (Table 2).

The topological characteristics of the compounds (Wiener indices) were calculated as described previously [20].

The framework structure of adamantane and its derivatives is responsible for their specific physical and chemical properties. The three-dimensional model of the adamantane molecule is a highly symmetrical structure with a low surface area and weak intermolecular interactions in the crystal lattice. On introducing various substituents, the molecular symmetry becomes lower and the physicochemical characteristics of the compounds, including their retention indices, change.

Table 1. Chromatographic characteristics of adamantane derivatives (T = 200°C)

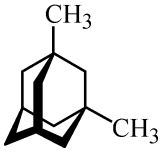
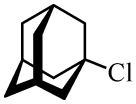
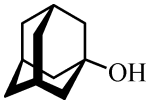
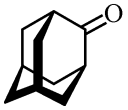
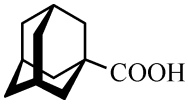
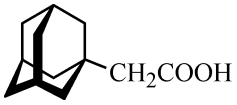
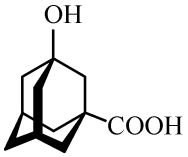
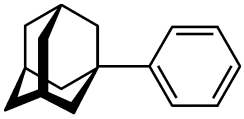
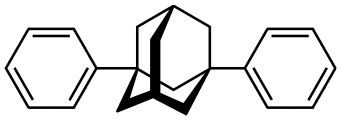
Compound no.	Compound	Structural formula	Adamantylsilicone				Apiezon L	
			I	δI_R	$-\Delta G$, kJ mol^{-1}	$\delta(\Delta G)_R$	I	δI_R
1	Adamantane		1188	–	13.96	–	1216	–
2	1,3-Dimethyladamantane		1207	8.5	15.03	0.54	1245	14.5
3	1-Chloroadamantane		1369	181	17.19	3.23	1355	139
4	1-Bromoadamantane		1460	272	18.68	4.72	1461	245
5	1-Adamantanol		1323	135	16.14	2.18	1333	117
6	2-Adamantanone		1378	190	17.02	3.06	–	–
7	Adamantane-1-carboxylic acid		1553	365	19.77	5.81	1513	297
8	Adamantane-1-acetic acid		1626	438	20.95	6.99	1498	282
9	Adamantane-1,3-diacetic acid		2041	426.5	27.57	6.81	–	–
10	1-Adamantanol-3-carboxylic acid		1743	555	21.35	7.39	–	–
11	1-Phenyladamantane		1796	608	24.16	10.16	–	–
12	1,3-Diphenyladamantane		2192	502	30.62	8.33	–	–

Table 1. (Contd.)

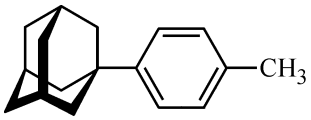
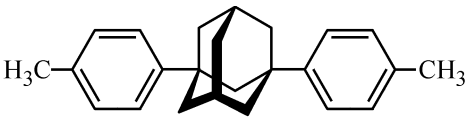
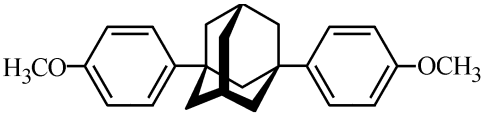
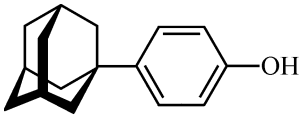
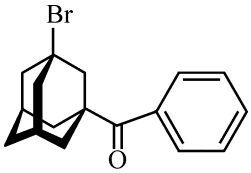
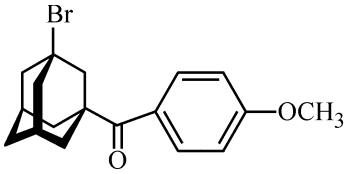
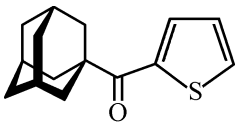
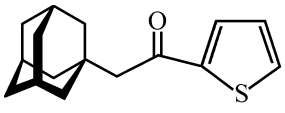
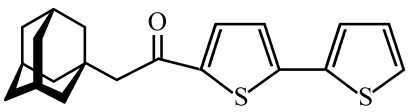
Compound no.	Compound	Structural formula	Adamantylsilicone				Apiezon L	
			I	δI_R	$-\Delta G$, kJ mol^{-1}	$\delta(\Delta G)_R$	I	δI_R
13	1-(*p*-Tolyl)adamantane		1855	667	25.62	11.69	–	–
14	1,3-Di(*p*-tolyl)adamantane		2354	583	33.27	9.655	–	–
15	1,3-Di(*p*-methoxyphenyl)adamantane		2447	629.5	34.79	10.42	–	–
16	4-(1-Adamantyl)-phenol		2061	873	27.89	13.93	–	–
17	3-Bromoadamant-1-yl phenyl ketone		1830	642	23.36	9.4	1951	735
18	3-Bromoadamant-1-yl *p*-methoxyphenyl ketone		2199	1011	28.99	15.03	2210	994
19	1-Adamantyl 2-thienyl ketone		2082	894	27.62	13.66	–	–
20	Adamant-1-ylmethyl 2-thienyl ketone		2156	968	28.77	14.81	–	–
21	Adamant-1-ylmethyl 2,2'-dithien-5-yl ketone		2331	1143	31.52	11.56	–	–

Table 2. Physicochemical and topological properties of adamantane derivatives

Compound no.	Compound	V_{vdW}, Å^3		MR, Å^3	log *P*	α, Å^3	μ, D	*W*
		Bondi method	HyperChem					
1	Adamantane	147	147	42.2	2.69	16.8	0	96
2	1,3-Dimethyladamantane	181	180	51.2	3.56	20.5	0.03	156
3	1-Chloroadamantane	161	161	46.9	2.60	18.7	2.03	118
4	1-Bromoadamantane	164	168	49.9	2.66	19.4	2.04	116
5	1-Adamantanol	155	155	43.9	1.45	17.4	1.30	122
6	2-Adamantanone	148	148	42.9	2.31	16.9	3.05	118
7	Adamantane-1-carboxylic acid	174	171	48.4	2.36	19.4	2.12	194
8	Adamantane-1-acetic acid	185	187	52.9	2.29	21.2	2.09	225
9	Adamantane-1,3-diacetic acid	235	229	63.7	1.89	25.6	2.15	513
10	1-Adamantanol-3-carboxylic acid	181	178	50.1	1.12	20.0	2.39	232
11	1-Phenyladamantane	219	220	66.8	4.34	26.5	0.32	342
12	1,3-Diphenyladamantane	292	294	91.3	5.99	36.1	0.33	804
13	1-(*p*-Tolyl)adamantane	236	237	71.8	4.81	28.3	0.06	412
14	1,3-Di(*p*-tolyl)adamantane	325	328	101.4	6.93	39.8	0.05	1052
15	1,3-Di(*p*-methoxyphenyl)adamantane	342	343	104.3	5.49	41.1	2.28	1339
16	4-(1-Adamantyl)phenol	227	227	68.6	4.06	27.1	1.38	463
17	3-Bromoadamant-1-yl phenyl ketone	259	259	79.9	3.85	31.0	4.36	547
18	3-Bromoadamant-1-yl *p*-methoxyphenyl ketone	285	285	86.4	3.60	33.5	1.86	743
19	1-Adamantyl 2-thienyl ketone	229	227	71.0	3.17	18.63	3.11	398
20	Adamant-1-ylmethyl 2-thienyl ketone	246	245	75.6	3.10	30.47	2.90	512
21	Adamant-1-ylmethyl 2,2'-dithien-5-yl ketone	309	310	99.4	3.84	40.38	3.23	860

It is known [12] that the C–H bond involving the tertiary carbon atom in the adamantane molecule is appreciably polarized under the action of strong polarizing agents. As a result, effective charges arise on the atoms of this bond. The adamantane core can accept an appreciable fraction of the electron density from the carbon atom and thus decrease its effective charge. A decrease in the charge on the carbon atom favors further polarization of the C–H bond under the action of polarizing agents (e.g., polar fragments of stationary phases in gas chromatography). It is assumed that the uptake of the electron density by the adamantane core is due to the overlap of the "rear" sides of the orbitals of the bridgehead carbon atoms, resulting in a direct contact of atoms that are not linked by a valence bond. This effect has been termed the cage effect [12]. Thus, the substituent effects can be transferred in the adamantane framework both through C–C bonds (*I* effect) and through the field (*F* effect) [21].

Previously we have examined the chromatographic retention of eight adamantane derivatives on a capillary column with cross-linked adamantylsilicone as a stationary phase (SP) [22]. In this study, we extended the range of adamantane derivatives and used silicone modified by grafting of the adamantyl radical to the base silicone matrix as a stationary phase. Despite that there is as yet no common opinion in the literature on the differences between cross-linked and grafted stationary phases, it is usually believed that cross-linking results in binding of particular groups of the polymer phase with each other to give a more stable macromolecular film, whereas grafting is chemical fixation of a stationary phase on the surface of a quartz capillary [23]. Thus, a grafted layer is a set of functional groups, grafted molecules, or substances covalently fixed on the surface. Its constituent elements are grafted molecules themselves, a part of the support base, and residual structural groups of the surface [24].

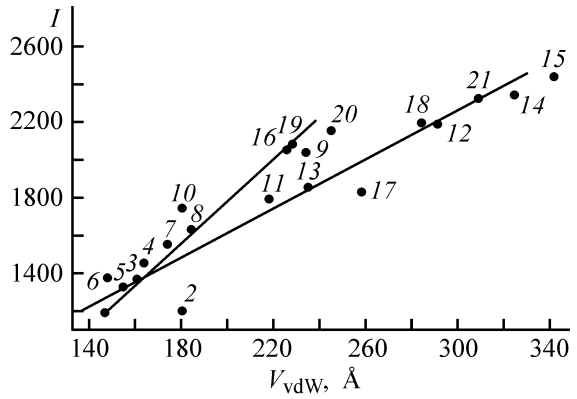


Fig. 1. Correlation between the van der Waals volumes of molecules, V_{vdW}, calculated by the Bondi method, and retention indices I of adamantane derivatives on adamantylsilicone. *Figures at points* are compound nos. in Table 1; the same for Figs. 2 and 3.

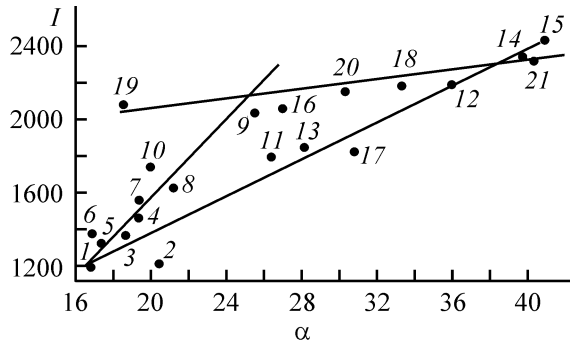


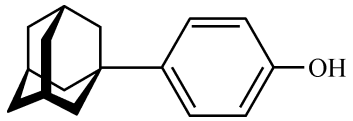
Fig. 2. Correlation between the molecular polarizabilities of adamantane derivatives, α, and their retention indices on adamantylsilicone I.

It has been shown previously [25] that, irrespective of the modification procedure, columns with adamantylsilicone stationary phases are weakly polar, but the polarity factors (especially those characterizing polar interactions) are somewhat higher for grafted adamantylsilicone.

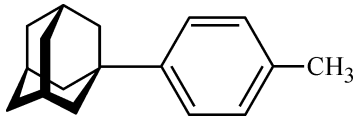
It is known that, in the case of nonpolar or weakly polar stationary phases, the chromatographic retention of sorbates is determined by dispersion forces; therefore, the relationship between the structure of compounds and their retention is based on the assumption that the free energies of sorption are additive and can be calculated by summation of the structural increments. Furthermore, the sorbates are, as a rule, eluted in such systems in the order of increasing molecular size; thus, the retention characteristics appreciably depend on the deformability of molecules and hence on their volume and polarizability.

The retention of adamantane and its derivatives is primarily determined by the presence of a bulky adamantane framework, by the nature and position of substituents (both directly participating in the retention and affecting the redistribution of the electron density within the adamantane core), and by the steric factor [14]. In the chromatographic system used, the adamantane fragments are present not only in sorbate molecules, but also in the structure of the stationary phase; therefore, the steric factor acquires a particular importance. Also, up to 50% of free silanol groups, accessible to molecules of different volumes, remain on the surface after the immobilization of the silicone SPs with any modifier [23]. Furthermore, the larger the grafted fragments (radicals or functional groups), the lower the grafting density. Therefore, residual silanol groups are apparently present in a certain amount in adamantylsilicone; these groups are capable of hydrogen bonding with the corresponding sorbates [25].

This assumption is confirmed by Table 1, which shown that substances capable of hydrogen bonding (hydroxy and carboxy derivatives of adamantane) have considerably higher RIs I than compounds capable of only dispersion interactions with the stationary phase (aryl and alkyl derivatives), at similar molecular volumes:



I = 2061, V = 227



I = 1855, V = 236

Furthermore, for adamantylsilicone, the contributions to the retention made by functional groups capable of hydrogen bonding are appreciably larger than those for Apiezon L. For example, the contributions of the OH group of 1-adamantanol are 135 and 117 units, respectively; for 4-(1-adamantyl)phenol, the contribution of the OH group on adamantylsilicone increases considerably, reaching 265 units.

Similar factors are apparently responsible for the increased contribution of the carboxy group on adamantylsilicone compared to Apiezon L: 365 and 297 units for adamantanecarboxylic acid, and 438 and 282 units for adamantylacetic acid, respectively, and also for the increased retention of haloadamantanes.

Figures 1 and 2 show that, on the whole, the retention indices of the adamantane derivatives vary in the same direction with the volume and polarizability of

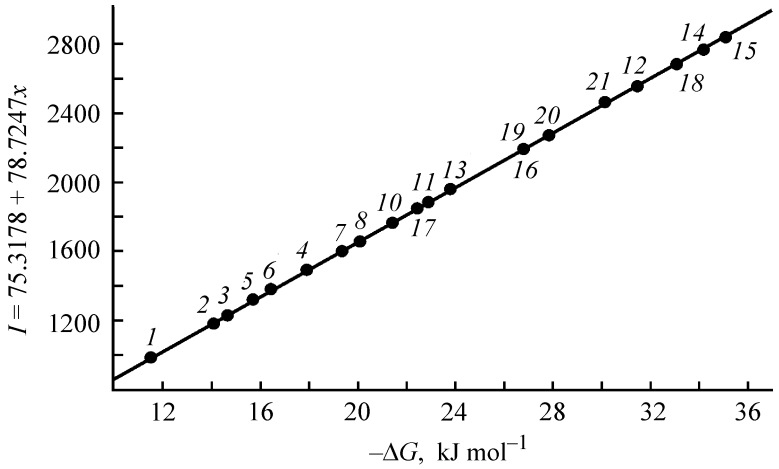


Fig. 3. Correlation between the retention indices I and differential molar free energy of sorption, ΔG, on adamantylsilicone (r = 1.0000, p = 0.0000).

the molecules. However, there is no common correlation, and the compounds are subdivided into several correlation groups consisting of adamantane derivatives that are retained by the stationary phase mainly through hydrogen bonding with residual silanol groups or dispersion interactions. A similar pattern was observed with cross-linked adamantylsilicone [22]; with the grafted SP, however, the correlation groups are manifested more clearly.

The adamantane fragments in the stationary phase considerably enhance the retention of the aromatic derivatives. As already noted, such a behavior is characteristic of systems in which the intermolecular interactions of the sorbate with the stationary phase are governed by the dispersion forces, which are determined by the volume and polarizability of the molecules.

The applicability of the linear free energy relationship to the retention characteristics of adamantane derivatives on adamantylsilicone is illustrated by the plot of the Kovats retention indices I vs. the differential Gibbs energy ΔG (Fig. 3).

The quantity ΔG characterizes the structural and sorption properties of a substance and the energy of its interaction with the stationary phase at a given temperature; therefore, the temperature is an important factor affecting the GLC retention. It is known that the energy of polar interactions considerably decreases with increasing temperature [21]. Despite that the retention with low-polarity adamantylsilicone is mainly governed by the dispersion interactions, free silanol groups in the starionary phase also play, as already noted, a certain role in the retention of polar molecules. The occurrence of specific interactions with the stationary phase results in a considerable decrease in the retention volume of polar sorbates with increasing temperature. The parameters of the equation describing the dependence of the retention volume on the reciprocal temperature (Table 3) show that the slope of the straight line [coefficient a in the equation $\log V_g^T = a(1000/T) - b$] for the hydroxy and carboxy derivatives of adamantane is somewhat larger than that for the other derivatives.

Also, it is known that the retention on nonpolar stationary phases can be characterized by a compensation effect, namely, by a linear correlation between

Table 3. Parameters of the equation $\log V_g^T = a(1000/T) - b$ for adamantane derivatives

Compound	a	b	r
Adamantane	1.568	1.743	0.985
1,3-Dimethyladamantane	1.463	1.436	0.968
1-Chloroadamantane	1.875	2.058	0.988
1-Bromoadamantane	1.922	1.985	0.992
1-Adamantanol	1.949	2.301	0.993
2-Adamantanol	2.025	2.350	0.994
2-Adamantanone	1.983	2.274	0.995
2,6-Adamantanedione	2.282	2.723	0.997
Adamantane-1-carboxylic acid	2.705	3.493	0.997
Adamantane-1-acetic acid	2.776	3.517	0.997
1-Adamantanol-3-carboxylic acid	3.246	4.456	0.999
1-Acetyladamantane	2.152	2.405	0.994
1-Phenyladamantane	2.610	2.845	0.993

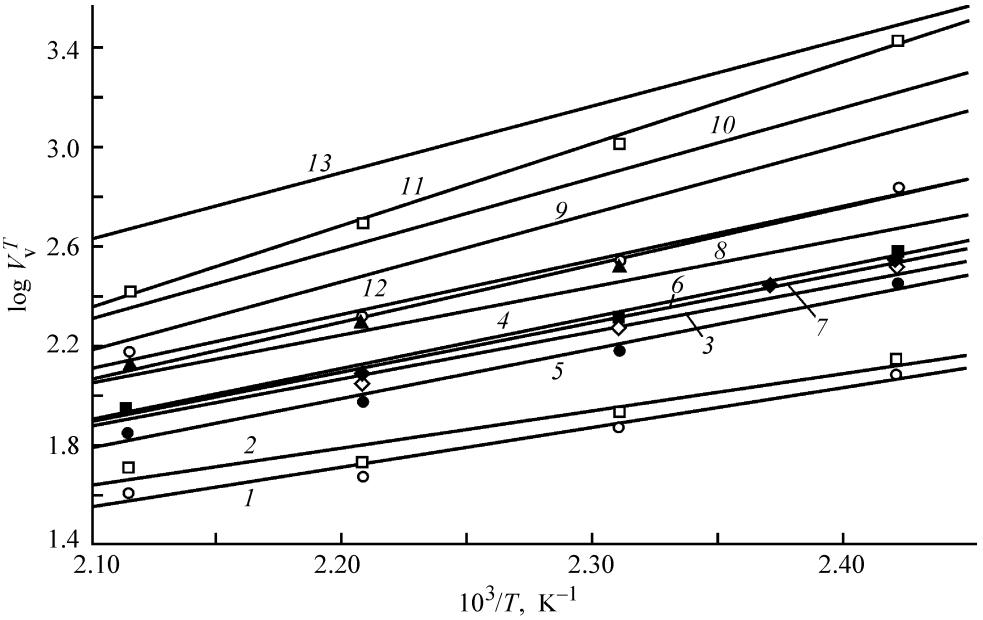


Fig. 4. Temperature dependence of log V_v^T for adamantane derivatives: (*1*) adamantane, (*2*) 1,3-dimethyladamantyane, (*3*) 1-chloroadamantane, (*4*) 1-bromoadamantane, (*5*) 1-adamantanol, (*6*) 2-adamantanol, (*7*) 2-adamantanone, (*8*) 2,6-adamantanedione, (*9*) adamantane-1-carboxylic acid, (*10*) adamant-1-ylacetic acid, (*11*) 1-adamantanol-3-carboxylic acid, (*12*) acetyladamantane, and (*13*) phenyladamantane.

ΔH^0 and ΔS^0, suggesting the similarity of the physicochemical processes in the series of the compounds under consideration [25]. Figure 4 shows that the dependences of log V_v^T on $1/T$ are linear for all the sorbates studied in the temperature range examined. These straight lines, when extrapolated, should intersect at a point corresponding to the compensation temperature. It follows from the compensation relationships that the retention parameters of sorbates of various structures should approach each other with increasing column temperature, which should make lower the separation selectivity.

Table 4. Parameters of the correlation equation $I = a + bx$ for adamantane derivatives

Group of compounds	X	a	b	r
Alkyladamantanes	V_{vdW}	108.1	7.1	0.97
	MR	274.8	21.1	0.98
	log P	338.6	302.4	0.97
	α	248.9	45.2	0.98
	log W*	–1284.1	1199.9	0.99
Hydroxy- and carboxyadamantanes	V_{vdW}	–147.4	9.6	0.97
	log MR	–5513.5	4155.7	0.99
	log P	4058.9	–1064.7	1.00
	log	–3726.5	4079.4	0.97
	log W	–1216.6	1218.9	0.99
Adamantyl ketones	V_{vdW}	1368.9	3.10	0.98
	MR	1387.6	9.8	0.97
	log$W$	267.8	693.5	0.97

* (W) Wiener index.

The correlations between the structural characteristics and chromatographic parameters determined by the type of intermolecular interactions in a chromatographic column are also examples of the linear free energy relationship as applied to adamantane derivatives. The coefficients of the correlation equations describing the relationships between the physicochemical and chromatographic characteristics of adamantane derivatives are listed in Table 4.

Such correlations can be used for predicting the chromatographic retention of substances and the properties of hypothetical molecules, for identifying compounds without references, for choosing a selective chromatographic system, etc.

CONCLUSIONS

(1) The chromatographic retention of polar compounds on adamantylsilicone is provided by the dispersion interaction with bulky adamantane fragments of the stationary phase and by specific interactions with the residual silanol groups of the base silicone matrix.

(2) The chromatographic behavior of functional derivatives of adamantane is determined by the linear free energy relationship and is characterized by a compensation effect.

ACKNOWLEDGMENTS

The authors thank I.K. Moiseev and A.Ya. Gerchikov for the submitted samples of the compounds and V.G. Berezkin for the submitted columns with adamantylsilicone.

REFERENCES

1. Shvekhgeimer, M.-G., *Usp. Khim.*, 1996, vol. 65, no. 7, pp. 603–647.
2. Mlinaric-Majerski, K. and Kragol, G., *Tetrahedron*, 2001, vol. 57, pp. 449–457.
3. May, P.W., Ashworth, S.H., Pickard, C.D.O., et al., *Phys. Chem. Commun.*, 1998, no. 4, pp. 1–4.
4. Merkle, R.C., *Nanotechnology*, 1997, no. 8, pp. 149–162.
5. Dahl, J.E., Moldowan, J.M., Peters, K.E., et al., *Nature*, 1999, vol. 399, pp. 54–57.
6. Schoell, M. and Carlson, R.M.K., *Nature*, 1999, vol. 399, pp. 15–16.
7. Herzog, U. and Rheinwald, G., *J. Organomet. Chem.*, 2001, vol. 628, pp. 133–143.
8. Miroshnichenko, E.A., Lebedev, V.P., and Matyushin, Yu.N., *Dokl. Ross. Akad. Nauk*, 2002, vol. 382, no. 4, pp. 497–499.
9. Mansoori, G.A., in *The Next Industrial Revolution: Proc. 1st Conf. on Nanotechnology*, 2002, vol. 2, pp. 53–59.
10. Takeushi, H., *Rev. Toyota CRDL*, 2001, vol. 36, no. 3, p. 9.
11. Korol'kov, D.V. and Sizova, O.V., *Zh. Obshch. Khim.*, 2003, vol. 73, no. 11, pp. 1881–1892.
12. Bagrii, E.I., *Adamantany: Poluchenie, svoistva, primenenie* (Adamantanes: Preparation, Properties, Applications), Moscow: Nauka, 1989.
13. Burkhard, J., Vais, J., Vodicka, L., and Landa, S., *J. Chromatogr.*, 1969, vol. 42, pp. 207–218.
14. Kurbatova, S.V., Arutyunov, Yu.I., Moiseev, I.K., and Kudryashov, S.Yu., *Zh. Fiz. Khim.*, 1998, vol. 72, no. 8, pp. 1485–1489.
15. Yang, S.S. and Gilpin, R.K., *J. Chromatogr.*, 1988, pp. 414–416.
16. Vigdergauz, M.S., Semenchenko, L.V., Ezrets, V.A., and Bogoslovskii, Yu.N., *Kachestvennyi gazokhromatograficheskii analiz* (Qualitative Gas-Chromatographic Analysis), Moscow: Nauka, 1978.
17. Grigor'eva, D.N., Vasil'ev, A.V., and Golovnya, R.V., *Zh. Anal. Khim.*, 1993, vol. 48, no. 7, pp. 1167–1173.
18. Onuchak, L.A., Bulanova, A.V., Egorova, K.V., and Arutyunov, Yu.I., *Nomenklatura v khromatografii* (Nomenclature in Chromatography), Samara: Samar. Univ., 1999.
19. Bondi, A., *J. Phys. Chem.*, 1964, vol. 68, no. 3, pp. 441–452.
20. Kurbatova, S.V., Finkel'shtein, E.E., Kolosova, E.A., et al., *Zh. Strukt. Khim.*, 2004, vol. 40, no. 1, pp. 150–157.
21. Dneprovskii, A.S. and Temnikova, T.I., *Teoreticheskie osnovy organicheskoi khimii* (Theoretical Principles of Organic Chemistry), Leningrad: Khimiya, 1979.
22. Konstantinova, K.K., Berezkin, V.G., Kurbatova, S.V., and Finkel'shtein, E.E., *Zh. Prikl. Khim.*, 2005, vol. 78, no. 9, pp. 1522–1526.
23. *High Resolution Gas Chromatography*, Hyver, K.J., Ed., Hewlett-Packard, 1989. Translated under the title *Vysokoeffektivnaya gazovaya khromatografiya*, Khaiver, K., Ed., Moscow: Mir, 1993.
24. Lisichkin, G.V., Fadeev, A.Yu., Serdan, A.A., et al., *Khimiya privitykh poverkhnostnykh soedinenii* (Chemistry of Grafted Surface Compounds), Moscow: Fizmatlit, 2003.
25. Konstantinova, K.K., Kurbatova, S.V., Kartashev, A.V., and Zimichev, A.V., *Izv. Vyssh. Uchebn. Zaved., Khim. Khim. Tekhnol.*, 2005, vol. 48, no. 10, pp. 77–83.

ISSN 1070-4272, Russian Journal of Applied Chemistry, 2006, Vol. 79, No. 8, pp. 1260–1265. © Pleiades Publishing, Inc., 2006.
Original Russian Text © L.N. Skvortsova, E.V. Petrova, M.A. Kiseleva, V.I. Otmakhov, 2006, published in Zhurnal Prikladnoi Khimii, 2006, Vol. 79, No. 8, pp. 1275–1279.

SORPTION AND ION-EXCHANGE PROCESSES

Optimization of the Conditions of Sorption Recovery and Concentration of Noble Metals on Anion Exchangers and Their Subsequent Determination in Geochemical Objects by Atomic-Emission Spectroscopy

L. N. Skvortsova, E. V. Petrova, M. A. Kiseleva, and V. I. Otmakhov

Tomsk State University, Tomsk, Russia

Received March 7, 2006

Abstract—Sorption of Au(III), Pt(IV), Pd(II), and Rh(III) ions on ANS-80, AN-108-4 macrocellular anion exchangers and on AV-17-10P macroporous anion exchanger from hydrogen chloride media was studied in relation to HCl concentration and time. The residual concentration of matrix elements in analytical concentrates of a real object was determined and their influence on the delivery of vapors of noble metals into the cloud of the arc discharge and on their excitation in the discharge was revealed. The conditions of recovery, concentration, and atomic-emission determination of noble metals were examined. The effect of matrix elements, combined with a number of supports (NaCl, CdO, TeO_3, Sb_2O_3), on the amplitude of analytical signals was evaluated.

DOI: 10.1134/S1070427206080088

When determining noble metals in geochemical and industrial objects with complex multicomponent composition, there is, as a rule, no way of obviating the stage of separation of matrix elements (ME) even in the case of high-sensitivity analytical methods (neutron-activation, mass-spectral, etc.). High sensitivity and determination accuracy can be achieved by rational combination of separation and concentration techniques with the potentialities and specific features of more accessible instrumental analytical procedures. In the authors' opinion, the optimal combination is that of atomic-emission spectroscopy with preliminary sorption recovery and concentration of microelements. Their detection limits can be lowered by choosing those conditions of spectral analysis of the concentrate which favor enrichment of the plasma of the light source with the elements being determined.

Earlier studies of application of sorption methods for recovery and concentration of noble metals were based on the ability of their chloro complexes to be firmly fixed by strongly basic anion exchangers [1]. However, chelate-forming ion exchangers containing electron-donor atoms of nitrogen or sulfur are more promising for selective recovery of noble metals [2–5].

The present study is concerned with weakly basic ANS-80 and AN-108-4 S- and N-containing macrocellular anion exchangers obtained by amination with ethylenediamine of copolymers of methyl acrylate with a long-chain cross-linking agent (divinyl sulfide and divinyl ether of diethylene glycol, respectively) and AV-17-10P macroporous ion exchanger. The physicochemical properties of the sorbents have been studied previously [6].

Upon sorption concentration of noble metals, base elements of natural objects were found in the ion-exchange concentrate. These elements can strongly affect the conditions of sample heating in the electrode crater, delivery of vaporized noble metals into the arc discharge cloud, and excitation in the cloud. In the study, the effect of matrix elements was examined in order to formulate recommendations concerning their content, and the joint effect of a number of supports and the residual amount of matrix elements was analyzed in order to achieve lower determination limits of noble metals.

EXPERIMENTAL

To chose the optimal conditions of quantitative recovery of noble metals (Au, Pt, Pd, Rh) with the aim of their concentration and separation from the base elements of the rock (Ca, Mg, Fe, Al, Na), their sorption from hydrochloric acid solutions was studied in the acidity range from 2 M to pH 3. This range of

Table 1. Effect of matrix elements on the intensity of spectral lines, $\log I_l$, and evaporation constants A of noble metals ($n = 5$, $P = 0.95$)

Element	λ, nm	Excitation potential, eV	mp, °C	$\log I_l$, on indicated support		A, g s^{-1}, on indicated support	
				GP	GP + ME	GP	GP + ME
Au	242.79	5.10	1063	1.3	0.4	0.030	0.021
Pd	342.10	4.58	1552	1.6	0.9	0.030	0.022
Pt	265.95	4.66	1769	1.4	0.8	0.027	0.021
Rh	343.49	3.61	1960	0.9	0.4	0.026	0.023

HCl concentrations is due to existence in solutions of this kind of stable chloro complexes of noble metals and an insignificant fraction of anionic forms of macrocomponents, and primarily Fe(III). Experiments were carried out in the static mode. Weighed portions of a sorbent (0.1 g) were poured over with 10 ml of a solution containing $n \times 10^{-4}$ M of a noble metal ion and a certain concentration of HCl. The necessary pH value was created by adding NaOH or HCl solutions, with monitoring with a pH meter. The solutions with the sorbent were kept until equilibrium was attained. The concentrations of Pd(II), Pt(IV), and Rh(III) ions in the equilibrium solution were determined by spectrophotometry with $SnCl_2$ [1], and that of Au(III), by anodic inversion voltammetry with a graphite electrode on the background of 1 M HCl. The loss of concentration was used to calculate the degree of recovery of noble metals, R (%).

The sorption of noble metal ions in the course of time was studied by a similar method without agitation of the solution and under agitation with a magnetic rabble. After a certain period of time, the sorbent was separated from the solution and the residual amount of a metal ion in the solution was determined. Then the degree of approach to equilibrium, $F = Q_\tau/Q_\infty$ was calculated, where Q_τ is the amount of metal ions absorbed by instant of time τ (mmol) and Q_∞ is the amount of metal ions absorbed by the instant of attainment of equilibrium (mmol).

The degree of sorption of the matrix elements of the rock was determined by atomic-emission spectroscopy in the analytical concentrate of a real object. A weighed portion of the rock (10 g) was ground in a ball mill, placed in a glassy-carbon pan, and calcined in a muffle furnace at 500°C for 3 h. Then 20 ml of H_2SO_4 (1 : 1) and the same amount of HF_{conc} were introduced into the sample and the mixture was evaporated to humid salts and cooled. The treatment with a mixture of acids was repeated without calcination. Further, 30 ml of aqua regia was added in portions. After evaporation, the residue was twice treated with 10 ml of HCl_{conc}. To a dry residue was added 40 ml of 6 M (50 ml 0.5 M) HCl and the mixture was heated to dissolution of the salts. The content of the glassy-carbon pan was transferred into a chemical vessel with distilled water, with the volume of water brought to 240 (250) ml. After all the dilutions, the concentration of HCl should be 1 M (0.1 M). A part of unremoved silicon compounds remained in the solution in the form of a precipitate. In 24 h, the solution was separated from the precipitation by decantation, 100 mg of an ion exchanger was introduced, and sorption was performed under agitation for 10 min on AN-108-4 (or for 2 h on AV-17-10P). Further, the ionite was separated from the solution by filtration and washed with an HCl solution of an appropriate concentration. The filter with the sorbent was placed in a quartz dish and acid ashing was performed first on a hot plate, with H_2SO_{4conc} added dropwise, and then in a muffle furnace at 500°C in the course of 1 h.

The content of matrix elements in the resulting analytical concentrate was determined by atomic-emission spectroscopy after its successive dilutions with a buffer suspension composed of a graphite powder and 3 wt % Na in the form of NaCl, with state standard samples SOG-21 [7]. Spectra were recorded on an ISP-30 spectrograph with a dc arc (12 A) as excitation source. Electrodes of common shape with crater dimensions of 4.5 × 3.6 mm were used. The electrode with a sample served as anode, the weighed portion of a substance was 15 mg. The content of sodium was determined in a solution of the ash residue on a PAZh-1 flame photometer.

To assess the influence exerted by the residual amount of the matrix elements (individual or combined with that of supports) on the atomic-emission determination of noble metals, curves of their evaporation were obtained by recording spectra on a moving photographic plate. The evaporation constants A of noble metals (g s^{-1}), proportional to the rate constants of their vaporization were calculated (Table 1)

Table 2. Effect of supports on the amplification coefficients of the spectral lines of noble metals $K = I_{(S+ME)}/I_{GP}$ ($n = 6$, $P = 0.95$)

Support	Ionization potential, eV	Melting point, °C	Boiling point, °C	Amplification coefficient Γ			
				Au	Pd	Pt	Rh
–	–	–	–	0.9	1.2	1.1	1.4
NaCl	5.13	800.8	1413	0.3	0.7	0.5	0.8
TeO_3	9.01	400	–	0.8	1.5	1.7	1.8
Sb_2O_3	8.64	655	1425	0.8	1.4	1.2	1.5
CdO	8.99	900 (decomp.)	–	0.9	1.3	1.2	1.4

using the quantitative interpretation of the evaporation curves, suggested by Raikhbaum [8]. The ratio of the intensities of two atomic lines of zinc (I_1-ZnI 307.6 and I_2-ZnI 328.2) was used to calculate by the formula $T = 18\,850/[\log(I_1/I_2) + 3.258]$ the effective temperature T (K) of the arc plasma. The electron concentration n_e in the plasma was found from the ratio of intensities of the ionic and atomic lines of magnesium (I_3-MgII 279.6 and I_4-MgI 278.0) by the formula $\log n_e = -\log(I_3/I_4) - 7.72(5040/T) + 3/2\log T + 15.754$ [9]. The thus found temperature and electron concentration were $T \pm 200$ K and $n_e \pm 0.2 \times 10^{15}$ cm^{-3} ($P = 0.95$). The influence exerted by the matrix elements and supports on the amplitude of the analytical signal from noble metals was studied on model samples prepared by introduction of oxides of base elements noble metals into the graphite powder in accordance with their content in the concentrates, and 3 wt % support in terms of the metal. For comparison purposes, samples without matrix elements and supports were used. The blackening density of the analytical lines of noble metals, whose parameters are listed in Table 2 [10], and of the nearby background were recalculated into intensities with the use of characteristic curves plotted with a nine-grade attenuator.

It was found that a high degree of recovery of noble metals by the sorbents studied is observed in the virtually entire range of acidities (Fig. 1). A certain decrease in the sorption of Rh(III) ions on the ANS-80 anion exchanger (Fig. 1a) and of Pt(IV) ions on the AV-17-10P resin (Fig. 1c) in a strongly acidic medium is, in all probability, due to the competing sorption of Cl^- ions. The reason for the lower absorption of Rh(III) by the AN-108-4 anion exchanger (Fig. 1b) and of Pt(IV) by AV-17-10P at pH 2–3 (Fig. 1c) is their hydrolysis leading to the formation of aqua chloro complexes with a lower effective charge. The high degree of recovery of Rh(III) ions by the ANS-80 anion exchanger under these conditions may be due to involvement of a sulfur atom in complexation with a noble metal ion. This assumption agrees with the results of [5]. It is advisable to use for quantitative recovery of noble metals in analysis of real objects the AN-108-4 macrocellular anion exchanger in a strongly acidic medium and AV-17-10P macroporous sorbent in 0.1 M HCl.

Figure 2 shows kinetic curves of sorption of noble metals under the optimal conditions of their quantitative recovery with and without solution agitation. The rate of sorption processes depends on the structure of ion exchangers. The time in which equilibrium is attained in Pt(IV) sorption by the AV-17-10P mac-

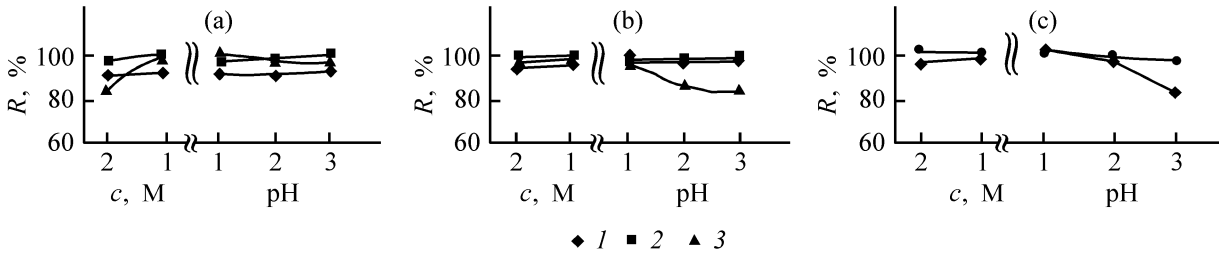


Fig. 1. Degree R of recovery of noble metals by (a) ANS-80, (b) AN-108-4, and (c) AV-17-10P ion exchangers from hydrochloric acid media vs. the acid concentration c and solution pH. $C_M = n \times 10^{-4}$ M, $m_{i.e} = 0.1$ g, $V = 10$ ml; the same for Fig. 2. (*1*) Pt, (*2*) Pd, and (*3*) Rh.

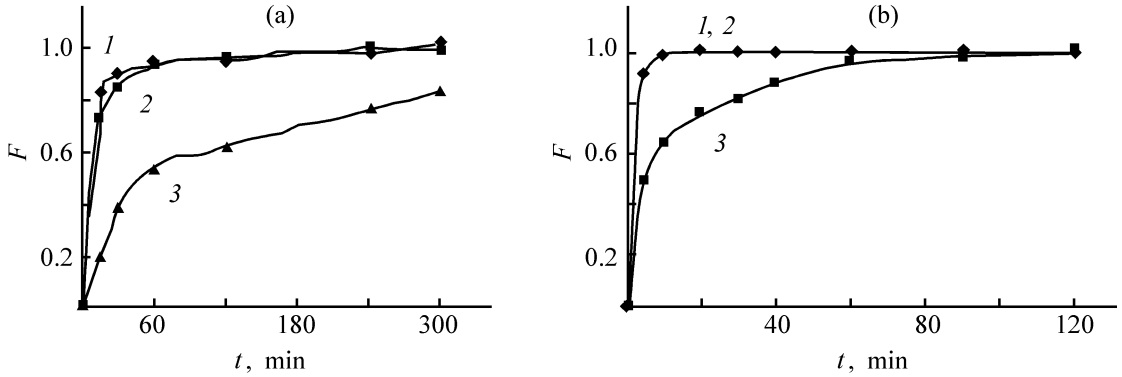


Fig. 2. Kinetic curves of sorption of (*1*) Pd(II) and (*2*, *3*) Pt(IV) by (*1*, *2*) AN-108-4 and (*3*) AV-17-10P ion exchangers (a) without solution agitation and (b) with agitation. (*F*) Degree of recovery and (*t*) time.

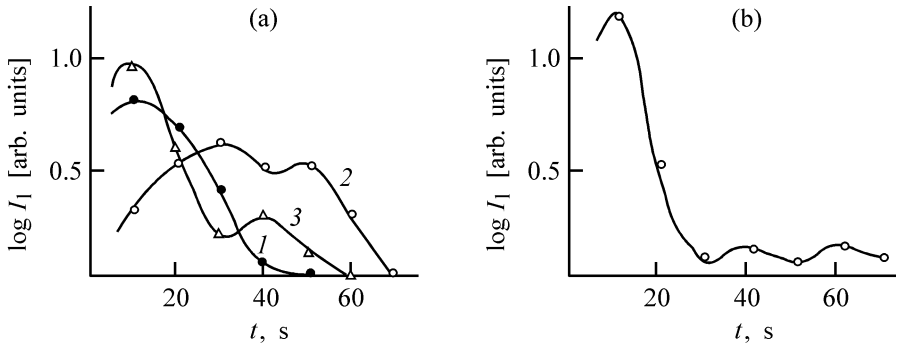


Fig. 3. Evaporation curves of (a) Pt on a support of (*1*) pure graphite powder, (*2*) graphite powder with a residual amount of matrix elements, and (*3*) graphite powder with matrix elements and TeO_3 support and (b) Te on a support of graphite powder with a residual amount of matrix elements. (I_l) Line intensity and (*t*) time.

roporous anion exchanger is 15 h, and decreases to 2 h under agitation (Fig. 2b). Macrocellular sorbents have improved kinetic properties because of the presence of long-chain cross-linking agents in their polymeric chain. Without solution agitation, a 90% absorption of Pt(IV) and Pd(II) ions is observed on the AN-108-4 anion exchanger already in 20 min. The sorption equilibrium is attained in 5 h. Sorption of noble metals in a hydrochloric medium on chelate-forming anion exchangers occurs in two stages [11]: first, the interaction occurs by the ion-exchange mechanism (functional groups are protonated under sorption conditions, pK_a 7.9–8.0), and then there occurs a rearrangement with incorporation of an amine group into the inner coordination sphere of the chloride complex of Pd(II) or Pt(IV), similarly the Andersen rearrangement. If the solution is agitated, the time of quantitative recovery of Pd(II) decreases to 10 min.

The support-collector of noble metals may contain, depending on the conditions of their concentration, various residual amounts of the matrix elements. When the AV-17-10P macroporous ion exchanger is used as a sorbent, the concentrate contains (wt %): 15–20 Ca, 5–15 Si and Al, 1–10 Na, Fe, and Mg, and also minor amounts (<1 wt %) of Mn and Ti. As the time in which equilibrium is attained in sorption of noble metals becomes longer, the residual content of the matrix elements grows and the interval of their variation, which also depends on the nature of an object being analyzed, is extended. Therefore, the sorption conditions should be chosen taking into account the effect of matrix elements on the impurities being controlled. It was found that presence of the residual amount of matrix elements, specified above, leads to a decrease in the arc temperature from 6370 to 5450 K and to an increase in the electron concentration in the plasma from 0.4×10^{15} to 5×10^{15} cm^{-3}. This is accounted for by the predominance in the concentrate of elements with low ionization potentials (Ca, Al, Na). The high values of the electron concentration diminish the ionization, which should lead to an increase in the intensity of the atomic lines of noble metals [9]. However, the results obtained in the study demonstrate that, in the presence of a considerable amount of matrix elements, low plasma temperatures are less favorable for atomization and excitation of noble metals. This is manifested in a change of the shape of the evaporation curves of noble metals in the presence of base elements (Fig. 3a, curves *1*, *2*). Their

maximum intensity decreases and shifts to longer exposures, and the time of total evaporation becomes longer. As a result, the evaporation rate of the elements being controlled falls and the analytical signals decrease by a factor of 1.5–2 for Pt, Pd, and Rh, and by a factor of 3.8 for Au, which has the highest ionization potential (Table 1). Therefore, it is preferable to perform the sorption concentration of noble metals on the AN-108-4 macrocellular anion exchanger, with the solution agitated and heated. This makes it possible to reduce the time in which equilibrium is attained to 10 min and to lower the content of matrix elements in the analytical concentrate by approximately a factor of 10. Under these conditions, the content of Ca, Al, and Si does not exceed 3–5 wt %, and that of Na, Mg, and Fe is not higher than 0.5–1.0 wt %.

The detection limits of noble metals in geochemical materials can be additionally lowered by introduction of supports into samples. A versatile support NaCl and oxides of readily vaporizable elements (Sb, Cd, Te) having low boiling points and high ionization potentials were studied (Table 2). Their choice was due to the presence in the concentrate of readily ionizable matrix elements (Ca, Al, Na), which affect, as shown previously, the excitation conditions. Compounds of some of these elements have been studied as collectors-coprecipitators of the elements to be determined, including noble metals, in analysis of pure substances [12].

The efficiency of the action of the supports and the residual amount of the matrix elements (Table 2) was evaluated by comparing the amplification coefficients K, which are numerically equal to the ratio of the intensities of the lines related to noble metals in the presence of matrix elements and supports to the intensity of similar lines of noble metals on a substrate of graphite powder ($K = I_{ME + S}/I_{GP}$). It was found that, in the presence of a minor residual amount of readily ionizable matrix elements (Na, Al, Ca), the intensity of lines of noble metals having lower ionization potentials (Rh, Pd) becomes higher owing to an increase in the electron concentration. Additional introduction of a readily ionizable NaCl support makes the spectral lines of noble metals weaker ($K < 1$). An effect of this kind, resulting from a decrease in the temperature of the arc plasma, has been observed previously in the case of an excess amount of matrix elements. In the presence of highly volatile elements, the amplification coefficients of the lines of Pt, Pd, and Rh exceed unity. However, the highest amplification coefficients are obtained in the presence of TeO_3. The nature of the experimentally observed amplification of the spectral lines of noble metals is not related in this case to changes in the parameters of the arc discharge plasma, because changes in T and n_e are insignificant in the presence of TeO_3. Highly volatile elements affect transport processes in the arc source. For example, tellurium evaporates at the first instants of arc burning and favors an increase in the height of primary peaks in the evaporation curves of noble metals, which points to their enhanced supply from the electrode rater into the discharge (Fig. 3a, curve *3*). Reactions in which volatile compounds are formed by noble metals are unlikely in the given case. Therefore, delivery of tellurium into the discharge zone leads, in all probability, to a strong change of the gas dynamic conditions in the electrode channel, and the TeO_3 vapor carries along vapors of noble metal admixtures. In the case of Au, which has the lowest melting and boiling points among all the noble metals (Table 1), rates of its evaporation in the presence of highly volatile supports are probably very high, which does not always lead to an increase in the intensity of spectral lines, because diffusion and convective processes become more important.

The results of the study were used to suggest a scheme for analysis of geological materials for the content of noble metals by atomic-emission spectroscopy, with their preliminary ion-exchange recovery and concentration. The detection limits calculated using the 3σ criterion fall in the range 2×10^{-7}–10^{-6} %, with S_r not exceeding 20%.

CONCLUSIONS

(1) It was found that quantitative concentration of noble metals and their most complete separation from matrix elements occurs on the AN-108-4 macrocellular anion exchanger from 1 M HCl solutions in the course of 10 min.

(2) It was demonstrated that matrix elements affect the intensity of the spectral lines of noble metals in atomic-emission spectroscopy: an increase in the content of matrix elements in the ion-exchange concentrate impairs the sensitivity of their determination. To make lower the detection limit of noble metals, it is suggested to use joint effective action of the residual amount of the matrix elements in the ash residue and of the TeO_3 support.

REFERENCES

1. Ginsburg, S.I., Ezerskaya, N.A., Prokof'eva, I.V., et al., *Analiticheskaya khimiya platinovykh metallov* (Analytical Chemistry of Platinum Metals), Moscow: Nauka, 1972.
2. Myasoedova, G.V. and Komozin, P.N., *Zh. Neorg. Khim.*, 1994, vol. 39, no. 2, pp. 280–288.

3. Shcherbinina, N.I., Pavlova, G.P., Myasoedova, G.V., et al., *Zh. Anal. Khim.*, 1995, vol. 50, no. 8, pp. 839–841.
4. Simanova, S.A., Kuznetsova, T.V., Belyaev, A.N., et al., *Zh. Prikl. Khim.*, 1999, vol. 72, no. 8, pp. 1276–1281.
5. Kholmogorov, A.G., Kononova, O.N., and Kachin, S.V., *Zh. Fiz. Khim.*, 1998, vol. 72, no. 9, pp. 1681–1685.
6. Kiseleva, M.A. and Skvortsova, L.N., *Sorbts. Khromatogr. Protsessy*, 2004, vol. 4, no. 6, pp. 82–85.
7. *GSO* (State Standard Sample) *4519-4523–89. Standard Graphite Samples (SOG-21 set).*
8. Raikhbaum, Ya.D., Loseva, A.F., and Luzhnova, M.A., *Zh. Prikl. Spektr.*, 1971, vol. 14, no. 4, pp. 571–574.
9. *Spektral'nyi analiz chistykh veshchestv* (Spectral Analysis of Pure Substances), Zil'bershtein, Kh.I., Ed., Leningrad: Khimiya, 1971.
10. Zaidel', A.N., Prokof'ev, V.K., Raiskii, S.M., et al., *Tablitsy spektral'nykh linii* (Tables of Spectral Lines), Moscow: Nauka, 1969.
11. Losev, V.N., Volkova, G.V., Maznyak, N.V., et al., *Zh. Anal. Khim.*, 2000, vol. 55, no. 2, pp. 144–147.
12. Pavlenko, L.I., Simonova, L.V., Vnukovskaya, G.L., et al., *Zh. Anal. Khim.*, 1987, vol. 42, no. 9, pp. 1598–1603.

ISSN 1070-4272, Russian Journal of Applied Chemistry, 2006, Vol. 79, No. 8, pp. 1266–1270. © Pleiades Publishing, Inc., 2006.
Original Russian Text © A.K. Pyartman, V.V. Lishchuk, V.A. Keskinov, 2006, published in Zhurnal Prikladnoi Khimii, 2006, Vol. 79, No. 8, pp. 1280–1284.

SORPTION AND ION-EXCHANGE PROCESSES

Extraction of Thorium(IV), Lantanum(III), and Yttrium(III) Nitrates with a Composite Solid Extractant Based on a Polymeric Support Impregnated with Trialkylamine

A. K. Pyartman, V. V. Lishchuk, and V. A. Keskinov

St. Petersburg State Technological Institute (Technical University), St. Petersburg, Russia

Received March 23, 2006

Abstract—Extraction of Th(IV), La(III), and Y(III) from aqueous solutions containing 0–4 M sodium nitrate with a composite solid extractant based on a polymeric support impregnated with trialkylamine (Alamine-336) was studied. The extraction isotherms were analyzed assuming that lanthanides and thorium are extracted with the solid extractant in the form of complexes $(R_3HN)_3[Ln(NO_3)_5]$ and $(R_3HN)_2[Th(NO_3)_6]$, respectively. The extraction constants were calculated. The joint extraction of Th(IV) and La(III) [Y(III)] with the solid extractant from aqueous salt solutions was studied.

DOI: 10.1134/S107042720608009X

Russian loparite, orthite, and monazite, along with rare-earth metals, usually also contain thorium and uranium as natural radioactive impurity metals. Therefore, the separation of thorium and uranium from rare-earth metals is a topical technological problem. This problem is usually solved by solvent extraction [1]. Another approach to solution of this problem is the use of composite solid extractants based on a porous support impregnated with a liquid extractant. This technique eliminates certain drawbacks characteristic of common solvent extraction procedures.

The extraction of rare-earth metals(III) [REM(III)] from aqueous solutions containing sodium nitrate (1–5 M) with a composite solid extractant (SE) based on a polymeric support impregnated with trialkylamine (Alamine-336) was studied in [1]. The extraction isotherms were processed assuming that the extractable complex $(R_3HN)_3[Ln(NO_3)_5]$ is formed in the solid extractant. No data have been reported on the joint extraction of La^{3+}, Th^{4+}, and Y^{3+} from aqueous solutions with the composite solid extractant. Since extraction of these metals with solid extractants is important from both scientific and practical viewpoints, we tried to fill this gap in this study.

We used a granulated composite solid extractant (Purolite Company) based on super cross-linked, poly(styrene–divinylbenzene) matrix impregnated with trialkylamine [TAA, (Alamine-336), general formula $(C_7H_{17}–C_9H_{19})_3N$]. Its specific volume was 2.50 ± 0.02 mol dm^{-3}. The Alamine-336 concentration in the composite solid extractant was 0.97 ± 0.01 mol dm^{-3}. The REM(III) concentration in the solid extractant and aqueous phase was determined by a technique similar to that reported in [2–4]. The metal nitrate concentration in SE (mol kg^{-1}) was recalculated to mol dm^{-3}, taking into account the density of the composite solid extractant.

The relative errors were within ± 0.5 % in preparing the solutions, and $\pm$ (1–3) and $\pm$ (1–5) rel. %, respectively, in determining REM(III) [Th(IV)] concentration in the liquid phase and SE. As a rule, each final result was the average of the results of no less than three experiments. The errors in parameter determination are given as standard deviations.

Figure 1 shows the extraction isotherm of nitric acid from aqueous solutions with SE at 298.15 K.

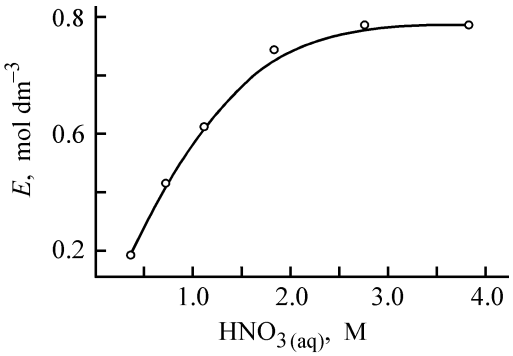


Fig. 1. Extraction isotherm of nitric acid with SE(TAA). (E) HNO_3 content in SE.

This isotherm flattens out due to saturation of the solid extractant with nitric acid. The limiting HNO_3 content in SE was 0.97 mol dm^{-3}, which corresponds to formation of stoichiometric TAA nitrate by the reaction

$$R_3N_{(o)} + HNO_{3(aq)} \rightleftarrows R_3NHNO_{3(o)}. \quad (1)$$

Before use for the extraction of Th(IV) and Ln(III) from aqueous solutions, the initial SE(TAA) was treated with 4 M HNO_3 to convert SE(TAA) into the salt form SE(TAA nitrate) and then was washed with water.

Figure 2a shows the extraction isotherms of Th(IV) from aqueous solutions containing $NaNO_3$ (0–4 M) with SE(TAA nitrate) at pH 1 and 298.15 K. As the $NaNO_3$ concentration in the aqueous phase increases, the Th(IV) concentration in SE grows and becomes close to $c_s/2$, where c_s is the TAA concentration in SE (0.97 ± 0.01 mol dm^{-3}). This fact suggests that, in saturation of SE(TAA nitrate) with thorium(IV) nitrate, the compound $(R_3NH)_2[Th(NO_3)_6]$ is formed.

The extraction of Th(IV) nitrate with TAA nitrate can be described by the equation of the following heterogeneous reaction:

$$Th^{4+}_{(aq)} + 4NO^-_{3(aq)} + 2R_3NHNO_{3(o)} \rightleftarrows (R_3NH)_2[Th(NO_3)_6]_{(o)}, \quad (2)$$

(aq) and (o) refer to aqueous and organic phases, respectively.

The extraction constant of Th with TAA can be calculated by the equation

$$K^{2,0}_{ex} = \frac{\{(R_3NH)_2[Th(NO_3)_6]\}_{(o)}}{\{Th^{4+}\}_{(aq)}\{NO^-_3\}^4_{(aq)} y^5_{\pm}\{R_3NHNO_3\}^2_{(o)}}, \quad (3)$$

where $\{...\}_0$ and $\{...\}_{(aq)}$ are the equilibrium concentrations of the components in the SE and aqueous phase, respectively, and $y_{\pm}$ is the mean ionic molar activity coefficient of Th(IV) nitrate in the aqueous phase.

The equilibrium Th concentrations in SE, calculated assuming the occurrence of reaction (2), (3) are listed in the table. The $y_{\pm}$ values used in these calculations were taken from [2]. The table shows that the calculated Th(IV) concentrations in the solid extractant agree with the experiment to within 1–2 rel.%. Thus, our model adequately describes the extraction of thorium(IV) nitrate from aqueous solutions with the solid extractant in the systems widely differing in the $Th(NO_3)_4$ concentration in both aqueous and solid extractant phases, with $\log K^{2,0}_{ex} = 4.30 \pm 0.05$.

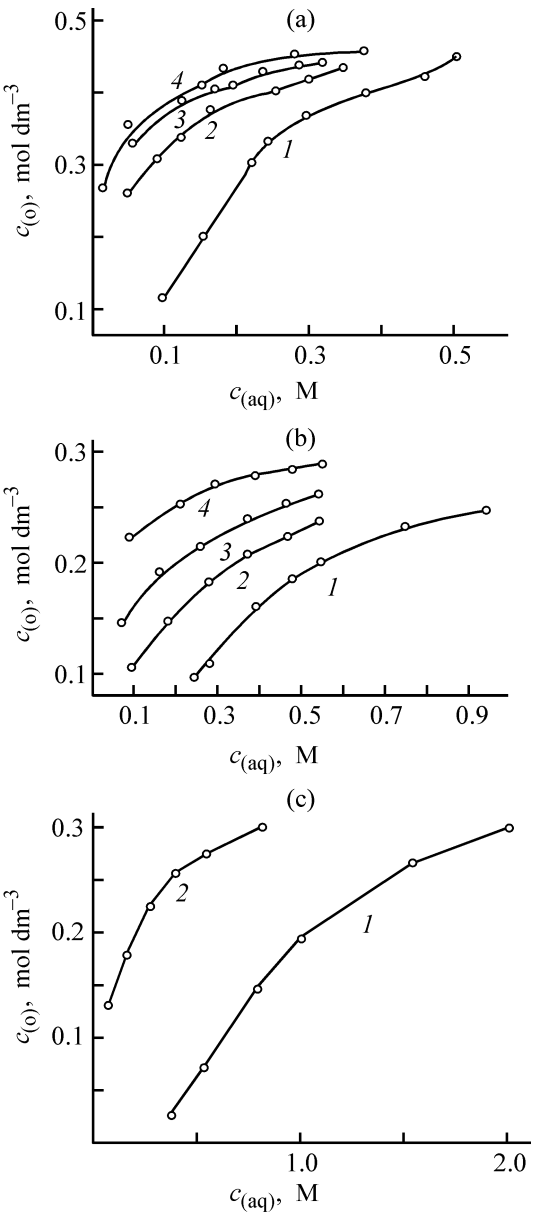


Fig. 2. Extraction isotherms of (a) thorium(IV), (b) lanthanum(III), and (c) yttrium(III) nitrates with SE from aqueous solutions in the absence and in the presence of sodium nitrate. ($c_{(aq)}$) thorium(IV), lantanum(III), or yttrium(III) nitrate concentration in the aqueous phase; ($c_{(o)}$) thorium(IV), lanthanum(III) or yttrium(III) nitrate concentration in SE. Sodium nitrate concentration in the aqueous phase, M: (a, b) (*1*) 0, (*2*) 1.0, (*3*) 2.0, and (*4*) 4.0; (*c*) (*1*) 0 and (*2*) 4.0.

The influence of the ionic strength of the aqueous phase ($I^{\Sigma} = 0.5\Sigma c_i Z_i^2$) on the concentration extraction constants K^2_{ex} can be estimated by the equation [1]

$$\log K^2_{ex}(I^{\Sigma}) = \log K^{2,0} + \Delta Z^2 F_{ex}(I^{\Sigma}) + 10\theta_1\{Th^{4+}\}_{(aq)} + \theta_2 c_{NaNO_3(aq)}, \quad (4)$$

Data on the extraction of thorium(IV), lanthanum(III) and yttrium(III) nitrates from aqueous solutions with SE(TAA) at T = 298.15 K, processed assuming the occurrence of reaction (2)*

$c_{(aq)}$	$c_{(o)}$	$c_{(o)}$(calc)	deviation, %	$\{R_3NHNO_3\}_{(o)}$, M	D_{ex}	$y_{\pm}$
M						
			Thorium(IV)			
0.099	0.059	0.0610	–3.46	0.849	0.60	0.281
0.155	0.158	0.1632	–3.28	0.644	1.02	0.244
0.225	0.273	0.2710	0.72	0.428	1.21	0.219
0.245	0.308	0.2944	4.41	0.381	1.26	0.214
0.298	0.348	0.3435	1.31	0.283	1.17	0.205
0.379	0.385	0.3926	–1.96	0.185	1.02	0.196
0.462	0.411	0.4234	–3.02	0.123	0.89	0.192
0.505	0.440	0.4347	1.19	0.101	0.87	0.191
			LanthanumIII)			
0.243	0.0980	0.0922	5.946	0.6935	0.40	0.240
0.281	0.1100	0.1119	–1.688	0.6344	0.39	0.233
0.394	0.1620	0.1609	0.673	0.4873	0.41	0.221
0.483	0.1860	0.1906	–2.495	0.3981	0.39	0.219
0.550	0.2020	0.2014	0.283	0.3657	0.37	0.208
0.750	0.2340	0.2317	0.967	0.2748	0.31	0.196
0.950	0.2480	0.2523	–1.728	0.2131	0.26	0.191
			Yttrium(III)			
0.373	0.0280	0.0253	9.765	0.8942	0.08	0.256
0.535	0.0710	0.0734	–3.447	0.7497	0.13	0.266
0.796	0.1480	0.1475	0.360	0.5276	0.19	0.277
1.002	0.1940	0.1946	–0.300	0.3863	0.19	0.297
1.546	0.2650	0.2687	–1.385	0.1640	0.17	0.397
2.005	0.2980	0.2969	0.374	0.0794	0.15	0.541

* $c_{(aq)}$ is the equilibrium thorium(IV), lanthanum(III), or yttrium(III) nitrate concentration in the aqueous phase; $c_{(o)}$, equilibrium thorium(IV), lanthanum(III), and yttrium(III) nitrate concentration in the organic phase; $c_{(o)}$(calc), the calculated equilibrium thorium(IV), lanthanum(III), and yttrium(III) nitrate concentration in the organic phase; deviation, means the deviation of the calculated values from the experimental data; $[R_3NHNO_3]_{(o)}$, equilibrium extractant concentration; D_{ex}, distribution ratio; and $\gamma_{\pm}$, mean ionic molar activity coefficients of thorium(IV), lantanum(III), or yttrium(III) nitrate in the aqueous phase.

where ΔZ^2 is the algebraic sum of the squared charge numbers of the ionic species participating the extraction equilibrium. For the extraction of Th(IV), $\Delta Z^2 = -20$; $F(I^{\Sigma})$ is a function of the ionic strength, e.g., $F(I^{\Sigma}) = -\alpha(I^{\Sigma})^{1/3}$; θ_1 and θ_2 are empirical parameters; $[Th^{4+}]_{(aq)}$ and c_{NaNO_3} are the equilibrium concentrations of Th(IV) and sodium nitrates in the aqueous phase.

The mathematical processing of the extraction isotherms of thorium(IV) nitrate was carried out with an algorithm reported in [2], taking into account the material balance equations and effect of the ionic strength on the extraction constant. The parameter a in the function $F(I^{\Sigma})$ was 0.155 ± 0.005 at $\{Th^{4+}\} < 0.7$ M and 0.139 ± 0.005 at $\{Th^{4+}\} > 0.7$ M. The other parameters were as follows: θ_1, 0.345 ± 0.005 at $\{Th^{4+}\} < 0.7$ and 0.258 ± 0.006 at $\{Th^{4+}\} > 0.7$; θ_2, 0 ± 0.005; and $\log K_{ex}^{2,0} = 4.30 \pm 0.06$.

Figures 2b, 2c show the extraction isotherms of La(III) and Y(III) nitrates from their solutions both in water and in aqueous sodium nitrate (0–4 M). Similarly to the case of Th(IV), the La(III) and Y(III) nitrate content in SE increases with the sodium nitrate concentration. The limiting La(III) and Y(III) nitrate concentration in SE is close to $c_s/3$. Therefore, we can suggest that the SE extracts REM nitrate in the form

of the $(R_3H)_3[Ln(NO_3)_6]$. Comparison of curves *1* in Figs. 2b and 2c shows that Ln(III) nitrate is better extracted with SE than Y(III) nitrate. The extraction of Y with SE in the absence of sodium nitrate occurs only at yttrium nitrate concentrations higher than 0.3 M (Fig. 2c). The extraction of REM(III) nitrates with TAA nitrate can be described by the equation of the following heterogeneous reaction:

$$Ln^{3+}_{(aq)} + 3NO^-_{3(aq)} + 3R_3NHNO_{3(o)} \rightleftarrows (R_3NH)_3[Ln(NO_3)_6]_{(o)}. \quad (5)$$

The extraction constant can be calculated by equation

$$K^{3,0}_{ex} = \frac{\{(R_3NH)_3[Ln(NO_3)_6]\}_{(o)}}{\{Ln^{3+}\}_{(aq)}\{NO^-_3\}^3_{(aq)}y^4_{\pm}\{R_3NHNO_3\}^3_{(o)}}. \quad (6)$$

The La(III) and Y(III) equilibrium concentrations in SE, calculated assuming the occurrence of reaction (5), are listed in the table. The $y_{\pm}$ values used in these calculations were published in [2, 3]. The table shows that the calculated La(III) and Y(III) concentrations in the solid extractant agree with the experiment to within 1–3 rel. %. Thus, our model adequately describes the extraction of La(III) and Y(III) nitrates from aqueous solutions with the solid extractant in the systems with widely different metal concentration in both aqueous and solid extractant phases. The values of $\log K^{3,0}_{ex}$ for La(III) and Y(III) were found to be 2.95 ± 0.05 and 1.20 ± 0.05, respectively.

The effect of the solution ionic strength on the concentration extraction constants K^3_{ex} of La(III) and Y(III) nitrates can be estimated by the equation

$$\log K^3_{ex}(I^{\Sigma}) = \log K^{0,3} + \Delta Z^2 F_{ex}(I^{\Sigma}) + 6\theta_1\{Ln^{3+}\}_{(aq)} + \theta_2 c_{NaNO_3(aq)}, \quad (7)$$

where $\Delta Z^2 = -12$, $a = 0.238 \pm 0.005$, θ_1 is equal to 0.451 ± 0.005 and 0.579 ± 0.006 for La and Y, respectively; θ_2 is equal to 0.400 ± 0.005 and 0.602 ± 0.005 for La and Y, respectively; $\log K^{3,0}_{ex}$ is 2.95 ± 0.05 and 1.20 ± 0.05 for La and Y, respectively.

We also studied the extraction of Th(IV) with SE in the presence of varied amounts of La(III) or Y(III) nitrates in the aqueous phase (Fig. 3a, 3b). It was found that, within the entire La(III) and Y(III) concentration range, these metals are not noticeably transferred into SE [(La(III) and Y(III) concentrations in the SE were lower than 0.01 mol dm^{-3}]. At the same time, similarly to extraction of Th(IV) in the presence of sodium nitrate (Fig. 2a), the Th(IV) concentration in SE increases with the La(III) and Y(III) nitrate concentration in the aqueous phase and becomes close to $c_s/2$.

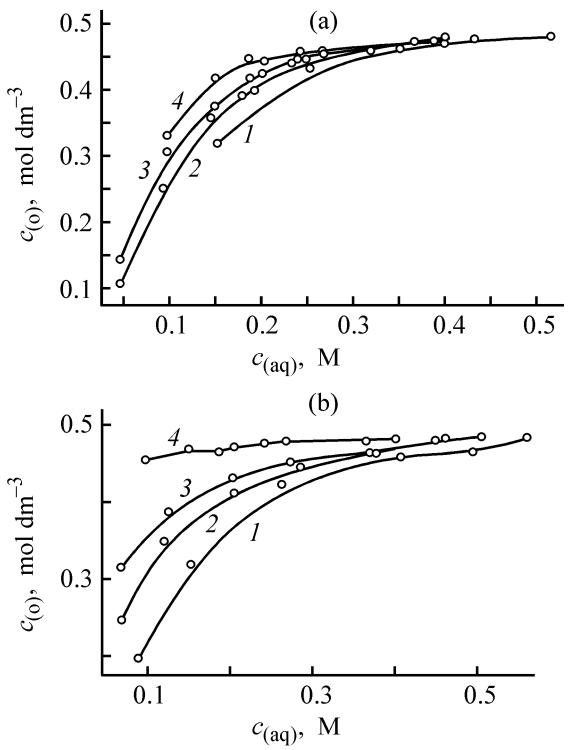


Fig. 3. Extraction of Th(IV) nitrate with SE ($c_{(o)}$) vs. equilibrium Th(IV) nitrate concentration ($c_{(aq)}$) in the aqueous phase containing (a) yttrium nitrate and (b) lanthanum nitrate. Y(III) and La(III) nitrate concentration in the initial aqueous solutions, M: (*1*) 0.1, (*2*) 0.2, (*3*) 0.3, and (*4*) 1.0.

The effect of varied ionic strength of the aqueous phase on the concentration extraction constants K^2_{ex} of Th(IV) nitrate from aqueous solutions containing La(III) or Y(III) nitrates was estimated by the equation

$$\log K^2_{ex}(I^{\Sigma}) = \log K^{0,2} + \Delta Z^2 F_{ex}(I^{\Sigma}) + 10\theta_1\{Th^{4+}\}_{(aq)} + 6\theta_2\{Ln^{3+}\}_{(aq)}, \quad (8)$$

where for $\Delta Z^2 = -20$, $a = 0.139 \pm 0.005$; for Y, $\theta_1 = 0.420 \pm 0.005$ and $\theta_2 = 0.315 \pm 0.005$; for La(III), $\theta_1 = 0.690 \pm 0.005$ and $\theta_2 = 0.300 \pm 0.005$ ($I^{\Sigma} < 7$) and $\theta_1 = 0.400 \pm 0.005$ and $\theta_2 = 0.265 \pm 0.005$ ($I^{\Sigma} > 7$); $\log K^{2,0}_{ex} = 4.30 \pm 0.06$.

Thus, our results show that treatment of concentrated aqueous solutions of REM(III) nitrates with a composite solid extractant based on a polymeric support impregnated with neat trialkylamine allows

their extractive purification to remove Th(IV) impuruties.

CONCLUSIONS

(1) In extraction of nitric acid from aqueous solution with a composite solid extractant based on a polymeric support impregnated with neat trialkylamine (SE), the limiting HNO_3 concentration in SE is 0.97 mol dm^{-3}, which corresponds to the formation of stoichiometric TAA nitrate.

(2) The extraction isotherms were analyzed assuming that lanthanides(III) and thorium(IV) are extracted with the solid extractant in the form of complexes $(R_3HN)_3[Ln(NO_3)_5]$ and $(R_3HN)_2[Th(NO_3)_6]$. The extraction constants were calculated; they decrease in the order Th(IV) > La(III) > Y(III).

(3) In joint extraction of Th(IV) nitrate and La(III) or Y(III) nitrate, La(III) and Y(III) are not noticeably transferred into the SE phase but the extraction of Th(IV) increases with the La(III) and Y(III) nitrate concentrations in the aqueous phase.

(4) The treatment of concentrated aqueous solutions of REM(III) nitrates with a composite solid extractant allows their purification to remove Th(IV) impuruties.

REFERENCES

1. Mikhailichenko, A.I., Mikhlin, E.B., and Patrikeev, Yu.B., *Redkozemel'nye metally* (Rare-Earth Metals), Moscow: Metallurgiya, 1987.
2. Pyartman, A.K., Keskinov, V.A., Mikhailenko, M.A., et al., *Radiokhimiya*, 2004, vol. 46, no. 3, pp. 240–242.
3. Pyartman, A.K., Kopyrin, A.A., Berinskii, A.E., and Keskinov, V.A., *Radiokhimiya*, 2000, vol. 43, no. 2, pp. 128–130.
4. Pribil, R., *Komplexometrie*, Prague: Chemapol, 1955.

ISSN 1070-4272, Russian Journal of Applied Chemistry, 2006, Vol. 79, No. 8, pp. 1271–1277. © Pleiades Publishing, Inc., 2006.
Original Russian Text © L.B. Belykh, Yu.Yu. Titova, V.A. Umanets, F.K. Shmidt, 2006, published in Zhurnal Prikladnoi Khimii, 2006, Vol. 79, No. 8, pp. 1285–1291.

CATALYSIS

Palladium Hydrogenation Catalysts Modified with Aluminum- and Phosphorus-containing Compounds and with Alcohols: Effect of Modifiers

L. B. Belykh, Yu. Yu. Titova, V. A. Umanets, and F. K. Shmidt

Irkutsk State University, Irkutsk, Russia

Received March 14, 2006

Abstract—The catalytic properties of nanosize catalysts derived from $Pd(acac)_2$ and triethylaluminum in hydrogenation of organic substrates were studied, and the optimal conditions for the catalyst preparation were found. The maximum observed on the plot of the catalyst specific activity vs. Al/Pd ratio was explained by experiments.

DOI: 10.1134/S1070427206080106

Transition metals and their complexes catalyze hydrogenation of unsaturated organic compounds with gaseous hydrogen; the process has numerous industrial applications [1, 2]. A particular place is occupied by palladium catalysts, whose properties significantly differ from those of catalysts containing Rh, Pt, Ru, Ni, or Cu [2]. Palladium is one of the most active metals in the hydrogenation of double bonds conjufated with an aromatic ring, such as Ar–C=C, Ar–C=O, or Ar–C=NR. Furthermore, Pd is one of the most selective metal catalysts in the hydrogenation of triple and conjugated double bonds and the most active metal in hydrogenolysis, i.e., reductive cleavage of C–X bonds. However, at low temperatures Pd is virtually inactive in the hydrogenation of the majority of aromatic rings and shows low activity in the hydrogenation of aliphatic ketones and aldehydes [2]. These characteristics determine the applications of palladium-based catalysts in chemo- and stereo-selective hydrogenation, hydrogenolysis, and dehydrogenation of various organic compounds.

Along with heterogeneous catalysts, hydrogenation catalysts based on transition metal complexes has attracted growing researchers' attention since the second half of the XXth century with the development of coordination catalysis. A particular place among such catalysts is occupied by Ziegler-type catalytic systems [3]. The majority of studies in this field concerned the nature and properties of hydrogenation catalysts based on β-diketonate, carboxylate, and cyclopentadienyl complexes of transition metals of the first row [4–10], and also the synthesis of metal nanoparticles by treatment with organoaluminum compounds [11–16].

The problems of the formation mechanism, phase state, and nature of hydrogenation-active species in Ziegler-type catalytic systems based on Pd(II) complexes and the properties of these systems have been studied to a lesser extent [17, 18] and are the subject of this paper.

EXPERIMENTAL

Solvents (toluene, benzene, hexane) were purified by standard procedures required for manipulations with organometallic compounds [19]. For more exhaustive drying, the solvents were additionally distilled from $LiAlH_4$ on a distillation column and were stored under Ar in sealed ampules over 4 Å molecular sieves.

Palladium bis(acetylacetonate) $Pd(acac)_2$ was prepared according to [20]. ^{1}H NMR, δ, ppm: 5.04 s (2H, CH), 1.76 s (12H, CH_3).

Commercial-grade triethylaluminum $AlEt_3$ was distilled in a vacuum; the fraction boiling at 48–49°C (1 mm Hg) was collected. ^{1}H NMR, δ, ppm: 1.22 t (9H, CH_3, ^3J = 8.24 Hz), 0.45 q (6H, ^3J = 8.24 Hz). The samples were stored in a glass ampule under Ar. Solutions of triethylaluminum in hexane were prepared in a Schlenk vessel under Ar.

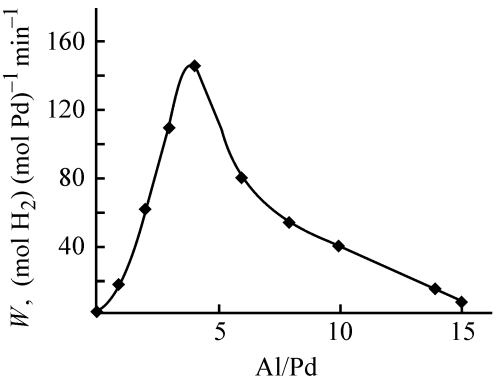


Fig. 1. Hydrogenation of styrene in the presence of the catalytic system $Pd(acac)_2$–$n AlEt_3$. $c_{Pd} = 5 \times 10^{-3}$ M, $n_{styrene}$ = 9 mmol, T = 30°C, P_{H_2} = 1 atm, solvent toluene; the same for Fig. 3. (W) Specific activity of the system.

The hydrogenation of the substrates was performed in a temperature-controlled glass vessel at 30°C and initial hydrogen pressure of 1 atm in the presence of the catalytic system formed in situ. To a solution of 0.01522 g (5×10^{-5} mol) of $Pd(acac)_2$ in toluene, placed in a temperature-controlled duck-shaped vessel, we added dropwise in a hydrogen flow a solution of $AlEt_3$ in hexane from a Schlenk vessel; the mixture was stirred for 5 min. The molar ratio $AlEt_3/Pd(acac)_2$ was varied from 2 to 16. The total solution volume was 10 ml. To the resulting brown-black mixture, we added a substrate whose hydrogenation was performed with vigorous stirring at the initial hydrogen pressure of 1 atm. The reaction progress was monitored volumetrically and by GLC. Experiments involving modification of the catalyst with triphenylphosphine and ethanol were performed similarly.

The NMR spectra were recorded on a Varian VXR-500S pulse spectrometer. The ^{31}P chemical shifts are given relative to 85% H_3PO_4.

A TEM examination of the samples was performed with a BS-300 microscope (Czechia). A drop of a solution was applied onto a supporting grid coated with a carbon film and was dried in an argon atmosphere. The recording conditions excluded melting and decomposition of the samples under electron beam.

The IR spectra of the precipitates were recorded on a Specord 75-IR spectrometer in the range 4000–400 cm^{-1} using KBr windows. Samples for recording the IR spectra were prepared in a box with an inert atmosphere as mulls in mineral oil preliminarily heat-treated to remove traces of moisture.

The catalytic properties of the Ziegler-type systems based on $Pd(acac)_2$ and $AlEt_3$ in the hydrogenation depend on numerous factors, in particular, on the Al/Pd molar ratio. The dependence of the specific activity in the hydrogenation of alkenes on the component ratio passes through a maximum at Al/Pd = 4 (Fig. 1).

A high activity of the $Pd(acac)_2$–$AlEt_3$ system at Al/Pd = 4 was also observed in the hydrogenation of other organic substrates: α-alkenes, alkynes, nitro and carbonyl compounds (Table 1). In particular, the specific activity W in hydrogenation of 1-hexene was 112 (mol H_2) (mol Pd)$^{-1}$ min^{-1}. The hydrogenation was accompanied by isomerization of 1-hexene into 2-hexene (*cis* + *trans*). At 99% conversion of 1-hexene, the reaction system contained 59% hexane, 33% *trans*-2-hexene, and 7% *cis*-2-hexene. The rates of hydrogenation of the terminal and internal double bonds differed by an order of magnitude; however, even under these conditions, 2-hexene fairly rapidly and quantitatively transformed into hexane under mild conditions (30°C, P_{H_2} = 1 atm). The high rate of the positional isomerization of the double bond was observed in the hydrogenation of 1,5-hexadiene whose

Table 1. Hydrogenation of organic substrates in the presence of the system $Pd(acac)_2$–$4AlEt_3$ ($c_{Pd} = 5 \times 10^{-3}$ M, 30°C, P_{H_2} = 1 atm, [substrate] : [Pd] = 182, solvent toluene)

Substrate	W, (mol H_2) (mol Pd)$^{-1}$ min^{-1}	Product, %
Styrene	145	Ethylbenzene 100
1-Hexene	112	Hexane 100
1,5-Hexadiene	77	1-Hexene 9.1, *trans*-2-hexene 43.7, *cis*-2-hexene 23.7, hexane 11.3*
Phenylacetylene	117	Ethylbenzene 100
Nitrobenzene	39	Aniline 97
Benzaldehyde	3	Benzyl alcohol 98, toluene 0.1**
Naphthalene	0	–

* At 99% conversion of 1,5-hexadiene. ** Solvent benzene.

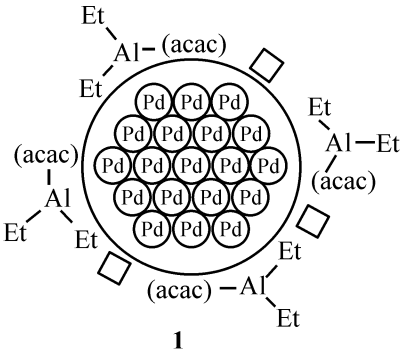
reduction is usually regarded as a model reaction of the hydrogenation of polyene compounds.

The hydrogenation of phenylacetylene in the presence of the catalytic system $Pd(acac)_2$–$AlEt_3$ occurs not only at a high rate, but also with a fairly high selectivity: 97% with respect to styrene at 96% conversion of phenylacetylene. No side reaction of di- and oligomerization of phenylacetylene was observed. The high selectivity of palladium catalysts in the hydrogenation of α-alkynes is due to a thermodynamic factor: considerably higher equilibrium constant of the coordination of α-alkyne, compared to alkene [21], with the active center. The $Pd(acac)_2$–$4AlEt_3$ system also shows high selectivity in the hydrogenation of benzaldehyde to benzyl alcohol, which is usually followed by hydrogenolysis of the $C_6H_5CH_2$–OH bond.

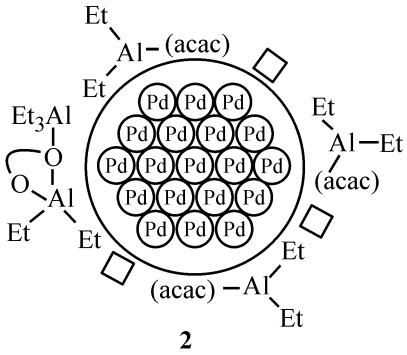
The observed dependence of the specific activity on the Al/Pd ratio is caused by several factors. Previously, when studying the reaction of $Pd(acac)_2$ with $AlEt_3$ in an inert atmosphere by ^1H NMR spectroscopy and electron microscopy, we have revealed three major facts [22]. First, the reduction of $Pd(acac)_2$ with triethylaluminum is quantitative at the ratio Al/Pd ≥ 3.5, rather than at Al/Pd = 2 as could be expected from the stoichiometric equation

$$Pd(acac)_2 + 2AlEt_3 = 1/xPd(O)_x + 2Al(acac)Et_2 + C_2H_4 + C_2H_6.$$

This is apparently due to side catalytic decomposition of triethylaluminum in the presence of Pd(0) nanoparticles. At Al/Pd ≥ 3.5, unchanged triethylaluminum remains in the reaction system. Second, the reduction of $Pd(acac)_2$ yields Pd(0) nanoparticles stabilized with $AlEt_2(acac)$ (**1**) and/or with adduct of $AlEt_2(acac)$ with $AlEt_3$ at Al/Pd ≥ 3.5 (**2**):



1



2

Third, the mean size of the Pd(0) nanoparticles depends on the Al/Pd ratio and decreases with an increase in the triethylaluminum concentration from 4.5 (Al/Pd = 4) to 1–2 nm at Al/Pd ≥ 8.

Thus, the rise in the specific activity of the $Pd(acac)_2$–$AlEt_3$ system in the initial portion of the curve (Fig. 1) is caused by an increase in the fraction of reduced palladium and in the dispersity of the microheterogeneous system. The nonlinear dependence of the styrene hydrogenation rate on the palladium concentration and a decrease in the reaction rate at Pd concentrations exceeding 10 mM suggest association of the active particles into less active aggregates and confirm the microheterogeneous nature of the catalyst (Fig. 2).

The hydrogenation of alkenes is a structure-insensitive reaction [23, 24]. Therefore, a decrease in the catalytic activity with a decrease in the size of Pd nanoparticles (Al/Pd > 4) suggests the appearance of a catalytic poison in the system. Unchanged $AlEt_3$ can act as such a poison. To confirm the inhibiting effect of $AlEt_3$ at high Al/Pd ratios, we studied the effect of

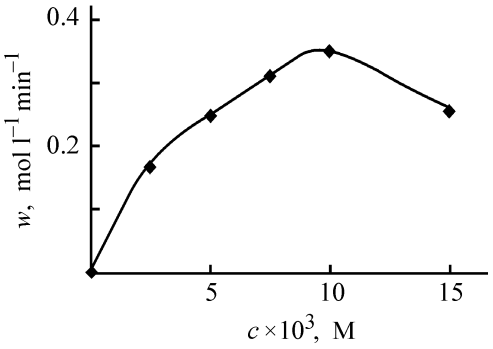


Fig. 2. Styrene hydrogenation rate w vs. the Pd concentration c. Al/Pd = 4, $n_{styrene}$ = 9 mM, 30°C, P_{H_2} = 1 atm, solvent toluene.

Table 2. Influence of the modifier on the specific activity of the $Pd(acac)_2$–$n AlEt_3$ system in the hydrogenation of styrene ($c_{Pd} = 5 \times 10^{-3}$ M, 30°C, $P_{H_2} = 1$ atm, [substrate]/[Pd] = 182, solvent toluene)

$\frac{AlEt_3}{Pd(acac)_2}$	Modifier X	$\frac{X}{Pd}$	W_1	W_2
			(mol H_2) (mol Pd)$^{-1}$ min^{-1}	
15	$OPPh_3$	2	2	19
4	C_2H_5OH	2	145	116
4		4	140	106
4		10	147	37
15		10	5	51
15		20	4	71
15		30	3	172
15		60	4	138
15		15	18**	90**

* (W_1, W_2) Specific activity before and after introduction of the modifier, respectively.

** Hydrogenation of phenylacetylene.

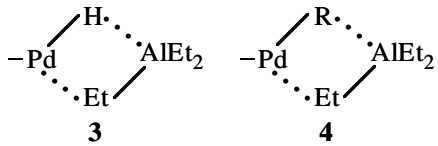
Table 3. Hydrogenation of phenylacetylene (PA) in the presence of the $Pd(acac)_2$–$n AlEt_3$ system ($c_{Pd} = 5 \times 10^{-3}$ M, 30°C, $P_{H_2} = 1$ atm, [substrate]/[Pd] = 182, solvent toluene)

Al/Pd	W, (mol H_2) (mol Pd)$^{-1}$ min^{-1}	
	–C≡C–	–C=C–
2	39	34
4	117	100
6	121	122
8	124	124
10	113	85
16	15	3

various modifying additives capable of binding $AlEt_3$ (Table 2).

It is known that organoaluminum compounds form stable 1 : 1 adducts with Lewis bases (e.g., ethers, amines) and react, with release of hydrocarbons, with water, alcohols, acids, and other proton-donor compounds. Therefore, we tested as modifiers the substances that should, on the one hand, bind excess triethylaluminum and, on the other hand, be relatively inert toward palladium. Among such compounds are alcohols and triphenylphosphine oxide $OPPh_3$. The ^{31}P NMR spectrum of the mixture from the reaction of equimolar amounts of $OPPh_3$ and $AlEt_3$ does not contain the signal from $OPPh_3$ ($\delta_P = 25$ ppm), but contains a signal at $\delta_P = 39$ ppm, which can be assigned to the adduct $Ph_3PO \cdot AlEt_3$ formed by the donor–acceptor interaction.

As follows from Table 2, addition of ethanol or triphenylphoshine oxide to the $Pd(acac)_2$–$AlEt_3$ catalytic system prepared in advance makes higher the hydrogenation rate. In particular, in the presence of $OPPh_3$ the rate of styrene hydrogenation increases by a factor of approximately 10. With additions of ethanol, even the performance of the most active catalytic system (Al/Pd = 4) is surpassed. Hence, the role of triethylaluminum is not restricted to the reduction of Pd(II) compounds. When in excess, $AlEt_3$ acts as a catalytic poison. The poisoning effect of $AlEt_3$ on the catalyst may be due to formation of surface compounds by the reaction of $AlEt_3$ with hydride **3** or alkyl **4** intermediates of the catalytic cycle:



3 **4**

As noted above, the donor power of α-alkynes is higher than that of alkenes. Therefore, the poisoning effect of triethylaluminum in the hydrogenation of phenylacetylene was observed at higher Al/Pd ratios (Table 3). However, the hydrogenation of α-alkynes is, in contrast to that of alkenes, a structure-sensitive reaction [24], and a question naturally arises: Can the observed drastic decrease in the rate of phenylacetylene hydrogenation at Al/Pd > 10 be attributed to the too strong adsorption of the substrate on small palladium particles? Addition of ethanol to the $Pd(acac)_2$–$15AlEt_3$ catalytic system prepared in advance led to an increase in the specific activity in the hydrogenation of phenylacetylene by a factor of 5. Hence, as in the case of alkenes, the major factor responsible for the decrease in the catalytic activity of the $Pd(acac)_2$–$AlEt_3$ system in the hydrogenation of phenylacetylene at high Al/Pd ratios is the inhibiting effect of triethylaluminum.

An opposite pattern was observed when ethanol was added to the $Pd(acac)_2$–$4AlEt_3$ system, which is the most active in the hydrogenation of styrene: The specific activity decreased with an increase in the alcohol concentration (Table 2). On adding ethanol, the system became aggregation-unstable, and a black precipitate formed. This fact indicates that the compounds $Al(OEt)_2(acac)$ and/or $Al(OEt)Et(acac)$ formed by the reaction of $AlEt_2(acac)$ with ethanol exhibit weaker

stabilizing power than does $AlEt_2(acac)$, which results in the aggregation of the palladium nanoparticles.

Taking into account the microheterogeneous nature of the catalyst based on $Pd(acac)_2$ and $AlEt_3$, one of the ways to enhance the catalytic activity is to decrease the palladium particle size. However, increasing the dispersity by adding more $AlEt_3$ leads to an opposite result because of the poisoning effect of excess triethylaluminum. The dispersity can be increased not only by taking the reductant in a higher concentration, but also by performing the catalyst synthesis by chemical condensation in the presence of a stabilizer; as stabilizer we used triphenylphosphine.

It is known that the complexation of triphenylphosphine with an equimolar amount of $Pd(acac)_2$ leads to the transformation of one of the acetylacetonate ligands from the O,O-chelate to the C^3-bound form, with the formation of the complex $Pd(acac)_2PPh_3$ [25]. At P/Pd < 1, the reaction mixture contains two complexes, $Pd(acac)_2$ and $Pd(acac)_2PPh_3$, and at P/Pd > 1, $Pd(acac)_2PPh_3$ and free triphenylphosphine.

Addition of triphenylphosphine to the $Pd(acac)_2$–$4AlEt_3$ before adding triethylaluminnum affects in a complex fashion the catalytic properties in hydrogenation. In particular, in the hydrogenation of styrene, as the P/Pd ratio is raised, the specific activity first increases (P/Pd = 0.25) relative to the unmodified catalyst, reaches a maximum at P/Pd = 1, and decreases to zero at P/Pd = 2 (Fig. 3). The catalyst prepared at P/Pd = 1 [i.e., by the reduction of $Pd(acac)_2 \cdot PPh_3$ with $AlEt_3$] is the most active; therefore, we studied in more detail the catalyst based on $Pd(acac)_2 \cdot PPh_3$–$AlEt_3$.

The ^{31}P NMR spectrum of the $Pd(acac)_2PPh_3$–$4AlEt_3$ system prepared in an inert atmosphere contains broadened signals from free triphenylphosphine ($\delta_P = -6$ ppm) and from PPh_3 coordinated to Pd in lower oxidation states (δ_P = 22, 16.4 ppm). A TEM examination of the reaction mixture revealed the presence of high-contrast palladium particles, among which particles 2.5 nm in diameter prevail (Fig. 4). The IR spectrum of the brown powder isolated from the reaction mixture contains bands of $AlEt_2(acac)$ [ν(C=O) + ν(C=C) 1585 and 1525 cm^{-1}; ν(C=C) + ν(C–CH_3) 1284, 1218 cm^{-1}; δ(Al–C–H) + ν(C–CH_3) 1187, 1104, 1047, 1010 cm^{-1}] and bands characteristic of out-of-plane bending vibrations of the C–H and C–C bonds in the monosubstituted benzene ring (706, 676, 450 cm^{-1}); this pattern indicates that both triphenylphosphine and diethyl(acetylacetonato)aluminum molecules act as stabilizers of palladium nanoparticles.

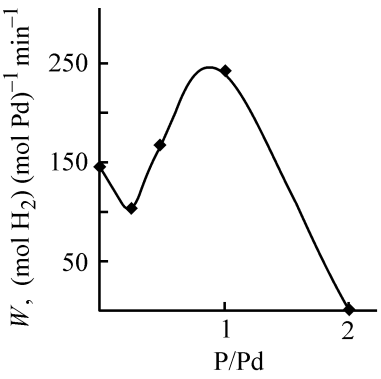
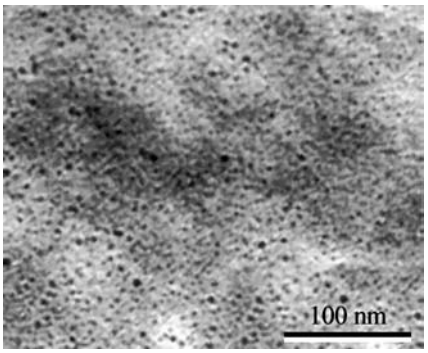


Fig. 3. Hydrogenation of styrene in the presence of the catalytic system $Pd(acac)_2$–$nPPh_3$–$4AlEt_3$.



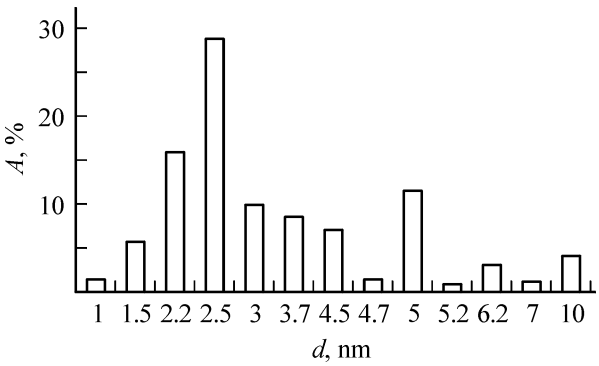


Fig. 4. Electron micrograph of the $Pd(acac)_2PPh_3$–$4AlEt_3$ system and particle size distribution (inert atmosphere). (*A*) Fraction of particles and (*d*) particle size; the same for Fig. 5.

The reaction of $Pd(acac)_2PPh_3$ with $AlEt_3$ in a hydrogen atmosphere yields benzene along with the above-mentioned products. This fact indicates that the catalyst formation is accompanied not only by the reduction of Pd(II) to Pd(0), but also by decomposition of the phosphine ligands. At P/Pd = 1, about half

Table 4. Formation of benzene in the course of preparation of a catalyst based on the $Pd(acac)_2$–$AlEt_3$ system modified with triphenylphosphine ($c_{Pd} = 5 \times 10^{-3}$ M, 30°C, P_{H_2} = 1 atm, solvent toluene)

$PPh_3/Pd(acac)_2$	C_6H_6/PPh_3 in indicated time, min	
	1	5
0.25	2.9	2.9
0.5	2.3	2.9
1.0	0.7	1.4
2.0	0.8	0.8

Table 5. Hydrogenation of styrene in the presence of the $Pd(acac)_2$–$4AlEt_3$ system modified with elemental P ($c_{Pd} = 5 \times 10^{-3}$ M, 30°C, P_{H_2} = 1 atm, [substrate]/[Pd] = 182, solvent toluene)

P/Pd	W, (mol H_2) (mol Pd)$^{-1}$ min^{-1}	
	$Pd(acac)_2$–P_4–$4AlEt_3$	$Pd(acac)_2$–$4AlEt_3$–P_4
0	145	145
0.2	147	155
0.3	155	163
0.5	31	49
1.0	0	0

of the phenyl groups of triphenylphosphine transformed into benzene (Table 4). The detection of broadened signals with δ_P = 22 and 16.4 ppm, which were observed when the reaction was performed in an inert atmosphere and were assigned to PPh_3 coordinated with Pd, indicates that a part of triphenylphosphine remained intact. The PPh_2 and PPh fragments formed by dephenylation of the phosphine ligands readily undergo further degradation, ultimately yielding palladium phosphides of various compositions.

It should be noted that the amount of benzene formed per mole of triphenylphosphine in the course of preparation of the $Pd(acac)_2$–$n PPh_3$–$4AlEt_3$ catalyst in hydrogen increased with a decrease in the P/Pd ratio (Table 4). A similar trend has been observed previously in reduction of $Pd(acac)_2$ in the presence of tertiary and primary phosphines [26, 27]. At P/Pd 0.25 or 0.5, triphenylphosphine decomposes virtually completely, i.e., palladium phosphides are formed, and the majority of Pd(0) passes into the form inactive in the hydrogenation.

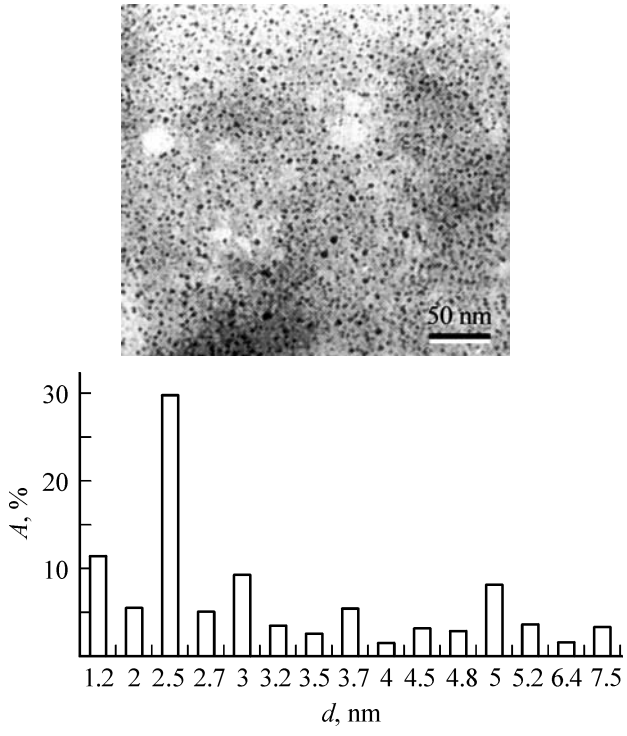


Fig. 5. Electron micrograph of the $Pd(acac)_2PPh_3$–$4AlEt_3$ system and particle size distribution (hydrogen atmosphere).

According to electron microscopic examination, the reaction of $Pd(acac)_2PPh_3$ with $AlEt_3$ (Al/Pd = 4) in a hydrogen atmosphere yields a polydisperse microheterogeneous system in which particles 2.5 nm in diameter prevail; the relative content of 1.2-nm particles increases (Fig. 5). Thus, on the one hand, modification of the catalytic system with phosphine in a hydrogen atmosphere leads to partial transformation of Pd into an inactive form as a result of decomposition of the phosphine ligands; on the other hand, addition of phosphine favors formation of smaller Pd(0) particles. A decrease in the palladium particle size is one of the factors responsible for the promoting effect of triphenylphosphine at P/Pd = 1.

Previously,we have put forward a hydrolysis, according to which palladium phosphides show no catalytic activity in the hydrogenation but act as a matrix for Pd(0) clusters which are actual hydrogenation catalysts [26]. To confirm this hypothesis, we performed additional experiments on modification of the catalytic system $Pd(acac)_2$–$4AlEt_3$ with elemental phosphorus. Irrespective of the order of phosphorus addition (before or after adding triethylaluminum), we observed at P/Pd ≥ 0.5 a decrease in the catalytic activity with an increase in the concentration of elemental phosphorus (Table 5). A slight increase in the specific activity at small additions of P may be due to changes in the catalyst dispersity.

CONCLUSIONS

(1) Examination of the conditions for preparing a Ziegler-type catalyst derived from palladium bis(acetylacetonate) and triethylaluminum and active in hydrogenation of unsaturated compounds and carbonyl and nitro groups showed that the role of triethylaluminum is not limited to the reduction of Pd(II). The complex $AlEt_2(acac)$ formed by the reaction of $AlEt_3$ with $Pd(acac)_2$ is a stabilizer of palladium nanoparticles. At high Al/Pd ratios, triethylaluminum acts as a catalytic poison.

(2) It was found that the modifying effect of ethanol depends on the Al/Pd ratio. At Al/Pd $\leq$ 4, ethanol makes the catalytic activity lower as a result of binding of the stabilizer and, as a consequence, of aggregation of nanoparticles. At high Al/Pd ratios, the promoting effect of ethanol is due to the adduct formation with the catalytic poison, $AlEt_3$.

(3) The nature of the modifying effect of triphenylphosphine on the catalytic properties of the Ziegler-type system $Pd(acac)_2$–$AlEt_3$ was examined. The formation of the hydrogenation catalyst in a hydrogen atmosphere is accompanied by decomposition of the phosphine ligands; the extent of this process increases with a decrease in the P/Pd ratio. The inhibiting or promoting effect of phosphine at P/Pd $\leq$ 1 depends on the ratio of two factors exerting opposite effects on the catalyst activity: transformation of palladium particles into an inactive form as a result of decomposition of phosphine ligands and decrease in the size of Pd(0) particles upon stabilization with phosphine.

REFERENCES

1. Colquhoun, H.M., Holton, J., Thomson, D.J., and Twigg, M.V., *New Pathways of Organic Synthesis: Practical Applications of Transition Metals*, New York: Plenum, 1984.
2. Blaser, H.-U., Indolese, A., Schnyder, A., et al., *J. Mol. Catal. A: Chemical*, 2001, vol. 173, pp. 3–18.
3. Ziegler, K., Gellert, H.G., Holzkamp, E., and Wilke, G., *Brennstoff Chem.*, 1954, vol. 35, p. 322.
4. Sloan, M.F., Matlack, A.S., and Bresloy, D.S., *J. Am. Chem. Soc.*, 1963, vol. 85, no. 24, pp. 4014–4018.
5. Kalechits, I.V. and Shmidt, F.K., *Kinet. Katal.*, 1966, vol. 7, no. 4, pp. 614–617.
6. Kalechits, I.V., Lipovich, V.G., and Shmidt, F.K., *Neftekhimiya*, 1966, vol. 6, pp. 813–816.
7. Lipovich, V.G., Shmidt, F.K., and Kalechits, I.V., *Kinet. Katal.*, 1967, vol. 8, no. 4, pp. 812–815.
8. Lipovich, V.G., Shmidt, F.K., and Kalechits, I.V., *Kinet. Katal.*, 1967, vol. 8, no. 6, pp. 1099–1103.
9. Shmidt, F.K., *Kataliz kompleksami metallov pervogo perekhodnogo ryada reaktsii gidrirovaniya i dimerizatsii* (Catalysis of Certain Hydrogenation and Dimerization Reactions by Complexes of Transition Metals of the First Row), Irkutsk: Irkutsk. Gos. Univ., 1986.
10. Savel'ev, S.R. and Noskova, N.F., *Usp. Khim.*, 1994, vol. 63, no. 11, pp. 995–1003.
11. *Active Metals: Preparation, Characterization, Application*, Furstner, A., Ed., Weinheim: VCH, 1995, pp. 339–376.
12. Duteil, A., Schmid, G., and Meyer-Zaika, W., *J. Chem. Soc., Chem. Commun.*, 1995, pp. 31–32.
13. Kozitsyna, N.Yu., Troitskii, S.Yu., Kryukova, G.N., et al., *Mendeleev Commun.*, 2003, p. 1.
14. Bonnemann, H., Brijoux, W., Brinkmann, R., et al., *Rev. Roum. Chim.*, 1999, vol. 44, nos. 11–12, pp. 1003–1010.
15. Bonnemann, H., Waldofner, N., Yautbold, H.-G., and Vad, T., *Chem. Mater.*, 2002, vol. 14, no. 3, pp. 1115–1120.
16. Shmidt, F.K., Nindakova, L.O., Shainyan, B.A., et al., *J. Mol. Catal. A: Chemical*, 2005, vol. 235, pp. 161–172.
17. Levkovskii, Yu.S., Ryutina, N.M., and Shmidt, F.K., *Kinet. Katal.*, 1980, vol. 21, pp. 797–800.
18. Khar'kova, E.M., Rozantseva, L.E., and Frolov, V.M., *Kinet. Katal.*, 1998, vol. 39, no. 3, p. 389.
19. Gordon, A.J. and Ford, R.A., *The Chemist's Companion. A Handbook of Practical Data, Techniques, and References*, New York: Wiley, 1972.
20. US Patent 3474464.
21. Tungler, A. and Fogassy, G., *J. Mol. Catal. A: Chemical*, 2001, vol. 173, pp. 231–247.
22. Belykh, L.B., Goremyka, T.V., Rokhin, A.V., et al., *Koord. Khim.*, 2005, vol. 31, no. 10, pp. 719–724.
23. Navalikhina, M.D. and Krylov, O.V., *Usp. Khim.*, 1998, vol. 67, no. 7, pp. 657–687.
24. Karpinski, Z., *Adv. Catal.*, 1990, vol. 37, pp. 45–57.
25. Baba, S., Ogura, T., and Kawaguchi, S., *Bull. Chem. Soc. Jpn.*, 1974, vol. 47, no. 3, pp. 665–668.
26. Shmidt, F.K., Belykh, L.B., and Goremyka, T.V., *Kinet. Katal.*, 2003, vol. 44, no. 5, pp. 683–691.
27. Belykh, L.B., Goremyka, T.V., and Shmidt, F.K., *Zh. Prikl. Khim.*, 2004, vol. 77, no. 5, pp. 774–778.

ISSN 1070-4272, Russian Journal of Applied Chemistry, 2006, Vol. 79, No. 8, pp. 1278–1281. © Pleiades Publishing, Inc., 2006.
Original Russian Text © S.Ya. Brichka, L.Yu. Kotel, G.P. Prikhod'ko, A.V. Brichka, 2006, published in Zhurnal Prikladnoi Khimii, 2006, Vol. 79, No. 8, pp. 1292–1295.

CATALYSIS

Synthesis of Carbon Nanotubes on Water-soluble Supports

S. Ya. Brichka, L. Yu. Kotel, G. P. Prikhod'ko, and A. V. Brichka

Institute of Surface Chemistry, National Academy of Sciences of Ukraine, Kiev, Ukraine

Received April 5, 2005; in final form, March 2006

Abstract—Gas-phase pyrolytic synthesis of carbon to give multilayer carbon nanotubes on Ni catalysts supported by NaCl and K_2SO_4 mineral water-soluble substrates was studied. The morphology of the nanotubes synthesized was examined.

DOI: 10.1134/S1070427206080118

The method of synthesis of carbon nanotubes (CNT) by chemical vapor deposition of carbon in a comparatively high yield is highly promising for introduction into large-tonnage industrial manufacture. The process of catalytic pyrolysis of carbon-containing reagents is affected by the choice of a catalyst, source of carbon, temperature, partial pressure of synthesis components, and nature of a catalyst support [1]. The key importance of the catalyst support consists in that nanosize particles of metals that belong to the iron subgroup can be formed on its surface, which is a necessary condition for growth of nanosize fibrous carbon structures (fibers, tubes). Use of silicon oxide (primarily that with a developed surface, of the MCM-41 type), silica gels, and zeolites as supports has been found effective for synthesis of CNT [2, 3]. According to the results of [4, 5], aluminum oxide has an advantage over the supports mentioned above, which is manifested in an increase in the yield of CNT. It is assumed that aluminum oxide exhibits catalytic activity in pyrolysis of hydrocarbons and thereby diminishes the formation of pyrolytic carbon on its surface. Syntheses of nanotubes with other catalyst supports carbon and magnesium oxide, have been described. Emphasis should be placed on the study [6], in which CNT was obtained with high selectivity and purity, with calcium carbonate used as support. The technique makes it possible to separate CNT from a catalyst on a support with diluted nitric acid in a single stage and to perform, as it was done in [7], partial purification of nanotubes to remove other forms of carbon.

To disadvantages of the catalyst supports described in the literature can be attributed the fact that their separation from the carbon fraction requires use of corrosive media (HF, HNO_3, HCl, H_2SO_4, $HClO_4$, and alkalis). These media react not only with the substrate and catalyst, but also with carbon nanotubes and the modifying components they contain, which makes lower their amount. Replacement of the conventional supports with novel ones of some other chemical nature will extend the existing synthetic potentialities of the method.

The aim of this study was to find conditions in which CNT can be synthesized with water-soluble catalyst supports, sodium chloride and potassium sulfate.

EXPERIMENTAL

We synthesized CNT using water-soluble substrates: salts of alkali metals, such as sodium chloride and potassium sulfate. A quartz boat was placed in a quartz horizontal flow-through reactor 42 mm in diameter. A layer of nickel(II) acetylacetonate [$Ni(acac)_2$] was deposited onto one half of the boat, and that of a thoroughly ground catalyst support, onto the other. In the inert atmosphere of argon, which served as transport gas, the temperature was gradually raised to 250–300°C and nickel(II) acetylacetonate (sublimation temperature 132°C) passed into the gaseous state. Its subsequent thermal decomposition resulted in that metal nanoparticles appeared on the whole surface of the water-soluble substrate and a carbon-containing gaseous component was formed in the volume of the reactor. After 0.5 h, a mixture of argon with acetylene (C_2H_2) was fed into the system in order to make higher the content of carbon in the reaction mixture, with the temperature raised to 600°C. After pyrolysis of acetylene continued for 20–30 min, the reactor was cooled to room temperature. The resulting carbon-containing composite, in

which black pyrolysis products, catalyst, and support were present, was treated under agitation with warm distilled water to remove the substrate, water-soluble salts. The carbon fraction was separated from the solution by centrifugation and used in further studies. Nanotubes were identified with a JEMOOCX-II transmission electron microscope.

There exist a rather large number of methods for production of catalysts for gas-phase pyrolytic synthesis of carbon nanotubes, and these methods rely on a variety of approaches. One of these is based on codeposition by hydrolysis of a mixture of precursors containing the active component and the component of a support: compounds of metals of the iron subgroup and silicon, aluminum, and magnesium, followed by reduction of the active component to give catalysts on the substrate surface. The support prevents aggregation of nanoparticles of the active metal and favors their more uniform distribution. A distinctive feature of another approach is that oxides with a large specific surface area, impregnated with solutions of metal salts, are used as substrates. The initial substrate has a prescribed structure and porosity, which allows control over the catalyst preparation procedure in the impregnation and reduction stages, with the catalyst formed on the matrix surface. Use of volatile catalyst precursors (e.g., organometallic compounds) enables synthesis of catalytically active substances by pyrolysis directly in the reaction zone and makes it possible to exclude any liquid medium from the process, i.e., synthesis of CNT is performed in the gas phase in all stages. Destruction of these precursors occurs at high temperatures (above 500°C) in an inert atmosphere to give catalyst nanoparticles on the substrate [8].

A most important stage of CNT synthesis is separation of the carbon fraction composed of CNT and other forms of carbon from the substrate with catalyst and further purification of the carbon fraction to remove admixtures of amorphous carbon and carbon nanoparticles. Acids commonly serve to dissolve the conventionally used catalyst supports. For example, the matrix, porous aluminum oxide, was dissolved in HF for 24 h in [9, 10] (in our opinion, full dissolution of such a substrate requires no less than 6 h). Further chemical purification of a CNT sample is based on the fact that the oxidation rate of nanotubes differs from that of more active admixtures of amorphous carbon and other forms of carbon. Thermal treatment of a carbon sample in air at 530°C results in that the loss of mass by the sample exceeds 60% and the content of CNT in the sample increases to 90%. Another purification method is based on treatment of a carbon-containing sample with a 30% HNO_3 solution. As a result, the $CaCO_3$ support and the Fe(II), Co(II) catalyst dissolve and carbon partly oxidizes. The treatment of a carbon sample with HNO_3 can be regarded as the most efficient method of CNT purification because of the high reactivity of pyrolytic carbon toward oxidation, compared with CNT, which enables deep purification of nanotubes.

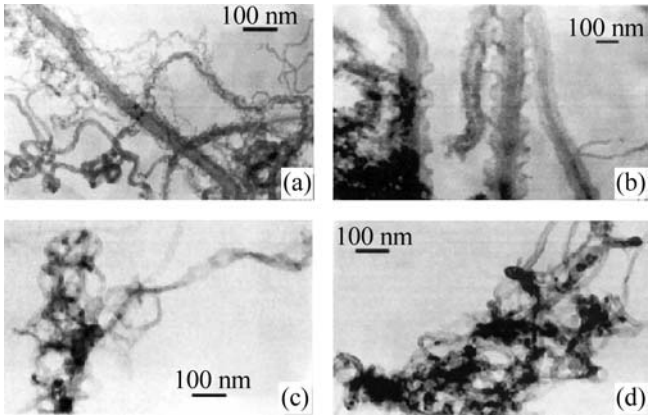


Fig. 1. (a–d) Electron micrographs of CNT with different diameters. Diameter (nm): (a) outer 5–28 and (b) inner 1–15.

Pyrolysis of various sources of carbon in an inert gas yields CNT at high temperatures, as a rule at 500–800°C. Therefore, a necessary requirement to supports of catalysts used in synthesis of CNT is their thermal stability up to temperatures exceeding the synthesis temperature. Thus, we chose salts with high melting points, NaCl (mp 801°C) and K_2SO_4 (mp 1076°C) as model water-soluble catalyst supports. The property of the substrates to dissolve in water imposed limitations on the choice of a source and method of catalyst deposition. The available acetylacetonates of metals of the iron subgroup, with sublimation points in the range 97–132°C and decomposition points of 150–400°C are convenient sources of catalysts and carbon, and the catalysts can be deposited from the gas phase without any aqueous medium. The use of acetylene in CNT synthesis made it possible to preclude a deficiency of carbon in the reaction mixture. Metal nanoparticles are probably formed in decomposition of acetylacetonate at 300°C, or there may occur a redox reaction between Ni(II) and C_2H_2 to give metallic nickel at higher temperatures (up to 600°C).

Figs. 1a–1d show typical electron micrographs of the CNT synthesized: fibers of various diameters. The distribution of CNT over outer diameters exhibits a clearly pronounced peak corresponding to nanotubes

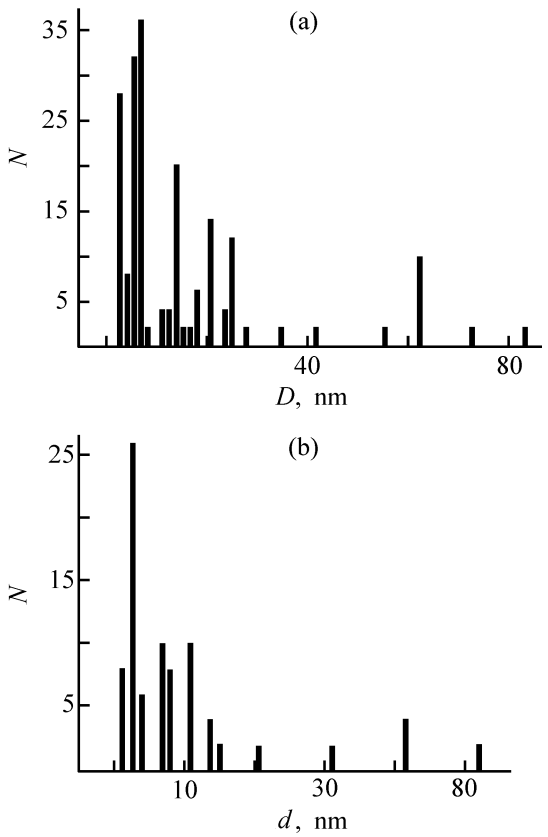


Fig. 2. Distribution of CNT over (a) outer (*D*) and (b) inner (*d*) diameters. (*N*) Number of nanotubes.

with a diameter of about 7 nm. Most of the nanotubes have diameters in the range 5–28 nm, which constitutes 89% of the total amount of the CNT synthesized (Fig. 2a). The diagram of the CNT distribution over inner diameters shows a peak corresponding to nanotubes with an inner diameter of 3 nm. Most of the nanotubes have diameters in the range from 1 to 15 nm, which constitutes 86% of the total amount of nanotubes (Fig. 2b). The minimum outer and inner diameters of the nanotubes are 3 and 1 nm, respectively, and the maximum diameters, 125 and 52 nm.

We may assume that the significant scatter of the diameters of carbon nanotubes, observed in this study, can be accounted for by the mechanism of formation of catalyst nanoparticles of different sizes and shapes on flat undeveloped surfaces of salt crystals. The mechanisms may strongly differ, depending on a technique used to synthesize a catalyst and on the nature of its support. Use of silicas as supports gives a narrower diameter distribution of nanotubes [2]. CNT with diameters of 10–35 nm could be synthesized with a Ni-catalyst supported by silica of the MCM-41 type, and those with diameters in the range 35–52 nm, with a Co-catalyst on the same support. The authors of [2] attributed this behavior to the uniform deposition of the catalysts on the surface of silicon oxide, which is achieved by the application of a method that consists in chemisorption of metal complex compounds, and by the ordered structure of MCM-41 with uniform pores.

The potential advantages of the method of synthesis of carbon nanotubes with water-soluble substrates consist in that the adverse influence exerted by corrosive media in the stage of support separation on the modifying component of nanotubes is eliminated. For example, dissolution of aluminum oxide, on which boron-containing CNT are synthesized, with hydrofluoric acid may lead to a chemical reaction with release of BF_3 and HBF_4 because of the formation of the energetically more favorable B–F bond. Consequently, the content of boron in CNT will decrease under these synthesis conditions, which is undesirable if, e.g., carbon nanotubes are used in lithium capacitors as an active filler. In [11], when creating a nanocomposite material in the form of CNT bimodified with nitrogen and nickel, we separated nanotubes from Al_2O_3 with NaOH under hydrothermal conditions, which was due to the solubility of nickel in acids. According to XPS data, a treatment of a sample with an alkali failed to completely dissolve the matrix and led to the formation of a $NiAl_2O_4$ admixture on the outer surface of CNT. A tendency in the industrial development is application of waste-free technologies. In synthesis of CNT with water-soluble catalyst supports, this goal is achieved by their repeated use in the chemical cycle upon recovery from solution.

CONCLUSION

A method for synthesis of carbon nanotubes with water-soluble catalyst supports was developed. The method allows regeneration of the catalyst supports via their recrystallization from aqueous solutions.

REFERENCES

1. Rakov, E.G., *Usp. Khim.*, 2001, vol. 70, no. 10, pp. 934–973.
2. Katok, K.V., Tertykh, V.A., Pavlenko, A.M., et al., *Magisterium Natsional'nogo universiteta "Kievo-Mogilyanskaya akademiya," Estestvennye nauki* (Magisterium of the "Kiev–Mohyla Academy" National University, Natural Sciences), 2004, issue 16, pp. 75–78.
3. Choi, K.H., Bourgoin, J.P., Auvray, S., et al.,

Surface Sci., 2000, vol. 462, nos. 1–3, pp. 195–202.

4. Cassell, A.M., Verma, S., Delzeit, L., et al., *Langmuir*, 2001, vol. 17, pp. 260–264.
5. Kukovecz, A., Konya, Z., Nagaraju, N., et al., *Phys. Chem. Chem. Phys.*, 2000, vol. 12, no. 13, pp. 3071–3076.
6. Seo, J.W., Couteau, E., Umek, P., et al., *New J. Phys.*, 2003, vol. 5, pp. 120.1–120.22.
7. Lobach, A.S., Spitsyna, N.G., Terekhov, S.V., et al., *Fiz. Tverd. Tela*, 2002, vol. 44, no. 3, pp. 457–459.
8. Rakov, E.G., *Usp. Khim.*, 2000, vol. 69, no. 1, pp. 41–59.
9. Brichka, S.Ya., Prikhod'ko, G.P., Brichka, A.V., et al., *Teor. Eksper. Khim.*, 2002, vol. 38, no. 2, pp. 107–109.
10. Brichka, S.Ya., Prikhod'ko, G.P., Sementsov, Yu.I., et al., *Carbon*, 2004, no. 42, pp. 2581–2587.
11. Brichka, S.Ya., Prikhod'ko, G.P., Brichka, A.V., et al., *Neorg. Mater.*, 2004, vol. 40, no. 12, pp. 1455–1458.

ISSN 1070-4272, Russian Journal of Applied Chemistry, 2006, Vol. 79, No. 8, pp. 1282–1285. © Pleiades Publishing, Inc., 2006.
Original Russian Text © L.Ya. Shteinberg, 2006, published in Zhurnal Prikladnoi Khimii, 2006, Vol. 79, No. 8, pp. 1296–1299.

SORPTION AND ION-EXCHANGE PROCESSES

Effect of Cocatalysts on the Reaction of 4-Nitrobenzoic Acid with Ammonia Catalyzed by Boric Acid

L. Ya. Shteinberg

Institute of Chemical Technology and Industrial Ecology, Scientific and Technical Establishment, Rubezhnoe, Lugansk oblast, Ukraine

Received March 1, 2006

Abstract—The effect of cocatalysts on the reaction of 4-nitrobenzoic acid with ammonia catalyzed by boric acid was studied.

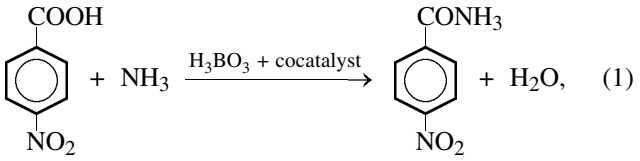
DOI: 10.1134/S107042720608012X

We have shown previously [1] that the system constituted by boric acid and PEG-400 (polyethylene glycol) efficiently catalyzes the formation of 4-nitrobenzamide in the reaction of 4-nitrobenzoic acid with ammonia. The reaction has been studied in various media, and it was suggested that PEG-400 acts as a cocatalyst, forming with boric acid a complex exhibiting enhanced acidity [2].

Since the acidity of boric acid is also enhanced in its interaction with other alcohols [3], it was of interest to examine their effect on the reaction in question.

This study deals with the effect of various cocatalysts on the activity of boric acid in the catalysis of the formation of 4-nitrobenzamide.

As cocatalysts we tested various polyhydric alcohols and polyethylene glycols (PEGs):



where cocatalyst is PEG-400, PEG-13, PEG-1000, PEG-2000, PEG-115, dibenzo-18-crown-6, ethylene glycol, diethylene glycol, triethylene glycol, or glycerol.

The reaction was performed in 1,2,4-trichlorobenzene, which proved to be one of the most convenient solvents ensuring high yield of 4-nitrobenzamide [2]. The cocatalyst performance was judged from the yield of 4-nitrobenzamide under equal other conditions. The results are listed in the table.

As can be seen from the table, not only PEG-400 (run no. 1) but also other PEGs (run nos. 2–7) are effective as cocatalysts. The PEG size affects their performance insignificantly. For example, the molecular weights of the PEGs used vary by more than

Yield of 4-nitrobenzamide in the presence of boric acid and various cocatalysts [solvent 1,2,4-trichlorobenzene, 170–175°C, reaction time 6 h (12 h), molar ratio 4-nitrobenzoic acid : boric acid : cocatalyst 1 : 0.02 : 0.009]

Run no.	Cocatalyst	Yield of 4-nitrobenzamide, %
1	PEG-400	69(97)
2	PEG-13	62(97)
3*	PEG-13	82
4	PEG-1000	45(93)
5	PEG-2000	58(95)
6	PEG-115	73(95)
7*	PEG-115	92
8	Dibenzo-18-crown-6	0
9	Ethylene glycol	0
10	Glycerol	0
11	Diethylene glycol	0
12*	〃	Traces
13	Triethylene glycol	0
14*	〃	60**
15	–	0

* In run nos. 3, 7, 12, and 14, we took 15 mol % cocatalyst and 33 mol % boric acid.

** Total yield of 4-nitropbenzamide and 4-nitrobenzoic acid esters, calculated from the amount of unchanged 4-nitrobenzoic acid. In parentheses are the yields of 4-nitrobenzamide at a reaction time of 12 h.

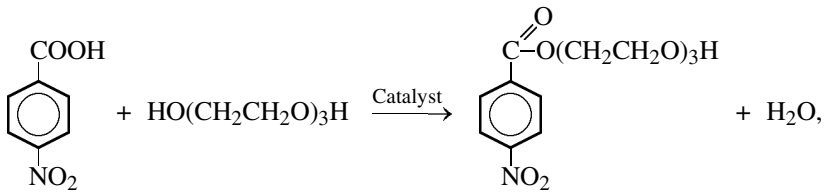
an order of magnitude, whereas the highest and the lowest yields of 4-nitrobenzamide differ by a factor of only 1.6. At the reaction time increased from 6 to 12 h, the yield of 4-nitrobenzamide becomes almost quantitative. The amounts of boric acid and cocatalysts, required to attain a high yield of 4-nitrobenzamide, may vary in a wide range (run nos. 2 and 3 with PEG-13, nos. 6 and 7 with PEG-115).

All the cocatalysts that proved to be effective well solubilize boric acid and are known as phase-transfer catalysts [4]. At the same time, dibenzo-18-crown-6 widely used in phase-transfer catalysis does not ensure formation of 4-nitrobenzamide (run no. 8).

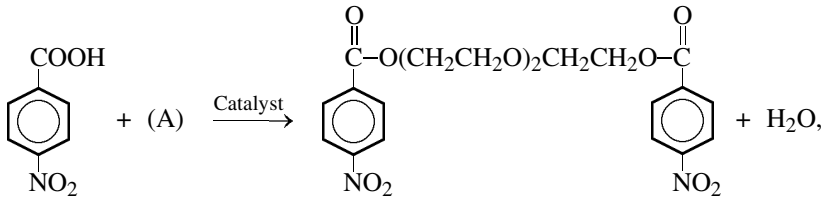
Systems constituted by boric acid and polyhydric alcohols (run nos. 9–11, 13) do not catalyze the reaction either. We, however, did obtain 4-nitrobenzamide with triethylene glycol and boric acid taken in a larger amount (run no. 14). However, one more compound is formed in this case along with the target product (TLC data: 4-nitrobenzoic acid, R_f = 0.54; 4-nitrobenzamide, R_f = 0.18; unknown compound, R_f = 0.82). This mixture melts at a lower temperature (150–170°C) than does 4-nitrobenzamide (mp 196–197°C [5]). The IR spectrum of this mixture contains, along with the 4-nitrobenzamide bands (1660, 3400, 3500 cm^{-1}), also bands at about 1720 and 1280 cm^{-1}, characteristic of esters [6]. Apparently, the product is a mixture of 4-nitrobenzamide and an ester formed from 4-nitrobenzoic acid and triethylene glycol.

It is not improbable that 4-nitrobenzamide is formed by aminolysis of such esters. To verify this assumption, we studied the esterification of 4-nitrobenzoic acid with triethylene glycol in the presence of various esterification catalysts. As solvent we used 1,2,4-trichlorobenzene, with *o*-xylene added to provide removal of the released water by azeotropic distillation. The reaction was performed to complete conversion of 4-nitrobenzoic acid (TLC monitoring); sulfuric acid and tetrabutoxytitanium, previously used for preparing 4-nitrobenzamide [1], were taken as catalysts.

We found that sulfuric acid and, to a lesser extent, tetrabutoxytitanium catalyze the esterification. A TLC analysis showed that, in the presence of sulfuric acid, the spot corresponding to 4-nitrobenzoic acid disappears after the 3-h reaction, and two new spots with R_f = 0.34 and 0.82 appear. In the presence of tetrabutoxytitanium, the reaction is slower; the product with R_f = 0.82 is formed first, and the spot of the starting 4-nitrobenzoic acid disappears only in 7 h, with the appearance of a spot with R_f = 0.34. The bottoms formed on distilling off the solvent contain products with the same R_f values. These products were identified by the IR spectrum as esters. Apparently, 4-nitrobenzoic acid reacts with both hydroxy groups of triethylene glycol to form mono- and diesters:



(2)



(3)

where the catalyst is H_2SO_4 or $Ti(OBu)_4$.

However, bubbling of ammonia for 4 h through the reaction mixture containing 4-nitrobenzoic acid esters did not give 4-nitrobenzamide (TLC analysis). Apparently, catalysis by the system constituted by boric acid and triethylene glycol is weak, and 4-nitrobenzamide is formed directly by the reaction of ammonia with 4-nitrobenzoic acid, rather than with its triethylene glycol esters.

The low performance of polyols as cocatalysts suggests that the formation of an acidic complex from

boric acid and an alcohol is not the decisive factor of the catalysis in contrast to what has been assumed previously [2].

It is known [3] that alcohols reacting with boric acid favor its extraction from aqueous solutions into low-polarity organic phases, such as toluene, decane, and *o*-xylene. Low-molecular-weight polyols, which are readily soluble in water, hardly promote the transfer of boric acid into low-polarity solvents. It is not improbable that, in the synthesis of 4-nitrobenzamide too, polyols, in contrast to PEGs, solubilize boric acid in 1,2,4-trichlorobenzene only weakly, and the catalysis becomes inefficient.

The amidation actually occurs in a multiphase system consisting of gaseous ammonia, a low-polarity solvent, and 4-nitrobenzoic and boric acids, which are poorly soluble in this solvent. Apparently, the added PEG initially forms an ester with boric acid, which is more soluble in the low-polarity medium and is the true amidation catalyst:

$$\rangle B{-}OH + H(OCH_2CH_2)_nOH \rightarrow \rangle B{-}O(CH_2CH_2O)_nH + H_2O. \quad (4)$$

At the same time, the role of PEG is hardly restricted to the solubilization of boric acid. We have shown previously [1] that tetrabutoxytitanium, which is readily soluble in nonpolar solvents, also catalyzes the synthesis of 4-nitrobenzamide only in the presence of PEG-400.

The boric acid ester formed can solubilize other molecules (ammonia, 4-nitrobenzoic acid, its ammonium salt) and play the role of a microreactor of a sort, forming a microphase with a high concentration of the reactants adsorbed on the PEG chain [7]. Boric acid can act as a center binding both the reactants and PEG molecules [8].

It is not improbable that other active catalysts of 4-nitrobenzamide synthesis (tetrabutoxytitanium, dimethyl hydrogen phosphite, phosphoric and phosphorous acids [1]) also form esters with PEG, which are subsequently involved in the catalysis.

The absence of free hydroxy groups capable of the reaction with boric acid and the high selectivity to the size of the transferred particles [9] can be responsible for the low catalytic activity of dibenzo-18-crown-6 in the synthesis of 4-nitrobenzamide.

EXPERIMENTAL

4-Nitrobenzoic and boric acids, *o*-xylene, 1,2,4-trichlorobenzene, ethylene glycol, diethylene glycol, triethylene glycol, tetrabutoxytitanium, ammonia, and PEG-400 were purified and used as described in [1, 2]. The other PEGs, dibenzo-18-crown-6, and sulfuric acid (technical and pure grade) were used without additional purification. Glycerol was dried over sodium sulfate and vacuum-distilled.

A chromatographic analysis of the mixtures and evaluation of the product purity were performed on Silufol UV-254 plates, eluents acetone–hexane and acetone–chloroform, development in the UV light. The IR spectra were recorded on a UR-20 spectrometer (KBr pellets). The procedures for the synthesis of 4-nitrobenzamide, analysis of the mixtures, and evaluation of the product purity were the same as in [1]; an additional amount of the target product was isolated from the reaction mixture by distilling off the solvent in a vacuum. Unchanged 4-nitrobenzoic acid was isolated by evaporation of the ammonia mother liquor to 10 ml, acidification with concentrated HCl to pH 1, filtration, and washing of the precipitate with 10 ml of water.

The esterification was performed in the amidation installation as follows. 4-Nitrobenzoic acid (2.0 g, 12.0 mmol), triethylene glycol (1.9 g, 12.7 mmol), and sulfuric acid (0.03 g, 0.3 mmol) or tetrabutoxytitanium (0.1 g, 0.3 mmol) were heated to 160–165°C in 30 ml of trichlorobenzene containing *o*-xylene; the *o*-xylene–water azeotrope was distilled off using a Dean–Stark trap. The reaction was performed until 4-nitrobenzoic acid was fully consumed (TLC monitoring). After that, the temperature was elevated to 170–175°C, and ammonia was bubbled for 4 h.

CONCLUSIONS

(1) The system constituted by boric acid and polyethylene glycol (PEG-400, PEG-13, PEG-115, PEG-1000, PEG-2000) is an effective catalytic system for synthesis of 4-nitrobenzamide by the reaction of 4-nitrobenzoic acid with ammonia.

(2) The effect of polyethylene glycols as cocatalysts is specific. Lower polyols and dibenzo-18-crown-6 used instead do not ensure formation of 4-nitrobenzamide.

(3) Triethylene glycol esters of 4-nitrobenzoic acid do not transform into 4-nitrobenzamide under the reaction conditions.

REFERENCES

1. Shteinberg, L.Ya., *Zh. Org. Khim.*, 2003, vol. 39, no. 7, pp. 1033–1036.

2. Shteinberg, L.Ya., *Zh. Prikl. Khim.*, 2005, vol. 78, no. 10, pp. 1745–1747.
3. Shvarts, E.M., *Vzaimodeistvie bornoi kisloty so spirtami i oksikislotami* (Reaction of Boric Acid with Alcohols and Hydroxy Acids), Riga: Zinatne, 1990.
4. Gol'dberg, Yu.Sh., *Izbrannye glavy mezhfaznogo kataliza* (Selected Chapters on Phase-Transfer Catalysis), Riga: Zinatne, 1989.
5. USSR Inventor's Certificate, no. 127 657, 1960.
6. Bellamy, L.J., *The Infra-Red Spectra of Complex Molecules*, New York: Wiley, 1957.
7. Pomogailo, A.D., *Polimernye immobilizovannye metallokompleksnye katalizatory* (Polymeric Immobilized Coordination Catalysts), Moscow: Nauka, 1988.
8. *Polymeric Reagents and Catalysts*, Ford, W.T., Ed., Washington: Amer. Chem. Soc, 1986. Translated under the title *Polimernye reagenty i katalizatory*, Ford, U.T., Ed., Moscow: Khimiya, 1991.
9. *Phase-Transfer Catalysis. New Chemistry, Catalysts, and Applications*, Starks, Ch.M., Ed., Washington, D.C.: Amer. Chem. Soc., 1987. Translated under the title *Mezhfaznyi kataliz: Khimiya, katalizatory i primenenie* (Phase-Transfer Catalysis: Chemistry, Catalysts, and Applications), Starks, Ch.M., Ed., Moscow: Khimiya, 1991.

ISSN 1070-4272, Russian Journal of Applied Chemistry, 2006, Vol. 79, No. 8, pp. 1286–1290. © Pleiades Publishing, Inc., 2006.
Original Russian Text © V.V. Tarasov, N.F. Kovalenko, N.E. Kruchinina, S.A. Shilin, 2006, published in Zhurnal Prikladnoi Khimii, 2006, Vol. 79, No. 8, pp. 1300–1304.

PROCESSES AND EQUIPMENT OF CHEMICAL INDUSTRY

Model of Heterogeneous Hydrodynamic Coagulation of Microdrops

V. V. Tarasov, N. F. Kovalenko, N. E. Kruchinina, and S. A. Shilin

Mendeleev Russian University of Chemical Technology, Moscow, Russia

Received October 5, 2005; in final form, January 2006

Abstract—The Eley–Rideal and Langmuir concepts of surface reactions were used to develop a model of heterogeneous hydrodynamic coagulation of diluted "oil-in-water" emulsions (0.1–2.0 vol %). The mathematical model was verified, and factors that govern the coagulation rate were revealed.

DOI: 10.1134/S1070427206080131

Coagulation and flocculation [1] are widely used in practice for purification of wastewater to remove dispersed particles. Recently, the method of heterogeneous hydrodynamic coagulation (HHC) has been receiving a large development effort because its use can markedly raise the drop size in emulsions stable against sedimentation and accelerate their separation by a factor of 100–200. The HHC procedure and the apparatus used were described in [2, 3]. The same publications described a method for preparation of emulsions comparatively stable against sedimentation, whose light absorption decreased by no more than 10–15% per day. In [2], basic kinetic data, used in the present study to verify the model developed, were obtained.

The HHC mechanism is based on the Deryagin–Landau–Verwey–Overbeek (DLVO) theory [4]. The kinetic energy of correctly organized emulsion flows favors overcoming of potential barriers in the DLVO curve [4], which accelerates the coagulation process. Adsorption of droplets on the apparatus walls probably leads to formation of large droplet aggregates (clusters). A part of a cluster grown is split-off under the action of incident vortices (pulsations). In our opinion, the maternal part of the cluster is smaller in size than the split-off daughter part. Having become not attached to wall, the latter comes under the influence of the Archimedes force and ascends into the comparatively "quiet" part of the fluid in the apparatus. As a result, a certain part of coarsened clusters is removed from the HHC process in the form of transparent (in the case of coalescence) or nontransparent (in the absence of coalescence) drops. The walls and other immobile parts of the apparatus "work" as size converters: small drops arrive to leave coarse.

The aim of our study was to develop a mathematical model of HHC and verify its validity.

EXPERIMENTAL

We used as fluids being dispersed Midel 7131 transformer oil, I-40 machine oil, olive oil, and decane [5].

It is reasonable to assume that the stage of adsorption of microdrops on a solid surface is a necessary stage of HHC. Coagulation becomes a rather probable process because flows of droplets attack at a high velocity the surface of a solid, especially in the case when they have a considerable affinity to this surface. Presence of coarse drops of a second organic solvent facilitates coagulation. Coarse drops can even lead to disappearance of the latent period frequently accompanying the development of HHC. In this study, we considered the process of surface coagulation without any additional solvent. In our opinion, the mechanism suggested includes the following stages [2]: formation of guiding (nucleating) centers from microdrops, surface coagulation of fine drops with the guiding centers, interaction of the guiding centers with coarse drops (coalescence) or with pulsations of the moving fluid, detachment of coarsened drops or drop clusters from the solid surface, and secondary disintegration of coarsened drops or decomposition of drop clusters. The last of the processed listed above is undesirable and should be minimized.

Figure 1 shows how guiding centers are formed and "grown" coarse drops are detached from these centers under attack by other drops or fluid pulsations. The interaction of an adsorbed drop with a drop that attacks the former from the bulk is the basis for further consideration or the so-called Eley–Rideal process.

Formation of clusters from a set of droplets is an energetically favorable process because the droplets associate to form contacts with one another. This leads to a decrease in the free surface energy. Let us use the Eley–Rideal concepts based on the Langmuir theory, which have already been successfully used in description of the kinetics of surface reactions [6, 7]. We mean the so-called SV mechanism: the interaction between a droplet (molecule) in the adsorbed state and a droplet (molecule) incident from the bulk [6, 7]:

$$r = \mathrm{d}x/\mathrm{d}t = -kax\theta = -kaxx/(x + b) = -kax^2/(x + b). \quad (1)$$

Let us consider the irreversible process. The mass rate of the process, r, has dimensionality of grams per square centimeter per second. We assume that the rate at which the drop concentration x decreases is proportional to the concentration itself, to the fraction θ of the surface of walls of flown-around solid bodies (dimensionless), occupied by adsorbed drops, and to the specific surface area a of contact between the phases (cm^{-1}). The rate constant k has dimensionality of the mass-transfer coefficient ($cm\ s^{-1}$).

The quantity k is constant only in the particular case of the kinetic mode. In the transition and diffusion modes, the rate coefficient k is not a constant, being a function of the hydrodynamic conditions, $k = f(\mathrm{Re}, \mathrm{Sc})$. The dimensionless quantity θ is calculated by the Langmuir isotherm equation.

Let us consider the first case, when the adsorption of drops on the solid surface is strong. In this case, $b \ll x$ (b is a coefficient having dimensionality of the mass concentration of drops, $g\ cm^{-3}$). Then, $r = \mathrm{d}x/\mathrm{d}t = -kax$. Integrating over the interval from x_0 to x, we obtain

$$-\ln(x/x_0) = kat \quad \text{or} \quad \ln(x_0/x) = kat. \quad (2)$$

In the second case of $b \gg x$ at any t, when the adsorption of droplets is very weak,

$$r = \mathrm{d}x/\mathrm{d}t = -kax\theta = -kab^{-1}x^2, \quad (3)$$

$$(x^{-1} - x_0^{-1}) = kab^{-1}. \quad (4)$$

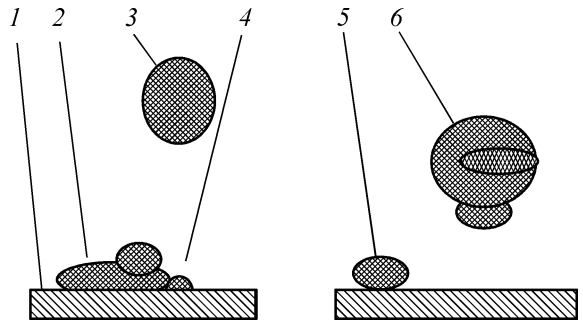


Fig. 1. Schematic of the attack on a guiding center of coagulation by a coarse drop: (*1*) Solid, (*2*) guiding center (drop or droplet cluster), (*3*) attacking drop of an organic substance, (*4*) microscopic droplet, (*5*) residue of the guiding center, and (*6*) detached coagulate (cluster).

At a direct proportionality between x and A we have

$$(A^{-1} - A_0^{-1}) = ka\alpha^{-1}b^{-1}t, \quad (5)$$

where A and A_0 are the colorimetrically measured light absorptions.

In this case, both parts of the equality are dimensionless. It is the dimensionless equation of this kind that is convenient for use. The coefficient α has a dimensionality inverse to that of b.

In the third case of the same model, when none of the terms of the Langmuir denominator can be neglected (which frequently occurs in experiments), we have the equation

$$\ln(A_0/A) + \alpha b(A^{-1} - A_0^{-1}) = kat. \quad (6)$$

The quantity ka has dimensionality of inverse time (s^{-1}). All the terms of Eq. (6) are also dimensionless.

The linearity in the coordinates $\ln(A_0/A) + \alpha b(A^{-1} - A_0^{-1}) = f(t)$ indicates that, on the one hand, the HHC mechanism is valid, and, on the other, αb is close to unity. It is known that, in a homogeneous process, the coagulation rate constant is independent of the hydrodynamics and the equation has a simple form [8]:

$$c^{-1} - c_0^{-1} = -(K_0/2)t, \quad (7)$$

where $c^{-1} - c_0^{-1}$ is the difference of the inverse running and initial concentrations.

In this case, the coagulation rate constant is well described by the dependence $K_0 = 8k_BTc_c/3\mu$ [8],

Table 1. Experimental values of light absorption A in extraction of "oil" emulsion droplets at varied rotation speed n of 10 smooth discs

n, rpm	Olive oil		I-40 oil		Midel 7131		Decane	
	τ, min	A	t, min	A	τ, min	A	t, min	A
2200	0.0	1.05	0.0	1.00	0.0	1.20	0.0	1.20
	3.5	0.89	3.0	0.85	5.0	0.57	2.0	0.45
	7.5	0.75	7.0	0.68	10.0	0.40	7.0	0.25
	15.0	0.62	15.0	0.46	15.0	0.37	15.0	0.21
1100	0.0	1.02	0.0	0.95	0.0	1.20	0.0	0.89
	3.5	0.90	3.0	0.88	5.0	0.70	2.0	0.45
	7.5	0.80	7.0	0.80	10.0	0.52	7.0	0.28
	15.0	0.67	15.0	0.66	15.0	0.44	15.0	0.22
700	0.0	1.05	0.0	1.05	0.0	1.10	0.0	1.20
	3.5	0.96	3.0	0.98	5.0	0.85	2.0	0.90
	7.5	0.89	7.0	0.90	10.0	0.68	7.0	0.59
	15.0	0.81	15.0	0.80	15.0	0.59	15.0	0.40
500	0.0	1.00	0.0	0.96	0.0	1.10	0.0	0.82
	3.5	0.96	3.0	0.93	5.0	0.95	2.0	0.71
	7.5	0.92	7.0	0.90	10.0	0.85	7.0	0.58
	15.0	0.86	15.0	0.85	15.0	0.78	15.0	0.46
400	0.0	1.02	0.0	0.93	0.0	1.05	0.0	1.00
	3.5	0.98	3.0	0.91	5.0	0.95	2.0	0.93
	7.5	0.95	7.0	0.90	10.0	0.88	7.0	0.83
	15.0	0.91	15.0	0.88	15.0	0.85	15.0	0.71

where k_B is the Boltzmann constant; T, absolute temperature; and $c_c \approx 1$, effective concentration. Thus, the equations of heterogeneous hydrodynamic coagulation, (4) and (5), and the equation of homogeneous coagulation, (7), are identical in form, but have coefficients with different physical meanings.

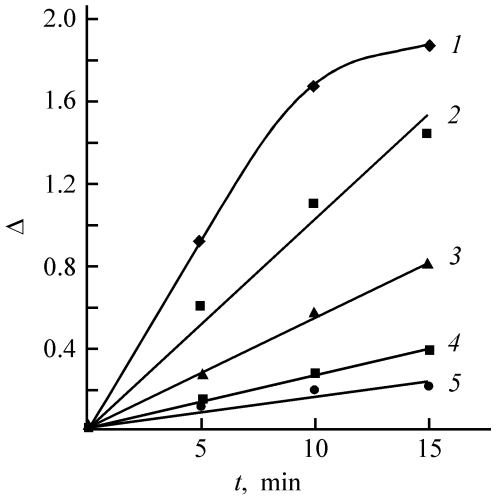


Fig. 2. Dependence $\Delta = f(t)$ in the case of coagulation of a microscopic emulsion of Midel 7131 fluid. (t) Coagulation time. Rotation speed of discs (rpm): (*1*) 2200, (*2*) 1100, (*3*) 700, (*4*) 500, and (*5*) 400.

Verification of the SV model. The relative root-mean-square deviation of the results obtained (Δ) was 12%, which points to a sufficiently good reproducibility. The basic model is verified using the data of [2]. Equations (4) and (5) make it possible to check the simplest coordinate metrics, which will be further named the plot of the Δ–t function. If the HHC concepts developed are correct, the kinetic curves will be straight lines in the coordinates $\Delta = (A^{-1} - A_0^{-1}) = (\alpha^{-1}b^{-1}ka)t$. It is important that there should not occur any repeated disintegration of drops. Such a situation is possible at degrees of purification of about 70–75%.

Let us use Table 1, which was compiled using the data of [2]. Table 1 lists all the quantities necessary for verifying the model. In addition, it contains the quantity n, rotation speed of a rotor with discs (rpm). The data of Table 1 are represented by the linear plots $\Delta = (A^{-1} - A_0^{-1}) = (\alpha^{-1}b^{-1}ka)t$, which indicates that the model is correct and the SV mechanism is valid [Eqs. (4), (5)].

In Fig. 2, the functions $\Delta = f(t)$ are plotted for the Midel 7131 fluid at all disc rotation speeds listed in Table 1.

Table 2. Cumulative data on the kinetics of HHC of various emulsions in relation to the rotor rotation speed n

n, rpm	Equation for the HHC rate			
	olive oil	I-40 oil	Midel 7131	Decane
400	$\Delta = 0.0038t$, $R^2 = 0.956$	$\Delta = 0.0077t$, $R^2 = 0.979$	$\Delta = 0.0184t$, $R^2 = 0.997$	$\Delta = 0.0262t$, $R^2 = 0.996$
500	$\Delta = 0.0088t$, $R^2 = 0.996$	$\Delta = 0.0107t$, $R^2 = 0.998$	$\Delta = 0.0248t$, $R^2 = 0.995$	$\Delta = 0.0622t$, $R^2 = 0.994$
700	$\Delta = 0.0198t$, $R^2 = 0.995$	$\Delta = 0.0185t$, $R^2 = 0.983$	$\Delta = 0.0531t$, $R^2 = 0.997$	$\Delta = 0.1106t$, $R^2 = 0.988$
1100	$\Delta = 0.0309t$, $R^2 = 0.996$	$\Delta = 0.0340t$, $R^2 = 0.991$	$\Delta = 0.0962t$, $R^2 = 0.987$	Nonlinear
2200	$\Delta = 0.0793t$, $R^2 = 0.994$	$\Delta = 0.044t$, $R^2 = 0.983$	Nonlinear	"

As expected, we have for olive oil and I-40 oil straight lines that pass through the origin of coordinates in the whole interval of t, whereas in the case of decane, such a linearity is only observed up to $A < 1.5$ (not shown in Fig. 2). This can be attributed to reversibility of the process and to secondary disintegration. It is noteworthy that, while the value of Δ is lower than 1.4–1.6, the $\Delta = f(t)$ plots are linear. This fact is particularly clearly manifested for the emulsion of Midel 7131 fluid (Fig. 2) and in the case of the decane–water system. In the case of Midel 7131, only a single line, and specifically the steepest, is abruptly curved after $\Delta = 1.6$, which corresponds to a degree of purification to remove drops as high as 70%. The confidence factors of the approximation of plots like those shown in Fig. 2 are very close to unity, which points to a good adequacy of the SV model.

The slope of the $\Delta = f(t)$ plots is the HHC rate coefficient. This slope depends on the disc rotation rate, which points to the diffusion and transition modes.

Table 2 lists the results of processing of kinetic curves by Eq. (5) for all the four fluids. The aim of this processing is to find a full set of equations for the HHC rate. The confidence factors of the approximation lie in the interval $R^2 = 0.994 - 0.956$. It is clear from the data obtained that there is a linear relationship between the HHC rate coefficient and the disc rotation speed (Fig. 3).

We obtained, instead of straight lines in log–log coordinates (observed in the case of mass-transfer processes), straight lines in the natural coordinates φ–n, where n is the disc rotation speed, and φ, the slope of the $\Delta = f(t)$ plot. The HHC rate coefficients were too strongly dependent on the rotor rotation speed. Presumably, the HHC rate coefficients reflect, in contrast to the rate constants of homogeneous coagulation, not only the physical properties of fluids, but also the inertia properties of elements of the fluids, including "oil" drops. This is the principal distinctive feature of the concepts of the HHC kinetics, we developed, from those described by Fuks and Reist [8] and recommended for consideration of the kinetics of homogeneous coagulation.

If we use the known criterial equations that relate the Sherwood numbers to the Reynolds and Schmidt numbers, in an attempt to find the parametric sensitivity p in the equation $\mathrm{Sh} = \mathrm{const}\,\mathrm{Re}^p\mathrm{Sc}^q$, then we obtain too high values of p, up to 2.90 in the case of I-40 oil. Generally speaking, we never obtained p values lower than 1.05. Such a behavior is not characteristic of "purely diffusion" processes, for which p is in the range 0.5–0.8. Consequently, the HHC rate coefficients should be regarded as integrated factors reflecting both the physicochemical (molecular) and hydrodynamic (inertia) properties of the systems.

Thus, we obtained a definite proof that the SV model is valid. Its natural limitation is that it disregards the reversibility of the process, manifested in the repeated disintegration of drops. This disintegration can be accounted for by an additional term in the differential equation (1); however, this complicates the simple form of the analytical equation.

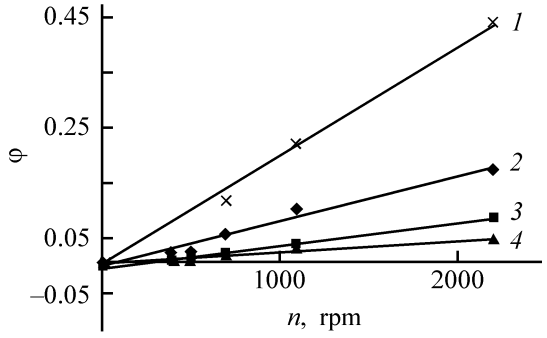


Fig. 3. Slope φ of the functions $\Delta = f(t)$ vs. the disc rotation speed n. Type of emulsion: (*1*) decane, (*2*) Midel 7131, (*3*) I-40 oil, (*4*) olive oil.

CONCLUSIONS

(1) A mathematical model of the kinetics of heterogeneous hydrodynamic coagulation of emulsions with particle size of 1–5 μm and concentration of 0.1–2.0 vol % was developed.

(2) The mathematical model of the kinetics of heterogeneous hydrodynamic coagulation was constructed on the basis of Eley–Rideal equations which coincide in form with the kinetic equations of homogeneous coagulation, but have coefficients with a different physical meaning.

(3) A strong, untypical of mass-transfer processes, dependence of the kinetics of heterogeneous hydrodynamic coagulation on the flow velocities of the emulsions being separated relative to the apparatus walls was found.

REFERENCES

1. *Coagulation and Flocculation: Theory and Applications*, Dobias, B., Ed., New York: Marcel Dekker, 1993.
2. Dudko, K.V., Ogunmoela, T.O., and Tarasov, V.V., *Uspekhi v khimii i khimicheskoi tekhnologii* (Advances in Chemistry and Chemical Technology), Moscow: Ross. Khim. Tekhnol. Univ., 2003, vol. 17, no. 12(37), pp. 36–46.
3. Tarasov, V.V., Dudko, K.V., and Dobrokhlop, K.A., *Nauchnaya sessiya MIFI – 2004: 3-e nauchno-innovatsionnoe sotrudnichestvo: Sbornik nauchnykh trudov* (Scientific Session of the Moscow Institute of Engineering Physics in 2004: 3rd Scientific-Innovational Collaboration: Coll. of Sci. Works), Moscow, 2004, part 1, pp. 69–70.
4. Deryagin, V.V., *Teoriya ustoichivosti kolloidov i tonkikh plenok* (Stability Theory of Colloids and Thin Films), Moscow: Nauka, 1986.
5. Tarasov, V.V., Kruchinina, N.E., Shilin, S.A., and Shchedrova, N.I., *Zh. Prikl. Khim.*, 2006, vol. 79, no. 6, pp. 954–957.
6. Tarasov, V.V., Yagodin, G.A., and Pichuginyu, A.A., *Kinetika ekstraktsii neorganicheskikh veshchestv. Itogi nauki i tekhniki: Neorganicheskaya khimiya* (Kinetics of Extraction of Inorganic Substances, Advances of Science and Technology: Inorganic Chemistry), Moscow: VINITI, 1984.
7. Tarasov, V.V. and Yagodin, G.A., *Ion Exchange and Solvent Extraction*, New York: Marcel Dekker, 1988, pp. 141–223.
8. Reist, P.C., *Introduction to Aerosol Science*, New York: MacMillan, 1984.

ISSN 1070-4272, Russian Journal of Applied Chemistry, 2006, Vol. 79, No. 8, pp. 1291–1296. © Pleiades Publishing, Inc., 2006.
Original Russian Text © L.S. Litvinova, N.G. Bel'nikevich, 2006, published in Zhurnal Prikladnoi Khimii, 2006, Vol. 79, No. 8, pp. 1305–1310.

MACROMOLECULAR CHEMISTRY AND POLYMERIC MATERIALS

A Study of the Relationship between the Thermodynamic Quality of Mobile Phases and Their Strength for the Critical Conditions of Liquid Chromatography of Polystyrenes

L. S. Litvinova and N. G. Bel'nikevich

Institute of Macromolecular Compounds, Russian Academy of Sciences, St. Petersburg, Russia

Received March 9, 2006

Abstract—The relationship between the thermodynamic quality of mobile phases and their strength ε was studied for the critical conditions of liquid chromatography. The chromatography of reference polystyrene samples was carried out in the adsorption and exclusion modes, and also under critical conditions, with binary mobile phases and a silica gel column used. The thermodynamic quality of solvent mixtures with respect to one another was evaluated by the intrinsic viscosity [η].

DOI: 10.1134/S1070427206080143

Liquid chromatography under critical conditions (LCCC) is a promising method for analysis of polymers with various types of molecular polydispersity. A common LCCC strategy is to suppress the separation selectivity for one of molecular characteristics (usually, molecular weight), which provides separation by another parameter [1–11].

An important specific feature of LCCC is the necessity for fine adjustment of interactions within the system. This is achieved by careful selection of both mobile and immobile phases for the polymer systems studied and by varying the temperature of the experiment. Another distinctive feature of LCCC is that mixed solvents are used as mobile phases. As a rule, this is a mixture of adsorption-active and adsorption-inactive solvents. Thus, ternary polymer systems (a polymer in a binary solvent) are widely used in LCCC.

In liquid chromatography, the distribution coefficient K_d is related to a change in the Gibbs energy ($-\Delta G$) for polymer–solvent–adsorbent systems [1, 12]:

$$-\Delta G = RT \ln K_d = -\Delta H + T\Delta S, \qquad (1)$$

where $-\Delta H$ is a change in the enthalpy; ΔS, change in entropy upon transition of a macromolecule from the interparticle (free) volume into the immobile phase; T, temperature (K); and R, gas constant.

It follows from Eq. (1) that $\Delta H = T\Delta S$ for $K_d = 1$. Consequently, the change in the entropy at the critical point, when a macromolecule passes from solution into the adsorbent, is compensated for by a change in the enthalpy corresponding to the interaction between the macromolecule and active centers of the adsorbent.

It is important that the critical conditions can be created for the same polymer–adsorbent combination in mixtures of different solvents.

Because a macromolecule competes with solvent molecules for the active centers of the adsorbent, changes in the macromolecule–adsorbent interactions are due to a change in the interaction between the mobile phase and the adsorbent, provided that the system is in equilibrium. The interaction of the mobile phase with the adsorbent and the polarity of the former can be evaluated using Snyder's parameters: solvent strength ε^0 [13] and polarity index P' [14].

A specific feature of polymers is that the molecular conformation (i.e., intramolecular interactions determining the coil size in solution) depends on properties of a solvent, specifically, on its thermodynamic quality. It can be assumed that the conformational changes in solution, which can be evaluated by the intrinsic viscosity [η] [15], may be a reason for changes in the chromatographic behavior of macromolecules.

Table 1. Mark–Kuhn–Hauwink parameters K and α, Snyder's parameters P' and ε^0, and values of the Flory–Huggins constant χ and of the second virial coefficient A_2 for individual solvents

Solvent	α [16]	$K \times 10^3$, ml g^{-1}, [16]	T, °C	P' [14]	$\varepsilon^{0*}_{SiO_2}$ [13]	χ [16]	$A_2 \times 10^4$, mol cm^3 g^{-2} [16]
MEK	0.64	17.1	35	4.7	0.39	0.491	1.00
	0.635	19.5	25				
THF	0.713	12.5	25	4.0	0.346	0.4645	4.00
Toluene	0.71	12.6	35	2.4	0.22	0.456	3.29
	0.71	13.4	25				
CCl_4	0.7	15	25	1.6	0.139	0.463	2.60
Cyclohexane	0.5	82	34	0.2	0.031	0.5	0.93 (35°C)
	0.5	76	35				

* $\varepsilon^0_{SiO_2} = 0.77\varepsilon^0_{Al_2O_3}$.

Thus, the chromatographic system is sufficiently fully described in analysis of polymers by three parameters: K_d, [η], and ε (where ε is the strength of a mixture of solvent), which are accessible both to evaluation or measurement and to study of their mutual influence. The critical conditions with constant K_d are ideally suitable for analysis of the mutual influence of the parameters ε and [η]. The best suitable object for a study of this kind is a model polymer, polystyrene (PS), for which the thermodynamic quality of individual solvents has been long and thoroughly studied [16] (Table 1).

It should be noted that, recently, there have been reports in which different concepts concerning the relationship between the thermodynamic quality of a mixed solvent and its strength under dynamic conditions were presented. For example, it has been shown previously that, in LCCC, the polarity of binary mobile phases, necessary for reaching the point of enthalpy-entropy compensation, increases as the thermodynamic quality of such mobile phases is improved [17–19]. In these studies, the thermodynamic quality of a solvent was evaluated by the intrinsic viscosity, with the polarity of solvent mixtures described by Snyder's polarity index P' [14].

When studying the chromatographic behavior of PS on silica gel in mixed mobile phases composed of a solvent and a precipitating agent (hexane), the authors of [20, 21] came to a conclusion that the critical conditions cannot be related to the thermodynamic property of mobile phases, specifically, to values of the Mark–Kuhn–Hauwink parameter α. They also compared the solution strengths ε, calculated for critical formulations by an empirical formula [21], with the hydrodynamic radii of the molecules. When analyzing the results mentioned above, Macko and Hunkeler also noted that the critical conditions are independent of the thermodynamic quality of a solvent.

Thus, in view of the wide variety of opinions concerning the influence of the thermodynamic quality of a solvent on the energy characteristics of the polymer–adsorbent interaction in LCCC conditions, we found it appropriate to carry out an additional study.

EXPERIMENTAL

We used reference PS samples (Waters Co,) with molecular weights M of 1.4 to 2600 kg mol^{-1} ($M_w/M_n \le 1.1$, where M_w is the mass-average molecular weight, and M_n, number-average molecular weight) and PS samples with M of 120 and 460 kg mol^{-1} ($M_w/M_n \le 1.15$).

As reference samples in thin layer chromatography (TLC) served polynuclear aromatic hydrocarbons: benzo[α]pyrene (98%, Fluka Chemie, Switzerland), chemically pure scintillation naphthalene (Reakhim), and coronene (99%, Aldrich).

As solvents were used cyclohexane ("for spectroscopy" grade, Merck, Darmschtadt, Germany), pure carbon tetrachloride, analytically pure toluene, and pure methyl ethyl ketone (MEK) (Reaktiv, St. Petersburg, Russia), all of which were additionally purified by distillation. Tetrahydrofuran (Reaktiv) was distilled over KOH immediately prior to use.

Liquid chromatography was performed on a KhZh-1309 microcolumn chromatograph equipped with refractometric and photometric detectors. The results of analysis were recorded and processed using the Mul'tikhrom software (Ampersend, Russia). Mixed mobile phases were prepared by weighing components with an accuracy of no less than 0.1%.

Table 2. Chromatographic data for PS with M = 1.6–2600 kg mol^{-1}, Snyder's parameters for solvent mixtures, and viscometric data for PS with M = 120 and 460 kg mol^{-1}

Solvent mixture	Composition of the mobile phase at the critical point	Snyder parameters		[η], dl g^{-1}, for PS with indicated M, kg mol^{-1}	
		P'	ε	460 (25°C)	120 (35°C)
Toluene/CCl_4	39.89/60.11	2.04	0.220	1.15	0.48
Cyclohexane/Toluene	21.02/78.98	1.89	0.215	1.14	0.48
CCl_4/MEK	99.70/0.30	1.60	0.141	1.15	0.48
Cyclohexane/MEK	89.76/10.24	0.65	0.082	0.66	0.35
Cyclohexane/THF	88.58/11.42	0.58	0.091	0.71	0.35

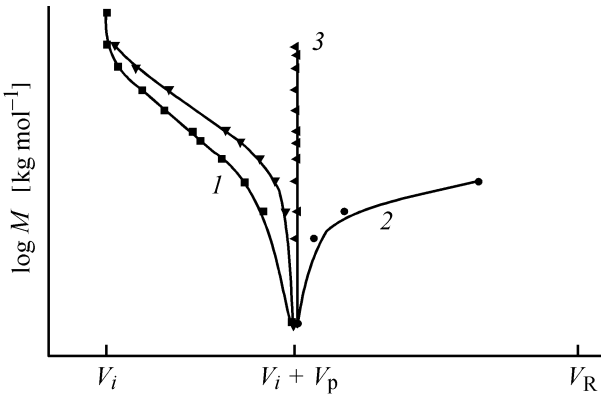
A 0.5 × 300 mm fluoroplastic column packed with Biospher psi 300 spherical silica gel with a particle size of 5 μm (Labio, Prague, Czechia) was equipped with a water jacket. The column temperature was maintained at 35 ± 0.05°C with a water thermostat. The concentration of PS samples dissolved in the corresponding mobile phase and introduced into the column was 1 mg ml^{-1}; sample volume, 0.1 μl, flow rate of the mobile phase, 4 μl min^{-1}.

The thin layer chromatography was performed on 10 × 10 cm Sorbfil and PTSKh-AF-V-UF (Sorbpolimer, Krasnodar, Russia) plates. After the plates were activated at 105°C for 45 min, solutions of the test compounds in hexane (1 mg ml^{-1}) were deposited with a calibrated capillary (1 μl) (Camag, Switzerland) at a distance of 1 cm from the plate edge. The chromatography was performed in a saturated or unsaturated N-chamber containing 10 ml of a mobile phase (hexane or mixed solvents of composition listed in Table 2). UV_{254} and UV_{366} lamps were used detect the chromatographic zones of polynuclear hydrocarbons. The error of R_F determination (relative standard deviation) did not exceed 5% at n = 3 repetitions.

The intrinsic viscosity [η] of PS solutions in mixed solvents (including the LCCC compositions) was measured by the standard method [22] in a capillary Ubellohde viscometer at 25 ± 0.05 and 35 ± 0.05°C. The outflow time of the solvent was no less than 100 s. PS samples were dissolved in solvent mixtures obtained by mixing the starting components in various volume ratios.

We used five different solvents for PS. Their ability to enhance or hinder PS adsorption was determined in a set of preliminary experiments by TLC. Cyclohexane and CCl_4 were chosen as solvents that favor PS adsorption, whereas THF, MEK, and toluene were used to suppress PS adsorption. Tetrahydrofuran, CCl_4, and toluene are good solvents for PS [16]. The quality of MEK is somewhat poorer [16], and cyclohexane is a theta-solvent at 35°C. Some parameters of the solvents used in the study are listed in Table 1.

We obtained dependences in the log M–V_R (V_R is the retained volume) for the cases of adsorption, exclusion, and critical conditions for various compositions of binary mobile phases. The calibration dependences for the three modes of liquid chromatography are shown schematically in the figure. The critical conditions were determined for five different mobile phases: toluene/CCl_4, cyclohexane/toluene, cyclohexane/THF, cyclohexane/MEK, and CCl_4/MEK. Mixtures composed of a solvent and a precipitating agent were not used in order to prevent occurrence of the precipitation chromatographic mode, because ambiguous results would be obtained otherwise. In all cases, the fact that the critical composition was reached was confirmed graphically by the point of



Schematic of calibration dependences in the log M–V_R coordinates for three modes of liquid chromatography: (*1*) exclusion, (*2*) adsorption, and (*3*) critical. (V_i) Interparticle (or dead) volume, (V_p) pore volume, and (V_R) retained volume.

intersection of the dependences of the retained volume on the composition of the mobile phase [23].

It should be particularly emphasized that the attainment of critical conditions itself is presumably determined by the thermodynamic property of the solvent: the higher the quality of a solvent, the more difficult task is obtaining a calibration plot corresponding to critical conditions. In other words, the width of the critical region depends on the thermodynamic quality of the solvent. In the case in question, it was particularly difficult to determine the critical conditions for the CCl_4/MEK mixture; A 1% change in the composition of the mobile phase resulted in that the chromatographic mode changed from adsorption to exclusion. Snyder's parameters were calculated for the critical compositions of the mobile phases, solvent strengths ε were measured, and the intrinsic viscosities were determined for PS with $M = 120$ and 460 kg mol^{-1} at 35 and 25°C, respectively.

As already noted, some authors [10, 20, 21] give preference, when comparing solvent–polymer interactions, to the exponent α. In the present study, the intrinsic viscosities were used to characterize the thermodynamic quality of solvent mixtures. The choice of this parameter was due to the ease of its experimental determination, as well as to its accuracy and sensitivity. It can be readily shown that the error in determining the intrinsic viscosity is an order of magnitude smaller than that in determining the exponent α, because at least two methods are to be used in the latter case. Making and substantiating the choice of the parameter responsible for the thermodynamic quality of solvent mixtures used in chromatographic conditions were described in more detail in [15].

To evaluate solvent properties, Snyder introduced two parameters: polarity index P' [14] and solvent strength ε^0 [13]. The polarity index P' reflects the ability of a solvent to interact with certain polar test compounds. This index is independent of the properties of the adsorbent, but allows a comparative estimate of solvent polarities. The parameter ε^0 is the relative energy of interaction of solvent molecules with the surface of the adsorbent [13]. The parameters P' and ε^0 are known for most of individual solvents [13, 14, 24]. Moreover, it was shown in [25] that these parameters correlate with each other for pure solvents and such adsorbents as silica gel and aluminum oxide. The correlation is only violated for alcohols and acids, which tend to form hydrogen bonds.

The polarity indices are commonly calculated for solvent mixtures by the additive formula $P' = \Sigma P_i \varphi_i$, where P_i are Snyder's polarity indices for pure components, and φ_i, their volume fractions in the mixture [26]. A more complicated task is calculation of the solvent strength ε for mixtures [13, 24, 27–29]. The reason is that the concentrations of mixture components in the solution bulk and on the surface of the adsorbent do not coincide, with the experimental determination of the latter under dynamic adsorption conditions remaining an unsolved problem.

Calculated values of the solvent strength ε for some mixtures can be found in the literature. Certain experimental data are used to calculate ε [13]. One of the most important parameters is the adsorbent activity. Apparently, the activities may be different even for adsorbents of the same chemical nature. A certain, the most probable in the opinion of those performing a calculation, value of the activity is, as a rule, used in calculations: 1 [21], 0.57 [26], or 0.83–0.66 [13]. Even this simple example shows that the strengths ε calculated by different authors will not coincide.

A more reliable way to determine ε for mixtures is the experimental technique, also developed by Snyder. In our study, values of ε for mixed solvents were calculated from retention factors R_F for polynuclear hydrocarbons, with R_F found using TLC.

Data on the critical compositions of the mobile phases, values of the parameters P' and ε, and intrinsic viscosities for PS are listed in Table 2. The following tendency can be seen: thermodynamically good solvents have high P' and ε; in other words, the better the thermodynamic quality of a mobile phase, the higher P' and ε for compositions corresponding to the critical conditions of liquid chromatography.

It is known that, in solvents of good thermodynamic quality, the temperature dependence of the viscosity is very weak [22, 30]. When the solvent quality deteriorates, the dependence becomes more pronounced. However, differences in intrinsic viscosity remain insignificant in a narrow temperature range. The data obtained confirm this conclusion. It was demonstrated in [19] for a mixture of poor thermodynamic quality, cyclohexane/MEK, that [η] weakly depends on temperature in the range from 25 to 35°C. This solvent mixture is the worst in thermodynamic regard. Consequently, it is admissible to compare results of chromatographic experiments at 5°C with viscometric data obtained at 35 and 25°C.

As can be seen in Table 2, a correlation between P' and ε is also observed for mixed solvents. In ad-

dition, mixtures with high thermodynamic quality have high Snyder's parameters and solvent strengths. Consequently, the same tendency as that in TLC is preserved in the column chromatography [17–19].

Let us consider the reasons why the results of the present study disagree with the conclusions made in [20, 21]. We chose for consideration the results of these authors because just their data were processed and discussed by Macko and Hunleker [10]. As already noted, Baran et al. [21] reported that the critical conditions are in no way related to the thermodynamic quality of a solvent. Possibly, such a conclusion resulted, in part, from an unsuccessful choice of binary mobile phases. First, the precipitation mechanism cannot be completely ruled out for such mixed mobile phases as hexane/MEK and hexane/ethyl acetate because the exponent α is lower than 0.5 for critical compositions [20]. Therefore, the authors of [21] took into account only three of the five mobile phases represented in their study. Second, mixtures with very close properties were studied. At least Snyder's parameters are very close for the critical compositions of these mixtures [1.9, 1.7, 1.7 [21]). In addition, the adsorbent activity was taken to be unity ($\alpha = 1$) when calculating the solvent strength. However, Baran et al. [21] found that the hydrodynamic radii of macromolecules are unequal under critical conditions reached in different mixtures. This points to the corresponding difference in the conformations of macromolecules. The authors of [10] calculated ε for the same mixtures by a simplified method [26] and came to the conclusions coinciding with those in [21].

Let us consider specific features of the behavior of the macromolecule–adsorbent interactions in the case when the solvent quality is improved. For small molecules in the absence of specific interactions, an increase in the solvent strength commonly leads to a decrease in retention. For polymers, however, K_d may remain unchanged as the adsorption activity of the solvent increases. This phenomenon can be attributed to unfolding of the chain and to an increase in the number of contacts of a macromolecule with the adsorbent surface. As the solvent quality is improved, intramolecular interactions become weaker and hinder to a lesser extent the unfolding of the polymer chain on the adsorbent surface. As a result, the number of contacts of the macromolecule with the adsorbent grows. The rise in the number of contact, in turn, leads to preservation of the values of K_α.

CONCLUSIONS

(1) The calibration dependences of V_R on $\log M$ were used to find the compositions of binary solvent mixtures that correspond to the critical conditions of liquid chromatography of polystyrene on a silicate adsorbent.

(2) Snyder's polarity indices P' were calculated, solvent strengths ε were experimentally determined by thin-layer chromatography, and intrinsic viscosities were measured for polystyrene with M_w = 120 and 460 kg mol^{-1}.

(3) The thermodynamic quality of the solvent, evaluated by the intrinsic viscosity for polystyrene, was correlated with Snyder's parameters P' and ε and a conclusion was made that, in chromatography of polystyrene on a silicate adsorbent, the strength of the mobile phase and its polarity are the higher, the better the thermodynamic quality of a binary mixture.

REFERENCES

1. Belenkii, B.G., Gankina, E.S., Tennikov, M.B., and Vilenchik, L.Z., *J. Chromatogr.*, 1978, vol. 147, pp. 99–110.
2. Gorbunov, A.A. and Skvortsov, A.M., *Vysokomol. Soedin., Ser. A*, 1988, vol. 30, no. 4, pp. 895–899.
3. Gorbunov, A.A., Skvortsov, A. M., Trathnigg, B., et al., *J. Chromatogr.*, 1998, vol. 798, pp. 187–201.
4. Litvinova, L.S., Kever, E.E., Melenevskaya, E.Yu., and Zgonnik, V.N., *Zh. Fiz. Khim.*, 1995, vol. 69, no. 9, pp. 1657–1663.
5. Entelis, S.G., Evreinov, V.V., and Gorshkov, A.V., *Adv. Polym. Sci.*, 1986, vol. 76 (32), pp. 129–175.
6. Entelis, S.G., Evreinov, V.V., and Kuzaev, A.I., *Reaktsionnosposobnye oligomery* (Reactive Oligomers), Moscow: Khimiya, 1985.
7. Zimina, T.M., Kever, J.J., Melenevskaya, E.Y., and Fell, A.F., *J. Chromatogr.*, 1992, vol. 593, pp. 233–241.
8. Pasch, H. and Trathnigg, B., *HPLC of Polymers*, Berlin: Springer, 1999.
9. Macko, T., Hunkeler, D., and Berek, D., *Macromolecules*, 2002, vol. 35, pp. 1797–1804.
10. Macko, T. and Hunkeler, D., *Adv. Polym. Sci.*, 2003, vol. 163, pp. 61–136.
11. Chang, T., *Adv. Polym. Sci.*, 2003, vol. 163, pp. 1–60.
12. Glökner, G., *Polymer Characterization by Liquid Chromatography*, New York: Elsevier, 1987.
13. Snyder, L.R., *Principles of Adsorption Chromatography*, New York: Marcel Dekker, 1968.
14. Snyder, L.R., *J. Chromatogr. Sci.*, 1978, vol. 16, pp. 223–234.
15. Bel'nikevich, N.G., Litvinova, L.S., and Budtov, V.P., *Zh. Prikl. Khim.*, 2005, vol. 78, no. 6, pp. 997–1002.
16. Brandrup, J. and Immergut, E.H., *Polymer Handbook*, New York: Wiley, 1989.

17. Litvinova, L.S. and Bel'nikevich, N.G., *13th Bratislva Int. Conf. on Polymers "Separation and Cheracterization of Macromolecules," July 4–9*, 1999, p. 135.
18. Litvinova, L., Bel'nikevich, N., and Tyihak, E., *J. Planar Chromatogr.*, 2000, vol. 13, no. 2, pp. 149–151.
19. Litvinova, L.S. and Bel'nikevich, N.G., *J. Chromatogr., Ser. A*, 2003, vol. 1005, pp. 165–176.
20. Baran, K., Laugier, S., and Cramail, H., *Macromol. Chem. Phys.*, 1999, vol. 200, pp. 2074–2079.
21. Baran, K., Laugier, S., and Cramail, H., *J. Polym. Anal. Charact.*, 2000, vol. 6, pp. 123–145.
22. Budtov, V.P., *Fizicheskaya khimiya rastvorov polimerov* (Physical Chemistry of Polymer Solutions), St. Petersburg: Khimiya, 1992.
23. Cools, P., Herk, A., German, A.L., and Staal, W., *J. Liquid Chromatogr.*, 1994, vol. 17, nos. 14–15, pp. 3132–3134.
24. Snyder, L.R. and Glaich, J.L., *J. Chromatogr.*, 1981, vol. 248, pp. 165–182.
25. Geiss, F., *Fundamentals of Thin Layer Chromatography (Planar Chromatography)*, Heidelberg: Hüthig, 1987.
26. Palamareva, M.D. and Palamarev, H.E., *J. Chromatogr.*, 1989, vol. 477, pp. 235–248.
27. Snyder, L.R. and Poppe, H.J., *Chromatogr.*, 1980, vol. 184, pp. 363–413.
28. Snyder, L.R. and Glaich, J.L., *J. Chromatogr.*, 1981, vol. 214, pp. 1–19.
29. Snyder, L.R., *High-Performance Liquid Chromatography*, Horváth, Cs., Ed., New York: Acad., 1983, vol. 3, pp. 157–223.
30. Tsvetkov, V.N., Eskin, V.E., and Frenkel', S.Ya., *Struktura makromolekul v rastvorakh* (Structure of Macromolecules in Solutions), Moscow: Nauka, 1964.

ISSN 1070-4272, Russian Journal of Applied Chemistry, 2006, Vol. 79, No. 8, pp. 1297–1300. © Pleiades Publishing, Inc., 2006.
Original Russian Text © K.M. Imanbekov, E.E. Ergozhin, 2006, published in Zhurnal Prikladnoi Khimii, 2006, Vol. 79, No. 8, pp. 1311–1314.

MACROMOLECULAR CHEMISTRY AND POLYMERIC MATERIALS

Aminovinylpyridine Ion-Exchange Resins

K. M. Imanbekov and E. E. Ergozhin

Bekturov Institute of Chemical Sciences, Ministry of Education and Science of the Republic of Kazakhstan, Almaty, Kazakhstan

Received March 1, 2006

Abstract—Highly permeable aminovinylpyridine ion-exchange resins are synthesized by the reaction of epoxy/polyvinylpyridine prepolymers with aliphatic amines. Synthetic conditions are optimized and physicochemical and sorption characteristics of the resulting polyelectrolytes are examined.

DOI: 10.1134/S1070427206080155

Development of advanced ion-exchange processes stimulates research in the area of synthesis of pyridine-containing polycondensation polymers with desired physicochemical and adsorption properties.

In this context, simple routes to ion-exchange resins of the Ional series have been developed, based on condensation of allyl glycidyl ether with polyethylenimine and poly(2-methyl-5-vinylpyridine) [1] or of aliphatic amines and 2-methyl-5-vinylpyridine with epichlorhydrin [2], and their sorption characteristics with respect to noble and polyvalent metals have been reported [3, 4].

In this study, we synthesized aminovinylpyridine ion-exchange resins by condensation of prepolymers based on various epoxy compounds and poly(2-methyl-5-vinylpyridine) with aliphatic di- and polyamines and characterized the physicochemical and sorption properties of the products.

EXPERIMENTAL

Di- and polyamines (DPA) were purified as follows. Hexamethylenediamine (HMDA) was vacuum-distilled under Ar at 100°C and 2 mm Hg (mp 41–42°C); polyethylenepolyamine (PEPA) (MW 285, c_N 23%) and polyethylenimine (PEI) (MW 10×10^3, c_N 32%) were allowed to stand over granulated NaOH for six days. Poly(2-methyl-5-vinylpyridine) (PMVP) (MW 30×10^3) was prepared by radical polymerization of 2-methyl-5-vinylpyridine [5].

Di-, tri-, and tetraglycidyl epoxy derivatives of aniline, resorcinol, and ethylene glycol (DGA, DGER, DGEE), *m*- and *p*-aminophenols (T*m*-AP, T*p*-AP), *p*-phenylenediamine (TGE*p*-PDA), diaminodiphenylmethane (TGEM), diaminodiphenyl oxide (TGEO), and benzidine (TGEB) were prepared as in [6].

The ion-exchange resins were synthesized by polycondensation of 15% PMVP in ethanol with an epoxy compound (EC) at 50–70°C for 3–5 h (until the epoxy group content decreased by half). Then an aliphatic DPA was added and the mixture was allowed to stand for 2 h. The reaction mixture was poured on a tray and the solvent was removed. The resulting gel was cured at 80–100°C for 3–5 h, crushed, and screened to obtain the 0.25-mm fraction. Prior to addition of an aliphatic DPA, the residual epoxy groups were determined by argentometric back-titration according to GOST (State Standard) 12497–78.

The physicochemical characteristics of the resins were studied using the standard procedures [7, 8]. The IR spectra of the starting reagents, intermediates, and final products were recorded on a Specord M80 spectrophotometer (Carl Zeiss, Germany) using the KBr technique or with samples placed between KRS-5 glasses. The electronic absorption spectra were recorded on a Jasco instrument, model 7850 (Japan).

Sorption of V, Mo, and W was carried out from solutions of sodium metavanadate, molybdate, and tungstate in the static and dynamic modes. The speciation of the adsorbed metals was determined by IR spectroscopy.

The model reaction between EC and PMVP was studied IR- and UV-spectroscopically with an equimolar mixture of DGEE and 4-ethylpyridine (4EP) [9]. After 1 h of heating at 70°C, the initially trans-

Table 1. SEC and swellability of resins based on PMVP and PEI with DGA (1) and TGEM (2), as influenced by the starting reagents and their ratio

PMVP : EC : PEI molar ratio	V_{sp}, ml g^{-1}		SEC (0.1 N HCl or NaCl), mg-equiv g^{-1}			PMVP : EC : PEI molar ratio	V_{sp}, ml g^{-1}		SEC (0.1 N HCl or NaCl), mg-equiv g^{-1}		
	1	2	HCl (1)	HCl (2)	NaCl (2)		1	2	HCl (1)	HCl (2)	NaCl (2)
3 : 1 : 2	5.4	4.0	6.1	6.5	0.5	1 : 1 : 3	5.3	4.1	7.4	7.3	0.8
3 : 1 : 1	4.2	3.2	5.8	6.0	1.0	2 : 1 : 3	6.0	4.5	7.7	7.2	0.8
2 : 1 : 2	3.6	3.0	7.0	6.8	1.2	3 : 1 : 3	6.5	6.0	8.0	7.5	0.5

Table 2. SEC (0.1 N HCl) of resins, as influenced by the temperature and duration of the reaction of PMVP : TGEB with PEPA and PEI

SEC_{HCl}, mg-equiv g^{-1}						SEC_{HCl}, mg-equiv g^{-1}					
T, °C (5 h)			τ, h (80°C)			T, °C (5 h)			τ, h (80°C)		
60	80	100	3	5	7	60	80	100	3	5	7
PMVP : TGEB : PEPA = 2 : 1 : 2						PMVP : TGEB : PEI = 2 : 1 : 2					
5.8	6.2	6.3	5.5	6.3	6.3	6.0	6.6	6.7	5.9	6.6	6.6

Table 3. SEC of resins, as influenced by the structure of DPA (molar ratio of starting reagents 2 : 1 : 3)

PMVP : EC : DPA anion-exchanger	c_N in resin, %	SEC (0.1 N HCl), mg-equiv g^{-1}	c_N in resin, %	SEC (0.1 N HCl), mg-equiv g^{-1}	c_N in resin, %	SEC (0.1 N HCl), mg-equiv g^{-1}
	HMDA		PEPA		PEI	
TG*p*-PDA	9.75	6.6	10.20	7.0	10.42	7.3
TGEM	8.86	5.7	9.00	6.3	9.27	6.6
TGEO	8.80	5.5	9.00	6.3	9.30	6.5

parent liquid turned to yellow, and the IR intensities of the out-of-plane vibrations of C–H bonds (822 cm^{-1}) in 4EP and of the bands of the epoxy ring in DGE (920 cm^{-1}) decreased by half, which was accompanied by the appearance of new bands of 4-ethylpyridinium at 1560 and 1640 cm^{-1}, whose intensity increased during heating. The UV spectrum of the prepolymers formed by the condensation of DGE with 4EP shows a strong absorption of the pyridinium salt near 254 nm.

To optimize the synthesis of the ion exchangers, we studied under similar conditions the effects of the reagent ratio, temperature mode, and time of curing of PMVP/EC prepolymers with aliphatic DPA on the static exchange capacity (SEC) and swellability V_{sp} of the resulting resins.

As in the case of the reaction between 4EP and DGEE, the condensation of PMVP with DGA or TGEM was performed in isopropanol at 70°C for 3 h to 50% consumption of the epoxy groups. Further curing of the prepolymer in the presence of PEI at 80°C for 5 h produced ion-exchange resins demonstrating simultaneously the properties of aliphatic and heterocyclic polyamines with SEC (0.1 N NaCl) ranging from 0.5 to 1.2 mg-equiv g^{-1}. In the case TGEM, at the reagent ratio of (1–3) : 1 : (3–1), the resulting resins demonstrate a limited swellability (3.0–4.5 ml g^{-1}) (Table 1).

Tables 2 and 3 show that 80°C and 5 h are the optimal temperature and time for the reaction of PMVP/TGEB prepolymers with PEPA. Further increase in temperature and time resulted in the SEC loss

Table 4. Heat resistance of resins in hot water (48-h treatment)

Anion exchanger	SEC (0.1 HCl), mg-equiv g^{-1}				SEC loss, %, at indicated temperature, °C		
	initial	after treatment at indicated temperature, °C					
		80	100	120	60	100	120
PMVP : DGA : PEI = 3 : 1 : 1	5.8	5.7	5.6	5.6	1.7	4.5	4.5
PMVP : DGEP : PEI = 1 : 1 : 3	6.5	6.4	6.3	6.2	1.5	3.0	4.6
PMVP : T*m*-AP : PEI = 1 : 1 : 3	5.6	5.6	5.5	5.4	0	1.8	3.6
PMVP : T*p*-AP : PEI = 1 : 1 : 3	5.2	5.2	5.0	5.0	0	3.9	3.9
PMVP : TGEO : PEI = 2 : 1 : 2	6.5	6.5	6.4	6.3	0	1.5	3.0

in the final product. The yield of the PEPA-based products is above 80%, and, in the case of PEPA, 95%. Among the di- and polyamines used, PEI appeared to be the most efficient aminating agent, which can be attributed to its branched structure and higher nitrogen content. Raising the curing temperature from 60 to 100°C and the curing time to 5 h favored an increase in SEC. The minimal capacity of the resins was attained in 5–7 h at 80°C.

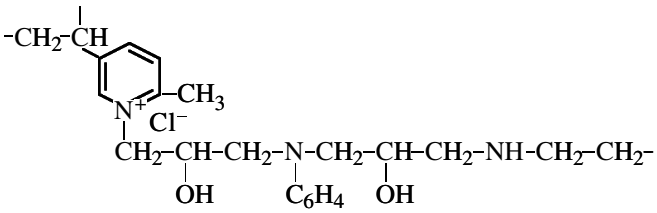
Therefore, it follows from our results that the optimal conditions for synthesis of aminovinylpyridine ion exchangers based on PMVP, aromatic EC, and DPA are as follows: temperature of synthesis of PMVP/EC prepolymers 70°C (3 h); curing in the presence of aliphatic DPA at 80°C for 5 h; and PMVP : EC : DPA molar ratio (1–3) : 1 : (2–3), depending on the nature of the starting reagents. Further increase in the amount of aliphatic polyamines promoted the formation of weakly cross-linked polyelectrolytes. Among the aliphatic DPA, PEI is the most efficient aminating agent because of the branched structure and high nitrogen content.

Generally, thermal degradation of anion-exchange resins first involves aliphatic NH groups, which is reflected primarily in SEC loss. Therefore, the heat resistance was determined in hot water from the SEC loss after 48-h treatment at 80, 100, and 120°C. The SEC loss in these experiments was within 5% (Table 4).

The IR spectra of the resulting polyelectrolytes show the characteristic bands of the pyridine and benzene rings and the bands due to stretching and bending vibrations of the NH groups of the aliphatic amines at 1460, 1500–1560, 1472–1530, 1600–1640, and 3472 cm^{-1}, but no characteristic bands of the epoxy ring at 760 and 848 cm^{-1}. Also we found the bands due to asymmetric (2940 cm^{-1}) and symmetric (2840 cm^{-1}) vibrations of the CH_2 groups. The appearance of the pyridinium absorption band at 1532 cm^{-1} is consistent with the published IR data on strongly basic commercial anion exchangers VP-1Ap and VP-100 [10].

The polyelectrolytes obtained in this study demonstrate a high chemical resistance. Thus, the SEC_{HCl} loss after treatment of the PMVP : TGEB : PEPA and PMVP : TGEB : PEI resins with 5 N H_2SO_4 and NaOH for 30 min at 100°C was within 5%, and that after treatment with 10% H_2O_2 for 24 h at 25°C, within 10–15%.

Our results suggest the following structure for the resulting polyelectrolytes:



It is known that the aminovinylpyridine ion exchangers are characterized by higher sorption capacity as compared to the commercial vinylpyridine sorbents based on divinylbenzene [4, 11]. Therefore, it was interesting to study the sorption of vanadium, molybdenum, and tungsten polyanions. In our experiments, the sorption efficiency with PMVP : TGEB : PEI = 2 : 1 : 3 increased in acidic and weakly acidic solutions. The maximal SEC was observed at pH 1.0–2.4 (1650 mg V_2O_5/g), 1.6–2.5 (1500 mg Mo/g), and 2.0–3.5 (1340 mg W/g). Under optimal conditions, the V, Mo, and W ions were completely recovered in 15, 45, and 72 h, respectively. The IR spectra of the resins after sorption contain new bands assigned to the polyanions: $Mo_7O_{24}^{6-}$ (860, 895–900, 930 cm^{-1}),

$H_2V_{10}O_{28}^{4-}$ (960 cm^{-1}), and $W_{12}O_{41}^{2-}$ (broadening of the adsorption bands at 770–800, 895–900, and 950–1000 cm^{-1}).

In studying the Mo sorption isotherms, the maximal SEC (1780 mg Mo/g) was observed at a metal concentration of 5 g l^{-1}. Under similar conditions, the maximal SEC of commercial anion-exchange resin VP-1Ap was reported to be only 700 mg Mo/g [11].

In passing a model solution containing 1.5 g Mo/l (pH 2.0) through a column with a diameter to height ratio of 1 : 15, the breakthrough of the Mo ions was observed after passing 75 volumes of the eluate per unit volume of the resin. In this case, the dynamic exchange capacity is 1000 mg Mo/g. The degree of Mo desorption with 12% ammonia amounts to 98%. The desorption efficiency loss in the sorption/desorption cycles was within 0.5–1.0% only after the third cycle.

To conclude, successive reactions of di-, tri-, and tetraglycidyl compounds with PMVP and PEI allow preparation of ion-exchange resins bearing the amino, pyridine, and pyridinium groups. The products demonstrate such useful properties as high heat resistance and resistance to oxidizing agents and concentrated acids. The presence of the aliphatic amino groups improves the flexibility and complexing power of the polyelectrolytes. In this case, the use of epoxy compounds of various structures allows effective control over the size of the channels in the polymer network and its permeability for V, Mo, and W ions [1, 11].

CONCLUSIONS

(1) Aminovinylpyridine ion-exchange resins are synthesized by polycondensation of epoxy compounds with poly(2-methyl-5-vinylpyridine) at 70°C (3 h) followed by curing of the resulting prepolymer in the presence of aliphatic di- and polyamines for 5 h at 80°C at a reagent ratio of (1–3) : 1 : (2–3), depending on the starting components.

(2) The loss in the static exchange capacity (0.1 N HCl) after treatment with 5 N H_2SO_4 and NaOH and hot water, characterizing the chemical and heat resistance of the resulting resins, is within 5%.

(3) The UV and IR spectra of the model compounds and final products suggest the formation of heterolytic pyridine, pyridinium, and aliphatic amino groups in successive reactions of the epoxy compounds with poly(2-methyl-5-vinylpyridine) and di- and polyamines.

(4) The ion-exchangers obtained demonstrate high permeability for vanadium, molybdenum, and tungsten polyanions from solutions at pH 1.5–3.5. In this case, the dynamic exchange capacity of the resin based on PMVP : TGEB : PEI is 1000 mg Mo/g, and the degree of Mo desorption with 12% ammonia is 98%.

REFERENCES

1. Chalov, T.K., Highly Permeable Polyelectrolytes and Ion-Exchange Membranes Based on Certain Oxygen- and Nitrogen-Containing Compounds, *Doctoral Dissertation*, Almaty, 2005.
2. KZ Prepatent 5928.
3. Ergozhin, E.E., Kenzhaliev, B.K., Chalov, T.K., et al., *Tsvetn. Met.*, 2005, no. 2, pp. 43–46.
4. Imanbekov, K.I., Nusipova, A.M., and Erkasov, R.Sh., *Izv. Vyssh. Uchebn. Zaved., Ser. Khim. Khim. Tekhnol.*, 1998, vol. 41, no. 2, pp. 122–124.
5. Korshak, V.V., Zubakova, L.B., and Zhovnirovskaya, A.B., *Vysokomol. Soedin., Ser. A*, 1968, vol. 10, no. 7, pp. 1618–1632.
6. Menligaziev, E.Zh., Novel Highly Permeable Polyfunctional Anion Exchangers, *Doctoral Dissertation*, Alma-Ata, 1989.
7. *GOSTs* (State Standards) *10898–84, 10898–2.74, 10898–5.84: Ion-Exchangers: Physicochemical Testing Techniques; GOST 10896–78: Preparation for Testing*; *GOST 20255.1–89: Methods for Determination of the Static Exchange Capacity*.
8. Polyanskii, N.G., Gorbunov, G.V., and Polyanskaya, N.L., *Metody issledovaniya ionitov* (Methods for Testing Ion Exchangers), Moscow: Khimiya, 1976.
9. Imanbekov, K.I., Highly Permeable Ion Exchangers Based on Certain Derivatives of Pyridine, Di- and Tetraglycidyl Ethers of Dihydroxybenzenes, and Diamines, *Doctoral Dissertation*, Alma-Ata, 1987.
10. Stupin, N.P., Dmitrochenkova, T.S., Zhukova, N.G., et al., *Plast. Massy*, 1983, no. 7, p. 59.
11. Shatalov, V.V., Kharina, T.P., Balanovskii, N.V., et al., *Khim. Tekhnol.*, 2000, no. 7, pp. 19–23.

ISSN 1070-4272, Russian Journal of Applied Chemistry, 2006, Vol. 79, No. 8, pp. 1301–1305. © Pleiades Publishing, Inc., 2006.
Original Russian Text © O.G. Al'tshuler, L.A. Sapozhnikova, G.N. Al'tshuler, 2006, published in Zhurnal Prikladnoi Khimii, 2006, Vol. 79, No. 8, pp. 1315–1319.

MACROMOLECULAR CHEMISTRY AND POLYMERIC MATERIALS

Sulfonic Cation Exchangers Based on Immobilized *cis*-Calix[4]resorcinolarenes

O. G. Al'tshuler, L. A. Sapozhnikova, and G. N. Al'tshuler

Kemerovo Branch, Institute of Solid State Chemistry and Mechanochemistry, Siberian Division, Russian Academy of Sciences, Kemerovo, Russia

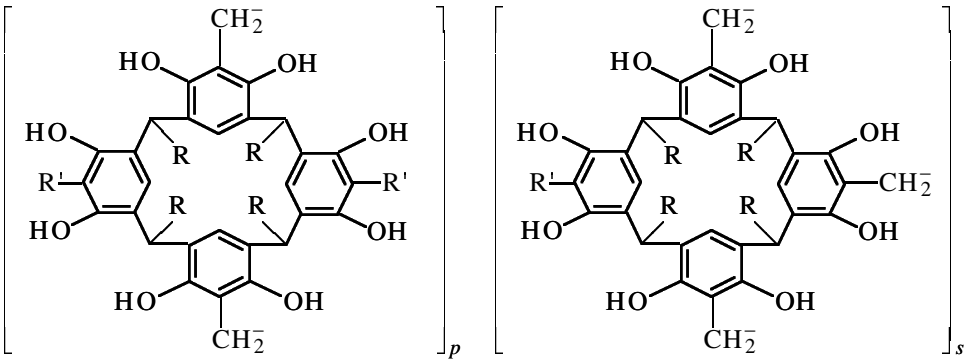
Received March 24, 2006

Abstract—New sulfonic cation exchangers based on immobilized calix[4]resorcinolarenes were prepared. Their ion-exchange properties toward Na^+, Cu^{2+}, $[Pd(NH_3)_4]^{2+}$, In^{3+}, and Sn^{4+} ions were studied in a wide pH range, and their chemical stability was examined.

DOI: 10.1134/S1070427206080167

Previously, we have prepared new network polymers containing immobilized calix[4]resorcinolarenes [1–5]. These polymers can act as biomimetics [1, 2], nanoreactors for catalytic hydrogenation processes [6, 7], solid polyelectrolytes [8], and weakly acidic cation exchangers [1, 2, 9]. The ion-exchange and ionophore properties of network polymers based on immobilized calix[4]resorcinolarenes are due to the presence of phenolic (resorcinol) OH groups capable of ionization in alkaline solutions (pH > 7). The selectivity of the cation exchange can be enhanced by introducing carboxy [9], phosphate [10], or furyl(hydroxy)methyl [4] functional groups into the monomeric units of immobilized calixarenes.

In this study, we prepared novel bifunctional cation exchangers **I** and **II** by sulfonation of network polymers based on immobilized calix[4]resorcinolarenes. The monomeric units of **I** and **II** contain macrorings of two kinds:



where R = CH_3, R' = SO_3H (**I**); R = Ph–SO_3H, R' = H (**II**).

One of the macrorings is incorporated in the chain via two bridging CH_2 groups, and the other macroring, via three bridging CH_2 groups, forming a network structure. Cation exchangers **I** and **II** contain strongly acidic SO_3H groups dissociating with the release of protons in a wide pH range (pH 0–14) and weakly acidic phenolic OH groups.

The goal of this study was to prepare cation exchangers **I** and **II** and determine of their main ion-exchange characteristics (cation-exchange capacity, potentiometric titration curves).

EXPERIMENTAL

Calix[4]resorcinolarenes immobilized in the phase of network polymers (polytetramethylcalix[4]resor-

cinolarene or polytetraphenylcalix[4]resorcinolarene) were prepared by resol polycondensation of *cis*-tetramethylcalix[4]resorcinolarene or *cis*-tetraphenylcalix[4]resorcinolarene with formaldehyde, as described in [4].

Cation exchanger **I** was prepared by two-step sulfonation of a network polymer, polytetramethylcalix[4]resorcinolarene. Polytetramethylcalix[4]resorcinolarene (4 g, 5 mmol) was kept for 24 h in 20 ml of dichloroethane, after which 25 ml of concentrated (98%) sulfuric acid was added, and the mixture was heated for 5 h at 98°C, with the evaporation of the released water. The sulfonated product was dried in air. Then repeated sulfonation with a 3 : 2 (*v*/*v*) mixture of 98% sulfuric acid and oleum (25% free SO_3 in 98% sulfuric acid) at 98°C was performed. Dry cation exchanger **I** in the H form was thus obtained in the form of dark brown granules of irregular shape; yield 3.4 g (85%).

Cation exchanger **II** was prepared by two-step sulfonation of polytetraphenylcalix[4]resorcinolarene. The polymer (6 g, 5 mmol) in the form of spherical granules 0.05–0.5 mm in diameter was kept for 24 h in 30 ml of dichloroethane, after which 30 ml of 90% sulfuric acid was added, and the mixture was heated for 5 h at 90°C, with the evaporation of the released water. The sulfonated product was dried in air. Then repeated sulfonation with a mixture of concentrated sulfuric acid and oleum at 90°C was performed. Dry cation exchanger **II** in the H form was thus obtained in the form of spherical granules 0.05–0.5 mm in diameter; yield 3.8 g (63%).

Table 1. Enthalpies of formation $\Delta_f H^0_{298}$, enthalpies of reaction (1) ΔH^0_n, and enthalpies of separate steps of reaction (1) $\Delta\Delta H^0_n = \Delta H^0_n - \Delta H^0_{n-1}$, calculated by the MNDO/PM3 method*

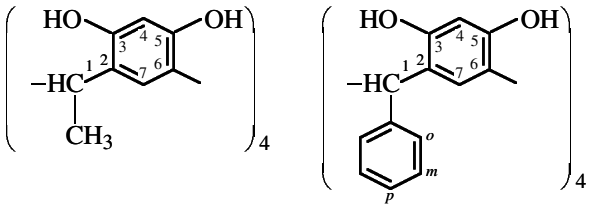
Compound	$\Delta_f H^0_{298}$	ΔH^0_n	$\Delta\Delta H^0_n$
	kJ mol^{-1}		
Sulfonation of **III** at aromatic rings of tetraresorcinol belt			
LH_4	–1207.9		
$LH_3 \cdot SO_3H$	–1666.7	104.8	104.8
$LH_2 \cdot (SO_3H)_2$	–2133.6	201.5	96.7
Sulfonation of **IV** at pendant benzene rings			
LH_4	–629.7		
$LH_3 \cdot SO_3H$	–1130.2	63.1	63.1
$LH_2 \cdot (SO_3H)_2$	–1640.5	116.3	53.2
$LH \cdot (SO_3H)_3$	–2151.3	169.1	52.8
$L \cdot (SO_3H)_4$	–2665.9	218.1	49.0

* $\Delta_f H^0_{298}(H_2SO_4) = -787.1$, $\Delta_f H^0_{298}(H_2O) = -223.6$ kJ mol^{-1}.

Cation exchangers **I** and **II** were conditioned by the standard procedure [11]. The FTIR and DRIFT spectra were recorded on a Tensor-27 Fourier transform IR spectrometer (Bruker Optics). The FTIR spectra were measured with polymer samples pelletized with KBr, and the DRIFT spectra, with preliminarily ground samples, using a diffuse reflection unit. The procedures for determination of the dynamic ion-exchange capacity and for potentiometric titration of the resins were described in [1, 2, 5].

The sulfur content of the cation exchanger samples was determined according to [12]. Quantum-chemical calculations were performed by the MNDO semiempirical method with PM3 parametrization of the Hamiltonian, using MOPAC 2000 program included in the Chem 3D Ultra 9.0 software package (CambridgeSoft Corporation).

Let us consider the thermodynamic probability (and site) of the electrophilic attack by a sulfonated agent of *cis-meta*-cyclophanoctols **III** and **IV** modeling the monomeric units of the polymers, polytetramethylcalix[4]resorcinolarene or polytetraphenylcalix[4]resorcinolarene, respectively.



III **IV**

Assume that the sulfonation of **III** and **IV** occurs by a reversible reaction

$$LH_4 + nH_2SO_4 \rightleftarrows LH_{4-n}(SO_3H)_n + nH_2O, \quad (1)$$

where LH_4 is **III** or **IV**.

A quantum-chemical calculation showed that the most favorable sulfonation site in **III** is position 4 in each aromatic ring of the tetraresorcinol belt of the meta-cyclophanoctol. Monosulfo derivatives of **IV** can contain a sulfo group in the *p*- or *m*-position of the pendant benzene rings, because sulfonation of the resorcinol rings is less energetically favorable. The incorporation of a SO_3H group into each pendant benzene ring of **IV** is the most probable.

The minimal calculated enthalpies of formation $\Delta_f H^0_{298}$ of **III** and **IV** and of their sulfonation products, and also the enthalpies of reaction (1) are listed in Table 1.

Table 1 shows that sulfonation reaction (1) should be endothermic, with ΔH 97–105 kJ per mole SO_3H in sulfonation of **III** at the tetraresorcinol belt and 49–63 kJ per mole SO_3H in the sulfonation of **IV** at the pendant phenyl groups. Naturally, elevated temperatures are required to promote the reaction. The thermodynamic probability of reaction (1) decreases with an increase in the number of SO_3H groups in the reaction products. In going to cation exchangers **I** and **II**, the pattern changes: In the tetraresorcinol fragmnent, only one or two SO_3H groups can be introduced per macroring, because the other positions favorable for the electrophilic attack (4-positions in **III** and **IV**) are already occupied by the bridging CH_2 groups of the polymeric chains. Based on the analysis of model reaction (1), we developed procedures for preparing sulfonic cation exchangers **I** and **II**.

The FTIR spectra of the polymers are shown in Fig. 1. In the transmission spectra of the samples, there are broad bands at about 3400 cm^{-1}, corresponding to intramolecular hydrogen bonds in diols. The band at 2850 and the doublet at 2940 and 2920 cm^{-1} are due to the C–H vibrations in aliphatic hydrocarbons. The band at 1600 cm^{-1} belongs to stretching vibrations in the benzene ring. Sulfonated polymers **I** and **II** additionally contain bands at 1196, 1145, and 1000 cm^{-1} (stretching vibrations of the sulfo group) and long-wave bands at 570 cm^{-1} in the sulfonated polymer derived from **III** (*o*-substitution [13]) and at 590 and 540 cm^{-1} in the sulfonated polymer derived from **IV** (vibrations of the C–S bond between the sulfo group and benzene ring). The vibration band of the benzene ring is broadened (doublet at 1591 and 1610 cm^{-1} in the spectrum of the sulfonated polymer derived from **IV**).

The bands observed for **I** and **II** in the FTIR and DRIFT spectra are similar.

The potentiometric titration curves of **I** and **II** (Fig. 2) have a stepped shape due to the presence in the monomeric units of both strongly acidic sulfo groups fully dissociating even in acid solutions and phenolic OH groups dissociating at pH > 7. Thus, compounds **I** and **II** are bifunctional cation exchangers.

Analysis of the material balance shows that protons of all the sulfo groups and four of eight OH groups (one OH group per resorcinol fragment) in the monomeric units of **I** and **II** are involved in the ion exchange. The latter fact is associated with a large difference between the ionization constants of resorcinol (pK_{a1} = 9.15, pK_{a2} = 11.33 [14]).

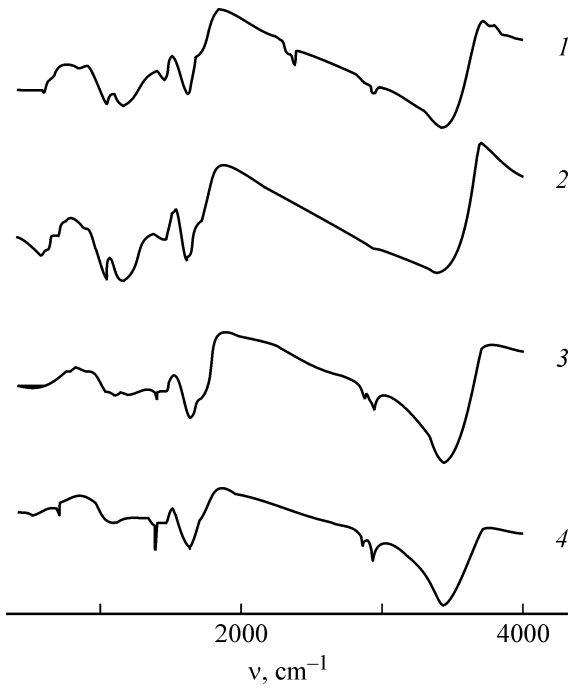


Fig. 1. FTIR spectra of (*1*) **I**, (*2*) **II**, (*3*) polytetramethylcalix[4]resorcinolarene, and (*4*) polytetraphenylcalix[4]-resorcinolarene. (ν) Wavenumber.

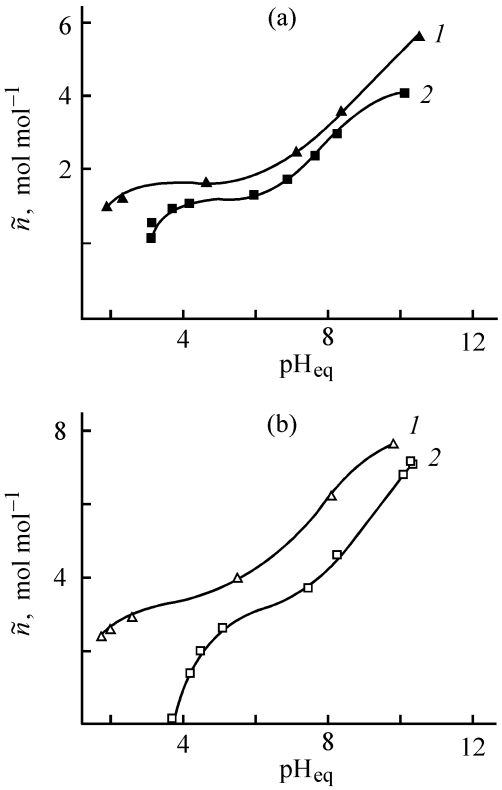


Fig. 2. Potentiometric titration curves of cation exchangers (a) **I** and (b) **II** with aqueous KOH solutions (*1*) with and (*2*) without salts added. (ñ) Amount of cations sorbed by the cation exchanger per macroring of the monomeric unit.

Table 2. Characteristics of sulfonic cation exchangers based on immobilized *cis*-calix[4]resorcinolarenes

Cation exchanger	Sulfur content of polymer, %		Total dynamic cation-exchange capacity, mg-equiv g^{-1} resin in H form					
	elemental analysis	in SO_3H groups	0.1 N NaOH	0.01 N NaCl	0.01 N $CuCl_2$	0.01 N $InCl_3$	0.01 N $SnCl_4$	0.01 N $[Pd(NH_3)_4]Cl_2$
I	8.1 ± 0.2	5.9 ± 0.2	6.47 ± 0.10	1.85 ± 0.05	1.86 ± 0.05	1.85 ± 0.05	1.85 ± 0.05	–
II	7.7 ± 0.2	7.8 ± 0.2	5.65 ± 0.10	2.45 ± 0.05	2.45 ± 0.05	2.45 ± 0.05	2.45 ± 0.05	2.45 ± 0.05

The characteristics of the sulfonic cation exchangers based on immobilized *cis*-calix[4]resorcinolarenes are given in Table 2. Table 2 shows that the sulfonation of network polymers based on calix[4]resorcinolarenes yields sulfonic cation exchangers **I** and **II** containing strongly acidic SO_3H groups. The total ion-exchange capacity of **I** and **II** (for 0.1 N NaOH) is 6.47 and 5.65 mg-equiv g^{-1} dry polymer in the H form, respectively, which considerably exceeds the cation-exchange capacity of the nonsulfonated polymers, polytetramethylcalix[4]resorcinolarene and polytetraphenylcalix[4]resorcinolarene (5.0 and 3.8 mg-equiv g^{-1} [4]).

The sorption capacities for chlorides of alkali, rare, and nonferrous metals and tetraamminepalladium in neutral and acidic solutions correspond to the content of sulfo groups in **I** and **II**. Under these conditions, the sorption capacity of the corresponding nonsulfonated polymers [1, 2] is zero. The working range of **I** and **II** is $0 < pH < 14$.

The sulfur content in **I**, according to elemental analysis, exceeds the calculated value corresponding to the content of SO_3H groups in the polymer. Since the sulfonation of polytetramethylcalix[4]resorcinolarene occurs under more severe conditions (which may lead to formation of sulfones [15]), a part of S atoms in **I** may be incorporated in bridging SO_2 groups. The SO_3H groups in **I** are, apparently, in the 4-position (between two OH groups of the resorcinol fragment), because the band at 570 cm^{-1} in the FTIR spectrum of **I**, according to [13], corresponds to the *o*-substitution in the sulfonation of aromatic rings. The dynamic ion-exchange capacity shows that resin **I** contains no more than two SO_3H groups per macroring, and the content of SO_3H groups following from the potentiometric titration curve (Fig. 2a) is 1.6 per macroring.

The sulfur content of **II** and its capacity for strongly acidic groups show that the whole amount of sulfur in **II** is in the form of four sulfo groups at the pendant phenyl rings (approximately one sulfo group per phenyl ring).

Sulfonic cation exchangers **I** and **II** have important service characteristics. Resins **I** and **II** exhibit the dynamic ion-exchange capacity for strongly acidic SO_3H groups in a wide pH range in sorption of both Na^+ cations and multicharged cations of Cu^{2+}, $[Pd(NH_3)_4]^{2+}$, In^{3+}, and Sn^{4+}. The capacity for cation exchange with phenolic OH groups is fully preserved in both resins. Apparently, the functional groups (OH, SO_3H) belonging to the same macroring of the monomeric unit of **I** and **II** preserve in the polymeric phase the well-known capacity of calixarenes [16] for complementary stereoelectronic interactions with substrate molecules (metal cations in our case). In this context, we expect that sulfonic cation exchangers **I** and **II** can show high selectivity due to formation of ensembles of multicharged cations and ionic groups belonging to the same macroring.

Cation exchangers **I** and **II** are chemically stable in the range $0 < pH < 14$. Comparison of the FTIR and DRIFT spectra of **I** and **II** shows that their surface is resistant to oxidation in air. The chemical resistance of cation exchangers **I** and **II** to alkalis, acids, and oxidants and their high dynamic ion-exchange capacity in a wide pH range determine the possibility of using these resins in various branches of industry for separation of electrolyte mixtures, recovery of nonferrous and rare metals from multicomponent systems, and exhaustive demineralization of water, and also as catalyst supports.

CONCLUSIONS

(1) Novel sulfonic cation exchangers were prepared by sulfonation of network polymers derived from *cis*-tetramethylcalix[4]resorcinolarene or *cis*-tetraphenylcalix[4]resorcinolarene.

(2) The IR spectra, elemental analysis, potentiometric titration curves, and sorption characteristics of these cation exchangers confirm the presence of strongly acidic sulfo groups and weakly acidic phenolic hydroxy groups. Each macroring of the monomeric

unit of the polymer contains one to four SO_3H groups and eight OH groups. The total dynamic cation-exchange capacity (mg-equiv g^{-1}) of the sulfonic cation exchangers based on *cis*-calix[4]resorcinolarenes **I** and **II** is, respectively, 6.47 and 5.65 for 0.1 N NaOH, and 1.85 and 2.45 for 0.01 N NaCl, $CuCl_2$, $InCl_3$, $SnCl_4$, and $[Pd(NH_3)_4]Cl_2$.

(3) The high ion-exchange capacity for multicharged ions and the chemical stability in a wide pH range make the sulfonic cation exchangers based on immobilized *cis*-calix[4]resorcinolarenes suitable for separation of multicomponent electrolyte mixtures, for exhaustive demineralization of water, and for use as catalyst supports.

REFERENCES

1. Al'tshuler, G.N., Sapozhnikova, L.A., and Abramova, L.P., *Izv. Ross. Akad. Nauk, Ser. Khim.*, 1998, no. 11, pp. 2214–2216.
2. Al'tshuler, G.N., Fedyaeva, O.N., and Ostapova, E.V., *Izv. Ross. Akad. Nauk, Ser. Khim.*, 2000, no. 8, pp. 1475–1477.
3. Al'tshuler, G.N., Fedyaeva, O.N., Sapozhnikova, L.A., and Ostapova, E.V., *Vysokomol. Soedin., Ser. B*, 2001, vol. 43, no. 4, pp. 755–759.
4. Altshuler, H., Ostapova, E., Fedyaeva, O., et al., *Macromol. Symp.*, 2002, vol. 181, pp. 1–4.
5. Ostapova, E.V., Al'tshuler, O.G., Sapozhnikova, L.A., and Al'tshuler, G.N., *Zh. Fiz. Khim.*, 2003, vol. 77, no. 5, pp. 909–913.
6. Al'tshuler, G.N. and Sapozhnikova, L.A., *Zh. Prikl. Khim.*, 2004, vol. 77, no. 11, pp. 1914–1916.
7. Al'tshuler, G.N. and Sapozhnikova, L.A., *Zh. Strukt. Khim.*, 2004, vol. 45, appendix, pp. 178–180.
8. Al'tshuler, G.N., Ostapova, E.V., and Evdoshenko, A.A., *Zh. Prikl. Khim.*, 2006, vol. 79, no. 1, pp. 82–84.
9. Shinohara, T., Wakisaka, S., Ohto, K., and Inouc, K., *Chem. Lett.*, 2000, no. 6, pp. 640–641.
10. Alexandratos, S.D. and Natesan, S., *Macromolecules*, 2001, vol. 34, pp. 206–210.
11. Marhol, M., *Ion Exchangers in Analytical Chemistry. Their Properties and Use in Inorganic Chemistry*, Prague: Academia, 1982.
12. Lebedeva, A.I. and Novozhilov, I.V., *Zh. Anal. Khim.*, 1961, vol. 16, pp. 223–225.
13. Semushkin, A.M., Yakovlev, V.A., and Ivanova, E.V., *Infrakrasnye spektry pogloshcheniya ionoobmennykh materialov* (Infrared Absorption Spectra of Ion-Exchange Materials), Leningrad: Khimiya, 1980.
14. *Khimicheskaya entsiklopediya* (Chemical Encyclopedia), Moscow: Bol'shaya Ross. Entsiklopediya, 1994, vol. 4, p. 418.
15. Andersen, K.K., *Comprehensive Organic Chemistry. The Synthesis and Reactions of Organic Compounds*, Barton, D. and Ollis, W.D., Eds., Oxford: Pergamon, 1979. Translated under the title *Obshchaya organicheskaya khimiya*, Moscow: Khimiya, 1983, vol. 5, pp. 508–564.
16. Cram, D.J., Hye-Eyn Kim, S.K., Knoler, C.B., et al., *J. Am. Chem. Soc.*, 1988, vol. 110, pp. 2229–2237.

ISSN 1070-4272, Russian Journal of Applied Chemistry, 2006, Vol. 79, No. 8, pp. 1306–1311. © Pleiades Publishing, Inc., 2006.
Original Russian Text © M.I. Abdullin, T.V. Gainullina, O.S. Kukovinets, A.R. Khalimov, N.N. Sigaeva, R.R. Muslukhov, M.A. Kayumova, 2006, published in Zhurnal Prikladnoi Khimii, 2006, Vol. 79, No. 8, pp. 1320–1325.

MACROMOLECULAR CHEMISTRY AND POLYMERIC MATERIALS

Synthesis and Properties of Epoxy Derivatives of Syndiotactic 1,2-Polybutadiene

M. I. Abdullin, T. V. Gainullina, O. S. Kukovinets, A. R. Khalimov, N. N. Sigaeva, R. R. Muslukhov, and M. A. Kayumova

Bashkir State University, Ufa, Bashkortostan, Russia

Institute of Organic Chemistry, Ufa Scientific Center, Russian Academy of Sciences, Ufa, Bashkortostan, Russia

Received November 25, 2005; in final form, March 2006

Abstract—Samples of modified 1,2-polybutadiene were prepared by the reaction of the polymer with peracetic acid or *tert*-butyl hydroperoxide in the presence of a catalyst, hexacarbonylmolybdenum. The hydrodynamic characteristics of dilute solutions and the rheological properties of concentrated solutions of the starting and epoxidized polydiene in hydrocarbon solvents were studied. The Huggins constant K_χ, second virial coefficient A_2, root-mean-square size of macromolecular coils $(\overline{R^2})^{1/2}$, and the enthalpy, entropy, and Gibbs energy of activation of the viscous flow of solutions of the starting and modified polydiene were estimated.

DOI: 10.1134/S1070427206080179

According to published data, addition to polymeric formulations of polydienes, including 1,2-polybutadiene (1,2-PB), that contain a small amount of epoxy units in the backbone and pendant chains improves the properties of the compounds and expands the field of their application [1–6]. In particular, 1,2-PB containing 5–8% oxirane oxygen is used for preparing compounds with enhanced flame resistance and improved sealing properties [7] and as a component of paint-and-varnish materials [8] and of compounds whose rigidity does not change with time and the elasticity and high adhesive power are preserved under moist conditions [9].

Here we suggest a new approach to the synthesis of epoxy derivatives of syndiotactic 1,2-PB, allowing introduction of a prescribed amount of epoxy groups into the polydiene macromolecules.

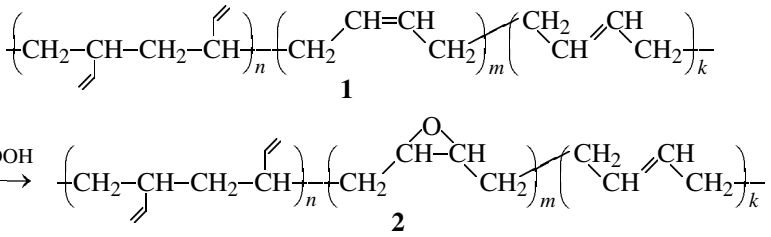
As starting polymer we chose syndiotactic 1,2-PB with a Mooney viscosity of 30. The polymer had the following characteristics: flow point T_f = 105°C, glass transition point T_g = –15°C, $M_n = 71.6 \times 10^3$, M_w/M_n = 1.8 (M_n and M_w/M_n were determined by GPC), degree of crystallinity 30%, content of 1,2 and 1,4 units 84 and 16%, respectively.

Epoxidation of syndiotactic 1,2-PB was performed in benzene; the epoxidizing agent was peracetic acid prepared in situ by the treatment of solution acetic acid with a concentrated H_2O_2. The thus synthesized epoxy derivatives of syndiotactic 1,2-PB were characterized by ^{1}H (300 MHz) and ^{13}C (75.47 MHz) NMR spectroscopy. The degree of modification of 1,2-polydiene was determined by comparing its NMR spectra with those of the starting polymer [10]. The signals were assigned using the COSY H–H and COSY C–H 2*D* correlation spectroscopy.

The formation of epoxy groups in the macromolecules of syndiotactic 1,2-PB was confirmed by the presence of weak doublets at 55.89 and 55.65 ppm in the ^{13}C spectra and of an unresolved group of signals at 2.7–2.9 ppm in the ^{1}H spectra, with the chemical shifts typical of epoxy groups [11]. Simultaneously the ^{13}C triplets at 27.57, 27.43, and 27.35 ppm and doublets at 127.8–130.3 ppm, corresponding to the C atoms in the *cis* units formed by 1,4 polymerization, decreased in intensity relative to the starting polydiene.

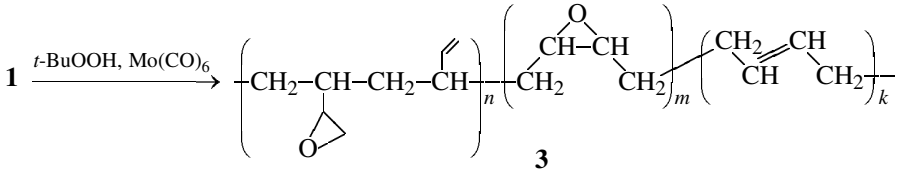
The experimental results show that the epoxidation of syndiotactic 1,2-PB with peracetic acid mainly involves the >C=C< double bonds in the 1,4-*cis* units of the backbone. This is apparently due to a higher nucleophilicity of these bonds compared to those in the 1,2 units [12]. The NMR spectra of modified syndiotactic 1,2-PB are consistent with the relatively low degree of epoxidation of the polymer upon its treat-

ment with peroxyacetic acid: With this agent, only up to 4–5% of the double bonds in the macromolecule of syndiotactic 1,2-PB are converted into epoxy groups (Table 1). Thus, the formation of oxirane groups in macromolecules of syndiotactic 1,2-PB in its epoxidation with peracetic acid follows the scheme



Epoxidation of syndiotactic 1,2-PB with *tert*-butyl hydroperoxide in the presence of $Mo(CO)_6$ [13] showed an essentially different pattern. In this case, the pendant vinyl groups of the polydiene macromolecules were epoxidized too. The modification was performed in benzene at 20°C. The degree of functionalization was controlled by the amount of the epoxidizing agent added (up to a twofold excess relative to the content of the >C=C< bonds in the macrochains). We prepared epoxy derivatives of syndiotactic 1,2-PB containing up to 9% epoxy groups (Table 1).

The ^{13}C NMR spectra of the polymer modified by treatment with *tert*-butyl hydroperoxide contain, along with the signals from the C atoms of the epoxy groups in the backbone, also stronger signals: a triplet at 57.9 ppm and doublets at 56.36 and 56.88 ppm, with large coupling constants $^1J(^{13}C–^1H)$ 172, 174, and 168 Hz. This fact unambiguously indicates that the vinyl >C=C< bonds are also converted into epoxy groups. The presence in the COSY C–H spectra of the cross peaks of these signals with the proton signals at 2.6–3.0 ppm additionally confirms that the vinyl groups in the macromolecules of syndiotactic 1,2-PB are involved in the epoxidation:



Thus, the course of epoxidation of syndiotactic 1,2-PB strongly depends on the epoxidizing agent. Peracetic acid is insufficiently reactive for the epoxidation of the nonactivated pendant vinyl group. As a result, only the >C=C< bonds of the backbone, and only those with the *cis* configuration, are involved in the epoxidation with this agent. In the epoxidation of 1,2-PB with *tert*-butyl hydroperoxide in the presence of $Mo(CO)_6$, the epoxy groups are formed both from pendant vinyl groups and from the >C=C< bonds in the backbone. The optimal degree of functionalization can be attained by varying the reaction conditions.

We studied the physicochemical properties of syndiotactic 1,2-PB epoxidized with *tert*-butyl hydroperoxide in the presence of $Mo(CO)_6$. We examined how the content of epoxy groups in the 1,2-polydiene macromolecules affects the intrinsic viscosity [η] of the modified polymer in CCl_4. From the concentration dependence of the reduced viscosity η_r, we calculated [14] the Huggins constants K_χ.

Table 1. Epoxidation of syndiotactic 1,2-PB with peracetic acid and *tert*-butyl hydroperoxide in the presence of $Mo(CO)_6$ in benzene at 20°C

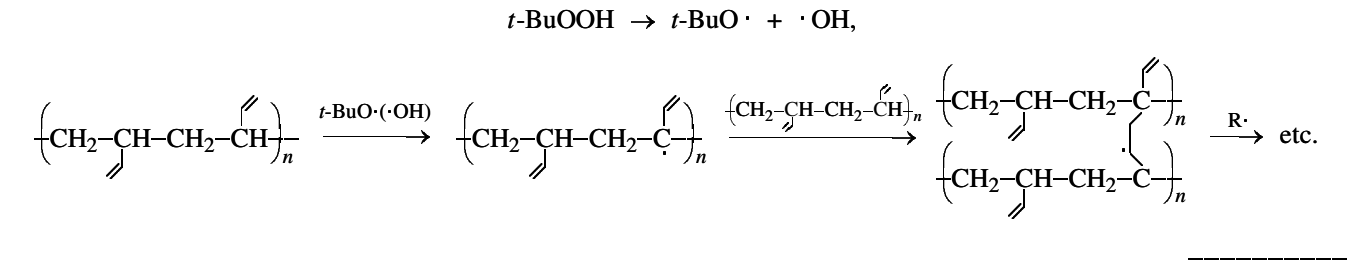
Degree of functionalization of >C=C< bonds,* %		Calculated degree of functionalization of >C=C< bonds in 1,2-PB, %
peracetic acid	*tert*-butyl hydroperoxide	
–	1.5	2.5
1.7	2.3	5.0
2.3	6.0	12.5
3.8	7.4	15.0
4.6	8.9	17.5

* Determined by elemental analysis and functional analysis for epoxy groups.

Table 2 shows that an increase in the degree of epoxidation of syndiotyactic 1,2-PB results in that the intrinsic viscosity of the polymer grows and K_χ decreases. The observed effect is apparently caused by an increase in the mean molecular weight of 1,2-PB (M_w was determined from the light scattering) upon its modification and by a change in the thermodynamic affinity of the polymer for the solvent upon introduction of polar groups into the macromolecules.

We calculated A_2 and $(\overline{R^2})^{1/2}$ for the starting and modified polydiene. We found that an increase in the degree of epoxidation of 1,2-PB results in an increase in [η] and M_w and a decrease in A_2 (Table 2). As a rule, a decrease in A_2 leads to a regular decrease in $(R^2)^{1/2}$ [15]. In the epoxidation of syndiotactic 1,2-PB with *tert*-butyl hydroperoxide in the presence of $Mo(CO)_6$, $(\overline{R^2})^{1/2}$ decreases only at a relatively low degree of functionalization of the polymer (up to ~1.5%), which is apparently due to worse, compared to the starting polymer, thermodynamic affinity of the modified polymer for the solvent and, as a result, to the more compact conformation of the modified macromolecules. However, when the content of the epoxy fragments in the 1,2-PB macromolecules exceeds 2%, a decrease in A_2 is accompanied, by contrast, by an increase in $(\overline{R^2})^{1/2}$ (Table 2).

The observed contradiction is only apparent and is caused by side reactions involving the macromolecules, such as formation of branchings and interchain cross-links by the reactions with peroxy radicals formed in the reaction mixture in the course of epoxidation of the polydiene with *tert*-butyl hydroperoxide:



The formation of structures of this kind in the polymer causes an increase in its mean molecular weight, which leads to an increase in the root-mean-square radius of its coils $(R^2)^{1/2}$ with simultaneous worsening of the thermodynamic affinity for the solvent. Thus, two trends compete: a decrease in the size of the macromolecular coil due to a decrease in the thermodynamic affinity of the macromolecules for the solvent upon an increase in the content of epoxy groups, on the one hand, and an increase in the coil size due to side reactions leading to the formation of branchings and occurring in the epoxidation of 1,2-PB with *tert*-butyl hydroperoxide in the presence of $Mo(CO)_6$, on the other hand.

Table 2. Hydrodynamic and molecular characteristics of syndiotactic 1,2-PB, starting and epoxidized with *tert*-butyl hydroperoxide in the presence of $Mo(CO)_6$ (CCl_4, 20°C)

Degree of epoxidation, %	K_χ	[η], dl g^{-1}	$M_w \times 10^{-5}$	$A_2 \times 10^4$	$(\overline{R^2})^{1/2} \times 10^{-3}$
0	0.98	1.48	3.4	0.80	0.9
1.5	0.94	1.47	4.5	0.50	0.7
3.7	0.91	1.52	8.0	0.30	0.8
6.1	0.89	1.57	8.6	0.20	1.0
8.9	0.68	1.59	13.0	0.15	1.8

With an increase in the polymer concentration in the solution, the mean distance between the macromolecules decreases. As a result, the probability of collision of the macrochains in the course of their random motion and of formation of associates and molecular networks increases. The strength and ordering of the fluctuation structures in polymer solutions can be evaluated from the properties of concentrated solutions, in particular, from the solution viscosity under a shear stress [16].

The rheological properties of solutions of syndiotactic 1,2-PB and its modified derivatives were studied with a Reotest-2M rotary viscometer. We determined how the viscosity η of concentrated (1–10 g dl^{-1}) toluene solutions of syndiotactic 1,2-PB and its epoxy derivatives depends on the shear rate. These data furnish information on the conformation and intermolec-

ular interaction of the macrochains. For modified syndiotactic 1,2-PB containing 2.3 and 8.9% epoxy fragments, we obtained the log–log plots of the viscosity vs. the shear stress (Fig. 1). The curves obtained consist of two portions corresponding to the highest Newtonian (η_0) and effective (η_{eff}) viscosities (regions *A* and *B*, respectively); this pattern is characteristic of non-Newtonian fluids. The lack of the third portion corresponding to the region of the lowest Newtonian viscosity is typical of solutions of flexible-chain polymers [16].

Processing of the experimental results with Frenkel–Eyring's equation (1) allows determination of the activation parameters of the viscous flow, which furnish information on the strength and ordering of molecular structures present in the solution:

$$\eta_0 = A \exp(\Delta G_{vf}/RT), \quad (1)$$

where η_0 is the highest Newtonian viscosity; ΔG_{vf}, activation free energy of the viscous flow; R, gas constant; T, temperature; and A, a coefficient.

If we assume $A = 10^{-4}$ Pa s [15], the calculation of the activation parameters is simplified, and Eq. (1) takes the form

$$\Delta G_{vf} = 2.303RT \log(\eta_0/10^{-4}). \quad (2)$$

The difference between the activation enthalpy of viscous flow, ΔH_{vf}, characterizing the strength of structural bonds and the activation Gibbs energy ΔG_{vf} is the activation entropy of viscous flow (multiplied by temperature) [17]:

$$T\Delta S_{vf} = \Delta H_{vf} - \Delta G_{vf}; \quad (3)$$

then

$$\log \eta_0 = \log 10^{-4} - \Delta S_{vf}/(2.303R) + \Delta H_{vf}/(2.303RT), \quad (4)$$

where ΔS_{vf} is the activation entropy of viscous flow, associated with the ordering of the structure.

From Eq. (2) we can calculate the potential ΔG_{vf}, and from the dependence of $\log \eta_0$ on $1/T$, the activation enthalpy of viscous flow, ΔH_{vf}. The quantities ΔG_{vf} and ΔH_{vf}, calculated from the experimental data for solutions of syndiotactic 1,2-PB and its epoxy derivatives (Fig. 2), are relatively low and, on the whole, typical of flexible-chain polymers [15]; they show that the strength of structural bonds in the derivatives of syndiotactic 1,2-PB is rather low.

The concentration dependences of the activation enthalpy of viscous flow, ΔH_{vf}, of toluene solutions

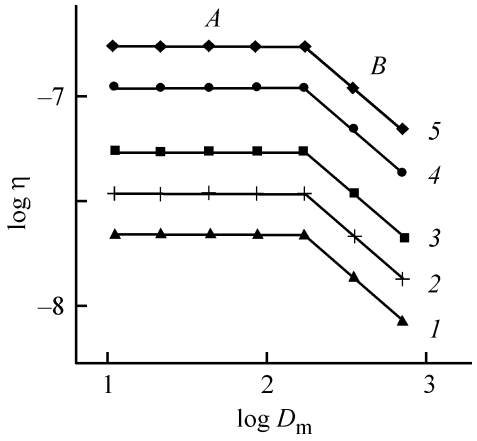


Fig. 1. Viscosity η vs. the shear stress D_m (log–log plot) for a toluene solution of syndiotactic 1,2-PB containing 8.9% epoxy groups (20°C). Polymer concentration, g dl^{-1}: (*1*) 2.0, (*2*) 4.0, (*3*) 6.0, (*4*) 8.0, and (*5*) 10.0. (*A*) Region of the highest viscosity and (*B*) region of effective viscosity.

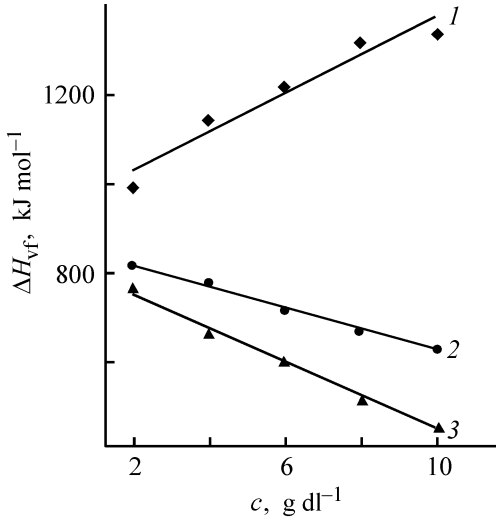


Fig. 2. Activation enthalpy of viscous flow ΔH_{vf} vs. the concentration c of toluene solutions of syndiotactic 1,2-PB and its epoxidized derivatives. Content of epoxy groups in the modified polydiene, %: (*1*) 0, (*2*) 2.3, and (*3*) 8.9; the same for Figs. 3 and 4.

of syndiotactic 1,2-PB and its epoxy derivatives show that ΔH_{vf} decreases upon introduction of epoxy groups to the greater extent, the higher the content of oxirane rings in the macromolecules (Fig. 2). For the modified 1,2-PB, ΔH_{vf} decreases with an increase in the polymer concentration in the solution, whereas for the starting polymer the trend is the opposite. This fact indicates that the bonding strength in associates of the macromolecules containing oxirane groups is lower, compared to the starting polydiene. A decrease in the activation enthalpy of viscous flow with an in-

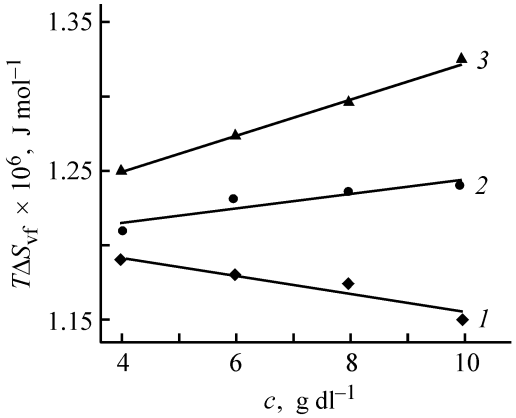


Fig. 3. Activation entropy of viscous flow $T\Delta S_{vf}$ of toluene solutions of syndiotactic 1,2-PB and its epoxy derivatives vs. the polymer concentration c.

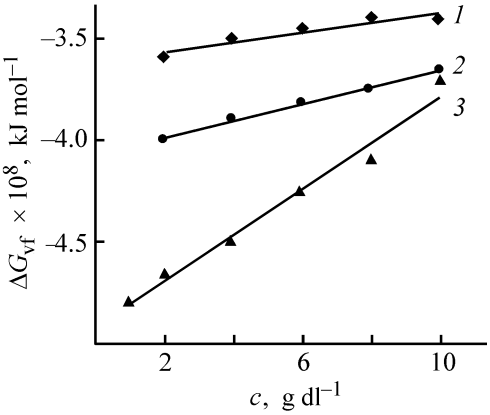


Fig. 4. Activation Gibbs energy of viscous flow ΔG_{vf} of toluene solutions of syndiotactic 1,2-PB and its epoxy derivatives vs. the polymer concentration c.

crease in the content of epoxy groups in the modified syndiotactic 1,2-PB should be attributed to worsening of the affinity of the polymer for the solvent with an increase in the content of epoxy fragments in the macrochains and formation of branched structures.

When a shear stress is applied to solutions of syndiotactic 1,2-PB and its epoxy derivatives, the unrolling of macromolecular coils and molecular orientation prevail, and the system becomes more ordered in the flow. For the starting polydiene, the activation entropy of viscous flow, $T\Delta S_{vf}$, steadily decreases with an increase in the polymer concentration (Fig. 3). For solutions of epoxidized 1,2-PB, the trend is the opposite (Fig. 3) and is caused by hindered unrolling and orientation of macromolecular coils under shear stress, due to the appearance of branched structures upon epoxidation.

The activation Gibbs energy of viscous flow, ΔG_{vf}, increases with the concentration of the starting 1,2-PB (Fig. 4), which is caused by an increase in ΔH_{vf} and a decrease in ΔS_{vf}. This trend should be attributed to profound structurization of the solution at relatively high concentrations of the polymer. Introduction of epoxy groups leads to a decrease in ΔG_{vf} relative to the starting 1,2-PB (Fig. 4), which indicates that the bonding strength in associates of the macromolecules containing oxirane groups is lower, compared to the macrochains of the starting syndiotactic 1,2-PB and hence is more favorable for formation of uniform polymer compositions.

CONCLUSIONS

(1) Syndiotactic 1,2-polybutadiene can be subjected to chemical modification by epoxidation with peracetic acid or with *tert*-butyl hydroperoxide in the presence of $Mo(CO)_6$. Treatment of the polymer with peracetic acid results in epoxidation of the >C=C< bonds in the *cis* units of the backbone only, whereas treatment with *tert*-butyl hydroperoxide in the presence of $Mo(CO)_6$ results also in epoxidation of pendant vinyl groups and thus ensures a higher degree of modification of the polymer.

(2) Epoxidation of syndiotactic 1,2-polybutadiene with *tert*-butyl hydroperoxide in the presence of $Mo(CO)_6$ is accompanied by an increase in the mean molecular weight of the polymer due to formation of branchings and cross-links in the reactions with peroxy radicals.

(3) The activation enthalpies ΔH_{vf} and Gibbs energies ΔG_{vf} of viscous flow of solutions of syndiotactic 1,2-polybutadiene and its epoxy derivatives show that the strength of structural bonds in associates of the macromolecules in concentrated solutions is relatively low.

REFERENCES

1. RF Patent 2221816.
2. Kryuk, T.V., Mikhal'chuk, V.M., Volyanskaya, R.I., et al., *Vopr. Khim. Khim. Tekhnol.*, 2002, no. 3, pp. 73–76, 264.
3. JPN Patent 57-12037.
4. US Patent 1323761.
5. US Patent 6515094.
6. Petti, Z., Mormile, P., Abbatge, M., et al., *J. Mod. Opt.*, 2000, vol. 47, no. 4, pp. 581–585.
7. JPN Patent 53-112955.
8. JPN Patent 55-38991.
9. JPN Patent 58-25324.

10. Abdullin, M.I., Kukovinets, O.S., Kayumova, M.A., et al., *Vysokomol. Soedin., Ser. B*, 2004, vol. 46, no. 10, pp. 1774–1778.
11. Ionin, B.I., Ershov, B.A., and Kol'tsov, A.I., *YaMR-spektroskopiya v organicheskoi khimii* (NMR spectroscopy in Organic Chemistry), Leningrad: Khimiya, 1983.
12. Osamu, H., Tooru, T., Hideo, K., and Haruo, U., *Kobunshi Rombunshu*, 1980, vol. 37, no. 3, pp. 195–198.
13. USSR Inventor's Certificate, no. 1 584 325.
14. Semchikov, Yu.D., *Vysokomolekulyarnye soedineniya* (Macromolecular Compounds), Moscow: Akademiya, 2003.
15. Rafikov, S.R., Budtov, V.P., and Monakov, Yu.B., *Vvedenie v fizikokhimiyu polimerov* (Introduction to Physical Chemistry of Polymers), Moscow: Nauka, 1978.
16. Tverdokhlebova, I.I., *Konformatsiya makromolekul* (*viskozimetricheskii metod otsenki*) (Conformation of Macromolecules (Viscometric Methods of Evaluation)), Moscow: Khimiya, 1981.
17. Tager, A.A., *Fizikokhimiya polimerov* (Physical Chemistry of Polymers), Moscow: Khimiya, 1978.

ISSN 1070-4272, Russian Journal of Applied Chemistry, 2006, Vol. 79, No. 8, pp. 1312–1315. © Pleiades Publishing, Inc., 2006.
Original Russian Text © I.P. Dobrovol'skaya, M.V. Mokeev, Yu.N. Sazanov, A.V. Gribanov, T.E. Sukhanova, 2006, published in Zhurnal Prikladnoi Khimii, 2006, Vol. 79, No. 8, pp. 1326–1329.

MACROMOLECULAR CHEMISTRY AND POLYMERIC MATERIALS

Variation of Supramolecular Structure of Heat-Resistant Polyimide Films during Thermal Treatment

I. P. Dobrovol'skaya, M. V. Mokeev, Yu. N. Sazanov, A. V. Gribanov, and T. E. Sukhanova

Institute of Macromolecular Compounds, Russian Academy of Sciences, St. Petersburg, Russia

Received April 21, 2006

Abstract—Variation of the supramolecular structure of heat-resistant polyimide films in the course of high-temperature treatment was studied by X-ray diffraction analysis and NMR spectroscopy in solids.

DOI: 10.1134/S1070427206080180

A wide range of practical applications of polyimide (PI) films in various branches of industry arouses unremitting scientific interest in carbonization of polyimides. It was shown [1] that high-temperature treatment of polyimides yields crosslinked carbo- and heterocyclic structures. These chemical transformations of macromolecules favor formation of structures having a series of new characteristics and also leads to a high carbon residue in carbonization (up to 50–70%). Subsequent publications have shown [2–4] that the characteristics of carbonized polyimides depend on the chemical structure of the initial polymer, its supramolecular structure, conditions of thermal treatment, and other process parameters. A study of variations of the supramolecular structure of polyimide films in the course of their thermal treatment can give additional data both on thermochemical processes and on expected properties of composite materials based on these films.

In this study, we examined variations of the supramolecular structure of heat-resistant films based on polyimide PM during thermal treatment and the influence of the chemical structure of the polyimide on the type of these variations.

EXPERIMENTAL

The PI PM films were prepared from a solution of polyacrylic acid (PAA), with the subsequent thermal imidization. The film thickness was 20 μm. Pyrolysis was performed in the dynamic mode in an inert medium; the heating rate was 20 deg min^{-1}.

The studies by scanning electron microscopy were performed on a Tesla BS-350 electron microscope; X-ray diffraction measurements, on a DRON-1.5 and KRM devices (Kratky collimation; Cu_{K_α} radiation). The ^{13}C NMR spectra in solids were recorded at room temperature on a Bruker CXP-100 spectrometer using the magic angle spinning (MAS) and cross-polarization (CP) techniques.

The pyrolysis kinetics of the PI PM films was studied at 500°C and keeping time of 1 and 6 h.

The large-angle X-ray diffraction patterns of the initial PI PM films and films pyrolyzed at various temperatures are shown in Fig. 1. The broadening of

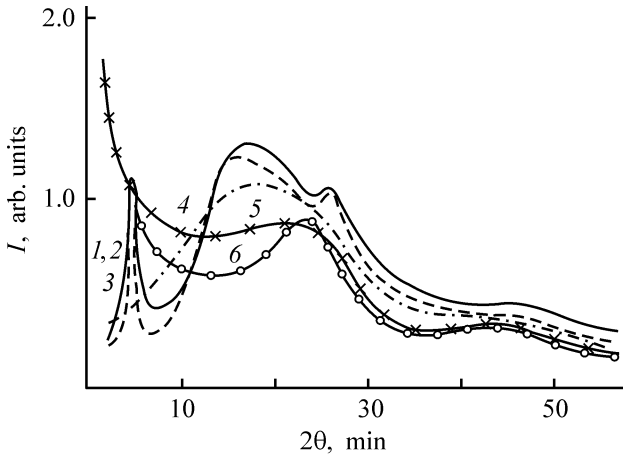


Fig. 1. Large-angle X-ray diffraction patterns of PI PM films: (*1*) initial and (2–6) pyrolyzed at various temperatures. Heat treatment temperature, °C: (*2*) 500, (*3*) 550, (*4*) 600, (*5*) 750, and (*6*) 850. (*I*) Intensity and (2θ) angle.

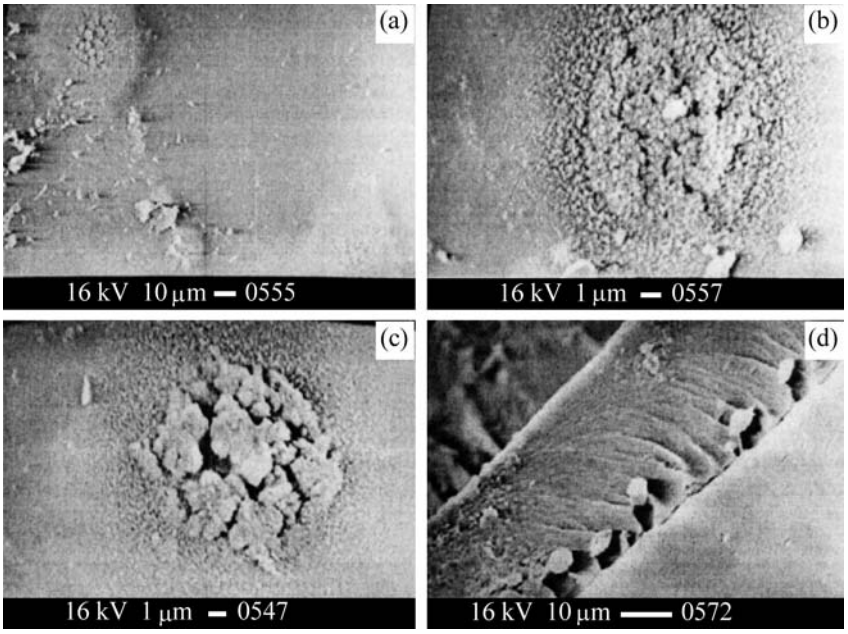


Fig. 2. Photomicrographs of a PI PM film pyrolyzed at 600°C: (a–c) surface and (d) chip in liquid nitrogen.

the reflections in both radial and azimuthal directions in the powder patterns of the initial films suggests the absence of orientation of macromolecules in the film samples and low ordering of the crystallites. A similar structure of crystallites is retained up to 550°C, which follows from the shapes of the X-ray diffraction patterns of the heat treated films.

The main signals in the ^{13}C NMR spectrum of the solid polymer undergo no significant changes up to 550°C, which confirms the constancy of the macromolecule structure. In addition, data of X-ray photoelectron spectroscopy indicate that the main degradation processes in the film studied develop above 550°C [5]. At a pyrolysis temperature of 600°C, the reflections typical of PI PM disappear in the X-ray powder patterns of the films and the carbon reflection (002) appears (Fig. 1, curve *4*). Heating is favorable for formation of turbostratic carbon stacks and, as a consequence, for an increase in the intensity of reflection (002) and decrease in its half-width (curves *5*, *6*). The ^{13}C NMR spectra of pyrolyzed PM samples suggest that heating of the polymer to 600°C causes significant transformation of the polymer chain and strongly alters its structure. At 900°C, the spectrum transforms into a singlet at 123 ppm, corresponding to a polyaromatic turbostratic carbon structure.

The variation of the density heterogeneity of the PI PM films was estimated by the small-angle X-ray scattering. Analysis of the small-angle scattering curves of the initial and pyrolyzed PI PM films shows that the initial films have a weak, virtually degenerated small-angle reflection, which is also preserved after pyrolysis at 550°C. The intensive development of the carbonization process results in disappearance of this reflection (at 600°C) and significant increase in the diffuse scattering above 700°C. This suggests a strong density heterogeneity in the film, caused by the presence of elements of the turbostratic structure, and also the presence of pores with a size of several nanometers to tens of nanometers.

A comparison of the results of large- and small-angle X-ray diffraction analyses suggests that thermal degradation of polyimide PM films begins in less ordered amorphous areas, similarly to the development of pyrolysis of hydrated cellulose fibers and thermal oxidation of polyacrylonitrile fibers [6, 7].

Scanning electron microscopy gives interesting information on the development of the pyrolysis of the PI PM film samples at the micrometer level. The photomicrographs of PI PM films imidized at 400°C, which were used as starting samples for the subsequent pyrolysis and carbonization, are smooth and flat both on the support side and on the free surface. A cleavage made in liquid nitrogen shows the presence of a dense surface layer and a more friable core subjected to scores and exfoliations in little failure at low temperatures. This pattern is in good agreement with numerous published data, in particular [6, 8], for polyimide films and fibers.

The nonuniformity of pyrolysis development at the microlevel is seen in the photomicrographs of the surface of films pyrolyzed at 600°C (Fig. 2).

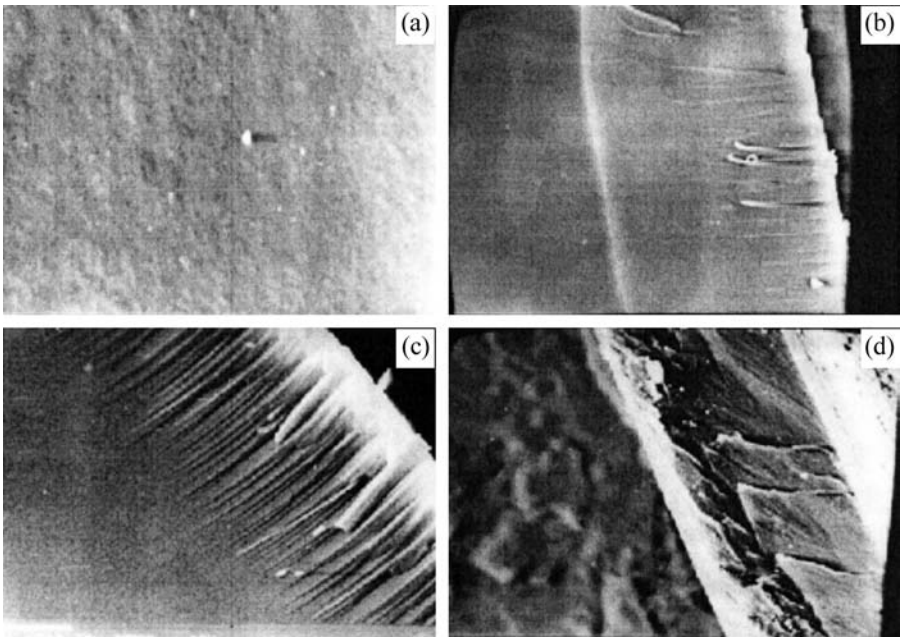


Fig. 3. Photomicrographs of a PI PM film pyrolyzed at 800°C. (a) Surface and (b)–(d) cleavage in liquid nitrogen.

The nucleation sites of the new carbon structure are several micrometers in size and, in turn, consist of finer formations with a size of 1–0.1 μm. The volatile products of polymer decomposition leave the reaction area through the channels clearly visible on the cleaved surfase of the film sample pyrolyzed at 600°C (Fig. 2d).

In carbonization at 700–800°C, the sample is compacted and micropores and cracks are healed, which follows from the photomicrographs of the surface of the PI PM film carbonized at 800°C. This surface is flat and uniform and does not contain no so coarse (of micrometers size) pores and cracks (Fig. 3). It is well known that, in the course of carbonization, the initial sample is subjected to shrinkage, which can reach from 5 to 15–25%.

A large number of parallel cracking strips is seen on the cleaved surface of the carbonized film (Fig. 3). This suggests a layered structure of carbon films based on PI PM.

The carbonized film samples were very little, which did not allow determination of their physicomechanical characteristics.

The heterogeneity of development of the thermal degradation of polyimide films was confirmed in a study of their isothermal pyrolysis.

The large-angle X-ray diffraction patterns of the films pyrolyzed at 500°C in the isothermal mode show that variation of the heating time in a wide range (up to 6 h) does not noticeably affect the shape of the X-ray diffraction patterns. This suggests a high thermal stability of the crystal structure of the PI PM films. At the same time, the intensity of small-angle X-ray scattering increases with the pyrolysis time. The presence of a small-angle X-ray reflection suggests the regular alternation of areas with different densities (large periods) with a size of $c \approx 15.0$–17.0 nm.

In the NMR spectra, the amorphous areas contribute to the signals as broadened pedestals, which is caused by the heterogeneity of the local surrounding of the carbon atoms. In thermal treatment of the PI PM samples, the lines corresponding to the diphenyl oxide fragment are narrowed. This is caused by the conformation ordering of the benzene cores of the macromolecules in the most ordered crystalline areas. In the amorphous areas, where mutual disordering of the chains hampers these processes, thermal degradation with release of thermolysis products is possible. This gives the heterogeneous structure detected by small-angle X-ray scattering.

The increase in the intensity of the small-angle scattering suggests that the density heterogeneity of the structure becomes more pronounced. Since the crystal structure remains unchanged in this process, it can be concluded that thermal degradation of the polymer is localized in intercrystallite amorphous areas, with their density decreasing.

To estimate the influence of phenylene rings in polyimide macromolecule on the structural features of carbonized films, the films based on PI PP were subjected to pyrolysis and carbonization. This polymer contains one phenylene ring in the macromolecule unit, while the PI PM macromolecule contains two phenylene rings.

The large-angle X-ray diffraction patterns of the PI PP films pyrolyzed at 500°C under isothermal conditions show that, as in the case of pyrolysis of PI PM films, the diffraction pattern does not change at this temperature. This fact suggests that the crystal structure of PI PP film does not change during isothermal pyrolysis for various periods (up to 6 h).

As follows from the results of small-angle X-ray diffraction measurements, the intensity of small-angle X-ray scattering significantly decreases as the heating time increases to 6 h, which suggests an equalization of the densities of various structural elements with sizes of 1–5 nm. Therefore, it can be concluded that, in contrast to the PI PM film, the supramolecular structure becomes more compact in pyrolysis of a film based on PI PP.

Comparison of small-angle scattering data for PI PM and PI PP films shows that PI PP films have a significantly higher density heterogeneity of supramolecular structure, compared to PI PM. This is evidently caused by the increased rigidity of the PI PP macromolecule due to the absence of "oxygen hinge" between phenyl rings. This significantly decreases the mobility of PI PP and hampers ordering in formation of the film structure. The presence of the –O– hinge group in the polymer structure results in that thermal degradation of the polymer chain starts from this bond [9]. The onset of homolytic degradation of benzimide rings and formation of interchain crosslinking are observed in the same temperature range. The absence of a "hinge" in the chain hampers rearrangement of macromolecules, recorded as line narrowing in the ^{13}C NMR spectra of PI PM. This is supported by a decrease in the intensity of small-angle X-ray scattering with increasing pyrolysis time. The thermal degradation of macromolecules makes higher the mobility of intermediates, which, in turn, can assist to structural rearrangements resulting in that the density heterogeneity decreases. It is likely that the latter causes the decrease in the intensity of small-angle X-ray scattering in pyrolysis of PI PP films.

A high heterogeneity of the hypomolecular structure of the PI PP films and the intensive processes on both molecular and supramolecular levels, which occur in the course of pyrolysis, exert a strong influence on the structure and characteristics of these films. The films based on this polymer and carbonized at 900°C had low strength and high brittleness.

CONCLUSIONS

(1) The crystalline regions of PM polyimide films have high heat resistance up to 550°C. In the amorphous regions, thermolysis and carbonization of the sample are accompanied by an increase in the heterogeneity on the nanometer level.

(2) An increase in the molecular mobility of macromolecules of a PP polyimide film in comparison with a PM film leads to higher heterogeneity of the density of the film; its carbonization is accompanied by equalization of the densities of structural elements with a size of 1–5 nm.

REFERENCES

1. Gribanov, A.V. and Sazanov, Yu.N., *Zh. Prikl. Khim.*, 1997, vol. 70, no. 6, pp. 881–902.
2. Gribanov, A.V., Sazanov,Yu.N., Beloborodova, E.V., and Fedorova, G.N., *Zh. Prikl. Khim.*, 1999, vol. 72, no. 3, pp. 467–473.
3. Gribanov, A.V. and Sazanov, Yu.N., *Zh. Prikl. Khim.*, 2000, vol. 73, no. 3, pp. 465–469.
4. Gribanov, A.V. and Sazanov, Yu.N., *Zh. Prikl. Khim.*, 2000, vol. 73, no. 10, pp. 1705–1709.
5. Sazanov, Yu.N., Stepanov, N.G., Shibaev, L.A., et al., *Acta Polym.*, 1998, vol. 39, no. 8, pp. 431–434.
6. Dobrovol'skaya, I.P., Slutsker, L.I., Chereiskii, Z.Yu., and Utevskii, L.E., *Vysokomol. Soedin., Ser. A*, 1975, vol. 17, no. 7, pp. 1555–1559.
7. Dobrovol'skaya, I.P., Utevskii, L.E., and Varshavskii, V.Ya., *Vysokomol. Soedin., Ser. B*, 1978, vol. 20, no. 12, pp. 909–911.
8. Sukhanova, T.E., Structuring and Morphology of Oriented Polyimides and Fiber Composites Based on These, *Doctoral Dissertation*, St. Petersburg, 2000.
9. Gribanov, A.V., Sazanov, Yu.N., and Mokeev, M.V., *Zh. Prikl. Khim.*, 2002, vol. 75, no. 4, pp. 620–624.

ISSN 1070-4272, Russian Journal of Applied Chemistry, 2006, Vol. 79, No. 8, pp. 1316–1320. © Pleiades Publishing, Inc., 2006.
Original Russian Text © O.B. Kucherenko, C. Kohlert, E.A. Sosnov, A.A. Malygin, 2006, published in Zhurnal Prikladnoi Khimii, 2006, Vol. 79, No. 8, pp. 1330–1333.

MACROMOLECULAR CHEMISTRY AND POLYMERIC MATERIALS

Synthesis and Properties of Polyvinyl Chloride Films with Modified Surface

O. B. Kucherenko, C. Kohlert, E. A. Sosnov, and A. A. Malygin

St. Petersburg State Technological Institute, St. Petersburg, Russia
Klöeckner Pentaplast GmbH & Co. Kg, Montabaur, Germany

Received March 10, 2006

Abstract—Atomic-force microscopy was used to study structural chemical transformations on the surface of polyvinyl chloride films subjected to modification with compounds based on acrylic acid derivatives, with preliminary activation of the polymer surface with a corona discharge.

DOI: 10.1134/S1070427206080192

Polymeric materials, e.g., polyvinyl chloride (PVC), find wide use in various industries, e.g., as components of modern packaging materials, owing to such properties as transparence, low density, and chemical stability.

It is [1] known that use of various methods of surface modification and, in particular, of those in which various functional groups and fragments of a different chemical nature are introduced into macromolecules enables control over properties of materials and favors considerable expansion of their application areas. To raise the surface activity of polymers, various physical treatments of a polymer: laser or UV irradiation, corona discharge, etc. are used prior to, or together with chemical modification [2]. The processes occurring in this case, result in that a positive or negative charge (electret effect) or new functional groups that can enter into chemical interactions with other modifying agents appear on the surface.

A promising way to improve the adhesion properties of polymers are various types of surface treatment, which should create stable active centers. As treatments of this kind can be classed vapor-phase chemical modification and, in particular, chemical vapor deposition onto the surface of a solid polymeric matrix of organic structures that make higher its polarity [3].

The aim of the present study was to examine chemical transformations that occur in PVC under the action of a corona discharge and upon the subsequent interaction with derivatives of acrylic and metacrylic acids and to analyze the influence of the surface organic structures synthesized on the adhesion properties of PVC.

EXPERIMENTAL

As objects of study served 200–300-μm-thick PVC films of Pentaprint brand (manufactured by Klöeckner Pentaplast GmbH). The surface of a prescribed composition was formed using a procedure based on the treatment of the polymer surface with a flow of charged particles and chemical vapor deposition of organic structures, derivatives of acrylic and methacrylic acids. The choice of the modifying agents was due to the necessity for use of a combination of substances that can enter into a photochemical chain reaction of polymerization, initiated on the polymer surface in the course of offset printing. To reveal the effect of modification on the PVC properties, the surface structure and free surface energy of the starting and final products were studied by atomic-force microscopy (AFM) [4].

Organic acryl structures were synthesized on a Coating Star industrial installation (Ahlbrandt GmbH, Germany), shown schematically in Fig. 1. A PVC film was modified in a reactor *1*, in which a corona discharge *2* was initiated in the range 2.0–2.5 W cm^{-1} at room temperature and atmospheric pressure. Vapors of reagents were delivered at a pressure of $(1.5–2.0) \times 10^5$ Pa and temperature of 35–38°C via systems for mixing (*3*) and spraying (*4*) into reactor *1* into the atmosphere of corona discharge *2*.

To preclude any rise in temperature in the reactor and in the corona discharge zone, a cooling system *5* was used. As modifying agents were used benzotriazole, polyethylene diacrylate, morpholine monoacrylate, and 6-ethoxy methacrylate. The results of surface modification with low-molecular-weight reagents were assessed by the degree of polarity and changes in the surface morphology of films.

The surface energy of PVC was studied on a DSA 100 instrument (Kruess GmbH), which measures the surface wetting angle for two control liquids with known surface tension energy in the dynamic mode. The supply rate of the control liquids was 8–10 μl min^{-1}. The free surface energy was calculated by the Owens–Wendt–Rabel–Kaelble method [5]:

$$\sigma_s = \sigma_{sl} + \sigma_l \cos\theta,$$

where σ_s is the surface energy of the solid phase, which depends on the angle θ of wetting of the solid by the liquid phase chosen for measurements, on the surface tension energy of the liquid phase (σ_l), and on the free energy of the solid–liquid interface (σ_{sl}).

The state of the initial surface and changes of its topography upon coating deposition were studied on a Solver P47 Pro scanning probe microscope (NT–MDT, Russia)[1] by the AFM technique in the tapping mode in air, with an NSG-01 silicon cantilever used. The samples were scanned in two modes, which yielded various kinds of information about the structure and properties of a material by measuring (i) topography and (ii) phase contrast. The latter approach revealed differences in the composition of different parts of the sample surface by analyzing data on the phase shift of the amplitude-frequency characteristic of the cantilever as a result of adhesion interactions [6].

It is known that irradiation of polymeric insulators with flows of charged particles results in a buildup of positive or negative charge [7, 8] on their surface and generates polar functional groups, such as carboxy, carbonyl, and hydroxy groups, as well as amino groups [9]. The aim of such a physical treatment of the polymer surface is to produce polar active centers that can be involved in chemisorption in deposition of subsequent layers, lamination, or printing. The stability and concentration of active centers of this kind is a function of the surface Gibbs free energy, which, in turn, depends on the chemical composition and structure of the polymeric material and its phase state [10].

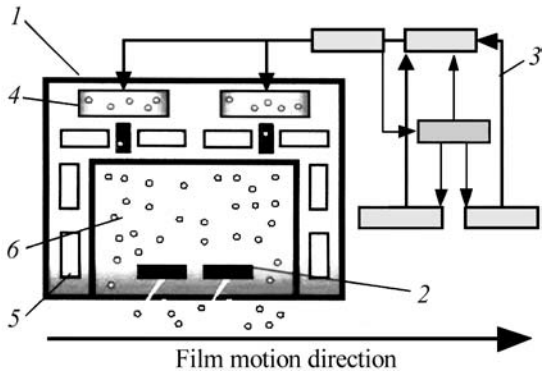


Fig. 1. Schematic of the installation for surface modification of PVC films. (*1*) Reactor, (*2*) electrodes and the corona discharge zone, (*3*) system for mixing and delivery of reagents, (*4*) system for spraying of the reagents, (*5*) reactor cooling system, and (*6*) area of coating deposition.

The table lists the results obtained in measuring the free surface energy of the initial and modified PVC. It follows from the data in the table that surface modification gives rise to new active centers and, accordingly, leads to comparatively high surface polarities. Prolonged measurements (up to 150 days) suggest that the modified surface is stable. The insignificant changes in the surface energy of modified films can be attributed to relaxation of active centers that did not enter into the reaction of chemical de-

Free surface energy of modified PVC films* (initial PVC: σ_g = 36.89 mN m^{-1}, σ_{pol} = 0.60 mN m^{-1}, σ_{disp} = 39.29 mN m^{-1})

τ, day	σ, mN m^{-1}		
	σ_g	σ_{pol}	σ_{disp}
0	44.35	5.29	39.06
12	44.35	5.19	39.16
9	44.15	4.37	39.78
33	43.80	4.45	39.35
62	42.13	4.28	37.85
90	41.35	4.59	37.75
148	41.96	3.95	38.00

[1] Studies carried out at the Shared Center "Chemical Assembly of Nanomaterials" at St. Petersburg State Technological Institute (Technological University).

* σ_g is the free surface energy of a film; σ_{pol}, its polar component; and σ_{disp}, its dispersion component in accordance with the Antonov formula $\sigma_g = \sigma_{pol} + \sigma_{disp}$.

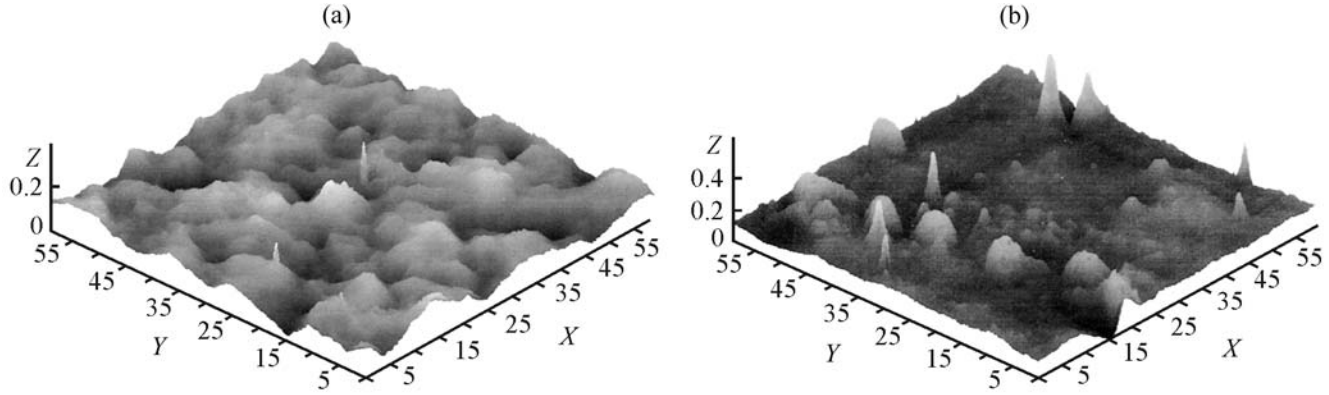


Fig. 2. 3*D* reconstruction of the surface of a PVC film. Film: (a) initial and (b) that modified with derivatives of acrylic and methacrylic acids in a corona discharge.

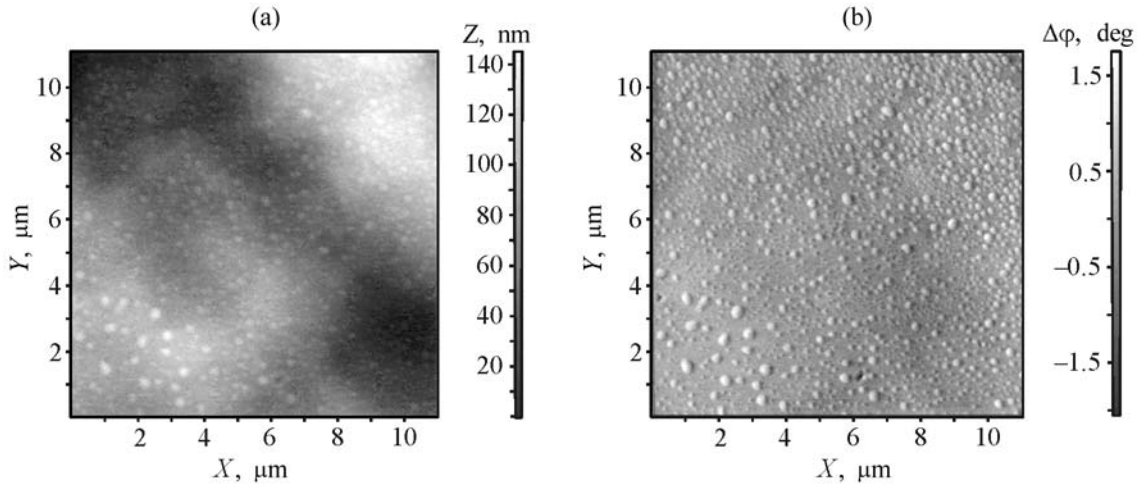


Fig. 3. AFM reconstruction of the surface of a PVC film. (a) Topography and (b) phase-contrast mode.

position or to gradual neutralization in interaction with air of charged particles produced upon preliminary treatment of the surface with a corona discharge.

A study of the surface morphology of the initial PVC by the AFM method (Fig. 2a) revealed that the film has a sufficiently smooth surface with a roughness determined in accordance with DIN 4768 equal to 2–5 nm. Irregularly arranged rounded projections 150–200 nm in diameter and 10–20 nm high are observed over the entire surface (Fig. 3a). At the same time, surface scanning in the phase-contrast mode did not reveal any differences in adhesion properties between different parts of the surface (Fig. 3b), which indicates that the chemical composition and properties of the entire surface of the initial PVC film are uniform.

Chemical modification of a PVC film with a mixture of derivatives of acrylic and metacrylic acids in a corona discharge leads to a significant change in the topography of the material (Fig. 2b): separate structures of irregular shape, 8–15 μm in size and up to 0.5 μm high, appear on the surface in addition to smooth areas. At the same time, the surface roughness remains virtually unchanged (20–30 nm) as compared with the initial PVC.

A scanning in the phase-contrast mode revealed that chemical modification of a PVC film results in that two types of areas with different levels of the adhesion interaction with the silicon cantilever appear on its surface (Fig. 4). Comparison of the surface morphology and data obtained in scanning in the phase-contrast mode shows that the volume structures appearing on the surface have a chemical nature different from that of PVC and presumably belong to the organic coating formed as a result of this treatment. The polyvinyl chloride film is covered with the organic coating nonuniformly: areas with the initial

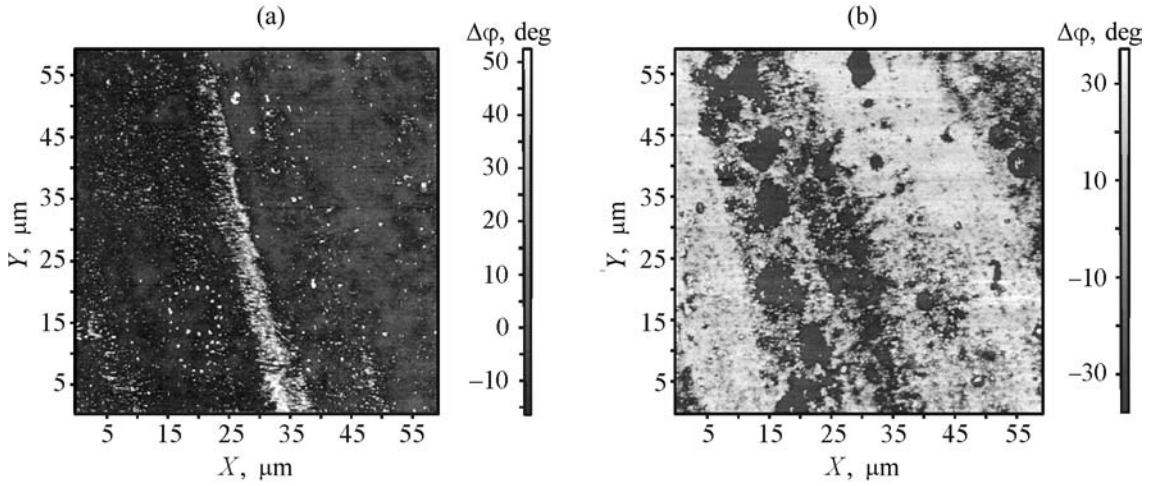


Fig. 4. AFM reconstruction of the surface of a modified PVC film. Phase-contrast mode. (a, b) Areas with different degrees of the surface coverage by modifying agents. *Light areas*, PVC; *dark areas*, coating deposited in a corona discharge.

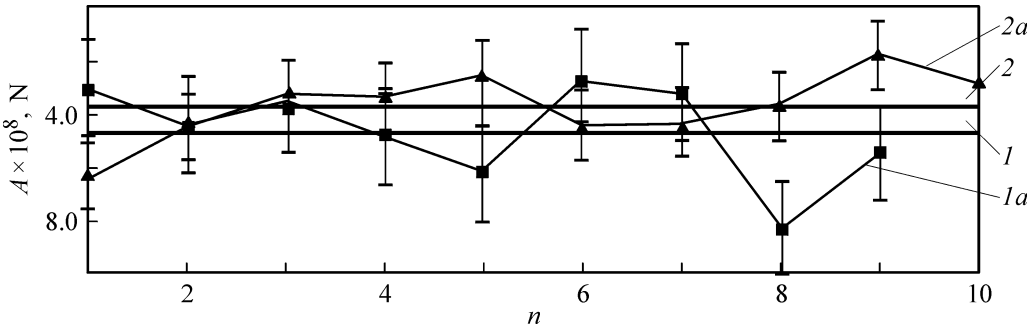


Fig. 5. Comparison of adhesion forces *A* of the surface of (*1, 1a*) initial and (*2, 2a*) modified PVC. (*n*) Number of measurements. (*1a, 2a*) Results of measurements of the adhesion force of the PVC surface; (*1, 2*) averaged adhesion force.

PVC film virtually completely covered with a newly formed of average thickness 100 nm (Fig. 4a) and those partly exposed (Fig. 4b) are observed.

The effect of chemical modification on the adhesion properties of the surface was assessed by a change in the interaction of the surface with an offset printing ink. Black and orange industrial offset inks of Sicpa brand with a high absorption coefficient of UV light were used for this purpose. It should be noted that offset printing is a complex physical process, which occurs at a high rate and imposes stringent requirements to the quality and structure of the surface of a solid support. It is known that the film surface is wetted by the ink in the initial stage of deposition. Then a photochemical chain reaction of polymerization is initiated by UV irradiation, which results in that offset inks are hardened and retained on the polymer surface by forces of the atomic-molecular interaction, which appear between the liquid and solid phases in the course of wetting [2, 9]. Figure 5 shows adhesion curves for the initial and modified PVC surfaces. The differences in the adhesion interaction forces between these two kinds of surfaces suggest that forces of not only physical, but also chemical, covalent nature exist in the case of a chemically modified surface. This confirms once more that organic functional groups interact with molecules of the solid-phase PVC surface.

CONCLUSIONS

(1) The results obtained in a physicochemical study of the products formed in interaction of a gaseous mixture of derivatives of acrylic and metacrylic acids with polyvinyl chloride films made it possible to suggest that organic functional structures are chemically grafted to reactive centers created by preliminary treatment of the polymer surface with a corona discharge.

(2) A study of the properties of the modified surface in offset printing and its analysis by atomic-force microscopy revealed that the grafted functional groups

are involved in the photochemical chain reaction of radical polymerization and the adhesion properties of the polymer toward the inks used in practice are improved.

REFERENCES

1. Malkov, A.A., Malygin, A.A., and Trifonov, S.A., *Metod molekulyarnogo naslaivaniya – osnova noveishei pretsizionnoi tekhnologii* (Method of Molecular Layering as a Basis for Newest Precision Technology), Available from VINITI, 1992, St. Petersburg, no. 2205-V92.
2. Wertz, K.W., *Praxishandbuch moderne Beschichtungen*, Hanser, 2001.
3. Povstugar, V.I., Kodolov, V.I., and Mikhailova, S.S., *Stroenie i svoistva poverkhnosti polimernykh materialov* (Surface Structure and Properties of Polymeric Materials), Moscow: Khimiya, 1988.
4. Malygin, A.A., *Zh. Prikl. Khim.*, 1996, vol. 69, no. 10, pp. 1585–1593.
5. Elias, H.-G., *Makromolekule*, Viley-VCH, 2000.
6. Magonov, S.M., Elings, V., and Whangbo, M.-H., *Surf. Sci.*, 1997, vol. 375, nos. 2–3, pp. L385–L391.
7. Rychkov, A.A., Rychkov, D.A., and Trifonov, S.A., *Polimernye dielektriki* (Polymeric Insulators), St. Petersburg: OOO Knizhnyi Dom, 2005.
8. Rychkov, A.A., Boitsov, V.G., and Shvets, B.B., *Proc. 9th Int. Symp. Electrets (ISE-9)*, Shanghai, 1996, pp. 89–92.
9. Doerfler, H.-D., *Springer*, 2002, pp. 827–863.
10. Bartenev, G.M. and Frenkel', S.Ya., *Fizika polimerov* (Physics of Polymers), Leningrad: Khimiya, 1990.

ISSN 1070-4272, Russian Journal of Applied Chemistry, 2006, Vol. 79, No. 8, pp. 1321–1324. © Pleiades Publishing, Inc., 2006.
Original Russian Text © E.N. Popova, A.L. Didenko, V.M. Svetlichnyi, V.E. Yudin, E.A. Kaidash, E.S. Vasil'eva, O.V. Tolochko, D.W. Li, D. Kim, 2006, published in Zhurnal Prikladnoi Khimii, 2006, Vol. 79, No. 8, pp. 1334–1336.

MACROMOLECULAR CHEMISTRY AND POLYMERIC MATERIALS

Synthesis and Properties of Films of a Polyimide Filled with Ferromagnetic Nanoparticles

E. N. Popova, A. L. Didenko, V. M. Svetlichnyi, V. E. Yudin, E. A. Kaidash, E. S. Vasil'eva, O. V. Tolochko, D. W. Li, and D. Kim

Institute of Macromolecular Compounds, Russian Academy of Sciences, St. Petersburg, Russia
St. Petersburg State Polytechnic University, St. Petersburg, Russia
Korea Institute of Machinery and Materials, Changwon, South Korea

Received March 23, 2006

Abstract—Film-forming polyimide nanocomposites containing 5 to 20 wt % nanoparticles were prepared from ferromagnetic Fe/Fe_3O_4 nanoparticles and a polyimide derived from 4,4'-bis(4-aminophenoxy)diphenyl sulfone and 1,3-bis(3,4-dicarboxyphenoxy)benzene dianhydride. The mechanical properties and magnetization of the nanocomposite samples were studied in relation to the nanoparticle concentration.

DOI: 10.1134/S1070427206080209

Introduction of nanosized inorganic fillers into polymers yields novel materials, so-called nanocomposites [1, 2]. With the progress of nanotechnologies, major attention is given to the development of new nanocomposites based on carbon-containing, metallic, or ceramic nanoparticles. These materials can be used for preparing protective antifriction coatings, components for high-frequency magnetic shields, and articles exhibiting optical, conducting, and other properties [3–5].

Polyimides (PIs), thanks to their high mechanical properties and heat resistance [6, 7], are of particular interest as a polymeric base for nanocomposites. Imide-containing magnetic composites filled with 75–100-μm magnetic particles (Nd–Fe–B) were prepared by a specially developed procedure involving synthesis in a melt [8–10]. This procedure makes it possible to prepare magnetic plastics at lower temperatures (220–240°C), compared to compacting of the corresponding polymeric composites at 350°C, using the powder metallurgy techniques, and to avoid oxidation of ferromagnetic particles. The use of a new kind of nanoparticles, magnetic iron nanoparticles in an oxide shell, will allow preparation of elastic highly heat-resistant magnetic nanocomposites under the conditions of traditional two-step procedure for synthesis of polyimides [11].

The goal of this study was to examine the possibility of introduction of magnetic iron nanoparticles in an oxide shell into a polyimide matrix and to analyse the mechanical and magnetic properties of the resulting materials in relation to the filler content.

EXPERIMENTAL

Fe/Fe_3O_4 nanoparticles were prepared by chemical vapor condensation [1]; they consist of an iron (Fe) core encapsulated in a 2–4-nm-thick magnetite (Fe_3O_4) shell [12]. These nanoparticles have an approximately spherical shape with a diameter of 15–25 nm (Fig. 1).

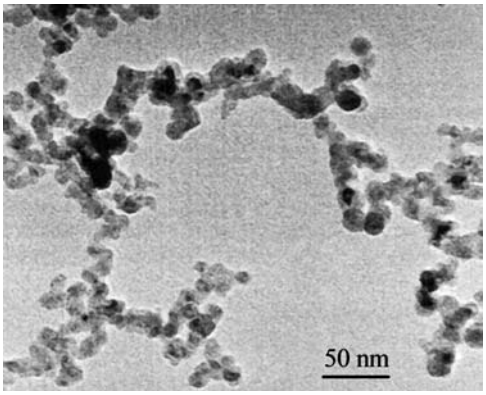
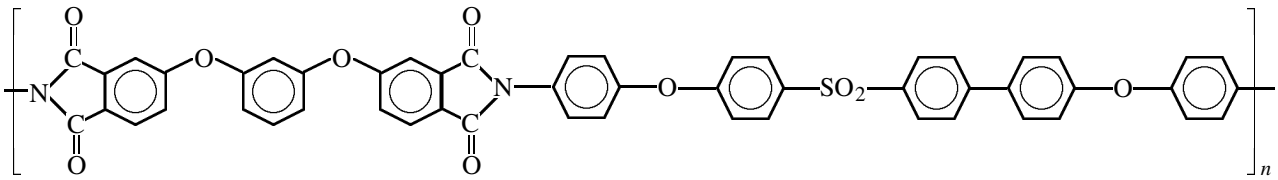


Fig. 1. Photomicrographs of Fe/Fe_3O_4 nanoparticles.

As a polymeric matrix of the composite material we used the polyimide derived from 4,4'-bis(4-aminophenoxy)diphenyl sulfone and 1,3-bis-(3,4-dicarboxyphenoxy)benzene dianhydride (PI P-SOD) [13]; its structural formula is given below:



The nanocomposite was prepared as follows. A round-bottomed flask was placed in an ultrasonic bath (40 kHz) equipped with a stirrer and a tube for feeding Ar. The flask was charged with the solvent, *N*-methyl-2-pyrrolidone (MP), in which the required amount of Fe/Fe_3O_4 nanoparticles (5–30 wt % relative to PI, depending on the desired concentration of the nanoparticles in the polyimide film) was dispersed for 1 h by ultrasonic treatment combined with stirring. Then the diamine, 4,4'-bis(4-aminophenoxy)diphenyl sulfone (SOD), was added. After the added diamine completely dissolved, an equimolar amount of 1,3-bis-(3,4-dicarboxyphenoxy)benzene dianhydride (P) was added, and the solution was stirred for 2 h in an argon flow, with the ultrasonic treatment continued until the dianhydride complete dissolved. The resulting solution of the prepolymer, polyamido acid (PAA), was applied onto glass plates as a thin layer. After the solvent evaporation at 60°C for 24 h, 40 ± 5-μm-thick PAA films were obtained; these films were subsequently imidized by stepwise heating (100°C, 1 h; 200°C, 1 h; 250°C, 1 h).

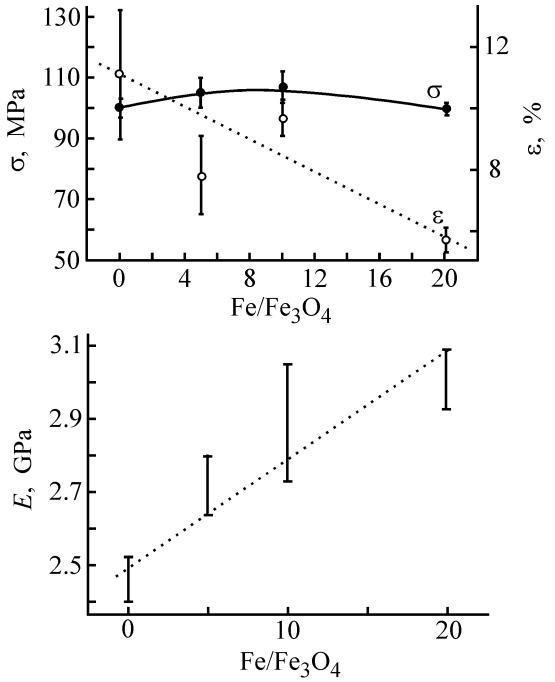


Fig. 2. Properties of samples of polyimide nanocomposites P-COD/Fe/Fe_3O_4 vs. the content (wt %) of the nanoparticles in the polyimide matrix. (σ) Ultimate tensile strength, (ε) relative elongation, and (*E*) Young's modulus.

The mechanical properties (tensile strength σ, Young's modulus *E*, and break elongation ε) of the film samples of the polyimide–metal nanocomposites were determined with a UMIV-3 tensile-testing machine (Russia). Samples of nanocomposites for mechanical tests were films of the following dimensions: thickness 40 ± 5 μm, width 2 mm, and base length 30 mm. Tensile tests were performed at room temperature in the active-loading mode at a rate of 1 mm min^{-1}.

The magnetic properties of the films were studied in fields of up to 10 kOe by vibration magnetometry using a Lakeshore 7400 standard magnetometer.

An optical microscopic examination of nanocomposite specimens revealed no inclusions or aggregates of the metallic powder, visible at ×500 magnification, at a filler content of up to 20 wt %. At the Fe/Fe_3O_4 content increased to 30 wt %, it appeared impossible to obtain a homogeneous distribution of the particles in the polymer matrix. The material is optically transparent at a filler content of 0 to 10 wt %.

Figure 2 shows how the mechanical properties of the nanocomposite films vary with the filler content. With an increase in the filler concentration, the film strength, 105 ± 2 MPa, remains unchanged within the measurement error. With an increase in the Fe/Fe_3O_4 concentration, the break elongation of the films somewhat decreases (from 11 to 6%), but remains sufficiently high to avoid brittle failure at bending. It should also be noted that, as the filler content is

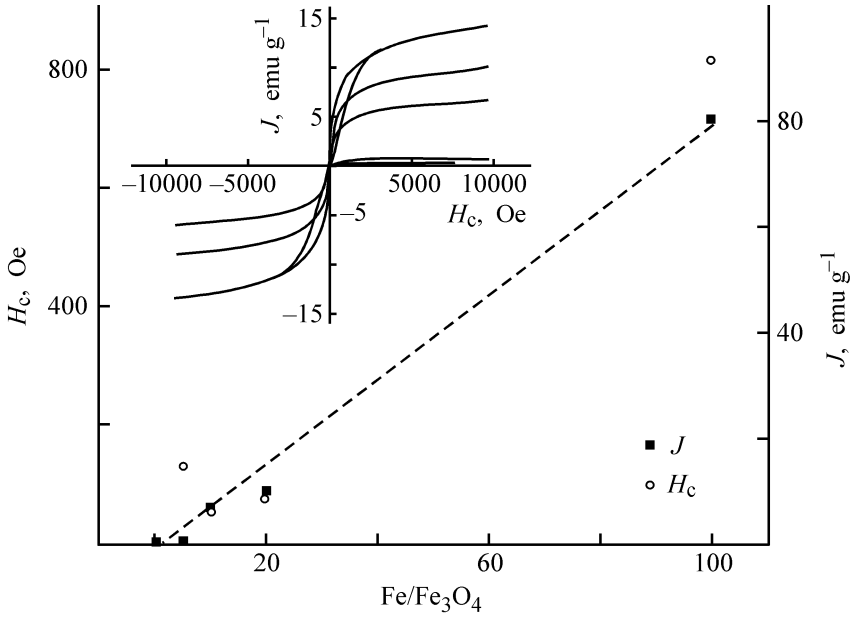


Fig. 3. Maximal magnetization J and coercivity H_c of samples of polyimide nanocomposites P-SOD/Fe/Fe_3O_4 vs. the filler content. Inset: characteristic hysteresis loops of the nanocomposites containing 20, 10, and 5 wt % nanoparticles.

raised from 0 to 20 wt %, Young's modulus increases from 2.4 to 3 MPa, with the elastic properties preserved.

The influence of the filler content on the maximal specific magnetization and coercivity of the composite material is illustrated by Fig. 3. The points corresponding to the initial nanoparticles (100% Fe/Fe_3O_4) are given for comparison. The inset shows the characteristic hysteresis loops.

The maximal specific magnetization of the material linearly increases with the concentration of ferromagnetic particles in the polyimide matrix. The coercivity of the nanocomposite is considerably lower than that of the initial powder and shows no definite correlation with the filler content. Apparently, at random orientation of single-domain particles and at their fixed arrangement in the polymer matrix, the coercivity will depend on the particle orientation (easy magnetization axis) relative to the measurement field, whereas at predominant orientation along the field it will have a maximum. In our experiment, the particles were oriented randomly, and, therefore, there was no pronounced correlation between the coercivity and filler content. Apparently, to obtain a high-coercivity material, it is necessary to provide definite orientation of particles in the matrix, e.g., by curing the polymer in a magnetic field.

CONCLUSION

Flexible ($\varepsilon \leq 10\%$) films of nanocomposites containing 5 to 20 wt % ferromagnetic Fe/Fe_3O_4 nanoparticles in a matrix of the polyimide derived from 4,4'-bis(4-aminophenoxy)diphenyl sulfone and 1,3-bis(3,4-dicarboxyphenoxy)benzene dianhydride were prepared. With an increase in the filler concentration, the magnetization of the film samples linearly increases, and Young's modulus grows from 2.4 to 3.0 GPa.

ACKNOWLEDGMENTS

The study was financially supported by the Russian Foundation for Basic Research (project no. 04-03-32470).

REFERENCES

1. Gubin, S.P., Koksharov, Yu.A., Khomutov, G.B., and Yurkov, G.B., *Usp. Khim.*, 2005, vol. 74, no. 6, pp. 539–574.
2. Vaia, R.A., Tolle, T.B., Schmitt, G.F., et al., *SAMPE J.*, 2001, vol. 37, no. 6, p. 24.
3. Pomogailo, A.D., Rozenberg, A.S., and Uflyand, I.E., *Nanochastitsy metallov v polimerakh* (Metal Nanoparticles in Polymers), Moscow: Khimiya, 2000.
4. Vora, R.H., Pallathadka, P.K., Goh, S.H., et al.,

Macromol. Mater. Eng., 2003, vol. 288, no. 4, pp. 337–356.

5. Fischer, N., *Mater. Sci. Eng.*, 2003, vol. 23, pp. 763–772.
6. Wilson, D., Stengenberger, H.D., and Hergenrother, P.M., *Polyimides*, New York: Chapman and Hall, 1990.
7. Sroog, C.E., *Prog. Polym. Sci.*, 1991, vol. 16, pp. 561–694.
8. Yudin, V.E., Otaigbe, J.U., Bui, T.X., and Svetlichnyi, V.M., *J. Appl. Polym. Sci.*, 2003, vol. 88, pp. 3151–3158.
9. Yudin, V.E., Otaigbe, J.U., Bui, T.X., and Svetlichnyi, V.M., *J. Appl. Polym. Sci.*, 2006, vol. 100, pp. 478–485.
10. Choi, C.J., Tolochko, O., and Kim, B.K., *Mater. Lett.*, 2002, vol. 56, no. 3, pp. 289–294.
11. Bessonov, M.I., Koton, M.M., Kudryavtsev, V.V., and Laius, L.A., *Poliimidy – klass termostoikikh polimerov* (Polyimides: a Class of Heat-Resistant Polymers), Leningrad: Nauka, 1983.
12. Choi, C.-J., Kim, B.-K., Tolochko, O., and Li-Da, *Rev. Adv. Mater. Sci.*, 2003, vol. 5, no. 5, pp. 487–492.
13. Yudin, V.E., Divoux, G.M., Otaigbe, J.U., and Svetlichnyi, V.M., *Polymer*, 2005, vol. 46, pp. 10866–10872.

ISSN 1070-4272, Russian Journal of Applied Chemistry, 2006, Vol. 79, No. 8, pp. 1325–1328. © Pleiades Publishing, Inc., 2006.
Original Russian Text © V.M. Misin, A.I. Kuzaev, M.V. Misin, 2006, published in Zhurnal Prikladnoi Khimii, 2006, Vol. 79, No. 8, pp. 1337–1340.

MACROMOLECULAR CHEMISTRY AND POLYMERIC MATERIALS

Preparation and Characteristics of Thin Films of Phenyl-containing Polyacetylenes

V. M. Misin, A. I. Kuzaev, and M. V. Misin

Institute of Biochemical Physics, Russian Academy of Sciences, Moscow, Russia
Institute for Problems of Chemical Physics, Russian Academy of Sciences, Chernogolovka, Moscow oblast, Russia

Received March 7, 2006

Abstract—Colored thin films with a thickness of 0.1–10 μm were prepared by the vacuum sputtering of phenyl-containing polyacetylenes. The mechanism of formation of ordered films was analysed. The characteristics of the films were studied and possible fields of their application were outlined.

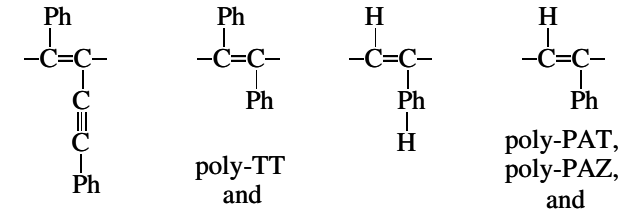
DOI: 10.1134/S1070427206080210

The specific features of molecular structure and electrophysical, optical, and magnetic characteristics of polyacetylenes necessitate use of new procedures for production of various new materials based on homo- and copolymers of substituted acetylenes and acetylenecontaining oligomers [1–3]. For example, new approache have made it possible to prepare high-temperature composites and ceramics with carborane-containing acetylenesiloxanes [4], reactive elastomers containing two types of the C=C bonds using propyne and allene [5], films based on (*p*-*tert*-butyl-*o*,*o*'-dimethylphenyl)acetylene polymer allowing separation of oxygen and nitrogen [6], and liquid crystals based on acetylene-containing macromonomers [7].

Here we report first data on the formation of uniform thin films by vacuum sputtering of various polyphenylacetylenes. We also discuss the characteristics of films and possible fields of their application. The starting substances were polymers of diphenyldiacetylene (poly-DPDAC), *p*-diethynylbenzene (poly-DEBA), phenylacetylene (poly-PAT, poly-PAZ, poly-PAAC), and tolan (poly-TT and poly-TA) prepared by various procedures. The last letter (last letters in the case of poly-PAAC) in the abbreviation denotes the synthesis procedure: thermal polymerization (T), polymerization in the presence of acetylacetonate (AC), and anionic (A), Ziegler (Z), or cobalt-containing (C) catalysts.

EXPERIMENTAL

The polymers were synthesized by the following procedures: poly-DPDAC [8], poly-PAT [9], poly-PAZ [10], poly-PAAC [11], poly-TT [12], poly-TA [13], and poly-DEBA [14]. The initial polymers have the following structure of units:



Sputtering was performed on a VUP-2 vacuum setup at a pressure of 6.65×10^{-2}–1.33×10^{-3} Pa.

The molecular weights and molecular-weight distribution of polymers were studied on a Waters GPH-200 liquid chromatograph with styrogel columns. The solvent, tetrahydrofuran, was fed at a flow rate of 1 ml min^{-1}; temperature 25°C.

The photoelectric sensitivity was studied in the electrophotographic mode [15].

The quality of thin films and the rate of their preparation depended on the polymer type, vaporizer temperature, distance between the support and vaporizer, and residual pressure. An increase in the residual pressure (vacuum deterioration) resulted in that the sublimation rate decreased or the process terminated. The sublimation temperature was in the range 280–400°C for linear polymers and 500–700°C for cross-linked polymers (poly-DEBA); it was governed by the degradation temperature of the polymers. It was 10–15°C lower than the temperature of the onset of weight loss, determined from the TGA curve.

Raising the heater temperature resulted in an increase in the pyrolysis rate, rise in the flow of molecular fragments, and deterioration of the quality of the resulting film: appearance of loose areas and surface heterogeneity. A decrease in temperature below the optimum decelerated the film formation. Under the given conditions, the optimal distance between the heater and the support was 5–7 cm. An increase in the distance decelerated the process. A decrease in the distance significantly deteriorated the quality of the resulting film because of its contamination with coarse polymer particles carried away with the pyrolyzate flow, detectable even visually.

Certain difficulties arose in operation with soluble or thinly cross-linked poly-DEBA. Because of the strong exothermic effects arising from scission of the C≡C bonds, the polymer was scattered in the course of pyrolysis, and the quality of the thin film deteriorated. To prevent this phenomenon, the heater temperature was raised more slowly.

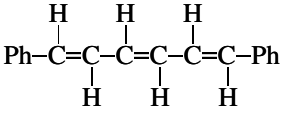
When the above-mentioned optimal conditions were observed, uniform colored (brown, light brown, yellow) thin films with a thickness of 0.1–10 μm were obtained on the supports of polished quartz, silicon, and aluminum. The polyphenylacetylene films had higher mechanical strength and adhesion to the support than the films prepared from a solution. All the films except the films from DEBA, were soluble in organic solvents, except alcohols and alkanes. This allowed us to monitor changes in the molecular weights of the polymers after their sublimation.

The coincidence of the IR spectra of the initial polymers and sputtered films in the range 400–3400 cm^{-1} suggests preservation of the basic molecular structure of the polymers after their sublimation and condensation. This fact confirms that the pyrolysis proceeds with the formation of volatile intermediate fragments consisting of 1–2 polymer units. This conclusion is consistent with the volatility of the low-molecular-weight compounds modeling the units of the polymers studied (stilbene, bp 123–125°C; 1,2,3,4-tetraphenyl-1,3-butadiene, bp 183–184°C; 1,6-diphenyl-1,3,5-hexatriene, bp 201–202°C):



stilbene

1,2,3,4-tetraphenyl-1,3-butadiene



1,6-diphenyl-1,3,5-hexatriene

Table 1. Molecular weight of polymers forming sputtered films

Polymer	$\overline{M}_n$	$\overline{n}^*$	$\overline{M}_w$	$\overline{n}^*$	$\overline{M}_w/\overline{M}_n$
Poly-TT:					
initial	1310	7.4	4990	28.1	3.79
after sublimation	1190	6.7	1440	8.1	1.20
Poly-TA:					
initial	1300	7.4	1460	8.2	1.11
after sublimation	1230	6.9	1340	7.5	1.09
Poly-PAT:					
initial	1400	13.8	1700	16.8	1.25
after sublimation	980	9.6	1210	11.9	1.23

* Average number of units in polymers.

A consideration of the number-average ($\overline{M}_n$) and weight-average ($\overline{M}_w$) molecular weights and also polydispersity $\overline{M}_w/\overline{M}_n$ of both the initial and sputtered polymers (Table 1) revealed certain specific features: (1) low-molecular-weight fractions are absent in all the initial samples; (2) all the initial polymers and polymeric sublimation products have unimodal molecular-weight distribution; (3) $\overline{M}_n$, $\overline{M}_w$, and $\overline{M}_w/\overline{M}_n$ decrease for all the polymeric sublimation products; (4) the polydispersity significantly decreases after the sublimation; and (5) the higher the initial $\overline{M}_n$ and $\overline{M}_w$ values, the greater the decrease in $\overline{M}_n$ and $\overline{M}_w$, i.e., the molecular weights are equalized.

These results confirm the assumption that, in sublimation, the initial polymer chains are first cleaved into identical short fragments (1–2 units). Then, short fragments diffuse into the gas phase toward the support. Finally, under the conditions preventing random recombination of these fragments, low-defective polymer chains with decreased polydispersity $\overline{M}_w/\overline{M}_n$ are formed at the supports. Thin films formed by this way from polyarylacetylenes are more ordered than films prepared by other procedures. Actually, it has been found [16] that the drift mobility of current carriers in these sputtered layers increases by many orders of magnitude, from 10^{-5} to 0.07–0.1 $cm^2\,V^{-1}\,s^{-1}$. The increase in the carrier drift mobility was attributed in [16] to ordering of the molecular structure and to the corresponding decrease in the concentration of deep traps for carriers.

The electron microscope images of thin polymer films (surface replicas) showed that the films have a dense uniform surface disturbed only when the sput-

tering conditions deviated from the optimum. The resulting uniform films can be suitable for various applications.

We studied some characteristics of thin films of polyphenylacetylenes, which can determine their possible application areas. We found that the polymer films have a photoelectric sensitivity. Some results of an electrographic study of thin films prepared on an aluminum support are presented in Table 2. An incandescent lamp of 1×10^3 lux was used as a light source. The increased photoelectric sensitivity of the layers based on poly-DPDAC is accounted for by the polyacene character of the intramolecular structure of the polymer molecules forming sputtered a poly-DPDAC film [8].

The sputtered films based on poly-TT were studied as protective coatings for electronics. For this purpose, we used test elements of three types: (1) devitrified glass supports with an applied photosensitive film based on PbCdS; (2) devitrified glass supports with active components with a size of 50, 125, 250, and 500 μm^2, formed by photosensitive film based on PbCdS; and (3) silicon plates with a thin SiO_2 layer and the subsequent Si_3N_4 layer with sputtered aluminum strips.

The protective characteristics of the sputtered films were tested by tenfold cyclic temperature action (from –60 to +60°C) on the samples at standard humidity and keeping time of 30 min. For the elements tested, uncoated and coated with the sputtered films, we measured and compared the following characteristics: dark resistance, photocurrent multiplied by the photoresistor resistance under conditions of short exposure, and noise voltage. It was shown that the photoresistor resistance increases after applying the polymer film; the main parameters of photoresistors (intensity of photosignal, signal-to-noise ratio) are improved or remain unchanged.

The features of the chemical structure of molecules forming sputtered films were the cause of their unusual behavior under UV irradiation under various conditions. It was found that fairly short UV irradiation of sputtered films in a vacuum through a phototemplate results in the appearance of a latent image due to intermolecular cross-linking of polymers in irradiated areas. After heating of the layers in a vacuum at the optimal temperature of 200–350°C, the nonirradiated non-cross-linked part of the polymers is evaporated. As a result, a visible contrast image is formed. This image does not appear if the development temperature is raised above the optimum because of the simultaneous degradation and evaporation of the cross-linked areas.

Table 2. Photoelectrical sensitivity of sputtered films

Polymer	Charge potential, V	Half-life of charge potential, s	
		in darkness	in light
Poly-DPDAC	410	120	35
Poly-PAT	290	225	175
Poly-PAZ	320	120	72

By contrast, prolonged UV irradiation of sputtered films through a phototemplate in air results in the disappearance of the areas of sputtered layers at the points of exposure to light and in the appearance of a contrast positive image. This process is accounted for by formation of ozone from atmospheric oxygen under UV irradiation and subsequent oxidation of unsaturated bonds of sputtered polymers by ozone. In this case, according to the rate constants of the reactions of ozone with organic compounds [17], the most probable is ozone attack on the C=C bonds of polyene chains.

Rate constants of the reactions of ozone with compounds

Compound	k, $1\ mol^{-1}\ s^{-1}$
Ethylbenzene	0.4
Phenylacetylene	60
Styrene	3×10^5
Stilbene	1.8×10^5
1,4-Diphenylbutadiene	9×10^4
1,2,3,4-Tetraphenylbutadiene	8×10^4
Poly-PAT	1.4×10^3

Actually, only the degradation of polyene chromophores (i.e., the main chains of polyphenylacetylenes) forming sputtered films gives rise to a visible image. This mechanism is additionally confirmed by the following fact. By applying some low-molecular-weight compounds, which model polyphenylacetylene units and readily react with ozone (stilbene. 1,6-diphenyl-1,3,5-hexatriene), to the support, we also obtained films though of lower quality. An image appeared on these films under prolonged UV irradiation.

Thus, sputtered films of polyphenylacetylenes are the first real example of the previously unknown class of photoresists, which can be both negative and positive, depending on the treatment conditions. These films can be used as visualizing materials for dry photolythography, a new promising approach in production of microelectronics items. Development and use of such technologies will allow elimination of solvents or etching agents. We believe that the sen-

sitivity of sputtered thin films can be improved by introducing fragments that enhance the photosensitivity of the materials.

CONCLUSIONS

(1) Uniform ordered colored films with a thickness of 0.1–10 μm were obtained on quartz, silicon, and aluminum supports by vacuum sputtering of polyphenyldiacetylene, poly-*p*-diethynylbenzene, and polytolan.

(2) It was shown that the polydispersity of polymers forming thin layers decreases in comparison with that of the initial polymers.

(3) It was found in the electrophotographic mode that the thin films of polymers have a photoelectric sensitivity.

(4) It was demonstrated that, under various conditions of UV irradiation, the polymer chains in the film cross-link or are broken with ozone. This results in appearance of images at the support surface.

REFERENCES

1. Berlin, A.A., Geiderikh, M.A., Davydov, B.E., et al., *Khimiya polysopryazhennykh sistem* (Chemistry of Polyconjugated Systems), Moscow: Khimiya, 1972.
2. Chauser, M.G., Rodionov, Yu.M., Misin, V.M., and Cherkashin, M.I., *Usp. Khim.*, 1976, vol. 45, no. 4, pp. 695–741.
3. Misin, V.M. and Cherkashin, M.I., *Usp. Khim.*, 1985, vol. 54, no. 6, pp. 956–1008.
4. US Patent 5483017.
5. Nakano, M., *Chem. Chem. Ind.*, 1999, vol. 52, pp. 1286–1289.
6. Yoshida, T., Abe, Y., Masuda, T., and Higashimura, T., *J. Polym. Sci., Ser. A*, 1996, vol. 34, no. 11, pp. 2229–2236.
7. Kong Xiangxing, Wan Xinhua, Kwok Hoi Sing, et al., *J. Polym. Sci., Ser. A*, 1998, vol. 16, no. 2, pp. 185–192.
8. Glagolev, N.N., Misin, V.M., Zaichenko, N.L., et al., *Vysokomol. Soedin., Ser. A*, 1986, vol. 28, no. 10, pp. 2123–2128.
9. Berlin, A.A., Blyumenfel'd, L.A., and Cherkashin, M.I., *Vysokomol. Soedin.*, 1959, vol. 1, pp. 1361–1363.
10. Noguchi, H. and Kambara, S., *J. Polym. Sci., Ser. B*, 1963, vol. 1, pp. 553–559.
11. Simionescu, C. and Dumitrescu, S., *Makromol. Chem.*, 1970, vol. 136, pp. 47–64.
12. Kisilitsa, P.P., Cherkashin, M.I., and Berlin, A.A., *Izv. Akad. Nauk SSSR, Ser. Khim.*, 1967, no. 9, pp. 1959–1965.
13. Misin, V.M., Kisilitsa, P.P., Bolondaeva, N.I., and Cherkashin, M.I., *Vysokomol. Soedin., Ser. A*, 1976, vol. 18, no. 8, pp. 1726–1732.
14. Misin, V.M. and Cherkashin, M.I., *Vysokomol. Soedin., Ser. B*, 1976, vol. 23, no. 2, pp. 130–131.
15. Scaffert, R.M., *Electrography*, London: Focal, 1965.
16. Berlin, A.A., Bakh, R.A., Merkulov, E.I., et al., *Izv. Akad. Nauk SSSR, Ser. Khim.*, 1969, no. 10, p. 2345.
17. Razumovskii, S.D. and Zaikov, G.E., *Ozon i ego reaktsii s organicheskimi soedineniyami (Kinetika i kataliz)* (Ozone and Its Reaction with Organic Compounds (Kinetics and Catalysis)), Moscow: Nauka, 1974.

ISSN 1070-4272, Russian Journal of Applied Chemistry, 2006, Vol. 79, No. 8, pp. 1329–1332. © Pleiades Publishing, Inc., 2006.
Original Russian Text © A.V. Sidorovich, Yu.N. Sazanov, O.E. Praslova, N.V. Bobrova, A.V. Novoselova, D.M. Kostycheva, L.A. Nud'ga, 2006, published in Zhurnal Prikladnoi Khimii, 2006, Vol. 79, No. 8, pp. 1341–1344.

MACROMOLECULAR CHEMISTRY AND POLYMERIC MATERIALS

Thermomechanical Properties of Composite Films of Polyacrylonitrile with Chitin and Chitosan

A. V. Sidorovich, Yu. N. Sazanov, O. E. Praslova, N. V. Bobrova, A. V. Novoselova, D. M. Kostycheva, and L. A. Nud'ga

Institute of Macromolecular Compounds, Russian Academy of Sciences, St. Petersburg, Russia

Received April 13, 2006

Abstract—Composite films were prepared from polyacrylonitrile synthesized by anionic and radical polymerization and combined with chitin or chitisan. The thermomechanical properties of the films were examined. The compatibility of polyacrylonitrile synthesized by radical polymerization with chitosan was studied by DSC over a wide temperature range 140–280°C.

DOI: 10.1134/S1070427206080222

In [1, 2] we examined the thermochemical reactions of blends of polyacrylonitrile (PAN) with chitin (CT) and chitosan (CTS) at temperatures within the range 0–900°C and demonstrated the possibility and promise of preparation of composite materials based on synthetic acrylonitrile polymers and CTS. This study was focused on preparation of films based on PAN synthesized by anionic and radical polymerization and modified with polysaccharides CT and CTS.

EXPERIMENTAL

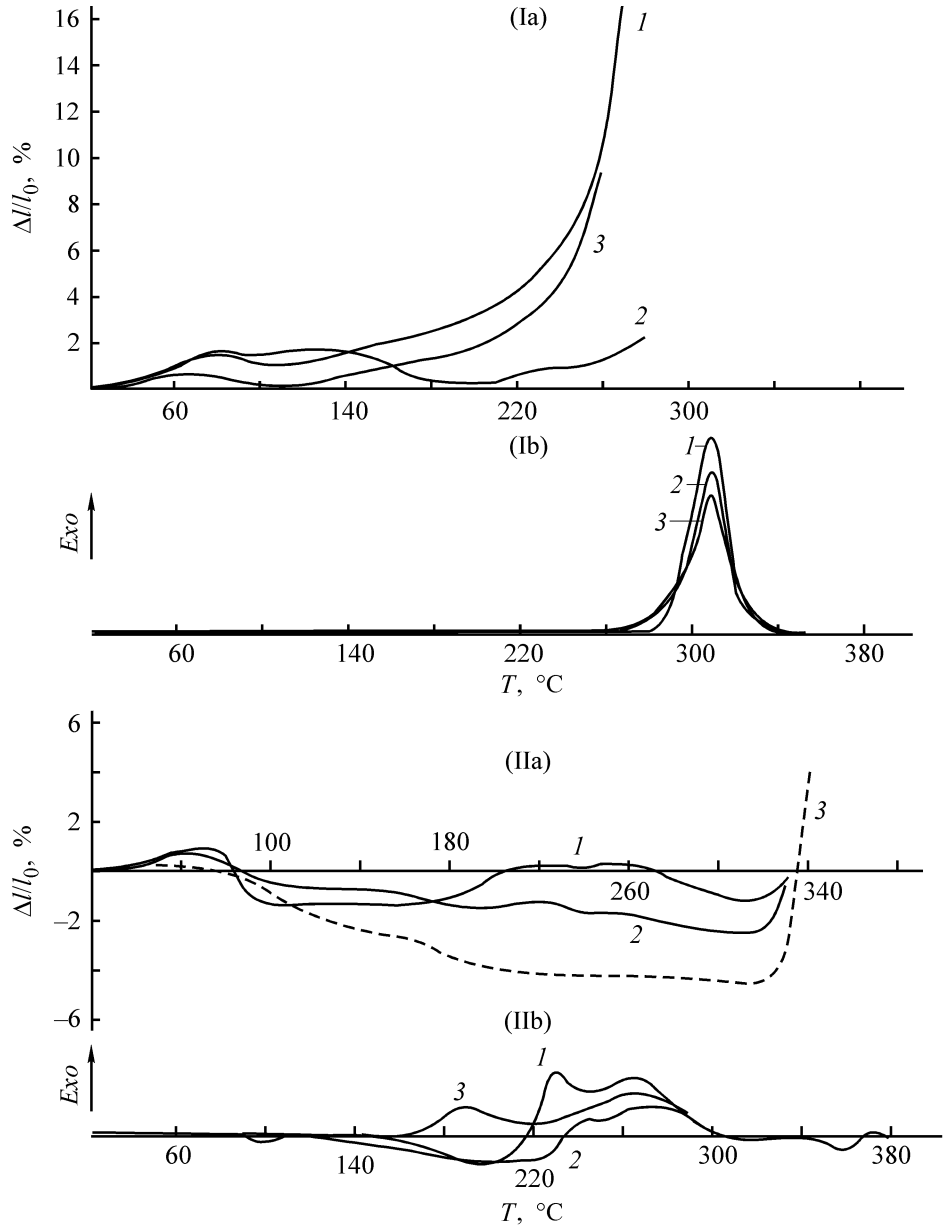
We used previously characterized [1] acrylonitrile polymers R-PAN and A-PAN synthesized by radical (initiator $K_2S_2O_8$–$Na_2S_2O_8$) and anionic (initiator lithium alkoxide, in toluene) polymerization, respectively, as well as chitin and chitosan obtained from a crab shell: CT (ash content 1%) and CTS (degree of deacetylation 0.79), molecular weights 282 and 245 kD, respectively. The CT and CTS powders were partially dissolved by heating for 1 h at 140°C in dimethylformamide solutions of PAN at the 1 : 1 ratio (by weight) of the starting blend components. Films were cast from these solutions after filtration and dried at room temperature for three days. The content of CT and CTS in the films was calculated from the difference of the weights of their introduced and returned amounts.

The mechanical characteristics of the films (ultimate tensile strength, Young modulus, and elongation at break) were determined on a UMIV-3 universal setup at an extension rate of 5 mm min^{-1}, sample size of 35×2 mm, distance between the grips of 25 mm, and film thickness of 30–40 μm. The strength was calculated for the initial cross section of the sample. The Young modulus was determined at a strain of 1%. Results of 10 measurements were averaged.

The dilatometric measurements were carried out with a setup on which the changes of the longitudinal sizes of the films can be determined accurately to within 0.01 μm when heating the samples (30×4 mm, d = 40 μm) at a rate of 10 deg min^{-1} at temperatures within the range 20–400°C and a tensile stress of 3 kg cm^{-2}.

The calorimetric measurements in the same temperature range were carried out in a DSM-2M differential scanning microcalorimeter at a scanning rate of 16 deg min^{-1} and threshold sensitivity of 0.04 mW.

Since preparation of films based on PAN synthesized by radical and anionic polymerization entails a number of technological difficulties, we attempted to modify PAN with chitin and chitosan. To this end, we developed the conditions for preparation of composite films with satisfactory strength properties. The table lists the deformation and strength characteristics of the films formed by the basic polymer, AN, and its composites with CT and CTS of the formulations indicated. The data for experiment nos. 7 and 8 were identical to those for the A-PAN–BA copolymer containing 5% butyl acrylate. In all cases, the strength characteristics of the films were deteriorated to a certain extent in the presence of chitin



(a) Thermomechanical curves at the tensile stress of 3 kg cm^{-2} and (b) DSC curves of the films. ($\Delta l/l_0$) Relative size change and (T) temperature. (I) (*1*) A-PAN, (*2*) A-PAN + CT, and (*3*) A-PAN + CTS. (II) (*1*) R-PAN, (*2*) R-PAN + CT, and (*3*) R-PAN + CTS.

and chitosan. This can be due to a high-temperature (140°C) treatment of mixed polymer solutions from which the films were cast.

Figures Ia and Ib demonstrate the thermomechanical properties of films of A-PAN, A-PAN + CT, A-PAN + CTS. It is seen that, in the initial stage of the heat treatment (20–140°C), when the residual solvent is being eliminated (thereby increasing the probability of intermolecular interaction), the size of the films changes insignificantly. With a rise in temperature to above 140°C, the elongation of the A-PAN and A-PAN + CTS films increases, and films pass from the hyperelastic to the viscous-flow state, which is followed by break at 260°C. The break of the films corresponds to the onset of the A-PAN thermal cyclization (Fig. Ib) with T_{max} = 320°C. The appearance of the exothermic peaks suggests that this process is not complicated by other chemical reactions, i.e., the energy release is due to the cyclization reaction only. The ΔH parameters were estimated at 1060,

Composition and strength of the films

Experiment no.	Film composition	Ultimate tensile strength σ, MPa	Elongation at break ε, %	Young modulus *E*, MPa
1	R-PAN	72	2.6	3600
2	R-PAN + CT 6%)	52	2.0	3000
3	R-PAN + CTS 6%)	48	2.0	3000
4	A-PAN	65	2.7	3500
5	A-PAN + CT (12%)	55	2.2	2600
6	A-PAN + CT (20%)	45	1.5	3500
7	A-PAN · BA	65	3.3	3000
8	A-PAN · BA + CT (6%)	64	1.8	3300

770, and 690 kJ g^{-1} for A-PAN, A-PAN + CT, and A-PAN + CTS, respectively. Earlier, we have observed a similar phenomenon of fluidity in the thermograms of the films of anionic PAN synthesized in DMF [3]. This is, evidently, due to the structural and molecular-weight heterogeneity, stereoblock structure, and presence of nitrile groups with a high dipole moment, which make possible gradual formation of associates, mainly double helices, by the A-PAN macromolecules in solution. Interaction between them is much weaker than that between the A-PAN macromolecules inside the coils. The observed phenomena of the viscous-flow state of the A-PAN and A-PAN + CTS films, as well as the absence of heat effects (DSC) up to 260°C, suggest that no prominent intermolecular valence interactions occur in these films. The thermodilatogram of the A-PAN + CT film (Fig. I, curve *2*) shows a different pattern. The fact that the film length remains unchanged under these conditions suggests a significant amount of chemical intermolecular cross-links. The lack of a peak of exothermic effect on the corresponding DSC curve suggests that the cross-links appear during the heat treatment of the starting mixed solution (140°C, 1 h).

As to interaction with the polysaccharides examined, the R-PAN, as well as the R-PAN + CT and R-PAN + CTS, films have complex thermodilatograms and DSC curves (Figs. IIa, IIb). This is due to the known molecular-weight and structural heterogeneity of R-PAN, as well as to the presence of a significant amount of oxygen-containing fragments of the initiator in its macromolecules. The DSC curve of the R-PAN films after heat treatment exhibits two exothermic peaks and one endothermic peak (Fig. II, curve *1*).

The thermodilatogram of the same film showed that the initial heating stage (removal of the residual solvent) is characterized by insignificant absorption of energy, possibly due to the solvent evaporation. Above 200°C, chemical processes with a significant exothermic effect (T_{max} = 230°C) occur. The film elongation, which began earlier (180–200°C), ceases (Fig. II, curve *1*). The film length remains unchanged under heating to 270°C, whereupon the film contracts as a result of the thermal cyclization (250–300°C).

The chemical processes occurring in the R-PAN films during the heat treatment also occur in the composite films, now with the polysaccharide macromolecules involved. It should be noted that a gradual and more intensive contraction in comparison to the R-PAN film (Fig. IIa, curves *2*, *3*), observed in the thermodilatograms of the composite films, is partly due to the chemical intermolecular interactions already in the stage of preparation of mixed solutions (140°C, 1 h). The A-PAN + CT composite film (Fig. IIb, curve *2*) shows a weakly pronounced endothermic effect at 140–240°C due to removal of the residual solvent and an exothermic effect (240–300°C) corresponding to the R-PAN cyclization. A different DSC curve is exhibited by the R-PAN + CTS blend, for which oxidation reactions, clearly involving the amino groups of CTS, are observed at 190°C. In the same temperature range, this film contracts more intensively (Fig. IIa, curve *3*).

Notably, the thermocyclization of R-PAN in the composite films proceeds in the conventional temperature range (250–300°C), but with a much smaller heat effect, and is accompanied by a weakly pronounced contraction of the film. This suggests that this reaction involves a much smaller number of nitrile groups. Hence, some of them were already spent earlier in intermolecular interactions of the CN groups with the functional groups (>C=O, $–NH_2$, –OH, etc.), which can occur either in the concomitant impurities, or in the co-components, or in the molecular structure of the polymer proper. This is confirmed by the thermomechanical characteristics of sample no. 7 (see table).

Thus, the nature of the thermocyclization peak is indicative of the purity of the sample examined and of the presence/absence of structural defects in it. Moreover, the width of the thermocyclization peak allows judging of the molecular-weight homogeneity of PAN. This conclusion is consistent with our previous DTA data for the AN polymers synthesized under various conditions [4].

We showed that attaining the desired properties of the PAN-based composite materials being developed (semiconductor and carbon fibers) requires taking into account the structural and chemical features of the polymeric components used.

CONCLUSIONS

(1) Films with high deformation and strength characteristics were prepared from polysaccharides chitin and chitosan, combined with polyacrylonitrile.

(2) Polyacrylonitrile synthesized by radical polymerization enters into thermochemical reactions with the polysaccharide at 140–280°C, to form a composite.

REFERENCES

1. Sazanov, Yu.N., Novoselova, A.V., Amsharov, K.Yu., et al., *Zh. Prikl. Khim.*, 2005, vol. 78, no. 5, pp. 810–813.
2. Sazanov, Yu.N., Novoselova, A.V., Nud'ga, L.A., et al., *Zh. Prikl. Khim.*, 2005, vol. 78, no. 8, pp. 1344–1348.
3. Sidorovich, A.V., Praslova, O.E., Novoselova, A.V., and Zgonnik, V.N., *Zh. Prikl. Khim.*, 2004, vol. 77, no. 5, pp. 825–830.
4. Novoselova, A.V., Zgonnik, V.N., Sazanov, Yu.N., et al., *Vysokomol. Soedin., Ser. A*, 1992, vol. 34, no. 3, pp. 59–63.

ISSN 1070-4272, Russian Journal of Applied Chemistry, 2006, Vol. 79, No. 8, pp. 1333–1337. © Pleiades Publishing, Inc., 2006.
Original Russian Text © A.Yu. Solov'ev, A.P. Shiryaev, B.Ya. Basin, L.K. Shataeva, 2006, published in Zhurnal Prikladnoi Khimii, 2006, Vol. 79, No. 8, pp. 1345–1349.

MACROMOLECULAR CHEMISTRY AND POLYMERIC MATERIALS

A Membrane Bioreactor with Immobilized Proteinase

A. Yu. Solov'ev, A. P. Shiryaev, B. Ya. Basin, and L. K. Shataeva

Institute of Macromolecular Compounds, Russian Academy of Sciences, St. Petersburg, Russia
Plazmofil'tr Private Company, St. Petersburg, Russia

Received March 22, 2006

Abstract—A procedure was developed for layer-by-layer immobilization of terrilytin proteolytic enzyme on track membranes and flat-membrane blocks. The hydrolysis of fibrinogen and casein was studied, and the possibility of using such a structure as an enzymatic bioreactor was demonstrated.

DOI: 10.1134/S1070427206080234

The development and use of bioreactors of a new generation with immobilized hydrolytic enzymes remains a topical problem of the modern fine biotechnology [1]. On the one hand, it is necessary to optimize the immobilization procedure, because the known methods of enzyme incorporation into a gel decrease the catalytic performance of the immobilized substance. This is due to hindered diffusion of the substrate and product in the gel phase; furthermore, this immobilization procedure is inapplicable at all to macromolecular substrates [2]. On the other hand, the bioreactor design should allow continuous specific hydrolysis of macromolecular viscous substrates and colloids whose solutions cannot be filtered [3]. Column bioreactors with enzymes immobilized on porous granular supports are unsuitable for treatment of such systems.

The most promising approach to the development of a modern enzymatic bioreactor involves immobilization of enzymes on microfiltration membranes and use of the design developed for membrane microfilters operating in the tangential filtration mode [4, 5].

Track membranes (TMs) based on poly(ethylene terephthalate) are widely used today in microfiltration of virus suspensions, fractionation of colloidal solutions, and also in new equipment for practical medicine. Previously, we have studied the microfiltration of viscous solutions of high-molecular-weight polysaccharides on PFM-800 plasmofilters using TM based on poly(ethylene terephthalate) as filtration material [4]. The PFM-800 unit is commercially produced for medicine and can be used without changes in the design as a support for immobilization of hydrolytic enzymes [6]. Preliminary studies have shown that some macromolecules (serum albumin, SA; heparin; urokinase) preserve their native structure and biological activity in the sorbed state on the surface of a TM based on poly(ethylene terephthalate) [7].

This study was aimed to develop a membrane bioreactor [in particular, a method for immobilization of terrilytin (microbial proteinase) on membranes of the plasmofilter] and to estimate the activity of the immobilized enzyme toward viscous solutions of macromolecular proteins, casein and fibrinogen.

EXPERIMENTAL

To develop an enzymatic bioreactor, we used track membranes with a rated pore size of 0.5 μm and PFM-800 plasmofilters based on these membranes (Plazmofil'tr Private Company, St. Petersburg).

As a hydrolytic enzyme we used terrilytin, a microbial proteinase preparation permitted for use in medical practice for therapy [8]. Terrilytin is a single-chain glycosylated protein with a molecular weight of about 27 kDa and isoelectric point at pH 4.6.

The enzymatic activity of terrilytin was determined by the method described above, with 1% solution of Hammersten-grade casein from Reanal in 0.05 M phosphate buffer (pH 7.6) as a substrate [9]. After a treatment of casein with proteinase at 37°C for 10 min, high-molecular-weight proteins were precipitated with 5% trichloroacetic acid (TCA), and the optical density of the TCA-soluble hydrolysis products was determined at λ = 280 nm. The activity of the enzyme was expressed in proteolytic units (PUs).

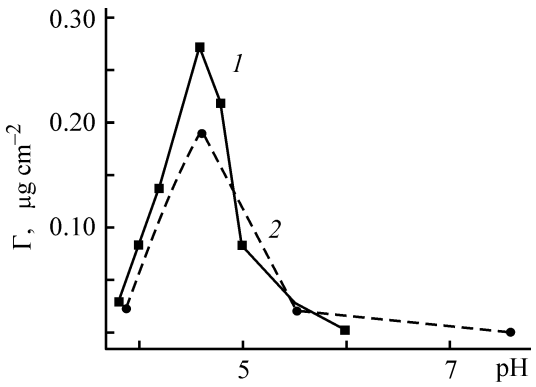


Fig. 1. Sorption capacity Γ of track membranes for (*1*) terrilytin and (*2*) serum albumin vs. solution pH.

The specific activity of the sample used in this study was 2 PU mg^{-1}, or 25 PU (mg protein)$^{-1}$.

The protein concentration was determined spectrophotometrically with the Coomassie reagent at λ = 595 nm [10].

To find the optimal conditions for immobilization of terrilytin on the surface of track membranes, we studied the pH dependence of the TM sorption capacity under static conditions by the procedure described previously [11].

To attain firm immobilization of terrilytin, we preliminarily modified the TM surface by the sorption of SA at pH 5.6 from a 1 mg ml^{-1} protein solution. It is known that SA is sorbed on the TM surface owing to hydrophobic interactions; as a result, the membrane surface acquires polyampholytic properties. After thorough washing of the membrane with a salt buffer solution to remove the free protein, terrilytin was sorbed onto the layer of sorption-bound albumin following the procedure described in [12], to obtain a two-layer protein coating. For irreversible fixation of this coating on the TM surface, the proteins were linked with each other by glutaraldehyde (GA) [13]. The immobilization of the enzyme on the PFM-800 membrane unit was performed similarly, by successive circulation of the above-mentioned solutions through the substrate and product chambers. It has been shown previously that successive deposition of monomolecular layers onto the TM surface does not noticeably affect the TM hydrodynamic characteristics. The filtering surface area of TMs in the plasmofilter was 800 cm^2, and the TM thickness, 10 μm; thus, the total volume of the phase with the immobilized enzyme (catalyst phase) inside the bioreactor was 0.8 cm^3.

The proteolytic activity of terrilytin immobilized on membranes was measured under static conditions. A 1-dm^2 piece of the membrane was kept in 10 ml of a 1% casein solution for 30 min at 37°C, with continuous rocking of the weighing bottle. Then the membrane was withdrawn from the solution and transferred into another weighing bottle with a fresh substrate solution and kept there for another 30 min. This procedure was repeated two times to monitor the affinity desorption of the immobilized enzyme with the substrate solution.

The proteolytic activity of terrilytin immobilized on a PFM-800 unit was measured under the dynamic conditions. A substrate solution was recirculated in the substrate chamber under a pressure head of 0.5 kPa at a pumping rate of 0.6 l h^{-1}. In the process, a part of the solution was filtered in the tangential mode through the filter to the hydrolyzate (product) chamber at a rate of 0.2 l h^{-1}. The volume of the circulating solution was kept constant by adding a fresh portion of the substrate. At 5-min intervals, the filtered solution was sampled, and its spectrophotometric analysis was performed to determine the content of TCA-soluble products (λ = 280 nm). As substrates for the hydrolysis in the bioreactor we used aqueous solutions of casein and fibrinogen (2.2 mg ml^{-1}). The choice of fibrinogen was governed by the fact that, according to our previous data, terrilytin shows maximal specific activity toward triple-helix structural proteins, such as collagen, fibrin, elastin, and fibrinogen [11, 14]. The fibrinogen hydrolysis products were collected at the reactor outlet, and the capability of the product to form a fibrin clot under the action of thrombin was monitored [15]. The error in measuring the activity of terrilytin in the free and immobilized states did not exceed 10 and 16%, respectively.

It is known that all the polymer surfaces are sorption-active toward hydrophilic or hydrophobic components present in solution, depending on the morphology and chemical composition of the polymer surface. We have shown previously that the sorption capacity of the surface of a TM based on poly(ethylene terephthalate) toward hydrophilic molecules is determined by the carboxy and hydroxy groups on the surface of these materials. In the case of irreversible physical adsorption, the sorbed macromolecules preserve their native conformation. Therefore, in sorption immobilization of enzymes on a polymer surface, their enzymatic activity can be preserved. However, upon a change in the external conditions (pH, ionic strength, presence of a displacing component), the enzyme is desorbed from the surface.

Figure 1 shows the dependence of the sorption capacity of a TM toward SA and terrilytin on pH of the protein solution. The best pH for the equilibrium sorption of these proteins on track membranes is 4.6 (isoelectric point of terrilytin).

Activity of immobilized terrilytin relative to casein at various immobilization procedures

Immobilization procedure	Enzyme amount, μg dm^{-2}	Calculated activity, PU dm^{-2}	Enzyme activity in statics, PU dm^{-2}	Percent ratio of activity to that calculated for standard conditions, %
TM~TRL*	20	0.5	0.35*	70
TM~(TRL)GA	20	0.5	0.28	56
TM~SA~TRL	11	0.28	0.44*	>100
TM~SA~(TRL)GA	11	0.28	0.38	>100

* In repeated measurements, the samples showed no enzymatic activity.

As can be seen from Fig. 1, the sorption capacity of intact track membranes for terrilytin at pH 4.6 is 0.2 μg cm^{-2}. With alkalization of the external solution, the enzyme desorption starts at pH 6 and is complete at pH 7.6, which does not allow use of this sorption-immobilized enzyme in neutral media, in which the enzyme is the most active [14].

An efficient method for firm immobilization of proteins on polymer surfaces is their fixation on a hydrophilic support, with the subsequent covalent cross-linking of the protein macromolecules with glutaraldehyde. The reaction involves formation of Schiff base fragments from primary amino groups of the protein and carbonyl groups of the aldehyde [16]:

$$\text{TM-terrilytin-NH}_2 + \text{HOC}-\text{CH}_2-\text{CH}_2-\text{CH}_2-\text{COH} + \text{H}_2\text{N-terrilytin-TM}$$

$$\rightarrow \text{TM-terrilytin-N=CH-CH}_2-\text{CH}_2-\text{CH}_2-\text{HC=N-terrilytin-TM}.$$

To make milder the conditions of the enzyme immobilization, terrilytin was also sorbed on TM with a deposited SA monolayer. The sorption capacity of the intact TM for terrilytin in the absence of SA is 0.2 μg cm^{-2}. For the TM preliminarily modified with SA, the sorption capacity for terrilytin is 0.1 μg cm^{-2}. In other words, the enzyme macromolecules are situated sufficiently far apart from each other on the sorption surface in the SA layer, which excludes the possibility of autolysis. In addition, SA makes the sorption surface more hydrophilic, which favors preservation of the native structure of the enzyme molecule.

Comparative evaluation of the enzymatic activity of terrilytin at various types of immobilization is made in the table, where TM~TRL denotes terrilytin sorption-immobilized on intact TM; TM~(TRL)GA, terrilytin sorption-immobilized on intact track membrane and cross-linked with glutaraldehyde; TM~SA~TRL, sorption-immobilized layers of SA and TRL without cross-linking; and TM~SA~(TRL)GA, the same after cross-linking with glutaraldehyde.

The higher, compared to the calculated value, level of the enzyme activity is due to different conditions of the activity measurement: The contact time of the immobilized enzyme with the substrate solution was 30 min, against 10 min as for the enzyme in solution. The only conclusion following from this fact is that the immobilization of the enzyme on the monomolecular SA layer, followed by the covalent cross-linking, ensures better preservation of the terrilytin activity than the covalent cross-linking of terrilytin directly sorbed on TM (see table).

The highest activity of the enzyme is preserved in joint sorption with albumin followed by chemical cross-linking with GA. This procedure was used in immobilization of terrilytin on the plasmofilter membranes. The design of the bioreactor is shown in Fig. 2.

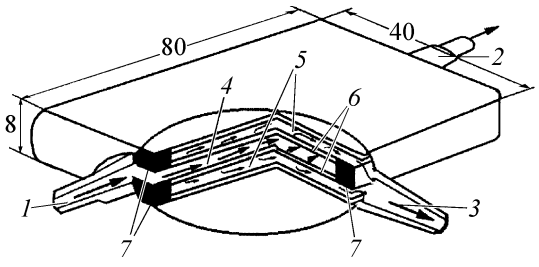


Fig. 2. Scheme and dimensions (mm) of the bioreactor: (*1*, *2*) tubes for inlet and outlet of the initial substrate solution, (*3*) outlet tube for the solution with hydrolysis products (filtrate), (*4*) chamber for pumping the substrate solution, (*5*) chamber for collecting the solution of hydrolysis products, (*6*) track membranes with immobilized terrilytin, and (*7*) sealant for sizing the reactor parts.

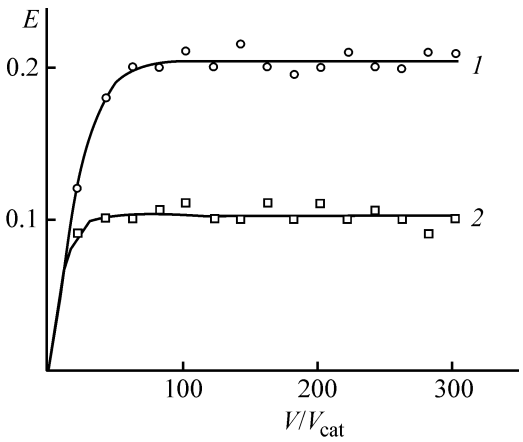


Fig. 3. Enzymatic activity of the bioreactor in hydrolysis of solutions of (*1*) casein and (*2*) fibrinogen. (*E*) Optical density of the solution at λ = 280 nm and (V/V_{cat}) volume of the substrate solution passed per unit volume of the catalytically active element of the bioreactor.

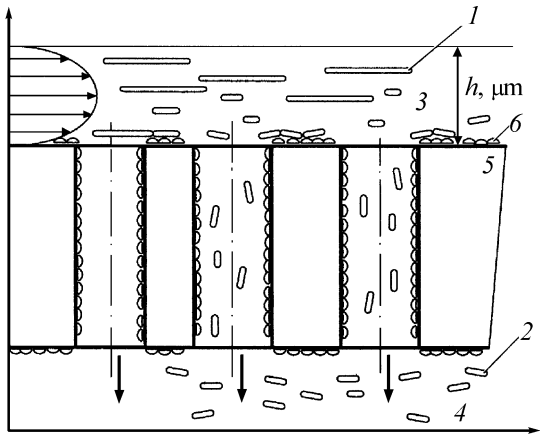


Fig. 4. Scheme of separation of the high-molecular-weight rigid-chain substrate from low-molecular-weight hydrolysis products in the mode of tangential microfiltration of a mixture of substrate and products at high shear rates in the slit chamber: (*1*) substrate, (*2*) products, (*3*) substrate chamber, (*4*) product chamber, (*5*) track membrane, and (*6*) terrilytin immobilized on the filtering and pore surfaces of the track membrane. (*h*) Slit height.

The PFM-800 plasmofilter can be used as a support for immobilization of enzymes and as a bioreactor for continuous hydrolysis of high-molecular-weight proteins. The hydrodynamic conditions in the substrate resource chamber at tangential filtration lift the diffusion limitations and provide continuous removal of the low-molecular-weight hydrolysis products, i.e., fractionation of the substrate and products. Figure 3 shows the dynamics of the proteolytic hydrolysis of casein and fibrinogen; it indicates that the hydrolysis occurs in the steady-state mode.

The most important advantage of the bioreactor developed is the combination of two processes in one unit: enzymatic hydrolysis of a high-molecular-weight rigid-chain substrate (fibrinogen) and simultaneous removal of lower-molecular-weight globular hydrolysis products. The product solution is fully free of fibrinogen: Addition of thrombin and an increase in the calcium concentration do not induce formation of fibrin clots [15].

Fractionation of the solution components with respect to the shape and molecular weight is due to the hydrodynamic conditions in the slit chamber of the substrate, in which the slit height is 100 μm and the viscous liquid flows at high shear rates. Under these conditions, the rigid-chain macromolecules are oriented along the direction of the solution flow, which is confirmed by dynamooptical measurements [17]. As shown previously [4], such a flow is accompanied not only by the orientation but also by the shift of the highest-molecular-weight components to the center of the restricted flow, to the region of the highest linear velocities. Then the tangential flow of the filtrate removes from the substrate chamber only the hydrolysis products, as shown in Fig. 4.

The use of natural proteins and their intermolecular complexes in the formation of polylayer coatings of bioreactors is of large interest from the viewpoint of basic and applied problems of biotechnology.

CONCLUSIONS

(1) A new procedure for immobilization of proteolytic enzyme terrilytin was suggested: application onto a layer of serum albumin sorbed on track membranes, followed by covalent cross-linking of these proteins with glutaraldehyde.

(2) Terrilytin was immobilized by this procedure on a PFM-800 membrane unit with a capacity of 0.1 μg per 1 cm^2 of the filtering surface, which allowed this unit to operate as an enzymatic bioreactor.

(3) The developed membrane reactor with immobilized terrilytin hydrolyzes casein and fibrinogen in the steady-state mode and shows an activity comparable to that of the free enzyme.

ACKNOWLEDGMENTS

The study was financially supported by the Foundation for the Support of the Domestic Science (project no. K-407).

REFERENCES

1. Cooper, J.W., Chen, J., Li, Y., and Lee, C.S., *Anal. Chem.*, 2003, vol. 75, no. 5, pp. 1067–1074.
2. *Biotekhnologiya* (Biotechnology), Egorov, N.S. and Samuilov, V.D., Eds., book 7: Berezin, I.V., Klyachko, N.L., Levashov, A.V., et al., *Immobilizovannye fermenty* (Immmobilized Enzymes), Moscow: Vysshaya Shkola, 1987.
3. Heath, C.A. and Belford, G., *Adv. Biochem. Eng. Biotechnol.*, 1992, vol. 47, no. 1, pp. 45–88.
4. Shataeva, L.K., Ryadnova, I.Yu., Potekhina, T.S., et al., *Zh. Prikl. Khim.*, 1999, vol. 72, no. 1, pp. 152–156.
5. Nagata, N., Herovis, K.J., Dziewulski, P., and Belfort, G., *Biotechnol. Bioeng.*, 1989, vol. 34, pp. 447–466.
6. RF Patent 2046647.
7. Solov'ev, A.Yu., Chernova, I.A., Shataeva, L.K., and Zelikson, B.M., *Effer. Terap.*, 2003, vol. 9, no. 3, pp. 62–65.
8. Mashkovskii, V.M., *Lekarstvennye sredstva. Posobie dlya vrachei* (Drugs. Textbook for Physicians), Moscow: Novaya Volna, 2005, 15th ed.
9. Samsonov, G.V., Shataeva, L.K., and Orlievskaya, O.V., *Dokl. Akad. Nauk SSSR*, 1972, vol. 206, no. 2, pp. 497–498.
10. Vredford, M.M., *Anal. Biochem.*, 1976, vol. 72, no. 12, pp. 248–252.
11. Zaikina, N.A., Shataeva, L.K., Elinov, N.P., and Samsonov, G.V., *Mycopathol. Mycol. Appl.*, 1975, vol. 56, no. 3, pp. 153–157.
12. Brynda, E., Houska, M., Jirouskova, M., and Dyr, J.E., *J. Biomed. Mater. Res.*, 2000, vol. 51, pp. 249–257.
13. Solov'ev, A.Yu., Brynda, E., Houska, M., et al., *Vysokomol. Soedin., Ser. A*, 2003, vol. 45, no. 9, pp. 1574–1579.
14. Shataeva, L.K., Orlievskaya, O.V., Chichkovskaya, G.V., and Samsonov, G.V., *Biokhimiya*, 1973, vol. 38, no. 6, pp. 169–174.
15. Vermilen, C., De Vrecer, R., and Verstraete, R., *Clin. Chim. Acta*, 1963, vol. 8, no. 4, pp. 418–424.
16. Kuznetsova, N.P., Gudkin, L.R., Kol'tsova, S.V., and Mishaeva, R.N., *Vysokomol. Soedin., Ser. A*, 1996, vol. 38, no. 10, pp. 1668–1673.
17. Shur, A.M., *Vysokomolekulyarnye soedineniya* (Macromolecular Compounds), Moscow: Vysshaya Shkola, 1981.

ISSN 1070-4272, Russian Journal of Applied Chemistry, 2006, Vol. 79, No. 8, pp. 1338–1340. © Pleiades Publishing, Inc., 2006.
Original Russian Text © S.I. Gusev, S.D. Zaitsev, Yu.D. Semchikov, O.G. Zakharova, 2006, published in Zhurnal Prikladnoi Khimii, 2006, Vol. 79, No. 8, pp. 1350–1352.

MACROMOLECULAR CHEMISTRY AND POLYMERIC MATERIALS

A Method for Determining the Molecular Weight of Hyperbranched Polymers

S. I. Gusev, S. D. Zaitsev, Yu. D. Semchikov, and O. G. Zakharova

Lobachevsky State University, Nizhni Novgorod, Russia

Received November 3, 2005; in final form, April 2006

Abstract—A method for determining the molecular weight of hyperbranched polymers is developed, based on the measurement of the area of the monolayer at the water/air interface.

DOI: 10.1134/S1070427206080246

Intensive studies in the area of dendrimers and hyperbranched polymers, which include applied research and are generally interdisciplinary (macromolecular chemistry–catalysis, macromolecular chemistry–medicine, etc.), have created a need for developing fairly simple and efficient methods for measuring molecular weights, similar to the viscometry in the case of linear polymers. A possible way is to measure the area of a close-packed monomolecular layer of rigid-spherical hyperbranched or dendritic macromolecules, using the Langmuir film balance.

The goal of this study was to develop a method for determining the size of macromolecules, as applied to hyperbranched dendritic polymers, poly(perfluorophenylenegermane) and poly(methyldiallylsilane).

Poly(perfluorophenylenegermane) (PPG) was among the first hyperbranched dendritic polymers prepared by a single-stage synthesis from the Flory monomer AB_3 [tris(pentafluorophenyl)germane (PG)] [1, 2]. The units of this polymer consist of perfluorinated aromatic rings bonded to the germanium atom, C_6F_4Ge and C_6F_5Ge, the latter being terminal. The ratio between units of these types is 1 : 2 [3], which corresponds to a regular branched structure with the formula $[(C_6F_5)_2Ge(C_6F_4)]_n$ (Fig. 1). Starting from the third generation, the shape of the macromolecules is nearly spherical, which is supported by the sedimentation data obtained with an ultracentrifuge [4]. The polymer demonstrates high heat resistance and clearly pronounced antifriction properties [5].

EXPERIMENTAL

PPG was synthesized as follows. To a solution of 1 g of PG in 10 ml of a solvent, the estimated amount of triethylamine in THF was added with stirring over a period of 5 min, and the reaction mixture was further stirred for 5 h at 25°C. The yield was 75–85%, and increased with $[Et_3N] : [PG]$ ratio. The resulting PPG was purified by twofold reprecipitation from THF with methanol and then vacuum-dried to constant weight. We obtained three PPG samples with

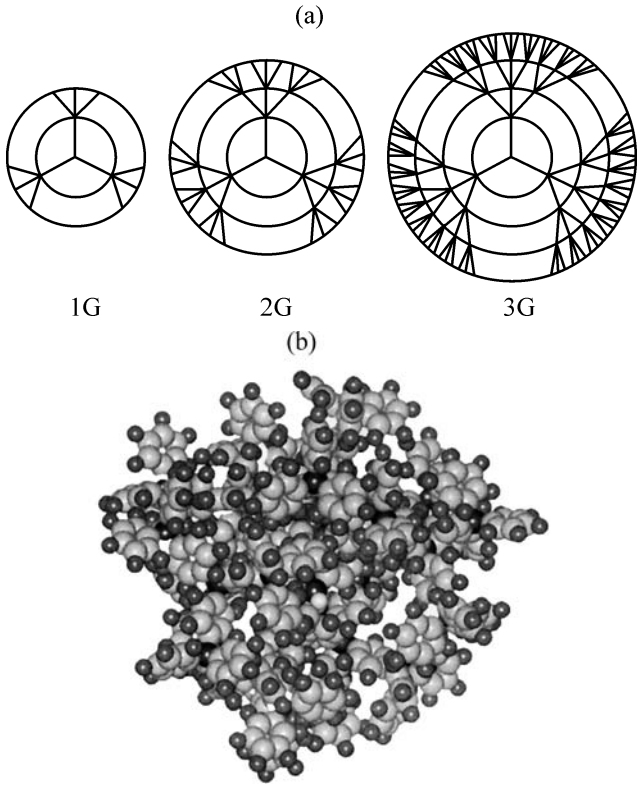


Fig. 1. (a) Chemical graph of the first to third generations and (b) scaled chemical model of hyperbranched PPG of the third generation.

MW 2×10^4, 3×10^4, and 8×10^4, determined by gel filtration and centrifugal sedimentation [4]. The surface pressure isotherms were obtained on a TsIDNP instrument, whose principle of operation and design have been described in detail elsewhere [6]. The surface pressure was measured by the Wilhelmy plate method. In order to approach the equilibrium conditions of formation of the monomolecular films, we used the discrete mode with intermittent interruption of the moving barrier for 10 min prior to each measurement. As a substrate, we used double-distilled water. The experiments were carried out at 20 ± 1°C. Chloroform was used as a solvent for PPG. The solution was applied onto water using a 50-μl syringe. Before the measurement, the surface covered with the polymer film was allowed to stand for 15 min, to remove the solvent. From the surface pressure isotherm, we determined A_0, the area occupied by 1 mg of PPG in the close-packed monolayer.

Figure 2 shows the surface pressure isotherms of hyperbranched PPG with MW 8×10^4. As can be seen, A_0 depends on the PPG concentration in the chloroform solution applied onto the water/air interface. For all the samples studied, the initial portion of this dependence is linear (Fig. 3). Therefore, we used in our calculations the parameter A_0^∞ obtained by extrapolation of A_0 to zero polymer concentration. From A_0 and the density of PPG ($\rho = 2.39$ g cm^{-3}) we estimated the effective thickness of the monolayer, equal to the effective diameter of the spherical macromolecule of PPG (d_{eff}):

$$h_{\text{eff}} = 1/\rho A_0,$$

To obtain a relationship between d_{eff} and MW, we employed computer simulation. Figure 1 shows the chemical graphs of the first three PPG generations, as well as the chemical model of the third generation obtained using the HyperChem code. Below are given the theoretical sizes of the PPG macromolecules d_{theor} for the first five generations and their molecular weights.

Generation no.	1	2	3	4	5
d_{theor}, nm	1.63	3.03	4.00	5.23	6.46
MW	2240	7200	22 200	67 200	202 000

This dependence is plotted in Fig. 4 along with the experimental data obtained using the Langmuir film balance for the PPG samples with molecular weights measured by gel filtration (with calibration by the centrifugal sedimentation data). The observed satisfactory agreement of the theoretical and experimental results suggests that the above procedure is well applicable to hyperbranched PPG.

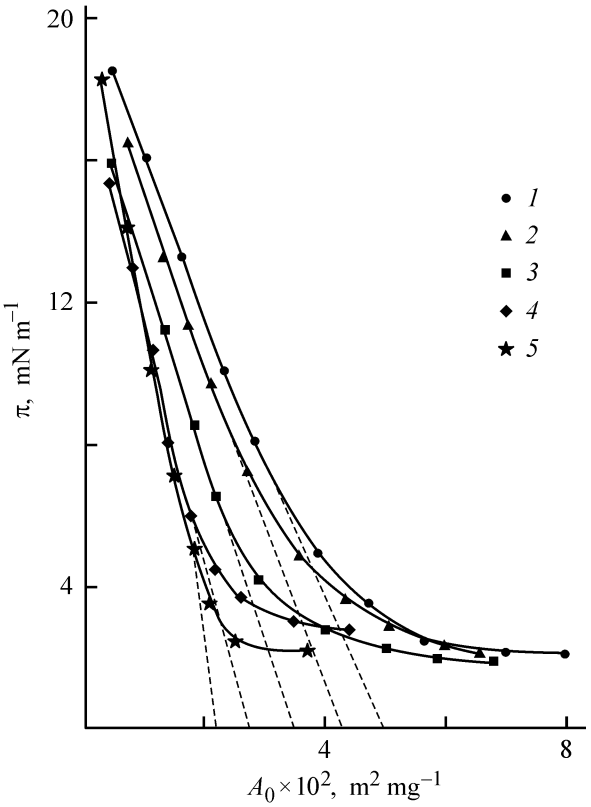


Fig. 2. Surface pressure isotherms of PPG (MW 8×10^4). (π) Surface pressure and (A_0) area occupied by 1 mg of PPG in the close-packed monolayer. PPG concentration (mg ml^{-1}): (*1*) 2, (*2*) 2.5, (*3*) 3, (*4*) 3.5, and (*5*) 4.

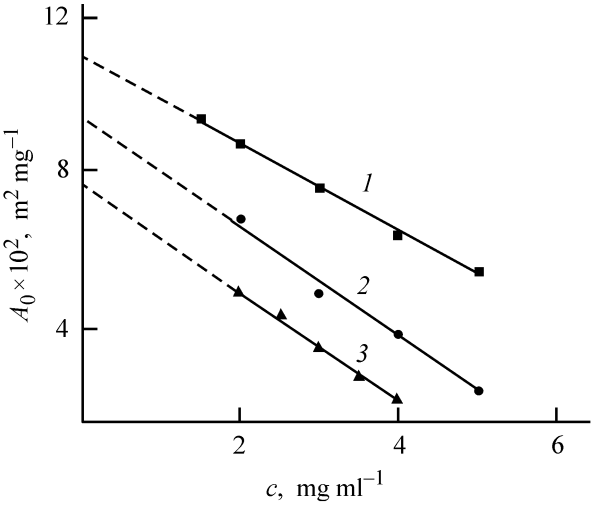


Fig. 3. Area occupied by 1 mg of PPG in the close-packed monolayer A_0 vs. PPG concentration c. MW $\times 10^4$: (*1*) 2, (*2*) 3, and (*3*) 8.

Similarly, we determined the size and MW of another hyperbranched polymer, poly(methyldiallyl-

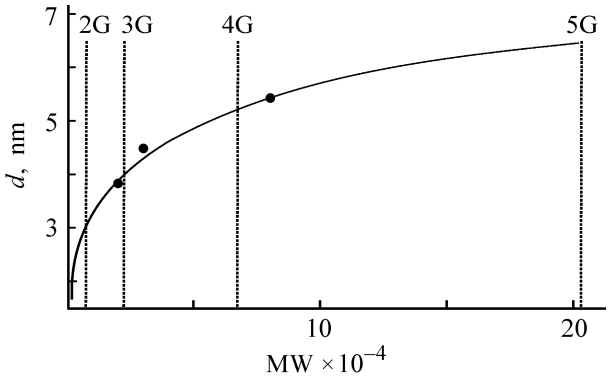


Fig. 4. Diameter d of hyperbranched PPG macromolecules vs. MW. *The solid line* represents the theoretical curve, and *the points*, experimental data. *The dotted lines* correspond to the generation number on the assumption of a regular structure.

silane), prepared by single-stage hydrosilylation [7]. For the polymer sample with MW 2.3×10^4 (determined by gel filtration), d_{eff} was found by the above procedure to be 7.0 nm. This value corresponds to MW 2.5×10^4, as obtained from the theoretical dependence of the diameter on MW, derived from the results of computer simulation, as in the case of PPG. In turn, this MW value corresponds to generation no. 6.6, i.e., to the imperfect seventh generation. Figure 4 shows that the structures of two of three PPG samples studied also have imperfect external generations. This phenomenon is typical of uncontrolled single-stage synthesis of hyperbranched polymers.

CONCLUSIONS

(1) The Langmuir film balance method was used to determine the size of two hyperbranched dendritic polymers, poly(perfluorophenylenegermane) and poly(methyldiallylsilane).

(2) The dependences of the diameter of the hyperbranched macromolecules on the molecular weight were obtained by computer simulation. The resulting theoretical dependences could be used to determine the molecular weight and generation number of dendritic polymers.

ACKNOWLEDGMENTS

The authors are grateful to A.M. Muzafarov for providing a sample of polymethyldiallylsilane.

The study was financially supported by the Russian Foundation for Basic Research (project no. 06-03-32872) and Federal Target Scientific and Technical Program "Research and Development in Priority Areas of Science and Technology in 2002–2006" (State contract no. 02.442.11.7487).

REFERENCES

1. Bochkarev, M.N., Silkin, V.B., Maiorova, L.P., et al., *Metalloorg. Khim.*, 1988, vol. 1, no. 1, pp. 196–200.
2. Bochkarev, M.N., Semchikov, Yu.D., Silkin, V.B., et al., *Vysokomol. Soedin., Ser. B*, 1989, vol. 31, no. 9, pp. 643–644.
3. Kir'yanov, K.V., Semchikov, Yu.D., Bochkarev, M.N., and Zaitsev, S.D., *Vysokomol. Soedin., Ser. A*, 2003, vol. 45, no. 5, pp. 715–722.
4. Zaitsev, S.D., Turshatov, A.A., Pavlov, G.M., et al., *Vysokomol. Soedin., Ser. B*, 2004, vol. 46, no. 8, pp. 1443–1448.
5. Silkin, V.B., Maiorova, L.P., Bochkarev, M.N., et al., *Vysokomol. Soedin., Ser. A*, 1990, vol. 32, no. 11, pp. 2346–1250.
6. Abramenko, Yu.M., Abramzon, A.A., Bening, G.P., and Leshchenko, M.Ya., *Kolloidn. Zh.*, 1987, vol. 49, no. 1, p. 122.
7. Drohman, C., Gorbatsevich, O., Muzafarov, A., and Moller, M., *Polym. Prepr.*, 1998, vol. 39, no. 1, p. 471.

ISSN 1070-4272, Russian Journal of Applied Chemistry, 2006, Vol. 79, No. 8, pp. 1341–1346. © Pleiades Publishing, Inc., 2006.
Original Russian Text © E.M. Tretenichenko, V.M. Datsun, L.N. Ignatyuk, L.A. Nud'ga, 2006, published in Zhurnal Prikladnoi Khimii, 2006, Vol. 79, No. 8, pp. 1353–1358.

MACROMOLECULAR CHEMISTRY AND POLYMERIC MATERIALS

Preparation and Properties of Chitin and Chitosan from a Hydroid Polyp

E. M. Tretenichenko, V. M. Datsun, L. N. Ignatyuk, and L. A. Nud'ga

Far-Eastern State Technical Fishery University (Dal'rybvtuz), Vladivostok, Russia
Institute of Macromolecular Compounds, Russian Academy of Sciences, St. Petersburg, Russia

Received March 30, 2006

Abstract—The chemical composition of *Obelia longissima* hydroid polyp from mariculture system fouling community was examined. Conditions for chitin recovery and chitosan preparation thereof were developed. The initial raw material, chitin, and chitosan were characterized by electron microscopy, infrared spectroscopy, and X-ray diffraction analysis. Also, certain qualitative characteristics of these materials were determined.

DOI: 10.1134/S1070427206080258

Various marine organisms are responsible for fouling of hydrobiotechnical systems for mariculture cultivation. Among them a significant proportion (12–32.2%) belongs to *Obelia longissima* (*Hydrozoa*) hydroid polyp. The skeleton of the hydroid polyp is formed by a chitinoid substance. Large volumes of the fouling organisms, as well as the possibility of cultivation of the polyp, make reasonable an elucidation of its suitability as a source of chitin [1, 2].

In this study we identified the chemical composition of the polyp skeleton, elucidated the possibility of recovery of chitin thereof, developed a method for preparation of a chitin derivative, chitosan, and comprehensively characterized the resulting products.

EXPERIMENTAL

We examined marine biological fouling organisms, uncrushed *O. longissima* and its processing products, chitin and chitosan.

Chitin was recovered by successive extraction of the concomitant substances from the chitin-containing raw material. Extraction of protein substances (deproteinization) was carried out in 4% aqueous sodium hydroxide at the raw material : alkali fluid ratio M = 1 : 4 and temperature of 95–97°C for 60 min. Demineralization was carried out with 4% hydrochloric acid at room temperature for 30 min at M = 1 : 4. The deproteinization and demineralization stages were twice repeated in succession.

Chitosan was obtained by base deacetylation with 50% aqueous sodium hydroxide at M = 1 : 5 and temperatures of 80, 100, and 120°C for 10, 30, and 60 min.

The moisture and ash contents, as well as the content of protein substances (by the Kjeldahl method) in the initial raw material were determined in accordance with GOST (State Standard) 7636–85. The amount of lipids was determined by extraction with petroleum ether according to GOST 13893–68.

The content of protein substances in chitin was determined on a Biochrom-30 (Cambridge) amino acid analyzer after sample preparation by acid hydrolysis [3, 4].

The kinematic viscosity of the chitosan solutions was determined according to the appropriate TU (Technical Specifications) [5].

The changes of the microsctructure of the initial raw material during treatment with acid and base agents, as well as those of the microstructure of chitin and chitosan, were monitored with an SEM LEO-430 scanning electron microscope at the ×400 magnification. The electrically conducting coating was applied by vacuum thermal sputtering of carbon [6].

The IR absorption spectra of chitin in KBr pellets were measured on a Spectrum BX-II (Perkin Elmer) spectrometer, and the IR spectra of the chitosan films on calcium fluoride supports, on a Vector-22 (Bruker) IR Fourier spectrometer.

Table 1. Chemical composition of *O. longissima* and other chitin sources

Raw material	Dry substance content, %				References
	protein	lipids	mineral substances	chitin	
O.longissima	43.2	0.2	11.6	44.9	–
Shell of:					
krill	25–30	1–3	20–22	25–30	[14]
crabs	14.7	1.0	34.5	35.3	[15]
shrimps	25.1	14.8	36.4	9.8	[15]
Calmar gladius	–	2–5	0.5–2	28–39.4	[14]
Hammarus crayfish	50–54	6–8.5	15–18	22–25	[14]
Dead bees	50–80	–	2–3	10–12	[16]
Fungi:					
Aspergillus niger	56.0	1.2	17.0	40.6	[17]
Aspergillus terricola	16.3	0.4	12.6	18.3	[18]

The content of free amino groups in chitosan was determined spectrophotometrically using tropeolin anionic dye [sodium 4-(2-hydroxy-1-naphthylazo)benzenesulfonate] in 1% acetic acid. It was estimated from the ratio of the intensity A_{1666} of the amide I absorption band to that of the band of the stretching vibrations of the hydoxy groups (A_{3440}) [7–9].

The molecular weight of the chitosan samples was determined viscometrically in 0.1 M aqueous acetic acid containing 0.2 M NaCl at 25°C [10–12]. The measurements were performed on an Ubbelohde viscometer [13] with a capillary diameter of 0.3 mm at 25 and 37°C. The chitosan concentration in solution was expressed in grams per cubic centimeter. The molecular weight was calculated by the formula [14]

$$[\eta] = 1.81 \times 10^{-3} M^{0.93}.$$

The X-ray diffraction patterns of the chitin and chitosan samples were measured on a DRON-2 diffractometer using Ni-filtered $Cu_{K_{\alpha 2}}$ radiation.

Table 1 compares the chemical composition of the raw material we used with those of other chitin-containing raw materials, taken from the literature.

As can be seen from Table 1, the content of chitin in the hydrobiont examined is 44.9%, which significantly exceeds that in the shells of a number of crustaceans. The content of protein substances is higher than that in the shell-containing raw materials, but the degree of mineralization is much lower. The content of lipids is insignificant (0.23%).

In the amount of chitin, *O. longissima* is superior to all the chitin sources from Table 1, including mycelial fungi. A comparatively low degree of mineralization makes this hydroid polyp a very promising source of chitin.

To find the best conditions for recovery of chitin, we treated the raw material by two schemes differing in the succession of deproteinization and demineralization stages and involving extraction of concomitant substances [15, 19]. In each scheme, we varied the number of treatment runs for the polyp. After each treatment run with acid and alkali and washing of the product, we determined the amount of the protein and mineral substances.

Scheme 1 involves two treatment runs with acid and base agents; the content of mineral substances is 0.3% (against 0.75% for one treatment run). At the same time, the protein content was about the same for procedures with one and two treatment runs, 12.53 and 11.06%, respectively.

In scheme 2, repeated treatment of chitin with acid and base agents was inefficient: The contents of protein and mineral substances were approqimately equal, 12.81 and 13.03 and 0.14 and 0.15%, respectively.

This makes reasonable the recovery of chitin by scheme 2 including one treatment run with alkali and acid in succession. The reason is the high content of protein in the initial raw material; removal of protein favors deeper demineralization. It should be noted that chitin is recovered from shell-containing raw materials by scheme 1 because of the high content of the mineral component in this raw material.

The chitin recovered consists of fine fibers, from white to light cream or light beige in color. The total

Table 2. Characteristics of chitosan in relation to the conditions of preparation from *O. longissima* chitin

Chitin quality parameter	Process temperature and duration, min								
	80°C			100°C			120°C		
	10	30	60	10	30	60	10	30	60
Degree of deacetylation, %	70.0	71.3	72.8	77.1	78.2	80.5	79.7	80.6	87.8
Molecular weight, kDa	660.0	610.0	572.3	550.3	510.0	420.1	449.2	414.8	274.1
Intrinsic viscosity, ml g^{-1}	500.1	452.2	410.8	400.4	350.0	310.0	327.9	304.5	207.1
Yield of chitosan, % of chitin	65.2	62.2	60.2	58.2	57.2	56.8	56.0	55.3	53.2
Kinematic viscosity, 10^{-4} m^2 s^{-1}	881.0	713.0	598.0	762.0	603.0	525.0	570.0	422.0	333.0

nitrogen content is 7.27% (against theoretical 6.90%). The fact that N_{tot} that we determined exceeds the theoretical value suggests the presence of residual protein; the mass fraction of chitin in the product is 92.2%.

Electron micrographs (Fig. 1b, 1c) show how the initial raw material is modified by treatment with acid and base agents. Before treatment with reagents (Fig. 1a), the skeleton of the polyp consists of 3–5 ring-shaped necks or has a smooth segment. The middle layer is obscured by the covering outer layer. Each treatment run with chemical reagents loosens the structure, making visible the middle layer (Figs. 1b, 1c). A small thickness (thin film) of the outer and inner layers of the skeleton, as well as of the skeleton proper, facilitates its deproteinization and demineralization during chitin recovery. This involves removal of the outer and inner layers and thinning of the middle layer of the skeleton, where longitudinal cords are prominent. The middle layer exhibits a fibrous structure comprised of a number of small vertical columns, each with transverse streakes. The small columns, evidently, consist of chitin fibers, in agreement with the data from [16]. That study involved an electron-microscopic examination of the chitin recovered from the cuticle of insects (locust, hornet), which contain uniform chitin fibers fixed in protein matrices, as well as fibrils aggregated into ordered layers.

The IR spectrum of the chitin recovered from the polyp contains absorption bands typical of the chitin of crustaceans [16]: band at 1640 and a shoulder at 1656 cm^{-1}, corresponding to the C=O groups of the acetamide moiety (amide I), as well as bands at 3267, 1554, and 712 cm^{-1}, belonging to the amide group (amide II).

The fact that, whatever the origin, chitin does not melt and dissolves in a limited number of aggressive or toxic solvents, makes preparation of films, fibers, and other items thereof a difficult task. More convenient for various applications (in medical, pharmaceutical, cosmetic, textile, paper, and other industries) is a chitin derivative, chitosan. It readily dissolves in dilute organic and monobasic mineral acids. Chitosan is typically prepared by alkaline treatment of chitin with heating [15, 20–23]. The alkali concentration, as well as the temperature and time of the process, depend on the kind of the raw material from which chitin was recovered.

Since the chitin we examined has a fine-fibered morphology, chitosan was recovered thereof under milder conditions, compared to those in recovering chitosan from crab chitin with a dense lamellar morphology. Chitin was treated with 50% aqueous sodium hydroxide at 80–120°C for 10–60 min. Table 2 summarizes the results.

Table 2 shows that, even at 80°C after 10 min, the degree of deacetylation (DD) was 70%, which is sufficient for complete dissolution of the product in 2% acetic acid. Raising the reaction temperature, like prolongation of the base treatment of chitin, causes a decrease in the DD, in parallel with a decrease in the molecular weight of chitosan and in the yield of the final

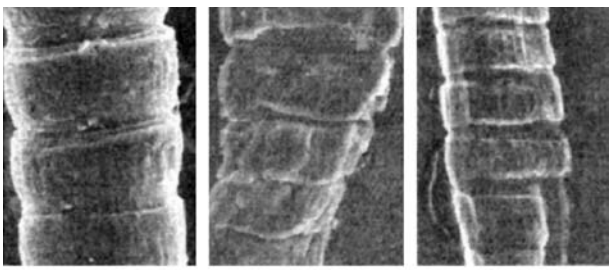


Fig. 1. Appearance and structure of the *O. longissima* skeleton: (a) section of the polyp stem, (b) after base treatment, and (c) after acid treatment (×400 magnification).

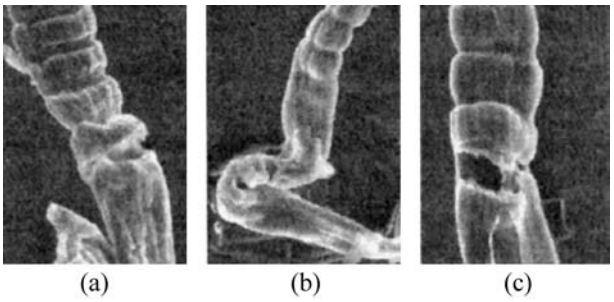


Fig. 2. Appearance and structure of chitosan obtained from *O. longissima* at τ = 60 min and temperature of (a) 80, (b) 100, and (c) 120°C (×400 magnification).

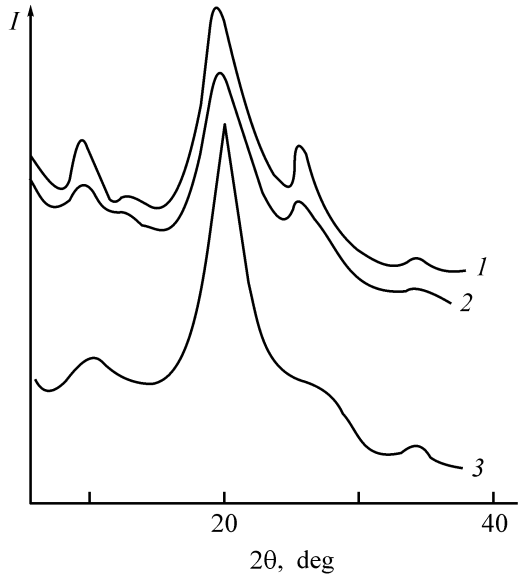


Fig. 3. X-ray diffraction patterns of chitosan obtained from *O. longissima* chitin at τ = 60 min and temperatures of (*1*) 80, (*2*) 100, and (*3*) 120°C. (*I*) Relative intensity and (2θ) reflection angle.

product. A decrease in the molecular weight is due to hydrolytic and oxidative degradation of the macromolecules, since the reaction was run in the presence of atmospheric oxygen. A decrease in the yield is due to the natural loss because of the elimination of the acetyl group, as well as to degradation to water-soluble oligomers, which are removed during purification of the product.

By varying the chitosan recovery conditions, it is possible to obtain a product with the desired DD of 70–87.8%, molecular weight of 270–660 kDa, and kinematic viscosity of $(333-881) \times 10^{-4}$ m^2 s^{-1}. Numerous application fields and different requirements imposed on chitosan give no way of specifying the optimality of these characteristics. Preparation of the most viscous chitosan solutions (881×10^{-4} m^2 s^{-1}) requires running the process at 80°C for 10 min. The resulting chitosan is identical in morphology and color to the initial chitin, namely, consists of fine fibers, from white to light cream or light beige in color.

The chitosan samples prepared at (a) 80, (b) 100, and (c) 120°C for 60 min were characterized by electron microscopy (Fig. 2), X-ray diffraction analysis (Fig. 3), and IR spectroscopy.

The electron micrographs of chitosan (Fig. 2) show that deacetylation of chitin leads to a general amorphization of the structure. A thin film of the middle layer of the skeleton is characterized by parallel arrangement of regular fibers with some gaps and disintegrations, which make visible an empty space inside the skeleton, suggesting the lack of protein.

The electron micrographs of the chitosan obtained at 120°C for 60 min (Fig. 2c) show that the particle surface is more uniform and is formed by wide fibrils and spherulites. The chitosan obtained at 80°C (Fig. 2a) exhibits a more defective and nonuniform structure with fine fibrils and spherulites and a lower degree of crystallinity, which agrees with published data [24–26].

An X-ray diffraction analysis of chitosan (Fig. 3) showed that it has the same crystal lattice as chitin, but is characterized by a lower degree of ordering of the macromolecules.

The reflections in the X-ray diffraction patterns of chitin and chitosan have identical positions, but those of chitosan are less intense. The diffraction patterns of chitosan consist of two fairly broad reflections at 2θ = 10° and 20°. The broadening of the reflections suggests lowering of the degree of ordering of the structure during deacetylation [26].

The diffraction patterns we obtained are similar to those of the chitosan samples obtained from crab, shrimp, and lobster shells [27, 28].

Figure 3 shows that, as the degree of deacetylation increases (curves *1*, *2*), the reflection at 2θ = 26.5° tends to decrease in intensity. It corresponds to the interplanar spacing of 0.334–0.343 nm and is the most intense third-order reflection (003) for chitin fibers. In curve *3*, the reflection in this range of angles disappears.

The changes in the X-ray diffraction pattern suggest that the samples with lower DDs (curves *1*, *2*) still contain fragments of ordered chitin. At higher DDs (samples with DD = 87.7%), this reflection degenerates, which suggests the lack of chitin fragments in

the chitosan structure; the residual acetamide groups are randomly spread along the macrochain and do not form an intrinsic structure. Similar changes in the X-ray diffraction patterns were observed in alkaline deacetylation of the chitin recovered from crab shell [29].

The IR spectra of the chitosan samples contain characteristic bands corresponding to vibrations of the carbonyl group of the acetamide moiety (amide I) at 1659–1660 cm^{-1}, bending vibrations of the amide groups (amide II) (NH and NH_2 groups) at 1552–1591 cm^{-1}, vibrations of carbonyl groups at 1377–1379 cm^{-1}, and vibrations of hydroxy groups at 3441–3450 cm^{-1}, which is consistent with published data [14, 29–31]. With DD increasing from sample 1 to sample 3, the absorption bands at 1659 and 1552–1591 cm^{-1} tend to decrease in intensity, which confirms removal of the N-acetyl groups. These bands are suggested for determination of the DD by IR spectroscopy [7–9].

CONCLUSIONS

(1) It was found that the hydroid polyp *Obelia longissima* contains up to 45% chitin and is weakly mineralized. Large volumes of *Obelia longissima* removed from mariculture systems and the possibility of its cultivation makes it suitable as a commercial source of chitin.

(2) A procedure for recovery of chitin from the hydroid polyp was suggested. It includes one treatment run with alkali for the raw material, followed by one treatment run with acid. Conditions for preparation of chitosan from chitin were developed.

(3) It was determined that the chitosan samples with deacetylation degrees of 70–87.7% and molecular weights of 270–660 kDa, prepared in the study, are soluble in dilute acids. The IR spectra and X-ray diffraction patterns of the chitin and chitosan samples correspond to those of the chitin and chitosan recovered from crab shells.

REFERENCES

1. Feofilova, E.P. and Tereshina, V.M., in *Materialy Pyatoi Vserossiiskoi konferentsii "Novye perspektivy v issledovanii khitina i khitozana"* (Proc. Fifth Russian Conf. "New Prospects in Studies of Chitin and Chitosan"), Moscow: Vseross. Nauchno-Issled. Inst. Rybnogo Khozyaistva i Okeanografii, 1999, pp. 76–78.
2. Tretenichenko, E.M., Datsun, V.M., and Maslennikov, S.I., in *Materialy III Mezhdunarodnoi nauchnoi konferentsii "Rybokhozyaistvennye issledovaniya mirovogo okeana"* (Proc. III Int. Scientific Conf. "Fishery Studies of the World Ocean"), May 19–21, 2005, Vladivostok: Dal'rybvtuz, 2005, pp. 3–4.
3. Bruggeman, I. and Erberdobler, H., *Z. Tierphysiol., Tierernahr., Futtermitteln*, 1967, vol. 22, no. 3, pp. 173–181.
4. Kozarenko, T.D., Zuev, S.N., and Mulyar, N.R., *Ionoobmennaya khromatografiya aminokislot* (Ion-Exchange Chromatography of Amino Acids), Novosibirsk: Nauka, 1981.
5. *TU* (Technical Specifications) *15-02 545–89: High-Molecular-Weight Chitosan for Commercial Processing: Technical Specifications.*
6. Mironov, A.A., Komissarchik, Ya.Yu., and Mironov, V.A., *Metody elektronnoi mikroskopii v biologii i v meditsine* (Electron Microscopy Methods in Biology and Medicine), St. Petersburg: Nauka, 1994.
7. Domzy, J.F. and Roberts, G.A.F., *Macromol. Chem.*, 1985, vol. 186, pp. 1671–1677.
8. Domard, A., *Int. J. Biol. Macromol.*, 1987, vol. 9, pp. 333–336.
9. Glazunov, V.P. and Gorbach, V.I., *Bioorg. Khim.*, 1999, vol. 25, no. 3, pp. 216–219.
10. Tsien Zhen Yuan, *Opredelenie molekulyarnykh vesov polimerov* (Determination of Molecular Weights of Polymers), Moscow: Inostrannaya Literatura, 1962.
11. Maghami, G.G. and Roberts, G.A.F., *Makromol. Chem.*, 1988, vol. 189, no. 1, pp. 195–200.
12. Davydova, V.N., Interaction of Bacterial Endotoxins with Chitosan, *Cand. Sci. Dissertation*, Vladivostok, 2000.
13. Freifelder, D.M., *Physical Biochemistry*, San Fracisco: Freeman, 1976.
14. *Khitin i khitozan: Poluchenie, svoistva i primenenie* (Chitin and Chitosan: Preparation. Properties, and Application), Skryabin, K.G., Vikhoreva, G.A., and Varlamov, V.P., Eds., Moscow: Nauka, 2002.
15. Datsun, V.M. and Safronova, T.M., *Khitin* (Chitin), Vladivostok: Dal'nevost. Gos. Univ., 1995.
16. Rudall, K.M. and Kenchington, W., *Biol. Rev.*, 1973, vol. 49, pp. 597–636.
17. Nud'ga, L.A., Ganicheva, S.I., Petrova, V.A., et al., *Zh. Prikl. Khim.*, 1997, vol. 70, no. 2, pp. 242–246.
18. Nud'ga, L.A., Petrova, V.A., Ganicheva, S.I., et al., in *Materialy Pyatoi Vserossiiskoi konferentsii "Novye perspektivy v issledovanii khitina i khitozana"* (Proc. Fifth Russian Conf. "New Prospects in Studies of Chitin and Chitosan"), Moscow: Vseross. Nauchno-Issled. Inst. Rybnogo Khozyaistva i Okeanografii, 1999, pp. 242–245.
19. Datsun, V.M., Investigation of the Composition and Development of a Technology for Rational Use of Antarctic Krill Waste, *Cand. Sci. Dissertation*, Moscow, 1981.
20. Falk, M., Smith, D.G., McLachlan J., and McInness, A.G., *Can. J. Chem.*, 1966, vol. 44, pp. 2269–2280.

21. Bykov, V.P. and Furman, D.I., in *Materialy Pyatoi Vserossiiskoi konferentsii "Novye perspektivy v issledovanii khitina i khitozana"* (Proc. Fifth Russian Conf. "New Prospects in Studies of Chitin and Chitosan"), Moscow: Vseross. Nauchno-Issled. Inst. Rybnogo Khozyaistva i Okeanografii, 1999, pp. 18–21.
22. Levan'kov, S.V., Kupina, N.M., and Blinov, Yu.G., in *Materialy Pyatoi Vserossiiskoi konferentsii "Novye perspektivy v issledovanii khitina i khitozana"* (Proc. Fifth Russian Conf. "New Prospects in Studies of Chitin and Chitosan"), Moscow: Vseross. Nauchno-Issled. Inst. Rybnogo Khozyaistva i Okeanografii, 1999, pp. 44–46.
23. *Metody khimiii uglevodov* (Methods of Carbohydrate Chemistry), Kochetkov, N.K., Ed., Moscow: Mir, 1967.
24. Nud'ga, L.A., Baklagina, Yu.G., Petropavlovskii, G.A., et al., *Vysokomol. Soedin., Ser. B*, 1991, vol. 33, no. 11, pp. 864–868.
25. Roberts, G.F.A., *Chitin Chemistry*, London: Macmillan, 1992.
26. Muzzarelli, R.A.A., *Chitin*, Oxford: Pergamon, 1997.
27. Sacurai, K., *Sen-i Gakkaishi*, 1985, vol. 41, pp. 361–363.
28. Yokota, H., *J. Polym. Sci., Part C: Polym. Lett.*, 1986, vol. 24, no. 6, pp. 423–426.
29. Braussignac, P., *Chim. Ind. - Jenie Chim.*, 1968, vol. 99, no. 9, pp. 1241–1247.
30. Rogovina, S.Z., Vikhoreva, G.A., Akopova, T.A., and Gorbacheva, I.N., *Vysokomol. Soedin., Ser. A*, 1997, vol. 39, no. 6, pp. 941–946.
31. Rogovina, S.Z., Akopova, T.A., Vikhoreva, G.A., et al., *Vysokomol. Soedin., Ser. A*, 1998, vol. 40, no. 8, pp. 1389–1393.

ISSN 1070-4272, Russian Journal of Applied Chemistry, 2006, Vol. 79, No. 8, pp. 1347–1349. © Pleiades Publishing, Inc., 2006.
Original Russian Text © K.G. Guliev, 2006, published in Zhurnal Prikladnoi Khimii, 2006, Vol. 79, No. 8, pp. 1359–1362.

MACROMOLECULAR CHEMISTRY AND POLYMERIC MATERIALS

Synthesis of a Self-Cross-Linking Copolymer from 2-Glycidyloxymethyl-1-(*p*-vinylphenyl)cyclopropane and Maleic Anhydride

K. G. Guliev

Institute of Polymeric Materials, National Academy of Sciences of Azerbaijan, Sumgaiyt, Azerbaijan

Received May 4, 2006

Abstract—Radical copolymerization of 2-glycidyloxymethyl-1-(*p*-vinylphenyl)cyclopropane with maleic anhydride in benzene was studied. The copolymerization constants, Alfrey–Price parameters, and complexation constant were calculated.

DOI: 10.1134/S107042720608026X

It is known that maleic anhydride (MA) forms molecular complexes with donor monomers, which promotes the formation of alternating copolymers [1]. The formation of donor–acceptor complexes was also detected in the copolymerization of MA with cyclic compounds [2–4].

This study was aimed to prepare a new self-cross-linking copolymer with epoxy and anhydride groups from 2-glycidyloxymethyl-1-(*p*-vinylphenyl)cyclopropane and maleic anhydride and to examine features of radical copolymerization in the system.

High physicomechanical and thermal parameters of thermosetting polymers with pendant glycidyl groups are mainly determined by their chemical structure. Therefore, synthesis of such polymers and elucidation of the structure–property relationships for them is a topical problem of polymer chemistry. A characteristic feature of such polymers is also their capacity for self-curing.

These polymers are most often cured with di-, tri-, and polyfunctional compounds applied as curing agents for ordinary epoxy resins.

EXPERIMENTAL

The monomer, 2-glycidyloxymethyl-1-(*p*-vinylphenyl)cyclopropane (M_1), was prepared according to [5] and had the following characteristics: bp 150–153°C/1 mm Hg, n_D^{20} 1.5220, d_4^{20} 1.04. Its purity, according to GLC analysis, was 99.9%.

The copolymerization of M_1 with MA was performed in benzene at 333 K, with AIBN as initiator (0.02 M).

The copolymers were precipitated with diethyl ether, filtered off, and vacuum-dried to constant weight. The copolymer composition was determined by potentiometric titration of anhydride groups; the structure was determined by IR spectroscopy. The copolymer yield was 87%.

Found, %: C 69.20, H 6.30, O 24.70.
$C_{19}H_{20}O_5$.
Calculated, %: C 69.51, H 6.10, O 24.39.

The copolymerization kinetics was studied by dilatometry.

To study the complexation of M_1 with MA, we prepared isomolar series of their solutions in dioxane and recorded the electronic absorption spectra on a Specord UV-VIS spectrometer in the range λ = 300–400 nm at 298 K. The dependence of the optical density on the MA content was examined in the range λ = 330–370 nm.

The total concentration of M_1 and MA was constant (0.2 M), and their ratio was widely varied.

The structure of the macromolecular chain of the copolymers isolated at various conversions and the content of the units of both monomers were studied by IR spectroscopy. The spectra contain bands at 1500 and 1605 cm^{-1}, characteristic of the benzene ring, at 1035–1045 cm^{-1}, characteristic of the cyclopropane group, and at 1740–1780 cm^{-1}, characteristic of the anhydride moiety.

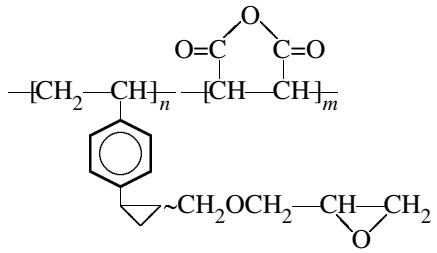
The IR spectrum of the monomer contains the absorption bands of the epoxy groups at 830–850 and

Table 1. Copolymerization of M_1 with MA (M_2) in benzene at 333 K ([M] = 0.5 M, [AIBN] = 0.1%)

$[M_1]$ in starting mixture, mol %	Yield, %	Acid number, mg KOH/g	Copolymer composition, mol %		r_1	r_2	r_1/r_2	Q_1	e_1
			M_1	M_2					
90	11.5	384	50.80	49.20	0.003	0.002	0.006	0.04	–1.16
75	7.3	388	50.20	49.80					
50	12.4	390	50.05	49.95					
25	6.4	394	49.90	50.10					
10	7.2	395	49.82	50.18					

1250–1260 cm^{-1} and those of the ether group at 1105–1110 cm^{-1}. These bands are fully preserved upon copolymerization. At the same time, the vinyl absorption bands at 1645 and 965 cm^{-1} disappear upon copolymerization.

The IR spectra and elemental analysis show that the polymerization involves the double bond of the vinyl group, with the cyclopropane and epoxy rings remaining intact:



This structure of the macromolecular chain units is confirmed by ^1H NMR spectroscopy. The ^1H NMR spectrum contains proton signals from the benzene ring (δ 6.85–7.25 ppm) and cyclopropane group (δ 0.75–1.75 ppm). The epoxy groups give signals at δ 2.5–3.0 ppm, and the anhydride groups, at δ 3.5 ppm.

The optical density of M_1 + MA solutions in dioxane at λ = 330–370 nm is plotted in Fig. 1 vs. the MA content. The plots pass through a maximum at a monomer ratio of 1 : 1.

This fact suggests formation of 1 : 1 molecular complexes in the M_1–MA system. The complexation can also be detected visually: On mixing solutions of M_1 and MA, the mixture becomes yellowish within 20–25 min, and the color becomes more intense in the course time (light yellow in 2 h).

Experiments on the copolymerization of M_1 with MA revealed the formation of a copolymer with a high degree of alternation of the monomeric units at any monomer ratio. From the ^1H NMR data, using the Ketelaar equation [6], we calculated the complexation constant: $K_e = 0.18 \pm 0.01$ $1\ mol^{-1}$.

The reactivities of M_1 and MA were evaluated using the Fineman–Ross method [7]. The results are listed in Table 1; they show that the monomers tend to undergo alternating copolymerization. The polarity (e) and specific activity (Q) parameters of M_1 were calculated by the Alfrey–Price scheme.

To elucidate the mechanism of formation of the alternating copolymer, we studied how the copolymerization rate depends on the composition of the reaction mixture and on the total concentration of the monomers (Fig. 2). The plot of the copolymerization rate vs.

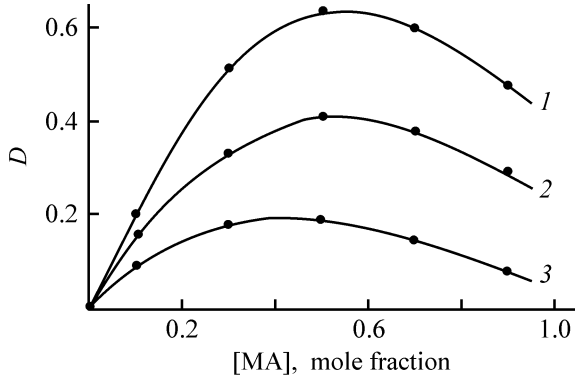


Fig. 1. Optical density D of M_1 + MA solutions in dioxane (total concentration 0.2 M) vs. the MA content in the mixture. λ, nm: (*1*) 350, (*2*) 355, and (*3*) 362.

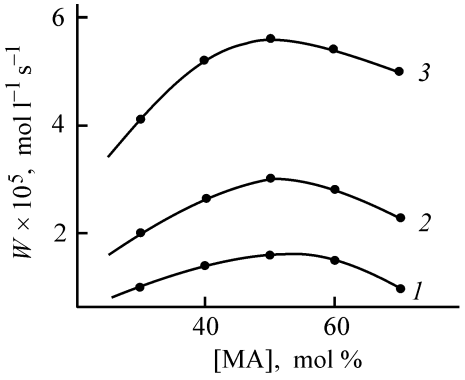


Fig. 2. Rate W of the copolymerization of M_1 with MA vs. the MA content in the monomer mixture. Total concentration of the monomers, M: (*1*) 0.4, (*2*) 0.6, and (*3*) 1.4.

Table 2. Physicochemical properties of M_1–MA copolymer (cross-linking temperature: numerator, 120°C, and denominator, 150°C; cross-linking time 6 h)

Parameter	Characteristic	Parameter	Characteristic
Gel fraction content, wt %	81/99	Specific impact resilience, kgf cm^{-1} cm^{-2}	19.5
Temperature of deformation onset under a load of 0.5 kg cm^{-2}, °C	288/352	Ultimate static bending strength, MPa	135–145
		Heat distortion point, °C	318
Water absorption in 24 h, %	0.05/0.01	Adhesion strength, MPa	10.5
Weight loss at 300°C in 24 h in air, wt %	5–6/3–4	Elasticity, %	12
		Photosensitivity, cm^2 J^{-1}	62.5

reaction mixture composition suggests that the chain propagation involves both free monomers and monomers bound in a complex [8]. Owing to the structural features, these copolymers have specific favorable properties [9]. The presence of polar groups and of pendant functional groups regularly arranged along the macrochain imparts to the copolymer high physicomechanical and thermal properties, and also other specific properties, including the capacity for self-cross-linking. This copolymer is highly photosensitive, as can be seen from its behavior under UV irradiation.

The copolymer prepared by the procedure suggested is capable of thermal cross-linking without addition of a cross-linking component or catalyst. Therefore, the copolymer exhibits high physicomechanical properties. The copolymer is readily cross-linked at 100–150°C in a time from 10 min to 6 h. The yield of the cross-linked fraction is 10–99%.

The cross-linking of the linear copolymer was monitored by comparison of the IR spectra of the samples before and after the heat treatment. We found that the intensities of the absorption bands of the anhydride and epoxy groups decrease in the course of the cross-linking. The properties of the cross-linked copolymer are given in Table 2.

The high adhesion of the copolymer prepared to metals and glass makes it suitable for preparing water-resistant coatings with high levels of hardness and elasticity. Our experiments show that the copolymer of 2-glycidyloxymethyl-1-(*p*-vinylphenyl)cyclopropane with maleic anhydride is cross-linked at a high rate, which allows preparation of materials with high physicomechanical and thermal properties. Furthermore, owing to structural features and polyfunctionality, the copolymer can be readily cross-linked by UV irradiation.

CONCLUSIONS

(1) The copolymerization of 2-glycidyloxymethyl-1-(*p*-vinylphenyl)cyclopropane with maleic anhydride occurs via complexation of the monomers.

(2) The monomers show a pronounced tendency toward alternation in the copolymer.

(3) The copolymer obtained is capable of thermal self-cross-linking.

REFERENCES

1. Kabanov, V.A., Zubov, V.P., and Semchikov, Yu.D., *Kompleksno-radikal'naya polimerizatsiya* (Coordination Radical Polymerization), Moscow: Khimiya, 1987.
2. Fukuda, H., Hirota, M., Endo, T., et al., *J. Polym. Sci., Polym. Chem. Ed.*, 1982, vol. 20, no. 11, pp. 2935–2939.
3. Guliev, A.M. and Guliev, K.G., *Vysokomol. Soedin., Ser. B*, 1985, vol. 27, no. 11, pp. 812–814.
4. Kalinina, F.E., Radnaeva, I.D., Magnonov, D.M., et al., *Polym. Sci., Ser. B*, 2004, vol. 46, nos. 5–6, pp.182–187.
5. Guliev, K.G., Ponomareva, G.Z., and Guliev, A.M., *Zh. Prikl. Khim.*, 2006, vol. 79, no. 3, pp. 497–500.
6. Ketelaar, I.A., Stolpe, C., Goudsmit, A., et al., *Recl. Trav. Chim. Pays-Bas*, 1952, vol. 71, no. 10, pp. 1104–1108.
7. Toroptseva, A.M., Belogorodskaya, K.B., and Bondarenko, V.M., *Laboratornyi praktikum po khimii i tekhnologii vysokomolekulyarnykh soedinenii* (Practical Laboratory Course of Chemistry and Technology of Macromolecular Compounds), Leningrad: Khimiya, 1972.
8. Georgiev, G.S., Golubev, V.B., and Zubov, V.P., *Vysokomol. Soedin., Ser. A*, 1978, vol. 20, no. 7, pp. 1608–1615.
9. Tanaka, Y., Atsukawa, M., Shimura, Y., et al., *J. Polym. Sci., Polym. Chem. Ed.*, 1975, vol. 13, no. 5, pp. 1017–1028.

ISSN 1070-4272, Russian Journal of Applied Chemistry, 2006, Vol. 79, No. 8, pp. 1350–1353. © Pleiades Publishing, Inc., 2006.
Original Russian Text © A.I. Vorob'eva, M.N. Gorbunova, V.Yu. Gusev, S.I. Kuznetsov, S.V. Kolesov, V.P. Begishev, A.G. Tolstikov, Yu.B. Monakov, 2006, published in Zhurnal Prikladnoi Khimii, 2006, Vol. 79, No. 8, pp. 1363–1366.

MACROMOLECULAR CHEMISTRY AND POLYMERIC MATERIALS

Copolymerization of *N*,*N*-Diallyl-*N*'-benzoylhydrazine with Acrylonitrile and Sulfur Dioxide

A. I. Vorob'eva, M. N. Gorbunova, V. Yu. Gusev, S. I. Kuznetsov, S. V. Kolesov, V. P. Begishev, A. G. Tolstikov, and Yu. B. Monakov

Institute of Organic Chemistry, Ufa Scientific Center, Russian Academy of Sciences, Ufa, Bashkortostan, Russia
Institute of Technical Chemistry, Ural Division, Russian Academy of Sciences, Perm, Russia

Received March 7, 2006

Abstract—Radical copolymerization of *N*,*N*-diallyl-*N*'-benzoylhydrazine with acrylonitrile and sulfur dioxide was studied. The kinetic features of the copolymerization of these systems were examined, the relative activities of the monomers were determined, and the structure of the resulting copolymers was elucidated.

DOI: 10.1134/S1070427206080271

Polyfunctional polymers based on nitrogen-, oxygen-, and sulfur-containing vinyl and allyl monomers are of doubtless interest owing to their complexing and flocculating properties and to a wide spectrum of biological activities. These compounds are used as flocculants, growth-stimulating agents in plant growing, drugs in cattle breeding, aftertanning agents in leather production, etc. [1–4]. At the same time, the range of monomers commercially available in Russia for the synthesis of such polymers by radical (co)polymerization is very limited. Therefore, application of industrial facilities intended for production of specialty products (in particular, hydrazine derivatives) to the synthesis of *N*-containing monomers and to production on their basis of new structural types of polyfunctional polymers is a topical problem. Previously we have shown that copolymers of diallylhydrazines with vinyl monomers and sulfur dioxide can be, in principle, obtained [5].

This study deals with the radical copolymerization of *N*,*N*-diallyl-*N*'-benzoylhydrazine (DABH) with acrylonitrile and sulfur dioxide.

EXPERIMENTAL

N,*N*-Diallyl-*N*'-benzoylhydrazine was prepared by the reaction of benzoylhydrazine with allyl chloride:

$$2CH_2{=}CH{-}CH_2{-}Cl + NH_2{-}NH{-}C(O){-}C_6H_5$$

$$\rightarrow (CH_2{=}CH{-}CH_2)_2{-}N{-}NH{-}C(O){-}C_6H_5 + 2HCl.$$

The synthesis conditions are described in [6]. The purity was checked by elemental analysis and ^{13}C NMR spectroscopy.

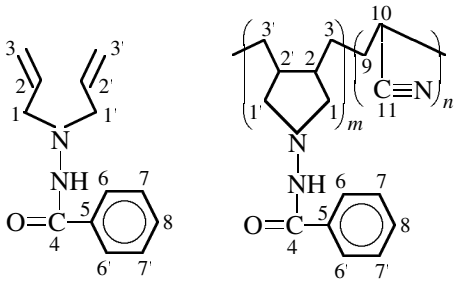
Elemental composition, %	C	H	N
Found	71.71	7.93	12.84
Calculated	72.22	7.41	12.96

The chemical shifts (δ, ppm) and multiplicities of signals in the ^{13}C NMR spectrum of DABH are listed in the table (the ^{13}C NMR spectrum of the DABH–SO_2 copolymer was reported in [5]).

The comonomer (acrylonitrile, AN), initiators [azobis(isobutyronitrile), AIBN; benzoyl peroxide, BP], and solvents (dimethyl sulfoxide, DMSO; methanol; acetone] were purified by standard procedures, and their characteristics agreed with reference data. Sulfur dioxide was dried by passing through concentrated H_2SO_4 and freshly calcined $CaCl_2$.

The copolymerization of DABH with AN and SO_2 was performed to low conversions in the bulk and in DMSO in the presence of AIBN in evacuated ampules (with AN) or in a glass reactor [7] (with SO_2). The reaction mixture temperature was 80°C. The polymers were purified by twofold reprecipitation from the solvent (DMSO) into the precipitant (methanol with AN, acetone with SO_2). The purified polymers were vacuum-dried to constant weight at 50°C. The composition of the copolymers was calculated from the results of elemental analysis.

Chemical shifts and multuplicities of ^{13}C NMR signals of DABH and its copolymers with AN



I **II**

Compound	Stereoisomer	C^1, $C^{2'}$	C^2, $C^{2'}$	C^3, $C^{3'}$	C^4	C^5	C^6	C^7	C^8	C^9	C^{10}	C^{11}
I	–	117.38 t	134.96 d	58.83 t	165.28 s	134.13 s	117.08 d	128.14 d	131.02 d			
II	*cis* *trans*	57.97 60.99 t	40.41 41.80 d	29.83 31.16 t	164.77 s	134.17 s	127.08 d	128.14 d	131.02 d	32.70 33.81 t	27.96 d	120.02 121.17 s

The NMR spectra were recorded on a Bruker AM-300 spectrometer at the operating frequency for ^{13}C of 75.46 MHz. The spectra were recorded in the broad-band proton decoupling and JMOD modes. DMSO-d_6 was used as solvent, and tetramethylsilane, as internal reference.

The UV spectra were measured with a Shimadzu UV-VIS-NIR 3100 spectrophotometer. The complexation was judged from the difference between the optical density of the solution of the monomer mixture and the sum of the optical densities of the solutions of the same monomers taken separately in the same concentrations. The composition of the complex was determined by the method of isomolar series [8].

DABH does not undergo radical homopolymerization in the presence of AIBN or BP and homopolymerizes only in the presence of H_3PO_4. Similar results (10% yield) were obtained in our previous study [5] of the homopolymerization of *N*,*N*-diallyl-*N*'-acetylhydrazine.

Our studies showed that DABH copolymerizes with AN in the presence of AIBN. The copolymerization of DABH (M_1) with AN (M_2) was studied at low conversions. Experiments showed that, irrespective of the conditions (in the bulk or in solution), the reaction yields copolymers with random distribution of the comonomer units in the polymer chain. The composition of the copolymers is plotted in Fig. 1 vs. the composition of the starting monomer mixtures. These data and the effective copolymerization constants calculated by the Mayo–Lewis method ($r_1 = 0$, $r_2 = 1.9 \pm 0.2$) indicate that DABH is considerably less active than AN. It is seen (Fig. 1) that the copolymers are enriched in the AN units in the entire range of the monomer ratios. Since the DABH molecule cannot add to a propagating radical with the DABH terminus, the copolymers cannot contain more than 50 mol % DABH units at any monomer ratio in the starting mixture.

A kinetic study of the copolymerization of DABH with AN at low conversions showed that an increase in the DABH content in the starting monomer mix-

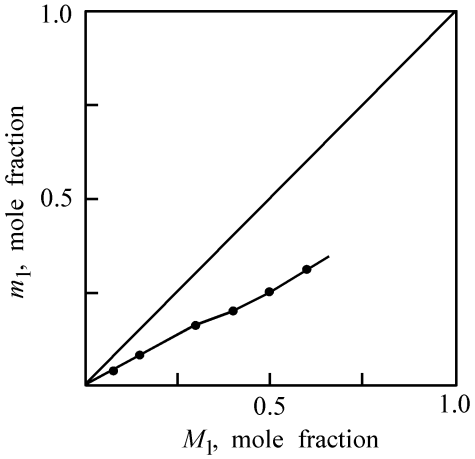


Fig. 1. Composition of DABH–AN copolymers vs. the composition of the initial monomer mixture. $[M_1 + M_2] = 2.2$, [AIBN] = 0.18 M; the same for Fig. 2. (M_1, m_1) Mole fractions of DABH in the starting mixture and copolymer, respectively.

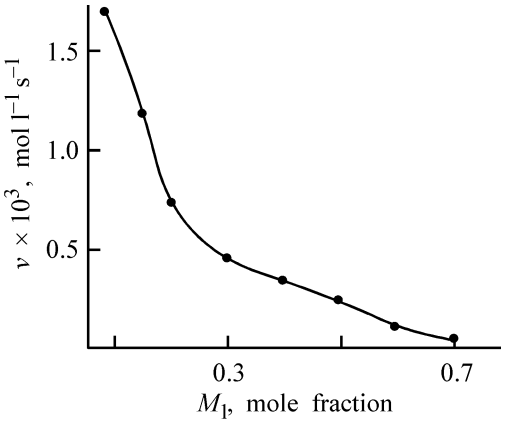


Fig. 2. Initial rate v of the copolymerization of DABH (M_1) with AN (M_2) vs. the composition of the starting monomer mixture. (M_1) Mole fraction of DABH in the starting mixture; the same for Fig. 3.

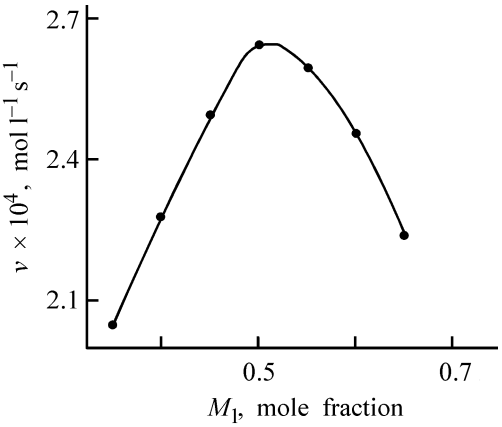


Fig. 3. Initial rate v of the copolymerization of DABH (M_1) with SO_2 (M_2) vs. the composition of the starting monomer mixture. $[M_1 + M_2] = 3.0$, [AIBN] = 0.18 M.

ture leads to a decrease in the reaction rate (Fig. 2), and at a DABH content exceeding 70 mol % the reaction is very slow.

DABH shows a considerably higher activity in the polymerization with SO_2, which exhibits high electron-withdrawing power. The copolymerization of DABH with SO_2 involves the formation of alternating copolymers of the equimolar composition, irrespective of the monomer ratio in the starting mixture, nature of the solvent (DMSO, methanol) and initiator (AIBN, BP), and reaction temperature (60–90°C). The constancy of the copolymer composition at any monomer ratios suggests that the copolymerization of DABH with SO_2 involves the formation of the complexes [DABH···SO_2]. To confirm these data, we studied this system by UV spectroscopy. We found that the electronic absorption spectra of DABH, SO_2, and their mixture in DMSO show noticeable deviations from the additivity: The sum of the optical densities of separately taken solutions of DABH and SO_2 differs from the optical density of the mixed solution, and the largest deviations from the additivity (0.8 in the D scale) are observed at the equimolar ratio of the monomers. These data confirm the occurrence of donor–acceptor interactions between the DABH and SO_2 molecules in the DMSO solution.

Although the reaction conditions do not affect the composition of the copolymers, they strongly affect the reaction rate and copolymer yield. In particular, in the copolymerization of DABH with SO_2 in DMSO at 80°C in the presence of 3 wt % AIBN, the copolymer yield is 70%, whereas with BP taken as initiator, virtually no copolymerization occurs under the same conditions.

The initial rate of the copolymerization of DABH with SO_2 as a function of the comonomer ratio passes through a maximum at the equimolar ratio of the monomers (Fig. 3). The decreased reaction rate at the monomer ratios differing from 1 : 1 is caused by the decreased concentration of the reactive complex in the system.

The overall activation energy of the copolymerization of DABH with SO_2, calculated from the Arrhenius plot using the data obtained for the range 60–90°C, is 103 ± 2 kJ mol^{-1}; this value is typical of radical polymerization.

The structures of the DABH copolymers obtained were studied by ^{13}C NMR spectroscopy. The spectra of the DABH–AN and DABH–SO_2 copolymers (see table) contain, along with the signals of carbon atoms of the –NH–C(O)–C_6H_5 group of the DABH unit, only three pairs of signals corresponding to two methylene groups and one methine group in two stereoisomeric structures, which is indicative of the symmetrical structure of the copolymers. Two pairs of low-field triplets correspond to the *cis*/*trans*-stereoisomeric carbon atoms C^1, $C^{1'}$ and C^3, $C^{3'}$, and the pair of doublets, to the stereoisomeric C^2 and $C^{2'}$ atoms. The chemical shifts and multiplicities of the signals show that the copolymerization of DABH involves opening of both double bonds and formation of symmetrical structures, five-membered pyrrolidine rings. The ratio of the *cis*/*trans*-stereoisomeric units of DABH in its copolymer with SO_2, estimated from the ^{13}C NMR spectrum, is approximately 4 : 1, whereas in the copolymer of DABH with AN, the *trans*-stereoisomeric units prevail.

The chemical shifts of the signals of the AN units in the spectrum of the DABH–AN copolymer virtu-

ally coincide with those in polyacrylonitrile (PAN) [9]. In the spectrum of the copolymer (recorded with broad-band proton decoupling), in contrast to the spectrum of PAN, the configuration multiplets of the pseudo-asymmetrical C^{10} atoms and the adjacent α-, β-C nuclei of the AN units are lacking. This fact indicates that the copolymer does not contain long AN blocks in a noticeable amount and has an ordered structure.

The copolymers obtained are soluble in DMSO and DMF and insoluble in other common solvents (methanol, acetone, tetrahydrofuran, benzene, ethyl acetate, etc.).

CONCLUSIONS

(1) *N*,*N*-Diallyl-*N*'-benzoylhydrazine copolymerizes with acrylonitrile in the presence of various radical initiators to form copolymers with random distribution of the comonomer units in the macromolecule. The relative activity of *N*,*N*-diallyl-*N*'-benzoylhydrazine is considerably lower than that of acrylonitrile, and the copolymers are enriched in the acrylonitrile units in the entire range of monomer ratios.

(2) *N*,*N*-Diallyl-*N*'-benzoylhydrazine copolymerizes with sulfur dioxide by the radical mechanism to form alternating copolymers of equimolar composition, irrespective of the monomer ratio in the starting mixture and reaction conditions. The reaction rate is the highest at the equimolar ratio of the monomers.

(3) The copolymerization of *N*,*N*-diallyl-*N*'-benzoylhydrazine is accompanied by intramolecular cyclization with the formation of pyrrolidine rings and involves both double bonds.

ACKNOWLEDGMENTS

The study was financially supported by the Russian Foundation for Basic Research (project no. 05-03-32097).

REFERENCES

1. Vorob'eva, A.I., Prochukhan, Yu.A., and Monakov, Yu.B., *Vysokomol. Soedin., Ser. C*, 2003, vol. 45, no. 12, pp. 2118–2136.
2. Boyarkina, N.M., Kryuchkov, V.V., Parkhamovich, E.S., et al., *Plast. Massy*, 1987, no. 8, pp. 17–20.
3. USSR Inventor's Certificate, no. 1425258.
4. RF Patent 2145978.
5. Vorob'eva, A.I., Gorbunova, M.N., Gusev, V.Yu., et al., *Zh. Prikl. Khim.*, 2004, vol. 77, no. 7, pp. 1174–1178.
6. Gusev, V.Yu., Vorob'eva, A.I., Radushev, A.V., et al., *Izv. Ross. Akad. Nauk, Ser. Khim.*, 2003, no. 12, pp. 2603–2605.
7. Vorob'eva, A.I., Vasil'eva, E.V., Gaisina, Kh.A., et al., *Vysokomol. Soedin., Ser. A*, 1996, vol. 38, no. 10, pp. 1663–1667.
8. Gur'yanova, E.N., Gol'dshtein, I.P., and Romm, I.P., *Donorno-aktseptornaya svyaz'* (Donor–Acceptor Bond), Moscow: Khimiya, 1973.
9. Berestova, S.S., Shchirets, V.S., Selikhova, V.I., et al., *Vysokomol. Soedin., Ser. B*, 1996, vol. 38, no. 9, pp. 1612–1613.

ISSN 1070-4272, Russian Journal of Applied Chemistry, 2006, Vol. 79, No. 8, pp. 1354–1359. © Pleiades Publishing, Inc., 2006.
Original Russian Text © D.N. Emel'yanov, N.V. Volkova, O.I. Sheronova, Z.G. Chernorukova, 2006, published in Zhurnal Prikladnoi Khimii, 2006, Vol. 79, No. 8, pp. 1367–1372.

MACROMOLECULAR CHEMISTRY AND POLYMERIC MATERIALS

Physicochemical Aspects of Preservation of Cellulose Paper with Polymers

D. N. Emel'yanov, N. V. Volkova, O. I. Sheronova, and Z. G. Chernorukova

Lobachevskii State University, Nizhni Novgorod, Russia

Received February 13, 2006

Abstract—The process of preservation of newspaper with aqueous solutions and dispersions of acrylic copolymers is considered from the instant of impregnation till removal of the polymeric preservative from paper.

DOI: 10.1134/S1070427206080283

Books and archival, artistic, and other materials on paper media are subject to intensive aging (and, occasionally, destruction), which may lead to their loss. Therefore, the process of their preservation and restoration as a porous colloid material should be based on fundamental scientific principles, with special preserving polymeric materials used.

The aim of this study was to examine the process of preservation of porous cellulose paper with water-soluble acrylic polymers. It was necessary to reveal fundamental aspects of impregnation and strengthening of news paper with polyacrylate solutions and find what structural changes occur in paper under the action of various factors.

EXPERIMENTAL

As paper preservatives served water-soluble copolymers of sodium salts (NaMAC, NaAC) of methacrylic (MAC) or acrylic acid (AC), whose backbone contains methyl acrylate (MA) or butyl acrylate (BA) as a second component. The composition of the copolymers is listed in Table 1. The copolymers were synthesized by radical polymerization of 20 wt % solutions of comonomers in water. For the copolymers obtained to exhibit a neutral reaction, a required amount of a 10% solution of sodium hydroxide was introduced into the reaction mixture, with pH adjusted to 7–7.5. The intrinsic viscosity was measured at 23°C in a 2 N aqueous solution of NaOH (the polyelectrolyte effect disappeared under these conditions). To impart biocide properties to paper, it was impregnated with polyacrylic biocide latexes. The latexes were synthesized by emulsion polymerization of methyl methacrylate (MMA) with BA and AC, and tributyltin methacrylate (TBTM) and zinc acetate methacrylate (AcZnMAC) were used as biocide components. The latexes of Sn- and Zn-containing copolymers were obtained in the presence of nonionogenic surfactants, emulsifying agents and water-soluble initiating agents [1].

As a preservation object served news paper manufactured by Balkhna pulp-and-paper combine [GOST (State Standard) 6445–74]. Paper is a capillary-porous colloid material. It has a heterogeneous structure constituted by interwoven cellulose fibers. The fibers have different lengths and their cross-section is the key factor determining the size of pores [2]. The average pore radius of the news paper under study was calculated from the rate of the capillary rise of water by the Washburn equation

$$\frac{dh}{dt} = \frac{2\sigma r \cos\theta}{8\eta h},$$

where h is height; t, time in which a fluid moves up in the capillary; σ and η, surface tension and viscosity of the fluid, respectively; θ, wetting angle; and r,

Table 1. Composition of water-soluble (co)polymers and characteristic viscosity [η] of their solutions

Composition of (co)polymers, wt %	[η], dl g^{-1}
21 MAC–79 NaMAC	0.79
poly-NaAC	0.45
96 NaAC–4 MA	1.47
93 NaAC–7 MA	1.15
90 NaAC–10 MA	1.29
96 NaAC–4 BA	0.93
94 NaAC–6 BA	0.70
92 NaAC–8 BA	0.96

capillary radius [3]. The average size of capillaries (pores) in news paper was found to be 78 nm.

The rate at which the polymeric solution penetrates into paper pores was evaluated by the method of capillary rise of the fluid along a paper sample 50 mm long and 10 mm wide, which was vertically suspended in a hermetically sealed vessel with a solution.

The physicomechanical properties of paper samples 10 mm wide and 80 mm long were tested at room temperature (~23°C) on an RMI-5 tensile-testing machine. Preliminarily, a polymeric solution was once deposited with a brush onto the paper surface along the sheet. Then, the solvent was removed from the paper in the convective-exchange mode at room temperature to constant weight of the sample.

The thermal aging of the paper samples under study was performed at 100 and 160°C in the course of 1–6 h; the thermooxidative destruction was carried out at 240°C, with changes in the sample weight monitored.

The microstructure of paper was examined with an MIM-7 microscope and a ×20 Huygens eye-piece. The image was magnified by a factor of 24.5 with an epiobjective with F-8.2 and A-0.37. The image was recorded with a portable video camera attached to the eye-piece and connected to a computer.

The study of the process of paper preservation included the following stages: (1) analysis of the rate of spontaneous impregnation (rise) of polymer solutions into pores of the paper; (2) examination of the effect of the composition of copolymers, their content in the impregnating solutions, and size of latex particles on the physicomechanical properties of reinforced paper; (3) study of the stability of paper preserved with polyacrylic copolymers against thermal, light, and biological treatments; (4) examination of the reversible removal of the preservative from paper.

Preservation of any porous body, including paper, begins with impregnation with a solution of a preservative, acrylic polymer in our case. It follows from Fig. 1 that, as the concentration of the impregnating polyacrylate solution increases, the viscosity η (mPa s) of this solution becomes higher and the rate V ($m^2\ s^{-1}$) of its capillary rise into the pores of the paper decreases. Both the increase in viscosity and decrease in the rate of solution penetration into paper are related to a change in the structuring of the polymer in solution. In a strongly diluted solution, the polymer is in the form of separate macrocoils, whereas in a moderately concentrated solution, these coils form coarse associates, which come in contact with one another in the concentrated solution to form a continuous structural network [4]. Consequently, the probability of

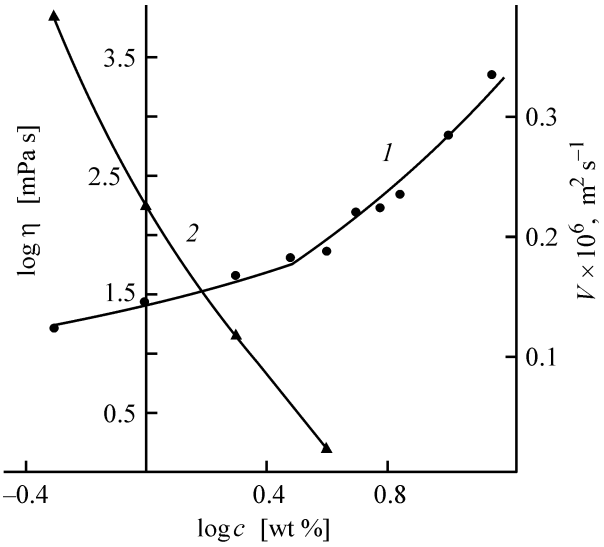


Fig. 1. (*1*) Viscosity η and (*2*) rate V of capillary rise of an aqueous solution of a copolymer composed of 96 wt % NaAC and 4 wt % MA into news paper vs. the concentration c of this solution.

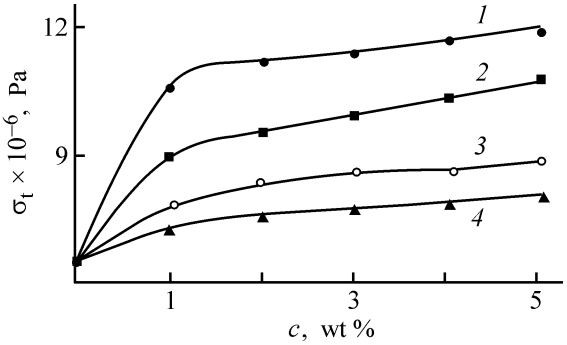


Fig. 2. Tensile strength σ_t of paper vs. the content c of impregnating solutions of copolymers of various compositions. Copolymer composition (wt %): (*1*) 96 NaAC + 4 MA, (*2*) 88 NaAC + 12 MA, (*3*) poly-NaAC, and (*4*) 96 NaAC + 4 BA.

penetration of coarse associates into the paper pores decreases, compared with that for separate macrocoils, whose size is very small. By contrast, a characteristic feature of latexes is that the rate of capillary rise of the fluid into paper pores increases with the size of colloid particles. For example, $V = 1.65 \times 10^{-6}\ m^2\ s^{-1}$ for water, $V = 0.75 \times 10^{-6}\ m^2\ s^{-1}$ for 1% latexes (40% TBTM–31% MMA–26% BA–3% AC) with a particle size of 90 nm , and $V = 0.95 \times 10^{-6}\ m^2\ s^{-1}$ for that with a particle size of 160 nm. Such a behavior of the latexes can be accounted for by the fact that it is more difficult for coarse particles to penetrate into the narrow paper capillaries, compared with finer particles.

An important result of paper preservation with a polymer is that its strength increases, compared with the initial paper. Figure 2 shows how the ten-

Table 2. Colloid-chemical parameters of MMA–BA latexes and tensile strength σ_t of news paper reinforced with latexes

Latex composition, wt %		Particle size, nm	Surface tension, erg cm^{-1}	Physical state of the film	$\sigma_t^* \times 10^{-5}$, Pa
MMA	BA				
80	20	58	72	Glassy	212
70	30	63	71	〃	230
60	40	61	70	〃	243
50	50	70	71	Elastic	259
40	60	76	76	〃	214
30	70	86	82	Sticky	202
20	80	108	83	〃	186
10	90	117	86	〃	178

* Paper samples treated with 5% latexes.

sile strength σ_t (Pa) of paper samples reinforced with various polyacrylic copolymers depends on the concentration of the impregnating polymeric solution. The strength properties of the reinforced paper are strongly affected by the copolymer composition: introduction of MA units into the poly-NaAC backbone raises, and that of BA units, lowers the strength characteristics of polymer-treated paper, compared with poly-NaAC. This is apparently due to the rigidity of the poly-NaAC film. Introduction of MA units makes the rigidity lower, and BA, in addition, imparts to the polymeric film a considerable elasticity. In treatment of paper with latexes, its strength properties also depend on the physical state of the polymeric film and on the size of latex particles (Table 2). The data in the table show that the highest strength is observed for paper samples treated with latexes whose particle size is comparable with the size of pores in paper and the polymer in the film is in the highly elastic state at room temperature. The influence exerted by the size of latex particles on the strength properties of paper is confirmed by measurements of the strength of paper treated with latexes of composition 40% TBTM–31% MMA–26% BA–3% AC. For example, the tensile strength of paper treated with a 5% latex with a particle size of 90 nm is 240×10^5 Pa, whereas for paper treated with a latex of the same concentration but having a particle size of 160 nm, the strength decreases to 180×10^5 Pa. It can be assumed that fine latex particles penetrate into paper pores between its fibers and glue the fibers thereby improving the strength of paper.

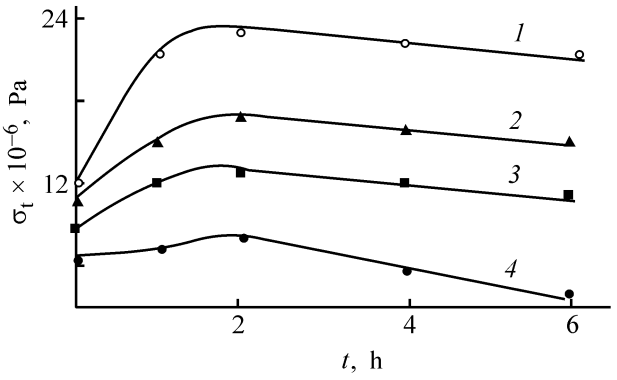


Fig. 3. Effect of the time t of thermal aging (T = 100°C) on the tensile strength σ_t of news paper samples treated with 2 wt % solutions of copolymers of various compositions. Copolymer composition (wt %): (*1*) 96 NaAC + 4 MA, (*2*) poly-NaAC, (*3*) 96 NaAC + 4 BA, and (*4*) paper wetted with water and dried at room temperature.

In the course of time, any paper is subject to aging, becomes fragile, is infested by microbes, looses whiteness, and changes composition. Various criteria are used to judge the paper aging. These are parameters related to mechanical, optical, and chemical properties of paper [5]. In the present study, the stability of paper samples treated with polyacrylic polymers against thermal aging was judged from changes in their strength parameters and from the loss of mass in the course of time under conditions leading to destruction of both the polyacrylate and cellulose. Figure 3 shows how the duration of heat treatment affects the strength of paper samples. It can be seen that the strength of all paper samples increases during 2 h, which is apparently due to evaporation of residual water serving as plasticizer of cellulose fibers of paper. The subsequent decrease in the strength of paper is, in all probability, due to aging of paper, with this process being faster for untreated paper, compared with that subjected to impregnation. This indicates that polyacrylates hinder aging of paper. A similar behavior of the strength of paper preserved with polyacrylates is observed at 160°C. The higher

Table 3. Biological activity of Sn- and Zn-containing copolymers of various compositions

Copolymer composition, mol %				Radius R of the inhibition zone for bacteria and microscopic fungi, mm					
MMA	BMA	TBTM	AcZnMAC	*E.coli*/ *A.niger*	*Prot.vul*/ *P.chryso-genum*	*Staph. auer*/ *Alt. alternata*	*Strep. Savil.*/ *Fus. monili forme*	*B.megater.*/ *Chaet. globosum*	Association of bacteria/ association of microfungi
20	70	10	0	0/6	1/5	0/4	0/5	3/5	0/7
20	65	10	5	3/7	3/5	5/6	6/5	7/7	2/8
20	63	10	7	5/8	3/7	8/7	10/6	8/7	3/10
20	60	10	10	7/10	5/7	10/8	11/8	8/10	5/12
20	70	0	10	7/0	6/0	9/1	11/0	9/2	6/0

stability of paper preserved with the acrylic polymers under study against high-temperature treatments is even more clearly indicated by the data in Fig. 4, which shows how the mass of paper samples varies under conditions of thermooxidative destruction of both the polymer and paper. As demonstrated by microstructural studies of paper samples (Fig. 5, thermal treatment leads to partial redistribution of the copolymer, and specifically its low-molecular-weight fractions, from coarse paper fibers (Fig. 5b) to fine fibrils (Fig. 5c), which protects from the action of heat.

Biocide tin- and zinc-containing latexes were tested for a wide spectrum of antimicrobial action. As test cultures served bacteria *Escherichia coli*, *Proteus vulgaris*, *Staphylococcus aureus*, *Streptococcus salivarius*, *Bacillus megaterium* and micromycetes *Aspergillus niger*, *Penicillium chrysogenum*, *Alternaria alternata, Fusarium moniliforme*, *Chaetomium globosum.* The choice of these cultures was determined by their predominance in biodestruction processes [6]. It follows from the data in Table 3 that Sn-containing copolymers are clearly pronounced fungicides, and Zn-containing copolymers, bactericides, whereas copolymers with Sn- and Zn-containing monomer units exhibit fungicide and bactericide activities simultaneously. It should also be noted that the bactericide activity of the copolymers studied toward associations of test cultures is lower than that toward each separate kind of bacteria, and the fungicide activity is, by contrast, higher toward associations of microscopic fungi, compared with their separate species. The mechanism of the biocide action of the copolymers obtained is due to splitting-off of their Sn- and Zn-containing pendant groups of hydrolysis products (hydroxides of tributyltin and zinc), which are lethal for various species of bacteria and microscopic fungi [1]. In this connection, the rate of release of hydrolysis products into the environment is 1.5–2.0 orders of magnitude lower than that in the case of low-molecular-weight biocides, which is undoubtedly ecologically important. It was found that paper treated with latexes of this kind is protected from the action of fungi, bacteria, and algae.

The latexes were tested and it was found that the preparations used do not adversely affect documents, preserve their authenticity, improve service properties of books, hinder their aging, and are harmless for users [7].

One of necessary conditions in preservation of any work of art is that the preservative should be removed from its material by prolonged storage ("reversibility" of preservation). In the present study, washing-out of acrylic polymers with water from paper samples impregnated with these polymers was examined both before and after thermal aging. The washing-out of

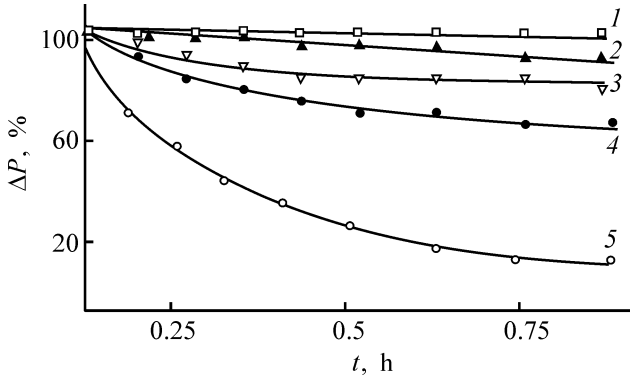


Fig. 4. Loss of mass, ΔP, by the paper–polymer composite in a time t of thermooxidative destruction at 240°C. Paper is impregnated with 2 wt % copolymer solutions. Copolymer composition (wt %): (*1*) 96 NaAC + 4 BA, (*2*) 96 NaAC + 4 MA, (*3*) 90 NaAC + 10 MA, (*4*) poly-NaAC, and (*5*) initial paper.

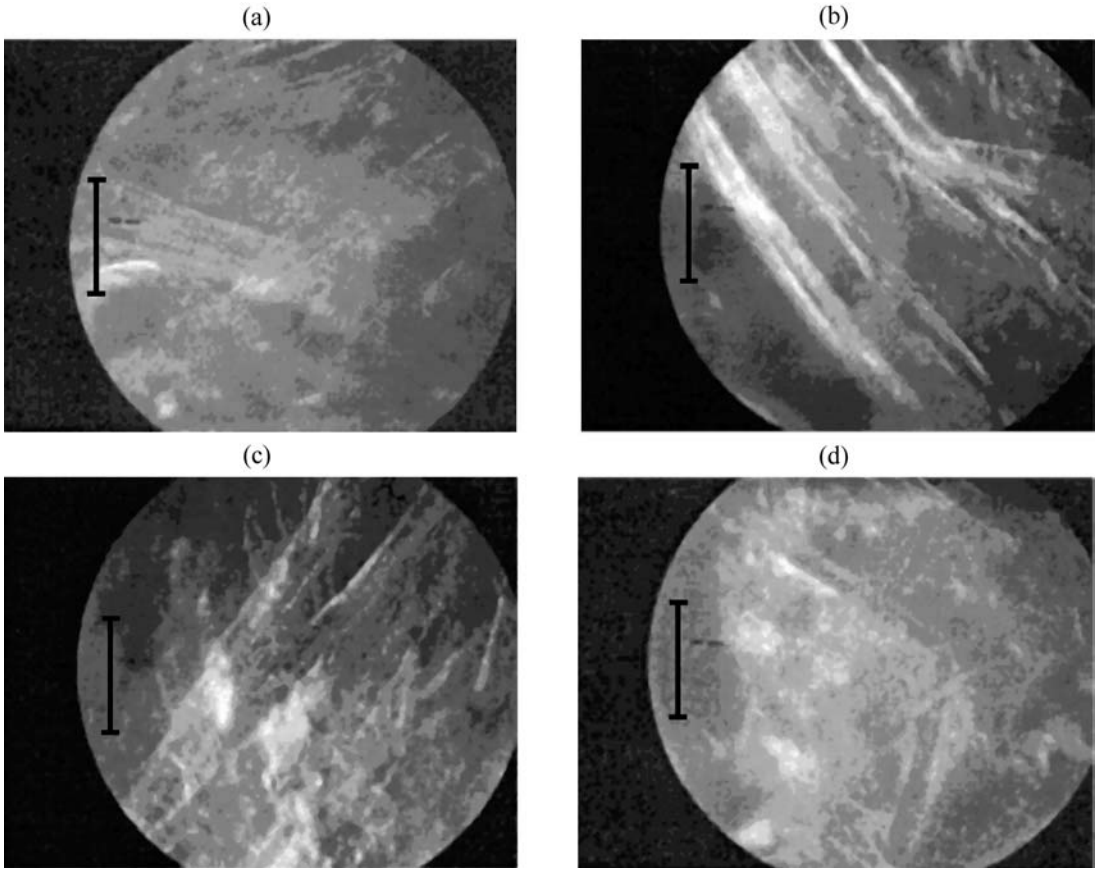


Fig. 5. Microstructure of news paper: (a) fibers of initial news paper and that (b) impregnated with a 5 wt % solution of the NaMAC copolymer, (c) impregnated with a 5 wt % solution of the NaMAC copolymer and aged at 100°C, and (d) with a 5 wt % solution of the NaMAC copolymer, aged at 100°C, and soaked in water for 24 h.

a polymer from paper sheets was judged from changes in their mass and in the microstructure of paper samples. It can be seen from Fig. 6. that the mass of paper samples impregnated and not impregnated with the polymer increases on their keeping in water for 1 h. This is due to capillary absorption of water by paper fibers and polymer. Further, during the subsequent 2–3 h, the mass of the samples dramatically decreases because of washing-out of the polymer from paper and diffusion of fine fibers into water. In the interval of 4–6 h from the beginning of the experiment, the mass of the samples again somewhat increases, probably because of penetration of water now into those fibers which were protected by the polymer before. The fact that the structure of a paper sample that was impregnated with the poly-NaAC copolymer, aged at 100°C for 6 h, and then soaked in water becomes more disordered, and the residual polymeric layer remaining on fibers becomes thinner. Analysis of Figs. 6 and 5d shows that the acrylic polymer protecting paper fibers does not chemically interact with cellulose even at high temperatures. Only a physical interaction (of adsorption type and via hydrogen bonds) is established between paper fibers and polyacrylate.

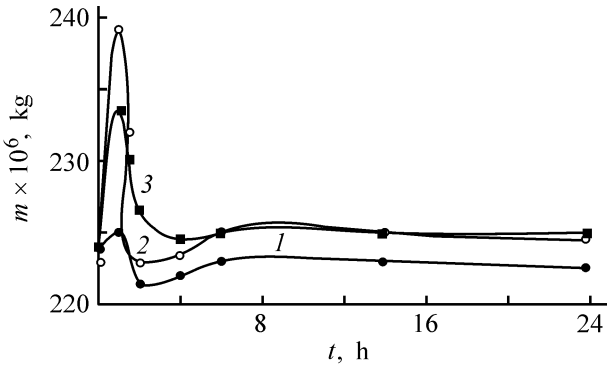


Fig. 6. Mass m of paper sample vs. the time t of their keeping in water. Paper: (*1*) initial, (*2*) treated with a 21 wt % solution of NaMAC copolymer, and (*3*) treated with the same polyacrylate solution, but subjected to thermal aging at 100°C for 2 h.

CONCLUSIONS

(1) The water-soluble acrylic polymers studied satisfy a number of requirements imposed by restorers on paper-preserving preparations. They are transparent and colorless, stable themselves, impart stability against thermal treatment to paper treated with these polymers, and, upon introduction of tin- and/or zinc-containing units, against biological destruction as well.

(2) The polyacrylates obtained reinforce paper and make it water-resistant, but can be removed from paper with water upon prolonged storage.

(3) The rate of penetration of a polymeric solution into paper pores depends on the relative sizes of paper pores and polymer particles (macrocoils or latex particles), as well as on the degree of structuring of the impregnating solution.

REFERENCES

1. Emel'yanov, D.N., Novospasskaya, N.Yu., Chernorukova, Z.G., et al., *Vestn. Nizhegorod. Univ. im. N.I. Lobachevskogo, Ser. Khim.*, Nizhni Novgorod, 2001, issue 1(3), pp. 14–18.
2. *Entsiklopediya polimerov* (Encyclopedia of Polymers), Kargin, V.A., Ed., Moscow: Sovetskaya Entsiklopediya, 1972, vol. 1, p. 292.
3. Voyutskii, S.S., *Fiziko-khimicheskie osnovy propityvaniya i impregnirovaniya voloknistykh materialov dispersiyami polimerov* (Physicochemical Foundations of Impregnation of Fibrous Materials with Polymer Dispersions), Leningrad: Khimiya, 1969.
4. Tager, A.A., *Fizikokhimiya polimerov* (Physical Chemistry of Polymers), Moscow: Khimiya, 1978.
5. Flyatte, D.M., *Bumazhn. Prom–st.*, 1988, no. 4, pp. 8–9.
6. Smirnov, V.F., *Vestn. Nizhegorod. Univ. im. N.I. Lobachevskogo, Ser. Biol.*, Nizhni Novgorod, 2001, issue 2, pp. 182–187.
7. Bondareva, T.F., Emel'yanov, D.N., and Smirnov, V.F., *Trudy Gosudarstvennogo Istoricheskogo Muzeya* (Trans. of State Historical Museum), Moscow, 2002, issue 129, pp. 91–93.

ISSN 1070-4272, Russian Journal of Applied Chemistry, 2006, Vol. 79, No. 8, pp. 1360–1364. © Pleiades Publishing, Inc., 2006.
Original Russian Text © S.G. Agaev, E.O. Zemlyanskii, A.N. Grebnev, S.V. Gul'tyaev, N.S. Yakovlev, 2006, published in Zhurnal Prikladnoi Khimii, 2006, Vol. 79, No. 8, pp. 1373–1378.

CHEMISTRY OF FOSSIL FUEL

Paraffin Deposition in Crude Oil Production and Depressor Additives for Paraffin Inhibition

S. G. Agaev, E. O. Zemlyanskii, A. N. Grebnev, S. V. Gul'tyaev, and N. S. Yakovlev

Tyumen State Oil and Gas University, Tyumen, Russia

Received August 4, 2005; in final form, March 2006

Abstract—Paraffin deposition on cold metallic surfaces in crude oil production, collection, and transportation is studied. Comparative analysis is made of the efficiencies of various paraffin inhibitors in West-Siberian paraffin oils. The mechanism of action of the additives is analyzed in relation to the phase and structural transitions in them in model systems.

DOI: 10.1134/S1070427206080295

Production of paraffin oils is complicated by increased hydraulic resistance and paraffin deposition (PD) in the production, collection, and transportation systems, resulting in death of oil field equipment [1]. The simplest and the most efficient solution of this problem is the use of depressor additives [2].

The goal of this study was to simulate the paraffin deposition in crude oil production and collection. We also made a comparative analysis of the efficiency of domestic and imported depressor additives in West-Siberian paraffin oils.

The experiments were carried out by the cold-rod method using a laboratory setup developed at the Tyumen Oil and Gas University [3]. As a simulated crude oil we used a hexane solution of Ceresin-80N [GOST (State Standard) 2488] and high-melting native paraffin deposits (NPD) collected from the Verkhnesalatskoe oilfield (Tomsk oblast, Russia). Certain physicochemical characteristics of the solid paraffins are given in Table 1.

Hexane as a model of liquid hydrocarbons of crude oil was selected taking into account that its boiling

Table 1. Physicochemical characteristics of solid paraffins in crude oil

Parameter	Solid paraffins					
	Ceresin -80N	PD	urea-bound paraffins		urea-unbound paraffins	
			from Ceresin	from PD	from Ceresin	from PD
Density at 20°C, kg m^{-3}	853.1	854.8	826.2	860.6	854.8	821.0
Zhukov's melting point, °C	79.0	91.2	86.4	95.5	67.8	70.8
Molecular weight, g mol^{-1}	812	882	767	911	832	834
Content of urea-bound paraffins, wt %	27	>61	–	–	–	–
Refractive index at 100°C:						
as prepared	1.4469	1.4492	1.4467	1.4463	1.4510	1.4497
after refining on silica gel	1.4419	1.4435	1.4457	1.4423	1.4483	1.4439
Refractive index difference	0.0050	0.0057	0.0010	0.0040	0.0027	0.0058
Content of paraffin-naphthene hydrocarbons,* wt %	98.0	91.0	99.5	92.4	95.4	89.7
Content of aromatic hydrocarbons,* wt %	2.0	9.0	0.5	7.6	4.6	10.3

* Content of paraffin-naphthene hydrocarbons was approximately determined by desorption from silica gel with petroleum ether, and that of aromatic hydrocarbons, as the difference between the initial sample weight and the estimated amount of paraffin-naphthene hydrocarbons.

point (68.7°C) falls within the range of temperatures that occur along the whole length of throughout most of the oil wells in Western Siberia. As a hot heat carrier we used water at its boiling point, and as a cold heat carrier, ethanol at a temperature inside the cold rod from –15 to +5°C. Such a combination of the solvent (hexane) and heat carriers provides boiling of the simulated crude oil in the working space, thus imitating the motion of the oil, its degassing, and the diffusion of solid paraffins from the bulk to the surface of the cold rod. The hot heat carrier : working mixture weight ratio was accepted to be 2.5 : 1, taking into account the design factors of the laboratory setup.

We studied the effects of the nature of solid paraffins and their concentration in the simulated crude oil, and also of the process temperature and time on the paraffin deposition on cold metallic surfaces.

The experimental techniques have been described elsewhere [3]. The process parameters were as follows: water temperature 100°C, ethanol temperature 0°C, temperature gradient in the working space 14.3 deg mm^{-1}, and deposition time 60 min. The solid paraffin content in *n*-hexane was varied from 2.5 to 30 wt %.

The waxing of the cold rod was characterized by the yield of the deposit in grams, as influenced by the solid paraffin content of hexane. The specific yield of the deposit, G_{sp}, was estimated as the weight of the deposit related to the unit surface area of the oil-wet surface of the cold rod per unit time (g m^{-2} h^{-1}).

Data on the waxing of the cold rod (Table 2) show that G_{sp} the with the initial content of solid paraffins.

The yield of secondary PDs from NPD systems is considerably higher than that from the simulated systems (Ceresin in *n*-hexane), the increase in the PD yield being more pronounced in the former case. For some of the deposits obtained we determined Zhukov's melting point (Table 2). The melting point of PDs appears to be considerably higher than that of the initial Ceresin and NPDs. The melting point of the deposits approaches that of solid paraffins capable of forming complexes with urea (Table 1).

Evidently, higher-melting solid paraffins with long aliphatic radicals are preferentially deposited on the cold rod. These are *n*-paraffins and paraffin-naphthene and alkylaromatic hydrocarbons with long aliphatic radicals. The presence of such alkylaromatic hydrocarbons in the deposits was confirmed by both urea dewaxing and liquid chromatography on silica gel (Table 1).

Table 2. Paraffin deposition from hexane solutions of high-molecular-weight solid paraffins on a cold rod (experimental conditions: cold heat carrier temperature 0°C, hot heat carrier temperature 100°C, deposition time 60 min, and temperature gradient in the working space 14.3 deg mm^{-1})

Paraffin concentration in *n*-hexane, wt %	*n*-Hexane solution of indicated paraffin			
	Ceresin		NPD	
	G_{sp}, g m^{-2} h^{-1}	mp of PD, °C	G_{sp}, g m^{-2} h^{-1}	mp of PD, °C
–	–	79.0*	–	91.2*
2.5	15.3	–	–	–
5.0	29.9	–	45.8	–
7.5	28.6	–	–	–
10	62.0	–	208.5	94.8
12.5	67.8	–	304.5	94.5
15	81.6	87.4	401.7	94.2
17.5	105.1	86.8	515	94.2
20	121.5	86.6	633.9**	94.0
22.5	147.5	87.4	–	–
25	173.2	86.5	–	–
27.5	220.3	87.0	–	–
30	253.4	87.2	–	–

* Melting point of the initial solid paraffins.

** Deposition at higher content of solid paraffins in hexane was unfeasible because of limitations caused by the design factors of the experimental setup.

Table 3. Specific yield of paraffin deposit from simulated solutions of Ceresin in *n*-hexane on a cold rod (Ceresin concentration 20 wt %; hot heat carrier temperature 100°C)

Cold heat carrier temperature, °C	Temperature gradient in working space, deg mm^{-1}	Deposition time, min	Specific yield, g m^{-2} h^{-1}
5	13.6	60	98.3
0	14.3	60	122.0
–5	15.0	60	128.8
–10	15.7	60	130.5
–15	16.4	60	125.4
0	12.5	5	37.3
0	12.5	10	50.8
0	12.5	15	61.0
0	12.5	20	64.4
0	12.5	30	79.6
0	12.5	40	101.7
0	12.5	50	113.6
0	12.5	60	122.0

We studied the influence of temperature and time on the paraffin deposition on the cold rod for the example of the systems with Ceresin in *n*-hexane (Table 3).

Table 4. Selected physicochemical characteristics of West-Siberian crude oils

Parameter	Oilfield	
	Tarkosalinskoe	Verkhnesalatskoe
Density at 20°C, kg m^{-3}	820	755
Content of solid paraffins with mp >52.5°C, wt %	6.5	23.7
Congelation point, °C	12	22
Silica gel resin content, wt %	1.02	0.46
Asphaltene content, wt %	0.51	Not detected

Table 5. Congelation temperature of West-Siberian crude oils in the presence of depressor additives

Depressor additive	Chemical nature of DA	Congelation temperature, °C, at indicated DA concentration, wt %						
		–	0.005	0.01	0.05	0.1	0.5	1.0
Tarkosalinskoe crude oil								
Visco-5351	–	12	–10	–12	–15	–14	–22	–13
Flexoil-WM	–	12	–1	–20	–25	–25	–12	–1
TyumII-77	Ester	12	–2	–3	–15	–15	–19	–4
DP-65	Polyamide	12	4	5	1	–11	–8	–8
SNPKh-4002	–	12	12	12	13	12	12	11
VPEA	Polyethylene wax	12	12	12	10	9	10	10
VPEN	〃	12	9	9	10	9	10	10
DPM-12/05	Polyurethane amido ether	12	9	5	–13	–12	–31	–30
DPM-18/05	Polyurethane ether	12	2	0	–9	–14	–25	–13
DN-MA	Polyalkyl methacrylate	12	–2	–3	–10	–13	–19	–15
DN-1	Alkyl methacrylate/polyalkyl acrylate copolymer	12	12	12	10	0	–1	–2
Verkhnesalatskoe crude oil								
Visco-5351	–	22	–9	–10	–9	–3	–2	–1
Flexoil-WM	–	22	22	10	10	10	9	9
TyumII-77-77	Ester	22	22	18	17	14	8	5
DP-65	Polyamide	22	22	22	22	18	9	9
SNPKh-4002	–	22	22	22	22	22	22	13
VPEA	Polyethylene wax	22	22	22	22	22	22	22
VPEN	〃	22	22	22	22	22	22	22
DPM-12/05	Polyurethane amido ether	22	21	21	21	21	–7	–28
DPM-18/05	Polyurethane ether	22	21	18	18	8	–11	–16
DN-MA	Polyalkyl methacrylate	22	12	9	1	2	0	–2
DN-1	Alkyl methacrylate/polyalkyl acrylate copolymer	22	13	14	13	13	12	10

Deposition of solid paraffins was carried out using the above-described procedure at varied temperature or deposition time, all other parameters being fixed.

Table 3 shows that the PD yield only slightly depends on the cold rod temperature, being controlled essentially by the deposition time. The PD yield increases with the deposition time. Therefore, under

the actual conditions, the exploitation time is the factor controlling the paraffin deposition on the internal walls of oil field equipment. The PD yield is controlled by the nature of solid paraffin, all other conditions being equal. High-molecular-weight high-melting solid paraffins, which apparently belong to hydrocarbons capable of forming complexes with urea, are preferentially deposited.

We also made a comparative study of the efficiency of domestic and imported depressor additives in two samples of West-Siberian crude oil from the Tarkosalinskoe (Tyumen oblast) and Verkhnesalatskoe (Tomsk oblast) oilfields. Certain physicochemical characteristics of these samples are listed in Table 4.

As depression additives we used imported Visco-5351 (Nalko Company) and Flexoil WM-1470 (Servo Champion Company), and domestic DN-1, DN-MA [4], TyumII-77 [5], DP-65 [6], SNPKh-4002, two polyethylene waxes from industrial wastes VPEN and VPEA [TU (Technical Specifications) 6-05-1837–82], and additives DPM-12/05 and DPM-18/05 synthesized at the Laboratory of Petrochemical Synthesis, Tyumen State Oil and Gas University.

The efficiency of depressor additives was characterized by the decrease in the oil congelation temperature over the concentration range of the additives 0.005–1.0 wt %. The oil congelation temperature was determined according to GOST (State Standard) 20287–91. The results (Table 5) show that, regardless of the crude oil sample, the most efficient additives are Visco-5351, Flexoil WM-1470, DN-MA, and TyumII-77. The additives DPM-12/05 and DPM-18/05 are also quite efficient. The efficiency of the additives depends primarily on the characteristics of crude oil, such as the content of solid paraffins, resins, and asphaltenes.

To elucidate the paraffin inhibiting mechanism, we determined the parameters of phase transitions [7] in several model systems [depression additives in RT kerosene (GOST 10227)] (Table 6). The phase transition parameters were also determined for paraffin deposits from Verkhnesalatskoe crude oil (mp 91.2°C), T-1 solid paraffin [mp 54.5°C (GOST 23683)], and Ceresin-80N (Table 6). In making decision on solid paraffins, we proceeded from the fact that specifically these kinds of solid paraffins, contained in crude oil, control paraffin deposition on oil field equipment.

The phase transitions and structurization in the course of cooling of the model systems were studied in relation to the content of solid paraffins and depressor additives in kerosene c_s The solid phase content was varied from 0.1 to 5 wt %. Using standard procedures, we determined the congelation temperature t_g (GOST 20287–91) and cloud point t_c (GOST 5066–91). Based on the dependences of t_g and t_c on c_s, we constructed the phase transition diagrams.

Table 6. Parameters of phase transitions and structurization factor in model systems containing solid paraffins of crude oil and depressor additives in kerosene

Product	$c_1^{'}$, wt %	T_{CSCC}, °C	r_2, g l^{-1} min^{-1}	S_{CDS}, deg wt %
Paraffin deposit	0.1	46	3.7	609.5
Ceresin-80N	0.3	37	3.6	568.4
T-1 paraffin	0.2	1	3.3	70.4
Visco-5351	0.1	–11	7.0	141.5
Flexoil WM-1470	0.1	–2	8.6	50.0
TyumII-77	0.13	10	7.0	324.0
DP-65	0.08	34	11.5	463.2
VPEA	0.30	32	4.8	517.4
VPEN	0.10	28	3.8	516.3

Three distinctive regions were found in the diagrams: (*1*) molecular-disperse state (MDS) of solid paraffins and additives in kerosene (region above t_c), (*2*) colloidal-disperse state (CDS) (region between t_g and t_c), and (*3*) quasisolid state (QSS) (region below t_g). The degree of structurization of the dispersed particles of solid paraffins and additives was characterized by the area of the CDS region S_{CDS} (the higher S_{CDS}, the lower the degree of structurization).

The phase transitions were characterized by the critical spontaneous crystallization concentration $c_1^{'}$, cloud point at this concentration t_{CSCC}, and solid phase accumulation rate r_2 above t_{CSCC} [4]. Data on S_{CDS} and phase transitions (Table 6) show that all the parameters of phase transitions of the depressor additives considerably differ from those of the solid paraffins.

The structurization factor S_{CDS} decreases in the order Flexoil WM-1470 > T-1 paraffin > Visco-5351 >> TyumII-77 > DP-65 >> VPEN > VPEA > Ceresin-80N > PD.

What is common to depressor additives Visco-5351, TyumII-77, and DP-65 and polyethylene waxes is that they are characterized by a small degree of structurization in the colloidal-disperse state region, compared to T-1 paraffin, suggesting a weak intermolecular interaction in the additives in the CDS re-

gion and a high lubricity of the DA molecules brought in contact with the crystals of solid paraffin in one way or another.

Comparison of data on the phase transitions in the solid paraffins and additives, on the one hand, and the efficiency of the depressor additives in the crude oil samples investigated, on the other hand, shows that the common feature of the most efficient imported depressor additives is that they have lower t_{CSCC} as compared to that of paraffin deposits. Evidently, these additives operate by essentially the adsorption (lubrication) mechanism controlled by the low surface tension at the interface between the solid paraffin surface and the dispersion medium, thus minimizing the consumption of the additives, which is determined only by their expenditure for the formation of a monolayer on the surface of the paraffin crystals.

What is common to additives TyumII-77 and DP-65 and the waxes is that their t_{CSCC} is close to that of solid paraffins. It follows from the fact of different efficiencies of the additives and waxes that the latter, as isomorphous compounds, act by the purely cocrystallization mechanism. Additives TyumII-77 and DP-65 operate, presumably, by the mixed cocrystallization/adsorption mechanism.

The results obtained show that Visco-5351, DN-MA, TyumII-77, DP-65, DPM-12/05, and DPM-18/05 may be recommended as effective depressor additives for Verkhnesalatskoe crude oil. DPM-12/05 and DPM-18/05 show promise also as additives produced from available raw materials. Because of the lack of available higher fatty alcohols and synthetic fatty acids, domestic additives DN-MA, TyumII-77, and DP-65 currently cannot be produced n Russia.

Flexoil-WM is currently used as a paraffin inhibitor in Verkhnesalatskoe crude. Changing this additive for Visco-5351 should reduce the consumption of additives at least by half (Table 5). Because of the nearly the same cost of these additives, the charges for the depressor additive will be reduced by half also. Furthermore, Visco-5351 is a considerably more efficient additive in relation to the depression of the congelation temperature. Therefore, its use should reduce not only the consumption of the additive, but also the frequency of paraffin removal from oil field equipment and collection systems. Changing Flexoil-WM for DPM-12/05 or DPM-18/05 is also economically sound, since the cost of the domestic additives is lower by about half, and the efficiency of, e.g., DPM-18/05, taken in amount of 0.5 wt %, is considerably higher.

REFERENCES

1. Sherstnev, N.I., Gurvich, L.M., Bulina, I.G., et al., *Primenenie kompositsii PAV pri ekspluatatsii skvazhin* (Application of Surfactant Mixtures in Exploitation of Oil Wells), Moscow: Nedra, 1988.
2. Agaev, S.G., Khalin, L.N., and Berezina, Z.N., *Neftepromysl. Delo*, 1996, no. 5, pp. 16–17.
3. Agaev, S.G., Berezina, Z.N., Khalin, L.N., and Kravchenko, G.V., *Izv. Vyssh. Uchebn. Zaved., Neft' Gaz*, 1997, no. 1, pp. 89–93.
4. Min'kov, V.A., Sopina, V.E., and Zakordonets, O.P., *Sintez polimernykh depressornykh prisadok dlya vysokoparafinistykh neftei* (Synthesis of Polymeric Depression Additives for Highly Paraffinic Crude Oils), Available from TsNIITEneftekhim, February 23, 1988, Shchebekino, no. 38-nkh88.
5. Agaev, S.G., Berezina, Z.N., Sheveleva, M.G., et al., *Khim. Tekhnol. Topl. Masel*, 1994, nos. 9–10, pp. 10–11.
6. Agaev, S.G. and Khalin, L.N., *Zh. Prikl. Khim.*, 1997, vol. 70, no. 11, pp. 1893–1896.
7. Agaev, S.G., Gurov, Yu.P., and Zemlyanskii, E.O., *Neftepererab. Neftekhim.*, 2004, no. 9, pp. 37–40.

ISSN 1070-4272, Russian Journal of Applied Chemistry, 2006, Vol. 79, No. 8, pp. 1365–1367. © Pleiades Publishing, Inc., 2006.
Original Russian Text © A.G. Morachevskii, E.Yu. Kolosova, L.B. Tsymbulov, 2006, published in Zhurnal Prikladnoi Khimii, 2006, Vol. 79, No. 8, pp. 1379–1381.

BRIEF COMMUNICATIONS

Activity of Iron and Nickel in the Copper-Rich Region of Compositions of the Copper–Iron–Nickel System in the Liquid State

A. G. Morachevskii, E. Yu. Kolosova, and L. B. Tsymbulov

St. Petersburg State Polytechnic University, St. Petersburg, Russia
"Institute Gipronikel'" Open Joint-Stock Company, St. Petersburg, Russia

Received July 4, 2006

Abstract—Activities of iron and nickel in the copper-rich part of the Cu–Fe–Ni system in the liquid state at 1350°C were calculated using model concepts from data on the boundary binary systems.

DOI: 10.1134/S1070427206080301

In the last two decades, calculation methods have been acquiring increasing importance in thermodynamic description of ternary and more complex liquid metallic systems. A larger part of the calculation techniques are based on the assumption that pair interactions in the systems consisting of three and more components give a major contribution to values of the integral thermodynamic functions of multicomponent systems. This makes it possible to describe with a sufficient reliability the concentration dependence of the thermodynamic characteristics of these systems, leaning only upon experimental data for boundary binary systems. A sufficiently good agreement between calculated and experimental data has been confirmed by the example of the iron–nickel–cobalt system [1].

Our previous publications reported calculations of integral molar thermodynamic characteristics of liquid alloys in the copper–iron–nickel system at 1600°C [2] and of the activity of copper in these alloys [3]. In this study, we compared calculated activities of iron and nickel (1350°C) in alloys of the Cu(1)–Fe(2)–Ni(3) ternary system with the available published experimental data on the activity of the components in the copper-rich part of the system [4, 5]. As it was done in [3], we used equations following from Toop's method [6] to calculate the activities of the components. Equation (1) was used for component 2 (iron), and equation (2), for component 3 (nickel).

$$\log \gamma_2 = \left[\frac{x_1}{1-x_2}\log \gamma_{2(1)} + \frac{x_3}{1-x_2}\log \gamma_{2(3)}\right]_{x_2} + (1-x_2)^2\left[\frac{\Delta G_{13}^{ex}}{2.303RT}\right]_{x_1/x_3},$$

$$\log \gamma_3 = \left[\frac{x_2}{1-x_3}\log \gamma_{3(2)} + \frac{x_1}{1-x_3}\log \gamma_{3(1)}\right]_{x_3} + (1-x_3)^2\left[\frac{\Delta G_{21}^{ex}}{2.303RT}\right]_{x_2/x_1}.$$

Here x_1, x_2, and x_3 are the mole fractions of the components in a liquid alloy; γ_2 and γ_3, activity coefficients of components 2 and 3 in a ternary alloy; and $\gamma_{i(j)}$, activity coefficient of component i in a boundary binary alloy i–j.

When calculating the activity coefficients of iron and nickel by Eqs. (1) and (2), we used the available published data on the boundary binary systems Cu–Fe, Fe–Ni, and Ni–Cu. A detailed analysis of studies concerned with the thermodynamic properties of liquid

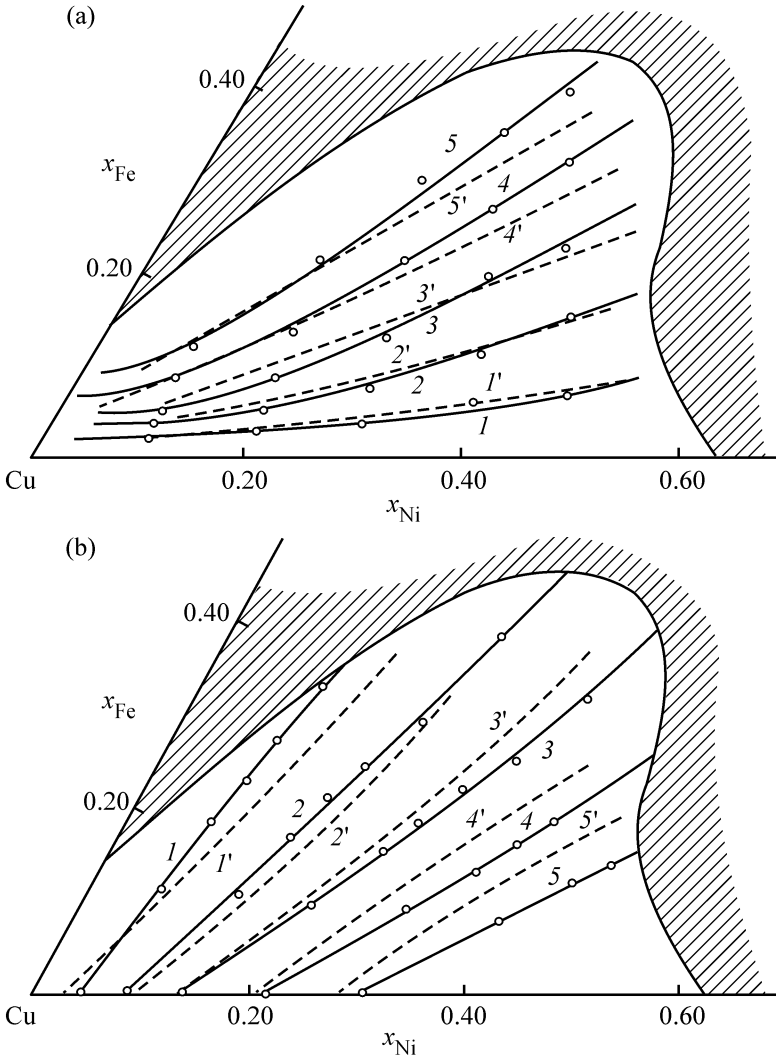


Fig. 1. Lines of equal activities of (a) iron and (b) nickel in liquid alloys of the Cu–Fe–Ni system at 1350°C. The solid lines were plotted by calculated points and the dashed lines were plotted in [5] on the basis of experimental data. Activity: (*1, 1'*) 0.1; (*2, 2'*) 0.2; (*3, 3'*) 0.3; (*4, 4'*) 0.4; and (*5, 5'*) 0.5. Standard state, pure liquid metals (iron and nickel in a supercooled state); the two-phase region is shaded.

alloys in these systems is given in [7]. For the calculations concerning the Cu–Fe system we used the data of [8], where the thermodynamic properties of liquid alloys were studied using the electromotive-force method and calorimetric measurements. These results are recommended as reference data in the monograph [9] and reference book [10]. The data of [8] on the activity of the components in liquid alloys agree with the results obtained in later studies of this system [11, 12].

When calculating the activity of the components of the ternary system, we used the data for the boundary Ni–Cu system, obtained by Kulkarni and Johnson [7, 14] by the electromotive-force method with an electrolyte exhibiting conduction by oxygen (ZrO_2 + 3 wt % of MgO). The thermodynamic properties of liquid alloys of the Fe–Ni system have been studied repeatedly, a detailed analysis of the results obtained can be found in [15]. In the calculations, we used the data from the reference book by Hultgren and coworkers [16] and from the monograph [9].

The activities of nickel and iron in the homogeneity region of liquid alloys of the Cu–Fe–Ni system at 1350°C, specified in [4, 5], for seven secants with a fixed ratio $x_{Ni} : x_{Cu}$ (when calculating γ_{Fe}) and $x_{Fe} : x_{Cu}$ (when calculating γ_{Ni}). As can be seen from the figure, the calculated isoactivity lines of iron and nickel rather well agree with the experimental results of the Japanese authors [4, 5]. The boundaries of the region of liquid alloys in the Cu–Fe–Ni system

at 1350°C, given in [4, 5] are close to those reported in reference publications [17].

CONCLUSION

The activities of iron and nickel at 1350°C in liquid alloys of the system Cu–Fe–Ni, calculated using model concepts, agree with the available published experimental data.

REFERENCES

1. Morachevskii, A.G., Tsymbulov, L.B., Kolosova, E.Yu., and Tsemekhman, L.Sh., *Zh. Prikl. Khim.*, 2005, vol. 78, no. 12, pp. 1963–1966.
2. Morachevskii, A.G., Fedorova, N.A., Tsymbulov, L.B., and Tsemekhman, L.Sh., *Zh. Prikl. Khim.*, 2003, vol. 76, no. 11, pp. 1801–1805.
3. Morachevskii, A.G., Tsymbulov, L.B., and Kolosova, E.Yu., *Zh. Prikl. Khim.*, 2004, vol. 77, no. 9, pp. 1438–1441.
4. Itagaki, K., Hino, M., Padagor, R.U., and Surapunt, S., *Ber. Bunsengesell. Phys. Chem.*, 1998, vol. 102, no. 9, pp. 1304–1308.
5. Fudjita, Y., Pagador, R.U., Higo, M., and Azakami, T., *J. Japan Inst. Metals*, 1997, vol. 61, no. 7, pp. 619–624.
6. Toop, G.W., *Trans. Met. Soc. AIME*, 1965, vol. 233, pp. 850–855.
7. Morachevskii, A.G., Ryabko, A.G., and Tsemekhman, L.Sh., *Termodinamika zhidkikh splavov sistemy nikel'–med'–zhelezo* (Thermodynamics of Liquid Alloys in the System Nickel–Copper–Iron), St. Petersburg: SPb. Gos. Politekhn. Univ., 2002.
8. Batalin, G.I., *Termodinamika zhidkikh splavov na osnove zheleza* (Thermodynamics of Liquid Alloys on the Basis of Iron), Kiev: Vyshcha Shkola, 1982.
9. Batalin, G.I. and Sudavtsova, V.S., *Izv. Akad. Nauk SSSR, Metally*, 1980, no. 2, pp. 45–49.
10. Belousov, G.I., Bakhvalov, S.G., Aleshina, S.N., et al., *Fiziko-khimicheskie svoistva zhidkoi medi i ee splavov: Spravochnik* (Physicochemical Properties of Liquid Copper and Its Alloys: Handbook), Yekaterinburg: Ural. Otd. Ross. Akad. Nauk, 1997.
11. Sorokin, M.L., Andryushechkin, N.A., and Nikolaev, A.G., *Izv. Vyssh. Uchebn. Zaved., Tsv. Metall.*, 1996, no. 6, pp. 10–14.
12. Turchanin, M.A. and Agraval, P.G., *Poroshk. Metall.*, 2001, nos. 7/8, pp. 34–53.
13. Morachevskii, A.G., Ryabko, A.G., and Tsemekhman, L.Sh., *Termodinamika zhidkikh splavov sistemy nikel'–med'–kobal't* (Thermodynamics of Liquid Alloys in the System Nickel–Copper–Cobalt), St. Petersburg: SPb. Gos. Politekhn. Univ., 2004.
14. Kulkarni, A.D. and Johnson R.E., *Met. Trans.*, 1973, vol. 4, pp. 1723–1727.
15. Morachevskii, A.G., Ryabko, A.G., and Tsemekhman, L.Sh., *Termodinamika zhidkikh splavov sistemy zhelezo–nikel'–kobal't* (Thermodynamics of Liquid Alloys in the System Iron–Nickel–Cobalt), St. Petersburg: SPb. Gos. Politekhn. Univ., 2004.
16. Hultgren, R., Desai, P., Hawkins, D., et al., *Selected Values of Thermodynamic Properties of Binary Alloys*, Ohio (USA): Metals Park, Amer. Soc. Met., 1973.
17. *Dvoinye i mnogokomponentnye sistemy na osnove medi: Spravochnik* (Copper-based Binary and Multicomponent Systems: Reference Book), Moscow: Nauka, 1979.

ISSN 1070-4272, Russian Journal of Applied Chemistry, 2006, Vol. 79, No. 8, pp. 1368–1370. © Pleiades Publishing, Inc., 2006.
Original Russian Text © A.I. Demidov, M.S. Kokhatskaya, 2006, published in Zhurnal Prikladnoi Khimii, 2006, Vol. 79, No. 8, pp. 1382–1384.

BRIEF COMMUNICATIONS

Thermodynamics of Reactions of Iron with Oxygen in the Presence of Water Vapor

A. I. Demidov and M. S. Kokhatskaya

St. Petersburg State Polytechnic University, St. Petersburg, Russia

Received July 4, 2006

Abstract—Changes in the standard Gibbs energies of the reactions of iron and iron oxides with pure oxygen and oxygen saturated with water vapor were calculated.

DOI: 10.1134/S1070427206080313

A study of the reactions of iron with oxygen at different humidities is of considerable interest for explaining the atmospheric corrosion of metal and for substantiating measures for corrosion protection [1, 2].

This study presents the results of a thermodynamic analysis of the reactions of iron with pure oxygen and oxygen saturated with water vapor. In performing the calculations, we used published data [3, 4] on changes in the standard Gibbs energies (see table). The reactions of iron with oxygen at a standard temperature of 298.15 K can be described by the following equations:

$$Fe + 1/2O_2 = FeO,\ \Delta G^0_{298} = -244.3\ kJ; \quad (1)$$

$$3Fe + 2O_2 = Fe_3O_4,\ \Delta G^0_{298} = -1014.2\ kJ; \quad (2)$$

$$2Fe + 3/2O_2 = Fe_2O_3,\ \Delta G^0_{298} = -741.0\ kJ. \quad (3)$$

The thermodynamic calculation of the standard Gibbs energies of reactions (1)–(3) per mole of a compound gives the most negative value for reaction (2) [5]. Consequently, the yield of the product in this reaction is the highest [5].

In calculation of reactions (1')–(3') per mole of oxygen, the most negative value of the change in the standard Gibbs energy was obtained for reaction (2'):

$$2Fe + O_2 = 2FeO,\ \Delta G^0_{298} = -488.6\ kJ; \quad (1')$$

$$3/2Fe + O_2 = 1/2Fe_3O_4,\ \Delta G^0_{298} = -507.1\ kJ; \quad (2')$$

$$4/3Fe + O_2 = 2/3Fe_2O_3,\ \Delta G^0_{298} = -494.0\ kJ. \quad (3')$$

In a thermodynamic analysis of heterogeneous condensed systems, the thermodynamic parameters are, as a rule, calculated per mole of the alloy or solution or per gram-atom of the constituted substance this compound [6, 7]. Therefore, we calculated the change in the standard Gibbs energy for the reactions of iron with oxygen per mole of the atoms of starting substances [reactions (1")–(3")]:

$$1/2Fe + 1/4O_2 = Fe_{0.5}O_{0.5},$$
$$\Delta G^0_{298} = -122.15\ kJ\ mol^{-1}; \quad (1")$$

$$3/7Fe + 2/7O_2 = Fe_{0.429}O_{0.571},$$
$$\Delta G^0_{298} = -144.89\ kJ\ mol^{-1}; \quad (2")$$

$$2/5Fe + 3/10O_2 = Fe_{0.4}O_{0.6},$$
$$\Delta G^0_{298} = -148.2\ kJ\ mol^{-1}. \quad (3")$$

As can be seen from the data presented, reaction (3") has a more negative change in the standard

Changes in the standard Gibbs energy of various substances and ions according to the data of [3, 4]

Formula	ΔG^0_{298}, kJ mol^{-1}	Formula	ΔG^0_{298}, kJ mol^{-1}
Fe	0	α-FeOOH	–490.0
FeO	–244.3	γ-FeOOH	–460.2
Fe_3O_4	–1014.2	O_2	0
Fe_2O_3	–741.0	H_2O	–237.2
$Fe(OH)_2$	–483.7	$Fe_3O_4 \cdot 4H_2O$	–1892.8
$Fe(OH)_3$	–694.5		

Gibbs energy. Consequently, the yield of the product in this reaction is the highest. The difference in the results obtained by thermodynamic analysis of reactions (1)–(3), (1')–(3'), and (1'')–(3'') is due to the fact that the Gibbs energy is an extensive quantity and its change is dependent on the number of substances involved in the reactions. Different numbers of moles were taken when writing the reactions per mole of a compound, and different numbers of moles of iron, when writing the reactions per mole of oxygen. When writing the reactions per mole of atoms of the starting substances, the total amount of these substances in all of the reactions considered was constant.

In turn, iron(II) oxide and a double iron(III)–iron(II) oxide can react with oxygen. When writing the reactions per mole of atoms of the starting substances, we obtain

$$3/7FeO + 1/14O_2 = Fe_{0.429}O_{0.571},$$
$$\Delta G^0_{298} = -40.19 \text{ kJ mol}^{-1}. \quad (4)$$

$$2/5FeO + 1/10O_2 = Fe_{0.4}O_{0.6},$$
$$\Delta G^0_{298} = -50.48 \text{ kJ mol}^{-1}. \quad (5)$$

$$2/15Fe_3O_4 + 1/30O_2 = Fe_{0.4}O_{0.6},$$
$$\Delta G^0_{298} = -12.97 \text{ kJ mol}^{-1}. \quad (6)$$

Iron(III) oxide can be reduced with iron to a double iron(III)–iron(II) oxide:

$$4/21Fe_2O_3 + 1/21Fe = Fe_{0.429}O_{0.571},$$
$$\Delta G^0_{298} = -3.74 \text{ kJ mol}^{-1}. \quad (7)$$

The reaction of double iron(III)–iron(II) oxide with iron shows a positive change in the standard Gibbs energy, and, consequently, has a small yield of the reaction product:

$$1/8Fe_3O_4 + 1/8Fe = Fe_{0.5}O_{0.5},$$
$$\Delta G^0_{298} = 4.62 \text{ kJ mol}^{-1}. \quad (8)$$

Thus, iron(III) oxide, which can be reduced to a double iron(III)–iron(II) oxide when brought in contact with iron, is the most stable compound in the Fe–O system. The oxide film formed on iron at room temperature can consist either of a single Fe_2O_3 layer, or of two layers, the outer Fe_2O_3 layer and the inner Fe_3O_4 layer. According to the data [8], oxide films formed on iron at room temperature consist of γ-Fe_2O_3 or of a cubic oxide, whose composition lies between pure γ-Fe_2O_3 and a 20%Fe_3O_4 + 80% γ-Fe_2O_3 mixture.

The reactions of double iron(III)–iron(II) oxide and iron(III) oxide with deoxygenated water, written per mole of atoms of the starting substances

$$[Fe_3O_4 + 4H_2O = 2Fe(OH)_3 + Fe(OH)_2] : 19,$$
$$\Delta G^0_{298} = 4.75 \text{ kJ mol}^{-1}. \quad (9)$$

$$[Fe_2O_3 + 3H_2O = 2Fe(OH)_3] : 14,$$
$$\Delta G^0_{298} = 4.54 \text{ kJ mol}^{-1}, \quad (10)$$

show small positive changes in the standard Gibbs energy, and, consequently, have a small yield of the reaction products.

In oxygen saturated with water vapor, oxidation of a double iron(III)–iron(II) oxide involves water:

$$[4Fe_3O_4 + O_2 + 6H_2O = 8\alpha\text{-FeOOH} + 4\gamma\text{-FeOOH}] : 48,$$
$$\Delta G^0_{298} = -17.29 \text{ kJ mol}^{-1}. \quad (11)$$

Thus, at a certain humidity and sufficient access of oxygen, Fe_2O_3, α-FeOOH, and γ-FeOOH can be formed on the oxidized surface of iron.

If iron is oxidized in the presence of water, then water is involved in the oxidation processes:

$$[Fe + 1/2O_2 + H_2O = Fe(OH)_2] : 5,$$
$$\Delta G^0_{298} = -49.3 \text{ kJ mol}^{-1}. \quad (12)$$

$$[3Fe + 2O_2 + 4H_2O = Fe(OH)_2 + 2Fe(OH)_3] : 19,$$
$$\Delta G^0_{298} = -48.63 \text{ kJ mol}^{-1}. \quad (13)$$

$$[2Fe + 3/2O_2 + 3H_2O = 2Fe(OH)_3] : 14,$$
$$\Delta G^0_{298} = -48.39 \text{ kJ mol}^{-1}. \quad (14)$$

The resulting iron(II) hydroxide is unstable and can be easily oxidized:

$$[4Fe(OH)_2 + O_2 = 2\gamma\text{-FeOOH} + 2Fe(OH)_3] : 22,$$
$$\Delta G^0_{298} = -17.03 \text{ kJ mol}^{-1}. \quad (15)$$

$$[4Fe(OH)_2 + O_2 = 4\gamma\text{-FeOOH} + 2H_2O] : 22,$$
$$\Delta G^0_{298} = -17.29 \text{ kJ mol}^{-1}. \quad (16)$$

Gamma iron metahydroxide is the first and the main crystalline product of iron corrosion in a low-corrosive atmosphere [1]. At a certain humidity, the hydroxides formed by reactions (12)–(15) can interact with each other to yield double iron(III)–iron(II) oxide tetrahydrate:

$$[Fe(OH)_2 + 2Fe(OH)_3 = Fe_3O_4 \cdot 4H_2O] : 19,$$
$$\Delta G^0_{298} = -1.06 \text{ kJ mol}^{-1} \quad (17)$$

or

$$[Fe(OH)_2 + 2\gamma\text{-FeOOH} = Fe_3O_4 + 2H_2O] : 13,$$
$$\Delta G^0_{298} = -6.50 \text{ kJ mol}^{-1}. \quad (18)$$

In turn, double iron(III)–iron(II) oxide tetrahydrate is oxidized by the reaction

$$[2(Fe_3O_4 \cdot 4H_2O) + 1/2O_2 = 6\alpha\text{-FeOOH} + 5H_2O] : 39,$$
$$\Delta G^0_{298} = -8.73 \text{ kJ mol}^{-1}, \quad (19)$$

with α-FeOOH crystallized [1]. α-Metahydroxide can be formed by the reaction:

$$[Fe(OH)_3 = \alpha\text{-FeOOH} + H_2O] : 7,$$
$$\Delta G^0_{298} = -4.67 \text{ kJ mol}^{-1}. \quad (20)$$

Thus, the results of the thermodynamic analysis performed confirm the experimentally established fact [1] that only α-FeOOH and γ-FeOOH are formed on the surface of iron at a certain humidity and sufficient access of oxygen.

REFERENCES

1. Kukurs, O., Upite, A., Khonzak, I., et al., *Produkty atmosfernoi korrozii zheleza i okraska po rzhavchine* (Products of Atmospheric Corrosion of Iron and Painting over Rust), Riga: Zinatne, 1980.
2. Uhlig, G.G. and Revie, R.W., *Corrosion and Corrosion Control: An Introduction to Corrosion Science and Engineering*, New York: Wiley, 1985.
3. Garrels, R.M. and Christ, C.L., *Solutions, Minerals, and Equilibria*, New York: Harper Row, 1965.
4. Sukhotin, A.M., *Fizicheskaya khimiya passiviruyushchikh plenok na zheleze* (Physical Chemistry of Passivating Films on Iron), Leningrad: Khimiya, 1989.
5. Gerasimov, Ya.I., Dreving, V.P., Eremin, E.N., et al., *Kurs fizicheskoi khimii* (Course of Physical Chemistry), Gerasimov, Ya.I., Ed., Moscow: Khimiya, 1969, vol. 1.
6. Sirota, N.N., *Fiziko-khimicheskaya priroda faz peremennogo sostava* (Physicochemical Nature of Variable-Composition Phases), Minsk: Nauka i Tekhnika, 1970.
7. Morachevskii, A.G., *Termodinamika rasplavlennykh metallicheskikh i solevykh sistem* (Thermodynamics of Molten Metallic and Salt Systems), Moscow: Metallurgiya, 1987.
8. *Oxydation des Metaux*, Benard, J., Ed., Paris: Gauthier-Villars, 1964, vol. 2.

ISSN 1070-4272, Russian Journal of Applied Chemistry, 2006, Vol. 79, No. 8, pp. 1371–1373. © Pleiades Publishing, Inc., 2006.
Original Russian Text © G. Khabdolda, V.I. Yamovoi, A.G. Berdin, K.M. Turdybekov, B.I. Tuleuov, P.V. Tarlykov, U.A. Baltaev, Yu.V. Gatilov, A.B. Ospanova, S.M. Adekenov, 2006, published in Zhurnal Prikladnoi Khimii, 2006, Vol. 79, No. 8, pp. 1385–1387.

BRIEF COMMUNICATIONS

Crystal and Molecular Structure of Tigogenin

G. Khabdolda, V. I. Yamovoi, A. G. Berdin, K. M. Turdybekov, B. I. Tuleuov, P. V. Tarlykov, U. A. Baltaev, Yu. V. Gatilov, A. B. Ospanova, and S. M. Adekenov

Institute of Phytochemistry, Ministry of Education and Science of the Republic of Kazakhstan, Karaganda, Kazakhstan

Novosibirsk Institute of Organic Chemistry, Siberian Division, Russian Academy of Sciences, Novosibirsk, Russia

Received April 12, 2006

Abstract—Tigogenin [(25R)-5α-spirostan-3β-ol] was isolated from *Digitalis lanata Ehrh.*, and its crystal and molecular structure was determined by single crystal X-ray diffraction.

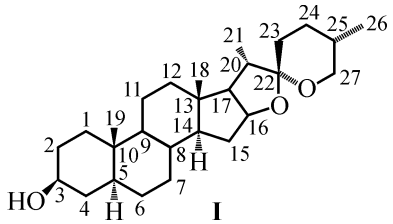
DOI: 10.1134/S1070427206080325

Digitalis lanata Ehrh. is one of promising sources of cardenolides [1]; it also contains steroid saponins [2]. Preparations from the *Digitalis lanata Ehrh*. tops are widely used in medicine as cardiotonic agents [3]. Tigogenin [(25R)-5α-spirostan-3β-ol] has been previously found in *Digitalis lanata Ehrh*. [4] and in some other plants [5, 6].

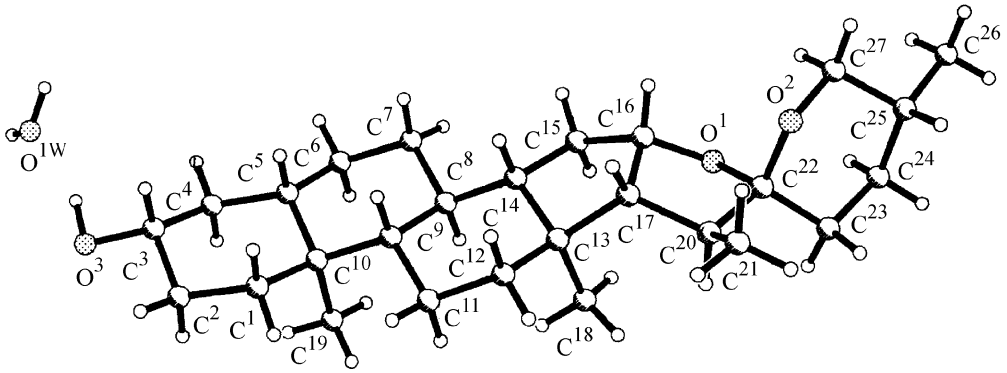
A TLC analysis and acid hydrolysis (5% H_2SO_4 in 1,3-dioxane–water, 1 : 1, 4 h, refluxing) showed that the tops of *Digitalis lanata Ehrh*., collected in the flowering period from the cultivated plants (herb seed growing nursery of the Institute of Phytochemistry, Ministry of Education and Science of the Republic of Kazakhstan, Karaganda), contain both tigogenin and, apparently, its glycosides.

The vegetable raw material was extracted with 70% ethanol; lipophilic components were removed from the extract by treatment with petroleum ether. Then the extract was hydrolyzed as described above. From the hydrolysis products, we isolated (25R)-5α-spirostan-3β-ol by column chromatography on alumina. The product was identified by its melting point and the melting point of its acetate [4].

We found no data on the crystal and molecular structure of **I** in the Cambridge Crystallographic Database [7], and, therefore, we studied its structure by single crystal X-ray diffraction.



I



Molecular structure of **I**.

Table 1. Bond lengths d in **I**

Bond	d, Å	Bond	d, Å
O^1–C^{22}	1.413(7)	C^{10}–C^{19}	1.533(7)
O^1–C^{16}	1.444(7)	C^{11}–C^{12}	1.537(7)
O^2–C^{27}	1.438(7)	C^{12}–C^{13}	1.518(8)
O^2–C^{22}	1.444(6)	C^{13}–C^{14}	1.529(7)
O^3–C^3	1.433(7)	C^{13}–C^{18}	1.544(7)
C^1–C^2	1.530(8)	C^{13}–C^{17}	1.548(7)
C^1–C^{10}	1.530(7)	C^{14}–C^{15}	1.531(7)
C^2–C^3	1.503(8)	C^{15}–C^{16}	1.528(7)
C^3–C^4	1.509(8)	C^{16}–C^{17}	1.551(8)
C^4–C^5	1.542(7)	C^{17}–C^{20}	1.533(8)
C^5–C^6	1.508(7)	C^{20}–C^{21}	1.519(8)
C^5–C^{10}	1.522(7)	C^{20}–C^{22}	1.527(8)
C^6–C^7	1.531(7)	C^{22}–C^{23}	1.500(7)
C^7–C^8	1.531(7)	C^{23}–C^{24}	1.542(10)
C^8–C^{14}	1.521(7)	C^{24}–C^{25}	1.506(9)
C^8–C^9	1.534(7)	C^{25}–C^{27}	1.521(9)
C^9–C^{11}	1.543(7)	C^{25}–C^{26}	1.535(11)
C^9–C^{10}	1.564(7)		

Table 2. Bond angles ω in **I**

Angle	ω, deg	Angle	ω, deg
$C^{22}O^1C^{16}$	105.7(4)	$C^{14}C^{13}C^{18}$	111.8(4)
$C^{27}O^2C^{22}$	112.8(5)	$C^{12}C^{13}C^{17}$	115.6(4)
$C^2C^1C^{10}$	113.9(5)	$C^{14}C^{13}C^{17}$	101.1(4)
$C^3C^2C^1$	111.8(5)	$C^{18}C^{13}C^{17}$	110.8(4)
$O^3C^3C^4$	107.9(5)	$C^8C^{14}C^{13}$	114.9(4)
$O^3C^3C^2$	112.1(5)	$C^8C^{14}C^{15}$	120.5(4)
$C^4C^3C^2$	110.5(5)	$C^{13}C^{14}C^{15}$	102.9(4)
$C^3C^4C^5$	111.2(5)	$C^{16}C^{15}C^{14}$	102.0(5)
$C^6C^5C^{10}$	113.5(4)	$O^1C^{16}C^{15}$	112.5(5)
$C^6C^5C^4$	113.0(5)	$O^1C^{16}C^{17}$	104.6(4)
$C^{10}C^5C^4$	113.0(5)	$C^{15}C^{16}C^{17}$	107.9(5)
$C^5C^6C^7$	111.7(5)	$C^{20}C^{17}C^{13}$	121.8(5)
$C^6C^7C^8$	112.0(5)	$C^{20}C^{17}C^{16}$	104.2(5)
$C^{14}C^8C^7$	111.0(4)	$C^{13}C^{17}C^{16}$	103.4(4)
$C^{14}C^8C^9$	109.3(4)	$C^{21}C^{20}C^{22}$	116.4(5)
$C^7C^8C^9$	111.1(4)	$C^{21}C^{20}C^{17}$	114.7(5)
$C^8C^9C^{11}$	111.0(4)	$C^{22}C^{20}C^{17}$	103.6(4)
$C^8C^9C^{10}$	113.2(4)	$O^1C^{22}O^2$	108.9(5)
$C^{11}C^9C^{10}$	113.8(4)	$O^1C^{22}C^{23}$	109.5(5)
$C^5C^{10}C^{19}$	108.2(4)	$O^2C^{22}C^{23}$	110.1(4)
$C^5C^{10}C^{11}$	111.4(5)	$O^1C^{22}C^{20}$	105.3(4)
$C^{19}C^{10}C^1$	109.3(5)	$O^2C^{22}C^{20}$	106.8(5)
$C^5C^{10}C^9$	107.1(4)	$C^{23}C^{22}C^{20}$	116.1(5)
$C^{19}C^{10}C^9$	110.2(4)	$C^{22}C^{23}C^{24}$	112.0(6)
$C^1C^{10}C^9$	110.6(4)	$C^{25}C^{24}C^{23}$	111.2(6)
$C^{12}C^{11}C^9$	112.4(5)	$C^{24}C^{25}C^{27}$	108.7(5)
$C^{13}C^{12}C^{11}$	112.1(5)	$C^{24}C^{25}C^{26}$	112.3(7)
$C^{12}C^{13}C^{14}$	108.4(4)	$C^{27}C^{25}C^{26}$	109.4(7)
$C^{12}C^{13}C^{18}$	108.9(4)	$O^2C^{27}C^{25}$	111.0(6)

The general view of the molecule of **I** is shown in the figure. The bond lengths (Table 1) are common, whereas the bond angles (Table 2) differ from the ideal tetrahedral values [8], varying from 101(4)° ($C^{14}C^{13}C^{17}$) to 121.8(5)° ($C^{20}C^{17}C^{13}$). All the six-membered rings have a slightly distorted chair conformation. For example, for $C^1C^2C^3C^4C^5C^{10}$ ΔC_S^{10} = 1.4° and $\Delta C_2^{1,10}$ = 1.8°; for $C^5C^6C^7C^8C^9C^{10}$ ΔC_S^7 = 2.0° and $\Delta C_2^{7,8}$ = 1.6°; for $C^8C^9C^{11}C^{12}C^{13}C^{14}$ ΔC_S^{14} = 0.9° and $\Delta C_2^{13,14}$ = 2.3°; for $O^2C^{22}C^{23}C^{24}C^{25}C^{27}$ ΔC_S^{24} = 3.7° and $\Delta C_2^{2,27}$ = 0.5°.

The heteroring $O^1C^{16}C^{17}C^{20}C^{22}$ has a conformation intermediate between a distorted envelope (with out-of-plane O^1 atom) and a distorted 1,22-half-chair (ΔC_S^1 = 8.3° and $\Delta C_2^{1,22}$ = 10.5°); the conformation of the five-membered ring $C^{13}C^{14}C^{15}C^{16}C^{17}$ is also intermediate between a distorted envelope (with out-of-plane C^{14} atom) and a distorted 13,14-half-chair (ΔC_S^{14} = 11.9° and $\Delta C_2^{13,14}$ = 8.3°). The methyl groups at C^{20} and C^{25} and the hydroxy group at C^3 are equatorial, whereas the methyl groups at C^{10} and C^{13} are axial.

The molecules in the crystal are linked in infinite ribbons oriented along the crystallographic axis $2_1(0, y, 0)$ by hydrogen bonds O^3–H $(x, y, z)\cdots O^{1W}$ (x, y, z) (∠OHO 160.98°; distances O^3–H = 0.98, $O^3\cdots O^1$ = 2.71, $H\cdots O^{1W}$ = 1.77 Å), O^{1W}–H^{1W} $(x, y, z)\cdots O^{2*}$ $(-2 - x, y - 0.5, -z)$ (∠OHO 163.02°; distances O^1–H^1 = 0.87, $O^1\cdots O^2$ = 2.89, $H\cdots O^2$ = 2.05 Å), and O^{1W}–H^{2W} $(x, y, z)\cdots O^{3**}$ $(-2 - x, y - 0.5, 1 - z)$ (∠OHO 175.04°; distances O^1–H^2 = 0.81, $O^3\cdots O^1$ = 2.79, $H\cdots O^3$ = 1.99 Å).

EXPERIMENTAL

The unit cell parameters and intensities of 2391 unique reflections were measured with a Bruker P4 diffractometer (Mo_{K_α} radiation, graphite monochromator, θ/2θ scanning, 2θ < 50°). The crystals are monoclinic; a = 10.282(7), b = 7.374(5), c = 16.637(11) Å, β = 94.72(5)°, V = 1257.1(1) Å^3, Z = 2 ($C_{27}H_{44}O_4$), d_{calc} = 1.143 g cm^{-3}, space group $P2_1$.

The structure was solved by the direct method and refined by the full-matrix least-squares method in the anisotropic approximation for all nonhydrogen atoms. The hydrogen atoms of water of hydration and hydroxy group were revealed by differential synthesis and refined in the isotropic approximation; the positions of the other H atoms were calculated geometrically and fixed in the rider model. In the calculations, we used 1467 reflections with $I > 2\sigma(\mathbf{I})$.

Table 3. Atomic coordinates in the structure of **I**

Atom	$x \times 10^4$	$y \times 10^4$	$z \times 10^4$	Atom	$x \times 10^4$	$y \times 10^4$	$z \times 10^4$
O^1	–6744(4)	–2675(5)	–2372(2)	C^{14}	–7888(5)	–1696(7)	–468(3)
O^2	–7659(3)	–1014(6)	–3465(2)	C^{15}	–7698(6)	–3210(8)	–1077(3)
O^3	–9409(5)	–3830(7)	4157(2)	C^{16}	–7771(6)	–2169(8)	–1873(3)
O^{1W}	–11111(7)	–3397(9)	4575(4)	C^{17}	–7517(5)	–137(8)	–1678(3)
C^1	–8305(6)	1125(7)	2247(3)	C^{18}	–5588(5)	–561(8)	–634(3)
C^2	–8461(6)	885(8)	3147(3)	C^{19}	–6446(5)	–1018(10)	2142(3)
C^3	–9361(6)	–660(8)	3302(3)	C^{20}	–6620(6)	489(8)	–2315(3)
C^4	–8905(6)	–2383(8)	2924(3)	C^{21}	–7005(7)	2278(9)	–2719(4)
C^5	–8775(6)	–2130(7)	2015(3)	C^{22}	–6560(5)	–1156(9)	–2869(3)
C^6	–8494(6)	–3878(7)	1591(3)	C^{23}	–5322(6)	–1387(11)	–3275(4)
C^7	–8553(6)	–3631(8)	675(3)	C^{24}	–5414(6)	–2964(12)	–3886(4)
C^8	–7689(5)	–2064(7)	434(3)	C^{25}	–6613(7)	–2796(10)	–4465(4)
C^9	–7972(5)	–327(7)	896(3)	C^{26}	–6808(8)	–4451(13)	–5022(5)
C^{10}	–7858(5)	–591(7)	1832(3)	C^{27}	–7798(7)	–2573(9)	–3984(4)
C^{11}	–7167(6)	1281(8)	611(3)	H^{1W}	–11620(70)	–4160(100)	4300(40)
C^{12}	–7356(6)	1560(8)	–307(3)	H^{2W}	–10970(80)	–4050(120)	4960(50)
C^{13}	–7062(5)	–150(7)	–767(3)	H^3O	–9940(80)	–1910(120)	4220(40)

The final divergence factors are as follows: R = 0.0615, ${}_WR_2$ = 0.1513. The structure was solved and refined using SHELXS-97 and SHELXL-97 software. The atomic coordinates are listed in Table 3.

(25R)-5α-Spirostan-3β-ol. The air-dry raw material (1 kg) of *Digitalis lanata* tops was extracted with 8 l of 96% ethanol. The extraction was performed four times. The extracts were combined and evaporated to dryness on a rotary evaporator at 45–50°C. A thick extract was obtained (490 g). The extract was dissolved in 1 l of a 2 : 1 water–ethanol mixture and treated with petroleum ether (6 × 500 ml) to remove nonpolar components. The water-soluble components were removed by extraction of the aqueous-alcoholic phase with isobutanol (5 × 500 ml). The isobutanol extract was evaporated to dryness, and residual isobutanol was removed by repeated dissolution of the residue in 96% ethanol, followed by vacuum evaporation of the solvent; the extract was dried in a water-jet-pump vacuum. A fraction (153.5 g) containing steroid glycosides was obtained. The isobutanol fraction was dissolved in 600 ml of a 1 : 1 1,3-dioxane–water mixture containing 5 wt % H_2SO_4; the solution was heated on a water bath at 95°C for 4 h. After that, the solution was diluted with 300 ml of a saturated aqueous NaCl solution, neutralized with 10% Na_2CO_3 to pH 7, and extracted with five 500-ml portions of isobutanol. The combined isobutanol extracts were washed with 300 ml of a saturated aqueous NaCl solution and vacuum-evaporated to dryness. The residue (87 g) was chromatographed on a column packed with 1.5 kg of alumina (Brockmann grade II, weight ratio of the sum of the components to the sorbent 1 : 17.5), using chloroform as eluent. White crystals of (25R)-5α-spirostan-3β-ol **I** were obtained; mp 209–211°C (ethanol), yield 0.52% based on the air-dry raw material. IR spectrum, KBr, ν_{max}, cm^{-1}: 900 (C–O in spirostanol system), 1050 (C–OH), 1620 (C=C), 2950 (CH), 3300–3500 (OH).

REFERENCES

1. Haack, E., Kaiser, F., and Springler, H., *Naturwissenschaften*, 1957, vol. 44, no. 2, pp. 633–634.
2. Tamura, K., Kobayashi, Y., and Torita, K., *Jpn. Med. J.*, 1948, no. 1, pp. 206–214.
3. Mashkovskii, M.D., *Lekarstvennye sredstva* (Drugs), Tashkent: Meditsina, 1987, part 1.
4. Lack, R., Newman, B.C., and Shoppee, C.W., *Aust. J. Chem.*, 1963, vol. 16, pp. 896–899.
5. Viqar, U.A., Fehmida, T.B., and Roshan, A., *Phytochemistry*, 1993, vol. 34, pp. 511–515.
6. Kubo, S., Mimaki, Y., Sashida, Y., et al., *Phytochemistry*, 1992, vol. 31, pp. 2445–2450.
7. *Cambridge Crystallographic Database: Release November 2003*, Cambridge.
8. Allen, F.H., Kennard, O., Watson, D.G., et al., *J. Chem. Soc., Perkin Trans. 2*, 1987, no. 12, pp. S1–S19.

ISSN 1070-4272, Russian Journal of Applied Chemistry, 2006, Vol. 79, No. 8, pp. 1374–1377. © Pleiades Publishing, Inc., 2006.
Original Russian Text © E.E. Ergozhin, T. Hirotsu, B.A. Mukhitdinova, S.A. Shoinbekova, A.I. Nikitina, G.N. Zhunusova, 2006, published in Zhurnal Prikladnoi Khimii, 2006, Vol. 79, No. 8, pp. 1388–1390.

BRIEF COMMUNICATIONS

Cationic Polymerization of Redox Monomers Derived from Monoethanolamine Vinyl Ether and Various Quinones

E. E. Ergozhin, T. Hirotsu, B. A. Mukhitdinova, S. A. Shoinbekova, A. I. Nikitina, and G. N. Zhunusova

Bekturov Institute of Chemical Sciences, Ministry of Education and Science of the Republic of Kazakhstan, Almaty, Kazakhstan

National Institute of Advanced Industrial Science and Technology–AIST, Tsukuba, Japan

Received February 21, 2006

Abstract—Cationic polymerization of redox monomers derived from monoethanolamine vinyl ether and various chlorinated quinones in aqueous–organic solutions in the presence of HCl was studied. Optimal reaction conditions were found, and the kinetic characteristics of the reactions were calculated.

DOI: 10.1134/S1070427206080337

The new redox monomers prepared from monoethanolamine vinyl ether (MEAVE) and chlorinated quinones (chloranil, CA; 2,3-dichloro-1,4-naphthoquinone, DCNPQ; 2,3-dichloro-5,6-dicyano-1,4-benzoquinone, DCDCQ) [1] can be classed with substituted vinyl ethers (VEs) CH_2=CHOR, namely, with ethanolamine VEs. It is known [2] that the polymerization activity of VEs depends on the structure of the organic residue. For example, aliphatic VEs polymerize considerably more readily than vinyl aryl ethers. Also, introduction of a halogen substituent into the monomer molecule enhances its activity in polymerization [2]. Furthermore, chlorine substituents significantly alter the properties of a polymer, especially its solubility and softening point, which are higher compared to the unsubstituted analog.

Vinyl alkyl ethers polymerize most readily under the action of ionic, in particular, acid catalysts [2]. It has been shown [3, 4] that radical homopolymerization of vinyl ethers occurs considerably more difficultly than the cationic polymerization. Therefore, it is interesting to study how the chemical structure of redox monomers affects their reactivity in cationic polymerization.

In this study, we examined the features of cationic polymerization of redox monomers in the DMF–water mixture in the presence of HCl.

EXPERIMENTAL

Redox monomers derived from MEAVE and chloranil (disubstituted derivative MEAVE–CA–MEAVE), MEAVE and 2,3-dichloro-1,4-naphthoquinone (MEAVE–DCNPQ), and MEAVE and 2,3-dichloro-5,6-dicyano-1,4-benzoquinone (MEAVE–DCDCQ) were prepared as described in [1].

The polymerization of the redox monomers was performed at 7–27°C for 2–7 h in DMF–water mixtures, volume ratio from 4 : 0 to 1 : 3, in the presence of HCl (0.07–0.61 M). The reaction progress was monitored by polarographic measurement of the concentration of the unchanged monomer and by gravimetric determination of the precipitated polymer.

The polarograms were recorded on a PU-1 polarograph in a temperature-controlled cell at 25 ± 0.5°C, using a mercury dropping electrode with the open-circuit capillary characteristic $m^{2/3}t^{1/2}$ = 4.38 $mg^{2/3}$ $s^{-1/2}$; the supporting electrolyte was a phosphate buffer solution (pH 7.4) in 25% DMF. Saturated calomel electrode was a reference electrode. The solutions were deoxygenated by bubbling of argon for 5 min.

Ethanolamine vinyl ethers are considerably less active than vinyl alkyl ethers in reactions occurring by the ionic mechanism [5], because of the pres-

Table 1. Optimal conditions of cationic polymerization of redox monomers

Monomer	DMF : H_2O (by volume)	$c_{monomer}$, g l^{-1}	c_{HCl}, M	T, °C	τ, h	Polymer yield, %
MEAVE–CA–MEAVE	1 : 2	20	0.11	21	2	96
MEAVE–DCNPQ	1 : 3	35	0.11	21	5	94
MEAVE–DCDCQ	1 : 2	25	0.29	21	5	83

ence of double bonds and two centers (O, N) capable of forming onium compounds. As indicated in [6], the relative activity increases with the enhancement of the electron-donor power of substituents. We found that, despite the fact that the quinones themselves [7] and their functional groups –C≡N, –Cl are strong electron acceptors, the redox monomers show capacity for cationic polymerization. The reaction was performed in DMF–water mixtures in the presence of HCl. We examined the influence of the water content, concentrations of the monomers and HCl (catalyst), and reaction temperature and time on the yield of the polymers (Fig. 1).

Figure 1 shows that these factors affect the cationic polymerization of MEAVE–CA–MEAVE, MEAVE–DCNPQ, and MEAVE–DCDCQ differently, with the last monomer showing a distinctive behavior. Its polymerization requires a higher HCl concentration. Table 1 shows the optimal conditions of the polymer synthesis by cationic polymerization, found from the experimental data.

Table 1 shows that MEAVE–DCDCQ is less reactive than the other redox monomers. To obtain more detailed quantitative data on their activity under optimal conditions, we studied the kinetics of the cationic polymerization of MEAVE–CA–MEAVE, MEAVE–DCNPQ, and MEAVE–DCDCQ.

To calculate the rate constants of the overall polymerization process, we determined the reaction order. We found that the cationic polymerization of the redox monomers is a first-order reaction with respect to the monomer, as indicated by the linear dependence of the logarithm of its concentration on the synthesis time. The rate constants of the cationic polymerization of the redox monomers, calculated from the first-

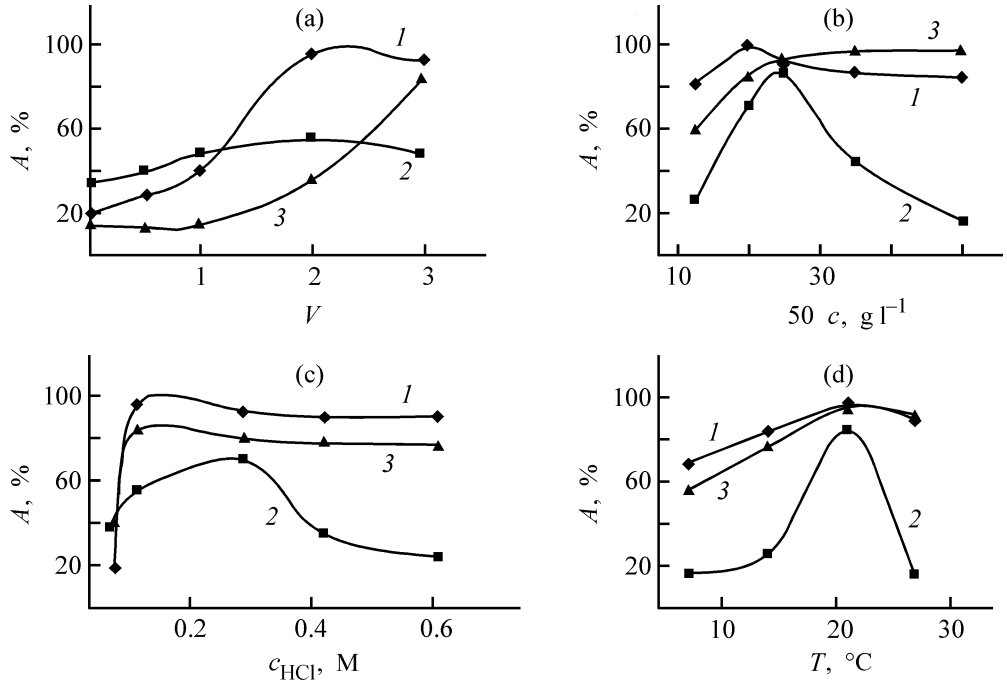


Fig. 1. Polymer yield A in the cationic polymerization vs. the (a) water : DMF volume ratio V, (b) monomer concentration c, (c) HCl concentration c_{HCl}, and (d) temperature T. (*1*) MEAVE–CA–MEAVE, (*2*) MEAVE–DCDCQ, and (*3*) MEAVE–DCNPQ.

Table 2. Kinetic characteristics of the cationic polymerization of redox monomers

T_{synth}, °C	Monomer	$k \times 10^3$, min^{-1}	E_a, kJ mol^{-1}	Monomer	$k \times 10^3$, min^{-1}	E_a, kJ mol^{-1}	Monomer	$k \times 10^3$, min^{-1}	E_a, kJ mol^{-1}
7	MEAVE–CA–	12.40	14.42	MEAVE–	2.72	63.32	MEAVE–	2.63	63.75
14	MEAVE	14.30		DCNPQ	5.20		DCDCQ	5.25	
21		16.80			10.68			11.35	

Table 3. Physicochemical characteristics of the chlorinated polymers synthesized

Monomer	η, dl g^{-1} (DMF, 25°C)	T_m, °C	SEC_{HCl}	RC	E_0, V
			mg-equiv g^{-1}		
MEAVE–CA–MEAVE	0.18–0.20	190	2.12	5.32	0.58
MEAVE–DCNPQ	0.10–0.12	172	2.60	5.88	0.39
MEAVE–DCDCQ	0.16–0.18	145	2.42	4.86	0.40

order rate equation [8], and the activation energies of the process, estimated from the Arrhenius dependence (Fig. 2b), are listed in Table 2.

Table 2 shows that all the redox monomers are active in the cationic polymerization. The most reactive is the disubstituted derivative of MEAVE and CA. With respect to the reactivity in the cationic polymerization, the monomers are ranked in the following order: MEAVE–CA–MEAVE > MEAVE–DCNPQ > MEAVE–DCDCQ.

The structure of the monomers affects not only their reactivity, but also the properties of the resulting polymers. Some physicochemical properties of the polymers prepared are given in Table 3.

The polymers are colored powders readily soluble in polar solvents. The low intrinsic viscosity is apparently due to the formation of oligomers, which is typical of vinyl ethers [4, 6]. Thanks to the relatively high redox capacity (RC), these polymers can find application in hydrometallurgy and other branches of industry as redox resins with complexing properties.

CONCLUSIONS

(1) Optimal conditions were found for the cationic polymerization of redox monomers derived from monoethanolamine vinyl ether and various chlorinated quinones in an aqueous–organic solution in the presence of HCl.

(2) The reaction kinetics was studied, and the rate constants and activation energies were determined. The disubstituted chloranil derivative is the most reactive.

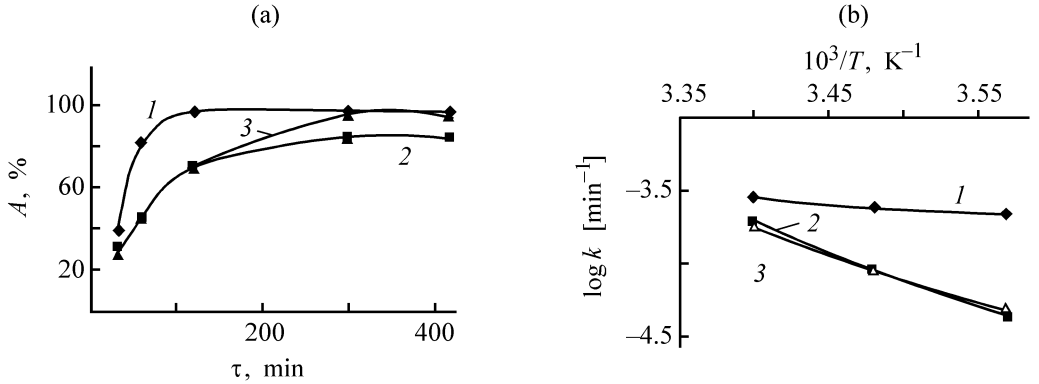


Fig. 2. (a) Polymer yield A vs. the synthesis time τ and (b) temperature dependence of $\log k$. (*1*) MEAVE–CA–MEAVE, (*2*) MEAVE–DCDCQ, and (*3*) MEAVE–DCNPQ.

ACKNOWLEDGMENTS

The study was financially supported by the International Science and Technology Center (ISTC) (grant no. K-604).

REFERENCES

1. Kazakh Patent 8813.
2. Vaculik, P., *Chemie Monomerů*, Prague: Československ. Akad. Ved, 1956, vol. 1.
3. Shostakovskii, M.F., *Prostye vinilovye efiry* (Vinyl Ethers), Moscow: Akad. Nauk SSSR, 1952.
4. Mikhant'ev, B.I., Mikhant'ev, V.B., Lapenko, V.L., and Voinova, V.K., *Nekotorye vinilovye monomery* (Some Vinyl Monomers), Voronezh: Voronezh. Univ., 1970.
5. Zhubanov, B.A., Shaikhutdinov, E.M., and Osadchaya, E.F., *Prostye vinilovye efiry v radikal'noi polimerizatsii* (Vinyl Ethers in Radical Polymerization), Alma-Ata: Nauka, 1985.
6. Erusalimskii, B.L. and Lyubetskii, S.G., *Protsessy ionnoi polimerizatsii* (Ionic Polymerization), Leningrad: Khimiya, 1974.
7. Pullman, B. and Pullman, A., *Quantum Biochemistry*, New York: Interscience, 1963.
8. Emanuel', N.M. and Knorre, D.G., *Kurs khimicheskoi kinetiki* (Course of Chemical Kinetics), Moscow: Khimiya, 1974.

ISSN 1070-4272, Russian Journal of Applied Chemistry, 2006, Vol. 79, No. 8, pp. 1378–1380. © Pleiades Publishing, Inc., 2006.
Original Russian Text © I.G. Silinskaya, A.V. Novoselova, Yu.N. Sazanov, A.V. Gribanov, I.N. Serov, V.I. Margolin, 2006, published in Zhurnal Prikladnoi Khimii, 2006, Vol. 79, No. 8, pp. 1391–1393.

BRIEF COMMUNICATIONS

Structuring of Polyacrylonitrile Solutions

I. G. Silinskaya, A. V. Novoselova, Yu. N. Sazanov, A. V. Gribanov, I. N. Serov, and V. I. Margolin

Institute of Macromolecular Compounds, Russian Academy of Sciences, St. Petersburg, Russia
AIRES Foundation for Development of New Medical Technologies, St. Petersburg, Russia

Received March 30, 2006

Abstract—Mechanisms of orientation for the solutions of polyacrylonitrile synthesized under conditions of radical and anionic polymerization were studied. The effect of the fractal-matrix structuring agent developed by the AIRES foundation on the correlation parameters of the solution density and average squared fluctuation polarizability, which can be used to determine how the supramolecular structure changes by "self-orientation" and "induced orientation" mechanisms, was analyzed.

DOI: 10.1134/S1070427206080349

Polyacrylonitrile (PAN) is one of the most important and widely industrially used polymers. It serves to obtain various polymeric materials with unique properties (thermal stability, strength, electrical conductivity, hydrophilicity, etc.). This is determined by specific structural features of the PAN molecule, whose quantitative and qualitative parameters depend on preparation techniques and methods of its modification [1, 2]. Various methods of acrylonitrile polymerization can be used to obtain polymers with predominance of 3*D* structures of atactic, isotactic, and syndiotactic types [3–5]. Stereoisomers of this kind possess various properties and differently behave in forming and under thermal treatment. The "wet" method is for the most part used in the industry to form PAN fibers, and, therefore, the spatial orientation of polymer chains of PAN in solution is important. As a rule, spinning solutions of PAN are oriented by mechanical treatment in fiber forming on a technological line.

The aim of this study was to orient PAN solutions of varied genesis with a fractal-matrix structuring agent (FMSA) developed by AIRES foundation. Previous studies have shown that FMSA exerts an orienting influence on the spatial organization of certain inorganic compounds in the liquid state [6–8]. A noticeable influence of the structure on the crystallization and polymorphism of the compounds studied has been revealed for the examples of water and metal salts and alloys.

EXPERIMENTAL

As starting objects served solutions of PAN in dimethylformamide (DMFA), produced by radical (R-PAN) and anionic (A-PAN) polymerization [9], with the solution concentration equal to 0.5%. The light-scattering method [10] was used to examine during 14 days the variation of the parameters $\overline{\eta}^2$ (average square of polarizability fluctuations) and α_v (correlation dimensions of the solution density at a given point). Two cuvettes were subjected to the action of FMSA, and two others served as controls.

The processes under study were affected with FMSA having the form of a complex curvilinear diffraction grating whose image was transferred by precision optical lithography onto optically polished glass substrates. A diffraction grating of this kind has a fractal-matrix topology in the form of a fractally assembled matrix comprising a set of self-similar units, each of which is a graphical image of a planar cross-section of a multilevel spatial geometric structure.

Figures 1a and 1b shows the experimentally found dependences of α_v and $\overline{\eta}^2$ on the time of keeping on FMSA and without it. It can be seen that, immediately after solution preparation, the system is microisotropic, with the value of $\overline{\eta}^2$ for R-PAN solutions exceeding that for A-PAN. This indicates that the R-PAN solution contains particles with larger heterogeneity dimensions, i.e., the R-PAN solution is more heterogeneous than the A-PAN solution. Hence follows

a conclusion that the supramolecular organizations of PAN solutions produced by radical and anionic polymerization are different. It is known [11] that R-PAN is characterize by larger molecular weight, broader molecular weight distribution, and a more pronounced branching, compared with A-PAN, and, therefore, it is these factors that lead to a higher heterogeneity of R-PAN solutions.

Further variation of the optical parameters of R-PAN and A-PAN solutions with the time of keeping at room temperature reflects the effect of FMSA on the supramolecular organization of PAN macromolecules in solution. A study of this effect demonstrated that the parameters $\overline{\eta}^2$ and α_v change with time, compared with the control experiments. It is well seen that the influence is exerted not only by the FMSA, but also by methods used to synthesize PAN. For example, the supramolecular structure remains unchanged during 14 days ($\overline{\eta}^2$ and α_v remain constant). During the same time, an R-PAN solution subjected to the action of FMS becomes more heterogeneous ($\overline{\eta}^2$ grows), whereas the heterogeneity dimensions (α_v) remain virtually unchanged and the solution structure remains isotropic.

In contrast to R-PAN, the control solution of A-PAN spontaneously changes its structure in the course of time. It becomes more heterogeneous and the heterogeneity dimensions decrease (α_v value falls), i.e., the supramolecular formations present in the initial solution become denser and more compact. This behavior of A-PAN solutions is in an agreement with (i) data on the stereoblock structure of A-PAN, which predetermines the high packing density, and (ii) with the formation, in solution, of associates having the form of a double helix via interaction of two nitrile groups of adjacent A-PAN chains and CN groups with α-atoms of hydrogen [12]. After the end of the testing period (14 days), measurements of the asymmetry of anisotropic light scattering by the control A-PAN solution demonstrate that the solution becomes anisotropic (α_n = 335 Å, $\delta^2 \times 10^9$ = 78). An additional specificity of the behavior of the control A-PAN solution is that the time dependence of $\overline{\eta}^2$ changes and becomes similar to that of an R-PAN solution subjected to the action of FMSA.

Thus, a kind of similarity between the temporal "self-organization" of A-PAN and the organizing effect of FMSA for the R-PAN solution is observed. The effect of FMSA on the A-PAN solution, judged from changes in $\overline{\eta}^2$ and α_v relative to that of the control sample, is less pronounced than that for the R-PAN solution. Probably, two competing tendencies associated with its orientation exist for the A-PAN solution. These are the self-organization well seen for the control sample and the organization "induced" by FMSA, for which large values of the anisotropic parameters are observed (α_n = 390 Å, $\delta^2 \times 10^9$ = 82). It can be assumed that the mechanism of orientation of the A-PAN solution under the action of FMSA differs from the mechanism of self-organization. However, the available experimental data are insufficient for a hypothetical substantiation of this difference.

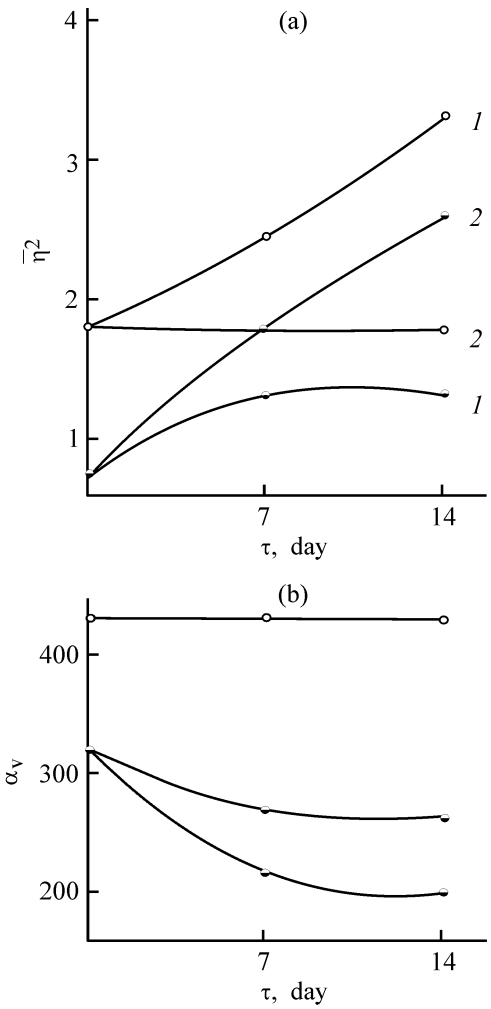


Fig. 1. (a) Average square of the polarizability, $\overline{\eta}^2$, and (b) α_v of R-PAN and A-PAN solutions vs. (*1*) time τ of keeping on FMSA. (*2*) Control run.

CONCLUSIONS

(1) A study by the light scattering method of the effects of organization of polyacrylonitrile solutions in relation to the keeping time, methods of polymer preparation, and action of the fractal-matrix structuring agent developed by the AIRES founda-

tion demonstrated that the polyacrylonitrile solutions produced by radical polymerization change their structure only under the action of the structuring agent to become more heterogeneous in the course of time, but their structure remains isotropic.

(2) Solutions of polyacrylonitrile produced by the anionic method undergo self-orientation in the course of time and their structural parameters change under the action of the structuring agent. Prolonged treatment with the structuring agent gives rise to anisotropic structures.

REFERENCES

1. Konkin, A.A., *Uglerodnye i drugie zharostoikie voloknistye materially* (Heat-resistant Fibrous Materials of Carbon and Other Types), Moscow: Khimiya, 1974.
2. Gribanov, A.V. and Sazanov, Yu.N., *Zh. Prikl. Khim.*, 2000, vol. 73, no. 1, pp. 465–469.
3. Khachaturov, A.S., Abramenko, E.A., Novoselova, A.V., et al., *Vysokomol. Soedin., Ser. B*, 1988, vol. 30, no. 6, pp. 891–896.
4. Novoselova, A.V., Zgonnik, V.N., Sazanov, Yu.N., et al., *Vysokomol. Soedin., Ser. A*, 1992, vol. 34, no. 3, pp. 59–63.
5. Kudryavtsev, G.I., *Armiruyushchie khimicheskie volokna dlya kompozitsionnykh materialov: Prakticheskoe rukovodstvo* (Reinforcing Chemical Fibers for Composites: Manual), Moscow: Khimiya, 1992.
6. Slesarev, V.I., Shabrov, A.V., Serov, I.N., and Alekseitsev, A.V., *Vestn. SPb. Gos. Med. Akad. im. Mechnikova*, 2002, vol. 3, pp. 124–138.
7. Serov, I.N., Zhabreev, V.A., and Margolin, V.I., *Fiz. Khim. Stekla*, 2004, vol. 30, no. 1, pp. 45–71.
8. Zhabreev, V.A., Luk'yanov, G.I., Margolin, V.I., et al., *Nanotekhnika*, 2005, no. 3, pp. 60–77.
9. Sazanov, Yu.N., Shirokov, N.A., and Goltsin, B.E., *Thermochim. Acta*, 1979, vol. 32, pp. 73–79.
10. Kallistov, O.V., Krivobokov, V.V., Kalinina, N.A., et al., *Vysokomol. Soedin., Ser. A*, 1985, vol. 37, no. 5, pp. 968–974.
11. Sazanov, Yu.N., Novoselova, A.V., Nud'ga, L.A., et al., *Zh. Prikl. Khim.*, 2005, vol. 78, no. 8, pp. 1344–1348.
12. Sazanov, Yu.N., Novoselova, A.V., and Amsharov, K.F., *Zh. Prikl. Khim.*, 2005, vol. 78, no. 5, pp. 810–813.

ISSN 1070-4272, Russian Journal of Applied Chemistry, 2006, Vol. 79, No. 8, pp. 1381–1383. © Pleiades Publishing, Inc., 2006.
Original Russian Text © Ch.Sh. Ibragimov, F.A. Novruzova, Kh.Sh. Gadzhiakhmedzade, F.R. Khalafov, 2006, published in Zhurnal Prikladnoi Khimii, 2006, Vol. 79, No. 8, pp. 1394–1396.

BRIEF COMMUNICATIONS

Kinetics of the Reaction of Polyisobutylene Modification with Acrylonitrile and Vinyl Acetate

Ch. Sh. Ibragimov, F. A. Novruzova, Kh. Sh. Gadzhiakhmedzade, and F. R. Khalafov

Institute of Chemical Problems, National Academy of Sciences of the Republic of Azerbaijan, Baku, Azerbaijan

Received December 1, 2005; in final form, March 2006

Abstract—Kinetic parameters of the reaction of polyisobutylene modification with acrylonitrile and vinyl acetate were calculated. The reaction rate constants were obtained for three temperatures, and the activation energies and the preexponential factor were determined for modification of polyisobutylene with acrylonitrile and vinyl acetate. The effect of the $AlCl_3$ concentration on the kinetic parameters of the reaction of polyisobutylene modification was studied.

DOI: 10.1134/S1070427206080350

The development of methods for modification of polyisobutylene (PIB) with polar monomers in the presence of Lewis acids opens up wide opportunities for control over its properties, which extends the synthetic capacity of polymer chemistry.

Polymers of isobutylene are large-tonnage products that find wide use in various areas of industry and technology. Polyisobutylene belongs to the class of saturated polyolefins, which determines their comparatively high stability against corrosive media (acids, alkalis).

It is a common knowledge that Lewis acids (Friedel–Krafts catalysts) are used in organic chemistry and carbocation polymerization of olefins and dienes as catalysts of electrophilic reactions. It has been found, however, that, under mild conditions (20–60°C), strong Lewis acids ($AlCl_3$, $AlEtCl_2$) cause activation of polyisobutylene and butyl caoutchouc by the free-radical mechanism [1–4]. EPR spectroscopy and quantum-chemical calculations confirmed that paramagnetic centers are formed in catalytic destruction of PIB [2, 3].

As evidence in favor of the radical-chain mechanism of destruction served results of calorimetric and ^{13}C NMR studies of samples of destructed PIB [5, 6], which demonstrated that polyolefins (?PIB) with branched structure are formed. The data obtained were used to develop a method for synthesis of isobutylene copolymers with polar monomers, acrylonitrile (AN) and vinyl acetate (VA) [7]. Therefore, construction of a kinetic model of PIB modification with AN and VA on the basis of the data obtained and calculation of the kinetic parameters of these processes seem to be necessary for solving the problem of development of a polymeric material on their basis.

The paper reports the results of kinetic studies of the reaction of PIB modification with polar monomers AN and VA in *n*-hexane in the presence of the acid $AlCl_3$ (Tables 1, 2).

The reaction rate is described by the equation

$$-\frac{\mathrm{d}([\mathrm{AN}]_0 - [\mathrm{AN}]_c)}{\mathrm{d}t} = k([\mathrm{AN}]_0 - [\mathrm{AN}]_c)([\mathrm{PIB}]_0 - [\mathrm{PIB}]_c), \quad (1)$$

which gives, with account of the initial conditions, the following equation for the rate constant of the reaction of PIB modification with acrylonitrile:

$$k = \frac{1}{t}\,\frac{1}{[\mathrm{AN}]_0 - [\mathrm{PIB}]_0}\ln\frac{[\mathrm{PIB}]_0([\mathrm{AN}]_0 - [\mathrm{AN}]_c)}{[\mathrm{AN}]_0([\mathrm{PIB}]_0 - [\mathrm{AN}]_c)}. \quad (2)$$

Here, $[AN]_0$ and $[PIB]_0$ are the initial concentrations of AN and PIB in the reaction mixture (g g^{-1}); $[AN]_c$ and $[PIB]_c$, concentrations of AN and PIB in the copolymer (g g^{-1}); and t, time (h).

Equations similar to (1) and (2) were also derived for the reaction of PIB modification with vinyl acetate. In this case, $[VA]_0$ and $[VA]_c$ are substituted for $[AN]_0$ and $[AN]_c$ in Eqs. (1), (2).

Table 1. Experimental kinetic data for the reaction of PIB modification with acrylonitrile and vinyl acetate {reaction with AN: amount of the solvent (hexane) 77.91 ($AlCl_3$ 1.8%) and 78.88 wt % ($AlCl_3$ 0.92%), $[PIB]_0$ = 6.12% and $[AN]_0$ = 14%; Reaction with VA: amount of the solvent (hexane) 80.77 ($AlCl_3$ 2.23%) and 81.93 wt % ($AlCl_3$ 0.76%), $[PIB]_0$ = 8% and $[VA]_0$ = 9%; the same for Table 2}

T, K	τ, h	$[AN]_c \times 10^3$, g g^{-1}		$[VA]_c \times 10^3$, g g^{-1}	
		c_{AlCl_3} = 1.8%	c_{AlCl_3} = 0.92%	c_{AlCl_3} = 2.23%	c_{AlCl_3} = 0.76%
293	0	0	0	0	0
	0.083	0.534	0.206	0.428	0.184
	0.167	1.078	0.416	0.863	0.337
	0.333	2.191	0.834	1.744	0.744
	0.5	3.344	1.259	2.641	1.119
	1.5	3.937	1.884	3.153	1.616
313	0	0	0	0	0
	0.083	0.581	0.231	0.469	0.216
	0.167	1.178	0.463	0.944	0.437
	0.333	2.400	0.934	1.909	0.878
	0.5	3.656	1.412	2.899	1.325
	1.5	4.344	2.131	3.456	1.881
333	0	0	0	0	0
	0.083	0.609	0.247	0.516	0.253
	0.167	1.228	0.494	1.041	0.509
	0.333	2.503	0.994	2.075	1.025
	0.5	3.825	1.503	3.200	1.550
	1.5	4.537	2.309	3.894	2.116

Table 2. Calculation of the kinetic parameters for the reaction of PIB modification with acrylonitrile and vinyl acetate

T, K	τ, h	c_{AlCl_3} = 1.8%			c_{AlCl_3} = 0.92%		
		k, h^{-1}	*A*, h^{-1}	*E*, J mol^{-1}	*k*, h^{-1}	*A*, h^{-1}	*E*, J mol^{-1}
				Acrylonitrile			
293	0	0	0	0	0	0	0
	0.083	0.771	2.63	3000	0.302	1.394	3760
	0.167	0.745	2.63	3000	0.303	1.394	3760
	0.333	0.775	2.63	3000	0.298	1.394	3760
	0.5	0.789	2.63	3000	0.287	1.394	3760
	1.5	0.319	2.63	3000	0.148	1.394	3760
313	0	0	0	0	0	0	0
	0.083	0.785	2.63	3000	0.352	1.394	3760
	0.167	0.816	2.63	3000	0.298	1.394	3760
	0.333	0.854	2.63	3000	0.334	1.394	3760
	0.5	0.873	2.63	3000	0.332	1.394	3760
	1.5	0.347	2.63	3000	0.169	1.394	3760
333	0	0	0	0	0	0	0
	0.083	0.861	2.63	3000	0.402	1.394	3760
	0.167	0.879	2.63	3000	0.335	1.394	3760
	0.333	0.891	2.63	3000	0.344	1.394	3760
	0.5	0.929	2.63	3000	0.352	1.394	3760
	1.5	0.371	2.63	3000	0.183	1.394	3760

Table 2. (Contd.)

T, K	τ, h	c_{AlCl_3} = 1.8%			c_{AlCl_3} = 0.92%		
		k, h^{-1}	A, h^{-1}	E, J mol^{-1}	k, h^{-1}	A, h^{-1}	E, J mol^{-1}
Vinyl acetate							
293	0	0	0	0	0	0	0
	0.083	0.466	2.417	4190	0.227	1.216	5206
	0.167	0.411	2.417	4190	0.223	1.216	5206
	0.333	0.425	2.417	4190	0.239	1.216	5206
	0.5	0.459	2.417	4190	0.230	1.216	5206
	1.5	0.177	2.417	4190	0.093	1.216	5206
313	0	0	0	0	0	0	0
	0.083	0.438	2.417	4190	0.243	1.216	5206
	0.167	0.439	2.417	4190	0.244	1.216	5206
	0.333	0.489	2.417	4190	0.216	1.216	5206
	0.5	0.497	2.417	4190	0.230	1.216	5206
	1.5	0.196	2.417	4190	0.105	1.216	5206
333	0	0	0	0	0	0	0
	0.083	0.546	2.417	4190	0.193	1.216	5206
	0.167	0.548	2.417	4190	0.262	1.216	5206
	0.333	0.525	2.417	4190	0.269	1.216	5206
	0.5	0.550	2.417	4190	0.253	1.216	5206
	1.5	0.224	2.417	4190	0.122	1.216	5206

The data in Table 1 were used to determine the reaction rate constants, activation energies E, and pre-exponential factors A for various concentrations of $AlCl_3$, and AN and VA monomers (Table 2). The activation energies E and pre-exponential factors A were determined using the Arrhenius equation.

Thus, it was found that, irrespective of the reaction stage, the rate constant remains constant within the experimental error of 1–6%. An increase in the catalyst content from 0.76 to 2.2 wt % results in that, at temperatures of 20, 40, and 60°C, the rate constants increase by factors of 2.59, 2.53, and 2.49, respectively, in the case of the reaction with AN and by factors of 1.9, 2.0, and 2.2 for the reaction with VA.

CONCLUSIONS

It was found that the activation energies of the reactions of polyisobutylene modification with acrylonitrile in the temperature range 20–60°C have the values E = 3760 (amount of the catalyst 0.92 wt %) and 3000 J mol^{-1} (amount of the catalyst 1.8%), and those in modification with vinyl acetate, E = 4190 (amount of the catalyst 2.23%) and 5206 J mol^{-1} (amount of the catalyst 0.76%) in the same temperature range.

REFERENCES

1. Khalafov, F.R., Novruzova, F.A., Ismailov, E.G., et al., *Vysokomol. Soedin, Ser. B*, 1990, vol. 32, no. 3, pp. 165–167.
2. Khalafov, F.R., Novrusova, F.A., Ismailov, E.G., and Krentsel, B.A., *Acta Polym.*, 1990, vol. 41, no. 4, pp. 226–229.
3. Khalafov, F.R., Novruzova, F.A., Faradzhev, G.M., et al., *Vysokomol. Soedin., Ser. A*, 1991, vol. 33, no. 12, pp. 2568–2573.
4. Khalafov, F.R., *Doctoral Dissertation*, Moscow, 1992.
5. Khalafov, F.R., Novruzova, F.A., Krentsel', B.A., et al., *Vysokomol. Soedin., Ser. B*, 1990, vol. 32, no. 3, pp. 194–196.
6. Khalafov, F.R., Novrusova, F.A., Krentsel, B.A., et al., *Acta Polym.*, 1990, vol. 43, no. 2, pp. 102.
7. RF Patent 2026307.

ISSN 1070-4272, Russian Journal of Applied Chemistry, 2006, Vol. 79, No. 8, pp. 1384–1385. © Pleiades Publishing, Inc., 2006.
Original Russian Text © A.P. Stankevičius, L.N. Janušiene, P.B. Terent'ev, M.S. Saprogoniene, 2006, published in Zhurnal Prikladnoi Khimii, 2006, Vol. 79, No. 8, pp. 1397–1398.

BRIEF COMMUNICATIONS

A Procedure for Preparing 4-Cyanofluoren-9-one

A. P. Stankevičius, L. N. Janušiene, P. B. Terent'ev, and M. S. Saprogoniene

Institute of Cardiology, Kaunas Medical University, Kaunas, Lithuania
Lomonosov Moscow State University, Moscow, Russia

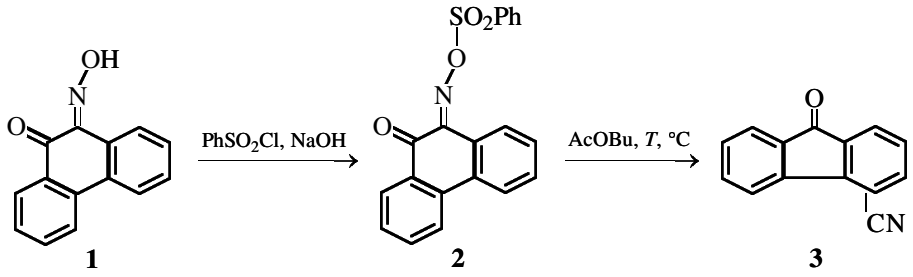
Received June 19, 2006

Abstract—A procedure was developed for preparing 4-cyanofluoren-9-one by intramolecular cyclization of 9,10-phenanthrenequinone monooxime benzenesulfonate.

DOI: 10.1134/S1070427206080362

Fluorenones, mainly 2- and 4-substituted, are widely used in electrophotography [1] and as drugs [2]. In particular, Grintsev et al. studied a series of fluorenones [3] and synthesized a novel antiviral agent, Florenal [4]. It is widely used in medical practice against herpesis and adenoviruses. However, the lack of facile routes to 4-substituted fluorenones hinders the development of this novel group of antiviral agents.

Fluorenones are usually prepared from 2-arylbenzoic acids by the Friedel–Crafts reaction or its modifications [1]. Even 2'-cyanodiphenyl-2-carboxylic acid in thionyl chloride forms, along with the corresponding acid chloride, also 4-cyanofluoren-9-one [2]. Experiments on the Beckmann rearrangement of the second kind of 9,10-phenanthrenequinone monooxime **1** have shown that suspensions of this compound in ether under the action of PCl_5 give 4-cyanofluoren-9-one **3** in a low yield [3]. Proceeding with studies of *o*-quinone monooxime sulfonates, we found that 9,10-phenanthrenequinone monooxime benzenesulfonate **2**, when melted (~215°C) or crystallized from ethyl acetate, forms traces of a new substance with mp 238–240°C (dec.), whose mass spectrum was consistent with the structure of 4-cyanofluoren-9-one. Prolonged refluxing of **2** in ethyl acetate or (which is better) in butyl acetate always gives fluorenone **3** in a good yield:



1 **2** **3**

An attempt to perform the reaction with 9,10-phenanthrenequinone monooxime propionate or benzoate resulted in the recyclization.

EXPERIMENTAL

The purity of the compounds was checked by TLC on Silufol UV-254 plates, solvent system tetrachloromethane–ethyl acetate, 3 : 1; the spots were developed with iodine vapor. The mass spectra were recorded on MAT-1303 and MAT-212 devices (Varian-MAT) at ionizing electron energies of 50 and 70 eV, respectively, with direct sample input. The elemental composition of the major ions was determined with an MAE-212 device at high resolution ($M/\Delta M$ = 10000).

9,10-Phenanthrenequinone monooxime 1 was prepared by the procedure described in [4]; mp 157°C. Mass spectrum, *m/z* (*I*, %): 223 (96), 207 (20), 206

(100), 179 (11), 178 (34), 177 (15), 166 (7), 165 (40), 164 (149), 163 (20), 151 (18).

9,10-Phenanthrenequinone monooxime benzenesulfonate 2. To a solution of 22.3 g (0.1 mol) of **1** and 17.66 g (0.1 mol) of benzenesulfonyl chloride in 50 ml of acetone was added, with cooling to 0–5°C, a solution of 4.8 g (0.12 mol) of NaOH in 50 ml of water. The mixture was stirred for 10 min and then diluted with 50 ml of cold water. The precipitate was separated by vacuum filtration, washed with ice-cold water, and dried at room temperature. Yield 21 g (78%); yellow-orange compound, mp 140–141°C (from methyl ethyl ketone); R_f = 0.58.

Found (%): C 66.27, H 3.41, N 3.92, S 8.54.
$C_{20}H_{13}NO_4S$.
Calculated (%): C 66.11, H 3.58, N 3.85, S 8.81.

Mass spectrum, *m*/*z* (*I*, %): 363 (6) M, 299 (4) (M – SO_2), 222 (7) (M – $PhSO_2$), 206 (100) (M – $PhSO_3$), 179 (11) (M – $PhSO_3$ – HCN), 178 (24) (M – $PhSO_3$ – CO), 177 (21), 163 (6), 151 (20), 141 (9), 77 (43).

9,10-Phenanthrenequinone monooxime propionate was prepared similarly to **2** from 4.46 g (0.02 mol) of **1** in 40 ml of acetone, 2.8 g (0.03 mol) of propionyl chloride, and 1.6 g (0.04 mol) of NaOH in 10 ml of water. Yield 4.45 g (80%), mp 109.5–110°C (acetonitrile), R_f = 0.46.

Found (%): C 73.40, H 4.65, N 4.86.
$C_{17}H_{13}NO_3$.
Calculated (%): C 73.11, H 4.69, N 5.02.

9,10-Phenanthrenequinone monooxime benzoate was prepared similarly to **2** from **1** and benzoyl chloride; yield 60%, mp 172–174°C (butanone), R_f = 0.70.

Found (%): N 4.32.
$C_{21}H_{13}NO_3$.
Calculated (%): N 4.28.

4-Cyanofluoren-9-one 3. A mixture of 3.63 g (0.01 mol) of **2** and 30 ml of anhydrous butyl acetate was refluxed on an oil bath at 100°C for 6 h until sulfonate **2** was completely consumed (chromatographic monitoring). The solvent was distilled off by half, the mixture was cooled, and the precipitate was separated by vacuum filtration and crystallized from benzene. Yield 1.23 g (60%), mp 238–240°C (published data: mp 240°C [1]), R_f = 0.43. Mass spectrum, *m*/*z* (*I*, %): 205 (100) M, 177 (57) (M – CO), 176 (8), 175 (5), 150 (17) (M – CO – HCN), 149 (5), 127 (4), 124 (3), 89 (10), 75 (16), 74 (9).

REFERENCES

1. Borsche, W. and Sander, W., *Ber.*, 1914, vol. 47, pp. 2815–2826.
2. Rapoport, H. and Williams, A.R., *J. Am. Chem. Soc.*, 1949, vol. 71, pp. 1774–1778.
3. Fuson, R., *Reactions of Organic Compounds: A Textbook for the Advanced Student*, New York: Wiley, 1962.
4. Terent'ev, P.B. and Stankiavicius, A.P., *Khim. Geterotsikl. Soedin.*, 1988, pp. 1518–1521.

ISSN 1070-4272, Russian Journal of Applied Chemistry, 2006, Vol. 79, No. 8, pp. 1386–1387. © Pleiades Publishing, Inc., 2006.
Original Russian Text © N.V. Maidanova, D.A. Rozental', 2006, published in Zhurnal Prikladnoi Khimii, 2006, Vol. 79, No. 8, pp. 1399–1400.

BRIEF COMMUNICATIONS

Asphalt Adsorption in Relation to the Surface Area of the Mineral Filler and Content of Aromatic Oils

N. V. Maidanova and D. A. Rozental'

St. Petersburg State Technological Institute (Technical University), St. Petersburg, Russia

Received April 24, 2006

Abstract—The composition and properties of asphalts were examined in relation to the time of keeping at 160°C of asphalt–granite and asphalt–gabbro-diorite blends. The time of filling of the filler surface with the adsorbed asphalt components was established. A criterion was suggested for estimating the properties of asphalt during preparation and pouring of asphalt concrete.

DOI: 10.1134/S1070427206080374

We have shown previously [1, 2] that oil asphalts are instable dispersion systems whose properties are modified by both storage and contact with mineral fillers. The reason is that the overall process of asphalt oxidation consists in that molecules of oils, which cannot form a solid phase under the oxidation conditions, are used to produce molecules of asphaltenes, which can form solid particles via association. The rate of formation of the asphaltene molecules significantly exceeds that of their association into supramolecular structures. As a result, the products yielded in arbitrarily terminated asphalt oxidation contain a certain amount of unassociated asphaltene molecules that tend to form a solid phase. This process also occurs at low temperatures, though at a lower rate, which modifies the asphalt structure. Hence, after storage for a certain period even at room temperature, the commercial characteristics of asphalt correspond to those of a more rigid brand.

When asphalt comes in contact with mineral fillers, especially at elevated temperatures, its liquid components are selectively adsorbed on the surface of the mineral material. This leads to a decrease in the amount of the dispersion medium in the nonadsorbed asphalt, thereby increasing its rigidity. The commercial characteristics of asphalts vary with the amount of their components adsorbed. Determination of the amount of the adsorbed asphalt is a labor-consuming and arbitrary process; it is more convenient to monitor its outcome from the change in such commercial characteristics of asphalts as penetration P_{25} and softening point T_s.

Evidently, adsorption is limited by two factors, the surface area and activity of the adsorbent and the amount of the asphalt components that can be adsorbed by this material (sorbent). The sorption capacities of granite (G) and gabbro-diorite (GD) (typical fillers for asphalt concrete) were examined in experiments with an 80 : 20 (wt %) blend of these fillers (2–3-mm granules) with BDUS 70/100 asphalt (after 6-month storage in a hermetically sealed flask, the penetration P_{25} was 41 dmm, and the softening point T_s, 60°C). Such an excess of asphalt should afford the necessary amount of sorbable components. Table 1 summarizes the results of our experiments.

Our results suggest that the adsorption equilibrium was established after a 2-h keeping. In this case, the limiting factor was the surface area of the ma-

Table 1. Modification of the properties of BDUS 70/100 asphalt brought in contact with granite and gabbro-diorite at 160°C

Keeping time, h	Granite		Gabbro-diorite	
	T_s, °C	P_{25}, dmm	T_s, °C	P_{25}, dmm
0	60	41	60	41
1	61	33	63	34
2	62	32	63	32
3	62	32	64	31
4	62	32	64	31
5	62	31	64	31

Table 2. Properties of asphalts at different times of keeping at 160°C

Filler	Keeping time, h											
	0		1		2		3		4		5	
	T_s, °C	P_{25}, dmm	T_s, °C	P_{25}, dmm	T_s, °C	P_{25}, dmm	T_s, °C	P_{25}, dmm	T_s, °C	P_{25}, dmm	T_s, °C	P_{25}, dmm
BDUS 70/100												
Granite	60	41	61	33	62	32	62	32	62	32	62	31
Gabbro-diorite	60	41	63	34	63	32	64	31	64	31	64	31
BDU 70/100												
Granite	56	55	58	42	59	39	60	38	60	37	60	37
Gabbro-diorite	56	55	58	42	59	41	59	40	60	40	61	39
Yaroslavl BND 60/90												
Granite	60	44	62	36	63	34	64	33	64	34	64	34
Gabbro-diorite	60	44	62	36	63	35	63	34	63	34	63	34
Ryazan BND 60/90												
Granite	52	62	54	50	56	48	56	46	56	43	56	41
Gabbro-diorite	52	62	53	48	56	47	56	45	56	42	56	41

Table 3. Component composition, wt %, of BDUS 70/100 asphalt, determined on an IATROSCAN MK-5 analyzer

Component group	Initial BDUS	Granite		Gabbro-diorite		Component group	Initial BDUS	Granite		Gabbro-diorite	
		2 h	5 h	2 h	5 h			2 h	5 h	2 h	5 h
Saturated	6.5	7.0	6.8	6.7	6.5	Resins	28.3	35.5	34.5	33.8	34.3
Aromatic	50.1	43.2	43.2	43.1	44.2	Asphaltenes	15.1	14.3	15.5	16.4	15.0

terials examined. To validate this conclusion, granite was transferred onto a screen after a 2-h keeping and, after excess asphalt completely drained off at 160°C, was once again placed in the reaction vessel, and a fresh portion of asphalt was added.

The asphalt isolated after a repeated 2-h keeping had the same quality characteristics as those before pouring into the reaction vessel.

Similar data were obtained for other asphalts (Table 2). Tables 1 and 2 show that the quality characteristics of asphalts were modified most profoundly after 2-h keeping at 160°C. To identify the asphalt components responsible for a such modification, the component composition of the initial asphalt was analyzed, as well as that of the asphalt after keeping for 2 and 5 h at 160°C with fillers. The results are summarized in Table 3. It is seen that the only component whose amount decreases is that constituted by aromatic oils. Hence, specifically this component is responsible for the adhesion between the asphalt and mineral materials.

CONCLUSIONS

(1) There exists an adsorption limit for asphalt–mineral filler system, which is determined by the specific surface area of the filler.

(2) Aromatic oils are the asphalt component responsible for its adsorption on mineral fillers.

(3) The change in the commercial characteristics of asphalt brought in contact with the mineral filler at elevated temperatures can be regarded as a criterion of modification of the properties of asphalt during preparation and pouring of asphalt concretes.

REFERENCES

1. Levchenko, E.S., Rozental', D.A., and Zalishchevskii, G.D., *Zh. Prikl. Khim.*, 2004, vol. 77, no. 3, pp. 521–522.
2. Levchenko, E.S., Influence of Mineral Fillers on the Properties and Composition of Asphalt, *Cand. Sci. Dissertation*, St. Petersburg, 2005.

ISSN 1070-4272, Russian Journal of Applied Chemistry, 2006, Vol. 79, No. 8, p. 1388. © Pleiades Publishing, Inc., 2006.
Original Russian Text © Editorial board, 2006, published in Zhurnal Prikladnoi Khimii, 2006, Vol. 79, No. 8, p. 1401.

ANNIVERSARIES

Professor Dmitrii Aleksandrovich Rozental' (To His 80th Birthday)

DOI: 10.1134/S1070427206080386

Dmitrii Aleksandrovich Rozental' was born on August 9, 1926, in Novosibirsk into the family of office workers. In 1933, Rozental's father was transferred to work in Leningrad as a senior hydrographer at Glavsevmorput' (Central Administration of the Northern Sea Route). The family moved to Leningrad. Rozental's mother became a senior comptroller at Lenkombank (Leningrad Commercial Bank).

Rozental's father was subjected to repressions in 1937 and died in 1941. He was rehabilitated in 1958.

In 1941, Dmitrii Aleksandrovich finished the seventh grade of secondary school. In April 1942, he was evacuated, together with his mother, to Tatarstan. In November 1943 he was enlisted in the Soviet army and served in air defense of the Far-Eastern front. In 1949, he finished tenth grade at the regional extramural secondary school in Ussuriisk.

After demobilization of 1950–1951, Dmitrii Aleksandrovich worked as collector at Leningrad Geological Prospecting Institute. Rozental' entered Lensovet Technological Institute in Leningrad in 1951, successfully graduated from the institute in 1956, and was recommended for postgraduate education. In 1960, he defended his candidate dissertation (technical sciences). He defended his doctoral dissertation in 1972 and became a professor in 1975. Dmitrii Aleksandrovich combines his pedagogical activities with research work. Rozental' has been given the rank of Honorary petrochemist of the USSR, he is a leading scientist in the field of structure and properties of heavy oil residues.

He has the badge of a resident of the besieged Leningrad.

During the forty-five years of his scientific activities, he has introduced new fundamental concepts concerning the oxidation and aging of bitumens, formation of asphaltenes, and their molecular and supramolecular structure. He elucidated the role of the adsorption factor in manufacture of asphalt concrete. Rozental' is the author of numerous formulations and technological procedures for production of polymer–bitumen formulations with a wide application area.



The results of Rozental's pedagogical and research activities are reflected in 280 publications and 34 inventor's certificates and patents. Thirty-two postgraduate students and applicants have defended their candidate dissertations under his supervision, he was a scientific consultant of an applicant who successfully defended his doctoral dissertation. Professor Rozental' has been cooperating with the editorial office of *Zhurnal Prikladnoi Khimii* (*Russian Journal of Applied Chemistry*) and has been refereeing and publishing articles devoted to bitumens and chemistry of high-molecular-weight compounds.

Rozental' was deputy head of the chair of technology of petrochemical and coal-chemical industries diring 20 years and headed the chair in 1990–1991.

Professor Rozental' has been decorated with government awards for his services as a soldier and pedagogue.

Dmitrii Aleksandrovich is a very well-wishing and responsive person, true friend, and patriot. Numerous generations of students, post-graduates, teachers, and research workers are thankful to him for help and support.

Staff members of the chair of technology of petrochemical and coal-chemical industries, St. Petersburg State Technological Institute

Editorial board staff members of the Editorial office of Zhurnal Prikladnoi Khimii

ISSN 1070-4272, Russian Journal of Applied Chemistry, 2006, Vol. 79, No. 8, pp. 1389–1390. © Pleiades Publishing, Inc., 2006.
Original Russian Text © A.G. Morachevskii, 2006, published in Zhurnal Prikladnoi Khimii, 2006, Vol. 79, No. 8, pp. 1402–1403.

BOOK REVIEWS

B. V. L'vov, *Termorazlozhenie tverdykh i zhidkih veshchestv* (Thermal Decomposition of Solid and Liquid Substances),

St. Petersburg: Politekhn. Univ., 2006, 278 pp.

DOI: 10.1134/S1070427206080398

Thermal decomposition of solid and liquid substances is a process that underlies most of natural phenomena and industrial technologies. Active studies of decomposition processes and attempts to explain their mechanism and kinetics were commenced in the second half of the XIX century and were continued in the subsequent years. The certain success achieved in understanding of thermal decomposition phenomena is associated with works of J. Van't-Hoff (1852–1911), S. Arrhenius (1859–1927), H. Hertz (1857–1894), I. Langmuir (1881–1957), and other prominent chemists and physicists.

The interesting monograph brought to readers' notice, written by B.V. L'vov (Polytechnic University, St. Petersburg), a known specialist in atomic-absorption spectroscopy, presents the results of many years' studies of the mechanism and kinetics of thermal decomposition of solid and liquid substances belonging to a wide variety of classes of compounds (crystal hydrates, oxides, hydroxides, nitrides, azides, nitrates, carbonates, sulfates). In the framework of the original approach based on a thermochemical analysis of the processes under study, developed by the author of the monograph, reliable kinetic characteristics have been obtained and the mechanism of reactions of thermal decomposition of the substances studied have been interpreted.

The book comprises a preface, list of abbreviations, introduction, fifteen chapters grouped into three parts, conclusion, and supplement. Bibliographic lists are given at the end of each chapter. The monograph has a subject index. The brief preface (pp. 7 and 8) notes that the monograph presents a new approach to the mechanism of decomposition reactions, their kinetics, and methodology of their examination. The approach is based on a thermochemical analysis of the process. This approach has been formed during the last 25 years on the basis of author's studies, with methods of electrothermal atomic-absorption spectroscopy, mass spectrometry, and thermal analysis. The results of L'vov's studies have been for the most part published in foreign journals (principally in Thermochimica Acta). Generalization and analysis of these studies within a single monograph should be considered rather useful and timely. The list of the accepted designations and abbreviations, given (pp. 9–11) after the preface, facilitates the reading of the monograph.

The introduction (pp. 12–22) specifies the main areas of industrial application of the results obtained in studies of the mechanism and kinetics of thermal decomposition of solid and liquid substances, describes the historical aspect of the development of research in this field, and briefly describes the purpose of the monograph and objectives of each of its parts.

The first part of the book (pp. 23–79) comprises three chapters describing the starting physicochemical concepts: mechanism, kinetics, and methodology, which are used in further presentation to interpret the specific features and fundamental aspects of the processes studied. The author proceeds from the concept that the decomposition of substances occurs in all cases by the common mechanism described by the scheme of congruent dissociative evaporation, which, in the case of formation of hardly volatile substances, includes an additional stage of their condensation. In addition to this fundamental concept, two assumptions are made. According to the first of these, primary decomposition products may differ from their equilibrium forms. According to the second assumption, the energy released in condensation of a hardly volatile product in the reaction zone, partly reduces the enthalpy of the full decomposition reaction. When discussing the kinetics of decomposition processes, the author gives preference to the approaches of Hertz, Knudsen, and Langmuir, compared with the most widely used Arrhenius equation and later dependences based on the theory of the transition state. L'vov convincingly demonstrated that Langmuir's evaporation equations open up far better opportunities for describing thermal decomposition processes, compared with other approaches. Comparison of three different methods that can be used to determine the enthalpy of the heterogeneous decomposi-

tion process (method of Arrhenius plots, method of the second law, and method of the third law) in accordance with the results of L'vov's studies shows that the method based on the third law of thermodynamics is beyond competition in every respect. It manyfold exceeds the other two methods in accuracy, adequacy of results, and productivity of measurements. These conclusions are in complete agreement with the opinion commonly accepted in data processing in equilibrium thermochemistry. The author analyzes the possible reasons why the third-law method has not found wide acceptance in studies of the kinetics of decomposition processes until very recently.

The second part of the book (pp. 80–161), which comprises nine chapters (from 4th to 12th), is devoted to interpretation and quantitative analysis of the effects, phenomena, and fundamental aspects of processes of thermal decomposition of various classes of substances. The author, in particular, discusses the relationship between the decomposition temperature and molar enthalpy of the process, the effect of various factors on the molar enthalpy, specific features of decomposition of carbonates in the presence of CO_2, and decomposition of crystal hydrates in the presence of H_2O vapor. Particular attention is given to the effect of self-cooling in endothermic reactions of thermal decomposition, to anomalous changes in the rate of dehydration of crystal hydrates upon an increase in the water vapor pressure (Topley–Smith effect), and to the effect of vapor condensation on the enthalpy. Of considerable interest are data on the influence exerted by the crystal structure of a substance on the composition of primary decomposition products and interpretation of the low values of the evaporation coefficients for quite a number of substances.

The third part of the monograph (pp. 162–254, chapters 13–15) describes apparatus for thermogravimetric measurements and the procedures involved and reviews the results obtained in studies of evaporation and thermal decomposition of a large group of widely diverse substances. Of importance is the section that discusses methods for evaluation of the absolute decomposition rate in relation to the type of the substance studied: crystals, powders, melts.

The final part of the monograph (pp. 254–258) makes certain general conclusions. Among the most important results directly associated with the concept of congruent dissociative evaporation, being developed by the author, the following can be mentioned: the fact that hardly volatile products appear in the gas phase at the instant of decomposition was established by mass spectrometry, the shape of kinetic curves was identified, and the mechanism of nucleation via formation of a hardly volatile product over the reagent surface was substantiated. The author gives a simple physical interpretation of the parameters of the Arrhenius equation for the evaporation process and revealed the relationship between the rate constant and the absolute evaporation rate.

It should be noted once again that the same thermal decomposition mechanism for different substances, Hertz–Langmuir evaporation model, and method based on the third law of thermodynamics underlie the approach developed by the author. The larger part of the whole body of experimental data has been obtained using the above-mentioned atomic absorption spectroscopy, mass spectrometry, and thermal analysis. L'vov's monograph is very well written, all the concepts put forward by the author are logically substantiated and experimentally confirmed. The author mentions as the most controversial issues the mechanism of energy transfer in condensation of a hardly volatile product to the reagent and the influence exerted by the crystal structure of the reagent on the composition of gaseous decomposition products.

The book is well published, includes 114 rather informative tables, and 43 figures. The total number of references for all the chapters is 474.

L'vov's monograph is of interest for a wide audience of specialists, and for researchers working in the field of physical chemistry, geochemistry, inorganic materials science, and metallurgy in the first place. The simplicity and clearness of presentation make it possible to recommend the book to postgraduates and senior students of the corresponding specialties.

A. G. Morachevskii

ISSN 1070-4272, Russian Journal of Applied Chemistry, 2006, Vol. 79, No. 8, pp. 1391–1392. © Pleiades Publishing, Inc., 2006.
Original Russian Text © A.G. Morachevskii, 2006, published in Zhurnal Prikladnoi Khimii, 2006, Vol. 79, No. 8, pp. 1403–1404.

BOOK REVIEWS

P. I. Chernousov, V. M. Mapel'man, and O. V. Golubev, *Metallurgiya zheleza v istorii tsivilizatsii: Uchebnoe posobie* (Metallurgy of Iron in the History of Civilization: Textbook), Moscow: Mosk. Inst. Stali Splavov, 2006, 350 pp.

DOI: 10.1134/S1070427206080404

The history of humankind is intimately associated with the development of manufacture of metals. Already in ancient times, people mastered extraction and processing of, first, native metals and then copper, its alloys, and iron. Metals and their alloys form foundation of the modern civilization and their consumption will continue to increase in the foreseeable future. A particular place, in occurrence and manufacture scale, among metals is occupied by iron, with which both the development of the material culture and the progress in all areas of public manufacture are closely connected. The textbook written by P.I. Chernousov and co-authors and published by Moscow Institute of Steel and Alloys summarizes evidence concerning the development of the metallurgy of iron, beginning from the ancient times and till the end of the medieval era (end of the XVI century).

The book comprises a preface, eight chapters, bibliographic list, and three supplements. In a very brief preface (p. 6), the authors emphasize the importance for future metallurgists of a historical study of their specialty in a relationship with the history of the society. The first chapter (pp. 7–62) is devoted to the origin of metallurgical industries and includes sections about use of metals in different periods of development of the civilization, use of the most widely occurring minerals in manufacture of metals, and gradual mastering of production of new metals and materials. To metals known from the ancient times belong gold, meteoritic iron, silver, lead, mercury, copper, tin, and some alloys (bronze, brass).

The second chapter (pp. 63–114) contains the available archeological evidence concerning the development of metallurgy in various civilizations of the Ancient World: Celts, Hetts, Etruscans, and discusses specific features of the development of metallurgy in Egypt, Assyria, Roman Empire, Ancient China, and Ancient India. The third chapter (pp. 115–146) describes the technologies used in the early stages of development of metallurgy (crucible melting, hearth melting, and simplest techniques for metal processing). Particular attention is given in the chapter to manufacture of metallic coins in various countries. The very brief fourth chapter (pp. 147–153) discusses the ancient metallurgical terminology. The fifth chapter (pp. 154–186) considers the advances in metallurgy in the Middle Age, depending on the type of iron ore deposits in different regions. The same chapter gives a detailed description of the use of metals for manufacture of various kinds of armor, armaments, and other articles of this kind.

The sixth chapter (pp. 187–211) is devoted to the development of high-quality metallurgy in the Middle Ages (VI–XVI centuries). The appearance of processes for corrosion protection of steel and for manufacture of high-quality armament steel (Damascus steel, forging and hardening of steel) is considered. In the seventh chapter (pp. 212–275), the authors describe the development of firearms and of the related cannon-casting industries (at the turn of the XV century).

The eighth chapter (pp. 276–290) contains evidence concerning the activities of known scientists of the Middle Age: Italian chemist and metallurgist V. Biringuccio (1480–1539) and German metallurgist and mineralogist G. Agricola (1494–1555). The former is the author of a classical work *The Pirotechnia* in ten books (1540), which contains a vast body of metallurgical and chemical evidence. In particular, methods for recovery of gold and silver, amalgamation technique, and method for synthesis of nitric acid are described. Agricola generalized in his treatise *De Re Metallica Libri XII* (Twelve Books on Metals, published posthumously in 1556) the many centuries' experience of recovery of metals from ores, developed foundations of processing of copper, lead, and silver ores, described preparation of a number of salts and technology of manufacture of glass, and described the fundamentals of assaying.

The bibliographic list (p. 291) includes references to 18 recent publications (1985–2005) of mostly popular-science type.

The supplements (pp. 292–349) include laboratory manuals, control questions, and a metallurgical crossword. The book is well published and equipped with clear illustrations and schemes. The use of studying the history of science and technology at technical higher-school institutions is beyond any doubt. As noted by the authors in the preface, the textbook under discussion is based on the course of lectures "The History of the Metallurgy of Iron," which has been delivered at Moscow Institute of Steel and Alloys since 1993. The textbook describes a huge period in the history of humankind, from the Stone Age till the late medieval era. Probably, it would be desirable that the introductory chapter for the textbook of this kind should be written by a specialist in the history of material culture of that time or archaeology. Reading the textbook under discussion creates an impression that is primarily based on popular-science publications.

The book by Chernousov, V.M. Mepel'man, and O.V. Golubev is approved by the educational-methodological association on education in metallurgy as a textbook for students of higher-school institutions training bachelors and licensed engineers specialized in metallurgy and physical materials science. As regards the manner of presentation, the book is well understandable for pupils of senior grades and students of technical schools.

A. G. Morachevskii

ISSN 1070-4272, Russian Journal of Applied Chemistry, 2006, Vol. 79, No. 9, pp. 1393–1402. © Pleiades Publishing, Inc., 2006.
Original Russian Text © V.N. Salimgareeva, S.V. Kolesov, 2006, published in Zhurnal Prikladnoi Khimii, 2006, Vol. 79, No. 9, pp. 1409–1418.

REVIEWS

Principles of Radiation Protection of Poly(Methyl Methacrylate)

V. N. Salimgareeva and S. V. Kolesov

Institute of Organic Chemistry, Ufa Scientific Center, Russian Academy of Sciences, Ufa, Bashkortostan, Russia

Received July 15, 2005

Abstract—Mechanisms of radiation aging of poly(methyl methacrylate) and methods for enhancing its resistance to high-energy radiation are considered.

DOI: 10.1134/S1070427206090011

Poly(methyl methacrylate) (PMMA) is one of the most important materials in production of structural-decorative elements in building, of machines and devices, of items for medicine, of consumer's goods, and also as structural material in nuclear and space engineering where it is exposed to ionizing radiation. Poly(methyl methacrylate) is also exposed to radiation in the course of radiation sterilization of medical equipment, which is a widely used procedure.

High-energy radiation induces changes in physical, physicomechanical, and chemical properties of polymeric materials, resulting in deterioration of their service characteristics [1, 2]. The radiation resisance of PMMA items requires enhancement. This goal can be accomplished by introducing special protecting additives (antirads) preventing the development of undesirable radiation-chemical reactions and this preventing or considerably reducing changes in the structure and properties of the polymer upon irradiation.

As radiation protectors are used aromatic hydrocarbons and aromatic amines, urea and thiourea derivatives, alkyl mercaptans, and organophosphorus and sulfur-containing heterocyclic compounds [1–5]. The range of compounds used for radiation protection of PMMA steadily expands; various methods are used for their introduction into polymeric items or incorporation into macromolecules [6–9]. Development of new approaches to the radiation stabilization of PMMA remains an urgent problem.

This review summarizes and correlates published data on the search for high-performance radiation-chemical inhibitors of PMMA aging and on the development of scientific principles of their choice and introduction into the polymer.

RADIATION AGING OF PMMA

Irradiation of a substance results in generation of free electrons, cations, and excited molecules. Transformations of these intermediates yield the second generation of active intermediate species (excited molecules, cations and anions, free radicals, radical ions) according to the scheme [4]

$$AB \rightarrow AB^+ + e,\ AB \rightarrow AB^*,\ AB^+ + e \rightarrow AB^*,$$

$$AB + e \rightarrow AB^-,\ AB^* \rightarrow A^\bullet + B^\bullet,\ AB^* \rightarrow AB^+ + e,$$

where the asterisk denotes electronically excited state.

Free-radical reactions make the major contribution to radiation-chemical transformations of polymers. The generation of primary radicals and subsequent radical chain processes are responsible [10] for the chemical cross-linking and degradation of macromolecules under γ-irradiation.

Irradiation of PMMA causes random cleavage of the backbone; the number of breaks is proportional to the radiation dose [1]. The contribution of depolymerization to the radiation-induced degradation is very small compared to pyrolysis involving the depolymerization by the radical-chain mechanism. The monomer, methyl methacrylate (MMA), is not released until the polymer is heated to 398 K and higher temperatures [11]. Simultaneous action of heat and radiation (irradiation with an electron beam at 498–598 K) causes thermal and radiation degradation. The gaseous products released in the process mainly consist of MMA [12]. The activation energy of the thermal degradation of PMMA decreases from E = 140 without irradiation to E = 5 kJ g^{-1} under irradiation [12].

The mechanism of radiation aging of PMMA was studied at low temperatures (≤100 K) with the aim to elucidate the primary events in the interaction of the radiation with the substance [10, 13, 14]. At these temperatures, the effect of secondary processes associated with the migration and diffusion of the primary active species is reduced to a minimum. At 77 K, low-molecular-weight radicals $\dot{C}HO$, $\dot{C}H_3$, and $\dot{C}OOCH_3$

are formed; they are indicative of the elimination and decomposition of the ester group and elimination of the methyl group. Macroradicals such as ~CH_2–$\dot{C}(COOCH_3)$–CH_2~ or ~CH_2–$C(CH_3)$–$(COO\dot{C}H_2)$~ [10] are also formed. Terminal radicals ~CH_2–$\dot{C}\cdot(COOCH_3)(CH_3)$ were not detected at low temperatures. They are formed either upon irradiation at temperatures above 250–270 K or on heating γ-irradiated PMMA samples [10]. The terminal macroradicals are stable at room temperatures and start to decay only at T ~350 K along the disproportionation pathway [15].

The mechanism of aging at $T \geq 273$ K is discussed in [16–26]. It is believed [18] that the radiation degradation of PMMA occurs in two steps one of which is fast,

$$M^*_{n+m} \rightarrow M_n + M_m, \quad (1)$$

and the other is slow:

$$M^{\bullet}_{n+m} \rightarrow M_n + M^{\bullet}_m, \quad (2)$$

where M^*_{n+m} is an excited or ionized polymer molecule, and $M^{\bullet}_{n+m}$, polymer radical arising from elimination of a pendant group from the polymer molecule.

In irradiation in air, reaction (2) is suppressed because of the reaction of the primarily formed radical $M^{\bullet}_{n+m}$ with O_2 molecules [18].

It is known that the structure and properties of irradiated polymers largely depend on the kind of the radiation. The radiation yield of degradation (G_S) of the polymer chain, defined as the number of breaks in the polymer chain per 100 eV of absorbed energy, is independent of the dose rate (varied in the range 2.2–18.0 kGy h^{-1}) but depends on the absorbed dose and kind of the radiation. In γ-irradiation of PMMA in a vacuum, G_S is 1.93 at room temperature and 1.63 at 333 K; in neutron irradiation, G_S is 1.09 both at room temperature and at 333 K [18, 27]. The degradation of PMMA under α-irradiation is less intense than under γ-irradiation. The ratio G_α/G_γ of the radiation yields of PMMA degradation and of free radicals under α- and γ-irradiation is 0.067 and 0.55, respectively [28].

When PMMA is irradiated at temperatures below 273 K to doses of up to 30 kGy, the radiation yield of the degradation is independent of temperature and equal to 1.5 [29]. In the interval 293–333 K, it is temperature-independent also [27].

For G_S at 77 K, different authors give the values from 1.2 to 2.2; the most probable value is 1.9 ± 0.3 [19, 30]. The scatter of these data is caused by different times of keeping the irradiated sample after the irradiation [30]. The terminal radicals formed by cleavage of the macromolecule can recombine. The recombination rate strongly affects the polymer properties, because it determines the rate of "healing" of damaged sites in macromolecules in reactions of radicals with the environment [10]. The total yield of radicals G_R at 77 K is 4.8, whereas the yield of breaks in the backbone is 0.5–1 [10] (G_R is the number of radicals arising upon absorption of the radiation energy of 100 eV). The effective activation energy of the radical recombination is 84 kJ mol^{-1} [10]. Decomposition of atactic PMMA in the temperature interval 273–453 K is characterized by $E_a \approx 4.2$ kJ mol^{-1}. This fact suggests that the mechanism of the chain break is monomolecular [31]. In the interval 273–173 K, E_a approaches zero [32, 33].

It is known that, when PMMA is irradiated at $T \leq 270$ K, the curve of macroradical accumulation flattens out. This trend is attributed to the decay of macroradicals in the course of irradiation: At sufficiently high absorbed doses, the polymer radicals are no longer isolated and can react with each other or with hydrogen atoms, and also take up mobile electrons [4, 10, 13]. The existence of limiting concentrations is also explained by the heat release in the recombination of two radicals, leading to the decay of the neighboring radical pairs, and also by radiation-induced microheating [10].

At $T \geq 300$ K, the concentration of macroradicals grows with an increase in the irradiation dose, reaches a maximum, then slowly decreases to a certain minimum, after which it increases again [16]. The ratio of the local concentration of radicals to their average concentration, $[R]_{loc}/[R]_{av}$, in PMMA is 10–100 [16], i.e., the distribution of radicals is nonuniform [10]. It is believed [16] that at $T > 273$ K the macroradicals are accumulated as clusters in the interglobular space.

Belichenko et al. [24] believe that initially (at $0.1 < D < 0.7$ kGy) degradation of macromolecules involves break of the "weak" bonds formed by radical polymerization in the bulk, after which, at $0.7 < D < 10$ kGy, "common" bonds start to break. Upon irradiation of PMMA to a dose of 10 kGy (T = 300 K), new bands appear in the spectrum at 325–330 and 420 nm, and the polymer becomes less transparent [25]. Taraban et al. [26] attributed these changes to the appearance of terminal alkyl (λ_{max} = 410–412 nm) and allyl (λ_{max} = 425 nm) macroradicals. The ESR spectra recorded immediately after the irradiation in a vacuum at room temperature are determined by the terminal alkyl macroradicals. After postradiation storage for

200–300 h, the signals of macroradicals of the allyl and polyenyl types become prevalent in the ESR spectra, i.e., the radicals undergo mutual transformations [26]. The appearance of allyl macroradicals in PMMA irradiated at $T \geq 253$ K is attributed to the decay of terminal radicals [16]. The PMMA degradation leading to a decrease in the molecular weight (MW) of the polymer is also associated with terminal radicals [16, 26].

Schnabel and Sotobayashi [19] showed that the initially broad molecular-weight (MWD) distribution of PMMA becomes narrower upon γ-irradiation at 293 K, and vice versa. In all the cases, the ratio $b = \overline{M}_w/\overline{M}_n$ (where $\overline{M}_w$ and $\overline{M}_n$ are the weight-average and number-average molecular weights, respectively) tends to a limit $b = 2$, which is attained at doses of about 100 kGy and corresponds to random MWD [18]. In the dose range 100–300 kGy, $G_S = 1.75$ [19]. Comparison of the amount of paramagnetic centers and number of radiation damage sites (final numbers of breaks determined from a decrease in the MW of the polymer upon irradiation) shows that radicals generated by the irradiation initiate the degradation [16]. Initiation of the degradation is enhanced with a decrease in the concentration of terminal radicals.

The radiation resistance of PMMA is determined by its morphology and supramolecular structure. It is known that the degradation of PMMA in the crystalline phase is less intense than in the amorphous phase [34]. γ-Irradiation of partially crystalline isotactic PMMA in air at 303 K leads to a decrease in the crystallinity with increasing dose (0.7–2.90 MGy) [23].

The isotactic polymer is more sensitive to irradiation than the syndiotactic polymer [35]. Changes in the chemical structure of polymeric molecules cause changes in the supramolecular structure of the polymer. Upon high-temperature (293, 353, 383 K) γ-irradiation of PMMA, the content of isotactic triads (mm) in the isotactic polymer decreases (from 0.98 in the nonirradiated polymer to 0.55 in the polymer irradiated to a dose of 500 Gy), and the content of syndiotactic (rr) and heterotactic (mr) triads increases (from 0 to 0.23 and from 0.02 to 0.22, respectively). The transformation of the isotactic polymer into the syndiotactic and atactic polymer in the crystalline state prevails over the chain break [34]. With an increase in the temperature, changes in the polymer tacticity become more pronounced [36]. The radiation-chemical yield of the chain break G_S in isotactic PMMA irradiated at 353 and 303 K is 18.6 [37] and ~15 events/100 eV [23], respectively.

In the course of the degradation, the macromolecule is broken into smaller fragments. As a result, the MW of the polymer decreases, its solubility increases, and the flow point decreases [2, 34, 38, 39]. Upon irradiation, the strength, transparency [1, 2], refractive index, and density of PMMA decrease (the density, from 1.187 to 1.185 g cm^{-3} at a dose of 100 kGy), and the dielectric permittivity passes through a maximum at a dose of 10 kGy [22]. The creep [40], mechanical loss tangent, dynamic elastic modulus, and low-frequency speed of sound [41] change. The dielectric loss tangent decreases to 10% upon irradiation in air to a dose of 500 kGy [42]. Changes in the refractive index, density, and dielectric constant upon X-ray irradiation are linear in the dose range 15–120 kGy at various temperatures [43].

The degradation of PMMA macromolecules deteriorating the physicomechanical properties of the polymer can be prevented or considerably reduced by introducing special additives, antirads, providing the radiation protection of polymeric materials.

RADIATION PROTECTION OF PMMA

Antirad additives can be subdivided into two groups with respect to the mechanism of their action. Additives of the first group ensure the energy transfer from the polymer to the additive without chemical changes in the polymer. In the process, the additive either dissipates the energy or undergoes transformations or decomposition. Antirad additives of the second groups can heal the damaged site.

If irradiation causes ionization of macromolecules, additive A can act as an electron donor or electron acceptor and participate in the charge transfer:

$$M^+ + A \xrightarrow{k_1} M + A^+,$$

whereas in the absence of an antirad the polymer molecules degrade:

$$M^+ + e \xrightarrow{k_2} M^* \rightarrow R_1^\bullet + R_2^\bullet.$$

The capability of compounds to inhibit the degradation of PMMA by this pathway is attributed in [44] to their ionization potentials: The rate constant ratio k_1/k_2 is higher for compounds with the lower ionization potential I. In the series tetramethylphenylenediamine–diphenyldiamine–*p*-nitroaniline–stilbene–naphthalene–benzophenone–benzoic acid, k_1/k_2 is 68.5, 56, 52, 46, 30, 24, and 10, and the ionization potentials

Table 1. Classes of antirads [5]

Radiolysis step	Protection mechanism	Class of antirads
Intra- and intermolecular transfer of absorbed ionizing radiation energy in the form of electronic excitation	(A) The electronic excitation energy taken up by the additive is dissipated as heat or long-wave electromagnetic radiation	Compounds containing aromatic fragments, aromatic hydrocarbons
Ionization of the molecule with formation of electron and ion, followed by recombination of geminal ions leading to excitation and dissociation of the molecule	(B) Electron is transferred to the polymeric ion without subsequent excitation (B') Electrons are accepted by the additive, and the probability of neutralization with formation of excited states decreases	Aromatic amines, diamines, polysubstituted phenols and polyphenols Nitro- and halo-substituted organic compounds, quinones, quinone imines
Bond cleavage, generation of free radicals, reactions of free radicals	(C) Transfer of hydrogen atom to the macroradical, reactions with free radicals with formation of inactive radicals and stable molecules	Aromatic amines and phenols, sulfur-containing compounds, phosphites, sterically hindered piperidine derivatives, spin traps

are 6.6, 7.25, 7.7, 7.95, 8.10, 9.45, and 9.5 eV, respectively. For PMMA, the charge transfer is energetically unfeasible, because the ionization potentials of these additives are lower than that of PMMA (I = 10.5 eV).

The arising macroradicals can be deactivated by the addition of antirads. It is known that aromatic compounds (anthracene, acridine) and quinones (benzoquinone, tetrachlorobenzoquinone) add to terminal radicals $\dot{C}H_2$–$C(CH_3)(COOCH_3)$ even at 100 K [45]. In degrading PMMA, additive A can link two terminal macroradicals and thus heal the radiation-induced damage:

$$R_n^{\bullet} + A + R_m^{\bullet} \rightarrow R_n\text{–A–}R_m.$$

Also possible are substitution reactions involving abstraction of an H atom by a polymeric radical from low-molecular-weight compounds containing labile C–H, N–H, and S–H bonds with the formation of a low-active radical:

$$AH + R_n^{\bullet} \rightarrow A^{\bullet} + R_nH.$$

In the abstraction of hydrogen atoms from phenols, amines, and mercaptans, the terminal radicals $\sim C(CH_3)(COOCH_3)\dot{C}H_2$ are more active than $\sim CH_2$–$\dot{C}(CH_3)(COOCH_3)$ [45].

The classes of antirads protecting the polymer by one or another mechanism are listed in Table 1 [5]. In addition, we should note deactivation of macroradicals in their reaction with radicals formed by radiolysis of the antirad (e.g., of sulfur-containing compounds) and restriction of the mobility of the macroradicals by cross-linking of the macromolecules. As seen from Table 1, the protection mechanism is determined by the type of compounds used as antirads.

Protection with aromatic compounds. One of the major quantities characterizing the radiation resistance of polymers and polymeric materials is the radiation-chemical yield of paramagnetic centers G_R, which is equal for PMMA at 77 K to 3.4 [46] or 4.8 [15] radicals per 100 eV. At 298 K, G_R is 2.6 [47]. Aromatic compounds introduced into PMMA decrease the yield of radicals and enhance the stability of the polymer [13]. On introducing 1 wt % pyrene, *p*-terphenyl, or benzene, the degradation (relative to pure PMMA) is 0.694, 0.694, and 0.886, respectively [48] (hereinafter, the content of antirads in PMMA is given in wt %). With *p*-terphenyl, the resistance of PMMA to γ-radiation is also enhanced: The number of breaks per macromolecule in the presence of 0.25% *p*-terphenyl decreases from 12.9 to 12.7 (at a dose of 42 kGy) [6].

Owing to their π-electron system, aromatic compounds such as anthracene, phenanthrene, benzanthracene, etc. [1] act as "energy sponges," absorbing the energy from the main substance being irradiated and dissipating this energy as heat or fluorescence. These substances provide intermolecular energy transfer and, in so doing, undergo no appreciable transformations. The majority of compounds used as luminescent additives in plastic scintillators based on this polymer [49] protect PMMA just by this mechanism. In the presence of naphthalene, *p*-terphenyl, 2,5-diphenyloxazole, 1,4-di[2-(5-phenyloxazolyl)]benzene (POPOP), or 1,1,3-trimethyl-3-phenylindan (TMPI), the concentration of radicals causing the degradation of the irradiated polymer decreases [6], and the thermomechanical properties do not change up to irradiation doses of 40 kGy (the flow point starts to decrease

at doses exceeding 40 kGy, and the glass transition point, at doses exceeding 250 kGy).

Calculations made using the data from [50] show that naphthalene introduced in an amount of 15% into the polymer in the course of its synthesis decreases from 11.5 to 4.4 the number of breaks arising in the macromolecule upon γ-irradiation to a dose of 42 kGy and limits the growth of the optical absorption and decrease in the light output [50]. The G_S of PMMA (determined from a decrease in the MW of the polymer) decreases from 0.79 to 0.35 on adding 12% naphthalene and to 0.26 on adding 10% pyrene [52].

The radioprotective effect on aging of PMMA is enhanced when additives are used in a combination. The number of breaks in PMMA containing 15% naphthalene and γ-irradiated to a dose of 42 kGy decreases to 4.2 on adding 0.2% POPOP [50]. In γ-irradiated PMMA containing 0.2% TMPI, the maximal concentration of paramagnetic centers is 1.2 times lower than in the polymer without this additive. The number of breaks per macromolecule upon irradiation to a dose of 42 kGy is 12.9 without additives and 2.2 with addition of 24% TMPI [6, 49]. On adding 0.01% POPOP to this formulation, it decreases further to 2.1; on adding 0.2% *p*-terphenyl, to 2.0; and on adding 0.01% POPOP + 0.2% *p*-terphenyl, to 1.9 [6]. Owing to a decrease in the amount of the radiolysis products in the presence of such antirads, the optical properties of PMMA upon γ-irradiation are deteriorated to a lesser extent than in their absence [49, 51].

The radiation-induced degradation of PMMA is inhibited by aromatic amines whose protective effect is attributed to the electron transfer from amines to the polymer being irradiated [53–55]. β-Naphthol and diphenyl ether also exert a protective effect. In their presence, the number of breaks decreases by a factor of 1.5–3.0 [54]. The radioprotector activity characterized by the relative protection coefficients [44] increases in the series trinitrobenzene–benzoic acid–benzophenone–naphthalene–chloranil–stilbene–*p*-nitroaniline–diphenylamine–tetramethyl-*p*-phenylenediamine.

Enhancement of the radiation resistance of a polymer by introducing aromatic compounds that are not incorporated into the macromolecule is external protection. The degradation can also be inhibited by incorporating appropriate units (aromatic rings) directly into the PMMA macromolecules, e.g., by copolymerization of MMA with styrene and α-methylstyrene (internal radiation protection).

The intramolecular protection (e.g., in copolymer of MMA with α-methylstyrene) is more efficient than intermolecular protection (in a mixture of PMMA with *n*-propylbenzene) [4]. The radiation-induced degradation of MMA–styrene copolymer (61 : 39 by moles) starts with the break of the backbone in MMA units with the generation of the free radicals ~CH_2–$\dot{C}(CH_3)(COOCH_3)$ [56]. Longer γ-irradiation results in the generation of radicals in the styrene units also, ~CH_2–$\dot{C}(C_5H_5)CH_2$~; the ratio of their concentration to that of the radicals in MMA units increases from 0 to 9. The viscosity-average molecular weight decreases during radiolysis more slowly, compared to pure PMMA, with increasing dose, and the yield of radicals in the polymer is lower [56]. In the copolymers, the excitation energy is transferred intramolecularly from MMA to styrene units. O'Donnell and Pomery [14] showed that about 50% of the excitation energy is dissipated on styrene units in styrene–MMA copolymer (51 : 49 by moles). The G_R values for the copolymer are lower than the additive value calculated for the given molar ratio of the comonomers. Whereas the yield of radicals in PMMA and polystyrene at 77 K is 0.58 ± 0.2 and 0.05 ± 0.02 per 100 eV, respectively, in the copolymer it is 0.18 per 100 eV [14]. Owing to the high radiation resistance, the 1 : 1 (by moles) styrene–MMA copolymer with additions of naphthalene (15%) and POPOP (0.2%) loses only 11% of the light output upon γ-irradiation to a dose of 40 kGy, whereas in PMMA with the same additives the loss is 25% [25].

There is no energy transfer between the polystyrene and PMMA molecules [57]. This fact, together with the incompatibility of the polymers, is apparently responsible for the lack of the protective effect of polystyrene in its blend with PMMA in γ-irradiation from a ^{60}Co source [58, 59].

In [7] we described the radioprotective properties of 1,4-phenylene-1,2-diphenylvinylene oligomer incorporated in PMMA as a comonomer. We found that the relative change in the flow point, $(T_f^0 - T_f)/T_f^0$, upon γ-irradiation to a dose of 10 kGy of the PMMA block sample containing this oligomer (1%) is 0.11, whereas for the polymer without additives this quantity is 0.19 (T_f^0 and T_f are the flow points of the nonirradiated and irradiated samples, respectively). The flow point of the irradiated polymer as a function of the stabilizer concentration passes through a maximum due to a change in the relative contributions of the inhibition and initiation of PMMA chain degradation with the oligomer and its radiolysis products [7]. At low concentrations of the stabilizer, virtually all the radicals formed by its decomposition are spent for the deactivation of the PMMA macroradicals. With an increase in the oligomer content, the increasing

amount of radicals start to participate in the degradation initiation.

Sulfur-containing compounds known as radioprotectors of biological systems also exert a protective effect on polymeric materials [3].

Protection with sulfur-containing compounds. One of specific properties of sulfur-containing compounds is the capability of bivalent sulfur atoms to protect the alkyl substituent in the molecule from the radiation impact. Sulfur exerts the protective effect not only on the adjacent atoms but also on molecules [60], including macromolecules. The protection mechanism may involve migration of the charge and/or excitation from the alkyl moiety to the sulfur atoms [13]. The possibility of the energy migration in this direction is due to the low energy of the excitation of the sulfur *d* orbitals (the sulfur atom has five vacant 3*d* orbitals which can accept more than eight electrons). The excitation of electrons to the *d* orbitals leads to the energy dissipation, which considerably reduces the probability of the bond dissociation. The effect of bivalent sulfur compounds on the PMMA aging may be due not only to the transfer of the energy or charge from the polymer to the additive, but also to the reaction of the additive with radicals. Owing to relatively easy homolysis of S–S and C–S bonds, these compounds generate the corresponding thiyl radicals. The most labile bonds are S–H in thiols, C–S in sulfides, and S–S in disulfides [61]. Aliphatic and aromatic compounds generate thiyl monoradicals, and sulfur-containing cyclanes generate biradicals capable of deactivating polymeric radicals responsible for the degradation [62].

The protective function of allylthiourea, di-*m*-tolylthiourea, dithienyl disulfide, and ethyl mercaptan was demonstrated in [1, 3, 4, 37]. The number of chain breaks in PMMA decreases on adding S-containing compounds. In PMMA without additive, γ-irradiated at 313 K to a dose of 100 kGy, this number is 12.0, whereas in the presence of 1.4% ethyl mercaptan it decreases to 3.3. When the irradiation is performed at 77 K, the number of breaks is 4.2 and 1.2, respectively [62].

The radioprotector activity of S-containing compounds depends on the procedure of their introduction not only into the polymeric formulation, but also into the macromolecule [47]. The presence of impurities of organosulfur compounds in PMMA containing 1,3,5,7-tetramethyl-2,4,6,8-tetrathiaadamantane (compound with highly stable rings) exerts no noticeable influence on the properties of the irradiated polymer [47]. The stabilizing effect of S-containing compounds is manifested only when they are incorporated into the macromolecule being protected.

Incorporation of sulfur-containing fragments in the PMMA macromolecule as terminal groups by polymerization of MMA in the presence of a chain-transfer agent, 3,5,7,9,9'-pentamethyl-1-mercapto-2,4,6,8-tetrathiaadamantane, and as pendant groups by copolymerization with 3,5,7,9,9'-pentamethyl-1-amethacryloylthio-2,4,6,8-tetrathiaadamantane slightly enhances the radiation resistance of the polymer. The quantities $(T_f^0 - T_f)/T_f^0$ of these samples after γ-irradiation to a dose of 50 kGy are equal, 0.20 (for the polymer without additive, 0.24) [47]. Sulfur(VI) compounds (sulfolanes) incorporated in the macromolecule as pendant groups do not alter the radiation resistanc of PMMA. Incorporation in the pendant group of a thioether fragment containing S(II), along with the sulfolane fragment [in copolymer of MMA with 3-methacryloyloxy-4-(1'-thia)hexyltetrahydrothiophene dioxide], appreciably enhances the stability: $(T_f^0 - T_f)/T_f^0$ decreases to 0.22 [47].

Sulfur(II) compounds exert the strongest protective effect when incorporated in the macromolecule backbone, as can be shown by the example of 3,6-dimethyl-1,4,5-trithiacycloheptane and elemental sulfur (S_8) [47, 63]. The quantity $(T_f^0 - T_f)/T_f^0$ for PMMA containing these additives (0.5%) and irradiated to a dose of 50 kGy is 0.11 and 0.15, respectively (without additive, 0.24) [47]. The radiation yield of radicals in PMMA at 305 K upon incorporation of 0.1% S_8 decreases from 2.9 to 1.9 per 100 eV [63]. In the presence of S_8, the number of radiation-damaged sites in the PMMA macromolecule after γ-irradiation to a dose of 80 kGy is smaller than the number of chain breaks responsible for the generation of radicals. Irradiation to a dose of 20 kGy causes 2.5 breaks per macromolecule, and 1.0 damaged site remains by the time of molecular weight determination. In the absence of the additive, 2.8 breaks formed upon irradiation give rise to 4.3 residual damaged sites, i.e., initiation of the degradation by radicals takes place [63]. Stabilization of the polymer in the presence of sulfur-containing additives is due to the recombination of terminal macroradicals with thiyl radicals formed by radiolysis [63]. Their reaction is more probable within one molecule. The restricted diffusion in solid samples and nonuniform distribution of the additive (present as an impurity) in the polymer complicate the contact of these radicals and require higher concentrations of antirads.

The polymer protection can also be accomplished by varying its structure.

Structural protection. Along with the chemical structure, the radiation resistance of a polymer is influenced by the structure and mobility of chains. A decrease in the mobility of macromolecules due to their cross-linking (occurring along with the degradation) under the action of γ-radiation is responsible [64] for the lower yield of chain breaks ($G_S \approx 2.41$) determined from a decrease in the molecular weight, compared to the value ($G_S = 2.82$) calculated from the volumes of the isolated gaseous products released from poly(cyclohexyl methacrylate).

Apparently, this mechanism is operative in the protection of PMMA by carboranes, which are relatively inert, thermally stable, electron-deficient boron compounds of polyhedral structure in which one or more boron atoms in the molecular core are replaced by carbon atoms [65, 66]. Addition of 10% 1,2-dibenzyl-*o*-carborane as a mechanical admixture to PMMA leads to an increase in its glass transition point upon γ-irradiation to a dose of 80 kGy from 369 to 389 K, which is attributed to cross-linking of the macromolecules in the course of irradiation, decreasing their segmental mobility. Cross-linking can also result from the reaction of the carborane or its radiolysis products with oxygen-containing ester groups (–$COOCH_3$) in PMMA [8]. Degradation is inhibited in the presence of the carborane, which is manifested in a less intense decrease in the flow point of the polymer compared to the polymer without additive: The flow point of PMMA containing 10% additive decreases from 570 to 480 K upon γ-irradiation to a dose of 10 kGy, whereas without additive it decreases to 460 K. The polymer protection is also provided, apparently, by the capability of carborane groups (and aromatic fragments) to absorb and dissipate the radiation energy owing to the presence of delocalized electrons.

The inhibition of the radiation-induced degradation of PMMA may due to cross-links that not only arise in the course of irradiation but also may be present initially. For example, copolymers of MMA with *trans*-1,2-dimethacryloyloxycyclohexane (DMCH) and 3,4-dimethacryloyloxysulfolane (DMS), whose macromolecules are cross-linked by cyclohexane and sulfolane groups, are more resistant to high-energy radiation than PMMA [67]. The flow point of the copolymers decreases under γ-irradiation considerably less intensely than that of PMMA [67]. The quantity $(T_f^0 - T_f)/T_f^0$ at an irradiation dose of 50 kGy is 0.24 for PMMA, 0.19 for its copolymer with DMS, and 0.20 for the copolymer with DMCH (comonomer content 2.75 mol %). In sulfolane groups, all the six valence electrons of the S atom participate in the formation of the S–O and C–S bonds in contrast to S(II) compounds, and there are no electrons capable of transition to the *d* level upon excitation. Therefore, the absorbed energy is not dissipated. The cyclohexane fragment contains no conjugated double bonds and therefore is also incapable of the redistribution of the absorbed energy. In radiolysis, these groups do not decompose into species capable to deactivate macroradicals. The stabilization of these copolymers is apparently due to structural features of their macromolecules.

Cross-links decrease the mobility of the macromolecules and favor stabilization of radicals; therefore, the concentrations and radiation yields of radicals in these copolymers are higher than in PMMA [67]. The cross-links hinder the decay of radicals both by thermal recombination (responsible for inhibition of degradation) and by disproportionation, and also by direct interaction with the radiation (leading to degradation of the polymer, e.g., by dissociation of the radicals with formation of stable molecules and hydrogen atoms recombining with the nearest radicals [13]). The rate constant of the decay of radicals in irradiated MMA–DMS copolymer by interaction with the radiation is 0.023 kGy^{-1}, whereas in straight PMMA it is 0.037 kGy^{-1} [20]. The activation energy of the decay of radicals by the bimolecular mechanism in PMMA is 110, and in the copolymer, 146 kJ mol^{-1}. The inhibition of the recombination of radicals in the copolymer is attributed to a decrease in their "rotational" mobility in the cage and in the probability of their escape from the cage [20]. Owing to the decreased mobility of macromolecules, radicals arising in one molecule cannot induce degradation of another molecule. In PMMA, $\dot{C}H_2$–$C(CH_3)(COOCH_3)$~ radicals can disappear by abstraction of an H atom from a neighboring chain [15]. The radicals arising in the process decompose:

$$\sim(CH_2\text{–}C(CH_3)(COOCH_3)\text{–}\dot{C}H\text{–}C(CH_3)(COOCH_3)\text{–}CH_2\sim$$

$$\rightarrow \sim CH_2\text{–}C(CH_3)(COOCH_3)\text{–}CH{=}C(CH_3)(COOCH_3)$$

$$+ \dot{C}H_2\text{–}C(CH_3)(COOCH_3)\sim.$$

Cross-links of macromolecules hinder these reactions. The stability of PMMA is considerably enhanced by cross-linking of the macromolecules with anthracene fragments in the copolymer of MMA with 9,10-dimethacryloyloxymethylanthracene (DMMA) owing to participation of the aromatic nuclei in the redistribution of the incident energy [67]. The radiation yield of radicals in this copolymer (per 100 eV) is

Table 2. Coefficients of PMMA protection with antirad additives*

Additive	*c*, %	*F*, %	Additive	*c*, %	*F*, %
Benzene	0.9, 2.7, 7.2	5, 13, 28	1-Naphthylamine	2.5	78
Naphthalene	0.8, 2.5, 5.3	15, 43, 58	2-Naphthylamine	3.3	73
Anthracene	2.1, 3.3	37, 57	Phenyl-2-naphthylamine	0.6, 0.9, 3.3	29, 52, 62
Phenanthrene	0.9, 2.1, 9.8	17, 35, 64	1,3,5-Trinitrobenzene	3.6, 5.4	18, 27
Diphenyl	2.2, 2.5	43, 56	2,4-Dinitrophenol	3.2	68
p-Terphenyl	0.1, 1.0	11, 31	2,4-Dinitroaniline	4.2	72
Benzanthracene	0.4, 2.2, 4.5	19, 55, 70	*N*,*N*'-Dimethylurea	10	15
Pyrene	0.1, 1, 5	4, 35, 56	Ethylurea	10	12
Triphenylmethane	5.2	71	Ethyl mercaptan	1.4, 2.9, 9.9	75, 83, 93
Phenol	2.7	52	Diphenylthiourea	3.6	69
1-Naphthol	5.5	82	Allylthiourea	10	57
2-Naphthol	5.3	24	Di-*m*-tolylthiourea	10	72
Benzophenone	3.4, 8.3	43, 60	*p*-Benzoquinone	5, 10	64, 70
Benzoic acid	2.9, 4.6, 7.2	33, 40, 52	Diphenylpicrylhydrazine	5	67
Aniline	10	59	8-Quinolinol	1, 5, 10	44, 54, 68
Diphenylamine	0.6, 3.3, 8.6	33, 63, 73	Triphenylphosphine	2.5	22
Triphenylamine	1	57	Triphenyl phosphite	2.7	56
N,*N*'-Dimethyl-*p*-phenylenediamine	1	45	Triphenyl phosphate	2.7	40
Tetramethyl-*p*-phenylenedioamine	0.7, 1.4, 2.5	36, 53, 63	TTA	0.5	0
TMPI	0.2, 25	2, 87	TTA–SH	0.5	57
POPOP	0.01	1.1	–	–	–
TMPI + POPOP	25 + 0.01	88	TTA–SC	0.5	57
TMPI + PPP	25 + 0.2	89	TTH	0.5	93
TMPI + POPOP + PPP	25 + 0.01 + 0.2	90	Elemental sulfur	0.1, 0.5	50, 78
DBOC	10	78	MSA	0.5	0
PDPV	0.5	58	DMS	0.5	42
DMCH	0.5	40	DMMA	0.5	79

* DBOC, dibenzyl-*o*-carborane; PDPV, oligo(1,4-phenylene-1,2-diphenylvinylene); DMCH, *trans*-1,2-dimethacryloyloxycyclohexane; DMMA, 9,10-dimethacryloyloxymethylanthracene; TTA, 1,3,5,7-tetramethyl-2,4,6,8-tetrathiaadamantane; TTA–SH, 3,5,7,9,9'-pentamethyl-1-mercapto-2,4,6,8-tetrathiaadamantane; TTA–SC, 3,5,7,9,9'-pentamethyl-1-methacryloylthio-2,4,6,8-tetrathiaadamantane; TTH, 3,6-dimethyl-1,4,5-trithiacycloheptane; MSA, 3-methacryloyloxytetrahydrothiophene dioxide; DMS, 3,4-dimethacryloyloxytetrahydrothiophene dioxide.

lower than in PMMA and copolymers of MMA with DMS and DMCH: 2.9 in PMMA, 3.0 in copolymer with DMS (2.75 mol %), 3.2 in copolymer with DMCH, and 1.4 in copolymer with DMMA [67]. The quantity $(T_f^0 - T_f)/T_f^0$ for the latter copolymer is as small as 0.15 upon γ-irradiation to a dose of 50 kGy [67]. To evaluate the relative performance of antirads in radiation protection, it is suggested to use the protection factors F (%) defined [1] as

$$F = (1 - r_0/r) \times 100,$$

where r_0 and r are the ionizing radiation energies required to attain the same radiation effect in the absence and in the presence of an antirad, respectively.

The protection factors of some antirads given in [5] and calculated from the experimental data of [6–8, 63, 67] are listed in Table 2. Table 2 shows that polycyclic hydrocarbons, aromatic amines, and sulfur-containing compounds exhibit high radioprotecting effect. A particular place among them is occupied by thiacyclanes. The protection factor of 70–93% is attained on their introduction into PMMA in concentrations 8–20 times lower than the concentrations of aromatic hydrocarbons providing the same effect.

CONCLUSION

Degradation processes occurring in poly(methyl methacrylate) under the action of high-energy radiations can be controlled by introducing into the polymer aromatic hydrocarbons, aromatic amines, carbo-

ranes, and sulfur-containing compounds. The radioprotective performance of these compounds depends on their capability to be incorporated in the polymer chain and on their arrangement in the chain. When structural units responsible for the radioprotecting effect are incorporated directly in the polymer chain, the protecting effect is stonger than when radioprotectors are introduced as mechanical admixtures that do not form chemical compounds with the macromolecule. Compounds incorporated in the polymer backbone are more effective antirads than those incorporated as terminal, pendant, or cross-linking groups.

REFERENCES

1. Charlesby, A., *Atomic Radiation and Polymers*, New York: Pergamon, 1960.
2. *Radiation Effects on Organic Materials*, Bolt, R.A. and Carrol, J.G., Eds., New York: Academic, 1963.
3. Romantsev, M.F., *Khimicheskaya zashchita organicheskikh sistem ot ioniziruyushchego izlucheniya* (Chemical Protection of Organic Systems from Ionizing Radiation), Moscow: Atomizdat, 1978.
4. Makhlis, F.A., *Radiatsionnaya fizika i khimiya polimerov* (Radiation Physics and Chemistry of Polymers), Moscow: Atomizdat, 1972.
5. Laricheva, V.I. and Suminov, S.I., *Problemy radiatsionnoi zashchity polimerov* (Problems of Radiation Protection of Polymers), Moscow: NIITEKhIM, 1985.
6. Leplyanin, G.V., Salimgareeva, V.N., Sannikova, N.S., and Kirichenko, G.N., *Khim. Vys. Energ.*, 1996, vol. 30, no. 6, pp. 424–427.
7. Salimgareeva, V.N., Leplyanin, G.V., Sannikova, N.S., and Rafikov, S.R., *Bashk. Khim. Zh.*, 1995, vol. 2, nos. 3–4, pp. 32–35.
8. Salimgareeva, V.N., Sannikova, N.S., Kolesov, S.V., and Leplyanin, G.V., *Zh. Prikl. Khim.*, 2002, vol. 72, no. 6, pp. 998–1002.
9. Salimgareeva, V.N. and Leplyanin, G.V., Abstracts of Papers, *III Bakhovskaya konferentsiya po radiatsionnoi khimii* (III Bakh Conf. on Radiation Chemistry), Moscow, 2000, p. 79.
10. Milinchuk, V.K., Klinshpont, E.R., and Pshezhetskii, S.Ya., *Makroradikaly* (Macroradicals), Moscow: Khimiya, 1980.
11. Bruk, M.A., Kondratova, M.V., Baranova, A.A., et al., *Vysokomol. Soedin., Ser. A–B*, 1999, vol. 41, no. 2, pp. 256–262.
12. Fiske, H.H., Merrill, E.W., and Vasa, N.K., *Polym. Eng. Sci.*, 1980, vol. 20, no. 18, pp. 1236–1241.
13. Pshezhetskii, S.Ya., Kotov, A.G., Milinchuk, V.K., et al., *EPR svobodnykh radikalov v radiatsionnoi khimii* (ESR of Free Radicals in Radiation Chemistry), Moscow: Khimiya, 1972.
14. O'Donnell, J.H. and Pomery, P.J., *J. Polym. Sci., Polym. Symp.*, 1976, no. 55, pp. 269–278.
15. Pikaev, A.K., *Sovremennaya radiatsionnaya khimiya: Tverdoe telo i polimery: Prikladnye aspekty* (Modern Radiation Chemistry: Solids and Polymers: Applied Aspects), Moscow: Nauka, 1987.
16. Rafikov, S.R., Ibragimov, Sh.Sh., Leplyanin, G.V., et al., *Khim. Vys. Energ.*, 1981, vol. 15, no. 4, pp. 333–337.
17. Ichikawa, T., *Nucl. Instr. Meth. Phys. Res. B*, 1995, vol. 105, nos. 1–4, pp. 150–153.
18. Egusa, S., Ishigue, K., and Tabata, Y., *Macromolecules*, 1979, vol. 12, no. 5, pp. 939–944.
19. Schnabel, W. and Sotobayashi, H., *Polym. J.*, 1976, vol. 8, no. 5, pp. 423–424.
20. Pivovarov, S.P., Poljakov, A.J., Rjabikin, Ju.F., et al., *Radiat. Eff.*, 1981, vol. 59, nos. 3–4, pp. 179–182.
21. Miguez, S.Y.C., Biasotto, M.E., Costa, M.E.E., and Bruno, T.M.I., *J. Appl. Polym. Sci.*, 2002, vol. 85, no. 4, pp. 886–895.
22. Gardner, D.G. and Toosi, M.T.A., *J. Appl. Polym. Sci.*, 1967, vol. 11, no. 7, pp. 1065–1078.
23. Kusy, R.P. and Greenberg, A.P., *Macromolecules*, 1978, vol. 11, no. 5, pp. 1051–1053.
24. Belichenko, A.S., Dyumaev, K.M., Maslyukov, A.P., et al., *Dokl. Akad. Nauk SSSR*, 1990, vol. 315, no. 6, pp. 1401–1404.
25. Nagornaya, A.A., Gunder, O.A., and Malinovskaya, S.A., in *Monokristally, stsintillyatory i organicheskie lyuminofory* (Single Crystals, Scintillators, and Organic Luminophores), Kharkov: Vses. Nauchno-Issled. Inst. Monokristallov, 1968, issue 3, pp. 167–170.
26. Taraban, V.B., Zhdanov, G.S., Smolyanskii, F.S., et al., *Khim. Vys. Energ.*, 1993, vol. 27, no. 5, pp. 46–50.
27. Izyumnikov, A.A. and Bol'bit, N.M., *Khim. Vys. Energ.*, 1996, vol. 30, no. 4, pp. 264–272.
28. Briskman, B.L. and Milinchuk, V.K., *Khim. Vys. Energ.*, 1989, vol. 23, no. 3, pp. 195–207.
29. Yoshida, H. and Ichikawa, T., *Radiat. Phys. Chem.*, 1995, vol. 46, nos. 4–6, pp. 921–924.
30. Charlesby, A., *Polymer*, 1964, vol. 5, no. 2, pp. 67–88.
31. Charlesby, A. and Moore, N., *Int. J. Appl. Radiat. Isot.*, 1964, vol. 15, no. 12, pp. 703–708.
32. Kroh, J. and Polovinska, A., *Bull. Acad. Polon. Sci.*, 1968, vol. 16, no. 8, pp. 425–428.
33. Wundrich, K., *J. Polym. Sci., Polym. Phys. Ed.*, 1973, vol. 11, no. 6, pp. 1293–1300.
34. Luo Yunxia, Guan Jinqiu, Yang Hong, et al., *Acta Polym. Sin.*, 1992, no. 4, pp. 385–390.

35. Sharma, V.K., Pethrick, R.A., and Affrossman, S., *Polymer*, 1982, vol. 23, no. 12, pp. 1732–1736.
36. Dong Limin, Hill David, J.T., O'Donnell, J.H., et al., *Macromolecules*, 1995, vol. 28, no. 10, pp. 3681–3691.
37. David, C., Fuld, D., and Geuskens, G., *Makromol. Chem.*, 1970, vol. 139, no. 9, pp. 269–276.
38. Kusy, R.P., Katz, M.J., and Turner, D.T., *Thermochim. Acta*, 1978, vol. 26, nos. 1–3, pp. 415–425.
39. Andullah, A.A., Al-Bayati, A.A., and Selman, A.A., *Indian J. Phys.*, 2002, vol. 76, no. 5, pp. 457–462.
40. Peschanskaya, N.N., Smolyanskii, A.S., and Surovova, V.Yu., *Vysokomol. Soedin., Ser. B*, 1992, vol. 34, no. 12, pp. 354–358.
41. Perepechko, I.I. and Mar'yasin, B.Ya., *Vysokomol. Soedin.*, 1978, vol. 20, no. 7, pp. 1601–1607.
42. Sauerbrey, H. von, *Koll. Z. Z. Polym.*, 1968, vol. 225, no. 2, pp. 121–124.
43. Toosi, M.T.A., *US Atomic Energy Comm., COO-1224-8*, 1965.
44. Borovkova, V.A. and Bagdasar'yan, Kh.S., *Khim. Vys. Energ.*, 1967, vol. 1, no. 1, pp. 340–345.
45. Butyagin, P.Yu., Dubinskaya, A.M., and Radtsig, V.A., *Usp. Khim.*, 1969, vol. 38, no. 4, pp. 593–623.
46. Kiryukhin, V.P. and Milinchuk, V.K., *Vysokomol. Soedin., Ser. A*, 1974, vol. 16, no. 4, pp. 816–820.
47. Salimgareeva, V.N., Leplyanin, G.V., Vorob'eva, A.I., and Rafikov, S.R., *Bashk. Khim. Zh.*, 1995, vol. 2, nos. 3–4, pp. 27–31.
48. Gardner, D.G. and Epstein, L.M., *J. Chem. Phys.*, 1961, vol. 34, no. 5, pp. 1653–1660.
49. Salimgareeva, V.N. and Kolesov, S.V., *Prib. Tekh. Eksp.*, 2005, no. 3, pp. 1–11.
50. Malinovskaya, S.A., Gunder, O.A., Generalova, V.V., et al., in *Monokristally, stsintillyatory i organicheskie lyuminofory* (Single Crystals, Scintillators, and Organic Luminophores), Kharkov: Vses. Nauchno-Issled. Inst. Monokristallov, 1969, issue 5, pp. 158–164.
51. Kolninov, O.V., Shelukov, J.P., Klinspont, E.R., et al., *Radiat. Phys. Chem.*, 1995, vol. 46, nos. 4–6, pp. 843–846.
52. Wundrich, K., in *Proc. 3rd Tihany Symp. on Radiation Chemistry*, Balatonfured–Tihany, 1972, Budapest, 1972, vol. 1, pp. 747–755.
53. Bagdasar'yan, Kh.S., Krongauz, V.A., and Kardash, N.S., *Dokl. Akad. Nauk SSSR*, 1962, vol. 144, no. 1, pp. 101–104.
54. Milyutinskaya, R.I. and Bagdasar'yan, Kh.S., *Zh. Fiz. Khim.*, 1964, vol. 38, no. 3, pp. 776–778.
55. Borovkova, V.A., Bagdasar'yan, Kh.S., Chepel', D.V., and Shemarov, F.V., *Khim. Vys. Energ.*, 1971, vol. 5, no. 4, pp. 337–339.
56. Torikai, A. and Fueki, K., *Polym. Degrad. Stab.*, 1984, vol. 6, no. 2, pp. 81–93.
57. Wilske, J. and Heusinger, H., *Radiochim. Acta.*, 1969, vol. 11, nos. 3–4, pp. 187–193.
58. Garrett, R.W., O'Donnell, J.H., Pomery, P.J., and Shum, E.C., *J. Appl. Polym. Sci.*, 1979, vol. 24, no. 12, pp. 2415–2418.
59. Lina Ivanla, S. de, Arayjo Elmo S. de, and Azevedo Walter M. de, *Rev. Quim. Technol.*, 2003, vol. 2, no. 2, pp. 35–39.
60. Panchvidze, M.V., Nanobashvili, E.M., and Dalakashvili, N.Z., *Izv. Akad. Nauk Gruz. SSR, Ser. Khim.*, 1977, vol. 3, no. 4, pp. 365–372.
61. Calvert, J.G. and Pitts, J.N., Jr., *Photochemistry*, New York: Wiley, 1966.
62. Ramakrishnan, V., Thompson, S., and Geynn, S., *Photochem. Photobiol.*, 1965, vol. 4, no. 5, pp. 907–915.
63. Rafikov, S.R., Ibragimov, Sh.Sh., Leplyanin, G.V., et al., *Vysokomol. Soedin., Ser. A*, 1981, vol. 23, no. 3, pp. 540–544.
64. Kumar Manmohan, Rao, M.H., and Rao, K.N., *Radiat. Phys. Chem.*, 1986, vol. 27, no. 3, pp. 219–223.
65. Grimes, R.N., *Carboranes*, New York: Academic, 1970.
66. *Uspekhi v oblasti sinteza elementoorganicheskikh polimerov* (Advances in Synthesis of Organoelement Polymers), Korshak, V.V., Ed., Moscow: Nauka, 1988.
67. Salimgareeva, V.N., Pivovarov, S.P., Kolesov, S.V., et al., *Zh. Prikl. Khim.*, 2004, vol. 77, no. 2, pp. 275–279.

ISSN 1070-4272, Russian Journal of Applied Chemistry, 2006, Vol. 79, No. 9, pp. 1403–1406. © Pleiades Publishing, Inc., 2006.
Original Russian Text © A.V. Vegera, A.D. Zimon, 2006, published in Zhurnal Prikladnoi Khimii, 2006, Vol. 79, No. 9, pp. 1419–1422.

INORGANIC SYNTHESIS AND INDUSTRIAL INORGANIC CHEMISTRY

Synthesis and Physicochemical Properties of Silver Nanoparticles Stabilized by Acid Gelatin

A. V. Vegera and A. D. Zimon

Moscow State University of Technology and Management, Moscow, Russia

Received July 8, 2006

Abstract—Silver nanoparticles were synthesized by the reduction of silver nitrate with sodium borohydride at widely varied concentrations of the starting reagents. A physicochemical study of the synthesized nanosystems was carried out. The stabilizing ability of acid gelatin in the systems under study was considered. The stability diagram in the coordinates initial concentration of silver nitrate–concentration of gelatin was constructed.

DOI: 10.1134/S1070427206090023

The preparation of stable concentrated aqueous dispersions with preset physicochemical properties, based on silver nanoparticles, is a necessary step in the development of nanostructural materials applied in microelectronics, electrochemistry, synthesis of electrooptical sensors, pigments, etc. Owing to the bactericidal properties of silver ions, its nanodispersions can form a basis for the development of new classes of bactericides and various medicinal substances.

The preparation of a disperse system with the required stability in time and resistance to the action of external factors remains the major problem. In this connection, our goal was to study how the conditions of the synthesis of silver nanoparticles affect the stability of silver nanodispersions. To characterize properties of the synthesized nanodisperse silver systems, we used a number of methods. The transmission electron microscopy and computer analysis of the resulting images of nanoparticles allowed us to determine the size distribution of particles under various synthesis conditions. The concentration of silver ions in the systems was determined by atomic absorption spectroscopy, and optical properties of silver nanodispersions, by spectrophotometry. The stability diagram of the silver nanoparticle sol was constructed using a combination of the three above-mentioned methods. The stability of the systems was determined in relation to two parameters: initial concentration of silver ions in the reaction mixture and concentration of gelatin in the dispersion medium.

EXPERIMENTAL

Silver nanoparticles were synthesized by the reduction of aqueous solutions of silver nitrate. The process follows the scheme

$$AgNO_3 + [\text{reductant}] \rightarrow \text{silver nanoparticles}.$$

In the study we used chemically pure grade silver nitrate (Reakhim). To make the constructed stability diagram of the system more reliable, we determined gravimetrically the metal content in the reagent. For this purpose, three weighed portions of the starting salt were heated in crucibles at 120°C to constant weight. Sample weights were measured accurate to 1×10^{-4} g. From the data obtained, we have found that the content of silver nitrate in the starting preparation was 83.00%. These data were confirmed by atomic adsorption spectroscopy.

As reductant we used chemically pure grade sodium borohydride (Reakhim) without additional purification; in the process, it is oxidized to borate. The following reaction scheme is presumed:

$$2AgNO_3 + 2NaBH_4 + 6H_2O \rightarrow 2Ag + 7H_2\uparrow + 2NaNO_3 + 2H_3BO_3.$$

As the stabilizer of silver nanoparticles we used photo A grade acid gelatin without additional purification (isoelectric point 4.9, average molecular weight 94 kDa). In all experiments we used double-distilled water.

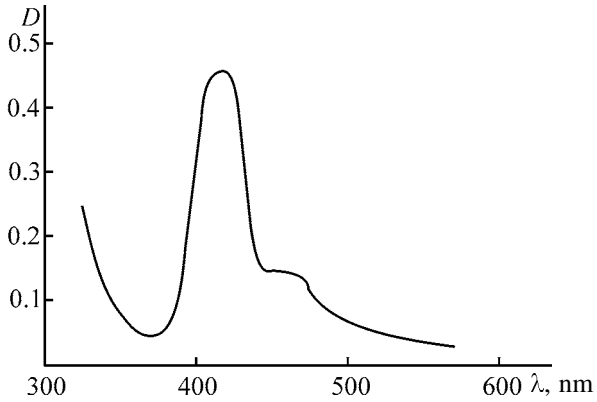


Fig. 1. Absorption spectrum of silver nanodispersion obtained at a gelatin concentration of 0.5% and the initial concentration of silver ions of 2×10^{-4} M. T = 293 K, pH 8.0; after 24-h storage. (D) Optical density and (λ) wavelength.

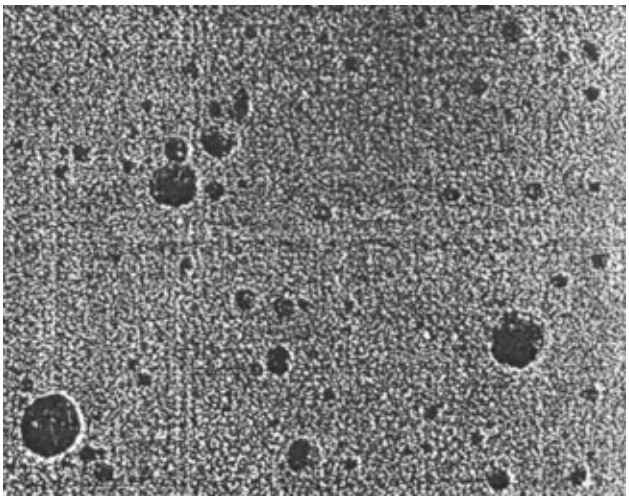


Fig. 2. Electron micrograph of silver nanoparticles. Initial concentration of silver nitrate 2×10^{-5} M, concentration of gelatin 0.5%; 3 h after the synthesis.

Physicochemical properties of silver nanoparticles. Properties of a colloidal solution, including that of silver nanoparticles, are determined by the possibility of coagulation and recrystallization, i.e., by the aggregation stability, and also by the sedimentation stability [1, 2] and the possibility of oxidation with atmospheric oxygen.

An examination of the published data [1, 2, 8, 9] showed that several methods can be used to describe the stability of silver nanodispersions in time. The visual observation can reveal preliminary and general trends in the relative stability of a dispersion under study. A change in the system color and(or) the formation of a precipitate can be detected. The average particle size correlates with the sol color. The color of silver nanoparticles varies from red (yellow-brown) to gray and even black. The visual observation can play a decisive role in studying the sedimentation stability.

The optical method based on recording the visible absorption spectrum of the system under study is one of reliable instrumental methods (Fig. 1). The occurrence of coagulation and recrystallization can be suggested when a shoulder or a new maximum appears in the long-wavelength part of the spectrum [3, 4]. A quantitative characteristic of the aggregation stability can be obtained by electron microscopy, which makes it possible to determine the distributions of particles with respect to the size and shape, and also to estimate the arrangement of nanoparticles in space (separate or coagulated particles) (Fig. 2).

In the system under study, several pathways of nanodispersion breakdown are possible, namely, the oxidation of metal particles accompanied by their dissolution, aggregation of particles, and also sedimentation.

A wide spectrum of silver sols was synthesized in the initial concentration range 1×10^{-5}–2×10^{-3} M. We will consider the results of studying physicochemical properties of the synthesized silver nanosystems. First of all, as the initial concentration of silver ions increases, the size of the forming nanoparticles and the range of their distribution in size increase from 3–9 nm for the 1×10^{-5} M concentration of silver ions to 5–50 nm for the concentration of 2×10^{-3} M. Let us consider specific features of silver sol depending on the initial concentration of the reagent (silver nitrate) in the concentration range 1×10^{-5}–1×10^{-4} M. The solution color changes from red to yellow within 10–14 days. Three hours after the synthesis, nanoparticles have the size from 3 to 9 nm, and the particle size distribution is normal. After 48 h, the distribution of nanoparticles in size changes. Particles of size 9 nm make up 48%. Due to the aggregation and recrystallization, the number of particles decreases from $(7.5 \pm 0.8) \times 10^{14}$ to $(1.1 \pm 0.5) \times 10^{14}$ particles per liter, i.e., by a factor of approximately 7.

At the initial silver concentration of 2×10^{-4}–3×10^{-4} M, the diameter of nanoparticles varies from 5 to 40 nm. The content of nanoparticles 15 nm in diameter is about 23%. After 3 months, the particle size distribution slightly changes. The range of the sizes is 5–50 nm. The most probable diameter is 20 nm (18% of such particles). The concentration of particles decreases from $(5.7 \pm 0.6) \times 10^{14}$ to $(2.1 \pm 0.5) \times 10^{14}$, i.e., by a factor of approximately 2.5. The system is more stable to aggregation than the previous system.

At the initial concentration of silver ions of 2×10^{-3} M, the initial size distribution of nanoparticles is asymmetric. The diameter of nanoparticles varies from 5 to 50 nm, and the most probable value is 30 nm (20% of particles). Coagulation structures consisting of large asymmetric particles and more symmetric small particles are formed (Fig. 3).

Stabilization of silver nanoparticle by gelatin. In time, the aggregation of nanoparticles occurs, their concentration decreases, and their size increases. The aggregation stability stability can be enhanced by adding gelatin. This additive substantially prevents the aggregation and reduces the average size of nanoparticles (particle size in the range from 3 to 17 nm).

The stability diagram of the synthesized silver nanodispersion consists of three regions (Fig. 4). In region *A*, the nanosystems show limited stability. In this region, the dispersion systems are broken down by oxidation (dissolution) of metallic particles under the action of oxygen dissolved in the dispersion medium. Region *B* is the area of stable systems. In region *C*, the systems are unstable. The stability is lost due to the coagulation and the subsequent sedimentation of the aggregates formed.

As the gelatin concentration increases, the stability of silver dispersion against oxidation (dissolution) increases. The properties of the adsorption layer play the decisive role. The curve separating regions *B* and *C* characterizes the increase in the system stability with increasing concentrations of gelatin and silver ions. The gelatin adsorption under these conditions (adsorbate concentration of 0.1–0.5% and adsorption surface area of 0.3–0.8 m^2 in 100 ml of the system) is polylayer [4]. When the gelatin mass is thickened in the adsorption layer, its concentration can increase to 30%.

According to the phase diagram of the gelatin–water system, such a change in the gelatin content results in the gel formation [5]. Gelatin gels envelop nanoparticles. The gelatin adsorption layer affects the mass-transfer process and the formation of other concentration gradients of the system components, in contrast to systems without gelatin. The surface-active properties of gelatin should also be taken into account. Its adsorption results in a decrease in the interfacial tension, which leads to overall lyophilization of the system.

The stability of the colloidal solution of nanoparticles depends on the concentration of silver ions in the starting solution. We chose two systems for the analysis, the first with the concentration of silver



Fig. 3. Electron micrograph of silver nanoparticles. Initial concentration of silver nitrate 2×10^{-3} M, concentration of gelatin 0.0%; 3 h after the synthesis.

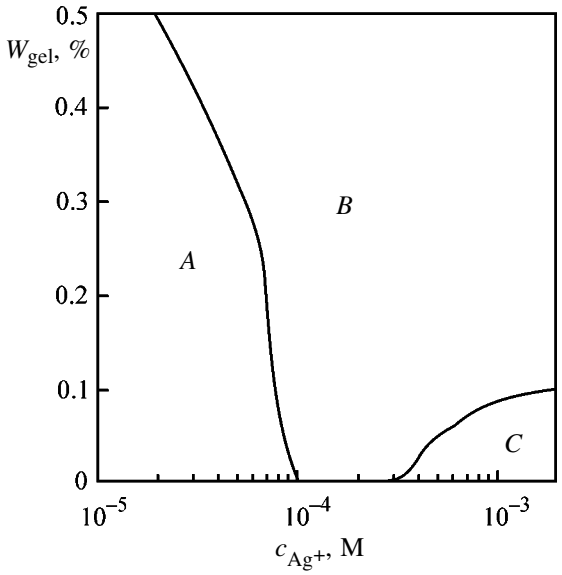


Fig. 4. Stability diagram of silver sol at T = 293 K and pH 8.0. Regions in the diagram: (*A*) relatively stable, (*B*) highly stable, and (*C*) unstable.

nitrate of 2×10^{-4} M, which corresponds to formation of the stable system (Fig. 4, region *B*), and the second, aggregation-unstable, with the concentration of 8×10^{-4} M (Fig. 4, region *C*).

The dependence of the concentration of silver ions in solution on the time elapsed after the synthesis of

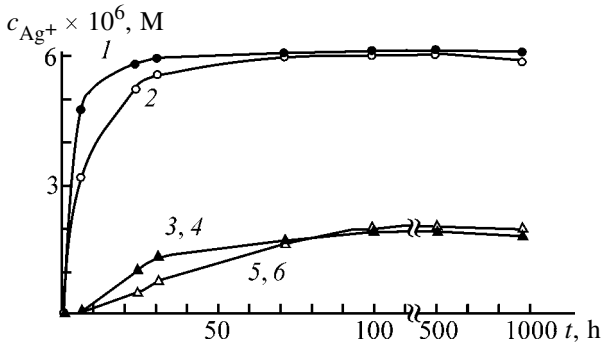


Fig. 5. Concentration of silver ions c as a function of the storage time t of nanodispersion samples with the initial content of silver ions of (*1, 3, 5*) 2×10^{-4} and (*2, 4, 6*) 8×10^{-4} M. Gelatin concentration, %: (*1, 2*) 0, (*3, 4*) 0.1, and (*5, 6*) 0.3. T = 293 K, pH 6.7.

nanoparticles is given in Fig. 5. In the system without gelatin with the initial concentration of 8×10^{-4} M, the content of free silver ions increases faster (Fig. 5, curve *2*) than in the system containing 2×10^{-4} M silver ions (Fig. 5, curve *1*). This trend agrees with the general dependence of kinetic parameters of chemical reactions on the initial concentration of the substance. It should be noted that equal Ag^+ concentrations, $(6.3 \pm 0.3) \times 10^{-6}$ M, are attained within 70 h in both systems.

The addition of gelatin to the system results in a sharp decrease in the concentration of silver ions (by a factor of approximately 3.5) in the systems with the initial concentrations of silver ions of both 2×10^{-4} and 8×10^{-4} M, and gelatin concentrations of 0.1% and 0.3% (curves *3, 5* and *4, 6*). A stationary concentration of silver ions was observed in the systems containing silver nanoparticles of different sizes.

In the presence of gelatin, during a certain initial period of time, free silver ions are not detected in the system (detection limit 1×10^{-7} M). Stationary concentrations are attained within 72 h. Irrespective of the initial concentrations of silver ions and gelatin, the quasi-equilibrium concentration of silver ions is the same, $(1.7 \pm 0.2) \times 10^{-4}$ M. Such a behavior of the system is apparently caused by the influence of the gelatin adsorption layer hindering the oxidation of metallic silver.

CONCLUSIONS

(1) The sizes and shapes of silver nanoparticles synthesized by the reduction of aqueous solutions of silver nitrate with sodium borohydride were determined by electron microscopy.

(2) The size distributions of nanoparticles in the range of the initial concentrations of silver nitrate of 10^{-5}–10^{-3} M were determined.

(3) The possibility of stabilization of the nanoparticles by acid gelatin was demonstrated.

(4) Aggregation- and sedimentation-stable nanodispersions were obtained at appropriate gelatin concentrations.

REFERENCES

1. Zimon, A.D., *Kolloidnaya khimiya. Agar* (Colloid Chemistry. Agar), Moscow, 2003.
2. Zimon, A.D., Vegera, A.V., and Pavlov, A.N., *Trudy XII mezhdunarodnoi nauchnoi konferentsii Moskovskogo gosudarstvennogo universiteta tekhnologii i upravleniya* (Proc. XII Int. Conf. of Moscow State Univ. of Technology and Management), Moscow, 2006, vol. 3, pp. 132–136.
3. Perner, M., Klar, T., Glosse, S., and Lemmer, G., *J. Luminescence*, 1998, vols. 76–77, pp. 181–184.
4. Sokolov, A.V., *Opticheskie svoistva metallov* (Optical Properties of Metals), Moscow: Fizmatgiz, 1961.
5. Izmailova, V.N., Yampol'skaya, G.P., and Summ, B.D., *Poverkhnostnye yavleniya v belkovykh sistemakh* (Surface Phenomena in Protein Systems), Moscow: Khimiya, 1988.
6. Lipatov, Yu.S., *Usp. Khim.*, 1981, vol. 1, no. 2, pp. 355–379.
7. Panarin, E.F., Pavlov, G.M., and Santuryan, Yu.G., *Khim. Farm. Zh.*, 1991, no. 3, pp. 68–70.
8. Kopeikin, V.V. and Panarin, E.F., *Dokl. Ross. Akad. Nauk*, 2001, vol. 380, no. 4, pp. 497–500.
9. Bogdanchikova, N.E., Zaikovskii, V.I., and Kolomiichuk, V.N., Colloidal Silver: Physicochemical Properties and Application, *Preprint*, Novosibirsk, 1992, pp. 15–30.
10. Pomogailo, A.D., *Usp. Khim.*, 1997, vol. 66, no. 8, pp. 750–791.

ISSN 1070-4272, Russian Journal of Applied Chemistry, 2006, Vol. 79, No. 9, pp. 1407–1412. © Pleiades Publishing, Inc., 2006.
Original Russian Text © G.M. Pavlov, A.S. Gubarev, I.I. Zaitseva, M.A. Sibileva, 2006, published in Zhurnal Prikladnoi Khimii, 2006, Vol. 79, No. 9, pp. 1423–1428.

PHYSICOCHEMICAL STUDIES OF SYSTEMS AND PROCESSES

Determination of Intrinsic Viscosity of Polyelectrolytes in Salt-Free Solutions

G. M. Pavlov, A. S. Gubarev, I. I. Zaitseva, and M. A. Sibileva

Fock Research Institute of Physics, St. Petersburg State University, St. Petersburg, Russia

Received June 5, 2006

Abstract—Comparative analysis of the methods for determination of the intrinsic viscosity of both neutral and polyelectrolyte molecules is made.

DOI: 10.1134/S1070427206090035

The intrinsic viscosity remains among the most significant molecular-hydrodynamic characteristics of polymers. A relatively simple and descriptive viscometric method is widely used in the molecular physics of polymers and rheology and technology of macromolecular compounds for studying polymer solutions [1–4].

The intrinsic viscosity $[\eta]$ is related to the molecular characteristics of a linear-chain macromolecule by the well-known Flory equation [1, 2]

$$[\eta] = \Phi\langle h^2\rangle^{3/2}/M, \quad (1)$$

where $\langle h^2\rangle$ is the mean-square chain length; M, molecular weight of the investigated sample or fraction; and Φ, Flory parameter (mol^{-1}).

Kuhn–Mark–Houwink–Sakurada relationship (2) is also widely used in the polymer science and technology [2, 5, 6]:

$$[\eta] = K_\eta M^a, \quad (2)$$

where a and K_η are the parameters tabulated for a variety of systems polymer–solvent [5].

Analysis and normalization of the Kuhn–Mark–Houwink–Sakurada relationships are presented in [7].

There is a number of extrapolation procedures allowing estimation of $[\eta]$ for neutral macromolecules [1, 4, 6]. The most common among them is the Huggins equation [8]

$$\eta_{sp}/c = [\eta] + k'[\eta]^2 c + ..., \quad (3)$$

where c is the polymer concentration in the solution ($g\ cm^{-3}$); $\eta_{sp} = \eta_r - 1 = (\eta/\eta_0) - 1$; η and η_0 are the dynamic viscosities of the solution and solvent, respectively; η_r and η_{sp}, relative and reduced viscosities of the solution; and k is the Huggins dimensionless parameter.

Kraemer equation (4) is considered in a combination with the Huggins equation [9]:

$$\ln \eta_r/c = [\eta] + k''[\eta]^2 c + ..., \quad (4)$$

where k'' is the Kraemer dimensionless parameter.

It should be pointed out that German researchers often prefer Schulz–Blaschke equation (5) to determine $[\eta]$ [10]:

$$\eta_{sp}/c = [\eta] + k_{sb}[\eta]\eta_{sp} + ... \quad (5)$$

Equations (3)–(5) cover the range of dilute polymer solutions with $\eta_r \le 2.5$ (Fig. 1a).

Recently Fedors has derived a relationship, linear over a wide concentration range ($1 < \eta_r < 100$), allowing determination of $[\eta]$ from the slope of the plot presented in Fig. 1b:

$$[2(\eta_r^{1/2} - 1)]^{-1} = ([\eta]c)^{-1} - ([\eta]c_m)^{-1}, \quad (6)$$

where c_m is the concentration corresponding to the maximally dense packing of rigid equivalent hydrodynamic spheres.

At the same time, it is well known [3, 4, 12] that the dynamic viscosity of a polymer over a wide concentration range can be written as

$$\eta = \eta_0 e^{[\eta]c}. \quad (7)$$

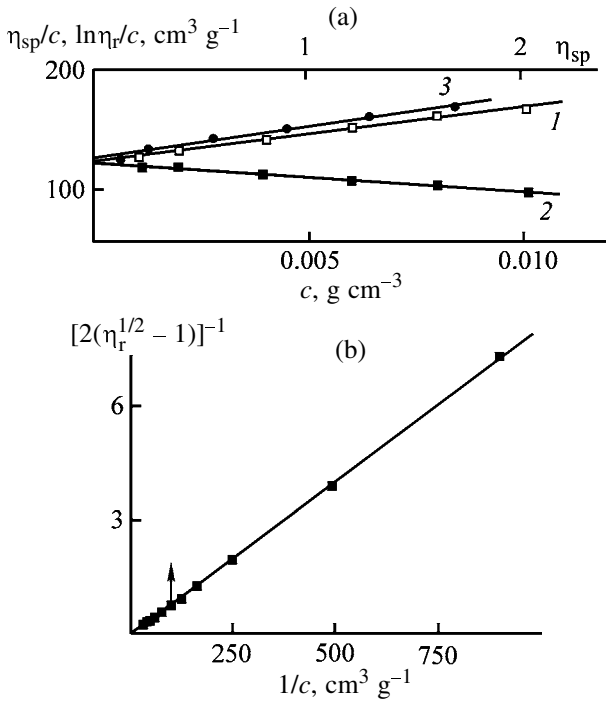


Fig. 1. Various methods for processing viscometric data for aqueous solutions of neutral PVP. (c) Concentration. (a) Concentration range in which $\eta_r \le 2.5$. Data processing according to (*1*) Huggins [Eq. (3)], (*2*) Kraemer [Eq. (4)], and (*3*) Schulz–Blaschke [Eq. (5)]. (b) Data processing by Fedors [Eq. (6)] over the entire concentration range. The arrow indicates the concentration at which $\eta_r = 2.5$. The range of dilute solutions is to the right of the arrow, and the range of moderate concentrations, to the left.

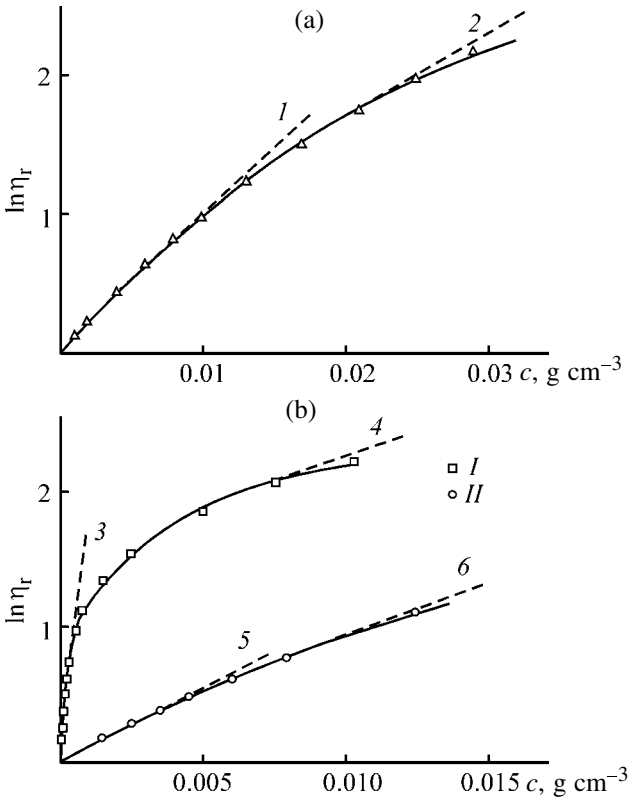


Fig. 2. Dependence of $\ln\eta_r$ on c for (a) PVP and (b) PSSN-1 solutions. (*I*) Aqueous salt-free solution and (*II*) 0.2 M NaCl. The slopes at given concentrations $c \times 10^2$ correspond to the following intrinsic viscosities $[\eta]^*$ (cm^3 g^{-1}): (a) (*1*) c = 0.6, $[\eta]^*$ = 95 and (*2*) c = 2.1, $[\eta]^*$ = 60; (b) (*3*) c = 0.021, $[\eta]^*$ = 1510 and (*4*) c = 0.76, $[\eta]^*$ = 70 (*I*); (*4*) c = 0.25, $[\eta]^*$ = 110 and (*6*) c = 0.87, $[\eta]^*$ = 75 (*II*).

It follows from Eq. (7) that $\partial\ln\eta_r/\partial c$ can be considered as the current intrinsic viscosity in any point of the dependence of $\ln\eta_r$ on c (Fig. 2) [12, 13]:

$$[\eta]^* \equiv \partial\ln\eta_r/\partial c. \quad (8)$$

It is clear that, at $c \to 0$, $[\eta]^*$ corresponds to the initial slope of the plot $\ln\eta_r$–c, coinciding with $[\eta]$ [Eq. (4)] for the isolated macromolecule.

At a finite polymer concentration, $[\eta]^*$ characterizes the specific volume occupied by the probe macromolecule placed into a solution with a uniform distribution of all other macromolecules. Such an approach can be considered as an experimental realization of the middle field concept. The $[\eta]^*$ changes with variation of the polymer concentration.

The method of determination of the intrinsic viscosity using Eq. (8) was employed in [12, 14] when analyzing the effect of compaction of the globules in flexible-chain polymers on passing to the moderate polymer concentration range in solvents of various thermodynamic quality, and also when interpreting the hydrodynamic behavior of rod-shaped macromolecules.

In our experiments we studied a sample of neutral poly(vinylpyrrolidone) (PVP, *MW* 400×10^3) [15]; samples of polystyrenesulfonates of various molecular weights: PSSN-1 (*MW* 920×10^3), PSSN-2 (*MW* 740×10^3), and PSSN-6 (*MW* 50×10^3) containing amino groups in each monomeric unit [16]; and a sample of sulfated *meta*-aromatic polyamide (*m*-PASA, *MW* 250×10^3) [17]. The viscosity was measured at 25°C on an Ostwald viscometer, and also on a Zimm–Crothers low-gradient viscometer [18, 19].

The table summarizes the results of processing of the viscometric data for PVP in water and for PSSN and *m*-PASA in 0.2 M NaCl. In the latter case, the primary polyelectrolytic effects in the PSSN and *m*-PASA chains are suppressed. It is seen that the $[\eta]$ values obtained by different methods [Eqs. (3)–(8)]

Intrinsic viscosity estimated by Eqs. (3)–(8) for poly(vinylpyrrolidone) in water and polystyrene sulfonates and sulfated *meta*-aromatic polyamide in 0.2 M NaCl at 25°C

Polymer/solvent	$[\eta]$, $cm^3\ g^{-1}$	k'	$[\eta]$	k''	$[\eta]$	k_{SB}	$[\eta]$	c_m, $g\ cm^{-3}$	$[\eta]^*$, $c \to 0$
	Eq. (3)		Eq. (4)		Eq. (5)		Eq. (6)		Eq. (8)
PVP/H_2O	123.0±0.9	0.31	121.8±0.4	0.15	126±2	0.21	122.3±0.3	0.19	122.6±0.5
PSSN-6/0.2 M NaCl	22.0±0.2	0.32	21.8±0.2	0.15	22.5±0.2	0.22	22.2±0.2	1.77	21.7±0.2
PSSN-2/0.2 M NaCl	118±1	0.29	115.3±0.3	0.16	119±1	0.21	116.4±0.5	0.26	108.7±0.8
PSSN-1/0.2 M NaCl	174±1	0.35	173.4±0.6	0.14	179±2	0.23	174.2±0.8	0.08	166.6±0.5
m-PASA/0.2 M NaCl	209±3	1.19	224±3	0.15	229±4	0.53	221±2	0.01	226±4

are in satisfactory agreement. For polyelectrolytes (charged macromolecules), at $\eta_r < 2.5$, Eqs. (3)–(5) are nonlinear. In salt-free solutions, it is difficult to estimate $[\eta]$. At low polyelectrolyte concentrations, $\ln \eta_r/c$ and η_{sp}/c increase with decreasing c as a result of the polyelectrolytic effect (Fig. 3). This effect is caused by the fact that, with dilution, the volume in which the counterions are spread increases, thus reducing the screening of the charges fixed on the chain and strengthening their mutual repulsion. As a result, the size of the polyion increases. Thus, with decreasing ionic strength of the solution μ, the chain size increases by virtue of electrostatic repulsion between the monomeric units [20, 21].

For weak polyelectrolytes, with further decreasing concentration, we observed a maximum in the concentration dependences of $\ln \eta_r/c$ and η_{sp}/c. The nature of this maximum was discussed in [22, 23]. The data related to the ascending portion of these dependences can be linearized using the Fuoss empirical relationship [20, 24]:

$$c/\eta_{sp} = [\eta]^{-1} + (B/[\eta])c^{1/2}. \quad (9)$$

In the coordinates c/η_{sp}–$c^{1/2}$, the portion cut off on the abscissa is considered as the reciprocal intrinsic viscosity of a polyelectrolyte. However, the Fuoss equation is not always valid (Fig. 4).

As a more reasonable procedure for the determination of $[\eta]$ of polyelectrolytes, the isoionic dilution method was suggested [20, 25, 26]. In this case, the initial salt-free solution is characterized by the ionic strength controlled by the polyelectrolyte concentration and by the degree of dissociation of ionic groups. The polyelectrolyte solution is diluted with a solution of a low-molecular-weight salt whose ionic strength is equal to that of the initial salt-free solution of the polyelectrolyte. In practice, the concentration of the low-molecular-weight salt is selected so that the dependence of η_{sp}/c (or $\ln \eta_r/c$) on c be linear. Under-

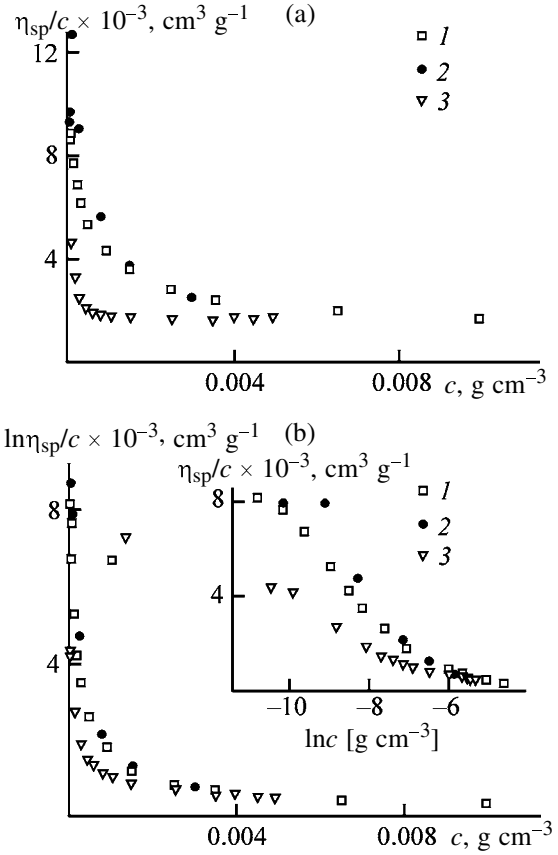


Fig. 3. Dependences of (a) η_{sp}/c and (b) $\ln \eta_r/c$ on c for polyelectrolytes in aqueous salt-free solutions. (*1, 2*) PSSN-1 and (*3*) *m*-PASA. Measuring technique: (*1, 3*) Ostwald capillary viscometer and (*2*) low-gradient rotary viscometer. In the insert (Fig. 3b), a logarithmic scale is used for the abscissa.

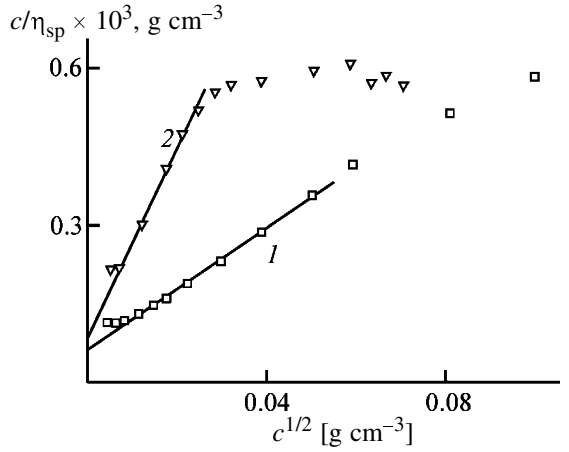


Fig. 4. Fuoss representation of data from Fig. 3: (*1*) PSSN-1 and (*2*) *m*-PASA.

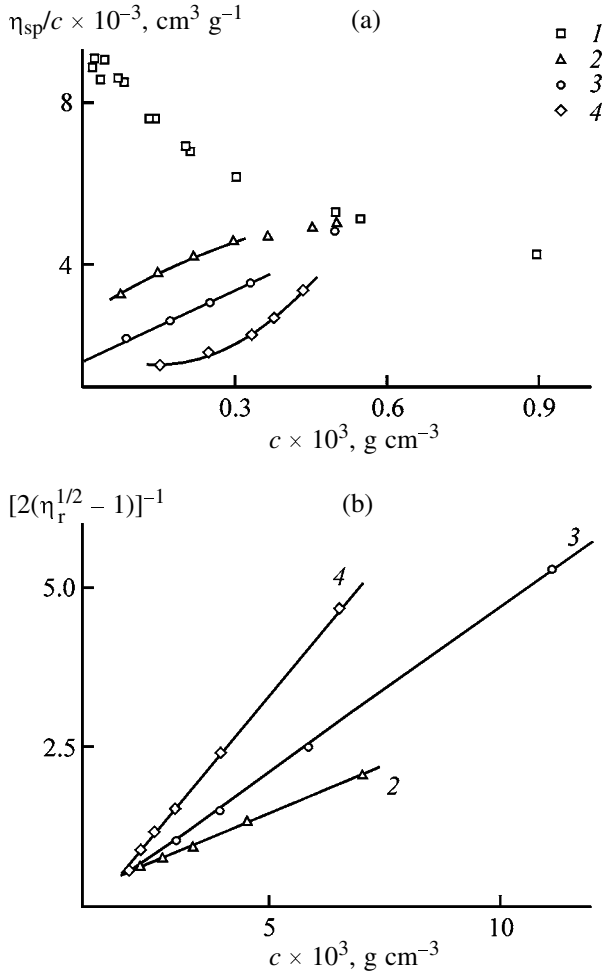


Fig. 5. (*1*) η_{sp}/c as a function of c in aqueous salt-free solution; (a) optimization of isoionic dilution conditions for PSSN-1 solution at the polymer concentration c = 0.5 mg cm^{-3} and (b) Fedors representation of data from Fig. 5a [Eq. (6)]. C_{NaCl}, mM: (*2*) 0.20 (undersalting of the buffer electrolyte), (*3*) 0.64 (isoionic dilution), and (*4*) 2.14 (oversalting of the buffer electrolyte).

or oversalting of the solvent distorts the linearity of the indicated dependences. The resulting dependences are well reproduced by second-order polynomials with opposite signs of the coefficients at c^2 (Fig. 5a). Therefore, the goal of optimization is to obtain a dependence with $\partial^2(\eta_{sp}/c)/\partial c^2 = 0$. In this case, the resulting dependence of η_{sp}/c (or $\ln \eta_r/c$) on c will be linear, allowing determination of $[\eta]$ at a fixed ionic strength.

We found that, in all cases of underestimation or overestimation of the ionic strength of the solvent containing a low-molecular-weight salt, and also in the case of isoionic dilution, the Fedors representations were linear (correlation factor $r > 0.9995$) over the entire concentration range of the polyelectrolyte (Fig. 5b). In this case, the dependence of thus obtained $[\eta]$ on the ionic strength was consistent with the dependence of the intrinsic viscosity obtained for flexible-chain polymers ($[\eta] \sim \mu^{-1/2}$) [27].

In our case, the NaCl concentration corresponding to the isoionic dilution was determined as an average between the concentrations meeting the conditions $\partial^2(\eta_{sp}/c)/\partial c^2 = 0$ and $\partial^2(\ln \eta_r/c)/\partial c^2 = 0$. The relative error of determination of this concentration was within 20%. Using the isoionic dilution method and Fedors representation, we determined $[\eta]$ of polystyrene sulfonate over the ionic strength range from 0.1 to 2.4 mM.

For PSSN-1, in the range of polyelectrolytic effects, very high intrinsic viscosities ($[\eta] > 2000$ cm^3 g^{-1}) are expected with isoionic dilution. In this case, the effect of the flow velocity gradient on the viscosity of the polymer solutions should be taken into account. This effect was examined on a Zimm–Crothers low-gradient viscometer [18]. The results are presented in Fig. 6 for the gradient range $0.1 \le g \le 7$ s^{-1}. The viscosity of the polymer solution appeared to be practically independent of the velocity gradient. The $\ln \eta_r$ values thus obtained are compared in Fig. 3 with the values obtained with the Ostwald capillary viscometer ($g \approx 700$ s^{-1}). As seen, these values are in satisfactory agreement.

As a rule, the concentration dependences of the relative viscosity in the salt-free solutions were measured with the Ostwald viscometer at 10–15 concentrations. At low concentrations, the concentration step was about 1×10^{-4}, and at high concentrations, 20×10^{-4} g cm^{-3}, allowing reliable determination of the slopes of the concentration dependences ($\partial \ln \eta_r/\partial c$) over the entire experimental concentration range including limiting dilution. With increasing polyelectro-

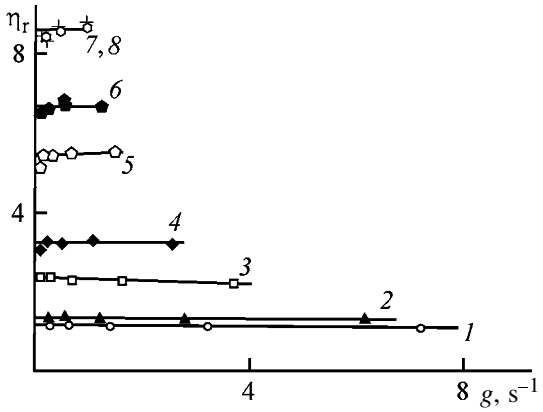


Fig. 6. Gradient dependences of the relative viscosity η_r in salt-free aqueous PSSN-1 solutions at various concentrations c (mg cm^{-3}): (*1*) 0.020, (*2*) 0.040, (*3*) 0.110, (*4*) 0.252, (*5*) 0.806, (*6*) 1.511, and (*7, 8*) 2.992. (*g*) Velocity gradient.

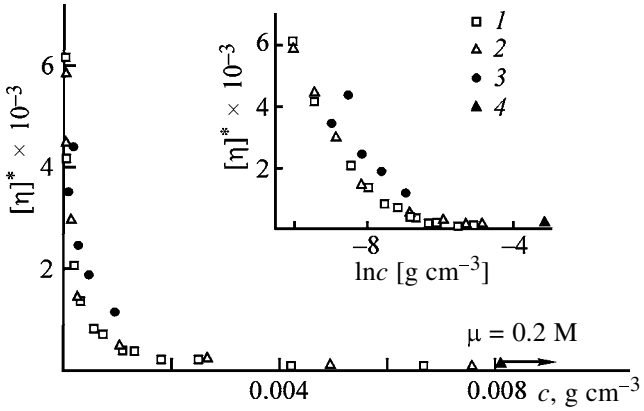


Fig. 7. Current intrinsic viscosity η^* as a function of the PSSN-1 concentration c in salt-free aqueous solution. (*1, 2*) Two independently prepared solutions, (*3*) intrinsic viscosity obtained in the isoionic dilution experiment, and (*4*) intrinsic viscosity obtained in 0.2 M NaCl. In the insert, logarithmic scale is used for the abscissa.

lyte concentration in water, the ionic strength of the solution increases, resulting in a decrease in the diameter of the globules and η^*. We have made a comparative analysis of $[\eta]^* = (\partial \ln \eta_r/\partial c)$ and $[\eta]$ obtained in the isoionic dilution experiment. These values appeared to be well consistent (Fig. 7).

Note also that $[\eta]$ obtained by the Fuoss extrapolation [when it is possible, i.e., when relationship (9) is linear] is, on the average, twice that obtained as $[\eta]^*_{c\to 0} = (\partial \ln \eta_r/\partial c)_{c\to 0}$, suggesting that the Fuoss extrapolation procedure provides overestimated volume occupied by the polyelectrolyte molecule at the infinite dilution in the absence of additional counterions.

To conclude, the viscometric data obtained in dilution of salt-free polyelectrolyte solutions were analyzed in terms of the current intrinsic viscosity using the Fedors and Fuoss relationships. Comparative analysis of the current intrinsic viscosity $[\eta]^* \equiv \partial \ln \eta_r/\partial c$ with the results obtained by the isoionic dilution method showed practical identity of the results obtained by these two methods. Therefore, in addition to the isoionic dilution method, we can recommend this considerably less time-consuming method for determination of the intrinsic viscosity of polyelectrolyte in salt-free solutions or at low ionic strengths.

CONCLUSION

The current intrinsic viscosity $[\eta]^* = \partial \ln \eta_r/\partial c$ proved to be an adequate parameter to describe the molecular properties of polyelectrolytes in salt-free solutions.

REFERENCES

1. Tsvetkov, V.N., *Zhestkotsepnye polimernye molekuly* (Rigid-Chain Polymeric Molecules), Leningrad: Nauka, 1986.
2. Fujita, H., *Polymer Solutions*, Amsterdam: Elsevier, 1990.
3. Vinogradov, G.V. and Malkin, A.Ya., *Reologiya polimerov* (Rheology of Polymers), Moscow: Khimiya, 1977.
4. Furukawa, J., *Physical Chemistry of Polymer Rheology*, Berlin: Springer, 2003.
5. *Polymer Handbook*, Brandrup, J. and Immergut, E.H., Eds., New York: Wiley, 1989, 3rd ed., vol. 1, pp. VII-61–VII-146.
6. Rabek, J.F., *Experimental Methods in Polymer Chemistry. Physical Principles and Applications*, Chichester: Wiley, 1980.
7. Pavlov, G.M., *Vysokomol. Soedin., Ser. A*, 2005, vol. 47, pp. 1872–1878.
8. Huggins, M.L., *J. Am. Chem. Soc.*, 1942, vol. 64, pp. 2716–2718.
9. Kraemer, F.O., *Ind. Eng. Chem.*, 1938, vol. 30, pp. 1200–1204.
10. Schulz, G.V. and Blaschke, F., *J. Prakt. Chem.*, 1941, vol. 158, pp. 130–135.
11. Fedors, R.F., *Polymer*, 1979, vol. 20, pp. 225–228.
12. Baranov, V.G., Brestkin, Yu.V., Agranova, S.A., et al., *Vysokomol. Soedin., Ser. B*, 1986, vol. 28, pp. 841–843.
13. Irzhak, V.I., in *Fizicheskie svoistva vyazkouprugikh polimerov* (Physical Properties of Viscoelastic Poly-

mers), Sverdlovsk: Ural'sk. Nauchn. Tsentr Akad. Nauk SSSR, 1981, pp. 76–81.

14. Baranov, V.G., Frenkel', S.Ya., Agranova, S.A., et al., *Vysokomol. Soedin., Ser. B*, 1987, vol. 29, pp. 745–748.
15. Pavlov, G.M., Panarin, E.F., Korneeva, E.V., et al., *Vysokomol. Soedin., Ser. A*, 1990, vol. 32, pp. 1190–1196.
16. Pavlov, G.M., Zaitseva, I.I., Gubarev, A.S., et al., *Zh. Prikl. Khim.*, 2006, vol. 79, no. 9, pp. 1506–1509.
17. Pavlov, G.M., Korneeva, E.V., Fedotov, Yu.A., et al., *Zh. Prikl. Khim.*, 1996, vol. 69, no. 5, pp. 824–828.
18. Frisman, E.V., Shchagina, L.V., and Vorob'ev, V.I., *Kolloidn. Zh.*, 1965, vol. 27, pp. 130–133.
19. Tsvetkov, V.N. and Korneeva, E.V., *Vestn. Leningr. Gos. Univ., Ser. Fiz. Khim.*, 1965, vol. 4, no. 22B, pp. 75–79.
20. Tanford, Ch., *Physical Chemistry of Macromolecules*, New York: Wiley, 1963.
21. Dobrynin, A.N. and Rubinstein, M., *Prog. Polym. Sci.*, 2005, vol. 30, pp. 1049–1118.
22. Eisenberg, H. and Pouyet, J., *J. Polym. Sci.*, 1954, vol. 13, pp. 85–93.
23. Nishida, K., Kaji, K., Kanaye, T., et al., *Polymer*, 2002, vol. 43, pp. 1295–1300.
24. Fuoss, R.M., *J. Polym. Sci.*, 1948, vol. 3, pp. 603–609.
25. Pals, D. and Hermans, J., *J. Polym. Sci.*, 1950, vol. 5, pp. 733–734.
26. Sakurada, I. and Ise, N., *Makromol. Chem.*, 1960, vol. 40, pp. 126–139.
27. Dautzenberg, H., Jaeger, W., Koetz, J. et al., *Polyelectrolytes*, Munich: Hauser, 1994.

ISSN 1070-4272, Russian Journal of Applied Chemistry, 2006, Vol. 79, No. 9, pp. 1413–1418. © Pleiades Publishing, Inc., 2006.
Original Russian Text © T.S. Bondarenko, E.S. Boichinova, 2006, published in Zhurnal Prikladnoi Khimii, 2006, Vol. 79, No. 9, pp. 1429–1434.

PHYSICOCHEMICAL STUDIES OF SYSTEMS AND PROCESSES

A Physicochemical Study of the Structure of Inorganic Electron and Ion Exchanger Based on Zirconium(IV), Molybdenum(VI), and Silicon(IV)

T. S. Bondarenko and E. S. Boichinova

St. Petersburg State Technological Institute, St. Petersburg, Russia

Received July 9, 2004; in final form, June 2006

Abstract—To elucidate the character of binding of water and hydroxy groups with a substance, the activation energy and the order of the dehydration reaction of an inorganic electron and ion exchanger based on zirconium(IV), molybdenum(VI), and silicon(IV) were calculated from the weight loss curve in the maximal loss region. To determine the structure of the synthesized electron and ion exchanger, its physicochemical properties were studied by X-ray phase analysis and electron microscopy.

DOI: 10.1134/S1070427206090047

To properly choose and efficiently perform the processes, it is necessary to calculate the parameters of sorption columns and the optimal amounts of sorbents absorbing various materials, which, in turn, requires knowledge of the physicochemical potential of the exchanger. We have shown previously that coprecipitation of zirconium(IV), molybdenum(VI), and silicon(IV) salts in a weakly acidic medium yields a compound differing from zirconium, molybdenum, and silicon oxides [1]. It was conventionally named zirconium silicomolybdate (ZSM). The synthesized granular product, according to IR and derivatographic data, is an individual inorganic compound containing residues of silicomolybdic heteropoly acid and exhibiting ion-exchange and redox properties, i.e., it is an inorganic electron and ion exchanger (EIE) [2]. The complicated IR spectrum and an ambiguous interpretation of thermal effects in the thermogravimetric curve called for a more detailed consideration of the ZSM dehydration, and the elucidation of the ZSM transformations and of the structure formation in the temperature regions corresponding to the main thermal effects required an X-ray phase analysis of samples and their electron microscopic examination.

The activation energy and reaction order (Table 1; Figs. 1, 2) for the ZSM dehydration suggest that the strengths of binding of water and OH groups in the exchanger are different. This assumption is supported by the comparison of the results of thermogravimetric analysis with certain published data (Tables 2, 3).

It was proved in [6] by IR spectroscopy that glassy tungsten-containing acids contain two types of H-bonds. Additional absorption frequencies related to nonequivalent water H-bonds were found in the spec-

Table 1. Calculated activation energy and reaction order for ZSM dehydration*

T, K	Weight loss W, mg	Transformation rate R, deg min^{-1}
395	4.40	184.60
418	10.00	198.80
440	16.00	121.42
483	20.00	238.60

* Reaction order n = 1.40, rate constant k = 1.59, activation energy E_a = 127.50 kJ mol^{-1}.

Table 2. Results of thermogravimetric analysis

Effect type	Temperature, °C		Weight loss by the end of effect, %
	effect peak	effect end	
Endo (–)	170	330	16.98
Endo (–)	390	460	3.59
Exo (+)	490	525	–
Endo (–)	550	570	>1
Endo (–)	620	725	–
Exo (+)	820	880	–
Endo (–)	980	990	6.36
Sharp weight loss above 1000°C			

Table 3. Results of derivatographic analysis of known compounds

Compound	Thermal effect		Process	References
	type	T, °C		
$ZrO_2 \cdot nH_2O$	Endo (–)	200–400	Dehydration	[3]
	Exo (+)	400–450	Metastable cubic structure	
	Exo (+)	650–850	Cubic → monoclinic	
	Endo (–)	1120–1190	Monoclinic → tetragonal	
Mixture of zirconium and molybdenum oxides	Endo (–)	100–300	Dehydration	[4]
	Exo (+)	400–550	Crystallization of oxides	
	Exo (+)	550–650	Chemical compound formation	
	Endo (–)	720–830	Polymorphous transition	
SM HPA (silicomolybdic heteropoly acid)	Endo (–)	112	Dehydration	[5]
	Endo (–)	150	Dehydration	
	Exo (+)	370	Crystallization of molybdenum oxide	
	Endo (–)	420	Decomposition into silicon and molybdenum oxides	

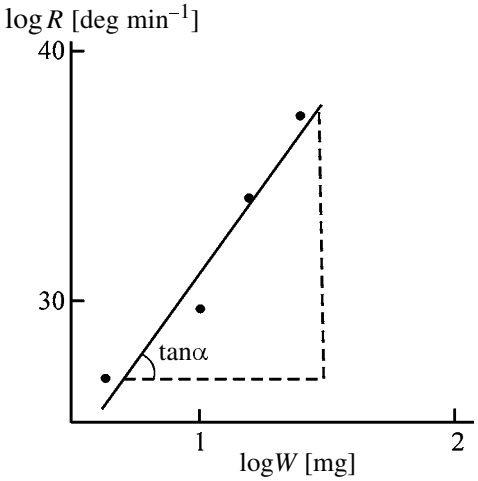


Fig. 1. Determination of the reaction order for ZSM dehydration. (R) Transformation rate and (W) weight loss.

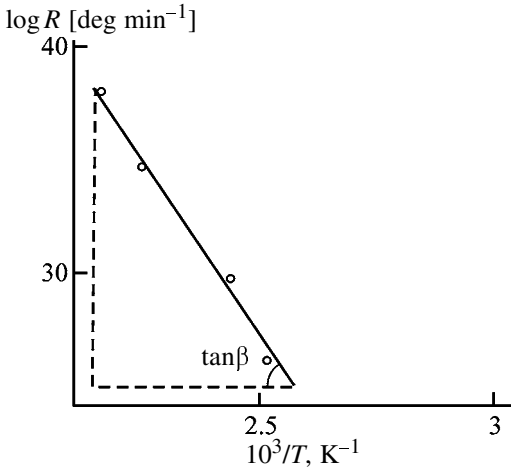


Fig. 2. Determination of the rate constant of ZSM dehydration. (R) Transformation rate and (T) temperature.

tra. In papers concerning dehydration of hydrated titanium dioxide and tin hydroxide [7, 8], it was also concluded that water and OH groups are bound with different strengths in the sorbents under study.

The nature of transformations in ZSM and the formation of a structure were judged from the diffraction patterns of an air-dry sample and samples subjected to the corresponding thermal treatment in the regions of peak temperatures (Fig. 3). The interplanar spacings calculated from the diffraction patterns are given in Table 4; the ZSM thermogravimetric curve, in Fig. 4; and the interplanar spacings of individual compounds, in Table 5.

Figure 4 shows that a crystalline phase appears only on heating to 490°C and higher temperatures. The diffuse character of reflections in the diffraction pattern suggests the presence of a considerable fraction of X-ray amorphous phases. A comparative analysis of the reflections in diffraction pattern *3* (Fig. 3) and interlayer spacings in the polymeric modification of molybdenum oxides and in molybdenum trioxide, and also of zirconium dioxide reveals appearance of diffraction maxima at reflection angles of 6°–8°, 11.65°, and 13.5°. The first of them is rather weak and two other are better pronounced and can be assigned to molybdenum trioxide. According to published data [4], the first line of MoO_3 is of a medium intensity, and two other lines are strong. Apparently, a superposition of thermal transformations associated with a change in the state of the heteropoly anion structure is observed against the background of the formed crystalline structure on heating of ZSM at 490°C. Two

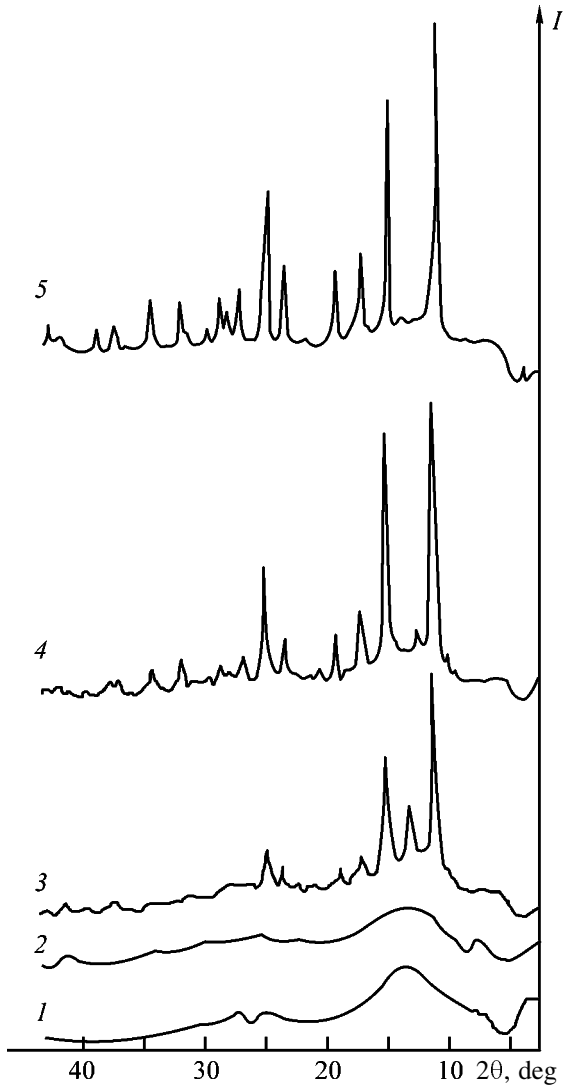


Fig. 3. ZSM diffraction pattern. (*I*) Relative intensity and (θ) reflection angle. (*1*) Drying temperature 20°C; precalcination temperature, °C: (*2*) 180, (*3*) 490, (*4*) 620, and (*5*) 820.

Table 4. Results of X-ray phase analysis of ZSM

θ, deg	sin θ	*d*, Å	*I*, rel. units
Calcination temperature 490°C			
11.65	0.2019	3.83	46
13.50	0.2334	3.29	17
15.50	0.2672	2.89	27
17.60	0.3024	2.55	10
19.40	0.3322	2.33	6
23.70	0.4019	1.92	8
25.15	0.4249	1.81	11
27.20	0.4571	1.69	7
Calcination temperature 620°C			
11.65	0.2019	3.83	53
15.50	0.2672	2.89	49
17.60	0.3024	2.55	15
19.40	0.3322	2.33	9
23.70	0.4019	1.92	11
25.15	0.4249	1.81	22
27.20	0.4571	1.69	7
28.25	0.4726	1.63	2
28.76	0.4813	1.60	4
31.85	0.5277	1.46	1
Calcination temperature 820°C			
11.65	0.2019	3.83	100
13.00	0.2385	3.23	7
15.50	0.2672	2.89	61
17.60	0.3024	2.55	19
19.40	0.3322	2.33	15
23.70	0.4019	1.92	17
25.15	0.4249	1.81	32
27.20	0.4571	1.69	13
28.25	0.4726	1.63	10
28.76	0.4813	1.60	11
31.85	0.5277	1.46	9
34.50	0.5664	1.36	10

crystalline forms, polymeric molybdenum oxide and molybdenum trioxide, are apparently formed, which is supported by the fact that the sample acquires a pink color with a metallic tint. The behavior of individual silicomolybdic heteropoly acid on heating has been described in [5] (Table 3). The intensive line at 11.65° most likely belongs to a mixture of both forms of the oxides. The crystalline phase is less clearly manifested at reflection angles of 25°–27°.

After calcination at a higher temperature (620°C), the polymeric form of molybdenum oxide predominates in the diffraction pattern (Figs. 3, curve 4), and the sample becomes violet. In this range, an endothermic effect appears in the derivatogam (Fig. 4) without a noticeable weight loss. Apparently, the oxygen content in the system changes at this temperature, Mo(VI) is partially reduced to Mo(V), and one modification of molybdenum oxide transforms into another. Furthermore, an endothermic effect can take place without weight loss if, e.g., a finely crystalline phase transforms into a coarsely crystalline phase. The reflections characteristic of molybdenum trioxide become weak and smoothed. The diffraction maxima at 6°–8° and 13.50° become poorly discernible. Most likely, an additional energy consumption is associated with the transformation of the finely crystalline fraction existing at a lower temperature into a coarsely crystalline fraction (broad peak at 18.50°, smeared at the base).

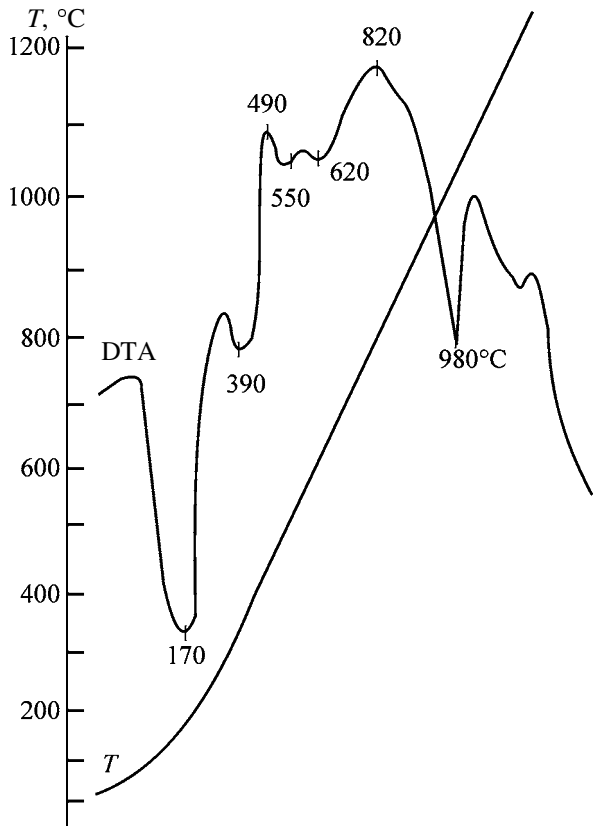


Fig. 4. Thermogravimetric curve of air-dry ZSM sample. (*T*) Temperature.

Table 5. Results of X-ray phase analysis of individual compounds

ZrO_2 [9]		Mo_xO_y-500 [4]		MoO_3 [4]	
I	*d*, Å	*I*	*d*, Å	*I*	*d*, Å
2	3.692	Strong	3.86	34	6.93
4	3.158	Medium	3.496	82	3.81
5	2.947	Strong	3.30	61	3.46
3	2.843	Medium	2.97	100	3.26
3	2.611	Weak	2.72	13	3.01
3	2.589	Medium	2.68	19	2.702
2	2.324	Weak	2.54	35	2.055
2	2.202	Medium	2.31	12	2.527
5	1.811	Weak	1.85	12	2.332
3	1.692	Weak	1.665	31	2.309
2	1.656	Weak	1.632	18	2.271
3	1.588	Weak	1.570	9	2.131
4	1.556			4	1.996
3	1.476			13	1.982
1	1.357			17	1.960
1	1.321			21	1.849
2	1.296			11	1.820
				17	1.733

The polymeric form of molybdenum oxide predominates and reflections of a mixture of modifications (monoclinic and tetragonal) of crystalline zirconium oxide become more distinct in the diffraction pattern of the ZSM sample obtained after calcination at 820°C. The sample transforms from a violet form into a white form with a grayish tint. The appearance of an exothermic effect in the thermogravimetric curve is associated most likely with the formation of a crystalline phase of zirconium oxide. Thus, the X-ray phase analysis shows that the character of the ZSM structure is retained on heating in the temperature range under study. The analysis also confirms that the compounds are individual and undergo complex phase transformations on heating.

The electron micrographs of the air-dry starting and reduced ZSM samples and of the samples regenerated from the reduced form have shown that all the three samples have a rather developed surface (Figs. 5a–5c). A predominantly finely porous structure with apparently smoothed parts is observed along with porous regions, which is clearly seen in the image of the sample oxidized again after regeneration. This conclusion agrees well with a low value of the total ZSM porosity of 0.02 $cm^3\ g^{-1}$ [9]. The apparent smoothness of surface regions is attributable to an insufficient magnification for microporous subjects studied in the microdiffraction mode. All the three abovementioned ZSM forms were studied. We were able to obtain a diffraction pattern only for the reduced ZSM sample (Fig. 5, Table 6). The interplanar spacings calculated from the diameters of rings point to a higher degree of crystallization of the reduced form, especially when we take into account the fact that the X-ray analysis is less sensitive compared to the electron microscopy.

EXPERIMENTAL

The activation energy and reaction order were calculated by the Freeman–Carroll method [10] for the part of the thermogravimetric curve corresponding to the heating to 200°C, where the weight loss is maximal (Fig. 4). The first endothermic peak is in the same region. The calculated data and plots are presented in Figs. 1, 2 and in Table 1. The calculations were performed as follows. Two dependences were constructed: $\log R$–$\log W$ and $\log R$–$1/T$. In both cases they are linear. The reaction order n was determined from the logarithmic dependence of the transformation rate on the weight using the slope of the straight line to the abscissa. The rate constant of the process k was

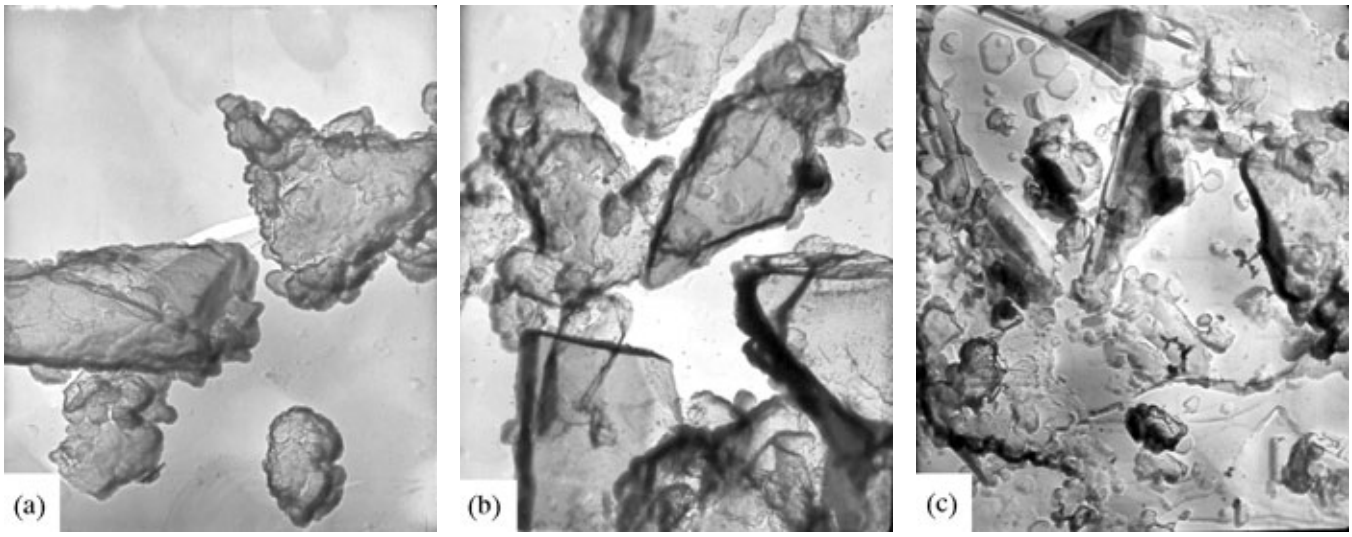


Fig. 5 . Electron micrographs of ZSM surface: (a) oxidized form, starting air-dry sample; (b) reduced form, air-dry sample; and (c) oxidized form regenerated from air-dry reduced form.

determined from the semilog dependence of the transformation rate on reciprocal temperature. According to the Arrhenius equation,

$$k = Ze^{E_a/RT},$$

where Z is the preexponential factor; E_a, activation energy of the process (kJ mol^{-1}); R, universal gas constant (J K^{-1} mol^{-1}); and T, absolute temperature (K).

From the above equation, we can find E:

$$\log k = E_a/2.303R \times 4.187.$$

The X-ray phase analysis was carried out on a DRON-2 diffractometer using nickel-filtered copper radiation. The diffraction patterns of the starting sample and the samples preliminary calcined at the temperatures corresponding to the main thermal effects in the thermogravimetric curve were recorded. The measurement rate was 3 deg min^{-1}. The error of the intensity determination was 3–5%. The reflection angles found from the diffraction pattern were transformed to interplanar spacings using Tolkachev's tables [11].

Table 6. Diffraction pattern of reduced ZSM form

Ring no.	Ring radius $2r$, mm	d, Å	Intensity
1	8.0	5.85	Strong, smeared
2	12.0	3.88	Strong, clear
3	18.0	2.59	Fairly clear
4	21.0	2.22	Weak, fairly clear
5	24.5	1.90	Weak, less clear
6	32.0	1.46	Weak, smeared
7	42.0	1.11	Weak, smeared

Parts of ZSM surface were detected as micrographs obtained by the method of carbon replicas with spraying or with extraction on an EVM-1000L electron microscope [12]. Magnification ×20 000. In the first case, hydrofluoric acid was used as a solvent, and in the second case it was a mixture of nitric and hydrochloric acids.

The samples of the reduced form and samples regenerated from this form were obtained by the technique described in [2].

The diffraction patterns were obtained in the microdiffraction mode [9]. As a standard for a device constant we used a plate of aluminum having a face-centered cubic lattice. Interplanar spacings d (Å) were calculated by the formula [13]

$$d = 46.6/2r,$$

where r is the radius (mm) and 46.6 is the device constant (mm Å).

CONCLUSIONS

(1) The calculations of the activation energy and the order of the reaction of zirconium silicomolybdate dehydration showed that binding energies of water and hydroxy groups are different.

(2) It was proved for the first time by X-ray phase analysis that zirconium silicomolybdate is an individual inorganic compound with its own structure.

(3) The surface structure of zirconium silicomolybdate was examined by electron microscopy, and the diffraction pattern of the reduced sample was obtained.

REFERENCES

1. Bondarenko, T.S. and Boichinova, E.S., *Zh. Prikl. Khim.*, 1985, vol. 58, no. 8, pp. 1746–1750.
2. Bondarenko, T.S. and Boichinova, E.S., *Zh. Prikl. Khim.*, 1992, vol. 65, no. 12, pp. 2677–2682.
3. Kuznetsov, A.K., Keler, E.K., and Fan' Fu-Kan, *Zh. Prikl. Khim.*, 1965, vol. 38, no. 2, pp. 233–235.
4. Denisova, N.E. and Boichinova, E.S., *Izv. Akad. Nauk SSSR, Neorg. Mater.*, 1967, vol. 3, no. 6, pp. 1049–1054.
5. Nikitina, E.A. and Buris, E.V., *Zh. Obshch. Khim.*, 1965, vol. 26, no. 3, pp. 622–625.
6. Derkach, L.V., Godonova, G.V., and Shafranskii, V.N., *Zh. Neorg. Khim.*, 1987, vol. 32, no. 5, pp. 1086–1088.
7. Evdokimova, L.I., Boichinova, E.S., and Brynzova, E.D., *Vliyanie nekotorykh uslovii polucheniya gidratirovannoi dvuokisi titana na ee ionoobmennye svoistva* (Influence of Some Conditions of Preparation of Hydrated Titanium Dioxide on Its Ion-Exchange Properties), Available from VINITI, Cherkassy, 1978, no. 2225178.
8. Parshutkin, V.V., Yaroslavtsev, A.B., and Prozorovskaya, Z.N., *Zh. Neorg. Khim.*, 1985, vol. 50, no. 1, pp. 56–59.
9. Bondarenko, T.S. and Boichinova, E.S., *Ionnyi obmen i ionometriya* (Ion Exchange and Ionometry), Belinskaya, F.A., Ed., St. Petersburg: Sankt-Peterb. Gos. Univ., 1995, issue 8, pp. 60–66.
10. *Termicheskii analiz polimerov* (Thermal Analysis of Polymers), Mukhlenov, I.P., Ed., Leningrad: Leningr. Tekhnol. Inst., 1981.
11. Tolkachev, S.S., *Tablitsy mezhploskostnykh rasstoyanii* (Tables of Interplanar Spacings), Leningrad: Khimiya, 1965.
12. Schimmel, G., *Elektronenmikroskopische Metodik*, Berlin: Springer, 1969.
13. Komissarova, L.N., Simanov, Yu.P., and Vladimirova, E.A., *Zh. Neorg. Khim.*, 1960, vol. 5, no. 7, pp. 1413–1417.

ISSN 1070-4272, Russian Journal of Applied Chemistry, 2006, Vol. 79, No. 9, pp. 1419–1422. © Pleiades Publishing, Inc., 2006.
Original Russian Text © I.D. Troshkina, Khaing Zo Naing, O.N. Ushanova, Vei P'o, A.A. Abdusalomov, 2006, published in Zhurnal Prikladnoi Khimii, 2006, Vol. 79, No. 9, pp. 1435–1438.

SORPTION AND ION-EXCHANGE PROCESSES

Recovery of Rhenium from Sulfuric Acid Solutions with Activated Coals

I. D. Troshkina, Khaing Zo Naing, O. N. Ushanova, Vei P'o, and A. A. Abdusalomov

Mendeleev Russian University of Chemical Engineering, Moscow, Russia

Received December 8, 2005; in final form, June 2006

Abstract—Equilibrium and kinetic characteristics of rhenium sorption from sulfuric acid solutions (pH 2) by activated coals produced from coal raw materials (China) were studied. Constants of the Henry equation describing isotherms of rhenium sorption by activated coals were calculated. The effective diffusion coefficients of rhenium in the coals were determined. The dynamic characteristics of rhenium sorption and desorption were determined for the activated coal with the best capacity and kinetic characteristics.

DOI: 10.1134/S1070427206090059

Metallic rhenium and its alloys and compounds have unique physicochemical properties, owing to which they are applied in various high-technology branches of industry [1]. The fact that rhenium is a rare metal, and hence its concentrations in ores are low, complicates its recovery.

The hydrometallurgical processing of rhenium-containing raw materials produces sulfuric acid solutions in which rhenium is in the form of perrhenate ions. It is recovered by sorption on weakly basic and strongly basic anion exchangers [2]. From dilute solutions, rhenium is sorbed with activated coals, which allows its deep recovery [2]. The best results are obtained in acid solutions (pH 2–3).

In this study we examined the sorption characteristics of activated coals (ACs) with respect to rhenium. The coals were produced from coal raw material by Ningxia Hui Autonomous Region Import and Export Corporation (China) [3]. The choice of these coals is caused by their rather high specific surface area and low cost.

EXPERIMENTAL

The main characteristics of the activated coals used are given in Table 1. The capacity properties of the coals were studied under static conditions at room temperature with model sulfuric acid solutions (rhenium concentration 0.1 g dm^{-3}, pH 2) at a phase ratio (g : dm^3) coal : solution (S : L) = 1 : 0.5. The time of contact of coals with the solution was no less than 8 days. Desorption was carried out with 8% ammonia solution at a phase ratio S : L = 1 : 0.06. The rhenium content in the aqueous phase was determined photocolorimetrically according to the standard technique [4].

We obtained the rhenium sorption isotherms by varying the rhenium concentration in solutions within the range 50–200 mg dm^{-3}. The isotherms were processed using the Henry equation [5].

The kinetics of rhenium sorption by activated coals from sulfuric acid solutions was studied by the method of limited solution volume under the conditions described above (rhenium concentration in the initial solution was 0.1 g dm^{-3}). The integral kinetic curves of rhenium sorption were obtained within the time of the sorbent contact with solution from 5 to 11 520 min (8 days).

The rhenium diffusion coefficients were calculated using the equation taking into account the half-conversion time $\tau_{0.5}$ [6]. These coefficients were calculated by the formula

$$\bar{D} = \frac{kR^2}{\pi\tau_{0.5}},$$

where $\bar{D}$ is the effective coefficient of rhenium diffusion from the sorbent (m^2 s^{-1}); k, a coefficient depending on the size and shape of the coal particle; R, radius of a particle or of a sphere equivalent to the particle [4] (m); and $\tau_{0.5}$, half-conversion time (s).

The dynamics of rhenium sorption from sulfuric

Table 1. Characteristics of activated coals

Activated coal	Ash content, no greater than, %	Moisture, no more than, %	Density, no less than, %	Capacity for iodine, mg g^{-1}	Bulk weight, g dm^{-3}
AC-1	14.58	3.26	93.5	1007	474
AC-2	8.22	7.28	95.8	–	456
AC-3	9.58	2.82	94.6	1060	430
AC-4	8.12	2.55	93.6	1058	435
AC-5	8.64	2.72	94.2	1026	485
AC-6	11.51	3.12	89.92	1039	511
AC-7	10.7	2.63	92.7	1114	375
AC-8	9.8	3.32	95.6	–	485
AC-9	9.23	2.97	95	–	454
AC-10	10.17	2.88	95.86	–	595
AC-11	9.93	3.01	93.2	932	476
AC-12	9.51	2.98	96.3	1016	415
AC-13	9.17	2.19	93.6	1066	390
AC-14	11.67	2	93	956	434
AC-15	11.48	4.72	92.3	924	503
AC-16	10.89	2.56	95.99	–	490

acid solutions (pH 2) by activated coals was studied in a column with the ratio of the coal bed height to the column diameter of 10 : 1; the solutions were passed at a rate of 17 specific (column) volumes h^{-1}; and the rhenium concentration in solution was 0.02 g dm^{-3}.

Table 2. Rhenium distribution at its sorption by activated coals from sulfuric acid solutions*

Activated coal	Sorption			Desorption	
	a, mg g^{-1}	K_d, cm^3 g^{-1}	α, %	K_d, g dm^{-3}	β, %
AC-1	30.3	767	61	22.5	58
AC-2	18.8	301	38	11.5	41
AC-3	31.5	852	63	11.0	40
AC-4	27.3	600	55	17.3	51
AC-5	27.8	625	56	17.6	51
AC-6	32.4	918	65	7.2	30
AC-7	31.5	851	63	3.4	17
AC-8	14.0	195	28	8.7	34
AC-9	21.4	373	43	12.5	43
AC-10	21.4	373	43	10.5	39
AC-11	24.5	480	49	17.9	51
AC-12	26.8	576	54	21.6	52
AC-13	12.0	158	24	21.5	57
AC-14	29.0	690	58	22.0	57
AC-15	28.8	678	58	11.3	40
AC-16	11.5	149	23	13.2	44

* (*a*) Weight capacity with respect to rhenium, (α) degree of sorption, and (β) degree of desorption.

The volume of activated coal in the column was 7 cm^3. The rhenium content was determined in the solution at the column outlet.

After the saturation of the coal with rhenium, it was washed with water to remove the residual initial solution. Rhenium was desorbed with an 8% ammonia solution, which was passed at a rate of 34 column volumes h^{-1}.

It is seen from the sorption–desorption characteristics of the coals (Table 2) that more than 50% of rhenium is recovered from solution by activated coals AC-1, -3, -4–7, -12, -14, and -15. Rhenium is efficiently eluted from coals AC-1, -4, -5, and -11–14. Thus, activated coals AC-1, -4, -5, -12, and -14 have the best sorption–desorption characteristics with respect to rhenium.

To compare the capacity characteristics with respect to rhenium in a wide range of its equilibrium concentrations, we have taken the rhenium sorption isotherms from sulfuric acid solutions (pH 2) with activated coals AC-1, -4, -5, -12, ad -14, and also with NORIT (the Netherlands) (for comparison), which exhibits high capacity (Fig. 1).

The resulting isotherms have a linear shape and are described by the Henry equation [4]. The Henry constants K (dm^3 g^{-1}) are given in Table 3.

The rate of rhenium sorption by the coals under study decreases in the order AC-4 > AC-12 > AC-1 > NORIT ≫ AC-14 > AC-5. The diffusion coefficients of activated coals are given in Table 4.

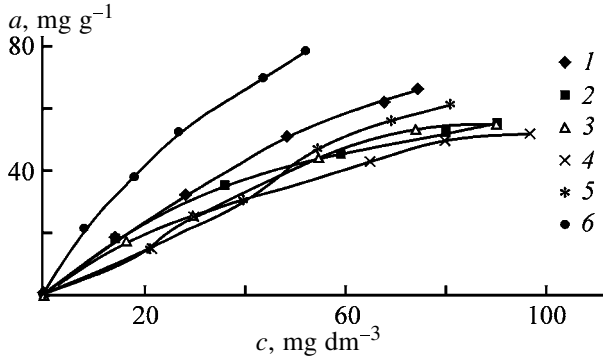


Fig. 1. Isotherms of rhenium sorption by activated carbons from sulfuric acid solutions (pH 2). (a) Weight capacity and (c) rhenium concentration in solution. Activated coal: (*1*) AC-1, (*2*) AC-4, (*3*) AC-5, (*4*) AC-12, (*5*) AC-14, and (*6*) NORIT.

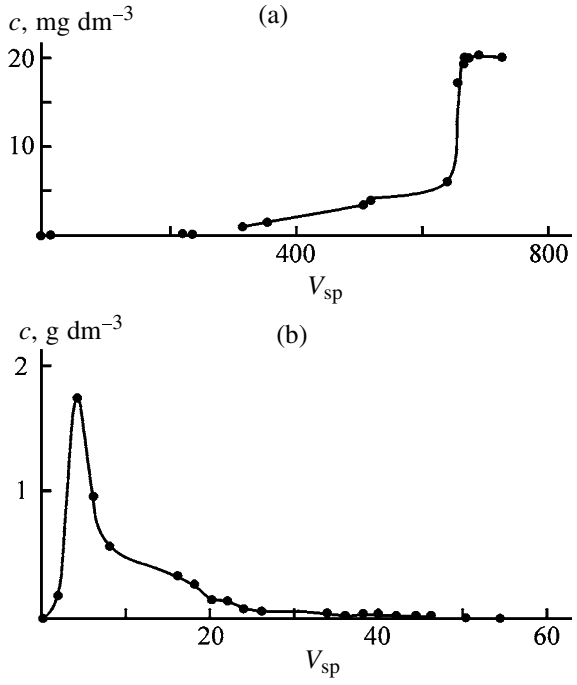


Fig. 2. (a) Breakthrough curve for rhenium sorptoin from sulfuric acid solution (pH 2) on AC-1 activated coal and (b) curve of rhenium desorption with 8% ammonia solution. (*c*) Rhenium concentration in solution and (V_{sp}) number of specific (column) volumes.

Table 3. Constants of the Henry equation

Activated coal	K, dm^3 g^{-1}	R^2	S
AC-1	0.90±0.06	0.986	2.9×10^{-3}
AC-4	0.66±0.06	0.978	7.5×10^{-3}
AC-5	0.69±0.07	0.967	10.5×10^{-3}
AC-12	0.57±0.03	0.989	1.8×10^{-3}
AC-14	0.77±0.03	0.993	6.9×10^{-4}
NORIT	1.6±0.21	0.948	22.4×10^{-3}

Table 4. Rhenium diffusion coefficients in activated coals

Activated coal	$\tau_{0.5}$, s	$\bar{D}$, m^2 s^{-1}
AC-1	780	1.3×10^{-11}
AC-4	480	2.6×10^{-11}
AC-5	1710	6.6×10^{-12}
AC-12	720	1.7×10^{-11}
AC-14	1800	7.1×10^{-12}
NORIT	1260	7.7×10^{-12}

For the AC-1 coal with the best sorption–desorption characteristics, we have taken the rhenium breakthrough curves (Fig. 2a) and desorption curves (Fig. 2b).

Figure 2a shows that rhenium is almost completely absorbed by AC-1 active coal from the first 320 specific volumes of the passed solution. The total dynamic exchange capacity for rhenium was 33 mg g^{-1}.

Rhenium is virtually completely washed out in a 20-column eluate volume, 80% of rhenium being concentrated in 3–5 column volumes.

We found that eluates with a rhenium concentration of 0.9–1 g dm^{-3} can be obtained by one sorption–desorption cycle when rhenium is recovered by AC-1 activated coal from a sulfuric acid solution (pH 2) containing 0.02 g dm^{-3} of rhenium.

We have carried out cyclic experiments on rhenium sorption–desorption by AC-1 activated coal under static conditions. Rhenium was sorbed from sulfuric acid solutions (pH 2) at a phase ratio (g ml^{-1}) S : L = 1 : 500; the desorption (two contacts) was carried out by 8% ammonia solution at a phase ratio S : L = 1 : 60. After three sorption–desorption cycles, the activated coal keeps its capacity characteristics: the degree of rhenium recovery (approximately 60%) has not changed.

CONCLUSIONS

(1) Among the examined activated coals (16 samples) produced from coal raw material (China), AC-1, -4, -5, -12, and -14 coals have the best sorption–desorption characteristics for rhenium extraction from sulfuric acid solutions.

(2) The use of AC-1 activated coal makes it possible to concentrate rhenium by a factor of 50 in one sorption–desorption cycle.

REFERENCES

1. Ellis, R., *Mining Mag*., 2004, Feb., pp. 32–33.
2. Korovin, S.S., Bukin, V.I., Fedorova, P.I., et al., *Redkie i rasseyannye elementy: Khimiya i tekhnologiya* (Rare and Scattered Elements: Chemistry and Technology), Moscow: MISiS, 2003.
3. *Catalog of Ningxia Hui Autonomous Region Import and Export Corporation* (China), 1999.
4. Borisova, A.V. and Ermakov, A.N., *Analiticheskaya khimiya reniya* (Analytical Chemistry of Rhenium), Moscow: Nauka, 1974.
5. Kel'tsev, N.V., *Osnovy adsorbtsionnoi tekhniki* (Fundamentals of Adsorption Technology), Moscow: Khimiya, 1984.
6. Smirnov, A.D., *Sorbtsionnaya ochistka vody* (Sorption Treatment of Water), Leningrad: Khimiya, 1982.

ISSN 1070-4272, Russian Journal of Applied Chemistry, 2006, Vol. 79, No. 9, pp. 1423–1427. © Pleiades Publishing, Inc., 2006.
Original Russian Text © N.I. Alekseev, O.V. Arapov, B.O. Bodyagin, V.V. Kudenko, E.V. Kustova, V.V. Samonin, K.N. Semenov, A.K. Sirotkin, N.A. Charykov, M.N. Chentsov, 2006, published in Zhurnal Prikladnoi Khimii, 2006, Vol. 79, No. 9, pp. 1439–1443.

SORPTION AND ION-EXCHANGE PROCESSES

Activation of the Carbon Component of Shungite-III and the Sorption Capacity of the Material for Hydrogen

N. I. Alekseev, O. V. Arapov, B. O. Bodyagin, V. V. Kudenko, E. V. Kustova, V. V. Samonin, K. N. Semenov, A. K. Sirotkin, N. A. Charykov, and M. N. Chentsov

Ioffe Physicotechnical Institute, Russian Academy of Sciences, St. Petersburg, Russia
Innovations by Leningrad Institutes and Enterprises, Private Company, St. Petersburg, Russia
St. Petersburg State Technological Institute, St. Petersburg, Russia
St. Petersburg State University, St. Petersburg, Russia

Received January 18, 2006

Abstract—The carbon material MNS, produced from shungite-III by successive alkaline and acid treatment, was studied. Cavitational treatment of an aqueous dispersion of the MNS material in the field of a standing acoustic wave converts a part of the substance into a material with a developed surface and a sorption capacity for hydrogen of up to 1.5%.

DOI: 10.1134/S1070427206090060

Development of inexpensive and reversible hydrogen accumulators is a topical task of modern science and technology because of the prospects for replacement (at least partial) of liquid fuels with hydrogen [1–3]. High hopes are pinned in this context on materials with considerable content of carbon nanotubes and other nanoparticles. However, on obtaining the first encouraging results [4–7] (not confirmed, but not refuted conclusively, either), an opinion was established that unmodified carbon nanoparticles can hardly provide a hydrogen accumulation level exceeding 1.5–2 wt % under atmospheric pressure [8]. With account of the high cost of carbon nanotubes, such a sorption capacity is insufficient for economically feasible applications. However, for an inexpensive material containing a nanocarbon component, e.g., industrial waste or abundant natural material, a capacity of 1–2% at 1 atm can be a starting figure for studies of the possible modifications of this material. The most promising, as regards the content of the nanocarbon component, among natural materials is shungite, which contains, together with noncrystalline carbon, also aluminosilicates and a minor amount of a bitumen-like organic material. Shungite-I [9] is the richest in carbon (up to 90%), but its cost is rather high, and resources, low. We believe that more promising for various applications, including hydrogen accumulation, is shungite-III with a carbon content of 30–40% [9] (the rest, 60–70%, is mainly constituted by aluminosilicates). The total amount of shungite rocks in the Onega basin exceeds 1 billion tons [10], and the resources of the largest Zazhoginskoe deposit are about 150 million tons.

The presence of the nanocarbon component (fulleroid structures of the type of multilayer nanotubes, nanobarrels, nanobulbs, etc.) in both shungite-I and shungite-III was first demonstrated in [11, 12]. As the shungite carbon as a whole, these structures are firmly bound to the aluminosilicate matrix [13], with both phases uniformly present even in a particle produced by micrometer grinding of a sample. Therefore, the application of shungites as catalyst supports [14], additives to concrete, etc. [15] is primarily based on grinding, rather than chemical treatment of the starting material. However, it is clear now that even a shungite of this kind is exceedingly promising.

An optimized technology for recovery of the carbon (hereinafter, nanocarbon) component of shungites markedly extends the potentialities of the resulting material, but does not lead to any significant rise in its cost.

The main technique for processing of the starting shungite-III included the following stages. A coarsely ground material (with particle size of up to several centimeters) was treated with molten NaOH in a graphite crucible at 500–520°C for 12 h in order to remove the aluminosilicate and silicate components.

Elemental chemical composition of the materials produced by chemical treatment of shungite-III

Processing method	Content, wt %								
	Na	Mg	Al	Si	S	Cl	K	Ca	Fe
Alkali without preliminary grinding and subsequent mild acid treatment (boiling HCl); MNS	0.5	<0.1	0.4	13.2	0.1	0.2	0.4	0.1	0.3
Treatment with HF/HNO_3 mixture without preliminary alkaline treatment	0.8	1.4	5.4	0.2	0.1	<0.1	0.5	2.2	0.8
Alkali with preliminary grinding to 50–100 μm, subsequent mild acid treatment (boiling HCl); MNS1	0.2	0.1	0.5	3.5	0.3	0.6	0.8	0.4	0.1

Further, the carbon phase was washed with water to remove trace amounts of the alkali and sieved to obtain a powder with grain sizes of 80–100 μm. The resulting material was subjected to a mild acid treatment in boiling nitric acid to remove metals, as well as metal oxides and poorly soluble salts, and to dissolve amorphous carbon and, partly, graphite, and washed with water to remove the residual acid.

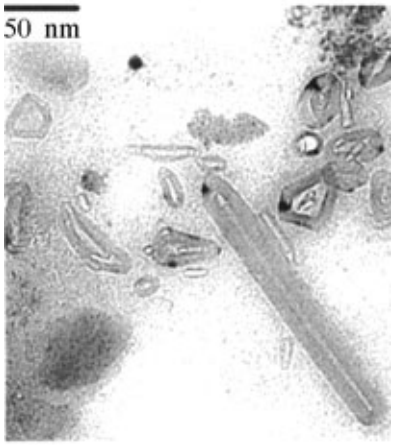


Fig. 1. TEM micrograph of modified shungite-III.

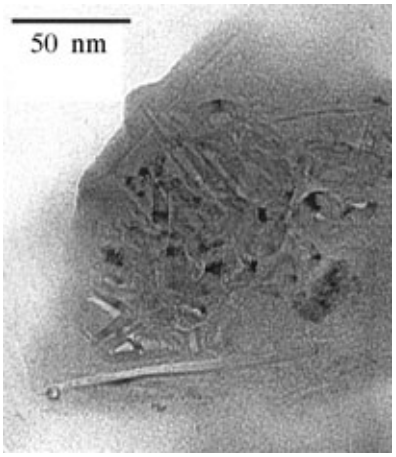


Fig. 2. TEM micrograph of a fragment of unmodified shungite-III.

The elemental composition of the thus obtained material (in what follows, MNS, modified nanoshungite) is presented in the table. It can be seen that, as a result of the treatment, the sample loses virtually the whole amount of aluminum, but retains a considerable amount of silicon (13 wt %). This content of Si yields the upper limit to the content of "concealed" carbon, judged from the approximate relative amounts of carbon and silicon in the starting shungite.

Typical electron micrographs of the nanostructures are shown in Fig. 1. The analysis was made on a JEOL JEM-100S transmission electron microscope (Japan) at magnifications of 10000–100000. Figure 1 illustrates a compact aggregation of nanoparticles nonuniformly distributed throughout the bulk of the material. It shows a hollow multilayer tube closed on both ends, with a large number of layers, channel diameter of about 3 nm, outer diameter of approximately 20 nm, and length of about 0.2 μm, and a set of nanobarrels and nonhollow nanobulbs. All the structures mentioned above are clearly separate from the silicate matrix. For comparison, Fig. 2 shows a fragment of the shungite material, which remained unsplit and has numerous fulleroid particles embedded in the aluminosilicate phase (naturally, the contrast of this micrograph is poorer than that of the preceding image).

The total amount of nanoparticles in the MNS material is up to 2%. The main structural motif of the rest of the carbon substance is constituted by short stacks of graphite-like layers [12]. Therefore, the carbon of this kind, which is different from that in

nanoparticles, is further designated as "graphite-like component," even though it is not subject to graphitization.

The possible enrichment of the MNS material with nanotubes and other nanoparticles must be due to removal of both this carbon and residual amounts of silicon. However, attempts of more thorough removal of silicon in order to improve the quality of the material proved to be inefficient. For example, treatment of the MNS material with a boiling $HF–HNO_3$ mixture (which is used, e.g., in decomposition of granites) results in that the amorphous and graphite components are effectively removed, as indicated by gravimetric measurements, but the amount of nanoparticles decreases dramatically. A similar pattern is observed in acid treatment of shungite not subjected preliminarily to the action of alkali, although silicon is removed in this case much more effectively (see table). The nanotubes preserved have a characteristic chopped structure, with the channels of the nanotubes not, nevertheless, cleaned (Fig. 3).

The possible reason for the inefficiency of the acid treatment is as follows. In contrast to nanoparticles synthesized in an arc or chemically grown by methods such as CVD [16] or HIPCO [17], shungite nanoparticles have the structure of imperfect, nearly amorphous fullerene caps [11, 12]. They are effectively destroyed by nitric and other strong acids. The nanoparticles are no less vulnerable than the graphite-like or amorphous component.

Similarly to the acid treatment, additional alkaline treatment of the MNS material fails to give positive results. The more effective removal of silicon is accompanied by a decrease in the amount of nanoparticles.

For example, a material richer in fulleroid particles and lower amount of silicates can be obtained from shungite-III, but this can only be done upon preliminary grinding of shungites to 50–100 μm. In this case, even a shorter alkaline treatment (three times in an hour) provides more effective removal of silicon than a three times longer treatment of unground shungite (see table). Also noticeable is the improvement of the material as regards the amount of nanoparticles, which now increases approximately twofold (to 3–4%).

The sorption capacity of MNS was studied by the volumetric method, using a version described, e.g., in [18]. The installation was intended for use in the static mode at pressures of up to 16 atm and temperatures of 20–30°C. The pressure drop in the gas medium upon introduction of a solid body was measured. A weighed portion of a shungite under study was placed in the adsorber and hydrogen was let-in from an auxiliary calibrated vessel (i.e., that in which the pressure, temperature, and volume were known). After equilibrium was attained by the system, the pressure in the adsorber and the amount of adsorbed hydrogen per unit mass of the sorbent were measured. The results obtained were used to plot hydrogen adsorption isotherms in the coordinates adsorption–absolute pressure.

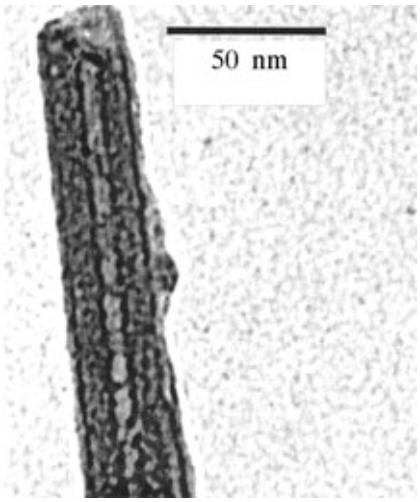


Fig. 3. Typical appearance of carbon nanotubes present in the shungite-based MNS material after an acid treatment with an $HF–HNO_3$ mixture.

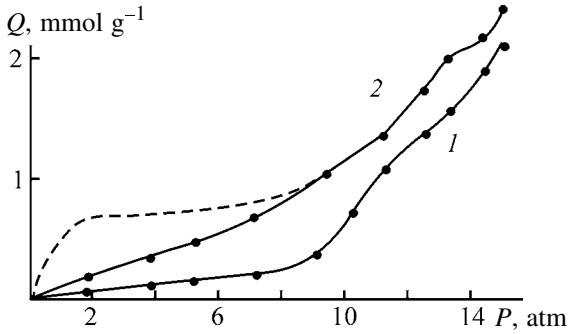


Fig. 4. Typical thermal desorption curves. (*Q*) Capacity and (*P*) pressure. Sample: (*1*) MNS and (*2*) MNS1. Dashed line, behavior observed for some MNS1 samples.

Typical thermal desorption curves are shown in Fig. 4 for MNS (curve *1*) and MNS1 (curve *2*) materials. At low pressures, curve *2* runs higher: at 2 atm the sorption capacity of the sample is about 0.05 wt %. If the whole capacity α_m is considered to be related to the nanocarbon component, then, in terms of this component, $\alpha_m \approx 1.2\%$, in agreement with the value commonly accepted for nanoparticles. Interestingly, a characteristic step was observed for some MNS1

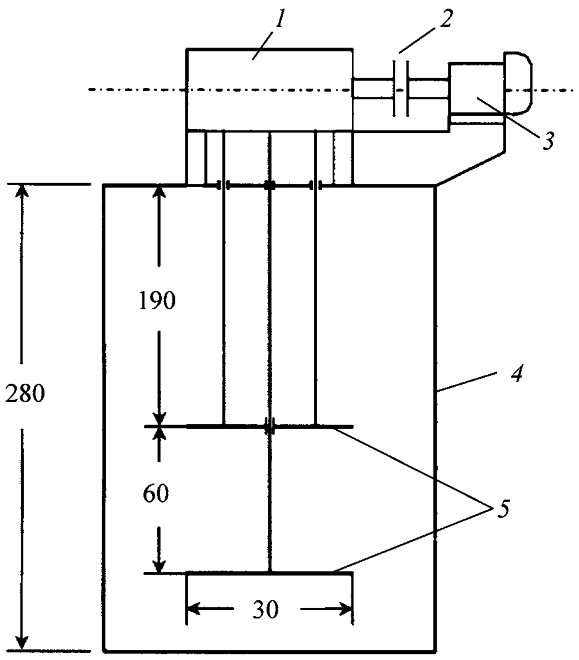


Fig. 5. Scheme of the vibrocavitational installation: (*1*) gearbox, (*2*) sleeve coupling, (*3*) UMT-22 electric motor, (*4*) frame, and (*5*) plates. The dimensions are given in millimeters.

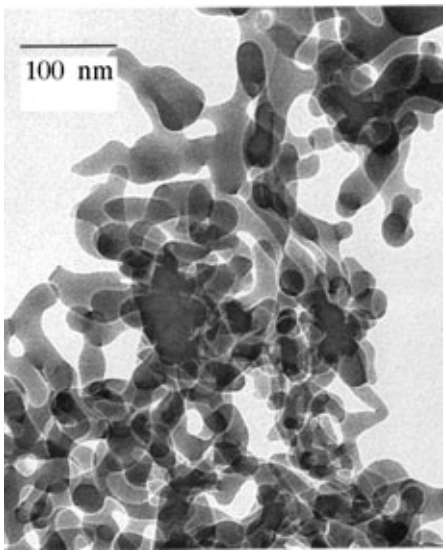


Fig. 6. TEM micrograph of a sample obtained upon vibrocavitational treatment of the MNS material.

samples at low pressures, and it seems natural to attribute it to the most actively sorbing component, the nanocarbon component. The height of the step in terms of the nanocarbon component may be as large as 3–4%, which corresponds to the best parameters for unmodified nanotube materials at moderate pressures.

Thus, the opportunity to use a shungite-based material for hydrogen accumulation may be furnished by separation of the nanocarbon component. However, the efficiency of such a separation is, as shown above, low. Nevertheless, attempts to stimulate the recovery of fulleroid particles from shungite yielded an unexpected side effect. In an experiment, an aqueous dispersion of a chemically treated shungite was placed in the field of a standing acoustic wave of rather low power (~60 W), which was created by plates oscillating in antiphase in water at a sonic frequency. The vibrocavitational installation for such treatment is shown schematically in Fig. 5. The total treatment time was 2.5 h. Then the suspension was allowed to settle and both fractions were analyzed: those settled at the bottom and floating on the surface. As can be seen from the electron micrograph of the floating fraction (Fig. 6), a totally different structure appears in addition to the usual shungite structure. Its "looseness" stands out: the structure is constituted by nanopores 5–20 nm in size and short wormlike projections 30–100 nm in size. A detailed study of the projection structure requires a resolution better than that available.

The structure of the material obtained is specific to shungite (e.g., a ground cathode deposit, enriched in nanotubes as a result of chemical treatment, formed a different nanoporous structure upon vibrocavitational treatment). The mechanism of its appearance may be as follows. In the course of a vibrocavitational treatment, part of graphitized stacks not fastened by the aluminosilicate matrix as a result of chemical etching fall out into the aqueous dispersion. After the action of the cavitator is complete, the energy of interaction between these stacks, associated with the dangling bonds at edges of graphite planes, must be at a minimum if the stacks are arranged "butt-to-butt" and further form a globule.

The share of the given fraction, floating up to the surface after each treatment session of the shungite material, does not exceed several percent so far, despite attempted optimization. Tentative measurements of the sorption capacity for hydrogen show that it reaches a value of 1.5% even under atmospheric pressure, the adsorption isotherm is of the Langmuir type, and the sorption process is reversible.

CONCLUSIONS

(1) Chemical treatment of shungite-III with a molten alkali and an acid can destroy to a considerable extent the carbon–silicon matrix and, simultane-

ously, preserve a large part of fulleroid (or nano-) structures contained in the starting shungite. In the process, the content of nanostructures not bound to silicon can be brought to the level of 1–2%.

(2) The method of treatment with preliminary grinding of shungite-III into ~100-μm fractions can raise the content of unbound nanostructures to 3–4%.

(3) The sorption capacity for hydrogen of the material produced upon such grinding and subsequent chemical treatment is high, but only conditionally, in terms of the nanocarbon component: 1.5–2 wt % at a pressure of 2 atm. However, real separation of fulleroid particles is difficult because of their high chemical activity, which does not noticeably differ from the chemical activity of the carbon component of shungites as a whole.

(4) A material with a high true sorption capacity for hydrogen (up to 1.5 wt %) can be produced from shungites by vibrocavitational treatment of preliminarily chemically modified shungite-III.

ACKNOWLEDGMENTS

The study was financially supported by the Federal Target Scientific and Technical Program "Research and Development in Priority Areas of Science and Technology for 2002–2006" (State Contract no. 02.467.11.7005, May 23, 2005) and by the International Science and Technology Center (grant no. 2769).

REFERENCES

1. Harris, P., *Carbon Nanotubes and Related Structures: New Materials for the Twenty-First Century*, Cambridge: Cambridge Univ. Press, 2001.
2. Loutfy, R.O., Moravsky, A., Franco, A., and Veksler, E., in *Prospectives of Fullerene Technology*, Osawa, E., Ed., London: Kluwer, 2002, pp. 327–340.
3. Schlapbach, L. and Zuttel, A., *Nature*, 2001, vol. 414, pp. 353–360.
4. Chambers, A., Park, C., Baker, R.T., and Rodrugues, N., *J. Phys. Chem. B*, 1998, vol. 102, pp. 4253–4257.
5. Chen, P., Wu, X., Lin, J., and Tan, K.L., *Science*, 1999, vol. 285, pp. 91–93.
6. Dillon, A.C., Jones, K.M., Bekkedahl, T.A., et al., *Nature*, 1997, vol. 386, pp. 377–379.
7. Yang, R., *Carbon*, 2000, vol. 38, pp. 623–634.
8. Eletskii, A.V., *Usp. Fiz. Nauk*, 2004, no. 11, pp. 947–964.
9. Sokolov, V.A., Kalinin, Yu.K., and Dyukkiev, E.F., *Shungity – novoe uglerodistoe syr'e* (Shungites, New Type of Carbon Raw Materials), Petrozavodsk: Karel'sk. Filial Akad. Nauk SSSR, 1984.
10. Mikhailov, V.P., *Uglerodsoderzhashchie formatsii v geologicheskoi istorii* (Carbon-Containing Formations in the Geological History), Petrozavodsk: Nauka, 1998, p. 47.
11. Rozhkova, N., *Prospectives of Fullerene Technology*, Osawa, E., Ed., London: Kluwer, 2002, pp. 237–252.
12. Zaidenberg, A.Z., Rozhkova, N.N., Kovalevsky, V.V., et al., *Mol. Mater.*, 1996, vol. 8, pp. 107–10.
13. Kovalevskii, V.V., *Neorg. Mater.*, 1994, vol. 39, pp. 28–32.
14. Grigorieva, E.N. and Rozhkova, N.N., *Russ. J. Appl. Chem.*, 2000, vol. 73, no. 4, pp. 600–605.
15. RF Patent 2097357.
16. Cassell, A., Franklin, N., Chan, E., et al., *J. Am. Chem. Soc.*, 1999, vol. 121, pp. 7975–7976.
17. Dai, H.J., Rinzler, A.G., Nicolaev, P., et al., *Chem. Phys. Lett.*, 1996, vol. 62, pp. 161–166.
18. Kel'tsev, N.V., *Osnovy adsorbtsionnoi tekhniki* (Fundamentals of Adsorption Technology), Moscow: Khimiya, 1984.

ISSN 1070-4272, Russian Journal of Applied Chemistry, 2006, Vol. 79, No. 9, pp. 1428–1431. © Pleiades Publishing, Inc., 2006.
Original Russian Text © V.V. Sidorchuk, 2006, published in Zhurnal Prikladnoi Khimii, 2006, Vol. 79, No. 9, pp. 1444–1447.

SORPTION AND ION-EXCHANGE PROCESSES

Specific Features of Modification of Activated Carbons with Steam and Hydrogen Peroxide Vapor at High Temperatures and Pressures

V. V. Sidorchuk

Institute of Sorption and Endoecological Problems, National Academy of Sciences of Ukraine, Kiev, Ukraine

Received February 14, 2006

Abstract—The effect of high-temperature treatment of activated carbons with water and hydrogen peroxide solutions on their pore structure, surface structure, and adsorption properties was studied.

DOI: 10.1134/S1070427206090072

It is known that steam treatment at 700–950°C is frequently used in the activation stage in preparing carbons from various raw materials [1–3]. Also, there is published evidence that the adsorption capacity of some carbon materials increases upon their modification in a flow of steam or as a result of treatment in an autoclave [4–6]. This apparently occurs both via development of a porous structure in these materials and because of an increase in the concentration of surface oxygen-containing functional groups [6, 7]. At the same time, no systematics studies concerned with this issue have been reported. Here we report certain results of autoclave modification of two carbons of different origins.

EXPERIMENTAL

Two kinds of carbons were subjected to vapor-phase treatment in a 45-ml autoclave: A2PS fruit-kernel carbon manufactured in Poland and SKN carbon prepared from an organic polymer. Distilled water, 10–30% aqueous solutions of hydrogen peroxide, and 10% aqueous ammonia served as modifying media. The treatment temperature was 250–350°C, and treatment duration, 3 h.

To calculate the pore structure parameters, nitrogen adsorption isotherms were measured with a Sorptomat instrument. These isotherms were used to determine by the methods described in [8] the following parameters: BET specific surface area, S_{BET}; surface area of micropores, S_{mi}, found by the de Boer method from *t*-plots; surface area of mesopores, S_{me}, determined by the Dollimore–Hill method; and volumes of micro- and mesopores, V_{mi} and V_{me}. Also, isotherms of adsorption of benzene and water vapor were obtained by gravimetry and used to calculate by the BET technique the specific surface area for benzene, $S_{C_6H_6}$ and the limiting-sorption pore volume for benzene, V_s, and to find the geometric surface area for water, S_g [9]. The adsorption of water vapor was also used to calculate the concentration of primary adsorption centers (PAC) [10]. The same installation served to measure adsorption isotherms of gaseous NH_3 and CO_2 in order to characterize the adsorption capacity of carbons in relation to the nature and concentration of functional groups on their surface.

Table 1 lists parameters of the porous structure of A2PS carbon upon its treatment at 250–350°C. It can be seen that, depending on the modification temperature and medium, a rather intricate pattern is observed and it is difficult to reveal any fundamental aspects. However, certain trends can be traced.

First, the specific surface area somewhat grows as the temperature and hydrogen peroxide concentration are made higher, because of the appearance of an additional microporosity, which is indicated by an increase both in the surface area of micropores by 120–200 $m^2 g^{-1}$ and in their volume by 0.05–0.07 ml g^{-1}. This is also indicated by the simultaneous steady rise in the combustion loss by the modified carbons to 10–12%. The micropore width was estimated [11, 12] to be 0.8–1.1 nm, and the mesopore size varied within the range 35–45 nm.

Second, the mesoporous component of the porosity (both S_{me} and V_{me}) remains virtually unchanged under the conditions studied, whence follows the con-

Table 1. Effect of the treatment conditions of A2PS carbon in an autoclave on its pore structure parameters

Treatment temperature, °C	Medium	S_{BET}	S_{mi}	S_{me}	$S_{C_6H_6}$	S_g	V_{mi}	V_{me}	V_s
		$m^2\ g^{-1}$					$ml\ g^{-1}$		
Starting sample		1054	767	264	1042	310	0.39	0.28	0.69
250	H_2O	1080	739	284	1068	413	0.40	0.29	0.71
	10% H_2O_2	1021	581	457	988	820	0.39	0.30	0.70
	20% H_2O_2	1170	915	240	1090	1095	0.44	0.28	0.72
	30% H_2O_2	1090	710	301	1052	1010	0.39	0.30	0.70
	10% NH_3	960	715	203	991	378	0.38	0.31	0.68
300	H_2O	1119	851	265	1090	639	0.41	0.30	0.71
	30% H_2O_2	1182	927	266	1101	1120	0.44	0.30	0.73
350	H_2O	1019	751	285	980	993	0.39	0.30	0.70
	30% H_2O_2	1250	1032	220	1201	1240	0.46	0.28	0.75

clusion that microporosity of carbon bodies is not converted into mesoporosity under hydrothermal condition, in contrast to oxide systems, in which this conversion is one of the principal aspects of hydrothermal modification of the pore structure. This is possibly due to difference between the mechanisms of porosity transformation in oxides and carbons. In highly dispersed oxide bodies, the pore structure parameters change through mass transfer over the surface and via solution and because of phase transformations at a constant mass of the solid. At the same time, treatment of carbons leads to intensive oxidation of the surface layer and partial gasification of the substance, with a decrease in the mass of the solid, i.e., a combustion loss by the carbons is observed, as in their activation [1, 2]. As indicated by the results of this study, the burning-out of carbon mostly occurs via appearance of new micropores, rather than at the surface of mesopores. At the same time, further oxidation is hindered by accumulation of gaseous products in the autoclave and decomposition of hydrogen peroxide. Therefore, a more significant change in porosity possibly requires a multiple treatment or an increase in the H_2O_2 concentration.

One more natural consequence of the oxidation of carbon is that the concentration of surface oxygen-containing groups considerably increases. The fact that the surface structures of the starting carbon and those modified under dissimilar conditions are different is demonstrated by the following experimental evidence.

(1) The difference between the values of S_{BET} and $S_{C_6H_6}$, on the one hand, and S_g, on the other, becomes less pronounced as the treatment temperature and H_2O_2 concentration are raised. This indicates that, simultaneously, the surface density of oxygen-containing groups increases and, consequently, the landing area for water molecules approaches the value characteristic of a hydroxylated surface [8].

(2) The shape of isotherms of water vapor adsorption changes after the treatment of carbons. Figure 1 shows that the adsorption isotherm for the starting sample is concave, i.e., belongs to type III by the BDDT classification, whereas upon modification in an autoclave, it tends to become a type-II isotherm with a convex shape in the initial portion [8].

To verify the assumptions made, the concentrations of PAC, which characterize the presence of just oxygen-containing functional groups on the carbon surface [10], were calculated from the isotherms of

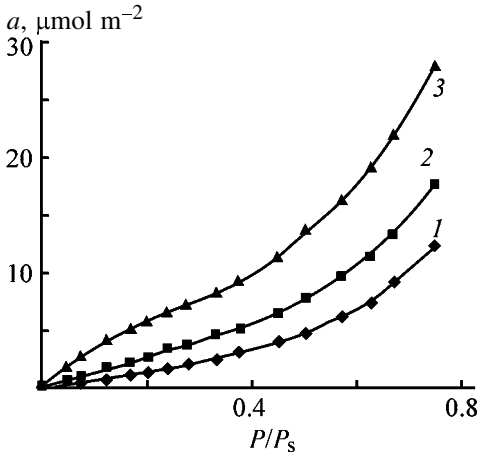


Fig. 1. Adsorption isotherms of water vapor at 20°C for A2PS carbon. (a) Adsorption and (P/P_s) relative pressure of water vapor. Sample: (*1*) starting, (*2*) steam-treated at 250°C, and (*3*) treated at 250°C with a 10% solution of hydrogen peroxide; the same for Fig. 2.

Table 2. Effect of the autoclave treatment temperature on the PAC concentration for A2PS and SKN carbons

Treatment temperature, °C	Medium	PAC concentration			
		A2PS		SKN	
		c, mmol g^{-1}	μ,* μmol m^{-2}	c, mmol g^{-1}	μ,* μmol m^{-2}
Starting sample		0.60	0.56	0.16	0.38
250	H_2O	0.69	0.64	–	–
	10% H_2O_2	0.79	0.77	0.23	0.40
	20% H_2O_2	2.02	1.72	0.89	1.70
	30% H_2O_2	3.63	3.33	1.56	3.16
	10% NH_3	0.54	0.56	0.18	0.42
300	H_2O	0.74	0.66	0.25	0.57
	30% H_2O_2	4.37	3.70	2.01	3.45
350	H_2O	0.79	0.77	0.29	0.64
	30% H_2O_2	1.20	0.96	0.48	1.40

* The value of μ was calculated by dividing the concentration c by the specific surface area found by BET from nitrogen adsorption isotherms.

water vapor adsorption. The data obtained for A2PS and SKN carbons are listed in Table 2. It can be seen that, as the treatment temperature and the concentration of the oxidizing agent are raised, the content of PAC on the surface of the carbons of both types steadily grows (both c and μ). The only exception is provided by samples modified with a 30% solution of hydrogen peroxide, for which a sharp decrease in the PAC concentration is observed upon treatment at 350°C, compared to the samples treated at 300°C. This may, in particular, be due to a more intensive H_2O_2 decomposition at the autoclave walls, rather than on the carbon surface, with a dramatic buildup of pressure at 350°C. Noteworthy is the fact that the absolute concentrations of PAC (per unit surface area) are, as a rule, rather close for both of the carbons under study upon treatment under identical conditions.

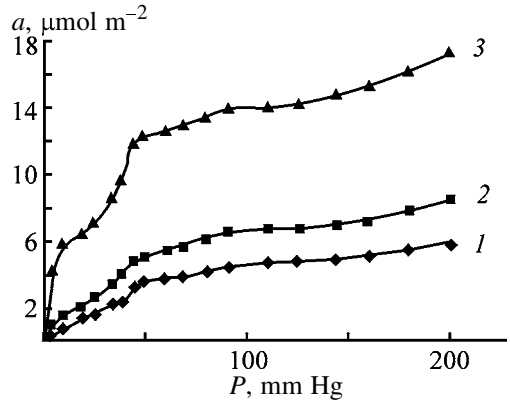


Fig. 2. Adsorption isotherms of gaseous ammonia at 20°C for A2PS carbon. (*a*) Adsorption and (*P*) ammonia pressure.

To elucidate the nature of the functional groups formed on the carbon surface in the course of treatment, the adsorption of gaseous ammonia and carbon dioxide was studied as suggested in [6]. The resulting absolute adsorption isotherms of gaseous NH_3 are shown for A2PS carbon in Fig. 2. The figure demonstrates a significant increase in the concentration of oxygen-containing groups upon modification with steam (curve *2*) and, especially, with a 10% solution of hydrogen peroxide (curve *3*), with the appearing functional groups having the acid nature. The steplike shape of the ammonia adsorption isotherms indicates that at least three types of acid adsorption centers are present on the surface of both starting and modified carbons and these centers are the most clearly pronounced upon modification of the carbon with an H_2O_2 solution. The strength of these acid centers corresponds to carboxy, phenolic, and lactone groups [1]. However, their unambiguous identification requires an additional study by other physicochemical methods.

As expected, treatments of carbon, including that in 10% ammonia, have virtually no effect on the surface concentration of basic groups.

CONCLUSIONS

The autoclave modification of activated carbons, and primarily that in hydrogen peroxide solutions, promotes noticeable development of their microporosity on raising the temperature and H_2O_2 concentration, with the mesoporosity remaining unchanged. Also, a significant rise in the concentration of acid functional

groups on the surface of carbons is observed in the process.

REFERENCES

1. Tarkovskaya, I.A., *Okislennyi ugol'* (Oxidized Carbon), Kiev: Naukova Dumka, 1981.
2. Fenelonov, V.B., *Poristyi uglerod* (Porous Carbon), Novosibirsk: Inst. Kataliza Sib. Otd. Ross. Akad. Nauk, 1995.
3. Ariyadejwanish, P., Tanthapanichakoon, W., Nakagawa, K., et al., *Carbon*, 2003, vol. 41, no. 1, pp. 157–164.
4. Nieh, G.-K. and Grow, D.T., *J. Colloid Interface Sci*., 1987, vol. 119, no. 1, pp. 280–285.
5. Turov, V.V., Gun'ko, V.M., Leboda, R., et al., *J. Colloid Interface Sci*., 2002, vol. 253, no. 1, pp. 23–34.
6. Leboda, R., Sidorchuk, V.V., and Skubiszewska-Zienba, J., *Mater. Chem. Phys*., 1994, vol. 39, no. 1, pp. 136–141.
7. Sidorchuk, V.V., *7th Eur. Congr. on Catalysis*, Sofia, August 28–September 1, 2005, p. 49.
8. Gregg, S.J. and Sing, K.S.W., *Adsorption, Surface Area, and Porosity*, New York: Academic, 1982, 2nd ed.
9. Dubinin, M.M., *Usp. Khim*., 1982, vol. 51, no. 7, pp. 1065–1074.
10. Vartapetyan, V.Sh., Dubinin, M.M., and Shumilina, E.B., *Izv. Ross. Akad. Nauk, Ser. Khim*., 1993, no. 1, pp. 54–56.
11. Tsunoda, R., *J. Colloid Interface Sci*., 1990, vol. 137, no. 2, pp. 563–570.
12. Stoeckli, H.F., Ballerini, L., and De Bernardini, S., *Carbon*, 1989, vol. 27, pp. 501–505.

ISSN 1070-4272, Russian Journal of Applied Chemistry, 2006, Vol. 79, No. 9, pp. 1432–1437. © Pleiades Publishing, Inc., 2006.
Original Russian Text © L.N. Grigor'ev, O.A. Shanova, 2006, published in Zhurnal Prikladnoi Khimii, 2006, Vol. 79, No. 9, pp. 1448–1453.

SORPTION AND ION-EXCHANGE PROCESSES

Chemisorption of Vapors of Organic Substances on a Modified Silica Gel

L. N. Grigor'ev and O. A. Shanova

St. Petersburg State Technological University of Plant Polymers, St. Petersburg, Russia

Received March 31, 2005; in final form, December 2005

Abstract—Experimental data on the equilibrium and dynamics of chemisorption of vapors of organic substances on a silica gel modified with color reagents are presented.

DOI: 10.1134/S1070427206090084

Adsorption, which mainly proceeds by the physical mechanism, is widely used in industry for treatment of discharged gases to remove vapors of organic substances [1]. In recent years, the adsorption-catalytic method has found application. This method employs not only industrial catalysts [2], but also chemically active adsorbents [3–6]. Chemically active adsorbents are widely used in sampling (concentration of contaminants) of gases for analysis and directly in analysis of gases by proximate techniques, of which the linear-coloristic method is the best known [7]. This method consists in the following. A certain volume of a gas to be analyzed is passed in an evacuated vessel through a bed of an adsorbent (commonly, silica gel) saturated with a color reagent, and the reaction of the color agent with the adsorbed contaminant results in that a band of width L_{st} proportional to the concentration c_0 of the contaminant being analyzed changes its coloration. For the method to be used in practice, it is sufficient to construct the calibration plot characterizing the dependence $c_0 = kL_{st}$ (k is the proportionality factor). However, the linear dependence of the concentration of a substance being determined on the width of the colored band is not observed, especially at low concentrations. In this case, the relative error in determining the contaminant concentration may be as large as 60% [8]. In this context, it is of interest to obtain information about specific features of chemisorption of contaminants in the sampling and analysis of gas samples by the linear-coloristic method. Such information could not only improve the method (by diminishing the determination error), but also provide additional insights into the adsorption process and lead to the development of methods for calculation of adsorption processes accompanied by a chemical reaction on the surface.

The aim of this study was to reveal specific features of chemisorption of vapors of organic substances on a silica gel modified with color reagents.

The choice of color reagents (substances that change their coloration in reaction with contaminants) for modification is due to their practical use in systems for sampling (concentration) and analysis of gases and to the resulting simplification of the experimental procedure: if color reagents are used, variations of the amount of an adsorbed substance can be monitored visually, by changes in the bed coloration.

KSKG silica gel of the $(0.11–0.16) \times 10^{-3}$-m fraction, preliminarily heat-treated at 473, 673, and 973 K, served as an adsorbent (color reagent carrier). The silica gel was prepared for experiments and modified by the procedure described in [9]. A sulfuric acid solution of potassium dichromate was used as a modifying agent for determining the concentration of ethanol; sulfuric acid solution of potassium iodate, for toluene; and sulfuric acid solution of chromium trioxide, for acetone and diethyl ether (DE). A flow of a vapor–air mixture (VAM) was passed, using a UG-2 gas analyzer [9], through a bed of a modified adsorbent (indicator powder) charged into a glass tube with an inner diameter of 0.0026 m. In the process, the time in which a band of prescribed width (0.005–0.020 m) acquired coloration was measured. To determine the degree of saturation of the indicator powder in relation to the sampling duration, a VAM flow with contaminant concentrations of 200, 400, 600, 800, and 1000 mg m^{-3} was passed through tubes with an indicator powder (bed height 0.080 m), with the process duration varied in the range 5–230 s. The amount of the absorbed contaminant was found from the gain in the weight of the indicator powder during an experi-

Table 1. Amount a of a substance adsorbed on modified (unmodified) silica gel

Silica gel treatment temperature, K	a, mg g^{-1}, at indicated adsorption temperature, K			
	333	353	333	353
	toluene		ethanol	
473	$a = 0.28c$ ($a = 0.87c$)	$a = 0.69c$ ($a = 0.42c$)	$a = 0.12c$ ($a = 1.10c$)	$a = 0.22c$ ($a = 0.35c$)
673	$a = 0.22c$ ($a = 0.70c$)	$a = 0.60c$ ($a = 0.40c$)	$a = 0.15c$ ($a = 0.82c$)	$a = 0.28c$ ($a = 0.33c$)
973	$a = 0.18c$ ($a = 0.70c^{0.85}$)	$a = 0.52c$ ($a = 0.33c^{0.95}$)	$a = 0.21c$ ($a = 0.68c$)	$a = 0.52c$ ($a = 0.26c$)

ment. With the specific features of gas sampling with a UG-2 gas analyzer taken into account, model VAMs were prepared in the static mode, with the error in VAM preparation not exceeding 2.8%.

The adsorption isotherms of the contaminant vapor were plotted using the results of chromatographic measurements [11] with a Chrom-5 chromatograph equipped with a heat-conductivity detector (carrier gas helium). Figure 1 shows a chromatogram of toluene on unmodified silica gel preliminarily heat-treated at 473 K. The reproducibility of the peak areas was 1.39% in the case of introduction of 1 μl of the contaminant and 10.62% for 0.06 μl. Figure 2 shows the adsorption isotherm of a toluene vapor, plotted using the data of Fig. 1 with account of the conditions in which the chromatogram was measured: column temperature 353 K, flow rate of helium under the working conditions 17.5 ml min^{-1}, weight of the adsorbent in the packed microcolumn 0.012 g.

Table 1 lists the data obtained in processing of chromatograms of toluene and ethanol on silica gel calcined at various temperatures in terms of the Freundlich equation: $a = kc^{1/n}$, where a is the amount of adsorbed substance (mg g^{-1}); c, its concentration in the gas (mg m^{-3}); and n, k, constants. The processing was done with chromatographic peaks whose areas corresponded to contaminant concentrations in the range 10–200 mg m^{-3} and temperatures of 333–353 K. These values are the most typical for industrial ventilation gases [12]. The relative error in calculation of a by the equations listed in Table 1 does not exceed 5.24%.

It can be seen in Table 1 that, in the examined interval of the concentrations of ethanol and toluene vapors, the isotherms are linear: the exponent $1/n$ is equal or close to unity. For unmodified silica gels, the constant k decreases as the adsorption temperature increases, and also as the temperature at which the starting silica gel is calcined becomes higher. Similar dependences are observed in adsorption of toluene on the modified silica gel; in adsorption of ethanol, however, the constant k increases with the silica gel calcination temperature. A probable reason is that the chemical component of the process in adsorption of

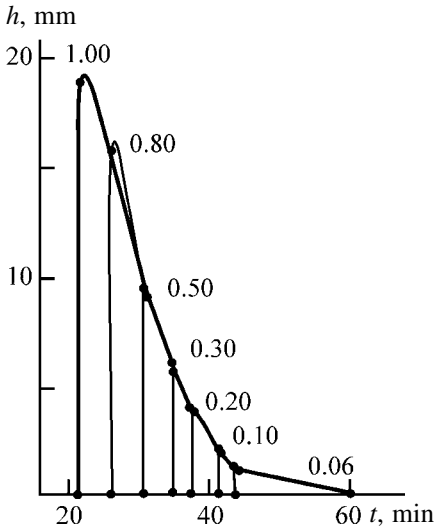


Fig. 1. Chromatogram of toluene on silica gel. (h) Peak height and (t) retention time. Figures at points denote the volume (μl) of a toluene sample introduced into the chromatograph vaporizer.

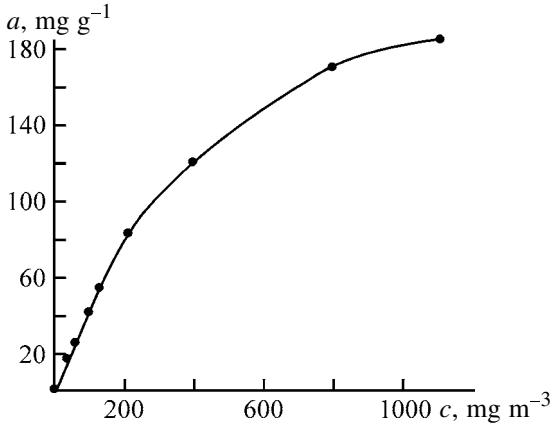


Fig. 2. Isotherm of adsorption a of the toluene vapor on silica gel. (a) Adsorbed amount of contaminant and (c) its concentration in the gas.

Table 2. Results of analysis of the ethanol vapor in air (L_{st} = 0.07 m, VAM volume V = 0.400 l, total time of VAM passing 4 min)

c_0, mg m^{-3}	l = 5 mm		l = 10 mm		l = 20 mm		L, mm
	τ, s	w, mm s^{-1}	τ, s	w, mm s^{-1}	τ, s	w, mm s^{-1}	
200	20.0	0.250	–	–	–	–	5
400	15.3	0.333	–	–	–	–	8
600	11.8	0.424	22.7	0.434	–	–	11
800	8.0	0.625	16.3	0.625	–	–	16
1000	5.0	1.000	10.0	1.000	21.0	0.952	22

* τ is the duration of coloring; w, linear velocity of the color change front in the bed; and L, width of the band of primary coloration.

toluene decreases as the concentration of the modifying agent becomes lower, which is favored by an increase in the temperature at which the silica gel is calcined. In addition, it is known that an elevated calcination temperature leads to formation of Si–O–Si siloxane bridges, which are not favorable to specific adsorption [13] of toluene (and do not promote the nonspecific adsorption, either). At the same time, no decrease in k is observed in the case of ethanol. This is presumably due to partial dissociation of siloxane bonds (at temperatures below 473 K) in adsorption on a calcined silica gel, which results in the formation of free radicals (≡Si–O$^{\bullet}$, ≡Si$^{\bullet}$) [14] with which ethanol can react.

Visual monitoring of how the coloration of the indicator powder varies in adsorption of vapors of ethanol, toluene, acetone, and DE from a VAM whose flow rate changed in the course of the experiment from the initial value to virtually zero demonstrated the following. The width of the colored band reaches its final value virtually at the initial instant of time, and then the coloration grows in intensity within the already formed colored band, with the most intense coloration observed in the first, along the VAM flow direction, portions of the bed.

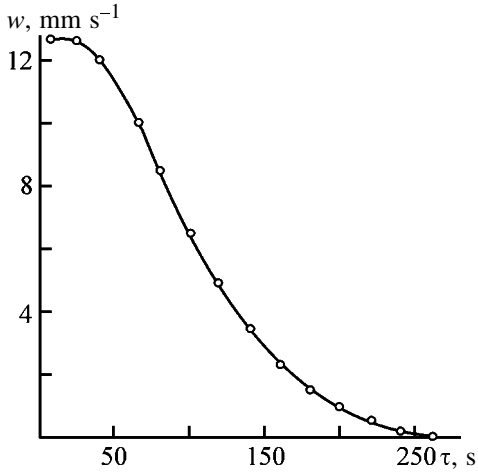


Fig. 3. Linear velocity w of the color change front in the bed of the indicator powder through which a VAM is passed vs. time τ.

The manner in which the sorbent coloration varies during the initial period of time after the VAM flow starts can be judged, in relation to the contaminant concentration, from the data in Table 2. These data suggest that the minimum time τ in which the primary coloration band is formed is 20 to 5 s for the concentrations c_0 ranging from 200 to 1000 mg m^{-3}, respectively.

Figure 3 shows that, at the initial instant of time (20 s) corresponding to the formation of the primary coloration band, the linear velocity of the color change front in the bed is virtually constant and has the maximum value. Further, the velocity decreases, which is accompanied by a decrease in the width of the color change band and, consequently, in the length of the mass-transfer zone. It is the variation of these parameters that is responsible, in the authors' opinion, for the above-mentioned deviation of the calibration plot from the straight line.

It has been shown previously [15] that the linearity of the calibration plot can be achieved if the rate at which the VAM flow is passed is maintained constant. It follows from Fig. 3 that this condition can be satisfied if the gas is sampled during a short time (20–25 s). In this case, the dependence $c_0 = k_0 l/\tau$ (where τ is the time in which a band of prescribed width is colored, and k_0 is the proportionality factor), which was suggested in [10] for the calibration plot, becomes substantiated. In view of the fact that, as follows from Fig. 1, τ should not be large, there is no need to pass the whole volume of the gas in its sampling for analysis and, for obtaining the desired result, it suffices to record the time in which the coloration changes in a band of a prescribed width l. In this case,

$l \ll L$ and, consequently, smaller amounts of fresh silica gel and modifying agent (color reagent) are necessary if the calibration plot in the c_0–l/τ coordinates is used to determine the contaminant concentration. This, in turn, leads to a decrease in the resistance of the VAM sampling system and allows use of electric aspirators instead of the commonly employed mechanical air-sampling devices of the bellows and piston types.

Figure 4 shows how the width of the colored band formed in the initial stage after the gas flow starts to be passed depends on the contaminant concentration.

The experimental results were processed using the Shilov–Mecklenburg equation in the following form:

$$c_0 = a_0/w\tau(l - h) = k'(l - h), \quad (1)$$

$$l = (c_0/k') - h, \quad (2)$$

where $k' = a_0/w\tau$ characterizes the amount of substance absorbed along the unit length of the sorbent when a unit volume of the gas is passed; a_0, amount of the contaminant absorbed when a primary colored band is formed; l, width of the band in which the coloration changes in time τ; h, unused bed height; and w, linear flow velocity of the gas in the free cross section of the tube filled with the sorbent.

The above formulas and data in Fig. 4 were used to find, for ethanol, toluene, acetone, and diethyl ether, values of h and k' (Table 3), which make it possible to determine the minimum width of the colored band for any c_0.

Also of interest in a study of the chemisorption of contaminants on the indicator powder is the time distribution ($\tau > 20$ s) of the concentrations of the substance being determined within the band in which coloration was formed at the initial instant of time.

The experimental and calculated data, presented in Table 4 and Fig. 5, made it possible to assess the manner in which the coloration of the adsorbent bed varies when the whole volume of VAM is passed through it. For example, the data for ethanol (V = 0.4 l) are given in Table 4.

A verification of whether the K_{eth} values belong to the same sample by the test [16]

$$Q = \frac{K_X - K_N}{K_M - K_1},$$

(K_X, questionable value of K; K_N, neighboring value of K; K_M and K_1, extreme values of K in a sample arranged in the order of increasing numerical values) demonstrated that all values of K belong to the same sample. The average value of K is (0.043 ± 0.005) s^{-1}.

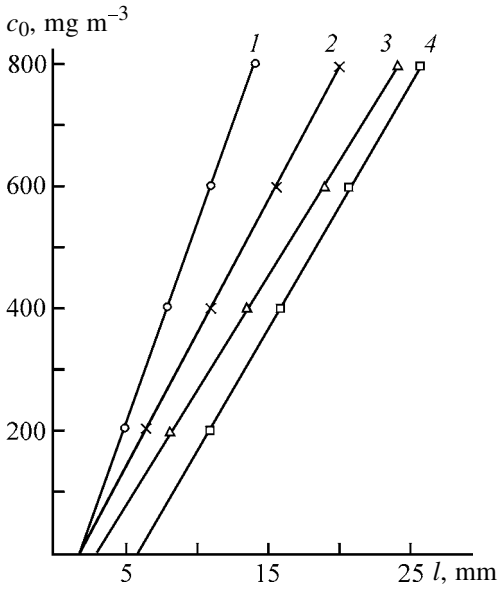


Fig. 4. Effect of the contaminant concentration c_0 on the width l of the colored band formed in the initial stage after the gas flow starts to be passed. (*1*) Ethanol, (*2*) diethyl ether, (*3*) toluene, and (*4*) acetone.

Thus, it can be taken that, in the concentration range 200–1000 mg m^{-3}, K is constant at a confidence level of 0.95.

Table 3. Values of h and k' for organic substances of various classes

Substance	h, mm	k', g m^{-3} m^{-1}
Ethanol	2.0	42.6
Toluene	2.5	36.4
Acetone	6.5	52.6
Diethyl ether	1.6	60.6

Table 4. Parameters of chemisorption of the ethanol vapor*

c_0, mg m^{-3}	ν, ml s^{-1}	v, ml	$K = \nu/v$, s^{-1}
200	0.00130	0.0265	0.050
400	0.00175	0.0424	0.041
600	0.00223	0.0583	0.038
800	0.00328	0.0848	0.038
1000	0.00530	0.1113	0.047

* ν is the flow rate; v, volume of the indicator powder in which the coloration changed; and K, rate constant of the coloration variation.

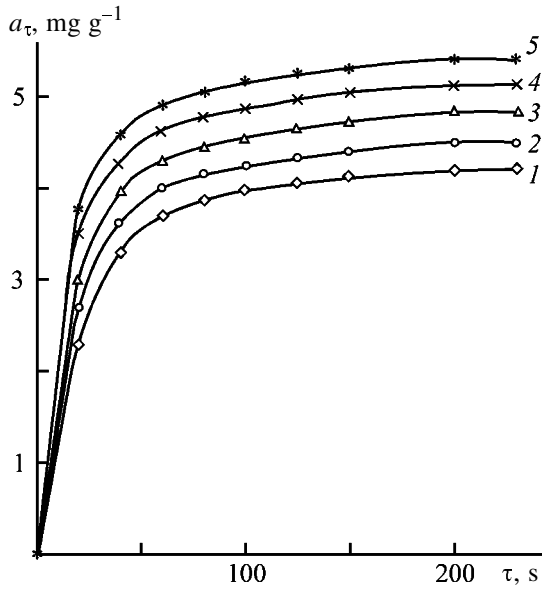


Fig. 5. Time distribution of the ethanol concentration (bed height l = 5 mm). (a_τ) Dynamic adsorption value and (τ) time during which the VAM flow is passed. c_0, mg m^{-3}: (*1*) 200, (*2*) 400, (*3*) 600, (*4*) 800, and (*5*) 1000.

Figure 5 shows how the amount of ethanol absorbed by the indicator powder varies with the initial concentration and time during which the VAM flow is passed.

The type of the curves in Fig. 5 allows the variation of the ethanol concentration in the indicator powder, a_τ, to be represented as the equation

$$a_\tau = a_0(1 - e^{-0.043\tau}), \quad (3)$$

where a_0 is the amount of ethanol absorbed by unit weight of the indicator powder for the time in which the whole volume of VAM is passed.

Equation (3) furnishes an opportunity to calculate the amount of adsorbed substance for different instants of time.

The aforesaid suggests, with account of the fact that the flow rate of VAM was varied in the experiments from the initial value to zero, the following: the resistance to the process from the gas phase is at a minimum because the value of K is independent of the linear velocity (flow rate) of the VAM and, in all probability, depends on the type of surface and color reagent, temperature, and presence of concomitant substances in the vapor–gas mixture.

Similarly to the example of ethanol, Eq. (3) is valid for other substances (K_{toluene} = 0.026, K_{acetone} = 0.032, K_{DE} = 0.034 s^{-1}).

It should be noted that expression (3) is valid at times longer than 20 s. In the initial period of time (0–20 s), when the fraction of the active surface is at a maximum, the rate of conversion (of change in coloration) is virtually independent of the concentration of the substance being determined.

For example, at the initial instant of formation of the coloration front, the expression for the conversion rate w has the form

$$w = 19.47c_0^{0.225}, \quad (4)$$

where 19.47 is the rate constant of color variation.

The maximum error of calculation by Eq. (4) is 5.31%.

CONCLUSIONS

(1) The rate constants of the Freundlich isotherm equation were determined for describing the adsorption of vapors of organic substances of various classes on unmodified silica gel and that modified with oxidizing agents, and the manner of their variation with the adsorption temperature and the temperature of calcination of the starting silica gel was revealed.

(2) It was found that, at temperatures in the range 60–80°C, the constant 1/n is independent of the type of contaminants and adsorption temperature, and the constant k decreases as the adsorption temperature is raised for all classes of substances. As the calcination temperature is raised, the constant k decreases for the unmodified silica gel, and decreases or increases in adsorption of, respectively, nonpolar (toluene) or polar (acetone, ethanol, diethyl ether) substances for the modified silica gel.

(3) The conditions under which vapors of toluene, ethanol, acetone, and diethyl ether are chemisorbed (minimum bed height of a modified silica gel; duration of coloration variation within a prescribed bed height) were determined. These conditions can be used in analytical determination of the concentrations of these substances in a vapor–air mixture by the linear-coloristic method at a lower inaccuracy of the final result.

(4) An equation was suggested for calculating the amount of a contaminant absorbed in chemisorption in relation to time and its concentration in the flow of a vapor–air mixture.

REFERENCES

1. Kel'tsev, N.V., *Osnovy adsorbtsionnoi tekhniki* (Fundamentals of Adsorption Technology), Moscow: Khimiya, 1984.

2. Toropkina, G.N., Kalinkina, L.I., and Kisarov, V.M., *Zh. Vses. Khim. O–va. im. D.I. Mendeleeva*, 1992, no. 1, pp. 33–42.
3. Solov'ev, S.A., Belokleitseva, G.M., and Vlasenko, V.M., *Zh. Prikl. Khim.*, 1992, vol. 65, no. 9, pp. 1921–1926.
4. Solov'ev, S.A., Belokleitseva, G.M., and Vlasenko, V.M., *Zh. Prikl. Khim.*, 1994, vol. 67, no. 9, pp. 1467–1470.
5. Grigor'ev, L.N., Petrova, E.V., and Cheperegin, G.G., *Zh. Prikl. Khim.*, 1995, vol. 68, no. 9, pp. 1510–1513.
6. Grigor'ev, L.N., Cherkashin, A.G., and Burenina, T.I., *Zh. Prikl. Khim.*, 1999, vol. 72, no. 10, pp. 1673–1676.
7. Peregud, E.A. and Gorelik, D.O., *Instrumental'nye metody kontrolya zagryazneniya atmosfery* (Instrumental Methods for Monitoring of Atmospheric Contaminants), Leningrad: Khimiya, 1981.
8. Murav'eva, S.I., Bukovskii, M.I., Prokhorova, E.K., et al., *Rukovodstvo po kontrolyu vrednykh veshchestv v vozdukhe rabochei zony. Spravochnoe izdanie* (Manual for Monitoring of Noxious Substances in the Atmosphere in the Working Zone: Reference Book), Moscow: Khimiya, 1991.
9. Peregud, E.A., Bykhovskaya, M.S., and Gernet, E.V., *Bystrye metody opredeleniya vrednykh veshchestv v vozdukhe* (Fast Methods for Determination of Noxious Substances in Air), Moscow: Khimiya, 1970.
10. Grigor'ev, L.N. and Shanova, O.A., *Zavod. Lab., Diagnost. Mater.*, 2003, vol. 69, no. 5, pp. 6–10.
11. *Eksperimental'nye metody v adsorbtsii i molekulyarnoi khromatografii* (Experimental Techniques in Adsorption and Molecular Chromatography), Nikitin, Yu.S. and Petrova, R.S., Eds., Moscow: Mosk. Gos. Univ., 1990.
12. Maksimov, V.F., Vol'f, I.V., Vinokurova, T.A., et al., *Ochistka i rekuperatsiya promyshlennykh vybrosov: Uchebnik dlya vysshikh uchebnykh zavedenii* (Treatment and Recuperation of Industrial Discharges: Textbook for Higher-School Institutions), Moscow: Lesnaya Prom–st., 1980.
13. Dei, R.E. and Kuznetsov, B.V., *Osnovnye problemy teorii fizicheskoi adsorbtsii: Trudy Pervoi Vsesoyuznoi konferentsii po teoreticheskim voprosam adsorbtsii* (Basic Problems of the Theory of Physical Adsorption: Proc. First All-Union Conf. on Theoretical Problems of Adsorption), Moscow: Nauka, 1970, pp. 178–180.
14. Strelko, V.V., *Adsorbtsiya i adsorbenty* (Adsorption and Adsorbents), Kiev: Naukova Dumka, 1974, issue 2, pp. 65–76.
15. Grigor'ev, L.N., Shanova, O.A., and Burenina, T.I., *Zhizn' Bezopasn.*, 2001, nos. 1–2, pp. 354–357.
16. Alekseev, R.I. and Korovin, Yu.I., *Rukovodstvo po vychisleniyu i obrabotke rezul'tatov kolichestvennogo analiza* (Manual for Calculation and Processing of Results of Quantitative Analysis), Moscow: Atomizdat, 1972.

ISSN 1070-4272, Russian Journal of Applied Chemistry, 2006, Vol. 79, No. 9, pp. 1438–1442. © Pleiades Publishing, Inc., 2006.
Original Russian Text © V.M. Nagirnyi, R.D. Apostolova, E.M. Shembel', 2006, published in Zhurnal Prikladnoi Khimii, 2006, Vol. 79, No. 9, pp. 1454–1458.

APPLIED ELECTROCHEMISTRY AND CORROSION PROTECTION OF METALS

Electrodeposition of Molybdenum Oxide and Its Structural Characteristics

V. M. Nagirnyi, R. D. Apostolova, and E. M. Shembel'

Ukrainian State University of Chemical Engineering, Dnepropetrovsk, Ukraine

Received November 10, 2005; in final form, April 2006

Abstract—The cathodic processes in electroplating of compact molybdenum oxide coatings onto supports made of 12Cr18Ni9Ti steel and aluminum are considered along with the physicochemical characteristics determining their service properties.

DOI: 10.1134/S1070427206090096

Electrolytic molybdenum oxide is a promising cathode material for lithium batteries, because it has satisfactory tendency to cycling and stable reversible capacity within 200–250 mA h g^{-1} [1]. The conditions of its preparation have been considered in [2, 3]. The electrosynthesis method is advantageous in that it allows preparation of both fine deposits and compact coatings on the support made of stainless steel or aluminum. This makes it possible to manufacture effective ballastless cathodes by the direct oxide deposition onto the body of the cell of a chemical power source.

In the above studies, problems concerning the mechanism of the cathodic deposition of oxide molecules, formation of molecular crystalline deposit, and its physicochemical characteristics were not considered. These data seem also useful for optimizing the synthesis conditions and refining the existing concepts in the field under consideration. This was the subject of the present study.

The electrochemical characteristics of the electrolytic molybdenum oxide are a subject of a separate study not considered here.

Test deposits were prepared in the form of compact coatings on smooth plates of $10 \times 20 \times 0.3$ mm size made of 12Cr18Ni9Ti steel and AMG-6 aluminum. The electrolysis was performed in saturated (0.2–0.25 M) and dilute (0.005–0.01 M) solutions (pH 6.5–7.0) of ammonium molybdate $(NH_4)_6Mo_7O_{24} \cdot 4H_2O$ at 80–85 and 20–25°C, respectively, and a cathodic current density of 3.5–7.0 mA cm^{-2}. Preliminarily, the steel plates were degreased with Vienna lime and activated in concentrated hydrochloric acid for 3–5 min. Aluminum plates were etched in a 5–6 M NaOH solution and activated in dilute HCl solution (1 : 4). The aluminum plates were loaded into the cell under the current. The polarization curves in the range I_c = 1–50 mA cm^{-2} were measured relative to a silver chloride reference electrode using a Ts-413 digital voltammeter. The partial curves were constructed on the basis of the nominal current efficiencies by molybdenum oxide (ox-Mo) (CE_{nom}) [3]. The adhesion and mechanical resistance of the deposits were determined qualitatively from the weight loss of the sample with an oxide coating after a 180° bending. The microstructure of the surface of the coatings (1.5–3.5 μm thick) on a 12Cr18Ni9Ti steel support was studied by the atomic-force microscopy (AFM) on a nanoscope. The phase composition of the deposits was determined by X-ray diffraction (CoK_α radiation, DRON-2 diffractometer). The chemical composition of the deposits was determined by thermogravimetric and spectral analyses.

The possibility of depositing ox-Mo in a quantitative yield by cathodic reduction during electrolysis of an aqueous solution of ammonium molybdate salt under the practicable conditions has been established in [2, 3]. The product containing the nonstoichiometric oxide compound of the composition $Mo_4O_{11} \cdot nH_2O$ as major component is deposited on the cathode [3]. This fact indicates that the discharge of MoO_4^{2-} ions and the phase transition with formation of the three-dimensional molecular lattice, which are the interrelated processes occurring on the cathode, have the complex kinetic character. The process starting from the molybdate ion discharge and terminating when a compact ox-Mo deposit is formed on the cath-

ode involves three steps: (1) discharge of MoO_4^{2-} ions and formation of the intermediate oxide radicals (MoO_2^+, MoO_2, MoO^-_3, and other radicals), (2) adsorption of intermediate oxide radicals on the cathode surface, and (3) simultaneous formation of a Mo_4O_{11} structural fragments and molecular crystal lattice.

The mechanism of this process is not clearly understood yet. At the same time, it is evident that it can be realized exclusively by multistep formation of a complex molecular compound ox-Mo.

The total (curve *1*) and partial polarization curves of the ox-Mo deposition (curves *3*–*5*, *5*') and hydrogen evolution (curve *2*) from ammonium molybdate solutions in the E–$\log I$ coordinates are shown in Fig. 1. All the dependences are strictly straight lines. The slopes and positions of the curves depend on the solution concentration and temperature. An increase in these parameters leads to a shift of the ox-Mo deposition curves toward lower cathode potentials (curves *3, 4*). The slope of the curves of the H_2 evolution from concentrated solution (curve *2*) and those of the ox-Mo deposition from concentrated solution (curves *3, 4*) is the same ($\partial E/\partial \log I$ = 0.58 V). For the curve of the ox-Mo deposition from dilute solution (curve *5*) this value is abnormally high (1.15 V). The partial curves of the ox-Mo deposition have an inflection whose position with respect to the $\log I$ axis depends on the solution concentration and temperature and corresponds to the limiting attainable current. The sections of the curves above the inflection points have different slopes corresponding to the rate at which the main process occurs in the limiting region under the given conditions of the electrolysis. The total curve *1* taken in dilute solution lies at a certain angle with respect to the partial H_2 evolution curve taken in the same solution. Hence, it follows that, in the limit, the main process is completely replaced by the H_2 evolution.

The high values of the slope coefficients of these dependences do not fit well into the known theory [4]. At the same time, satisfactory interpretation for the observed phenomenon can be given. For example, delayed migration, mainly via convection and molecular diffusion, of MoO_4^{2-} ions toward the cathode surface is likely to make the major contribution to the $\partial E/\partial \log I$ coefficient. This is clearly seen in the partial curve of ox-Mo deposition from dilute solution (curve *5*). The slope of the curve (1.15 V) decreases to 0.87 V after vigorous stirring of the solution (curve *5*'). Similar effect is attained with increasing solution concentration and electrolysis temperature (under other conditions equal). In this case, the corresponding dependences (curves *3, 4*) are shifted to lower cathode potentials and the slopes decrease to 0.58 V. Theoretically, this effect is substantiated by the known relationship of the electrochemical kinetics accompanied by concentration polarization [5]. The large slopes of the curves may also be due to the multistep character of the cathode process, typical of electrodeposition of some metals [6]. In the given case, the same role can be played by the filling of the cathode surface with adsorbed hydrogen, oxide molecules, and intermediate oxide radicals [4]. These factors, along with the mutual influence of conjugate cathodic reactions proceeding simultaneously, can also be responsible for the large slope of curve *2* of the H_2 evolution.

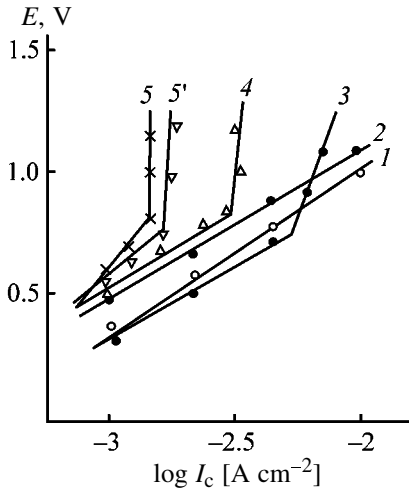


Fig. 1. Cathode potential E vs. $\log I_c$ of the molybdenum oxide deposition from ammonium molybdate solution (pH 6.5–7.0). Concentration of ammonium molybdate solution, M: (*1, 2, 5, 5*') 0.01 and (*3, 4*) 0.25. Curves: (*1*) total, (*2*) partial of H_2 evolution, (*5, 5*') partial of ox-Mo deposition at 20°C with and without stirring the solution, respectively, and (*3, 4*) partial of ox-Mo deposition at 80 and 20°C, respectively.

The complex kinetic behavior of the processes studied substantially impedes determination of the true value and character of the cathode polarization. Approximate estimate of the latter, based on the difference between the initial potential of the ox-Mo deposition (about –0.4 V) and the rest potential of the molybdenum oxide electrode on the 12Cr18Ni9Ti support (–0.12 V) in a 0.25 M test solution shows that the ox-Mo cathodic deposition proceeds at a fairly high polarization. Evidently, the MoO_4^{2-} ion discharge, whose rate largely depends on the intensity of the leading reaction of H_2 evolution, is the potential-determining stage in this case.

Approximate limiting thicknesses of ox-Mo coatings on 12Cr18Ni9Ti and aluminum supports, corresponding to break and complete failure of the sample along bending lines

Conditions of ox-Mo electrodeposition	Limiting coating thickness, μm, at indicated annealing temperature, °C			
	no annealing	180	250	350
Solutions:				
saturated	15–20	5–7	2–3	0.5–1.5
	45–55	25–30	10–15	5–7
dilute	10–15	3–5	1.5–3	0.5–1.0
	35–50	25–30	7–12	2–5

The Mo_4O_{11} molecule, primary product of the electrochemical phase transformation localized on the cathode surface, is a small three-dimensional unit "crystal" constituting the unit cell. Based on the atomic representation of the crystal nucleation, such a "crystal" may be considered as the initial crystallization center with a large excess of free energy [7]. The energy stability of the "center" and its fixation to the cathode surface are attained after applying an additional potential, which compensates the work spent for the destruction of the center. This "superpotential" simultaneously ensures spontaneous development of the nucleus to a certain size corresponding to the minimum of the free surface energy of the system. Apparently, this process is facilitated by the three-dimensional structure of oxide molecules. Indirectly, the superpotential may also be manifested in the higher slopes of the ox-Mo deposition curves.

Irrespective of preparation conditions, the ox-Mo coatings prepared on 12Cr18Ni9Ti steel supports have smooth black surface with a slight bluish tint. No visible defects such as cracks, voids, porosity, or thrown-on particles were found. The deposits prepared from saturated ammonium molybdate solutions at 80–85°C are slightly lustrous, and those prepared from dilute solutions on an aluminum support at low temperatures are relatively dull. The nonannealed deposits are compact coatings. Such coatings 20–25 μm thick on stainless steel support have fairly high mechanical resistance including that against mechanical abrasion. Heat treatment considerably deteriorates the coating characteristics.

The approximate values of the thickness of the electrolytic ox-Mo coatings on a stainless steel support, above which the sample is broken completely along the bending line, are presented in Table 1 as results of many tests. For the same coatings on aluminum support, these values are higher by a factor of 2–3, but are insufficiently reproducible. The values presented determine the limiting thickness of ox-Mo coating, above which the adhesion and mechanical resistance are zero for the given conditions of their deposition and subsequent heat treatment. The higher the annealing temperature, the smaller the coating thickness below which satisfactory adhesion and inner volume mechanical resistance are preserved. The impossibility of depositing thicker coatings may be caused by simultaneously occurring processes: coarsening of crystals upon annealling and weakening of bonds between grains along their boundaries owing to the different linear thermal expansion of the coating and the support. Along with this, the above characteristics of the nonannealed deposits may also get worse under the influence of the internal stresses, which increase and lead to a brittle failure with increasing coating thickness.

The morphology of the surface of the ox-Mo oxides studied is shown in Fig. 2. We found no strong correlation between the morphology, the nature of a solution, and the electrolysis conditions. Finely grained compact deposits are formed from hot saturated solutions of ammonium molybdate. More coarsely crystalline deposits are formed from dilute solutions and from solutions of sodium molybdate. However, the structure of both deposits, consisting of small poorly faceted crystals with random crystallographic orientation, differs insignificantly (Fig. 2a). With increasing temperature, the ordering of the deposit structure consisting in growth of coarser crystalline grains in a certain normal orientation takes place (Fig. 2b). The deposits heat-treated above 250°C are characterized by intense twinning of crystals with their clearly resolved layer-by-layer growth (Fig. 2c). This fact shows that, in the given case, the main mechanism of the formation of crystalline grains of the deposit is the normal layer-by-layer growth of the molecular crystalline aggregates-nuclei. The deposits heated above 600°C have coarsely crystalline structure consisting of ag-

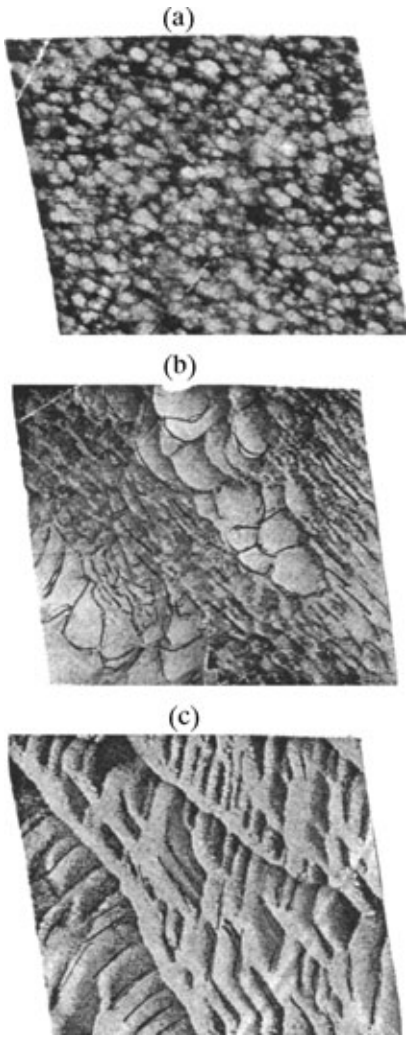


Fig. 2. Morphology of the surface of ox-Mo deposited from a 0.25 M ammonium molybdate solution: (a) drying at 20°C; annealing temperature in air, °C: (b) 280 and (c) 420. Magnification 50000.

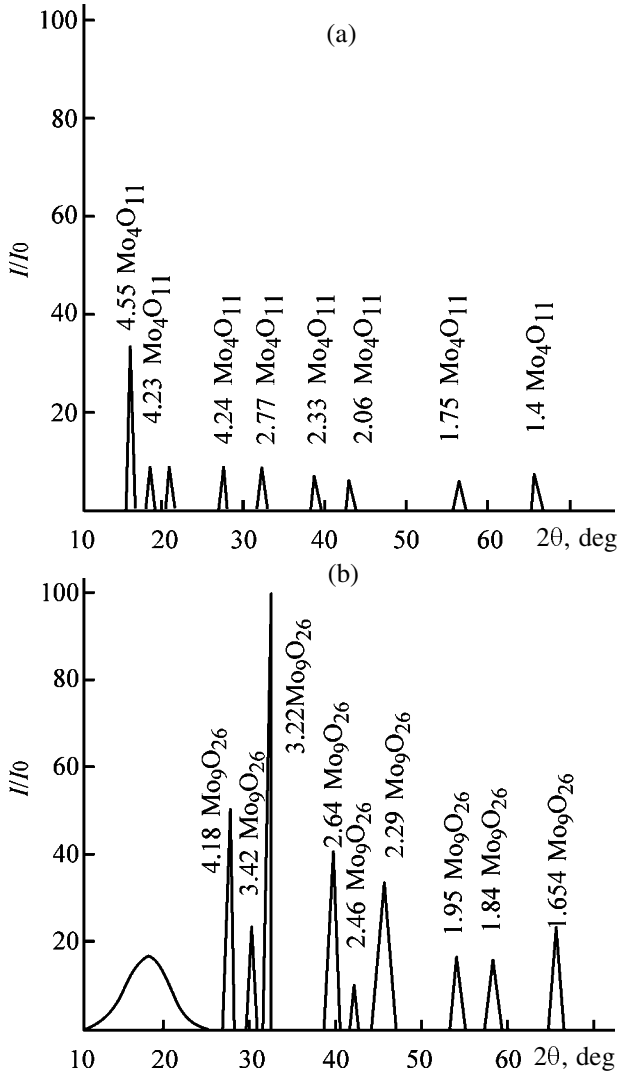


Fig. 3. X-ray diffraction patterns of electrolytic ox-Mo deposits obtained from a 0.25 M solution. (I/I_0) Relative intensity and (2θ) Bragg angle. (a) After drying at 20°C for 16 h and (b) after annealing at 260°C for 7 h. Interplanar spacings in Å are indicated.

glomerates of randomly oriented white grains with yellowish tint, typical of molybdenum(VI) oxide MoO_3, which is associated with the oxidation of the Mo_4O_{11} molecule with atmospheric oxygen by the reaction

$$Mo_4O_{11} + 1/2O_2 \xrightarrow{600°C} 4MoO_3.$$

According to the thermogravimetric and IR spectral analyses of the deposits studied, the chemical compound of the composition $MoO_x \cdot nH_2O$ (x is the homogeneity region within 2.75–2.88) may be present in them as the main phase. The amount of water of hydration lies within n = 1.33–1.35. The thermal effects observed in the differential thermogravimetric curve show that the main weight loss occurs within 160–180 and 260–300°C and is likely due to the removal of water and ammonia, part of which is incorporated in the deposit [8, 9].

According to the X-ray diffractoin analysis, molybdenum oxide is deposited on the cathode in the form of a nonstoichiometric intermediate oxide corresponding to the formula Mo_4O_{11} (Fig. 3a). The phase composition of the deposits can be affected by the electrolysis conditions. At increased values of the current density and pH, the additional phases, Mo_3O_8, Mo_3O_{23}, and Mo_9O_{26}, appear in the deposits, along with the indicated oxide phase. The reproducibility in this case, however, was poor. The deposits annealed

at 250°C and higher temperatures in air contain Mo_9O_{26} as the major phase, which is confirmed by intense reflections in the corresponding X-ray diffraction pattern (Fig. 3b). Evidently, this is associated with the absence of amorphous constituents of the deposits, which exist owing to the presence of hydrated oxide compounds. From this viewpoint, it is more correct in this case to consider electrolytic ox-Mo as a mixed system of the continuous oxide series MoO_x (x = 2.75–2.88). Nonetheless, thid does not exclude the possibility of controlling the phase composition of ox-Mo deposits by choosing appropriate electrolysis parameters and annealing conditions.

CONCLUSIONS

(1) Analysis of the total and partial E–$\log I$ dependences for molybdenum oxide deposition from ammonium molybdate solutions at different concentrations and temperatures shows that these parameters exert a decisive effect on the positions and slopes of the curves.

(2) The abnormally high $\partial E/\partial \log I$ values can be attributed to the delayed diffusion of MoO_4^{2-} ions and to the influence of concomitant factors of the cathodic process.

(3) The adhesion and mechanical resistance of molybdenum oxide electroplated on stainless steel or aluminum support is inversely proportional to the coating thickness and annealing temperature. The annealed deposits have more coarsely grained and more ordered structure. The chemical composition of the deposits changes upon annealing. The complex oxide compounds MoO_x transform into the homogeneous oxide MoO_3.

REFERENCES

1. Shembel', E., Apostolova, R., Nagirny, V., et al., *J. Solid State Electrochem*., 2005, vol. 9, no. 2, pp. 96–105.
2. Nagirny, V.M., Apostolova, R.D., Baskevich, A.S., et al., *Zh. Prikl. Khim*., 2000, vol. 73, no. 3, pp. 406–409.
3. Nagirny, V.M., Apostolova, R.D., Baskevich, A.S., et al., *Zh. Prikl. Khim*., 2000, vol. 73, no. 1, pp. 75–77.
4. Frumkin, A.N., Bagotskii, V.S., Iofa, Z.A., and Kabanov, B.N., *Kinetika elektrodnykh protsessov* (Kinetics of Electrode Processes), Moscow: Mosk. Gos. Univ., 1952.
5. Skorcheletti, V.V., *Teoreticheskaya elektrokhimiya* (Theoretical Electrochemistry), Leningrad: Goskhimizdat, 1959.
6. Bokris, J. and Conway, B.E., *Modern Aspects of Electrochemistry*, London: Butterworths, 1964.
7. Danilov, A.I. and Polukarov, Yu.M., *Usp. Khim*., 1987, vol. 56, no. 7, pp. 1082–1104.
8. Schleich, D.V., Chang, H.S., and Barberio, J.L., *Power Sources*, 1989, vol. 26, nos. 1–2, pp. 103–106.
9. Zhang, X., and French, R., *J. Electrochem. Soc*., 1996, vol. 145, no. 6, pp. 847–852.

ISSN 1070-4272, Russian Journal of Applied Chemistry, 2006, Vol. 79, No. 9, pp. 1443–1446. © Pleiades Publishing, Inc., 2006.
Original Russian Text © V.M. Nagirnyi, R.D. Apostolova, E.M. Shembel', 2006, published in Zhurnal Prikladnoi Khimii, 2006, Vol. 79, No. 9, pp. 1459–1462.

APPLIED ELECTROCHEMISTRY AND CORROSION PROTECTION OF METALS

Surface Morphology of Electrolytic Deposits of Vanadium, Cobalt, and Manganese Oxides

V. M. Nagirnyi, R. D. Apostolova, and E. M. Shembel'

Ukrainian State University of Chemical Engineering, Dnepropetrovsk, Ukraine

Received November 10, 2005; in final form, May 2006

Abstract—The surface morphology of V_2O_5, Co_2O_3, and MnO_2 electroplated under different electrolysis conditions was studied. The nature of the electrocrystallization of these materials was suggested on the basis of the analysis results.

DOI: 10.1134/S1070427206090102

Electrolytic deposition of compact coatings and dispersed deposits of vanadium and cobalt oxides and of two-phase systems based on manganese dioxide onto anode in a quantitative yield from aqueous solutions of appropriate salts was considered previously from the scientific and technological standpoints [1–5]. These oxide compounds are promising materials of lithium batteries. They have high electrochemical activity and a satisfactory tendency to cycling at stable and reasonably high reversible capacity [6, 7]. In the above studies, the electrosynthesis of the above materials was not considered in the aspect of the structural characteristics of the deposits obtained and the related phase formation processes. Here this problem was considered by analyzing the surface morphology of electrolytic V_2O_5, Co_2O_3, and MnO_2 deposits.

The deposits were prepared in the form of compact coatings 1.5–3.5 μm thick on smooth plates made of 12Cr18Ni9Ti steel (surface finishing grade 8). The surface morphology of the deposits was studied by atomic-force microscopy on a IIIa nanoscope (Digital Instruments). The compositions of the solutions for preparing deposits and the electrolysis parameters are given in the table.

The surface morphology of the deposits studied is shown in Fig. 1. All the deposits have a crystalline structure. The exception is vanadium oxide V_2O_5 prepared from solution no. 1 of oxovanadium sulfate, with fine-grained, nearly amorphous structure (Fig. 1a). In this case, a pronounced relief formed by accumulation of randomly projecting comb-like aggregates is observed on the V_2O_5 surface. Such a crystallization character is possible at continuous degeneration of crystals in the step close to the nucleation and may be favored by the high sorption capacity of V_2O_5 [8], which is responsible for the overgrowth of the deposited oxide molecules with atomic and molecular oxygen and with water molecules. The adsorption layer forming in the process impedes the three-dimensional growth of the crystalline nucleus because of hindered access of discharging VO^{2+} ions toward the active sites on the anode surface and retarded attachment of the forming oxide molecules to the nucleus.

When sodium ions are added to solution no. 1 (solution no. 2), the character of the V_2O_5 crystalliza-

Composition of solutions and electrolysis parameters for deposition of oxide compounds at 80–85°C

Oxide	Solution no.	Solution, M	pH	I_a, mA cm^{-2}
V_2O_5	1	$VOSO_4$ 0.25	1.8–2.0	7.5–10
	2	$VOSO_4$ 0.25, Na_2SO_4 0.15	1.8–2.0	7.5–10
	3	NH_4VO_{3sat}	6.0–6.5	3.0–3.5
	4	NH_4VO_{3sat}	5.5–6.0	3.5–4.0
Co_2O_3	5	$CoSO_4$ 0.025, $CoSO_4 \cdot 7H_2O$ 0.07	4.5–5.0	10–15
	6	$CoSO_4 \cdot 7H_2O$ 0.025 $Cr_2(SO_4)_3 \cdot 6H_2O$ 0.04	4.5–5.0	8.0–10
MnO_2	7	$MnSO_4 \cdot 5H_2O$ 0.45	2.0–2.5	10–12.5
	8	$MnSO_4 \cdot 5H_2O$ 0.20, $Cr_2(SO_4)_3 \cdot 6H_2O$ 0.40	2.0–2.5	8.5–10

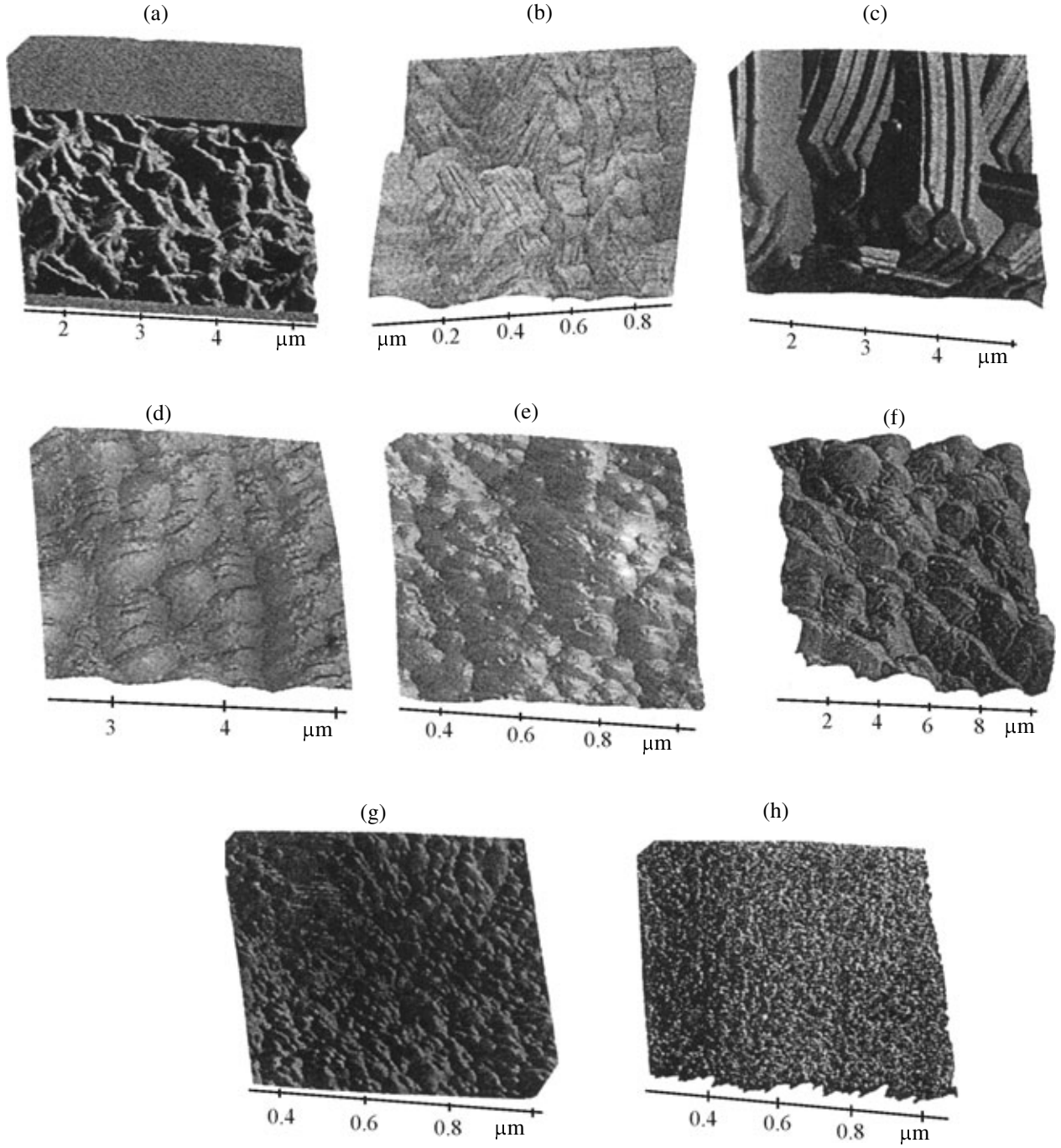


Fig. 1. Surface morphology of electrolytic deposits of V_2O_5, Co_2O_3, and MnO_2: (a) V_2O_5 formed from oxovanadium sulfate solutions; (b) the same as in (a), in the presence of Na^+ ions; (c) V_2O_5 deposited from ammonium metavanadate solutions; (d) the same as in (c), in the presence of Co^{2+} ions; (e) Co_2O_3 deposited from $CoSO_4$ solution; (f) MnO_2 deposited from sulfate solution; (g) the same as in (e), in the presence of Cr^{3+} ions; (h) the same as in (f), in the presence of Cr^{3+} ions in higher concentration.

tion and the structure of the anodic deposit change markedly (Fig. 1). The deposit has a crystalline structure consisting of densely packed crystals growing layer-by-layer in the form of well-defined steps. In this case, sodium atoms may participate in the formation of the energy barrier making the sorption activity of V_2O_5 molecules lower, which creates favorable conditions for the ordered crystal growth. The reaction of sodium ions with vanadium oxide forming on the anode yields a compound belonging to the class of

vanadium bronzes of the composition $Na_xV_2O_5$ (x = 0.23–0.28), which is confirmed by X-ray analysis of the deposits [9]. In this case, the formation of the deposit decelerates considerably, probably because of the hindered discharge of VO^{2+} ions due to a qualitative change in the energy state of the support [2].

Large-block crystalline deposits are formed on the anode from ammonium vanadate solution no. 3, with steps of crystal growth clearly edged and the sequentially superposed stacks having a smooth facet surface (Fig. 1c). The stacks have nearly the same thickness and are arranged so that their frontal facets are shifted at a nearly equal distance from each other. Such a structure suggests fairly fast development of primary two-dimensional crystalline aggregates growing in one plane, with the volume crystal growth by the sequential deposition of the molecular layers. This mechanism can be realized when the concentration conditions and the direction of growth of the step are strongly coordinated. In our case, this may be facilitated by the joint action of two mechanisms of the V_2O_5 formation:

coagulation

$$2HVO_3 \rightarrow V_2O_5 + H_2O$$

and electrochemical mechanisms:

$$2VO^{2+} + H_2O - 2e \rightarrow V_2O_5 + 6H^+ \text{ [3].}$$

The coagulation mechanism, which is mainly due to the electrostatic interaction, involves no energy consumption and promotes the crystal growth owing to direct formation of molecular crystalline aggregates on the anode surface. Their further growth is evidently provided via both the first and the second mechanisms. In this case, dark orange or brownish deposits are formed, unlike light orange crystalline V_2O_5 deposits formed by the traditional thermochemical method, which confirms the above suggestion.

In the presence of Co^{2+} ions (solution no. 4), the surface morphology of the V_2O_5 deposit electroplated from ammonium vanadate solution changes essentially (Fig. 1d). Break of the large-block structure of crystalline grains with simultaneous decrease in their size and transformation into the qualitatively new globular structure is responsible for this result. In the process, the deposits acquire a dark gray color. However, finely grained dark orange deposits are observed along the grain boundaries. These formations probably originate from the fact that, in the step close to the onset of nucleation, the growth of V_2O_5 crystals is suppressed by jointly deposited Co_2O_3 molecules. The presence of Co_2O_3 in these deposits was confirmed by X-ray diffraction analysis [3]. This makes it possible to consider these deposits as an interstitial solid solution of Co_2O_3 in V_2O_5. Probably, the globular structure of the deposits is formed owing to the fact that growth of V_2O_5 crystals is decelerated with adsorbing Co_2O_3 molecules and they are deposited between the growth steps at the limited supply of Co^{2+} ions toward the anode surface.

The Co_2O_3 deposits electroplated from solution no. 5 also tend to form spheroidal crystalline structures (Fig. 1d). This may be due to the fact that the strict geometry of the step growing at the frontal face of the crystal is broken at the limited and nonuniform supply of oxide molecules toward its active points. In this case, a certain role may be played by the structure of Co_2O_3 molecules, whose rhombic structure is likely to facilitate their packing in aggregation.

The MnO_2 deposits electroplated from solution no. 7 have a lamellar structure (Fig. 1d). Each "lamella" is a multilayer dense stack with projecting growth steps. Some of these superimposed steps form coarser crystalline grains. The size distribution of the lamellas over the deposit surface is fairly uniform. This structure suggests a specific mechanism of the phase formation, largely dependent on the structure of the oxide lattice. This lattice belongs to the γ-MnO_2 modification having a complex polymolecular rhombic structure. Therefore, it may be suggested that the nucleation and growth of MnO_2 crystals and the formation of the three-dimensional structure of the crystal lattice occur simultaneously. A two-dimensional nucleus, or layer, forming in the process is actually a three-dimensional formation with the height equal to the corresponding lattice parameter. If the crystal growth is a diffusion-controlled process, the limit of the oxide molecules formed electrochemically in the adjacent region of the solution will be rapidly exhausted, which will restrict the growth of molecular layers in the stack.

The introduction into the Co_2O_3 and MnO_2 electroplating solutions (solutions nos. 5, 7) of chromium ions (solutions nos. 6, 8, respectively), results in an essential change in the phase composition and crystal structure of the deposits. The crystalline grains become considerably finer, and the surface morphology changes. The Co_2O_3 deposits plated in the presence of Cr^{3+} ions consist of rather uniformly distributed fine aggregates in the form of layered petal-shaped stacks, with growth steps projecting on the end

faces (Fig. 1g). The crystalline grains have random crystallographic orientation. The formation of such a structure is likely due to the blocking of the frontal boundary of a growing stack with Cr_2O_3 molecules. As a result, its development is inhibited as the concentration of Co_2O_3 molecules in the growth zone decreases.

Increasing the concentration of the Cr^{3+} ions in the solution results in a marked change in the crystal structure of the deposits (cf. Figs. 1g and 1h, solution nos. 8 and 6). The deposits consist of fine close-packed pillared crystalline grains forming a fairly uniform surface. Apparently, the formation of this structure is due to a strong effect of jointly deposited Cr_2O_3 molecules on the formation and growth of nascent MnO_2 crystals. The Cr_2O_3 molecules confine the development of nuclei in layers in the longitudinal direction by blocking their frontal faces in the initial steps of the formation. This creates the favorable conditions for their sequential superposition and for the growth of pillared crystals in the direction normal to the electrode surface.

The analysis of the surface morphology of electrolytic V_2O_5, Co_2O_3, and MnO_2 deposits showed that the electrocrystallization of these oxides has a number of common features determining their crystal structure and the energy balance in their formation. For example, according to the voltammetric characteristics of the deposits [1–4], the corresponding anodic polarization, determined from difference between the potential of the onset of the oxide deposition and the standard electrode potential, lies within 0.07–0.15 V, decreasing in the order $Na_xV_2O_5 > Co_2O_3 > V_2O_5 > MnO_2$. This implies that the given oxide systems are deposited at a moderate overvoltage of the electrode process. The energy consumption in the process may be partly compensated at the expense of the energy liberated upon phase transformation. This effect may be associated with the influence of chemisorbed oxygen on the mechanism of the anodic deposition of the oxide, facilitating the electron transfer. For example, in the case of V_2O_5 formation, this process can occur by the scheme

$$VO^{2+} + (M–O) - e \rightarrow VO_2^+ + M,$$

$$VO^{2+} + VO_2^+ + 2(M–O) - e \rightarrow V_2O_5 + 2M;$$

and in the case of Co_2O_3 formation, by the scheme

$$Co^{2+} + (M–O) - e \rightarrow CoO^+ + M,$$

$$2CoO^+ + (M–O) \rightarrow Co_2O_3 + M.$$

Thus, the electrocrystallization of the oxide compounds under consideration is determined by the electrolysis conditions, on the one hand, and by the crystal lattice structure, on the other hand. This is clearly seen in the case of electrolytic V_2O_5, whose crystallization depends directly on the composition of a solution and electrolysis conditions. The correlation with the oxide crystal system is reflected in essentially different crystal structures of the corresponding electrolytic deposits.

CONCLUSIONS

(1) The morphology of the surface of electrolytic V_2O_5, Co_2O_3, and MnO_2 deposits was analyzed. The probable mechanisms responsible for the deposition and formation of the corresponding crystalline structures were suggested. It was assumed that a comparatively low overvoltage in formation of the oxides considered is due to the three-dimensional molecular structure facilitating crystal nucleation through the intermediate oxide radicals in the course of interaction with adsorbed oxygen.

(2) The formation of crystalline structures of the deposits depends on the electrolysis conditions and crystal lattice structure of the oxide.

REFERENCES

1. Apostolova, R.D., Nagirnyi, V.M., and Shembel', E.M., *Elektrokhimiya*, 1998, vol. 34, no. 7, pp. 778–784.
2. Shembel', E.M., Nagirnyi, V.M., and Apostolova, R.D., *Zh. Prikl. Khim.*, 2000, vol. 73, no. 3, pp. 409–412.
3. Nagirnyi, V.M., Apostolova, R.D., Baskevich, A.S., et al., *Zh. Prikl. Khim.*, 2001, vol. 74, no. 9, pp. 1429–1432.
4. Nagirnyi, V.M., Apostolova, R.D., Baskevich, A.S., et al., *Zh. Prikl. Khim.*, 2001, vol. 74, no. 9, pp. 1433–1437.
5. Nagirnyi, V.M., Apostolova, R.D., Baskevich, A.S., et al., *Zh. Prikl. Khim.*, 2002, vol. 75, no. 2, pp. 221–226.
6. Apostolova, R.D., Shembel', E.M., and Nagirnyi, V.M., *Elektrokhimiya*, 2000, vol. 36, no. 1, pp. 41–48.
7. Shembel, E., Apostolova, R., Nagirny, V., et al., *Power Sources*, 1999, vols. 81–82, pp. 480–488.
8. Goncharenko, *Elektrokhimiya vanadiya* (Vanadium Electrochemistry), Moscow: Metallurgiya, 1969.
9. Apostolova, R.D., Shembel', E.M., and Nagirnyi, V.M., *Elektrokhimiya*, 2001, vol. 37, no. 10, pp. 1205–1213.

ISSN 1070-4272, Russian Journal of Applied Chemistry, 2006, Vol. 79, No. 9, pp. 1447–1452. © Pleiades Publishing, Inc., 2006.
Original Russian Text © Kh.Kh. Gil'manov, A.A. Lamberov, E.V. Dement'eva, N.V. Romanova, S.V. Trifonov, A.V. Andryushkevich, R.Ya. Bikkulov, 2006, published in Zhurnal Prikladnoi Khimii, 2006, Vol. 79, No. 9, pp. 1463–1468.

CATALYSIS

Effect of the Paste Molding Pressure on the Activity of Iron Oxide Catalyst in Dehydrogenation of Methylbutenes

Kh. Kh. Gil'manov, A. A. Lamberov, E. V. Dement'eva, N. V. Romanova, S. V. Trifonov, A. V. Andryushkevich, and R. Ya. Bikkulov

Nizhnekamskneftekhim Open Joint-Stock Company, Nizhnekamsk, Tatarstan, Russia
Kazan State University, Kazan, Tatarstan, Russia
Kazan State Technological University, Kazan, Tatarstan, Russia

Received December 27, 2005; in final form, May 2006

Abstract—The effect of the paste molding pressure on the activity of an iron oxide catalyst in dehydrogenation of methylbutenes was studied. The study involved detailed analysis of the pore structure of the samples by mercury porosimetry and determination of the mode of the catalytic process (kinetic or diffusion control). The range of pore sizes in which dehydrogenation reactions occur was determined.

DOI: 10.1134/S1070427206090114

Olefins and alkylaromatic hydrocarbons are commonly dehydrogenated in the presence of iron oxide catalysts [1–4], which contain alkali metal ferrites as active components [5, 6]. It has been shown [7, 8] that dehydrogenation on an iron oxide catalyst proceeds under diffusion control and is limited by mass transfer in its porous system, i.e., by the rates of reagent supply and reaction product removal. Therefore, it is important to determine the optimal pore structure of iron oxide catalysts, which have low specific surface area (3–9 $m^2 g^{-1}$) and low porosimetric volume (0.1–0.5 $cm^3 g^{-1}$).

The porous structure is formed in all stages of catalyst synthesis, including that of molding of catalyst pastes. This stage predetermines not only the texture characteristics, but also the physicomechanical properties of the finished catalyst. However, published information on how the molding conditions affect the properties of iron oxide catalysts is insufficient [9, 10]. There are only patents [11, 12] which suggest that grains of various noncylindrical shapes (trifoliate, starlike, perforated, etc.) should be formed by extrusion in order to improve the efficiency of the catalysts.

The aim of this study was to examine the influence exerted by the molding pressure on the pore structure parameters of the iron oxide catalyst and on its catalytic properties.

EXPERIMENTAL

Catalyst samples were synthesized by "wet" mixing of the starting components containing iron oxide and compounds of potassium, magnesium, calcium, and other metals. Then the suspensions obtained were dried at 150–200°C, after which the powder was moistened to 10% humidity, weighed into 4-g portions, and molded on a Maekawa Testing Machine MFG hydraulic press at pressures of 50, 150, and 275 MPa. The samples (pellets 20 mm in diameter) were obtained at different compaction pressures but had the same chemical composition. After the compaction, the samples were calcined in air under the similar conditions.

The catalysts were tested in dehydrogenation of methylbutenes into isoprene. The tests were performed in a laboratory flow-through reactor with a catalyst charge of 40 cm^3 at reaction temperatures of 600–615°C, space velocity of methylbutenes equal to 1 h^{-1}, atmospheric pressure, dilution of the raw material with steam, and molar ratio $C_5H_{10} : H_2O$ = 1 : 20. The compositions of gaseous products and the isoamylene fraction were determined chromatographically on two gas–liquid chromatographs with heat-conductivity detectors, with subsequent processing of the analytical results. The accuracy with which the composition of the dehydrogenation products was determined was evaluated using methods of mathematical statistics [13], developed for a small number of determinations ($n < 30$). The relative root-mean-square error was ±2%.

To preclude condensation of C_5 hydrocarbons, the gaseous mixture was sampled for analysis into an aspirator with a brine of density 1.2. The aspirator

Table 1. Composition of the feed and products of the dehydrogenation at 600°C

Composition	Content, wt %								
	sample no. 1			sample no. 2			sample no. 3		
	feed	products		feed	products		feed	products	
		600°C	615°C		600°C	615°C		600°C	615°C
H_2	–	2.20	2.68	–	2.14	2.74	–	2.20	2.47
CH_4	–	0.53	0.68	–	0.46	0.84	–	0.57	0.70
CO_2	–	0.65	1.00	–	0.50	1.20	–	0.63	1.17
C_3H_8	–	0.38	0.56	–	0.30	0.56	–	0.33	0.50
C_4H_{10}	0.1	1.75	2.52	0.1	1.56	2.60	0.1	1.50	2.17
t-C_5H_{12}	0.7	0.63	0.60	1.4	1.06	1.08	0.3	0.20	0.20
n-C_5H_{12}	6.5	7.20	7.34	6.5	7.38	7.34	6.4	7.00	7.13
i-C_5H_{10}	84.4	41.15	32.28	83.7	41.48	33.24	84.1	39.07	33.30
n-C_5H_{10}	6.6	3.33	2.72	6.4	3.14	2.38	7.2	3.10	2.60
i-C_5H_8	1.7	39.03	47.06	1.8	39.3	45.46	1.9	42.10	46.90
n-C_5H_8	–	3.13	2.58	–	2.60	2.52	–	3.17	2.90
$K_{C_5H_{10}}$	–	51.24	61.70	–	50.44	60.30	–	53.54	60.40
$A_{C_5H_8}$	–	45.30	54.70	–	46.00	53.20	–	49.10	54.53
$S_{C_5H_8}$	–	86.80	87.40	–	89.30	87.10	–	89.70	89.00

was preliminarily filled with argon, so that the sample-to-argon ratio was 1 : 4. The composition of the gas was calculated with account of the dilution factor.

The composition of low-boiling gases (H_2, O_2, N_2, CH_4, and CO) was determined on a column packed with NaX molecular sieves, and that of the hydrocarbon mixture and CO_2, on a column with a sorbent composed of 30% TEGNM on a diatomite of the 0.16–0.25-mm fraction.

As the catalyst activity factor $A_{C_5H_8}$ (%) we took the yield of isoprene based on the methylbutenes passed, which was calculated by the formula

$$A_{C_5H_8} = \frac{c_{C_5H_8}(\text{gas.prod.})}{c_{C_5H_{10}}(\text{feed}) + c_{C_5H_8}(\text{feed})} \times 100.$$

As the selectivity factor by isoprene $S_{C_5H_8}$ (%) we took the yield of isoprene based on decomposed isoamylenes, calculated by the formula [14]

$$S_{C_5H_8} = \frac{c_{C_5H_8}(\text{gas.prod.})}{[c_{C_5H_{10}}(\text{feed}) + c_{C_5H_8}(\text{feed})] - c_{C_5H_8}(\text{gas.prod.})} \times 100.$$

The texture characteristics of the catalysts were studied by mercury porosimetery on a Micromeritics Auto-Pore 9200 instrument (the United States). The porosity ε of the catalysts was calculated from the pellet density ρ_c and the specific pore volume V_p by the formula $\varepsilon = \rho_c V_p$ [15].

The X-ray phase analysis (XPA) was performed on a DRON-2 diffractometer with CuK_α radiation and a monochromatic filter. The range of recording angles 2θ was 5°–60°.

The dehydrogenation of methylbutenes involves both the target (synthesis of isoprene) and side reactions (decomposition of isoamylenes and isoprene to give low-boiling hydrocarbons and coke) [16]. The results of the catalytic tests at dehydrogenation temperatures of 600 and 615°C of samples having the same chemical and phase composition (according to XPA), but molded at different pressures of 50 (sample no. 1), 150 (sample no. 2), and 275 MPa (sample no. 3), are listed in Table 1.

As follows from Table 1, the samples produced at pressures of 50 and 150 MPa exhibit approximately the same activity at a reaction temperature of 600°C, with the conversion of methylbutenes, $K_{C_5H_{10}}$, equal to 51.14 and 50.44 wt %. Raising the process temperature from 600 to 615°C is accompanied by a significant rise in $K_{C_5H_{10}}$ (by 10%). The selectivities to isoprene of sample nos. 1 and 2 are at the same level (~87%); however, their values differ from those ini-

Table 2. Experimental and calculated values of kinetic parameters

P, MPa	$K_{C_5H_{10}}$, wt %			k, h^{-1}			E_a, kJ mol^{-1}	β
	K_{600}	K_{610}	K_{615}	k_{600}	k_{610}	k_{615}		
50	51.2	58.2	61.7	0.72	0.87	0.96	122.8	1.33
150	50.4	57.0	60.3	0.70	0.84	0.92	125.3	1.34
275	53.54	57.4	60.4	0.77	0.85	0.93	65.8	1.22

Note: The target reaction of dehydrogenation of methylbutenes is first-order.

Table 3. Experimental and calculated values for finding the Thiele modulus

P, MPa	S_{sp}, $m^2\ g^{-1}$	V_p, $cm^3\ g^{-1}$	ε	R_{av}, μm	D_{eff}, $m^2\ h^{-1}$		$W_{C_5H_{10}}$, mol $m^{-2}\ h^{-1} \times 10^3$		Ψ	
					D_{600}	D_{615}	W_{600}	W_{615}	Ψ_{600}	Ψ_{615}
50	7.4	0.43	0.93	7.77	9.584	9.666	0.77	0.93	0.126	0.138
150	8.0	0.36	0.84	5.44	6.713	6.770	0.76	0.92	0.229	0.250
275	13.0	0.16	0.40	0.24	0.301	0.303	0.81	0.92	2.370	2.510

tially observed (at 600°C). The sample molded at 275 MPa exhibits a somewhat higher conversion of methylbutenes at 600°C, which increases by approximately 6.5% as the process temperature is raised to 615°C, without any change in the selectivity to isoprene. The differences between the increments in the conversion of methylbutenes, observed as the process temperature is elevated, suggest that the pressure of catalyst molding affects the nature of the rate-determining step of the reaction.

To determine the reaction mode (diffusion or kinetic control) and the kinetic parameters of the process, the following quantities were calculated: effective rate constant k, temperature coefficient β of the process rate, effective activation energy E_a, and Thiele modulus. The effective rate constant was calculated from the degree of conversion of methylbutenes to isoprene, $K_{C_5H_{10}}$, at temperatures of 600, 610, and 615°C [17], after which the effective activation energy was found by the graphical method [18]. The results of calculation of the kinetic parameters are listed in Table 2.

The Thiele modulus, whose value was used to determine the reaction mode, was calculated from the integral characteristics of the pore structure of the catalyst, found by mercury porosimetry: specific surface area S_{sp}, porosimetric volume V_p, and average pore radius R_{av}; also, the diffusion coefficient D_{eff} and the rate of dehydrogenation of methylbutenes, $W_{C_5H_{10}}$, at T = 600 and 615°C were calculated.

The results obtained (Table 3) demonstrate that the dehydrogenation of methylbutenes with samples molded at pressures of 50 and 150 MPa is diffusion-controlled ($\Psi < 0.5$) and the degree of surface utilization is close to unity [17], i.e., virtually the whole catalyst surface is involved in dehydrogenation of methylbutenes. At higher molding pressures (275 MPa), the process mode shifts to inner diffusion control ($\Psi > 2.5$), in which case the degree of surface utilization becomes considerably lower (~0.5–0.6) [14], and, according to the dependence reported in [19], the effective activation energy of the process corresponds to half the activation energy in the case of kinetic control (Table 2). It is for this reason that, in contrast to sample nos. 1 and 2, an increase in the reaction temperature by 15°C for sample no. 3 leads to a less pronounced rise in the conversion of methylbutenes.

Comparison of the integral texture characteristics of the samples (Table 1) suggests that the higher conversion of methylbutenes (at 600°C) for the sample molded at 275 MPa is due to its considerably larger specific surface area. Probably, an interval of optimal pore diameters in which the main reaction occurs must exist for the diffusion-controlled process. In this case, the process rate is proportional to S_{sp} corresponding to this range of pore diameters.

In order to study in more detail the effect of the pore structure on the mode of the reaction control and on kinetic parameters, the texture characteristics of the catalyst samples described above were analyzed.

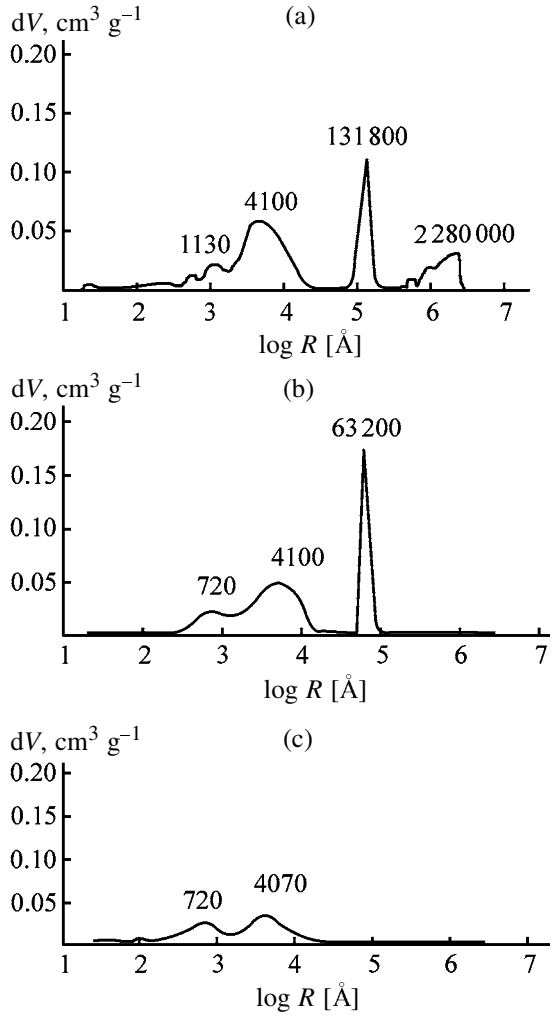


Fig. 1. Distributions of the pore volume over radii R for catalyst samples obtained by single-side compaction. Pressure, MPa: (a) 50, (b) 150, and (c) 275.

The porograms measured by mercury porosimetry for the samples studied are shown in Fig. 1. Three regions can be distinguished in the pore volume distribution for different pore radius intervals (Fig. 1, Table 4): fine-porous with $R < 0.2$ μm, medium-porous with the radii in the range 0.2–3.5 μm, and coarse-porous at $R > 3.5$ μm.

The starting sample no. 1 (P = MPa) has a polymodal pore structure with pore volume distribution peaks at radii of 228, 13.8, 0.41, 0.11, and 0.005 μm (Fig. 1a). The value of V_p is largely determined by pores with radii exceeding 3.5 μm (0.22 $cm^3 g^{-1}$), and S_{sp}, by pores with radii smaller than 0.2 μm (6.7 $m^2 g^{-1}$).

In the case of molding at 150 MPa (sample no. 2), the peak at R = 228 disappears from the porograms and, simultaneously, the peak at R = 13.18 μm shifts to smaller radii (6.32 μm), with its intensity increasing by 38%.

The disappearance of coarse pores and the appearance of additional pores with smaller radius lead to a 17% decrease in the porosimetric volume in the coarse-porous range and cause an insignificant change (<1%) in the specific surface area. In the medium-porous range, the intensity of the peak at R = 0.41 μm decreases, which leads to a significant (by 24%) decrease in the porosimetric volume at pore radii in the range 0.2–3.5 μm. In the range of fine pores, the peak at R = 0.11 μm shifts toward smaller radii (R = 0.07 μm), with the result that the specific surface area increases from 6.7 to 7.2 $m^2 g^{-1}$.

Thus, an increase in the molding pressure to 150 MPa strongly affects the transformation of pores in the medium- and coarse-porous ranges, but does not lead to significant changes in the integral characteristics V_p and S_{sp}. The latter may be due to densification of the material as a result of void disappearance and particle disintegration under the action of stresses and structural and shear deformations caused by the pressure applied [20]. Comparison of the results obtained in catalytic tests (Table 1) and analysis of the texture characteristics shows that transformation of pores with radii exceeding 3.5 μm has no effect on the activity of samples in dehydrogenation of methylbutenes. However, these pores strongly affect the physicomechanical properties of extrudates [21].

Molding of samples at a pressure of 275 MPa (sample no. 3) leads to disappearance of pores with $R > 3.5$ μm (0.02 $cm^3 g^{-1}$) and to a decrease in the intensity of the peak at R = 0.41 μm from 0.05 to 0.03 $cm^3 g^{-1}$. The polymodal pore structure becomes bimodal. A low-intensity peak appears in the range of fine pores at R = 0.009 μm, and the contribution of this peak to the specific surface area is 17.5% (2.28 $m^2 g^{-1}$). The increase in the molding pressure results in that S_{sp} at $R < 0.2$ μm grows by 43% (from 7.2 to 12.6 $m^2 g^{-1}$) and V_p at $R > 3.5$ μm falls by 90% (from 0.18 to 0.02 $cm^3 g^{-1}$) at an insignificant change in the sample density.

For a closer analysis of the pore structure, the range from 2 to 3000 nm was considered in more detail. The data obtained are listed in Table 5. It can be seen that the increase in the specific surface area with the molding pressure is due to formation of an additional number of pores at $R < 50$ nm, with more than 60% of S_{sp} accounted for by pores with $R < 5$ nm (8 out of 13 $m^2 g^{-1}$).

Table 4. Pore structure parameters of samples of catalysts for dehydrogenation of methylbutenes, found from mercury porosimetric data

P, MPa	S_{sp}, $m^2\ g^{-1}$	R_{av}, μm	R_{max}, μm	V_p, $cm^3\ g^{-1}$	Pore volume in indicated range of pore radii, μm			Specific surface area in indicated range of pore radii, μm		
					<0.2	0.2–3.5	>3.5	<0.2	0.2–3.5	>3.5
					$cm^3\ g^{-1}$/%			$m^2\ g^{-1}$/%		
50	7.4	7.77	13.18	0.43	0.08/18.6	0.14/29.6	0.22/47.6	6.71/90.7	0.66/8.9	0.02/0.21
150	8.0	5.44	6.32	0.36	0.07/20.3	0.10/28.6	0.18/50.3	7.25/90.5	0.68/8.6	0.07/0.8
275	13.0	0.24	0.41	0.16	0.09/53.7	0.06/37.5	0.02/11.3	12.59/96.8	0.36/2.8	0.00/0.0

Table 5. Distribution of the specific surface area with respect to pore radius ranges for samples obtained at different molding pressures

P, MPa	S_{sp}, $m^2\ g^{-1}$	Specific surface area in indicated range of pore radii, μm											
		2–3		3–5		5–15		15–50		50–100		100–3000	
		$m^2\ g^{-1}$	%	$m^2\ g^{-1}$	%	$m^2\ g^{-1}$	%	$m^2\ g^{-1}$	%	$m^2\ g^{-1}$	%	$m^2\ g^{-1}$	%
50	7.4	4.13	55.8	0.71	9.6	0.43	5.8	0.43	5.8	0.69	9.32	0.98	13.2
150	8.0	4.17	52.1	1.11	13.9	0.63	7.9	0.32	4.0	0.72	9.0	0.97	12.1
275	13.0	4.85	37.3	3.46	26.6	2.72	20.9	0.67	5.2	0.73	5.6	0.52	4.0

The data of Table 5 were used to find the "working" range of pore radii, for which the specific surface area is proportional to the conversion of methylbutenes. The conversion $K_{C_5H_{10}}$ correlates with S_{sp} for mesopores with radii in the range 15–50 nm. The specific surface area has too widely varying values at smaller radii (5–15 nm) and remains virtually unchanged at larger radii (50–100 nm).

At the same time, it may be suggested that the increase in S_{sp} at 5–15 nm gives rise to steric hindrance as a result of formation of a large number of pores with radii smaller than the "working" value and transfers the process from kinetically controlled to diffusion-controlled mode. Pores with radii smaller than 5 and larger than 50 nm do not affect the reaction control mode significantly.

CONCLUSIONS

(1) The paste molding pressure affects the parameters of the pore structure of a catalyst, and reaching a certain pressure (~250 MPa) leads to a shift from kinetically to diffusion-controlled process.

(2) It was suggested that the catalytic process mostly occurs in pores of radius 15–50 nm, which is indicated by the correlation between the conversion of methylbutenes and the specific surface area in this range of pore radii.

(3) The results of catalytic tests and the texture characteristics were compared and it was demonstrated that pores with radii smaller than 5 and larger than 50 nm affect the activity of the catalyst samples, but cannot govern their physicomechanical properties.

REFERENCES

1. RF Patent 2186619.
2. RF Patent 2127633.
3. US Patent 6184174.
4. RF Patent 999237.
5. Meima, G.R. and Menon, P.G., *Appl. Catal.*, 2001, vol. 212, pp. 239–245.
6. Kotel'nikov, G.R., Buyanov, R.A., and Strunnikova, L.V., Abstracts of Papers, *V Vsesoyuznaya konferentsiya "Termodinamika i tekhnologiya ferritov"* (V All-Union Conf. "Thermodynamics and Technology of Ferrites"), Ivano-Frankovsk, 1981, p. 135.
7. Krylov, O.V., *Geterogennyi kataliz* (Heterogeneous Catalysis), Moscow: Akademkniga, 2004.

8. Dadayan, K.A., Zagrafskaya, R.V., Karnaukhov, A.P., and Fenelonov, V.B., *Kinet. Katal.*, 1977, vol. 18, no. 6, pp. 1517–1524.
9. Furen, E.L., Gernet, D.V., Goroshko, O.N., and Gernet, O.D., *Kinet. Katal.*, 1971, vol. 12, no. 2, pp. 452–456.
10. Dis'ko, V.A., Karnaukhov, A.P., and Tarasova, D.V., *Fizikokhimicheskie osnovy sinteza oksidnykh katalizatorov* (Physicochemical Foundations of Synthesis of Oxide Catalysts), Novosibirsk: Nauka, 1978.
11. EP Patent 0 794 004.
12. RF Patent 2 167 711.
13. Aleskovskii, V.B. and Yatsimirskii, K.B., *Fiziko-khimicheskie metody analiza: Prakticheskoe rukovodstvo* (Physicochemical Methods of Analysis: Manual), Leningrad: Khimiya, 1971.
14. *TU* (Technical Specifications) *2173-134-05 766 801–2005: KDO Dehydrogenation Catalyst.*
15. Diyarov, I.N., Mal'kovskii, P.A., and Diyarov, I.I., *Metody issledovaniya geterogennykh katalizatorov: Uchebnoe posobie* (Methods for Study of Heterogeneous Catalysts: Textbook), Kazan: Kazan. Gos. Tekhnol. Univ., 2005.
16. Tyuryaev, I.Ya., *Teoreticheskie osnovy polucheniya butadiena i izoprena metodami degidrirovaniya* (Theoretical Foundations of Butadiene and Isoprene Synthesis by Dehydrogenation Methods), Kiev: Naukova Dumka, 1973.
17. Mukhlenov, I.P., Dobkina, E.I., Deryuzhkina, V.I., and Soroko, V.E., *Tekhnologiya katalizatorov* (Technology of Catalysts), Leningrad: Khimiya, 1979.
18. Samuilov, Ya.D. and Cherezova, E.N., *Reaktsionnaya sposobnost' organicheskikh soedinenii: Uchebnoe posobie* (Reactivity of Organic Compounds: Textbook), Kazan: Kazan. Gos. Tekhnol. Univ., 2003.
19. Boreskov, G.K., *Geterogennyi kataliz* (Heterogeneous Catalysis), Moscow: Nauka, 1986.
20. Generalov, M.B., *Mekhanika tverdykh dispersnykh sred v protsessakh khimicheskoi tekhnologii: Uchebnoe posobie* (Mechanics of Solid Disperse Media in Processes of Chemical Technology), Kaluga: Izd. N. Bochkarevoi, 2002.
21. Kotel'nikov, G.R., Patanov, V.A., and Buyanov, R.A., *Formovanie katalizatorov: Nauchnye osnovy proizvodstva katalizatorov* (Molding of Catalysts: Scientific Foundations of Catalyst Manufacture), Novosibirsk: Nauka, 1982.

ISSN 1070-4272, Russian Journal of Applied Chemistry, 2006, Vol. 79, No. 9, pp. 1453–1457. © Pleiades Publishing, Inc., 2006.
Original Russian Text © A.A. Lamberov, E.V. Dement'eva, Kh.Kh. Gil'manov, S.R. Egorova, N.V. Romanova, 2006, published in Zhurnal Prikladnoi Khimii, 2006, Vol. 79, No. 9, pp. 1469–1473.

CATALYSIS

Effect of the Paste Molding Pressure on the Mechanical Strength of an Iron Oxide Catalyst in the Dehydrogenation of Methylbutenes

A. A. Lamberov, E. V. Dement'eva, Kh. Kh. Gil'manov, S. R. Egorova, and N. V. Romanova

Kazan State University, Kazan, Tatarstan, Russia
Nizhnekamskneftekhim Open Joint-Stock Company, Nizhnekamsk, Tatarstan, Russia
Kazan State Technological University, Kazan, Tatarstan, Russia

Received December 27, 2005; in final form, May 2006

Abstract—The effect of the paste molding pressure on the physicomechanical and texture characteristics of catalysts was studied. An indirect criterion is suggested to evaluate the molding pressure in industrial extruders, whose optimal value ensures good physicomechanical properties of the catalysts and kinetic control over the catalyzed reaction. The results obtained were verified in paste molding on various industrial extruders, and this enabled the optimal choice of the molding equipment.

DOI: 10.1134/S1070427206090126

The preceding paper was concerned with the effect of the molding pressure on the activity of catalysts in the dehydrogenation of methylbutenes. It was shown that the molding pressure of the catalyst paste can predetermine the limiting stage of the process. An assumption was made that the dehydrogenation reaction mostly proceeds within the "working" pores of the catalyst, which have radii in the range from 15 to 50 nm. This is indicated by the correlation between the conversion of methylbutenes and the specific surface area S_{sp} in this range. An increase in the molding pressure results in that S_{sp} grows in the pore radius range 5–15 nm, which gives rise to steric hindrance caused by the formation of a large number of pores of size smaller than the "working" value and shifts the process from kinetic to diffusion control mode. Pores with radii exceeding 3.5 μm have no significant effect on the reaction control mode, but can determine the physicomechanical properties of the catalyst.

Iron oxide catalysts are used under industrial conditions in reactors with large unit power and charges exceeding 60 t. Therefore, one of the most important parameters of a catalyst is its mechanical strength, which is known to be determined by the chemical composition and pore structure. The latter, in turn, depends on the molding pressure of the catalyst paste, which can hardly be found for domestic industrial extruders.

The aims of this study were as follows: to find out how the molding pressure affects the pore structure and mechanical strength of iron oxide catalysts; to reveal an indirect criterion for evaluating the molding pressure in industrial extruders and substantiate its optimal values; and to verify the reliability of the results under industrial process conditions.

EXPERIMENTAL

Catalyst samples were synthesized by "wet" mixing [2] of the starting components containing iron oxide and compounds of potassium, magnesium, calcium, and other metals. Then the suspensions obtained were dried at 150–200°C, after which the powder was moistened and molded on a Maekawa Testing Machine MFG hydraulic press at pressures of 50, 150, and 275 MPa and on extruders of various types. The samples having the same chemical composition were calcined in air under identical conditions.

The cleavage strength was determined with a PPK-1 semiautomatic device with a knife with a blade width of 0.1 mm [3]. The cleavage strength coefficient K_G was calculated as the ratio of the breaking load to grain diameter or height of a catalyst pellet.

The texture characteristics of the catalysts were studied by mercury porosimetry (MP) on a Micromeritics Auto-Pore 9200 instrument (the United

Table 1. Physicomechanical and texture characteristics of catalyst samples molded by different methods

Sample no.	Molding device	P, MPa	S_{MP}, $m^2\ g^{-1}$	ΣV_{MP}, $cm^3\ g^{-1}$	ε	n	ρ, g cm^{-3}	K_G*
1	Hydraulic press	50	7.4	0.43	0.93	2	2.03	2.04
2	〃	100	–	–	–	–	2.26	2.53
3	〃	150	8.0	0.36	0.84	3	2.34	3.11
4	〃	200	–	–	–	–	2.49	3.38
5	〃	275	13.0	0.16	0.40	6	2.53	3.52
6	〃	300	–	–	–	–	2.54	3.81
7	Extruder no. 1		4.3	0.18	0.45	7	2.48	2.09
8	Extruder no. 2		9.6	0.13	0.36	8	2.76	3.07

* K_G is G/h, where h is the pellet height, for sample nos. 1–6, and G/d, where d is the grain diameter, for sample nos. 7 and 8.

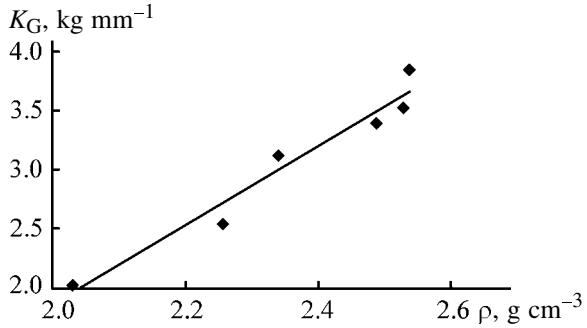


Fig. 1. Strength coefficient K_G vs. density ρ of the pelletized samples.

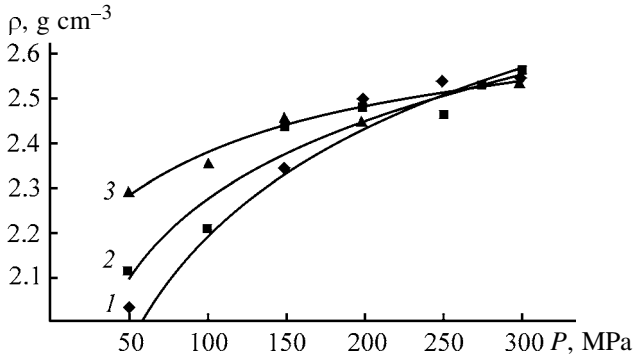


Fig. 2. Effect of the pressure P on the density ρ of the pelletized samples. Compaction time, s: (*1*) 3, (*2*) 15, and (*3*) 30.

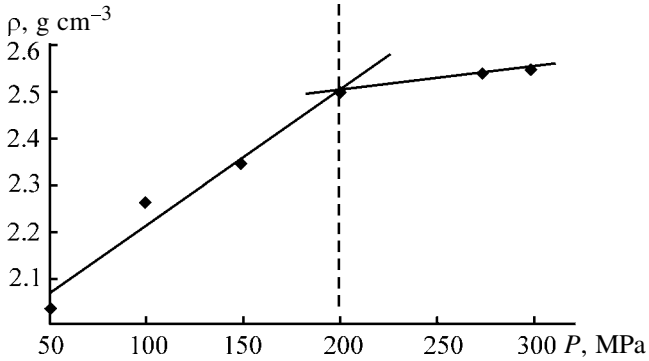


Fig. 3. Effect of the compaction pressure P on the density ρ of pelletized samples.

States). The porosity ε of the catalysts was calculated from the pellet density ρ_c and the specific pore volume V_p by the formula $\varepsilon = \rho_c V_p$ [4].

The physicomechanical and integral parameters of the pore structure of the catalyst samples obtained at different molding pressures P on a hydraulic press are listed in Table 1. As the parameter characterizing the mechanical strength was taken K_G, which allows comparison of pellets and grains. It can be seen from the dependence shown in Fig. 1 that, as the molding pressure is raised from 50 to 300 MPa, the pellet strength coefficient increases from 2.04 to 3.81 kg mm^{-1}, which is due to denser packing of catalyst particles. This is also indicated by data on the variation of the density ρ and porosity ε of the pellets obtained and of the number n of contacts between the particles [2], listed in Table 1. Because the dependence $K_G = f(\rho)$ is linear, the pellet density was taken as the main criterion for assessing how the molding pressure affects the pellet strength.

Important factors in pellet molding include not only the value of the compaction pressure, but also the duration τ of the action of this pressure on the material being compacted. This is indicated by the dependences of the pellet density on the molding pressure at τ = 3, 15, and 30 s (Fig. 2). It can be seen that, as the compaction time increases from 3 to 15 and 30 s at compaction pressures lower than 150 MPa, the catalyst paste is markedly densified, which results in that the density of the finished catalyst increases by a factor of approximately 1.2. At higher pressures (>150 MPa), the compaction time has virtually no effect on the density of the samples. Consequently, the time during which a load is applied to the catalyst paste will largely determine the texture of the finished catalyst at P < 150 MPa.

Figure 3 shows that the density–pressure dependence is described by a curve that tends to level-off and consists of two portions: that at P = 50–200 MPa,

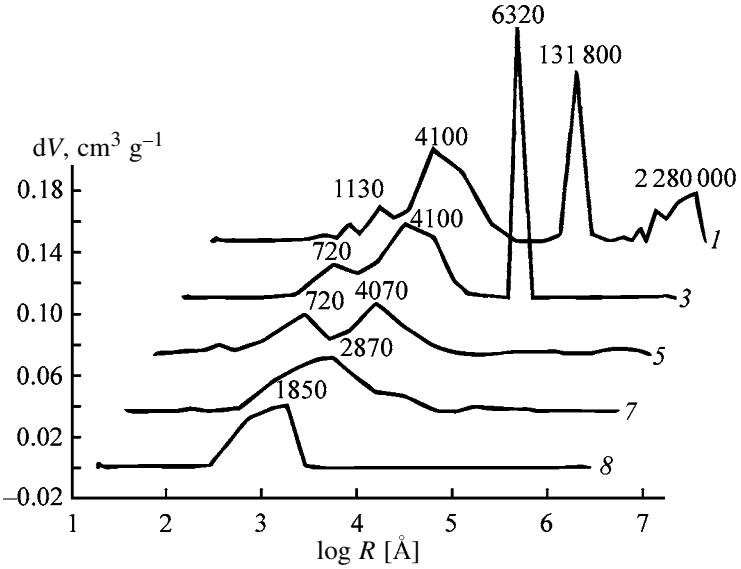


Fig. 4. Pore volume (V) distribution with respect to pore radii R for the catalyst samples obtained on the hydraulic press. Curve nos. are sample nos. in Table 1.

in which the pellet density varies in proportion to the pressure applied, and the portion at P = 200–300 MPa, in which the density variation is insignificant. These data indicate that the pore structure transforms in different ways, depending on the compaction pressure. Therefore, the texture characteristics of samples obtained at pressures lower (Table 2, sample nos. 1, 3) and higher (sample no. 5) than 200 MPa were analyzed by mercury porosimetry.

In the programs of the samples under study (Fig. 4), three regions of pore volume distributions can be distinguished at different pore radii (Table 2): fine-porous (R < 0.2 μm), medium-porous (R = 0.2–3.5 μm), and coarse-porous (R > 3.5 μm).

Sample no. 1, molded at a pressure of 50 MPa, has a polymodal structure. Macropores are observed in the coarse-porous region with peaks at radii of 228 ($\log R$ = 6.4) and 13 μm ($\log R$ = 5.1), whose joint contribution to the total porosimetric volume is 47.6% (0.22 $cm^3\ g^{-1}$). In the fine- and medium-porous regions, peaks in the pore volume distribution are observed at radii of 0.1 and 0.4 μm, which account for 0.08 and 0.14 $cm^3\ g^{-1}$, respectively.

As the compaction pressure is raised to 150 MPa (sample no. 3), the coarsest pores with radii of 228 and 13 μm disappear from the catalyst, and finer pores with R = 6.32 μm ($\log R$ = 4.8) appear, which account for 0.18 $cm^3\ g^{-1}$ in the total pore volume. The height of the peak at R = 0.4 μm decreases from 0.07 to 0.05 $cm^3\ g^{-1}$, with the porosimetric volume for pores with R = 0.2–3.5 μm decreasing from 0.14 to 0.10 $cm^3\ g^{-1}$.

Thus, pronounced transformations of coarse pores are observed at pressures of up to 200 MPa, which lead to a decrease in V_p by 18% for pore radii exceeding 3.5 μm. The changes observed may be due [5] to densification of the material being compacted via disappearance of voids and particle disintegration, which are caused by stresses and structural and shear deformations induced by the pressure applied.

The pore structure of a sample molded at a pressure exceeding 200 MPa (sample no. 5) becomes bimodal. The MP curves show no peaks at radii larger than 3.5 μm ($\log R \approx 4.5$). Raising the molding pressure leads to a decrease in the height of the peak in the medium-porous range at a radius of 0.41 μm, which is 0.06 $cm^3\ g^{-1}$ (37.5% of V_p), and to a 43% increase in S_{sp} at R < 0.2 μm (from 7.2 to 12.6 $m^2\ g^{-1}$). This is due to an elastoplastic compression of the porous agglomerate at pressures exceeding 200 MPa. The contacting surfaces approach to a distance not exceeding the action radius of intermolecular forces. Jointing bridges are intensively formed between particles and the surface area of the contacts formed increases [5].

Thus, a pellet density exceeding 2.49 $g\ cm^{-3}$ (Fig. 3, $P \geq 200$ MPa) is reached because of the disappearance of the coarse-porous component (R > 3.5 μm) in samples obtained at molding pressures higher than 200 MPa. Therefore, to obtain catalyst pellets with high physicomechanical parameters (K_G =

Table 2. Pore structure parameters of samples of catalysts for dehydrogenation of methylbutenes, as indicated by mercury porosimetry

Sample no.	S_{sp}, $m^2 g^{-1}$	R_{av}, μm	R_{max}, μm	V_p, $cm^3 g^{-1}$	Pore volume in indicated range of pore radii, μm			Specific surface area in indicated range of pore radii, μm		
					<0.2	0.2–3.5	>3.5	<0.2	0.2–3.5	>3.5
					$cm^3 g^{-1}$/%			$m^2 g^{-1}$/%		
1	7.4	7.77	13.18	0.43	0.08/18.6	0.14/29.6	0.22/47.6	6.71/90.7	0.66/8.9	0.02/0.2
3	8.0	5.44	6.32	0.36	0.07/20.3	0.10/28.6	0.18/50.3	7.25/90.5	0.68/8.6	0.07/0.8
5	13.0	0.24	0.41	0.16	0.09/53.7	0.06/37.5	0.02/11.3	12.59/96.8	0.36/2.8	0.00/0.0
7	4.3	0.22	0.29	0.18	0.09/50.0	0.09/47.2	0.01/5.0	3.91/90.9	0.40/9.3	0.00/0.0
8	9.6	0.13	0.18	0.13	0.13/94.6	0.00/0.8	0.00/0.8	9.60/100	0.01/0.00	0.00/0.0

3.38–3.81 kg mm^{-1}), the molding should be done at pressures of no less than 200 MPa.

At the same time, it has been shown previously [1] that a large number of fine pores with radii smaller than 15 nm appear in a sample in the stage of molding of the catalyst paste at P = 275 MPa (ρ = 2.53 g cm^{-3}), which shifts the catalytic process from the kinetic to diffusion control mode. It follows from the aforesaid that the optimal range of pressures for molding of the catalyst paste on a hydraulic press is 200–250 MPa, which corresponds to a pellet density of about 2.49–2.51 g cm^{-3}.

Under the industrial conditions, iron oxide catalysts are commonly molded on worm extruders, for which it is difficult to determine the molding pressure. As shown above, the pellet density can be used as a parameter that enables evaluation of the molding pressure. To verify the reliability of the results obtained under industrial conditions, grains were molded on two different extruders. The densities of the samples obtained were 2.48 (Table 1, sample no. 7) and 2.76 g cm^{-3} (Table 1, sample no. 8), which corresponds to molding pressures higher than 200 MPa. The lower values of the strength coefficients (2.09 and 3.07 kg mm^{-1}) for the extruded samples, compared to those pelletized, may be due to the fact that different methods were used to mold the catalyst paste. Probably, the shape of the curves describing the pore volume distribution with respect to pore radii for the extruded samples and pelletized catalyst (sample no. 5) is about the same. In order to examine the pore structure of sample nos. 7 and 8 in more detail, their texture characteristics were analyzed by mercury porosimetry.

Table 3. Kinetic, catalytic, and texture parameters of catalysts obtained on different extruders

Parameter*	Extruder no. 1	Extruder no. 2
$A_{C_5H_8}$, wt %	42.3	38.9
$S_{C_5H_8}$, wt %	87.9	85.6
Ψ	1.61	3.26
E_a, kJ mol^{-1}	64.6	49.4
S_{sp}, $m^2 g^{-1}$, in indicated range of pore radii (nm):		
5–15	0.52	0.66
15–50	0.22	0.21

* For formulas for calculating $A_{C_5H_8}$, $S_{C_5H_8}$, Ψ, and E_a, see [1].

The pore volume distributions with respect to pore radii are shown in Fig. 4. The extruded sample nos. 7 and 8 show a unimodal pore size distribution with peaks at R = 0.29 and 0.18 μm, respectively. As expected, the samples have virtually no pores with radii R > 3.5 μm, which predetermines their high density.

Sample no. 7, molded on extruder no. 1, has a total pore volume of 0.18 $cm^3 g^{-1}$ and specific surface area of 4.3 $m^2 g^{-1}$. Approximately equal contributions to the porosimetric volume are made by fine and medium pores (approximately 50% each). S_{sp} is 0.22 $m^2 g^{-1}$ in the "working" range of pore radii (15–50 nm) and 0.52 $m^2 g^{-1}$ at smaller radii (5–15 nm) (Table 3).

Sample no. 8, molded on extruder no. 2, has a porosimetric volume of 0.13 $cm^3 g^{-1}$ and specific surface area of 9.6 $m^2 g^{-1}$. The largest part (94.6%) of the porosimetric volume is distributed over the range of pore radii R < 0.2 μm. The specific surface area is 0.21 $m^2 g^{-1}$ in the range 15–50 nm (Table 3) and 0.66 $m^2 g^{-1}$ at pore radii of 5–15 nm, which suggests that steric hindrance appears and the catalytic process

is diffusion-controlled. To verify this assumption, the mode (diffusion or kineic control) of the dehydrogenation of methylbutenes was determined from the results of catalytic tests of the samples (Table 3) and from the integral characteristics of the pore structure (Table 1).

A calculation of the Thiele modulus (Table 3), which is used to determine the type of control over the catalytic process [2], demonstrated that the dehydrogenation on sample no. 7 proceeds under mixed control ($\Psi = 0.5–2.5$), and that on sample no. 8, under inner-diffusion control ($\Psi > 2.5$), which confirms the assumption made.

The higher catalytic activity of sample no. 7 (42.3%) may be due to the presence of an additional number of pores with radii in the range 0.2–3.5 μm, which is indicated by the value of the specific surface area (Table 2).

It is known that the activity of a catalyst decreases in the course of its operation, which is compensated for by raising the reaction temperature by 2–3°C every 20–100 h. Because a catalytic process occurring under kinetic control is more sensitive to a rise in temperature, it is preferable to mold the catalyst paste on extruder no. 1 to obtain extrudates with a density of 2.40–2.46 g cm^{-3}.

CONCLUSIONS

(1) The paste molding pressure affects the physicomechanical and texture characteristics of the catalysts obtained. The disappearance of pores with $R > 3.5$ μm at molding pressures $P > 200$ MPa leads to formation of high-strength catalysts.

(2) The catalyst molding pressure affects the type of control over the reaction. This is due to formation of pores with radii of 5–15 nm at high molding pressures (>250 MPa), which gives rise to steric hindrance and shifts the reaction from the kinetic to diffusion control mode.

(3) It was suggested to use the density of extrudates to control the catalyst molding pressure in industrial extruders. The optimal densities (for the given composition of the catalyst paste) fall within the range 2.40–2.46 g cm^{-3}, which provides high physicomechanical properties of the catalysts and kinetic control over the reaction.

(4) The results obtained were verified in paste molding on two different industrial extruders, demonstrated a high degree of reliability, and enabled the optimal choice of the molding equipment.

REFERENCES

1. Gil'manov, Kh.Kh., Lamberov, A.A., Dement'eva, E.V., et al., *Zh. Prikl. Khim.*, 2006, vol. 79, no. 9, pp. 1463–1468.
2. Mukhlenov, I.P., Dobkina, E.I., Deryuzhkina, V.I., and Soroko, V.E., *Tekhnologiya katalizatorov* (Technology of Catalysts), Leningrad: Khimiya., 1979.
3. *OST* (Branch Standard) *3 801 130–95: Catalysts for Hydrorefining: Testing Techniques.*
4. Diyarov, I.N., Mal'kovskii, P.A., and Diyarov, I.I., *Metody issledovaniya geterogennykh katalizatorov: Uchebnoe posobie* (Methods for Studying Heterogeneous Catalysts: Textbook), Kazan: Kazan. Gos. Tekh. Univ., 2005.
5. Generalov, M.B., *Mekhanika tverdykh dispersnykh sred v protsessakh khimicheskoi tekhnologii: Uchebnoe posobie* (Mechanics of Solid Disperse Media in Processes of Chemical Technology: Textbook), Kaluga: Izd. N. Bochkarevoi, 2002.

ISSN 1070-4272, Russian Journal of Applied Chemistry, 2006, Vol. 79, No. 9, pp. 1458–1462. © Pleiades Publishing, Inc., 2006.
Original Russian Text © V.S. Shmotin, A.S. Knyazev, A.I. Titkov, A.N. Salanov, O.V. Vodyankina, L.N. Kurina, 2006, published in Zhurnal Prikladnoi Khimii, 2006, Vol. 79, No. 9, pp. 1474–1478.

CATALYSIS

Effect of Iodine-Containing Promoter on the Catalytic Activity of Silver in the Course of Ethylene Glycol Oxidation

V. S. Shmotin, A. S. Knyazev, A. I. Titkov, A. N. Salanov, O. V. Vodyankina, and L. N. Kurina

Tomsk State University, Tomsk, Russia
Boreskov Institute of Catalysis, Siberian Division, Russian Academy of Sciences, Novosibirsk, Russia

Received March 3, 2006

Abstract—Surface morphology and catalytic properties of electrolytic silver crystals in partial oxidation of ethylene glycol into glyoxal were studied.

DOI: 10.1134/S1070427206090138

Glyoxal is widely used in industry for preparing high-quality paper, films, adhesives, various polycondensates, and pharmaceuticals [1]. Being the nearest analog of formaldehyde, glyoxal surpasses it in chemical properties. Partial oxidation of ethylene glycol on polycrystalline silver catalysts, performed in the continuous flow mode, is the most ecnomically feasible and facile procedure for preparing glyoxal. In this case, the alcohol conversion is as high as 90%, and the selectivity with respect to glyoxal reaches 55–60% [2, 3]. Promotion of the surface or introduction of certain additives into the reaction mixture with the subsequent treatment of the catalyst are the best ways to enhance the activity of the catalytic systems. Various promoters are used in catalysts for partial oxidation of organic compounds, e.g., alkali metals [4] and phosphorus-containing compounds [5]. The promoting effect of halogen-containing hydrocarbons on the partial oxidation of methanol to formaldehyde in the presence of silver catalysts was studied in [6, 7]. It was found that, with addition of microamounts of iodine-containing promoters into the reaction mixture, the alcohol conversion and yield of formaldehyde increase, whereas the yield of the products of deep oxidation decreases. Taking into account that the processes of partial oxidation of methanol and ethylene glycol are largely similar, in this study we examined the catalytic synthesis of glyoxal in the presence of ethyl iodide promoter.

EXPERIMENTAL

Silver crystals were prepared at the Institute of High-Temperature Electrochemistry (Ural Division, Russian Academy of Sciences, Yekaterinburg, Russia) by electrolysis of a $KNO_3 + NaNO_3 + AgNO_3$ melt in an open electrolysis bath using rotating cathode [8]. The crystal surface was finely cleaned by the procedure described elsewhere [9]. The catalyst was prepared by pressing of silver crystals with paraformaldehyde and subsequent annealing in an air flow at 650°C for 3 h.

The catalytic activity of silver was studied in a flow catalytic installation with a fixed catalyst bed by the procedure described in [10]. The height of the catalyst bed was 20 mm, and the reactor diameter was 16 mm. The gaseous and liquid products obtained in the course of oxidation were analyzed chromatographically [11, 12].

The surface morphology of the silver samples was studied using a JEOL 6460LV field-emission high-vacuum scanning electron microscope (energy of the primary electron beam 20 keV). To improve the image contrast, the sample surface was coated with gold (film thickness up to 0.05 μm).

Data on the partial oxidation of ethylene glycol into glyoxal in the absence of ethyl iodide and with its addition to the reaction mixture in relation to the oxygen content in the reaction mixture are plotted in Fig. 1a. The molar content of the promoter added was 6 ppm with respect to ethylene glycol. The oxygen/ethylene glycol (O_2 : EG) molar ratio was varied from 0.8 to 1.8. As seen, with increasing oxygen content in the promoter-free reaction mixture the alcohol conversion increases (Fig. 1a, curve *1*), whereas the selectivity of the glyoxal formation passes through a maximum (Fig. 1a, curve *3*). Addition of the promoter into the reaction mixture improves the selectivity with respect to the desired product in a broader range of

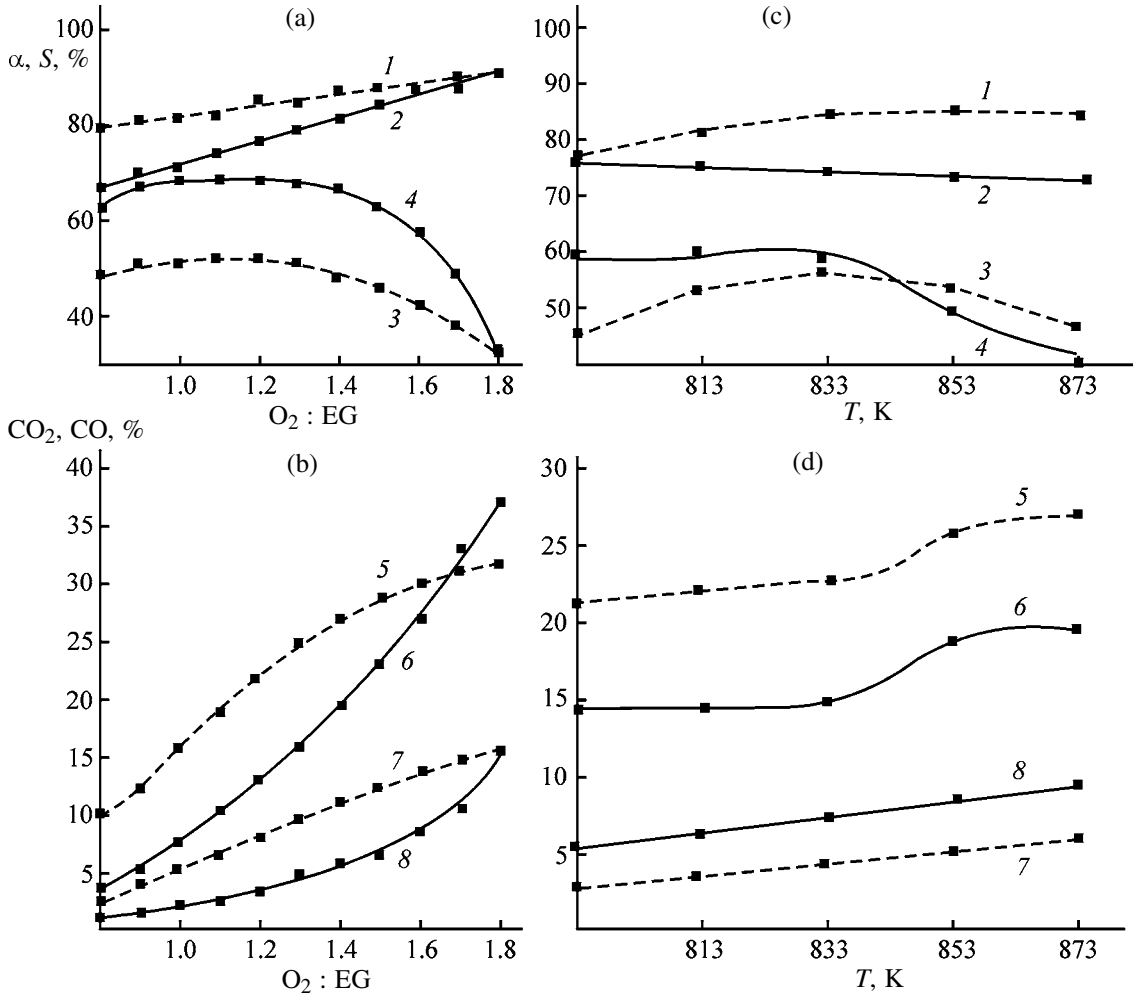


Fig. 1. (*1, 3, 5, 7*) Catalytic activity of silver catalyst without iodine-containing promoter and (*2, 4, 6, 8*) with addition of promoter into the reaction mixture as a function of the (a, b) O_2 : EG molar ratio and (c, d) temperature *T*. (α) (*1, 2*) Conversion of ethylene glycol; (*S*) (*3, 4*) selectivity with respect to glyoxal; yields of (*5, 6*) CO_2 and (*7, 8*) CO.

the compositions of the reaction mixture as compared to the initial sample (Fig. 1a, curve *4*).

It should be noted that, with addition of the iodine-containing promoter into the reaction mixture, the yields of the products of deep oxidation decrease (Fig. 1b), which is probably due to changes in the chemical composition of the silver crystal surface. Atomic iodine formed by the ethyl iodide decomposition is adsorbed on the silver surface and, occupying the adsorption centers, decreases adsorption of the oxygen atoms responsible for the deep oxidation [13]. This assumption is confirmed by certain decrease in the ethylene glycol conversion in the presence of the promoter (Fig. 1a, curve *2*).

The effect of temperature on the activity of the silver catalyst in the course of ethylene glycol oxidation is illustrated in Figs. 1c and 1d. As seen, with increasing temperature of treatment of the silver catalyst with the promoted reaction mixture, the selectivity with respect to glyoxal decreases (Fig. 1c, curve *4*), whereas the conversion of ethylene glycol remains essentially constant (Fig. 1c, curve *2*). This decrease in the selectivity with respect to glyoxal is probably due to the increasing rate of the iodine desorption from the catalyst surface and rearrangement of the centers of deep oxidation.

In the case of promoted reaction mixtures, the yields of the products of deep oxidation are lower than those in the promoter-free systems at the same temperatures (Fig. 1d). These data suggest that, in the presence of the promoter, the process is stable in the broader range of experimental conditions. On the whole, the silver catalyst in the presence of the iodine-containing promoter is characterized by higher yield

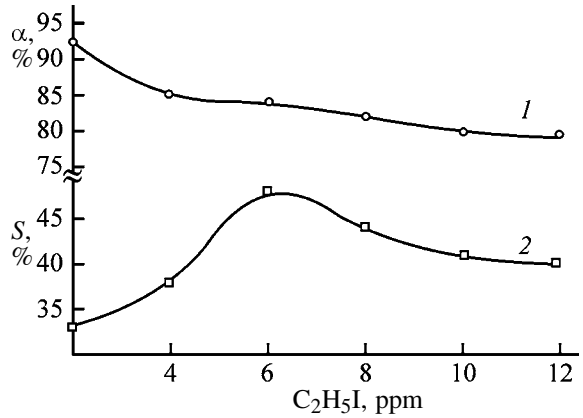


Fig. 2. Catalytic activity of silver as a function of the promoter (C_2H_5I) concentration in the reaction mixture (molar ratio to ethylene glycol). Composition of the reaction mixture: EG : O_2 : N_2 : H_2O 1.0 : 1.0 : 10.0 : 3.4, *T* 560°C. (α) (*1*) Conversion and (*S*) (*2*) selectivity.

of the desired product and high stability in a wide range of experimental conditions.

The dependence of the catalytic activity of silver on the content of the iodine-containing promoter in the reaction mixture is shown in Fig. 2. As seen (Fig. 2, curve *1*), the ethylene glycol conversion decreases with increasing promoter content in the reaction mixture. This is probably due to the fact that iodine competing with oxygen in the adsorption on the silver surface decreases the content of adsorbed atomic oxygen which provides selective oxidation of ethylene glycol. Also, poisoning of the catalyst surface with iodine due to excess removal of oxygen cannot be excluded.

The dependence of the selectivity with respect to glyoxal on the promoter concentration passes through a maximum, which is observed at a molar ratio of ethyl iodide to ethylene glycol of about 6 ppm (Fig. 2, curve *2*). This is probably due to the following reasons. At a molar ratio smaller than 6 ppm, the promoter content is insufficient for the selective conversion, i.e., at low concentrations of the promoter in the reaction mixture significant amounts of oxygen are retained on the catalyst surface in the form of surface oxide Ag_2^SO, which can participate in further oxidation of the final product by the following reaction:

$$C_2H_2O_2 + 3Ag_2O \rightarrow 2CO_2 + H_2O + 6Ag.$$

On the other hand, at molar ratios of ethyl iodide to ethylene glycol higher than 6 ppm, the catalyst activity decreases due to poisoning of both the oxidation centers on the silver surface participating in the deep oxidation and oxygen-containing centers of the O_α type participating in the selective oxidation of ethylene glycol into glyoxal. Participation of the O_α centers of adsorbed oxygen in the glyoxal formation was confirmed in [14].

Upon prolonged treatment of the catalyst with the reaction mixture containing ethyl iodide in amounts greater that 6 ppm, the process characteristics deteriorate owing to poisoning of the active centers on the silver surface. We studied the possibility of the regeneration of catalyst after prolonged treatment with the iodine-containing promoter. For this purpose, the spent catalyst was annealed in an air flow at 600°C. After this treatment, the experiments on the catalytic oxidation were repeated; the results are listed in the table.

Catalytic activity of the silver samples before and after regeneration; composition of the reaction mixture: EG : O_2 : N_2 : H_2O 1.0 : 1.0 : 10.0 : 3.4, *T* 560°C

Sample	Ethylene glycol conversion, %	Selectivity to glyoxal, %
Ag	90	55
Ag/I	80	66
Ag/I:		
prolonged treatment	70	45
after regeneration	80	64

As seen from the table, annealing in an air flow at 600°C ensures almost complete regeneration of the activity of the silver catalyst. This is probably due to the iodine desorption from the sample surface and regeneration of the centers of alcohol selective oxidation. Thus, we found that the catalyst activity can be enhanced by adding an iodine-containing promoter (ethyl iodide) and the spent silver catalyst can be readily regenerated.

An electron-microscopic examination was performed to study the mechanism of promotion of the iodine-containing additive and the effect of the reaction mixture containing ethyl iodide on the morphology of the silver catalyst. The surface of the initial sample is shown in Fig. 3a. The samples prepared by electrolysis of the silver nitrate melt are elongated particles (5–7 μm wide and 40–60 μm long). The particle surface is smooth and well-rounded along the edges. The structure of the sample surface is determined by the side topochemical processes occurring during electrolysis of the molten mixture of KNO_3, $NaNO_3$, and $AgNO_3$ [15].

The surface morphology of the silver catalysts strongly changes after treatment with both initial and promoted reaction mixtures (Figs. 3b and 3c). As seen, after treatment with the initial reaction mixture $EG : O_2 : N_2 : H_2O = 1.0 : 1.0 : 10.0 : 3.4$ at 873 K, channels 0.2–1.0 μm in diameter are formed on the silver catalyst surface (Fig. 3b), and their amount upon treatment in the presence of the iodine-containing promoter is significantly smaller (Fig. 3c). It was found [14, 16] that these channels are formed in the near-surface silver layers in the course of treatment due to the adsorption of C-containing reagents providing accumulation of the oxocarbon structures able to diffuse into the sample bulk with increasing temperature. Under the action of the oxygen-containing reaction mixture, the oxocarbon fibers formed in the near-surface layer are burnt out, causing formation of channels.

In accordance with the electron-microscopic data, prolonged contact of the catalyst with the reaction mixture leads to the formation of carbon deposits (particles about 2 μm long and 0.5 μm thick, Fig. 3d). This effect is due to the adsorption of carbon-containing reagents participating in the catalytic process [17]. Addition of ethyl iodide does not cause changes in the silver crystal morphology (Fig. 3e). No pronounced carbonization was observed after treatment under the conditions similar to that of the initial sample.

Moreover, we observed almost no adsorption of carbon structures, no formation of the carbonization products, and no development of channels upon treatment of silver with the iodine-containing reaction mixture. This is most probably due to a decrease in the content of oxygen adsorbed on the catalyst surface, which directly participates in carbonization, because no accumulation of the carbonization products on the silver surface is observed in the oxygen-free systems [14].

In the reaction of ethyl iodide with the oxidized silver surface, along with competitive adsorption, removal of the surface oxygen is also possible by the following reactions:

$$2Ag_2O + 4C_2H_5I \rightarrow 4AgI + 2C_4H_{10} + O_2,$$

$$\Delta G_{298} = -564 \text{ kJ};$$

$$Ag_2O + 2C_2H_5I \rightarrow 2AgI + 2C_4H_{10}O, \Delta G_{298} = -450 \text{ kJ}.$$

In a study of the interaction of ethyl iodide with the surface of a preoxidized silver single crystal, the reaction products (butane, diethyl ether) used in the ther-

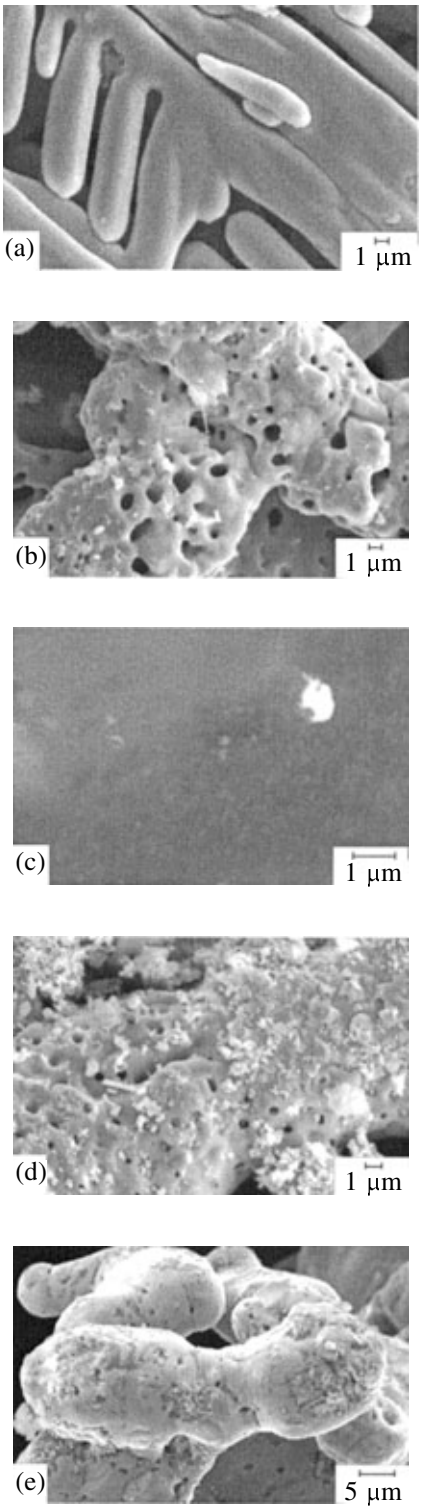


Fig. 3. Morphology of the silver catalyst surface: (a) initial sample, (b) sample treated with the initial reaction mixture, (c) catalyst treated with the promoted reaction mixture, (d) sample treated with the initial reaction mixture for a long period, and (e) sample treated with the promoted reaction mixture a long period.

mochemical calculations were detected by gas chromatography–mass spectrometry [18].

CONCLUSIONS

(1) The catalytic and physicochemical experimental data showed that addition of an iodine-containing promoter into the reaction mixture increases the selectivity with respect to glyoxal by 5–10%.

(2) The catalytic activity increases owing to a decrease in the contribution of the carbonization and profound oxidation in the presence of the iodine-containing additives.

(3) Promoter decreases the concentration of the centers of adsorbed oxygen responsible for the formation of carbonization products and occurrence of deep oxidation of ethylene glycol. In this case, the amount of oxygen participating in the selective conversion of alcohol decreases only slightly, leading to only insignificant decrease in the ethylene glycol conversion.

REFERENCES

1. Kon'kova, I.V. and Gritsan, V.I., *Glioksal': Svoistva, Primenenie* (Glyoxal: Properties, Application), Moscow: NIITEKhim, 1990.
2. Ioffe, I.I., Brodskii, M.S., and Tishchenko, M.S., *Metody proizvodstva glioksalya* (Methods of Glyoxal Production), Moscow: Nauka, 1964.
3. Vodyankina, O.V., Kurina, L.N., Petrov, L.A., et al., *Khim. Prom–st*., 1997, no. 12, pp. 802–807.
4. Lu, G. and Zuo, X., *Catal. Lett.*, 1999, vol. 58, pp. 67–70.
5. Knyazev, A.S., Sushkova, E.V., Vodyankina, O.V., et al., *Neftekhimiya*, 2003, vol. 43, no. 6, pp. 454–458.
6. Dai, W.-L., Liu, Q., Cao, Y., and Deng, J., *Appl. Catal*., 1998, vol. 175, pp. 83–88.
7. Dai, W.-L., Cao, Y., Deng, J., et al., *Catal. Lett*., 1999, vol. 63, pp. 49–57.
8. Ivanovskii, L.E., Rozanov, I.G., Zotin, I.V., and Khramov, A.P., *Rasplavy*, 1997, no. 2, pp. 51–69.
9. Knyazev, A.S., Vodyankina, O.V., Kurina, L.N., et al., *Zh. Prikl. Khim*., 2004, vol. 77, no. 1, pp. 43–47.
10. Vodyankina, O.V., Kurina, L.N., Izatulina, G.A., and Arkatova, L.A., *Zh. Prikl. Khim*., 1997, vol. 70, no. 12, pp. 2007–2009.
11. Lur'e, A.A., *Sorbenty i khromatograficheskie nositeli* (Sorbents and Chromatographic Supports), Moscow: Khimiya, 1972.
12. Medonos, V., Ruzicka, V., Kalina, Y., and Marnoln, A., *Coll. Czech. Chem. Commun*., 1968, vol. 33, no. 12, p. 4393.
13. Vodyankina, O.V., Kurina, L.N., Sudakova, N.N., and Izatulina, G.A., *Zh. Fiz. Khim*., 1998, vol. 72, no. 3, pp. 521–524.
14. Vodyankina, O.V., Kurina, L.N., Voronin, A.I., and Salanov, A.N., *Stud. Surf. Sci. Catal., Ser. B*, 2000, vol. 130, pp. 1775–1781.
15. Baraboshkin, A.N., *Elektrokristallizatsiya metallov iz rasplavlennykh solei* (Electrolytic Crystallization of Metals from Molten Salts), Moscow: Nauka, 1976.
16. Fromm, E. and Gebhardt, E., *Gase und Kohlenstoff in Metallen*, Berlin: Springer, 1976.
17. Vodyankina, O.V., Kurina, L.N., Voronin, A.I., et al., *J. Mol. Catal*., 2000, vol. 158, no. 1, pp. 381–387.
18. Wu, G., Stacchiola, D., Kaltchev, M., and Tysoe, W.T., *Surf. Sci*., 2000, vol. 463, pp. 81–92.

ISSN 1070-4272, Russian Journal of Applied Chemistry, 2006, Vol. 79, No. 9, pp. 1463–1472. © Pleiades Publishing, Inc., 2006.
Original Russian Text © O.V. Yatsenko, 2006, published in Zhurnal Prikladnoi Khimii, 2006, Vol. 79, No. 9, pp. 1479–1488.

ENVIRONMENTAL PROBLEMS OF CHEMISTRY AND TECHNOLOGY

Refined Estimates of the Effect of Jet Discharges from Launch Vehicles on the Kinetics of the Stratospheric Ozone

O. V. Yatsenko

Don State Technical University, Rostov-on-Don, Russia

Received November 15, 2004; in final form, April 2004

Abstract—The kinetic model of perturbations of the stratospheric ozone by propulsive jet discharges of modern launch vehicles was modified, which made it possible to refine theoretical estimates of the accompanying physicochemical processes and to improve the reliability and consistence of the basic parameters. The natural and artificial mechanisms of turbulent dissipation of the rocket trace in the stratosphere and their dependence on the altitude were taken into account. The mass–energy and specific characteristics of the propulsive jet discharges of rockets were factorized. The agents, factors, and mechanisms determining the scale, level, and dynamics of the perturbation of stratospheric ozone in launches of liquid-propellant launch vehicles were revealed and a small-scale kinetic–diffusion model was suggested for engineering estimates.

DOI: 10.1134/S107042720609014X

The stratosphere, or ozonosphere, is an atmospheric layer lying at altitudes of 15–50 km [1]. Preventing penetration of the ultraviolet solar radiation with wavelengths $\lambda \leq 300$ nm, this layer provides the existence of the present-day biosphere. The main agents absorbing the detrimental photons are molecular oxygen and ozone. Oxygen molecules O_2 (principal stratospheric absorber of UV photons with $\lambda \leq 220$ nm) is one of the main components of the atmosphere at these altitudes and its content cannot differ significantly from 21%, whereas O_3 is minor chemically active admixture whose relative concentration does not exceed 10^{-5} (a collective term minor gas components of the stratosphere, MGCS, is used for these substances [1]). It is of fundamental importance that the stratosphere is a multicomponent distributed dynamic system with strong chemical nonlinearity, multiscale transfer, and long-range radiative coupling, classified as dissipative (see scheme in Fig. 1). The evolution of systems of this kind is unstable and stochastic, and their response to external impacts may have a trigger nature [2]. Although the theory of dissipative dynamic systems is a priority area of mathematical research, the achievements made fail to satisfy the increased requirements of natural-science applications.

The modern economical activities involve risk of triggering the stratospheric processes into the alternate stable mode and thereby causing a global environmental disaster and extinction of the biosphere. Because the chemically active gases discharged by terrestrial industrial sources do not reach the stratospheric altitudes [1], the propulsive jets of launch vehicles seem to be one of the main artificial hazards to the ozone layer of the Earth.

The published results of experimental studies [3–9] are largely contradictory, which is due to the exceedingly complicated and interdisciplinary nature of the problem. When classifying the imperfections of modern models of evolution of the rocket trail in the stratosphere, the following should be distinguished: (1) incompleteness and thermochemical inconsistency of the kinetic schemes proper of (photo)reactions; (2) insufficiently detailed description of turbulent motions in that part of the ozonosphere which is perturbed by launch vehicles; and (3) contradictory evidence concerning the thermochemical parameters and, in particular, the degree of departure from equilibrium of the gas in the propulsive jets of launch vehicles. In addition, no attempts to construct versatile small-scale models of perturbation of the stratospheric O_3 in vehicle launches have been known, despite that models of this kind are exceedingly useful as a means of engineering evaluation of the environmental damages and risks accompanying the launches.

The aim of this study was to reveal processes, factors, and circumstances that determine the qualitative features and quantitative parameters of the influence exerted by rockets on the stratospheric ozone.

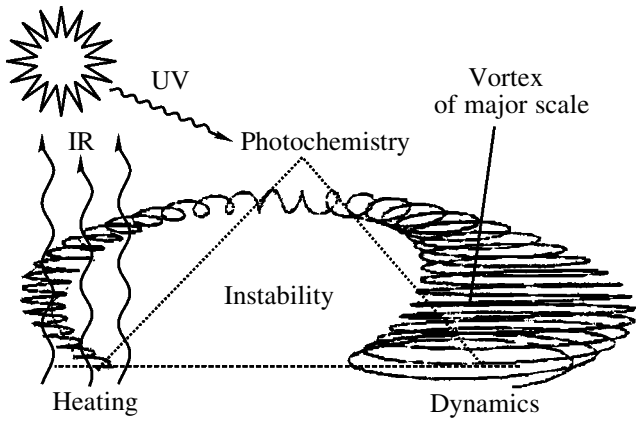


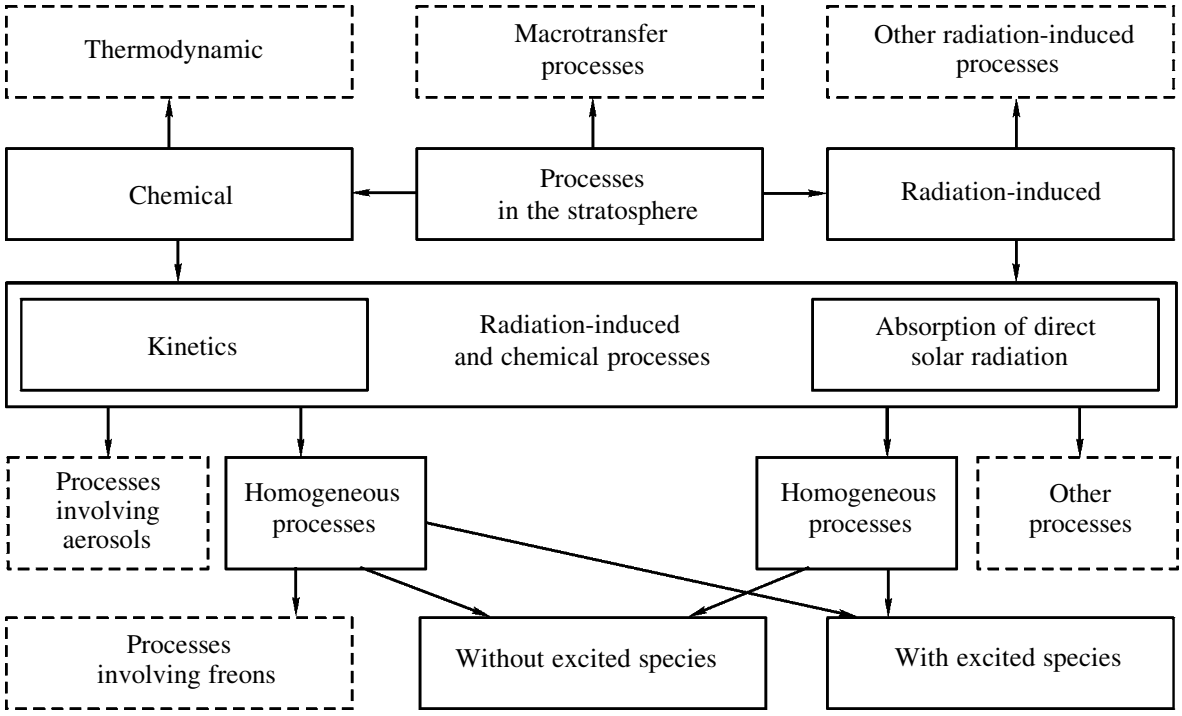
Fig. 1. Scheme of dissipative photochemical and mechanical processes in the ozonosphere.

This was done by means of theoretical analysis and systems synthesis based on computer simulations with high-resolution information models free of disadvantages 1–3. The problems solved in the framework of the research program specified above consist in construction of appropriate equations and reaction schemes, development of efficient methods for their numerical integration and asymptotic study, selection and systematization of the initial characteristics of the rocket trail, and factor analysis of detailed computer models of disturbed stratosphere and their subsequent "reduction" to minimum overall models suitable for fast, including scenario-type, assessments of the environmental consequences of rocket launches.

Model of a stratosphere perturbed by rocket jets. Thorough analysis [1, 10, 11] shows that the energy supply of all the stratospheric processes (Fig. 1) occurs via the photochemical cycle of ozone. This circumstance, in particular, accounts for the term "ozonosphere," equivalent to stratosphere. At the same time, this fact serves as a basis for setting up the physical or energetic hierarchy of processes and scales in construction of mathematical models of the ozonosphere dynamics. The characteristic parameters of the stratosphere are the density $0.001–0.1\rho_0$ (ρ_0 is the air density at the sea level) and concentration of ozone $10^{11} < [O_3] < 3 \times 10^{12}$ cm^{-3}, which is at a maximum at the altitude $H \approx 25$ km. In these conditions, the mean free path l of molecules is within the range 10^{-4}–10^{-2} cm, and the Knudsen number $Kn = l/L$ falls within the range 10^{-6}–10^{-4} for the minimum rocket trail scale $L = 1$ m, i.e., the dynamics of the ozonosphere perturbed by launch vehicles is adequately described by the models of a continuous medium and equilibrium chemical kinetics [12].

The computer simulations performed in this study are based on a detailed model of photochemical processes in the ozonosphere perturbed by rocket discharges. This model, successfully tested and described

Scheme 1.
Physicochemical processes in the ozonosphere perturbed by propulsive jets of launch vehicles



in detail in [13–15], includes more than 1100 (or 550 pairs of mutually reverse) elementary chemical reactions and 32 elementary photo processes involving photons in the spectral range λ = 180–740 nm. The structure and composition of the photochemical unit of the model are presented in Scheme 1. The unaccounted-for physicochemical processes (delimited by dashed lines in Scheme 1) can be included in the model when necessary, which is provided by the open structure of the photochemical unit and is supported by the means of automated kinetic modeling, developed by the author [16, 17]. The neglect of the atmospheric macroscopic transfer (winds, circulation, convection, large-scale turbulent diffusion) limits the adequacy of the model to the time interval corresponding to the so-called synoptic scale of ~10 days [1, 10]. At the same time, the very detailed photochemical unit [13, 15] can be used as an element of more intricate and versatile models.

Because the stratosphere is permanently stratified (temperature increases with altitude, which hinders vertical agitation), the turbulent transfer occurs virtually exclusively in the horizontal direction. Hence it is, in principle, appropriate to regard the overall rocket-induced perturbation of the ozonosphere as a superposition of perturbed dynamics of its separate layers. This circumstance makes it possible to reduce by a factor of at least N^2 the necessary volume of computation by dividing the stratosphere into N quasi-homogeneous zones along its height, and, as a result, the problem comes within the powers of modern computers. The technical problem of stratification of the ozonosphere dynamics is solved by "decoupling" of the kinetics of photoreactions and of the radiative transfer. If we denote the set of concentration variables $c_i(H, t)$ (subscript i designates a particular substance, i = 1, ..., I – 1) and temperature $T(H, t)$, which form a pseudovector, by $\theta(H, t)$, the kinetics of unperturbed ozonospheric (photo)reactions is described by the system of equations

$$d\theta/dt = f(\theta, t), \quad (1)$$

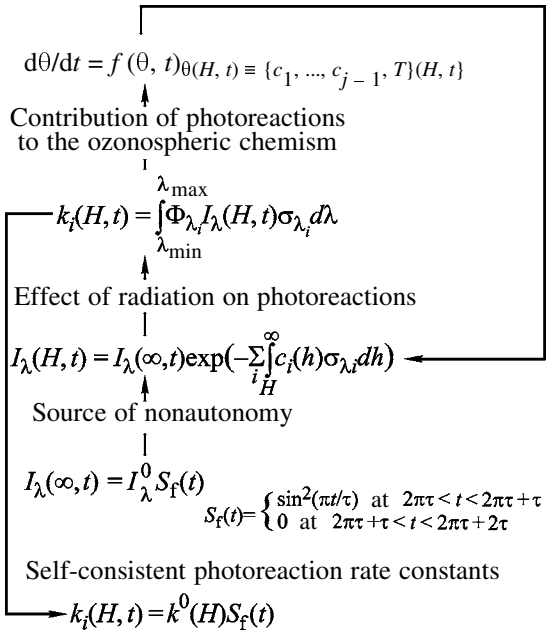
which implicitly includes, via the nonautonomy of the right-hand parts of (1), the field of solar radiation in the stratosphere. The iteration procedure, described in detail in [13, 15] and presented in Scheme 2, enables factorization of the altitude- and time-related components in the models of rate constants of the photoreactions

$$k_i(H, t) = k_i^0(H) S_f(t). \quad (2)$$

The altitude dependences of the photoconstants $k_i^0(H)$, amplitude I_λ^0, and averaged time dependence

Scheme 2.

Scheme of model stratification of the ozonosphere perturbed by rocket discharges via introduction of effective photoreaction constants



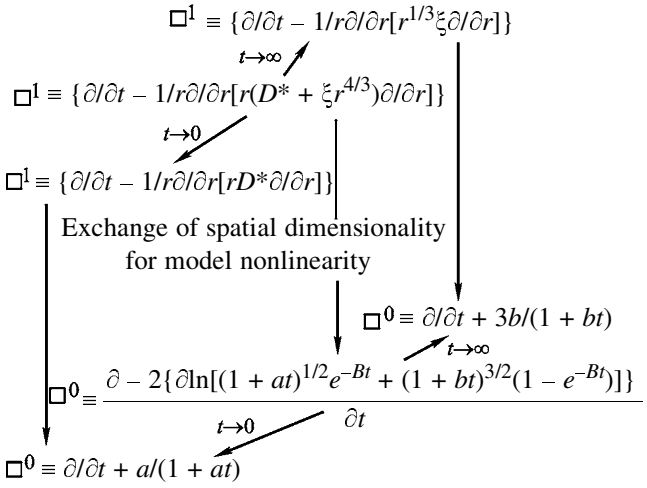
Note: $I_\lambda(H, t)$ is the intensity of direct solar radiation with wavelength λ at altitude H (20 to 50 km) at instant of time t; c_i, concentration of a substance decomposing in ith process; and σ_{λ_i} and Φ_{λ_i}, cross section and quantum yield of a photoreaction. Here, the common numbering of substances and photoreactions is used because, in the given case, each component decomposes in only a single process.

of the intensity of solar radiation [$S_f(t)$] were reported in [13–15].

An additional important improvement of, in particular, the models reported in [13–15] is associated with the refinement of the magnitude and altitude profile of the turbulent transfer coefficient ζ for the stratospheric conditions. In [13–15], this parameter of the stratosphere was assumed to be altitude-independent and was determined on the basis of the following considerations. Stratospheric gases, mainly ozone, almost fully absorb the solar radiation in the spectral range 200–300 nm. An energy of about 1.8×10^4 erg cm^{-2} comes every second to the ozonosphere with this radiation. The mass of a column in the stratosphere, with a base of area 1 cm^2, is about 100 g. With the alternation of day and night accounted for by the factor 1/2, we obtain an altitude-average dissipation of solar energy in the stratosphere $\langle\varepsilon\rangle$ = 90 cm^2 s^{-3} and an ozonosphere-average turbulent transfer coefficient $\langle\xi\rangle = \langle\varepsilon\rangle^{1/3}$ = 4.5 cm$^{2/3}$ s^{-1} [1, 18]. Relating these consideration to the experimentally

Scheme 3.

Hierarchy of models of the turbulent dissipation of the rocket trail in the ozonosphere



known [1] daily heating of the ozonosphere, $\Delta T(H)$, we obtain

$$D(H) = 15e^{H/16}[\mathrm{cm^2\ s^{-3}}],$$

$$\xi(H) \approx 2.5e^{H/48} \approx 1.4 + 0.11H\ [\mathrm{cm^{2/3}\ s^{-1}}]. \quad (3)$$

According to (3), the value of ξ at the upper boundary of the stratosphere is twice that at the lower boundary and equals 7 $\mathrm{cm^{2/3}\ s^{-1}}$. Relation (3) makes the model more realistic by refining the duration of smearing of the rocket trail by the atmospheric turbulence proper.

Model of evolution of a rocket trail in the stratosphere. If we assume that the flight of a launch vehicle does not directly distort the stable stratification and the radiation regime of the ozonosphere, the evolution of a rocket trail is described by a system of quasilinear differential equations [15] for the concentration-temperature field $\theta(r, t) \Leftarrow \theta_H(r, t) \Leftarrow \theta(r, H, t)$, which has, if we take into account (1), the form

$$\square^n\theta = f(\theta, t), \quad (4)$$

where $\square^n$ is the operator responsible for impurity dispersal in the box-type ($n = 0$) and spatially unidimensional ($n = 1$) centrally symmetric formulations; r, distance from the trajectory axis; and $f(\theta, t) \Leftarrow f(\theta_H, t)$, i.e., the altitude H is regarded as a parameter.

Model (4) of rocket trail dissipation is adequate upon termination of the impact-wave stage of its evolution or approximately a second after the fly-by of a launch vehicle [19]. It should also be noted that integration of the solution to (4) over the altitude does not involve any additional difficulties, because the trajectories of modern launch vehicles in the stratospheric part (up to altitudes of 42–45 km) are virtually vertical.

Analysis of the mechanisms of stratospheric [1, 18] and artificial, generated by a propulsive jet [20], turbulence makes it possible to construct a generalized model that adequately reflects the dynamics of the early and late stages of the evolution of a rocket trail. In this model, the differential evolution operators $\square^n$ have the form

$$\square^0 \equiv \frac{\partial - 2\{\partial \ln[(1 + at)^{1/2}e^{-Bt} + (1 + bt)^{3/2}(1 - e^{-Bt})]\}}{\partial t},$$
$$\square^1 \equiv \{\partial/\partial t - 1/r\partial/\partial r[r(D^* + \xi r^{4/3})\partial/\partial r]\}, \quad (5)$$

where r and t are the spatial and temporal variables, respectively; D^*, effective coefficient of quasimolecular diffusion, whose value (for modern launch vehicles $D^* \approx u_0 d \approx 10^8$ $\mathrm{cm^2\ s^{-1}}$, where $u_0 \approx 3 \times 10^5$ $\mathrm{cm\ s^{-1}}$ is the outflow velocity of propulsive gases; $d \approx 3 \times 10^2$ cm is the initial jet diameter) is many times the coefficient of truly molecular diffusion, D, which does not exceed 10^3 $\mathrm{cm^2\ s^{-1}}$ under the stratospheric conditions; $a = D^*/r_{\mathrm{ini}}^2$, $b = \xi(3r_{\mathrm{fin}}^{2/3})$, reciprocals of the characteristic swelling time of the trail cloud in the early and final stages of evolution; r_{ini} and r_{fin}, minimum radii of the trail cloud in the initial and final turbulent-diffusion stages of dissipation of the rocket trail; constant $B \approx (\xi/D^*)^{1/2}$ characterizes the rate of change of the dispersal mechanism, from that motivated by the kinetic energy of propulsive gases to the mechanism due to purely atmospheric motions.

In the early stage of dissipation of the rocket trail, when gas agitation is due to the residual energy of the propulsive jet, we have the starting asymptotic of turbulent motions [15] and

$$\square^0 \equiv \partial/\partial t + a/(1 + at),$$
$$\square^1 \equiv \{\partial/\partial t - 1/r\partial/\partial r[rD^*\partial/\partial r]\}. \quad (6)$$

After the dissipation of the trail cloud becomes associated with the energy balance of the atmospheric turbulence, these operators degenerate in another way. The corresponding asymptotic has the form [13–15]

$$\square^0 \equiv \partial/\partial t + 3b/(1 + bt),$$
$$\square^1 \equiv \{\partial/\partial t - 1/r\partial/\partial r[r^{7/3}\xi\partial/\partial r]\}. \quad (7)$$

Equations (5) degenerate into (6) at $Bt \ll 1$, and into (7) at $Bt \gg 1$. Taken together and arranged in a certain order, Eqs. (5)–(7) constitute the hierarchy of models of evolution of the rocket trail in the ozonosphere (Scheme 3).

As the initial conditions specifying model (5) should be chosen

$$\theta(0) = \theta_H + \Delta\theta_H \text{ at } r \le r_{ini} \text{ and } \theta(0) = \theta_H \text{ at } r > r_{ini},$$

$$\text{if } n = 0;\ \theta(r,0) = \theta_H + \Delta\theta \exp[-(r/r_{ini})^2] \text{ at } n = 1. \quad (8)$$

Relations (8) were derived on the assumption that the mass fraction of the impurity in the trail cloud is small. Below, we suggest a way to set the initial parameters of propulsion discharges of particular launch vehicles, which implements the idea of dividing the characteristics of primary rocket-induced perturbations of the ozonosphere into quantitative and qualitative.

Versatile model and real parameters of rocket discharges. The trajectories of all modern launch vehicles are closely similar in their stratospheric part: here, the close run of altitude–velocity dependences $v(H)$ of different rockets of the same purpose is meant. This statement is a result of an analysis of the trajectory data published in [4, 6, 8, 9, 21–24]. These data, plotted in Fig. 2, allow a simple approximation

$$v(H) \approx 25(H - 5) \text{ m s}^{-1}. \quad (9)$$

The universality of constraint (9) is due to the following. The phase portrait of a rocket trajectory, $v(H)$, is defined as a solution to a first-order ordinary differential equation. The structure of this equation is such that the solution is very smoothly dependent on two parameters. Endowed with the physical meaning of a thrust-to-weight ratio (possible acceleration typically equal to 30 ± 5 m s^{-2}) and the Lock number (ratio of aerodynamic to inertia forces, which is proportional to the mass of the launch vehicle to the 1/3 power and, consequently, shows a scatter by a factor of less than 2) of the rocket, these parameters virtually coincide for launch vehicles of different types. This is not surprising because those who develop aerospace facilities are forced to fit the common, and rather narrow, ranges of design parameters of engines and constructions in order to make compromise solutions satisfying a wide variety of contradictory requirements.

The extensive characteristic of a particular jet, the total per-second flow rate of combustion products, appears in the initial conditions of the problem of dissipation of the trail cloud via the parameter r_{ini}: as the power of a launch vehicle increases, the propulsion trail reaches in a longer time, and farther from the nozzle exit, the thermal gas-dynamic conditions chosen as those of universal nature. Using the theory of turbulent jets [20] and neglecting the impact-wave

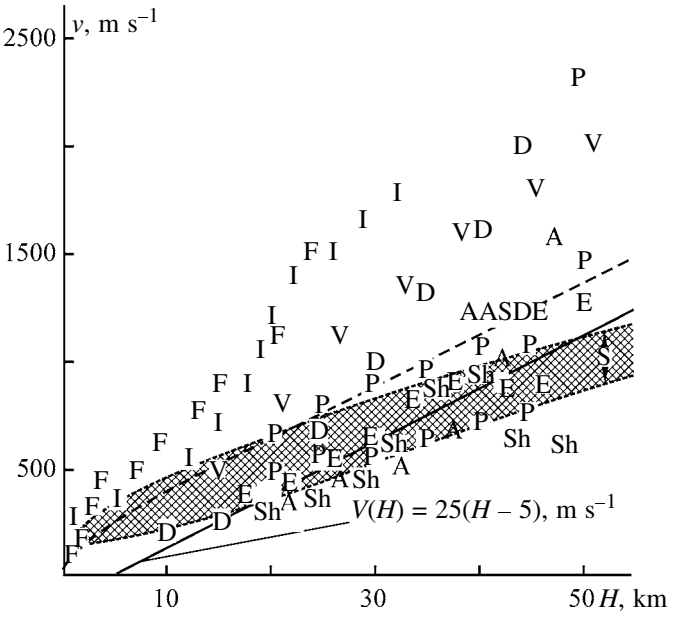


Fig. 2. Phase portraits of rocket trajectories according to [4, 6, 8, 9, 21–24]. (v) Velocity and (H) altitude. Launch vehicles: A, Ariane V; P, Proton; S, Saturn 5; Sh, Space Shuttle; E, Energiya. D, Dyna Soar rocket plane (descent dynamics). Aerophysical rockets: V, Viking 12; I, Aerobee; F, V-2 ballistic rocket. AASDE, approximate analytical solution to the dynamics equation of an averaged rocket.

processes in the near trail of a launch vehicle [19, 20], we can express r_{ini} as a function of the gas-dynamic parameters of the jet and concurrent flow:

$$r_{ini} = \left[\frac{[u_0 - v(H)]\dot{m}}{u_s^2 \rho_0}\right]^{1/2} e^{H/16}, \quad (10)$$

where $u_0 \approx 3700$ m s^{-1}, $u_s \approx 300$ m s^{-1}, and $\rho_0 \approx 1.29$ kg m^{-3} are, respectively, the outflow velocity of the propulsive jet, speed of sound in air, and density of the atmosphere near the Earth's surface; $\dot{m}$ is the per-second expenditure of fuel during the working period of the first stage of a launch vehicle.

When deriving formula (10), we assumed that the value of r_{ini} corresponds to the thermal gas-dynamic state of an expanded jet, in which the kinetic energy of its directed motion is at a level of 10% relative to the thermal energy of the surrounding atmospheric gases. It was also considered that the remaining 90% of the energy of the propulsive jet is transformed into heat by that time.

Combining (9) and (10), we obtain the altitude dependence of the initial radius of the rocket trail

$$r_{ini}(H, \dot{m}) \approx 0.1(3 - 0.03H)^{1/2} e^{H/16} (\dot{m})^{1/2}. \quad (11)$$

Energetic and ecological characteristics of first stages of modern launch vehicles

Type a launch vehicle (number and make of engines)	Fuel expenditure, kg s^{-1}	Content in propulsive jet, mole fraction, of indicated combustion product of rocket fuels				
		Cl_2	HCl	Al_2O_3	NO	OH
Proton, 6×RD-253	3200	–	–	–	7.6×10^{-3}	1.6×10^{-4}
Space shuttle, 3×SSME + 2×SRM	1600	–	–	–	3.0×10^{-4}	1.7×10^{-5}
	5800	5×10^{-4}*	0.13	0.18	2.4×10^{-4}	2.0×10^{-4}
Energiya, 4×RD-120 + 4×RD-170	1800	–	–	–	3.0×10^{-4}	1.6×10^{-5}
	9800	–	–	–	8.8×10^{-4}	2.1×10^{-4}
Ariane V	1900*	5×10^{-4}*	0.12	0.18	3×10^{-4}*	2.0×10^{-4}
Titan-IV	2250*	5×10^{-4}*	0.19	0.019	3×10^{-4}*	3.3×10^{-4}

* The parameters of the propulsive jets of launch vehicles were obtained by combination of data from various sources, with account of the common constraints (9)–(15).

Equation (11) factorizes the universal altitude–velocity and the specific extensive components of the initial conditions of the problem concerning the turbulent dissipation of a cylindrically symmetrical cloud of a chemically active impurity in the stratosphere.

The levels of the initial perturbation of the concentration–temperature field, $\Delta\theta \equiv \{\Delta c_i, \Delta T\}$, which are necessary for integration of the evolution equations (5)–(8) of the rocket trail, and the overall contamination and densification are evaluated by the formulas [15, 20] that express the conservation laws in the theory of submerged turbulent jets:

$$\Delta c_{i,H}(0,0)/\Sigma c_{i,H} = \Delta c_{i,H}(0)/\Sigma c_{i,H} \approx 1000/[\mu_i(145 - H) \times (H - 5)], \quad (12)$$

$$\Delta T_H/T_H \approx [u_0 - v(H)]/[v(H)] \approx (145 - H)/[4(H - 5)], \quad (13)$$

$$\Delta\rho/\rho_H = u_s^2/\{\pi[v(H)(u_0 - v(H))]\} \approx 40/[(145 - H)(H - 5)], \quad (14)$$

$$\Delta c/c = \Sigma\Delta c_{i,H}/\Sigma c_i \approx \Delta\rho/\rho \approx 40/[(145 - H)(H - 5)]. \quad (15)$$

The most widely used are two-component liquid rocket propellants (LRP) whose chemical energy is contained in substances or mixtures, fuel and oxidant, separately stored and fed into the combustion chamber. Typical liquid rocket fuels are liquid hydrogen, hydrazine N_2H_4, unsymmetrical dimethylhydrazine $N_2H_2(CH_3)_2$, kerosene T-1, and synthetic hydrocarbon fuel RJ-1, as well as Al and Mg dispersed in liquid fuels (present in fuels as free metals or hydrides AlH_3, MgH_2). As oxidants commonly serve liquid oxygen O_2, concentrated nitric acid HNO_3, or nitrogen tetraoxide N_2O_4 [21, 23, 24]. The products formed in the combustion of liquid rocket fuels include ozone-depleting species: NO, OH, and Al_2O_3.

Composite solid rocket propellants (CSRP) are based on an oxidant, commonly, ammonium perchlorate NH_4ClO_4, and more rarely, ammonium dinitramide $NH_4N(NO_2)_2$ and nitrates of alkali metals. As the main metallic fuel serves aluminum Al or AlH_3, with the mass fraction of the fuel in CSRP reaching 18%. In combustion, CSRP release, together with nitrogen and aluminum oxides, also ozone-depleting chlorine compounds, HCl and Cl_2.

It has been found [4–7, 13–15] that the stratospheric chemistry essentially differently "responds" to launches of liquid- and solid-propellant launch vehicles: in the former case, the perturbed ozonosphere comparatively rapidly relaxes to the initial (dynamic) state via local reactions, whereas in the latter, the relaxation is exceedingly slow and occurs exclusively via vertical transfer of untypical substances. Accordingly, simulation of these varieties of perturbation requires that specific approaches should be used. Similarly to the models from [4–7, 13–15], the set of models considered in this study is adapted to description of sharp, locally eliminable perturbations of the ozonosphere, i.e., those caused by launches of various liquid-propellant launch vehicles, which yield combustion products containing no chlorine compounds.

Considered together with formulas (8)–(15), the initial parameters of perturbation of the ozonosphere by various types of launch vehicles are readily combined into a table. The table summarizes the specific energetic and ecological parameters of the most widely used launch vehicles [4, 6, 8, 9, 21–24]. Because of the wide scatter of published data, the content of separate components in the rocket trail is given in the form of interval estimates. The reliability of these

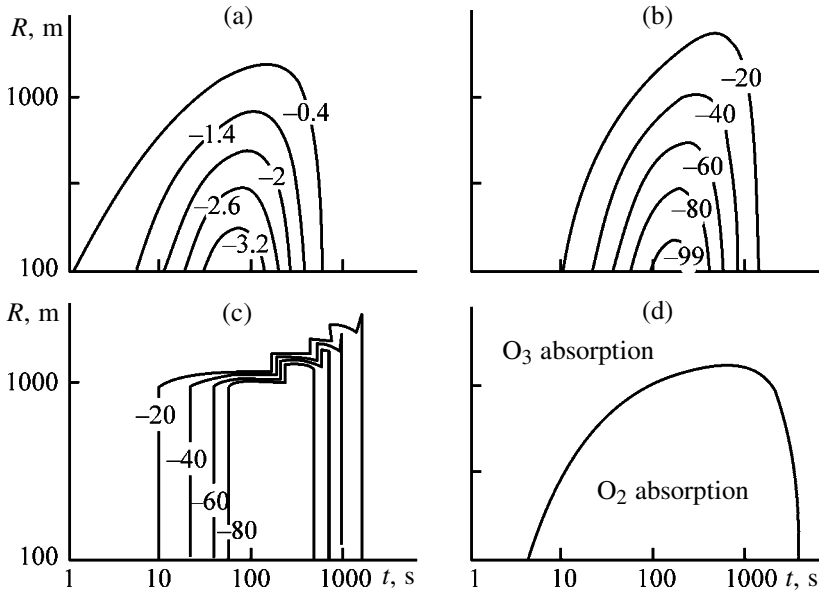


Fig. 3. Dynamics of an integral perturbation of stratospheric ozone (in percent relative to the unperturbed value) in a single launch of Proton launch vehicle. (*R*) Distance from the axis of the rocket trail and (*t*) time.

data well justifies the assumptions on which the estimates (8)–(15) are based.

It is noteworthy that the table lists the launch vehicles and substances that are the most important for the photochemistry of stratospheric ozone. If the estimates of the content of ozone-depleting substances in the primary rocket trail, made by different authors [4, 6, 8, 9, 21–24], show a wide scatter, preference is given either to better confirmed (both directly and indirectly) estimates or to those producing the least optimistic impact scenario. When it is impossible to range the reliability of published data [4, 6, 8, 9, 21–24], the table gives the upper bound. Because changes of the working modes of rocket engines cannot be correctly taken into account, either, data on the expenditure of fuel components and on the composition of combustion products are averaged. It is noteworthy that the tabulated content of NO and OH in discharges from liquid-propellant launch vehicles corresponds to the real nonequilibrium composition of combustion products, but exceeds by three to four orders of magnitude the equilibrium values previously used in a number of studies [5, 7]. As shown below, this refinement of previous estimates is the most important factor.

The launch of the main Russia's launch vehicle Proton is accompanied by discharge into the ozone layer of considerable amounts of NO, the main ozone-depleting species (factorial analysis of the model shows that hydroxide is of secondary importance in the given case). Analysis of recent domestic and foreign publications [4, 6, 8, 9] and the chemical composition of the propulsive jet, specially calculated by the author, indicate that the level of this specific factor was strongly underrated in previous estimates [5, 7]. The reason for this frequently occurring error is that nitrogen oxide forming in the combustion chamber does not have enough time to relax to the equilibrium concentration in the fast outflow from the nozzle. Therefore, the content of NO in the propulsive jet virtually coincides with that in the combustion chamber and, accordingly, is determined by thermodynamic parameters in the most thermally loaded part of the rocket engine. If this circumstance, first discovered by Zel'dovich and named "quenching" [25], is taken into account, the initial level of the NO-related perturbation is approximately four orders of magnitude higher, the spatial scale of the perturbed region increases by approximately $4^{1/2} = 2$ orders of magnitude, and the dispersal time becomes longer by $4^{1/3}$ orders of magnitude, i.e., by a factor of approximately 40. The result of a numerical integration of rate equations (4) and (5) with initial conditions (8)–(15) for a single launch of Proton launch vehicle (see table) is shown in Fig. 3.

The calculation is performed on the assumption that the combustion products have equilibrium (according to [7], Fig. 4a) and nonequilibrium (according to data in the table, Figs. 3b–3d) chemical composition. Separately are presented the computed detailed

kinetics of ozone depletion (Fig. 3b), its approximation with a small-scale model [15] (Fig. 3c), and the physical size of the ozone hole, the region in which molecular oxygen becomes the main absorber of the UV radiation with wavelengths λ = 221–235 nm (Fig. 3d).

The results of a detailed computer simulation, shown in Fig. 3, indicate that the impact is local and short (compared with the synoptic scale), which well justifies the assumptions made when constructing the model. An analysis of the results of the numerical experiment demonstrated that the principal refinement of the models of rocket-induced perturbations of the ozonosphere dynamics [5, 7] is due to taking into account the chemically nonequilibrium state of the propulsion gases, caused by quenching of NO. If the dynamic model and initial data, refined in this study, are used, the magnitude of the integral (across the entire thickness of the ozonosphere) perturbation increases by approximately one and a half orders of magnitude, and the time of relaxation of the stratosphere to the initial state and the transverse size of the ozone hole grow severalfold. This result is in good agreement with the above elementary estimates based on the conservation laws and properties of a developed turbulence, the dynamic mode of the stratosphere. The perturbation of ozone at any fixed altitude is stronger and shorter than the integral perturbation shown in Fig. 3. The refinement of the spatial profile of the ozone hole shows itself in a later stage, when the $[O_3]$ perturbation level becomes insignificant and comparable with diurnal, seasonal, or solar-activity variations. In this case, the addition of an artificial mechanism of dispersal of the trail cloud in the early stage of its evolution is more important that that refinement of the model which is associated with transition from the box dissipation scheme to that realistically distributed [$\square^0 \Rightarrow \square^1$ in the evolution equations (4), (5)]. The results obtained actually point to the priority of refining the models of the reactions between the rocket fuel components, with account of the gas dynamics in the nozzle and detailed data on mixing of the propulsive jet with air.

The practice of modern engineering-ecological calculations acutely needs methods for extension of the results of detailed computer simulations to a wide variety of similar situations without performing labor-consuming computations in each particular case. As applied to short-time ozonosphere perturbations caused by launches of liquid-propellant launch vehicles, this demand can be satisfied by analytical models suggested in [7] and further developed in [13, 15]. The numerical result obtained (Fig. 3b) is in good agreement with the two-component box model [15], in which ozone is decomposed by NO, and NO is decomposed on certain third species in parallel turbulent dispersal of both substances in the horizontal direction. Dropping the rearrangements reported in [15], we obtain the law of evolution of the whole amount of stratospheric ozone upon a rocket-induced perturbation:

$$[O_3](r,t) = \{[O_3]_0 + k_{O_3}[O_3]_{ph}[NO]_0/(k_{NO}[M]) \times [\exp(-k_{NO}[M]t) - 1]\}S^n(r,t),$$

$$S^n(r,t) = \begin{cases} \operatorname{sign}[r_{ini}^{2/3}(1+bt) - r^{2/3}]/(1+bt)^3 \text{ at } n = 0, \\ 6e^{-r^{2/3}/[(r_{ini}/6)^{2/3}(1+bt)]}/(1+bt)^3 \text{ at } n = 1. \end{cases} \quad (16)$$

In Eqs. (16), the subscript ph refers to unperturbed or background concentrations; k_{O_3} and k_{NO}, effective constants of ozone depletion in the set of reactions involving NO and loss of NO in reactions with various substances M; $S^n(r_{ini},0)$, initial distribution of impurity components (products of complete and incomplete combustion of liquid rocket fuels) in the stratosphere, which provides existence of self-simulating solutions to problem (16).

If (16) is regarded as a model of an overall perturbation of the ozonosphere by Proton liquid-propellant launch vehicle, it is necessary to find values of the effective kinetic coefficients. To do this, we use the calculated data in Fig. 3b and an appropriate optimization method. We use the least-squares procedure to find $k_{NO}[M] \approx 10^{-2}$ s^{-1} and $k_{O_3}[O_3]_{ph} \approx 10^{-4}$ s^{-1}, $[O_3]_0/[O_3]_{ph} \approx 0.01$–$0.03$, $[NO]_0/[O_3]_{ph} \approx 30$–$100$. The first two values are in good agreement with the results of [1, 10, 11], and the last two, with the stratosphere-average parameters of the primary rocket trail in the detailed model (4)–(15) (see table). To initialize Eqs. (16) using the results of computer simulations in terms of the detailed kinetic model (4), (5), (8)–(15), it was necessary to include r_{ini} in the set of fitting parameters. Variation of the initial size of the perturbed region makes it possible to take into account the asynchronous action of a launch vehicle on different layers in the stratosphere. The altitude-averaged value $r_{ini} \approx 1000$ m exceeds by an order of magnitude the local initial radius of the trail. This means that, as the launch vehicle reaches the upper boundary of the ozone layer, the size of the ozone hole has enough time to grow, across a considerable thickness of

lower-lying layers, to

$$R \sim \{\xi(H_{max} - H_{min})/v[(H_{max} + H_{min})/2]\}^{3/2} \approx 3 \times 10^2 \text{ m}. \quad (17)$$

This value is in good agreement with the result of identification (16) based on the results of detailed calculations (Fig. 3b); the difference of half an order of magnitude is readily accounted for by the neglect, in deriving (17), of the fact that the launch vehicle is comparatively slowly moving in the lower part of the stratosphere, where the main part of ozone is concentrated. The relative difference of the numerical results (Fig. 3b) from their approximation in terms of the small-scale model (16) does not exceed $3^{1/2}$, which points to simplicity and predictability of ozonosphere perturbations caused by launches of liquid-propellant launch vehicles.

It should be noted that the extensive characteristic of the discharge, $d\dot{m}/dt$, has effect only on the size of the perturbed region, whereas the content of ozone-depleting components (NO in the case in question) in the combustion products of liquid rocket fuels affects not only the size r_{ini} of the primary trail cloud, but also the peak perturbation level $[NO]_0/[O_3]_{ph}$.

However, the simplified approach cannot, despite the advantages mentioned above, completely replace a computer simulation of the process in terms of high-resolution models. This is due to the fact that the minimum model (16) is based on analytical solutions to systems of two quasilinear equations [15] and can serve as a convenient projection of real, strongly nonlinear systems of high dimension in a strictly limited range of parameters. When going beyond the admissible limits, the reduced model loses adequacy: such a complex dynamic system as the ozonosphere differently responds to impacts of the same type, but of different levels. The mechanism of rapid neutralization of weak external impacts, which exist in systems of this kind, fail when the impacts become too strong and the response (counteraction) is effected by more powerful and, simultaneously, more sluggish mechanisms. In the case in question, the small-scale model (16) is identified by the response of the detailed model to a strong impact and the kinetic parameters of the homeostatic mechanism of the corresponding level are calculated. It would be expected that the response of the simplified model to a weak impact will be delayed (computer calculations confirm this conclusion). If, however, the small-scale model is identified by the weakly perturbed dynamics of the detailed model (4)–(15), we run the risk of overlooking the organization of the ozonospheric homeostasis, which is responsible for the structural-dynamic integrity of the ozonosphere upon external destructive impacts and is characterized by a hierarchy of connectedness. Therefore, small-scale models of the type (16) are parametrically local: their purpose is to explain particular results, rather than to make long-term predictions.

CONCLUSIONS

(1) Taking into account the nonequilibrium state of the products formed in combustion of liquid rocket fuels is the main way to improve models of local impact of launch vehicles on the stratospheric ozone.

(2) The corresponding refinements of prototype models show that the degree of local ozone depletion in launches of Proton launch vehicle is close to 100%, rather than to 3%, and it is absolutely necessary to take into account the risk of biological objects being damaged by UV radiation near rocket trajectories.

(3) The situation with the key role of the chemically nonequilibrium state is "robust," i.e., it does not change on making the models more detailed, e.g., by incorporation of more realistic descriptions of the turbulence.

(4) The models of rocket-induced perturbations of the ozonosphere can be factorized with respect to extensive and specific parameters, which gives reason to "compress" the information and make engineering-ecological estimates by similarity methods.

(5) Taking into account the artificial or propulsive mechanism of dissipation of the rocket trail in the early stage of its evolution is the priority way to modify the model by detailing the spatial distribution of trail substances.

ACKNOWLEDGMENTS

The study was supported by the Russian Foundation for Basic Research (project no. 05-08-33 433-a).

REFERENCES

1. *Atmosfera: Spravochnik* (Atmosphere: Reference Book), Sedunov, Yu.S., Ed., Leningrad: Gidrometeoizdat, 1991.
2. Feigin, A.M., Konovalov, I.B., and Molkov, Y.I., *J. Geophys. Res.*, 1998, vol. 103, no. D19, pp. 25 447–25 460.

3. Burdakov, V.P., Elanskii, N.F., and Filin, V.M., *Vestn. Akad. Nauk SSSR*, 1990, no. 12, pp. 72–81.
4. Tishin, A.P., Aleksandrov, E.L., Rodionov, A.V., et al., *Khim. Fiz.*, 1993, vol. 12, no. 9, pp. 1184–1225.
5. Davletshin, R.F., Lokhov, G.M., and Yatsenko, O.V., *Pis'ma Zh. Tekh. Fiz.*, 1993, vol. 19, no. 19, pp. 5–9.
6. *Ekologicheskie problemy i riski vozdeistviya raketno-kosmicheskoi tekhniki na okruzhayushchuyu prirodnuyu sredu: Spravochnoe posobie* (Environmental Problems and Risks of Impact by Spacecraft on the Natural Environment: Reference Book), Adushkin, A.V., Ed., Moscow: Ankil, 2000.
7. Yatsenko, O.V., *Zh. Prikl. Khim.*, 2003, vol. 76, no. 11, pp. 1827–1833.
8. Jackman, C.H., Considine, D.B., and Fleming, E.L., *J. Geophys. Res.*, 1996, vol. 101, no. D7, pp. 12523–12529.
9. Jones, A.E., Bekki, S., and Pyle, J.A., *J. Geophys. Res.*, 1995, vol. 100, no. D8, pp. 16651–16660.
10. Brasseur, G.P. and Solomon, S., *Aeronomy of the Middle Atmosphere*, Dordrecht: Reidel, 1984.
11. McEwan, M.J. and Philips, L.F., *Chemistry of the Atmosphere*, London: Edward Arnold, 1975.
12. Hirschfelder, J.O., Curtiss, C.F., and Bird, R.B., *Molecular Theory of Gases and Liquids*, New York: Wiley, 1954.
13. Bakulin, V.N., Potopakhin, V.A., and Yatsenko, O.V., *Matem. Model.*, 2005, vol. 17, no. 8, pp. 81–94.
14. Yatsenko, O.V. and Ladosha, E.N., *Bezopasn. Zhiznedeyat.*, 2005, no. 8, pp. 31–35.
15. Yatsenko, O.V. and Ladosha, E.N., *Inzh. Ekol.*, 2005, no. 6, pp. 27–45.
16. Yatsenko, O.V., Computer Program Registration Certificate no. 2003612394, Moscow: Rospatent, 2003.
17. Yatsenko, O.V., Database Registration Certificate no. 2003620238, Moscow: Rospatent, 2003.
18. Kolesnichenko, A.V. and Marov, M.Ya., *Turbulentnost' mnogokomponentnykh sred* (Turbulence in Multicomponent Media), Moscow: Nauka, 1999.
19. Hemsch, M.J., *Tactical Missile Aerodynamics*, Nielsen, J.N., Ed., New York: Am. Inst. of Aeronautics, 1986.
20. *Teoriya turbulentnykh strui* (Theory of Turbulent Jets), Abramovich, G.N., Ed., Moscow: Nauka, 1984.
21. Feodos'ev, V.I. and Sinyarev, G.B., *Vvedenie v raketnuyu tekhniku* (Introduction to Missile Technology), Moscow: Oborongiz, 1961.
22. *Spravochnik po geofizike* (Handbook of Geophysics), Breus, T.K. and Vedes, L.F., Eds., Moscow: Nauka, 1965.
23. Vertregt, M., *Principles of Astronautics*, New York: Elsevier, 1966.
24. Aleshkov, M.N. and Zhukov, I.I., *Fizicheskie osnovy raketnogo oruzhiya* (Physical Foundations of Missile Warfare), Moscow: Voenizdat, 1965.
25. Zel'dovich, Ya.B., Sadovnikov, P.Ya., and Frank-Kamenetskii, D.A., *Okislenie azota pri gorenii* (Oxidation of Nitrogen in Combustion), Moscow: Akad. Nauk SSSR, 1947.

ISSN 1070-4272, Russian Journal of Applied Chemistry, 2006, Vol. 79, No. 9, pp. 1473–1477. © Pleiades Publishing, Inc., 2006.
Original Russian Text © S.A. Lobanov, V.Z. Poilov, 2006, published in Zhurnal Prikladnoi Khimii, 2006, Vol. 79, No. 9, pp. 1489–1493.

ENVIRONMENTAL PROBLEMS OF CHEMISTRY AND TECHNOLOGY

Treatment of Wastewater to Remove Ammonium Ions by Precipitation

S. A. Lobanov and V. Z. Poilov

Perm State Technical University, Perm, Russia

Received April 12, 2006

Abstract—The process of wastewater treatment to remove ammonium ions by precipitation in the form of ammonium magnesium phosphate was studied. The fundamental aspects of the chemical precipitation process were examined. The effect of various factors on the efficiency of wastewater treatment was experimentally analyzed.

DOI: 10.1134/S1070427206090151

At present, numerous industrial plants encounter the problem of wastewater treatment to remove ammonium ions. The large amount of ammonium nitrogen in industrial sewage leads to oxygen starvation of plants and adversely affects the flora and fauna of water reservoirs.

One of the most promising methods of wastewater treatment to remove ammonium ions is precipitation of ammonium in the form of insoluble ammonium magnesium phosphate hexahydrate (AMP), struvite $MgNH_4PO_4 \cdot 6H_2O$ (SP = 5.5×10^{-14} [1]). This method provides a high degree of purification and enables secondary use of ammonia, because AMP is a valuable product and can be used as a fertilizer [2]. At present, the operation of some sewage treatment facilities in various countries is based on removal of ammonium and phosphate ions from sewage by their precipitation as AMP. The precipitate obtained is in demand at the world market as an integrated mineral fertilizer [3, 4].

Available publications show that the high efficiency of wastewater treatment is achieved at pH 8–9 and a stoichiometric ratio of the reacting components, or at their minor excess [3, 4]. The most frequently used in wastewater treatment are magnesium chloride and soluble phosphates of alkali metals as precipitating reagents, and sodium hydroxide as an alkaline agent [4].

The fundamental aspects of the AMP crystallization process and the influence exerted on this process by various factors have been insufficiently studied. An analysis of this kind is necessary for control over the crystallization process and production of a precipitate with prescribed parameters. In view of the fact that wastewater is a multicomponent system, it is also necessary to take into account the effect of various impurity substances on wastewater treatment to remove ammonium ions, because some of these substances can impair the efficiency of the process. The role of impurities in AMP precipitation is played by ions of potassium and calcium. At a high content of calcium ions in wastewater, part of phosphate ions is consumed for formation of difficultly soluble calcium phosphates, which impairs the treatment efficiency [4]. In the presence of a large amount of potassium ions, they can substitute ammonium ions in AMP to form magnesium potassium phosphate $MgKPO_4 \cdot 6H_2O$ with identical structure and properties [5, 6]. In addition, the problem of wastewater treatment to remove ammonium ions is topical for plants manufacturing urea, and, therefore, a study of the influence exerted by urea impurity on the wastewater treatment process is of practical interest. It is known that urea can undergo hydrolysis in an alkaline medium to form ammonium ions, which may diminish the degree of wastewater purification.

The aim of this study was to analyze the fundamental aspects of chemical precipitation (crystallization) of AMP to give crystals with certain dispersity at a high degree of wastewater purification and to examine the effect of impurities on the degree of wastewater purification.

To study the wastewater treatment process, we analyzed the precipitation of AMP with sodium hydrophosphate, sodium hydroxide, and magnesium chloride. The precipitation occurred by the reaction

$$MgCl_2 + NH_4Cl + Na_2HPO_4 + NaOH + 5H_2O = MgNH_4PO_4 \cdot 6H_2O + 3NaCl.$$

Table 1. Results of experiments on wastewater treatment at various pH values and reagent modes

Run no.	Volume of solutions, $m^3\ m^{-3}$ wastewater		pH_{in}	pH_{fin}	$\tau_{c.r.}$*	$\tau_{c.p.}$**	c_{in} (NH_4^+)	c_{fin} (NH_4^+)	X, %	Precipitation mode
	Na_2HPO_4	$MgCl_2$			s		$g\ l^{-1}$			
1	1.00	1.00	7.85	5.72	180	10	2	0.761	61.9	Instantaneous supply of $MgCl_2$ into solutions of NH_4Cl and Na_2HPO_4
2	1.00	1.00	9.73	8.52	130	10	2	0.058	95.5	
3	1.00	1.00	10.42	10.26	40	2	2	0.087	95.6	
4	1.00	1.00	10.27	10.56	–	2	2	0.14	93.1	〃
5	1.00	1.00	12.38	12.29	–	2	2	1.18	59	〃
6	1.00	1.00	10.5	8.53	50	2	2	0.176	91.2	〃
7	1.00	1.00	10.33	8.01	110	10	2	0.133	93.3	Batched supply of $MgCl_2$ into solutions of NH_4Cl and Na_2HPO_4
8	1.00	1.00	6.86	8.12	70	2	2	0.176	91.2	Instantaneous supply of Na_2HPO_4 and NaOH into solutions of NH_4Cl and $MgCl_2$
9	1.00	1.00	6.54	8.68	150	15	2	0.127	93.6	Batched supply of Na_2HPO_4 and NaOH into solutions of NH_4Cl and $MgCl_2$
10	1.07	1.07	10.43	8.23	–	2	2	0.106	94.7	Instantaneous supply of $MgCl_2$ into solutions of NH_4Cl and Na_2HPO_4. Excess of reagents 6.7%
11	1.07	1.00	6.62	8.1	–	2	2	0.154	92.3	Instantaneous supply of Na_2HPO_4 and NaOH into solutions of NH_4Cl and $MgCl_2$. Excess of reagents 6.7%

* Time of reactoin completion. ** Time of chemical precipitation.

To a certain amount of a simulated wastewater solution with a 2 $g\ l^{-1}$ concentration of NH_4^+ ions in a transparent reactor placed in a nephelometer, we added with stirring a stoichiometric amount of an equimolar solution of sodium hydrophosphate (concentration 15.778 $g\ l^{-1}$), a certain amount of a 1% NaOH solution, and then a stoichiometric amount of a $MgCl_2$ solution (10.589 $g\ l^{-1}$) The resulting suspension was stirred for 20 min. In the course of the process, the pH value and transmission of light through the transparent reactor were recorded. In accordance with the reaction equation, the pH value decreases in the course of AMP precipitation, and this circumstance was used to judge the reaction rate from the variation of pH with time. The transmission of light through the reactor served to judge how the degree of chemical precipitation varies with time. The completion of the chemical reaction and chemical precipitation was judged from time dependences of the pH value and degree of chemical precipitation: as the time of completion of the process we took the time after which the pH value and degree of precipitation remained virtually unchanged. After keeping the suspension, the rate of sedimentation of the resulting precipitate was measured in the course of settling in a volumetric cylinder. After the settling, the suspension was filtered and the filtrate was analyzed for the content of ammonium ions. The precipitate was dried and subjected to chemical, optical-microscopic, and X-ray phase analyses.

The results of experiments in which the AMP precipitation was studied are listed in Table 1. At low pH values, the degree X of wastewater purification was not high (62%). At final pH values of 8.5 and more, higher degrees of purification (~95%) are achieved. This is due to the low solubility of AMP in alkaline media. As demonstrated by an analysis of the data on the rate of the chemical reaction, the AMP formation is complete in less than 3 min (Table 1), and the higher the pH value, the faster the reaction, which does not contradict the law of mass action. However, rather high pH values adversely affect the treatment efficiency. Table 1 shows that the degree of purification remains rather high (93%) at final pH 10.5 (run no. 4), whereas at pH 12.3 (run no. 5) it drastically decreases to 59%. Hence, it may be concluded that AMP is soluble in an excess of alkali. This does not contradict published evidence [1] that equilibrium is

reached at pH 10–11. The pH dependence of the degree of wastewater purification is shown in the figure. It can be seen that the maximum degree of purification is reached at pH 8.5–10.

The chemical precipitation is fast and virtually complete in 10 s (Table 1). As expected, the higher the pH value in the course of the reaction, the faster the formation of precipitate particles. This is due to a decrease in the solubility of AMP, observed on raising the pH to a certain value.

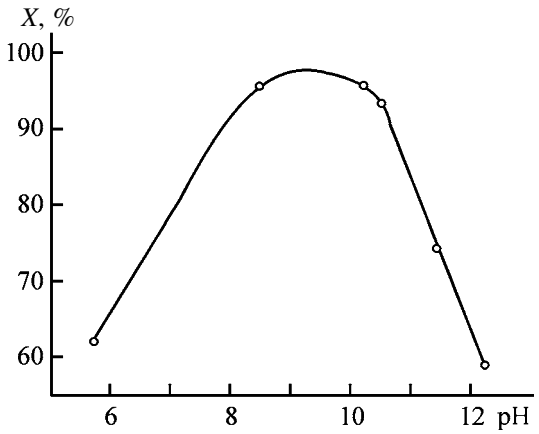
However, high pH values adversely affect the sedimentation rate because the alkaline medium leads to a low solubility of the precipitate and to a high supersaturation. This favors a high rate of nucleation and low rate of crystal growth, which, in turn, leads to the formation of a finely dispersed suspension whose settling and filtration are slow.

An optical microscopic analysis of the precipitates confirmed the results obtained in the study of the sedimentation rate of the suspensions. At low pH, a coarsely crystalline precipitate is formed, with prismatic and so-called twin crystals characteristic of AMP [8]. At higher pH values, fine needle-like crystals, which are commonly formed in the presence of free ammonia [8], are observed.

To create a minor supersaturation and obtain a coarsely crystalline precipitate, experiments with batch supply of reagents by a peristaltic pump at a rate of 8.5 $cm^3\ min^{-1}$ were performed at the optimal pH 8.5. Also, the order in which the reagents should be supplied was analyzed. In the case of a direct order of reagent supply, a solution containing Mg^{2+} ions was introduced into that containing NH_4^+ and PO_4^{3-} ions and an alkali. In the case of a reverse order of reagent supply, a solution containing PO_4^{3-} ions and an alkali was introduced into that containing NH_4^+ and Mg^{2+} ions.

The results of experiments with various modes of reagent supply showed that the degree of purification to remove ammonium ions was high and approximately equal (91–94%) in all the experiments (run nos. 6–9). The reaction was complete in 2–3 min in all the reagent supply modes. The chemical precipitation was fast, and in the experiments with instantaneous supply of reagents the maximum degree of crystallization was reached within less than 2 s. A longer time was necessary in the case of a gradual supply (10–15 s), which is due to the low rate of delivery of precipitants.

The highest sedimentation rate was observed for the suspension obtained with reverse batched supply of reagents. However, this suspension was polydisperse (contained both coarse and fine crystals), which was confirmed by optical microscopic examination. This is probably due to the fact that the pH value was low at the beginning of supply of a mixture of Na_2HPO_4 and NaOH solutions into the reaction vessel, which favored formation of a coarsely crystalline precipitate. As the reagents were introduced into the reaction mixture, the pH increased and this led to a high rate of nucleation and low rate of crystal growth and, consequently, to formation of a finely crystalline precipitate. A high sedimentation rate was also observed for the suspension obtained with instantaneous reverse supply of reagents, and this rate exceeded that in the case of a direct batched supply. The suspension obtained with a direct batched supply of reagents was finely dispersed and flocculent and had a low sedimentation rate. Thus, suspensions with unsatisfactory properties are formed in the case of a batched supply of reagents, and this hinders the suspension separation. Therefore, it is more appropriate to use the instantaneous supply of reagents.



Degree X of wastewater purification as a function of the final pH value in precipitation of AMP.

Also, experiments aimed to study the effect of an excess of precipitants with respect to ammonium in direct and reverse supply of reagents were carried out (run nos. 10 and 11). Table 1 shows that a higher degree of purification (95%) is achieved in the case of a direct supply of reagents in a minor excess (6.7%), i.e., with a $MgCl_2$ solution introduced into a mixture of NH_4Cl, Na_2HPO_4, and NaOH solutions.

Thus, the optimal treatment mode is that with direct instantaneous supply of precipitants in a minor excess with respect to ammonium ions. This mode provides both a high degree of wastewater purification (95%) and high rates of chemical precipitation and sedimentation of the resulting suspension. Further experiments devoted to analysis of the effect of vari-

Table 2. Results of experiments on wastewater treatment in the presence of impurities. Solution volume ($m^3\ m^{-3}$ wastewater): Na_2HPO_4 0.150 and $MgCl_2$ 0.027

pH_{in}	pH_{fin}	c_{in} (NH_4^+)	c_{fin} (NH_4^+)	X, %	Content of AMP in precipitate, %	Wastewater to be treated
		g l^{-1}				
10.95	7.99	2.06	0.097	95.3	95.3	No admixture
11.21	8.38	2.11	0.072	96.6	96.6	Admixture of urea, c_{ur} = 30 g l^{-1}
10.68	8.63	1.70	0.19	88.8	88.8	Admixture of K, c_{K^+} = 68 g l^{-1}
11.04	8.00	2.06	0.20	90.3	88.3	Admixture of Ca, $[Ca^{2+}]:[Mg^{2+}] = 0.25:1$
10.54	8.74	2.06	0.70	66.0	59.4	Admixture of Ca, $[Ca^{2+}]:[Mg^{2+}] = 1:1$

ous factors on the wastewater treatment process to remove ammonium ions were performed under the optimal conditions found.

An X-ray phase analysis of a precipitate obtained in the optimal mode confirmed that the precipitate is ammonium magnesium phosphate hexahydrate with a minor impurity of magnesium phosphate and hydrophosphate $Mg_3(PO_4)_2 \cdot 8H_2O$ and $MgHPO_4 \cdot 3H_2O$.

A study of the influence exerted by the initial concentration of ammonium ions on the treatment process revealed that wastewater containing ammonium ions in high concentration will be purified to a greater extent than low-concentrated wastewater. In addition, the AMP precipitate obtained in processing of highly concentrated wastewater is coarsely dispersed and its separation from the liquid phase in the stage of settling and filtration is simpler. It was found that the wastewater treatment at elevated temperatures (>80°C) leads to a low degree of purification (66%). This is due to an increase in the solubility of the AMP precipitate upon heating; furthermore, the precipitate obtained has a low sedimentation rate.

Experiments on AMP precipitation in the presence of impurities were performed in the optimal reagent mode at the optimal pH with saturated solutions of the precipitants taken in a 5% excess relative to the stoichiometry. Solutions of precipitants with the following content of the main component were used (%): Na_2HPO_4 solution 10.32, $MgCl_2$ solution 32, and NaOH solution 16. The results of the experiments on the wastewater treatment are listed in Table 2.

In a study of the influence exerted by a urea admixture on the wastewater treatment process, the simulated solution contained, in addition to ammonium ions, urea in a concentration of 30 g l^{-1}. The experiments performed (Table 2) demonstrated that urea is not noticeably hydrolyzed in alkaline solutions under the conditions specified during the time prescribed. The urea admixture does not affect the efficiency of wastewater treatment to remove ammonium ions and the process of chemical precipitation and sedimentation of the precipitate obtained. X-ray phase and optical microscopic analyses of the precipitate obtained in the presence of urea demonstrated that the precipitate was AMP hexahydrate virtually free of any impurity phases.

Presence of a large amount of potassium ions in wastewater (68 g l^{-1}) reduces the purification efficiency from 95 to 89% (Table 2). The precipitate obtained in this case is only 89% composed of AMP hexahydrate. An X-ray phase analysis of the precipitate demonstrated that no new phases and, in particular, $MgKPO_4 \cdot 6H_2O$ were present. Because magnesium potassium phosphate is formed under the same conditions as AMP, it may be assumed that magnesium potassium phosphate forms a solid solution with AMP, rather than a separate phase. Magnesium potassium phosphate hexahydrate is isostructural with AMP hexahydrate, both substances crystallize in the orthorhombic crystal system [6, 9], and the radius of the ammonium ion is close to that of the potassium ion. The precipitate obtained contains coarse prismatic and needle-like crystals, in contrast to the fine needle-like crystals characteristic of AMP, which resulted in a higher rate of sedimentation of the suspension obtained.

The strongest influence on the process of wastewater treatment to remove ammonium ions by precipitation of AMP is exerted by calcium ions. It has been found [10] that mostly AMP is formed in precipitation at ion concentration ratios $[Ca^{2+}] : [Mg^{2+}]$ in wastewater lower than 0.25 : 1. For comparison, experiments were performed at $[Ca^{2+}] : [Mg^{2+}] = 1 : 1$. It was found that at $[Ca^{2+}] : [Mg^{2+}] = 0.25:1$ the degree of wastewater purification decreased, but, nevertheless, remained fairly high (90%). An analysis of the precipitate formed in this case demonstrated that mostly AMP was formed (88%). At $[Ca^{2+}] : [Mg^{2+}] =$

1 : 1, the degree of wastewater purification drastically decreased (66%). An X-ray phase analysis demonstrated that the precipitates were mostly composed of AMP hexahydrate; however, the intensity of its lines was somewhat lower, compared to the pure substance. No lines associated with calcium phosphates were found. Because the precipitates contain low amounts of the main substance, it may be assumed that an X-ray amorphous calcium phosphate $Ca_3(PO_4)_2$ was formed in addition to struvite. An optical-microscopic analysis demonstrated that most of crystals had an indeterminate shape, different from the needle-like appearance characteristic of struvite.

It is known [4] that hydroxylapatite, having the lowest solubility product ($SP = 3.2 \times 10^{-59}$), is the most thermodynamically stable phase among all forms of calcium phosphate; however, intermediate phases, including amorphous calcium phosphate, can be formed in primary nucleation. A study of the formation rate of the precipitates demonstrated that, at $[Ca^{2+}] : [Mg^{2+}] = 0.25 : 1$, the reaction of AMP formation is fast (complete in 25 s), whereas at $[Ca^{2+}] : [Mg^{2+}] = 1 : 1$, the rate markedly decreases, suggesting the occurrence of a side reaction (formation of calcium phosphates). A small addition of Ca^{2+} has no effect on the sedimentation process. However, as the relative content of this additive increases, the sedimentation rate significantly decreases. This behavior can be accounted for by the nature of the precipitate formed (calcium phosphate).

CONCLUSIONS

(1) The maximum degree of wastewater purification to remove ammonium ions by precipitation of ammonium magnesium phosphate hexahydrate with sodium hydrophosphate and magnesium chloride (>95%) is reached at pH 8.5–10 and a minor excess of precipitants (5%).

(2) The optimal mode of precipitation of ammonium magnesium phosphate hexahydrate is that with direct instantaneous supply of reagents, which consists in that, first, Na_2HPO_4 and NaOH solutions are added to wastewater, and then a $MgCl_2$ solution. This way of reagent delivery provides a high degree of wastewater purification and high rates of chemical precipitation and sedimentation of the resulting precipitate of ammonium magnesium phosphate hexahydrate.

(3) Wastewater containing high concentrations of ammonium ions is purified better and the precipitate of ammonium magnesium phosphate hexahydrate, obtained in treatment of such a wastewater, is coarsely dispersed and its separation from the liquid phase in the stage of settling and filtration is simpler. Performing the process at elevated temperatures leads to a low degree of wastewater purification and to formation of a finely dispersed suspension of ammonium magnesium phosphate hexahydrate.

(4) Presence of high concentrations of urea in wastewater has no effect on the efficiency of its treatment. In the presence of potassium ions, the efficiency of wastewater treatment to remove ammonium ions decreases because of the partial consumption of precipitating agents for the formation of a magnesium potassium phosphate precipitate. The presence of a minor amount of Ca^{2+} ions in wastewater ($[Ca^{2+}] : [Mg^{2+}] = 0.25 : 1$) somewhat reduces the efficiency of wastewater treatment. At larger amounts of calcium ions in wastewater, the degree of purification markedly decreases because of the formation of calcium phosphate.

REFERENCES

1. Ohlinger, K.N., Young, T.M., and Schroeder, E.D., *Second Int. Conf. on Recovery of Phosphate from Sewage and Animal Wastes*, Amsterdam: Center for European Studies of Polyphosphates, March 12–13, 2001.
2. Grabovenko, V.A., *Proizvodstvo beskhlornykh kaliinykh udobrenii* (Manufacture of Chlorine-Free Potassium Fertilizers), Leningrad: Khimiya, 1980.
3. Parsons, S.A., Wall, F., Doyle, J., et al., *Environ. Technol.*, 2001, vol. 22, no. 11, pp. 1279–1286.
4. Regy, S., Mangin, D., Klein, J.P., and Lieto, J., *Phosphate Recovery by Struvite Precipitation in a Stirred Reactor*, Centre Europeen d'Etudes des Polyphosphates, 2002.
5. US Patent 4496526.
6. *X-ray Diffraction Data Cards*, Baltimore: ASTM, 1959, no. 20-685.
7. *Kratkaya khimicheskaya entsiklopediya* (Concise Chemical Encyclopedia), Knunyants, I.L., Ed., Moscow: Sov. Entsiklopediya, 1964, vol. 3.
8. Suschka, J., Kowalski, E., and Poplawski, S., *Study of the Effects of the Reactor Hydraulics on Struvite Precipitation at Municipal Sewage Works*, Centre Europeen d'Etudes des Polyphosphates, 2003.
9. *X-ray Diffraction Data Cards*, Baltimore: ASTM, 1959, no. 15-762.
10. Mitani, Y., Sakai, Y., Mishina, F., and Ishiduka, S., *Second Int. Conf. on Recovery of Phosphate from Sewage and Animal Wastes*, Amsterdam: Center for European Studies of Polyphosphates, March 12–13, 2001.

ISSN 1070-4272, Russian Journal of Applied Chemistry, 2006, Vol. 79, No. 9, pp. 1478–1484. © Pleiades Publishing, Inc., 2006.
Original Russian Text © E.D. Lodygin, V.A. Beznosikov, 2006, published in Zhurnal Prikladnoi Khimii, 2006, Vol. 79, No. 9, pp. 1494–1500.

ENVIRONMENTAL PROBLEMS OF CHEMISTRY AND TECHNOLOGY

^{13}C NMR and ESR Study of Structural and Functional Group Characteristics of Macromolecular Compounds of Soils

E. D. Lodygin and V. A. Beznosikov

Institute of Biology, Komi Scientific Center, Ural Division, Russian Academy of Sciences, Syktyvkar, Komi Republic, Russia

Received May 12, 2006

Abstract—The structure of macromolecular compounds of soils is studied by ^{13}C NMR and ESR. Data on the structural and functional group characteristics and paramagnetic activity of humus compounds may provide a basis for developing methodological approaches to parametric characterization of the environmental potential of the soil organic matter.

DOI: 10.1134/S1070427206090163

Characterization of the structure and functionalities of humus compounds, including the quantity into quality transformation, and development of theoretical principles for the soil organic matter are topical problems of the soil science. Studies of the structure of humic acids, including intramolecular ordering in systems that were previously considered as chaotic, may provide a basis for developing a quantitative approach to evaluation of the main environmental functions of soils.

Further progress of the chemistry of soil organic matter requires employment of up-to-date techniques for studying the molecular structure and functionalities of humus compounds (HCs) [1, 2]. The common methods ranging from characterization of the group and functional composition to examination of the properties of humus acids are arbitrary in many respects, resulting occasionally in discrepancy of both experimental results and their interpretation [3].

Therefore, in this study we examined the qualitative and quantitative composition of some molecular fragments of humic (HAs) and fulvic acids (FAs) by ^{13}C NMR and ESR.

EXPERIMENTAL

Humus compounds were studied with an example of soils of a microcatena (typical podzolic, podzolic surface-gleyic, and peaty-podzolic-gleyic soils), arable podzolic soil, and paleopedorelicts. The samples of paleopedorelicts were collected from the knap at the Maksimov Station of the Institute of Biology, Komi Science Center, Ural Division, Russian Academy of Sciences. The morphological description and physicochemical and biological characteristics of the investigated soils were reported elsewhere [4].

Samples of humic and fulvic acids were separated following Kononova and Bel'chikova [3]. The elemental analysis of HAs was determined on an EA 1110 CHNSO analyzer (Italy). The solid-state magic angle spinning (CPMAS) ^{13}C NMR spectra of humus compounds were recorded on a Bruker CXP-100 pulse NMR spectrometer (25.18 MHz). The ESR spectra were recorded on an SE/X2547 Radiopan spectrometer (microwave power in the cavity 20–40 mW; microwave frequency 9.372 GHz) using diphenylpicrylhydrazyl (DPPH) as a reference with fixed radical concentration. The concentration of paramagnetic centers in the samples was estimated relative to the reference peak intensity using the relationship $(\Delta H)^2 Y$, where ΔH and Y are the line width and amplitude, respectively. The absolute error of determination of the free radical concentration by ESR is 10–20% [5].

To study the structural features and functionalities of the organic matter of podzolic and peaty-podzolic-gleyic soils, we recorded the ^{13}C NMR spectra of HAs and FAs separated from the upper genetic horizons (Fig. 1).

As seen from Table 1, NMR spectroscopy allows identification of various functional groups and molecular fragments in HAs and FAs. The relative contents of the basic functional groups and molecular fragments of HAs and FAs were estimated from the NMR

spectra by integration of the areas under the corresponding peaks (Table 2).

Analysis of the ^{13}C NMR spectra of humus acids allowed assignment of chemical shifts to carbon atoms of various functional groups and molecular fragments of HAs and FAs (Table 1) [1, 4, 6, 7].

In analysis of the extensive information obtained from the ^{13}C NMR spectra, we used the aromaticity index defined as the ratio of the amount of the aromatic carbon atoms to the total amount of the aromatic and aliphatic carbon atoms [AR/(AR + AL)]. In this case, the signals of the aromatic carbon atoms were summed over the ranges 105–164 and 183–190 ppm [2, 8].

Comparative analysis of the molecular structures of humic and fulvic acids revealed that FAs are enriched with oxygen-containing fragments, which explains their higher solubility in water and mobility. High carboxy group content (up to 27.1%) causes high acid reactivity of FAs with respect to soil minerals, as well as the tendency to complexation with iron, aluminum, and other metal cations, resulting in the formation of soluble species. High content of the carbohydrate fragments (up to 23.2%) makes the FA molecules more preferable nutrient for soil microorganisms, as compared to HAs, the latter being constituted by more than half by aliphatic chains and aromatic fragments, so that their oxidation is less profitable [3].

The data obtained on the functionalities of humic acids show that, in all the soils studied, their structure considerably changes on passing from the organogenic to mineral horizon. Humic compounds of upper horizons (A_0 and O_1) demonstrate high aromaticity in both podzolic and peaty-podzolic-gleyic soils. The reason is that humus acids of the organogenic horizons are presented by not humic and fulvic acids proper, but by prohumic and profulvic acids, i.e., by the compounds that are still only slightly humified and preserve (at least partly) the molecular structure of the compounds composing the plant residues. Therefore, only the compounds extracted from the mineral horizons (A_1A_2h and A_2hg) represent, in fact, HAs and FAs.

Comparison of the molecular structure of HAs of variously hydromorphic soils shows that HAs extracted from podzolic soil are more enriched in aromatic fragments than HAs from peaty-podzolic-gleyic soil. Furthermore, for podzolic soil, we observed an increase in the fraction of oxygen-containing functional groups (COOR, C_{ar}=O, and C=O) in the HA molecules on passing from horizon A_0 to A_1A_2h. On the contrary, in peaty-podzolic-gleyic soil, the fraction of these groups decreases on passing from horizon O_1 to A_2hg (Table 2). The point is that, in podzolic soil, aerobic conditions typical of them favor oxidation reactions, while in peaty-podzolic-gleyic soil, in which anaerobiosis dominates, reduction reactions are preferable.

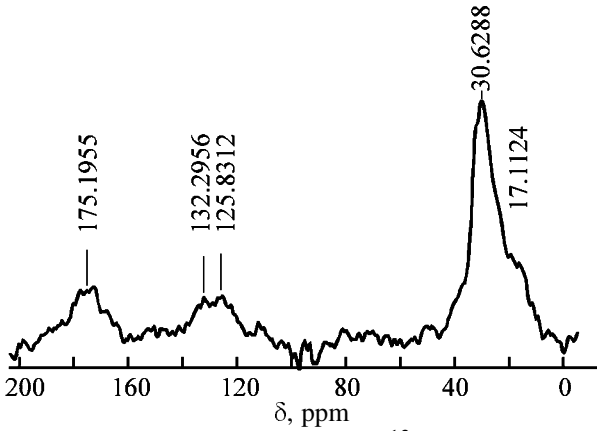


Fig. 1. Typical solid-state CPMAS ^{13}C NMR spectrum of humus compounds obtained with an example of humic acid separated from peaty-podzolic-gleyic soil (horizon A_2hg). (δ) Chemical shift; the same for Fig. 2.

The change in the functional group composition of FAs on passing from automorphic to hydromorphic soils is even more clearly pronounced. In this case, the tendency to increase in the aromaticity of FAs on passing from peaty-podzolic-gleyic soil to typical podzolic soil is preserved. The content of oxygen-containing groups also increases by 14.5% on passing from horizon A_0 to A_1A_2h in podzolic soil, but decreases by 5.2% in peaty-podzolic-gleyic soil on passing from horizon O_1 to A_2hg.

Thus, in podzolic soil, humification of plant

Table 1. ^{13}C chemical shifts in various molecular fragments of humus acids

δ, ppm	Molecular fragments
0–47	Aliphatic CH, CH_2, and CH_3 groups
47–60	C atoms of amino groups and –O–CH_3 moieties
60–105	CO groups of carbohydrates, alcohols, and ethers
105–144	C atoms of aromatic structures
144–164	C_{ar}–O of phenols
164–183	C atoms of carboxy groups
183–190	C=O groups of quinones
190–204	C=O groups of aldehydes and ketones

Table 2. Contents of molecular fragments in humic and fulvic acids, estimated from ^{13}C NMR data

Soil, horizon	Content of molecular fragments, %, in indicated range of chemical shift δ, ppm								Aromaticity, %
	0–47	47–60	60–105	105–144	144–164	164–183	183–190	190–204	
Humic acids									
Podzolic:									
A_0	22.4	8.1	12.8	33.5	10.0	11.3	0.5	1.4	44.0
A_1A_2h	40.7	8.6	8.9	18.8	7.1	12.1	1.7	2.1	27.6
Peaty-podzolic-gleyic:									
O_1	23.2	6.0	11.8	22.4	8.8	17.0	4.3	6.5	35.5
A_2hg	50.5	2.8	7.3	16.9	4.7	12.8	2.7	2.3	24.3
Fulvic acids									
Podzolic:									
A_0	23.3	6.6	23.2	18.6	7.4	19.6	0.6	0.7	26.6
A_1A_2h	25.1	6.4	18.6	10.3	4.2	25.0	3.2	7.2	17.7
Peaty-podzolic-gleyic:									
O_1	19.5	2.4	20.2	12.9	4.2	26.3	5.1	9.4	22.2
A_2hg	31.2	2.7	17.9	8.7	3.3	27.1	2.5	6.6	14.5

residues proceeds more intensively, promoting the formation of aggressive humus acids rich in oxygen-containing functional groups and aromatic fragments. On the contrary, humus compounds of peaty-podzolic-gleyic soil are characterized by lower aromaticity, consisting primarily of unoxidized aliphatic fragments, which, in combination with anaerobic conditions, favors gleyzation.

Comparative analysis of the experimental results obtained for humus acids of podzolic and peaty-podzolic soils of the north-east of the European part of Russia and of data on the functional group composition of humus compounds extracted from soils of other climatic zones showed that the investigated HA samples are richer in aromatic structures than spodisols (Spodic Cryosols), but poorer as compared to soils of south regions, such as grey forest soils and chernozems [1]. The indicated trends are associated with the humification rate: in north regions, this rate is lower, and in the south regions, higher, resulting in the latter case in the formation of more "mature" humus compounds [3].

To study the effect of farming, we examined HA samples extracted from horizon A_p of arable podzolic soil (Fig. 2). The effect of farming on the relative contents of functional groups and molecular fragments is shown in Fig. 3.

Comparison of data on the structure of HAs (Figs. 2, 3) shows that, on passing from virgin to arable podzolic soils, the total amount of aliphatic chains decreases, which is accompanied by an 8.4% increase in the aromatic fraction (aromaticity of HAs of arable soils is higher by a factor of 1.5). It was demonstrated that ploughing decreases the contents of COR groups of alcohols, ethers, and carbohydrates in the HA structure, which is due to the fact that farming enhances the microbiological activity, resulting in degradation of the readily hydrolyzable fraction of humus compounds consisting essentially of carbohydrate fragments.

Data on the functional group composition of the core of HAs of young soils and paleopedorelicts show (Fig. 3) that relict HAs differ significantly from young HAs. The 17% increase in the aromaticity of HAs of paleopedorelicts is accompanied by the increase in the fraction of oxidized fragments of both aliphatic (carbonyl and carboxy groups) and aromatic (phenolic and quinone fragments) nature. Furthermore, all the peaks in the ^{13}C NMR spectrum of relict HAs are relatively smoother, suggesting that the carbon skeleton of HAs in paleopedorelicts is characterized by higher thermodynamic stability and uniformity.

To determine the concentration of free radicals in humus compounds in relation to the degree of soil hydromorphism and amelioration, we recorded

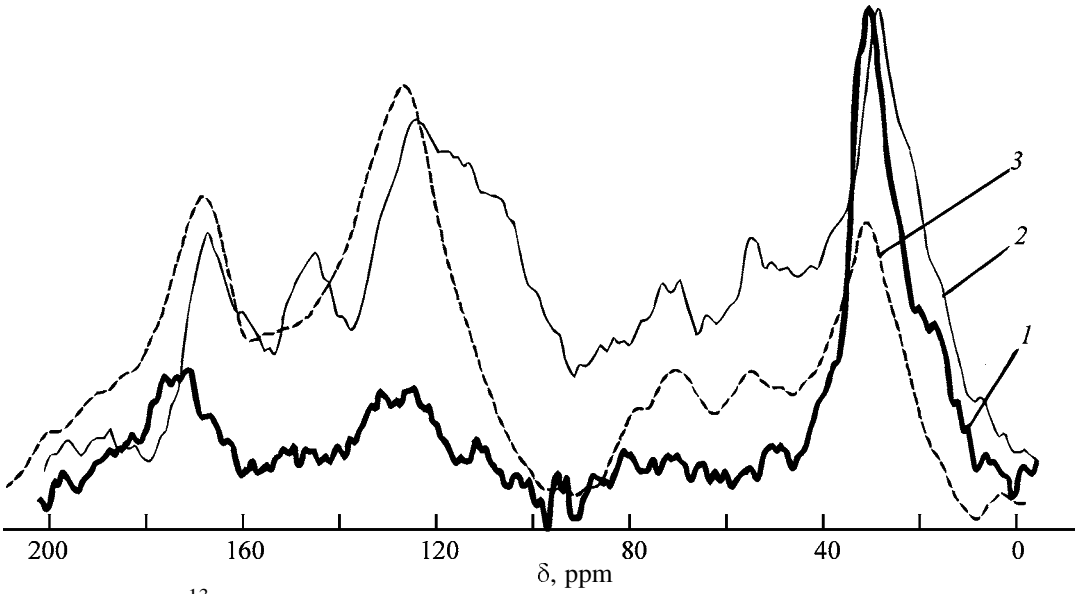


Fig. 2. Solid-state CPMAS ^{13}C NMR spectra of HA samples extracted from (*1*) virgin and (*2*) arable podzolic soils, and (*3*) paleopedorelict.

the ESR spectra of HAs and FAs. The spectra show a single broad peak with g = 2.003, clearly suggesting the presence of free radicals in the humus compounds. The indicated g factor is close to that of free electron (g = 2.0023), revealing either the occurrence of a strongly delocalized molecular orbital or of such state in which the orbital component of the magnetic moment of electron is close to zero [2, 9, 10]. The estimates made for the integral intensity of the absorption band allowed evaluation of the concentration of unpaired electrons in humus compounds. It was demonstrated that the concentration of paramagnetic centers in the HA molecules of peaty-podzolic-gleyic soil is nearly twice that in HAs of podzolic and podzolic surface-gleyic soils.

Figures 4 and 5 show the variation of the free radial concentration in HAs and FAs of variously hydromorphic soils. As can be seen (Fig. 4), the concentration of free radicals in HAs from any horizon of peaty-podzolic-gleyic soil increases with increasing soil moisture content. This is caused by the biohydrothermal conditions of humus formation in peaty-podzolic-gleyic soil, under which all the biochemical processes are inhibited, thus favoring the accumulation of free radicals in the HA molecules. In the three-component soil catena of the top soil (typical podzolic–podzolic surface-gleyic–peaty-podzolic-gleyic), podzolic surface-gleyic soil is found to be similar to typical podzolic soils in the concentration of paramagnetic centers in HAs and FAs. It was demonstrated that, for all the investigated soils, the free radical concentration in HAs decreases with the depth of the soil profile, suggesting higher thermodynamic stability of the HA molecules of the mineral horizons, as compared to HAs of the organogenic horizons. The only exception is HAs of the litter and peaty soil in which the free radical concentration is lower than in the underlying horizons. Evidently, this can be

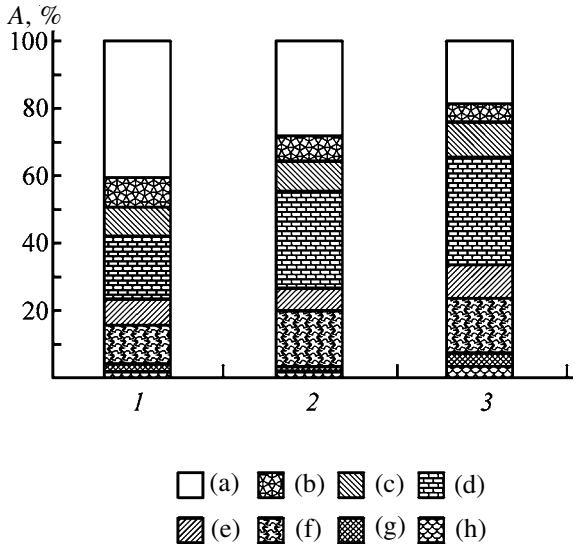


Fig. 3. Relative contents of structural fragments A in HA samples extracted from (*1*) virgin and (*2*) arable podzolic soils, and (*3*) paleopedorelict. (a) Aliphatic CH, CH_2, and CH_3 groups; (b) C atoms of amino groups and O–CH_3 structures; (c) COR groups of carbohydrates, alcohols, and ethers; (d) C atoms of aromatic structures; (e) C_{ar}–O of phenols; (f) COOR groups; (g) C_{ar}=O groups of quinones; and (h) C=O groups of aldehydes and ketones.

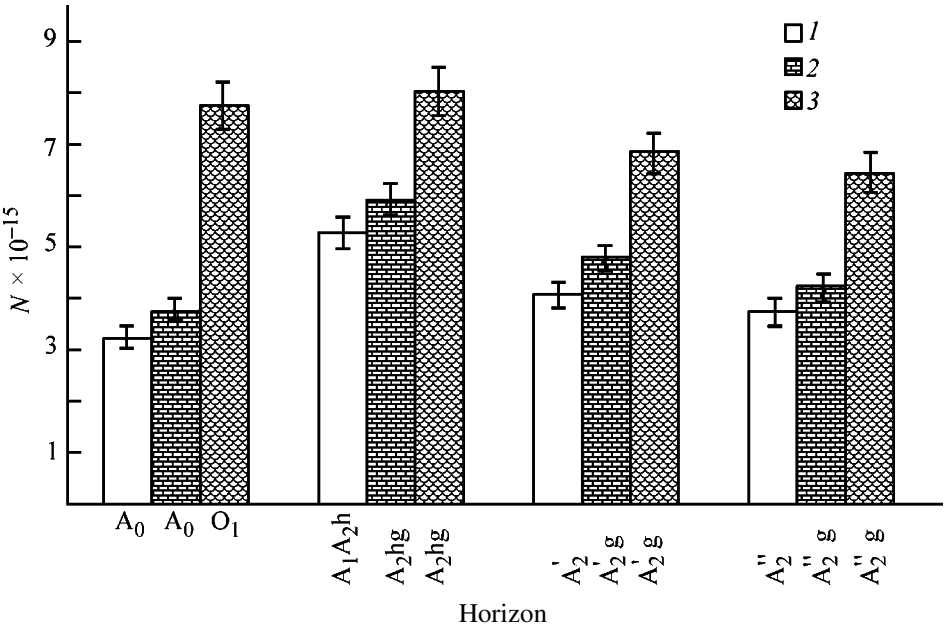


Fig. 4. Concentration of free radicals N in humic acids of variously hydromorphic soils: (*1*) podzolic, (*2*) podzolic surface-gleyic, and (*3*) peaty-podzolic-gleyic (n = 5, P = 0.95); the same for Fig. 5.

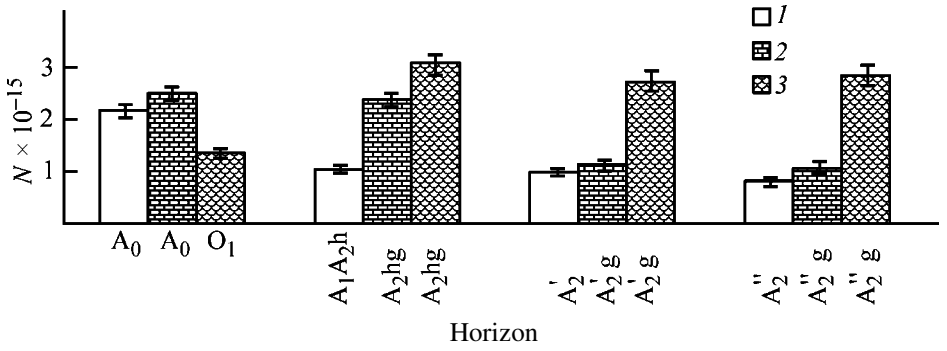


Fig. 5. Concentration of free radicals N in fulvic acids of variously hydromorphic soils.

attributed to the fact that these HAs are actually represented by prohumic acids, and the free radical content in their structure is caused primarily by the properties of the litter input. Somewhat different trends were observed for the FA samples (Fig. 5). In FAs of podzolic soils, the free radical concentration in the organogenic horizons is more than twice that in the mineral horizons. Therefore, it may be concluded that, in podzolic and podzolic surface-gleyic soils, FAs of the mineral horizons are more thermodynamically stable than those of the organogenic horizons.

In peaty-podzolic-gleyic soil, on the contrary, the amount of paramagnetic centers in FAs abruptly increases on passing from the organogenic (O_1) to mineral (A_2hg) horizon, and then slightly decreases with the depth of the soil profile, i.e., the trend in the variation of the free radical concentration in FAs and HAs of peaty-podzolic-gleyic soil with depth is similar.

To study the effect of farming on the concentration of free radicals in humus acids, we examined the HA and FA samples extracted from arable podzolic soil. The results show that ploughing has a stronger effect on the free radical concentration in FAs (Table 3).

Table 3 shows that the concentration of paramagnetic centers in HAs of the plough layer approximately corresponds to the mean concentration of free radicals in horizons A_0 and A_1A_2h. Unlike HAs, FAs of arable podzolic soil are less thermodynamically stable, demonstrating a stronger tendency to biodegradation. In turn, this causes more extensive transformation of the FA molecules in the course of soil

Table 3. Concentration of free radicals in humus acids

Soil, horizon	Free radical concentration $N \times 10^{-15}$, spin g^{-1}	
	HAs	FAs
Podzolic (virgin):		
A_0	3.24 ± 0.19	2.17 ± 0.13
A_1A_2h	5.26 ± 0.3	1.05 ± 0.06
Podzolic (arable), A_p	4.05 ± 0.24	Traces
Paleopedorelict, A_b	1.45 ± 0.09	Traces

improvement, resulting in a significant decrease of the free radical concentration (to trace amounts). There is no common view of the effect of soil improvement on the free radical concentration in humus acids. For example, Chukov believes that the concentration of paramagnetic centers in HAs is inversely proportional to their biothermodynamic stability and degree of humification, and in ploughing, the paramagnetic activity of humus compounds decreases [2]. The opinion of other researchers is that inclusion of residues of some crops in humus matter could increase the amount of free radicals [11].

Data on structural and functional group characteristics and paramagnetic activity of humus compounds may provide a basis for developing methodological approaches to parametric characterization of the environmental potential of the soil organic matter. Some attempts to develop such approaches for soils were made previously [2]. Our thought is that the environmental potential of the soil organic matter can be evaluated from combined data on the structural and functional group characteristics and paramagnetic activity of humus compounds.

CONCLUSIONS

(1) In the structure of humus acids we identified carboxy, carbonyl, and aliphatic groups of alcohols, ethers, and carbohydrates; and phenolic, quinone, and aromatic fragments. Aliphatic structures dominate in fulvic acids, and aromatic structures, in humic acids.

(2) Excessive moistening affects not only the amount of accumulated humus compounds, but also their molecular structure: in semihydromorphic peaty-podzolic-gleyic soil, it stimulates accumulation of humus compounds enriched in aliphatic structures. In combination with anaerobic conditions, the presence of unoxidized aliphatic fragments in the structure of humus acids promotes gleyzation. Soil development promotes transformation of the molecular structure of humus compounds, reflected in a relative increase in the fraction of aromatic fragments and decrease in the fraction of the carboxy and ester groups. As a result, acids become less aggressive, which favors their accumulation in the plough layer.

(3) Humic acids of paleopedorelicts are enriched in aromatic fragments and oxygen-containing functional groups, which is indicative of their thermodynamic stability.

(4) The concentration of free radicals in humic acids of the investigated soils is higher by a factor of 1.5–5 than that in fulvic acids. As a result, they demonstrate a strong tendency to polymerization and complexation by the radical mechanism. The concentration of paramagnetic centers in humic acids decreases with depth, suggesting higher stability of their molecules in the mineral horizons as compared to humic acids from the organogenic horizons.

(5) Farm production decreases the paramagnetic activity of humus compounds by more than 20% as compared to the corresponding virgin soils as a result of accumulation of more humified (more thermodynamically stable) compounds in the plough layer.

ACKNOWLEDGMENTS

The study was financially supported by the Presidium of the Russian Academy of Sciences (State Contract no. RES-3-7-05) and by the Russian Foundation for Basic Research (projects nos. 04-04-96015-r2004Urals, 04-04-49000).

REFERENCES

1. Chukov, S.N., *Pochvovedenie*, 1998, no. 9, pp. 1085–1093.
2. Chukov, S.N., *Strukturno-funktsional'nye parametry organicheskogo veshchestva pochv v usloviyakh antropogennogo vozdeistviya* (Structural and Functional Parameters of Soil Organic Matter under Human Impact), St. Petersburg: Sankt-Peterb. Gos. Univ., 2001.
3. Orlov, D.S., *Pochvovedenie*, 1998, no. 9, pp. 1049–1057.
4. Lodygin, E.D. and Beznosikov, V.A., *Geoderma*, 2005, vol. 127, nos. 3–4, pp. 253–262.

5. Neto, L.M., Nascimento, O.R., Talamoni, J., and Poppi, N.R., *Soil Sci*., 1991, vol. 151, no. 5, pp. 369–373.
6. Kanitskaya, L.V., Ivanova, N.V., Gorokhova, V.G., and Babkin, V.A., *Khim. Inter. Ustoich. Razv*., 1996, no. 4, pp. 275–279.
7. Kanitskaya, L.V., Medvedeva, S.A., Volchatova, I.V., and Babkin, V.A., *Khim. Inter. Ustoich. Razv*., 1997, no. 5, pp. 599–603.
8. Wershaw, R.L., Leenheer, J.A., Kennedy, K.R., and Noyes, T.I., *Soil Sci*., 1996, vol. 161, pp. 667–679.
9. Liang, B.C., Gregorich, E.G., Schnitzer, M., and Shulten, H.R., *Soil Sci. Soc. Am. J*., 1996, vol. 60, pp. 1758–1763.
10. Lodygin, E.D., Beznosikov, V.A., and Chukov, S.N., *Latv. Univ. Raksti*, 2005, no. 692, pp. 49–55.
11. Neto, L.M., Enrique, A.A., and Gomes, T.D., *Soil Sci*., 1994, vol. 157, no. 6, pp. 365–372.

ISSN 1070-4272, Russian Journal of Applied Chemistry, 2006, Vol. 79, No. 9, pp. 1485–1489. © Pleiades Publishing, Inc., 2006.
Original Russian Text © K.K. Kalnin'sh, S.G. Semenov, 2006, published in Zhurnal Prikladnoi Khimii, 2006, Vol. 79, No. 9, pp. 1501–1505.

MACROMOLECULAR CHEMISTRY AND POLYMERIC MATERIALS

Mechanism of Initiation of Cationic and Anionic Polymerization of Methylenecyclobutenes

K. K. Kalnin'sh and S. G. Semenov

Institute of Macromolecular Compounds, Russian Academy of Sciences, St. Petersburg, Russia
St. Petersburg State University, St. Petersburg, Russia

Received June 13, 2006

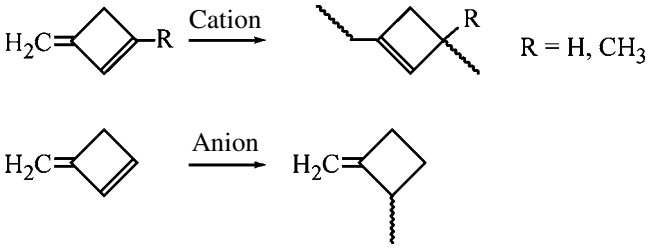
Abstract—The mechanism of initiation of cationic and anionic polymerization of methylenecyclobutenes, yielding different polymeric products, was studied quantum-chemically on the basis of electronic excitation in an elementary chemical process, using the formalism of free valence indices. In the cationic polymerization, the polymer chain consists of cyclobutene fragments linked by methylene bridges, and in anionic polymerization, of saturated cyclobutane fragments linked directly to each other and containing exocyclic methylene substituents.

DOI: 10.1134/S1070427206090175

Cationic and anionic polymerizations are traditionally belileved to occur by essentially different mechanisms. In the first case, the monomer molecule adds to the electrophilic carbon atom C^+ (C^+–X^- in the general case) of the propagating chain, and in the second case it is inserted into the C^-–Me^+ bond [2]. The cationic polymerization is initiated by Friedel–Crafts acid catalysts and Brønsted acids acting as electron acceptors, whereas anionic polymerization is initiated by electron-donor compounds, e.g., organolithium compounds. At the same time, both mechanisms have common features; their elementary process involves electron transfer (excitation) [3] giving rise to chemically active radical or radical ion species. Stable reaction products are formed by recombination of radical species in accordance with the free valence indices on atoms of the reacting molecules.

Previously we studied the mechanism of polymerization of 1-cyanobicyclobutane and 1-cyano-3-vinylbicyclobutane [4] involving thermal electronic excitation of monomer molecules into the low-lying biradical state. It is known that incorporation of cyclic fragments in a polymer chain increases the melting point and crystallinity and improves the mechanical properties of polymeric films, fibers, and structural materials [5]. Interesting possibilities for thermochemical and photochemical modification of polymers, in particular, for imparting to them electrical conductivity by doping with electron-donor or electron-acceptor admixtures, are provided by unsaturated C=C bonds present in the polymers.

This paper deals with a theoretical analysis of specific features of cationic and anionic initiation of polymerization of methylenecyclobutenes. In this case, the products formed with anionic and cationic initiators are different [5]:



The observed difference can be readily accounted for using the formalism of the free valence indices and assuming the electron transfer (excitation) in the elementary reaction step.

Ab initio quantum-chemical calculations of the electronic and steric structure and vibration spectra were made by restricted and unrestricted Fartree–Fock methods for closed (RHF) and open (ROHF) electronic shells using the GAMESS program package [6] (version pcGAMESS 6.2 [7]) in the 6-31G* basis set.

Chemical bonds between atoms are characterized by equilibrium internuclear distances and bond indices [8, 9]:

$$I_{A,B} = \mathrm{Spur}[(PS)_{AB}(PS)_{BA}], \quad (1)$$

where A and B are atom numbers.

Matrix P in formula (1) consists of coefficients of expansion of the electron density matrix $\rho(\mathbf{r}|\mathbf{r}')$ [10]

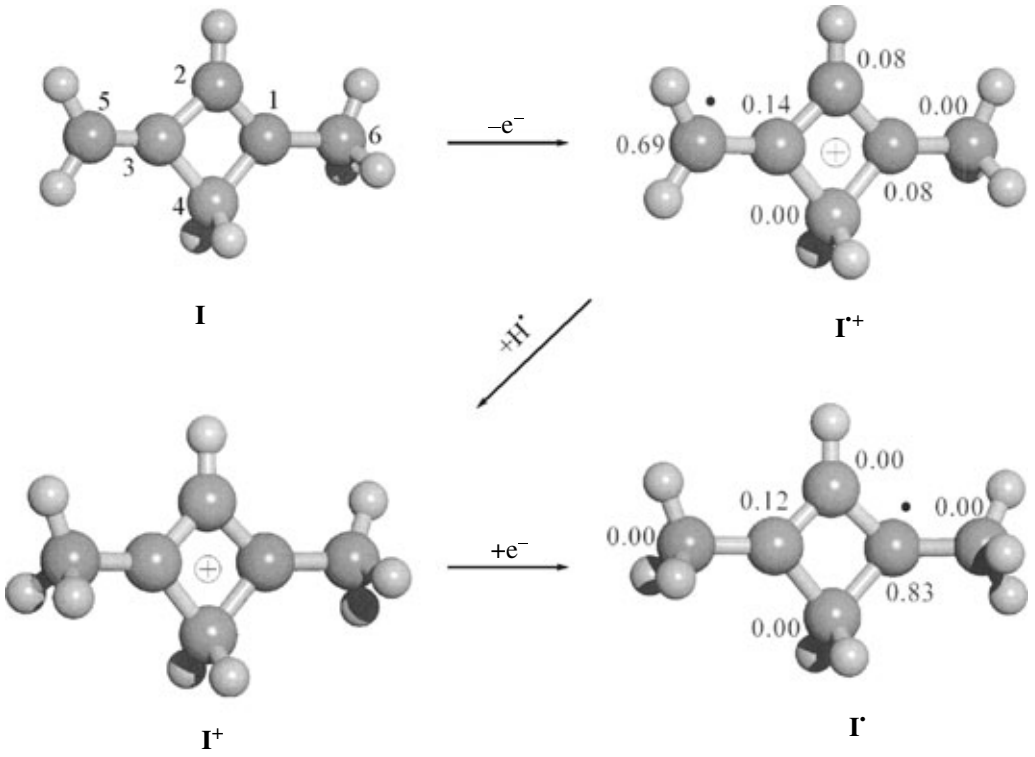


Fig. 1. Structure of primary intermediates of cationic polymerization of 1-methyl-3-methylenecyclobutene and distribution of the free valence in the triplet state.

in terms of pair products of atomic orbitals; S is a metric matrix. The diagonal elements of the matrix product PS are identified with the electronic populations of AOs, $n_a^{\mathrm{M}} = (PS)_{aa}$ [11, 12].

Comparison of the sum of the bond indices with the valence index suggested in [13],

$$V_A = \mathrm{Spur}[2(PS)_{AA} - (PS)_{AA}(PS)_{AA}] \quad (2)$$

allows determination of the free valence of each atom as the difference

$$F_A = V_A - \sum_{B(\neq A)} I_{AB}. \quad (3)$$

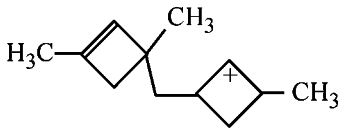
The indices F_A, designated as D_A, were suggested for the first time in [14] without connection with the valence indices V_A.

Another quantity of interest is the total valence of a molecule or radical, defined as the sum of the valences of atoms minus doubled sum of the indices of the intraradical chemical bonds [15]:

$$V_{\mathrm{mol}} = \mathrm{Spur}(2PS - PSPS) = \sum_A (V_A - \sum_{B(\neq A)} I_{AB}) = \sum_A F_A = F_{\mathrm{mol}}. \quad (4)$$

In accordance with formula (4), free valences F_{A} are additive quantities characterizing the distribution of the total valence of a chemical compound (free radical or excited molecule) and revealing its reactive centers. Not also that the same quantity $V_{\mathrm{mol}} = F_{\mathrm{mol}}$ is obtained from the alternative formula defining the valence of an atom represented as a region of a real three-dimensional space [16].

Cationic polymerization of 1-methyl-3-methylenecyclobutene. Cationic (acid) initiation involves as the first step oxidation of the monomer (1-methyl-3-methylenecyclobutene **I**) to radical cation $\mathbf{I}^{\bullet+}$, which in the second step recombines with the oxidant-initiator in the form of free radical (in Fig. 1, with the hydrogen atom $H^{\bullet}$). Then the resulting cation $\mathbf{I}^{+}$, which is a strong electron acceptor, oxidizes another molecule of monomer **I** to form a diradical cation pair $\mathbf{I}^{\bullet}\mathbf{I}^{\bullet+}$. Recombination of its constituent radicals in accordance with the free valence distribution (Fig. 1) gives as the reaction product 1-methyl-3-methylenecyclobutene dimer in the cationic form, $\mathbf{II}^{+}$:



$\mathbf{II}^{+}$

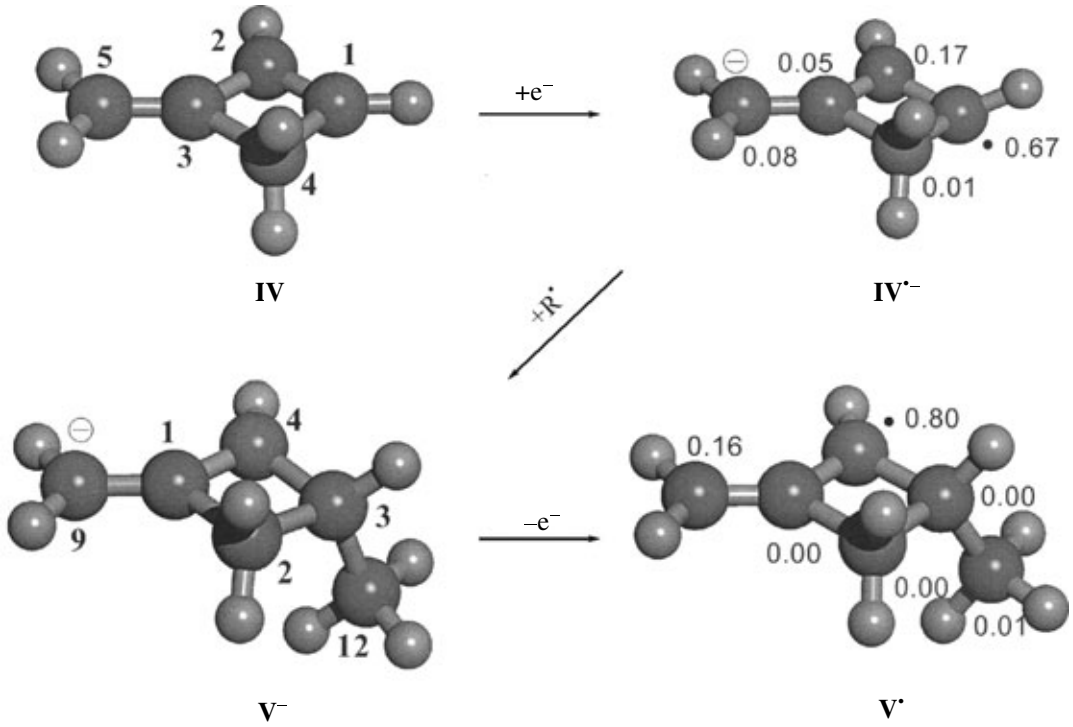
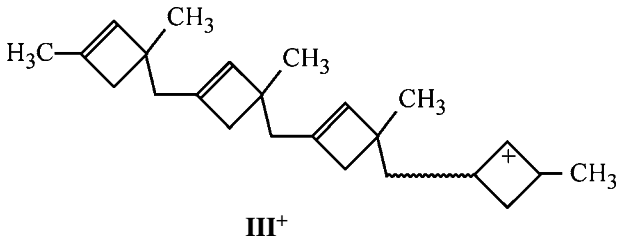


Fig. 2. Structure of primary intermediates of anionic polymerization of methylenecyclobutene and distribution of the free valence in the triplet state. Structures **V** and **V•** are shown with methyl radical as R•.

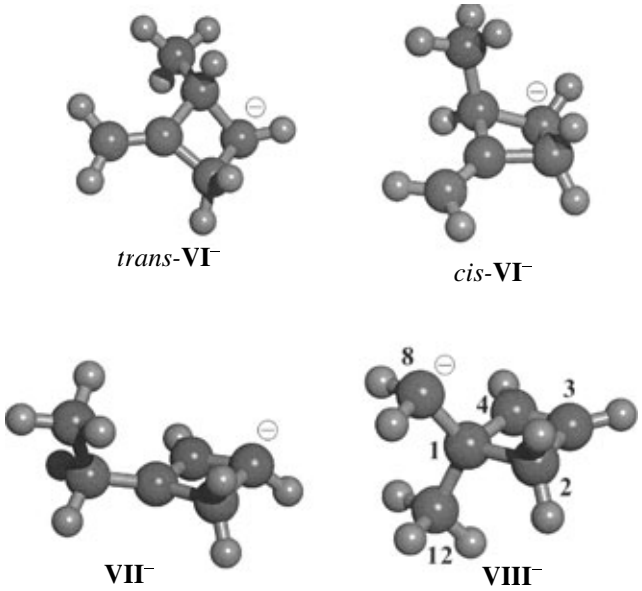
At a sufficiently high concentration of the monomer in solution, dimeric cation $\mathbf{II}^+$ can oxidize new molecules of 1-methyl-3-methylenecyclobutene, with the propagation of the polymer chain by the mechanism shown in Fig. 1. The resulting polymer consists of cyclobutene fragments linked by methylene bridges:



$\mathbf{III}^+$

Anionic polymerization of methylenecyclobutenes. Anionic initiation with organolithium compounds LiR involves as the first step reduction of the monomer (methylenecyclobutene **IV**) to radical anion $\mathbf{IV}^{\bullet -}$. In the second step, radical anion $\mathbf{IV}^{\bullet -}$ recombines with radical R• (methyl radical in Fig. 2). In accordance with the free valence distribution, this should lead to the formation of anion $\mathbf{V}^-$.

Alternative pathways of addition of radical R• lead to the isomeric anions *trans*-$\mathbf{VI}^-$, *cis*-$\mathbf{VI}^-$, $\mathbf{VII}^-$, and $\mathbf{VIII}^-$ (Fig. 3) whose energies are higher than that of anion $\mathbf{V}^-$ in a vacuum by 22.5, 24.4, 23.8, and 33.6 kcal mol^{-1}, respectively. Taking into account the hydrocarbon medium as a polarizable continuum (PCM) with the dielectric characteristics of heptane alters these differences insignificantly: to 21.6, 23.2, 22.7, and 31.2 kcal mol^{-1}, respectively. Thus, both



trans-$\mathbf{VI}^-$ *cis*-$\mathbf{VI}^-$ $\mathbf{VII}^-$ $\mathbf{VIII}^-$

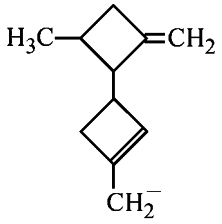
Fig. 3. Structure of anions $\mathbf{VI}^-$, $\mathbf{VII}^-$, and $\mathbf{VIII}^-$ (one of two possible enantiomers is shown).

Charges on carbon atoms in methylenecyclobutene **IV** and intermediates $\mathbf{V}^-$ and $\mathbf{VIII}^-$ (for atom numbering, see Figs. 2 and 3)

Species	C^1	C^2	C^3	C^4	C^5	C^8	C^9	C^{12}
IV	–0.20	–0.17	**+0.10**	–0.36	–0.48			
$\mathbf{V}^-$	+0.24	–0.35	–0.11	–0.42			**–0.67**	–0.44
VIII	+0.04	–0.31	–0.23	–0.12		**–0.61**		–0.44

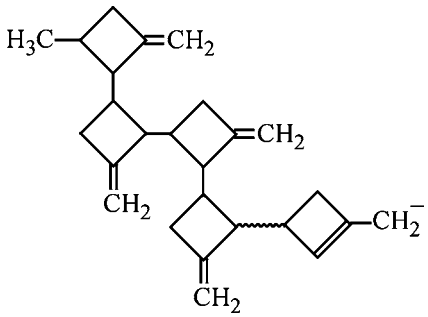
methods for determination of the possible products of the radical recombination, use of the free valence indices and direct calculation of the energy of the products, give the same result: Anion $\mathbf{V}^-$ should be the only reaction product.

Then anion $\mathbf{V}^-$ as a strong electron donor reduces another molecule of monomer **IV** to give a diradical anion pair $\mathbf{V}^{\bullet}\mathbf{V}^{\bullet-}$. The recombination of its constituent radicals in accordance with the free valence distribution (Fig. 2) leads to methylenecyclobutene dimer in the anionic form $\mathbf{IX}^-$:



$\mathbf{IX}^-$

At a sufficiently high concentration of the monomer in solution, dimeric anion $\mathbf{IX}^-$ can reduce new molecules of methylenecyclobutene, with the propagation of the polymer chain by the mechanism similar to that shown in Fig. 2. The resulting polymer, in agreement with the experimental data [5], consists of cyclobutane fragments linked directly to each other and containing exocyclic methylene groups:



$\mathbf{X}^-$

It should be noted that, when the reaction centers in the anionic polymerization of methylenecyclobutene **IV** are revealed on the basis of atomic charges (see table), in accordance with popular views, formation of anion $\mathbf{VIII}^-$ would be expected; the energy of this species is considerably higher than that of $\mathbf{V}^-$, and therefore its formation is improbable. If anion $\mathbf{VIII}^-$ were formed despite its relatively high energy, the largest (in the absolute value) negative charge in it (–0.61) would be localized on the exocyclic C^8 atom (Fig. 3), and, according to the charge control principle, the chain would propagate just at this atom.

Application of the charge control principle to anionic intermediate $\mathbf{V}^-$ leads to the same erroneous conclusion that the exocyclic carbon atom is incorporated in the backbone. Indeed, in $\mathbf{V}^-$, the C^9 atom bears the largest (in the absolute value) negative charge (–0.69) (Fig. 2). However, according to the experimental data [5], actually reactive in the polymerization of methylenecyclobutene **IV** is the C^4 atom characterized by the largest free valence (0.80) in radical intermediate $\mathbf{V}^{\bullet}$ arising from the intermolecular electron transfer.

CONCLUSIONS

(1) The role of electron transfer between the monomer and initiator as primary elementary step of the anionic and cationic polymerization is demonstrated by the example of methylenecyclobutenes.

(2) The structure of the polymer predicted on the basis of a quantum-chemical calculation of the free valence indices in radical intermediates of the anionic and cationic polymerization is consistent with the experimental data.

(3) Two procedures for quantum-chemical determination of the reaction product, by calculation of the free valence of the radical intermediates and by direct calculation of the energies of the expected products, give the same result.

REFERENCES

1. Kennedy, J.P., *Cationic Polymerization of Olefins: A Critical Inventory*, New York: Wiley, 1975.
2. Szwarc, M. and Van Beylen, M., *Ionic Polymerization*

and Living Polymers, New York: Chapman and Hall, 1993.

3. Kalnin'sh, K.K., *Elektronnoe vozbuzhdenie v khimii* (Electronic Excitation in Chemistry), St. Petersburg: Sankt-Peterb. Gos. Univ. Tekhnol. i Dizaina, 1998.
4. Kalnin'sh, K.K. and Semenov, S.G., *Zh. Prikl. Khim.*, 2005, vol. 78, no. 7, pp. 1157–1164.
5. Hall, H.K., Jr. and Ykman, P., *J. Polym. Sci., Macromol. Rev.*, 1976, vol. 11, pp. 1–44.
6. Schmidt, M.W., Baldridge, K.K., Boatz, J.A., et al., *J. Comput. Chem.*, 1993, vol. 14, no. 11, pp. 1347–1363.
7. Granovsky, A.A., http://classic.chem.msu.su/gran/gamess/index.html.
8. Giambiagi, M., Giambiagi, M., Grempel, D.R., and Heymann, C.D., *J. Chim. Phys.*, 1975, vol. 72, no. 1, pp. 15–22.
9. Giambiagi, M.S. de, Giambiagi, M., and Jorge, F.E., *Z. Naturforsch. (a)*, 1984, vol. 39, pp. 1259–1273.
10. McWeeny, R., *Rev. Mod. Phys.*, 1960, vol. 32, no. 2, pp. 335–369.
11. McWeeny, R., *J. Chem. Phys.*, 1951, vol. 19, pp. 1614–1615.
12. Mulliken, R.S., *J. Chem. Phys.*, 1955, vol. 23, pp. 1833–1840.
13. Dmitriev, I.S. and Semenov, S.G., *Kvantovaya khimiya – ee proshloe i nastoyashchee: Razvitie elektronnykh predstavlenii o prirode khimicheskoi svyazi* (Quantum Chemistry—Its Past and Present: Development of Electronic Concepts of the Nature of Chemical Bond), Moscow: Atomizdat, 1980.
14. Takatsuka, K., Fueno, T., and Yamaguchi, K., *Theor. Chim. Acta*, 1978, vol. 48, pp. 175–183.
15. Tulub, A.V. and Semenov, S.G., *Valentnost' (Sovremennye aspekty staroi problemy)* (Valence (Modern Aspects of Old Problem)), Leningrad: Znanie, 1989.
16. Semenov, S.G., *Vestn. Leningr. Gos. Univ.*, 1987, no. 11, pp. 97–101.

ISSN 1070-4272, Russian Journal of Applied Chemistry, 2006, Vol. 79, No. 9, pp. 1490–1493. © Pleiades Publishing, Inc., 2006.
Original Russian Text © G.M. Pavlov, I.I. Zaitseva, A.S. Gubarev, I.I. Gavrilova, E.F. Panarin, 2006, published in Zhurnal Prikladnoi Khimii, 2006, Vol. 79, No. 9, pp. 1506–1509.

MACROMOLECULAR CHEMISTRY AND POLYMERIC MATERIALS

Diffusion-Viscometric Analysis and Conformational Characteristics of Sodium Polystyrenesulfonate Molecules

G. M. Pavlov, I. I. Zaitseva, A. S. Gubarev, I. I. Gavrilova, and E. F. Panarin

Fock Research Institute of Physics, St. Petersburg State University, St. Petersburg, Russia
Institute of Macromolecular Compounds, Russian Academy of Science, St. Petersburg, Russia

Received June 5, 2006

Abstract—Samples of sodium polystyrenesulfonate of molecular weights varying in a 20-fold range were synthesized. The hydrodynamic behavior of the samples was studied in a 0.2 M NaCl solution in which the initial polyelectrolyte effects are suppressed. Relationships between the molecular weight and the translational friction coefficient and intrinsic viscosity were obtained. The theory describing the hydrodynamic behavior of wormlike chains with taking into account both the percolation effects and the excluded-volume effects was applied to estimation of the length of the statistical segment and the cross section of the sodium polystyrenesulfonate molecules in 0.2 M NaCl solution.

DOI: 10.1134/S1070427206090187

Ionic macromolecules, polyelectrolytes, play an important role in animate nature and in various industrial processes [1–4]. Studies of polyelectolytes are of great interest, since their macromolecules are represented by chains with variable equilibrium rigidity governed by the linear charge density, ionic strength of solution, and the structure of the monomeric unit. Recently the interest in studies of charged macromolecules increased again; new theoretical approaches were developed that describe the behavior of this class of polymers, more complex than neutral polymers [1–6]. At the same time, systematic quantitative studies of the molecular characteristics and properties of polyelectrolytes are much less in number than those in the databank describing the behavior of neutral polymers.

In this study we extended the scope of many-year studies of water-soluble polymers and examined the hydrodynamic and molecular characteristics of sodium polystyrene-4-sulfonate (SPSS).

EXPERIMENTAL

Polymerization of styrene-4-sulornate was carried out in an H_2O : DMF = 1 : 1 solution at 60°C for 24 h with various concentrations of AIBN in sealed ampules. The resulting polymer was precipitated into acetone and dried in a vacuum to constant weight.

The hydrodynamic characteristics were studied in 0.2 M NaCl solution. The translational diffusion was studied in a Tsvetkov's diffusometer [12] by the classical method of formation of solution–solvent boundary, which was fixed at regular intervals with a polarization interferometer [12, 13]. The diffusion interferograms were processed by the maximal ordinate and area method [12]. The diffusion coefficient $D = (\Delta\sigma^2/\Delta t)/2$ was estimated from the slope of the experimental dependences of the variance σ^2 of the diffusion boundary on the time of experiment t (Fig. 1).

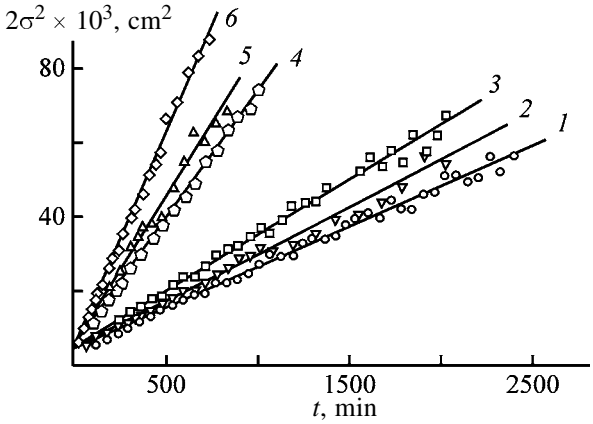


Fig. 1. Dependence of the variance of the diffusion boundary σ^2, cm^2, on the diffusion time t, min, for sodium polystyrene sulfonate samples in 0.2 M NaCl solution at 25°C. Figures at straight lines correspond to sample nos. in the table; the same for Figs. 2 and 3.

Polymerization conditions for sodium styrene-4-sulfonate in H_2O : DMF = 1 : 1, hydrodynamic characteristics of sodium polystyrenesulfonate samples in 0.2 M NaCl solution, and their molecular weights

Sample no.	Solution concentration	AIBN	Yield	$D_0 \times 10^7$, $cm^2\ s^{-1}$	$\Delta n/\Delta c$	[η]	k'	$M_{D_\eta} \times 10^{-3}$, g mol^{-1}
	%				$cm^3\ g^{-1}$			
1	40	0.2	65	0.90	0.142	172	0.34	920
2	30	0.2	55	1.10	0.123	117	0.40	740
3	29	0.3	90	1.25	0.143	117	0.29	500
4	12	0.5	90	2.85	0.147	43.5	0.33	115
5	20	3	99	3.25	0.142	29.8	0.31	110
6	17	5	99	4.75	0.145	22.0	0.32	50

The table presents the refractive index increment $\Delta n/\Delta c$, estimated from the average areas enclosed by the diffusion curves (Fig. 2). The average refractive index increment $\Delta n/\Delta c$ was estimated at 0.144 ± 0.002 $cm^3\ g^{-1}$. The intrinsic viscosities [η] were determined from the Huggins plots [12] $\eta_{sp} = [\eta] + k'[\eta]^2 c$ (Fig. 3), where $h_{sp} \equiv (\eta - \eta_0)/\eta_0 = (t - t_0)/t_0$; η and η_0, viscosity of the solution and solvent, respectively; and t and t_0, time of flow of the solution and solvent in an Ostwald viscometer, respectively.

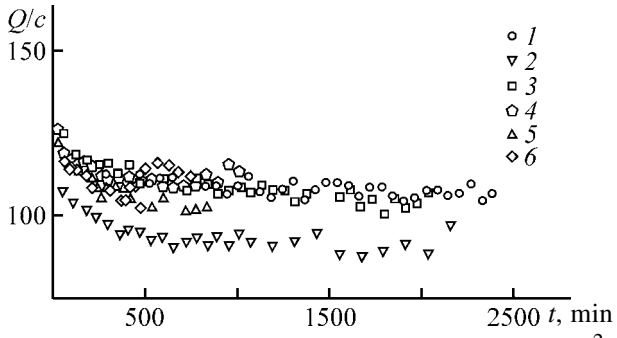


Fig. 2. Area enclosed by the interference curve of Q, cm^2, divided by the polymer concentration c, g cm^{-3}, vs. the diffusion time t.

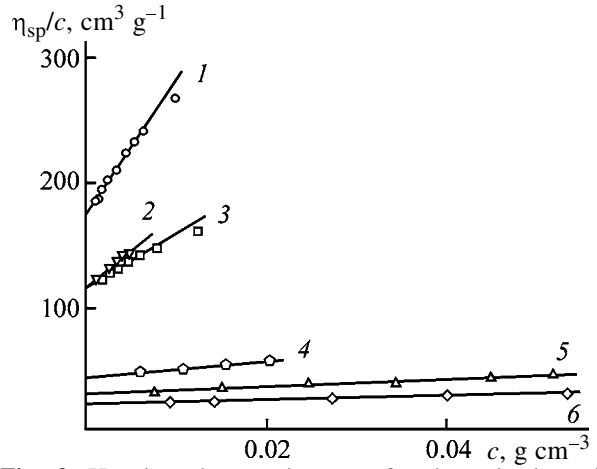


Fig. 3. Huggins plots η_{sp}/c vs. c for determination of the intrinsic viscosity of sodium polystyrenesulfonate in 0.2 M NaCl solution at 5°C.

The intrinsic viscosities [η] and the Huggins parameters k' are presented in the table. The average k' was estimated at 0.32 ± 0.02.

Based on the translational diffusion coefficient D_0 and the intrinsic viscosity [η], using the concept of hydrodynamic invariant A_0 and the average A_0 for flexible-chain polymers of 3.2×10^{-10} g $cm^2 \times (s^2\ deg\ mol^{1/3})^{-1}$ [12], we estimated the molecular weights of the samples examined using the relationship

$$M_{D_\eta} = (A_0 T/\eta_0 D_0)^3/[\eta],$$

where T is absolute temperature, and η_0, viscosity of the solvent (in our case, $\eta_0 = 0.91 \times 10^{-2}$ P).

In calculation of the molecular weight M we used the [η] values expressed in 100 $cm^3\ g^{-1}$ units. Figure 2 shows that the areas enclosed by the diffusion curves weakly change with the diffusion time (after the first 3 h of diffusion), which indicates that the samples are relatively monodisperse.

Analysis of the log–log plots of M vs. D_0 and M vs. [η] (Fig. 4) yields a relationship similar to the Kuhn–Mark–Houwink–Sakurada relationship for sodium polystyrenesulfonate molecules in 0.2 M NaCl solution at 25°C:

$$[\eta] = 1.17 \times 10^{-2} M^{0.69 \pm 0.06} \quad (r = 0.9849),$$

$$D_0 = 2.18 \times 10^{-4} M^{-(0.57 \pm 0.02)} \quad (r = -0.9977).$$

In view of the error in determination, the exponents relating the intrinsic viscosities and the diffusion coefficients b_η and b_D to the molecular weight satisfy the relationship $|b_D| = (b_\eta + 1)/3$, typically valid for linear polymer homologs.

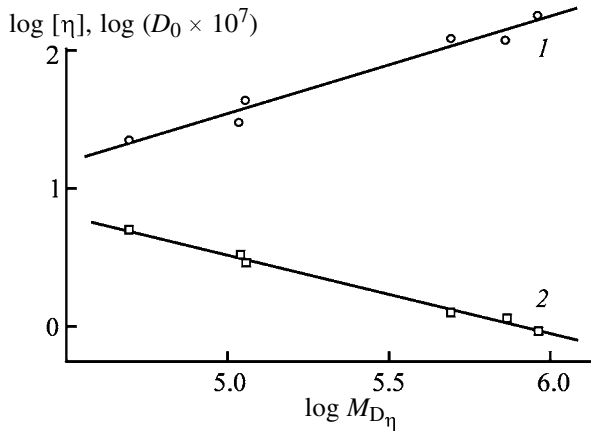


Fig. 4. Kuhn–Mark–Houwink–Sakurada plots (*1*) $\log[\eta]$–$\log M_{D_\eta}$ and (*2*) $\log(D_0 \times 10^7)$–$\log M_{D_\eta}$ for sodium polystyrenesulfonate in 0.2 M NaCl solution at 25°C.

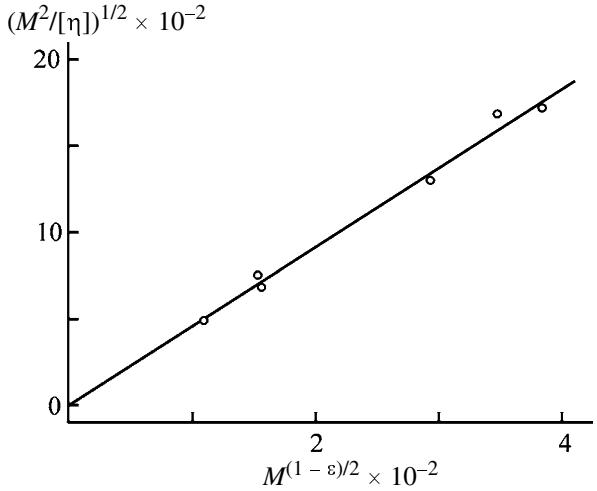


Fig. 5. $(M^2/[\eta])^{1/3}$–$M^{(1-\varepsilon)/2}$ plot at $\varepsilon = 0.133$, used for estimation of the Kuhn segment length and the hydrodynamic diameter d of the sodium polystyrenesulfonate molecules.

The resulting relationship for [η] agrees well with the similar relationship obtained by Takahashi et al. [14] for polytstyrenesulfonate in 0.1 M NaCl solution. They estimated the molecular weights at $2300 < M_w \times 10^{-3} < 400$ by the static light scattering method.

We will attribute the fact that the exponents b_η and $|b_D|$ differ from 0.50 to long-range effects in the SPSS chains. We estimated the parameter $\varepsilon = 2(|b_D| - 1) = (2b_\eta - 1)/3$ describing the thermodynamic quality of the solvent at 0.133 ± 0.007, on the average, and used it in the subsequent interpretation of the hydrodynamic characteristics. The length of the Kuhn statistical segment and the hydrodynamic cross section of the macromolecule were determined by the relationship

$$(M^2\Phi_0/[\eta])^{1/3} = [3/(1-\varepsilon)(3-\varepsilon)](M_L^{(1+\varepsilon)/2}/A^{(1-\varepsilon)/2})M^{(1-\varepsilon)/2} + (M_L P_0/3\pi)[\ln A/d - (3A/d)^{-1} - \varphi(\varepsilon)], \quad (1)$$

where $\Phi_0 = 2.87 \times 10^{23}$ mol^{-1} is the Flory viscosity parameter; $P_0 = 5.11$, hydrodynamic Flory parameter; M_L, weight of the unit length of the polymeric chain; A, statistical segment length; d, hydrodynamic diameter of the chain; and $\varphi(\varepsilon) = 1.431 + 2.64\varepsilon + 4.71\varepsilon^2$ [15].

The relationship (1) was obtained by substituting the $[s]N_A P_0 = (M^2\Phi_0/[\eta])^{1/3}$ variables in the equation describing the dependence of the sedimentation coefficient of a wormlike necklace, taking into account the long-range effects and the intramolecular percolation (Gray–Bloomfield–Hearst theory) [16]. Relationship (1) was first suggested for interpretation of the viscometric data for polyvinylpyrrolidone [7], whereupon it was successfully applied to other polymeric systems [8–11].

Figure 5 presents the plot corresponding to relationship (1). The points are fitted by a straight line with a good linear correlation ($r = 0.9946$). This straight line is described by the following parameters: slope $dy/dx = 4.5 \pm 0.2$ and intersept $-67 < y_0 < 59$. Using the weight of the unit length of the chain $M_L = 206/(2.52 \times 10^{-8}) = 8.17 \times 10^9$ g cm^{-1} mol^{-1}, we estimate from the slope the statistical segment length $A = 3.9 \pm 0.4$ nm. The intersept y_0 is determined with a large scatter, and the parameter $3\pi/M_L P_0) \times (M^2\Phi_0/[\eta])^{1/3}_{M\to 0}$ was estimated at ca. 50% of $\varphi(\varepsilon) = 1.842$. Therefore, the cross section of the SPSS molecules is estimated in this case with a large error, $d = 0.9 \pm 0.6$ nm.

The estimated A parameter for SPSS is 2 times that for the macromolecules of unsubstituted polystyrene (PS). In discussion of this value we will take into account, above all, the electrostatic component of A.

The polyelectrolyte theory [17, 18] considers two characteristic lengths, the Bjerrum radius λ_B and the Debye–Hückel radius of shielding $æ^{-1}$. The Bjerrum radius $\lambda_B = (e^2/4\pi\varepsilon_0\varepsilon kT)$ characterizes the shielding effect of the solvent. The Debye–Hückel shielding radius $k^{-1} = (8\pi\lambda_B\mu)^{-1/2}$ is the distance covered by the effect of the electric field of an individual charge, placed in a medium containing other charges. Here, e is the elementary charge; ε_0, dielectric constant; ε, dielectric permittivity of the medium; k, Boltzmann constant; T, absolute temperature; $\mu = (1/2)\Sigma n_i Z_i^2$, ionic strength of solution; n_i, number of ith ions per unit volume; and Z_i, charge of ith ion in e units.

For solutions of salts of univalent ions $\mu = c_s \times 10^{-3} N_A$ cm^{-3}, where c_s is the molar concentration of the salt. In our case, $c_s = 0.2$ M, $\lambda_B = 0.71$ nm, and $æ^{-1} = 0.68$ nm. The charges occurring at a distance $l < æ^{-1}$ along the chain are responsible for additional electrostatic short-range effects, which cause the chain rigidity to increase by A_{el}. The latter depends on the linear charge density and the ionic strength of the solution. A linear polyelectrolyte is characterized by the dimensionless parameter Q_{el}, which is the product of the Bjerrum radius and the linear charge density (Z/L) : $Q_{el} = (\lambda_B Z)/L$. The general expression for A_{el} was obtained by Odijk [19]; at $L/æ^{-1} \gg 1$ and $Q_{el} > 1$ it takes a simple form $A_{el} = æ^{-2}/2\lambda_B$.

In our case, $Q_{el} \approx 2.8$, and the electrostatic component of the statistical segment length A_{el} was estimated at 0.35 nm. In the case of polyelectrolytes, the concept of additivity of the chain rigidity is considered [17, 18]. The total equilibrium rigidity of a chain is the sum of the structural and electrostatic components: $A = A_{str} + A_{el}$. It is seen that the electrostatic component contributes with approximately 10% to the total length of the statistical segment ($A \approx 4$ nm). Thus, we estimated the structural component A_{str} at ≈ 3.6 nm. The fact that A_{str} for SPSS chains exceeds that for chains of unsubstituted PS ($A \approx 2$ nm) [20] suggests that the SPSS chains are characterized by more hindered rotation than PS and/or that the theory of polyelectrolytes underestimates the contribution from the electrostatic short-range effects to the statistical segment length. Elucidation of this question requires further quantitative studies, in particular, over a wide range of ionic strengths.

CONCLUSIONS

(1) A number of samples of sodium polystyrene sulfonates with molecular weights within $50 < M \times 10^{-3}$ g mol^{-1} < 920 were synthesized by radical polymerization of sodium styrene-4-sulfonate.

(2) Kuhn–Mark–Houwink–Sakurada relationships were obtained for 0.2 M NaCl solution; the Kuhn statistical segment length A was estimated at 3.9 nm, and the hydrodynamic diameter of chains d, at 0.9 nm.

(3) It terms of modern theories of polyelectrolyte solutions, the electrostatic contribution to the statistical segment length does not exceed 10%.

REFERENCES

1. Dautzenberg, H., Jaeger, W., Koetz J., et al., *Polyelectrolytes: Formation, Characterization, Application*, Munich: Chemie, 1994.
2. *Handbook of Polyelectrolytes and Their Applications*, Tripathy, S.K., Kumar, J., and Nalwa, H.S., Eds., California: Am. Science, 2002, vols. 1–3.
3. Holm, C., Rehahn, M., Oppermann, W., and Ballauff, *M. Adv. Polym. Sci*., 2004, vol. 166, pp. 1–27.
4. Volk, N., Vollmer, D., Schmidt, M., et al., *Adv. Polym. Sci*., 2004, vol. 166, pp. 29–65.
5. Dobrynin, A.V. and Rubinstein, M., *Prog. Polym. Sci*., 2005, vol. 30, pp. 1049–1118.
6. Grosberg, A.Yu., Nguyen, T.T., and Shklovskii, B.I., *Rev. Modern Phys*., 2002, vol. 74, no. 4, pp. 329–345.
7. Pavlov, G.M., Panarin, E.F., Korneeva, E.V., et al., *Vysokomol. Soedin., Ser. A*, 1990, vol. 32, no. 6, pp. 1190–1192.
8. Pavlov, G.M., Korneeva, E.V., Mikhailova, N.A., et al., *Vysokomol. Soedin., Ser. A*, 1993, vol. 35, pp. 1647–1651.
9. Pavlov, G.M., Korneeva, E.V., Jumel, K., et al., *Zh. Prikl. Khim*., 2000, vol. 73, no. 6, pp. 992–996.
10. Pavlov, G.M., Korneeva E.V., Ebel', K., et al., *Vysokomol. Soedin., Ser. A*, 2004, vol. 46, no. 10, pp. 1732–1737.
11. Pavlov, G.M., Panarin, E.F., Korneeva, E.V., et al., *Prog. Colloid Polym. Sci*., 2006, vol. 131, pp. 134–140.
12. Tsvetkov, V.N., *Zhestkotsepnye polimernye molekuly* (Rigid-Chain Polymeric Molecules), Moscow: Nauka, 1986.
13. Levedev, A.A., *Izbrannye trudy* (Selected Works), Leningrad: Nauka, 1974.
14. Takahashi, A., Kato, T., and Nagasawa, M., *J. Phys. Chem*., 1967, vol. 71, no. 7, pp. 2001–2010.
15. Pavlov, G.M., *Prog. Colloid Polym. Sci*., 2002, vol. 119. pp. 149–157.
16. Gray, G., Bloomfield, V., and Hearst, J., *J. Chem. Phys*., 1967, vol. 46, no. 4, pp. 1493–1500.
17. Mandel, M., *Polyelectrolytes: Science and Technology*, Hara, M., Ed., New York: Dekker, 1993, pp. 1–75.
18. Barrat, J.-L. and Joanny, J.-F., *Adv. Chem. Phys*., 1996, vol. 94, pp. 1–39.
19. Odijk, T.J., *Polym. Sci., Polym. Phys. Ed*., 1977, vol. 15, pp. 477–482.
20. Tsvetkov, V.N., Eskin, V.E., and Frenkel, S.Ya., *Struktura makromolekul v rastvorakh* (Structure of Macromolecules in Solutions), Moscow: Nauka, 1964.

ISSN 1070-4272, Russian Journal of Applied Chemistry, 2006, Vol. 79, No. 9, pp. 1494–1499. © Pleiades Publishing, Inc., 2006.
Original Russian Text © A.V. Ten'kovtsev, L.V. Abramova, M.M. Dudkina, 2006, published in Zhurnal Prikladnoi Khimii, 2006, Vol. 79, No. 9, pp. 1510–1515.

MACROMOLECULAR CHEMISTRY AND POLYMERIC MATERIALS

Supramolecular Polymeric Complexes of Calix[8]arenes

A. V. Ten'kovtsev, L. V. Abramova, and M. M. Dudkina

Institute of Macromolecular Compounds, Russian Academy of Sciences, St. Petersburg, Russia

Received March 17, 2006

Abstract—Formation of ionic complexes of calix[8]arenes with polymers of various basicities was studied, and previously unknown ternary polymeric complexes of calix[8]arenes of the ion–ion (polymer–calixarene–uranyl ion) and ion–hydrophilic molecule–hydrophobic molecule (polymer–calixarene–fullerene) types were prepared.

DOI: 10.1134/S1070427206090199

Calixarenes exhibit unique properties from the viewpoint of the host–guest complex chemistry [1, 2]. Firstly, methods have been developed for facile synthesis of calixarenes of the required size under properly chosen condensation conditions. Secondly, calixarenes have internal cavities of different size formed by a belt of phenyl rings; these cavities are capable to accommodate a guest molecule of a definite size, which allows their use in molecular recognition. It should be noted that calixarenes form complexes both with neutral organic molecules and with ions. Furthermore, calixarenes can be readily functionalized, which allows variation of their affinity for a guest molecule. Finally, expenses for the preparation of calixarenes from *p*-substituted phenols and formaldehyde are relatively low, which is an important factor for practical applications. For example, calixarenes can be used as specific ligands in analytical chemistry, sensor techniques, medical diagnostics, and synthesis of new materials in supramolecular chemistry.

For many technical applications, it is desirable to combine in one sample the useful properties of both calixarenes and polymers. Synthesis of polymers based on calixarenes is a challenging problem, because these are polyhomofunctional compounds and preparation of di- and monofunctionalized derivatives suitable as monomers for polymerization or polycondensation is difficult. However, the presence in calixarenes of functional groups capable of deprotonation (e.g., hydroxy groups) suggests the possibility of formation of ionic complexes of calixarenes with basic polymeric carriers.

In this study we examined the possibility of preparation of binary and ternary complexes of calixarenes with ionic monomers of various basicities. As investigation objects we chose octa-*p-tert*-butylcalix[8]arene and octa-*p*-nitrocalix[8]arene, polymers of various basicities (polyalkyleneacetamidines and poly-4-vinylpyridine), and fullerene C_{60} and uranyl ions UO_2^{2+} as guest species. The choice of the guest species was governed by the complementarity of their size and the size of the calix[8]arene cavity, and also by the pronounced tendency of many calixarene derivatives to form complexes with uranyl cation. Owing to the latter property, sulfo derivatives of calixarenes were suggested as a sensor element [3] in determination of the uranium content in radiochemical production wastes.

EXPERIMENTAL

p-tert-Butylphenol, paraform, and solvents were used without additional purification. To prepare the complexes, we used polyamidines ($M_w = 2 \times 10^3$, $M_w/M_n = 2.2$) and poly-4-vinylpyridine (Acros, $M_w = 1.6 \times 10^4$).

The NMR spectra were recorded on Bruker AC200 (200 MHz) and Bruker AC300 (300 MHz) spectrometers from solutions in DMSO and chloroform. The UV spectra were taken with Varian Cary 100 and SF-26 spectrophotometers. The luminescence spectra were excited with the nitrogen laser radiation (λ = 337 nm, pulse length 6–8 ns) and were recorded during the persistence time of 1 μs after the excitation pulse at T = 300 K. To measure the linear-optical properties of the samples, we used a Nd–garnet pulse laser with the emission wavelength of 1.06 μm. The laser operated in the modulated Q-factor mode; the

pulse length was 15 ns. The dynamic light scattering was measured with a Brookhaven BI-200SM goniometer and a Brookhaven BI-9000AT correlator. As a light source we used a He–Ne laser (λ = 632.8 nm).

***p*-Nitrocalix[8]arene.** To 10 ml of a 1 : 1 mixture of 65% HNO_3 and 98% H_2SO_4, cooled to +3°C, 1 g (7.7×10^{-4} mol) of *p-tert*-butylcalix[8]arene [4] is gradually added with stirring, keeping the temperature of the reaction mixture in the interval 3–5°C. The product is precipitated by adding 40 ml of water. The yellow precipitate is treated with 20 ml of boiling methanol; the solution is cooled and filtered. This treatment is repeated two times. By so doing, two fractions (soluble and insoluble in methanol) are obtained. As follows from the ^1H NMR data, the fraction soluble in methanol is a mixture of partially degraded or incompletely substituted cyclic and acyclic products. The fraction insoluble in methanol is the target product; yield 0.25 g (27%), mp >360°C. ^1H NMR spectrum (300 MHz, DMSO, 25°C), δ, ppm: 7.97 s (2H, C_{ar}–H), 5.13 br (1H, OH), 4.00 s (2H, CH_2).

Ternary complex poly-1,8-octamethyleneacetamidine–octa-*p*-nitrocalix[8]arene–$UO_2(OH)_2$. Nitrocalix[8]arene (0.02 g, 1.6×10^{-5} mol) is dissolved in 2 ml of acetone, and $UO_2(OH)_2$ (0.015 g, 0.5×10^{-4} mol) is suspended in 2 ml of acetone. Mixing of the solution and suspension results in formation of a soluble binary complex. To the resulting solution, 2 ml of an alcoholic solution of poly-4-vinylpyridine (0.06 g, 0.5×10^{-3} mol) is added. The ternary complex is isolated on cooling as a dark orange precipitate. Films of the complex are obtained by casting onto a rotating support (3000 rpm, 30 s).

Ternary complex polymer–calixarene–fullerene. Such ternary complexes can be prepared by two procedures differing in the order of combining the components.

(1) A solution of *p-tert*-butylcalix[8]arene and poly-1,8-octamethyleneacetamidine (1.2×10^{-3} mol) (calixarene : polymer ratio 1 : 40) in ethanol is prepared. A polymer film is prepared by casting onto a rotating support. After drying over concentrated H_2SO_4, the film is placed in a hot 1.5×10^{-3} M solution of fullerene (2 mg) in toluene (2 ml). The ternary complex is formed within 24 h as a gray-brown film. The product is extracted with two 2-ml portions of boiling toluene and vacuum-dried.

(2) Fullerene (1 mg) is dissolved in 2 ml of toluene on refluxing for 2 h. To the refluxing solution, 2 mg of *p-tert*-butylcalix[8]arene is added to obtain a 1.5×10^{-3} M solution. The solution is filtered while hot and allowed to slowly cool over a period of 24 h. The black precipitate is separated by centrifugation and dissolved in 5 ml of toluene. A polymer film is prepared by casting a solution of 0.2068 g (1.2×10^{-3} mol) of poly-1,8-octamethyleneacetamidine in 1.2 ml of alcohol onto a rotating support; the film is dried over concentrated H_2SO_4, placed in the hot solution of the calixarene–fullerene complex (see above), and allowed to stand for 4–6 h in a closed weighing bottle. The ternary complex is formed as a gray-brown film. The product is extracted with two 2-ml portions of boiling toluene and vacuum-dried.

Octa-*p-tert*-butylcalix[8]arene was prepared as described in [4] by the condensation of *p-tert*-butylphenol with paraform in the presence of sodium oxide. According to published data, the simplest route to octa-*p*-nitrocalix[8]arene is *ipso* nitration of octa-*p-tert*-butylcalix[8]arene with acetyl nitrate [5] or with a mixture of anhydrous HNO_3 and H_2SO_4 [6]. However, we failed to reproduce these procedures. In the case of nitration with acetyl nitrate, it appeared impossible to add the reagent to a solution of octa-*p-tert*-butylcalix[8]arene in methylene chloride because of extremely low solubility of the macrocycle in this solvent (in agreement with data of [4]). Nitration of octa-*p-tert*-butylcalix[8]arene under the conditions described in [6] yields octa-*p*-nitrocalix[8]arene heavily contaminated with decomposition products; the suggested purification procedure, reprecipitation from 2 M Na_2CO_3 into dilute HCl, results in tarring and total decomposition of octa-*p*-nitrocalix[8]arene. In this connection, we suggested a modification of this method, allowing preparation of the desired compound in a reasonable yield (up to 30%). We found that *ipso* nitration does not occur at temperatures below 3°C, whereas above 10°C the reaction becomes uncontrollable and leads to the ring opening. When the reaction is performed in the interval 5–7°C, >97% pure octa-*p*-nitrocalix[8]arene can be isolated by selective extraction with methanol.

The possibility of preparing double polymer–calixarene complexes was examined with octa-*p-tert*-butylcalix[8]arene and octa-*p*-nitrocalix[8]arene as calixarene components, and polyoctamethyleneacetamidine and poly-4-vinylpyridine, differing in the basicity of nitrogen-containing moieties, as polymer components.

p-tert-Butylcalix[8]arene is insoluble in ethanol but soluble in an alcoholic solution of polyamidine (pK ~11), which suggests the deprotonation of the macrocycle and formation of an ionic bond between the calixarene and polymer. As seen from Fig. 1, in a rel-

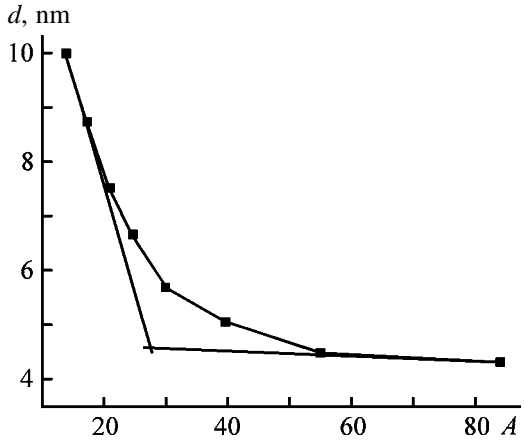


Fig. 1. Diameter d of particles of polyoctamethyleneacetamidine–octa-*p*-*tert*-butylcalix[8]arene complex as a function of the polymer : macrocycle ratio A.

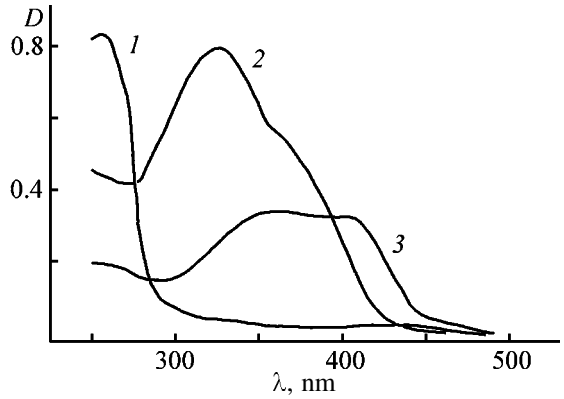


Fig. 2. Absorption spectra of (*1*) polyoctamethyleneacetamidine, (*2*) octa-*p*-nitrocalix[8]arene, and (*3*) their complex. (D) Optical density and (λ) wavelength; the same for Figs. 3 and 5.

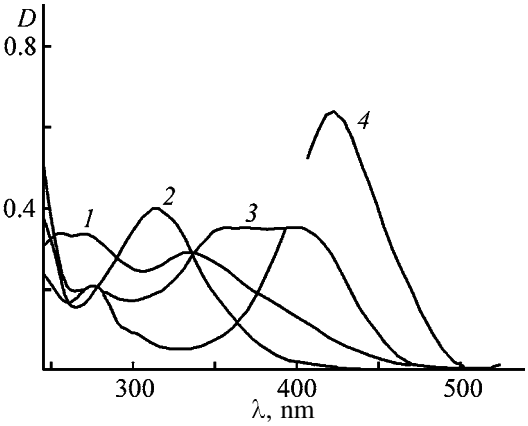


Fig. 3. Absorption spectra of octa-*p*-nitrocalix[8]arene at pH (*1*) 6.0, (*2*) 0, (*3*) 9.7, and (*4*) 13.

atively wide range of calixarene : polyamidine ratios (up to 1 : 40, counting for functional groups), no colloidal particles are formed, which suggests monodeprotonation of the macrocycle and formation of a comb-shaped ionic complex. Apparently, owing to the steric factors associated with the size and shape of the calixarene, the maximal capacity of the polymer for the calixarene should be considerably lower than the theoretical value (1 mol of polymer units per mole of calixarene). Polarization-optical examination of the complexes shows that the system becomes two-phase at polymer : calixarene ratios less than 30 : 1, which is in good agreement with the dynamic light scattering data.

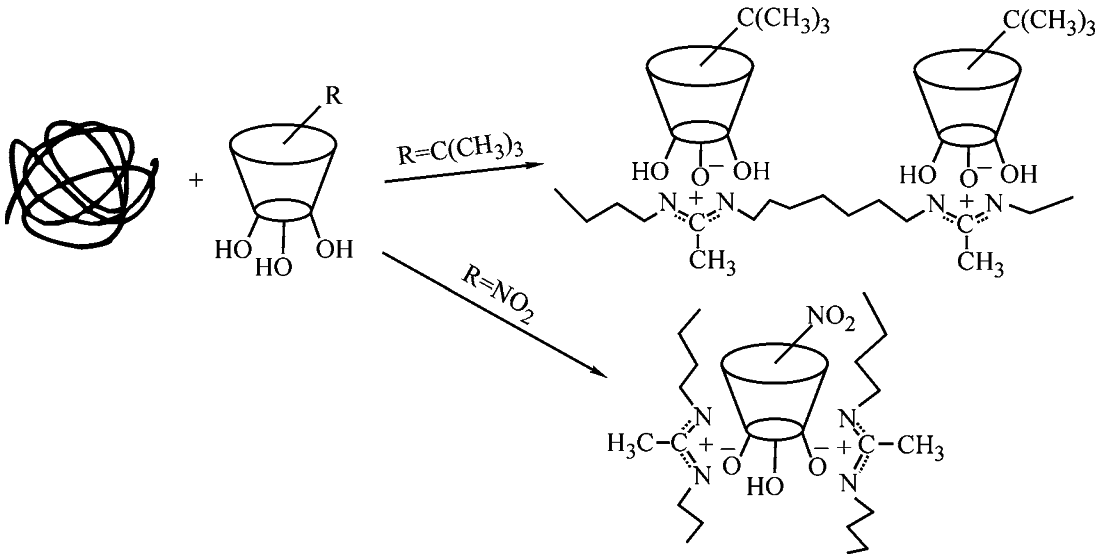
Mixing of an alcoholic solution of poly-4-vinylpyridine with *p*-*tert*-butylcalix[8]arene does not lead to their reaction, because of insufficient basicity of the polymer (pK ~9).

Octa-*p*-nitrocalix[8]arene (pK_1 <0, pK_2 2.6, pK_3 7.2 [6]) is sparingly soluble in ethanol (~3.2×10^{-3} M). On mixing alcoholic solutions of the macrocycle and a polymer (both polyamidine and poly-4-vinylpyridine), a polymer–calixarene complex precipitated, suggesting the binding of the polymer with the calixarene via several hydroxy groups and formation of a three-dimensional ionic network. Figure 2 shows the spectra of the starting polyamidine, octa-*p*-nitrocalix[8]arene, and their complex in DMF solutions. As seen, the spectrum of the complex differs essentially from those of the components, confirming the ionic interaction in the system. Figure 3 shows that the electronic spectra of octa-*p*-nitrocalix[8]arene depend on pH strongly and in a complex fashion, suggesting successive deprotonation of several hydroxy groups. It should be noted that the number of deprotonated groups in the nitrocalix[8]arene molecule is as follows [6], at pH 0, 0; at pH 6.0, 1; at pH 9.7, 2 or 3; and at pH 13.0, 4 or more. Comparison of the electronic spectrum of the complex with those of octa-*p*-nitrocalix[8]arene suggests that the interaction involves two or three hydroxy groups of the macrocycle.

Thus, our data show that variation of the basicity of the polymer and acidity of the hydroxy groups of calixarene can lead to the formation of both comb-shaped and cross-linked structures (Scheme 1).

The possibility of formation of ternary ion–ion complexes in a calixarene–polymer–metal ion system was examined with the system poly-4-vinylpyridine–octa-*p*-nitrocalix[8]arene–UO_2^{2+} as example. The choice of this system was governed by the fact that the less acidic octa-*p*-*tert*-butylcalix[8]arene does not form sufficiently stable complexes with uranyl ion, as judged from the identity of the luminescence spectra of a mechanical mixture of octa-*p*-*tert*-butylcalix[8]-arene and the residue after evaporation of a solution of

Scheme 1. Formation of binary complexes



the components in DMSO–ethanol. However, the reaction of an alcoholic solution of octa-*p*-*tert*-butylcalix[8]arene with $UO_2(OH)_2$ is accompanied by the dissolution of $UO_2(OH)_2$, formation of a 1 : 1 complex (according to elemental analysis), and disappearance of the characteristic luminescence spectrum of the uranyl ion, consisting of several well-resolved lines (Fig. 4). The high acidity of octa-*p*-nitrocalix[8]arenes (first, $pK_1 < 0$, and second, pK_2 2.6, dissociation steps) suggests that two hydroxy groups of the macrocycle act as anionic ligands for UO_2^{2+}, four less acidic OH groups act as donor–acceptor ligands, and the remaining two phenolic groups do not participate in the complexation. It should be noted that the equivalence of all the hydroxy groups of the macrocycle does not allow us to clearly distinguish the role of each particular OH group of the calixarene in the complexation.

On mixing alcoholic solutions of the polyamidine and UO_2^{2+}–octa-*p*-nitrocalix[8]arene complex, the ternary complex UO_2^{2+}–octa-*p*-nitrocalix[8]arene–polyamidine precipitates. Its qualitative composition is suggested by a broad band with a maximum at about 500 nm, appearing in the luminescence spectrum (Fig. 4). The appearance of the luminescence is probably associated with the electron density redistribution in the interaction of the UO_2^{2+}–octa-*p*-nitrocalix[8]-arene complex with highly basic polyamidine, resulting in the deprotonation of the hydroxy groups of the macroring that are not involved in ionic bonding with uranyl ions (Scheme 2).

The possibility of preparing ternary polymeric complexes of calixarenes in which the components are bound by a combination of ionic and hydrophilic–hydrophobic interactions was examined with the octa-*p*-*tert*-butylcalix[8]arene–poly-1,8-octamethyleneacetamidine–C_{60} system as example. The complexes were prepared by two pathways: treatment of the octa-*p*-*tert*-butylcalix[8]arene–poly-1,8-octamethyleneacetamidine complex with a boiling solution of fullerene in toluene and treatment of the polyamidine with a hot solution of the calixarene–fullerene complex in toluene. Both procedures yielded the ternary complexes. Figure 5 shows the electronic spectra of the binary complexes fullerene–octa-*p*-*tert*-butylcalix[8]arene and poly-1,8-octamethyleneacetamidine–octa-*p*-*tert*-butylcalix[8]arene and of the ternary complex. It is seen that the spectrum of the ternary complex fuller-

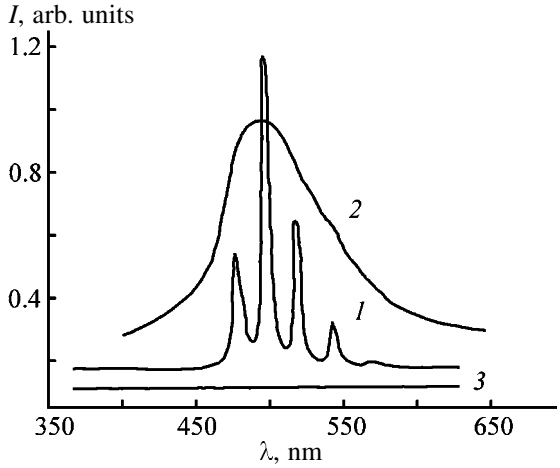
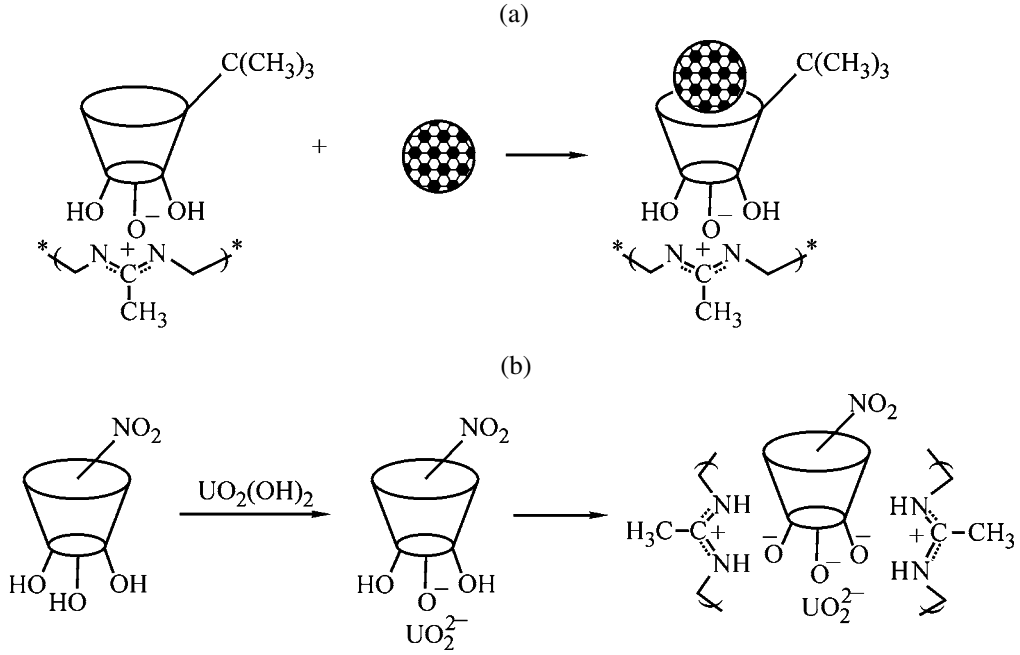


Fig. 4. Luminescence spectra of (*1*) uranic acid, (*2*) complex of UO_2^{2+} with octa-*p*-nitrocalix[8]arene, and (*3*) ternary complex UO_2^{2+}–octa-*p*-nitrocalix[8]arene–polyoctamethyleneacetamidine. (*I*) Intensity and (λ) wavelength.

Scheme 2. Formation of ternary (a) hydrophilic-hydrophobic and (b) ion–ion complexes



ene–poly-1,8-octamethyleneacetamidine–octa-*p-tert*-butylcalix[8]arene is a superposition of the spectra of the binary complexes. This fact indicates that both procedures allow preparation of ternary complexes combining the ionic and hydrophobic–hydrophilic binding of the components (Scheme 2).

Both procedures for preparing the ternary complex yield a stable film resistant to the action of boiling hydrocarbons (toluene, xylene) but partially degrading under the action of boiling ethanol. Such a behavior is also indicative of the formation of a ternary complex, taking into account the fact that the fullerene–*p-tert*-butylcalix[8]arene complex is soluble in toluene and decomposes in polar solvents [7].

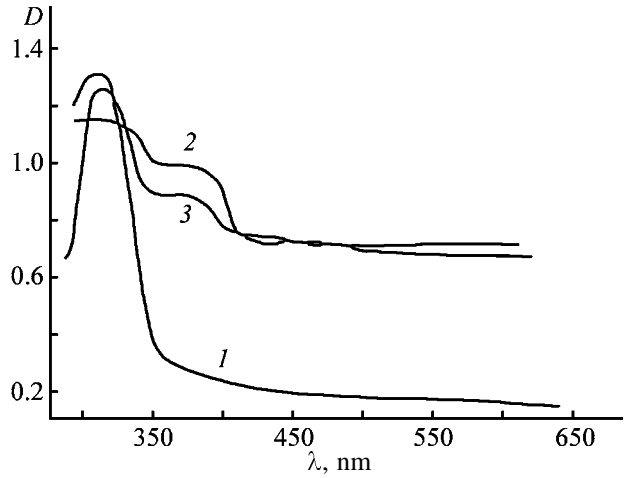


Fig. 5. Electronic spectra of the binary complexes (*1*) fullerene–octa-*p-tert*-butylcalix[8]arene and (*2*) poly-1,8-octamethyleneacetamidine–octa-*p-tert*-butylcalix[8]arene; (*3*) spectrum of the ternary complex.

Thus, calixarenes are capable of forming ternary complexes by simultaneous interactions with the functional groups of ionic polymers and guest molecules; the acidity–basicity ratio for the polymer–calixarene system strongly affects the possibility of formation of ion–ion and ion–hydrophobic component–hydrophilic component supramolecular structures. We believe that the suggested route to polymer systems containing fullerenes can find use in the development of new materials for optoelectronics and of polymeric sensors for environmental monitoring.

CONCLUSION

The formation of ionic complexes by interaction of ionic polymers with calix[8]arenes was studied in relation to the basicity of functional groups of the polymer and acidity of those of the macrocycle. The possibility of formation of ternary supramolecular complexes ion–ion (polymer–calixarene–uranyl ion) and ion–hydrophilic component–hydrophobic component (polymer–calixarene–fullerene) was shown.

ACKNOWLEDGMENTS

The authors are grateful to Prof. F. Böhme (Institute of Polymer Research, Dresden, Germany) for sub-

mission of samples of polyamidines and to Prof. H. Tenhu (University of Helsinki, Finland) for the assistance in the experiments.

The study was financially supported by the Russian Foundation for Basic Research (project no. 06-03-32044-a).

REFERENCES

1. Asfari, Z., Boehmer, V., Harrowfield, J., and Visens, J., *J. Inclus. Phenom. Macrocyclic Chem.*, 2002, vol. 43, nos. 1–2, pp. 149–151.
2. Redshow, C., *Coord. Chem. Rev.*, 2003, vol. 244, no. 1, pp. 45–70.
3. Li, Q., Callahan, H., and Collins, G.E., *Chem. Commun.*, 2000, no. 10, pp. 1913–1914.
4. Gutsche, C.D., *Org. Synth.*, 1990, coll. vol. 8, pp. 80–82.
5. Kumar, S., Kurur, N.D., Chawla, H.M., and Varadarajan, R., *Synth. Commun.*, 2001, vol. 31, no. 5, pp. 775–779.
6. Bunzli, J.-C. and Ihrenger, F., *Inorg. Chim. Acta*, 1996, vol. 246, no. 3, pp. 195–205.
7. US Patent 5711927.

ISSN 1070-4272, Russian Journal of Applied Chemistry, 2006, Vol. 79, No. 9, pp. 1500–1505. © Pleiades Publishing, Inc., 2006.
Original Russian Text © L.M. Kalyuzhnaya, L.I. Kutsenko, E.B. Karetnikova, E.N. Vlasova, A.M. Bochek, 2006, published in Zhurnal Prikladnoi Khimii, 2006, Vol. 79, No. 9, pp. 1516–1521.

MACROMOLECULAR CHEMISTRY AND POLYMERIC MATERIALS

Sorption of Vapors of Organic Solvents with Cyanoethyl Hydroxyethyl Cellulose

L. M. Kalyuzhnaya, L. I. Kutsenko, E. B. Karetnikova, E. N. Vlasova, and A. M. Bochek

Institute of Macromolecular Compounds, Russian Academy of Sciences, St. Petersburg, Russia

Received June 9, 2006

Abstract—The interaction of cyanoethyl hydroxyethyl cellulose with acetone, methylene chloride, and trifluoroacetic acid in the temperature range 10–50°C was studied by the solvent vapor sorption technique. The temperature and concentration dependences of the Flory–Huggins parameter for polymer–solvent interaction χ_1 and the mechanism of the structural rearrangement in the systems were determined.

DOI: 10.1134/S1070427206090205

Growing attention is paid today to studying the structure and physicochemical characteristics of polymers having increased rigidity of macrochains and able to form mesophase on dissolution in appropriate solvents. It is well known [1] that cellulose ethers can form both lyotropic and thermotropic liquid crystals (LCs). Hydroxyethyl (HEC) and hydroxypropyl cellulose (HPC) are typical representatives of such ethers. It was shown [2] that HEC forms lyotropic cholesteric LC and thermotropic LC only in the case of high molar substitution (7–8 mol oxirane per glucose unit). It is assumed that introduction of bulky substitutes into anhydroglucose units of cellulose increases the equilibrium rigidity of macrochains of the polymer due to decreasing mobility of anhydroglucose units (vibration amplitudes) relative to the β-glucoside bond. Cyanoethylation of cellulose and HEC (introduction of strongly polar groups into cellulose macromolecules and, in the case of HEC, at unsubstituted hydroxy groups of anhydroglucose units and, probably, at terminal primary OH groups of hydroxyethyl substituents) is an efficient way to increase the equilibrium rigidity of macrochains and alter the intermolecular interaction between them.

Despite extensive experimental and calculated data obtained on lyotropic polymeric LC systems [1–3], the thermodynamic features of the interaction of cellulose ethers with solvents were not adequately studied.

Experimental determination of complete phase diagrams for systems of this type using only one instrumental method is difficult. Additional problems arise from the existence of higher and lower critical solution temperatures in solutions of some cellulose derivatives in a series of solvents. The structural features of anisotropic solutions and ranges of phase transitions are studied by polarization microscopy. Sorption methods can also give information on the structure and molecular dynamics of LC polymers [4]. It should be noted that any structural transitions in a polymer sample are necessarily reflected in the shape of absorption curves of a sorbate. Thus, studying features of solvent vapor sorption is a necessary link between studying the behavior of macromolecules in solutions and the supramolecular structure and physicomechanical characteristics of polymers in solids.

In this study we examined the features of formation of an ordered LC mesophase by cyanoethyl hydroxyethyl cellulose in concentrated solutions in a series of organic solvents. To elucidate the features of mesophase formation and interaction of polymer with the solvent, we evaluated various thermodynamic parameters from the experimental data on sorption.

EXPERIMENTAL

Cyanoethyl hydroxyethyl cellulose (CEHEC) samples were synthesized under laboratory conditions by cyanoethylation of HEC with acrylonitrile according to the procedure described previously [5–7]. We used commercial HEC with degree of polymerization DP = 900 and molar substitution MS = 2.0. On completion

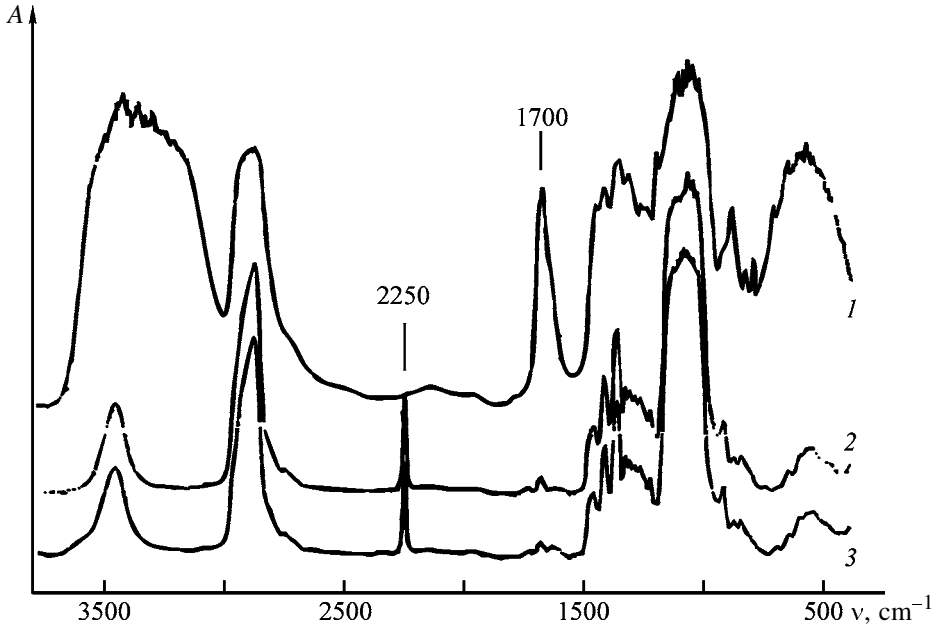


Fig. 1. Fourier IR spectra of films: (*1*) HEC from a solution in TFAA, (*2*) CEHEC from a solution in methylene chloride, and (*3*) CEHEC from a solution in TFAA. (*A*) Absorption and (ν) wavenumber.

of the synthesis, the CEHEC samples were washed to remove alkali with 10% aqueous acetic acid, water, and ethanol, after which the samples were dried to constant weight and analyzed for the nitrogen content by the Kjeldahl method [8]. The degree of substitution with respect to cyanoethyl groups was evaluated by the formula

$$DS = \frac{216y}{1400 - 53y}, \quad (1)$$

where y is the nitrogen content (wt %), 216 is the molecular weight of HEC unit, and 53 is the increase in the molecular weight of HEC upon addition of one cyanoethyl group.

We used a CEHEC sample with MS with respect to ethylene oxide of 2.0 and degree of substitution with respect to cyanoethyl groups DS = 2.0.

CEHEC formation was also proved by Fourier IR spectroscopy. The IR spectra of the samples were recorded in films on a Bruker FS-88 spectrophotometer.

As the main method of the study we used commonly accepted sorption measurements with a high-vacuum McBain balance with a sensitivity of the quartz spiral of 0.5–0.7 mg mm^{-1}. The sorption kinetics was measured under isobaric–isothermal conditions in films prepared by isothermal evaporation of the solvent from 1% polymer solutions. The film thickness was 50–100 μm. The residual content of the solvent in the films did not exceed 0.02 wt %.

The X-ray diffraction patterns of the initial CEHEC samples and those after sorption of the solvent vapor were obtained by small-angle scattering of polarized light. Changes in the X-ray patterns were observed in polarized light using an MIN-8 microscope. The polaroids were crossed at an angle of 45°.

The rheological characteristics of the solutions were studied at 20°C on a Rheotest-2 rheoviscometer with a cylinder–cylinder operating unit in the range of shear stress τ 3–600 Pa.

As sorbates we used the solvents in which CEHEC forms a lyotropic phase: acetone, methylene chloride, and trifluoroacetic acid (TFAA). The CEHEC films were prepared from the same solvents. These solvents interact with functional groups of CEHEC by different mechanisms: dispersion and dipole-dipole interactions and hydrogen bonding [9]. Thus, the specific interactions of solvent molecules with various functional groups can promote rearrangement of polymer macrochains to form an ordered LC structure of the polymer matrix.

The Fourier IR spectra of the samples of HEC and CEHEC films prepared from polymer solutions in the solvents studied are shown in Fig. 1. In the IR spectrum of HEC, there is an absorption band at 1700 cm^{-1} which suggests that, in dissolution of HEC in trifluoroacetic acid (TFAA), trifluoroacetate groups replace primary OH groups [10]. This is also typical for unsubstituted cellulose in its dissolution in TFAA.

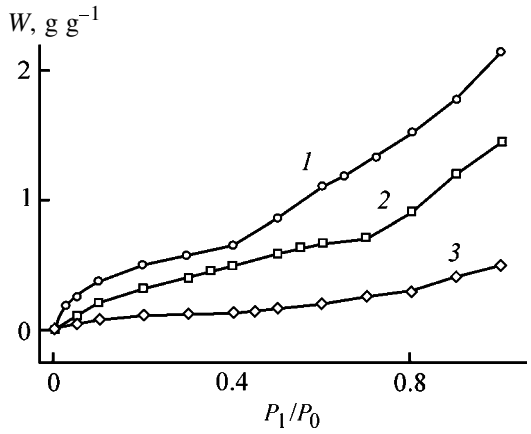


Fig. 2. Isotherms of solvent vapor sorption with CEHEC films. (W) Amount of solvent sorbed with polymer and (P/P_0) relative vapor pressure. Solvent: (*1*) TFAA, (*2*) methylene chloride, and (*3*) acetone; the same for Figs. 3–6.

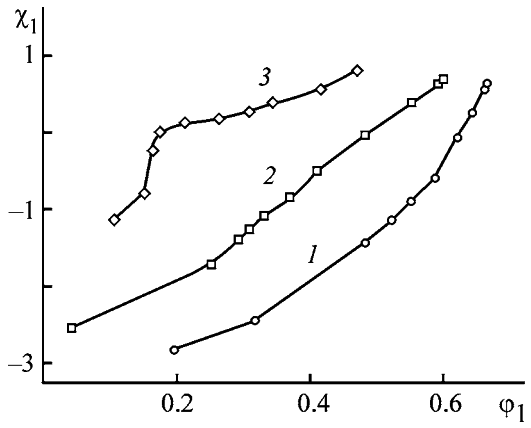


Fig. 3. CEHEC–solvent interaction parameter χ_1 as a function of the volume fraction φ_1 of the solvent.

To remove unstable trifluoroacetic substituents, the films should be treated with water. In the IR spectra of CEHEC, an absorption band appears in the range 2240–2250 cm^{-1}. This band belongs to stretching modes of the CN group, which suggests the presence of cyanoethyl groups in the polymer.

In introduction of cyanoethyl groups into HEC macromolecule, the intensity of the absorption band of OH groups significantly decreases and its shape changes (range 3000–3700 cm^{-1} for free OH groups of the polymer and OH groups bound by intra- and intermolecular hydrogen bonds). This is caused by a small amount of residual unsubstituted hydroxy groups. The absence of the absorption band at 1700 cm^{-1} in the IR spectrum of the CEHEC film prepared from a TFAA solution suggests that most of the primary OH groups remaining in anhydroglucose units and terminal OH groups of hydroxyethyl substituents were substituted in the course of cyanoethylation of HEC. Therefore, in the course of dissolution of CEHEC and TFAA, unstable trifluoroacetate substituents are not formed, in contrast to cellulose and HEC [10]. Therefore, the experimental data obtained were further interpreted assuming no chemical transformations of CEHEC in its interaction with the solvent vapor.

The sorption isotherms were obtained from the equilibrium amounts of the solvent sorbed in the sample at 20°C and the corresponding pressures of the solvent vapor. For all the solvents the S-shaped sorption isotherms [11] are observed (Fig. 2). It is seen that, with respect to the amount of the sorbed substance, the solvents can be ranked in the order TFAA > methylene chloride > acetone.

According to the Flory–Gibbs–Di Marcio theory [12] considering formation of ordered structures in the polymer–solvent system, variation of the thermodynamic affinity of the polymer for the solvent with the temperature and solution concentration significantly affects the ability of the system to pass into the LC state. The influence of the above factors on the formation of a mesophase in CEHEC was studied by sorption of the solvent vapor.

The polymer–solvent interaction parameter χ_1 was evaluated from the classical Flory–Huggins equation [10]

$$\ln a_1 = \ln(1 - \varphi_2) + \varphi_2 + \chi_1\varphi_2^2, \qquad (2)$$

where a_1 is the solvent activity governed by the relative pressure of the solvent vapor and φ_1 and φ_2^2 are the volume fractions of the solvent and polymer, respectively.

The volume fraction of the polymer in swollen samples φ_2 was evaluated by the relationship

$$\varphi_2 = \frac{1}{1 + (d_2/d_1)W}, \qquad (3)$$

where d_2 and d_1 are the densities of the dry polymer and solvent, respectively, and W is the amount of solvent absorbed with the polymer (grams of solvent per gram of dry polymer).

The dependences of the polymer–solvent interaction parameter χ_1 on the volume fraction of the solvent absorbed by polymer are shown in Fig. 3. With increasing solvent concentration, the quantities $\chi_1 = f(\varphi_1)$ change sign from negative to positive, which is in good agreement with published data for a series of

cellulose ethers [11–13]. Apparently, as in the case of some other cellulose derivatives [14], the negative values of χ_1 are caused by the microporous structure of CEHEC films and adsorption in micropores. In this case, the most porous structure is typical for CEHEC films prepared from TFAA.

At the saturated vapor pressure of the solvents, the Flory–Huggings interaction parameters are 0.63 for TFAA, 0.68 for methylene chloride, and 0.8 for acetone. We found that TFAA molecules are more active with respect to the polymer in comparison with acetone and methylene chloride molecules. All the three solvents can interact with functional groups of CEHEC by the dispersion and dipole–dipole mechanism and through formation of hydrogen bonds. The dipole moments of the solvents increase in the order methylene chloride < TFAA < acetone (1.5 < 2.3 < 2.7). Contrary to methylene chloride and TFAA, acetone molecules can be only proton acceptors in formation of hydrogen bonds with functional groups of the polymer. It should also be noted that TFAA molecules form stronger hydrogen bonds than do methylene chloride molecules. The presence of a small amount of hydroxy groups in CEHEC and a large amount of polar groups (hydroxyethyl, cyanoethyl) suggests that the solvents used interact with the functional groups of the polymer predominantly by the dispersion mechanism and hydrogen bonding. In the case of dipole–dipole interactions, it should be expected that the activity of acetone should be higher than that of methylene chloride (based on dipole moments).

From the rheological characteristics of the polymer solutions, we determined the concentration conditions for the formation of lyotropic LC in the CEHEC–solvent system. The solutions of CEHEC in TFAA up to a concentration of 15 wt % behave as ordinary isotropic systems (Fig. 4). At a concentration above 15 wt %, the viscosity of the solutions decreases, which is typical for transition into the LC state [1]. The critical concentration corresponding to the maximum in the concentration dependence of the viscosity, is taken as the concentration at which LC is formed in the solution. Under these conditions, two processes start to compete in the flow: shear ordering of the domains formed and further packing of chains to form domains. When accumulation of LC domains becomes predominant, the viscosity starts to increase again with increasing concentration of the solution. In methylene chloride solutions, LC domains are formed in CEHEC at a concentration of 20 wt %, which is higher than in TFAA. In the concentration range

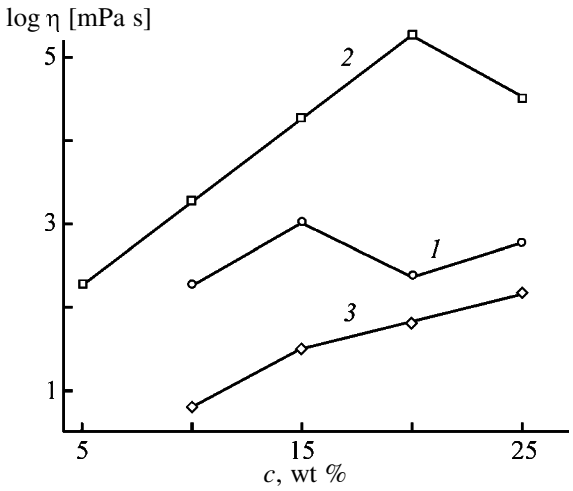


Fig. 4. Dependence of log η on solution concentration *c*.

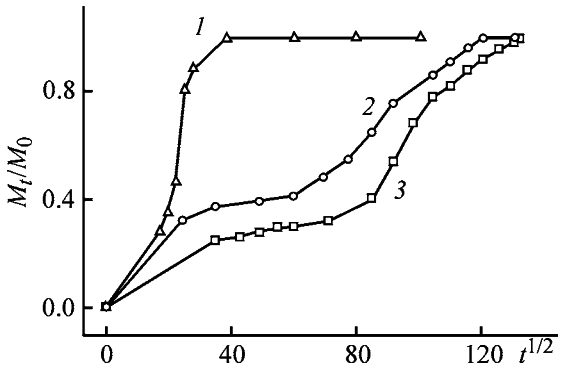


Fig. 5. Kinetic curves of solvent vapor sorption by CEHEC at 20°C and the saturated vapor prassure.

studied, we did not observe transition into the LC state in acetone solutions. It is likely that the lyotropic phase is formed at a higher concentration of the polymer.

Any structural transformations are inevitably reflected in the shape of the kinetic curves of the sorbate adsorption with the polymer. The kinetic curves of the solvent vapor sorption at the saturated vapor pressure at 20°C are shown in Fig. 5. It is seen that with TFAA the standard S-shaped curve is observed, whereas with methylene chloride and acetone there are two portions in the kinetic curves (two stages of sorption). Abnormal sorption kinetics can be caused by both relaxation processes in rearrangement of the polymeric structure under the action of the solvent and by the nonequilibrium structure of the polymer matrix [4, 18, 19].

It can be assumed that, in the systems studied, there are two mechanisms of structural rearrangement of polymer macrochains. In the CEHEC–TFAA system, this rearrangement is a transition from the perfect

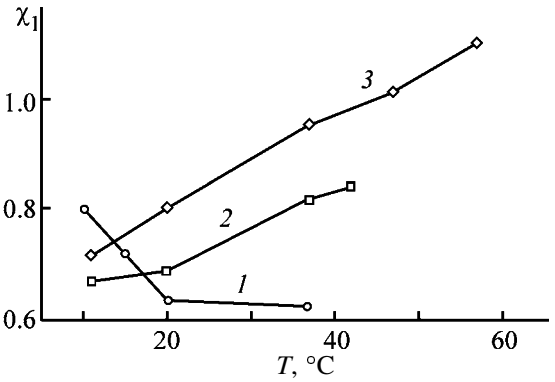


Fig. 6. Polymer–solvent interaction parameter χ_1 as a function of temperature T.

LC structure to the isotropic state (from the evidence of the X-ray study, the CEHEC films prepared from TFAA have the most perfect packing in the mesophase). In the systems CEHEC–methylene chloride and CEHEC–acetone, the mesophase formation becomes complete (i.e., in placing of the polymer into the medium causing swelling, the nonequilibrium bent macromolecules become straight and the ordering of the mesophase system increases) [20, 21]. The initial structure of the CEHEC films and the film structure after the sorption of the solvents were studied by small-angle scattering of polarized light. The analysis of the radial distribution of the intensity and radial scattering angle θ at azimuthal scattering angles μ 0° and 90° showed that the intensity monotonically decreased with increasing θ from zero and higher values (i.e., it was established that the mesophase is characterized by four-petal reflections of small-angle light scattering with the intensity uniformly decreasing with the radial angle). As in the case of cyanoethyl cellulose [16], disordered fibrillar anisotropic formations whose optical axis does not coincide with the direction of the longest axis of fibrils are responsible for diffraction. In this case, the most ordered structure is observed in the initial CEHEC films prepared from solutions in TFAA. After sorption of TFAA vapor, this structure becomes diffuse. On the contrary, in acetone and methylene chloride solutions the ordering in the initial films is lower than that after sorption of solvent vapor, which confirms the above assumption on different mechanisms of structural rearrangement in the systems studied.

To characterize the features of formation of liquid-crystalline state, it is of interest to study the temperature dependence of the thermodynamic affinity of solvents for the polymer (Fig. 6). The amount of the sorbed solvent as a function of temperature was determined at saturated vapor pressure (the solvent activity is 1). In sorption of acetone and methylene chloride vapors with CEHEC, the amount of the sorbed solvent decreases and the polymer–solvent interaction parameter χ_1 increases with heating. Such trends indicate that these systems have a lower critical temperature of solution.

The opposite pattern is observed for sorption of TFAA: the amount of the sorbed solvent increases with heating and the interaction parameter χ_1 decreases, which, in turn, indicates that the system has an upper critical temperature of solution.

Thus, the specific interactions of solvents with various functional groups of CEHEC (as in the case of cellulose acetates [22]) result in formation of polymer materials with different supramolecular structures from the same cellulose ether.

CONCLUSIONS

(1) Sorption studies of the thermodynamic features of formation of liquid-crystalline order in concentrated solutions of cyanoethyl hydroxyethyl cellulose in acetone, methylene chloride, and trifluoroacetic acid in the range 10–50°C show that the systems cyanoethyl hydroxyethyl cellulose–acetone and cyanoethyl hydroxyethyl cellulose–methylene chloride have a lower critical temperature of solution. The system cyanoethyl hydroxyethyl cellulose–trifluoroacetic acid has an upper critical temperature of solution.

(2) There are two different mechanisms of structural rearrangement in the systems cyanoethyl hydroxyethyl cellulose–acetone and cyanoethyl hydroxyethyl cellulose–methylene chloride: for cyanoethyl hydroxyethyl cellulose–trifluoroacetic acid, transition from perfect liquid-crystalline structure into isotropic state and for cyanoethyl hydroxyethyl cellulose–methylene chloride, completion of the mesophase during sorption of the solvent.

(3) Variation of the solvent from which cyanoethyl hydroxyethyl cellulose film is prepared and the action of vapor of various solvents during sorption provide a possibility of preparing polymer materials with different characteristics from the same cellulose ether.

REFERENCES

1. Kulichikhin, V.G. and Golova, L.K., *Khim. Drev.*, 1985, no. 3, pp. 9–27.
2. Lavrenko, P.N., Strelina, I.A., Magarik, S.Ya., and Kutsenko, L.I., *Vysokomol. Soedin., Ser. A*, 1995, vol. 37, no. 12, pp. 2007–2012.

3. Chalykh, A.E., Gerasimov, V.K., and Avgonova, F.A., *Vysokomol. Soedin., Ser. A*, 2001, vol. 43, no. 7, pp. 1134–1139.
4. Buntjakov, A.S. and Averyanova, R.M., *J. Polym. Sci., Ser. C*, 1972, vol. 38, pp. 109–112.
5. Bochek, A.M., Petropavlovskii, G.A., Kutsenko, L.I., and Karetnikova, E.B., *Zh. Prikl. Khim.*, 2000, vol. 73, no. 1, pp. 152–155.
6. Kutsenko, L.I., Petropavlovskii, G.A., Karetnikova, E.B., et al., *Zh. Prikl. Khim.*, 2000, vol. 73, no. 4, pp. 652–656.
7. Petropavlovsky, G.A., Bochek, A.M., Kutsenko, L.I., et al., *Cellulose Chem. Technol.*, 2000, vol. 34, nos. 1–2, pp. 63–70.
8. Klimova, V.A., *Osnovnye mikrometody analiza organicheskikh soedinenii* (Main Micromethods of Analysis of Organic Componds), Moscow: Khimiya, 1967.
9. Timofeeva, G.N. and Aver'yanova, R.M., *Vysokomol. Soedin., Ser. A*, 1982, vol. 24, no. 11, pp. 2268–2274.
10. Geddes, A.I., *J. Polym. Sci.*, 1956, vol. 22, no. 100, pp. 31–39.
11. Aitken, C.L., Koros, W.J., and Paul, D.R., *Macromolecules*, 1992, vol. 25, no. 13, pp. 3424–3434.
12. Bartenev, G.M. and Zelenev, Yu.V., *Kurs fiziki polimerov* (Course of Polymer Physics), Leningrad: Khimiya, 1976.
13. Tager, A.A., *Osnovy ucheniya o rastvorakh neelektrolitov* (Fundamentals of the Theory of Nonelectrolyte Solutions), Yekaterinburg: Ural. Gos. Univ., 1993.
14. *Cellulose and Cellulose Derivatives*, Bikales, N.M. and Segal, L., Eds., New York: Wiley, 1971, part IV. Translated under the title *Tsellyulosa i ee proizvodnye*, Moscow: Mir, 1974, pp. 433–450.
15. Tager, A.A., Tsilipotkina, M.V., and Reshet'ko, D.A., *Vysokomol. Soedin., Ser. A*, 1975, vol. 17, no. 11, pp. 2566–2570.
16. Kutsenko, L.I., Kalyuzhnaya, L.M., Karetnikova, E.B., et al., *Zh. Prikl. Khim.*, 1993, vol. 66, no. 2, pp. 386–392.
17. Samsonov, G.V., Trostyanskaya, E.V., and El'kin, G.E., *Ionnyi obmen. Sorbtsiya organicheskikh veshchestv* (Ion Exchange. Sorption of Organic Substances), Leningrad: Nauka, 1969.
18. Rogers, C.E., in *Physics and Chemistry of the Organic Solid State*, Fox, D., Labes, M., and Weissberger, A., Eds., New York: Wiley, 1965, vol. 2. Translated under the title *Problemy fiziki i khimii tverdogo sostoyaniya organicheskikh soedinenii*, Moscow: Mir, 1968, pp. 293–326.
19. Chalykh, A.E., *Vysokomol. Soedin., Ser. C*, 2001, vol. 43, no. 12, pp. 2304–2320.
20. Papkov, S.P., *Ravnovesie faz v sisteme polimer–rastvoritel'* (Phase Equilibrium in the Polymer–Solvent System), Moscow: Khimiya, 1981.
21. Frenkel, S.Ya., *Pure Appl. Chem.*, 1974, vol. 38, no. 1/2, pp. 117–128.
22. Shipovskaya, A.B. and Timofeeva, G.N., *Vysokomol. Soedin., Ser. A*, 2001, vol. 43, no. 7, pp. 1237–1244.

ISSN 1070-4272, Russian Journal of Applied Chemistry, 2006, Vol. 79, No. 9, pp. 1506–1508. © Pleiades Publishing, Inc., 2006.
Original Russian Text © E.E. Ergozhin, T. Hirotsu, B.A. Mukhitdinova, S.A. Shoinbekova, A.I. Nikitina, N.I. Razuvaeva, 2006, published in Zhurnal Prikladnoi Khimii, 2006, Vol. 79, No. 9, pp. 1522–1524.

MACROMOLECULAR CHEMISTRY AND POLYMERIC MATERIALS

Cationic Polymerization of a Derivative of Allylamine and 1,2-Naphthoquinone

E. E. Ergozhin, T. Hirotsu, B. A. Mukhitdinova, S. A. Shoinbekova, A. I. Nikitina, and N. I. Razuvaeva

Bekturov Institute of Chemical Sciences, Ministry of Education and Science of Kazakhstan Republic, Almaty, Kazakhstan

National Institute of Advanced Industrial Science and Technology, AIST, Tsukuba, Japan

Received May 12, 2006

Abstract—Cationic polymerization of a monomer derived from allylamine and 1,2-naphthoquinone was studied by polarography. The optimum conditions and kinetic characteristics of the process were found.

DOI: 10.1134/S1070427206090217

Allyl monomers form a wide class of fairly accessible compounds with various functional groups: –OH, $–NH_2$, –COOR, and –C≡H [1, 2]. Therefore, their conversion into polymer products at acceptable rates is of practical importance. The activity of allyl compounds is mainly governed by the substituent in the chain. For example, attempts to prepare polymers from diallylamine or diallylalkylamine using radical initiators failed [3]. Introduction into diallylamines of substituents containing electron-acceptor groups directly bonded to the nitrogen atom enhances the reactivity of monomers in radical polymerization. Kabanov and coworkers [3] explain this fact by displacement of the π-electron density under the action of electron-acceptor substituents, which causes activation of the allyl bond. It is well known [2, 4] that quinones have electron-acceptor power; therefore, the derivative of allylamine and 1,2-naphthoquinone [5] should be more active than the initial monomer which polymerizes at a low rate and only at radiation initiation.

This paper deals with a polarographic study of the polymerization of a monomer derived from allylamine and 1,2-naphthoquinone in the presence of hydrochloric acid.

EXPERIMENTAL

The monomer derived from allylamine and 1,2-naphthoquinone (AA–1,2-NPQ) was synthesized by the procedure described previously [5].

We used concentrated hydrochloric acid of ultrapure grade, d 1.179 g cm^{-3}. Dimethylformamide (DMF) was purified by the procedure described in [6].

The redox monomer was polymerized by the ampule method in the presence of hydrochloric acid in a DMF–water mixture. A weighed portion of AA–1,2-NPQ was placed into a glass ampule, DMF and hydrochloric acid were added, and, after dissolution of the monomer, water was added. The reaction conditions were varied in the following limits: temperature, 7–28°C; duration, 0.5–5.0 h; monomer concentration, 10–50 g l^{-1}; c_{HCl}, 0.04–0.29 M; and H_2O : DMF volume ratio, (0–3) : 1. The reaction course was judged from the concentration of unreacted monomer, which was determined polarographically. The polarograms were recorded with a phosphate buffer solution (pH 7.4) in 25% DMF in a temperature-controlled cell at 25°C on a PU-1 polagraph using mercury dropping electrode with a capillary characteristic at open circuit $m^{2/3}t^{1/6}$ = 4.38 mg$^{2/3}$ s$^{-1/2}$. AA–1,2-NPQ was determined from the wave with a half-wave potential $E_{1/2}$ = –0.54 V, whose amplitude is in direct proportion to monomer concentration in the range 10^{-4}–10^{-3} M.

Contrary to vinyl monomers readily polymerizing under the action of radical initiators to macromolecular compounds, monoallyl monomers with the general formula CH_2=CH–CH_2–X polymerize by the radical mechanism at extremely low rates with formation of oligomeric products [1, 2]. Allyl radicals add to low-active double bond of the monomer at a high rate only at a temperature higher than 300–400°C or under a pressure of 5–20 kbar and also under the action of γ-irradiation.

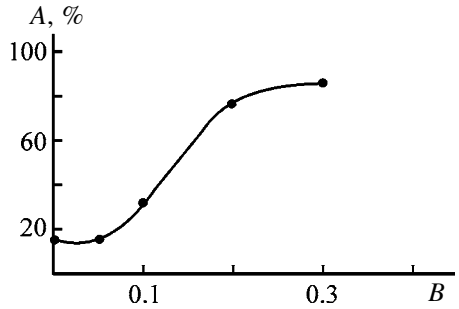


Fig. 1. Influence of water on the polymer yield *A* in cationic polymerization of AA–1,2-NPQ. c_{mon} = 20 g l^{-1}, c_{HCl} = 0.10 M, 21°C, 5 h. (*B*) Volume ratio H_2O : DMF.

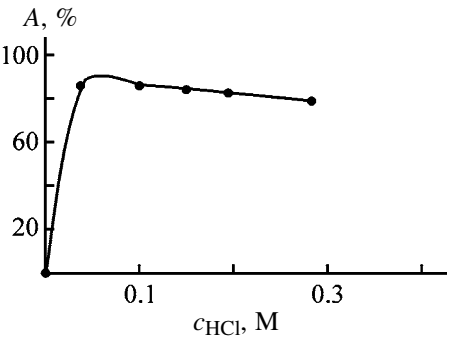


Fig. 2. Conversion of AA–1,2-NPQ in cationic polymerization as a function of the catalyst amount c_{HCl}. c_{mon} = 20 g l^{-1}, H_2O : DMF = 3 : 1, 21°C, 5 h. (*A*) Polymer yield, the same for Fig. 4.

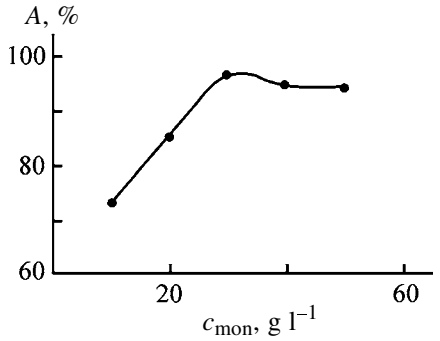


Fig. 3. Polymer yield *A* as a function of monomer concentration c_{mon} in cationic polymerization. c_{HCl} = 0.04 M, H_2O : DMF = 3 : 1, 21°C; the same for Fig. 4.

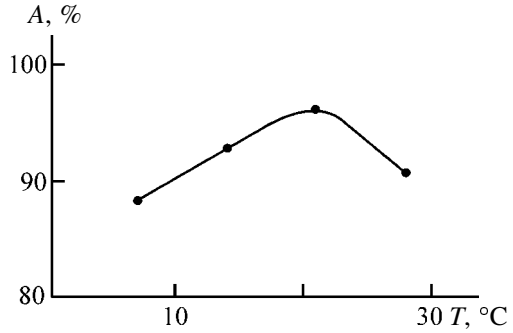


Fig. 4. Influence of temperature *T* on the conversion of AA–1,2-NPQ in its cationic polymerization.

It is well known [1, 2] that, on adding protonic acids to allyl monomers, the rates of their radical polymerization and molecular weights of the resulting polymers significantly increase. In this case, the reaction is initiated predominantly by the radiation-chemical procedure, since many of the initiators used readily undergo heterolytic decomposition in the presence of protonic acids. Reservation of the radical nature of the process is confirmed by the fact that the reaction occurs only in the presence of a source of free radicals and is inhibited by radical inhibitors.

A possibility of polymerization of AA–1,2-NPQ monomer in the presence of hydrochloric acid without radical initiators was established and the process conditions were studied (Figs. 1–5).

Figure 1 shows that, due to its proton-donor power, water activates polymerization of AA–1,2-NPQ. Apparently, the chain propagation constant increases as a result of formation of H-complexes of the monomer and propagating AA–1,2-NPQ radicals with water molecules [2]. Figure 2 shows that the polymer is formed with the maximum yield in the presence of 0.04 M HCl and further increase in the amount of the catalyst results in insignificant decrease in the yield. Figures 3 and 4 show that polymerization of AA–1,2-NPQ proceeds better at its concentration in the solution of 30 g l^{-1} and at a temperature of 21°C. Insignificant dependence of the process yield on temperature (Fig. 4) suggests that the activation energy of this reaction should be low. Figure 5 shows that polymerization of AA–1,2-HPQ proceeds at a fairly high rate in the first 0.5 h and then the process decelerates.

Thus, the polymer is formed with the maximum yield of 96% in the presence of 0.04 M HCl at a

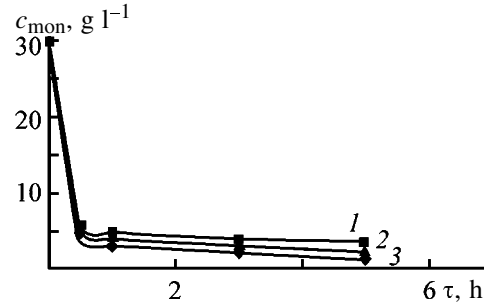


Fig. 5. Kinetics of expenditure of AA–1,2-NPQ monomer c_{mon} in cationic polymerization at various temperatures. H_2O : DMF = 3 : 1, c^0_{mon} = 30 g l^{-1}, c_{HCl} = 0.04 M. (τ) Time. Temperature, °C: (*1*) 7, (*2*) 14, and (*3*) 21.

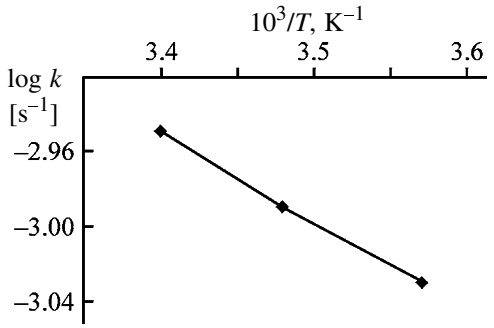


Fig. 6. Logarithm of the rate constant of cationic polymerization of AA–1,2-NPQ $\log k$ as a function of reciprocal temperature T.

volume ratio H_2O : DMF = 3 : 1, monomer concentration of 30 g l^{-1}, temperature of 21°C, and synthesis duration of 5 h.

The kinetics of AA–1,2-NPQ polymerization under optimum conditions was studied. The kinetic curves (Fig. 5) show that the process is first-order with respect to the monomer concentration. We evaluated the reaction rate constants at various temperatures using the appropriate equation [6] and determined the activation energy (see table) from the Arrhenius plot (Fig. 6).

As we assumed, the activation energy of this reaction was fairly low. Hence, the monomer synthesized from allylamine and 1,2-naphthoquinone shows a high reactivity in polymerization. Since the reaction occurs in the absence of radical initiators and is activated by hydrochloric acid, we can conclude that the reaction occurs by the cationic mechanism [8]. The resulting polymer is a dark cherry-brown powder with mp 152°C and $[\eta]$ = 0.12 dl g^{-1}. Its redox capacity with respect to 0.1 N solution of $Fe_2(SO_4)_3$ is 2.9 mg-equiv g^{-1}.

Thus, a new redox polymer containing groups capable of redox reactions (>C=O) and complex formation (–NH–) was synthesized by cationic polymerization under mild conditions. The possible areas of its application are hydrometallurgy (for separation and concentration of metal ions), water treatment (for removal of oxygen and chlorine), chemical industry (for purification and removal of organic compounds), and medicine [9, 10].

Kinetic characteristics of cationic polymerization of AA–1,2-NPQ monomer

T, K	k, s^{-1}	$\log k$	E_{act}, kJ mol^{-1}
280	0.00094	–3.03	
287	0.00102	–2.99	8.65
294	0.00112	–2.95	

CONCLUSIONS

(1) The optimal conditions of cationic polymerization of a derivative of allylamine and 1,2-naphthaquinone were found.

(2) The kinetics of this reaction was studied, and the reaction constants and activation energy were evaluated.

ACKNOWLEDGMENTS

This work was financially supported by the International Science and Technology Center (grant no. K-604).

REFERENCES

1. Vorob'eva, Yu.A., Prochukhan, Yu.A., and Monakov, Yu.B., *Vysokomol. Soedin., Ser. C*, 2003, vol. 45, no. 12, pp. 2118–2136.
2. Kabanov, V.A., Zubov, V.P., and Semchikov, Yu.D., *Kompleksno-radikal'naya polimerizatsiya* (Radical Complex Polymerization), Moscow: Khimiya, 1987.
3. Matsoyan, S.G., Pagosyan, R.M., Dzhigamen, A.O., and Mushegyan, A.V., *Vysokomol. Soedin.*, 1963, vol. 5, no. 6, pp. 854–860.
4. Pullman, B. and Pullman, A., *Quantum Biochemistry*, New York: Interscience, 1963.
5. Kazakhstan Patent 9729.
6. Weissberger, A. and Proskauer, E.S., *Organic Solvents. Physical Properties and Methods of Purification*, Riddick, J.A. and Toops, E.E., Eds., New York: Interscience, 1955.
7. Emanuel', N.M. and Knorre, D.G., *Kurs khimicheskoi kinetiki* (Course of Chemical Kinetics), Moscow: Vysshaya Shkola, 1969.
8. Shur, A.M., *Vysokomolekulyarnye soedineniya* (Macromolecular Compounds), Moscow: Vysshaya Shkola, 1981.
9. Cassidy, H.G. and Kun, K.A., *Oxidation–Reduction Polymers (Redox Polymers)*, Interscience, 1965.
10. Ergozhin, E.E. and Mukhitdinova, B.A., *Okislitel'novosstanovitel'nye ionoobmenniki* (Redox Ion Exchangers), Almaty: RIO VAK RK, 2000.

ISSN 1070-4272, Russian Journal of Applied Chemistry, 2006, Vol. 79, No. 9, pp. 1509–1513. © Pleiades Publishing, Inc., 2006.
Original Russian Text © R.M. Islamova, Yu.I. Puzin, V.A. Kraikin, A.A. Fatykhov, U.M. Dzhemilev, Yu.B. Monakov, 2006, published in Zhurnal Prikladnoi Khimii, 2006, Vol. 79, No. 9, pp. 1525–1528.

MACROMOLECULAR CHEMISTRY AND POLYMERIC MATERIALS

Controlling the Polymerization of Methyl Methacrylate with Ternary Initiating Systems

R. M. Islamova, Yu. I. Puzin, V. A. Kraikin, A. A. Fatykhov, U. M. Dzhemilev, and Yu. B. Monakov

Institute of Organic Chemistry, Ufa Scientific Center, Russian Academy of Sciences, Ufa, Bashkortostan, Russia
Ufa State Technical University of Oil, Ufa, Bashkortostan, Russia
Institute of Petroleum Chemistry and Catalysis, Russian Academy of Sciences, Ufa, Bashkortostan, Russia

Received April 26, 2006

Abstract—The effect of ternary initiating systems benzoyl peroxide–ferrocene–3,6-bis(*o*-carboxybenzoyl)-*N*-isopropylcarbazole and benzoyl peroxide–di-η^5-indenylzirconium dichloride–3,6-bis(*o*-carboxybenzoyl)-*N*-isopropylcarbazole on the radical polymerization of methyl methacrylate and on the heat resistance and microstructure of the resulting polymers was examined.

DOI: 10.1134/S1070427206090229

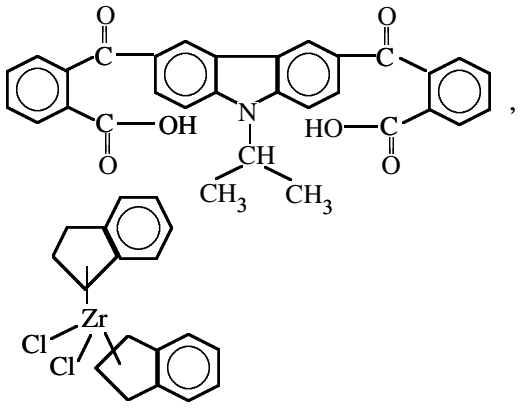
The main goal of macromolecular chemistry is preparation of polymeric materials with required properties. This goal can be accomplished by performing the process in the presence of initiating systems that contain, along with other components, organometallic compounds [1]. Organic compounds of transition metals find growing use not only as catalysts of ionic-coordination polymerization of olefins and dienes, but also as agents controlling the radical polymerization of vinyl monomers [2].

It is known [3–5] that the use of certain metallocenes (ferrocene, titanocene dichloride, etc.) in combination with initiators [benzoyl peroxide, azobis(isobutyronitrile)] not only accelerates the polymerization, but also allows preparation of poly(methyl methacrylate) (PMMA) with a narrower molecular-weight distribution and increased content of syndiotactic seqeunces in the polymer chain.

At the same time, study of initiating systems containing heteroaromatic diketo carboxylic acids showed that they, especially 3,6-bis(*o*-carboxybenzoyl)-*N*-isopropylcarbazole, catalyze the decomposition of benzoyl peroxide [6]. The effect of 3,6-bis(*o*-carboxybenzoyl)-*N*-isopropylcarbazole on the microstructure of the polymer is so strong that it is manifested at concentrations 1–2 orders of magnitude lower than the peroxide concentration and exceeds the effect of metallocene systems [3, 4, 6, 7].

However, peroxide–nitrogen-containing compound systems are characterized by deceleration of the polymerization [8], which makes them hardly suitable for commercial production of polymeric materials. It can be expected that combination of a metallocene and a nitrogen-containing compound in one initiating system would not only preserve their stereoregulating functions but also accelerate the polymerization and improve the thermal characteristics of the polymers obtained.

Here we report on the radical polymerization of methyl methacrylate (MMA) initiated by ternary systems benzoyl peroxide (BP)–3,6-bis(*o*-carboxybenzoyl)-*N*-isopropylcarbazole (DCN)–ferrocene (FC) and BP–DCN–di-η^5-indenylzicronium dichloride (DIZD) and on the heat resistance and microstructure of the resulting polymers.



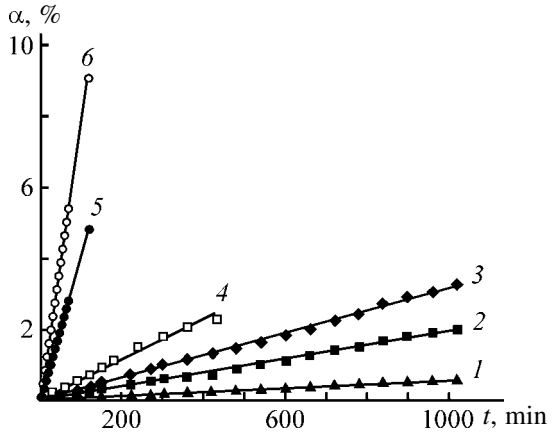


Fig. 1. Kinetic dependences of polymerization of methyl methacrylate at 60°C in the presence of additives (M): (*1*) 1×10^{-4} DCN, (*2*) 1×10^{-3} DIZD, (*3*) none, (*4*) 1×10^{-3} DIZD + 1×10^{-4} DCN, (*5*) 1×10^{-3} ferrocene + 1×10^{-4} DCN, and (*6*) 1×10^{-3} ferrocene. Initiator benzoyl peroxide, 1×10^{-3} M. (α) Conversion and (*t*) time.

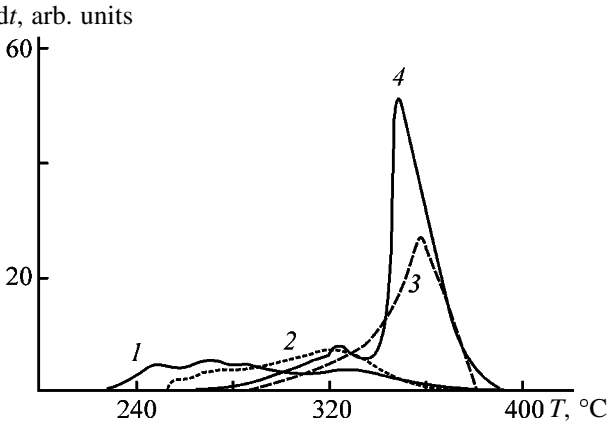


Fig. 2. DTG curves of poly(methyl methacrylate) prepared at 30°C in the presence of 1×10^{-3} M benzoyl peroxide. (d*m*/d*t*) Weight loss rate and (*T*) temperature. Additive, M: (*1*) none, (*2*) 1×10^{-3} DIZD, (*3*) 1×10^{-3} DIZD + 1×10^{-3} DCN, and (*4*) 1×10^{-3} FC + 1×10^{-4} DCN.

EXPERIMENTAL

MMA was shaken with a 5–10% KOH solution to remove the stabilizer, washed with water to neutral reaction, dried over $CaCl_2$, and double-distilled in a vacuum. Benzoyl peroxide was recrystallized three times from methanol and dried at room temperature in a vacuum to constant weight; mp 108°C (dec.). Ferrocene was prepared as described in [9] and purified by sublimation. 3,6-Bis(*o*-carboxybenzoyl)-*N*-isopropylcarbazole was prepared and purified by the procedure described in [10]. Diindenylzirconium dichloride was prepared according to [11] and purified by sublimation.

The polymerization was performed in the bulk [12]; the temperature was maintained with an accuracy of ±0.05°C.

Dynamic TGA was performed on a Q-1000 derivatograph (MOM) in air; heating rate 5 deg min^{-1}, sample weight 100 mg.

The content of syndio- and isotactic sequences in the macromolecules was determined by ^1H NMR spectroscopy [13–15] on a Bruker AM-300 device; solvent $CDCl_3$, operating frequency 300 MHz.

Experiments on the polymerization of MMA initiated by ternary systems BP–FC–DCN and BP–DIZD–DCN showed that, in the entire temperature range studied (30–60°C), the initial reaction rate increased relative to the samples without additives (Fig. 1). The polymerization initiated by the BP–FC–DCN system was considerably faster than that initiated by the binary system BP–DCN. However, the reaction rate was considerably lower compared to the polymerization initiated by the binary system BP–FC (Fig. 1). Apparently, the metallocene exerts a predominant effect on the kinetic parameters of the process.

The apparent activation energy of the polymerization in the presence of the BP–FC–DCN system, calculated from the temperature dependence of the rate constant, appeared to be 12±0.5 kJ mol^{-1}, which is appreciably lower than in the initiation with BP only (80 kJ mol^{-1}) [16] or with the BP–FC system (48.3 kJ mol^{-1}) [17]). The ternary initiating system decreases primarily the activation energy of the polymerization initiation, because the activation energies of the chain propagation and termination are insignificant.

A study of the MMA polymerization initiated by the BP–DIZD–DCN system revealed a synergistic effect of the additives, caused by the competition for the coordination sites of the Zr atom and by the mutual influence of the additives as ligands. The MMA polymerization initiated by the BP–DIZD–DCN system is conbsiderably faster than that initiated by the BP–DIZD or BP–DCN system (Fig. 1). The apparent activation energy of the polymerization is 50 kJ mol^{-1}. Hence, in this case we can speak of formation of a ternary initiating system.

Polymers prepared with ternary initiating systems BP–FC–DCN and BP–DIZD–DCN exhibit high heat resistance and stereoregular structure.

Both ferrocene and DIZD, when added to the initiating system BP–DCN, appreciably enhance the heat resistance of the PMMA obtained. The temperature of the decomposition onset ($T_{o.d}$) increases by approximately 40–50°C compared to the polymers prepared without additives (Fig. 2).

The use of ternary systems BP–FC–DCN and BP–DIZD–DCN results in the disappearance of the low-temperature peak from the DTG curves of the poly(methyl methacrylate) obtained (Fig. 2). Apparently, the additives affect the polymer degradation in the low-temperature step. The PMMA degradation occurs very rapidly within a narrow temperature range (280–380°C) and is accompanied by heat release, according to DTA (Fig. 3). The exothermic peak in the DTA curves of the samples prepared with the DIZD-containing initiating system is observed only at synthesis temperatures of 30 and 45°C.

The heat resistance of PMMA prepared with the ternary initiating systems is higher ($T_{o.d}$ is higher by 20–30°C) than that of PMMA prepared with the binary systems [6, 14] (Fig. 2). An increase in the ferrocene concentration at a fixed content of DCN and BP results in an increase in the temperature of the decomposition onset, which tends to a certain limit (Fig. 4). A different pattern is observed with an increase in the DCN concentration. Addition of 0.5×10^{-4} M DCN to the polymerizing system increases $T_{o.d}$ of PMMA. However, further increase in the DCN concentration causes a decrease in the heat resistance (Fig. 4b). The $T_{o.d}$ of PMMA prepared using the benzoyl peroxide–DIZD–DCN system does not appreciably change with an increase in the DIZD content in the polymerizing system. The effect of DCN on the heat resistance of the polymer is the same as with the FC–DCN–BP system. The relative increase in $T_{o.d}$ as a function of the temperature of the MMA polymerization is maximal for the polymers prepared at 30°C and minimal for those prepared at 60°C, with both ternary initiating systems.

An increase in the heat resistance of PMMA prepared in the presence of a metallocene and a tertiary amine can be due to a decrease in the amount of unsaturated terminal groups formed as a result of chain termination by disproportionation [18, 19], and also to formation of more stable metallocene and diketo carboxylic acid fragments on the ends of the polymer chain. Furthermore, the stabilizing effect of a diketo carboxylic acid on the depolymerization of PMMA was noted previously [6].

Examination of the structure of PMMA macromolecules formed in the simultaneous presence of a metallocene (ferrocene, DIZD) and a tertiary amine (DCN) revealed an increased content (up to 70%, see table) of the syndiotactic structures. The polymers prepared using the ternary systems have a noticeable content of isotactic fragments. This fact suggests that not only free radicals but also radicals bound in a

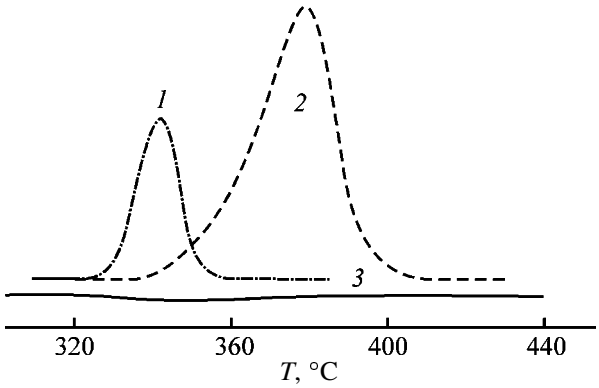


Fig. 3. DTA curves of poly(methyl methacrylate) prepared at 45°C in the presence of 1×10^{-3} M benzoyl peroxide. (*T*) Temperature. Additive, M: (*1*) 1×10^{-3} DIZD + 1×10^{-4} DCN, (*2*) 1×10^{-3} FC + 1×10^{-4} DCN, and (*3*) none.

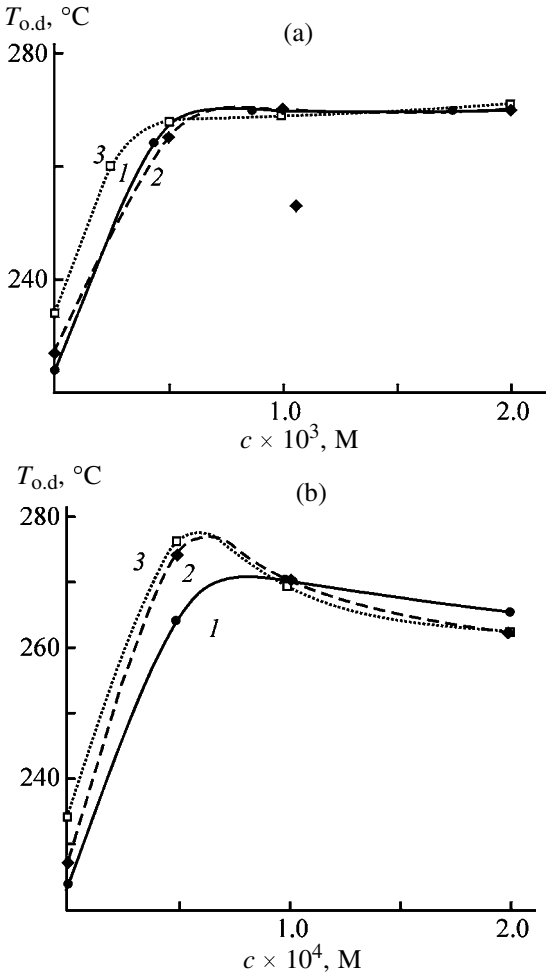


Fig. 4. Decomposition onset temperature $T_{o.d}$ of PMMA (a) prepared in the presence of 1×10^{-3} M benzoyl peroxide and 1×10^{-4} M DCN as a function of ferrocene concentration *c* and (b) prepared in the presence of 1×10^{-3} M benzoyl peroxide and 1×10^{-3} M FC as a function of DCN concentration *c*. Synthesis temperature, °C: (*1*) 60, (*2*) 45, and (*3*) 30.

Microstructure of poly(methyl methacrylate) prepared in the presence of ternary initiating systems at various synthesis temperatures. Initiator: 1×10^{-3} M benzoyl peroxide

T, °C	[ferrocene] × 10^3	[DIZD] × 10^3	[DCN] × 10^4	Content of indicated triads, %		
	M			syndio	hetero	iso
60	0	0	0	56.0	42.0	2.0
	1.0	0	1.0	62.4	33.2	4.4
	0	1.0	0	58.3	36.0	5.7
	0	1.0	1.0	62.1	31.3	6.6
45	1.0	0	1.0	63.0	31.9	5.1
	0	1.0	0	65.0	31.7	3.3
	0	1.0	1.0	66.2	28.1	5.7
30	1.0	0	1.0	68.0	30.3	1.7
	0	1.0	0	69.3	28.9	1.8
	0	1.0	1.0	71.5	27.1	1.4

complex are formed in the system, initiating the polymerization [20]. Hence, the polymerization of MMA in the presence of the FC–DCN and DIZD–DCN systems occurs by the radical complex mechanism. Apparently, the stereospecificity of the MMA polymerization in the systems under consideration is primarily due to interaction between the components of the initiating systems.

CONCLUSION

A study of ternary initiating systems allows not only acceleration of the methyl methacrylate polymerization but also preparation of polymers with enhanced heat resistance and regular microstructure.

ACKNOWLEDGMENTS

The study was financially supported by the Russian Foundation for Basic Research (project no. 05-03-32087) and Foundation for the Support of Scientific Schools (project no. NSh-728.2003.3).

REFERENCES

1. Matkovskii, P.E., *Radikal'nye stadii v reaktsiyakh kompleksnykh metalloorganicheskikh i metallotsenovykh katalizatorov i ikh rol' v polimerizatsii* (Radical Steps in Reactions of Complex Organometallic and Metallocene Catalysts and Their Role in Polymerization), Chernogolovka: Inst. Problem Khimicheskoi Fiziki, Ross. Akad. Nauk, 2003.
2. Grishin, D.F., Shchepalov, A.A., Telegina, E.V., et al., *Vysokomol. Soedin., Ser. A*, 2005, vol. 47, no. 6, pp. 943–951.
3. Puzin, Yu.I., Yumagulova, R.Kh., and Kraikin, V.A., *Eur. Polym. J.*, 2001, vol. 37, no. 9, pp. 1801–1812.
4. Kolesov, S.V., Yumagulova, R.Kh., Prokudina, E.M., et al., *Vysokomol. Soedin., Ser. B*, 2003, vol. 45, no. 2, pp. 324–328.
5. Grishin, D.F., Semenycheva, L.L., Telegina, E.V., et al., *Izv. Ross. Akad. Nauk, Ser. Khim.*, 2003, no. 2, pp. 482–484.
6. Galinurova, E.I., Aromatic Diketo Carboxylic Acids in Radical Polymerization of Vinyl Monomers, *Cand. Sci. Dissertation*, Ufa, 2003.
7. Puzin, Yu.I., Prokudina, E.M., Yumagulova, R.Kh., et al., *Dokl. Ross. Akad. Nauk*, 2002, vol. 386, no. 1, pp. 69–71.
8. Pravednikov, A.N., Stavrova, S.D., Chikhaeva, I.P., et al., *Plast. Massy*, 1980, no. 12, p. 10.
9. Agronomov, A.E. and Shabarov, Yu.S., *Laboratornye raboty v organicheskom praktikume* (Laboratory Works in Organic Chemistry), Moscow: Khimiya, 1974.
10. Puzin, Yu.I., Egorov, A.E., and Kraikin, V.A., *Eur. Polym. J.*, 2001, vol. 37, no. 6, pp. 1165–1173.
11. Samuel, E. and Setton, R., *J. Organomet. Chem.*, 1965, no. 4, p. 156.
12. Gladyshev, G.P., *Polimerizatsiya pri glubokikh stepenyakh prevrashcheniya i metody ee issledovaniya* (Polymerization at High Conversions and Methods for Studying It), Alma-Ata: Nauka, 1968.
13. Lyalikov, Yu.S., *Fiziko-khimicheskie metody analiza* (Physicochemical Methods of Analysis), Moscow: Khimiya, 1973.
14. Mironov, V.A. and Yankovskii, S.A., *Spektroskopiya v organicheskoi khimii* (Spectroscopy in Organic

Chemistry), Moscow: Khimiya, 1985.

15. Yutaka Isobe, Tamaki Nakano, and Yoshio Okamoto, *J. Polym. Sci.*, 2001, vol. 39, no. 9, pp. 1463–1474.
16. *Entsiklopediya polimerov* (Polymer Encyclopedia), Moscow: Sovetskaya Entsiklopediya, 1974, vol. 2.
17. Kraikin, V.A., Ionova, I.A., Puzin, Yu.I., et al., *Vysokomol. Soedin., Ser. A*, 2000, vol. 42, no. 9, pp. 1569–1573.
18. Grassie, N. and Scott, G., *Polymer Degradation and Stabilisation,* Cambridge: Cambridge Univ. Press, 1985.
19. Grassie, N., *Chemistry of High Polymer Degradation Processes*, London: Butterworths, 1956.
20. Kabanov, V.A., Zubov, V.P., and Semchikov, Yu.D., *Kompleksno-radikal'naya polimerizatsiya* (Radical Complex Polymerization), Moscow: Khimiya, 1987.

ISSN 1070-4272, Russian Journal of Applied Chemistry, 2006, Vol. 79, No. 9, pp. 1514–1517. © Pleiades Publishing, Inc., 2006.
Original Russian Text © N.V. Khitrich, I.I. Seifullina, Yu.K. Epimakhov, P.A. Ivanchenko, 2006, published in Zhurnal Prikladnoi Khimii, 2006, Vol. 79, No. 9, pp. 1529–1533.

MACROMOLECULAR CHEMISTRY AND POLYMERIC MATERIALS

Influence of Cobalt(III) Dimethyldithiocarbamate Complexes on Styrene Polymerization Initiated by *tert*-Butyl Perbenzoate

N. V. Khitrich, I. I. Seifullina, Yu. K. Epimakhov, and P. A. Ivanchenko

Mechnikov National University, Odessa, Ukraine

Received March 1, 2006

Abstract—Kinetic features of radical polymerization of styrene initiated by *tert*-butyl perbenzoate in the presence of tris(*N,N*-dimethyldithiocarbamato)cobalt(III) (CoL_3) and its adduct with iodine ($CoL_3 \cdot 2I_2$) were studied. The optimal concentration ratios of the activators and *tert*-butyl perbenzoate, providing fast styrene polymerization at 338–368 K, were determined.

DOI: 10.1134/S1070427206090230

Previously we prepared tris(*N,N*-dimethyldithiocarbamato)cobalt(III) (CoL_3) [1] and its molecular complex with iodine ($CoL_3 \cdot 2I_2$) [2]. The structure of these complexes and their physicochemical properties were determined. This paper continues the study of the synthesis, structure, and properties of these complexes. The goal of this study was to examine the catalytic effect of these complexes on the decomposition of initiators under the conditions of radical polymerization of styrene. This study was stimulated by the following facts.

First, organic compounds containing dithiocarbamate groups are effective agents for living polymerization. They are iniferters, i.e., compounds that simultaneously initiate, transfer, and terminate chains [3, 4].

Second, cobalt(III) dithiocarbamates can be reduced to cobalt(II) compounds or can be oxidized to cobalt(IV) complexes [5–7]. For example, CoL_3 is electrochemically oxidized in acetonitrile by the mechanism [6]

$$CoL_3 \rightleftarrows [CoL_3]^+ + e^-,$$

$$2[CoL_3]^+ \rightarrow [Co_2L_5]+ + \text{oxidized ligand},$$

$$[Co_2L_5]^+ + 2CH_3CN \rightarrow CoL_3 + [CoL_2(CH_3CN)_2]^+.$$

The products, CoL_3 and $[CoL(CH_3CN)_2]^+$, can be repeatedly oxidized. Therefore, cobalt(III) dithiocarbamates can catalyze decomposition of organic initiators, thus accelerating polymerization of vinyl monomers initiated by these systems. However, no data on the use of CoL_3 and $CoL_3 \cdot 2I_2$ for this purpose are reported. Since $CoL_3 \cdot 2I_2$ contains weakly bound molecular iodine, which is an active scavenger of free radicals [8], this complex can both inhibit and catalyze styrene polymerization.

The aim of this study was to examine the influence of $Co[S_2CN(CH_3)_2]_3$ and $Co[S_2CN(CH_3)_2]_3 \cdot 2I_2$ complexes on styrene polymerization initiated by different compounds, to reveal the difference in the kinetic features of the polymerization, and to determine the optimal polymerization conditions at moderately low temperatures. The results of this study can be used to decrease the power consumption and the possibility of occurrence of side reactions.

EXPERIMENTAL

Styrene was treated with 10% KOH to remove hydroquinone, washed with water to neutral washings, dried over $CaCl_2$, and fractionally distilled in Ar at a pressure of 1.3 kPa.

Tris(*N,N*-dimethyldithiocarbamato)cobalt(III) was prepared by the reaction of cobalt(II) chloride with a stoichiometric amount of sodium *N,N*-dimethyldithiocarbamate in an aqueous solution. The product was recrystallized twice from a chloroform–ethanol mixture [1]. The molecular complex $CoL_3 \cdot 2I_2$ was prepared by the reaction of CoL_3 with a threefold excess of iodine in a chloroform–diethyl ether mixture [2]. The content of the main compound in *tert*-butyl perbenzoate (TBPB) was 97.5%.

The kinetics of bulk styrene polymerization was studied dilatometerically [9]. The concentration of cobalt(III) complexes and *tert*-butyl perbenzoate was 10^{-4}–10^{-3} and 10^{-2}–10^{-1} M, respectively. Polymerization was performed at 338, 353, and 368 ± 0.1 K. The polymerization rate under the steady-state condi-

tions was calculated from the slope of the degree of polymerization (S) vs. time (τ) curves using the Excel software.

To determine the molecular weight, polystyrene samples obtained at 20% conversion of the monomer were reprecipitated twice from a benzene solution with methanol and dried to constant weight in a vacuum at room temperature. The intrinsic viscosity of benzene solutions of the polymers was measured on an Ubbelohde viscometer at 298 ± 0.1 K. The molecular weight of polystyrene was calculated by the Mark–Kuhn–Houwink equation $[\eta] = KM^{\alpha}$, where $K = 2.7 \times 10^{-4}$, $\alpha = 0.66$ [10].

The electronic absorption spectra of the solutions of the polymerization systems were recorded on a Specord UV–VIS spectrophotometer in 1-cm quartz cells.

To determine the most effective initiation system, we studied first the influence of typical commercial initiators on the rate of styrene polymerization in the presence of CoL_3. We found that the polymerization rate and the polystyrene molecular weight remained virtually the same when 2,2-azobisisobutyronitrile (AIBN) and dicumyl peroxide were used as the initiators. The polymerization decelerates in the presence of benzoyl peroxide and accelerates when TBPB or isopropylbenzene hydroperoxide is used as the initiator. Subsequent experiments were performed using TBPB as an effective initiator. Styrene polymerization in the presence of this initiator is faster that that in the presence of isopropylbenzene hydroperoxide, all other conditions being the same.

A kinetic study of styrene polymerization initiated by CoL_3–TBPB (**I**) and $CoL_3 \cdot 2I_2$–TBPB (**II**) systems showed that the shape of the initial portions of the kinetic curves was determined by both the qualitative composition and the quantitative ratio of the components of the initiating systems (Fig. 1).

(1) The first steps of the polymerization initiated by system **I** in which the TBPB concentration was substantially higher than that of CoL_3 (Fig. 1, curve *2*) were slightly slower than in the polymerization initiated by TBPB without CoL_3 (Fig. 1, curve *1*). Then the polymerization accelerates, reaching a high constant rate up to a monomer conversion of >75%, without pronounced gel effect.

(2) The kinetic curves became S-shaped with increasing CoL_3 concentration in the system (Fig. 1, curve *3*). As in the first case, the initial polymerization steps were somewhat slower compared to the initiation by TBPB without CoL_3. Polymerization substantially accelerated with time and then gradually decelerated.

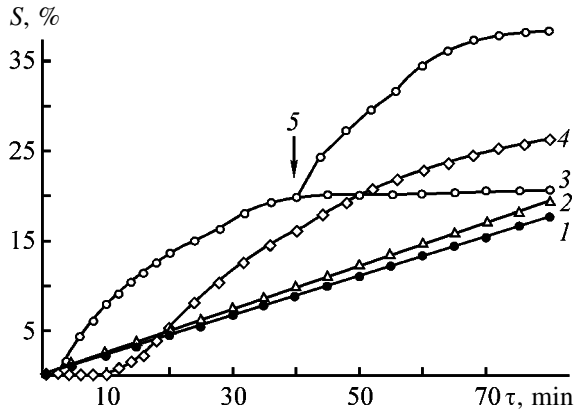


Fig. 1. Kinetic curves of styrene polymerization at 368 K. TBPB concentration 5×10^{-2} M. (S) Degree of polymerization and (τ) time. Concentration of cobalt(III) complexes, M: (*1*) 0, (*2*) 2.5×10^{-3} CoL_3, (*3*) 10^{-4} CoL_3, and (*4*) 2.5×10^{-3} $CoL_3 \cdot 2I_2$; (*5*) additional introduction of TBPB.

(3) The feature of the polymerization initiated by system **II** is a well-defined inhibition period during which no polymerization is observed (Fig. 1, curve *4*). After the completion of this time, the shape of the polymerization curves was similar to that of the kinetic curves of styrene polymerization initiated by system **I**.

Analysis of these data suggests that the insignificant deceleration of styrene polymerization in the first steps is due to the reaction of CoL_3 with TBPB (or its decomposition product) to form reactive intermediates [CoL_3···TBPB] which generate free radicals in the system more readily than does TBPB, thus accelerating the polymerization. The occurrence of the reaction of CoL_3 with TBPB (or its decomposition products) is unambiguously proved by changes in the ESR spectra of solutions of the initiating systems in styrene (Fig. 2), recorded immediately after their preparation and after heating at 368 K for 5–15 min (onset time of the polymerization acceleration).

The electronic absorption spectra of the freshly prepared solutions (Fig. 2, curves *1, 2*) contain weak bands at ~15 600 cm^{-1} assigned to hte $^1A_{1g} \rightarrow {}^1T_{1g}$ transition typical for low-spin octahedral cobalt(III) complexes. The shoulder at ~21 000 cm^{-1} in the spectrum of **I** is due to the second spin-allowed $^1A_{1g} \rightarrow {}^1T_{2g}$ transition. In the case of system **II**, the band of this transition is obscured by the band of free iodine formed by partial dissociation of $CoL_3 \cdot 2I_2$. Strong bands in the short-wave region are due to intraconfigurational transitions in the central atoms and to

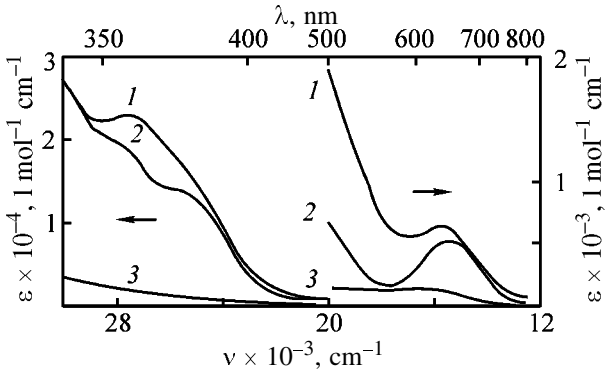


Fig. 2. Electronic absorption spectra of solutions of the initiating systems in styrene. Concentrations, M: cobalt(III) complexes 2.5×10^{-3} and TBPB 5×10^{-2}. (ε) Molar extinction coefficient, (*n*) wavenumber, and (λ) wavelength. (*1*) $CoL_3 \cdot 2I_2$–TBPB, (*2*) CoL_3–TBPB immediately after preparation of the solutions, and (*3*) $CoL_3 \cdot 2I_2$–TBPB or CoL_3– TBPB after heating of the solutions at 368 K for 15 and 5 min, respectively.

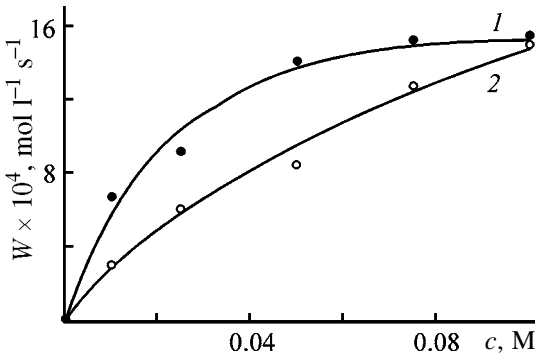


Fig. 3. Rate of styrene polymerization *W* initiated by (*1*) CoL_3–TBPB and (*2*) $CoL_3 \cdot 2I_2$–TBPB systems at 368 K as a function of the TBPB concentration *c*. Concentration of cobalt(III) complexes 2.5×10^{-3} M.

charge transfer between the cobalt atom and the dithiocarbamate group. In the case of system **II**, these bands are masked by a strong charge-transfer band at ~27800 cm^{-1} typical for complexes of thiocarbonyl compounds with iodine.

Heating of the solutions of the initiating system causes the hypsochromic shift of the *d–d* bands and the hypochromic effect for all the bands. The spectra of the solutions of systems **I** and **II** become similar (Fig. 2, curve *3*), which suggests formation of [CoL_3···TBPB] intermediates in both cases.

When the concentration of cobalt(III) dimethyldithiocarbamate complexes in the initiating system increases, the polymerization accelerates and then decelerates with time (Fig. 1, curve *3*). The higher the $c_{Co(III)} : c_{TBPB}$ ratio, the sharper is deceleration of styrene polymerization at the smaller conversion. We suggest that the polymerization decelerates owing to fast consumption of TBPB. To confirm this assumption, a small amount of TBPB was added to one of the dilatometers after deceleration of the polymerization. This resulted in acceleration of the process (Fig. 1, curve *5*). Hence, [CoL_3···TBPB] intermediates formed by the reaction of CoL_3 with TBPB (or its decomposiiton products) catalyze the generation of radicals after introduction of additional portions of TBPB. The S shape of the kinetic curves of polystyrene accumulation under the conditions when the rates of formation and consumption of [CoL_3···TBPB] intermediates are comparable indicates that these intermediates are involved in the polymerization.

The well-defined inhibition period observed when the polymerization is initiated by system **II** (Fig. 1, curve *4*) is caused by the presence of molecular iodine (radical "counter") formed by dissociation of $CoL_3 \cdot 2I_2$. This assumption is confirmed by the shape of its electronic spectrum (Fig. 2, curve *1*) and by our previous data [2]. The induction period is directly proportional to the concentration of $CoL_3 \cdot 2I_2$ and inversely proportional to the TBPB concentration and temperature. The constancy of the $c_{CoL_3 \cdot 2I_2}/\tau_{inhib}$ ratio suggests that iodine is consumed only in reaction with primary radicals generated by the TBPB decomposition. After the end of the inhibition period (complete consumption of molecular iodine), the polymerization accelerates and occurs similarly to the polymerization initiated by system **I**. Thus, $CoL_3 \cdot 2I_2$ both inhibits and catalyzes the TBPB decomposition, which allows the control over the kinetics and temperature of the first polymerization steps.

Polymerization of styrene accelerates with increasing TBPB concentration in systems **I** and **II** at a constant content of the cobalt(III) dimethyldithiocarbamate complexes (Fig. 3). At the same time, the dependence of the polymerization rate on the concentration of these complexes at a constant content of TBPB passes through a maximum (Fig. 4) at $c_{CoL_3} : c_{TBPB}$ and $c_{CoL_3 \cdot 2I_2} : c_{TBPB}$ ratios of 1 : ~20 and 1 : ~30, respectively. The molecular weight of polystyrene decreases from 1.38×10^5 to 2.2×10^4 with an increase in the content of the cobalt(III) complexes in the initiating systems (Fig. 5). Apparently, the cobalt(III) complexes are involved at least in catalysis of TBPB decomposition and in termination of the polymeric chains. The fact that the rate of styrene polymerization initiated by the CoL_3–AIBN system and the molecular weight of the resulting polymer are similar to those in the presence of AIBN without CoL_3 suggests that CoL_3 has no effect on the chain propagation.

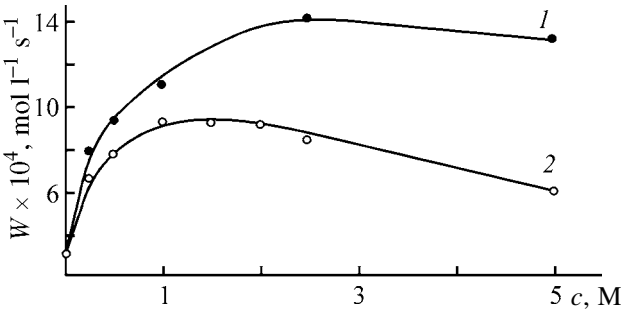


Fig. 4. Rate of styrene polymerization W initiated by (*1*) CoL_3– TBPB and (*2*) $CoL_3 \cdot 2I_2$–TBPB systems at 368 K as a function of the concentration of the cobalt(III) complexes. TBPB concentration 5×10^{-2} M.

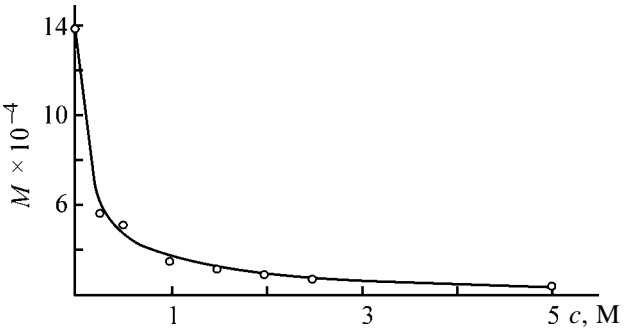


Fig. 5. Molecular weight of polystyrene M as a function of the $CoL_3 \cdot 2I_2$ concentration c. Polymerization temperature 368 K, 20% conversion, TBPB concentration 5×10^{-2} M.

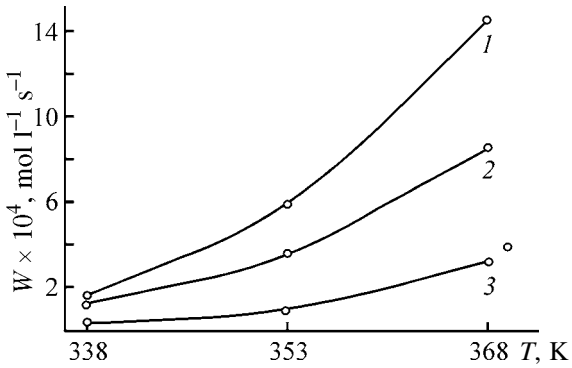


Fig. 6. Rate of styrene polymerization W initiated by (*1*) CoL_3– TBPB and (*2*) $CoL_3 \cdot 2I_2$–TBPB systems, and (*3*) by straight TBPB as a function of temperature T. TBPB concentration 5×10^{-2} M, concentration of cobalt(III) complexes 2.5×10^{-3} M.

The temperature dependence of the styrene polymerization rate (Fig. 6) clearly demonstrates the advantage of initiating systems **I** and **II** over straight TBPB. As seen from Fig. 6, in the presence of these systems styrene rapidly polymerizes at moderately low temperatures. The apparent activation energy of the polymerization in the presence of TBPB and systems **I** and **II** is 93, 76, and 69 kJ mol^{-1}, respectively.

CONCLUSIONS

(1) The kinetic features of bulk styrene polymerization initiated by CoL_3– and $CoL_3 \cdot 2I_2$–*tert*-butyl perbenzoate systems are determined by the qualitative composition of the components of the initiating systems and their quantitative ratio.

(2) Reactive intermediates [CoL_3–*tert*-butyl perbenzoate], which readily generate free radicals in the system and can be repeatedly used, provide fast styrene polymerization.

(3) The $CoL_3 \cdot 2I_2$–*tert*-butyl perbenzoate system inhibits the first steps of styrene polymerization owing to formation of molecular iodine by dissociation of $CoL_3 \cdot 2I_2$ and then catalyzes the process.

(4) The cobalt(III) dimethyldithiocabamate complexes are effective catalysts of *tert*-butyl perbenzoate decomposition into free radicals. Initiating systems containing these complexes can be used to catalyze styrene polymerization at moderately low temperatures. The optimal activator-to-*tert*-butyl perbenzoate concentration ratios for the CoL_3–*tert*-butyl perbenzoate and $CoL_3 \cdot 2I_2$–*tert*-butyl perbenzoate systems are 1 : ~20 and 1 : ~30, respectively.

REFERENCES

1. Khitrich, M.V. and Seifullina, I.I., *Visn. Odes'k. Nats. Univ., Vip. 2: Khimiya*, 2000, vol. 5, pp. 27–32.
2. Khitrich, N.V., Seifullina, I.I., and Starikova, Z.A., *Zh. Neorg. Khim.*, 2002, vol. 47, no. 1, pp. 85–91.
3. Korolev, G.V. and Marchenko, A.P., *Usp. Khim.*, 2000, vol. 69, no. 5, pp. 447–475.
4. Otsu, T. and Matsumoto, A., *Adv. Polym. Sci.*, 1998, vol. 136, pp. 75–137.
5. Bond, A.M., Hendrickson, A.R., Martin, R.L., et al., *Inorg. Chem.*, 1983, vol. 22, no. 23, pp. 3440–3446.
6. Alden, A.J., Bond, A.M., Colton, R., et al., *J. Electroanal. Chem.*, 1998, vol. 447, pp. 155–171.
7. Webster, R.D., Heath, G.A., and Bond, A.M., *J. Chem. Soc., Dalton Trans.*, 2001, no. 21, pp. 3189–3195.
8. Denisov, E.T., *Kinetika gomogennykh khimicheskikh reaktsii* (Kinetics of Homogeneous Chemical Reactions), Moscow: Vysshaya Shkola, 1988.
9. *Praktikum po fizike i khimii polimerov* (Practical Course on Physics and Chemistry of Polymers), Kurenkov, V.F., Ed., Moscow: Khimiya, 1990.
10. Rafikov, S.R., Pavlova, S.A., and Tverdokhlebova, I.I., *Metody opredeleniya molekulyarnykh vesov i polidispersnosti vysokomolekulyarnykh soedinenii* (Procedures for Determining Molecular Weights and Polydispersity of Macromolecular Compounds), Moscow: Akad. Nauk SSSR, 1963.

ISSN 1070-4272, Russian Journal of Applied Chemistry, 2006, Vol. 79, No. 9, pp. 1518–1521. © Pleiades Publishing, Inc., 2006.
Original Russian Text © B.M. Ginzburg, D.G. Tochil'nikov, A.A. Shepelevskii, A.M. Leksovskii, Sh. Tuichiev, 2006, published in Zhurnal Prikladnoi Khimii, 2006, Vol. 79, No. 9, pp. 1534–1537.

MACROMOLECULAR CHEMISTRY AND POLYMERIC MATERIALS

Tribological Properties of Polytetrafluoroethylene Modified with Fullerene Black in Dry Sliding Friction

B. M. Ginzburg, D. G. Tochil'nikov, A. A. Shepelevskii, A. M. Leksovskii, and Sh. Tuichiev

Institute of Problems of Mechanical Engineering, Russian Academy of Sciences, St. Petersburg, Russia
Ioffe Physicotechnical Institute, Russian Academy of Sciences, St. Petersburg, Russia
Tajik State National University, Dushanbe, Tajikistan

Received April 27, 2006

Abstract—The effect of fullerene black introduced (after extraction of light fullerenes from the black with toluene) into polytetrafluoroethylene F-4 on its wear resistance and antifriction properties in sliding over steel at contact pressures in the range 0.2–2.0 MPa was studied.

DOI: 10.1134/S1070427206090242

Polytetrafluoroethylene (PTFE) is one of the best antifriction polymeric materials [1]. However, its use is restricted by cold flow and poor wear resistance. Introduction of various solid fillers into PTFE leads to a certain compromise: the wear resistance increases at a certain deterioration of antifriction properties. Composites based on PTFE are used in manufacture of plain bearings, guiding devices, and seals, including those working without additional lubrication in vacuum and corrosive media [1].

It was shown in [2–4] that introduction of fullerene C_{60} into liquid lubricating oils improves their antifriction and wear-resistant properties in sliding friction of metals. Moreover, introduction of fullerene blacks into oils (even upon extraction of most of fullerenes from the blacks) also markedly improves the tribological properties of lubricants [3]. The possible reason is that a large amount of fullerenes, especially higher fullerenes, remains in the black upon extraction of the larger part of fullerenes with aromatic solvents [5]. Use of various blacks of other origins produces no effects of this kind. At the same time, the fullerene black is a considerably less expensive material than pure fullerenes and, upon extraction of fullerenes, is a waste from the fullerene production, which has not found wide use so far.

The aim of this study was to examine the effect of fullerene black on the tribological properties of PTFE; it was intended to use fullerene black from which fullerenes were already extracted as additive to materials in order to obtain data on the possibility of its practical application.

EXPERIMENTAL

We used as starting materials for tribological tests polytetrafluoroethylene F-4 [GOST (State Standard) 10007–80]. The starting fullerene black was obtained in electric-arc plasma by the Krätschmer–Huffman method [6]. Extraction with toluene as a solvent was used to recover from the black an 8% amount of a mixture of fullerenes (mostly C_{60} and C_{70} in a 75 : 25 ratio). The fraction of residual fullerenes remaining in the fullerene black after the extraction, found by additional prolonged extraction, did not exceed 0.2–0.3%. However, published data suggest that the residual amount of higher fullerenes remaining after primary extraction with toluene in the black we used (designated as FB) is rather high [5, 7].

We introduced 1 wt % FB into the bulk of F-4 in conformity with the same technical specifications which were used in introduction of coal coke and production of F-4K20 material [TU (Technical Specification) 6-05-1412–76]. As shows practical experience [8], there is no point in introducing fullerene C_{60} or a fullerene black into lubricants in an amount exceeding 1–3 wt %. Part of samples were coated with a thin film of fullerene C_{60} by drying a toluene solution of C_{60} directly on the sample surface. The thickness of this film, evaluated by the concentration of the solu-

tion and the area being coated, did not exceed 1 μm. It was natural to assume that such a thin film will be rapidly worn-out in friction, and only the effect of residual amounts of fullerene C_{60} in the gap of the tribocontact on the process of further friction and wear would be expected to occur.

The study was performed on a standard 2070 SMT-1 roller friction machine. A sample being tested had the form of a flat plate with a rectangular cross section and thickness of 10 mm. A roller 46 mm in diameter and 16 mm wide, made of 18Kh2NChMA (GOST 4543–71) chromium–nickel–molybdenum steel and rotating at 400 rpm, which corresponded to a linear sliding velocity of 1 m s^{-1}, was brought to the plate. The roller always exceeded the sample in width.

Two schemes of the initial friction contact were used. In scheme A, the initial cylinder–plane contact between counter bodies was created along the generatrix of the mobile cylindrical roller. Further, a normal load F_N, maintained constant during the entire test (300 s), was applied to the sample and all the tribological characteristics measured were related to this load. In scheme B, a wear groove of area 30–50 mm^2 was preliminarily produced on the sample surface, so that further tests were performed on conformal counter bodies with a worn-in friction contact. A steadily increasing normal load F_N was applied to a sample. The test duration at each load was 300 s. The tests were carried out without lubrication (dry friction mode). Other details of the procedure used to measure tribological characteristics have been described previously [9].

Figure 1 shows dependences of the friction coefficient on the contact pressure for the starting F-4 samples and those filled with a fullerene black, obtained using test scheme B. It can be clearly seen that, upon introduction of the fullerene black, the friction coefficient decreases in the whole range of pressures studied.

Similar results were obtained in tests by scheme A. In addition, longer tests were performed by scheme A (during 30 min) at various initial loads. At each load, the friction coefficient is always smaller (by a factor of 1.2–1.6) for black-filled samples, compared with samples of pure F-4 (Fig. 2).

Introduction of fullerene black FB markedly reduces the volume wear. A similar conclusion that the antiwear properties are improved by introduction of the black can be made on the basis of other wear characteristics. For example, the linear wear intensity

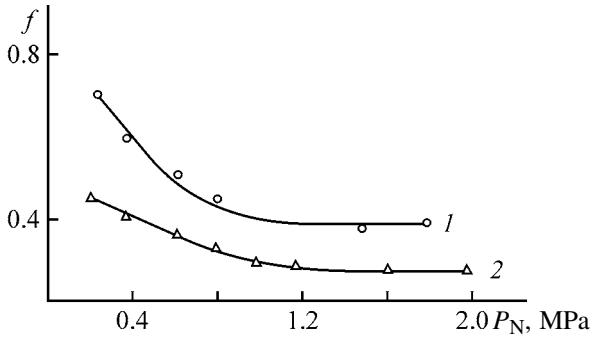


Fig. 1. Sliding-friction coefficient f of F-4 fluoroplastic over steel vs. normal pressure P_N in a friction contact. (*1*) Starting F-4 and (*2*) F-4 + 1% FB; the same for Fig. 2.

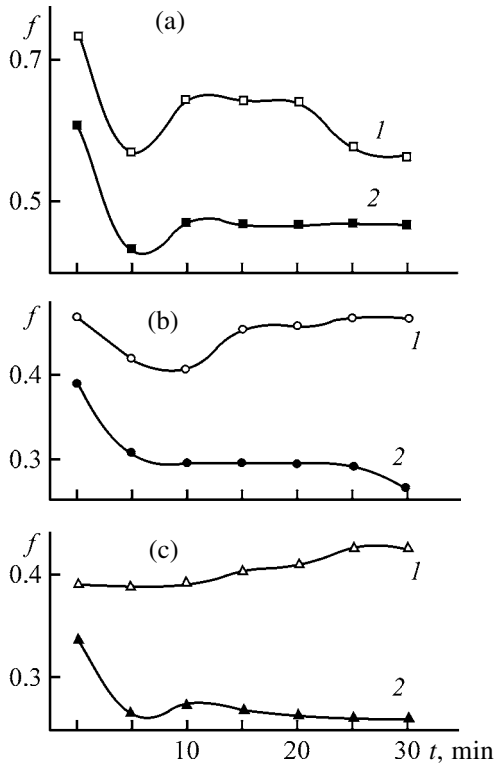


Fig. 2. Sliding-friction coefficient f of F-4 fluoroplastic over steel vs. testing time t at initial loads on the linear constant, F_N, of (a) 40, (b) 120, and (c) 200 N.

I_h is the smallest for F-4 fluoroplastic filled with a fullerene black in the entire range of pressures studied.

The I_h–P_N curves are S-shaped, which is characteristic of transitions between two different wear mechanisms. However, I_h is directly proportional to the contact pressure, rather than being constant, even within the same wear mechanism. Therefore, the wear process is better characterized, in our opinion, by the energy-related wear intensity I_W [10–12], which is equal to the volume worn-out upon expenditure of unit energy.

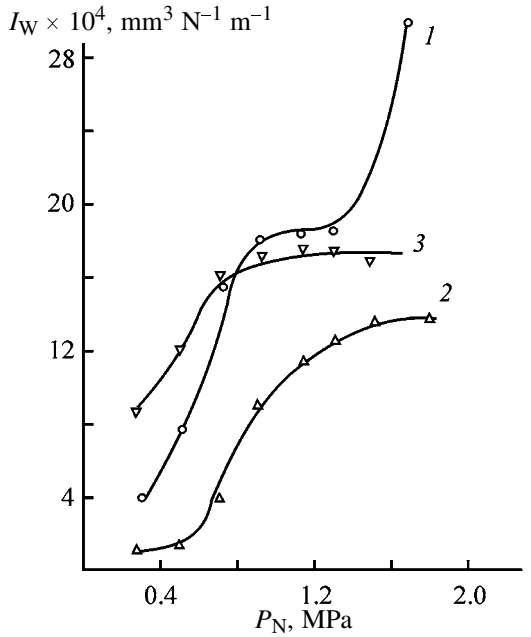


Fig. 3. Energy-related wear intensity I_W vs. normal pressure P_N on a friction contact in dry sliding friction over steel of (*1*) F-4, (*2*) F-4 + 1% FB, and (*3*) F-4 coated with a thin layer of C_{60} fullerene.

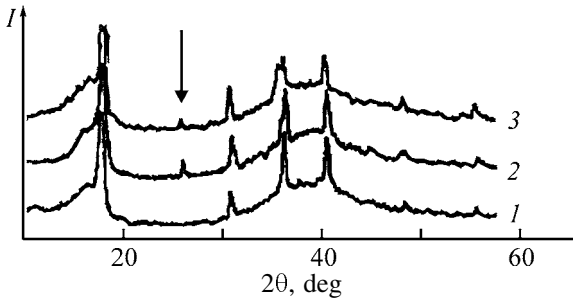


Fig. 4. Wide-angle X-ray diffraction patterns of (*1*) F-4, (*2*) F-4 + 1% FB, and (*3*) F-4 + 3% FB. CuK_α radiation. The arrow shows the reflection corresponding to the strongest 002 reflection from the graphite lattice. (*I*) Reflection intensity and (2θ) Bragg angle.

The constancy of I_W values, frequently observed experimentally on varying the external conditions, is the criterion of a constant wear mechanism. At a given friction path L, the values of I_W and I_h are related by [11, 12]

$$I_W(L) = I_h(L)/f(L)P_N(L).$$

All the dependences of I_W on the contact pressure (Fig. 3) flatten out, which characterizes transition to a mode with a constant wear mechanism. However, only in curve *1* this is followed by a steep rise in I_W at high pressures. In the rest of the cases, the transition to intensive wear, characteristic of scuffing, is apparently shifted to higher pressures, and, therefore, is not seen in the range of the pressures used. This extends the range of working pressures, which should be attributed to the positive effect of fullerenes.

It was assumed previously [2, 3] that, owing to their quasispherical shape, molecules of C_{60} fullerene can serve as a kind of molecular "rollers" on friction surfaces and thereby favor a decrease in the friction and wear coefficients. Further studies of friction surfaces demonstrated that the mechanism of action of C_{60} fullerene in a mineral oil consists in that it initiates formation on friction surfaces of a thin protective polymeric film composed of naphthene and paraffin oligomers present in oils [13, 14]. However, the present study is concerned with dry friction and, consequently, the mechanism by which the wear resistance of F-4 is improved should be different. It should be noted here that fullerene black is present in the F-4 matrix as a separate phase; because of the small amount of the black, only the strongest 002 reflection from the lattice of graphite contained in the black slightly appears in the X-ray diffraction patterns of the samples studied (Fig. 4).

It is known that mechanical degradation of polymer chains occurs at mouths of the forming cracks in mechanical disintegration of polymers. A similar process apparently occurs in mouths of numerous cracks leading to formation of wear particles. The degradation generates free radicals, which can readily add to fullerene molecules to form a fullerene–polymer network. The fact that the polymer radicals formed by thermal degradation of polymers readily react with C_{60} has been demonstrated by numerous examples (polystyrene, polymethyl methacrylate, polyethylene glycol, and poly-*N*-vinylpyrrolidone) [15, 16]. Therefore, the formation of a network from PTFE and fullerenes is rather probable. Consequently, it may be assumed that microscopic cracks that appear in the course of tests close up (are healed) at fullerene molecules because of their high electron-acceptor capacity, rather than go around the fullerene-containing particles as ordinary inclusions. The chain-type free radicals generated by mechanical degradation of F-4 are bound to fullerene molecules by covalent bonds.

It follows from general considerations that the better the properties of the starting material, the lower the efficiency of additives aimed to improve these properties. An effect of this kind with respect to antifriction and antiwear properties was observed upon introduction of fullerene-containing additives into liquid lubricating oils. Therefore, the improvement of the antifriction properties of F-4 fluoroplastic upon

introduction of fullerene black opens up prospects for improvement of tribological properties of other polymeric materials (polyamides, polyimides, epoxy resins, other fluoroplastics, etc.) that are used in friction units [1], but do not possess such good antifriction properties as F-4.

CONCLUSIONS

(1) Introduction of 1 wt % fullerene black (after extraction of light fullerenes from the black with toluene) into the highly antifriction material F-4 leads to an additional decrease in the dry sliding friction coefficient of F-4 over steel by 25–35% at contact pressures in the range 0.2–2.0 MPa. The antiwear properties of F-4 are also noticeably improved upon introduction of fullerene black. Introduction of fullerene black can be recommended for F-4 working as an antifriction material in dry sliding friction units.

(2) The dependences of the energy-related wear intensity on the contact pressure, $I_W(P_N)$ have a flat region within which the wear mechanism is invariable in the corresponding pressure range. Introduction of fullerene black extends the flat region of $I_W(P_N)$ and shifts it to higher pressures, i.e., the load-bearing capacity of the friction unit is raised.

(3) The improvement of the antifriction properties of F-4 fluoroplastic upon introduction of fullerene blacks opens up prospects for enhancement of the antifriction properties of other polymeric materials used in friction units.

ACKNOWLEDGMENTS

The study was carried out in the framework of scientific program no. 14 (coordinator Acad. I.G. Goryacheva) of basic research of the Division of Power Engineering, Machine Building, Mechanics, and Control Processes, Russian Academy of Sciences. It was supported by the International Science and Technology Center (project T-1145).

REFERENCES

1. *Polimery v uzlakh treniya mashin i priborov: Spravochnik* (Polymers in Friction Units of Machines and Instruments: Reference Book), Chichinadze, A.V., Ed., Moscow: Mashinostroenie, 1988, 2nd ed., revised and supplemented.
2. Ginzburg, B.M., Tochil'nikov, D.G., Kireenko, O.F., and Bulatov, V.P., *Pis'ma Zh. Tekh. Fiz.*, 1995, vol. 21, no. 22, pp. 62–66.
3. Ginzburg, B.M., Kireenko, O.F., Tochil'nikov, D.G., and Bulatov, V.P., *Pis'ma Zh. Tekh. Fiz.*, 1995, vol. 21, no. 23, pp. 35–38.
4. Ginzburg, B.M., Tochil'nikov, D.G., and Bulatov, V.P., *Trenie Iznos*, 1997, vol. 18, no. 2, pp. 235–239.
5. Beer, F., Gufel, A., Martin, K., et al., *J. Mater. Chem.*, 1997, vol. 7, no. 8, pp. 1327–1330.
6. Krätschmer, W. and Huffman, D.R., *Phil. Trans. Roy. Soc. London, A*, 1993, vol. 343, no. 1667, pp. 33–38.
7. Smart, C., Eldridge, B., Reuter, W., et al., *Chem. Phys. Lett.*, 1992, vol. 188, no. 1, pp. 171–176.
8. Ginzburg, B.M., Budtov, V.P., Kireenko, O.F., et al., *Problemy mashinovedeniya: Sbornik trudov Inst. problem mashinovedeniya Ross. Akad. Nauk* (Problems of Machine Science: Coll. of Works of the Inst. of Problems of Mechanical Engineering, Russian Acad. Sci.), Bulatov, V.P., Ed., St. Petersburg: Nauka, 2005, pp. 189–222.
9. Tochil'nikov, D.G. and Ginzburg, B.M., *Vopr. Materialoved.*, 2002, no. 31(3), pp. 39–48.
10. Fleisher, G., *Schmierungstechnik*, 1973, vol. 4, pp. 9–15.
11. Kozyrev, Yu.P., Ginzburg, B.M., Priemskii, N.D., et al., *Wear*, 1994, vol. 171, pp. 71–75.
12. Kozyrev, Yu.P., Ginzburg, B.M., Priemskii, N.D., et al., *Trenie Iznos*, 1993, vol. 14, no. 4, pp. 759–764.
13. Shepelevskii, A.A., Shibaev, L.A., Ginzburg, B.M., and Bulatov, V.P., *Zh. Prikl. Khim.*, 1999, vol. 72, no. 7, pp. 1198–1203.
14. Ginzburg, B.M., Kireenko, O.F., Baidakova, M.V., and Solov'ev, V.A., *Zh. Tekh. Fiz.*, 1999, vol. 69, no. 11, pp. 113–116.
15. Ginzburg, B.M., Pozdnyakov, A.O., Zgonnik, V.N., et al., *Pis'ma Zh. Tekh. Fiz.*, 1996, vol. 22, no. 4, pp. 73–77.
16. Shibaev, L.A., Antonova, T.A., Vinogradova, L.V., et al., *Zh. Prikl. Khim.*, 1998, vol. 71, no. 5, pp. 835–841.

ISSN 1070-4272, Russian Journal of Applied Chemistry, 2006, Vol. 79, No. 9, pp. 1522–1525. © Pleiades Publishing, Inc., 2006.
Original Russian Text © B.N. Dudkin, V.P. Krivoshapkin, E.F. Krivoshapkina, 2006, published in Zhurnal Prikladnoi Khimii, 2006, Vol. 79, No. 9, pp. 1538–1541.

MACROMOLECULAR CHEMISTRY AND POLYMERIC MATERIALS

Effect of Aluminum Oxide Nanoparticles on the Properties of Urea–Formaldehyde Resin

B. N. Dudkin, V. P. Krivoshapkin, and E. F. Krivoshapkina

Institute of Chemistry, Komi Scientific Center, Ural Division, Russian Academy of Sciences, Syktyvkar, Komi Republic, Russia

Received April 20, 2006

Abstract—The efficiency of aluminum oxide nanoparticles as a sorbent for removing residual formaldehyde from urea–formaldehyde resin was studied.

DOI: 10.1134/S1070427206090254

Urea–formaldehyde resins (UFRs) are large-tonnage commercial products widely used in production of wood chipboards (WCs), amino- and foam plastics, decorative paper-laminated plastics, synthetic veneer sheet, and moisture-resistant paper, and also in textile industry. However, application of these materials for interior finish and furniture production is restricted by strong liberation of toxic formaldehyde in the course of service of these articles [1]. To decrease the free formaldehyde content, sorbents are introduced into the resin. These sorbents should strongly chemisorb formaldehyde and should be compatible with urea–formaldehyde resins.

Introduction of finely divided silica into UF adhesive substantially decreases the formaldehyde release into the environment [2]. For this purpose, silica sol prepared by acid treatment of "liquid glass" (technical-grade sodium metasilicate) was used. Silica particles strongly sorb up to 15 wt % of formaldehyde released in curing of UF adhesive, and formaldehyde liberation in the course of the use of the resins does not exceed the maximum permissible concentration (MPC). A decrease in MPC of formaldehyde in production and domestic premises make the requirements for UFR materials more stringent. The UFR production process should solve this problem.

Sorbents used for this purpose should rapidly and irreversibly sorb formaldehyde even when the system contains no strong acids, bases or oxidizing agents capable of decomposing the resin structure [3]. In this connection, silica is not optimal sorbent since its surface silanol groups are strongly acidic (pK 2) [4]. Hence, introduction of silica particles with strongly acidic surface can result in premature curing of the resin or its structural degradation.

Since aluminol groups of alumina are moderately strong acids and bases and have no destructive effect on the resin, alumina is a more promising sorbent for residual formaldehyde. Previously we found [5] that alumina sol irreversibly sorbs formaldehyde owing to formation of strong bonds with it. In addition, alumina sol is well compatible with UFR. Formaldehyde is incompletely desorbed form the sol under rigorous conditions. The product of reaction of alumina and formaldehyde, treated in a vacuum (3×10^{-3} Pa) at 220°C, contains approximately 20% organic component.

In this study we examined the influence of alumina nanoparticles used as sorbent of free formaldehyde on the properties of UFR.

An aqueous formaldehyde solution used in production of UFR contains an equilibrium mixture on monomeric formaldehyde and polyoxymethylene glycols $HO(CH_2O)_nH$ [6]. These compounds readily interact with the OH groups of finely divided particles of alumina sol [7], thus providing good compatibility of the polymeric UFR matrix and alumina nanoparticles. Since the carbonyl group of formaldehyde is highly nucleophilic, formaldehyde readily enters into addition reactions. The monomer polymerizes in the presence of almost all base catalysts. Adsorption of formaldehyde on the surface of alumina particles involves acid–base interaction of the surface OH groups with formaldehyde oligomers on the pseudoliquid interface to form strong bonds [8]. Formation of the organic film at the interface decreases the interface

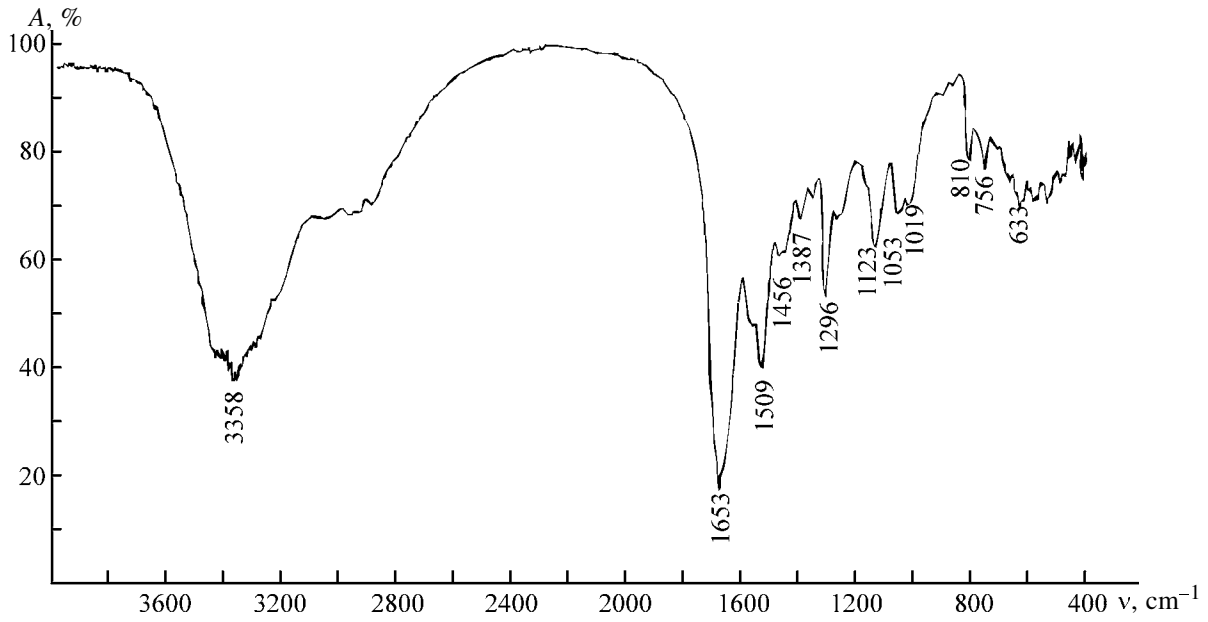


Fig. 1. IR Fourier spectrum of UFR containing alumina particles. (*A*) Transmission and (ν) wavenumber.

surface energy at the liquid-solid boundary, and the loose fractal structure of alumina sol [9] favors absorption of formaldehyde oligomers in the bulk of the sorbent to form interpenetrating polymer networks. It should be noted that materials in which the organic component forms a cross-linked structure in the primary network structure of the inorganic component or vice versa or in which both components form interpenetrating network structure with covalent or ionic bonds are of great interest [10].

Several compounds can be formed in the urea–formaldehyde system. The content of these compounds is determined by the process parameters. Complex structure of UFR is caused by high functionality of urea (4) and formaldehyde (2), which favors formation of diverse condensation products [11]. Polycondensation of urea and formaldehyde in moderately basic solutions yields methylol urea derivatives (mono- and dimethylolurea) which polymerize in neutral or weakly acidic solutions to form cross-linked polymers. The presence of alumina particles with the above properties should promote formation of these polymers.

Sorption of formaldehyde on the nanoparticle surface is accompanied by hydrophobic–hydrophilic effects caused by interactions between the surface and formaldehyde oligomers. The stability of the resulting structure is determined by the balance of these forces.

The number and the frequency of the bands in the IR spectrum of UFR are similar to those in the typical spectrum described in [12]. In the presence of alumina particles, the bands of the NH and C=O groups in the spectrum of UFR are shifted toward the long waves owing to formation of bonds between these groups and the alumina surface.

The photomicrographs of UFR containing alumina nanoparticles (ω = 5%, transmitted light, magnification 400) are shown in Fig. 2. The samples have fairly uniform microstructure; the components are uniformly distributed in the material.

The microstructure of UFR prepared in the presence of aluminum isopropoxide (Fig. 3a) substantially differs from that described above. The sample contains relatively large blocks with a highly uniform structure. We suggest that the blocks are formed owing to the presence of the alcohol which is a chain-



Fig. 2. Photomicrograph of UFR containing alumina particles.

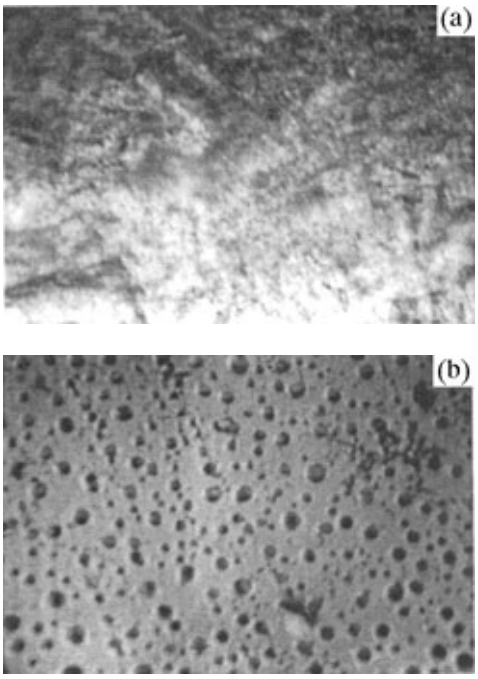


Fig. 3. Microstructure of UFR prepared using (a) aluminum isopropoxide (transmitted light, magnification 400) and (b) aluminum salt (reflected light, magnification 400), alumina content ω = 10%.

transfer agent. The other reason is hydrophobic interaction of formaldehyde oligomers and the alkoxide hydrolysis products, leading to the formation of compact microconstituents of the structure [13], which minimize the contact with the medium. These microstructures can be considered as hydrophobic areas consisting of associates of hydrophobic molecules. The presence of interface between the blocks is a disadvantage of the material.

Polymerization of UFR containing more than 8% alumina nanoparticles yields a milk-white solid. The sample is brittle and tends to exfoliate owing to the segregation of the inorganic salt in some areas. The photomicrograph of the exfoliated surface, taken by optical microscopy in the transmitted light, is shown in Fig. 3b.

The UFR samples prepared by the procedures described in the Experimental section exhibit different stability with respect to water. The weight loss in 2 days of the resin free of alumina particles and of the alumina-containing resins prepared by hydrolysis of the salt and of aluminum isopropoxide is 23, 17, and 9%, respectively. These data correlate well with the content of free formaldehyde in the samples, which is 0.01 and 1.1% in the resin containing alumina nanoparticles and free of them, respectively.

The free formaldehyde content in UFR samples modified with alumina particles is lower by two orders of magnitude than that in the reference samples and by an order of magnitude compared to the published data [14].

EXPERIMENTAL

We used 5–10-nm alumina particles prepared by chemical condensation in a solution. To modify the resin with alumina nanoparticles, a powder prepared by hydrolysis of an aluminum salt in an ammonia formaldehyde solution was introduced into the reaction mixture. The product is spontaneously dispersed in an aqueous formaldehyde solution. The weight fraction of alumina in UFR was determined by the weighed portion of the preparation.

Modified UFR was prepared from formaldehyde containing alumina nanoparticles by the procedure described in [15]. To a formaldehyde solution, ammonia was added to pH 7. Urea (1/2 of the total amount) was added at continuous stirring and heating. The remaining amount of urea was added in portions. The urea : formaldehyde molar ratio was 1 : 2. Water was distilled off, and the syrupy liquid was applied onto a plastic support. The resin was polymerized at 50°C for more than a day. The product had no formaldehyde odor. The concentration (ω) of Al_2O_3 particles in UFR samples ranged from 5 to 10%.

Modification of UFR with alumina nanoparticles using aluminum isopropoxide was performed by the following procedure. To a formaldehyde solution, an ammonia solution was added. Then aluminum isopropoxide was added dropwise. A flaky precipitate that formed in the solution disappeared on stirring, and a sol was formed. A white syrupy liquid was obtained after heating with continuous stirring. To this product, urea was added as described above. The resin was polymerized at 50°C for more than a day. The product had no formaldehyde odor. The alumina content (ω) in the samples was 0.1, 0.4, 0.8 and 1.5%. The samples are water-insoluble bluish or milk white plates in transmitted light, depending on the alumina content.

CONCLUSION

Alumina nanoparticles prepared by sol–gel procedure effectively sorb free formaldehyde in urea–formaldehyde resins, thus decreasing their toxicity.

REFERENCES

1. Leonovich, A.A., Kovrizhnykh, L.P., Korneev, V.I., et al., *Zh. Prikl. Khim.*, 2002, vol. 75, no. 8, pp. 1363–1365.
2. Maslosh, V.Z., Kotova, V.V., and Maslosh, O.V., *Zh. Prikl. Khim.*, 2003, vol. 76, no. 3, pp. 498–501.
3. Maslosh, V.Z., Kotova, V.V., and Maslosh, O.V., *Zh. Prikl. Khim.*, 2002, vol. 75, no. 8, pp. 1396–1397.
4. Huertas, F.J., Lei Chou, and Wollast, R., *Geochim. Cosmochim. Acta*, 1998, vol. 62, no. 3, pp. 417–431.
5. Dudkin, B.N., Krivoshapkin, V.P., and Luksha, V.G., *Kolloidn. Zh.*, 2006, vol. 68, no. 1, pp. 46–50.
6. Balashov, A.L., Danov, S.M., Krasnov, V.L., et al., *Zh. Obshch. Khim.*, 2002, vol. 72, no. 5, pp. 797–801.
7. Ryazanov, M.A. and Dudkin, V.N., *Kollodn. Zh.*, 2004, vol. 66, no. 6, pp. 807–810.
8. Ogorodnikov, S.K., *Formal'degid* (Formaldehyde), Leningrad: Khimiya, 1984.
9. *Sovremennye problemy fizicheskoi khimii* (Modern Problems of Physical Chemistry), Moscow: Granitsa, 2005.
10. Pomogailo, A.D., Rozenberg, A.S., and Uflyand, I.E., *Nanochastitsy metallov v polimerakh* (Metal Nanoparticles in Polymers), Moscow: Khimiya, 2000.
11. Odian, G., *Principles of Polymerization*, New York: McGraw-Hill, 1970.
12. Kuptsov, A.Kh. and Zhizhin, G.N., *Fur'e-KR and Fur'e-IK spektry polimerov* (Raman and IR Fourier Spectra of Polymers), Moscow: Fizmatlit, 2001.
13. Kessler, Yu.M. and Zaitseva, A.L., *Sol'vofobnye effekty* (Solvophobic Effects), Leningrad: Khimiya, 1989.
14. *Entsiklopediya polimerov* (Encyclopedia of Polymers), Moscow: Sov. Entsiklopediya, 1977, vol. 1–3.
15. Losev, I.P. and Fedotova, O.Ya., *Praktikum po khimii vysokopolimernykh soedinenii* (Laboratory Course on Chemistry of Highly Polymeric Compounds), Moscow: Goskhimizdat, 1962.

ISSN 1070-4272, Russian Journal of Applied Chemistry, 2006, Vol. 79, No. 9, pp. 1526–1531. © Pleiades Publishing, Inc., 2006.
Original Russian Text © O.A. Ermolovich, A.V. Makarevich, 2006, published in Zhurnal Prikladnoi Khimii, 2006, Vol. 79, No. 9, pp. 1542–1547.

MACROMOLECULAR CHEMISTRY AND POLYMERIC MATERIALS

Effect of Compatibilizer Additives on the Technological and Performance Characteristics of Biodegradable Materials Based on Starch-Filled Polyethylene

O. A. Ermolovich and A. V. Makarevich

Belyi Institute of Mechanics of Metal–Polymer Systems, National Academy of Sciences of Belarus, Gomel, Belarus

Received June 16, 2005; in final form, January 2006

Abstract—The deformation and strength characteristics, as well as rheological properties and biodegradability of film materials prepared by hot pressing and slot extrusion methods from polyethylene–plasticized starch–compatibilizer blends were examined. Polyethylene with grafted itaconic acid served as compatibilizer. The formulation and technological parameters of preparation of biodegradable film materials were optimized to meet the technical performance criteria.

DOI: 10.1134/S1070427206090266

The need to solve the problem of contamination of the environment with industrial and domestic plastic waste (packaging and agricultural films, containers, disposables, etc.) stimulated, in particular, the development of biodegradable polymeric materials (BPMs). Waste BPM products are capable of degradation when exposed to natural factors (soil and atmospheric microorganisms, ultraviolet radiation) and water-soluble chemical reagents [1–3].

A large group of BPMs is based on biopolymers belonging to polysaccharides, as well as on their composites with synthetic thermoplastics. Polysaccharides are isolated from renewable plant (corn, potato, and rice starchs, cellulose) and animal (chitin, chitosan) raw materials [4, 5]. An important place in the BPM group of interest is occupied by composites based on starch (St) and polyethylene (PE).

Nonpolar PE is thermodynamically incompatible with polysaccharides whose macromolecules contain polar groups [6]. This is responsible for the fact that an increase in the St content deteriorates the process parameters, above all, the fluidity of PE/St melts, as well as the physicomechanical characteristics of the products thereof. At the same time, the St concentration in a blend with PE should be fairly high to make the composite biodegradable. The development of BPMs combining high biodegradability with good deformation and strength characteristics still remains an important problem in materials science and polymer composite technology.

One way to solve this problem is to use starch-filled composites of functionalized PE, with polar functional groups grafted to its macromolecules, as the polymeric binder. Today, reactive extrusion of polymers is actively introduced into industry [6]. For example, PE is chemically modified by grafting polar vinyl monomers (maleic anhydride, itaconic acid, etc.) to the PE macromolecules occurring in the viscous-flow state [7]. The macromolecules of modified PE contain carboxy groups and exhibit enhanced thermodynamic compatibility with the polar polysaccharide filler, which intensifies the interphase interactions. The mechanism of the latter is virtually not understood; this is a multifactor physicochemical process affecting the structural organization and properties of composites [8]. Chemical reactions between the carboxy groups grafted to the PE macromolecules and the hydroxy groups of St and the plasticizer [typically, glycerol (Gl)] can proceed via formation of ester and hydrogen bonds (the energy parameters of the latter are determined, in particular, by the proton-donating and proton-accepting powers, as well as by the concentration of the reacting groups).

Full replacement of PE by expensive functionalized PE in BPM like PE/plasticized starch (PSt) is economically unfavorable. In this study we suggested compatibilization of the PE/PSt blend by introducing functionalized PE as the third component of the blend (compatibilizer). Polymeric compatibilizers are reactive copolymers or chemically modified polymers

X–Z (where Z is a long-chain reactive segment or a functional group attached to the main chain) that can compatibilize the polymeric pair of X and Y provided that Z can chemically react with polymer Y [6]. This will increase the concentration of the biopolymeric filler in the composite and, hence, the biodegradability of the latter without deteriorating its physicomechanical characteristics.

In this study we established the physicochemical and technological relationships in formation of PE/PE–itaconic acid (ItA)/PSt film composites having a high biodegradability and good deformation and strength characteristics.

EXPERIMENTAL

The base for hot-pressed film BPMs was 16 803–070 brand powdered LDPE; the compatibilizer was functionalized PE with grafted itaconic acid [TU RB (Technical Specifications of Belarus Republic) 03 535 279.015–97]; and the biodegradable filler was native corn St [GOST (State Standard) 7697–82)].

Starch was dried at 110°C for 5 h and introduced into PE in concentrations from 5 to 50 wt %. Technological, in particular, rheological, characteristics of mixed PE/St melts were poorer than those of PE melts, evidently, because of a large grain size of St and its low compatibility with PE. The workability of the compositions was improved by plasticization with glycerol. The choice of Gl as plasticizer was dictated by its high plasticizing power with respect to St and a satisfactory plasticizing power with respect to PE, as well as nontoxicity and a fairly high thermal stability [9]. The Gl concentration in the compositions was constant, 10 wt %. The polymer blends were prepared in two stages: (1) mixing St with the plasticizer to obtain a homogeneous mass and (2) mixing PSt with LDPE and PE with grafted ItA (PE–ItA). The film samples were prepared by hot pressing on a hydraulic press with heated plates (pressing temperature 180 ± 5°C, pressure 10–15 MPa) or by reactive extrusion on a Haake Rheocord 90 single-screw extruder equipped with a sheet die (temperature range over the cylinder zones and on the sheet die of the extruder 160–180°C).

The deformation and strength parameters of the BPMs were determined according to GOST 14 236–81 on an Instron (the United States) tensile-testing machine at a sample extension rate of 5 mm min^{-1} at 25°C. Before testing, the samples were kept for 24 h in a desiccator over silica gel.

The melt flow index (MFI) was measured on an IIRT-AM (GOST 11 645–73) extrusion plastometer at a load of 5 kg at 190°C. After drying, the granules of the compositions were charged into the heated cylinder of the setup and kept for 4 min before application of the load. The melt flow index was determined by the formula

$$\mathrm{MFI} = m600/\tau,$$

where m is the weight of the melt that flows out from the cylinder within time τ, s.

The MATIR IR spectra of the composite BPMs and their components were recorded on a Nicolet 5700 IR Fourier spectrophotometer. The components were analyzed as granules (PE, PE–ItA), powder (St), or liquid (Gl), and the composites, as films formed by hot pressing.

The microstructure of the samples was examined by scanning electron microscopy (a CamScan-4 microscope).

Biodegradation of the composite film BPMs was examined by microbiological testing. Strains of *Aspergillus (A.) niger, Penicillium (P.) funiculosum, Trichoderma viride, Azotobacter sp., Bacillus megatherium, Bacillus brevis*, and *Pseudomonas sp.* microorganisms, available from the collection of the St. Petersburg Pharmaceutical Institute, served as test cultures. These microorganisms were recommended by GOST 9.049–91 for testing the bioresistance of polymeric materials. The microbial strains were cultivated for tests on a Czapek agar [10].

First, we identified the most active degrader microorganisms for BPMs. The film samples examined were most rapidly fouled with mycelium of *A. niger* and *P. funiculosum* microscopic fungi. In subsequent experiments we used *A. niger* culture. According to GOST 9.049–91, *A. niger* was cultivated for 28 days in Petri dishes with BPM placed in them on an agar lawn. We recorded the broadening in time of the zone covered with mycelium of *A. Niger* formed over the sample perimeter.

Figure 1a presents the ultimate tensile strength σ and the relative elongation at break ε of the films pressed from PE/PSt binary polymeric blends vs. the filler concentration c. It is seen that the parameters σ and ε of the film samples monotonically decrease with increasing c. This trend is due, evidently, to an increase in their imperfection. Apparently, extension causes the composite samples to fail at the interface of poorly compatible binder and filler phases, and the

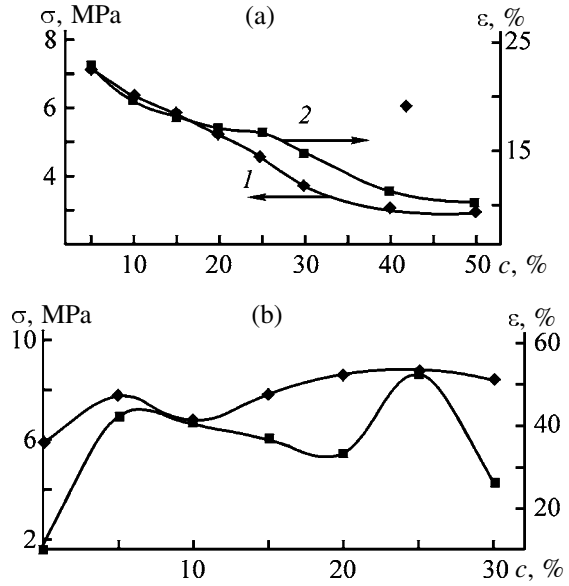


Fig. 1. (*1*) Ultimate tensile strength σ and (*2*) relative elongation at break ε of (a) PE/PSt film samples vs. St concentration *c* and (b) PE/PE–ItA/25 wt % St film samples vs. PE–ItA concentration *c*. (a) Glycerol content in the samples 10 wt %.

surface area of the interfaces increases with increasing St concentration.

To estimate the deformation and strength characteristics of the films pressed from the PE/PE–ItA/PSt ternary blends as influenced by the compatibilizer concentration, the content of St in them was fixed at 25 wt %, ensuring high degradability of the materials. We examined the deformation and strength characteristics σ, ε of the films in relation to the PE–ItA concentration (Fig. 1b). It is seen that, with increasing content of the compatibilizer, the ultimate tensile strength of the films passes through a flat maximum corresponding to c = 20–30 wt %. This is, evidently, due to formation at the PSt–binder interfaces of a new phase involving PE–ItA. An increase in c to 20 wt % is accompanied by a directly proportional increase in σ owing to strengthening of the interfaces. At c = 20–30 wt %, the strength of the films is virtually constant, since further increase in the number of the bonds between PSt and LDPE does not lead to strengthening of the interfaces. At c > 30 wt %, the strength begins to decrease by exponent. This is due to an increase in the content of the PE–ItA component in the composition, less strong than LDPE. Because of enhanced barrier properties of the compatibilizer, this adversely affects the biodegradability of the materials.

The maxima in the plot of the elasticity of the films are also due to formation of a new phase between the PSt particles and the binder. Increase in the elasticity up to concentrations c of 8–9 wt % is due to strengthening of the interfaces, which is responsible for ever more active participation of the binder in deformation of the samples. At c = 8 wt %, the strength reserve of LDPE is exhausted, and rigid binder–filler interfaces are involved into film deformation, thereby decreasing ε. At 20 < c < 25 %, ε tends to increase, since a new factor, increase in the content of the LDPE + PE–ItA polymeric phase at a fixed PSt concentration of 25 wt %, begins to operate. A subsequent (c > 25 wt %) decrease in the elasticity of the films is due to the fact that the properties of the composition are dominated by those of the PE–ItA compatibilizer.

Thus, 25 wt % can be considered as the optimal concentration of PE–ItA in the compositions examined, ensuring satisfactory deformation and strength properties of the hot-pressed BPM films.

In the subsequent series of experiments we compared the σ and ε parameters of the film samples in which PE–ItA was absent (Fig. 1) or present in a constant concentration (25 wt %) (see table), and the St content increased at the expense of a decrease in the PE concentration. Comparison of the data in Fig. 1 and in the table suggests that, at a constant St concentration, the compatibilized composites surpass noncompatibilized samples in the mechanical strength and elasticity. Thus, increase in the PE–ItA concentration in the PE/PSt blends to a certain level allows the degree of filling of the composites with the biodegradable filler to be increased without substantially deteriorating their strength.

Poorer deformation and strength parameters of the composites prepared by pressing compared to those prepared by extrusion can be attributed to imperfection of their structure. This is due, above all, to aggregation of the polysaccharide filler particles and nonuniform distribution of the aggregates over the polymeric pressed matrix. By contrast, the structure of the samples prepared by extrusion is distinguished by high uniformity, with the binder macromolecules oriented in the extrusion direction, as suggested by the electron-microscopic data. Evidently, this is specifically responsible for a high tensile strength and elasticity of the films prepared by extrusion.

The technological properties of the compositions were estimated from the MFI. In the absence of compatibilizer, the MFI of the PE/PSt blends with a high filler (starch) content was 0.15–0.22 g $(10\ \text{min})^{-1}$, which is markedly lower than that of melts of commercial thermoplastics (for various LPDE brands

Melt flow indices (MFIs) of the PE/PE–ItA/St/Gl polymeric compositions and deformation and strength characteristics of films thereof

BPM composition, wt %	MFI, g (10 min)$^{-1}$		σ, MPa		ε, %	
	A	B	A	B	A	B
PE (100)	7.00 ± 0.04	1.63 ± 0.05	8.7 ± 4.2	9.0 ± 0.6	410.0 ± 5.1	450.0 ± 3.1
PE/PE–ItA(25)/St(*X*)/Gl(10), *X*:						
5	17.9 ± 0.9	1.00 ± 0.07	9.3 ± 3.3	18.4 ± 2.2	10.2 ± 2.1	134.2 ± 5.0
10	19.5 ± 0.8	0.7 ± 0.1	7.0 ± 3.6	10.6 ± 3.6	25.0 ± 5.4	114.2 ± 2.1
15	14.0 ± 0.9	0.50 ± 0.05	6.6 ± 2.3	8.9 ± 2.8	25.2 ± 7.2	77.2 ± 5.2
20	11.5 ± 0.8	0.50 ± 0.05	5.9 ± 3.4	7.6 ± 2.3	38.9 ± 3.2	56.3 ± 7.9
25	5.8 ± 2.1	1.4 ± 0.1	5.7 ± 3.4	7.0 ± 4.4	45.2 ± 5.1	61.4 ± 15.2
30	7.6 ± 1.1	0.4 ± 0.2	3.4 ± 2.7	5.3 ± 2.4	20.1 ± 2.6	50.0 ± 7.4

* Samples prepared by (A) hot pressing and (B) extrusion.

prepared by extrusion, this parameter varies within 0.3–2 g (10 min)$^{-1}$ [11]). The dependence of MFI *y*, g (10 min)$^{-1}$, on the St concentration *x*, %, for binary PE/PSt blends is satisfactorily described by the linear correlation (r = 0.86)

$$y = 22.23 - 0.54x.$$

The compatibilized PE/PE–ItA/PSt compositions are characterized by appreciably higher MFI parameters that noncompatibilized samples (see table). An increase in the St content in the former at the PE–ItA concentration fixed at 25 wt % causes the MFI of the composite melts to decrease, though to a technologically acceptable level.

Thus, the experimental data we obtained suggest that the ternary PE/PE–ItA/PSt blends differ favorably from the binary PE/PSt blends in the MFI and the deformation and strength characteristics of films thereof. The reason is, evidently, the favorable effect of the compatibilizer on the compatibility of the blend components and structure of the composite films. At the PE–ItA concentrations of 25 wt % in the PE/PE–ItA/PSt blends, the composites exhibit the highest MFI and the best deformation and strength characteristics over a wide range of the St concentration. This makes the blends with optimized formulation suitable for extrusion processing into film BPMs.

We assumed that improvement of the parameters of interest for the PE/PE–ItA/PSt composites relative to PE/PSt samples is due to the fact that, in the presence of the compatibilizer, the interphase interactions are intensified via involvement of the polar groups of the PE–ItA and St molecules. The diphilic PE–ItA molecules in the compositions are, evidently, localized at the PE/PSt interface with their polar groups oriented toward the filler surface. The oxygen-containing groups in the PE–ItA molecules are able of both physicochemical and chemical interaction with the functional groups in St and Gl. These assumptions were confirmed by an IR study of the molecular structure of the composites.

Extensive interpretation of the vibrational spectra of the composites of interest and their components was beyond the scope of this study. We analyzed selected spectral ranges in which the expected chemical reactions of the components could be manifested.

We compared the IR spectra of PSt, PE, and PE–ItA samples, as well as of the binary PE/PSt and PE–ItA/PSt and ternary PE/PE–ItA/PSt blends (Fig. 2). The spectra essentially differ in the frequency range 1600–1800 cm^{-1} (Fig. 2a), where the characteristic absorption bands of the carbonyl groups (in particular, in carboxylic acids, esters) are usually manifested, and also in the 1000–1300 cm^{-1} range (Fig. 2b), where the bands of the stretching vibrations of the C–O–C bond in ethers and esters can appear [12].

The spectrum of PE–ItA (Fig. 2a, curve *4*) contains the absorption band ν(C=O) at 1743 cm^{-1}, apparently belonging to the stretching vibrations of the carboxy groups of itaconic acid grafted to the PE macromolecules. The carboxy groups are, evidently, hydrogen-bonded, as suggested by the shift of their ν(C=O) band to lower frequencies [13]. In the spectrum of the initial PE (Fig. 3a, curve *2*), the ν(C=O) band belonging to the oxidized form of the polymer [14] is weakly manifested. The vibrational spectrum of PSt (Fig. 2a, curve *1*) contains no characteristic absorption bands in the range of interest. At the same time, the IR spectrum of the binary PE–ItA/PSt blend (Fig. 2a, curve *5*) contains, along with the absorption band with

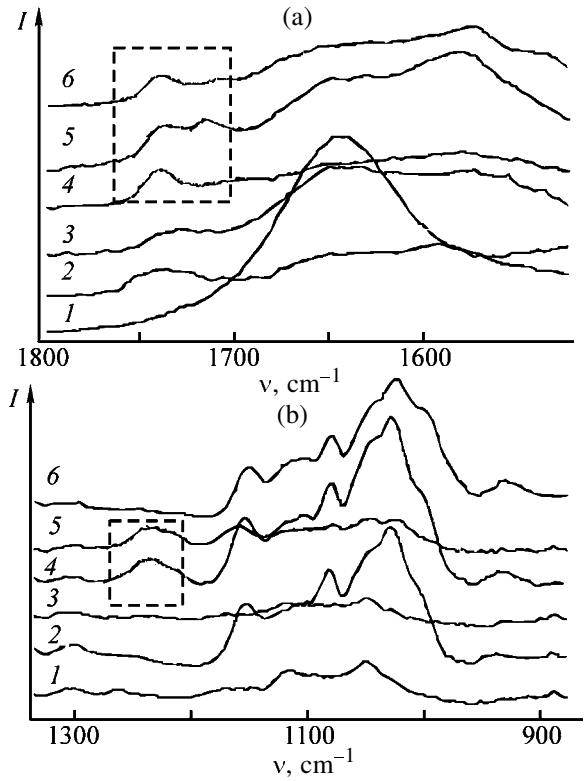


Fig. 2. IR spectra of the compositions and their components in various frequency ranges. (*I*) Intensity and (ν) wavenumber. (a) 1500–1880 cm^{-1}: (*1*) PSt, (*2*) PE, (*3*) PE/PSt, (*4*) PE–ItA, (*5*) PE–ItA/PSt, and (*6*) PE/PE–ItA/PSt; (b) 900–1300 cm^{-1}: (*1*) PE, (*2*) PE/PSt, (*3*) PE–ItA, (*4*) PE–ItA/PSt, (*5*) PE–ItA/Gl, and (*6*) PE/PE–ItA/PSt.

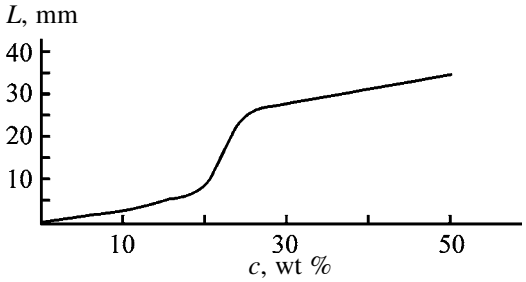


Fig. 3. Width *L*, mm, of the zone of fouling of the PE/PSt film samples with *A. niger* mycelium vs. the St concentration *c* after 7 days of cultivation.

a maximum at 1740 cm^{-1}, a new band at 1720 cm^{-1}. The latter band, probably, corresponds to ν(C=O) of the ester groups formed by the chemical reaction of PE–ItA and PSt. This reaction, most likely, involves the carboxy groups of PE–ItA and hydroxy groups of Gl, as well as of St. The ν(C=O) band of the carboxy groups of PE–ItA participating in esterification does not disappear completely, but decreases in intensity. Hence, despite excess of the esterification agent (PSt), esterification proceeds only partially. The fact that the carboxy groups of the PE-grafted itaconic acid are chemically bound to the hydroxy groups of Gl and St is confirmed by the appearance in the spectra of PE–ItA/PSt and PE–ItA/Gl blends (Fig. 2b, curves *4* and *5*) of the absorption band corresponding to the stretching vibrations ν(C–O–C) of the ester groups at 1230 cm^{-1}. The spectra of the PE/PE–ItA/PSt ternary blend (Figs. 2a, 2b, curves *6*) contain both (though less pronounced) characteristic absorption bands of ester groups [ν(C=O) at 1720 cm^{-1} and ν(C–O–C) at 1230 cm^{-1}]. Thus, the IR data suggest chemical bonding of the polysaccharide filler and compatibilizer in the composites examined. IR monitoring of the possible compatibilization by hydrogen bonding of the molecules of the components of the compatibilized blends [15] proved to be a complicated task because of overlap of the characteristic bands of the hydroxy groups in these molecules. Hydrogen bonding is suggested by a low-frequency shift of the bands corresponding to the stretching vibrations of the carboxy groups of the PE–ItA molecules and the ester groups formed at the PE–ItA/PSt interface.

The microbiological experiments revealed a rapid (manifested even on the third day) growth of the *A. niger* mycelium over the surface of starch-flled PE films. By contrast, no fouling was observed for the PE samples. The results obtained on the seventh day (Fig. 3) suggest correlation between the *A. niger* growth intensity and the St concentration in the PE/PSt film samples. Introduction of the compatibilizer into the PE/PSt compositions insignificantly accelerated biodegradation of the film samples thereof.

It can be assumed that degradation of the starch-filled composite films by *A. niger* soil fungus is due to the mechanical impact by the proliferating mycelium, as well as to the chemical impact of the microbial metabolites on the polymeric components of the films. The metabolites are secreted by the growing fungus and promote degradation of the macromolecules. With time going, the material becomes an ever more accessible feed source for the microorganisms.

CONCLUSIONS

(1) Filling of polyethylene with starch, a biodegradable polysaccharide agent, sharply decreases the fluidity of the polymer melt, whose viscosity grows with increasing concentration of starch in the polyethylene–starch blend. Introduction into this blend of a compatibilizer, polyethylene with grafted itaconic acid, causes the fluidity of the composite melt to increase to technologically acceptable levels. This

allows easy processing of the polyethylene/polyethylene with grafted itaconic acid/plasticized starch compositions into films on standard extrusion equipment. Also, the physicomechanical characteristics of the biodegradable film polymeric materials prepared from the compatibilized compositions are significantly improved.

(2) Satisfactory technological parameters (melt uniformity and fluidity) of the polyethylene/polyethylene with grafted itaconic acid/plasticized starch compositions with the optimized formulation (St 20–25 wt %, PE–ItA 25 wt %), as well as high performance characteristics (tensile strength, elasticity, and biodegradability) of the films thereof make these compositions suitable as the basis for preparation of biodegradable film polymeric materials and other biodegradable items intended for short-term application.

(3) Examination of the structure of the compositions showed that better technological and physicomechanical parameters of the compatibilized composites examined (compared to noncompatibilized composites) are due to a better compatibility of their components, owing to more intense physicochemical interactions and arising chemical interactions at the polymer binder–compatibilizer–biodagradable filler interface.

REFERENCES

1. Vasnev, V.A., *Vysokomol. Soedin.*, 1997, vol. 39, no. 12, pp. 2073–2089.
2. Fomin, V.A. and Guzeev, V.V., *Plast. Massy*, 2001, no. 2, pp. 42–46.
3. Suvorova A.I., Tyukova I.S., and Trufanova, E.I., *Usp. Khim.*, 2000, vol. 69, no. 5. pp. 454–503.
4. Bugorkova, V.S. et al., *Plast. Massy*, 1988, no. 4, p. 40.
5. Larionov, V.G., *Plast. Massy*, 1993, no. 4, pp. 36–38.
6. Baranov, A.O., Kotova, A.V., Zelenetskii, A.N., and Prut, E.V., *Usp. Khim.*, 1997, vol. 66, no. 10, pp. 972–984.
7. Pesetskii, S.S., Jurkowski, B., Krivogus, Y.M., and Kelar, K., *Polymer*, 2001, vol. 42, pp. 469–475.
8. Lipatov, Yu.S., *Sintez i modifikatsiya polimerov* (Synthesis and Modification of Polymers), Moscow: Nauka, 1976.
9. Barshtein, R.S., Kirilovich, V.I., and Nosovskii, Yu.E., *Plastifikatory dlya polimerov* (Plasticizers for Polymers), Moscow: Khimiya, 1982.
10. *Metody izucheniya pochvennykh mikroorganizmov i ikh metabolitov* (Methods of Studying Soil Microorganisms and Their Metabolites), Krasil'nikov, N.A., Ed., Moscow: Mosk. Gos. Univ., 1966.
11. Molchanov, Yu.M., *Fizicheskie i mekhanicheskie svoistva polietilena, polipropilena i poliizobutilena* (Physical and Mechanical Properties of Polyethylene, Polypropylene, and Polyisobutylene), Riga: Zinatne, 1966.
12. Dechant, J., Danz, R., Kimmer, W., *et al.*, *Ultrarotspektroskopische Untersuchungen an Polymeren*, Berlin: Akademie, 1972.
13. Bikiaris, D. and Panayiotou, C., *J. Appl. Polym. Sci.*, 1998, vol. 70, pp. 1503–1521.
14. Tarutina, L.I. and Pozdnyakova, F.O., *Spektral'nyi analiz polimerov* (Spectral Analysis of Polymers), Leningrad: Khimiya, 1986.
15. Gordon, A.J. and Ford, R.A., *The Chemist's Companion. A Handbook of Practical Data, Techniques, and References*, New York: Wiley–Interscience, 1972.

ISSN 1070-4272, Russian Journal of Applied Chemistry, 2006, Vol. 79, No. 9, pp. 1532–1537. © Pleiades Publishing, Inc., 2006.
Original Russian Text © I.M. Lipatova, N.V. Losev, A.A. Yusova, 2006, published in Zhurnal Prikladnoi Khimii, 2006, Vol. 79, No. 9, pp. 1548–1553.

MACROMOLECULAR CHEMISTRY AND POLYMERIC MATERIALS

Mechanical Degradation of Gelatinized Starch Upon Hydroacoustic Treatment

I. M. Lipatova, N. V. Losev, and A. A. Yusova

Institute of Solution Chemistry, Russian Academy of Sciences, Ivanovo, Russia

Received April 26, 2006

Abstract—Mechanical degradation of gelatinized starch upon hydroacoustic treatment in a rotary pulse installation was studied by spectrophotometry of the iodine–starch complexes and analysis of the concentrations of the terminal reducing groups. The energy efficiency of hydroacoustic and ultrasonic mechanical degradation was estimated.

DOI: 10.1134/S1070427206090278

Starch is widely used in various branches of industry not only for preparing gel-like accessory (thickening, gluing, binding, finishing, etc.) materials, but also as environmentally safe precursor of new preparations. When gel-like materials are prepared from starch products, it is necessary to break down its primary structure formed by swollen starch granules, and when starch is used as a precursor for organic and enzymatic synthesis, its preliminary depolymerization (liquation) is required. These processes can be enhanced by hydroacoustic treatment (HA treatment) using rotary pulse installations (RPIs), which provides a significant decrease in the preparation time and total energy consumption and excludes chemical and enzymatic cleaving agents [1–3]. Cavitation and high shear stresses are the decisive factors enhancing the hydromechanical, physicochemical, and chemical processes upon HA treatment [4–6]. The contribution of each factor to hydroacoustic pulverization of starch hydrogel granules was studied in [6]. However, chemical effects of HA treatment such as degradation of starch macromolecules were not taken into account in that study.

In this study we examined some relationships of mechanical degradation of gelatinized starch treated in a rotary pulse installation and the possibility of predicting the process, taking into account the imparted mechanical energy.

EXPERIMENTAL

Experiments were performed with corn starch [GOST (State Standard) 7697–82]. The starch hydrogels for subsequent mechanical treatment were prepared by heating a starch suspension on a water bath at 90°C for 15 min.

The starch hydrogels were treated on a laboratory RPI whose working chamber is formed by a stator and a rotor, both equipped with special units. The gap between the rotating and stationary elements of the working chamber at a given rotation rate determines the tangential stresses in the treated liquid-phase material. The rotation rate was varied in the 1000–5000 rpm range, which corresponds to the shear rate gradient of $(0.5–17.4) \times 10^4$ s^{-1}.

The starch hydrogels were exposed to ultrasonic treatment in a UZDN-2T disintegrator (22 kHz). The volume density of the acoustic energy determined by the calorimetric procedure was 1.34 W cm^{-3}.

The content of the water-soluble fraction A (%) in the starch was determined by hot extraction; the extract composition was analyzed spectrophotometrically using complexation with iodine. The optical densities of the solutions were measured on a Spekol-221 spectrophotometer (λ 400 nm).

The viscosity of the initial and mechanically treated starch hydrogels was measured with a VPZh-2 capillary viscometer at 80°C in accordance with GOST 33–66.

Study of the mechanical degradation of the gelatinized starch is complicated by the fraction and phase heterogeneity of the starch hydrogels, by the presence of various impurities [7, 8], and by impossibility of monitoring the process using common viscometric procedures. The latter problem is due to the fact that the mechanical treatment provides degradation of the

initial hydrogel, which decreases its viscosity. In this study, the degradation of starch hydrogels upon HA treatment in RPI was studied by two complementary methods: spectrophotometry of the iodine–starch complexes and analysis of the concentrations of the terminal reducing groups.

It is known that corn starch consists of amylopectin (75%) and linear amylose (25%). The iodine complexes of corn starch amylose and amylopectin are characterized by the absorption bands at 620 and 540 nm, respectively. Superposition of these two spectra gives the spectrum with a peak at 590 nm, which corresponds to the product of interaction between iodine and starch. Degradation of starch fractions shifts λ_{max} toward higher frequencies [9]. The degree of degradation in the mechanically treated starch was evaluated using the experimental calibration curve $\lambda_{max} = f(P)$ obtained in [9] and plotted in Fig. 1. The absorption spectra of the iodine–starch complexes of (*1*) initial hydrogel and (*2*) hydrogel treated in RPI for 60 s at a shear rate gradient of 1.1×10^5 s^{-1} are shown in Fig. 2. As seen, the mechanical treatment of the starch hydrogels affects the spectra of their iodine complexes; we observed a decrease and a hypsochromic shift of the absorption maxima and an increase in the absorption in the 520–550 nm range.

Changes in the absorption spectra of iodine–starch complexes reflect changes caused by the mechanical treatment in the amylose and amylopectin starch fractions. The most informative are the spectra of the iodine complexes of the water-soluble fraction prepared by hot extraction of the initial and acoustically treated starch hydrogels. The water-soluble fraction involves predominantly the macromolecules of amylose (most soluble starch fraction), which is confirmed by the absorption maximum at λ_{max} 614–618 nm. The degree of polymerization of corn starch amylose reaches 900–1000. It is known that the mechanical degradation of any polymer is a nonrandom process. It is believed [10] that, in the course of mechanical degradation, the longest macromolecules are broken first, predominantly in their middle. Hence, mechanical degradation of a linear amylose molecule can cause only an insignificant hypsochromic shift of the absorption maximum in the spectra of the iodine–amylose complex. An increase in the absorption in the short-wave range suggests accumulation of short amylose chains formed by elimination of side L- and S-chains of amylopectin. These side chains are the amylose fragments with the degree of polymerization less than 50 [10], and their complexes with iodine exhibit

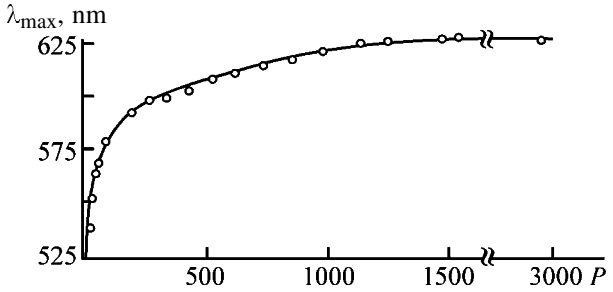


Fig. 1. λ_{max} in the absorption spectra of the iodine–amylose complexes as a function of the degree of amylose polymerization *P*.

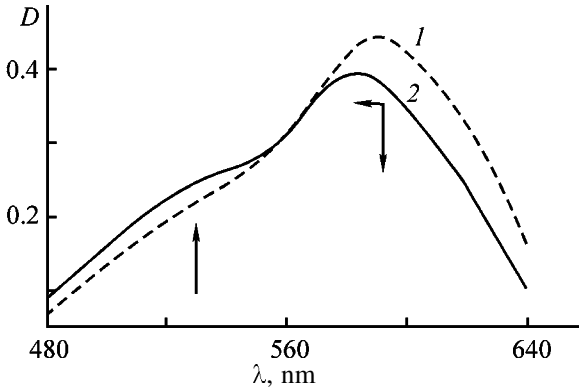


Fig. 2. Absorption spectra of starch hydrogels: (*1*) initial and (*2*) hydroacoustically treated in RPI (γ 1.1×10^5 s^{-1}, *t* 60 s). (*D*) Optical density and (λ) wavelength.

the absorption spectra with $\lambda_{max} < 550$ nm (Fig. 1). The ratio of the optical densities D_{530}/D_{max} can be used for quantitative evaluation of the degree of mechanically induced debranching of amylopectin.

The hypsochromic shifts of the absorption maximum λ_{max} and D_{530}/D_{max} ratios in the absorption spectra of iodine–amylose complexes (water-soluble fraction), and also the concentrations of the terminal reducing groups and viscosities of the treated hydrogels, in relation to the time of mechanical treatment in RPI of 3 and 8% starch solutions, are listed in the table. As seen, the content of the reducing groups in the treated hydrogels first increases due to the breakdown of macromolecules across the glycoside bonds and then decreases with increasing treatment time. This is probably due to the mechanically activated oxidation of the forming terminal aldehyde groups. In accordance with the experimental data, even in first seconds of the mechanical treatment, the absorption maximum λ_{max} shifts from 617 to 602 nm ($\Delta\lambda_{max}$ 15 nm) in the spectra of the iodine–amylose complexes, which corresponds to a decrease in the degree of amylose polymerization from 890 to 430. No changes in the absorption spectra were observed upon

Properties of starch hydrogels in relation to the time t of mechanical treatment

t, s	λ_{max}, nm	D_{530}/D_{max}	Relative viscosity μ/μ_0	Optical density D	Content of reducing groups, c_R, wt %
			c_{st} = 3 wt %		
0	616.7	0.51	1	1.38	0.071
4	601.9	0.58	0.575	0.92	0.074
10	598.8	0.60	0.412	0.70	0.077
20	598.5	0.61	0.373	0.69	0.080
30	598.6	0.62	0.364	0.68	0.081
60	598.1	0.62	0.336	0.68	0.140
90	599.0	0.60	0.328	0.74	0.142
120	599.3	0.60	0.306	0.79	0.137
150	599.7	0.59	0.289	0.84	0.137
180	600.0	0.59	0.274	0.92	0.136
			c_{st} = 8 wt %		
0	611.9	0.49	1	1.84	0.074
4	592.4	0.54	0.226	1.46	0.099
10	590.5	0.56	0.132	1.42	0.111
20	589.9	0.58	0.081	1.40	0.133
30	590.2	0.57	0.079	1.37	0.150
60	590.0	0.57	0.076	1.38	0.151
90	589.5	0.56	0.070	1.36	0.148
120	588.6	0.57	0.064	1.37	0.140
150	587.4	0.57	0.062	1.37	0.133
180	587.0	0.57	0.058	1.37	0.126

longer mechanical treatment (up to certain level), which suggests attainment of the degradation limit.

It should be noted that hydrogels of different concentrations show essentially different changes in the characteristics with time. For example, at a lower hydrogel concentration (3 wt %), λ_{max} (after initial decrease and attainment of a certain plateau) again slightly decreases with increasing treatment time. The optical density of 3% hydrogels, after the initial decrease at the start of the treatment due to the breakdown of starch grains, then increases again with increasing treatment time. As shown in [12], this behavior is probably associated with the phase transformations in the hydrogel caused to the shear stresses. Most probably, short chains act as nucleating centers of the solid phase [13].

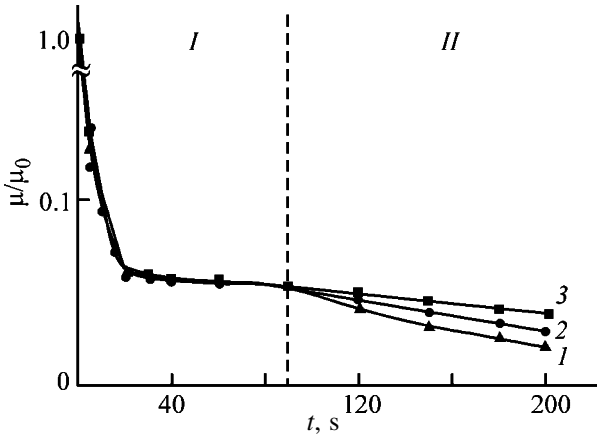


Fig. 3. Relative viscosity μ/μ_0 of the starch hydrogel (9 wt %) as a function of treatment time t in RPI. Temperature, °C: (*1*) 70, (*2*) 40, and (*3*) 20. Steps: (*I*) mechanical degradation and (*II*) activated hydrolysis.

Phase transitions (appearance of turbidity) lead to a decrease in the content of the short chains in the amylose fraction recovered by hot extraction; as a result, the absorption maximum in the spectra of the iodine–amylose complexes again shifts to the long-wave region. For hydrogels with a higher starch content (c > 7 wt %), showing weaker tendency to phase transitions, $\Delta\lambda_{max}$ monotonically decreases with increasing treatment time.

The dependences of the viscosity of 9% starch hydrogel on the time of mechanical treatment, recorded at three different temperatures, are shown in Fig. 3. As seen, even in the first seconds of mechanical treat-

ment, the hydrogel viscosity sharply decreases; then, after reaching a certain value, it remains constant for some time, and in this period all the curves recorded at various temperatures of mechanical treatment coincide. With a further increase in the treatment time, the hydrogel viscosities decrease at a rate growing with an increase in the temperature. This experimental fact can be accounted for as follows. Small amounts of hydrogen peroxide formed by cavitation of aqueous solutions of organic compounds in air can oxidize these organic compounds. As a result, carboxy groups are accumulated in the system owing to mechanically activated oxidation of starch and organic impurities. For example, no increase in the amount of carboxy groups was observed upon mechanical treatment for 4–30 s, whereas after treatment for 60 s the content of the carboxy groups increased from 0.07 (initial starch) to 0.15% (treated hydrogel). Under the cavitation conditions, even insignificant amounts of carboxy groups catalyze hydrolytic degradation of starch. Cavitation causes formation of the starch macroradicals which, in contrast to valence-saturated macromolecules, are hydrolyzed even at pH 6.5 [14]. Hence, our experimental data allow us to distinguish two steps of degradation of the gelatinized starch exposed to HA treatment in the presence of air. The time periods corresponding to different steps of the degradation are shown in Fig. 3.

The first step (Fig. 3, *I*) is the step of only mechanical promotion of the starch degradation (mechanical degradation proper), characterized by the independence of the process rate from temperature, attainment of the degradation limit, and nonrandom degradation course.

The occurrence of nonrandom degradation, i.e., predominant breakdown of the longest macromolecular chains in their middle, is confirmed by the constant width of the absorption bands in the spectra of the iodine–amylose complexes, because in the case of random degradation the width of the spectral band should increase due to the random distribution of the chain length.

The second step (Fig. 3, *II*) is the step of mechanically activated hydrolysis, whose characteristics are the positive temperature coefficient, random character of the process, absence of the degradation limit, and dependence on pH of the medium.

The dependence on pH of the medium apparently explains the separation of the steps in time, because accumulation of some minimal amount of the carboxy groups and attainment of the required pH require certain time (pH of the initial hydrogel 7.5). This step may be autocatalytic.

As shown previously, in the course of single-cycle treatment in RPI, the gelatinized starch was exposed to only short HA treatment for a period shorter than 1 s. Therefore, the first mechanically activated step of degradation is of particular importance from the practical viewpoint. We consider it proved that the degradation at the beginning of treatment of the starch hydrogel with concentrations of 5–9% proceeds through mechanical activation, e.g., it proceeds predominantly due to cavitation (acoustic component) and shear stresses. It was of interest to reveal the decisive factor at various concentration of starch in the hydrogels. For this purpose, the process was performed simultaneously in the RPI working chamber and in the ultrasonic disintegrator.

Mathematical treatment of the absorption spectra of iodine–amylose complexes using the experimental dependences of λ_{max} and extinction coefficients on the degree of amylose polymerization [9] allowed us to evaluate changes in the degree of polymerization of amylose chains and to calculate the number of breaks of macromolecular chains in starch hydrogels of various concentrations caused by HA treatment in the RPI working chamber.

At low starch concentrations (1–3 wt %), the mechanoacoustic yields calculated as the ratio of the number of breaks to the amount of the absorbed acoustic energy using Eq. (1) was 0.03–0.05 breaks per 100 eV:

$$G = \frac{c(P^{-1} - P_0^{-1}) \times 100 N_A}{W_{ac} t}, \quad (1)$$

where c is the starch concentration in the hydrogel (wt %), P and P_0 are the initial and final degrees of the starch polymerization, N_A is the Avogadro number, W_{ac} is the acoustic capacity (W), and t is the time of the mechanical treatment (s).

Approximately the same mechanoacoustic yields were obtained at ultrasonic treatment of these hydrogels in the UZDN-2T ultrasonic disintegrator. This result suggests that, at small starch concentrations, the ultrasonic cavitation is the major factor causing the degradation of starch macromolecules. At HA treatment of hydrogels with the starch concentration exceeding some critical limit (4 wt %), at which the fluctuation physical network can appear in the starch, the yields calculated only from the amount of the absorbed ultrasonic energy increase proportionally to the hydrogel viscosity, which sharply grows with an

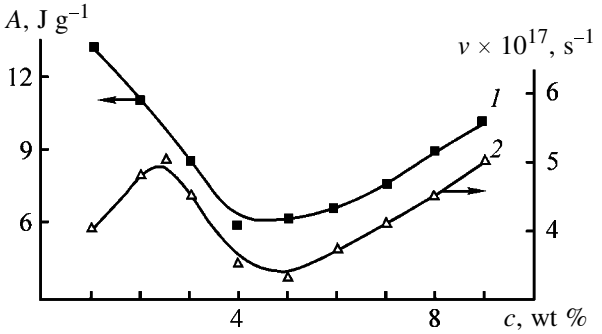


Fig. 4. (*1*) *g* Factor *A* and (*2*) rate of mechanical degradation *v* as functions of the starch concentration *c* in hydrogels upon HA treatment in RPI (γ 1.1×10^5 s^{-1}, *t* 4 s).

increase in their concentration. This fact suggests that, with increasing viscosity of starch hydrogels, the contribution of the shear stresses to the degradation increases.

To predict the process of mechanical degradation of gelatinized starch upon hydroacoustic treatment, it is necessary to evaluate the dependences of the degradation rate on the amount of the absorbed mechanical energy. Taking into account the strong dependence of this process on the starch concentration in hydrogels, we used the volume density of the total mechanical energy divided by starch concentration as the energy parameter of the HA treatment (*g* factor):

$$g = E_m t/Vc, \quad (2)$$

where E_m is the mechanical energy (J) and *V* is the volume of the RPI working chamber (ml).

As seen from Eq. (2), *g* factor is the amount of the total mechanical energy per unit weight of the polymer. The values of *g* factor for hydroacoustic treatment were calculated from the total energy of ultrasonic and shear contribution using the following equation:

$$g = \frac{l}{cV}\left[W_{ac} + \frac{\pi^3 n^2 \mu R_r^2 h(R_r + R_s)}{900\delta}\right], \quad (3)$$

where *n* is the rotor rotation rate (rpm), R_r and R_s are the radii of the rotor and stator, respectively (m), δ is the radial gap (m), and μ is the dynamic viscosity (Pa s^{-1}).

The dependences of the calculated *g* factor and rate of mechanical degradation (number of breaks in macromolecules per second) on the starch concentration in hydrogels is shown in Fig. 4. As seen, these dependences show similar trends. The deviation at low starch concentrations can be accounted for as follows. Starch hydrogels are microheterogeneous systems with swollen starch grains as the dispersed phase particles. Breakdown of these swollen particles in starch hydrogels into smaller fragments probably promotes degradation processes occurring simultaneously. It is known that the efficiency of the cavitation grinding of the disperse systems decreases with decreasing concentration of dispersed phase particles, due to the effect of the probability factor [15]. As a result, there is no correlation between the number of the chain breaks and *g* factor at low concentrations of starch hydrogels. Since the final λ_{max} values of the iodine–amylose complexes are independent of the presence of radical acceptors and the degree of polymerization of amylose becomes constant after attainment of a certain degradation limit, the contribution of the radical mechanism to the initiation of degradation is insignificant.

CONCLUSIONS

(1) At short hydroacoustic treatment of starch hydrogels at concentrations exceeding the critical concentration of gelation, cavitation and shear stresses are the decisive factors of mechanical degradation.

(2) The degree of degradation initiated by hydroacoustic treatment of starch hydrogels is determined by the total mechanical energy absorbed per unit weight of the polymer.

(3) Two steps of mechanical degradation of gelatinized starch at hydroacoustic treatment in the presence of air can be distinguished: mechanical initiation and activated hydrolysis.

ACKNOWLEDGMENTS

This study was financially supported by the Russian Foundation for Basic Research (project no. 06-08-96506).

REFERENCES

1. Lipatova, I.M., Sedova, I.L., Ermolaeva, N.A., et al., *Textile Chemistry*, Moryganov, A.P., Ed., New York: Nova Science, 1998, pp. 265–271.
2. Mukhina, V.P., Iglamova, N.A., Smolentsev, A.V., and Levin, Ya.A., *Khran. Pererab. Sel'khozsyr'ya*, 2003, no. 3, pp. 38–41.
3. Lipatova, I.M., Makarova, L.I., Losev, N.V., et al., *Izv. Vyssh. Uchebn. Zaved., Teknol. Tekstil'n. Prom–sti.*, 2002, no. 3, pp. 58–62.

4. Losev, N.V., Makarova, L.I., and Lipatova, I.M., *Zh. Prikl. Khim.*, 2003, vol. 76, no. 6, pp. 1025–1029.
5. Badikov, Yu.V., *Tekhnika i tekhnologiya gidroakusticheskogo vozdeistviya v protsessakh khimicheskoi tekhnologii* (Equipment and Processes of Hydroacoustic Treatment in Chemical Technology), Ufa: Reaktiv, 2001.
6. Lipatova, I.M., Losev, N.V., Yusova, A.A., et al., *Starch: From Polysaccharides to Granules, Simple and Mixture Gels*, Yuryev, V.P., Tomasik, P, and Ruck, H., Eds., New York: Nova Science, 2004, pp. 171–185.
7. Suvorova, A.I., Tyukova, I.S., and Trufanova, E.I., *Usp. Khim.*, 2000, vol. 69, no. 5, pp. 494–503.
8. Andreev, N.R., *Osnovy proizvodstva nativnykh krakhmalov* (Fundamentals of Production of Native Starches), Moscow: Pishchepromizdat, 2001.
9. Rikhter, M., Augustat, S., and Schierbaum, F., *Ausgewählte Methoden der Stärkechemie*, Leipzig: Fachbuchverlag, 1968. Translated under the title *Izbrannye metody issledovaniya krakhmala*, Moscow: Pishchevaya Prom–st., 1975, pp. 105–140.
10. Basedow, A.M., Ebert, K.T., and Fobhag, E., *Makromol. Chem.*, 1978, vol. 179, no. 10, pp. 2565–2568.
11. Hizukuris, S., *Carbohydr. Res.*, 1985, vol. 141, pp. 295–306.
12. Lipatova, I.M., Yusova, A.A., Blokhina, S.V., and Moryganov, A.P., *Zh. Prikl. Khim.*, 2001, vol. 74, no. 9, pp. 1517–1521.
13. Kadykova, E.L., and Gubina, S.M., *Zh. Prikl. Khim.*, 1992, vol. 65, no. 4, pp. 891–895.
14. Petryaev, E.P., Shadyro, O.I., Kovalenko, N.I., and Boltrameyuk, V.V., *Vestsi Akad. Navuk Bel. SSR, Ser. Fiz.-Energ. Navuk*, 1984, no. 3, pp. 80–84.
15. Matsievich, E.B. and Butyagin, P.Yu., *Kolloidn. Zh.*, 1958, vol. 20, no. 5, pp. 665–673.

ISSN 1070-4272, Russian Journal of Applied Chemistry, 2006, Vol. 79, No. 9, pp. 1538–1541. © Pleiades Publishing, Inc., 2006.
Original Russian Text © L.A. Zemnukhova, S.V. Isai, E.D. Shkorina, N.G. Busarova, T.V. Kafanova, 2006, published in Zhurnal Prikladnoi Khimii, 2006, Vol. 79, No. 9, pp. 1554–1557.

MACROMOLECULAR CHEMISTRY AND POLYMERIC MATERIALS

Composition of Lipids in Wastes from Rice and Buckwheat Production

L. A. Zemnukhova, S. V. Isai, E. D. Shkorina, N. G. Busarova, and T. V. Kafanova

Institute of Chemistry, Far-Eastern Division, Russian Academy of Sciences, Vladivostok, Russia
Pacific Institute of Bioogranic Chemistry, Far-Eastern Division, Russian Academy of Sciences, Vladivostok, Russia

Received March 1, 2006

Abstract—The lipid composition of the waste fine fraction (dust) from rice and buckwheat production was studied.

DOI: 10.1134/S107042720609028X

Efficient utilization of vegetable wastes with exhaustive recovery of valuable components is an important problem of modern chemistry [1–9].

Rice and buckwheat husk accumulated at plants for groats production usually contains particle of size less than 2 mm (2–11 wt %) consisting of fruit shells, corns, and rice husking product (dust). The weight and chemical composition of fine fractions in the waste depends on the plant strain and on the processes and equipment used. Analysis of the fine fractions of such wastes suggests the possibility of preparing from them more valuable products: drugs [10], food additives [11], rice oil [12], phytin [13], γ-oryzanol antioxidant [14], and others [15].

This study continues our systematic research concerning the chemical composition of wastes from rice

Table 1. Composition and content of total lipids in wastes from rice (RH) and buckwheat (BH) production*

Sample	TL yield, wt %	Composition	
		NLs	PLs
RH-14	1.65	Wax, FAMEs (traces), TGs, free FAs, fatty alcohols, phytosterols, DGs, MGs, MGDG	PC, PI
RH-13	1.80	〃	PC, PI
RH-15	1.45	〃	PC, PI, PS
RH-16	1.54	Wax, FAMEs (traces), TGs	PE, PS
BH-1	0.97	Wax, FAMEs (traces), TGs, free FAs, fatty alcohols, phytosterols, DGs, MGs, MGDG	PC, PE, PI, PS, PG, SQDG
BH-11	1.90	〃	PC, PE, PS, lyso-PC, PI, PG
BH-6	1.40	Wax, TGs, FAMEs (traces), fatty alcohols, phytosterols, DGs, MGDG	PC, PE, PS, PI
BH-7	2.08	Wax, TGs, FAMEs (traces), fatty alcohols, phytosterols, DGs, MGDG	PC, PE, PS, PI
BH-7**	2.12	Wax, TGs, FAs, fatty alcohols, phytosterols, DGs, MGDG	PC, PE, PS, PI
BH-8	2.46	DGs, MGs, MGDG	PC, PE, PS, PI
BH-8**	2.20		PC, PE, PS, PI
BH-9	2.24		PC, PE, PS, PI
Soybeans	2.43	Wax, TGs, free FAs, fatty alcohols (traces), phytosterols, DGs, MGs	PC, PE, PS, PI, PG, SQDG, DGTS

* FAMEs, fatty acid methyl esters; TGs, triglycerides; FAs, fatty acids; DGs, diglycerides; MGs, monoglycerides; MGDG, monogalactosyl diacyl glyceride; PI, phosphatidyl inositol; PC, phosphatidyl choline; PS, phosphatidyl serine; PE, phosphatidyl ethanolamine; PG, phosphatidyl glycerol; SQDG, sulfoquinovosyl diacyl glyceride; DGTS, diacylglycerotrimethylhomoserine.
** Particle size less than 1 mm.

and buckwheat production [1–3, 6, 7, 13], aimed to develop an efficient scheme of their processing, and deals with the composition of the lipid fractions.

EXPERIMENTAL

Samples of rice husk (RH) and buckwheat husk (BH) were taken in 2001–2004 from corn husking plants. Samples were sieved, and the fraction with the particle size ≤1.5 mm was taken. As reference materials we used soybeans (a well studied material [16]) and oat dust from Amur oblast.

All the samples were analyzed for the content of total lipids (TLs) and fatty acids (FAs). Among TLs, we determined neutral (NLs) and polar (PLs) lipids. The weighed portion of the raw material for the TL recovery was 20 g.

The TL extraction was performed with ethanol and chloroform following the Bligh–Dyer procedure [17]. The qualitative composition of TLs was determined by uni- and two-dimensional TLC on commercial Sorbfil plates (100 × 100 mm, silica gel STKh-1A sorbent, grain size 5–17 μm, silica sol binder, aluminum support).

To separate TLs, we used the solvent system hexane–diethyl ether–formic acid, 80 : 20 : 2. The lipids were identified using reference samples and by comparing the R_f values with the published data [18, 19].

The chromatograms were developed using both specific and nonspecific (sulfuric acid in methanol) agents. Polar lipids were separated by two-dimensional micro-TLC on 5 × 5-cm Sorbfil plates in the solvent systems chloroform–acetone–methanol–formic acid–water, 100 : 40 : 20 : 20 : 3 and acetone–benzene–formic acid–water, 200 : 30 : 3 : 10.

The qualitative composition of phospholipids (PLs) in TLs was determined spectrophotometrically [20, 21].

The TL content in the examined RH and BH samples is given in Table 1. Their yield is 1.45–1.80% for RH and 0.97–2.46% for BH. The soybean sample contains 2.43% TLs. Experiments show that the TL yield depends primarily on the amount of corn particles in the waste, i.e., on the technology for removing flower films from rice and buckwheat corns.

Analysis shows that all the samples have a similar set of NLs (Table 1).

For rice waste, on the whole, the list of NLs coincides with data of [22]. However, we additionally detected unidentified lipids in RH (R_f 0.23 and 0.34)

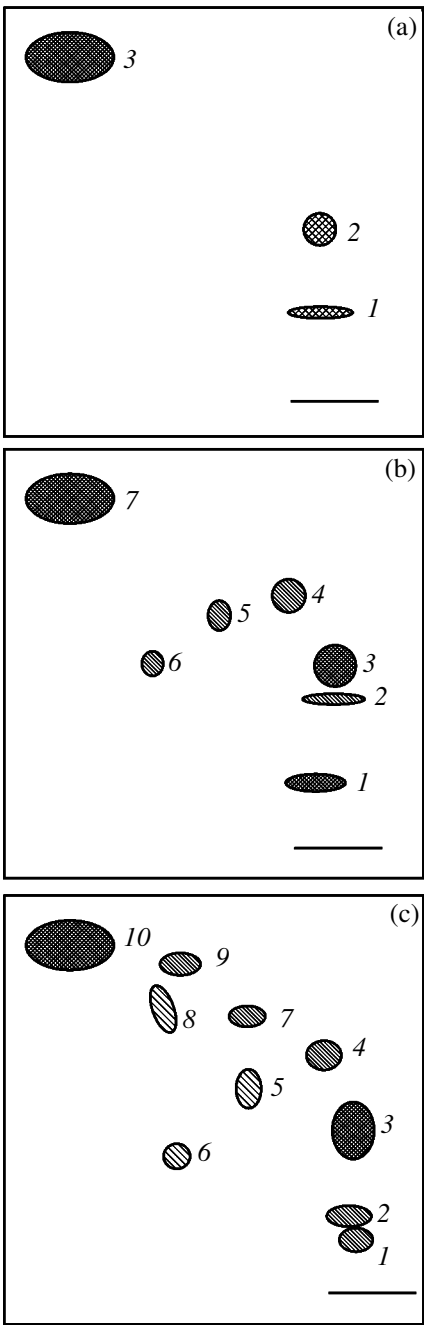


Fig. 1. Two-dimensional micro-TLC of polar lipids of (a) RH-13, (b) BH-1, and (c) soybean samples. (a) (*1*) Phosphatidyl inositol, (*2*) phosphatidyl choline, and (*3*) monogalactosyl diglycerides; (b) (*1*) phosphatidyl inositol, (*2*) phosphatidyl serine, (*3*) phosphatidyl choline, (*4*) phosphatidyl ethanolamine, (*5*) phosphatidyl glycerol, (*6*) sulfoquinovosyl diacyl glyceride, and (*7*) monogalactosyl diglycerides; (c) (*1*) phosphatidyl inositol, (*2*) phosphatidyl serine, (*3*) phosphatidyl choline, (*4*) phosphatidyl ethanolamine, (*5*) phosphatidyl glycerol, (*6*) sulfoquinovosyl diacyl glyceride, (*7*) diacylglycerotrimethylhomoserine, (*8*, *9*) unidentified lipids, and (*10*) monogalactosyl diglycerides.

Table 2. Content of phospholipids in rice and buckwheat husk samples

Sample	TL content, wt %	PL yield (based on TLs)	
		mg	wt %
RH-14	1.65	0.57	0.22
RH-13	1.80	0.37	0.12
RH-15	1.45	0.27	0.32
RH-16	1.54	0.68	0.22
BH-1	0.97	0.95	0.49
Soybeans	2.43	4.41	1.20

and in BH (R_f 0.25 and 0.23) samples. The qualitative composition of the set of neutral lipids in RH and BH is similar to that in the reference sample, soybeans. In BH-6 and BH-7 samples we found increased content of wax.

The qualitative composition of phospholipids (PLs) determined by two-dimensional micro-TLC (Figs. 1a–1c, Table 1) indicates that the rice processing waste contains two representatives of the PL group: phosphatidyl choline (PC) and phosphatidyl inositol (PI). The set of PLs in the buckwheat waste is more diverse, and the content of some components is even higher than in soybean PLs [16]. For example, soybeans contain only traces of PI, whereas in buckwheat husk its content is as high as that of PC. Thus, the buckwheat production waste can be considered as a quite real source for preparative recovery of the individual PI fraction.

In all the RH and BH samples studied, the major component is a glycolipid, monogalactosyl diacyl glyceride (MGDG). The composition of the acyl residues R_1 and R_2 was not studied. However, it is known that the length and degree of unsaturation of the chains in the acyl groups affect the chromatographic mobility of glycerides [23]. Since in TLC separation of glycolipids (GLs) and PLs MGDG forms a single spot (Figs. 1a–1c, spots *3*, *7*, and *10*, respectively), the acyl residues R_1 and R_2 in this component are presumably similar. This result can be used for preparing a homogeneous MGDG compound from rice production waste in which the set of PLs is minimal compared to BH and soybeans.

The content of phospholipids in the samples is given in Table 2.

The fatty acids (FAs) were analyzed by GLC on an Agilent 6850 Series device. Fatty acid methyl esters (FAMEs) were prepared as described in [21]. An HP-5MS capillary column was used; l = 30 m, d = 0.25 mm, stationary phase 5% phenyl methyl siloxane, carrier gas He, flow rate 25 ml min^{-1}, column temperature 220°C. Mass-spectrometric analysis of FAMEs was performed on a Hewlett–Packard device (HP 6890 GC, HP 5973 MSD).

Up to 12 fatty acids were detected in rice and buckwheat wastes (Table 3). The major components are palmitic acid (16:0) and C_{18} acids. The similar FA composition was found in bran of Japanese rice strains [24]. In contrast to RH and BH, oat dust (Table 3) is characterized by a high content of eicosenoic acid (20:1). Thus, the set of FAs in rice and buckwheat

Table 3. Content of major fatty acids

Sample	Major FAs,* % of total FAMEs											
	14:0	16:0	16:1	18:0	18:1^8	18:1^{12}	18:2	20:0	20:1	20:2	22:0	24:0
RH-13	Traces	33.98	Traces	3.10	51.08	Traces	3.45	Traces	4.91	3.47	Traces	Traces
RH-14	0.89	30.95	″	5.96	29.01	1.48	2.85	4.68	3.46	9.66	5.85	5.08
BH-1	0.58	24.48	0.42	2.52	36.88	2.05	24.61	1.96	2.42	3.64	Traces	N/d
BH-11	1.27	29.39	0.60	5.18	29.56	1.81	3.76	4.24	2.65	9.31	5.61	6.24
BH-6	Traces	18.85	Traces	3.81	44.88	N/d	24.01	0.76	0.50	6.01	0,67	0.45
BH-7	4.61	48.34	N/d	7.26	20.04	Traces	7.87	4.12	2.34	4.48	Traces	0.40
BH-7**	Traces	27.25	Traces	5.20	43.15	″	16.13	1.13	5.25	Traces	1.23	0.55
BH-8	″	35.84	″	7.82	26.31	″	20.74	1.98	0.98	3.96	1.49	0.71
BH-8**	″	16.74	″	1.72	40.28	N/d	35.71	0.70	3.12	N/d	0.80	0.80
BH-9	3.61	28.29	″	3.85	44.68	1.97	6.23	2.52	4.88	1.05	2.65	Traces
Oat dust	Traces	39.88	0.29	4.39	31.77	0.99	3.45	0.35	14.09	3.85	0.28	0.24

* Acid: (14:0) myristic, (16:0) palmitic, (16:1) palmitooleic, (18:0) stearic, (18:1) oleic (superscript indicates double bond position), (18:2) linoleic, (20:0) arachic, (20:1) eicosenoic, (20:2) eicosadienoic, (22:0) docosanoic, and (24:0) tetracosanoic.
** Particle size less than 1 mm; (N/d) not detected.

production wastes is diverse and can be of interest for preparation of lipid products with the known content of individual acids. Modern achievements in the development of new lipid products with improved biological and physicochemical properties [25] show that unsaturated FAs are responsible for the most important therapeutic and prophylactic effects.

Thus, the major lipid components of wastes from rice and buckwheat production are monogalactosyl diacyl glycerides and phospholipids, which are important biologically active substances. Since such compounds are in demand in medicine and in food and pharmaceutical industry and the cost of individual products is relatively high, it seems appropriate to recover them in the course of integrated processing of rice and buckwheat production wastes.

CONCLUSIONS

(1) The content of total lipids in rice and buckwheat production wastes was determined; it varies in the range 0.97–2.46% relative to the dry matter weight depending on the kind of plants. The compositions of polar and neutral lipid fractions and the content of phospholipids (0.12–0.49 wt % relative to total lipids) were determined.

(2) The qualitative composition of the phospholipids was studied. Rice waste contains two phospholipids (phosphatidyl choline and phosphatidyl inositol), and buckwheat waste, up to six components depending on the plant strain. All the samples are characterized by a high content of monogalactosyl diacyl glyceride.

(3) The composition and content of fatty acids in rice and buckwheat husk were studied. Twelve fatty acids were detected; the major components are palmitic acid (16:0) and C_{18} acids.

REFERENCES

1. Zemnukhova, L.A., Fedorishcheva, G.A., Egorov, A.G., and Sergienko, V.I., *Zh. Prikl. Khim.*, 2005, vol. 78, no. 2, pp. 324–328.
2. Zemnukhova, L.A., Shkorina, E.D., and Fedorishcheva, G.A., *Zh. Prikl. Khim.*, 2005, vol. 78, no. 2, pp. 329–333.
3. Zemnukhova, L.A., Sergienko, V.I., Davidovich, R.L., et al., *Vestn. Dal'nevost. Otd. Ross. Akad. Nauk*, 1996, no. 3, pp. 82–87.
4. Dudkin, M.S. and Ozolina, S.A., *Khim. Prirodn. Soedin.*, 1976, no. 4, pp. 417–419.
5. Brylev, A.N., Adylov, D.K., Tukhtaeva, G.G., et al., *Khim. Prirodn. Soedin.*, 2001, no. 6, pp. 488–489.
6. Zemnukhova, L.A., Tomshich, S.V., Mamontova, V.A., et al., *Zh. Prikl. Khim.*, 2004, vol. 77, no. 11, pp. 1901–1904.
7. Zemnukhova, L.A, Tomshich, S.V., Shkorina, E.D., and Klykov, A.G., *Zh. Prikl. Khim.*, 2004, vol. 77, no. 7, pp. 1192–1196.
8. Dudkin, M.S., Ozolina, S.A., and Darman'yan, N.G., *Khim. Drev.*, 1976, no. 3, pp. 33–35.
9. Moryganov, A.P., Zakharov, A.G., and Zhivotin, V.V., *Ross. Khim. Zh.*, 2002, vol. 46, no. 1, pp. 58–66.
10. Kaputskii, F.N. and Yurkshtovich, T.L., *Lekarstvennye preparaty na osnove proizvodnykh tsellyulozy* (Medicinals Based on Cellulose Derivatives), Minsk: Universitetskoe, 1989.
11. Aleinikov, I.N., Sergeev, V.N., Rusakov, A.V., and Aganyan, V.E., *Pishch. Ingred.: Syr'e Dobavki*, 2001, no. 1, pp. 30–31.
12. Sugano, M. and Tsuji, E., *J. Nutr.*, 1997, vol. 127, pp. 5215–5245.
13. Kolzunova, L.G., Zemnukhova, L.A., Fedorishcheva, G.A., et al., *Zh. Prikl. Khim.*, 2000, vol. 73, no. 10, pp. 1644–1651.
14. Kim, J.Sh., Godber, J.S., King, J.M., and Pringawiwatrul, W.J., *J. Am. Oil Chem. Soc.*, 2001, vol. 78, no. 7, pp. 669–685.
15. Govindarao Venneti, M.H., *J. Sci. Ind. Res.*, 1980, vol. 39, no. 9, pp. 495–515.
16. Wu, Y. and Wang, T., *J. Am. Oil Chem. Soc.*, 2003, vol. 80, no. 2, pp. 127–132.
17. Bligh, E.G. and Dyer, W.J., *Can. J. Biochem. Physiol.*, 1959, vol. 37, pp. 911–917.
18. Christie, W.W., *Lipid Analysis: Isolation, Separation, identification and Structural Analysis of Lipids*, London, 1973, pp. 153–154.
19. Kates, M., *Techniques of Lipidology. Isolation, Analysis, and Identification of Lipids*, New York: North-Holland, 1972.
20. Svetashev, V.I. and Vaskovsky, V.E., *J. Chromatogr.*, 1972, vol. 67, pp. 376–378.
21. Hartman, L., Lago, C.H., and Regino, N., *Lab. Pract.*, 1973, vol. 22, pp. 475–476.
22. Lam, H.S. and Proctor, A., *J. Am. Oil Chem. Soc.*, 2004, vol. 81, no. 4, pp. 385–388.
23. Khotimchenko, S.V., *Lipidy morskikh vodoroslei-makrofitov i trav: Struktura, raspredelenie, analiz* (Lipids of Marine Algae-Macrophytes and Grasses: Structure, Distribution, Analysis), Vladivostok: Dal'nauka, 2003.
24. Goffman, F.D., Pinson, S., and Bergman, C., *J. Am. Oil Chem. Soc.*, 2003, vol. 80, no. 5, pp. 485–490.
25. Neklyudov, A.D. and Ivankin, A.N., *Prikl. Biokhim. Mikrobiol.*, 2002, vol. 38, no. 5, pp. 469–481.

ISSN 1070-4272, Russian Journal of Applied Chemistry, 2006, Vol. 79, No. 9, pp. 1542–1545. © Pleiades Publishing, Inc., 2006.
Original Russian Text © M.V. Shishonok, V.I. Shadrina, 2006, published in Zhurnal Prikladnoi Khimii, 2006, Vol. 79, No. 9, pp. 1558–1561.

MACROMOLECULAR CHEMISTRY AND POLYMERIC MATERIALS

Recovery of Wool from Flax Fibers Using Nitric Acid

M. V. Shishonok and V. I. Shadrina

Belarussian State University, Minsk, Belarus

Received June 4, 2006

Abstract—The principal possibility of preparing wool from cottonized flax fibers using nitric acid both in the course of cooking and in the bleaching step was studied. The influence of the nitric acid concentration and cooking time on the extent of flax delignification was examined.

DOI: 10.1134/S1070427206090291

About 12% of cellulose is produced in the world from annual plants, including flax [1]; according to estimates [2], by 2010 this share can reach 19.8%. For Belarus and Russia, flax is a domestic raw material capable to replace imported cotton. National and international programs concerning integrated processing of flax are being realized in Germany, Finland, Denmark, Sweden, and the United States [3].

Flax contains from 60 to 90% cellulose; the lignin content varies from 2 to 5%, reaching 37% in flax boon [3, 4]. Only long flax fibers, accounting for only 1/5 of the total, are suitable for production of high-quality textiles; the remaining flax fibers are short and are either processed to obtain heat-insulating materials or burnt [5]. At the same time, short fibers are a valuable source of cellulose. Thus, recovery of cellulose from substandard flax fibers with the aim to produce useful materials (in particular, wool) is an urgent problem. Flax wool is characterized by high sorption activity, hygroscopicity, antiseptic and hemostatic properties, and good air permeability [6]; it is even more hygroscopic than cotton wool [6].

Only 1/3 of wool consumed in Russia is produced at domestic plants; the raw material is expensive cotton [7]. The demand of Belarus for wool is about 2000 t annually. The use of local resources, primarily flax, would allow partial replacement of imported cotton fibers.

Flax fiber is produced in industry by alkaline cooking followed by hypochlorite bleaching [8]. From the economical and environmental viewpoints, Ryzhkov [8] considers it appropriate to replace chlorine-containing agents by peracetic acid. Methods for production of flax wool by oxidative bleaching with complexones [9] and by reductive cooking of flax followed by peroxide bleaching in an alkaline medium [10] have been patented.

It is known [11–15] that nitric acid is an excellent delignifying agent for nonwood fibrous raw materials, such as straw of cereals, cane, or manioc. Reaction of nitric acid with lignin involves electrophilic substitution in the aromatic ring (nitrosation, nitration), electrophilic displacement, aliphatic substitution, addition, and oxidation [11]. The thus modified lignin is extracted with a dilute alkali solution. According to Nikitin [11], 3–5% HNO_3 is the most suitable for cooking of nonwood plant materials. It was shown previously [13] that the optimal HNO_3 concentration for nitric acid cooking of rye straw is 2.0%. As for flax fibers, we found no systematic data on the recovery of flax cellulose with nitric acid; only superficial information about delignification of flax with nitric acid was available [3].

This study deals with optimization of the conditions of nitric acid cooking of flax fibers with the aim to obtain wool.

EXPERIMENTAL

As starting material we used cottonized flax fibers (Groniteks State Unitary Enterprise, Grodno, Belarus). The weight fraction of boon and foreign impurities in the cottonized fiber was 1.0%, and the mean fiber length, 30.0 mm. The lignin content was 6.2%; Kapp number, 18.1; content of pentosans, 3.7%; and ash residue, 1.4%. Nitric acid delignification of fibers involved impregnation of the flax fiber with an aqueous HNO_3 solution (for 30 min at liquid : solid ratio of 20 ml g^{-1} and room temperature), cooking of the swollen fibers in the same HNO_3 solution at 60°C,

Table 1. Results of delignification of flax fiber with HNO_3 solutions of various concentrations (cooking time 2 h)

HNO_3 concentration	Cellulose yield	Lignin content [17]	Kapp number [18]	DD, %
%				
2.0	83	3.7	8.3	51.1
3.0	80	3.6	7.9	54.2
4.0	78	2.7	7.0	66.7
5.0	81	2.7	7.0	65.3

and extraction of the modified lignin with a 1% NaOH solution (2 h, 80°C, liquid : solid ratio 20 ml g^{-1}). After the cooking and extraction, the pulp was washed with hot water to neutral reaction. The cooking and extraction were performed in a temperature-controlled flask equipped with a reflux condenser.

We varied the HNO_3 concentration (2, 3, 4, 5%) and cooking time (1, 2, 3, 4, 5 h). All the experiments on studying the influence of the HNO_3 concentration and cooking time on the extent of delignification were performed under identical conditions of impregnation and extraction. These conditions were a fortiori favorable for the nitric acid delignification [13, 16].

The lignin content in the samples was determined by Komarov's modification of Klasson's method [17], and also from the Kapp number [18]. The degree of delignification (DD, %) of flax fibers was calculated by the formula [19]

$$DD = 100 - YL/L_{in},$$

where DD is the degree of delignification, %: Y, cellulose yield, %; and L_{in} and L, lignin content in the fiber before and after the treatment, respectively (%).

The content of pentosans in the samples was determined by the TAPPI standard method [20], and the α-cellulose content [21] and ash residue [22], by according to the corresponding state standards.

The degree of polymerization (DP) of cellulose was determined from the viscosity of its solution in Cadoxen [23]. The water-retaining power (WRP) was evaluated in accordance with [24].

Experiments on flax fiber cooking at varied HNO_3 concentration were performed for 2 h at 60°C. When planning the experiment, we tried to minimize the cooking temperature, because elevated temperatures stimulate undesirable hydrolytic degradation of cellulose. The choice of the temperature is based on the data that the mean glass transition point of dry lignin is 195°C, and in lignin with 27.1% moisture content it decreases to 90°C [25]. Aqueous HNO_3 solution apparently plasticizes lignin more strongly than does water and decreases the glass transition point of lignin to a still greater extent. It is reasonable to assume that lignin in an HNO_3 solution at 60°C gets devitrified and passes into a hyperelastic state. Hence, reactive centers of lignin become more accessible, and the reactivity of lignin as a whole increases.

The extent of delignification was evaluated by three parameters: residual lignin content, Kapp number, and degree of delignification. The results are listed in Table 1.

Table 1 shows that delignification with dilute (2–5%) HNO_3 solutions provides high (up to 83%) yield of unbleached cellulose. After cooking with 4–5% HNO_3, the lignin content decreases by a factor of more than 2: from 6.2% in the initial fiber to 2.7%. The maximal degree of delignification calculated from the yield and residual lignin content is 66.7%. The cellulose hardness, i.e., the capability for bleaching determined by the Kapp number, also regularly decreases (by 1.3 units) with an increase in the acid concentration (Table 1).

Thus, upon cooking with 4–5% acid, the hardness of flax fibers decreases by a factor of approximately 2.6 relative to the initial value. Since the Kapp number characterizes the residual lignin content, the agreement between the results of the two independent methods of lignin determination [17, 18] confirms their reliability. Thus, the HNO_3 concentration of 4.0% is sufficient to provide relatively high degree of delignification.

The next step of our experiment involved examining the influence of the cooking time on the extent of delignification, at the HNO_3 concentration of 4.0%. We found that the influence of the cooking time on the yield of flax cellulose is insignificant. Even after prolonged cooking (4–5 h), the yield remained as high as 77–78%.

The dependence of the residual lignin content in

Table 2. Characteristics of flax wool

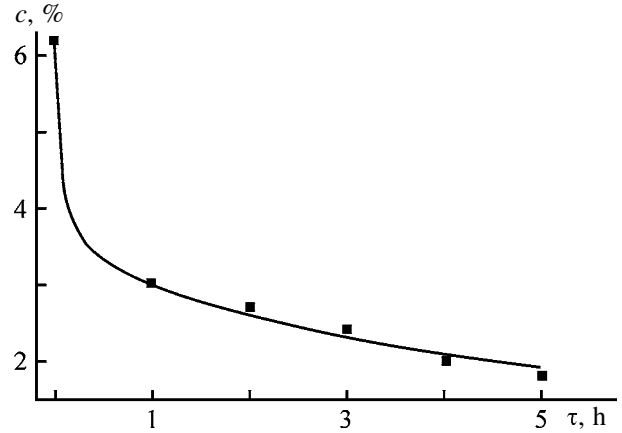
Delignification procedure	Yield, %	Lignin content, %	Kapp number	α-Cellulose content, %	Content of pentosans, %	DL, %	DP	WRP, %
Nitric acid	70	1.5	2.6	91.0	2.9	83	1300	52
Alkaline	75	1.8	–	95.0	3.4	78	2000	42

unbleached flax fiber on the time of cooking in 4% HNO_3 is plotted in the figure. It is seen that the kinetics of the nitric acid delignification of flax is characterized by the fast initial step. Within the first minutes of cooking, the lignin content in the fiber decreases by a factor of almost 2, after which the process decelerates. After 4 h, the residual lignin content in the unbleached cellulose is 2.0, and after 5 h, 1.8%, i.e., it decreases by a factor of approximately 3.5 relative to the initial fiber.

With increasing cooking time, the degree of flax delignification regularly increases, reaching 74.8% in 4 h and growing insignificantly after 5 h. Naturally, the cellulose hardness decreases upon 4–5-h cookings (by a factor of ~3.4 relative to the initial fibers).

Further study involved preparation of wool from flax fibers delignified under the optimal cooking conditions (HNO_3 concentration 4.0%, cooking time 4 h).

Preparation of wool proper involves bleaching of unbleached flax cellulose, i.e., removal of residual lignin. The activity of nitric acid toward lignin and the selectivity of its action provide relatively low content of residual lignin (2.0%) even after the first cooking step. Owing to its efficiency, it is also appropriate to use nitric acid treatment in the step of bleaching of flax cellulose. Correspondingly, we developed a delignification scheme involving both nitric acid cooking and nitric acid bleaching. This approach was suggested and tested previously in delignification of rye straw [13].



Kinetic curve of nitric acid delignification of flax fiber: (*c*) lignin content and (τ) cooking time.

We suggest a three-step scheme of bleaching of flax cellulose obtained by nitric acid treatment. The first step is treatment of unbleached fibers with 20% nitric acid followed by alkaline extraction of modified lignin; the second step is final bleaching with hydrogen peroxide; and the third step is souring with acetic acid. To generate nitrogen oxides which intensify delignification, we added reductants (sodium nitrite, sodium sulfite) to nitric acid in the first bleaching step. It is appropriate to combine the second step, final bleaching of the fiber with hydrogen peroxide, with the step of alkaline extraction of modified lignin. The third step (souring) is performed to neutralize the medium and, as noted in [12], to stabilize the cellulose whiteness.

The wool quality was evaluated by its chemical purity (content of residual lignin, pentosans, and α-cellulose) and hygroscopicity, and also by the mean degree of polymerization of cellulose. As reference material we used flax wool recovered from the same cottonized fibers by alkaline delignification at the Groniteks enterprise (a part of a semicommercial batch). The characteristics of flax wool prepared by our procedure (nitric acid process) and of Groniteks wool are compared in Table 2.

Table 2 shows that the yield of wool prepared by nitric acid delignification is about 70%, which is close to the yield of the semicommercial wool (75%). Semicommercial wool is characterized by a somewhat higher content of pentosans, i.e., by lower chemical purity. On the whole, the wool prepared by our procedure appreciably surpasses the semicommercial material in the extent of delignification evaluated by the residual lignin content and DD.

An important characteristic of wool is the degree of polymerization of cellulose. Low-molecular-weight fractions of cellulose decrease the strength and adhesiveness of the fibers. According to the State Standard [26], the weight fraction of short fibers and so-called "dust" in wool should not exceed 0.2%. Low-molecular-weight fractions of cellulose may induce inflammations caused by penetration of short fibers inside

a wound. It should be noted that cotton wool prepared by alkaline delignification contains 95% α-cellulose, i.e., 95% high-molecular-weight fractions, and in this parameter it surpasses the sample prepared by the nitric acid procedure (Table 2). The lower content of high-molecular-weight fractions in the nitric acid treated sample is apparently caused by degradation of cellulose in the course of bleaching. Upon removal of the major fraction of lignin in the cooking step, the cellulose structure becomes more accessible to attack of agents causing degradation.

The mean degreee of polymerization of the resulting nitric acid flax cellulose is 1300 (Table 2). The degree of polymerization of flax cellulose recovered by nitric acid delignification in [2] (the treatment conditions are not indicated) is as low as 400–450. The relatively high degree of polymerization of flax cellulose in our experiment shows that we actually found acceptable conditions for the nitric acid delignification of flax fibers. Indeed, the suggested scheme provides high selectivity of the reactions of nitric acid with the lignin–polysaccharide complex and limits the acid-catalyzed hydrolytic degradation of cellulose in the cooking step.

Medical wool is used as exudate absorbent and a reservoir of liquid medicinals. In engineering and in homes, the use of wool as wiping and moisture-collecting material is of no less importance. Table 2 shows that flax wool prepared by nitric acid delignification considerably surpassed in the water-retaining power the wool prepared by alkaline delignification: 52% against 42%. This result is quite predictable, because nitric acid treatment causes appearance of cracks on the fiber surface [27], which, apparently, enhances the water-retaining power.

CONCLUSIONS

(1) The suggested scheme of nitric acid delignification followed by nitric acid bleaching of cottonized flax fibers ensures high yield of chemically pure wool with a high hygroscopicity.

(3) The main parameters of the wool prepared by the suggested procedure are similar to or exceed the parameters of the semicommercial flax wool.

REFERENCES

1. Bowyer, J.L. and Stockmann, V.E., *Forest Product J.*, 2001, vol. 49(193), pp. 10–21.
2. Pande, H., *Unasylva*, 1998, vol. 51, no. 1, p. 44.
3. http://www.textileclub.ru/index.php&option=articles&task=viewarticle&artid=360&Itc.
4. Petrova, S.N., Volkova, I.Yu., and Zakharov, A.G., *Zh. Prikl. Khim.*, 2003, vol. 76, no. 8, pp. 1382–1385.
5. Barmin, M.I., Grebenkin, A.N., Boiko, A.I., et al., *Izv. Vyssh. Uchebn. Zaved., Khim. Khim. Tekhnol.*, 2004, vol. 47, no. 3, pp. 156–158.
6. http://www.apteka.ua/archives/479/21668.html.
7. http://www.regnum.ru/news/tumen/565827.html.
8. Ryzhkov, A.I., *Tekstil'n. Khim.*, 1998, no. 3(15), pp. 64–67.
9. RF Patent 2194107.
10. RF Patent 2175363.
11. Nikitin, V.M., *Teoreticheskie osnovy delignifikatsii* (Theoretical Principles of Delignification), Moscow: Lesnaya Prom–st., 1981.
12. Nepenin, N.N. and Nepenin, Yu.N., *Tekhnologiya tsellyulozy* (Cellulose Technology), vol. 3: *Ochistka, sushka i otbelka tsellyulozy: Prochie sposoby proizvodstva tsellyulozy* (Purification, Drying, and Bleaching of Cellulose: Other Procedures for Cellulose Production), Moscow: Ekologiya, 1994.
13. Shishonok, M.V., Torgashov, V.I., Gert, E.V., et al., *Cellulose Chem. Technol.*, 1997, vol. 31, nos. 5–6, pp. 425–438.
14. Ngamveng, J.N. and Ndikontar, M., *Cellulose Chem. Technol.*, 1990, vol. 31, no. 4, p. 523.
15. Abou-State, M.A., Helmy, S.A., and El-Sherbini, A.M., *Cellulose Chem. Technol.*, 1986, vol. 20, no. 4, pp. 421–428.
16. Andaburskii, S.I., *Khim. Drev.*, 1978, no. 3, pp. 8–11.
17. Obolenskaya, A.V., Shchegolev, V.P., Akim, G.L., et al., *Prakticheskie raboty po khimii drevesiny i tsellyulozy* (Practical Works on Wood and Cellulose Chemistry), Moscow: Lesnaya Prom–st., 1965.
18. Starostenko, N.P. and Demchenkov, P.A., *Tekhnologiya tsellyulozno-bumazhnogo proizvodstva: Rukovodstvo k laboratornym rabotam* (Technology of Pulp and Paper Production: Laboratory Manual), Leningrad: Vsesoyuznyi Zaochnyi Lesotekhnicheskii Inst., 1964.
19. Petrova, S.N., Volkova, I.Yu., Lebedeva, T.N., and Zakharov, A.G., *Izv. Vyssh. Uchebn. Zaved., Khim. Khim. Tekhnol.*, 2003, vol. 46, no. 1, pp. 84–85.
20. *TAPPI Standard Method T–223–os62*.
21. *GOST* (State Standard) *6840–54.*
22. *GOST* (State Standard) *18461–93*.
23. Bolotnikova, L.S., *Zh. Prikl. Khim.*, 1966, vol. 39, no. 1, pp. 176–180.
24. Fahmy, Y. and Mobarak, F., *Sven. Papperstidn. Ach. Svenpappersförädlingstidskr. A*, 1971, vol. 74, no. 1, pp. 2–9.
25. Fengel, D. and Wegener, G., *Wood (Chemistry, Ultrastructure, Reactions)*, Berlin: Walter de Gruyter, 1984.
26. *GOST* (State Standard) *5556–81*.
27. Gert, E.V., Matyul'ko, A.V., Shishonok, M.V., et al., *Zh. Prikl. Khim.*, 2003, vol. 76, no. 4, pp. 616–620.

ISSN 1070-4272, Russian Journal of Applied Chemistry, 2006, Vol. 79, No. 9, pp. 1546–1549. © Pleiades Publishing, Inc., 2006.
Original Russian Text © N.B. Ivanenko, A.A. Ivanenko, E.V. Molodkina, E.B. Nosova, A.E. Zeimal', Yu.A. Zavoda, 2006, published in Zhurnal Prikladnoi Khimii, 2006, Vol. 79, No. 9, pp. 1562–1565.

CHEMISTRY OF FOSSIL FUEL

Direct Atomic-Absorption Determination of the Ni and V Content in Oil

N. B. Ivanenko, A. A. Ivanenko, E. V. Molodkina, E. B. Nosova, A. E. Zeimal', and Yu. A. Zavoda

St. Petersburg State University, St. Petersburg, Lyumeks NPF AP, St. Petersburg, Russia

Received April 20, 2006

Abstract—A direct (without sample pretreatment) atomic-absorption method of V and Ni determination in oil with electrothermal atomization and Zeeman correction of background was developed.

DOI: 10.1134/S1070427206090308

About 30 metals were detected in oil, among which V, Ni, Fe, Cu, Al, Cr, and Zn are the most abundant. Vanadium and nickel were the first metals detected in oil. The content of these metals in oil can reach tenth parts of percent, which makes recovery of vanadium and nickel from oil economically attractive [1]. Approximately 40% of vanadium and nickel exist in oil as vanadyl and nickel porphyrins and are concentrated in oil fractions with boiling points above 300°C, i.e., in raw material of catalytic cracking, black oil, and tar [2]. The presence of vanadium and nickel in these fractions is undesirable because of catalyst poisoning and corrosion of boiler parts with vanadium(V) oxide, which is formed in the course of fuel combustion.

Vanadium and nickel compounds are the most hazardous among all metals discharged into the environment from petrochemical plants. They have toxicological, immunopathological, and carcinogenic effect on a human body.

The vanadium and nickel content in oil and in its heavy fractions is usually determined by various instrumental methods [3, 4]. There is a standard method of vanadium determination [5], in which oil samples are preliminarily treated with concentrated sulfuric and nitric acids, or elemental sulfur, or samples are burnt. The ash is treated with acids, which is followed by photometric determination of vanadium as a tungstate complex at 436 nm. The standard method of determination of metals in oil in the United States involves oil sample treatment with concentrated sulfuric acid, followed by heating to 525°C in muffle, or sample dissolution in a complex mixture of aromatic solvents. The final determination is performed on atomic absorption spectrometers with flame atomization or on atomic emission spectrometers with inductively coupled plasma [6].

In this study, we developed a method of vanadium and nickel determination in oil on a atomic absorption spectrometer with electrothermal atomization and Zeeman correction of the background.

EXPERIMENTAL

An MGA-915 Zeeman atomic absorption spectrometer produced by Lyumeks Limited Liability Company, Massman graphite cells with L'vov's platform, and 5–50 mm^3 single-channel pipettes (batcher) were used; the measurement error did not exceed 5%.

We used a 1 g dm^{-3} aqueous solution of nickel [GSO (State Reference Sample) 8001–93(8003–96), Water Research and Control Center], a 0.1 g dm^{-3} aqueous solution of vanadium (GSO 7267–96, Ural Research Institute of Metrology), distilled water [GOST (State Standard) 6709–72], double-distilled water (the metal content should not exceed 30% of the lower boundary of the interval determined), ultrapure grade palladium nitrate (10 g dm^{-3}) as a modifier, ultrapure grade concentrated nitric acid (GOST 11 125–84), and calibration solutions of Ni and V(IV) (10 and 20 μg dm^{-3}) prepared in double-distilled water.

To plot the calibration dependence of the analytical signal on the element weight, before each measurement 20 mm^3 of a 1 g dm^{-3} modifier solution was introduced with a batcher into a graphite cell of the MGA-915 atomic absorption spectrometer and dried for 40 s at 110°C. Then the required volume (5–

40 mm^3) of 10 μg dm^{-3} nickel and vanadium calibration solutions and 30–40 mm^3 of 20 μg dm^{-3} calibration solutions were introduced. Then, the corresponding integral analytical signals were measured; each measurement was repeated 5 times with calculation of the arithmetic mean.

The calibration dependences were plotted for each element. These dependences are linear within the 100–800 pg range for vanadium and within the 40–80 pg range for nickel.

For oil sample preparation, a 0.1–0.2-g oil sample was dissolved in heptane (~5 cm^3). The solution was quantitatively transferred into a 10 cm^3 volumetric flack, and heptane was added to the mark.

Then, 20 mm^3 of modifier solution with a metal concentration of 1 g dm^{-3} was introduced into a graphite cell with the batcher and dried for 40 s at 110°C, and then 5 mm^3 of an oil sample diluted with heptane depending of the expected metal content was introduced. Then the measurement was performed in accordance with the selected mode of the spectrometer operation.

Atomic absorption analysis of oil is complicated by noises generated by sample components, e.g., chemical effects or high level of nonselective absorption. The latter is caused by broad-band molecular absorption of evaporated components of the sample or light scattering on the particles of the products of the matrix decomposition [7]. To take into account nonselective absorption in atomic absorption spectrometers with electrothermal atomization, various background corrections are used; Zeeman correction realized in MGA-915 spectrometer is the most efficient [8, 9].

However, background correction in the analysis of complex objects is insufficient. Optimization of the temperature–time program of furnace heating and chemical modification should also be used. In our study, both approaches were applied simultaneously.

In spite of numerous papers on successful application of modifiers, modifiers for metal determination in a specific matrix in most cases are still chosen empirically [7]. We studied three modifiers: palladium(II) nitrate, hydrogen hexachloroplatinate(IV), and magnesium nitrate (in a concentration of 1 g dm^{-3}). The first two compounds are readily reduced to the elemental state on the surface of the graphite furnace. They form intermetallic compounds with V and Ni, which provides elevation of the pyrolysis temperature. Magnesium nitrate forms high-temperature oxide in the course of the pyrolysis in the furnace zone that does not contact graphite; this oxide provides thermal stabilization of nickel and vanadium oxides. The maximal analytical signal of V and Ni, maximal temperature of pyrolysis, and minimal nonselective absorption were obtained with palladium(II) nitrate used as modifier. Probably, this modifier provides more complete ashing of the oil organic matrix.

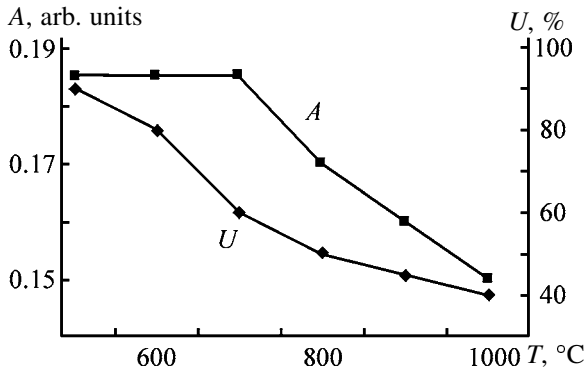


Fig. 1. Dependence of the analytical signal A and the level of the nonselective absorption U on the pyrolysis temperature T for Ni.

Properly chosen mode of the oil sample drying is of great importance for attaining well reproducible results. The temperature and drying duration depend on the solution type. In the case of heptane, we chose the temperature of 60°C and drying time of 40 s.

The pyrolysis stage in many respects determines the accuracy of the analysis and elimination of nonselective absorption. The dependence of the integral analytical signal on the pyrolysis temperature is shown in Fig. 1. Insufficient temperature of the pyrolysis does not allow complete decomposition of the organic matrix, whereas too high pyrolysis temperature leads to partial loss of the elements. As seen from Fig. 1, at 700°C for both nickel and vanadium the ratio between the analytical signal and nonselective absorption is optimal.

The optimal temperature of the nickel and vanadium atomization stage is the minimal temperature producing the maximal analytical signal. At lower temperature, atomization of the oil sample is incomplete, which decreases the analysis sensitivity. At too high temperature, the loss of vaporous nickel and vanadium atoms is observed. This decreases the intensity of the analytical signal and, moreover, drastically shortens the lifetime of the graphite atomizer. The dependence of the integral analytical signal of V and Ni on the atomization temperature is shown in Fig. 2.

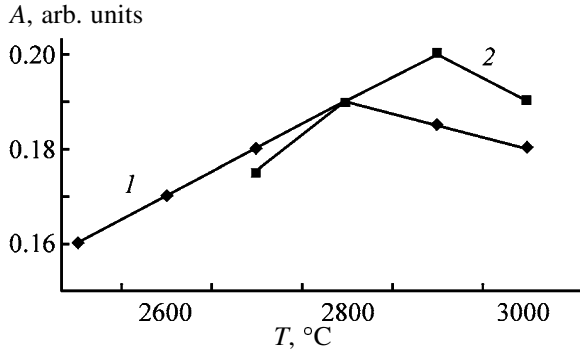


Fig. 2. Dependence of analytical signal A of (*1*) nickel and (*2*) vanadium on the atomization temperature T.

As seen, the optimal atomization temperature is 2900°C for vanadium and 2800°C for nickel.

The optimal temperature–time parameters of the analysis of oil samples are listed in Table 1. To determine the error characteristics of the method, we used the reference sample (RS) of oil composition SRM 1634-c (producer NIST, the United States). The vanadium and nickel content in it is 28.20 and 17.25 mg kg^{-1}, respectively, at standard deviation of the analysis of 0.21 (RS no. 1). To cover the whole interval of V and Ni contents, we also used the sample diluted with heptane by a factor of 2, 4, 5, 10, 20, 50, and 100 (RS nos. 2–8, respectively).

The interval of the measured contents was 0.3–28.2 and 0.2–3.5 mg kg^{-1} for vanadium and nickel, respectively. The random component of the error was estimated from 10 replicate determinations. The characteristics of the random component of the error are listed in Table 2., where $\bar{c}$ is mean content of V and Ni in RS, and S_r, relative standard deviation of the analysis results.

As seen, for vanadium concentration ranges 0.3–0.6 and 0.6–28.2 mg kg^{-1}, the relative standard deviation does no exceed 15 and 10%, respectively, and for nickel it amounts to 20 and 12% within the concentration ranges 0.2–0.4 and 0.45–3.5 mg kg^{-1}, respectively. The fixed component of the error was determined using the above RSs of the oil composition. The results obtained are shown in Table 3, where c_{cf}

Table 1. Optimal temperature–time parameters of the process

Mode	V, λ = 318.4 nm		Ni, λ = 232 nm	
	t, s	T, °C	t, s	T, °C
Drying, volume 5–40 mm^3	40	60	40	60
Pyrolysis	30	700	30	700
Atomization	1.5	2900	1.5	2800
Cleaning	1.5	2950	1.5	2850
Pause	70	–	50	–

Table 2. Characteristics of the error random component in the measurements of V and Ni concentration in oil

Element	RS no.	$\bar{c}$, mg kg^{-1}	S_r, %
V	1	28.46	6.4
	2	13.85	9.3
	3	7.22	10.4
	5	2.75	9.2
	7	0.62	12.3
	8	0.29	13.7
Ni	4	3.46	7.0
	5	1.77	10.8
	6	1.01	9.0
	7	0.42	11.9
	8	0.20	20.0

Table 3. Fixed error in measurements of V and Ni concentration (P = 0.95, n = 10)

Element	Sample no.	c_{cf}, mg kg^{-1}	c, mg kg^{-1}	S	θ, mg kg^{-1}	t_c
V	1	28.20	28.46	1.82	0.28	0.26
	2	14.10	13.85	1.29	–0.25	0.59
	3	7.05	7.22	0.75	0.17	0.64
	5	2.82	2.75	0.25	–0.07	0.48
	7	0.56	0.62	0.08	0.06	0.48
	8	0.28	0.29	0.04	0.01	0.08
Ni	4	3.45	3.43	0.24	–0.02	0.14
	5	1.75	1.77	0.16	0.02	0.15
	6	0.88	1.01	0.11	0.13	1.05
	7	0.35	0.42	0.05	0.05	0.57
	8	0.18	0.20	0.04	0.04	0.21

Table 4. Results of determination of Ni and V concentrations in oil (P = 0.95, n = 6)

Deposit, oil well no.	Concentration ±Δ, mg kg^{-1}	
	vanadium	nickel
Asar, 49	3.17 ± 0.34	9.70 ± 0.62
Burmasha, 3	1.64 ± 0.12	2.40 ± 0.28
Zhetybai, 1068	0.80 ± 0.08	16.80 ± 1.20

is the content of the element in RS in accordance with the certificate; c, measured content of the element in RS; S, standard deviation of the replicate measurements; and $\theta = c - c_{cf}$ and t_c are the calculated values of the Student test for the confidence level $P = 0.95$ and the number of replicate measurements 10.

Table 3 shows that the calculated Student test for $P = 0.95$ and the number of degrees of freedom $f = n - 1 = 9$ within the whole range of metal contents for both V and Ni does not exceed the tabulated value $t_{0.95,9} = 2.26$. Hence, the fixed component of the method error is insignificant. Thus, the method proposed for the direct determination of V and Ni in oil provides correct and well reproductible results. The content of vanadium and nickel was determined by this method in samples of various oils (Table 4).

CONCLUSION

A method of the direct atomic-absorption determination of vanadium and nickel in oil was developed. This method can be recommended for express determination of V and Ni in oil.

REFERENCES

1. Sitnikova, G.Yu. and Davydova, S.A., *Neftekhimiya*, 1992, vol. 32, no. 5, pp. 387–397.
2. Manovyan, A.K., *Tekhnologiya pervichnoi pererabotki nefti* (Technology of Primary Oil Processing), Moscow: Khimiya, 2001.
3. Anikina, N.A., *Zavod. Lab: Diagn. Mater.*, 1998, no. 8, p. 12.
4. Bukhbinder, G.L., Shabanova, L.N., and Gil'bert, E.N., *Zh. Anal. Khim.*, 1988, vol. 43, no. 7, pp. 1323–1328.
5. *GOST* (State Standard) *10364–90: Oil and Oil Products. Method of Vanadium Determination*, Moscow: Izd. Standartov, 2002.
6. *Standard Test Method for Determination of Ni, V, Fe in Crude Oils and Residual Fuels by ICP Atomic Emission Spectrometry*, p. 5.
7. Pupyshev, A.A., *Prakticheskii kurs atomno-absorptsionnogo analiza* (Practical Course of Atomic Absorption Analysis), Yekaterinburg: Ural'sk. Politekh. Inst., 2003.
8. Sholupov, S.E. and Ganeyev, A.A., *Spectrochim. Acta, Part B*, 1995, vol. 50, no. 10, pp. 1227–1236.
9. Ganeev, A.A., Sholupov, S.E., Timofeev, A.D., and Ivankov, V.M., *Zh. Anal. Khim.*, 1995, vol. 50, pp. 648–654.

ISSN 1070-4272, Russian Journal of Applied Chemistry, 2006, Vol. 79, No. 9, pp. 1550–1551. © Pleiades Publishing, Inc., 2006.
Original Russian Text © V.V. Rogozhin, E.Yu. Anan'eva, 2006, published in Zhurnal Prikladnoi Khimii, 2006, Vol. 79, No. 9, pp. 1566–1567.

BRIEF COMMUNICATIONS

Mechanism of Chemical Deposition of Nickel–Boron Coatings in Tartrate–Glycine Solutions

V. V. Rogozhin and E. Yu. Anan'eva

Nizhni Novgorod State Technical University, Nizhni Novgorod, Russia

Received April 17, 2006

Abstract—The effect of glycine additive on the deposition of nickel–boron coatings from tartrate–glycine solutions was studied.

DOI: 10.1134/S107042720609031X

Nickel–boron coatings, compared to nickel–phosphorus coatings, are more resistant to high temperatures in air, show better barrier properties against diffusion of metal atoms of the substrate, and can be subjected to high-quality soldering and welding.

At the same time, wide practical application of borohydride solutions, recommended for chemical deposition of nickel–boron coatings by GOST (State Standard) 9308–84, is seriously impeded by the presence of ethylenediamine constituent, which is a known carcinogen, and by the use of heavy metal salts as stabilizing additives. The compositions of tartrate–glycine solutions of chemical nickel plating have been recommended in [1–3].

In this study, we examined how glycine additive affects the mechanism of the deposition of nickel–boron coatings from the above solutions. The initial solution was tartrate–glycine solution [2] containing (g l^{-1}) nickel sulfate 25, K–Na tartrate 50, glycine 50, sodium hydroxide 80, sodium borohydride 1.0, and stabilizers. A nickel–boron coating containing about 3.0% boron is deposited from such solution at an average rate of 7–9 μm in 30 min.

EXPERIMENTAL

The electrochemical study was performed in a standard YaSE-2 cell using PI-50 and P-5848 potentiostats. The coating thickness was calculated from the gain in the coating weight per visible surface of the electrode. Mercury oxide electrode was used as reference. The potentials were recalculated relative to standard hydrogen electrode. The experiments were performed at 85°C for 30 min.

The electrochemical mechanism of the chemical deposition of nickel–boron alloy from tartrate–glycine solution was confirmed by the dependence of the nickel plating rate on the potential, which passes through a maximum (Fig. 1). The deposition rate is maximal in the vicinity of the compromise potential of chemical nickel plating, when the steps of cathodic deposition of the coating and anodic oxidation of the reductant are kinetically compensated. These steps are actually interrelated: the shift of the electrode potential to the negative direction from the compromise potential of the chemical nickel plating considerably decreases the rate of the coating deposition. Acceleration of the external electroplating of the coating is far from compensating the decrease in the rate of the chemical process.

Evidently, this fact indicates that the adsorbed reductant, borohydride, whose reactivity in the region of electronegative potentials is decreased, exhibits the

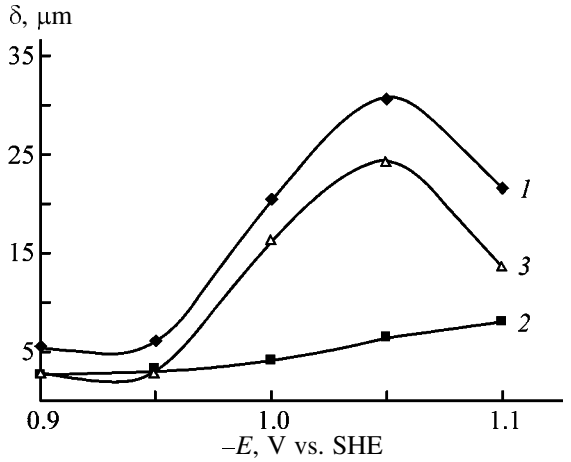


Fig. 1. Coating thickness δ in nickel deposition from initial solution vs. potential *E*. (*1*) Total curve; partial curves: (*2*) external electroplating and (*3*) chemical deposition.

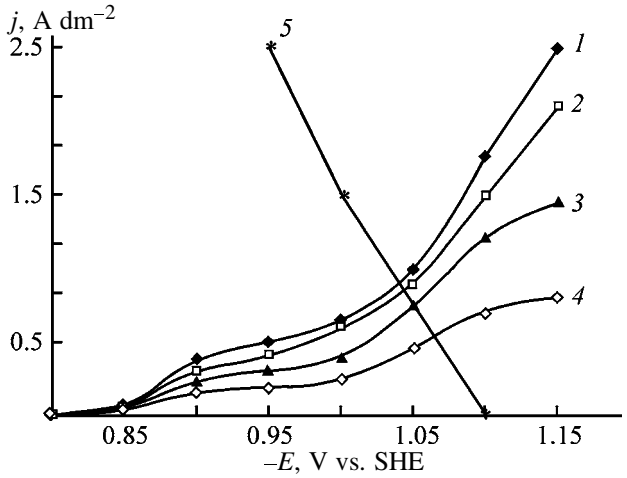


Fig. 2. Polarogram of the chemical nickel plating. (*j*) Current density and (*E*) potential. (*1–4*) Cathodic curves (solutions without borohydride) at glycine concentration, g l^{-1}: (*1*) 25, (*2*) 50, (*3*) 75, and (*4*) 100; (*5*) anodic curve (solution without nickel salt).

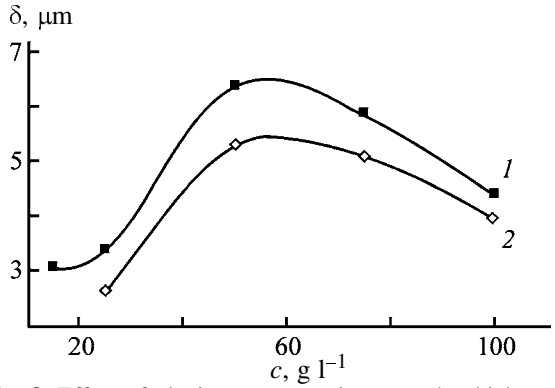


Fig. 3. Effect of glycine concentration *c* on the thickness δ of the nickel–boron coatings. Thickness, μm: (*1*) experimental and (*2*) calculated from conjugation of the cathodic and anodic curves.

inhibiting effect, which should be taken into account in electrochemical simulation of steps of the chemical nickel plating process.

Variations of the rate of the nickel partial deposition with varying the potential are considerably more pronounced in solutions without reductant, which shows that the reductant inhibits the cathodic deposition of nickel at electronegative potentials (Fig. 2). In this case, the rate of the nickel deposition is markedly affected by the glycine concentration in the solution, which, as additional ligand for nickel ions, considerably increases the rate of the chemical deposition of nickel–boron coatings. Glycine, taken in optimal concentrations (40–60 g l^{-1}), facilitates the cathodic nickel deposition (Fig. 2) not only owing to the formation of a [Ni(Tart)(Gly)] complex but also owing to rearrangement of the dense part of the electrical double layer with increasing ψ' potential, as it was shown previously in [4].

A possibilty of stepwise simulation of the deposition of nickel–boron coatings based on the conjugation of cathodic and anodic steps is confirmed by the fact that the coating thicknesses calculated from the currents at the point of intersection of the polarization curves of its cathodic and anodic model steps (Fig. 2) and the actual thicknesses of the coatings prepared by the chemical nickel deposition from solutions differing in the glycine concentrations are close (Fig. 3). The latter thickness also passes through a maximum at a glycine concentration of 40–60 g l^{-1}.

In the course of the chemical nickel deposition, its compromise potential first passes a peak at about 20 mV, which is evidently due to the difficulty in formation of a new phase, and then gradually shifts toward positive potentials, attaining the steady-state values of –1040 to –1050 mV. This shift may be accounted for by consumption of adsorbed particles of the reductant and by retardation of surface adsorption stages.

CONCLUSION

The chemical nickel deposition in tartrate–glycine solutions proceeds by the electrochemical mechanism based on the conjugation of the anodic (borohydride oxidation) and cathodic (nickel deposition) steps. The latter process is affected by the glycine additive, which, on the whole, determines the rate of the chemical nickel deposition.

REFERENCES

1. Plokhov, V.A., Rogozhin, V.V., and Flerov, V.N., *Zashch. Met.*, Moscow, 1985, no. 9, pp. 976–978.
2. Rogozhin, V.V., Abstracts of Papers, *Ezhegodnaya Vserossiiskaya nauchno-prakticheskaya konferentsiya "Gal'vanotekhnika, obrabotka poverkhnosti i ekologiya 2002"* (Annual All-Russian Scientific and Practical Conf. "Electroplating, Surface Treatment, and Ecology 2002"), Moscow: 2002.
3. Flerov, V.N., Prusov, Yu.V., Rogozhin, V.V., and Kurnoskin, G.A., *Sbornik trudov NGTU "Razrabotka ekonomichnykh protsessov khimicheskoi metallizatsii radioelektronnykh detalei"* (Coll. of Works of Nizhni Novgorod State Technical Univ. "Development of Effective Processes for Chemical Metal Plating of Radioelectronics Parts), Nizhni Novgorod, 2003, vol. 39, no. 1, pp. 70–76.
4. Ryabov, E.I., Naumov, V.I., and Rogozhin, V.V., *Izv. Vyssh. Uchebn. Zaved., Khim. Khim. Tekhnol.*, 1992, vol. 35, no. 1, pp. 102–106.

ISSN 1070-4272, Russian Journal of Applied Chemistry, 2006, Vol. 79, No. 9, pp. 1552–1554. © Pleiades Publishing, Inc., 2006.
Original Russian Text © V.M. Lembrikov, L.V. Konyakhina, V.V. Volkova, G.P. Zhavoronkova, B.T. Kunin, 2006, published in Zhurnal Prikladnoi Khimii, 2006, Vol. 79, No. 9, pp. 1568–1570.

BRIEF COMMUNICATIONS

Density of Organic Phases in the Extraction System Tributyl Phosphate–Phosphoric Acid

V. M. Lembrikov, L. V. Konyakhina, V. V. Volkova, G. P. Zhavoronkova, and B. T. Kunin

Voskresensk Research Institute of Fertilizers and Phosphoric Acid, Joint-Stock Company, Voskresensk, Moscow oblast, Russia
Ivanovo State University of Chemical Technology, Ivanovo, Russia

Received January 11, 2006

Abstract—Data on the density of phosphoric acid solutions in crude TPB and TBP-based commercial extractant for purification of wet-process phosphoric acid are tabulated over the phosphoric acid concentration range 0.62–27.74 wt % (recalculated to P_2O_5).

DOI: 10.1134/S1070427206090321

One of the methods for purification of wet-process phosphoric acid (WPPA) is extraction with organic solvents. At the Voskresensk Institute of Fertilizers and Phosphoric Acid (Voskresensk, Moscow oblast, Russia), an industrial process has been developed for purification of WPPA by TBP extraction [1]. The process conditions (reagent consumption, temperature, and compositions of the liquid phases) were reported elsewhere [2]. In this process, phase separation in the pulsating columns and settlers is accomplished under the action of gravity, i.e., the driving force of the process is the density difference between the organic and aqueous phases.

In this study, we report the densities of phosphoric acid solutions in the commercial TPB-based extractant. The major impurities in the extraction system are as follows (wt %): sulfate (0.056), fluorine-containing compounds (0.035), humics (0.15), and other foreign compounds present in WPPA produced from Khibiny concentrate and transferred into TBP in the course of extraction. For comparison, we measured the density of crude TBP solutions [3] and commercial phosphoric acid (analytically pure grade).

The phosphoric acid concentration in the solutions was varied from 0.62 to 27.74 wt % (recalculated to P_2O_5). The acid concentration was determined potentiometrically [4].

The density of solutions was measured pycnometrically over the temperature range 10–70°C. In the experiments, the temperature was controlled to within 0.5°C.The results are summarized in Tables 1 and 2.

The graphical analysis and data processing showed that the temperature dependence of the density can be described by the Mendeleev equation [5]

$$\rho_t = \rho_{23}(1 - k\Delta t), \quad (1)$$

where ρ_t and ρ_{20} are the densities (g cm^{-3}) at a given temperature (°C) and 20°C; Δt is the temperature difference (t – 20) (°C); and k, expansion modulus of the liquid.

Tables 1 and 2 present the expansion modulus of phosphoric acid solutions in the extractant and TBP, estimated by Eq. (1). In fact, this is the mean cubic expansion coefficient α for the temperature ranges 10–20, 20–30, 20–40°C, etc. [6]. The graphical (see figure) and mathematic treatment of the k values revealed that the concentration dependence of k fits Eq. (2) for the solutions obtained by saturation of the process extractant and Eq. (3) for the solutions obtained by saturation of crude TBP with commercial phosphoric acid:

$$k \times 10^3 = 1.3444 - 0.054c_{P_2O_5}, \quad (2)$$

$$k \times 10^3 = 0.9046 - 0.0071c_{P_2O_5}, \quad (3)$$

where k is the expansion modulus and $c_{P_2O_5}$, phosphoric acid concentration in the solution, recalculated to P_2O_5 (wt %).

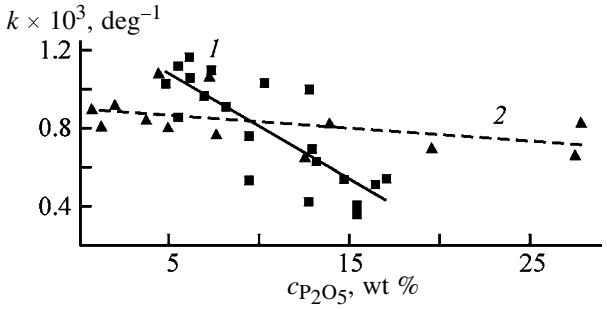
Previously [2], using data obtained in the course of

Table 1. Density of phosphoric acid solutions ρ in commercial extractant

P_2O_5, wt %	20°C		30°C			40°C			50°C		
	ρ, g cm^{-3}		ρ, g cm^{-3}		$k \times 10^3$, deg^{-1} [Eq. (1)]	ρ, g cm^{-3}		$k \times 10^3$, deg^{-1} [Eq. (1)]	ρ, g cm^{-3}		$k \times 10^3$, deg^{-1} [Eq. (1)]
	experiment	Eq. (4)	experiment	Eq. (6)/(7)		experiment	Eq. (6)/(7)		experiment	Eq. (6)/(7)	
4.7	1.020	1.018				0.999	0.996/1.001	1.030			
5.4	1.023	1.024				1.000	1.002/1.006	1.120	0.997	0.992/0.997	0.850
6.1	1.032	1.029				1.008	1.008/1.012	1.160	0.999	0.998/1.003	1.060
6.86	1.036	1.035	1.026	1.025/1.027	0.965						
7.3	1.039	1.039				1.016	1.019/1.022	1.100			
8.08	1.045	1.045							1.016	1.017/1.019	0.920
9.35	1.054	1.055	1.046	1.046/1.047	0.760				1.037	1.028/1.029	0.530
10.20	1.059	1.062				1.037	1.045/1.045	1.038			
12.72	1.091	1.082	1.080	1.074/1.074	1.010	1.076	1.067/1.065	0.690	1.077	1.060/1.056	0.420
13.08	1.117	1.084							1.096	1.063/1.059	0.630
14.58	1.106	1.096	1.100	1.090/1.089	0.540						
15.38	1.116	1.103	1.112	1.097/1.095	0.360	1.107	1.091/1.086	0.400			
16.37	1.120	1.110				1.108	1.100/1.094	0.500			
17.00	1.115	1.115							1.097	1.101/1.090	0.540

Table 2. Density of phosphoric acid solutions ρ in crude TBP

P_2O_5, wt %	10°C			20°C		40°C			70°C		
	ρ, g cm^{-3}		$k \times 10^3$, deg^{-1} [Eq. (1)]	ρ, g cm^{-3}		ρ, g cm^{-3}		$k \times 10^3$, deg^{-1} [Eq. (1)]	ρ, g cm^{-3}		$k \times 10^3$, deg^{-1} [Eq. (1)]
	experiment	Eq. (7)		experiment	Eq. (5)	experiment	Eq. (7)		experiment	Eq. (7)	
0.62					0.986				0.942	0.942	0.890
1.15					0.990	0.974	0.972	0.800			
1.43				0.993	0.992						
1.96					0.997				0.953	0.952	0.920
3.64					1.010	0.993	0.992	0.840			
4.06				1.011	1.013						
4.42	1.027	1.025	1.080		1.016						
4.86					1.020				0.979	0.975	0.800
6.55				1.035	1.033						
7.15					1.038	1.016	1.020	1.060			
7.61	1.050	1.051	0.770		1.042						
12.56					1.081				1.046	1.037	0.650
13.53				1.087	1.089						
13.79					1.091	1.073	1.074	0.820			
19.29				1.139	1.135						
19.49					1.137	1.121	1.119	0.700			
20.41					1.144				1.100	1.101	0.770
27.47					1.201				1.162	1.158	0.650
27.74	1.210	1.211	0.830	1.200	1.203						



Expansion modulus k of phosphoric acid solutions in (*1*) commercial extractant and (*2*) crude TBP as a function of the acid concentration (wt %, recalculated to P_2O_5).

long-time service of the semicommercial plant, we have demonstrated that the phosphoric acid concentration in the extractant can be described by Eq. (4):

$$c_{P_2O_5} = 127\rho_{20} - 124.64, \quad (4)$$

For the solutions in crude TBP, we obtained relationship (5):

$$c_{P_2O_5} = 125\rho_{20} - 122.62, \quad (5)$$

where $c_{P_2O_5}$ is the phosphoric acid concentration in the organic solutions, recalculated to P_2O_5 (wt %).

From Eqs. (1)–(5), we obtain Eq. (6) for the density of process solutions of phosphoric acid in the extractant, and Eq. (7) for simulated solutions of phosphoric acid in TBP:

$$\rho_t = \frac{c_{P_2O_5} + 124.64}{127}[1 - (1.3444 - 0.054c_{P_2O_5})\Delta t \times 0.001], \quad (6)$$

$$\rho_t = \frac{c_{P_2O_5} + 122.62}{125}[1 - (0.9046 - 0.0071c_{P_2O_5})\Delta t \times 0.001]. \quad (7)$$

The results obtained using these equations are given in Tables 1 and 2, respectively. It should be pointed out that these equations are similar, having close coefficients. Table 1 shows that the difference between the densities estimated by Eqs. (6) and (7) is within 1%, being generally 0.3%. This fact suggests that the occurrence of the above-indicated amounts of impurities in the process solutions has no significant effect on the density of phosphoric acid solutions in TBP, and, therefore, the estimates can be made by both Eqs. (6) and (7).

CONCLUSION

Analytical expressions are derived for the dependences of the density of phosphoric acid solutions in tri-*n*-butyl phosphate on the temperature and composition of the organic phase over the temperature range 10–70°C and the range of the P_2O_5 concentration in the organic phase from 0.62 to 27.74 wt %.

REFERENCES

1. Lembrikov, V.M., Konyakhina, L.V., Nikitin, V.G., and Volkova, V.V., *Khim. Tekhnol.*, 2004, no. 8, pp. 4–8.
2. Lembrikov, V.M., Konyakhina, L.V., Volkova, V.V., Nikitin, V.G., et al., *Khim. Tekhnol.*, 2005, no. 6, pp. 2–5.
3. *TU* (Technical Specifications) *2435-305-05 763 458–01: Crude Tributyl Phosphate*.
4. Skornyakova, R.A., Konyakhina, L.V., and Tokmakova, T.V., *Ekspress informatsiya: Otechestvennyi proizvodstvennyi opyt* (Express Information: Domestic Industrial Experience), Ser.: *Metody analiza i kontrolya kachestva produktsii* (Methods for Analysis and Quality Control of Products), Moscow: NIITEKhim, 1985, no. 6, pp. 20–22.
5. Kireev, V.A., *Kurs fizicheskoi khimii* (Course of Physical Chemistry), Moscow: Khimiya, 1975.
6. *Spravochnik khimika* (Chemist's Handbook), Nikol'skii, B.P., Ed., Moscow: Khimiya, 1966, vol. 1.

ISSN 1070-4272, Russian Journal of Applied Chemistry, 2006, Vol. 79, No. 9, pp. 1555–1558. © Pleiades Publishing, Inc., 2006.
Original Russian Text © Yu.G. Khabarov, L.A. Pes'yakova, A.V. Kolygin, 2006, published in Zhurnal Prikladnoi Khimii, 2006, Vol. 79, No. 9, pp. 1571–1574.

BRIEF COMMUNICATIONS

Nitrosation of Lignosulfonic Acids for Their Colorimetric Determination

Yu. G. Khabarov, L. A. Pes'yakova, and A. V. Kolygin

Arkhangelsk State Technical University, Arkhangelsk, Russia

Received December 21, 2006; in the final form, April 2006

Abstract—The kinetics of lignosulfonic acid nitrosation in the presence of acetic and nitric acids used for generation of nitrous acid in combination with sodium nitrite was studied as applied to colorimetric determination of lignosulfonic acids.

DOI: 10.1134/S1070427206090333

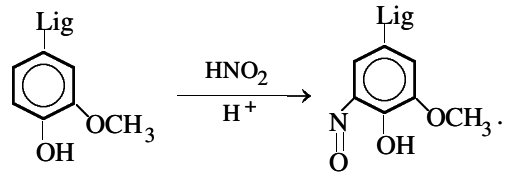
Owing to high reactivity under mild conditions, nitrous acid is widely used in organic synthesis and analysis. Organic compounds of various types can be prepared using nitrous acid [1–3]. Certain organic reactions are catalyzed by nitrous acids [4, 5]. Vast material on the chemistry of nitroso and nitro compounds was summarized in monographs and reviews [6–9].

Numerous organic compounds can be identified by the reaction with nitrous acid: phenols (Liebermann's reaction), amines, amino acids and amino acridines, acid acylides, xylidines, naphthols, nitro compounds, alcohols, sulfanilamides, and thiols. These methods were summarized and considered in detail by Korenman in [10].

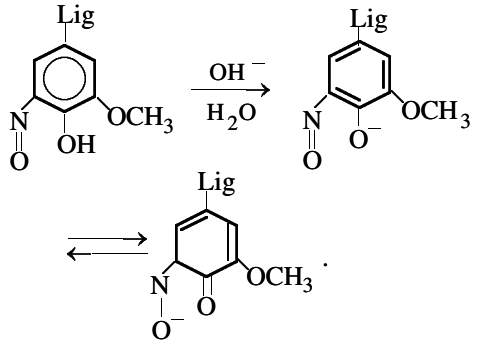
Nitrous acid and nitrites are widely used in lignin chemistry [11]. The possibility of using nitrous acid for cellulose bleaching was discussed in [12]. Nitrosated lignosulfonic acids (LSAs) are chelating agents for biogenic metal cations [13–15]. Nitrous acid is used for determining lignins in both solid and liquid media.

A method for determining wood pulp content in paper composites was developed by Gogotov et al. [16]. According to this technique, a paper composite is nitrosated at 60°C for 30 min at 6% sodium nitrite consumption and then the ratio of the reflection and scattering coefficients of the paper composite is measured at 430 nm.

Currently lignosulfonic acids are determined by the Pearl–Benson's method developed in the 1940s [17]. This method is widely used in many countries [18–23]. In this method, sulfite liquor or wastewater to be analyzed is treated with nitrous acid generated by acidification of aqueous sodium nitrite with acetic acid. The resulting solution is alkalized, kept for 15 min, and then the lignosulfonic acid content is determined from the optical density at 430 nm. The light absorption in this system is caused by the colored nitrosated sulfonic acid derivatives formed by the following reactions. In the first step, lignosulfonic acid is nitrosated by the S_E reaction



On alkalization, the phenolic groups of nitrosated lignosulfonic acid are ionized to form the anion stabilized by conjugation.



A method for quantitative determination of LSA based on its nitrosation was suggested in [24]. According to this method, the solution to be analyzed is

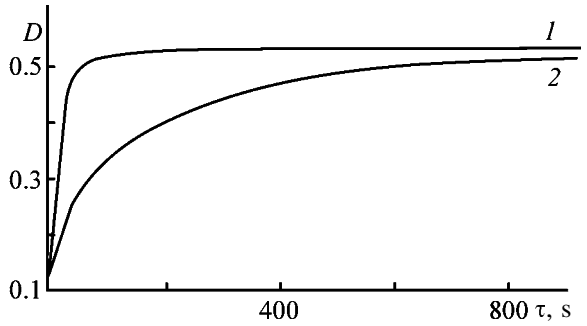


Fig. 1. Variation of the optical density of LST solution in the course of nitrosation with nitrous acid generated from sodium nitrite in combination with (*1*) nitric acid and (*2*) acetic acid. λ = 440 nm.

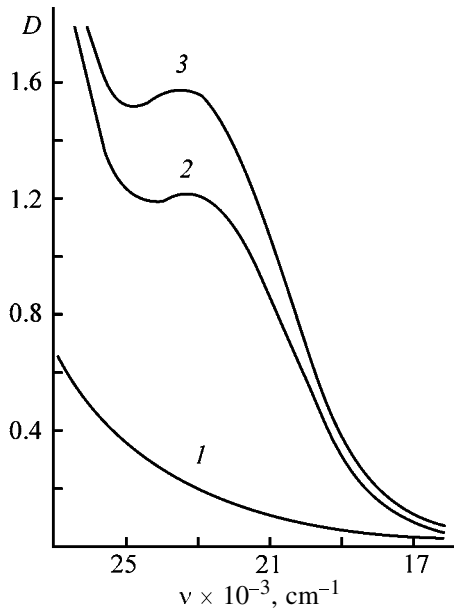


Fig. 2. Electronic spectra of (*1*) alkalized solution of LST and solution of LST after its nitrosation with nitrous acid generated from sodium nitrite in combination with (*2*) acetic acid and (*3*) nitric acid. λ = 440 nm. (ν) Wavenumber.

subjected to short treatment with hot nitric acid, and then the optical density is determined at 315–340 nm. It was found that, in LSA nitration at room temperature, the optical density of the solution changes with time, which is typical of catalytic reactions. The sigmoid-shape kinetic curve of this reaction consists of three separate portions. Within the first portion, the optical density remains virtually constant. The second portion of the kinetic curve is characterized by a sharp increase in the optical density. Within the third portion, the optical density reaches a maximum and then remains constant. We believe that this complicated kinetic pattern is caused by the fact that nitric acid is not only electrophilic but also oxidizing agent. The LSA oxidation with nitric acid yields nitrous acid which readily reacts with lignosulfonic acid. We found that, on adding sodium nitrite to the reaction mixture in the amount less than 1% of the total LSA content, the LSA nitrosation was accelerated and the kinetic curve lost its sigmoidal shape [25]. In this connection, it was of interest to elucidate how replacement of acetic acid used in the Pearl–Benson's method with nitric acid affects the LSA colorimetric determination.

EXPERIMENTAL

Aqueous sodium nitrite (10%), aqueous nitric acid (10%), aqueous acetic acid (10%), and aqueous ammonia (2 M) used in the experiments were prepared from chemically pure grade chemicals. The aqueous stock solution of lignosulfonate (LST) containing 10 mg ml^{-1} LST was prepared from powdered LST produced by the Kotlas Pulp and Paper Combine.

The colorimetric determination of LST was carried out as follows. Aqueous sodium nitrite (2 ml), distilled water (50 ml), and nitric acid (2 ml) were successively placed into a 100-ml volumetric flask. After keeping for a certain time, this mixtute was alkalized with aqueous ammonia, and the volume was brought to the mark with distilled water. The optical density of solutions was measured on a KFK 2MP photocolorimeter at 440 nm in 10-mm optical cells.

The kinetic of LST nitrosation was studied without alkalization of the reaction mixture. The electronic spectra were recorded on a Specord 200 spectrophotometer at 20-s intervals. The total electronic spectra were recorded on a Specord M 40 spectrophotometer.

First of all, we studied how LST nitrosation with nitrous acid generated from sodium nitrite in combination with nitric and acetic acid depends on the reaction time. In these experiments, the reagent concentrations were identical. The kinetic curves shown in Fig. 1 indicate that, in the presence of acetic acid, the optical density at 440 nm increases gradually with time, whereas in the case of nitric acid the optical density reaches a maximum within 1 min and then does not noticeably change.

The electronic spectra (Fig. 2) show that the nature of the acid used for the generation of nitrous acid affects not only the nitrosation kinetics but also the characteristics of the nitrosated products. The solution of LST nitrosated in the presence of nitric acid has a noticeably higher optical density than that nitrosated in the presence of acetic acid. At the same time,

Table 1. Calibration plot parameters, $c = a + bD$

Method	Calibration parameters		Pair correlation factor
	a	b	
Pearl–Benson's	–0.046	0.43	0.991
Our	–0.019	0.37	0.999

Table 2. Reproducibility of determination of the optical density of solutions of LST nitrosated by different methods

Run no.	Pearl–Benson's method			Our method		
	D_{av}	rms*	V,** %	D_{av}	rms*	V,** %
1	0.198	0.002	1.2	0.173	0.004	2.1
2	0.269	0.002	0.6	0.271	0.013	4.9
3	0.308	0.003	1.1	0.344	0.012	3.6
4	0.373	0.008	2.1	0.482	0.011	2.3
5	0.537	0.010	1.9	0.624	0.007	1.2
6	0.675	0.018	2.6	0.773	0.012	1.5
7	0.738	0.028	3.8	0.888	0.014	1.6
8	0.817	0.029	3.5	1.019	0.070	6.9
9	0.978	0.015	1.6	–	–	–

* (rms) Root-mean-square deviation.
** Variation coefficient.

Table 3. LST determination error

Method	D_{440}	LST content, mg ml^{-1}		Error, %
		introduced	found	
Our	0.334	0.108	0.105	3.2
	0.625	0.207	0.212	2.5
	0.767	0.260	0.265	1.8
	0.919	0.328	0.321	2.1
	1.068	0.396	0.376	5.0
Mean determination error				2.9
Pearl–Benson's	0.408	0.127	0.130	1.9
	0.737	0.235	0.271	15.1
	0.800	0.268	0.298	11.0
	0.996	0.372	0.382	2.7
	1.027	0.405	0.396	2.3
Mean determination error				5.0

with both acids the absorption maximum occurs near 23000 cm^{-1}.

It was found in special experiments that, for both nitric and acetic acids, the optical density of solutions in the course of LST nitrosation is described by the Bouguer–Lambert–Beer law within the entire concentration range.

The calibration plot of c vs. D [c is LST concentration and D, optical density] was constructred for a series of solutions with known LST concentration after nitrosation. As seen from Table 1, the slope b in our calibration plot is smaller than that in the calibration plot constructed using the Pearl–Benson's method. This fact means that our method is more sensitive with respect to LST.

The reproducibility of the LST determination by our method was evaluated from the results of three replicate experiments. The small values of the variation coefficients show that the reproducibility in the optical density determination is good (Table 2).

The LSA determination error was evaluated from the comparison of the LSA content in reference solutions prepared in advance and its value obtained photometrically after LSA nitrosation. Each determination was triply repeated. Table 3 shows that, as compared to the Pearl–Benson's method, our technique ensures more accurate LSA determination.

CONCLUSION

Use of nitric acid in combination with sodium nitrite ensures complete nitrosation of lignosulfonic acids within 1 min and increases both the sensitivity and accuracy of their colorimetric determination.

REFERENCES

1. Yukel'son, I.I., *Tekhnologiya osnovnogo organicheskogo sinteza* (Technology of Basic Organic Synthesis), Moscow: Khimiya, 1968.
2. Stepanov, B.I., *Vvedenie v khimiyu i tekhnologiyu organicheskikh krasitelei* (Introduction to Chemistry and Technology of Organic Dyes), Moscow: Khimiya, 1977.
3. Gorelik, M.V. and Efros, L.S., *Osnovy khimii i tekhnologii aromaticheskikh soedinenii* (Fundamentals of Chemistry and Technology of Aromatic Compounds), Moscow: Chemistry, 1992.
4. Ingold, C.K., *Structure and Mechanism in Organic Chemistry*, Ithaca: Cornell Univ. Press, 1969.
5. Topchiev, A.V., *Nitrovanie uglevodorodov i drugikh organicheskikh soedinenii* (Nitration of Hydrocarbons and Other Organic Compounds), Moscow: Akad. Nauk SSSR, 1956.
6. *The Chemistry of the Nitro and Nitroso Groups*, Feuer, H., Ed., New York: Interscience, 1969, part 1.

7. *The Chemistry of the Nitro and Nitroso Groups*, Feuer, H., Ed., New York: Interscience, 1970, part 2.
8. *Comprehensive Organic Chemistry. The Synthesis and Reactions of Organic Compounds*, Barton, D. and Ollis, W.D., Eds., vol. 2: *Nitrogen Compounds*, Oxford: Pergamon, 1979.
9. Belyaev, E.Yu. and Gidaspov, B.V., *Aromaticheskie nitrozosoedineniya* (Aromatic Nitroso Compounds), Leningrad: Khimiya: 1988.
10. Korenman, I.M., *Fotometricheskii analiz: Metody opredeleniya organicheskikh soedinenii* (Photometric analysis: Methods for Determining Organic Compounds), Moscow: Khimiya, 1975, 2nd ed.
11. Gogotov, A.F., *Khim. Inter. Ustoich. Razv*., 1999, vol. 7, no. 3, pp. 223–227.
12. Gogotov, A.F., *Khim. Rast. Syr'ya*, 1999, no. 1, pp. 89–97.
13. RF Patent 2 165 936.
14. Khabarov, Yu.G. and Koshitina, N.N., *Sixth Eur. Workshop on Ligno Cellulosics and Pulp "Advances in Lignocellulosics Chemistry Towards High Quality Processes and Products,"* Bordeaux (France), 2000, pp. 391–393.
15. US Patent 5 169 931.
16. Gogotov, A.F., Zakazov, A.N., and Babkin, V.A., *Khim. Rast. Syr'ya*, 2001, no. 2, pp. 39–46.
17. Pearl, I.A. and Benson, H.K., *Paper Trade J*., 1940, vol. 111, pp. 235–236.
18. Roffael, E. and Schaller, K., *Wochenbl. Papierfabr*., 1972, vol. 100, nos. 11–12, pp. 417–418.
19. Ganin, G.I. and Kaplin, V.T., *Gidrokhim. Mater*., 1984, vol. 90, pp. 89–100.
20. Leithe, W., *Die Analyse der organischen Verunreinigungen in Trink-, Brauch-, und Abwassern*, Stuttgart: Wissenschaftliche, 1972.
21. *Unifitsirovannye metody issledovaniya kachestva vody: Soveshchanie rukovoditelei vodokhozyaistvennykh organov stran-chlenov SEV* (Standardized Methods for Studying Water Quality: Meet. of Managers of Hydroeconomic Organizations of COMECON Countries), part 1: *Metody khimicheskogo analiza vod* (Methods for Chemical Analysis of Waters), Moscow, 1977, 3rd ed.
22. Barnes, C.A., Hrutfiord, B.F., Livingston, A., et al., *TAPPI*, 1963, vol. 46, no. 6, pp. 347–351.
23. *Unifitsirovannye metody analiza vody* (Standardized Methods for Water Analysis), Lur'e, Yu.Yu., Ed., Moscow: Khimiya, 1971.
24. Khabarov, Yu.G., Brovko, O.S., and Pes'yakova, L.A., in *III Vserossiiskaya konferentsiya "Khimiya i tekhnologiya rastitel'nykh veshchestv"* (III Russian Conf. "Chemistry and Technology of Plant Compounds"), Saratov: Saratov. Gubernsk. Torgovo-Prom. Palata, 2004, pp. 336–338.
25. Khabarov, Yu.G., Kamakina, N.D., and Pes'yakova, L.A., in *Materialy Mezhdunarodnoi konferentsii "Fizikokhimiya lignina"* (Proc. Int. Conf. "Lignin Physical Chemistry"), Arkhangelsk: Arkahgel'sk. Gos. Tekh. Univ., 2005, pp. 237–238.

ISSN 1070-4272, Russian Journal of Applied Chemistry, 2006, Vol. 79, No. 9, pp. 1559–1560. © Pleiades Publishing, Inc., 2006.
Original Russian Text © N.I. Polezhaeva, I.V. Polezhaeva, V.A. Levdanskii, V.A. Fedorov, 2006, published in Zhurnal Prikladnoi Khimii, 2006, Vol. 79, No. 9, pp. 1575–1576.

BRIEF COMMUNICATIONS

Thermal Oxidative Degradation of a Composition Based on a Polyester Resin and Tetramethylammonium Chloride

N. I. Polezhaeva, I. V. Polezhaeva, V. A. Levdanskii, and V. A. Fedorov

Sibirean State Technological University GOU VPO, Krasnoyarsk, Russia

Received March 10, 2006

Abstract—Thermal oxidative degradation of a composition based on a polyester resin modified with rosin and tetramethylammonium chloride and its use as a flux for low-temperature solder pastes were studied.

DOI: 10.1134/S1070427206090345

This work continues the studies [1–3] on the development of formulation of corrosion-inactive, low-temperature solder pastes based on polyester resin modified with rosin and quaternary ammonium salts.

Tetramethylammonium chloride (TMAC) was taken as a flux. 2 g of TMAC was added to 15 g of polyester resin modified with rosin and synthesized as described in [1]. The components were thoroughly mixed.

The characteristics of thermal oxidative degradation of both the composition and flux were determined by dynamic thermogravimetry [4]. To determine more precisely the temperature of the decomposition onset, along with TG curve, we recorded the DTG and DTA curves for both the substance studied and an inert reference (Figs. 1a and 1b). Measurements were performed with an MOM Q-1000 derivatograph (Hungary) in the programmed heating mode. A 0.03-g sample was heated in a platinum crucible in air, at a heating rate of 10 deg min^{-1}. The sensitivities were as follows: balance, 50 mg; DTA galvanometer, 1/3; and DTG galvanometer, 1/10.

We found that the polyester resin + TMAC composition decomposes in air within the 70–650°C

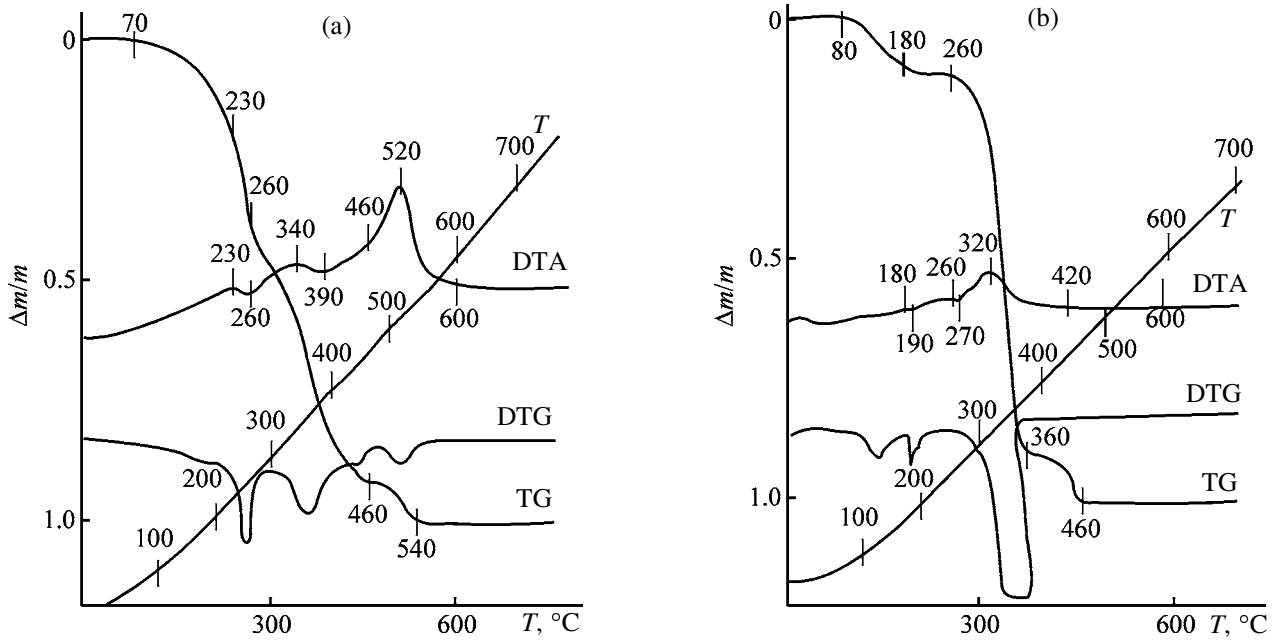


Fig. 1. Derivatogram of the (a) composition based on polyester resin and tetramethylammonium chloride and (b) tetramethylammonium chloride. ($\Delta m/m$) Relative weight loss and (T) temperature.

range in 3 steps (Fig. 1a). The first step at 70–230°C corresponds to elimination of the solvent and unbound water, residual alcohol, and unsaponifiable substances boiling in this temperature range. The second step at 260–340°C is caused by simultaneous endothermic decomposition of TMAC (Fig. 1b) and exothermic oxidation of the part of the products formed. The third step corresponds to a complex process with the characteristic temperature of 460 (temperature of the onset of the exothermic peak in the DTA curve corresponding to the onset of oxidation) and 520°C. The peak at 520°C reflects oxidation of gaseous products formed by thermal decomposition of the polyester resin [1].

The DTG and DTA curves of TMAC show that it decomposes within the 100–320°C range (Fig. 1b). This indicates that TMAS can be used as a flux of solder pastes with a fritting temperature of 320°C.

The study of solder pastes containing 15% polyester resin, 2% TMAC, and 83% solder powder showed that they correspond to GOST (State Standard) V 20.39.304–76 and OST (Branch Standard) 4GO 033000 [5].

CONCLUSIONS

(1) It was shown by dynamic thermogravimetry that the composition based on a polyester resin and tetramethylammonium chloride is stable with respect to thermal oxidative degradation.

(2) This composition meets the requirements to low-temperature solder pastes.

REFERENCES

1. Polezhaeva, N.I., Polezhaeva, I.V., Levdanskii, V.A., et al., *Zh. Prikl. Khim.*, 2001, vol. 74, no. 4, pp. 684–685.
2. Polezhaeva, N.I., Polezhaeva, I.V., Levdanskii, V.A., and Kuznetsov, B.N., *Zh. Prikl. Khim.*, 2002, vol. 75, no. 4, pp. 689–690.
3. Polezhaeva, N.I. Polezhaeva, I.V., Levdanskii, V.A., and Kuznetsov, B.N., *Zh. Prikl. Khim.*, 2003, vol. 76, no. 6, pp. 1042–1044.
4. Wendlandt, W.Wm., *Thermal Methods of Analysis*, New York: Wiley–Interscience, 1974.
5. *OST* (Branch Standard) *4GO 033000: Fluxes and Solder for Soldering. Composition, Properties, Application Area.*

ISSN 1070-4272, Russian Journal of Applied Chemistry, 2006, Vol. 79, No. 9, pp. 1561–1563. © Pleiades Publishing, Inc., 2006.
Original Russian Text © L.G. Eliseeva, M.N. Eliseev, T.I. Kuzichkina, I.M. Potapova, D.S. Lychnikov, A.I. Sapozhnikova, N.V. Berlova, 2006, published in Zhurnal Prikladnoi Khimii, 2006, Vol. 79, No. 9, pp. 1577–1579.

BRIEF COMMUNICATIONS

Determination of the Molecular Force Constants of Colloid Particles

L. G. Eliseeva, M. N. Eliseev, T. I. Kuzichkina, I. M. Potapova, D. S. Lychnikov, A. I. Sapozhnikova, and N. V. Berlova

Plekhanov Russian Academy of Economics, Moscow, Russia
Skryabin State Academy of Veterinary Medicine and Biotechnology, Moscow, Russia
Far-Eastern State Academy of Economics and Management, Vladivostok, Russia

Received June 7, 2006

Abstract—The possibility of analysis of the shape of colloid particles in solutions of latex and French and Moldovan wines with a flow-type ultramicroscope and digital photo camera was studied. The micrographs taken can be used to determine distances between particles by comparison with particle radii found by an independent method. The concepts of Deryagin–Landau–Vervey–Overbeek's physical theory of stability of colloid systems were used to calculate the molecular force constants for wine particles.

DOI: 10.1134/S1070427206090357

Analysis of the shape of colloid particles is a topical problem of colloid science, because the stability, colloid characteristics, and other parameters of colloid systems depend on the particle shape. However, it has been impossible to determine the shape of particles in their natural environment because of the lack of appropriate equipment. Moreover, the light scattered by particles is, according to the known concepts, a result of its diffraction on particles when its wavelength is comparable with their radius. In this case, particles in the field of vision of an ultramicroscope are represented by diffraction rings and their shape is indeterminate.

In the study, the particle size and interparticle distances in finely dispersed structures were determined using micrographs taken with modern digital cameras.

The colloid particles in the field of vision of the ultramicroscope were photographed with a NIKON 5600 digital camera. As the object of photographing served calibrated colloid latex particles with radii of 600 and 1000 nm, obtained from the All-Russia Institute of Synthetic Rubbers (VNIISK) and particles from Cabernet wine produced in France and Moldova in 2004. All samples of latexes and wines were diluted 10^7-fold to make convenient observation of separate particles.

The ultramicroscope was equipped with a solid-state laser source of light with a power of 5 mW and wavelength λ = 630 nm.

Figure 1 shows micrographs of latex and wine particles in the field of vision of the microscope. Latex particles of size 600 and 1000 nm can be clearly seen. These particles have a regular spherical shape. Also seen are wine particles of irregular shape. Figure 2 shows a micrograph of a particle from French Cabernet wine, which is composed of several smaller particles. These particles are enveloped with a substance

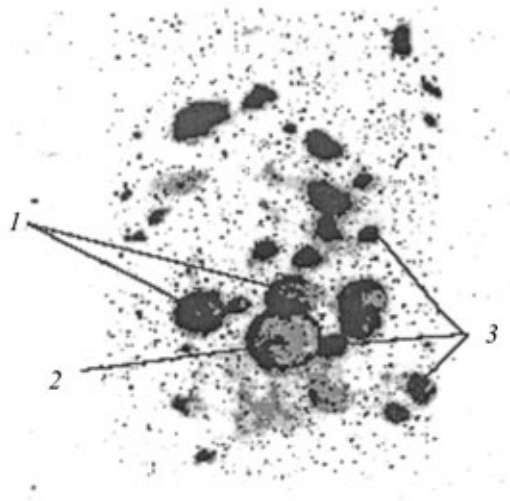


Fig. 1. Micrograph of colloid particles of a calibrated latex, with R = (*1*) 600 and (*2*) 1000 nm, and (*3*) of Cabernet wine.

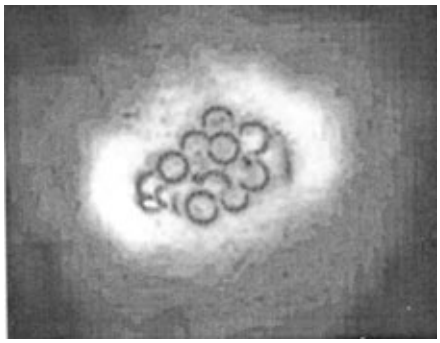


Fig. 2. Micrograph of a particle from French wine, composed of smaller particles, in the field of vision of the flow-type ultramicroscope.

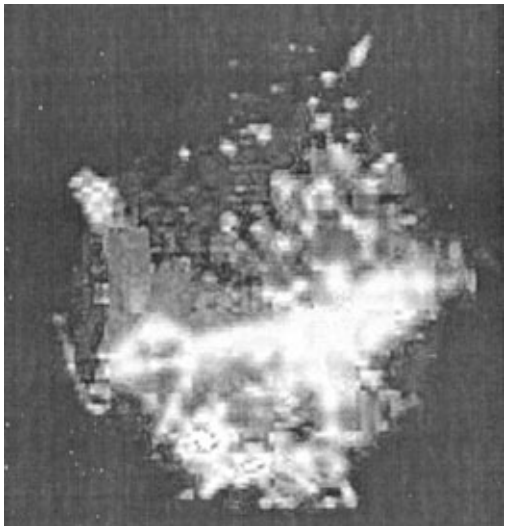


Fig. 3. Micrograph of an aggregate of particles from Cabernet wine (Moldova) after prolonged keeping at 55°C. Aggregate radius ~2000–2500 nm.

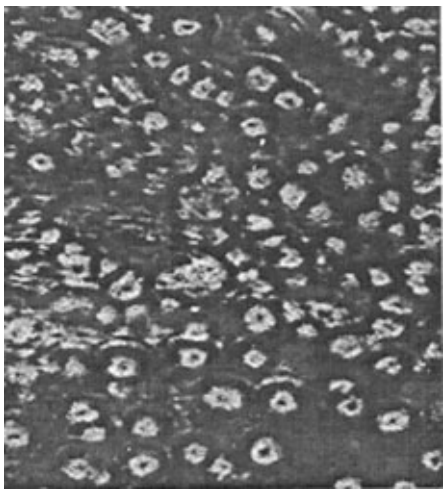


Fig. 4. Micrograph of latex particles of radius 1000 nm, taken with an MBI optical microscope (×20 objective, ×15 eyepiece).

that possibly serves as a surface layer stabilizing colloid particles in the wine. The fine particles in this aggregate are separated by spaces of width close to one tenth of the radius of these particles, whose most probable size is 120 nm [1]. This circumstance gives reason to state that, in accordance with Deryagin–Landau–Vervey–Overbeek's physical theory of stability of colloid systems (DLVO), particle aggregation occurs in the second, farther situated potential minimum in the curve of the interaction between particles vs. the interparticle distance.

Figure 3 shows a micrograph of a similar aggregate in Moldovan wine, composed of several tens of particles. The micrograph clearly shows the irregular shape of the aggregate, caused by the chaotic arrangement of the constituent particles. At the same time, chains of fine particles (~100–200 nm) are rather clearly seen in the micrograph. These chains have contacting lateral surfaces and form a primary aggregate of size smaller than that in Fig. 3.

In the micrographs presented, latex and wine particles have sizes close to the wavelength of the laser light sources. Despite the strong dilution, latex and wine particles still create a luminous background, which is superimposed on the coherent laser light and favors formation of particle images as in the ordinary optical photography. Probably, the optical image of particles is superimposed on the diffraction pattern formed by the same particles illuminated with coherent laser light. To verify this assumption, latex particles were photographed with an MBI microscope (×20 objective, ×15 eyepiece) (Fig. 4). Latex with a particle size of 1000 nm was sandwiched between a cover glass and a slide separated by a distance of 4–5 μm. The micrograph shows particles of virtually regular shape; however, their image was too small even at a high magnification of the object. Therefore, it was impossible to determine whether a surface layer was present.

Let us use the micrographs obtained to evaluate the molecular force constant (Hamaker constant A_{121}) from the potential energy of the farther potential minimum in the particle interaction curve, i.e., the overall constant determined by the interaction of a colloid particle of wine with water particles. In accordance with the DLVO theory, this energy can be found from the expression

$$U \approx -A_{121}R/12h, \quad (1)$$

where A_{121} is the Hamaker constant (J); R, particle radius (m); and h, interparticle distance (m).

Hence the Hamaker constant can be found as

$$A_{121} = 12Uh/R. \quad (2)$$

At $U = 3kT = 4.15 \times 10^{-23}$ J, a value characteristic of the second potential energy minimum, $h = 10 \times 10^{-9}$ m, and $R = 150 \times 10^{-9}$ m, the Hamaker constant $A_{121} \approx 1 \times 10^{-20}$ J. This value is in good agreement with the results of other studies [2].

The Hamaker constant directly related to the substance of a wine particle, A_{11}, can be calculated using Deryagin's concept [3], i.e.,

$$A_{121} = (A_{11}^{1/2} - A_{22}^{1/2})^2,$$

where A_{11} and A_{22} are the Hamaker constants for the substance of a particle and water, respectively: $A_{22} = 4.38 \times 10^{-20}$ J [3].

Hence follows that the Hamaker constant for the substance of a wine particle $A_{11} = 9.6 \times 10^{-20}$ J.

This value of the Hamaker constant is characteristic of colloid particles that contain oxides of metals [4], e.g., of iron and other metals, which find their way into wine from soil or wine-containing vessels.

CONCLUSIONS

Photographing of particles with a flow-type ultramicroscope gives a clearer notion of particle sizes in colloid systems, makes it possible to calculate some constants, and reveals structural features of particle aggregates and surface layers enveloping the particles.

REFERENCES

1. Polozhishnikova, M.A., Perelygin, O.N., and Lychnikov, D.S., *Trudy XII Mezhdunarodnoi konferentsii po spinovoi elektronike i girovektornoi elektrodinamike* (Proc. XII Int. Conf. on Spin Electronics and Gyrovector Electrodynamics). Moscow–Firsanovka, Publ. UNC-1 MPEI(TU), 2003, pp. 380–386.
2. Kononova, M. and Guilmitova, I., Abstracts of Papers, *Russ. Acad. Sci. X Int. Conf.*, Moscow, 1992, p. 96.
3. Deryagin, B.V., Churaev, N.V., and Muller, V.M., *Poverkhnostnye sily* (Surface Forces), Moscow: Nauka, 1985.
4. Visser, J., *Adv. Colloid Interface Sci.*, 1972, vol. 3, pp. 331–363.

ISSN 1070-4272, Russian Journal of Applied Chemistry, 2006, Vol. 79, No. 10, pp. 1565–1570. © Pleiades Publishing, Inc., 2006.
Original Russian Text © M.V. Maslova, L.G. Gerasimova, 2006, published in Zhurnal Prikladnoi Khimii, 2006, Vol. 79, No. 10, pp. 1585–1590.

INORGANIC SYNTHESIS AND INDUSTRIAL INORGANIC CHEMISTRY

A Study of the Composition of Solid Phases Formed in the Reaction of Titanite with Phosphoric Acid

M. V. Maslova and L. G. Gerasimova

Tananaev Institute of Chemistry and Technology of Rare Elements and Mineral Resources, Kola Scientific Center, Russian Academy of Sciences, Apatity, Murmansk oblast, Russia

Received March 24, 2006

Abstract—The composition and structure of titanium phosphate products formed in decomposition of titanite with phosphoric acid were studied. The sorption capacity of the products obtained for alkali and alkaline-earth elements was determined. The possibility of using phosphate products as titanium-containing pigment fillers was examined.

DOI: 10.1134/S1070427206100016

Titanium phosphates are widely known synthetic products used in manufacture of high-quality white paper and light-resistant plastics and serving as fillers for industrial rubber articles, building materials, and paints and as sorbents for radionuclides and ions of heavy and nonferrous metals. Each of the above-listed application fields of the product imposes certain requirements on its composition and structure, which are largely determined by the starting components and synthesis conditions [1–3]. In particular, three types of titanium phosphate with layered structure are known, which belong to ion-exchange materials. Titanium phosphate of the α-phase contains only HPO_4^{2-} groups and the formula of this compound can be represented as $Ti(HPO_4)_2 \cdot H_2O$ [4]. In the γ-phase, phosphorus(V) is present in $H_2PO_4^-$ and PO_4^{3-} groups and the composition of the phosphate corresponds to the formula $Ti(H_2PO_4)(PO_4) \cdot 2H_2O$ [5]. The third type of titanium phosphates belongs to oxo-hydroxo forms of general formula $TiO(OH)(H_2PO_4) \cdot 2H_2O$ [6]. Specific features of the layered structure of the phosphates are manifested in that protons that can be substituted by cations are situated between layers. Half of the protons form hydroxonium ions with water, and the other half, hydrogen bridges with atoms of the neighboring layer [7]. The different types of bonding of protons in the sorbent matrix predetermine their different abilities to be substituted.

As a rule, layered titanium phosphates are produced from sulfuric (hydrochloric) acid titanium-containing solutions by introduction of phosphoric acid and subsequent keeping of the reaction mass under boiling [8–10]. In the present study, we obtained titanium phosphate phases (TPP) by reacting the titanite mineral ($CaTiSiO_5$) with phosphoric acid [11, 12]. The aim of our study was to examine the composition and properties of TPP in relation to the conditions of their synthesis.

EXPERIMENTAL

Titanite $CaTiSiO_5$ was decomposed with 40–80% phosphoric acid, with the titanite-to-H_3PO_4 mass ratio in the starting mixture varied within s : l = 1 : (2–3) (in terms of 100% H_3PO_4) and the process performed in the boiling mode in the course of 12 h. The liquid and solid phases were separated by vacuum filtration of the reaction mass. Their substance composition was determined by chemical analysis. The specific surface area of the titanium phosphate solid phases (TPP) was determined by BET on a Flowsorb II 2300 electronic analyzer with degassing at 100°C for 2 h. An X-ray phase analysis (XPA) was performed with a DRON-3 instrument in Cu_{K_α} radiation. A thermogravimetric analysis of the samples was carried out in quartz test tubes at 20–980°C at a heating rate of 90 deg min^{-1}. Spectroscopic studies were performed on a UR-20 IR spectrometer.

We tested the sorption properties of the products under static conditions. For this purpose, we added to 20 ml of a solution containing 10^{-3} M of the metal ion a weighed portion of a modified sample in an amount corresponding to the mass ratio s : l = 1 : 200. We used a 0.1 N solution of NaCl as a sup-

Composition of precipitates formed in decomposition of titanite with phosphoric acid

H_3PO_4, wt %	Content of main components in the precipitate, wt %			
	TiO_2	P_2O_5	CaO	SiO_2
80	21.04	38.48	1.04	16.77
70	23.76	36.77	2.0	18.24
60	24.6	34.27	3.67	19.06
50	27.3	32.31	5.05	19.6
40	27.7	31.95	5.13	20.36

porting electrolyte. The components were brought in contact for 2 h, after which the spent material was separated from the solution by filtration. The residual content of cations in the filtrate was determined and the extent of absorption of the element was calculated (in percent). The basic technical properties characteristic of the filler were determined by the techniques described in GOST (State Standard) 9808–84.

In the reaction of titanite with phosphoric acid, the crystal lattice of the mineral disintegrates and its components are converted to compounds having different solubilities in a phosphoric acid medium and in water. The precipitate formed is composed of several phases. One of these is an acid salt of composition corresponding to the formula $Ca(H_2PO_4)_2 \cdot H_2O$. Titanium(IV) forms a hydrophosphate $Ti(HPO_4)_2 \cdot H_2O$, and silicon, amorphous silica $SiO_2 \cdot nH_2O$. On treating the precipitate with water, $Ca(H_2PO_4)_2 \cdot H_2O$ completely passes into the aqueous phase. XPA data confirmed that calcium(II) is present in a washed precipitate is in particles of the undecomposed titanite. The table lists the compositions of washed precipitates (in terms of oxides) obtained in decomposition of titanite with H_3PO_4 of various concentrations.

Titanium(IV) present in the precipitate can be in the form of both TPP and particles of an undecomposed mineral. The degree of binding of titanium(IV) in TPP was calculated with account of the fact that the $TiO_2 : P_2O_5$ molar ratio in TPP is 1 : 1. The excess (not bound to P_2O_5) titanium(IV) is contained in particles of the undecomposed titanite. The extent to which titanium(IV) passes into the phosphate phase approaches 100% with a 80% H_3PO_4 and does not exceed 50% in the case of 40% H_3PO_4 (Fig. 1). Based on an analysis of structural bonds in the crystal lattice of titanite, we can conclude that, in acid treatment, bound titanium cannot dissolve faster than the calcium compound and silicon in silicon-oxygen tetrahedra cannot be activated before the Ti and Ca structural bonds are ruptured. Apparently, the Ti-cation is activated in the course of leaching-out of calcium(II), and this activation is accompanied by the formation of TPP, including that on the surface of grains of the mineral.

It was noticed that the degree of leaching-out of calcium(II) increases and, consequently, the diffusion drift of titanium(IV) to the mineral grain surface becomes faster as the acid concentration is raised. If diluted phosphoric acid is used in the decomposition process, the diffusion of titanium ions to the grain surface is hindered by the slow disintegration of calcium bonds in the structure (Fig. 2). The amount of phosphorus(V) bound to titanium(IV) increases with the content of phosphoric acid (Fig. 3). The amount of phosphoric acid did not exceed in all the experiments its stoichiometrically necessary consumption for formation of calcium and titanium(IV) phosphates. Therefore, it may be assumed that the initial content

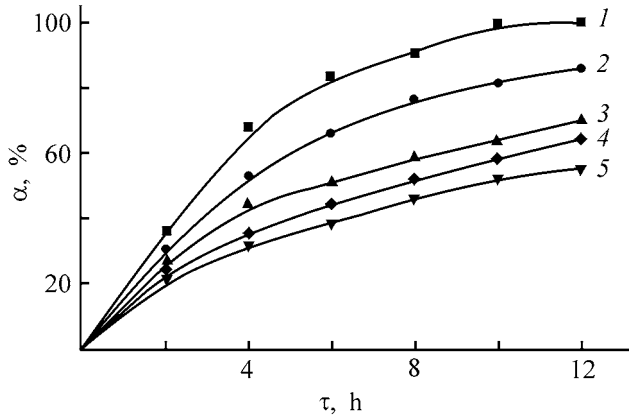


Fig. 1. Degree of binding of TiO_2 into TPP, α, vs. the process duration τ. H_3PO_4 content (wt %): (*1*) 80, (*2*) 70, (*3*) 60, (*4*) 50, and (*5*) 40.

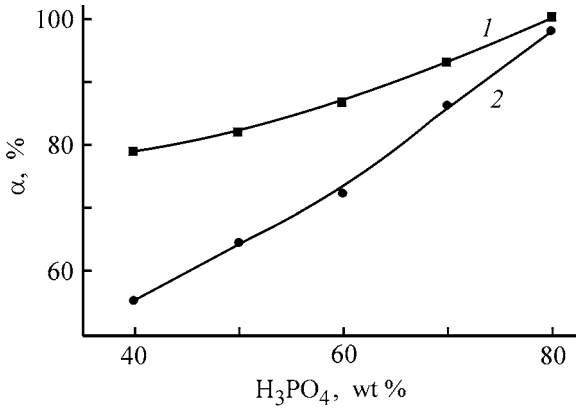


Fig. 2. Degree of binding of (*1*) CaO and (*2*) TiO_2 into TPP, α, vs. the H_3PO_4 content. Process duration 12 h.

of phosphoric acid predetermines the completeness of decomposition of the mineral.

The precipitates obtained were subjected to crystal-optic, thermogravimetric, and X-ray phase analyses and studied by IR spectroscopy.

Crystal-optical studies of TPP washed to remove calcium(II) demonstrated that, irrespective of the concentration of phosphoric acid, it is composed of $Ti(HPO_4)_2 \cdot H_2O$ and particles of undecomposed titanite and, in addition, contains amorphous silica.

The presence of two endothermic effects in the DTA curves in Fig. 4, which correspond to temperatures of 212–215 and 532–538°C and are accompanied by loss of mass, indicates that there occurs steplike dehydration of TPP. A calculation based on the TG and DTG curves demonstrated that 0.5 mol H_2O is removed below 215°C, and additional 0.5 mol H_2O, upon heating to 550–580°C. Apparently, the samples under study contain two kinds of water, which are retained in the product with different extents of firmness. The fact that the hydrogen ion is retained up to high temperatures may be only due to its presence in phosphate groups. The dehydration process presumably includes stages of removal of hydrate H_2O and water formed in condensation of acid phosphate groups. The exothermic effect at 864–873°C, which is not accompanied by any change in mass, is due to the formation of crystalline titanium diphosphate of composition TiP_2O_7. The titanium phosphate phases formed at initial H_3PO_4 contents of 50 and 40 wt % show a number of endothermic effects in the range 270–400°C. These effects are due to dehydration of hydroxy groups bound to silicon, which is formed in various modifications under the conditions specified.

The IR spectra of air-dry TPP in Fig. 5 contain high-intensity bands at 3600–3000 cm^{-1}, which are associated with stretching vibrations of water molecules and hydroxy groups, and also bands at 1600 cm^{-1}, which correspond to deformation vibrations of water molecules. To vibrations of the P–O bond of the tetrahedral PO_4^{3-} ion belong strong absorption bands at 1000 and 580 cm^{-1}. The broadening of the band at 1000 cm^{-1} is due to superposition of vibrations of SiO_4 tetrahedra. The weak band at 700 cm^{-1} can be attributed both to vibrations of the O–P–O bonds in the PO_4^{3-} ion and to active vibrations of O–Ti–O in the octahedral group of titanium. The absorption bands at 550–450 cm^{-1} are associated with deformation vibrations of P–O and Ti–O groups [13].

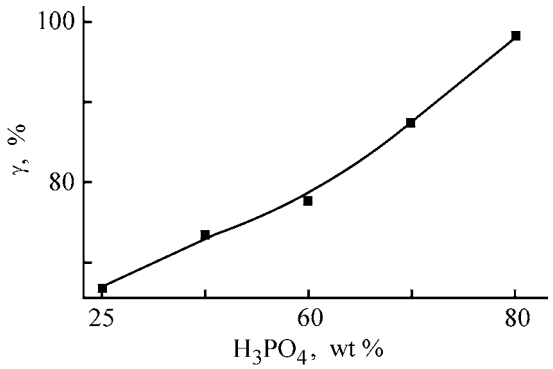


Fig. 3. Degree of P_2O_5 binding, γ, relative to the stoichiometry vs. the content of H_3PO_4.

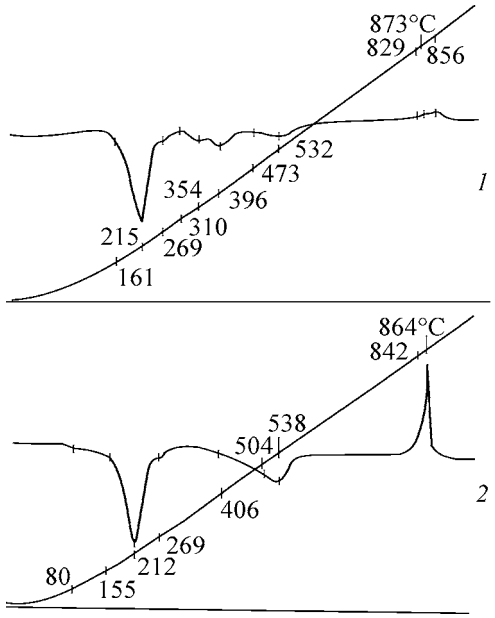


Fig. 4. Thermogram of the precipitate formed in decomposition of titanite with H_3PO_4. H_3PO_4 content (wt %): (*1*) 50 and (*2*) 80; the same for Fig. 5.

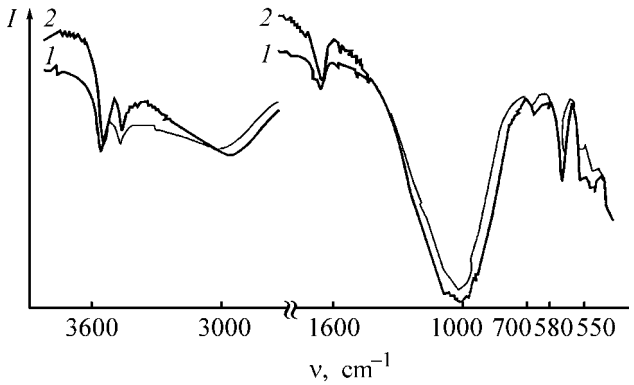


Fig. 5. IR spectra of products formed in decomposition of titanite with H_3PO_4. (*I*) Intensity and (ν) wavenumber.

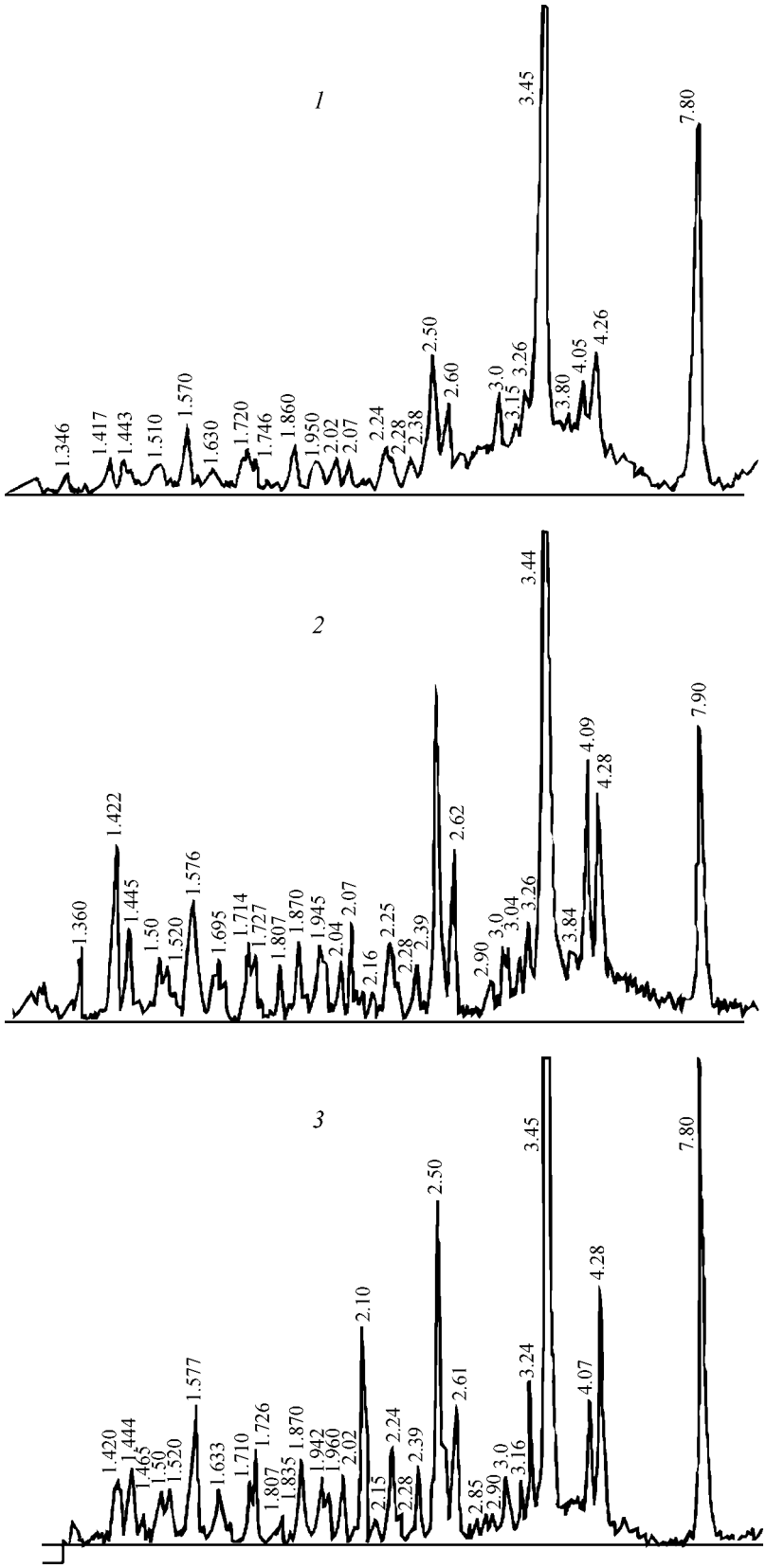


Fig. 6. X-ray diffraction patterns of the product formed in decomposition of titanite with H_3PO_4. H_3PO_4 content (wt %): (*1*) 40, (*2*) 60, and (*3*) 80.

According to XPA, all the TPP samples calcined at 850°C contain, in addition to the main crystalline phase (TiP_2O_7), an admixture of the titanite mineral, and its amount is the higher, the lower the H_3PO_4 concentration at which the product was synthesized. The air-dry product is a crystalline substance of composition $Ti(HPO_4)_2 \cdot H_2O$ (Fig. 6). Lowering the concentration of phosphoric acid in TPP synthesis results in that the intensities of the main reflections decrease and weak peaks disappear. On the whole, the diffraction pattern indicates that, irrespective of TPP synthesis conditions, the phase compositions remains virtually the same, but the packing order of layers and the type of internal bonds change. Presumably, the main phase $Ti(HPO_4)_2 \cdot H_2O$, contained in TPP, can be identified as the known layered α-phase of titanium phosphate. The hydrated silica phase is not involved in the formation of the structure of titanium phosphate and is an inert component in the precipitate formed in the reaction of titanite with H_3PO_4.

The specific surface area of TPP varies within the range 35–70 $m^2\ g^{-1}$, and the pore volume, within 0.1–0.2 $cm^3\ g^{-1}$. Lowering the H_3PO_4 content leads to an increase in the specific surface area of the product.

Figure 7 presents data on the sorption capacity of TPP for ions of alkali and alkaline-earth elements. It can be seen that the products obtained with 50–60 wt % H_3PO_4 effectively sorb cations. More severe synthesis conditions favor formation of compact precipitates, which impairs their sorption properties. The precipitates formed with dilute phosphoric acid contain up to 20–25% undecomposed mineral, which also makes lower their sorption capacity. It was noticed that the transfer of the sorbent to the sodium form by treatment with a NaOH solution and the subsequent grinding lead to an increase in the sorption capacity of the material. The maximum degree of sorption is 98% for Cs^+ ions and 79% for Sr^{2+}. The possible explanation of the lower degree of sorption for strontium(II) is that Cs^+ ions are sorbed in the whole volume of a sorbent particle, whereas sorption of Sr^{2+} probably occurs mainly on its surface.

To find out whether TPP can be used as pigment filler, we calcined it at 550–600°C and then ground the material in a vibration mill. These operations, successively, make the precipitate structure denser and raise the dispersity of its particles, which brings the values of such pigment parameters as oil (moisture) capacity and covering power to the required values. A sample of the pigment filler was successfully tested in a dry building mixture instead of the expensive titanium dioxide.

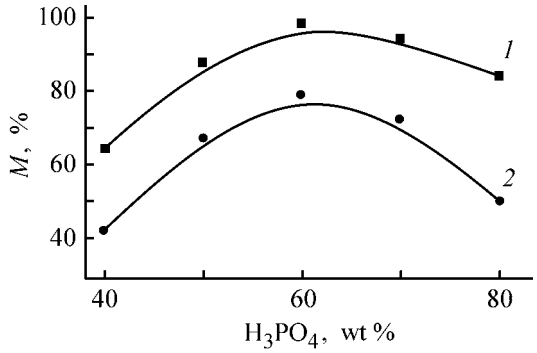


Fig. 7. Sorption capacity of TPP for (*1*) Cs^+ and (*2*) Sr^{2+} ions. (*M*) Degree of absorption of metal ions and ($[H_3PO_4]$) acid content.

CONCLUSIONS

(1) The reaction of titanite with phosphoric acid under boiling conditions leads to conversion of the components of the mineral to compounds with different types of behavior in an aqueous solvent, which enables effective separation of titanium(IV) and calcium(II).

(2) Titanium(IV) is formed as a layered titanium hydrophosphate, $Ti(HPO_4)_2 \cdot H_2O$. Hydrated silicon oxide remaining in the precipitate, together with titanium hydrophosphate, after separation of calcium(II) is not involved in the formation of the structure of the precipitate, being only its inert component.

(3) The formulation composed of titanium hydrophosphate and hydrated silicon dioxide has a rather high sorption capacity for cations of alkali and alkaline-earth elements and its thermal treatment yields a high-quality pigment filler.

(4) The data obtained can serve as a physicochemical substantiation of the choice of technological parameters in phosphoric acid processing of titanite, a waste product formed in integrated processing of apatite-nepheline ores.

REFERENCES

1. Clearfield, A. and Roberts, B.D., *Inorg. Chem.*, 1988, vol. 27, pp. 3237–3242.
2. Marireles-Torres, P., Olivera-Pastor, P., Jimenez-Lopez, A., et al., *J. Mater. Chem.*, 1991, vol. 1, pp. 319–325.
3. Bereznitski, Y., Jaroniec, M., Bortun, A.I., et al., *J. Colloid Interface Sci.*, 1997, vol. 191, pp. 442–448.

4. Alberti, G., Cardini-Galli, P., Costanino, U., et al., *J. Inorg. Nucl. Chem.*, 1967, vol. 29, pp. 571–575.
5. Allulli, S., Ferragina, C., Ginestra, A., et al., *J. Inorg. Nucl. Chem.*, 1977, vol. 39, pp. 1043–1048.
6. Li, Y.J. and Whittingham, M.S., *Solid State Ionics*, 1993, vol. 63–65, pp. 391–396.
7. Materova, E.A., *Neorganicheskie ionoobmennye materialy* (Inorganic Ion-Exchange Materials), Leningrad: Len. Gos. Univ., 1974, issue 1.
8. Clearfield, A., *Eur. J. Solid State Inorg. Chem.*, 1991, vol. 28, p. 37.
9. Bortun, A.I., Jaimez, E., Llavona, R., et al., *J. Mater. Res. Bull.*, 1995, vol. 30, no. 4, pp. 413–420.
10. Llavona, R., Garsia, J.R., Suarez, M., et al., *Thermochim. Acta*, 1985, vol. 8b, pp. 281–286.
11. Maslova, M.V., Gerasimova, L.G., Okhrimenko, R.F., et al., *Khim. Tekhnol.*, 2005, no. 1, pp. 37–40.
12. RF Patent 2 235 685.
13. Nakamoto, K., *Infrared Spectra of Inorganic and Coordination Compounds*, New York: John Wiley & Sons, 1963.

ISSN 1070-4272, Russian Journal of Applied Chemistry, 2006, Vol. 79, No. 10, pp. 1571–1575. © Pleiades Publishing, Inc., 2006.
Original Russian Text © E.S. Plokhov, M.G. Mikhalenko, S.V. Plokhov, 2006, published in Zhurnal Prikladnoi Khimii, 2006, Vol. 79, No. 10, pp. 1591–1595.

SORPTION AND ION-EXCHANGE PROCESSES

Ion-Exchange Recovery of Nickel(II) from Wash Water Formed in Electroless Plating in Acid Hypophosphite Solutions

E. S. Plokhov, M. G. Mikhalenko, and S. V. Plokhov

Nizhni Novgorod State Technical University, Nizhni Novgorod, Russia

Received May 26, 2005; in final form, March 2006

Abstract—Kinetic aspects of extraction of Ni(II) ions with KU-2-8 cation-exchange resin in the Na^+ form from wash water produced in electroless nickel-plating were studied. The optimal conditions and parameters of ion-exchange purification and regeneration of the cation-exchanger were determined.

DOI: 10.1134/S1070427206100028

Despite the undeniable advantages of Ni–P coatings [1–3], a wider industrial application of processes for their deposition from acid hypophosphite solutions is hindered by the formation of large amounts of liquid nickel-containing waste [4], mostly constituted by spent plating solutions and wash water. The amount of this waste can be reduced to a minimum by integrated solution of the following problems: use of effective stabilizers in solutions for electroless nickel-plating, optimization of the plating and electrolyte adjustment conditions and of the composition of the adjusting solution used in plating, development of technologies for recovery and utilization of components from spent solutions and wash water [5]. The best technical and economic effect is achieved by purification of wash water to remove nickel(II) ions. It is known that joint use of ion exchange and electrolysis, with preliminary sorption treatment of wash water with activated carbon, is advisable for recovery of heavy metals ions from wash water [6–10].

The aim of this study was to determine the fundamental kinetic aspects and the optimal conditions and parameters of ion-exchange recovery of Ni(II) from wash water after electroless nickel-plating in acid hypophosphite solutions.

As objects of study served model solutions and industrial wash water of the following composition ($g\ l^{-1}$): $NiSO_4 \cdot 7H_2O$ 0.3–1.25 (in terms of nickel ions), sodium hypophosphite (NaH_2PO_2) 2.0, sodium phosphite (NaH_2PO_3) 0.4, sodium acetate 2.2, and CH_3COOH 3. The pH value was 4.5. The electrolyte temperature was $20 \pm 2°C$. The concentrations of impurity metal ions [Cu(II), Zn(II), Fe(III), and Sn(II)] in wash water were very low because of the short time of use of electroless nickel-plating solutions, which did not allow their quantitative determination. Removal of these ions was not considered in this study and they were not introduced into model solutions, because they had virtually no effect on the results of ion-exchange recovery of nickel(II). No stabilizer (thiourea, 0.0005 $g\ l^{-1}$) was introduced, either, into model solutions, because wash water is subjected to sorption treatment before ion exchange and this completely extracts the stabilizing agent from it.

The ion-exchange recovery of Ni(II) from wash water was studied on a laboratory setup comprising a glass column with an inner diameter of 0.019 m. The ratio of the inner diameter of the column to the height of a bed of the swollen ion exchanger was 1 : 9. The mass of the KU-2-8 cation exchanger in the Na^+ form in the column was 21.89 g. The concentration of nickel cations in wash water and in eluates was determined by spectrophotocolorimetry [11] and atomic-absorption spectroscopy [12] on SF-26 and SF-115 Saturn spectrophotometers, respectively. The relative determination error did not exceed ±2%.

Wash water produced in electroless nickel-plating in acid hypophosphite solutions contains nickel(II) in several cationic forms. Together with simple hydrated Ni^{2+} aqua-complex ions, $[Ni(H_2O)_n]^{2+}$ (n = 1–6) are present in the wash water, the most stable of which is the complex ion with octahedral structure [13].

The ion-exchange purification was performed to remove all kinds of nickel ions without separation. For this purpose, the cation exchanger was used in

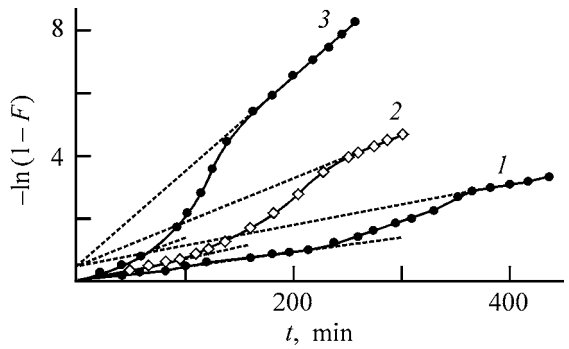


Fig. 1. Dynamic curves of nickel(II) sorption on KU-2-8 cation exchanger in the Na^+ form. (F) Degree of saturation of the ion exchanger and (t) time. Initial nickel(II) concentration in wash water ($g\ l^{-1}$): (*1*, *2*) 0.75 and (*3*) 1.25. Flow rate of wash water ($m^3\ m^{-2}\ h^{-1}$): (*1*) 0.5 and (*2*, *3*) 1.0.

the Na^+ form. The preferable use of the salt form of the ion exchanger, compared with the H^+ form, is due to the subsequent electrochemical treatment of eluates. The electroreduction of nickel(II) to metal from strongly acidic eluates requires a considerable expenditure of sodium hydroxide for bringing their pH to 2.0 [9]. This disadvantage can be avoided by using the cation exchanger in the salt form.

We studied the fundamental kinetic aspects of the ion-exchange recovery of nickel(II) from washing solutions with KU-2-8 cation exchanger in the Na^+ form by the dynamic method. For this purpose, we determined experimentally the dependences of the Ni(II) concentration after the ion exchanger on the time t during which the wash water was passed at various initial concentrations of metal ions in the liquid phase and various rates of its flow across the ion-exchanger bed (outlet ion exchange curves). From these dependences, we calculated dynamic curves of sorption of nickel(II) ions, plotted in the $-\ln(1 - F)$–t coordinates ($F = Q/Q_\infty$ is the degree of saturation of the ion exchanger, Q and Q_∞ are the running and limiting masses of the metal ions being recovered). The values of Q were determined by graphical integration of the outlet ion exchange curves, and the value of Q_∞, by extrapolation of the $Q = f(t)$ dependences to $t \to \infty$. Some of the dynamic sorption curves are shown in Fig. 1. Other sorption curves were of a similar shape. According to the ion-exchange theory, the presence of linear portions with different slopes in the dynamic sorption curves at low ($F \le 0.05$) and high ($F \ge 0.8$) degrees of saturation of the cation exchanger indicates that the process is outer- and inner-diffusion-controlled, respectively [14]. Hence, the ion exchange occurs, on the whole, under conditions of a mixed-diffusion kinetics. At low degrees of saturation of the cation exchanger, the ion-exchange recovery of Ni(II) is controlled by outer diffusion, i.e., by the mass transfer of metal ions from the bulk of the liquid phase to the surface of the ion exchanger. At high F values the inner diffusion (mass transfer of metal ions in the bulk of the ion exchanger) becomes the limiting stage.

The above conclusion about the nature of the limiting stage was additionally confirmed by calculation of the effective diffusion coefficient of nickel ions. For this purpose, we used the so-called basic equation of the inner-diffusion kinetics [15], which has for simple models of ion-exchanger particles (sphere, plate, and cylinder) the form

$$\ln(1 - F) = Bt - \ln A. \quad (1)$$

Here A and B are coefficients dependent on the diffusion mode.

Application of expression (1) is justified at $F \ge 0.8$. The extrapolation of linear portions of the sorption curves at high degrees of saturation of the ion exchanger to the ordinate axis (Fig. 1) gives 0.607 for coefficient A. This allows us to describe the ion-exchange process using the mathematical model of "a sphere with a shell" with $A = 0.61$ [15] and coefficient B given by

$$B = D\pi^2/R^2. \quad (2)$$

Here D is the effective diffusion coefficient of the ion being sorbed ($cm^2\ s^{-1}$), and R, the average grain radius of the ion exchanger, 0.125 cm.

The effective diffusion coefficient can be calculated by expression (2) if coefficient B is known.

We found coefficient B from expression (1) as the slope of linear portions of the experimental sorption curves (Fig. 1) at high degrees of saturation of the ion exchanger. The values of D, calculated by formula (2), were $(1.7–7.5) \times 10^{-7}$ $cm^2\ s^{-1}$, which corresponds in order of magnitude to the mixed-diffusion control over the ion-exchange process [14]. It is important to note that the theory of ion exchange under conditions of mixed-diffusion kinetics is not fully elaborated, and the equation of the inner-diffusion kinetics, which is used to describe the process, is exact only in static conditions. Therefore, the calculated values presented here should be regarded as qualitative.

The parameters of the ion-exchange recovery of Ni(II) from wash water can be improved under con-

ditions of mixed-diffusion kinetics and a cation exchanger of standard brand with known properties only by affecting the outer-diffusion stage, whose effectiveness depends mainly on the initial concentration of nickel ions in the liquid phase and on the rate at which they are passed across the ion-exchanger bed. As the parameters of the ion-exchange process serve the dynamic exchange capacity (DEC) and the breakthrough capacity (BC). The dynamic exchange capacity is the maximum mass of Ni(II) ions retained by 1 kg of a swollen ion exchanger in the given conditions of wash water flow, and BC, the maximum mass of Ni(II) ions retained by 1 kg of the swollen ion exchanger until nickel(II) appears after the cation exchanger [7].

The fact that the outer-diffusion stage contributes to the control over the process allows us to explain the dependences of DEC and BC on the flow rate U of wash water across the cation-exchanger bed (Fig. 2a), which were obtained by integrating the outlet ion exchange curves. An increase in the flow rate diminishes the time of contact of each elementary volume of wash water with the cation exchanger, which must make the ion-exchange parameters smaller. At the same time, the increase in the flow rate reduces the depth of the diffusion layer, which leads to a rise in the DEC and BC. Apparently, with U raised to 1.0 $m^3 m^{-2} h^{-1}$, the time of contact between the phases is sufficient and the key factor is the depth of the diffusion layer. Therefore, an increase in DEC and BC is observed. For flow rates higher than 1.0 $m^3 m^{-2} h^{-1}$, the key factor is the contact time, whose deficiency results in a decrease in the ion-exchange parameters. Consequently, the flow rate of 1.0 $m^3 m^{-2} h^{-1}$ corresponding to the maximum values of DEC and BC (33.0 and 19.7 g kg^{-1}, respectively) is the optimal for Ni(II) recovery.

The dependences of DEC and BC on the initial Ni(II) concentration in wash water, $c_{Ni\ (II)}$, obtained from outlet cation-exchange curves, also had maxima at 0.75 g l^{-1} (Fig. 2b). The constancy of the flow rates of wash water ensured that the diffusion layer depth and the time of contact between the phases were invariable. Under these conditions, the ion exchange parameters are affected by the contact time and by the gradient of Ni(II) concentration in the diffusion layer. An increase in $c_{Ni\ (II)}$ to 0.75 g l^{-1} makes the gradient of Ni(II) concentration in the diffusion layer higher and, at a sufficient contact time, causes a rise in DEC and BC. Further increase in the initial Ni(II) content of the liquid phase and in the concentration gradient occurs under the conditions of an insufficient contact time. Furthermore, the increase in

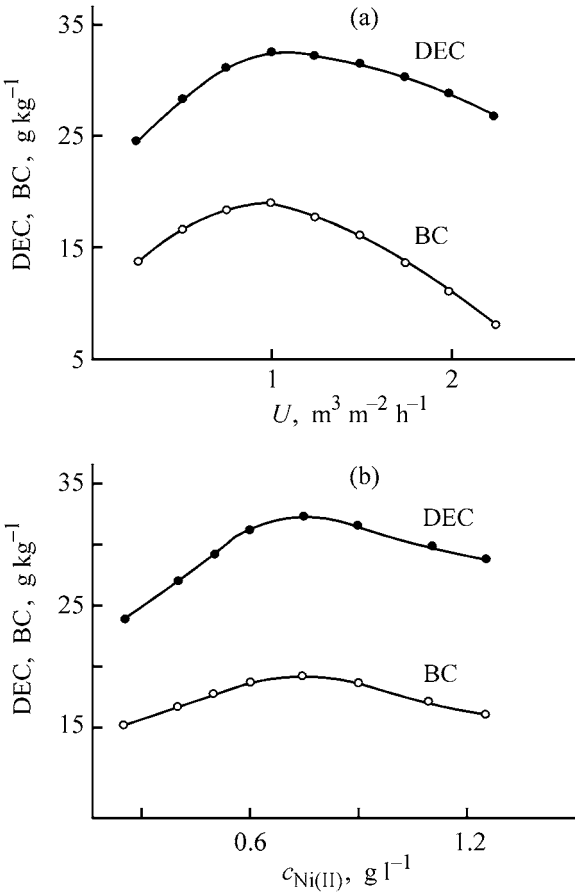


Fig. 2. Dependences of DEC and BC on (a) flow rate U of wash water and (b) concentration $c_{Ni(II)}$ of nickel ions in the water. KU-2-8 cation exchanger in the Na^+ form; Ni(II) concentration 0.75 g l^{-1}; (a) flow rate of wash water 1.0 $m^3 m^{-2} h^{-1}$.

the concentration enhances the ion–ion interaction (repulsion) of hydrated nickel-containing ions at the phase boundary. All these factors result in that DEC and BC decrease at Ni(II) concentrations higher than 0.75 g l^{-1}. Hence, the initial Ni(II) concentration of 0.75 g l^{-1} in wash water is the optimal value for ion-exchange recovery of metal ions.

The maxima in the dependences of DEC and BC on U and on the concentration have been observed previously [6–8, 10] when studying the ion-exchange recovery of heavy metal ions from wash water produced in various electrochemical processes (copper-, zinc-, nickel-, and chromium-plating). In [16], the basic equation of inner-diffusion kinetics (1) was transformed. A mathematical analysis of the resulting expression demonstrated that, under the conditions of mixed-diffusion kinetics, the dependences of DEC and BC on the flow rate and concentration must exhibit maxima because of the variation of the contact time,

Mass of nickel(II) recovered in regeneration

Na_2SO_4, g l^{-1}	Mass of nickel(II), g, recovered in indicated time, h				
	0.66	1.33	4.0	7.0	21.0
25	0.035	0.067	0.070	0.082	0.084
50	0.048	0.066	0.074	0.078	0.086
100	0.062	0.070	0.074	0.086	0.092
150	0.057	0.065	0.068	0.070	0.072

diffusion layer depth, and concentration gradient within this layer. Apparently, the same can be done with the basic equation of outer-diffusion kinetics. However, solution of this problem is beyond the scope of the present study.

The ion exchanger saturated in optimal conditions was regenerated with sodium sulfate solutions. By analogy with the saturation, the regeneration efficiency mainly depends on the concentration of the eluent and on its flow rate across the ion-exchanger bed.

The effect of eluent concentration on the regeneration efficiency was studied by the static method. For this purpose, equal weighed portions of the cation exchanger (4.0 g) were poured-over with Na_2SO_4 solutions of various concentrations, provided that the amount of anhydrous sodium sulfate was the same in all the experiments (12.5 g). The mass of Ni(II) removed from the cation exchanger by a certain instant of time was determined by chemical analysis of the liquid phase.

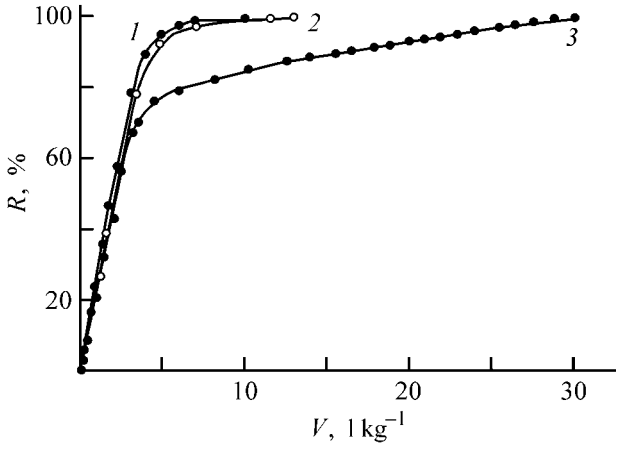


Fig. 3. Dependence of the degree of regeneration, *R*, of the cation exchanger on the volume *V* of the eluent solution passed. Na_2SO_4 concentration 100 g l^{-1}. Flow rate of the solution (m^3 m^{-2} h^{-1}): (*1*) 0.25, (*2*) 0.5, and (*3*) 1.0.

It is seen from the table that, at any instant of time, the largest mass of Ni(II) recovered from the cation exchanger corresponds to the Na_2SO_4 concentration of 100 g l^{-1}. Therefore, a solution containing 100 g l^{-1} of the eluent was considered the optimal for regeneration.

Experiments on regeneration in various hydrodynamic conditions allowed us to determine the optimal flow rate of the eluent across the cation-exchanger bed. It is 0.25 m^3 m^{-2} h^{-1} (Fig. 3), because at this flow rate the minimal volume of the eluent is expended for the complete regeneration, and the highest degree of regeneration degree is achieved. Use of flow rates lower than 0.25 m^3 m^{-2} h^{-1} is technologically inexpedient.

The ion exchange is a reversible process [14, 15], i.e., the regeneration can be regarded as saturation of the cation exchanger in the Ni^{2+} form with Na(I) ions. Therefore, the explanation of the extremal behavior of the dependences of regeneration parameters on the concentration of the eluent solution and on its flow rate is analogous to that in the case of nickel(II) recovery from wash water.

Analysis of curve *1* (Fig. 3) shows that, to save chemicals, reduce the regeneration time, and obtain eluates with a higher Ni(II) concentration (6.0 g l^{-1}), the regeneration should be carried out not completely, but to a 90% degree of regeneration, because this requires only a half of the eluent volume necessary for the complete regeneration. The reduction of the degree of regeneration of the ion exchanger will diminish DEC and BC by 10% in the case of a multiple use of the cation exchanger. This should be taken into account when designing ion-exchange equipment.

The results obtained in this study can be used to tackle with ecological problems of factories that employ processes of electroless nickel-plating and to design local systems for wash water purification with utilization of the metal recovered.

CONCLUSIONS

(1) It was found that the ion-exchange recovery of Ni(II) with the KU-2-8 cation exchanger in the Na^+ form from wash water produced in electroless metal plating in an acid hypophosphite electrolyte occurs under conditions of mixed-diffusion kinetics and is described by a mathematical model of "a sphere with a shell." At low degrees of saturation of the ion exchanger, the limiting stage is that of outer diffusion, whereas at high degrees of saturation, the process is controlled by the inner-diffusion stage.

(2) The optimal conditions and parameters of the ion-exchange recovery of metal ions from wash water produced in electroless nickel-plating were determined on a laboratory setup: initial Ni(II) concentration in the liquid phase 0.75 g l^{-1}; flow rate of the liquid phase across the cation-exchanger bed 1.0 $m^3 m^{-2} h^{-1}$; regeneration of the ion exchanger with a solution of 100 g l^{-1} Na_2SO_4, which flows at a rate of 0.25 $m^3 m^{-2} h^{-1}$ across the ion-exchanger bed, to a 90% degree of regeneration with a single use of the eluent to give eluates containing 6.0 g l^{-1} of nickel ions and 85 g l^{-1} of sodium sulfate.

(3) A physicochemical explanation was given for the experimental dependences of the dynamic exchange capacity and the breakthrough capacity on the flow rate of the solutions across the cation-exchanger bed and on the initial nickel(II) concentration in these solutions. The maximum values of the dynamic exchange capacity and the breakthrough capacity were found to be 33.0 and 19.7 g kg^{-1} of the ion exchanger, respectively.

REFERENCES

1. Nikandrova, L.I., *Khimicheskie sposoby polucheniya metallicheskikh pokrytii* (Chemical Methods for Deposition of Metallic Coatings), Leningrad: Mashinostroenie, 1971.
2. Shalkauskas, M. and Vashkyalis, A., *Khimicheskaya metallizatsiya plastmass* (Electroless Metal Plating of Plastics), Leningrad: Khimiya, 1977.
3. Sviridov, V.V., *Khimicheskoe osazhdenie metallov iz vodnykh rastvorov* (Chemical Deposition of Metals from Aqueous Solutions), Minsk: Universitskoe izd., 1988.
4. Vishenkov, S.A., *Khimicheskie i elektrokhimicheskie sposoby osazhdeniya metallopokrytii* (Chemical and Electrochemical Methods for Deposition of Metallic Coatings), Moscow: Mashinostroenie, 1975.
5. Plokhov, S.V., Torunova, V.I., Plokhov, V.A., et al., *Zh. Prikl. Khim.*, 1998, vol. 71, no. 11, pp. 1909–1910.
6. Plokhov, S.V., Vinogradov, S.N., Ershov, D.A., et al., *Zh. Prikl. Khim.*, 1999, vol. 72, no. 7, pp. 1154–1157.
7. Plokhov, S.V., Barinova, N.A., and Mikhalenko, M.G., *Zh. Prikl. Khim.*, 2001, vol. 74, no. 1, pp. 79–82.
8. Plokhov, S.V., Matasova, I.G., Utkin, V.A., et al., *Zh. Prikl. Khim.*, 2002, vol. 75, no. 6, pp. 967–970.
9. Plokhov, S.V., Kuzin, D.V., and Mikhalenko, M.G., *Izv. Vyssh. Uchebn. Zaved., Khim. Khim. Tekhnol.*, 2001, vol. 44, no. 6, pp. 104–106.
10. Plokhov, S.V., and Mikhalenko M.G., *Izv. Vyssh. Uchebn. Zaved., Khim. Khim. Tekhnol.*, 2002, vol. 45, no. 5, pp. 155–156.
11. Lur'e, Yu.Yu. and Rybnikov, A.I., *Khimicheskii analiz proizvodstvennykh stochnykh vod* (Chemical Analysis of Industrial Wastewater), Moscow: Khimiya, 1974.
12. *GOST* (State Standard) *22 001–87, Reagents and Special-Purity Grade Substances: Method of Atomic-Absorption Spectroscopy: Determination of Admixtures of Chemical Elements*, Moscow: Izd. Standartov, 1986.
13. Akhmetov, N.S., *Obshchaya i neorganicheskaya khimiya* (General and Inorganic Chemistry), Moscow: Vysshaya Shkola, 1981.
14. Ashirov, A., *Ionoobmennaya ochistka stochnykh vod, rastvorov i gazov* (Ion-Exchange Purification of Wastewater, Solutions, and Gases), Leningrad: Khimiya, 1983.
15. Kokotov, Yu.A. and Pasechnik, V.A., *Ravnovesiya i kinetika ionnogo obmena* (Equilibria and Kinetics of Ion Exchange), Leningrad: Khimiya, 1970.
16. Trigub, V.I. and Plokhov, S.V., *Pis'ma Zh. Tech. Fiz.*, 2005, vol. 31, no. 7, pp. 32–39.

ISSN 1070-4272, Russian Journal of Applied Chemistry, 2006, Vol. 79, No. 10, pp. 1576–1580. © Pleiades Publishing, Inc., 2006.
Original Russian Text © A.Yu. Shvykin, V.V. Platonov, V.A. Proskuryakov, K.B. Chilachava, S.I. Podshibyakin, 2006, published in Zhurnal Prikladnoi Khimii, 2006, Vol. 79, No. 10, pp. 1596–1600.

SORPTION AND ION-EXCHANGE PROCESSES

Sorption Capacity of Acetylacetonated Humin-Like Compounds with Respect to Cations of Heavy Metals

A. Yu. Shvykin, V. V. Platonov, V. A. Proskuryakov, K. B. Chilachava, and S. I. Podshibyakin

Leo Tolstoy State Pedagogical University, Tula, Russia
St. Petersburg State Technological Institute, St. Petersburg, Russia

Received April 25, 2006

Abstract—A method of synthesis of acetylacetonated humin-like compounds was developed. The effect of modification on the sorption capacity of humin-like compounds with respect to heavy metals was studied.

DOI: 10.1134/S107042720610003X

Humic substances (HS) have been studied for more than 200 years, and the number of papers devoted to the chemical structure, biological activity and practical applcation of HS and humin-like compounds (HLC) steadily grows, especially in the recent years. Economically developed countries, such as the United States, Germany, Canada, etc. make large investments in these studies. The interest of chemists and soil scientists in more complete and detailed studies of HS and HLC is caused by several reasons. Firstly, HS and HLC are of natural origin and positively affect the growth and evolution of plants. Therefore, these substances and complex fertilizers on their base find growing use in agriculture. Secondly, HS and HLC exhibit a pronounced pharmaceutical activity and can be used as highly active antioxidants, immunomodulators, biostimulants, bactericidal, antiviral, and antiumor preparations. Thirdly, due to their unique ability to bind heavy metals and radionuclides, HS and HLC can be used to solve environmental problems. In this conntext, growing attention is given to complexation HS and HLC with metal ions. For instance, it was found that small amounts of HS and HLC almost completely inhibit toxic influence of heavy metals on microorganisms and plants, even at high metal concentrations. HS and HLC similarly affect pesticides and transform them into inactive forms gradually decomposing into nontoxic compounds. Thus, due to high protecting activity with respect to the above pollutants and toxic substances, HS and HLC can be used for purification of subsoil water, soil, and atmosphere to remove heavy metals, radionuclides, and pesticides. In this context, studies aimed to enhance the complexing ability of HS and HLC with respect to heavy metal ions by chemical modification are of interest. A wide spectrum of synthetic macromolecular β-dicarbonyl compounds that can form stable polychelates with Cu, Fe, Co, Ni, Ca, Zn, Th, UO_2^{2+}, and rare-earth metal (REM) ions have been prepared [1]. However, introduction of β-dicarbonyl fragments, and, in particular, acetylacetone (AA) fragment into HS and HLC has not been described. At the same time, such a modification of HS and HLC would enhance the ability of HS and HLC to sorb metal ions.

The goal of our study was to develop a method for introduction of AA fragment into tea HLC structure and to examine the sorption capacity of the initial and modified HLC with respect to heavy metal ions.

The probable modification pathway is chloromethylation of HS and HLC, followed by nucleophilic substitution of chlorine by β-diketone fragments, in particular, AA. The choice of tea HLC as a subject of the study is firstly caused by the fact that they, in contrast to peat, coal, and sapropelic HS, have almost no mineral fraction that could affect the sorption activity of modified HLC. Secondly, tea HLC have a higher content of phenolic groups and lower average molecular weight, which suggests their higher reactivity as compared to the above HS in the stage of chloromethylation of the initial HLC and weaker steric hindrances in the stage of acetylacetonation of chloromethylated HLC.

EXPERIMENTAL

The objects of this study were HLC recovered from tea, chloromethylated HLC prepared by two methods (ChMHLC-1 and ChMHLC-2), and acetylacetonated HLC (AAHLC-1 and AAHLC-2) prepared from these intermediates.

To isolate HLC, a sample (~4 g) of black tea (preliminarily purified to remove bitumens by extraction with toluene for 8 h in a Soxhlet apparatus) was treated with 450 ml of 0.1 M KOH in a 1-l Erlenmeyer flask under stirring with a mechanical stirrer at 90°C (water bath) for 1 h. Then, the solution was allowed to stay for 2 h and then was centrifuged for 10–15 min (8000 rpm). The residue in the flask was treated with a fresh portion of 0.1 M KOH (450 ml), and the above procedure was repeated two times. All the centrifugates, which are brown-black solutions of HLC potassium salts, were combined and a 6 M HCl solution was added to pH ~2. In so doing, HLC was separated as a brown voluminous precipitate. It was centrifuged (8000 rpm), separated from the reddishbrown acidic solution of fulvic acid, washed with distilled water to pH ~5, and dried in a vacuum desiccator or a Fischer pistol in a vacuum at 60°C to constant weight. The HLC obtained (~2.5 g) were ground in an agate mortar and stored as a fine brown powder in a weighing bottle with a ground-glass stopper. A 19.9-g portion of tea HLC was prepared by this method.

Chloromethylation was performed by two methods: (1) without catalyst by heating a mixture of HLC with 40% formalin and concentrated hydrochloric acid, with bubbling gaseous HCl and (2) with $ZnCl_2$ as a catalyst. The reaction equations are as follows:

$$\text{HLC-H} + CH_2O + HCl \xrightarrow{H^+,\ \text{HCl solution}} \text{HLC}{-}CH_2Cl + H_2O,$$

$$\text{HLC-H} + CH_2O + HCl \xrightarrow{ZnCl_2,\ CCl_4} \text{HLC}{-}CH_2Cl + H_2O.$$

In the first case, to a mixture of the initial HLC (3 g) with $HCl_{(conc.)}$ (ρ = 1.19 g ml^{-1}, 12.6 ml) (weight ratio of HLC to HCl solution 1 : 5) in a 50-ml Erlenmeyer flask at stirring with a magnetic stirrer, we added 0.4 ml of 40% formalin (ρ = 1.071 g ml^{-1}) at a HLC to formalin weight ratio of 7 : 1. A strong flow of gaseous HCl (prepared by the reaction of concentrated sulfuric acid with dry NaCl) was bubbled for 2 h through this mixture at 60°C and continuous stirring. A precipitate of chloromethylated HLC (ChMHLC-1) was filtered through a fine-pore Schott filter no. 4 under vacuum, repeatedly washed with distilled water to pH 7, and dried to constant weight in a vacuum desiccator over anhydrous $CaCl_2$ at 20°C. As a result, 2.1303 g of ChMHLC-1 was prepared as a fine brown powder.

In the second case, to an HLC suspension (3 g) in dry CCl_4 (40 ml) in a 100-ml three-necked flask equipped with a reflux condenser with a $CaCl_2$ tube, a tube for supply of gaseous HCl, and a magnetic stirrer, we added with stirring paraformaldehyde (0.43 g) [weight ratio of HLC to $(CH_2O)_n$ = 7 : 1] and anhydrous $ZnCl_2$ (0.175 g) (weight ratio of HLC to $ZnCl_2$ = 40 : 1). A strong flow of gaseous HCl (prepared by the reaction of concentrated sulfuric acid with dry NaCl) was bubbled through this mixture with continuous stirring for 2 h. A precipitate of chloromethylated HLC (ChMHLC-2) was filtered through a fine-pore Schott filter no. 4 under vacuum, washed with dry CCl_4, and then repeatedly washed with distilled water to pH 7 and dried to constant weight in a vacuum desiccator over anhydrous $CaCl_2$ at 20°C. As a result, 2.4281 g of ChMHLC-2 was prepared as a fine brown powder.

The ChMHLC-1 and ChMHLC-2 intermediates were treated with Na-AA obtained by treatment of AA with sodium ethylate in dehydrated ethanol:

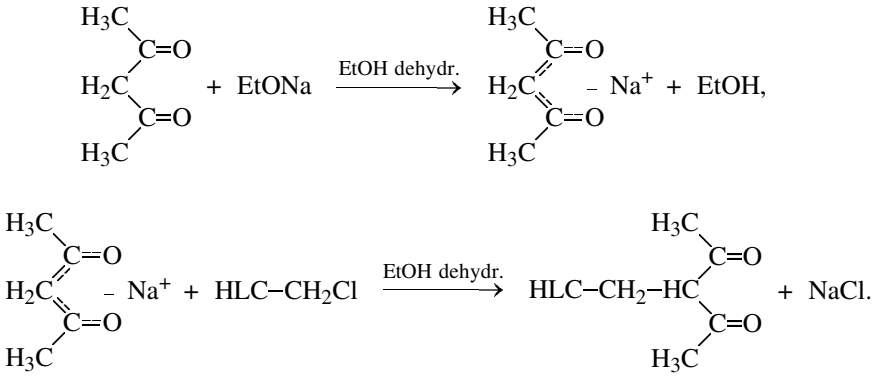


Table 1. Elemental analysis of the initial HLC, ChMHLC-1, 2, and AAHLC-1, 2

Sample	Content, wt %			
	C	H	N	O(+Cl)
Initial HLC	49.59	4.93	3.36	42.12
ChMHLC-1	47.61	4.76	3.14	44.49
ChMHLC-2	43.67	4.43	2.71	49.19
AAHLC-1	48.78	5.45	3.02	42.75
AAHLC-2	47.18	6.50	2.34	43.98

Table 2. Metal ion concentrations before and after treatment with initial and acetylacetonated HLC

Cations	Concentration, mg l^{-1}			
	initial solutions	initial HLC	AAHLC-1	AAHLC-2
Pb^{2+}	212.4	31.2	5.1	2.2
Cd^{2+}	104.3	104.2	52.2	21.2
Cu^{2+}	61.3	58.1	3.4	1.0
Mn^{2+}	60.5	59.2	56.4	52.5
Zn^{2+}	62.7	60.2	36.0	25.0

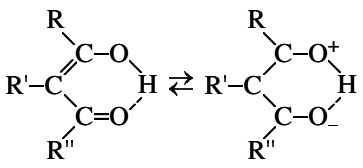
A solution of sodium ethylate in dehydrated ethanol was prepared by dissolving sodium (0.4242 g) in dehydrated ethanol (9.22 ml) in a 50-ml Erlenmeyer flask. To an EtONa solution, AA (1.89 ml) was added with stirring. The mixture appreciably warmed up, and after cooling, white NaAA crystals precipitated. The suspension obtained was heated to 60°C under stirring with a magnetic stirrer. The NaAA crystals dissolved to form a transparent solution containing about 30 wt % NaAA. To this solution, ChMHLC-1 or ChMHLC-2 (2 g; weight ratio of ChMHLC-1, 2 : NaAA = 8 : 9) was added with stirring. The reaction mixture was stirred at 60°C for 5 h, and then an AHLC-1, 2 precipitate was filtered through a fine-pore Schott filter no. 4 under vacuum and washed three times with dehydrated EtOH, three times with 10% HCl, and then with distilled water to pH 7. The resulting AAHLC-1 and AAHLC-2 samples were dried to constant weight in a vacuum desiccator over anhydrous $CaCl_2$. The weights of AAHLC-1 and AAHLC-2 samples, which are fine light brown powders, were 2.0066 and 1.7069 g, respectively.

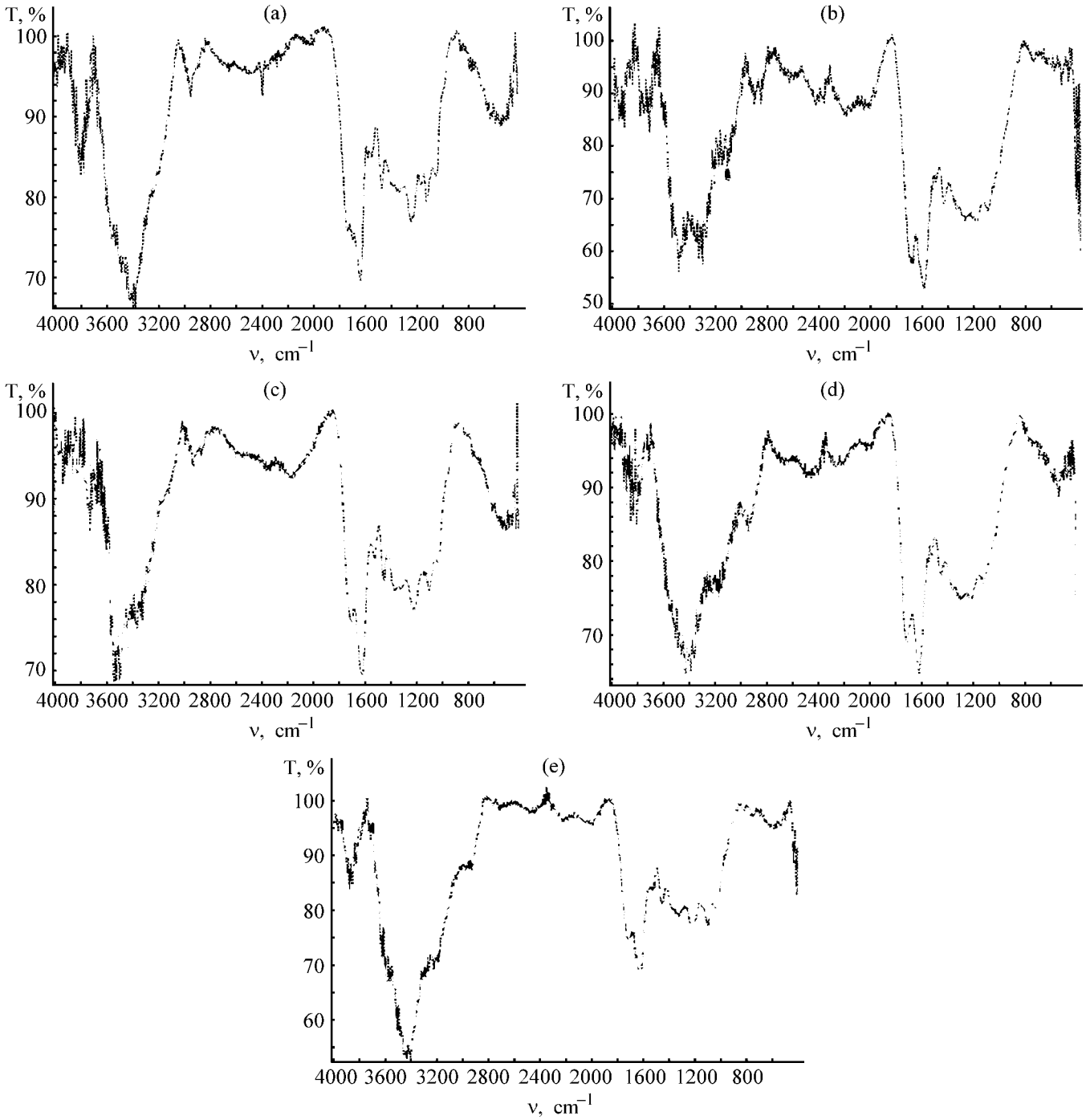
The elemental analysis of the initial HLC, ChMHLC-1, 2, and AAHLC-1, 2 was performed on a Carlo Erba-1100 gas-chromatographic analyzer. The results obtained are listed in Table 1.

The complexing ability of AAHLC-1, 2 and initial HLC with respect to heavy metal ions was measured. 0.2-g samples of HLC, AHLC-1 and AHLC-2 were stirred with a magnetic stirrer for 2 h in a 50-ml Erlenmeyer flask with 8 ml of ~0.001 M $ZnSO_4$, $MnSO_4$, $CuSO_4$, $Pb(NO_3)_2$, and $CdCl_2$ solutions. Then the precipitates of HLC and AHLC-1, 2 were filtered through a Schott filter no. 4 under vacuum, and the filtrates and initial salt solutions were analyzed on a Saturn-1 atomic absorption spectrometer. The results obtained are listed in Table 2.

The IR Fourier spectra of ChMHLC-1 and ChMHLC-2 (Figs. 1b, 1c) show, as compared to the initial HLC (Fig. 1) an increase in the intensity of bands at 2916 and 2860 cm^{-1} for ChMHLC-1 and at ~2925 cm^{-1} for ChMHLC-2, belonging to C–H_2 stretching vibrations of methylene groups [2], which suggests that the content of $-CH_2-$ fragments in ChMHLC-1 and ChMHLC-2 becomes higher. For ChMHLC-2, the band at 2925 cm^{-1} overlaps with a broad band at 3650–3000 cm^{-1} belonging to stretching vibrations of –OH and –NH groups associated by H bonds [2]. In addition, the spectra of ChMHLC-2 and especially ChMHLC-1 contain a doublet at 420 and 440 cm^{-1} of C–Cl stretching vibrations. The IR data are confirmed by elemental analysis (Table 1), which shows that, compared to HLC, in ChMHLC-1 and especially ChMHLC-2, the content of C, H, and N decreases, whereas the total content of O and Cl increases. All the above facts confirm the incorporation of $-CH_2Cl$ groups into the HLC structure. The changes are more pronounced for ChMHLC-2 due to more rigorous chloromethylation conditions, since the aprotic Lewis acid $ZnCl_2$ in anhydrous CCl_4 is a stronger catalyst of the electrophilic chloromethylation reaction than H^+ in aqueous HCl.

In the IR spectra of AAHLC-1 and AAHLC-2 as compared to the initial HLC (Fig. 1), the band of the carbonyl group at 1717 cm^{-1} shifts to 1703 and 1691 cm^{-1}, respectively (Figs. 1d, 1e) and grows in intensity. The intensity of the band at 1616 cm^{-1} increases for AAHLC-1 and especially AAHLC-2. This band belongs to the enol form of β-dicarbonyl systems with an intramolecular hydrogen bond [3–5]:





IR Fourier spectra of humin-like compounds. (T) Transmission and (ν) wavenumber. Compound: (a) initial HLC, (b) ChMHLC-1, (c) ChMHLC-2, (d) AAHLC-1, and (e) AAHLC-1.

At the same time, as compared to ChMHLC-1 and ChMHLC-2 (Figs. 1b, 1c), for AAHLC-1 and AAHLC-2, the intensity of the broad band at 3600–3000 cm^{-1} grows, which corresponds to an increase in the content of OH groups associated by hydrogen bond in AAHLC-1 and AAHLC-2 as compared to ChMHLC-1 and ChMHLC-2. This is connected with an additional contribution into the total absorption of –OH and –NH– groups in ChMHLC-1 and ChMHLC-2, made by the OH group of the enol form of the β-dicarbonyl system introduced into HLC [3–5]. It should be noted that, in the IR spectra of AAHLC-1 and AAHLC-2, the doublet at 420, 440 cm^{-1} is preserved, suggesting an in-

complete substitution of chloromethyl groups in ChMHLC-1 and ChMHLC-2 by AA fragments. These IR data are confirmed by elemental analysis (Table 1), which shows that in AAHLC samples (especially, in AAHLC-2), the content of carbon and especially hydrogen increases, whereas the content of nitrogen and total content of oxygen and chlorine decrease as compared to ChMHLC. The above is the evidence of substitution (incomplete) of chloromethyl groups in ChMHLC-1 and ChMHLC-2 by AA fragments. The higher content of AA fragments in AAHLC-2 as compared to AAHLC-1 corresponds to higher content of chloromethyl groups in ChMHLC-2 as compared to ChMHLC-1.

The initial HLC (Table 2) sorb Pb^{2+} ions the most actively. The metal concentration in the solution decreases after sorption by a factor of 6.8. With respect to other ions, especially to Cd^{2+} and Mn^{2+}, HLC show a lower sorption capacity. AAHLC (especially AAHLC-2) exhibit substantially higher sorption capacity. After sorption with AAHLC-1, the Pb^{2+} concentration decreases by a factor of 41.6, and with AAHLC-2, by a factor of 96.6; concentration of Cd^{2+}, Cu^{2+}, Mn^{2+}, and Zn^{2+}, by factor of 2.0 and 4.9; 18.0 and 61.3; 1.1 and 1.2; and 1.7 and 2.5, respectively. These results show that AA fragments introduced into the initial HLC substantially enhance their complexing ability with respect to metal ions (except Mn^{2+}), especially in the case of AAHLC-2. Along with the IR data, this fact shows that the concentration of AA fragments in Aahlc-2 is higher than in AAHLC-1. As seen, the sorption capacity of AAHLC-2 is higher than that of AAHLC-1 by a factor 1.4–3.4.

The results obtained suggest that, to prepare AAHLC with the highest sorption capacity for heavy metal ions, it is preferable to use $ZnCl_2$ as a catalyst in anhydrous CCl_4 in the stage of synthesis of ChMHLC.

Because of the substantial increase in the sorption capacity of AAHLC in comparison with the initial HLC, the above-described method of the chemical modification can be recommended for obtaining sorbents based on HS and HLC with a high sorption capacity for heavy metal ions. Such preparations can be used for recovery of precious metals (REE, platinum metals, etc.) from solutions formed in processing of ores, fuel ashes, waste piles, wastewater, etc., and also as detoxicants.

CONCLUSIONS

(1) A new method of chemical modification of tea HLC was developed, based on introduction into the HLC structure of an acethylacetone fragment via chloromethylated intermediates.

(2) The IR and analytical data confirm the incorporation of chloromethyl fragments into the initial HLC structure, with their subsequent partial substitution by acetylacetone fragments.

(3) To achieve a more complete chloromethylation of HLC, followed by ChMHLC acetylacetonation, the use of paraformaldehyde in the stage of chloromethylation in the presence of Lewis acids, for e.g., $ZnCl_2$ is preferable over the use of formalin in aqueous HCl.

(4) Acetylacetonated HLC have a substantially higher sorption capacity for heavy metal ions as compared to the initial HLC.

(5) The method developed for chemical modification of HLC can be recommended for preparing acetylacetonated HLC with a high sorption capacity for heavy metal ions, which can be used in technology, ecology, and pharmacology.

REFERENCES

1. Davydova, S.L. and Barabanov, V.A., in *Teoreticheskaya i prikladnaya khimiya β-diketonatov metallov* (Theoretical and Applied Chemistry of Metal β-Diketonates) Moscow: Nauka, 1985, pp. 121–124.
2. Becker, H., Berge, W., Domschke, G., et al., *Organicum. Organisch-chemisches Grundprakticum*, Berlin: VEB Deutscher Verlag, 1990, Bd. 1, 2.
3. Nakanishi, K., *Infrared Absorbtion Spectroscopy*, Tokyo: Nankido, 1962.
4. Silverstein, R.M., Clayton, G.C. and Morril, T.C., *Spectrometric Identification of Organic Compounds*, New York: John Wiley and Sons, 1974.
5. Kazitsyna, L.A. and Kupletskaya, N.B., *Primenenie UF-, IK-, YaMR- i mass-spektroskopii v organicheskoi khimii* (Application of UV, IR, NMR, and Mass Spectrometry in Organic Chemistry), Moscow: Mosk. Gos. Univ., 1979, pp. 72–77, 212–215.

ISSN 1070-4272, Russian Journal of Applied Chemistry, 2006, Vol. 79, No. 10, pp. 1581–1587. © Pleiades Publishing, Inc., 2006.
Original Russian Text © V.V. Platonov, A.A. Khadartsev, A.Yu. Shvykin, D.V. Prokopchenkov, V.A. Proskuryakov, T.V. Chestnova, 2006, published in Zhurnal Prikladnoi Khimii, 2006, Vol. 79, No. 10, pp. 1601–1607.

SORPTION AND ION-EXCHANGE PROCESSES

Chemical Compositions of Extracts of Organic Matter of Schungite Rock form Zazhogino Deposit of Karelian Transonega Region

V. V. Platonov, A. A. Khadartsev, A. Yu. Shvykin, D. V. Prokopchenkov, V. A. Proskuryakov, and T. V. Chestnova

Leo Tolstoy State Pedagogical University, Tula, Russia
Tula State University, Tula, Russia
St. Petersburg State Technological Institute, St. Petersburg, Russia

Received April 25, 2006

Abstract—The organic matter of schungite rock from the Zazhogino Deposit of Karelian Transonega region was extracted in the sequential mode. The extract composition was determined by several modern physicochemical methods.

DOI: 10.1134/S1070427206100041

Schungite is a unique rock containing fullerenes [1, 2]. A wide number of diseases, including cancer, have been cured with schungite water and schungite preparations for a period of many years [3]. However, the cause of these unique biological properties is virtually not understood. One of the main explanations is the presence of fullerenes of the schungite composition. However, the fullerene content in the organic matter of schungite rock (OMSR) is low (up to 2 wt %), and the therapeutic action of schungite cannot be only due to the presence of fullerenes. All biologically active compounds of both OMSR and the mineral constituent of schungite rock (SR) should be taken into account.

One of the efficient methods for studying organic matter of caustobioliths, especially their low-molecular weight fraction containing components of different chemical nature, is extraction [4–8].

In this study, we examined for the first time the chemical composition of the extracts of OMSR (from Zazhogino Deposit of Karelian Transonega region) obtained by sequential extraction with organic solvents of gradually increasing polarity.

EXPERIMENTAL

Initial SR was ball-milled to 70–90 μm, placed in a Teflon vessel, and thoroughly stirred in 40% hydrofluoric acid at 20°C for 6 h. The solid was repeatedly washed with distilled water by decanting to pH ~7, filtered on a Buchner funnel under a reduced pressure, and dried at 100°C to constant weight. The OMSR content of the product enriched with organic matter (OM) was determined by thermal gravimetric analysis. Elemental analysis shows that the OMSR content in SR increases from 30.21 to 82.00 wt % after treatment with an HF solution. The elemental composition of OMSR (wt % daf) is as follows: C 95.45, H 0.30, N 0.60, O + S 3.65.

The organic fraction of the schungite rock was successively extracted form a weighed portion of the enriched schungite rock (100 g) in a Soxhlet apparatus with hot *n*-hexane, toluene, chloroform, acetone, ethanol, and acetic acid. The extraction was performed until the refractive index of the extract became equal to that of the initial solvent. The solvents were removed from the extracts. The residue was dried in a vacuum to constant weight and weighed to determine the yield. This procedure was used to prepare hexane, toluene, chloroform, and acetone extracts. The ethanol and acetic acid extracts were prepared by a different procedure described below. The elemental composition of each extract and the content of functional groups in the extracts were determined. The extracts were also analyzed by emission spectroscopy, atomic absorption analysis,

cryoscopy, and Fourier IR and UV-Vis spectroscopy. The toluene and chloroform extracts were methylated with an ether solution of diazomethane and then analyzed by gas chromatography-mass spectrometry (GC-MS) [9–13].

Ethanol was removed from the extract under a reduced pressure. Yellow oil with floating brown crystals was obtained. The extract yield was 1.44 wt % based on OMSR. Acetone was added to the extract. The oil fraction dissolved. The solvent was decanted, and the remaining crystals were washed with two portions of acetone. The brown crystals were dissolved in methanol. The solution was quantitatively transferred into a weighing bottle, and the solvent was removed in a vacuum. The yield of brown crystals (fraction no. 1) was 0.16 wt % based on OMSR. The combined acetone extracts were dried in a vacuum. A light yellow oil with a small amount of yellow crystals was obtained. The oil was separated from the crystals by decantation. The oil yield was 1.20 wt % based on OMSR (fraction no. 2). The remaining yellow crystals were dissolved in methanol. The solution was quantitatively transferred into a weighing bottle, and the solvent was removed in a vacuum. The yield of yellow crystals (fraction no. 3) was 0.08 wt % based on OMSR.

The yield of acetic acid extract was 1.90 wt % based on OMSR. To isolate the organic fraction from the extract, it was evaporated in a vacuum to ~50 mol and was diluted with distilled water to the total volume of 1 l. The resulting solution was extracted with chloroform (5x100 ml). The chloroform extracts were combined. Chloroform was distilled off, and then the small amount of AcOH was removed in a vacuum. The residue was dissolved in chloroform, and the solution was quantitatively transferred into a weighing bottle. The solvent was evaporated under a reduced pressure. The yield of the organic fraction of the acetic acid extract was 0.18 wt % based on OMSR. After the extraction, the aqueous phase was evaporated to dryness on a water bath. The weight of the brown residue was 1.41 g.

The yield of the hexane extract was 0.22 wt % based on OMSR. Absorption bands of the following structural fragments were identified in the IR Fourier spectrum (ν, cm^{-1}):

the absence of absorption in the range 900–650 suggests a nonaromatic structure of the hexane extract. The spectra of aromatic and heteroaromatic compounds contain in this range strong bands of out-of-plane bending vibrations of C–H bonds and bending vibrations of the rings, which usually correlate with the substitution type. The strong bands of carbon skeleton vibrations of aromatic and heteroaromatic compounds lie in the range 1600–1300;

naphthene structures containing probably aromatic rings (970–980, 980, 1950), and also cyclic hydrocarbons (3420–3140, 1110, 1060, 2966, 2931, 2854, 1464, 1377, 720) with short (C ≤ 4) alkyl substituents (720–740, 3030–3020, 1464–1590, 650–910) and substituents with unsaturated bonds (3050, 1642, 1600, 980, 880, 820);

aromatic rings (3000–3100, 1500–1600, a number of bands in the ranges 900–1200 and 650–900); isolated (650–900, 905–1200) and fused (3030–3080, 1500, 1600, 1500–1580, 1450–1500, 1125–1175, 1070–1100, 1000–1070) aromatic rings;

oxygen-containing heterocycles (3125–3165, 1565, 1015–1030, 845–870, 740–800); quinoid (1642, 1675, 1655–1622, 1642–1690), keto (1695, 1705, 1749, 1715, 1100), and carboxy (3500–3580, 1749–1800, 1280–1377, 1075–1190) groups;

pyrrole rings (3490–3400, 1565, 1500).

The yield of the toluene extract was 0.22 wt % based on OMSR.

The Fourier IR spectrum of the toluene extracts contains the following bands of structural fragments (ν, cm^{-1}):

alkanes: $\nu^{as}_{CH_3}$ (2880.0–2853.2), $\delta^{as}_{CH_3}$ (1462.2–1430.0 and 1385.0–1377.2); $\nu^{as}_{CH_2}$ (2940.0–2921.3), $\nu^{s}_{CH_2}$ (2870.0–2845.0), δ_{CH_2} (1491.5–1462.2); rocking vibrations (ρ) of $-(CH_2)_n-$ (742.8–720.0), ν_{CH} (2921.3–2880.0), δ_{CH} (1340.0); ν_{C-C} (1600.3–1515.0); alkenes R–CH=CH_2 (3095.0–3075.0; 1660.0–1645.0; 892.9–885.0); RR'C=CH_2 (3095.0–3075.0, 1660.0–1645.0, 892.9–885.0); R–CH=CH–R' (3045.0–3010.0; 1665.0–1635.0, 730.0–660.0); alkenes (3074.2, 1645.0, 720.0, 742.8, 660.0, 885.0, 892.9, 905.0, 985.0);

aromatic rings (3080.0–3030.0, 1625.0–1580.0, 1515.0–1462.2, 1462.2–1440.0);

alcohols and phenols (3552.5–3467.9, ν_{OH}, intermolecular hydrogen bonds in dimers; 3600.8–3420.0, ν_{OH}, intramolecular hydrogen bonds);

ketones R–CO–R' (1729.2–1700.0, $\nu_{C=O}$), esters R–COOR' (1750.0–1729.2), acid amides (3552.5–3200.0, 3467.9–3100.0); pyrrole, indole, pyridine, quinoline, piperidine heterocycles (3309.5–3367.5, 3367.5, 3325.0, 3347.5, 3467.9, 1491.9, 1285.2–1377.2, 742.8).

The yield of the chloroform extract was 0.04 wt % based on OMSR.

The Fourier IR spectrum of the chloroform extracts contains the following bands (ν, cm^{-1}):

alkanes: $\nu^{as}_{CH_3}$ (2880.0–2853.2), $\delta^{as}_{CH_3}$ (1461.1–1420.0, 1385.0–1377.2); $\nu^{as}_{CH_2}$ (2940.0–2923.3), $\nu^{s}_{CH_2}$ (2870.0–2853.5), δ_{CH_2} (1490.0–1461.1); rocking vibrations (ρ) of $-(CH_2)_n-$ (745.0–720.0); ν_{CH} (2923.3–2880.0); δ_{CH} (1340.0); ν_{C-C} (1600.0–1500.0); alkenes (3074.2, 1630.0, 720.0, 745.0, 660.0, 885.0, 905.0, 950.0);

aromatic rings (3074.2–3030.0; 1630.0–1580.0, 1512.2–1461.1; 1461.1–1440.0);

alcohols and phenols (3664.7–3572.9, ν_{OH}, free OH group; 3541.8–3455.8, ν_{OH}, intermolecular hydrogen bonds in dimers; 3411.9–3196.5, ν_{OH}, intermolecular hydrogen bonds in polyassociates; 3594.4–3411.9, ν_{OH}, intramolecular hydrogen bond); ν_{C-O} (phenol) (1220.0); primary (1060.0) and secondary (1207.9) hydroxy group of alcohols;

ketones, $\nu_{C=O}$ (1726.7–1700.0); acid amides (3541.8–3196.5; 3455.8–3102.0); pyrrole, indole, pyridine, quinoline, piperidine heterocycles (3313.8–3370.5, 3358.0, 3340.7, 3472.5, 1461.1, 1280.0–1377.5, 720.0–770.0); quinones (1635.0–1680.0); diketones (1729.2); carboxylic acids (3000.0–2500.0, 1600.3, 1630.0, 1462.2, 1491.5, 1300–1200).

The Fourier IR spectrum of the acetone extract contains the following bands (ν, cm^{-1}):

alkanes: $\nu^{as}_{CH_3}$ (2960.4), $\nu^{s}_{CH_3}$ (2868.4), $\delta^{as}_{CH_3}$ (1431.0), $\nu^{s}_{CH_3}$ (1381.1), $\nu^{as}_{CH_2}$ (2915.2), $\nu^{s}_{CH_2}$ (2852.7); CH_2 (1470.0, scissors vibrations); $-(CH_2)_n$ ($n \geq 4$) rocking vibrations (728.8);

aromatic rings (3037.4, 3046.0, 3072.4, 3088.0, 1537.5, 1520.0, 1580.0, 1600.0); fused aromatic systems (1650.0–1600.0, 1537.5–1431.0); 1,2,4-substituted (1284.9–1180.0, 1180.0–1120.0; 1071.5–1040.0, two bands);

alcohols and phenols [599.7–3516.5, ν_{OH}, intermolecular and intramolecular hydrogen bonds, e.g., for polyhydric alcohols (1,2–diols); π-hydrogen bond]; ν_{C-O} (phenol) (1200.0); secondary OH (1100.0–1071.5); primary OH (1040.0); δ_{OH} (1284.9): ketones (1727.2), quinones (1650.0–1680.0); diketones (1727.2), carboxylic acids (3013.8–2500.0, 1727.2, 1431.0, 1300–1200.0); acid amides (3046.0–3205.3, 1650.0, 3434.5, 3307.4, 1284.9); R–CO–SH (1727.2);

pyrrole, indole, pyridine, quinoline, piperidine heterocycles (3307.7–3368.8, 3360.9, 3339.9, 3338.9, 3461.4, 1431.0, 1381.1–1284.9, 728.8).

The Fourier IR spectrum of fraction 1 of the ethanol extract contains the following bands (ν, cm^{-1}):

alkanes: $\nu^{as}_{CH_3}$ (2978.3), $\nu^{s}_{CH_3}$ (2886.9), $\delta^{as}_{CH_3}$ (1402.1), $\delta^{s}_{CH_3}$ (2946.8), $\nu^{as}_{CH_2}$ (2850.0), $\nu^{s}_{CH_2}$ (1402.1, CH_2 scissors vibrations); 740.0, $-(CH_2)_n$ rocking vibrations);

aromatics rings (3007.7, 3040.1; 1515.0, 1550.0, 1580.0, 1635.4), mainly fused rings (1650.0–1635.4; 1550.0–1470.0), with short alkyl substituents (1280.0–1150.0; 1150.0–1109.3; 1060–1044.7); δ_{C-C} [out-of-plane, ring (685.0)]; δ_{OH} (out-of-plane, OH groups) (650.0); δ_{OH} (in-plane) (1340.0);

alcohols and phenols [3601.6–3509.1, ν_{OH}, intermolecular and intramolecular hydrogen bonds, e.g., for polyhydric alcohols (1,2-diols), π-hydrogen bond]; ν_{C-O} (phenol) (1229.1); secondary OH (1100.0–1080.0); primary OH (1044.7); δ_{OH} (1280.0), ketones (1734.7), quinones (1635.4–1680.0); diketones (1724.7), carboxylic acids (3007.7–2508.5; 1635.4; 3438.9; 3320.3; 1280.0; 1229.1); acid amides (3040.1–3235.9; 1635.4; 3438.9; 3320.3; 1280.0; 1229.1); R–CO–SH (1724.7);

pyrrole, indole, pyridine, quinoline, piperidine heterocycles (3320.3–3364.4; 3354.9; 3320.3, 3377.3, 3482.5; 1402.1, 1470.0, 1340.0, 1280.0, 740.0, 780.0).

The Fourier IR spectrum of fraction 2 of the ethanol extract contains the following bands (ν, cm^{-1}):

alkanes: $\nu^{as}_{CH_3}$ (2958.6), $\nu^{s}_{CH_3}$ (2885.1), $\delta^{as}_{CH_3}$ (1404.2), $\delta^{s}_{CH_3}$ (1368.1), $\nu^{as}_{CH_2}$ (2950.9), $\nu^{s}_{CH_2}$ (2850.0); CH_2 scissors vibrations (1404.2, 1460.0); $-(CH_2)_n$ ($n \geq 4$) rocking vibrations (745.6);

aromatic rings (3010.3, 3035.5; 3056.0, 3075.9, 1635.8, 1520.0, 1580.0) mainly fused rings (1650.0–1635.8, 1560.0–1480.0), with short alkyl substituents (1282.1–1113.5, 1150.0–1141.7; 1060.0–1041.7); δ_{C-C} (out-of-plane, rings) (680.1);

alcohols and phenols (3601.5–3505.0, ν_{OH}, intermolecular and intramolecular hydrogen bonds); ν_{C-O} (phenol) (1230.0); secondary OH (1230.0); primary alcoholic hydroxy group (1041.7); δ_{OH} (in-plane) (1368.1), δ_{OH} (out-of-plane) (680.1); ketones (1727.9), quinones (1635.4–1680.0); diketones (1727.9), carboxylic acids (3010.3–2500.0; 1635.8; 3441.0, 3320.3, 1282.1, 1230.0);

pyrrole, indole, pyridine, quinoline, piperidine heterocycles (3320.3–3377.1, 3334.3, 3377.1, 3492.0, 1404.2; 1460.0, 1480.0, 1282.1; 745.6); ν^{s}_{C-O-C} (aliphatic, 1109.3; aromatic, aryl alkyl ethers, 1080.0–1041.7); $\nu_{C=C}$ (in *cis*-vinyl ethers) (1635.8); ν_{C-O} (alicyclic 5- or 6-membered ring) (1041.7–1080.0).

The Fourier IR spectrum of fraction 3 of the ethanol extract contains the following bands (ν, cm^{-1}):

alkanes: $\nu^{as}_{CH_3}$ (2960.0), $\nu^{s}_{CH_3}$ (2885.5), $\delta^{as}_{CH_3}$ (1464.2), $\delta^{s}_{CH_3}$ (1367.6), $\nu^{as}_{CH_2}$ (2944.0), $\nu^{s}_{CH_2}$ (2872.5); CH_2 scissors vibrations (1464.2); $-(CH_2)_n$ rocking vibrations (745.5);

aromatic rings (3061.0, 3027.9, 3084.3, 1580.4, 1637.1, 1601.1), mainly fused rings (1680.0–1637.1, 1530.0–1580.4; 1530.0–1464.2), with short alkyl substituents (1287.0–1173.9; 1173.9–1123.7; 1040.8–1073.2); δ_{C-C} (out-of-plane ring vibrations) (651.8, 680.0);

alcohols and phenols (3606.0–3522.4, ν_{OH}, intermolecular and intramolecular hydrogen bond); ν_{C-O} (phenol) (1287.0, 1230.0); primary OH (1040.8) and secondary OH (1230.0, 1287.0) of alcohols; δ_{OH} (in-plane) (1367.6), δ_{OH} (out-of-plane) (651.3, 680.0); ketones (1727.7), quinones (1637.1–1680.0); diketones (1727.7), carboxylic acids (3010.3–2500.0; 1637.1, 1464.2, 1480.0, 1394.0, 1300.0–1200.0), acid amides (3027.9–3249.7, 1637.1, 3427.5, 3475.0, 3325.4, 1287.0, 1230.0);

pyrrole, indole, pyridine, quinoline, and piperidine heterocycles (3325.4–3365.5; 3352.9, 3392.8, 3497.7; 1447.3, 1464.2, 1287.0, 745.5); ν^{s}_{C-O-C} (aliphatic, 1123.7; aromatic, aryl alkyl ethers, 1073.2–1040.8); $\nu_{C=C}$ (in vinyl ethers) (1637.1); ν_{C-O} (alicyclic 5- or 6-membered ring) (1040.8–1073.2).

The Fourier IR spectrum of the organic fraction of the acetic acid extract contains the following bands (ν, cm^{-1}):

alkanes: $\nu^{as}_{CH_3}$ (2950.0), $\nu^{s}_{CH_3}$ (2880.0), $\delta^{as}_{CH_3}$ (1435.5), $\delta^{s}_{CH_3}$ (1371.9), $\nu^{as}_{CH_2}$ (2923.3), $\nu^{s}_{CH_2}$ (2851.4); CH_2 scissors vibrations (1435.5; 1460.0); $-(CH_2)_n$ rocking vibrations (720.0, 747.5);

aromatic rings (3021.5, 3046.7, 3060.0, 1530.0, 1560.0, 1580.0, 1638.0, 1659.9, 1600.0), mainly fused rings (1680.0–1638.0, 1530.0–1580.0, 1530.0–1435.0), with short alkyl substituents (1230.4, 1180.0, 1124.9, 1140.3); δ_{C-C} (out-of-plane ring vibrations) (603.9, 680.0);

alcohols and phenols (3602.3–3509.2, ν_{OH}, intermolecular and intramolecular hydrogen bonds); ν_{C-O} (phenol) (1230.4); primary OH (1044.3) and secondary OH (1230.4, 1280.0) of alcohols; δ_{OH} (in-plane) (1371.9), δ_{OH} (out-of-plane) (650.0, 680.0); ketones (1746.0), quinones (1638.0–1659.9, 1680.0); diketones (1746.0), carboxylic acids (3021.5–2522.0; 1638.0, 1435.5, 1371.9, 1300.0–1200.0); acid amides (3021.5–3257.4, 1638.0, 3423.3, 3408.6, 3465.4, 1230.4, 1280.0); aliphatic (1124.9), aromatic and aryl alkyl ethers (1080.0–1044.3, ν_{C-O-C}); vinyl ethers (1638.0, $\nu_{C=C}$); alycyclic 5- and 6-membered rings (1044.3–1080.0, ν_{C-O});

pyrrole, indole, pyridine, quinoline, and piperidine heterocycles (3304.2– 3372.9, 3353.2, 3388.5, 3483.0, 1435.5, 1230.4, 1280.0, 747.5).

The content of carboxylic acids in this extract is higher. Fractions 1 and 2 of the ethanol extract contain larger amounts of phenols, alcohols, and ketones.

The IR Fourier spectra of OMSR extracts are shown in Fig. 1.

As determined by gas chromatography-mass spectrometry (GC-MS), the methylated toluene extract contains the following compounds (Fig. 2):

alkanes: 2-methyldecane, tridecane, tetradecane, pentadecane, hexadecane, heptadecane, octadecane, 2,6,10-trimethylpentadecane, nonadecane, 2,6,10,14-

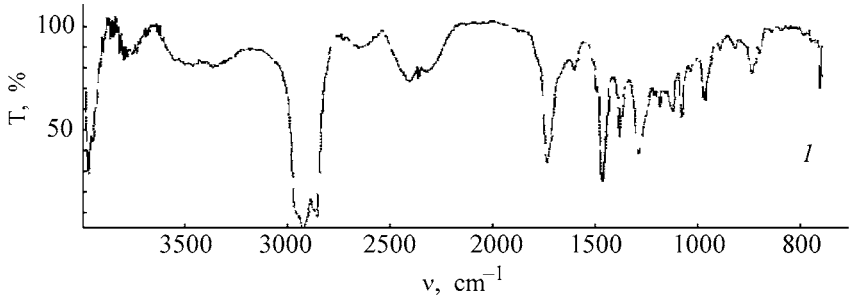


Fig. 1. Fourier IR spectra of (*1*) toluene, (*2*) chloroform, (*3*) acetone, (*4*) ethanol (fraction 1), (*5*) ethanol (fraction 2), (*6*) ethanol (fraction 3), and (*7*) acetic acid extracts of OMSR. (T) Transmission and (ν) wavenumber.

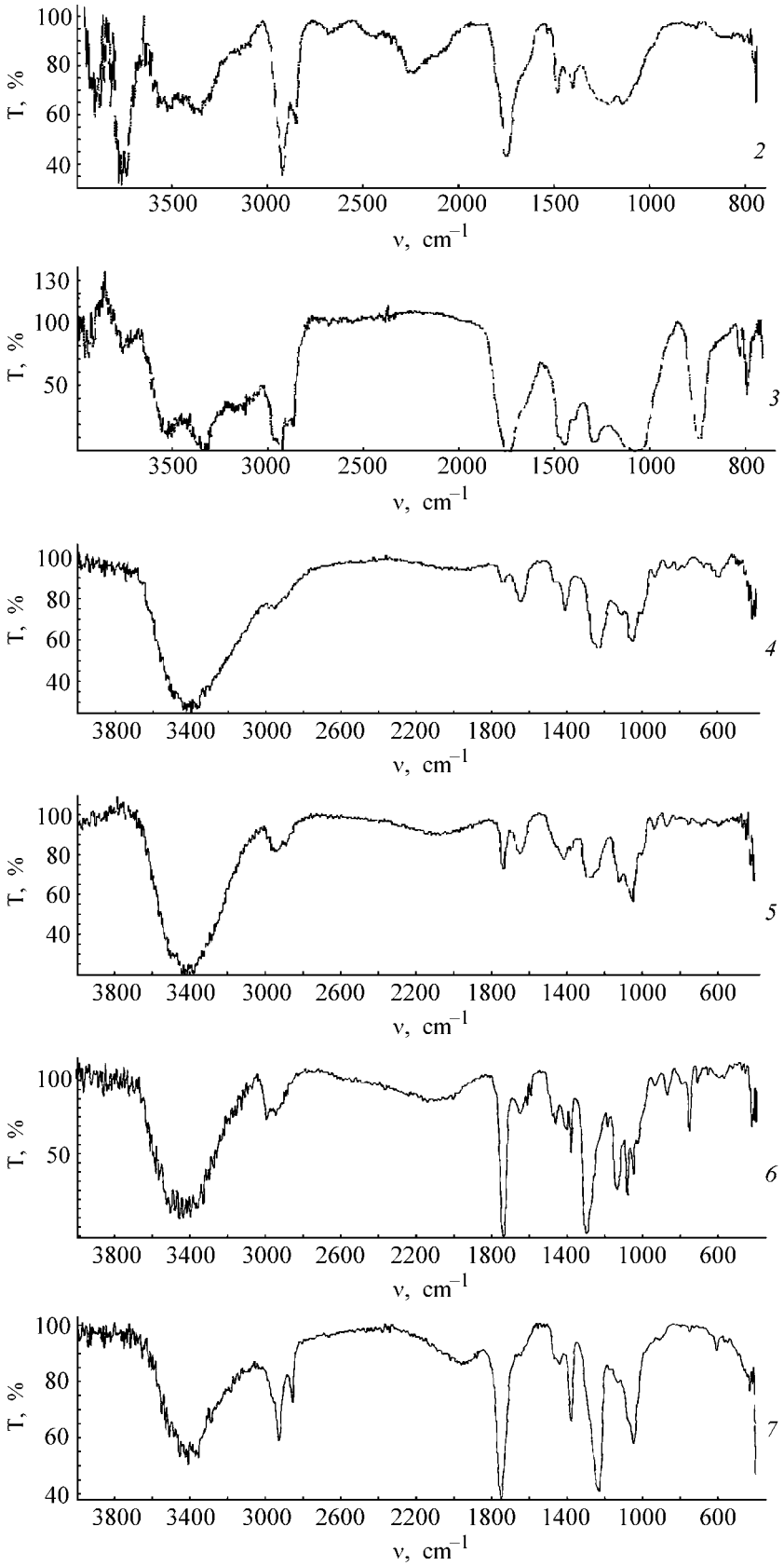

T, %
100
80
60
40
3500 3000 2500 2000 1500 1000 800
ν, cm⁻¹
2
T, %
130
100
50
3500 3000 2500 2000 1500 1000 800
ν, cm⁻¹
3
T, %
100
80
60
40
3800 3400 3000 2600 2200 1800 1400 1000 600
ν, cm⁻¹
4
T, %
100
80
60
40
3800 3400 3000 2600 2200 1800 1400 1000 600
ν, cm⁻¹
5
T, %
100
50
3800 3400 3000 2600 2200 1800 1400 1000 600
ν, cm⁻¹
6
T, %
100
80
60
40
3800 3400 3000 2600 2200 1800 1400 1000 600
ν, cm⁻¹
7

Fig. 1. (Contd.)

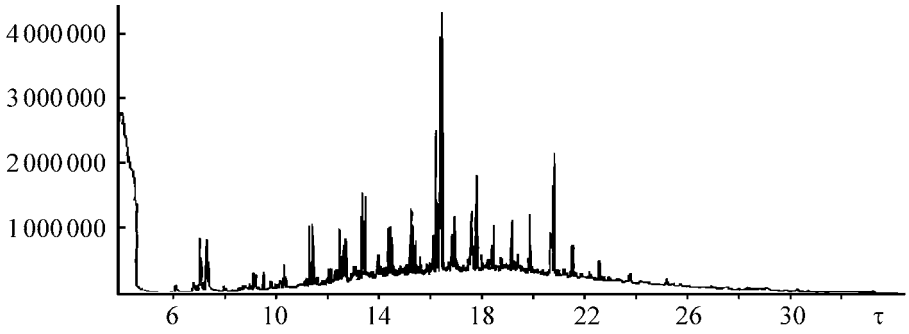


Fig. 2. Chromatogram of methylated toluene extract of OMSR.

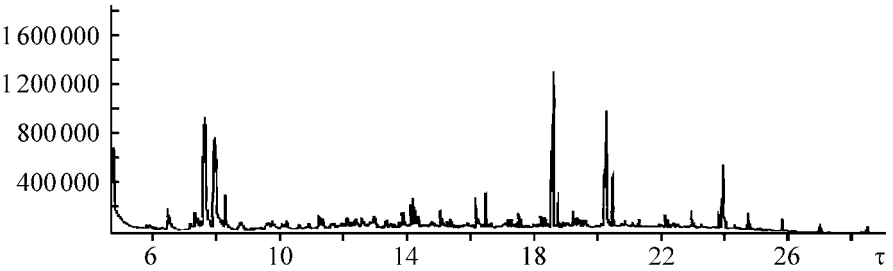


Fig. 3. Chromatogram of methylated chloroform extract of OMSR. The results of GCMS are consistent with the IR Fourier spectra of some extracts.

tetramethylpentadecane, eicosane, 2,6,10-14-tetramethylhexadecane, heneicosane, docosane, tricosane, tetracosane, pentacosane, heptacosane, and octacosane:

alkenes: 1-dodecene, 1-tetradecene, 1-hexadecane, 1-octadecene, and 1-nonadecene;

cycloalkanes: cyclododecane and cycloeicosane;

methyl esters of saturated carboxylic acids: octanoic, decanoic, dodecanoic, hexadecanoic, octadecanoic, and heptacosanoic acids;

methyl esters of unsaturated carboxylic acids: methyl octadec-8-enoate;

aromatic alcohols (benzyl alcohol), methyl ethers of phenols (2-methylphenol, 3-methylphenol, 4-methylphenol), fused aromatic compounds (1,2,3,4-tetrahydronaphthalene, 1-methylnaphthalene, 2-methylnaphthalene, and 2,6-dimethylnapthalene).

The GC-MS analysis of the methylated chloroform extract showed the presence of the following compounds (Fig. 3):

alkanes: hexadecane, docosane, tricosane, tetracosane, pentacosane, hexacosane, heptacosane, octacosane, and nonacosane;

methyl esters of saturated carboxylic acids: nonanoic, decanoic, undecanoic, dodecanoic, tridecanoic, tetradecanoic, pentadecanoic, hexadecanoic, octadecanoic, and eicosanoic acids;

methyl esters of unsaturated carboxylic acids: hexadec-7-enoic, hexadec-8-enoic, and octadec-8-enoic acids;

dimethyl esters of saturated dicarboxylic acids: octanedioic and nonanedioic acids;

esters of fused aromatic acids (methyl 1-phenanthrenecarboxylate).

Thus, OMSR from the Zazhogino Deposit of Karelian Transonega region is a complex multicomponent mixture of aliphatic, hydroaromatic, aromatic, and heterocyclic compounds. It consists of saturated, unsaturated, and aromatic acids, alcohols, ketones, ethers, esters, phenols, derivatives of pyrrole, indole, thiophene, and furan, alkaloids and steroids, and organometallic complexes.

CONCLUSIONS

(1) The structural features of the mobile phase of the organic matter of schungite rock form the Zazhogino Deposit of Karelian Transonega region were studied in detail for the first time by modern physicochemical methods including elemental analysis, emission spectral analysis, atomic absorption and X-ray

fluorescence spectroscopy, quantitative analysis of functional groups, cryoscopy, Fourier IR and UV-Vis spectroscopy, gas chromatography-mass spectrometry, and sequential extraction with solvents of different polarities.

(2) The mobile phase consists mainly of long-chain alkanes, alkenes, hydroaromatic, aromatic, and heterocyclic compounds. The main functional groups are carboxy, keto, and phenolic groups. The main heterocyclic compounds present in the organic fraction are derivatives of pyrrole, indole, and acridine.

REFERENCES

1. Polevaya, M.A., *Shungit – volshebnyi kamen' zdorov'ya: Mineral'nye vody: Shungit: Sapropel'* (Schungite: A Magic Stone of Health: Mineral Water: Schungite: Sapropel), St. Petersburg: Ves', 2004, pp. 11–21.
2. Sidorov, L.N., Yurovskaya, M.A., et al., *Fullereny: Uchebnoe posobie* (Fullerenes: Textbook), Moscow: Ekzamen, 2005, p. 42.
3. Kalinin, Yu.K. Subbotina, T.I., Tuktamyshev, I.I., et al., *Shungit – kamen' zdorov'ya: Informatsionnyi listok* (Schungite: A Stone of Health: Information Sheet), Tula: Tul'skii Poligrafist, 2003, pp. 8–10.
4. Marzec, A. and Sobkowiak, M., *Erdol und Kohle-Ergas. Petrochemie*, 1981, vol. 34, no. 1, pp. 38–43.
5. Vahraman, M., *Fuel*, 1970, vol. 49, no. 1, pp. 5–16.
6. Imuta, K., *Report of the National Research Inst. for Pollution and Resources*, 1978, no. 10, pp. 1–122.
7. Yokoyama, S., Yamamoto, Y., and Takeya, G., *Menryo Kyokai Shi*, 1970, vol. 49, pp. 932–935.
8. Huston, J.L., Studier, M.H., and Scott, R.G., *Fuel*, 1974, vol. 53, no. 2, pp. 139–140.
9. Mironov, V.A. and Yankovskii, S.A., *Spektroskopiya v organicheskoi khimii* (Spectroscopy in Organic Chemistry), Moscow: Khimiya, 1985.
10. Nakanishi, K., *Infrared Absorption Apectroscopy*, Tokyo: Nankido, 1962.
11. Silverstein, R.M., Bassler, G.C., and Morrill, T.C., *Spectrometric Identification of Organic Compounds*, New York: Wiley, 1974.
12. Kazitsyna, L.A., and Kupletskaya, N.B., *Primenenie UF-, IR-, NMR- i mass-spektroskopii v organicheskoi khimii* (Use of UV, IR, NMR, and Mass Spectroscopy in Organic Chemistry), Moscow: Mosk. Gos. Univ., 1979.
13. Chapman, J.R., *Practical Organic Mass Spectrometry*, Chichester: Wiley, 1985.

ISSN 1070-4272, Russian Journal of Applied Chemistry, 2006, Vol. 79, No. 10, pp. 1588–1592. © Pleiades Publishing, Inc., 2006.
Original Russian Text © S.V. Krupin, E.S. Krivtsova, V.P. Barabanov, 2006, published in Zhurnal Prikladnoi Khimii, 2006, Vol. 79, No. 10, pp. 1608–1612.

SORPTION AND ION-EXCHANGE PROCESSES

Adsorption of Water-Soluble Polyelectrolytes of Varied Nature on Mineral Adsorbents

S. V. Krupin, E. S. Krivtsova, and V. P. Barabanov

Kazan State Technical University, Kazan, Tatarstan, Russia

Received March 29, 2006; in final form, May 16, 2006

Abstract—The adsorption behavior of water-soluble polyelectrolytes on mineral and synthetic adsorbents was analyzed. The effect of ionic strength, pH value, and hydrophobic interaction on the adsorption transfer of macrochains to the solid surface, determined by the conformation state of the macrochains and the electrokinetic potential of the adsorbent, was studied for model and industrial polyelectrolytes and adsorbents of varied acid-base nature.

DOI: 10.1134/S1070427206100053

The adsorption of macromolecular compounds from solutions on a solid surface underlies a number of technological processes (flocculation and purification of industrial wastewater, selective separation of disperse systems, structuring of soils, oil displacement, and restriction of water inflow in oil production) and plays an important role in the formation of properties of polymeric composite materials. In this context, the adsorption behavior of polyelectrolytes at a phase boundary is of independent scientific and practical interest [1].

The main goal of the present communication is to discuss the adsorption of industrial polyelectrolytes used in oil production to restrict the inflow of water and raise the extraction of oil from oil strata. Here, the principal factor is adsorption of polyelectrolytes from aqueous solutions by the porous bodies of a water-bearing stratum and an oil stratum strongly flooded in "secondary" extraction of oil by its displacement with water.

EXPERIMENTAL

As the closest models of industrial polyelectrolytes were used polyacids: polyacrylic, polymethacrylic, and polyfluoroacrylic.

Polyacid samples were obtained by preparative synthesis. Preparations of industrial copolymers (GIPAN, METASOL, and AMIFLOK) were produced from industrial samples reprecipitated from aqueous solutions with isopropanol and purified by dialysis. Selected parameters of the polyelectrolytes are listed in the table.

Parameters of the polyelectrolytes

Polyelectrolyte	pK_{char}	Hydrophobicity	$M \times 10^{-4}$, g mol^{-1}
Polyacrylic acid (PAA)	6.4	2	3.0
Polymethacrylic acid (PMAA)	7.0	3	4.2
Polyfluoroacrylic acid (PFAA)	3.2	0.5	4.2
Hydrolyzed polyacrylonitrile (GIPAN) MRTU (Interrepublican Technical Specifications) 6-01-166–67	6.5	2	5.3
Copolymer of methacrylamide with sodium methacrylate (METASOL) TU (Technical Specification) 6-01-1172–78	6.0	3	8.0
Copolymer of methacrylamide with diethylaminoethyl methacrylate (AMIFLOK) TU 6-01-1238–80	7.1	4.4	9.6

The adsorption behavior of the water-soluble polyelectrolytes mentioned above was analyzed using solid adsorbents of synthetic and mineral origin. The effect of the ionic strength of a solvent and hydrophobic interactions on the adsorption transfer of macrochains from aqueous solutions to a solid surface, determined by the conformation state of the macrochains, their surface activity, and the electric polarity of the adsorbent (dispersed phase of a complex colloid system), was studied for synthesized and industrial polyelectrolytes of varied acid-base nature.

As adsorbents served medium-dispersed and highly dispersed materials of varied colloid chemical nature: (1) quartz sand supplied to a glass-making plant, GOST (State Standard) 22551–77, composed of 98% silicon dioxide and 2% metal oxides (mostly iron and titanium), with a predominant particle size 0.25–0.075 mm (97%); (2) aerosil of A-175 brand, GOST 14022–77), specific surface area 175 ± 25 $m^2 g^{-1}$ (by BET); composition (%): silicon dioxide 99.9, titanium dioxide 0.03; average particle size 10–40 nm; electrokinetic potential at pH 3–8 in the range 0–70 mV; (3) pigments in the form of highly dispersed powders: TiO_2 (d = 0.2–0.80 μm), ZnS (d = 1–3 μm), $BaSO_4$ (d = 1–3 μm), and MgO; (4) microbiological cover glass degreased in solvents and steam-treated for 2 h.

The adsorption of polyelectrolytes was studied by interferometry [2]. The initial and equilibrium concentrations of dilute polyelectrolyte solutions were determined with an ITR-2 interferometer; the adsorption equilibrium was attained not later than in 72 h.

The free energy of adsorption of polyelectrolytes contains an electrostatic component (free energy of the electric double layer in adsorption of charged parts of a macrochain on a charged surface, dependent on polarization effects). Therefore, it has been shown [2–6] that the adsorption of water-soluble polyelectrolytes must depend on the charge density in the macrochain, surface charge density of the adsorbent, ionic strength and pH value of the solution, and acid-base nature of the polyelectrolyte and adsorbent.

A previous analysis of the adsorption isotherms of polybases, polyacids, and their copolymers [2, 7–10] has shown that, in a certain range of polyelectrolyte concentrations, the isotherms show "negative adsorption," which is due to competing adsorption of water and a polymer on the adsorbent surface. In this case, virtually no relaxation processes occur in water and it is capable of instantaneous orientation, with the appropriate end of its dipole facing the adsorbent surface. In addition, the adsorption of polybases on negatively charged surfaces obeys the Rebinder rule of polarity equalization and is described by a high affinity isotherm. At the same time, polymers with acid groups predominant in the macrochain diminish the adsorption from aqueous solutions. This occurs because the affinity of polyelectrolytes for water is enhanced as a result of an increase in the fraction of dissociated groups in macromolecules. The adsorption of polybases on silicon-containing adsorbents can be regarded as a reaction in which polymer-colloid complexes with the ionized surface of silicon dioxide are formed [11–14] or as chemisorption via formation of ionic bonds between the macromolecular coil and the matrix of silicon dioxide.

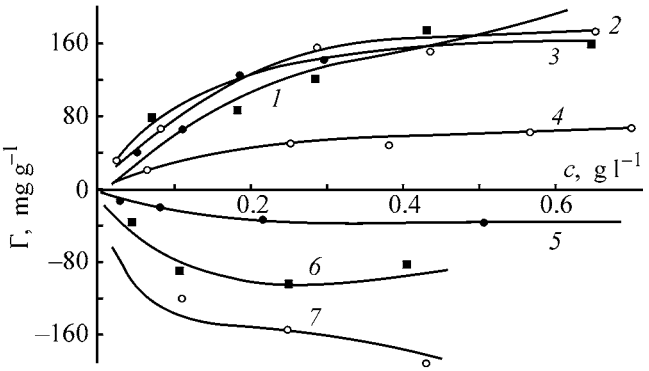


Fig. 1. Adsorption isotherms of (*1–3*) AMIFLOK and (*4–7*) GIPAN on adsorbents of varied nature. (Γ) Adsorption and (*c*) polyelectrolyte concentration; the same for Figs. 2–4. Adsorbent: (*1*) TiO_2, (*2*, *7*) MgO, (*3*, *5*) ZnS, (*6*) $BaSO_4$, and (*4*) anion-exchanger.

In view of the aforesaid, the adsorption of polyacids and polybases on various adsorbents of acid (oxides, sulfides) and basic (anion exchanger) nature was studied (Fig. 1). Here, the apparent factor is the leveling action of water on the nature of the "acid" adsorbents, which consists, in accordance with the Ken rule, in that a negative charge is imparted to the adsorbent. The role of ionic interactions is illustrated the most clearly by adsorption of hydrolyzed polyacrylonitrile on the anion exchanger, which has a basic nature in water.

In addition, it was found that the influence exerted by the electrostatic component on the interaction between a polyelectrolyte and an adsorbent is well manifested at various contents of carboxyl groups in the polyelectrolyte. Judging from the adsorption isotherms and from the wetting angles of polyelectrolyte

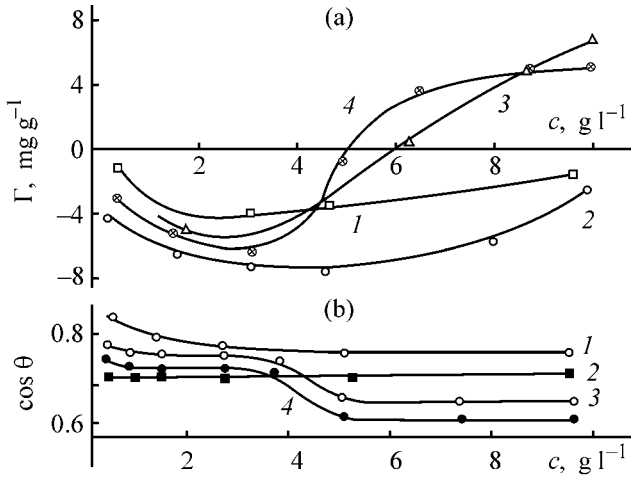


Fig. 2. Isotherms of (a) adsorption of GIPAN with varied content of carboxyl groups and (b) wetting of the glass surface. (cos θ) Cosine of the wetting angle of the polyelectrolyte on the surface. Adsorbent, quartz sand. Content of carboxyl groups (mol %): (*1*) 20, (*2*) 35, (*3*) 55, and (*4*) 67.

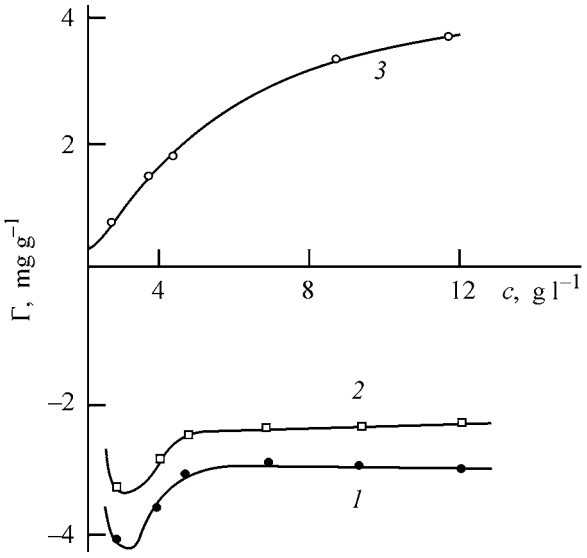


Fig. 3. Isotherms of adsorption of GIPAN with and without addition of iron(III) chloride on quartz sand. (*1*) In the absence of $FeCl_3$; in the presence of $FeCl_3$ at the following ratios with GIPAN: (*2*) 1 : 10 and (*3*) 1 : 2.

solutions on glass surfaces (Fig. 2), an increase in the number of carboxyl groups at a degree of hydrolysis exceeding 50% leads to the following: the ionic strength of the system grows, macrochains undergo coiling, and the adsorption becomes higher because of the counter-ionic binding, lower lyophylization of macrochains, and poorer wetting of the glass surface [16].

A study of the influence exerted by the concentration of triple-charged iron cations in solution on the adsorption of GIPAN from aqueous solutions on quartz sand demonstrated that the adsorption isotherm passes from negative to positive adsorption (Fig. 3). In order to assess the role of the structure of carboxyl-containing polyacids, the adsorption of polyacids was compared with that of industrial copolymers of acid type. In doing so, primary attention was focused on the relationship between the adsorption and the hydrophilic-hydrophobic balance in macromolecules, which is reflected in the value of the dissociation constant of acid groups and in the hydrophobicity of polychains [17]. The hydrophobicity is characterized by the ratio between the numbers of hydrophobic ($–CH_3$, $–CH_2–$, –CH=, –H–) and hydrophilic (–COOH, –COONa, $–CONH_2$) groups in a unit of the macromolecule. The necessary evidence is presented in the table.

The highest sensitivity to the hydrophilic-hydrophobic ratio was manifested in the adsorption azeotropy [2]. On passing from PAA to PMAA (Fig. 4) or to PFAA, the adsorption azeotropy in aqueous solutions disappears, but this occurs for different reasons: the isotherm of PFAA adsorption lies in the range of negative values, and that of PMAA adsorption, at positive values. Apparently, the large ionogenic capacity of PFAA, which can be judged from the characteristic dissociation constant pK_{char}, and the low hydrophobicity lead to a more pronounced repulsion of PFAA macroions and to negative charging of the surface of pyrogenic silicon dioxide (aerosil A-175). At the same concentration of adsorption centers on the adsorbent, this predetermines the considerably lower adsorption of PFAA, compared with PAA. In addition, the nature of the isotherm of PFAA adsorption can be accounted for by the increased energy of hydrogen bonding between the fluorine atoms of the polyacid and the hydrogen of water (about 42 kJ mol^{-1} [15]), which hinders adsorption of PFAA on aerosil.

The differences in the adsorption behavior of PMAA and PAA on aerosil cannot be accounted for by differences in the ionization of macromolecules at identical constants of electrolytic dissociation. However, the fact that the adsorption isotherm is of a high-affinity type for PMAA in the case of like charges of the adsorbate and adsorbent can be only due to the presence of a strong hydrophobic component in macromolecular coils of PMAA, which leads to a more compact conformation of macrocoils and to an increase in its adsorption. The similar relationship between the adsorption isotherms of GIPAN and METASOL also confirms the assumption made. The hydrophobic

nature of interaction in adsorbed layers of PMAA, MAA–MMA (copolymer of methacrylic acid with methyl methacrylate), and mixed adsorbed layers of polyacids with a surfactant is indicated by the relatively low activation energies of breakdown of these interactions, equal to several kilojoules per mole and comparable with the energy necessary for rupture of a small number of noncovalent bonds [16, 17].

The effect of hydrophobicity on the adsorption can also be judged from the amount of limiting adsorption and from the degree of filling of the adsorbent surface. The limiting adsorption of PAA on aerosil, equal to 63 mg g^{-1}, is reached at a concentration c_{eq} = 0.7 g/100 cm^3. The calculated value of the limiting adsorption in the case of formation of a monomolecular layer for PAA was 142 mg g^{-1}, whence follows that the degree of surface filling by PAA macromolecules is 0.45. A comparison of the experimental and calculated values of the limiting adsorption for PAA, equal to 82 and 168 mg g^{-1}, respectively, made it possible to evaluate the degree of surface filling to be 0.51. Comparison of the degrees of filling and values of the limiting adsorption of PAA and PMAA points to a higher surface activity of PMAA and higher density of filling of its surface, which is due to the hydrophobic interaction.

The calculated limiting adsorption was found using the formula

$$\Gamma_\infty = \frac{MS_{sp}}{\pi R_s^2 N_A},$$

where M is the molecular weight of the polymer (g mol^{-1}); S_{sp}, specific surface area of the adsorbent (175 m^2 g^{-1} for aerosil); R_s, macrocoil radius (m); and N_A, Avogadro number.

The macrocoil radius R_s was found from the root-mean-square distance between macrocoil ends $(h^{-2})^{1/2}$, using the relation $R_s = 0.36(h^{-2})^{1/2}$. In turn, the value of $(h^{-2})^{1/2}$ was calculated by the formula

$$(h^{-2})^{1/2} = (K_0/\Phi_0)^{1/2} M^{1/2},$$

where Φ_0 is the Flory coefficient equal to 2.84×10^{23} mol^{-1}. Because, according to published data [18], K_0 for PAA and PMAA is 1×10^{-3} and 0.6×10^{-3}, respectively, the macrocoil radius was found to be 4.4 and 4.8 nm.

CONCLUSIONS

(1) The enhancement of the ionization capacity of a polyacid results in the predominance of Coulomb repulsion forces, which hinders the adsorption of the polyacid on the like-charged surface, whereas the hydrophobic interaction in polyelectrolyte molecules favors a more compact conformation of macrochains, lessens the effectiveness of the Coulomb repulsion, and leads to an increase in the adsorption of polyelectrolytes on a like-charged surface.

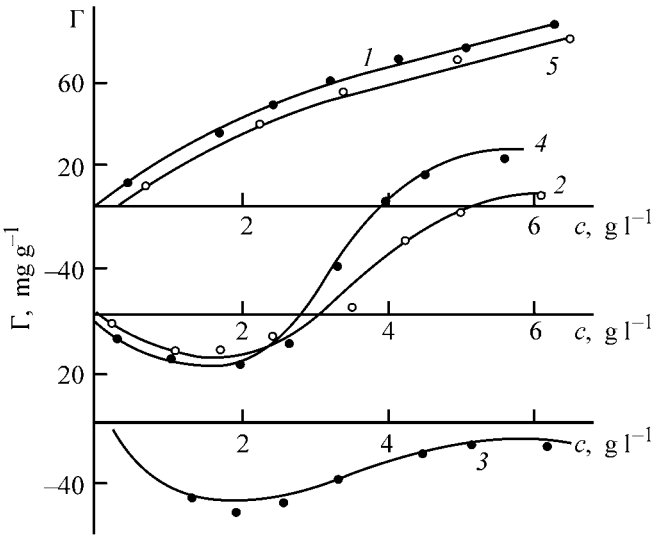


Fig. 4. Isotherms of adsorption of (*1*) PMAA, (*2*) PAA, (*3*) PFAA, (*4*) GIPAN, and (*5*) METASOL from aqueous solutions on aerosil.

(2) Analysis of experimental data on adsorption of industrial polyelectrolytes and of polymeric acids or polybases, which are, respectively, closely similar or antagonistic to the polyelectrolytes both in structure and acid-base properties and in principal characteristics, suggests that it is most advantageous to use copolymers with a sufficiently high hydrophobicity and basicity to restrict the inflow of water in oil wells.

(3) METASOL and AMFILOK should be recognized as best satisfying the requirements imposed, because they have the highest hydrophobicity; in addition, being a polybase salt, AMFILOK can compete for ionic bonding with the electrostatically negative matrix of oil-containing rock.

REFERENCES

1. Muslimov, R.Kh., *Sovremennye metody povysheniya nefteizvlecheniya, proektirovanie, optimizatsiya i otsenka effektivnosti* (Modern Ways To Improve Oil Extraction: Designing, Optimization, and Efficiency Assessment), Kazan: Fen, 2005.
2. Barabanov, V.P., Krupin, S.V., and Shaidullin, K.Sh., *Kolloid. Zh.*, 1981, vol. 43, no. 3, pp. 551–553.

3. Hesselink, F.T., *Adsorption from Solution at the Solid/Liquid Interface*, Parfitt, G.D. and Rochester, C.H., Eds., New York: Academic, 1983. Translated under the title: *Adsorbtsiya polielektrolitov iz razbavlennogo rastvora: Adsorbtsiya iz rastvorov na poverkhnosti verdykh tel*, Moscow: Mir, 1963, pp. 435–473.
4. Lyklema, J.J., Fleer, G.J., and Scheutjens, J.M.H.M., *Kolloid. Zh.*, 1987, vol. 49, no. 2, pp. 211–216.
5. Frich, H. and Stillinger, F., *J. Phys. Chem.*, 1962, vol. 66, no. 5, pp. 823 – 830
6. Hesselink, F.T., *J. Colloid Interface Sci.*, 1977, vol. 60, no. 3, pp. 448 – 466.
7. Sharifullin, I.L., Krupin, S.V., and Barabanov, V.P., *Kolloid. Zh.*, 1986, no. 2, pp. 383 –386.
8. Krupin, S.V., Sharifullin, I.L., Sidorov, I.A., and Savina, T.R., *Zh. Prikl. Khim.*, 1987, vol. 40, no. 9, pp. 2134 –2137.
9. Krupin, S.V., Polovnyak, V.K., Barabanov, V.P., and Sharifullin, I.L., *Zh. Prikl. Khim.*, 1987, vol. 40, no. 10, pp. 2316 –2321.
10. Sharifullin, I.L., Krupin, S.V., and Barabanov, V.P., *Available from ONIITEKhIM*, 1984, Cherkassy, no. 763 khp 184.
11. Shaidullin, K.Sh., Krupin, S.V., and Barabanov, V.P., Bibliogr. *Ukazatel' "Deponirovannye rukopisi"* (Bibliographic Index "Deposited Manuscripts"), 1980, no. 11, p. 94: Bibliography: 5 Titles Available from NIITEKhIM, 1980, Cherkassy, no. 691 khp D80.
12. Barabanov, V.P., Krupin, S.V., Shaidullin, K.Sh., and Danilova, S.A., Abstracts of Papers, *XII Mendeleevskii s"ezda po obshchei i prikladnoi khimii* (XII Mendeleev Congress on General and Applied Chemistry), Moscow: Nauka, 1981, p. 152.
13. Frolov, Yu.G., Krivoshchepov, A.F., and Samoilova, L.I., *Uspekhi kolloidnoi khimii* (Advances in Colloid Chemistry), Tashkent: Fan, 1987, pp. 199 –214.
14. Samuilova, L.V., Structuring in Highly Concentrated Suspensions of Quartz with a Silica Hydrosol and Polyelectrolytes, *Cand. Sci. Dissertation*, Moscow, 1985.
15. Karapet'yants, M.Kh. and Drakin, S.I., *Stroenie veshchestva* (Structure of Substances), Moscow: Vysshaya Shkola, 1970.
16. Izmailova, V.N., Nefedova, E.N. Tulovskaya, Z.D., and Yampol'skaya, G.P., *Kolloid. Zh.*, 1981, vol. 43, no. 1, pp. 161–164.
17. Musabekov, K.B., Zhubanov, B.A., Izmailova, V.N., and Summ, B.D., *Mezhfaznye sloi polielektrolitov* (Interphase Layers of Electrolytes), Alma-Ata: Nauka, 1987.
18. Bekturov, E.A. and Bakauova, Z.Kh., *Sinteticheskie vodorastvorimye polimery v rastvorakh* (Synthetic Water-Soluble Polymers in Solutions), Alma-Ata: Nauka, 1981.

ISSN 1070-4272, Russian Journal of Applied Chemistry, 2006, Vol. 79, No. 10, pp. 1593–1599. © Pleiades Publishing, Inc., 2006.
Original Russian Text © G.R. Anpilogova, A.I. Vorob'eva, S.A. Onina, R.A. Khisamutdinov, Yu.I. Murinov, Yu.B. Monakov, 2006, published in Zhurnal Prikladnoi Khimii, 2006, Vol. 79, No. 10, pp. 1613–1620.

SORPTION AND ION-EXCHANGE PROCESSES

Vinyl 2-Hydroxyethyl Sulfide Polymers and Their Sorption Properties with Respect to Transition Metals

G. R. Anpilogova, A. I. Vorob'eva, S. A. Onina, R. A. Khisamutdinov, Yu. I. Murinov, and Yu. B. Monakov

Institute of Organic Chemistry, Ufa Scientific Center, Russian Academy of Sciences, Ufa, Bashkortostan, Russia

Received May 30, 2006

Abstract—Vinyl 2-hydroxyethyl sulfide (VHES) homopolymer and the homopolymer and vinyl 2-hydroxyethyl sulfide-acryl amide copolymer cross-linked by bisacrylamide were prepared by radical polymerization. The sorption of Au(III), Ag(I), Pd(II), Pt(IV), Hg(II), Pb(II), Fe(III), Ni(II), Cu(II) on these polymers under the static conditions was studied in relation to the solution pH. The polymers are highly selective and efficient sorbents for Au(III), Ag(I) and Hg(II).

DOI: 10.1134/S1070427206100065

Vinyl 2-hydroxyethyl sulfide (VHES), as well as alklyl vinyl sulfides [1], is a promising monomer for directed synthesis of functionalized polymers [2–4]. This monomer can be selectively prepared in high yield by the procedure described in [5, 6]. Radical copolymerization of VHES with acrylic monomers [2], *N*,*N*-dimethyl-*N*,*N*-diallylammonium chloride [3], and *N*-vinylpyrrolidone [4] in the presence of azobis(isobutyronitrile) (AIBN) has been studied. Simple procedures for preparing these copolymers have been developed. The copolymers consist of randomly distributed monomeric units and are soluble in water or acid aqueous solution.

It is known [7–11] that complexing sorbents containing dialkyl sulfide and alkyl 2-hydroxyethyl sulfide functional groups selectively sorb Au(III), Pd(II), and Pt(IV) from hydrochloric acid solutions Ag(I) and Pd(II) from nitric acid solutions and Hg(II) from nitric and hydrochloric acid solutions at room temperature. Hydrophilic sorbents with primary amide groups effectively and selectively sorb Hg(II) from hydrochloric and acetic acid solutions [12–14]. Therefore, preparation of VHES polymers insoluble in water and study of their sorption properties with respect to *d* metals are of interest.

The aim of this study was to prepare water-insoluble VHES homopolymer, VHES homopolymer cross-linked by *N*,*N*-methylenebisacrylamide, and VHES–acrylamide (AA) copolymer cross-linked by *N*,*N*-methylenebisacrylamide and to examine their sorption properties with respect to nonferrous, heavy, and noble metals.

EXPERIMENTAL

Vinyl 2-hydroxyethyl sulfide was prepared by vinylation of 2-mercaptoethanol with acetylene by the procedure described in [5]; bp 74–75°C (9 mm Hg), n_D^{20} 1.5220, d_4^{20} 1.0612. The purity of the monomer was determined by GLC, and by IR and NMR spectroscopy [2]. The properties of all the monomers, AIBN, and solvents purified by the conventional procedures were consistent with published data.

Our preliminary experiments showed that VHES readily polymerizes in the presence of AIBN both in the bulk and in a DMSO solution, with the polymerization being fast (up to 20% per hour) and proceeding to deep (about 70%) conversion.

VHES homopolymer (Table 1, polymer no. 1), VHES homopolymer cross-linked by *N*,*N*-methylenebisacrylamide (bis-AA) (no. 2), and VHES–acrylamide (AA) copolymer cross-linked by bis-AA (no. 3) were prepared by radical polymerization in the bulk (no. 1) or in solution (nos. 2, 3) under a reduced pressure in the presence of AIBN as an initiator. The total monomer concentration in the initial solu-

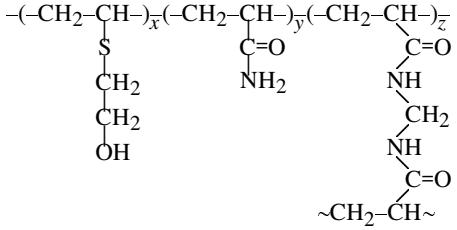
Table 1. Preparation conditions of PVHES and cross-linked PVHES and VHES–acrylamide copolymer

Polymer no.	Composition of the initial monomer mixtures, mol % (wt %)			Solvent	c_{AIBN}, wt %	T, °C	τ, h	Yield, %
	VHES	AA	bis-AA					
1	100	–	–	In the bulk	1.5	70	4.5	71
2	93.02	–	6.98 (10.0)	Acetone	1.0	80	5.0	61
3	35.33	57.88	6.79 (11.8)	DMSO	0.01	60	4.8	72

Table 2. Composition, limiting static sorption capacity for Ag(I), and thermal stability of polymers

Polymer no.	Mole fraction of monomeric units in polymer*			E^S, (mg-atom) g^{-1}	$LSSC^{Ag}$, mmol g^{-1}	T_{do}, °C
	VHES, x	AA, y	bis-AA, z			
1	1.00	–	–	9.37	8.86**	270
2	0.84	–	0.16	7.43	6.70	255
3	0.35	0.53	0.12	3.79	3.75	252

* Monomeric units:



** The limiting static sorption capacity (LSSC) of PVHES for Ag(I) was measured at $[HNO_3]$ = 1 M.

tions used to prepare polymers 2 and 3 was 50 and 35%, respectively. Polyvinyl 2-hydroxyethyl sulfide (PVHES) was precipitated three times from a methanol solution with acetone; the cross-linked polymers were washed three times with acetone and then with water and acetone. The purified polymers were dried in a vacuum at 50°C to constant weight. The weight yield of the polymers was determined (Table 1). The composition of the polymers and the content of sulfide groups ES (Table 2) were calculated from the results of elemental analysis.

The thermal stability of the polymers was studied in air by thermal analysis on an MOM Q-1500D derivatograph (Hungary) operating in the dynamic mode. The heating rate was 5 deg min^{-1}. Al_2O_3 was used as reference. The intrinsic viscosity [η] of the homopolymer was measured in DMSO on a Ubbelohde viscometer at 25°C. The IR spectra of the polymers were recorded on a Specord M 80 spectrometer (4000 – 400 cm^{-1}, Nujol).

The metal sorption was studied by the static procedure at the initial concentration of metal ions c_0^M = 0.0050 ± 0.0002 M, room temperature 20 ± 1°C, and vigorous agitation (WL-1 bench shaker). The sorption of Ag(I) was studied in the dark. The LSSC of the polymers for Ag(I) and Hg(II) was determined in 0.1 M HNO_3 at c_0^M = 0.49 and 0.10 M, respectively, at s : l = 1 : 100. The experiments were performed with intermittent agitation for τ = 10 days.

Solutions of metal salts were prepared by dissolution of weighed portions of $CuCl_2 \cdot 2H_2O$, $AgNO_3$, $Hg(NO_3)_2$ (analytically pure grade); $NiCl_2 \cdot 6H_2O$ (chemically pure grade); $FeCl_3 \cdot 6H_2O$, $Pb(NO_3)_2$, $PdCl_2$, $H_2PtCl_6 \cdot {}_6H_2O$ (pure grade) in HCl or HNO_3 solutions of required concentrations. Acetate solutions of Hg(II) were prepared by dilution of 0.10 M $Hg(NO_3)_2$ solution in 0.1 M HNO_3 in the presence of definite amounts of acetic acid and (or) sodium acetate. The pH of weakly acidic solutions was measured on a bench digital OP-211/1 pH meter with a combined glass electrode. The concentration of Ni(II), Cu(II), Pb(II), Pt(IV), and Ag(I) in the solutions was determined by atomic absorption spectroscopy on a Hitachi 506 spectrophotometer; the Pd(II) concen-

tration, by the spectrophotometic procedure using tin chloride [15]; Fe(III) concentration, by the spectrophotometric procedure using KCNS [16] on a Specord spectrophotometer; and the Hg(II) concentration, by the Volhard method [17]. The static sorption capacity was calculated as difference between the metal concentrations in the solution before and after sorption with an error no more than 5%.

The polymers consist of small (1) colorless or (2, 3) white irregular-shaped particles. The elemental analysis of the homopolymer is fairly consistent with the theoretical composition.

Found, %: C 45.91, H 7.76, S 30.04.
Calculated, %: C 46.11, H 7.76, S 30.77.

The atactic structure of the polymer follows from its ^{13}C NMR spectrum [2]. The intrinsic viscosity ($[\eta] = 0.3$ dl g^{-1}) of PVHES suggests its relatively high molecular weight. PVHES is soluble in DMSO, DMF, methanol, and also in concentrated HNO_3 (with decomposition) and HCl. The polymer is insoluble in acetone, ethanol, THF, chlorinated hydrocarbons, benzene, and water, and moderately concentrated HCl (≤5 M) and HNO_3. PVHES is a film-forming compound. It readily swells in aqueous solutions and exhibits a significant adhesion to glass. Its particles readily agglutinate owing to the high density of OH groups forming hydrogen bonds. The adhesion and film-forming properties of PVHES allow its application for preparing surface-layered sorbents with the silica gel or glass inert core.

We found that introduction of 10 wt % cross-linking agent (bis-AA) into the monomer mixture is sufficient for preparing a polymer free of the disadvantages of PVHES. Polymer nos. 2 and 3 (Table 1) exhibit no adhesion and cohesion properties and moderately swell in aqueous solutions.

The presence of the comonomeric units in the structure of the cross-linked polymers was confirmed by elemental analysis and IR spectroscopy. The IR spectra of the polymers were assigned according to [18]. A broad medium-intensity band with a complex shape at 3304 cm^{-1} in the spectrum of polymer no. 2 is due to stretching vibrations of the O–H bonds of ethanol and N–H bonds of secondary amide groups bound with hydrogen bonds. In the spectrum of polymer no. 3, this band is observed at 3320 cm^{-1} and is more intense owing to the contribution of ν_{as}(NH) vibration of the primary amide groups; the band at 3192 cm^{-1} is assigned to ν_s(NH) of the primary amide groups associated with hydrogen bonds. The moderate amide I band at 1650–1648 cm^{-1} and the less intense amide II band of the secondary amide groups of the cross-link at 1532–1520 cm^{-1} are observed in the spectra of polymer nos. 2 and 3. The strong amide I band at 1676 cm^{-1} and less intense amide II band as a shoulder at 1616 cm^{-1} are present in the spectrum of polymer no. 3. The weak amide III band of secondary amide groups at 1284 cm^{-1} and medium-intensity ν(C–O) band of primary alcoholic groups at 1048–1044 cm^{-1} are observed in the spectra of polymer nos. 2 and 3.

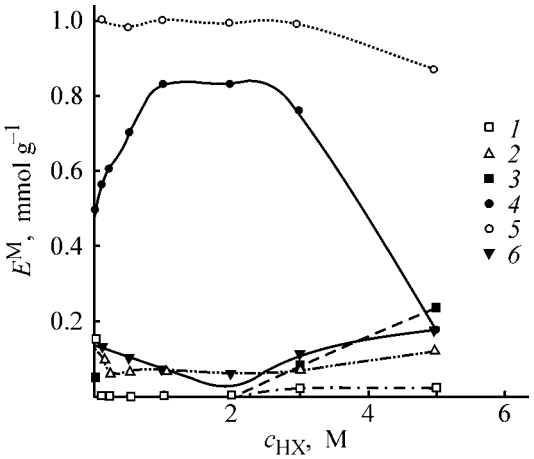


Fig. 1. Sorption capacity E^M of poly(vinyl 2-hydroxyethyl sulfide) for (*1*) Fe(III), (*2*) Pd(II), (*3*) Cu(II), (*4*) Ag(I), (*5*) Au(III), and (*6*) Pt(IV) vs. the concentration c_{HX} of nitric [Ag(I)] or hydrochloric acid.

The application field of the cross-linked polymers is restricted by the resistance of the bisacrylamide cross-link to hydrolysis (pH 1–11 [19]). The onset temperature of intense decomposition T_{do} of cross-linked polymers is somewhat lower than that of the homopolymer (Table 2).

Our preliminary experiments showed that the equilibrium sorption of Cu(II), Fe(III), Ni(II), and Pb(II) and pseudoequilibrium sorption of Pt(IV) on the homopolymer at pH ≥ 1 are attained within no more than 1–2 h. The equilibrium sorption of Pd(II) is reached in more than 24 h. We studied the sorption properties of PVHES with respect to metal ions in related to the acidity of the initial solution. At room temperature, Au(III) and Ag(I) are quantitatively sorbed with high distribution coefficients from solutions with acid concentrations lying in the range 0.1–5 M. However, Pd(II) and Pt(IV) are sorbed less effectively under these conditions. Base metals are sorbed with low distribution coefficients at pH 1, and Cu(II) and Fe(III) at $c_{HCl} \geq 3$ M (Fig. 1, Table 3). The negligible sorption of Cu(II) and Fe(III) in this range is probably due to anion exchange of anionic

Table 3. Degree of recovery and distribution coefficients of metal ions at s : l = 1 : 200 and τ = 4 h

Polymer no.	Metal ion	Acid concentration, M; pH	Recovered, %	K_d, ml g^{-1}
1	Au(III)	0.1–5 HCl	100–86.5	∞–1281
	Ag(I)	1–2 HNO_3	83.0	1000
	Pd(II)	0.1 HCl	9.8	22
	Pt(IV)	0.1 HCl	13.2	30
	Cu(II)	pH 4.31	4.8	10
		3 HCl	8.0	18
		5 HCl	23.3	61
	Fe(III)	pH 2.53	15.5	37
		3–5 HCl	4.0	4
	Ni(II)	pH 5.01	8.3	18
		0.1 HCl	2.0	4
	Pb(II)	pH 4.23	13.7	32
		0.1 HNO_3	5.5	12
2	Au(III)	0.1 HCl	99.0	19 800
	Pd(II)	0.1 HCl	98.3	11 606
	Fe(III)	pH 2.53	10.0	22
		0.1 HCl	6.6	7
	Hg(II)	pH 1.52 (HNO_3)	90.5	1913
3	Au(III)	0.1 HCl	98.4	12 000
	Pd(II)	0.1 HCl	45.6	168
	Pt(IV)	0.1 HCl	50.0	200
	Cu(II)	pH 4.67	9.4	21
		pH 2.89	15.6	37
		0.1 HCl	9.9	22
	Fe(III)	pH 2.53	10.0	22
		0.1 HCl	4.1	9
	Hg(II)	pH 1.52 (HNO_3)	45.6	167

complexes $[CuCl_4]^{2-}$ and $[FeCl_4]^-$ on partially protonated sulfide groups of the polymer [20]. The yellow color of the Cu(II) and Fe(III) complexes sorbed from strongly acidic solutions is typical of the anionic complexes of these metals [21]. The higher sorption of Cu(II), compared to that of Fe(III), is caused by electroselective anion exchange of differently charged anions $[CuCl_4]^{2-}$ and $[FeCl_4]^-$ in solutions dilute with respect to the metal ion [22].

The dependence of the sorption capacity of PVHES for Ag(I) on the HNO_3 concentration (Fig. 1) is typical of sorbents containing dialkyl sulfide functional groups reacting with Ag(I) by the following scheme:

$$-CH_2-CH- + Ag^+ + NO_3^- \rightleftarrows -CH_2-CH-$$
$$\quad\quad\quad

This assumption is indirectly confirmed by an increase in the pH of the solution to 2.64 after Ag(I) sorption from 0.05 M $AgNO_3$ at pH_0 4.65, s : l = 1 : 100 for τ = 6 days. It should be noted that pH of water (5.66) does not change after contact with the sorbent under the similar conditions.

The substantial decrease in E^{Ag} at the HNO_3 concentration exceeding 2 M (Fig. 1) is due to partial oxidation of the sulfide groups to the sulfoxide groups forming weaker complexes with Ag(I) [7]. The resistance of the sulfide groups of PVHES to oxidation with HNO_3 is somewhat higher than that of linear poly(methylene monosulfide) and styrene-divinylbenzene sorbent with grafted dialkyl sulfide groups ($c \le 1$ M HNO_3) [11, 23], which is probably due to steric hindrances caused by branching of the alkyl radical in the α-position with respect to the S atom [7].

The $LSSC^{Ag}$ of PVHES is significantly higher than that of known sorbents with lower content of sulfide groups, e.g. polyhydroxymacrothiacyclane (5.33 mmol g^{-1} [7]), and sorbents with grafted sulfide groups [23]. The $LSSC^{Ag}$ decreases in the order no. 1 > no. 2 > no. 3 in accordance with the decrease in the content of the sulfide groups E^S (Table 2).

The sorption of Pd(II) on the homopolymer and sorbent no. 3 is comparable with that of Pt(IV) (Fig. 1, Table 3). By contrast, the sorption capacity for Pd(II) of the known sorbents containing dialkyl sulfide groups and having no branching in the α-position with respect to the S atom [7, 9] and of nonbranched dialkyl sulfides [8, 20] at room temperature is significantly higher than that for Pt(IV). This is probably due to the steric effect of the α-branched hydrocarbon radical on the kinetics of Pd(II) sorption. The E^{Pt} of PVHES remains constant (0.14 mmol g^{-1}) and E^{Pd} increases from 0.11 to 0.42 mmol g^{-1} with the sorption time increasing from 2 to 6 h at c_0^M = 0.010 M, [HCl] = 0.1 M, and s : l = 1 : 200. It is known that square planar complexes $[PdCl_4]^{2-}$ react with low-molecular-weight dialkyl sulfides by the association mechanism of ligand exchange. The kinetics of association reactions is very sensitive to steric hindrances. The reaction of $[PdCl_4]^{2-}$ with α-branched dialkyl sulfides is substantially decelerated [7]. Reactions of ligand substitution in octahedral $[PtCl_6]^{2-}$ ions occur by the dissociation mechanism. In this case, the α-branching of the radical has virtually no effect on the complexation rate [7]. Hence, the time required for attainment of the equilibrium Pt(IV) sorption and E^{Pt} for this sorbent are comparable with those for Pt(IV) sorption on poly(ethylene monosulfide) from weakly acidic solutions with the same Pt(IV) concentration at low temperatures (E^{Pt} = 0.15 mmol g^{-1}, 30°C) [24]. Association of the alcoholic groups by interchain hydrogen bonds probably produces additional steric hindrance, since a decrease in the concentration of interchain hydrogen bonds owing to the cross-linking leads to increase in the efficiency of sorption recovery of Pd(II) and Pt(IV), with K_d remaining about the same (Table 3, polymer nos. 2, 3).

Table 4. Sorption properties of polymer nos. 2 and 3 with respect to Hg(II)

Polymer no.	$LSSC^{Hg}$, mmol g^{-1}	$LSSC^{Hg} : E^S$	E^{Hg}, mmol g^{-1}, in CH_3COONa solution, M	
			0.1	1.0
2	3.80	1 : 1.95	1.80	1.52
3	2.01	1 : 1.89	1.38	0.94

The distribution coefficients of Au(III), Pd(II), and Pt(IV) between polymer nos. 2 and 3 and hydrochloric acid solutions are high. These metals can be selectively separated from Cu(II) and Fe(III) which are sorbed insignificantly. The efficiency of Hg(II) recovery from nitric acid solutions by sorption on the cross-linked polymers is comparable with that of Pd(II) recovery from a hydrochloric acid solution (Table 3).

We studied Hg(II) sorption from nitrate and acetate solutions on the cross-linked polymers at s : l = 1 : 600, particle size of the sorbent d = 0.020–0.0315 cm (Fig. 2), agitation rate of 400 rockings/min, and sorption time of 24 h (Table 4, Figs. 3, 4).

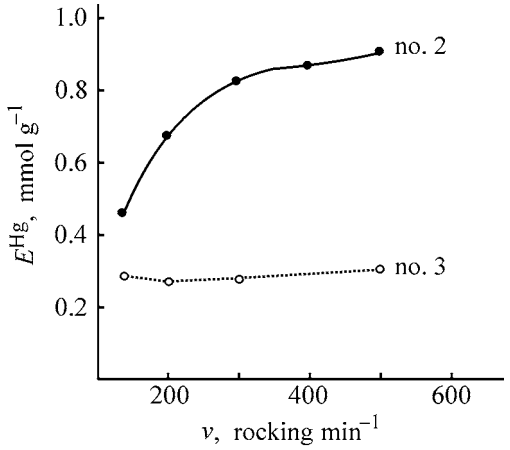


Fig. 2. Sorption capacity E^{Hg} of polymer nos. 2 and 3 at pH 1.52 (HNO_3) and τ = 30 min vs. the agitation rate ν.

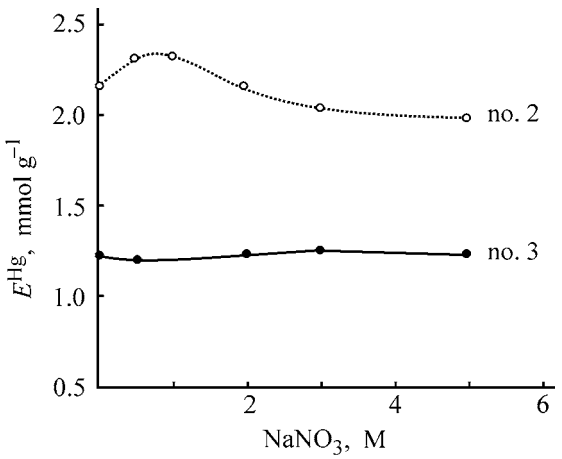


Fig. 3. Sorption capacity E^{Hg} of polymer nos. 2 and 3 in 0.01 M HNO_3 vs. the $NaNO_3$ concentration.

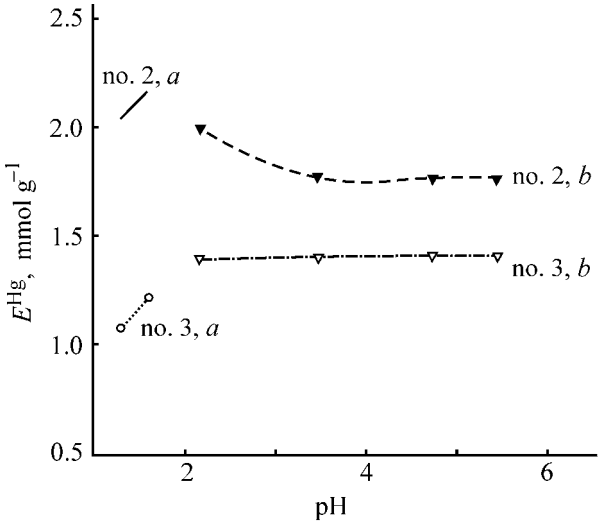


Fig. 4. Sorption capacity E^{Hg} of polymer nos. 2 and 3 in (*a*) nitrate and (*b*) 0.1 M acetate buffer vs. pH.

The rate of Hg(II) sorption from a nitrate solution on polymer no. 2 is controlled by internal diffusion even at high agitation rates (Fig. 2). The fact that the rate of Hg(II) sorption on polymer no. 3 is independent of the stirring rate (Fig. 2) suggests that the external diffusion has no effect on the rate of Hg(II) recovery. The time required for attainment of the equilibrium Hg(II) sorption from a nitrate solution at pH 1.52 on polymer nos. 2 and 3 is τ_e = 1.3 and 1.4 days, respectively; the half-time of the equilibrium sorption is $\tau_{0.5}$ = 1.5 and 5 h, respectively. The τ_e and $\tau_{0.5}$ for polymer no. 3 at s : l = 1 : 200 decrease to 24 and 2 h, respectively. This fact indirectly suggests high diffusion resistance of the polymer layer containing metal complexes.

The efficiency of Hg(II) recovery from nitrate and acetate solutions and the $LSSC^{Hg}$ are higher for polymer no. 2 (Tables 3, 4; Figs. 3, 4) with higher content of thioether groups E^S (Table 2). The $LSSC^{Hg} : E^S$ ratio for polymer nos. 2 and 3 (Table 4) suggests formation of sorption complexes with Hg : S = 1 : 2 under the saturation conditions. Based on this data, we suggested the following mechanism of sorption of cationic Hg(II) species prevailing in nitric acid solutions at pH 1–2 [25]:

$$2R_1SR_2 + Hg^{2+} + 2NO_3^- \rightarrow Hg(R_1SR_2)_2(NO_3)_2.$$

As in the case of Hg(II) extraction with thioethers [26], high concentrations of weakly coordinating anion NO_3^- insignificantly affect the efficiency of Hg(II) recovery with the cross-linked polymers from nitric acid solutions (Fig. 3). When the concentration of acetate ions forming relatively strong complexes with Hg(II) substantially increases, the efficiency of Hg(II) recovery decreases owing to the competing formation of anionic complexes $Hg(CH_3COO)_3^-$ and $Hg(CH_3COO)_4^{2-}$ in the solution. A similar trend was observed with the chloride concentration increasing in the course of Hg(II) extraction with thioethers from hydrochloric acid solutions [27]. This effect can be used, e.g., to desorb Hg(II) with a hot concentrated solution of CH_3COOH which does not induce hydrolysis of the amide bonds [12–14].

The fact that the efficiency of the Hg(II) sorption by cross-linked polymers at a constant ionic strength (0.1 M acetate buffer) is independent of pH in the range examined (Fig. 4, curves no. 2, *b*, no. 3, *b*) confirms the coordination of the sulfide groups to the metals. The slight decrease in the sorption capacity of polymer no. 2 for Hg(II) in going from nitrate to acetate solutions is due to the formation of acetate complexes of Hg(II) in the solution (Fig. 4, curves no. 2, *a*, no. 2, *b*). An increase in the sorption capacity of polymer no. 3 with increasing pH in going to the acetate solutions (curves no. 3, *a*, no. 3, *b*) suggests that the primary amide groups partially form Hg(II) complexes by the mechanism similar to that of Hg(II) sorption by cross-linked polyamide sorbents from acetate solutions at pH 2.6–6.2 [12, 13]:

$$n\mathrm{RC(O)NH_2} + \mathrm{Hg(CH_3COO)_2} \rightleftarrows (\mathrm{RC(O)NH})_n\mathrm{Hg(CH_3COO)_{2-n}} + n\mathrm{CH_3COOH},$$

where n = 1, 2.

CONCLUSIONS

(1) High-molecular-weight VHES homopolymer and the homopolymer and vinyl 2-hydroxyethyl sul-

fide–acryl amide copolymer cross-linked by bis-AA were prepared by radical polymerization. The polymers selectively sorb noble metal ions and Hg(II).

(2) The homopolymer is a highly efficient sorbent for Au(III) in hydrochloric acid solutions and for Ag(I) in nitric acid solutions. The low sorption capacity of the homopolymer for Pd(II) is probably due to the influence exerted on the kinetics of Pd(II) sorption by the steric hindrances caused by α-branching of the hydrocarbon radical and by the high concentration of the alcoholic groups associated by interchain hydrogen bonds. Silver(I) can be completely separated from Pb(II) at $c_{HNO_3} > 0.1$–5 M; Au(III), Pd(II), Pt(IV) can be selectively separated from Ni(II) at $c_{HCl} = 0.1$–5 M and from Cu(II) and Fe(III) at $c_{HCl} = 0.1$–3 M.

(3) In nitric acid solutions, Ag(I) reacts with the thioether groups of PVHES to form a sorption complex of the composition $Ag : S : NO_3^- = 1 : 1 : 1$ under the saturation conditions. Formation of Ag(I) chelates with alkyl 2-hydroxyethyl sulfide groups of polymer nos. 1–3 in 0.1 M HNO_3 is possible.

(4) The cross-linked polymers effectively sorb cationic Hg(II) species from nitric acid solutions with pH 1–1.6 to form the $Hg : S = 1 : 2$ sorption complexes with the thioether groups under the saturation conditions. A high $NaNO_3$ concentration and high acidity (pH 2.2–5.5) of 0.1 M acetate buffer have virtually no effect on the Hg(II) sorption. The efficiency of Hg(II) recovery decreases when the concentration of the acido ligands (acetate ions) forming strong anionic complexes with Hg(II) substantially increases. In 0.1 M acetate buffers, the reaction of Hg(II) with the primary amide groups of polymer no. 3 by the proton substitution mechanism is also possible.

REFERENCES

1. Sviridova, A.V. and Prilezhaeva, E.N., *Usp. Khim.*, 1974, vol. 43, no. 3, pp. 519–536.
2. Vorob'eva, A.I., Onina, S.A., Muslukhov, R.R., et al., *Vysokomol. Soedin., Ser. B*, 2003, vol. 45, no. 4, pp. 700–704.
3. Vorob'eva, A.I., Onina, S.A., Musina, I.D., et al., *Vysokomol. Soedin., Ser. B*, 2004, vol. 46, no. 2, pp. 364–368.
4. Vorob'eva, A.I., Onina, S.A.,, Kolesov, S.V., et al., *Vysokomol. Soedin., Ser. B*, 2004, vol. 46, no. 7, pp. 1239–1243.
5. Amosova, S.V., Atavin, A.S., and Trofimov, B.A., *Izv. Akad. Nauk SSSR, Ser. Khim.*, 1967, vol. 3, pp. 619–623.
6. Trofimov, B.A., *Geteroatomnye proizvodnye atsetilena* (Heteroatomic Derivatives of Acetylene), Moscow: Nauka, 1981.
7. Murinov, Yu.I., Maistrenko, V.N., and Afzaletdinova, N.G., *Ekstrakysiya metallov S,N-organicheskimi soedineniyami* (Extraction of Metals with *S,N*-Organic Compounds), Moscow: Nauka, 1993.
8. Nikolaev, A.V., Fokin, A.V., Kolomiets, A.F, et al., *Izv. Sib. Otd. Akad. Nauk SSSR, Ser. Khim. Nauk*, 1977, no. 4, issue 2, pp. 49–54.
9. Nikolaev, A.V., Gribanova, I.I., Vasil'eva, A.A., et al., *Izv. Sib. Otd. Akad. Nauk SSSR, Ser. Khim. Nauk*, 1977, no. 12, issue 5, pp. 58–64.
10. Rafikov, S.R., Nikitin, Yu.N., Bikbaeva, G.G., et al., *Dokl. Akad. Nauk SSSR*, 1980, vol. 253, no. 3, pp. 644–647.
11. Anpilogova, G.R., Kondrat'eva, E.V., Afzaletdinova, N.G., et al., *Zh. Neorg. Khim.*, 1996, vol. 41, no. 3, pp. 447–452.
12. Bicak, N. and Sherrington, D.C., *React. Funct. Polym.*, 1995, vol. 27, no. 3, pp. 155–161.
13. Bicak, N., Sherrington, D.C., and Senkal, B.F., *React. Funct. Polym.*, 1999, vol. 41, nos. 1–3, pp. 69–76.
14. Bicak, N., Sherrington, D.C., Sungur, S., and Tan, N., *React. Funct. Polym.*, 2003, vol. 54, nos. 1–3, pp. 141–147.
15. Ginzburg, S.I., Ezerskaya, N.A., Prokof'eva, I.V., et al., *Analiticheskaya khimiya platinovykh metallov* (Analytical Chemistry of Platinum Metals), Alimarin, I.P., Ed., Moscow: Nauka, 1972.
16. Charlot, G., *Les Methods de la Chemie Analytique. Analyse quantitative Minerale, Quatrieme Edition*, Paris: Masson, 1961.
17. Gladyshev, V.P., Levitskaya, S.A., and Filippova, L.M., *Analiticheskaya khimiya rtuti* (Analytical Chemistry of Mercury), Moscow: Nauka, 1974.
18. Silverstein, R.M., Clayton, G.C. and Morril, T.C., *Spectrometric Identification of organic compounds*, New York: Wiley and Sons, 1974.
19. Lur'e, A.A., *Khromatograficheskie materialy* (Chromatographic Materials), Moscow: Khimiya, 1978.
20. Chekushin, V.S. and Borbat, V.F., *Ekstraktsiya blagorodnykh metallov sul'fidami i sul'foksidami* (Extraction of Noble Metals with Sulfides and Sulfoxides), Moscow: Nauka, 1984.
21. Cotton, F.A. and Wilkinson, G., *Advanced Inorganic Chemistry*, New York: Interscience, 1966.
22. Vol'dman, G.M., *Osnovy ekstraktsionnykh i ionoobmennykh protsessov gidrometallurgii* (Main Principles of Extraction and Ion-Exchange Processes of Hydrometallurgy), Moscow: Metallurgiya, 1982.
23. Nikolaev, A.V., Fokin, A.V., Anshits, N.N., et al., *Izv. Sib. Otd. Akad. Nauk SSSR, Ser. Khim. Nauk*, 1978, no. 2, issue 1, pp. 50–54.
24. Bikbaeva, G.G., Nikitin, Yu.E., Gavrilova, A.A., et al., *Zh. Neorg. Khim.*, 1984, vol. 29, no. 4, pp. 1010–1015.
25. Moreno-Gutiurrez, B.Y. and Olgunin, M.T., *J. Radioanal. Nucl. Chem.*, 2003, vol. 256, no. 2, pp. 345–348.
26. Nikolaev, A.V., Torgov, V.G., and Gil'bert, E.N., *Izv. Sib. Otd. Akad. Nauk SSSR, Ser. Khim. Nauk*, 1967, no. 14, issue 6, pp. 120–122.
Sevdizh, D. and Meider, H., *J. Inorg. Nucl. Chem.*, 1977, vol. 39, no. 8, pp. 1409–1413.

ISSN 1070-4272, Russian Journal of Applied Chemistry, 2006, Vol. 79, No. 10, pp. 1600–1604. © Pleiades Publishing, Inc., 2006.
Original Russian Text © A.V. Yakovlev, S.L. Zabud'kov, E.V. Yakovleva, A.I. Finaenov, 2006, published in Zhurnal Prikladnoi Khimii, 2006, Vol. 79, No. 10, pp. 1621–1625.

APPLIED ELECTROCHEMISTRY AND CORROSION PROTECTION OF METALS

A Study of the Possibility of Anodic Oxidation of Suspensions Formed by Dispersed Graphite and Nitric Acid

A. V. Yakovlev, S. L. Zabud'kov, E. V. Yakovleva, and A. I. Finaenov

Engels Technological Institute, Saratov State Technical University, Engels, Saratov oblast, Russia

Received June 15, 2006

Abstract—The dispersion stability of graphite–HNO_3 suspensions was studied in relation to the acid concentration, dispersity of the graphite powder, and solid-to-liquid phase ratio. The relative electrical resistivity was determined for the same system.

DOI: 10.1134/S1070427206100077

Chemical or electrochemical oxidation of graphite in nitric acid electrolytes is a necessary stage in synthesis of graphite intercalation compounds (GIC) processed into thermally expanded graphite. The main advantage of the electrochemical method is the possibility of obtaining a product with highly uniform composition and properties [1–3]. The continuous-operation equipment developed for electrochemical oxidation of dispersed graphite [4, 5] is based on pressing of the anode paste to the current lead to provide electronic conduction in the bulk of the electrode in motion of the paste in the interelectrode gap. Despite the sufficient reliability of the electrolyzer and the possibility of its automatic operation [5], the apparatus has low output capacity and is complicated in exploitation. A way to improve the output capacity of the apparatus and to simplify its design is to eliminate clamping, for which purpose it has been suggested to use electrically conducting graphite–HNO_3 mixtures with a sufficient electrical conductivity. Apparently, only paste-like mixtures with a predominant solid phase will exhibit electronic conduction. At the same time, anodic oxidation of graphite–acid suspensions to give graphite intercalation compounds by the reaction [6]

$$24nC + 3HNO_3 = C^+_{24n}NO^-_3 2HNO_3 + H^+ + e, \quad (1)$$

where n is the number of a GIC stage, requires a sufficient amount of the acid in the mixture for the maximum possible filling of the graphite matrix with the intercalate. In this study, graphite–HNO_3 mixtures will be named "suspensions" at any component ratio. Because the electrochemical oxidation of graphite in solutions with water content exceeding 20% yields graphite nitrate of second and higher stages [7], the mass ratio of graphite and HNO_3 in the suspension should be no less than 1 : 3. An excess of the liquid phase will lead to stratification of the suspension and to loss of the electric contact between graphite grains, and its deficiency, to nonuniform distribution of the components and to formation of electrolytically uncoupled graphite particles, which will eliminate regions of this kind from the electrochemical process. Therefore, the principal characteristics determining the possibility of anodic oxidation of graphite–acid suspensions will be the dispersion stability and electrical conductivity of a suspension.

This communication presents the results obtained in a study of the electrical conductivity and dispersion stability of graphite–HNO_3 suspensions in relation to the components ratio (s : l), graphite dispersity, and acid concentration.

EXPERIMENTAL

The suspensions studied were prepared from disperse graphite powders of GT OSCh brand [GOST (State Standard) 1891–78, special purity grade] with ash content of 0.1% and particle size in the range 200–250 μm and of Chinese manufacture (GB/T standard 3518–95, ash content 0.2%, particle size 250–300 μm). The choice of the graphite brands was due to their predominant use in modern techniques for synthesis of GIC. As electrolytes served 59 and 30% solutions of nitric acid of chemically pure grade [TU (Technical Specification) 701–89E].

The stratification of the suspensions was examined in a measuring cylinder of diameter 1.5 cm and height 10 cm (GOST 1770–74). The height of the liquid phase column and the total height of the mixture were measured at 10-min intervals until their constant ratio was attained. The instant of stratification of the suspension was judged from the appearance of the liquid phase on the surface of graphite particles after the keeping time specified above.

The degree of densification and the under-pressure electrical conductivity of dry graphite powders were studied in a special cell equipped with mobile punches bearing current leads (Fig. 1).

The electrical conductivity of graphite powders and suspensions was measured in a polymethyl methacrylate cell with two flat vertical platinum electrodes with a working surface area of 1 cm^2 and interelectrode spacing of 1.5 cm. To perform anodic polarization of the suspension electrode and suppress electronic conduction via graphite, the platinum cathode was embedded in a diaphragm material (polypropylene filtering cloth).

After the graphite powder or a graphite–HNO_3 suspension was charged into the cell, a direct current of 2.2 to 15 mA was passed (P-5848 potentiostat) with the ohmic voltage drop on the cell recorded with a Shch-1413 digital dc voltmeter. The voltage drop across the cell did not reach values at which Faraday reactions can occur. This was confirmed by the linear run of the dependences of the voltage across the cell on the current strength. The acid was introduced into the suspension with a microbatcher with an accuracy of 0.02 ml.

In the range currents at which Ohm's law was obeyed for the circuit, the electrical conductivity was calculated by the formula

$$\chi = Il/US,$$

where χ is the electrical conductivity (S cm^{-1}); I, current strength (A); U, voltage (V); S, electrode area (cm^2); and l, interelectrode spacing (cm).

A potentiostatic (P-5848 potentiostat) treatment of graphite–HNO_3 suspensions pressed at a load of 0.2 kg cm^{-2} was performed in a special three-electrode cell [1]. The current was recorded in the course of time with a KSP-4 recording potentiometer with an accuracy of 0.1 mA.

The standard silver chloride electrode of EVL-1M1 brand served as a reference electrode in all the electrochemical measurements, and, in what follows, all the potentials are given relative to this electrode.

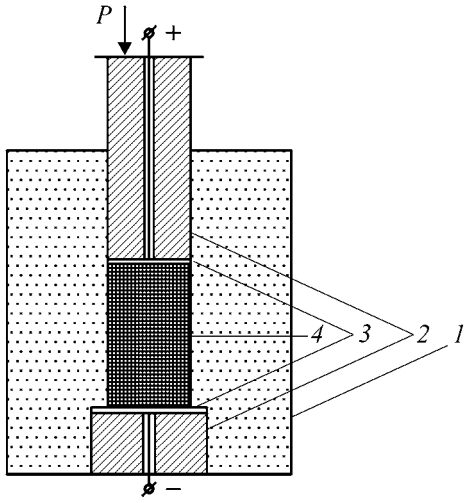


Fig. 1. Schematic of a cell for measuring the electrical conductivity and volume of graphite powders: (*1*) Polymethyl methacrylate case, (*2*) steel punches, (*3*) platinum current leads, and (*4*) graphite powder.

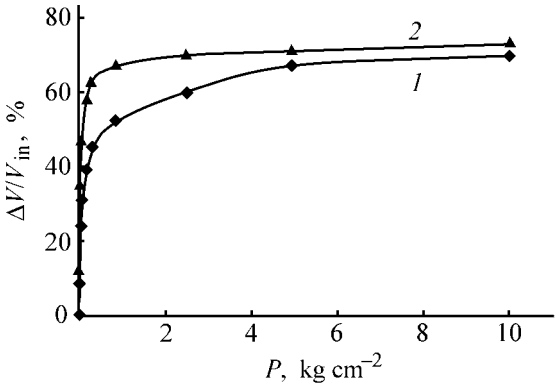


Fig. 2. Degree of densification of the graphite powder, $\Delta V/V_{in}$, under the action of the external pressure P. V_{in}, volume of the graphite powder in the absence of external pressure, $\Delta V = V_{in} - V$; V, volume of the graphite powder under an external pressure. Graphite: (*1*) Chinese and (*2*) GT.

All the experiments were carried out at a constant temperature of 298 ± 1 K.

The electrical conductivity of dry dispersed graphites is considerably lower than that of single crystals, which is due to the fact that the contact resistance between separate graphite particles is high because of their chaotic orientation in the volume. The electrical conductivity of graphite powders was determined under the action of an external pressure to provide contact between graphite particles. A considerable densification of the graphite powder is observed as the pressure is gradually raised to $P \approx 0.5$ kg cm^{-2} (Fig. 2). Further increase in the pressure on GT has virtually no effect on its bulk volume, whereas coarser

Table 1. Composition and properties of suspensions formed by graphite and an HNO_3 solution in the equilibrium state

Figure no.	Graphite brand	HNO_3 content, wt %	$m_{gr} : m_a$ ratio (s : l)	Graphite : HNO_3	Suspension density, g cm^{-3}	$\chi_{suspension} : \chi_{acid}$
			g g^{-1}			
1	Chinese	30	1 : 1.15	1 : 0.35	1.24	3.2
2	GT OSCh		1 : 1.45	1 : 0.44	1.10	3.2
3	Chinese	59	1 : 1.27	1 : 0.75	1.47	3.2
4	GT OSCh		1 : 1.70	1 : 1.00	1.34	3.2

particles of the Chinese graphite continue to be densified, which is probably due to mechanical dispersion of particles oriented perpendicularly to the plane of action of the external load. The pressure clamping the graphite powder to the anode current lead, which should provide an electronic contact between separate particles and the anode, but, at the same time, should allow uniform distribution of the electrolyte throughout the electrode, was 0.2–0.5 kg cm^{-2} [1]. The electrical conductivity measured at this clamping pressure was 0.51 S cm^{-1} for GT-1 and 0.53 S cm^{-1} for Chinese graphite.

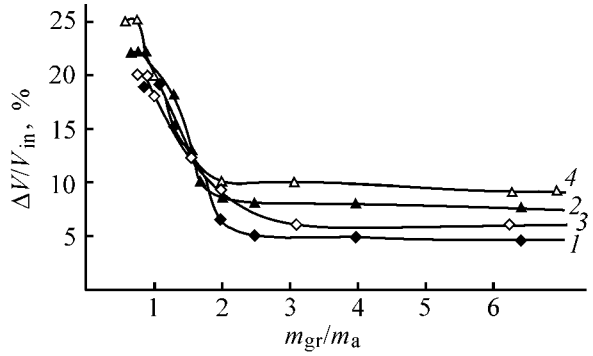


Fig. 3. Degree of densification of the suspension, $\Delta V/V_{in}$, vs. the graphite-to-acid mass ratio m_{gr}/m_a. V_{in}, volume of the graphite powder in the absence of acid; $\Delta V = V_{in} - V$; V, volume of the graphite powder upon addition of the acid. Graphite: (*1*, *3*) Chinese and (*2*, *4*) GT OSCh. HNO_3 content (wt %): (*1*, *2*) 30 and (*3*, *4*) 59; the same for Fig. 4.

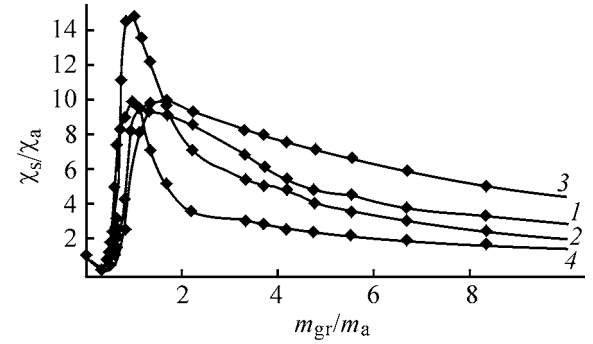


Fig. 4. Relative electrical conductivity of suspensions formed by graphite and HNO_3 solution, χ_s/χ_a, vs. the mass ratio of their components.

When graphite is wetted with the acid, the suspension volume remains, irrespective of the acid concentration, virtually unchanged until a mass ratio s : l = 1 : 0.5 is reached. As the amount of the liquid phase grows, the suspension volume considerably increases. It should be noted that complete wetting of coarser graphite particles (Chinese graphite) requires a substantially smaller amount of the acid, irrespective of its concentration, than wetting of GT graphite (Fig. 3). Measurements of the electrical conductivity of all the suspensions under study in conditions of dispersion stability at the maximum content of the liquid phase revealed an increase in its value by a factor of 3.2, compared with the corresponding acid solution (Table 1), which points to the existence of an electronic component in the electrical conductivity. However, the available data on the dispersion stability of suspensions are insufficient for making a final conclusion about the possibility of electrochemical synthesis of GIC with their use. This is because these data fail to provide a complete understanding of the electrochemical behavior of the suspensions (ionic and electronic components in a suspension) in relation to the solid-to-liquid phase ratio.

Measurements of the electrical conductivity of graphite–HNO_3 suspensions (Fig. 4) confirmed that the contact between particles of dispersed graphite is improved upon their wetting with HNO_3 solutions. In this case, the agglomeration of coarse particles of Chinese graphite, which improves the electronic contact between the particles, occurs considerably faster, which is indicated by the higher values of the electrical conductivity of the suspensions (Fig. 4, curves *1*, *3*). The maximum values of the electrical conductivity of the suspensions based on Chinese graphite are reached at a mass ratio s : l ≈ 1 : 0.66 (curves *1*, *3*), whereas in the suspensions based on GT, the maximum electrical conductivity is obtained at s : l ≈ 1 : 1

Table 2. Electric capacity in potentiostatic treatment of dispersed graphite electrodes

Electrode	Graphite brand	Q, mA h g^{-1}, in indicated time, min		
		200	250	300
Clamped	Chinese	60	90	120
	GT	75	110	150
Suspension-type	Chinese	15	25	40
	GT	40	70	100

Note. E = 2.1 V.

(curves *2*, *4*). The shift of the maximum values of electrical conductivity to a higher content of the liquid phase in the suspensions, observed for the finer particles of GT graphite, is presumably due to the more porous, compared with Chinese graphite, structure of the agglomerates and to larger specific surface area of graphite particles. The anomalously high values of electrical conductivity, observed for suspensions formed by GT graphite and 30% HNO_3 (curve *2*), are probably due to the largest area of contact between graphite particles, which leads to a more effective charge transfer. Such a favorable, for improvement of the electric contact, orientation may result both from a chemical interaction of the surface groups on GT graphite with the 30% solution of HNO_3 and from the action of the field generated by H_3O^+ and NO_3^- ions. The absence of an interaction of this kind in the 59% solution of HNO_3 can be attributed to a change in the structure of the acid. For example, according to the data of [8], the acid has a structure similar to that of NO_2OH esters and is characterized by a considerable decrease in the degree of dissociation, compared with less concentrated solutions.

Further dilution of the suspension with nitric acid leads to a decrease in the electrical conductivity because of the stratification of the suspension and increased share of the ionic component in charge transfer.

The kinetics of anodic processes was examined under potentiostatic polarization of suspension electrodes prepared in accordance with the results obtained (Table 1, Fig. 4) in a 59% solution of HNO_3. With account of the side processes involving the acid, the amount of acid molecules in the suspensions formed by graphite and 30% HNO_3 (Table 1) is insufficient for II-stage GIC to be formed by reaction (1), and, therefore, the kinetics of anodic reactions in this system was not analyzed. Previously, the potential of anodic polarization of a clamped graphite electrode in a 59% solution of HNO_3 and the electric capacity providing formation of a GIC with a high degree of thermal expansion have been found to be 2.1 V and 200–300 mA h g^{-1} [1]. Comparison of the results of a potentiostatic synthesis in a cell with a clamped electrode [1] (Fig. 5, curves *3*, *4*) with those of an electrochemical treatment of a suspension electrode (Fig. 5, curve *1*, *2*) shows that the currents are 1.5–4 times higher in the latter case (Table 2). This confirms the existence of an electronic contact between graphite particles, which is only formed when the content of liquid phase is optimized and graphite particles agglomerate under the action of surface tension forces. The fact revealed demonstrates that the true surface area of the carbon material, involved in the electrochemical process, is considerably larger in the suspension electrode. Graphite particles in the suspension remain mobile to a certain extent, which allows them to change their spatial orientation under the action of current. In the process, an electron can pass across the acid films adsorbed on the surface of carbon particles, i.e., the electron transfer is accompanied by a jump across the "liquid phase." The initial rise in current (Fig. 5) is presumably

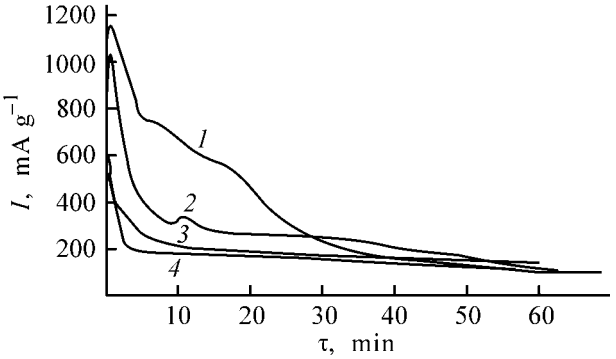


Fig. 5. Potentiostatic curves of anodic oxidation (E = 2.1 V) of dispersed graphite electrodes in a 59% solution of HNO_3. (*I*) Current strength and (τ) time. (*1*, *2*) Suspension electrode and (*3*, *4*) pressed electrode (P = 0.2 kg cm^{-2}). Graphite: (*1*, *3*) Chinese and (*2*, *4*) GT.

due to an increase in the electronic conductivity of the suspension electrode through reorientation and densification of graphite particles. The process of graphite intercalation after the completion of the induction period is accompanied by a steep decrease in current (Fig. 5). The volume expansion of graphite particles in GIC formation leads to densification of the suspension and, further, the currents for the suspension and pressed electrodes virtually coincide.

It can be seen from the results obtained (Fig. 5, Table 2) that the rate of anodic reactions is higher, on both suspension and pressed electrodes, for Chinese graphite, despite its smaller specific surface area. In this case, the kinetics of the electrochemical processes is determined by the contact resistance between graphite grains in the suspension bulk. This is confirmed by the fact that the difference in the anode currents during the first 20 min of anodic polarization is small (10%) for a clamped electrode (Fig. 5, curves *1*, *2*) and considerable (up to 200%) for the suspension electrode (curves *3*, *4*).

CONCLUSIONS

(1) It was shown that, in principle, anodic oxidation of dispersed graphite materials can be performed in suspensions with nitric acid and the suspension component ratio at which electrons are removed from graphite particles was determined.

(2) It was found that the rate of anodic processes in a 59% solution of HNO_3 is 1.5–4 times higher on a graphite suspension electrode, compared with the clamped electrode, and depends on the dispersity of the starting carbon powder.

(3) The experimental data were obtained, which create good prerequisites to improvement and simplification of the electrochemical technique for synthesis of graphite intercalation compounds.

REFERENCES

1. Yakovlev, A.V. and Finaenov, A.I., *Zh. Prikl. Khim.*, 1999, vol. 72, no. 1, pp. 88–91.
2. Yaroshenko, A.P., Popov, A.F., and Shapranov, V.V., *Zh. Prikl. Khim.*, 1994, vol. 67, no. 2. C. 204–211.
3. Yakovleva, E.V., Yakovlev, A.V., and Finaenov, A.I., *Zh. Prikl. Khim.*, 2002, no. 10, pp. 1632–1638.
4. Finaenov, A.I., Apostolov, S.P., Krasnov, V.V., and Nastasin, V.A., *Zh. Prikl. Khim.*, 1999, vol. 72, no. 5, pp. 767–772.
5. RF Patent 2 142 409.
6. Rudorff, W. and Hofmann, U., *Z. Anorg. Allg. Chem.*, 1938, vol. 238, no. 1, pp. 1–50.
7. Scharff, P., Xut, Z.-Y., Stump, E., and Barteczko, K., *Carbon*, 1991, vol. 29, no. 1, pp. 31–37.
8. Beskov, S.D., Kochetkova, L.I., and Mukanov, I.P., *Uch. Zap. Mosk. Gos. Ped. Inst. im. V.I. Lenina*, 1962, no. 181, issue 2, pp. 241–254.
9. Yakovlev, A.V., Finaenov, A.I., Nikitina, L.E., and Apostolov, S.P., *Zh. Prikl. Khim.*, 1999, vol. 72, no. 4, pp. 589–593.

ISSN 1070-4272, Russian Journal of Applied Chemistry, 2006, Vol. 79, No. 10, pp. 1605–1608. © Pleiades Publishing, Inc., 2006.
Original Russian Text © I.I. Obraztsova, G.Yu. Simenyuk, N.K. Eremenko, 2006, published in Zhurnal Prikladnoi Khimii, 2006, Vol. 79, No. 10, pp. 1626–1629.

APPLIED ELECTROCHEMISTRY AND CORROSION PROTECTION OF METALS

Effect of the Nature of a Reducing Agent on Properties of Ultradisperse Copper Powders

I. I. Obraztsova, G. Yu. Simenyuk, and N. K. Eremenko

Kemerovo Branch, Institute of Solid-State Chemistry and Mechanochemistry, Siberian Division, Russian Academy of Sciences, Kemerovo, Russia

Received March 29, 2006

Abstract—Ultradisperse copper powders were produced by reduction of copper sulfate with glycerol, *L*-ascorbic acid, sodium hypophosphite, glucose, and hydrazine. The influence exerted by the nature of a reducing agent on the size-related parameters and physicochemical properties of the powders was studied.

DOI: 10.1134/S1070427206100089

One of the main current issues of modern science and technology is production of electrically conducting ultradisperse powders (UDPs) of copper. Numerous methods for synthesis of copper UDPs are known, which enable wide variation of their dispersity and properties. However, the problem of synthesis of copper UDPs with controlled particle size distribution, which can be used to create materials with nearly metallic electrical conductivity, remains topical. Composite materials of this kind find wide application in electronics for development of electrically conducting glues and pastes used in low-temperature soldering of device elements and in assembly of integrated circuits and flexible printed-circuit boards.

Previously, methods for synthesis of copper UDPs by reduction of copper sulfide with glycerol have been developed and patented [1, 2]. It was shown in [3] that chemical modification of copper UDPs makes it possible to obtain from these UDPs formulations possessing increased stability (of epoxy type, more than 10 years; of novolac type, more than 6 years) and low electrical resistivity (10^{-6}–10^{-7} Ω m).

It has been shown that it is preferable to carry out reduction of various copper salts with sodium hypophosphite and hypophosphorous acid in the water–hexanol system, rather than in an aqueous medium [4]. This is so because hexanol adsorbed on the surface of UDPs leads to an increase in their stability and electrical conductivity by blocking the surface of copper particles and thereby preventing their oxidation by atmospheric oxygen. It was also demonstrated that additional treatment of copper UDPs with formic acid makes them more stable and electrically conducting.

The present communication reports the results obtained in an experimental study of copper sulfide reduction with various reducing agents. The influence exerted by the nature of the reducing agent on the dispersity, stability, and electrical conductivity of copper powders is analyzed.

Five different reducing agents were chosen for copper by analysis of published data. These are glycerol, *L*-ascorbic acid, sodium hypophosphite, *D*-glucose, and hydrazine.

EXPERIMENTAL

The results obtained in reduction of copper salts with sodium hypophosphite have been described in sufficient detail [1–4]. The reduction with glycerol was carried out by the procedure described in [1]. The reaction of copper sulfate with sodium hypophosphite was performed by the method reported in [4]. The procedure used to reduce copper salts with ascorbic acid was described in [5].

The reduction with glucose was carried out in an alkaline medium by the technique reported in [6]. Copper sulfate and glucose were dissolved in separate vessels. A minor amount of an alkali (NaOH, KOH) was introduced into the glucose solution to bring the solution pH to 8–9. The copper sulfate solution was heated to 80–90°C. Then the glucose solution was gradually poured in the copper sulfate solution under permanent agitation and the mixture heated to 80–90°C. A red precipitate was formed in 40–50 min. The precipitate was separated from the solution, treated with formic acid to remove copper oxides, and stored in a 0.05% solution of stearic acid in ethanol.

Results obtained in reduction of copper sulfate with various reducing agents*

Sample no.	Reducing agent	t_r, °C	τ_r, min	S_{sp}, $m^2 g^{-1}$	D_{Cu_2O}	D_{Cu}	D_{max}	D_{av}
					nm			
1	Glycerol	180–185	180	0.51	–	85	1.29	1.46
2	*L*-ascorbic acid	30–40	12	2.82	–	52	1.28	1.45
3	Sodium hypophosphite	80–85	10	4.70	34	42	1.28	1.42
4	*D*-glucose	80–90	45	1.71	29	48	1.21	1.41
5	Hydrazine sulfate	70–80	15	6.00	56	64	1.17	1.41

* t_r and τ_r, temperature and duration of the reduction reaction.

The reduction with hydrazine was performed by analogy with the procedure described in [7]. Copper sulfate and hydrazine sulfate solutions were prepared separately. A 1 M solution of an alkali (NaOH, KOH) was poured in a hydrazine sulfate solution to bring its pH to 8–9 and then the hydrazine solution was gradually poured in the copper sulfate solution under permanent agitation and heated to 70–80°C for 15–20 min. The copper powder was washed with water and treated with a 1% solution of hydroquinone and 0.05% solution of stearic acid in ethanol to improve its stability against oxidation and aggregation, as recommended previously [1].

In order to examine the influence exerted by the nature of a reducing agent on the properties of copper UDPs, both organic (glycerol, *L*-ascorbic acid, *D*-glucose) and inorganic (hypophosphorous acid, sodium hypophosphite, hydrazine sulfate) reagents were used. The interaction with these reducing agents occurs under various conditions (see table). As a result, the physicochemical and electrical properties of the ultradisperse copper powders obtained vary widely.

The physicochemical properties of the resulting ultradisperse copper powders were studied. The average sizes of copper(I) oxide crystallites, D_{Cu_2O} and metallic copper, D_{Cu}, were found from the spectra of X-ray phase analysis (XPA) in Fig. 1 by Scherrer formulas [8]. The specific surface area S_{sp} of the powders was determined by the BET technique from adsorption of argon. The most probable (D_{max}) and statistical-average (D_{av}) diameters of primary particles were calculated from the particle size distribution functions [9]. The results obtained are listed in the table.

Figure 2 shows the first maxima of mass particle-size distribution functions D_m, calculated from

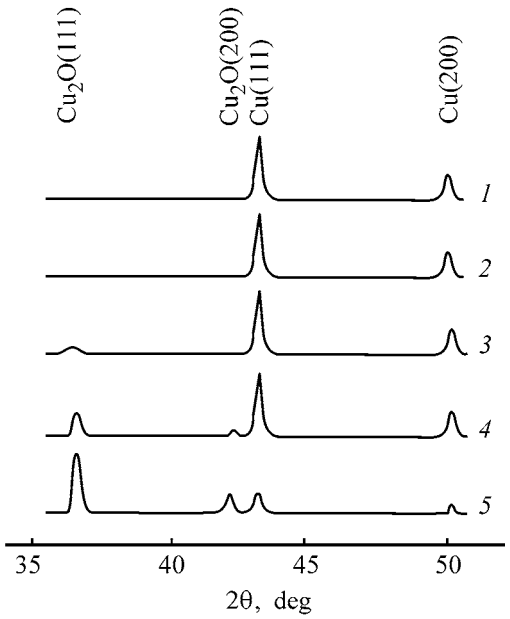


Fig. 1. Spectra obtained in X-ray phase analysis of ultradisperse copper powders (2θ) Bragg angle. (*1–5*) Sample numbers in the table; the same for Figs. 2, 3.

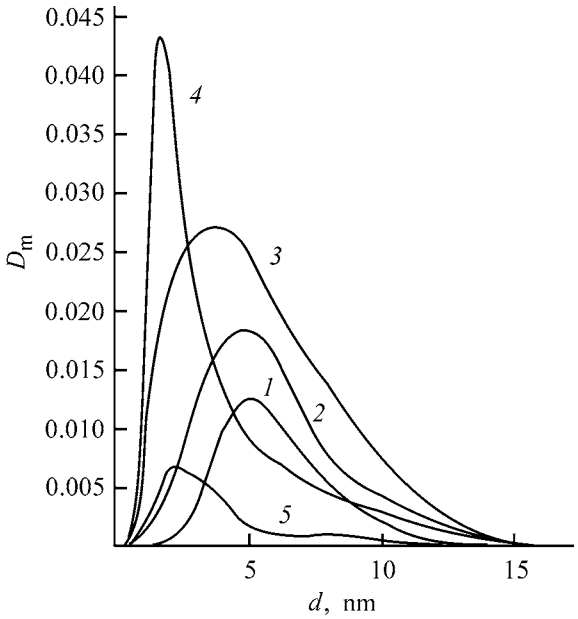


Fig. 2. First maxima of mass particle-size distribution functions $D_m(d)$, calculated from small-angle scattering curves. (d) Particle diameter.

small-angle scattering curves by special procedures [10].

It can be seen from the results presented above that copper powders produced by reduction with glycerol and *L*-ascorbic acid have the largest particle sizes according to small-angle scattering data and contain a virtually zero amount of Cu_2O.

It is apparent that, as the specific surface area of the powders grows, the content of copper(I) oxide in these powders increases. The only exception is sample no. 4, produced by reduction with *D*-glucose. This sample has a specific surface area smaller than that of copper powders synthesized by reduction with sodium hypophosphite and *L*-ascorbic acid, but contains a larger amount of copper(I) oxide. This is presumably due to the fact that the first peak in the particle size distribution curves (Fig. 2) is shifted for sample no. 4 to smaller sizes and has smaller values of D_{max} and D_{av} than sample nos. 2 and 3. Thus, a clearly pronounced correlation between the values of D_{maz} and D_{av}, on the one hand, and the content of copper(I) oxide, on the other, is observed for samples represented in the table.

The electrical conductivity σ and stability of copper powders were evaluated by changes in the electrical resistivity ρ (ρ = 1/σ) of formulations with SF-010 phenol-formaldehyde novolac resin (with 80% metallic phase). The electrical resistivity of the formulations was measured in the dc mode (12 V, 2.5 mA) at a temperature of 20–25°C. The results obtained are presented in Fig. 3.

It can be seen that the electrical conductivity and stability of the powders are in an agreement with the data on their dispersity: the larger the most probable (D_{max}) and statistical-average (D_{av}) particle diameters, the higher their stability and electrical conductivity. For example, the electrical conductivity was the highest for copper powders obtained by reduction of copper sulfate with glycerol (sample no. 1), which have the smallest specific surface area, largest D_{max} and D_{av}, and, according to XPA spectra, the lowest content of impurities, which is accounted for by the process conditions. Somewhat lower is the electrical conductivity of copper powders produced by reduction with *L*-ascorbic acid (sample no. 2). The electrical conductivity is the lowest for powders reduced with *D*-glucose and hydrazine (sample nos. 4 and 5), which have the smallest primary particles and the highest content of copper(I) oxide impurity.

It can also be seen from the table that the most probable and statistical-average diameters are close

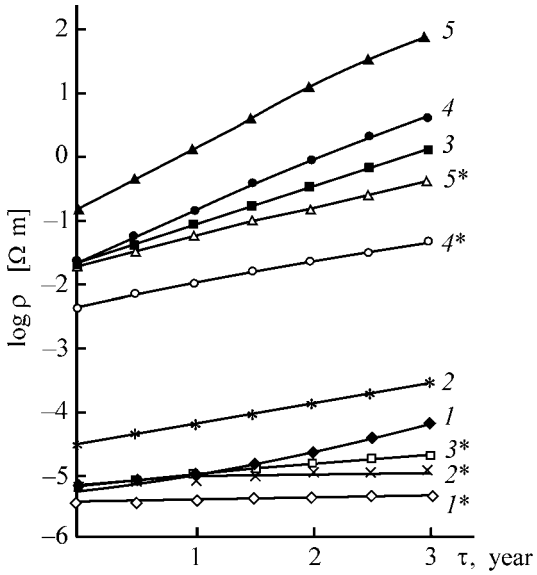


Fig. 3. Effect of the nature of a reducing agent on the variation of the electrical resistivity ρ of formulations composed of copper UDP and novolac resin with time τ. (*1–5*) Before treatment with HCOOH and (*1*–5**) after the treatment. (*1*, *1**) Glycerol, (*2*, *2**) *L*-ascorbic acid, (*3*, *3**) sodium hypophosphite, (*4*, *4**) *D*-glucose, and (*5*, *5**) hydrazine.

for copper UDPs produced by reduction with glycerol, *L*-ascorbic acid, and sodium hypophosphite. It is this circumstance that is, in all probability, responsible for the fact that UDPs reduced with sodium hypophosphite and *L*-ascorbic acid become comparable with the samples reduced with glycerol if appropriate stabilizing agents are used. The enhanced stability of UDPs produced by reduction with *L*-ascorbic acid and sodium hypophosphite may also be due to unreacted molecules of the reducing agent, which are adsorbed on the UDP surface. In the case of reduction with hydrazine, the electrical conductivity is several orders of magnitude lower, even if stabilizing agents are used, and the powders are unstable in the course of time. This is presumably due to their substantially larger specific surface area (see table, sample no. 5), which leads to enhanced oxidation of the copper powder in air.

It was found that additional treatment of copper UDPs with formic acid leads to a considerable increase in the electrical conductivity and stability of the ultradisperse powders produced by reduction of copper sulfate with glycerol (Fig. 3, curve *1**), *L*-ascorbic acid (*2**), and sodium hypophosphite (*3**). However, the electrical conductivity of the powders produced by reduction with *D*-glucose and hydrazine is several orders of magnitude lower even upon treat-

ment with formic acid (curves *4** and *5**, respectively) and they are unstable in the course of time.

CONCLUSIONS

(1) A comparison of the physicochemical properties of ultradisperse powders produced by reduction with various reducing agents revealed that glycerol, *L*-ascorbic acid, and sodium hydrophosphite are the most effective reducing agents for synthesis of stable copper powders with high electrical conductivity.

(2) It was shown that the nature of a reducing agent affects the size-related parameters and physicochemical properties of the powders obtained, which determines their stability and electrical properties.

ACKNOWLEDGMENTS

The authors thank V.A. Polyboyarov (Institute of Solid-State Chemistry and Mechanochemistry, Siberian Division, Russian Academy of Sciences) for determining the specific surface area of the powders, V.G. Dodonov (Kemerovo State University) for analysis of the powders by the small-angle scattering method, and V.M. Pugachev (Kemerovo State University) for recording XPA spectra.

REFERENCES

1. RF Patent 2031759.
2. RF Patent 2115516.
3. Obraztsova, I.I., Simenyuk, G.Yu., and Eremenko, N.K., *Zh. Prikl. Khim.*, 2002, vol. 75, no. 11, pp. 1772–1775.
4. Obraztsova, I.I., Simenyuk, G.Yu., and Eremenko, N.K., *Zh. Prikl. Khim.*, 2004, vol. 77, no. 4, pp. 386–390.
5. Obraztsova, I.I., Simenyuk, G.Yu., and Eremenko, N.K., *Zh. Prikl. Khim.* (in press).
6. Nichiporenko, O.S., Pomosov, A.V., and Naboichenko, S.S., *Poroshki medi i ee splavov* (Powdes of Copper and Its Alloys), Moscow: Metallurgiya, 1988, pp. 173–174.
7. Shalkauskas, M. and Vashkyalis, A., *Khimicheskaya metallizatsiya plastmass* (Chemical Metallization of Plastics), Leningrad: Khimiya, 1985.
8. Kovba, L.M., *Rentgenografiya v neorganicheskoi khimii* (X-ray Analyses in Inorganic Chemistry), Moscow: Mosk. Gos. Univ., 1991, pp. 230–238.
9. *Fizika tverdogo tela: Metody polucheniya tverdykh tel i issledovaniya ikh struktury. Kniga 1. Laboratornyi praktikum* (Solid-State Physics: Methods For production of Solids and Study of Their Structure, Book 1, Laboratory Course), Khokhlov, A.F., Ed., Moscow: Vysshaya Shkola, 2001, pp. 141–154.
10. Dodonov, V.G., *Z. Kristallogr., Supplied Issue*, 1991, no. 4, p. 102.

ISSN 1070-4272, Russian Journal of Applied Chemistry, 2006, Vol. 79, No. 10, pp. 1609–1611. © Pleiades Publishing, Inc., 2006.
Original Russian Text © Zh.M. Kebadze, L.Sh. Kakuriya, G.P. Gobechiya, 2006, published in Zhurnal Prikladnoi Khimii, 2006, Vol. 79, No. 10, pp. 1630–1632.

APPLIED ELECTROCHEMISTRY AND CORROSION PROTECTION OF METALS

Effect of the Dispersity of Components of a Cathode Mixture on Discharge Characteristics of a Leclanché Cell

Zh. M. Kebadze, L. Sh. Kakuriya, and G. P. Gobechiya

Agladze Institute of Inorganic Chemistry and Electrochemistry, Tbilisi, Georgia

Received January 11, 2006; in final form, July 13, 2006

Abstract—The effect of dispersity of electrolytic manganese dioxide and of an electrically conducting additive to the cathode mixture on the discharge capacity of chemical power cells of the manganese–zinc system with a salt electrolyte was studied.

DOI: 10.1134/S1070427206100090

The most widely occurring type of chemical power cells (CPC) are primary cells of the manganese–zinc (MZ) system [1, 2]. By the end of the last century, the annual per capita consumption in the United States and Japan was 15 cells, and the present-day world production of cells of this system is 46 billion [3, 4] In view of the fact that utilization of worked-out primary CPC is still not carried out worldwide, a large amount of noxious substances contained in these cells find their way into the environment [2]. Thus, making the service life of CPC longer may aid in solving not only technical and economical, but also ecological problems.

At present, 140 years after it was developed, the Leclanché cell, a salt-type CPC of the MZ system $Zn/NH_4Cl/MnO_2$, retains its high practical importance. This is due to its low cost, high reliability and safety, convenient manufacturing technology, and wide application area. However, the electrical characteristics of the Leclanché cell are assessed as only acceptable or satisfactory [1, 2]. In the last decades, the rise in the specific energy capacity of CPC of the MZ system with a salt electrolyte lagged behind that for CPC with an alkaline electrolyte, which was, naturally, reflected on the production: during this time the number of manufactured alkaline cells exceeded that of saline cells [4]. It has been shown previously [5] that the Leclanché cell has not exhausted its potentialities in improvement of its electrotechnical characteristics.

The aim of this study was to demonstrate the possibility of a more effective use of the influence exerted by the dispersity of components of the cathode mixture on the discharge capacity of galvanic cells.

Experiments were performed with saline cells of the MZ system of R12 (336) standard size. The CPS were fabricated under laboratory conditions from materials and articles used in the industry, with all the technological conditions satisfied [1, 6]. Electrolytic manganese dioxide (EMD) of first grade [7], manufactured in Rustavi (Georgia), was used as the active cathode material. The composition of the dry cathode mixture was as follows (wt %): EMD 80, graphite 16.5, and carbon black 3.5. Each CPC batch comprised seven R12 galvanic cells. The CPC were discharged at room temperature in the continuous mode through a constant external resistance of 3.33 Ω to a final voltage of 0.67 V. The total internal resistance was calculated from discharge parameters [8].

EXPERIMENTAL

The mechanism of electrochemical reduction of MnO_2 in various electrolytes, associated with diffusion and concentration polarization in the solid phase, determines a dependence of the extent of utilization of the active substance on its particle size [1, 8]. It is known [9] that the particle size of the positive electrode of a CPC of the manganese–zinc system with an alkaline electrolyte strongly affects the electrochemical characteristics of the cells. Experiments demonstrating that the amount of electric energy produced by a cell is independent of the size of EMD particles in the salt electrolyte have been performed in a rather narrow range of dispersities of the active substance [10].

Table 1. Fraction composition of EMD and graphite powders

Sieve mesh, mm	EMD sample no.					Graphite sample no.	
	1	2	3	4	5	6	7
	under sieve, %						
0.200	100					86	97
0.160	96	100				72	94
0.100	83	87	100			39	89
0.063	65	66	80	100		16	82
0.050	30	40	42	52	100	7	74

Table 2. Discharge of R12 CPC through an external resistance of 3.33 Ω

Voltage, V		Discharge energy, W h	Coefficient of MnO_2 utilization, %
open-circuit	average over discharge		
1.69	0.867	0.902	32.8
1.68	0.873	0.981	35.5
1.68	0.890	1.125	39.9
1.69	0.852	0.915	33.9
1.68	0.845	0.814	30.0

Moreover, the composition of samples that have been tested in electrochemical cells did not correspond to the relative masses of components in the cathode mixture of the standard Leclanché cell [1, 6]. The electrochemical characteristics of CPC of the MZ system are strongly affected by the amount and quality of carbon materials added to the cathode mixture to raise its electrical conductivity [9, 11, 12]. Various types of carbon materials produced by modern techniques (carbon fiber, colloidal and thermally expanded graphite, etc.) are successfully used in technical electrochemistry and, in particular, in fabrication of certain types of CPC [13–16]. The macro- and microcharacteristics of these materials (structural defects, dispersity, porosity, and specific surface area) are important for their effective use.

The influence exerted by the EMD dispersity on the discharge capacity of Leclanché cells was studied with five samples of EMD powder with different fraction compositions. The elemental (flaky) graphite used in CPC manufacture or the low-ash graphite produced by processing of flaky graphite was added to the cathode mixture, together with acetylene black, as a conducting material [6].

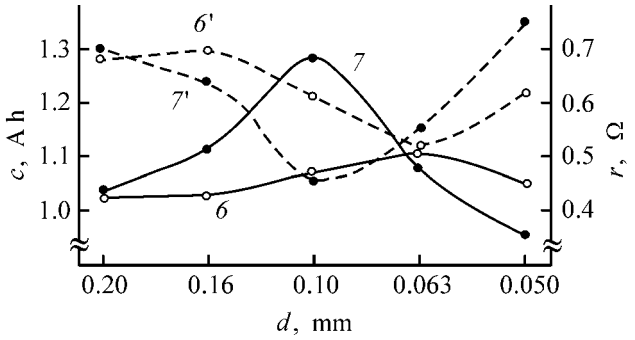


Fig. 1. (*6*, *7*) Discharge capacity and (*6*', *7*') internal resistance of R12 cells of the MZ system vs. the dispersity of the EMD powder. (*c*) Discharge capacity, (*r*) resistance, and (*d*) sieve mesh. Cells fabricated with the use of (*6*, *6*') elemental graphite and (*7*, *7*') low-ash graphite.

Table 1 lists results of a sieve analysis of EMD powder samples (nos. 1–5, no. 1 standard sample [7]) and the elemental (no. 6) and low-ash (no. 7) graphite. The EMD samples were obtained by sieving the starting product through the corresponding sieves.

According to the data of Table 1, the dispersity of the low-ash graphite is higher than that of the elemental graphite. This is particularly noticeable in comparison of fine fractions.

Table 2 lists some discharge characteristics of R12 galvanic cells fabricated from the above EMD samples and the low-ash graphite. The use of the latter as an electrically conducting additive to the cathode mixture, instead of the elemental graphite, raised by, on average, 13% the utilization coefficient of the active substance. The manner in which this coefficient varies is reflected in Table 2, which shows that the discharge capacity of the cells depends on the EMD dispersity (see Fig. 1, curves *6*, *7*). In both cases, the curve describing this dependence passes through a maximum. This is probably due to variation of the ohmic and diffusion characteristics inherent in porous electrodes [2, 17], of which type is the cathode of the CPC of the MZ system, fabricated by powder compaction. Presumably, the above characteristics of the porous electrode degrade, beginning with a certain degree of EMD dispersity, as the size of particles and pores in the electrode decreases. Another possible reason for the observed dependence of the electric capacity of the cells on the dispersity of the active substance is the tendency toward an increase in the con tact electrical resistance, caused by processes that occur at points of contact between EMD and graphite particles in operation of the cell [1]. This interpretation can be confirmed by the fact that the internal electrical resistance of the cell varies as the EMD

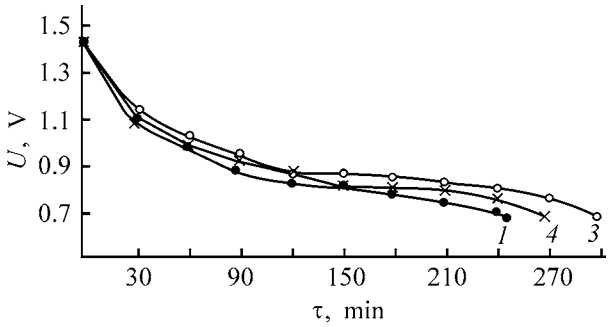


Fig. 2. Discharge curves of R12 cells of the MZ system, fabricated using (*1*, *4*) elemental and (*3*) low-ash graphite. (*U*) Voltage and (τ) time. Digits at the curves correspond to EMD sample nos. in Table 1.

dispersity increases. It can be seen from Fig. 1 that this resistance first decreases and then increases with both the elemental (curve *6*') and lowash (curve *7*') graphite used. The maximum discharge capacity of cells fabricated with the low-ash graphite exceeds by 16% that of cells fabricated using the elemental graphite. One more fact of importance is that the maximum capacity of the cell with the low-ash graphite was obtained for an EMD powder with particle size larger (Table 1, sample no. 3) than that in the case of the elemental graphite (sample no. 4). Thus, use of the low-ash graphite can lower the cost of EMD grinding by diminishing the energy expenditure.

Figure 2 shows discharge curves of the best R12 cells fabricated using the low-ash (curve 3) and elemental (curve *4*) graphite as additive to EMD samples (Table 1, sample nos. 3 and 4, respectively). The figure also shows curve *1*, which corresponds to cells based on the EMD powder of the standard fraction composition (Table 1, sample no. 1) and the elemental graphite. To the discharge curves *3* and *4* corresponds an increase in the discharge capacity of the cells by 24% for the low-ash graphite and by 8% for the elemental graphite, respectively. The results obtained may be due not only to the high dispersity of the low-ash graphite, but also to its other advantages: lower content of ash (by approximately a factor of 25) and impurities (on average, by a factor of 10), compared with the elemental graphite [6]. This circumstance determines the high content of carbon and, accordingly, the high electrical conductivity of the low-ash graphite, and just this was reflected in the data on the internal resistance of CPC (Fig. 1, curves *6*', *7*').

CONCLUSIONS

(1) The standard requirements to the fraction composition of EMD are not optimal for salt CPC of the MZ system and require adjustment toward a higher dispersity of the powder.

(2) Use of EMD with the optimal dispersity and the low-ash graphite as an additive to the cathode mixture improves the discharge capacity of Leclanché cell of R12 standard size by 22–25%.

REFERENCES

1. Varypaev, V.N., Dasoyan, M.A., and Nikol'skii, V.A., *Khimicheskie istochniki toka* (Chemical Power Cells), Moscow: Vysshaya Shkola, 1990.
2. *Khimicheskie istochniki toka: Spravochnik* (Chemical Power Cells: Reference Book), Korovin, N.V. and Skundin, A.M., Eds., Moscow: Mosk. Energet. Inst., 2003.
3. Takei, T., Tanaka, H., Miyazawa, T., et al., *Progr, Batteries Battery Mater.*, 1998, vol. 17, pp. 303–313.
4. Korovin, N.V., *Elektrokhim. Energet.*, 2003, vol. 3, no. 4, pp. 163–168.
5. Kebadze, Zh.M., Kakuriya, L.Sh., and Pruidze, V.P., *Elektrokhim. Energet.*, 2005, vol. 5, no. 4, pp. 242–245.
6. Dam'e, V.N. and Rysukhin, N.F., *Proizvodstvo pervichnykh khimicheskikh istochnikov toka* (Manufacture of Primary Chemical Power Cells), Moscow: Energoizdat, 1981.
7. *GOST* (State Standard) *25823–83: Manganese Dioxide for Chemical Power Cells*, 1983.
8. Nalesnik, O.I., *Obshchaya teoriya khimicheskikh istochnikov toka* (General Theory of Chemical Power Cells), Tomsk: Tomsk. Politekhn. Inst., 1985.
9. Urfer, A., Lawrance, G.A., and Swinkels, D.A.J., *J. Appl. Electrochem.*, 2001, vol. 31, pp. 341–347.
10. Kononov, Yu.S., Zhizhaev, A.M., and Patrushev, V.V., *Zh. Prikl. Khim.*, 2003, vol. 76, no. 6, pp. 1039–1041.
11. Andersen, T.N., Mischler, G.A., and Howard, W.F., *J. Appl. Electrochem.*, 2003, vol. 33, pp. 717–723.
12. Fialkov, A.S., *Elektrokhimiya*, 2000, vol. 36, no. 4, pp. 389–413.
13. Varentsov, V.K., *Intensifikatsiya elektro-khimicheskikh protsessov: Sbornik nauchnykh trudov* (Intensification of Electrochemical Processes: Coll. of Sci. Works), Moscow: Nauka, 1988, pp. 94–118.
14. Danilov, M.O. and V'yunova, N.V., *Zh. Prikl. Khim.*, 2000, vol. 74, no. 11, pp. 1897–1898.
15. Takei, T., Yamamoto, Y., Akinori, I., et al., *Progr. Batteries Battery Mater.*, 1998, vol. 17, pp. 319–325.
16. Finaenov, A.I., Krasnov, V.V., Trifonov, A.I., et al., *Elektrokhim. Energet.*, 2003, vol. 3, no. 3, pp. 107–118.
17. Fioshin, M.Ya. and Smirnova, M.G., *Elektrokhimicheskie sistemy v sinteze khimicheskikh produktov* (Electrochemical Systems in Synthesis of Chemical Products), Moscow: Khimiya, 1985.

ISSN 1070-4272, Russian Journal of Applied Chemistry, 2006, Vol. 79, No. 10, pp. 1612–1616. © Pleiades Publishing, Inc., 2006.
Original Russian Text © V.I. Korchagin, P.T. Poluektov, 2006, published in Zhurnal Prikladnoi Khimii, 2006, Vol. 79, No. 10, pp. 1633–1637.

ENVIRONMENTAL PROBLEMS OF CHEMISTRY AND TECHNOLOGY

Integrated Utilization of Spent Ion-Exchange Resins in Wastewater Treatment and in Polymer Composites

V. I. Korchagin and P. T. Poluektov

Voronezh State Technological Academy, Voronezh, Russia

Received May 25, 2006

Abstract—The possibility of recovery of contaminants (soaps of resin and fatty acids, Leukanol, and finely dispersed rubber) from spent synthetic ion-exchange resins in the stage of treatment of wastewater formed in production of synthetic rubbers and latexes, which polymer composites obtained, was studied.

DOI: 10.1134/S1070427206100107

The increasing volumes of industrial and household water consumption, deterioration of quality of natural water, organization of recycling water supply and local water treatment systems, and also the fact that the regulations concerning the water quality become more and more stringent, lead to higher consumption of ion-exchange resins. With this tendency preserved, the global demand for these materials will steadily increase; however, the problem of their utilization after repeated use remains unsolved.

Among widespread kinds of polymer wastes are spent synthetic cation exchangers having the form of a three-dimensional copolymer of styrene and divinylbenzene with grafted functional groups, which lose the ion-exchange power during operation. It is well known [1] that ion-exchange treatment of aqueous solutions involves various reactions yielding sparingly soluble, weakly dissociated, and complex compounds.

A no less important problem is treatment of wastewater formed in production of synthetic rubbers and latexes. This wastewater is a dilute colloidal system containing difficultly removable finely dispersed particles of quality standard rubber and concomitant organic components, such as potassium soaps of resin and fatty acids entering into the composition of rosin or tall oil, and also the nonbiodegradable Leukanol (Table 1).

The specific features of the polymer matrix and functional groups of spent ion exchangers, in combination with the properties of elastomers and surfactants present in wastewater, formed the basis for the development of an integrated process for reprocessing of waste cation-active resins and the efficient treatment of wastewater, with utilization of its valuable components.

As an object of study we used pure and spent cation exchangers: gel-like KU-2 × 8 and macroporous KU-23 with a specific surface area of 35 $m^2 g^{-1}$. The content of metal ions in the spent cation exchangers was 35–45 mg per gram of cation exchanger, predominantly in the form of iron ions (up to 25 mg per gram of cation exchanger). The ion-exchange resins were ground in a ball mill and also in a 1A27 disintegrator produced by the EKS (Riga, Latvia) with an efficiency of 2.0 kg h^{-1} and rotation rate of 8000 rpm, which allowed preparation of a filler with a particle size of up to 5 μm.

Table 1. Characteristics of wastewater formed in production of SKS-30ARK(M) rubber

Parameter	Parameter value	
	before treatment	after treatment
pH	4.9–6.5	7.0–8.5
COD, mg O_2 per 1 dm^3	1500–7500	80–200
BOD, mg O_2 per 1 dm^3	320–960	60–120
Polymer, mg dm^{-3}	35–1200	5–15
Suspended substances, mg dm^{-3}	90–300	5–20
Total content of salts of resin and fatty acids, mg dm^{-3}	175–280	10–20
Leukanol, mg dm^{-3}	90–350	Less than 2
Styrene, mg dm^{-3}	3–45	Absent

The content of Leukanol, oligomeric product of condensation of naphthalenesulfonic acid and formaldehyde with $n = 2–10$, in the solution was determined with an SF-46 spectrophotometer. The UV spectrum of Leukanol contains absorption bands peaked at 227 and 235 nm. The relative error of measurement of the Leukanol content was 5.0% [2].

The content of soaps of resin and fatty acids was determined by direct titration with alkali after the extraction of these acids from the acidified serum with diethyl ether [3].

The characteristic of the total contamination with organic substances, chemical oxygen demand (COD), was determined by the procedure [3] involving oxidation of organic compounds with an excess of potassium dichromate in a sulfuric acid solution, with heating in the presence of silver sulfate as a catalyst. The excess potassium dichromate was determined by titration with a solution of iron(II) sulfate, and the amount of potassium dichromate spent for the oxidation of organic substances was found from the difference.

The surface tension in the wastewater to be treated was determined tensimetrically on a Du Nouy device.

The physicochemical principles of wastewater treatment to remove polymer pollutants are presented in [4]. However, removal of concomitant components with the use of a finely dispersed waste formed in water treatment, spent KU-2 cation exchanger, was not considered [5].

The studies showed that addition of a finely dispersed spent cation exchanger in an amount of 0.1–1.5 g per gram of the polymer into rubber-containing wastes with vigorous stirring for 5–10 min ensures its uniform distribution over the wastewater volume. After the liquid-phase combination of the polymer phase with the finely dispersed cation exchanger, we performed their joint coagulation in a weakly acidic medium with the commonly used coagulant, aluminum sulfate or iron(III) chloride. The coagulation in an alkaline medium can be performed with a mineral powder, waste from production of building materials, whose major components are calcium oxide (70–95 wt %) and magnesium oxide (5–8%).

With the mineral powder, the filled latex system coagulates at pH 12.0 ± 0.5, and with aluminum sulfate or iron(III) chloride, at pH 3.5 ± 0.5, which is caused by the hydrolysis of the coagulants in the aqueous medium and release of OH^- and H^+ ions, respectively.

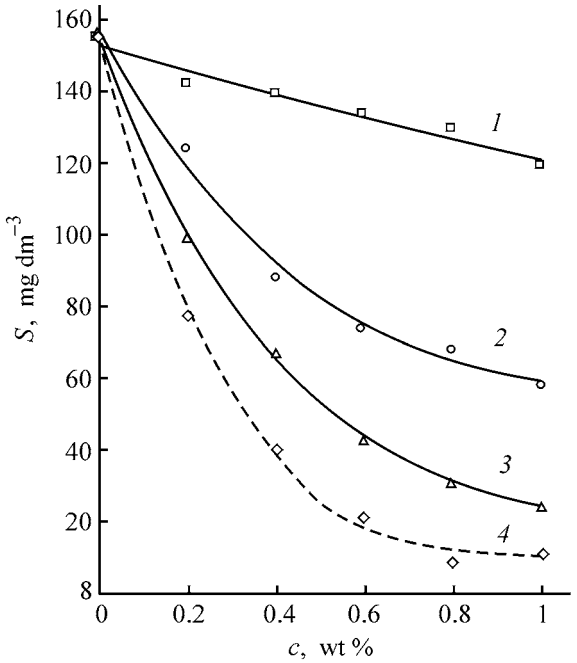


Fig. 1. Content of rosin soaps (surfactant) in the simulated waste vs. the concentration of the added cation exchanger with various structural characteristics. (*S*) Content of rosin soaps, and (*c*) concentration of cation exchanger. Gel cation exchanger KU-2 in the simulated wastes: (*1*) fresh and (*2*) spent. Spent macroporous cation exchanger KU-23: (*3*) simulated waste and (4) simulated waste containing 1.0 g dm^{-3} mineral powder.

It should be noted that a high degree of purification judget from COD, without using a spent cation exchanger is observed with aluminum sulfate or iron(III) sulfate as a coagulant, which is consistent with the Schulze–Hardy rule according to which the coagulating effect is exhibited by the counter-ion, and this effect increases with its charge.

Addition of milled ion-exchange resins to the latex wastewater causes a decrease in the COD upon coagulation, which is due to additional recovery of soaps of resin and fatty acids and also Leukanol. Figure 1 shows that the use of a spent ion-exchange resin, KU-2 cation exchanger belonging to the sorbents with a gel structure and high degree of neutralization of sulfo groups (more than 50%), allows the content of resin and fatty acids in the simulated waste to be decreased. The sorption power with respect to the surfactant significantly increases when using a spent macroporous cation-exchanger KU-23.

It is well known [6] that the volume of gel ion-exchange resins increases upon swelling, and coarse organic ions or uncharged molecules can penetrate into the space between the polymer chains of their network structure (matrix). In this case, coarse organic ions

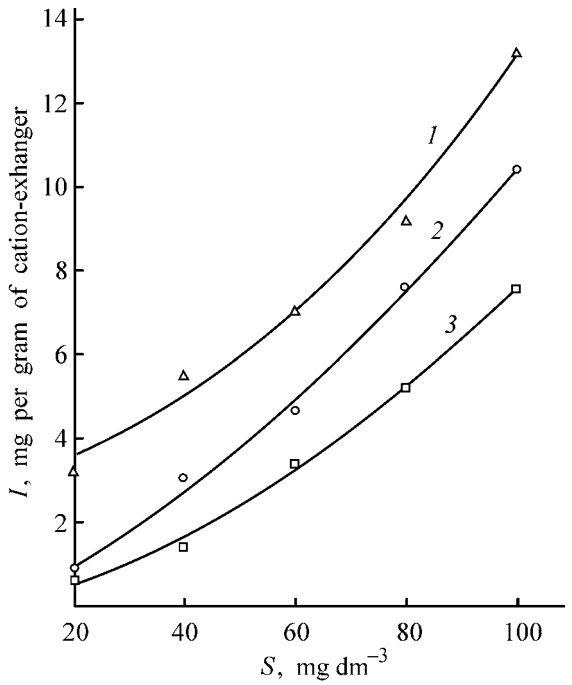


Fig. 2. Sorption isotherms of Leukanol in relation to the dispersity of cation exchangers and their structural characteristics. (*I*) Specific sorption power and (*S*) Leukanol content. Cation-exchanger: (*1*) macroporous (KU-23) and (*2*, *3*) gel-like (KU-2). Particle size of cation exchanger, μm: (*1*, *2*) 5–20 and (*3*) 80–100.

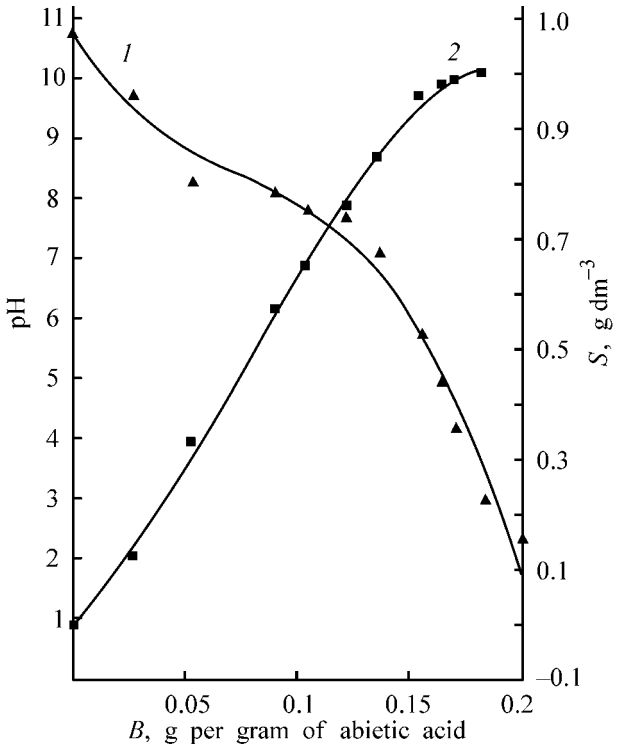
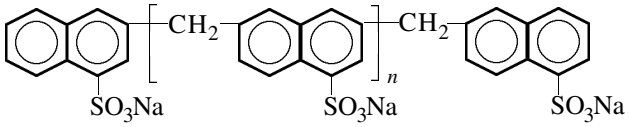


Fig. 3. Influence of the sulfuric acid expenditure *B* on (*1*) pH and (*2*) content of abietic (resin) acid in aqueous solution, *S*.

can be not only absorbed with ion-exchange materials as a result of substitution for inorganic counter-ions of ion exchangers, but also firmly retained as a result of adsorption [1].

Therefore, the regeneration of ion-exchange resins used for treatment of water containing various types of surfactants and macromolecular compounds is severely complicated.

However, this factor, negative at first glance, can be useful in our case as providing irreversible recovery of ionized surfactant molecules and Leukanol from wastewater with likely charged particles of spent resins KU-2 and KU-23. This fact is of particular importance for removal of highly toxic nonbiodegradable detergent Leukanol, which is an oligomeric polyelectrolyte with the general formula



The presence of Leukanol in wastewater prevents its treatment at biological treatment facilities.

The studies showed that the sorption power of the cation exchanger with respect to Leukanol does not noticeably depend on the impurity content, i.e., on the extent of charge compensation in the cation exchanger, and is determined by its structure and degree of dispersion (Fig. 2).

The recovery of soaps of resin and fatty acids from wastes with a spent cation exchanger as a sorbent and a mineral powder or aluminum sulfate [or iron(III) chloride] as a coagulant, is due to the following factors. The first of these is conversion of soaps of resin and fatty acids to their Ca^{2+} and Mg^{2+} salts, which are poorly soluble in water, using the mineral powder, i.e., calcium and magnesium oxides, which favors the formation of macromolecular globules and, as a consequence, sorption interaction with the network structure of the KU-2 gel-like cation exchanger. Second, with iron(III) chloride or aluminum sulfate used in a medium with pH 3.5 ± 0.5 (Fig. 3), poorly soluble salts of resin and fatty acids with the ions of these metals can be formed and, the emulsifiers based on rosin and fatty acids transform into low-polarity acids, which are sorbed by the inner and outer surfaces of particles of the swollen cation exchanger.

The above facts suggest that resin and fatty acids are better sorbed by the cation-exchanger surface, which is confirmed by the decrease in the surface ten-

sion (Fig. 4) in conversion of soaps in wastewater. However, coagulation in an acidic medium can result in secondary contamination with metal ions present in the spent ion-exchange resin via partial regeneration of the ion-exchange resin, which complicates the use of spent cation exchangers as adsorbents of organic compounds from acidic medium.

The degree of compensation of the fixed charge affects the sorption power of the surfactant, i.e., the spent cation exchanger loses the ion-exchange power because of the formation of weakly dissociated compounds, which is accompanied by the loss of polarity by functional groups.

However, spent ion-exchangers do not completely lose the functional power. For example [1], the commonly used procedures of water treatment at heat and electric power plants allow utilization of, at most approximately 50% of the total exchange capacity of ion exchangers.

Milling of spent cation-exchangers allows partial regeneration of their functionality, which, in turn, causes a decrease in the adsorption power with respect to anionic surfactants. However, addition of a coagulant solution or suspension to a latex system filled with a cation exchanger is accompanied by ion exchange between the fixed ions and cations of the coagulant in alkaline medium, which allows neutralization of charges of fixed ions and increase in the sorption power (Fig. 1).

All the components of coagulated latex wastes, including Leukanol present in the form of separate molecules, interact with the surface of the finely dispersed adsorbent. As a result of adsorption, the total contamination with respect to COD and the surface tension decrease (Fig. 4).

In liquid-phase filling of latex wastes with spent cation exchangers, the concomitant components are recovered, i.e., the wastewater is purified (Table 1) and a filled polymer system is obtained. The filled rubber composition is separated from the waste using a vibrosieve with subsequent mechanical and thermomechanical dehydration. The resulting vulcanized rubbers based on the polymer composite have characteristics comparable with those of the elastomers filled with Kerogen-70, which is well known as organomineral filler of rubber stocks (Table 2).

Analysis of the physicomechanical characteristics shows that the impurities present in spent cation exchangers do not noticeably affect these characteristics.

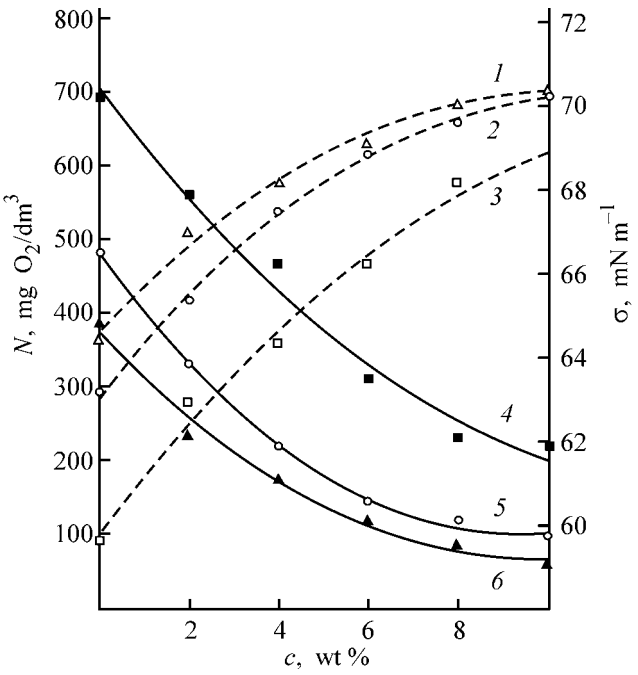


Fig. 4. COD N and surface tension σ vs. the concentration of spent KU-2 cation exchanger in the waste, c, with the initial content of the polymer of 10 g dm^{-3}, upon treatment with various coagulants. (*1–3*) Surface tension and (*4–6*) COD. Coagulant: (*1*, *6*) iron(III) chloride, (*2*, *5*) aluminum sulfate, and (*3*, *4*) mineral powder.

CONCLUSIONS

(1) Milled spent cation exchanger exhibits adsorption power with respect to anionic surfactants (soaps of resin acids and synthetic fatty acids) and also to oligomeric polyelectrolyte, Leukanol.

(2) In utilization of a spent cation exchanger, it is appropriate to recover soaps of resin and fatty acids in an alkaline medium.

Table 2. Influence of the filler type on the physicomechanical characteristics of vulcanized rubbers (composition of rubber stock, wt parts: rubber 100, filler 40, stearin 2, zinc white 5, Captax 3, and sulfur 2)

Filler type	Ultimate tensile stress, MPa	Tear resistance, kN m^{-1}	Shore hardness, *A*, arb. units
P-234 carbon black	8.3	56	64
Technical-grade chalk	2.3	12	42
Kerogen	6.1	42	46
Initial KU-2	5.4	36	52
Spent KU-2	5.9	38	54

(3) Preparation of polymer composites in waste treatment reduces the impact of wastes on the environment and expands the sources of raw materials.

REFERENCES

1. Ashirov, A., *Ionoobmennaya ochistka stochnykh vod, rastvorov i gazov* (Ion-Exchange Treatment of Wastewaters, Solutions, and Gases), Leningrad: Khimiya, 1983.
2. Yakubenok, E.F., Poluektov, P.T., Svatikov, V.P., et al., *Proizv. Ispol'z. Elastom.*, 1991, no. 9, pp. 3–4.
3. Lur'e, Yu.Yu., *Analiticheskaya khimiya promyshlennykh stochnykh vod* (Analytical Chemistry of Industrial Wastewaters), Moscow: Khimiya, 1984.
4. Poluektov, P.T. and Korchagin, V.I., *Proizv. Ispol'z. Elastom.*, 1998, no. 4, pp. 11–13.
5. RF Patent no. 2271335.
6. Koganovskii, A.M. and Klimenko, N.A., *Fiziko-khimicheskie osnovy izvlecheniya poverkhnostno-aktivnykh veshchestv iz vodnykh rastvorov i stochnykh vod* (Physicochemical Principles of Recovery of Surfactants from Aqueous Solutions and Wastewaters), Kiev: Naukova Dumka, 1978.

ISSN 1070-4272, Russian Journal of Applied Chemistry, 2006, Vol. 79, No. 10, pp. 1617–1620. © Pleiades Publishing, Inc., 2006.
Original Russian Text © S.A. Lobanov, V.Z. Poilov, A.V. Sofronova, 2006, published in Zhurnal Prikladnoi Khimii, 2006, Vol. 79, No. 10, pp. 1638–1641.

ENVIRONMENTAL PROBLEMS OF CHEMISTRY AND TECHNOLOGY

Wastewater Purification To Remove Ammonium Ions by the Oxidation Method

S. A. Lobanov, V. Z. Poilov, and A. V. Sofronova

Perm State Technical University, Perm, Russia

Received March 10, 2006

Abstract—Wastewater purification to remove ammonium ions and carbamide by oxidation with hypochlorites of alkali and alkaline-earth metals was studied. The effect of various factors on the degree of purification was examined experimentally.

DOI: 10.1134/S1070427206100119

At present, the problem of wastewater purification to remove ammonium ions is encountered by numerous of industrial plants. The large amount of ammonium nitrogen in wastewater leads to oxygen starvation of plants and adversely affects the flora and fauna of the water basin.

Various methods [1] can be used in wastewater purification to remove ammonium ions. However, the majority of these methods have a number of drawbacks, which restricts their application. One of widely applied methods of purification of wastewater with low content of ammonium ions is the oxidative method. Ozone and chlorine can be used as oxidizing agents; however, their use involves gross expenditure and severe hazard. Hypochlorites of alkali and alkaline-earth metals can also be used [2]. In this case, a preliminary adjustment of wastewater pH to initial values of 8–10.5 with an alkaline agent or a buffer mixture is necessary. After that, a treatment with hypochlorite ions is carried out using hypochlorites of alkali or alkaline-earth metals (NaClO or $Ca(ClO)_2$) in amounts equivalent to, or exceeding by 5%, the equivalent content of ammonia or ammonium salts in wastewater. The oxidation proceeds in a liquid homogeneous medium to form a gaseous final product [3]:

$$2NH_4OH + 3NaClO = N_2 + 3NaCl + 5H_2O,$$

$$4NH_4OH + 3Ca(ClO)_2 = 2N_2 + 3CaCl_2 + 10H_2O.$$

As a result, toxic ammonium ions are replaced with sodium or calcium ions.

The method is simple in use, does not require development of special installations (necessary in ozonization), and provides a high degree of purification. Unlike chlorine and ozone, solutions of sodium or calcium hypochlorites are safe and less expensive, because they are formed as waste in catching of chlorine from discharge gases at soda and magnesium plants. Owing to such advantages, this method has found industrial application.

In the present study, we carried out a technological analysis in order to develop the optimal modes of wastewater purification to remove ammonium ions NH_4^+ by the oxidation method. The aim of the study was to determine the degree of wastewater purification to remove NH_4^+ under various chemical and technological conditions, such as temperature (for summer and winter conditions), pH of the medium, and amount of an oxidizing agent.

The following procedure was used in the experiments. A 100-ml portion of wastewater with a preliminarily determined content of ammonium ions was poured in a temperature-controlled reaction vessel. Then, using a separating funnel, we poured in a calculated amount of the solution of an oxidizing agent. The mixture was continuously agitated for a prescribed time. To determine the degree of water purification to remove ammonium ions, we sampled the reaction mixture to determine the content of NH_4^+ and ClO^- ions at certain intervals of time. We used wastewater from nitrogen-fertilizer plants, formed in the carbamide production. Sodium and calcium hypochlorites were used as oxidizing agents. Sodium hypochlorite was manufactured by Bereznikovo chemical combine under brand name Belizna (Whiteness) and contained 78 g l^{-1} of active chlorine ClO^-. As cal-

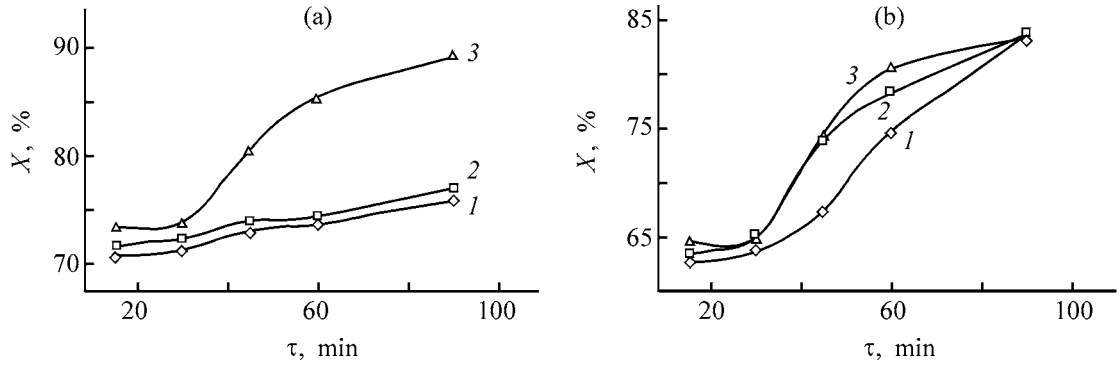


Fig. 1. Degree of wastewater purification, X, vs. time τ at various temperatures. Purification: (a) with sodium hypochlorite and (b) with calcium hypochlorite; the same for Figs. 2 and 3. Temperature (°C): (*1*) 0, (*2*) 20; (*3*) 30.

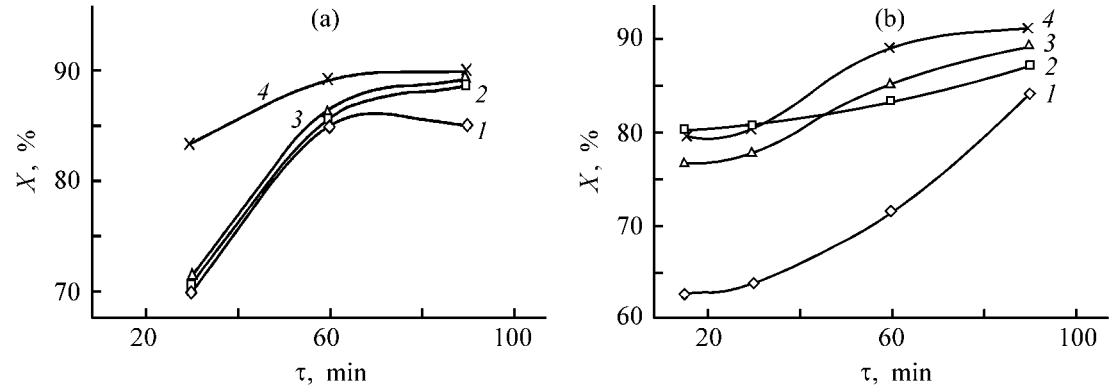


Fig. 2. Degree of wastewater purification, X, vs. time τ at various temperatures and an excess amount of the oxidizing agent. Temperature (°C): (*1*, *2*) 20 and (*3*, *4*) 30. Excess of the oxidizing agent (%): (*1*, *3*) 20 and (*2*, *4*) 40.

cium hypochlorite was used a clarified solution produced as a waste by the gas-purification station of Solikamsk magnesium plant. The content of active chlorine ClO^- was 66.48 g l^{-1}.

The dependences of the degree of purification of a wastewater containing 8.16 g l^{-1} of ammonium ions on time and temperature [stoichiometric consumption of NaClO and $Ca(ClO)_2$] at pH 8.5 are shown in Fig. 1. It can be seen that the effective purification time (T 20 and 30°C) is 60 min. After this time, the oxidation reaction continues, but its rate is low and the degree of purification varies only slightly. An increase in temperature results in that a higher degree of wastewater purification is achieved in a shorter time owing to the higher oxidation rate.

Comparing the action of oxidizing agents (Fig. 1), we can note that the degree of wastewater purification at 30°C is higher with sodium hypochlorite as compared with calcium hypochlorite, whereas at lower temperatures (0 and 20°C), the degree of wastewater purification with sodium hypochlorite is lower.

With $Ca(ClO)_2$, the final degree of purification, X (reached after 1.5 h), is virtually the same both at 30°C and at 0 and 20°C. Thus, calcium hypochlorite better oxidizes ammonium ions than sodium hypochlorite at low temperatures. Possibly, this is due to the presence of iron(III) impurity ions in the calcium hypochlorite solution, which accelerate the oxidation of ammonium ions.

We also found that the presence of an excess amount of the oxidizing agent also affects the completeness of wastewater purification to remove NH_4^+ ions (Fig. 2).

It can be seen from the time dependence of the degree of purification (Fig. 2) that the degree of purification increases with temperature and with the excess of hypochlorite. In the presence of an excess of hypochlorite, the reaction is more intensive even at the very beginning of the purification process and the degree of purification is higher, as demonstrated by the higher X values already after 30 min after the beginning of the process.

It is necessary to note that the maximum degree of wastewater purification to remove ammonium ions under the conditions specified in the experiments under discussion (Figs. 1 and 2) was 89–91%. At

Table 1. Results of wastewater purification with a calcium hypochlorite solution with preliminary neutralization of the wastewater with hydrochloric acid

τ, min	Wastewater without acidification (pH 8.5)		Fast neutralization (acidification to pH 5)		Neutralization within 1 h	
	$c_{NH_4^+}$, g l^{-1}	X, %	$c_{NH_4^+}$, g l^{-1}	X, %	$c_{NH_4^+}$, g l^{-1}	X, %
30	0.561	78.8	0.400	84.9	–	–
60	0.480	81.8	0.240	90.9	0	100
90	0.450	83.0	0.220	91.7	–	–

the same time, chemical analyses demonstrated that the efficiency of use of active chlorine in the oxidation process is higher and reaches 95–98%. This shows that a part of the oxidizing agent is consumed for oxidation of impurity components in wastewater. Carbamide is among such components. An analysis of the wastewater composition indicated that the content of carbamide considerably exceeds that of ammonium ions. In all probability, a part of hypochlorites enter into the following reactions with carbamide [4]

$$CO(NH_2)_2 + 3NaClO = 3NaCl + N_2 + CO_2 + 2H_2O,$$

$$2CO(NH_2)_2 + 3Ca(ClO)_2 = 3CaCl_2 + 2N_2 + 2CO_2 + 4H_2O.$$

For comparison purposes and for revealing the influence exerted by the presence of carbamide on the completeness of wastewater purification to remove ammonium ions, we carried out experiments with a model solution free of carbamide admixtures. The model solution was prepared by diluting a concentrated aqueous solution of ammonia. To compare the results, we prepared a solution containing 8.14 g l^{-1} of NH_4^+, which corresponds to the concentration of NH_4^+ in wastewater. The experiments were carried out at 20°C with a varied amount of the oxidizing agent introduced into wastewater. The results of these experiments are shown in Fig. 3.

It is seen from Fig. 3 that the degree of purification of the model solution to remove NH_4^+ ions is higher than that for the industrial wastewater. These data confirm that the oxidizing agent is partly consumed for side reactions in wastewater purification. Therefore, it is expedient to preliminarily decompose carbamide immediately before the subsequent purification with hypochlorites.

Carbamide is known [5] to be decomposed in acid media by the reaction

$$CO(NH_2)_2 + 2HCl + H_2O = 2NH_4Cl + CO_2.$$

In this context, we carried out experiments on treatment of wastewater containing 2.65 g·l^{-1} of NH_4^+ first with hydrochloric acid to pH 5 and then with calcium hypochlorite. In one experiment, the neutralization with hydrochloric acid was fast, and in the other, the neutralized solution was kept for 60 min. Then the wastewater was treated with a clarified solution of calcium hypochlorite. The volume ratio of the oxidizing agent solution to wastewater was 0.110. The results of the experiments are listed in Table 1. For com-

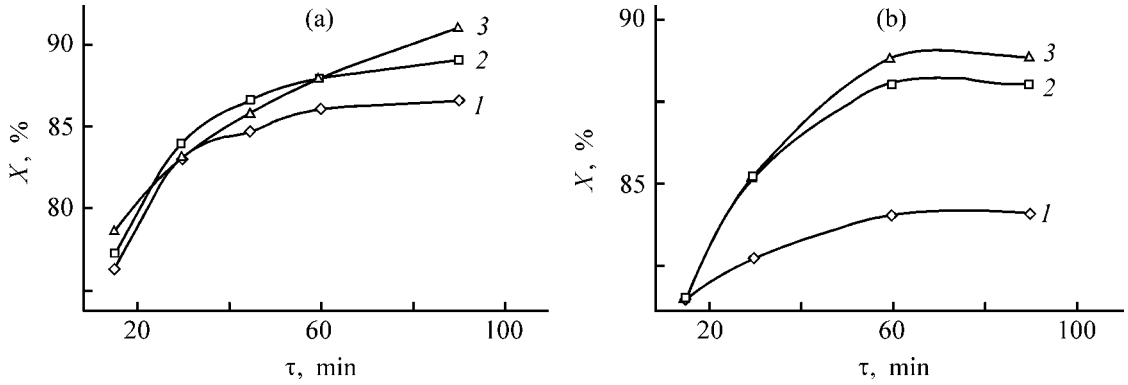


Fig. 3. Degree of purification of model wastewater, X, vs. time τ at varied excess of the oxidizing agent. Excess of the oxidizing agent (%): (*1*) 0, (*2*) 5, and (*3*) 20.

Table 2. Parameters of purification of water containing 0.530 g l^{-1} of ammonium ions at pH 5

Residual content, mg l^{-1}			Degree of wastewater purification, %	
NH_4^+	$CO(NH_2)_2$	ClO^-	to remove $CO(NH_2)_2$	to remove NH_4^+
1.1	320	0	98.93	99.79
1.7	341	0	98.86	99.68
0	36	0	99.88	100

parison, we carried out experiments on wastewater purification without preliminary neutralization (acidification with hydrochloric acid).

Analysis of the experimental data in Table 1 demonstrates that, with preliminarily neutralization of wastewater with hydrochloric acid for 60 min and the subsequent water treatment with calcium hypochlorite, 100% of ammonium ions are removed from wastewater. In the case of fast neutralization of wastewater with hydrochloric acid (for 30 min) and subsequent treatment of wastewater with calcium hypochlorite, carbamide contained in wastewater has not enough time to decompose, and the degree of wastewater purification to remove ammonium ions is 91.7%. Nevertheless, the degree of purification with calcium hypochlorite of wastewater acidified to pH 5 is higher than that at pH 8.5.

Similar experiments on neutralization with hydrochloric acid in wastewater purification were carried out with water containing 0.530 g l^{-1} of ammonium ions and 30 g l^{-1} of carbamide. The expenditure of the calcium hypochlorite solution was 0.25 m^3 per 1 m^{-3} of sewage. The duration of wastewater treatment with hydrochloric acid and calcium hypochlorite was 60 and 90 min, respectively. The results of these experiments on wastewater purification are listed in Table 2.

The data in Table 2 demonstrate that wastewater purification by the technique described above makes it possible to reduce the concentration of carbamide in wastewater to 36 mg l^{-1} (degree of purification 99.88%) and that of ammonium ions to 0–1.7 mg l^{-1} (degree of purification 99.68–100%). The residual concentration of hypochlorite ions in wastewater is zero.

CONCLUSIONS

(1) At high initial concentrations of ammonium ions in wastewater, an increased expenditure of NaClO and $Ca(OCl)_2$, which depends on the initial concentration of ammonium ions and carbamide, is required for achieving a high degree of purification by oxidation.

(2) Under winter conditions of purification (0°C), the rate of oxidation slightly decreases, which leads to a lower degree of purification or requires a longer duration of the process (up to 60–90 min).

(3) The carbamide impurity present in wastewater is oxidized by hypochlorites of alkali and alkaline-earth metals, which results in a decrease in the degree of water purification to remove ammonium ions by approximately 10%. Purification of water with high content of carbamide impurity requires that an excess amount of hypochlorites of alkali and alkaline-earth metals should be added, which enables purification of contaminated water to remove not only ammonium ions, but also carbamide.

(4) Preliminary adjustment of the pH of discharged solutions with high content of ammonium ions and carbamide makes it possible to raise the degree of water purification to remove ammonium ions by 10%. At a longer treatment duration, wastewater purification by this technique makes it possible to reduce the concentration of carbamide to 36 mg l^{-1} (degree of purification 99.88%) and that of ammonium ions to 0–1.7 mg l^{-1} (degree of purification 99.68–100%). In this case, the residual concentration of hypochlorite ions in wastewater is zero.

REFERENCES

1. Proskurjakov, V.A. and Shmidt, L.I., *Ochistka stochnykh vod khimicheskoi promyshlennosti* (Wastewater Purification in Chemical Industry), Leningrad: Khimiya, 1977.
2. US Patent 4 137 166.
3. Kudryavskii, Yu.P., *Tsv. Metall.*, 1997, nos. 8–9, pp. 46–48.
4. Gorbunov, S.A., *Cand. Sci. (Chem.) Dissertation*, Perm: Perm Gos. Tekhn. Univ., 2005.
5. *Kratkaya khimicheskaya entsiklopediya* (Concise Chemical Encyclopedia), Knunyants, I.L., Ed., Moscow: Sovetskaya Entsiklopediya, 1964.

ISSN 1070-4272, Russian Journal of Applied Chemistry, 2006, Vol. 79, No. 10, pp. 1621–1625. © Pleiades Publishing, Inc., 2006.
Original Russian Text © E.G. Mamedov, 2006, published in Zhurnal Prikladnoi Khimii, 2006, Vol. 79, No. 10, pp. 1642–1646.

ORGANIC SYNTHESIS AND INDUSTRIAL ORGANIC CHEMISTRY

Asymmetric Diels-Alder Reaction between Acrylates and Cyclopentadiene in the Presence of Chiral Catalysts

E. G. Mamedov

Institute of Petrochemical Processes, National Academy of Sciences of Azerbaijan, Baku, Azerbaijan

Received August 17, 2005; in final from, March 2006

Abstract—Asymmetric Diels-Alder reaction between cyclopentadiene and alkyl and cycloalkyl acrylates in the presence of new chiral catalysts, $BBr_3 \cdot MentOEt$, $AlCl_2OMent$, BBr_2OMent, and $BBr(OMent)_2$, was studied. Optically active bicyclo[2.2.1]hept-2-ene-5-carboxylates were synthesized. The influence of the reaction conditions on the total and optical yields and on the stereoselectivity of the adducts synthesized was examined.

DOI: 10.1134/S1070427206100120

The asymmetric catalysis is currently under rapid development. The number of publications on this subject and the finance assigned to development of this line tend to increase [1–3]. Organic reactions performed in the presence of chiral catalysts underlie modern asymmetric synthesis. A key issue for achievement of high results in this field is directed synthesis of new efficient optically active catalysts [4].

Norbornene and its saturated analogue norbornane are essential fragments of many important natural compounds [5]. Today, synthesis of new compounds containing these moieties attracts the researchers' attention [6–8]. Synthesis of representatives of this class of compounds in the optically active form is of certain theoretical and practical interest.

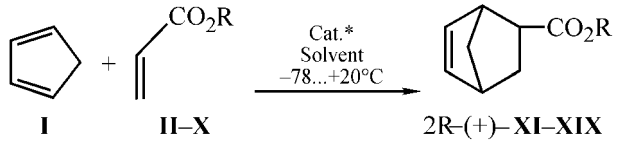
Among the promising lines of synthesis of optically active norbornene derivatives is the asymmetric Diels-Alder reaction (ADAR) in the presence of chiral catalysts. We described the first example of ADAR with $BF_3 \cdot MentOEt$ as chiral catalyst in [9]. That study laid the foundations of an efficient method of synthesis of optically active derivatives of norbornene by ADAR, which was further developed [10, 11] using optically active methyloxy- and bornyloxyaluminum dichlorides.

Here we report the results of examination of ADAR between acrylates and cyclopentadiene (CPD) in the presence of chiral catalysts, aimed at preparation of optically active norbornene derivatives.

Chiral B- and Al-containing complex catalysts were synthesized from natural *l*-(–)menthol; their characteristics are listed in Table 1.

All chiral catalysts are well soluble in organic solvents (CH_2Cl_2, CCl_4, $CHCl_3$, C_6H_6, C_5H_5Cl, $C_6H_5CH_3$) and can be used as homogenous catalysts.

Optically active norbornenecarboxylates **XI**–**XIX** are prepared by ADAR according to the scheme



I **II–X** 2R–(+)–**XI–XIX**

where R = Et (**II**, **XI**), *n*-Pr (**III**, **XII**), *i*-Pr (**IV**, **XIII**), *n*-Bu (**V**, **XIV**), *i*-Bu (**VI**, **XV**), *t*-Bu (**VII**, **XVI**),

Table 1. Characterization of chiral catalysts

Catalyst	Initial compound	bp, °C (*P*, mm Hg)	$[\alpha]_D^{20}$, deg	Reference
$BBr_3 \cdot MentOEt$	MentOEt	187–188 (1)	–99.3	–
$AlCl_2OMent$	*l*-(–)-MentOH	181–182 (1)	–73.5	[10]
BBr_2OMent	*l*-(–)-MentOH	185–187 (1)	–78.5	–
$BBr(OMent)_2$	*l*-(–)-MentOH	191 (1)	–91.7	–

Table 2. Constants and elemental analysis data for compounds of optically active norbornenecarboxylates **XI**–**XIX**

Compound	bp °C (P, mm Hg)	n_D^{20}	d_D^{20}	Found, %		Formula	Calculated, %	
				C	H		C	H
XI	127–128 (15)	1.4805	1.038	71.19	8.97	$C_{10}H_{14}O_2$	72.28	9.03
XII	130–132 (25)	1.4795	1.0262	73.02	8.10	$C_{11}H_{16}O_2$	73.33	8.89
XIII	100–101 (10)	1.4630	0.9958	72.90	8.30	$C_{11}H_{16}O_2$	73.33	8.89
XIV	115–117 (10)	1.4602	0.9771	73.91	9.56	$C_{12}H_{18}O_2$	74.23	9.28
XV	104–105 (10)	1.4615	0.9794	73.50	8.89	$C_{12}H_{18}O_2$	74.23	9.28
XVI	101–103 (10)	1.4645	0.9889	75.22	8.99	$C_{12}H_{18}O_2$	74.23	9.28
XVII	115–117 (20)	1.5521	0.9780	74.16	8.13	$C_{13}H_{18}O_2$	75.72	8.73
XVIII	118–120 (20)	1.5526	0.9789	75.69	9.24	$C_{14}H_{20}O_2$	76.36	9.09
XIX	144–146 (5)	1.5261	0.9785	76.53	8.20	$C_{14}H_{18}O_2$	77.06	8.25

Table 3. Isomeric composition and total and optical yields of **XI**–**XIX** in relation to the reaction conditions

Dienophile	T, °C	Solvent	Catalyst	Catalyst : dienophile molar ratio	Yield of **XI**–**XIX**, %	Isomeric composition, %		Optical yield	$[\alpha]_D^{20}$, EtOH, deg
						endo	*exo*		
III	20	CH_2Cl_2	BBr_2OMent	0.25	88	94	6	35	+24.8
III	–10	CH_2Cl_2	BBr_2OMent	0.25	87	95	5	45	+31.9
III	–40	CH_2Cl_2	BBr_2OMent	0.25	87	96	4	50	+35.3
III	–70	CH_2Cl_2	BBr_2OMent	0.25	85	99	1	92	+67.5
III	–78	CH_2Cl_2	BBr_2OMent	0.25	82	99	1	94	+68.2
II	20	CH_2Cl_2	BBr_2OMent	0.25	88	96	4	35	+24.8
IV	20	CH_2Cl_2	$AlCl_2OMent$	0.25	89	96	4	35	+24.8
V	20	CH_2Cl_2	$AlCl_2OMent$	0.25	89	95	5	36	+25.5
VI	20	CH_2Cl_2	$AlCl_2OMent$	0.25	89	95	5	35	+24.8
VII	20	CH_2Cl_2	$AlCl_2OMent$	0.25	89	95	5	36	+25.5
VIII	20	CH_2Cl_2	$AlCl_2OMent$	0.25	88	96	4	36	+25.5
IX	20	CH_2Cl_2	$AlCl_2OMent$	0.25	89	96	4	36	+25.5
X	20	CH_2Cl_2	$AlCl_2OMent$	0.25	88	95	5	35	+24.8
III	–10	CH_2Cl_2	BBr_2OMent	0.5	88	96	4	45	+31.9
III	–10	CH_2Cl_2	BBr_2OMent	0.75	89	97	3	45	+31.9
III	–70	CH_2Cl_2	$AlCl_2OMent$	0.25	86	98	2	90	+63.8
III	–70	CH_2Cl_2	$BBr_3MentOEt$	0.25	85	98	2	91	+64.8
III	–70	CH_2Cl_2	$BBr(OMent)_2$	0.25	85	98	2	91	+64.8
IV	20	$C_6H_5CH_3$	BBr_2OMent	0.25	84	97	3	45	+31.9
IV	20	CCl_4	BBr_2OMent	0.25	83	98	2	45	+31.9
IV	20	$CHCl_3$	BBr_2OMent	0.25	84	98	2	45	+31.9
IV	20	C_6H_5Cl	BBr_2OMent	0.25	83	97	3	45	+31.9

cyclopentyl (**VIII**, **XVII**), cyclohexyl (**IX**, **XVIII**), and cyclohex-3-enyl (**X**, **XIX**).

The reaction was run in a wide temperature range from –78 to 20°C in a CH_2Cl_2 or $C_6H_5CH_3$ solution. The catalyst-to-dienophile molar ratio was varied from 0.25 to 0.75. The physicochemical characteristics of adducts **XI**–**XIX** synthesized are listed in Table 2.

We examined how various reaction parameters affect the isomeric composition, as well as optical and chemical yields of the compounds synthesized. The results are summarized in Table 3.

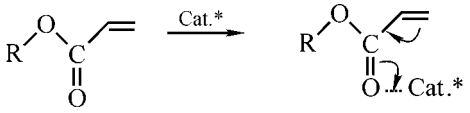
A mixture of *endo* and *exo* isomers of **XI**–**XIX** was separated by preparative chromatography. The amount of *exo* isomers was negligible; therefore, only *endo* isomers of the adducts were collected, and their optical activity was examined.

Table 3 shows that, in contrast to the noncatalyzed asymmetric Diels-Alder reaction of CPD with acrylic

diphenophiles, for which a temperature change insignificantly affects the optical yield of the adducts [12], the optical yield of **XI**–**XIX** significantly increases at lower temperatures in the presence of the chiral catalysts of interest. The optical yield of adduct **XII** with *endo* configuration, synthesized at –78°C, is as high as 94%.

On lowering the temperature, the stereoselectivity of the reaction increases, and the total yield of the adducts decreases. An increase in the content of chiral catalysts does not noticeably affect the optical yield of **XI**–**XIX**, but the total yield increases insignificantly. Table 3 also shows that the optical and total yields of the end products are virtually unaffected by the solvent.

At the reaction parameters within the limits examined, *endo* isomers of the adducts are preferentially formed. The isomeric composition of these adducts was determined by gas liquid chromatography. We found that all the Diels-Alder reactions between CPD and acrylates yield adducts with a positive rotation sign, as in the case of ADAR in the presence of Lewis acids [13]. The catalytic action of chiral catalysts can be attributed to formation of their complex with dienophiles **II**–**X**. The resulting electron deficiency on the multiple bond in dienophiles facilitates their reaction with CPD:

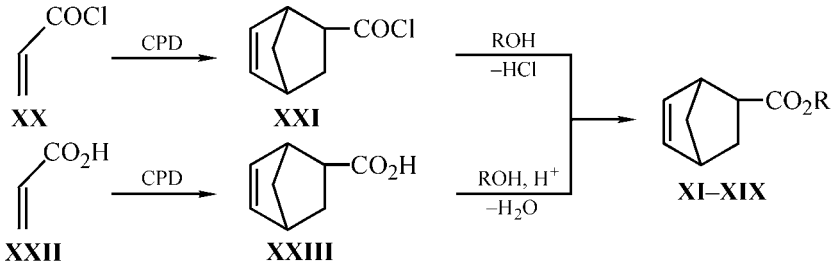


Here Cat.* is a chiral catalyst.

This is confirmed by a shift of the absorption band ν(C=O) from 1730 to 1640 cm^{-1} on passing from dienophiles to their complexes with chiral catalysts. These data are consistent with our observation that the absorption band of the C=O group of methacrylate is shifted from 1730 to 1630 cm^{-1} under the action of BBr_3, which suggests complexing between the catalysts and dienophiles.

All the physicochemical data for adducts **XI**–**XIX** synthesized by different procedures are identical.

The composition and structure of the compounds synthesized were confirmed by independent synthesis:



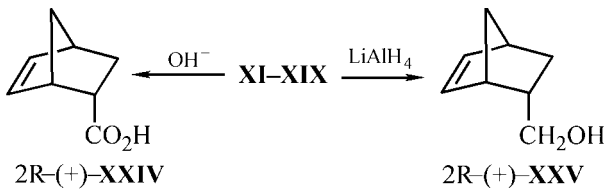
where R = Et, *n*-Pr, *i*-Pr, *n*-Bu, *i*-Bu, *t*-Bu, cyclopentyl, cyclohexyl, cyclohex-3-enyl.

The composition and structure of adducts **XI**–**XIX** were confirmed by their IR and ^1H NMR spectra.

In the IR spectra of the norbornenecarboxylates synthesized, the absorption bands of the ethylene moiety are observed at 1575–1550 and 3064–3040 cm^{-1} [ν(C=C), ν(C–H)]. The unusual position of the first absorption band is attributed to the strained state of the double bond [14]. The ν(C–H) absorption is characteristic of norbornenes, which distinguishes them both from alkenes with the terminal double bond (3080 cm^{-1}) and from cyclohexene (3024 cm^{-1}).

More information can be derived from the ^1H NMR spectra of nonbornenes derivatives. The spectra of the esters synthesized contain characteristic signals due to protons of the double bond of the norbornene moiety at 5.8–6.2 ppm. The signals from protons of the olefin moieties of the *exo* isomers are close because of the spatial remoteness from magnetically anisotropic groups of the substituent. The signals from *endo* isomers are significantly nonequivalent because of the shorter distance from the substituent situated on the rear side of the bicyclic moiety. The bridgehead protons appear at 2.6–2.9 ppm as a multiplet.

To determine the optical yield of the chiral compounds **XI**–**XIX**, they were converted either to **XXIV** by base hydrolysis or to **XXV** by reduction with $LiAlH_4$:



The optical yield of **XI**–**XIX** was determined by comparing the specific rotation of the *endo*-bicyclo[2.2.1]-hept-5-ene-2-carboxylic acid **XXIV** or 2-hydroxymethylbicyclo[2.2.1]hept-5-ene **XXV** synthesized with those of the corresponding enantiomerically pure sample described by Berson et al. [15]. Based on the correlation of the optical rotation sign of compounds with the known configuration [15], the relative configuration of **XI**–**XIX** was determined to be 2R–(+) for all the adducts with *endo* configuration.

EXPERIMENTAL

The IR spectra were measured on a UR-20 spectrophotometer at 4000–400 cm^{-1}, and the ^1H NMR spectra, on a Tesla BS-48 (80 MHz) spectrometer in CCl_4 with hexamethyldisiloxane as internal reference. The optical rotation was measured on a Perkin–Elmer-141 polarimeter and on a Spektropol-1 spectropolarimeter. Preparative separation was carried out on 900 × 0.8-cm columns packed with Porovina + 5% polyethylene glycol adipate; evaporator and column temperature, 240 and 170°C, respectively; carrier gas (nitrogen) flow rate 200 $cm^3\ min^{-1}$; flame-ionization detector; a Varian-Aerograph chromatograph. Chromatographic analysis of the compounds we synthesized was performed and their purity was determined with an LKhM-8MD chromatograph with a thermal-conductivity detector; 300 × 0.3-cm column with 5% Porovina on Dinokhrom II; carrier gas (helium) flow rate 40 $cm^3\ min^{-1}$; column and evaporator temperature, 145 and 240°C, respectively.

Acryloyl chloride **XX** was prepared by the known procedure [16].

The starting alkyl and cycloalkyl acrylates **II**–**X** were prepared by the reactions of acryloyl chloride with the corresponding alcohols [17].

The chiral catalysts were prepared by the known procedures: $BBr_3 \cdot$ MentOEt [16], $AlCl_2$OMent, BBr_2OMent, and BBr(OMent)$_2$ [18]. Alkyl and cycloalkylbicyclo[2.2.1]hept-2-ene-5-carboxylates **XI**–**XIX** were prepared by the reactions of CPD with the corresponding acrylates. To a 0.05 M solution of acrylate in 20 ml of CH_2Cl_2, 0.0125 mol of chiral catalyst in 10 mol of CH_2Cl_2 was added at a prescribed temperature. Next, 0.05 M of freshly distilled CPD in 10 ml CH_2Cl_2 was added dropwise with stirring.

After stirring for 0.5 h, the mixture was treated with a dilute HCl solution, washed with distilled water, and dried over $MgSO_4$. After the solvent was evaporated, the residue was vacuum-distilled (for conditions and results see Table 3).

Independent synthesis. Bicyclo[2.2.1]hept-2-ene-5-carboxylic acid chloride **XXI** [17] and bicyclo-[2.2.1]hept-2-ene-5-carboxylic acid **XXIII** [19] were prepared by known procedures. Independent synthesis of **XI**–**XIX** was carried out by the reactions of chloride **XXI** or acid **XXIII** with the corresponding alcohols. All the physicochemical characteristics of compounds **XI**–**XIX** prepared by independent synthesis are identical to those of the compounds prepared by condensation of CPD with acrylates **II**–**X** (Table 2).

CONCLUSIONS

(1) Asymmetric Diels-Alder reaction of alkyl and cycloalkyl acrylates with cyclopentadiene in the presence of chiral catalysts $BBr_3 \cdot$ MentOEt, $AlCl_2$OMent, BBr_2OMent, and BBr(OMent)$_2$ yields optically active norbornenecarboxylates with R–(+) configuration.

(2) As temperature is lowered, the optical yield of norbornenecarboxylates tends to grow and reaches 94% at –78°C; with increasing temperature, the total yield tends to grow, and the stereoselectivity, to fall.

(3) An increase in the content of the chiral catalyst does not noticeably affect the optical yield, but the total yield tends to increase; the solvent only slightly affects the optical and total yields of the adducts.

REFERENCES

1. Pavlov, V.A., *Usp. Khim.*, 2004, vol. 42, no. 12, pp. 1269–1304.
2. Murzin, D.Yu., Myaki-Arvela, P., and Salmi, T., *Kinet. Katal.*, 2003, vol. 44, no. 3, pp. 353–364.
3. Stinson, S.C., *Chem. Eng. News*, 1999, no. 1, pp. 101–106.
4. Gavrilov, K.N., Bondarev, O.G., and Polosukhin, A.I., *Usp. Khim.*, 2004, vol. 73, no. 7, pp. 726–756.
5. Potapov, V.M., *Stereokhimiya* (Stereochemistry), Moscow: Khimiya, 1988.
6. Kas'yan, L.I., Okovityi, S.I., Bombushkar', M.F., et al., *Zh. Org. Khim.*, 2000, vol. 36, no. 2, pp. 218–228
7. Kas'yan, L.I., Tarabara, I.N., Kas'yan, A.O., et al., *Zh. Org. Khim.*, 2002, vol. 38, no. 1, pp. 29–35.
8. Kas'yan, A.O., Golodaeva, A.V., and Tsygankov, A.V., *Zh. Org. Khim.*, 2002, vol. 38, no. 11, pp. 1661–1669.

9. Guseinov, M.M., Akhmedov, I.M., and Mamedov, E.G., *Azerb. Khim. Zh.*, 1976, no. 1, pp. 46–48.
10. JPN Patent 53–138926, *Ref. Zh. Khim.*, 1981, no. 19, 19N81P.
11. Bao, J. and Walf, D., *J. Am. Chem. Soc.*, 1993, vol. 115, no. 9, pp. 3814–3815.
12. Farmer, R.F., and Hamer, J., *J. Org. Chem.*, 1966, vol. 31, no. 7, pp. 2418–2419.
13. Mamedov, E.G., *Zh. Org. Khim.*, 2001, vol. 37, no. 2, pp. 230–235.
14. Zefirov, N.S. and Sokolov, V.I., *Usp. Khim.*, 1967, vol. 36, no. 2, pp. 243–268.
15. Berson, J.A., Remaninck, A., Suzuki, S., et al., *J. Amer. Chem. Soc.*, 1961, vol. 83, no. 8, pp. 3986–3997.
16. Weigand-Hilgetag, *Organisch-Chemische Experimentierkunst*, Hilgetag, H.G. and Martini, A., Eds. Leipzig: Johann Ambrosius Barth, 1964, 3d Ed.
17. Akhmedov, I.M., Mamedov, E.G., Kyazimov, E.A., et al., *Azerb. Khim. Zh.*, 1980, no. 5, p. 5155.
18. Mamedov, E.G., *Azerb. Khim. Zh.*, 2001, no. 3, pp. 27–31.
19. Nody, C.D., *J. Amer. Chem. Soc.*, 1954, vol. 76, no. 11, pp. 2907–2910.

ISSN 1070-4272, Russian Journal of Applied Chemistry, 2006, Vol. 79, No. 10, pp. 1626–1628. © Pleiades Publishing, Inc., 2006.
Original Russian Text © L.A. Badykova, R.Kh. Mudarisova, G.S. Khamidullina, Kh.K. Aminev, I.M. Borisov, Yu.B. Monakova, 2006, published in Zhurnal Prikladnoi Khimii, 2006, Vol. 79, No. 10, pp. 1647–1649.

ORGANIC SYNTHESIS AND INDUSTRIAL ORGANIC CHEMISTRY

Modification of Arabinogalactan and Its Oxidized Forms with *p*-Aminosalicylic Acid

L. A. Badykova, R. Kh. Mudarisova, G. S. Khamidullina, Kh. K. Aminev, I. M. Borisov, and Yu. B. Monakova

Institute of Organic Chemistry, Ufa Scientific Center, Russian Academy of Sciences, Ufa, Bashkorkostan, Russia

Bashkir State Medical University, Ufa, Bashkorkostan, Russia

Republican Antitubercular Dispensary, State Institution of Public Health, Ufa, Bashkorkostan, Russia

Received May 11, 2006

Abstract—The reaction of arabinogalactan and its oxidized forms with an antitubercular agent, *p*-aminosalicylic acid, was studied. The reaction conditions, chemical composition, and some physicochemical characteristics of the modified compounds were examined.

DOI: 10.1134/S1070427206100132

Arabinogalactan (AG) is a natural water-soluble polysaccharide whose macromolecules have a branched structure and a molecular weight of approximately 40 000. Arabinogalactan has a wide spectrum of biological activity and exhibits immunomodulating, antimutagenic, gastroprotective, and antimicrobial properties. Its specific types of biological activity, combined with a high membranotropism and dispersive power open wide avenues for using AG in medicine and other fields [1–3]. Arabinogalactan is readily subjected to various physical and chemical modifications allowing adjustment of its physicochemical characteristics. For example, modification of AG with medical products is one of the ways for production of more perfect forms of drugs [3–5]. Binding of drugs with AG provides prolonged effect and significantly reduces the toxicity of the initial drugs owing to a decrease in the total amount of a drug for a course of treatment [6].

In this study we examined modification of AG and its low-molecular-weight oxidized forms with an antitubercular agent, *p*-aminosalicylic acid (*p*-ASA) [7].

EXPERIMENTAL

We used AG with a molecular weight of 40 000, recovered by aqueous extraction from Siberian larch wood [8]. Extraction and purification of AG to remove water-soluble phenolic compounds was performed on a polyamide sorbent [8]. In so doing, an aqueous polysaccharide solution containing trace amounts of flavonoids was obtained. The ratio of the residues of galactose and arabinose in the polymer is 5.6 : 1 [9]. The oxidative functionalization of AG was performed by oxidation of its aqueous-peroxide solutions with molecular oxygen in a glass bubble-type reactor. The volume of the reaction mixture was 10 ml. After the reaction completion, the polymeric form of oxidized AG was separated from the oligomeric form by precipitation with acetone. The oligomeric form was recovered from the supernatant by distillation of acetone and water, which was followed by drying of the product in a vacuum. The analysis of the functional groups of AG and polymeric (AG_{pol}) and oligomeric (AG_{ol}) forms was described in [10, 11].

The IR spectra of the samples in mineral oil were recorded on a Specord M-80 spectrophotometer. The optical density was determined on a Specord M-40 spectrophotometer; pH of the solutions was measured on an ANION 4100 pH-meter and adjusted by adding 0.1 M NaOH. The specific rotation $[\alpha]_D^{25}$ was measured on a Perkin–Elmer polarimeter (model 141).

The modified compounds were synthesized by the reaction of *p*-ASA with AG and its oxidized

Table 1. Characteristics of AG, AG_{pol}, and AG_{ol} modified with *p*-ASA

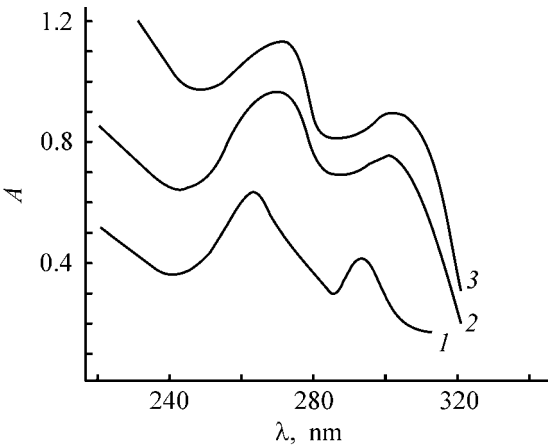
Compound	α_D^{20}	IR spectrum ν, cm^{-1}	Appearance
AG	+11.9	3600–3150 (OH), 1740–1710 (COOH), 1152–1080 (C–O)	White powder
AG_{pol}	+8.4	3600–3050 (OH), 1750–1715 (COOH), 1150–1072 (C–O)	Yellowish powder
AG_{ol}	+5.3	3600–3150 (OH), 1760–1720 (COOH), 1130–1090 (C–O)	Brown amorphous substance
AG + *p*-ASA	+13	3450–3020 (OH), 1740–1710 (COOH), 1580 (Ph), 1150–1070 (C–O)	Gray-violet powder
AG_{pol} + *p*-ASA	+9	3550–3015 (OH), 1710–1740 (COOH), 1580 (Ph), 1140–1070 (C–O)	Light violet powder
AG_{ol} + *p*-ASA	+10	2950–2850 (OH), 1760–1720 (COOH), 1580 (Ph), 1040–950 (C–O)	Black amorphous substance

species in water at pH 7–8 [12, 13]. The synthesis procedure was as follows: 1 g of the polysaccharide or oligosaccharide (5.55 base-mmol) was dissolved in 20 ml of distilled water. *p*-ASA in an amount of 0.85 g (5.55 mmol) was suspended in 20 ml of water and pH was adjusted to 7–8. A *p*-ASA solution was added dropwise to a polysaccharide solution, with vigorous stirring at 25°C. The reaction was carried out for 3 h. After the reaction completion, the product was precipitated with ethanol and recrystallized from water into ethanol; the precipitate was separated and washed three times with ethanol and then with diethyl ether and dried in a vacuum. It was shown by thin-layer chromatography (TLC) that the products purified by the above procedure were individual compounds and contained no mechanical impurities of *p*-ASA. The TLC of the complexes was performed on Silufol plates in the systems of solvents *n*-butanol : pyridine : water 6 : 4 : 5; ninhydrin was used as a developer.

The resulting modified compounds of the initial AG (AG + *p*-ASA) and its oxidized species (AG_{pol} + *p*-ASA, AG_{ol} + *p*-ASA) were studied by IR and UV spectroscopy; the rotation angles were determined (Table 1). In the IR spectra of the compounds, there is a shift of the absorption peak in the range 3600–3100 cm^{-1} (OH stretching modes) by 20–50 cm^{-1} and a low-frequency shift of the absorption peaks of stretching modes of the ether C–O bond of pyranose and furanose rings in the range 1200–1100 cm^{-1} by 10–15 cm^{-1}, suggesting also the formation of intermolecular hydrogen bonds between *p*-ASA and polysaccharide molecules. In addition, in the range 1500–1750 cm^{-1}, the intensity of absorption band at 1750 cm^{-1} caused by vibrations of the carbonyl groups decreases, and an absorption band with a medium intensity, caused by vibrations of the benzene ring of *p*-ASA, appears at 1580 cm^{-1}.

In the electronic spectrum of *p*-ASA in aqueous solution at pH 7 and [*p*-ASA] = 10^{-4} M, there are two absorption peaks: at 266 and 298 nm (see figure). The electronic spectra of the reaction products are characterized by the bathochromic shift of the absorption peak to 270 and 303 nm. Solutions of polysaccharides do not absorb in this range.

The main functional groups of AG and its oxidized species are hydroxy and carboxy groups. The amino group in *p*-ASA can interact with carboxy groups of the polysaccharide. In an acidic medium, when dissociation of carboxy groups is suppressed, there is no interaction between polysaccharides and *p*-ASA. In alkaline medium at pH 7 and higher, when carboxy groups of polysaccharides are present in the solution in the form of carboxylate anions and amino groups in *p*-ASA, in the protonated form, modified compounds are formed. Therefore, it can be assumed that the reaction between AG, AG_{pol}, and AG_{ol} with *p*-ASA follows the scheme



Electronic spectra of aqueous solutions of (*1*) *p*-ASA, (*2*) AG + *p*-ASA, and (*3*) AG_{pol} + *p*-ASA. (*A*) Optical density and (λ) wavelength. Concentration (M): (*1*) 1×10^{-3} and (*2, 3*) 1×10^{-4}.

Table 2. Influence of conditions of AG, AG_{pol}, and AG_{ol} modification with *p*-ASA on the content of drug in the modified form

Molar ratio AG : *p*-ASA	τ, h	*T*, °C	Content of *p*-ASA, mol per mole of AG, AG_{pol}, and AG_{ol}
AG + *p*-ASA (mol COOH : mol AG = 0.047)			
1 : 1	0.5	20	0.01
1 : 1	1	20	0.01
1 : 1	2	20	0.02
1 : 1	4	20	0.02
1 : 0.5	24	20	0.01
1 : 1	24	20	0.02
1 : 1	3	25	0.02
1 : 1	3	60	0.02
1 : 1	3	90	0.02
AG + *p*-ASA (mol COOH : mol AG_{pol} = 0.12)			
1 : 0.1	4	20	0.07
1 : 1	4	20	0.12
AG + *p*-ASA (mol COOH : mol AG_{ol} = 0.76)			
1 : 0.1	4	20	0.12
1 : 1	4	20	0.21

$$AG\text{–}COOH + H_2N\text{–}C_7O_3H_5 \rightarrow AG\text{–}COO^{-+}H_3N\text{–}C_7O_3H_5,$$

where AG–COOH is AG, AG_{pol}, and AG_{ol}; H_2N–$C_7O_3H_5$ is *p*-ASA.

All the resulting modified compounds are readily soluble in water and DMSO, but insoluble in acetone, alcohols, and ether.

We studied the influence of the conditions of AG, AG_{pol}, and AG_{ol} modification with *p*-ASA on the content of the drug in the modified form (Table 2).

Table 2 shows that the keeping time and heating from 0 to 90°C do not affect significantly the *p*-ASA content of the resulting product. The *p*-ASA content in the compounds synthesized increased with the molar ratio [AG] : [*p*-ASA], and also does so an passing from AG to AG_{pol} and AG_{ol}. This is evidently caused by the higher content of carboxy groups in the oxidized samples of the biopolymer. In AG, there are 4.7 carboxy groups per 100 molecules of the polysaccharide, whereas in the polymer fraction their content is 12, and in the oligomer fraction, 76 per 100 molecules. Hence, the content of carboxy groups in the oligomer fraction is higher than that in the initial AG by approximately a factor of 15, and in the polymer fraction, by a factor of 3, which is in good agreement with data on the content of *p*-ASA in the compounds studied.

We found that, among the compounds studied, AG + *p*-ASA and AG_{ol} + *p*-ASA have high tuberculostatic activity in vitro against pathogenic mycobacteria, AG and AG_{pol} + *p*-ASA exhibit moderate activity, and under the action of AG_{pol} and AG_{ol} the growth of tuberculosis mycobacteria is partially suppressed.

CONCLUSIONS

A correlation between the concentration of carboxy groups in polysaccharides and the drug content in the modified compounds was elucidated. Depending on the polysaccharide fraction, we obtained modified compounds containing 1.4, 8.5, and 16.0% drug. In the course of modification, the protonated amino group of *p*-aminosalicylic acid reacts with carboxylate ions of AG.

ACKNOWLEDGMENTS

This study was financially supported by the program of the Presidium of the Russian Academy of Sciences "Basic Research for Medicine," scientific program of the Federal Education Agency "Development of the Scientific Potential of the Higher School," and also by the State Scientific and Technological Program of the Republic of Bashkorkostan for the years 2005–2007 (contract no. 419-X).

REFERENCES

1. Ovodov, Yu.S., *Bioorg. Khim.*, 1998, vol. 24, no. 7, pp. 483–501.
2. Arifkhodzhaev, A.O., *Khim. Prirodn. Soedin.*, 2000, no. 3, pp. 185–197.
3. Antonova, G.F. and Usov, A.I., *Bioorg. Khim.*, 1984, no. 10, pp. 1664–1669.
4. Kiyohara, H. and Yamada, H., *Carbohydr. Res.*, 1989, vol. 193, no. 10, pp. 173–192.
5. Ovodov, Yu.S., Ovodova, R.G., and Loenko, Yu.N., *Khim. Prirodn. Soedin.*, 1983, no. 6, pp. 675–694.
6. Plate, N.A. and Vasil'ev, A.E., in *Fiziologicheski aktivnye polimery* (Physiologically Active Polymers), Moscow: Khimiya, 1986.
7. Mashkovskii, M.D., *Lekarstvennye sredstva* (Drugs), Kharkov: Torsing, 1997, vol. 2.
8. Antonova, G.F. and Tyukavkina, N.A., *Khim. Drev.*, 1976, no. 4, p. 60.
9. Tyukavkina, N.A. and Antonova, G.F., *Izv. Sib. Otd. Akad. Nauk SSSR*, 1969, no. 9, issue 4, pp. 112–116.
10. Borisov, I.M., Shirokova, E.N., Mudarisova, R.Kh., et al., *Izv. Ross. Akad. Nauk, Ser. Khim.*, 2004, no. 2, pp. 305–311.
11. Borisov, I.M., Shirokova, E.N., Babkin, V.A., et al., *Dokl. Ross. Akad. Nauk*, 2002, vol. 383, pp. 774–777.
12. Virnik, A.D., Khomyakov, K.P., and Skokova, I.F., *Usp. Khim.*, 1975, no. 7, pp. 1280–1302.
13. Mudarisova, R.Kh., Badykova, L.A., Tolstikova, T.G., et al., *Zh. Prikl. Khim.*, 2005, vol. 78, no. 10, pp. 1721–1724.

ISSN 1070-4272, Russian Journal of Applied Chemistry, 2006, Vol. 79, No. 10, pp. 1629–1633. © Pleiades Publishing, Inc., 2006.
Original Russian Text © A.P. Malyshev, K.V. Shirshin, O.A. Kazantsev, A.P. Sivokhin, I.V. Zhiganov, A.E. Kuznetsov, 2006, published in Zhurnal Prikladnoi Khimii, 2006, Vol. 79, No. 10, pp. 1650–1654.

ORGANIC SYNTHESIS AND INDUSTRIAL ORGANIC CHEMISTRY

Effect of Reactant Association on Addition of Tertiary Amines to Acrylic Acid in Aqueous Solutions

A. P. Malyshev, K. V. Shirshin, O. A. Kazantsev, A. P. Sivokhin, I. V. Zhiganov, and A. E. Kuznetsov

Dzerzhinsk Polytechnic Institute, Nizhni Novgorod State Technical University, Dzerzhinsk, Nizhni Novgorod oblast, Russia

Received January 24, 2006

Abstract—The formation of betaines by the reaction of tertairy amines (*N*,*N*-dimethyl-*N*-2-hydroxyethylamine, *N*,*N*-dimethylaminoethyl methacrylate, *N*-methylmorpholine, *N*,*N*-dimethylaminopropionitrile, 1,4-diazabicyclo[2.2.2]octane) with acrylic acid in aqueous solutions in a wide concentration range was studied. The concentration effects observed were interpreted taking into account the association of the starting reagents.

DOI: 10.1134/S1070427206100144

Carboxy betaines are components of many cosmetics and pharmaceutical preparations [1]. In many cases, it is appropriate to prepare β-betains in a single step by nucleophilic addition of tertiary amines to the activated C=C bond in acrylic acid. Water is a convenient solvent for such reactions [2]. Previously, we have examined the reaction of a series of trialkylamines with acrylic acid in dilute and moderately concentrated aqueous solutions [3, 4]. From the practical viewpoint, it is appropriate to use as high concentrations of reactants as possible; however, specific features of betaine formation from amines and acrylic acid in concentrated aqueous solutions have not been studied yet.

Recent papers give more and more indications that (meth)acrylic monomers in aqueous soilutions tend to form stable molecular associates which can strongly affect the chemical properties of these compounds. In particular, studies of the hydrolysis of aminoalkyl and hydroxyalkyl methacrylates (*N*,*N*-dimethylaminoethyl and 2-hydroxyethyl methacrylates) have shown that the association of the monomers results in abnormal acceleration or inhibition of the reaction in concentrated solutions [5, 6]. Another consequence of the association of amine-containing (meth)acrylic esters or amides in water is the possibility of spontaneous radical polymerization under certain conditions [7, 8]. A study of the radical homopolymerization of acrylic acid (AA) in aqueous solutions also revealed a significant effect of the monomer self-association on the rate constant of chain propagation [9].

In this study, we examined the effect of reactant association on the nucleophilic addition of tertiary amines to AA to give betaines:

$$CH_2{=}CHCOOH + NRR'R'' \rightleftarrows RR'R''\overset{+}{N}CH_2CH_2COO^-,$$

where NRR'R" = $(CH_3)_2NCH_2CH_2OH$ (DMAE), $(CH_3)_2NCH_2CH_2OCOC(CH_3){=}CH_2$ (DMAEM), $H_3C{-}N\langle\rangle O$ (MeM), $(CH_3)_2N(CH_2)_3CN$ (DMAPN), $N(CH_2CH_2)_3N$ DABCO.

As amines we chose compounds containing, along with the reacting amino group, additional N- and O-containing functional groups: *N*,*N*-dimethyl-*N*-2-hydroxyethylamine (DMAE), *N*,*N*-dimethylaminoethyl methacrylate (DMAEM), *N*-methylmorpholine (MeM), *N*,*N*-dimethylaminopropionitrile (DMAPN), asnd 1,4-diazabicyclo[2.2.2]octane (DABCO). The additional functional groups considerably increase the solubility of amines and their salts in water, which allowed syntheses in aqueous solutions in a wide concentration range. Furthermore, according to [10], the energies of intermolecular associative interactions involving hydroxy, etser, ether, nitrile, and amino groups are essentially different. Therefore, we expected that comparison of the activities of polyfunctional amines in the betaine formation would furnish additional information on the effect of these interactions on the reaction in question.

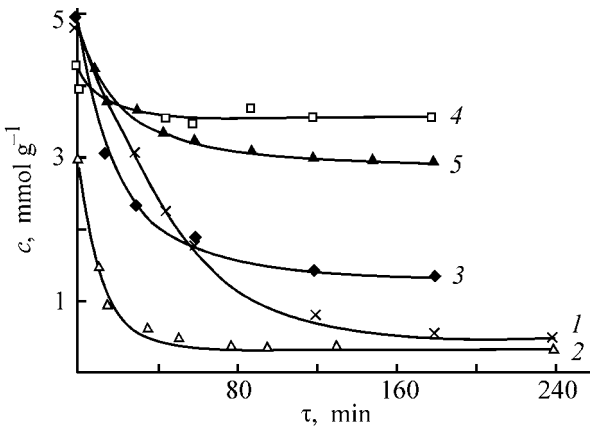


Fig. 1. Variation of the reactant concentration c with time τ. Amine: (*1*) DMAPN, (*2*) DABCO, (*3*) DMAE, (*4*) DMAEM, and (*5*) MeM; the same for Figs. 2, 3, and 5.

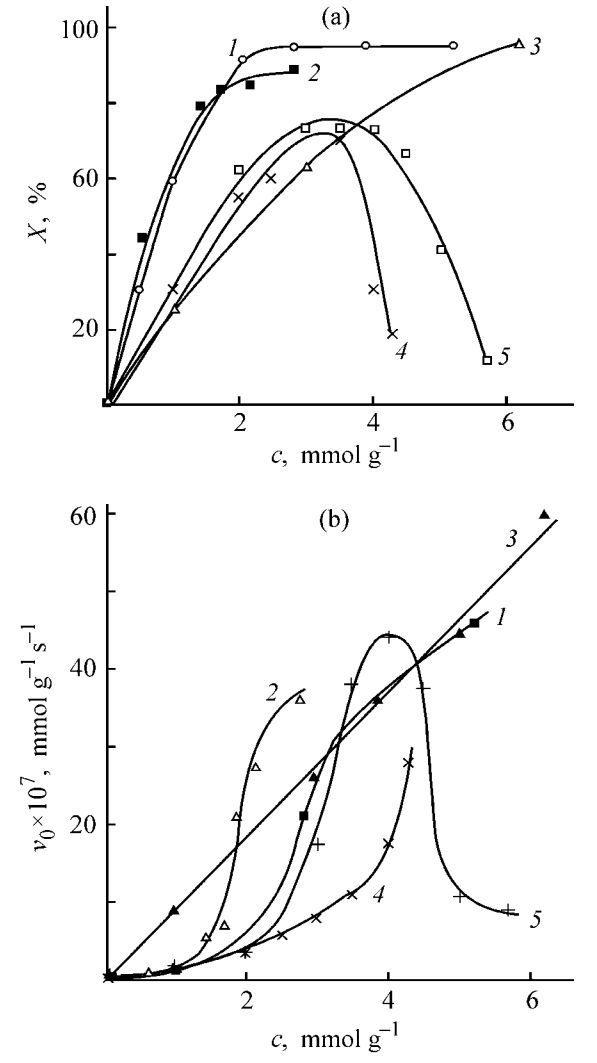


Fig. 2. (a) Equilibrium conversion X and (b) initial reaction rate v_0 vs. the reactant concentration c.

EXPERIMENTAL

The reaction of AA with tertiary amines was performed at 50°C and equimolar ratio of the reactants. Hydroquinone (0.5 wt % relative to AA) was added to the reaction mixtures to prevent radical polymerization. The reactant concentrations in aqueous solution were varied from 1 to 6 mmol g^{-1} (with DABCO, the maximal concentration was 3 mmol g^{-1}; at higher concentrations, the system became heterogeneous).

Addition of tertiary amines to AA was monitored by a decrease in the concentration of the C=C bonds determined by bromide–bromate titration. The specific viscosity of the reactants was measured with an Ubbelohde viscometer (d_c 0.34, 0.56, and 0.73 mm; 25°C). The ^{1}H NMR spectra were recorded on a Varian Gemini-300 Fourier spectrometer (300 MHz), solvent D_2O, reference DMSO.

3-(*N*,*N*-Dimethyl-*N*-hydroxyethylammonio)propionate. To 18.2 g of a 76% solution of AA in water, containing 0.07 g of hydroquinone, we added 17.1 g of DMAE. The resulting mixture was heated at 50°C for 5 h. After the reaction completion, water was distilled off in a vacuum, and the residue was washed with acetone. The product was vacuum-dried (20–40°C, 2 mm Hg) to constant weight. Yield 24.8 g (80.1%). The product contained no C=C bonds and no acid groups.

Found, %: N 8.58.
Calculated, %: N 8.70.

^{1}H NMR spectrum, δ, ppm: 3.34–3.39 ($-CH_2N^+$); 2.85 (CH_3N^+); 2.55–2.64 ($-C\underline{H}_2OH$, $-CH_2COO^-$).

The addition of amines to AA is an equilibrium reaction throughout the examined range of initial concentrations of the reactants. Figure 1 shows typical kinetic curves of consumption of the reactants at their high concentrations. Figures 2a and 2b show the dependences of the equilibrium conversion and initial reaction rate on the initial reactant concentration. The following trends can be revealed. As the initial concentrations are raised in the range 0–1.5 mmol g^{-1} for amines containing no oxygen (DMAPN, DABCO), the equilibrium conversion sharply increases, reaches a maximum (88–95%) at the initial concentration of about 2.5 mmol g^{-1}, and does not noticeably change with further increase in the concentration.

A different pattern is observed with the oxygen-containing amines. In the experiments with DMAE, the equilibrium conversion monotonically grows with

Inductive (σ^*) and steric (R_s) constants of substituents R, R', R" in the starting amines (N^* is the reaction center)

Amine	NRR'R"	$\Sigma\,\sigma^*$	$\Sigma\,-R_s$
DMAE	$(CH_3)_2N^*CH_2CH_2OH$	0.20	5.83
DMAEM	$(CH_3)_2N^*CH_2CH_2OCOC(CH_3)=CH_2$	0.5	6.33
MeM	$CH_3N^*(CH_2CH_2)_2O$	0.67	6.23
DABCO	$N^*(CH_2CH_2)_3N$	–	4.43
DMAPN	$(CH_3)_2N^*CH_2CH_2C\equiv N$	0.8	6.02

the initial solution concentration (with a minor deviation from linearity) and reaches almost 100% at the maximal concentration (actually, for neat reactants without solvent). With DMAEM and MEM, the equilibrium conversion first increases in the initial concentration, passes through a maximum, and then sharply decreases at concentrations exceeding 3.2 mmol g^{-1}.

The dependences of the initial rates on the reactant concentration also vary with the amine structure. This dependence is approximately linear with DMAE, passes through a pronounced maximum with MeM, is close to exponential with DMAEM, and is S-shaped with DMAPN and DABCO.

It has been shown previously [3, 4] that, in dilute solutions at approximately equimolar reactant ratio, the relative activity of various tertiary amines in reactions with AA is determined by the steric accessibility and nucleophilicity of the nitrogen atom. To evaluate these parameters for the amines examined in this study, we used the inductive (σ^*) and steric (R_s) constants of substituents, calculated according to [11, 12]. These procedures were developed for systems with a four-coordinate carbon atom as a reaction center. However, previous studies of *N*-alkylation of tertiary amines have shown that this approach also gives adequate results when applied to systems with a nitrogen atom as reaction center [13].

The constants listed in the table show that the amines chosen are similar in the steric accessibility and nucleophilicity of the reaction centers. Therefore, in accordance with the previously developed concepts, the amines should not essentially differ in the reactivity toward AA. Thus, the concentration effects observed cannot be interpreted in terms of the traditional concept of nucleophilic reactions of amines. We attribute the abnormal dependences of the initial rate of betaine formation and equilibrium conversion on the initial reactant concentration to intermolecular interactions of reactant molecules with the formation of various associates.

Therefore, the next step of our study was concerned with the association of amines in aqueous solutions in the presence of acids. In these experiments, AA was replaced with acetic acid to preclude betaine formation. We obtained the viscosity–concentration dependences (VCDs) for solutions of amine acetates (Fig. 3). It is known [14] that the occurrence and features of intermolecular interactions in solutions can be judged from the VCDs. Pronounced deviations of the VCDs from the linearity, observed with all the amines, suggest the occurrence of the association. Figure 3 shows that the VCDs of the salts of all the amines except DABCO exhibit pronounced maxima. According to [14, 15], maxima in the viscosity isotherms correspond to the formation of stable complexes in the system. To evaluate the relative capability of the amine salts for association, we cal-

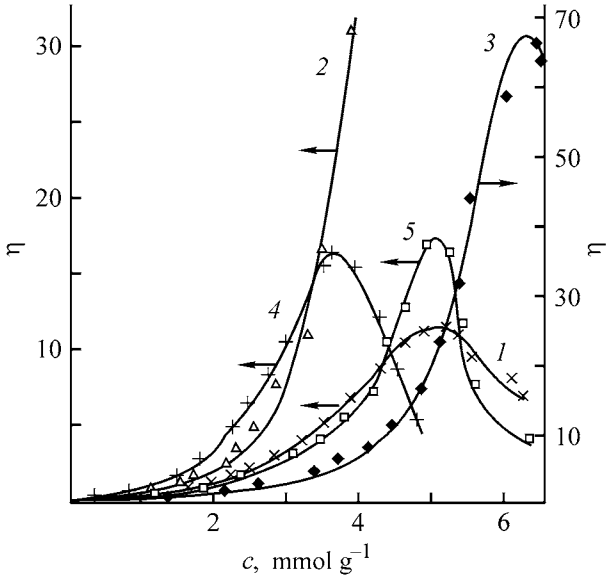


Fig. 3. Specific viscosity η of aqueous solutions of amine acetates at 25°C vs. the concentration *c*.

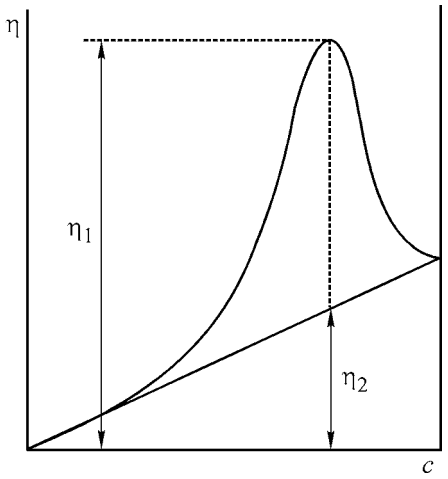


Fig. 4. Determination of η_1 and η_2 for calculating the association factor α.

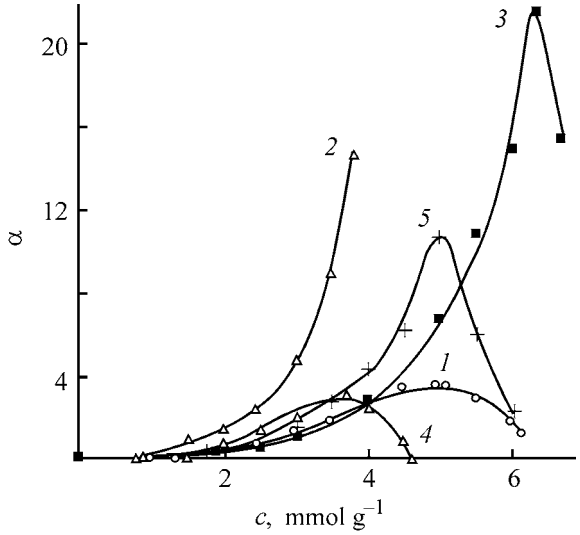


Fig. 5. Association factor α at 25°C vs. the concentration of amine acetates, *c*.

culated the association factor α reflecting the extent of deviation of the VCD from the linearity:

$$\alpha = (\eta_1 - \eta_2)/\eta_2,$$

where η_1 is the actual specific viscosity of an amine salt at a given concentration, and η_2 is the specific viscosity at the same concentration, estimated by extrapolation of the initial linear portion of the VCD (Fig. 4).

Figure 5 shows the dependences of α on the amine salt concentration. It is seen that DABCO and DMAE show the strongest tendency toward association, and DMAEM and DMAPN, the weakest tendency. Thus, the amines chosen are similar in the nucleophilicity and steric accessibility of reaction centers in the isolated molecules, but strongly differ in the tendency toward association in the presence of acids. In this context, it is reasonable to assume that the factor responsible for significant differences in the betaine formation kinetics is the effect of the association on the local concentration, accessibility, and reactivity of active centers of the reactants. Our results show that the association can both accelerate and inhibit the reaction.

In particular, it is known [16] that form linear aggregates alcohols in aqueous solutions. It is reasonable to assume that DMAE or its salt, containing a hydroxy group, also tend to form such associates. Apparently, the local concentration of the reactants in such associates increases, which facilitates their reaction. As a result, the concentration, initial rate, and equilibrium conversion proportionally increase.

Shibalovich et al. [17] measured the surface tension of aqueous solutions of DMAEM and its salts and showed that these compounds exhibit surface activity even in relatively dilute solutions. Hence, associates of micellar rather than linear type are more probable for DMAEM salts. It should be noted that, at concentrations less than 1.8 mmol g^{-1} (relatively dilute solutions), the dependences of the specific viscosity and reaction rate on the amino ester concentration are approximately linear. At concentrations exceeding 2 mmol g^{-1}, both the viscosity of the reaction mixtures and the initial reaction rate sharply increase, i.e., the association of the starting amine salts favorably affects the betaine formation. A sharp decrease in the equilibrium conversion in highly concentrated solutions (>3.5 mmol g^{-1}) is apparently due to formation in the course of the reaction of stable heteroassociates of the starting reactants and betaines, in which the mutual arrangement of the unchanged amino groups and C=C bonds is unfavorable for the reaction.

Data for the MeM–AA system show that, in this case, the reaction rate and viscosity of the system grow virtually linearly as the reactant concentration is raised to 2 mmol g^{-1}, and in the concentration range 2–4 mmol g^{-1} the growth accelerates. With a further increase in the concentration, the initial rate, equilibrium conversion, and viscosity sharply decrease. This fact may be due to the formation in highly concentrated solutions of stable homoassociates of the starting amine salts and heteroassociates of amine salts with the forming betaines, with the mutual arrangement of the amino group and C=C bond in these associates being unfavorable for the reaction.

With DABCO and DMAPN containing no oxygen atoms, the molecular "packing" in the homo- and

heteroassociates is favorable, according to the experimental data, for the betaine formation. Therefore, with an increase in the initial concentration to above 1.0 – 1.5 mmol g^{-1}, the initial reaction rate and viscosity of the mixture demonstrate virtually synchronous accelerated growth, without a decrease in the equilibrium conversion.

CONCLUSIONS

(1) The effect of the initial reactant concentration on the nucleophilic addition of tertiary amines to acrylic acid in aqueous solutions was examined.

(2) With an increase in the initial reactant concentration, the initial reaction rate grows linearly (*N*,*N*-dimethyl-*N*-2-hydroxyethylamine), exponentially (*N*,*N*-dimethylaminoethyl methacrylate), in the S-shaped mode (*N*,*N*-dimethylaminopropionitrile, 1,4-diazabicyclo[2.2.2]octane), or passes through a maximum followed by a sharp decrease (*N*-methylmorpholine).

(3) With an increase in the initial reactant concentration, the equilibrium conversion monotonically grows to reach maximal values (*N*,*N*-dimethyl-*N*-hydroxyethylamine, *N*,*N*-dimethylaminopropionitrile, 1,4-diazabicyclo[2.2.2]octane) or passes through a maximum followed by a sharp decrease (*N*,*N*-dimethylaminoethyl methacrylate, *N*-methylmorpholine).

(4) Salts of tertiary amines in aqueous solutions tend to form associates; their structure determines the course of the reaction of betaine formation.

REFERENCES

1. Abramzon, A.A., *Poverkhnostno-aktivnye veshchestva: Sintez, analiz, svoistva, primenenie: Uchebnoe posobie dlya vuzov* (Surfactants: Synthesis, Analysis, Properties, Applications: Textbook for Higher Schools), Leningrad: Khimiya, 1988.
2. Suminov, S.I. and Kost, A.N., *Usp. Khim.*, 1969, vol. 38, no. 11, pp. 1933–1963.
3. Kazantsev, O.A., *Doctoral Dissertation*, Yaroslavl, 1998.
4. Le Berre, A. and Delacroix, A., *Bull. Soc. Chim. Fr.*, 1973, nos. 7–8, pp. 2404–2408.
5. Kuznetsova, N.A., Kazantsev, O.A., Shirshin, K.V., et al., *Zh. Prikl. Khim.*, 2003, vol. 76, no. 7, pp. 1150–1153.
6. Kazantsev, O.A., Shirshin, K.V., Sivokhin, A.P., et al., *Zh. Prikl. Khim.*, 2003, vol. 76, no. 8, pp. 1333–1335.
7. Kazantsev, O.A., Kuznetsova, N.A., Shirshin, K.V., et al., *Vysokomol. Soedin., Ser. A*, 2003, vol. 45, no. 4, pp. 572–580.
8. Kazantsev, O.A. and Shirshin, K.V., *Polymer*, 2004, vol. 45, no. 15, pp. 5021–5029.
9. Lazhik, I., Beuermann, S., and Buback, M., *Macromolecules*, 2003, vol. 36, no. 25, pp. 9355–9363.
10. Irzhak, V.I., Korolev, G.V., and Solov'ev, M.E., *Usp. Khim.*, 1997, vol. 66, no. 2, pp. 179–200.
11. Galkin, V.A., Cherkasov, A.R., Sayakhov, R.D., et al., *Zh. Obshch. Khim.*, 1995, vol. 65, no. 4, pp. 458–468.
12. Galkin, V.A., Sayakhov, R.D., and Cherkasov, R.A., *Usp. Khim.*, 1991, vol. 60, no. 8, pp. 1617–1644.
13. Kazakov, S.A., Kazantsev, O.A., Shirshin, K.V., et al., *Zh. Org. Khim.*, 2000, vol. 36, no. 3, pp. 363–369.
14. *Rastvoritel' kak sredstvo upravleniya khimicheskim protsessom* (Solvent as a Means To Control a Chemical Process), Fialkov, Yu.Ya., Ed., Leningrad: Khimiya, 1990.
15. Arutyunyan, R.S., Grigoryan, V.V., Egoyan, R.V., et al., *Arm. Khim. Zh.*, 1988, vol. 41, no. 6, pp. 323–327.
16. Berlin, P.A., Levina, M.A., Chirkov, Yu.N., et al., *Kinet. Katal.*, 1993, vol. 34, no. 4, pp. 640–644.
17. Shibalovich, V.G., Efimova, D.Yu., and Nikolaev, A.F., *Plast. Massy*, 2000, no. 3, pp. 25–27.

ISSN 1070-4272, Russian Journal of Applied Chemistry, 2006, Vol. 79, No. 10, pp. 1634–1638. © Pleiades Publishing, Inc., 2006.
Original Russian Text © T.G. Dzherayan, A.V. Rudnev, V.P. Morgalyuk, 2006, published in Zhurnal Prikladnoi Khimii, 2006, Vol. 79, No. 10, pp. 1655–1659.

MACROMOLECULAR CHEMISTRY AND POLYMERIC MATERIALS

Capillary Electrophoretic Study of Synthesis of Polyhexamethyleneguanidine

T. G. Dzherayan, A. V. Rudnev, and V. P. Morgalyuk

Vernadsky Institute of Geochemistry and Analytical Chemistry, Russian Academy of Sciences, Moscow, Russia

Received December 21, 2005; in final form, April 2006

Abstract—Synthesis of polyhexamethyleneguanidine hydrochloride was studied by capillary electrophoresis. A procedure for determining the reaction components was developed.

DOI: 10.1134/S1070427206100156

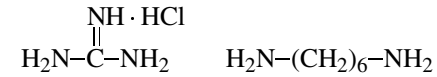
Presently, control of microbial pathogens (human and animal infectious agents) is a very topical problem. It has been demonstrated that water-soluble salts of the high-molecular-weight polycationic compound, polyhexamethyleneguanidine hydrochloride (PHMG), show high biocidal activity against pathogenic microorganisms and low toxicity [1, 2]. However, their application as biocidal agents, especially in medical practice, requires a high quality of the polymer, since admixtures of the initial monomers of guanidine hydrochloride (GHC) and hexamethylenediamine (HMDA) impart toxic and allergic properties to the product. It has also been demonstrated [1] that, in some cases, the biocidal characteristics of the product are dependent on the preparation procedure. Therefore, to control the course of the synthesis and to elucidate the sources of the biocidal activity loss, it was necessary to develop a procedure for prompt analysis of the product and to determine the reaction mechanism.

It is known that capillary electrophoresis (CE) is successfully used for separation and determination of such high-molecular-weight compounds as oligonucleotides, oligopeptides, and oligisaccharides [3, 4]. For example, CE has been used to separate polycationic dendrimers of polyaminoamides with various charge/molecular weight ratios [5].

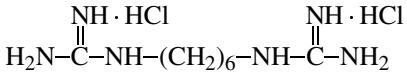
The goals of this study included were to optimize the conditions of separation and determination of polymeric forms of PHMG (properties of the samples varied, depending on the synthetic conditions) and starting reagents used for its synthesis (GHC and HMDA), determine the reaction mechanism of synthesis, and searching for the ways to monitor the course of the synthesis.

EXPERIMENTAL

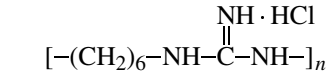
As samples for analysis we used PHMG, GHC, HMDA, and also 1,6-diguanidinohexane dihydrochloride (1,6-DGH):[1]



GHC HMDA



1,6-DGH



PHMG

Buffer solutions with pH 6.86 and 9.18 were prepared from NaH_2PO_4/Na_2HPO_4 and $Na_2B_4O_7 \cdot 10H_2O$ standard titrants, using double-distilled water.

For analysis we used a Kapel-105 capillary electrophoresis system (Lumex, St. Petersburg, Russia) equipped with a variable-wavelength UV detector (wavelength range 190–380 nm) and hydraulic sample injection system. We used a quartz capillary

[1] Samples were synthesized and purified at the Institute of Ecotechnological Problems, Moscow, Russia.

(inner diameter 75 μm, outer diameter 375 μm, total length 59 cm, distance to the detector 50 cm) with a polyimide outer protection coating (Composite Metal Services, Worcester, UK). The experiments were carried out at 25°C.

Based on analysis of the UV spectra of the compounds under study, we selected 200 nm as a working wavelength. The best peak resolution was obtained at a working voltage of 20 kV (current 20–50 μA). To refresh the active surface of the capillary, it was rinsed with 0.1 M NaOH, double-distilled water, and the buffer solution after each analysis. The electrophoregrams were recorded in the cathodic space of the capillary. Experimental data were processed using MultiChrom software package for Windows-95/98/NT. The concentration of the analyte in the injected sample was controlled by varying the injection time t and pressure in the injection system p. In making a calibration curve, the desired concentration of the analyte in reference samples was provided by varying the values of p and t (their product was proportional to the analyte concentration in the sample).

The CE method is based on the differentiated migration of components of the sample dissolved in a conducting buffer solution within a narrow capillary under the influence of the applied electric field. The separation is controlled by two factors [6]. First, the electrophoretic mobility of analytes, μ, depends on the size and charge of the ions to be separated. The electrophoretic velocity is written as

$$V = \mu E = zFE/6\pi\eta r N_a, \quad (1)$$

where E is the field strength; z, effective charge; r, Stokes radius of the ion; F, Faraday number; η, viscosity of the electrolyte solution; and N_a, Avogadro number.

Second is that, on applying an external electric field, the negatively charged inner surface of the quartz capillary attracts the counterions from the mobile layer, providing a driving force for a electroosmotic flow (EOF). Since, in our case, the analytes are positive ions, their migration velocity along the capillary is the sum of the EOF and electrophoretic velocities [Eq. (1)]. The electromigration velocity was controlled by varying pH and ionic strength of the buffer solution, i.e. the factors that govern the ζ potential of the surface of the quartz capillary and, therefore, the EOF velocity. In our experiments, it was demonstrated that, in analysis of PHMG and the starting reagents for its synthesis, the optimal conditions are the ionic strength from 0.02 to 0.05 M and pH 6–9.

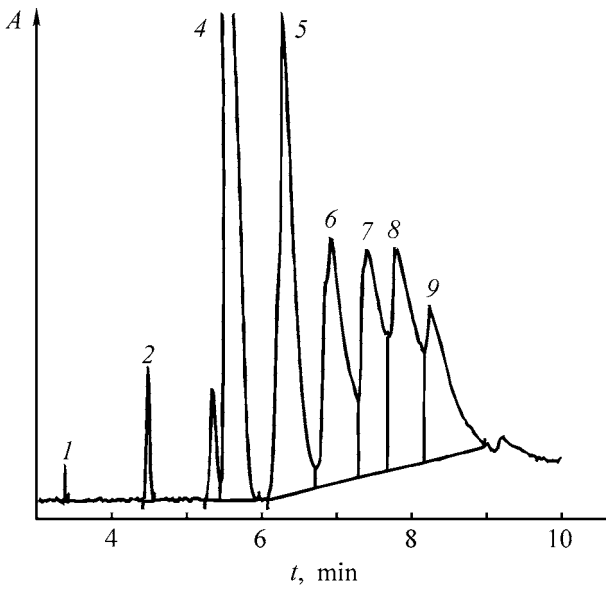


Fig. 1. Electrophoregrams of the mixture of PHMG and starting reagents for its synthesis. Hydrodynamic injection time of the sample 5 s at 30 mbar; 20 mM NaH_2PO_4/Na_2HPO_4 buffer (pH 6.86). Sample composition (mg ml^{-1}): GHC 0.1, HMDA 5.0, 1,6-DGH 1.0, and PHMG 2.0. (*A*) Peak intensity and (*t*) time; the same for Figs. 2, 3. Peak assignments: (*1*, *3*) HMDA, (*2*) GHC, (*4*) PHMD + 1,6-DGH + HMDA, and (*5*–*9*) PHMD oligomers.

A study of the kinetics of the polycondensation of GHC and HMDA [1] showed that, at the equimolar reagent ratio, water-soluble linear PHMG with MW of about 2500 is formed (mean number of units n = 13–14). At a slight molar excess of HMDA, MW increases, and branched or 3*D* polymers can be formed.

In developing a procedure for analysis of PHMG, an important criterion is the possibility of simultaneous determination of the initial reagents used in its synthesis. The typical electrophoregrams of individual GHC and HMDA, PHMG, and 1,6-DGH are shown in Fig. 1. The most difficult was to analyze HMDA, since it gives a weak peak in the electrophoregram, probably because of a low molar extinction coefficient at 200 nm (optimal wavelength selected for identification and determination of the other components). It is known [7] that HMDA, being a strong base, readily absorbs carbon dioxide from air and demonstrates a tendency toward association in solutions. Therefore, it may be suggested that, in the electrophoregram, HMDA will give three peaks corresponding to the cationic species (dicarbonate and carbonate) and dimers. This suggestion is supported by the electrophoregrams of commercial HMDA and HMDA di-

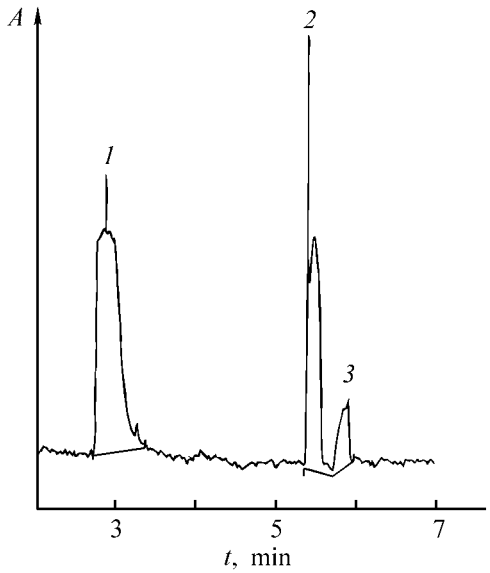


Fig. 2. Electrophoregram of HMDA. Hydrodynamic injection time of the sample 20 s; 20 mM $Na_2B_4O_7 \cdot 10H_2O$ buffer (pH 9.18); HMDA concentration in the sample 5.0 mg ml^{-1}. Peak assignments: (*1*) HMDA dihydrochloride, (*2*) HMDA hydrochloride, and (*3*) HMDA dimer.

hydrochloride specially prepared for this purpose (Fig. 2). Using the standard additive method, we assigned peak no. 2 in the electrophoregram to guanidine hydrochloride (Fig. 1).

In considering the reaction mechanism it was logical to suggest that, in synthesis of PHMG, 1,6-DGH is formed as one of the oligomers, i.e., that the polycondensation proceeds by two quite similar mechanisms *a* and *b*:

$$n\mathrm{H_2N{-}(CH_2)_6{-}NH_2} + n\mathrm{H_2N{-}\underset{\underset{\mathrm{NH\cdot HCl}}{\|}}{C}{-}NH_2} \rightarrow \mathrm{NH_2{-}[(CH_2)_6{-}NH{-}\underset{\underset{\mathrm{NH\cdot HCl}}{\|}}{C}{-}NH{-}]_n} + \mathrm{NH_3}, \quad a$$

$$n\mathrm{H_2N{-}(CH_2)_6{-}NH_2} + (n+1)\mathrm{H_2N{-}\underset{\underset{\mathrm{NH\cdot HCl}}{\|}}{C}{-}NH_2} \rightarrow \mathrm{NH_2{-}\underset{\underset{\mathrm{NH\cdot HCl}}{\|}}{C}{-}NH{-}[(CH_2)_6{-}NH{-}\underset{\underset{\mathrm{NH\cdot HCl}}{\|}}{C}{-}NH{-}]_n} + (n+1)\mathrm{NH_3}. \quad b$$

In the case with $n = 1$, 1,6-DGH is formed by mechanism *b*. To identify 1,6-DGH among the oligomers, this compound and PHMG were analyzed as individual components, and then their electrophoregrams were compared with those of the mixture of 1,6-DGH, DGC, HMDA, and PHMG (Fig. 1). The peaks were assigned using the standard additive method. For example, on addition of 1,6-DGH, the area of the first peak of PHMG increased by the value corresponding to the peak area of the additive, suggesting that it is 1,6-DGH that is responsible for the first peak in the electrophoregram of PHMG, which is consistent with mechanism *b*. As can be seen from the above scheme, the content of guanidine fragments in the oligomers is higher if they are formed by mechanism *b*, which can be considered among the possible explanations for the change in the biocidal activity of the resulting PHMG. It is known [1] that the biocidal activity of PHMG is caused by the presence of the guanidine groups, and the decrease in the biocidal activity of the product can be attributed to the fact that, in this case, the polycondensation proceeds preferentially by mechanism *a*.

In macromolecular chemistry, by oligomers are meant molecularly uniform substances, which are intermediate in molecular weight (from 500 to 5000) and chemical properties between polymers and monomers [8]. In their physical properties, oligomers differ significantly from each other, allowing their separation into individual compounds. Oligomers with higher MW, whose properties are closer to those of polymers, cannot be separated because of the similarity of their physical properties. In our case, the PHMG oligomers have different MW and, accordingly, different molecular sizes. However, only in the case of polycondensation by mechanism *b*, they will have different effective charges and, therefore, different migration rates in the electric field [see Eq. (1)].

In the case of mechanism *a*, the charge to MW ratio is a constant independent of the molecular size; all the oligomers will have the same electrophoretic mobility, and they can be separated only by, e.g., gel electrophoresis or through modification of the buffer solution by additon of appropriate solvents [3, 9, 10].

As mentioned above, the polycondensation product PHMG has a mean unit number of 13–14. Figure 1 shows the electrophoregram of oligomers formed by mechanism *b* as a series of five peaks corresponding to the first five oligomers with considerably different z/MW ratios (for 1,6-DGH z/MW = 2 at $n = 1$), which gradually decrease with increasing n. The other oligomers of this series are represented by a group of unresolved peaks. To increase the separation selectivity, we added solvents (methanol and acetonitrile) into the mobile phase. With acetonitrile, we

Results of determination of PHMG and starting reagents for its synthesis (n = 5, P = 0.95) (determination conditions: λ = 200 nm; I = 30–50 μA; U = 20 kV; pH 9.18)

Analyte	Introduced, mg ml^{-1}	Found, mg ml^{-1}	S_r	Detection limit, mg ml^{-1}	Linearity range of CC, mg ml^{-1}	CC equation*	r
GHC	0.500	0.504 ± 0.008	0.014	0.002	0.006–0.5	$S = 0.472c$	0.999
1,6-DGH	0.250	0.250 ± 0.015	0.050	0.002	0.005–0.5	$S = 2.65c + 0.015$	0.999
HMDA	0.400	0.390 ± 0.018	0.039	0.0035	0.007–0.5	$S = 1.359c + 0.002$	0.994
PHMG	0.300	0.297 + 0.019	0.053	0.002	0.005–0.05	$S = 14.71c + 0.686$	0.999
Oligomer:							
1	–	–	–	0.0018	0.005–0.05	$S = 8.25c + 0.028$	0.996
2	–	–	–	0.0015	0.005–0.05	$S = 2.29c + 0.027$	0.997
3	–	–	–	0.0016	0.005–0.05	$S = 22.96c + 0.027$	0.997
4	–	–	–	0.0018	0.005–0.05	$S = 52.94c + 0.004$	0.996

* (S) Peak area equal to the product of the optical density by the time, min; (c) concentration, mg ml^{-1}; (r) correlation coefficient; and (S_r) relative standard deviation.

obtained an electrophoregram containing resolved peaks of 16 oligomers (Fig. 3).

The sum of the peak areas (each being the function of the product of the optical density by the time) is the integral signal of the sum of PHMG oligomers. This sum and the signals of the first four oligomers are linear functions of the PHMG concentration (see table). The table also includes the linearity range of the calibration curves (CCs) and detection limits for the compounds studied, the latter being estimated from the peak area (signal/noise = 3).

To monitor the synthesis, samples were taken 20, 30, and 40 min after the beginning of the reaction. Figure 4 shows the evolution of the concentrations of the PHMG oligomers in the course of synthesis. The amounts of the lower oligomers formed by mechanism b initially decreases, reaching a constant value in about 30–40 min, i.e., by the end of the reaction, when the liberation of ammonia is virtually completed. Therefore, the course of the process and the quality of the resulting product can be monitored by the evolution of the concentration of the lower oligomers.

CONCLUSIONS

(1) The mixture of the starting toxic reagents (hexamethylenediamine and guanidine hydrochloride) and their polycondensation products (polyhexamethyleneguanidine hydrochloride and its oligomers) can be separated by capillary electrophoresis.

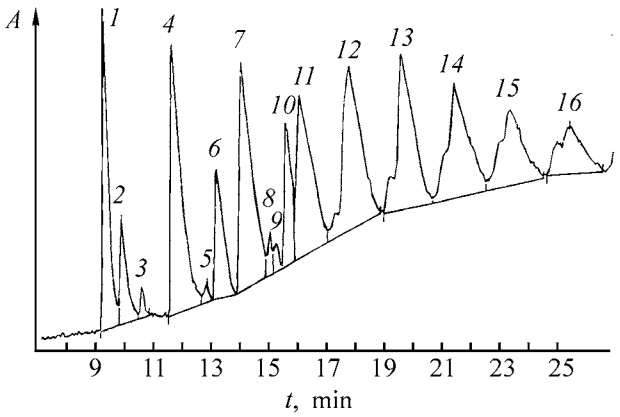


Fig. 3. Electrophoregram of PHMG. Hydrodynamic injection time of the sample 5 s at 30 mbar; 10 mM NaH_2PO_4/Na_2HPO_4 buffer (pH 6.86) + acetonitrile (1 : 1 v/v); PHMG concentration in the sample 1 mg ml^{-1}. For explanations, see text.

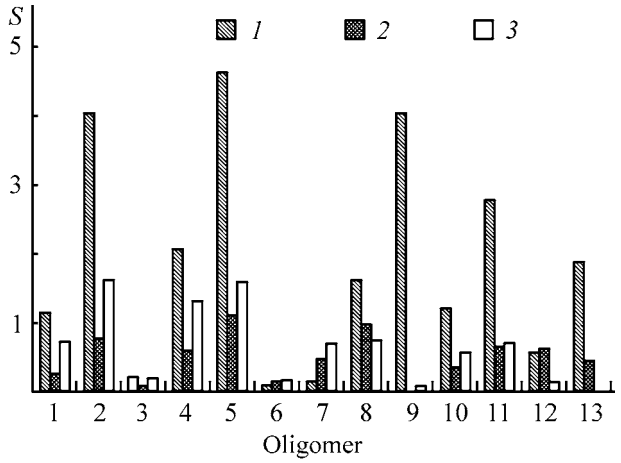


Fig. 4. Evolution of the concentrations of PHMG oligomer nos. 1–13 in the course of synthesis. (S) Peak area. Time (min): (*1*) 20, (*2*) 30, and (*3*) 40.

(2) A procedure is developed for quantitative analysis of polyhexamethyleneguanidine hydrochloride, its oligomers, and the starting reagents used in the synthesis.

(3) The course of the synthesis and the quality of the resulting polyhexamethyleneguanidine hydrochloride can be monitored by the decrease in the concentration of the lower oligomers.

ACKNOWLEDGMENTS

The authors are grateful to P.A. Gembitskii (IETP, Moscow) and A. R. Timerbaev (GEOKhI RAS, Moscow) for valuable discussions.

REFERENCES

1. Efimov, K.M., Gembitskii, P.A., and Snezhko, A.G., *Dezinfekts. Delo*, 2000, no. 4, p. 28.
2. Gembitskii, P.A. and Vointseva, I.I., *Polimernyi biotsidnyi preparat poligeksametilenguanidin* (Polymeric Biocidal Agent Polyhexamethyleneguanidine), Zaporozh'e: Poligraf, 1998.
3. Nikashina, V.A., Kats, E.M., Zotova, V.I., Danilina, N.I., et al., Abstracts of Papers, *Mezdunarodnyi kongress "Voda: ekologiya i tekhnologiya"* (Int. Congress "Water: Ecology and Technology"), vol. 2, Moscow, September 6–9, 1994, p. 518.
4. Foret, F., Krivankova, L., and Bocek, P., *Capillary Zone Electrophoresis*, Weinheim: VCH, 1993.
5. *Rukovodstvo po kapillyarnomu elektroforezu* (Guide of Capillary Electrophoresis), Moscow: TsNIITEI Traktorsel'khozmash, 1968.
6. Shi, X., Banyai, I., Lesniak, W.G., et al., *Electrophoresis*, 2005, vol. 26, p. 2949.
7. Tomilov, A.P. and Smirnov, S.K., *Adiponitril i geksametilendiamin* (Adiponitrile and Hexamethylenediamine), Moscow, 1974.
8. Strepikheev, A.A., Derevitskaya, V.A., and Slonimskii, G.L., *Osnovy khimii vysokomolekulyarnykh soedinenii* (Principles of Macromolecular Chemistry), Moscow: Khimiya, 1967.
9. Sarmini, K. and Kenndler, E.J., *Chromatogr., A*, 1997, vol. 792, p. 3.
10. Masselter, S.M. and Zemann, A.J., *Anal. Chem.*, 1995, vol. 67, p. 1047.

ISSN 1070-4272, Russian Journal of Applied Chemistry, 2006, Vol. 79, No. 10, pp. 1639–1642. © Pleiades Publishing, Inc., 2006.
Original Russian Text © I.R. Saifullina, G.A. Chiganova, S.V. Karpov, V.V. Slabko, 2006, published in Zhurnal Prikladnoi Khimii, 2006, Vol. 79, No. 10, pp. 1660–1663.

MACROMOLECULAR CHEMISTRY AND POLYMERIC MATERIALS

Preparation of Composite Films with Silver Nanoparticles and Their Fractal Aggregates in a Polymeric Matrix

I. R. Saifullina, G. A. Chiganova, S. V. Karpov, and V. V. Slabko

Department of Physics of Nanophase Materials, Krasnoyarsk Scientific Center, Siberian Division, Russian Academy of Sciences, Krasnoyarsk, Russia

Kirenskii Institute of Physics, Siberian Division, Russian Academy of Sciences, Krasnoyarsk, Russia

Krasnoyarsk State Technical University, Krasnoyarsk, Russia

Received February 13, 2006

Abstract—Conditions were examined for preparation of film materials with polyacrylamide matrix, promising for optical applications and containing both single silver particles and their fractal aggregates.

DOI: 10.1134/S1070427206100168

Nanocomposite materials containing metal nanoparticles in polymeric matrices have unique optical properties [1–3] and open up new prospects for nanophotonics. This concerns both the fractal-structured nanocomposites or highly ordered colloid systems and composite media with random-uniform distribution of single metal nanoparticles in the matrix [1, 2]. In particular, nanocomposites containing fractal silver aggregates are regarded as one of the most promising types of photochromic media for polychrome recording of information with large storage times [1, 4].

One of the problems arising in preparation and application of metal nanocomposites is the rather low reproducibility of many synthesis methods [2]. In this context, development and improvement of methods for preparation of polymeric nanocomposites still remains an important applied task. Among the simplest methods ensuring uniform distribution of a metal in the matrix is preparation of metal sols by reduction of metal ions, followed by introduction of the sol into a monomer solution and its polymerization.

In this study, we prepared polymeric films, suitable for optical examinations and applications and containing both single silver nanoparticles and fractal aggregates of nanoparticles.

EXPERIMENTAL

Silver hydrosols were prepared from silver nitrate and sodium borohydride solutions. Low-concentration ion-stabilized sols were prepared by the procedure described in [5, 6] by mixing 10^{-3} M solution of $AgNO_3$ and 2×10^{-3} M solution of $NaBH_4$, precooled to 273 K, in a 1:3 (by volume) ratio. The initial temperature of the system was 283 K; next, the system was heated to 333 K and cooled to room temperature. The degree of silver reduction was estimated from the silver ion concentration determined by Folgard's method [7]; as references served standard solutions of silver nitrate, reducing agent, and deionized silver sols, obtained in the presence of a high-molecular-weight stabilizing agent poly-*N*-vinyl-pyrrolidone (PVP) and passed through columns packed with ion exchangers. Silver ions were reduced virtually completely upon heating the sol for 10 min at 333 K; the silver content was 0.003 wt %. The sols stabilized with PVP were prepared by a similar procedure, with a polymer solution preliminarily introduced ($M \approx 20 \times 10^5$) into a silver nitrate solution. The PVP content of the resulting system was 10^{-6} M.

Electron-microscopic examinations with a JEM-100 CX microscope showed that aggregated particles were virtually lacking in the sols. The reduction of silver ions in the presence of PVP decreased to a certain extent, from 18 [5] to 12 nm, the numeric-average particle diameter; the range of particle sizes changed from 5–33 [5] to 2–25 nm.

The electrophoretic mobility of the silver particles was measured by macroelectrophoresis in a Ken instrument at 293 K and a current source voltage of

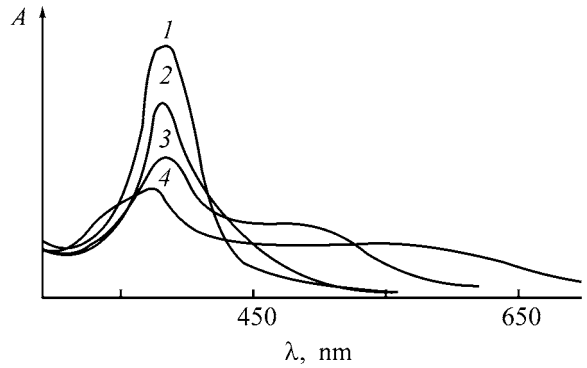


Fig. 1. Evolution of the absorption spectrum of the silver-borohydride hydrosol (*1*) freshly prepared and (*2–4*) with addition of pyridine responsible for the formation of fractal aggregates, at increasing periods of time elapsed after the addition [6]. (*A*) Absorption and (λ) wavelength.

100 V. The lateral liquid was a dispersion centrifugate or solution of potassium nitrate (10^{-3} M). The absorption spectra of the sols were determined on an SF-20 spectrophotometer. We used chemically pure-grade reagents and double-distilled water.

Uniform composition materials suitable for preparation of optical elements are obtained from polymer glasses with addition of nanoparticles of various chemical compositions. The concentration of the dispersed additives in the polymeric binder is typically no greater than 0.1 wt % [2]. Preparation of such nanocomposites requires stabilization of the available metal sols (since the electrostatic factor alone does not ensure the aggregation stability of the sols with such a metal concentration), as well as the controlled aggregate formation in the system. Linear polymers are widely used for stabilization of metal particles; the appropriate length of their chains, exceeding the range action of van der Waals attraction forces between the nanoparticles, is attained at the molecular weight of the polymer over 10^4 because the root-mean-square distance between the ends of a linear polymer chain $(r^2)^{1/2} \approx 0.06M^{1/2}$ [2, 8]. Ion-stabilized sols with a silver content of 0.003 wt %, prepared by Heard [5] and Creighton [6], have a yellow color both in the absence and presence of PVP. This corresponds to localization of the plasmon absorption peak at 400–430 nm; the appearance of the absorption spectra and the half-width of the peak are typical of sols containing single silver particles with a size of 5–30 nm [1, 5].

In the course of slow aggregation of the ion-stabilized silver sols by gradual neutralization of the surface charge (upon addition of pyridine replacing the potential-determining anions), the color of the silver sol successively changes from yellow to red and then to blue-gray [6]. In the absorption spectrum of the sol, the intensity of the absorption peak corresponding to single silver particles decreased, and a long-wave wing appeared covering the entire visible and a part of the IR spectral range (Fig. 1). We discussed the reasons for the evolution of the absorption spectra of the metal sols in [1, 9].

Our measurements revealed a fairly high electrophoretic rate for negatively charged silver particles obtained in the absence of polyvinylpyrrolidone (3.3×10^{-8} m^2 V^{-1} s^{-1}) and the lack of a charge for particles formed in the presence of a nonionic polymer. This suggests localization of the electric double layer within the adsorption layer of the stabilizer [10]. The thickness of the diffusion layer of counter ions, λ, on the surface of the particles in the sol was calculated by the expression

$$\lambda^{-1} = æ = (2F^2I/\varepsilon\varepsilon_0RT)^{1/2}.$$

Here, F is the Faraday constant; I, ionic strength of solution; ε, dielectric constant of the medium; ε_0, permittivity of free space; R, gas constant; and T, temperature.

The ionic strength of the solution $I = 1/2(\Sigma\, c_{0i}Z_i^2)$ (c_{0i} is the ion concentration, and Z_i, ion charge) was estimated taking into account the fact that, for sodium borohydride, the number of single-charged ions does not change as a result of hydrolysis and reduction reaction. The parameter λ for the sol was estimated at 7.6 nm; consequently, the thickness of the polymer layers does not exceed this value.

The sols stabilized with PVP, containing up to 0.15 wt % silver, were obtained at the same ratio of the reactants as in the case of low-concentration sols. The resulting dark brown sols were diluted to a silver concentration of 0.003 wt % for spectral and electrophoretic examinations. The electrophoretic measurements showed that the particles were not charged. The spectral characteristics of the diluted sols corresponded to those of low-concentration sols with single silver nanoparticles. The sols did not change their yellow color upon addition of 1 M KNO_3 or NaCl solution, upon heating and boiling. Even combined action of the electrolyte and boiling did not change the absorption spectra of the sols. Thus, under the actual conditions, stabilization with PVP of a high molecular weight yields highly stable sols with single silver nanoparticles.

Poly-*N*-vinylpyrrolidone is also used for stabilization of sols and simultaneous reduction of silver

ions in aqueous alcoholic solutions in preparation of the pharmacological agent Poviargol [11, 12]. Bogdanchikova et al. [13] showed that, in Poviargol, silver particles 1–2 nm in size are dominating; the second maximum in the particle-size distribution corresponds to the diameter of 70 nm. The electron-microscopic examinations by Panarin et al. [11] showed that Poviargol contains silver nanoparticle aggregates comprising from several to thousand grains each. Particle aggregation in the course of preparation of such systems (with the sedimentation stability of the sols preserved) is confirmed by their spectral characteristics [1]. The main distinctive features of the resulting systems are evidently due to the use of a strong reducing agent and a high-molecular-weight PVP: PVP with a molecular weight of 12.6×10^3 serves as the basic protective polymer in Poviargol [12].

Among the matrices used for development of new nanocomposites based on polymers with silver nanoparticles are polyacrylamide gels [2, 14]. Silver nanoparticles are obtained both in situ (with simultaneous photoreduction of Ag^+ ions and photocopolymerization of a monomer mixture) and by incorporation of cryochemically synthesized silver nanoparticles into polyacrylamide gels [2, 14]. For preparation of similar systems upon introducing polyvinylpyrrolidone-stabilized sol with silver nanoparticles, we used an aqueous solution of the 3 : 1 (by volume) monomer mixture of acrylamide and *N*,*N*'-methylene-bis-acrylamide. Copolymerization was initiated by introduction of the potassium persulfate–*N*,*N*,*N*',*N*'-tetramethylethylenediamine redox system. The silver concentration in the resulting composite medium based on polyacrylamide was 0.1 wt %. In the first stage of film preparation, the mixture was applied, in the initial phase of its viscosity growth, to a glass substrate and kept at room temperature. The optical characteristics of the films corresponded to those observed in absorption of single silver particles. However, prolonged removal of moisture in the course of slow drying of the films was responsible for the gradual appearance of local nonuniformities deteriorating the optical transparency. The reproducibility of the results virtually was not improved upon additional keeping of the films in a drying box at 330 K or in a desiccator with hygroscopic agents. Reproducible preparation of optically uniform films whose characteristics remain virtually unchanged for a long time can be achieved with semi-permeable membranes, used in dialysis, as substrates and by removing moisture with a water-jet pump. Such films can be stored without changes for over 2 years after preparation.

When introduced in an amount insufficient for total coverage of the surface of all the particles, the stabilizer can be nonuniformly distributed over particles [15]. Therefore, for preparation of a uniform system with fractal silver aggregates it is desirable to provide controlled formation of aggregates of particles with the surface entirely covered with the stabilizer. This fractal structure of the aggregates is manifested in the spectra by a significant long-wave broadening of the plasmon absorption band. The maximal broadening of the band in the spectrum corresponds to the minimal thickness of the polymer layers between the particles.

To obtain sols with optical characteristics corresponding to those of fractal silver aggregates, we used a protein-based stabilizer casein used for preparation of the pharmacological agent silver colloid (Collargol). Electron-microscopic examinations by Bogdanchikova et al. [13] showed that, in Collargol solutions, the particle size varies within 1–12 nm with d_{max} of 5 and 12 nm. Spectral examinations of the low-concentration silver sol with a casein stabilizer (c_{Ag} = 0.003 wt %) showed that the sol contains predominantly single silver particles and an insignificant fraction of microaggregates composed of several particles. The latter is indicated by a slightly increased width of the plasmon resonance, 100–120 nm, against 70–90 nm in silver sols with high electrostatic stabilization.

Partial astabilization of a sol based on Collargol is achieved by introducing an alkali. The negatively charged particles of the dispersed phase preserved the electrophoretic mobility in 0.2 M NaOH, while, at such ionic strengths, the particles with electric double layer (prepared in the absence of stabilizers) have a zero electrophoretic mobility. This suggests that the surface electrical characteristics of the particles are totally determined by the protein macromolecules: The isoelectric point of ampholytic casein corresponds to pH 4.7; with increasing pH, the negative charge tends to increase due to dissociation of the functional groups by the acid mechanism [16].

In the absence of light irradiation accelerating silver particle aggregation [1, 3], the spectral characteristics of the freshly prepared partially astabilized yellow sol remain unchanged for 1–2 weeks. Upon solar irradiation, the absorption spectra of the sol exhibit a slow evolution corresponding to thinning of the stabilizer layers between the neighboring particles of the aggregate. The precipitate formed 5 days after the light irradiation has a clear violet tint. This suggests that the adsorption layers preventing formation of dense silver particle aggregates of gray color are preserved [1, 5].

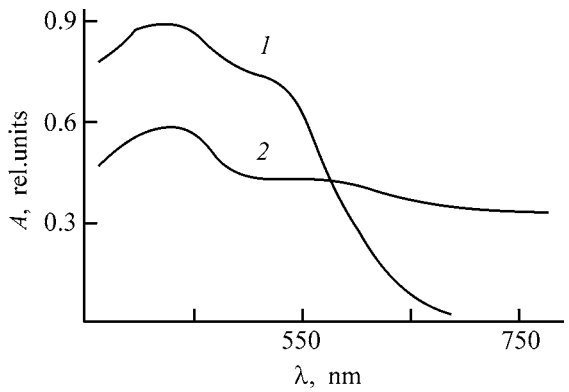


Fig. 2. Absorption spectrum of the silver sol prepared on the basis of Collargol. (*A*) Absorption and (λ) wavelength. Aggregation phase: (*1*) intermediate and (*2*) developed.

To accelerate the formation of fractal structures, the solution temperature was raised, which also decreased the relative amount of the alkali used for astabilization of the sols. The experimental conditions we selected for preparation of a sol with a silver concentration over 0.1 wt % and optical characteristics corresponding to the developed phase of the fractal aggregate formation were as follows. The sol with casein stabilizer (containing 0.07 wt % silver) was prepared by mixing on a magnetic stirrer at 330 K for 0.5 h, followed by the introduction of an alkali solution to the concentration of 0.03 M and evaporation on a water bath at 365 K till the system volume decreased by a factor of 1.5. The absorption spectra of such sols at tenfold dilution have an extended wing in the long-wavelength part of the visible spectral range (Fig. 2), which corresponds to the absorption spectra of sols with fractal silver aggregates [1].

The differential absorption spectra of the films based on polyacrylamide were, on the whole, close to those of the fractal silver aggregates. Prolonged storage of such films prepared on a substrate made of semi-permeable membranes with prompt removal of moisture results in a certain decrease/narrowing of the plasmon absorption band of the incorporated silver aggregates. This effect deserves special examination.

CONCLUSION

The methods for preparation of stable silver hydrosols stabilized with a high-molecular-weight nonionic polymer and silver hydrosols with fractal aggregates of nanoparticles and a protein stabilizer on the surface, as well as the methods for preparation of polymeric films containing fractal aggregates of nanoparticles, can be used for development of new photochromic materials.

ACKNOWLEDGMENTS

This study was financially supported by the Russian Foundation for Basic Research [project nos. 05-03-32642a and RNPVSh (Development of Scientific Potential of High School) 2.1.1.1814].

REFERENCES

1. Karpov, S.V. and Slabko, V.V., *Opticheskie i fotofizicheskie svoistva fraktal'no-strukturirovannykh zolei metallov* (Optical and Photophysical Properties of Fractal-Structured Metal Sols), Novosibirsk: Sib. Otd. Ross. Akad. Nauk, 2003.
2. Pomogailo, A.D., *Usp. Khim.*, 1997, vol. 66, no. 8, pp. 750–791.
3. Roldugin, V.I., *Usp. Khim.*, 2000, vol. 69, no. 10, pp. 899–923.
4. Safonov, V.P., Shalaev, V.M., Markel, V.M., et al., *Phys. Rev. Lett.*, 1998, vol. 80, no. 5, pp. 1102–1105.
5. Heard, S.M., Grieser, F., Barrachclough, C.G., and Sanders, I.V., *J. Colloid. Interface Sci.*, 1983, vol. 93, no. 2, pp. 545–555.
6. Creighton, J.A., Blatchford, C.G., and Albrecht, M.G., *J. Chem. Soc., Faraday II*, 1979, vol. 75, p. 790.
7. Kreshkov, A.P., *Osnovy analiticheskoi khimii* (Basics of Analytical Chemistry), Moscow: Khimiya, 1976, vol. 2, p. 30.
8. Napper, D.H., *Polymeric Stabilization of Colloidal Dispersions*, London: Academic, 1983.
9. Karpov, S.V., Bas'ko, A.L., Popov, A.K., and Slabko, V.V., *Kolloid. Zh.*, 2000, vol. 62, no. 6, pp. 773–783.
10. Baran, A.A., *Polimersoderzhashchie dispersnye sistemy* (Polymer-containing Disperse Systems), Kiev: Naukova Dumka, 1986.
11. Panarin, E.F., Pavlov, G.M., and Santuryan, Yu.G., *Khim.-Farm. Zh.*, 1991, no. 3, pp. 68–70.
12. Kopeikin, V.V. and Panarin, E.F., *Dokl. Ross. Akad. Nauk*, 2001, vol. 380, no. 4, pp. 479–500.
13. Bogdanchikova, N.E., Zaikovskii, V.I., Kolomiichuk, V.N., et al., Silver Colloid: Physicochemical Properties and Application, *Preprint*, Novosibirsk, 1992, pp. 15–30.
14. Sergeev, G.B., *Nanokhimiya* (Nanochemistry), Moscow: Mosk. Gos. Univ., 2003.
15. Kuz'mina, G.L., Girfanova, T.F., Martynov, G.A., and Muller, V.M., *Kolloid. Zh.*, 1976, vol. 38, no. 4, pp. 795–800.
16. Chernikov, M.P., *Proteoliz i biologicheskaya tsennost' belkov* (Proteolysis and Biological Value of Proteins), Moscow: Meditsina, 1975.

ISSN 1070-4272, Russian Journal of Applied Chemistry, 2006, Vol. 79, No. 10, pp. 1643–1646. © Pleiades Publishing, Inc., 2006.
Original Russian Text © E.S. Sashina, A.V. Vnuchkin, N.P. Novoselov, 2006, published in Zhurnal Prikladnoi Khimii, 2006, Vol. 79, No. 10, pp. 1664–1667.

MACROMOLECULAR CHEMISTRY AND POLYMERIC MATERIALS

A Study of the Thermodynamics of Chitosan Interaction with Polyvinyl Alcohol and Polyethylene Oxide by Differential Scanning Calorimetry

E. S. Sashina, A. V. Vnuchkin, and N. P. Novoselov

St. Petersburg State University of Technology and Design, St. Petersburg, Russia

Received April 28, 2006

Abstract—Chitosan/polyvinyl alcohol and chitosan/polyethylene oxide blend films were prepared by coagulation from solutions. The interaction energy density B and interaction parameter χ_{12} of the components were estimated from the change in the melting point of the synthetic component in the blends.

DOI: 10.1134/S107042720610017X

Because of its biological activity and polyelectrolyte behavior, chitosan finds wide application as powders, gels, films, and fibers [1]. Mechanical characteristics of chitosan-based materials can be improved by chemical modification of the polymer or blending with other polymers. Blends of chitosan with cellulose [2], polyelectrolytes [3–6], polyvinyl alcohol (PVA) [7, 8], and polyethylene oxide (PEO) [9] have been studied. It was demonstrated that addition of such flexible-chain polymers as PVA and PEO improves the mechanical characteristics of the films. The indicated polymers are biologically inert, which is important for medical applications of the polymer blends. In preparation of the blends, functional groups of chitosan interact with the hydroxy groups of PVA and the ether groups of PEO. Furthermore, an important factor is the increase in the packing density of the macromolecules in blends through filling of the cavities in the rigid structure of chitosan by flexible macromolecules.

It may be suggested that the hydroxy groups of PVA can form stronger hydrogen bonds with the OH and NH_2 groups of chitosan than the less polar ether groups of PEO. However, PEO, has a smaller size of the macromolecule and can provide a denser packing in filling the cavities of the chitosan structure. Therefore, we made a comparative study of the compatibility of chitosan with the indicated flexible-chain polymers under similar conditions. To eliminate the solvent effect on the interaction between the components having different solubilities and solution temperatures we used, in estimation of the interaction parameter the DSC data obtained for the blend films. This method is widely used to characterize the compatibility on the basis of data on the change in the glass transition and melting points of the components in the blends [10]. Evaluation of the compatibility from the glass transition point is complicated by the facts that the peak corresponding to glass transition of PVA in the blends is superimposed with the broad peak due to the evaporation of the bound water, and that the glass transition of PEO occurs below –50°C. Therefore, we selected as a parameter the melting point of the synthetic component in the blend. An additional argument in favor of this decision is that the effects of the conformation and H bonding of the synthetic component on the interaction with the chitosan molecules are insignificant at the melting point.

EXPERIMENTAL

In the experiments, we used chitosan purchased from Dalwoo-Chitosan Co. Ltd. (Korea) (degree of deacetylation 95%; moisture content 7.5%; viscosity at 25°C of 2% solution in 2% acetic acid 30.8 mPa s), polyvinyl alcohol (Merck) (mean MW 45000), and polyethylene oxide (Merck) with MW 35000.

The polymers were dissolved in 2% acetic acid at 80°C with stirring to obtain a clear solution of the desired concentration. The resulting solution was then vacuum-filtered (Buchner funnel) through a glass

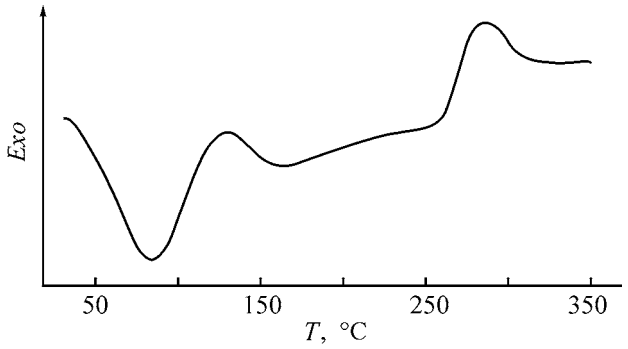


Fig. 1. DSC curve of the chitosan film. (*t*) Temperature.

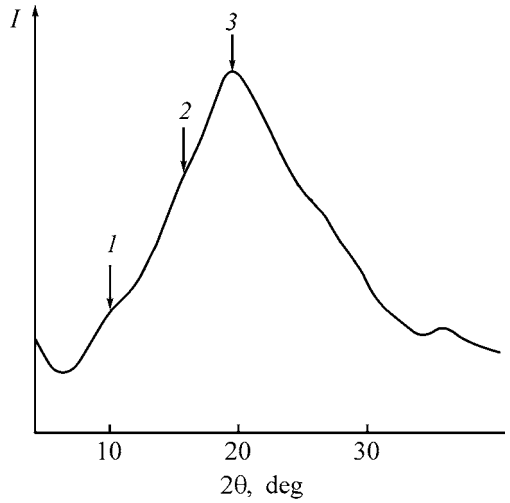


Fig. 2. X-ray diffraction pattern of the chitosan film. (*I*) Intensity and (2θ) Bragg angle. *d*: (*1*) 8.92725, (*2*) 5.67584, and (*3*) 4.58004.

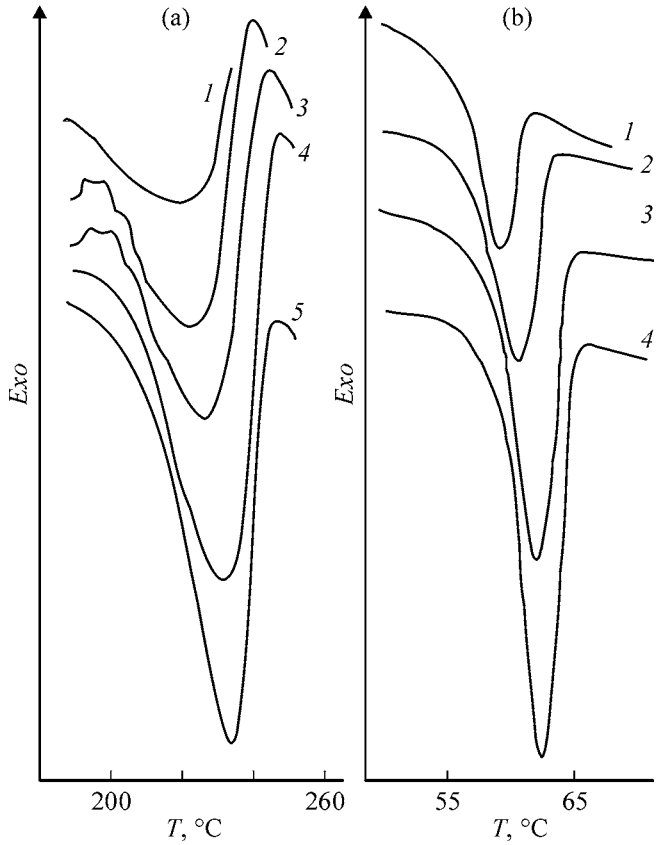


Fig. 3. Change in the melting point *t* of (a) PVA and (b) PEO in blends with chitosan. (a) Chitosan : PVA: (*1*) 30 : 70, (*2*) 50 : 50, (*3*) 70 : 30, (*4*) 90 : 10, and (*5*) 100 : 0. (b) Chitosan : PEO: (*1*) 30 : 70, (*2*) 50 : 50, (*3*) 70 : 30, and (*4*) 100 : 0.

filter no. 1. Stock polymer solutions were mixed in the required ratio for 1 h with continuous stirring.

Films were prepared by pouring the solutions onto a foil, which was followed by removing the solvent. The resulting films were 40–60 μm thick.

A thermal analysis of the films was carried out on a Netzsch-Geraetebau GmbH Thermal Analysis scanning calorimeter with heating from 30 to 500°C at a rate of 10 deg min^{-1} under nitrogen.

X-ray diffraction patterns were obtained on a Bruker D8 Advance diffractometer.

To characterize the interpolymer interaction, we used DSC data obtained for the blend films. The compatibility of the polymers was assessed with the melting point depression of the synthetic component serving as a parameter. The DSC curve of chitosan (Fig. 1) shows endothermic peaks associated with removal of adsorbed water (83°C) and glass transition (158.2°C).

The onset of thermal degradation of the chitosan film is observed at 251°C. The thermal degradation in nitrogen is exothermic, and the corresponding peak is observed at 280°C.

The observed broad endothermic glass transition peak and the lack of distinct peaks in the X-ray diffraction pattern of the chitosan film (Fig. 2) suggest an essentially amorphous supramolecular structure of the polymer obtained under the experimental conditions.

The DSC curves of PVA and PEO, obtained in this study, are typical of these polymers [11], so they are not presented here. The endothermic effects of melting were observed at 223.7 and 62°C for PVA and PEO, respectively. In the blends with chitosan, the melting points of the synthetic polymers steadily decreased with increasing chitosan content, and, at a chitosan : synthetic polymer ratio of 90 : 10, the thermal effects of melting were not detected at all. The change in the melting points of the synthetic polymers in the blends with chitosan is shown in Figs. 3a and 3b.

Table 1. Melting point of synthetic polymers in blends with chitosan

Polymer content, wt %	Melting point, °C		Polymer content, wt %	Melting point, °C	
	PVA	PEO		PVA	PEO
100	223.7	62.0	50	216.8	60.1
90	221.4	Not determined	30	208.7	59.4
70	218.0	60.3	10	Not determined	Not determined

Table 2. Thermodynamic parameters of interaction in blends of chitosan with synthetic polymers

Blend	B, cal cm^{-3}	χ_{12}
Chitosan–PVA	–3.3	–0.348 (T_m = 223.7°C)
Chitosan–PEO	–0.81	–0.13 (T_m = 62°C)

A similar effect of depression of the melting point has been reported for blends of well-compatible polymers [12–18]. The melting points of the synthetic components in the blends with chitosan are listed in Table 1.

Thermodynamically, the melting point depression is due to the exothermic effect of interpolymer interaction. Since chitosan occurs in our case essentially in the amorphous state, the interaction parameter was estimated from the dependence of the melting point depression ΔT_m in the amorphous polymer/crystalline polymer blend on the interpolymer interaction energy [19]:

$$\Delta T_m = T_m^0 - T_m = T_m^0(V_{2u}/\Delta H_{2u})B\nu_1^2, \qquad (1)$$

where the subscripts 1 and 2 refer to chitosan and synthetic polymers, respectively; T_m^0 is the melting point of the straight synthetic polymer; T_m, melting point of the synthetic polymer in the blend; ν, volume fraction; V_u, molar volume of the polymer unit; and B, interaction energy density of two polymers.

The interpolymer interaction energy density is related to the interaction parameter χ_{12} by

$$B = RT_m^0(\chi_{12}/V_{1u}). \qquad (2)$$

where R is the gas constant.

It follows from Eq. (2) that the dependence ΔT_m on χ_{12} should be linear, originating from the zero point. From the DSC data we obtained the concentration dependences of ΔT_m (Fig. 4) for the blends of chitosan with PVA and PEO. In estimating the volume fractions of the components, we used the density of amorphous chitosan of 1.5 g cm^{-3} [1], the density of PVA melt of 1.29 g cm^{-3} [16, 17], and that of PEA melt of 1.09 g cm^{-3} [18]. The densities of the polymer melts were taken because the interaction parameters were to be estimated at the melting point. The curves in Fig. 4 intersect the ordinate at 2.4 and 1.5°C for chitosan–PVA and chitosan–PEO blends. Such a deviation from the zero point is within the range typical of compatible polymers (0.5–2.5°C), and should be attributed to the residual entropy effect [12, 19]. In estimating parameter B, we used the $\Delta T_m/\nu_1^2$ ratio obtained from the plots in Fig. 4 (35 and 5.45 for PVA and PEO, respectively); V_u was estimated from the MW to density ratio; and the $\Delta H_{2u}/V_{2u}$ values were taken from [16–18] (45.4 and 49.7 cal cm^{-3}, for PVA and PEO, respectively). The estimated interaction energy densities B and interaction parameters χ_{12} are listed in Table 2.

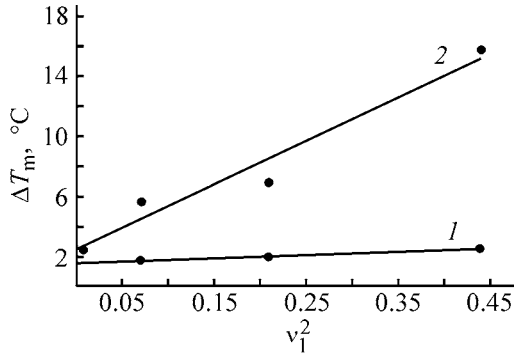


Fig. 4. ΔT_m of (*1*) PEO and (*2*) PVA vs. the volume fraction of chitosan in the blend, ν_1^2.

CONCLUSIONS

(1) Negative values of B and χ_{12} suggest that, in chitosan–polyvinyl alcohol and chitosan–polyethylene oxide blends, the interaction between dissimilar macromolecules is more preferable than that between similar ones. The compatibility of the polymers is provided by strong H bonding between the functional groups of their macromolecules.

(2) Comparison of the interaction parameters in chitosan–polyvinyl alcohol and chitosan–polyethylene oxide blends reveals that the functional groups of chitosan interact with the OH groups of polyvinyl alcohol more strongly than the ether groups of polyethylene oxide.

REFERENCES

1. *Khitin i khitozan: Poluchenie, svoistva i primenenie* (Chitin and Chitosan: Preparation, Properties, and Applications), Skryabina, K.G., Vikhoreva, G.A., and Varlamova, V.P., Eds., Moscow: Nauka, 2002.
2. Suvorova, A.I., Tujkova, I.S., and Borisova, T.S., *Chemie-Ingenier-Technik*, 2001, vol. 73, no. 4, p. 621.
3. Sashina, E.S. and Novoselov, N.P., *Zh. Prikl. Khim.*, 2005, vol. 78, no. 3, pp. 493–498.
4. Kweon, H., Ha, H.C., Um, I., and Park, Y.H., *J. Appl. Polym. Sci.*, 2001, vol. 80, pp. 928–934.
5. Ageev, E.P., Vikhoreva, G.A., Gal'braikh, L.S., et al., *Vysokomol. Soedin., Ser. A*, 1998, vol. 40, no. 7, pp. 1198–1204.
6. Simsek-Ege, F., Bond, G.M., and Stringer, J., *J. Appl. Polym. Sci.*, 2003, vol. 88, no. 2, pp. 346–351.
7. Mukhina, V.P., Pastukhov, N.V., Semchikov, Yu.D., et al., *Vysokomol. Soedin., Ser. A*, 2001, vol. 43, no. 10, pp. 1797–1804.
8. Bel'nikevich, N.G., Bobrova, N.V., Bronnikov, S.V., et al., *Zh. Prikl. Khim.*, 2004, vol. 77, no. 2, pp. 316–320.
9. Alekseev, V.L., Kel'berg, E.A., Bronnikov, S.V., and Evmenenko, G.A., *Vysokomol. Soedin., Ser. B*, 2001, vol. 43, no. 10, pp. 1856–1860.
10. *Polymer Blends*, Paul, D.R. and Newman, S., Eds., New York: Academic, 1978, vol. 1.
11. Brandrup, Y., Immergut, E.M., and Grulke, E.A., *Polymer Handbook*, New York: Wiley, 1999.
12. Ziska, J.J., Barlow, J.W., and Paul, D.R., *Polymer*, 1981, vol. 22, no. 6, pp. 918–923.
13. Harris, J.E., Goh, S.H., Paul, D.R., and Barlow, J.W., *J. Appl. Polym. Sci.*, 1982, vol. 27, no. 6, pp. 839–844.
14. Aubin, M., Bedard, Y., Morrissette, M.-F., and Prud'homme, R.E., *J. Polym. Sci., Polym. Phys. Ed.*, 1983, vol. 21, no. 2, pp. 233–237.
15. Runt, J.P., *Macromolecules*, 1981, vol. 14, no. 3, pp. 420–424.
16. Nishio, Y. and Manley, R.S., *Macromolecules*, 1988, vol. 21, no. 8, pp. 1270–1277.
17. Nishio, Y., Haratani, T., and Takahashi, T., *Macromolecules*, 1989, vol. 22, no. 19, pp. 2547–2549.
18. Nishio, Y., Hirose, N., and Takahashi, T., *Polym. J.*, 1989, vol. 21, no. 4, pp. 347–351.
19. Paul, D.R., Barlow, J.W., Bernstein, R.E., and Wahrmund, D.C., *Polym. Eng. Sci.*, 1978, vol. 18, no. 9, pp. 1225–1229.

ISSN 1070-4272, Russian Journal of Applied Chemistry, 2006, Vol. 79, No. 10, pp. 1647–1650. © Pleiades Publishing, Inc., 2006.
Original Russian Text © I.A. Novakov, O.Yu. Kovaleva, Yu.V. Shulevich, A.V. Navrotskii, V.P. Volodina, Yu.B. Monakov, 2006, published in Zhurnal Prikladnoi Khimii, 2006, Vol. 79, No. 10, pp. 1668–1671.

MACROMOLECULAR CHEMISTRY AND POLYMERIC MATERIALS

Molecular Characteristics and Hydrodynamic Behavior of Polyelectrolyte–Surfactant Complexes in Chloroform

I. A. Novakov, O. Yu. Kovaleva, Yu. V. Shulevich, A. V. Navrotskii, V. P. Volodina, and Yu. B. Monakov

Volgograd State Technical University, Volgograd, Russia
Institute of Organic Chemistry, Ufa Scientific Center, Ufa, Bashkortostan, Russia

Received June 14, 2006

Abstract—Molecular characteristics of polyelectrolyte complexes of the ultrahigh-molecular-weight poly(*N*,*N*-dimethyl-*N*-benzyl-*N*-methacryloyloxyethyl)ammonium chloride with oppositely charged surfactants in chloroform were studied by centrifugal sedimentation and viscometry. The effect of oil-soluble surfactants on the hydrodynamic properties of the complexes was examined.

DOI: 10.1134/S10704272061000181

The interaction of polyelectrolytes (PEs) with oppositely charged micelle-forming surfactants produces amphiphilic polymer–colloid complexes whose solubility in aqueous and organic solvents can be controlled by varying the hydrophilic-hydrophobic balance [1–4]. In this case, polyelectrolyte complexes (PECs) of various compositions and molecular organizations can be formed, depending on the initial reagent ratio [5]. At the equimolar PE/surfactant ratio, stoichiometric PECs (SPECs) are formed, which are insoluble in aqueous solvents. Bobrov et al. [6] have demonstrated that SPECs are amphiphilic because of the presence of polar and nonpolar fragments in their structure, namely ionic groups of PEs and surfactants, and hydrophobic aliphatic radicals of surfactants arranged into the lamellar micelles.

A study of the hydrodynamic behavior of SPECs based on amphiphilic anions and ultrahigh-molecular-weight poly(*N*,*N*-dimethyl-*N*-benzyl-*N*-methacryloyloxyethyl)ammonium chloride (PDMBMAC) in chloroform and methanol showed an abnormal concentration dependence of the reduced viscosity η_r [7]. Such a behavior is typical of polyelectrolytes, suggesting the presence of an effective charge on the chains even in weakly polar solvents.

Additional hydrophobization of SPEC, caused by the presence of the benzyl radical in the polyelectrolyte unit and of hydrocarbon chains of a surfactant, is expected to provide preferential solubility of the complex in nonpolar solvents by virtue of solvation of the indicated fragments of SPEC. However, we have demonstrated previously [7] that the PDMBMAC-based complexes are insoluble in hydrocarbon solvents, and that an increasing fraction of hydrocarbons in mixtures with chloroform promotes compaction of the macromolecular globules.

It may be suggested that the effect of compaction is compensated by weakening of the ion–ion interactions as a result of association of polar groups of the complex with other amphiphilic compounds, e.g., oil-soluble surfactants (OSSs) characterized by low hydrophiliclipophilic balance. In this case, the shielding of the polar groups should make SPECs soluble in a wider spectrum of solvents, including hydrocarbon solvents, thus expanding the applicability range of SPECs.

In this study, we examined the effect of oil-soluble surfactants on the hydrodynamic properties of stoichiometric complexes of the ultrahigh-molecular-weight PDMBMAC in chloroform.

EXPERIMENTAL

Ultrahigh-molecular-weight PEs were synthesized by polymerization of quaternary salts of vinylpyridines and aminoalkyl esters of acrylic and methacrylic acids to form poly(1,2-dimethyl-5-vinyl)pyridinium methyl sulfate (P-1,2-DM-5-VPMS), poly(*N*,*N*,*N*-trimethyl-

Table 1. Molecular and conformation characteristics of PEs ([NaCl] = 0.1 M; T = 20°C)

PE	[η], dl g^{-1}	$A_2 \times 10^4$, cm^3 mol g^{-2}	$M_W \times 10^{-6}$	R_G	l_k^{el}
				nm	
P-1,2-DM-5-VPMS	4.65	2.3	3.85	140	30
PDMBMAMS	6.89	2.9	12.2	229	29
PDMBMAC	5.67	1.9	13.6	162	13

N-methacryloyloxyethyl) ammonium methyl sulfate (PDMBMAMS) [8], and poly(*N*,*N*-dimethyl-*N*-methacryloyloxyethyl)ammonium chloride (PDMBMAC) [7].

Molecular properties of the complexes were characterized using static laser light scattering. The molecular weight MW of the PE samples and mean-square radius of gyration R_G were determined by Zimm's double extrapolation procedure [9]. The error of MW determination was within 10%. The Kuhn electrostatic segment was evaluated according to [10] on the suggestion that, in aqueous PE solutions, the contribution of the bulk interactions is negligible as compared to that caused by the electrostatic interactions:

$$l_k^{el} = 6R_g^2/L,$$

where L is the contour length of the chain.

Anionic surfactants, sodium dodecyl sulfate SDS (chemically pure grade, Merck) and Volgonat-emul'gator (VE) [mixture of sodium salts of alkylsulfonic acids RSO_3Na, R = C_{16}–C_{18}, Khimprom Joint-Stock Company, Volgograd, Russia; STP (Enterprise Standard) 2480-282-05 763 458 – 99], were recrystallized from ethanol.

The stoichiometric polyelectrolyte complexes were prepared by mixing components in aqueous solutions with vigorous stirring [7]. The composition of PECs, φ, was characterized by the ratio of the number of diphilic surfactant ions in PEC to the number of PE units in the polymeric complex (φ = $[surfactant]_{PEC}/[PE]_{PEC}$). This value was determined from the results of elemental analysis for sulfur and nitrogen.

Molecular characteristics of the resulting SPECs were determined by centrifugal sedimentation, using an MOM Model 3180 analytical ultracentrifuge (Hungary) at a rotation speed of 30 000 rpm. The sedimentation constants S_0 were determined by extrapolation to zero concentration. The molecular weight $M_{S\eta}$ was determined according to [9]. The M_{calc} value was estimated from MW of the initial PE and PEC composition.

Maleic and stearic acids (oil-soluble surfactants) were used without further purification.

The viscosity of the SPEC solutions in chloroform was measured with an Ubbelohde viscometer (capillary diameter 0.34 mm).

In addition to the solvent effect, the chemical structure of the PE elementary unit influences the solubility of SPECs in nonpolar solvents [2]. An increase in the hydrophobicity of the units of the initial PE makes higher the solubility of the complexes. In this connection, it was necessary to compare molecular and conformation characteristics of a series of ultrahigh-molecular-weight polyelectrolytes.

Table 1 shows that PDMBMAC has lower A_2, Kuhn electrostatic segment B, and radii of gyration R_G and equivalent hydrodynamic sphere R_H, compared to P-1,2-DM-5-VPMS and PDMBMAMS, which suggests the occurrence of intramolecular hydrophobic interactions caused by the presence of the benzyl radical, which is also reflected in the solubility and hydrodynamic behavior of this PE in various solvents [11]. Such a high molecular weight (13.6×10^6) and the presence of the bulky benzyl radical in the structure of PDMBMAC open the door for preparation of ultrahigh-molecular-weight SPECs soluble in low-polar organic solvents.

In all cases, the sedimentograms of the complexes in chloroform showed a single-peak profile. Since PDMBMAC is insoluble in chloroform in the absence of amphiphilic anions, the SPEC does not dissociate into the initial components, but occurs as an individual compound.

Table 2 shows that $M_{S\eta}$ of the PDMBMAC-based hydrophobic complexes in chloroform is $(3.0–4.4) \times 10^7$, and M_{calc}, $(2.7–3.2) \times 10^7$. Keeping in mind the polydispersity of the initial PE sample, one may suggest that the estimated $M_{S\eta}$ values are close to the M_{calc} obtained by taking into consideration MW of

Table 2. Molecular characteristics of hydrophobic PDMBMAC-based complexes in chloroform (T = 20°C; ω = 30000 rpm)

Sample	φ	[η], dl g^{-1}	$S_0 \times 10^{13}$, s	$M_{S\eta} \times 10^{-7}$	$M_{calc} \times 10^{-7}$	R_H^S, nm
PDMBMAC–VE	0.84	1.72	30.77	3.73	2.91	78
	1.10	4.12	25.45	4.28	3.16	115
	1.07	4.30	26.39	4.36	3.16	112
PDMBMAC–SDS	0.80	3.90	24.10	2.97	2.67	95
	0.83	4.41	30.39	3.90	2.71	108
	1.00	4.80	24.21	4.43	2.93	111

the initial PE and the composition of PEC, φ, and also that SPEC does not form intermolecular associates in chloroform.

Table 2 shows that the radii of equivalent hydrodynamic spheres, R_H^S, of the SPECs obtained are about 100 nm, indicating that chloroform can solvate both the polar and nonpolar fragments of SPEC. As a result, the SPEC macromolecules in chloroform occur as loose swollen globules.

It may be suggested that the weakening of ion–ion interactions in the SPEC structure, as well as the solubility in hydrocarbon solvents, occur by virtue of association of the complexes with other amphiphilic compounds with clearly pronounced hydrophobic behavior. Such compounds can be oil-soluble surfactants (OSSs) having a low hydrophobic–lipophilic balance and a considerable solubility in organic solvents. Taking into consideration the presence of polar groups in the OSS structure, one may expect that its association with the ester groups of SPEC will weaken the intermolecular interactions.

Figure 1 shows how the concentration dependence of the reduced viscosity η_r of complex in chloroform is influenced by addition of oleic and stearic acids.

The concentration dependence of η_r of the complex without addition of OSS (Figs. 1a, 1b) shows that, over the SPEC concentration range 0.3–0.12 g dl^{-1}, SPEC behaves as an uncharged polymer (η_r decreases from 5.3 to 4.6 dl g^{-1}). Further decrease in the SPEC concentration initiates unfolding of the macromolecule as a result of electrostatic repulsion of the charges formed on the chain, which leads to an increase in the reduced viscosity to 4.7–4.9 dl g^{-1}.

Analysis of the concentration dependences of η_r of the solutions of the complex in the presence of OSSs reveals that, in all the systems investigated, the reduced viscosity increases with the OSS concentration (Fig. 1a, curves *2–4*; Fig. 1b, curves *2*, *3*). These curves are similar in shape to the concentration dependence of η_r, obtained without addition of OSS (Figs. 1a, 1b, curves *1*). However, the curves obtained in the presence of OSS are arranged above curve *1*, and η_r is higher by a factor of 1.3–1.5 than that obtained without OSS. Evidently, introduction of OSS weakens the ion–ion interactions in the complex by virtue of the solvation of the esteric fragments of SPEC. As a result, the intermolecular interaction between the solvent and the complex strengthens, providing further swelling of the SPEC globules.

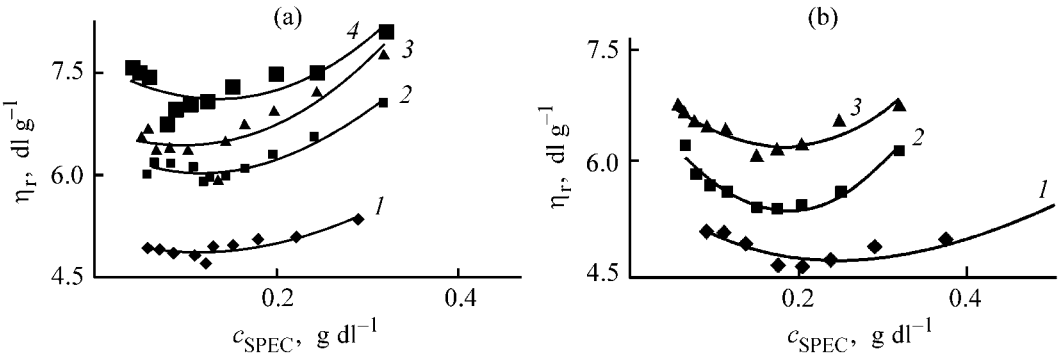


Fig. 1. Reduced viscosity η_r vs. the PDMBMAC–SDS concentration c_{SPEC} in chloroform in the presence of (a) oleic and (b) stearic acids. c_{OSS}/c_{SPEC}: (*1*) 0, (*2*) 5, (*3*) 10, and (*4*) 15.

Table 3. Reduced viscosity η_r of the complex in chloroform at various c_{OSS}/c_{SPEC} ratios

Complex	MSS	c_{OSS}/c_{SPEC}	η_r^*, dl g^{-1}	Complex	MSS	c_{OSS}/c_{SPEC}	η_r^*, dl g^{-1}
PDMBMAC–VE	Stearic acid	0	4.3	PDMBMAC–SDS	Stearic acid	0	4.8
		5.0	7.1			5.0	5.6
		10.0	7.2			10.0	6.4
	Maleic acid	0	4.3		Maleic acid	0	4.8
		2.0	2.9			5.0	6.1
		5.0	3.2			10.0	6.4
		15.0	4.9			15.0	7.0
		37.5	7.6				

* (η_r) Reduced viscosity in chloroform at c_{SPEC} = 0.1 g dl^{-1}.

A study of the effect of c_{OSS}/c_{SPEC} on η_r in chloroform (Table 3) showed that an increase in the OSS concentration also leads to a rise in the reduced viscosity of SPEC in chloroform by a factor of 1.6–1.8.

In modern engineering, polymers are widely used to raise the viscosity of aqueous and organic systems. High molecular weights and equivalent hydrodynamic sphere radii (about 100 nm) of the polyelectrolyte complexes obtained in this study suggest that they could be efficient agents to control rheological properties of nonpolar liquids.

CONCLUSIONS

(1) Molecular characteristics of stoichiometric polyelectrolyte complexes based on ultra-high-molecular-weight poly(*N*,*N*-dimethyl-*N*-benzyl-*N*-methacryloyloxyethyl)ammonium chloride in chloroform are studied. The complexes are characterized by extremely large molecular weight [MW $(3.0-4.4) \times 10^7$], equivalent hydrodynamic sphere radius R_H^S of about 100 nm, and do not form intermolecular associates.

(2) Introduction of oil-soluble surfactants into chloroform solutions of the complexes promotes solvation of ion pairs and polar fragments and provides further swelling of the globules and high viscosity indices, thus expanding their applicability as modifiers of the rheological properties of process fluids.

REFERENCES

1. Goddard, E.D. and Ananthapadmanabhan, K.P., *Interactions of Surfactants with Polymers and Proteins*, New York: CRC, 1993.
2. Bakeev, K.N., Yan Min Shu, Zezin, A.B., and Kabanov, V.A., *Dokl. Ross. Akad. Nauk*, 1993, vol. 332, no. 4, pp. 450–453.
3. Lezov, A.V., Mel'nikov, A.B., Kolomiets, I.P., et al., *Vysokomol. Soedin., Ser. A*, 1995, vol. 37, no. 11, pp. 1904–1909.
4. Bakeev, K.N., Yang M. Shu, Zezin, A.B., et al., *Macromolecules*, 1996, vol. 29, no. 4, pp. 1320–1325.
5. Zakharova, Yu.A., Otdel'nova, M.V., Aliev, I.I., et al., *Kolloidn. Zh.*, 2002, vol. 64, no. 2, pp. 170–175.
6. Bobrov, A.B., Skorikova, E.E., Sul'yanov, S.N., et al., *Vysokomol. Soedin., Ser. A*, 1997, vol. 39, no. 4, pp. 627–631.
7. Kovaleva, O.Yu., Navrotskii, V.A., Shulevich, Yu.V., et al., *Zh. Prikl. Khim.*, 2005, vol. 78, no. 7, pp. 1211–1214.
8. Novakov, I.A. and Navrotskii, V.A., *Vysokomol. Soedin.*, 2002, vol. 44, no. 9, pp. 1660–1676.
9. Rafikov, S.R., Budtov, V.P., and Monakov, Yu.B., *Vvedenie v fizikokhimiyu rastvorov polimerov* (Introduction into Physical Chemistry of Polymer Solutions), Moscow: Nauka, 1978.
10. Grosberg, A.Yu. and Khokhlov, A.R., *Statisticheskaya fizika makromolekul* (Statistical Physics of Macromolecules), Moscow: Nauka, 1989.
11. Kotlyarevskaya, O.O., Navrotskii, V.A., Orlyanskii, M.V., et al., *Vysokomol. Soedin.*, 2005, vol. 47, no. 3, pp. 508–514.

ISSN 1070-4272, Russian Journal of Applied Chemistry, 2006, Vol. 79, No. 10, pp. 1651–1654. © Pleiades Publishing, Inc., 2006.
Original Russian Text © V.A. Zayats, A.N. Nikolaevskii, T.A. Filippenko, O.P. Kniga, G.A. Tikhonova, 2006, published in Zhurnal Prikladnoi Khimii, 2006, Vol. 79, No. 10, pp. 1672–1674.

MACROMOLECULAR CHEMISTRY AND POLYMERIC MATERIALS

Fundamental Aspects of Initiated Oxidation of Tridecane and Polyethylene in Solutions

V. A. Zayats, A. N. Nikolaevskii, T. A. Filippenko, O. P. Kniga, and G. A. Tikhonova

Donetsk National University, Donetsk, Ukraine

Zavod Donplast OOO, Dontesk, Ukraine

Received March 29, 2006

Abstract—Specific features of the initiated oxidation of polyethylene and its low-molecular-weight analogue tridecane, associated with the occurrence of the process in the short-chain mode, were studied.

DOI: 10.1134/S1070427206100193

Action of aggressive factors and, primarily, atmospheric oxygen and temperature leads to degradation of polymers. Stabilizers are used to preserve the service characteristics of polymers. A search for new, more effective inhibitors of oxidative degradation of polymeric materials is an important theoretical and practical problem. Tentative evaluation of the antioxidation activity of substances is commonly performed on test systems, which simplifies solution of practical stabilization problems and makes it possible to abandon the inefficient empirical trial-and-error method of search for antioxidants (AO).

The aim of this study was to compare the fundamental kinetic aspects of initiated oxidation of polyethylene (PE) and its low-molecular-weight analogue, long-chain hydrocarbon tridecane (TD), in solutions of chlorobenzene (CB) and dichlorobenzene (DCB) to reveal the potentialities of the tridecane–chlorobenzene system as a test system in studies of the antioxidant stabilization of polyolefins.

EXPERIMENTAL

Industrial high-pressure polyethylene (M = 40000) was used in the study. The solvents were purified to remove impurities by the procedure described in [1], with subsequent distillation. The oxidation initiators (I), azodiisobutyronitrile (AIBN) for TD and dicumyl peroxide (DCP) for PE, were purified by recrystallization from ethanol and dried in a vacuum. The oxidation rate W_{O_2} was determined from the oxygen uptake in the initial stage of the reaction by gasometry, which can measure the oxygen absorption rate in the range 12×10^{-8}–1×10^{-4} mol l^{-1} s^{-1}. To provide the kinetic control, the oxidation was carried out at low concentrations of the substrates (PE, up to 8 wt %), partial oxygen pressure of 600 mm Hg, and vigorous agitation with a magnetic rabble at a rate of 200–250 rpm.

The AIBN-initiated oxidation of tridecane in a chlorobenzene solution was performed at 353 K, and PE was oxidized at 383 K. Experiments with neat chlorobenzene demonstrated that no oxygen absorption is observed at 353 K, whereas at 383 K, CB is oxidized at a rather fast rate ($W_{O_2} = 8 \times 10^{-7}$ mol l^{-1} s^{-1} [2]). Therefore, the more stable dichlorobenzene, which is not oxidized at these temperatures, was used to dissolve the polymer.

The influence exerted by the initiator concentration on the rate of oxygen uptake in oxidation of TD and PE was studied (see table). It has been shown previously [3] that, at low rates of initiation in an inert solvent, when rather long chains would be expected for establishing the polymer oxidation mechanism, the reaction rate is negligibly low. To reach noticeable oxidation rates, considerable initiator concentrations were used, with the initiation rates varying within the range $(1–6) \times 10^{-7}$ mol l^{-1} s^{-1}. Under these oxidation conditions, the length ν of the kinetic chain is ~6–7 units for TD and less than 4 units for PE, i.e., the oxidation involves short chains.

In the liquid-phase radical-chain oxidation of hydrocarbons [4], the process rate is first-order with respect to the substance and half-order with respect to the initiator, with the chain length varying from sev-

Oxygen uptake rate W_{O_2} and the kinetic chain length ν in initiated oxidation of tridecane and polyethylene in solutions ([TD] = 0.82 M, [PE] = 38 g l^{-1})

Oxidation substrate	T, K	Initiator	$[I] \times 10^{-2}$, M	$W_i \times 10^7$	$W_{O_2} \times 10^6$	ν
				mol l^{-1} s^{-1}		
TD	353	AIBN	0.61	1.32	0.9	6.8
			1.22	2.65	1.9	7.2
			1.82	3.95	2.7	6.8
			2.43	5.27	3.3	6.3
			3.04	6.60	4.1	6.2
PE	383	DCP	1.5	1.61	0.6	3.9
			2.7	2.88	1.1	3.8
			3.5	3.75	1.4	3.8
			4.5	4.82	1.6	3.4

eral tens to thousands of units. For short chains [4–7], more complex dependences are observed as a result of the involvement of low-molecular-weight radicals (of initiator or solvent) in chain termination. In this case, the kinetic equation of the chain process with short chains has the form

$$W_{O_2} = k_2[RH](W_i/k_6)^{1/2} + aW_i, \quad (1)$$

where a is a coefficient that accounts for release of oxygen in chain termination and its uptake in initiation reactions; [RH], concentration of the oxidation substrate; W_i, initiation rate; $W_i = 2ek_d[I]$; e, initiation efficiency; k_d, rate constant of thermal decomposition of the initiator [8, 9]; k_2, k_6, constants of further propagation and quadratic termination of chains, respectively.

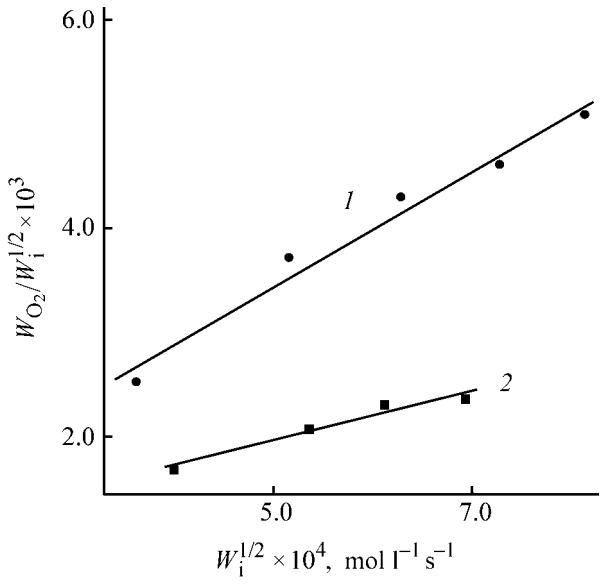


Fig. 1. Effect of the initiation rate W_i on the oxygen uptake rate W_{O_2} in oxidation of (*1*) tridecane and (*2*) polyethylene. (*1*) T = 355 K, [TD] = 0.82 M; (*2*) T = 383 K, [PE] = 38 g l^{-1}.

The data on the oxygen uptake rate at a varied initiation rate, obtained in the study (see table), are linearized in the coordinates of Eq. (1), $W_{O_2}/W_i^{1/2}$ vs. $W_i^{1/2}$ (Fig. 1). This behavior corresponds to oxidation of the long-chain hydrocarbon tridecane and polyethylene in the short-chain range, in contrast to [2], where a linear dependence of W_{O_2} on $W_i^{1/2}$ was observed in *n*-decane oxidation initiated with dicumyl peroxide.

The oxidizability parameter $k_2/k_6^{1/2}$ was found from Fig. 1 by extrapolation to the origin of coordinates: for TD at 353 K this parameter is 3.0×10^{-4} $(l\ s^{-1}\ mol^{-1})^{1/2}$. This value is an order of magnitude lower than those determined previously [3, 6] for benzene and cumene, in agreement with the lower oxidation reactivity of secondary C–H bonds, compared with those of tertiary type.

The fact that the fundamental aspects of initiation of TD and PE oxidation are identical shows that the kinetic schemes of oxidation of the polymer and its low-molecular-weight analogueare are similar.

The effect of raising the substrate concentration [RH] on the process kinetics is shown in Fig. 2. It can be seen that a nonlinear dependence of W_{O_2} on [RH] is observed at low TD and PE concentrations. The same curves were obtained for polymer solutions in [2, 5, 10–12], and this was attributed by the authors

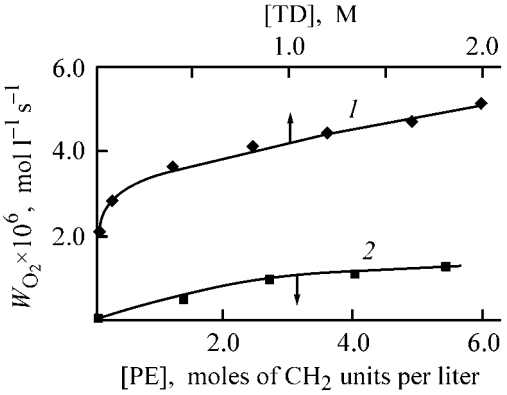


Fig. 2. Rate of initiated oxidation, W_{O_2}, of (*1*) tridecane and (*2*) polyethylene vs. the concentrations of the substrates, [TD] and [PE]. (*1*) T = 353 K, [AIBN] = 3.04×10^{-2} M; (*2*) T = 383 K, [DCP] = 2.7×10^{-2} M.

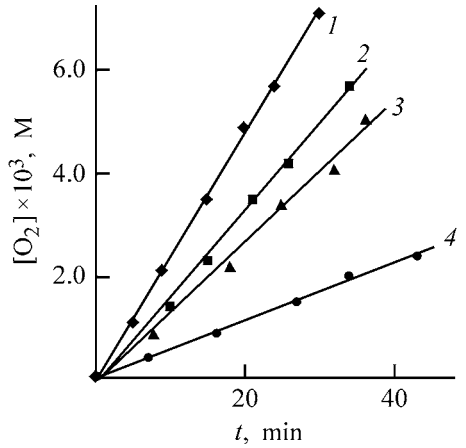


Fig. 3. Kinetic curves of oxygen uptake $[O_2]$ in oxidation of tridecane in a chlorobenzene solution in the presence of ionol. T = 353 K; [AIBN] = 3.04×10^{-2}, [TD] = 0.82 M. (*t*) Time; the same for Fig. 4. [AO] $\times 10^3$ (M): (*1*) 0, (*2*) 1.0, (*3*) 5.0, and (*4*) 10.0; the same for Fig. 4.

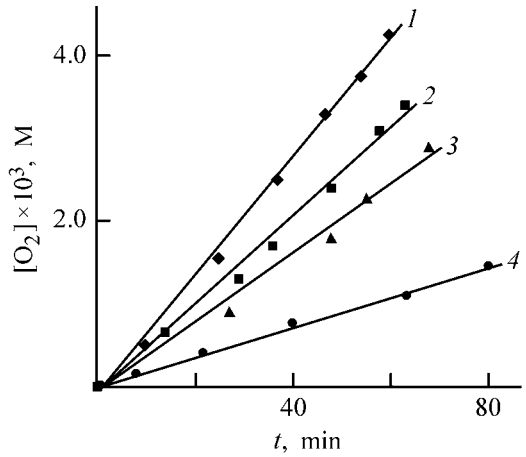


Fig. 4. Kinetic curves of oxygen uptake $[O_2]$ in oxidation of polyethylene in a dichlorobenzene solution in the presence of ionol. T = 383 K; [DCP] = 2.7×10^{-2} M, [PE] = 38 g l^{-1}.

of [11, 12] to solution structuring via aggregation processes that occur as the concentration of polymers increases. However, a similar behavior is observed in oxidation of tridecane (Fig. 2) and other low-molecular-weight hydrocarbons [2, 5, 6]. The nonlinear dependence of W_{O_2} on [RH] is attributed both to conjugated oxidation of the substrate and chlorobenzene [2], which occurs as a result of chain transfer to the solvent (neat CB is not oxidized at 353 K) and to specific oxidation at short chains with account of the intramolecular isomerization [7], i.e., of the relay mechanism of migration of a free valence along the polymer chain.

A comparison of the kinetics of TD and PE oxidation in solutions in the presence of ionol, a classical inhibitor of free-radical processes, also demonstrated that the results obtained in these two cases are identical. The kinetic curves of oxygen uptake by the substrates at varied antioxidant concentrations are shown in Figs. 3, 4. The run of the kinetic curves indicates that there is no induction period of oxidation. It should also be noted that ionol exerts an inhibiting action only at sufficiently high concentrations, which is characteristic of short-chain oxidation processes.

CONCLUSIONS

(1) The study demonstrated that, in initiated oxidation of tridecane in chlorobenzene and polyethylene in dichlorobenzene with molecular oxygen, similar kinetics of the processes are observed, including those in the presence of an inhibitor.

(2) It was shown that the tridecane–chlorobenzene system can serve as a test system adequately modeling the oxidation of polyethylene in solution and can be used in a search for new, more effective inhibitors of polyethylene oxidation.

REFERENCES

1. Weisberger, A., Proskauer, E.S., Riddick, J.A., and Toops, E.E., *Organic Solvents*, New York: Wiley, 1955.
2. Shilov, Yu.B. and Denisov, E.T., *Kinet. Kataliz*, 1973, vol. 14, no. 2, pp. 306–312.
3. Guk, A.F., Ermilov, S.P., and Tsepalov, V.F., *Kinet. Kataliz*, 1972, vol. 13, no. 1, pp. 86–91.
4. Denisov, E.T., *Okislenie i destruktsiya karbotsepnykh polimerov* (Oxidation and Degradation of Carbochain Polymers), Leningrad: Khimiya, 1990.
5. Opeida, I.A. and Zalevskaya, N.M., *Vysokomol.*

Soedin., Ser. A, 1976, vol. 18, no. 10, pp. 2270–2274.

6. Guk, A.F. and Tsepalov, V.F., *Kinet. Kataliz*, 1973, vol. 14, no. 2, pp. 322–327.
7. Kucher, R.V. and Opeida, I.A., *Sookislenie organicheskikh veshchestv v zhidkoi faze* (Cooxidation of Organic Substances in the Liquid Phase), Kiev: Naukova Dumka, 1989.
8. Antonovskii, V.L., *Organicheskie perekisnye initsiatory* (Organic Peroxide Initiators), Moscow: Khimiya, 1972.
9. Denisov, E.T., *Konstanty skorosti gomoliticheskikh zhidkofaznykh reaktsii* (Rate Constants of Homolytic Liquid-Phase Reactions), Moscow: Nauka, 1971.
10. Azizov, A.A., *Khim. Khim. Tekhnol.*, 2003, vol. 46, no. 4, pp. 110–113.
11. Kulish, E.I., Gerchikov, A.Ya., Chirko, K.S., et al., *Vysokomol. Soedin., Ser. B*, 2004, vol. 46, no. 2, pp. 349–353.
12. Kulish, E.I., Gerchikov, A.Ya., Kolesov, S.V., et al., *Zh. Prikl. Khim.*, 2005, vol. 78, no. 3, pp. 490–492.

ISSN 1070-4272, Russian Journal of Applied Chemistry, 2006, Vol. 79, No. 10, pp. 1655–1659. © Pleiades Publishing, Inc., 2006.
Original Russian Text © Yu.V. Bondar', 2006, published in Zhurnal Prikladnoi Khimii, 2006, Vol. 79, No. 10, pp. 1675–1679.

MACROMOLECULAR CHEMISTRY AND POLYMERIC MATERIALS

Specific Features of Sulfonation of Poly(Glycidyl Methacrylate) Chains Radiation-Chemically Grafted to Nonwoven Polypropylene

Yu. V. Bondar'

Institute of Environmental Geochemistry, Kiev, Ukraine

Received March 24, 2006

Abstract—Sulfonation of poly(glycidyl methacrylate) chains radiation-chemically grafted to nonwoven polypropylene was performed with sodium hydrosulfite in a water–dimethylformamide solution. Recommendations are given on optimization of the synthesis of a sorption-active hydrophilic polypropylene material bearing strongly acidic sulfo groups.

DOI: 10.1134/S107042720610020X

Nonwoven polypropylene materials are widely used in sorption processes as an adsorbing filtration material. In particular, polypropylene filters, are successfully used thanks to their fibrous structure and to the chemical resistance of the polypropylene base, for catching of microparticles from industrial gas discharges, for purification and separation of petroleum products, liquid chemicals, organic liquids, dyes, pigments, inks, pharmaceuticals, foodstuffs, etc. [1]. The range of possible applications of these materials can be extended by purposeful modification of the hydrophobic, chemically inert polypropylene base. Radiation-chemical technologies and, in particular, radiation-induced graft polymerization, find growing use for this purpose [2, 3]. This method allows introduction of polymer chains with the desired functional groups into an inert polymer matrix both by single-step grafting of appropriate monomers and by grafting of a precursor monomer followed by polymer-analogous transformations.

Because of the limited number of available vinyl monomers with functional groups, the second pathway seems extremely promising. An appropriate precursor monomer is glycidyl methacrylate (GMA), a vinyl monomer containing an epoxy ring which is readily opened under the action of acids, alcohols, and amines [4]. The following polymeric materials have been prepared under laboratory conditions by polymer-analogous reactions involving epoxy rings in grafted poly(glycidyl methacrylate) (PGMA) chains: those containing phosphoric acid groups [5], hydroxylamino and amino groups [6, 7], thiol groups [8], sulfonate groups [9–11], and iminodiacetic acid fragments [12]. However, none of these papers considered issues concerning the optimal density of grafted PGMA chains, efficiency of conversion of epoxy rings in GMA into functional groups, and stability of the functional groups in adsorption processes. The diversity of problems solved using polymeric adsorbents necessitates further search for the best synthesis procedures and a comprehensive study of the properties of the materials prepared.

The goal of this study was to perform a detailed analysis of the sulfonation of grafted PGMA chains and choose of the best conditions for preparing a sorption-active hydrophilic polypropylene material containing strongly acidic sulfo groups.

EXPERIMENTAL

Experiments were performed with a nonwoven material made of polypropylene fibers with radiation-chemically grafted PGMA chains; its preparation procedure is described elsewhere [13]. The PGMA chains were further modified with sodium hydrosulfite in a water–dimethylformamide solution at a weight ratio $NaHSO_3$: water : DMF = 2 : 7 : 3 at 70°C. The chemicals, sodium hydrosulfite (Aldrich) and dimethylformamide (DMF) (Merck, Germany), were used without additional purification.

The density S_{R-SO_3Na} (mmol g^{-1}) of sulfonate groups formed by conversion of the epoxy rings in PGMA was determned by gravimetric analysis (from the weight gain after the reaction):

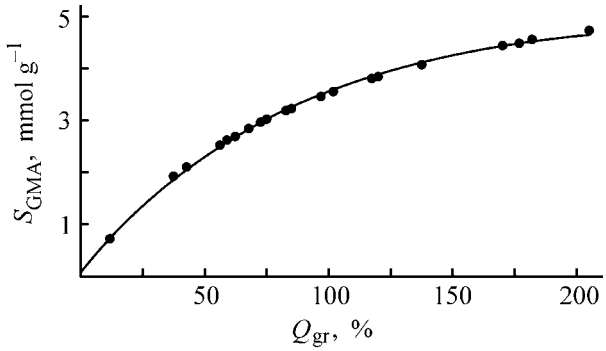


Fig. 1. Density S_{GMA} of grafted PGMA chains vs. the degree of GMA graft polymerization, Q_{gr}.

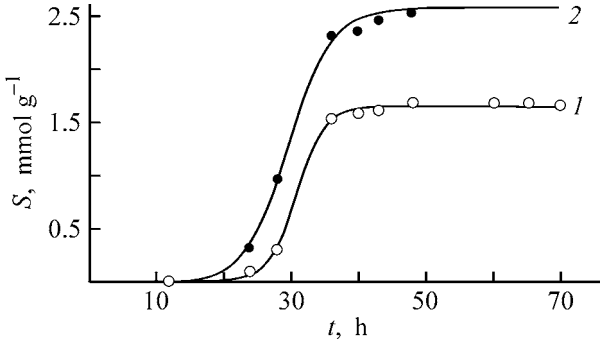


Fig. 2. Influence of the sulfonation time t on the density of the introduced sulfonate groups, S. Degree of GMA grafting, %: (*1*) 40 and (*2*) 180.

$$S_{R\text{–}SO_3Na} = \frac{m_2 - m_1}{m_2 M_{NaHSO_3}} \times 1000,$$

where m_1 is the weight of the grafted sample; m_2, weight of the sulfonated sample in the Na form; and M_{NaHSO_3}, molecular weight of $NaHSO_3$ (104).

The presence of functional groups was judged from the IR spectra recorded on a Perkin–Elmer Golden Gate Single Reflection ATR spectrometer.

The cation-exchange capacity $S_{R\text{–}SO_3Na_t}$ (mmol g^{-1}) reflecting the actual density of sulfonate groups formed by opening of epoxy rings in grafted PGMA chains was calculated from the back-titration results [14].

The adsorption properties of the sulfonated material were determined from the adsorption of Cu^{2+} ions from an aqueous solution of $CuCl_2 \cdot 2H_2O$ at pH 3.8. The content of Cu^{2+} ions in solution was determined with an atomic absorption spectrometer (UNICAM 989, UK).

The amount of metal ions adsorbed by unit weight of the dry modified material, S_m (mmol g^{-1}), was calculated by the formula

$$S_m = \frac{c_0 - c}{W} V,$$

where c_0 and c are the concentrations of metal ions in solution (mmol ml^{-1}) before and after adsorption, respectively; V, volume of the solution being analyzed (ml); and W, adsorbent weight (g).

The procedure for preparing a polymeric sulfonic cation exchanger by conversion of epoxy rings in grafted PGMA chains, considered in numerous papers [9–11], involved three steps: (1) GMA grafting, (2) sulfonation, and (3) hydrolysis. For example, Sasagawa et al. [10] performed sulfonation of porous polyethylene membranes with grafted PGMA chains (degree of grafting 200%, density of grafted chains 10 mmol g^{-1}) in a solution of the composition sodium sulfite : isopropanol : water = 10 : 15 : 75 at 80°C for 0.5–6 h. Since the maximal molar degree of conversion of epoxy rings in GMA into sulfonate groups did not exceed 28%, the unchanged epoxy rings were additionally subjected to hydrolysis in 0.5 M H_2SO_4 (80°C, 2 h). Similar conditions were used in [9, 11].

This sulfonation procedure has apparent advantages over other methods for sulfonation of polymeric materials: The process is fairly simple and easy to control; it allows preparation of a hydrophilic material with high density and prescribed localization of functional (sulfonate) groups.

In our study, the hydrophilic cation-exchange fabric bearing sulfonate groups was prepared in a two-step experiment involving radiation-induced graft polymerization of GMA onto a nonwoven polypropylene support, followed by sulfonation.

The specific features of radiation-induced graft polymerization of PGMA chains onto nonwoven polypropylene support were considered in [13]. By varying the absorbed dose, the temperature and time of grafting, the reaction medium, and the inhibitor concentration, we obtained a nonwoven polypropylene material with a widely varying density of grafted chains (Fig. 1).

The sulfonation with sodium hydrosulfite in aqueous-alcoholic solutions (water–methanol, ethanol, isopropanol) at 70°C failed, but water–dimethylformamide and water–dimethyl sulfoxide solutions appeared to be suitable for sulfonation at this temperature.

The kinetics of sulfonation of PGMA chains was monitored by the increase in the density of the sulfonate groups $S_{R\text{–}SO_3Na}$ (mmol g^{-1}), calculated from the sample weight gain after the reaction. The kinetic curves for two samples with degrees of grafting of 40 (curve *1*) and 180% (curve *2*) are shown in Fig. 2.

A specific feature of the sulfonation is a long induction period (about 20 h) followed by rapid sulfonation and then by flattening-out of the kinetic curve as the maximal conversion of the epoxy rings is attained. Figure 2 shows that the time in which the kinetic curve reaches a plateau depends on the degree of grafting: it is 48 h for the first sample (curve *1*) and 60 h for the second sample (curve *2*). The maximal densities of the sulfonate groups in these samples (plateau level) were 1.6 and 2.5 mmol g^{-1}, respectively.

To study in detail the correlation between the density of the sulfonate groups introduced and the degree of GMA grafting, we chose the reaction time of 70 h, in which the plateau is attained for all the samples.

At low degrees of grafting (Fig. 3, curve *2*), the densities of sulfonate groups, calculated by the gravimetric analysis, grow with the degree of grafting, but the curve slope noticeably decreases at degrees of grafting exceeding 50%. Such a pattern is attributable to the following: at low degrees of grafting, the major fraction of PGMA chains is grafted onto the surface of the polymeric matrix, whereas at high degrees of grafting, the amount of chains grafted onto internal layers increases. Apparently, surface epoxy rings are more accessible to conversion, whereas at high degrees of grafting, their primary conversion may hinder the conversion of the internal GMA epoxy rings.

The density of sulfonate groups, calculated from the back-titration data, is also plotted in Fig. 3 (curve *1*). As noted above, the density of sulfonate groups determined by back-titration, reflects the actual content of sulfonate groups in the sample. Figure 3 shows that, at low degrees of grafting, the curves of the density of the sulfonate groups, plotted on the basis of gravimetric and back-titration data, virtually coincide, whereas at higher degrees of grafting, the gravimetric method gives appreciably overestimated results. This fact suggests the occurrence of another reaction, along with the sulfonation, leading to weight gain. Such a side reaction can be only the hydrolysis of epoxy rings to give diols.

Figure 4 shows the IR spectra of the samples. The IR spectra of nonwoven polypropylene with grafted PGMA chains (Fig. 4, spectrum *2*) contain absorption bands at 1730 (C=O), 1300–1100 (C–O–C), and also 1260, 950–815, and 760 cm^{-1} (epoxy ring). After sulfonation for 70 h, the bands of the epoxy ring at 1260 and 950–815 cm^{-1} disappear irrespective of the degree of GMA grafting (Fig. 4, spectra *3*, *4*), and a new band, characteristic of OH vibrations, appears at 3400 cm^{-1} as well as the absorption bands

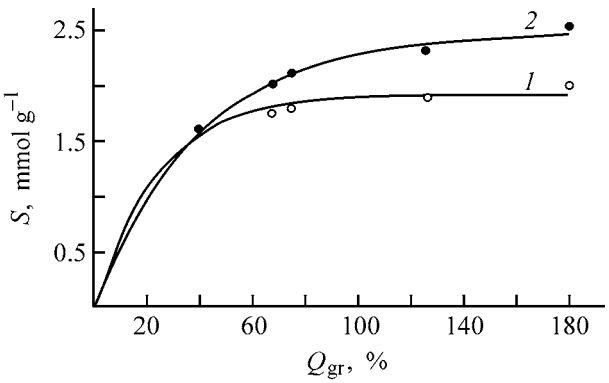


Fig. 3. Density of the introduced sulfonate groups *S*, calculated from (*1*) back-titration and (*2*) gravimetric data, vs. the degree of GMA grafting Q_{gr}.

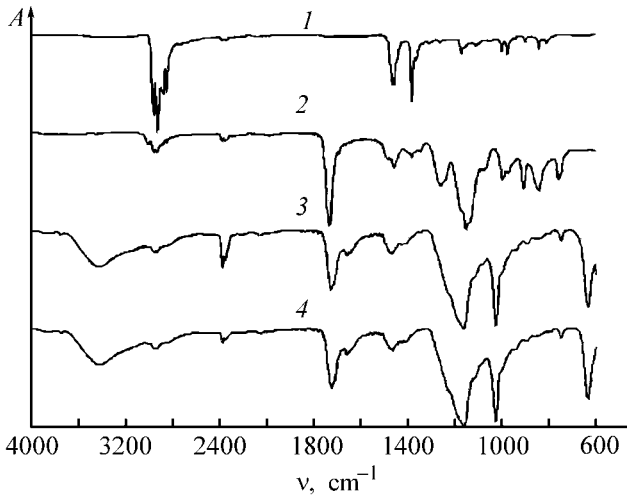


Fig. 4. IR spectra of the (*1*) initial nonwoven polypropylene, (*2*) nonwoven polypropylene with grafted PGMA chains, and (*3*, *4*) sulfonated samples with the degree of GMA grafting of 180 and 40%, respectively. (*A*) Transmission and (ν) wavenumber.

of sulfonate groups at 1150, 1030, and 670 cm^{-1}. The presence of an extremely weak peak of the epoxy ring at 760 cm^{-1} after sulfonation for 70 h can be accounted for by the possible, despite that the radiation grafting of GMA occurs at the acrylic group, also minor involvement of epoxy rings in the formation of cross-links [15]. The IR spectra of samples subjected to incomplete sulfonation (30–40 h) contained absorption bands assignable to vibrations of epoxy rings, hydroxy groups, and sulfonate groups.

Thus, the curves of the density of sulfonate groups vs. the degree of GMA grafting, plotted using the back-titration and gravimetric data, show that, in

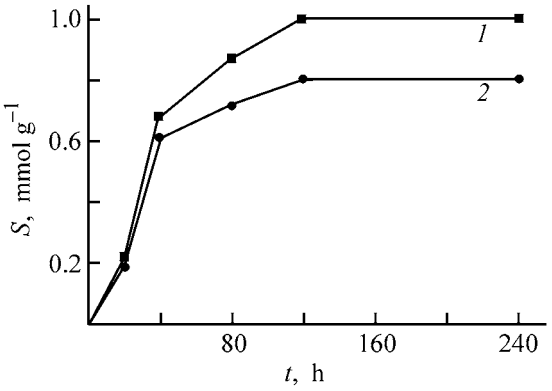


Fig. 5. Kinetic curves of adsorption of Cu^{2+} ions on the cation-exchange polypropylene material bearing sulfonate groups, synthesized in this study. (*S*) Amount of metal ions adsorbed per unit weight of the dry modified material and (*t*) time. Density of sulfonate groups, mmol g^{-1}: (*1*) 20 and (*2*) 1.67.

the course of sulfonation, the epoxy rings are opened not only in the desired reaction but also in a side reaction of diol formation (hydrolysis). The IR spectra of the samples, recorded at different stages of the reaction, confirm this conclusion. The sulfonation ends in complete conversion of the epoxy rings (plateau in the curve). Samples subjected to incomplete sulfonation (stopped before reaching the plateau) contained unchanged epoxy rings along with sulfonate and hydroxy groups; these samples were hydrophobic. After the plateau is reached, with the complete conversion of the epoxy rings into sulfonate and hydroxy groups, the samples become hydrophilic.

The results obtained are of practical significance. Apparently, to prepare an effective sorbent (cation exchanger), it is necessary to take samples with medium degrees of GMA grafting, since further increase in the degree of grafting does not lead to any appreciable increase in the density of sulfonate groups. For example, samples with a 70% degree of grafting will have the same ion-exchange capacity as those with a 170% degree of GMA grafting. This fact is particularly important in the case of synthesis of polymeric adsorbents, since high degrees of graft polymerization often lead to decreased strength of the polymeric support.

For two samples (ion-exchange capacity 2.0 and 1.67 mmol g^{-1}; degrees of grafting of 180 and 70%, respectively), taken in the H form, we determined the adsorption capacity for Cu^{2+} ions in adsorption from an aqueous salt solution. The results presented in Fig. 5 show that the equivalent adsorption capacity of the samples for Cu^{2+} ions is close to the ion-exchange capacity determined by back-titration. The exchange kinetics is fast, i.e., the cation-exchange material will be efficient in sorption processes.

CONCLUSIONS

(1) A cation-exchange material bearing sulfonate groups was prepared by radiation-induced graft polymerization of glycidyl methacrylate on a nonwoven polypropylene support, followed by the sulfonation with sodium hydrosulfite in a water–dimethyl sulfoxide solution at 70°C.

(2) The sulfonation kinetics was studied. The sulfonation ends in the plateau stage in complete conversion of the epoxy rings. The plateau is reached in 40–70 h, depending on the degree of glycidyl methacrylate grafting.

(3) The epoxy ring opening occurs along two pathways: introduction of sulfonate groups and formation of diols (hydrolysis of epoxy rings).

(4) Samples subjected to incomplete sulfonation (with the reaction was stopped before the plateau is reached) contain unchanged epoxy rings along with sulfonate and hydroxy groups. After the plateau is reached, all the epoxy rings are completely converted into the sulfonate and hydroxy groups, and only in this case, the samples become hydrophilic.

(5) To prepare an effective sulfonic cation exchanger, it is appropriate to take samples with medium degrees of glycidyl methacrylate grafting, because further increase in the degree of grafting does not lead to any appreciable increase in the density of sulfonate groups.

REFERENCES

1. *Filter and Filtration Handbook*, Dickenson, Ch., Ed., Elsevier Advanced Technology, FBIM, 1991, 3rd ed.
2. Kato, K., Uchida, E., Kang, E., et al., *Prog. Polym. Sci.*, 2003, vol. 28, no. 2, pp. 209–259.
3. Ivanov, V.S., *Radiatsionnaya khimiya polimerov* (Radiation Chemistry of Polymers), Leningrad: Khimiya, 1988.
4. Roberts, J.D. and Caserio, M.C., *Basic Principles of Organic Chemistry*, Amsterdam: Benjamin, 1964.
5. Choi, S.H. and Nho, Y.C., *Anal. Sci. Technol.*, 1999, vol. 12, no. 1, pp. 7–12.
6. Lee, K.P., Kang, H.J., Joo, D.L., and Choi, S.H.,

Radiat. Phys. Chem., 2001, vol. 60, nos. 4–5, pp. 503–511.

7. Choi, S.H., Nho, Y.C., Kim, G.T., *J. Appl. Polym. Sci.*, 1999, vol. 71, pp. 643–650.
8. Miyazaki, K., Hisada, K., and Hori, T., *Transaction*, 2000, vol. 156, no. 5, pp. 227–233.
9. Kim, M. and Saito, K., *React. Funct. Polym.*, 1999, vol. 40, no. 3, pp. 275–279.
10. Sasagawa, N., Saito, K., Sugita, K., et al., *J. Chromatogr. A*, 1999, vol. 848, pp. 161–168.
11. Kim, M. and Saito, K., *Radiat. Phys. Chem.*, 2000, vol. 57, pp. 167–172.
12. Choi, S.H. and Nho, Y.C., *J. Appl. Polym. Sci.*, 1999, vol. 71, pp. 999–1006.
13. Bondar', Yu.V., Kim, Kh.D., and Lim, I.D., *Zh. Prikl. Khim.*, 2005, vol. 78, no. 5, pp. 827–830.
14. Kreshkov, A.P., *Osnovy analiticheskoi khimii* (Principles of Analytical Chemistry), Moscow: Khimiya, 1970, vol. 2.
15. Evtushenko, E.G. and Vishev, Yu.V., *Khim. Vys. Energ.*, 1990, vol. 24, no. 2, pp. 122–127.

ISSN 1070-4272, Russian Journal of Applied Chemistry, 2006, Vol. 79, No. 10, pp. 1660–1665. © Pleiades Publishing, Inc., 2006.
Original Russian Text © A.I. Men'shikova, T.G. Evseeva, K.S. Inkin, Yu.O. Skurkis, S.S. Ivanchev, 2006, published in Zhurnal Prikladnoi Khimii, 2006, Vol. 79, No. 10, pp. 1680–1685.

MACROMOLECULAR CHEMISTRY AND POLYMERIC MATERIALS

Bifunctional Monodisperse Microspheres of Copolymers of Methyl Methacrylate and *N*-Vinylformamide

A. I. Men'shikova, T. G. Evseeva, K. S. Inkin, Yu. O. Skurkis, and S. S. Ivanchev

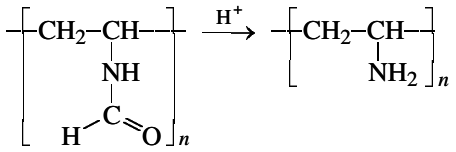
Institute of Macromolecular Compounds, Russian Academy of Sciences, St. Petersburg, Russia

Received June 21, 2006

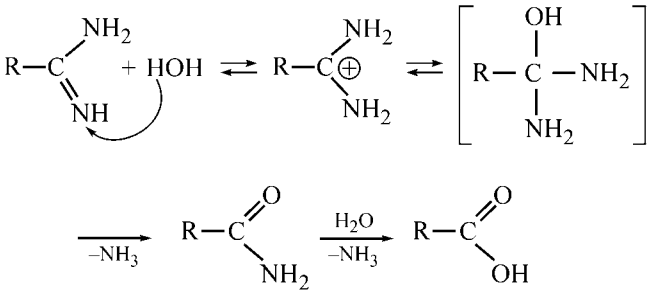
Abstract—Emulsion copolymerization of methyl methacrylate and *N*-vinylformamide in the presence of azo initiators and dextran as a polymeric stabilizer was analyzed with the aim to prepare monodisperse polymer microspheres with a polyfunctional surface. Hydrolysis of comonomer units and cationic groups of the initiator residues in the surface layer of the particles to give amphoteric surfaces containing carboxy and amino groups was studied. The optimal conditions of formation of monodisperse microspheres with diameter varied in the 340 – 660 nm range and the conditions of their hydrolysis, which allow direct control of the amount and nature of functional groups on their surface, were found.

DOI: 10.1134/S1070427206100211

At present, polystyrene particles with carboxy or aldehyde surface groups for covalent binding of bioligands are the most widely used corpuscular carriers in latex test-systems [1–4]. However, owing to the diversity of the chemical structures of biologically specific ligands and the necessity to preserve their biologically active conformation after linking, a search for new ways to introduce other functional groups in the surface layer is a topical task. The binding of amino groups to the particle surface by copolymerization of styrene with *N*-vinylformamide (VFA), initiated with 2-azobis(2-methylpropanamidine) (AMP) and followed by hydrolysis of the amide groups, was studied in [5]:



Due to protonation of the amino groups and also amidine groups of the initiator residues at the ends of the polymer chain, the surface of these particles was positively charged in a wide pH range. Moreover, the presence of carboxy groups on the particle surface, whose ionization provides inversion of the surface charge sign at pH ≥ 10, was observed. These carboxy groups can be formed by hydrolysis of the residues of AMP initiator [6, 7]:



Thus, the surface layer of the resulting particles contains both acid and base groups. This type of a polyfunctional surface provides multiple covalent, coordination, and ion-ion interactions with biological ligands; as a result, their structure and amphoteric properties become similar to those of corpuscular biological objects (cells and viruses). Addition of dextran and its derivatives, which provides formation of structures from the protein and polysaccharide fragments simulating the surface membranes of the cells and viruses, opens up additional opportunities for design of the carrier particle surface [8–11]. Biologically compatible polymers less hydrophobic than polystyrene are preferable as polymeric supports. This approach decreases the probability of nonspecific hydrophobic interactions proceeding simultaneously with immunochemical reactions and allows in vivo use of these supports for transportation of drugs and vaccines. As shown previously [9–11], particles of

Conditions of polymerization of MAA and VFA and properties of the resulting particles

Run no.	Initial pH	VFA, wt %	Initiator	Salt (10^{-2} M)	Particle diameter, μm	ζ Potential, mV		Surface concentration of weakly acidic and basic groups, μg-equiv m^{-2}
						after synthesis	after 5-month storage	
1	5.50	–	AMP	–	325	21	7	0.76
2	6.00	5	AMP	–	350	38	9	1.09
3	6.65	–	AMP	–	360	25	33	0.97
4	6.35	5	AMP	–	375	29	13	1.48
5	5.97	10	AMP	–	(Coagulum)	–	–	–
6	6.18	–	AIP	–	400	43	11	0.41
7	5.94	5	AIP	–	385	37	17	0.77
8	6.00	10	AIP	–	350	18	16	0.49
9	4.84	10	AIP	KH_2PO_4	470	34	15	2.31
10	5.30	15	AIP	–	573	12	12	1.37
11	5.14	20	AIP	–	593	11	11	1.74
12	4.85	20	AIP	KH_2PO_4	600	11	11	2.29

* All the measurements were carried out in 0.001 M NaCl at pH 6.7.

poly(methyl methacrylate) (PMMA) with a carboxylated surface, prepared in the presence of dextran or its carboxylated derivatives, meet these requirements. In this study, we examined the emulsion copolymerization of methyl methacrylate (MMA) and VFA in the presence of dextran and cationic initiators with the aim to prepare monodisperse copolymer particles with a polyfunctional surface and to found conditions of their surface hydrolysis to obtain amphoteric surfaces containing carboxy and amino groups.

Methyl methacrylate (Ekros Joint-Stock Company, St. Petersburg, Russia) and VFA (98.5%, BASF Corp.) were purified by distillation by standard procedures. The cationic azo initiators, such as 2-azobis[2-(imidazolidinyl-2)propane] (AIP) and 2-azobis(2-methylpropanamidine), purchased from Waco Pure Chemical Industries Ltd. (Japan), and the fraction of dextran hydrolyzate produced by *Leuconostoc Mesnteroids* bacteria with molecular weight 60000 ± 10000, prepared at the Chemical-Pharmaceutical Academy (St. Petersburg, Russia) were used without additional purification. All the solutions were prepared using double-distilled water.

The emulsion copolymerization of MMA with VFA was carried out at 338 ± 1 K in the presence of dextran (0.2 wt % relative to water) in accordance with the procedure described elsewhere [2]. The VFA concentration in the monomer mixture was varied from 0 to 20 wt %, the ratio of the monomer mixture to the aqueous solution was 1 : 10, and the solution pH was varied within 4.8–6.7. The reaction was initiated with AIP or AMP (0.2 wt %).

The particle diameters in the resulting latexes were measured with a JEM 100 S electron microscope (JEOL, Japan). After triple washing to remove water-soluble fraction by centrifugation and intermediate dispersion, the total surface concentration of the carboxy and amino groups was determined by conductometric titration.

The electrophoretic mobility of the copolymer particles prepared under various conditions was determined by standard microphoresis in 10^{-3} M NaCl solutions in a wide pH range. Using experimental data, ζ potentials of the particles were calculated by the Smoluchowski equation.

The properties of particles formed by emulsion polymerization were studied in relation to the nature of the initiator, content of VFA in the monomer mixture, initial pH of the reaction mixture, and content of KH_2PO_4 additive (see table).

An electron microscopic examination of the latexes prepared showed a high monodispersity of the particles of PMMF and copolymers of MMA and VFA [P(MMA–VFA)] formed in the course of emulsifier-free emulsion polymerization in the presence of cationic azo initiators (Fig. 1). The particle size increases with the pH of the reaction mixture because the degree of protonation of the cationic groups of the initiator residues on the particle surface decreased and, consequently, so did the height of the electrostatic barrier preventing aggregation of the primary nuclei at the beginning of the synthesis (see table and Figs. 1a, 1b).

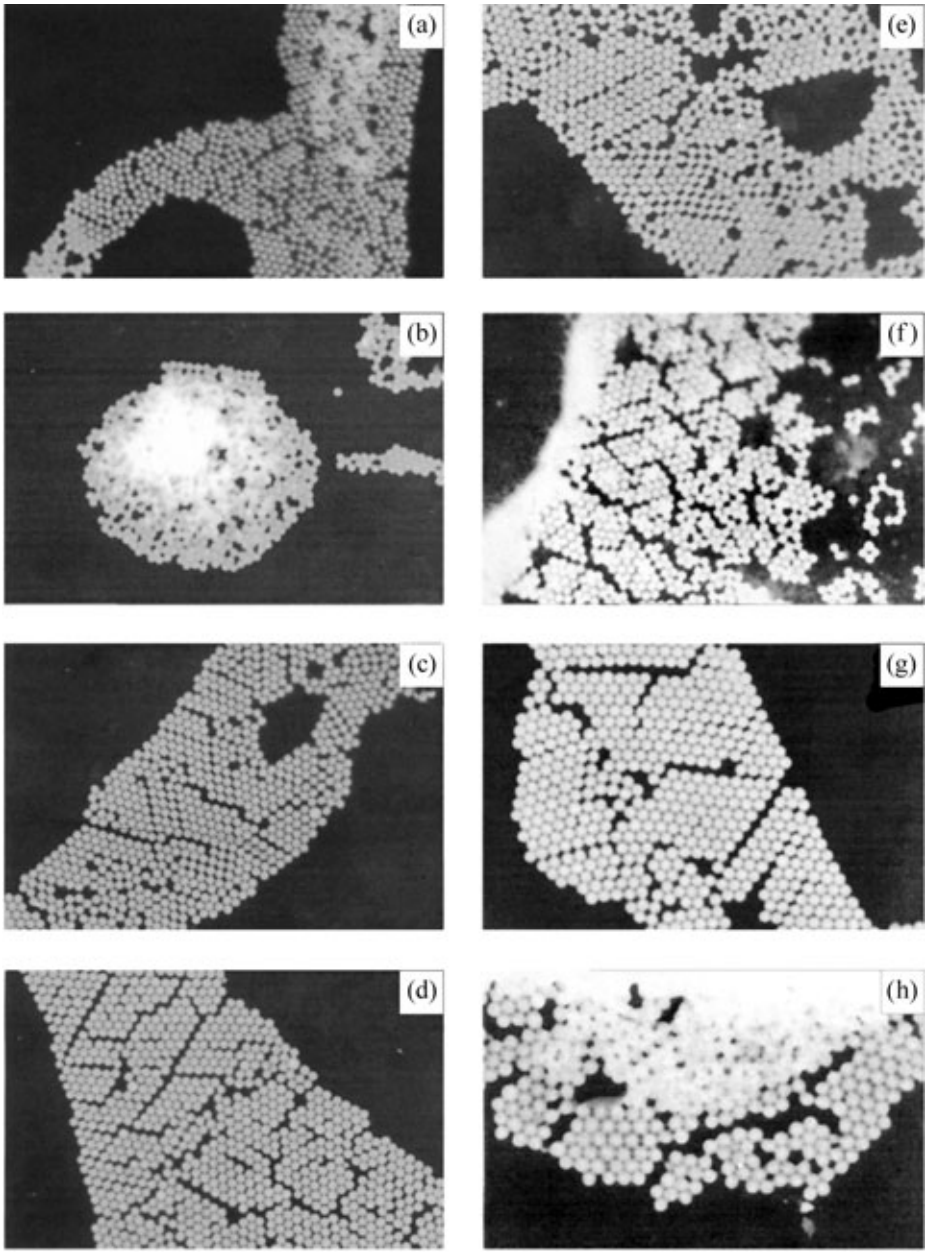


Fig. 1. Electron micrographs: (a–c) PMMA particles prepared in the presence of AMP initiator at pH (a, b) 5.5 and (c) 6.65 [(b) after hydrolysis]; (d–h) P(MMA–VFA) particles prepared in the presence (d) of AMP initiator and 5 wt % VFA and (e–h) of AIP initiator and (e) 5, (f, g) 10, and (h) 15 wt % VFA, (e, f, g) in the absence and (h) in the presence of KH_2PO_4 (0.01 M).

It should be noted that addition of VFA to the reaction mixture in the presence of AMP increases the diameter of the resulting P(MMA–VFA) particles as compared to PMMA particles (see table, run nos. 1–4, Fig. 1d). Moreover, on adding even 5 wt % VFA, the positive ζ potentials of the particles noticeably increase owing to the hydrolysis of this comonomer to form amino groups. However, with the VFA content of the monomer mixture increasing above 5 wt %, the resulting latex coagulated in the course of polymerization in the presence of AMP (run no. 5).

Immediately after the synthesis, the latexes of PMMA (sample no. 1) and of the copolymer of MMA with BFA (5 wt %) (sample no. 2) were hydrolyzed in the presence of 0.15 M HCl at 70–80°C for 24 h [5] to prepare amino groups in the surface layer of the styrene–VFA copolymer particles. However, this treatment led to coagulation of the latexes, which

is probably due to the hydrolysis of not only VFA units to form amino groups, but also initiator terminal groups to form carboxy groups. When weakly acidic and weakly basic groups are simultaneously present in the surface layer, the total surface charge of the particles and the electrostatic barrier of the latex stability both decrease.

Owing to the heterocyclic structure, the imidazole groups are more stable against hydrolysis than the amidine groups in AMP [6, 7]. Hence, we used in our further experiments the AIP initiator with imidazole groups to provide a positive charge of the latex particles. This allowed us to decrease the coagulum formation in the course of copolymerization. We found that the (co)polymerization in the presence of AMP decreased pH of the reaction mixture to 4.0–4.5, whereas in the case of AIP, the acidification was stronger and the pH of the final latex frequently reached 3.5. As a result, the positive ζ potential of the PMMA and P(MMA–VFA) particles prepared with AIP was significantly higher (see table, run nos. 6, 7), which provided their stronger electrostatic stabilization.

It should be noted that substitution of AIP for AMP in initiation of MMA copolymerization with VFA (5 wt %) causes an additional increase in the diameter of the particles formed (run nos. 2, 7), which is probably due to the difference in the rates of degradation of these initiators. The half-life of AMP is 10 h at 57°C, whereas for AIP, the same half-life is observed at about 61°C [12]. Thus, AIP causes a decrease in the rate of initiation and thus in the effective concentration of radicals in the reaction mixture, which, in turn, leads to an increase in the size of the resulting polymer–monomer particles (PMPs) as compared to the initiation of polymerization with AMP under the same conditions.

The AIP initiator increases the content of VFA in the monomer mixture from 5 to 20 wt % without any decrease in the latex stability. This allowed us to evaluate the effect of this hydrophilic comonomer on the particle size (see table, run nos. 7, 8, 10, 11; Figs. 1e, 1f, 1g). We found that, with the VFA content increasing to 10 wt %, the particle diameter slightly decreases. As, however, the VFA content increases to 15–20 wt %, the particle size strongly grows, with the narrow size distribution preserved (Fig. 2). The dependence observed is probably due to two opposite trends. On the one hand, a certain increase in the positive surface charge of a particle upon addition of small amounts of VFA decreases their size and, on the other, enrichment of the oligomer chains with VFA fragments at the beginning of the experiment decreases their surface activity and, thus, impairs their stabilizing performance. As a result, coarser particles are formed at high VFA concentrations, (Fig. 1h), with a simultaneous decrease in the positive ζ potential (see table). This is due to the enrichment of the surface layer of the resulting particles with polymeric chains containing predominantly VFA units. The conformation mobility of these chains at the water–polymer interface is high; as a result, the comparatively smooth and hydrophobic surface of PMMA particles is substituted by the "haired" hydrophilic surface of the copolymer particles. In this case, the ionic groups may be distributed and partially neutralized by counterions in the bulk of the lengthy hydrophilic surface layer; as a result, the charge at the phase sliding boundary and the ζ potential decrease.

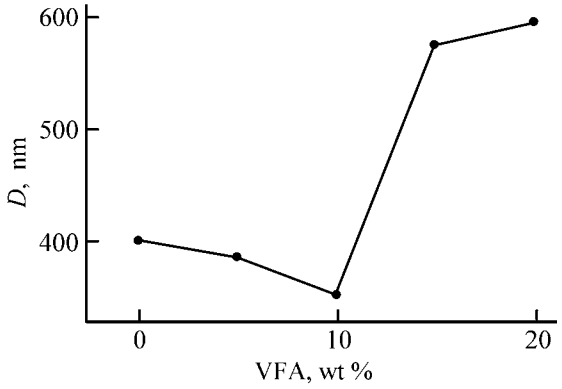


Fig. 2. Diameter of the P(MMA–VFA) particles D vs. the VFA content of the monomer mixture.

The size of the forming particles of a prescribed copolymer composition is usually controlled by varying the ionic strength of the reaction mixture. Indeed, raising the ionic strength of the reaction mixture by adding KH_2PO_4 (10^{-2} M) increases the particle diameter (see table, run nos. 8, 9, 11, 12). As, however, the content of the VFA units in the copolymer increases, this effect disappears owing to a rise in the hydrophilicity of the particle surface. It should be noted that the initial solution becomes more acidic in the presence of KH_2PO_4 and a larger amount of imidazole groups on the particle surface become protonated. This can exert an opposite effect on the size of the resulting particles by compensating for an increase in their diameter. When added to the reaction mixture, KH_2PO_4 also makes higher the content of the surface groups, because the shielding of the surface groups by counterions increases with the ionic strength of a dispersion medium and, in turn, their lateral repulsion decreases, which has been shown previously for a monofunctional carboxylated surface [10, 11].

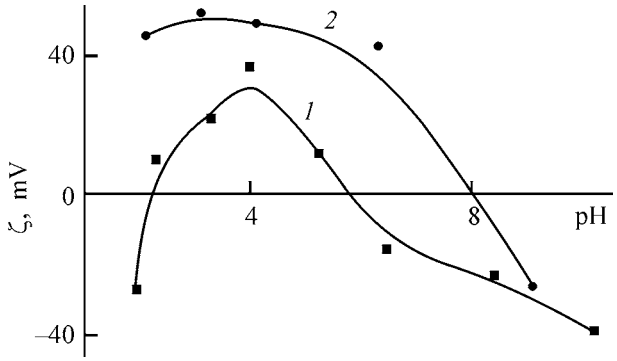


Fig. 3. ζ Potential of particles of PMMA latex prepared in the presence of initiators (*1*) AMP (run no. 1) and (*2*) AIP (run no. 6) vs. the solution pH; 10^{-3} M NaCl supporting electrolyte. Run nos. are the same as in the table; the same for Figs. 4, 5.

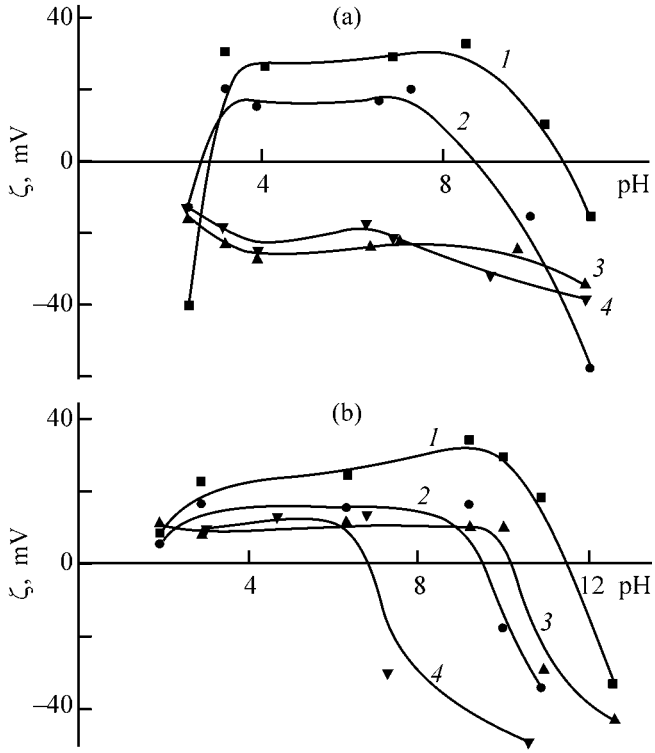


Fig. 4. ζ Potential of particles of (a) PMMA (run no. 3) and (b) P(MMA–VFA-5) latexes (run no. 4) prepared in the presence of AMP initiator (*1*) immediately after preparation and after storage for (*2*) 1, (*3*) 2, and (*4*) 3 days, vs. the solution pH.

Since certain differences were found in the products of polymerization of MMA and its copolymerization with VFA in the presence of AMP and AIP, we studied how the initiator we used affects the stability of the surface characteristics of PMMA and P(MMA–VFA) particles in their storage and subsequent treatment. We found that the surface charge of the resulting particles remained positive after storage for five months at 4°C for all the latexes prepared in the presence of any cationic azo initiator (see table). The ζ potential is more positive in the case of AIP, whose imidazole groups are more stable against hydrolysis.

However, as can be seen from the pH dependences of the ζ potential, an inversion of the potential sign is observed (Figs. 3–5). This suggests that the surface of PMMA and P(MMa–VFA) is enriched with carboxy groups owing to the hydrolysis of the terminal groups of the cationic azo initiators. In the case of the AIP initiator, the loss of the cationic groups upon hydrolysis was smaller than that with AMP (Fig. 3).

In keeping of latexes in acidic and alkaline solutions the PMMA particles retain positive charge for only 1 day (Fig. 4a), whereas addition of the VFA comonomer, whose units are hydrolyzed to form additional amino groups [13], expands the pH range in which the particle surface retains its charge for several days. For example, P(MMA–VFA-5) particles retain their positive charge for a week; the charge slightly decreases in neutral and weakly acidic solutions (Fig. 4b).

With increasing VFA content and upon addition of KH_2PO_4 buffer (10^{-2} M), the positive ζ potential of the resulting particles decreases (Fig. 5). Apparently, both factors favor synthesis of particles with more hydrophilic and, thus, more easily hydrolyzed surface, because the increase in the ionic strength leads to transfer of VFA from the reaction mixture into the polymer–monomer particles and to enrichment of the surface hydrophilic chains with the VFA fragments. In these chains, not only terminal groups of the initiator, but also MMA units can be hydrolyzed. A similar effect is observed as the VFA content in the monomer mixture increases from 15 to 20 wt %. As a result, inversion of the surface charge of the particles prepared under these conditions in acidic and alkaline solutions proceeds more rapidly.

Thus, we found that emulsifier-free emulsion copolymerization of MMA and VFA, initiated by cationic azo initiators in the presence of dextran, yields monodisperse particles 320–660 nm in diameter with a hydrophilic surface layer. The subsequent hydrolysis of the comonomer units and cationic groups of the initiator residues leads to the formation of the amphoteric surface containing both carboxy and amino groups. Taking into account the biocompatibility of the polymer matrix of these particles, structural similarity of their surface to that of cell membranes, and the possibility of their hydrolysis, we can expect that

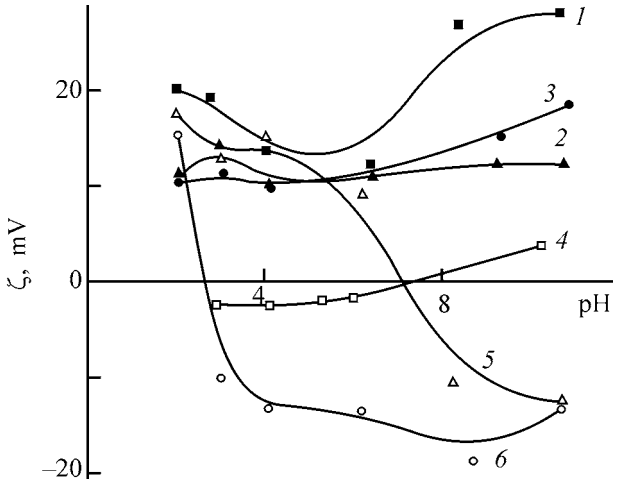


Fig. 5. ζ Potential of particles of (*1*, *4*) P(MMA–VFA-15) (run no. 10) and P(MMA–VFA-20) latexes [(*2*, *5*) run no. 11 and (*3*, *6*) run no. 12] prepared in the presence of AIP initiator (*1*, *2*, *4*, *5*) in the absence and (*3*, *6*) in the presence of KH_2PO_4, (*1*–*3*) immediately after preparation and (*4*–*6*) after storage for 1 day, vs. the solution pH.

these particles would be more efficient carriers of immunological reagents in vivo than the previously described PMMA particles modified with carboxymethyl dextran [10, 11].

CONCLUSIONS

(1) Emulsifier-free emulsion copolymerization of methyl methacrylate and N-vinylformamide in the presence of cationic azo initiators and dextran yields monodisperse microspheres 320–660 nm in diameter with positive surface charge in neutral and weakly acidic solutions.

(2) Comonomer ratio, nature of the cationic azo initiators, initial solution pH, and addition of the salt buffer significantly affect the diameter of the resulting particles, their ζ potential, and possibility of inversion of the surface charge sign.

(3) Hydrolysis in acidic and alkaline solutions of the *N*-vinylformamide units to form amino groups, which proceeds simultaneously with the hydrolysis of the amidine or imidazole groups of the initiator residues and of the ester groups of methyl methacrylate to form carboxy groups, leads to the formation of the hydrophilic amphoteric particle surface. Enrichment of the monomer mixture with *N*-vinylformamide and addition of sodium dihydrophosphate buffer enhance the hydrolysis of the resulting groups to form carboxy groups in the surface layer.

ACKNOWLEDGMENTS

This study was financially supported by the Russian Foundation for Basic Research (project no. 04-03-33080) and by the Scientific Program "Synthesis and Study of Macromolecules and Macromolecular Structures of New Generations" Department of Chemistry and Material Science of the Russian Academy of Sciences.

REFERENCES

1. Prokopov, N.I., Gritskova, I.A., Cherkasov, V.R., and Chalykh, A.E., *Usp. Khim.*, 1996, vol. 65, no. 2, pp. 178–1992.
2. Lishanskii, I.S., Men'shikova, A.Yu., Evseeva, T.G., et al., *Vysokomol. Soedin.*, 1991, vol. 33, no. 6, pp. 413–416.
3. Men'shikova, A.Yu., Evseeva, T.G., Peretolchin, M.B., et al., *Vysokomol. Soedin., Ser. A*, 2001, vol. 43, no. 4, p. 607.
4. Men'shikova, A.Yu., Evseeva, T.G., Chekina, N.A., and Ivanchev, S.S., *Zh. Prikl. Khim.*, 2001, vol. 74, no. 10, pp. 1677–1683.
5. Xu, J., Timmons, A.B., and Pelton, R., *Colloid. Polym. Sci.*, 2004, vol. 282, pp. 256–263.
6. Goodwin, J.W., Ottewill, R.H., Pelton, R., et al., *Brit. Polym. J.*, 1978, vol. 10, no. 9, pp. 173–180.
7. Goodwin, J.W., Ottewill, R.H., and Pelton, R., *Colloid Polym. Sci.*, 1979, vol. 257, no. 1, pp. 61–69.
8. Bakeeva, I.V., Borodina, .A., and Gritskova, I.A., *Vysokomol. Soedin., Ser. B*, 1997, vol. 39, no. 5, pp. 868–871.
9. Men'shikova, A.Yu., Evseeva, T.G., Chekina, N.A., and Ivanchev, S.S., *Zh. Prikl. Khim.*, 2001, vol. 74, no. 3, pp. 478–482.
10. Men'shikova, A.Yu., Evseeva, T.G., Chekina, N.A., et al., *Vysokomol. Soedin., Ser. A*, 2003, vol. 45, no. 4, pp. 623–630.
11. Men'shikova, A.Yu., Evseeva, T.G., Chekina, N.A., et al., *Prog. Colloid Polym. Sci.*, 2003, vol. 123, pp. 68–72.
12. Waco Pure Chemical Industries Ltd. (Japan), http://www.wakochem.co.jp/specialty/waterazo/index.htm
13. Yamamoto, K., Imamura, Y., Nagatomo, E., et al., *Appl. Polym. Sci.*, 2003, vol. 89, no. 5, pp. 1277–1283.

ISSN 1070-4272, Russian Journal of Applied Chemistry, 2006, Vol. 79, No. 10, pp. 1666–1668. © Pleiades Publishing, Inc., 2006.
Original Russian Text © M.L. Eritsyan, L.A. Gyurdzhyan, L.T. Melkonyan, G.V. Akopyan, 2006, published in Zhurnal Prikladnoi Khimii, 2006, Vol. 79, No. 10, pp. 1686–1688.

MACROMOLECULAR CHEMISTRY AND POLYMERIC MATERIALS

Copolymers of Acrylic Acid with Urea

M. L. Eritsyan, L. A. Gyurdzhyan, L. T. Melkonyan, and G. V. Akopyan

Abovyan State Pedagogical University, Yerevan, Armenia

Received March 24, 2006

Abstract—Composition and rheological characteristics of aqueous solutions of acrylic acid/urea copolymers were studied, including the composition dependences of the equivalent conductivity and viscosity.

DOI: 10.1134/S1070427206100223

There is only limited information on copolymers of acrylic acid (AA) and urea (Ur) [1]. These branched copolymers are poorly soluble in common organic solvents. Srivastava and Majki [1] have demonstrated that AA/Ur copolymers are formed by the radical mechanism via addition of the vinyl radical of AA to the carbonyl group of urea. Together with the radical polymerization, some condensation reactions occur, resulting in branching of the copolymers.

To our knowledge, there is no information on the composition of AA/Ur copolymers and their characteristics, such as rheology of aqueous solutions, conductivity, etc. To characterize the composition of AA/Ur copolymers, we first determined their copolymerization constants. Then we examined the dependence of the molecular weight MW of the copolymers on the AA/Ur molar ratio in the monomer mixture, and also the rheology and conductivity of their aqueous solutions.

All the experiments on radical polymerization were carried out at a constant AA concentration of 2 M.

The copolymerization constants r_1 and r_2 were estimated using the classic Fineman–Ross equation for the case with no interaction between the urea-derived radical with the corresponding monomer (r_2) [2].

$$f = r_1 F + 1, \quad (1)$$

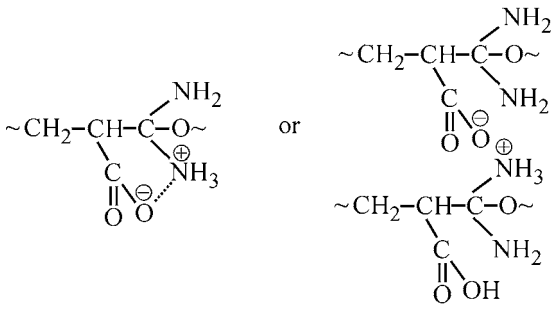
$$r_1 = K_{1,1}/K_{1,2}, \quad (2)$$

$$F = [\mathrm{AA}]/[\mathrm{Ur}], \quad (3)$$

where $f = a/b$; a and b are the AA and Ur units in the copolymer; $K_{1,1}$ and $K_{1,2}$, addition rate constants the AA radical to its monomer and Ur; and [AA] and [Ur], monomer concentrations.

The copolymerization constant r_1 was estimated from the Fineman–Ross plot (Fig. 1) to be 4 ± 0.1.

Results on r_1 and r_2 reveal that, in the copolymer, each Ur unit adjoins microblocks of the AA units. In synthesis of the copolymer of a given composition and structure, one may expect salt formation as a result of the interaction between the carboxy group of AA with the amino group of Ur. Such an interaction can be both intra- and intermolecular:



The resulting copolymer films were analyzed for ionic groups by IR spectroscopy. The spectra clearly

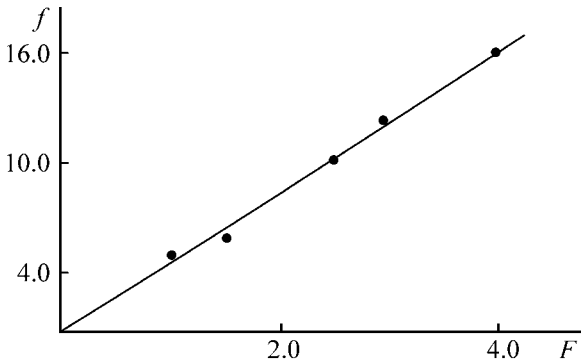
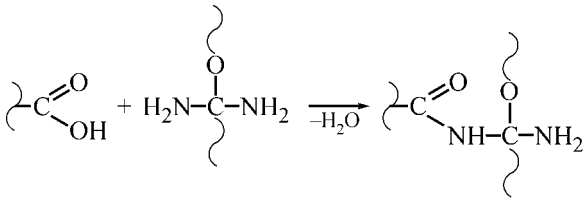


Fig. 1. Polymerization factor f from Eq. (1) vs. the AA/Ur molar ratio F.

show the bands at 1560–1640 cm^{-1} due to adsorption of the $\overset{+}{N}H_3$ and $H-C\overset{O}{\overset{//}{\underset{O^-}{\backslash}}}$ groups.

The bands at 1200–1280, 1710–1730, and 3400–3450 cm^{-1} are assigned to the –C–O–C–, $-C\overset{O}{\overset{//}{\underset{OH}{\backslash}}}$, and $-NH_2$ groups. The bands at 1695–1705 cm^{-1} suggest the presence of the $(-\underset{\underset{O}{\|}}{C}-NH-R-)$ group, which can be formed in the copolymer through the interaction between the –COOH and $-NH_2$ groups:



The presence of ionic groups will undoubted by provide higher conductivity of aqueous solutions of the copolymers, as compared to the polyacrylic acid reference. In this context, we studied the composition dependence of the equivalent conductivity of aqueous solutions of the copolymers. Figure 2 shows that the conductivity increases with the fraction of urea units in the copolymers, to reach a maximum at $F = 1$.

Then we studied the rheological properties of the copolymers prepared at $F = 2.5$, as influenced by temperature. We determined the concentration dependence of the reduced viscosity η_{sp}/c (c is the copolymer concentration in water) (Fig. 3).

The occurrence of a peak in the η_{sp}/c–c curves can be attributed to structural features of the polyelectrolytes under study, in which the degree of unfolding of the globules in water depends not only on the molecular weight of the copolymer, but also on the degree of dissociation of the ion pairs formed in the interaction of the carboxy and amino groups of the AA and Ur units, respectively. Such a viscosity anomaly is well documented [3, 4]. The clearly pronounced peaks in the curves (Fig. 3) suggest that the macromolecular chain, being in the maximally unfolded state, has an increased viscosity. Therefore, the unfolding threshold of such polyelectrolyte globules depends on both the temperature and copolymer concentration (Fig. 3).

The data on the molecular weights of the copolymers, as influenced by the initial AA/Ur molar ratios, are given in the table.

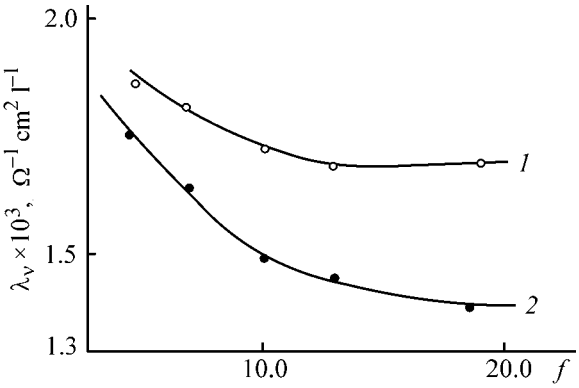


Fig. 2. Equivalent conductivity λ_v of aqueous copolymer solutions vs. their composition f. Solution concentration (wt %): (*1*) 0.5 and (*2*) 1. λ_v (PAA) (Ω^{-1} cm^2 l^{-1}): (*1*) 1.55×10^3 and (*2*) 1.28×10^3.

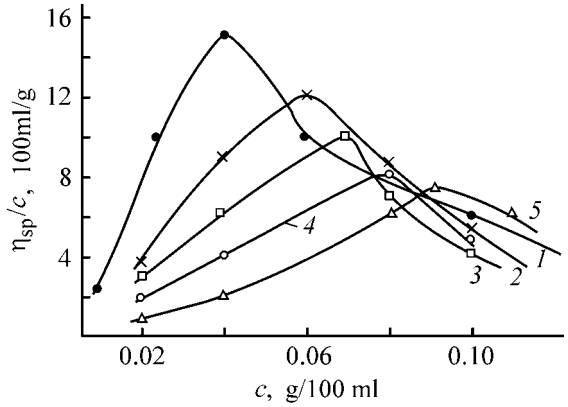


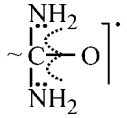
Fig. 3. Reduced viscosity η_{sp}/c of the copolymers in water vs. the concentration c. Temperature (°C): (*1*) 1.25, (*2*) 2.35, (*3*) 3.45, (*4*) 4.55, and (*5*) 5.65.

The results show that, at low F, i.e., with increasing Ur concentration in the initial mixture of the monomers, not only MW decreases, but also the copolymer yield. Therefore, in this case, urea serves as a polymer chain length regulator. The regulating capacity of urea is caused by the higher stability of its radicals (compared to the AA radical), which demonstrate lower rate of addition to the AA monomer. The sta-

Molecular weight of copolymers at various F

AA/Ur molar ratio	Copolymerization time, min	Conversion, %	$\overline{M} \times 10^{-4}$
1.0	25.0	8.7	3.2
1.5	19.0	9.5	4.5
2.5	17.0	11.5	5.7
3.0	15.0	12.0	6.0
3.9	10.0	15.0	7.5

bility of the Ur radical is due to the mesomeric effect occurring between the unpaired electron of the oxygen atom and the free electron pair of the amine nitrogen:



EXPERIMENTAL

Acrylic acid was distilled, and the fraction with bp 141°C at 760 mm Hg (n_D^{20} = 1.4224) was taken. Urea was recrystallized from alcohol, washed with chloroform and ether several times, and dried to constant weight at 45–50°C in a vacuum oven, to obtain a product with mp 132.7°C. $(NH_4)_2S_2O_8$ was recrystallized from ethanol.

In copolymerization, the initiator concentration was maintained constant (1 wt % of the total molar content of the monomers). The copolymerization of AA and Ur was carried out in water at 70 ± 0.03°C in 50-ml reactors. After the completion of the reaction, the resulting copolymers were precipitated by adding ethanol (AA and Ur remain in solution). The precipitate was filtered off, washed several times with ethanol, and dried to constant weight.

The IR spectra of the copolymers (film obtained from 6% aqueous solution of the copolymer) were recorded on a Specord 75-IR spectrophotometer.

To characterize the composition of the copolymers, the concentration of the carboxy groups was determined by titration with 0.1 N aqueous NaOH, with phenolphthalein as an indicator. From these data, the amount of the carboxy groups m (g) was estimated as

$$m = \frac{V \times 0.1 \times 72}{10^3},$$

where V is the volume of NaOH (ml) consumed for titration.

The molecular weight of the copolymers was determined ebullioscopically [5]:

$$M = \frac{E \times 10^3}{\Delta T} \frac{g_2}{g_1},$$

where E is the ebullioscopic constant of water (0.52); g_2 and g_1, weight amounts of the copolymer and water (g); and ΔT, difference between the boiling points of the solution and solvent (water).

The viscosity of the aqueous copolymer solutions was determined using Ostwald and Ubbelohde capillary viscometers [4]. In this case, demineralized water was used.

CONCLUSIONS

(1) Acrylic acid/urea copolymers of various compositions were prepared and the copolymerization constants were determined.

(2) The rheological properties of acrylic acid/urea copolymers were studied. The concentration dependence of the reduced viscosity η_{sp}/c shows an anomalous behavior, which is probably due to structural and conformation features of the polyelectrolytes investigated.

(3) The dependence of the equivalent conductivity of the acrylic acid/urea copolymers on their composition is studied. The highest conductivity was observed for the copolymers with nearly equivalent proportion of the acrylic acid and urea units.

REFERENCES

1. Srivastava, P.R. and Majki, S.S., *Oriental J. Chem.*, 1998, vol. 14, no. 1, pp. 7–12.
2. Bagdasar'yan, Kh.S., *Teoriya radikal'noi polimerizatsii* (Theory of Radical Polymerization), Moscow: Nauka, 1966.
3. Bigelow, C.C. and Cragg, L.H., *Canad. J. Chem.*, 1958, vol. 33, p. 199.
4. Rafikov, S.V., Pavlova, S.A., and Tverdokhlebova, I.I., *Metody opredeleniya molekulyarnykh vesov i polidispersnosti vysokomolekulyarnykh soedinenii* (Methods for Determination of Molecular Weight and Polydispersity of Macromolecular Compounds), Moscow: Akad. Nauk SSSR, 1963.
5. Balezin, S.A., *Praktikum po fizicheskoi i kolloidnoi khimii* (Practical Course of Physical and Colloid Chemistry), Moscow: Prosveshchenie, 1964, pp. 42–51.

ISSN 1070-4272, Russian Journal of Applied Chemistry, 2006, Vol. 79, No. 10, pp. 1669–1672. © Pleiades Publishing, Inc., 2006.
Original Russian Text © L.K. Altunina, B.N. Manzhai, M.S. Fufaeva, 2006, published in Zhurnal Prikladnoi Khimii, 2006, Vol. 79, No. 10, pp. 1689–1692.

MACROMOLECULAR CHEMISTRY AND POLYMERIC MATERIALS

Mechanical and Thermal Properties of Cryogels and Foamed Cryogels Produced from Aqueous Solutions of Poly(vinyl alcohol)

L. K. Altunina, B. N. Manzhai, and M. S. Fufaeva

Institute of Petrochemistry, Siberian Division, Russian Academy of Sciences, Tomsk, Russia

Received May 19, 2006

Abstract—The effect of sodium chloride and technical-grade carbon (carbon black) on the mechanical and thermal properties of cryogels and foamed cryogels produced from homogeneous and heterogeneous (foamed) solutions of poly(vinyl alcohol) was studied.

DOI: 10.1134/S1070427206100235

Aqueous solutions of poly(vinyl alcohol) (PVA) are transformed after a freeze-thaw cycle from their viscous-flow state to become elastic polymeric bodies capable of large reversible deformations. Cryogels formed under conditions of solvent crystallization are thermally reversible, but their melting point is several tens of degrees higher than the gelation point. The mechanical and thermal properties of the forming PVA cryogels depend on the composition and concentration of the components of the starting solution, on the molecular weight of the polymer and degree of its acetylation, and on modes and methods of cryogenic treatment of the starting solutions [1].

Cryogels have found wide use in biotechnologies, medicine, and technological processes for extraction and transportation of oil [2]. Recently, of increasing practical importance have been foamed cryogels (FCG) [3], which can be used, in particular, for thermal insulation of mouths of production oil wells in order to prevent precipitation of paraffin deposits. It seems that a promising way is to use cryogels and foamed cryogels to prevent degradation of the cryolite zone as a result of global warming-up and technologically induced processes in the northern climatic zone. Their application would be particularly important for improvement of the stability of antifiltration elements of water-retaining structures in water storage basins and for soil reinforcement.

EXPERIMENTAL

To develop the optimal method for production of cryogels and foamed cryogels, it is necessary to have full, to the maximum possible extent, information about molecular characteristics and specific rheological features of the behavior of starting PVA solutions. The methods of capillary and rotational viscometry were used to study the viscous properties of varied-concentration solutions of a PVA sample having an average molecular weight M = 74000 and containing in its structure residual acetate groups in an amount of 1%. The presence in the PVA chain of a certain amount of acetate groups hindering cryogelation is an inevitable result of the industrial manufacture of PVA from polyvinyl acetate [4]. It was found experimentally that solutions of the sample chosen for study, with the molecular parameters specified above, can form cryogels at a polymer concentration of no less than 5 g dl^{-1}. In starting solutions of this kind, a continuous fluctuation network of macromolecules is formed, and its presence is confirmed by the fact that the Weissenberg effect is observed in these solutions.

At concentrations higher than 5 g dl^{-1}, aqueous PVA solutions are typical non-Newtonian (pseudoplastic) fluids, whose viscosity depends on the shear rate. Making lower the temperature of polymer solutions to 0°C leads to a rise in their viscosity without loss of flowability. It should be noted that the viscosities of the starting solutions virtually coincide with

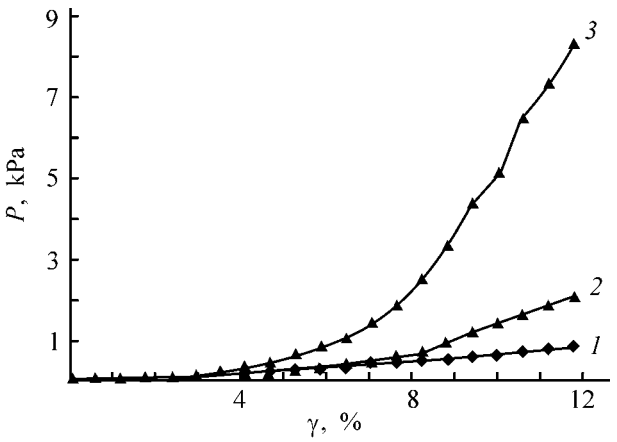


Fig. 1. Stress P vs. strain γ for cryogel samples with various PVA concentrations. c_{PVA} (g dl^{-1}): (*1*) 5, (*2*) 10, and (*3*) 16.

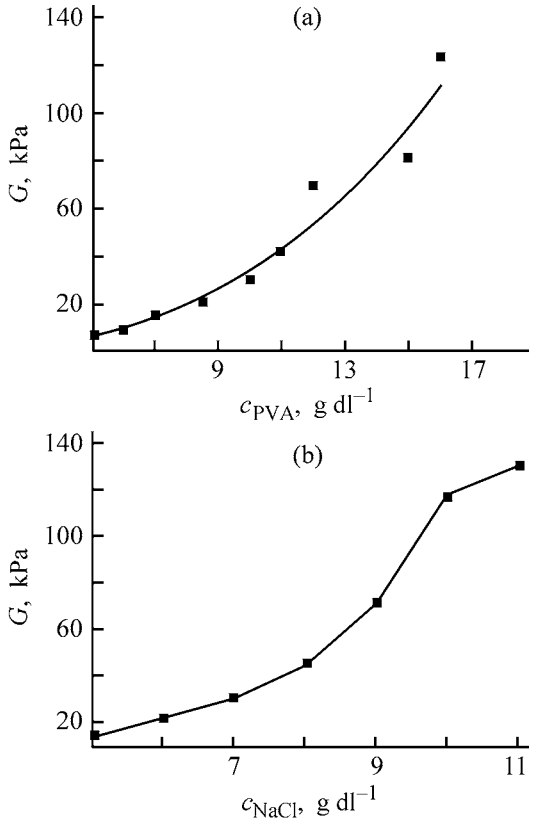


Fig. 2. Elastic modulus G of cryogels vs. concentrations of (a) PVA (c_{PVA}) and (b) sodium chloride (c_{NaCl}) at c_{PVA} = 5 g dl^{-1}.

the viscosities of solutions preliminarily subjected to low-temperature gelation and subsequent thermal melting. This feature emphasizes the total reversibility of the process of cryotropic gelation and the absence of irreversible structural changes in PVA molecules on performing a freeze-thaw cycle with the solutions.

To obtain cryogels, aqueous PVA solutions of various concentrations (5 to 16 g dl^{-1} with a step of 1 g dl^{-1}) were poured in cylindrical cells and frozen at T = –22°C for 20 h. Then they were thawed at T = 20°C in the course of 4 h and the resulting elastic cryogel samples were deformed to a strain γ and the stress P was measured. The results obtained are shown in Fig. 1.

It can be seen that the stress–strain curve clearly shows two different portions. The existence of these regions in the rheological curves is a consequence of the dual, with entropy- and energy-related components, nature of the elasticity of polymeric bodies. At small strains, which transfer the macromolecular coils of the polymer network of the cryogel from the more probable state to that with a lower probability, the dominant factor is the change in entropy. Upon further deformation of the sample, the chemical bond lengths and valence angles in polymer chains somewhat change, and, as a result, the elastic modulus (slope of the curve) noticeably increases. Figure 2a shows elasticity moduli of cryogels formed from polymer solutions of various concentrations and strained (compressed) by 10%.

It follows from Fig. 2a that, as the PVA concentration is raised from 5 to 16 g dl^{-1}, the elastic modulus strongly increases from 5 to 120 kPa. Of the highest practical value in use of cryogel as construction materials are samples with the lowest content of the structuring component, PVA. It is known from the literature that low-molecular-weight components adversely affect the mechanical properties of cryogels. However, presence of some of them, e.g., sodium chloride [5], in the starting polymer solutions favors strengthening of the cryogels obtained. The results of measurements of the elasticity moduli of PVA solutions with a concentration of 5 g dl^{-1} and varied content of sodium chloride are shown in Fig. 2b.

It can be seen that, as the NaCl concentration is raised from 5 to 11 g dl^{-1}, the elastic modulus of the cryogels increases from 15 to 130 kPa. It should be noted that the elastic modulus of the starting two-component cryogel produced from an aqueous PVA solution (c_{PVA} = 5 g dl^{-1}) is 5 kPa (Fig. 2a). It was found experimentally that further increase in the sodium chloride concentration is inadvisable because of the "salting-out" of the polymer from the solution and the corresponding decrease in the mechanical strength of the cryogels obtained.

In processes of cryotropic gel formation and use of the samples obtained, it is necessary to know the heat conductivity coefficients, whose values for the start-

ing solutions and the cryogels formed are listed in the table.

It follows from the table that the dissolution of the polymer in water leads to a considerable decrease in the heat conductivity coefficients λ_{PVA} of the polymer solutions, compared with the neat solvent (λ_W = 0.62 W K^{-1} m^{-1}), and the structuring of solutions into cryogels is accompanied by further decrease in the heat conductivity coefficient.

It is known that an effective way to reduce the heat conductivity coefficient of a material is to saturate it with a gas. Therefore, a gas phase was introduced into homogeneous PVA solutions to improve the thermal properties of cryogels, and, because of the foam formation, foamed cryogels were obtained after a freeze–thaw cycle. Gas-saturated formulations with a foam ratio of 2 were formed by bubbling air through a Schott filter into aqueous PVA solutions of various concentrations. The heat conductivity coefficient of the foam is substantially lower than that of the polymer solution [6]. As a result, the cooling and subsequent freezing of a gas-saturated formulation is considerably slower than that of the polymer solution. Therefore, starting foams stable in the course of time are necessary for synthesis of foamed cryogels. Measurements of the time of foam settling demonstrated that the foam stability increases with the polymer concentration in the solution (Fig. 3). However, even the polymer solution with the highest concentration (c_{PVA} = 10 g dl^{-1}) has a foam destruction time shorter than half an hour (1500 s), which is obviously insufficient for the process of full freezing of the foamed sample to be complete. Any further increase in the concentration of the polymer in the solution is inadvisable because it leads to a pronounced increase in the solution viscosity and makes impossible formation of a finely dispersed foam from this solution. Therefore, a powder of finely dispersed technical-grade carbon (carbon black) was introduced into the aqueous formulation containing PVA (c_{PVA} = 5 g dl^{-1}) and sodium chloride (c_{NaCl} = 11 g dl^{-1}) in order to make more stable the starting foam.

Introduction of a solid phase into the foam leads to localization of gas bubbles by the flotation mechanism on hydrophobic particles of carbon black, which results in a decrease in the surface energy of the three-phase system, compared with the starting two-phase system. As a result, stable foams are formed, which do not settle during 24 h. Raising the carbon black content of the foamed cryogels from 3 to 7% is accompanied by an increase in the elastic modulus from 4 to 50 kPa because of the structural-mechanical reinforcement of walls of gas cells with finely dispersed particles of carbon black (Fig. 4a).

Heat conductivity coefficient of PVA solutions with various concentrations and of the cryogels produced from these solutions

c_{PVA}, g dl^{-1}	λ_{PVA}	λ_{FCG}
	W K^{-1} m^{-1}	
0	0.62	–
5	0.42	0.33
6	0.40	0.33
9	0.37	0.33
10	0.36	0.33
16	0.35	0.33

The elastic properties of foamed cryogels that are produced from aqueous solutions upon a single freezing and contain PVA (c_{PVA} = 5 g dl^{-1}), sodium chloride (c_{NaCl} = 11 g dl^{-1}), and carbon black (c = 7%)

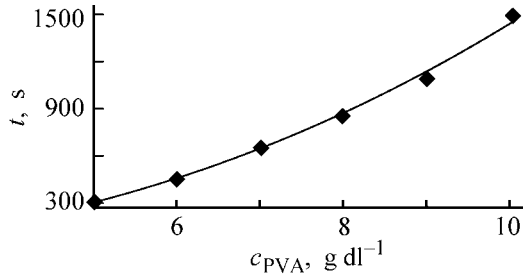


Fig. 3. Settling time t of a foam produced from aqueous PVA solutions with various concentrations c_{PVA}.

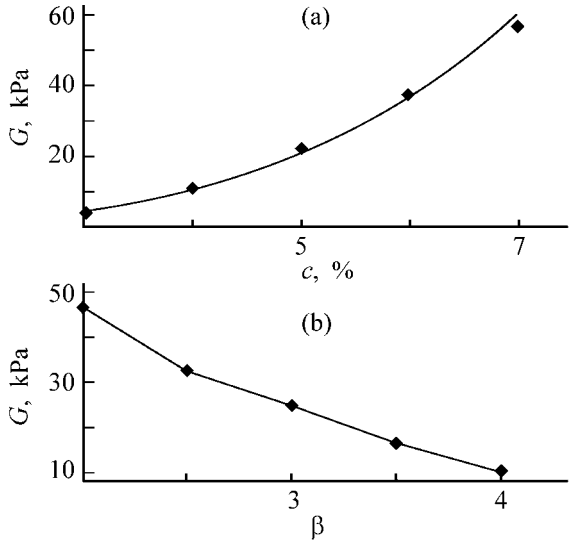


Fig. 4. Elastic modulus G of a foamed cryogel vs. (a) carbon black content c and (b) foam ratio β. (b) Solution composition: PVA 5 g dl^{-1}, NaCl 11 g dl^{-1}, carbon black 7%.

are strongly deteriorated as the foam ratio increases (Fig. 4b). As the ratio β of the starting foam increases from 2 to 4, the elastic modulus of the foamed cryogel decreases from 50 to 10 kPa. Presumably, foamed cryogels with low foam ratios (β = 2) can be used under practical conditions.

The heat conductivity coefficient was found experimentally for a foamed cryogel with a foam ratio β = 2 and the composition: PVA 5 g dl^{-1}, NaCl 11 g dl^{-1}, carbon black 7%, and water 77 g dl^{-1}. The following value was obtained: $\lambda_{FCG} = 0.25$ W K^{-1} m^{-1}, which is in a satisfactory agreement with the value calculated by the Manegold formula $\lambda_{FCG} = 2\lambda_W/3\beta + (\beta - 1/\beta)\lambda_G$. Thus, introduction of the gas phase into the continuous matrix of the cryogel improves the heat-insulating properties of the material.

Laboratory studies of the chemical stability of cryogels at a temperature of 20°C for 72 h demonstrated that they retain their stability when in contact with distilled and mineralized (Senoman) water, as well as with alkaline solutions and hydrocarbon liquids of different polarities (hexane, acetone, oil). Cryogel samples are also stable in acid media with pH > 1 and decompose only in concentrated sulfuric or hydrochloric acid. A gravimetric study of the stability of a foamed carbon-reinforced plastic in air revealed that it tends to be dehydrated. Removal (evaporation) of water leads to loss of elasticity by a cryogel sample, which is accompanied by its deformation and a decrease in its volume.

The mechanical properties of a foamed cryogel directly depend on the working temperature of articles made of this material, which should not exceed its melting point. Measurements of the melting points of cryogels and foamed cryogels of various compositions demonstrated that they are virtually independent of the content of PVA (5–16 g dl^{-1}) and carbon black (3–7%) and fall within the range $T \approx 73$°C, but presence of the salt has a strong effect. For example, the melting point increases from 97 to 110°C as the concentration of sodium chloride is raised from 5 to 11 g dl^{-1}.

CONCLUSIONS

(1) Introduction of technical-grade carbon (carbon black) into a polymer solution raises the stability of the foam produced from this solution and favors structural-mechanical reinforcement of the walls of gas cells in the resulting foamed cryogel.

(2) Sodium chloride makes higher the elastic modulus and the melting point of cryogels and foamed cryogels.

(3) Introduction of a gas phase into the polymer matrix leads to a decrease in the elastic modulus of the material, but its heat-insulating properties are markedly improved.

REFERENCES

1. Lozinskii, V.I., *Usp. Khim.*, 1998, vol. 67, no. 7, pp. 641–655.
2. Lozinskii, V.I., *Usp. Khim.*, 2002, vol. 71, no. 6, pp. 559–585.
3. Lozinsky, V.I. and Damshkaln, L.G., *J. Appl. Polym. Sci.*, 2001, vol. 82, pp. 1609–1619.
4. Ushakov, S.N., *Polivinilovyi spirt i ego proizvodnye* [Poly(vinyl alcohol) and Its Derivatives], Moscow: Akad. Nauk SSSR, 1960.
5. Lixing, Dai, Kohshuke, Ukai, Sharif, Mohammad Shaheen, and Kazuo, Yamaura, *Polymer Internat.*, 2002, vol. 51, pp. 715–720.
6. Tikhomirov, V.K., *Peny: Teoriya i praktika ikh polucheniya i razrusheniya* (Foams: Theory and Practice of Their Formation and Disintegration), Moscow: Khimiya, 1983.

ISSN 1070-4272, Russian Journal of Applied Chemistry, 2006, Vol. 79, No. 10, pp. 1673–1680. © Pleiades Publishing, Inc., 2006.
Original Russian Text © A.N. Krasovskii, M.G. Potashev, V.N. Filippov, S.S. Mnatsakanov, 2006, published in Zhurnal Prikladnoi Khimii, 2006, Vol. 79, No. 10, pp. 1693–1700.

MACROMOLECULAR CHEMISTRY AND POLYMERIC MATERIALS

Scale Invariance of Viscosity and Cluster Structure of Epoxy Formulations

A. N. Krasovskii, M. G. Potashev, V. N. Filippov, and S. S. Mnatsakanov

St. Petersburg State University of Cinema and Television, St. Petersburg, Russia

Received June 7, 2006

Abstract—The concentration dependences of the relative viscosity of epoxydiane resins (M_n = 400–650) in solutions of monoglycidyl esters, Cardura and Laproxide, and of the dynamic viscosity of filled epoxy formulations in a shear flow were studied. The optimal concentrations of the formulation components and structural parameters of the fractal aggregates of oligomers and clusters of pigment (filler) particles were calculated in the approximation of the cluster lattice model.

DOI: 10.1134/S1070427206100247

A study of the concentration dependences of the viscosity and structure of epoxydiane oligomers (EO) in solutions is of particular interest in view of the wide use of epoxy formulations for deposition of protective and anticorrosion coatings onto metals [1, 2]. To systems of this kind, in particular, belong formulations based on low-molecular-weight epoxydiane resins (M_n = 400–650), monoepoxy compound Cardura, and pigments and fillers [1].

As is known [3–5], the conditions under which a continuous fluctuation network of entanglements between macromolecules is formed in EO solutions are determined by the molecular weight M and concentration c of the oligomers and by the solvent polarity [6]. Such a network disintegrates at shear rates $g > 160$ s^{-1} [2]. It has been shown previously [3, 5] that the initial slope $[\eta]$ of concentration dependences of the relative viscosity $\eta_{rel}(c)$ of EO in solutions with chloroform, plotted in the $\ln \eta_{rel} - c$ coordinates, increases with the molecular weight M. The $\eta_{rel}(c)$ curves may be of two types. In the case when the size of EO molecules does not exceed the length of the statistical Kuhn segment (degree of polymerization DP ≈ 5) [2, 6], the condition $[\eta]_c/[\eta] \geq 1$, where $[\eta]_c = d\ln \eta_{rel}/dc$ ($c > 0$) is the current intrinsic viscosity, is valid for the $\eta_{rel}(c)$ curves. For $\eta_{rel}(c)$ curves of the second type, the condition $[\eta]_c/[\eta] < 1$ is satisfied. The hydrodynamic behavior of such EO (DP > 5) in solutions is similar to that of flexible-chain macromolecules with a large number of statistical Kuhn segments [5, 6].

Studies of the concentration dependences of the relative viscosity, $\eta_{rel}(c)$, and of the intensity of quasi-elastic scattering of light in EO solutions have shown [3–5] that discrete aggregates (associates) [7] and an infinite cluster of EO molecules [8] are formed in EO solutions. According to [4, 5], the minimum in the dependences of the Rayleigh scattering of light in solutions of ED-20 epoxydiane resin ($M_n \approx 400$) in Cardura is due to the formation of an infinite cluster of EO molecules at the critical concentration c^* = 52%. On introduction of epoxidized caoutchouc (EC, $M_n \approx 1000$), whose molecules can also be incorporated in the infinite cluster containing ED-20 and Cardura molecules, into a solution of the ED-20 resin in Cardura, such a cluster is formed at a threshold percolation probability $p_c \approx 0.69$, c^* (ED-20) = 48%, and c (EC) = 16% [4, 8].

As is known [9], the viscosity η of concentrated polymer solutions shows a power dependence on the concentration c and molecular weight M of macromolecules: $\eta \sim c^{\beta} M^{3.4}$, where β is a constant [10]. It would be expected [10] that, upon introduction of pigment (filler) particles into an oligomer solution, the infinite (fractal) cluster of such particles is formed at the critical particle concentration c_p, which corresponds to a threshold percolation probability $p_c \approx 0.31$ in a simple cubic lattice [8]. In accordance with the cluster lattice model [10], the viscosity η of a filled formulation will increase with the concentration c_p by the law: $\eta \sim c_p^{\beta}$ [9], and the exponent β will change jumpwise near the critical value c_p^*. In this case,

Table 1. Molecular parameters of epoxy oligomers* (298 K)

Sample no.	Oligomer	$M_n \pm 5\%$	E.n., %	[η], $cm^3\ g^{-1}$	η, Pa s	σ, $mN\ m^{-1}$
1	YD-128S	410	20.9	2.5/3.2	22.2	52.4
2	YD-136	630	13.6	4.5/4.8	6.2**	56.2
3	Cardura E-10P	250	17.2	–	0.035	30.6
4	Laproxide-702	520	8.4	–	0.101	34.6

* E.n., epoxide number; σ, surface tension at the liquid–air phase boundary. The values of [η] are given for solutions in Cardura (numerator) and Laproxide (denominator). For the mixture of YD-128S and YD-136 resins (mass ratio 2.9 : 1) dissolved in Cardura, [η] = 2.9 $cm^3\ g^{-1}$.

** Viscosity of a 80% solution of sample no. 2 in *o*-xylene.

the elastic modulus E of the filled epoxy formulation must also grow in accordance with the expression obtained for filled caoutchoucs: $E \sim \Delta c_p^t$, where $\Delta c_p = c_p - c_p^*$ ($c_p > c_p^*$) and $t = 1.8$ [8, 10].

The 3*D* structure of filled epoxy polymers [11] obtained by curing of epoxy formulations with amines [12] is characterized by alternation of regions with different densities of cross-link sites in the chemical network of a cross-linked polymer and different distributions of pigment (filler) particles [13]. The strength properties of polymers of this kind depend on the density of cross-link sites in the chemical network [2] and pigment (filler) concentration c_p [11]. According to the authors' data, the reduced relative elongation $\Delta l/lE$ (E is the elastic modulus) of films of a filled polymer produced by curing a formulation based on ED-20 epoxydiane resin, Cardura [4], and a mixture of pigments (fillers) shows an extremum near the critical concentration $c_p^* \approx 31$ vol % (Fig. 1).

It should be noted that development of the physicochemical principles of making up an epoxy formulation with an active solvent [1, 4], which are based on the cluster lattice model [8, 10], is topical for reliable substantiation of the prescribed composition of formulations of this kind [14] and promising for improvement of the strength and protective properties of epoxy polymers [11, 12].

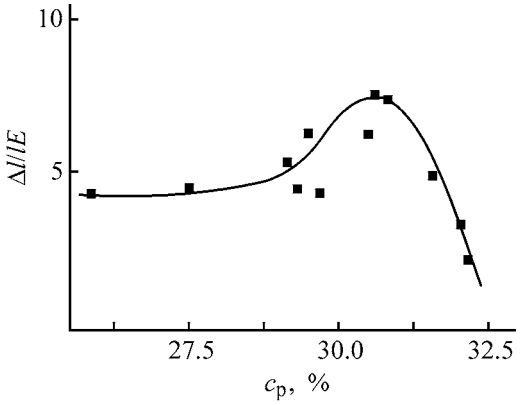


Fig. 1. Reduced relative elongation $\Delta l/lE$ of films of the epoxy polymer vs. volume concentration c_p of pigments and fillers. Film thickness 400 μm.

For this purpose, the concentration dependences of the relative viscosity of epoxydiane resins (M_n = 400–650) in solutions of monoglycidyl esters and the rheological behavior of filled epoxy formulations in shear flow were studied. The structural parameters of fractal aggregates of EO and clusters of pigment (filler) particles and the critical (prescribed) concentrations of the components of the epoxy formulation were calculated in terms of the cluster lattice model.

EXPERIMENTAL

As objects of study served the following commercial samples: YD-128S and YD-136 epoxydiane resins (Kykdo Chemicals); Cardura E-10P, monoglycidyl ester of Versatic acid, with the total number of carbon atoms equal to 10 (Shell Chemicals) [1]; and Laproxide, monoglycidyl ester of oligooxypropylene triol [4]. Some parameters of sample nos. 1–4 are listed in Table 1.

The concentration dependences of the relative viscosity $\eta_{rel}(c)$ of YD-128S and YD-136 epoxydiane resins (Table 1, sample nos. 1 and 2) and of their mixtures dissolved in Cadura and Laproxide were measured with an Ubbellohde capillary viscometer (shear rate $g = 100\ s^{-1}$) [6] at concentrations in the range c = 5–60 wt % and temperature of 298 K. The $\eta_{rel}(c)$ curves were plotted in the $\ln \eta_{rel}(c)$–$[\eta]c$ coordinates, where $[\eta]c$ is a dimensionless parameter

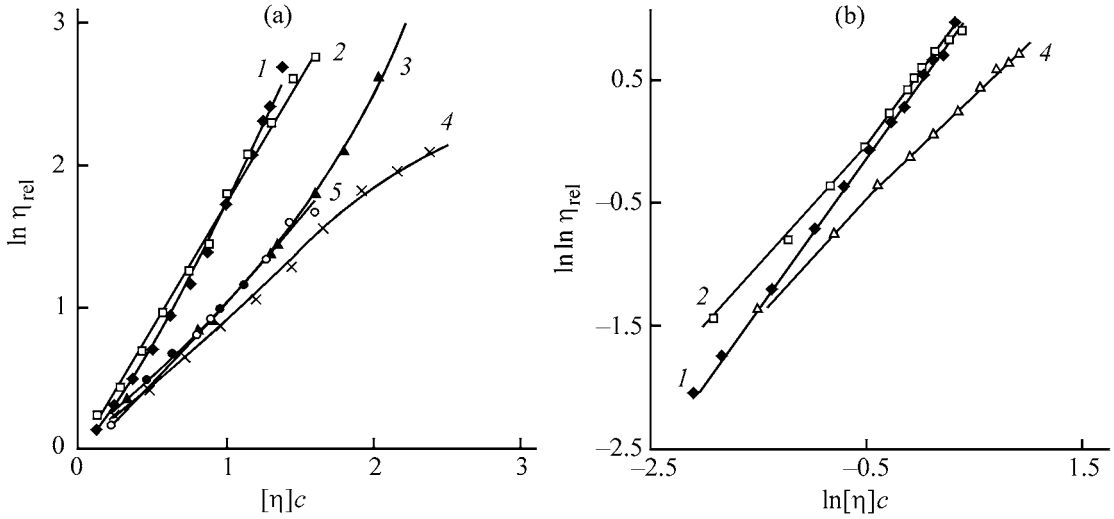


Fig. 2. Relative viscosity η_{rel} of epoxydiane resins (*1*, *5*) YD-128S and (*3*, *4*) YD-136 and (*2*) their mixture (mass ratio 2.9 : 1) in solutions in (*1–3*) Cardura and (*4*, *5*) Laproxide vs. the dimensionless parameter $[\eta]c$ in the coordinates (a) $\ln \eta_{rel}$–$[\eta]c$ and (b) $\ln\ln \eta_{rel}$–$\ln [\eta]c$, 298 K.

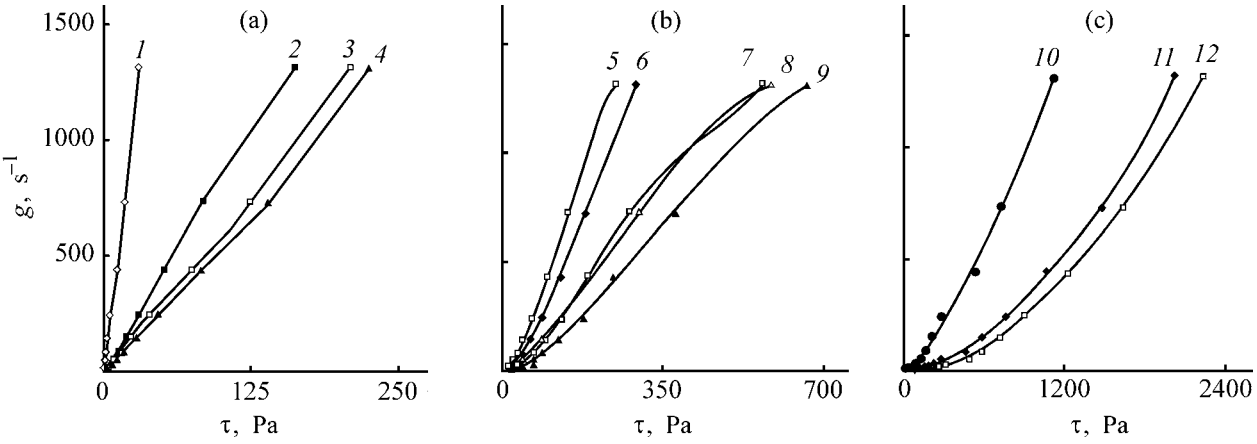


Fig. 3. Flow curves g–τ of epoxy formulations. Temperature 298 K. Sample nos.: (*1–4*) 5–8, (*5–9*) 9–13, and (*10–12*) 14–16 (Table 3).

and c is concentration (g cm^{-3}) (Fig. 2). The intrinsic ($[\eta]$) and current intrinsic ($[\eta]_c$) viscosities were calculated from the $\eta_{rel}(c)$ curves by the expression $[\eta]_c = d\ln \eta_{rel}/dc$ at $c \to 0$ and $c > 0$, respectively [3, 6] (Table 1).

Filled epoxy formulations were prepared using an anticorrosive red iron oxide pigment (RIO, TR-303 brand, Czech Republic) [15] with a particle size of 5 μm and Microtalc filler (GShM, Tal'kon) [16] with a particle size $d \le 40$ μm. Samples of the formulations were prepared by mixing RIO pigment and Microtalc with YD-128S and YD-136 epoxydiane resins and Cardura. Into a paste composed of RIO pigment in Cardura, prepared in a bead mill, was introduced a mixture of YD-128S and YD-136 resins and Cardura (Table 3, sample no. 5), in which Microtalc was dispersed. The concentration c_{RIO} of RIO pigment in sample nos. 6–16 was 11%, and the concentration c_p of Microtalc was varied from 10 to 40%.

The flow curves $g(\tau)$ of filled epoxy formulations were measured on a Rheotest-2 rotational viscometer at shear rates g = 3–1312 s^{-1} and shear stresses τ = 3–2200 Pa in the temperature range 298–333 K (Fig. 3). When determining the viscosity η of epoxy formulations from flow curves $g(\tau)$, it was assumed that the dynamic viscosity $\eta(g)$ varies by the power law $\eta = Kg^{n-1}$, where K is a constant, and n, flow index [9]. The $\eta(g)$ curves are linear in log–log coordinates $\ln \eta$–$\ln g$ at g = 3–81 s^{-1} (Fig. 4), which makes it possible to calculate the flow index n from the slope of the linear portion of $\eta(g)$ curves and the initial viscosity η^0 of formulations at g = 1 s^{-1} and to obtain dependences of the initial viscosity η^0 and flow index n on the Microtalc concentration c_p (Table 3).

Table 2. Parameters of aggregates of molecules of epoxydiane resins in solutions in Cardura and Laproxide (298 K)*

System	$c < c^*$		$c > c^*$		c^*, % (±1%)	ρ (± 0.02)	σ(c^*), mN m^{-1}
	α	D	α	D			
YD-128S–Cardura	1.25	1.33	1.42	1.24	42 (1.05)	0.70	29.2
YD-128S–Laproxide	1.05	1.46	1.14	1.40	67 (2.1)	–	–
YD-136–Cardura	0.96	1.53	1.40	1.25	24 (1.1)	0.60	31.2
YD-136–Laproxide	0.97	1.52	1.15	1.40	25 (1.2)	0.55	35.3
YD-128S–YD-136–Cardura	1.10	1.43	0.85	1.62	41.5 (1.2)	0.69	32.0

* In the YD-128S–YD-136–Cardura system, the mass ratio of YD-128S and YD-136 resins is 2.9 : 1. Values of the parameter $[\eta]c$ are given in parentheses. σ(c^*) is the surface tension at the interface between the solution of an epoxydiane resin and air at the critical concentration c^*.

Table 3. Composition, initial viscosity η^0 (g = 1 s^{-1}), flow index n of formulations, and fractal dimension D and lattice density of clusters of RIO and Microtalc particles Sample nos. 5–15, 298 K

Sample no.	Component concentration c, wt %				η^0, Pa s	n ± 7%	D ± 7%	ρ ±3%
	YD-128S	YD-136*	Cardura	$c_{RIO} + c_p$ (c_p)				
5	52.4	18.2(4.5)	24.9	0 (0)	0.44	0.00	–	0.72
6	46.4	16.2(4.1)	22.3	11 (0)	3.2	0.02	1.78	0.67
7	41.2	14.4(3.6)	19.8	21 (11)	5.4	0.04	1.78	0.51
8	38.6	13.5(3.4)	18.5	26 (15)	6.8	0.04	1.78	0.48
9	36.0	12.6(3.1)	17.3	31 (20)	8.5	0.04	2.45	0.42
10	33.4	11.6(2.9)	16.1	36 (25)	10	0.07	2.45	0.49
11	32.1	11.2(2.8)	15.4	38.5 (27.5)	11	0.22	2.45	0.56
12	30.8	10.7(2.7)	14.8	41 (30)	12.2	0.42	2.45	0.71
13	29.5	10.3(2.5)	14.2	43.5 (32.5)	17.8	0.40	1.07	0.64
14	28.2	9.8(2.4)	13.5	46 (35)	31.7	0.31	1.07	0.36
15	26.9	9.4(2.3)	12.9	48.5 (37.5)	73.5	0.24	1.07	0.19
16	25.6	8.9(2.2)	12.3	51 (40)	131	0.12	1.07	0.11

* YD-1236 resin was introduced into the formulation as a 80% solution in *o*-xylene (concentration of *o*-xylene is given in parentheses). c_p is the mass concentration of Microtalc.

The lattice density ρ of aggregates of EO molecules in solution and of clusters of solid particles was calculated by the expression $\rho = \omega^{\alpha}([\eta]/[\eta]_c)^{\alpha/(\alpha-1)}$, where ω = 0.637 is the coefficient of random packing of rigid spheres [8, 13], and α is the exponent similar to that in the expression for the intrinsic viscosity $[\eta] \sim M^{\alpha}$ [6] (Table 2). The lattice density ρ of clusters of pigment (filler) particles was calculated using the values $[\eta]_c = d\ln(\eta^0/\eta)/dc_p$, where η^0 and η are the initial viscosities of a filled formulation and of a mixture of resins in a solution in Cardura, respectively (Table 3).

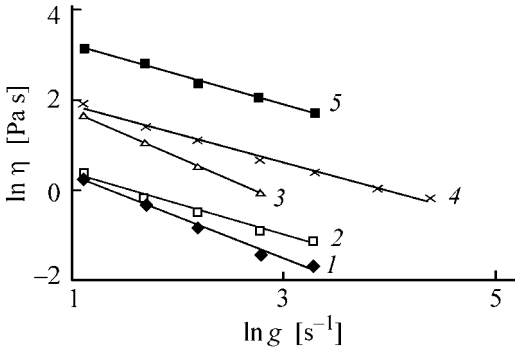


Fig. 4. Dynamic viscosity η vs. shear rate g in the ln η–ln g coordinates at 298 K. Sample no.: (*1*) 5, (*2*) 8, (*3*) 10, (*4*) 12, and (*5*) 15.

As can be seen from the data obtained (Fig. 2), the concentration dependences of the relative viscosity $\eta_{rel}(c)$ of epoxydiane resins in solutions in Cardura and Laproxide follow the expression $\ln\eta_{rel} = ([\eta]c)^{\alpha}$, where $\alpha = (3 - D)/D$, and D is the fractal dimension of aggregates of EO molecules [5, 13]. For the systems studied, with the exception of solutions of YD-136 resin in Laproxide, the $\eta_{rel}(c)$ curves plotted in the $\ln\eta_{rel}$–$[\eta]c$ coordinates lie above the bisector of the angle formed by the coordinate axes The point

of intersection of two linear portions of the $\eta_{rel}(c)$ curves plotted in the $\ln\ln\eta_{rel}$–$\ln[\eta]c$ coordinates corresponds to the critical concentration c^* of formation of an infinite cluster of EO molecules in solutions [5], and the values of the parameters α and D can be calculated from the slope of the linear portions of these curves [13] (Fig. 2b, Table 2).

Analysis of the values of the parameters α and D, obtained for solutions of YD-128S resin in Cardura and Laproxide (Table 2), shows that $\alpha > 1$ ($D < 1.5$) in two regions: $c < c^*$ and $c > c^*$. The corresponding $\eta_{rel}(c)$ curves belong to the case when EO molecules are smaller in size than the statistical Kuhn segment [2]. In the first portion of the $\eta_{rel}(c)$ curves for solutions of YD-136 resin in Cardura and Laproxide, $\alpha \le 1$ ($D \approx 1.5$) (Fig. 2a). These curves can be related to the case when the size of EO molecules only slightly exceeds the length of the statistical segment [2, 5]. For a mixture of YD-128S and YD-136 resins (mass ratio 2.9 : 1) dissolved in Cardura, $\alpha = 1.1$ ($D \approx 1.4$ (in the range $c < c^*$, and, therefore the average size of EO molecules in this mixture of resins is only slightly smaller than the length of the statistical segment [2].

Passing from dilute ($c < c^*$) to concentrated ($c > c^*$) solutions of epoxydiane resins leads to a change in the parameters α and D and in the density ρ of EO aggregates near the critical concentration c^* [3, 13]. In solutions of YD-128S resin and of a mixture of YD-128S and YD-136 resins in Cardura, the construction of an infinite cluster is complete at a lattice density of aggregates, $\rho_c \approx 0.69$, which is confirmed by the presence of absolute and local minima in the surface-tension curves $\sigma(c)$ at the liquid–air interface [8] (Fig. 5). The minima in the $\sigma(c)$ curves for solutions of these resins occur because the second derivative of the free Gibbs energy with respect to concentration, d^2F/dc^2, is zero [17]. They coincide on the concentration scale with the corresponding values of c^*.

The flow curves $g(\tau)$ of filled epoxy formulations can be conditionally divided into three groups differing in the rate at which the initial viscosity η^0 and yield stress τ_0 [9, 18] vary with the increasing concentration c_p of Microtalc (Fig. 3, Table 3). The first group of $g(\tau)$ curves are of pseudo-Newtonian type [9] and show a slight rise in η^0 and τ_0 at $c_p \le 15\%$ and ($c_{RIO} + c_p$) = 0–26% (Fig. 3a, sample nos. 5–8).

The flow curves of Bingham type [9], assigned to the second (Fig. 3b) and third (Fig. 3c) groups of formulation samples, have two portions, which are linear on the logarithmic scale. The first $g(\tau)$ portion at $g <$ 150 s^{-1} corresponds to a pseudoplastic flow of a viscous fluid, and the second at $g > 150$ s^{-1}, to a flow of cross-link sites of the fluctuating network of EO entanglements [9, 18]. The slope m_1 of the first portion of the $g(\tau)$ curves for the third group of samples steeply falls as the concentration c_p of Microtalc becomes higher, and the slope m_2 of the second portion in the curves of this group, increases jumpwise (Fig. 6). The bend in these curves at $g < 150$ s^{-1} indicates that strong hydrogen bonds are formed between EO molecules and filler particles [15].

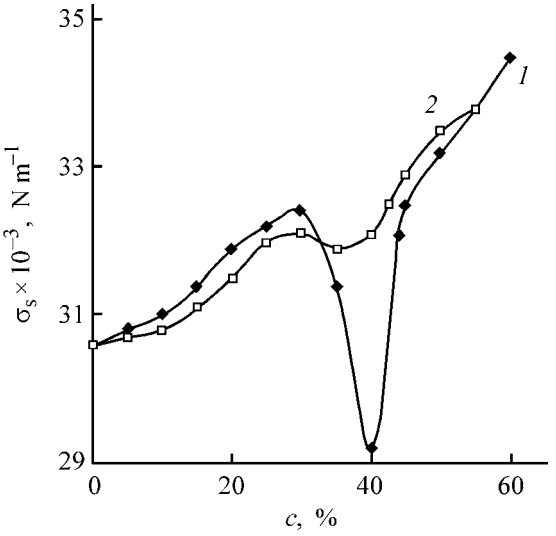


Fig. 5. Surface tension σ_s at the interface between a solution of an epoxydiane resin and air vs. the mass concentration c of (*1*) YD-128S resin and (*2*) mixture of YD-128S and YD-136 resins in Cardura at 298 K.

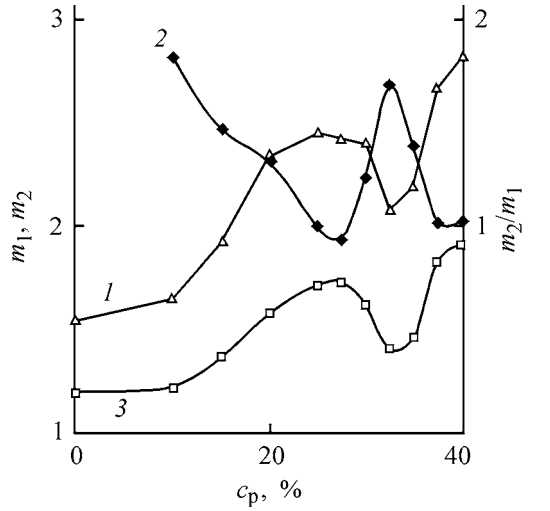


Fig. 6. Slopes of (*1*) first (m_1, $g < 150$ s^{-1}) and (*2*) second (m_2, $g > 150$ s^{-1}) linear portions of the flow curves $g(\tau)$ and (*3*) the ratio of these slopes, m_1/m_2, vs. the mass concentration c_p of Microtalc, 298 K.

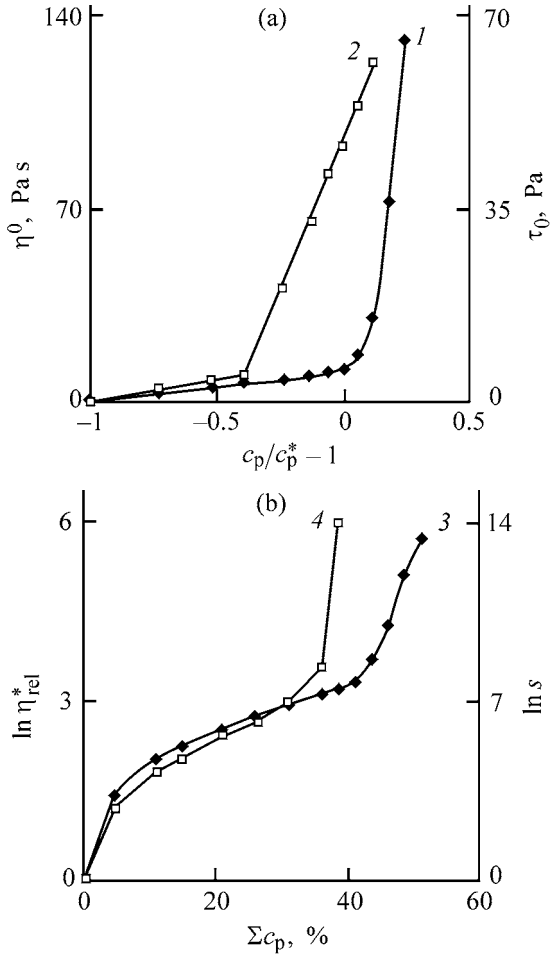


Fig. 7. (a) (*1*) Initial viscosity η^0 and (*2*) yield stress τ_0 vs. the parameter $(c_p/c_p^* - 1)$; (b) (*3*) reduced viscosity $\eta_{rel}^* = \eta^0/\eta$ and (*4*) degree of aggregation of pigment (filler) particles vs. the concentration Σc_p of the pigment and filler, at 298 K. c_p, critical Microtalc concentration, equal to 30%; η, viscosity of a mixture of resins in solution.

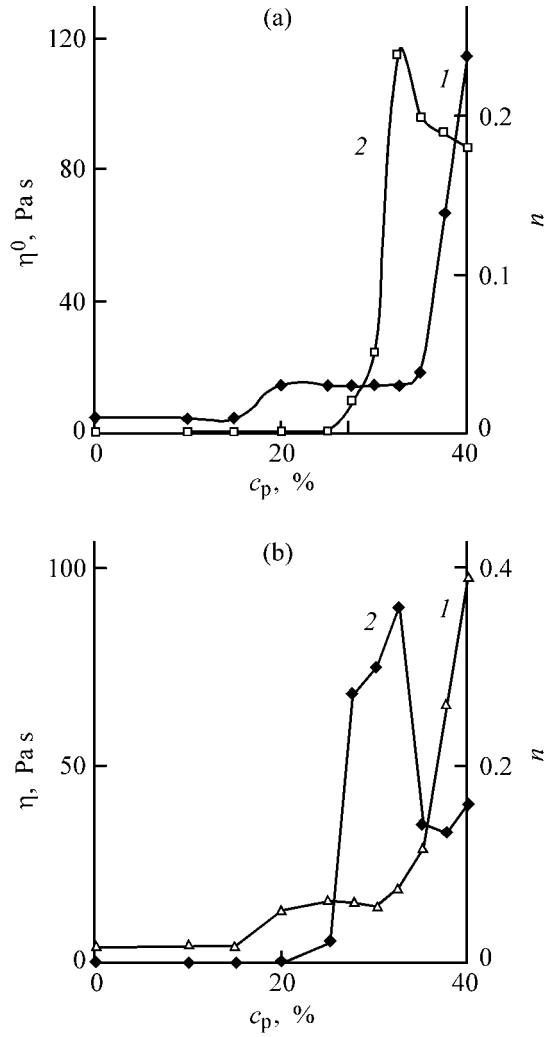


Fig. 8. (*1*) Initial viscosity η^0 and (*2*) flow index n of the formulations vs. the Microtalc concentration c_p. Temperature (K): (a) 323 and (b) 333.

The flow curves $g(\tau)$ show at $c_p = 20$–35% a steep rise in the yield stress τ_0 in accordance with the expression $\tau_0 \sim |c_p - c_p^*|^t$, where c_p^* is the critical Microtalc concentration, equal to 30% (Fig. 7, Table 3). Such a variation of the yield stress τ_0 near c_p^* is similar to the behavior of the elastic modulus E and the value of τ_0 in polymeric gels above the gelation threshold [10, 18], and the calculated value $t = 1.8$ coincides with the theoretical estimate of t [8].

As follows from the $\eta^0(c_p)$ curve, the initial viscosity η^0 of the formulations is virtually independent of temperature and Microtalc concentration c_p in the range $c_p = 20$–30%, but in the range $c_p = 32.5$–40%, the value of τ^0 increases jumpwise (Figs. 7, 8). The concentration dependence of the logarithm of the viscosity η^0 is of the power-law type: $\ln\eta^0 \sim c_p^{\alpha}$, where $\alpha = (3 - D)$ and D is the fractal dimension of clusters formed by pigment (filler) particles [8, 10]. As the critical concentration c_p^* of formation of an infinite cluster [8] of pigment (filler) particles can be taken a value of 30%, because the fractal dimension D of clusters is about 1.8 at $c_p = 15\%$ and reaches a value of approximately 2.5 in the range $c_p = 20$–30% (Table 3). The scaling of the dynamic viscosity η of the formulations at $c_p > c_p^*$ is due to relaxation of the irreversible deformation of an anomalously viscous fluid [9] and to disintegration of a continuous fluctuation network of entanglements of EO molecules [18]. The dynamic processes occurring in formulations of this kind ($c_p > c_p^*$) at low shear rates g lead to disintegration of the infinite cluster ($D \approx 2.5$) of filler particles into discrete clusters ($D \approx 1.1$) (Figs. 6, 7).

The concentration dependences of the flow index n of filled formulations have the form of delta functions [8]. The value of n is close to zero at $c_p \le 20\%$, increases jumpwise near the critical concentration $c_p^* = 30\%$, and falls as c_p grows in the range $c_p > 30\%$ (Table 3, Fig. 8). Such a run of the $n(c_p)$ curves is due to an unlimited increase in the degree of aggregation, s, of pigment (filler) particles near c_p^* (Fig. 7). The peak in the $n(c_p)$ curves corresponds to the threshold lattice density of clusters of pigment (filler) particles, $\rho \approx 0.69$, and the corresponding state of the formulation is similar to a dense solution of solid spheres at the percolation threshold [10, 14]. The disintegration of the infinite cluster of pigment (filler) particles into discrete clusters at $c_p > c_p^*$ leads to a sharp decrease in the lattice density ρ, fractal cluster dimension D, and flow index n of filled formulations (Table 3).

The volume concentration of the pigment and filler in the formulations was calculated by the expression $\Sigma c_p = (c_{RIO} + c_p)/\rho_c$ [1], where c_{RIO} and c_p are the mass concentrations of RIO and Microtalc, respectively; and ρ_c is the sample density. The volume density ρ_c of sample no. 12 (Table 3) is 1.34 g cm^{-3}, and $\Sigma c_p \approx 31$ vol %, which coincides with the critical particle concentration in the infinite cluster in the case of a simple cubic lattice [8].

Tests of the protective and anticorrosion properties of coatings obtained on metals by curing of filled epoxy formulations with amines [11] revealed that the best results are achieved at pigment and filler concentration in a formulation equal to 31 vol % (Table 3, sample no. 12). On introduction of a stoichiometric amount of tetrafunctional amine, Mannich base (M_n = 250) [14], into a formulation of this kind, the total mole fraction of YD-128S and YD-136 resins and Cardura in the organic phase of the formulation is $\Sigma m_i \approx 0.69$, and that of the amine curing agent, $m \approx 0.31$. The composition of sample no. 12 can be taken as a prescribed composition because the component concentrations satisfy the criterion of percolation in a simple cubic lattice [4, 8].

As is known [11, 12], the mechanical, protective, and thermal properties of an epoxyamine polymer depend on the density of cross-link sites in the chemical network [20]. Such a network is composed of quadruply and triply connected sites containing fragments of amine molecules [19], with fragments of molecules of epoxydiane resins and Cardura constituting intersite chains [2] and the coil part of the chemical network of the cross-linked polymer [12]. The concentration of epoxydiane resins, Cardura, and amine, as well as the formulation curing conditions, predetermine the structural parameters of the network [19, 20].

The most uniform chemical network is formed, according to the authors' data, in curing of sample no. 12. The cross-link sites of such a network and pigment (filler) particles constitute a continuous 3D network of the polymer [20], which can be represented as two embedded infinite clusters [8]. The lattice density of these clusters, which reflect the continuous small-scale chemical network of the polymer and the uniform large-scale physical network of pigment (filler) particles distributed within regions with lowered local density of cross-link sites of the chemical network [10, 20], is close to the critical values of 0.69 and 0.31, respectively [8].

It is this cluster structure of the chemical and physical networks that provides the high mechanical, protective, and anticorrosion parameters of a filled epoxy polymer (Fig. 1). In particular, 400-μm-thick films produced by curing of sample no. 12 (Table 3) have an ultimate tensile strength of about 30 MPa, elastic modulus $E \approx 900$ MPa, and maximum relative elongation $\Delta l/l = 7\%$.

Thus, the physicochemical principles to be used in making up epoxy formulations were developed with the help of the cluster lattice model. These principles make it possible to substantiate the prescribed composition of the formulations and to provide high strength and protection parameters of epoxy polymers and coatings [14].

CONCLUSIONS

(1) The optimal (prescribed) concentrations of formulation components and the structural parameters of molecule aggregates and pigment (filler) clusters were calculated in the approximation of the cluster lattice model for the example of a formulation containing low-molecular-weight epoxydiane resins, a monoepoxy compound Cardura, red iron oxide pigment and filler (Microtalc).

(2) It was shown that the yield stress τ_0 of the filled epoxy formulation varies in accordance with the expression $\tau_0 \sim |c_p - c_p^*|^t$, where c_p^* is the critical Microtalc concentration and $t = 1.8$. The initial viscosity η^0 of the formulation is a power function of the concentration c_p of pigment (filler) particles: $\ln \eta^0 \sim c_p^{(3-D)/D}$, where D is the fractal dimension of particle clusters. The scaling of the viscosity η^0 in a shear flow of the filled formulation in the range $c_p > c_p^*$ is due to the irreversible dynamic degradation of the continuous

fluctuation network of entanglements between oligomer molecules, which leads to disintegration of the infinite cluster ($D \approx 2.5$) of pigment (filler) particles into discrete clusters ($D \approx 1.1$).

(3) In the filled formulation, the degree of aggregation of pigment (filler) particles shows an unlimited rise near the threshold value c_p^* and the lattice density of particle clusters reaches the maximum value of ~0.69 and then sharply falls in the range $c_p > c_p^*$, which predetermines the extremal behavior of the flow index curves $n(c_p)$. The corresponding state of the formulation is close to that of a dense solution of solid spheres at the percolation threshold.

(4) Tests of the mechanical and protective properties of coatings produced by curing of the filled epoxy formulation with amines demonstrated that these properties are the best pronounced at a pigment (filler) concentration $c_p \approx 31$ vol %, which coincides with the threshold value c_p^*. These data make it possible to state the physicochemical principles to be used in making up these formulations and to substantiate their prescribed composition.

REFERENCES

1. *Paint and Surface Coatings: Theory and Practice*, Lambourne, R., Ed., New York: Wiley, 1988.
2. Markevich, M.A., Structural-Chemical Aspects of Processes in which Epoxydiane Oligomers and 3*D* Polymers on Their Base are Formed, *Doctoral Dissertation*, Chernogolovka, 1986.
3. Krasovskii, A.N., Kharlampiev, A.A., and Krasheninnikov, V.A., *Vysokomol. Soedin., Ser. A*, 1997, vol. 39, no. 2, pp. 250–258.
4. Krasovskii, A.N., Kharlampiev, A.A., and Plodistyi, A.B., *Zh. Prikl. Khim.*, 1997, vol. 70, no. 4, pp. 661–669.
5. Krasovskii, A.N., Kharlampiev, A.A., and Tkach, V.P., *Zh. Prikl. Khim.*, 1997, vol. 70, no. 7, pp. 1165–1174.
6. Tsvetkov, V.N., Eskin, V.E., and Frenkel', S.Ya., *Struktura makromolekul v rastvorakh* (Structure of Macromolecules in Solutions), Moscow: Nauka, 1964.
7. Demidov, V.N., *Dokl. Akad. Nauk*, 2004, vol. 394, no. 2, pp. 218–221.
8. Feder, J., *Fractals*, New York: Plenum, 1988.
9. Vinogradov, G.V. and Malkin, A.Ya., *Reologiya polimerov* (Rheology of Polymers), Moscow: Khimiya, 1977.
10. De Genne, P.G., *Scaling Concepts in Polymer Physics*, New York: Cornell University, 1979.
11. Lipatov, Yu.S., *Fiziko-khimicheskie osnovy napolneniya polimerov* (Physicochemical Foundations of Polymer Filling), Moscow: Khimiya, 1991.
12. Chernin, I.Z., Smekhov, F.M., and Zherdyaev, Yu.M., *Epoksidnye polimery i kompozitsii* (Epoxy Polymers and Formulations), Moscow: Khimiya, 1982.
13. Krasovskii, A.N., Novikov, D.V., Filippov, V.N., et al., *Zh. Prikl. Khim.*, 2003, vol. 76, no. 2, pp. 304–312.
14. Hare, C.H., *Protective Coatings, Fundamentals of Chemistry and Composition*, London: Technology Publishing Company, 2001.
15. Odlyanitskaya, V.S., Agafonov, G.I., Kashina, L.A., et al., *Lakokras. Mater. Ikh Primenenie*, 1988, no. 2, pp. 18–19.
16. Kuleshov, I.D., *Lakokras. Mater. Ikh Primenenie*, 2002, no. 12, pp. 4–8.
17. Filippov, V.N., Application of the Cluster Lattice Model to Substantiation of Concentration and Kinetic Modes of Deposition of Polyesterimide and Epoxy Phenol Coatings, *Cand. Sci. Dissertation*, St. Petersburg, 2004.
18. Krasovskii, A.N., Andreeva, A.I., Urina, M.A., et al., *Zh. Nauchn. Prikl. Fotogr.*, 1996, vol. 41, no. 5, pp. 26–35.
19. Bershtein, V.A. and Egorov, V.M., *Differentsial'naya skaniruyushchaya kalorimetriya v fiziko-khimii polimerov* (Differential Scanning Calorimetry in Physical Chemistry of Polymers), Leningrad: Khimiya, 1990.
20. Krasovskii, A.N., Novikov, D.V., and Filippov, V.N., *Zh. Prikl. Khim.*, 2004, vol. 77, no. 8, pp. 1382–1388.

ISSN 1070-4272, Russian Journal of Applied Chemistry, 2006, Vol. 79, No. 10, pp. 1681–1685. © Pleiades Publishing, Inc., 2006.
Original Russian Text © S.F. Sen'ko, Yu.P. Snitovskii, 2006, published in Zhurnal Prikladnoi Khimii, 2006, Vol. 79, No. 10, pp. 1701–1705.

MACROMOLECULAR CHEMISTRY AND POLYMERIC MATERIALS

Adhesion of Polyimide Films to Microelectonic Article Components

S. F. Sen'ko and Yu. P. Snitovskii

Physicotechnical Institute, National Academy of Sciences of Belarus, State Scientific Establishment, Minsk, Belarus
Belarus State University of Informatics and Radioelectronics, Educational Establishment, Minsk, Belarus

Received April 13, 2006; in final form, June 5, 2006

Abstract—Reactions between polypyromellitamido acid and component materials of microelectronic articles were examined by thermogravimetric analysis. Modes of modification of the surfaces of semiconductor structures to be used in formation of a system of interconnections with polyimide as interlayer insulator to obtain a high adhesion between the layers via their chemical reactions.

DOI: 10.1134/S1070427206100259

The miniaturization of the active elements of microelectronic articles and the ensuing increase in the degree of integration are responsible for the fact that a steadily growing area of the crystal (chip) is occupied by electric interconnections. An increase in the length of interconnections, with a simultaneous decrease in their cross section, leads to a pronounced rise in both the resistance and capacitance. This strongly limits the speed of response of devices.

A possible solution to this problem is to create multilevel interconnections, which, in, turn, give rise to many other problems. The most significant among them are breaks of the interconnecting paths and disturbance of the continuity of the insulator films at steps of the topological profile.

This problem can be tackled with by using films of organic insulators and, in particular, polyimides [1–4] ensuring the required planarity and continuity of the coatings. However, polyimides are chemically inert compounds and do not enter into chemical reactions with components of microelectronic articles (Si, SiO_2, Al, Al_2O_3, etc.), used for fabrication of interconnection systems. This results in an unsatisfactory adhesion of the films of the multilayer system and gives no way of obtaining the required parameters of the structures being manufactured.

Lee et al. [5] suggested to raise increasing the adhesion by forming an independent intermediate layer based on γ-aminopropyltriethoxysilane. Its hydrolysis yields silicon dioxide with attached amino groups, which react with the functional groups of polyamido acid to form a chemical bond between the film and the substrate. However, the method of preparation of such a film does not satisfy the requirements of microelectronics as regards the purity, defectiveness, carbon content, and other characteristics. Yih et al. [6] introduced various additives directly into the polyimide formulation, but this markedly affected the insulation quality. It should be noted that all the above-described options only partially, rather than cardinally, solve the problem.

Babaevskii et al. [7] found that physicochemical modification of thin polyimide films and coatings by plasmochemical treatment and treatment in hexamethyldisilasane vapor affects the nature of the bonds, surface and bulk properties, and nature of inter-phase interaction across the whole width of the films. We suggested that the grains in the films should be predominantly oriented in the (110) plane to improve the adhesion of aluminum films to other layers [8].

Today, the mostly used organic interlevel insulators are polypyromellitimide (PI) films. A characteristic feature of their preparation procedure is that a film of polypyromellitamido acid (PAA) is formed on the semiconductor substrate and is converted to polyimide by heat treatment. In contrast to PI, the PAA macromolecules contain chemically active functional groups –COOH and –NH–, which can, under certain conditions, react with the materials of the contacting layers and provide adhesion between them.

Diverse physicochemical processes are used to form the multilevel interconnection system for micro-

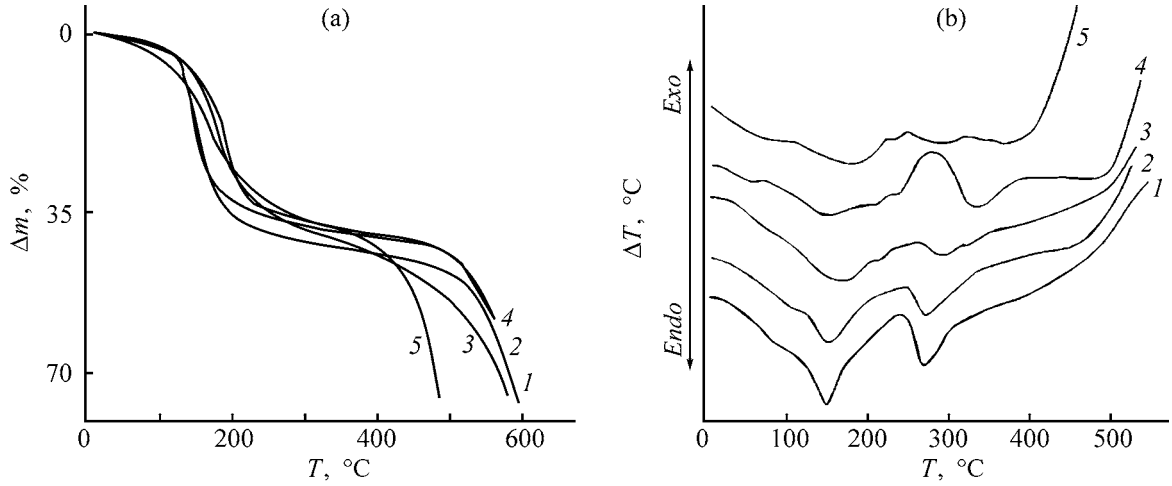


Fig 1. (a) TG and (b) DTA curves for PAA, PAA + silicon, PAA + silicon oxide, PAA + aluminum, PAA + aluminum oxide for different weighed portions. (Δm) Mass loss, and (T) temperature. Weighed portion, mg: (*1*) 62.7 PAA, (*2*) 53.1 PAA + 6.3 silicon, (*3*) 45.4 PAA + 5.8 silicon dioxide, (*4*) 39.5 PAA + 6.9 aluminum, and (*5*) 35.2 PAA + 4.7 aluminum oxide. Heating rate 10 deg min^{-1}.

electronic articles, thus creating certain prerequisites for ensuring such conditions. High-temperature processes (>550°C) are absolutely unacceptable because of the possible degradation of the Al–Si contacts, and, in the case of shallow *p–n* junctions, to failures caused by short circuit of aluminum with the active region of the device.

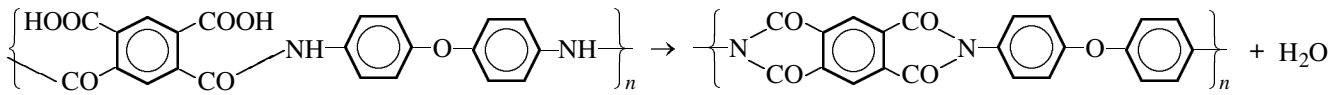
In this study, we examined chemical reactions of PAA with component materials of microelectronic articles and attempted to develop processes for modifying the surfaces of semiconductor structures and surface of polyimide films to provide a strong chemical bonding with the contacting layers and a high adhesion between them.

EXPERIMENTAL

In thermal analysis, we used a neat (without additives) solution of PAA in dimethylformamide (DMF) and its blends with powdered Si, SiO_2, Al, and Al_2O_3. The weighed portions were 62.7 mg of the PAA solution in DMF (henceforth, PAA), 53.1 mg of PAA with 6.3 mg of silicon, 45.4 mg of PAA with 5.8 mg of silicon dioxide, 39.5 mg of PAA with 6.9 mg of aluminum, and 35.2 mg of PAA with 4.7 mg of aluminum oxide.

A thermal analysis was carried out on an OD-102 derivatograph in the temperature range 20–600°C at a heating rate of 10 deg min^{-1} in a self-generated atmosphere. All the additives were finely ground powders; to prevent overlapping of curves we took different weighed portions of PAA. The adhesion of PI was monitored by the previously described procedure [9], as well as visually with an MMU-3 microscope.

Figure 1a demonstrates the TG, and Fig. 1b, the DTA curves for PAA, PAA + silicon, PAA + silicon dioxide, PAA + aluminum, and PAA + aluminum oxide blends. The thermogravimetric characteristics of PAA have been rather extensively examined and described [3]. The imidization proceeds by the scheme



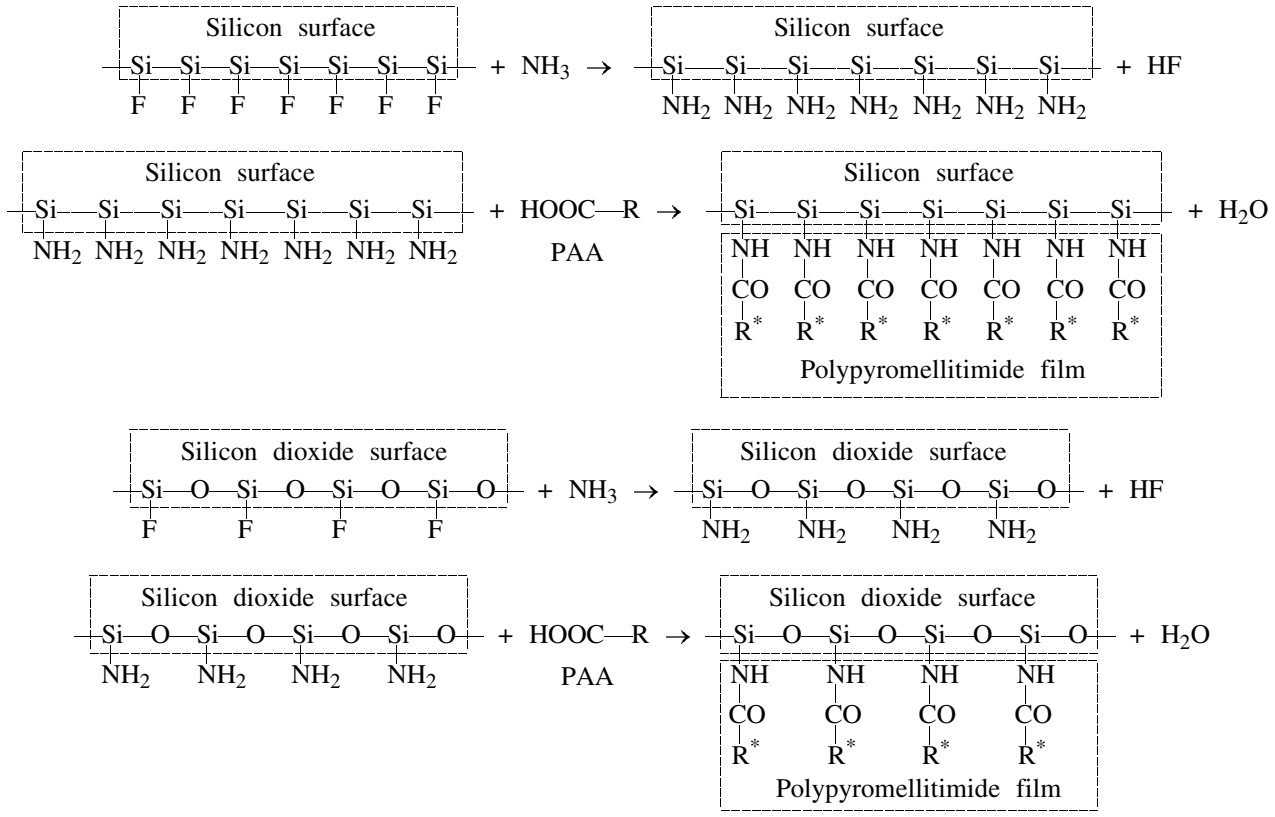
In the first stage, at temperatures within the range 20–120°C (curve *1*), there is insignificant mass loss due, probably, to intermolecular interaction of the PAA macromolecules and partial release of the solvent and imidization water from the polyamido acid solution. In the second stage (120–160°C), the release of the solvent and water is accelerated, possibly due to superposition of the continuing growth of the molecular weight and the beginning intramolecular cyclization into imide rings. This agrees well with the boiling point of DMF (~153°C) and with the occurrence of an endothermic peak in the DTA curve. Since the onset of imidization coincides with the release of the solvent, there is no additional step in the mass loss curve.

As the temperature increases, the release of volatile products is decelerated to a certain extent at 160–500°C and then accelerated at 500–600°C.

The peak in the DTA curve at 250–300°C is virtually not accompanied by any change in the sample mass. Bessonov et al. [1] attribute the improvement of the mechanical properties upon heating at 200–300°C to restoration of the molecular weight of polyamido acid (supposedly, via reactions at terminal groups). Also, cross-linking of the macromolecules is possible.

Silicon and silicon dioxide (curves *2* and *3*) virtually do not affect the thermogravimetric characteristics of PAA. A small shift of the solvent loss peak in the DTA curve to higher temperatures and smoothening of the corresponding step in the TG curve for the PAA + silicon dioxide blend is, most probably, due to sorption–desorption of the solvent released and imidization water by silicon dioxide. The TG and DTA curves suggest that PAA does not enter into chemical reactions with silicon or silicon dioxide, which gives no way of obtaining an acceptable adhesion of the PI film to these materials without taking additional measures.

The process we developed for modification of the silicon dioxide and silicon surfaces ensures formation of a monolayer of amino groups on their surface. The process includes two stages. The first stage involves treatment of the surface in a fluorine-containing plasma and formation of a monolayer of fluorine atoms. The Si–F chemical bond is unstable; it is immediately hydrolyzed in the presence of trace amounts of moisture. Therefore, it is necessary to monitor the process and the purity of the reagents. Treatment of the surface with gaseous ammonia results in the replacement of fluorine atoms by amino groups. Modification does not require high temperatures, and the Si–NH_2 chemical bond is fairly stable. During the subsequent formation of the polyimide film, the –NH_2 functional groups on the substrate surface enter into a chemical reaction with –COOH groups in PAA macromolecules. Thus, the film being formed is "fastened" to the substrate surface by –CO–NH– bonds. The –CO– group belongs to the macromolecule of the film being formed, and the –NH– group, to the modified surface. A strong chemical bond is formed between the film and the substrate, which ensures their mutual adhesion. This method is suitable for a silicon substrate and a substrate coated with polycrystalline silicon, silicon dioxide, silicides, and similar silicon compounds. The process occurs at the film–substrate interface exclusively and does not deteriorate the electrical characteristics of the resulting insulation. Below given are the schemes of the occurring chemical reactions:



Formation of the adhesion bonds and intramolecular cyclization of PAA proceed simultaneously and compete with each other. The residual R of the polyamido acid macromolecule, the educt, is converted to a residual of the polyimide macromolecule in the reaction products and is designated as R^*.

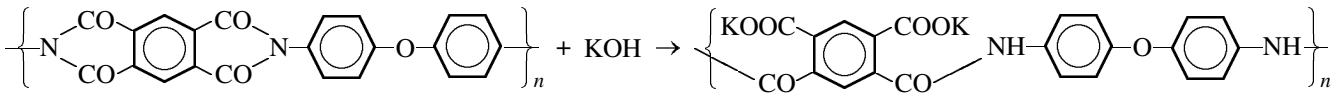
As is known, the cyclization of PAA begins even at its drying temperature but does not go to completion. The reason is the growing rigidity of the macromolecules, which presents a spatial hindrance to approach of the reacting functional groups [1]. Therefore, a significant proportion of the functional groups and, in particular, –COOH, are not involved in the formation of imide rings in this stage and, despite the predominant occurrence of the processes considered, prtovides formation of the adhesion bonds.

In the presence of aluminum and aluminum oxide (curves *4* and *5*, respectively), the thermogravimetric characteristics of PAA are modified as follows. The solvent loss peaks are shifted to higher temperatures; this shift is more pronounced for the PAA + aluminum oxide blend, which can also be due to sorption–desorption of the solvent and water. The endothermic effect for the PAA + aluminum blend at 250–300°C is virtually completely compensated for by the exothermic effect in the same temperature range. This process does not affect the mass change, which suggests chemical reactions between the polymer and aluminum. Chemical reactions between PAA and metals were also noted by Bessonov et al. [1]. For the PAA + aluminum oxide blend, the steps in the TG curve are markedly smoothened, and the DTA peaks are rather weakly manifested, which suggests the predominant occurrence of adsorption processes. Intensive interaction in this blend begins only at 400°C, and the thermal stability of the polyimide being formed decreases by ca. 100°C. This is, probably, due to decomposition of the polymer under the action of aluminum oxide exhibiting amphoteric properties.

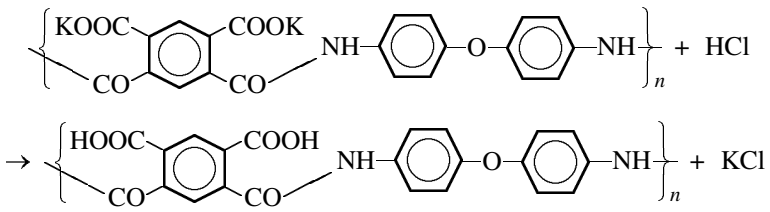
As is known, aluminum is immediately oxidized in air to form on its surface a thin oxide film. The thickness of this film depends on the storage time and conditions and can attain ca. 10 nm. Therefore, formation of a polyimide film on the surface of the aluminum-coated structure should be preceded by cleaning (a kind of "refreshing" of the surface) to remove the oxide immediately before application of PAA. The choice of the temperature modes for treatment of the polyamido acid film applied to the structure with aluminum in order to convert it into polyimide should also take into account the temperature range of interaction between PAA and the metallic substrate. Prolonged primary drying of the PAA film at a temperature below 250°C, leads not only to evaporation of the solvent, but also to a significant imidization without chemical reactions with the metallic base. Subsequent heat treatment of the structure at the temperature of the reaction between PAA and the metal (above 250°C) does not lead to formation of a sufficient number of adhesion bonds, since, by this moment, the concentration of the functional groups becomes too low.

Thus, polyamido acid actively reacts with aluminum at temperatures above 250°C, while polyimide is known to be inert toward aluminum [3]. Thus, an acceptable adhesion of metallized coatings to unmodified polyimide is unattainable in principle. At the same time, adhesion of polyimide films to metallized surfaces is typically fairly satisfactory. Therefore, it is reasonable to carry out surface modification of polyimide into polyamido acid in order to obtain good adhesion of the metal films to polyimide.

The process we developed for surface modification of the polyimide film into polyamido acid can include one or two stages. In the two-stage process, the polyimide film is initially treated with a dilute alkali solution (e.g., KOH). This results in opening of the imide rings to give salts of the polyamido acid and alkali by the scheme:



In this context, the most important aspect is termination of the process at a proper time, when it is complete on the surface and has not spread deep inside the polyimide film, as this will degrade the film. This termination is achieved by using dilute (to 1%) solutions of alkali and by maintaining the temperature within 15–30°C. The second stage consists in treatment of the resulting film in an acid solution, with the salts regenerated to the initial PAA by the scheme



Heat treatment after formation of the interconnection pattern leads to reaction of the resulting PAA with the metal film to form a strong –COO–Al chemical bond. PAA that does not react with aluminum (between the interconnecting paths) is converted back to polyimide.

In the one-stage process, the treatment was carried out in a solution of a weak base. Upon subsequent washing in water, the salts formed in the film are hydrolyzed to polyamido acid. The choice of the method for surface modification of polyimide into polyamido acid is dictated by the specific process conditions and the possibility of combining the treatment of polyimide with other operations, e.g., removal of the photoresist, opening of contact windows.

Monitoring of adhesion of the polyimide films prepared by the processes we developed showed that the film does not peel-off in peeling tests. Visual monitoring of opening of contact windows in hydrofluoric acid solutions also showed that the film does not peel-off at the contact window edges. Monitoring of adhesion of the metal film to polyimide did not reveal peeling-off for the aluminum interconnecting paths. The results we obtained were used for developing a process for fabrication of a multilevel system of interconnections in integrated circuits.

CONCLUSION

Processes were developed for modification of the surfaces of semiconductor structures, as well as of the surface of polyimide films, that provide chemical reactions between the polyimide films and the contacting layers to achieve a high mutual adhesion.

REFERENCES

1. Bessonov, M.I., Koton, M.M., Kudryavtsev, V.V., and Laius, L.A., *Poliimidy–klass termostoikikh polimerov* (Polyimides: a Class of Thermostable Polymers), Leningrad: Nauka, 1983.
2. Harada, Yasoo, Matsumoto, Fumio, and Nakakado, Takashi, *Solid State Science and Technology*, 1983, vol. 130, no. 1, pp. 129–134.
3. Wilson, A.M., *Thin Solid Films*, 1981, vol. 83, no. 2, pp. 145–163.
4. Sen'ko, S.F. and Snitovskii, Yu.P., *Tr. Mezhnatsional'nogo soveshchaniya "Radiatsionnaya fizika tverdogo tela"* (Proc. of XI Int. Workshop "Radiation Physics of Solid State"), Sevastopol', June 25–30, 2001, Moscow, 2001, pp. 310–311.
5. Lee, Y.K., Craig, J.D., and Pye, W.E., *Proc., 4th Bien. Univ. Gov. Int. Microelectron. Symp., Starkville, 1981*, New York, 1981, pp. 30–39.
6. Yih, Jie, Ye, Yu-Feng, and Wang, Zong-Gvang, *Europ. Polym. J.*, 1998, vol. 34, no. 12, pp. 1839–1843.
7. Babaevskii, P.G., Zhukov, A.A., and Zhukova, S.A., *Mikrosistem. Tekhn.*, 2004, no. 5, pp. 2–6.
8. Snitovskii, Yu.P., *Neorg. Mater.*, 2005, vol. 41, no. 8, pp. 922–927.
9. *GOST* (State Standard) *15140–78: Paint and Varnish Materials. Methods of Determination of Adhesion*, Moscow: Izd. Standartov, 1978.

ISSN 1070-4272, Russian Journal of Applied Chemistry, 2006, Vol. 79, No. 10, pp. 1686–1689. © Pleiades Publishing, Inc., 2006.
Original Russian Text © N.I. Afanas'ev, T.F. Lichutina, M.A. Gusakova, G.F. Prokshin, A.P. Vishnyakova, D.A. Sukhov, O.Yu. Derkacheva, 2006, published in Zhurnal Prikladnoi Khimii, 2006, Vol. 79, No. 10, pp. 1706–1709.

MACROMOLECULAR CHEMISTRY AND POLYMERIC MATERIALS

Estimation of the Content and Assessment of Structural Transformations of Residual Lignin and Resin in Deciduous Kraft Pulp by Fourier IR Spectroscopy

N. I. Afanas'ev, T. F. Lichutina, M. A. Gusakova, G. F. Prokshin, A. P. Vishnyakova, D. A. Sukhov, and O. Yu. Derkacheva

Institute of Environmental Problems of the North, Ural Division, Russian Academy of Sciences, Arkhangelsk, Russia

St. Petersburg State Technological University of Plant Polymers, St. Petersburg, Russia

Received June 14, 2006

Abstract—Variation of the amount, composition, and structure of the residual lignin and resin in pulp samples from kraft cooking of birch and aspen woods and their blend with addition of distilled tall oil was studied by Fourier IR spectroscopy.

DOI: 10.1134/S1070427206100260

The use of deciduous wood, including birch and aspen wood, in production of kraft pulp involves so-called "resin problems," since the content of neutral substances (styrenes, waxes) in the extractive substances is 25–30%, and that of fats (mainly glycerides of unsaturated linoleic and oleic acids), 50–60%; these substances tend to readily transform in storage and production [1].

It is well known that, in cooking, the resin content in deciduous pulp can be decreased by adding various surfactants, among them products of wood chemistry [2].

We studied the possibility of using distilled tall oil (DTO) and its acidic components for this purpose. It has been shown previously [3, 4] that, in separate and combined kraft cooking of birch and aspen wood with addition of DTO, the content of resinous substances and residual lignin can be decreased by 30–40%.

To obtain fundamentally new data, we used in this study a noninvasive method, Fourier IR spectroscopy. This method is the most informative and allows determination of not only the content, but also structural transformations of the residual lignin in situ, without its recovery from fibers [5–7]. Here, we describe the results of using this method for studying changes in the composition and structure of residual lignin in pulp samples from kraft cooking of birch and aspen wood and their blends with DTO as an additive.

EXPERIMENTAL

The study was performed with samples of sound birch (Betula pubesceus) and aspen (Populus tremula) woods: age 25–35 years, stem diameter without bark 20 cm. For cooking we used hand-made chips of the following dimensions (mm): length 25–30, width 20–25, and thickness 2–3.

The content of extractive substances in birch and aspen sawdust was the same, 2.5%. The lignin content determined by the sulfuric acid method was 20.0% in birch wood and 20.4% in aspen wood; the pulp content determined by the nitric acid–alcohol method was 45.6 and 50.6%, respectively.

The kraft cookings were performed using white liquor (sulfide content 30%) in the same temperature–time mode (heating to 170°C over a period of 120 min, cooking at 170°C for 60 min) in a set of six pressure vessels. The prescribed expenditure of active alkali in the Na_2O units relative to absolutely dry wood charged into pressure vessels was 17 wt %. After the cooking was complete, the pulp was squeezed, washed on a filter with hot water, and dried in air; then the pulp yield and resin content were determined (the latter, by extraction with methylene chloride); the content of the residual lignin was determined by the sulfuric acid method, following the standard procedures [8].

Table 1. Yield and content of residual lignin and resin in pulp samples

Sample no.	Sample characteristics	Recovery from wood, %		Pulp yield, %	Content in pulp, %	
		lignin	resin		lignin	resin
	Pulp:					
1	from kraft cooking of birch wood without additives	93.4	81.0	47.2	2.7	0.43
2	extracted with methylene chloride	93.4	100.0	47.2	2.7	0.00
3	from cooking with addition of 3 wt % DTO	95.9	81.0	45.7	1.8	0.49
4	from kraft cooking of aspen wood without additives	97.6	95.4	51.6	0.95	0.37
5	extracted with methylene chloride	97.6	100.0	51.6	0.95	0.00
6	from cooking with addition of 3 wt % DTO	97.5	81.0	51.7	1.0	0.16
7	from kraft cooking of a blend (birch : aspen 50 : 50) without additives	95.3	89.2	52.0	1.8	0.52
8	extracted with methylene chloride	95.3	100.0	52.0	1.8	0.00
9	from cooking of the blend with addition of 3 wt % DTO	96.4	88.5	50.9	1.4	0.6

To obtain the Fourier IR absorption spectra, the pulp samples were prepared in the form of thin pellets of diameter 13 mm and weight 2–4 mg by direct pressing of fibers in a press mold without addition of KBr. Before recording the spectra on a Bruker IFS25IR Fourier spectrophotometer, the samples were purged for 5 h in the cell compartment of the spectrophotometer, which allowed improvement of the spectrum quality due to a decrease in the intensity of absorption bands of atmospheric water and water adsorbed on the fiber surface.

The characteristics of the pulp samples from separate kraft cookings of birch (sample nos. 1–3) and aspen (sample nos. 4–6) wood and from cooking of a blend of birch and aspen chips (sample nos. 7–9) are listed in Table 1.

Table 1 shows that 93–97% of lignin and 81–90% of resin, recovered from wood in kraft cooking, are in black liquor. The ratios of the content of residual lignin and resin DTO were 2.7 : 0.43 and 1.8 : 0.49 in the pulp obtained in cooking of birch wood without additives and with addition of 3 wt %; 0.95 : 0.37 and 1.0 : 0.16 in that produced in cooking of aspen wood; and 1.8 : 0.52 and 1.4 : 0.6 in that formed in cooking of the blend. These ratios show that the content of lignin and resin in the pulp after cooking with addition of distilled tall oil decreases in such a manner that their ratio in the pulp after recovery varies insignificantly or remains the same as in the cooking without additives.

In the data listed in Table 1, it is assumed that the resin substances are completely recovered from pulp in the extraction and the residual content of lignin, which is insoluble in methylene chloride under the conditions of determination of the resin content, remains the same.

The variations in the ratios of the contents of residual lignin and resin in the pulp after kraft cooking of birch and aspen woods and their mixture without addition and with addition of 1, 2, and 3% DTO (see Fig. 1) illustrate the main differences in the influence

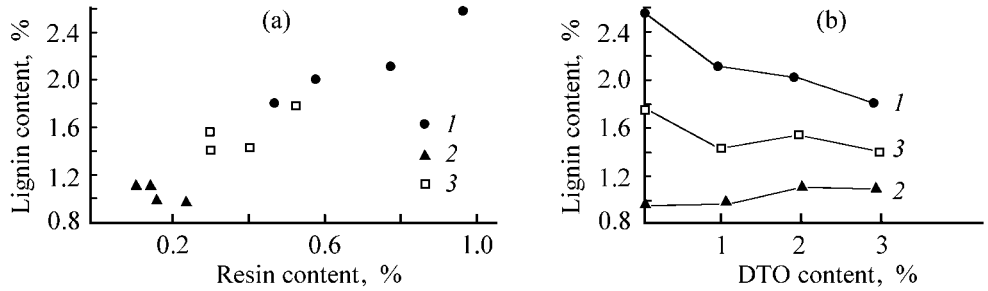


Fig. 1. Variation of the content of residual lignin and resin in the pulp after cooking of (*1*) birch and (*2*) aspen wood and (*3*) their blend (a) without and (b) with addition of DTO.

Table 2. Relative intensities of the absorption bands of residual lignin in the Fourier IR spectra of the pulp

Sample no.	1740	1600	1510	G/S 1515/1502	1540 cm^{-1}
	cm^{-1}				
1	0.07	2.00	0.53	1.2	0.037
2	0.03	2.15	0.56	1.3	0.018
3	0.13	1.90	0.16	1.5	0.056
4	0.06	1.75	0.38	1.6	0.006
5	0.15	1.90	0.40	1.7	0.001
6	0.16	1.70	0.26	1.6	0.004
7	0.09	2.00	0.28	1.3	0.023
8	0.07	1.90	0.26	1.6	0.034
9	0.14	1.85	0.20	1.5	0.021
Error	0.02	0.03	0.02	0.1	0.003

exerted by increasing amounts of DTO on the decrease in the content of lignin and resin. In cooking of aspen wood without additives, the minimum content of lignin and resin was reached, and, with increasing amount of additives, it did not noticeably vary. In cooking of a blend of birch and aspen wood (50 : 50), the average content of lignin and resin (curve *3*) was mainly governed by the fraction of the birch wood.

To obtain new data on the composition of the samples studied, we recorded their Fourier IR spectra in the range 1450–1800 cm^{-1}, in which the characteristic bands of guaiacyl and syringyl rings of lignin, resin residues, uronic acids, and other components predominantly lie.

The spectra of all the samples contain a weak band of carbonyl groups (C=O) at 1740 cm^{-1} and characteristic bands at approximately 1600, 1540, and 1510 cm^{-1}, related to various vibration modes of aromatic structures of the residual lignin. A mathematical processing for improvement of the spectral resolution (deconvolution and differentiation) showed that the band in the range of 1510 cm^{-1} is a superposition of two bands at 1515 and 1502 cm^{-1} related to vibrations of guaiacyl (G) and syringyl (S) aromatic rings.

Data on the relative intensities of characteristic bands of lignin aromatic structures and carbonyl groups in the spectra of the pulp samples (Table 2) allow estimation of changes in the content and structure of residual lignins, caused by addition of distilled tall oil and extraction of resinous substances with methylene chloride.

Comparison of the intensity of the bands at 1600 and 1510 cm^{-1} shows that the strongest changes are observed with the band at 1510 cm^{-1} and, hence, with the content of aromatic rings of lignin in the structure of the kraft pulp samples. The intensity of the band at 1600 cm^{-1} varied in the same direction as the intensity of the band at 1510 cm^{-1}, but its variations were significantly less pronounced. The intensity of this band shows a good total correlation with the parameter of Clason lignin. The relative intensity of the band at 1600 cm^{-1} closely correlates (r 0.98) with the content of the residual lignin in the pulp, which confirms the possibility of using Fourier IR spectroscopy for development of a sensitive quantitative spectral method of noninvasive analysis for the lignin content at its low content in the pulp.

In the course of delignification, the most pronounced changes in the spectra are associated with tensities of the bands at 1600, 1515, and 1502 cm^{-1}; a decrease in the in the behavior of their intensities depends on the kind of a sample.

The most pronounced differences were observed in the ratios between the intensities of the absorption bands of guaiacyl (G) rings at 1515 cm^{-1} and syringyl (S) rings at 1502 cm^{-1} and, hence, in the content of these structural units in residual lignins (Table 2, parameter G/S). Based on these ratios, it can be noted that the content of guaiacyl structures in the residual lignin of kraft aspen pulp was, on the average, higher than that in the residual lignin of birch pulp and the highest content of guaiacyl structures was observed in the pulp samples with addition of 3 wt % DTO.

The intensities of weak bands at 1740 and 1540 cm^{-1} decrease in the sample of birch pulp after deresination and increase in the sample obtained with addition of 3% DTO. This fact suggests that these bands of lignin overlap with the bands of resinous substances of pulp. The intensity of the absorption band at 1740 cm^{-1} is somewhat higher than that of the band at 1540 cm^{-1}, which is caused by the apparent superposition of the absorption bands of lignin and uronic acids whose content in the pulp is significantly higher than that of esters of neutral resinous substances and carbonyl groups in them. The practical use of these bands for monitoring changes in the content and composition of resin in the samples is, however, difficult because of the above features.

CONCLUSION

The high correlation coefficient of the relative intensity of the characteristic band of lignin with

the content of residual lignin and high the sensitivity of these bands to changes in the content of guaiacyl and syringyl structures allowed quantitative estimation of the content of residual lignin and assessment of its structural transformations in kraft birch and aspen pulp by Fourier IR spectroscopy in situ without its recovery from wood fibers.

REFERENCES

1. Lysogorskaya, N.P., Protskii, A.N., and Dem'yantseva, E.Yu., *Materialy nauchno-prakticheskoi konferentsii "Dostizheniya i problemy varki i otbelki tsellyulozy"* (Proc. of Scientific and Practical Conf. "Advances and Problems of Pulp Cooking and Bleaching"), St. Petersburg, 2003, pp. 37–40.
2. Rikhter, N.E., Leonovich, A.A., and Borilkevich, Z.I., *Bumazhn. Prom–st.*, 1988, no. 10, pp. 5–6.
3. Afanasjev, N., Proshkin, G., Vishnjakova, A., et al., Abstracts of Papers, *Int. Conf. "Eighth European Workshop on Lignocellulosics and Pulp,"* Riga, 2004, pp. 465–468.
4. Prokshin, G.F., Afanas'ev, N.I., Vishnyakova, A.P., et al., Abstracts of Papers, *Mezhdunarodnaya konferentsiya "Fizikokhimiya lignina"* (Int. Conf. "Physical Chemistry of Lignin"), Arkhangelsk, 2005, pp. 165–168.
5. Sukhov, A.V., Derkacheva, O.Yu., Komarov, V.I., and Kazakov, Ya.V., *Lesn. Zh.*, 1994, no. 3, pp. 99–104.
6. Derkacheva, O.Yu., Sukhov, A.V., and Fedorov, A.V., Abstracts of Papers, *Mezhdunarodnaya konferentsiya "Fizikokhimiya lignina"* (Int. Conf. "Physical Chemistry of Lignin"), Arkhangelsk, 2005, pp. 177–180.
7. Sukhov, A.V., Derkacheva, O.Yu., and Komarova, G.V., Abstracts of Papers, *Mezhdunarodnaya konferentsiya "Fizikokhimiya lignina"* (Int. Conf. "Physical Chemistry of Lignin"), Arkhangelsk, 2005, pp. 235–257.
8. Obolenskaya, A.V., El'nitskaya, Z.P., and Leonovich, A.L., *Laboratornye raboty po khimii drevesiny i tsellyulozy* (Laboratory Works on Chemistry of Wood and Pulp), Moscow: Ekologiya, 1991.

ISSN 1070-4272, Russian Journal of Applied Chemistry, 2006, Vol. 79, No. 10, pp. 1690–1695. © Pleiades Publishing, Inc., 2006.
Original Russian Text © L.A. Zemnukhova, O.V. Brovkina, N.A. Didenko, L.E. Kryukova, V.V. Bespalova, E.D. Shkorina, 2006, published in Zhurnal Prikladnoi Khimii, 2006, Vol. 79, No. 10, pp. 1710–1714.

MACROMOLECULAR CHEMISTRY AND POLYMERIC MATERIALS

Kinetics of Bleaching of Rice Straw and Husk with Potassium Peroxoborate

L. A. Zemnukhova, O. V. Brovkina, N. A. Didenko, L. E. Kryukova, V. V. Bespalova, and E. D. Shkorina

Institute of Chemistry, Far-Eastern Division, Russian Academy of Sciences, Vladivostok, Russia

Received March 23, 2006

Abstract—The kinetics of bleaching with potassium peroxoborate of waste from rice production (straw and husk), untreated and treated with water, acid, and sodium hydroxide, was studied.

DOI: 10.1134/S1070427206100272

Production of husked rice groats involves formation of large-tonnage wastes. These wastes can be a source for production of various types of products for chemical, medical, food, textile, paper, construction, and other branches of industry [1–5]. Rice straw has long been used as a raw material for production of the cellulose material [6]. Development of environmentally safe procedures for bleaching of lignocellulose materials without using chlorine-containing reagents is a topical problem [7–9].

This study proceeds with examination of wastes from rice production and considers the possibility of using potassium peroxoborate (PPB) for bleaching of rice straw (RS) and husk (RH).

EXPERIMENTAL

We chose for the study the RS and RH samples prepared from rice of the Darii-8 strain cultivated in Primorskii krai in 2002 [10]. The straw was milled to particles with a length of 3–5 cm, the husk was fractionated, and particles with a size of no less than 2 mm were taken. The raw material was washed with water and dried at 60°C. The content of inorganic and organic components of the initial raw material has been determined previously [2–4] and is as follows (%): 12 and 88% for RS and 20 and 80%, respectively, for RH.

As a bleaching agent we used PPB containing 20% available oxygen O_{av} whose synthesis is described in [11]. We studied the effect of PPB on the samples of the initial raw materials and their residues after treatment (extraction) with water, hydrochloric acid (1 N), and sodium hydroxide (1 N) at the volume ratio solid : liquid = 1 : 13, treatment duration of 1 h, and temperature of 90°C. The residual raw materials after the extraction of soluble substances were filtered off, washed with water, and dried to constant weight at 60°C. The composition of the extracts was studied in [4]. The samples were bleached at the optimal temperature of 95°C, with the concentration of PPB varied from 6 to 12 g l^{-1}, and the process duration, from 5 to 60 min.

The rate of PPB decomposition was estimated from variation of the O_{av} content in the solution, determined by permanganatometric titration [12], and was calculated from the ratio $\ln[c_0/(c_0 - c_x)]$, where c_0 is the initial concentration of O_{av} in the solution, and $(c_0 - c_x)$ is the concentration of available oxygen undecomposed by the time τ. The rate constants of O_{av} decomposition were evaluated from the rate equation of a first-order reaction [13]. The bleaching power of PPB was estimated on a Specol device by the procedure described in [14]; freshly calcined magnesium oxide was used as reference. We analyzed the spectrophotometric curves of the reflection coefficient ρ in the wavelength range 400–700 nm. The results are listed in Tables 1 and 2 and shown in Figs. 1–4.

Initial (untreated) RS. The parameters of thermal decomposition of aqueous solutions of PPB in

Table 1. Decomposition of aqueous solutions of potassium peroxoborates in bleaching of rice straw and husk (T = 95°C, τ = 60 min)

Sample no.	System	c_{PPB}, g l^{-1}	pH	Logarithm of O_{av} decomposition rate in solution $\ln[c_0/(c_0 - c_x)]$				$k \times 10^{-3}$, s^{-1} (degree of O_{av} decomposition, %)			
				5 min	15 min	30 min	60 min	5 min	15 min	30 min	60 min
1	PPB	6	9.2	–	0.89	1.26	1.51	–	0.99	0.69	0.42
				–					(79.45)	(85.77)	(88.93)
2	RS(init) + PPB	6	9.2	–	0.62	1.85	2.07	–	0.69	1.03	0.58
			9.4					–	(73.12)	(92.10)	(93.68)
3	PPB	12	8.9	0.121	1.66	2.44	3.05	0.40	1.84	1.35	0.85
								(11.46)	(81.03)	(91.31)	(95.26)
4	RS(init) + PPB	12	8.9	0.053	2.07	2.89	3.45	0.18	2.30	1.61	0.96
			9.6					(5.14)	(87.35)	(94.47)	(96.84)
5	RS(H_2O) + PPB	12	9.5	0.052	1.20	2.76	–	0.17	1.33	1.53	-
			10.5					(5.14)	(69.96)	(93.68)	–
6	RS(HCl) + PPB	12	8.9	0.016	1.66	2.20	2.35	0.05	1.84	1.22	0.65
			9.8					(1.98)	(81.03)	(89.93)	(90.51)
7	RS(NaOH) + PPB	12	8.9	0.02	0.81	1.44	2.07	0.067	0.90	0.80	0.58
			9.7					(1.58)	(55.73)	(76.29)	(87.35)
8	RH(init) + PPB	12	9.2	0.024	2.01	2.64	–	0.08	2.22	1.64	–
			10.4					(2.37)	(86.56)	(92.89)	–
9	RH(H_2O) + PPB	12	9.0	0.069	1.66	2.07	–	0.23	1.84	1.15	–
			10.2				–	(6.72)	(81.03)	(87.35)	–
10	RH(HCl) + PPB	12	9.2	0.02	1.01	1.05	1.25	0.067	1.12	0.58	0.35
			9.2					(1.98)	(63.64)	(65.22)	(71.54)
11	RH(NaOH) + PPB	12	9.3	0.095	1.37	1.84	3.05	0.32	1.52	1.02	0.85
			9.3					(9.10)	(74.71)	(84.19)	(95.26)

the course of RS bleaching are listed in Table 1. The kinetic curves illustrating the linear dependence of the O_{av} concentration on time are shown in Fig. 1.

The results obtained suggest that, as the PPB concentration in aqueous solution increases, the rate of O_{av} decomposition grows both in the presence of RS and without it; in the process, the solution pH varies in the range 8.9–9.6. The decomposition of O_{av} proceeds more actively in the first 30 min.

Depending on the PPB concentration and bleaching duration, the rate constants of O_{av} decomposition decrease from 0.99×10^3 to 0.42×10^3 and from 1.84×10^3 to 0.85×10^3 s^{-1} (Table 1; Fig. 1, curves *1*, *3*), respectively. The degree of O_{av} decomposition by the end of bleaching for these systems is 88.93 and 95.26%. In the presence of RS, both the reaction rate and the rate constant of O_{av} decomposition increase (Fig. 1, curves *2*, *4*). By the end of peroxide bleaching (τ = 60 min), the rate constants of O_{av} decomposition decrease to 0.58×10^3 (Table 1, sample no. 2) and 0.96×10^3 s^{-1} (Table 1, sample no. 4). The degree of O_{av} decomposition is 93.68 and 96.84%, respectively.

Treated RS. Analysis of the kinetic characteristics of thermal decomposition of PPB solutions in

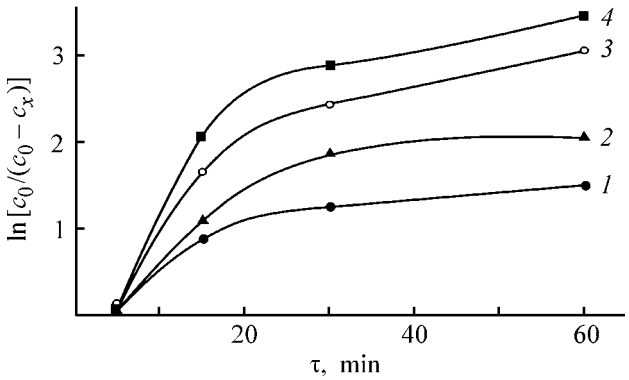


Fig. 1. Kinetic curves in the coordinates $[\ln(c_0/c_0 - c_x)]$–time τ of thermal decomposition of O_{av} in solutions containing PPB and RS. (c_0) Initial concentration of O_{av} in the solution, wt % and (c_x) concentration of O_{av} in the solution at the time τ; the same for Figs. 2 and 3. (*1*, *3*) PPB of various concentrations without plant raw materials (Table 1, samples nos. 1, 3); (*2*, *4*) in bleaching of the initial RS (samples nos. 2, 4).

Table 2. Physicochemical characteristics of the material being bleached and its solutions (T = 95°C, τ = 60 min)

Sample no.	System	Weight loss after bleaching, %	c_{PPB}, g l^{-1}	Solution before/after bleaching	
				pH	solution color*
1	PPB	–	6	9.2/9.2	Colorless
2	RS(init) + PPB	12.6	6	9.2/9.4	Light straw-colored
3	PPB	–	12	8.9/8.9	Colorless
4	RS(init) + PPB	21.6	12	8.9/9.6	Weak yellow tint
5	RS(H_2O) + PPB	–	12	9.5/10.5	Green tint/deep yellow with green tint
6	RS(HCl) + PPB	24.0	12	8.9/9.8	Golden yellow with green tint
7	RS(NaOH) + PPB	9.0	12	8.9/9.7	Yellow tint
8	RH(init) + PPB	–	12	9.2/10.4	Yellow tint/golden color
9	RH(H_2O) + PPB	–	12	9.0/10.2	Yellow tint/slightly yellow with green tint
10	RH(HCl) + PPB	18.2	12	9.2/9.2	Slightly yellow tint
11	RH(NaOH) + PPB	19.6	12	9.3/9.3	Green tint

* Color of transparent solution after removal of the bleached raw material.

the presence of treated RS samples (Table 1, Fig. 2) shows that the bleaching of raw materials depends on the procedure of their pretreatment (aqueous, acidic, or alkaline). For example, the rate constants of O_{av} decomposition in bleaching of RS treated with acid or alkali by the end of peroxide bleaching are 0.65×10^3 and 0.58×10^3 s^{-1} (Table 1, sample nos. 6, 7). In this case, the degree of PPB decomposition is 90.51 and 87.35%, respectively, which is lower than that in decomposition of pure PPB (95.26%).

In the course of bleaching of RS pretreated with water, acid, or alkali, the solution color and pH (in the range 8.9–10.5), and also the weight of the cellulose product (≤24%) after bleaching vary depending on pretreatment of straw (Table 2).

A comparison of the effect of PPB on RS shows that the maximum rate of O_{av} decomposition in the solution is observed in bleaching of the initial RS and the minimum rate, for RS treated with NaOH (Fig. 2, curves *2*, *5*). With respect to the influence of the procedure of preextraction of soluble substances from straw on the rate of PPB decomposition in the course of bleaching, the samples of raw materials can be ranked in the following order: RS(init) > RS(H_2O) > RS(HCl) > RS(NaOH).

Rice husk. The RH bleaching with PPB proceeds somewhat differently (Table 1, Fig. 3), compared to

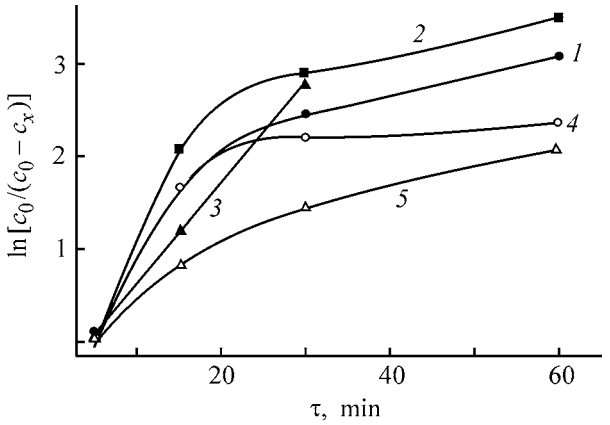


Fig. 2. Kinetic curves in the coordinates $[\ln(c_0/c_0 - c_x)]$–time of thermal decomposition of O_{av} τ in solutions containing PPB and RS. (*1*) Without RS (Table 1, sample no. 3); RS: (*2*) initial (sample no. 4), (*3*) treated with H_2O (sample no. 5), (*4*) treated with HCl (sample no. 6), and (*5*) treated with NaOH (sample no. 7).

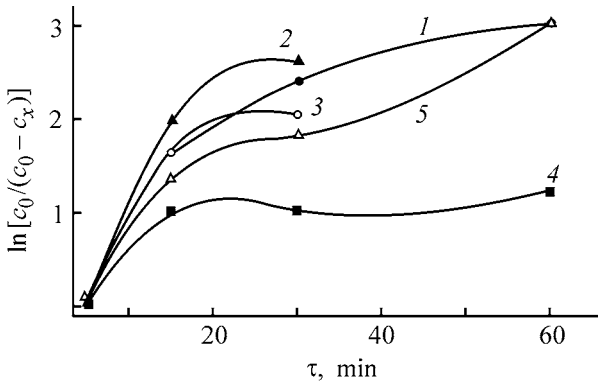


Fig. 3. Kinetic curves in the coordinates $[\ln(c_0/c_0 - c_x)]$–time τ of thermal decomposition of O_{act} in solutions containing PPB and RS. (*1*) Without husk (Table 1, sample no. 3); RH: (*2*) initial (sample no. 8), (*3*) treated with H_2O (sample no. 9), (*4*) treated with HCl (sample no. 10), and (*5*) treated with NaOH (sample no. 11).

straw bleaching and depends on the procedure of husk pretreatment.

The kinetic curves of thermal decomposition of PPB show that the maximum rate of O_{av} decomposition is attained, as in the experiments with RS, in bleaching of the initial RH (Fig. 3, curve *2*), and the minimum rate, in bleaching of the husk subjected to acid treatment (not alkaline, as for RS) (Fig. 3, curve *4*). With respect to variation of the rate of O_{av} decomposition in bleaching with PPB, the raw materials can be ranked in the following order, depending on the pretreatment procedure: RH(init) > RH(H_2O) > RH(NaOH) > RH(HCl).

The degree of O_{av} decomposition in the PPB solution is 65.22% for RH(HCl) and 84.19% for RH(NaOH) (Table 1). The maximum degree of O_{av} decomposition is observed in bleaching of RH(init): 92.89%.

A comparison of the rate constants of PPB decomposition (Table 1) shows that they are close in bleaching of the initial samples of RH and RS, 2.22×10^3 and 2.30×10^3 for τ = 15 min and 1.64×10^3 and 1.61×10^3 s^{-1} for τ = 30 min, respectively, and decrease with increasing duration of PPB action on the raw materials, irrespective of the pretreatment procedure.

Bleaching of RH subjected to alkaline or acid treatment proceeds without changes in the solution pH (Table 2), contrary to the solutions with the initial RH or RH treated with water, in which pH changes from 9.0 to 10.4. After bleaching, the weight of the cellulose product decreases, depending on the procedure of pretreatment of the raw materials, to 19.6%.

Thus, the study of bleaching of wastes from rice production with PPB shows that, in the presence of untreated RS and RH, the constant of O_{av} decomposition increases, whereas in the case of RS and RH pretreated with water and acid and alkali solutions, the rate constant of O_{av} decomposition decreases.

The spectrophotometric curves recorded before and after bleaching of the samples (Fig. 4, curves *1–4*) show that the reflection coefficient of bleached samples of RH and RS, ρ, increases. The highest ρ is observed for RS subjected to acid treatment and RH treated with alkali (Fig. 4, curves *2*, *4*). These data correlate with the maximum concentration of water-soluble substances extracted from raw material during its pretreatment and subsequent bleaching (Table 2).

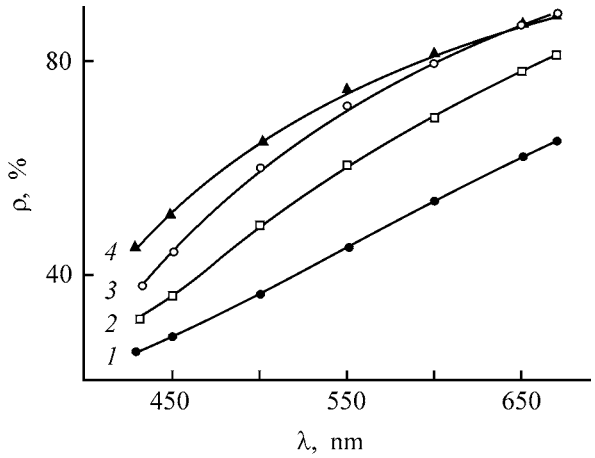


Fig. 4. Reflection coefficient ρ vs. wavelength λ for the samples of raw materials (Table 1) without and after bleaching. (*1*) Initial unbleached RH, (*2*) RH treated with NaOH and bleached with PPB (sample no. 11), (*3*) RS treated with NaOH and bleached with PPB (sample no. 7), and (*4*) RS treated with HCl and bleached with PPB (sample no. 6).

Thus, our study demonstrated that the use of PPB as a bleaching agent for wastes from rice production (straw and husk) is not only possible, but also efficient. The necessary condition for improvement of the whiteness of fibrous intermediates is pretreatment: acid for straw and alkaline for husk; in this case, RS is bleached more efficiently than RH. This pretreatment of the raw material is favorable for milder bleaching, due to the decrease in the rate of O_{av} decomposition in the solution. The data obtained allow recommendation of potassium peroxoborate in design of a new chlorine-free procedure for synthesis of cellulose-containing materials from wastes formed in rice production.

The kinetic studies of bleaching of plant raw materials with potassium peroxoborate were performed in the pH range 8.9–13 (the pH was adjusted by adding a NaOH solution to the system) for the systems with the best whiteness index, PBB + RS(HCl) and PPB + RH(NaOH). The results obtained are listed in Table 3.

The results of our study show that the pH affects the O_{av} decomposition in solution more strongly than does an increase in the bleaching duration. In the pH range 8.9–13, the O_{av} decomposition accelerates during a short period of time (τ = 5 min) for all the systems. The increase in pH from 10 to 12 in sys-

Table 3. Influence of pH on the rate constant of potassium peroxoborate decomposition in bleaching of rice straw and husk (T = 95°C, τ = 30 min)

Sample no.	System	pH	$k \times 10^{-3}$, s^{-1}			Degree of O_{av} decomposition, %		
			5 min	15 min	30 min	5 min	15 min	30 min
1	PPB without RS	8.9	0,40	1.84	1.35	11.46	81.03	91.31
		10.0	3.80	2.70	2.13	68.09	91.5	97.87
		12.0	7.70	3.06	1.86	90.07	93.62	96.45
		13.0	8.83	3.33	1.86	92.91	95.04	96.45
2	PPB + RH(NaOH)	9.3	0.32	1.52	1.02	9.10	74.71	84.19
		10.0	3.42	1.78	1.28	64.19	68.79	90.08
		12.0	7.93	3.51	2.14	90.77	95.71	97.87
		13.0	8.50	3.95	2.36	92.20	97.16	98.58
3	PPB + RS(HCl)	8.9	0.05	1.84	1.22	1.98	81.03	89.93
		10.0	1.11	2.64	1.59	28.37	90.78	94.33
		12.0	10.01	3.71	2.14	95.04	95.82	97.87
		13.0	11.37	4.08	1.98	96.74	97.45	97.23

tems 1 and 2 (Table 3) leads to a rise in the rate constants of decomposition by more than a factor of 2 (3.80×10^3 and 7.70×10^3, and 3.42×10^3 and 7.93×10^3 s^{-1}, respectively). The degree of O_{av} decomposition in the solution at given pH values is 68.09 and 90.07% for PPB without plant raw materials and 64.19 and 90.77% in bleaching of RH treated with alkali solution.

In bleaching of RS treated with HCl solution, a similar change in the solution pH results in an increase in the rate constant of O_{av} decomposition by an order of magnitude (1.11×10^3 and 10.01×10^3 s^{-1}, respectively, at pH 10 and 12, τ = 5 min). In this case, the degree of O_{av} decomposition is 28.37 and 95.04%, respectively.

Further increase in the solution pH to 13 only slightly affects the rate constants of decomposition for all the systems studied, since the available oxygen has decomposed practically completely. Therefore, an increase in the bleaching duration to 30 min at the same pH decreases the rate constant of O_{av} decomposition.

Thus, our studies showed that a pH not exceeding 12 is optimal for bleaching of plant raw materials.

CONCLUSIONS

(1) The kinetics of the thermal decomposition of high-peroxide potassium peroxoborate containing 20% of available oxygen in aqueous solutions in the course of bleaching of rice straw and husk was studied in relation to the type of raw materials, procedure of its pretreatment, solution pH, and process duration. It was found that potassium peroxoborate is efficient for bleaching of wastes from rice production.

(2) The straw treated with a solution of hydrochloric acid (the rate constant of available oxygen decomposition varies from 0.05×10^3 to 0.65×10^3 s^{-1}) and husk treated with alkali solution (the rate constant varies from 0.32×10^3 to 0.85×10^3 s^{-1}) are the most susceptible to oxidation. The optimum time interval of bleaching of the raw materials is 30 min.

REFERENCES

1. Sergienko, V.I., Zemnukhova, L.A., Egorov, A.G., et al., *Ross. Khim. Zh.*, 2004, vol. 48, no. 3, pp. 116–122.
2. Zemnukhova, L.A., Fedorishcheva, G.A., Egorov, A.G., and Sergienko, V.I., *Zh. Prikl. Khim.*, 2005, vol. 78, no. 2, pp. 324–328.
3. Zemnukhova, L.A., Egorov, A.G., Fedorishcheva, G.A., et al., *Neorg. Mater.*, 2006, vol. 42, no. 1, pp. 27–32.
4. Zemnukhova, L.A., Tomshich, S.V., Mamontova, V.A., et al., *Zh. Prikl. Khim.*, 2004, vol. 77, no. 11, pp. 1901–1904.
5. Kolzunova, L.G., Zemnukhova, L.A., Fedorishcheva, G.A., et al., *Zh. Prikl. Khim.*, 2000, vol. 73, no. 10, pp. 1644–1651.
6. Nelepin, Yu.N., *Tekhnologiya tsellyulozy* (Cellulose Production), Moscow: Lesn. Prom–st., 1990, vol. 2.
7. Medvedeva, E.N., Neverova, N.A., Khindy, S.O., et al., *Khim. Rast. Syr'ya*, 2001, no. 3, pp. 17–21.
8. Karetnikov, N.V., Pen, R.Z., Byvshev, A.V., and Taraban'ko, V.E., *Khim. Rast. Syr'ya*, 2002, no. 2, pp. 21–24.

9. Kolmakova, O.A., Pen, R.Z., Shapiro, I.L., et al., *Khim. Rast. Syr'ya*, 2003, no. 1, pp. 21–24.
10. Zemnukhova, L.A., Fedorishcheva, G.A., Egorov, A.G., et al., *Agrarn. Nauka*, 2005, no. 3, pp. 13–15.
11. Chernyshov, B.N., Brovkina, O.V., Kavun, V.Ya., and Pashnina, E.V., *Zh. Neorg. Khim.*, 1996, vol. 41, no. 11, pp. 1798–1802.
12. *GOST* (State Standard) *R 50672–94: Household Chemical Goods. Procedure of Determination of Weight Fraction of Available Oxygen: State Standards: Index*, Moscow: Izd. Standartov, 1996, vol. 3.
13. Emanuel', N.M. and Knorre, D.G., *Kurs khimicheskoi kinetiki* (Course of Chemical Kinetics), Moscow: Vysshaya Shkola, 1984.
14. *OST* (Branch Standard) *6-15-1616–90: Household Bleachers. Procedure of Determination of Bleaching Power: State Standards: Index*, Moscow: Izd. Standartov, 1996, vol. 3.

ISSN 1070-4272, Russian Journal of Applied Chemistry, 2006, Vol. 79, No. 10, pp. 1696–1699. © Pleiades Publishing, Inc., 2006.
Original Russian Text © L.K. Mal'kevich, L.Ya. Tsarik, 2006, published in Zhurnal Prikladnoi Khimii, 2006, Vol. 79, No. 10, pp. 1715–1719.

MACROMOLECULAR CHEMISTRY AND POLYMERIC MATERIALS

Wastes from Woodworking Industry as a Filler for a Cable Sheathing Compound

L. K. Mal'kevich and L. Ya. Tsarik

Irkutsk State University, Irkutsk, Russia

Received December 16, 2006

Abstract—The suitability of an alternative filler for a cable polyvinyl chloride plastic compound was studied. Physicomechanical, chemical, and relaxation properties and inflammability of plastic compound were analyzed in relation to the filler content.

DOI: 10.1134/S1070427206100284

Composites of wood and polyvinyl chloride (PVC) can be subdivided into two groups: composites based on polyvinyl chloride plastic and on plastic compounds [1]. Highly-filled composites for building industry have been developed [2].

As fillers for cable sheathing compounds we tested wastes from woodworking industry (WWI). The main attention was focused on the O-40 cable plastic compound for wire and cable sheaths, which is the product of deep processing of PVC.

In this study, we examined the effect of a filler alternative to chalk, the waste from woodworking industry, and developed the formulations of this plastic compounds.

EXPERIMENTAL

Fine sawdust (WWI) was taken because of its practical importance as filler of polymeric materials [3]. Fine sawdust meets the requirements to the fillers, such as filler purity, absence of inclusions, high dispersity, light color (which does not affect the pigment color), chemical stability, and low specific density.

Six formulations with various contents of sawdust filler were prepared under the conditions close to those used in the component ratios in these samples are listed in Table 1. The formulations with WWI filler were developed on the basis of the compositions of commercial plastic compounds containing suspension polyvinyl chloride of S 7058-M brand as binder. This binder is a homogeneous white powder without smell and taste; it is used in production of light- and heat resistant cable sheathing compounds, high-strength pipes, specialty linoleum, plasticized films, and artificial leather. Dioctyl phthalate (DOP), which is the main plasticizer for PVC, is a transparent colorless

Table 1. Component content in the composition

Sample no.	Composition, wt %						
	PVC	DOP	chalk	WWI	LOS	CaSt	Sb_2O_3
1	55	41.5	0	–	2	1	0.5
2	52.4	39.3	5.2	–	1.6	1	0.5
3	47	36	14	–	1.5	1	0.5
4	43	32.5	22	–	1	1	0.5
5	40	30	28	–	1	0.7	0.5
1	55	41.5	–	0	2	1	0.5
2	52.4	39.3	–	5.2	1.6	1	0.5
3	49.7	37.3	–	10	1.5	1	0.5
4	47	36	–	14	1.5	1	0.5
5	45	34	–	18	1.5	1	0.5
6	43	32.5	–	22	1	1	0.5

Table 2. Strength and relative elongation of the samples in comparison with GOST

Sample no.	Strength, MPa	Relative elongation, %
Chalk:		
1	11.19	332
2	11.66	322
3	12.53	319
4	12.73	303
5	12.89	265
Sawdust:		
1	11.3	330
2	10.8	289
3	9.7	263
4	9.6	258
5	9.2	221
6	9.1	218
Grade in accordance with GOST:		
extra	11.7	300
first	10.7	280

Table 3. Chemical stability of the samples containing chalk and sawdust*

Sample no.	On heating			At room temperature for 24 h					
	NaOH 40%	H_2SO_4 45%	HNO_3 60%	NaOH 40%	H_2SO_4 45%	HNO_3 60%	CH_3COOH 70%	NH_4OH	mixture of organic solvents
Chalk:									
1	S	S	S	S	S	S	S	S	S
2	S	S	S	S	S	S	S	S	S
3	S	S	R	S	S	S	S	S	S
4	S	S	U	S	S	S	S	S	S
Sawdust:									
1	S	S	S	S	S	S	S	S	S
2	S	S/B**	S	S/C	S	S/C	S	S	S
3	S/C***	S/B	S/C	S/C	S/B	S/C	S	S	S
4	S/C	S/B	S/C	S/C	S/B	S/C	S	S	S
5	S/C	S/B	S/C	S/C	S/B	S/C	S	S	S
6	S/C	S/B	S/C	S/C	S/B	S/C	S	S	S

* S, R, and U means stable, relatively stable, and unstable. ** Sawdust particles turn black. *** Solution is yellowish.

oily liquid with slight odor; bp 340°C (6 mm Hg), mp –40°C. The separated chalk (white powder) was used as filler for S 7058–M PVC. Light and thermal stabilization of PVC was performed using lead oxosulfate (LOS) $PbO \cdot PbSO_4 \cdot H_2O$ (white powder, mp 977°C, ρ 7.0–7.1, insoluble in water, greases, and oils). Calcium stearate $(CH_3(CH_2)_{16}COO)_2Ca$ (CaSt) is a PVC stabilizer, which can be used as a lubricant at PVC processing (white nontoxic powder, mp 175°C, density of technical-grade product 1.035). Antimony(III) oxide Sb_2O_3 (special-purpose fire-retardant additive) shifts the ignition point of PVC by 10°C. The sawdust (WWI) consists of yellowish particles (0.2–1.0 mm size and 11% moisture content).

Also, formulations were modified with various technological additives (lubricants, odorants), which, being added in amounts even smaller than the stabilizers, do not affect the polymer properties.

The resulting formulations were exposed to extrusion treatment at the laboratory of the Sayanskkhimplast Joint-Stock Company, and their strength and relative elongation at break were measured in accordance with GOST (State Standard) 11 262–80. In the course of the tests, the load and relative elongation at break were measured.

The chemical stability of the samples to various aggressive liquids was studied; three samples of each plastic compound were placed in 40% NaOH, 45% H_2SO_4, 60% HNO_3, 70% CH_3COOH, NH_4OH and some household solvents; after 1-day exposure, changes in the samples were analyzed.

In this study, we examined the effect of the new filler on the inflammability of the plastic compound, using sample no. 3 with chalk, and nos. 3 and 4 with sawdust. The inflammability group of the samples was determined in accordance with GOST 12.1.044–89 on an OTM device. The combustion delay was measured with a stopwatch at the instant of attainment of the self-combustion. The electrical resistivity of the coke residues of the burnt polymer materials was measured using an experimental setup consisting of a press, a press mold, and an ohmmeter.

The relaxation properties upon deformation of the composites were studied on a tensile-testing machine in accordance with the procedure described elsewhere [4].

The optimal composition of OP-40 sheathing compound is as follows (wt %): PVC 43.75, DOP 31.65, chalk 22.2, LOS 1.18, CaSt 0.8, and Sb_2O_3 0.42. In the first stage of the study, we examined the samples with different contents of chalk. New formulations were prepared by substitution of chalk with fine sawdust (Table 1).

The results of the first stage of our study showed a direct dependence of the compound properties on the content of the common filler (chalk). The data on the strength and relative elongation are listed in Table 2. Comparison of the results for the composites containing sawdust with GOST showed that sample nos. 3–6 (Table 1) are unsuitable for preparing sheathing compounds.

Changes in the sample properties after chemical treatment are shown in Table 3. Among the samples

Table 4. Time τ of attainment of the indicated combustion gas temperature

Sample no.	Time τ, s, of attainment of attainment of indicated temperature, °C					
	200	250	300	350	400	600
3, chalk	66	79	84	88	90	100
3, sawdust	52	70	81	87	91	99
4, sawdust	71	86	91	105	107	113

containing chalk, sample no. 4 with the highest chalk content appeared to be the most unstable to nitric acid. Sample nos. 1 and 2 are the most stable to chemical treatment, but sample no. 1 contains no chalk. All the samples containing sawdust were stable to degradation. Thus, addition of the sawdust filler does not affect the chemical properties of the plastic compound, whose integrity and initial shape do not change in both concentrated acids and alkalis. This phenomenon is independent of the sawdust content. When immersed in concentrated solutions, the sawdust either becomes charred in concentrated sulfuric acid or swells in NaOH and HNO_3; as a result, the solution acquires the natural color of the wood fiber. The optimal chemical properties (i.e., the highest chemical stability) among the samples containing the new filler are exhibited by sample no. 2.

Polyvinyl chloride cable plastic compound is designed to prepare wire and cable sheaths that operate, depending on the plastic compound brand and design of the wire and cable, at temperatures of –60 to +70°C, and to 105°C for IT-105 compound. It is known that the main disadvantage of many plastics is their instability under heat treatment. Soft PVC plastics (plasticized PVC, plastisols) contain considerably larger amounts of more inflammable plasticizing agents than do rigid plastics (polyvinyl chloride plastic). In this study, we examined inflammabil-ity of materials in relation to the content of the new filler using sample no. 3 with chalk and nos. 3 and 4 with sawdust (Table 1).

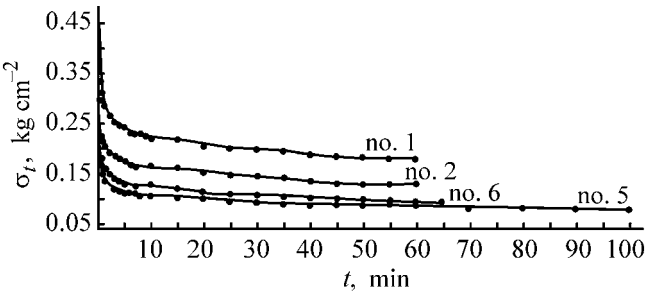


Fig. 1. Stress relaxation curves for sample nos. 1, 2, 5, and 6 containing sawdust. (σ_t) Stress and (t) time.

The combustion delay for the samples studied was as follows, s: no. 3 (chalk) 17, no. 3 (sawdust) 14, and no. 4 (sawdust) 13. With increasing combustion delay, the inflammability of the material decreases. As seen, the combustion delay decreases in the series of samples studied, which is obviously due to the increasing content of the combustible material in the PVC composite. As can be seen from the test for the inflammability group, the weight loss of all the three samples exceeded 60% [76.3, 86.7, and 85.8% for sample nos. 3 (chalk), 3 (sawdust), and 4 (sawdust), respectively], i.e., the resulting composites belong to the class of highly inflammable and combustible materials. The maximal temperatures of the flue gas and the time of their attainment are listed in Table 4. With increasing sawdust content, the time of the sample heating becomes longer. This is probably due to the fact that the sawdust particles, being charred upon heating, form some "insulation" barrier preventing transport of the pyrolysis products into the combustion area. The heat is also consumed for the release of water and its evaporation. The water vapor hinders diffusion of atmospheric oxygen to the combustion area, and thus decelerates degradation.

The electrical resistivity of the coke residue of the polymeric materials was as follows (mΩ): 25, 1000, and 500 for sample nos. 3 (chalk), 3 (sawdust), and 4 (sawdust), respectively. The slowest temperature increase was observed for sample no. 4, and its specific electrical resistivity is lower than that of sample no. 3.

The equilibrium and relaxation moduli and relaxation time of the samples containing chalk were E_∞ 0.28–0.45 kg cm^{-2}, E_{rel} 0.675–1.17 kg cm^{-2}, and τ 6.1–9.3 s. The experimental data on the samples containing sawdust are shown in Fig. 1. The equilibrium and relaxation moduli and relaxation time of the samples containing sawdust were E_∞ 0.28–0.39 kg cm^{-2}, E_{rel} 0.66–0.90 kg cm^{-2}, and τ 8.4–14.4 s.

On adding solid fillers, the mobility of macromolecules in the boundary layer decreases due to steric hindrance caused by the solid surface and interaction of the polymer with this surface. This changes the re-

laxation properties. A decrease in the molecular mobility upon filling makes longer the average relaxation time; it increases with the degree of filling and filler dispersity and with decreasing flexibility of macromolecules.

Since addition of the filler not only changes the properties of the composite but also reduces its price, we calculated the per ton cost of all the samples. Sample no. 4 was the least expensive among the composites containing chalk. Since the sawdust is a waste from woodworking industry (i.e., no special production is required), only the transport charges should be taken into account in production of plastic compounds filled with sawdust. Sample no. 6 with the highest content of sawdust is the least expensive material.

It should be noted that sample no. 4 is the least expensive among all the composites studied, though its stability with respect to chemical treatment is the lowest. Hence, composite no. 4 can be used for preparing plastic compounds to be used in nonaggressive media, and this production would be profitable. Plastic compounds prepared from composite nos. 1 and 2 (Table 1) can operate in aggressive media, but it should be noted that the strength of sample no. 1 corresponds only to the first grade, and plastic compound prepared from these composites would require greater capital investments.

The composites were selected taking into account not only the economic parameters but also the plastic compound properties. In this study, the compound quality of the plastic was evaluated using only two parameters (strength and relative elongation at break) taken from GOST 5960–72 for the plastic compound of O–40 brand. Chemical characteristics also affect the sample quality. Thus, the quality of a plastic compound was assessed in our studies by its strength, relative elongation, and chemical stability. All these three parameters are summarized in Fig. 2 relative to sample no. 1, whose strength, relative elongation, and chemical stability were taken as unity.

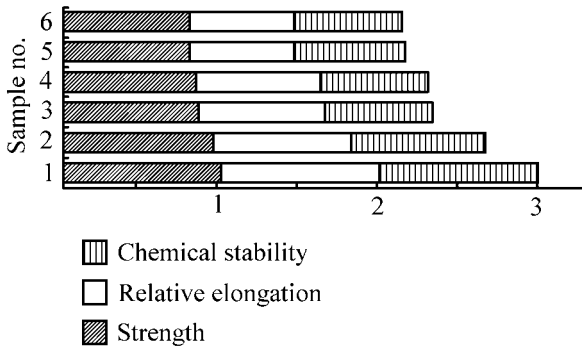


Fig. 2. Mechanical properties and chemical stability of the samples Sample no. 1–6.

As can be seen from Fig. 2, sample no. 1 exhibits the best properties, but it contains no filler, which is an essential drawback, because the filler is an obligatory component of the plastic compounds. Among all the other samples, sample no. 2 containing sawdust (5.2 wt %) is the best (Table 1).

CONCLUSIONS

Polyvinyl chloride is compatible with a new filler, waste from woodworking industry. Sawdust can be used as a filler of O-40 plastic compound. The effect of the filler content on the properties of the plastic compound was examined.

REFERENCES

1. Sangalov, Yu.L., Krasumina, N.A., and Il'yasova, A.I., *Khim. Prom–st.*, 2002, no. 3, pp. 1–10.
2. Tikhonov, N.N., *Plast. Massy*, 2000, no. 9, pp. 41–43.
3. Vorob'eva, G.Yu., *Khimicheskaya stoikost' polimernykh materialov* (Chemical Stability of Polymeric Materials), Moscow: Khimiya, 1981.
4. Antipina, A.D., Banatskaya, M.I., Baranovskii, V.Yu., et al., *Praktikum po vysokomolekulyarnym soedineniyam* (Practical Course of Macromolecular Compounds), Moscow: Khimiya, 1985.

ISSN 1070-4272, Russian Journal of Applied Chemistry, 2006, Vol. 79, No. 10, pp. 1700–1704. © Pleiades Publishing, Inc., 2006.
Original Russian Text © B.A. Zaitsev, G.I. Khramova, I.D. Shvabskaya, I.V. Balanina, 2006, published in Zhurnal Prikladnoi Khimii, 2006, Vol. 79, No. 10, pp. 1720–1724.

MACROMOLECULAR CHEMISTRY AND POLYMERIC MATERIALS

Alkali Resistance of Cured Rolivsans and Glass-Reinforced Plastics Based on Them

B. A. Zaitsev, G. I. Khramova, I. D. Shvabskaya, and I. V. Balanina

Institute of Macromolecular Compounds, Russian Academy of Sciences, St. Petersburg, Russia

Received April 25, 2006

Abstract—The effect of strongly alkaline media on the strength and heat resistance of thermosetting polymers and plastics prepared by thermal transformations of Rolivsans (cross-linking and cyclizing polyfunctional aromatic ethers with terminal styrene and methacrylate groups) was studied.

DOI: 10.1134/S1070427206100296

Rolivsans, thermosetting castable resins of a new type, are used for preparing various polymeric and composite materials highly resistant to heat and to aggressive agents, including hot sulfuric acid and solutions of HF [1–7]. Rolivsans are low-viscosity (containing no solvents) unsaturated monomer–oligomer systems formed by chemical transformations of di[4-(1-hydroxyethyl)phenyl] ether with methacrylic acid, catalyzed by strong acids [3, 8–10].

When heated to 120–250°C and higher temperatures, Rolivsans are cured to form heat-resistant network polymers. The first step of thermal curing (120–170°C) involves three-dimensional radical copolymerization of unsaturated monomeric and oligomeric components via terminal methacrylate and styrene-like (vinylaromatic) groups, to give a primary polymer network. Heating to 170–220°C induces cleavage of methacrylate cross-links to give, first, methacrylic acid units and then tetralone and anhydride units (polycyclization) in the course of solid-phase rearrangements. The formation of the final heat-resistant structure of cured Rolivsans is complete at 240–260°C; the resulting nonporous polymers and plastics exhibit high hardness and heat resistance [11–13].

It is known that common heat-resistant heterocyclic polymers (e.g., aromatic polyimides, bismaleimides, polycyanurates), which are widely used in modern engineering, show poor hydrolytic stability, especially in alkaline media [14, 15]. The practical interest in alkali-resistant polymeric materials is also associated with the use of rods of glass-reinforced plastics based on polyester resins in concrete structures in building. These rods have certain advantages over the common steel reinforcement. However, concretes and cements undergo hydration in the course of service, which gives rise to an alkaline medium (pH ~12) exerting a prolonged destructive effect on the polyester binder [7].

We expected that the high cross-linking density and high content of aromatic and tetralone rings in the structure of cured Rolivsans would enhance the hydrolytic stability of these thermosets and of reinforced plastics based on them. To evaluate the alkali resistance of these materials, we examined their behavior in alkaline solutions.

EXPERIMENTAL

Experiments were performed with Rolivsan samples prepared according to [10]. Their characteristics are listed in Table 1. Exclusion liquid chromatography of Rolivsan samples was performed with a Waters gel permeation chromatograph at 20°C, using columns packed with Ultrastyrogel (500 Å) and toluene as eluent. The number-average molecular weights $\bar{M}_n$ were determined with a Hitachi–Perkin–Elmer 115 vapor osmometer. The unsaturation of the samples was evaluated with an ADS-3 ozonizer at 0°C, solvent CCl_4.

The cured (cast) samples were prepared by casting into brass molds, and glass-reinforced plastics, by hot pressing of T-10-80 glass fabric sheets impregnated with Rolivsans in a mold at a pressure of 1 kgf cm^{-2}, followed by thermal curing in the temperature range 150–260°C at a heating rate of 5 and 7 deg h^{-1}. The shear elastic modulus G' and mechanical loss

Table 1. Characteristics of Rolivsan samples

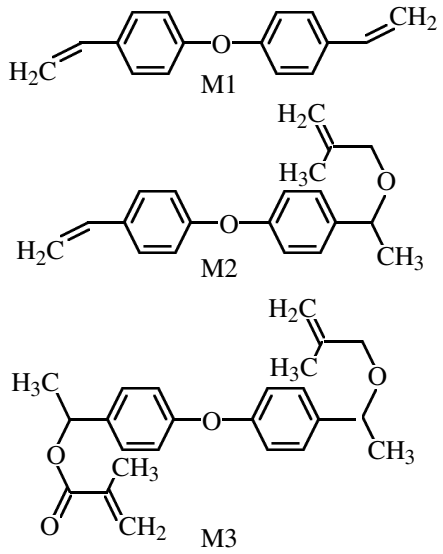
Composition	Component content, wt %					>C=C<*	$\overline{M}_n$	n_D^{20}	η^{25}, cP
	M1	M2	M3	OL	$Ar(OH)_n$				
I	14 ± 3	16 ± 4	20 ± 4	49 ± 5	1 ± 0.1	0.55	450	1.599	3800
II	14 ± 3	23 ± 4	23 ± 4	39 ± 5	1 ± 0.1	0.56	420	1.592	2500

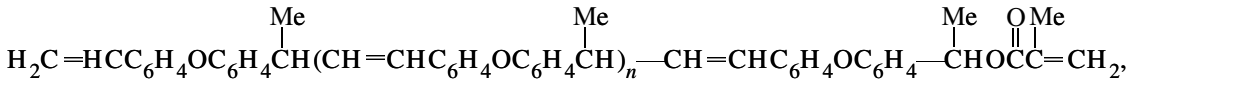
* Mol >C=C< per 100 g of product.

tangent tan δ were measured with a reverse torsion pendulum with an oscillation frequency of 0.25–0.50 Hz in the temperature range 15–400°C; the sample size was (36–38) × (4.2–5.6) × (1.7–2.0) mm.

To test the samples for alkali resistance, we prepared a standard alkaline buffer (pH 12) from aqueous solutions of NaOH (0.1 M), NH_2CH_2COOH (0.1 M), and NaCl (0.1 M). The samples were cut into 40 × 2.5 × (1.0–1.5)-mm strips, weighed, and placed in flasks containing alkaline buffer solutions; each flask was connected to a reflux condenser and to a tube packed with CaO to prevent penetration of CO_2 into the system in the course of prolonged tests. Samples were kept in the alkaline solution at room temperature; for prompt evaluation of the hydrolytic stability, samples were additionally heated at the boiling point (~102°C) for a definite time. Then the samples were washed with distilled water, dried to constant weight, and weighed, after which the breaking bending stress was measured and compared to the initial value.

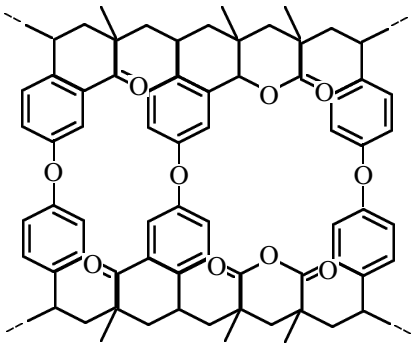
As shown in [3, 9–11], Rolivsans consist of the following unsaturated aromatic compounds:





and also of antioxidants (products of alkylation of phenolic compounds with monomers M1 and M2 and with oligomer OL).

Thermal transformations of Rolivsans and their components M2 and M3 (cross-linking, polycyclization) yield thickly cross-linked glassy polymers having the following polycyclic structure [11, 13]:



Preliminarily finely divided (powdered) samples of cured Rolivsan and a model polymer prepared by three-dimensional polymerization of M2 were treated with aqueous–dioxane solutions of KOH at the boiling point for 7 h. An IR study of the samples before and after the treatment confirmed the stability of the chemical structure (backbones, tetralone units, diphenyl oxide bridges) of the cured Rolivsan and model polymer (poly-M2), despite severe testing conditions [3, 16].

The characteristics of the initial Rolivsans used for preparing glassy (nonporous) polymers and glass-reinforced plastics are listed in Table 1. Tables 2 and 3 show how alkaline solutions affect the strength of the block polymers and glass-reinforced plastics prepared from Rolivsans of various compositions. To accelerate the hydrolytic degradation, samples were kept for various intervals of time at room temperature and additionally at the boiling point of the alkaline solution.

Table 2. Effect of the alkaline medium (pH 12) on the strength of cured Rolivsans

Conditions of alkaline treatment, time, days/T, °C	τ^*, days (years)	σ_b^{20}, MPa	C,** %	Weight gain, %	σ_b^{20}, MPa	C,** %	Weight gain, %	σ_b^{20}, MPa	C,** %	Weight gain, %
	Composition I***				Composition II***			Composition I****		
–	0 (0)	145 ± 6	100	0.0	130 ± 7	100	0.0	80 ± 10	100	0.0
10/20 + 1/102	270 (0.74)	152 ± 10	105	1.8	145 ± 15	112	2.1	–	–	–
17/20 + 2.2/102	560 (1.54)	140 ± 10	97	1.9	100 ± 10	77	2.1	–	–	–
105/20 + 6/102	1640 (4.5)	–	–	–	–	–	–	66 ± 2	83	2.2

* Time of alkaline treatment at 20°C (semiquantitative estimation by the van't Hoff rule [19]), calculated from the preset conditions of accelerated alkaline aging of polymer samples at 20 and 102°C.

** Relative strength $C = 100\sigma_t^{20}/\sigma_0^{20}$, where σ_t^{20} and σ_0^{20} are the breaking bending stresses before and after alkaline treatment, respectively.

*** Cured at a heating rate of 5 deg h^{-1}.

**** Cured at a heating rate of 7 deg h^{-1}.

It could be expected [15] that alkaline treatment would induce hydrolytic degradation leading to a decrease in the strength of network polymers and plastics prepared by curing of Rolivsans. However, it should be borne in mind that cured Rolivsans having a high network density and containing mainly low-polarity units and groups do not noticeably swell in water and weakly swell in the majority of common solvents [3, 17, 18]. Therefore, the effect of an alkaline buffer solution containing surfactants on the strength of the polymers and plastics could be primarily associated with the adsorption of surfactants [15]. The subsequent hydrolytic degradation occurred mainly under the external diffusion–kinetic control, i.e., in the surface layers of the polymer sample.

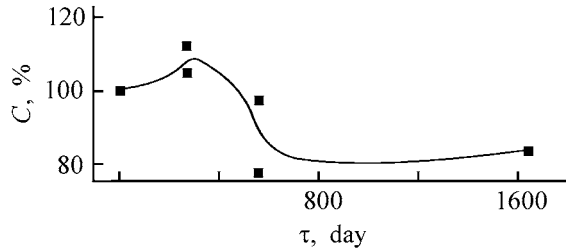


Fig. 1. Relative strength C of cured Rolivsans vs. time τ of their treatment with an aqueous buffer solution (pH 12) at 20°C, according to data from Table 2.

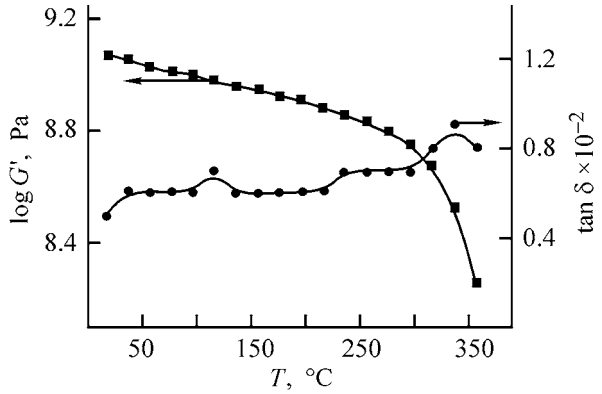


Fig. 2. Dynamic shear modulus log G' and mechanical loss tangent tan δ vs. temperature T for composition II thermally cured at a heating rate of 5 deg h^{-1}.

Table 2 shows that a combined (accelerated) action of the alkaline solution by alternating prolonged keeping at room temperature and boiling (equivalent time of testing at 20°C, estimated by the van't Hoff rule [19], varies from 9 months to 4.5 years) does not lead to failure of the thermosets. The cast samples still preserve a high strength. Furthermore, the strength even appreciably increases during the first 9 months of alkaline treatment, after which it starts to gradually decrease, i.e., the relative strength passes through a maximum (Fig. 1). A similar effect of an original increase in strength under the action of chemically active media has been described in the literature [15]. In the given case, this can be explained as follows. As can be seen from the results of a dynamic mechanical analysis (DMA) (Fig. 2), cured Rolivsans are rigid (low mechanical loss tangent) and have high heat resistance (~340°C). Apparently, they contain microcracks which give rise, under an applied force, to increased local stresses and appearance of a main crack, which causes

Table 3. Effect of alkaline medium (pH 12) on the strength of glass-reinforced plastics based on Rolivsans

Conditions of alkaline treatment, time, days/T, °C	τ, days (years)	σ_b^{20}, MPa	C, %	σ_b^{250}, MPa	C, %	σ_b^{20}, MPa	C, %	σ_b^{250}, MPa	C, %
	Composition I*					Composition I**			
–	0 (0)	620 ± 40	100	280 ± 15	100	620 ± 50	100	350 ± 25	100
105/20 + 6/102	1641 (4.5)	400 ± 50	65	320 ± 15	114	300 ± 50	48	260 ± 10	74

* Cured at a heating rate of 7 deg h^{-1}.

** Cured at a heating rate of 5 deg h^{-1}.

failure of the sample. Thus, microcracks impair the strength of a sample whose external layers are subject to extension at bending. Base hydrolysis induces cleavage of ester cross-links and opening of anhydride rings on the sample surface, which decreases the network density and improves the deformation-strength properties of the surface layers. Such a chemical modification of the surface does not promote formation of new microcracks but, by contrast, leads to erosion of the edges of the already existing microcracks. In the process, the local stresses decrease and become more uniformly distributed over the sample surface. The decrease in the breaking force with the further progress of degradation (hydrolysis) is apparently due to a decrease in the cross section of the polymer sample.

As expected, glass-reinforced plastics were found to be more sensitive than the block (unfilled) polymers to the effect of an alkali medium (Table 3), because the reinforcing aluminoborosilicate glass fibers of the glass fabric (E glass) degrade under the action of acids and alkalis [20]. Nevertheless, glass-reinforced plastics still retain no less than a half of their initial strength (σ_0^{20} 20) after prolonged treatment (~4.5 years) with an alkaline solution. Apparently, the access of an alkali to glass fibers coated with the binder (cured Rolivsan) is strongly hindered. Table 3 also shows that the breaking bending stresses of the glass-reinforced plastic before and after the alkaline treatment, with loading at 250 (σ_0^{250}, σ_t^{250}) and 20°C (σ_0^{20}, σ_t^{20}), essentially differ. It was noted above that a decrease in the polymer network density and erosion of microcracks in the surface layers after alkaline treatment lead to a decrease in the local glass transition points and, as a result, to the surface plasticization in high-temperature tests. Therefore, a seemingly unexpected trend is observed (Table 3): The hydrolytic degradation of the plastic can result in an appreciable enhancement of its high-temperature strength (or in its slight decrease).

CONCLUSIONS

(1) Heat-resistant network polymers and plastics prepared by thermal curing of Rolivsans exhibit high hydrolytic resistance in a strongly alkaline medium. After keeping at 20°C for 105 days, combined with refluxing at 102°C for 6 days in aqueous-alkaline buffer solutions (pH 12), the plastics still retain approximately 50–80% of their initial bending strength.

(2) Alkaline treatment under certain conditions noticeably enhances the strength of cured Rolivsans and glass-reinforced plastics based on them. The effect is caused by partial hydrolytic degradation of cross-links in the surface layers of the plastics, leading to a decrease in the polymer network density, in the concentration of microcracks (with their partial elimination), and in the local glass transition points. As a result, surface plasticization is observed, increasing the breaking bending stress in high-temperature tests.

REFERENCES

1. Zaitsev, B.A., Khramova, G.I., Dantsig, L.L., et al., *Plast. Massy*, 1981, no. 9, pp. 12–13.
2. Zaitsev, B.A., Khramova, G.I., Tsygankova, G.S., et al., *Mekh. Kompoz. Mater.*, 1982, no. 5, pp. 775–778.
3. Zaitsev, B.A., Regular Trends in Formation, Structure, and Properties of Heat-Resistant Network Polyarylenes, *Doctoral Dissertation*, Leningrad, 1983.
4. Zaitsev, B.A., in *Sintez, struktura i svoistva polimerov* (Synthesis, Structure, and Properties of Polymers), Leningrad: Nauka, 1989, pp. 66–77.
5. Zaitsev, B.A., *Polym. Mater. Sci. Eng.*, 1992, vol. 66, pp. 70–71.
6. Zaitsev, B.A., Abstracts of Papers, *XVI Mendeleevskii s''ezd po obshchei i prikladnoi khimii* (XVI Mendeleev Congr. on General and Applied Chemistry), St. Petersburg, May 25–29, 1998, Moscow, 1998, no. 2, pp. 304–305.

7. Zaitsev, B.A., Tsygankova, T.S., and Khramova, G.I., Abstracts of Papers, *VII Mezhdunarodnaya konferentsiya po khimii i fizikokhimii oligomerov "Oligomery-2000"* (VII Int. Conf. on Chemistry and Physical Chemistry of Oligomers "Oligomers-2000"), Perm, September 4–8, 2000, Moscow–Perm–Chernogolovka, 2000, p. 330.
8. Zaitsev, B.A., Khramova, G.I., and Dantsig, L.L., *Vysokomol. Soedin., Ser. A*, 1982, vol. 24, no. 12, pp. 2467–2474.
9. Zaitsev, B.A., Dantsig, L.L., and Khramova, G.I., *Zh. Org. Khim.*, 1983, vol. 19, no. 11, pp. 2340–2349.
10. Zaitsev, B.A., Khramova, G.I., and Tsygankova, T.S., *Zh. Prikl. Khim.*, 2003, vol. 76, no. 4, pp. 658–662.
11. Zaitsev, B.A., Abstracts of Papers, *VIII Mezhdunarodnaya konferentsiya po khimii i fizikokhimii oligomerov "Oligomery-2002"* (VIII Int. Conf. on Chemistry and Physical Chemistry of Oligomers "Oligomers-2002"), Chernogolovka, September 9–14, 2002, Moscow–Chernogolovka, 2002, p. 193.
12. Zaitsev, B.A., Khramova, G.I., and Tsygankova, T.S., *Zh. Prikl. Khim.*, 2003, vol. 76, no. 10, pp. 1708–1714.
13. Zaitsev, B.A., Khramova, G.I., Tsygankova, T.S., et al., *Plast. Massy*, 2003, no. 10, pp. 23–25.
14. Buhler, K.-U., *Spezialplaste*, Berlin: Akademie, 1978.
15. Moiseev, Yu.V. and Zaikov, G.E., *Khimicheskaya stoikost' polimerov v agressivnykh sredakh* (Chemical Resistance of Polymers in Aggressive Media), Moscow: Khimiya, 1979.
16. Zaitsev, B.A., Khramova, G.I., Tsygankova, T.S., et al., *Acta Polym.*, 1985, vol. 36, no. 10, pp. 527–530.
17. Zaitsev, B.A., Kiseleva, R.F., Garkavi, S.L., and Kalyuzhnaya, L.M., *Mekh. Kompoz. Mater.*, 1986, no. 4, pp. 590–594.
18. Zaitsev, B.A., Kiseleva, R.F., and Garkavi, S.L., *Crosslinked Epoxides*, Sedlacek, B. and Kahovek, J., Eds., Berlin: Walter de Gruyter, 1987, pp. 517–524.
19. Eremin, E.N., *Osnovy khimicheskoi kinetiki* (Fundamentals of Chemical Kinetics), Moscow: Vysshaya Shkola, 1976.
20. *Handbook of Composites*, Lubin, G., Ed., New York: Van Nostrand Reinhold, 1982.

ISSN 1070-4272, Russian Journal of Applied Chemistry, 2006, Vol. 79, No. 10, pp. 1705–1708. © Pleiades Publishing, Inc., 2006.
Original Russian Text © A.V. Boldashevskii, Zh.K. Tukhmetova, Sh.B. Kasenova, S.M. Adekenov, A. Nukhuly, B.K. Kasenov, A.M. Gazaliev, S.D. Fazylov, 2006, published in Zhurnal Prikladnoi Khimii, 2006, Vol. 79, No. 10, pp. 1725–1727.

BRIEF COMMUNICATIONS

Thermochemistry of Potassium Morpholinodithiocarbamate

A. V. Boldashevskii, Zh. K. Tukhmetova, Sh. B. Kasenova, S. M. Adekenov, A. Nukhuly, B. K. Kasenov, A. M. Gazaliev, and S. D. Fazylov

Institute of Phytochemistry, Karaganda, Republic of Kazakhstan
Institute of Organic Synthesis and Coal Chemistry, Karaganda, Republic of Kazakhstan
Pavlodar University, Pavlodar, Republic of Kazakhstan

Received March 24, 2006

Abstract—Results of thermochemical studies of a new compound, potassium morpholinodithiocarbamate, are presented. The enthalpies of its solution in water at various dilutions and the specific heat at 173–348 K were examined by the experimental methods of isothermal and dynamic calorimetry.

DOI: 10.1134/S1070427206100302

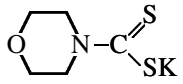
Bioactive substances forming the basis of medicinals are of particular importance for the human life. To compounds of this kind also belong morpholine derivatives, which occupy a prominent place among the known analgesics, antiarrythmatics, antidepressants, etc. [1].

Studies of the thermodynamic properties of bioactive substances and their derivatives are of high theoretical and practical importance for their directed synthesis and for revealing the relationship between their structural and energy-related characteristics.

In this context, we performed a calorimetric study to determine the enthalpies of solution in water of a new compound, potassium morpholinodithiocarbamate, and its specific heat in the temperature range 173–348 K.

EXPERIMENTAL

The sample under study was potassium morpholinodithiocarbamate[1] of chemically pure grade, T_{decomp} = 230°C, empirical formula $C_5H_8NOS_2K$, molecular weight 201.3434. The structural formula of the compound is as follows:



The enthalpy of solution of this compound was studied on a DAK-I-IA automated differential calorimeter under isothermal conditions (25°C) at various dilutions (1 : 18000, 1 : 36000, and 1 : 72000 moles of compound per moles of water). The theory and practice of calorimetric studies was described in detail in [2–5]. The technical parameters of the calorimeter are as follows: working temperature range 25–200°C, ampule volume 8 cm^3, sensitivity in the mode of a direct measurement of the thermal electromotive force not worse than 0.012 μV, error in measurement of heat effects not exceeding 2.0%. Heat effects were recorded with a KSP-4 potentiometer, and also using an IP-4 precision integrator. The time of preliminary thermostating was 2 h. The substance under study was placed in a metallic ampule, which was inserted into a metallic cartridge with the solvent.

The operation of the device was checked by measuring the enthalpy of solution of thrice recrystallized KCl at dilutions of 1 : 1600, 1 : 2400, and 1 : 3200 (moles of salt per moles of water). The value obtained at 25°C, ΔH_{sol} = 17780 ± 262 J mol^{-1}, is in a good agreement with the reference values reported in [6, 7].

The experimental errors and the homogeneities of their variances were calculated using the Student and Cochran criteria [8].

The significance level of the criteria employed was 5%. The regression line had the following parameters:

[1] Synthesized at the Institute of Organic Synthesis and Coal Chemistry, Karaganda, Republic of Kazakhstan.

Table 1. Enthalpy of solution of potassium morpholinodithiocarbamate in water at various dilutions

Dilution (moles of compound per moles of water)	Weighed portion of $C_5H_8NOS_2K$, g	ΔH_{sol}, J	ΔH^m_{sol}, kJ mol^{-1}
1 : 18000	0.0031	1.0853	70.49
	0.0031	1.0907	70.84
	0.0031	1.0733	69.71
	0.0031	1.0744	69.78
	0.0031	1.0938	71.04
	$\Delta\overline{H}^m_1 = 70.37 \pm 0.75$		
1 : 36000	0.0015	0.4952	66.47
	0.0015	0.4921	66.05
	0.0015	0.4901	65.78
	0.0015	0.4911	65.92
	0.0015	0.4935	66.24
	$\Delta\overline{H}^m_2 = 66.09 \pm 0.34$		
1 : 72000	0.0008	0.2487	62.59
	0.0008	0.2459	61.89
	0.0008	0.2473	62.24
	0.0008	0.2482	62.47
	0.0008	0.2454	61.76
	$\Delta\overline{H}^m_3 = 62.19 \pm 0.45$		

$a_0 = 1.820$, $b_0 = 22.41$, $a = 1.780$. The sought-for regression equation has the form

$$Y = 1.780 + 22.41x.$$

The linearity hypothesis is satisfied by the inequality $F_{exp} = 40.97 < 243.9$.

As the optimal confidence probability was chosen $\alpha = 0.95$.

Table 1 lists the results of a calorimetric analysis of the enthalpies of solution in water of the compound under study.

As can be seen in Table 1, an endothermic effect is observed in dissolution of potassium morpholinodithiocarbamate in water, which demonstrates predominance of the energy of the crystal lattice over that of solvation of the constituent ions of the compound.

Further, the experimentally obtained average values of the enthalpies of solution of the compound under study at the specified dilutions were extrapolated to infinite dilution to calculate the standard enthalpy of solution of the compound in an infinitely diluted aqueous solution. According to [9], $\Delta H^m_{sol} = f\sqrt{m}$ (m is the molal concentration). Based on the data obtained, we found that the dependence of the enthalpy of solution (kJ mol^{-1}) of potassium morpholinodithiocarbamate on the molal concentration is described by the expression

$$\Delta H^m_{sol} = 54.18 + 295.17\sqrt{m}. \quad (1)$$

The standard enthalpy of solution of $C_5H_8NOS_2K$ in an infinitely diluted aqueous solution is 54.2 ± 0.4 kJ mol^{-1}.

The specific heat of potassium morpholinodithiocarbamate was studied with an IT-S-400 dynamic calorimeter in the temperature range 173–348 K. Liquid nitrogen was used as a cooling agent. The duration of measurements covering the whole temperature range, including experimental data processing, was about 2.5 h. The maximum rated error of the device was ±10%. The device was calibrated by determining the thermal conductivity K_{th} of the heat meter [10, 11]. For this purpose, several runs were performed with a copper sample and empty ampule.

The specific heat was measured in accordance with the technical characteristics of the device at intervals of 25 K.

A sample to be studied was placed in the metallic ampule of the measuring cell and heated by the continuous flow of heat through the heat meter. The time lag of the ampule temperature with respect to the base temperature was measured at intervals of 25 K.

As in the case of calibration, five parallel runs were performed with the compounds under study at each temperature (at 25-K intervals). The results obtained were averaged and processed by the methods of mathematical statistics [8].

At each measurement temperature, the root-mean-square deviation $\overline{\delta}$ was calculated for the averaged values of the specific heat, and the random component of the error, $\mathring{\Delta}$, was determined for molar values of the specific heat.

The results obtained in the study of the specific heat are listed in Table 2.

Table 2. Specific heat ($C_p \pm \bar{\delta}$) and mole heat capacity ($C_p^0 \pm \mathring{\Delta}$) of potassium morpholinodithiocarbamate

T, K	$C_p \pm \bar{\delta}$, J g^{-1} K^{-1}	$C_p^0 \pm \mathring{\Delta}$, J mol^{-1} K^{-1}	T, K	$C_p \pm \bar{\delta}$, J g^{-1} K^{-1}	$C_p^0 \pm \mathring{\Delta}$, J mol^{-1} K^{-1}
173	0.6977 ± 0.0138	140 ± 8	273	0.8596 ± 0.0231	173 ± 13
198	0.7244 ± 0.0208	146 ± 12	298.15	0.9955 ± 0.0268	200 ± 15
223	0.7557 ± 0.0198	152 ± 11	323	1.0673 ± 0.0224	215 ± 13
248	0.8148 ± 0.0163	164 ± 9	348	1.1047 ± 0.0281	222 ± 16

The data in Table 2 were used to derive the equation describing the temperature dependence of the specific heat of the compound in the temperature range under study (J mol^{-1} K^{-1})

$$C_p^0 = -(86.3 \pm 5.84) + (825.7 \pm 55.9) \times 10^{-3}T + (25.1 \pm 1.70) \times 10^5 T^2. \quad (2)$$

To calculate the standard enthalpy of formation of potassium morpholinodithiocarbamate, we first estimated its standard heat of combustion by the Karas and Frost methods [12], which are the best suitable for taking into account the contributions of various groups to the heat of combustion. The averaged enthalpy of combustion of $C_5H_8NOS_2K$ in the liquid state, found by these two methods, is –3024 ± 82 kJ mol^{-1}.

Using the average value of the enthalpy of combustion by the reaction

$$2C_5H_8NOS_2K_{(l)} + 17.5O_{2(g)} = 10CO_{2(g)} + 8H_2O_{(l)} + N_{2(g)} + 4SO_{2(g)} + K_2O_{(s)} - \Delta H^0_{comb} \quad (3)$$

we calculated, on the basis of the Hess cycle, the value of $\Delta_f H^0_{298.15}$ for $C_5H_8NOS_2K_{(l)}$, equal to –541.3 kJ mol^{-1}. The values of $\Delta_f H^0_{298.15}$ for $CO_{2(g)}$, $H_2O_{(l)}$, $N_{2(g)}$, $SO_{2(g)}$, and $K_2O_{(s)}$, necessary for the calculation, were taken from the reference book [13].

In view of the fact that $C_5H_8NOS_2K$ is in the crystalline state at 298.15 K, it was necessary to calculate its standard enthalpy of formation in the solid state. For this purpose, the melting heat of the compound under study was evaluated [14]:

$$\Delta H_m / T_m = 20.72 \times 10^{0.00324M}. \quad (4)$$

The value of ΔH_m, found for $C_5H_8NOS_2K$ by Eq. (5), is 46.8 kJ mol^{-1}.

Using the equation

$$\Delta_f H^0_{298.15} C_5H_8NOS_2K_{(s)} = \Delta_f H^0_{298.15} C_5H_8NOS_2K_{(l)} - \Delta H_m, \quad (5)$$

we calculated the standard enthalpy of formation of crystalline potassium morpholinodithiocarbamate to be –588.2 kJ mol^{-1}.

CONCLUSIONS

(1) The enthalpy of solution of a new morpholine derivative, potassium morpholinodithiocarbamate, in water was studied and its standard enthalpy of solution in an infinitely diluted aqueous solution was determined (54.2 ± 0.4 kJ mol^{-1}).

(2) The method of dynamic calorimetry was used to measure the temperature dependence of the specific heat of $C_5H_8NOS_2K$ in the temperature range 173–348 K), C_p^0 (298.15 K) was found, and the equation describing the dependence $C_p^0 \sim f(T)$ for the compound in this temperature range was derived.

(3) The enthalpies of combustion (–3024 ± 82 kJ mol^{-1}) and melting (46.8 kJ mol^{-1}) and the standard heats of formation of liquid (molten) (–541.3 kJ mol^{-1}) and crystalline (–588.2 kJ mol^{-1}) potassium morpholinodithiocarbamate were calculated using indirect methods.

The data on the thermochemical and thermodynamic properties of the new morpholine derivative, obtained in this study, are of interest for physicochemical modeling of the technology of development of medicinals and for determining their structural, energetic, and bioactivity characteristics.

REFERENCES

1. Lukevich, E., *Khim. Geterotsikl. Soedin.*, 1985, no. 6, pp. 723–734.
2. Skuratov, S.M., Kolesov, V.P., and Vorob'ev, A.F., *Termokhimiya* (Thermochemistry), Moscow: Mosk. Gos. Univ., 1964, vol. 1.
3. Calvet, E. and Prat, H., *Microcalorimétrie. Applications physico-chemiques et biologiques*, Paris: Masson, 1956.
4. Topor, N.D. and Suponitskii, Yu.L., *Usp. Khim.*, 1984, no. 9, pp. 1425–1462.

5. Poslednie dostizheniya mikrokalorimetrii (Recent Advances in MIcrocalorimetry), *Zh. Fiz. Khim.*, 1959, no. 6, pp. 1161–1175.
6. Mishchenko, K.P. and Poltoratskii, G.M., *Termodinamika i stroenie vodnykh nevodnykh i rastvorov elektrolitov* (Thermodynamics and Structure of Aqueous and Nonaqueous Electrolyte Solutions), Leningrad: Khimiya, 1976.
7. Glushko, V.P., *Termicheskie konstanty veshchestv: Spravochnik* (Thermal Constants of Substances: Reference Book), Moscow: Nauka, 1982, issue 10, part 2.
8. Spiridonov, V.P. and Lopatkin, A.A., *Matematicheskaya obrabotka eksperimental'nykh dannykh* (Mathematical Processing of Experimental Data), Moscow: Mosk. Gos. Univ., 1970.
9. Krestov, G.A., *Termodinamika ionnykh protsessov v rastvorakh* (Thermodynamics of Ionic Processes in Solutions), Leningrad: Khimiya, 1984.
10. Platunov, E.S., *Teplofizicheskie izmereniya v monotonnom rezhime* (Thermal Measurements in the Monotonic Mode), Moscow: Energiya, 1973.
11. *Tekhnicheskoe opisanie i instruktsii po ekspluatatsii IT-S-400* (Description and Operating Instructions for IT-S-400 Device), Aktyubinsk: Aktyub. Zavod Etalon, 1986.
12. Kazanskaya, A.S. and Skoblo, V.A., *Raschety khimicheskikh ravnovesii* (Calculations of Chemical Equilibria), Moscow: Vysshaya shkola, 1974.
13. Viktorov, V.V., *Metody vychisleniya fiziko-khimicheskikh velichin i prikladnye raschety* (Methods for Calculation of Physicochemical Quantities and Applied Calculations), Moscow: Khimiya, 1977.
14. Ryabin, V.A., Ostroumov, M. A., and Svit, T.F., *Termodinamicheskie svoistva veshchestv: Spravochnik* (Thermodynamic Properties of Substances: Reference Book), Leningrad: Khimiya, 1977.

ISSN 1070-4272, Russian Journal of Applied Chemistry, 2006, Vol. 79, No. 10, pp. 1709–1711. © Pleiades Publishing, Inc., 2006.
Original Russian Text © E.S. Stromova, V.N. Pak, 2006, published in Zhurnal Prikladnoi Khimii, 2006, Vol. 79, No. 10, pp. 1728–1730.

BRIEF COMMUNICATIONS

Acceleration of the Diffusion of Aqueous $CoCl_2$ Solutions in Porous-Glass Membrane in the Presence of Alkali Metal Chlorides

E. S. Stromova and V. N. Pak

Hertzen State Pedagogical University, St. Petersburg, Russia

Received June 29, 2006

Abstract—The diffusion coefficients of a 0.1 M aqueous solution of cobalt(II) chloride in a porous-glass membrane with a predominant pore radius of 45 nm in the presence of 0.5–3.0 M of lithium, potassium, and cesium chlorides were determined. Specific features of the influence exerted by the type of accompanying electrolytes on the rate of diffusion transport of $CoCl_2$ were considered.

DOI: 10.1134/S1070427206100314

Commonly, the diffusion rate of electrolytes in microporous glass membranes is markedly lower than that in free solutions [1–7]. This fact is reflected by several reports [4–6] of the "size" dependence of the diffusion coefficient on the radius of transport channels, r_p:

$$D = D_0 \exp(-K_p/r_p). \quad (1)$$

Here D_0 is found by the extrapolation $r_p \to \infty$ and the parameter K_p characterizes the effective thickness of the near-wall structured solution layer with hindered diffusion.

At the same time, it is possible that the membrane transport of water–salt solutions can be considerably accelerated by introduction of accompanying electrolytes having high diffusion mobility. To the authors' knowledge, this opportunity has not been subjected to reliable experimental verification. The reason is, in part, that the results of such a verification would hardly be obvious, primarily because of the decrease in the activity of the main substance in the presence of accompanying substances.

This study is concerned with the influence exerted by the nature and concentration of 1 : 1 electrolytes (LiCl, KCl, and CsCl) on the rate of diffusion mass-transfer of cobalt(II) chloride in porous-glass membrane. The existence of Co^{2+} cations in aqueous solutions in the form of stable hexa-aqua complex $[Co(H_2O)_6]^{2+}$, possibility of their direct photometric determination, and negligibly small adsorption on the silica surface [8] strongly simplify the formulation and solution of the problem by making it possible to distinguish the nature and concentration of supporting electrolytes as the main potential factors influencing the diffusion coefficient.

The porous-glass membrane with a predominant pore radius r_p = 45 nm and porosity δ = 31.3% was hermetically fixed between the feeding and receiving cells. Working solutions with a constant concentration of $CoCl_2$ (0.5 M) and a concentration of alkali metals within the range 0.5–3.0 M were used. The dynamics of the diffusion transport of $CoCl_2$ was judged from the results of a direct photometric determination of the amount of Co^{2+} ions in the receiver cell at a wavelength λ_{max} = 510 nm [9]. It is important to note that the profile of the absorption band peaked at 510 nm was completely preserved over the entire range of concentrations of the supporting electrolytes on both sides of the membrane, which indicates that the form of the $[Co(H_2O)_6]^{2+}$ cation being transferred remains unchanged. The diffusion was measured at 20°C under continuous agitation of the solutions. A steady-state flow across the membrane was attained in all cases 20–30 min after the beginning of a run. The fact that linear time dependences of the amount of $CoCl_2$ transferred, Q–τ, were observed made it possible to determine the diffusion rate and diffusion coefficients by using the first Fick's law

$$dQ/d\tau = DS\delta\Delta c/h. \quad (2)$$

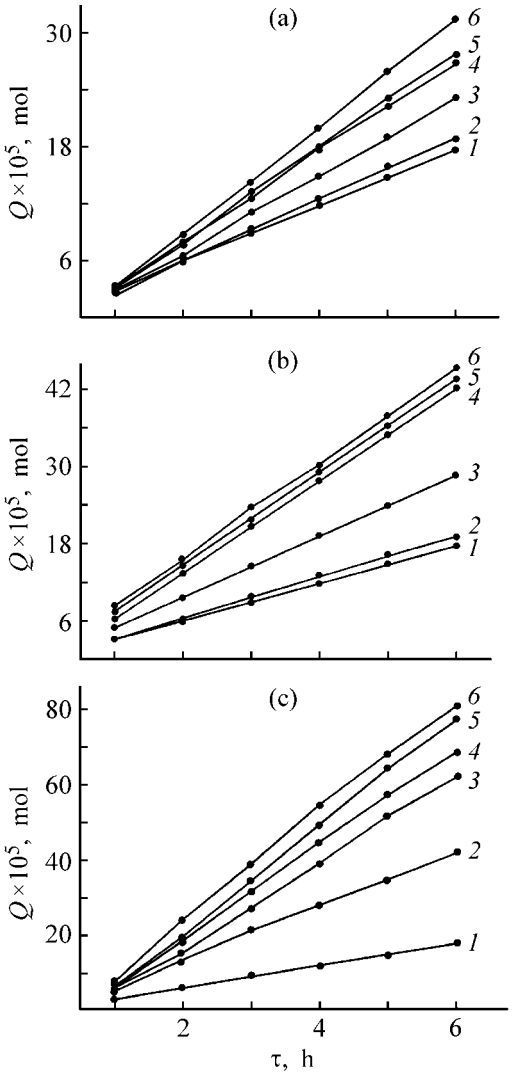


Fig. 1. Amount Q of $CoCl_2$ transferred across the membrane vs. time τ for (*1*) its 0.5 M solution and for solutions containing (a) LiCl, (b) KCl, and (c) CsCl. Solution concentration (M): (*2*) 0.5, (*3*) 1.0, (*4*) 1.5, (*5*) 2.0, and (*6*) 3.0.

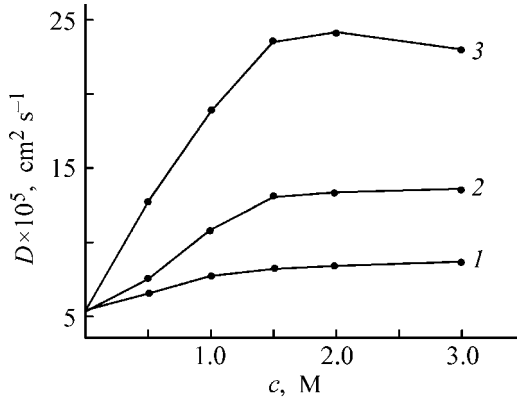


Fig. 2. Membrane diffusion coefficient D of cobalt(II) chloride vs. concentration c of (*1*) LiCl, (*2*) KCl, and (*3*) CsCl solutions.

Here $S\delta$ is the free cross-section of a membrane, equal to its geometric area with a correction for the porosity; $\Delta c/h$, the difference of solution concentrations before and after the membrane of thickness h.

Because the $CoCl_2$ concentration in the receiving cell, $c_{out} \sim 10^{-3}$ M, was considerably lower than that in the feeding cell (c_{in}), the gradient in Eq. (2) was taken in all the experiments to be $\Delta c/h \cong (c_{in} - c_{out})/h \cong c_{in}/h$.

The kinetic dependences in Fig. 1 reflect the reliably recorded acceleration of the diffusion of cobalt(II) chloride, caused by an increase in the concentration of the supporting electrolytes. The degree of their activating action strongly increases in the order LiCl–KCl–CsCl, which provides in the last case an increase in the rate of the $CoCl_2$ transport across the membrane by more than a factor of 4. The character and extent of the influence exerted by alkali metal chlorides on the $CoCl_2$ mobility is even more clearly reflected by the dependences shown in Fig. 2. The increase in the diffusion coefficient, caused by the presence of supporting electrolytes, is more than considerable and, on the whole, corresponds to the increase in their intrinsic mobility in the above order, which is determined by the decrease in the effective size of hydrated cations [10]. Thus, it is apparent that cobalt chloride is involved in the high-intensity diffusion flow of the accompanying salts, and this involvement is the more pronounced, the higher their concentration.

It should be noted that, in all cases, the $CoCl_2$ diffusion coefficient mainly increases within the range bounded by the concentration of the supporting electrolytes (~1.5 M) (Fig. 2). This feature is to a certain extent consistent with the known decrease in the viscosity of aqueous KCl solutions in thin quartz capillaries, which ceases at a concentration of about 1 M [11, 12]. This gives reason to believe that the principal factor governing the nature of diffusion and the degree of its acceleration is the specific interaction of salts of alkali metals with water in the pore space of the membrane. It is well known [10] that the viscosity of free CsCl solutions is lower at any concentration than that of water; the K^+ cation causes only a weakly pronounced disintegration of its structure, whereas Li^+ is a positively hydrated ion. Accordingly, the run and relative positions of the curves describing the dependences of the membrane diffusion coefficient of $CoCl_2$ on the concentration of supporting electrolytes (Fig. 2) are determined by the decrease in the viscous resistance of pore solutions and by the increase in diffusion mobility in the order LiCl–KCl–CsCl.

CONCLUSIONS

(1) An increase in the concentration of alkali metal chlorides in the range 0.5–3.0 M is accompanied by acceleration of the $CoCl_2$ diffusion transport in glass membrane, and the degree of this acceleration grows in the order Li–Cl–KCl–CsCl.

(2) The most probable factor responsible for the influence exerted by accompanying electrolytes on the mass transfer of $CoCl_2$ is the specific interaction of alkali-metal cations with water from the pore space of the membrane.

REFERENCES

1. Mazurin, O.V. and Antropova, T.V., *Fiz. Khim. Stekla*, 1986, vol. 12, no. 4, pp. 507–510.
2. Antropova, T.V., Tsyganova, T.A., and Krylova, N.L., *Fiz. Khim. Stekla*, 1990, vol. 16, no. 5, pp. 732–737.
3. Voloshina, O.S., Burkat, T.M., and Pak, V.N., *Zh. Fiz. Khim.*, 2000, vol. 74, no. 6, pp. 1099–1102.
4. Pak, V.N., Nepomnyashchii, A.V., Burkat, T.M., and Mal'kova, S.V., *Zh. Prikl. Khim.*, 2002, vol. 75, no. 12, pp. 1959–1962.
5. Pak, V.N., Nepomnyashchii, A.V., and Burkat, T.M., *Zh. Fiz. Khim.*, 2003, vol. 77, no. 11, pp. 1979–1982.
6. Pak, V.N., Nepomnyashchii, A.V., Burkat, T.M., and Kun, Sh.R., *Zh. Fiz. Khim.*, 2005, vol. 79, no. 9, pp. 1411–1414.
7. Pak, V.N., Stromova, E.S., Lobov, B.I., and Levkin, A.N., *Zh. Prikl. Khim.*, 2006, vol. 79, no. 3, pp. 363–366.
8. Pak, V.N., Tikhomirova, I.Yu., Burkat, T.M., and Lobov, B.I., *Zh. Fiz. Khim.*, 1999, vol. 73, no. 11, pp. 2024–2028.
9. Liver, A.B.P., *Inorganic Electronic Spectroscopy*, Amsterdam: Elsevier, 1984.
10. Lilich, L.S. and Khripun, M.K., *Rastvory kak khimicheskie sistemy* (Solutions as Chemical Systems), Leningrad: Khimiya, 1990.
11. Deryaguin, B.V. and Churaev, N.V., *Langmuir*, 1987, vol. 3, no, 5, pp. 607–612.
12. Aitkuliev, K., Sobolev, V.D., and Churaev, N.V., *Kolloid. Zh.*, 1985, vol. 47, no. 4, pp. 647–651.

ISSN 1070-4272, Russian Journal of Applied Chemistry, 2006, Vol. 79, No. 10, pp. 1712–1714. © Pleiades Publishing, Inc., 2006.
Original Russian Text © S.V. Ivanov, V.V. Trachevskii, O.S. Titova, L.A. Zozulya, 2006, published in Zhurnal Prikladnoi Khimii, 2006, Vol. 79, No. 10, pp. 1731–1733.

BRIEF COMMUNICATIONS

Prognostication of Aging of Polymeric Composite Materials

S. V. Ivanov, V. V. Trachevskii, O. S. Titova, and L. A. Zozulya

National University of Aviation, National Academy of Sciences of Ukraine, Kiev, Ukraine

Received April 13, 2006; in final form, June 21, 2006

Abstract—Experimental data demonstrate that a study of accelerated aging can enable prognostication of the working capacity and storage life of polymeric formulations used in aircraft components on the basis of changes in thermogravimetric constants of these polymeric formulations.

DOI: 10.1134/S1070427206100326

To determine whether or not promising polymeric composite materials can be used in aircraft components, it is necessary to know, with account of exploitation requirements, their real service and storage life.

Only prolonged full-scale tests give reliable results in assessment of the aging of polymeric composites, but, frequently, these results are out of date by the time they are obtained. A way to make aging studies of polymeric formulations shorter is to intensify the action of climatic factors and develop accelerated laboratory techniques simulating various climatic conditions [1].

To perform scientifically substantiated accelerated studies, it is necessary to make a quantitative assessment of the correlation between the effect of climatic factors and changes in physicochemical and, consequently, performance characteristics of a polymeric composite material.

Despite the wide variety of diverse factors that impair the durability and working capacity of polymeric aircraft components, the key role is attributed to the action of radiation, temperature, and oxygen on the polymeric composites [2, 3].

Chemical transformations that occur in polymers in the course of aging mainly belong to the following two processes: structuring and destruction of macromolecules in a material. The first process leads to cross-linking of separate chains of the polymer to give 3*D* structures. This improves the strength of the polymeric composite, but it becomes rigid and brittle and loses elasticity, which, naturally, results in loss of the required performance characteristics. The second process, destruction, leads to rupture of molecular chains and reduces the molecular weight of the polymer, with the result the polymeric composite becomes soft and sticky and loses its mechanical strength and, consequently, fails to satisfy the performance requirements. Therefore, the basic problem of stability of a polymeric composite against aging should be assessed on the basis of changes in its chemical structure under the action of ambient conditions (ionizing radiation, temperature, oxygen).

In this study, we chose as an object of analysis a polymeric formulation composed of a copolymer of vinyl chloride and vinyl acetate (A–15–OM), urethane prepolymer (SKU–PFL), and triisocyanate (TT–75), at an NCO/OH ratio of 1.2. We introduced diphenylsilanediol (DPSD) into the polymeric formulation as an additional cross-linking compound.

We chose as a criterion for assessing changes in the chemical structure the effective activation energy E_A of thermooxidative destruction of the polymeric formulation, found from thermogravimetric characteristics.

The thermogravimetric characteristics were determined in a dynamic thermogravimetric analysis (DTG), combined with differential thermal analysis (DTA), on an MOM derivatograph (Hungary) in air, with the temperature raised at a rate of 2.5–5°C/min in the range 100 – 600°C. The kinetic parameters of thermooxidative destruction were determined by a procedure we developed.

The working capacity of the polymeric composite was assessed on the basis of changes in tribological parameters determined by the required performance under severe climatic conditions.

To confirm our choice, we studied how the cross-linking compound DPSD, which allows purposeful modification of the structure of the polymeric composite, affects the thermooxidative destruction of the formulation. This was done by analysis of changes in the effective activation energy (see figure).

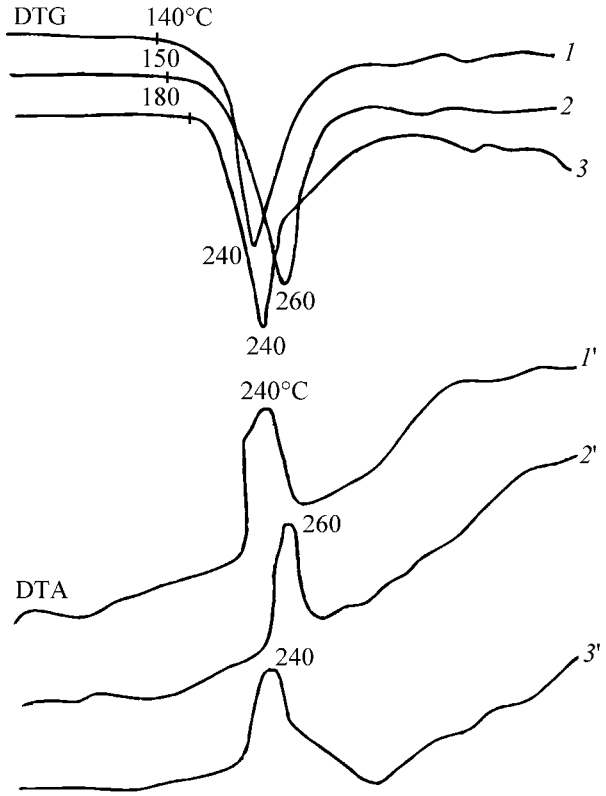
As can be seen from the figure, introduction of a DPSD additive changes the shape of the thermogravimetric curves and shifts the temperature peaks, which indicates that the structure of the polyurethane formulation changes and, consequently, so does the effective activation energy of thermooxidative destruction.

An additional, particularly important factor is that the introduction of a cross-linking compound affects both the structure of the composite being formed and the working capacity of polymeric aircraft components. The experimental results we obtained are listed in Table 1.

It can be seen from Table 1 that the modification of the physicochemical properties of the polymeric formulation upon introduction of the cross-linking compound changes the activation energy of thermooxidative destruction of the formulation.

In addition, the working capacity of the polymeric composite under severe climatic conditions also changes, with there existing a certain activation energy below which the working capacity of the polymeric formulation starts to fall steeply and its physicochemical properties degrade. Therefore, it was of interest to find out whether derivatographic analysis can be used to prognosticate the durability or service life of polymeric formulations by determining how the activation energy changes in the course of destruction of a polymeric formulation in its accelerated aging under heating or irradiation and by extrapolating the rate or time of the reaction to real aging conditions.

Previous studies have shown that polymeric composites subjected to the action of ionizing radiation change their physicochemical properties and, consequently, their working capacity under severe climatic conditions. Therefore, it was of interest to analyze



Thermogravimetric curves for a polyurethane formulation with varied content of DPSD. DPSD content (wt %): (*1*, *1'*) 0, (*2*, *2'*) 10, and (*3*, *3'*) 15.

changes in the activation energy of thermooxidative destruction of a polymeric formulation under exposure to ionizing radiation (Co^{60} gamma photons). Table 2 lists the experimental data we obtained.

It can be seen that the ionizing radiation causes accelerated aging of the polymeric formulation and changes its structure, and it is this fact that leads to a decrease in the activation energy of thermooxidative destruction.

Thus, the results we obtained demonstrate that processes of accelerated aging can be studied in order to prognosticate the service capacity and storage life

Table 1. Activation energy of thermooxidative destruction of SKU-100 formulation and its working capacity at varied content of the cccross-linking compound

DPSD, %	Hardness, rel. units	E_A, kJ mol^{-1}	Working capacity, cycles
0	0.40	165.7	15
5	0.55	215.6	1000
10	0.73	246.9	1500
15	0.70	256.0	1500

Table 2. Effect of irradiation on the working capacity and activation energy of thermooxidative destruction of SKU-100 polymer formulation

Irradiation dose, Gy	E_A, kJ mol^{-1}	Working capacity, cycles
0	246.98	1500
50	229.67	1500
100	185.66	1000
250	105.37	<10

Table 3. Changes in the activation energy of destruction of polymeric formulations in accelerated aging

Formulation	State of a sample	E_A, kJ mol^{-1}	Working capacity, cycles
SKU–BDM	Initial	148.1	1000
	500 Gy	68.0	<10
SKU–PFL-100	Initial	189.8	1500
	500 Gy	134.4	?????
SKU–PFL-3	Initial	186.94	1500
	500 Gy	169.94	1500

of polymeric composites for aircraft components on the basis of changes in the effective activation energy of thermooxidative destruction of the corresponding polymeric composite materials.

Table 3 lists the results obtained in a study of how the activation energy of thermooxidative destruction changes in the course of accelerated aging of polymeric formulations.

As can be seen from Table 3, the activation energy decreases in accelerated aging, and does so to varied extent for different polymeric materials. Therefore, the results obtained make it possible to prognosticate the real service life of polymeric composites in aircraft components by comparing the activation energies obtained with those determined previously for known polymeric formulations. Thus, the procedure we developed can be used for comparative evaluation of the time during which the performance characteristics of polymeric formulations are preserved. This should be done by establishing a correlation between the accelerated and natural aging processes.

In addition, analysis of the results obtained suggests that the derivatographic technique allows identification of aircraft components by the composition of a polymeric formulation and enables prognostication of the performance characteristics of polymeric formulations of the same composition. This is so because there exists a clearly pronounced correlation between the results of assessment of the working capacity of a polymeric formulation and its activation energy of thermooxidative destruction. The results obtained in the study were confirmed by full-scale tests of aircraft components.

CONCLUSIONS

(1) A correlation was established between the working capacity and storage life of polymeric composites, on the one hand, and changes in derivatographic constants, on the other.

(2) It was shown that changes in the effective activation energy of thermooxidative destruction of polymeric formulations in accelerated aging can be used to prognosticate the time during which the performance characteristics of the aircraft components fabricated from these formulations are preserved.

REFERENCES

1. Pavlov, N.N., *Starenie plastmass v estestvennykh i iskusstvennykh usloviyakh* (Aging of Plastics under Natural and Artificial Conditions), Moscow: Khimiya, 1982.
2. Ermak, A.A., Tkachev, S.M., et al., *Khim. Tekhnol. Topl. Masel*, 2005, no. 10, pp. 42–44.
3. Bystritskaya, E.V., Karpuzin, O.N., and Kryuchkov, A.A., *Vysokomol. Soedin., Ser. B*, 2006, vol. 48, no. 2, pp. 370–375.

ISSN 1070-4272, Russian Journal of Applied Chemistry, 2006, Vol. 79, No. 10, pp. 1715–1717. © Pleiades Publishing, Inc., 2006.
Original Russian Text © V.F. Burdukovskii, D.M. Mognonov, 2006, published in Zhurnal Prikladnoi Khimii, 2006, Vol. 79, No. 10, pp. 1734–1736.

BRIEF COMMUNICATIONS

Mechanism of the Rearrangement of Polyarylene Benzimidoates into *N*-Phenyl-Substituted Polyaramides and Poly(*N*-arylenebenzamides)

V. F. Burdukovskii and D. M. Mognonov

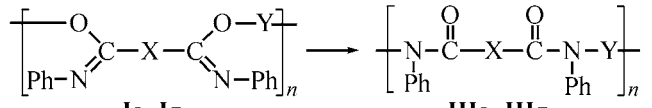
Baikal Institute of Nature Management, Siberian Division, Russian Academy of Sciences, Ulan-Ude, Buryatia, Russia

Received April 7, 2006; in final form, May 23, 2006

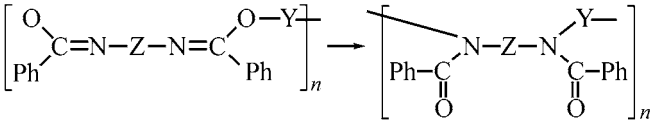
Abstract—The mechanism of the rearrangement of polyarylene benzimidoates into *N*-phenyl-substituted aromatic polyamides and poly(*N*-arylenebenzamides) was studied.

DOI: 10.1134/S1070427206100338

Previously we have studied macromolecular rearrangements of polyarylene benzimidoates (PABIs) [1, 2] heated to 260–340°C without solvent or to 240°C in diphenyl ether. Depending on the PABI structure, the reaction products are either *N*-phenyl-substituted aromatic polyamides (*N*-PAPAs) or poly(*N*-arylenebenzamides) (P-*N*-BAs). The transformation follows the schemes



Ia–Ig **IIIa–IIIg**



IId–IIk **IVd–IVk**

where X = *p*-C_6H_4 (**a**), *m*-C_6H_4 (**b**), (*p*-$C_6H_4)_2O$ (**c**); Y = *p*-C_6H_4 (**d**), *m*-C_6H_4 (**e**), (*p*-$C_6H_4)_2CMe_2$ (**f**), (*p*-$C_6H_4)_2SO_2$ (**g**); Z = *p*-C_6H_4 (**h**), *m*-C_6H_4 (**i**), (*p*-$C_6H_4)_2O$ (**j**), (*p*-$C_6H_4)CH_2O$ (**k**). Hereinafter, the first literal index in the compound designations refers to fragment X in compounds **I** and **III** and fragment Z in compounds **II** and **IV**, and the second literal index, to fragment Y.

The resulting polymers exhibit high resistance to thermal oxidative degradation, good solubility, and relatively low softening point. The structures of the polymers were confirmed by instrumental methods, but the reaction mechanism remained unclear. Therefore, the goal of this study was to elucidate the mechanism of the rearrangement of PABIs into *N*-PAPAs and P-*N*-BAs.

To this end, we mixed compounds **Ia**–**Id** and **IIk**–**IIf** in a 1 : 1 ratio. The rearrangement was performed in diphenyl ether for 20 h at 240°C. The reaction product was subjected to thermomechanical analysis (Fig. 1). Two transitions to the viscous-flow state were revealed in the TMA curve. Taking into account that the depolymerization and cross-linking did not occur, block copolymers were absent initially and were not formed in the process, and the polymer was fully X-ray-amorphous, these two transitions should be assigned to the glass transitions of the two polymers [3, 4]. The artificially prepared analogous blend of the rearrangement products showed an essentially similar TMA curve, suggesting the intramolecular reaction mechanism. Otherwise, a single random co-

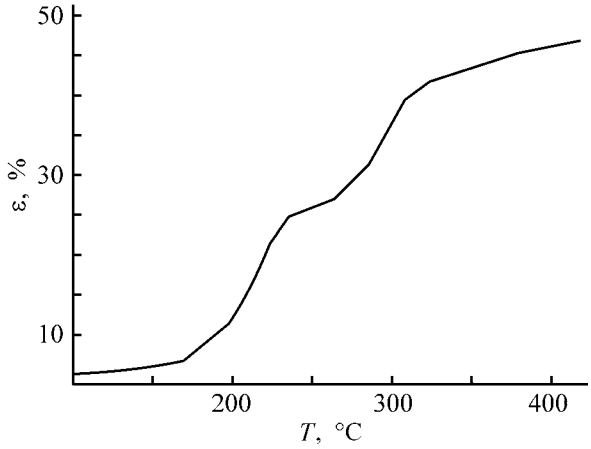


Fig. 1. TMA curve: (ε) strain and (*T*) temperature.

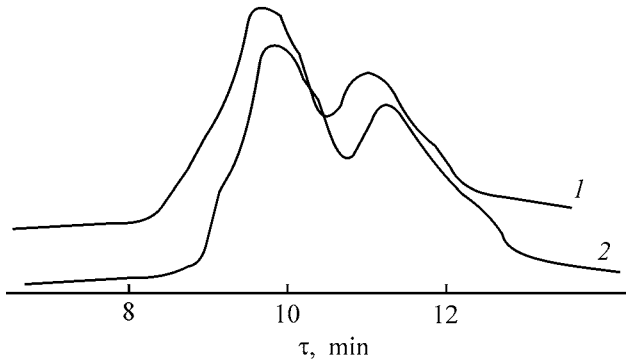


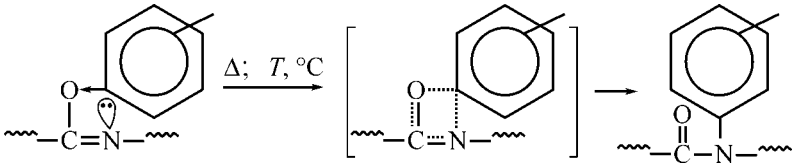
Fig. 2. Gel chromatograms of (*1*) PABI **Ic**–**Ie** and (*2*) its rearrangement product, *N*-PAPA. (τ) Time.

polymer would be obtained, and the TMA curve would show a single glass transition point.

We examined PABI **Ic**–**Ie** and its rearrangement product, *N*-PAPA, by gel permeation chromatography (Fig. 2). The GPC curve of PABI shows a characteristic bimodal molecular-weight distribution, which does not change essentially in going to *N*-PAPA. Furthermore, the polymers have virtually equal molecular weights: M_w 29 120 and 28 970, M_n 16 850 and 16 300 for the PABI and *N*-PAPA, respectively. Thus, the rearrangement does not involve cleavage of the polymer chain.

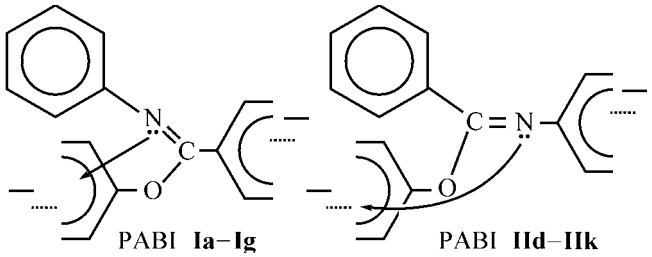
A model compound, benzanilimino ester, also undergoes an intramolecular rearrangement into *N*-phenylbenzamide by the known mechanism of the Chapman rearrangement [5].

These facts show that the mechanism of the rearrangement of the low- and high-molecular-weight compounds is similar and starts with the nucleophilic attack on the aromatic ring by the nitrogen atom. The nitrogen migrates by the intramolecular pathway via a four-membered transition state:



The rearranging fragment of a macromolecule can form such a transition state if it is compact and the chain is flexible.

In view of the aforesaid, it becomes clear why PABIs **I** rearrange more slowly (see table) than PABIs **II**. The main difference between these polymers is in the position of the rearranging fragment in the polymer chain:



PABI **Ia**–**Ig** PABI **IId**–**IIk**

PABIs **I** rearrange more slowly because the reactive fragment is oriented along the chain, whereas in PABIs **II** it is more compact; furthermore, the pendant group is more mobile than units in the back-bone [6].

Our results show that, in diphenyl ether, more flexible polymers rearrange faster than more rigid polymers, whereas in the melt, the rigid polymers rearrange faster.

EXPERIMENTAL

A thermomechanical analysis was performed on a Zetlin device at a constant load of 0.08 MPa and heating rate of 5 deg min^{-1}.

The X-ray phase analysis was performed on a D-8 Advance diffractometer (Bruker AXS), Cu_{K_α} radiation, graphite monochromator.

Gel permeation chromatography of polymers was performed on a Waters chromatograph, using columns packed with U-Styrogel Linear; refractometric detector, solvent tetrahydrofuran, T = 20°C, flow rate 0.3 mol min^{-1}; Maxima data processing system, calibration against polystyrene references.

The PABIs were prepared in a 50-ml three-necked flask equipped with a stirrer and inlet and outlet tubes for argon. The flask was successively charged in an argon flow with 0.01 mol of bisphenol and *N*-methyl-2-pyrrolidone; the mixture was homogenized. Then 0.02 mol of triethylamine and 0.01 mol of imidoyl chloride were added with vigorous stirring. The homogenized reaction mixture was heated to 170–180°C. After the lapse of 17–18 h, the product was precipitated into 2% aqueous ammonia, filtered off, washed

Conditions of PABI rearrangement and degree of conversion, γ

PABI	In melt			In solution		PABI	In melt			In solution	
	reaction conditions		γ, %	reaction conditions: T=240°C; τ, h	γ, %		reaction conditions		γ, %	reaction conditions: T=240°C; τ, h	γ, %
	T, °C	τ, h					T, °C	τ, h			
Ia–Id	340	14	92.4	12	76.6	**IIh–IId**	340	17	90.1	14	73.9
Ia–Ie	330	14	93.6	11	81.4	**IIh–IIe**	340	17	89.7	14	79.2
Ia–If	310	14	90.3	11	84.0	**IIh–IIf**	290	17	88.3	14	87.1
Ia–Ig	340	13	93.8	12	79.6	**IIh–IIg**	320	16	90.2	14	78.8
Ib–Id	340	14	95.5	11	76.1	**IIi–IId**	350	17	89.1	13	73.9
Ib–Ie	330	14	91.3	11	78.8	**IIi–IIe**	330	18	88.3	14	76.4
Ib–If	290	13	89.9	10	92.5	**IIi–IIf**	260	16	89.6	12	95.8
Ic–Id	300	14	90.4	11	85.4	**IIi–IIg**	290	16	92.0	13	89.6
Ic–Ie	300	14	91.6	10	93.4	**IIj–IId**	340	16	87.4	13	80.2
Ic–If	260	13	90.5	10	96.8	**IIj–IIe**	340	16	90.5	13	84.5
Ic–Ig	280	13	93.6	10	92.6	**IIj–IIf**	280	16	87.9	12	96.6
						IIj–IIg	300	17	91.3	12	90.3

with a 1% solution of sodium bisulfite and with water, and vacuum-dried at 60–70°C to constant weight.

P-*N*-BAs and *N*-PAPAs were prepared by rearrangement of the corresponding PABIs in an Ar atmosphere in a melt and in DPE.

CONCLUSIONS

(1) The rearrangement of polyarylene benzimidoates in the melt and in diphenyl ether occurs by the intramolecular mechanism, without cleavage of the polymer chain and similarly to the rearrangement of the model benzanilimino ester, whose mechanism consists in the nucleophilic substitution in the aromatic ring.

(2) In diphenyl ether, more flexible polymers rearrange faster than more rigid polymers, whereas in the melt, more rigid polymers rearrange faster.

ACKNOWLEDGMENTS

The study was supported by the Federal Target Scientific and Technical Program (State Contract no. 02.442.11.7270) and by a grant for young scientists of the Republic of Buryatia in the field of new materials.

REFERENCES

1. Burdukovskii, V.F., Mognonov, D.M., Botoeva, S.O., and Mazurevskaya, Zh.P., *Vysokomol. Soedin., Ser. B*, 2006, vol. 48, no. 4, pp. 709–713.
2. Burdukovskii, V.F., Mognonov, D.M., Botoeva, S.O., and Mazurevskaya, Zh.P., *Zh. Prikl. Khim.*, 2006, vol. 79, no. 3, pp. 437–439.
3. Teitel'baum, B.Ya., *Termomekhanicheskii analiz polimerov* (Thermomechanical Analysis of Polymers), Moscow: Nauka, 1979.
4. Hirooka, M. and Kato, T., *J. Polym. Sci. B*, 1974, vol. 12, pp. 31–37.
5. Vatsuro, K.V. and Mishchenko, G.L., *Imennye reaktsii v organicheskoi khimii* (Named Reactions in Organic Chemistry), Moscow: Khimiya, 1976.
6. Fabulyak, F.G., *Molekulyarnaya podvizhnost' polimerov v poverkhnostnykh sloyakh* (Molecular Mobility of Polymers in Surface Layers), Kiev: Naukova Dumka, 1983.

ISSN 1070-4272, Russian Journal of Applied Chemistry, 2006, Vol. 79, No. 10, pp. 1718–1720. © Pleiades Publishing, Inc., 2006.
Original Russian Text © R.Kh. Mudarisova, E.I. Kulish, R.M. Zinatullin, N.E. Tamindarova, S.V. Kolesov, S.N. Khunafin, Yu.B. Monakov, 2006, published in Zhurnal Prikladnoi Khimii, 2006, Vol. 79, No. 10, pp. 1737–1739.

BRIEF COMMUNICATIONS

Films of Chitosan-based Complexes with Controlled Release of Levomycetin

R. Kh. Mudarisova, E. I. Kulish, R. M. Zinatullin, N. E. Tamindarova, S. V. Kolesov, S. N. Khunafin, and Yu. B. Monakov

Institute of Organic Chemistry, Ufa Scientific Center, Russian Academy of Sciences, Ufa, Bashkortostan, Russia
Bashkir State University, Ufa, Bashkortostan, Russia
Bashkir State Medical University, Ufa, Bashkortostan, Russia

Received April 26, 2006

Abstract—Complexation between chitosan and Levomycetin antibiotic and the possibility of formation of complexes of stoichiometric composition was studied.

DOI: 10.1134/S107042720610034X

Because of the low toxicity and biological activity, natural polysaccharides, chitin and chitosan, are of particular interest for medical applications [1–4]. Owing to its film-forming ability, chitosan can be used to produce coatings for temporal protection and treatment of wounds and burns [5, 6]. Recent studies have shown that chitosan is promising as a polymer matrix, carrier of medicinals, which makes their action longer and toxicity lower [7, 8]. In this context, synthesis of chitosan complexes with medicinals exhibiting antimicrobial activity for treatment of burns and open is an urgent task.

The aim of this study was to examine the complexation of chitosan (CTS) and the antimicrobial preparation Levomycetin (LM) and to obtain on their basis films with controlled release of the active medicinal.

EXPERIMENTAL

CTS obtained from shells of Far-Eastern crabs with initial number-average degree of polymerization (P_n) of 860, degree of deacetylation in the range 70–75%, and humidity of 4.5% was used in the study. Levomycetin, a pharmaceutical preparation, was taken without additional purification (as purchased). The IR spectra were recorded on a Specord-M 80 spectrophotometer in KBr pellets and in films. The ^{1}H NMR spectra were measured in an HCl solution in D_2O on a Bruker AM 300 instrument. The UV spectra of the samples in 1% acetic acid were measured on a Specord M-40 spectrophotometer. The pH values of the solutions were determined with an ANION 4100 pH-meter. The specific rotation [α_D^{25}] was measured on a Model 141 Perkin–Elmer polarimeter. The compounds synthesized were purified to remove unreacted levomycetin by double reprecipitation from solution into isopropyl alcohol, with the subsequent washing of the precipitate with isopropyl alcohol. Films were produced from a solution of the CTS–LM complex with a 1 : 1 molar ratio of components in 1% acetic acid by casting on glass with subsequent drying in air at room temperature. A three-layer film was produced by successive castings on glass of a 2% solution of chitosan, a 2% solution of CTS–LM complexes (at 1 : 1 molar ratio), and again a 2% chitosan solution. After each casting, the substrate was dried in air at 25°C and, finally, the resulting three-layer film was heated at 80°C for 1.5 h. To study the release of the medicinal, the films were placed in a test tube filled with a 0.01 N KOH solution (10 ml, pH 10). The release of the medicinal was monitored with a Specord M-40 spectrophotometer by the absorption band at λ = 260 nm.

Levomycetin is a broad-spectrum antibiotic [9]. It has the structure of a neutral compound containing no charged groups, which makes impossible any specific ionic interaction between LM and the polymer matrix under study. However, the presence of two hydroxy and one amide groups enables formation of hydrogen bonds between the medicinal and chitosan.

The electronic spectrum of LM at its concentration of 1×10^{-4} M in 1% acetic acid contains one absorption peak at 270 nm. On addition of a comparable amount of chitosan to the solution, the intensity of the LM absorption peak increases and its position shifts to shorter wavelengths by 8–10 nm. The spectral changes indicate that chitosan affects the electron system of LM and a complex compound is formed. It was found using the isomolar series method [10] that the ratio of the stoichiometric coefficients for the CTS–LM complex is 1 : 1 (Fig. 1). The complexation constant (β_c) was calculated by the method of molar ratios [10] to be $(2.4 \pm 0.3) \times 10^4$ l mol^{-1}.

The complexes of CTS with LM were isolated, purified, and studied by IR, UV, and ^{1}H NMR spectroscopies; their angles of rotation were also determined. The electronic spectra of the polymer complexes show a shift of the absorption peak of LM in the CTS–LM complex to lower wavelengths, compared with that in the LM spectrum (λ_{max} = 258–260 and 270 nm, respectively). Chitosan has no absorption in this spectral range. The absorption bands at 1730 cm^{-1}, characteristic of stretching vibrations of the carbonyl group of substituted amine, and at 1580 cm^{-1}, associated with stretching vibrations of the benzene ring in LM, appear in the IR spectra of the complexes. In addition, the IR absorption peaks of OH groups are shifted to lower frequencies by 30–50 cm^{-1} (3250–3150 cm^{-1}), and those of C–O groups of glycoside, by 10–15 cm^{-1} (1200–1000 cm^{-1}). This confirms that intermolecular hydrogen bonds are formed between the molecules of the medicinal and chitosan. Comparison of the ^{1}H NMR spectra of CTS, LM, and CTS–LM complex shows that the proton signals from the complex are shifted downfield (σ_H 3.21 ppm for the complex and 3.01 ppm for CTS). In this case, the redistribution of the electronic density, caused by the complexation, results in the downfield shift of the H^2 peak. The values of the specific rotation [α_D^{25}] were determined for CTS, LM, and CTS–LM complex to be +23.0, +3.5, and +1.0, respectively.

Changing the molar ratio between the components of the complex from 1 : 0.25 to 1 : 3 and raising the time and temperature of complexation affect the content of the medicinal in the reaction products only slightly (Table 1).

The kinetics of LM release was monitored by the accumulation of the medicinal in a KOH solution. On submerging CTS–LM films (one- and three-layer) in an aqueous–alkaline solution, their swelling occurs. A typical kinetic curve of LM release from a one-layer CTS–LM film formed at 25°C is shown in Fig. 2.

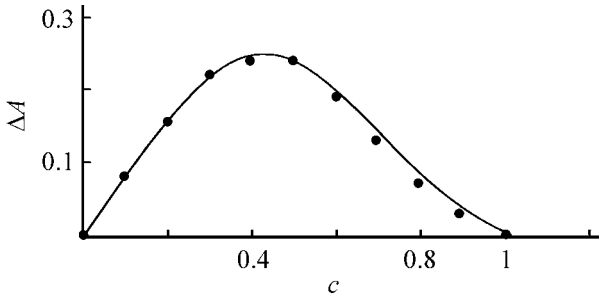


Fig. 1. Isomolar diagram. [CTS] + [LM] = 5×10^{-4} M, pH 4.1, l = 1 cm. (ΔA) Change in optical density, $c = c_{LM}/(c_{LM} + c_{CTS})$.

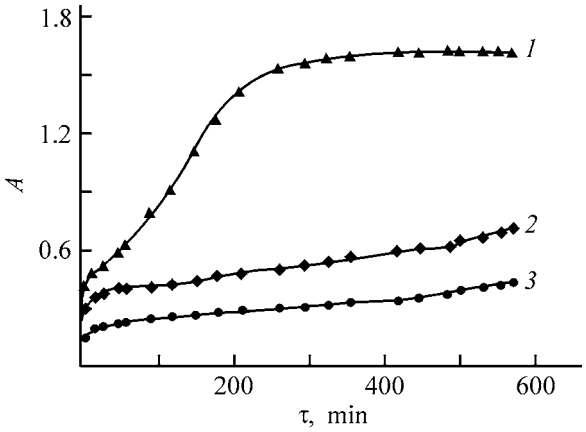


Fig. 2. Kinetic curves of LM release from films based on the CTS–LM complex. (A) Optical density and (t) time. Film: (*1*) one-layer (T = 25°C), (*2*) three-layer (T = 80°C), and (*3*) one-layer (T = 80°C).

The complete release of LM from this film takes 6.5 h. The time of complete release of LM is about 12 days for a three-layer film and markedly decreases (to about 7 days) for a heated one-layer film. At the same time, the complete release of LM from a film prepared

Table 1. Influence of the complexation conditions on the content of the medicinal in reaction products

CTS–LM molar ratio	τ, h	T, °C	LM content of the complex, %
1 : 1	2	60	0.8
1 : 1	6	60	1.3
1 : 1	10	60	1.4
1 : 1	24	60	1.7
1 : 0.25	6	60	1.2
1 : 0.5	6	60	1.3
1 : 2	6	60	0.8
1 : 3	6	60	1.2
1 : 1	6	20	0.7
1 : 1	6	40	1.0
1 : 1	6	90	1.4

Table 2. Dependence of the effective rate constants of LM release on the conditions of formation of films based on the CTS–LM complex

Film	T, C°	$k_{eff} \times 10^{-3}$, s^{-1}
One-layer	25	–4.30
"	80	–1.10
Three-layer	80	–0.87

by mechanical mixing of 2% acetate solutions of LM and CTS takes 30 min. The effective rate constant of LM release (Table 2) was found by plotting the kinetic curves in the coordinates of the equation

$$\ln [A]_t = \ln [A]_0 - k_{eff}\tau,$$

where A is the optical density, and τ, the time of LM release.

It can be seen from the data of Table 2 that the rate of LM release is higher for films formed at 25°C. Probably, a decrease in the rate of release from heated films is due to structural changes in the polymer matrix in the course of the heat treatment. Thus, the rate of LM release from the films depends on their preparation conditions.

The experimental data obtained show that use of polymer coatings based on CTS–LM complexes provides quite acceptable terms of a continuous release of the medicinal into a wound, i.e., allows a prolonged action of the medicinal during several days.

CONCLUSIONS

In a study of some aspects of complexation between chitosan and Levomycetin, the conditions of controlled release of the medicinal from a polymer coating were chosen and the formation of complexes of the stoichiometric composition was revealed.

ACKNOWLEDGMENTS

The study was in part financially supported by the Foundation for Support of Leading Scientific Schools (grant no. NSh 728.2003.3.), Scientific Program of the Federal Agency for Education "Development of the Scientific Potential of the High School" (project no. UP.05.01.008), and State Scientific-Technical Program of the Republic of Bashkortostan for the years of 2005–2007 (contract no. 419-X).

REFERENCES

1. Suzuki, K., Mikami, T., and Okawa, Y., *Carbohydr. Res.*, 1986, vol. 151, pp. 403–408.
2. Dubinskaya, A.M. and Dobrotvorskaya, A.E., *Khim-Farm. Zh.*, 1989, no. 5, pp. 623–628.
3. Galiaskarova, G.G., Mullagaliev, I.R., and Monakov, Yu.B., *Bashkir. Khim. Zh.*, 1996, vol. 3, nos. 5–6, pp. 3–12.
4. *Chitin and Chitosan: Sources, Chemistry, Biochemistry, Physical Properties and Application*, Anthonsen, T., Ed., London: Elsevier, 1990.
5. JPN Patent 62-43 129.
6. US Patent 4 952 618.
7. JPN Patent 59-27 827.
8. JPN Patent 61-268 626.
9. Mashkovskii, M.D., *Medicinals*, Kharkov: Torsing, 1997, vol. 2.
10. Bulatov, I.P. and Kalinkin, M.I., *Prakticheskoe rukovodstvo po fotometricheskim metodam analiza* (Manual on Photometric Analysis), Leningrad: Khimiya, 1986.

ISSN 1070-4272, Russian Journal of Applied Chemistry, 2006, Vol. 79, No. 10, pp. 1721–1722. © Pleiades Publishing, Inc., 2006.
Original Russian Text © M.G. Voronkov, S.V. Basenko, R.G. Mirskov, S.N. Adamovich, 2006, published in Zhurnal Prikladnoi Khimii, 2006, Vol. 79, No. 10, p. 1740.

BRIEF COMMUNICATIONS

Synthesis of High-Purity Tris(trimethylsilyl) Borate

M. G. Voronkov, S. V. Basenko, R. G. Mirskov, and S. N. Adamovich

Favorskii Institute of Chemistry, Siberian Division, Russian Academy of Sciences, Irkutsk, Russia

Received June 5, 2006

Abstract—A method was developed for synthesis of high-purity tris(trimethylsilyl) borate by reaction of trimethylacetoxysilane with powdered boric acid.

DOI: 10.1134/S1070427206100351

Tris(trimethylsilyl) borate $B(OSiMe_3)_3$ (TMSB) is used as a monomer and comonomer in production of polyorganyl borosiloxane caoutchoucs for improving their technical parameters, as a catalyst for polymerization processes, and as an adsorbent of neutrons. It is recommended as a means of protection of surfaces subjected to action of an electric arc and as a half-product in synthesis of silicon-and-boron-containing compounds [1]. High-purity TMSB has been suggested by the authors for use in the microelectronic technology for plasmochemical deposition of thin layers of boron-doped silicon dioxide, with a boron content of 1.5 to 10 wt % [2].

Previously, TMSB has been synthesized in a 20% yield by heating hexamethyldisiloxane with B_2O_3 in an autoclave at 350°C or by boiling trimethylchlorosilane with H_3BO_3 (yield 26.5%) [3].

The yield of TMSB could be raised to 81% on heating hexamethyldisilthiane with boric acid to 120°C [4]. However, use of the difficultly accessible and foul-smelling hexamethyldisilthiane is unfeasible for industry. The reaction of hexamethyldisilazane with ammonium borate in a solvent [5] or with boric acid at 110–120°C in the course of 10 h [6] produced TMSB in 40 and 72% yields, respectively.

To be used in micro- and optoelectronics, TMSB should be of special purity. This forced the authors to develop a method for synthesis of high-purity TMSB by heating trimethylacetoxysilane with powdered boric acid of chemically pure grade at 110°C:

$$B(OH)_3 + 3MeCOOSiMe_3 \rightarrow B(OSiMe_3)_3 + 3MeCOOH.$$

A mixture of 20 g (0.15 mol) of trimethylacetoxysilane and 3 g (0.05 mol) of finely ground boric acid of chemically pure grade was heated at 110°C for 1 h. After acetic acid was evaporated (8.4 g, 97%), the residue was distilled in a vacuum. The yield of TMSB was 7.95 g (95%), bp 70°C (19 mm Hg), $n_d^{20} = 1.3865$, in agreement with published data [3]: bp 48°C (5 mm Hg), $n_d^{20} = 1.3860$.

According to GLC data, TMSB purified by rectification in a vacuum on a quartz column is free of even trace amounts of organic impurities. According to the results of an atomic-absorption analysis, the content of metals (Na, K, Ca, Fe, Ni, Co, etc.) does not exceed 10^{-5}–10^{-6} wt % for each of the metals.

CONCLUSION

A method for synthesis of high-purity tris(trimethylsilyl) borate for micro- and optoelectronics in a 92% yield was developed. The method is based on the reaction of trimethylacetoxysilane with powdered boric acid of chemically pure grade at 110°C for 1 h, with the subsequent purification of the product by rectification in a vacuum.

ACKNOWLEDGMENTS

The study was supported by the Council for Pre-

sidential grants of the Russian Federation (project no. NSh-4575.2006.3).

REFERENCES

1. Voronkov, M.G., Maletina, E.A., and Roman, V.K., *Geterosiloksany* (Heterosiloxanes), Novosibirsk: Nauka, Sib. Otd., 1984.
2. Voronkov, M.G., Sulimin, A.D., Yachmenev, V.V., et al., *Dokl. Akad. Nauk SSSR*, 1978, vol. 241, no. 6, p. 1363.
3. Voronkov, M.G. and Zgonik, V.N., *Zh. Obshch. Khim.*, 1957, vol. 27, no. 6, p. 1476.
4. Lebedev, E.P., Reisfel'd, V.O., and Baburina, V.A., *Zh. Obshch. Khim.*, 1974, vol. 44, no. 4, p. 787.
5. Voronkov, M.G. and Yarosh, O.G., *Zh. Obshch. Khim.*, 1972, vol. 42, no. 9, p. 20.
6. Voronkov, M.G., Mirskov, R.G., Chernova, V.G., and Ivanova, N.P., *Zh. Obshch. Khim.*, 1981, vol. 51, no. 7, p. 1678.

ISSN 1070-4272, Russian Journal of Applied Chemistry, 2006, Vol. 79, No. 10, pp. 1723–1725. © Pleiades Publishing, Inc., 2006.
Original Russian Text © S.E. Mamedov, E.I. Akhmedov, F.Sh. Kerimli, M.I. Makhmudova, 2006, published in Zhurnal Prikladnoi Khimii, 2006, Vol. 79, No. 10, pp. 1741–1743.

BRIEF COMMUNICATIONS

Influence of Phosphorus Content on Physicochemical and Catalytic Properties of H-Pentasil in *m*-Xylene Isomerization and Toluene Methylation

S. E. Mamedov, E. I. Akhmedov, F. Sh. Kerimli, and M. I. Makhmudova

Baku State University, Baku, Azerbaijan

Received February 21, 2006

Abstract—Physicochemical and catalytic properties of H-pentasils in *m*-xylene isomerization and toluene methylation were studied.

DOI: 10.1134/S1070427206100363

Control of the zeolite pore size and acid properties by elimination of the strongest acidic centers and by variation of their nature is one of probable ways to modify the catalytic and molecular-sieve properties of zeolites. Chemical modification of the zeolite surface with compounds of B, Mg, P, Si, etc. [1–3], which have a para-orienting effect upon the activity of zeolite catalysts in transformations of aromatic hydrocarbons, is promising in this respect.

Since pentasil-type high-silica zeolites offer wide opportunities in oil refining, it is interesting to study how modification of such zeolites with a phosphorus compound will affect their catalytic and physicochemical characteristics in *m*-xylene isomerization and toluene methylation.

EXPERIMENTAL

Pentasil-type zeolite with a SiO_2/Al_2O_3 molar ratio of 58 was used. It was converted into the NH_4 form by ion exchange as in [4] and then into the H form by thermal decomposition of the NH_4 form for 4 h at 500°C. Catalysts modified with 0.5–4 wt % phosphorus were prepared by impregnation of the zeolite H form with ammonium hydrophosphate for 6 h at 80°C. The samples were dried in air for 16 h, then for 4 h in a desiccator at 110°C, and finally calcined in a muffle for 4 h at 550°C.

The catalysts obtained were subjected to chemical analysis, X-ray phase analysis, and adsorption analysis and studied by IR spectroscopy.

The IR spectra were recorded on a Specord spectrophotometer. Zeolites were compacted into thin pellets containing 6–8 mg of the substance per square centimeter. Before adsorption, they were heated in a vacuum for 2 h at 500°C. Adsorption of pyridine was performed at room temperature and saturated vapor pressure. The IR spectra in the region of aluminosilicate framework vibrations were recorded with samples pelletized with KBr. Adsorption measurements were performed by the method described in [4].

The experiments were performed on a flow-type device with a fixed catalyst bed (4 cm^3), in a plug-flow reactor, at atmospheric pressure within the 250–450°C range, volumetric flow rate of the raw material of supply 1 h^{-1}, and m-$C_6H_4(CH_3) : H_2$ and $C_7H_8 : CH_3OH : H_2$ molar ratios of 3 : 1 and 2 : 1 : 2, respectively. The reaction products were analyzed chromatographically [5].

The X-ray phase analysis showed that the crystalline structure of the zeolite is preserved during modification with ammonium hydrophosphate. The IR study confirmed this conclusion. In the region of aluminosilicate framework vibrations (400–1300 cm^{-1}), which are the most sensitive to the degree of crystallinity of the zeolite, the bands of the external Si–O– bonds at 550–560 and 790–800 cm^{-1} remain virtually unchanged upon modification with phosphorus. An increase in the intensity of the high-frequency branch of the asymmetrical stretching band (1000–1100 cm^{-1}) may be due to interaction of phosphorus atoms with structural aluminum atoms [6].

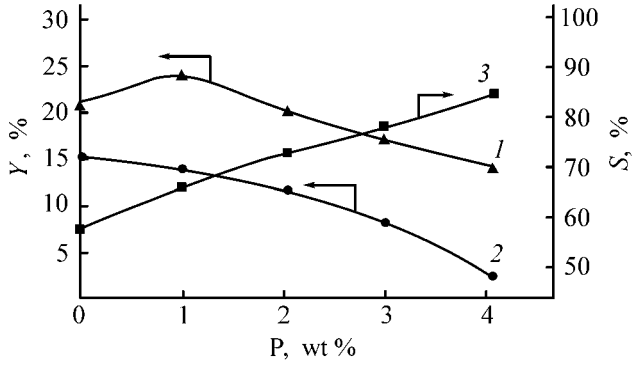


Fig. 1. Yield Y of (*1*) *p*-xylene and (*2*) *m*-xylene, and (*3*) selectivity S with respect to *p*-xylene vs. the phosphorus content of H-pentasil.

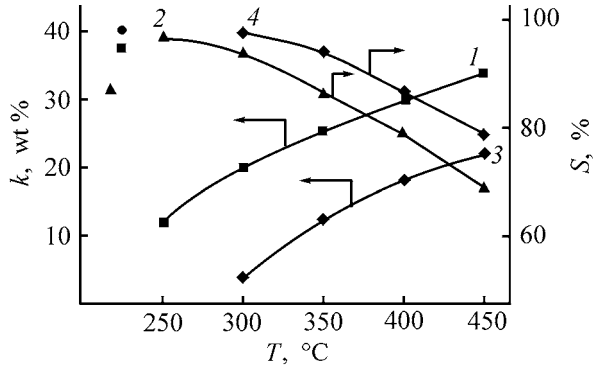


Fig. 2. Conversion k of (*1*) *m*-xylene and (*3*) toluene, and selectivity S with respect to *p*-xylene vs. temperature T in (*4*) isomerization of *m*-xylene and (*2*) methylation of toluene.

Analysis of the activity and selectivity of the modified catalysts shows that the phosphorus content strongly affects the *m*-xylene isomerization and toluene methylation. As can be seen from Fig. 1, the yield of *p*-xylene somewhat grows as the phosphorus content increases to 1.0 wt %. At a phosphorus content higher than 2 wt %, the *p*-xylene content noticeably decreases, but the para-selectivity substantially increases (from 70 to 85%). A different trend is observed for *o*-xylene. An increase in the phosphorus content decreases the *o*-xylene content within the entire range of phosphorus contents and, especially at those higher than 2 wt %. For example, the *o*-xylene yield decreases from 12.0 to 1.2% when the phosphorus content is raised from 2 to 4%. In this case, the condensate is enriched in *p*-xylene, i.e., the selectivity with respect to *p*-xylene formation increases.

Adsorption of water and benzene vapors on H-pentasils (HP) modified with phosphorus (P/P_s = 0.1, T = 20°C)

Zeolite	Adsorption, $cm^3\ g^{-1}$	
	H_2O	G_6H_6
NP	0.078	0.046
0.5% P/NP	0.071	0.040
1.0% P/NP	0.059	0.031
2.0% P/NP	0.043	0.023
3.0% P/NP	0.018	0.0084
4.0% P/NP	0.0083	0.0037

The temperature dependence of the *m*-xylene and toluene conversion and selectivity with respect to *p*-xylene on H-pentasil modified with 4 wt % phosphorus is shown in Fig. 2. As seen, a decrease in the conversion of *m*-xylene and toluene is accompanied by an increase in the para-selectivity of the catalyst. At 250°C and 12% conversion of the aromatic hydrocarbon, the selectivity with respect to *p*-xylene reaches 95%. This shows that *p*-xylene is the primary product of *m*-xylene isomerization and toluene methylation on the phosphorus-containing zeolite.

The differences in the distribution of the products of *m*-xylene isomerization and toluene methylation and in the selectivity of the reaction on modified pentasils become more understandable when the results obtained are considered from the viewpoint of control of the reaction rate by diffusion into the volume. Reactions in zeolites occur with the diffusion rate determined by the shape and size of both the reacting molecules and zeolite channels (configuration diffusion) [5]. In this case, the increased selectivity with respect to *p*-xylene can be accounted for by the higher diffusion rate of *p*-xylene molecules, which have a smaller kinetic diameter than molecules of *m*- and *o*-xylenes, in the channels of the modified pentasil.

Indeed, the modification with phosphorus is accompanied by a chemical reaction with the zeolite, as judged from a substantial decrease in the intensity of absorption of zeolite OH groups in the IR spectra of the modified samples as compared to the initial zeolite. In addition, polymeric structures of –P–O–P– type probably appear during modification [6], along with PO_4 fragments formed in reactions of phosphorus compounds with zeolite OH groups, which undoubtedly affects the accessibility of the zeolite channels. This, in turn, decreases the zeolite sorption capacity (see table) and is reflected in molecular-sieve properties of pentasil in reactions sensitive to the pore size: *m*-xylene isomerization and toluene methylation.

It is known that a change in the number and strength of acid centers is the main reason for variation of the catalytic activity of zeolites [7]. Since the isomerization is catalyzed by Brønsted acid centers faster than by Lewis centers, a decrease in the Brønsted acidity and a change in the ratio of Brønsted to Lewis acidic centers will affect the catalyst activity [8].

The IR spectra of the initial zeolite and that modified with ammonium hydrophosphate (Fig. 3) show that the band at 3615 cm^{-1} in the region of the stretching vibrations of the strongly acidic bridging OH groups is observed in the spectra of all the samples studied. Its intensity substantially decreases with an increase in the phosphorus content of the sample. This fact suggests that phosphorus partially dealuminates the zeolite and thus neutralizes acid centers situated at entrances into channels or at their intersections [6]. Thus, modification of zeolites with phosphorus decreases the total concentration of hydroxy groups.

In the region of pyridine bending vibrations (1440–1700 cm^{-1}), the spectra of all the samples contain the following pyridinium ion (PyH^+) bands: a band at 1550 cm^{-1} corresponding to Brønsted acid centers (B centers), band at 1450 cm^{-1} belonging to Lewis acid centers (L centers), and band at 1490 cm^{-1}, belonging to B and L centers; their intensity decreases with the phosphorus content increasing from 1.0 to 4.0 wt %. Thus, not only the amount of strong acid centers decreases, but also the ratio of L to B centers increases more substantially, which is probably a reason for the change in the activity and selectivity of the catalysts modified with phosphorus.

Thus, our study showed that modification with phosphorus affects not only the concentration, but also the nature and properties of the active centers in zeolite. In addition, the zeolite channels become narrower. All these facts affect the adsorption and diffusion characteristics of the catalysts, which largely determine the high selectivity with respect to formation of *p*-xylene.

CONCLUSION

Chemical modification of H-pentasil with ammonium hydrophosphate redistributes acid centers and decreases the zeolite sorption capacity. The ratio of Lewis to Brønsted acid centers increases and the zeolite channels become narrower, which makes higher the catalyst selectivity with respect to *p*-xylene.

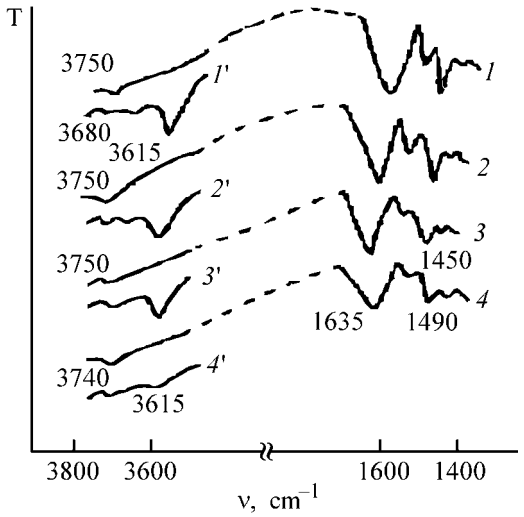


Fig. 3. IR spectra of H-pentasils modified with phosphorus and heated in a vacuum at 500°C for 2 h. (*1*) H-pentasil; P (wt %): (*2*) 1.0, (*3*) 2.0, and (*4*) 4.0. (*1'–4'*) After pyridine adsorption at 20°C for 1 h and desorption at 200°C. (ν) Wavenumber.

REFERENCES

1. Romannikov, V.N. and Ione, K.G., *React. Kinet. Catal. Lett.*, 1993, vol. 51, no. 1, pp. 151–154.
2. Chen Nai, Y., *Ind. Eng. Chem. Res.*, 2001, vol. 40, no. 20, pp. 4157–4161.
3. Young, L.B., Butter, S.A., and Kaeding, W.W., *J. Catal.*, 1982, vol. 76, no. 2, pp. 418–421.
4. Mamedov, S.E., *Nefrekhimiya*, 1998, vol. 38, no. 1, pp. 60–63.
5. Mamedov, S.E., Aminbekov, A.F., and Mamedov, A.B., *Nefrekhimiya*, 1998, vol. 38, no. 2, pp. 107–110.
6. Kubasov, A.A., Kitaev, L.E., Koldysheva, E.M., et al., *Kinet. Katal.*, 1988, vol. 29, no. 4, pp. 1016–1020.
7. Spiridonov, S.E., Khadzhiev, S.N., Yaralov, N.G., and Limova, T.V., *Kinet. Katal.*, 1986, vol. 27, no. 1, pp. 201–204.
8. Chulin, G.D., Khusid, E.L., Lupina, M.I., et al., *Kinet. Katal.*, 1987, vol. 28, no. 5, pp. 1211–1216.

ISSN 1070-4272, Russian Journal of Applied Chemistry, 2006, Vol. 79, No. 10, pp. 1726–1728. © Pleiades Publishing, Inc., 2006.
Original Russian Text © O.V. Bakbardina, I.Yu. Pukhnyarskaya, M.A. Gazalieva, S.D. Fazylov, E.M. Makarov, 2006, published in Zhurnal Prikladnoi Khimii, 2006, Vol. 79, No. 10, pp. 1744–1746.

BRIEF COMMUNICATIONS

Synthesis and Fungicidal Activity of *S*-Amino Derivatives of *O*-Alkyldithiocarbonic Acids

O. V. Bakbardina, I. Yu. Pukhnyarskaya, M. A. Gazalieva, S. D. Fazylov, and E. M. Makarov

Institute of Organic Synthesis and Coal Chemistry of the Republic of Kazakhstan, Limited Liability Company, Karaganda, Kazakhstan

Research Institute of Plant Protection, Almaty, Kazakhstan

Received November 2, 2005

Abstract—*S*-Amino derivatives of *O*-alkyldithiocarbonic acid were prepared by oxidative condensation of certain alkaloids with sodium xanthates. Some of the compounds synthesized exhibit fungicidal activity.

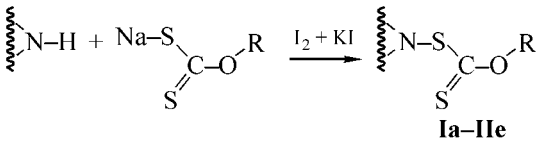
DOI: 10.1134/S1070427206100375

Alkali metal xanthates are widely used as additives to lubricating oils [1], flotation agents for dressing of various mineral ores [2], and complexing agents [3]. Their effect on the central nervous system and on redox processes in a human body has been examined [4].

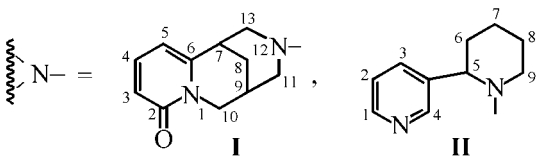
The properties of numerous sodium xanthate derivatives showing promise for development of new pesticides have been studied [5]. However, no data are available on the compounds derived from sodium xanthates and natural alkaloids anabasine and cytisine, whose insecticidal and fungicidal properties are well known [6].

Therefore, we studied the oxidative condensation of cytisine and anabasine with a series of sodium xanthates.

The oxidative condensation of sodium xanthates, prepared according to [7], with cytisine and anabasine was performed in an aqueous solution in the presence of I_2 (in 20% KI solution) by the scheme



Ia–IIe



I **II**

where R = C_2H_5 (**a**), C_3H_7 (**b**), $(CH_3)_2CH$ (**c**), C_4H_9 (**d**), $(CH_3)_2CHCH_2$ (**e**).

To determine the optimal reaction conditions, we examined the influence of temperature on the yield of the target products. With compound **Ia** as an example, we performed a series of experiments at temperatures varied in the range 0–80°C.

We found that the highest yield of **Ia**, 86%, is attained at 40°C. At lower temperatures, sodium xanthates are oxidized too slowly, and the yield of **Ia** decreases to 12%; at higher temperatures (60–80°C), the products form an intractable tar. As for the influence exerted by the structure of the alkyl substituent in sodium xanthates, the yields of the target products decrease with an increase in its size and with its branching: C_2H_5– > C_3H_7– > $(CH_3)_2CH$– > C_4H_9– > > $(CH_3)_2CHCH_2$–.

The yields of the anabasine derivatives are considerably lower than those of the cytisine derivatives. This trend may be due to the presence of a bulky pyridyl fragment with a conjugated system in the α-position of the piperidine ring in anabasine. As shown in [8], the anabasine molecule can exist in the form of two stable equatorial conformers produced by rotation of the pyridyl and piperidyl substituents about the C–C bond linking the two rings. At a certain steric orientation of the pyridyl fragment, its π-electron system can interact with the lone electron pair of the piperidyl nitrogen atom, thus decreasing the reactivity of the anabasine molecule.

Yields, physicochemical constants, and elemental analyses of **Ia**–**Ie** and **IIa**–**IIe**

Compound	mp, °C	Yield, %	Found, %			Empirical formula	Calculated, %		
			C	H	N		C	H	N
Ia	67–68	86.0	54.19	5.81	9.03	$C_{14}H_{18}N_2O_2S_2$	54.23	5.93	9.12
Ib	81–82	80.5	55.56	6.17	8.64	$C_{15}H_{20}N_2O_2S_2$	55.61	6.20	8.68
Ic	77–78	78.1	55.56	6.17	8.64	$C_{15}H_{20}N_2O_2S_2$	55.61	6.20	8.68
Id	121–122	63.4	56.80	6.51	8.28	$C_{16}H_{22}N_2O_2S_2$	56.92	6.61	8.31
Ie	109–110	45.1	56.80	6.51	8.28	$C_{16}H_{22}N_2O_2S_2$	56.92	6.61	8.31
IIa	72–73	60.3	60.30	6.38	9.93	$C_{13}H_{18}N_2OS_2$	55.41	6.43	9.97
IIb	84–85	54.7	54.70	6.76	9.46	$C_{14}H_{20}N_2OS_2$	56.84	6.82	9.58
IIc	71–72	52.8	54.70	6.76	9.46	$C_{14}H_{20}N_2OS_2$	56.84	6.82	9.58
IId	101–102	46.3	48.30	7.09	9.03	$C_{15}H_{22}N_2OS_2$	50.15	7.16	9.14
IIe	93–94	42.2	48.30	7.09	9.03	$C_{15}H_{22}N_2OS_2$	50.15	7.16	9.14

Compounds **Ia**–**Ie** and **IIa**–**IIe** are crystalline substances readily soluble in many organic solvents.

The structures of **Ia**–**Ie** and **IIa**–**IIe** were confirmed by IR and ^{1}H NMR spectroscopy, and their compositions, by elemental analysis. The IR spectra of **Ia**–**Ie** and **IIa**–**IIe** contain strong bands in the range 1135–1130 cm^{-1}, assigned to the C=S bond [9], and bands at 796–816 cm^{-1} characteristic of C–S stretching vibrations [9].

In the NMR spectra of **Ia**–**Ie**, the protons of the alkaloid core give signals in the expected regions of the spectrum [10]. Three groups of low-field signals belong to protons of the α-pyridone ring. The signals at 7.20 ppm correspond to H^2 ($J_{H^2H^3}$ 8.0 Hz), and a doublet at 6.32 ppm, to H^1 ($J_{H^1H^2}$ 10.0 Hz). A complex multiplet at 3.20–4.40 ppm corresponds to the axial and equatorial protons at C^7. The H^8 protons appear as a doublet at 2.38 ppm. The H^4 and H^6 protons give a group of lines in the range 2.98–3.10 ppm. The methylene H^5 protons appear as a complex multiplet centered at 1.96 ppm. The methyl group of the alkoxy fragment gives a multiplet at 1.18 ppm, and the methylene group, at 4.08 ppm.

Comparison of the spectra of **Ia**–**Id** with that of the starting cytisine shows that the signals of the protons at C^8 and $C^{8'}$ are appreciably shifted. This is apparently due to the fact that the lone electron pair of the adjacent nitrogen atom, occupying the equatorial position in cytisine, becomes axial on replacement of the hydrogen atom by the xanthate group. As a result, the delocalization of the lone electron pair to the antibonding orbital of the C–H bond becomes possible, which results in a stronger shielding of these protons.

In the ^{1}H NMR spectra of **IIa**–**IIe**, the signals of the pyridine ring protons H^1, H^2, H^3, and H^4 are observed in the low field. The H^1 proton gives a doublet at 8.80 ppm; H^4, a doublet at 8.79 ppm; H^3, a quartet at 8.10 ppm; and H^2, a quartet at 6.74 ppm. The methylene protons of the piperidine ring gives a complex multiplet at 3.47–3.80 ppm; the methine proton, a signal at 3.92–4.05 ppm; and the methylene protons remote from the N atom, a multiplet at 1.8–2.5 ppm.

Some of compounds **Ia**–**Ie** and **IIa**–**IIe** were tested for the fungicidal activity. *Fusarium oxysporum* and *Botrytis cinerea* phytopathogenic fungi were used as test cultures. The fungicidal activity was evaluated by the intensity of development of microorganisms on the cultural medium, compared to control experiments without addition of the xanthate derivatives.

We found[1] that *S*-(*N*-anabasinyl) derivative of *O*-isopropoxydithiocarbonic acid **IIc**, tested in vitro, shows a pronounced fungicidal activity against *Botrytis cinerea* (69–74% growth suppression). This compound also showed a pronounced activity against *Fusarium oxysporum* (56–67% growth suppression).

The results were confirmed by biological test statements. Compound **IIc** was recommended for further comprehensive studies as a promising pesticide for agriculture.

EXPERIMENTAL

The IR spectra were recorded on an Avatar-320 spectrometer (KBr pellets), and the ^{1}H NMR spectra, on a Tesla BS-587 spectrometer (operating frequency 80 MHz, C_6D_6, internal reference HMDS). The melting points were determined with a Boëtius heating

[1] Tests were performed at the Research Institute of Plant Protection, Almaty.

stage. The reaction mixtures were analyzed, and the product purity checked, by TLC on Silufol UV-254 plates (eluent benzene–acetone, 1 : 1 by volume).

***S*-(*N*-Cytisinyl) *O*-ethyl dithiocarbonate Ia.** A 0.25-l round-bottomed flask equipped with a mechanical stirrer and a dropping funnel was charged with 0.6 g (0.003 mol) of cytisine and 0.52 g (0.003 mol) of sodium xanthate in 30 ml of water. Then the mixture was heated to 40°C, and a saturated solution of iodine in 20% aqueous KI was added dropwise with stirring. The precipitate was filtered off and recrystallized from EtOH–H_2O (1 : 1).

***S*-(*N*-Anabasinyl) *O*-ethyl dithiocarbonate IIa** was prepared similarly from 0.5 g (0.003 mol) of anabasine and 0.52 g (0.003 mol) of sodium xanthate in 30 ml of water.

The other alkaloid xanthate derivatives were prepared similarly; their characteristics are listed in the table.

CONCLUSIONS

(1) *S*-Amino derivatives of *O*-alkyldithiocarbonic acids were prepared by oxidative condensation of cytisine and anabasine with sodium xanthates.

(2) It was found that *S*-(*N*-Anabasinyl) *O*-isopropyl dithiocarbonate exhibits pronounced fungicidal activity.

REFERENCES

1. Fal'kovskaya, A.A., Oberfel'd, M.Sh., Kheifets, E.M., Rapoport, I.B., et al., *Prisadki k maslam* (Additives to Oils), Moscow: Khimiya, 1966.
2. Otrozhdennova, L.A., Efimov, G.A., Pudov, V.F., et al., *Obogashch. Rud*, 1977, no. 2, pp. 6–10.
3. Campaigne, E. and Nargund, P.K., *J. Med. Chem.*, 1964, vol. 7, no. 2, pp. 132–135.
4. Hornemann, U., Iguchi, K., Vu, Y.V., and Rozlovski, J.F., *J. Org. Chem.*, 1983, no. 25, pp. 5026–5033.
5. Mel'nikov, N.N., *Pestitsidy: Khimiya, tekhnologiya i primenenie* (Pesticides: Chemistry, Technology, and Applications), Moscow: Khimiya, 1987.
6. Orekhov, A.P., *Khimiya alkaloidov* (Chemistry of Alkaloids), Moscow: Akad. Nauk SSSR, 1955.
7. Dawert, F., Reuther, K.H., and Born, F., *Chem. Ber.*, 1960, vol. 93, p. 3064.
8. Gazaliev, A.M., Zhurinov, M.Zh., and Fazylov, S.D., *Novye bioaktivnye proizvodnye alkaloidov* (New Bioactive Alkaloid Derivatives), Almaty: Gylym, 1992.
9. Bellamy, L.J., *Advances in Infrared Group Frequencies*, London: Methuen, 1968.
10. Kazitsyna, L. and Kupletskaya, N.B., *Primenenie UF, IK i YaMR spektroskopii v organicheskoi khimii* (Application of UV, IR, and NMR Spectroscopy to Organic Chemistry), Moscow: Vysshaya Shkola, 1971.

ISSN 1070-4272, Russian Journal of Applied Chemistry, 2006, Vol. 79, No. 10, pp. 1729–1730. © Pleiades Publishing, Inc., 2006.
Original Russian Text © G.A. Mandrov, M.Yu. Klimovich, A.N. Pukh, 2006, published in Zhurnal Prikladnoi Khimii, 2006, Vol. 79, No. 10, pp. 1747–1748.

BRIEF COMMUNICATIONS

Clarification of Coal-Clay Disperse Systems with Modified Polyacrylamide Flocculant

G. A. Mandrov, M. Yu. Klimovich, and A. N. Pukh

Institute of Coal and Coal Fuel Chemistry, Siberian Division, Russian Academy of Sciences, Kemerovo, Russia
Kemerovo Branch, Institute of Chemistry of Solids and Mechanochemistry, Siberian Division, Russian Academy of Sciences, Kemerovo, Russia

Received February 10, 2006

Abstract—Modification of polyacrylamide under mild conditions was studied.

DOI: 10.1134/S1070427206100387

Wastes from ore dressing enterprises, concentrated in sludge precipitation tanks of various designs and in sludge ponds, occupy large fields and pollute surface and underground waters and open reservoirs. From the safety viewpoint, processing of finely dispersed coal sludge from sludge ponds and precipitation tanks should improve the environmental situation around ore dressing enterprises.

One of the key problems of flotation is precipitation of fine (smaller than 30 μm) particles, which pass, in the case of modern processing procedures, into the final tailings with the mineral component. Owing to the absence of inexpensive and efficient reagents for concentration of coal fines by flotation, low-ash wastes are discharged into precipitation tanks, which causes of additional loss of the coal combustible mass.

In this study, we examined the possibility of enhancing the flocculation activity of domestic polyacrylamide (PAA), which is the most widely used flocculant with a well-developed production technology.

EXERIMENTAL

A large number of parameters that affect the structure formation in the course of polymer modification should be taken into account. Because of this circumstance, preparation of modified PAA with specified flocculation properties by the reaction of PAA with reactive monomers is a rather difficult problem. These parameters include the type and distribution of charged groups in the polymer chain, chain length, charge density, degree of branching and microstructure of macromolecules, polymer-monomer molar ratio, pH of the medium, temperature, pressure, etc. [1].

Taking into account the above factors, we chose the modification pathway making the structure more branched. PAA was modified with α-propylene chlorohydrin (1-chloro-2-propanol). The reaction of the initial PAA (molecular weight 1×10^6) with the above reagent was performed by the procedure reported in [2]. The resulting modified polyacrylamide (MPAA) was tested in clarification of coal-clay disperse systems. For these purpose, we used coal sludges from the sludge dump of the processing plant, which contains a mixture of coking coals of K, KO, and KS brands. These sludges were preliminarily concentrated using a hydrosizer [3]. The hydrosizer allows preparation of an enriched coal concentrate with permissible ash content and increased ash content in the rock material. After treatment of the coal suspension with the initial ash content A^d = 32.5% in the hydrosizer, we obtained a concentrate with ash content A^d = 10–11%. Then, the coal-clay suspension was treated with a flocculant. The initial coal sludge was sieved (mesh size 800 μm), and, after treatment in the hydrosizer, we obtained a coal-clay suspension with a mean geometrical diameter of particles of the dispersed phase of 2.25 μm (Fig. 1).

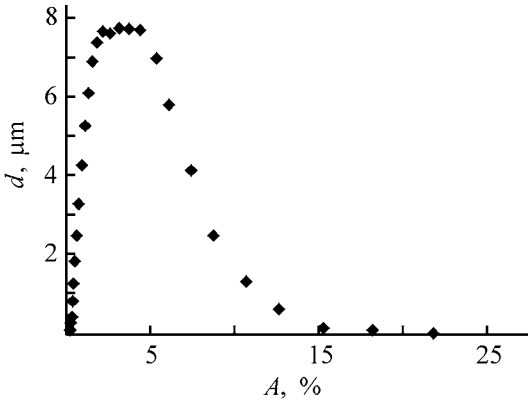


Fig. 1. Particle size distribution of the coal-clay suspension. (*d*) Particle diameter and (*A*) number of particles.

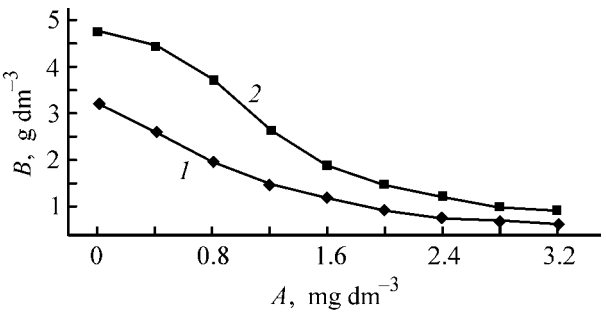


Fig. 2. Weight of the dry residue, *B*, in the clarified coal-clay suspension vs. the flocculant concentration *A*. Flocculant: (*1*) MPAA and (*2*) PAA.

The size distribution of the coal particles was determined on an Analysette-22 device.

The major mineral component of the coal-clay suspension is the clay material. The concentration process of the coal sludge in the laboratory hydrosizer is characterized by the following parameters (%): ash content in the initial coal sludge, A^d 32.6; ash content in the concentrate, A^d 10.5; ash content in the washed coal-clay suspension, A^d 67.8; water content of the concentrate, W^a 23; water content of the flocculated precipitate, W^a 25; yield of the dry concentrate, X_α 78; and yield of the dry coal-clay dispersion, X_α 17.

The flocculation activity of PAA and MPAA was evaluated by the procedure described elsewhere [4]. The dependence of the weight of the dry residue in the clarified coal-clay suspension on the content of flocculant is shown in Fig. 2. As seen, the flocculation activity increases on passing from PAA to MPAA. The flocculation process, as influenced by the flocculation activity of polymers, was described using the following mathematical model. Changes in the content of the solid phase (SP) in the coal-clay suspension with time in the course of treatment with a flocculant are described by

$$dc/dt = -Kcc_f, \quad (1)$$

where $c = c(t)$ is the total content of the solid phase (SP) in the coal-clay suspension (g dm^{-3}); c_f, flocculant concentration (mg dm^{-3}); and K, scaling factor, generally dependent on the total concentration of the solid phase and on the flocculant concentration.

The same equation can be written for each ith fraction of the SP particles, with c_i substituted for c. By integrating Eq. (1) at $t = 0$ and $c = c_0$, we obtained the following equation:

$$c = c_0 e^{-Kc_f t}, \quad (2)$$

where $\tau = 1/Kc_f$ is the relaxation time, i.e., the time in which the content of SP decreases by a factor of e.

The particle size distribution of the coal-clay suspension (Fig. 1) shows that the size of the SP particles is in the range of applicability of the Stokes law [5]. Our calculations using Eq. (2) for a flocculant concentration of 0.4 mg dm^{-3} (Fig. 2) show a decrease in the SP content by a factor of 1.8 and 3.1 in 102 and 53 s for PAA and MPAA, respectively. Analysis of the experimental and calculated data shows that the modified flocculant increases the rate of SP precipitation.

CONCLUSION

Modification of polyacrylamide with α-propylene chlorohydrin enhances the flocculation properties of the modified polymer, which can be used to clarify the return water in concentration of coal sludges with a hydrosizer.

REFERENCES

1. Mende, M., Petzold, G., and Buchhammer, H., *Colloid Polym. Sci.*, 2002, vol. 280, pp. 342–351.
2. Shevchenko, T.V., Ul'rikh, E.V., Yakovchenko, M.A., et al., *Kolloid. Zh.*, 2004, vol. 66, no. 6, pp. 840–843.
3. US Patent 5 609 256.
4. Mandrov, G.A., Klimovich, M.Yu., amd Pukh, A.N., *Estestv. Tekh. Nauki*, 2006, no. 1(21), pp. 290–294.
5. Kouzov, P.A., *Osnovy analiza dispersnogo sostava promyshlennykh pylei i izmel'chennykh materialov* (Principles of the Dispersion Composition of Industrial Dusts and Milled Materials), Leningrad: Khimiya, 1987.

ISSN 1070-4272, Russian Journal of Applied Chemistry, 2006, Vol. 79, No. 10, pp. 1731–1735. © Pleiades Publishing, Inc., 2006.
Original Russian Text © A.G. Morachevskii, 2006, published in Zhurnal Prikladnoi Khimii, 2006, Vol. 79, No. 10, pp. 1749–1753.

Henri Étienne Sainte-Claire Deville (To 150th Anniversary of the Development of the First Industrial Method for Production of Aluminum)

DOI: 10.1134/S1070427206100399

A French scientist, Professor Henri Étienne Sainte-Claire Deville is among the most outstanding chemists of the second half of the XIX century. A member of Paris Academy of Sciences (since 1861), president of the French Chemical Society (1863) and foreign corresponding member of Imperial St. Petersburg Academy of Sciences (since 1869), he laid foundations of quite a number of scientific areas, primarily in the field of applied inorganic chemistry. One of the main deeds of the scientist is the development of the first industrial method for production of aluminum (1856).

At the turn of the XIX century (1800), A. Volta (1745–1827), an Italian physicist, created the first chemical current source (Volta's column battery) and thereby opened up wide opportunities for analysis of the effect of electric current on various substances. One of the best known researchers of the early XIX century, English physicist and chemist H. Davy (1788–1829), a member of London Royal Society (since 1803) and honorary foreign member of St. Petersburg Academy of Sciences (since 1826), was among the first to commence electrochemical experiments. Having carried out a detailed study of the decomposition of water, Davy was the first to isolate metallic potassium (1807) and sodium (1808) by electrolysis of their molten hydroxides. Davy's studies aroused considerable interest and further served as a basis for development of industrial techniques for production of these metals. Later, Davy isolated barium, strontium, calcium, and magnesium by electrolysis of their molten hydroxides, but failed to obtain aluminum from its oxygen-containing compounds.

Aluminum was first isolated in the free state at the beginning of 1825 by a Danish physicist H.C. Oersted (1777–1851), who developed methods for obtaining aluminum chloride and for reduction of aluminum with a potassium amalgam. Metallic aluminum was obtained in a small amount from the forming aluminum amalgam by distillation without access of air. In 1827, a German physicist F. Wöler (1800–1882)



continued Oersted's experiments by replacing potassium amalgam with metallic potassium in the vapor state. Wöler's studies lasted long and only by 1845 the first stage in the history of aluminum was complete: although the metal was not obtained in a compact form, its amount was sufficient for determining its basic physical and chemical properties.

Thus, Davy was the first to formulate the task of obtaining in the free state an as yet unknown metal, named by him, in advance, aluminum. Oersted was the first to obtain aluminum, but he did not study its properties and did not specify the conditions of his experiments. Wöler not only isolated aluminum, but also determined its most important properties.

It was necessary to find a method for industrial manufacture of the metal and to specify areas of its practical use. This task was successfully accomplished in 1854, nine years after the final Wöler's work, by Henry Sainte-Claire Deville, who used the less expensive and more accessible sodium instead of potassium.

H. Sainte-Claire Deville was born on March, 11, 1818, in the island of Saint-Thomas (Virgin Islands, West-Indies) into the family of the French consul and, simultaneously, ship owner. He received his primary classical education in Paris and finished a medical institute in the same city (doctor of medicine, 1843). Even earlier, however, H. Sainte-Claire Deville took a great interest in chemistry, primarily under the influence of lectures delivered by professor L. Thenard (1777–1857, member of Paris Academy of Sciences since 1810, honorary foreign member of St. Petersburg Academy of Sciences since 1826), organized a private chemical laboratory, published in 1839 his first scientific study in the field of chemistry of natural compounds, and carried out a number of additional studies in this area.

In 1845, H. Sainte-Claire Deville occupied, by recommendation of Thenard, the position of a professor of chemistry and, simultaneously, became dean of a faculty at the University of Besanc'on (eastern France), one of the oldest universities of the country (founded in 1423).

An excellent experimenter, H. Sainte-Claire Deville continued, together with teaching and despite the lack of appropriate conditions, his scientific activities. The first years of his work were devoted to organic chemistry; however, already in 1849 he performed an original inorganic synthesis, obtained nitric anhydride by treating fry silver nitrate with chlorine. Having done so, he dispelled the opinion of that time that monobasic acids have no anhydrides.

In 1851, a French chemist A. Balard (1802–1876, member of Paris Academy of Sciences since 1844) was elected a professor at Collége de France, and H. Sainte-Claire Deville, who already became known by that time, occupied his position at Ecole Normale Superieure in Paris. This educational institution was engaged in training of teachers for secondary schools and, unfortunately, did not have sufficient conditions for scientific work. H. Sainte-Claire Deville did much for improvement of the laboratory improvement. He worked at Ecole Normale Superieure for for thirty years. It is during this period of time that all his diverse scientific studies were performed. In 1851–1853, H. Sainte-Claire Deville paid a considerable attention to improvement of methods for analysis of minerals and, in particular, silicates and carbonates. This refined the scientist's concepts concerning reactions at high temperatures in inorganic systems and gave him an impetus to devise and improve methods for production of metals and their purification to remove impurities. Based primarily on works of his predecessors, Davy, Oersted, and Wöler, H. Sainte-Claire Deville set to study aluminum. By that time, metallic potassium became less expensive and more accessible, which allowed H. Sainte-Claire Deville to perform large-scale experiments. Accounts of these experiments were rendered to Paris Academy of Sciences in 1854 and aroused a considerable interest. Professor J.B.A. Dumas (1800–1884, member of Paris Academy of Sciences, foreign corresponding member of St. Petersburg Academy of Sciences since 1845), a prominent scientist and public figure, demonstrated samples of aluminum and described properties of the metal to Emperor Napoleon III (1808–1873, Emperor of France in 1852–1870). Beginning from that time, H. Sainte-Claire Deville's works aimed to devise an industrial technology for manufacture of aluminum were fully financed by the State. A major success was that potassium was replaced, as a reducing agent, with metallic sodium, which is considerably simpler and safer in use. To reduce the cost of sodium, H. Sainte-Claire Deville developed a new technology for its manufacture. A mixture of anhydrous sodium carbonate, coal, and chalk was heated in tubular iron furnaces, with sodium produced in the vapor state and condensed in a cooler. This method was considerably more economical than that used before, in which sodium hydroxide served as the raw material. Another important achievement was that the readily volatile aluminum chloride was replaced with the double salt $AlCl_3 \cdot NaCl$. To obtain this salt, dry chlorine was passed over hot mixture of alumina, sodium chloride, and coal. The double aluminum sodium chloride formed in the vapor state was condensed and cooled.

It should be noted that metallic aluminum can be obtained from the double salt $AlCl_3 \cdot NaCl$ by electrolysis. This possibility was noticed in 1854, virtually simultaneously and independently, by H. Sainte-Claire Deville and R.W. Bunsen (1811–1899, foreign member of St. Petersburg Academy of Sciences), a professor of Heidelberg University in Germany. The equipment used by both researchers in studies of electrolysis of a molten double chloride was nearly the same: experiments were performed in porcelain crucibles at about 200°C. In Bunsen's studies, both electrodes were made of carbon, whereas H. Sainte-Claire Deville used a carbon anode and a platinum cathode. Aluminum was deposited as a thin layer on the platinum cathode and was scraped-off at regular intervals of time and remelted. H. Sainte-Claire Deville attempted to obtain aluminum by electrolysis of other molten electrolytes, but, at that time, such experiments could not go beyond the laboratory scale, because it was impossible to produce considerable amounts of electric power. Nevertheless, H. Sainte-

Claire Deville's experiments in France and Bunsen's in Germany undoubtedly affected the later development of an industrial technology for manufacture of aluminum by electrolysis of cryolite–alumina melts (1886).

In the middle of the XIX century, the chemical technique for industrial manufacture of aluminum was the only possible. Beginning in 1856, more than 200 tons of the metal was produced during more than thirty years by reduction of aluminum chloride in the form of the double salt $AlCl_3 \cdot NaCl$ by the method devised by H. Sainte-Claire Deville, and the price of the metal was steadily decreasing. Already at the World Exhibition in Paris in 1855, chemically produced aluminum was demonstrated as a commercial product. Twelve aluminum slugs of the metal, with a total weight of 12 kg, were demonstrated. At a regular meeting of the French Academy of Sciences on October 13, 1856, professor Dumas reported that production of aluminum went beyond the stage of research and became an industrial process. France was the first country that set up production of aluminum on the industrial scale.

Originally, the alumina necessary for production of the $AlCl_4 \cdot NaCl$ salt was obtained by calcination of ammonium alum $NH_4Al(SO_4)_2 \cdot 12H_2O$; later, bauxites served as the raw material. Bauxites were processed into alumina by a method close to the present-day sintering technique. Crushed bauxite was mixed with powdered soda and the mixture was calcined in a flame surface to give sodium aluminate. The mass extracted from the furnace was leached with water, and the resulting pure solution of sodium aluminate was treated with carbon dioxide under agitation, with an aluminum hydroxide precipitate formed.

The history of discovery of aluminum and its industrial production by H. Sainte-Claire Deville's method were described in a monograph by Debard [1] and in later publications [2–4]. The contribution of Oersted and Wöler to the development of the aluminum production technology was considered in detail by Goldschmidt [5, 6].

H. Sainte-Claire Deville was primarily a scientist and a pedagogue. Together with teaching at Ecole Normale Superieure, he delivered lectures on chemistry at Paris University (Sorbonne) in 1853 to 1866, by invitation of professor Dumas. After the industrial manufacture of aluminum was organized, H. Sainte-Claire Deville continued intensive scientific studies of processes for isolation of other elements. Because sodium and aluminum became well accessible, the scientist used these elements as reducing agents. In a joint study with Wöler, H. Sainte-Claire Deville obtained by reduction of boron oxide with sodium an amorphous modification of boron in the form of a powder. Soon after, having changed the experimental conditions and using aluminum as a reducing agent, he obtained boron in the crystalline form and synthesized boron nitride. By reduction of silicon chloride vapor with aluminum, H. Sainte-Claire Deville obtained crystals of silicon (1856). Later (1863), the scientist suggested a faster and more convenient method for production of crystalline silicon from its fluorosilicate. By treating potassium fluorotitanate with a sodium vapor in the atmosphere of hydrogen, H. Sainte-Claire Deville and Wöler obtained titanium [7]. To perform high-temperature studies, H. Sainte-Claire Deville designed and fabricated laboratory furnaces using various kinds of fuel. During the period of his intensive scientific activities (1850–1880), he was a leading specialist in high-temperature inorganic chemistry.

In 1859–1861, H. Sainte-Claire Deville and his closest co-worker H.G. Debray (1827–1888, member of Paris Academy of Sciences since 1877) took part, at request of the Russian government, in the development of methods for refinement of Ural platinum. A Russian academician, B.S. Jacoby (1801–1874), acted as intermediate in the negotiations. Thirty-two kilograms of crude platinum, 16 kg of platinum in the form of coins minted in Russia, and 8 kg of crude iridium were shipped to France. The French scientists devised a method for refining platinum and isolating platinum group metals. They were the first to fuse platinum in a considerable amount (12–15 kg), and to obtain platinum ingots. A detailed report on the accomplished work was published in Russia in Gornyi Zhurnal (Mining Journal) [8]. Studies by H. Sainte-Claire Deville and Debray in the field of refining of platinum group metals were highly appreciated by specialists. Commissioned by the International Committee for Weights and Measures, they fabricated international prototypes of the meter and kilogram from a platinum alloy with 10% iridium (1872).

In 1857, H. Sainte-Claire Deville commenced studies in the field of thermal dissociation of substances, which were later recognized as classical. According to a Russian scientist N.N. Beketov (1827–1911, academician of St. Petersburg Academy of Sciences since 1886), who worked at H. Sainte-Claire Deville's laboratory during a business trip (1858), these studies "constituted a historical epoch in the development of chemistry" [9, 10]. In his paper "On dissociation or spontaneous decomposition of substances under

the action of heat" [11], which became widely known, the scientist demonstrated that, when heated, steam does decompose into oxygen and hydrogen. In his later studies (1859–1861), H. Sainte-Claire Deville noted that water vapor decomposes not only at the melting point of platinum (1750°C), but also at that of silver (950°C) [9]. In a series of lectures on this subject, published in Paris in 1866, the scientist suggested that "the phenomenon of spontaneous decomposition of water ... should be named dissociation." According to H. Sainte-Claire Deville, this definition refers only to those cases in which "decomposition occurs partially and at a temperature lower than that corresponding to a complete disintegration of the compound," i.e., the cases of reversible decomposition, whose products again interact when the forces causing the decomposition are removed [9]. In an experimental study of equilibria, H. Sainte-Claire Deville suggested and successfully used the method of their "quenching." The studies of the French scientist, devoted to thermal dissociation, were of primary importance for the further development of the theory of thermal equilibria.

In the Russian scientific literature, H. Sainte-Claire Deville's studies in the field of thermal dissociation were first analyzed by V.F. Alekseev (1852–1919) in "Essay on the Modern State of Chemical Mechanics" [12]. The scientific activities of Alekseev were considered in a previous publication by Morachevsii [13]. H. Sainte-Claire Deville's works exerted a strongest influence on the development of experimental research and their thermodynamic assessment.

The main results of H. Sainte-Claire Deville's scientific activities can be briefly formulated as follows.

He developed and implemented on the industrial scale a chemical method for manufacture of aluminum (reduction of the double salt $AlCl_3 \cdot NaCl$ with metallic sodium);

independently of Bunsen, demonstrated the possibility of aluminum recovery at low temperatures by electrolysis of chloroaluminate melts;

together with Wöler, was the first to isolate boron, silicon, and titanium in pure form and obtained some compounds of these elements;

widely used metallic sodium as a reducing agent and developed a method for its production, which markedly reduced its price; was the first to use aluminum as a reducing agent;

made a major contribution to the development of a laboratory equipment that enabled high-temperature studies;

together with Debray, developed a technology for platinum refinement with recovery of platinum group metals and was the first to fuse platinum;

discovered the phenomenon of thermal dissociation.

Owing to H. Sainte-Claire Deville's efforts, the chemical laboratory at Ecole Normale Superieure became one of the best known European scientific centers, visited by scientists from various countries. Students were actively involved in research, especially in studies of dissociation processes. The scientific legacy of the scientist is huge. In addition to being engaged in the above-mentioned principal areas of research, H. Sainte-Claire Deville carried out numerous studies in analytical chemistry and performed high-temperature syntheses of a large number of minerals (apatite, ruby, sapphire, zircon, etc.).

In October 1876, H. Sainte-Claire Deville suffered a severe loss, his elder brother Charles (born in 1814), a specialist in geology and meteorology and member of the French Academy of Sciences, died. The brothers were on very friendly terms, they together leaved their parents in West-Indies in 1828 and came to Paris. Despite the difference in age, they together received their secondary education. The loss of the brother strongly affected H. Sainte-Claire Deville's health and mental state. He died on July 1, 1881, at Boulogne sur Seine not far from Paris and was buried near his brother. The commemoration speech at the meeting of the French Academy of Sciences on July 4, 1881, was delivered by Louis Pasteur (1822–1895, member of numerous academies of the world, honorary foreign member of St. Petersburg Academy of Sciences), an outstanding chemist and microbiologist and a close friend of H. Sainte-Claire Deville [14].

Among the known publications, that by Gernez [15] describes the life and scientific and pedagogical activities of H. Sainte-Claire Deville in most detail. More concise evidence can be found in [7], brief articles [16, 17], and encyclopedias and biographical reference books. A popular description of certain episodes of H. Sainte-Claire Deville's life is contained in a book by M. Manolov [18].

REFERENCES

1. Debard, R., *Alyuminii, ego proizvodstvo i primenenie* (Aluminum, Its Manufacture and Use), Leningrad: Goskhimtekhizdat, 1932.
2. Mashovets, V.P., *Elektrometallurgiya alyuminiya* (Electrometallurgy of Aluminum), Moscow: Metallurgizdat, 1938.
3. Belyaev, A.I., *Tr. In–ta Istorii Estestvozn. Tekhn.*, 1959, vol. 20, pp. 3–152.

4. Kaluzhskii, N.A. and Taits, A.Yu., *Otechestvennaya metallurgiya alyuminiya – ot pervykh shagov do promyshlennogo proizvodstva 1825–1932 gg*. (Domestic Metallurgy of Aluminum: from First Steps to Industrial Manufacture, 1825–1932), Moscow: Metallurgiya, 1991.
5. Goldschmidt, K., *Z. Angew. Chemie*, 1925, vol. 38, no. 47, pp. 1057–1058.
6. Goldschmidt, K., *Z. Angew. Chemie*, 1926, vol. 39, no. 11, pp. 375–376.
7. Oesper, R.E. and Lemay, P., *Chymia*, 1950, vol. 3, pp. 205–221.
8. Sainte-Claire Deville, H. and Debray, H.G., *Gornyi Zh.*, 1861, no. 4, pp. 32–94; no. 5, pp. 237–280; no. 6, pp. 400–459.
9. Solov'ev, Yu.I., *Ocherki po istorii fizicheskoi khimii* (Essays on History of Physical Chemistry), Moscow: Nauka, 1964.
10. *Istoriya ucheniya o khimicheskom protsesse. Vseobshchaya istoriya khimii* (History of the Theory of the Chemical Process, General History of Chemistry), Moscow: Nauka, 1981.
11. Sainte-Claire Deville, H., *Compt. Rend.*, 1857, vol. 45, pp. 857–861.
12. Alekseev, V.S., *Gornyi Zh.*, 1884, vol. 1, pp. 369–398.
13. Morachevskii, A.G., *Ocherki ob uchenykh-khimikakh SanktPeterburga. XIX vek i pervaya polovina XX veka* (Essays about Scientists-Chemists of St. Petersburg, XIX Century and First Half of the XX Century), St. Petersburg: Politekhn. Univ., 2004.
14. Pasteur, L., *Compt. Rend.*, 1881, vol. 93, pp. 6–9.
15. Gernez, M.D., *Ann. Sci. Ecol. Normale Superieure*, 1894, vol. 11. Supplement, pp. 3–70.
16. *Nature*, 1881, no. 7 (July), pp. 219–221.
17. Leicester, H.M., *Dictionary of Scientific Biography*, Gillespil, Ch.C., Ed., New York: Charles Scrilner's and Sons, 1980, pp. 77–78.
18. Manolov, K., *Velikie khimiki* (Outstanding Chemists) (Translation from Bulgarian), in 4 vols., Moscow: Mir, 1986, vol. 1, 3rd ed.

A. G. Morachevskii

ISSN 1070-4272, Russian Journal of Applied Chemistry, 2006, Vol. 79, No. 10, p. 1736. © Pleiades Publishing, Inc., 2006.
Original Russian Text © G.E. Zaikov, 2006, published in Zhurnal Prikladnoi Khimii, 2006, Vol. 79, No. 10, p. 1754.

INFORMATION

Scientific Legacy of N.N. Semenov: A Breakthrough into the Future

DOI: 10.1134/S1070427206100405

The title of this article fully corresponds to the name of the International conference devoted to the 110th anniversary of Academician N.N. Semenov (1896–1986). Over 800 scientists and students took part in this conference.

Semenov was the founder and permanent head of the Institute of Chemical Physics, Academy of Sciences of the USSR, in 1931–1986. In 1956 he (jointly with S. Hinschelwood) was awarded a Nobel Prize for the development of the theory of branched chain reactions. He had been publishing these works since 1928. Semenov was one of the founders of chemical physics and biochemical physics as sections of natural sciences. He significantly contributed to the development of chemical kinetics as a tool for studying mechanisms of chemical and biochemical processes.

The conference was organized by the Russian Academy of Sciences (RAS), Ministry of Education and Science of the Russian Federation, Lomonosov State University in Moscow (MGU), Moscow City Government, Semenov Foundation for Science Development, and Joint Institute of Chemical Physics (OIKhF).

The conference proceeded according to a two-day program on April 14–15, 2006 (Semenov was born on April 16, 1896).

On the first day, the conference proceeded in the Big Hall of the Russian Academy of Sciences. The opening of the conference was attended by leading scientists of the Russian Federation and representatives of UNESCO and Moscow Government. A large number of telegrams were addressed to the conference and, in particular, that the from President of the Russian Federation V.V. Putin.

Four plenary presentations were held on the first day of the conference.

RAS Academician V.E. Fortov devoted his presentation to the development of chemical physics under extreme conditions. Prof. J.-M. Lehn (France) characterized the current status of supramolecular chemistry, chemical physics, and chemical kinetics. Prof. J Polanyi (Canada) presented modern views in the field of quantum chemistry and chemical kinetics of gas-phase processes. Special interest was evoked by the presentation of RAS Academician V.P. Skulachev, concerned with radical forms of oxygen (mithochondrias and aging processes), and its discussion.

On the second day, the conference proceeded in the Big Hall of the main building of MGU. There were two sessions. The morning session included three plenary presentations and one discussion. RAS Academician A.E. Shilov delivered a lecture on some modern achievements in chemical physics and biomimetics. The second presentation was concerned with problems of light, energy, and natural photosynthesis (M. Gretzel, Switzerland). The presentation by S. Sarisiftsy, Austria, was focused on problems of accumulation of solar energy and its transformation into electricity (organic solar batteries). This was followed by round table debates on the subject "Fundamental science for power generation" (it should be reminded that Semenov for many years headed in the USSR the Scientific Council for solar energy accumulation).

The evening session on the second day of the conference included presentations on the prospects for development of high school (universities and institutes). It should be mentioned that Semenov established in 1944 the Chair of Chemical Kinetics at the Chemical Faculty of MGU and headed it till 1986. Two presentations concerning the future of higher education in various countries were made by Prof. R. Loughline, US.

The session concluded with round table debates on the subject "Higher Education in XXI Century", whose participants suggested diversified (occasionally, conflicting) ideas.

As a part of the conference, a number of events were organized:

informal meeting of Russian and foreign scientists with Russian young scientists and students;

meetings of Nobel Prize Laureates with representatives of the Semenov International Foundation for Science Development;

exhibition devoted to the 110th anniversary of Academician Semenov at the MGU Museum in the New Library building.

The conference demonstrated that the ideas and solutions suggested by Semenov in his time were further developed by many scientists from various countries.

G.E. Zaikov

ISSN 1070-4272, Russian Journal of Applied Chemistry, 2006, Vol. 79, No. 10, p. 1737. © Pleiades Publishing, Inc., 2006.
Original Russian Text © G.E. Zaikov, M.I. Artsis, N.N. Madyuskin, 2006, published in Zhurnal Prikladnoi Khimii, 2006, Vol. 79, No. 10, p. 1755.

INFORMATION

All-Russia Conference of Young Scientists and Second School "Oxidation, Oxidative Stress, and Antioxidants"

DOI: 10.1134/S1070427206100417

The All-Russia Conference of Young Scientists and Second School "Oxidation, Oxidative Stress, and Antioxidants" was held on June 1–3, 2006, at the Semenov Institute of Chemical Physics, Russian Academy of Sciences (IKhF RAN). It was devoted to the 90th anniversary of Academician N.M. Emanuel' and the 110th anniversary of his teacher, Nobel Prize Laureate Academician N.N. Semenov.

The conference was organized by IKhF RAN, Emanuel' Institute of Biochemical Physics (IBKhF RAN), and Institute of Problems of Chemical Physics, Russian Academy of Sciences (IPKhF RAN). The Organizing Committee was headed by Academician A.A. Berlin, Director of IKhF, and Corresponding Member of the Russian Academy of Sciences (RAS), S.D. Varfolomeev, Director of IBKhF. Over 100 scientists from 15 research centers of CIS took part in the conference.

The session was opened by Academician A.A. Berlin who made a presentation devoted to the 110th anniversary of Academician Semenov. A special attention was given to the school created by Semenov, disciples of this school, and their contribution to science. The discussion on oxidation processes included a presentation by G.E. Zaikov (IBKhF RAN), focused on the practical implementation of the results of the research conducted by Academician N.M. Emanuel' and his disciples (Research–Development–Production).

On the second day of the work of the conference, 4 plenary presentations were made, devoted to the development of ideas and views concerning the role of free radicals and peroxide oxidation in biology and medicine (E.B. Burklakova, IBKhF RAN); reactivity of antioxidants of radical reactions (E.T. Denisov, IPKhF RAN); role of nitrogen oxides in oxidation processes (A.F. Vanin, IKhF RAN); and theoretical and applied aspects of the chemistry of phenolic antioxidants (V.B. Volevaya, IBKhF RAN).

Young scientists prepared numerous poster presentations, whose discussion was followed by an extensive discussion of the subject "What is antioxidant," headed by Burlakova and O.T. Kasaikina, IKhF RAN.

On the third day of the work of the conference, two sessions were held. At the morning session, S.D. Varfolomeev, RAS Corresponding Member, made a presentation concerning the role of enzymes in the development and suppression of oxidative stress. The presentation by Kasaikina was focused on the oxidation of complex multicomponent systems, with a special emphasis on pro- and antioxidative effects, and that by N.P. Pal'mina (IBKhF RAN), on the peroxide oxidation of lipids by biological membranes. The morning session concluded with another poster session.

During the evening session, the conference participants heard and discussed presentations devoted to the antioxidative properties of natural components of cells in vitro and in vivo (L.N. Shishkina, IBKhF RAN); synergism and antagonism in mixed compositions of bioantioxidants (N.M. Storozhok, Medical Academy, Tyumen); and numerical analysis of the chemical reaction mechanism of the α-tocopherol-inhibited peroxidation of methyl linoleate (L.A. Tavadyan, Nalbandyan Institute of Chemical Physics, National Academy of Sciences of Armenia, Yerevan). The last presentation was focused on the kinetic significance of individual stages of the processes.

This was followed by an analysis and discussion of all the poster presentation made at the conference (a total of nearly 70), mostly prepared by young scientists. All these presentations concerned various aspects of the kinetics and mechanism of oxidation of organic compounds of various classes (with both low and high molecular weight). The general discussion at this session was aimed to decide what is a more efficient pathway for stabilization: deactivation of radicals or nonradical utilization of peroxides with deactivation of catalysts (enzymes). The conclusion was that each factor plays a significant role, and its share depends on the nature of organic compounds and catalysts.

The work of the conference demonstrated that young people are gradually returning to science; the scientific level of the presentations corresponds to the current world standard.

The conference participants decided to hold the next conference in 2008 at IKhF RAN and IBKhF RAN.

G.E. Zaikov, M.I. Artsis, and N.N. Madyuskin

ISSN 1070-4272, Russian Journal of Applied Chemistry, 2006, Vol. 79, No. 10, pp. 1738–1739. © Pleiades Publishing, Inc., 2006.
Original Russian Text © A.G. Morachevskii, 2006, published in Zhurnal Prikladnoi Khimii, 2006, Vol. 79, No. 10, pp. 1756–1757.

REVIEWS

Sadykov, S.B., *Avtoklavnaya pererabotka nizkosortnykh tsinkovykh kontsentratov* (Autoclave Processing of Low-Grade Zinc Concentrates),

Yekaterinburg: Ural. Otd. Ross. Akad. Nauk, 2006, 541 pp.

DOI: 10.1134/S1070427206100429

In the scale of its manufacture, zinc occupies the third place among nonferrous metals, being exceeded in this regard only by aluminum and copper. The demand for zinc steadily grows; the main areas of its use are as follows: deposition of protective coatings, and primarily those on steel articles; manufacture of brass, bronze, and alloys for die casting; and production of chemical goods.

The favorable situation in the world market of zinc promotes development of additional facilities for its manufacture from domestic raw materials in the Republic of Kazakhstan. In the construction of the Balkhash zinc plant with an annual design output of 100 thousand tons of zinc, the unique technology of autoclave leaching, previously not used in Kazakhstan or other CIS countries, has been implemented. The book by S.B. Sadykov, which probably should be better classed with industrial-technological literature, covers three principal areas: (i) analysis of the present-day state of world's production of zinc with account of the role played by autoclave hydrometallurgy, (ii) examination of the potentialities of the autoclave leaching in decomposition of low-grade zinc concentrates, and (iii) search for optimal solutions in the implementation of the new technological process.

Sadykov's book, published under scientific editorship of S.S. Naboichenko, a known specialist in hydrometallurgy and corresponding member of the Russian Academy of Sciences, comprises an introduction, six chapters grouped into three parts, conclusion, and three supplements. The brief introduction (pp. 3–5) formulates the problems discussed in the book. The first part of the book (chs. 1, 2; pp. 7–110) starts with a discussion of the situation in the world market as of the beginning of 2004. The state of production in the countries that are leading manufacturers of zinc is considered, as well as that in the CIS countries and, separately, in Kazakhstan, where the main manufactures of zinc is OAO Kaztsink. This company, organized in January 1997, performs the whole production cycle, from geological surveys to mining works, mining and dressing of the ore, and metallurgical processing of the concentrate to give zinc and lead as final products. In 2004, Kaztsink company manufactured 279 thousand tons of refined zinc. All plants of the company are situated on the territory of the Republic of Kazakhstan. The first part of the book also analyzes in detail the experience gained in autoclave processing of zinc concentrates at a number of foreign plants (Canada, Germany, Japan).

The second part of the book (chs. 3–5, pp. 113–411) discusses the results of studies of the autoclave technology for processing of zinc concentrates in Kazakhstan (Kazakhmys plant). The autoclave leaching is based on the interaction of components of a crushed concentrate with sulfuric acid and oxygen to give the corresponding sulfates and elementary sulfur. The author presents the results of numerous experiments with both single- and double-stage leaching. All the experimental data obtained are presented with exhaustive completeness, including numerous analysis of various products (solutions and solid phases) to determine a large number of elements and material balances of the leaching stages. The good agreement between the data for zinc, copper, iron, lead, and sulfur in input and output materials in autoclave leaching indicates that the procedures used for sampling and analysis are reliable. Also considered are the results of laboratory studies (ch. 3) and large-scale tests (ch. 4). The same part of the book gives a general description of a design of a plant for processing of zinc concentrates by the autoclave technology (ch. 5).

The third part of the book (ch. 6, pp. 413–494) describes in detail the implementation of the technology including the autoclave leaching at Balkhash zinc plant in the pre-startup period.

In the conclusion (pp. 413–494), the author emphasizes once more that nonferrous metallurgy is one of the leading branches of industry in the economy of

the Republic of Kazakhstan. The increasing demand for zinc in the world market makes feasible industrial use of zinc concentrates of comparatively poor quality, with a lowered content of zinc (40–45%) and increased content of copper (3–5%) and lead (1–3%). In accordance with the foreign technological practice, it is advisable to use, when processing concentrates of this kind, the autoclave leaching with the subsequent purification of the resulting solutions to remove impurities and electrolysis in the final stage.

Supplements I, II, and III (pp. 515–527, 528–540, and 541–579) present, respectively, the generalized results of stand tests of autoclave leaching of the zinc concentrate at Kazakhmys plant, per-operation balances of the autoclave-hydrometallurgical technology for manufacture of zinc, and technological regulation for processing of solutions produced in autoclave leaching.

The author summarized and discussed a vast material of technological nature. The book is well published and includes a large number of tables, as well as technological schemes and photographs. The book is primarily intended for engineers and technicians at plants and research and design institutions engaged in use and development of hydrometallurgical technologies. It may be of use for students of metallurgical specialties in the pregraduate stage. Sadykov has accomplished a large and valuable work.

A. G. Morachevskii

ISSN 1070-4272, Russian Journal of Applied Chemistry, 2006, Vol. 79, No. 11, pp. 1741–1751. © Pleiades Publishing, Inc., 2006.
Original Russian Text © A.V. Yakovlev, A.I. Finaenov, S.L. Zabud'kov, E.V. Yakovleva, 2006, published in Zhurnal Prikladnoi Khimii, 2006, Vol. 79, No. 11, pp. 1761–1771.

REVIEWS

Thermally Expanded Graphite: Synthesis, Properties, and Prospects for Use

A. V. Yakovlev, A. I. Finaenov, S. L. Zabud'kov, and E. V. Yakovleva

Engels Technological Institute, Saratov State Technical University, Engels, Saratov oblast, Russia

Received April 13, 2006

Abstract—Results obtained in synthesis of thermally expanded graphite by chemical and electrochemical methods with sulfuric and nitric acids are summarized. The possibility of controlling the properties of thermally expanded graphite compounds in electrochemical synthesis is demonstrated. The existing and promising application areas of thermally expanded graphite are analyzed.

DOI: 10.1134/S1070427206110012

Graphite and various composite materials based on graphite, including graphite intercalation compounds (GICs), are widely used in a variety of fields of science, technology, and industry. Some GICs with acids and salts are used to obtain thermally expanded graphite (TEG), which has the form of a foamed carbon structure [1] and is used to produce low-density carbon materials and articles [2–6]. Similarly to graphite, TEG is chemically inert and heat-resistant. Its electrical conductivity and thermal conductivity are determined by the porous structure of the material and may widely vary [7–9]. An important distinction of TEG from all other powder-like carbon materials is its ability to form carbon articles without any binder. Thermally expanded graphite is well rolled into a flexible graphite foil [10], compacted into gaskets and seal rings [11–13], and introduced into the composition of multifunctional composites [14–17]. Thanks to a unique combination of properties of the material and to the possibility of their purposeful modification, seals, linings, catalysts, adsorbents, fireproofing composites, flexible heaters, and many other TEG-based articles are rather widely used in modern high-tech industries. The high chemical and thermal stability, combined with controllable electrical and thermal conductivity, porosity, and developed specific surface area create prerequisites for development of multifunctional materials.

The general principle underlying various methods for production of TEG consists in intercalation of substances or compounds, which either are themselves converted into gases upon rapid heating or give gaseous decomposition products, into the interlayer spaces of graphite [18, 19].

Numerous methods for GIC synthesis have been developed [20–22]. They are commonly subdivided into chemical (including vapor- or gas-phase synthesis and liquid-phase intercalation) and electrochemical, including galvanostatic or potentiostatic oxidation.

According to [23], the stages of GIC are the following: (1) transport of a substance to be introduced to the surface of the graphite host; (2) its adsorption by the surface, accompanied by separation of the substance to be introduced from that serving as a transporting agent; (3) intercalation into the host; (4) diffusion within the host; and (5) reaction between different intercalation stages.

Rudorff [24, 25] determined the fundamental aspects of the process of acid intercalation of graphite. The main specific feature of the process is the stepwise intercalation and the necessary presence of an oxidizing agent. The chemical model of GIC formation presumes occurrence of conjugated reactions of oxidation and intercalation [24]:

$$pC + [Ox] \rightarrow C_p^+ + [Ox]^-, \quad (1)$$

$$C_p^+ + A^- + m\mathrm{HA} \rightarrow C_pA^- \cdot m\mathrm{HA}. \quad (2)$$

The necessity for presence of an oxidizing agent is due to the low redox potentials of systems containing most of the acids being introduced, which cannot withdraw electrons from the graphite network. An exception is provided by nitric and perchloric acids, which are self-intercalating agents [26]. Initially, the oxidizing agents change the composition of oxygen-containing surface functional groups (SFGs) at terminal atoms of graphite layers [7, 19, 27]. The transfer

of electrons from graphite networks lowers the Fermi level of graphite, and the C_p^+ macrocation is formed in the carbon layers [reaction (1)]. The change in the SFG composition and the presence of charge on the graphite planes favor wedging of the interplanar spaces at edges of a carbon particle, which creates conditions for electrostatic drawing-in of acid anions [reaction (2)], i.e., for the direct occurrence of the intercalation process.

A particular place among acceptor GICs is occupied by compounds with sulfuric and nitric acids, graphite bisulfate and graphite nitrate. This is due to their high practical importance, because they serve as starting products for synthesis of thermally expanded graphite. The chemical method for synthesis of graphite bisulfate consists in oxidation of graphite with an H_2SO_4 solution additionally containing an oxidizing agent (Ox) [28, 29]:

$$24n\mathrm{C} + \mathrm{Ox}^z + m\mathrm{H_2SO_4} \rightarrow \mathrm{C}_{24n}^+ \cdot \mathrm{HSO_4^-} \cdot (m-1)\mathrm{H_2SO_4} + \mathrm{HOx}^{(z-1)}. \quad (3)$$

As oxidizing agents can serve a wide variety of compounds: CrO_3, $K_2Cr_2O_7$, $(NH_4)_2S_2O_8$, HNO_3, $KMnO_4$, H_2O_2, O_3, etc. The rate of formation and the stage of the resulting graphite bisulfate depend on the H_2SO_4 concentration and on the nature and content of the oxidizing agent in the solution [24, 29–31]. The dynamics of graphite bisulfate formation, with such oxidizing agents as HNO_3 and $KMnO_4$ involved, was studied for the first time by the potentiometric method in [32, 33]. Plateaus at potentials of 1.0 and 1.3 V (vs. SHE) were observed on the potentiometric curves obtained during chemical synthesis. These plateaus correspond, according to the results of X-ray phase analysis (XPA), to the formation of stage III of graphite bisulfate and to transformation of stage II of graphite bisulfate into stage I.

The mechanism of graphite nitrate formation by chemical oxidation in 96% nitric acid was described in [34]. The sequence of reactions, with account of the adsorption and reduction of HNO_3, formation of graphite macrocations, and their neutralization via penetration of NO_3^- into the interlayer space, can be represented as the following set of reactions:

$$\mathrm{HNO_3} \rightarrow \mathrm{HNO_{3(ads)}}, \quad (4)$$

$$2\mathrm{HNO_{3(ads)}} \rightleftarrows \mathrm{H_2O} + \mathrm{NO_{3(ads)}^-} + \mathrm{NO_2^+}, \quad (5)$$

$$\mathrm{NO_{2(ads)}^+} + n\mathrm{C} \rightarrow n\mathrm{C}^+ + \mathrm{NO_{2(ads)}}, \quad (6)$$

$$\mathrm{NO_{2(ads)}} \rightarrow \mathrm{NO_{2(g)}}, \quad (7)$$

$$n\mathrm{C}^+ + \mathrm{NO_{3(ads)}^-} + m\mathrm{HNO_{3(ads)}} \rightarrow \mathrm{C}_n^+ \cdot \mathrm{NO_3^-} \cdot m\mathrm{HNO_3}. \quad (8)$$

Reaction (5) in the adsorbed form is similar to the well-known dissociation of pure HNO_3 and gives rise to strongly electrophilic nitronium ions NO_2^+. Reaction (6) shows that the NO_2^+ ion captures an electron from the graphite lattice to be desorbed as NO_2 [reaction (7)]. As a result, graphite acquires a positive charge and draws in nitrate ions with solvate HNO_3 ligands to become electrically neutral.

As regards the possible composition of the resulting graphite nitrate, published evidence is contradictory [28, 34–37], in contrast to that for graphite bisulfate. According to the data for graphite nitrate, its composition is described by the general formula also characteristic of other graphite compounds with acids: $C_{24n}^+ \cdot NO_3^- \cdot 2HNO_3$, where n = 1, 2, 3, ... are intercalation stages. In addition, X-ray and electron diffraction analyses revealed that a small number of water molecules forming their own sublattice are present between carbon layers [37]. The ideal stoichiometry for this case is $C_{4.3n}HNO_3 \cdot mH_2O$ for nth stage, where $m < 0.07$ [37], which agrees with the chemical analysis data.

In [38–42], a strict correlation between the redox potential of a system under study and the number of a stage of the forming GIC was revealed by potentiometry for the graphite–H_2SO_4–Ox and graphite–HNO_3–H_2O systems. In addition, the concentration ranges in which various stages of graphite bisulfate and graphite nitrate are formed were determined. Under the conditions of chemical synthesis, the threshold intercalation concentrations of the acids are approximately 63% for H_2SO_4 and 75% for HNO_3. Weaker acids, e.g., H_3PO_4 and $H_4P_2O_7$, can be intercalated into the graphite host only at a 100% concentration of an acid [24]. Weak protonic acids, e.g., H_3BO_3, cannot be intercalated into graphite.

The chemical method is rather technologically and instrumentally simple [28]. However, changes in the concentration of an acid and, to a greater extent, in that of the oxidizing agent in the course of intercalation predetermine inhomogeneity of the graphite nitrate composition and make synthesis difficultly controllable. In addition, the compounds obtained are contaminated with the oxidizing agent and products of its reduction. This circumstance, combined with the high concentration of the acids, requires a gross expenditure of water for hydrolysis and washing of the final product.

To conclude the consideration of the liquid-phase method for synthesis of acceptor-type GIC, it can be

stated that the presence of an oxidizing agent and the effect of its potential on the degree of intercalation indicate that GICs are synthesized by the electrochemical mechanism.

The electrochemical method has a number of advantages over the chemical technique: it is environmentally safer, the compound obtained is not contaminated with the oxidizing agent and products of its reduction, and synthesis can be performed in a controlled mode, which makes it possible to obtain with high precision a product of the required composition and diminishes the expenditure of the acid. The electrochemical synthesis is used to produce GICs with inorganic and organic acids, such as H_2SO_4, HNO_3, $HClO_4$, H_2SeO_4, $HReO_4$, CF_3COOH, and HCOOH [24, 25, 43–48].

The electrochemical synthesis of graphite bisulfate is based on anodic oxidation of graphite in H_2SO_4 solutions of a sufficient concentration. The following stages of the synthesis can be distinguished [24, 28, 35, 49, 50].

(1) Induction period, i.e., SFG oxidation accompanied by buildup of stresses in carbon networks and their wedging from the sample surface.

(2) Introduction of the intercalate, which consists in electrochemical formation of carbon macrocations and diffusion of acid ions and molecules into interlayer spaces:

$$nC - e \rightarrow C_n^+ \xrightarrow{3.5H_2SO_4} C_n^+HSO_4^- \cdot 2.5H_2SO_4 + H^+, \quad (9)$$

to the point of maximum saturation of the graphite host ($C_{21}^+ \cdot HSO_4^- \cdot 2.5H_2SO_4$).

(3) Overoxidation of stage I graphite bisulfate with partial deformation of carbon layers by one of the following reactions [49, 51, 52]:

$$C_{24}^+HSO_4^- \cdot 2.5H_2SO_4 \rightarrow 2C_{12}^+ \cdot 2HSO_4^- \cdot 1.5H_2SO_4 + H^+ + e, \quad (10)$$

$$C_{24}^+HSO_4^- \cdot 2H_2SO_4 \rightarrow C_{24}^+ \cdot 0.5S_2O_8^{2-} \cdot 2H_2SO_4 + H^+ + e, \quad (11)$$

$$C_{24}^+HSO_4^- \cdot 2H_2SO_4 \rightarrow 3(C_8^+ \cdot HSO_4^-) + 2H^+ + 2e. \quad (12)$$

According to [53, 54], overoxidation in the presence of a sufficient amount of H_2O_2 in the electrolyte may lead to formation of graphite oxide $C_n^+(OH)^- \cdot yH_2O$.

(4) Oxidation of water to oxygen released in the form of O_2, CO, and CO_2 [55]. In moderately concentrated H_2SO_4 solutions, this stage may occur in parallel to the first three, with a number of soluble organic compounds as possible products of carbon oxidative breakdown [54]. The rate of GIC formation decreases with the H_2SO_4 concentration [36, 56].

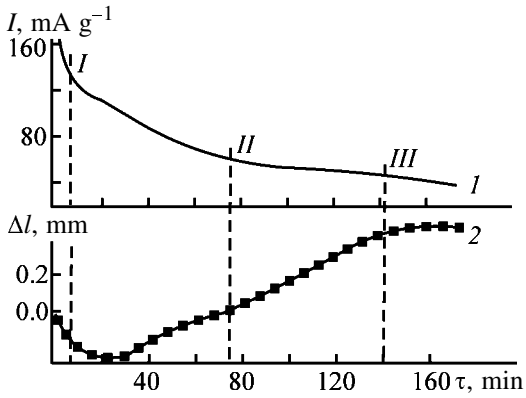


Fig. 1. Variation of (*1*) current *I* and (*2*) piston shift Δl with time τ in potentiostatic synthesis [E_a = 2.42 V (vs. SHE)] of graphite bisulfate in 96% H_2SO_4.

The above-described fundamental aspects of the electrochemical synthesis of graphite bisulfate have been mainly revealed in preparative experiments with samples of pyrolytic graphite. Taking into account that dispersed natural graphite is predominantly used to obtain thermally expanded graphite, we made a comprehensive study of electrochemical intercalation of graphite electrodes in sulfuric and nitric acid electrolytes.

An induction period was experimentally revealed from variation of the thickness of the graphite layer in anodic treatment in sulfuric acid (Fig. 1) [57]. It corresponds to the time elapsed before dashed line *I*. In this stage, the friction force between carbon particles becomes weaker and the graphite layer is densified (Fig. 1, negative Δl) due to oxidation of surface groups and to charging of the electrical double layer. Then, anodic intercalation leads to an increase in interlayer spacings and, accordingly, to a rise in the volume of graphite particles and to an upward shift of the piston (graphite layer thickness increases). XPA data confirm that the graphite bisulfate phase is absent during the induction period [57].

According to [58, 59], the potentials of formation of various stages of graphite bisulfate from dispersed graphite somewhat exceed analogous values for GICs synthesized from pyrolytic graphite [49, 50] (Table 1). The possibility of synthesis of various stages of graphite bisulfate by anodic treatment of dispersed graphite and of their subsequent "overoxidation"

Table 1. Formation potentials of graphite bisulfates of various stages in anodic oxidation of graphite in 96% H_2SO_4

Stage of graphite bisulfate	Potential, V (vs. SHE)		
	pyrolytic graphite		GT-1 graphite [58, 59]
	[50]	[49]	
III	1.11–1.18	1.11–1.18	1.02–1.27
II	1.17–1.45	1.19–1.47	1.29–1.52
I	1.45–1.95	>1.47	1.70–2.02

Table 2. Effect of the specific amount of the electricity passed on the properties of compounds synthesized in galvanostatic anodic treatment of dispersed graphite (I = 200 mA g^{-1}) in 96% H_2SO_4

Q, mA h g^{-1}	Stage according to XPA	Sample weight gain, %	E_{st},* V
20	IV + graphite	8.0	0.94
40	III	14.3	1.02
60	II	19.2	1.29
80	II	25.8	1.45
100	I + II	34.1	1.56
150	I + II	35.8	1.69
200	I + II	47.5	1.84
250	I	48.4	1.84
300	I	47.0	1.85
400	I	48.2	1.85
500	I + oxide	50.2	1.86
600	I + oxide	47.8	1.88

* Steady-state graphite potential after switching off the current.

(Table 2) to give oxide-like structures was demonstrated in [58, 59].

According to the results obtained in [58, 59], the kinetics of anodic processes on a dispersed graphite

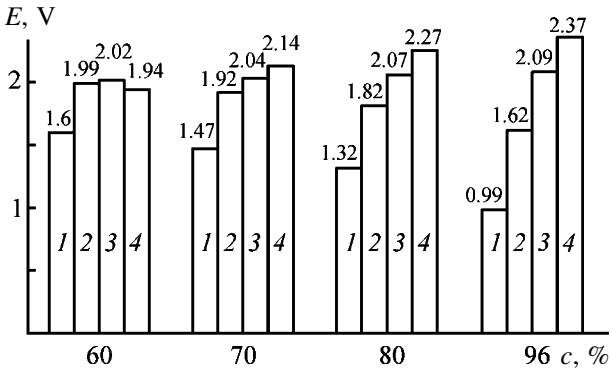


Fig. 2. Potentials E of (*1*) intercalation onset, (*2*) formation of stage I graphite bisulfate, (*3*) its overoxidation, and (*4*) oxygen evolution vs. the H_2SO_4 concentration c.

Table 3. Formation potentials of graphite nitrates of various stages in anodic oxidation of pyrolytic graphite in 65% HNO_3 according to [64]

Stage of graphite nitrate according to XPA	E, V (vs. SHE)	Q, mA h g^{-1}	Sample weight gain, %
I + oxide	1.84	90	35
II	1.67	60	27
III	1.54	35	22
IV	1.52	30	18

electrode in concentrated H_2SO_4 mostly depends on the anode potential, whereas the composition and properties of the compounds obtained are governed by the amount of the electricity passed. In electrochemical synthesis of graphite bisulfate, the distribution of the overall anode current among intercalation, overoxidation, and oxygen evolution processes is strongly affected by the concentration of the sulfuric acid electrolyte [50, 58, 60–62]. Despite certain contradictions in interpretation of experimental data, it is possible to reveal general aspects, which consist in a shift of the threshold intercalation potential and of the formation potentials of graphite bisulfates of various stages in the positive direction with dilution of the electrolyte (Fig. 2). Thus, it can be stated that an increase in the fraction of water in the electrolyte favors anodic overoxidation of graphite bisulfate to give compounds that approach graphite oxide in their properties.

Of no less importance is the effect of temperature on the electrochemical intercalation of graphite. According to [60], the threshold intercalation potential and the potentials of stage conversion (III → II and II → I) steadily increase (at a rate of 1.9–2.8 mV K^{-1}), together with the intercalation rate, in electrochemical synthesis of graphite bisulfate in 96% H_2SO_4 as temperature is raised from 0 to 80°C. A similar trend was observed in [61, 63].

In electrochemical synthesis of graphite nitrate, all the basic aspects of stages of anodic oxidation are the same as in the case of graphite bisulfate. According to [64], graphite nitrates of various stages can be synthesized by anodic oxidation of graphite (Table 3).

According to [64–66], electrochemical oxidation of graphite can yield graphite nitrate of classical composition in HNO_3 solutions with concentrations of no less than 55–65%. In these electrolytes, formation of graphite nitrate stages has been recorded only upon a short-time anodic treatment, with an amount of electricity passed in the process not exceeding

Table 4. Variation of the volume of a dispersed graphite electrode with time in anodic potentiostatic treatment in 13.5 M HNO_3

E_a, V (vs. SHE)	Change in volume, %, by indicated time, min						
	5	20	50	100	150	250	420
2.3	0	3	25	40	44	44	44
2.0	0	1	11	29	40	61	52

60 mA h g^{-1}. An increase in the amount of electricity yields defective structures of the type of graphite oxide, which can be formed in HNO_3 solutions that contain about 20% H_2O [54]. In the opinion of Shapranov and Yaroshenko [54], intercalation and hydrolysis occur in 20–55% HNO_3 solutions simultaneously, which favors oxidation of a sample, e.g., by the reaction

$$C^+_{24n}\cdot NO^-_3\cdot 2HNO_3 + 3yH_2O$$

$$\rightarrow C^+_{24n}\cdot(1 - y)NO^-_3\cdot yOH^-\,2(1 - y)HNO_3\cdot 2yH_2O, \quad (13)$$

where $y < 1$.

The electrochemical method allows use of more dilute HNO_3 solutions for GIC synthesis [67, 68]. In particular, graphite nitrate can be obtained at concentrations in the range 1–70% [68]. To obtain GIC, dispersed graphite was subjected to polarization with anodic current in the range 0.5–4.0 A, with 66–440 mA h g^{-1} imparted. However, the publication cited presents only evidence of general technological nature, with no data on the occurring chemical processes and chemical composition of GIC reported.

The analysis made in our studies confirmed that the electrochemical oxidation of graphite in 59% HNO_3 occurs in stages similar to those described for graphite bisulfate. In particular, it was confirmed that there exists an induction period whose duration becomes somewhat shorter as the anodic polarization potential is raised [69]. A strong increase in the volume of the graphite electrode is due to intercalation and GIC formation. After the intercalation process is complete and the volume of the graphite anode ceases to grow, currents corresponding to overoxidation of the GIC formed continue to be observed in the potentiostatic curves (Table 4).

At higher anode potentials, an increase in the volume of the graphite electrode upon conversion of graphite into GIC becomes faster, but the strongest swelling is, by contrast, observed at lower potentials (2.0 V is the potential of oxygen evolution in 59% HNO_3 [70]). This circumstance can be understood with account of the fact that the probability of formation of graphite oxide grows with the anode potential. The theoretically possible (as determined by the interplanar spacings) increase in the graphite volume upon formation of graphite bisulfate should be 30% larger than that upon conversion of graphite into graphite oxide. Consequently, it may be assumed that graphite nitrate subject to hydrolysis is predominantly formed at E_a = 2.0 V, and compounds of the type of graphite oxide, at E_a = 2.3 V.

Thus, it has been shown experimentally that the qualitative composition of the products of anodic oxidation of graphite is determined by the electrolyte concentration, specific amount of the electricity passed, and potential of anodic polarization. In this context, it is preferable to perform electrochemical synthesis of GIC in the potentiostatic mode [71], which makes the process more controllable, diminishes gas evolution, and saves electric power by 10 to 50%.

After determining the dynamics of the electrochemical treatment process at different anodic polarization potentials [72], it becomes possible to find the minimum necessary time of anodic treatment to give GICs of various compositions (Table 5). The theoretical amount of electricity necessary for graphite nitrate formation was determined using the Faraday law. It should be noted that, in anodic oxidation of graphite, the current efficiency does not exceed 65% and markedly decreases at potentials exceeding the oxygen evolution potential (1.8–2.0 V) [70]. As follows from Table 5, synthesis of GIC is only possible at $E_a > 1.8$ V even at a low intercalate concentration. The theoretical value of Q necessary for overoxidation of GIC is about 380 mA h g^{-1}. It would be expected that, in anodic treatment of graphite, the electrical conductivity will substantially decrease upon conversion of GIC into graphite oxide. This will lead to a dramatic fall of currents and will eliminate part of the graphite anode from the process. According to [54], electrochemical synthesis of a graphite oxide of the composition $C_8O_2(OH)_2$ is virtually impossible. In-

Table 5. Time necessary for imparting the theoretically necessary capacity Q_{theor} in synthesis of GICs of various compositions at different potentials E of anodic treatment of graphite in 59% HNO_3

Charge of macrocation	Q_{theor}, mA h g^{-1}	Time, min, at indicated E, V (vs. SHE)								
		1.7	1.8	1.9	2.0	2.1	2.2	2.3	2.4	2.5
C_8^+	350	–	–	–	–	–	–	240	180	150
C_{12}^+	93	–	–	–	–	68	38	33	30	25
C_{18}^+	46	–	54	33	30	25	18	16	15	11
C_{27}^+	31	–	30	19	17	13	9	9	8	6
C_{36}^+	23	–	13	9	8	6	4	4	4	3

deed, even imparting $Q > 800$ mA h g^{-1} leads only to formation of intermediate forms of graphite oxide ($C_{24n}^+ \cdot OH^- \cdot 2H_2O$, where $n < 1$) because of a decrease in the current efficiency and an increase in the resistivity of the compounds obtained. In addition, prolonged anodic polarization makes higher the probability that hydrolysis will occur directly in the course of GIC synthesis [reaction (13)].

The available experimental data on the mechanism and conditions of electrochemical synthesis of GIC made it possible to formulate the basic principles of development of continuous reactors for synthesis of GIC with acids from dispersed graphite [73]. The originality of the design consists in that the gap between the anode current lead and the diaphragm on the rotating drum has a variable width (Fig. 3). The narrowest gap (compression zone) corresponds to the induction period of the reaction, and its further widening, to GIC synthesis accompanied by an increase in volume. Graphite and the forming GIC are transported along the gap by retractable blades. The blades are pushed out of the drum by springs or by spokes connecting diametrically opposite blades into pairs, with a special slide guide mounted in the upper part of the electrolyzer. This installation can use as an electrolyte both sulfuric and nitric acids. The electrode and structural materials for both systems were experimentally selected. It is recommended to use in sulfuric acid the 12Cr18Ni10Ti stainless steel as a stable material [74]. Titanium is an appropriate structural material and as a cathode in nitric acid electrolytes [75]. Platinum or platinum-plated titanium should be necessarily used as the anode current lead [76]. The diaphragm can be made of a polyvinyl chloride filter cloth, which is inert toward corrosive media and possesses high retentive properties. The attenuation coefficient of diaphragms of this kind does not exceed 2.5–4. The tests performed confirmed the working capacity and high reliability of the design and the possibility of performing GIC synthesis in a continuous automated mode [77]. Alternative reactor designs, which enable GIC synthesis from nonstratifying graphite–acid suspensions, have also been developed [78, 79].

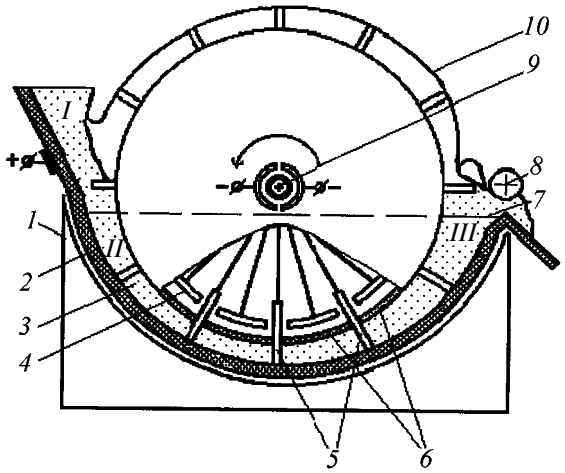


Fig. 3. Schematic of a drum electrolyzer: (*1*) electrolyzer case, (*2*) anode current lead, (*3*) graphite bed, (*4*) cathode, (*5*) blades, (*6*) diaphragm, (*7*) electrolyte level, (*8*) GIC remover, (*9*) shaft, and (*10*) blade guide. (*I–III*) Zones of charging, compression, and GIC discharge, respectively.

GICs synthesized by the chemical and electrochemical methods contain residual amounts of acids and oxidizing agents, both directly in their composition and on the surface in the form of adducts. To remove the residues, GIC are washed with water to pH 5–7. The specific expenditure of water for washing of graphite nitrate and graphite bisulfate is about 100 and 600 ml per gram of the product, respectively. As a result, the intercalating layer is totally replaced with hydroxide ions and water [29]:

$$C_{24n}^+ \cdot A^- \cdot 2HA + 3H_2O \rightarrow C_{24n}^+ \cdot OH^- \cdot 2H_2O + 3HA. \quad (14)$$

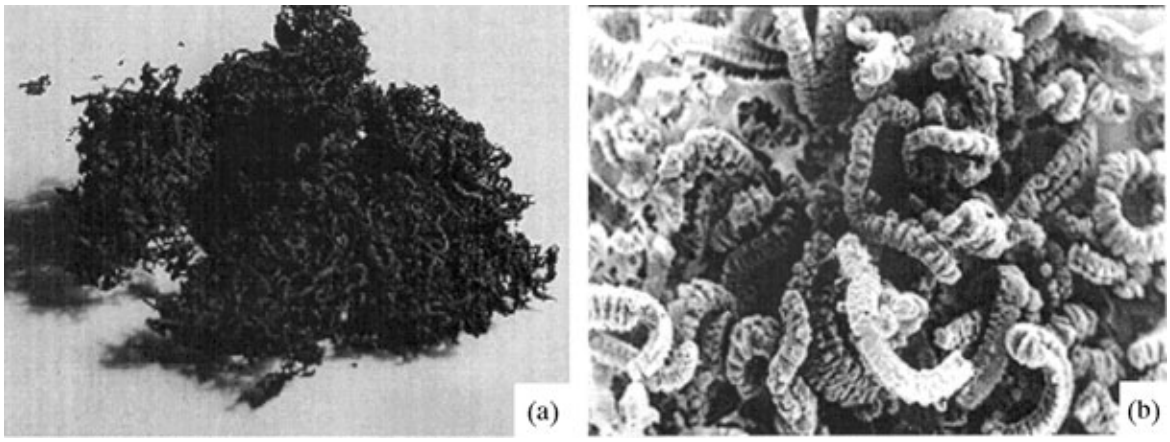


Fig. 4. Thermally expanded graphite. Magnification: (a) 1 and (b) 20.

In addition, a GIC containing sulfur or nitrogen in the highest oxidation state can, when brought in contact with water, oxidize it with an increase in the oxygen concentration in the GIC. Oxygen can be present in various carbonyl, carboxy, and phenol groups on the surface of the graphite host or can form covalent bonds with neighboring carbon atoms. The thus produced and dried at 60–100°C hydrolyzed GICs (HGICs) are used to obtain thermally expanded graphite.

The mechanism of thermal expansion of GIC still remains a matter of discussion [80–84]. Makhorin et al. [80] assumed that carbon networks break down after fast removal of a certain amount of intercalating particles from the interlayer space of the graphite host, with neighboring planes disintegrated. In [81, 82], the process of thermal expansion of graphite was regarded as a phase transition caused by removal of the intercalating agent from GIC. The degree of foaming depends on the synthesis conditions and composition of the resulting GIC, as well as on the structure and size of particles of the starting carbon raw material. Chung [81] believes that the size of grains of the starting graphite should exceed 75 μm, with the crystallite size of no less than 75 nm. It is assumed most frequently that fast heating of GIC gives rise to a pressure (280–720 atm) between layers of carbon networks in graphite [83], and this pressure has a dispersing effect. Deintercalation of the graphite host occurs via layer edges and the existing defects, with the layers ruptured and shifted. At high heating rates this leads to formation of foam-like structures. An increase in the dispersity and defectiveness of graphite leads to a decrease in the internal interlayer pressure and, consequently, to a decline in the degree of expansion.

According to [84], the expansion originally involves cleavage of crystallites along the *c*-axis into thin packets-ribbons consisting of a small number of atomic planes, with their simultaneous deformation, to give a 3D folded structure. The resulting wormlike and cylindrical particles have a closed surface, within which residual decomposition products are contained (Fig. 4). The wormlike shape of particles of foamed graphite is due to opening of planar carbon networks wedged at the edge surface of a crystallite by surface groups. The basic technological characteristic of TEG is its bulk density d_{TEG}, which largely depends on preparation conditions and may vary widely, from 1–5 to 20–100 g dm^{-3} [7, 8, 80, 85]. According to experimental data, there exists a certain relationship between the composition of a GIC and its capacity for thermal expansion (Fig. 5). The greatest practical demand is for TEG with bulk densities of less than 7 g dm^{-3}. In addition, electrochemical oxidation of graphite in HNO_3 has been used to obtain GIC that can be thermally expanded even at 200–250°C to give a TEG with a bulk density of less than 2 g dm^{-3} [86].

At present, the overwhelming fraction (up to 50000 tons per year) of TEG is processed into a flexible graphite foil and compacted articles (see the

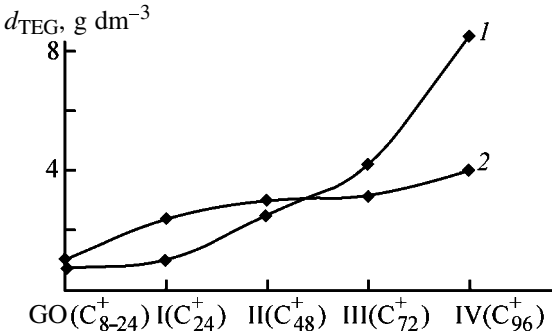
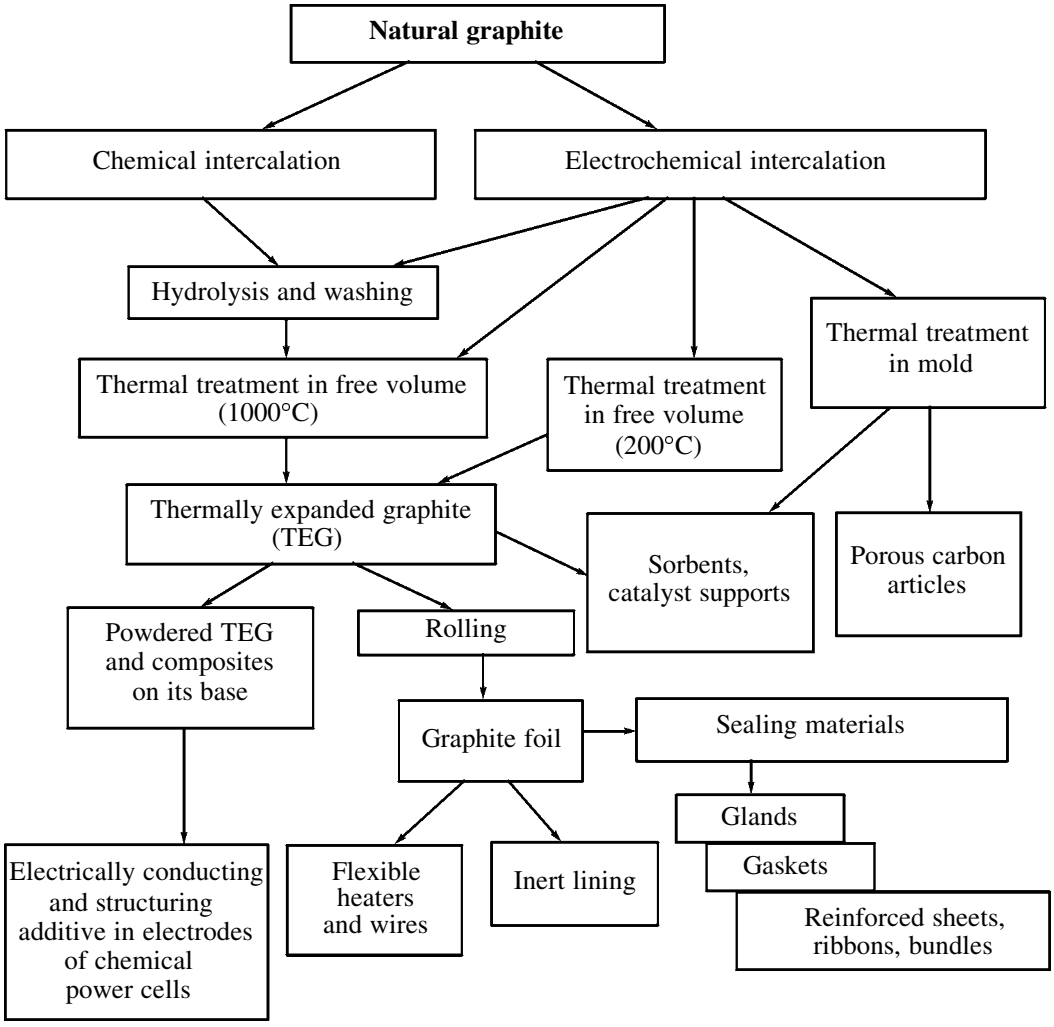


Fig. 5. Bulk density d_{TEG} of thermally expanded graphite in relation to the macrocation composition and GIC stage. (*1*) Graphite bisulfate and (*2*) graphite nitrate.

General scheme of synthesis of thermally expanded graphite and its subsequent processing into articles and materials



general scheme of synthesis and processing of TEG). The foil is obtained on a set of rolls in the same cycle with thermal treatment without introduction of a binder. This yields roll materials with a thickness of 0.15–1.5 mm, density of 0.7–1.3 g cm^{-3}, tensile strength of 4–7 MPa, and electrical resistivity of $(0.3–0.7)\times10^{-4}$ Ω m [10]. Owing to their high inertness toward corrosive media and thermal stability, combined with elasticity and plasticity, TEG-based materials everywhere replace such conventional sealing and laying materials as asbestos, Poronite, fluoroplastic, copper, and lead. Their use is especially effective in chemical and oil-and-gas machine building [12], fuel-and-energy complex [13, 87], and municipal service, which provides a decrease in the accident rate, diminishes the expenditure for equipment repairing, and improves the environmental safety.

It is known [14, 88] that TEGs are used as electrically conducting and structuring additives in electrodes of lithium chemical power cells to improve their specific characteristics; fluorination of TEG yields active reagents of chemical power cells; and their modification with metals serves to control their thermal and electrical conductivity [90]. According to [91, 92], TEG powders are effective adsorbents of oil products (sorption capacity 10–80 g g^{-1}) and certain metal cations (sorption capacity for hardness cations 0.42 mg-equiv g^{-1} [93]). The possibility that carbon materials, including TEG, can be used as catalysts and catalyst supports was reported in [94].

The most promising way to make articles of TEG, with its highly porous structure preserved, is thermal expansion of GIC in a gas-permeable mold with prescribed dimensions (chemical compaction). In this case, fabrication of articles of complex shape, with the density, porosity, and other properties of the material controlled, becomes possible because of the spatial

entanglement of particles of the expanding graphite [15, 89]. The above properties can be varied by changing the filling factor of the mold. In addition, the article properties can be varied widely by introducing carbon fibers and binders (pitch, phenol tars, metal oxides) into GIC before thermal treatment or by reinforcing the host produced from TEG with pyrocarbon from the gas phase [15]. A particular type of application is characteristic of composites containing intercalated graphite. The process of its thermal expansion under the action of open flame or heating results in the formation of a noncombustible thermally insulating coating, with simultaneous evolution of CO and CO_2, which decelerates and suppresses burning. Composites of this kind in the form of roll materials, pastes, and varnishes have been named active fireproofing materials [5, 17]. The presently manufactured domestic materials are used to protect electric cables, fabricate fire-resistant doors and partitions, and fireproof building constructions.

CONCLUSION

Comprehensive studies of the electrochemical synthesis of graphite intercalation compounds to be processed into thermally expanded graphite, design of a novel equipment for continuous anodic treatment of a dispersed carbon material, and its implementation as working laboratory and industrial installation revealed real prerequisites for the development of a new highly efficient technology that can yield thermally expanded graphite with controllable properties for various fields of science and technology.

REFERENCES

1. Fialkov, A.S., *Uglerod: Mezhsloevye soedineniya i kompozity na ego osnove* (Carbon: Interlayer Compounds and Composites Based on Carbon), Moscow: Aspekt, 1997.
2. Fialkov, A.S. and Malei, L.S., in *Elektrougol'nye i metallokeramicheskie izdeliya dlya elektrotekhniki* (Electric-Carbon and Metal–Ceramic Articles for Electrical Engineering), Moscow: Energoatomizdat, 1985, pp. 65–72.
3. Makhorin, K.E., Kozhan, A.P., Veselov, V.V., et al., *Khim. Tekhnol.*, 1987, no. 2, pp. 43–49.
4. USSR Inventor's Certificate no. 1662926.
5. Yaroshenko, A.P. and Savos'kin, M.V., *Zh. Prikl. Khim.*, 1995, vol. 68, no. 8, pp. 1302–1306.
6. Setton, R., *Synth. Met.*, 1988, vol. 23, no. 1–4, pp. 467–473.
7. Komarova, T.V., Puzyreva, E.V., and Puchkov, S.V., *Tr. Mosk. Khim.-Tekhnol. Inst. im. D.I. Mendeleeva*, 1986, vol. 141, pp. 75–83.
8. Chernysh, I.G. and Buraya, I.D., *Khim. Tverd. Topl.*, 1990, no. 1, pp. 123–127.
9. Bondarenko, S.G., Rykova, L.A., Statyukha, G.A., et al., *Khim. Tverd. Topl.*, 1988, no. 4, pp. 141–143.
10. RF Patent 2038337.
11. Antonov, A.N., Timonin, V.A., Fedoseev, S.D., and Makevnina, L.F., *Khim. Tverd. Topl.*, 1984, no. 1, pp. 114–117.
12. Kirshnek, R., *Khim. Neftegaz. Mashinostr.*, 2000, no. 8, pp. 31–33.
13. Avdeev, V.V. and Ulanov, G.A., *Materialy seminara-soveshchaniya "Problemy nadezhnosti ekspluatatsii i obnovleniya osnovnykh fondov tekhnologicheskikh ustanovok NPZ i puti ikh resheniya"* (Proc. Workshop "Problems of Reliability of Exploitation and Upgrade of Technological Installations at Oil Refineries and Ways to Their Solution"), Moscow, February 6–8, 2001, Moscow: TsNIITEneftekhim, 2001, pp. 88–91.
14. Barsukov, V.Z., Khomenko, V.G., Motronyuk, T.I., and Antonenko, P.A., Abstracts of Papers, *1-aya Mezhdunarodnaya konferentsiya "Uglerod: fundamental'nye problemy nauki, materialovedenie, tekhnologiya"* (1st Int. Conf. "Carbon: Fundamental Problems of Science, Materials Science, and Technology"), Moscow, October 17–19, 2002, Moscow: Ratmir-Vest, 2002, p. 55.
15. Avarbe, R.G., Karpov, O.P., Kondrasheva, L.M., et al., *Zh. Prikl. Khim.*, 1996, vol. 69, no. 12, pp. 2068–2070.
16. Yakovlev, A.V., Finaenov, A.I., Zabud'kov, S.L., and Nastasin, V.A., in *Sbornik nauchnykh trudov 3-go Vserossiiskogo seminara s mezhdunarodnym uchastiem "Toplivnye elementy i energoustanovki na ikh osnove"*, (Proc. 3rd All-Russia Workshop with Int. Participation "Fuel Cells and Power Installations Based on Fuel Cells"), Yekaterinburg, January 31–February 3, 2006, pp. 165–167.
17. Godunov, I.A., *Pozharn. Bezopasn.*, 2001, no. 3, pp. 199–201.
18. Chalykh, E.F., Zhitov, B.N., and Korolev, Yu.G., *Tekhnologiya uglegrafitovykh materialov* (Technology of Carbon–Graphite Materials), Moscow: Nauka, 1981.
19. Puzyreva, E.V., Komarova, T.V., and Fedoseev, S.D., *Khim. Tverd. Topl.*, 1982, no. 2, pp. 119–121.
20. Herold, A., *Mater. Sci. Eng.*, 1977, vol. 31, pp. 1–16.
21. Herold, A., *Physical Chemistry of Materials, Layered Structures, Intercalated Materials*, Levy, F., Ed., Dordrecht, 1979, vol. 6, pp. 323–421.

22. Ebert, L.B., *Ann. Rev. Mater. Sci*., 1976, vol. 6, pp. 181–211.
23. Anderson Axdal, S.H. and Chung, D.D.L., *Carbon*, 1987, vol. 25, no. 3, pp. 377–389.
24. Rudorff, W. and Hofmann, U., *Z. Anorg. Chem*., 1938, vol. 238, no. 1, pp. 1–50.
25. Rudorff, W., *Z. Phys. Chem*., 1939, vol. 45, no. 14, pp. 42–69.
26. Herold, A., *NATO ASY Ser*., 1987, vol. 172, ser. B, pp. 3–45.
27. Van der Plas, T., *Physical and Chemical Aspects of Adsorbents and Catalysts*, Linsen, B.G., Ed., London: Academic, 1970. Translated under the title *Stroenie i svoistva adsorbentov i katalizatorov*, Moscow: Mir, 1973, pp. 436–481.
28. Yaroshenko, A.P., Popov, A.F., and Shapranov, V.V., *Zh. Prikl. Khim*., 1994, vol. 67, no. 2, pp. 204–211.
29. Nikol'skaya, I.V., Fadeeva (Sorokina), N.E., Semenenko, K.N., et al., *Zh. Obshch. Khim*., 1989, vol. 59, no. 12, pp. 2653–2659.
30. Daioh, H. and Mizutani, Y., *Tanso*, 1985, no. 123, pp. 177–179.
31. Shapranov, V.V. and Yaroshenko, A.P., Abstracts of Papers, *1-aya Vsesoyuznaya konferentsiya "Khimiya i fizika soedinenii vnedreniya"* (1st All-Union Conf. "Chemistry and Physics of Intercalation Compounds") Rostov-on-Don, September 23–25, 1990, p. 25.
32. Inagaki, M., Iwashita, N., and Kouno, E., *Carbon*, 1990, vol. 28, no. 1, pp. 49–56.
33. Iwashita, N. and Inagaki, M., *Synth. Met*., 1989, vol. 34, pp. 139–144.
34. Forsman, N.S., Vogel, F.L., Carl, D.E., and Hofmann, J., *Carbon*, 1978, vol. 16, pp. 269–271.
35. Ubbelohde, A.R. and Lewis, F.A., *Grafit i ego kristallicheskie soedineniya* (Graphite and Its Crystal Compounds), Moscow: Mir, 1965.
36. Fuzzellier, H., Melin, J., and Herold, A., *Mater. Sci. Eng*., 1977, vol. 31, pp. 91–94.
37. Touzain, P., *Synth. Met*., 1979/80, no. 1, pp. 3–11.
38. Avdeev, V.V., Monyakina, L.A., Nikol'skaya, I.V., et al., *Mol. Cryst. Liq. Cryst*., 1994, vol. 244, pp. 115–120.
39. Avdeev, V.V., Monyakina, L.A., Nikol'skaya, I.V., et al., *Carbon*, 1992, vol. 30, no. 6, pp. 825–827.
40. Carr, K.E., *Carbon*, 1970, vol. 8, no. 2, pp. 153–166.
41. Ubbelohde, A.R. and Lewis, F.A., *Graphite and Its Crystal Compounds*, Oxford: Clarendon Press, 1960.
42. Monyakina, L.A., Avdeev, V.V., Nikol'skaya, I.V., et al., *Zh. Fiz. Khim*., 1995, vol. 69, no. 5, pp. 926–930.
43. Rudorff, U., *Adv. Inorg. Chem. Radiochem*., 1959, vol. 1, pp. 223–266.
44. Avdeev, V.V., Tverezovskaya, O.A., Sorokina, N.E., et al., *Mol. Cryst. Liq. Cryst*., 2000, vol. 340, pp. 131–136.
45. Petitjean, D., Furdin, G., Herold, A., and Dupont Pavlovsky, N., *Mol. Cryst. Liq. Cryst*., 1994, vol. 244, pp. 213–218.
46. Scharff, P., *Z. Naturforsh. (b)*, 1989, vol. 44, no. 7, pp. 772–777.
47. Bourelle, E., Douglade, J., and Metrot, A., *Mol. Cryst. Liq. Cryst*., 1994, vol. 244, pp. 227–232.
48. Kang, F., Leng, Y., and Zhang, T.-Y., *Carbon*, 1997, vol. 35, no. 8, pp. 1089–1096.
49. Metrot, A. and Fischer, J.E., *Synth. Met*., 1981, vol. 3, nos. 3–4, pp. 201–207.
50. Fuji, R., *Osaka Kogyo Gidzyutsu Sikendzi Hokoku*, 1978, vol. 353, pp. 1–66.
51. Metrot, A., *Synth. Met*., 1983, vol. 7, no. 3, pp. 177–184.
52. Shioama, H. and Fuji, R., *Carbon*, 1987, vol. 25, no. 6, pp. 771–774.
53. Horn, D. and Boehm, H.R., *Z. Anorg. Allg. Chem*., 1979, vol. 456, pp. 117–129.
54. Shapranov, V.V. and Yaroshenko, A.P., in *Khimiya i fizika uglya* (Chemistry and Physics of Coal), Kiev, 1991, pp. 56–74.
55. Tarasevich, M.R., *Elektrokhimiya uglerodnykh materialov* (Electrochemistry of Carbon Materials), Moscow: Nauka, 1984.
56. Press, M.D., Savost'yanova, N.A., and Yurkovskii, I.M., *Khim. Tverd. Topl*., 1990, vol. 1, pp. 128–131.
57. Finaenov, A.I., Krasnov, V.V., Trifonov, A.I., et al., *Elektrokhim. Energet*., 2003, vol. 3, no. 3, pp. 107–118.
58. Apostolov, S.P., Krasnov, V.V., Avdeev, V.V., and Finaenov, A.I., *Izv. Vyssh. Uchebn. Zaved., Khim. Khim. Tekhnol*., 1997, vol. 40, no. 1, pp. 113–117.
59. Apostolov, S.P., Krasnov, V.V., and Finaenov, A.I., *Zh. Prikl. Khim*., 1997, vol. 70, no. 4, pp. 602–607.
60. Kang, F., Leng, Y., Zhang, T.-Y., et al., *J. Phys. Chem. Solids*, 1996, vol. 57, no. 6–8, pp. 883–888.
61. Metrot, A. and Fuzellier, H., *Carbon*, 1984, vol. 22, pp. 131–133.
62. Beck, F. and Krohn, H., *Synth. Met*., 1986, vol. 14, no. 1–2, pp. 137–149.
63. Fiang, J. and Beck, F., *Carbon*, 1992, vol. 30, no. 2, pp. 223–228.
64. Scharff, P., Xut, Z.-Y., Stump, E., and Barteczko, K., *Carbon*, 1991, vol. 29, no. 1, pp. 31–37.
65. Sorokina, N.E., Maksimova, N.V., and Avdeev, V.V., *Neorg. Mater*., 2001, no. 4, pp. 1–7.
66. Wessbecher, S.D. and Jamsk, E., *Synth. Met*., 1992, vol. 46, no. 2, pp. 137–146.

67. USSR Inventors Certificate no. 1 609 744.
68. US Patent 3 323 869.
69. Yakovleva, E.V., Yakovlev, A.V., and Finaenov, A.I., *Zh. Prikl. Khim.*, 2002, no. 10, pp. 1632–1638.
70. Yakovlev, A.V., Finaenov, A.I., Nikitina, L.E., and Apostolov, S.P., *Zh. Prikl. Khim.*, 1999, vol. 72, no. 4, pp. 589–593.
71. Yakovlev, A.V. and Finaenov, A.I., *Zh. Prikl. Khim.*, 1999, vol. 72, no. 1, pp. 88–91.
72. Yakovlev, A.V., Finaenov, A.I., Yakovleva, E.V., and Zabud'kov, S.L., *Vestn. Saratov. Gos. Tekh. Univ.*, 2003, no. 1, pp. 113–120.
73. Finaenov, A.I., Apostolov, S.P., Krasnov, V.V., and Nastasin, V.A., *Zh. Prikl. Khim.*, 1999, vol. 72, no. 5, pp. 767–772.
74. Nastasin, V.A., Savel'eva, E.A., and Finaenov, A.I., *Izv. Vyssh. Uchebn. Zaved., Khim. Khim. Tekhnol.*, 2000, vol. 43, no. 5, pp. 106–108.
75. Zabud'kov, S.L., Yakovlev, A.V., and Finaenov, A.I., *Vestn. Saratov. Gos. Tekh. Univ.*, 2005, no. 1, pp. 85–91.
76. Zabud'kov, S.L., Yakovlev, A.V., Nastasin, V.A., and Finaenov A.I., Abstracts of Papers, *3-ya Mezhdunarodnaya konferentsiya "Uglerod: fundamental'nye problemy nauki, materialovedenie, tekhnologiya"* (3rd Int. Conf. "Carbon: Fundamental Problems of Science, Materials Science, and Technology"), Moscow, 2004, p. 103.
77. RF Patent 2 142 409.
78. RF Patent 2 264 983.
79. RF Patent 2 263 070.
80. Makhorin, K.E., Kozhan, A.P., and Veselov, V.V., *Khim. Tekhnol.*, 1985, no. 2, pp. 3–6.
81. Chung, D.D.L., *Proc. 7th Int. Thermal Expansion Symp.*, Chicago, November 7–10, 1972, Publ. 1982, pp. 32–44.
82. Anderson, S.H. and Chung, D.D.L., *Carbon*, 1984, vol. 22, no. 3, pp. 253–263.
83. Stevens, R.E., Ross, S., and Wesson, S.P., *Carbon*, 1973, vol. 11, pp. 525–630.
84. Yurkovskii, I.M., Smirnova, T.Yu., and Malei, L.S., *Khim. Tverd. Topl.*, 1986, no. 1, pp. 127–131.
85. USSR Inventor's Certificate no. 767 023.
86. RF Patent 2 233 794.
87. Biryukov, D.B., Voronin, V.P., Zroichikov, N.A., and Ulanov, G.A., *Elektr. Stantsii*, 2000, no. 5, pp. 31–34.
88. Kurenkova, M.Yu., in *Materialy III Mezhdunarodnogo simpoziuma "Prioritetnye napravleniya v razvitii khimicheskikh istochnikov toka"* (Proc. III Int. Symp. "Priority Areas of Development of Chemical Power Cells"), Ivanovo–Ples: Ivanov. Gos. Khim.-Tekhnol. Univ., 2004, pp. 23–26.
89. Avarbe, R.T., Karpov, O.P., Kondrasheva, L.M., et al., *Zh. Prikl. Khim.*, 1996, vol. 69, no. 12, pp. 2065–2067.
90. Mattsui, L.Yu., Tsaregradskaya, T.L., Vovchenko, L.L., et al., *Perspekt. Mater.*, 2002, no. 4, pp. 79–83.
91. Savos'kin, M.V., Yaroshenko, A.P., Mochalin, V.N., and Panchenko, B.V., *Zh. Prikl. Khim.*, 2003, vol. 76, no. 6, pp. 936–938.
92. Savos'kin, M.V., Yaroshenko, A.P., Shologin, V.I., and Galushko, L.Ya., *Zh. Prikl. Khim.*, 2003, vol. 76, no. 7, pp. 1213–1215.
93. Yakovleva, E.V., Yakovlev, A.V., Finaenov, A.I., and Finaenova, E.V., *Zh. Prikl. Khim.*, 2004, vol. 77, no. 11, pp. 1833–1835.
94. Stiles, A.B., *Catalyst Supports and Supported Catalysts. Theoretical and Applied Concepts*, Boston: Butterworths, 1987.
95. USSR Inventor's Certificate no. 1 515 202.

ISSN 1070-4272, Russian Journal of Applied Chemistry, 2006, Vol. 79, No. 11, pp. 1752–1756. © Pleiades Publishing, Inc., 2006.
Original Russian Text © D.V. Cherednichenko, E.V. Vorob'eva, N.P. Krut'ko, P.D. Vorob'ev, 2006, published in Zhurnal Prikladnoi Khimii, 2006, Vol. 79, No. 11, pp. 1772–1776.

INORGANIC SYNTHESIS AND INDUSTRIAL INORGANIC CHEMISTRY

Control over Wetting of Potassium Chloride by Water-Soluble Polymers

D. V. Cherednichenko, E. V. Vorob'eva, N. P. Krut'ko, and P. D. Vorob'ev

Institute of General and Inorganic Chemistry, National Academy of Sciences of Belarus, Minsk, Belarus

Received November 2, 2005

Abstract—The wetting of the potassium chloride surface by water-soluble polymers and polymer–surfactant complexes, which is highly important for granulation of potassium chloride, was studied. The efficiency of the wetting process was analyzed using a polymer–surfactant combination in comparison with individual polymers.

DOI: 10.1134/S1070427206110024

At present, the international market of mineral fertilizers imposes the following basic requirements on their physicomechanical properties: the grain size of a fertilizer should have a narrow distribution; the grains should be spherical and have a smooth surface, high crushing and wear resistance, low moisture content, resistance to caking, high resistance to moisture absorption, and low dust content [1–3]. A permanent problem in manufacture of potassium fertilizers and, especially, in their shipping to consumers is dusting of potassium chloride. Dust fractions of fertilizers are released into the atmosphere in handling, make difficult the work of the service personnel, contaminate the environment, and deteriorate the quality of fertilizers in storage.

Finely grained flotation potassium chloride presently manufactured by Belarus'kalii Production Association, Republican Unitary Enterprise, contains a considerable amount of dust particles. The dusty fraction is delivered together with the main product to compaction. The presence of dust, whose surface is hydrophobized by amines (organic reagents used in the industrial process), complicates compaction, lowers the output capacity, raises the energy expenditure, and impairs the quality of grains. The problem can be solved by separating the dust and performing granulation to obtain a commercial product. The granulation consists of a set of physicochemical and physicomechanical processes that provide formation of particles with certain size, shape, structure, and physical properties. Various methods for granulation of dispersed materials are known; however, the only presently existing way to granulate potassium fertilizers is compaction [4–7]. The efficiency of granulation is determined by the process parameters and by use of binder liquids. In a comparison of techniques used for granulation of dispersed systems (compaction and pelletizing), the authors of [3–5] believe that use of effective binder additives is especially important in pelletizing because of the absence in this case of any external pressure in the granulation process.

The interaction of a binder liquid with particles of the dispersed phase begins with surface wetting. A good wetting, which provides a fuller contact over a large surface area, predetermines the high efficiency of the binding action of an additive. In the general case, the wetting is governed by the properties of a liquid (viscosity, density, surface tension) and a material (capillary radius, nature of the substance, state of the surface). The properties of the material (dustlike fractions of flotation potassium chloride), namely, its high dispersity and hydrophobic surface, require a specific approach to the choice of binder materials. Experiments demonstrated that, in the case in question, use of the conventional binders based on water-soluble polymers (polyvinyl alcohol, carboxymethyl cellulose, polyvinyl acetate) is inefficient. According to electron-microscopic data, grains formed from finely dispersed potassium chloride are inhomogeneous and have the form of a combination of dust particles and clots of a polymer binder.

The aim of this study was to examine the possibility of control over wetting of potassium chloride by using complexes based on water-soluble polymers and surfactants of varied nature.

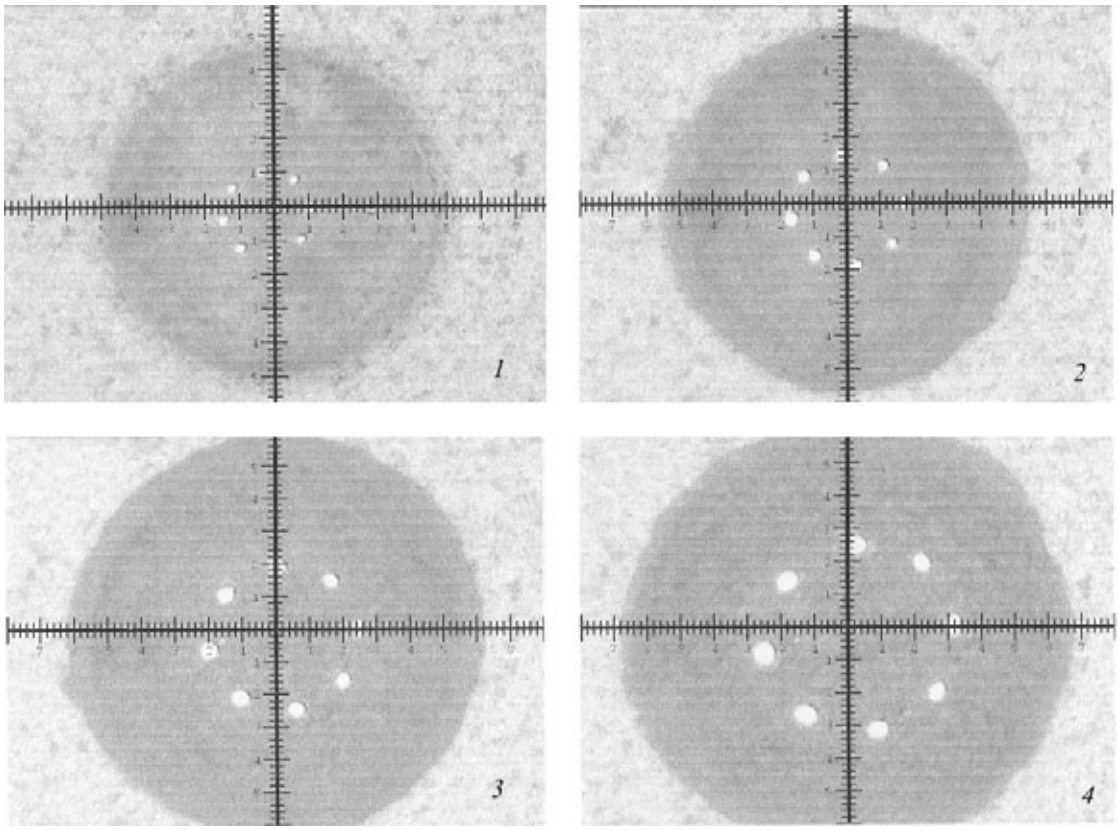


Fig. 1. Variation of the diameter of a drop on the KCl surface with time. Time t, min: (*1*) 0, (*2*) 1.5, (*3*) 3, and (*4*) 4.5.

EXPERIMENTAL

As water-soluble polymers were used commercial samples of acrylamide (co)polymers of Praestol brand (Stockhausen, Germany): nonionic polyacrylamide (N) and anionic (A) and cationic (C) polyelectrolytes. The anionic polyelectrolytes were high-molecular-weight copolymers (molecular weight of 14×10^6 according to manufacturer's data) of acrylamide with sodium acrylate, with a 20% content of ionic units. The cationic polyelectrolytes, copolymers of acrylamide with trimethylammoniopropylacrylamide chloride had a molecular weight of about 9×10^6 and contained 20% ionic units.

Oxyethyl alcohol was used as a nonionic surfactant (S_N); sodium octanesulfonate, as anionic surfactant (S_A); and cetylpyridium chloride, as cationic surfactant (S_C).

Potassium chloride of chemically pure grade, used in the study, was ground to a finely dispersed state corresponding in particle size to the dustlike fraction (1200–1500 $cm^2\ g^{-1}$). The surface of potassium chloride was hydrophobized with aliphatic amine chlorides of Flotigam S brand. Creating a monomolecular layer at a specific surface area of about 100 $cm^2\ g^{-1}$ requires about 20 g of amine per ton of potassium chloride [8]; for finely dispersed fractions this amount is 270–300 g t^{-1}. At amine doses of 50, 100, and 200 g t^{-1}, the fraction of the hydrophobized surface is 15–20, 30–35, and 60–70%, respectively. According to laboratory tests, the industrial samples of the dustlike fraction contained 60 to 270 g t^{-1} of amine.

To evaluate the efficiency of wetting of the potassium chloride surface, a procedure for estimating the spreading velocity of drops of the same volume over the surface of densified finely dispersed material was developed. Samples of potassium chloride ground to the state of a dust (fraction with a particle size of less than 0.2 mm) were prepared under identical conditions (humidity, temperature, time, and force of compaction). The variation of the drop diameter was recorded by measurements under a Telemik-1 microscope (Russia–Japan) with a tenfold magnification at certain intervals of time, and the velocity of drop spreading over the surface was evaluated (Fig. 1). The wetting efficiency (D_w) was calculated as the ratio between the spreading velocity of a drop of

Table 1. Efficiency of surface wetting by aqueous solutions of mixtures of polymers and surfactants of varied nature (the efficiency of wetting by individual polymers is taken as unity)

Polymer/surfactant ratio	Wetting efficiency							
	$A–S_A$	$A–S_N$	$N–S_A$	$N–S_N$	$N–S_C$	$C–S_A$	$C–S_N$	$C–S_C$
1 : 0.005	1.0	1.02	1.02	1.09	1.01	1.11	1.03	1.0
1 : 0.01	1.0	1.09	1.03	1.12	1.02	1.15	1.06	1.01
1 : 0.05	1.02	1.14	1.05	1.20	1.04	1.20	1.11	1.03
1 : 0.1	1.03	1.15	1.09	1.25	1.07	1.32	1.15	1.03
1 : 0.5	1.03	1.17	1.11	1.27	1.10	1.54	1.17	1.03
1 : 1	1.02	1.19	1.13	1.34	1.12	1.76	1.17	1.02
1 : 1.5	1.03	1.19	1.13	1.35	1.12	1.76	1.18	1.03

a liquid under study to that of a drop of distilled water over the sample surface.

The interaction in systems based on polymers and surfactants was studied by viscometry (using an Ostwald viscometer with a capillary diameter of 0.63 mm) and by measuring the surface tension by the ring detachment method to within ± 0.2 mJ m^{-2}. In the experiments, the same volume of a surfactant solution of varied concentration was added to a certain volume of a polymer solution of prescribed concentration, at various relative amounts of polar groups of the polymer and a surfactant.

The wetting of the hydrophobized surface of potassium chloride with distilled water and polymer solutions was evaluated in relation to the amount of amine. It was found that the spreading velocity of drops sharply decreases at an amine content of 300 g t^{-1}, i.e., under the conditions of virtually complete hydrophobization of the surface. Therefore, the effect of reagents (polymers, surfactants, and mixtures of these) on the wetting efficiency was studied at the maximum content of amine (300 g t^{-1}).

The adsorption layers formed by amine chlorides on the surface of potassium chloride contain surface-active ions with hydrophobic radicals directed away from the surface. In treatment of potassium chloride with water-soluble polymers, this hinders surface wetting and prevents uniform distribution of polymer solutions. To improve the wetting, a preliminarily prepared mixture of aqueous solutions of polymers and surfactants of varied nature was used. Mixing of solutions of an anionic polyelectrolyte and cationic surfactant leads, at any component ratio, to precipitation. Therefore, the rheological and surface-active properties and the wetting efficiency were not studied for this system.

Table 1 lists data characterizing the wetting efficiency of the potassium chloride surface by aqueous solutions of polymers mixed with surfactants. It can be seen that the wetting efficiency increases to varied extent for all combinations of polymers with surfactants, with the exception of $A–S_A$ and $C–S_C$ mixtures. The wetting efficiency is the highest with the oppositely charged polymer and surfactant and with nonionic components ($N–S_N$). Addition of even an insignificant amount of a surfactant to the polymer (polymer/surfactant ratio = 1 : 0.005) leads to an increase in the wetting efficiency by 9–11%. It may be assumed that the improvement of the wetting capacity is due to interaction between components and to formation of polymer–surfactant complexes. As the ratio of the interacting groups of the components starts to exceed 1 : 1, the wetting efficiency remains virtually unchanged, which indicates that there exists a limiting degree of interaction of the components.

It is known that, in wetting of powdered materials, drops expand in all directions and fill pores between separate particles. At invariable properties of the material and wetting conditions, the rate of capillary suction is determined by the properties of the liquid and, in particular, by its viscosity and surface tension [3, 5]. Therefore, the rheological and surface-active properties of solutions of polymers and their mixtures with surfactants of varied nature were studied.

It was found that the viscosity of aqueous solutions of a mixture of a cationic polyelectrolyte and anionic surfactant decreases relative to that of the starting polymer (by a factor of more than 3 at the equimolar polymer/surfactant ratio) (Table 2). As there is no dilution in the system (the surfactant concentration changes at an invariable volume), the changes observed may be due to interaction between the components and to complexation. As the concentration

of the surfactant in the mixture increases, its adsorption on oppositely charged polymer macromolecules becomes more pronounced. This is accompanied by a decrease in the polyelectrolyte charge and in the size of polymer macromolecules and by the resulting lowering of the viscosity of the solutions. A decrease in viscosity is also observed on mixing aqueous solutions of a nonionic polymer with a nonionic surfactant (Table 2). In this case, the change in the viscosity of the mixture, compared with the individual polymer, is due to interaction of the nonionic groups of the components via hydrogen bonds.

A comparison of the rheological properties of $A–S_N$, $N–S_A$, $N–S_C$, and $C–S_N$ mixtures and individual polymers demonstrated that the viscosity decreases, on the average, by 10% at a component ratio of 1 : 1. Taking into account that polymer macromolecules contain 20% ionic groups, the rest of the groups can be involved in formation of hydrogen bonds with surfactant molecules.

It is known [9] that the macromolecules are hydrophobized and their surface activity increases in complexation as a result of the interaction between the hydrophilic groups of the polymers and surfactants (electrostatic or via hydrogen bonds). In the case in question, studies revealed a decrease in the surface tension of aqueous solutions of polymers upon addition of a surfactant. In treatment of potassium chloride, the aqueous solution of the polymer–surfactant complex comes in contact with the salt. The presence of the low-molecular-weight surfactant affects the surface-active properties of the polymer complex. In this context, the effect of the salt in various concentrations on the surface tension of solutions of 1 : 1 polymer complexes was studied (Table 3).

As seen from Table 3, the surface tension of the solutions decreases as the concentration of the low-molecular-weight salt becomes higher. This is due to a change in the solvent (water) structure, a decrease in the degree of hydration of complex species, and the resulting enhancement of their adsorption on the potassium chloride surface [10]. As the concentration of the low-molecular-weight electrolyte is raised to 20%, the surface tension of the solutions grows, which may be due to rearrangement of the complex species, but remains lower than that of the aqueous solutions.

Figure 2 shows magnified images of drops of an aqueous solution of a polymer and of a mixture of the cationic polyelectrolyte and anionic surfactant (1 : 1 ratio of ionic groups), taken at regular intervals of time (2 min).

Table 2. Variation of the relative viscosity of aqueous solutions of polymer–surfactant mixtures with the ratio of the ionic groups of the components (the viscosity of the individual polymers is taken as unity)

Polymer/surfactant ratio	Relative viscosity	
	$C–S_A$	$N–S_N$
Polymer (no surfactant)	1.0	1.0
1 : 0.005	0.96	0.98
1 : 0.01	0.90	0.92
1 : 0.05	0.82	0.90
1 : 0.1	0.75	0.88
1 : 0.5	0.55	0.85
1 : 1	0.30	0.79
1 : 1.5	0.28	0.80

Table 3. Effect of the low-molecular-weight electrolyte (potassium chloride) on the surface tension of solutions of polymer–surfactant complexes (1 : 1)

KCl concentration in solution, %	Surface tension of solutions of complexes, mJ m^{-2}			
	$C–S_A$	$N–S_N$	$A–S_N$	$C–S_N$
0	66.1	65.6	70.0	67.9
0.1	62.6	61.9	64.7	64.1
0.5	60.5	59.8	61.7	63.2
1.0	59.8	58.7	60.6	64.1
3.0	60.5	58.9	59.8	64.9
5.0	61.1	59.9	60.2	65.3
10.0	62.1	60.9	60.6	65.8
20.0	63.5	62.6	62.7	68.3

The drop of the aqueous solution of the complex (Fig. 2a) wets the potassium chloride surface better than does that of the individual polymer (Fig. 2b). The presence of the surfactant favors distribution of the liquid over the surface, which improves the binding properties of the polymer in further processing (granulation) of potassium chloride.

The results obtained were used in practice in granulation of a finely dispersed flotation potassium chloride. The introduction of surfactants into the solution of a polymer binder improved the grain strength by a factor of 2.5 and raised the output of the target fraction by 12% on average.

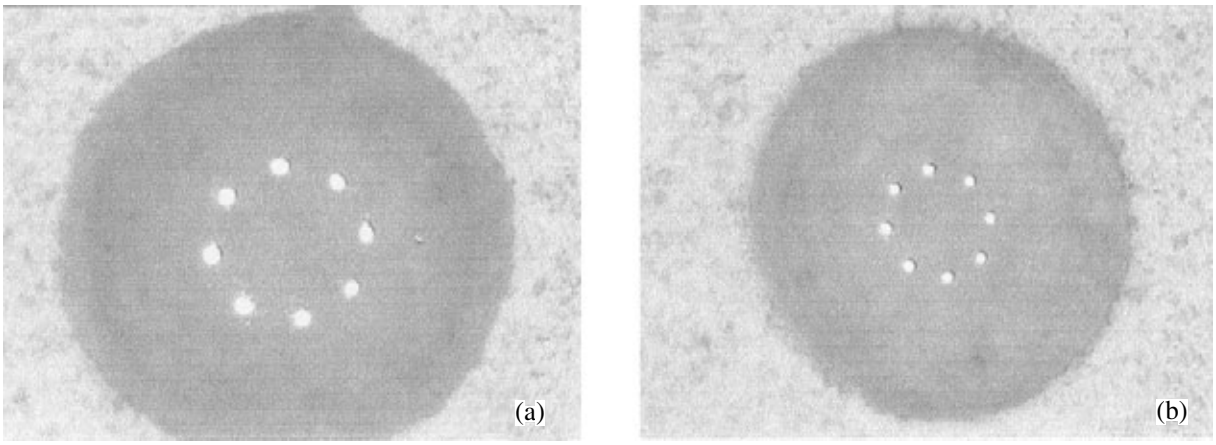


Fig. 2. Photographs of drops of (a) 1 : 1 C–S_A mixture and (b) aqueous solution of C.

CONCLUSIONS

(1) The wetting efficiency of the hydrophobized surface of finely dispersed potassium chloride by aqueous solutions of polymeric binders increases if complexes based on polymers and surfactants are used. This is due to a change in the colloid-chemical properties of the solutions: decrease in viscosity and increase in surface activity.

(2) Surfactants serve as a kind of interlayer between the hydrophobic surface of potassium chloride particles and the hydrophilic solution of a binder, which has a positive effect in the stage of component mixing on the distribution of the binder over the particle surface and, further, on the physicomechanical properties of fertilizer grains.

REFERENCES

1. *Galurgiya: Teoriya i praktika* (Mineral-Salt Production: Theory and Practice), Sokolov, I.D., Ed., Leningrad: Khimiya, 1983.
2. Golovkov, B.Yu., Lomakin, A.G., and Reibman, L.A., *Kalii v proshlom, nastoyashchem i budushchem* (Potassium in the Past, Present, and Future), St. Petersburg, 2001.
3. Klassen, P.V. and Grishaev, I.G., *Osnovy tekhniki granulirovaniya* (Fundamental of Ganulation Technology), Moscow: Khimiya, 1982.
4. Klassen, P.V. and Grishaev, I.G., *Osnovnye protsessy tekhnologii mineral'nykh udobrenii* (Basic Processes of the Technology of Mineral Fertilizers), Moscow: Khimiya, 1990.
5. Pietsch, A. and Wolfgang, V., *Agglomeration Processes: Phenomena, Technologies*, 2002.
6. Ufimtsev, V.M., *Gorn. Zh.*, 1997, nos. 11–12, pp. 220–226.
7. Vilesov, N.G., *Protsessy granulirovaniya v promyshlennosti* (Granulation Processes in Industry), Kiev: Tekhnika, 1976.
8. Pavlyuchenko, M.M., *Kaliinye soli i metody ikh pererabotki* (Potassium Salts and Methods for Their Processing), Minsk: Akad. Nauk Bel. SSR, 1963.
9. Shaikhutdinov, E.M., Abdiev, K.Zh., Zhursumbaeva, M.B., and Khusain, S.Kh., *Kolloidn. Zh.*, 2001, vol. 63, no. 6, pp. 850–854.
10. Dikhtievskaya, L.V. and Mozheiko, F.F., *Dokl. Nats. Akad. Nauk Bel.*, 1999, vol. 43, no. 5, pp. 58–61.

ISSN 1070-4272, Russian Journal of Applied Chemistry, 2006, Vol. 79, No. 11, pp. 1757–1760. © Pleiades Publishing, Inc., 2006.
Original Russian Text © V.V. Guzeev, A.N. D'yachenko, 2006, published in Zhurnal Prikladnoi Khimii, 2006, Vol. 79, No. 11, pp. 1777–1780.

INORGANIC SYNTHESIS AND INDUSTRIAL INORGANIC CHEMISTRY

Autoclave Breakdown of Zircon with Ammonium Fluorides

V. V. Guzeev and A. N. D'yachenko

Tomsk Polytechnic University, Tomsk, Russia

Received March 30, 2006; in final form, June 2006

Abstract—Autoclave breakdown of zircon with ammonium fluorides was studied.

DOI: 10.1134/S1070427206110036

Zircon is one of the main mineral sources of zirconium materials, but the technology of its breakdown and processing is still labor-consuming, and much efforts are made to improve it.

The classical industrial methods of breaking down zirconium concentrates are sintering with fluosilicates and chlorination. Numerous studies summarized in [1] were devoted to zircon fluorination; however, it did not gain industrial application. The fluoride technology allows the scheme of the zirconium product processing to be reduced considerably, but high cost and corrosive behavior of HF and F_2, and also SiF_4 liberation restrain industrial application of these reagents.

In this study we examined the autoclave breakdown of zircon with ammonium fluorides.

Unlike fluorine and hydrogen fluoride, ammonium fluorides are very convenient to use, as these are solid crystalline substances under normal conditions. Ammonium fluorides can be obtained from metal fluorides by the action of ammonia water, which is the basis for conversion and recycling of ammonium fluorides.

Ammonium fluoride is known to react slowly with zircon [2, 3]. At temperatures below 240°C, the reaction rate is negligible and the degree of breakdown is unsatisfactory for the industrial use, whereas at higher temperatures ammonium fluoride evaporates with decomposition.

Here we report new data on the zircon breakdown with ammonium fluoride and hydrofluoride.

The essence of the method consists in the reaction of zircon with ammonium fluoride or hydrofluoride under isochoric conditions (in an autoclave), after which the reaction products are separated by sublimation to give zirconium tetrafluoride and dioxide. The advantage of ammonium fluorides over other fluorinating agents consists in their convenient physicochemical properties allowing their regeneration and recycling.

The experiments were carried out with zircon samples from Tugan deposit of Tomsk oblast.

The reactions of zircon with ammonium fluoride and hydrofluoride were studied under isochoric conditions in a 100 cm^3 stainless steel autoclave. A weighed portion of zircon with a grain size of 0.074 mm was placed in the autoclave together with a weighed portion of ammonium fluoride taken in a 20% excess in relation to the stoichiometric amount calculated for the reaction

$$ZrSiO_4 + 13NH_4F = (NH_4)_3ZrF_7 + (NH_4)_2SiF_6 + 8NH_3 + 4H_2O.$$

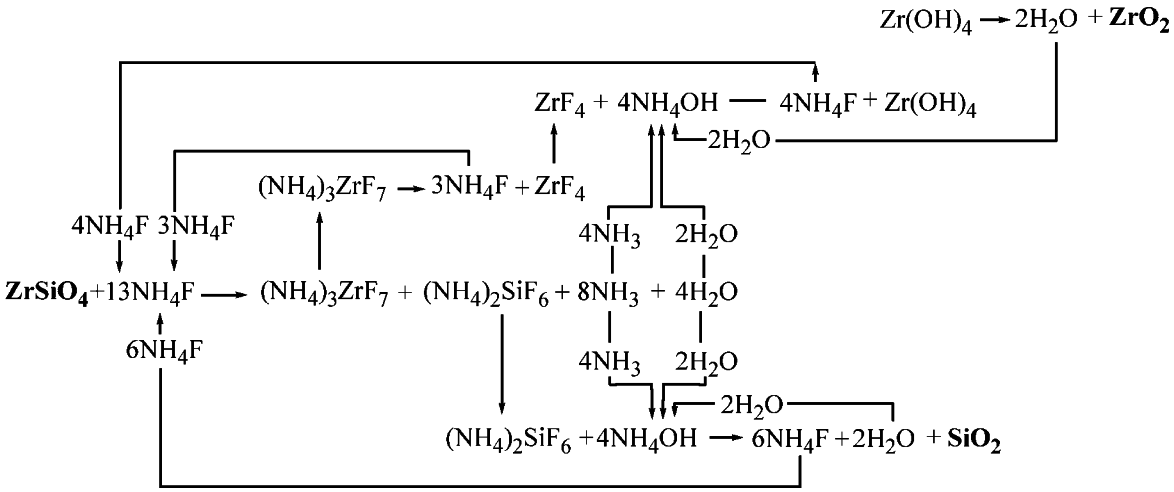
The autoclave was heated to 150, 200, 250, 300, 350, and 400°C and kept at these temperatures for 0.5, 1, 2, and 4 h.

After opening the autoclave, its content was transferred into a crucible and calcined for 30 min at 400°C to remove by sublimation unchanged NH_4F and formed $(NH_4)_2SiF_6$. The residue in the crucible was a mixture of unchanged $ZrSiO_4$ and NH_4ZrF_5, to which 5 ml of concentrated sulfuric acid was added, and the mixture was kept until H_2SO_4 vapor disappeared. Zirconium in the form of $ZrOSO_4$ solution was leached with water from the formed cake, converted to zirconium dioxide, and weighed to determine the degree of conversion.

The same procedure was used to study the reaction of ammonium hydrofluoride with zircon

$$2ZrSiO_4 + 13NH_4F\cdot HF = 2(NH_4)_3ZrF_7 + 2(NH_4)_2SiF_6 + 3NH_3 + 8H_2O.$$

Scheme 1.



The data on the kinetics of zircon breakdown with ammonium fluoride are given in Fig. 1, which contains two series of curves: the first corresponds to temperatures below ammonium fluoride boiling point and the second, to elevated temperatures.

The standard mathematical treatment of the kinetic data showed that the curves for 150, 200, and 250°C are described with an adequate accuracy by Gray–Weddington's, and the curves for 300, 350 and 400°C, by Crank–Ginstling–Brounshtein's equation.

The rate equation for the range 150–250°C is

$$\alpha = 1 - [1 - 10^{-3}\exp(-17\,000/RT)\,t]^3.$$

The activation energy E_A is 17 kJ mol^{-1}, which corresponds to the diffusion control, the preexponential factor $k_0 = 10^{-3}$ s^{-1}, and the gas constant R = 8.31.

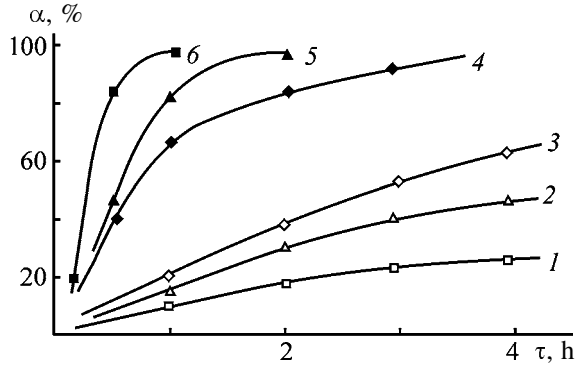


Fig. 1. Kinetic curves for the reaction of ammonium fluoride with zircon under isochoric conditions. (α) Degree of conversion degree and (τ) time; the same for Fig. 2. Temperature, °C: (*1*) 150, (*2*) 200, (*3*) 250, (*4*) 300, (*5*) 350, and (*6*) 400.

The rate equation for the range 300–400°C is

$$1 - 1/3\,\alpha(1 - \alpha)^{1/3} = \exp(-5500/RT)\,t.$$

The activation energy E_A = 55 kJ mol^{-1}, which corresponds to the kinetic control, the preexponential factor k_0 = 1 s^{-1}, and the gas constant R = 8.31. Material streams and material balance were calculated in accordance with Scheme 1.

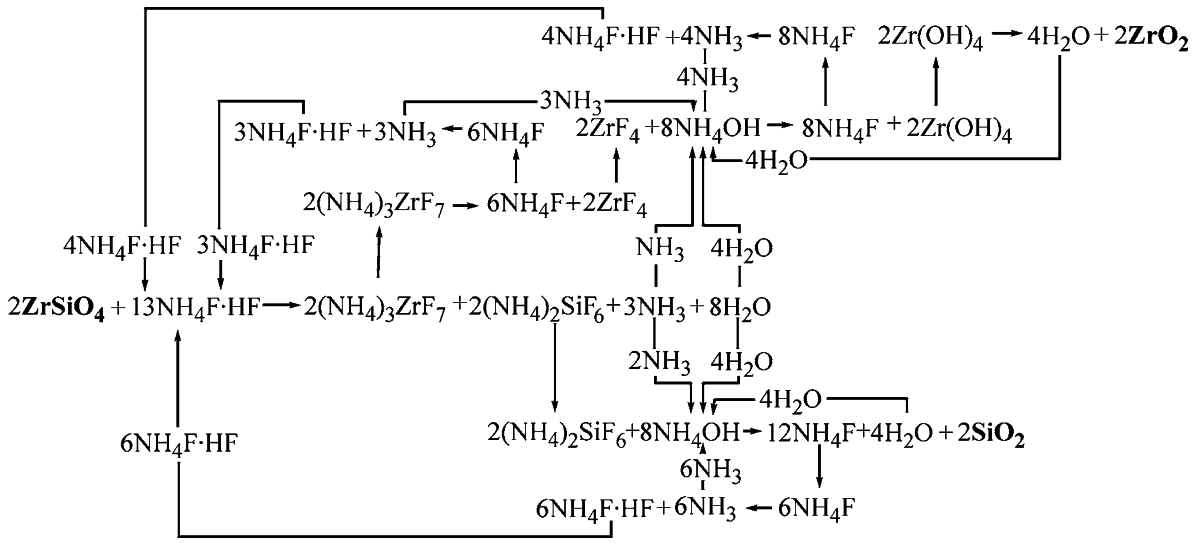
Scheme 1 clearly illustrates the breakdown of zircon with ammonium fluoride and the formation of complexes followed by their hydrolysis and ammonium fluoride regeneration. Uniqueness of ammonium fluorides consists in the fact that their melt is the most powerful fluorinating agent reacting with zircon to form zirconium and silicon complex fluorides. Zirconium tetrafluoride and ammonium hexafluorosilicate are easy to separate by sublimation. After separation, the fluorides are subjected to hydrolysis with ammonia. Ammonium fluoride is regenerated, and oxides are precipitated from the solution. Unlike ammonium fluoride melt, its solution is inert and does not react with oxides.

The experimental dependences of the conversion α on time and temperature for the breakdown of zircon with ammonium hydrofluoride are given in Fig. 2. The kinetic curves are linearized most accurately by Yander's equation

$$\alpha = 1 - \{1 - [6.6\exp(-54\,000/RT)\,\tau]^{1/3}\}^3.$$

The preexponential factor is k_0 = 6.6 s^{-1}, and the activation energy calculated from the Arrhenius equation is E_A = 54 kJ mol^{-1}, which indicates that the process is kinetically controlled and temperature

Scheme 2.



exerts a decisive effect on its rate. Scheme 2 of material streams in the breakdown of zircon with ammonium hydrofluoride is given below.

The above-given experimental data allow us to suggest the optimal process parameters: with $NH_4F \cdot HF$, the conversion higher than 95% is reached at 300°C within 1.5 h and at 400°C, within less than 0.5 h [4].

When NH_4F was used, an elevated pressure was developed in the autoclave. The heating of ammonium fluoride is known to result in its thermal dissociation into ammonia and hydrogen fluoride, which increases the total pressure in the system [5].

The pressure of the mixture of HF and NH_4F vapors calculated by the Mendeleev–Clapeyron equation considerably exceeds the actual pressure owing to the condensation of the mixture of hydrogen fluoride and ammonia at a temperature below 240°C and also owing to considerable deviations of the behavior of this mixture from that of an ideal gas to which theoretical calculations are applicable.

To determine the real pressure which is developed under the considered conditions, we have carried out special experiments.

The temperature dependence of the vapor pressure was studied for two substances: ammonium fluoride and hydrofluoride. In a 100 cm^3 autoclave, 10 g of salt was placed, and the system was sealed and gradually heated to 350°C with continuous monitoring of the pressure with an MTP-1M manometer. The plots of the vapor pressure of ammonium fluoride and hydrofluoride are given in Fig. 3.

Apparently, the use of ammonium fluoride at high temperatures is not appropriate because high pressures arise and hence more sophisticated equipment is required; therefore, the use of ammonium hydrofluoride is the most efficient. As follows from Fig. 3, the vapor pressure of ammonium hydrofluoride at 300°C does not exceed 45 atm, which allows its use in the technology of the zircon breakdown with ammonium hydrofluoride. A considerable experience of using high-pressure devices in the industrial synthesis of ammonia and in the transportation of natural gas has been accumulated.

The temperature of 300°C is optimal for implementation of the process, as relatively low temperature will not cause strong corrosion of the instrumentation even at a long reaction time (4 h).

A distinctive feature of the zircon breakdown with ammonium hydrofluoride is the complete regeneration

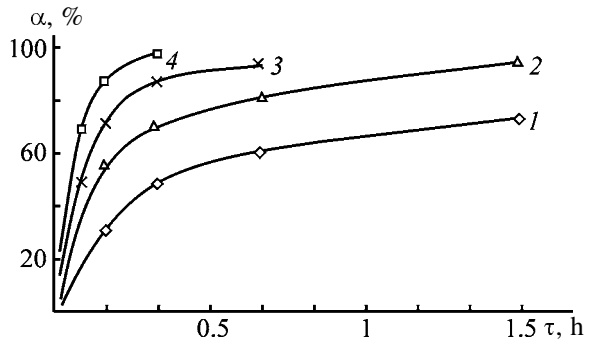


Fig. 2. Kinetic curves for the reaction of ammonium hydrofluoride with zircon. Temperature, °C: (*1*) 250, (*2*) 300, (*3*) 350, and (*4*) 400.

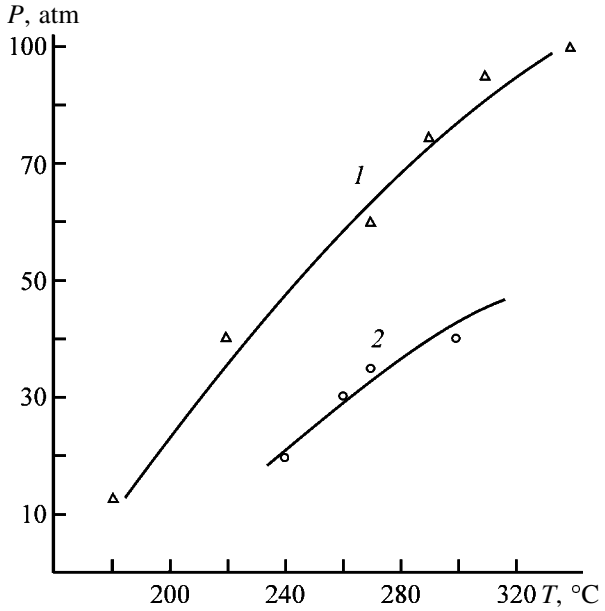


Fig. 3. Dependence of vapor pressure P of (*1*) ammonium fluoride and (*2*) ammonium hydrofluoride on temperature T under isochoric conditions in 100 cm^3 of air.

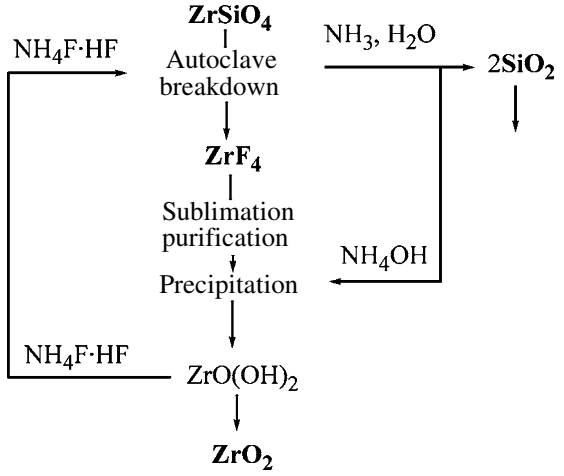
of ammonium fluoride, which makes the process economically attractive and environmentally safe.

The formed ammonium fluosilicate sublimes at temperatures above 320°C and is removed from the mixture [6].

Heating to 300°C removes unchanged ammonium fluoride from the mixture. As the temperature is increased, $(NH_4)_2ZrF_6$ decomposes to zirconium tetrafluoride, and ammonia and hydrogen fluoride are liberated.

The overall process of ammonium fluoride breakdown of zircon is shown in Scheme 3.

Scheme 3.



In the suggested scheme, the number of operations is minimized and complete recycling of the reagents is provided. Among disadvantages of the scheme is certain complexity of the instrumentation of the main process, ammonium fluoride breakdown of zircon, which is caused by the buildup of high pressure under isochoric conditions. The corrosive action of ammonium fluoride on stainless steel can be reduced by adding sodium fluoride [7]; however, the use of sodium fluoride will pose a problem of its regeneration and removal from the products.

CONCLUSIONS

(1) Optimal parameters of zircon breakdown with ammonium fluoride and hydrofluoride in an autoclave under isochoric conditions were found. In the case of ammonium hydrofluoride, the 95% decomposition at 300°C is reached within 1.5 h, and a pressure of 45 atm is developed in the system.

(2) The overall scheme of the cycle of zircon breakdown with the regeneration of ammonium fluoride and production of zirconyl hydroxide was suggested.

REFERENCES

1. Rikhvanov, L.P., Kropatin, S.S., Babenko, S.A., et al., *Zirkon-il'menitovye rossypnye mestorozhdeniya kak potentsial'nyi istochnik razvitiya Zapadno-Sibirskogo regiona* (Zircon–Ilmenite Gravel Deposits as a Potential Source of the Development of the Western Siberia Region), Kemerovo: Sars, 2001.
2. Mel'nichenko, E.I., Krysenko, G.F., Epov, D.G., and Ovsyannikova, A.A., *Zh. Prikl. Khim.*, 1994, vol. 67, no. 5, pp. 737–741.
3. Mel'nichenko, E.I., *Ftoridnaya pererabotka redkometall'nykh rud Dal'nego Vostoka* (Fluoride Processing of Rare-Metal Ores of the Far East), Vladivostok: Dal'nauka, 2002.
4. RF Patent 2 211 804.
5. Rakov, E.G., *Khimiya i tekhnologiya neorganicheskikh ftoridov: Uchebnoe posobie* (Chemistry and Technology of Inorganic Fluorides: Tutorial), Moscow: Mosk. Khim.-Tekhnol. Inst. im. D.I. Mendeleeva, 1990.
6. Mel'nichenko, E.I., Epov, D.G., Krysenko, G.F., et al., *Zh. Prikl. Khim.*, 1996, vol. 69, no. 8, pp. 1248–1250.
7. Zotikov, V.S., Kobulashvili, G.Sh., and Semenyuk, E.Ya., Abstracts of Papers, *VIII Vsesoyuznyi simpozium po khimii neorganicheskikh ftoridov* (VIII All-Union Symp. on the Chemistry of Inorganic Fluorides), Moscow: Nauka, 1987, p. 154.

ISSN 1070-4272, Russian Journal of Applied Chemistry, 2006, Vol. 79, No. 11, pp. 1761–1764. © Pleiades Publishing, Inc., 2006.
Original Russian Text © V.N. Lebedev, 2006, published in Zhurnal Prikladnoi Khimii, 2006, Vol. 79, No. 11, pp. 1781–1784.

INORGANIC SYNTHESIS AND INDUSTRIAL INORGANIC CHEMISTRY

Sulfate-Containing Zirconium Dioxide Powders Made of Products of Baddeleyite Processing

V. N. Lebedev

Tananaev Institute of Chemistry and Technology of Rare Elements and Mineral Raw Materials, Kola Scientific Center, Russian Academy of Sciences, Apatity, Murmansk oblast, Russia

Received March 16, 2006

Abstract—Manufacture of sulfate-containing zirconium dioxide powders from basic zirconium sulfate, zirconium disulfate, and ammonium sulfatozirconate, which are sulfate-containing products of processing of baddeleyite concentrate, was studied.

DOI: 10.1134/S1070427206110048

Zirconium dioxide nanopowders are used for manufacturing specialty ceramics, catalysts, sorbents, and other materials with special properties. Such materials are commonly obtained from zirconium oxychloride or oxynitrate, with composition and properties of the products obtained dependent on both the starting salts and the method of powder preparation. Different crystalline modifications can be formed even in the stage of precipitation at prolonged boiling of hydrolysis precipitates or in an autoclave [1, 2]. The metastable cubic and tetragonal phases of zirconium dioxide are formed by the thermal dehydration below 380–400°C and transform into the stable monoclinic phase at higher temperature [3]. The temperature of the phase transitions and the properties of powders depend on the preparation conditions and on the presence of stabilizing impurities such as water, cationic, and anionic impurities [4–6].

In catalysis, ZrO_2 modified with sulfate groups came into use relatively recently. The modified ZrO_2 exhibits superacid properties, and its high specific surface area (of the order of 100 $m^2 g^{-1}$) is retained on heating [7–9]. Therefore, we consider in this study the manufacture of powders in which the content of SO_4^{2-} ions can be controlled by the starting materials. As starting materials were used products of processing of baddeleyite concentrate, i.e., basic zirconium sulfate (BZS), zirconium disulfate (ZDS), and ammonium sulfatozirconate (ASZ) [10, 11]. ZrO_2 obtained from zirconium oxychloride (ZOC) was used for comparison. The above products were separated by breakdown of baddeleyite concentrate with sulfuric acid or by sintering with calcium carbonate. The content of the impurities in BZS and ZOC was about 1×10^{-3}–1×10^{-4} wt %, and that in ZDS and ASZ, 1×10^{-1}–1×10^{-2} wt %. The basic zirconium sulfate was precipitated at the $SO_4^{2-} : ZrO_2$ molar ratios (m.r.) of 0.8, 0.6, and 0.45.

Zirconium oxides were prepared by heating hydroxides or sulfate-containing products at 380–800°C. The hydroxides were washed to remove sulfate ions to various extents, or the sulfate-containing products were heated without washing. According to data of the thermal analysis, the sulfates decompose in the range 600–800°C [12]. Zirconium hydroxides were prepared by back precipitation. To do this, a sample of zirconium-containing precipitate was introduced into a calculated amount of a 5% ammonia solution. The zirconium hydroxide precipitate thus obtained are pseudocrystalline and easy to filter [13]. The pulp was stirred for 2 h at pH 9, stored for 24 h to remove the possible products of incomplete hydrolysis, and washed to remove sulfate ions. The hydroxides were dried at 120°C for 12 h. Then, they were treated in a 0.1–1.0 M H_2SO_4 solution for 12 h to be saturated with sulfate groups.

The products obtained were subjected to X-ray phase analysis (DRON-1 diffractometer, CuK_α radiation). The specific surface area was calculated from the isotherms of low-temperature adsorption of nitrogen (BET). The content of the sulfate ions (counting on SO_3) in the samples was determined by X-ray fluorescence analysis (FRA-1 analyzer).

The monitored parameters of the samples heat-treated for 3 h are listed in Table 1.

Table 1 shows that the sintering of all samples, except for ASZ, yields zirconium dioxide powders

Table 1. Results of heat treatment of sulfate-containing zirconium products

Sample	Treatment temperature, °C							
	600		650			750		
	SO_3, wt %	phase	SO_3, wt %	phase	S, $m^2 g^{-1}$	SO_3, wt %	phase	S, $m^2 g^{-1}$
ZDS	60.2	ZDS	46	ZDS + am	–	4.3	m(70%) + t	26.9
ASZ	45.8	am*	28.6	t(85%) + m + ram	28.5	3.0	m(60%) + t	68.5
BZS (0.45)	20	″	5.5	m(75%) + t	56.8	2.9	m	36.1
BZS (0.6)	22.2	″	5.9	m(78%) + t	59.4	2.5	m(83%) + t	37.4

* (am) X-ray amorphous, (m) monoclinic, and (t) tetragonal; the same for Tables 2–4.

Table 2. Specific surface area and phase composition of washed samples of zirconium hydroxide and zirconium dioxide. Treatment time 3 h

Precursor	Treatment temperature, °C							
	120		380		600		800	
	S, $m^2 g^{-1}$	phase	S, $m^2 g^{-1}$	phase	S, $m^2 g^{-1}$	m-ZrO_2,* %	S, $m^2 g^{-1}$	m-ZrO_2, %
BZS (m.r. 0.45)	n.d.**	am	49	t	48	40	11	97
BZS (m.r. 0.6)	175	″	38	t	32	10	9	97
BZS (m.r. 0.8)	n.d.	″	n.d.	t	2.2	2	1.8	98
ASZ	165	″	44	t	30	0	16	90
ZDS	190	″	41	m	40	100	31	98
ZOC	n.d.	″	84	t	55	15	26	100

* (m-ZrO_2) Concentration of the monoclinic phase in the samples.
** (n.d.) No data.

with the predominant amount of the monoclinic phase, which makes them of little use for catalysis [8]. In addition, the specific surface area of the sintered samples is low. The sulfur(VI) removal is maximal within 600–750°C. Most of sulfur(VI) ions are not removed from zirconium disulfate and ammonium sulfatozirconate after treatment at 650°C for 3 h.

The data obtained on heating the washed hydroxide samples of the different origins are presented in Table 2. Note that the hydroxides obtained by the addition into an ammonia solution of BZS, ASZ, and, to a lesser extent, of ZOC and ZDS, more readily settle and are easier to filter than those obtained by the direct neutralization of solution. The samples obtained from BZS and ASZ and dried at 120°C are powders, those obtained from ZOC, slightly sintered, and those converted from ZDS are glassy and more hydrated.

The hydroxides with sulfate history, prepared by the same method and treated at 380°C for 6 h, crystallize in different modifications. The hydroxides obtained from BZS, ASZ, and ZOC crystallize in the standard low-temperature cubic or tetragonal modification, whereas those obtained from ZDS transform into the monoclinic modification at 380°C, i.e., the phase transition temperature is abnormally low.

The surface area of the samples dried at 120°C is approximately the same (165–190 $m^2 g^{-1}$). Therefore, it is unlikely to attribute the above distinctions to the "dimensional" factor [4]. The phase transition temperature can be largely affected by the presence of impurities. In our case, however, the factor determining the phase composition is the history of samples, because the impurity concentrations in ZDS and ASZ are close.

The heat treatment accompanied by the loss of water results in the formation of crystallites. As a result, the specific surface area of the powders decreases. The surface area of the ZDS sample treated below 800°C decreases to a lesser extent, which is likely due to the constancy of the phase composition. The surface area of the sample obtained from BZS with a molar ratio of 0.45 is retained up to 600°C.

Table 3. Characteristics of heat-treated samples incompletely washed to remove sulfate ions

Precursor	SO_3, wt %	Treatment temperature, °C				
		380	600		750	
		phase	S, $m^2 g^{-1}$	m-ZrO_2, %	S, $m^2 g^{-1}$	m-ZrO_2, %
BZS (m.r. 0.45)	5.6	am + t	75	4	34	16
BZS (m.r. 0.6)	2.9	t	63	2	30	20
ASZ	10.4	am	74	2	29	10
	4.2	am + t	39	8	18	8
ZDS	11.2	am	24	60	31	85
	5.6	"	29	42	27	80

Note that the specific surface area directly correlates with the content of the monoclinic phase in samples obtained from BZS and treated at 600°C. The sample from ZOC has the largest specific surface area which, however, decreases to a greater extent on heating.

The phase composition in heat treatment and the specific surface area of the samples incompletely washed to remove sulfate ions are presented in Table 3.

The data obtained for hydroxides washed to remove sulfate ions to different extents show that the presence of sulfate ions in hydroxides shifts the zirconium dioxide crystallization to higher temperatures (Table 3). The sulfate-containing samples, except for ZDS, sintered at 600°C have the larger specific surface areas than their washed analogs. With increasing concentration of the sulfate ions, the specific surface area increased. These samples were mostly in the tetragonal modification up to 750°C, but their specific surface area, however, noticeably decreased. Thus, the effect exerted by the presence of sulfate groups in hydroxides is essentially the same as that observed in modification of the dried hydroxides with sulfuric acid.

Table 4. Characteristics of samples treated with H_2SO_4

Precursor	Characteristics of ZrO_2 powders		
	SO_3, wt %	phase	S, $m^2 g^{-1}$
BZS (m.r. 0.45)	4.5–6.0	t + 2–4% m-ZrO_2	94–108
BZS (m.r. 0.6)	5.4	t	59
BZS (m.r. 0.8)	5.6	t	16
ASZ	7.1	t	73.8
ZDS	6.2	t + 30% m-ZrO_2	45
ZOC	4.3–7.9	t	68–82

The characteristics of the zirconium dioxide samples obtained by saturating hydroxides with H_2SO_4 and sintering them at 600°C for 3 h are presented in Table 4. As seen from the table, the treatment of hydroxides with sulfuric acid results in an increase in the specific surface area of the samples and leads to stabilization of the tetragonal phase. The surface area of the powders obtained from BZS increases in the same proportion as in the samples not treated with sulfuric acid. The sample obtained from BZS at the minimal $SO_4^{2-} : ZrO_2$ molar ratio has the largest surface area. For hydroxides prepared from the BZS precursor (at the molar ratio of 0.45) and for those prepared from the ZOC precursor, the concentration of the acid in the saturated solution was varied within 0.1–1.0 M. After sintering, the concentration of sulfate groups and the specific surface area varied within the range indicated in Table 4, with rather large data scattering. In all cases, we failed to attain the characteristics presented for ZOC in [9]. In [9], hydroxides were obtained by the direct precipitation from a solution. However, in our study, the dried samples obtained by the same method were glassy and had the lower specific surface area. As in other cases, the sample obtained from ZDS stands out, as containing the monoclinic phase, though in a somewhat smaller amount.

CONCLUSIONS

(1) The characteristics of the products obtained by heat treatment of zirconium disulfate, ammonium sulfate zirconate, and basic zirconium sulfate, which are sulfate-containing products of processing of baddeleyite concentrate, were studied. Zirconium dioxide, mainly of monoclinic modification, was formed by decomposition of sulfates at 650–750°C. The specific surface area varied from 68 $m^2 g^{-1}$ with ammonium

sulfatozirconate precursor to 28 $m^2 g^{-1}$ with zirconium disulfate precursor.

(2) The presence of incompletely removed sulfate ions in hydroxides with a sulfate history increases the temperature of the onset of the zirconium dioxide crystallization, the temperature of its transformation from the tetragonal into the monoclinic phase, and the specific surface area.

(3) The sulfate-containing zirconium dioxide powders with the largest specific surface area (94–108 $m^2 g^{-1}$) were obtained from samples of basic zirconium sulfate at the molar ratio $SO_4^{2-} : ZrO_2 = 0.45$. The advantage of this method of manufacturing powders is good filterability of hydroxides and more efficient removal of chloride ions by washing in deposition of basic zirconium sulfate.

REFERENCES

1. *Physical and Chemical Aspects of Adsorbents and Catalysts*, Linsen, B.G., Ed., New York: Academic, 1970.
2. Kolen'ko, E.V., Maksimov, V.D., Garshev, A.V., et al., *Zh. Neorg. Khim.*, 2004, vol. 49, no. 8, pp. 1237–1242.
3. Komissarova, L.N., Simanov, Yu.P., and Vladimirova, Z.A., *Zh. Neorg. Khim.*, 1960, vol. 5, no. 7, pp. 1413–1417.
4. Oleinikov, N.N., Murav'eva, G.P., and Pentin, I.V., *Zh. Neorg. Khim.*, 2002, vol. 47, no. 5, pp. 754–764.
5. Shevchenko, A.V., Dudnik, E.V., Ruban, A.K., et al., *Poroshk. Metall.*, 2001, nos. 11–12, pp. 9–18.
6. Garvie, R.S., *J. Phys. Chem.*, 1978, vol. 82, no. 2, pp. 218–224.
7. Lunin, V.V., Badina, E.Yu., Kuznetsova, N.N., and Tarakulova, A.O., *Zh. Fiz. Khim.*, 1990, vol. 64, no. 10, pp. 2777–2782.
8. Ivanov, A.V. and Kustov, L.M., *Ross. Khim. Zh.*, 2000, vol. 44, no. 2, pp. 21–52.
9. Kuznetsov, P.N., Kuznetsova, L.I., Zhizhaev, A.M., et al., *Khim Tekhnol.*, 2004, no. 1, pp. 2–6.
10. Kolenkova, M.A., Shumenko, V.I., Dorokhina, M.N., and Safuanova, N.A., *Novoe otechestvennoe zirkonievoe syr'e i sposoby ego pererabotki* (New Domestic Zirconium Raw Materials and Methods for Their Processing), Moscow: TsNIItsvetmet Ekonomiki i Informatsii, 1980.
11. Lebedev, V.N., Lokshin, E.P., and Mel'nik, N.A., *Zh. Prikl. Khim.*, 2003, vol. 76, no. 2, pp. 190–195.
12. Godneva, M.M., Popova, R.A., Motov, D.L., et al., *Zh. Neorg. Khim.*, 1974, vol. 19, no. 1, pp. 17–22.
13. Zaitsev, L.M., Zabelin, V.N., Sakharov, V.V., et al., *Zh. Neorg. Khim.*, 1972, vol. 17, no. 1, pp. 60–65.

ISSN 1070-4272, Russian Journal of Applied Chemistry, 2006, Vol. 79, No. 11, pp. 1765–1768. © Pleiades Publishing, Inc., 2006.
Original Russian Text © I.V. Zatovskii, A.A. Babarik, N.S. Slobodyanik, 2006, published in Zhurnal Prikladnoi Khimii, 2006, Vol. 79, No. 11, pp. 1785–1788.

INORGANIC SYNTHESIS AND INDUSTRIAL INORGANIC CHEMISTRY

Mixed Phosphates $K_2M^{III}M^{V}(OPO_4)_2$: Heterovalence-Substituted Analogs of $KTiOPO_4$

I. V. Zatovskii, A. A. Babarik, and N. S. Slobodyanik

Shevchenko Kiev National University, Kiev, Ukraine

Received May 11, 2006

Abstract—A series of heterovalence-substituted analogs of $KTiOPO_4$ of the general composition $K_2M^{III}M^{V}(OPO_4)_2$ (M^{III} = Cr, Fe, In; M^{V} = Nb, Ta) were synthesized by crystallization from melts and by solid-phase reactions. Influence of the nature of tri- and pentavalent metals on the conditions of preparation and on the features of phase formation of substituted mixed phosphates was examined. The compounds obtained were characterized by X-ray diffraction analysis and by diffuse reflection spectroscopy.

DOI: 10.1134/S107042720611005X

Considerable interest in studying properties and preparing crystals of double phosphates with the $KTiOPO_4$ (KTP) structure does not weaken for more than 30 years. This is caused by unique nonlinear-optical and ferroelectric properties of KTP crystals [1]. Studies in this direction can be conventionally subdivided into applied and basic. The purpose of the applied studies is a search for conditions of KTP crystal growth and preparation of materials for laser technique on their basis [2]. Basic studies are aimed to reveal correlations between the composition, structure, and properties of KTP structural analogs [3, 4].

Compounds with a three-dimensional anionic sublattice of the general composition $AMOBO_4$, consisting of infinite chains of MO_6 octahedra linked in a certain mode by BO_4 tetrahedra, are usually assigned to structural analogs of KTP. In this case, a system of channels is formed, in which compensating cations of alkali or alkaline-earth metals are accommodated. Recently a considerable number of KTP analogs were synthesized by homo- and heterovalence substitution: $ATiOBO_4$ (A = Li, Na, K, Rb, Cs, Ag, Tl; B = P, As) [5–11], $AMOBO_4$ (A = Na, K, Rb, Ag, Tl; M = Sb, Nb, Ta; B = Ge, Si) [12–20]. Specific features of structures and properties of these compounds are appreciably affected by the nature of the transition metal forming their framework, by the nature of the tetrahedral anion BO_4, and by features of the charge-compensating cation.

Here we consider regular trends in formation of heterovalence-substituted KTP analogs $K_2M^{III}M^{V}(OPO_4)_2$ (M^{III} = Cr, Fe, In; M^{V} = Nb, Ta) by crystallization from melts and by solid-phase reactions. The phosphates synthesized have been characterized by X-ray phase analysis and diffuse reflection spectroscopy. Specific features of the preparation and crystallization of these compounds in relation to the nature of structure-forming metals and to the ratio of their ionic radii are discussed.

EXPERIMENTAL

Heterovalence-substituted KTP analogs were prepared by crystallization of potassium phosphate melts in the systems K_2O–P_2O_5–$M^{III}_2O_3$–$M^{V}_2O_5$ (M^{III} = Cr, Fe, In; M^{V} = Nb, Ta), and also by solid-phase reactions. As initial components we used analytically pure grade potassium phosphates KPO_3 and $K_4P_2O_7 \cdot 4H_2O$ and ultrapure and analytically pure grade oxides Nb_2O_5, Ta_2O_5, Fe_2O_3, Cr_2O_3, and In_2O_3.

When heterovalence-substituted KTP analogs were synthesized by crystallization from melts, the K/P ratio was varied from 1.10 to 1.55. The total weight content of oxides of metals in oxidation states V and III was set over a wide range (depending on their joint solubility) for M^{III}/M^{V} ratios from 0.5 to 3.0. Ground initial charges were placed in platinum crucibles and heated to 1000–1150°C. In most cases, the oxides completely dissolved within 3–8 h under isothermal conditions. The required tantalum(V) content in the systems was reached by adding K_2TaF_7 to homogeneous K_2O–P_2O_5–$M^{III}_2O_3$ melts at 900°C. The result-

Table 1. Conditions of solid-phase synthesis of heterovalence-substituted phosphates $KM^{III}_{0.5}Nb_{0.5}OPO_4$

Compound	Temperature, °C (time, h) of stepwise heat treatment
$KFe_{0.5}Nb_{0.5}OPO_4$	600 (5); 700 (3); 850 (6)
$KCr_{0.5}Nb_{0.5}OPO_4$	600 (5); 800 (5); 1000 (5); 1000 (10)
$KIn_{0.5}Nb_{0.5}OPO_4$	600 (5); 800 (5); 1000 (10)

ing melts were crystallized by cooling to 650–750°C at a rate of 10–50 deg h^{-1}. Phase formation processes were controlled by optical microscopic monitoring of samples of the melts. After the crystallization completion, fluxes were removed, and the resulting phases were washed with hot water or with solutions of inorganic acids.

To carry out solid-phase reactions in K_2O–P_2O_5–$M^{III}_2O_3$–Nb_2O_5 systems, we took stoichiometric amounts of metal oxides and potassium metaphosphate according to the equation

$$4KPO_3 + M^{III}_2O_3 + Nb_2O_5 \rightarrow 2K_2M^{III}Nb(OPO_4)_2,$$

The starting components were thoroughly ground, placed in platinum crucibles, and heated for 5 h at 600°C, after which the temperature was raised in 100°C steps to 1000–1130°C depending on the composition of the initial charge (Table 1). After each step, the charge was ground and the degree of conversion was evaluated by X-ray phase analysis.

The elemental composition of the resulting phosphates was determined by X-ray fluorexcence analysis (an Elvax Light spectrometer) and by flame photometry (an FPL-1 photometer). The X-ray diffraction patterns of products of solid-phase reactions and of powders of individual compounds were recorded on a DRON-3.0 diffractometer using CuK_α radiation (λ = 1.54178 Å). The electronic diffuse reflection spectra were taken on a UV-VIS Specord M-40 spectrophotometer in the range 11 000–40 000 cm^{-1}.

Generally, the crystallization areas of heterovalence-substituted KTP analogs $K_2M^{III}M^{V}(OPO_4)_2$ in potassium phosphate melts are limited by K/P and M^{III}/M^{V} ratios. At the same time, the regions and conditions of phase formation of pure compounds are considerably affected by the nature of a heterovalence pair of substituting metals and by the ratio of their ionic radii. Mixed phosphates $K_2M^{III}M^{V}(OPO_4)_2$ are formed of prismatic crystals with various extent of the development of base edges, which is typical for the growth of $KTiOPO_4$ crystals [21]. Conditions of the phase formation of mixed $K_2M^{III}M^{V}(OPO_4)_2$ phosphates in the course of their synthesis by spontaneous crystallization are given in Table 2.

When preparing melts in systems K_2O–P_2O_5–$M^{III}_2O_3$–Na_2O_5 (M^{III} = Cr, Fe, In), we found that the solubility of tantalum oxide in a melt considerably depends not only on the initial K/P ratio, but also on the nature of the trivalent metal present in the system. Therefore, we failed to reach homogeneity of some of the systems. Crystallization of such melts does not allow preparation of pure compounds.

The crystallization of $K_2M^{III}M^{V}(OPO_4)_2$ phosphates in iron-containing systems K_2O–P_2O_5–Fe_2O_3–$M^{V}_2O_5$ (M^{V} = Nb, Ta) is observed at the ratios K/P = 1.20–1.40 and the content of oxides in the liquid phase of 17–25 wt %. When the concentration of oxides decreases at this K/P ratio, the melts tend to vitrify. Also, the crystal phase is not formed in melts at K/P > 1.45, whereas at K/P < 1.20 the $K_2Fe_{1.5}\cdot Nb_{0.5}(PO_4)_3$ phosphate isostructural to langbeinite crystallizes [22].

The crystallization areas of phosphates with the KTP structure from the melts K_2O–P_2O_5–$M^{III}_2O_3$–$M^{V}_2O_5$ (M^{III} = Cr, In; M^{V} = Nb, Ta) are observed only in the case of the niobium-containing system. Mixed phosphate $K_2CrNb(OPO_4)_2$ is formed in melts at the ratio K/P = 1.25–1.37 in the range 860–820°C. In this case, when Cr_2O_3 is used as the initial component, preparation of a homogeneous reaction product

Table 2. Areas and conditions of crystallization of heterovalence-substituted KTP analogs from potassium phosphate melts

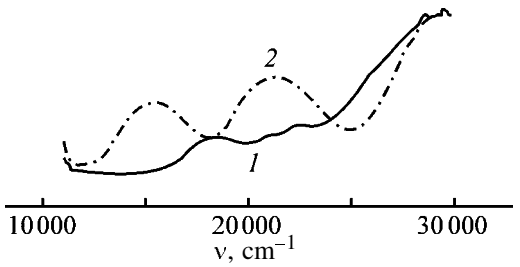
Compound	Ratio of components in melt	Temperature of crystal formation, °C	Color of crystals
$K_2NbFe(OPO_4)_2$	K/P = 1.2–1.4; Nb/Fe = 1; Fe/P = 0.28	860–820	Dark red
$K_2FeTa(OPO_4)_2$	K/P = 1.3; Fe/Ta = 2–3; Fe/P = 0.37	800–680	Bright red
$K_2CrNb(OPO_4)_2$	K/P = 1.25–1.37; Cr/Nb = 1; Cr/P = 0.13	860–820	Dark green
$K_2InNb(OPO_4)_2$	K/P = 1.5; In/Nb = 1; In/P = 0.13	860–780	Colorless

Table 3. Unit cell parameters of mixed phosphates, structural analogs of $KTiOPO_4$

Compound	Unit cell parameters, Å			V, Å^3
	a	b	c	
$K_2FeNb(OPO_4)_2$	10.66(5)	12.97(2)	6.46(1)	897.30(3)
$K_2FeTa(OPO_4)_2$	10.67(2)	12.96(2)	6.43(1)	890.07(2)
$K_2CrNb(OPO_4)_2$	10.67(0)	12.91(3)	6.42(9)	884.35(3)
$K_2InNb(OPO_4)_2$	10.79(5)	13.02(9)	6.58(9)	924.39(6)
$KTiOPO_4$	10.616(5)	12.814(6)	6.404(2)	871.16(64)

is considerably hampered, because of a low solubility of chromium(III) oxide in potassium phosphate melts even at 1150°C, which is caused by the formation of the double diphosphate $KCrP_2O_7$ on the surface of Cr_2O_3. The use of chromium orthophosphate $CrPO_4$ as the primary reaction product makes it possible to reach the equilibrium more quickly and to obtain $K_2CrNb(OPO_4)_2$ in the pure state. A decrease in the K/P ratio in the chromium-containing system to <1.20 leads to the crystallization of only $KCrP_2O_7$, and an increase in the K/P ratio to >1.40 in air results in partial $Cr^{3+} \rightarrow Cr^{6+}$ oxidation in the melt and, as a consequence, in the glass formation. The synthesis of $K_2InNb(OPO_4)_2$ is possible only in a very narrow range of ratios K/P = 1.47–1.52. At lower K/P ratios, joint crystallization of this compound and the mixed phosphate $K_2In_{1.5}Nb_{0.5}(PO_4)_3$ is observed [22].

Conditions of solid-phase synthesis of heterovalence-substituted phosphates $K_2M^{III}_{0.5}Nb(OPO_4)_2$ (M^{III} = Fe, Cr, In) considerably differ for various trivalent metals (Table 2). According to the IR data, the products of the primary heat treatment (600–800°C) are mixtures of phosphates always containing the double diphosphate $KM^{III}P_2O_7$. In the case of the iron-containing system, the formation of the phase $KFe_{0.5}Nb_{0.5}OPO_4$ at 850°C is complete within 6 h. Higher temperatures of 1000 and 1130°C are necessary to prepare pure $KIn_{0.5}Nb_{0.5}OPO_4$ and $KCr_{0.5}Nb_{0.5}OPO_4$, respectively. This difference in the synthesis conditions is attributable to different reactivities of double diphosphates $KM^{III}P_2O_7$ formed in the first stage of the reaction between KPO_3 and a metal(III) oxide.



Electronic diffuse reflection spectra of heterovalence-substituted KTP analogs. (ν) Frequency. (*1*) $K_2FeNb(OPO_4)_2$ and (*2*) $K_2CrNb(OPO_4)_2$.

The unit cell parameters for the KTP structural analogs obtained were calculated form the powder X-ray diffraction data. The X-ray patterns were analyzed using the least-squares iteration method applied to identity periods of structural models based on the $KTiOPO_4$ structural data [8] and also on our structural data for single crystals. All the phosphates synthesized crystallize in the orthorhombic system, and their unit cell volume increases as the ionic radius of the triple-charged metal ions increases (Table 3).

The local coordination surrounding of *d* metals in heterovalence-substituted phosphates $KFe_{0.5}Nb_{0.5}OPO_4$ and $KCr_{0.5}Nb_{0.5}OPO_4$ was studied by electronic diffuse reflection spectroscopy. The resulting spectra (see figure) suggest the octahedral oxygen surrounding of Fe^{3+} (d^5) and Cr^{3+} (d^3) ions. For the [FeO_6] chromophore, all the *d–d* transitions are spin- and Laporte-forbidden [23] and hence appear in the spectra as weak bands: $^6A_{1g} \rightarrow {}^4T_{1g}$ (ν = 26500 cm^{-1}, weak); $^6A_{1g} \rightarrow {}^4T_{2g}$ (ν = 22500 cm^{-1}, weak); $^6A_{1g} \rightarrow {}^4A_{1g}$ and $A_{1g} \rightarrow {}^4E_{1g}$ (ν = 18100 cm^{-1}, merged in a very weak common band). The charge-transfer band $Fe^{3+} \rightarrow O^{2-}$ is the strongest in the spectrum of $KFe_{0.5}Nb_{0.5}OPO_4$, which is caused by a rather strong electron-acceptor power of Fe^{3+} ions. In the diffuse reflection spectrum of $KCr_{0.5}Nb_{0.5}OPO_4$, three strong bands caused by *d–d* electronic transitions are observed: $^4A_2 \rightarrow {}^4T_2$ (ν = 25000 cm^{-1}, strong); $^4A_2 \rightarrow {}^4T_1(F)$ (ν = 18000 cm^{-1}, strong); and $^4A_2 \rightarrow {}^4T_1(P)$ (ν = 11900 cm^{-1}, strong). This pattern suggests almost regular octahedral surrounding of chromium atoms in the [CrO_6] chromophore [23].

CONCLUSIONS

(1) Features of the phase formation of heterovalence-substituted KTP analogs $K_2M^{III}M^{V}(OPO_4)_2$

(M^{III} = Cr, Fe, In; M^{V} = Nb, Ta) under conditions of the crystallization from a melt and of a solid-phase reaction were determined. The nature of M(III) ions essentially affects the conditions of formation of these compounds.

(2) The unit cell parameters of the phosphates synthesized were calculated from the powder X-ray diffraction data. These compounds crystallize in the orthorhombic system.

(3) The local coordination surrounding of *d* metals in the phosphates $KFe_{0.5}Nb_{0.5}OPO_4$ and $KCr_{0.5}Nb_{0.5}OPO_4$ was studied by electronic diffuse reflection spectroscopy.

REFERENCES

1. Yanovkii, V.K. and Voronkova, V.I., *Phys. Status Solidi (A)*, 1986, vol. 93, p. 665–668.
2. Bierlein, J.D. and Vanherseele, H.J., *J. Opt. Soc. Am. B*, 1989, vol. 6, pp. 622–633.
3. Slobodyanik, N.S., *Doctoral (Chem.) Dissertation*, Kiev, 1987.
4. Nagornyi, P.G., *Doctoral (Chem.) Dissertation*, Kiev, 1998.
5. Nagornyi, P.G., Kapshuk, A.A., Stus', N.V., and Slobodyanik, N.S., *Zh. Neorg. Khim.*, 1991, vol. 36, no. 11, pp. 2766–2768.
6. Zumsteg, F.C., Bierlein, J.D., and Gier, T.E., *J. Appl. Phys.*, 1976, vol. 47, pp. 4980–4985.
7. Phillips, M.L.F., Harrison, W.T.A., and Stucky, G.D., *Proc. SPIE – Int. Soc. Opt. Eng.*, 1991, vol. 84, pp. 1561–1565.
8. Masse, R. and Grenier, J.C., *Bull. Soc. Fr. Miner. Cristallogr.*, 1971, vol. 94, pp. 437–440.
9. Cheng, L.K., Cheng, L.T., Galperin, J., et al., *J. Cryst. Growth*, 1994, vol. 137, pp. 107–115.
10. El Brahimi, M. and Durand, J., *Rev. Chim. Miner.*, 1986, vol. 23, pp. 146–153.
11. Loiacono, G.M., Loiacono, D.N., and Stoizenberger, R.A., *J. Cryst. Growth*, 1993, vol. 131, pp. 323–330.
12. Crosnier, M.-P., Guyomard, D., Verbaere, A., and Piffard, Y., *Eur. J. Solid State Inorg. Chem.*, 1990, vol. 27, pp. 845–854.
13. Pagnoux, C., Guyomard, D., Verbaere, A., et al., *C. R. Acad. Sci. Paris, Ser. II*, 1991, vol. 312, pp. 611–615.
14. Pagnoux, C., Favard, J.-F., Verbaere, A., et al., *C. R. Acad. Sci. Paris, Ser. II*, 1992, vol. 314, pp. 115–155.
15. Butashin, A.V., Mil', B.V., Mosunov, A.V., and Stefanovich, S.Yu., *Zh. Neorg. Khim.*, 1994, vol. 39, no. 9, pp. 1433–1437.
16. Belokoneva, E.L., Mil', B.V., and Butashin, A.V., *Izv. Akad. Nauk SSSR, Neorg. Mater.*, 1991, vol. 27, pp. 1708–1713.
17. Favard, J.-F., Verbaere, A., Piffard, Y., and Tornoux, M., *C. R. Acad. Sci. Paris, Ser. II*, 1992. vol. 315, pp. 305–310.
18. Belokoneva, E.L. and Mil', B.V., *Zh. Neorg. Khim.*, 1992, vol. 37, no. 2, pp. 252–256.
19. Belokoneva, E.L. and Mil', B.V., *Zh. Neorg. Khim.*, 1992, vol. 37, no. 5, pp. 502–505.
20. Mil', B.V., Butashin, A.V., and Stefanovich, S.Yu., *Zh. Neorg. Khim.*, 1993, vol. 38, no. 6, pp. 874–876.
21. Bolt, R.J. and Bennema, P., *J. Cryst. Growth*, 1990, vol. 137, pp. 329–340.
22. Zatovskii, I.V., Slobodyanik, N.S., Ushchapivskaya, T.I., et al., *Zh. Prikl. Khim.*, 2006, vol. 79, no. 1, pp. 12–17.
23. Lever, A.B.P., *Inorganic Electronic Spectroscopy*, Amsterdam: Elsevier, 1984.

ISSN 1070-4272, Russian Journal of Applied Chemistry, 2006, Vol. 79, No. 11, pp. 1769–1774. © Pleiades Publishing, Inc., 2006.
Original Russian Text © N.N. Khimich, Yu.L. Zub, L.A. Koptelova, T.S. Mashchenko, E.P. Troshina, M.G. Voronkov, 2006, published in Zhurnal Prikladnoi Khimii, 2006, Vol. 79, No. 11, pp. 1789–1794.

INORGANIC SYNTHESIS AND INDUSTRIAL INORGANIC CHEMISTRY

Synthesis and Optical Properties of Nanohybrids in the System Constituted by Silica and Lanthanide Phosphoramide Complexes

N. N. Khimich, Yu. L. Zub, L. A. Koptelova, T. S. Mashchenko, E. P. Troshina, and M. G. Voronkov

Grebenshchikov Institute of Silicate Chemistry, Russian Academy of Sciences, St. Petersburg, Russia
Institute of Surface Chemistry, National Academy of Sciences of Ukraine, Kiev, Ukraine

Received March 13, 2006

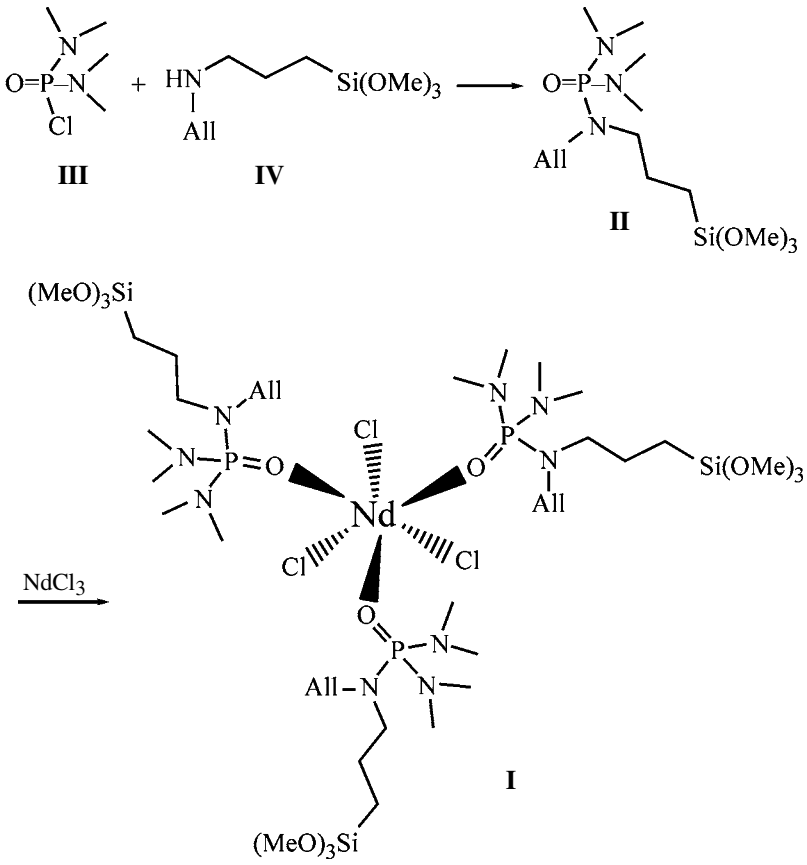
Abstract—Sol–gel process of hydrolytic polycondensation of tetramethoxysilane with trimethoxysilyl derivatives of lanthanide phosphoramide complexes was studied in order to obtain photoluminescent organic–inorganic hybrid materials.

DOI: 10.1134/S1070427206110061

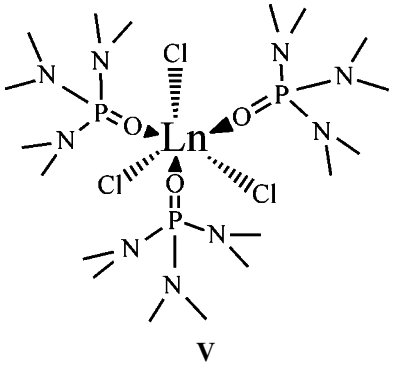
Compounds of rare-earth elements (REE) are extensively used in analytical chemistry, electroplating, photooptics, and optoelectronics. The wide spectral range of emission (200 nm to 5 μm) in interaction of lanthanide derivatives with light makes them irreplaceable as nonlinear-optical and fiber-optic materials and elements of lasing media [1]. For practical use of REE derivatives in optics, they are introduced into chemically and thermally stable optically transparent coatings and materials. One of the most convenient methods for synthesis of hosts of this kind is the sol–gel process [2, 3] yielding silica matrices and, in particular, polycondensation of tetraalkoxysilanes [4]. An important disadvantage of such matrices is the high content of hydroxy groups and water molecules, which leads to strong quenching of photoluminescence (PL) from REE derivatives [5]. Therefore, introduction of lanthanides into a SiO_2 host in the form of their inorganic salts requires high-temperature treatment with special dehydrating reagents, e.g., Freons [6]. The simplest way to eliminate these labor-consuming procedures is to isolate REE from hydroxy quenching of PL via complexation with various organic ligands.

Complexes of lanthanides with various ligands have been synthesized (with 1,10-phenathroline and 2,2'-bipyridine [7], 4,4,5,5,5-pentafluoro-1-phenyl-1,3-pentanedione [8], 4,4,4-trifluoro-1-(2-thienyl)-1,3-butanedione [9], 2-pyridinecarboxaldehyde benzoylhydrazone [10], polyoxycarboxylic acids [11]). Introduction of transition elements into a silica matrix formed via hydrolytic polycondensation of tetraalkoxysilane does not present any difficulties [12–15]. Of particular interest from the standpoint of materials science are systems in which lanthanides complexes and silica are chemically bound [5, 16–19]. This improves the functional properties of the system via formation of organic–inorganic hybrids and guarantees uniform distribution of REE throughout the matrix. The formation of a chemical bond between silica and the REE complex is provided by use of ligands containing functional groups and application of special cross-linking agents [4]. As organic ligands are commonly used 5-amino-1,10-phenanthroline [16–18], 2-aminobenzoic acid [19], 2,6-pyridinedicarboxylic acid [5], etc.

In this study, organic–inorganic hybrids in the system Ln^{3+}–SiO_2 were synthesized using a derivative of hexamethylphosphoric triamide (HMPA) as a complexing agent and neodymium as REE. The choice of this ligand is not accidental. On the one hand, the synthesis and structure of complexes of salts of all REE with HMPA have been well studied [20], and on the other, use of complexes of this kind makes it possible to synthesize silica glasses in which the lanthanide ion is encapsulated in an inorganic phosphate fragment [22]. Previously unknown trimethoxysilyl derivative **II** of HMPA was synthesized as a ligand for preparing REE phosphoramide complexes chemically bound to the silica host:



The sol–gel method, hydrolytic polycondensation of tetramethoxysilane (TMOS) and complex **I**, was used to produce organic–inorganic hybrids with various concentrations of the organic component. The chemical binding of these reagents provided uniform distribution of the neodymium salt throughout the silica matrix. For comparison purposes, we synthesized composites in which the role of the organic component was played by the previously known complex of Nd^{3+} with HMPA [20, 21]:



V

Preliminary results of this study have been reported previously [23].

EXPERIMENTAL

The open porosity W_{op} and apparent density d_{app} of the composites obtained was determined by the Archimedes method for samples that did not crack in drying or measurements. The hardness of the samples was measured with a PMT-3 microhardness meter. Derivatograms were obtained with a Q-1500D derivatograph at temperatures of up to 1000°C at heating rate of 20 deg min^{-1}. The content of SiO_2 in composites **VIa**–**VIi** was found by thermal analysis. An electron-microscopic study of the gels was performed on an EM-125 instrument at an accelerating voltage of 75 kV by the method of cellulose–carbon replicas prepared on the surface of freshly cleaved samples. The pore structure of the samples was examined by studying adsorption–desorption isotherms of ethanol on a McBain spring vacuum balance [24]. ^1H and ^{13}C NMR spectra were obtained on a Bruker DPX-300 instrument at working frequencies of 300.13 and 75.5 MHz, respectively, with TMS as internal reference. UV spectra were measured on a Specord M40 instrument. Luminescence spectra were measured under sample illumination with light of argon (λ =

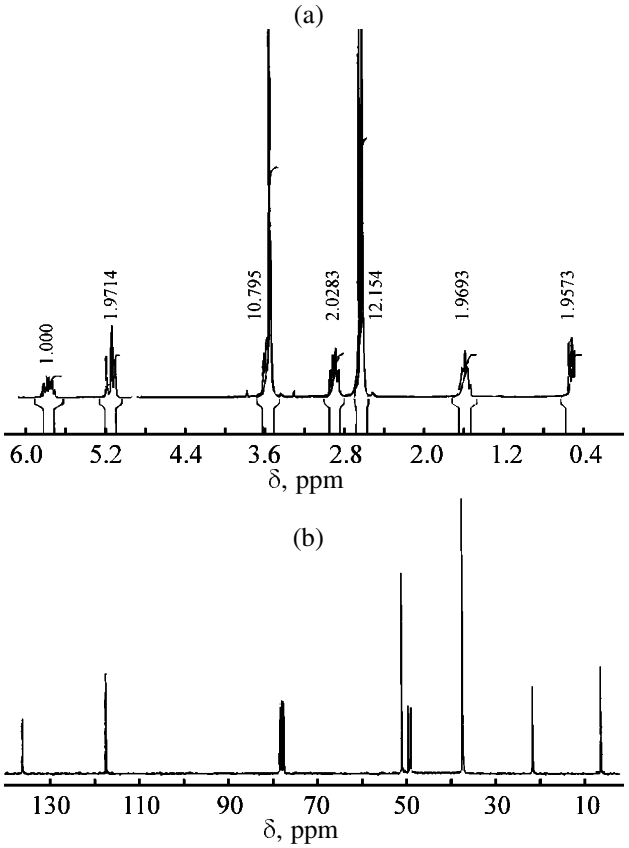


Fig. 1. (a) ^{1}H and (b) ^{13}C NMR spectra of compound **I**. (δ) Chemical shift.

337 nm) and krypton (λ = 580 nm) lasers, with detection by an optical analyzer.

Trimethoxysilylpropyl derivative **II** of phosphoric acid triamide was prepared by the reaction of tetramethylphosphorodiamidic chloride **III** [25] with 3-trimethoxysilylpropyl-*N*-allylamine **IV** [26] by the following procedure. A mixture of 3.9 g of chloride **III**, 5.0 g of amine **IV**, and 1.81 g of anhydrous pyridine in 100 ml of anhydrous petroleum ether (bp 70–110°C) was agitated for 5 days at 30°C under argon. The mixture was cooled and kept at 0°C for 24 h, after which the precipitate formed was filtered off and the filtrate was evaporated in a water-jet-pump vacuum and distilled to give 4.0 g (40%) of a colorless viscous oil [bp 128–130°C (0.01 mm Hg)]. The structure of the compound obtained was confirmed by ^{1}H and ^{13}C NMR data (Fig. 1).

In sol–gel synthesis of nanohybrids in the system Nd^{3+}–SiO_2, 4 equiv of water was added dropwise under vigorous agitation to a solution of TMOS (1 equiv) and REE complex in acetic acid (1 equiv). The resulting solutions were poured into hermetically sealed polypropylene test tubes and kept at 70°C for



Fig. 2. Electron micrograph of gel **VIc**. Magnification 60000.

2 days. Further, the hermetic stoppers of the tubes were replaced with stoppers with apertures (aperture diameter about 1 mm) and humid gels were dried for 24 h at 70°C, 24 h at 100°C, and 48 h at 120°C. The temperature was raised at a rate of 5 deg min^{-1}. Depending on the structure and content of an REE complex (1, 5, 10, 15, and 20 wt %), a number of composites were obtained (**VIa**–**VIi**, see table). The samples with a high content of the REE complex (**VIc**–**VIe**, **VIg**–**VIi**) were used in physicomechanical studies, and those with a low content of REE [0.5–1 wt % (**VIb, VId**)], in analysis of the luminescent properties of the materials obtained.

The structure of samples **VIa**–**VIi** is virtually the same (see Fig. 2). At the same time, composites **VIa**–**VId** formed via chemical binding of the components of the system are transparent (similarly to the starting SiO_2 gel, sample **VIa**); their density and

Density and microhardness of the samples synthesized (**VIa**–**VIi**)

Organic complex, wt %	Sample	Density, g cm^{-3}	Microhardness, kg mm^{-2}
I:			
0	**VIa**	1.407	62.7
5	**VIc**	1.415	123.5
10	**VId**	1.809	162.4
20	**VIe**	1.729	205.0
V:			
5	**VIg**	1.450	77.3
10	**VIh**	1.429	97.0
20	**VIi**	1.753	60.9

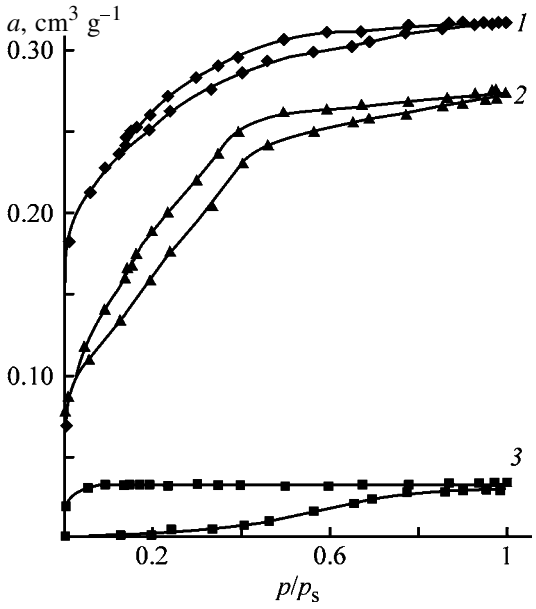


Fig. 3. Adsorption–desorption isotherms of ethanol at 18°C on composites **VIa**, **VId**, and **VIh**. (*a*) Adsorption and (p/p_s) relative vapor pressure. Sample: (*1*) **VIa**, (*2*) **VId**, and (*3*) **VIh**.

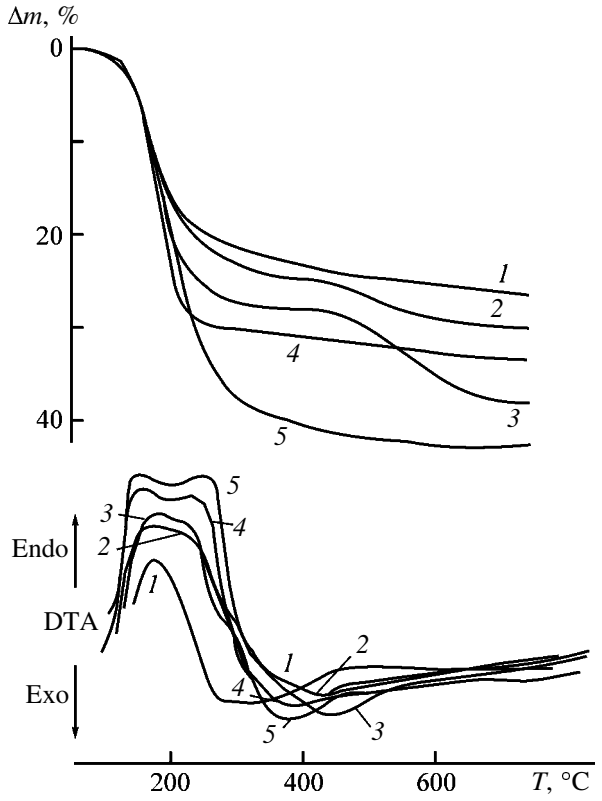


Fig. 4. DTA and TG curves for composites **VIa**, **VId**, **VIe**, **VIh**, and **VIi**. (Δm) Weight loss and (T) temperature. Composite: (*1*) **VIa**, (*2*) **VId**, (*3*) **VIe**, (*4*) **VIh**, and (*5*) **VIi**.

microhardness grow with an increase in the content of the organic component.

By contrast, composites **VIf**–**VIi** formed without chemical binding of the components of the sol–gel system are opaque and opalescent, and the increase in the content of the organic component has virtually no effect on the mechanical properties of the materials.

Figure 3 shows adsorption–desorption isotherms of ethanol at 18°C on composites **VIa**, **VId**, and **VIh**. These data can be used to calculate the specific surface area S and pore radius r for gel **VIa** and hybrids **VId, VIh**:

Sample	**VIa**	**VId**	**VIh**
S, $m^2\ g^{-1}$	530	10	360
r, nm	0.7	–	0.7

Apparently, the formation of a nanocomposite in which the organic and inorganic components are chemically bound is accompanied by virtually complete disappearance of porosity (i.e., pores visible in Fig. 2 for composite **VId** are not empty). In contrast to composite **VId**, in which the REE complex is uniformly distributed in the SiO_2 host because of the chemical binding to the matrix, association of REE molecules is observed for composite **VIh**. As a result, heterogeneities leading to loss of transparence by the system are formed in the composite.

Thermal analysis curves for a number of the composites synthesized (Fig. 4) allow certain conclusions about the structure of the hybrids formed. The range 100–200°C corresponds to intensive weight loss caused by evaporation of ethanol, excess acetic acid, water, methyl acetate, etc. [27]. The range 200–280°C apparently corresponds to removal of phosphoramide, primarily from composites **VIh** and **VIi**, because the intensity of the DTA effects for these composites substantially exceeds that for composites **VId** and **VIe**. The exothermic peaks of composites **VId** and **VIe** (Fig. 4, curves *2, 3*) are shifted to higher temperatures, compared with the exothermic peaks of composites **VIh** and **VIi** (curves *4, 5*). This fact suggests that hybrids whose components are not bound chemically (**VIh, VIi**) are only a mechanical mixture of the starting reagents, whereas hybrids **VId** and **VIe** exhibit a coordination Ln–O–P and Ln–N–P. Therefore, according to the weight loss curves, the organic component of the composite in hybrids **VId** and **VIe** burns-out at considerably higher temperatures.

Figure 5 shows UV spectra of a methanol solution of complex **I** (Fig. 5a) and of organic–inorganic hybrid **VId** containing 10 wt % phosphoramide com-

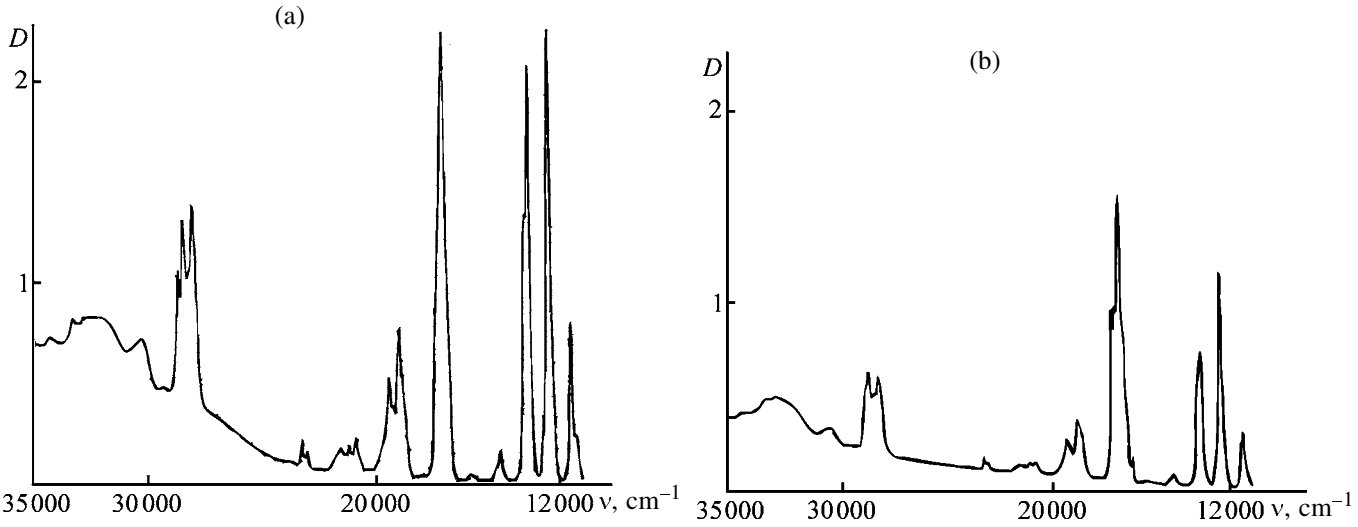


Fig. 5. UV spectra of (a) methanol solution of complex **I** and (b) organic–inorganic hybrid **VId** containing 10 wt % phosphoramide complex. (*D*) Absorption and (ν) wavenumber.

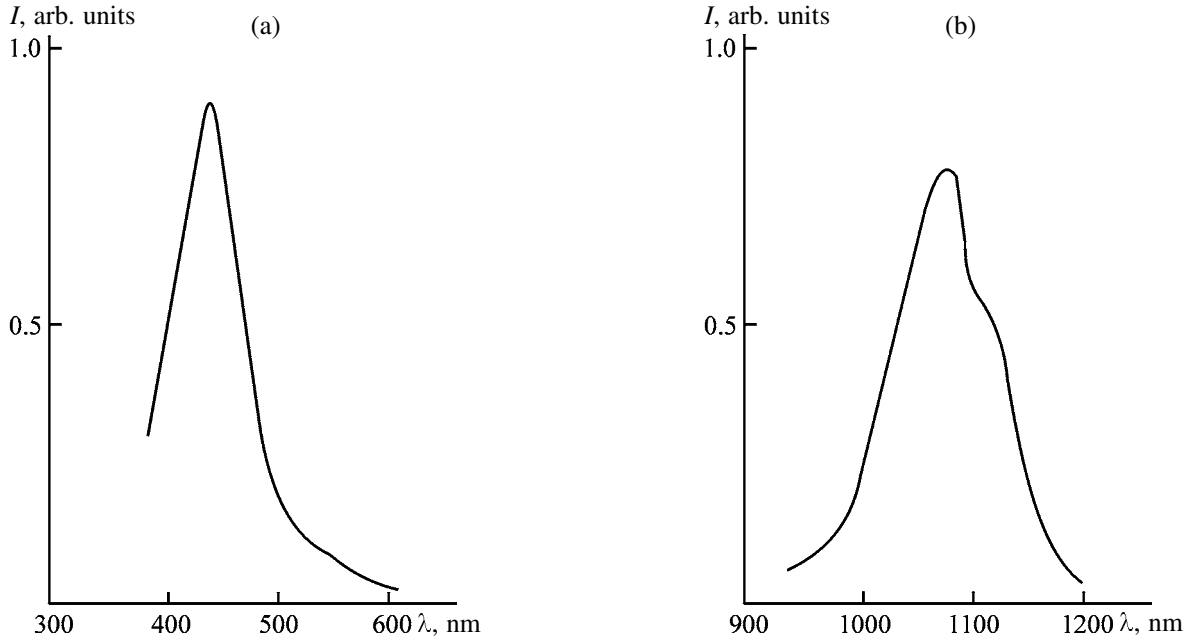


Fig. 6. PL of composite **VIb** containing complex **I** in an amount of 1 wt %. (*I*) Intensity and (λ) wavelength. The curves were obtained with sample exposure to (a) UV (λ = 337 nm) and (b) red (λ = 580 nm) light.

plex (Fig. 5b). Comparison of Figs. 5a and 5b shows good optical properties of the silica matrix synthesized. Preliminary data obtained in a study of the PL from composite **VIb** containing 1 wt % complex **I** are shown in Fig. 6. The curves in Figs. 6a and 6b were obtained with sample exposure to UV light (λ = 337 nm) and red light (λ = 580 nm), respectively.

CONCLUSIONS

(1) The hydrolytic polycondensation of tetramethoxysilane and lanthanide *N*-allyl-*N*-3-trimethoxysilylpropyl-*N*',*N*',*N*'',*N*''-tetramethylphosphoric triamide complex can be used to obtain photoluminescent materials in a system constituted by a lanthanide complex and silica.

(2) The formation of a nanohybrid via chemical binding of the components of the system provides uniform distribution of a lanthanide in the matrix.

(3) Encapsulation of the Nd^{3+} ion via complexation with a derivative of hexamethylphosphoric triamide prevents luminescence quenching under the

action of hydroxy groups of the xerogel matrix and water molecules.

ACKNOWLEDGMENTS

The authors thank St. Petersburg Scientific Center, Russian Academy of Sciences, for the financial support of the study.

REFERENCES

1. Kaminskii, A.A. and Antipenko, B.M., *Mnogourovnevye funktsional'nye skhemy kristallicheskikh lazerov* (Multilevel Functional Schemes of Crystalline Lasers), Moscow: Nauka, 1989.
2. Brinker, C.J. and Scherrer, G.W., *Sol–Gel Science: the Physics and Chemistry of Sol–Gel Processing*, San Diego: Academic, 1990.
3. *Handbook of Sol–Gel Science and Technology*, vol. 1: *Sol–Gel Processing*, Hiromitsu Kozuku, Ed., Boston: Kluwer, 2005.
4. Khimich, N.N., *Fiz. Khim. Stekla*, 2004, vol. 30, no. 5, pp. 586–603.
5. Lai, D.C., Dunn, B, and Zink, J.I., *Inorg. Chem.*, 1996, vol. 35, pp. 2152–2154.
6. Malashkevich, G.E., Poddenezhny, E.N., Melnichenko, I.M., et al., *Acta Phys. Polon. A*, 1996, vol. 90, no. 2, pp. 419–421.
7. Van Staveren, D.R., Haasnoot, J.G., Manotti-Lanfredi, A.M., et al., *Inorg. Chim. Acta*, 2000, vol. 307, pp. 81–87.
8. Sareen, V. and Gupta, R., *J. Fluorine Chem.*, 1996, vol. 76, pp. 149–150.
9. Pode, R.B., *Phys. Status Solidi (a)*, 1998, vol. 170, pp. 137–144.
10. Paschalidis, D.G., Tossidis, I.A., and Gdaniec, M., *Polyhedron*, 2000, vol. 19, pp. 2629–2637.
11. Giroux, S., Aury, S., Henry, B., and Rubini, P., *Eur. J. Inorg. Chem.*, 2002, pp. 1162–1168.
12. Ferrari, M. and Armellini, C., *J. Sol–Gel Sci. Technol.*, 2000, vol. 19, nos. 1–3, pp. 569–572.
13. Sviderskii, V.A., Voronkov, M.G., Klimenko, V.S., and Klimenko, S.V., *Zh. Prikl. Khim.*, 1997, vol. 70, no. 10, pp. 1698–1703.
14. Sviderskii, V.A., Voronkov, M.G., Klimenko, V.S., and Klimenko, S.V., *Zh. Prikl. Khim.*, 2001, vol. 74, no. 7, pp. 1137–1141.
15. Khimich, N.N., Aleksandrova, E.L., Goikhman, V.Ya., and Koptelova, L.A., *Fiz. Khim. Stekla*, 2003, vol. 29, no. 4, pp. 555–561.
16. Binnemans, K., Lenaerts, P., Driesen, K., and Görller-Walrand, C., *J. Mater. Chem.*, 2004, vol. 14, pp. 191–195.
17. Li, H.R., Lin, J., Fu, L.S., et al., *Micropor. Mesopor. Mater.*, 2002, vol. 55, pp. 103–107.
18. Li, H.R., Fu, L.S., Lin, J., and Zhang, H.J., *Thin Solid Films*, 2002, vol. 416, pp. 197–200.
19. Wang, Q.-M. and Yan, B., *Inorg. Chem. Commun.*, 2004, vol. 7, pp. 747–750.
20. Skopenko, V.V., Zub, Yu.L., Tsivadze, A.Yu., et al., *Koord. Khim.*, 1985, vol. 11, no. 2, pp. 182–189.
21. Skopenko, V.V., Zub, Yu.L., and Kapshuk, A.A., *Zh. Neorg. Khim.*, 1984, vol. 29, no. 3, pp. 582–597.
22. Zub, Yu.L., Gamza, T.F., and Khimich, N.N., Abstracts of Papers, *Int. Conf. on Nanoparticles, Nanostructures, and Nanocomposites*, St. Petersburg (Russia), 2004, p. 118.
23. Khimich, N.N., Alexandrova, E.L., and Zub, Yu.L., Abstracts of Papers, *Int. Conf. "Sol–Gel Materials'04, Research, Technology, Applications,"* Wroclaw (Poland), 2004, p. 54.
24. Venzel', B.I. and Svatovskaya, L.G., *Fiz. Khim. Stekla*, 1994, vol. 20, no. 4, pp. 523–528.
25. Walsh, E.N. and Toy, A.D.F., *Inorg. Synth.*, 1963, vol. 7, pp. 71–73.
26. Speier, J.L., Roth, C.A., and Ryan, J.W., *J. Org. Chem.*, 1971, vol. 36, no. 21, pp. 3120–3126.
27. Khimich, N.N., Venzel', B.I., and Koptelova, L.A., *Zh. Prikl. Khim.*, 2004, vol. 77, no. 2, pp. 294–298.

ISSN 1070-4272, Russian Journal of Applied Chemistry, 2006, Vol. 79, No. 11, pp. 1775–1778. © Pleiades Publishing, Inc., 2006.
Original Russian Text © I.A. Bakhtina, M.S. Khristenko, N.G. Andreeva, L.F. Komarova, 2006, published in Zhurnal Prikladnoi Khimii, 2006, Vol. 79, No. 11, pp. 1795–1798.

PHYSICOCHEMICAL STUDIES OF SYSTEMS AND PROCESSES

A Study of the Effect of Molecule Fragmentation Method on the Accuracy of Estimation of Phase Equilibria in Terms of the UNIFAC Model

I. A. Bakhtina, M. S. Khristenko, N. G. Andreeva, and L. F. Komarova

Polzunov Altai State Technical University, Barnaul, Russia

Received May 4, 2005; in final form, September 2006

Abstract—Application of the UNIFAC model to calculation of the liquid–vapor equilibrium in binary subsystems of the mixture of butyl alcohol, butyl Cellosolve, ethylene glycol, butyl carbitol, and diethylene glycol with different ways of molecule fragmentation into group constituents was considered. The optimal way of fragmentation was suggested.

DOI: 10.1134/S1070427206110073

In development of processes for separation of substances by distillation and extraction, it is necessary to have experimental data on liquid–vapor and liquid–liquid phase equilibria in binary and multicomponent subsystems of a mixture under study. If these data are lacking, the UNIFAC group model [1] can be used to estimate phase equilibria from the properties of pure substances.

To calculate liquid–vapor and liquid–liquid equilibria using the UNIPAC model, it is necessary to do the following: (i) fragment molecules into group constituents; (2) reduce the geometric parameters for each group constituent: volume parameter R_s and surface parameter Q_s; and (3) compose the matrix of parameters of the group interaction a_{mn}, a_{nm}.

The accuracy of estimation of a phase equilibrium is governed by the way in which molecules are fragmented into group constituents [2–4].

This study is concerned with the influence exerted by the method of molecule fragmentation on the accuracy of estimation of the phase equilibrium. A real industrial mixture formed in manufacture of butyl Cellosolve at Kazan'orgsintez Joint-Stock Company [5] was taken as a model.

The mixture includes the following components: butyl alcohol (BA), ethylene glycol (EG), butyl Cellosolve (BCe), butyl carbitol (BCa), and diethylene glycol (DEG). Among these compounds are monohydric (BA) and dihydric alcohols (EG, DEG) and ethers (BCe, BCa).

In simulation of the vapor–liquid equilibrium (VLE) using UNIFAC, it is necessary to take into account, wherever possible, specific features of each type of molecules of the mixture components and the mutual influence of their group constituents [2]. For example, formation of intermolecular hydrogen bonds is characteristic of such strongly associated molecules as alcohols. The so-called proximity effect of the ether and alcohol functional groups is observed in molecules of dihydric alcohols, e.g., diethylene glycol, and their ethers. At the same time, molecules of Cellosolves can form not only intermolecular but also intramolecular hydrogen bonds [3]. Let us consider alternative ways of fragmentation of molecules into group constituents.

Alternative 1: separation of the EG molecule into the DOH (OH–CH_2–CH_2–OH) group. For this type of fragmentation, the group interaction parameters a_{mn} and a_{nm} in [3, 4] are different. Therefore, we simulated phase equilibria using a_{mn}, a_{nm} from these references: DOH [3] and DOH [4].

Alternative 2 (for monohydric alcohols and ethers): separation of the –CH_2–CH_2–OH group [3, 4]: $n(CH_3)$–$n(CH_2)$–$n(CH_2O)$–$n(CH_2$–CH_2–OH).

Alternative 3: separation of the –OH group [3, 4]: $n(CH_3)$–$n(CH_2)$–$n(CH_2O)$–n(OH).

Alternative 4: separation of the ether group –O– [2]: $n(CH_3)$–$n(CH_2)$–n(O)–n(COH).

The values of the dimensionless geometric param-

Table 1. Geometric parameters of groups

Parameter	Group							
	$-CH_3$	$-CH_2-$	$-CH_2O$	–OH	–COH	–O–	$-CH_2OH$	–DOH
Q_s	0.85	0.54	0.78	1.20	1.12	0.24	1.66	2.25
R_s	0.90	0.67	0.92	1.00	1.20	0.24	1.88	2.41

eters R_s and Q_s coincide in all references [2–4] and are listed in Table 1 for the alternatives considered.

Alternative 5: separation of the ether group –O–, differs from alternative 4 in that the geometric parameters R_s and Q_s were found using the quasichemical group model [3].

This model rests on the Barker–Guggenheim theory [6] and represents a molecule as a sum of contact regions of different types. For example, two contact regions are distinguished in the hydroxy group, –O– and –H–, with

$$R_{OH} = R_O + R_H, \quad (1)$$

$$Q_{OH} = Q_O + Q_H. \quad (2)$$

Such a separation reflects the ability of the hydroxy group to form one hydrogen bond via the hydrogen atom and two bonds via the oxygen atom. The ether group is also separated into a contact region –O–.

However, the quasichemical Barker's model cannot be used in VLE simulation, because the group interaction parameters are not determined for all the components in terms of this model. We used the quasichemical Barker's model only in part, i.e., we used the model only to determine the geometric parameters R_s and Q_s. Published data [4] were taken for the $-CH_3$, $-CH_2-$, and –O– groups, and for the –OH group the parameters R_s and Q_s were calculated from data furnished by the quasichemical group model by formulas (1), (2). The parameters for alternative 5 are listed in Table 3.

Table 2. Geometric parameters calculated in terms of the quasichemical group model

Parameter	Group			
	$-CH_3$	$-CH_2-$	–O–	–COH(OH)
Q_s	0.68	0.43	0.19	0.90
R_s	0.72	0.54	0.20	0.96

VLE was simulated using a software package developed at Karpov Research Physicochemical Institute. The VLE was simulated using the UNIFAC model at 6–10 experimental points uniformly distributed over the entire concentration range.

The estimation accuracy was evaluated by root-mean-square discrepancies between the experimental and calculated data for the liquid–vapor equilibrium [7–9]. The resulting root-mean-square deviations of the boiling points of the mixtures, ΔT_{rms} (°C), and vapor compositions, Δy_{rms} (mol %), in binary mixtures are listed in Table 4 for all the alternatives.

As seen from Table 4, the fragmentation by alternative 1 (with the ethylene glycol molecule represented by a single subgroup) shows the largest error and can be considered unsatisfactory. Alternative 2 also exhibits gross errors.

Consequently, fragmentation of the molecules into larger subgroups containing two or more functional groups fails to give satisfactory results in VLE calculations in terms of the UNIFAC model. Finer fragmentation of the molecules (alternatives 3–5) furnishes better results.

The VLE simulation in systems that have no thermodynamic limitations on separation and are constituted by molecules of strongly different sizes yielded satisfactory and comparable accuracies of estimation of the phase equilibrium by alternatives 3–5. At the same time, the smallest root-mean-square discrepancies between the calculated and experimental boiling points and vapor compositions are obtained using alternative 5, and, therefore, this alternative is preferable.

In mixtures with molecules of components differing in size only slightly, as in the BCe–BCa system and in azeotropic mixtures such as BCe–EG (tangential azeotrope), ERG–BCa, and BCa–DEG (minimal azeotropes), alternatives 3–5 give different VLE estimations, especially at high concentrations of the low-boiling component, i.e., in the region in which separation of mixtures into individual components is difficult.

Table 3. Matrix of group interaction parameters a_{mn}, a_{nm} (K)

Group	–CH_3	–CH_2	–CH_2O	–OH	–COH	–O–	–CH_2OH	–DOH [3]	–DOH [4]
–CH_3	0.00	0.00	251.50	986.50	931.20	472.60	737.50	5890.00	3025.00
–CH_2–	0.00	0.00	251.50	986.50	931.20	472.60	737.50	5890.00	3025.00
–CH_2O	83.36	83.36	0.00	237.70	–	–	42.00	–	–
–OH	156.40	156.40	28.06	0.00	–	–	–	–332.00	–319.00
–COH	169.70	169.70	–	–	0.00	–204.60	–	–	–
–O–	2160.00	2160.00	–	–	–13.44	0.00	–	–	–
–CH_2OH	–87.93	–87.93	70.00	–	–	–	0.00	–	–
–DOH [3]	154.20	154.20	–	268.80	–	–	–	0.00	–
–DOH [4]	140.00	140.00	–	267.60	–	–	–	–	0.00

Table 4. Root-mean-square deviations of boiling points and vapor compositions in binary systems

System	Pressure P, mm Hg	Alternative											
		1 [3]		1 [4]		2		3		4		5	
		ΔT_{rms}, °C	Δy_{rms}, %	ΔT_{rms}, °C	Δy_{rms}, %	ΔT_{rms}, °C	Δy_{rms}, %	ΔT_{rms}, °C	Δy_{rms}, %	ΔT_{rms}, °C	Δy_{rms}, %	ΔT_{rms}, °C	Δy_{rms}, %
BA–3BCe [7]	760	–	–	–	–	0.97	0.75	0.85	0.72	0.36	0.49	0.37	0.47
BA–EG [7]	760	1.93	1.71	1.89	1.69	–	–	1.59	1.03	1.78	1.11	0.59	0.23
BA–BCa [7]	760	–	–	–	–	3.95	2.31	2.37	1.81	2.26	1.37	1.07	0.64
BA–DEG [8]	120	–	–	–	–	–	–	0.89	0.09	0.97	0.67	0.87	0.09
BCe–EG [7]	10	3.54	4.93	7.62	10.41	–	–	1.76	2.08	1.62	1.95	1.03	1.54
BCe–BCa [8]	760	–	–	–	–	2.29	3.10	2.21	2.18	2.33	2.59	1.57	1.90
BCe–DEG [7]	760	–	–	–	–	4.49	1.99	2.80	0.89	1.12	0.40	1.10	0.43
EG–BCa [9]	20	2.62	5.73	6.67	13.36	–	–	1.27	2.26	1.35	2.47	0.76	1.54
EG–DEG [7]	20	3.89	5.58	3.62	5.23	–	–	0.39	0.37	0.36	0.42	0.37	0.31
BCa–DEG [7]	2	–	–	–	–	3.18	2.06	0.93	1.55	0.82	1.37	0.57	0.92

Table 5. Root-mean-square deviations of boiling points and vapor compositions in ternary systems

System	Pressure P, mm Hg	Alternative					
		3		4		5	
		ΔT_{rms}, °C	Δy_{rms}, %	ΔT_{rms}, °C	Δy_{rms}, %	ΔT_{rms}, °C	Δy_{rms}, %
BA–BCe–BCa	760	0.7	2.05	0.8	1.98	0.5	1.95
BA–EG–BCa	760	0.6	2.12	0.5	2.16	0.3	2.12
BA–BCe–EG	40	1.3	2.37	1.1	2.42	0.9	2.27
BCe–EG–BCa	40	0.9	3.14	0.7	2.98	0.6	2.85
BCe–EG–DEG	40	0.7	1.54	0.8	1.45	0.5	1.38
BCe–BCa–DEG	40	1.2	1.96	1.1	1.88	0.8	1.85
EG–BCa–DEG	40	0.9	1.28	0.8	1.15	0.7	1.08

With alternative 3, the azeotrope compositions in the EG–BCa and BCa–DEG systems are shifted by 3.5–4.3 mol %. With alternatives 4 and 5, the compositions are reproduced, with the root-mean-square errors for the boiling point and vapor composition equal to 0.8–1.4°C and 1.4–2.5 mol % for alternative 4 and to 0.6–0.8°C and 0.6–1.5 mol % for alternative 5.

To verify the reliability of the binary interaction parameters, we simulated VLE in ternary systems. The calculated and previously obtained experimental data [10] were compared, and the results obtained are listed in Table 5.

Thus, the minimum discrepancies between the calculated and experimental values were obtained with alternative 5. It may be suggested that using the geometric parameters of the quasichemical model with separation of contact regions makes it possible to reflect orientation effects and association and to take into account the formation of inter- and intramolecular bonds by alcohol and Cellosolve molecules, respectively.

CONCLUSIONS

(1) Fragmentation of molecules into large constituents containing three or more functional groups fails to provide satisfactory results in simulation of the vapor–liquid equilibrium in terms of the UNIFAC model. Finer fragmentation of molecules furnishes better results.

(2) The type of fragmentation of molecules into group constituents in systems that are composed of molecules strongly different in size and have no thermodynamic limitations on separation has virtually no effect on the accuracy of estimation of the liquid–vapor phase equilibrium in terms of the UNIFAC model.

(3) The effect of the type of fragmentation of molecules into group constituents on the accuracy of estimation of the vapor–liquid equilibrium in terms of the UNIFAC model is the most pronounced for difficultly separable (azeotropic and close-boiling) mixtures. The ether group –O– should be separated in molecules of such mixtures: [$n(CH_3)$–$n(CH_2)$–n(O)–n(COH)]. When determining the geometric parameters R_s and Q_s, it is advisable to separate the contact region –O– in the ether group and contact regions –O– and –H– in the hydroxy group.

REFERENCES

1. Gmehling, J., Rasnussen, P., and Fredenslung, A., *Ind. Eng. Chem. Process Des. Develop*., 1982, vol. 21, no. 1, pp. 118–120.
2. Bakhtina, I.A., Development of a Low-Waste Technology for Manufacture of Butyl Cellosolve, *Cand. Sci. Dissertation*, Barnaul, 1998.
3. Reid, R.G., Prausnitz, J.M., and Sherwood, T.K., *The Properties of Gases and Liquids*, New York: McGraw-Hill, 1977.
4. *Termodinamika ravnovesiya zhidkost'–par* (Thermodynamics of Liquid–Vapor Equilibrium), Morachevskii, A.G., Ed., Leningrad: Khimiya, 1989.
5. Barker, J.A., *Chem. Phys*., 1952, vol. 20, pp. 1526–1530.
6. Wales, S.M., *Phase Equilibria in Chemical Engineering*, Boston: Butterworths, 1985.
7. Bakhtina, I.A., Khristenko, M.S., and Komarova, L.F., *Zh. Prikl. Khim*., 1998, vol. 71, no. 6, pp. 907–910.
8. Kogan, V.B., Fridman, V.M., and Kafarov, V.V., *Ravnovesie mezhdu zhidkost'yu i parom* (Liquid–Vapor Equlibrium), Moscow: Nauka, 1966.
9. *Ravnovesie zhidkost'–par* (Liquid–Vapor Equilibrium), Bogomol'nyi, A.M., Ed., Leningrad: Khimiya, 1987.
10. Bakhtina, I.A., Khristenko, M.S., and Komarova, L.F., *Zh. Prikl. Khim*., 1998, vol. 71, no. 6, pp. 1078–1080.

ISSN 1070-4272, Russian Journal of Applied Chemistry, 2006, Vol. 79, No. 11, pp. 1779–1784. © Pleiades Publishing, Inc., 2006.
Original Russian Text © V.P. Korolev, 2006, published in Zhurnal Prikladnoi Khimii, 2006, Vol. 79, No. 11, pp. 1799–1804.

PHYSICOCHEMICAL STUDIES OF SYSTEMS AND PROCESSES

Thermodynamic Properties of Ternary Systems: Calculation of Standard Enthalpies of Solvation of Triols, Diols, and a Series of Their Ethers in Water–Methanol Mixed Solvent

V. P. Korolev

Institute of Chemistry of Solutions, Russian Academy of Sciences, Ivanovo, Russia

Received January 11, 2006

Abstract—An equation for the standard enthalpy of solvation of a compound in a binary solvent is derived. The enthalpies of solvation in water–methanol mixtures are estimated for 1,3-propane- and 1,6-hexanediols, 1,2,4-butane- and 1,3,5-pentanetriols, 2-methoxy- and 2-propoxyethanols, and diethylene glycol. The enthalpy of solvation of 1,2-dimethoxyethane in the water–methanol mixed solvent is determined experimentally.

DOI: 10.1134/S1070427206110085

Development of empirical and semiempirical methods for calculation of physicochemical and thermodynamic characteristics of solutions is important for prediction of properties of the solution on the basis of characteristics of its components.

In this study we examined the system water–methanol as a mixed solvent, because it is widely used in various processes, as being characterized by a broad range of solvency and solvating activity. Note also that the correlation between the host–guest complexation constant and properties of the solvent was first reported just for the water–methanol mixed solvent [1].

As solutes we considered such compounds as glycerol, diols, and their ethers up to 1,2-dimethoxyethane (fragment of polyether). Mixtures containing the indicated components are currently intensively studied by various methods [2–9]. It is worth noting that polyhydric alcohols currently attract attention as protein stabilizers and cryobioprotectors.

The characteristics of the solvents (water and methanol) and solutes, required for our calculations, are summarized in Table 1. Among them the key parameter is the cohesion energy density p (kJ cm^{-3}). The compounds were selected so that two of them (glycerol and ethylene glycol) have p higher than that of methanol, two have p close in value to methanol, and two have p considerably lower than that of methanol.

Let us consider alternative calculation procedures.

A. ESTIMATION OF THERMODYNAMIC CHARACTERISTICS OF TERNARY SYSTEMS FROM DATA FOR INDIVIDUAL COMPONENTS

Following the Scatchard–Hildebrand theory, the standard enthalpy of solvation (SES) of a nonelectrolyte A in a solvent S can be estimated by Eq. (1) [12]:

$$\Delta H^0(\mathrm{S,A}) = V_\mathrm{A} p_\mathrm{S} - 2V_\mathrm{A}(p_\mathrm{A}p_\mathrm{S})^{1/2} - RT, \qquad (1)$$

where V_i is the molar volume and p_i, cohesion energy density calculated using Eq. (2)

$$p_i = (\Delta_\mathrm{vap} H_i^0 - RT)/V_i, \qquad (2)$$

where $\Delta_\mathrm{vap}H_i^0$ is the heat of vaporization; R, gas constant; and T, absolute temperature [12–16].

If S represents a binary mixture, in estimating the

Table 1. Properties of compounds at 25°C

Compound	V, cm^3 mol^{-1} [10]	$\Delta_\mathrm{vap}H^0$, kJ mol^{-1} [11]	p, kJ cm^{-3}
Water	18.1	44.0	2.29
Methanol	40.7	37.8 [12]	0.868
Glycerol	73.2	91.7	1.22
Ethylene glycol	55.9	67.7	1.17
Diethylene glycol	95.4	83.4	0.848
1,4-Butanediol	88.6	76.5	0.835
2-Ethoxyethanol	97.4	48.2	0.469
1,2-Dimethoxyethane	104.5	36.4 [9]	0.325

Table 2. Experimental [11] and theoretical [Eq. (1)] standard enthalpies of solvation (kJ mol^{-1}) of glycerol and 1,4-butanediol in water (1)–methanol (2) mixtures at 25°C

x_2	p_{mix}	Glycerol		1,4-Butanediol	
		$-\Delta H^0_{exp}$	$-\Delta H^0_{calc}$	$-\Delta H^0_{exp}$	$-\Delta H^0_{calc}$
0	2.29	97.2	79.6	86.6	44.6
0.05	2.15	95.1	82.6	83.6	50.1
0.10	2.01	93.2	84.6	81.2	54.0
0.20	1.78	91.1	87.9	77.8	60.8
0.30	1.59	90.4	90.0	76.7	65.8
0.50	1.31	90.0	91.7	76.2	71.7
0.75	1.05	89.6	91.3	75.9	75.4
1.0	0.87	90.1	89.6	76.2	76.4

cohesion energy density we will neglect its excess parameters, H^E_{12} and V^E_{12}:

$$p_S = p_{mix} = (x_1\Delta_{vap}H^0_1 + x_2\Delta_{vap}H^0_2 - RT)/(x_1V_1 + x_2V_2), \quad (3)$$

where x_i is the mole fraction.

Experimental [11] and theoretical [calculated by Eq. (1) on the condition that $p_S = p_{mix}$] standard enthalpies of solvation of glycerol and 1,4-butanediol in water–methanol mixtures are given in Table 2. For both compounds in methanol, the theoretical results agree well with the experiment. Therefore, SES of diols and triols in methanol can be estimated theoretically with a precision well comparable with that of the experiment. In the case of glycerol, the experimental values are well consistent with the experimental results over a wide concentration range (x_2 = 0.3–1.0). In going from glycerol to 1,4-butanediol, i.e., to the compound with a lower cohesion energy density, this range is considerably narrower. In both cases, the maximal discrepancy was observed in water as a solvent. It should be pointed out that, for 2-ethoxyethanol, having even lower cohesion energy density than glycerol or 1,4-butanediol (Table 1), the error of determination of SES by Eq. (1) is fairly high even in straight methanol (ΔH^0_{exp} = –47.2 kJ mol^{-1} [11]; ΔH^0_{calc} = –42.2 kJ mol^{-1}). Therefore, calculation by procedure A is limited by both the solvent composition and the nature of solute.

B. ESTIMATION OF THERMODYNAMIC CHARACTERISTICS OF TERNARY SYSTEMS FROM DATA FOR BINARY SYSTEMS

In this case, we should know SES values of compound A in components of the mixed solvent ΔH^0_1 and ΔH^0_2, determined experimentally or theoretically.

The enthalpy of solvation of a compound in a mixed solvent ΔH^0 can be estimated by Eq. (4) [15]:

$$\Delta H^0 = g_1\Delta H^0_1 + g_2\Delta H^0_2, \quad (4)$$

where g_i is the weight factor ($g_1 + g_2 = 1$).

Kustov et al. [15] derived an equation for the weight factor using the Scatchard–Hildebrand theory:

$$g_2 = \frac{\varphi_2(p_2 - p_1) - 2p_3^{1/2}\{[p_1 + \varphi_2(p_2 - p_1)]^{1/2} - p_1^{1/2}\}}{p_2 - p_1 - 2p_3^{1/2}(p_2 - p_1^{1/2})}, \quad (5)$$

where φ_i is the volume fraction of the ith component [$\varphi_2 = x_2V_2(x_1V_1 + x_2V_2)^{-1}$; $\varphi_1 = 1 - \varphi_2$], and subscript 3 refers to the solute.

Note that the weight factor g also reflects such a characteristic of the solute as its cohesion energy density p_3. It is easy to see that, for the hypothetical case with $p_3 = 0$, $g_2 = \varphi_2$. Actually, $p_3 \neq 0$ and $g_2 > \varphi_2$ (Table 3).

Taking our previous results [16] into account, in this study we use a new relationship for the enthalpies of solvation of nonelectrolytes in binary solvents:

$$\Delta H^0 = \varphi_1\Delta H^0_1 + \varphi_2H^0_2 + V_3p^E_{at}, \quad (6)$$

where p^E_{at} is the excess cohesion energy density of the binary solvent, estimated in the athermic approximation [16],

$$p^E_{at} = p_{at} - p_{id}, \quad (7)$$

$$p_{at} = (x_1\Delta_{vap}H^0_1 + x_2\Delta_{vap}H^0_2 - RT)/(x_1V_1 + x_2V_2 + V^E_{12}), \quad (8)$$

$$p_{id} = (x_1\Delta_{vap}H^0_1 + x_2\Delta_{vap}H^0_2 - RT)/(x_1V_1 + x_2V_2). \quad (9)$$

The cohesion energy density of an ideal mixture can be estimated also by Eq. (10) [16]:

$$p_{id} = \varphi_1p_1 + \varphi_2p_2. \quad (10)$$

The sum of the first two terms in Eq. (6) represents the additive (by φ) contribution to SES, and the third term, the deviation of SES from the additivity. Note that the first term in Eq. (1) corresponds to the heat of cavity formation in solvent S in solvation of compound A. It follows from comparison of the first term in Eq. (1) and the third term in Eq. (6) that it is the energy of cavity formation that represents the nonad-

Table 3. Experimental [11] and theoretical [calculated by Eqs. (1), (12)] standard enthalpies of solvation (kJ mol^{-1}) of compounds in water (1)–methanol (2) mixtures at 25°C [g_2 is estimated by Eq. (5)]

Composition		Glycerol				Ethylene glycol			
x_2	φ_2	g_2	$-\Delta H^0_{exp}$	$-\Delta H^0_4$	$-\Delta H^0_{12}$	g_2	$-\Delta H^0_{exp}$	$-\Delta H^0_4$	$-\Delta H^0_{12}$
0.05	0.11	0.293	95.1	95.1	94.9	0.260	72.6	72.5	72.5
0.10	0.20	0.509	93.2	93.6	93.3	0.454	70.6	71.0	71.1
0.20	0.36	0.835	91.1	91.3	91.1	0.750	67.9	68.7	69.0
0.30	0.49	1.036	90.4	89.8	89.8	0.938	67.6	67.3	67.8
0.50	0.69	1.206	90.0	88.6	89.0	1.113	67.4	65.9	66.7
0.75	0.87	1.172	89.6	88.9	89.3	1.118	66.8	65.9	66.5
Composition		1,4-Butanediol				2-Ethoxyethanol			
x_2	φ_2	g_2	$-\Delta H^0_{exp}$	$-\Delta H^0_4$	$-\Delta H^0_{12}$	g_2	$-\Delta H^0_{exp}$	$-\Delta H^0_4$	$-\Delta H^0_{12}$
0.05	0.11	0.168	83.6	84.9	83.6	0.135	62.2	63.3	61.8
0.10	0.20	0.298	81.2	83.5	81.5	0.242	58.7	61.5	58.9
0.20	0.36	0.510	77.8	81.3	78.5	0.425	53.6	58.4	54.8
0.30	0.49	0.663	76.7	79.7	76.8	0.564	51.0	56.1	52.2
0.50	0.69	0.853	76.2	77.7	75.4	0.760	49.9	52.8	49.5
0.75	0.87	0.966	75.9	76.6	75.4	0.911	49.2	50.2	48.6

ditive (on the volume fraction scale) contribution to the enthalpy of solvation of the compound in the mixed solvent. Therefore, the enthalpy of interaction of the solute with the binary solvent is additive with respect to the volume fraction. Thus, Eq. (6) indirectly correlates with the theoretical equation (1).

It should be pointed out that Eqs. (4) and (6) are of particular interest in view of the fact that they include no empirical coefficients. Each of these equations includes ΔH^0_1 and ΔH^0_2, i.e., the terms reflecting the interaction of the solute with the solvent components. Equation (4) takes into account [via the weight factor (5)] the cohesion energy density of the solute p_3. Equation (6) includes the characteristics of the solute (V_3) and binary solvent [V^E_{12}, Eq. (8)].

In order to use Eq. (6), one should obtain the analytical relationship p^E_{at} vs. φ. This dependence is reproduced with a high correlation coefficient r by a symmetrical parabola:

$$p^E_{at}\ (\text{J cm}^{-3}) = (212 \pm 1)\varphi_1\varphi_2,\ r = 0.999. \qquad (11)$$

Taking Eq. (6) into account, we finally obtain:

$$\Delta H^0 = \varphi_1 \Delta H^0_1 + \varphi_2 \Delta H^0_2 + 212 V_3 \varphi_1\varphi_2. \qquad (12)$$

The experimental SES values of compounds in water–methanol mixtures are given in Table 3 in comparison with the theoretical values, and the average (for six compositions) moduli of the absolute errors $\delta H^0_{av} = \Sigma \mid \Delta H^0_{calc} - \Delta H^0_{exp} \mid /6$ (kJ mol^{-1}) are presented below.

Equation no.	(4)	(12)
Glycerol	0.6	0.4
Ethylene glycol	0.7	0.5
1,4-Butanediol	2.1	0.4
2-Ethoxyethanol	3.0	0.7

For the most hydrophilic compounds, glycerol and ethylene glycol, characterized by high cohesion energy density (Table 2), the enthalpies of solvation estimated by Eqs. (4) and (12) are well consisted with the experimental values (δH^0_{av} = 0.4–0.7 kJ mol^{-1}). The situation changes in going to the less hydrophilic compounds, 1,4-butanediol and 2-ethoxyethanol. These compounds have considerably lower cohesion energy densities as compared to glycerol or ethylene glycol. As a result, for 1,4-butanediol, the calculation error decreases by a factor of 5 in going from Eq. (4) to Eq. (12). For 2-ethoxyethanol, the calculation error decreases to nearly the same extent. Therefore, in these cases, Eq. (4) is inferior to Eq. (12) in the accuracy. However, it should be pointed out that Eq. (4) includes no characteristics of the binary mixture (Y^E_{12}).

Equation (12) reproduces the experimental values for all four solutes at nearly the same accuracy. In

Table 4. Experimental and theoretical [Eq. (12)] standard enthalpies of solvation (kJ mol^{-1}) of compounds in water (1)–methanol (2) mixtures at 25°C

x_2	1,3-Propanediol		1,6-Hexanediol		1,2,4-Butanetriol		1,3,5-Pentanetriol	
	$-\Delta H^0_{exp}$	$-\Delta H^0_{calc}$	$-\Delta H^0_{exp}$	$-\Delta H^0_{calc}$	$-\Delta H^0_{exp}$	$-\Delta H^0_{calc}$	$-\Delta H^0_{exp}$	$-\Delta H^0_{calc}$
0	80.6	80.6	98.7	98.7	103.3	103.3	109.3	109.3
0.05	78.1	78.1	94.6	94.8	100.6	100.6	106.1	106.1
0.10	75.9	76.3	91.8	92.0	98.5	98.6	103.8	103.8
0.20	72.9	73.8	87.7	88.1	96.0	95.9	101.0	100.6
0.30	72.2	72.3	85.8	85.9	95.0	94.4	99.5	98.9
0.50	71.8	71.0	85.0	84.2	94.4	93.4	98.8	97.8
0.75	71.4	70.9	85.0	84.4	94.2	93.8	98.7	98.2
1.0	71.5	71.5	85.6	85.6	94.8	94.8	99.5	99.5

the subsequent, we will analyze only Eq. (12), including predictability tests.

Equation (12) was tested for several of solutes from the diol and triol series (Table 4). There are no published data on SES of such compounds in water–methanol mixtures other than those presented in Table 3. The "experimental" solvation enthalpies of 1,3-propanediol (V = 72.5 cm^3 mol^{-1} [18]) and 1,6-hexanediol were determined by linear interpolation and extrapolation with respect to the carbon atoms of data of Table 3 for ethylene glycol and 1,4-butanediol. The molar volume of 1,6-hexanediol (mp 42°C), obtained by linear extrapolation of data for 1,3-propane- and 1,4-butanediols, is 120.8 cm^3 mol^{-1}. Note that the standard enthalpy of hydration of 1,6-hexanediol, given in monograph [19], is –94.2 kJ mol^{-1}. This quantity appears to be strongly underestimated by its absolute value. Indeed, according to [19], the difference between the enthalpies of hydration of 1,4-butanediol and 1,5-pentanediol is 6, and between 1,5-pentanediol and 1,6-hexanediol, only 1.2 kJ mol^{-1}, which is doubtful, since for higher homologs, the contribution of the CH_2 group is a constant value. Therefore, the standard enthalpy of hydration that we give in Table 4 for 1,6-hexanediol appears to be more realistic than that reported in [19].

The "experimental" SES values of 1,2,4-butane- and 1,3,5-pentanetriols were estimated on the assumption that the contribution of the CH_2 group to the enthalpy of solvation of the triols with terminal OH groups is the same as for the corresponding diols. Using this assumption, we estimated the molar volumes of 1,2,4-butanetriol (89.3 cm^3 mol^{-1}) and 1,3,5-pentanetriol (105.4 cm^3 mol^{-1}). Table 4 demonstrates reasonable agreement between the "experimental" and theoretical [calculated by Eq. (12)] standard enthalpies of solvation. The δH^0_{av} estimated for six water–methanol mixtures is 0.5 kJ mol^{-1} for 1,3-propanediol and 0.4 kJ mol^{-1} for three other compounds (Table 4). In this connection, it would be interesting to calculate SES of erythritol and, possibly, other polyhydric alcohols using Eq. (12).

Table 5. Theoretical [estimated by Eq. (12)] standard enthalpies of solvation (kJ mol^{-1}) of 2-methoxyethanol (MOE), 2-propoxyethanol (POE), and diethylene glycol (DEG) in water (1)–methanol (2) mixtures at 25°C

x_2	MOE	POE	DEG
0	60.4	70.0	97.5
0.05	57.1	65.8	94.0
0.10	54.5	62.7	91.4
0.20	50.8	58.3	87.8
0.30	48.4	55.5	85.5
0.50	45.8	53.0	83.4
0.75	44.7	52.4	82.9
1.0	44.5	52.9	83.4

Glycols and their ethers as well are widely used in technology. Mixtures containing these components are being intensively studied. The estimated SES values of two ethylene glycol ethers in water–methanol mixtures are given in Table 5. The enthalpies of hydration of 2-methoxy- and 2-propoxyethanols were taken from [19]. The contribution of the CH_2 group to SES of alkoxyethanols in methanol was taken equal to that of 1-alkanols. The molar volume of 2-propoxyethanol (114.6 cm^3 mol^{-1}) was estimated from the published data for 2-ethoxy- and 2-butoxyethanols [10].

It is accepted that, because of their simple molecular structure, polyethylene glycols are well suited as models for studying structuring of water in solutions of macromolecules [4]. The strong hydration of poly-

ethylene glycols is caused primarily by their topology [4]. The available set of experimental data allows estimation of SES of diethylene glycol in water–methanol mixtures. This compound has a relatively high cohesion energy density (p = 0.848 kJ cm^{-3} [20]). Taking into account the excellent quality of calculation (Table 2) of the enthalpy of solvation of 1,4-butanediol (p = 0.835 kJ cm^{-1}) in methanol, SES of diethylene glycol in methanol also was estimated by Eq. (1). The resulting SES (–83.4 kJ mol^{-1}) is only slightly lower in the absolute value than that of 1,6-hexanediol (–85.6 kJ mol^{-1}) (Table 4). However, SES of diethylene glycol in methanol is considerably less negative than that of its isomer, 1,2,4-butanetriol [–94.8 kJ mol^{-1} (Table 4)]. The standard enthalpy of hydration of diethylene glycol was estimated from its heat of solution in water (–14.1 kJ mol^{-1} [21]) using Eq. (12). The results are given in Table 5. It would be interesting to perform such a calculation for, e.g., triethylene glycol and tetraethylene glycol, but, unfortunately, the required data are not available.

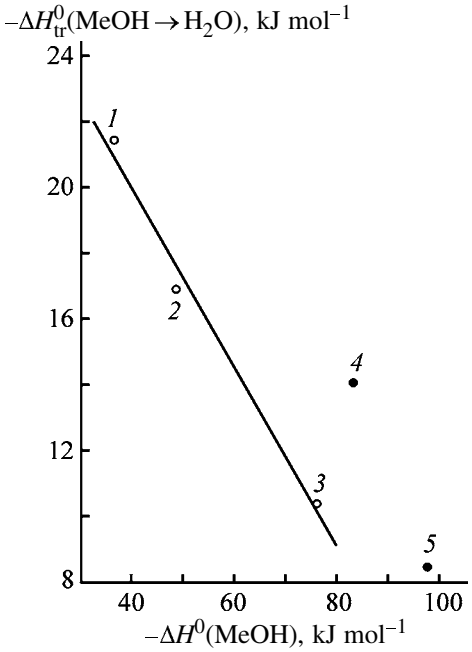
Our results show that Eq. (12) reproduces well SES of ethylene glycol and its monoethyl ether (2-ethoxyethanol) in methanol. It may be suggested that the theoretical data obtained for 2-methoxyethanol are sufficiently reliable (Table 5). However, one cannot be sure that Eq. (12) provides good quality of calculation of ethylene glycol dimethyl ether (1,2-dimethoxyethane). This compound in the liquid state is an aprotic solvent having a low cohesion energy density (p = 0.325 kJ cm^{-3}), which is typical of ethers. Therefore, in this study we have measured the enthalpies of solution of 1,3-dimethoxyethane in water–methanol mixtures using the same experimental procedure as in [9]. The moisture content in methanol (chemically pure grade) was below 0.1 wt %. From the heats of solution, we estimated the enthalpies of solvation of 1,2-dimethoxyethane for various ether concentrations (Table 6). The heats of solution are not presented in Table 6, since it is easy to calculate them by summing the enthalpies of solvation with the heat of vaporization of 1,2-dimethoxyethane (Table 1). Table 6 also includes the values estimated by Eq. (12). The molar volume can be found in Table 1. In water-rich mixtures ($x_2 \le 0.3$, $\varphi_2 \le 0.5$), the theoretical results agree well with the experiment. In the methanol-rich mixtures ($\varphi_2 > 0.5$), the calculation error is noticeably higher. Generally, analysis of the results obtained (Tables 3, 4, 6) reveals that Eq. (12) provides quite reliable SES for dilute solutions of methanol in water ($x_2 \le 0.1$), i.e., in the composition range where hydrophobic interactions and related structural transformations of the solutions are clearly pronounced.

Table 6. Experimental and theoretical [Eq. (12)] standard enthalpies of solvation (kJ mol^{-1}) of 1,2-dimethoxyethane in water (1)–methanol (2) mixtures at 25°C

$m \times 10^3$	x_2	$-\Delta H^0_{exp}$	$-\Delta H^0_{calc}$
35	0	57.9	57.9
47	0.05	53.4	53.5
42	0.10	49.9	50.1
48	0.20	44.9	45.1
49	0.29	41.5	42.1
52	0.52	39.6	38.1
76	0.75	38.2	36.8
92	1.0	36.5	36.5

(m) Molality of DME.

The main goal of this study was to obtain SES theoretically. Nevertheless, I would like to draw attention of readers to a feature of the behavior of the investigated compounds in water and methanol. 1,2,4-Butanetriol and diethylene glycol, on the one hand, and 1,4-butanediol, 2-ethoxyethanol, and 1,2-dimethoxyethane, on the other hand, are structural isomers. On changing the hydroxy group for the ether oxygen, both the standard enthalpies of hydration and SES in methanol become less negative. However, in this case, the standard heats of transfer of the solutes from methanol to water become more negative, as shown in the figure. As can be seen, the less negative the SES



Standard enthalpies of solvation of compounds in methanol and of their transfer from methanol to water: (*1*) 1,2-dimethoxyethane, (*2*) 2-ethoxyethanol, (*3*) 1,4-butanediol, (*4*) diethylene glycol, and (*5*) 1,2,4-butanetriol.

of the compound in methanol, the more negative is its heat of transfer from methanol to water. We attribute this trend to the fact that, in solvation of the investigated compounds, methanol behaves as a stronger base (acceptor of the hydrogen bond), while water, as a stronger acid (donor of the hydrogen bond).

CONCLUSIONS

(1) An equation for the standard enthalpies of solvation of compounds in the water–methanol mixtures is derived.

(2) The enthalpies of solvation in water–methanol mixtures are estimated for 1,3-propane- and 1,6-hexanediols, 1,2,4-butane- and 1,3,5-pentanetriols, 2-methoxy- and 2-propoxyethanols, and diethylene glycol.

(3) The enthalpy of solvation of 1,2-dimethoxyethane in the water–methanol mixtures is determined experimentally.

REFERENCES

1. Spenser, J.N., Mihalick, J.E., Paul, I.M., et al., *J. Solution Chem.*, 1994, vol. 23, no. 6, pp. 711–720.
2. De Haan, A., Fisher, K., Haacke, M., et al., *J. Chem. Eng. Data*, 1997, vol. 42, no. 5, pp. 875–881.
3. Huot, J.-Y., Battistel, E., Lumry, R., et al., *J. Solution Chem.*, 1988, vol. 17, no. 7, pp. 601–636.
4. Rudan-Tasik, D. and Klofutar, C., *J. Mol. Liq.*, 2003, vols. 103–104, pp. 187–200.
5. Awwad, A.M., *J. Chem. Thermodyn.*, 1986, vol. 18, no. 5, pp. 443–445.
6. Martin, M.C., Cocero, M.J., and Mato, R.B., *J. Chem. Eng. Data*, 1994, vol. 39, no. 3, pp. 535–537.
7. Reddy, V.K., Reddy, K.S., and Krishnaiah, A., *J. Chem. Eng. Data*, 1994, vol. 39, no. 3, pp. 615–617.
8. Kulikov, M.V. and Trutneva, E.Yu., *Izv. Ross. Akad. Nauk, Ser. Khim.*, 1997, no. 9, pp. 1592–1599.
9. Kustov, A.V., Antonova, O.A., and Korolev, V.P., *J. Solution Chem.*, 2002, vol. 31, no. 8, pp. 671–680.
10. Marcus, Y., *Ion Solvation*, New York: Wiley, 1985.
11. Batov, D.V., Antonova, O.A., Egorova, N.G., and Korolev, V.P., *Zh. Obshch. Khim.*, 1996, vol. 66, no. 2, pp. 214–221.
12. Hallen, D., Nilsson, S.-O., Rothschild, W., and Wadsö, I., *J. Chem. Thermodyn.*, 1986, vol. 18, no. 5, pp. 429–442.
13. Krishnan, C.V. and Friedman, H.L., *J. Phys. Chem.*, 1971, vol. 75. no. 23, pp. 3598–3606.
14. Sivolozhskaya, Yu.A., Potkina, N.L., and Korolev, V.P., *Zh. Obshch. Khim.*, 2000, vol. 70, no. 9, pp. 1492–1498.
15. Kustov, A.V., Bekeneva, A.V., and Korolev, V.P., *Izv. Vyssh. Uchebn. Zaved., Khim. Khim. Tekhnol.*, 2002, vol. 45, no. 4, pp. 44–48.
16. Korolev, V.P., *Zh. Obshch. Khim.*, 1998, vol. 68, no. 2, pp. 188–195.
17. Afanas'ev, V.N., Efremova, L.S., and Volkova, T.V., *Fiziko-khimicheskie svoistva binarnykh rastvoritelei: Vodosoderzhashchie sistemy* (Physicochemical Properties of Binary Solvents: Water-Containing Systems), Ivanovo: Inst. Khimii Nevodnykh Rastvorov Akad. Nauk SSSR, 1988, part 1.
18. Matsumoto, Y., Touhara, H., Nakanishi, K., and Watanabe, N., *J. Chem. Thermodyn.*, 1977, vol. 9, no. 8, pp. 801–805.
19. Belousov, V.P. and Panov, M.Yu., *Termodinamika vodnykh rastvorov neelektrolitov* (Thermodynamics of Aqueous Nonelectrolyte Solutions), Leningrad: Khimiya, 1983.
20. Chastrette, M., *Can. J. Chem.*, 1985, vol. 63, no. 12, pp. 3492–3496.
21. Dohnal, V., Roux, A.N., and Hynek, V., *J. Solution Chem.*, 1994, vol. 23, no. 8, pp. 889–900.

ISSN 1070-4272, Russian Journal of Applied Chemistry, 2006, Vol. 79, No. 11, pp. 1785–1792. © Pleiades Publishing, Inc., 2006.
Original Russian Text © K.V. Titova, V.P. Nikol'skaya, V.V. Buyanov, O.B. Pudova, N.L. Kulinchik, 2006, published in Zhurnal Prikladnoi Khimii, 2006, Vol. 79, No. 11, pp. 1805–1812.

PHYSICOCHEMICAL STUDIES OF SYSTEMS AND PROCESSES

Dependence of the Stability of Peroxo Solvates on Their Structural and Thermochemical Characteristics and on the Chemical Properties of the Starting Salts

K. V. Titova, V. P. Nikol'skaya, V. V. Buyanov, O. B. Pudova, and N. L. Kulinchik

Institute of Problems of Chemical Physics, Russian Academy of Sciences, Chernogolovka, Moscow oblast, Russia
State Research Institute of Biological Instrument Making, Federal State Unitary Enterprise, Moscow, Russia

Received April 7, 2006

Abstract—Data on the dependence of the stability of peroxo solvates on their structural and thermochemical characteristics and on the chemical properties of the starting salts, carriers of hydrogen peroxide, are summarized and correlated.

DOI: 10.1134/S1070427206110097

It is common knowledge that hydrogen peroxide in aqueous solutions and in solid compounds is prone to catalytic decomposition. Hydrogen peroxide itself, present in the associated state in concentrated solutions and in the form of associates with water in dilute solutions, is a reasonably stable substance. The existing methods of the H_2O_2 purification to remove catalytic impurities make use of any stabilizers unnecessary. Stabilizers are added only when exhaustive purification of hydrogen peroxide is economically inexpedient [1].

The stability of hydrogen peroxide coordinated to salts, i.e., of peroxo solvates, can be affected by foreign impurities. Also, unlike the stability of free H_2O_2, it can depend on their intrinsic physicochemical properties, such as the degree of structural changes in H_2O_2 molecules upon coordination, binding energy of hydrogen peroxide, and chemical properties of the solvated salt.

Here we attempt to summarize and correlate the data on effect of the above characteristics on the stability of peroxo solvates, which may be useful for further studies in this field.

Peroxo solvates, as solid forms of hydrogen peroxide, are promising oxidants, oxygen sources in portable respiration apparatus, and whiteners. The high decontaminating activity found recently for some compounds of this class made it possible to develop on their basis environmentally friendly disinfectants with broad-spectrum antimicrobial action [2].

EXPERIMENTAL

Peroxo solvates were synthesized by the reaction of the starting anhydrous or hydrated salts with a 30–35% solution of hydrogen peroxide taken in different excess over the stoichiometry [3]. Water and the excess H_2O_2 were removed at 20°C in a vacuum or with a flow of heated air over the solution [2]. The solvates were analyzed for the content of hydrogen peroxide by permanganatometric titration. The thermograms were recorded on an HTP-64 device and a Q-1500D derivatograph (Pt–Pt/Rh thermocouple, Al_2O_3 reference). The heating rate was 5 deg min^{-1}. The degree of dissociation was determined for the peroxo solvate samples kept at a prescribed temperature for 2 h in a vacuum. The evolved hydrogen peroxide was frozen in a trap cooled with liquid nitrogen and then analyzed. The thermochemical data were obtained by the dissolution method. The enthalpies of solution were measured in rocking calorimeters equipped with an isothermal shell [4, 5]. The devices were calibrated before and after the dissolution of the sample. The accuracy of the determination was checked by the enthalpies of solution of KCl and $KClO_4$. The samples of the substances under study were placed into preliminarily weighed thin-walled ampules with ground-glass joints. The ampules were filled with a substance in a dry box. The ampules were evacuated, resealed, and weighed again on a Bunge balance with an accuracy of 2×10^{-6} g. To initiate dissolution, the ampules were broken.

Table 1. Crystallographic parameters of peroxo solvates

Solvate	Bond length, Å			Angle, deg		References
	O–O	O–H	F(O)···H–O	OOH	dihedral	
$Na_2CO_3 \cdot 1.5H_2O_2$	1.43–1.49	0.95	2.52–2.66	100	125, 170	[9, 10]
$KF \cdot H_2O_2$	1.44–1.54	0.84–1.07	2.45–2.60	62–133	≤110	[6]
$KF \cdot 2H_2O_2$	1.469–1.473	0.797–0.970	2.57–2.84	95.2–101.3	88.0, 95.3	[11]
$RbF \cdot H_2O_2$	1.488	0.68–0.71	2.51–2.54	92–106	94.5	[12]
$M_2C_2O_4 \cdot 2H_2O_2$, M = Li, Na	144–149	–	2.56–2.80	95–108	93–180	[13, 14]
H_2O_2	1.453	0.988	–	102.7	90.2	[15]

The structure of $KF \cdot H_2O_2$ was determined by the method described in detail in [6]. The kinetic parameters of the peroxo solvate decomposition were determined from the decomposition curves taken under the isothermal conditions and calculated using the Kolmogorov–Erofeev equation [7, 8]. The degree of decomposition in one year at 25°C was found by extrapolating the degrees of decomposition obtained from the kinetic curves to low temperatures using the $\log \eta$ vs. $1/T$ curve. The peroxo solvate samples were stored for a long time at 20 ± 2°C in closed polymeric vessels. The other methods and procedures, not presented here, are described in [3].

Effect of structural changes in H_2O_2 molecules, occurring upon coordination to anions, on the peroxo solvate stability. In most of the peroxo solvates studied, the crystal lattice is formed by layers of ions and H_2O_2 molecules. In the peroxo solvate $Na_2CO_3 \cdot 1.5H_2O_2$, Na^+ and CO_3^{2-} ions are present as separate layers. Each H_2O_2 molecule forms H bonds with oxygen atoms of two different CO_3^{2-} ions. The CO_3^{2-} anion is thus involved in three hydrogen bonds. The peroxo solvate contains two different types of H_2O_2 molecules. These are bent (dihedral angle 125°) and nearly planar molecules (dihedral angle 170°). In a bent molecule, each oxygen atom interacts with two Na^+ cations, and in a planar molecule, with one cation. The H_2O_2 molecules in the $Na_2CO_3 \cdot 1.5H_2O_2$ lattice, unlike ionic components, do not occupy definite positions. Both planar and bent molecules occupy different positions with the same probability, forming bonds with two or one Na^+ cation [9, 10].

The structure of $KF \cdot H_2O_2$ is also layered. Three layers differing in the compositions are formed in $KF \cdot H_2O_2$: a homoatomic layer of K^+ cations, a heteroatomic layer of K^+ and F^- ions, and a heteroatomic layer of H_2O_2 molecules and F^- anions. The homo- and heteroatomic layers form an alternating sequence (K^+, F^-)–(H_2O_2, F^-)–(K^+)–(H_2O_2, F^-)–(K^+, F^-)–(H_2O_2, F^-)–(K^+)–(H_2O_2, F^-)... along the *a*-axis, and the heteroatomic layers form a sequence (K^+, F^-)–(H_2O_2, F^-)–(K^+, F^-)–(H_2O_2, F^-) along the *b*-axis [6].

The structure of $KF \cdot 2H_2O_2$ consists of (K^+) and (H_2O_2, F^-) layers [11]. The tetragonal structure of $Rb \cdot H_2O_2$ is formed by layers that have the same composition along the *a*- and *b*-axes and are arranged in the same sequence, coinciding with the sequence of layers along the *a*-axis in $KF \cdot 2H_2O_2$ [12]. Each F^- ion in the structure of fluoride peroxo solvates forms two ($KF \cdot H_2O_2$, $Rb \cdot H_2O_2$) or three ($KF \cdot 2H_2O_2$) hydrogen bonds.

The crystallographic parameters of the peroxo solvates are presented in Table 1. As seen, the lengths of the O–O and O–H bonds and the O–O–H bond angles in free hydrogen peroxide change only slightly after the coordination to salts. The same is true for the hydrogen bond parameters (distance O(F)···H–O lies within 2.51–2.84 Å). The dihedral angles change to a considerably greater extent. The largest angles are observed in $Na_2CO_3 \cdot 1.5H_2O_2$. Of 12 hydrogen peroxide molecules constituting the unit cell, eight molecules have a dihedral angle of 125°, whereas in the remaining four molecules this angle is 170°.

It may be suggested that the bonds between H_2O_2 and CO_3^{2-} in $Na_2CO_3 \cdot 1.5H_2O_2$ are somewhat stronger owing to larger opening of hydrogen peroxide dihedral angles. Sarin et al. [11] inferred that the dihedral angle is the most sensitive parameter to the surrounding of H_2O_2 molecules, because it is connected with the change in the potential energy of hydrogen peroxide molecules at rotation of hydroxy groups with respect to each other. The enthalpy of formation of $Na_2CO_3 \cdot 1.5H_2O_2$ from the components is considerably higher in the absolute value than for other peroxo solvates (–93.8 kJ mol^{-1}) [16–18]. The loss of H_2O_2 by the solvate at 25°C in 1 year, estimated from the degrees of decomposition determined from the kinetic curves

Table 2. Thermochemical data for peroxo solvates [3] and some hydrates [19]

Reaction	$-\Delta H$ of reaction, kJ mol^{-1}	$-\Delta H$ of binding 1 mol H_2O_2(g), kJ
$Na_2CO_3(s) + 1.5H_2O_2(g) = Na_2CO_3 \cdot 1.5H_2O_2(s)$	140.70	93.80
$KF(s) + H_2O_2(g) = KF \cdot H_2O_2(s)$	85.53	85.53
$KF(s) + 2H_2O_2(g) = 2KF \cdot H_2O_2(s)$	156.23	78.13
$KF(s) + 3H_2O_2(g) = 3KF \cdot H_2O_2(s)$	221.39	73.80
$NH_4F(s) + H_2O_2(g) = NH_4F \cdot H_2O_2(s)$	72.20	72.20
$Na_2HPO_4(s) + 2H_2O_2(g) = Na_2HPO_4 \cdot 2H_2O_2(s)$	155.89	77.90
$Na_4P_2O_7(s) + 3H_2O_2(g) = Na_4P_2O_7 \cdot 3H_2O_2(s)$	235.10	78.40
$KF \cdot H_2O_2(s) + H_2O_2(g) = KF \cdot 2H_2O_2(s)$	70.88	70.88
$KF \cdot 2H_2O_2(s) + H_2O_2(g) = KF \cdot 3H_2O_2(s)$	65.03	65.03
$Na_2CO_3(s) + H_2O(g) = Na_2CO_3 \cdot H_2O(s)$	58.60	58.60
$KF(s) + H_2O(g) = KF \cdot H_2O(s)$	53.5	53.5

in the interval 100–125°C by extrapolation to lower temperatures, is $7 \cdot 10^{-4}$%. The crystal structure of $KF \cdot H_2O_2$ has also a characteristic feature. In the majority of solvate H_2O_2 molecules, except for one molecule, H(29)–O(29)–O(30)–H(30) [6], hydrogen atoms form an acute angle with respect to the O–O bond. Such configuration suggests the existence of O···H–O intramolecular bonds. Thus, in $KF \cdot H_2O_2$ crystals the majority of H_2O_2 molecules form not only intermolecular bonds O–H···F, but also intramolecular bonds O–H···O. This makes the $KF \cdot H_2O_2$ crystal structure fundamentally different from the structures of other peroxo solvates and may be responsible for its stability. The enthalpy of formation of $KF \cdot H_2O_2$ from H_2O_2(g) and KF is lower in the absolute value (–85.5 kJ mol^{-1}) than of that of $Na_2CO_3 \cdot 1.5H_2O_2$. For this reason, the H_2O_2 loss in 1 year is correspondingly larger (4×10^{-2}%). The examples of $Na_2CO_3 \cdot 1.5H_2O_2$ and $KF \cdot H_2O_2$ show that the solvate structure exerts a certain effect on their stability. However, this effect may be partially or completely leveled off by the effect of the chemical properties of the starting salts.

Dependence of the stability of peroxo solvates on their thermochemical characteristics. The enthalpies of reactions of salts with hydrogen peroxide and the energies of binding of 1 mol of H_2O_2(g) with the corresponding salt are given in Table 2. As seen, the enthalpies of coordination of H_2O_2 are fairly high in the absolute value, varying from –93.8 for $Na_2CO_3 \cdot 1.5H_2O_2$ to –65.0 kJ mol^{-1} for the addition of 1 mol of H_2O_2 to $KF \cdot 2H_2O_2$.

For certain salts, the enthalpy of solvation is higher than the enthalpy of hydration. For example, the enthalpy of hydration of Na_2CO_3 by 1 mol of H_2O(g) is –58.6 kJ mol^{-1} and that of KF, –53.5 kJ mol^{-1}, which is by a factor of 1.5 lower than the enthalpy in solvation of these salts with H_2O_2(g).

Apparently, stability of peroxo solvates toward dissociation is largely determined by the H_2O_2 binding energy. The decomposition pathway through dissociation may be insignificant or predominant. The dissociation can occur simultaneously with the irreversible decomposition of H_2O_2 or may be the only stage of the solvate decomposition. In the latter case, the H_2O_2 decomposition will occur in the gas phase as a typical heterogeneous gas-phase reaction catalyzed by the reactor surface. The degrees of dissociation in the overall process of the peroxo solvate decomposition in a vacuum at different temperatures are given in Table 3.

The direct dependence of the degree of dissociation α_{dis} on the H_2O_2 binding energy ΔH_{bind} is observed for peroxo solvates of potassium and ammonium fluorides at 60°C and for the other solvates ($Na_2HPO_4 \cdot 2H_2O_2$, $Na_2CO_3 \cdot 1.5H_2O_2$, $KF \cdot H_2O_2$), at 100°C (see figure). The solvate $Na_4P_2O_7 \cdot 3H_2O_2$, with a considerably lower degree of dissociation at 100°C, drops out of the latter series.

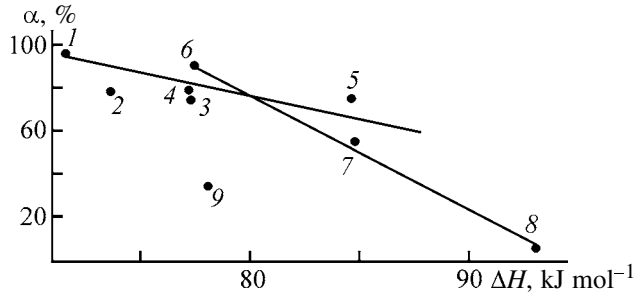
Table 4 shows how the H_2O_2 binding energy correlates with the kinetic parameters of the peroxo solvate decomposition. As seen, sodium carbonate peroxo solvate having the highest H_2O_2 binding energy is the fourth in the decomposition rate constant. In actual practice of storage, the nonstabilized solvate $Na_2CO_3 \cdot 1.5H_2O_2$ is unstable. Coarse, well-edged $Na_2CO_3 \cdot 1.5H_2O_2$ crystals stored for 15 days in closed reservoirs do not loss available oxygen [3], whereas samples obtained under conventional laboratory conditions decompose within a rather short time of storage (loss of H_2O_2 after 1 year is 60%) [19].

Table 3. Dissociation of peroxo solvates in a vacuum ($p = 10^{-3}$ mm Hg, $\tau = 2$ h)

Solvate	T, °C	Overall degree of decomposition η, %	Decomposition through dissociation	Irreversible decomposition
			% of η	
$Na_2CO_3 \cdot 1.5H_2O_2$	100	90	5	95
$KF \cdot H_2O_2$	60	4	77	23
	80	18	75	25
	100	59	55	45
$KF \cdot 2H_2O_2$	40	45	90	10
	60	58	75	25
	80	83	72	28
$KF \cdot 3H_2O_2$	40	61	95	5
	60	82	77	23
	80	100	61	39
$NH_4F \cdot H_2O_2$	40	45	88	12
	60	100	95	9
$Na_2HPO_4 \cdot 2H_2O_2$	60	7	74	26
	80	91	95	5
	100	99	91	9
$Na_3PO_4 \cdot 3H_2O_2$	60	74	62	38
	80	94	55	45
	100	95	54	46
$Na_4P_2O_7 \cdot 3H_2O_2$	80	2	48	52
	100	17	35	65
	120	97	23	77

Table 4. Kinetic parameters of thermal decomposition of peroxo solvates

Solvate	Decomposition temperature, °C	Initial stage, η	$K \times 10^3$, min^{-1}, at 115°C		Calculated loss of H_2O_2, %/year	ΔH of binding H_2O_2(g), kJ mol^{-1}
			K_1	K_2		
$Na_2CO_3 \cdot 1.5H_2O_2$	100–125	0.07–0.80	8.2	9.8	7.0×10^{-4}	93.8
$KF \cdot H_2O_2$	90–125	0.01–0.12	1.2	0.8	4.0×10^{-2}	85.5
$NH_4F \cdot H_2O_2$	70–90	0.04–0.40	–	–	–	72.2
			4.2 (90°C)	1.45 (90°C)		
$Na_2HPO_4 \cdot 2H_2O_2$	100–120	0.10–0.50	12.0	8.3	5.1×10^{-4}	77.9
$Na_4P_2O_7 \cdot 3H_2O_2$	115–135	0.04–0.06	4.0	1.1	2.0×10^{-4}	78.4



Degree of dissociation α of peroxosolvates vs. H_2O_2 binding energy ΔH: (*1*) $NH_4F \cdot H_2O_2$, (*2*) $KF \cdot 3H_2O_2$, (*3, 6*) $Na_2HPO_4 \cdot 2H_2O_2$, (*4*) $KF \cdot H_2O_2$, (*5, 7*) $KF \cdot H_2O_2$, (*8*) $Na_2CO_3 \cdot 1.5H_2O_2$, and (*9*) $Na_4P_2O_7 \cdot 3H_2O_2$.

$KF \cdot H_2O_2$ is the second in the H_2O_2 binding energy, but it surpasses well $Na_2CO_3 \cdot 1.5H_2O_2$ in the decomposition rate constant under isothermal conditions and belongs to the most stable compounds among the peroxo solvates studied. The loss of H_2O_2 in 1 year is 1.5%.

Ammonium fluoride peroxo solvate markedly differs from $KF \cdot H_2O_2$ in the stability and character of decomposition. The low H_2O_2 binding energy in the solvate (72.2 kJ mol^{-1}) causes it to decompose under the isothermal conditions within 70–90°C. At the same time, the solvate is fairly stable in storage (less than 4% H_2O_2 is lost in 1 year). The degree of its dis-

sociation in a vacuum reaches 95% even at 60°C. Evidently, the solvate decomposes virtually completely owing to the dissociation.

Assuming that the decomposition rate constant in the longest portion of the kinetic curve at the same temperature (115°C) is the most adequate criterion for comparing the peroxo solvate stability (Table 4), we obtain that the order in which the stability of peroxo solvates decreases (see below) differs from the order in which the H_2O_2 binding energy decreases: $KF \cdot H_2O_2$, $K_2 = 0.8$; $Na_4P_2O_7 \cdot 3H_2O_2$, $K_2 = 1.1$; $Na_2CO_3 \cdot 5H_2O_2$, $K_1 = 8.2$; $Na_2HPO_4 \cdot 2H_2O_2$ $K_1 = 12.0$.

The effect of the H_2O_2 binding energy on the peroxo solvate stability should be considered in more detail. Naturally, the small value of the energy means that the solvate stability is low. In this case, however, its decomposition through dissociation followed by decomposition of hydrogen peroxide outside the solid phase prevents the formation of a catalytically active film of a solution on the surface of crystals and makes the solvate fairly stable, as shown by the example of ammonium fluoride peroxo solvate.

At a high H_2O_2 binding energy, a part of hydrogen peroxide should irreversibly decompose in the solid phase concurrently with the dissociation, and the solvate stability will be largely determined by the properties of the solution film being formed. For example, in the case of $KF \cdot H_2O_2$, the irreversible decomposition of the solvate in the solid phase yields a neutral film of the solution.

Sodium carbonate peroxo solvate characterized by the highest H_2O_2 binding energy decomposes through dissociation at relatively high temperatures only slightly, and the major pathway is the catalytic decomposition of H_2O_2 in a highly alkaline medium formed by a film of the solution on the surface of the solid phase.

Thus, the solvate stability depends to a considerably greater extent on the chemical properties of the salt, hydrogen peroxide carrier, than on any other parameters.

Effect of chemical properties of salts coordinating hydrogen peroxide on the peroxo solvate stability. In the peroxo solvates studied, the starting salts, hydrogen peroxide carriers, are not oxidized upon solvation. Although products of carbonate oxidation, so-called true percarbonates, exist, they are formed by electrolysis of concentrated carbonate solutions or by other reactions that do not involve CO_3^{2-} anion [20]. Since salts are solvated by hydrogen peroxide owing to the formation of hydrogen bonds between H_2O_2 and the anions, it may be suggested that the water of hydration coordinated to cations can be retained in the peroxo solvates. However, even in salts hydrated with a large amount of water, $KF \cdot 2H_2O$, $NaHPO_4 \cdot 12H_2O$, $Na_4P_2O_7 \cdot 10H_2O$, and $Na_2SO_4 \cdot 10H_2O$, the water of hydration is not retained after the hydrogen peroxide coordination. Exceptions are hydrated oxalate peroxo solvates $[C(NH_2)_3]_2C_2O_4 \cdot 2H_2O \cdot H_2O_2$ and $[C(NH_2)_3]_2C_2O_4 \cdot 0.5H_2O \cdot 0.5H_2O_2$ [21], for which crystallographic data were obtained. The existence of hydrated peroxo solvate of sodium sulfate, $Na_2SO_4 \cdot 0.5H_2O_2 \cdot H_2O$, found as the bottom phase in the Na_2SO_4–H_2O_2–H_2O system at –20°C in [22] and at 20 and 35°C in [23], was not confirmed by the structural data. Thus, the effect exerted by the chemical properties of salts on the peroxo solvate stability must be considered assuming that the peroxo solvates do not contain water of hydration and any derivatives of the salts.

All peroxo solvates are hygroscopic. They absorb water from air to form a microscopic film of the solvate solution on the surface of crystals. The more concentrated the solution, the higher the solubility of the solvate in water. The comparison of the solubilities in water for Na_2CO_3 and $Na_2CO_3 \cdot 1.5H_2O_2$, and for KF and $KF \cdot H_2O_2$ shows that the hydrogen peroxide coordination to salt affects the solubility only slightly (Table 5). Thus, a film of a relatively concentrated solution will be always formed upon absorption of water vapor by the peroxo solvate. In such solution, the H_2O_2 stability, responsible for the stability of the peroxo solvate itself, depends on two factors acting in the opposite directions. The first refers to the acid properties of a solution film, and the second, to the stabilizing property of the solvated salt, its ability to transform microimpurities present in the salts, mainly transition metals or other compounds, into the catalytically inactive state with respect to H_2O_2. It should be noted, however, that various mechanisms responsible for the stabilization of hydrogen peroxide by a particular substance were suggested, but no satisfactory explanation has been found for this effect [1]. The only true conclusion consists in that peroxo solvate stabilization involves purification of both the starting substances and solutions from which a solvate is crystallized, and also their protection from microimpurities. In some cases as, e.g., with sodium percarbonate, the ready solid solvate is protected against moisture to prevent formation of an alkaline film of solution.

Data on the solubility of the starting salts and peroxo solvates are presented in Table 5, along with the pH values of their solutions. As seen, the pH values for the solutions of the starting salt and its solvate

Table 5. Solubility and pH of solutions of salts and their peroxo solvates

Compound	Solubility, wt % (T, °C) [reference]	pH (c, wt %), 20°C [reference]	Stabilizing effect
Na_2CO_3	6.86 (0) [24] 44.5 (100)	11.5 (1.1) [25]	–
$Na_2CO_3 \cdot 1.5H_2O_2$	10.5 (0) [28] 12.8 (26)	10.4 (10) [3, 21] 10.5 (10)	–
KF	92.3 (18) [24] 150.0 (80)	7.1 (1.0) [27]	–
$KF \cdot H_2O_2$	51.1 (0) [26] 60.7 (20)	6.8 (1.0) [27]	–
NH_4F	74.1 (10) [25] 62.8 (20)	6.3 (1.0) (experimental)	–
$NH_4F \cdot H_2O_2$	–	6.1 (1.0) (experimental)	–
Na_2HPO_4	Soluble (0) [24] 104.1 (100)	9.2 (1.4) [25, 28] 8.9 (1.0)	+
$Na_2HPO_4 \cdot 2H_2O_2$	–	9.2 (5) (experimental)	+
Na_3PO_4	10.5 (15) [24] 77.0 (100)	12.0 (1.6) [25, 28] 12.1 (1)	+
$Na_3PO_4 \cdot 3H_2O_2$	–	11.7 (1.5) (experimental)	+
$Na_4P_2O_7$	[24]	10.2 (1.0) [28]	+
$Na_4P_2O_7 \cdot 3H_2O_2$	–	9.9 (1.0) [28]	+

differ slightly (for example, 7.1 and 6.8 for 1% solutions of KF and $KF \cdot H_2O_2$, respectively). With growing concentration, the pH of the KF solution increases considerably (pH 8.0 for a 10% solution), whereas for $KF \cdot H_2O_2$ solution the increase is slight (pH 7.0 for a 10% solution) [26]. Evidently, the effect in coordination of a weakly acidic component, H_2O_2, to highly alkaline salts will be even less significant, especially at high and medium concentrations.

All the peroxo solvates studied can be subdivided into three groups with respect to the extent to which their stability is affected by the chemical properties of the starting salt. The first group includes solvates of salts that form essentially neutal solutions. The second group includes peroxo solvates of salts forming alkaline solutions and exhibiting no stabilizing properties. Peroxo solvates derived from salts that form alkaline salts but, at the same time, exhibit pronounced stabilizing properties with respect to hydrogen peroxide constitute the third group. The first group includes peroxo solvates of potassium and ammonium fluorides, and, probably, of rubidium and cesium fluorides. The pH of solutions of these salts and solvates ranges from 7.8 (65% $KF \cdot H_2O_2$ solution) to 6.1 (1% $NH_4F \cdot H_2O_2$ solution) [27, 28].

Peroxo solvates of potassium and ammonium fluorides, as all peroxo solvates, are hygroscopic. They absorb water from the air without loss of H_2O_2, which made it possible to determine their hygroscopic points [3]. Solutions of solvates are also stable. A saturated solution of $KF \cdot H_2O_2$ decomposes at 20°C at an average rate of $0.1\% \cdot day^{-1}$ (observation time 5 days). The moistened samples are also stable: $KF \cdot H_2O_2$ after taking up 10 wt % water does not loss available oxygen for 75 days. Thus, we can state that the main parameter determining the stability of these compounds is the neutral character of their solutions. A microscopic film formed by a solution on the solvate surface does not exert a catalytic effect on the boundary layer of the solid solvate. Therefore, the solvate $KF \cdot H_2O_2$ with a high H_2O_2 binding energy and presence of an intramolecular hydrogen bond shows extremely high stability, even in the absence of intrinsic stabilizing activity. The solvate does not noticeably lose hydrogen peroxide after 5 years of storage. Its annual loss does not exceed 0.1%. The developed $KF \cdot H_2O_2$ disinfectants containing some additives lose no more than 8% of H_2O_2 after 10 years of storage [2].

The second group includes peroxo solvates of carbonates. The solvates in the solid state are unstable. Highly alkaline solutions of $Na_2CO_3 \cdot 1.5H_2O_2$ are also unstable, because pH of their 10% solution is 10.4 (pH of 1% solution of the carbonate itself is 11.5). A 10 wt % $Na_2CO_3 \cdot 1.5H_2O_2$ solution after 1 day of storage at 20°C loses 12.2% of H_2O_2 [3]. Alkaline solutions of carbonate peroxo solvates on the surface of solid crystals not only promote the hy-

drogen peroxide decomposition but also convert impurities of transition metal compounds into the hydroxides, which have extremely high catalytic activity. It was found [3] that fresh $Fe(OH)_3$ added to $K_2CO_3 \cdot 3H_2O_2$ in an amount of 5×10^{-5}% increases the rate constant of the solvate decomposition to the same extent as does the addition of Fe_2O_3 in an amount of 4×10^{-2}%, higher by three orders of magnitude. Thus, carbonate peroxo solvates, unlike phosphate peroxo solvates, do not have intrinsic stabilizing properties. Therefore, carbonate peroxo solvates moistened with the formation of a highly alkaline film of solution are examples of how the low stabilizing properties of the structure and the high H_2O_2 binding energy are leveled off virtually completely by the chemical properties of the starting salt, a hydrogen peroxide carrier.

Unlike carbonate peroxo solvates, phosphate peroxo solvates of the third group, despite highly alkaline properties, exert a stabilizing effect on aqueous solutions of hydrogen peroxide [1] and on its solid forms, including sodium percarbonate. More than 200 patents are published concerning $Na_2CO_3 \cdot 1.5H_2O_2$ stabilization, with a majority of them using sodium pyrophosphate, its derivatives, and mixtures with other compounds [3]. Although $Na_2CO_3 \cdot 1.5H_2O_2$ is unstable in the pure form, addition of appropriate stabilizers enhances its stability to the level allowing its use as bleaching agent in multicomponent detergents [20]. According to [1], phosphates as a class of compounds are the best stabilizers and the only substances that can be recommended for H_2O_2 stabilization. We found no data about the difference in the stabilizing abilities of sodium pyrophosphate and phosphates of different degrees of substitution. At the same time, it is known that the $P_2O_7^{4-}$ ion in an aqueous solution even at 20°C is hydrolyzed to HPO_4^{2-} [28]. This fact suggests that disubstituted and, apparently, fully substituted phosphates do possess, though to a lesser extent than pyrophosphates, the stabilizing properties with respect to H_2O_2.

Among the phosphate peroxo solvates studied, the most alkaline is a solution of $Na_3PO_4 \cdot 5H_2O_2$ (pH of 1.5% solution is 11.7; pH of 1% phosphate solution 12.1). Apparently, the high alkalinity of the peroxo solvate solution at its low stabilizing activity is the main reason for the low stability of $Na_3PO_4 \cdot 5H_2O_2$.

Disubstituted sodium phosphate, like its peroxo solvate, is less alkaline. In the decomposition rate constant, $Na_2HPO_4 \cdot 2H_2O_2$ is the closest to $Na_2CO_3 \cdot 1.5H_2O_2$. It should be noted that the lower alkalinity of its solutions in comparison with $Na_2CO_3 \cdot 1.5H_2O_2$ solutions and the lower H_2O_2 binding energy lead to the fact that $Na_2HPO_4 \cdot 2H_2O_2$ in the degree of dissociation in a vacuum surpasses well sodium carbonate peroxo solvate (91% against 5% at 100°C).

Sodium pyrophosphate peroxo solvate is less alkaline than $Na_2HPO_4 \cdot 2H_2O_2$ (pH of 1% $Na_4P_2O_7$ solution is 10.8 and pH of the solvate solution of the same concentration, 9.6). At the same time, $Na_4P_2O_7 \cdot 3H_2O_2$ in the decomposition rate constant is close to the most stable solvate $KF \cdot H_2O_2$. This is certainly due to the stabilizing effect of the $P_2O_7^{4-}$ anion. However, $Na_4P_2O_7 \cdot 3H_2O_2$, stable under ambient conditions, irreversibly decomposes in a vacuum, with the degree of decomposition larger compared to $Na_2HPO_4 \cdot 2H_2O_2$ and $KF \cdot H_2O_2$. The degree of decomposition at 100°C is as follows (%): 65 for $Na_4P_2O_7 \cdot 3H_2O_2$, 45 for $KF \cdot H_2O_2$, and 9 for $Na_2HPO_4 \cdot 2H_2O_2$. This fact suggests that the solution on the surface of crystals of pyrophosphate peroxo solvate, because of the growth of its concentration in the course of evacuation, becomes more alkaline; as a result, the degree of the irreversible decomposition of H_2O_2 increases.

CONCLUSIONS

(1) The stability of peroxo solvates largely depends on the chemical properties of salts, H_2O_2 carriers. First of all, it depends on their acidity and on the ability of the solvated salt to neutralize or bind catalytically active foreign impurities.

(2) For neutral salts (KF, NH_4F) the binding energy is the major factor determining the degree of decomposition of their peroxo solvates through dissociation.

REFERENCES

1. Schumb, W.C., Satterfield, Ch.N., and Wentworth, R.L., *Hydrogen Peroxide*, New York: Chapman and Hall, 1955.
2. Buyanov, V. V., Nikol'skaya, V.P., Pudova, O.B., et al., *Peroksosol'vaty v dezinfektologii* (Peroxo Solvates in Disinfectology), Chernogolovka: Inst. Problem Khimicheskoi Fiziki, Ross. Akad. Nauk, 2000.
3. Titova, K.V., Buyanov, V.V., and Nikol'skaya, V.P., *Koordinatsionnye soedineniya peroksida vodoroda* (Coordination Compounds of Hydrogen Peroxide), Chernogolovka: Inst. Problem Khimicheskoi Fiziki, Ross. Akad. Nauk, 2000.
4. Titova, K.V., Kon'kova, T.S., Matyushin, Yu.N., and Rosolovskii, V.Ya., *Izv. Akad. Nauk SSSR, Ser. Khim.*, 1989, no. 2, pp. 247–250.

5. Krivtsov, N.V. and Titova, K.V., *Zh. Neorg. Khim.*, 1993, vol. 38, no. 10, pp. 1741–1742.
6. Titova, K.V., D'yachenko, O.A., Grintsenko, V.V., and Shilov, G.V., *Izv. Ross. Akad. Nauk, Ser. Khim.*, 1993, no. 1, pp. 38–43.
7. Titova, K.V., Kolmakova, E.I., and Rosolovskii, V.Ya., *Zh. Neorg. Khim.*, 1983, vol. 28, no. 8, pp. 1922–1927.
8. Titova, K.V., Kolmakova, E.I., and Rosolovskii, V.Ya., *Zh. Neorg. Khim.*, 1989, vol. 34, no. 12, pp. 3016–3020.
9. Adams, J.M. and Pritchard, R.G., *Acta Crystallogr., Sect. B*, 1977, vol. 33, no. 12, p. 3650.
10. Carrondo, M.A.A.F. de C.T., Griffith, W.P., Jones, D.P., and Scapski, A.S., *J. Chem. Soc., Dalton Trans.*, 1977, no. 23, pp. 2323–2327.
11. Sarin, V.A., Dudarev, V.Ya., Dobrynina, T.A., et al., *Kristallografiya*, 1976, vol. 21, no. 5, pp. 929–936.
12. Sarin, V.A., Dudarev, V.Ya., Dobrynina, T.A., et al., *Kristallografiya*, 1977, vol. 22, no. 5, pp. 982–987.
13. Pedersen, B.F. and Pedersen B., *Acta Chim. Scand.*, 1964, vol. 18, pp. 1454–1468.
14. Pedersen, B.F., *Acta Chim. Scand.*, 1969, vol. 23, pp. 1871–1877.
15. *Gmelins Handbuch der anorganischen Chemie*, Sauerstoff, 1966, system no. 3, issue 7, p. 2257.
16. Kirpichev, E.P., Rubtsov, Yu.I., Titova, K.V., and Rosolovskii, V.Ya., *Zh. Neorg. Khim.*, 1983, vol. 28, no. 7, pp. 1858–1860.
17. Titova, K.V., *Zh. Neorg. Khim.*, 1999, vol. 44, no. 6, pp. 925–930.
18. Yanush, A.V., *Khim. Prom–st.* (Kiev), 1964, no. 4, p. 18.
19. Karapet'yants, M.Kh. and Karapet'yants, M.L., *Osnovnye termodinamicheskie konstanty neorganicheskikh i organicheskikh veshchestv* (Fundamental Themodynamic Constants of Inorganic and Organic Substances), Moscow: Khimiya, 1968.
20. Titova, K.V., Kolmakova, E.I., and Rosolovskii, V.Ya., *Fizikokhimicheskie svoistva i sposoby stabilizatsii* $Na_2CO_3 \cdot 1.5H_2O_2$ (Physicochemical Properties and Stabilization Techniques of $Na_2CO_3 \cdot 1.5H_2O_2$), Available from VINITI, Moscow, 1984, no. 1254–84.
21. Vol'nov, I.I. and Antonovskii, V.L., *Peroksidnye proizvodnye i addukty karbonatov* (Peroxy Derivatives and Carbonate Adducts), Moscow: Nauka, 1985.
22. Vol'nov, I.I. and Kolotova, E.I., *Zh. Neorg. Khim.*, 1959, vol. 4, no. 9, pp. 2143–2145.
23. Peni, S. and Ferry, H., *J. Chem. Soc.*, 1955, no. 9, p. 3056.
24. *Spravochnik khimika* (Chemist's Handbook), Nikol'skii, B.P., Ed., Leningrad: Khimiya, 1951, vol. 2.
25. Lazarev, A.I. and Kharlamov, I.P., *Analiz metallov: Spravochnik* (Metal Analysis: Handbook), Moscow: Metallurgiya, 1983.
26. Titova, K.V., Karzhavina, G.P., Nikol'skaya, V.P., et al., *Zh. Neorg. Khim.*, 2003, vol. 48, no. 5, pp. 849–853.
27. Titova, K.V., Nikol'skaya, V.P., Buyanov, V.V., and Pudova, O.B., *Zh. Neorg. Khim.*, 2005, vol. 50, no. 1, pp. 133–136.
28. Nekrasov, B.V., *Osnovy obshchei khimii: uchebnoe posobie dlya studentov vtuzov* (Fundamentals of General Chemistry: Textbook for Higher Technical School Students), Moscow: Nauka, 1973.
29. Titova, K.V., Nikol'skaya, V.P., Buyanov, V.V., and Pudova, O.B., *Zh. Neorg. Khim.*, 2005, vol. 50, no. 4, pp. 704–706.

ISSN 1070-4272, Russian Journal of Applied Chemistry, 2006, Vol. 79, No. 11, pp. 1793–1797. © Pleiades Publishing, Inc., 2006.
Original Russian Text © M.V. Maslova, L.G. Gerasimova, R.F. Okhrimenko, A.S. Chugunov, 2006, published in Zhurnal Prikladnoi Khimii, 2006, Vol. 79, No. 11, pp. 1813–1817.

SORPTION AND ION-EXCHANGE PROCESSES

Composition of Ion-Exchange Materials Based on Titanium Phosphate

M. V. Maslova, L. G. Gerasimova, R. F. Okhrimenko, and A. S. Chugunov

Tananaev Institute of Chemistry and Technology of Rare Elements and Mineral Raw Materials, Kola Scientific Center, Russian Academy of Sciences, Apatity, Murmansk oblast, Russia
St. Petersburg State Technological Institute, St. Petersburg, Russia

Received May 4, 2006

Abstract—Composition and structure of synthetic ion-exchange materials based on titanium phosphate were studied. The materials were synthesized from titanium(IV), phosphorus(V), and silicon(IV) reagents taken in various concentrations, using various modes of the synthesis and treatment of the precursors. The dependence of the ion-exchange properties of the final products on the composition of the precursors was examined.

DOI: 10.1134/S1070427206110103

High sorption characteristics of ion-exchange materials based on elements of Groups III–IV of the periodic table attract attention of chemists and ecologists. Insoluble iron, aluminum, titanium, and zirconium oxyhydroxides, phosphate compounds of transition elements, and compositions based on them belong to this class of ion exchangers. They exhibit high resistance to chemical agents, heat, and radiation, and also selectivity with respect to a number of ions. The selectivity is determined by the structure of an ion exchanger matrix and by the nature of functional groups capable of ion exchange.

Titanyl phosphates $TiOHPO_4 \cdot xH_2O$ are also highly selective materials. Methods for preparing this sorbent and its properties have been described in detail [1–4]. Most frequently, a titanyl phosphate intermediate product (precursor) is synthesied by precipitation from solutions of titanium(IV) salts with orthophosphoric acid. Another procedure is based on the treatment of freshly precipitated titanium(IV) oxyhydroxide with orthophosphoric acid [5]. More rarely, the synthesis is carried out from dilute solutions of reagents (sol–gel method) [6, 7]. The subsequent treatment of precursors involves transformation of a sorption material into a state convenient for the efficient use. There are data on the preparation of precursors with a mixed composition, e.g., of hydrated titanium phosphates containing silicon compounds. Such products can be readily granulated with the formation of porous sorbent matrices, which makes it possible to accelerate the exchange processes and enhance the selectivity to multiply charged ions. It is possible to vary sorption properties during the preparation of the compositions by varying the precursor composition and the mode of its synthesis [8].

Here we report new data on the composition of sorbents based on titanyl phosphate. As a raw material for their production we used concentrates, products of integrated processing of apatite–nepheline ores, in particular, a concentrate containing titanite (calcium titanosilicate $CaTiSiO_5$), and also nepheline and apatite concentrates. The principal flowsheet of production of the sorbents and the process features have been published in several works and patented [9–12].

EXPERIMENTAL

Finely dispersed titanite concentrate was mixed with a sulfuric acid solution (H_2SO_4 concentration 550 g l^{-1}, weight ratio s : l = 1 : 1.65), and the reaction mixture was heated with stirring for 7 h at 105–110°C [13]. Under these conditions, titanium(IV) is leached from the mineral and passes into the sulfuric acid liquid phase (a titanium solution). The synthesis of a composite titanyl phosphate precursor and its subsequent treatment were carried out by the known technique [14]. A phosphoric acid silicate solution obtained by the reaction of nepheline with 15% phosphoric acid and containing 60 g l^{-1} of SiO_2 was added to a titanium solution heated to 70–80°C. Then phosphoric acid was added in an amount corresponding to

Synthesis conditions, composition, and main characteristics of the synthesized ion-exchange materials

Sample	Synthesis conditions*	Composition	Characteristic of structure	S_{sp}, $m^2\ g^{-1}$
I	H_3PO_4 30%	$TiO_2 \cdot 0.5P_2O_5 \cdot 3.0H_2O$	X-ray amorphous	60.5
II	H_3PO_4 60%	$TiO_2 \cdot 0.75P_2O_5 \cdot 3.0H_2O$	Finely crystalline	95.5
III	H_3PO_4 30%, $TiO_2 : SiO_2 = 1 : 0.25$ (mol)	$TiO_2 \cdot 0.5P_2O_5 \cdot 0.16SiO_2 \cdot 2.5H_2O$	X-ray amorphous	85.9
IV	H_3PO_4 60% $TiO_2 : SiO_2 = 1 : 0.25$ (mol)	$TiO_2 \cdot 0.75P_2O_5 \cdot 0.16SiO_2 \cdot 2.75H_2O$	Finely crystalline	122.3

* For all the samples $TiO_2 : P_2O_5 = 1 : 1$ (mol).

the molar ratios of the components given in the table. The resulting suspension was kept for 12 h, after which the precipitate was filtered off and washed with 5% phosphoric acid and distilled water to pH 4.5. The product washed to remove the residual mother liquor was dried at 60°C.

The specific surface areas of the sorbent samples were determined by the BET method on a Flowsorb II 2300 electronic analyzer; the samples were degassed for 2 h at 140°C. The thermogravimetric analysis of the samples placed in quartz test tubes was performed in the range 20–980°C with heating at a rate of 9 deg min^{-1}. The X-ray phase analysis of the samples was carried out on a DRON-2 diffractometer (CuK_α radiation). The IR spectra of the samples were recorded on a UR 20 IR spectrometer in the range 400–4000 cm^{-1}. The pH-metric titration was carried out with an I-120.2 ionomer; the initial and equilibrium concentrations of metal ions in solution were determined by standard techniques on a Perkin–Elmer FT-IR 200 spectrometer.

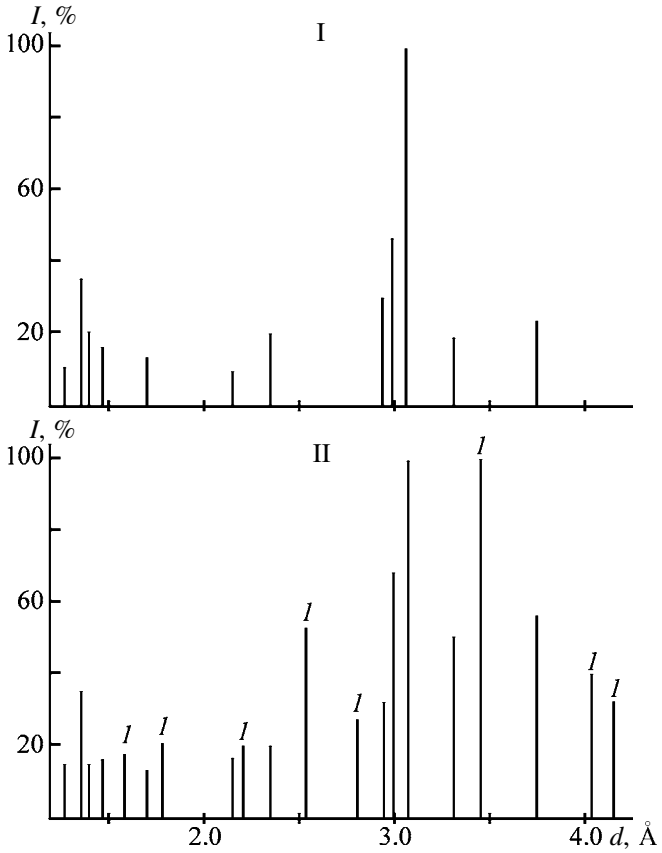


Fig. 1. X-ray diffraction patterns of products I and II dehydrated at 280°C. (*I*) Intensity and (*d*) interplanar spacing. (*1*) Phase corresponding to the composition $TiO(H_2PO_4)_2$.

According to the X-ray data, air-dry precursors have an X-ray amorphous or finely crystalline structure depending on the synthesis conditions (see table). Products I and III dehydrated at 280°C have the composition $TiOHPO_4$, and products II and IV are mixtures containing $TiOHPO_4$ and $TiO(H_2PO_4)_2$ (Fig. 1). The phosphoric acid concentration does not affect the rate of the solid phase formation. However, an increase in its concentration leads to increasing crystallinity of the precipitate. Judging from the specific surface areas, particles of crystalline precipitates show weaker tendency to sticking during heat treatment than particles of amorphous precipitates. Two endothermic effects at 165–170 and 312–326°C accompanied by a weight loss were detected in the DTA curves (Fig. 2). The presence of two effects indicates that the dehydration is stepwise. However, as the TG curve shows, samples containing no silicon component have a higher content of both water of crystallization and water released from the condensation of acid phosphate groups. Two exothermic effects without weight loss refer to the formation of titanium pyrophosphate (TiP_2O_7). The shift of the effects of the titanium pyrophosphate formation toward lower temperatures for the silicon-containing precipitate is presumably associated with the formation of solid solutions of titanium pyrophosphate with SiO_2.

The IR spectra of the precipitates under study (Fig. 3) are practically identical and contain strong broad bands in the range 3600–3100 cm^{-1} belonging

to stretching vibrations of water and OH groups, and also less strong bands belonging to bending vibrations of OH^- groups (1630 cm^{-1}). Strong bands in the region of 1000 cm^{-1} correspond to asymmetric vibrations of P–OH bonds, and bands in the region of 650–750 cm^{-1}, to vibrations of titanium polyhedra [15]. It is known that the Si–O–Ti bond is manifested in the region of 960 cm^{-1} [16] and can overlap with the vibrations of P–OH groups.

To determine the nature of bonding between titanium and silicon in the precursors under study, we used the known technique based on the determination of active and passive OH^- groups [17]. According to this technique, two processes occur successively when a suspension sample reacts with potassium fluoride: fast substitution of fluoride ions for terminal OH^- groups bonded to titanium and silicon and slow cleavage of the bridging bonds. We found the number of OH^- groups graphically from the intersection with the ordinate axis of the tangent to the flat portion of the curve corresponding to the range 0–30 min for active OH^- groups and 1–5 h for passive OH^- groups. The experimental data obtained were interpreted from this point of view.

Both terminal and bridging OH^- groups are absent from samples I and II. As such products were synthesized without silicate component, we can conclude that titanium(IV) species do not polymerize to form –Ti–O–Ti– chains, and the precursor matrix is formed by multiple repetition of the events of bonding between titanyl ions and phosphate groups. Both active and passive OH^- groups are determined in silicon-containing samples III and IV (Fig. 4). As we found that titanium(IV) in the synthesized products does not contain terminal OH^- groups, the formation of –Si–O–Ti– bonds seems improbable. The OH^- groups found in the composite sorbents can be assigned only to silanol groups (Si–OH). The number of terminal OH groups for samples III and IV is the same, 0.05 mol of OH^- per mole of SiO_2. Bridging –Si–O–Si– bonds are formed by cross-linking of silicon hydroxo complexes by OH^- groups with the formation of species with a friable structure, as seen from the specific surface area. The use of dilute phosphoric acid for the synthesis of products leads to the formation of silica particles hydrated to a greater extent; hence, the number of passive OH^- groups in such products is considerably larger.

The results obtained allow us to state that sorbents I and II represent hydrated titanyl hydrophospates free from hydroxy groups. Composite sorbents III and IV consist of two phases. Particles of hydrated silicon

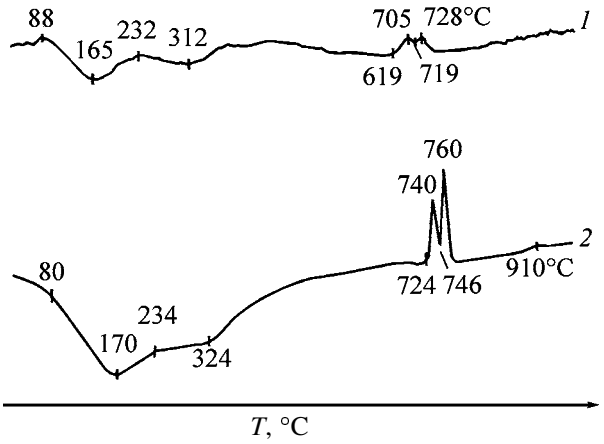


Fig. 2. Thermograms of the synthesized samples. (*T*) Temperature. (*1*) Composite sorbent and (*2*) titanyl phosphate.

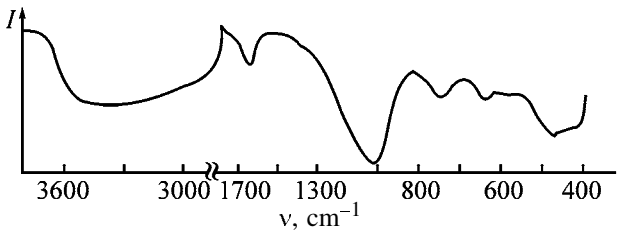


Fig. 3. IR spectrum of titanyl phosphate. (*I*) Intensity and (ν) wavenumber.

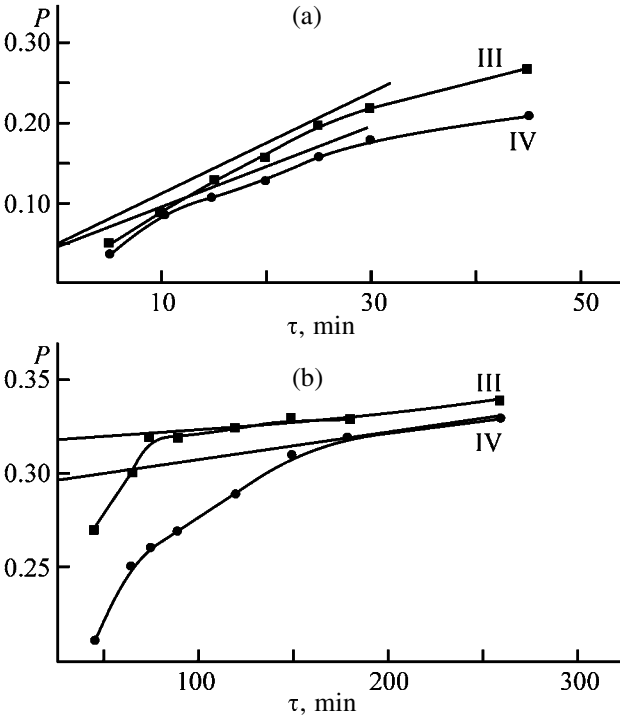


Fig. 4. Variation of the content *P* of (a) active and (b) passive OH^- groups relative to the SiO_2 content in composite sorbents. (τ) Process duration.

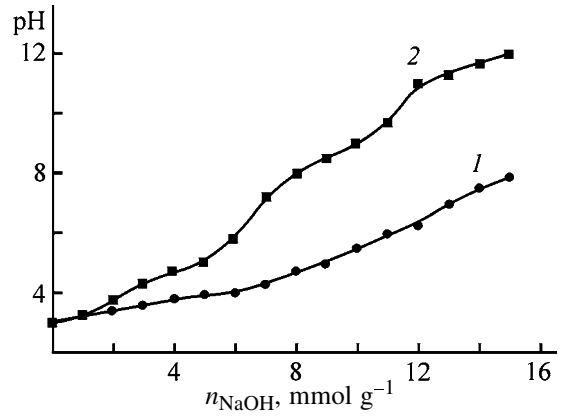


Fig. 5. Curves of pH-metric titration of titanyl phosphate samples of (*1*) X-ray amorphous and (*2*) crystalline structure. (n_{NaOH}) Amount of NaOH.

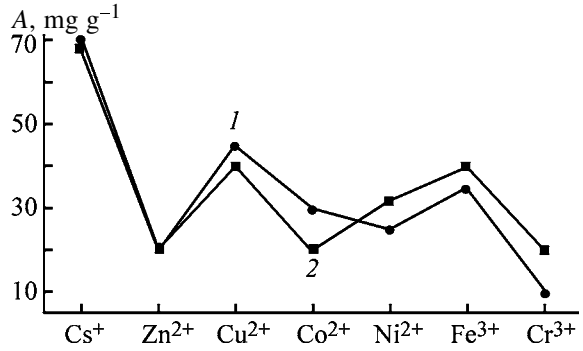


Fig. 6. Sorption activity A of (*1*) titanyl phosphate and (*2*) composite sorbent to metal cations.

oxide (HSO) are rather evenly distributed in a titanyl phosphate matrix exceeding them in weight.

In the curve of pH-metric titration of sample II (Fig. 5), there are two clear pH jumps, which, apparently, correspond to the first and second steps of the dissociation of phosphate groups. The curve of pH-metric titration of sample I is a monotonically ascending curve suggesting continuous dissociation of all the possible functional groups.

The total ion-exchange capacity of the synthesized materials varies within narrow limits, 3.12–3.22 mg-equiv g^{-1}. In addition to HPO_4 groups, the sorbents obtained using 60% phosphoric acid also contain strongly acidic ion-exchange groups making a 15–20% contribution to the total ion-exchange capacity.

The influence of the structure on the ion-exchange properties was found when studying the sorption activity of the materials (Fig. 6). For this purpose, the precursors were dried at 60°C and then treated for 24 h with a 100 g l^{-1} Na_2CO_3 solution. To maintain constant pH 6, the sorption was carried out in the presence of an acetate buffer solution.

The sorption activity of the materials under study decreases in the following order: for titanyl phosphate, Cs(I) > Cu(II) > Fe(III) > Co(II) > Ni(II) > Zn(II) > Cr(III); for the composite sorbent, Cs(I) > Cu(II) > Fe(III) = Ni(II) > Co(II) = Zn(II) = Cr(III).

We found that both types of the synthesized ion-exchange materials exhibit a high selectivity to cesium cations.

The above series of selectivity to transition metals do not correlate with the sequence of crystal-chemical radii of the ions. It is known that an ion exchanger has the strongest affinity for a metal ion when active groups of the ion exchanger form stable complexes with counterions. Therefore, iron(III) cations having the smallest ionic radius and, hence, the largest hydration shell should have the lowest sorption ability. However, due to the formation of a strong coordination bond of a sorbed ion with oxygen in the sorbent structure (Ti=O), sorption of iron(III) ions increases. Chromium(III) ions with a developed hydration shell have the lowest ability to penetrate into sorbent pores, and the ion exchange proceeds basically due to the active groups concentrated on the sorbent surface.

Different sorption behavior of cobalt(II) and nickel(II) ions is of interest, as there is a problem of the separation of these elements in the case of liquid radioactive waste treatment. The Ni^{2+} ion has a smaller ionic radius (0.69 Å) than Co^{2+} (0.74 Å); hence, it is more strongly hydrated and more difficultly penetrates into a sorbent. This dependence is observed when the elements are sorbed on titanyl phosphate. In the case of a composite sorbent, the series undergoes partial inversion. We believe that this is possible only if active sites of the HSO surface make a certain contribution.

As found previously, the composite sorbent is a mixture of two phases, titanyl phosphate and HSO, evenly distributed throughout the sorbent volume. In aqueous solutions, SiO_2 has active sites with a variable charge, appearing as a result of protonation or deprotonation of surface hydroxy groups. The degree of the protonation of the surface sites depends on pH of a medium and is a surface characteristic of an oxide. It is known that, in the region of neutral pH, silanol groups of silicon oxide are charged negatively [18], and the deprotonation reaction on surface sites can be presented as $\equiv SiOH \rightleftarrows \equiv SiO^- + H^+$. Surface $[\equiv SiOH]^0$ and $[\equiv SiO]^-$ groups are potential ligands, i.e., they can form surface complexes with an ion of the adsorbed metal as an acceptor; $[\equiv SiO]^-$ is a more

active ligand than $[\equiv SiOH]^0$ [19]. In view of the aforesaid, we can assume that the deprotonated active sites of silanol groups play a noticeable role in sorption processes due to specific adsorption of metal ions. When studying the adsorption of cations of polyvalent metals on quartz, Tikhomolova and Urakova [20] found that Ni(II) is adsorbed more actively than Co(II), which agrees with our data. Nickel(II) ions are adsorbed by the donor–acceptor mechanism, and the bond in such complex is rather strong [21]. Complexes of Co(II) with monodentate ligands having an oxygen atom as a donor center, as a rule, are labile [22].

The data of our studies were confirmed by the results of semicommercial trials on the treatment of highly saline radioactive solutions from the Leningrad Atomic Power Plant and of liquid wastes from the Plant of Art Paints of St. Petersburg.

CONCLUSIONS

(1) The study of how the conditions of the synthesis of titanyl phosphate precursors of ion-exchange materials affect their phase composition and structure showed that an increase in the phosphoric acid concentration promotes the formation of a titanyl phosphate solid phase with a crystalline matrix, which is formed by multiple repetition of the events of bond formation between titanyl ions and phosphate groups.

(2) Species in the titanyl phosphate precursor containing hydrated silicon oxide are additionally bound together by the formation of –Si–O–Si– bridging bonds, which promotes the formation of a solid phase with a friable structure. The higher the phosphoric acid concentration, the larger the specific surface area of the precipitate particles.

(3) The silicate component in the composite sorbents makes a certain contribution to sorption processes due to specific adsorption of metal cations on active centers of hydrated silicon oxide.

(4) The synthesized ion-exchange materials have relatively high exchange capacity for Cs^+, Cu^{2+}, Fe^{3+}, Co^{2+}, and Ni^{2+} ions and, as the trials showed, can be used for the treatment of industrial sewage and liquid radioactive solutions.

ACKNOWLEDGMENTS

This study was financially supported by the Leading Scientific Schools grant (no. NSh-4383.2006.3).

REFERENCES

1. Mitchenko, T.E., Belyakov, V.N., Roitenberg, A.M., et al., *Zh. Prikl. Khim.*, 1986, vol. 59, no. 7, pp. 1440–1443.
2. Dranitsina, N.V., Egorov, Yu.V., and Fominykh, E.V., *Izv. Akad. Nauk SSSR, Neorg. Mater.*, 1970, no. 12, pp. 2178–2182.
3. Bortun, A., Jaimez, E., Llavona, R., et al., *Mater. Res. Bull.*, 1995, vol. 30, no. 4, pp. 413–420.
4. Bereznitski, Y., Jaroniec, M., Bortun, A., et al., *J. Colloid Interface Sci.*, 1997, vol. 191, pp. 442–448.
5. Lokshin, E.P., Ivanenko, V.I., Udalova, I.A., et al., *Radiokhimiya*, 2003, vol. 45, no. 4, pp. 357–361.
6. Egor'kova, O.V., Orlova, A.I., Pet'kov, V.I., et al., *Radiokhimiya*, 1996, vol. 38, no. 6, pp. 481–483.
7. Sharygin, L.M., Kalyagina, M.L., and Borovkov, S.I., *Zh. Prikl. Khim.*, 2005, vol. 78, no. 2, pp. 229–234.
8. Materova, E.A., in *Neorganicheskie ionoobmennye materialy* (Inorganic Ion-Exchange Materials), Leningrad: Leningr. Gos. Univ., 1974, issue 1, pp. 56–65.
9. Gerasimova, L.G., Maslova, M.V., Okhrimenko, R.F., and Belyavskii, A.T., *Khim. Tekhnol.*, 2004, no. 2. pp. 13–17.
10. Gerasimova, L.G., Matveev, V.A., Maslova, M.V., et al., *Tsvetn. Met.*, 2005, no. 3, pp. 87–91.
11. Gerasimova, L.G., Maiorov, V.A., Maslova, M.V., et al., *Al'ternat. Energet. Ekol.*, 2005, no. 2, pp. 39–41.
12. RF Patent 2207980.
13. RF Patent 2179528.
14. Gerasimova, L.G., Maslova, M.V., and Lazareva, I.V., *Obogashch. Rud*, 2005, no. 4, pp. 31–33.
15. Nakamoto, K., *Infrared Spectra of Inorganic and Coordination Compounds*, New York: Wiley, 1963.
16. Deo, G., Turek, A., Wachs, I., et al., *Zeolites*, 1993, vol. 13, pp. 365–373.
17. Biryuk, L.I., Goroshchenko, Ya.G., Khandros, E.L., et al., *Ukr. Khim. Zh.*, 1973, vol. 39, no. 3, pp. 504–506.
18. Parks, G., *Chem. Rev.*, 1965, vol. 65, pp. 177–183.
19. Aleksandrova, L.K. and Tikhomolova, K.P., *Kolloidn. Zh.*, 1988, vol. 50, no. 1, pp. 100–107.
20. Tikhomolova, K.P. and Urakova, I.N., *Zh. Prikl. Khim.*, 2002, vol. 75, no. 6, pp. 913–919.
21. Cotton, F.A. and Wilkinson, G., *Advanced Inorganic Chemistry*, New York: Interscience, 1966.
22. Spice, J.E., *Chemical Binding and Structure*, New York: Macmillan, 1964.

ISSN 1070-4272, Russian Journal of Applied Chemistry, 2006, Vol. 79, No. 11, pp. 1798–1801. © Pleiades Publishing, Inc., 2006.
Original Russian Text © A.N. Kalimgulova, M.A. Parfenova, A.D. Ulendeeva, N.K. Lyapina, R.A. Khisamutdinov, Yu.I. Murinov, 2006, published in Zhurnal Prikladnoi Khimii, 2006, Vol. 79, No. 11, pp. 1818–1821.

SORPTION AND ION-EXCHANGE PROCESSES

Keto Sulfides Derived from *tert*-Dodecyl Mercaptan and Their Extractive Power with Respect to Palladium(II) and Gold(III)

A. N. Kalimgulova, M. A. Parfenova, A. D. Ulendeeva, N. K. Lyapina, R. A. Khisamutdinov, and Yu. I. Murinov

Institute of Organic Chemistry, Ufa Scientific Center, Russian Academy of Sciences, Ufa, Bashkortostan, Russia

Received May 12, 2006

Abstract—γ-Keto sulfide concentrates were prepared by alkylthiomethylation of propanone, butanone, and acetophenone with technical-grade *tert*-dodecyl mercaptan and other sufur-containing substances, and their extractive power with respect to palladium(II) and gold(III) from hydrochloric acid solutions (chloroform as diluent) was studied.

DOI: 10.1134/S1070427206110115

Polyfunctional sulfides and petroleum sulfides and sulfoxides are promising extractants for recovery and separation of a number of radioactive, rare, trace, and nonferrous metals [1]. γ-Keto sulfides [2] prepared by alkylthiomethylation (ATM) of ketones with mercaptans [3] are accessible extractants., A method for the synthesis of γ-keto sulfide concentrates based on natural mercaptan mixtures with prevalent content of C_1–C_6 carbon chains was developed recently [4]. To obtain high-molecular-weight keto sulfides by ATM of propanone, technical-grade *tert*-dodecyl mercaptan was used as a sulfur-containing component [5] (Salavatnefteorgsintez Open Joint-Stock Company).

In this study, γ-keto sulfide (hereinafter γ is omitted for brevity) concentrates were prepared by ATM of propanone, butanone, and acetophenone with a technical mixture of C_{12}–C_{18} mercaptans (TM), and the extractive power of these concentrates with respect to palladium(II) and gold(III) recovered from hydrochloric acid solutions was examined.

Industrial mixtures of isomeric C_{12}–C_{18} mercaptans were used as sulfur-containing reagents. TM-1 (M = 190) is a mixture of $C_{12}H_{25}SH$ tertiary isomers (96–97%) and $C_{12}H_{24}$ *tert*-isoolephins (3–4%). TM-2 (M = 330), along with $C_{12}H_{25}SH$ tertiary isomers (8%) and $C_{12}H_{24}$ *tert*-isoolephins (8%), contains high-molecular-weight mercaptans, sulfides, and disulfides (25.0, 26.3, and 8.6%, respectively) and unidentified compounds (about 24%) [6].

Keto sulfide concentrate I was prepared by alkylthiomethylation of propanone with a mixture of formaldehyde and TM-1. TM-2 was used to prepare keto sulfide concentrates II, III, and IV by alkylthiomethylation of propanone, butanone, and acetophenone, respectively.

Synthesis procedure. Aqueous formaldehyde and appropriate ketone were added dropwise to TM-1 or TM-2 with vigorous stirring. The formaldehyde : ketone : sodium hydroxide (15% aqueous solution) molar ratio per mole of mercaptan sulfur was 1.2 : 1.2 : 1.2. Sodium hydroxide solution was diluted with ethyl alcohol in 1 : 1 volume ratio. The mixture was stirred for 3 h at 50°C, washed with 10% HCl, and then extracted with chloroform (3 × 25 ml). Extracts were washed with water (1 : 1 by volume), dried with $MgSO_4$, and chloroform was distilled off. In the concentrates I–IV, we determined total, sulfide, and mercaptan sulfur [7, 8]. The mercaptan conversion was monitored by determination of mercaptan and sulfide sulfur by potentiometric titration [8]. Formation of keto sulfides was confirmed by ν(C=O) bands at 1716–1720 cm^{-1} in the IR spectra of the products. The data of the chemical analysis of products are listed in the table. The maximal content of total (12.8 wt %) and sulfide (12.2 wt %) sulfur was found in concentrate I, which corresponds to 94% content of sulfides. In concentrates II, III, and IV, the content of sulfide sulfur amounts to 89.9, 76.7, and 87.6% of total sulfur, respectively (see table). The concentrates obtained are mixtures of keto sulfides. Concentrates I–IV contain mono- (67, 18, 47, and 26%, respective-

Chemical analysis of ketosulfide concentrates based on TM-1 and TM-2 prepared by alkylthiomethylation of ketones

Ketosulfide concentrate (ketone)	Content, wt %						*M*
	C	H	S				
			total	mercaptan	sulfide	disulfide	
TM-1	71.80	13.00	14.2	13.4	Absent	Absent	90
I (propanone)	70.59	11.87	12.8	Absent	12.20	Absent	305
TM-2	77.58	13.53	8.6	4.6	3.50	0.89	330
II (propanone)	77.69	13.06	8.56	0.40	7.70	0.77	380
III (butanone)	76.52	13.10	8.6	Absent	6.60	1.54	380
IV (acetophenone)	78.40	12.65	8.1	0.46	7.10	1.34	390

ly) and bis(alkylthiomethyl)-substituted (27, 29, 0, and 21%, respectively) ketones and initial compounds (hydrocarbons and organosulfur compounds) [6].

The extractive power of keto sulfide concetrates I–IV was compared with that of petroleum sulfides V and concentrates of C_6–C_{10} keto sulfides VI in which the extractive powers of different components are averaged. Petroleum sulfides V [9] are mixtures of monocyclothiaalkanes (50%), di-, tri-, and tetracyclothiaalkanes (18%), thiophenes (25%), thiaindans, thiaalkanes, and cycloalkyl sufides (6%). Keto sulfide concentrate VI is a mixture of aliphatic keto and diketo sulfides C_6–C_{10} [10].

Palladium(II) and gold(III) were extracted from 0.5 M hydrochloric acid solutions. The palladium concentration was varied within the 0–0.008 M range, and that of gold, within the 0–0.005 M range. All the extractant solutions had equal contents of sulfide sulfur. The solutions of keto sulfide concentrates in chloroform with sulfide sulfur content of 0.005 and 0.0025 M were used for palladium and gold, respectively. The extraction was performed in temperature-controlled separating funnels at 25°C and 1 : 1 volume ratio of aqueous to organic phase . The extraction equilibrium is reached within 20 min for palladium(II) and 7 min for gold(III).

Backwashing of gold(III) and palladium(II) from the organic phase was performed with 5% aqueous solutions of sodium sulfite and thiourea, respectively, for 3 min. After washing with 0.5 M hydrochloric acid, the extractants are suitable for the further use. The initial concentration of metal ions was determined spectrophotometrically with a Specord M40 spectrophotometer; palladium(II) with tin(II) chloride [11], and gold(III) as $AuCl_4^-$ ion at 313 nm with a calibrating plot [12]. The equilibrium concentrations of metal ions in raffinates were determined by atomic absorption spectrophotometry on a Hitachi 508 spectrometer. Aqueous solutions of Pd(II) and Au(III) were burned in an acetylene–air flame. Lamps with a hollow cathode made of metals to be determined served as monochromatic light sources with analytical wavelengths of 247.6 and 242.8 nm for Pd and Au, respectively. The error of the metal concentration determination was 5–10 rel %.

The steep slopes of the initial parts of the extraction isotherms (Figs. 1, 2) show that the keto sulfide

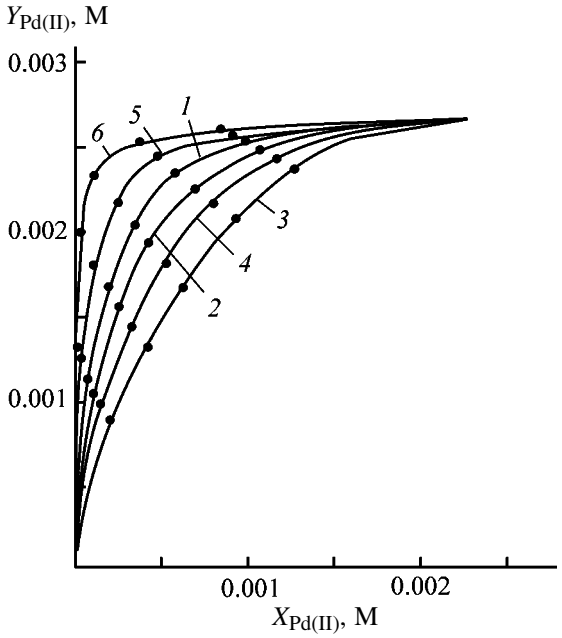


Fig. 1. Isotherms of palladium(II) extraction from 0.5 M HCl solutions with 0.005 M solutions of keto sulfide concentrates in chloroform at 25°C. $X_{Pd(II)}$ and $Y_{Pd(II)}$ are equilibrium concentrations of metal ion in the raffinate and extract, respectively (M); the same for Fig. 2. Extractant: (*1*) *tert*-C_{12}; (*2–4*) sum of *tert*-C_{12}, C_{15}, and C_{18}; (*5*) petroleum sulfides; (*6*) C_6–C_{10} mixture; the same for Fig. 2.

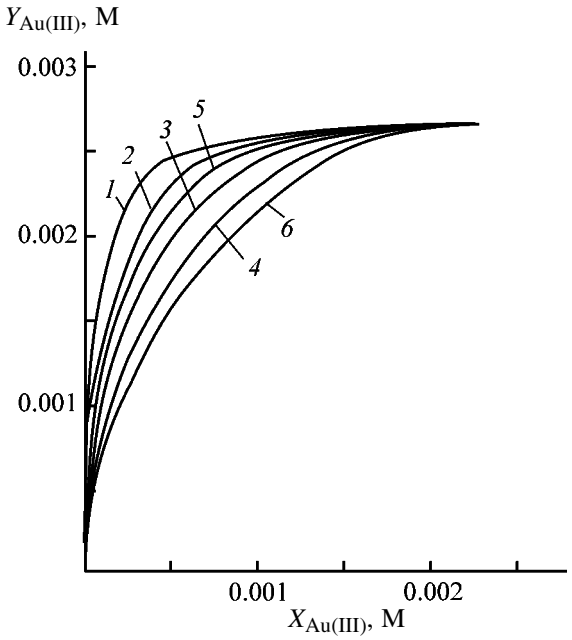


Fig. 2. Isotherms of palladium(II) extraction from 0.5 M HCl solutions with 0.0025 M solutions of keto sulfide concentrates in chloroform at 25°C.

concentrates studied efficiently recover metal ions from moderately acidic aqueous solutions. Concentrates of keto sulfides I and II based on TM-1, TM-2, and propanone are better extractants than III and IV. Product I based on TM-1 is a better extractant than II, which may be associated with the higher molecular weight of keto sulfide in the latter case. The extractive power in the series of concentrates II, IV, and III based on TM-2 and propanone, acetophenone, and butanone, respectively, decreases. A decrease in the extractive power of III and IV as compared to II may be due to elevated content of disulfide sulfur in III and IV (see table). The ratio of mono- and disubstituted ketones probably also affects the extractive power. In the saturation region, the extraction isotherms of palladium(II) with I and II differ from the isotherms with V and VI insignificantly; however, extraction with low-boiling keto sulfides is more efficient than extraction with high-boiling keto sulfides I–IV. The extractive power of petroleum sulfides V with respect to palladium(II) is lower than that of keto sulfides VI and higher than that of keto sulfides based on C_{12}–C_{18}.

For I–VI, the solvate number found by the saturation method is equal to 2 for palladium(II), and hence extraction is accompanied by formation of coordination compounds $PdCl_2L_2$ in the organic phase. At the same time, the slopes of the extraction isotherms show that palladium(II) recovery increases in the order III < IV < II < I < V < VI. Higher extractive power of IV as compared to III is probably caused by the effect of the phenyl substituent in the keto sulfide molecule.

It follows from the gold(III) extraction isotherms (Fig. 2) that its solvate number with I–VI is equal to 1. No reduction of Au(III) during extraction was observed. The extractive power increases in the order VI < IV < III < V < II < I. The extractive power of petroleum sulfides with respect to gold(III) is lower then that of keto sulfides I–IV and VI.

Taking into account the stability and accessibility of the technical-grade TMs for obtaining keto sulfides with high extractive power with respect to palladium(II) and gold(III), we can recommend to use keto sulfide concentrates I and VI in the analytical and hydrometallurgical practice.

CONCLUSIONS

(1) Concentrate of keto sulfides I based on TM-1 (yield 94%) with a high content of keto sulfides (12.2 wt % sulfide sulfur) and no impurities is the most efficient extractant of palladium(II) and gold(III).

(2) The use of low-boiling C_6–C_{10} keto sulfides is preferable for palladium(II) recovery.

REFERENCES

1. Murinov, Yu.I., Maistrenko, V.N., and Afzaletdinova, N.G., *Ekstraktsiya metallov S,N-organicheskimi soedineniyami* (Metal Extraction with S,N-Organic Compounds), Moscow: Nauka, 1993.
2. Potapov, V.V., Khisamutdinov, R.A., Murinov, Yu.I., et al., *Zh. Prikl. Khim.*, 2001, vol. 74, no. 7, pp. 1070–1074.
3. Dronov, V.I. and Nikitin, Yu.E., *Usp. Khim.*, 1985, vol. 54, no. 6, pp. 941–955.
4. Ulendeeva, A.D., Compounds of "Residual" and "Active" Sulfur of Petroleum and Gas Condensates, *Doctoral Dissertation*, Ufa, 1998.
5. Kalimgulova, A.N., Parfenova, M.A., Ulendeeva, A.D., and Lyapina, N.K., *Bashk. Khim. Zh.*, 2004, vol. 11, no. 1, pp. 88–89.
6. Parfenova, M.A., Ulendeeva, A.D., Galkin, E.G., et al., *Neftekhimiya*, 2005, no. 1, pp. 60–62.
7. Klimova, V.A., *Osnovnye mikrometody analiza organicheskikh soedinenii* (Basic Micromethods of Analysis of Organic Compounds), Moscow: Khimiya, 1967.

8. Rubinshtein, I.A., Kleimenova, Z.A., and Sobolev, E.P., in *Metody analiza organicheskikh soedinenii nefti, ikh smesei i proizvodnykh* (Methods of Analysis of Petroleum Organic Compounds, Their Mixtues, and Derivatives), Moscow: Akad. Nauk SSSR, 1960, vol. 1, pp. 74–87.
9. Lyapina, N.K., Obolentsev, R.D., Nikitina, V.S., et al., *Khim. Tekhnol. Topl. Masel*, 1971, no. 12, pp. 5–7.
10. Ulendeeva, A.D., Baeva, L.A., Vasil'eva, E.V., and Lyapina, N.K., *Neftekhimiya*, 1996, vol. 36, no. 3, pp. 266–273.
11. Ginzburg, S.I., Ezerskaya, N.A., Prokof'eva, I.V., et al., *Analiticheskaya khimiya platinovykh metallov* (Analytical Chemistry of Platinum Metals), Moscow: Nauka, 1972.
12. Vydra, F. and Celikovsky, J., *Chem. Listy*, 1957, vol. 51, pp. 768–770.

ISSN 1070-4272, Russian Journal of Applied Chemistry, 2006, Vol. 79, No. 11, pp. 1802–1807. © Pleiades Publishing, Inc., 2006.
Original Russian Text © A.K. Pyartman, V.A. Keskinov, V.V. Lishchuk, A.V. Konstantinova, V.V. Belova, 2006, published in Zhurnal Prikladnoi Khimii, 2006, Vol. 79, No. 11, pp. 1822–1826.

SORPTION AND ION-EXCHANGE PROCESSES

Extraction of Th(IV), La(III), and Y(III) Nitrates with a Composite Solid Extractant Based on a Polymeric Support Impregnated with Trialkylmethylammonium Nitrate

A. K. Pyartman, V. A. Keskinov, V. V. Lishchuk, A. V. Konstantinova, and V. V. Belova

St. Petersburg State Technological Institute (Technical University), St. Petersburg, Russia
Institute of General and Applied Chemistry, Russian Academy of Sciences, Moscow, Russia

Received May 29, 2006

Abstract—Extraction of Th(IV), La(III), and Y(III) from aqueous solutions containing 0–4 M sodium nitrate with a composite solid extractant based on a polymeric support impregnated with trialkylmethylammonium nitrate (Aliquat-336) was studied. The extraction isotherms were analyzed assuming that lanthanides and thorium are extracted with the solid extractant in the form of complexes $(R_4N)_2[Ln(NO_3)_5]$ and $(R_4N)_2[Th(NO_3)_6]$, respectively. The extraction constants were calculated. The joint extraction of Th(IV) and La(III) [Y(III)] with the solid extractant from aqueous salt solutions was studied.

DOI: 10.1134/S1070427206110127

Russian loparite, orthite, and monazite, along with rare-earth metals, usually contain also thorium and uranium as natural radioactive impurity metals. Therefore, the separation of thorium and uranium from rare-earth metals is an urgent technological problem. This problem is usually solved by solvent extraction [1]. Another approach to solution of this problem is the use of composite solid extractants based on a porous support impregnated with a liquid extractant. This technique eliminates certain drawbacks characteristic of common solvent extraction procedures.

The extraction of rare-earth metals(III) [REM(III)] from aqueous solutions containing sodium nitrate (1–5 M) with a composite solid extractant (SE) based on a polymeric support impregnated with trialkylmethylammmonium nitrate (Aliquat-336) was studied in [2]. The extraction isotherms were processed assuming formation of the extractable complex $(R_4N)_2 \cdot [Ln(NO_3)_5]$ in the solid extractant.

No data have been reported on extraction of Th(IV), La(III) and Y(III) nitrates from aqueous solutions containing sodium nitrate with the composite solid extractant based on a polymeric support impregnated with neat trialkylmethylammonium nitrate. Since extraction of these metals with solid extractants is important from both scientific and practical viewpoints, in this study we tried to fill this gap.

The granulated composite solid extractant Purolite D4384 MD 1/5 based on super-cross-linked poly(styrene–divinylbenzene) matrix impregnated with Aliquat-336 [general formula $(C_8H_{17}–C_{10}H_{21})_3CH_3NNO_3$] was used. Its specific volume was 1.93 ± 0.02 dm^3 kg^{-1}. The Aliquat-336 content in the composite solid extractant was 2.33 ± 0.02 mol dm^{-3}. The REM(III) and Th(IV) content in the solid extractant and aqueous phase was determined by the technique similar to that reported in [2–5]. The metal nitrate content in SE (mol kg^{-1}) was recalculated to mol dm^{-3} taking into account the density of the composite solid extractant.

The relative errors in determining REM(III) [Th(IV)] concentration in the aqueous and SE phases were $\pm$(1–3) and $\pm$(1–5) rel. %, respectively. As a rule, each final result was the average from the results of no less than three experiments. The errors in parameter determination are given as the standard deviations.

Figure 1a shows the extraction isotherm of thorium(IV) nitrate from aqueous solutions containing $NaNO_3$ (0–4 M) with SE at pH 1 and 298.15 K. With increasing $NaNO_3$ concentration in the aqueous phase, the thorium content in SE increases and becomes close to $c_s/2$, where c_s is the Aliquat-336 concentration in SE (2.33 ± 0.02 mol/dm^{-3}). This fact suggests

that, in saturation of SE (Aliquat-336) with thorium nitrate, the compound $(R_4N)_2[Th(NO_3)_6]$ is formed.

The extraction of Th(IV) nitrate with TAA nitrate can be described by the equation of the following heterogeneous reaction:

$$Th^{4+}(aq) + 4NO_3^-(aq) + 2R_4NNO_3(o) \rightleftarrows (R_4N)_2[Th(NO_3)_6](o), \quad (1)$$

where (aq) and (o) refer to the aqueous phase and SE, respectively.

The effective extraction constants of Th with Aliquat-336 can be calculated by the equation

$$K_{ex}^{2,0} = \frac{c_{(R_4N)_2[Th(NO_3)_6](o)}}{c_{Th^{4+}(aq)} c_{NO_3^-(aq)}^4 \gamma_\pm^5 c_{R_4NNO_3(o)}^2}, \quad (2)$$

where $c_{i(o)}$ *and* $c_{i(aq)}$ are the equilibrium concentration of components in SE and aqueous phase, respectively, and $\gamma_\pm$ is the mean ionic molar activity coefficient of Th(IV) nitrate in the aqueous phase.

The equilibrium Th concentrations in SE, calculated assuming the occurrence of reaction (1), are listed in the table. The $\gamma_\pm$ values used in these calculations were taken from [3]. The table shows that the calculated Th(IV) concentrations in the solid extractant reasonably agree (within 1–4%) with the experiment. Thus, our model adequately describes the extraction of thorium(IV) nitrate from aqueous solutions with the solid extractant in the systems widely differing in the $Th(NO_3)_4$ concentration in both aqueous and solid extractant phases, with $\log K_{ex}^{2,0} = 2.95 \pm 0.05$.

The influence of the ionic strength of the aqueous phase ($I^\Sigma = 0.5\Sigma c_i Z_i$) on the concentration extraction constants K_{ex}^2 can be estimated by the equation [2]

$$\log K_{ex}^2(I^\Sigma) = \log K_{ex}^{2,0} + \Delta Z^2 F(I^\Sigma) + 10\theta_1 c_{Th^{4+}(aq)} + \theta_2 c_{NaNO_3(aq)}, \quad (3)$$

where ΔZ^2 is the algebraic sum of the charge numbers squared of the ionic species participating in the extraction equilibrium. For the extraction of Th(IV), $\Delta Z^2 = -20$; $F(I^\Sigma)$ is a function of the ionic strength of aqueous solution, e.g., $F(I^\Sigma) = -a(I^\Sigma)^{1/3}$; θ_1 and θ_2 are empirical parameters; $c_{Th^{4+}}$ and c_{NaNO_3} are the equilibrium concentrations of Th(IV) and sodium nitrates in the aqueous phase.

The mathematical treatment of the extraction isotherms was carried out with an algorithm reported in

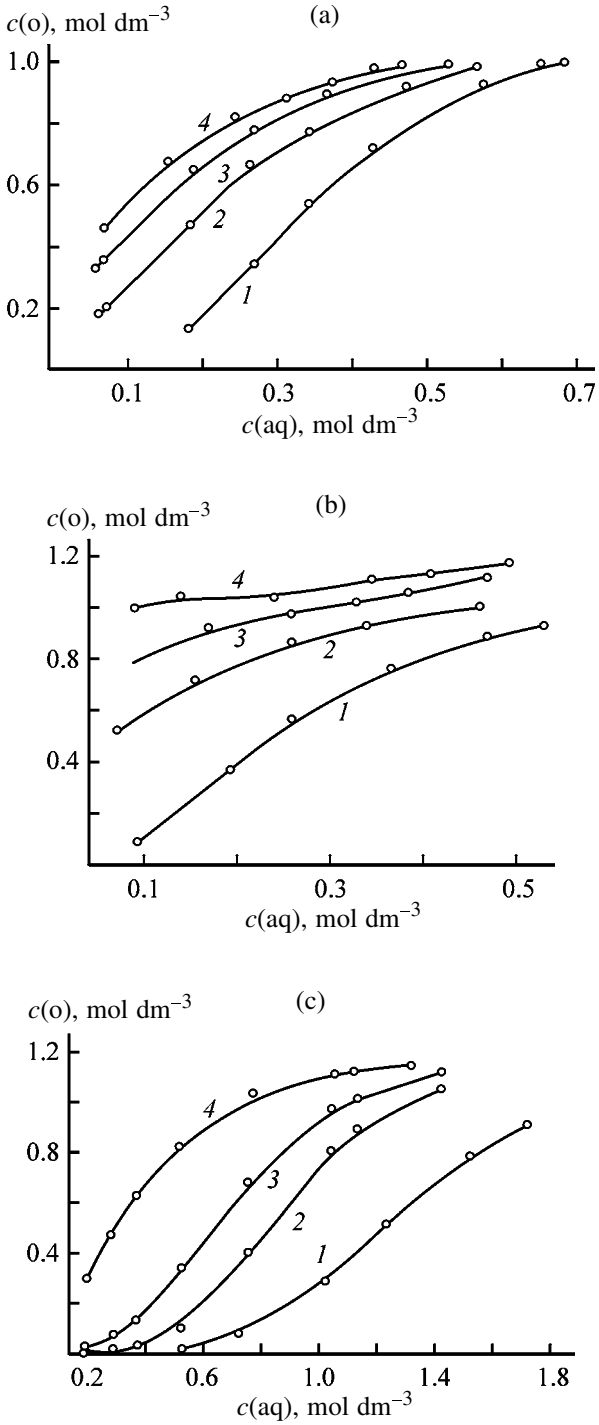


Fig. 1. Extraction isotherms of (a) thorium(IV), (b) lanthanum(III), and (c) yttrium(III) nitrates from aqueous solutions in the absence and in the presence of sodium nitrate with SE (Aliquat-336). [c(aq)] Th(IV), Ln(III), and Y(III) nitrate concentration in the aqueous phase; [c(o)] Th(IV), Ln(III), and Y(III) nitrate concentration in solid extractant; the same for Figs. 2 and 3. Sodium nitrate concentration, mol dm^{-3}: (*1*) 0, (*2*) 1.0, (*3*) 2.0, and (*4*) 4.0.

Results of mathematical processing of data on the extraction of thorium(IV), lanthanum(III), and yttrium(III) nitrates from aqueous solutions with SE(Aliquat-336) at T = 298.15 K

c(aq)	c(o)	c(o) (calc)	Deviation, %	$\{R_4NNO_3\}$(o), mol dm^{-3}	D_{ex}	$\gamma_{\pm}$
mol dm^{-3}						
Thorium(IV)						
0.181	0.132	0.1298	1.67	2.070	0.73	0.233
0.271	0.345	0.3512	–1.79	1.628	1.27	0.209
0.345	0.540	0.5401	–0.01	1.250	1.57	0.199
0.429	0.720	0.7157	0.59	0.899	1.68	0.193
0.576	0.925	0.9174	0.82	0.495	1.61	0.192
0.654	0.990	0.9842	0.58	0.362	1.51	0.194
0.683	0.998	1.0041	–0.61	0.322	1.46	0.196
Lanthanum(III)						
0.093	0.085	0.0875	–2.98	2.155	0.91	0.311
0.192	0.370	0.3767	–1.82	1.576	1.93	0.254
0.259	0.565	0.5581	1.23	1.214	2.18	0.236
0.367	0.760	0.7669	–0.91	0.796	2.07	0.223
0.469	0.890	0.8930	–0.34	0.544	1.90	0.219
0.529	0.930	0.9273	0.29	0.475	1.76	0.210
Yttrium(III)						
0.529	0.020	0.0219	–9.51	2.286	0.04	0.266
0.723	0.080	0.0757	5.31	2.178	0.11	0.271
1.025	0.290	0.2936	–1.24	1.743	0.28	0.300
1.234	0.517	0.5139	0.60	1.302	0.42	0.332
1.525	0.787	0.7870	0.01	0.756	0.52	0.392
1.725	0.910	0.9181	–0.89	0.494	0.53	0.446

Note: c(aq) is the equilibrium concentration of thorium(IV), lanthanum(III), or yttrium(III) nitrate in the aqueous phase; c(o), equilibrium concentration of thorium(IV), lanthanum(III), or yttrium(III) nitrate in the organic phase; c(o) (calc), calculated equilibrium concentration of thorium(IV), lanthanum(III), or yttrium(III) nitrate in the SE phase; deviation means the deviation of the calculated values from the experimental data; $[R_4NNO_3](o)$, equilibrium extractant concentration; D_{ex}, distribution ratio; and $\gamma_{\pm}$, mean ionic molar activity coefficient of thorium(IV), lantanum(III), or yttrium(III) nitrate in the aqueous phase.

[1], taking into account the material balance equations. The prameter a in function $F(I^{\Sigma})$ is equal to 0.155 ± 0.005 at $c_{Th}^{4+} < 0.7$ mol dm^{-3} and 0.139 ± 0.005 at $c_{Th}^{4+} > 0.7$ mol dm^{-3}. Within these thorium concentration ranges θ_1 is 0.345 ± 0.005 and 0.258 ± 0.006, respectively; $\theta_2 = 0 \pm 0.005$.

Figures 1b and 1c show the extraction isotherms of La(III) and Y(III) nitrates from aqueous solutions containing $NaNO_3$ (0–4 M) with SE at pH 2. It is seen that, with increasing $NaNO_3$ concentration in the aqueous phase, the REM content in the SE increases and becomes close to $c_s/2$. This fact suggests that, in saturation of SE(Aliquat-336) with REM nitrate, the compound $(R_4N)_2[Ln(NO_3)_5]$ is formed. The efficiency of extraction of La(III) nitrate is higher than that of Y(III) nitrate. The extraction of Y(III) with SE in the absence of sodium nitrate occurs only at the equilibrium concentration of Y(III) nitrate in the aqueous phase higher than 0.5 mol dm^{-3} (Fig. 1c).

The extraction of REM nitrate with Aliquat-336 can be described by the equation of the following heterogeneous reaction:

$$Ln^{3+}(aq) + 3NO_3^-(aq) + 2R_4NNO_3(o) \rightleftarrows (R_4N)_2[Ln(NO_3)_5](o). \quad (4)$$

The extraction constants of Ln(III) nitrate with Aliquat-336 can be calculated by the equation

$$K_{ex}^{2,0} = \frac{c_{(R_4N)_2[Ln(NO_3)_5](o)}}{c_{Ln^{3+}(aq)} c_{NO_3^-(aq)}^3 \gamma_{\pm}^4 c_{R_4NNO_3(o)}^2}. \quad (5)$$

The equilibrium concentrations of La(III) and Y(III) in the solid extractant, calculated by Eqs. (4) and (5) using $\gamma_\pm$ taken from [2, 3], are listed in the table. The calculated values fairly well agree with the experiment, i.e., our model adequately describes the extraction of REM nitrates from aqueous solutions with the solid extractant; $\log K_{ex}^{2,0}$ is equal to 3.00 ± 0.05 for La and 0.40 ± 0.05 for Y. The extraction constant of La(III) and Th(IV) are close but considerably exceed the extraction constant of Y(III).

The effect of the ionic strength of the aqueous phase on the concentration extraction constants K_{ex}^2 of La(III) and Y(III) nitrates can be expressed by the equation

$$\log K_{ex}^2(I^\Sigma) = \log K_{ex}^{2,0} + \Delta Z^2 F(I^\Sigma) + 6\theta_1 c_{Ln^{3+}(aq)} + \theta_2 c_{NaNO_3(aq)}, \quad (6)$$

where $\Delta Z^2 = -12$, $a = 0.238\pm0.005$, $\theta_1 = 0.451\pm0.005$ for La and 0.579 ± 0.006 for Y; $\theta_2 = 0.400\pm0.005$ for La and 0.602 ± 0.005 for Y.

The joint extraction of Th(IV) and Y(III) nitrates from aqueous salt solutions with SE was also studied. Figure 2 shows the extraction isotherms of Th(IV) nitrate from aqueous solutions containing varied amounts of yttrium nitrate. We found that Y(III) nitrate is not noticeably extracted in the presence of Th(IV) nitrate [Y(III) concentration in the SE phase is less than 0.005 mol dm^{-3}]. With increasing yttrium nitrate concentration in the aqueous phase, the Th(IV) nitrate content in SE becomes close to $c_s/2$ as in the case of extraction of Th(IV) nitrate from $NaNO_3$ containing no Y(III) (Fig. 1a).

The effect of the ionic strength of aqueous solution on the extraction constant K_{ex}^2 of Th(IV) nitrates from its aqueous solutions containing yttrium nitrate is described by the equation

$$\log K_{ex}^2(I^\Sigma) = \log K_{ex}^{2,0} + \Delta Z^2 F(I^\Sigma) + 10\theta_1 c_{Th^{4+}(aq)} + 6\theta_2 c_{Y^{3+}(aq)}, \quad (7)$$

where $\Delta Z^2 = -20$, $a = 0.139\pm0.005$, $\theta_1 = 0.420\pm0.005$, and $\theta_2 = 0.315\pm0.005$.

The joint extraction of Th(IV) and La(III) nitrate from aqueous salt solutions with SE was studied in relation to the Th(IV) nitrate equilibrium content in the aqueous phase at different La(III) nitrate concentrations in the initial solution (Fig. 3).

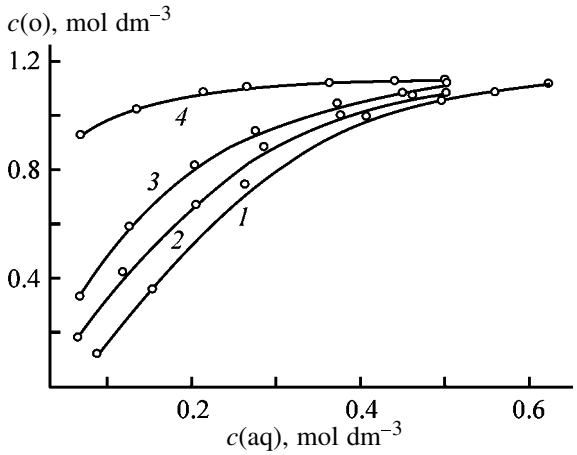


Fig. 2. Th(IV) concentration in the SE vs. its equilibrium concentration in aqueous solutions containing yttrium nitrate. Yttrium nitrate content in the initial aqueous solution (mol dm^{-3}): (*1*) 0.1, (*2*) 0.2, (*3*) 0.3, and (*4*) 1.0.

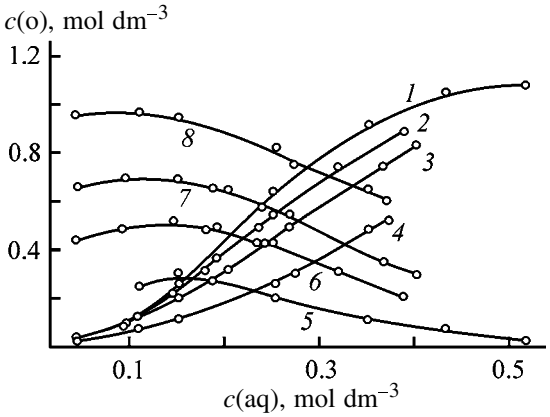


Fig. 3. Extraction of (*1–4*) thorium and (*5–8*) lanthanum nitrate with SE based on Aliquat-336 vs. the equilibrium thorium nitrate concentration in the aqueous phase. Lanthanum nitrate concentration in the initial aqueous solution, mol dm^{-3}: (*1, 5*) 0.1, (*2, 6*) 0.2, (*3, 7*) 0.3, and (*4, 8*) 0.5.

As seen from Fig. 3, in this system both metals are extracted with SE. At thorium(IV) nitrate concentration in the aqueous phase below 0.3 mol dm^{-3}, the extraction of lanthanum(III) nitrate prevails and the La(III) nitrate concentration in the SE increases with an increase in its concentration in the aqueous phase. At the Th(IV) nitrate concentration in the aqueous phase exceeding 0.3 mol dm^{-3}, its extraction predominates and the Th(IV) nitrate content in the SE decreases with increasing La(III) nitrate content in the initial solution (Fig. 3).

The effect of the ionic strength of the aqueous phase on the concentration constant of extraction K_{ex}^2 of Th(IV) nitrate from aqueous solution containing

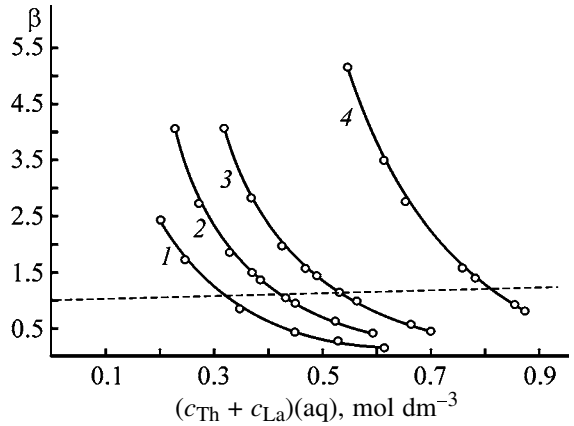


Fig. 4. La/Th separation factor β vs. the total equilibrium concentration of La + Th nitrates in the aqueous phase $(c_{Th} + c_{La})$(aq). La(III) nitrate concentration in the initial solution, mol dm^{-3}: (*1*) 0.1, (*2*) 0.2, (*3*) 0.3, and (*4*) 0.5.

thorium and lanthanum nitrates is expressed by the equation

$$\log K_{ex}^{2}(I^{\Sigma}) = \log K_{ex}^{2,0} + \Delta Z^2 F(I^{\Sigma}) + 10\theta_1 c_{Th^{4+}(aq)} + 6\theta_2 c_{La^{3+}(aq)}, \quad (8)$$

where $\Delta Z^2 = -20$, $a = 0.139 \pm 0.005$, $\theta_1 = 0.690 \pm 0.005$, $\theta_2 = 0.300 \pm 0.005$ at $I^{\Sigma} < 7$ and $\theta_1 = 0.400 \pm 0.005$, $\theta_2 = 0.265 \pm 0.005$ at $I^{\Sigma} > 7$, $\log K_{ex}^{2,0} = 2.95 \pm 0.06$.

The concentration constant of extraction of La(III) from aqueous solutions containing Th(IV) and La(III) nitrate can be calculated by Eq. (8). In this case, $\Delta Z^2 = -12$, $a = 0.238 \pm 0.005$, $\theta_1 = 0.500 \pm 0.005$, $\theta_2 = 0.500 \pm 0.05$; $\log K_{ex}^{2,0} = 3.00 \pm 0.06$.

Figure 4 shows dependence of the separation factor of lanthanum from thorium on the total equilibrium concentration of Th(IV) and La(III) nitrates in the initial aqueous solution containing variable amounts of La(III) nitrate. It is seen that the La/Th separation factor β significantly depends on both the total content of these metals in solution and their ratio. The highest La/Th separation factor (β = 5) is attained at low thorium nitrate and high lanthanum nitrate concentrations in the aqueous phase. For certain systems, β becomes equal to unity, i.e., the separation of La from Th disappears (see the boundary line of inversion of the separation factor in Fig. 4). At low equilibrium lanthanum nitrate concentration and high thorium nitrate concentration in the aqueous phase, the Th/La separation factor becomes equal to approximately five. The expression for the La/Th separation factor can be obtained by combination of Eq. (2) and Eq. (5):

$$\beta_{La/Th} = \frac{K_{ex,La}^{2,0} \gamma_{La\pm}^{4}}{K_{ex,Th}^{2,0} c_{NO_3^-(aq)}^{5} \gamma_{Th\pm}^{5}}. \quad (9)$$

This equation shows that, at small difference between the extraction constants of La and Th nitrates, the La/Th separation factor is controlled by the concentration of nitrate anion in the aqueous phase and the ratio of the mean ionic molar activity coefficients of La^{3+} and Th^{4+} risen to the corresponding power.

The composite solid extractant based on a polymeric support impregnated with neat trialkylmethylammonium nitrate can be used for purification of concentrated solution of La(III) nitrate to remove Th(IV) impurities, and, vice versa, for purification of concentrated solutions of Th(IV) nitrate to remove La(III) impurities. This solid extractant is also suitable for purification of Y(III) nitrate to remove Th(IV) nitrate impurities.

CONCLUSIONS

(1) The extraction isotherms of REM(III) and Th(IV) nitrate with a composite solid extractant based on a polymeric support impregnated with trialkylmethylammonium nitrate can be analyzed assuming that lanthanides and thorium nitrates are extracted in the form of complexes $(R_4N)_2[Ln(NO_3)_5]$ and $(R_4N)_2[Th(NO_3)_6]$, respectively. The extraction constants were calculated.

(2) In joint extraction of Th(IV) and Y(III) nitrates from aqueous salt solutions with a solid extractant, Y(III) nitrate is not noticeably extracted in the presence of Th(IV) nitrate. With increasing Y(III) nitrate concentration in the aqueous phase, the extraction of Th(IV) nitrate with the solid extractant increases.

(3) In joint extraction of Th(IV) and La(III) nitrates from aqueous salt solutions containing different amounts of Th(IV) and La(III), both metals are recovered with the solid phase, and the La/Th separation factor significantly depends on the Th(IV) and La(III) concentration and the Th(IV) : La (III) ratio in the aqueous phase.

(4) The composite solid extractant based on the polymeric support impregnated with neat trialkylmethylammonium nitrate can be used for purification of concentrated solution of La(III) nitrate to remove Th(IV) impurities, and, vice versa, for purification of concentrated solutions of Th(IV) nitrate to remove La(III) impurities. This extractant is also suitable for

purification of Y(III) nitrate to remove Th(IV) nitrate impurities.

ACKNOWLEDGMENTS

This study was financially supported by the Russian Foundation for Basic Research (project no. 04-03-32 580).

REFERENCES

1. Mikhailichenko, A.I., Mikhlin, E.B., and Patrikeev, Yu.B., *Redkozemel'nye metally* (Rare-Earth Metals), Moscow: Metallurgiya, 1987.
2. Pyartman, A.K., Keskinov, V.A., Mikhailenko, M.A., et al., *Radiokhimiya*, 2004, vol. 46, no. 3, pp. 240–242.
3. Pyartman, A.K., Kopyrin, A.A., Berinskii, A.E., and Keskinov, V.A., *Radiokhimiya*, 2000, vol. 42, no. 2, pp. 128–130.
4. Přibil, R., *Analytical Applications of EDTA and Related Compounds*, Oxford: Pergamon, 1972.
5. Pyartman, A.K., Lishchuk, V.V., and Keskinov, V.A, *Radiokhimiya*, 2006, vol. 48, no. 3, pp. 252–255.

ISSN 1070-4272, Russian Journal of Applied Chemistry, 2006, Vol. 79, No. 11, pp. 1816–1819. © Pleiades Publishing, Inc., 2006.
Original Russian Text © V.I. Dzhabarov, A.A. Knyazev, Yu.G. Galyametdinov, 2006, published in Zhurnal Prikladnoi Khimii, 2006, Vol. 79, No. 11, pp. 1836–1839.

APPLIED ELECTROCHEMISTRY AND CORROSION PROTECTION OF METALS

Lanthanide Tris(β-diketonates) as Ionophores for Chloride Ion-Selective Electrodes

V. I. Dzhabarov, A. A. Knyazev, and Yu. G. Galyametdinov

Kazan State Technological University, Kazan, Tatarstan, Russia

Received April 26, 2006

Abstract—Lanthanide tris(β-diketonates) were used as ionophores for plasticized polymer membranes of ion-selective electrodes. Electrochemical properties of the membranes were characterized, and the possibility of their use as components of chloride ion-selective electrodes was studied.

DOI: 10.1134/S1070427206110140

Surface waters and wastewaters are analyzed using various chemical, physical, and physicochemical methods. Currently used analytical methods and devices for monitoring the composition of surface waters and wastewaters are either too expensive or insufficiently prompt. There is a great need in developing sensors for prompt analysis of the ionic composition of aqueous solutions, including chemical sensors such as electrodes with ion-selective plasticized membranes. The use of ion-selective membrane electrodes is confined by the complexity of synthesis of sufficiently selective and sensitive ionophores as their basic components. Among the most efficient ionophores used in ion-selective electrodes are quaternary ammonium salts [1–3], vitamin B_{12} derivatives [4], metal porphyrins [5–7], and fluorinated polyethers [8].

Because of their high selectivity, ionophores based on lanthanide tris(β-diketonates) are of particular interest [9]. However, there is only limited information on the dependences of the selectivity and other electrode characteristics of these compounds on the composition and properties of aqueous solutions.

In this study we used lanthanide tris(β-diketonates) as ionophores for plasticized polymer membranes of ion-selective electrodes for prompt analysis of various aqueous systems for chloride.

EXPERIMENTAL

Lanthanide tris(β-diketonates) were synthesized from the corresponding lanthanide chlorides and β-diketones (Aldrich). For preparation of the membranes, we used THF after purification.

Tris(1,1,1-trifluoro-2,4-pentanedionato)europium (TPE). An aqueous-alcoholic solution containing 9 ml of H_2O and 9 ml of 95% EtOH was heated to 50°C. $EuCl_3 \cdot 6H_2O$ (0.122 g, 0.33 mmol) was added with stirring to obtain a clear solution. To the resulting solution, 1,1,1-trifluoro-2,4-pentanedione (0.154 g, 1 mmol) was added, and pH was adjusted to 6.5 by adding ammonia dropwise. White crystals were filtered off and vacuum-dried over P_2O_5. Yield 0.147 g (68%); mp 142–146°C.

Found, %: C 28.58, H 2.19, O 19.78, F 26.99, Eu 24.19.

$C_{15}H_{14}O_7F_9Eu$.

Calculated, %: C 28.63, H 2.24, O 17.79, F 27.17, Eu 24.15.

IR (ν, cm^{-1}): 1620 (C=O), 1280 (C–F), and 410 (Eu–O).

Tris(4,4,4-trifluoro-1-phenyl-1,3-butanedionato)-europium (PBE) was prepared by adding dropwise $EuCl_3 \cdot 6H_2O$ (0.216 g, 1 mmol) to a hot alcoholic solution containing 4,4,4-trifluoro-1-phenyl-1,3-butanedione (0.122 g, 0.33 mmol) with stirring. Then aqueous ammonia was added to adjust pH to 6.5. The precipitated white solid was filtered off, washed with alcohol, and vacuum-dried over P_2O_5. Yield 0.493 g (59.18%); mp 130–134°C.

Found, %: C 45.11, H 2.57, O 12.08, F 21.41, Eu 19.03.

$C_{30}H_{18}O_6F_9Eu$.

Calculated, %: C 45.17, H 2.59, O 12.04, F 21.44, Eu 19.06.

IR (ν, cm^{-1}): 1660 (C_6H_5), 1622 (C=O), 1282 (C–F), and 414 (Eu–O).

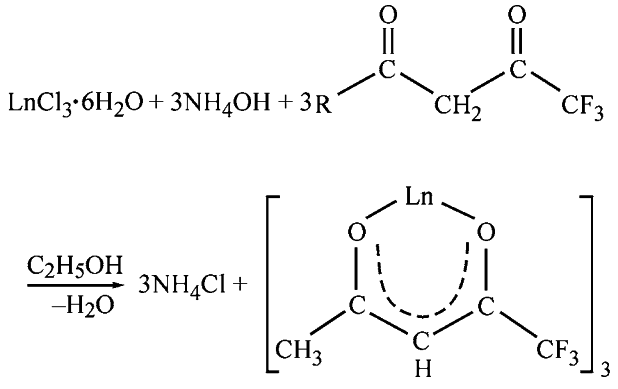
The IR spectra were recorded on a Perkin–Elmer 16 PC FTIR spectrometer using the KBr technique.

The ion-selective membranes were prepared as follows: PVC powder (0.01923 g, 31 wt %), ionophore (0.002 g, 3.3 wt %), sodium tetraphenylborate as a lipophilic ionic additive (0.0002 g, 0.3 wt %), and dioctyl phthalate as a plasticizer (0.03917 g, 64.7 wt %) were dissolved in THF in a 20-ml weighing bottle. The components were weighed on a VLR-20 balance to within 5×10^{-5} g. The resulting solution was cast into a glass mold 1 cm in diameter and allowed to stand for 24 h until complete removal of THF. As a result, an elastic transparent membrane 0.3–0.5 mm thick was obtained.

From the membrane, a circle 6–7 mm in diameter was cut off and then glued to the face of a PVC tube 50 mm long and 5 mm in diameter using a solution of PVC in THF as an adhesive. 0.01 M NaCl was used as an inner electrolyte. The inner electrode (AgCl/Ag) was fixed inside the PVC tube using silicone paste. Three membrane electrodes were prepared for each ionophore.

The potentiometric measurements were carried out with a pH-150 pH–millivoltmeter.

Using the procedure described in [10], we synthesized four complexes with the general formula LnL_3 (Ln = Dy, Eu; L = 1,1,1-trifluoro-2,4-pentanedionate, 4,4,4-trifluoro-1-phenyl-1,3-butanedionate). The route to the tris(β-diketonates) is shown in the scheme below.



The complexes were synthesized in aqueous–alcoholic solutions. The solution with the precipitated solid was stirred for 15 min and then the precipitate was filtered off. All the complexes are white, except for dysprosium tris(1,1,1-trifluoro-2,4-pentanedionate) which is pale-orange.

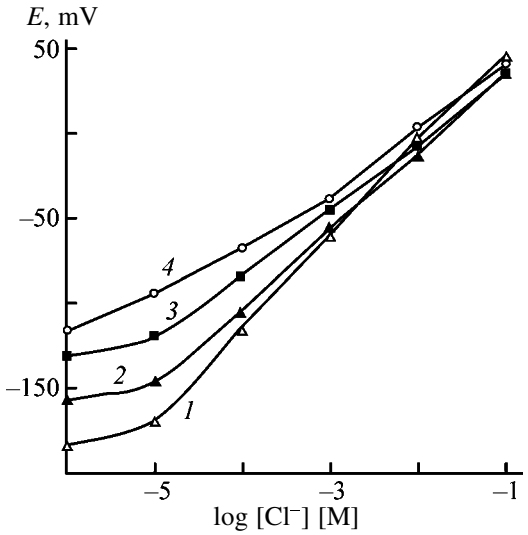


Fig. 1. emf E as a function of the chloride concentration. Ionophore: (*1*) PBE, (*2*) TPE, (*3*) PBD, and (*4*) TPD.

The structure of the complexes was derived from the elemental composition and IR spectra.

The ionophore-based membranes were prepared according to the procedure described in [9].

The emf vs. log[Cl] curves for the investigated electrodes are presented in Fig. 1. The highest slope of the electrode function was obtained for the PBE-based membrane (54 mV/decade). The detection limit of this electrode with respect to the chloride ion was found to be 10^{-5} M. The slopes of the electrode function of the other electrodes are as follows (mV/decade): 34 dysprosium tris(1,1,1-trifluoro-2,4-pentanedionate) (TPD), 34 dysprosium tris(4,4,4-trifluoro-1-phenyl-1,3-butanedionate) (PBD), and 46 TPE.

To characterize the selectivity of the membranes, we performed potentiometric measurements in NaCl solutions containing foreign anions such as I^-, Br^-, ClO_4^-, CH_3COO^-, NO_3^-, CO_3^{2-}, and SO_4^{2-}. The results obtained for the PBE-based electrode are given in Fig. 2.

The PBE-based electrode demonstrates the highest selectivity among the electrodes studied. For all the electrodes, the most interfering anion was bromide ($\log K_{A/B} = -1.6$).

The selectivity coefficients of the PBE-based electrode were determined at constant concentration of interfering anions (10^{-2} M) and variable concentration of chloride. In the table, the selectivity coefficients of our PBE-based electrode are compared with published data for electrodes based on various ionophores [8, 9,

Selectivity coefficients $K_{A/B}$ for membranes with various ionophores

Interfering ion B	$\log K_{A/B}$ for indicated ionophore				
	(5,10,15,20-tetraphenylporphyrinato)Mn(III) chloride [11]	trisdodecylmethylammonium chloride [12]	MC [8]	europium tris(2,2-dimethyl-6,6,7,7,8,8,8-heptafluorooctane-3,5-dionate) [9]	PBE
I^-	+2.4	+2.8	+2.3	–2.71	–2.0
Br^-	+0.9	+0.6	+1.0	–1.19	–1.6
ClO_4^-	–3.6	+4.6	–2.8	–2.94	–3.0
NO_3^-	+1.2	–	–2.7	–3.34	–3.0
CO_3^{2-}	–	–	–	–3.97	–2.9
SO_4^{2-}	–	–	–	–4.02	–3.2

11, 12]. As seen, the PBE-based electrode demonstrates higher selectivity with respect to the chloride ion.

Since pH of natural waters and, particularly, process solutions can vary over a wide range, we studied the pH effect on the electrode function of the PBE-based electrode (Fig. 3). As seen, the pH effect is insignificant over the pH range from 5 to 9, allowing the use of this electrode for environmental monitoring.

We also studied the stability of the potential of the PBE-based electrode in time. It was demonstrated that the electrode potential in 0.01 M NaCl is stable for 2 months.

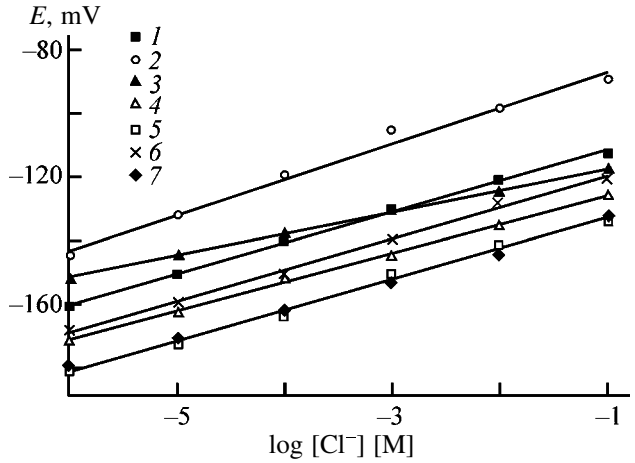


Fig. 2. emf E as a function of the chloride concentration for the PBE-based electrode in solutions containing interfering anions: (*1*) I^-, (*2*) Br^-, (*3*) ClO_4^-, (*4*) CH_3COO^-, (*5*) NO_3^-, (*6*) CO_3^{2-}, and (*7*) SO_4^{2-}.

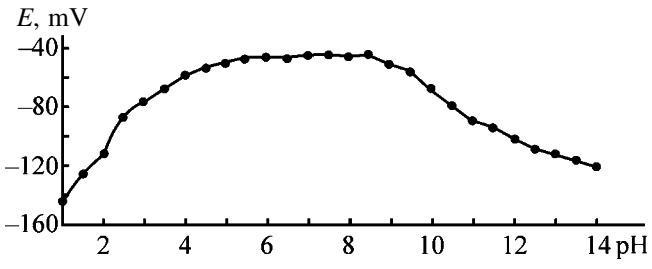


Fig. 3. emf of PBE electrode E as a function of pH.

CONCLUSION

The investigated lanthanide tris(β-diketonates) can be used as ionophores for membranes of ion-selective electrodes. All the ionophores studied demonstrate high selectivity and sensitivity over a wide concentration range and low detection limit with respect to the chloride ions. The best electrode characteristics were obtained with europium tris(4,4,4-trifluoro-1-phenyl-1,3-butanedionate). Electrode with this ionophore can be used a chloride-sensitive sensor for analysis of various aqueous systems.

ACKNOWLEDGMENTS

The study was financially supported by the Russian Foundation for Basic Research (project 04-03-32923).

REFERENCES

1. Worting, V.J., Johonson, D.M., and Bachas, L.G., *Anal. Chem.*, 1990, vol. 62, no. 14, pp. 1506–1509.
2. Nomura, S., *Analyst*, 1995, vol. 120, pp. 503–504.
3. Ozawa, S., Miyagi, H., Sahibata, Y., et al., *Anal. Chem.*, 1995, vol. 68, pp. 4149–4152.
4. Schulthess, P., Ammann, D., Simon, W., et al., *Helv. Chim. Acta*, 1984, vol. 67, pp. 1026–1032.

5. Park, S.B., Matuszewski, W., Meyerhoff, M.E., et al., *Electroanalysis*, 1991, no. 3, p. 909.
6. Wang, E. and Meyerhoff, M.E., *Anal. Lett*., 1993, vol. 26, p. 1519.
7. Badr, I.H.A., Meyerhoff, M.E., and Hassan, S.S.M., *Anal. Chim. Acta*, 1996, vol. 321, pp. 11–19.
8. Siswanta, D., Takenaka, J., Suzuki, T., et al., *Chem. Lett*., 1997, p. 195.
9. Rakest, K.M., Kaur, I., Kaur, R., et al., *Anal. Chem*., 2004, vol. 76, pp. 7354–7359.
10. Lyle, S.J. and Witts, A.D., *Inorg. Chim. Acta*, 1971, no. 5, p. 481.
11. Simon, W., Kondo, Y., Buhrer, T., et al., *Pflugers. Arch*., 1989, vol. 414, p. 663.
12. Chaniotakis, N.A., Chasser, A.M., and Meyerhoff, M.E., *Anal. Chem*., 1988, vol. 60, pp. 185–188.

ISSN 1070-4272, Russian Journal of Applied Chemistry, 2006, Vol. 79, No. 11, pp. 1820–1824. © Pleiades Publishing, Inc., 2006.
Original Russian Text © V.I. Karavaev, I.L. Korobova, Yu.V. Litovka, 2006, published in Zhurnal Prikladnoi Khimii, 2006, Vol. 79, No. 11, pp. 1840–1843.

APPLIED ELECTROCHEMISTRY AND CORROSION PROTECTION OF METALS

Calculation of the Most Uniform Electroplated Coating with Account of Changes in the Concentration of Electrolyte Components

V. I. Karavaev, I. L. Korobova, and Yu. V. Litovka

Tambov State Technical University, Tambov, Russia

Received May 6, 2006

Abstract—The problem of optimization of the electroplating process by the nonuniformity criterion with account of the effect of changes in the concentration of electrolyte components on the polarization is formulated and solved.

DOI: 10.1134/S1070427206110152

One of the most important quality parameters of an electroplated coating is the uniformity of metal distribution over the article surface. The uniformity depends on the configuration of an electrolytic cell (shape, size, and relative position of electrodes) and on the electrochemical component (polarization phenomena). The effect of these factors on the coating uniformity has been extensively studied [1, 2]. However, the influence of the concentration of electrolyte components on the polarization and, consequently, on the uniformity of electroplated coatings has been insufficiently studied. At the same time, the concentration of electrolyte components varies with time because of the carry-over of the electrolyte with processed articles, consumption of these components by electrochemical and chemical reactions, and electrolyte evaporation.

In many cases, the polarization strongly depends on the concentration of the electrolyte components. It was shown in [3] that the concentration of ammonium ions affects the run of the overall polarization curves in electrodeposition of a nickel–molybdenum alloy. In [4], polarization curves obtained at various concentrations of lead ions in the cyanide electrolyte in electrodeposition of gold were reported. It was demonstrated in [5–8] that polarization curves depend on the concentration of various electrolyte components in zinc-, cadmium-, tin-, rhodium-, nickel-, and silver-plating. In all of these examples, the overvoltage changes by 10–20% when the concentration of electrolyte components varies.

In this study, the influence exerted by the concentration of electrolyte components on the coating uniformity is examined and electrical parameters of the electroplating bath that provide the highest coating uniformity at varied electrolyte concentration are sought for.

The coating nonuniformity factor R is defined by the formula

$$S_c = \frac{1}{S_c}\int_{S_c}\frac{\delta(x, y, z) - \delta^{min}}{\delta^{min}}dS_c, \qquad (1)$$

where S_c is the cathode surface area; $\delta(x, y, z)$, coating thickness at a certain point of the cathode, with the coordinates (x, y, z); and δ^{min}, minimum coating thickness on the cathode.

The optimization problem is formulated as follows.

Let the concentration of a component that affects the polarization be c at a certain instant of time (the concentration can be measured or calculated in terms of a mathematical model [9]). It is necessary to find the voltage U applied to the bath, at which the coating nonuniformity (1) is at a minimum.

To relate the criterion R to the concentration c, we use a set of equations of the mathematical model, which will have the following form.

The coating thickness at a certain point (x, y, z) on the cathode surface S_c is calculated by the formula derived from the Faraday law:

$$\delta(x, y, z) = \frac{E\, i(x, y, z)\, \eta\, \tau}{\rho}, \qquad (2)$$

where E is the electrochemical equivalent of the substance; τ, process duration; ρ, substance density; $i(x, y, z)$, current density at a point (x, y, z) of the article; and η, cathode current efficiency.

The current density at the electrodes is calculated by Ohm's law in the differential form:

$$i(x, y, z) = -\chi \frac{\partial \varphi(x, y, z)}{\partial n} \Big| S_c, \quad (3)$$

where χ is the electrical conductivity of the electrolyte; φ, potential of the electric field; n, normal to the surface S_c of the cathode at a point (x, y, z); $\partial\varphi(x, y, z)/\partial n$, vector of the field of potentials in the normal direction.

The potential distribution over the volume of the electrolytic cell satisfies the Laplace equation

$$\partial^2\varphi(x, y, z)/\partial x^2 + \partial^2\varphi(x, y, z)/\partial y^2 + \partial^2\varphi(x, y, z)/\partial z^2 = 0. \quad (4)$$

The boundary conditions for Eq. (4) have the form:

(1) at the electrolyte–insulator interface:

$$\partial^2\varphi(x, y, z)/\partial n \,|\, S_b = 0, \quad (5)$$

where S_b is the insulator surface.

This equation means that no current flows through the insulator, i.e., there is no potential difference across the interface with the insulator.

(2) at the electrolyte–anode interface:

$$\varphi(x, y, z) + F_a[i(x, y, z)] \,|\, S_a = U, \quad (6)$$

where $F_a[i(x, y, z)]$ is a function of the anodic polarization; S_a, anode surface; and U, voltage across the anode and cathode.

(3) at the electrolyte–cathode interface:

$$\varphi(x, y, z) - F_c[i(x, y, z), c] \,|\, S_c = U, \quad (7)$$

where $F_c[i(x, y, z), c]$ is a function of the cathodic polarization.

The coating thickness is subject to the following limitation:

$$\delta(x, y, z) \geq \delta^{min}. \quad (8)$$

The basic equation for calculation of the electric field in the electrolyte is the Laplace equation. To obtain the distributions of the potentials and coating thickness, we use a combination of the methods of upper relaxation [10] and simple iterations [11] to provide that the boundary conditions (6) and (7) are satisfied.

We are going to search for the optimal solution by the method of internal penalty functions [12].

Let us consider as an example of implementation of the procedure suggested the problem of calculation of the most uniform coating for zinc plating in an alkaline electrolyte.

The experimental plots of cathodic polarization curves $F_c^{exp}(i, c)$ obtained at various zinc concentrations c in an alkaline electrolyte used in the experiments were reported in [5]. In calculations, it is more convenient to have an approximating analytical expression. Let us seek the approximating function in the form of a polynomial of two variables $F_c^{calc}(c, i) = a_1 + a_2c + a_3ci + a_4ci^2 + a_5c^2 + a_6c^2i + a_7i + \ldots$. The coefficients a_c of the polynomial are found by minimizing the error function ε (%):

$$\varepsilon = \{n^{-1}\sum_{j=1}^{n}[F_c^{exc}(j) - F_c^{calc}(j)]^2/[F_c^{exc}(j)]^2\}^{1/2} \times 100,$$

where j is the number of a point on a plot; n, number of points; $F_c^{exp}(j)$ and $F_c^{calc}(j)$, experimental and calculated values of the function.

Raising the number of terms in the polynomial and its order, we obtain an error ε smaller than 10% (10% is the accuracy of the MIP-10 nondestructive testing device for measuring the coating thickness, used to verify the adequacy of the mathematical model).

The result of the approximation is a follows:

$$F_c^{calc}(c, i) = -1.29 + 0.795c - 0.016ci - 0.00996ci^2 - 1.642c^2 + 1.6c^2i - 0.288i, \quad (9)$$

with $\varepsilon = 3.75\%$.

The plot of the approximating function obtained is shown in Fig. 1.

To confirm the adequacy of the analytical mathematical model we constructed, we compared the results of calculation of the coating thickness on cathodes-articles with the experimental data we obtained.

The relative root-mean-square error Δ (%) was calculated by the formula

$$\varepsilon = \{n^{-1}\sum_{j=1}^{n}[\delta^{exc}(i) - \delta^{calc}(i)]/\delta^{exc}(i)\}^{1/2} \times 100, \quad (10)$$

where i is the point number; n, number of points; δ^{exp}

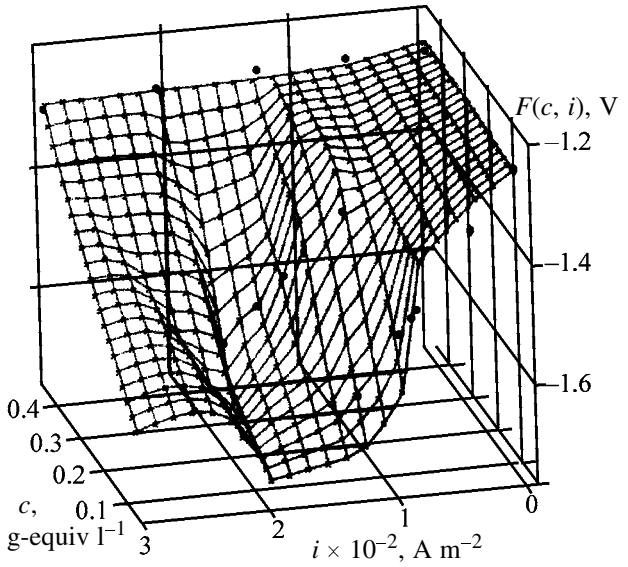


Fig. 1. Plot of the approximating function $F(c, i)$ obtained. (i) Current density and (c) Zn(II) concentration.

and δ^{calc}, experimental and calculated coating thicknesses at ith point.

In the first experiment, a zinc coating was deposited in an industrial electroplating bath. The electrolytic cell had dimensions of 750 × 1100 × 1300 mm; electrolyte level 1120 mm; four rectangular 250 × 500-mm anodes, with a 250 × 370-mm part submerged in the electrolyte; cathode, planar rectangular 270 × 140-mm plate (Fig. 2a); temperature 17°C; current strength 25 A; voltage 1.25 V; coating deposition time 20 min; electrolyte composition (g l^{-1}): ZnO 8–10, NaOH 140–150, Ekomet Ts1 3–4, and Na_2CO_3 35–40. The coating thickness was measured with an MIP-10 nondestructive testing device.

The following values were used in the calculation: current efficiency 100%, zinc density 7133 kg m^{-3}, electrical conductivity 0.118 Ω^{-1} cm^{-1} (found experimentally), electrochemical equivalent 3.39×10^{-7} kg (A s)$^{-1}$, ZnO concentration taken to be 9 g l^{-1} (0.221 g-equiv l^{-1}).

The conditions of the second experiment were as follows: 750 × 1100 × 1300-mm electrolytic cell, electrolyte level 1120 mm; two rectangular 230 × 500-mm anodes and two rectangular 270 × 500-mm anodes (the latter two extend beyond the electrolyte level and, therefore, their height is regarded to be 370 mm); cathode 1 in the form of a 90 × 140-mm angle and cathode 2, as a 50 × 190-mm angle (Fig. 2b); temperature 17°C; current strength 25 A; voltage 3 V; coating deposition time 30 min; electrolyte composition

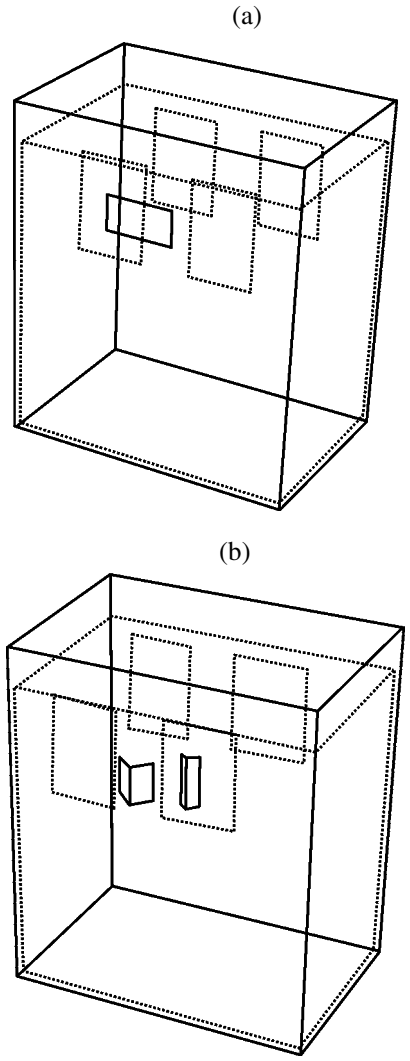


Fig. 2. Schematic of the electroplating bath. Experiment: (a) first and (b) second.

(g l^{-1}): ZnO 10–11, NaOH 170–180, Na_2CO_3 43–44. The coating thickness on the first article (90 × 140-mm angle) was measured. This article is constituted by two identical plates mounted at an angle of 90°. The coating thickness was measured with an MIP-10 nondestructive testing device.

The following values were used in the calculation: current efficiency 100%, zinc density 7133 kg m^{-3}, electrical conductivity 0.118 Ω^{-1} cm^{-1} (found experimentally), electrochemical equivalent 3.39×10^{-7} kg (A s)$^{-1}$, ZnO concentration taken to be 10.5 g l^{-1} (0.258 g-equiv l^{-1}).

In the calculations, the anodic polarization function $F_a[i(x, y, z)] = 0$, i.e., the anodic overvoltage was taken to be zero.

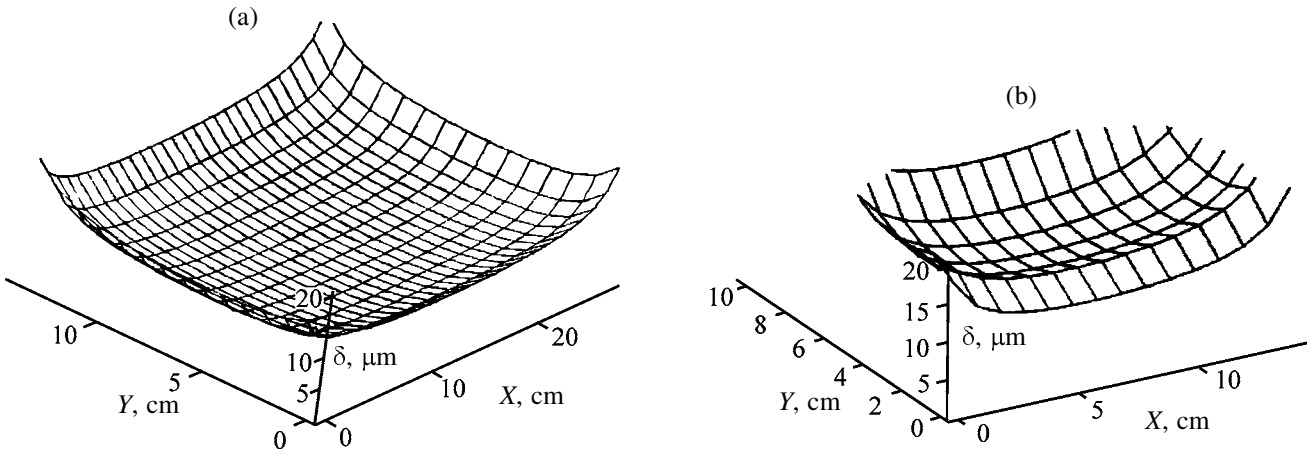


Fig. 3. Calculated coating thickness distribution $\delta(X, Y)$ (a) in the first experiment and (b) in the second experiment (first plate of the 90 × 140-mm angle).

Figures 3a and 3b show the coating thickness distribution over the cathode surface, calculated in terms of the mathematical model for the first and second experiments, respectively. The experimental and calculated coating thickness distributions over the cathode surface for a section with a plane parallel to $x0\delta$ are shown in Figs. 4a and 4b. Comparison of the calculated and experimental coating thicknesses at different points of the articles being coated shows their good agreement. The error calculated by formula (10) was 12.808% for the first experiment and 12.161% for the second, which indicates that mathematical model has a practically acceptable accuracy and is adequate.

It should be noted that the current density i is the current density at a cathode point (x, y, z), rather than the average current density. In the first experiment, for example, the current density $i^{min} = 0.7$ A dm^{-2} for a point with the minimum coating thickness $\delta^{min} = 4$ μm and $i^{max} = 3$ A dm^{-2} for the point with the maximum coating thickness $\delta^{max} = 17$ μm.

On confirming the validity of the model, we found the optimal voltage to be applied to the bath.

The problem was solved using the geometric parameters taken from the first experiment at various concentrations c_{ZnO}. The minimum coating thickness was taken to be 9 μm [8], and the time of coating deposition was 20 min. We obtained the following optimal voltages and the corresponding nonuniformity factors:

ZnO concentration, g l^{-1}	U, V	δ^{min}, μm	R_{min}
17.5	1.83	9.871	0.58038
9.0	2.03	9.911	0.5802962
6.0	2.21	9.952	0.580176

Thus, the voltage that provides the minimum nonuniformity varies rather strongly with the concentration (within 10–20%).

The effect of a change in the concentration can be illustrated as follows. If, for example, we use $U = 1.83$ V, calculated for $c_{ZnO} = 17.5$ g l^{-1}, then the minimum coating thickness and nonuniformity factor will be $\delta^{min} = 8.281$ μm and $R_{min} = 0.5806289$ at $c_{ZnO} = 9$ g l^{-1}, and $\delta^{min} = 7.968$ μm and $R_{min} = 0.5806933$ at $c_{ZnO} = 6$ g l^{-1}.

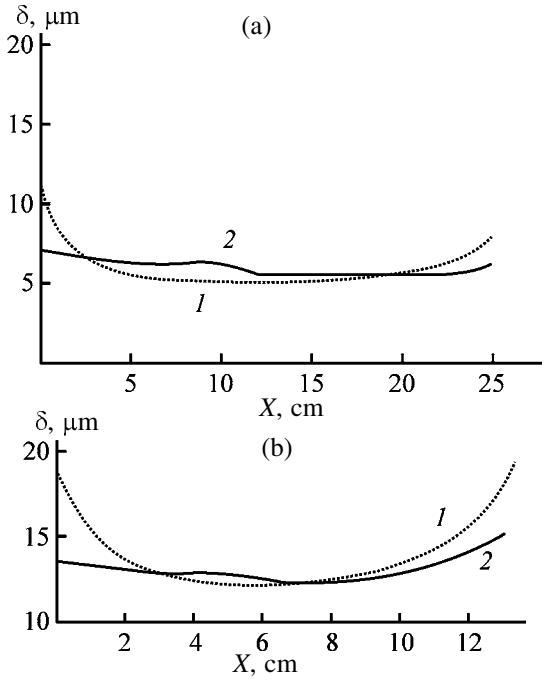


Fig. 4. Coating thickness δ along the X axis at (a) $Y = 6$ cm in the first experiment and (b) $Y = 4$ cm in the second experiment (first plate of the 90 × 140-mm angle). (*1*) Calculation and (*2*) experiment.

CONCLUSIONS

(1) The adequacy of the mathematical model developed is confirmed.

(2) Disregarding the influence exerted by changes in concentration on the polarization may lead to essentially negative results, such as deterioration of the coating uniformity and failure to satisfy the limitation on the minimum coating thickness.

REFERENCES

1. Kadaner, L.I., *Ravnomernost' gal'vanicheskikh pokrytii* (Uniformity of Electroplated Coatings), Kharkov: Khar'k. Gos. Univ., 1961.
2. Ivanov, V.T., *Elektrokhimiya*, 1972, vol. 8, pp. 1654–1658.
3. Kuznetsov, V.V., Pavlov, M.R., Cheleneva, S.A., and Kudryavtsev, V.A., *Elektrokhimiya*, 2005, vol. 41, pp. 83–89.
4. Bek, R.Yu. and Shuraeva, L.I., *Elektrokhimiya*, 2004, vol. 40, pp. 805–809.
5. Kudryavtsev, N.T., *Elektroliticheskie pokrytiya metallami* (Electrolytic Metal Coatings), Moscow: Khimiya, 1979.
6. Lainer, V.I., *Sovremennaya gal'vanotekhnika* (Modern Electroplating), Moscow: Metallurgiya, 1967.
7. Vainer, Ya.V. and Dasoyan, M.A., *Tekhnologiya elektrokhimicheskikh pokrytii* (Technology of Electrochemical Coatings), Leningrad: Mashinostroenie, 1972.
8. Mel'nikov, P.S., *Spravochnik po gal'vanopokrytiyam v mashinostroenii* (Reference Book of Electroplated Coatings in Machine Building), Moscow: Mashinostroenie, 1991.
9. Litovka, Yu.V., *Zh. Prikl. Khim.*, 1997, vol. 70, pp. 1631–1637.
10. Samarskii, A.A. and Nikolaev, E.S., *Metody resheniya setochnykh uravnenii* (Methods for Solution of Finite-Difference Equations), Moscow: Nauka, 1978.
11. Boyarinov, A.N. and Kafarov, V.V., *Metody optimizatsii v khimicheskoi tekhnologii* (Optimization Methods in Chemical Technology), Moscow: Khimiya, 1975.
12. Himmelblau, D.M., *Applied Nonlinear Programming*, New York: Wiley, 1972.

ISSN 1070-4272, Russian Journal of Applied Chemistry, 2006, Vol. 79, No. 11, pp. 1825–1828. © Pleiades Publishing, Inc., 2006.
Original Russian Text © V.V. Volynskii, A.V. Lopashev, I.A. Kazarinov, S.V. Grishin, N.A. Solov'ev, 2006, published in Zhurnal Prikladnoi Khimii, 2006, Vol. 79, No. 11, pp. 1844–1847.

APPLIED ELECTROCHEMISTRY AND CORROSION PROTECTION OF METALS

Processing of Cadmium(II) Wastes from Battery Industry

V. V. Volynskii, A. V. Lopashev, I. A. Kazarinov, S. V. Grishin, and N. A. Solov'ev

AIT Plant, Joint-Stock Company, Saratov, Russia
Saratov State University, Saratov, Russia

Received February 1, 2006

Abstract—Procedures allowing the use of cadmium electrodes from worked-out nickel–cadmium batteries as a secondary raw material in manufacture of the active paste for negative electrodes were developed and tested under industrial conditions at AIT Plant.

DOI: 10.1134/S1070427206110164

The presently wide use and predictable high demand for alkaline nickel–cadmium batteries (NCBs) for industrial and household applications necessitate a search for economically efficient and environmentally safe methods for their utilization. Practical experience shows that one of ways to tackle this problem is to process the components of the active paste of alkaline NCBs to enable their repeated use [1]. The economic expediency of processing of the nickel oxide electrode is beyond any doubt, whereas the possible expenditure for storage, utilization, or processing of cadmium electrodes diminishes the commercial attraction of projects of this kind.

As a starting component of the active paste for the cadmium electrode serves CdO obtained by sublimation and oxidation of metallic Cd (Cd_{met}) in a cadmium-burning furnace at 700–800°C [2, 3]. On mixing CdO with activating additives, the content of Cd(II) in the active paste of cadmium electrodes varies from 40 to 70%, depending on the formula used in fabrication of active pastes [2, 3]. Metallic cadmium used to obtain CdO should conform to the requirements of GOST (State Standard) 1467–93, imposed on cadmium of Kd0 brand. The cost of Cd_{met} is determined by that of the cadmium-containing raw material and by the method used to produce Cd_{met} from this raw material. The high percentage content of Cd(II) in the active paste of cadmium electrodes suggests that their processing after the end of the service life of alkaline NCB is economically expedient. Simultaneously, this diminishes the probability of environment contamination by toxic cadmium compounds, which makes apparent the positive environmental aspect of this procedure.

Methods for processing of worked-out NCB electrodes are known; however, they do not allow repeated use of the raw material containing nickel and cadmium for production of components of active pastes [4, 5]. For example, worked-out electrodes of alkaline nickel–iron (cadmium) batteries are fused at 1450–1575°C to give nickel in the form of an alloy with iron [6]. A disadvantage of this method is that cadmium and nickel cannot be separated because Cd(II) is partly reduced at these temperatures, passes into the gaseous state, and is oxidized and carried away by discharge gases into the atmosphere, thereby contaminating the environment.

The aim of this study was to develop an economically efficient and environmentally safe technique for production of CdO from the active paste of cadmium electrodes of worked-out alkaline NCB by improving the efficiency of Cd_{met} recovery from the electrodes, diminishing the discharge of hazardous materials into the environment, and lowering the laboriousness and energy capacity of the process.

EXPERIMENTAL

To solve the problem formulated above, a laboratory installation for distillation of Cd_{met} was fabricated. It is shown schematically in Fig. 1. The installation operates on the pyrometallurgical principle, which consists in that cadmium waste is mixed with a reducing agent, with the subsequent heating of the mixture (stock) in an electric furnace without access of air [6].

Experiments were carried out with a stock containing 71.2% Cd(II). The component composition of the

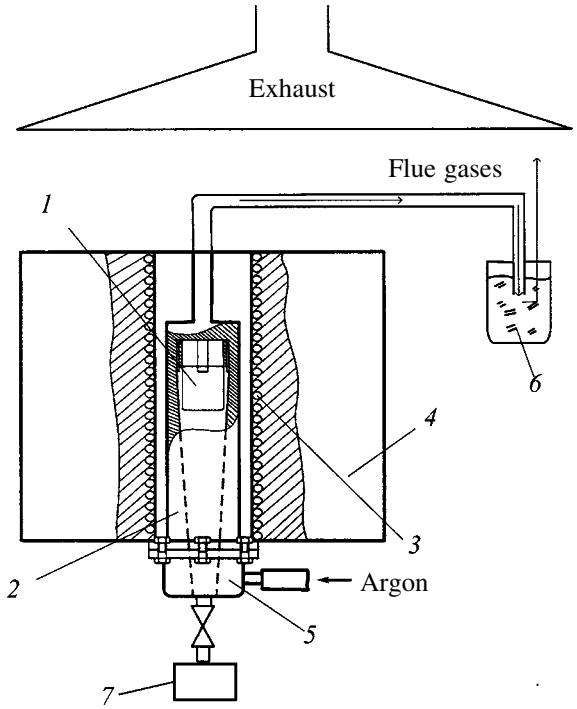


Fig. 1. Schematic of the installation for reduction of waste Cd(II): (*1*) reactor vessel, (*2*) solution, (*3*) heater, (*4*) furnace, (*5*) Cd_{met} collector, (*6*) water seal, and (*7*) dispenser vessel.

stock and the optimal conditions of the distillation process were found experimentally. As a criterion of quality of the process served such parameters as the reduction rate and recovery of Cd_{met}. It was found that these parameters strongly depend on the amount of stock present in the reaction zone. As can be seen in Fig. 2a, the reduction rate increases with the amount of stock in the working zone, whereas the recovery of Cd_{met} shows an opposite behavior (Fig. 2b).

The results of a chemical analysis of the stock after

Chemical composition of the stock with waste Cd(II) after distillation

Distillation	Content, %		
	Cd_{tot}	Ni_{tot}	Fe_{tot}
Primary	25	5.2	0.4
Secondary	0.06	58.4	0.3

primary and secondary distillation are listed in the table. The high residual content of Cd(II) in the stock after the primary distillation points to its incomplete recovery. However, repetition of the process enables virtually total reduction and recovery of Cd_{met} from the stock. The active pastes subjected to distillation contain nickel, and, therefore, the stock is enriched with this component in the course of thermal treatment.

Further, an industrial water-cooled groove furnace for processing of waste cadmium(II) was designed with account of the results obtained in the study and fabricated (Fig. 3).

The furnace includes a charging chamber *1*, into which trays with the stock containing waste cadmium(II) are introduced. For convenience of charging, guiding rollers are mounted in the chamber. The door opening is sealed in the closed state with a rubber cord laid in a groove on the chamber door. An inspection window and an air cylinder *2* are situated on the edge surface of the charging chamber. The cylinder is intended for pushing the trays into the preliminary condensation chamber *3*. The preliminary condensation chamber is separated from the charging chamber with a shutter attached to the shaft of an air cylinder *4*, which is opened immediately before pushing in the trays. When closed, the shutter prevents discharge of hot flue gases into the shop at the instant when a tray

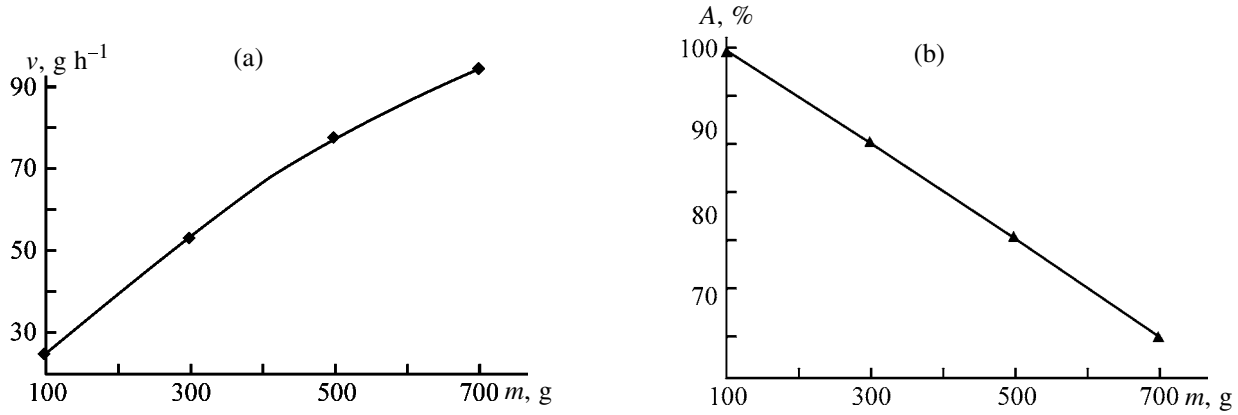


Fig. 2. (a) Cd_{met} recovery rate v and (b) recovery A of metallic cadmium vs. the amount m of stock in the reaction zone.

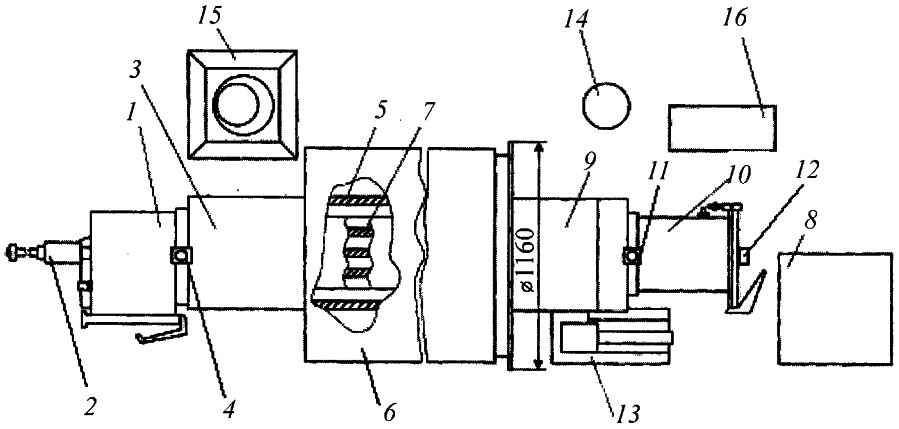


Fig. 3. Industrial water-cooled groove furnace for processing of waste cadmium(II). For explanations, see text.

with a stock is introduced into the charging chamber. The chamber walls are cooled by a water jacket.

A tray is moved from the preliminary condensation chamber into the muffle *5* of the heating chamber *6*. The muffle lying on the base frame is welded from 8-mm-thick sheets of 12Cr18Ni10Ti stainless steel. The heat insulation of the muffle is made of lightweight refractory bricks and kaolin wool. At joints with the charging chamber the muffle is rigidly attached to the frame. The opposite end of the muffle is mounted on a movable support and can shift via thermal elongation. To make molten Cd_{met} or its vapors move in a certain direction, the muffle is inclined at an angle of 2° by the frame, with rotation by 5° about the muffle axis. Thermocouples are fixed in the central part of the upper and lower surfaces of the muffle. A heater *7* is mounted in a metallic case within the muffle. The furnace is heated by electric current passed through a heater in the form of a Nichrome wire coil on a ceramic tube. For insulation from the case, each of the coils of the three-phase heater is placed in a large-diameter ceramic tube. The tubes are mounted in sections of a hermetically sealed metallic box, which prevents Cd_{met} vapor from coming in contact with the heater. To monitor the reaction course and provide the prescribed reaction conditions, two more thermocouples are fixed on the inner surface of the upper plate of the heater. The analog signal from temperature sensors is converted on the real-time basis by a personal computer on the control stand *8* into the digital form, analyzed, and further used to operate thyristor controllers in order to maintain a prescribed temperature.

At the exit from the heating chamber, the muffle is jointed with the Cd_{met} vapor condensation chamber *9* and unloading chamber *10*. Two air cylinders are mounted in the unloading chamber, one *11* serves to move the carriage with a tray to be unloaded, and the other *12* controls the shutter hermetically separating the unloading and condensation chambers. Cd_{met} reduced by carbon arrives in the form of a vapor to the condensation chamber, to be cooled there and to be delivered into a discharge chamber equipped with its own ribbon heater and thermocouple. From the discharge chamber, liquid cadmium runs down into water in the collector tank *13*, to form droplike particles.

The charging and unloading chambers are blown-through with argon from cylinder *14* in automatic mode. Because the working atmosphere in the heating chamber is reductive in the steady state, the whole heating chamber is blown-through with argon only at the beginning or end of furnace operation via charging and unloading chambers. The furnace is equipped with argon supply system. The operation of the gas pipes is monitored with three rotameters mounted on the gas panel. Flue gases are discharged through a water seal *15*. By changing the water level in the water seal, a necessary excess pressure can be created in the chambers. To maintain a certain air pressure in the system of control over air cylinders, the furnace is equipped with an autonomous compressor *16*.

The heating chamber and the charging and unloading chambers with condensation chambers are mounted on three separate frames welded from rectangular tubes. The power unit, gas distribution unit, air preparation unit, and water collector are mounted on the inner side of the frame and closed with decorative panels on their faces.

To distill off Cd_{met} according to the procedure developed, cadmium(II)-containing waste is screened,

separated from the metallic component, and mixed with P324 carbon (GOST 7885–86) [0.020 – 0.200 kg of carbon per 1 kg of Cd(I) contained in the active paste]. The resulting mixture is charged in batches in the continuous mode into the heating chamber of the furnace and kept at 650 –1100°C without access of oxygen, with the charging interval determined for each batch with account of the time of its keeping at a prescribed temperature for 5–15 h. The output capacity of the furnace is, on the average, about 95 kg of Cd_{met} per 24 h and varies, depending on the type of waste being processed, in the range 70 –120 kg in 24 h. In this case, the electric energy actually consumed by the furnace does not exceed values of about 7 kW h. The Cd_{met} obtained fully conforms in the content of impurities to the requirements of GOST 1467–93, imposed on cadmium of Kd0 brand:

Impurity	Content, %
Fe	0.0004
Pb	0.001
Cu	0.001
Ni	<0.001
Zn	0.001
Tl	<0.002
Mn	–

Gaseous reaction products, a mixture or carbon monoxide and carbon dioxide, pass through the water seal and are discharged into the environment without additional purification. Further, Cd_{met} is sublimed in a cadmium-burning furnace and oxidized with atmospheric oxygen to CdO. The resulting CdO is mixed with activating additives and used to fabricate cadmium electrodes for NCBs. The residual carbon containing cadmium compounds in an amount of 25 to 0.06% is accumulated and used to prepare subsequent portions of a mixture of carbon with the active paste of cadmium electrodes of worked-out NCBs.

The technique suggested allows use of cadmium electrodes of worked-out alkaline NCB as a secondary raw material for production of CdO without use of toxic reagents; no industrial wastewater or environmentally hazardous gas discharges are formed.

CONCLUSIONS

(1) The technique suggested for utilization of cadmium electrodes of worked-out nickel–cadmium batteries provides a high efficiency of recovery of the expensive Cd_{met} for repeated use with any impact on the environment.

(2) Presently, the technique can only be used to process the industrial cadmium(II) waste from the battery industry in order to prevent its accumulation and to diminish the production cost of articles.

REFERENCES

1. Erkel, J. van, Deelen, C.L. van, Kamphuis, B.A., and Visser, A.J., *Report on Conf.*, Geneva (Switzerland), September 1994, pp. 133–136.
2. Dasoyan, M.A., Novoderezhkin, V.V., and Tomashevskii, F.F., *Proizvodstvo elektricheskikh akkumulyatorov* (Manufacture of Electric Batteries), Moscow: Vysshaya shkola, 1965.
3. Dasoyan, M.A., *Khimicheskie istochniki toka* (Chemical Power Cells), Leningrad: Energiya, 1969.
4. USSR Inventor's Certificate no. 711 137.
5. USSR Inventor's Certificate no. 539 087.
6. Chizhikov, D.M., *Kadmii* (Cadmium), Moscow: Nauka, 1967.

ISSN 1070-4272, Russian Journal of Applied Chemistry, 2006, Vol. 79, No. 11, pp. 1829–1834. © Pleiades Publishing, Inc., 2006.
Original Russian Text © M.G. Veliev, N.M. Agaev, M.I. Shatirova, A.Z. Chalabieva, G.D. Geidarova, S.S. Alieva, 2006, published in Zhurnal Prikladnoi Khimii, 2006, Vol. 79, No. 11, pp. 1848–1854.

APPLIED ELECTROCHEMISTRY AND CORROSION PROTECTION OF METALS

Allylacetylenes and Their Derivatives as Inhibitors of Steel Corrosion in Sulfuric Acid

M. G. Veliev, N. M. Agaev, M. I. Shatirova, A. Z. Chalabieva, G. D. Geidarova, and S. S. Alieva

Institute of Polymeric Materials, Azerbaijan National Academy of Sciences, Sumgait, Azerbaijan

Received August 3, 2005; in final form, March 2006

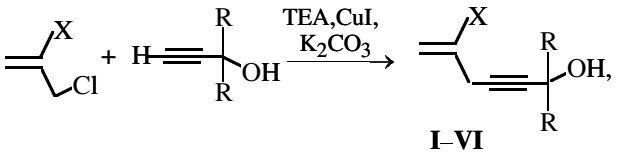
Abstract—New functionalized derivatives of allylacetylenes were prepared, and their ability to inhibit corrosion of St.3 low-carbon steel in 5 N sulfuric acid was studied. The effectiveness of inhibition of steel corrosion was studied in relation to the structure of acetylene derivatives, their concentration, and temperature of acidic medium.

DOI: 10.1134/S1070427206110176

Functionalized unsaturated compounds are efficient inhibitors of the steel acid corrosion [1–4]. Acetylene derivatives strongly decelerate corrosion of steel in hydrochloric acid [5–9]. The multiple bonds with mobile π electrons determine high adsorption and protective properties of acetylene compounds. It was found that inhibition of the acid corrosion of steel with allylacetylenes only slightly depends on the nature of functional groups and substituents at unsaturated bonds; the decisive effect is exerted by acetylene and ethylene bonds.

Proceeding with studies of high-performance acid inhibitors, in this work we prepared new allylacetylenes and their derivatives and studied their inhibition properties in 5 M sulfuric acid in relation to the structure (nature of substituents).

Previously [10, 11] we studied the reaction of alkenyl halides with monosubstituted primary and tertiary acetylenic alcohols in the presence of EtMgBr/CuCl and NH_4Cl/CuCl, which are not universal reagents for preparing the corresponding allylacetylenic alcohols in a high yield. In this study, allylacetylenic alcohols **I**–**VI** were prepared by reaction of alkenyl halides with the corresponding monosubstituted acetylenylcarbinols in dimethylformamide (DMF) in the presence of copper iodide, triethylamine (TEA), and potassium carbonate:



I–VI

where X = R = H (**I**); X = H, R = CH_3 (**II**); X = CH_3, R = H (**III**); X = R = CH_3 (**IV**); X = Cl, R = H (**V**); X = Cl, R = CH_3 (**VI**).

The other functionalized allylacetylene derivatives **VII**–**XXII** were prepared from appropriate alcohols **I**–**VI** in accordance with procedures given in [10–12] (Scheme 1), where X = R = H (**VII**), X = CH_3, R = H (**VIII, XI, XIV, XVII, XIX; X**) = Cl, R = H (**IX**); X = Cl, R = CH_3 (**X**); X = R = CH_3 (**XII, XV, XVIII, XX, XXI**); X = H, R = CH_3 (**XIII, XVI**, and **XXII**).

The physicochemical properties of compounds **I**–**XXII** are listed in Table 1. The structure and composition of the resulting compounds were studied by thin-layer (TLC) and gas–liquid (GLC) chromatography and by IR and ^1H NMR spectroscopy (Table 2) [10, 11, 13].

As seen from Scheme 1, the resulting allylacetylenes can be divided in two groups: (a) primary and tertiary alcohols of allylacetylene series and (b) ethers and esters of allylacetylene compounds, also containing functional groups.

When choosing the inhibitor structure, we took into account the fact that multiple (double and especially triple) bonds and functional groups [OH, $OCOCH_3$, $OCH(OC_2H_5)CH_3$] provide efficient adsorption of the compounds on the steel surface with the formation of a protective film decelerating the corrosion.

EXPERIMENTAL

The IR spectra were recorded on a UR-20 spectrophotometer in the 4000–400 cm^{-1} range (thin

Table 1. Properties of allylacetylenes and their derivatives **I–XXII**

Compound	Yield, %	bp, °C (*P*, mm Hg)	n_D^{20}	d_4^{20}	Found, %			Formula	Calculated, %		
					C	H	Cl(N)		C	H	Cl(N)
I	74.2	80–81 (18)	1.4762	0.9373	74.81	8.46	–	C_6H_8O	74.97	8.38	–
II	80.7	70–71 (12)	1.4596	0.8997	77.50	9.63	–	$C_8H_{12}O$	77.37	9.74	–
III	82.9	92–94 (13)	1.4765	0.9284	76.46	9.30	–	$C_7H_{10}O$	76.32	9.15	–
IV	85.3	86.5–87 (13)	1.4625	0.8839	78.01	10.34	–	$C_9H_{14}O$	78.21	10.21	–
V	68.5	71–72 (0.5)	1.4820	1.0680	55.30	5.10	27.20	C_6H_7ClO	55.19	5.41	27.15
VI	78.6	64–65 (0.5)	1.4770	1.0428	60.45	6.80	22.20	$C_8H_{11}ClO$	60.55	6.99	22.34
VII	82.4	84–85 (10)	1.4540	0.9769	69.68	7.13	–	$C_8H_{10}O_2$	69.54	7.30	–
VIII	85.8	95–96 (10)	1.4590	0.9700	71.18	7.79	–	$C_9H_{12}O_2$	71.02	7.95	–
IX	79.1	72–73 (0.5)	1.4720	1.1209	55.60	5.18	20.63	$C_8H_9ClO_2$	55.67	5.25	20.54
X	70.1	69–70 (0.5)	1.4660	1.0659	59.70	6.60	17.50	$C_{10}H_{13}ClO_2$	59.86	6.53	17.67
XI	75.2	60–61 (1)	1.4591	0.9287	72.55	9.86	–	$C_{11}H_{18}O_2$	72.48	9.95	–
XII	80.1	58–59 (1)	1.4572	0.9075	74.30	10.35	–	$C_{13}H_{22}O_2$	74.24	10.54	–
XIII	78.8	115–116 (1)	1.4767	1.0445	61.22	7.80	16.51	$C_{11}H_{17}ClO_2$	60.97	7.90	16.36
XIV	63.2	122–123 (1)	1.4894	1.0818	59.19	7.43	17.60	$C_{10}H_{15}ClO_2$	59.26	7.46	17.49
XV	67.1	123–124 (1.5)	1.4780	1.0293	62.39	8.19	15.55	$C_{12}H_{19}ClO_2$	62.46	8.30	15.36
XVI	85.2	78–79 (1)	1.4841	0.9539	73.40	8.92	–	$C_{11}H_{16}O_2$	73.30	8.94	–
XVII	66.4	98–99 (1.5)	1.4820	0.9843	72.19	8.55	–	$C_{10}H_{14}O_2$	72.26	8.49	–
XVIII	78.2	86–87 (1)	1.4665	0.9666	74.31	9.15	–	$C_{12}H_{18}O_2$	74.19	9.33	–
XIX	82.2	145–146 (1.5)	1.4878	0.9505	70.04	10.32	6.00	$C_{14}H_{23}NO$	70.19	10.44	5.85
XX	66.6	124–125 (1.5)	1.4674	0.9236	71.69	10.75	5.30	$C_{16}H_{28}NO$	71.80	10.84	5.23
XXI	72.1	104–105 (0.5)	1.4556	0.9467	71.20	9.71	–	$C_{15}H_{24}O_3$	71.39	9.59	–
XXII	76.1	89–90 (1)	1.4584	0.9620	70.68	9.29	–	$C_{14}H_{22}O_3$	70.55	9.30	–

Table 2. ^{1}H NMR and IR data for **I–XXII**

Compound	^{1}H NMR, δ, ppm	IR, ν, cm^{-1}
V	5.20 s, 5.55 s (2H, CH_2=C), 3.10 s (2H, CH_2), 4.05 s (2H, CH_2O), 3.80 br.s (1H, OH)	630, 1395, 1650, 2230, 3100, 3350
VI	5.15 s, 5.45 s (2H, CH_2=C), 3.05 s (2H, CH_2), 1.40 s [6H, $(CH_3)_2$], 3.90 br.s (1H, OH)	650, 1400, 1645, 2225, 3010, 3400
VII	4.90–5.43 m (2H, CH_2=C), 5.50–6.00 m (1H, C=CH), 2.85–3.05 m (2H, CH_2), 4.50–4.70 m (2H, CH_2O), 2.00 s (3H, $COCH_3$)	875, 990, 1160, 1248, 1656, 1746, 2235, 3010
VIII	4.75 s, 4.90 s (2H, CH_2=C), 1.75 s (3H, CH_3), 2.85 s (2H, CH_2), 4.55 s (2H, CH_2O), 2.10 s (3H, $COCH_3$)	890, 910, 1175, 1645, 1740, 2240, 3100
IX	5.10 s, 5.60 s (2H, CH_2=C), 3.15 s (2H, CH_2), 4.10 s (2H, CH_2O), 2.08 s (3H, $COCH_3$)	640, 1170, 1246, 1380, 1656, 1745, 2235, 3090
X	5.15 s, 5.80 s (2H, CH_2=C), 3.10 s (2H, CH_2), 1.53s [6H, $(CH_3)_2$], 1.96 s (3H, $COCH_3$)	660, 1135, 1250, 1395, 1660, 1740, 2220, 3010
XI	4.70 s, 4.96 s (2H, CH_2=C), 1.80 s (3H, CH_3), 2.72 s (2H, CH_2), 4.45 s (2H, CH_2O), 4.40 q (1H, OCH), 3.26 q (2H, OCH_2), 1.15 d (3H, CH_3CH), 1.00 t (3H, C$H_3$$CH_2$)	885, 915, 1095, 1160, 1410, 1655, 2235,
XII	4.76 s, 4.87 s (2H, CH_2=C), 1.75 s (3H, CH_3), 2.86 s (2H, CH_2), 1.40 s [6H, $(CH_3)_2$], 4.42 q (1H, OCH), 3.30 q (2H, OCH_2), 1.17 d (3H, CH_3CH), 1.05 t (3H, C$H_3$$CH_2$)	890, 920, 1100, 1175, 1645, 2240, 3100
XIII	4.90–5.40 m (2H, CH_2=C), 5.60–6.10 m (1H, C=CH), 2.75–3.05 m (2H, CH_2), 1.30 s [6H, $(CH_3)_2$], 3.30–3.70 m (4H, CH_2, CH_2Cl), 375–4.00 m (1H, CH–O), 2.35 br.s (1H, OH)	725, 880, 910, 1170, 1670, 2235, 3100, 3400

Table 2. (Contd.)

Compound	^{1}H NMR, δ, ppm	IR, ν, cm^{-1}
XIV	4.80 s, 4.95 s (2H, CH_2=C), 1.80 s (3H, CH_3), 2.90 s (2H, CH_2), 4.15 t (2H, CH_2O), 3.45 d (2H, CH_2Cl), 3.55 d (2H, OCH_2), 3.90 m (1H, CHO), 3.10 br.s. (1H, OH)	730, 885, 905, 1165, 1660, 2245, 3010, 3380
XV	4.85 s, 4.70 s (2H, CH_2=C), 1.70 s (3H, CH_3), 2.75 s (2H, CH_2), 1.36 s [6H, $(CH_3)_2$], 3.40, 3.55 m (4H, CH_2Cl, CH_2), 3.65 m (1H, OCH), 3.15s (1H, OH)	726, 890, 990, 1170, 1665, 2230, 3100, 3400
XVI	4.86–5.38 m (2H, CH_2=C), 5.57–6.05 m (1H, C=CH), 2.70–3.05 m (2H, CH_2), 1.38 s [6H, $(CH_3)_2$], 3.65–3.80 m (2H, OCH_2), 2.85–3.00 m (1H, CHO), 2.30–2.65 m (2H, CH_2)	880, 910, 950, 1180, 1248, 1660, 2235, 3010, 3065
XVII	4.80 s, 4.95 s (2H, CH_2=C), 1.86 s (3H, CH_3), 2.90 s (2H, OCH_2), 4.20 t (2H, CH_2O), 3.50 m (2H, CH_2), 3.05 m (1H, OCH), 2.45–2.70 m (2H, OCH_2)	885, 915, 950, 990, 1170, 1255, 1640, 2225, 3010, 3065
XVIII	4.70 s, 4.90 s (2H, CH_2=C), 1.70 s (3H, CH_3), 2.86 s (2H, CH_2), 1.30 s [6H, $(CH_3)_2$], 3.45 m (2H, CH_2), 2.90 m (1H, OCH), 2.30–2.65 m (2H, OCH_2)	890, 910, 953, 1167, 1250, 1645, 2210, 3060, 3100
XIX	4.75 s, 4.86 s (2H, CH_2=C), 1.76 s (3H, CH_3), 2.88 s (2H, CH_2), 4.10 t (2H, CH_2O), 3.20–3.60 m (1H, CH, 2H, CH_2), 2.33–2.65 q [6H, $N(CH_2)_3$], 1.36 s [6H, $(CH_3)_2$]	886, 990, 1180, 1650, 2230, 2785, 3010, 3400
XX	4.70 s, 4.95 s (2H, CH_2=C), 1.70 s (3H, CH_3), 2.85 s (2H, CH_2), 1.35 s [6H, $(CH_3)_2$], 3.25–3.65 m (3H, CH, CH_2), 2.30–2.60 q [6H, $N(CH_2)_3$], 1.30 s [6H, $(CH_3)_2$]	890, 985, 1160, 1655, 2240, 2786, 3100, 3450
XXI	4.73 s, 4.92 s (2H, CH_2=C), 1.80 s (3H, CH_3), 2.30 s (2H, CH_2), 1.35 s [6H, $(CH_3)_2$], 3.30–3.65 m (2H, OCH_2), 2.80–3.00 m (1H, CHO), 2.40–2.70 m (2H, CH_2O), 1.38 s [6H, $(CH_3)_2$]	880, 915, 1045, 1175, 1650, 2230, 3100
XXII	4.80–5.40 m (2H, CH_2=C), 5.55–6.00 m (1H, C=CH), 2.75–2.90 m (2H, CH_2), 1.32 s [6H, $(CH_3)_2$], 3.25–3.60 m (2H, OCH_2), 2.95–3.15 m (1H, CHO), 2.30–2.65 m (2H, CH_2O), 1.36 s [6H, $(CH_3)_2$]	885, 990, 1050, 1150, 1640, 2235, 3010

Note: The data for compounds **I**–**IV**, which are not included in the table, are given in [10].

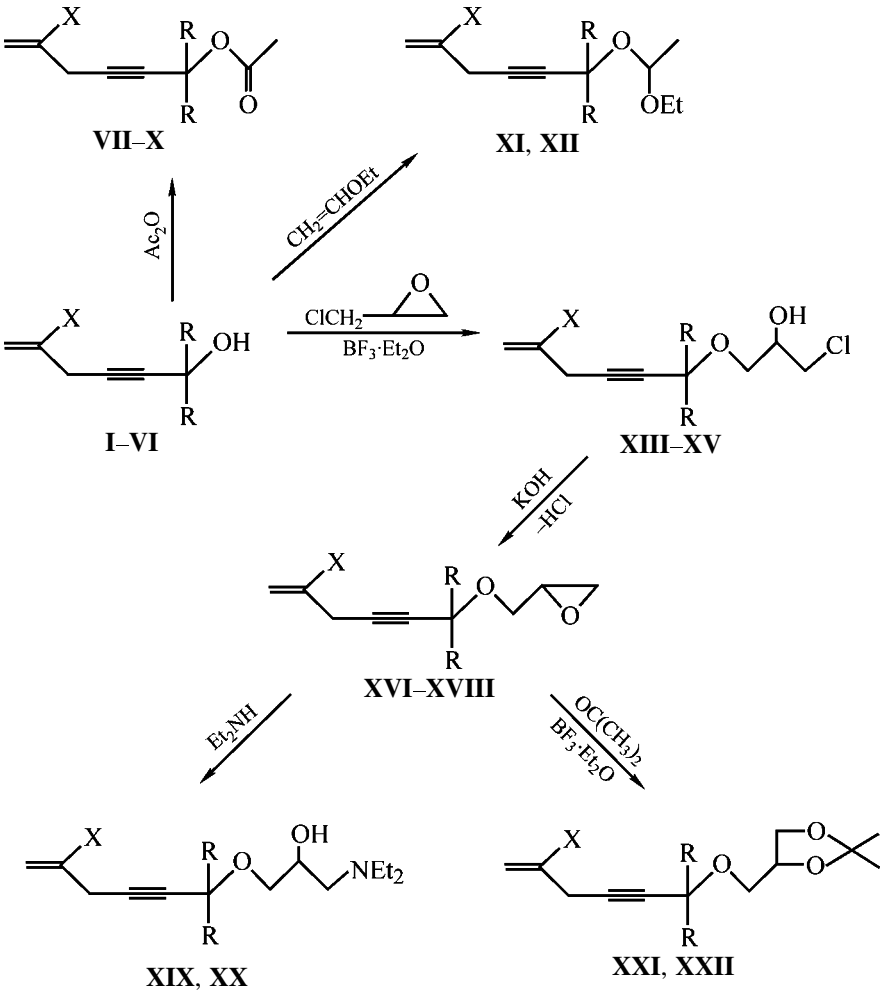
layer). The ^{1}H NMR spectra were recorded on a Tesla BS-487 B spectrometer (80 MHz) in carbon tetrachloride solutions using HMDS internal reference. The purity of the resulting compounds was controlled by thin-layer chromatography using Silufol UV-254 plates in various solvent mixtures and by gas–liquid chromatography on an LKhM-8 MD-5 device.

The physicochemical properties and spectra of compounds **I**–**XXII** are listed in Tables 1 and 2.

To prepare primary and tertiary allylacetylenic alcohols **I**–**VI**, dimethylformamide (100 ml), K_2CO_3 (1.5 g), CuI (9.5 g), and triethylamine (0.5 ml) were placed in a three-necked flask and stirred for 15–20 min in a nitrogen flow at 50°C. Appropriate acetylene compound (propargyl alcohol or dimethylethynylcarbinol) (0.05 mol) was added, the reaction mixture was stirred for 2 h, and then appropriate alkenyl halide (allyl chloride, 2,3-dichloropropene, methallyl chloride) (0.1 mol) was added dropwise. The resulting mixture was stirred for an additional 8 h at 50–55°C. After cooling, the mixture was washed with water and extracted with ether. The ether layer was separated, dried with $MgSO_4$, and evaporated in a vacuum. The yield of products **I**–**VI** was 65–80%. The physicochemical properties of the resulting compounds were close to those of the compounds prepared by the published procedure [10].

1-Acetoxy-5-hexen-2-yne VII. Acetic anhydride (4.1 g, 0.04 mol) was added with stirring to a mixture of allylacetylenic alcohol **I** (2 g, 0.02 mol) and concentrated sulfuric acid (0.1 ml) at 6–9°C, and the reaction mixture was left overnight. Then, the mixture was stirred for 1.5 h on heating to 65–70°C. After cooling, the reaction mixture was diluted with water, neutralized with K_2CO_3, and extracted with ether. The ether layer was dried ($MgSO_4$) and evaporated in a vacuum to yield compound **VII**.

Scheme 1.



Compounds **VIII**–**X** were prepared by similar procedures using alcohols **III, V**, and **VI**.

2-Methyl-7-oxa-8-ethoxy-1-nonen-4-yne XI. Hydrochloric acid (33%, 0.3 ml) was added with stirring at 11°C to a mixture of allylacetylenic alcohol **III** (0.06 mol) and vinyl ethyl ether (0.06 mol). The flask was intermittently shaken; in so doing, the temperature of the reaction mixture increased to 42°C. The reaction mixture was left overnight. Then, the reaction mixture was neutralized and extracted with ether. The ether layer was dried (K_2CO_3), the solvent was evaporated in a vacuum, and compound **XI** was isolated by vacuum sublimation.

Acetal **XII** was prepared by a similar procedure using alcohol **IV**.

3-Chloro-1-(1,1-dimethyl-5-hexen-2-ynyloxy)-propan-2-ol XIII. Epichlorohydrin (4 g, 0.043 mol) was added with stirring at 0–5°C to allylacetylenic alcohol **II** (12.4 g, 0.1 mol) containing boron trifluoride etherate (0.1 ml). The reaction mixture was stirred for 4 h at 25°C, and compound **XIII** was isolated by vacuum distillation.

Chlorohydrins **XIV** and **XV** were prepared by similar procedures from alcohols **III** and **IV**.

1-(1,1-Dimethyl-5-hexen-2-ynyloxy)-2,3-epoxypropane XVI. Powdered KOH (8.4 g, 0.15 mol) was added with stirring at 8–10°C to a solution of chlorohydrin **XIII** (10.8 g, 0.05 mol) in ether (60 ml). The reaction mixture was stirred for 3 h at 12–14°C. After common work-up and removal of the solvent, compound **XVI** was isolated by vacuum distillation.

Epoxides **XVII, XVIII** were prepared similarly from chlorohydrins **XIV** and **XV**.

1-(5-Methyl-5-hexen-2-ynyloxy)-3-diethylamino-propan-2-ol XIX. A mixture containing epoxide **XVII** (3 g, 0.018 mol) and diethylamine (6.5 g, 0.5 mol) was stirred in the presence of water (2 ml)

Table 3. Allylacetylene inhibitors of steel corrosion in 5 M H_2SO_4

Compound	Inhibitor concentration, g l^{-1}	Corrosion rate, g m^{-2} h^{-1}			Degree of corrosion protection, %		
		40	60	80	40	60	80
I	0.5	5.7	11.4	8.4	86.2	93.3	98.7
	1.0	3.1	9.1	5.3	92.5	94.6	99.2
III	0.5	5.7	46.5	11.4	86.3	72.7	98.3
	1.0	3.8	24.3	9.7	90.8	85.7	98.5
V	0.5	6.3	33.4	17.5	84.8	80.4	97.4
	1.0	4.2	21.7	8.6	90.1	87.2	98.7
VII	0.5	5.3	13.9	10.4	95.4	91.0	98.4
	1.0	1.9	5.4	5.5	91.0	96.8	99.2
VIII	0.5	3.3	13.0	5.3	92.6	92.4	99.2
	1.0	2.4	4.7	1.1	96.2	97.4	98.8
XI	0.5	0.3	1.1	1.3	99.2	99.3	99.8
	1.0	0.2	0.6	0.6	99.4	99.7	99.9
XII	0.5	1.35	3.3	21.0	96.7	98.0	98.0
	1.0	2.0	2.6	3.8	95.1	98.4	99.7
XIX	0.5	1.34	6.2	3.8	96.8	95.8	93.1
	1.0	2.2	3.6	2.4	93.9	97.9	96.7
XX	0.5	3.8	3.3	7.9	93.1	97.9	98.8
	1.0	2.4	2.1	4.5	96.7	98.9	99.6
XXI	0.5	4.36	10.3	14.0	88.9	94.0	97.2
	1.0	2.60	5.0	10.6	94.6	96.0	98.4

for 8 h at 50°C, then dioxane (about 10 ml) was added to obtain the homogeneous mixture; in so doing, the temperature of the reaction mixture increased. The mixture was heated at 40°C for 3 h. Then it was extracted with ether and the ether layer was dried (K_2CO_3). The solvent was removed in a vacuum and compound **XIX** was isolated by vacuum distillation.

Amino alcohol **XX** was prepared similarly from epoxide **XVIII**.

2,2-Dimetyl-4-(3,3,7-trimethyl-2-oxo-7-octen-4-ynyl)-1,3-dioxolane XXI. Epoxide **XVI** (1.8 g, 0.01 mol) was added to a mixture of acetone (8,1 g, 0.14 mol) containing boron trifluoride etherate (1.8 g, 0.01 mol); in so doing, the temperature of the reaction mixture increased. After storage for 24 h, the reaction mixture was treated with a saturated aqueous solution of K_2CO_3, and the organic layer was separated and dried ($MgSO_4$). The solvent was removed in a vacuum and 1,3-dioxolane **XXI** was isolated by vacuum distillation.

1,3-Dioxolane **XXII** was prepared similarly from epoxide **XVIII**.

Among all the allyl derivatives prepared, ten compounds (namely, **I, III, V, VII, VIII, XI, XII, XIX–XXI**) were studied as inhibitors of the acid corrosion of steel in 5 N H_2SO_4.

The inhibition effect of compounds was studied by gravimetric procedure simulating the conditions of acidic etching of steel and rolled metal. Before experiments, the specimens ($30 \times 20 \times 3$ mm) were cleaned on a polishing device with rubber discs, degreased with acetone, and stored for 1 day in a desiccator. The inhibitor concentration was 0.5–1.0 g l^{-1}; the required temperature of the acid medium of 40, 60, or 80°C was maintained with a thermostat. The experimental results listed in Table 3 show that all the above compounds are highly effective inhibitors of steel corrosion in sulfuric acid.

Along with studying the protective properties of compounds, we also tried to evaluate the correlation between the structure of organic compounds and their inhibiting performance and to determine the role of various functional groups in the total protection effect.

As seen, all the allylacetylenes studied exhibit pronounced activity in inhibition of the acid corrosion of steel. The degree of steel corrosion protection Z is 84–99%.

The compounds with normal structure with a terminal alcohol group **I, III**, and **V** are highly effective inhibitors. Substitution of the hydrogen atoms with chlorine atom and methyl groups slightly decreases the inhibiting performance of compounds **V** and **III** as

compared to **I**. Allylacetylenes **VII** and **VIII** with a terminal acetoxy group are also effective inhibitors. Addition of the methylene group at the double bond enhances the inhibition properties at 40 and 60°C, but *Z* remains almost unchanged at 80°C.

Substitution of two hydrogen atoms with methyl groups (acetals **XI, XII**) slightly decreases the inhibiting performance of allylacetylenes. The protective effectiveness of amino alcohols **XIX** and **XX** is ambiguous.

On the whole, our experimental results suggest that functionalized allylacetylenes are highly effective inhibitors of the acid corrosion of steel; with increasing concentration of inhibitors their protection effect increases.

The performance of inhibitors increases with increasing temperature of the corrosion medium (especially at 80°C), which is probably due to the activation of chemisorption of the particles and molecular fragments on the metal surface. On substitution of methyl groups for hydrogen atoms, the structure of inhibitors becomes more branched, which hinders their adsorption on the metal surface and thus ordering in the resulting protective film. We assumed that the protection effect of allylacetylenes as inhibitors of the acid corrosion of steel is due to the π-electron interaction of the double and triple bonds with metal, resulting in the formation of chemisorption bonds at elevated temperatures. The contribution of the other fragments to corrosion inhibition is not decisive, because the overall inhibition effect is extremely high.

CONCLUSIONS

(1) Methods were developed for preparing primary and tertiary allylacetylenic alcohols in high yields by the reaction of alkenyl halides with the corresponding monosubstituted acetylenic alcohols in the presence of copper(I) iodide, triethylamine, and potassium carbonate in dimethylformamide.

(2) A series of functionalized allylacetylenes prepared are highly effective inhibitors of steel corrosion in 5 N sulfuric acid. The inhibition effect is primarily determined by the presence of double and triple bonds and is virtually independent of the nature of functional groups.

(3) With increasing temperature of the reaction mixture and concentration of the inhibitor, the protection effect increases.

REFERENCES

1. Rozenfel'd, I.L., *Ingibitory korrozii* (Corrosion Inhibitors), Moscow: Khimiya, 1977.
2. Podobaev, N.I. and Avdeev, Ya.G., *Zashch. Met*., 2002, vol. 38, no. 1, pp. 51–56.
3. Kukharev, B.F., Stankevich, V.K., Klimenko, G.R., et al., *Zh. Prikl. Khim*., 2000, vol. 73, no. 1, pp. 181–163.
4. Podobaev, N.I. and Avdeev, Ya.G., *Zashch. Met*., 2001, vol. 37, no. 1, pp. 19–23.
5. Agaev, N.M., Veliev, M.G., Geidarova, G.D., et al., *Zashch. Met*., 1996, vol. 32, no. 1, pp. 101–103.
6. Agaev, N.M., Veliev, M.G., Geidarova, G.D., et al., *Neft' Gas*, 1993, no. 3, pp. 36–38.
7. Veliev, M.G., Alekperov, N.A., Agaev, N.M., et al., Abstracts of Papers, *I Bakinskaya mezhdunarodnaya konferentsiya po neftekhimii* (I Baku Int. Conf. on Petroleum Chemistry), Baku, 1994, p. 212.
8. RF Patent 2056406.
9. Agaev, N.M., Preparation of Inhibitors of Hydrogen Sulfide and Bacterial Corrosion of Steel Under the Conditions of Petroleum Production, *Doctoral Dissertation*, Lviv, 1998.
10. Veliev, M.G., Shatirova, M.I., Chalabiev, Ch.A., et al., *Zh. Org. Khim*., 1995, vol. 31, no. 1, pp. 58–63.
11. Veliev, M.G., Akperova, E.G., Shatirova, M.I., et al., *Azerb. Khim. Zh*., 2003, no. 3, pp. 41–46.
12. Veliev, M.G., Shatirova, M.I., and Nadirova, M.I., Abstracts of Papers, *6-e soveshchanie po khimicheskim reaktivam* (6th Meet. on Chemical Reagents), Baku, October 5–9, 1993, p. 80.
13. Gordon, A.J. and Ford, R.A., *The Chemist's Companion. A Handbook of Practical Data, Techniques and References*, New York: Wiley–Interscience, 1972.

ISSN 1070-4272, Russian Journal of Applied Chemistry, 2006, Vol. 79, No. 11, pp. 1835–1838. © Pleiades Publishing, Inc., 2006.
Original Russian Text © R.O. Azizov, M. Rakhmatov, Kh.M. Nazarov, 2006, published in Zhurnal Prikladnoi Khimii, 2006, Vol. 79, No. 11, pp. 1855–1859.

APPLIED ELECTROCHEMISTRY AND CORROSION PROTECTION OF METALS

Composition and Properties of Boronized Gas-Thermal Coatings Made of Low-Carbon Steels

R. O. Azizov, M. Rakhmatov, and Kh. M. Nazarov

Osimi Tajik Technical University, Dushanbe, Tajikistan

Received April 21, 2006

Abstract—The structure and durometric and anticorrosive properties of gas-thermal coatings deposited by sputtering of steel wires, with subsequent modification by boronizing, were studied.

DOI: 10.1134/S1070427206110188

The problem of reliability and durability of machine and mechanism elements can be successfully solved by creating new highly efficient processes and composite materials. The most versatile method for production of composite materials is deposition of coatings. This technique is of primary importance in reclamation of worn articles and units and can bring the article size to required values. Using materials with required properties for coating deposition, it is possible to prolong the service life of a reclaimed article as compared to a new one. A particular place among the wide variety of techniques for regeneration of worn working surfaces of machine units is the method of gas thermal spraying (GTS) [1, 2]. The advantages of GTS consist in the simplicity and relatively low cost of the process and in the possibility of deposition of coatings with prescribed protective properties [3].

A possible efficient way to improve the performance of GTS coatings is to form high-strength surface layers with gradient structure, using economical methods of chemical-thermal treatment, which is of indubitable scientific and practical interest. This study is concerned with the influence exerted by boronizing of GTS coatings composed of Sv 08 low-carbon steel on their structural state, microhardness, and corrosion resistance.

EXPERIMENTAL

The study was carried out on $30 \times 30 \times 5$-mm samples made of sheet steel 10. Prior to deposition of a gas-thermal coating, the samples were subjected to abrasive-blast treatment to activate the surface layer and to impart a certain roughness to this layer.

Coatings of Sv 08 low-carbon steel taken in the form of a wire of diameter d = 2 mm were deposited by electric-arc metallization and flame spraying on TERKO installations (manufactured by INDMASh NANB). The wire feed velocity was 0.4 m min^{-1}, air flow rate, 60 m^3 h^{-1}, and gas expenditure (propane–butane), 0.011 kg h^{-1}. Upon deposition, the coatings had thicknesses of 0.6–0.7 mm, which were brought by grinding to 0.5 mm.

Thermal-diffusion saturation was performed by boronizing in powder media of compositions listed in Table 1. The time and temperature of saturation were 1073–1173 K and 1–6 h. The samples were cooled after the thermal-diffusion hardening to room temperature together with the container.

Metallographic studies were carried out with a Unimet optical microscope; a Micromet II microhardness meter was used in durometric measurements (load 0.49 N). The phase and structural transformations in modified coating layers were examined by X-ray diffraction analysis on a DRON 3.0 diffractometer in monochromated CoK_α radiation. The standard PDF file was used in phase analysis.

A corrosion-electrochemical study was carried out on a PI 50.1.1 potentiostat with an LKD 4-002 *XY* recorder in a 3% NaCl solution. A silver chloride electrode served as reference, and a platinum electrode, as auxiliary electrode. Also, forward and back sweep curves were measured at a potential sweep rate of 2 mV s^{-1}. The study was performed using the procedure described in [4].

The boronizing of an Sv 08 steel coating is accompanied by formation of deep diffusion layers with a thickness of up to 300–320 μm, which have a relatively high microhardness. The distribution of the

Table 1. Compositions of powder mixtures for alloying of gas-thermal coatings

Boronizing	Content, wt %							Activating agent, wt %
	Al_2O_3	Cr_2O_3	B_2O_3	Ni	Al	ZrO_2	Fe	
Single-phase	8	9	23	10	22	3	25	1 NH_4BF_4
Two-phase	25	15	25	5	27	3	–	0.5 NH_4BF_4, 0.5 AlF_3

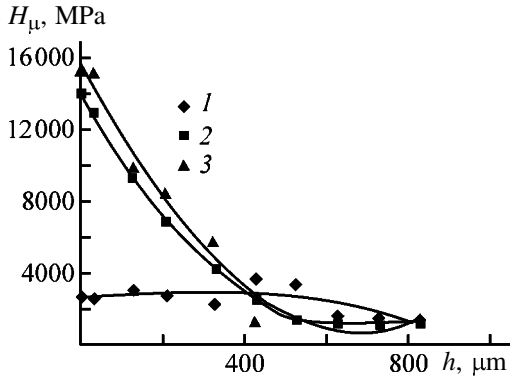


Fig. 1. Distribution of the microhardness H_μ of coatings across the layer thickness h. (*1*) Sv 08, initial state; boronizing: (*2*) single-phase and (*3*) two-phase.

microhardness across the boronized layer is shown in Fig. 1.

Boron-modified coatings have a multilayer structure including two boride zones and a diffusion-porosity zone. The results of an X-ray phase analysis indicate that mostly iron borides FeB are formed in the 30–50-μm-thick surface layer having a microhardness of 14500–16000 MPa (Fig. 2).

Figures 3 and 4 show how the thickness h of the diffusion layers on boronized GTS Sv 08 steel coatings and the thickness of the boronized layer obtained on monolithic steel depend on the time t and temperature T of boronizing.

The time necessary for Fe_2B nucleation is determined by the activity of a saturating medium. For

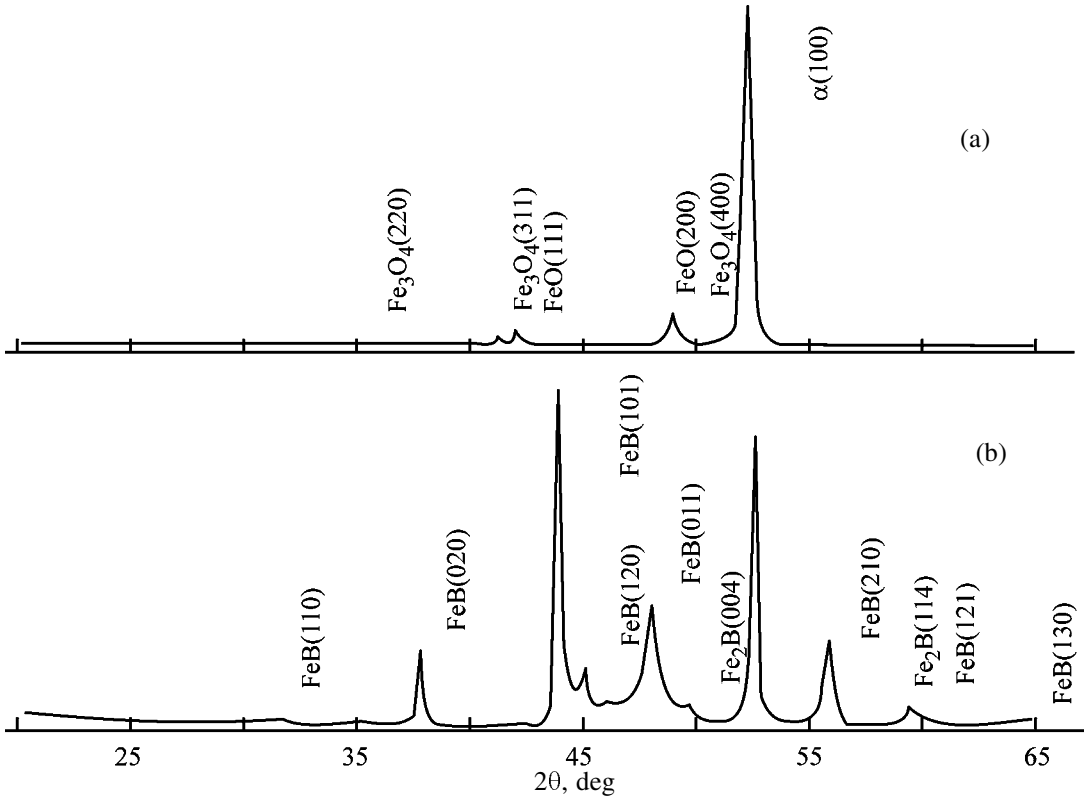


Fig. 2. X-ray diffraction pattern illustrating the phase composition of Sv 08 steel coatings. (2θ) Bragg angle. (a) Initial state (flame spraying) and (b) that upon boronizing.

example, this time does not exceed several minutes in boronizing in a melt of borax with 40 wt % B_4C. This time is sufficient for a developed zone of a solid solution of boron to be formed in the support.

The saturation of the samples was studied at temperatures of 1073, 1123, and 1173 K. During the first hour, the kinetic curves (Fig. 4) show high rates of formation of the boride layer and a nearly linear time dependence of the thickness. As the thickness of the saturated layer increases, the curves gradually pass into a parabola. The boride layer formed in the initial stages of the process is presumably composed of FeB.

An X-ray phase analysis of samples boronized to varied extent indicated that the phase composition of the boride layers is determined by the chemical composition of the saturating powder mixtures (Fig. 2). The true rate of saturation of the samples with boron was found by graphical analysis of the curve describing the dependence of the thickness of the boride layer on time t. For this purpose, tangents were drawn at several points of the curve. Further, their slopes were used to find the true saturation rate v ($\mu m\ h^{-1}$):

$$v_s = \tan\varphi.$$

The activation energy Q_a was calculated from the slope of the $\log k$–$1/T$ dependence by the formula

$$Q_a = 2.3R\tan\alpha,$$

where R is the gas constant, and α is the tangent slope.

The kinetic and energetic parameters of the saturation of the samples with boron are listed in Table 2.

The main task in the structural study of the sprayed coatings was to examine the kinetics of formation of diffusion layers on the surface of gas-thermal coatings, which affect the protective properties of the coatings. The structure of a coating composed of Sv 08 steel not subjected to any additional hardening treatment has the form of flattened particles with oxide films and separate poorly coated regions on the periphery. The transition zone has no region of interaction between the sprayed particles and the base metal. The coating has small characteristic closed pores.

The multilayer structure of a sprayed coating subjected to single-phase thermal-diffusion boronizing is shown in Fig. 5b. The outer unetchable layer of the coating, with a thickness of about 120–140 μm, has a needle-like structure characteristic of the boronizing process. At a larger depth lies a layer having no distinct boundaries between the sprayed particles. This layer is formed via reduction of oxide films in the

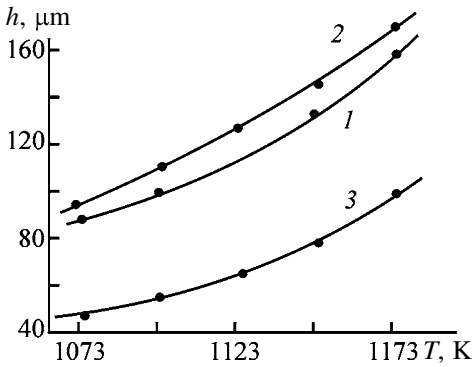


Fig. 3. Thickness h of the boride layer on GTS coatings vs. the saturation temperature T. (*1, 2*) Single- and two-phase boronizing of sprayed Sv 08 steel and (*3*) monolithic steel 10.

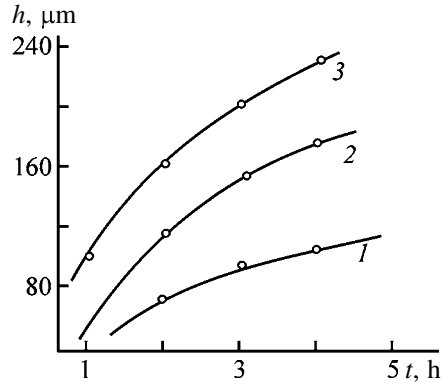


Fig. 4. Thickness h of the boride layer vs. the saturation time t (two-phase boronizing). Saturation temperature (K): (*1*) 1073, (*2*) 1123, and (*3*) 1173.

course of thermal-diffusion saturation. The deepest is the 180–250-μm-thick unreacted layer of the coating. Pores in the upper and lower layers of the main coating differ in size and shape, which points to a certain mechanism of diffusion in thermal treatment of the sprayed coating in a powder saturating medium.

The sprayed coating hardened by two-phase boronizing (Fig. 5c) has a denser structure, compared to the untreated coating. A specific feature of this coat-

Table 2. Kinetic and energetic parameters of the saturation process

Material	Boronizing temperature, K	v_s, $\mu m\ h^{-1}$	Q, $kJ\ mol^{-1}$
Steel 10	1073	12	
monolithic	1123	18	95.6
substrate	1173	30	
GTS	1073	20	
coating	1123	29	69.5
Sv 08	1173	40	

Table 3. Corrosion rate of steel coatings deposited by various methods

Sample no.	Coating deposition method	Coating material	Type of saturation	I_{cor}, A m^{-2}	k_{cor}, g m^{-2} h^{-1}
1	No coating	Steel 10	No saturation	0.0089	0.00610
2	Electric arc	Sv 08	No saturation	0.0069	0.00476
3	Electric arc	Sv 08	Single-phase boronizing	0.0072	0.00497
4	Flame	Sv 08	Two-phase boronizing	0.0070	0.00483

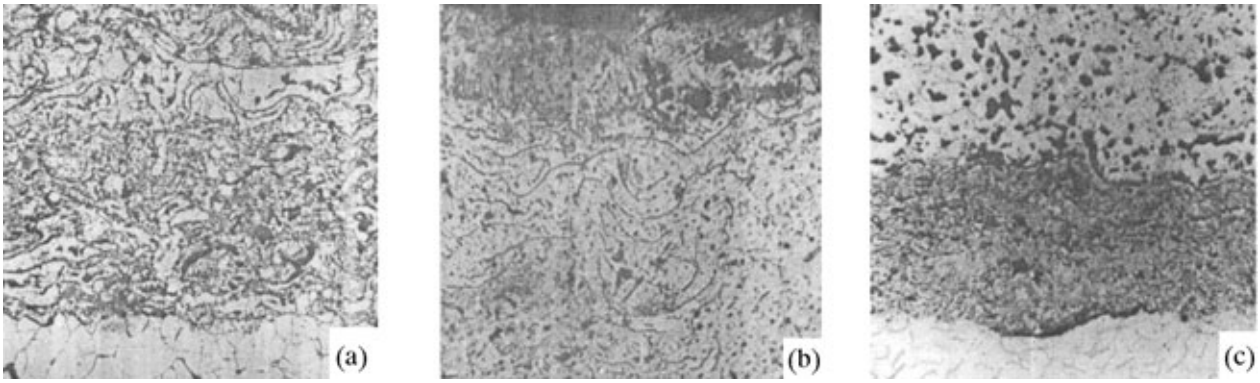


Fig. 5. Microstructure of GTS coatings (×100 magnification). (a) Sprayed coating in the initial state and (b, c) coatings subjected to single- and two-phase boronizing.

ing is the presence of comparatively coarse pores and a deep transition zone (about 80–90 μm).

The protective properties of hardened GTS coatings were examined. An analysis of the time dependence of the corrosion potential demonstrated that the potentials of the samples shift in the course of time into the negative region. At the same time, the surface potentials of the coating material become more positive, which indicates that the passivation properties of the samples studied are improved.

The saturation of the sprayed low-carbon steel coatings with boron leads to a decrease in the corrosion current density and, accordingly, in the corrosion rate of the samples (Table 3). Upon the boronizing, the corrosion current density reaches values of 0.0047–0.0049 A m^{-2}.

Thus, thermal-diffusion saturation by boronizing makes it possible to improve the critical parameters to such an extent that the coating can spontaneously pass into the passive state under the passivating action of those oxidizing components which are present in a corrosive medium under natural conditions.

CONCLUSIONS

(1) A study of the mechanism by which a boride layer is formed revealed that thermal-diffusion saturation of sprayed coatings in powder media results in that the defectiveness of phase boundaries, leading to an increase in the actual contact area and activating the chemical interaction between the contacting materials, decreases dramatically. The true saturation rate is about 12–40 μm h^{-1}, and the value of the apparent activation energy of the saturation process (69.5–95.6 kJ mol^{-1}) indicates that the saturation is diffusion-controlled.

(2) It was found that sprayed coatings modified with boron have a multilayer structure constituted by two boride zones of total thickness 300–320 μm and a diffusion-porosity zone. Iron boride FeB is formed in the 30–50-μm-thick surface layer. FeB has a microhardness of 14 500–16 000 MPa and simultaneously can serve as a corrosion-protective layer.

REFERENCES

1. Kudinov, V.V. and Bobrov, G.V., *Nanesenie pokrytii napyleniem: Teoriya, tekhnologiya i oborudovanie* (Coating Deposition by Spraying: Theory, Technology, and Equipment), Moscow: Metallurgiya, 1992.
2. Vityaz', P.A., Ivashko, V.S., and Il'yushchenko, A.F., *Teoriya i praktika naneseniya zashchitnykh pokrytii* (Theory and Practice of Deposition of Protective Coatings), Minsk: Belorusskaya Nauka, 1998.
3. Vityaz', P.A., Azizov, R.O., and Belotserkovskii, M.A., *Uprochnenie gazotermicheskikh pokrytii* (Hardening of Gas-Thermal Coatings), Minsk: Bestprint, 2004.
4. Ganiev, I.N., Yunusov, I., and Krasnoyarskii, V.V., *Zh. Prikl. Khim.*, 1987, vol. 60, no. 9, pp. 2119–2123.

ISSN 1070-4272, Russian Journal of Applied Chemistry, 2006, Vol. 79, No. 11, pp. 1839–1843. © Pleiades Publishing, Inc., 2006.
Original Russian Text © A.P. Savost'yanov, V.G. Bakun, 2006, published in Zhurnal Prikladnoi Khimii, 2006, Vol. 79, No. 11, pp. 1860–1864.

CATALYSIS

Relationship between the Selectivity of the Fischer–Tropsch Process and Type of Pore Structure of Cobalt Catalysts

A. P. Savost'yanov and V. G. Bakun

Southern-Russia State Technical University (Novocherkassk Polytechnic Institute), Novocherkassk, Rostov oblast, Russia

Received April 13, 2006

Abstract—The dependence of the selectivity and output capacity of the Fischer–Tropsch process with respect to liquid and solid hydrocarbons on pore structure parameters of a catalyst was determined for the example of a cobalt catalyst produced by impregnation of a preformed aluminosilicate support. The results obtained are analyzed in terms of the diffusion–kinetic theory.

DOI: 10.1134/S107042720611019X

In synthesis of hydrocarbons from CO and H_2 by the Fischer–Tropsch method, a three-phase system constituted by a gas (reactants and reaction products), liquid (C_{11+} reaction products), and solid (catalyst) is formed in the reaction zone. Accumulation of condensed hydrocarbons in catalyst pores may lead to a decrease in the rate of delivery of the reactants (CO and H_2) to the active centers of the catalyst or that of removal of synthesis products to the outer surface of the catalyst and into the flow core.

There is contradictory published evidence concerning the relationship between the diffusion and kinetic factors of the process. The activation energies are 30–125 kJ mol^{-1} [1–6]. E_a = 65–75 kJ mol^{-1} for coarse grains (1–3 mm) and 125 kJ mol^{-1} for fine grains (0.11–0.18 mm) [2, 3]. According to the results obtained in the differential reactor of a flow-through circulation installation [5], E_a = 30–69 kJ mol^{-1} for 0.25–1.0-mm metallic (Ni, Ru, Rh, Co) catalysts on γ-Al_2O_3 supports. For example, a conclusion has been made that the key factors responsible for the selectivity of a catalyst in the Fischer–Tropsch process are its porosity and particle size, which control the relative rates of mass-transfer of the reactants, readsorption of α-olefin, and chemical interaction [2, 3].

It has been shown [7, 8] that synthesis of various hydrocarbon fractions at a pressure of 0.9 MPa on a catalyst with a grain size of 3–4 mm is governed by the occurrence of different diffusion stages of the process: outer-diffusion for C_5–C_{60} hydrocarbons and inner-diffusion for ceresine (C_{60+}). The possibility of controlling the selectivity with respect to liquid and solid hydrocarbons by varying the pore structure parameters of a catalyst has been revealed for the example of coprecipitated cobalt catalysts [9, 10]. However, the pore structure of catalysts of this type is governed both by the support and by the secondary pore structure whose nature largely depends on a number of additional factors (support size, coprecipitation conditions, etc.).

Of interest is a study of model catalysts, for which the effect of only a single factor, predominant pore radius, on the conversion efficiency for various groups of hydrocarbons could be traced. Catalysts produced by impregnation of preformed supports of the same chemical composition are convenient in this regard.

EXPERIMENTAL

AS-37 amorphous aluminosilicate was used as a support. The pore structure was transformed by hydrothermal treatment at a pressure of 1–1.2 MPa for 72 and 164 h (designated as ASM.72 and ASM.164, respectively) and at 8 MPa for 4 h (ASM.R8) in a 5 dm^3 autoclave. The catalysts were prepared by impregnation of a support dried at 250°C with a 55% cobalt nitrate solution at 70°C to complete saturation (impregnation time 30 min). The catalyst was dried and calcined in air to a final temperature of 300°C. A catalyst with a grain size of 2–3 mm was used in the study. The catalyst was reduced with hydrogen at 380–400°C and space velocity of hydrogen equal to 3000 h^{-1} for 30–40 min until 50–55% of cobalt was reduced. The degree of cobalt reduction was determined by volumometry. The specific surface area of

Table 1. Parameters of catalysts on an aluminosilicate support

Support	Cobalt content, %	Specific surface area, $m^2\ g^{-1}$	Pore volume, $cm^3\ g^{-1}$	Pore diameter, nm
AS-37	18.7	70	0.06	4
ASM.72	18.3	72	0.30	8
ASM.164	19.7	86	0.35	12
ASM.R8	18.9	53	0.45	80

Table 2. Contraction of synthesis gas C and yield Y (calculated for normal conditions) of C_{5+} hydrocarbons

T, °C	Parameter	Catalyst pore diameter D, nm			
		4	8	12	80
170	C, %	17	16	20	3
	Y, $g\ m^{-3}$	37	48	82	0
180	C, %	16	21	31	5
	Y, $g\ m^{-3}$	40	59	96	0
190	C, %	22	26	38	6
	Y, $g\ m^{-3}$	40	50	96	15
200	C, %	28	32	48	14
	Y, $g\ m^{-3}$	32	40	94	25
210	C, %	31	42	57	16
	Y, $g\ m^{-3}$	30	38	66	21
220	C, %	40	45	64	24
	Y, $g\ m^{-3}$	12	29	55	0
230	C, %	43	51	61	37
	Y, $g\ m^{-3}$	3	6	22	0

the reduced catalyst was measured chromatographically from thermal desorption of argon. The pore structure of the unreduced catalyst was analyzed by mercury porosimetry, i.e., the size and volume of pores with diameters of 2 nm and more were determined.

Hydrocarbons were synthesized from CO and H_2 in a 30 cm^3 flow-through reactor under atmospheric pressure from an industrial synthesis gas with an H_2 : CO ratio of 2.1. The content of impurities in the feed was as follows (vol %): CO_2 8, CH_4 2, and N_2 2. The gaseous reaction products were analyzed by chromatography on two columns: C_1–C_5 were separated using Chromosorb with *n*-heptadecane as active phase; N_2, CO_2, CO, and CH_4 were separated on NaX zeolite. The composition of liquid products was determined by gas–liquid chromatography on a column with Apiezon L on Chromosorb P (flame-ionization detector, carrier gas helium).

The duration of uninterrupted tests of the catalyst in a single mode was as long as 24–48 h. No significant changes in the catalyst activity were observed in the process.

The catalysts have about the same content of cobalt, 18.3–19.7% (Table 1). The pore diameter of the catalysts varies from 4 to 80 nm. Support modification with steam leads to an insignificant increase in the surface area of the catalyst, which can be attributed, despite that the pores become larger, to an increase in the pore size. Experimental data on the catalytic properties of Co/AS systems are listed in Table 2.

An increase in the diameter of catalyst pores to 8 nm is sufficient for an increase in the C_{5+} yield by 10 $g\ m^{-3}$ at 170–210°C, but fails to improve significantly the conversion of the starting substances into reaction products. Upon an increase in the catalyst pore diameter to 12 nm, the specific surface area is about the same (72 and 85 $m^2\ g^{-1}$), but the efficiency of synthesis grows because of the increase in contraction, and synthesis can be performed purposefully, with high selectivity with respect to C_5–C_{20} hydrocarbons. In the presence of this catalyst, the highest yield of C_{5+} hydrocarbons is obtained (82–96 $g\ m^{-3}$) and the maximum conversion of the reaction gas mixture (48–64%) is reached at 200–230°C. Structural differences between the catalysts are reflected in the composition of the hydrocarbons synthesized (Table 3).

The products obtained on the Co/ASM catalysts have an increased content of branched olefins and paraffins C_8–C_{14} and lower content of paraffins C_{15}–C_{18}.

Figures 1 and 2 show the calculated performances of the catalysts in conversion of CO and synthesis of C_{5+}. It can be seen that the performance of the catalyst in CO conversion steadily increases with temperature, whereas that in synthesis of liquid hydrocarbons passes through a maximum in the temperature range 190–210°C.

The activation energy of CO hydrogenation (Fig. 3) on catalysts with a predominant pore diameter of 4–12 nm is virtually constant and equal to 55 $kJ\ mol^{-1}$. An increase in the average pore diameter to 80 nm makes it possible to diminish the diffusion limitations and to bring the process closer to the kinetic control (E = 84 $kJ\ mol^{-1}$). In this case, the selectivity with respect to C_{5+} substantially decreases, as it was noted above. As the pore size grows from 4 to 12 nm, the

Table 3. Composition of hydrocarbons

Catalyst	Olefins, %	Paraffins, %					Paraffins of normal structure, %				
		C_5–C_7	C_8–C_{10}	C_{11}–C_{14}	C_{15}–C_{18}	C_{19+}	C_5–C_7	C_8–C_{10}	C_{11}–C_{14}	C_{15}–C_{18}	C_{19+}
Co/AS	7	1	27	34	22	3	1	23	35	20	3
Co/ASM.72	15	3	21	41	16	4	2	11	26	14	4
Co/ASM.164	18	3	21	38	17	3	5	12	32	15	2

activation energy of C_{5+} synthesis in the temperature range 170–200°C increases from 23 to 58 kJ mol^{-1} (Fig. 4).

Thus, it was found that the hydrogenation of CO and selectivity with respect to C_{5+} are strongly affected by diffusion factors. However, their influence is ambiguous. The acceleration of reactant transport with an increase in pore diameter hinders readsorption of olefins and diminishes the performance with respect to high-molecular-weight products. The latter is confirmed by the increased content of olefins in products synthesized on catalysts with a high degree of transformation of the pore structure and, accordingly, with large pore diameter (Table 3). The content of olefins is 7% on the Co/AS catalyst and 15 and 18% on catalysts with pore diameters of 8 and 12 nm, respectively.

All the catalysts had virtually the same composition and the study was carried out in a comparatively narrow temperature range. Therefore, it can be suggested that the formation mechanism of primary intermediates remains the same and the gross differences in the process selectivity are due solely to the features of the pore structure of the catalysts. In this context, it is advisable to verify the applicability of concepts of the kinetic–diffusion model of the process, suggested in [3].

The diffusion and kinetic factors are related to structural characteristics of a catalyst by the Thiele modulus. The second factor χ depends only on the

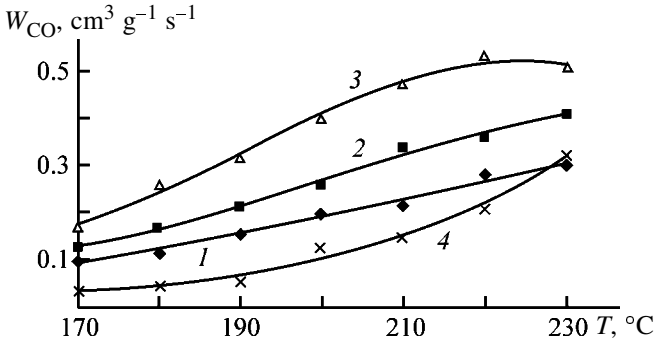


Fig. 1. Catalyst performance W_{CO} in CO conversion vs. temperature T for catalysts with different predominant pore diameters D. Pore diameter (nm): (*1*) 4, (*2*) 8, (*3*) 12, and (*4*) 80; the same for Figs. 2–4.

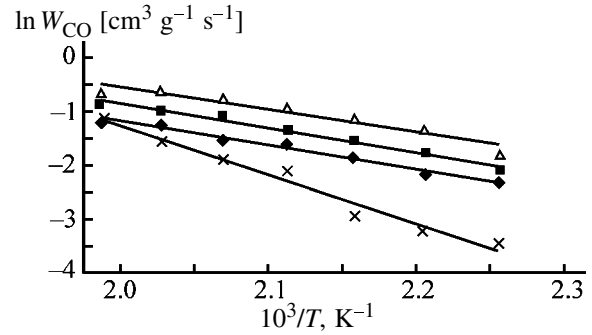


Fig. 3. Logarithm of catalyst performance in CO conversion, ln W_{CO}, vs. temperature T.

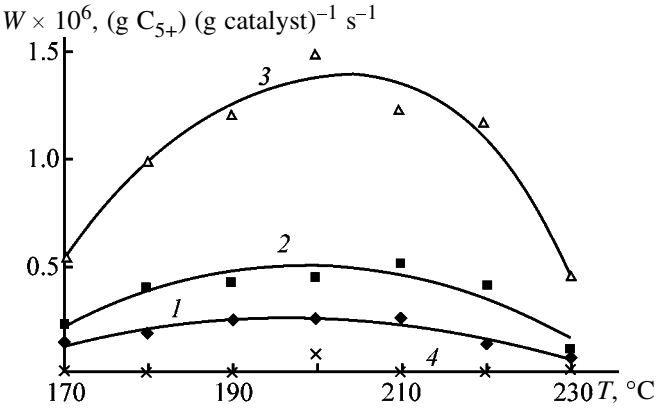


Fig. 2. Catalyst performance W in synthesis of C_{5+} vs. temperature T for catalysts with different predominant pore diameters D.

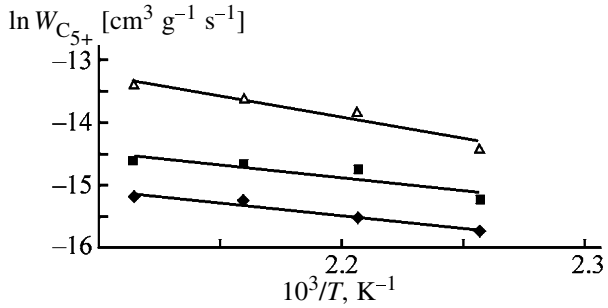


Fig. 4. Logarithm of catalyst performance in synthesis of C_{5+}, ln $W_{C_{5+}}$, vs. temperature T.

Table 4. Activity of Co/AS catalysts with varied pore structure (P = 0.9 MPa, feed space velocity 94–100 h^{-1})

d, nm	T_{synth}, °C	C, %	Yield of hydrocarbons, g m^{-3}			
			CH_4	C_2–C_4	C_{5+}	total
4	181	43	32	16	94	142
88	197	52	35	18	73	126

structural characteristics of the catalyst:

$$\chi = R_0^2 \varphi \theta_m / r_p, \quad (1)$$

where R_0 is the grain radius; φ, relative porosity; θ_m, density of Co distribution (g-at. Co/m^2); and r_p, pore radius (m).

The results obtained by processing the experimental data for temperatures of 190, 200, and 210°C in terms of Eq. (1) are shown in Fig. 5. These data are close to the recommended values of the structural factor [3].

Catalysts on the untreated (pore diameter 4 nm) and modified (pore diameter 8 nm) aluminosilicate were tested in synthesis of hydrocarbons under elevated pressure (Table 4).

Differences in the nature of the pore structure of the catalysts are manifested in the amount and composition of synthesis products. A considerably smaller amount of C_{5+} hydrocarbons was obtained on the catalyst with a predominant pore radius of 8 nm.

When predicting the way of development of theoretical concepts concerning formation of cobalt catalysts with controllable selectivity with respect to liquid and solid hydrocarbons, it can be assumed that these concepts may be based on determining the extent of utilization of the active surface of the catalysts. The Thiele modulus makes it possible to take into account both the kinetic and structural factors affecting the extent of surface utilization. The first, kinetic factor is largely determined, as regards the Fischer–Tropsch process, by the state of cobalt on the surface and primarily by its dispersity and by the electronic interaction in the Co–Co_xO_y–support system [11].

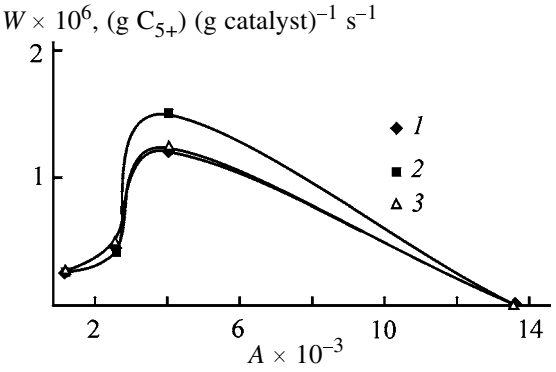


Fig. 5. Effect of the structural factor A on the performance W of the catalysts in C_{5+} synthesis at different temperatures. Temperature (°C): (*1*) 190, (*2*) 200, and (*3*) 210.

The second, structural factor, which combines the grain size and porosity, relates the time necessary for readsorption of primary α-olefins to their mass-transfer within the catalyst grain and, in the end, to the process selectivity with respect to separate groups of hydrocarbons.

When considering the concept suggested, it is necessary to analyze the arising contradictions. In particular, the chemical nature of a support cannot, at first sight, affect the process selectivity in this case. However, numerous data point to the opposite [12].

In our opinion, the contradiction is eliminated if we take into account the following. First, the chemical nature of the support affects the interaction in, and properties of, the $CoCo_xO_y$–support system in accordance with the two-center model of the active center [11]. Second, the structural factor of the Thiele modulus contains as parameter the Co distribution density, i.e., a quantity close in physical meaning to the dispersity of the active component.

CONCLUSIONS

(1) The activation energy of CO hydrogenation on catalysts with a pore diameter of 4–12 nm is virtually the same (55 kJ mol^{-1}). An increase in the average pore diameter to 80 nm diminishes the diffusion limitations and brings the process closer to kinetic control (E = 84 kJ mol^{-1}), with the selectivity with respect to C_{5+} decreasing dramatically. The activation energy of synthesis of condensed hydrocarbons (C_{5+}) grows from 23 to 58 kJ mol^{-1} as the pore size increases from 4 to 12 nm. The products synthesized on catalysts with a high degree of transformation of the pore structure contain a 2.5 times larger amount of olefins.

(2) With the conditions governing the dispersed

state of cobalt, its electronic interaction in the Co–Co_xO_y–support system, and the structural factor (χ in the Thiele modulus) determined, it is possible to control the activity and selectivity of cobalt catalysts for synthesis of hydrocarbons from CO and H_2.

REFERENCES

1. Rapoport, I.B., *Iskusstvennoe zhidkoe toplivo (khimiya i tekhnologiya)* (Synthetic Liquid Fuel (Chemistry and Technology)), Moscow: Gos. Nauchno-Tekh. Izd. Neftyanoi i Gorno-Toplivnoi Literatury, 1955.
2. Jglesia, E., Stuart, L. Soled, Baumgartner, J.E., and Reyes, S., *Top. Catal*., 1995, no. 2, pp. 17–27.
3. Jglesia, E., Stuart, L. Soled, Baumgartner, J.E., and Reyes, S., *J. Catal*., 1995, vol. 153, pp. 108–122.
4. Golodets, G.I., Pavlenko, N.V., and Tripol'skii, A.I., *Kinet. Katal*., 1987, vol. 28, no. 4, pp. 883–887.
5. Lahtinen, J., Anraki, T., and Somorjai, C., *Catal. Lett*., 1994, vol. 25, pp. 241–250.
6. Kiperman, S.L., *Osnovy khimicheskoi kinetiki v geterogennom katalize* (Fundamentals of Chemical Kinetics in Heterogeneous Catalysis), Moscow: Khimiya, 1979.
7. Savost'yanov, A.P., Bakun, V.G., Budtsov, V.S., and Taranushich, V.A., *Khim. Tverd. Topl*., 2001, no. 3, pp. 78–84.
8. Savost'yanov, A.P., Budtsov, V.S., and Taranushich, V.A., in *Sovremennye problemy khimicheskoi tekhnologii neorganicheskikh veshchestv: Sbornik nauchnykh trudov Mezhdunarodnoi nauchno-tekhnicheskoi konferentsii* (Modern Problems of Chemical Technology of Inorganic Substances: Proc. Int. Scientific and Technical Conf.), Odessa, 2001, pp. 137–140.
9. Taranushich, V.A., Savost'yanov, A.P., Mezhov, V.D., and Bakun, V.G., *Izv. Sev.-Kavk. Nauchn. Tsentra Vyssh. Shk., Tekh. Nauki*, 1983, no. 3, pp. 65–68.
10. Lapidus, A.L., Budtsov, V.S., Savost'yanov, A.P., et al., *Neftekhimiya*, 1991, vol. 31, no. 5, pp. 626–629.
11. Minachev, Kh.M., Lapidus, A.L., and Krylova, A.Yu., *Khim. Tverd. Topl*., 1993, no. 6, pp. 7–20.
12. Slivinskii, E.V., Kuz'min, A.E., Abramova, A.V., et al., *Neftekhimiya*, 1998, vol. 38, no. 4, pp. 243–268.

ISSN 1070-4272, Russian Journal of Applied Chemistry, 2006, Vol. 79, No. 11, pp. 1844–1848. © Pleiades Publishing, Inc., 2006.
Original Russian Text © V.P. Zakharov, 2006, published in Zhurnal Prikladnoi Khimii, 2006, Vol. 79, No. 11, pp. 1865–1869.

PROCESSES AND EQUIPMENT OF CHEMICAL INDUSTRY

Synthesis of Antiagglomeration Agent Based on Calcium Stearate for Synthetic Rubbers in Tubular Apparatus

V. P. Zakharov

Bashkir State University, Ufa, Bashkortostan, Russia

Received November 25, 2005; in final form, April 2006

Abstract—Formation of an antiagglomeration agent for synthetic rubbers, based on an aqueous suspension of calcium stearate, by the reaction a highly concentrated solution of calcium chloride (up to 40 wt %) and a dilute solution of potassium stearate (up to 5 wt %) in a small tubular apparatus of diffuser–confuser design was studied.

DOI: 10.1134/S1070427206110206

An integral stage in large-tonnage manufacture of synthetic rubbers by polymerization in solution is isolation of the polymer [1, 2]. To remove residual amounts of the solvent and unchanged monomer, the reaction mixture is treated, on reaching the required conversion and decomposing the catalyst, with live steam in the stage of aqueous degassing. To prevent coalescence of the polymer crumb in the deaerator and to reduce the viscosity of process flows in the degassing stage, an antiagglomeration agent is introduced into the reaction mixture in the form of a dilute suspension [1, 2]. Because of the formation of a loose precipitate, low-soluble calcium carboxylates and, in particular, calcium stearate are most frequently used as antiagglomeration agents. Particles of the antiagglomeration agent prevent agglomeration of the polymer crumb and enable its transportation to the drying stage by forming a structural-mechanical barrier [3] at the interface between the aqueous phase and the polymer. Apparently, the antiagglomeration capacity of the aqueous suspension of calcium stearate and, in the end, its expenditure and residual content in the finished product (at an expenditure of 7.5 kg of stearic acid and 1.5–2.5 kg of calcium chloride per ton of the polymer, the content of the antiagglomeration agent in the polymer should not exceed 1.1 wt %) are largely determined by the granulometric composition of particles of the active substance.

Under industrial conditions, calcium stearate is obtained just before introduction into a polymer solution (freshly prepared antiagglomeration agent) by the two-stage scheme (St = $C_{17}H_{35}COO$) [1, 2]:

$$HSt + KOH \longrightarrow KSt + H_2O,$$

$$2KSt + CaCl_2 \xrightarrow{Fast} CaSt_2\downarrow + 2KCl.$$

In the second stage, an irreversible reaction of ion exchange occurs at a high rate to give the solid phase (condensation method for synthesis of disperse systems) [3]. As a consequence, the granulometric composition of the suspension of the antiagglomeration agent can be affected by varying the conditions under which the reaction of potassium stearate and calcium chloride is performed.

Under industrial conditions, the antiagglomeration agent based on calcium stearate is obtained directly in the pipeline for circulating water. The content of stearic acid in the solution is 4.3–5.3 wt %, at an average flow rate of 3 $m^3 h^{-1}$ and temperatures of up to 75°C. The content of $CaCl_2$ in the aqueous solution is 2–3 wt %, at an average flow rate of 1.8 $m^3 h^{-1}$ and temperatures of 20–25°C. The content of calcium stearate in the resulting solution does not exceed 5 wt %. The low motion velocities of the starting solutions in their mixing in the pipeline (not exceeding 0.1 m s^{-1} at a total flow rate of 1.2 to 8 $m^3 h^{-1}$) predetermine the poor efficiency of reagent mixing and lead to formation of rather coarsely dispersed particles (diameter about 100–500 μm [4]).

The aim of the present study was to examine the fundamental aspects of variation of the granulometric composition of particles of the calcium stearate suspension with the conditions under which aqueous solutions of potassium stearate are reacted with $CaCl_2$.

The high rate of the reaction under consideration and the formation of the solid phase necessitate vigor-

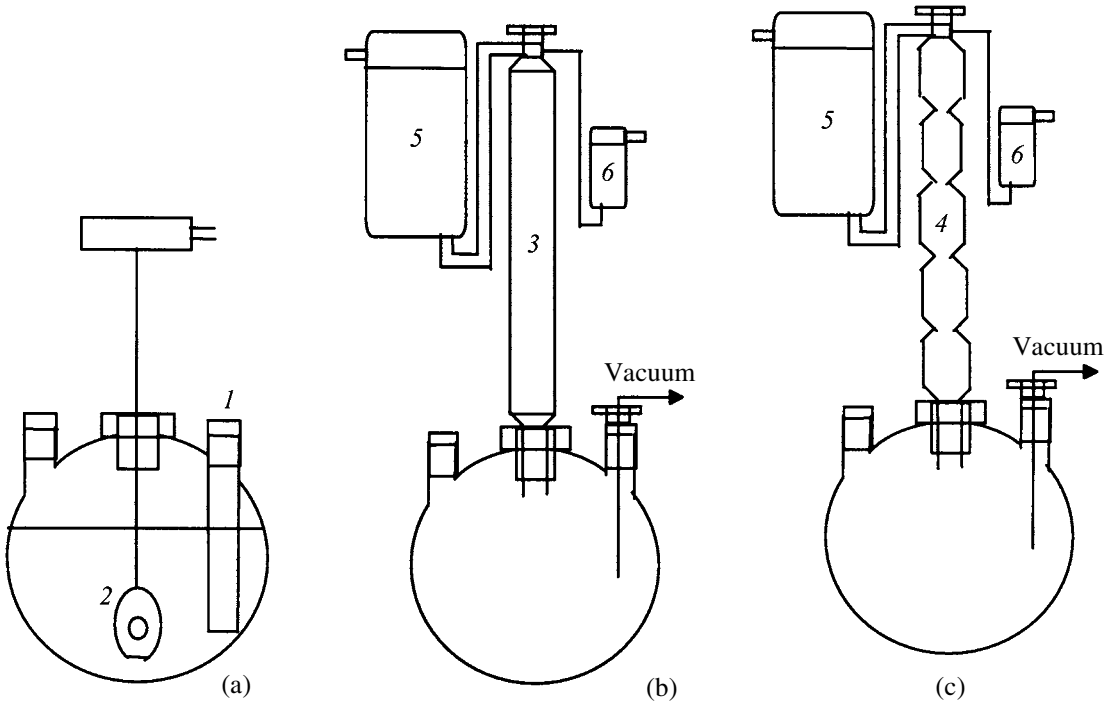


Fig. 1. Schematic of the experimental installation for synthesis of the antiagglomeration agent based on calcium stearate: (*1*) reflecting partition and (*2*) mechanical stirrer; tubular turbulent apparatus: (*3*) cylindrical and (*4*) of diffuser–confuser design; vessel: (*5*) for KSt and (*6*) for $CaCl_2$.

ous agitation of the reaction mixture directly in the reaction zone, which is significantly smaller in size. For this purpose, calcium stearate was synthesized in tubular turbulent apparatus of cylindrical and diffuser–confuser design [5, 6]. Potassium stearate was reacted with $CaCl_2$ in various reaction devices. The first is a volume apparatus (vessel) with a mechanical stirrer (~2000 rpm, method 1), with an additional turbulizing device (reflecting partition) mounted in the bulk of the reaction mixture to create intense turbulent agitation in the vertical direction (Fig. 1a). The second and third are tubular turbulent apparatus of cylindrical (Fig. 1b, method 2) and diffuser–confuser (Fig. 1c, method 3) designs [7]. The tubular apparatus for synthesis of calcium stearate had the following dimensions: diameter of the wide part (diffuser) 24 mm, that of the narrow part (confuser) 10 mm, length of the diffuser–confuser section 48 mm, overall reactor length ~480 mm, and diffuser opening angle $45° \pm 5°$.

To reduce the viscosity of the aqueous solution of potassium stearate, it was preliminarily heated to 75°C. The granulometric composition of the suspension was analyzed by the microscopic method, with a differential particle-size distribution curve plotted and then the average integral diameter and polydispersity factor calculated [7].

Of particular importance in the condensation method for synthesis of a disperse system are local concentration supersaturations of a poorly soluble reaction product, which serve as nucleation centers of the solid phase. Therefore, we primarily studied the effect of the concentration of reactants and reaction products on the granulometric composition of the suspension of the antiagglomeration agent. Raising the concentration of $CaCl_2$ at a fixed content of potassium stearate in the aqueous solution leads to a decrease in the particle size (Fig. 2). In this case, a significant change in the diameter occurs at the content of $CaCl_2$ in water of up to 2–3 wt %. In addition, the suspension particle size steadily decreases on passing from method 1 to method 2, and further to method 3, which correlates with the increase in the intensity of turbulent agitation [5, 6]. A similar influence is exerted on the granulometric composition of the antiagglomeration agent by changes in the concentration of the aqueous solution of potassium stearate (Fig. 3). However, the dependences are in this case smoother, without any pronounced breaks, and the particle diameter steadily decreases as the concentration of the starting reagent becomes higher. This is apparently due to the increased viscosity of the potassium stearate solution, which is also the reason for the fact that

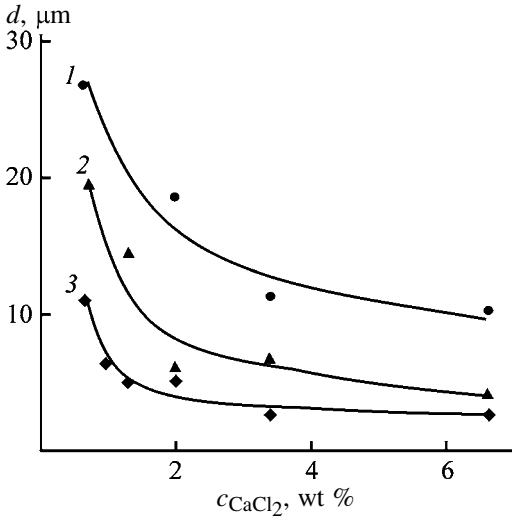


Fig. 2. Suspension particle diameter d vs. the $CaCl_2$ content c_{CaCl_2}. (*1*) Volume apparatus; tubular turbulent apparatus: (*2*) cylindrical and (*3*) of diffuser–confuser design; the same for Fig. 4. c_{KSt} = 5 wt %.

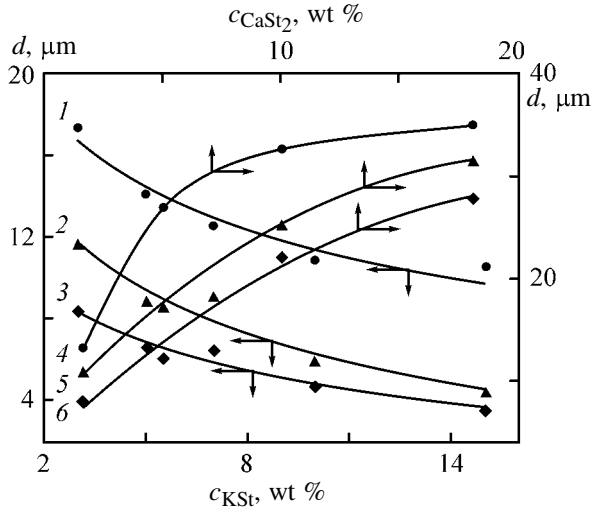


Fig. 3. Suspension particle diameter d vs. (*1–3*) KSt content c_{KSt} (c_{CaCl_2} = 2 wt %) and (*4–6*) $CaSt_2$ content. (*1, 4*) Volume apparatus; tubular turbulent apparatus: (*2, 5*) cylindrical and (*3, 6*) of diffuser–confuser design.

the limiting content of the reagent does not exceed 15 wt %. At a fixed ratio of the reactant concentrations, an increase in the content of the solid phase in the resulting calcium stearate suspension results in that the particle size grows (Fig. 3). In all cases, particles with the minimum, under certain experimental conditions, diameter are obtained when the reaction is carried out in the tubular turbulent apparatus of the diffuser–confuser design.

The dependences obtained can be attributed to variation of the ratio between the rates of nucleation and crystal growth. An increase in the concentration of one of the reactants at fixed low content of the other leads to a rise in the rate of solid phase nucleation because zones of local supersaturation, which are the driving force of formation of a new phase, appear in the reaction mixture. A decrease in the concentration of the second reactant provides a low rate of particle growth because of the diffusion limitations on motion of molecules from the bulk of the aqueous phase to the crystal surface, which, in the end, leads to a decrease in the particle size of the suspension. Apparently, it is advisable to use in manufacture of synthetic rubbers solutions of potassium stearate with its content not exceeding 5 wt % and a concentrated $CaCl_2$ solution. In view of the fact that the solubility of $CaCl_2$ in water is about 50 wt % (at 30°C), it is advisable to work with solutions containing up to 40 wt % $CaCl_2$ to obtain a finely dispersed suspension of the antiagglomeration agent and preclude premature crystallization of $CaCl_2$ on walls of the process equipment. Use of a small tubular turbulent apparatus of the diffuser–confuser design leads to an increase in the nucleation rate via intensive micromixing in the reaction zone, with the crystal growth rate growing to a lesser extent, which leads to a significant change in the granulometric composition of the suspension formed.

It should be noted that the formation of a structural-mechanical barrier via adsorption of calcium stearate particles in stabilization of the polymer crumb in the degassing stage depends to a greater extent on the particle size, and to a lesser extent on the particle size distribution. Data on changes in the polydispersity factor are not presented here, because the changes revealed in [7] for the case of synthesis of barium sulfate are similar to those for systems based on calcium stearate. Homogeneous systems with the minimum possible, under the experimental conditions, polydispersity factor are synthesized in tubular turbulent apparatus of diffuser–confuser design.

It is well known [3] that all disperse systems show poor aggregation stability because of the developed phase boundary surface and uncompensated surface energy. In addition, calcium stearate passes under industrial conditions, before being directly introduced into a polymer solution in the degassing stage, through a number of process units (pipeline, buffer vessel, etc.). This is accompanied by partial settling and inevitable agglomeration of particles. Therefore, it seemed appropriate to estimate the probability of agglomeration of freshly prepared calcium stearate upon keeping for varied time without agitation. For this purpose, we modeled under laboratory conditions the

processes that occur in real systems when a freshly prepared suspension is kept and partial settling of the reaction mixture is caused by gravity forces.

In keeping a suspension produced by methods 1–3, particles of the solid phase become coarser despite the low content of KSt and $CaCl_2$ (≤ 5 wt %) in the disperse systems obtained (Fig. 4). For particles formed in the volume mixing apparatus by method 1, the increase in size is about 30% after 40 min of keeping without agitation. Virtually no further changes occurred in the granulometric composition of calcium stearate. Because of the small initial size of suspension particles obtained in tubular turbulent apparatus of cylindrical and diffuser–confuser designs, they become virtually 4 times larger in 60 min. However, the final particle size of suspensions preliminarily produced in a tubular turbulent apparatus of diffuser–confuser design (method 3) and kept in the absence of agitation remains smaller than that for methods 1 and 2. Thus, agglomeration of solid phase particles is possible in motion of a suspension of a freshly prepared antiagglomeration agent through units of the process equipment before the degassing stage. The decrease in the antiagglomeration capacity of a more coarsely disperse suspension of calcium stearate may lead to an inadmissible increase in the content of the antiagglomeration agent in the finished product. The experimental data obtained (Fig. 4) indicate that additional fragmentation of particles of the antiagglomeration agent based on calcium stearate is necessary prior to using the suspension for stabilization of polymer crumb in the deaerator.

A hydrodynamic treatment of a suspension preliminarily produced and kept for a certain time in a volume apparatus with an additional turbulizing device leads to an only slight decrease in the particle size of the disperse phase (Fig. 5). A decrease in the particle size is observed upon a hydrodynamic treatment in cylindrical tubular apparatus. The thus treated suspension has a particle size of the active substance comparable with that obtained in the case of in situ synthesis (freshly prepared without preliminary keeping) in a volume apparatus with an additionally installed turbulizing device (Fig. 5, curve *5*). Motion of a preliminarily kept suspension in a tubular turbulent apparatus of diffuser–confuser design leads, because of strong shear deformations caused by the continuous phase, to formation of particles not exceeding in size those produced in situ in a volume apparatus (Fig. 5, curve *3*).

It should be noted that treatment by methods 1–3 of a suspension kept for varied time leads to the same

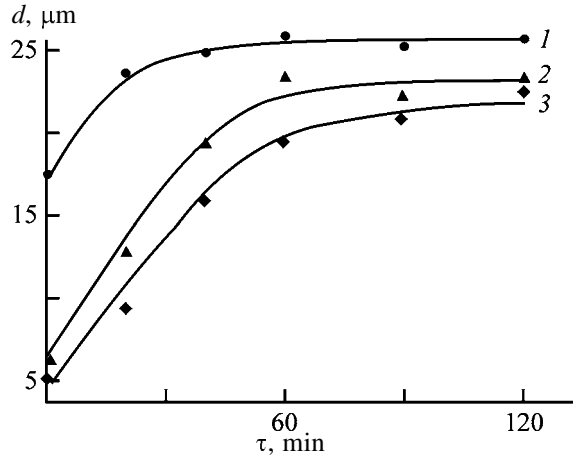


Fig. 4. Suspension particle diameter d vs. time τ of keeping without agitation. c_{KSt} = 5 wt %, c_{CaCl_2} = 2 wt %.

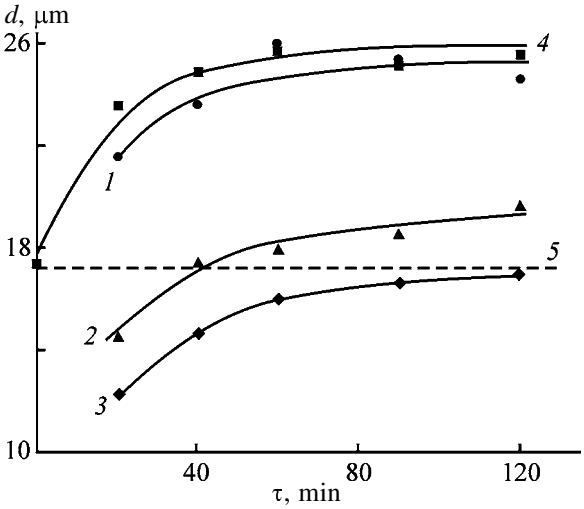


Fig. 5. (*4*) Diameter d of particles obtained in the volume apparatus vs. the time τ of keeping the suspension without agitation. Treatment of preliminarily obtained particles in (*1*) volume apparatus, (*2, 3*) tubular turbulent apparatus of (*2*) cylindrical and (*3*) diffuser–confuser design; (*5*) in situ synthesis.

decrease in particle size. This is manifested in a parallel shift of the plots describing the dependence of the particle size of calcium stearate on the keeping time for various synthesis conditions (Fig. 5, curves *1–3*) with respect to that for "aging" of the antiagglomeration agent (Fig. 5, curve *4*). This indicates that the shear deformations caused by the continuous phase govern the fragmentation of preliminarily obtained and kept suspension particles, with the intensity of the hydrodynamic action being the highest, among the reaction devices considered, for the tubular apparatus of diffuser–confuser design.

It should be noted that satisfying the industrial conditions in synthesis of the antiagglomeration agent

based on calcium stearate in tubular turbulent apparatus makes it possible to obtain an aqueous suspension with pH 10.5–12. Analysis of published data [1] shows that this pH value of the solution is the optimal both for stabilization of the polymer crumb and for recovery of the unreacted monomer and solvent from the reaction mixture in the degassing stage.

Thus, optimization of the reactant concentration in synthesis of calcium stearate based antiagglomeration agent for synthetic rubbers enables effective control over the granulometric composition of the active substance. All other conditions being the same, a suspension with the minimum possible, under the experimental conditions, particle size of the solid phase can be obtained in a small tubular turbulent apparatus of diffuser–confuser design. Variation of the reactant concentrations, combined with improvement of the type and design of the reaction device, make it possible to achieve the maximum ratio of the nucleation and crystal growth rates and, as a result, to obtain calcium stearate particles with high antiagglomeration capacity. The possibility of obtaining a high-quality product and the absence of mechanical agitating devices and mobile elements confirm that tubular turbulent apparatus of diffuser–confuser design are advantageous for production of an antiagglomeration agent based on calcium stearate for synthetic rubbers.

Performing the reaction of aqueous solutions of potassium stearate with calcium chloride in tubular turbulent apparatus provides a stoichiometric reaction course and shorter residence time of the reaction mixture in the apparatus. The latter factor precludes deposition of particles on walls of the process equipment and, as a result, leads to longer overhaul period, lower metal intensity of the process in the smaller reactor, lower energy consumption by the process because of the removal of mechanical stirrers from the process scheme, and higher dispersity of the antiagglomeration agent suspension obtained.

CONCLUSIONS

(1) The reaction of a concentrated solution of calcium chloride (up to 40 wt %) with a dilute solution of potassium stearate (up to 5 wt %) gives a calcium chloride based antiagglomeration agent for synthetic rubbers, which has a developed specific surface area of the phase boundary and high antiagglomeration capacity.

(2) An antiagglomeration agent with the minimum particle size of the solid phase is formed in a tubular turbulent apparatus of diffuser–confuser design both at the instant of synthesis and under a hydrodynamic treatment of a preliminarily obtained and aged aqueous suspension.

ACKNOWLEDGMENTS

The study was financially supported by the Russian Foundation for Basic Research (project no. 05-03-97903), Foundation for Support of the National Science, and Presidential Grant of the Russian Federation (no. MD-1427.2005.3).

REFERENCES

1. Kirpichnikov, P.A., Beresnev, V.V., and Popova, L.M., *Al'bom tekhnologicheskikh skhem osnovnykh proizvodstv promyshlennosti sinteticheskogo kauchuka* (Album of Flowsheets for Basic Production Facilities of the Industry of Synthetic Rubber), Leningrad: Khimiya, 1986.
2. Bashkatov, T.V. and Zhitalin, Ya.L., *Tekhnologiya sinteticheskikh kauchukov* (Technology of Synthetic Rubbers), Leningrad: Khimiya, 1987.
3. Shukin, E.D., Pertsov, A.V., and Amelina, E.A., *Kolloidnaya khimiya* (Colloid Chemistry), Moscow: Vysshaya Shkola, 1992.
4. RF Patent 2190592.
5. Berlin, Al.Al., Minsker, K.S., and Dyumaev, K.M., *Novye unifitsirovannye energo- i resursosberegayushchie vysokoproizvoditel'nye tekhnologii povyshennoi ekologicheskoi chistoty na osnove trubchatykh turbulentnykh reaktorov* (New Unified Energy- and Resource-Saving High-Performance Technologies of Enhanced Environmental Safety on the Basis of Tubular Turbulent Reactors), Moscow: NIITEKhIM, 1996.
6. Minsker, K.S., Berlin, Al.Al., Zakharov, V.P., and Zaikov, G.E., *Fast Liquid-Phase Processes in Turbulent Flows*, Netherlands: Brill, 2004.
7. Zakharov, V.P., Minsker, K.S., Sadykov, I.V., et al., *Zh. Prikl. Khim.*, 2003, vol. 76, no. 8, pp. 1302–1305.

ISSN 1070-4272, Russian Journal of Applied Chemistry, 2006, Vol. 79, No. 11, pp. 1849–1852. © Pleiades Publishing, Inc., 2006.
Original Russian Text © R.B. Bayatyan, B.E. Bayatyan, L.A. Saakyan, 2006, published in Zhurnal Prikladnoi Khimii, 2006, Vol. 79, No. 11, pp. 1870–1873.

ORGANIC SYNTHESIS AND INDUSTRIAL ORGANIC CHEMISTRY

Liquid-Phase Oxidation of Bromovinyl Compounds with Molecular Oxygen

R. B. Bayatyan, B. E. Bayatyan, and L. A. Saakyan

Expert Center of the Republic of Armenia, Yerevan, Armenia
Geratsi Yerevan State Medical University, Yerevan, Armenia

Received June 16, 2005; in final form, March 2006

Abstract—Liquid-phase oxidation of bromovinyl compounds with the aim to obtain the corresponding α-bromo acids was studied.

DOI: 10.1134/S1070427206110218

α-Bromo acids and their derivatives are of interest as intermediates in the synthesis of drugs, insecticides, fungicides, plasticizers, and stabilizes of polymers and α-amino acids against thermal oxidative degradation [1–5].

Data on liquid-phase oxidation of bromovinyl compounds are scarce [6–10]. Demole [6, 7] reported only qualitative data on the liquid-phase oxidation of bromovinyl compounds; Pericas and Serratosa [8] studied the stereochemistry of liquid-phase oxidation with molecular oxygen of certain 1-bromo-1,2-diisopropoxyethenes and showed that these compounds are very sensitive to oxygen. In particular, bubbling of oxygen through a dilute solution of 1-bromo-1,2-diisopropoxyethene in pentane results in an exothermic reaction; the oxidation is complete in 1.5 h. The reaction product, isopropyl isopropoxybromoacetate, was isolated in 87% yield by distillation after removing the solvent. Oxidation of 1,2-dibromo-3,3-diphenylmethylene-1,2-cyclobutene with molecular oxygen in benzene [9] occurs at the endocyclic double bond, with the migration of a bromine atom. The kinetics of autooxidation of tribromoethene in chlorobenzene at 303 and 313 K was studied by monitoring the oxygen uptake rate [10]. The reaction was shown to occur by the branched radical-chain mechanism; its major final stable products were bromooxirane and dibromoacetic anhydride. A probable mechanism of the autooxidation of tribromoethene was suggested.

Previously we studied the oxidation with molecular oxygen of a series of 1,1-dichloro- and 1,1-dibromochlorovinyl compounds and found that the reactions were highly selective and gave α-haloacyl chlorides in high yields [11–22]. It seemed interesting to study oxidation with molecular oxygen of bromovinyl compounds, with the aim to compare the results and discuss the general mechanism of oxidation of halovinyl compounds.

Proceeding with studies on oxidation of halovinyl compounds, we examined the oxidation of 1,2-dibromoethene **I** (1 : 4 *cis/trans* isomer mixture), tribromoethene **II**, tetrabromoethene **III**, β,β-dibromostyrene **IV**, and α,β,β-tribromostyrene **V**.

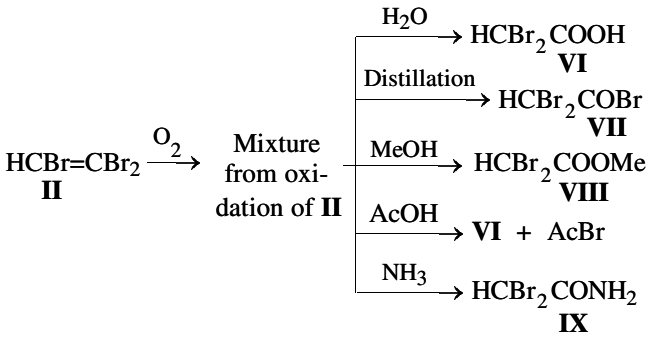
Experiments were performed on a laboratory installation in the temperature range 20–100°C at an oxygen feeding rate of 2–5 $1\,h^{-1}$.

The experiments revealed formation of bromooxiranes in the early oxidation steps; their content reaches 45–60% (determined iodometrically) at 70–80% conversion. Upon distillation, they transform into α-bromoacyl bromides. The only product of oxidation of **I** is dibromoacetic acid **VI**. A more detailed study of the oxidation of **II** with oxygen showed that pentabromoethane was also formed (15–20%) along with dibromoacetyl bromide **VII**. The amount of pentabromoethane depended on the oxidation conditions. For example, its formation was suppressed by increasing reaction temperature and oxygen feeding rate. This result can be attributed to partial removal of the released free bromine from the reaction mixture. However, the formation of free bromine does not appreciably affect the yield of **VII** (80–90% at 100% conversion).

Free bromine can be formed in the system by the reaction of HBr with peroxides accumulating in the

mixture, or by photochemical decomposition of **II** and its oxidation products.

Whereas direct distillation of the reaction mixture from the oxidation of **II** yielded acid bromide **VII**, treatment of the same mixture with water, acetic acid, alcohols, and ammonia yielded the corresponding products **VI**, **VIII**, and **IX**:



Oxidation of tetrabromoethene **III** gave tribromoacetyl bromide in high yield.

Under the similar conditions, the oxidation of **IV** and **V** gave bromo- and dibromophenylacetyl bromides, respectively, in 70–80% yields; as compared to **II**, these compounds are oxidized very slowly, i.e., the oxidation rate is strongly affected by the aromatic substituent.

The structure and purity of the compounds were checked by comparison of their physicochemical constants with the published data, and also by GLC.

The most interesting feature of liquid-phase oxidation of bromovinyl compounds with oxygen is high selectivity of the reaction at temperatures below 70°C, with the formation of α-bromoacyl bromides. With an increase in the temperature, the oxidation rate increases insignificantly, but the selectivity is lost, and other products, including polymers, are formed along with acyl bromides.

EXPERIMENTAL

The starting bromovinyl compounds **IV** and **V** were prepared according to [23], and **I**–**III**, by modified procedures from [24]; their physicochemical constants agree with the published data.

The starting compounds and final products were analyzed with a Tsvet-800 chromatograph equipped with a thermal conductivity detector; 3000 × 3-mm glass column, stationary phase E-301 + polyethylene glycol adipate (5% each) on Inerton Super (0.16–0.20 mm), column temperature 50–250°C, carrier gas He (40–60 ml min^{-1}).

***cis,trans*-1,2-Dibromoethene I.** A 250-ml flask equipped with a reflux condenser and a thermometer was charged with 172.9 g of 1,1,2,2-tetrabromoethane and 36.5 g of dimethylformamide, after which 14 g of iron powder was gradually added. The reaction was exothermic, and the reaction mixture, if necessary, was cooled with water. After the reaction completion, the mixture was distilled to give 86.7 g (93%) of a mixture of *cis*- and *trans*-dibromoethenes **I** in a 1 : 4 ratio (GLC data); bp 102–105°C (680 mm Hg), D_4^{20} = 2.2754, n_D^{20} = 1.5458 [25].

Tribromoethene II. A mixture of 16 g of NaOH, 20 ml of water, 2 g of a 50% aqueous solution of Katamin AB, and 148.3 g of 1,1,2,2-tetrabromoethane was stirred for 2 h at 25–30°C. The organic layer was separated and dried over $CaCl_2$; distillation gave 95.3 g (90%) of tribromoethene **III**, bp 53–55°C (10 mm Hg), D_4^{20} = 2.7080, n_D^{20} = 1.6040 [26]. The product purity (GLC data) was 99.2%.

Tetrabromoethene III was prepared similarly to **II** from 169.8 g of pentabromoethane; yield 126.8 g (92%), bp 100–102°C (16 mm Hg), crystallizes during distillation, mp 55–56°C (from ethanol) [27]. The product purity (GLC data) was 98.6%.

α-Bromoacyl bromides. A glass reactor 35 mm in diameter and 1 m high, equipped with a porous bubbler, an efficient reflux condenser, and a sampler was charged with dibromovinyl compounds freshly distilled from P_2O_5 (0.01 mol %); the vessel was placed in a thermostat. The temperature of 70°C was maintained, and technical-grade oxygen was fed at a rate of 2–4 l h^{-1}. Before entering the vessel, oxygen was purified by passing through two U-shaped tubes, one of which was packed with $CaCl_2$, and the other, with KOH, through a Tishchenko bottle with P_2O_5, and through a trap. All the parts of the system were connected with rubber tubes. The reaction completion was judged from the disappearance of the peak of the starting bromovinyl compound in the GLC pattern.

Oxidation of 1,2-dibromoethene I. A mixture of *cis*- and *trans*-dibromoethenes **I** (18.6 g) was oxidized with oxygen (3 l h^{-1}) at 30°C for 20 h. Vacuum distillation of 10 g of the oxidation products gave 7.4 g (74%) of dibromoacetic acid, bp 68–69°C (2 mm Hg). This compound gradually crystallizes on storage at 20°C; mp 48°C [28].

Oxidation of tribromoethene II. The reactor was charged with 3.5 kg of tribromoethene **II** and heated to 70°C; at this temperature, oxygen was fed (15–20 l h^{-1}) for 250 h. We obtained 3.69 kg of oxidation products. Vacuum distillation of their 300-g portion

gave 205.9 g (80%) of dibromoacetic anhydride **VII**, bp 77–80°C (10 mm Hg), D_4^{20} = 1.8236, n_D^{20} = 1.5480 [29].

Dibromoacetic acid VI. Water (1.5 l) was slowly added with cooling and stirring to 2100 g of the oxidation products of **II**. The mixture was allowed to stand at 20°C for 12 h, after which the insoluble fraction (287.5 g, tetrabromoethene : pentabromoethane = 95.8 : 4.2) was separated from the aqueous layer. Acetic acid (200 ml) was added to the aqueous layer, and the mixture was distilled under reduced pressure (water-jet-pump vacuum); the residue was distilled in a vacuum. Acid **VI** was obtained; yield 1219.2 g (88% based on converted **II**), bp 128–130°C (16 mm Hg), crystallizes in the course of distillation, mp 46°C [28].

Methyl dibromoacetate VIII. A three-necked flask equipped with a dropping funnel, a thermometer, and a reflux condenser was charged with 150 g of oxidation products of **II**, and 30 ml of absolute methanol was slowly added with cooling and stirring from a dropping funnel. After completion of the exothermic reaction and release of HBr, excess methanol was removed, and the residue was distilled. Ester **VIII** was obtained; yield 108.2 g (87%), bp 178–180°C (680 mm Hg), D_4^{20} = 1.8711, n_D^{20} = 1.9137 [29].

Oxidation of tetrabromoethene III. The reactor was charged with 68.9 g of **III** and heated to 90°C; at this temperature, oxygen was fed (2.5–3 $l\,h^{-1}$) for 90 h. We obtained 71.8 g of oxidation products. Vacuum distillation of their 16.8-g portion gave 13.2 g (79%) of tribromoacetic anhydride, bp 90–92°C (12 mm Hg), D_4^{20} = 2.6510, n_D^{20} = 1.8518 [30].

Tribromoacetic acid X. Water (15 ml) was slowly added with cooling to 20 g of oxidation products of **III**; the mixture was allowed to stand at 20°C for 12 h, and excess water was removed in a water-jet-pump vacuum. The residue was recrystallized from ethanol; yield of **X** 13.8 g (84%), mp 129–131°C [30].

Ethyl tribromoacetate XI. Absolute ethanol (15 ml) was slowly added from a dropping funnel with cooling (water–ice) to 20 g of oxidation products of **III**. After completion of the exothermic reaction, excess ethanol was distilled at reduced pressure, and the residue was distilled; yield of **XI** 15.9 g (88%), bp 148–150°C (70 mm Hg), D_4^{20} = 2.1105, n_D^{20} = 1.5349 [29].

Tribromoacetamide XII. Gaseous ammonia was passed through a solution of 8 g of oxidation products of **III** in 20 ml of absolute toluene until the ammonia uptake ceased. The precipitate was filtered off, washed with water, and air-dried. Yield of **XII** 5.2 g (78%), mp 119–120°C (from ethanol) [31].

Oxidation of β,β-dibromostyrene IV. The reactor was charged with 26.2 g of dibromostyrene **IV** and heated to 70°C. At this temperature, oxygen was fed (5 $l\,h^{-1}$) for 180 h. Distillation of 10 g of the oxidation products gave 7.4 g (74%) of phenylbromoacetic anhydride **XIII**, bp 140–143°C (20 mm Hg), D_4^{20} = 1.8557, n_D^{20} = 1.6000 [32].

Phenylbromoacetic acid XIV. A mixture of 10 g of oxidation products of **IV** and 10 ml of water was allowed to stand at 20°C for 12 h. Low-boiling products were evaporated in a water-jet-pump vacuum, and the residue was vacuum-distilled. Yield of acid **XIV** 5.9 g (77%), mp 84°C (from ethanol) [23].

Ethyl phenylbromoacetate XV: bp 141–143°C (8 mm Hg), D_4^{20} = 1.4165, n_D^{20} = 1.5415 [32].

Phenylbromoacetamide XVI: mp 146°C (from water) [32].

Oxidation of α,β,β-tribromostyrene V. Similarly to the oxidation of **IV**, 24 g of **V** was oxidized with oxygen for 250 h. Water (20 ml) was added to 20 g of the oxidation products, and the mixture was allowed to stand at 20°C for 12 h. After evaporation of water and recrystallization of the residue from petroleum ether, 10.9 g (72%) of phenyldibromoacetic acid **XVII** was obtained; mp 102–104°C (from CCl_4 : petroleum ether = 1 : 1) [23].

CONCLUSIONS

(1) Liquid-phase oxidation of bromovinyl compounds with oxygen in the range 20–100°C was studied, and conditions for selective preparation of α-bromoacyl bromides were found. The primary oxidation products are bromooxiranes; their maximal content in the oxidation products reaches 60%. In the course of distillation, hydrolysis, alcoholysis, aminolysis, and acidolysis, bromooxiranes quantitatively transform into the corresponding α-bromo carboxylic acid derivatives.

(2) Oxidation of some bromovinyl compounds with molecular oxygen yields, along with α-bromoacyl bromides, also the product of addition of bromine to the double bond. Aromatic substituents at the double bond considerably decrease the rate of oxidation of bromovinyl compounds.

(3) Liquid-phase oxidation of bromovinyl compounds occurs exclusively at the double bonds. The bromooxiranes formed in the process are insufficiently

reactive to induce side reactions (cleavage of the double bond or allyl oxidation).

REFERENCES

1. Mel'nikov, N.N. and Baskakov, Yu.L., *Khimiya gerbitsidov i regulyatorov rosta rastenii* (Chemistry of Herbicides and Plant Growth Regulators), Moscow: Goskhimizdat, 1962.
2. Tinius, K.A., *Plastifikatory* (Plasticizers), Moscow: Khimiya, 1964.
3. US Patent 2262686.
4. US Patent 3671641.
5. JPN Patent 26930.
6. Demole, E., *Ber.*, 1879, vol. 12, no. 2, pp. 2245–2248.
7. Demole, E., *Bull. Soc. Chim. Fr.*, 1880, vol. 34, no. 2, pp. 201–203.
8. Pericas, M.A. and Serratosa, F., *Tetrahedron Lett.*, 1978, vol. 49, pp. 4969–4970.
9. Toda, F., Ishihara, H., and Akadi, K., *Tetrahedron Lett.*, 1969, vol. 30, pp. 2531–2534.
10. Khachatryan, A.G., Bayatyan, B.E., Saakyan, R.G., et al., *Arm. Khim. Zh.*, 2001, vol. 54, nos. 1–2, pp. 24–31.
11. Bayatyan, B.E. and Ovasapyan, V.A., Abstracts of Papers, *3-ya Respublikanskaya konferentsiya "Organicheskii sintez"* (3rd Republican Conf. "Organic Synthesis"), Yerevan, 1997, p. 13.
12. USSR Inventor's Certificate no. 368227.
13. Shakhnazaryan, G.M. and Bayatyan, B.E., *Zh. Prikl. Khim.*, 1974, vol. 47, no. 5, pp. 1178–1189.
14. Shakhnazaryan, G.M. and Bayatyan, B.E., *Arm. Khim. Zh.*, 1979, vol. 32, no. 2, pp. 149–150.
15. Shakhnazaryan, G.M. and Bayatyan, B.E., *Zh. Prikl. Khim.*, 1979, vol. 52, no. 10, pp. 2307–2310.
16. Shakhnazaryan, G.M. and Bayatyan, B.E., Abstracts of Papers, *VII Vsesoyuznaya konferentsiya po khimii organicheskikh peroksidov* (VII All-Union Conf. on Chemistry of Organic Peroxides), Volgograd, 1980, p. 132.
17. Shakhnazaryan, G.M., Bayatyan, B.E., and Avoyan, R.S., *Neftekhimiya*, 1984, vol. 24, no. 4, pp. 531–536.
18. Shakhnazaryan, G.M., Bayatyan, B.E., and Avoyan, R.S., *Arm. Khim. Zh.*, 1986, vol. 39, no. 1, pp. 49–52.
19. Bayatyan, B.E., Movsisyan, K.A., and Vardanyan, R.L., Abstracts of Papers, *Vsesoyuznaya konferentsiya "Kinetika-90"* (All-Union Conf. "Kinetics-90"), Yaroslavl, 1990, p. 19.
20. Bayatyan, B.E. and Voskanyan, E.S., Abstracts of Papers, *IV Respublikanskaya konferentsiya "Organicheskii sintez"* (IV Republican Conf. "Organic Synthesis"), Yerevan, 1998, p. 18.
21. Bayatyan, B.E., Khachatryan, L.A., Asatryan, N.L., et al., Abstracts of Papers, *V Respublikanskaya konferentsiya "Organicheskii sintez"* (V Republican Conf. "Organic Synthesis"), Yerevan, 1999, p. 40.
22. Bayatyan, B.E., Mikaelyan, A.R., Voskanyan, E.S., et al., Abstracts of Papers, *V nauchnaya konferentsiya "Khimicheskaya nauka Armenii na poroge XXI veka"* (V Scientific Conf. "Chemical Science of Armenia on the Eve of the XXI Century"), Yerevan, 2000, p. 121.
23. Shakhnazaryan, G.M. and Gukasyan, A.O., *Arm. Khim. Zh.*, 1983, vol. 36, no. 6, pp. 370–373.
24. Bayatyan, B.E., *Cand. Sci. Dissertation*, Yerevan, 1987.
25. Anschutr, R., *Lieb. Ann.*, 1983, vol. 221, no. 1, pp. 133–156.
26. William, M., *J. Am. Chem. Soc.*, 1912, vol. 34, no. 2, pp. 286–290.
27. Nekrassow, A.S., *Ber.*, 1927, vol. 60, no. 7, pp. 1756–1758.
28. Shakhnazaryan, G.M., *Arm. Khim. Zh.*, 1974, vol. 27, no. 3, pp. 177–181.
29. Shaffer, L., *Ber.*, 1871, vol. 4, no. 2, pp. 366–372.
30. Biltz, H., *Ber.*, 1920, vol. 35, no. 2, pp. 1533–1537.
31. Weidel, H. and Gruber, M., *Ber.*, 1877, vol. 10, no. 7, pp. 1138–1157.
32. Ivanov, D. and Spasov, A., *Arhiv. Hem. Farm.*, 1934, vol. 8, no. 1, pp. 8–10.

ISSN 1070-4272, Russian Journal of Applied Chemistry, 2006, Vol. 79, No. 11, pp. 1853–1856. © Pleiades Publishing, Inc., 2006.
Original Russian Text © R.F. Khamidullin, N.Yu. Bashkirtseva, A.I. Abdullin, I.I. Akhmetov, 2006, published in Zhurnal Prikladnoi Khimii, 2006, Vol. 79, No. 11, pp. 1874–1877.

ORGANIC SYNTHESIS AND INDUSTRIAL ORGANIC CHEMISTRY

Polyethylene Glycol Monomethyl Ethers as the Main Component of Brake Fluid

R. F. Khamidullin, N. Yu. Bashkirtseva, A. I. Abdullin, and I. I. Akhmetov

Kazan State Technological University, Kazan, Tatarstan, Russia

Received March 24, 2006

Abstract—The main physicochemical properties of polyethylene glycol monomethyl ethers in a wide temperature range were determined. The effect exerted on the main quality indices of brake fluids by the introduction of polyethylene glycol monomethyl ethers borates was studied. The use of these ethers as the main component of DOT-5.1 brake fluids was analyzed.

DOI: 10.1134/S107042720611022X

Brake fluids (BFs) are used to transfer energy to the actuating mechanism in the hydraulic drive of the brake assembly of a car and to remove heat from the brake disks. The modern requirements to BFs are determined by FMVSS 116 (DOT) American federal motor vehicle safety standards [1].

According to this standard, BFs are subdivided into three classes: DOT-3, DOT-4, and DOT-5.1. The main requirements to these BFs are high operation temperatures, good low-temperature and viscosity–temperature properties, physical and chemical stability, protection of metals from corrosion, inactivity with respect to mechanical rubber articles, and lubricating effect. Some requirements of FMVSS 116 (DOT) are summarized in Table 1.

The boiling point is the main parameter determining the maximal operation temperature of a hydraulic drive of a brake assembly. Boiling point of most of brake fluids decreases in the course of their operation owing to high hygroscopicity of the fluids. In practice, the advantages of high-boiling BFs are actually useful when the fluids are frequently replaced.

Thus, a high boiling point of BF does not ensure its efficiency under hard operation conditions. Hence, not only "dry" equilibrium reflux boiling point (ERBP) of BF but also wet equilibrium reflux boiling point (WERBP) of BF containing 3.5% water [1] is determined. The WERBP corresponds to the temperature at which the liquid will boil after its operation in a hydraulic drive of a brake assembly of a vehicle for 1.5–3 years.

The viscosity–temperature properties of brake fluids should provide their efficiency in a wide temperature range. At low temperatures the fluid should be movable. To ensure reliable operation of a hydraulic drive of the brakes in summer time or in the South, the saturated vapor pressure of the fluid should be low and its boiling point should be sufficiently high [2].

Analysis of the available literature [3–5] revealed growing use of glycols or their derivatives, in particular, di-, tri-, and tetraethylene glycol monoalkyl ethers [3–8], in the last decade as the main components of BFs. To increase the boiling point of both wet and dry liquid, tris(methyl glycol) borates are introduced in BF [9, 10]. At the present time, Russian analogs of DOT-3 and DOT-4 brake fluids are widely used in Russia. Since the motor vehicle safety standards become tougher, the requirements to brake fluids become more stringent. Therefore, preparation of a BF of DOT-5.1 grade meeting these requirements is an urgent problem. However, no detailed data are available in the literature on physicochemical properties of tris(methyl glycol) borates of both pure polyethylene

Table 1. Some requirements of FMVSS 116 (DOT)

Quality index	DOT-3	DOT-4	DOT-5.1
Boiling point, °C:			
dry fluid	205	230	260
wet fluid	140	155	180
Kinematic viscosity, $mm^2 s^{-1}$, at −40°C no higher than	1400	1800	900

Table 2. Main physicochemical properties of the examined ethers

Ether	ERBP, °C	WERBP, °C	Kinematic viscosity at –40°C, $mm^2 s^{-1}$	*T*, °C	Density, g cm^{-3}	Dynamic viscosity, mPa s	Refractive index
MeDEG	193.2	134.0	72.6	20	1.0211 (1.0211 [11])	4.19	1.4261 (1.4263 [11])
				40	1.0059	2.74	
				60	0.9907	1.86	
				80	0.9731	1.19	
MeTEG	235.3	145.1	281	20	1.0494 (1.0494 [11])	7.44	1.4368 (1.4370 [11])
				40	1.0428	4.2	
				60	1.0217	2.77	
				80	1.0054	1.89	
MeTetraEG	298.0	151.0	–	20	1.0659	11.39	1.4448 (1.4452 [11])
				40	1.0505	6.42	
				60	1.0326	3.87	
				80	1.0182	1.61	
BMeTEG	332.0	203.0	–	20	1.0804	19.11	1.4434
				40	1.0653	9.52	
				60	1.0465	5.66	
				80	1.0295	4.04	

glycol monomethyl ethers and their mixtures with tris(methyl glycol) borates, as well as on the influence of the degree of boration of the initial compounds on the boiling point and viscosity of BF.

The aim of this study was to determine how additions of borates affects the boiling point and low-temperature viscosity of brake fluids.

EXPERIMENTAL

Diethylene glycol monomethyl ether (MeDEG), triethylene glycol monomethyl ether (MeTEG), and tetraethylene glycol monomethyl ether (MeTetraEG) were isolated from polyoxide-101 in accordance with TU (Technical Specifications) 2422-027-56649936–01 and were purified by repeated vacuum distillation on a bench unit at a residual pressure of 2–5 mm Hg. The purity (99%) was determined by comparison of their main physicochemical properties with the published data and by chromatographic analysis. The results are presented in Table 2.

Chromatographic analysis was performed on a Tsvet-500 chromatograph. We used a 2-m steel column 3 mm in diameter packed with PEG-20M on a Chromaton and a flame ionization detector with a sensitivity of 1×10^{-7}. The flow rate of hydrogen, carrier gas (nitrogen), and air was 30, 30, and 300 ml min^{-1}, respectively. The temperature of the vaporizer and junction chamber of the detector was 170 and 180°C, respectively. The temperature in the course of the analysis was automatically changed from 110 to 200°C at a rate of 10 deg min^{-1}. The temperature was controlled by a BU-125 control unit of the chromatograph with an accuracy of ±0.1°C.

The density was determined pycnometrically according to GOST (State Standard) 3900–85. The kinematic viscosity measured on a VPZh-3 viscometer (GOST 33–82) was converted into the dynamic viscosity. The substances were controlled thermostatically in a UT2/77 thermostat with an accuracy of ±0.05°C. The densities and dynamic viscosities of the pure ethers are summarized in Table 2.

The boiling points were measured in accordance with the MFVSS 116 standard [1]. The results are presented in Table 2 and in the figure.

The borates were prepared by conventional esterification on a vacuum bench unit consisting of a round-bottom flask used for distillation of the polymerization products, adapter with a reflux condenser, and a receiver for liberating water. The initial compounds were boric acid (GOST 9656–75) and MeTEG. These substances taken in a required ratio were placed in the reaction flask. The flask was evacuated to a residual pressure of 10–20 mm Hg. The reaction mixture

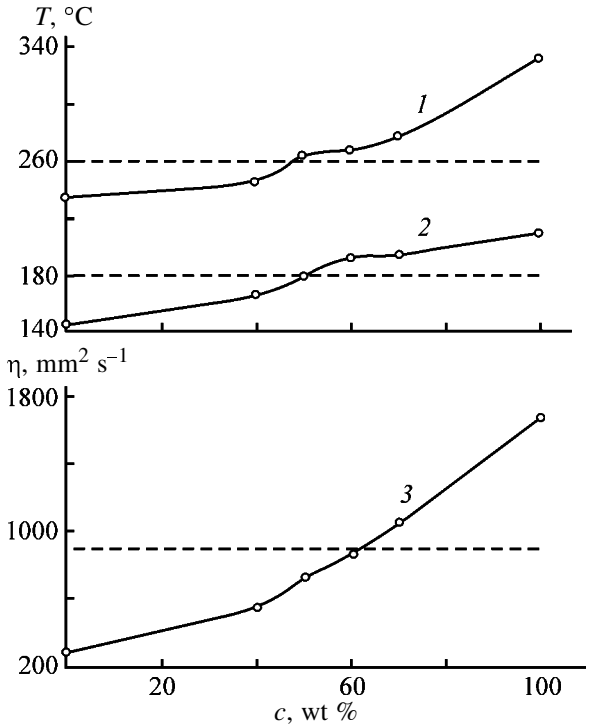


Fig. 1. (*1*) ERBP and (*2*) WERBP (*T*, °C) and (*3*) kinematic viscosity η at –40°C as functions of the concentration of tris(methoxyethoxyethoxyethyl)borate in MeTEG *c*.

was continuously stirred by a nitrogen flow fed through a capillary. The flask was gradually (over a period of 1.5–2.0 h) heated to 120°C, and the liberated water was distilled off.

As seen from Table 2, the temperature dependence of the density and viscosity of pure ethers monotonically decreases in the series MeDEG–MeTEG–MeTetraEG. The density and viscosity increase, probably due to densification of the structure (an increase in the degree of association) and increase in the number of intermolecular hydrogen bonds. The ERBP of MeTetraEG meets the requirements for DOT-5.1 BF. However, this ether freezes at –40°C. MeTEG, in turn, has good low-temperature viscosity but unsatisfactory boiling point. Oxyethylated additives have a negative effect on the properties of BF: the low-molecular-weight additives decrease the boiling point and the additives with higher molecular weight increase the low-temperature viscosity. Thus, MeTEG has good ERBP and low-temperature properties and can be used as the main component of BF.

To eliminate the negative effect of water and to increase the boiling point, borate esters of alkylene glycol monoethers were added to BF [9, 12]. The borate additive is readily hydrolyzed by water present in BF, binding this water and thus increasing the boiling point of a wet fluid [6]. However, since the viscosity of borate esters is high, introduction of large amounts of these compounds is undesirable. The main advantage of brake fluids containing borate esters is insignificant change of their physical properties in the presence of moisture. Esters of boric acid not only bind water but also have good lubricating and corrosion-preventing properties.

As noted above, an increase in the fraction of borate esters of methoxypolyethylene glycols in a brake fluid increases its boiling point. We studied the influence of methoxyethylene glycol borates on boiling points of their mixtures with individual polyethylene glycol monomethyl ethers. The content of tris(methoxyethoxyethoxyethyl) borate (BEMeTEG) ranged from 0 to 100%.

As seen from the figure, the kinematic viscosity of the mixtures monotonically increases with increasing borate content. The maximal permissible kinematic viscosity in accordance with FMVSS 116 (900 $mm^2 s^{-1}$) is reached at the borate content of about 60 wt %. The ERBP and WERBP of brake fluids containing this amount of borate are 260 and 180°C, respectively, which meets the FMVSS 116 (DOT) requirements.

CONCLUSIONS

(1) A mixture of triethylene glycol monomethyl ether with its full borate ester can be used as the main component of DOT-5.1 brake fluid. The ERBP, WERBP, and low-temperature viscosity of this BF meet the FMVSS requirements.

(2) To meet the FMVSS requirements to boiling points and low-temperature properties, the content of tris(methoxyethoxyethoxyethyl)borate in its mixture with triethylene glycol monomethyl ether should be in the range 55–60 wt %.

REFERENCES

1. *FMVSS* (Federal Motor Vehicle Safety Standards) *116: Car Brake Fluids*, USA, 1999.
2. Manusadzhyants, O.I. and Smal', F.V., *Avtomobil'nye ekspluatatsionnye materialy* (Car Operating Materials), Moscow: Transport, 1981.
3. US Patent 4371448.
4. RF Patent 2174536.
5. RF Patent 2087528.

6. Brusyantsev, N.V., *Ekspluatatsionno-tekhnicheskie svoistva i primenenie avtomobil'nykh topliv, smazochnykh materialov i spetszhidkostei* (Operation-Technical Properties and Application of Car Fuels, Lubricants, and Special Fluids), Moscow: Avtotransizdat, 1963.
7. Danilov, A.V., *Vvedenie v khimmotologiyu* (Introduction to Chemical Motor Science), Moscow: Tekhnika, 2003.
8. RF Patent 2 159 760.
9. US Patent 3 925 223.
10. US Patent 4 116 846.
11. Knunyants, I.L., *Khimicheskii entsiklopedicheskii slovar'* (Chemical Encyclopedia), Moscow: Nauka, 1983, 2nd ed.
12. Shvarts, E.M., *Kompleksnoe soedinenie bora s polioksisoedineniyami* (Boron Complex with Polyoxy Compounds), Riga: Zinatne, 1968.

ISSN 1070-4272, Russian Journal of Applied Chemistry, 2006, Vol. 79, No. 11, pp. 1869–1874. © Pleiades Publishing, Inc., 2006.
Original Russian Text © B.A. Zhubanov, V.D. Kravtsova, R.F. Mukhamedova, K.Kh. Bekmagambetova, 2006, published in Zhurnal Prikladnoi Khimii, 2006, Vol. 79, No. 11, pp. 1890–1895.

MACROMOLECULAR CHEMISTRY AND POLYMERIC MATERIALS

New Polymer Systems Based on Alicyclic Polyimides

B. A. Zhubanov, V. D. Kravtsova, R. F. Mukhamedova, and K. Kh. Bekmagambetova

Bekturov Institute of Chemical Sciences, Ministry of Education and Science of Kazakhstan Republic, Almaty, Kazakhstan
Almaty Institute of Power Engineering and Communications, Almaty, Kazakhstan

Received March 24, 2006

Abstract—Specific features of modification of some alicyclic polyimides with polyamido acids derived from aromatic tetracarboxylic acid dianhydrides were studied. The possibility of preparing new polymer systems with improved characteristics was demonstrated.

DOI: 10.1134/S1070427206110255

Recently there has been a considerable progress in modification of polymers with various additives and fillers. A promising approach to the development of new polymeric materials with high physicomechanical characteristics and good processability, including materials based on polyimides, is blending of polymers belonging to the same or different classes [1–4].

Published papers mainly concern aromatic polyimides. At the same time, alicyclic polymers are also of interest for various branches of engineering. In particular, they are promising materials for multilayer dielectrics in stacks of multiintegrated circuits, for production of enameled wires, film insulators, etc. [5–8]. However, these polymers, as compared to the aromatic analogs, exhibit insufficiently high physicomechanical characteristics. These characteristics can be improved by modification with various polymers.

The main goal of this study was to examine specific features of modification of polyimides containing tricyclodecene fragments in the backbone with polyamido acids derived from aromatic tetracarboxylic acid dianhydrides.

EXPERIMENTAL

The starting compounds and solvents were purified by standard procedures. The IR spectra were recorded on an IR-25 spectrometer. Polymer samples were prepared as 3–5-μm films.

The reduced viscosities of 0.5% solutions of the polyimides were measured with an Ubbelohde viscometer at 25°C in dimethylformamide (DMF). Thermogravimetric analysis of the polymers was performed with a TGA SDTA Mettler Toledo device at a heating rate of 8 deg min^{-1}. The temperatures of the onset of the polymer decomposition ($T_{o.d}$) were calculated from the TGA curves.

The physicomechanical (tensile strength, relative elongation) and dielectric (dielectric loss tangent, permittivity) characteristics were studied under standard conditions by known procedures [9, 10].

Dianhydrides were prepared by the Diels–Alder reaction upon UV irradiation of saturated solutions of maleic anhydride in appropriate hydrocarbons in the presence of acetophenone as sensitizer. Tricyclo-[4.2.2.$0^{2,5}$]dec-7-ene-3,4,9,10-tetracarboxylic acid dianhydride (photoadduct of benzene and maleic anhydride, AB) was prepared in a temperature-controlled quartz glass vessel by irradiation of a solution of 196.00 g (2.0 mol) of maleic anhydride in 1000 ml of benzene containing 24.12 g (0.2 mol) of acetophenone with a PRK-2M mercury quartz lamp for 15 h. In the course of irradiation, a white crystalline precipitate formed; it was filtered off, recrystallized from propionic anhydride, washed with dry diethyl ether, and vacuum-dried at 80–90°C to constant weight. Yield 80% based on maleic anhydride.

9-Oxotricyclo[4.2.$1^{1,6}0^{2,5}$]nonane-3,4,7,8-tetracarboxylic acid dianhydride (photoadduct of furan and maleic anhydride, AF) was prepared by irradiation of the monoanhydride prepared beforehand from furan and 193.24 g (2.0 mol) of maleic anhydride, performed for 10 h in 1000 ml of dioxane containing 24.12 g (0.2 mol) of acetophenone. Yield of AF 84.5%.

Melting points, °C: AB 350–352 and AF 408–410.

The composition and structure of the dianhydrides were determined by elemental analysis and IR spectra.

AB. Found, %: C 61.40; H 3.70; esterification number (EN) 137.03.
$C_{14}H_{10}O_6$. Calculated, %: C 61.33; H 3.65; EN 137.07.

AF. Found, %: C 54.60; H 3.12; EN 131.80.
$C_{12}H_8O_7$. Calculated, %: C 54.56; H 3.03; EN 132.01.

IR spectra, cm^{-1}: 1500 (benzene ring), 1775–1780, 1835–1840 (anhydride groups [11]).

The dianhydrides derived from fluoro- and chlorobenzene and maleic anhydride (AFB, ACB) were prepared by the procedures described in [7, 12].

The solvent, *N*-methyl-2-pyrrolidone (MP), was dried over 4A molecular sieves.

Unmodified polyimides were prepared in the presence of catalytic amounts of triethylamine. The polyimide derived from AB and 4,4'-diaminodiphenyl ether (DADPE) was prepared as follows: A three-necked flask equipped with a stirrer and an inlet tube for an inert gas was charged with 13.70 g (0.05 mol) of the dianhydride, 10.00 g (0.05 mol) of DADPE, and 3.55 g (15 wt % of the sum of the monomers) of triethylamine, after which 71.1 ml of MP was added. The flask with the reaction solution was placed on an oil bath (T = 50°C). The mixture was stirred for 15 min, after which the temperature was raised to 160°C over a period of 20 min, and the mixture was stirred for an additional 4.5 h. After cooling to room temperature, films were cast from the solution, or the polymer was precipitated into acetone (chemically pure grade); the resulting precipitate was washed with two portions of acetone and dried in a vacuum oven at 80–90°C to constant weight. The polyimides derived from AFB and ACB were prepared similarly.

The elemental analysis of the precipitated polymers gave consistent results. Polyimide films were prepared by casting 25% MP solutions of the precipitated polyimides onto glass surfaces; to remove the solvent, the films were first predried by heating in a vacuum oven to 80°C for 0.3 h and then additionally heat-treated in the temperature range 80–300°C in air for 1.0 h.

Syntheses of polyimides in the presence of catalytic amounts of polyamido acids derived from pyromellitic and benzophenonetetracarboxylic acid dianhydrides were performed similarly.

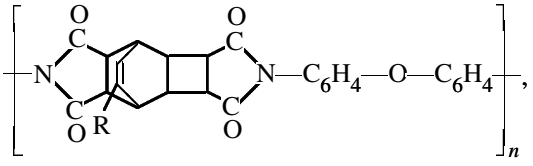
Polyamido acids (PAAs) derived from AB and AF (25 wt % solutions in dimethylacetamide) were prepared at equimolar ratio of the components at 25°C in 1.5 h. Heat treatment of the films prepared from blends of homopolyamido acids was performed at 80–300°C in a vacuum (2×10^{-2} hPa) for 2.0 h.

The prepolymers derived from pyromellitic and benzophenonetetracarboxylic acid dianhydrides were prepared by well-known procedures; polymer yield 98.5–99.0%.

Polymer blends of the polyimide derived from AB and DADPE with polyamido acids were prepared as follows: 10–25% solutions of the prepolymers, taken in an amount corresponding to the required PI–PAA ratio, were added at room temperature to a solution of the polyimide. The mixture was stirred for 1.5 h at room temperature, after which films were cast. The films were dried in the temperature range 80–300°C in air for 1.5 h. The degree of imidization was evaluated from the IR spectra.

Published data show that the choice of one or another modification procedure is governed by the nature and purpose of the polymer, and also by other factors. The widely used route to new polymers and polymer systems is chemical modification; it allows purposeful control of the formation of the material structure. A primising approach to the development of new polymers and polymer systems involves the use of various macromolecular compounds [1–4, 13, 14].

In particular, properties of polymer blends can be improved and their stability enhanced by performing the synthesis of one of the polymers in the presence of the other polymer as a matrix; at its definite content, this matrix can affect the formation rate, structure, and molecular weight of the target product. In is study, we used other approaches: mechanically blending polymers of different nature or performing the synthesis of alicyclic polyimides of the general formula



where R = H, F, Cl, in the presence of catalytic amounts of the second polymeric component (P2).

As a first step in examining the possibility of modification of polyimides with tricyclodecene fragments in the backbone, we considered the effect of polyamido acids derived from aromatic and alicyclic tetracarboxylic acid dianhydrides. These substances were added to a solution of a ready polyimide with ~100% degree of imidization. We found that different prepolymers exert different effects on the properties

Table 1. Properties of the polyimide derived from AB and DADPE and modified with various polyamido acids

Property	PAA			No PAA added
	AB	PMDA	BZP	
Tensile strength, MPa	130	180	135	100–110
Elongation, %	27	40	35	15–17
Elastic modulus, MPa	4100	3500	–	4400
Dielectric loss tangent (1 KHz)	0.001	0.001	0.001	0.001
Volume resistivity, Ω m	1.6×10^{15}	5.1×10^{15}	3.2×10^{15}	2.2×10^{15}
Dielectric permittivity	2.2–2.6	2.7–2.9	3.0–3.3	2.2–2.6
Softening point, °C:				
of prepolymer	150	100	110	155
of polyimide	300	310	300	No softening
$T_{o.d}$ in air, °C	370	375	370	370
Intrinsic viscosity, dl g^{-1}, in DMF	1.52	1.92	1.71	1.21

of the polyimide being modified; in the process, the concentration of the second component (P2) should also be controlled. Monitoring of the intrinsic viscosity [η] of the polyimide derived from AB and DADPE (PI_{AB}) in the presence of various polyamido acids showed that higher viscosities are attained when the PAA derived from 4,4'-diaminodiphenyl ether and pyromellitic dianhydride (PAA_{PMDA}) is added to the polyimide solution, and somewhat lower viscosity is attained with the PAA derived from benzophenonetetracarboxylic acid dianhydride (PAA_{BZP}); the optimal concentration of the second component is 10 wt %. With a further increase in the P2 content in the reaction mixture, the solution becomes turbid, and at 12–15 wt % content of P2 the phase segregation and coagulation of the polymer occur, i.e., the polymers are thermodynamically compatible up to a certain limit.

Some properties of the polyimide prepared by heat treatment of a blend containing 10 wt % PAA are given in Table 1. Introduction of polyamido acids into a polyimide solution yields a new polymer system with the intrinsic viscosity of 1.52 to 1.92 dl g^{-1}; whereas in the case of the polyamido acid derived from the same components (PAA from AB and DADPE) the elemental composition remains unchanged, with the PAA derived from pyromellitic or benzophenonetetracarboxylic acid dianhydride the resulting polymers differ in the composition and properties from the starting polymers and presumably have the structure of interpenetrating polyimide networks.

The completion of the transformation of the amido acid fragments into imide rings was judged from the IR spectra. The spectrum of the final polyimide did not contain bands characteristic of amido acid units (about 3280, 1670, 1540 cm^{-1}) but contained characteristic bands of imide rings [1780 (doublet with 1720), 1380, 730 cm^{-1}] [11].

For PIs derived from AFB and ACN with DADPE, the intrinsic viscosity reached, respectively, 2.10 and 1.75 dl g^{-1} with addition of PAA_{PMDA}, and 1.84 and 1.55 dl g^{-1} with addition of PAA_{BZP}; the tensile strength and elongation increased by 20–30%, and the dielectric characteristics changed insignificantly.

It should be noted that it is hardly possible to judge the interactions between the polymeric components from the IR spectra, because the major bands in the spectra of the alicyclic and aromatic polyimides are essentially the same (the only distinction is the band of the C=C bond at about 1620 cm^{-1} in the spectra of polyimides derived from tricyclodecenetetracarboxylic acid dianhydride). As noted above, in this case we took advantage of the elemental analysis.

As noted above, higher values of the viscosity, tensile strength, and elongation are attained for polyimide films containing PI_{PMDA}. The intrinsic viscosity of the new polymer system prepared in the presence of PAA_{BZP} is somewhat lower. It should be noted that introduction into a ready polyimide of the prepolymer of the similar structure also leads to a certain increase in the viscosity and other characteristics. Similar effects were also observed with the PIs derived from AFB and ACB.

One more procedure for modification of polyimides is based on the use of blends of polyamido acids [5, 15]. In this study, with the aim to enhance the heat resistance of alicyclic polyimides, we used mechanical blending of PAA_{AB} with the PAA derived from

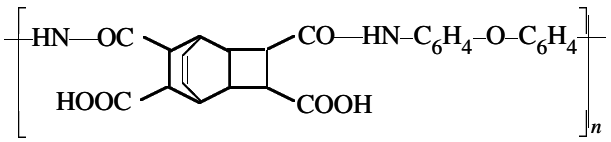
Table 2. Properties of polyimides prepared from AB–DADPE and AF–DADPE polyamido acids

Polymer	Initial blend composition, wt %		[η], dl g^{-1} (DMF, 25°C)	$T_{o.d}$ in air, °C	Tensile strength, MPa	Elongation, %
	PAA_{AB}	PAA_{AF}				
PI-1	100	0	1.21	370	100	15–17
PI-2	80	20	1.28	375	100	15–17
PI-3	60	40	1.37	385	100	17–20
PI-4	40	60	1.44	395	105	20–22
PI-5	20	80	1.46	405	110	20–22
PI-6	0	100	1.62	420	120	20–22

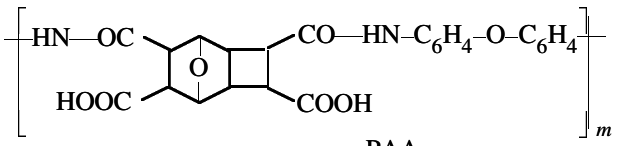
Table 3. Properties of polyimides prepared from AB–DADPE and PDMA–DADPE polyamido acids

Polymer	Initial blend composition, wt %		[η], dl g^{-1} (DMF, 25°C)	$T_{o.d}$ in air, °C	Tensile strength, MPa	Elongation, %
	PAA_{AB}	PAA_{PMDA}				
PI-1	100	0	1.21	370	100	15–17
PI-2	95	5	1.48	375	150	28–34
PI-3	90	10	1.54	375	155	32–35
PI-4	80	20	1.57	375	157	35–37
PI-5	60	40	1.60	380	158	36–39
PI-6	40	60	1.64	385	160	37–39
PI-7	20	80	1.68	387	165	38–40
PI-8	10	90	1.70	390	170	38–40
PI-9	5	95	1.74	395	170	40–44
PI-10 [5]	0	100	1.6–1.8	420	180–220	50–70

DADPE and AF. The furan structure of AF ensures higher thermal characteristics of the polymers [16, 17]. The properties of polyimides prepared by heat treatment of blends with various contents of polyamido acids of the general formulas



PAA_{AB}



PAA_{AF}

are listed in Table 2. it is seen that the intrinsic viscosity increases monotonically; the temperature parameters also gradually change. In going from the polymer prepared from the blend containing 20 wt % PAA_{AF} to the polymer with a higher content of this component, the decomposition onset temperature increases; for example, for the PI prepared with 80% PAA_{AF} (PI-5), $T_{o.d}$ is 405°C, whereas for PI-2 (20 wt % PAA_{AF}) it is 375°C.

Similar measurements were performed with the polyimides prepared from blends of PAAs derived from AB and PMDA. The properties of the polymers prepared by mechanical blending of alicyclic and aromatic polyamido acids are given in Table 3.

Data for PI-2 in Table 2 deserve particular attention. The physicomechanical characteristics of this polymer are considerably improved relative to PI-1: Introduction of only 5 wt % PMDA increases the tensile strength of a 40–45-μm film by 50 MPa and the elongation, by a factor of 2. With a further increase in the PAA_{PMDA} content in the starting blend, the properties of the polyimides change monotonically and more gradually.

Polyamido acids derived from alicyclic and aromatic tetracarboxylic acid dianhydrides can also be used as catalysts of the polycondensation in polar aprotic solvents of the amide type. We showed previously that MP is a suitable solvent for preparing by one-step polycondensation polyimides derived from tricyclo-

Table 4. Conditions for the synthesis of the polyimide derived from AB and DADPE in the presence of PAA

PAA	C_{mon}, wt %/C_{cat}, wt %	T, °C	Time, h	[η], dl g^{-1} (DMF, 25°C)
PMDA	40/1.5	170	4.0	1.73
BZP	40/1.5	180	5.0	1.51
AB	40/2.0	180	5.0	1.40

decenetetracarboxylic acid dianhydrides and various diamines, because the higher boiling point of this solvent is favorable for the process. The optimal conditions for the synthesis of PIs derived from AB in the presence of various prepolymers are listed in Table 4.

For the chlorinated and fluorinated polyimides prepared under the similar conditions, [η] was 1.58–1.92 dl g^{-1}.

Table 4 shows that, when an alicyclic polyimide is prepared in the presence of catalytic amounts of aromatic polyamido acids, [η] is somewhat lower compared to the procedure involving introduction of PAA into ready polyimide solutions (Table 1). However, in this case the viscosities of the PIs are also fairly high, i.e., the second polymer plays the role of not only a catalyst but also a polymeric matrix on which a polymer with improved properties is formed. The tensile strength of the polyimide films is 136–140 MPa, and the breaking elongation, 25–30%.

Certain dielectric characteristics of the new polymer systems deserve particular discussion. It is known that polyimides containing alicyclic fragments have lower dielectric permittivity compared to their aromatic analogs [6]. This is also true for the polyimides derived from tricyclodecenetetracarboxylic acid dianhydrides that we developed [7, 12]. For example, the dielectric permittivity ε of polyimide films prepared from the alicyclic polyimide derived from AB and DADPE is intermediate between that of the homopolymers: $\varepsilon(PI_{PMDA}) = 3–3.5$, $\varepsilon(PI_{AB}) = 2.2–2.6$, ε of the polyimide prepared with 10% PAA_{PMDA} is 2.7–2.9, and ε of the polyimide prepared with 2–3% PAA_{PMDA} is 2.5–2.7. At catalytic preparation of the alicyclic polyimide in the presence of polypyromellitic acid, ε is 2.4–2.7. The dielectric permittivity of the fluorinated PI is somewhat lower, and that of the chlorinated polyimide, higher than that of PI_{AB}: 1.8–2.1 and 1.9–2.2, respectively [8, 18]. The other characteristics (dielectric loss tangent, volume resistivity, electrical strength) are similar to those of aromatic polyimides.

To conclude, the best characteristics of the polymers are attained at their modification with polyamido acids introduced into PI solutions. The observed improvement of the properties of the alicyclic polyimide in the presence of polyamido acids may be due to the following factors: on the one hand, an increase in the size of the macromolecular globule and "loosening" of the structure; on the other hand, apparently, more complete reaction of the functional groups with each other.

Thus, modification with other polymers allows improvement of properties of alicyclic polyimides.

CONCLUSIONS

(1) Experiments on modification of polyimides derived from tricyclodecenetetracarboxylic acid dianhydrides with aromatic and alicyclic polyamido acids showed that higher viscosity and better physicomechanical characteristics are attained by modification of alicyclic polyimides with the polyamido acid derived from pyromellitic dianhydride.

(2) In one-step preparation of polyimides in the presence of prepolymes, the prepolymers exert a catalytic and plasticizing effect.

REFERENCES

1. Neverov, V.M., Chvalun, S.N., Blackwell, D., et al., *Vysokomol. Soedin., Ser. A*, 2000, vol. 42, no. 3, pp. 450–461.
2. Vygodskii, Ya.S., Sakharova, A.A., and Matieva, A.M., *Vysokomol. Soedine., Ser. A*, 2000, vol. 42, no. 3, pp. 538–541.
3. Nikalaichyk, H.V., Martsinkevich, A.A., Prokopchuk, N.R., and Krutko, E.T., Abstracts of Papers, *Third Int. Symp. on Polyimides and Other High Temperature Polymers: Synthesis, Characterization, and Applications*, Orlando, December 17–19, 2003, p. 21.
4. Yokota, R., Horiuchi, R., Kochi, M., et al., *J. Polym. Sci., Polym. Lett.*, 1988, vol. 26, no. 5, pp. 215–222.
5. Bessonov, M.I., Koton, M.M., Kudryavtsev, V.V., and Laius, L.A., *Poliimidy – klass termostoikikh polimerov* (Polyimides: A Class of Heat-Resistant Polymers), Moscow: Khimiya, 1983.

6. Rusanov, A.L., Stadnik, T.A., and Müllen, K., *Usp. Khim.*, 1999, vol. 68, no. 8, pp. 760–772.
7. Zhubanov, B.A., Kravtsova, V.D., and Bekmagambetova, K.H., *J. Polym. Sci.*, 2003, vol. 45/3-B, no. 4, pp. 78–81.
8. Zhubanov, B.A., Kravtsova, V.D., Bekmagambetova, K.Kh., and Akhmettaev, D.D., *Elektrotekhnika*, 1998, no. 11, pp. 57–60.
9. Kalinina, L.S., Motorina, M.A., Nikitina, N.I., and Khachapuridze, N.A., *Analiz kondensatsionnykh polimerov* (Analysis of Condensation Polymers), Moscow: Khimiya, 1984.
10. Bradulina, L.G., Gavrilova, N.D., Vygodskii, Ya.S., and Matieva, A.M., *Vysokomol. Soedin., Ser. B*, 1999, vol. 41, no. 5, pp. 901–905.
11. Kazitsyna, L.A. and Kupletskaya, N.B., *Primenenie UF-, IK-, YaMR- i mass-spektroskopii v organicheskoi khimii* (Applications of UV, IR, NMR, and Mass Spectroscopy to Organic Chemistry), Moscow: Mosk. Gos. Univ., 1979.
12. Zhubanov, B.A., Kravtsova, V.D., and Mukhamedova, R.F., *Zh. Prikl. Khim.*, 2004, vol. 77, no. 11, pp. 1853–1857.
13. Yudin, V.E., Svetlichnyi, V.M., Gubanova, G.N., et al., *Vysokomol. Soedin., Ser. A*, 2002, vol. 44, no. 2, pp. 257–267.
14. Kudaikulova, S., Musapirova, Z., Sobarina, N., et al., *Eur. Chem.-Technol. J.*, 2004, vol. 6, no. 1, pp. 7–10.
15. Smirnova, V.E., Garmonova, T.I., Baklagina, Yu.G., et al., *Vysokomol. Soedin., Ser. A*, 1985, vol. 27, no. 9, pp. 1954–1961.
16. Zapadinskii, B.I., Liogon'kii, B.I., and Berlin, A.A., *Usp. Khim.*, 1973, no. 11, pp. 2037–2072.
17. Sadykov, B.B., Polyimides Derived from Furan Compounds, *Cand. Sci. Dissertation*, Alma-Ata, 1984.
18. Akhmettaev, D.D., Bekmagambetova, K.Kh., Zhubanov, B.A., and Kravtsova, V.D., in *IV Mezhdunarodnyi simpozium "Elektrotekhnika – 2010 god"* (IV Int. Symp. "Electrical Engineering: Year 2010"), Moscow, May 20–23, 1997, part 1, pp. 173–177.

ISSN 1070-4272, Russian Journal of Applied Chemistry, 2006, Vol. 79, No. 11, pp. 1875–1878. © Pleiades Publishing, Inc., 2006.
Original Russian Text © B.A. Zhubanov, G. Meiirova, M.B. Umerzakova, K.B. Erzhanov, N.B. Kurmankulov, B.A. Ismailov, D.A. Kasymbekova, A. Kabyl, 2006, published in Zhurnal Prikladnoi Khimii, 2006, Vol. 79, No. 11, pp. 1896–1899.

MACROMOLECULAR CHEMISTRY AND POLYMERIC MATERIALS

Preparation of Phytoactive Polymers Derived from Mono- and Bispiperidols with Growth-Stimulating Properties

B. A. Zhubanov, G. Meiirova, M. B. Umerzakova, K. B. Erzhanov, N. B. Kurmankulov, B. A. Ismailov, D. A. Kasymbekova, and A. Kabyl

Bekturov Institute of Chemical Sciences, Ministry of Education and Science of Kazakhstan Republic, Almaty, Kazakhstan

Research and Production Center of Cattle Breeding and Veterinary Science, Ministry of Agriculture of Kazakhstan Republic, Almaty, Kazakhstan

Received May 19, 2006

Abstract—Optimal conditions for the synthesis of phytoactive polymers from mono- and bispiperidols and maleic anhydride copolymers were found. The growth-stimulating activity of these polymers was tested on arid cultures.

DOI: 10.1134/S1070427206110267

To improve the germinating capacity of seeds and enhance the resistance of plants to natural stress factors, synthetic biologically active substances (BASs) improving the formation of the root system and accelerating the growth and development of plants are used along with phytohormones. It is apparently preferable to use polymeric growth regulators exhibiting prolonged effect, high biological efficiency at small dosages, and single action in the vegetation period.

In this study, with the aim to obtain phytoactive polymers stimulating the growth of plants, including arid cultures, we examined the immobilization of 1,4-bis[*N*-(2-ethoxyethyl)-4-hydroxypiperid-4-yl]buta-1,3-diyne (Kaz-4) and 1,2,5-trimethyl-4-dimethoxyphosphorylpiperid-4-ol (Fospinol, ASA) with 1,4-bis-(1,2,5-trimethyl-4-hydroxypiperid-4-yl)buta-1,3-diyne (Akpinol, AE) on maleic anhydride copolymers. It is known that Fospinol affects to a greater extent the growth of tops, whereas Akpinol stimulates the root formation; therefore, the development of a polymeric plant growth regulator containing both these piperidols is of interest from both scientific and practical viewpoint.

Biologically active polymers were prepared by polymer-analogous transformations in a dimethyl sulfoxide solution. As starting polymers we used copolymers of maleic anhydride with styrene (Styromal, StMA) and with acrylic acid (AAMA). These copolymers, which are mainly alternating [1], allow immobilization of a BAS uniformly along the macromolecular chain. This feature allows prediction of the properties of phytoactive polymers being synthesized and facilitates further standardization and certification of agricultural agents based on them.

EXPERIMENTAL

To prepare a mixed polymeric monoester of Akpinol, Fospinol, and Styromal, a 1.212-g portion of StMA (0.006 mol) was charged into a two-necked flask equipped with a stirrer and was dissolved in 9.5 ml of DMSO at 60°C within 5–10 min. After the StMA dissolved completely, the temperature was raised to 90°C, and 0.7532 g (0.003 mol) of Fospinol and 0.4 ml (0.003 mol) of triethylamine (TEA) were added. Two hours later, 0.996 g (0.003 mol) of Akpinol, 9.1 ml of DMSO, and 0.4 ml (0.003 mol) of TEA were added. The reaction mixture concentration was 15 wt %, and total reaction time, 4.5 h. After the lapse of the prescribed time, the synthesis was stopped, and the polymer solution was slowly poured while hot into a precipitant mixture (150 ml of acetone, 30 ml of isopropyl alcohol, and 20 ml of 8% KOH solution in isopropyl alcohol). The mixture was allowed to stand for 15 min, after which the precipitate was filtered off at reduced pressure, washed on the filter with isopropyl alcohol, and filtered once more. The precipitate was transferred into a Petri dish and dried first at room temperature and then in a vacuum oven at 35°C

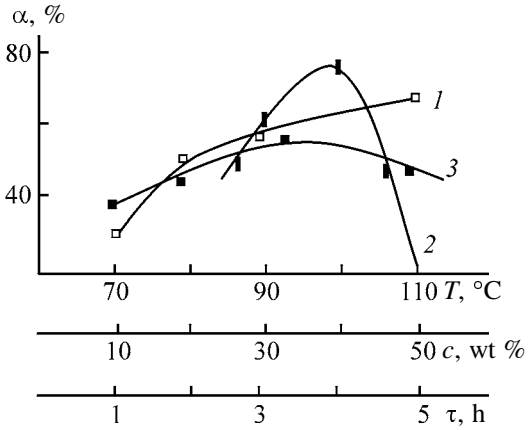


Fig. 1. Degree of immobilization α of a BAS on the copolymer as a function of the (*1*) reactant concentration *c*, (*2*) temperature *T*, and (*3*) reaction time τ.

to constant weight. Yield 2.701 g. The degree of immobilization determined by potentiomeric titration was 75 mol %. The IR spectrum contained a new band at 1710 cm^{-1} (ester groups).

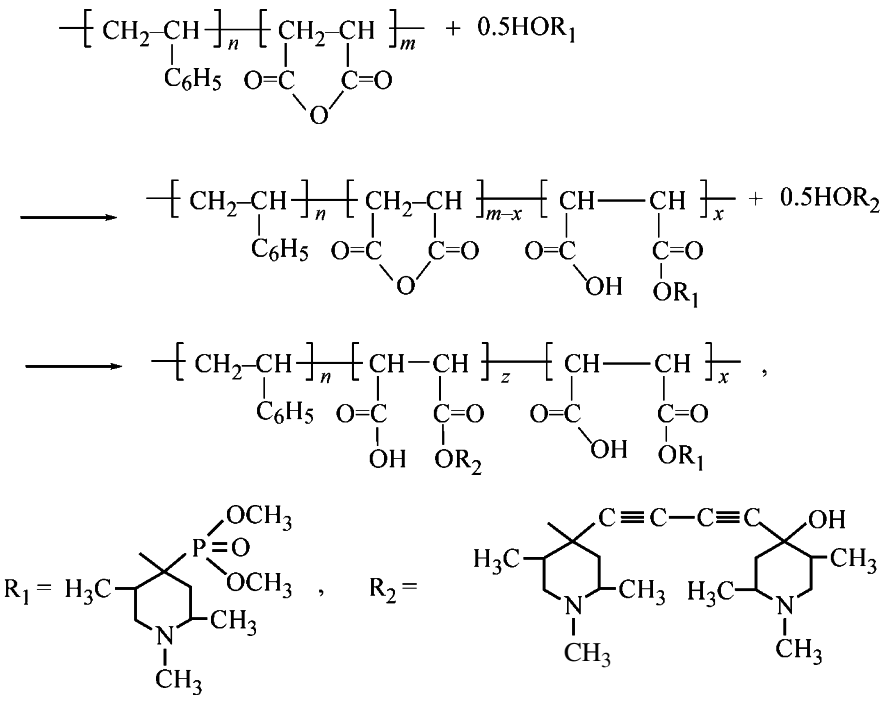
The biologically active polymers derived from Kaz-4 and Akpinol were prepared similarly.

The styrene–maleic anhydride copolymer (Kaustik Research and Production Association, molecular weight 40 000) was purified to remove residual monomer by reprecipitation from cyclohexane into petroleum ether and then was subjected to additional anhydridization in a vacuum at 200°C. The IR spectrum contained bands at 1770–1850 and 1080–1220 cm^{-1} (anhydride ring). The content of anhydride groups was 39 mol %.

Akpinol and Fospinol (submitted by the Laboratory of Chemistry of Physiologically Active Compounds, Bekturov Institute of Chemical Sciences, Ministry of Education and Science of Kazakhstan Republic) were used without additional purification. The physical constants agreed with the published data [2].

The amount of anhydride groups and degree of immobilization were determined by procedures described in [3].

The IR spectra of the starting and synthesized compounds were recorded on a Jasco IR-810 spectrometer (Japan) in KBr pellets against pure KBr pellet in the range 4000–400 cm^{-1}. The reactions of StMA with Fospinol and Akpinol followed the scheme



The reactant ratio was calculated per mole of elementary unit containing anhydride ring: copolymer : ASA : AE = 1.0 : 0.5 : 0.5. The IR spectrum confirmed the formation of an ester bond, and elemental analysis confirmed the presence of P and N.

To determine the optimal synthesis conditions, we examined the effect of various factors on the degree of immobilization of BAS on the copolymer.

Figure 1 shows how the degree of immobilization

of ASA and AE on StMA depends on the temperature, reaction time, and concentration of the reactants. With an increase in the concentration of the reaction solution to 30 wt %, the BAS content increases to 67.4 mol % (curve *1*). However, at this concentration the mixture becomes viscous, which prevents complete removal of the unchanged reactants. Therefore, it is not appropriate to use higher concentrations. The temperature dependence (curve *2*) passes through a maximum, and this point is shifted toward higher temperatures compared to experiments on immobilization of each BAS taken separately [2]. The highest degree of immobilization, 77.1 mol %, is attained at 100°C. An increase in the reaction time (Fig. 1, curve *3*) leads to a gradual increase in the BAS content. The maximal degree of immobilization is attained in the 4-h reaction.

The influence exerted on the degree of immobilization of phytoactive substances by the reaction time in the presence and in the absence of a catalyst and at different temperatures was examined in more detail; the results are shown in Fig. 2. The molar ratio of the reactants, copolymer : BAS : catalyst, was 1 : 1 : 1; the concentration, 15 wt %; and the temperature, 75 and 90°C.

At 75°C (Fig. 2, curve *1*), the maximal degree of immobilization (35.6%) is attained in 4 h. As the temperature is raised to 90°C (curve *2*), the degree of immobilization increases to 51.3%, and the effective time of BAS binding decreases to 3 h. Addition of TEA as catalyst (curve *3*) increases the degree of BAS immobilization to 57.3 mol %. The difference between the BAS amounts in the absence and in the presence of TEA is minor, which confirms the previously revealed capability of piperidols (in particular, ASA) for autocatalysis [2]. Figures 1 and 2 show that the temperature dependence of the degree of BAS immobilization passes through a maximum. A decrease in the content of immobilized BAS with an increase in the temperature above the optimal level is caused by the fact that esterification is an equilibrium process, and on reaching the maximal conversion the reverse process starts to prevail.

We determined the degree of immobilization of each piperidol separately. The results are given in the table. It is seen that addition of TEA increases the binding of the first component: ASA reacts almost completely within 4 h, and the degree of immobilization is 48.3 mol %, whereas the AE content is as low as 9.0%. In the absence of TEA, as seen from the table, the maximal content of ASA in the polymer decreased to 31.5%, but the degree of AE immobilization increased to 19.8 mol %. At 75 and 90°C, in the absence of the catalyst, the trend was similar; in the initial period (1–2 h), the content of both BASs was comparable, but in the subsequent period the amount of bound ASA increased and that of bound AE decreased. Thus, by varying the reaction conditions, it is possible to control the BAS ratio in the bioactive polymer.

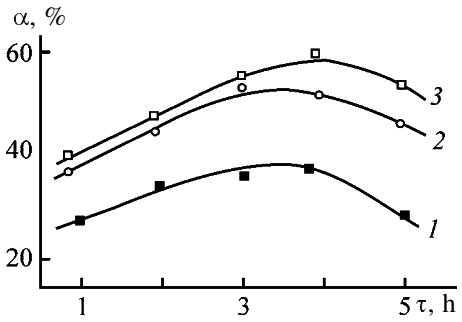


Fig. 2. Degree of immobilization α as a function of the reaction time τ at (*1*) 75 and (*2*, *3*) 90°C (*1*, *2*) in the absence and (*3*) in the presence of the catalyst.

The immobilization of Kaz-4 on StMA was studied similarly. The optimal conditions appeared to be as follows: copolymer : BAS ratio 1 : 1, 85–90°C, 3.5 h, concentration of the reactants 15–20 wt %. Under these conditions, the degree of immobilization determined by potentiometric titration was 35.4%. Addition of 1 mol of TEA per anhydride group increased this parameter to 54.0 mol %.

The use of AAMA as polymeric carrier allowed

Influence of the reaction temperature and time on the degree of BAS immobilization

T, °C	τ, h	Degree of immobilization, mol %		
		Fospinol	Akpinol	total
75	1	13.8	27.6	41.4
	2	19.1	33.3	52.4
	3	20.7	34.6	55.3
	4	25.3	35.6	60.9
	5	15.0	28.9	43.9
90	1	21.4	47.1	68.5
	2	30.6	50.5	81.1
	3	31.5	51.3	82.8
	4	28.9	47.9	76.8
	5	22.2	40.0	62.2
90 (in the presence of TEA)	1	38.4	39.3	77.7
	2	43.8	42.3	86.1
	3	48.5	48.6	97.1
	4	56.0	49.3	105.3

preparation of a water-soluble Kaz-4 polyester. We found that binding of Kaz-4 with AAMA occurs under milder conditions: concentration of the reactants 15–20 wt %, 75°C, 2.5 h; the maximal BAS content was 80.6 wt %, which is 1.5 times higher compared to the immobilization on StMA.

We also examined the influence of the TEA content on the degree of immobilization of Akpinol on AAMA. We found that, in the absence of a catalyst, the amount of the active substance did not exceed 46.0%. With introduction of the catalyst into the reaction mixture, the degree of BAS binding increased and reached 98.0% on adding 1 mol of TEA per mole of anhydride groups. At larger amounts of the catalyst, the degree of immobilization calculated from the nitrogen content exceeds 100%, which can be due only to binding of the catalyst with the carboxy group of the copolymer. Therefore, in the next step of our study we examined how the copolymer : BAS ratio affects the degree of binding of Akpinol which also contains tertiary nitrogen. We found that maximal immobilization of Akpinol (58.5 mol %) was attained at the AAMA : Akpinol ratio of 1 : 2.5. Then we examined how the amount of the immobilized substance depends on the reaction mixture concentration, temperature, and time. We found that the biopolymer with the maximal degree of binding of Akpinol with AAMA is obtained at 90–100°C in 3 h at the reaction mixture concentration of 30 wt %.

The IR spectrum of this polymer suggests the formation between the piperidol and copolymer of an ester bond (1717 cm^{-1}) and an ionic bond (absorption bands of the carboxylate ion at 1573 cm^{-1} and of the quaternary nitrogen moiety at 2528 cm^{-1}).

The character of BAS bonding with the polymer matrix suggests that, when this preparation will be used as aqueous solutions, the active agent will be released in time. The process will start with fast hydrolysis of the ionic bond (since the initial acid and base are relatively weak), which will be followed by slow hydrolysis of the ester bond. Furthermore, in contrast to Styromal-based polymeric BASs, the AAMA-based substances are soluble in water, apparently due to carboxy groups present in the copolymer. This fact makes it unnecessary to convert the polymeric BASs into potassium salts (this procedure is done with polymeric biostimulants based on maleic anhydride copolymers, in particular StMA, to make them water-soluble).

The biopolymers prepared were tested for the germination energy and germinating capacity of corns. The polymeric growth regulators showed higher, compared to the monomeric analogs, biological activity; the highest germination capacity was attained upon treatment with a 0.001% solution of polymeric Akpinol (87.3%).

The field tests showed that the biopolymer containing two growth regulators is more active than polymeric Akpinol. The polymeric growth regulators developed can be used for presowing treatment of seeds in cultivation of arid cultures (crops, saxaul) under semidesert conditions on alluvial sandy soils.

CONCLUSIONS

(1) Phytoactive polymers derived from 1,4-bis[*N*-(2-ethoxyethyl)-4-hydroxypiperid-4-yl]buta-1,3-diyne and 1,2,5-trimethyl-4-dimethoxyphosphorylpiperid-4-ol (Fospinol) with 1,4-bis(1,2,5-trimethyl-4-hydroxypiperid-4-yl)buta-1,3-diyne (Akpinol) were prepared. The optimal conditions for immobilization of these compounds on copolymers of maleic anhydride with styrene and methacrylic acid were found: copolymer : BAS : catalyst ratio 1 : 1 : 1, reation time 2.5–4 h, concentration of the reactants 15–30 wt %, temperature 90–100°C depending on the nature of the starting compounds.

(2) Tests of the polymers synthesized showed that the biopolymer prepared by immobilization of Akpinol with Fospinol on maleic anhydride–styrene copolymer is the most active.

REFERENCES

1. Meirova, G., Boiko, G.I., and Zhubanov, B.A., *Izv. Minist. Obraz. Nauki Resp. Kaz., Nats. Akad. Nauk Resp. Kaz., Ser. Khim.*, 2001, no. 6, pp. 114–119.
2. Meirova, G., Water-Soluble Regulators of Plant Growth and Development, Based on Piperidol Derivatives, *Cand. Sci. Dissertation*, Almaty, 1997.
3. Meirova, G., Umerzakova, M.B., Mukhamedova, R.F., and Zhubanov, B.A., *Vestn. Kaz. Nats. Univ., Ser. Khim.*, 2003, no. 3(31), pp. 231–234.

ISSN 1070-4272, Russian Journal of Applied Chemistry, 2006, Vol. 79, No. 11, pp. 1879–1883. © Pleiades Publishing, Inc., 2006.
Original Russian Text © S.S. Nikulin, O.N. Chernykh, 2006, published in Zhurnal Prikladnoi Khimii, 2006, Vol. 79, No. 11, pp. 1900–1905.

MACROMOLECULAR CHEMISTRY AND POLYMERIC MATERIALS

Modification of Styrene-Containing Polymer with Pinane. Possible Applications of the Product

S. S. Nikulin and O. N. Chernykh

Voronezh State Forestry Engineering Academy, Voronezh, Russia

Received March 24, 2006

Abstract—The influence of high-temperature treatment on the properties of a styrene-containing polymer prepared from by-products of polybutadiene production was studied. The use of the products in production of emulsion rubbers and for protecting treatment of wood materials was examined.

DOI: 10.1134/S1070427206110279

Polymers prepared by emulsion (co)polymerization occupy a prominent place in world industry [1–4]. Emulsion polymerization does not require hazardous, inflammable, and explosive organic solvents and yields polymers with good physicomechanical properties. Studies are continued to improve the process for production of polymers by emulsion (co)polymerization and to extend the assortment of these polymers.

Polymers can be prepared in a high yield by (co)polymerization of wastes and by-products of petrochemical industry with styrene in a solution or in the bulk in the presence of both ionic and radical initiators [5, 6]. Hence, preparation of artificial aqueous dispersions of these polymers is promising. This procedure is based on fine mechanical dispersion of a polymer in an aqueous phase containing surfactants as stabilizers. Then the solvent is distilled off and the resulting dispersion is introduced into a latex. The possibility of such modification was demonstrated in [7, 8].

The substantial disadvantage of the process developed in our previous study [7, 8] is the use of a 50–70% hydrocarbon solution of the low-molecular weight polymer for preparing dispersions. In this case, an additional step, distillation of the hydrocarbon solvent from the aqueous polymer dispersion, is required. Since the polymers prepared from petrochemical wastes are solid under the ordinary conditions, a hydrocarbon solvent is required to prepare the aqueous polymer dispersion. Hydrocarbon solvents such as toluene, xylene, Nefras (commercial solvent based on butylbenzene), etc. are used to dissolve these polymers. This additional step complicates the process and decreases its efficiency. In addition, the problem of recovery and processing of these solvents arises. To eliminate the use of a hydrocarbon solvent or to decrease its content in an aqueous polymer dispersion, the molecular weight of the polymers should be decreased and solid polymers should be converted into an oil. For this purpose, the polymers prepared from wastes and by-products of petrochemical industry are subjected to thermal oxidative treatment.

It this study we examined the influence of thermal oxidative treatment in the presence of pinane hydroperoxide on the properties of a low-molecular-weight styrene-containing polymer prepared from polybutadiene production wastes. We also studied the possibility of using the product as an additive to emulsion rubber and for protecting treatment of wood materials.

EXPERIMENTAL

First we determined the molecular weight of styrene-containing low-molecular weight polymer (SLMWP) treated at 100±2°C in the presence of pinane hydroperoxide (PH). The thermal oxidative treatment was performed by the following procedure.

A reactor equipped with a stirrer was charged with 100 g of a toluene solution of SLMWP containing 70–75 wt % of bound styrene. PH in amount of 0, 1.0, 2.0, and 3.0 wt % of the initial SLMWP was added to the solution with continuous stirring. The reaction mixture was heated to 100±2°C. The total time of the process was 30 h. Samples of the reaction mixture were taken at regular intervals, their molecular weight $\overline{M}_v$ was measured viscometrically, and the acid number was determined analytically. After treatment completion, the solvent and other low-boiling fractions were distilled off from the product.

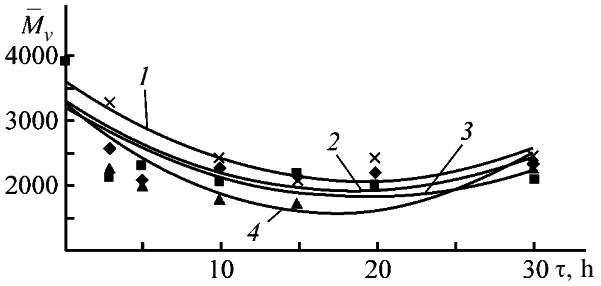


Fig. 1. Molecular weight $\overline{M}_v$ of SLMWP as a function of the time of thermal oxidative treatment τ. (*1*) Without PH and with (*2*) 1.0, (*3*) 2.0, and (*4*) 3.0 wt % of PH; the same for Fig. 2.

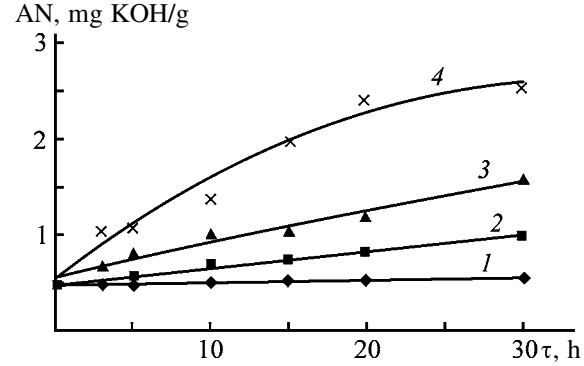


Fig. 2. Acid number AN as a function of the time of thermal oxidative treatment τ.

The molecular weight of the polymer decreases after the high-temperature (100°C) treatment of SLMWP in the presence of PH within the first 15–18 h (Fig. 1). This fact suggests that the thermal treatment involves mainly oxidative degradation to form products with oxygen-containing functional groups.

Degradation of SLMWP macromolecules can be considered as oxidative degradation of the units containing double bonds with preservation of styrene blocks [9, 10].

An increase in the acid number from 0.4–0.6 to 2.3–3.0 mg KOH/g in the whole temperature range (Fig. 2) confirms this assumption. The minimal viscosity and molecular weight are attained in 15–18 h. Then the viscosity and molecular weight of the system gradually increase, which can be due to prevalence of the cross-linking over degradation.

Low-molecular-weight polymers can cross-link to form oxygen-containing bridges.

Introduction of an additional amount of pinane hydroperoxide has a positive effect on the SLMWP modification: the molecular weight decreases to a greater extent (intensification of degradation) and the acid number increases.

Thus, our experimental data show that the properties of the products of thermal oxidative degradation can be controlled by the amount of PH added and the treatment duration. Polymers with minimal molecular weight can be prepared by treatment in the presence of 3.0 wt % PH for 15–18 h. To obtain polymers with an increased content of oxygen-containing groups (increased polarity) and a higher molecular weight, longer treatment (30 h) is required.

The molecular-weight characteristics of the initial and modified SLMWP are presented in Table 1.

Table 1. Molecular weight and content of SLMWP fractions before and after thermal oxidativer treatment*

$\overline{M}_w \times 10^{-3}$	Content of fractions, %	
	initial SLMWP	modified SLMWP
>300	0.11	–
200–300	0.19	–
100–200	0.64	–
50–100	1.57	–
20–50	4.33	–
10–20	4.92	–
5–10	4.18	0.08
3–5	13.00	1.17
1–3	31.33	20.08
0.5–1	28.96	59.26
<0.5	7.77	19.41

* According to the results of gel-permeation chromatography, SLMWP has the following molecular-weight parameters: initial, $\overline{M}_n$ = 1200, $\overline{M}_w$ = 6830, $\overline{M}_v$ = 4420, $\overline{M}_z$ = 84 173, $\overline{M}_w/\overline{M}_n$ = 5.68, $\overline{M}_z/\overline{M}_w$ = 12.33; modified, $\overline{M}_n$ = 720, $\overline{M}_w$ = 890, $\overline{M}_v$ = 850, $\overline{M}_z$ = 1260, $\overline{M}_w/\overline{M}_n$ = 1.24, $\overline{M}_z/\overline{M}_w$ = 1.42.

As seen from Table 1, the content of high-molecular-weight fraction sharply decreases, the content of the low-molecular-weight fraction increases, and the polydispersity ($\overline{M}_w/\overline{M}_n$) decreases.

As shown above, polymers prepared from petrochemical wastes can be used as fillers of emulsion polymerization rubbers, in tire and industrial rubber production, and as agents increasing the hydrophobicity and strength of wood and wood-containing articles. We tested for these applicxation SLMWP treated at high temperature in the presence of PH. We also examined the influence of the modified SLMWP on the properties of rubber, rubber stocks, vulcanizates, and wood fiberboards (WFB).

First we prepared an aqueous oligomer–antioxidant emulsion (AOAE) of modified SLMWP. A stable emulsion was obtained in the presence of emulsifiers on a unit equipped with a high-speed stirrer. An antioxidant was added to a toluene solution of modified

SLMWP and PN-6 oil (petroleum oil containing up to 14 wt % paraffin–naphthene hydrocarbons and up to 19 wt % light and up to 65 wt % medium aromatic hydrocarbons; this oil is widely used in production of extended rubbers). The mixture was stirred at 50–60°C for 0.5–2.0 h. Our preliminary results showed that no stable aqueous emulsion was formed in the presence of PN-6 oil and unmodified SLMWP without a solvent. Since these products are highly viscous, special equipment should be used for dispersing them. To prepare a stable emulsion, 20% of a solvent (toluene) was added to unmodified SLMWP and NP-6 oil.

An aqueous dispersion of SLMWP modified with PH can be prepared without introduction of a hydrocarbon solvent, since the products are oily liquids whose molecules have hydrophilic oxygen-containing functional groups.

Since the oxidative treatment of SLMWP with PH is performed in toluene, antioxidants used in production of emulsion rubber should be dissolved in an oxidized SLMWP solution prior to distillation of the solvent and low-molecular-weight products. As a result, the antioxidant will be uniformly distributed an SLMWP. Then, the solution of oxidized SLMWP and an antioxidant was emulsified and the low-molecular fraction was distilled off.

We found that the fairly uniform emulsion satisfactorily stable to phase separation can be prepared at the emulsifier content (rosin soap) of approximately 6.0 wt % and Leukanol content of 0.5 wt % relative to the dispersed phase. The content of the dispersed phase after distillation of the low-boiling fraction was 35–40 wt %.

The stable AOAE was mixed with SKS-30 ARK rubber latex and the resulting mixture was coagulated by the conventional procedure using a sodium chloride solution as a coagulating agent and a sulfuric acid solution as an acidifier [11]. The polymer content in the rubber matrix was 2.0, 3.0, 4.0, 5.0, and 6.0 wt % of the rubber and the antioxidant content was 1.2 wt % of the rubber.

Our results showed that introduction of AOAE increases the productivity of the process and results in uniform distribution of the filler in the bulk of the rubber matrix.

We prepared rubber stocks containing SLMWP samples and studied their physicomechanical properties. The optimal content of modified SLMWP in the matrix of SKS-30 ARK rubber is approximately 3.0 wt %. The strength of the vulcanizates decreases by 20–30% at the content of modified SLMWP in the rubber matrix increased to 5.0 wt %. The use of this rubber in critical articles is undesirable. However, rubber stocks with high SLMWP content can be used for preparing less critical articles such as rugs etc.

Modified SLMWP is an oily liquid whose properties are close to those of common widely used industrial oils. We performed a comparative study of the influence of SLMWP, SLMWP subjected to thermal oxidative degradation, and PN-6 oil on the properties of the rubber stocks and vulcanizates (Table 2).

Our tests of rubber stocks and vulcanizates prepared from SKS-30 ARK butadiene–styrene rubber showed that the properties of the samples containing initial and oxidized SLMWP were better than those of the samples containing PN-6 oil.

Among the positive properties of the composites are deceleration of a decrease in their strength with time, which is due to more uniform distribution of the antioxidant in the rubber matrix. In addition, the thermal resistance of the composite is enhanced.

An increase in the thermal aging coefficient is probably caused by encapsulation of the antioxidant in the areas on microheterogeneous concentration of the modified polymer. This is due to the fact that the solubility of amine and phenolic antioxidants in low-molecular-weight and more polar oxidized SLMWP is higher than that in the matrix of high-molecular-weight and low-polarity butadiene–styrene rubber. As a result, sites with high antioxidant concentrations appear in the bulk of the rubber. The concentration of the antioxidant in these sites decreases during their migration to the sample surface. Thus, this procedure for introducing antioxidants enhances the resistance of rubber articles to thermal oxidative aging and is an example of the efficient use of expensive antioxidants [12].

The next step of this study was to impregnate wood fiberboards (WFBs) with oxidized SLMWP.

The use of SLMWP treated with PH for this purpose is based on the assumption than the functional groups formed in the course of oxidation can react with the functional groups of wood components (cellulose, hemicellulose, and lignin) to form both chemical and hydrogen bonds. Formation of these bonds decreases the washout of a coating from an article in the course of its operation. The possibility of this interaction was demonstrated in our previous study [13] where a low-molecular-weight copolymer of the bottoms from styrene distillation and maleic anhydride was used for impregnation.

Table 2. Properties of rubber stocks and vulcanizates prepared from SKS-30 ARK rubber. Vulcanization time 60 min; temperature 143°C; the content of PN-6 oil and of initial and oxidized SLMWP 3.0 wt %

Property	SKS-30 ARK (reference*)	NP-6 oil	Initial SLMWP	Oxidized SLMWP
Mooney viscosity [MB 1 + 4 (100 OS)], arb. units:				
rubber	59.0	52.0	55.0	54.0
rubber stock	70.0	61.0	63.0	65.0
Weight fraction of VTS-150 antioxidant, %	1.2	1.2	1.2	1.2
Weight fraction, %:				
free organic acids	5.6	5.8	6.2	6.3
soap of organic acids	0.09	0.11	0.10	0.11
ash	0.21	0.20	0.19	0.22
Weight loss after drying at 105°C, %	0.18	0.19	0.21	0.24
Nominal stress at 300% elongation, MPa	11.0	9.3	9.9	10.8
Nominal tensile strength, MPa	25.8	19.8	23.6	24.8
Relative elongation at break, %	630	660	610	680
Elongation set, %	16	18	12	14
Rebound elasticity, %:				
20°C	38	39	35	40
100°C	48	48	50	46
Shore hardness *A*, arb. units	67	57	68	65
Thermal resistance with respect to:				
nominal tensile strength, MPa	7.8	7.9	11.1	8.9
relative elongation at break, %	120	160	180	290
Aging coefficient (100°C, 72 h) with respect to:				
nominal strength	0.60	0.61	0.68	0.70
relative elongation	0.32	0.35	0.38	0.37

* Reference sample of rubber stock and vulcanizate prepared from SKS-30 ARK rubber.

High-temperature treatment with PH of styrene-containing SLMWP prepared from polybutadiene production wastes sharply decreases the content of high-molecular-weight fractions and increases the content of low-molecular-weight fractions (Table 1). It should be noted that SLMWP penetrates in conductive elements of wood and gets bound with them in the course of the treatment of wood-containing materials.

The treatment was performed as follows. The WFB samples were weighed, immersed in an impregnation bath containing SLMWP subjected to thermal oxidative treatment in the presence of ~10% dryer, and kept for 1 min. Impregnation was performed at 60°C with subsequent heating at 160°C for 3 h. We chose these conditions on the basis of the known procedure for protecting treatment of wood materials by polymers prepared from petrochemical by-products [13, 14]. For impregnation we used SLMWP heated at 100°C for 17–20 h in the presence of 3.0 wt % PH.

Introduction of dryer accelerates both formation and decomposition of hydroperoxides. Intense reactions with atmospheric oxygen occur in the surface layers. In the depth of the composite, the contribution of the oxidation processes decreases owing to restricted oxygen access, and the contribution of high-temperature polymerization increases. These reactions are activated by various radicals present in the system.

Formation of films is inevitably accompanied by oxidative degradation to form compounds with carbonyl, carboxy, and hydroxy groups. The number of functional groups capable of interacting with reactive groups of lignin and cellulose increases. The probability of these processes is particularly high in the surface layers under conditions of film formation on exposure to air.

Our experimental results show that the treatment enhanced the stability of the WFB shape, its resistance to water and high humidity, and the mechanical properties (Table 3). Visual inspection of WFB sections showed a uniform distribution of oxidized SLMWP in the bulk of the board and filling of manufacturing

Table 3. Experimental properties of WFB samples treated with oxidized SLMWP

Property	Experiment	Reference*
Bending strength, MPa	25.6	17.8
Water absorption, %	23.9	36.5
Swelling in the thickness, %	17.1	25.7

* Reference WFB samples without treatment.

defects and of micro- and macropores. The polymer framework formed from three-dimensionally cross-linked styrene-containing SLMWP and the products of its reaction with wood components decreases the formaldehyde release from the articles prepared using phenol– or urea–formaldehyde resins as the binder.

Protective treatment of wood materials with SLMWP prepared from by-products and wastes from petrochemical industry not only improves their properties but also solves environmental problems.

CONCLUSION

High-temperature treatment of low-molecular-weight styrene-containing copolymer prepared from by-products of polybutadiene production decreases the molecular weight of the polymer and increases the content of oxygen-containing functional groups. The modified polymer can be used in production of extended rubbers and for protective treatment of wood materials.

REFERENCES

1. Eliseeva, V.I., Ivanchev, S.S., Kuchanov, S.L., and Lebedev, A.V., *Emul'sionnaya polimerizatsiya i ee primenenie v promyshlennosti* (Emulsion Polymerization and Its Indistrial Application), Moscow: Khimiya, 1976.
2. Erkova, L.N. and Chechik, O.S., *Lateksy* (Latexes), Leningrad: Khimiya, 1983.
3. Kirpichnikov, P.A., Averko-Antonovich, L.A., and Averko-Antonovich, Yu.O., *Khimiya i teknologiya sinteticheskogo kauchuka* (Chemistry and Technology of Synthetic Rubber), Leningrad: Khimiya, 1987.
4. Averko-Antonovich, Yu.A., Omel'chenko, R.Ya., Okhotina, N.A., and Ebich, Yu.R., *Teknologiya rezinovykh izdelii: Uchebnoe posobie dlya vyzov* (Technology of Rubber Articles: Textbook for Institutes of Higher Education), Kirpichnikov, P.A., Ed., Leningrad: Khimiya, 1991.
5. Nikulin, S.S., Shein, V.S., Zlotskii, S.S., et al., *Otkhody i pobochnye produkty neftekhimicheskikh proizvodstv – syr'e dlya organicheskogo sinteza* (Wastes and By-Products of Petrochemical Industry as a Raw Material for Organic Synthesis), Moscow: Khimiya, 1989.
6. Nikulin, S.S., Butenko, T.P., Ryl'kov, A.A., et al., *Perspektivy ispol'zovaniya kubovykh ostatkov proizvodstv vinilaromaticheskikh monomerov* (Prospects for Using Bottoms from Production of Vinylaromatic Monomers), Moscow: TsNIITEneftekhim, 1996.
7. Filimonova, O.N., Nikulin, S.S., Sedykh, V.A., and Khokhlova, O.A., *Proizv. Ispolz. Elastom.*, 2001, no. 1, pp. 3–9.
8. Filimonova, O.N., Nikulin, S.S., Sedykh, V.A., and Khokhlova, O.A., *Kauchuk Rezina*, 2003, no. 3, pp. 13–16.
9. Lemaev, N.V. and Zaboristov, V.N., *Destruktivnye metody pererabotki otkhodov elastomerov* (Destructive Methods for Processing Elastomer Wastes), Moscow: TsNIITEneftekhim, 1985.
10. Pchelintsev, V.V., *Termookislitel'naya destruktsiya dienovykh kauchukov* (Thermal Oxidative Degradation of Diene Rubbers), Moscow: TsNIITEneftekhim, 1986.
11. Raspopov, I.V., Nikulin, S.S., Garshin, A.P., et al., *Sovershenstvovanie oborudovaniya i tekhnologii vydeleniya butadien-(α-metil)stirol'nykh kauchukov iz lateksov* (Improvement of the Equipment and Processes for Recovering Butadiene–(α-Methyl)Styrene Rubbers from Latexes), Moscow: TsNIITEneftekhim, 1997.
12. Legotski, P. and Kavun, S.M., in *VI Rossiiskaya nauchno-prakticheskaya konferentsiya "Syr'e i materialy dlya rezinovoi promyshlennosti. Ot materialov k izdeliyam"* (VI Russian Scientific and Practical Conf. "Raw and Auxiliary Materials for Rubber Industry. From Materials to Articles"), Moscow, 1999, pp. 141–143.
13. Nikulin, S.S., Sakhokiya, I.A., Dmitrenkov, A.I., et al., *Izv. Vyssh. Uchebn. Zaved., Stroitel'stvo*, 2001, no. 1, pp. 39– 45.
14. Nikulin, S.S., Filimonova, O.N., and Oleinikova, O.N., *Zh. Prikl. Khim.*, 2003, vol. 76, no. 7, pp. 1185–1188.

ISSN 1070-4272, Russian Journal of Applied Chemistry, 2006, Vol. 79, No. 11, pp. 1884–1889. © Pleiades Publishing, Inc., 2006.
Original Russian Text © V.E. Smirnova, I.V. Gofman, G.N. Gubanova, A.I. Grigor'ev, A.L. Didenko, V.E. Yudin, V.M. Svetlichnyi, T.E. Sukhanova, 2006, published in Zhurnal Prikladnoi Khimii, 2006, Vol. 79, No. 11, pp. 1906–1911.

MACROMOLECULAR CHEMISTRY AND POLYMERIC MATERIALS

Influence of Zone Stretching on the Properties of Semicrystalline Thermoplastic Polyimide

V. E. Smirnova, I. V. Gofman, G. N. Gubanova, A. I. Grigor'ev, A. L. Didenko, V. E. Yudin, V. M. Svetlichnyi, and T. E. Sukhanova

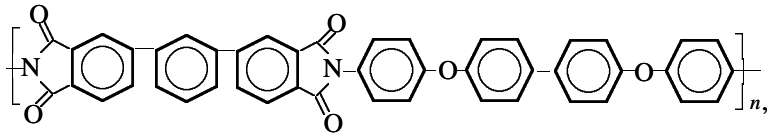
Institute of Macromolecular Compounds, Russian Academy of Sciences, St. Petersburg, Russia

Received June 27, 2006

Abstract—The effect exerted on the crystallizability of semicrystalline polyimide by zone stretching at a temperature above the glass transition point was studied.

DOI: 10.1134/S1070427206110280

Polyimides (PIs) whose macromolecules contain "hinge" heteroatoms in the diamine and dianhydride components (PI classification group 4 [1]), having an even number of benzene rings in the diamine component of the elementary unit, can occur in amorphous or semicrystalline state, depending on the conditions of synthesis of the corresponding prepolymers, polyamido acids (PAAs), and conditions of their thermal cyclization [1, 2]. A characteristic feature of the crystalline state of the most of PIs is its irreversibility: After heating above the melting point, the sample becomes amorphous, and the crystallinity is not regained after the subsequent heat treatment. A distinctive feature of the thermoplastic polyimide ROdPO of the structure



which was the subject of this study, is the ability for recrystallization after melting. This makes it suitable as a semicrystalline matrix of composite materials with carbon fibers as filler [3, 4].

Previously [3, 4] we examined the crystallizability and recrystallizability of these PIs as influenced by the molecular weight of the PAA, introduction into PI of oligoamides of identical chemical structure, and temperature modes of imidization, melting of the crystalline phase, and recrystallization.

To analyze how the characteristics of the crystalline structure of semicrystalline PIs are influenced by the above-mentioned factors, it is necessary to prepare highly oriented polymer films with oriented crystalline phase. However, highly crystalline films of this polymer are characterized by very low breaking elongations, which substantially restricts the possibilities of their orientation stretching.

As known, many carbochain polymers, both amorphous and semicrystalline with low degrees of crystallinity, are able of crystallization in the course of the orientation stretching [5]. This allows preparation of materials with oriented crystalline phase directly during such stretching.

In this study we examined the ability of ROdPO for crystallization under uniaxial stretching conditions at temperatures above the glass transition point.

EXPERIMENTAL

The PAAs were synthesized by polycondensation of a mixture of 1,3-bis(3',4- dicarboxyphenoxy)benzene dianhydride and 4,4'-bis(4'-aminophenoxy)biphenyl in a polar solvent, *N*-methyl-2-pyrrolidone, at 25°C. Our experiments were performed with PI film samples prepared from two types of PAA:

PAA-1 with $M_w \approx 150000$, prepared at the equimolar ratio of the reactants, and PAA-2 characterized by a decreased molecular weight $M_w \approx 23500$ [6]. The latter parameter was achieved at a nonstoichiometric dianhydride : diamine ratio of 0.97 : 1.00 with addition of 0.06 mol of phthalic anhydride to block excess terminal amino groups.

The PI films were prepared by casting the PAA solutions onto glass substrates and drying at 60°C for 5 h. Thermal cyclization of the films was carried out in two modes. Mode 1 involved stepwise temperature rise from 50 to 300°C (step of 50°C, keeping time at each step 15 min, heating rate between steps 3 deg min^{-1}). Cyclization mode 2 followed the above-described procedure to 110°C, whereupon the temperature was jumpwise raised to 280°C (crystallization point of ROdPO), and then slowly (over a period of 2 h) raised to 300°C. According to [1], both these modes allow complete conversion of the prepolymer to PI.

The molecular orientation of the samples was carried out by uniaxial stretching on a setup with an Utyuzhok contact heater. The hot-zone temperature was varied from the glass transition point to the crystallization point of the PI, namely, from 215 to 280°C. The optimal temperature affording the maximal degree of stretching is 250°C. The sample passed the heated zone at a velocity of 3.5 cm min^{-1}. The stretching was performed by a multistep procedure. Each step increased the degree of stretching by 50%.

The mechanical properties of the initial and oriented samples were examined using dynamic methods and tests in the uniaxial stretching mode. The temperature dependences of the dynamic Young modulus and the mechanical loss of the samples were determined on a setup described in [7] at a frequency of 660 Hz. The main characteristic reflecting the changes in the structural parameters of the samples, prepared under different conditions, was the dynamic Young modulus measured at room temperature. The reason was that an increase in the modulus, caused by the stretching, is governed by the degree of uniaxial molecular orientation or crystallinity [8]. The deformation and strength properties were determined in the uniaxial stretching mode for samples shaped as stripes with a 1×20 mm working segment. The tests were carried out on a UTS 10 (UTStestsysteme, Germany) tensile-testing machine. During tests, the sample stretching diagram was recorded; the results of the tests allowed determination of the strength σ_t and breaking elongation ε_b. The stress relaxation at isometric heating of the oriented films was determined on a UMIV-3 setup.

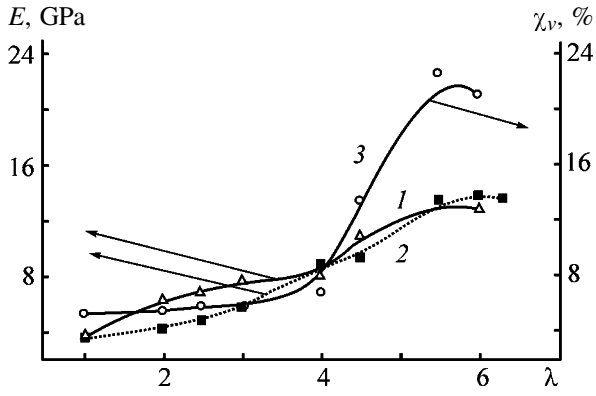


Fig. 1. (*1, 2*) Dynamic Young modulus E of the ROdPO films prepared from PAA-1 and (*3*) degree of crystallinity χ_v of the PI films prepared from PAA-1 as functions of the degree of stretching λ. Stretching temperature, °C: (*1*) 215 and (*2, 3*) 250.

The density of the samples was determined by the flotation method in a toluene–carbon tetrachloride mixture at 20°C. The experimental densities of the samples examined and densities of the amorphous phase (density after melting) of ROdPO, determined by this method, were used for estimating the degree of crystallinity of the samples by the formula [1]

$$\chi_v = \frac{\rho - \rho_a}{0.11\rho_a},$$

where χ_v is the volume degree of crystallinity; ρ, density of the sample; and ρ_a, density of the amorphisized sample.

Differential scanning calorimetric (DSC) examination of the initial and oriented samples was carried out on a DSM-2M (Specialized Designing Bureau, Pushchino) differential scanning calorimeter at a heating rate of 8 deg min^{-1}. The enthalpy of the transitions was calibrated with $KClO_4$ as reference.

The degree of crystallinity and characteristics of the transition to the oriented state for the initial film and the sample with the maximal degree of stretching were examined by X-ray diffraction analysis using a VIP-50–60 high-voltage power source, a PRF-1 X-ray accessory, and a URK-3 X-ray chamber, as well as on a DRON-3 diffractometer. We utilized Ni-filtered CuK_α radiation.

Figure 1 presents the dynamic moduli and degree of crystallinity as functions of the degree of stretching at 215 and 250°C of the films prepared from PAA-1

Mechanical properties, degree of crystallinity, shrinkage, and DSC data for the initial and oriented films

Characterization of the sample preparation procedure				Film properties						
PAA	imidization mode	T_{str}, °C	λ	E, GPa	ΔH_{melt}, J g^{-1}	mp, °C	χ_v, %	σ_t, MPa	ε_b, %	L_0/L_1
PAA-1	2	–	1	3.7	7.2	317	5	127	120	–
	2	215	4.5	11.0	–	–	10	–	–	1.53
	2	250	4.5	9.2	–	–	13	571	18	1.46
	2	250	6.3	13.5	17.6	318	20	–	–	–
	2	Annealing 280°C	–	8.0	24.7	319	25	–	–	–
PAA-2	2	–	1.0	4.6	32.0	322	36	–	–	–
	1	–	1.0	3.7	8.0	322	5	123	89	–
	1	215	4.5	9.5	15.0	318	13	–	–	1.60
	1	250	4.5	6.3	16.0	318	15	292	16	1.24
	1	280	4.5	4.0	11.3	320	8	–	–	–
	2 and amorph. 380°C	250	5.5	5.75	29.8	316	–	–	–	–
	2 and amorph. 380°C	215	4.5	10.5	20	317	12	–	–	–

by mode 2. Our previous studies [3] showed that a high molecular weight of PAA-1 decreases the crystallizability of the polymer in the isotropic state. Indeed, the initial (not subjected to orientation) films prepared by mode 2 are distinguished by very low degrees of crystallinity (see table), although it was shown previously [2, 3] that specifically this mode is favorable for crystallization. However, subsequent stretching of such films by a factor of 4 and over is accompanied by a significant increase in the strength, a decrease in the breaking elongation, and increases in the dynamic modulus and density (see table). This suggests enhanced molecular orientation and degree of crystallinity. It should be noted that the dependences of the modulus on the degree of stretching change very little with the stretching temperature.

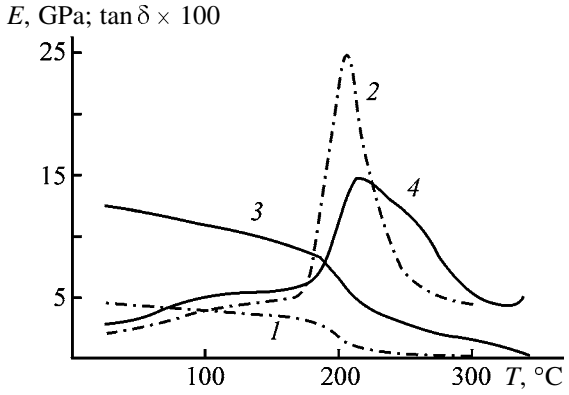


Fig. 2. Temperature dependences of (*1, 3*) the dynamic modulus E and (*2, 4*) mechanical loss tangent tan δ of the samples prepared from PAA-1, cyclized by mode 2. Sample: (*1, 2*) initial and (*3, 4*) stretched by a factor of 6.3 at 250°C.

The DSC curves showed that stretching by a factor of 6.3 of the PI sample prepared by mode 2 causes the enthalpy of melting to increase by a factor of 2.4 (see table). This can be due to an increase in the degree of crystallinity in the course of the orientation stretching.

Figure 2 presents the temperature dependences of the dynamic Young modulus and the mechanical loss tangent of the initial PI film prepared by mode 2 and the same film subjected to orientation stretching by a factor of 6.3 at 250°C. At temperatures above T_g, the modulus of the initial sample approaches that of the amorphous sample in a softened state, and that of the oriented sample is preserved up to the melting point at a significantly higher level. The mechanical loss tangent of the initial sample exhibits a narrow maximum near the softening points; the loss tangent maximum of the oriented sample is much broader, it is shifted by 10°C to higher temperatures and is asymmetric, with a shoulder near the melting points. It should be noted that such a pattern of variation of these parameters was observed for the orientation crystallization of polyethylene terephthalate [9].

Figure 3 presents the stress relaxation curve for the oriented sample at isometric stretching. It is

typical for oriented systems: With approaching the glass transition point of the polymer, the stresses in the sample significantly increase due to disorientation of the macromolecules. However, after the transition to the devitrified state, the stresses in the sample do not exhibit such a sharp decrease: The high-temperature branch of the relaxation curve contains a prominent shoulder; the stresses continue to decrease up to the melting point of RODPO. This run of the relaxation curve suggests that significant concentrations of the crystalline phase occur in the sample after the orientation stretching.

To increase the degree of crystallinity, the sample with the maximal degree of stretching was annealed for 2 h in the free state at the crystallization temperature, 280°C, which was accompanied by shrinkage of the sample and a decrease in the Young modulus (see table). At the same time, such heat treatment caused the enthalpy of melting and the degree of crystallinity (estimated from the density of the sample) to increase. The degree of crystallinity of this sample was estimated by X-ray diffraction analysis at 30%.

The PI films prepared from PAA-2 exhibit a noticeable dependence of the degree of crystallinity on the temperature and time mode of cyclization. A jumpwise mode of imidization (mode 2) allows preparation of films with a high degree of crystallinity (see table), but these samples were brittle and could not be subjected to orientation stretching. Upon heating to temperatures no higher than 320°C, these samples preserve the ability for recrystallization, but after heating to higher temperatures this ability in the isotropic state disappears [3]. To prepare oriented PI films cyclized from PAA-2 in the jumpwise mode, the initial samples with a high degree of crystallinity were amorphisized at 380°C, whereupon they were subjected to orientation stretching at 215 and 250°C.

Cyclization of PAA-2 in the jumpwise mode (mode 1) yielded films with high breaking elongations (see table) and a low degree of crystallinity. For these films, orientation stretching was achieved even in the initial state at different temperatures.

Figure 4 presents the dynamic moduli as functions of the degree of stretching at 215 and 250°C for RODPO films of two types prepared from PAA-2: imidized by mode 1 and by mode 2 with subsequent amorphization. The samples stretched at softening points (215°C) are characterized by significantly higher moduli than those stretched at 250°C. The dependences obtained for the initial samples prepared by mode 1 and those amorphisized after imidization by mode 2 and stretched at identical temperatures are close. The DSC data and the densities of these samples suggest close enthalpies of melting and crystallinities of the samples stretched at 215 and 250°C (see table, Fig. 5). Therefore, high moduli of the samples stretched at 215°C reflect, above all, a higher degree of molecular orientation, rather than a higher crystallinity compared to the films oriented at 250°C. This

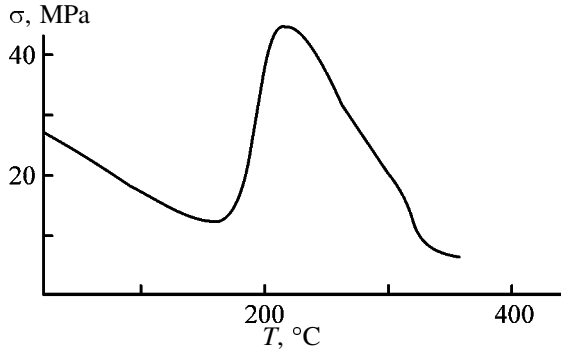


Fig. 3. Stress relaxation σ for isometric heating of the RODPO film from PAA-1, preliminarily stretched at 250°C by a factor of 6.3.

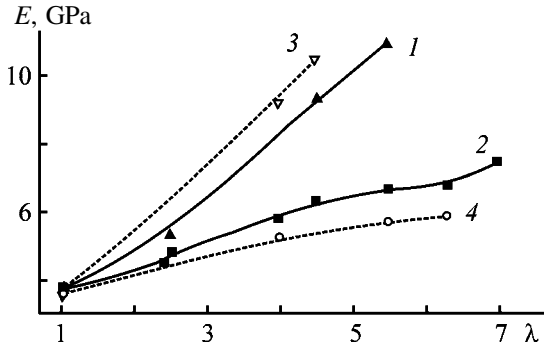


Fig. 4. Dynamic moduli *E* of the (*1, 2*) initial and (*3, 4*) amorphisized at 380°C RODPO films from PAA-2 as functions of the degree of stretching λ at (*1, 3*) 215 and (*2, 4*) 250°C.

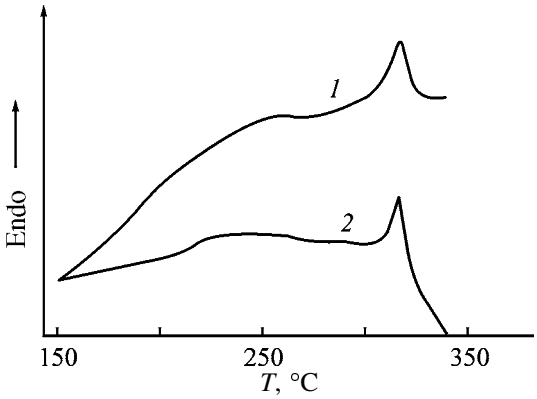


Fig. 5. DSC thermograms of the RODPO films from PAA-2, amorphisized at 380°C and subsequently stretched (*1*) by a factor of at 4.5 at 215°C and (*2*) by a factor of 5.5 at 250°C. (*T*) Temperature.

fact is confirmed by measurements of the enthalpy of disorientation of the amorphisized samples stretched at different temperatures (Fig. 5). The DCS thermograms clearly suggest thermoinduced disorientation of the preliminarily stretched samples. For samples stretched at 215°C by a factor of 4.5, this process is observed at 180–280°C and is characterized by the disorientation enthalpy of 92 J g^{-1}. For the film stretched by a factor of 5.5 at 250°C (the same process is realized at 200–280°C) we revealed a substantially lower enthalpy of disorientation, 32.5 J g^{-1}.

The influence of zone stretching on orientation of the amorphous phase was estimated from the results of the relaxation tests, as well as from measuring the shrinkages of the preliminarily oriented films as a result of heating at a temperature exceeding the stretching temperature by 5°C (see table). As known, stretching of a polymer film at temperatures above the glass transition point is realized via two kinds of strain: reversible hyperelastic and irreversible plastic strain. The former strain is realized via stretching of the macromolecules, orientation of their segments along the direction of the applied stress, and the latter, by mutual slipping of the macromolecules. Thus, the degree of molecular orientation, achieved during such stretching, is proportional specifically to the hyperelastic strain of the polymer. The plastic component of the strain should increase with increasing stretching temperature and decreasing molecular weight.

The fraction of the hyperelastic component of the strain can be estimated from the shrinkage of preliminarily stretched samples, arising from their subsequent heating at a temperature above the stretching temperature. We took specifically this approach. The shrinkage was estimated as the ratio of the length of the oriented samples before annealing L_0 to that after annealing L_1. The remainder of the strain of the sample during stretching is accounted for by plastic strain. The tabulated shrinkages of the samples stretched under different conditions to identical degrees suggest an increase in the fraction of plastic strain for the samples prepared from low-molecular-weight PAA (PAA-2) with rising stretching temperature. This agrees well with the Young moduli of the samples stretched at different temperatures. Our data confirm the fact that stretching of the samples prepared from PAA-2 at 215°C affords a higher molecular orientation than stretching to the same degrees at 250°C.

The shrinkages and elasticity moduli of the samples prepared from PAA-1 and stretched to identical degrees at 215 and 250°C are close. Hence, the hyperelastic strains in stretching at both temperatures are also close. It should be noted that, at high-temperature stretching of these samples, the hyperelastic strains are higher than those of the samples prepared from low-molecular-weight PAA-2 (see table).

The strength characteristics of the films prepared from PAA-1 and PAA-2 in the initial state are very close. However, upon stretching at 250°C by a factor of 4.5, these films substantially differ in the strengths (see table). Higher strengths of the stretched ROdPO samples prepared from PAA-1 suggest a higher degree of their molecular orientation.

Our results show that the orientation stretching substantially affects the crystallizability of the ROdPO polyimide samples. Such treatment of the films causes the degree of crystallinity of the PI to increase at temperatures below the crystallization point. This afforded a high degree of crystallinity for the samples prepared from high-molecular-weight PAA-1, whose crystallizabilty in the isotropic state is very low. The tabulated data suggest that stretching of these samples affords a higher degree of crystallinity than for the samples of PAA-2 stretched under identical conditions.

Further increase (above 250°C) in the temperature of stretching did not enhance the degrees of stretching, molecular orientation, and crystallinity of ROdPO. The table presents the parameters of the sample stretched to the prefailure state at the crystallization temperature (280°C). The enthalpy of melting, the Young modulus, and the degree of crystallinity of this sample proved to be lower than those of the samples stretched to the same degree at 250°C. This effect is due to the fact that, at so high temperatures, intensive relaxation processes occur in the sample directly during stretching.

Our studies showed that, taking into account all the competing processes occurring in the course of zone stretching, such as molecular orientation, crystallization, and relaxation, a multistep stretching at 250°C at the above-mentioned rate is the optimal mode for preparation of samples with the maximal degree of crystallinity.

The samples prepared by stretching in this mode were examined by wide-angle X-ray diffraction analysis. Figure 6 presents the X-ray diffraction patterns of the initial film prepared from PAA-2, imidized by mode 2 and crystallized in the isotropic state (Fig. 6a), as well as of the film prepared from PAA-1, imidized by the same mode and crystallized in the course of a sixfold stretching at 250°C (Fig. b).

Figure 6a shows that the initial film prepared by

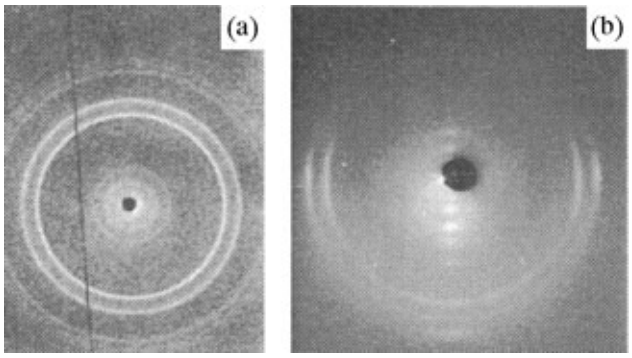


Fig. 6. X-ray diffraction patterns of the sample crystallized (a) in isotropic state and (b) during stretching by a factor of 6.3 at 250°C.

the above-described procedure is a nonoriented film and occurs in a semicrystalline state. The film subjected to a sixfold stretching is also semicrystalline. The degree of orientation of the crystallites is fairly low. Against the background of continuous rings, areas of increased intensity are prominent at the X-ray diffraction pattern equator within 30°. The orientation stretching of the weakly crystallized initial film causes the degree of crystallinity to increase, but the orientation of the crystalline phase proper is insignificant.

It can be assumed that the molecular orientation in the PI examined proceeds by orientation of the segments of the macromolecules in the amorphous phase, and a weak orientation of the crystallites is due to a low anisotropy of the shape of the crystalline domains.

CONCLUSIONS

(1) Orientation stretching at temperatures above the glass transition point to degrees of stretching above 4 noticeably increases the degree of crystallinity of the films of thermoplastic semicrystalline RODPO polyimide. This effect is observed both for the samples prepared from low-molecular-weight polyamido acids, whose degree of crystallinity in the isotropic state can be widely varied by varying the temperature–time mode of cyclization, and for the samples prepared from high-molecular-weight polyamido acids.

(2) This procedure is suitable for crystallization of samples preliminarily amorphisized at a high temperature, which do not crystallize in the isotropic state.

(3) Zone stretching does not afford significant orientation of the crystallites.

REFERENCES

1. Bessonov, M.I., Koton, M.M., Kudryavtsev, V.V., and Laius, L.A., *Poliimidy – klass termostoikikh polimerov* (Polyimides: A Class of Heat-Resistant Polymers), Leningrad: Nauka, 1983.
2. Smirnova, V.E., Bessonov, M.I., Florinskii, F.S., and Baklagina, Yu.G., *Vysokomol. Soedin., Ser. B*, 1971, vol. 13, no. 7, pp. 531–534.
3. Yudin, V.E., Svetlichnyi, V.M., Gubanova, G.N., et al., *J. Appl. Polym. Sci.*, 2002, vol. 83, pp. 2873–2882.
4. Yudin, V.E., Svetlichnyi, V.M., Gubanova, G.N., et al., *Polyimides and Other High Temperature Polymers: Synthesis, Characterization, and Applications*, Mittal, K., Ed., Utrecht: VSP, 2003, vol. 2, pp. 523–532.
5. Berestneva, G.L., Tsvankin, D.Ya., and Kozlov, P.V., *Vysokomol. Soedin.*, 1961, vol. 3, no. 12, pp. 1787–1790.
6. Silinskaya, I.G., Svetlichnyi, V.M., Kalinina, M.A., et al., *Vysokomol. Soedin., Ser. A*, 2006, vol. 48, no. 8, pp. 1383–1390.
7. Polikarpov, Yu.I., Rudakov, A.P., and Bessonov, M.I., *Zavod. Lab.*, 1976, vol. 42, no. 12, pp. 1517–1519.
8. Ward, I.M., *Mechanical Properties of Solid Polymers*, New York: Wiley, 1971.
9. Ferry, J.D., *Viscoelastic Properties of Polymers*, New York: Wiley, 1961.

ISSN 1070-4272, Russian Journal of Applied Chemistry, 2006, Vol. 79, No. 11, pp. 1890–1895. © Pleiades Publishing, Inc., 2006.
Original Russian Text © S.V. Usachev, A.S. Osipov, G.I. Kostrykina, T.I. Irkhina, N.B. Tantsova, E.G. Fedorova, 2006, published in Zhurnal Prikladnoi Khimii, 2006, Vol. 79, No. 11, pp. 1912–1917.

MACROMOLECULAR CHEMISTRY AND POLYMERIC MATERIALS

Specific Features of Separate and Joint Mastication of Natural and 1,4-*cis*-Butadiene Rubbers in the Presence of Dibenzoylaminodiphenyl Disulfide

S. V. Usachev, A. S. Osipov, G. I. Kostrykina, T. I. Irkhina, N. B. Tantsova, and E. G. Fedorova

Yaroslavl State Technical University, Yaroslavl, Russia
Yaroslavl Tire Plant, Joint-Stock Company, Yaroslavl, Russia

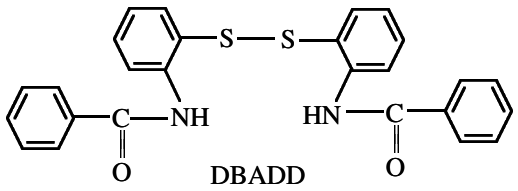
Received May 19, 2006

Abstract—Variation of the molecular structure characteristics and properties of natural and 1,4-*cis*-polybutadiene rubbers (gel content, molecular weight, degree of branching of macromolecules, viscosity) in the course of their separate and joint mastication in the presence of dibenzoylaminodiphenyl sulfide as mastication accelerator or without it was studied.

DOI: 10.1134/S1070427206110292

Natural rubber (NR) and its blends with other rubbers (e.g., *cis*-butadiene rubber, SKD) are widely used in rubber industry, in particular, for production of treads and sidewalls of R-type tyres. Industrial processing of NR is more labor- and power-consuming than that of synthetic rubbers, because it requires preliminary mastication with the aim to decrease the molecular weight and viscosity to the level suitable for processing into rubber stocks and semifinished products on the existing equipment. With polymer blends, the viscosity of compounds can be significantly decreased owing not only to a decrease in the molecular weight of rubber macromolecules, but also to formation of a specific structure. The causes of such a decrease in the viscosity of blends consisting of different rubbers are described in detail [1]. The most pronounced decrease in the viscosity of NR–SKD blends, measured at shear rates less than 100 s^{-1}, is observed at their ratios in the range from 80/20 to 50/50 [2]. However, in view of the free-radical nature of mechanochemical reactions, we should take into account the possibility of recombination of free radicals [3], which can lead to an increase in the molecular weight and decrease in the mastication effect.

It is well known that the molecular weight of rubbers can be decreased by introducing special additives, so-called chemical mastication accelerators [3, 4]. In this connection, it is appropriate to study specific features of joint mastication of NR and SKD in the presence of a commercially used additive, dibenzoylaminodiphenyl disulfide (DBADD), and without it.



DBADD

The commercial name of the accelerator is Pepton-22. It is a light yellow crystalline powder melting at 136–143°C [5].

EXPERIMENTAL

Experiments were performed with RSS-1 NR (Indonesia), SKD [GOST (State Standard) 14924–73], and an NR–SKD blend (1 : 1). The mastication of NR, SKD, and their blends was performed on Lb 320 160/160 laboratory rollers with addition of DBADD (0.3 wt % relative to rubber) or without it. The clearance between the rollers was 2.3 mm at a friction of 1 : 1.14. The mastication was performed for 5, 10, and 15 min. DBADD mastication accelerator was added in all the cases on the second minute after the rubbers adhere to the roller at the initial rubber temperature of 35°C. In the course of mastication, the rubber temperature increased to 75–80°C.

To evaluate changes in the rubber structure, we determined viscometrically at 25°C the intrinsic vis-

Table 1. Influence of the rolling time and DBADD content on the properties and molecular characteristics of NR, SKD, and their 1 : 1 blend

Sample	τ, min	Weight fraction of gel, %	Mooney viscosity, Mooney units	[η], dl g^{-1}	K_H, (dl g^{-1})$^{-2}$
NR:					
without DBADD	0	18.23	95.0	4.78	1.00
	5	3.33	77.5	4.20	0.3
	10	3.06	69	3.43	0.34
	15	1.68	58	2.40	0.80
with DBADD	5	4.43	66	3.32	0.57
	10	3.45	54.5	2.33	0.96
	15	1.55	44	2.64	0.33
SKD:					
without DBADD	0	3.95	–	2.52	0.14
	5	2.83	45	2.46	0.18
	10	2.11	46	2.39	0.28
	15	3.11	45	2.36	0.33
with DBADD	5	2.74	48.9	2.06	0.67
	10	3.30	49.8	2.18	0.49
	15	3.19	48.8	2.20	0.39
NR + SKD					
without DBADD	5	5.56	72.3	3.27	0.59
	10	4.19	73.9	3.17	0.72
	15	4.19	58.2	2.36	0.74
with DBADD	5	4.18	72.2	2.95	0.80
	10	3.46	71.3	2.97	0.53
	15	5.12	70.6	3.20	0.63

cosity [η] of the sol fraction soluble in toluene. From the slope of the linear concentration dependence of the reduced viscosity, we determined the branching coefficient from which we calculated the Huggins constant K_H characterizing the degree of macromolecule banching [6].

The content of the gel (insoluble fraction) was determined by two methods: from the weight of the residue on the filter and from the difference in the solution concentrations before and after filtration. From these data, we determined the constant of mechanical degradation K_σ and the degree of degradation φ [3]. The degradation constant was calculated by the equation

$$(\eta_t - \eta_\infty)/(\eta_0 - \eta_\infty) = \exp(-K_\sigma t), \quad (1)$$

where η_0, η_t, and η_∞ are the intrinsic viscosities of the rubber before rolling, after the treatment for time t, and after the 60-min treatment (limiting degradation).

The degree of degradation was calculated as

$$\varphi = (\eta_0 - \eta_t)/(\eta_0 - \eta_\infty). \quad (2)$$

The viscosity of rubbers and their blends was determined on a Mooney shear disk viscometer and evaluated in Mooney units (1 Mooney unit = 0.0846 N m) [7].

Table 1 shows how the rolling time τ and DBADD content affect the properties and molecular characteristics of NR, SKD, and their blends, and Table 2 shows how these factors affect the constant of mechanical degradation and degree of degradation of these materials.

An increase in the time of NR mastication without chemical accelerator is accompanied by a monotonic decrease in the gel content, intrinsic viscosity, and Mooney viscosity. The degree of degradation grows monotonically, but there is no definite trend in variation of the degree of branching: In the case of NR, it first decreases upon mastication for 5 min and then gradually increases. This may be due to the development of nonlinear degradation [3]. On the whole, the changes observed are consistent with the well-known views [8] that the viscosity of polymers in the condensed state of macromolecules decreases with a decrease in the gel content and in the molecular weight and with an increase in the degree of branching.

Table 2. Influence of the rolling time and DBADD content on the constant of mechanochemical degradation K_α and degree of degradation φ of NR and SKD

Sample	τ, min	K_σ, min	φ
NR:			
without DBADD	5	0.120	0.24
	10		0.57
	15		0.88
with DBADD	5	0.15	0.57
	10		0.90
	15		0.81
SKD:			
without DBADD	5	0.008	0.039
	10		0.078
	15		0.095
with DBADD	5	0.013	0.256
	10		0.191
	15		0.182

Addition of DBADD mastication accelerator noticeably increases the rate and degree of degradation of NR and SKD macromolecules. At the same time, more pronounced decrease in molecular weight (MW) at a mastication time of 5 and 10 min results in increased branching of macromolecules in the sol fraction and higher gel content in the masticated rubber. For example, after mastication of NR for 5 min, the branching of the macromolecules is characterized by the Huggins constant of 0.57 $(\text{dl g}^{-1})^{-2}$ and gel content in the masticated rubber of 4.43%; after rolling for 10 min, these parameters become 0.96 $(\text{dl g}^{-1})^{-2}$ and 3.45%, respectively. Longer rolling (15 min) results in a certain increase, rather than decrease, in the molecular weight; in the process, the degree of branching and gel content sharply decrease: from 0.96 to 0.33 $(\text{dl g}^{-1})^{-2}$ and from 3.45 to 1.55%, respectively. The Mooney viscosity monotonically decreases. Larger branching of macromolecules observed in the initial period of mastication in the presence of mastication accelerator indicates that the major pathways of deactivation of polymeric radicals in the initial period of the process are their recombination and reaction with nondegraded macromolecules, rather than addition of the sulfide radical of DBADD. Longer mastication results in more uniform distribution of the mastication accelerator and hence in higher probability of the reaction of polymeric radicals with DBADD. The high melting point of DBADD also plays a certain role, impeding its dispersion at the mastication temperature of 75–80°C.

Thus, mastication of NR for 15 min without mastication accelerator results in the formation of a rubber structure with decreased MW and increased branching of macromolecules. In the presence of DBADD, a decrease in the molecular weight is accompanied by a decrease in the polymer chain branching.

An increase in the time of SKD mastication without accelerator to 15 min results in monotonic but slight decrease in the molecular weight, with the Huggins constant increasing (from 0.14 to 0.33). The gel content in the initial period of the mastication decreases, but after the treatment for 15 min somewhat increases. The observed changes in the structure do not lead to noticeable changes in the Mooney viscosity. Addition of the mastication accelerator leads to a more noticeable decrease in the molecular weight of SKD rubber, with a considerable increase in the Huggins constant (to 0.67). An increase in the mastication time to 10 and 15 min results in a certain increase, rather than decrease, in the molecular weight. At the same time, the degree of branching of the macromolecules decreases to 0.39, and the gel content in the masticated rubber somewhat increases. The trends in the kinetics of degradation and branching of SKD and NR show certain analogy determined, as noted above, by decelerated dispersion of the mastication accelerator in the rubber matrix due to high melting point of its crystals.

Joint mastication of NR and SKD without mastication accelerator leads to a decrease in the intrinsic viscosity of the rubber blend, indicative of a decrease in the MW of the elastomeric components. The intrinsic viscosity of the rubber blend is close to the additive value. At the same time, macromolecules in the ash are characterized by increased degree of branching relative to the sum of the contributions of the components at the separate mastication. The masticated rubbers are characterized by the increased gel content, which imparts to them higher Mooney viscosity. Apparently, higher branching of macromolecules in the sol fractions is due to recmobination of chain radicals of NR and SKD, and also to the presence of fragments of the three-dimensional structure of the initial gel, which is broken down during mastication. Somewhat lower degree of the gel degradation may be caused by the lower shear stress in the initial period of the mastication, due to a decrease in the initial viscosity of the combined system [1].

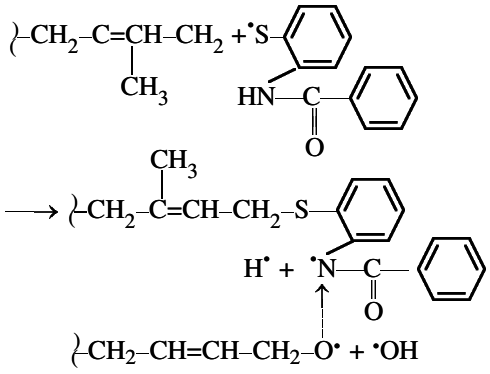
The effect of DBADD on the elastomer blend is similar to its effect in mastication of each rubber taken separately. More pronounced decrease in the MW in the initial period of the process (the intrinsic viscosity decreases from 3.27 in rolling without accelerator to

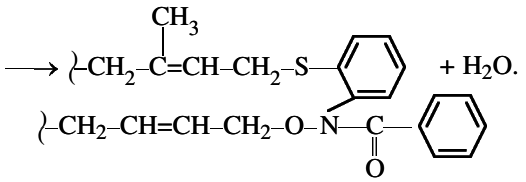
2.97 in the presence of DBADD) is accompanied by its increase with an increase in the mastication time. Initially high values of the Huggins constant decrease in the course of the mastication. At the same time, the gel content in the masticated rubber increases.

In joint mastication of NR and SKD both in the presence of DBADD and without it, the degree of branching of macromolecules and the gel content in the masticated rubber are higher than in mastication of the rubbers taken separately. This fact indicates that the role of the recombination of polymeric radicals and their reaction with macromolecules in rubber blends is more significant. It was interesting to additionally estimate the probability of the reaction of chain radicals belonging to different elastomers. To this end, the sol fraction of 1 : 1 NR + SKD blends masticated in the presence of DBADD and without it (rolling time 15 min) was dried and subjected to quantitative analysis by pyrolytic gas chromatography (Biokhrom-1 chromatograph):

Masticated rubber	NR/SKD rubber content in sol fraction, %
Without DBADD	50/50
With DBADD	55/45

These data show that, in the mastication without DBADD, the ratio of the rubbers in the sol fraction and hence in the gel is equal to their initial ratio. This fact suggests (though tentatively) formation of a chemical bond NR–SKD, which also follows from the stronger branching of the blended masticated rubber. In the joint mastication of NR and SKD with DBADD, a part of the macromolecules becomes incorporated in the gel structure. This fact also suggests that the joint mastication of NR and SKD is accompanied by chemical reaction of the chain radicals of different elastomers. The following scheme of formation of a chemical bond between polyisoprene and polybutadiene radicals in the presence of DBADD can be suggested:





The primary or peroxy radical of polyisoprene reacts with *o*-benzoylaminophenylthio radical to form macromolecules incorporating an amine-type antioxidant. Hydroperoxides of butadiene rubber, forming successively or simultaneously, readily decompose into products to form low-molecular-weight and chain radicals [3, 4]. These radical chemically bind the amine radical which is already bound chemically to a polyisoprene macromolecule. Repeated degradation of the linked chains can lead to an increase in their molecular weight, branching, and gel formation. The sequence of the reactions of polyisoprene or polybutadiene radicals with DBADD is apparently random. Thus, on the one hand, DBADD accelerates the mastication of *cis*-1,4-polyisoprene and *cis*-1,4-polybutadiene whose addition favors a decrease in MW; on the other hand, DBADD is an antioxidant and acts oppositely, promoting formation of interpolymers and enhancing the interactions at phase boundaries of different rubbers. It should also be noted that this accelerator is the most effective at treatment temperatures in the range 80–140°C [9]. This is apparently associated with its high melting point. In the course of mastication in closed rubber mixers and preparation of rubber stocks, rubbers are subject to simultaneous action of the mechanical and thermal energy. The temperature of extended rubber stocks in their preparation in closed rubber mixers increases to 160°C and more [5], which should lead to prevalence of processes leading to a decrease in the molecular weight.

In this study we examined the possibility of preparing rubber stocks with NR and performing the mastication directly in the step of stock preparation. Under industrial conditions, we prepared tread rubber stocks from nonmasticated NR in combination with SKD (85/15), with addition of 0.3 wt % DBADD in the first step of compounding. The properties of the experimental rubber stocks and vulcanized products were compared with those of the commercial product of the same composition in which NR was taken as P-3 masticated rubber prepared in a rubber mixer without mastication accelerator. The experimental and commercial rubber stocks were prepared under the same conditions. Their technological properties appeared to be the same. At the same time, vulcanized

Table 3. Physicomechanical parameters of vulcanized rubber stocks prepared by joint mastication of NR with SKD in the presence of DBADD

Parameter	Reference	Experimental value
Nominal tensile strength, MPa	171	187
Rebound elasticity, 20°C/100°C, %	38/50	41/56
Endurance at repeated 150% extension, thousands of cycles	35.1	53.7
Coefficient of resistance to thermal aging* at 100°C, 48 h, with respect to:		
nominal strength	0.73	0.84
relative elongation	0.58	0.69
tear resistance	0.70	0.97
De Matthias head buildup, T, °C:		
before aging	123	111
after aging at 100°C, 48 h	142	128
Mir-1 abradability, $m^3\ TJ^{-1}$:		
before aging	80	62.2
after aging at 100°C, 48 h	133.9	110.5
Schopper abradability, mm^3	64	58

* The coefficient of resistance to thermal aging is defined as the ratio of the indicated parameter before aging to that after aging.

products from experimental rubber stocks exhibit higher values of certain parameters (Table 3), in particular, higher elasticity, higher endurance at repeated extension, and lower heat buildup, which is attributable to weaker branching of NR macromolecules, at a considerably higher content of NR compared to SKD. Experimental rubbers have also a higher coefficient of resistance to thermal aging and wear. In this case, DBADD behaves as an aging inhibitor. According to [10], stabilizers incorporated in the polymer chain decrease the abradability of rubbers. Also possible is a positive effect of stronger bonding between the phases, due to formation of interpolymers of types NR–SKD and NR–DBADD–SKD.

CONCLUSIONS

(1) In separate mastication of natural and 1,4-*cis*-butadiene rubbers without using dibenzoylaminodiphenyl disulfide as mastication accelerator, the molecular weight monotonically decreases and the degree of branching of the macromolecules increases. In the presence of this mastication accelerator, the pattern is different.

(2) In joint mastication of natural and 1,4-*cis*-butadiene rubbers in the presence of dibenzoylaminodiphenyl disulfide and without it, the degree of branching of the macromolecules, gel content, and Mooney viscosity of the masticated rubbers are higher than the sum of the contributions of the components, determined at their separate mastication.

(3) Joint mastication of natural and 1,4-*cis*-butadiene rubbers can be combined in one step with the preparation of extended rubber stocks in closed rubber mixers in the presence of dibenzoylaminodiphenyl disulfide. The resulting stocks exhibit the required processing characteristics, and the physicomechanical properties of the resulting vulcanizates are improved owing to weaker branching of natural rubber macromolecules, incorporation of an *o*-benzoylaminophenylthio fragment, behaving as amine-type antioxidant, in the macromolecules, and stronger bonding between the polymer phases owing to formation of interpolymers.

REFERENCES

1. Kuleznev, V.N., *Smesi polimerov* (Polymer Blends), Moscow: Khimiya, 1980.
2. Folt, V.I. and Smith, L.W., Rheology of Blends, *Rubber Chemistry and Technology*, 1973, vol. 46, pp. 1193–1209.
3. Baramboim, N.K., *Mekhanokhimiya vysokomolekulyarnykh soedinenii* (Mechanochemistry of Macromolecular Compounds), Moscow: Khimiya, 1978.
4. Simionescu, C. and Opreo, C., *Mecanochimia Comusilor Macromoleculari*, Bucharest: Academiei, 1967.
5. Koshelev, F.F., Kornev, A.E., and Bukanov, A.M., *Obshchaya tekhnologiya reziny* (General Technology

of Rubber), Moscow: Khimiya, 1978, 4th ed.

6. Serenson, W.R. and Campbell, T.W., *Preparative Methods of Polymer Chemistry*, New York: Interscience, 1961.
7. Zakharov, N.D., Zakharkin, O.A., Kostrykina, G.I., et al., *Laboratornyi praktikum po tekhnologii reziny: uchebnoe posobie dlya vuzov* (Laboratory Manual on Rubber Technology: Textbook for Higher Schools), Moscow: Khimiya, 1988, 2nd ed.
8. Vinogradov, G.V. and Malkin, A.Ya., *Reologiya polimerov* (Rheology of Polymers), Moscow: Khimiya, 1977.
9. Betts, G.E., Karmin, B.K., Eitingon, I.I., et al., *Kauchuk Rezina*, 1960, no. 5, pp. 24–27.
10. Il'ina, E.A., Role of Chemical Factors in Wear Failure of Vulcanized Rubbers, *Cand. Sci. Dissertation*, Moscow, 1977.

ISSN 1070-4272, Russian Journal of Applied Chemistry, 2006, Vol. 79, No. 11, pp. 1896–1901. © Pleiades Publishing, Inc., 2006.
Original Russian Text © E.V. Gert, V.I. Torgashov, O.V. Zubets, F.N. Kaputskii, 2006, published in Zhurnal Prikladnoi Khimii, 2006, Vol. 79, No. 11, pp. 1918–1923.

MACROMOLECULAR CHEMISTRY AND POLYMERIC MATERIALS

Combination of Oxidative and Hydrolytic Functions of Nitric Acid in Production of Enterosorbents Based on Carboxylated Microcrystalline Cellulose

E. V. Gert, V. I. Torgashov, O. V. Zubets, and F. N. Kaputskii

Research Institute of Physicochemical Problems, Belarussian State University, Minsk, Belarus

Received March 1, 2006; in final form, May 2006

Abstract—A single-stage procedure was developed for preparing carboxylated microcrystalline cellulose from native cellulose in 45–55% nitric acid acting as a deposited form of catalyst of cellulose oxidation, nitrogen(IV) oxide, and as a selective reagent partially hydrolyzing cellulose.

DOI: 10.1134/S1070427206110309

According to the results of clinical trials in gastroenterology and detoxication therapy [1–3], carboxylated microcrystalline cellulose (CMCC) in the form of gels of its salt species [4] is an efficient enterosorbent with clearly pronounced coating and antiulcerogenic effects. The necessity of developing this type of enterosorbents stems from the following reasons. Widespread carbon enterosorbents cannot substitute in full measure enterosorbents of polysaccharide nature, food fibers adapted to human digestive system in the overall course of evolution. Traditional use of natural polyuronides in enterosorption is complicated by the possibility of accumulation of toxic substances from the biosphere in the vegetation period [5]. As regards high degree of chemical purity, among polysaccharides not digested in a human body, microcrystalline cellulose (MCC) deserves particular attention. In its production, foreign impurities accumulated predominantly in the structurally disordered component of the fiber precursor are removed together with this component in the course of hydrolytic cleavage of the fiber to so-called limited degree of polymerization (DP) [6].

Microcrystalline cellulose is widely used as a filler in production of many drugs, as a dietetic additive decreasing the caloric value of the food ration, and also as a remedy for removal of a dross from gastrointestinal tract. The possibility of using MCC in pharmaceutical and food industry is significantly widened by its unique ability to form stable thixotropic gels under the action of high shearing dynamic stresses on 5–20% aqueous dispersions [6]. However, the efficiency of MCC as enterosorbent is limited by the absence of ion-exchange groups that are contained in pectins and polysaccharides of seaweed (laminarin, carraginan).

Previously [1] CMCC was prepared by oxidation of cellulose with nitrogen(IV) oxide at room temperature in the gas phase followed by hydrolysis of the oxidized fiber to the microcrystalline state with a mixture of boiling dilute nitric and nitrous acids formed upon addition of the calculated amount of water into the oxidizing system. Implementation of this two-stage procedure allowing production of CMCC of high quality (increased stability, whiteness, and gel-forming ability) involves technical and environmenyal problems caused by direct use of a highly volatile (bp 21.2°C), toxic, and deleterious nitrogen(IV) oxide catalyzing the oxidation. First of all, consideration must be given to the problems of transportation and storage of nitrogen(IV) oxide. These problems can be largely solved using a "deposited" form of nitrogen(IV) oxide, in particular, nitric acid capable of generating the oxidation catalyst in situ under certain conditions of the reaction with cellulose. The aim of this study was testing of this approach to synthesis of CMCC and also comparison of the physicochemical characteristics of the resulting products.

EXPERIMENTAL

As in the previous study [1], the initial material for the synthesis of CMCC was bleached coniferous sulfite cellulose of the SS type (Bratsk Pulp and Paper

Plant) in the form of pulp which was cut into fragments 1×1 cm in size before charging into the reactor. The initial concentration of nitric acid of pure grade produced by the Azot Production Association (Grodno) was 59%.

The experiments were performed in a temperature-controlled glass reactor equipped with a reflux condenser, a thermometer, and a stirrer. The reaction products were repeatedly squeezed and washed to completely remove nitrate ions (test with diphenylamine). For analysis, a part of the resulting CMCC was dried at 60°C, milled in a mortar, and fractions passing through a sieve with a cell size of 100 μm were taken. For preparing hydrogels, we used the moist form of CMCC (washed and squeezed). The content of carboxy groups in CMCC was determined by the barium acetate method [7]. The content of "bound" nitrogen in the form of nitrate ester groups was determined by the Kjeldahl method [8]. The IR spectra of the samples pressed in KBr pellets were recorded on a Specord 75 IR spectrophotometer.

The X-ray patterns of the samples were recorded on an HZG-4a diffractometer (CuK_α radiation, Ni filter) at a scanning rate of the scintillation quantum counter of 1 deg min^{-1}. The samples for recording were prepared in the form of plane discs of the same weight by pressing.

The morphology of particles of dispersed phase of hydrogels was studied with an EM-125K transmission electron microscope. A drop of 10% hydrogel was diluted to a slightly opalescent suspension, which was irradiated with ultrasound (a UZDN-2T unit), applied to the surface of freshly split mica, and dried. The samples for examination were prepared by the method of palladium–carbon replicas.

The sorption of Methylene Blue with CMCC hydrogels (recalculated to dry substance) was determined from the residual concentration of the dye in the solution with a KFK-2UKhL 4.2 photoelectric colorimeter (λ = 450 nm, green filter). A calibration curve of the dependence of the solution optical density on the dye concentration was plotted preliminarily. The weight of the dry sorbent in all cases was approximately 0.3 g, the volume of the dye solution of the given concentration was 50 ml, and solution pH was 6.5–7.0.

The synthesis of oxidized powder-like cellulose using only HNO_3 without auxiliary additives (e.g., $NaNO_2$) stimulating formation of the oxidation catalyst, nitrogen dioxide, was described in Heuser's monograph [9]. In that monograph, with the reference to an earlier publication (*Berichte*, 1899, vol. 32, p. 2592), it was suggested that under heating of cotton with 49% HNO_3 nitrogen oxides are vigorously released and cellulose is oxidized with simultaneous conversion of the fiber into a powder-like substance.

These data were used previously for production of uniformly oxidized structurally disordered powder cellulose with a fairly high content of carboxy groups (12.3–18.3 wt %)[1] [10]. For this purpose, cellulose was preactivated with 68.5% HNO_3 to form a Knecht adduct which was oxidized with the same acid diluted to 55% concentration. Incorporation of HNO_3 molecules into the cellulose crystal lattice in the activation stage provided a high rate and uniformity of oxidation and, correspondingly, decrystallization of the initial material.

The aim of this work was to design a single-stage procedure of synthesis of a material combining ion-exchange properties with the characteristics of MCC, first of all, gel-forming ability. It is evident that solving this problem is possible only under conditions of intercrystalline reaction of cellulose with HNO_3 in which oxidation of crystalline grains is limited with their surface. This predetermines fairly low degree of cellulose oxidation excluding transformation of the reaction into intracrystalline reaction. Decrystallization of the initial material under conditions of intracrystalline reactions adversely affects the yield and morphology of the final product [1, 10]. The content of carboxy groups in previously synthesized CMCC preparations that showed high efficiency in enterosorption [1–4] did not exceed 4.8 wt %, which is comparable with the content of free carboxy groups in pectins.

Considering published data [9, 10], we tested the conditions of the reaction of cellulose with HNO_3 that seemed to be appropriate for our case. The curve describing accumulation of carboxy groups in the reaction of cellulose with 55% HNO_3 at 70°C is shown in Fig. 1. As seen, the course of oxidation is typical for heterogeneous transformations of cellulose, whose degree is limited by low accessibility of the crystalline "component" of the fiber. The results of our experiments are presented in the table; they show that increases in the HNO_3 concentration, temperature, and the reaction duration promote two parallel processes: cellulose oxidation and its hydrolytic cleavage. Accumulation of carboxy groups in cellulose is accompanied by a decrease in the yield of the final product. This can be explained by the fact that high rate and degree of hydrolytic cleavage of cellulose stimu-

[1] Theoretically, at oxidation of the sixth carbon atom of all anhydroglucose units of cellulose, the content of COOH groups is 25.57 wt %.

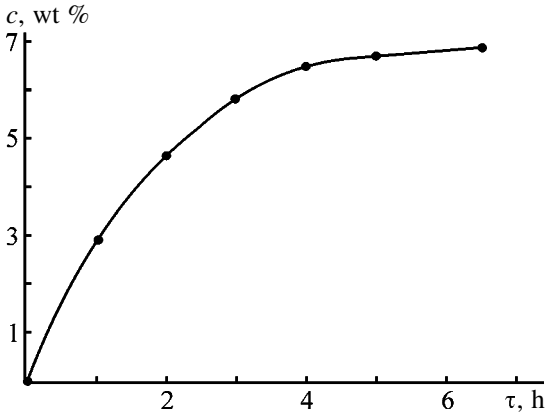


Fig. 1. Kinetic curve of cellulose oxidation in 55% HNO_3 at 70°C and liquid : solid ratio of 15 ml g^{-1}. (*c*) Content of COOH groups and (τ) time.

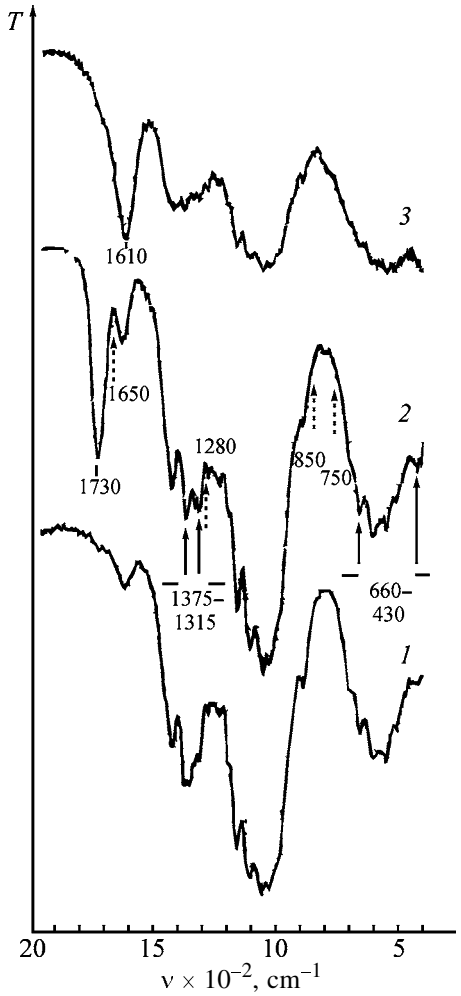


Fig. 2. IR spectra. Sample: (*1*) initial cellulose, (*2*), (*3*) H- and Na-CMCC with 5.8% content of carboxy groups. (*T*) Transmission and (ν) wavenumber.

Influence of HNO_3 concentration, reaction duration, and temperature on the degree of cellulose oxidation and yield of the final product at liquid : solid ratio of 15 ml g^{-1}

HNO_3 concentration, %	Reaction duration, h	*T*, °C	Content of COOH groups, wt %	Yield, %
45	3	70	3.5	83
45	5	70	4.3	79
50	3	70	4.8	80
50	5	70	5.5	76
50	5	60	3.6	82
55	3	70	5.8	75
55	3	60	3.5	83

late oxidation, since the hydrolysis products act as reducing agents additionally (along with temperature) promoting formation of nitrogen dioxide in the system [11]. The activation energy of heterogeneous acid hydrolysis of cellulose is fairly high (approximately 150 kJ [12]); therefore, its rate strongly depends on temperature. A decrease in the reaction temperature from 70°C to 60°C noticeably increases the yield of the final product and, correspondingly, weakens factors stimulating the oxidation (see table). The reaction of cellulose with fairly strong HNO_3 under the conditions presented in the table gives the oxidized product in a high yield (75–83%) comparable to the adequate yield of the ordinary MCC from wood cellulose by the classic scheme of recovery with dilute boiling mineral acids [6]. This fact indirectly suggests formation of the microcrystalline form of oxidized cellulose, although, according to published data [6], the hydrolytic selectivity with respect to structurally disordered areas of cellulose fiber is typical for dilute (2–3 N) boiling mineral acids, first of all HCl.

In the IR spectra of the resulting products (Fig. 2), there is an absorption band at 1730 cm^{-1} belonging to the C=O stretching modes of carboxy groups and typical for monocarboxy cellulose. Its intensity regularly increases with increasing content of COOH groups determined by the barium acetate method. Extremely low intensity or practical absence of absorption bands at 1650, 1280, 850, and 750 cm^{-1} in the spectra are indicative of trace content of nitrate ester groups in the samples. Analysis by the Kjeldahl method showed that the sample prepared under the most severe reaction conditions (55% HNO_3, 70°C, 3 h) contains approximately 0.3% bound nitrogen, which is in the limits of the determination error. It is likely that nitrate ester groups are removed from the final products in the course of partial hydrolysis of cellulose. In the spectra of the samples of oxidized cellulose, the absorption

bands in the range 1315–1375 cm^{-1} and in the low-frequency range 400–700 cm^{-1}, interpreted as the "crystallinity" bands [13, 14], are more pronounced in comparison with the spectrum of the initial cellulose. Thus, the synthesized monocarboxy cellulose surpasses the initial cellulose in the degree of crystallinity, which, considering the weight loss of 17–25% in the reaction with HNO_3 (see table), can be due only to the formation of a microcrystalline structure.

The conclusions based on the IR data are confirmed by data of the X-ray phase analysis (Fig. 3). The reflections in the X-ray pattern of the acidic form (H-CMCC) are stronger and more discrete than those in the X-ray pattern of the initial cellulose, which is quite natural for the transition from cellulose to its microcrystalline modification free of the structurally disordered component. An additional cause of increasing crystallinity of the reaction products of cellulose with HNO_3 can be cellulose refining due to its hydrolytic cleavage in oxidizing medium. These hydrolysis conditions should, in particular, promote additional oxidation of carbonyl groups. The cellulose refining is visually manifested in a noticeable increase in the whiteness of the final products in comparison with the initial cellulose. An increase in the crystallinity of cellulose upon introduction of carboxy groups (disturbing the regularity in the structure of macromolecules) is a strong evidence of localization of these groups at the crystallite grain surface.

The hydrogel state is the most efficient form of CMCC allowing realization of its sorption and, in particular, cation-exchange potential in full measure [1]. In addition, it is convenient for production of CMCC compositions with vitamins, minerals, biologically active fatty components, microorganism strains, drugs, and thus for design of new drug forms, including those with a prolonged effect (ointments, microcapsules) [2–4].

The acidic form of the reaction products of cellulose with HNO_3 (H-CMCC) is able to form stable hydrogels under conditions of using special high-speed (approximately 20000 rpm) mixers of the cutting type. Only applying a high shearing dynamic load provides disaggregation of microcrystals required for formation of a stable cohesive dispersion system. As regards gel formation, the behavior of H-CMCC differs only slightly from that of the ordinary MCC. A well-known procedure facilitating gel formation of MCC is addition of 8–10 wt % of water-soluble Na-carboxymethyl cellulose in the final stage of the synthesis [6]. This additive coats microcrystals, playing a role of peculiar "barrier" substance preventing

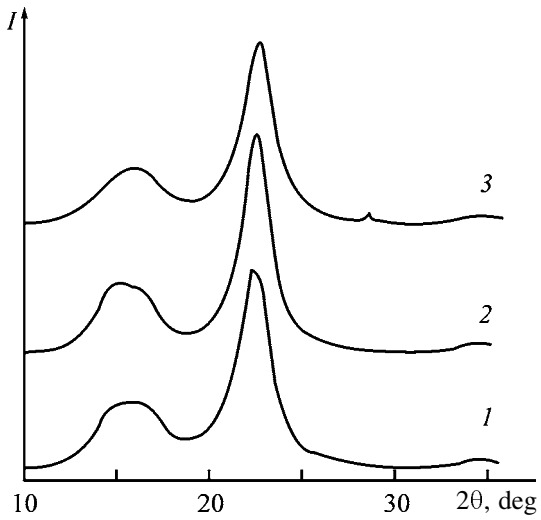


Fig. 3. X-ray patterns. Sample: (*1*) initial cellulose; (*2, 3*) H- and Na-CMCC, respectively, with 5.8% content of carboxy groups. (*I*) Relative intensity and (2θ) Bragg angle.

formation of stable associates in synthesis of dry MCC and promoting disaggregation of microcrystals when dispersing their associates in an aqueous medium.

Hydrogels are formed extremely readily in conversion of H-CMCC into salt forms, sodium or lithium salts. High-speed mixers are not required, ordinary domestic mixers are quite sufficient. The hydrogels were prepared in neutralization of moist (washed and squeezed) H-CMCC with a solution of alkali metal hydroxide under stirring. The amount of hydroxide required for neutralization was determined based on the content of carboxy groups in H-CMCC. The completeness of salt formation follows from a comparison of the IR spectra of dry samples of H-CMCC and Na-CMCC (Fig. 2). The strong absorption band at 1730 cm^{-1} in the spectrum of H-CMCC, caused by the C=O stretching modes of carboxy groups, practically completely disappears. Instead, a strong band at 1610 cm^{-1} corresponding to stretching modes of carboxylate groups [15] appears in the spectrum of Na-CMCC. Conversion of H-CMCC into NaCMCC is accompanied by significant weakening of the above-mentioned bands of cellulose "crystallinity." Under the experimental conditions with low-speed mixers we obtained creamy hydrogels containing 10 ± 0.5 wt % CMCC salt with pH 6.5–7.0.

The Na-CMCC hydrogels prepared do not show any signs of settling in storage for many months at a temperature of approximately 5°C. They have clearly pronounced thixotropy: they are structured with time, losing fluidity, but become fluid after shaking.

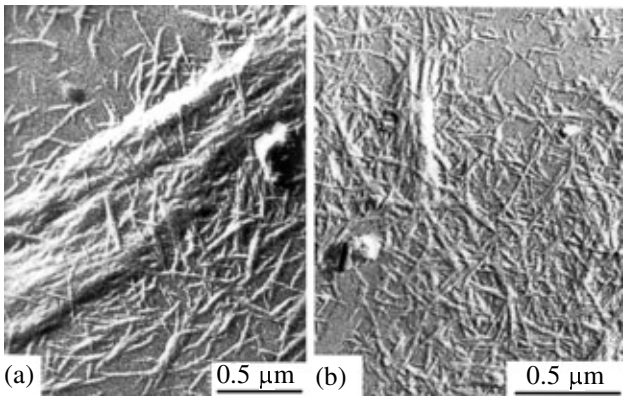


Fig. 4. Electron micrographs of particles of dispersed phase of (a) H-CMCC and (b) Na-CMCC hydrogels with 5.8% content of carboxy groups.

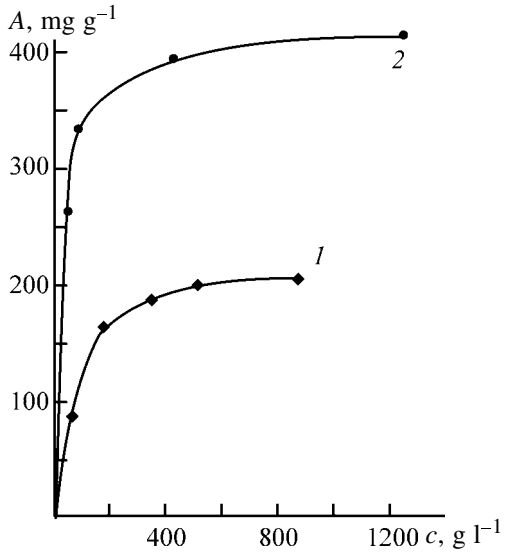


Fig. 5. Sorption isotherms of MB with 10% (*1*) H-CMCC and (*2*) Na-CMCC hydrogels with 5.8% content of carboxy groups. (*A*) Sorption and (*c*) equilibrium concentration.

In drying of thin layers of Na-CMCC hydrogels, dull films readily subjected to powdering are formed. The consistence of hydrogels formed by the salt forms of CMCC depends not only on the polymer concentration in the system but also on the disintegration conditions (intensity and duration). For example, substitution of a high-speed Warring blender (20000 rpm) for low-speed blender even at short disintegration results in obtaining a uniform cream-like nonfluid mass. This fact allows stable gel-like consistence to be attained in a wide range of concentrations of CMCC salt in the system (higher than 1 wt %).

Conversion of the acidic form of CMCC into a Na salt results in noticeable weakening and broadening of the reflections in the X-ray pattern of cellulose (Fig. 3), which is in good agreement with diffusion of the "crystallinity bands" in the IR spectra of Na-CMCC (Fig. 2). Broadening of interference peaks is caused by a decrease in the crystallite size and an increase in the lattice defectivity. This concerns first of all the least interrelated (101) reflection planes in the three-dimensional lattice of cellulose ($2\theta \approx 15°$), to which predominant penetration of reactants is most probable [16]. The decrease in the size and increase in the concentration of defects of H-CMCC crystallites is accompanied by strong hydrophilization of their surface due to salt formation and formation of a water-soluble sol-like fraction from a part of oxidized macromolecules of the surface layer. From the experimental estimation, approximately 10 wt % of water-soluble material is present in the Na-CMCC hydrogel containing 5.8% carboxy groups. This fraction plays the role of a "barrier" between microcrystals and facilitates their disaggregation in dispersion of aqueous Na-CMCC suspension to the hydrogel state.

The electron-microscopic examination of particles of the dispersed phase of H- and Na-CMCC hydrogels undoubtedly confirms their microcrystalline morphology (Fig. 4). Disintegration of an aggregate of H-CMCC microcrystals, holding microfibril shape, to separate elements is illustrated in Fig. 4a. The stability of MCC hydrogels is reached even upon release of approximately 30% of individual microcrystals from their aggregates [6]. The Na-CMCC samples (Fig. 4b) are characterized by more convincing crystalline morphology than the H-CMCC samples, since the degree of disintegration and homogeneity of the dispersed phase of their hydrogels is significantly higher. The above data on the yield and structure of the reaction products of cellulose with 45–55% HNO_3 strongly suggest that not only dilute boiling mineral acids but also fairly strong acids at low temperature show hydrolytic selectivity with respect to structurally disordered cellulose fiber.

The sorption activity of CMCC was estimated with respect to a bulky organic cation, Methylene Blue (MB), under the conditions described in [1].

Under the same conditions, the maximum sorption of MB with powdered H-CMCC sample containing 3% carboxy groups is approximately 30 times higher than the sorption with powdered MCC sample [1]. MB is mostly absorbed by the cation-exchange mechanism. Hydrogels have the highest sorption power recalculated to dry substance, which is due to the maximum accessibility of their active centers. The sorption isotherms of MB with 10% H- and Na-CMCC hydrogels with 5.8% content of carboxy groups are shown in Fig. 5. As expected, the sorption

isotherms are described by the Langmuir equation. The salt forms of CMCC apparently surpass acidic forms in the sorption power. This logically follows from the high degree of their ionization. Account must be taken of the fact that NaCl is formed in the reaction of Na-CMCC macroions with MB in the form of hydrochloride. The product of the reaction of H-CMCC with MB · HCl is HCl, a strong acid shifting the ion-exchange equilibrium toward the initial substances. The maximum sorption of MB with Na-CMCC hydrogel with 5.8% content of carboxy groups is 420 mg g^{-1}, which corresponds to 101% of the total exchange capacity. This result is in good agreement with published data [1], where the maximum sorption of MB with Na-CMCC hydrogel with 4.8% content of carboxy groups was 390 mg g^{-1}. For the above reasons, the sorption power of H-CMCC is more than 2 times lower than that of Na-CMCC hydrogel (Fig. 5). The degree of utilization of its exchange capacity is 48%.

Thus, as judged from the chemical composition, phase and morphologic states, and gel-forming and cation-exchange power of the materials studied, with respect to the most important physicochemical characteristics they are identical to those synthesized previously using gaseous nitrogen(IV) oxide [1].

CONCLUSIONS

(1) The conditions of using 45–55% nitric acid as a "deposited form" of nitrogen(IV) oxide for selective oxidation of cellulose at the sixth carbon atom of the anhydroglucose ring with simultaneous selective hydrolytic cleavage of structurally disordered areas of the fiber were determined.

(2) Examination by IR spectroscopy, X-ray phase analysis, and transmission electron microscopy shows that the resulting materials are microcrystals of cellulose modified with carboxy groups localized at the surface.

(3) Conversion of the acidic form of the samples into the salt forms (sodium or lithium) is accompanied by strong hydrophilization of microcrystals and formation of a water-soluble fraction from a part of oxidized macromolecules of the surface layer, which facilitates preparation of stable thixotropic gels.

REFERENCES

1. Gert, E.V., Torgashov, V.I., Zubets, O.V., and Kaputskii, F.N., *Cellulose*, 2005, vol. 12, no. 5, pp. 517–526.
2. Zubets, O.V., Torgashov, V.I., Larchenko, L.V., et al., Abstracts of Papers, *Mezhdunarodnaya nauchnaya konferentsiya "Novye lekarstvennye sredstva: sintez, tekhnologiya, farmakologiya, klinika"* (Int. Scientific Conf. "New Drugs: Synthesis, Technology, Pharmacology, Clinic"), Minsk, 2001, pp. 53–54.
3. Torgashov, V.I., Zubets, O.V., Kaputskii, F.N., and Gert, E.V., Abstracts of Papers, *Mezhdunarodnaya nauchnaya konferentsiya "Novye lekarstvennye sredstva: sintez, tekhnologiya, farmakologiya, klinika"* (Int. Scientific Conf. "New Drugs: Synthesis, Technology, Pharmacology, Clinic"), Minsk, 2001, pp. 147–148.
4. Torgashov, V.I., Gert, E.V., Zubets, O.V., and Kaputskii, F.N., Abstracts of Papers, *Mezhdunarodnaya nauchnaya konferentsiya "Novye lekarstvennye sredstva: sintez, tekhnologiya, farmakologiya, klinika"* (Int. Scientific Conf. "New Drugs: Synthesis, Technology, Pharmacology, Clinic"), Minsk, 2001, pp. 148–149.
5. Orlov, A.A., *Sb. Nauchn. Tr. Inst. Lesa Nats. Akad. Nauk Bel.*, 2004, issue 61, pp. 239–243.
6. Battista, O.A., *Microcrystal Polymer Science*, New York: McGraw-Hill, 1975.
7. *Kontrol' proizvodstva khimicheskikh volokon: Spravochnoe posobie* (Monitoring of Production of Chemical Fibers: A Handbook), Pakshver, A.B. and Kokin, A.A., Eds., Moscow: Khimiya, 1967.
8. Cheronis, N.D. and Ma, T.S., *Organic Functional Group Analysis by Micro and Semimicro Methods*, New York: Interscience, 1964.
9. Heuser, E., *Textbook of Cellulose Chemistry for Students in Technical Schools and Universities as Well as for Cellulose Experts*, New York: McGraw-Hill, 1924.
10. Gert, E.V., Shishonok, M.V., Zubets, O.V., et al., *Vysokomol. Soedin., Ser. A*, 1995, vol. 37, no. 7, pp. 1130–1136.
11. Becker, H., Berger, W., Domschke, G., et al., *Organikum: Organisch-chemisches Grundpraktikum*, Berlin: Wissenschaften, 1976, vol. 2.
12. Korol'kov, I.I., *Perkolyatsionnyi gidroliz rastitel'nogo syr'ya* (Percolation Hydrolysis of Plant Raw Materials), Moscow: Lesn. Prom–st., 1978, 2nd ed.
13. Nelson, M.L. and O'Connor, R.T., *J. Appl. Polym. Sci.*, 1964, vol. 8, pp. 1311–1324.
14. Michell, A.J., *Cellulose Chem. Technol.*, 1974, vol. 8, pp. 439–441.
15. Ermolenko, I.N., *Spektroskopiya v khimii okislennykh tsellyuloz* (Spectroscopy in Chemistry of Oxidized Celluloses), Minsk: Akad. Nauk Bel. SSR, 1959.
16. Goikhman, A.Sh. and Solomko, V.P., *Vysokomolekulyarnye soedineniya vklyucheniya* (Macromolecular Intercalation Compounds), Kiev: Naukova. Dumka, 1982.

ISSN 1070-4272, Russian Journal of Applied Chemistry, 2006, Vol. 79, No. 11, pp. 1902–1906. © Pleiades Publishing, Inc., 2006.
Original Russian Text © N.E. Kotel'nikova, E.L. Lysenko, R. Serimaa, K. Pirkkalainen, U. Vainio, A.L. Shakhmin, N.N. Saprykina, V.K. Lavrent'ev, D.A. Medvedeva, N.P. Novoselov, 2006, published in Zhurnal Prikladnoi Khimii, 2006, Vol. 79, No. 11, pp. 1924–1928.

MACROMOLECULAR CHEMISTRY AND POLYMERIC MATERIALS

Cellulose Matrix as a Nanoreactor for Preparing Nanoparticles of Nickel and Its Oxides Using Hydrazine Dihydrochloride as Reductant

N. E. Kotel'nikova, E. L. Lysenko, R. Serimaa, K. Pirkkalainen, U. Vainio, A. L. Shakhmin, N. N. Saprykina, V. K. Lavrent'ev, D. A. Medvedeva, and N. P. Novoselov

Institute of Macromolecular Compounds, Russian Academy of Sciences, St. Petersburg, Russia
State University of Technology and Design, St. Petersburg, Russia
University of Helsinki, Helsinki, Finland
Prikladnaya Khimiya Russian Scientific Center, Federal State Unitary Enterprise, St. Petersburg, Russia

Received May 24, 2006

Abstract—A matrix of microcrystalline cellulose was used as a nanoreactor for the reduction of Ni(II) ions with hydrazine dihydrochloride.

DOI: 10.1134/S1070427206110310

Numerous polymeric nanocomposites with preset physicochemical properties [1], containing stabilized metal (Ag, Cu, Ni, Pt, Pd, etc.) nanoparticles [2–7], have been prepared by now. Nanoparticles of some metals, e.g., Ni, impart fo polymeric nanocomposites magnetic and catalytic properties [8]; however, the preparation of Ni(0) nanoparticles is complicated because Ni metal is readily oxidized [9].

Recently the interest in preparation of metal nanoparticles in ordered solid matrices (nanoreactors) increased, because in these matrices, in contrast to polymer solutions, significant aggregation of nanoparticles can be avoided [1]. Among promising nanoreactors is cellulose, a natural polymer characterized by a highly porous system of conjugated fibers. It has a large specific surface area and is successfully used as a solid matrix for intercalation of transition metal (Ag, Pt, Pd, Cu) nanoparticles [10–12]. Papers on the intercalation of Ni nanoparticles into natural polymers (in particular, cellulose) are few [13, 14]. Ishiyama et al. [13] reported on the preparation of 5–21-nm particles of Ni and its oxide in a gel membrane of cellulose acetate by thermal decomposition of the membrane after the intercalation of Ni^{2+} ions.

This paper continues our studies of the use of a cellulose matrix as a nanoreactor for intercalation of nanoparticles of zero-valent metals (in particular, Ni) and their oxides [15]. Nanocomposites based on cellulose and nickel can be used in catalysis and also as magnetic and conducting materials.

EXPERIMENTAL

Cellulose samples containing nanoparticles of Ni(0) or its oxides were prepared by diffusion of Ni^{2+} ions into a cellulose matrix from a solution of nickel nitrate $Ni(NO_3)_2 \cdot 6H_2O$, followed by reduction of Ni^{2+}. As a matrix we used microcrystalline cellulose (MCC) prepared by acid hydrolysis according to [10]; it was a powder with the particle size less than 0.06 mm and moisture content not exceeding 1 wt %. As a reductant for Ni^{2+} we used hydrazine dihydrochloride $N_2H_4 \cdot 2HCl$ (Reaktiv Joint-Stock Company, St. Petersburg). It is known that nickel ions are reduced with $N_2H_4 \cdot 2HCl$ only in alkaline solutions containing complexing anions at a large excess of the reductant and elevated temperatures [16].

A 1-g sample of MCC was vigorously stirred with 20 ml of a 0.05 or 0.1 M citrate solution of nickel nitrate for 1 h; the diffusion temperature was varied from 20 to 95°C. The $C_m(C_6H_5O_7^{3-})/C_m(Ni^{2+})$ ratio was 1 : 1. Citrate ions served as ligands for Ni^{2+} ions, preventing the precipitation of nickel hydroxide in a strongly alkaline medium; also, being sorbed on the forming metal particles and imparting to them a negative charge, they prevented the particle aggregation.

Nickel content in the bulk and on the surface of MCC-Ni samples and crystallite size of Ni and MCC

Sample no.	Temperature of Ni^{2+} diffusion, °C	Ni content, wt %		Crystallite size (XPA), nm	
		in the bulk (elemental analysis)	on the surface (XPES)	MCC	Ni(0)
1	20	6.9	31.5	7.5 ± 0.3	10.8 ± 1.0
2	70	7.4	17.4	7.5 ± 0.3	12.3 ± 1.0
3	95	10.0	18.7	7.4 ± 0.3	13.5 ± 1.0

To a suspension obtained after the diffusion of Ni^{2+}, we added with vigorous stirring a solution prepared by dissolving a weighed portion of $N_2H_4 \cdot 2HCl$ in 20 ml of 3 M NaOH. The $N_2H_4 \cdot 2HCl$ concentration in this solution was varied from 0.5 to 4 M, so that the molar ratio $C_m(N_2H_4 \cdot 2HCl)/(C_m(Ni^{2+})$ (MR) was varied from 5 to 40. The reduction was performed at 95°C for 0.5–2 h.

After the reduction, the precipitate was separated on a glass frit and washed with water and ethanol. The washing completeness was judged from the neutral reaction of the wash waters and negative reaction for the Ni^{2+} ions with dimethylglyoxime [17]. The samples after vacuum drying at 40°C were powders of the color varying from light green to black. All the chemicals used in the synthesis were of pure or analytically pure grade. The nickel-containing cellulose materials obtained by this procedure are hereinafter designated as MCC-Ni.

The nickel concentration in the bulk of MCC-Ni samples was determined by elemental analysis, and that on the sample surface, by X-ray photoelectron spectroscopy (XPES). The oxidation state of Ni on the fiber surface was also determined by XPES. The sample structure, nickel oxidation state in the bulk of cellulose, and changes in the chemical composition were studied by X-ray phase analysis (wide-angle X-ray scattering, XPA) and IR Fourier spectroscopy. The procedures for sample preparation and calculations are described elsewhere [10]. The morphology of MCC-Ni samples and the nickel particle size and particle-size distribution were studied by scanning electron microscopy (SEM) [15].

The experimental conditions strongly affect both the amount of Ni intercalated into the MCC matrix and its oxidation state in MCC-Ni samples. For example, as the temperature of Ni^{2+} diffusion into the MCC matrix in the first step of the process was increased from 20 to 95°C, the amount of the intercalated nickel after the subsequent reduction appreciably increased (from 6.9 to 10.0 wt %) at any $C_m(N_2H_4 \cdot 2HCl)/C_m(Ni^{2+})$. A similar trend was observed when $NaBH_4$ and KH_2PO_2 were used as reductants [15].

Another factor strongly affecting the Ni content in the final products is the reductant concentration. As the MR was increased from 5 to 40, the Ni content in the bulk of MCC increased until the maximal value of 10.0 wt % was attained. An increase in the reductant concentration also favors the reduction of Ni^{2+} to Ni(0). It is known that the color of the samples obtained characterizes the oxidation state of Ni in the samples [18]. An increase in the MR from 5 to 40 led to a change in the sample color from light green or greenish-brown, caused by the presence of $Ni(OH)_2$, to light gray (at MR = 15) and then dark gray (at MR = 20 and over), characteristic of finely dispersed Ni(0). Thus, the reduction of Ni^{2+} to Ni(0) is possible only at a high concentration of the reductant, hydrazine dihydrochloride (MR ≥ 15–40). The maximal amount of nickel introduced into the cellulose matrix (10.0 wt %) corresponds to 0.289 mol of Ni per mole of MCC units. With $NaBH_4$ and KH_2PO_2 used as reductants, the maximal Ni content (molar ratio to MCC units) was 0.315 and 0.358 (11.1 and 12.8 wt %), respectively [15]. All these values are close, i.e.,

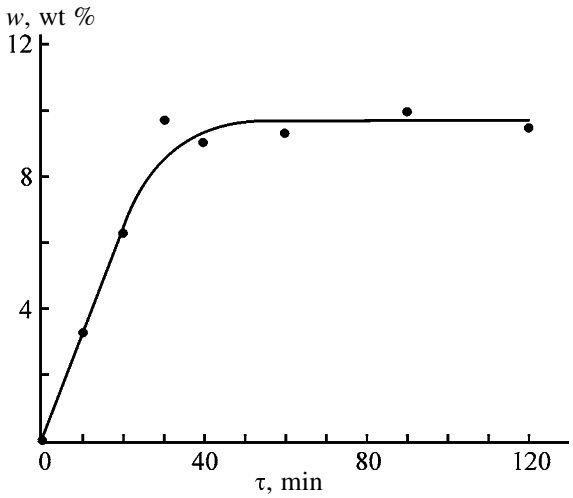


Fig. 1. Kinetic curve of Ni^{2+} reduction with $N_2H_4 \cdot 2HCl$. $C_m(Ni^{2+})$ 0.1 M, MR = 30, diffusion and reduction temperature 95°C. (*w*) Ni content and (τ) time.

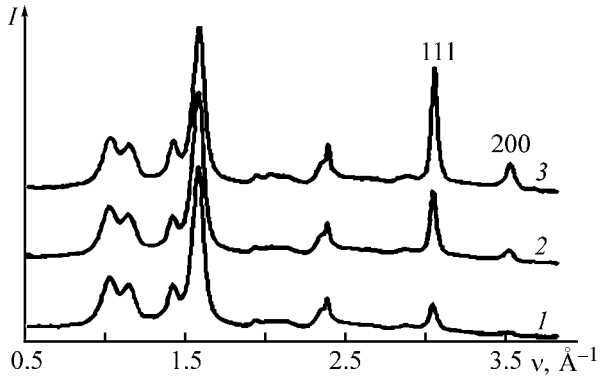


Fig. 2. Diffraction patterns of MCC-Ni sample nos. 1–3 prepared at MR = 30; reduction temperature 95°C. (*I*) X-ray scattering intensity and (ν) scattering angle. (*1–3*) Sample nos. 1–3 (see table), respectively; the same for Fig. 3.

about 1 mol of Ni was intercalated per 3 cellulose units with all the three reductants.

One of the major factors affecting the nickel content in the final products is the reduction time. The dependence of the nickel content in MCC-Ni samples on the reduction time (Fig. 1) shows that the equilibrium content of Ni in the MCC matrix is attained in 0.5 h and does not further change in the subsequent 1.5 h. The apparent rate constant of the pseudo-first-order reaction under these experimental conditions (the reaction was performed at MR = 30), calculated from the semilog plot, was $k = 2.7 \times 10^{-2}$ min^{-1}. The lower the MR, the slower the reduction. At MR = 20, the reaction rate decreases by a factor of approximately 3. It should be noted that the rate of the Ni^{2+} reduction with $N_2H_4 \cdot 2HCl$ exceeded by an order of magnitude the rate of its reduction with KH_2PO_2 reported in [15].

As shown above, an increase in the reductant concentration leads to a proportional increase in the Ni content in the bulk and to the reduction of Ni^{2+} to Ni(0). This was confirmed by XPA. The scattering curves of samples prepared at MR = 20 contained strong reflections of nickel oxide in the region of 2θ 36.8° and 42.9° and weak reflections of Ni(0) in the region of 2θ 44.3° and 51.2° ([111] and [200], respectively). With an increase in the MR to 30, the X-ray scattering curves of MCC-Ni samples differing only in the temperature of diffusion of Ni^{2+} into the MCC matrix (Fig. 2) contained Ni(0) reflections, and their intensity was proportional to the nickel content in the sample. This fact indicates that Ni(0) was the major nickel form in the bulk of these samples. The mean size of the crystallites, determined from the [111] reflections, was 10.8–13.5 nm (see table). Thus, XPA

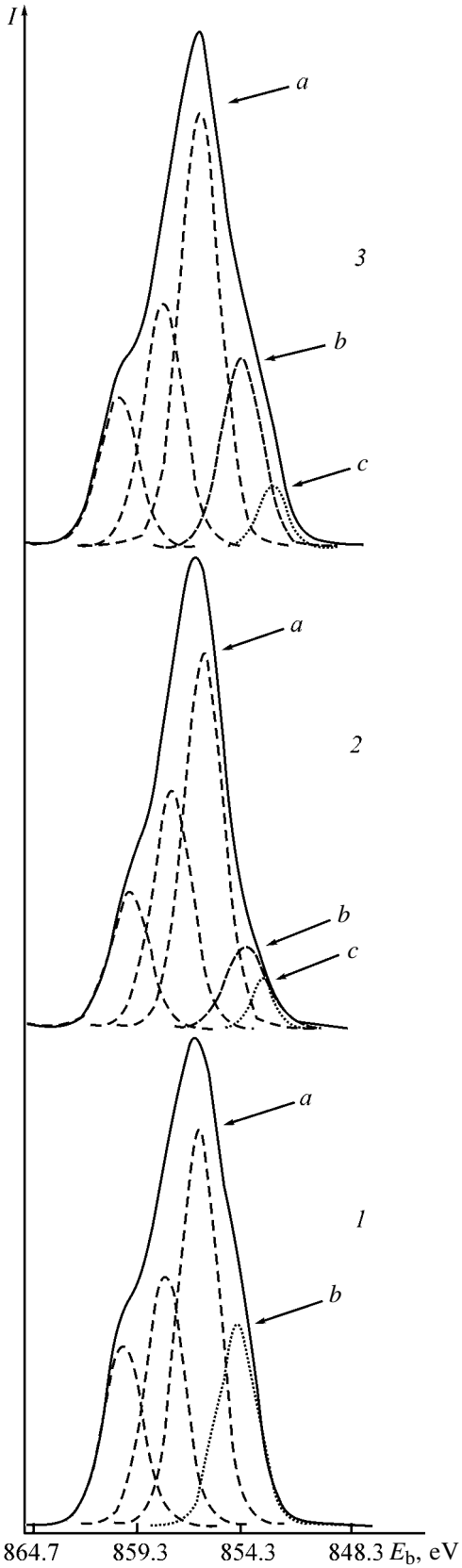


Fig. 3. XPE spectra of MCC-Ni sample nos. 1–3: (*I*) Intensity and (E_b) binding energy.

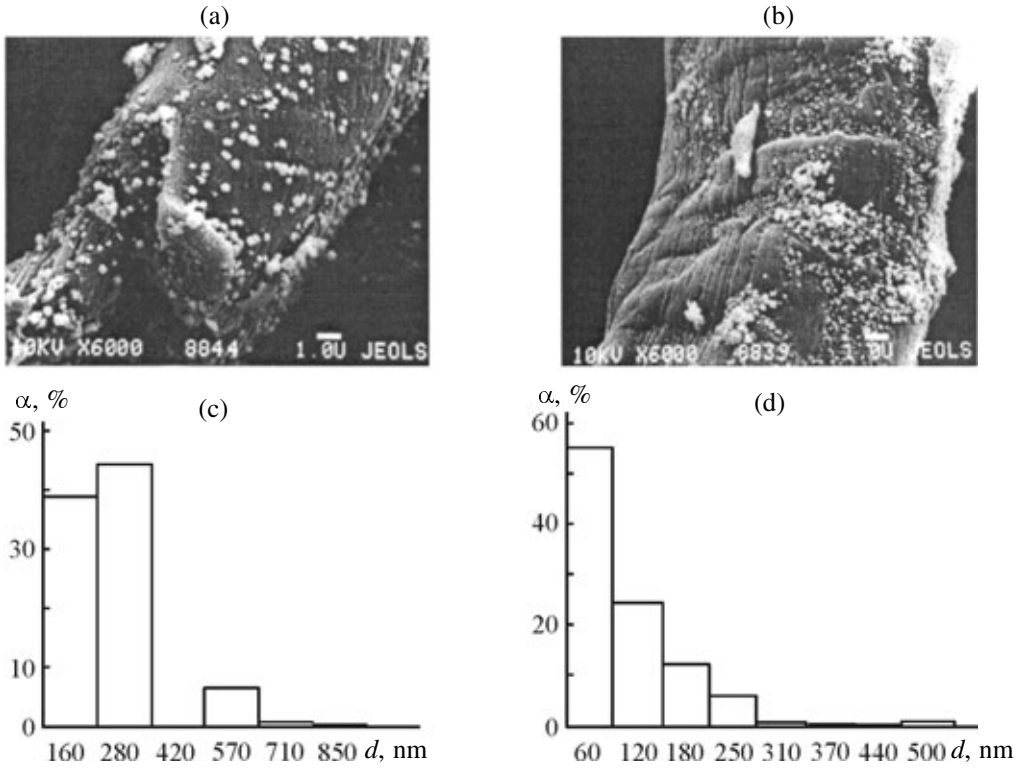


Fig. 4. Electron micrographs of MCC-Ni sample nos. (a) 1 and (b) 2; histograms of the distribution of Ni nanoparticles on the surface of sample nos. (c) 1 and (d) 2 with respect to the particle diameter. (α) Fraction of particles and (*d*) particle diameter.

confirmed the presence of the nanodispersed crystalline phase of Ni(0) in the bulk of the samples.

As in the case of reduction of Ni^{2+} with $NaBH_4$ and KH_2PO_2, the formation of nickel nanoparticles in the cellulose matrix did not affect the MCC crystal structure. The structural morphology of cellulose I, characteristic of MCC, was preserved, and the size (width) of MCC crystallites in MCC-Ni samples was close to that in the initial MCC (7.4 ± 0.1 nm, see table).

Thus, by intercalation of nickel in an MCC matrix we prepared MCC-Ni nanocomposites containing in the bulk mainly Ni(0) nanoparticles; the Ni oxidation state and crystallite size depended on the experimental conditions and primarily on the reductant concentration.

A comparison of the IR Fourier spectra of the MCC-Ni (at the maximal Ni content in the bulk) samples with that of the initial MCC revealed a minor decrease in the intensity of the absorption band at 3000–3600 cm^{-1} belonging to the stretching virbations of OH groups participating in inter- and intramolecular hydrogen bonds. Apparently, intercalation of Ni into a cellulose matrix is accompanied by cleavage of a small amount of hydrogen bonds on the surface of cellulose fibrils, followed by their redistribution.

The nickel concentration on the surface of fibers, determined by XPES, exceeds by a factor of 1.8–4.6 the nickel content in the bulk (see table). The ratio of redox forms on nickel on the surface is also different. Figure 3 shows the XPE spectra of the Ni $2p_{3/2}$ line and the resolution of spectral lines into four or five major components in MCC-Ni sample nos. 1–3. The components correspond to the Ni $2p_{3/2}$ binding energy in Ni_2O_3 (E_b = 856.7 eV, components *a*), NiO (E_b = 854.8 eV, components *b*), and Ni(0) (E_b = 853.4 eV, components *c*) [19]. The Ni(0) content on the fiber surface in sample nos. 2 and 3 (2.8 and 4.1 wt %, respectively) is considerably lower than that of nickel oxides. The high content of nickel oxides on the sample surface is due to the high susceptibility of Ni(0) nanoparticles to oxidation with atmospheric oxygen [9]. Thus, the samples obtained are not uniform in the chemical composition of nickel on the surface. It should be noted that the spectra of all the samples have also components with higher binding energies (858.0 and 860.4 eV, about 10%) which cannot be assigned to the above-noted nickel compounds. These may be electronic satellites [19]. Thus, an XPES study shows that the MCC-Ni nanocomposites prepared by reduction of Ni^{2+} ions in a cellulose matrix have a

variable content of nanoparticles of Ni(0) and nickel oxides on the surface of MCC fibes.

The distribution of nanoparticles of Ni(0) and nickel oxides on the surface of MCC-Ni samples is shown in the electron micrographs of MCC-Ni sample nos. 1 and 2 (Figs. 4a, 4b) and in the histograms of the nickel particle-size distribution (Figs. 4c, 4d). In most cases, nanoparticles of Ni(0) and its oxides have a globular shape and are nonuniformly distributed on the surface. In some cases, nanoparticles form giant agglomerates (however, few in number). The majority of nanoparticles in sample no. 1 (>55%) have a size within 160–280 nm (Fig. 4c). Contrary to sample no. 1, the majority (about 80%) of nanoparticles in sample no. 2 have a size of about 60 nm (Fig. 4d). Sample nos. 1 and 2 were prepared at the same MR, but the diffusion of Ni^{2+} into the MCC matrix was performed at 20 and 70°C, respectively. These results show that an increase in the diffusion temperature (see table) favors formation of smaller nanoparticles of Ni and its oxides on the surface. As a rule, the size and size distribution of nanoparticles are the decisive factors governing the applicability of materials containing nanoparticles. The results of reduction of Ni^{2+} in a cellulose matrix with $N_2H_4 \cdot 2HCl$ show that nanoparticles of Ni(0) and its oxides on the surface have a smaller size than those obtained by reduction with other solvents, in particular, KH_2PO_2 [15], whereas the size of Ni(0) crystallites in the bulk does not depend essentially on the kind of reductant used (cf. data from [13, 14]).

Thus, by reduction of Ni^{2+} in an MCC matrix with $N_2H_4 \cdot 2HCl$ we found that the temperature of the Ni^{2+} diffusion into the matrix and the reductant concentration are the major factors affecting the formation of nanoparticles of Ni(0) and its oxides of widely varied size in the bulk and on the surface of MCC fibers.

CONCLUSIONS

(1) Powdered cellulose materials with the maximal content of intercalated nickel of 10.0 wt % were prepared by reduction of Ni^{2+} ions in a cellulose matrix with hydrazine dihydrochloride.

(2) The presence of nanoparticles of Ni(0) and its oxides in the bulk of the cellulose matrix was confirmed by XPA.

(3) The distribution of nanoparticles of Ni(0) and its oxides on the surface of microcrystalline cellulose fibers was studied by SEM, and the qualitative composition and oxidation state of nickel on the surface, by XPES.

REFERENCES

1. Tret'yakov, Yu.D., Lukashin, A.V., and Eliseev, A.A., *Usp. Khim.*, 2004, vol. 73, no. 9, pp. 974–998.
2. Davis, S.C., Klabunde, K.J., and Stephen, C., *Chem. Rev.*, 1982, vol. 82, no. 2, pp. 153–208.
3. Clair, A.K.St. and Taylor, L.T., *J. Appl. Polym. Sci.*, 1983, vol. 28, no. 7, pp. 2393–2400.
4. Mayer, A.B. and Mark, J.E., *Macromol. Sci. Pure Appl. Chem.*, 1997, vol. 34A, no. 11, p. 2151.
5. Gubin, S.P. and Kosodubskii, I.D., *Usp. Khim.*, 1983, vol. 52, no. 8, pp. 1350–1364.
6. Schulze, W. and Abe, H., *Faraday Soc. Symp.*, 1980, no. 14, pp. 87–93.
7. Petrov, Yu.I., *Fizika malykh chastits* (Physics of Small Particles), Moscow: Nauka. 1982.
8. Gubin, S.P., *Zh. Vseross. Khim. O–va. im. D.I. Mendeleeva*, 2000, vol. 44, no. 6, pp. 23–31.
9. Ershov, B.G., *Ross. Khim. Zh.*, 2001, vol. 45, no. 3, pp. 20–30.
10. Kotel'nikova, N.E., Wegener, G., Paakkari, T., et al., *Zh. Obshch. Khim.*, 2003, vol. 73, no. 3, pp. 447–464.
11. Kotelnikova, N.E., Paakkari, T., Serimaa, R., et al., *Macromol. Symp.*, 1999, vol. 138, pp. 175–180.
12. Kotelnikova, N.E., Kotelnikov, V.P., Nikonorova, N.I., and Serimaa, R., Abstracts of Papers, *Int. Symp. "Nanochemistry: New Approaches to Creation of Polymeric Systems with Specific Properties,"* Tashkent, 2003, p. 36.
13. Ishiyama, J.-I., Shirakawa, T., Kurokawa, Y., and Imaizumi, S., *Angew. Makromol. Chem.*, 1988, vol. 156, no. 2548, pp. 179–185.
14. He, J., Kunitake, T., and Nakao, A., *Chem. Mater.*, 2003, no. 15, pp. 4401–4406.
15. Lysenko, E.L., Kotel'nikova, N.E., and Novoselov, N.P., in *Sbornik trudov aspirantov SPGUTiD* (Coll. of Papers by Postgraduate Students of the St. Petersburg State Univ. of Technology and Design), St. Petersburg: Sankt-Peterb. Gos. Univ. Tekhnologii i Dizaina, 2005, no. 10, pp. 182–187.
16. Korovin, N.V., *Gidrazin* (Hydrazine), Moscow: Khimiya, 1980.
17. Alekseev, V.N., *Kurs kachestvennogo khimicheskogo polumikroanaliza* (Course of Qualitative Chemical Semimicroanalysis), Moscow: Khimiya, 1973.
18. *Khimicheskaya entsiklopediya* (Chemical Encyclopedia), Knunyants, I.L., Ed., Moscow: Sov. Entsiklopediya, 1961, vol. 5, pp. 455–466.
19. Moulder, J.F., Stickle, W.F., Sobol, P.E., and Vomben, K.D., *Handbook of X-ray Photoelectron Spectroscopy*, Eden Prairie: Physical Electronic, 1995.

ISSN 1070-4272, Russian Journal of Applied Chemistry, 2006, Vol. 79, No. 11, pp. 1907–1911. © Pleiades Publishing, Inc., 2006.
Original Russian Text © M.F. Radenkov, P.Ts. Cherkezova, V.K. Dikov, F.D. Radenkov, 2006, published in Zhurnal Prikladnoi Khimii, 2006, Vol. 79, No. 11, pp. 1929–1933.

MACROMOLECULAR CHEMISTRY AND POLYMERIC MATERIALS

Modification of Polymeric Matrix of Polyester Fiber-Glass Materials with Powder Polyamide and Epoxy Resin

M. F. Radenkov, P. Ts. Cherkezova, V. K. Dikov, and F. D. Radenkov

Institute of Polymers, Bulgarian Academy of Sciences, Sofia, Bulgaria
Medical University, Varna, Bulgaria
Technical University, Sofia, Bulgaria

Received March 1, 2006

Abstract—The possibility of improving the quality of polyester fiber-glass products prepared by environmentally safe low-pressure procedures by modification of the polymeric matrix with moderate amounts of polycaproamide powder in combination with small amounts of epoxy resin was studied.

DOI: 10.1134/S1070427206110322

Owing to high strength, small specific density, and low cost, polyester fiber-glass materials reinforced with glass fabrics are excellent and widely used structural materials [1]. To increase the area of special-purpose applications, the quality of fiber-glass products (in particular, dimensional accuracy and dimensional stability) should be improved with preservation of their low cost. For this purpose, various procedures of chemical and physicochemical modification can be used [2, 3]. These methods can provide required results and can be realized without significant investments and material expenses.

In this work we studied the possibility of improving the direct low-pressure procedures for molding fiber-glass articles with a relatively small content (30–35%) of glass fibers. These procedures include the resin transfer molding (RTM), membrane procedures, cold pressing, etc. These environmentally safe procedures seem very promising. However, products prepared using these procedures have certain drawbacks such as high shrinkage and deformability.

To eliminate these drawbacks, moderate amounts of polycaproamide powder in combination with small amounts of epoxy resin (ER) are often added to unsaturated polyester resins.

EXPERIMENTAL

In this work we used Viapal UP 4627E/61 brand unsaturated polyester resin (UPER) (Vianova company, Austria); methyl ethyl ketone peroxide initiator (MEKPO) (Peroximon 41 brand, ATO company, France); 50% phthalate solution; cobalt octoate $Co(Ot)_2$ (Accelerator NZ 495, AKZO company, Holland); 6% phthalate solution containing Co(II) ions (1%); glass fabric (GF) (R12-500 9631 brand, Ahlstrom company, Finland) with a surface density of 500 g cm^{-2} woven of glass fibers of E glass (tex 1200) brand with orientation of 55.5 and 44.5% along the warp and weft, respectively; polyamide powder (PAP) (Vidakhim company, Bulgaria) with a particle size of 0.5–10 μm (after additional milling); epoxy resin (ER) (Epoks 1 brand) without plasticizer (Lakprom company, Bulgaria) with content of epoxy groups of 14%; and 2,4,6-dimethylaminotribenzylphenol (DMATBP) accelerator (Araldit Y060 brand, Ciba–Geigy company, Switzerland).

Powdered polyamide 6 was prepared by precipitation from solutions [4–7]; the precipitate consist of agglomerated particles of 60–200 μm size. Before studies, it was additionally powdered on a high-speed cutter-type mill. The size of finely dispersed PAP varied from 0.5 to 10.0 μm with the predominant fraction of 3–5 μm size.

The resin compositions were prepared from UPER, appropriate amount of PAP, ER (10% with respect to PAP), and DMATBP (10% with respect to ER). After thorough dispersion of the filler, a 1% solution of $CoOt_2$ and a 3% solution of MEKPO were added successively with vigorous stirring. The resin composite was quickly poured over the surface of glass-fabric reinforcement designed as a stack of four GF pieces

placed in the matrix cavity. The mold was closed with a punch and pressed for 35 min at 0.3 MPa. Using this procedure of cold pressing, we prepared the fiber-glass plates (250 × 25 × 4 mm) reinforced with orthogonally oriented glass fabrics with 35% content of the glass fibers. The density of the fiber-glass composite was 1405 kg m^{-3}. After removal from the mold, the plates were heated at 120°C for 24 h. Then, using a diamond saw, we prepared the specimens of the required sizes for each test procedure. The ends of the specimens, which were clamped with the dynamometer clips, were thickened with the plates of the same material glued at both sides of the sample.

To determine the degree of shrinkage, the size of the thermally treated plates was compared with the mold size. Deformations and strains of the plate surface were evaluated visually.

The tensile and bending strengths of the samples were studied on a TT-DM/INSTRON 85 dynamometer in accordance with ISO-527 and ISO-178. The impact resilience was measured on an CEACT 645/000 unit according to ISO-179 (after Charpy without notches).

In the course of curing, the volume of UPER decreases by 8%. Shrinkage of the polyester materials is due to the complex of interrelated chemical, rheological, and physicochemical processes. The shrinkage of the composites decreases with increasing filler content.

UPER composite is cured owing to free-radical polymerization, which occurs in several stages under various thermodynamic, rheological, and concentration conditions, which is reflected in the heterogeneity of the three-dimensional polymer network. This gives rise to internal stresses in the fiber-glass products and their elevated shrinkage and deformations.

The fiber-glass objects of stable shapes with elevated size accuracy and small internal stress are commercially produced using liquid or powdered polymer additives. For example, some of them are thermoplastic powders chemically inert to UPER, whereas the others are liquid rubbers, which, copolymerizing with UPER, form elastic blocks in the three-dimensional network [1].

The mechanism of the effect of these modifying agents is different. For example, polyvinyl, polyacrylate, and other thermoplastic powders are well wetted by liquid resins; in this case some of them partially swell under the effect of styrene contained in the resin. Modifying agents provide both quantitative and qualitative changes in the fiber-glass plastic shrinkage: the content of the twisting agent decreases and surface interaction occurs between UPER and the solid phase of the modifying agent in the course of polymerization. In the process, the effect of adsorption structuring is observed, which promotes formation of the three-dimensional network closer to the equilibrium steric structure. This procedure is associated with the adhesion contact between two phases in the polymer matrix. It is believed that the modifying agent grains, limited by the boundary polymeric layers, become the centers of relaxation microareas which partially compensate internal stresses in the cured composite and stresses appearing during operation of the fiber-glass plastic articles.

The other mechanism is associated with the copolymerization of UPER and liquid rubber. The rubber fragments are incorporated in the three-dimensional polymer network as elastic blocks, which at various stages of polyester cross-linking relieve the internal stresses and the shrinkage and deformation caused by them.

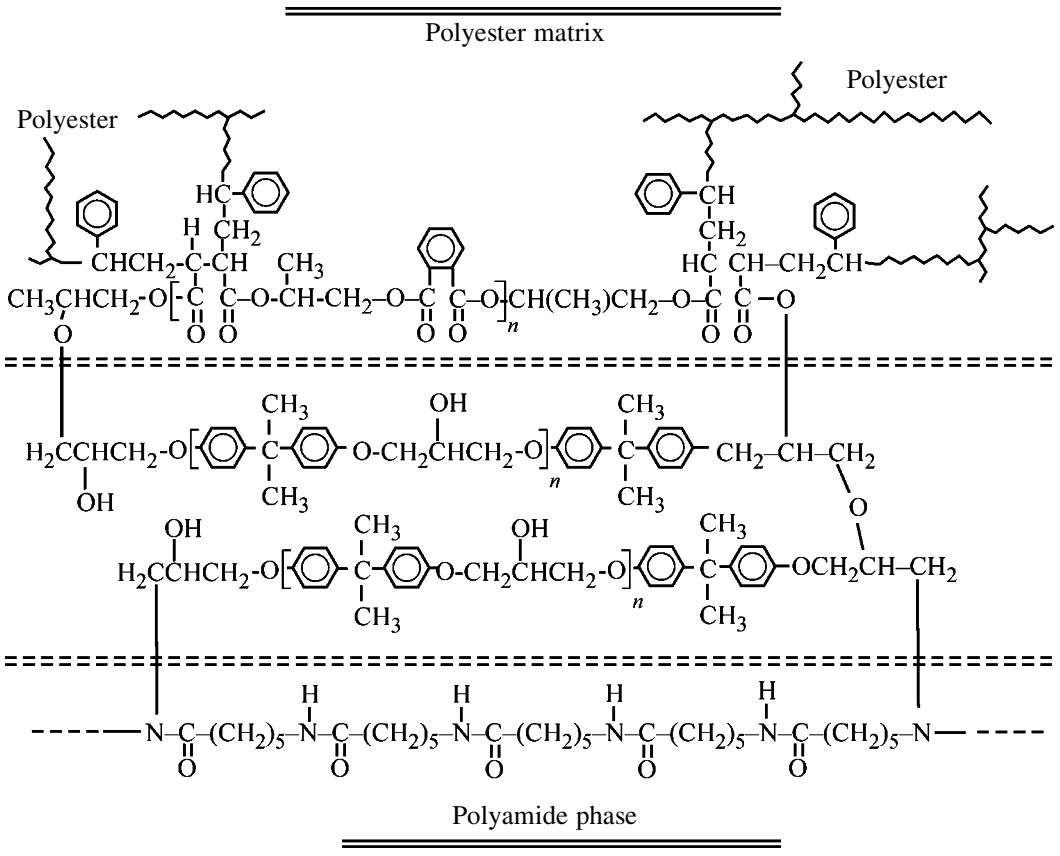
Using these concepts of the mechanism of the shrinkproofing agents, we developed a new approach [8, 9] based on formation of soft (low-elastic-modulus) microparticles in the polymeric matrix. In accordance with this approach, such microparticles enhance adhesion between the polymeric binder and reinforcing fibers in the stage of composite formation. In the course of operation, these soft particles act as structural nodes relieving stresses that appear under the effect of external forces.

The aim of this study was to design aggregate microcenters in the polymeric matrix of fiber-glass composites. In accordance with the Gibbs law, in all stages of the composite formation epoxy resin is deposited on the surface of polyacrylamide particles forming a shell around them. It acts as an intermediate layer between polyamide and polyester phases in the polymer matrix. It is known that the epoxy rings are able to participate in the addition polymerization with active hydrogen of amide groups [10]. Under the conditions of the exothermic stage of UPER curing and thermal treatment of the composite articles, the epoxy shell is grafted to the polyamide surface. At the same time, the epoxy groups of the external layer react with a multitude of carboxy groups contained in UPER. The internal layers of the epoxy resin are also partially linked owing to the hydroxy groups present in the polymer and formed upon grafting of the external layers to polyamide and polyester. Since the interactions of the epoxy and hydroxy groups are relatively weak, the resulting network is friable and hyperelastic.

Based on the above considerations, we assumed

that the epoxy shell of the polyamide particle consists of three layers: (1) grafted to polyamide surface, (2) internal weakly linked, and (3) chemically grafted to polyester surface (see scheme).

Fragment of the chemical structure of a three-component aggregate of epoxy shell of polyamide particles



Owing to their structure, the heterogeneous microareas of the aggregate grains of the modifying agent act as efficient relaxation centers relieving internal stresses and dissipating certain fraction of energy of the external forces.

The effect of the above modification is confirmed by the data on mechanical properties, shrinkage, and deformation of fiber-glass plastic articles (Fig. 1). For the convenience, the modifying agent concentration in Figs. 1 and 2 is expressed through the concentration of PAP. It is assumed that it corresponds to the content of ER taken in 1 : 10 ratio with respect to PAP.

As seen from Fig. 1, with increasing content of the modifying agent the shrinkage of the fiber-glass plastic plates decreases nonlinearly. At small concentrations, the effect is more pronounced. For example, at the PAP content of 3–4 wt % the "Low shrink" accuracy grade is attained. The effect becomes less pronounced with increasing PAP concentration to

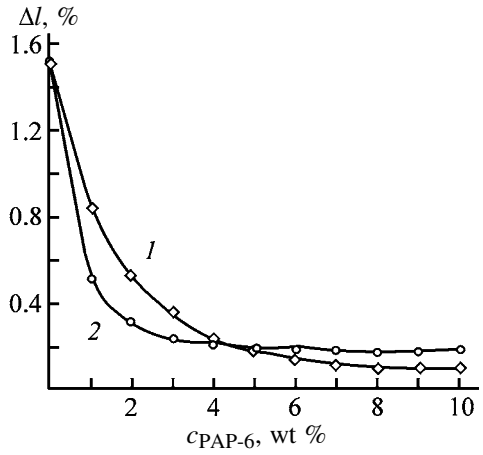


Fig. 1. Linear shrinkage Δl of fiber-glass plastic plates along the (*1*) warp and (*2*) weft of the reinforcing fabric as a function of the modifying agent concentration c_{PAP-6} in the UPER.

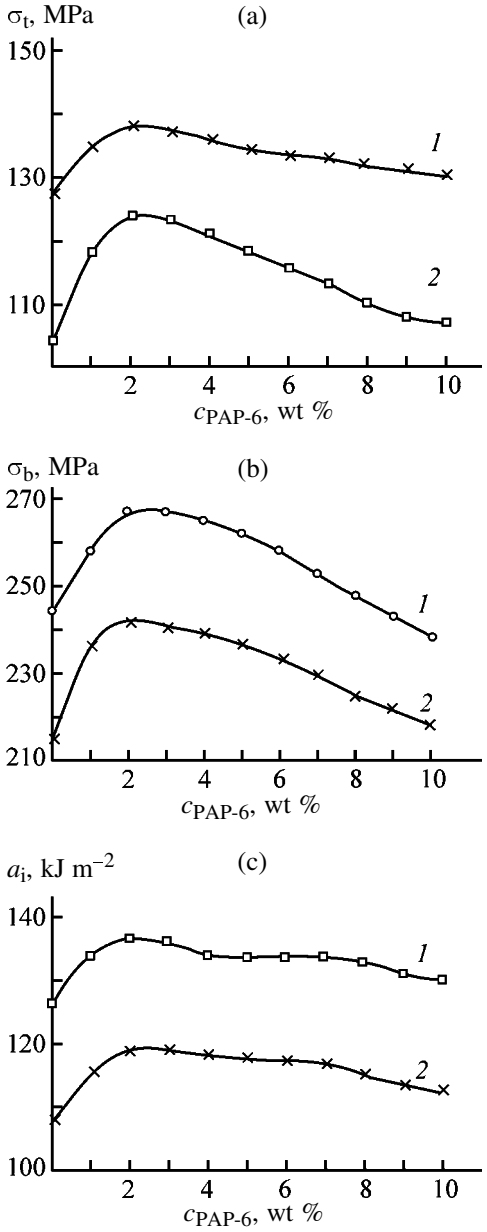


Fig. 2. (a) Tensile strength σ_t, (b) bending strength σ_b, and (c) impact resilience a_i of the fiber-glass plastic plates along the (*1*) warp and (*2*) weft of the reinforcing fabric as functions of the modifying agent concentration $c_{PAP\text{-}6}$ in the UPER.

≥5 wt %, and to prepare the objects with "Low profile" accuracy grade the content of PAP in UPER should be increased to 6–8 wt %. Moreover, along with decreasing shrinkage, no deformation and cracking of the resulting fiber-glass plastic plates was observed.

The data on the effect of modification on the mechanical properties of fiber-glass plastics are of particular importance from both the theoretical and practical viewpoints.

As seen from Fig. 2a, the tensile strength at small concentrations of the modifying agent increases by 10 and 15% along the warp and weft, respectively. With increasing content of the modifying agent in the matrix, its strength decreases but remains still higher as compared to the unmodified composites.

At small concentrations of the modifying agent (1–4 wt % PAP-6), the increase in the strength of fiber-glass composites is more pronounced. With increasing content of ER and PAP, their strength gradually decreases and at maximal degree of filling (10 wt % PAP) it is comparable with that of unmodified fiber-glass plastic materials (Fig. 2b).

The dependence of the impact resilience of the fiber-glass plastic on the concentration of the modifying agent is similar (Fig. 2c). Our experimental data showed that in all the cases the strength of the resulting materials along the warp is higher than that along the weft. This fact may be due to the decisive effect of the content of the glass fibers on the strength of the reinforced plastics as compared to the effect of other strengthening factors.

Our experimental data showed that, with increasing content of PAP modifying agent to 10 wt % and ER to 1 wt %, the scatter in the mechanical properties of the specimens cut out from plates of similar compositions decreases by a factor of 2.

CONCLUSIONS

(1) Fiber-glass plastic articles with decreased shrinkage were prepared. At 3 wt % content of the polyamide powder, the shrinkage of the resulting composite is 0.2–0.25%, which corresponds to the "Low shrink" accuracy grade. With increasing content of the modifying agent to 6–8 wt %, the shrinkage of the fiber-glass composite decreases to 0.10–0.15%, which corresponds to the "Low profile" accuracy degree.

(2) The articles of the modified composite do not deform irrespective of their shape and thickness.

(3) The tensile and bending strengths and impact resilience of the modified materials increases with increasing concentration of the modifying agents, and small amounts of the modifying agents are more efficient.

(4) The mechanism of modification, based on the

hybridization of the polymer matrix, is proposed. In accordance with this approach, microheterogeneities in the form of aggregate micronodes are formed in the network of the polymer matrix, which act as the relaxation centers compensating internal stresses in the fiber-glass plastic and dissipating certain fraction of the mechanical stresses caused by external forces.

REFERENCES

1. *Handbook of Plastic Materials and Technology*, Rubin, I., Ed., New York: Wiley, 1990.
2. Lubin, G., *Handbook of Composites*, New York: Reinhold, 1982.
3. Parker, E.E., Peffer, J.K., Schildknecht, C.E., and Skeist, I., *Polymerization Processes*, New York: Wiley, 1977.
4. Pishev, D., Gankov, N., Angelova, N.I., et al., *Khim. Ind.* (Sofia), 1983, vol. 7, pp. 295–296.
5. Pishev, D.I., Gankov, N.P., Angelova, N.I., et al., *Plast. Massy*, 1985, no. 6, pp. 50–51.
6. Angelova, N.I., Pishev, D.I., and Gankov, N.P., *Lakokras. Mater. Ikh Primen.*, 1986, no. 4, pp. 65–66.
7. BUL Inventor's Certificate 36707.
8. Radenkov, F., Anastasov, M., Dikov, V., and Zhelyazkov, Zh., Extended Abstracts, *VII mezhdunarodna konferentsiya po mekhanike i tekhnologii na kompozitnite materiali* (VII Int. Conf. on Mechanics and Technology of Composites), Sofia, 1994, pp. 174–179.
9. Radenkov, F., Anastasov, M., Dikov, V., and Zhelyazkov, Zh., Extended Abstracts, *VII mezhdunarodna konferentsiya po mekhanike i tekhnologii na kompozitnite materiali* (VII Int. Conf. on Mechanics and Technology of Composites), Sofia, 1994, pp. 180–183.
10. BUL Inventor's Certificate 33809.

ISSN 1070-4272, Russian Journal of Applied Chemistry, 2006, Vol. 79, No. 11, p. 1912. © Pleiades Publishing, Inc., 2006.
Original Russian Text © G.E. Zaikov, M.I. Artsis, N.N. Madyuskin, 2006, published in Zhurnal Prikladnoi Khimii, 2006, Vol. 79, No. 11, pp. 1934–1935.

INFORMATION

The 3rd International Conference on Times of Polymers

DOI: 10.1134/S1070427206110334

The 3nd International Conference on Times of Polymers (TOP) was held in Italy from June 18 to 22, 2006.

About 150 scientists from 22 countries (Algeria, Argentina, Bahrein, Brazil, Canada, Chile, China, France, Georgia, Greece, Iran, Israel, Italy, Kuwait, Mexico, Portugal, Russia, Slovak Republic, Switzerland, Taiwan, the United States, and Venezuela) participated in the Conference. They represented 65 research centers.

The Conference provided a forum for scientists and engineers throughout the world interested in the timescales of polymer and composite processing, structure, and properties. The Conference's motto was "Research, Development, Production."

As time is the driving concept in the polymer science community, the Conference included sessions on various topics and provided opportunities for exchanging ideas and opinions on both fundamental science and industry-relevant subjects such as viscoelasticity, thin films, nanocomposites, organic electronics (OLED, OTFT), polymer-based sensors, industrial rheology, durability/degradation, processing, biomaterials, cultural heritage, and fracture and yielding.

The Conference Program included a plenary lecture, 11 invited presentations, 50 oral contributions from participants, and the same number of poster presentations.

The plenary lecture entitled Nanomechanical Measurements of Polymers in the Vicinity of the Glass Transition: Question about T_g and Enhanced Surface Dynamics was presented by G.B. McKenna (the United States).

The eleven invited lectures were as follows: (1) Timescales of Mechanically Stimulated Glassy Polymers [A. D'Amore (Italy)]; (2) Dynamics of Nanoparticles for Biomedical Applications [J. Mijovic (the United States)]; (3) Control of the Macromolecular Architecture during Reactive Processing [F. Ciardelli (Italy)]; (4) Computer Simulations of Radical Polymerization at Unusual Conditions [A.R. Khoklov (Russia)]; (5) Reinvestigating Polymer Oxidation Processes by New Tools [G. Montaudo (Italy)]; (6) Comparison of the Viscoelastic Bulk and Shear Moduli [S.L. Simon (the United States)]; (7) Modelling and Experimental Characterization of Hydrothermoelastic Stress in Polymer Matrix Composites [A. Vautrin (France)]; (8) Water Diffusion in Glassy Polymers and Their Silica Hybrids: an Analysis of State of Water Molecules and of the Effect of Tensile Stress [G. Mensitieri (Italy)]; (9) Large Area Processing of All Organic Electronic Systems Combining Nanoscale Imprinting and Inkjet Printing Technologies [F. Zenhausern (the United States)]; (10) Chain Entanglement in Thin Free-Standing Polymer Films [K. Dalnoki-Veress (Canada)]; and (11) The Effect of Solvents (Plasticizers) on PVC Degradation [G.E. Zaikov (Russia)].

Oral and poster presentations covered such topical problems as development of conducting polymeric and composite materials as well as materials having semiconductor properties; biopolymers and their medical applications; new methods for polymer characterization (including chemiluminescence); relaxation phenomena in polymers and composites; liquid-crystalline polymers (preparation and characterization); and reactions in solid polymers under pressure and shear stress (reactions in extruders).

Several presentations were devoted to filled polymers (preparation and characterization), inorganic and organic polymers and their blends, dyeing of polymers and the contribution of chemical additives in the behavior of polymeric materials, degradation and stabilization of polymers, flame retardation in polymers, novel environmentally friendly fire retardants, "smart" polymers and their properties, polymeric hydrogels and their applications in medicine and farming, structure and properties of various polymers, diffusion of multicomponent systems (electrolytes) in a solid polymer, nanopolymers (preparation and characterization), mechanical properties of composite materials, prediction of the service and storage life of polymeric and composite materials, and biochemical synthesis as a novel approach to preparation of polymers.

The Conference revealed that synthesis, properties, and applications of polymers, polymer blends, polymer composites, and filled polymers continue to be topical basic and applied problems.

Proceedings of the Conference will be published as a special issue of the European Polymer Journal.

The next Conference Times of Polymers-IV will be held in July, 2006 at the same place.

G. E. Zaikov, M. I. Artsis, and N. N. Madyuskin

ISSN 1070-4272, Russian Journal of Applied Chemistry, 2006, Vol. 79, No. 12, pp. 1913–1918. © Pleiades Publishing, Inc., 2006.
Original Russian Text © V.Yu. Dolmatov, 2006, published in Zhurnal Prikladnoi Khimii, 2006, Vol. 79, No. 12, pp. 1937–1941.

INORGANIC SYNTHESIS AND INDUSTRIAL INORGANIC CHEMISTRY

Development of a Rational Technology for Synthesis of High-Quality Detonation Nanodiamonds

V. Yu. Dolmatov

Tekhnolog FGUP SKTB, St. Petersburg, Russia

Received February 9, 2005; in final form, June 2006

Abstract—Concepts concerning the structure of detonation nanodiamonds were generalized on the basis of data reported in previous publications. The pH value of the nanodiamonds in an aqueous suspension was determined. The mechanism of the longest stage, washing of nanodiamonds with water to remove excess acidity, was considered. A novel method for substantially improving the quality of nanodiamonds and the stability of aqueous suspensions of nanodiamonds was suggested.

DOI: 10.1134/S1070427206120019

The task of achieving a high purity of detonation nanodiamonds and preparing stable nanosize suspensions is a key issue for successful application of nanodiamonds in various areas of science and technology. However, due attention has not been given to this question because of the complexity of these problems. This study is devoted to generalization of concepts about the structure of nanodiamonds and to practical solution of the above problems.

Detonation nanodiamonds (average size 4–6 nm) are exceedingly complex objects having, at least, a three-layer structure [1–3]. Each particle (cluster) contained in aggregates is a set of constituent elements.

(1) A core composed of carbon atoms (sp^3 hybridized) bound into a cubic crystal structure characteristic of diamond includes 70–90% of carbon atoms and has, according to X-ray data, a size of 40–60 Å; the core contains 2.5–2.8 wt % nitrogen as substitution atoms [4].

(2) An intermediate carbon sheath of thickness 4–10 Å, which envelops the core, is composed of X-ray-amorphous carbon structures, and may contain 10–30% of carbon atoms of the cluster [5]. The sheath composed of sp^2-hybridized carbon is inhomogeneous. It is believed [2] that the inner layer of this sheath, immediately adjacent to the diamond core, is composed of continuous layers of onion-like carbon. Above the inner layer are situated, within the same sheath, fragmented graphite-like monolayers. This amorphous carbon sheath has a porous structure, contains numerous defects and discontinuous regions of structural carbon formations, and may include a minor amount of heteroatoms incorporated into the sheath in the course of detonation synthesis and chemical purification.

(3) Surface layer containing, in addition to carbon atoms, also other heteroatoms forming a broad spectrum of widely diverse functional groups. The amount of heteroatoms may be as large as 10% relative to the total mass of a particle, and oxygen may constitute their larger part [6]. Hydrogen contained in functional groups and nitrogen rather uniformly distributed over all layers of nanodiamonds are revealed in minor amounts. The major place is occupied by oxygen-containing groups (hydroxy, carboxyl, ketone, lactone, etc.).

In view of the fact that the core and its intermediate sheath are nearly wholly composed of carbon, all the heteroatoms (except nitrogen) are concentrated in the surface layer and their content in the surface layer is about 50%, i.e. [7], nanodiamond particles are not a purely carbon material. Moreover, carbon itself is present in the product simultaneously in several modifications, and only one of these corresponds to the structure of diamond.

The structure and quantitative characteristics of the core and intermediate carbon sheath of nanodiamonds are formed in the course of detonation synthesis [3, 7]. The outer sheath determines the relationship between the nanodiamond cluster and the environment. It is this sheath that forms the interface and

is involved in the interaction with the ambience. Its structure and composition may strongly depend on how nanodiamonds are recovered, purified, and stored. The ultrasmall size of particles results in that the role of surface interphase interactions becomes exceedingly important. It is these interactions that largely predetermine macroscopic characteristics of nanodiamonds and their consumer properties. The presence of highly polar and reactive groups concentrated in a small volume at the surface predetermines the strong impact of nanodiamond particles on the environment.

The existing methods for production of nanodiamonds, which are based on detonation synthesis, can actually yield only a raw carbon material, diamond stock, in which nanodiamonds are contained [1, 8]. The diamond stock also includes graphite-like structures and amorphous destructured chains of carbon atoms bearing numerous functional groups. It also contains technological impurities (metals and metal derivatives: carbides, oxides). The chemical methods used to recover nanodiamonds from the raw carbon material and purify them actually newly form the surface sheath [9].

From the standpoint of modeling, it is more appropriate to represent nanodiamond particles as a cross-linked rigidly structured polymer, whose internal skeleton is formed by saturated carbon bonds and the surface is saturated with highly polar groups, rather than as a small nanodiamond crystal with defective surface. The 3*D* skeleton provides concentration of a large amount of organic products within a very small volume. As a result, a strong field of impact on the environment can be created and the structuring action of nanodiamond particles is manifested. Nanodiamonds are a unique material owing to their intermediate position between inorganic and organic products. It is this circumstance that determines their particular place among ultradisperse materials and those related to nanocarbon (fullerenes, nanotubes, carbyne).

The most efficient and high-output-capacity technique for chemical purification of detonation nanodiamonds (ultradisperse diamonds, UDD) consists in treating the detonation diamond stock with dilute nitric acid under pressure (up to 100 atm) at high temperatures (240–260°C) [10]. With this method, it is possible to achieve a UDD purity of 99% and more at a residence time of diamond stock in the high-pressure and high-temperature zone as short as 30–40 min. This technology has been successfully implemented in Russia, China, and Belarus. However, despite the high quality of nanodiamonds and high output capacity of the reactor unit, the rate-determining stage is the seemingly simple last operation, washing of nanodiamonds to remove the acid and soluble impurities. This process takes as long as four to five days, which strongly affects the output capacity of the stage of chemical purification as a whole.

EXPERIMENTAL

Nanodiamonds were produced at Tekhnolog FGUP SKTB by detonation decomposition of a trinitrotoluene–hexogen alloy containing 40 wt % TNT (TNT/hexogen 40/60) in a nonoxidizing gas medium, with the explosive charge (0.6 kg) placed in a water envelope. The water : explosive ratio was 6 : 1. The diamond-containing stock obtained upon an explosion was subjected to nitric acid purification [10]. The product formed upon the nitric acid purification was subjected to ammonia thermolysis. The nanodiamonds obtained were of the UDD-TAN brand. According to TU (Technical Specification) 05 121 441-275–95, UDD-TAN should contain (wt %): main substance (nanodiamonds) ≥96.5, oxidizable carbon ≤2.5, and incombustible impurities ≤1.0; with the pH of the aqueous suspension in the range 5–8.

The pH of the aqueous suspension or of the clarified water layer (containing no nanodiamonds) was measured with a pH-121 pH-meter (ESL 43-07 glass electrode and EVL-1 M 3.1 silver chloride reference electrode).

The sedimentation rate of the solid phase (nanodiamonds) was determined in a 1-l glass cylinder by examining the motion of the interface between clarified water and thickened suspension in the course of time.

The thermolysis (treatment of weakly acidic nanodiamond suspensions having pH ~2.5 with ammonia, followed by heating) was carried out in a 10-l titanium autoclave equipped with a stirrer. The autoclave should sustain temperatures of up to 280°C and pressures of up to 500 atm. Aqueous ammonia was added to a nanodiamond suspension and the pH of the suspension was brought to 10.5–12.0. Then the weakly alkaline suspension was charged into the autoclave (charge 60–80% of the total volume), heated to 230°C, and kept for 2–3 h. After the keeping the suspension was cooled and the excess pressure was relieved. The pH value of the resulting nanodiamond suspension was 7–8.

The content of the main substance in the nanodiamond suspension was determined by taking an aliquot of the suspension (10–20 ml) and evaporating it to dryness. Then the percentage content of nanodiamonds was calculated.

When considering issues associated with washing of nanodiamonds to remove water-soluble impurities, control over the washing efficiency, and aggregation conditions, it is necessary to take into account that nanodiamonds have their own noticeable acidity determined by the presence of carboxyl groups on their surface.

A suspension of pure nanodiamonds in water cannot be neutral and should be acidic (Fig. 1). Two layers are formed in sedimentation of a nanodiamond suspension: lower thickened and upper clarified (nanodiamond-free water). A distinction should be drawn between the suspension acidities in these layers. The acidity of the lower thickened layer is determined by the overall effect of acid groups of nanodiamonds and acid agents dissolved in water, and that of the clarified layer, only by dissolved products.

Measurements of the pH value and titration in decantation of the upper clarified layer of the suspension make it possible to judge the content of acid impurities, and the difference in acid content between the thickened and clarified layers can be used to evaluate the contribution of nanodiamonds to the total acidity of the medium. At an acid content of the upper layer exceeding 0.5% (pH ~ 1), there is virtually no difference in acidity between the upper and lower layers. However, with further washing (pH > 3), the difference between the total acidities grows fast to become as large as orders of magnitude (Fig. 2). Nanodiamond particles should behave in water as a poorly soluble weak organic acid, which is the case in actual practice. Consequently, it is impossible to obtain a neutral nanodiamond suspension without use of neutralizing alkaline agents.

The acid properties are primarily manifested in the aggregative and sedimentation stability of aqueous suspensions. This circumstance is of fundamental importance for the technology of nanodiamond purification, because all the known variants include treatment with strong acids.

Commonly, acids are removed by washing with water. Free settling of a nanodiamond suspension in the course of its washing to remove acids or ammonia water (in the case of neutralization of acids) yields suspensions thickened to 5–7% in terms of nanodiamonds. After that, further settling virtually terminates (at least that observed visually) in the absence of considerable concentrations of salt-forming impurities. The sedimentation rate in dilute suspensions corresponds to a settling velocity of particles about 1 μm in size. The time sufficient for sedimentation of

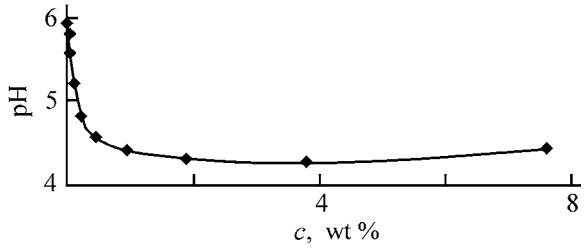


Fig. 1. pH of a washed nanodiamond suspension vs. content *c* of nanodiamonds.

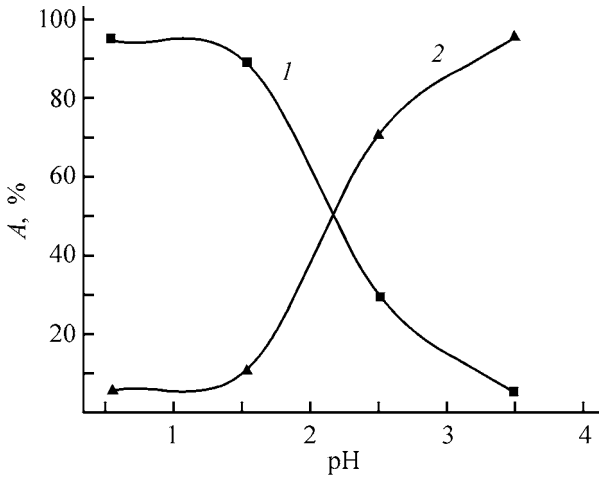


Fig. 2. Distribution of the overall acidity *A* of the nanodiamond suspension among nanodiamonds and the aqueous phase at different pH values of the medium. Fraction of the overall acidity: (*1*) in the aqueous phase and (*2*) on nanodiamonds.

the main part of nanodiamond particles to form a thickened aqueous suspension at pH < 2 is 12–24 h. The content of nanodiamond particles at the maximum thickening (5–7 wt %) is well reproducible. The interface between the thickened and clarified layers remains distinct. Presumably, the value of 5–7 wt % should be considered a characteristic value.

Physically, this can be interpreted as follows. At the given concentration, water in a thickened suspension is in the zone of structuring action of nanodiamond particles. As a result, water forms solvation shells that tightly envelop nanodiamond particles or aggregates of particles and are retained in the near field of these particles. The key role in the transfer of the structuring action is presumably played by ionic mechanisms and hydrogen bonds. It is known that, in the absence of foreign impurities, the surface of nanodiamond particles in aqueous suspensions is negatively charged, which is determined by the large number of oxygen-containing polar groups, and primarily hydroxy and carboxyl groups. However, in solutions

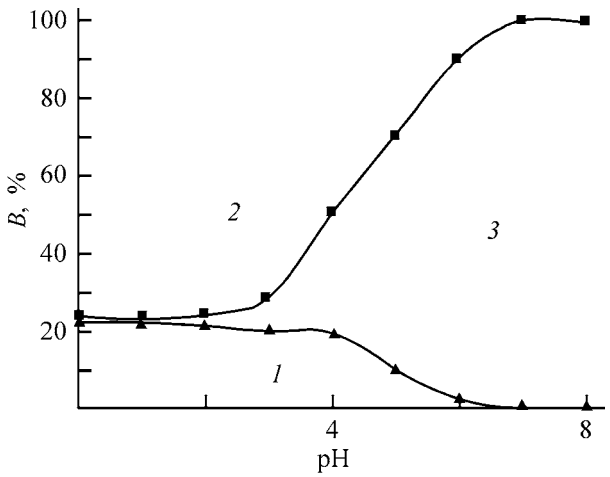


Fig. 3. Stratification of the nanodiamond suspension in settling in relation to the pH of the medium. Settling time 24 h, initial concentration of the nanodiamond suspension 1%. (*B*) Fraction of thickened suspension in the whole volume. (*1*) Thickened layer, (*2*) clarified layer, and (*3*) unsettling UDD suspension.

of strong acids (e.g., nitric acid), the surface of nanodiamonds should take on a positive charge because of the chemisorption and physical sorption of hydroxonium ions. As the concentration of nitric acid in the aqueous medium decreases in the course of washing, which is well monitored by pH values, the concentration of the thickened layer decreases and the interface between the clarified and thickened layers is smeared (Fig. 3). The interface smearing is due to a decrease in the amount of the electrolyte (acid) in the aqueous suspension in the course of nanodiamond washing. As a result, coarse aggregates partly disintegrate, with the remaining ions predominantly concentrated in the hydrospheres of nanodiamonds. Visually, this is observed as a decrease in the degree of thickening and boundary smearing (Fig. 3) ("hanging" effect).

Centrifugation accelerates the process of UDD concentration in the thickened layer (to 12–14% at pH < 2), but this is only effective for strongly acidic media. At pH values close to 7, the centrifugation efficiency falls dramatically and the "hung-up" suspension is not clarified completely.

It was shown that, after a fourth washing of acid nanodiamonds with water (with the ratio between the thickened layer of nanodiamonds and pure water maintained constant at 1 : 4), the content of HNO_3 in the suspension is 0.18–0.25 wt % (pH 1.8–2.0), and that after a fifth washing, 0.07–0.10 wt % (pH 2.2–3.0). Further washing to remove such an insignificant amount of HNO_3 is inadvisable because the suspension starts to "hang" and the waiting time increases dramatically. To prevent hang-up on reaching a pH value of 1.5–2.5, it is advisable to neutralize the acid remaining in solution and acid groups on the surface of nanodiamond particles with ammonia water, with the pH value of the medium changed abruptly from acidic (content of nitric acid in the suspension 0.1–0.3 wt %) to weakly alkaline (pH 9–10). In this case, the excess of ammonia water in the suspension is only 0.025 wt % even at pH 10.

The advantages of treatment of a nanodiamond suspension with ammonia water are as follows: (i) ammonium salts of nitric and nitrous acids are well soluble in water and are readily removed (in one or two washings), together with the clarified layer from the thickened nanodiamond suspension; (ii) excess of ammonia water is easily evaporated in the form of ammonia; and (iii) NH_4^+ ion, which has the smallest ionic radius among alkaline agents, readily penetrates into meso- and micropores of nanodiamond aggregates and neutralizes trace amounts of mineral acids, present there.

The weakly alkaline reaction of the suspension in the presence of an excess amount of ammonia water and the presence of ammonium salts (electrolyte) provide a sufficiently fast stratification (in two or three washings) and thickening of nanodiamonds in the lower layer to approximately 8 wt %, and, in some cases, even to 12 wt %.

However, no chemical purification, or even treatment of sufficiently well washed nanodiamonds with ammonia water under common conditions can significantly change the situation as regards the amount of nitrogen oxides contained in meso- and micropores of nanodiamond aggregates; these oxides are difficult to remove even under strong heating.

This problem can be solved, with the nanodiamond aggregates simultaneously made smaller, by heating a weakly acidic nanodiamond suspension neutralized with ammonia water at 200–240°C for 30 min. The following processes occur in the given medium at high temperature (and pressure).

(1) The salts formed on the surface, and primarily NH_4NO_3 and NH_4NO_2, readily diffuse into the aqueous solution.

(2) Most part of NH_4NO_3 and NH_4NO_2 starts to vigorously decompose at 200–240°C to give gaseous products and water by reactions (1) and (2); nitrogen(I) oxide formed by reaction (1) further decomposes to nitrogen by reaction (3), and nitrogen oxides

brought in contact with the excess ammonia water are converted to nitrogen and water:

$$NH_4NO_3 \rightarrow N_2O + 2H_2O, \quad (1)$$

$$NH_4NO_2 \rightarrow N_2 + 2H_2O, \quad (2)$$

$$N_2O \rightarrow N_2 + 0.5O_2, \quad (3)$$

$$N_2O_3 + 2NH_3 \rightarrow 2N_2 + 3H_2O. \quad (4)$$

(3) Vigorous gas evolution results in that nanodiamond aggregates 350–500 nm in size disintegrate to 10–100-nm aggregates, with harmless products, such as nitrogen and water, released.

(4) There also occurs a rather full desorption of nitrogen oxides from the surface of nanodiamonds (especially from internal pores) to give an excess amount of ammonia water in hydrolysis in water of ammonium nitrate and nitrite.

(5) Cooling of the nanodiamond suspension and its washing (two or three times) to remove residual amounts of ammonium salts and ammonia water yield a colloid-stable highly concentrated (10–12 wt %) aqueous nanodiamond suspension with low viscosity and high fluidity, which makes it highly technologically convenient for further use.

(6) The enhanced desorption of inorganic and organic impurities from the surface of nanodiamond particles in the presence of ammonia water at high temperatures and pressures and the subsequent washings result in that the purity of nanodiamonds is as high as 99.5 wt % in some cases.

The purity of nanodiamonds was determined by the conventional method (indirectly) from the difference between 100% and the total content of impurities (incombustibles and readily oxidizable carbon) in nanodiamonds.

For example, the total content of incombustibles in a well-washed (seven washings with water) batch of nanodiamonds of the UDD-STV brand (TU 05 121 441-275–95) is 0.95 wt % (see table), whereas the same batch of nanodiamonds, neutralized with ammonia water to pH 7.3, subjected to thermolysis at 230°C and then twice washed with water (UDD-TAN brand) contains only 0.4 wt % incombustibles.

After the thermolysis, the nanodiamond suspension contains an excess amount of ammonia water (pH ≥ 7) and a certain amount of ammonium salts, and, therefore, it is sedimentation-unstable. This circumstance facilitates its 2–3-fold washing with water.

Content of incombustibles in samples of an aqueous nanodiamond suspension (according to atomic-absorption spectroscopy)

Element	Content of elements in indicated brand of nanodiamonds, wt %		
	UDD-STV*	UDD-TAN*	Standard nanodiamonds**
Iron	0.15	0.1	0.1
Chromium	0.07	0.05	0.5
Silicon	0.3	0.1	0.15
Aluminum	0.005	0.001	0.01
Sodium	0.03	0.003	0.05
Potassium	0.002	0.002	0.002
Copper	0.005	0.002	0.003
Calcium	0.002	0.002	0.01
Magnesium	0.005	0.003	0.005
Manganese	0.001	Not found at a detection limit of 5×10^{-4} wt %	0.001
Titanium	0.01	0.005	0.002
Lead	0.001	0.001	0.001
Σ	0.58	0.27	0.84
Incombustible residue, %	0.95	0.4	1.4

* Manufactured by Tekhnolog FGUP SKTB.

** Manufactured by RFYaTs–VNIITF. Analysis of nanodiamonds made by S.I. Chukhaeva (RFYaTs–VNIITF, Snezhinsk).

The resulting suspension can be stored for years, but the pH of the medium gradually decreases to 4.5, which corresponds to the pH value of pure nanodiamonds. In storage, the size of nanodiamond aggregates increases from 10–100 to 150–300 nm.

CONCLUSIONS

(1) The basic properties of nanodiamonds, which characterize this product as a new formation combining all the possible forms of carbon atoms with various hybridizations into a single ensemble, are described. Nanodiamonds can be regarded as a material intermediate between inorganic and organic products.

(2) Washing of nanodiamonds to remove acids is a complicated task. At pH > 3, the acidity of the suspension is determined by the intrinsic acidity of sur-

face oxygen-containing groups on nanodiamonds. The pH of aqueous media containing well-washed nanodiamonds (1–10 wt %) is 4.4–4.5.

(3) The maximum content of gravitationally thickened nanodiamond suspensions in a daily (conventional) technological cycle of washing is as high as 5–7 wt %.

(4) A novel method is suggested for conditioning of nanodiamonds, which consists in that a weakly acidic aqueous nanodiamond suspension (pH 2–2.5) is treated with ammonia water and then heated to 200–240°C for 30 min.

REFERENCES

1. Volkov, K.V., Danilenko, V.V., and Elin, V.I., *Fiz. Goreniya Vzryva*, 1990, vol. 26, no. 3, pp. 123–125.
2. Aleksenskii, A.E., Baidakova, M.V., Vul', A.Ya., and Siklitskii, V.A., *Fiz. Tverd. Tela*, 1999, vol. 41, no. 4, pp. 740–743.
3. Dolmatov, V.Yu., *Usp. Khim.*, 2001, no. 7, pp. 687–708.
4. Kulakova, I.I., *7-ya Mezhdunarodnaya konferentsiya "Porodorazrushayushchii i metalloobrabatyvayushchii instrument – tekhnika i tekhnologiya ego izgotovleniya i primeneniya," Ukraina, Krym, poselok Morskoe, 19–24 sentyabrya 2004 g.* (Proc. 7th Int. Conf. "Rock-destroying and Metal-working Tools: Technology of Their Fabrication and Use," Ukraine, Crimea, Morskoe Settl., Sptember 19–24, 2004), Kiev, 2004, pp. 156–160.
5. Dolmatov, V.Yu. and Fujimura, T., *Sverkhtverd. Mater.*, 2001, no. 6, pp. 34–41.
6. European Patent 1 288 162.
7. Dolmatov, V.Yu., *Ul'tradispersnye almazy detonatsionnogo sinteza* (Ultradisperse Diamonds Produced by Detonation Synthesis), St. Petersburg: SPb. Gos. Ped. Univ., 2003.
8. RF Patent 2 230 702.
9. Gubarevich, T.M., Dolmatov, V.Yu., Pyaterikov, V.F., et al., *Zh. Prikl. Khim.*, 1992, vol. 65, no. 11, pp. 2512–2516.
10. RF Patent 2 109 683.

ISSN 1070-4272, Russian Journal of Applied Chemistry, 2006, Vol. 79, No. 12, pp. 1919–1923. © Pleiades Publishing, Inc., 2006.
Original Russian Text © E.V. Shkol'nikov, 2006, published in Zhurnal Prikladnoi Khimii, 2006, Vol. 79, No. 12, pp. 1942–1946.

PHYSICOCHEMICAL STUDIES OF SYSTEMS AND PROCESSES

Thermodynamic Characterization of the Amphoterism of Solid Oxides MO in Aqueous Media

E. V. Shkol'nikov

St. Petersburg State Forestry Academy, St. Petersburg, Russia

Received October 2, 2006

Abstract—Thermodynamic method was used to calculate, with account of the formation of hydroxo complexes, the molar solubilities of crystalline and amphoteric oxides MO as functions of the pH value of an aqueous-alkaline nonoxidizing medium at 25°C and constants of heterogeneous equilibria in water and alkaline and acid media for amphoteric metal MO, where M is Be, Mn–Zn, Cd, Hg, Sn, or Pb.

DOI: 10.1134/S1070427206120020

Previously, the thermodynamic method has been used to calculate the effect of the pH value on the molar solubility of solid hydroxides $M(OH)_2$ and their amphoterism in aqueous media has been characterized. Of interest is a thermodynamic calculation of the solubility of solid oxides MO, where M is Be, Sn, Pb, Cd, and 3*d*-elements from Mn to Zn, in an aqueous alkaline medium.

Crystalline and amorphous oxides are widely used in manufacture of ceramics and glasses, mineral paints and enamels, oxide electrodes and catalysts, in metallurgy, semiconductor electronics, and medicine [3–6]. As products of real dehydration of hydroxides, solid oxides can be obtained by heating of hydroxides in an inert medium. Anhydrous oxides are produced by burning of metals in oxygen or by pyrolysis of carbonates, oxalates, and nitrates [4–6].

Ionic-covalent oxides MO are frequently formed with defective crystal structure and, depending on the preparation method and conditions, have noticeable homogeneity regions and show differences in coloration and chemical activity [5, 6].

The amphoteric nature of the oxides MO is poorly understood, and quantitative data on their solubility in aqueous media are rather scarce and frequently contradictory [3–7]. For example, according to the reference book [7], the metal oxides under consideration are poorly soluble (PbO, HgO) or virtually insoluble in water, all react with acids, and only BeO (in fusion), ZnO, and PbO react with alkalis. According to [4], a white precipitate of $Sn(OH)_2$, soluble in acids and alkalis, is readily transformed to dark amphoteric oxide SnO upon heating. Dehydration of the white precipitate of $Pb(OH)_2$ yields red α-PbO at 100°C and yellow oxide β-PbO at lower temperatures. Both modifications are dissolved in acids and concentrated alkalis [4]. According to [5], the BeO oxide reacts under heating with acids and alkalis, CoO is amphoteric with predominance of basic properties, and MnO reacts with alkalis under strong prolonged heating. According to [6], black oxide α-SnO and red α-PbO with a tetragonal structure are amphoteric with predominance of basic properties. Brown cubic modification of CdO, black monoclinic CuO, and gray-green cubic modification α-CoO form, when fused with alkalis, cadmate, cuprates, and cobaltites(II). Black iron(II) oxide reacts with acids and alkaline solutions, but upon calcination, its chemical and pyrophoric activity decreases. Uncalcined hexagonal oxide α-BeO is hygroscopic, and that calcined below 500°C readily reacts with acids, and more difficultly, with alkali solutions [6].

The procedure described in [1] was used to perform a thermodynamic calculation of the solubility of crystalline and amorphous oxides MO in pure water and aqueous alkaline medium (with addition of NaOH) at pH 7–15 and 25°C. The standard Gibbs energies of formation of ions in aqueous solutions, ΔG_f^0, necessary for calculation of thermodynamic solubility constants K_s^0 (SP = $a_{M^{2+}} a_{OH^-}^2$) were taken from [8], and the Gibbs energies of formation of solid oxides at 298 K, from reference books [7, 9, 10]. The molar solubility of MO in pure water and aqueous solutions

Table 1. Thermodynamic parameters of dissolution of amorphous and crystalline oxides in water and alkali at 25°C

Composition	pK_s^0		H_2O			NaOH		s, M, in 1 M NaOH
	calculation	[13]	pH^0	s^0, M	$[M(OH)_2]$, M	pH_{opt}	ps_{min}	
α-BeO	20.37	–	8.12	2.3×10^{-6}	1.0×10^{-6}	8.9	5.87	0.041
α-SnO	26.65	26.2	7.01	2×10^{-6}	1.9×10^{-6}	7.1	5.71	0.058
α-PbO	15.29	–	9.54	5.8×10^{-5}	2.1×10^{-5}	10.25	4.46	0.042
β-PbO	15.12	–	9.62	7.8×10^{-5}	3.2×10^{-5}	10.25	4.28	0.063
MnO	9.54	9.48	11.05	1.37×10^{-3}	2.2×10^{-4}	12.0	3.25	0.020
FeO	15.38	15.4	8.99	5.5×10^{-6}	1×10^{-8}	10.8	7.18	4.8×10^{-5}
α-CoO	14.74	14.73	9.22	1.4×10^{-5}	3.8×10^{-6}	10.95	5.32	6.6×10^{-4}
α-NiO	15.51	15.53	8.94	4.9×10^{-6}	3.1×10^{-7}	10.2	6.40	3.3×10^{-4}
CuO*	20.06	–	7.45	1.4×10^{-7}	2×10^{-9}	9.9	9.19	2.3×10^{-4}
CuO	20.58	20.40	7.26	1×10^{-7}	1.4×10^{-9}	9.9	9.70	7×10^{-5}
ZnO*	16.55	16.66	8.75	7.7×10^{-6}	2.8×10^{-6}	10.2	5.48	0.015
ZnO	16.82	16.83	8.68	6×10^{-6}	1.9×10^{-6}	10.2	5.64	0.011
CdO*	12.21	–	10.1	1.1×10^{-4}	2.8×10^{-5}	11.6	4.34	6.4×10^{-4}
CdO	12.99	–	9.81	4.3×10^{-5}	4.6×10^{-6}	11.6	5.13	1.1×10^{-4}
α-HgO	25.49	–	7.03	2.2×10^{-4}	2.2×10^{-4}	8.85	3.66	2.6×10^{-4}
β-HgO	25.55	25.42	7.02	1.9×10^{-4}	1.9×10^{-4}	8.85	3.72	2.3×10^{-4}

* Amorphous powder.

of NaOH was calculated, taking into account the ionic strength of the solution and the formation of mononuclear hydroxo complexes, from reference data [11], and that for iron(II), cobalt(II), and copper(II), from the data of [12] by the generalized equation

$$s = c_M = \frac{K_s^0}{f_{M^{2+}} f_{OH^-}^2} \sum_{i=0}^{n} \beta_i [OH^-]^{i-2}.$$

Here, the constant K_s^0 characterizes the heterogeneous chemical equilibrium (2); $f_{M^{2+}}$, f_{OH^-}, molar activity coefficients of M^{2+} and OH^- ions; and $\beta_0 = 1$, β_1, β_2, β_3, β_4, general stability constants of the hydroxo complexes MOH^+, $M(OH)_2$, $M(OH)_3^-$, and $M(OH)_4^{2-}$ [average values $\beta_1 = 2.4 \times 10^6$, $\beta_2 = 4.2 \times 10^{10}$, and $\beta_3 = 7.9 \times 10^{13}$ were taken for lead(II)]. The molar solubility of MO in a 1 M solution of NaOH was calculated using a simplified formula, $s = 1.06 K_s^0 \Sigma \beta_i$.

The equilibrium concentration of free OH^- anions and the pH^0 value of saturated solutions of oxides in pure water (indicated by arrows in the figure) were found by solving a system of, as a rule, three equations [1], using Cardano's method for a reduced cubic equation. For the oxides SnO, PbO, and CuO, a system of four equations was solved with account of the formation of, respectively, the $Sn(OH)_3^-$, $Pb(OH)_3^-$ [11], and $Cu_2(OH)_2^{2+}$ complexes [12].

The heterogeneous reaction MO(s) + H_2O(l) = $M(OH)_2$(s) does not proceed to any noticeable extent in standard conditions [3–6] for the MO oxides under consideration (ΔG_{298}^0 varies from –18 kJ mol^{-1} for MnO to +10 kJ mol^{-1} for CuO, in contrast to the ionic oxides CaO, SrO, and BaO, for which ΔG_{298}^0 of the reaction mentioned above is in the range from –58 to –64 kJ mol^{-1}). For this reason, formation of solid hydroxides $M(OH)_2$ was disregarded in the calculations. The contribution from neutral $M(OH)_2$ complexes to the molar solubility in pure water ranges from 0.2% for FeO to 99% for HgO.

The results of the calculations are listed in Table 1, in which $pK_s^0 = -\log K_s^0$; s^0, total molar solubility of solid oxides in water; and $[M(OH)_2]$, equilibrium molarity of neutral complexes in aqueous solutions of oxides at 25°C.

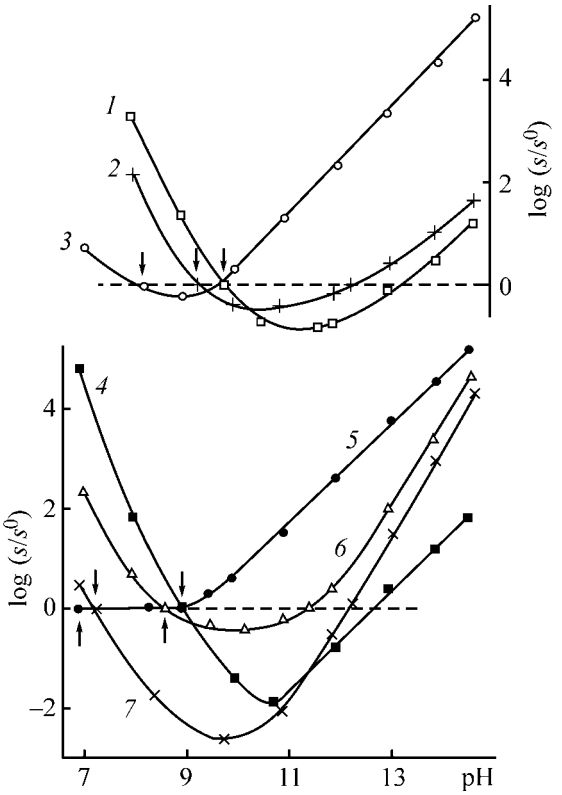
It can be seen from Table 1 that there is a satisfactory agreement between the pK_s^0 values calculated in this study and taken from [13]. For a number of oxides, K_s^0 was calculated for the first time. The solubility of amorphous oxides, as well as that of amorphous hydroxides [1, 2], is higher than that of crystal-

line modifications. The solubility (Table 1) and chemical activity of finely dispersed yellow α-modification of HgO markedly exceeds that of the red crystalline modification β-HgO having a more ordered rhombic structure [4–6]. The experimental values of the solubility in pure water at 25°C are as follows: 2.4×10^{-4} and 2.3×10^{-4} M for α-HgO and β-HgO, respectively [7]; $\sim 3 \times 10^{-5}$ and $\sim 6 \times 10^{-5}$ M for α-PbO and β-PbO [4]; and 4×10^{-5} M for CoO [6].

Calculation of the average ligand number $\bar{n}$ in hydroxo complexes (Bjørrum function) at pH 15 gives values in the range 2.5–4 for all the oxides in Table 1, which indicates that the amphoterism condition $\bar{n} > 2$ is satisfied for these oxides, in contrast to basic oxides MgO, CaO, SrO, and BaO ($\bar{n} < 2$). The minimum solubility of oxides MO is observed at the optimal concentration of OH^- ions, for which the mole fraction of neutral complexes $M(OH)_2$ in the alkaline solution is the highest. This condition was used to find, as it was done in [1], pH_{opt} and then s_{min}. The values of $ps_{min} = -\log s_{min}$ at 25°C are listed in Table 1. The figure shows a strong (85- and 500-fold) negative effect of common OH^- ions on the solubility of, respectively, FeO and CuO oxides in the alkali (curves *4* and *7*). For SnO, similarly to HgO [1] and $Sn(OH)_2$ [2], the effect of common OH^- ions is virtually zero (see figure, curve *5*). The figure shows on the logarithmic scale dependences of the ratio of molar solubilities of a number of oxides in an alkaline medium and pure water on the pH value of the medium at 25°C.

A comparative evaluation of the amphoterism of the oxides was based on the ratio ($A > 1$) of their molar solubilities in an alkaline medium with pH 14.7 (5 M NaOH solution) and in pure water. As follows from the data in Table 2, the amphoterism parameter A of stable crystalline oxides MO decreases as the element M replaced in the order Be → Sn → Zn → Cu → Pb → Ni → Mn → Fe ≈ Co → Cd → Hg. This series mainly differs from that established for hydroxides $M(OH)_2$ [2] in the position of Be and Pb, which is due to the low value of s^0 for the polymeric oxide BeO, compared with s^0 for PbO (Table 1). The amphoterism parameter A of amorphous oxides ZnO (4.5×10^4), CuO (3.9×10^4), and CdO (77) markedly exceeds that for crystalline modifications (Table 2). The amphoterism parameter and molar solubility of stable oxides MO (except ZnO, α-SnO, and CuO) markedly exceed the corresponding values for stable hydroxides $M(OH)_2$ [1, 2].

The molar solubility of stable crystalline oxides in a 5 M NaOH solution at 25°C decreases in the order



Ratio of molar solubilities in an aqueous-alkaline medium (s) and in pure water (s^0) vs. the pH value of the medium at 25°C. Oxide: (*1*) CdO, (*2*) α-CoO, (*3*) α-BeO, (*4*) FeO, (*5*) α-SnO, (*6*) ZnO, and (*7*) CuO.

α-BeO → MnO → α-SnO → ZnO → α-PbO → CuO → α-NiO–CdO → α-CoO → FeO ≈ β-HgO from 0.51 M for α-BeO to 3×10^{-4} M for FeO and β-HgO. The solubility of the oxides, beginning with CuO,

Table 2. Amphoterism parameters of stable crystalline oxides in aqueous media at 25°C

Oxide	A	pH_b	B	C_b	C_a
α-BeO	2.2×10^5	9.6	1.5	1.1	0.65
α-SnO	1.47×10^5	7.5	0.5	1.0	0.45
ZnO	4×10^4	11.5	2.8	1.4	1.5
CuO	1.5×10^4	12.3	5.0	1.6	1.1
α-PbO	3.4×10^3	10.8	1.3	0.9	1.2
α-NiO	3.1×10^2	11.9	3.0	0.88	1.9
MnO	2.8×10^2	12.6	1.6	1.1	1.8
FeO	55	12.8	3.8	0.93	1.9
α-CoO	48	12.3	3.1	0.70	1.7
CdO	33	13.0	3.2	0.87	1.8
β-HgO	1.6 [1]	~13	~6	0.04	~0.3

* Parameters: $A = s(\text{pH } 14.7)/s^0$, pH_b at $s_b = s^0$, $B = pH_b - pH^0$, $C_b = |\Delta ps_b/\Delta pH|$, $C_a = \Delta ps_a/\Delta pH$.

Table 3. Thermodynamic constants of heterogeneous equilibria for stable crystalline oxides in water [(1)–(5)] and in alkaline [(6), (7)] and acid [(8), (9)] media

Oxide	pK_{298} values for indicated equilibria								
	(1)	(2)	(3)	(4)	(5)	(6)	(7)	(8)	(9)
α-BeO	10.91	20.37	15.8	27.5	5.35	1.8	–0.51	–2.90	–7.60
α-SnO	16.09	26.65	14.76	–	5.76	0.77	–	2.10	–1.29
α-PbO	9.04	15.29	15.27	–	4.47	1.28	–	–4.95	–12.73
MnO	6.13	9.54	15.73	–	3.76	1.74	–	–7.86	–18.45
FeO	10.89	15.38	19.38	–	7.99	5.39	–	–3.10	–12.57
α-CoO	10.26	14.74	–	–	5.42	–	–	–3.73	–13.31
α-NiO	11.25	15.51	–	–	6.38	–	–	–2.74	–12.49
CuO	14.56	20.58	19.21	32.33	8.88	5.22	4.35	0.57	–7.35
ZnO	11.80	16.82	17.3	29.53	5.75	3.26	1.55	–2.19	–11.15
CdO	9.09	12.99	17.43	–	5.37	3.44	–	–4.89	–14.98
β-HgO	14.96	25.55	18.53	–	3.74	4.54	–	0.97	–2.43

under the conditions specified does not exceed 0.12 g l^{-1}. Raising the solubility requires heating in more concentrated alkaline solutions and, in the case of the readily oxidized oxides, FeO, MnO, and CoO, also the presence of a reducing atmosphere [5, 6]. Despite the high value of the basic amphoterism parameter A, the solubility of the oxides CuO and α-NiO in a 5 M NaOH solution is low (1.5×10^{-3} M) because of the low values of s^0 and s_{min} (Table 1) and influence of other parameters (Table 2) supplementing the characterization of the amphoterism of the oxides. Table 2 lists, in addition to the amphoterism parameter A, also the pH_b values at which the negative effect of common OH^- ions is completely compensated for upon addition of NaOH by the positive contribution of hydroxo complexes to the solubility of oxides ($s_b = s^0$). The lower the pH_b value, the smaller the amounts of the alkali added and its concentrations necessary for the solubility of an oxide to increase, compared with that in pure water. The lowest pH_b values were observed for the amphoteric oxides α-SnO and α-BeO, which also have the highest values of parameter A, and the highest pH_b values, for CdO and HgO with weak manifestation of amphoterism (Table 2). Parameter B, equal to ($pH_b - pH^0$) determines the range of pH values in which $s < s^0$ is the lowest for α-SnO and the highest for CuO and HgO (see figure and Table 2). Parameters C_b and C_a, equal to $|\Delta ps_b/\Delta pH|$ and $\Delta ps_a/\Delta pH$, respectively, characterize the rate at which the solubility increases as the pH value is varied upon addition of NaOH ($pH > pH_b$) or $HClO_4$ ($pH < pH^0$). The amphoteric oxides SnO, ZnO, PbO, and BeO, which have increased values of parameter C_b and low pH_b, dissolve to a noticeable extent even in 1–2 M NaOH [3, 5]. By contrast, the oxides NiO, FeO, CoO, and CdO, which have high values of parameter C_a, readily dissolve in acids [3–5], but very difficultly and in small amounts in highly concentrated alkalis [3, 5, 6].

Similarly to hydroxides [2], amphoteric oxides with chemical bonds close in ionicity [1] to the O–H bond can shift the equilibrium of water ionization and add hydroxide ions or protons in aqueous media to give the corresponding ions. Therefore, the comparative characterization of the acid-base properties of the stable crystalline oxides was supplemented with a calculation of thermodynamic parameters, ΔG^0_{298} and pK_{298} (K equilibrium constant), for heterogeneous reactions in a saturated aqueous solution:

$$MO(c) + H_2O(l) \rightleftarrows MOH^+(s) + OH^-(s), \quad (1)$$

$$MO(c) + H_2O(l) \rightleftarrows M^{2+}(s) + 2OH^-(s), \quad (2)$$

$$MO(c) + H_2O(l) \rightleftarrows H^+(s) + HMO_2^-(s), \quad (3)$$

$$MO(c) + H_2O(l) \rightleftarrows 2H^+(s) + MO_2^{2-}(s), \quad (4)$$

$$MO(c) + H_2O(l) \rightleftarrows M(OH)_2(s). \quad (5)$$

The results obtained in calculation of pK_{298}, based on the data of [7–12], are listed in Table 3, whence follows that, with the exception of α-SnO [the constant of equilibrium (3) exceeds that of equilibrium (1)], the basic properties of the amphoteric oxides MO dominate over the acid properties. The same

conclusion follows from a calculation of pK_{298} for chemical equilibria in alkaline and acid media:

$$MO(c) + OH^-(s) \rightleftarrows HMO_2^-(s), \quad (6)$$

$$MO(c) + 2OH^-(s) \rightleftarrows MO_2^{2-}(s) + H_2O(l), \quad (7)$$

$$MO(c) + H^+(s) \rightleftarrows MOH^+(s), \quad (8)$$

$$MO(c) + 2H^+(s) \rightleftarrows M^{2+}(s) + H_2O(l). \quad (9)$$

It can be seen from Table 3 that SnO, PbO, BeO, and ZnO are best soluble in alkalis, and MnO, CdO, PbO, and CoO, in acids. According to equilibrium (5), formation of neutral complexes $M(OH)_2$ in dissolution of solid oxides in water is the most probable for HgO and the least so for CuO, FeO, and NiO.

CONCLUSIONS

(1) The thermodynamic method was used to calculate, taking into account the formation of hydroxo complexes, the effect of the pH value of the aqueous-alkaline nonoxidizing medium on the molar solubility at 25°C of solid oxides MO, where M is Be, Sn, Pb, Cd, Hg, and 3*d* elements Mn–Zn.

(2) It was found that the amphoterism condition (average ligand number in hydroxo complexes $\bar{n} > 2$ at pH 14–15) is satisfied for the oxides studied and their amphoterism is evaluated (parameter *A* increases from 1.6 for HgO to 2.2×10^5 for BeO).

(3) It was shown that the solubility in aqueous media and the amphoterism parameter *A* of the oxides decreases on passing from an amorphous to a stable crystalline modification. The molar solubility and amphoterism parameter of stable oxides MO, except ZnO, α-SnO, and CuO, substantially exceed those of stables hydroxides $M(OH)_2$.

(4) A calculation of the thermodynamic constant of heterogeneous acid-base equilibria in aqueous media for stable crystalline oxides MO demonstrated that the basic properties predominate and are the most pronounced in MnO, CdO, and FeO and the weakest in HgO. Only in SnO, similarly to $Sn(OH)_2$ [2], weak acid properties predominate over weak basic properties.

REFERENCES

1. Shkol'nikov, E.V., *Zh. Prikl. Khim.*, 2004, vol. 77, no. 8, pp. 1271–1274.
2. Shkol'nikov, E.V., *Zh. Prikl. Khim.*, 2005, vol. 78, no. 11, pp. 1819–1823.
3. Nekrasov, B.V., *Osnovy obshchei khimii* (Principles of General Chemistry), St. Petersburg, 2003, vols. 1, 2.
4. Remy, H., *Treatise on Inorganic Chemistry*, Amsterdam: Elsevier, 1956, vols. 1, 2.
5. Akhmetov, N.S., *Obshchaya i neorganicheskaya khimiya* (General and Inorganic Chemistry), Moscow: Vysshaya Shkola, 1988.
6. *Khimicheskaya entsiklopediya* (Chemical Encyclopedia), Knunyants, I.L. and Zefirov, N.S., Eds., Moscow: Bol'shaya Rossiiskaya Entsiklopediya, 1988–1998, vols. 1–5.
7. Efimov, A.I., et al., *Svoistva neorganicheskikh soedinenii: Spravochnik* (Properties of Inorganic Compounds: Reference Book), Leningrad: Khimiya, 1983.
8. Vasil'ev, V.P., *Termodinamicheskie svoistva rastvorov elektrolitov* (Thermodynamic Properties of Electrolyte Solutions), Moscow: Vysshaya Shkola, 1982.
9. Karapet'yants, M.Kh. and Karapet'yants, M.L., *Osnovnye termodinamicheskie konstanty neorganicheskikh i organicheskikh veshchestv* (Principal Thermodynamic Constants of Inorganic and Organic Substances), Moscow: Khimiya, 1968.
10. *Termodinamicheskie svoistva individual'nykh veshchestv* (Thermodynamic Properties of Individual Substances), Glushko, V.P., Ed., Moscow: Nauka, 1979–1981, vols. 1–4.
11. Lur'e, Yu.Yu., *Spravochnik po analiticheskoi khimii* (Handbook of Analytical Chemistry), Moscow: Khimiya, 1989.
12. Fishtik, I.F. and Vataman, I.I., *Termodinamika gidroliza ionov metallov* (Thermodynamics of Hydrolysis of Metal Ions), Kishinev: Shtiintsa, 1988.
13. Kumok, V.N., Kuleshova, O.M., and Karabin, L.A., *Proizvedeniya rastvorimosti* (Solubility Products), Novosibirsk: Nauka, 1983.

ISSN 1070-4272, Russian Journal of Applied Chemistry, 2006, Vol. 79, No. 12, pp. 1924–1929. © Pleiades Publishing, Inc., 2006.
Original Russian Text © Yu.G. Tselishchev, V.A. Val'tsifer, O.G. Vasil'eva, 2006, published in Zhurnal Prikladnoi Khimii, 2006, Vol. 79, No. 12, pp. 1947–1952.

PHYSICOCHEMICAL STUDIES OF SYSTEMS AND PROCESSES

Capillary Moisture Content of a Number of Powders of Varied Nature

Yu. G. Tselishchev, V. A. Val'tsifer, and O. G. Vasil'eva

Institute of Technical Chemistry, Ural Division, Russian Academy of Sciences, Perm, Russia

Received April 21, 2006; in final form, September 2006

Abstract—The moisture content of a number of powders of varied nature, kept in a medium with 100% humidity, was studied. The volume of capillary fluid "bridges" between particles of powdered materials was evaluated.

DOI: 10.1134/S1070427206120032

Storage and processing of a powder under real conditions are accompanied by its moistening via adsorption of water vapor from the ambience onto the surface of particles and its capillary condensation in pores of the material. These processes lead to formation of fluid "bridges" between powder particles and give rise to capillary forces between the particles [1–5], which strongly affect the properties of powders and dispersed formulations based on these powders. The amount of moisture absorbed by a powder depends on various parameters of the material and ambience, size and shape of particles, their wettability, "free volume" of the powdered material, ambient temperature and humidity, etc.

The aim of this study was to evaluate the amount of moisture absorbed by powders of varied nature as a manifestation of their capillary properties and, in particular, capillary condensation of water vapor from the humid ambience in pores of the material and the contribution to the water content from the volume of fluid bridges between particles of powdered materials. In solving the problem formulated above, we used a previously developed calculation model for determining the capillary forces between powder particles [6–8], which also makes it possible to find the amount of capillary moisture in fluid bridges between the particles.

It is known that capillary forces occur in any powder in its storage in a humid medium [1–4]. These forces are generated under the action of capillary condensation of water vapor in the spaces between particles, described by the Kelvin equation. The fluid condensed between the particles takes the form of a bridge with a meniscus (Fig. 1) curved by the interaction between fluid molecules with one another and with dispersed particles, with an additional pressure ΔP created in the fluid. According to the Laplace equation, this pressure is given by

$$\Delta P = \sigma(1/r_1 + 1/r_2), \quad (1)$$

where σ is the surface energy (tension) of the fluid at the phase boundary; r_1 and r_2, curvature radii of the principal mutually perpendicular sections of the fluid surface.

The dependences obtained for calculating the capillary forces and its components in the general form are as follows

$$F_c = F_{c1} + F_{c2} = f(D_p, \theta, \sigma, h, \alpha, C, \Phi_p), \quad (2)$$

where F_c, F_{c1}, F_{c2} are the capillary force and its components, caused by the surface tension of the fluid

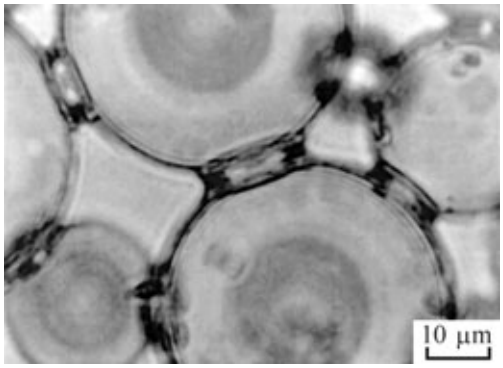


Fig. 1. Micrograph of glass microspheres with fluid bridges between particles.

Table 1. Geometrical and physical parameters of powders

Material	Particle size, μm	Particle shape	Contact angle, deg	Free volume		Coordination number of particles
				bulk	densified	
A-380 aerosil	0.005–0.040	Nearly spherical	58	0.97	0.91	1
MG	30–50	Spherical	49	0.57	0.46	6
MPh	20–40	"	61	0.6	0.47	6
ASD-4 aluminum	1–10	"	65	0.72	0.54	5
TiO_2	0.2–1	Grainy	55	0.79	0.67	4
ZnO	0.5–2	"	48	0.94	0.77	3
MgO	0.2–0.5	"	39	0.94	0.78	3

* For the free volume of a densified powder.

and the Laplace pressure; D_p, particle size; θ, angle of contact between the fluid and particle surface; h, distance between particles; α_f, angle characterizing the fluid volume V_f in a bridge; C, coordination number; and Φ_p, particle shape.

The results of our microscopic studies make it possible to approximate the meniscus of the fluid bridge by a circular arc of radius r [8]. With account of this circumstance, the fluid volume enclosed between particles is defined as a volume of a figure produced in revolution of a circular arc of radius r, minus the volume of particles immersed in the fluid:

$$V_f = 2\pi \int_{y_1}^{y_2} [f(y)]^2 dy - V_c, \quad (3)$$

where $f(y)$ is the equation describing the curve forming the surface of revolution; y_1 and y_2, integration limits defined as the ordinates of the lower and upper points of the perimeters of particle wetting by the fluid; and V_c, volume of particles submerged in the fluid.

If there is no mass exchange of fluid between the medium and the "bridge," then, in accordance with the Kelvin equation, we obtain

$$\Delta P = \frac{\ln(p_1/p_2)\rho_f R_g T}{2M}, \quad (4)$$

where p_1 and p_2 are the saturated vapor pressures of the fluid over curved and planar surfaces, respectively; ρ_f, fluid density; R_g, universal gas constant; T, temperature; and M, molecular weight of the fluid.

Solving Eqs. (1)–(4) by numerical methods, we obtain the capillary pressure, capillary forces, and volume of the fluid bridge with account of various particle parameters. The calculations demonstrated that the region in which the model we suggested is valid is restricted to a certain limiting volume of the fluid ($V_{f.\,max}$ or $\alpha_{f.\,max}$) [6], on exceeding which the neighboring bridges between contacting particles merge.

EXPERIMENTAL

The experimental amount of moisture absorbed was determined for powders differing in the nature of the solid phase and in the particle size and shape. We also examined the following materials: aerosil of A-380 brand; finely dispersed oxides of titanium (anatase), zinc, and magnesium (light magnesia); aluminum of ASD-4 brand; and hollow glass (MG) and phenol-formaldehyde (MPh) microspheres. The values of the parameters characterizing the powdered materials under study are listed in Table 1.

Preliminarily dried powder samples were placed in desiccators with a certain humidity set with saturated aqueous solutions of various salts and were kept there until an equilibrium state was attained. The gain in the mass of the powdered materials depended not only on the adsorption of moisture on the samples and its capillary condensation, but also on the possible chemical interaction of the material of particles with moisture and gaseous components of the ambience. Therefore, we also evaluated the contribution of the capillary component to the overall increase in the powder mass. The study was performed at the following relative air humidities: 31, 84, 98, and 100%.

According to the experimental data, the powder mass increases to the greatest extent at high, nearly

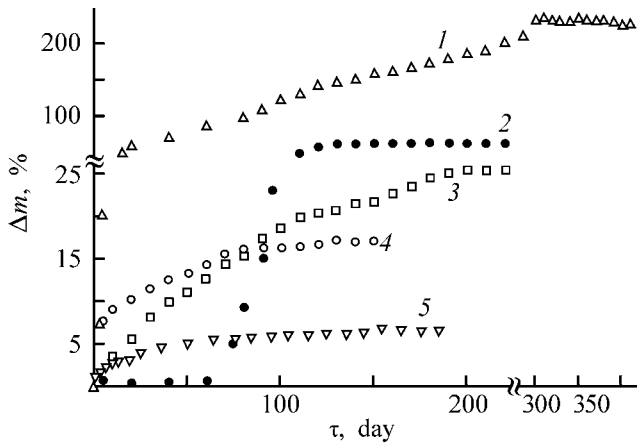


Fig. 2. Mass gain Δm by various powdered materials vs. the time τ of their residence in a humid medium (relative humidity 100%). (*1*) A-380 aerosil, (*2*) ASD-4 aluminum, (*3*, *4*) glass and phenol-formaldehyde microspheres, and (*5*) titanium oxide.

100%, relative humidities of the medium. This is in a qualitative agreement with the results of calculations by the previously obtained dependences and by Eqs. (1)–(4) for determining the volume of the fluid bridge between powder particles. In accordance with these results, further studies of the moisture content of the powders, including the capillary content, were carried out for the maximum relative humidity of the medium, 100%. The dynamics of mass gain by the materials under study is illustrated by Fig. 2.

It can be seen that the equilibrium values of the mass gain by the powders, as also the time in which these values are reached, strongly vary with the material of powder particles. According to the data obtained, the highest rate of mass gain by the majority of powdered materials is observed in the initial stage, whose duration does not exceed several days. The equilibrium state is reached by the powder mass during a significantly longer time.

The distinctive run of the curve describing the moistening of the ASD-4 aluminum powder is probably due to the influence of the oxide film on the particle surface. In this case, the initial stage of moistening is governed by the large contact angle between the oxide film and water and corresponds to a low moistening of the material, and further stages are determined by the gradual disintegration of the oxide film, which leads to a steep rise in the powder mass because of the chemical interaction between aluminum and water. Figure 2 does not show data for powders of zinc and magnesium oxides, for which the chemical interaction of the particle material with moisture and gaseous components of the ambience is, according the data of [9, 10] and results of thermogravimetric measurements, the key factor in the mass gain by the powders. Nevertheless, it is beyond any doubt that these powders also contain a certain amount of capillary-bound water, which depends on the relation between rates of adsorption and capillary condensation of moisture, on the one hand, and those of chemical reactions, on the other.

It can be seen from Fig. 2 that the highest absorption capacity (229%) is observed for A-380 aerosil, which is mainly determined by the large adsorption surface area of the material (380 $m^2 g^{-1}$). In addition, the nearly spherical shape of the contacting particles favors formation of small pores between the particles, and, according the Kelvin equation, a greater amount of capillary condensation of moisture vapor is observed in these pores. This assumption is confirmed by the results obtained by Ur'ev [11], who, in particular, studied the effect of the particle size on the structuring of dispersed materials. The rather large amount of moisture absorbed by microspheres (MG and MPh) is due to the low density of hollow particles (300 kg m^{-3}). The absolute amounts of moisture absorbed by microspheres and titanium oxide can be considered rather close if we take into account their relative densities (300 and 3700 kg m^{-3}) and insignificantly differing contact angles.

Moisture adsorbed by a powder is initially concentrated in spaces between contacting particles and forms fluid bridges. Here, we mean by the contact between particles not only direct contact of their surfaces, but also their arrangement at a certain distance from one another, which, however, does not lead to disintegration of the fluid bridge [6]. As small bridges between particles are formed, the fluid starts to fill coarser pores and voids in the powder, the volume of the fluid (or α_f) starts to exceed $V_{f.\,max}$ ($\alpha_{f.\,max}$), and this process may occur during a long time. The large amounts of moisture absorbed by these powders can be only understood if we take into account the decisive contribution of the capillary condensation of water vapor in spaces between particles and within pores of the material to its overall moisture content. To verify this assumption, we carried out thermogravimetric and differential-thermal studies of powders and, in particular, determined the relationship between the temperature *T*, changes in mass (thermogravimetry, TG), rate of changes in mass (differential thermogravimetry, DTG), and differential-thermal changes (differential-thermal analysis, DTA) in the samples on an MOM Q-1500D derivatograph (Hungary). The TG and DTA

Table 2. Moisture content parameters of powders

Material	Change in sample mass, %		Calculated moisture mass, %	
	in moistening	in desorption (T = 150°C)	in capillary bridges	pore filling***
A-380 aerosil	201 (229)*	197 (98)**	21.2	480–1540
MG	25.5	19.9 (78)**	6.3	280–440
MPh	17	12 (70)	3.9	330–560
ASD-4 aluminum	65	11 (17)	2.1	43–95
TiO_2	2.5 (6.6)	1.5 (60)	1.9	55–100
ZnO	18 (60)	9 (50)	3.0	60–275
MgO	115	29 (25)	13.9	100–438

* Steady-state values of the mass gain by the samples in a humid medium, provided that their equilibrium values were not attained during thermogravimetric studies.

** Decrease in the sample mass relative to the amount of absorbed substances.

*** Amount of moisture needed to fill pores in a powder upon a change in its free volume from that of a densified powder to that of a bulk material (Table 1).

curves of humid powders composed of A-380 aerosil and glass microspheres are shown in Fig. 3.

These curves were obtained in the dynamic mode at a low sample heating rate of 2.5 deg min^{-1}. The TG and DTA curves for phenol-formaldehyde spheres are qualitatively similar to those for glass microspheres and are not shown for this reason. To compare the amounts of moisture sorbed and desorbed by the powders, the values of these parameters were determined relative to the mass of dry materials. The experimental data in Table 2 characterize the mass gain (loss) by the powders as a result of absorption (desorption) of not only moisture as the main component responsible for changes in the mass of most of the samples studied, but also, as a rule, of minor amounts of other components contained in the humid ambience. It was found that aerosil loses 98% of moisture it absorbed, on being heated to 150°C, and 99% at 300°C. For glass microspheres, the loss of moisture at these temperatures is 78 and 90%, respectively. The loss of capillary moisture by phenol-formaldehyde microspheres is somewhat lower, 70% at 150°C. On further heating, a loss of mass is also observed, which starts to be determined by thermal destruction of the material of the particles as 255°C is reached (Fig. 4). An indication of the moisture loss by the samples is the endothermic peak at temperatures close to 100°C, well-pronounced in the DTA curves.

Most of the other samples studied also show a characteristic strong decrease in mass on reaching temperatures of 100°C and more (Fig. 4). It can be seen that the TG curves of the samples represented in the figure are more intricate than those in Fig. 3. To refine the run of the dependences and the manner in which

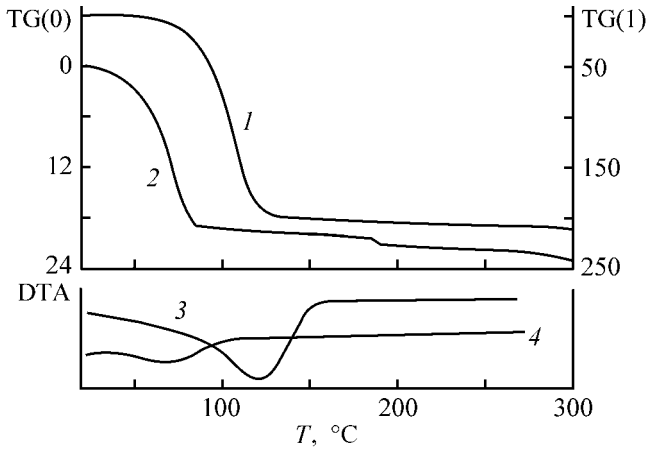


Fig. 3. TG and DTA curves for humid powders. (TG) Change in powder mass and (T) temperature; the same for Fig. 4. Powder: (*1*, *3*) A-380 aerosil and (*2*, *4*) glass microspheres.

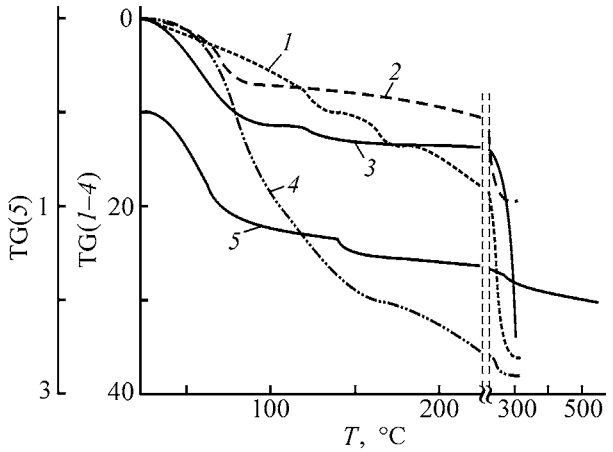


Fig. 4. TG curves for humid powders. Powder: (*1*) ASD-4 aluminum, (*2*, *4*, *5*) zinc, magnesium, and titanium oxides; and (*3*) phenol-formaldehyde microspheres.

the sample mass changes, we carried out additional TG experiments under quasi-isothermal conditions, which provide a higher selectivity of the reactions accompanied by changes in sample mass. The data obtained confirmed the type of the TG curves for all the samples represented in Figs. 3, 4.

The multiple-step run of the TG curves in Fig. 4 has different explanations for different samples. For example, the mass loss of 17% relative to the amount of moisture absorbed by the ASD-4 aluminum powder at temperatures below 150°C (Table 2) is mostly due to loss by the sample of physically adsorbed moisture and capillary moisture. The portions of mass loss at higher temperatures are associated with the loss of water molecules by aluminum hydroxides and, further, with the formation of aluminum oxide, which is confirmed by the data of [10, 11].

For humid MgO and ZnO powders, the multiple-step run of the TG curves is accounted for not only by the processes listed above, but also by transformations under the action of high temperatures of other chemical compounds: hydroxides and carbonates formed in these materials when they are kept in a humid medium [10–12].

The run of the TG curve of powdered titanium oxide, which is chemically inert toward the components of a natural humid ambience, is affected by another factor. Although a greater amount of moisture absorbed by the powder is evaporated or desorbed below 130°C (Fig. 4, Table 2), the remaining amount of water in the powder is still rather significant (40%). This is possibly due to the fact that a titanium oxide pigment was chosen for the study as a nontoxic material widely used in various industries, which, however, contains various, including water-soluble, impurities. These impurities, which find their way into the product from raw materials, are formed as by-products in synthesis, and are specially introduced into the material in manufacture to impart to it necessary properties [12–17], affect its adsorption-desorption properties. This assumption is also applicable, to a certain approximation, to other powders under study: zinc and magnesium oxides. However, revealing the composition of frequently insignificant admixtures in the powders under consideration and determining the properties of these admixtures, their effect, and mechanisms of formation and decomposition of the supposed compounds is beyond the scope of our study and cannot affect its main conclusions.

According to the experimental data in Table 2 and Figs. 3 and 4, the fraction of the capillary-bound water exceeds, for most of the samples, 50% of the amount of moisture and other components of the humid ambience, absorbed by the samples. We estimated by calculation the amount of moisture capillary-condensed in fluid bridges between particles (Table 2). The calculation was based on the data from Table 1 and on theoretical relations [6–8] and Eqs. (1)–(4) for determining the volume of a fluid bridge. It can be seen that, for all the samples, the calculated amounts of the capillary moisture contained in the bridges are lower than the corresponding experimental values. This discrepancy can be explained in several ways. The most important of these is that moisture is condensed in a powdered material not only in narrow spaces between contacting particles to form fluid bridges, which is accounted for by the calculational model we developed ($V_f \le V_{f.\,max}$), but also in the free volume of the powder, which includes coarser pores and voids and may reach considerable values. A substantial amount of moisture is also accumulated within agglomerates formed in a moisture-containing powder. This assumption is in an agreement with the results of [18–22]. It was also shown in [21, 22] that larger agglomerates have a higher porosity, compared with smaller agglomerates. Consequently, powders with higher porosity contain a greater amount of large particle agglomerates and, accordingly, a greater amount of moisture bound within these agglomerates.

We also estimated the amount of moisture necessary for complete filling of pores in a powder. The calculated ranges of variation of the moisture content with the experimentally determined free volume of the powder (Table 1) changing from a densified to a bulk powder are listed in Table 2. It can be seen that the amount of adsorbed and capillary-bound moisture in the powders is considerably smaller than our calculated values, which are, to be sure, rather specific and approximate parameters for the moisture forms in the powders, analyzed here. If, however, we only qualitatively explain the essence of the phenomena we observed, these data can characterize, to a certain approximation, the adsorption and capillary properties of the powders under study.

A next, though less significant explanation of the discrepancy between the calculated and experimental values is that the moisture adsorbed by the powder is originally concentrated on the particle surface to form polymolecular layers of the fluid [18, 19, 23]. The amount of this moisture is commonly small, compared with that of the capillary condensate. However, it can substantially increase at a higher dispersity of powder particles (e.g., for nanoparticles) and the accordingly larger specific surface area of the material.

The fraction of the forms of bound moisture under consideration, of adsorbed and capillary types, is the greater, the larger the free volume of the material, the higher the air humidity and particle dispersity, and the better their wettability. The effect of these factors on the powder properties is the most clearly manifested for A-38 aerosil.

Our study revealed that the method we suggested for calculating the amount of capillary fluid in a powdered material cannot be used to find the absolute amount of the capillary moisture in the powder because it is difficult to determine the shape and size of pores in the material and the type of contact between its particles. To solve this problem, it is necessary to carry out additional studies with a comprehensive account of the relationship between various parameters of powdered materials and of the ambient medium. The calculation method can qualitatively estimate the effect of certain parameters of particles and the ambience, such as dispersity of particles and their contact angle, humidity of the ambience, and free volume of the powder, on its capillary moisture content.

CONCLUSIONS

It was shown that the amount of moisture adsorbed by the powders under study from the ambience at its high humidity and capillary-bound in fluid bridges between contacting particles is considerably smaller than the amount of capillary moisture contained in pores of the material.

REFERENCES

1. Zimon, A.D. and Andrianov, E.I., *Autogeziya sypuchikh materialov* (Autohesion of Bulk Materials), Moscow: Metallurgiya, 1978.
2. Kel'tsev, N.V., *Osnovy adsorbtsionnoi tekhniki* (Principles of Adsorption Technology), Moscow: Khimiya, 1984.
3. Fuji, M., Machida, K., Watanabe, T., and Chikazawa, M., *World Congress on Particle Technology 3, July 6–9, 1998*, Brighton, UK, CD-ROM published, 65.
4. Wensik, E.J.W., Hoffmann, A.C., and Apol, M.E.F., *World Congress on Particle Technology 3, July 6–9, 1998*, Brighton, UK, CD-ROM published, 64.
5. Xu, L., Lio, A., Hu, J., et al., *J. Phys. Chem.*, 1998, vol. 102, no. 3, pp. 540–548.
6. Tselishchev, Yu.G. and Val'tsifer, V.A., *Khim. Fiz. Mezoskopiya*, 1999, vol. 1, no. 1, pp. 14–21.
7. Tselishchev, Yu.G., Val'tsifer, V.A., and Klyachkin, Yu.S., *Kompozitsionnye materialy na osnove dispersnykh chastits* (Composites Based on Diaspersed Particles), Yekaterinburg: Ural. Otd. Ross. Akad. Nauk, 1994, pp. 83–87.
8. Tselishchev, Yu.G. and Val'tsifer, V.A., *Kolloid. Zh.*, 2003, vol. 65, no. 3, pp. 418–423.
9. *Spravochnik khimika* (Chemist's Handbook), Nikol'skii, B.P., Ed., Leningrad: Khimiya, 1971, vol. 2.
10. *Khimicheskaya entsiklopediya* (Chemical Encyclopedia), Knunyants, I.L., Ed., Moscow: Bol'shaya Ross. Entsiklopediya, 1992, vol. 3.
11. Ur'ev, N.B., *Vysokokontsentrirovannye dispersnye sistemy* (Highly Concentrated Disperse Systems), Moscow: Khimiya, 1980.
12. Orlova, O.V. and Fomicheva, T.N., *Tekhnologiya lakov i krasok* (Technology of Lacquers and Paints), Moscow: Khimiya, 1990.
13. *Entsiklopediya polimerov* (Encyclopedia of Polymers), Kabanov, V.A., Ed., Moscow: Sov. Entsiklopediya, 1974, vol. 2.
14. Khazin, L.G., *Dvuokis' titana* (Titanium Dioide), Leningrad: Khimiya, 1970.
15. Livshits, M.L. and Pshiyalkovskii, B.I., *Lakokrasochnye materialy* (Paint-and-Varnish Materials), Moscow: Khimiya, 1982.
16. Verzhbitskii, F.R., *Vysokochastotno-termicheskii analiz* (High-Frequency-Thermal Analysis), Irkutsk: Irkutsk. Univ., 1986.
17. *Svyaznaya voda v dispersnykh sistemakh* (Bound Water in Disperse Systems), Kiselev, V.F. et al., Eds., Moscow: Mosk. Gos. Univ., 1970, issue 1.
18. Karnaukhov, A.P., in *Metody issledovaniya struktury vysokodispersnykh i poristykh tel* (Methods for Structural Studies of Highly Dispersed and Porous Bodies), Moscow: Akad. Nauk SSSR, 1958, pp. 71–85.
19. Isirikyan, A.A., in *Metody issledovaniya struktury vysokodispersnykh i poristykh tel* (Methods for Structural Studies of Highly Dispersed and Porous Bodies), Moscow: Akad. Nauk SSSR, 1958, pp. 85–96.
20. Pertsov, V.T. and Shmit'ko, E.I., *Izv. Vyssh. Uchebn. Zaved., Stroit. Arkhitektura*, 1997, no. 6, pp. 45–49.
21. Bruder, M.L., Koumarioyi, I., and Gargio–Rubio, L.H., *World Congress on Particle Technology 3, July 6–9, 1998*, Brighton, UK, CD-ROM published, 16.
22. Fedors, R.F. and Landel, R.F., *Powder Technol.*, 1979, vol. 23, no. 2, pp. 219–223.
23. Radushkevich, L.V., in *Metody issledovaniya struktury vysokodispersnykh i poristykh tel* (Methods for Structural Studies of Highly Dispersed and Porous Bodies), Moscow: Akad. Nauk SSSR, 1958, pp. 60–71.

ISSN 1070-4272, Russian Journal of Applied Chemistry, 2006, Vol. 79, No. 12, pp. 1930–1934. © Pleiades Publishing, Inc., 2006.
Original Russian Text © N.V. Grishatova, V.F. Ur'yash, A.E. Gruzdeva, N.V. Novoselova, 2006, published in Zhurnal Prikladnoi Khimii, 2006, Vol. 79, No. 12, pp. 1953–1957.

PHYSICOCHEMICAL STUDIES OF SYSTEMS AND PROCESSES

A Calorimetric Study of the Enthalpy of Enzymatic Hydrolysis of Components of a Product from Vegetable Raw Materials for Enteral Feeding

N. V. Grishatova, V. F. Ur'yash, A. E. Gruzdeva, and N. V. Novoselova

Research Institute, Lobachevskii State University, Nizhni Novgorod, Russia
Fitograd ZAO, Nizhni Novgorod, Russia
Ekstramed OOO, Nizhni Novgorod, Russia

Received September 27, 2006; in final form, September 2006

Abstract—The enthalpy of hydrolysis of potato starch and some starch-containing components of Lider-1 nutrition product for enteral (tube) feeding in the presence of α-amylase enzyme was studied on a DAK-1-1 differential microcalorimeter.

DOI: 10.1134/S1070427206120044

Full-value, balanced, and ecologically pure nutrition is a powerful factor in improving the peoples' health and enhancing the protective function of an organism. An important role in these processes is played by biologically active additives. This particularly refers to food products for enteral feeding, in which case a patient cannot feed on his (her) own, e.g., because of a cranial or maxillary injury. The action of such biologically active additives largely depends on the degree of assimilation by a human organism of valuable substances contained in these additives. In this context, development of an instrumental technique for evaluating the completeness of food digestion in a human organism is a topical task. In recent years, thermodynamic methods have been finding increasing use in solution of biochemical and biological problems. For example, attempts have been made to characterize enzymatic reactions and processes involving various proteins, cells, and cell communities by changes in the basic thermodynamic functions, entropy, enthalpy, and Gibbs function [1–5]. However, studies of this kind are few in number.

A calorimetric technique has been used to determine the enthalpy in our studies of the reaction of enzymatic hydrolysis of some polysaccharides, which models the process that occurs in the gastrointestinal tract of a human in food digestion [6–9]. In addition, we measured the specific heat of potato starch and its constituents, amylase and amylopectin, in the range 6–230 K and calculated their thermodynamic characteristics (enthalpy, entropy, and Gibbs energy) [10].

In the present study, we determined the enthalpy of hydrolysis of potato starch and some starch-containing components of Lider-1 nutrition product for enteral (tube) feeding[1] in the presence of the α-amylase enzyme.

EXPERIMENTAL

We studied potato starch of Ekstra brand [GOST (State Standard) 7699–78] with 13.6 wt % H_2O in the air-dry state. It contained 33.5 wt % amylase and 66.5 wt % amylopectin [10].

Lider-1 preparation includes the following starch-containing components (wt %): germinated wheat 7.76, potato 15.52, apple 23.72, and carrot 3.10 [TU (Technical Specification) 9160-002-39232318–97, TU 9164-001-39232318–01, TU 9197-018-39232318–01). They were prepared using a unique technique of cryogenic grinding, developed at Biofit ZAO (Nizhni Novgorod) [12–14]. The air-dry samples of vegetable products contained 4–6 wt % water.

α-Amylase (α-1,4-glucose-4-glucanohydrolase, KFZ 2.1.1), also named dextrinogenamylase or gly-

[1] The formulation of the product has been developed at Fitograd ZAO (Nizhni Novgorod) [11].

cogenase, belongs to enzymes that are involved in catabolic reactions.

It is an endoamylase, which favors rupture of intramolecular α-1,4-glucoside bonds of amylase and amylopectin and leaves intact the α-1,6-glucoside bonds of the latter. Therefore, starch is mostly hydrolyzed in the presence of α-amylase to low-molecular weight dextrins and a certain amount of maltose.

The enzyme was extracted from a cattle pancreas and had the form of a white powder produced by sublimation drying.[2]

According to [15], the optimal medium for amylase is an alkaline medium (e.g., in the small intestine), whose pH is controlled by sodium hydrocarbonate contained in the human intestinal juice. Therefore we adjusted the pH value to 8.3 with $NaHCO_3$. The optimal temperature of enzymatic process is in the range 303–313 K [16]. Therefore, we carried out experiments at a temperature of 310 K, close to the normal temperature of the human body. The amylolytic activity of α-amylase was determined colorimetrically (λ = 590 nm), as recommended in [17], using the Lachema biotest (AMS-50), and the specific activity of the enzyme was found to be 2260 E ml^{-1}.

The energy-related effects accompanying the hydrolysis of starch and starch-containing vegetable products in the presence of α-amylase were measured with a DAK-1-1 differential microcalorimeter (of the Thiane–Calve type [3]). This device can continuously record release and absorption of very small amounts of heat at some temperature in the range 298–373 K during a long period of time [18]. The control-and-calibration unit of the microcalorimeter can give 11, varied in steps, values of power in the range 8×10^{-5}–4×10^{-3} W in heaters of any of the cells, provide a prescribed temperature mode of operation in the temperature range specified, and ensure isothermal experimental conditions. The minimum and maximum measurable power was 1×10^{-6} and 3×10^{-1} W, respectively.

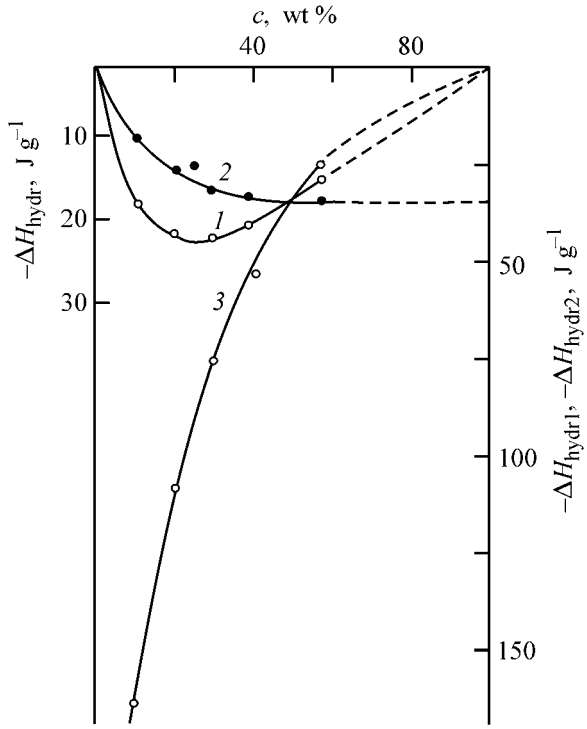
A sample of a vegetable product (0.1–0.25 g) was sealed in a thin-walled glass ampule and a liquid modeling the stomach medium, the optimal for the action of α-amylase, was poured in a preliminarily sterilized metallic ampule of the calorimetric cell. As noted above, the solution had a pH value of 8.3, which was maintained with $NaHCO_3$. A 0.02–0.1-g portion of α-amylase was dissolved in 4 ml of this solution. The metallic ampules were closed with Teflon stoppers. After a thermal equilibrium was attained between the cells of the calorimeter (at 310 K), the reagents were mixed by breaking the glass ampule with a pin and agitating the mixture. The energy obtained was corrected for heat effects accompanying the ampule breaking, reagent agitation, and solvent evaporation. These values were found in preliminary experiments to be 0.02–0.05 J (ampule breaking) and 0.005–0.03 J (agitation). The calorimeter was calibrated with electric current [13, 18]. An electric current of certain power was passed through the heater of a calorimetric cell, the amount of heat released in the heater was found from the Joule–Lenz formula, and the corresponding peak was recorded on the chart strip of the self-recorder. The time was measured with a stopwatch with an accuracy of 0.1 s.

To evaluate the measurement error and check the experimental procedure for absence of systematic errors, we determined the integral enthalpy of solution of chemically pure KCl in twice-distilled water. The concentration of KCl solutions in water was varied from 0.003 to 0.1 mol per 1000 g. To pass from the KCl solutions under study to a solution with a molality of 0.278, we used a value of the enthalpy of dilution (concentration) equal to 360 J mol^{-1} [19]. The experiments were performed under the same conditions as the experiments aimed to determine the enthalpy of the reaction of enzymatic hydrolysis under study. It was found that the error of separate measurements of the enthalpy of KCl solution in water is 4%, and the error in determining the average value does not exceed 2% at a confidence probability of 95%. Our results coincided with reliable published data for 310 K (160.20 ± 0.30 kJ mol^{-1}) to within these values [19].

Differential curves of heat release or heat absorption provide information about the rate of energy release or absorption and the area delimited by the curve and the time axis corresponds to the amount of energy accompanying the process under study. Using the calibration curve for the given experiment, we found the change in enthalpy in the process studied by the weighing method [3]. The process was considered to be complete when the differential curve reached the zero level.

The enthalpy of hydrolysis, ΔH_{hydr}, was found for starch and cryopowders in the air-dry state and recalculated per gram of the dry (anhydrous) process. In addition, we compared the values we obtained for the enthalpy of their hydrolysis with the enthalpy of enzymatic hydrolysis of the same components, but

[2] The enzyme was delivered by the Research Institute of Antibiotics and Enzymes (St. Petersburg).



Enthalpy of enzymatic hydrolysis of air-dry starch. (*c*) Amylase content. For explanation, see text.

subjected to thermal drying and mechanical crushing. This made it possible to evaluate the degree of digestion of the products preserved by different methods. The values obtained were compared with the enthalpy of mixing of the products with an aqueous solution of $NaHCO_3$ (pH 8.3) that contained no enzyme, ΔH_{mix}.

Published data were available only for the enthalpy of mixing of starch and water [20], and, therefore, we measured the enthalpy of its mixing with the aqueous solution of $NaHCO_3$ (pH 8.3). This process is accompanied by an exothermic effect. The contribution to the negative enthalpy of mixing of starch and an aqueous solution of $NaHCO_3$ comes not only from the enthalpy of hydration of starch macromolecules by molecules of water, but also from the negative enthalpy of transformation of starch from the glassy state to the hyperelastic state upon its mixing with water. This is the so-called excess enthalpy of the glassy state [21–24]. In our experiments, the fraction of starch in the final solution varied from 2 to 5 wt %. The value found for ΔH_{mix} of the process of starch mixing with an aqueous solution of $NaHCO_3$ in this concentration range was –88…103.5 J g^{-1} starch. This value coincides within the experimental error with the published value of the enthalpy of mixing of starch and water [20]. The enthalpy of mixing of α-amylase (0.6 wt %) and an aqueous solution of $NaHCO_3$ (pH 8.3) was found to be 12.3 J g^{-1} amylase.

The values obtained for the enthalpy of hydrolysis of air-dry starch (13.6 wt % H_2O) in the presence of α-amylase, ΔH_{hydr}, calculated per gram of the mixture are shown in the figure (curve *1*). The same figure presents the values of ΔH_{hydr} recalculated per gram of starch (ΔH_{hydr1}, curve *2*) and per gram of amylase (ΔH_{hydr2}, curve *3*). A correction for water contained in the air-dry starch (13.6 wt %) was made and the values obtained were recalculated to anhydrous starch. The results obtained are listed in Table 1. As can be seen in the figure and Table 1, this process is exothermic and the value of ΔH_{hydr} is three times smaller than the enthalpy of mixing of starch and water [20]. The resultant value of ΔH_{hydr} includes the exothermic enthalpy of mixing of starch and water, endothermic enthalpy of rupture of glucoside bonds in macromolecules of amylase and amylopectin, enthalpy of formation of hydroxy groups in the products, and exothermic enthalpy of hydration of the products formed.

Table 1. Experimental enthalpies of hydrolysis of dried starch with an aqueous solution of $NaHCO_3$ (pH 8.3) in the presence of α-amylase at 310 K

Mass, g		Amylase content, wt %	Q_{tot},* J	ΔH_{hydr}	ΔH_{hydr1}	ΔH_{hydr2}
starch	amylase			J g^{-1}		
				mixture	starch	amylase
0.1662	0.0233	12.29	3.8206	20.16	22.99	164.0
0.1736	0.0501	22.40	5.4984	24.57	31.67	109.7
0.1443	0.0715	33.13	5.3896	24.97	37.35	75.38
0.0679	0.0503	42.55	2.7024	22.86	39.79	53.72
0.0472	0.0548	53.72	1.8863	18.51	39.96	34.42
0.0790	0.1238	61.07	3.1109	15.34	39.39	25.12

* Q_{tot}, amount of energy released in an experiment.

Table 2. Enthalpy of hydrolysis, ΔH_{hydr}, of cryopowders, crushed vegetable products, and Lider-1 preparation in the presence of α-amylase at 310 K

Product	$-\Delta H_{hydr}$, J g^{-1} dry product
Germinated wheat:	
cryopowder	41.8
crushed	36.8
Potato:	
cryopowder	38.9
crushed	25.9
Apple:	
cryopowder	23.0
crushed	20.9
Carrot:	
cryopowder	14.2
crushed	10.5
Lider-1	13.8

Table 3. Enthalpy of mixing, ΔH_{mix}, of cryopowders, crushed vegetable products, and Lider-1 preparation with an aqueous solution of $NaHCO_3$ (pH 8.3) at 310 K

Product	$-\Delta H_{mix}$, J g^{-1} air-dry product	$-\Delta H_{mix}$, J g^{-1} dry product
Germinated wheat:		
cryopowder	37.2	39.7
crushed	35.1	37.2
Potato:		
cryopowder	33.9	36.0
crushed	22.2	23.4
Apple:		
cryopowder	19.1	19.9
crushed	17.6	18.4
Carrot:		
cryopowder	10.6	11.3
crushed	7.83	8.20
Lider-1	9.20	9.62

Tables 2 and 3 list the enthalpies of hydrolysis of vegetable products with an aqueous solution of $NaHCO_3$ (pH 8.3) in the presence of α-amylase and the enthalpies of mixing of some of these products with the aqueous solution of $NaHCO_3$ in the absence of α-amylase.

It can be seen from these tables that the enthalpies in question are negative. At the same time, ΔH_{hydr} exceeds ΔH_{mix} in absolute value. The difference exceeds the error in determining the enthalpies. The fact that a tendency opposite to that for starch is observed in this case indicates that more complex processes accompany the enzymatic hydrolysis of starch in real vegetable products. According to [25], α-amylase attacks the starch grain in a vegetable process and loosens its surface to form channels and grooves, i.e., leads to a kind of grain disintegration into parts. In our opinion, this makes it possible to evaluate by the enthalpy of hydrolysis the accessibility of starch in a vegetable product in relation to the type of its treatment. As can be seen from the data in Tables 2, 3, the values of ΔH_{hydr} and ΔH_{mix} are close for a sample of crushed germinated wheat, i.e., starch in the crushed sample is inaccessible to the enzyme.

It is important that the enthalpy of hydrolysis of cryopowders is more negative (by a factor of 1.2–1.5), compared with thermally dried and mechanically crushed samples. This indicates that starch in cryopowders is more accessible to the enzyme, compared with mechanically crushed vegetable products. Thus, it may be assumed that both the cryopowders and Lider-1 preparation, in which they are contained, will be better digested and assimilated by a human organism. ΔH_{hydr} of Lider-1 preparation was calculated from the additive contributions of the enthalpies of hydrolysis of the cryopowders it contains, with account of their content in the preparation. It was found to be –14.6 J g^{-1} dry product. This value is close to that found experimentally: ΔH_{hydr} = –13.8 J g^{-1} dry product (Table 2).

CONCLUSIONS

(1) It was shown that the enthalpy of hydrolysis of products prepared using the cryogenic grinding method and of thermally dried and mechanically ground samples is negative. The enthalpy of hydrolysis of cryopowders is more negative (by a factor of 1.2–1.5) than that of thermally dried and mechanically ground samples. Thus, starch in cryopowders is more accessible to the enzyme, compared with the mechanically ground vegetable products.

(2) The enthalpy of enzymatic hydrolysis of Lider-1 preparation was calculated from the additive contributions of the enthalpies of hydrolysis of the constituent cryopowders, with account of their contents in the preparation. It was demonstrated that the assimilability of products for enteral feeding can be evaluated by the additive contributions of the enthalpies of enzymatic hydrolysis of the components of these products. This provides objective criteria for assessing the quality of food additives and enables

deliberate selection of those better digested and assimilated by a human organism.

ACKNOWLEDGMENTS

The study was financially supported by the Foundation for Assistance to Small Innovative Enterprises (state contract no. 1574r/21008, May 23, 2002).

REFERENCES

1. *Biochemical Thermodynamics*, Jones, M., Ed., Amsterdam: Elsevier, 1979.
2. Kalous, V. and Pavlicek, Z., *Biofizicheskaya khimiya* (Biophysical Chemistry), Moscow: Mir, 1985, (Russian translation from Czech.).
3. Calve, E. and Pratt, *A., Mikrokalorimetriya: Primenenie v fizicheskoi khimii i biologii* (Microcalorimetry in Physical Chemistry and Biology), Moscow: Inostrannaya Literatura, 1963.
4. Gustafsson, L., *Thermochim. Acta*, 1991, vol. 193, pp. 145–171.
5. Boling, E.A., Blanchard, G.G., and Russel, W.J., *Nature*, 1973, vol. 241, no. 5390, pp. 472–473.
6. Ur'yash, V.F., Gruzdeva, A.E., Novoselova, N.V., et al., *Trudy III Mezhdunarodnoi NTK "Pishcha. Ekologiya. Chelovek," Moskva. 2–3 iyunya 1999* (Proc. III Int. Sci.-Techn. Conf. "Food, Ecology, Humans," Moscow, June 2–3, 1999), Moscow, 1999, p. 64.
7. Ur'yash, V.F., Grishatova, N.V., Gruzdeva, A.E., et al., *Trudy IV Vserossiiskoi NPK po primeneniyu biologicheski aktivnykh dobavok k pishche, Nizhni Novgorod, 20–21 iyunya 2001* (Proc. IV All-Russia SCi.-Techn. Conf. on Use of Biologically Active Additives to Food, Nizhni Novgorod, June 20–21, 2001), Nizhni Novgorod. 2001, pp. 20–21.
8. Ur'yash, V.F., Grishatova, N.V., Novoselova, N.V., et al., *Trudy VII Mezhdunarodnoi konferentsii po problemam sol'vatatsii i kompleksoobrazovaniya v rastvorakh, Ivanovo. 8–11 oktyabrya 2001* (Proc. VII Int. Conf. on Problems of Solvation and Complexation in Solutions, Ivanovo, October 8–11, 2001), Ivanovo, 2001, pp. 57–58.
9. Ur'yash, V.F., Novoselova, N.V., Grishatova, N.V., and Gruzdeva, A.E., *Trudy XIV Mezhdunarodnoi konferentsii po khimicheskoi termodinamike, Sankt-Peterburg, 1–5 iyulya 2002* (Proc. XIV Int. Conf. on Chemical Thermodynamics, St. Petersburg, July 1–5, 2002), St. Petersburg, 2002, p. 406.
10. Ur'yash, V.F., Gruzdeva, A.E., Kokurina, N.Yu., et al., *Zh. Fiz. Khim.*, 2004, vol. 78, no. 5, pp. 796–804.
11. Rakhmanov, R.S. and Gruzdeva, A.E., *Trudy VII Mezhdunarodnogo kongressa po parenteral'nomu i enteral'nomu pitaniyu, Moskva, 22–24 oktyabrya 2003* (Proc. VII Int. Congr. on Parenteral and Enteral Feeding, Moscow, October 22–24, 2003), Moscow 2003, pp. 81–82.
12. RF Patent 2110194.
13. RF Patent 2124300.
14. RF Patent 2124847.
15. Radbil', O.S., *Farmakoterapiya v gastroenterologii: Spravochnik* (Pharmacotherapy in Gastroenterology: Reference Book), Moscow: Meditsina, 1991.
16. Green, N.P.O., Stout, G.W., and Taylor, D.J., *Biological Science 1 & 2*, Cambridge: University, 1997.
17. *Metody biokhimicheskogo issledovaniya rastenii* (Methods for Biochemical Studies of Plants), Ermakov, A.I., Ed., Leningrad: Agropromizdat, 1987.
18. Gal'perin, L.N., Kolesov, Yu.R., Mashkinov, L.B., and Germer, Yu.E., *Trudy VI Vsesoyuznoi konferentsii po kalorimetrii, Tbilisi, 17–19 sentyabrya 1973* (Proc. VI All-Union Conf. on Calorimetry, Tbilisi, September 17–19, 1973), Tbilisi, 1973, pp. 539–543.
19. Mishchenko, S.P. and Poltoratskii, G.M., *Termodinamika i stroenie vodnykh i nevodnykh rastvorov elektrolitov* (Thermodynamics and Structure of Aqueous and Nonaqueous Electrolyte Solutions), Leningrad: Khimiya, Len. Otd., 1976.
20. Tsvetkov, V.G., Kaimin', I.F., Ioelovich, M.Ya., and Prokhorov, A.V., *Termodinamika organicheskikh soedinenii: Mezhvuzovskii sbornik* (Thermodynamics of Organic Compounds: Intercollegiate Coll. of Works), Gorki: Gork. Gos. Univ., 1982, pp. 54–60.
21. Jenkel, E. and Gorke, K., *Z. Elektrochemie*, 1956, vol. 60, no. 6, pp. 570–587.
22. Meerson, S.I., *Kolloid. Zh.*, 1969, vol. 31, no. 3, pp. 421–426.
23. Tager, A.A., *Vysokomolek. Soedin., Ser. A*, 2004, vol. 13, no. 2, pp. 4676–484.
24. Tsvetkov, V.G. and Tsvetkova, L.Ya., *Zh. Fiz. Khim.*, 1979, vol. 53, no. 7, pp. 1822–1824.
25. Gracheva, I.M. and Krivova, A.Yu., *Tekhnologiya fermentnykh preparatov* (Technology of Enzyme Preparations), Moscow: Elevar, 2000.

ISSN 1070-4272, Russian Journal of Applied Chemistry, 2006, Vol. 79, No. 12, pp. 1935–1939. © Pleiades Publishing, Inc., 2006.
Original Russian Text © T.Yu. Gumerov, A.F. Dobrynina, R.A. Yusupov, V.P. Barabanov, 2006, published in Zhurnal Prikladnoi Khimii, 2006, Vol. 79, No. 12, pp. 1958–1962.

PHYSICOCHEMICAL STUDIES OF SYSTEMS AND PROCESSES

Coagulation in Lipid- and Protein-containing Systems

T. Yu. Gumerov, A. F. Dobrynina, R. A. Yusupov, and V. P. Barabanov

Kazan State Technological University, Kazan, Tatarstan, Russia

Received March 16, 2006

Abstract—The behavior of real disperse systems with organic impurities was examined under conditions of destabilization by inorganic coagulants. A number of physicochemical methods of analysis and a simulation method were used to identify the character and type of the complexes formed and to calculate their stability constants.

DOI: 10.1134/S1070427206120056

Real colloid systems in wastewater from industrial enterprises are complex multcomponent systems. The data on the stability of lipid- and protein-containing systems [1, 2] need adequate systematization.

In this study, we optimized the conditions of removal of lipid- and protein-containing impurities from wastewater with inorganic coagulants.

EXPERIMENTAL

We examined disperse systems in wastewater from meat processing enterprises.[1] The main characteristics of the disperse systems are listed in Table 1. It is seen that all of them exceed the levels prescribed by the existing standards by an order of magnitude.

As coagulants served aluminum sulfate [GOST (State Standard) 12966–85], aluminum chloride [TU (Technical Specifications) 102612–88], and iron(III) chloride (GOST 4147–74).

We used the Soxhlet [3], Kjeldahl [4], and IR Fourier spectroscopic methods [5] for physicochemical analysis. The optimal concentrations of the coagulants were determined on the basis of the sedimentation analysis data in combination with measurements of the optical density of the solutions. The composition of the compounds in the system and the constants of equilibria involving them were determined by potentiometric titration and simulation [6]. An IR Fourier spectroscopic study showed that the samples of both disperse systems (KMC, SMC) contain nearly identical sets of absorption bands (Fig. 1). The absorption band intensities were estimated from the optical densities, using the band at 1600 cm^{-1} as internal reference.

The IR Fourier spectra contain a broad absorption band at 3300–3348 cm^{-1} corresponding to stretching vibrations of the NH groups. A group of bands at 3000–2850 cm^{-1} is associated with the absorption of

Table 1. Main characteristics of the disperse systems

System	pH	COD	BOD_5	Particulates	Lipids	Proteins
				mg l^{-1}		
KMC	6.5–7.0	2000	1770	800	800	234
SMC	6.5–7.0	1990	1520	100	374	155
Standard*	6.5–8.5	265	177	186	10	0

* Hygienic standards and regulations. Concentration of harmful substances in wastewater: Order of the Head of the City of Kazan Administration no. 917 of May 15, 2000.

[1] Kazan Meat Combine (KMC) and Sviyaga Meat Combine (SMC).

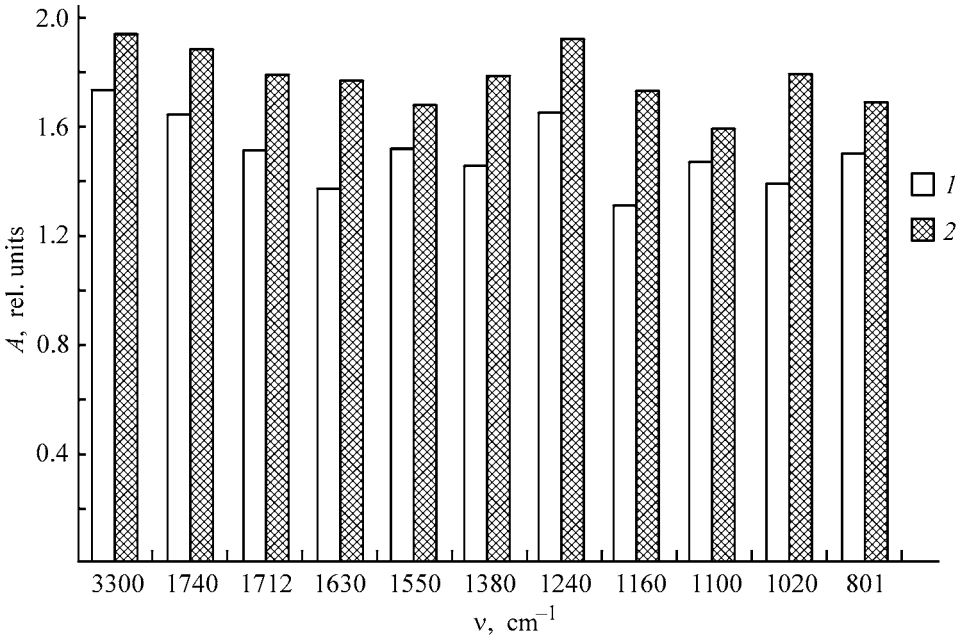


Fig. 1. Histogram of the content of the protein and lipid groups A in the wastewater samples. (ν) Absorption frequency. (*1*) SMC and (*2*) KMC.

methylene (CH_2) and methyl (CH_3) groups in the paraffin and naphthene moieties. The absorption at 1742 cm^{-1} corresponds to carbonyl groups (C=O) in esters, and that at 1710 cm^{-1}, to the same groups in acids.

The IR spectra of both the systems suggest a close similarity between their structural and group compositions (Fig. 1).

To select the optimal concentrations, samples of both the systems were subjected to sedimentation analysis and optical density measurements [7]. Figure 2

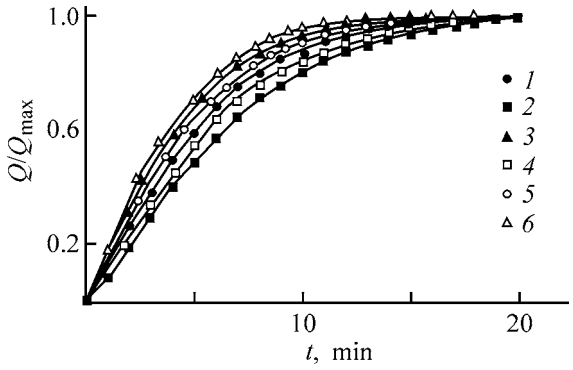


Fig. 2. Sedimentation curves of the samples of water from the overall discharge, plotted in the Q/Q_{max}-vs.-t coordinates. (Q, Q_{max}). Running and maximal masses of the sediments on the torsion balance dish, respectively, and (t) exposure time. Content, %: (SMC) (*1*) 0.03 $Al_2(SO_4)_3$, (*2*) 0.0125 $AlCl_3$, (*3*) 0.025 $FeCl_3$; (KMC) (*4*) 0.02 $AlCl_3$, (*5*) 0.04 $Al_2(SO_4)_3$, and (*6*) 0.03 $FeCl_3$.

shows the optimal concentrations of the coagulants, derived from the sedimentation analysis data. It is seen that the iron(III) and aluminum salts differ in the coagulating power. Upon introduction of iron(III), the chloride sedimentation proceeds at a higher rate than that in the case of the aluminum salts. The coagulating powers of the aluminum salts with respect to disperse phases having close structural and group compositions are virtually identical. Minor differences in the performance of the coagulants based on Al(III) may be due to complexation during hydrolysis in the dispersion medium and to quantitative differences in the chemical composition of the initial blends. At low doses of the coagulants introduced, iron(III) chloride surpasses in performance the coagulants based on Al(III) [$FeCl_3 > Al_2(SO_4)_3 \approx AlCl_3$].

To explain the influence exerted by the dispersion medium on the coagulating power of the coagulants, we converted the potentiometric titration curves obtained to the plots of the formation function: $n_L = (c_{NaOH}V_{NaOH})/(c_{salt}V_{salt})$ vs. pH of solution [8]. The curves in Fig. 2 were obtained at the optimal concentrations of the coagulants, derived from the sedimentation analysis data. In contrast to the curves obtained at lower concentrations of the coagulants, the converted potentiometric titration curves obtained under these conditions (Fig. 3) exhibit characteristic ascending sections due to the formation of compounds containing OH^- ions. Treatment of the potentiometric titration curves using the simulation method [9] al-

Table 2. Composition of the compounds and overall equilibrium constants in the Al(III)–H_2O–OH^-–Cl^-, SO_4^{2-}, and Fe(III)–H_2O–OH^-–Cl^- systems* (concentration, M: $AlCl_3$ 9.374×10^{-5}, $Al_2(SO_4)_3$ 4.5×10^{-5}, and $FeCl_3$ 9.252×10^{-5})

Composition of compounds M [Al(III), Fe(III)], $L(OH)^-$		Code	Constant		Step (total) equilibrium constants log β and solubility constants pK_s			n_{OH^-}
			Al(III)	Fe(III)	Al(III)		Fe(III)	
					Cl^-	SO_4^{2-}	Cl^-	
Basis series of compounds B (hydroxides)	ML	B1	K1	KC1	7.7	7.8	10	1.00
	ML2	B2	K2	KC2	7.7	7.8	10	2.00
	ML3	B3	K3	KC3	3.8	4.0	5	3.00
	ML3s	B3S	K3S	KC3S	7.2	7.2	7.5	3.00
	ML4	B4	K4	KC4	2.0	3.0	3.0	4.00
Polynuclear compounds P	M2L	P1.0	KPB0XB1		2.3	2.3	3.8	0.50
	M4L3	P2.0	KP2B0XB1XB2		–	–	15.5	0.75
	M3L5	P2.3	KPB1X2B2		15.2	15.2	18.0	1.67
	M3L5s	P2.3S	KPB1X2B2S		0.5	0.5	–	1.67
	M6L12	P2.5	KPB2X5B2		33.0	33.0	28.0	2.00
	M6L12s	P2.5S	KPB2X5B2S		21.0	21.0	21.0	2.00
	M32L64	P4.4	KP32B2		–	–	(140)	2.00
	M32L70	P4.5	KP32B2X6L		–	–	(180)	2.20
	M40L100	P5.0	KP40B2XB3		–	–	(186)	2.50
	M2L5	P2.6	KP2B2XL		10.0	10.0	–	2.50
	M2L5s	P2.6S	KP2B2XLS		1.4	1.4	–	2.50
	M3L8	P2.7	KP3B2X2L		16.0	16.0	–	2.67
	M4L11	P2.8	KP4B2X3L		22.0	22.0	–	2.75

* Order of indexing of complexes: (1) K is the step stability constant of the complex; (2) X, addition sign (the plus or minus sign cannot be used because of the incompatibility in programming); 3) B, the most stable series of a complex, termed the basis series of the complex (in this study, hydroxo complexes); the digit to the right of symbol B denotes the compound no. in these series [e.g., B0 corresponds to Al^{3+}, B1, to $AlOH^{2+}$, B2, to $Al(OH)_2^+$, etc.]; the digit to the left of symbol B, the number of the particles added; and C, the accompanying series of the complex compound; (4) P, polynuclear compounds; and (5) S, sediments.

lows determination of the type, amount, and distribution pattern for the Al(III) and Fe(III) complexes formed. Table 2 shows that complexing during hydrolysis of the aluminum and iron(III) salts involves formation of a series of polynuclear compounds.

The higher coagulation activity of $FeCl_3$ compared to $Al_2(SO_4)_3$ and $AlCl_3$, can be due to formation of complexes with higher stability constants. For example, compounds of Fe(III) include complexes ML, ML2, ML3, and ML4 from the basis series with higher stability constants as compared to similar complexes of Al(III) (Table 2). Polynuclear compounds of Fe(III) and Al(III) differ in both stability and composition. Polynuclear compounds of Fe(III) form an M2L complex similar to that of Al(III), with higher stability constants [log β 3.8 for Fe(III) against 2.3 for Al(III)] and a series of new complexes, differing from those of Al(III) in composition: M32L64, M32L70, and M40L100. The stability constants of these complexes (from 146 to 186) suggest possible formation of stable polymeric Fe(III) compounds. In the scheme of formation of the main complexes in the Al(III)–H_2O–OH^-–Cl^- and Fe(III)–H_2O–OH^-–Cl^- systems, protein

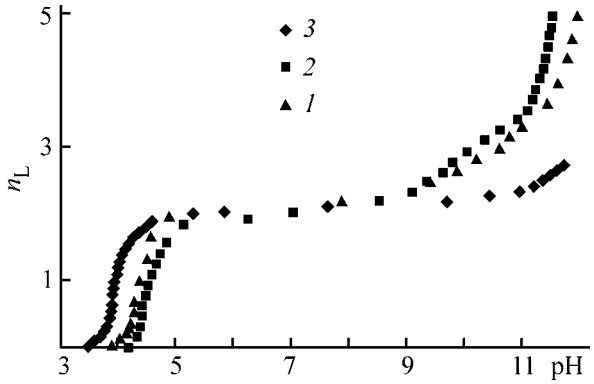
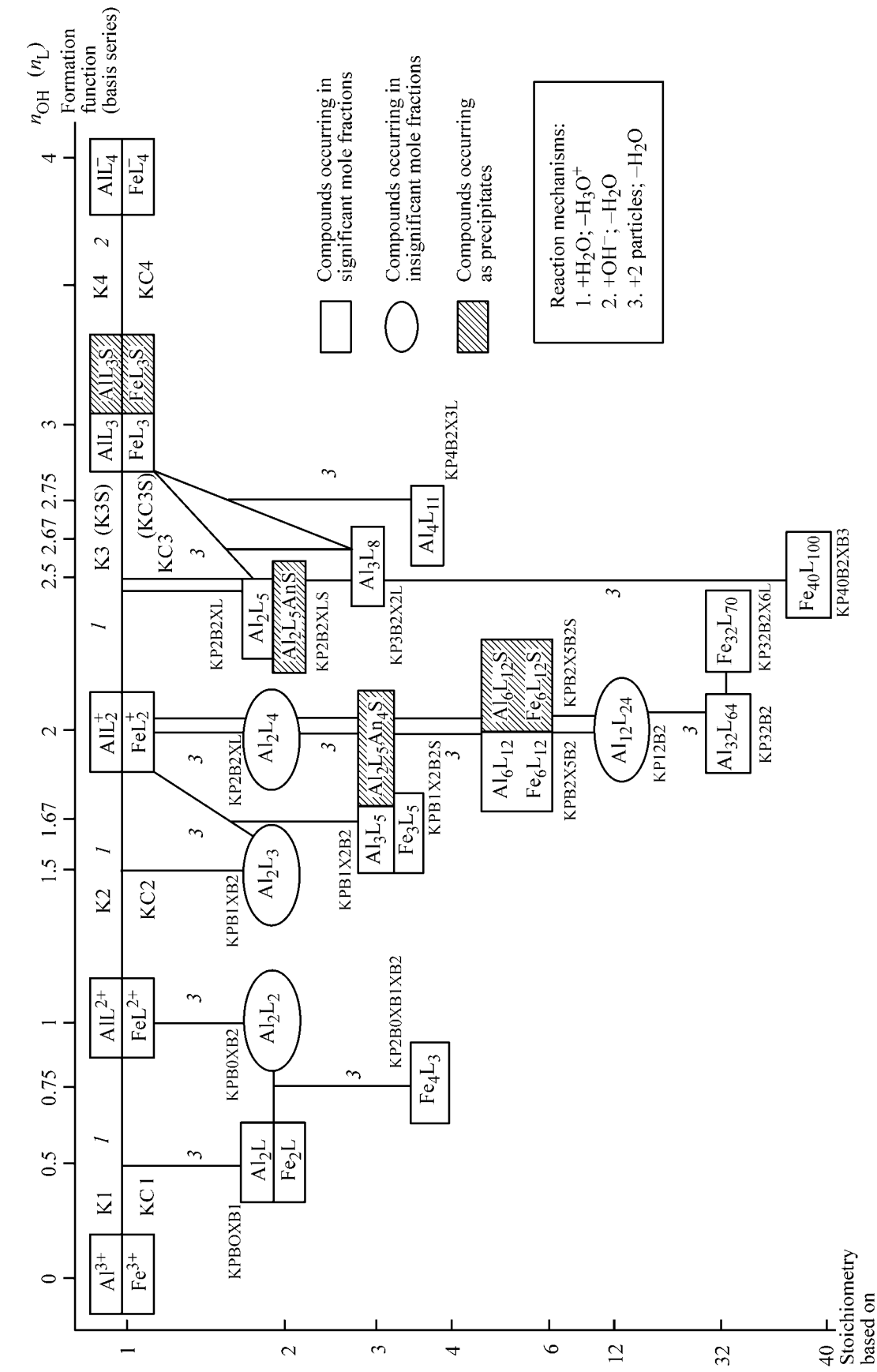


Fig. 3. Experimental curves of potentiometric titration of the solutions of the coagulants with a standard NaOH solution (0.05 M), converted to the plots of the formation function n_L vs. pH. Concentration, $c \times 10^5$, M: (*1*) 9.374 $AlCl_3$, (*2*) 4.5 $Al_2(SO_4)_3$, (*3*) 9.252 $FeCl_3$.



Formation of main complexes in the Al(III)–H_2O–OH^-–Cl^- and Fe(III)–H_2O–OH^-–Cl^- systems.

and lipid impurities are removed from the wastewater at pH 6.2–7.1. Under these conditions, the coagulants occur in solutions as stable complexes M6L12 and M6L12S for aluminum salts and M32L64 and M32L70 for iron(III) chloride with a higher degree of polymerization at the formation function $n_L = 2$.

CONCLUSIONS

(1) The behavior of disperse systems containing protein and lipid impurities under the action of coagulants, Al(III) and Fe(III) salts was studied. The optimal concentrations of the coagulants were determined by sedimentation analysis.

(2) It was shown that, for disperse systems containing protein and lipid impurities with comparable structural and group compositions, the coagulating power of the Fe(III) and Al(III) salts varies as $FeCl_3 > Al_2(SO_4)_3 \approx AlCl_3$.

(3) It was demonstrated that the presence of polynuclear compounds with close quantitative characteristics for coagulants based on Al(III) and of polynuclear compounds with higher stability constants for Fe(III) can be among the factors determining the effect of coagulants on disperse systems.

REFERENCES

1. Becherikova, A.K. and Tarasova, T.V., *Izv. Vyssh. Uchebn. Zaved., Khim. Khim. Tekhnol.*, 2000, vol. 43, no. 1, pp. 84–89.
2. Stepanova, N.V., Konovalova, I.N., Vasilevskaya, P.B., and Bereza, I.G., *Voda Ekol.*, 2000, no. 2, pp. 25–30.
3. *Sparavochnik po obshchei biologii* (Reference Book on General Biology), Filippovich, Yu.B., Ed., Moscow: Prosveshchenie, 1982.
4. Pleshkov, B.P., *Praktikum po biokhimii rastenii* (Practical Course of Plant Biochemistry), Moscow: Kolos, 1968.
5. Bellamy, L.J., *The Infra-red Spectra of Complex Molecules*, New York: John Wiley, 1957.
6. Yusupov, R.A., Movchan, N.I., Abzalov, R.F., and Smerdova, S.G., *Zh. Fiz. Khim.*, 2000, vol. 74, no. 4, pp. 625–629.
7. Faizullina, G.G., Colloid and Chemical Features of the Coagulation and Flocculation Processes in Lipid-Containing Systems, *Cand. Sci. Dissertation*, Kazan, 2003.
8. Yusupov, R.A. and Mikhailov, O.V., *Zh. Neorg. Khim.*, 2002, vol. 47, no. 7, pp. 1177–1179.
9. Yusupov, R.A., *Doctoral Dissertation*, Kazan, 2003.

ISSN 1070-4272, Russian Journal of Applied Chemistry, 2006, Vol. 79, No. 12, pp. 1940–1942. © Pleiades Publishing, Inc., 2006.
Original Russian Text © O.A. Besedina, A.N. Eremenko, N.V. Kiridenko, I.I. Obraztsova, E.S. Samchinskaya, 2006, published in Zhurnal Prikladnoi Khimii, 2006, Vol. 79, No. 12, pp. 1963–1965.

SORPTION AND ION-EXCHANGE PROCESSES

Adsorption Properties of Ultradispersed Diamonds

O. A. Besedina, A. N. Eremenko, N. V. Kiridenko, I. I. Obraztsova, and E. S. Samchinskaya

Kemerovo Branch, Institute of Solid-State Chemistry and Mechanochemistry, Siberian Division, Russian Academy of Sciences, Kemerovo, Russia

Received December 8, 2005; in final form, May 2006

Abstract—The adsorption capacity of ultradispersed diamonds for synthetic dyes and medicinal preparations was studied.

DOI: 10.1134/S1070427206120068

Recently, the interest has substantially increased in the field of special-purpose adsorption materials that possess improved properties and are intended for analytical separation of substances, synthesis of ultrapure materials and preparations, fast removal of impurities from liquids and gases, and operation under severe conditions, e.g., at high temperatures and large mechanical loads and in aggressive media.

Particularly stringent requirements are imposed on adsorbents and ion exchangers on their base that are developed for medical purposes. There exists a large demand for hemo- and enterosorbents and application sorbents that can adsorb toxins and carry ions, medicinals, and enzymes necessary for an organism. Carbon sorbents are most widely used in medicine. At present, carbon therapeutic methods constitute a broad and rapidly developing discipline, whose impact on the practice and results of curing may be rather important.

Previous studies have shown that the adsorption properties of detonation-produced ultradispersed diamonds (UDD) compare well with the adsorption properties of numerous carbon sorbents [1], and, moreover, UDD have a number of advantages: they posses a large specific surface area, have a plentiful of electrons on the diamond surface (multiple radical-donor), show nanometer dimensions, bear a large number of oxygen-containing functional groups, have chemically inert grains and hydrophilic surface and do not show any carcinogenic, mutagenic, or toxic properties [2].

The present study is concerned with the possibility of using as medical adsorbents the UDD produced by separation of ultradispersed diamonds by acid treatment of a detonation-produced carbon-containing stock under mild conditions in the presence of metal salts. UDD of this kind are distinguished by a high degree of purification and stable particle size scatter (3–4 nm) and are not subject to graphitization upon prolonged storage or use [3, 4].

It has been found previously that high-temperature treatment of UDD in a flow of hydrogen or argon leads to virtually complete removal of protonogenic surface groups and to an increase in the sorption capacity because of the active diamond skeleton [1]. Thus, UDD can be used both as carrier of medicinals, which does not cause their destruction, and as a means of removal of toxins from a human organism, e.g., in hemoperfusion.

EXPERIMENTAL

Information about the applicability of a sorbent to detoxication of an organism is provided by analysis of its adsorption capacity in aqueous solutions. As test substances are used synthetic dyes, whose molecules have dimensions close to those of biological substances serving as objects of medical studies, but are more stable and convenient in handling [5]. The adsorption capacity of UDD was evaluated by studying the adsorption of the following dyes: Methylene Blue (M = 344), Bromocresol Purple (M = 540), and Indigo Carmine (M = 466). The choice of dyes as test substances is based on the similarity in size and structure between their molecules and molecules of such preparations as antitumor medicinals of alkylating nature and soporifics belonging to the group of barbiturates.

Table 1. Amount of dye adsorption for various forms of ultradispersed diamonds

Dye	Molecular weight	Amount of adsorption, mg g^{-1}, at indicated modification temperature, °C						
		Starting UDD	argon			hydrogen		
			400	600	800	400	600	800
Methylene Blue	344	1.72	17	24	103	58	103	137
Bromocresol Purple	540	14	16	19	18	19	19	19
Indigo Carmine	460	4	6	9	89	9	9	

The dye concentrations were determined by photocolorimetry on a FEK-56N device. The amount of adsorption was evaluated for Luminal (Phenobarbital) preparation, whose removal from a human organism is an important detoxication problem.

This study is concerned with the ability of UDD to adsorb on their surface medicinals of the most important groups used for therapeutic purposes: (1) ampicillin, an antibiotic of the penicillin series with a broad action spectrum, quantitatively determined by acid–base titration [6]; (2) euphyllin (salt of theophylline with ethylenediamine), an alkaloid of the purine series, whose application in medicine is based on its stimulating effect of the nerve system, quantitatively determined in terms of ethylenediamine by acid–base titration [7]; (3) papaverine hydrochloride, an alkaloid of the isoquinoline series, exhibiting a high spasmolytic activity, quantitatively determined by acid–base titration in nonaqueous media [7]; (4) norsulfazol, a sulfanilamide preparation widely used in curing of inflammatory processes, quantitatively determined by nitritometry [8]; and (5) Phenobarbital (Luminal), a barbiturate exhibiting, together with a soporific effect, an antispasmodic action, quantitatively determined by acid–base titration in nonaqueous media [6].

An UDD, whose purification and preparation has been described by the authors previously [3, 4], was used in the study.

The amount of adsorption was determined under static conditions at room temperature [5, 9]. A dry UDD powder (0.5 g) was placed in 50 ml of a solution of a substance under study. The following solvents were used: distilled water for all the dyes, ampicillin, euphyllin, and norsulfazol; 50% ethanol for papaverine hydrochloride; and 95% ethanol for Phenobarbital. The choice of solvents was governed by the analytical procedure used to determine a substance [6–8]. After a sorbent–solution system reached equilibrium, the residual concentration of the sorbate was determined.

The adsorption capacities of unmodified UDD and UDD calcined in a flow of argon at 400, 600, and 800°C and in a flow of hydrogen at the same temperatures (modified UDD) were studied.

It was found experimentally that the maximum amount of adsorption corresponds to the following dye concentrations (mg ml^{-1}): Methylene Blue 1.9×10^{-2}, Bromocresol Purple 0.92, and Indigo Carmine 9.0×10^{-2}. The data obtained in determining the amount of dye adsorption for various kinds of modified UDD are listed in Table 1.

The experiments performed demonstrate that high-temperature modification of UDD improves their adsorption capacity. A significant increase in the amount of adsorption is observed for Methylene Blue. It should be noted that the adsorption capacity of unmodified UDD for Bromocresol Purple exceeds that for the other dyes; however, it is virtually unaffected by modification. The effect of thermal treatment of UDD on the sorption of Bromocresol Purple is also insignificant. Thus, it may be assumed that presence of acid groups on the surface of UDD does not noticeably affect the adsorption process and the adsorption capacity increases upon modification because of the coarsening of pores in UDD aggregates.

The results obtained in determining the adsorption of Methylene Blue demonstrate that UDD is a more effective adsorbent than carbon hemosorbents studied previously. For example, the maximum amount of adsorption is 137 mg g^{-1} for UDD and only 31 mg g^{-1} for AR-3 industrial carbon [10].

The amounts of adsorption of the medicinal substances were determined using pelletized pharmaceutical preparations. The content of the substances under study was monitored by pharmacopoeial techniques

Table 2. Adsorption of medicinal preparations

Medicinal preparation	Molecular weight	c_{in}, mg ml^{-1}	Adsorption, mg g^{-1}, for indicated modification temperature, °C					
			argon			hydrogen		
			400	600	800	400	600	800
Ampicillin	349	1.8	42	52	741	54	88	
Euphyllin (in terms of ethylenediamine)	60	1.6	25	44	50	19	48	82
Papaverine hydrochloride	376	2.6	41	51	74	60	70	86
Norsulfazol	255	1.3	10	32	46	6	32	52
Phenobarbital	232	9.2	–	22	15	–	33	21

[6–8]. The amounts of adsorption of the medicinal preparations are listed in Table 2.

It can be seen from Table 2 that, as in the case of dyes, the specific adsorption of the medicinal preparations strongly varies with UDD modification conditions and reaches the highest values, except for Phenobarbital, when there are virtually no surface groups on the UDD surface (thermal treatment at 800°C). UDD samples modified at 400°C in a flow of argon have a higher adsorption capacity than those calcined at the same temperature in a flow of hydrogen. As the treatment temperature is raised, the situation changes: the best adsorption properties are observed for UDD samples modified at 600 and 800°C in a flow of hydrogen. Presumably, the presence of protonogenic surface groups hinders the adsorption process, because these groups are most completely removed in modification in a flow of hydrogen at higher temperatures. A considerable increase in adsorption is observed for norsulfazol.

The results obtained in determining the adsorption capacity of UDD for the medicinal preparations show that UDD is a more effective sorbent that AR-3 industrial carbon. The maximum adsorption capacity for Phenobarbital is 33 mg g^{-1} for UDD and only 12 mg g^{-1} for AR-3 industrial carbon [10].

It should be noted that both for medicinal preparations and for dyes there is no unambiguous dependence of the amount of adsorption on the molecular weight of a substance.

CONCLUSIONS

(1) Ultradispersed diamonds possess a sufficient adsorption capacity for some medicinal preparations and show promise for use in medicine.

(2) Thermal treatment of ultradispersed diamonds in a flow of argon or hydrogen improves their adsorption capacity.

(3) Thermal treatment of ultradispersed diamonds at 800°C in a flow of hydrogen is the most effective method for raising their adsorption capacity.

REFERENCES

1. Eremenko, A.N., Besedina, O.A., and Obraztsova, I.I., *Zh. Prikl. Khim.*, 2004, vol. 77, no. 12, pp. 1956–1959.
2. Dolmatov, V.Yu., *Usp. Khim.*, 2001, vol. 70, no. 7, pp. 687–708.
3. RF Patent 2081821.
4. Obraztsova, I.I. and Eremenko, A.N., *Zh. Prikl. Khim.*, 2003, vol. 76, no. 3, pp. 443–445.
5. Nikolaev, V.G. and Strelko, V.V., *Gemosorbtsiya na aktivirovannykh uglyakh* (Hemosorption on Activated Carbons), Kiev: Naukova Dumka, 1979.
6. Pohloudek-Fabini, R. and Beyrich, Th., *Organische Analyse*, Leipzig: Geest und Portig, 1975. Translated under the title *Organicheskii analiz*, Leningrad: Khimiya, 1961.
7. *Farmakopeya. Ministerstvo zdravookhraneniya SSSR. Gosudarstvennaya Farmakopeya SSSR* (Pharmacopoeia, Ministry of Public Health of the USSR, State Pharmacopoeia of the USSR), Moscow: Medgiz, 1961, 9th ed.
8. Melent'eva, G.A. and Antonova, L.A., *Farmatsevticheskaya khimiya* (Pharmaceutical Chemistry), Moscow: Meditsina, 1985.
9. Nikolaev, V.G., *Metod gemokarboperfuzii v eksperimente i klinike* (Method of Hemocarboperfusion in Experiment and Clinical Practice), Kiev: Naukova Dumka, 1984, p. 16.
10. Strelko, V.V., Galinskaya, V.I., Davydov, V.I., et al., *Adsorbtsiya Adsorbenty*, 1976, no. 4, pp. 29–37.

ISSN 1070-4272, Russian Journal of Applied Chemistry, 2006, Vol. 79, No. 12, pp. 1943–1946. © Pleiades Publishing, Inc., 2006.
Original Russian Text © R.R. Daminev, E.I. Bakhonina, Yu.K. Dmitriev, R.N. Zagidullin, M.M. Muratov, L.F. Tukhvatullina, 2006, published in Zhurnal Prikladnoi Khimii, 2006, Vol. 79, No. 12, pp. 1966–1969.

SORPTION AND ION-EXCHANGE PROCESSES

Reactivation of a Solid Carbon-Containing Adsorbent, Graton, in a Microwave Electromagnetic Field

R. R. Daminev, E. I. Bakhonina, Yu. K. Dmitriev, R. N. Zagidullin, M. M. Muratov, and L. F. Tukhvatullina

Sterlitamak Branch, Ufa State Technical University of Oil, Sterlitamak, Bashkortostan, Russia
Kaustik ZAO, Sterlitamak, Bashkortostan, Russia

Received July 5, 2005; in final form, July 2006

Abstract—Results of experimental studies of reactivation of a graphite packing, Graton, in a microwave electromagnetic field are presented.

DOI: 10.1134/S107042720612007X

Adsorbents are widely employed in purification of gases and liquids to remove impurities [1]. Their use requires periodic regeneration, removal of adsorbed substances from adsorbent pores [1]. For example, electrochemical decomposition of a sodium amalgam on a carbon-containing packing with a developed surface area (Graton or graphilite) is used at organochlorine plants[1]. The packing serves as an anode, and sodium amalgam, as a cathode. The sodium amalgam is produced in the reaction of sodium with mercury: sodium is recovered from brine in discharge of Na^+ ions at the mercury cathode of a chlorine electrolyzer:

$$Na^+ + e + nHg \rightarrow NaHg_n.$$

Decomposition of the sodium amalgam with water is the second stage in manufacture of sodium hydroxide. In the process, NaOH and H_2 are formed, and mercury is regenerated and returned into the electrolyzer:

$$NaHg_n + H_2O \rightarrow NaOH + 1/2H_2 + nHg.$$

In electrochemical decomposition of the amalgam, reduction and oxidation processes occur separately and involve the current-conducting surface, which accepts electrons from the reducing agent, $NaHg_n$, and transfers them to the oxidizing agent, H_2O:

$$NaHg_n \rightarrow Na^+ + e + nHg,$$

$$H_2O + e \rightarrow OH^- = 1/2H_2.$$

The process of amalgam decomposition can be made tens of times faster if it is directed by the electrochemical pathway. For this purpose, it is necessary to diminish the hydrogen overvoltage. The most pronounced effect is achieved when hydrogen evolution occurs on a material with a lower overvoltage, brought in electric contact with mercury, rather than on mercury itself.

The amalgam is decomposed in vertical cylindrical apparatus (VCA) filled with a graphite packing (Fig. 1).

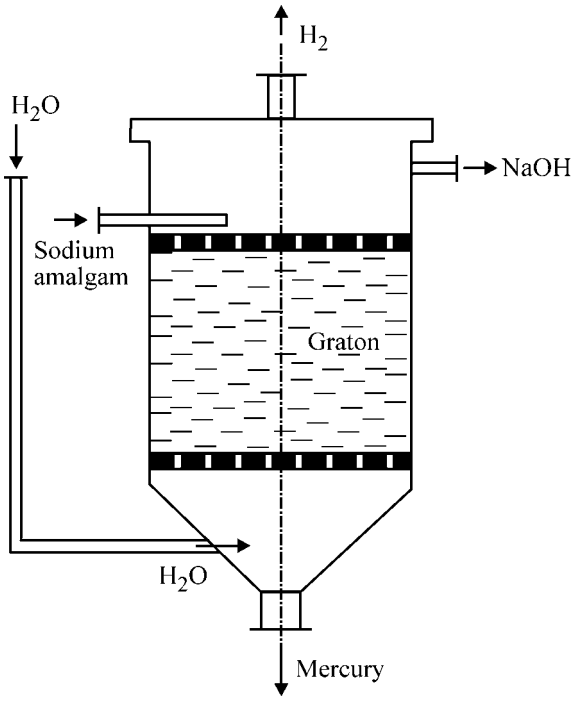


Fig. 1. Schematic of a VCA for decomposition of a sodium amalgam.

[1] Kaustik ZAO, Sterlitamak.

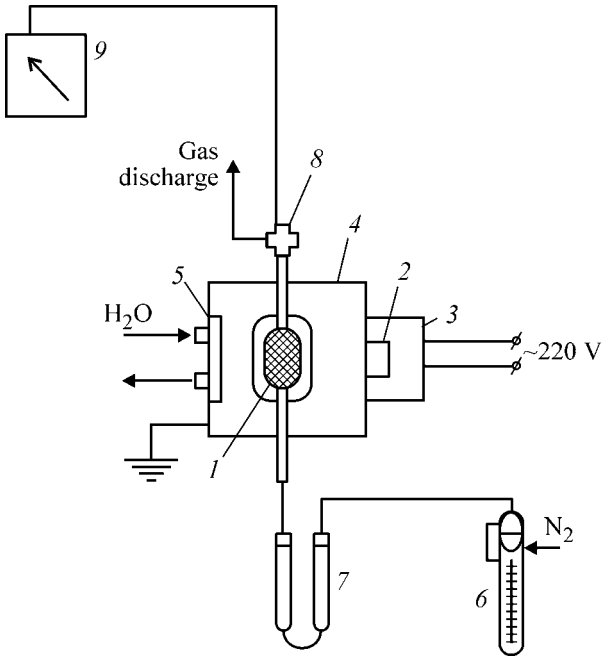


Fig. 2. Schematic of a laboratory microwave installation. (*1*) Reactor (150 cm^3), (*2*) magnetron, (*3*) power unit, (*4*) resonator, (*5*) load, (*6*) rheometer, (*7*) dehumidifier, (*8*) thermocouple, and (*9*) potentiometer.

Vigorous hydrogen evolution occurs on its surface. Such a system, constituted by a packing, a sodium amalgam, and water, operates as a short-circuited cell in which the packing serves as a cathode, and the amalgam, as an anode.

The content of sodium in the amalgam is 0.5×10^{-2} to 0.5 wt % (weak amalgam at the VCA outlet, ≤0.005–0.05 wt % sodium; and strong amalgam at the VCA inlet, ≤0.5 wt %).

At present, Graton packing (pellets 15–20 mm in diameter and 10–15 mm high) are used to fill VCA. Graton is a graphite packing with titanium carbide (up to 30%), which is added to make lower the hydrogen overvoltage.

A deposit of magnesium, calcium, and iron hydroxides, carbonates and sulfates is formed on the Graton surface. The exchange current decreases because a part of the surface is eliminated from the process of electrochemical decomposition of the amalgam. Therefore, the packing is periodically regenerated. At present, this is done under industrial conditions by washing with an HCl solution (5 wt %). This procedure is labor-consuming, has a low efficiency, and is ecologically unsafe.

The degree of filling of the packing material with adsorbed final and intermediate products of the electrochemical reaction depends on the state of the electrically conducting surface. For the sodium amalgam to be decomposed efficiently, a developed adsorbing surface of the packing is necessary. The exchange current decreases because adsorbed molecules of surface deposits screen a part of the packing surface. The catalytically active surface may constitute only a minor fraction of the whole adsorbing surface, and even a small amount of catalytic poisons may suppress the surface activity, with the adsorption capacity reduced only slightly.

Thus, to provide the electrocatalytic activity of palletized graphite packings (Graton, graphilite), it is necessary to preserve and maintain their porosity by regenerations at regular intervals of time, with blocking of active centers precluded.

To reactivate such a catalyst-adsorbent as Graton, it is necessary to desorb reaction products from pores. This is presently done for the most part by thermal methods. For example, thermal reactivation of AG-5 activated carbon saturated with elementary sulfur in oxidation of hydrogen sulfide by sulfur dioxide on a catalyst, activated carbon, has been reported [1]. According to [1], only 35% of sulfur contained in the carbon is extracted in 2 h at 200°C, and about 90% of sulfur is removed during the same time at 300°C. The thermal reactivation is carried out as follows. Spent carbon heated to 150°C is charged into a regenerator and is suspended there by overheated steam delivered into the regenerator from below. Before being fed into the regenerator, the steam is heated to 500°C in a superheater [1]. This treatment results in that reaction products and impurities are removed from pores of the spent carbon.

This method has a number of disadvantages: inefficient delivery of energy by steam via convective heat exchange; high energy expenditure for heating of steam to 500°C; formation of waste gases (toxic products of fuel combustion in the steam superheater) and wastewater (condensed steam), contaminated with desorbed reaction products.

The authors suggest to improve the efficiency and ecological safety of the reactivation of the adsorbent and the duration of its work between regenerations and to raise its activity by microwave (ν = 2450 MHz) heating of the adsorbent in a flow of an inert gas (nitrogen).

Figure 2 schematically shows a laboratory microwave installation for adsorbent reactivation. Graton containing up to 80 wt % carbon and about 20 wt % TiC was used in the experiments.

The graphite packing (Graton) was calcined, without any preliminary washing, at 400–450°C for 1–1.5 h in a bed of graphite particles in a laboratory reactor having a working volume of 150 cm^3 (Fig. 2). After a thermal treatment cycle was complete, the furnace was switched off and the packing cooled down in the inert gas. After the temperature of the packing decreased to 30–40°C, Graton was discharged from the reactor into a dry hermetical vessel.

The process occurred in reactor *1* (Fig. 2) under the action of a microwave electromagnetic field produced by microwave generator (magnetron) *2*, fed by high voltage from power unit *3*. To absorb the microwave radiation reflected from the walls of resonator *4*, a matching load *5* was installed within the working chamber (resonator). The load had the form of a horizontal cylindrical glass (quartz) vessel with flowing-through water. The air-cooling of the magnetron was provided by a ventilator built in the case of the microwave furnace. The power unit was energized from a two-phase three-line ac supply (220 V, 50 Hz).

Figure 3 shows how the volume of evolved hydrogen depends on the duration of sodium amalgam decomposition.

Introduction into the Graton bed (particle size 10 mm) of finer particles of a solid substance, filler, with particle size not exceeding 3 mm, e.g., of the same adsorbent, Graton, leads to an increase in the bulk density of the adsorbent and to a higher degree of conversion of the electromagnetic power into heat. After an experiment is complete, the filler is separated from Graton by sieving (5 mm mesh). The effect of the bulk density of a sample on its heating (temperature) at a fixed power (750 W, 2450 MHz) is illustrated below:

Change in bulk density, g cm^{-3}	Rise in sample temperature, °C
0.5	8.5
0.10	22
0.15	27
0.2	30

As can be seen from these data, an increase in the bulk density by 0.2 g cm^{-3} (from 1.03 to 1.23 g cm^{-3}) leads to a rise in the Graton temperature by 30°C (from 420 to 450°C). An increase in the amount of the substance by a certain amount in a unit volume favors transformation of a greater amount of microwave power into heat in the Graton bed. However,

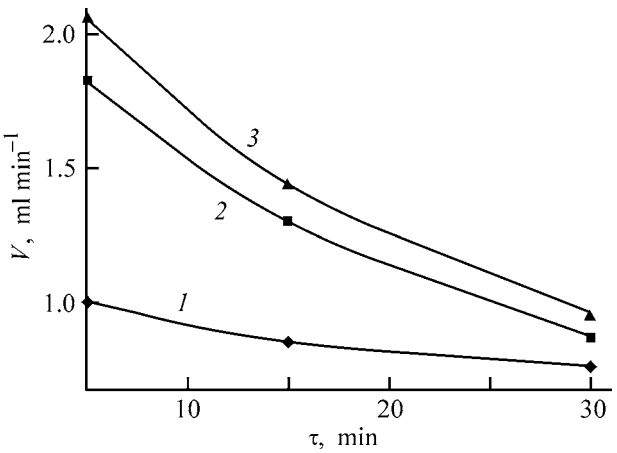


Fig. 3. Volume *V* of evolved hydrogen vs. the duration τ of decomposition of the sodium amalgam. Graton packing: (*1*) fresh, (*2*) reactivated by the conventional method, and (*3*) reactivated in a microwave field.

the temperature stabilizes at a certain mass of the substance and starts to decrease as the mass grows further.

The results obtained in studying the reactivation of the Graton graphite packing in a microwave field are presented in Fig. 3. It can be seen that, upon calcination of a spent packing in a microwave field (curve *3*), the rate of hydrogen evolution increases, compared with the case of a packing reactivated by the conventional method (curve *2*) and even with that of afresh (unused) packing (curve *1*).

The reactivation of the packing occurs as follows. In thermal regeneration without access of air, salts and bases adsorbed on the packing surface are decomposed and desorbed. Being evaporated, the desorbed substances raise the porosity of the graphite packing, i.e., make its active surface area larger. In the case of a highly intense evaporation of desorbed substances, observed under the action of microwave radiation on the adsorbent, the porosity of the graphite packing and, consequently, the active surface area increase to a greater extent.

Introduction of a solid substance that effectively converts the microwave power into heat, e.g., graphite with finer grains, into the packing (Graton) bed will enable these particles to act not only as an insulating material that provides accumulation of heat in the regeneration zone, but also as an absorber of desorbed substances, because the highest sorption capacity is observed just for powdered substances. As graphite particles of this kind can serve, in particular, particles of crushed Graton (with a size of up to 3 mm).

Application of the reactivation technique developed in this study improves the activity of the Graton graph-

ite packing by 14.3% [2]. This, in turn, makes longer the service life of the adsorbent between regenerations, raises its absorption capacity, and improves the efficiency of the process using the thus reactivated adsorbent.

CONCLUSIONS

It was shown that the reactivation technique developed raises the activity of the Graton graphite packing by 14.3%. This, in turn, improves the efficiency of the process employing the adsorbent reactivated in this way.

REFERENCES

1. Lukin, V.D. and Antsypovich, I.S., *Regeneratsiya adsorbentov* (Regeneration of Adsorbents), Leningrad: Khimiya, 1983.
2. RF Patent 2241538.

ISSN 1070-4272, Russian Journal of Applied Chemistry, 2006, Vol. 79, No. 12, pp. 1947–1951. © Pleiades Publishing, Inc., 2006.
Original Russian Text © A.A. Sheremet, S.S. Ermakov, 2006, published in Zhurnal Prikladnoi Khimii, 2006, Vol. 79, No. 12, pp. 1970–1974.

APPLIED ELECTROCHEMISTRY AND CORROSION PROTECTION OF METALS

Combined Standardless Electrochemical Method for Determination of Lead(II), Copper(II), and Cadmium(II) in Aqueous Solutions

A. A. Sheremet and S. S. Ermakov

St. Petersburg State University, St. Petersburg, Russia

Received August 1, 2006

Abstract—A combined standardless method (no calibration of the device against standard solutions or use of the method of additives is required) for determination of lead, copper, and cadmium in aqueous solutions is suggested. The method operates on principles of inversion voltammetry and potentiostatic coulometry. It is convenient for automated analysis of technological solutions and wastewater from electroplating and hydrometallurgical shops.

DOI: 10.1134/S1070427206120081

The inversion voltammetry (IVA) is one of the most sensitive analytical techniques. The high sensitivity of IVA is primarily due to the fact that the scheme of analysis includes a stage of pre-electrolysis, i.e., electrolytic concentration of a substance on the electrode. The stage of electrolysis is also included by another analytical technique, controlled-potential coulometry (CPC). The sensitivity of the latter method is lower, but it does not require calibration of the devices, i.e., it is not necessary to construct calibration plots or to use the method of additives. A condition for correct application of IVA is that the concentration c^0 of a substance being determined should remain unchanged in the bulk of the solution. Commonly, this is achieved by using a sufficiently large volume of a solution being analyzed and a small area of the working electrode. The latter circumstance predetermines a low pre-electrolysis current, which virtually does not change the analyte concentration in the solution bulk in the stage of its electrolytic concentration.

By contrast, the potentiostatic coulometry is based on measurements in which the analyte concentration varies with time. This occurs because the substance being determined is transformed under the action of electric current in electrolysis of a solution. Therefore, large-area electrodes are used in coulometry, and attempts are made to minimize the volume of a solution being analyzed.

The experimental conditions of IVA and CPC can be represented as follows.

For the IVA method:

$$\left.\begin{aligned} c(t) &= c^0 = \text{const}, \\ i_\text{d}^0 &= Kc, \\ i_\text{d} &= i_\text{d}^0 = \text{const}, \end{aligned}\right\} \quad (1)$$

$$V/S \to \infty, \quad (2)$$

For the CPC method:

$$\left.\begin{aligned} c(t) &= c^0 e^{-kT}, \\ i_\text{d}(t) &= Kc(t), \\ i_\text{d}(t) &= i_\text{d}^0 e^{-kT}, \end{aligned}\right\} \quad (3)$$

$$V/S \to 0, \quad (4)$$

Here, c^0 is the concentration of a substance being determined in solution; t_d^0, limiting diffusion current corresponding to the volume concentration c^0; $i_\text{d}(t)$, limiting diffusion current at an instant of time t; t, electrolysis duration; V, solution volume; and S, electrode area.

The advantage of IVA and CPC is the simplicity of measurements by these techniques, which is especially convenient under industrial conditions. However, IVA requires that the measuring device should be preliminarily calibrated or the method of additives should be used. The CPC technique is free of this disadvantage, which makes automated measurements less complicated.

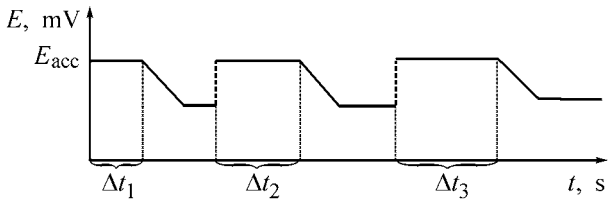


Fig. 1. Time diagram of variation of the potential in the combined electrochemical method. (E) Electrolysis potential and (t) electrolysis duration.

To improve the sensitivity of analysis by the CPC method and make it faster, it has been suggested to use thin-layer cells [1] or porous electrodes [2–4] in order to diminish the ratio between the volume of a solution being analyzed and the electrode area. In these studies, solution electrolysis was performed to complete, as postulated by the authors, recovery of the substance and, further, its amount was calculated by the Faraday law.

Several variants of inversion methods, which allow standardless electrochemical determination of analytes in solution, have been suggested [5–10]. The authors of [5, 6] used the potentiometric analytical procedure: they created by pre-electrolysis an amalgam of a metal being determined of a known concentration and then used the quasi-equilibrium potential of the $M(Hg)/M^{n+}$ system to calculate the concentration of the analyte in solution.

An inversion-chronopotentiometric variant of the standardless electrochemical method of analysis has been suggested [7]. This method is based on a multiple-cycle dissolution of a metal from an amalgam obtained in the pre-electrolysis stage and subsequent finding of a charge Q_∞ corresponding to complete recovery of the substance from solution. Further, the amount of the analyte in solution is found from the Faraday law.

A similar technique, named "dynamic coulometry" by the authors, was suggested in [8, 9]. This method can take into account the charging current of the electric double layer.

A combined electrochemical method based on fundamental aspects of inversion voltammetry was developed in [10]. The general principle of this technique is that it combines the advantages of IVA and potentiostatic coulometry. The latter is used to supplement the high sensitivity of IVA with an opportunity to make an analysis without standards.

The scheme of an electrochemical experiment, suggested in [10], includes three successive stages of IVA measurements (Fig. 1). The stage of electrolytic accumulation is performed three times during three different intervals of time: Δt_1, Δt_2, and Δt_3. The time is chosen in such a way that $(\Delta t_2 - \Delta t_1) = (\Delta t_3 - \Delta t_2)$. Further, the quantities of electricity, Q_1, Q_2, and Q_3, that correspond to the times of pre-electrolysis (Δt_1, Δt_2, and Δt_3) are found by integrating the current of metal ionization from the amalgam over time. This measurement procedure makes it possible to find the quantity of electricity Q_∞ that is necessary for complete electrodeposition on the electrode of the substance being determined, by using the Meites formula

$$Q_\infty = \frac{Q_2^2 - Q_1 Q_3}{2Q_2 - (Q_1 + Q_3)}. \quad (5)$$

Further, it is rather simple to calculate the amount of the substance in solution by the Faraday law, and, with the solution volume known, to find the concentration of the analyte.

The present study is concerned with the possibility of simultaneous determination of ions of lead, copper, and cadmium, which are metals most frequently used in electrolytic metallurgy, by the combined standardless electrochemical method.

The inversion-voltammetric measurements were performed on a PU-1 polarograph (ZIP, Moscow) with an AKV-07 transducer (Akvilon NPKF, Moscow) and on an AKV-07MK voltammetric analyzer with Polar-4.0 software (Akvilon NPKF, Moscow) in the dc and ac modes. Solutions with various concentrations of copper and cadmium ions were prepared from solutions of 10- and 1-g l^{-1} state standard samples (GSO 7255 and GSO 6690, respectively), using reagents of chemically pure and analytically pure grades and twice-distilled water. The measurements were carried out on a mercury-graphite film electrode rotated at a speed of 1000 rpm in the accumulation stage. A solution of composition (M): 1×10^{-4} $Hg(NO_3)_2$ + 5×10^{-2} HCl + 1×10^{-4} HNO_3, was used as a supporting electrolyte. The pre-electrolysis in IVA measurements was performed at a potential of –1.3 V, with a silver chloride reference electrode. To produce an electrochemical cell with a variable volume, a polyethylene terephthalate cylinder 20 mm in diameter and 20 mm high was glued with a sealing compound into the central part of a standard cell, glassy carbon crucible of volume 50 ml. The volume was further controlled by introduction of glassy-carbon inserts. Thus, the working volume of the cell could be varied from 5 to 1 cm^3. Measurements in larger volumes (20 ml) were carried out in the standard cell. The area of the working electrodes was

0.071 and 0.385 cm^2, which corresponded to diameters of the working surface of the electrodes equal to 3 and 7 mm, respectively. To satisfy the condition of a complete dissolution of the metal from the amalgam, slow (2–5 mV s^{-1}) potential sweep rates were used [10].

The first part of our study was aimed to verify whether or not principles of potentiostatic coulometry are satisfied in the method we suggested for the example of copper and cadmium and to find the coulometric constant k, which is a most important quantity characterizing the measurement conditions because it is related to the solution volume, electrode area, and hydrodynamic conditions of electrolysis [12]:

$$k = DS/V\delta, \quad (6)$$

where δ is the thickness of the diffusion layer.

For this purpose, we studied how the concentrations of these ions vary with the electrolysis duration and solution volume.

The dependence of the concentration variation rate on the electrolysis duration was studied as follows. The electrolysis was performed in a solution of a supporting electrolyte containing 5×10^{-8} M Cd^{2+} in the course of 2 min. The dissolution was carried out in a background solution containing no Cd^{2+} ions. Then a copper-containing solution was again subjected to electrolysis and then copper was dissolved in a background solution. The successive electrolyses led to variation of the concentration of metal ions in the solution. The height of the ionization peak of cadmium was used to determine its concentration in the solution. A similar experiment was carried out for a solution containing copper ions. The dependence of the volume concentration of cadmium(II) and copper(II) on the electrolysis duration is shown in Fig. 2, and the dependence of the fraction η of the substance being recovered on the electrolysis duration, in Fig. 3. The fraction of the substance being recovered was calculated by the formula

$$\eta = (c_i - c_{i+1})/c^0.$$

If we plot the data of Fig. 2 in the coordinates $\log(c/c^0)$–t, we obtain a linear dependence described by the equation $\log(c/c^0) = -kt$ (Fig. 4), which corresponds to condition (3). For comparison, the same figure shows a similar dependence for lead, plotted using the data of [10]. The dependences in Fig. 4 were used to find the coulometric constants for cadmium and copper: $k_{Cd} = 5.8 \times 10^{-3}$ s^{-1} and $k_{Cu} = 5.4 \times 10^{-3}$ s^{-1}. Because the coulometric constant depends on the solution volume, its value was reduced to a volume of 1 ml. The constant for lead under the same conditions, $k_{Pb} = 5.5 \times 10^{-3}$ s^{-1}, was found in [10]. The close values of the constants found for different ions point to a good reproducibility of the measurement results, because, as follows from Eq. (6), the values

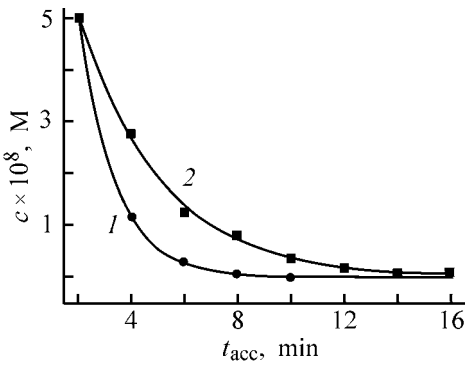


Fig. 2. Volume concentration c of (*1*) copper(II) and (*2*) cadmium(II) vs. the electrolysis duration t_{acc}. $c^0_{Cu} = c^0_{Cd} = 5 \times 10^{-8}$ M, $V = 5$ ml; the same for Fig. 3.

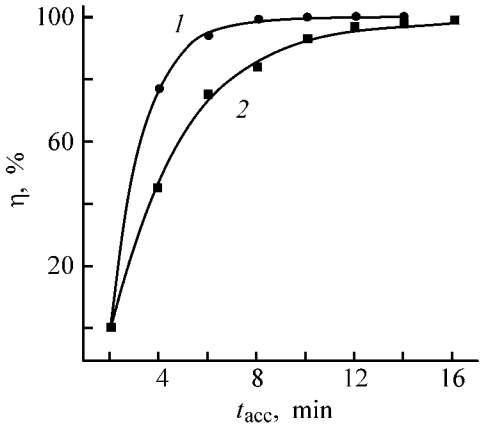


Fig. 3. Fraction of substance recovered, η, vs. the electrolysis duration t_{acc}. (*1*) Cu(II) and (*2*) Cd(II).

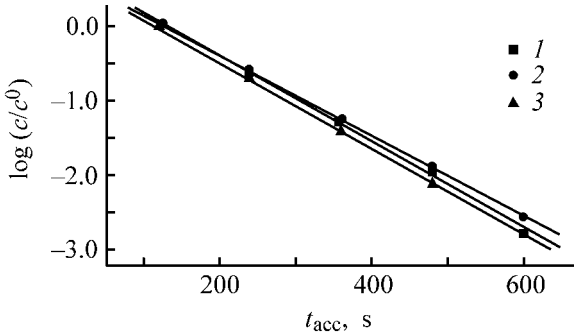


Fig. 4. Dependence of the logarithm of the normalized concentration, $\log(c/c^0)$, on the accumulation time t_{acc}, plotted using the data of Fig. 3. (*1*) Cd(II), (*2*) Cu(II), and (*3*) Pb(II) [10]; the same for Fig. 5.

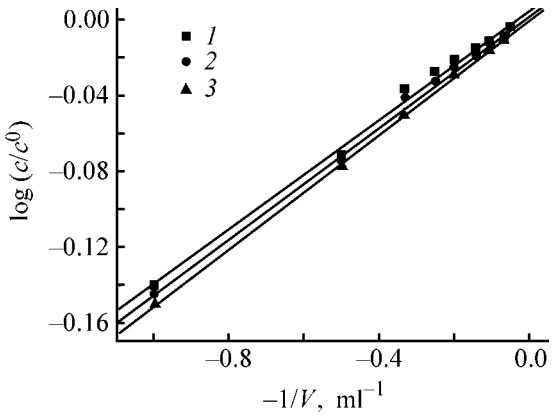


Fig. 5. Logarithm of the normalized concentration, $\log(c/c^0)$ on the volume V of the solution being analyzed. Accumulation time t_{acc} = 5 min, $c^0_{Cu} = c^0_{Cd} = c^0_{Pb} = 5 \times 10^{-8}$ M.

of the constants will differ at the same experimental conditions (solution volume, electrode area, and agitation conditions) in line with the diffusion coefficients.

It follows from condition (3) and Eq. (6) that, in electrolysis of a solution, the concentration will depend on the solution volume at a certain t, and this dependence is linearized in the coordinates $\log(c/c^0)$–$1/V$. Figure 5 shows the dependences of the concentration of copper and cadmium in solution on the volume of the solution being analyzed, which are linear in the coordinates $\log(c/c^0)$–$1/V$. The accumulation time was the same in all the measurements, and the volume was varied from 1 to 20 ml. For comparison, Fig. 5 also shows the same dependence for lead, plotted using the data of [10].

The experimental data we presented above indicate that the basic principles of potentiostatic coulometry are satisfied under the chosen measurement conditions. Therefore, we tested in the next stage of our study the applicability of the combined electrochemical method to determination of copper and cadmium, and also of copper, lead, and cadmium simultaneously present in a solution.

Cadmium was determined in a supporting electrolyte solution into which a known amount of Cd(II) ions was introduced in the concentration range 1×10^{-8}–1×10^{-7} M. Then measurements were made in accordance with the scheme in Fig. 1, the corresponding quantities of electricity (Q_1, Q_2, Q_3) were calculated, and Q_∞ was found using formula (5). The accumulation times (Δt_1, Δt_2, Δt_3) were 4, 6,

Table 1. Results of determination of cadmium and copper ions in aqueous solutions of various concentrations

Element being determined	Introduced $c \times 10^8$, M	Q_∞, μC, theor.	Found $c \times 10^8$, M	Q_∞, μC, calc.	V, ml	Standard relative deviation, %
Cd	3.50	20.263	3.03	17.54		
			3.51	20.32	3	0.2
			3.47	20.09		
	5.00	28.95	5.04	29.85		
			5.20	30.11	3	2.8
			4.86	28.14		
	10.00	96.50	9.3	89.75		
			10.3	99.40	5	1.0
			10.7	103.26		
Cu	1.00	9.65	1.03	9.94		
			1.02	9.84	5	3.3
			1.05	10.13		
	3.00	28.95	3.03	29.29		
			3.02	29.17	5	5.5
			3.45	33.32		
	5.00	48.25	5.07	48.92		
			4.86	46.90	5	1.4
			5.15	49.70		
	10.00	96.50	10.2	98.43		
			10.9	105.18	5	3.0
			9.8	94.57		

Table 2. Results of determination of cadmium and copper ions simultaneously present in solution

Introduced $c \times 10^8$, M		Q_∞, μC, theor.		Found $c \times 10^8$, M		Q_∞, μC, calc.		Standard relative deviation, %	
Cd	Cu	Cd	Cu	Cd	Cu	Cd	Cu	Cd	Cu
5.00		48.25		5.05	5.03	48.73	48.54	1.0	0.6
				5.10	5.08	49.21	49.02	2.0	1.6
				5.07	5.09	48.92	49.11	1.4	1.8

Table 3. Results of determination of cadmium, lead, and copper ions simultaneously present in solution

Element being determined	Number of measurements	Introduced $c \times 10^8$, M	Q_∞, μC, theor.	Found $c \times 10^8$, M	Q_∞, μC, calc.	Standard relative deviation, %
Cd	3	5.00	48.25	5.30	51.7	11.1
				4.51	45.1	
				6.86	66.2	
Pb	3	5.00	48.25	5.16	49.8	14.8
				6.06	58.5	
				6.00	57.2	
Cu	3	5.00	48.25	4.81	46.4	11.2
				6.32	60.9	
				5.54	53.4	

and 8 min, respectively, in all measurements. Knowing the quantity of electricity, necessary for a complete recovery of a substance, we calculated the content of cadmium and its concentration in the solution by the Faraday law. The measurement results are listed in Table 1.

Similar measurements were made for solutions containing ions of copper(II) (Table 1), copper(II) and cadmium(II) simultaneously (Table 2), and copper(II), cadmium(II), and lead(II) simultaneously (Table 3).

CONCLUSION

The results presented indicate that standardless determination of copper(II) and cadmium(II) is possible both in the case of their individual or joint presence in solution and in the case when lead(II) is also present.

REFERENCES

1. Eliseeva, L.V. and Kabanova, O.L., *Zh. Anal. Khim.*, 1973, vol. 28, pp. 1710–1713.
2. Beinrohr, E., *Accreditation Quality Assurance*, 2001, vol. 6, pp. 321–325.
3. Jurica, L., Manova, J., Dzurov, A., et al., *Fresenius J. Anal. Chem.*, 2000, vol. 366, pp. 260–265.
4. Beinrohr, E., Dzurov, J., and Annus, J., *Fresenius J. Anal. Chem.*, 1998, vol. 362, pp. 201–207.
5. Galceran, J., Companys, E., and Puy, J., *Electroanal. Chem.*, 2004, vol. 566, pp. 95–109.
6. Companys, E. Cecilia, J., Codina, G., et al., *Electroanal. Chem.*, 2005, vol. 576, pp. 21–32.
7. US Patent 5 891 322.
8. Sokolkov, S.V. and Zagorodnyuk, P.N., *Zh. Ross. Khim. O–va im. D.I. Mendeleeva*, 2001, vol. 45, p. 57314.
9. RF Patent 2 199 734.
10. Ermakov, S.S. and Chekmeneva, E.N., Abstracts of Papers, *2-ya Vserossiiskaya Konferentsiya "Analiticheskie pribory", Sankt-Peterburg, 27 iyunya–1 iyulya 2005 g.* (2nd All-Russia Conf. "Analytical Instruments," St. Petersburg, June 27–July 1, 2005), St. Petersburg, 2005, p. 172.
11. Meites, L., *Anal. Chem.*, 1959, vol. 31, pp. 1285–1296.
12. Budnikov, G.K., Maistrenko, V.N., and Vyaselov, M.R., *Osnovy sovremennogo elektrokhimicheskogo analiza* (Fundamentals of Modern Electrochemical Analysis), Moscow: Mir, 2003.

ISSN 1070-4272, Russian Journal of Applied Chemistry, 2006, Vol. 79, No. 12, pp. 1952–1956. © Pleiades Publishing, Inc., 2006.
Original Russian Text © O.V. Karlova, I.A. Kedrinskii, E.A. Chudinov, M.V. Yakovleva, 2006, published in Zhurnal Prikladnoi Khimii, 2006, Vol. 79, No. 12, pp. 1975–1979.

APPLIED ELECTROCHEMISTRY AND CORROSION PROTECTION OF METALS

A Negative Carbon Electrode in an Electrolyte Containing Sulfur Dioxide

O. V. Karlova, I. A. Kedrinskii, E. A. Chudinov, and M. V. Yakovleva

Siberian State Technological University, Krasnoyarsk, Russia
Istochnik Battery Institute OAO, St. Petersburg, Russia

Received August 10, 2006

Abstract—The possibility of replacing the electrolyte based on imported ethylene carbonate with a domestic SO_2-containing electrolyte based on propylene carbonate was considered for the example of operation of the negative electrode of a lithium–ion battery.

DOI: 10.1134/S1070427206120093

The standard electrolyte for lithium–ion batteries commonly contains ethylene carbonate (EC), which is not presently produced in Russia. At the same time, it has been shown in the development of primary lithium power sources that SO_2-containing electrolytes based on propylene carbonate (PC) can form on carbon electrodes surface layers similar in properties to those produced by EC-containing electrolytes [1]. However, the existence and stability of intercalation/deintercalation of lithium ions into/from the carbon matrix with a surface layer formed by SO_2 has not been studied.

To actualize the possibility of using a SO_2-containing electrolyte, it was necessary to complete studies of the electrochemical behavior of carbon materials in SO_2-containing electrolytes and to demonstrate the stability of operation of not only negative, but also positive electrodes and of the cell as a whole.

This study is concerned with the behavior of the carbon electrode in a PC-based electrolyte containing SO_2. It was established that the main characteristics determining the working capacity of a negative carbon electrode in a lithium ion battery are the expenditure of electricity for the formation of surface layer during the first charging, preservation of the surface layer on the charged and discharged electrode and on that subjected to cycling, stability of charging-discharge characteristics, and charge preservation in storage (self-discharge).

EXPERIMENTAL

We used as active material a powdered spectrally pure graphite (SPG) with grain size $d \le 40$ μm. The carbon of this type was used for two reasons. First, it is the standard material [TU (Technical Specification) 16-538-240–74] produced in Russia. Second, this material contains, by virtue of its main application, no impurities of spectrally active elements, which makes impossible a number of reactions leading to an irreversible immobilization of lithium ions. The electrode paste had the standard composition (%): SPG 85, acetylene black 5, and binder 10. As binder was used FP-42D or F2-ME. The electrodes fabricated contained about 2 mg cm^{-2} SPG. A 1 M solution of $LiClO_4$ in PC, with an SO_2 content of 13–20, served as the electrolyte. The electrolyte volume in the cell was 2.5 ml. The humidity of the electrolyte, as determined by the Fischer titration method, was 100 ppm. A plate of metallic lithium served as the counter electrode, so that the cell of composition C/Li was, in fact, subjected to electrolysis. The electrolysis was performed at $i = 0.06 - 0.127$ mA cm^{-2} of the apparent surface area (35.3–75.0 mA g^{-1} of carbon).

In the first charging, a surface layer responsible for the working capacity of an electrode in a battery is formed on the electrode surface. It should be noted that the first-cycle charging curve of the SPG electrode in the SO_2-containing electrolyte is well reproducible. The charging curves obtained by continuous electrolysis and by the method of static coulometric titration [2] in similar electrolytes (PC, 1 M $LiClO_4$, 13% SO_2 and PC : DME = 7 : 3, 0.6 M $LiClO_4$, 17% SO_2) are presented in Fig. 1. It can be seen that the curves largely coincide, especially in the region corresponding to reduction of sulfur dioxide.

The first-cycle charging curve plotted in the coordinates $(E_0 - E)$–$\ln[Q_0/(Q_0 - Q)]$ and E–$\log[(\tau^{1/2} - t^{1/2})/t^{1/2}]$, which correspond to SO_2 reduction and intercalation of lithium ions into the electrode matrix, is analyzed in Figs. 2, 3. The upper part of the curve at potentials of 2.5–1.5 V well correlates with SO_2 reduction. The inflection at a potential of 1.5 V corresponds to a change of the mechanism, and, according to the data of Fig. 3, this change characterizes a transition of the process to intercalation of lithium ions. This process is mainly complete by a potential of 0.2 V. Thus, the quantity of electricity corresponding to the inflection in the charging curve is spent for formation of a surface layer. It constitutes about 200 mA h g^{-1}

The studies performed demonstrated that, in the first-cycle charging, the content of water in the electrolyte decreases. The quantity of electricity spent for the electrochemical reduction of water was calculated from the difference of the water content of the electrolyte before the beginning and at the end of the first cycle of charging to be 3×10^{-10} mA h. It was found from this value of the capacity and from the corresponding electrode mass and its specific surface area that the products of water reduction will cover less than 0.01% of the electrode surface. Thus, we can state that the presence of the initial amount of water would not affect the shape and extent of the charging curve.

The preservation of surface layer on a charged and discharged electrode in the course of time and on an electrode subjected to cycling is an important property responsible for the working capacity of a lithium ion battery. It can be defined as the stability of the surface passivity reactions of electrochemical reduction. As an important indication that the passivity is disturbed can serve expenditure of electricity for reduction of the surface layer in a charging cycle that follows the discharge cycle, i.e., the case when the inequality $Q_{ch} > Q_{dis}$ (irreversible loss of capacity) holds. This loss is the most clearly pronounced in charging/discharge of an electrode stored after discharge in a zero-current state. Table 1 lists the irreversible loss in relation to the storage time of a discharged electrode before the following charging.

As can be seen from Table 1, the properties of the surface layer are fully preserved during 24 h of storage. The loss of the irreversible capacity appears upon a more prolonged storage. In this case, the process develops linearly with time and constitutes about 1% per day of the total capacity spent for the formation of the surface layer during the first charging.

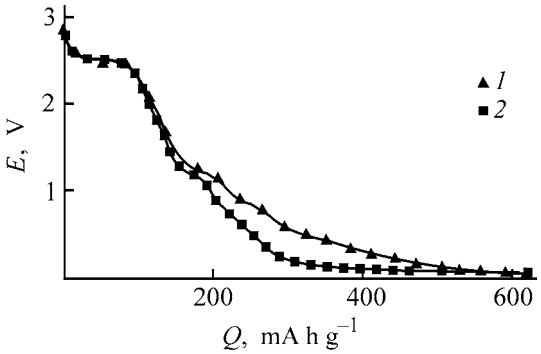


Fig. 1. First-cycle charging curves in various electrolytes. (E) Potential, (Q) capacity; the same for Figs. 2, 4; Electrolyte: (*1*) PC : DME = 7 : 3, 0,6 M $LiClO_4$, and 17% SO_2; (*2*) PC, 1 M $LiClO_4$, and 13% SO_2.

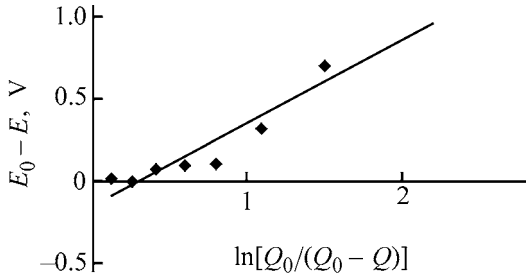


Fig. 2. $(E_0 - E)$–$\ln[Q_0/(Q_0 - Q)]$ dependence. SPG, 0.6 M $LiClO_4$, PC : DME = 7 : 3, 17% SO_2; the same for Fig. 3.

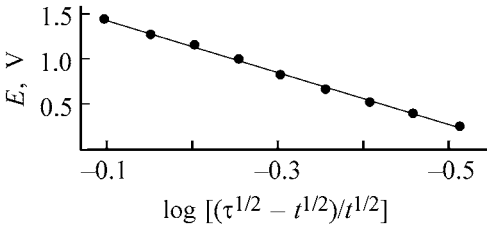


Fig. 3. E–$\log[(\tau^{1/2} - t^{1/2})/t^{1/2}]$ dependence.

A possible reason for the appearance of an irreversible loss is dissolution of the main surface layer component, lithium dithionite [1]. Another reason may be decomposition of the dithionite to give a thiosulfate. On

Table 1. Irreversible loss in relation to time of storage of the electrode in a discharged state

Cycle no.	Storage time, h	Q_i, mA h g^{-1}	Loss, % relative to Q of the first charging
1	2	3	4
37	10	0	0
46	17	0	0
57	28	0	0
75	112	7	3.5
58	158	15	7.5
51	220	26	13

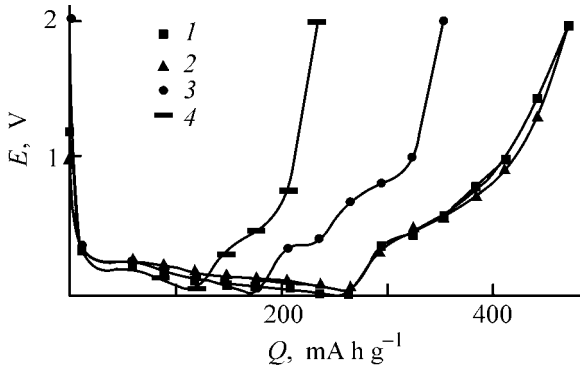


Fig. 4. Typical charging–discharge curves. Current density: (*1*) 35, 12th cycle; (*2*) 50, 54th cycle; (*3*) 75, and (*4*) 90.

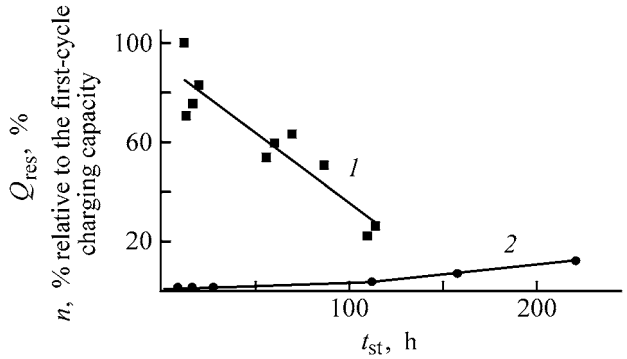


Fig. 5. Comparison of (*1*) residual capacity Q_{res} with the loss in a surface layer n in relation to the storage time t_{st}.

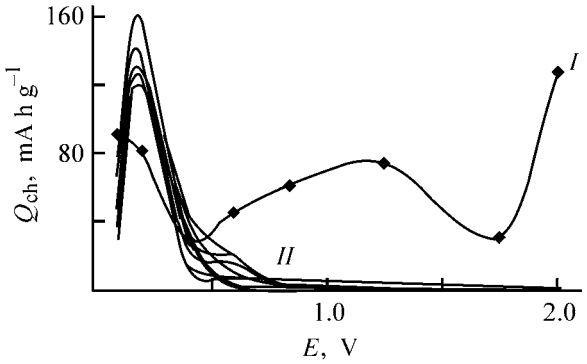


Fig. 6. Distribution of the charging capacity Q_{ch} over the ranges of potentials E. Cycle: (*I*) 1, (*II*) 10, 12–15, 17–19, and 36.

the assumption that the dissolution of the surface layer components is the main reason for the expenditure of electricity for additional charging in operation of a negative electrode, it would be expected that this phenomenon should be diminished at a smaller electrolyte volume.

The stability of the charging–discharge characteristics was determined by cycling an experimental C/Li cell during more than 100 cycles. Figure 4 shows the successively obtained charging–discharge curves for the 12th and 54th cycles, along with the curves measured at different current densities.

As can be seen from Fig. 4, the results are well reproducible at current densities of 35–50 mA g^{-1}. The stable discharge capacity obtained under the indicated electrolysis conditions (200–210 mA h g^{-1}) was retained during the entire period of cycling. The SPG cannot be classed by these values with high-capacity carbons. However, it is well suitable for studies concerned with the fundamental aspects of the behavior of a carbon electrode in SO_2-containing electrolytes.

The charge preservation in storage (self-discharge) is an important electrode characteristic predetermining the retention of a charge imparted to the electrode in the course of time in a stored battery. The dependence of the discharge capacity on the time of storage of a charged electrode is shown in Fig. 5. It can be seen that there is a clearly manifested correlation between the capacity retained by the electrode and the time of its storage in a charged state. Beginning with 20 h of storage this decrease is satisfactorily described by the equation $Q_{day}(\%) = -0.5T + 90$, which corresponds to a daily loss of capacity by about 10%.

To elucidate the reasons for the electrode self-discharge, we superimposed on the plot of self-discharge in Fig. 5 the plot reflecting the disintegration of the surface layer, expressed in the fraction of accumulated irreversible capacity (percent relative to the capacity after the first cycle of charging). Comparison of these curves shows that there is no correlation between the amount of self-discharge and the extent of disintegration of the surface layer. Moreover, the whole self-discharge process occurs within the region in which there is virtually no disintegration of the surface layer. In this context, the self-discharge mechanism requires an independent analysis.

Comparison of the SPG characteristics with the properties of carbons used in commercial products, such as the carbon of the FGC brand (Repsol), shows that a 1 M solution of $LiClO_4$ PC in PC/SO_2 can be used as electrolyte instead of a 1 M solution of $LiPF_6$ in EC/DEC. Also of interest are some other properties of the SPG electrode, observed in a study of the C/Li cell.

The processes occurring in intercalation-deintercalation of lithium ions in the carbon matrix can be judged from the ranges of potentials in which the charging and discharge capacities are formed. As can be seen from Fig. 6, a major part of the charging

capacity is imparted in a narrow range of potentials (0.2–0.4 V). This shows that, as expected in selecting the SPG as the active material, there is no irreversible binding of lithium ions to active centers of impurities in the carbon matrix. The fact that the first charging curve has a significantly different shape reflects the formation of a surface layer.

At the same time, there is no characteristic occurrence range for the discharge capacities. A common feature of all the discharge curves is that the discharge starts at potentials exceeding 0.2 V. The reason is that the potential of the charging curve includes the sum of the potential drops associated with the ohmic and polarization resistances. On switching the circuit to charging, the potential is shifted by 0.2–0.25 V and discharge begins just after this shift.

Information about the influence exerted by the charging–discharge current density on the specific capacity of the electrode makes it possible to optimize the conditions of these processes both by a reasonable choice of the load and by use of the best suitable operation modes of the charging device.

To obtain these data, the charging (and discharge) was performed in separate cycles of the experiment at three current densities: 0.06, 0.1, and 0.127 mA cm^{-2} (35.3; 58.8, and 75.0 mA g^{-1}). Comparison of the portions in which the current density is changed with those of increased Q_i values does not show any noticeable correlation. Thus, it can be stated that the charging–discharge current density has no effect on fluctuations of the irreversible expenditure of electricity in cycling.

The results of an analysis of the charging–dischage curves obtained at various current densities (Fig. 4) are listed in Table 2 as the specific discharge capacity in relation to the discharge current density.

As can be seen from the data presented, the efficiency of the charging–discharge process strongly decreases as the current density increases. Two characteristic features should be noted. At lower current densities the charging capacity is higher, but the efficiency is less than 100%. At higher current densities, the capacity is lower, but the efficiency is 100%.

Comparison of the charging and irreversible capacities shows that the observed decrease in the reversible capacity is a combined effect of the decrease in the charging capacity and the increase in the irreversible capacity (decrease in efficiency). It may be assumed that, as the current density becomes higher, the gradient of concentration in the electrode matrix, from the surface layer into the electrode bulk, gradually increases. In other words, the diffusion flow has not enough time to distribute the intercalated lithium ions throughout the volume of particles constituting the electrode. As a result, the saturation of the surface layer occurs earlier at higher charging current densities and the charging capacity decreases. Accordingly, the whole amount of lithium ions has not enough time to deintercalate and remains in the electrode bulk, which is manifested as an increase in the irreversible capacity.

Table 2. Specific characteristics in relation to current density

I		Q_{ch}	Q_{dis}	Efficiency %	Charge/discharge ratio X
mA g^{-1}	mA cm^{-2}	mA h g^{-1}			
35	0.06	264	206	80	0.7/0.55
50	0.10	264	206	80	0.7/0.55
75	0.127	176	176	100	0.5/0.5
90	0.20	118	118	100	0.3/0.3

The charging current is determined by the design of the charging device. Apparently, its parameters should be determined on the basis of the consumer requirements. Let us consider these requirements for the example of a mobile phone battery. There are two conflicting parameters: weight-size and recharging frequency. If we choose a low charging current density, we should use an excess amount of the cathode material in the battery, which makes it heavier and larger. Choosing a high current density, we force a consumer to charge the power source more frequently. It is a developer's choice.

CONCLUSIONS

(1) A propylene carbonate electrolyte containing SO_2 can be prepared from domestic materials, and its cost will be considerably lower than that of imported electrolytes based on ethylene carbonate. The surface layer formed in the first cycle of charging as a product of SO_2 reduction is similar in properties to the layer formed in electrolytes containing ethylene carbonate.

(2) The expenditure of electricity for loss in the form of irreversible capacity in prolonged cycling of the electrode is zero or insignificant.

(3) The solubility of the components of the surface layer in storage of a discharged electrode is low and, to a first approximation, the self-discharge of a charged electrode is admissible.

(4) The specific capacity of the electrode strongly depends on the charging and discharge current densities. The optimal modes of electrode operation are suggested.

(5) The reproducible operation of a carbon electrode in the electrolyte under consideration is confirmed by its cycling for more than 100 cycles.

(6) Analysis of the charging–discharge characteristics of a carbon electrode in propylene carbonate electrolyte containing SO_2 shows that this electrolyte can be used for development of a long-lived electrode for a lithium ion battery.

ACKNOWLEDGMENTS

The study was supported by the Russian Foundation for Basic Research (project no. 05-03-08 191-ofi_a).

REFERENCES

1. Shembel™, E.M. and Radyushkina, K.A., *Elektrokhimiya*, 1998, vol. 34, pp. 683–688.
2. Kedrinskii, I.A., Podalinskii, Yu.A., and Chudinov, E.A., Abstract of Papers, *8th Int. Frumkin Symp. "Kinetics of Electrode Processes,"* Moscow: Frumkin Inst. Fiz. Khim. Elektrokhim., Ross. Akad. Nauk, 2005, p. 121.

ISSN 1070-4272, Russian Journal of Applied Chemistry, 2006, Vol. 79, No. 12, pp. 1957–1963. © Pleiades Publishing, Inc., 2006.
Original Russian Text © V.N. Esenin, A.A. Stepanov, L.I. Denisovich, 2006, published in Zhurnal Prikladnoi Khimii, 2006, Vol. 79, No. 12, pp. 1980–1987.

APPLIED ELECTROCHEMISTRY AND CORROSION PROTECTION OF METALS

Electrochemical Procedure for Express Evaluation of the Corrosion Effect of Aqueous Glycol Solutions on Metals

V. N. Esenin, A. A. Stepanov, and L. I. Denisovich

Nesmeyanov Institute of Organoelement Compounds, Russian Academy of Sciences, Moscow, Russia

Received March 1, 2006

Abstract—Electrochemical procedure for express evaluation of the corrosion effect of aqueous glycol solutions on the metallic construction materials for cooling systems was studied. This procedure was used to develop new coolant formulations.

DOI: 10.1134/S107042720612010X

Efficient corrosion protection of metals is one of decisive factors determining prolonged and safe operation of various apparatus, installations, and industrial equipment. To select the most appropriate procedures for corrosion protection, preliminarily tests are necessary with the aim to develop measures for prevention or restriction of metal corrosion under the action of an aggressive medium.

At present, the data on the corrosion effect of antifreezing aqueous glycol solutions on the metallic construction materials of various heat-exchange apparatus (in particular, cooling systems of the internal-combustion engines) are of particular importance. Obviously, control over the state of polymetallic construction materials under the action of aggressive media, development of new coolant compositions on water–glycol basis, and prompt quality control of commercial products require an express and reliable evaluation of the corrosion effect of liquids on various structural materials. Such data can be obtained in preliminarily tests on corrosion effect of liquids using an appropriate express procedure.

However, an analysis of published data showed that any appropriate procedure of these preliminarily tests is lacking. At present, the corrosion effect of liquids is often evaluated using procedures of gravimetric and electrochemical analyses.

The tests with electrochemical control are performed both without external polarization [1] and using external polarization of electrodes [2, 3]. Well-developed series of electrochemical procedures for evaluation of the metal corrosion also involves the method of polarization resistance and coulostatic procedure [4, 5]. The data on electrochemical impedance allow detailed analysis of the corrosion mechanism [6], and the procedure of impedance spectroscopy is the most widely used for studying the corrosion behavior of metals [7]. Computer techniques for recording and processing of experimental results promote development of various pulse procedures to study corrosion phenomenon and, in particular, the pulse galvanostatic method [8, 9].

Among all the above electrochemical procedures, only the Evans method of corrosion diagrams [10] allows study of the direct contact corrosion in polymetallic systems. This rather complex procedure involves recording of curves of anodic and cathodic polarization for each metal of the multielectrode system, their combined processing, and plotting of the resulting corrosion diagram, from which the maximum possible current strength is determined. Then, using the known surface areas of the metal electrodes and neglecting the ohmic loss, the corrosion rate is calculated. It is assumed that the cathode remains unchanged and the rate of the anode corrosion is proportional to the strength of the local current.

However, a study of the contact corrosion by the above procedure has significant drawbacks, because it disregards the self-dissolution of the anode

and cathode, which strongly affects the corrosion processes in many cases. Moreover, certain contradiction is inherent in the Evans diagram, because, in the case of a completely polarized system, the difference of potentials of the anode and cathode is zero, whereas the strength of the local current in the absence of electromotive force reaches a maximum value.

Experimental data obtained using gravimetric methods seem to be more reliable for studying the corrosion behavior of metals at their prolonged storage in aggressive media, especially in the course of the corrosion processes changing with time.

A series of international [11, 12] and Russian [13, 14] gravimetric procedures can be used to evaluate the corrosion effect of antifreezing and process liquids. The procedure with gravimetric control [GOST (State Standard) 28 084 – 89] is the most reliable and widely used domestic laboratory method for evaluation of the corrosion effect of aqueous glycol solutions on metals. However, owing to the prolonged analysis time (336 h) and significant measurement errors (up to 28–50%, depending on the metal nature), this procedure is unacceptable for express evaluation of the metal corrosion.

Thus, the aim of this study was to develop a proximate laboratory method combining a certain promptness of electrochemical methods with the simplicity and reliability of gravimetric analysis and to study the corrosion effect of the aqueous glycol solutions on polymetallic construction materials for cooling systems of internalcombustion engines.

EXPERIMENTAL

Plates (50 × 25 × 3 mm) of St. 3 steel (GOST 380), GH-190 cast iron (normal VAZ 52 205), AK6M2 aluminum alloy (GOST 1583), M-1 copper (GOST 859), POS-35 solder [TU (Technical Specifications) 48-13-10], and L-63 brass (GOST 931) were polished and degreased, and their electrochemical behavior was studied in a 50% solution of monoethylene glycol (MEG) in water containing anhydrous sodium sulfate (148 mg l^{-1}), sodium chloride (165 mg l^{-1}), and sodium hydrocarbonate (138 mg l^{-1}) at 20 ± 2°C.

The tests were carried out in a specially designed electrochemical cell in the form of a 150-ml cylindrical vessel with a plastic lid equipped with electrode holders (one at the center for a cathode and three for anodes at equal distances from each other and from the center, with the anode holders short-circuited). Standard metal plates with a working surface area of 10 cm^2 were used as anodes, and a carbon rod (18 mm in diameter), as a cathode.

The current of the electrochemical couple was measured with an M 198/2 microammeter. Simultaneously, we measured, using a digital high-resistance voltmeter Shch 1413, changes in the electrode potentials of metals with time both in the absence of electrical contacts between them and in couples short-circuited through an external low-resistance conductor. We used a silver chloride reference electrode.

In accordance with a gravimetric procedure (GOST 28 084–89), to simulate the galvanic couples operating under the real conditions, three metallic plates are connected with each other (e.g., copper–brass–solder and steel–cast iron–aluminum) and kept in a corrosive medium studied for 336 h, and then the corrosion effect is determined from the changes in the sample weights. In our approach to the development of the express evaluation, the same set of metal samples were placed in the solution for galvanostatic treatment for a certain time in which the metals were subjected to anodic dissolution. This should strongly decrease the time of corrosion tests. The corrosion effect of the liquid in question was determined from the changes in the sample weights; in this case, the nature of corrosion (e.g., selective, intercrystallite pitting, etc.) was disregarded. We selected the mode of galvanostatic dissolution of the metals because the electrochemical methods with external potentiostatic polarization, which are frequently used in laboratory practice to study the corrosion processes, are rather convenient but require a sophisticated laboratory equipment.

To substantiate this approach, we first studied the anodic polarization of the metal samples in question in the aqueous glycol solution in the potentiostatic mode and found that the current in the electrolytic cell varied insignificantly (by no more than ±10%) with time in a fairly wide range of potentials (0.5–10.0 V). This result indicates that corrosion tests can be performed in the galvanostatic mode.

For further substantiation, it is also necessary to simulate anodic dissolution of the materials studied in the aqueous glycol solutions containing corrosion inhibitors in such a mode that would give results comparable with the gravimetric data according to GOST 28 084 – 89. For this purpose, we studied the dependence of the weight loss by individual standard metal samples in aqueous MEG solution at given current densities. We found that this dependence is linear

Table 1. Metal corrosion loss in aqueous glycol solutions at different current densities

Current density, mA cm^{-1}	Corrosion loss, mg					
	solder	copper	brass	aluminum	steel	cast iron
0.25	4.4* 4.2			0.6 0.8		
0.5	9.0 8.3	3.0 3.0	2.9 3.0	1.1 1.7	5.1 5.2	5.3 5.2
1.0	17.2 16.5	5.9 6.0	5.8 6.0	1.8 3.4	10.5 10.4	10.6 10.4
1.5	25.6 24.8	9.0 8.9	9.1 9.0	1.7 5.0	15.5 15.6	16.0 15.6
2.0	34.8 33.0	11.8 11.9	12.0 12.0	1.6 6.7	21.0 20.8	21.1 20.8
2.5	42.6 41.3	15.0 14.9	15.2 15.0		25.9 26.0	26.5 26.0
3.0	52.1 49.5	17.8 17.9	17.6 18.0	1.6 10.1	30.6 31.2	31.8 31.2
4.0		23.9 23.8	23.9 24.0	2.0 13.4	40.9 41.6	
5.0				1.7 16.7		53.8 52.0

* Experimental and calculated data are given in the numerator and denominator, respectively.

in a fairly wide range of current densities (Fig. 1), and, except the aluminum sample, reasonably agreed with the calculated data listed in Table 1.

The above data unambiguously suggest that only anodic dissolution of metals acting as working electrodes is observed, and the weight loss by the metal samples corresponds to the corrosion rate.

The certain discrepancy between the experimental and calculated data for aluminum in a wide range of current densities is probably due to the formation of a compact oxide films on the metal surface, which prevents aluminum dissolution. Actually, the experimental results and calculated values of the weight loss of the aluminum samples coincide at low current densities (i = 0.25 mA cm^{-2}) within the measurement error. However, with increasing current density ($i \geq$ 1.0 mA cm^{-2}), the deviation between the experimental and calculated values grows. The weight loss becomes independent of the current densities and, beginning with $i \geq 3.0$ mA cm^{-2}, an "cut-off" of the aluminum anode is observed (Fig. 2).

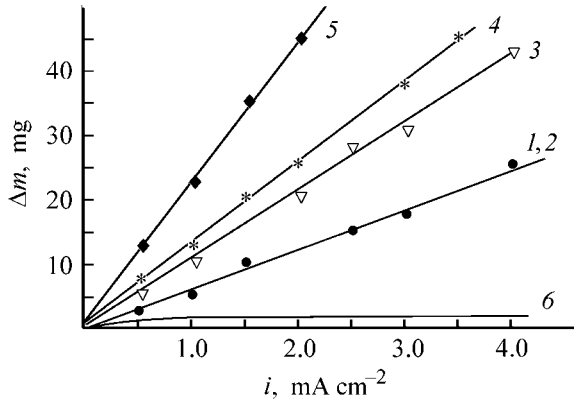


Fig. 1. Metal corrosion loss Δm vs. the current density i. Metal: (*1, 2*) Brass, (*3*) steel, (*4*) cast iron, (*5*) solder, and (*6*) aluminum.

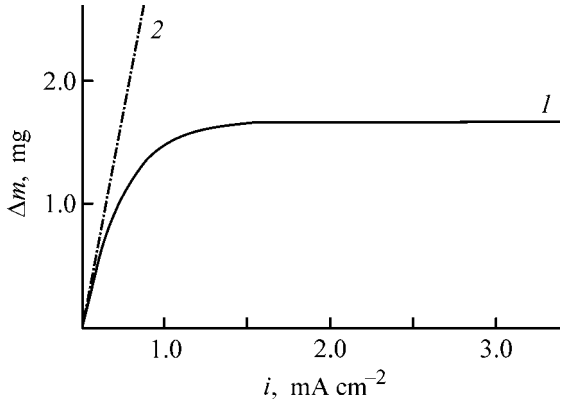


Fig. 2. Aluminum corrosion loss Δm vs. the current density i in the course of anodic polarization. Data: (*1*) experimental and (*2*) calculated.

Table 2. Corrosion weight loss by copper, brass, and solder samples in various electrolysis modes in the CC–water mixture

Test no.	i, mA cm^{-2}	τ, min	Weigh loss by anode, mg		
			copper	brass	solder
1	5.0	60	12.0	28.8	22.8
2	1.0	60	0.0	0.0	3.2
3	1.5	60	0.9	0.2	4.0
4	3.0	30	1.8*	2.0*	1.8*
5	–	–	1.3**	2.9**	1.7**

* Average over 20 tests.

** Gravimetric data.

Table 3. Corrosion loss by aluminum, steel, and cast iron samples at their anodic polarization in the CC–water mixture

i, mA cm^{-2}	τ, min	Weigh loss, mg		
		aluminum	steel	cast iron
2.0	60	0.0	0.0	0.0
3.0	60	0.0	0.0	0.0
7.0	120	0.0	6.1	10.0

This behavior of aluminum can be accounted for by the fact that, in the course of anodic polarization, aluminum oxidation proceeds simultaneously with the metal ionization on the electrode. With increasing polarization, the degree of the surface oxidation increases and at a certain current density (or potential) an oxide film completely covers the electrode surface. The diffusion of aluminum ions into solution through the oxide film becomes hindered, and the rate of anodic dissolution decreases. As a result of these two opposite factors, the rate of aluminum anodic dissolution remains nearly constant, being almost independent of the current density.

In view of the above data, we performed two series of experiments. In the first series, copper, brass, and solder were connected in parallel as anodes, and an inert material (graphite) was used as a cathode. The electrolyte was a Procor 3000 coolant concentrate (CC) (PEUGEOT, France) diluted with water to a 1 : 1 volume ratio, whose corrosion effect on the metal materials was reliably determined using standard gravimetric methods (GOST 28 084 – 89). As optimal, we used the electrolysis mode providing a corrosion weight loss by the metal samples that was comparable with the loss in gravimetric tests; the results are listed in Table 2.

As can be seen from Table 2, a decrease in the sample weight in the course of anodic dissolution strongly depends on the current density, i.e., on the anode potential. At low current densities (and, accordingly, at low potentials) the solder dissolution is mainly observed, which is probably due to the lower standard potential of tin. High currents densities ($i \geq 3.0$ mA cm^{-2}) allow simulation of the gravimetric data (test nos. 1, 4). To minimize changes in the surface state and, thus, in the surface area upon dissolution of the sample, we chose the following optimal conditions of the corrosion tests: 3.0 mA cm^{-1} current density and 30 min test time.

Electrochemical simulation of corrosion using the other three metals (steel–cast iron–copper) as anodes appeared to be difficult. Tests on the anodic dissolution in the CC–water mixture (as in the above case of anodic dissolution of aluminum in the aqueous glycol solution) of a separate aluminum plate, as well as of the aluminum plate connected in parallel with iron and steel plates, showed that no dissolution of aluminum occurred even at high current densities (Table 3). At the same time, the gravimetric data showed that the loss of aluminum in given system was about 2.5 mg.

It has been found previously [15–19] that the effective dissolution rate of various metals in aqueous solutions cannot be fitted by the exponential dependence of the current density on the potential, which is untypical of electrochemical processes. The current densities were higher than the expected values, which suggests that another process of metal dissolution occurs concurrently with electrochemical process. It was experimentally observed in the range of cathodic polarization as a deviation of the anodic partial current density from the Tafel dependence toward high current densities. The rate of partial anodic dissolution at a stronger cathodic polarization was almost independent of the potential. These experimental facts suggest that this process, occurring simultaneously with the electrochemical reaction, is chemical dissolution. In the case of cathodic polarization it becomes predominant, because the anodic partial current density exponentially decreases with increasing negative potential. A similar abnormal dissolution has been observed for several other metals, including aluminum [20]. The tendency of metals to dissolve in this way is associated with their electronic structure, and the chemical dissolution is due to direct reaction between the metal and water.

Indeed the metal actively dissolves with vigorous hydrogen evolution on the electrode surface in cath-

odic polarization of the aluminum sample in both aqueous and aqueous glycol solutions. The dependence of the corrosion weight loss by aluminum on the current density is shown in Fig. 3.

Significant difference between the types of behavior of aluminum in its cathodic dissolution in water and an aqueous glycol solution is probably due to the changes in the structure of the electric double layer upon adsorption of ethylene glycol, whose molecules can form compact shielding film owing to the planar arrangement on the electrode surface [21, 22]. Moreover, ethylene glycol (similarly to other polyatomic alcohols) strongly increases the viscosity of solutions and hinders the diffusion stages of the cathodic reactions [23].

Thus, cathodic polarization of aluminum in aqueous glycol solutions causes dissolution of the oxide film on the surface of the metal and is accompanied by its chemical corrosion. Based on the above data, the model of the corrosion behavior of the steel–cast iron–aluminum in aqueous glycol solutions can be described as that of a three-electrode system in which the aluminum plate acts as cathode, and steel and cast iron plates, as anodes.

Corrosion currents in the aluminum–steel and aluminum–cast iron couples were observed when studying the corrosion behavior in the short-circuited steel–cast iron–aluminum system in an aqueous glycol solution without external polarization (Fig. 4, curves *5*, *6*). Our experimental results showed that, after keeping the given electrochemical system in the aqueous glycol solution for 12–15 h, the aluminum sample becomes a cathode with respect to both steel and cast iron samples. This suggests that the use of aluminum cathode to determine the corrosion effect of aqueous glycol solutions on metals is quite reasonable. To determine the possibility of simulation of the gravimetric tests, we performed the electrolysis of the CC–water mixture, using an aluminum cathode and an anode consisting of the steel and cast iron plates connected in parallel; the results are listed in Table 4.

As can be seen from Table 4, at a current density i = 7.0 mA cm^{-2} the corrosion metal loss is high, and the results are insufficiently reproducible, whereas at i = 5.0 mA cm^{-2}, our experimental results well agree with the gravimetric data. Thus, the operation conditions for electrochemical simulation of the aluminum corrosion were as follows: current density 5.0 mA cm^{-2} and time 60 min.

For the electrochemical procedure, the relative total error of our experimental results at a confidence level P = 0.95 for all the metals studied does not exceed

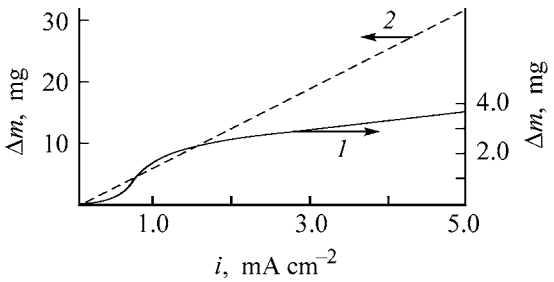


Fig. 3. Aluminum corrosion loss Δm vs. the current density i in the course of cathodic polarization. Polarization: in (*1*) MEG : water (1 : 1) solution and (*2*) water.

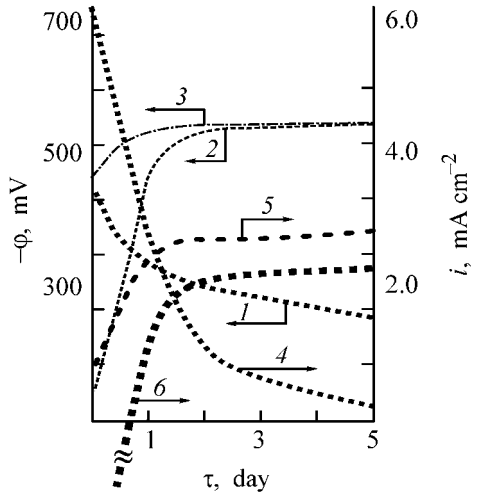


Fig. 4. Electrode potentials φ and current density i in the short-circuited aluminum–cast iron–steel system vs. time τ. Potential of: (*1*) aluminum, (*2*) steel, and (*3*) cast iron; current density in the contact couple: (*4*) steel–cast iron, (*5*) aluminum–cast iron, and (*6*) aluminum–steel.

± 15%, whereas for the gravimetric method, it is greater in accordance with GOST 28 084 – 89: ± 28% for copper, brass, aluminum, cast iron, and steel and ± 50% for solder.

Table 4. Corrosion weight losses by aluminum (cathode) and steel and cast iron (anode) samples in the CC–water mixture

i, mA cm^{-2}	τ, min	Weigh loss, mg		
		aluminum	steel	cast iron
7.0	60	3.2 4.6	2.3 2.9	3.3 5.4
5.0	60	4.9 2.5* 2.5**	0.8 0.8* 0.5**	3.8 1.8* 1.5**

* Average over 20 tests.

** Gravimetric data.

Table. 5. Corrosion weight loss by metals in 50% aqueous solutions of TOSOL–TORSA and TOSOL-AM concentrate

Test procedure	Weight loss, mg					
	solder	copper	brass	aluminum	steel	cast iron
TOSOL–TORSA						
Galvanostatic	16.8 ± 2.6	3.1 ± 0.4	3.4 ± 0.5	2.5 ± 0.3	2.3 ± 0.3	2.6 ± 0.2
Gravimetric	15.3 ± 3.2	2.6 ± 1.1	2.1 ± 0.4	2.1 ± 0.7	2.5 ± 1.1	2.8 ± 1.2
TOSOL-AM						
Galvanostatic	3.3	8.1	3.2	3.2	1.4	2.1
Gravimetric	4.5	7.0	4.0	5.1	1.9	2.3

Table 6. Effect of inhibitors on the corrosion loss by metals in 50% aqueous MEG solutions

Solution component	Weight loss, mg					
	solder	copper	brass	aluminum	steel	cast iron
Without additives	17.4	3.2	3.4	4.3	22.1	34.6
$Na_2HPO_4 \cdot 12H_2O$	1.4	3.7	3.9	2.5	0.3	2.6
$Na_2B_4O_7 \cdot 10H_2O$	27.4	5.1	3.1	0.7	11.0	6.8
$Na_2B_4O_7 \cdot 10H_2O$, $Na_2HPO_4 \cdot 12H_2O$	25.9	3.2	3.0	1.3	1.3	1.7
Sodium benzoate	7.8	3.9	4.1	3.4	5.1	6.6
Sodium benzoate, sodium tetraborate	4.4	3.5	2.9	3.3	3.3	2.0

Thus, our experimental data allow us to suggest a procedure for express analysis of corrosion processes, involving galvanostatic dissolution of metals in the medium under study in the course of 30–60 min and gravimetric control of the corrosion weight loss.

The suitability of this express procedure for studying the corrosion effect of various coolants was tested using industrial TOSOL–TORSA concentrate (TU 6-15-2007–98, Bulgar-Sintez Joint-Stock Company, Kazan, Russia) and widely used TOSOL-AM concentrate (TU 6-02-751–86). The metal samples were tested in 50% aqueous solutions of coolants, which were prepared from their concentrates by direct dilution with water. The results obtained using our express method were compared (Table 5) with the averaged data furnished by the gravimetric method (GOST 28084–89).[1]

[1] Experimental data were obtained at the State Research Institute no. 25, Laboratory and Test Department, AVTOVAZ Joint-Stock Company (Togliatti, Russia) and Center of Laboratory Installations, Kazan'orgsintez Joint-Stock Company (Kazan, Tatarstan, Russia).

As can be seen from Table 5, the corrosion losses in both liquid systems determined by two methods well agree with each other. This fact shows that our method is suitable for express evaluation of the corrosion effect of glycol aqueous solutions on construction materials for cooling systems of internal-combustion engines.

Our method was used to evaluate the performance of the corrosion inhibitors with the aim to develop new coolant formulations. For example, a significant drawback of the TOSOL–TORSA coolant concentrate, whose main components are disodium hydrogen phosphate and sodium tetraborate, is the relatively high corrosion activity with respect to solder. At the same time, TOSOL-AM concentrate containing sodium benzoate and tetraborate (corrosion inhibitors) exhibits no corrosion activity toward the solder (Table 6). It was suggested that addition of sodium benzoate to the TOSOL–TORSA coolant would improve its anticorrosive properties toward solder.

Table 6 illustrates the effect of corrosion inhibitors used in the coolant concentrates in similar concentrations on the corrosion behavior of metals in aqueous

Table 7. Effect of sodium benzoate on the corrosion weight losses by metals in 50% aqueous solution of TOSOL–TORSA concentrate

Sodium benzoate, wt %	Weight loss, mg					
	solder	copper	brass	aluminum	steel	cast iron
0.00	16.8	3.1	4.4	2.5	2.3	2.6
0.10	3.9	3.0	3.8	2.6	2.9	2.7
0.20	2.9	3.1	3.5	2.8	2.5	2.1
0.20*	2.6	2.7	3.2	0.8	3.4	2.5

* Measurements were performed in accordance with GOST 28084–89.

glycol solutions. As can be seen from Table 7, the corrosion loss of solder strongly decreases with addition of sodium benzoate (≥0.1 wt%) to 50% aqueous solution of commercial TOSOL-TORSA concentrate.

CONCLUSIONS

(1) An electrochemical procedure based on galvanostatic dissolution of metals was developed for preliminarily express evaluation of the corrosion effect of aqueous glycol solutions on metallic construction materials for cooling systems.

(2) This method can be used to evaluate the performance of corrosion inhibitors.

REFERENCES

1. Electrochemical Method for Evaluation of the Rates of Contact Metal Corrosion, *Report of the State Inter Departmental Commission on the Tests of Fuels, Oils, Lubricants, and Special Liquids*, Moscow: 1986, no. 23/1-169.
2. Levin, A.I., *Teoreticheskie osnovy elektrokhimii* (Theoretical Bases of Electrochemistry), Moscow: Metallurgiya, 1972.
3. Batrakov, V.P. and Polupanov, V.L., *Elekrokhimiya*, 1975, vol. 11, no. 6, pp. 919–923.
4. Mansfeld, F., *Corrosion*, 1974, vol. 30, no. 1, pp. 92–94.
5. Susuki, M. and Sato, I., *Werstoff Korros.*, 1980, vol. 31, no. 4, pp. 364–370.
6. Stoinov, Z.B. and Grafov, B.M., *Elektrokhimicheskii impedans* (Electrochemical Impedance), Moscow: Nauka, 1991.
7. Safonov, V.A., *Elekrokhimiya*, 1993, vol. 29, no. 1, pp. 152–154.
8. Glas, G.K., Page, C.L., and Short, N.R., *Corros. Sci.*, 1993, vol. 35, pp. 1585–1591.
9. Law, D.W., Millard, S.G., and Bungey, J.H., *Corrosion*, 2000, vol. 56, pp. 48–51.
10. Evans, U.R., *Metallic Corossion, Passivity and Protection*, London: Arnold, 1946.
11. *ASTM D-1384*: "Standard Test method for Corrosion Test for Engine Coolants in Glassware."
12. *Werkstoffprufung*, Blumenauer, H., Ed., Leipzig: Grundstoffindustrie, 1976. Translated under the title *Ispytanie materialov: Spravochnik*, Bernshtein, M.L., Ed., Moscow: Metallurgiya, 1979.
13. *GOST* (State Standard) *6243–75: Emulsions and Pastes, Test methods*, Moscow: Izd. Standartov, 1975.
14. *GOST* (State Standard) *28084–89: Cooing Antifreezing Liquids, General Technical Specifications*, Moscow: Izd. Standartov, 1989.
15. Florianovich, G.M. and Kolotyrkin, Ya.M., *Dokl. Akad. Nauk SSSR*, 1964, vol. 157, no. 2, pp. 422–426.
16. Kolotyrkin, Ya.M. and Florianovich, G.M., *Zashch. Met.*, 1965, vol. 1, pp. 7–12.
17. Florianovich, G.M.,Agladze, T.R., Sokolova, L.A., et al., *Elektrokhimiya*, 1973, vol. 9, no. 7, pp. 988–995.
18. Kolotyrkin, Ya.M. and Florianovich, G.M., *Z. Phys. Chem.*, 1966, vol. 231, pp. 145–148.
19. Knyazheva, V.M., Kolotyrkin, Ya.M., and Kruchkovskaya, A.A., *Zashch. Met.*, 1970, vol. 6, pp. 265–269.
20. Kuznetsova, O.P., Grubenko, T.V., and Zhuk, N.P., *Zashch. Met.*, 1975, vol. 11, pp. 321–324.
21. Kuznetsov, Yu.I., Oleinik, S.V., and Rozenfel'd, I.L., *Elektrokhimiya*, 1981, vol. 17, no. 6, pp. 942–945.
22. Dzhaparidze, Dzh.I., *Elektrokhimiya*, 1977, vol. 13, no. 5, pp. 668–671.
23. Rozenfel'd, I.L., Persiantseva, V.P., and Kuznetsov, Yu.I., *Zashch. Met.*, 1970, vol. 6, pp. 677–681.

ISSN 1070-4272, Russian Journal of Applied Chemistry, 2006, Vol. 79, No. 12, pp. 1964–1968. © Pleiades Publishing, Inc., 2006.
Original Russian Text © Yu.K. Pirskii, V.S. Kublanovskii, D.V. Shevchenko, V.N. Kokozei, 2006, published in Zhurnal Prikladnoi Khimii, 2006, Vol. 79, No. 12, pp. 1988–1992.

APPLIED ELECTROCHEMISTRY AND CORROSION PROTECTION OF METALS

Catalytic Electroreduction of Oxygen on Products of Pyrolysis of Heterobimetallic Complexes of Zinc

Yu. K. Pirskii, V. S. Kublanovskii, D. V. Shevchenko, and V. N. Kokozei

Vernadskii Institute of General and Inorganic Chemistry, National Academy of Sciences of Ukraine, Kiev, Ukraine

Taras Shevchenko National University, Kiev, Ukraine

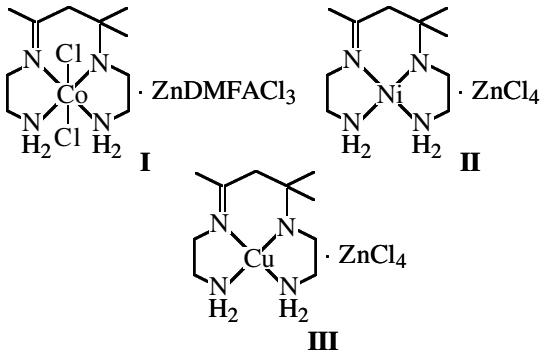
Received August 2, 2006

Abstract—Electrocatalysts for reduction of oxygen were synthesized from AG-3 activated carbon promoted with pyrolized heterobimetallic complexes $[CoLCl_2]$ $[ZnDMFACl_3]$ and $[ML][ZnCl_4]$ (M = Cu^{2+}, Ni^{2+}; L = 4,6,6-trimethyl-1,9-diamino-3,7-diaza-nona-3-ene). The optimal conditions of synthesis of the catalysts, which affect the efficiency of oxygen electroreduction, were found and the activity series of the catalyst in relation to the nature of the second metal was determined.

DOI: 10.1134/S1070427206120111

Use of binuclear or heteropolynuclear complexes as precursors in synthesis of reduction electrocatalysts provides better and more stable characteristics in fuel cells and chemical power cells, compared with mononuclear complex compounds [1–3]. The interest in catalysts based on polynuclear complexes is exhibited by scientists in many countries of the world [4]. Catalysts based on mononuclear complexes [5] of phthalocyanine, porphyrin, and some other chelate complexes with *d*-elements are well known, the most active catalysts have been obtained on the basis of cobalt complexes.

Catalysts are commonly synthesized by adsorption of a complex on the support surface, with its subsequent thermal treatment in an inert atmosphere. Pyrolysis in an inert atmosphere of complexes that incorporate ligands coordinated to central atoms via oxygen atoms yields electrocatalysts having active centers in the form of nonstoichiometric metal oxides on the surface of the carbon support [1]. In contrast to spinels, these oxides are more active because they form nanostructures on the support surface, whereas spinels are crystals with poor electrical conductivity [6]. Complexes with ligands coordinated to the central atom via nitrogen atoms enable imitation of pyropolymers produced on the basis of N_4-complexes [7]. They approach in electrical activity the known complexes, but are less expensive in manufacture than porphyrin and phthalocyanine complexes of *d*-elements. Use of heterobimetallic complexes combining different *d*-metals and ligands will make it possible to obtain new high-efficiency electrocatalysts for oxygen reduction and replace some expensive or noble metals. As shown in [3], heteropolynuclear complexes with copper and zinc are good precursors for high-efficiency catalysts, and, therefore, the following heterobimetallic complexes produced by direct template synthesis [8] were used to obtain electrocatalysts for oxygen reduction:



where $[CoLCl_2]$ $[ZnDMFACl_3]$ (**I**) and $[ML][ZnCl_4]$ [M = Ni^{2+} (**II**), Cu^{2+} (**III**); L = 4,6,6-trimethyl-1,9-diamino-3,7-diaza-nona-3-ene].

The aim of this study was to examine the influence exerted by the nature of the second metal in heterobimetallic complexes of zinc (Zn^{2+}–M, where M = Cu^{2+}, Ni^{2+}, Co^{2+}) in the reaction of oxygen reduction on

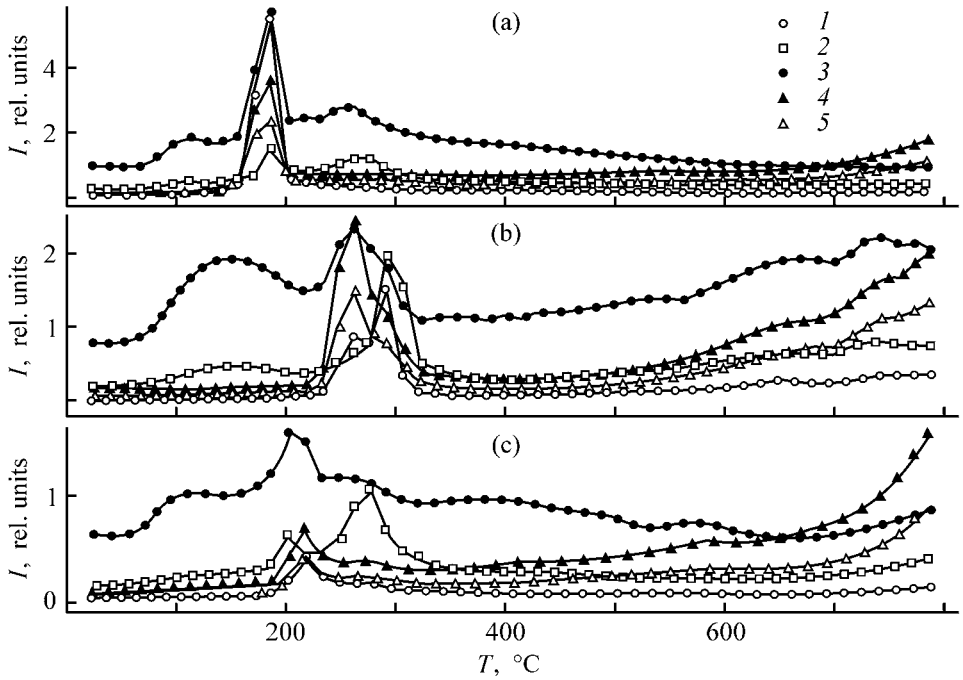


Fig. 1. Thermodesorption mass spectra of the complexes (a) [CoL] [$ZnDMFACl_3$], (b) [NiL][$ZnCl_4$], and (c) [CuL][$ZnCl_4$] in a vacuum at a residual pressure of 10^{-6} Pa and heating rate of 10 deg min^{-1}. (*I*) Ionic current and (*T*) heating temperature. *m/z*: (*1*) 15, (*2*) 17, (*3*) 18, (*4*) 28, and (*5*) 29.

the electrocatalytic properties of catalysts produced by the thermal method.

EXPERIMENTAL

To obtain electrocatalysts, heterobimetallic complexes of zinc, **I**–**III**, were synthesized by direct template synthesis [8]. The complexes were dissolved in dimethylformamide and adsorbed on AG-3 high-porosity carbon with a dispersity of less than 50 μm and specific surface area of 850 $m^2 g^{-1}$ (measured by BET). Then, the carbon materials with deposited complex compounds were thermally treated at various temperatures (in the range 200–800°C) in the atmosphere of argon. For this purpose, a 100-mg portion of AG-3 carbon with an adsorbed complex was placed in a tubular quartz furnace through which argon was permanently passed and was gradually heated to a prescribed temperature and kept under these conditions for 1 h. The samples were thermally treated at temperatures of 200, 400, 600, and 800°C and then their catalytic activity in the reaction of oxygen electroreduction was studied.

To determine the composition of products formed in pyrolysis of complexes on the surface of the carbon support, thermal analysis of complexes **I**–**III** was made on a Q-1500D derivatograph (MOM, Hungary). The analysis was performed under the following conditions: weighed portion 500 mg, TG galvanometer sensitivity 500, phase transformations fixed in the range 10–800°C at a heating rate of 5 deg min^{-1} in the atmosphere of argon. Freshly calcined Al_2O_3 served as reference. In a thermal analysis with a large amount of a complex at 180–220°C, the contents of the platinum crucible were ejected because of the pronounced exothermic effect with destruction of the ligand 4,6,6-trimethyl-1,9, diamino-3,7-diaza-nona-3-ene. Therefore, thermal analysis was performed for all the samples in the presence of Al_2O_3 taken in the proportion Al_2O_3 : complex = 0.04 g : 0.16 g. The final products of pyrolysis were analyzed for the content of hydrogen, nitrogen, and carbon, with the result of analysis of the starting complexes taken into account.

The starting complexes were examined by the method of thermal desorption with mass-spectrometric analysis of the species being desorbed on an MX-1302 mass spectrometer under the following conditions: heating temperature 20–800°C, heating rate 10 deg min^{-1} residual pressure 10^{-6} Pa, weighed portion of a complex 1 mg.

The thermal destruction of complex **I** begins with decomposition of dimethylformamide at 50–180°C, which corresponds to loss of 15.1% of the total mass of the complex. In this temperature range, the mass spectrometer records products of pyrolysis, such as NH_4^+, NH_3, CH_3^+. The thermodesorption mass spectra of complex **I** are shown in Fig. 1a. Because the spec-

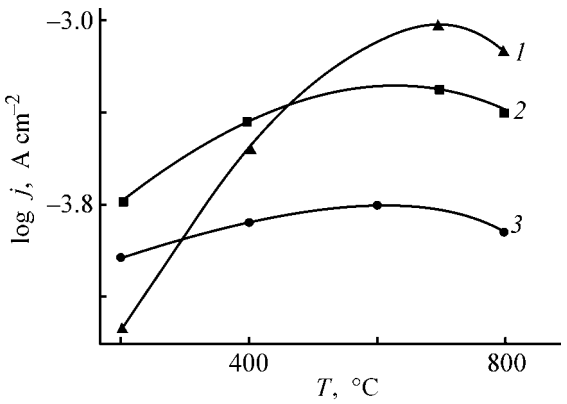


Fig. 2. Rate of oxygen electroreduction on catalysts formed by pyrolysis of heterobimetallic complexes on AG-3 in a 1 M KOH solution at 20°C vs. the pyrolysis temperature *T*. (*j*) Current density. Potential $E = -0.1$ V relative to Ag/AgCl reference electrode. Complex: (*1*) [CuL][$ZnCl_4$], (*2*) [NiL][$ZnCl_4$], and (*3*) [CoL][$ZnDMFACl_3$].

tra are rather intricate, Fig. 1 shows for all the complexes only selected data for species with *m*/*z* less than 29. The mass-spectra clearly show the temperature ranges in which the intensity of pyrolysis of the complexes under study is the highest. At 180–220°C occurs partial decomposition of the ligand (4,6,6-trimethyl-1,9-diamino-3,7-diaza-nona-3-ene) and the thermogravimetric curve demonstrates a considerable loss of mass (12.2%). The mass spectra reveal splitting-off of the following species: NH_4^+, NH_3, CH_3^+, $CH–NH_2^+$, $CH–NH^+$, $CH_2–CH_2^+$, etc. Some of the species desorbed add a Cl^- ion to form species with *m*/*z* exceeding 36. Molecular Cl_2 formed in pyrolysis may be present in decomposition products in minor amounts, with *m*/*z* of 69, 70, 71. In the following stage of pyrolysis (220–280°C) continues decomposition of the ligand and zinc oxide starts to be formed. In the range 280–620°C occurs full decomposition of the organic ligand to give the final product in the form of a mixture $CoCl_2$ + ZnO, which is confirmed by the results of elemental and thermal analyses.

The thermolysis of complex (**III**) begins with decomposition of 4,6,6-trimethyl-1,9-diamino-3,7-diaza-nona-3-ene. In the temperature range 100–240°C, the mass spectrometer records (Fig. 1c) such desorption products as NH_4^+, NH_3, CH_3^+, $CH–NH_2^+$, $CH–NH^+$, $CH_2–CH_2^+$ and chlorine-containing species with heavier mass (loss of mass was 15.1% of the total mass of the complex). At 240–550°C, the decomposition of the organic ligand is complete (37.6%) to give pyrolysis products containing $ZnCl_2$ and fragments of a compound of copper and nitrogen.

Complex (**I**) is more thermally stable. Its destruction also begins with decomposition of the ligand L in the range 130–320°C (15.1%). The decomposition products are similar for complexes **I**–**III** (Fig. 1b). In the range 320–710°C, the decomposition of the ligand L is complete (43.1%) to give pyrolysis products in the form of a mixture Ni + $ZnCl_2$.

The substances obtained were analyzed in the reaction of electrochemical reduction of oxygen in a three-electrode electrochemical cell (with 1 M KOH solution and separated cathode and anode spaces) by the method of the "floating" gas-diffusion electrode [9] at 20°C. The floating gas-diffusion electrode had the form of a pellet of hydrophobized acetylene black containing 30 wt % polytetrafluoroethylene, with a mass of 300 mg, density of 0.95 g cm^{-3}, diameter of 10 mm, and thickness of 2 mm, compacted under a pressure of 5–7 MPa. A nickel-wire current lead was embedded in the pellet. A layer of an electrocatalyst under study, with a particle size of less than 20 μm, was deposited in an amount of 1 mg cm^{-2} onto the electrode surface and compacted under a pressure of 5–6 MPa. This amount of the catalyst provided a kinetic mode of the electrochemical reaction [10]. The catalyst was retained on the surface of the support by adhesion forces. Polarization curves were measured in the potentiostatic mode on a PI-50-1.1 potentiostat with a step of 10 mV. The current was recorded with an M 2020 milliammeter.

The activity was evaluated by the current of oxygen reduction, observed at a potential of –0.10 V, and by the slope of the polarization curve, $\partial E/\partial \log j$ (b_1; b_2). The kinetic characteristics of oxygen electroreduction on the catalyst, obtained in the study, are listed in the table. Dependences of the rate of oxygen electroreduction at a constant potential $E = -0.1$ V on the temperature at which the electrocatalysts based on heterobimetallic complexes were synthesized are shown in Fig. 2. It can be seen from Fig. 2 and the table that the highest current of oxygen reduction is observed for the catalysts obtained from heterobimetallic complexes of copper and zinc at 700°C. It is known that electrocatalysts produced from porphyrin and phthalocyanine complexes [5, 11, 12] at $T \le 800$°C form active centers in which the MN_4 structure is preserved, and its chemical bonding with the carbon support is assumed.

Thus, 700–800°C is the optimal temperature range for production of active catalysts from complexes based on copper–zinc heterobimetallic complexes, which decompose in an inert atmosphere on the carbon surface and, probably, also form metal-and-nitrogen-

Kinetic parameters* of electrocatalytic reduction of oxygen on catalysts formed by pyrolysis of heterobimetallic Zn^{2+}–M complexes (M = Cu^{2+}, Ni^{2+}, Co^{3+}) in 1 M KOH at 20°C

Catalyst	T, °C	E_{st}, V	j_0, A cm^{-2}	$\partial E/\partial \log j$, V	
				b_1	b_2
AG-3	–	–0.094	1.2×10^{-9}	0.045	0.110
Cu–Zn(AG-3)	200	–0.105	5.6×10^{-8}	0.049	0.114
	400	–0.049	3.5×10^{-6}	0.049	0.115
	700	–0.045	7.5×10^{-6}	0.060	0.098
	800	–0.046	4.4×10^{-6}	0.060	0.098
Ni–Zn(AG-3)	200	–0.110	5.7×10^{-7}	0.050	0.117
	400	–0.052	8.1×10^{-7}	0.049	0.108
	700	–0.084	1.4×10^{-6}	0.049	0.115
	800	–0.075	3.2×10^{-7}	0.047	0.118
Co–Zn(AG-3)	200	–0.031	3.2×10^{-7}	0.053	0.116
	400	–0.021	9.5×10^{-7}	0.054	0.116
	700	–0.087	3.0×10^{-6}	0.053	0.115
	800	–0.069	1.0×10^{-6}	0.052	0.117

* j_0, exchange current density; b_1, b_2, slopes of steady-state polarization curves.

containing pyrolysis products bound to the carbon surface. In this case, the most active electrocatalysts for oxygen reduction are formed from Cu–Zn complexes. For catalytic compositions Zn–Co, catalytically active centers are formed at 600°C, as also in the case of oxygen-containing complexes [1–2], which give pyrolysis products in the form of nonstoichiometric oxides. The presence of oxygen in complex **I** contained in dimethylformamide favors formation of various oxide structures on the surface of the carbon support, which provides the electrocatalytic effect of oxygen reduction.

In the case of complex **II**, Ni and $ZnCl_2$, which show weak activity in the reaction of oxygen reduction, are formed in pyrolysis products. The highest current of oxygen reduction at –0.10 V is observed for catalysts synthesized at 700°C from a bimetallic Zn–Cu complex: 1.72 mA cm^{-2} (b_1 = 60 mV, b_2 = 100 mV). Next in activity are the compositions Zn–Co (1.68 mA cm^{-2}, b_1 = 55 mV, b_2 = 115 mV) and Zn–Ni (0.91 mA cm^{-2}, b_1 = 50 mV, b_2 = 110 mV) obtained at 600°C.

The steady-state polarization curves of oxygen reduction on catalysts synthesized at 600°C in the atmosphere of argon are shown in Fig. 3. It can be seen that the change in the steady-state potentials of the catalysts relative to the substrate is approximately 0.10 V. The positive shift of the steady-state polarization curves relative to AG-3 is 0.12 V for catalysts with Zn–Cu, 0.10 V for Zn–Co, and 0.08 V for Zn–Ni; the slopes $\partial E/\partial \log j$ for the catalysts formed on the basis of heterobimetallic complexes are close to those for AG-3 activated carbon. This indicates that the mechanisms of oxygen electroreduction are similar in these cases. The slopes suggest that the electroreduction of oxygen occurs by the single-electron mechanism with slowed-down addition of a first electron and via the stage of formation of hydrogen peroxide, which is characteristic of activated carbons [13]. The kinetic parameters of oxygen electroreduction on catalysts produced from heterobimetallic complexes (see table) show that the highest exchange

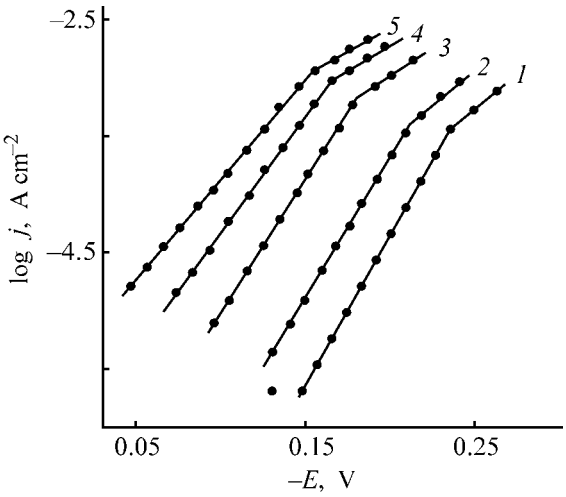


Fig. 3. Potentiostatic polarization curves of oxygen electroreduction, measured on a substrate of hydrophobized carbon black in a 1 M KOH solution at 20°C on catalysts formed by pyrolysis of heterobimetallic complexes on AG-3 at 600°C. (*j*) Current density and (*E*) electrode potential. (*1*) Hydrophobized carbon black, (*2*) AG-3 carbon, (*3*) Ni–Zn(AG-3), (*4*) Co–Zn(AG-3), and (*5*) Cu–Zn(AG-3).

currents are observed for the electrocatalyst obtained from the Zn–Cu complex (**III**) at 700°C. Thus, the electrocatalysts prepared from complex (**III**) are more electrically active than (**I**)–(**III**) complexes because their active centers contain a metal and nitrogen bound to surface carbon atoms, as also in the case of pyropolymers [5]. The slopes of the steady-state polarization curves lie within the ranges: b_1 = 0.04–0.06 V, b_2 = 0.10–0.12 V.

The electrocatalysts obtained can be used in metal-air chemical power cells, fuel cells, and sensors.

CONCLUSIONS

(1) The highest activity is characteristic of catalysts synthesized in thermal destruction of heterobimetallic complexes in the temperature range 500–700°C in the atmosphere of argon.

(2) The catalytic activity of the catalysts for oxygen reduction, prepared on the basis of heterobimetallic complexes of zinc, decreases in the order Zn–Cu > Zn–Co > Zn–Ni.

ACKNOWLEDGMENTS

The study was performed in the framework of the INTAS program (project no. 03-51-4532) and was financially supported by the State Foundation for Basic Research of the Ministry of Education and Science of Ukraine.

REFERENCES

1. Kublanovskii, V.S. and Pirskii, Yu.K., *Zh. Prikl. Khim.*, 2001, vol. 74, no. 7, pp. 1041–1044.
2. Pirskii, Yu.K., Levchuk, Ya.N., Reiter, L.G., and Kublanovskii, V.S., *Ukr. Khim. Zh.*, 2003, vol. 69, no. 3, pp. 77–80.
3. Rudchenko, A.V., Pirskii, Yu.K., Nesterova, O.V., and Kokozei, V.N., *Ukr. Khim. Zh.*, 2004, vol. 70, nos. 9–10, pp. 61–63.
4. Soriaga, M.P., *Chem. Rew.*, 1990, vol. 90, no. 5, pp. 771–793.
5. Tarasevich, M.R., Radyushkina, K.A., and Zhutaeva, G.V., *Elektrokhimiya*, 2004, vol. 40, no. 11, pp. 1369–1383.
6. Efremov, B.N. and Tarasevich, M.R., *Elektrokataliz i elektrokataliticheskie protsessy. Sbornik nauchnykh trudov* (Electrocatalysis and Electrocatalytic Processes. Coll. of Sci. Works), Kiev: Naukova Dumka, 1986, pp. 44–71.
7. Pirskii, Yu.K. and Prokopchuk, A.L., *Ukr. Khim. Zh.*, 2003, vol. 69, no. 3, pp. 72–75.
8. Ukrainian Patent 51 007.
9. Shteinberg, G.V., Kukushkina, I.A., Bagotskii, V.S., and Tarasevich, M.R., *Elektrokhimiya*, 1979, vol. 15, no. 4, pp. 527–532.
10. Chizmadzhev, Yu.A., Markin, V.S., Tarasevich, M.R., and Chirkov, Yu.G., *Makrokinetika protsessov v poristykh sredakh* (Macrokinetics of Processes in Porous Media), Moscow: Nauka, 1971.
11. Tarasevich, M.R., Radyushkina, K.A., and Bogdanovskaya, V.A., *Elektrokhimiya porfirinov* (Electrochemistry of Porphyrins), Moscow: Nauka, 1991.
12. Tarasevich, M.R., Beketaeva, L.A., Efremov, B.N., et al., *Elektrokhimiya*, 2004, vol. 40, no. 5, pp. 612–622.
13. Tarasevich, M.R., *Elektrokhimiya uglerodnykh materialov* (Electrochemistry of Carbon Materials), Moscow: Nauka, 1984.

ISSN 1070-4272, Russian Journal of Applied Chemistry, 2006, Vol. 79, No. 12, pp. 1969–1972. © Pleiades Publishing, Inc., 2006.
Original Russian Text © R.I. Yurchenko, I.S. Pogrebova, T.N. Pilipenko, T.E. Shubina, 2006, published in Zhurnal Prikladnoi Khimii, 2006, Vol. 79, No. 12, pp. 1993–1997.

APPLIED ELECTROCHEMISTRY AND CORROSION PROTECTION OF METALS

Corrosion-Protective Properties of 1-Phenacylmethyl-2-arylcarbamido(arylthiocarbamido)pyridinium Bromides

R. I. Yurchenko, I. S. Pogrebova, T. N. Pilipenko, and T. E. Shubina

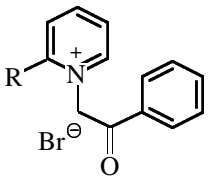
Kievskii Politekhnicheskii Institut National Technical University of Ukraine, Kiev, Ukraine

Received May 11, 2006

Abstract—Inhibiting effect of 1-phenacylmethylpyridinium bromides containing urea or thiourea substituents in the pyridinium ring on steel and zinc corrosion in sulfuric acid solutions was studied.

DOI: 10.1134/S1070427206120123

We found in [1, 2] that 1-phenacylmethylpyridinium bromides (**I**) are inhibitors of steel acid corrosion:

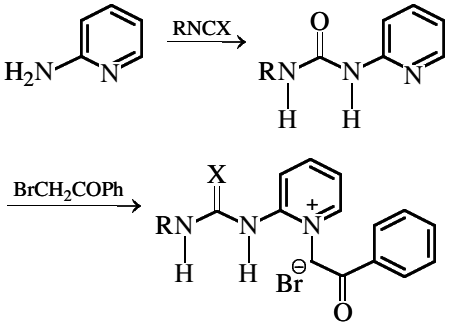


I

Introduction into the second position of the pyridinium ring in **Ia** (R = H) of an amino group (compound **Ib**, R = NH_2) enhances the inhibiting effect, whereas transformation of **Ib** into 1-phenacylmethyl-2-benzamidopyridinium bromide (**Ic**) substantially weakens it because of a decrease in the electron density on the nitrogen atom of the amino group. A different behavior is shown by amides [**I**; R = R_1CONH] in which substituents R_1 contain groups that can be independently involved in adsorption on the metal surface. Introduction of MeO group into the *p*-position of the phenyl ring of the benzamide group of compound **Ic**, or replacement of the latter with a heterylamide group (R = $HetCONH_2$) enhances the inhibiting effect as compared to **Ic**.

In this study, we considered, in order to further examine of the correlation between the structure and inhibiting effect of pyridinium salts, 1-phenacylmethyl-2-arylcarbamidopyridinium bromides (**II**) and -2-arylthiocarbamidopyridinium bromides (**III**). As known [3], many urea and thiourea derivatives are efficient inhibitors of acid corrosion of iron and steels. In addition, taking into account that arylurea and arylthiourea fragments of these compounds, similarly to phenacyl and pyridinium fragments, can be involved in adsorption, we may expect that compounds **II** and **III** should have a strong inhibiting effect on the steel acid corrosion.

The compounds studied were prepared by the reaction between 2-aminopyridine with the corresponding arylisocyanates or arylisothiocyanates, followed by alkylation of the compounds obtained with ω-bromoacetophenone:



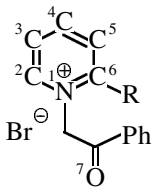
where X = O, R = (**a**) C_6H_5, (**b**) 4-$CH_3C_6H_4$, (**c**) 4-ClC_6H_4 (**II**); X = S, R = (**a**) C_6H_5 and (**b**) 4-$CH_3OC_6H_4$ (**III**).

The structures of compounds synthesized were confirmed by IR and NMR spectra.

EXPERIMENTAL

1-(2-Oxo-2-phenylethyl)-2-(3-phenylcarbamido)-pyridinium bromide (**IIa**), 1-(2-oxo-2-phenylethyl)-2-[3-(4-methylphenyl)carbamido]pyridinium bromide (**IIb**), 1-(2-oxo-2-phenylethyl)-2-[3-(4-chlorophenyl)-carbamido]-pyridinium bromide (**IIc**), 1-(2-oxo-2-

Table 1. Effective charges q in compounds of the general formula



Compound	R	q									
		N^1	C^2	C^3	C^4	C^5	C^6	O^8	N^8	$O(S)^9$	N^{10}
Ib	N^8H_2	–0.351	0.059	–0.274	–0.133	–0.279	0.466	–0.573	–0.801	–	–
IIa	$N^8HCO^9N^{10}HC_6H_5$	–0.328	0.056	–0.259	–0.138	–0.247	0.478	–0.568	–0.680	–0.624	–0.652
IIb	$N^8HCO^9N^{10}HC_6H_4CH_3$-4	–0.328	0.056	–0.260	–0.138	–0.248	0.478	–0.566	–0.679	–0.626	–0.651
IIc	$N^8HCO^9N^{10}HC_6H_4Cl$-4	–0.344	0.053	–0.264	–0.136	–0.257	0.473	–0.580	–0.668	–0.623	–0.613
IIIa	$N^8HCS^9N^{10}HC_6H_5$	–0.319	0.054	–0.249	–0.142	–0.231	0.477	–0.571	–0.660	–0.152	–0.592
IIIb	$N^8HCS^9N^{10}HC_6H_4O^{11}CH_3$-4*	–0.319	0.054	–0.250	–0.143	–0.232	0.478	–0.570	–0.660	–0.161	–0.595

* For O^{11} q = –0.506.

Table 2. Inhibition coefficients γ and degrees of corrosion protection Z for 08 KP steel in 3 M H_2SO_4 in the presence of 1×10^{-2} M 1-phenacylmethylpyridinium bromides **I**–**III**

Compound	γ	Z, %	γ	Z, %	γ	Z, %	γ	Z, %
	20°C		40°C		60°C		80°C	
Ib [1]	23.70	95.78	29.02	96.55	200.32	99.50	144.60	99.30
Ic [2]	2.60	61.54	4.78	79.08	17.20	94.19	12.00	91.66
IIa	28.10	96.44	61.83	98.38	517.25	99.81	124.13	99.19
IIb	30.00	96.67	86.91	98.85	528.56	99.81	210.53	99.53
IIc	12.75	92.16	22.23	95.50	218.71	99.54	117.97	99.15
IIIa	29.17	96.57	73.54	98.64	634.30	99.84	147.15	99.32
IIIb	39.13	97.44	136.50	99.27	731.85	99.86	162.90	99.39

phenylethyl)-2-[3-phenylthiocarbamido]pyridinium bromide (**IIIa**), and 1-(2-oxo-2-phenylethyl)- 2-[3-(4-methoxyphenyl)thiocarbamido]pyridinium bromide (**IIIb**). A mixture of 2-aminopyridine (0.02 M), appropriate isocyanate or thiocyanate, and dioxane (15 ml) was refluxed for 2 h. The reaction mixture was treated with a small amount of water, left overnight, and then the precipitate was separated. Then, a mixture containing equimolar amounts (0.0015 mol) of one of the compounds obtained, ω-bromacetophenone, and 15 ml of ethyl acetate was refluxed for 3 h, and the precipitate formed was separated. Yields (%) and boiling points (°C): **IIa**, 81, 205–207; **IIb**, 85, 242–244; **IIc**, 87, 253–255; **IIIa**, 80, 227–229; and **IIIb**, 80, 220–222, respectively.

The corrosion tests were performed by a commom procedure [1] with 08 KP steel and Ts0 zinc with a working surface area of 14×10^{-4} and 5.76×10^{-4} m^2, respectively. The steel samples were kept in 3 M H_2SO_4 at 20°C for 24 h, at 40 and 60°C for 2 h, and at 80°C for 1 h, and the zinc samples, in 0.5 M H_2SO_4 at 20°C for 0.5 h. The efficiency of metal protection was evaluated by the inhibition coefficient $\gamma = K_M/K'_M$ and degree of protection $Z = [(K_M - K'_M)/K_M] \times 100\%$, where K_M and K'_M (g m^{-2} h^{-1}) are the gravimetric corrosion indices in pure and inhibited acid solutions, respectively. Voltammetric measurements with steel and zinc were performed in the potentiodynamic mode after stabilization of the free corrosion potential E_c at a scanning rate of 2 mV s^{-1}.

Quantum-chemical calculations performed by the procedure from [4, 5] showed that the effective charges on the nitrogen atom of the amino group directly bonded to the pyridine ring in ureas **II**, thioureas **III**, and compound **Ic** (Table 1) differ only

slightly and are substantially lower than those in **Ib**. These results suggest that the inhibiting effect of the 1-phenacylmethylpyridinium bromides studied should be close to the effect of **Ic** and substantially lower than that of **Ib**.

The results of the corrosion test showed that compounds **II** and **III** are efficient inhibitors of steel acid corrosion (Table 2). The efficiency of the protection effect substantially increases as temperature is elevated to 60°C. This is in agreement with the hypothesis of specific adsorption of 1-phenacylmethylpyridinium bromides on the surface of steel, developed in [1, 2, 6]. Ureas (**II**) and thioureas (**III**) are characterized by the stronger anticorrosion effect as compared not only to compound **Ic**, but also to **Ib**. For instance, in the presence of **IIa** and **IIIa**, γ for steel is higher by a factor of 1.2 at 20°C and by a factor of 2.6 and 3.2, respectively, at 60°C than that in the presence of **Ib**. Electron-donor groups CH_3 and CH_3O introduced in the *p*-position of the phenyl ring of **IIa** and **IIIa** enhance the protective properties of these compounds, whereas the chlorine atom decreases them. An increase in the temperature to 80°C is accompanied, as for the other compounds of this type, by a small decrease in the inhibiting effect, probably caused by desorption of the inhibitor from the metal surface due to the elevated rate of its dissolution. The above results show that our compounds are, indeed, efficient inhibitors of the steel corrosion, whose corrosion-protective activity is mainly caused by the presence of arylurea and arylthiourea groups responsible for adsorption and inhibition.

Being efficient inhibitors of steel acid corrosion, compounds **II** and **III** only slightly inhibit the corrosion of zinc in 0.5 M H_2O_4, and compound **IIIa** at its low concentrations even stimulates the corrosion (Table 3). The decrease in the protective properties of **Ia**, **IIa**, and **IIIa** for zinc, compared to steel, is probably caused by involvement of these compounds in catalytic evolution of hydrogen due to discharge of their protonated forms.

In accordance with modern views [7], the catalytic evolution of hydrogen in acid media in the presence of nitrogen-containing organic compounds capable of protonation can proceed by the scheme

$$B + H^+ = BH^+,$$

$$BH_s^+ + e = BHs,$$

$$BH_s = B_s + 1/2H_2,$$

$$B_s + H_s^+ = BH_s^+,$$

where B and B_s are molecular forms and BH^+ and BH_s^+, protonated forms in the solution bulk and on the metal surface, respectively. Depending on a particular metal and on the structure and concentration of the inhibitor, the above reactions can either accelerate (due to easier hydrogen elimination) or decelerate the corrosion (due to inhibiting effect of protonated and molecular forms of compounds).

It is known that the discharge of hydroxonium ions on the zinc surface is characterized by high activation energy, whereas regeneration of BH_s^+ cations proceeds fairly rapidly due to the presence of activated hydrogen ions (H_s^+) in the electric double layer. Therefore, during zinc corrosion in the acid medium, the above processes usually decrease the hydrogen overvoltage and the inhibiting effect of the nitrogen-containing compounds [7]. On the steel surface, these processes are complicated, because the activation energy of the hydroxonium ion discharge on the surface of *d* metals is relatively low and regeneration of BH_s^+ is slow due to the ability of nitrogen atoms to interact with unoccupied *d* orbitals of iron [7]. This fact accounts for the high inhibiting effect of the compounds studied in the steel corrosion in sulfuric acid solution and for its substantial decrease in the case of zinc. For instance, at 20°C in the presence of **IIa** or **IIIa** (1×10^{-2} M), the rate of steel corrosion decreases by a factor of 28 and 29, respectively, whereas that of zinc corrosion, by only a factor of 2.3 (Tables 1, 3). In the presence of **Ib** (1×10^{-2} M) containing amino group at 20°C, the steel corrosion is inhibited by a factor of 24, and zinc corrosion, by a factor of 3, whereas unsubstituted 1-phenacylmethylpyridinium bromide (**Ia**) containing no protonation centers in the pyridinium ring virtually equally inhibits the corrosion of steel [1] and zinc (Table 4).

Quantum-chemical calculations showed that the negative charges on oxygen and sulfur atoms in

Table 3. Inhibition coefficients γ and degrees of corrosion protection, *Z*, for Ts0 zinc in 0.5 M H_2SO_4 in the presence of 1-phenacylmethylpyridinium bromides **IIa** and **IIIa** at 20°C

Concentration, M	γ	*Z*, %	γ	*Z*, %
	compound **IIa**		compound **IIIa**	
1×10^{-2}	2.34	57.26	2.27	55.94
4×10^{-3}	1.85	45.95	1.80	44.44
1.6×10^{-3}	1.70	41.17	0.88	–
6.4×10^{-4}	1.62	38.27	0.84	–

Table 4. Inhibition coefficients γ and degrees of corrosion protection, *Z*, for 08 KP steel in 3 M H_2SO_4 and for Ts0 zinc in 0.5 M H_2SO_4 in the presence of 1×10^{-2} M compounds **I**

R	γ	*Z*, %	γ	*Z*, %
	08 KP Steel		Ts0 Zinc	
H	11.30	91.10	12.52	92.01
H_2N	23.70	95.80	2.91	65.64
PhNHCONH	28.10	96.44	2.34	57.26
PhNHCSNH	29.17	96.57	2.27	55.94

the arylurea and arylthiourea groups that can be directly involved in the protonation amounts to –0.15229, –0.16143 and –0.62322, –0.62615, respectively. Therefore, in going from urea (**IIa**) to thiourea (**IIIa**) derivatives, the bond strength in the protonated arylthiourea group can decrease, which should facilitate catalytic evolution of hydrogen on zinc and hence decrease the protective effect of this group. This assumption is confirmed by the fact that at a concentration of 1.6×10^{-3} M compound **IIa** increases the overvoltage of the hydrogen evolution on zinc, whereas **IIIa** decreases it (Fig. 1a); compound **IIa** slightly inhibits zinc corrosion in 0.5 M H_2SO_4, whereas **IIIa** stimulates it (Table 3).

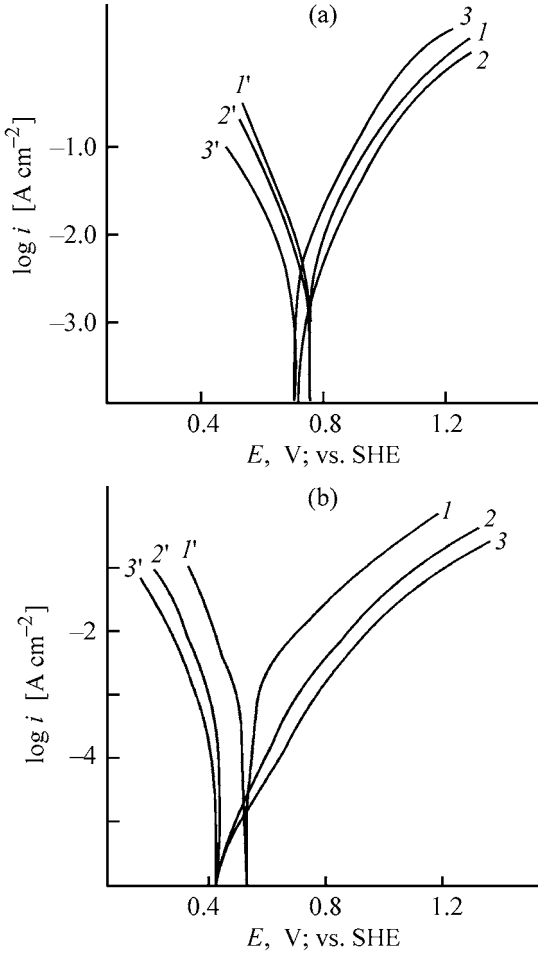


Fig. 1. (*1*–*3*) Catodic and (*1'*–*3'*) anodic polarization curves recorded (a) on Ts0 zinc in 0.5 M H_2SO_4 and (b) on 08 KP steel in 3 M H_2SO_4 at 20°C in the presence of 1.6×10^{-1} M of compounds **IIa** or **IIIa**. (*i*) Current density and (*E*) potential. (*1*, *1'*) none, (*2*, *2'*) **IIa**, and (*3*, *3'*) **IIIa**.

At the same time, the bulk and surface concentration of the molecular species of compounds capable of chemisorption on steel can increase from ureas (**II**) to thioureas (**III**) due to interaction with the metal surface of their arylurea and arylthiourea groups. This should inhibit catalytic evolution of hydrogen on steel and noticeably enhance its protection. This suggestion is in good agreement with the fact that compound **IIIa** increases the overvoltage of hydrogen evolution (Fig. 1b) and, correspondingly, is more efficient inhibitor of steel corrosion than the related urea **IIa** (Table 2).

CONCLUSIONS

(1) Arylurea and arylthiourea groups in the pyridinium ring of 1-phenacylmethylpyridinium bromides are responsible for the high level of their corrosion-protective effect in steel corrosion in 3 M sulfuric acid solution at 20–80°C.

(2) The compounds studied are ineffective as inhibitors of zinc acid corrosion, which is caused by catalytic evolution of hydrogen due to discharge of their protonated species.

REFERENCES

1. Yurchenko, R.I., Pogrebova, I.S., Pilipenko, T.N., and Kras'ko, E.M., *Zh. Prikl. Khim.*, 2003, vol. 76, no. 11, pp. 1814–1818.
2. Yurchenko, R.I., Pogrebova, I.S., Pilipenko, T.N., and Shubina, T.E., *Zh. Prikl. Khim.*, 2004, vol. 77, no. 7, pp. 1132–1135.
3. Reshetnikov, S.M., *Ingibitory kislotnoi korrozii metallov* (Inhibitors of Acid Corrosion of Metals), Leningrad: Khimiya, 1986.
4. Becke, A.D., *J. Chem. Phys.*, 1993, vol. 98, p. 5648.
5. Frisch, M.J., Trucks, G.W., Schlegel, H.B., et al., *GAUSSIAN*, Inc., Pittsburgh PA: Gaussian, 1999.
6. Yurchenko, R.I., Pogrebova, I.S., Pilipenko, T.N., and Shubina, T.E., *Zh. Prikl. Khim.*, 2006, vol. 79, no. 7, pp. 1110–1114.
7. Antropov, L.I. and Pogrebova, I.S., *Itogi Nauki, Ser.: Korroz. Zashch. Korroz.*, Moscow: VINITI Akad. Nauk SSSR, 1973, vol. 2, pp. 27–112.

ISSN 1070-4272, Russian Journal of Applied Chemistry, 2006, Vol. 79, No. 12, pp. 1973–1981. © Pleiades Publishing, Inc., 2006.
Original Russian Text © N.A. Samoilov, I.A. Mnushkin, O.A. Mnushkina, 2006, published in Zhurnal Prikladnoi Khimii, 2006, Vol. 79, No. 12, pp. 1998–2006.

PROCESSES AND EQUIPMENT OF CHEMICAL INDUSTRY

Theoretical Study of Ethylene Glycol Synthesis in a Reaction-Rectification Column

N. A. Samoilov, I. A. Mnushkin, and O. A. Mnushkina

Ufa State Technical University of Oil, Ufa, Bashkortostan, Russia
Peton OOO, Ufa, Baskortostan, Russia

Received February 21, 2006

Abstract—Principles of construction of a mathematical model of a reaction-rectification column for ethylene glycol synthesis are considered. Some specific features of the operation of the reaction-rectification column are analyzed. The correctness of the assumptions and limitations of the model is substantiated and the adequacy of the model is assessed.

DOI: 10.1134/S1070427206120135

Recently, interest has increased in development of reaction-rectification apparatus [1] combining a chemical process with separation of the reaction products, which markedly simplifies the technological scheme and diminishes the capital expenditure for construction of installations and optimization of the process as a whole [2–6]. Reaction-rectification columns can be used in such processes as etherification, hydrolysis, oxidation, alkylation, and isomerization, in which the chemical stage occurs in the range of boiling points of components of the reaction mixture on several contact mass-exchange devices of the column [1]. As an example of a process of this kind can serve production of ethylene glycol via direct hydration of ethylene oxide

$$C_2H_4O + H_2O \rightarrow HO–C_2H_4–OH. \quad (1)$$

Simultaneously with the target reaction occur side reactions of glycols with ethylene oxide to give diethylene glycol

$$C_2H_4O + HO–C_2H_4–OH \rightarrow HO–C_2H_4–O–C_2H_4–OH, \quad (2)$$

triethylene glycol

$$C_2H_4O + HO–C_2H_4–O–C_2H_4–OH \rightarrow HO–C_2H_4–O–C_2H_4–O–C_2H_4–OH \quad (3)$$

and tetraethylene glycol

$$C_2H_4O + HO–C_2H_4–O–C_2H_4–O–C_2H_4–OH \rightarrow HO–C_2H_4–O–C_2H_4–O–C_2H_4–O–C_2H_4–OH \quad (4)$$

To suppress the side reactions, ethylene glycol is synthesized in the liquid phase at elevated temperatures (about 200°C) and pressures (1.5–2 MPa) in the presence of water.

The technological scheme of the process is rather cumbersome and includes, in addition to the reactor, three evaporation installations for removal of excess water from the reaction mixture and a unit of rectification columns for removal of admixtures of di-, tri-, and tetraethylene glycol from the commercial ethylene glycol. All the components of the reaction mixture are successively evaporated and condensed, and only tetraethylene glycol is obtained from the bottom of the last rectification column in the liquid phase. This intricate technological scheme can be, in principle, replaced with a single apparatus, a reaction-rectification column [7, 8].

A specific feature of the operation of a reaction-rectification column in synthesis of ethylene glycol is the possibility of circulating the excess water within the column at a virtually total conversion of ethylene oxide and the resulting operation of the upper part of the column in the virtually total reflux mode (Fig. 1), which improves the fractionation efficiency [9].

Simulation of the operation of a reaction-rectification column is complicated by the fact that the reaction and rectification processes are commonly calculated by different methods. The rectification process is, as a rule, calculated by predetermined statics models based on the concept of a theoretical plate, which provide attainment of equilibrium between the contacting vapor and liquid during a conditionally infi-

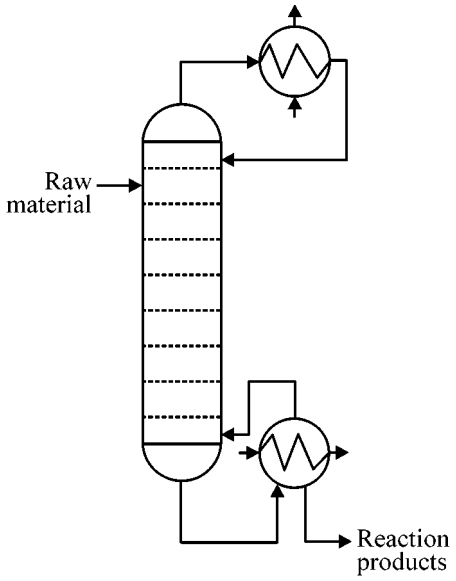


Fig. 1. Schematic of a reaction-rectification column.

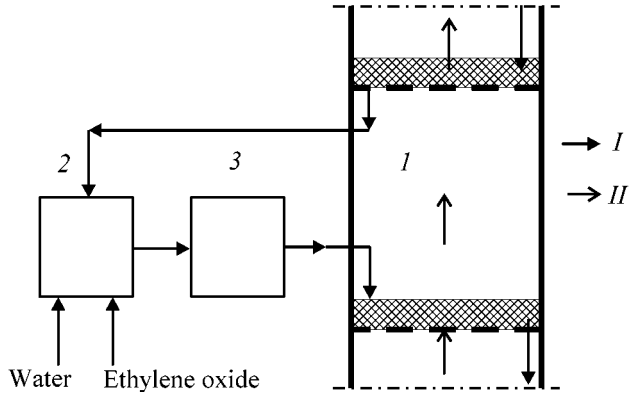


Fig. 2. Flow chart in calculation of the reaction zone of a reaction-rectification column. (*1*) Fractionating part, (*2*) mixing of flows of the raw material and recirculating water, and (*3*) reaction part. (*I*) Liquid flows and (*II*) vapor flows.

nite contact time. This makes unnecessary use of such difficultly determined characteristics as the phase boundary area, mass-transfer coefficient, and hydrodynamic structure of flows in a real contact device, which can only be obtained in full-scale experimental studies of the process. At the same time, simulation of a chemical process requires that its kinetics should be taken into account. The two approaches to solution of the problem can be united in a single combined static-kinetic model of operation of the reaction-rectification column.

The combined static-kinetic model is based on the rectification process in a complex composite column equivalent to any system of simple columns [10]. In the construction of this model, it was assumed that the raw material is introduced into each theoretical plate and the vapor and liquid phases are partly or totally removed from the plate after the mass exchange is complete; these phases are removed as final products or introduced as raw materials into other theoretical plates of the composite column. Such a construction of the model made it possible to simultaneously calculate the whole system of columns of the installation, which enabled optimization of the system as a whole. This model of the theoretical plate, as applied to the problem of calculation of the reaction-rectification column, considered here, was supplemented with units of mixing of the raw-material and circulating flows, and the chemical transformation on the theoretical plate simultaneously serving as the reaction device (Fig. 2) was calculated. In this case, it is possible to remove the reflux (mainly containing the circulating water) from a higher-lying plate and mix it with raw-material flows of ethylene oxide ($F0_{J,1}$) and water ($F0_{J,2}$), with the subsequent chemical reaction and separation of the reaction products both on the *J*th (reaction) plate and on other fractionating plates of the column. In this context, two calculation techniques are combined when calculating the column: statics of fractionation on the theoretical plate, which provides determination of the quality of the products of separation in the vapor–liquid system via mass exchange, and kinetics of the chemical process on the reaction plate, which makes it possible to determine the composition of the reaction products in the reaction mixture and the time necessary for achieving the acceptable degree of conversion of the raw material.

The reaction-rectification column can be effectively used only if the following two limitations are overcome: (i) the reaction duration should not exceed the residence time of the flows in the reaction zone of the column (necessary limitation); and (ii) the composition of the reaction mixture obtained in the reaction zone should provide the acceptable purity of the target product discharged from the column bottom (sufficient limitation).

The following assumptions were made in the development of the mathematical model of the reaction-rectification column: hydrodynamics of the contact device is described by the plug-flow model; relative volatility of the components of the mixture being separated, relative to the reference component, is taken to be constant along the column height; as the reference component is taken ethylene glycol, the boundary component of a mixture being fractionated: water with a minor admixture of organic substances goes to the top part of the column, and ethylene glycol

with admixture of water and higher glycols, products of side reactions, to the bottom part of the column.

The mathematical model of the reaction-rectification process on a contact device comprises three units: mixing unit, unit of the chemical reaction kinetics, and rectification statics unit.

The model of the unit of mixing of a balance amount of the raw material with the circulating water (reflux) coming from a higher-lying plate and containing a minor admixture of all the components of the reaction mixture, in which the initial amount $GR_{J,I}$ of each of the six components (ethylene dioxide, water, ethylene glycol, diethylene glycol, triethylene glycol, tetraethylene glycol) delivered into the reaction unit is determined, is constructed in the form of material-balance equations of the unit

$$GR_{J,I} = B_{J-1}x_{J-1,I} + FO_{J,I}, \quad (5)$$

Here, B_{J-1} and $x_{J-1,\,I}$ are the amount and composition of the reflux removed from the higher-lying plate.

The model of the reaction unit comprises a system of differential equations that account for the influence exerted by the hydrodynamic situation on the kinetics of the chemical process for all the components of the reaction mixture:

$$\left.\begin{aligned}
\frac{dx_{1,R}}{d\tau} &= -K_1x_{1,R}x_{2,R} - K_2x_{1,R}x_{3,R} - K_3x_{1,R}x_{4,R} - K_4x_{1,R}x_{5,R} - W\frac{dx_{1,R}}{dl},\\
\frac{dx_{2,R}}{d\tau} &= -K_1x_{1,R}x_{2,R} - W\frac{dx_{2,R}}{dl},\\
\frac{dx_{3,R}}{d\tau} &= -K_1x_{1,R}x_{2,R} - K_2x_{1,R}x_{3,R} - W\frac{dx_{3,R}}{dl},\\
\frac{dx_{4,R}}{d\tau} &= -K_2x_{1,R}x_{3,R} - K_3x_{1,R}x_{4,R} - W\frac{dx_{4,R}}{dl},\\
\frac{dx_{5,R}}{d\tau} &= -K_3x_{1,R}x_{4,R} - K_4x_{1,R}x_{5,R} - W\frac{dx_{5,R}}{dl},\\
\frac{dx_{6,R}}{d\tau} &= -K_4x_{1,R}x_{5,R} - W\frac{dx_{6,R}}{dl},
\end{aligned}\right\} \quad (6)$$

Here, $x_{1,R}$, ..., $x_{6,R}$ are the concentrations of ethylene dioxide, water, ethylene glycol, diethylene glycol, triethylene glycol, tetraethylene glycol, respectively (mole fractions); τ, reaction duration (s); W, motion velocity of the reaction mixture (m s^{-1}); l, path of the reaction mixture in the reaction zone (m); K_1–K_4, rate constants of reactions (1)–(4).

The reaction rate constants were calculated by the Arrhenius reaction

$$K_M = K_{M,0}\exp(-E_M/RT), \quad M = 1, 2, 3, 4, \quad (7)$$

where $K_{M,0}$ and E_M are the pre-exponential factor and activation energy for Mth reaction; T, process temperature; and R, universal gas constant.

The values of $K_{M,0}$ and E_M for reactions (1)–(4) were taken from [11]. In the calculation of the reaction unit, the amount E_J of the reaction products arriving to Jth plate were determined. The model of the rectification statics yielded the composition $Z_{J,I}$ of the mixture formed on a plate after mixing of the raw material introduced (reaction mixture) with flows of vapor and liquid coming from the lower- and higher-lying plates:

$$Z_{J,I} = \frac{L_{J-1}x_{J-1,I} + V_{J+1}y_{J+1,I} + F_Jx_{J,I}}{L_{J-1} + V_{J+1} + F_J}. \quad (8)$$

Further, the fraction of E_J of the vapor removed from the starting mixture was calculated

$$E_J = \frac{P_J}{F_J + L_{J-1} + V_{J+1}} \quad (9)$$

and the phase equilibrium constant $K_{E,J}$ of the reference component at which the prescribed fraction is achieved was found from the condition

$$\sum_{I=1}^{6} x_{J,1} = \sum_{I=1}^{6} \frac{Z_{J,I}}{1 + E_J(A_I K_{E,J} - 1)} = 1. \quad (10)$$

This made it possible to calculate, from the com-

Table 1. Calculated composition of the residue from the column bottom at the maximum yield of ethylene glycol (water : ethylene glycol ratio 6 : 1)

T, K	τ, min	Residue composition, mole fraction			
		ethylene glycol	diethylene glycol	triethylene glycol	tetraethylene glycol
373	181.2	0.8822	0.1081	0.09198	0.00531
393	64.0	0.8801	0.1098	0.09488	0.00556
413	24.2	0.8794	0.1104	0.09586	0.00564
433	9.7	0.8794	0.1104	0.09586	0.00564
453	4.1	0.8794	0.1104	0.09586	0.00564
473	1.9	0.8794	0.1104	0.09586	0.00564
493	0.9	0.8794	0.1104	0.09586	0.00564

position $x_{J,I}$ of the liquid phase, the composition $y_{J,I}$, of the vapor phase:

$$y_{J,I} = A_I K_{E,J} x_{J,I}, \quad (11)$$

where A_I are the volatilities of the mixture components, related to the reference component.

The phase equilibrium constant of the reference component was used to calculate the temperature T_J of the product on the theoretical plate:

$$T_J = [B_E/\log(P_c K_{E,J}) - A_E] + C_E. \quad (12)$$

where P_c is the pressure in the column; A_E, B_E, and C_E, constants of the Antoine equation for calculation of the saturated vapor pressure for the reference component.

The chemical stage of the process was calculated by the first-order Runge–Kutta method, with kinetic curves obtained for all the components of the reaction mixture and the time determined in which the maximum yield of ethylene glycol is reached.

The rectification stage was calculated by the relaxation method, with the column filled with pure water as the initial condition in solving the problem. The input data used in the calculation include setting the number of theoretical plates, mole vapor fluxes P_J ascending from each plate, positions at which raw materials are charged into the column, and the amount and composition of the raw material. The solution algorithm of the problem exhibits fast convergence (duration of computer calculation of a variant of the column operation is 1–2 h) at a high accuracy of the calculation (the integration step in calculating the chemical stage of the process is 0.0001 min at a reaction duration of 1.5–0.5 min; the equilibrium constant of the reference component is determined in calculating the rectification statics with an accuracy of 0.00001). The calculation of the problem is complete at discrepancies of $\leq 10^{-8}$ mole fraction between the compositions of the vapor ($x_{J,I}$) and liquid ($y_{J,I}$), obtained in two neighboring iterations on all plates of the column.

In mathematical calculation of the synthesis of ethylene glycol in the reaction-rectification column, the possibility was considered of overcoming the abovementioned limitations and the adequacy of the assumptions made both in the stage of chemical transformation of the raw material used to produce ethylene glycol on the reaction plate of the rectification column and in further fractionation of the reflux.

The process of synthesis of ethylene glycol was analyzed taking into account the formation of the byproducts, di-, tri-, and tetraethylene glycol, in a wide range of process temperatures and water : ethylene oxide ratios, because detailed published data are only available for a limited range (from zero to two parts of water per one part of ethylene oxide). Under industrial conditions, this ratio is about 6 : 1 [11].

A calculation of the reaction mixture compositions for obtaining ethylene glycol in maximum yield at a water : ethylene oxide ratio of 6 : 1, characteristic of industrial conditions, demonstrated that the yield of the product is virtually independent of the hydration temperature, 12.5–12.7 mol %. An increase in temperature in the range 373–493 K leads to a decrease in the concentration of unreacted ethylene oxide by nearly three orders of magnitude, with an insignificant acceleration of side reactions, because the rate constants of the side reactions and the target reaction are mutually proportional [11]. A calculation of the composition of the residue formed in the rectification column in full separation of unreacted water from the glycols formed demonstrated that high-purity ethylene glycol cannot be obtained at a water : ethylene dioxide ratio of 6 : 1 in the starting raw material (Table 1). It is necessary to introduce, in addition to the reaction-rectification column, a unit for fractionation of glycols, as it is commonly done in the industry. In this case, an increase in the temperature at which the chemical process is performed has virtually no effect on the quality of residue formed in the rectification column, but leads to a significant decrease in the reaction duration: from 182 min at 373 K to 0.9 min at 493 K.

Raising the water : ethylene oxide ratio within the range 2–100 leads to a considerable increase in the concentration of ethylene glycol (from 68 to 99 mol %) in the residue obtained at the column bot-

Table 2. Effect of the water : ethylene oxide ratio on the calculated composition of the residue from the column bottom at the maximum yield of ethylene glycol and temperature of 473 K

Water : ethylene oxide ratio	Residue composition, mole fraction			
	ethylene glycol	diethylene glycol	triethylene glycol	tetraethylene glycol
2 : 1	0.6799	0.2448	0.06312	0.01212
6 : 1	0.8794	0.1104	0.09586	0.00564
19 : 1	0.9585	0.0403	0.001154	0.0000217
29 : 1	0.9728	0.0267	0.000498	0.0000061
99 : 1	0.9918	0.0081	0.000045	0.0000004

Table 3. Effect of the reflux : ethylene oxide ratio and column pressure on the column diameter *d* and residence time *t* of the liquid on a real plate

Column pressure, MPa	Vapor flux, kg m^{-2} h^{-1}	Reflux : ethylene oxide ratio									
		10 : 1		30 : 1		50 : 1		70 : 1		90 : 1	
		d, m	*t*, min	*d*, m	*t*, min	*d*, m	*t*, min	*d*, m	*t*, min	*d*, m	*t*, min
0.1	4345	2.30	1.26	3.98	1.26	5.13	1.26	6.07	1.26	6.89	1.26
0.5	8899	1.60	0.586	2.78	0.586	3.59	0.586	4.25	0.586	4.81	0.586
1.0	11925	1.38	0.423	2.40	0.423	3.10	0.423	3.67	0.423	4.16	0.423
1.5	14218	1.27	0.351	2.20	0.351	2.84	0.351	3.36	0.351	3.81	0.351
2.0	15962	1.20	0.306	2.07	0.306	2.68	0.306	3.17	0.306	3.59	0.306

tom (Table 2). Thus, the limitation on the purity of ethylene glycol obtained in the rectification column can be overcome by proper choice of the water : ethylene oxide ratio in the starting raw material.

A simulation of the synthesis of ethylene glycol also demonstrated that an increase in temperature can make markedly shorter the synthesis duration, with the high purity of the final product preserved, if the starting raw material (water : ethylene oxide = 1 : 1) is mixed with the reflux removed from the upper-lying plate and circulated in the column.

The water : ethylene oxide ratio recommended on the basis of the results of simulation is (30 – 40) : 1, because further increase in the content of water fails to give any noticeable positive effect and only leads to a higher energy expenditure for the process (Fig. 3).

The possibility of providing the necessary residence time of the reaction mixture in the reaction zone on the rectification plate of the column was assessed by calculating the synthesis kinetics of ethylene glycol. The calculations demonstrated that, at a temperature of 493 K and a water : ethylene oxide ratio at the onset of the reaction equal to 29.3 : 1 (initial C_2H_4O concentration in the reaction mixture 0.033 mole fraction), ethylene oxide is virtually completely consumed to a level of 0.0746×10^{-3} mole fraction in 0.5 min, with concentrations of 0.0167×10^{-5} and 0.04×10^{-8} mole fraction reached in 1 and 1.5 min, respectively. The virtually total absence of ethylene oxide in the reaction mixture suppresses side reactions. The real residence time of the reflux flow in the reaction zone was calculated by the Souders–Brown method [12] by determining the column diameter *D* and the admissible vapor flux on a real plate of the column in the reaction zone, G_g (kg m^{-2} h^{-1}):

$$G_g = 0.305C\sqrt{\rho_V(\rho_L - \rho_V)}, \qquad (13)$$

where ρ_V and ρ_L are the densities of the vapor and liquid flows in the column, respectively, and *C* is a coefficient.

The residence time of the reaction mixture on a real fractionating plate of the reaction-rectification column was calculated for a throughput of 6.2 ton h^{-1} for ethylene glycol in a wide range of reflux : ethylene oxide ratios and column pressures (Table 3). The cal-

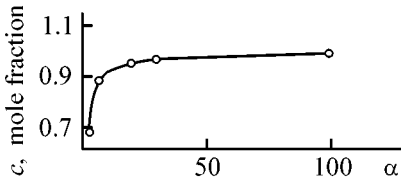


Fig. 3. Maximum concentration *c* of ethylene glycol in the potential residue of the column vs. the water : ethylene oxide ratio α in the starting raw material at a temperature of 493 K in the reaction zone.

Table 4. Relative volatilities A_I, $A_{I,t}$, and $A_{I,b}$ of the components of the system at various column pressures P

Component	P = 0.1 MPa			P = 0.5 MPa		
	A_I	$A_{I,t}$	$A_{I,b}$	A_I	$A_{I,t}$	$A_{I,b}$
Ethylene oxide	208.5	640.1	67.9	66.8	168.5	28.5
Water	26.4	47.3	14.7	14.5	23.7	8.9
Ethylene glycol	1	1	1	1	1	1
Diethylene glycol	0.154	0.126	0.188	0.203	0.146	0.283
Triethylene glycol	4.2×10^{-2}	2.6×10^{-2}	6.6×10^{-2}	6.7×10^{-2}	4.5×10^{-2}	10×10^{-2}
Tetraethylene glycol	4.4×10^{-3}	1.5×10^{-3}	12.6×10^{-3}	13×10^{-2}	5.2×10^{-3}	3.2×10^{-2}
Component	P = 1 MPa			P = 1.5 MPa		
	A_I	$A_{I,t}$	$A_{I,b}$	A_I	$A_{I,t}$	$A_{I,b}$
Ethylene oxide	40.8	94.2	17.7	30.5	66.8	13.9
Water	11.2	17.4	7.1	9.5	14.6	6.2
Ethylene glycol	1	1	1	1	1	1
Diethylene glycol	0.245	0.169	0.356	0.279	0.189	0.413
Triethylene glycol	8.4×10^{-2}	5.7×10^{-2}	12.3×10^{-2}	9.6×10^{-2}	6.6×10^{-2}	14×10^{-2}
Tetraethylene glycol	2.1×10^{-2}	9.2×10^{-3}	4.8×10^{-2}	2.8×10^{-3}	1.3×10^{-3}	2.1×10^{-2}

culations demonstrated that the residence time of the reaction mixture on a real plate is independent of the reflux : ethylene oxide ratio and decreases as the column diameter becomes smaller. A comparison of the residence time of the reaction mixture on a series of real plates with the necessary reaction duration demonstrated (Fig. 4) that it is the most appropriate to perform the process at a sufficiently high temperature and pressure in the reaction zone. At temperatures of 475–493 K, one to three real plates are sufficient for the reaction, i.e., the reaction virtually completely occurs on a single theoretical plate. The reaction requires 3–5 real plates at 450–475 K, up to 20 real plates at 425–450 K, and 30–40 real plates at 400–425 K. Thus, the limitation concerning the correspondence of the residence times of flows in the reaction zone of the column to the reaction duration in the reaction-rectification column can be overcome by proper choice of the temperature and pressure in the reaction zone.

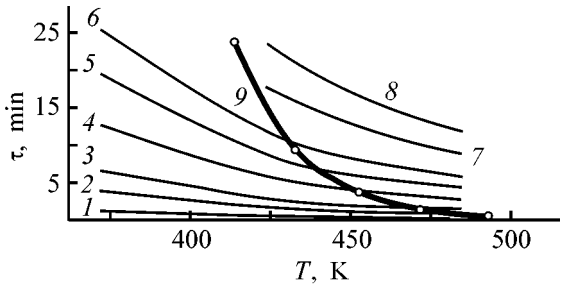


Fig. 4. Effect of temperature T and number of real plates in the reaction zone on the residence time τ of the reaction mixture in the column. Number of plates: (*1*) 1, (*2*) 3, (*3*) 5, (*4*) 10, (*5*) 15, (*6*) 20, (*7*) 30, and (*8*) 40; (*9*) effect of temperature on the reaction duration.

At a column diameter larger than 2 m, the hydrodynamics of the real rectification plate can be described by the plug-flow hydrodynamic model at a number of mixing members (e.g., tray caps) in the vapor–liquid system exceeding ten [13]. Thus, the description of the hydrodynamics in the reaction zone in terms of the plug-flow model taken into account by the system of equations (6) is quite adequate. The formal duration of the reaction in which ethylene glycol is synthesized, calculated in terms of the kinetic model, will be also valid for the process performed on a real contact device. This is so because, in this case, the model of the kinetics of the chemical reaction coincides in form with the mathematical model of the reaction plate, which takes into account both the kinetics and hydrodynamics of the stationary process.

An analysis of the assumption that the relative volatilities of the components are constant along the column height demonstrated that, in view of the significant difference between the saturated vapor pressures of the components of the system, the conventional procedure taking into account the average relative volatility A_I as

$$A_I = \sqrt{A_{I,b}A_{I,t}} \qquad (14)$$

[$A_{I,b}$ and $A_{I,t}$ are the relative volatilities at temperatures of the bottom and top parts of the column, respectively (Table 4)] leads to a gross error in calculat-

Table 5. Profile of temperature distribution over plates of the reaction-rectification column at a pressure of 0.1 MPa

Plate no.	Temperature at column plates, K		
	in calculation of relative volatilities A by (14)	with A taken to be separately constant in the upper and lower halves of the column	according to [9]
Top temperature 373 K (in discharge of pure water: actually, 0.9999 mole fraction of water the reflux)			
1	384.12	372.24	372.2
2	384.41	372.48	373.5
3	384.41	372.48	373.5
4	384.50	373.16	374.1
5	386.79	405.89	391.2
6	414.78	440.63	448.1
7	461.63	465.99	468.7
Bottom temperature 470 K (in discharge of pure ethylene glycol: actually, 0.9765 mole fraction of ethylene glycol in the residue)			

Table 6. Composition of nonequilibrium counter flows of vapor and liquid on neighboring plates of the reaction-rectification column (column pressure 0.5 MPa, reflux : ethylene oxide ratio at the inlet of 3rd theoretical plate 50 : 1)

Component	Composition of counter flows			
	between 1st and 2nd plates		between 7th and 8th plates	
	liquid	vapor	liquid	vapor
Ethylene oxide	2.529448×10^{-6}	2.528886×10^{-6}	1.46414×10^{-11}	1.4921×10^{-11}
Water	0.9999515	0.99990670	0.13059	0.132864
Ethylene glycol	3.599192×10^{-5}	3.599089×10^{-5}	0.8649360	0.8629011
Diethylene glycol	1.264544×10^{-8}	1.264509×10^{-8}	4.45336×10^{-3}	4.21003×10^{-3}
Triethylene glycol	1.35198×10^{-11}	1.35195×10^{-11}	2.058291×10^{-5}	1.72148×10^{-5}
Tetraethylene glycol	1.38167×10^{-15}	1.38194×10^{-15}	6.695805×10^{-8}	4.02859×10^{-8}

ing the temperature profile along the column height. In this case, the calculated product temperature on top plates of the column is overestimated, and that on bottom plates, underestimated with respect to the real values. For example, in a column operating at a pressure of 0.1 MPa and water content of the vapor upflowing from the top plate equal to 0.9999 mole fraction, the calculated top temperature of the top part of the column was 384.1 K, instead of the real value of 373 K. Therefore, the relative volatilities were taken, in simulating the operation of the reaction-rectification column, to be constant throughout the upper and lower halves of the column, but determined by the temperatures of the top and bottom parts of the column, respectively. This made it possible to obtain a more precise temperature profile along the column height (Table 5). Thus, the assumption that relative volatilities are constant along the column height is sufficiently correct in the modification accepted.

A simulation of the operation of a reaction-rectification column demonstrated that the compositions of the nonequilibrium counter flows of vapor and liquid are rather close for neighboring plates (Table 6). This corresponds to operation of the apparatus in the total reflux mode. A specific feature of the operation of the column is that the quality of the residue obtained is virtually independent of the number of theoretical plates, beginning with five or six. This is so because an increase in the number of plates between the input of raw materials and discharge of the residue leads to formation of a kind of a constant-concentration zone on a number of theoretical plates, and the tem-

Table 7. Effect of the number of theoretical plates on the variation of temperature T and the concentrations of water (x_2) and ethylene glycol (x_3) in the liquid phase downflowing from plates of the reaction-rectification column (column pressure 0.1 MPa, reflux : ethylene oxide ratio at the inlet of 3rd plate 90 : 1)

Plate no.	Parameter	Number of plates in the column			
		6	8	10	12
1	x_2	0.9999901	0.9999916	0.9999916	0.9999916
	x_3	6.42501×10^{-6}	4.9808×10^{-6}	4.97333×10^{-6}	4.97343×10^{-6}
	T	372.24	372.24	372.24	372.24
2	x_2	0.9996935	0.9997638	0.9997642	0.9997642
	x_3	3.04005×10^{-4}	2.35713×10^{-4}	2.35357×10^{-4}	2.35376×10^{-4}
	T	372.26	372.24	372.24	372.24
3	x_2	0.985711	0.9888626	0.9888790	0.9888788
	x_3	1.41865×10^{-2}	1.10364×10^{-2}	1.10199×10^{-2}	1.10202×10^{-2}
	T	372.52	372.45	372.45	372.45
4	x_2	0.8595069	0.9881128	0.9888635	0.9888674
	x_3	0.1403606	1.17861×10^{-2}	1.10354×10^{-2}	1.10315×10^{-2}
	T	375.17	372.47	372.45	372.45
5	x_2	0.1226969	0.9542174	0.98881579	0.98883245
	x_3	0.8756662	4.56777×10^{-2}	1.17401×10^{-2}	1.15735×10^{-2}
	T	415.55	373.14	372.47	372.47
6	x_2	9.45093×10^{-3}	0.6499565	0.9858908	0.9883142
	x_3	0.9812574	0.3498251	1.40071×10^{-2}	1.15838×10^{-2}
	T	465.76	405.97	390.13	390.13
7	x_2		0.1150408	0.9540226	0.9881598
	x_3		0.8833290	4.58725×10^{-2}	1.17381×10^{-2}
	T		440.84	397.83	397.09
8	x_2		8.78999×10^{-3}	0.6486488	0.9859213
	x_3		0.9820252	0.3511326	1.39766×10^{-2}
	T		466.02	405.01	397.13
9	x_2			0.1144457	0.9544424
	x_3			0.8839234	4.54527×10^{-2}
	T			440.93	397.82
10	x_2			7.73897×10^{-2}	0.6514865
	x_3			0.9820768	0.3483957
	T			466.04	405.92
11	x_2				0.1157427
	x_3				0.8826284
	T				440.74
12	x_2				8.85012×10^{-2}
	x_3				0.9819659
	T				465.99

perature and composition of vapor and liquid flows in this zone are virtually constant (Table 7). This situation additionally confirms that the reaction can be performed on several plates without any significant effect of the reaction on the fractionation in this zone.

To assess the adequacy of the model developed, the operation of a reaction-rectification column for synthesis of ethylene glycol was calculated and the flow rates of the raw material, vapor, and liquid on the plates were obtained, which virtually coincided with the data reported in [9]. The calculated profiles of temperatures and concentrations of the boundary components of the system (water and ethylene glycol), being separated, along the column height in a wide range of

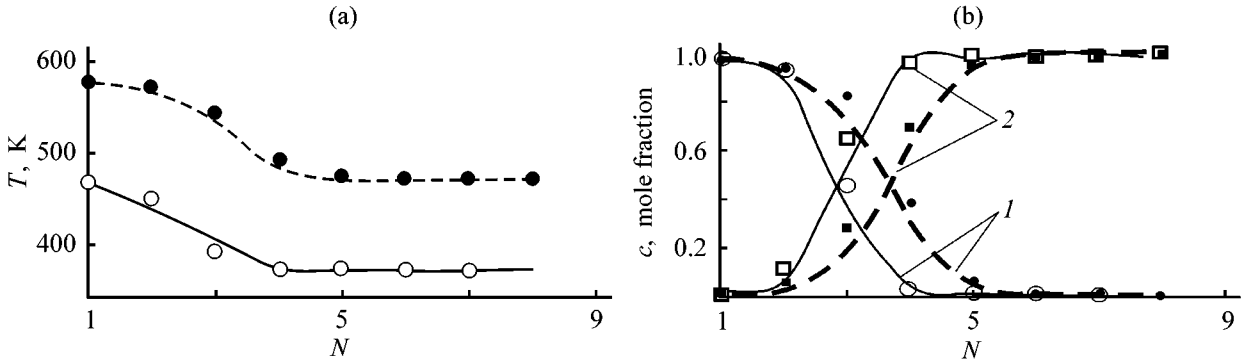


Fig. 5. Variation of (a) temperature T and (b) concentration c of (*1*) ethylene glycol and (*2*) water over plates of the reaction-rectification column. (N) Plate number. *Solid lines*, calculation in terms of the model at a pressure of 0.1 MPa; *dashed lines*, calculation by the model at a pressure of 1.5 MPa; *points*, data of [9].

pressures (Fig. 5) demonstrated an acceptable coincidence with the data of [9]. This circumstance can serve as a correct qualitative substantiation of the adequacy of the combined static-kinetic model of the reaction-rectification column, developed in this study.

CONCLUSIONS

(1) The principles of formation of a combined static-kinetic mathematical model of a reaction-rectification column were considered for the example of ethylene glycol synthesis.

(2) The possibility of obtaining high-purity ethylene glycol in a reaction-rectification column was substantiated.

(3) Ways for overcoming the limitations on synthesis of ethylene glycol in a reaction-rectification column were described.

(4) The correctness of the assumptions made in developing the mathematical model of the apparatus was substantiated.

(5) The adequacy of the combined static-kinetic model of the reaction-rectification column was confirmed.

REFERENCES

1. Astarita, G., *Mass Transfer with Chemical Reaction*, Amsterdam: Elsevier, 1967.
2. Okasinski, M.J. and Doherty, M.F., *Ind. Eng. Chem. Research*, 1998, no. 7, pp. 2821–2836.
3. Buzad, G. and Doherty, M.F., *Computers Chem. Eng.*, 1995, no. 4, pp. 395–412.
4. Cardoso, M.F., Salcedo, R.L., and Feyo de Azevedo, S., *Computers Chem. Eng.*, 1996, no. 9, pp. 1065–1080.
5. Venkataraman, S., Chan, W.K., and Boston, J., *Chem. Eng. Progress*, 1990, no. 8, pp. 45–53.
6. Chang, Y.A. and Seader, J.D., *Computers Chem. Eng.*, 1988, no. 12, pp. 1243–1257.
7. Stein, E., Kienle, A.R.J., Mohl, K.D., et al., *Computers Chem. Eng. (Suppl.)*, 1999, vol. 23, p. S903.
8. Ciric, A.R. and Gu, D., *Am. Inst. Chem. Eng. J.*, 1994, no. 9, pp. 1479–1486.
9. Cardoso, M.F., Salcedo, R.L., Feyo de Azevedo, S., et al., *Chem. Eng. Sci.*, 2000, vol. 55, pp. 5059–5078.
10. Kondrat'ev, A.A. and Samoilov, N.A., *Zh. Prikl. Khim.*, 1997, vol. 70, no. 9, pp. 1512–1517.
11. Dyment, O.N., Kazanskii, K.S., and Miroshnikov, F.M., *Glikoli i drugie proizvodnye okisei etilena i propilena* (Glycols and Other Derivatives of Ethylene and Propylene Oxides), Moscow: Khimiya, 1976.
12. Skoblo, A.I., Tregubova, I.A., and Molokanov, Yu.K., *Protsessy i apparaty neftepererabatyvayushchei i neftekhimicheskoi promyshlennosti* (Processes and Apparatus of Oil Refining and Petrochemical Industry), Moscow: Gostoptekhizdat, 1982.
13. Kafarov, V.V., *Metody kibernetiki v khimii i khimicheskoi tekhnologii* (Methods of Cybernetics in Chemistry and Chemical Technology), Moscow: Khimiya, 1976.

ISSN 1070-4272, Russian Journal of Applied Chemistry, 2006, Vol. 79, No. 12, pp. 1982–1985. © Pleiades Publishing, Inc., 2006.
Original Russian Text © E.A. Dikusar, N.A. Zhukovskaya, O.G. Vyglazov, 2006, published in Zhurnal Prikladnoi Khimii, 2006, Vol. 79, No. 12, pp. 2007–2010.

ORGANIC SYNTHESIS AND INDUSTRIAL ORGANIC CHEMISTRY

Synthesis of Esters of *D*,*L*-, *D*(+)-, and *L*(–)-Camphor Oximes: Structure–Odor Correlation

E. A. Dikusar, N. A. Zhukovskaya, and O. G. Vyglazov

Institute of Physical Organic Chemistry, National Academy of Sciences of Belarus, Minsk, Belarus
Tereza Inter Limited Liability Company, Moscow, Russia

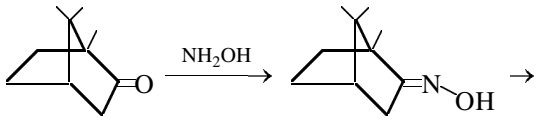
Received April 13, 2006

Abstract—Esters of *D*,*L*-, *D*(+)-, and *L*(–)-camphor oximes were synthesized, and the correlation between their structure and odor was examined.

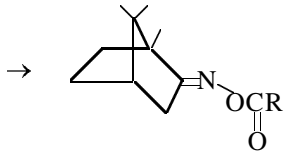
DOI: 10.1134/S1070427206120147

Examination of the correlation between the tints and scents of fragrance compounds and odorants, on the one hand, and structures of fragments of natural compounds used in the synthesis of these substances, on the other hand, is a topical problem of fragrance chemistry [1–3].

In this study we developed a convenient procedure for preparing esters of *D*,*L*-, *D*(+)-, and *L*(–)-camphor oximes and examined the correlation between their odor and structure:



I, **II**, **III** **IV**, **V**, **VI**



VIIa–**VIIv**, **VIIIa**–**VIIId**, **IXa**–**IXd**

I, **IV**, **VII**: *D*,*L*-camphor and its oxime and esters, respectively; **II**, **V**, **VIII**: *D*(+)-camphor and its oxime and esters, respectively; **III**, **VI**, **IX**: **L**(–)-camphor and its oxime and esters, respectively; **VII**, **VIII**, **IX**: R = Me (**a**), Et (**b**), Pr (**c**), $CHMe_2$ (**d**), Bu (**e**), CH_2CHMe_2 (**f**), $(CH_2)_4Me$ (**g**), $(CH_2)_5Me$ (**h**), $(CH_2)_6Me$ (**i**), $(CH_2)_7Me$ (**j**), $(CH_2)_8Me$ (**k**), $(CH_2)_{11}Me$ (**l**), $(CH_2)_{16}Me$ (**m**), $CHBrCCl{=}CCl_2$ (**n**), $(CH_2)_2C(O)OMe$ (**o**), C_6H_{11}-cyclo (**p**), C_6H_5 (**q**), C_6H_4Cl-2 (**r**), $C_6H_3Cl_2$-2,4 (**s**), $CH_2OC_6H_3Cl_2$-2,4 (**t**), $C_6H_4NO_2$-3 (**u**), $C_6H_4NO_2$-4 (**v**), $C_6H_3(NO_2)_2$-3,5 (**w**).

Camphor oxime esters **VIIa**–**VIIv**, **VIIIa**–**VIIId**, and **IXa**–**IXd** were prepared by the reactions of **IV**–**VI** with appropriate alkane- or arenecarboxylic acid anhydrides or chlorides in absolute hexane or benzene. The reactions with carboxylic acid chlorides were performed in the presence of pyridine. The reactant ratio was stoichiometric (1 : 1 or 1 : 1 : 1). By these reactions, the starting oximes **IV**–**VI** were converted to the corresponding esters **VIIa**–**VIIw**, **VIIIa**–**VIIId**, and **IXa**–**IXd** in yields of 88–92%.

Camphor oxime esters **VIIa**–**VIIw**, **VIIIa**–**VIIId**, and **IXa**–**IXd** are colorless liquids or crystalline substances (crystallizing from hexane) (Table 1). The esters do not require additional purification, contain no admixtures of the starting compounds, benzene, and pyridine, and are suitable for direct use in fragrance and food industry [4]. The purity of the compounds was 97–98% according to the ^{1}H NMR spectra.

The structure and properties of camphor oxime esters **VIIa**–**VIIv**, **VIIIa**–**VIIId**, and **IXa**–**IXd** were confirmed by elemental analysis, cryoscopic determination of the molecular weight (Table 1), and ^{1}H NMR, IR, and UV spectroscopy.

The IR spectra of **VIIa**–**VIIv**, **VIIIa**–**VIIId**, and **IXa**–**IXd** contain the following characteristic absorption bands (ν, cm^{-1}): 3020–2800 (CH_{Alk}), 1780–1750 (C=O), 1670–1660 (C=N), 1100–1220 (C–O), and 910–1000 (N–O).

The UV spectra of **VIIa**–**VIIv**, **VIIIa**–**VIIId**, and **IXa**–**IXd** show an absorption peak at 208 nm (ε 4000) assigned to the C=N–O fragment.

In the ^{1}H NMR spectra of **VIIa**–**VIIv**, **VIIIa**–**VIIId**, and **IXa**–**IXd**, the methyl groups of the bicyclic core

Table 1. Properties of camphor oxime esters **VIIa**–**VIIw**, **VIIIa**–**VIIId**, and **IXa**–**IXd**

Ester	Yield, %	mp, °C	Found, %			Formula	Calculated, %			*M*	
			C	H	N		C	H	N	found	calculated
VIIa	90	16–17	69.32	9.50	6.90	$C_{12}H_{19}NO_2$	68.87	9.15	6.69	201.6	209.3
VIIb*	92	–	70.28	9.50	6.32	$C_{13}H_{21}NO_2$	69.92	9.48	6.27	216.8	223.3
VIIc*	88	–	71.16	10.03	5.60	$C_{14}H_{23}NO_2$	70.85	9.77	5.90	229.3	237.3
VIId*	89	–	71.10	9.95	5.56	$C_{14}H_{23}NO_2$	70.85	9.77	5.90	226.7	237.3
VIIe*	88	–	71.92	10.14	5.22	$C_{15}H_{25}NO_2$	71.67	10.02	5.57	240.4	251.4
VIIf*	88	–	71.88	10.20	5.30	$C_{15}H_{25}NO_2$	71.67	10.02	5.57	242.8	251.4
VIIg*	88	–	72.75	10.33	5.07	$C_{16}H_{27}NO_2$	72.41	10.25	5.28	251.6	265.4
VIIh*	90	–	73.41	10.62	4.80	$C_{17}H_{29}NO_2$	73.07	10.46	5.01	266.5	279.4
VIIi*	88	–	73.98	10.81	4.52	$C_{18}H_{31}NO_2$	73.67	10.65	4.77	282.1	293.4
VIIj*	89	–	74.60	11.03	4.23	$C_{19}H_{33}NO_2$	74.22	10.82	4.56	295.9	307.5
VIIk*	88	–	75.05	11.04	4.10	$C_{20}H_{35}NO_2$	74.72	10.97	4.36	309.0	321.5
VIIl*	88	–	76.18	11.49	3.59	$C_{23}H_{41}NO_2$	75.98	11.37	3.85	340.2	363.6
VIIm	92	27–28	77.65	11.94	3.37	$C_{28}H_{51}NO_2$	77.54	11.85	3.23	408.7	433.7
VIIn**	89	94–95	40.67	4.35	3.45	$C_{14}H_{17}NBrCl_3O_2$	40.27	4.10	3.35	400.2	417.6
VIIo*	90	–	64.38	8.37	4.65	$C_{15}H_{23}NO_4$	64.04	8.24	4.98	272.5	281.4
VIIp*	88	–	73.82	9.96	4.78	$C_{17}H_{27}NO_2$	73.61	9.81	5.05	270.8	277.4
VIIq	88	64–65	75.54	7.97	4.87	$C_{17}H_{21}NO_2$	75.25	7.80	5.16	259.3	271.4
VIIr**	90	83–84	67.05	6.72	4.28	$C_{17}H_{20}Cl_2$	66.77	6.59	4.58	297.6	305.8
VIIs**	90	93–94	60.62	5.80	3.87	$C_{17}H_{19}NCl_2O_2$	60.01	5.63	4.12	329.0	340.3
VIIt**	90	–	58.77	5.91	3.50	$C_{18}H_{21}NCl_2O_3$	58.39	5.72	3.78	354.1	370.3
VIIu	89	85–86	64.60	6.35	8.89	$C_{17}H_{20}N_2O_4$	64.54	6.37	8.86	302.3	316.4
VIIv	90	110–111	64.73	6.45	8.80	$C_{17}H_{20}N_2O_4$	64.54	6.37	8.86	301.9	316.4
VIIw	92	127–128	57.13	5.22	11.89	$C_{17}H_{19}N_3O_6$	56.51	5.30	11.63	345.2	361.4
VIIIa	91	16–17	69.24	9.34	6.45	$C_{12}H_{19}NO_2$	68.87	9.15	6.69	202.4	209.3
VIIIb*	89	–	70.20	9.57	6.20	$C_{13}H_{21}NO_2$	69.92	9.48	6.27	211.6	223.3
VIIIc*	89	–	71.10	9.943	5.58	$C_{14}H_{23}NO_2$	70.85	9.77	5.90	225.7	237.3
VIIId*	88	–	71.14	9.86	5.71	$C_{14}H_{23}NO_2$	70.85	9.77	5.90	228.0	237.3
IXa	91	17–18	69.04	9.20	6.61	$C_{12}H_{19}NO_2$	68.87	9.15	6.69	204.7	209.3
IXb*	92	–	70.12	9.59	6.14	$C_{13}H_{21}NO_2$	69.92	9.48	6.27	209.3	223.3
IXc*	90	–	71.10	9.94	5.62	$C_{14}H_{23}NO_2$	70.85	9.77	5.90	228.6	237.3
IXd*	88	–	71.05	9.80	5.65	$C_{14}H_{23}NO_2$	70.85	9.77	5.90	224.1	237.3

* d_{20}^{20}, n_D^{20}; 1.0813, 1.4856 (**VIIb**); 1.0114, 1.4798 (**VIIc**); 0.9301, 1.4688 (**VIId**); 0.9793, 1.4814 (**VIIe**); 1.0488, 1.4725 (**VIIf**); 0.9189, 1.4734 (**VIIg**); 0.8963, 1.4762 (**VIIh**); 0.9310, 1.4722 (**VIIi**); 0.9459, 1.4778 (**VIIj**); 1.0409, 1.4748 (**VIIk**); 0.8664, 1.4752 (**VIIl**); 1.0558, 1.4892 (**VIIo**); 0.8668, 1.5048 (**VIIp**); 1.1789, 1.5385 (**VIIt**); 1.0809, 1.4855 (**VIIIb**); 1.0120, 1.4800 (**VIIIc**); 0.9310, 1.4690 (**VIIId**); 1.0805, 1.4854 (**IXb**); 1.0110, 1.4792 (**IXc**); 0.9300, 1.4692 (**IXd**).

** Found, calculated, respectively (%): Br + Cl 44.62, 44.61 (**VIIn**); Cl 11.5, 11.59 (**VIIr**); Cl 20.38, 20.84 (**VIIs**); Cl 18.79, 19.15 (**VIIt**).

give three characteristic singlets at 0.78–1.20 ppm, and the CH proton, a singlet at 2.20–2.30 ppm.

The IR, UV, and ^{1}H NMR spectra of **VIIa**–**VIIv**, **VIIIa**–**VIIId**, and **IXa**–**IXd** contain characteristic absorption bands and signals confirming the expected structure of the ester fragments [5].

A number of the compounds prepared have a pleasant odor[1] with various strong tints (Table 2). Of particular interest are compounds **VIIc**–**VIIi** having fruit–berry scents with various notes. With an increase in the size of the alkyl radical, the scent becomes more intense, changing from berry to fruit. Further increase in the size of the alkyl radical in the series **VIIj**–**VIIq** leads to disappearance of the fruit–berry scent and appearance of a wood scent with camphor notes and various tints; in this series, the odor intensity decreases. Particularly attractive among these derivatives are **VIIk** and **VIIo**, having popular odors of ozone and sweet leather. Esters **VIIn** and **VIIr**–**VIIw** have no odor because of low volatility. A very interesting fact for perfumery is the pronounced musk note in *D*-cam-

[1] Organoleptic evaluation of scents of **IV**–**VI**, **VIIa**–**VIIv**, **VIIIa**–**VIIId**, and **IXa**–**IXd** was performed by the Tasting Council at the Accredited Analytical Laboratory of the Tereza Inter Limited Liability Company (Moscow).

Table 2. Specific rotation and odor of camphor oximes IV–VI and their esters **VIIa–VIIm**, **VIIo–VIIq**, **VIIIa–VIIId**, and **IXa–IXd**

Compound	$[\alpha]_D^{20}$, deg	Odor
IV	0	Meat, animal, with potato and fried onion tint
V	–42.1	Meat, with fruit–camphor note and valerian tint
VI	+42.2	Camphor, sweet, with guelder-rose berry tint and spicy note
VIIa	0	Weak fruit-berry with cranberry– wine tint
VIIb	0	Wood–camphor with ambergis note
VIIc	0	Bright berry with ashberry– cranberry tint and bitter note
VIId	0	Sweet cranberry with light note of peach peel
VIIe	0	Red berry with wood and chilling note
VIIf	0	Wine–berry with camphor– grass note
VIIg	0	Intense berry–fruit, notes of cranberry and quince
VIIh	0	Sour fruit, with green apple note
VIIi	0	Moderate fruit–berry with mature apple note
VIIj	0	Moderate fruit–wood with animal–musk note
VIIk	0	Seaweed, ozone, sea breeze with fruit–flower note
VIIl	0	Wood–camphor with musk note
VIIm	0	Wood–camphor with anisic note
VIIo	0	Wood–leather with camphor– ambergis note
VIIp	0	Mild berry–camphor with smoke note
VIIq	0	Spicy, camphor–grass, resinous note
VIIIa	–38.4	Camphor–wood, coniferous note
VIIIb	–37.0	Wood–camphor, sour fruit note
VIIIc	–27.6	Wood–berry, note of guelder-rose berries with camphor tint
VIIId	–27.7	Wood–camphor, sweet leather note
IXa	+39.1	Camphor–wood, musk note
IXb	+38.5	Sour berry with musk tint
IXc	+26.9	Green and sour fruit with musk note
IXd	+27.2	Fruit–wood with peach peel note

phor esters **IXa–IXd**, in contrast to wood–camphor notes in the related *L*-camphor esters **VIIIa–VIIId** or berry–fruit notes in *D,L*-camphor esters **VIIa–VIId**. It should be noted that the presence of sweetish notes in the scents of *D* enantiomers of esters **IXa–IXd** and their absence in the scentes of *L* enantiomers **VIIIa–VIIId** well correlate with the presence and absence of these notes in the odors of the starting oximes **VI** and **V**, respectively.

EXPERIMENTAL

The IR spectra were recorded on a Protege-460 IR Fourier spectrometer (Nicolet) in a thin film or in KBr, and the UV spectra, on a Specord UV-Vis spectrometer from 1×10^{-4} M solutions in methanol. The ^{1}H NMR spectra were measured on a Tesla BS-587A spectrometer (100 MHz) from 5% solutions in $CDCl_3$; the chemical shifts were determined relative to internal TMS. The specific rotation was measured with an SM-2 device (3.5% solutions in 96% ethanol). The molecular weights were determined cryoscopically in benzene.

As starting compounds we used 96% *D,L*-camphor (mp 175–177°C; $[\alpha]_D^{20} = 0°$, $c = 10$, EtOH) (**I**), 98% *D*(+)-camphor (mp 179–181°C; $[\alpha]_D^{20} = +44.1°$, $c = 10$, EtOH) (**II**), 99% *L*(–)-camphor (mp 178–180°C; $[\alpha]_D^{20} = -43.0°$, $c = 10$, EtOH) (**III**). *D,L*-, *D*(+)-, and *L*(–)-camphor oximes **IV–VI** (pure *E* isomers) were prepared by the reaction of *D,L*-, *D*(+)-, and *L*(–)-camphor **I–III** with a threefold excess of hydroxylamine in ethanol [6, 7].

Carboxylic acid chlorides were prepared by refluxing the corresponding carboxylic acids with a 1.5-fold excess of $SOCl_2$ in benzene. We used freshly distilled carboxylic acid chlorides and absolute hexane, benzene, and pyridine.

Camphor oxime alkanoates VIIa–VIId, VIIIa–VIIId, and IXa–IXd. A 0.01-mol portion of *D,L*-, *D*(+)-, or *L*(–)-camphor oxime was mixed with

0.01 mol of an appropriate acyl chloride. The mixture was hermetically sealed and allowed to stand for 24–48 h at 20–23°C with intermittent careful shaking. Then the mixture was dissolved in 50 ml of hexane, transferred into a separating funnel, thoroughly washed with water and 20% NaCl to suppress formation of an emulsion, and washed with two or three portions of 5% $NaHCO_3$. The organic layer was separated and filtered through a paper filter. The hexane was removed in a vacuum at a bath temperature not exceeding 30°C.

Camphor oxime carboxylates VIIe–VIIw. A solution of 0.01 mol of pyridine in 10 ml of benzene was added to a solution of 0.01 mol of *D*,*L*-camphor oxime **IV** and 0.01 mol of an appropriate alkanoyl or aroyl chloride in 50 ml of benzene; in the process, the mixture was agitated by shaking the reaction flask. The mixture was hermetically sealed and allowed to stand for 10–12 h at 20–23 h with intermittent careful shaking. Then the mixture was transferred into a separating funnel, thoroughly washed with water and 20% NaCl solution to suppress formation of an emulsion, and washed with two or three portions of 5% $NaHCO_3$. The organic layer was separated and filtered through a paper filter. Benzene was removed in a vacuum at a bath temperature not exceeding 30°C. Compounds **VIIm**, **VIIn**, **VIIq–VIIs**, and **VIIu–VIIw** were crystallized from hexane.

CONCLUSIONS

(1) A convenient procedure was developed for preparing *D*,*L*-, *D*(+), and *L*(–)-camphor oxime esters in 88–92% yields.

(2) Some of the compounds prepared can be of interest as components for fragrance industry and available fragrance compounds.

REFERENCES

1. Ohloff, G, *Scent and Fragrances*, Berlin: Springer, 1994.
2. Ohloff, G. and Thomas, C.C., *Comment in Gustation and Olfaction*, New York: Academic, 1971.
3. Thomas, C.C., *Molecular Basis of Odor*, Springfield, 1970.
4. Sarafanova, L.A., *Pishchevye dobavki: Entsiklopediya* (Food Additives: Encyclopedia), St. Petersburg: GIRD, 2003.
5. Dikusar, E.A., Kozlov, N.G., Zhukovskaya, N.A., and Moiseichuk, K.L., *Khim. Prirodn. Soedin.*, 2004, no. 2, pp. 154–156.
6. Cottingham, R.W., *J. Org. Chem.*, 1960, vol. 25, no. 9, pp. 1473–1476.
7. *Dictionary of Organic Compounds*, Heilborn, I. and Banbury, H.M., Eds., New York: Eyre and Spottiswoode, 1934. Translated under the title *Slovar' organicheskikh soedinenii*, Moscow: Inostrannaya Literatura, 1949, pp. 384–385.

ISSN 1070-4272, Russian Journal of Applied Chemistry, 2006, Vol. 79, No. 12, pp. 1986–1989. © Pleiades Publishing, Inc., 2006.
Original Russian Text © M.G. Shcherban', T.Yu. Nasretdinova, N.A. Kladova, A.V. Radushev, T.B. Bubyakina, 2006, published in Zhurnal Prikladnoi Khimii, 2006, Vol. 79, No. 12, pp. 2011–2013.

ORGANIC SYNTHESIS AND INDUSTRIAL ORGANIC CHEMISTRY

Effect of Strong Electrolytes on Surface Activity of Aqueous 1,1-Dimethyl-1-alkylhydrazinium Chloride in Aqueous Solutions

M. G. Shcherban', T. Yu. Nasretdinova, N. A. Kladova, A. V. Radushev, and T. B. Bubyakina

Perm State University, Perm, Russia

Institute of Technical Chemistry, Ural Division, Russian Academy of Sciences, Perm, Russia

Received July 3, 2006

Abstract—The effect of electrolytes on the surface activity of aqueous anionic (1,1-dimethyl-1-alkylhydrazinium chloride homologues with the C_{10}–C_{18} alkyl radical) and nonionic (Neonol AF 9-12) surfactants in aqueous solutions was studied.

DOI: 10.1134/S1070427206120159

1,1-Dimethyl-1-alkylhydrazinium chloride homologues with C_{10}–C_{18} (DMAHCs) alkyl radicals belong to the quaternary hydrazinium salts (QHS). These compounds are efficient surfactants strongly decreasing the surface tension at the water-air interface [1]. Along with the surface activity, DMAHCs also exhibit other kinds of chemical and biochemical activity. For example, these compounds are antiseptics, corrosion inhibitors, and biocides [3, 4]. 1,1-Dimethyl-1-alkylhydrazinium chloride with the alkyl C_{12} and C_{14} radicals (commercial brand ChGS-1214) is applied as an effective collector in flotation of an insoluble residue of silicate and carbonate minerals in leaching of KCl from potassium-containing ores [5]. The consumption of ChGS-1214 in flotation of the insoluble mineral residue is two times less than that of commonly used collectors [6]; DGS-1214 is also less toxic. Owing to the higher selectivity in separation of the mineral residue, ChGS-1214 can be used without frothing [4]. However, to elucidate whether or not ChGS-1214 can be used for flotation of minerals from their suspensions in concentrated aqueous KCl, its surface activity in relation to ionic strength of aqueous solutions should be examined. Such data are lacking. In this study, we attempted to fill this gap.

EXPERIMENTAL

1,1-Dimethyl-1-alkylhydrazinium chloride homologues of the general formula $[R(CH_3)_2NNH_2]Cl$ (R = C_nH_{2n+1}, n = 10, 12, 14, 16, 18, and n = 12 + n = 14 mixture) were prepared by quaternization of 1,1-dimethylhydrazinium with primary chloroalkanes [7]. The main substance content determined by a modified method reported in [8] was no less than 96%. For comparison, nonionic surfactant Neonol AF 9-12 was also studied.

The surface tension at the interface between an aqueous DMAHC solution and air was determined stalagmometrically [9], and calculated by the formula

$$\sigma_x = (\sigma_0 m_x n_0)/(m_0 n_x), \quad (1)$$

where σ_x and σ_0 are the surface tensions of the solution tested and water, respectively (mN m^{-1}); m_x and m_0 are the weights of aqueous DMAHC and water that flowed out from the stalagmometer (g); n_x and n_0 are the number of drops of aqueous DMAHC and water that flowed out from the stalagmometer.

The surface tension of the model solutions containing KCl (1.34 M), NaCl (3.73 M), and varied DMAHC concentration was also measured stalagmometrically. The electrolyte content of these solutions was close to that in the saturated process solutions used to recover KCl by flotation [6].

The values of the surface tension at the water–air interface were taken from [10]. All the data reported hare were obtained by averaging the results of three

Effect of strong electrolytes on the solubility and CMC of solutions of cationic DMAHC {$[R(CH_3)_2NNH_2]Cl$} and neutral (AF 9-12) surfactants

Reagent	Solubility, g l^{-1}		σ_{min}, mN m^{-1}		CMC, g l^{-1}			
					H_2O		solution of NaCl + KCl	
	H_2O	solution of NaCl + KCl	H_2O	solution of NaCl + KCl	CMC_1	CMC_2	CMC_1	CMC_2
R:								
$C_{10}H_{21}$	>333	25	40	25	6.6	15.5	0.7	11.1
$C_{12}H_{25}$	–	20	36	23	2.0	10.0	1.3	10.0
$C_{14}H_{29}$	–	<0.1	34	23	0.8	12.5	–	–
$C_{16}H_{33}$	20	<0.1	34	–	0.4	0.6	–	–
$C_{18}H_{37}$	2	–	66	–	0.003	0.02	–	–
C_{12}, C_{14}	>100	1	35	23	2.8	38.9	0.3	13.4
Neonol 9-12	20	18	35	30	0.4	2.4	0.3	2.7

or four replicate measurements. The experiments were carried out at 20°C.

We found that addition of a strong electrolyte (1.34 M KCl or 3.73 M NaCl) to an aqueous surfactant solution significantly decreases its surface tension at the interface between the aqueous electrolyte and air as compared to a surfactant solution without electrolytes. For aqueous DMAHC with R = C_{10} and C_{12} containing NaCl + KCl, σ_{min} was 25 and 23 mN m^{-1}, respectively, whereas in the absence of these electrolytes the surface tension was 35 mN m^{-1} [1] (see table).

Figure 1 shows that, in going from a solution of DMAHC in distilled water to an electrolyte-containing aqueous DMAHC solution, the slope of the initial portion of the surface tension isotherm significantly increases. We believe that one of the reasons for this effect is partial dehydration of the polar groups of the surface-active cations in the presence of the electrolyte, which salts-out the surfactant and decreases its solubility. For example, the solubility of DMAHC with R = C_{10} and C_{12} decreases in the presence of an electrolyte from 300 to 20 g l^{-1}. The other DMAHC homologues added to water even in minor amounts form a separate phase. Therefore, the surface tension isotherms of the salt solutions were not studied for these surfactants. The solubilities of DMAHCs in both distilled water and the model electrolyte solutions, and also the critical micelle concentrations (CMC) are listed in the table. The CMC values were calculated from the plot of the logarithm of the surface tension vs. the electrolyte concentration. In this plot, the CMC is manifested as a point at which the curved portion of the plot transforms into a straight line parallel to the abscissa axis [11].

We found that addition of a strong electrolyte to the aqueous surfactant decreases both CMC_1 and CMC_2. This means that, in the presence of a strong electrolyte, the micellization power of the surfactant increases. A similar pattern has been observed on adding a strong electrolyte to aqueous sodium dodecyl sulfate [12]. Serdyuk and Chervontseva [12] believe that this phenomenon is due to the fact that, in the course of micellization, the surfactant dissociation and the micell charge decrease, and micelles tend to aggregate and form supramicellar structures. As a result, the viscosity of the aqueous surfactant increases at surfactant concentrations exceeding CMC_2.

Neonol AF 9-12 and ChGS-1214 used as collectors in flotation treatment of potassium-containing ores

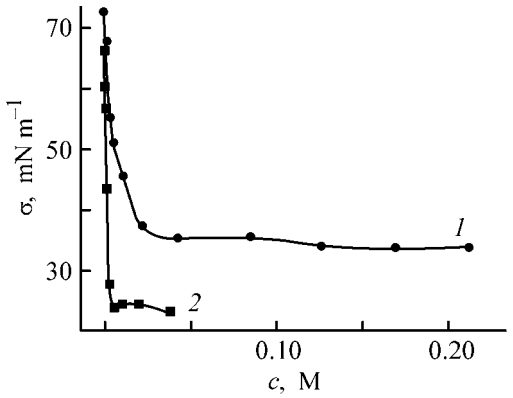


Fig. 1. Surface tension isotherms of solutions of DMAHCs (R = $C_{12}H_{25}$) in (*1*) distilled water and (*2*) model electrolyte solution. (σ) Surface tension and (*c*) electrolyte concentration.

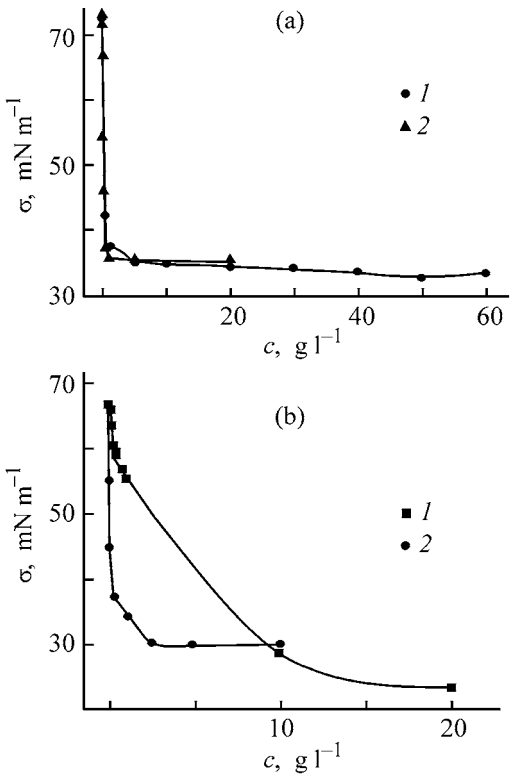


Fig. 2. Surface tension isotherms of (*1*) ChGS-1214 and (*2*) Neonol AF 9-12 in (a) distilled water and (b) model KCl + NaCl solution. (σ) Surface tension and (*c*) surfactant concentration.

exhibit virtually identical surface activities. Their surface tension isotherms in distilled water virtually coincide and σ_{min} is approximately 35 mN m^{-1} for both surfactants (Fig. 2a). On adding an electrolyte to both aqueous surfactants, the minimal surface tension decreases (Fig. 2b), but for Neonol AF 9-12 this effect is weaker (σ_{min} ~ 30 mN m^{-1}) than for ChGS-1214 (σ_{min} ~ 23 mN m^{-1}). The CMC values of both Neonol AF 9-12 and ChGS-1214 in the model electrolyte-containing solution and distilled water are virtually equal. These features are typical of this kind of surfactants.

If the surfactant counterion is identical to one of the ions of the electrolyte added, the effect of the counterion concentration c_i on CMC is determined by the equation [13]

$$\ln \mathrm{CMC} = \mathrm{const} - K_g \ln c_i, \qquad (2)$$

where K_g is a dimensionless constant. Its physical sense is explained below.

In association of ionic surfactant molecules into a micelle, they overcome the repulsion between similarly charged ions. When long-chain micelle-forming ions is accomodated on the micelle surface, the integral work against the electrostatic repulsion is $e\varphi_0$. However, in the presence of counterion, the electric charge of the micelle-forming ion becomes smaller than elementary charge. Therefore, the effective electrostatic work of association of a long-chain micelle-forming molecule with a micelle is $K_g\varphi_0 e$, where $K_g < 1$. Thus, K_g characterizes the effect of a counterion on the electrostatic energy of micelle formation [13].

The addition of electrolyte suppresses the factors hindering the micelle formation. This effect is manifested as a decrease in CMC_1 and CMC_2 for both the individual surfactants and their mixtures (see table).

In aqueous solutions of neutral nonionic surfactants, the micelle formation occurs without electrostatic interactions. Therefore, introduction of electrolytes weakly influences the CMC of Neonol AF 9-12.

Figure 2b shows that, at surfactant concentration exceeding 10 g l^{-1}, ChGS-1214 is a stronger surfactant than Neonol AF 9-12. This is manifested as a higher surface tension and lower CMC.

CONCLUSIONS

(1) On adding electrolytes to aqueous solutions containing 1,1-dimethyl-1-alkyl hydrazinium chloride homologues, their minimal surface tension decreases by a factor of two as compared to the initial aqueous solutions; the solubility of the surfactant and the critical micellization concentration sharply decrease due to a decrease in the degree of surfactant dissociation. At the same time, the electrolytes virtually do not affect the related characteristics of Neonol AF 9-12 nonionic surfactant.

(2) In the series of 1,1-dimethyl-1-alkyl hydrazinium chloride homologues, ChGS-1214 exhibits higher surface activity in concentrated aqueous NaCl + KCl than the nonionic surfactant Neonol AF 9-12.

REFERENCES

1. Shcherban', M.G., Radushev, A.V., Nasretdinova, T.Yu., et al., *Zh. Prikl. Khim.*, 2004, vol. 77, no. 11, pp. 1861–1864.
2. RF Patent 2245244.
3. Tul'bovich, B.I., Kazakova, L.V., Radushev, A.V., et al., *Neft. Khoz.*, 1995, no. 11 pp. 44–45.
4. Aleksandrova, G.A., Prokhorova, G.A., Lesnov, A.E., et al., *Khim.-Farm. Zh.*, 1995, vol. 29, no. 11, pp. 22–24.

5. RF Patent 2 123 893.
6. Titkov, S.N., Mamedov, A.I., and Solov'ev, E.I., *Obogashchenie kaliinykh rud* (Dressing of Potassium-Containing Ores), Moscow: Nedra, 1982.
7. RF Patent 2 074 174.
8. Siggia, S. and Hanna, Dj.G., *Kolichestvennyi organicheskii analiz po funktsional'nym gruppam* (Quantitative Organic Analysis for Functional Groups), Khimiya, 1983.
9. Shchukin, E.D., Amelina, E.A., and Pertsov, A.V., *Kolloidnaya khimiya* (Colloid Chemistry), Moscow: Mosk. Gos. Univ., 1982.
10. Ravdel', A.A. and Ponomareva, A.M., *Kratkii spravochnik fiziko-khimicheskikh velichin* (Concise Handbook of Physicochemical Quantities), Leningrad: Khimiya, 1983, 8th ed.
11. Aivazov, B.V., *Praktikum po khimii poverkhnostnykh yavlenii i adsorbtsii* (Practical Course of Chemistry of Surface Phenomena and Adsorption), Moscow: Vysshaya Shkola, 1973.
12. Serdyuk, A.I. and Chervontseva, N.N., *Kolloidn. Zh.*, 1979, vol. 35, no. 5, pp. 833–837.
13. Abramov, A.A., Kol'tsov, S.I., and Murashev, I.A., *Zh. Fiz. Khim.*, 1982, vol. 56, no. 1, pp. 86–89.

ISSN 1070-4272, Russian Journal of Applied Chemistry, 2006, Vol. 79, No. 12, pp. 1990–1993. © Pleiades Publishing, Inc., 2006.
Original Russian Text © N.G. Krupnova, V.N. Kurskaya, G.N. Chervyakova, V.A. Fomin, 2006, published in Zhurnal Prikladnoi Khimii, 2006, Vol. 79, No. 12, pp. 2014–2017.

ORGANIC SYNTHESIS AND INDUSTRIAL ORGANIC CHEMISTRY

Ester Interchange of Methyl Methacrylate with Fractions of Higher Fatty Alcohols

N. G. Krupnova, V. N. Kurskaya, G. N. Chervyakova, and V. A. Fomin

Kargin Research Institute of Polymers, Federal State Unitary Enterprise, Dzerzhinsk, Nizhni Novgorod oblast, Russia

Received May 30, 2006

Abstract—Optimal conditions were found for preparing higher alkyl methacrylates by ester interchange of methyl methacrylate with fractions of higher alcohols.

DOI: 10.1134/S1070427206120160

Higher esters of unsaturated carboxylic acids find wide application [1, 2]. The particular interest in these monomers is due to their easy conversion into macromolecular compounds used as viscosity and depression additives to mineral oils and fuels [3–6], components of adhesive formulations [7], agents for treating textile and paper [8], plasticizers [8], lubricants [9], and components of paint-and-varnish coatings [10].

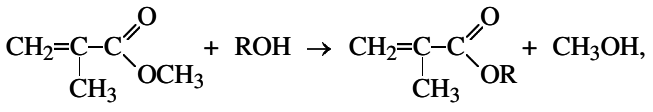
It is well known that synthesis of higher alkyl methacrylates by esterification of methacrylic acid in the presence of acid catalysts [11] is accompanied by substantial tarring of both the starting reagents and the reaction products, which requires additional expenses for purification and isolation of the target products. Furthermore, washing of higher alkyl methacrylates with alkaline solutions in the course of their isolation results in that stable, difficultly settling emulsions are formed, which results in major loss of the desired esters and yields a large amount of concentrated wastewater.

To eliminate the problems that arise in the synthesis and isolation of higher alkyl methacrylates by esterification, it seems appropriate to examine the possibility of preparing these compounds by ester interchange of methyl methacrylate with higher aliphatic alcohols in the presence of base catalysts, allowing the reaction to be performed virtually without formation of tar and by-products.

This paper deals with the preparation of higher alkyl methacrylates by ester interchange, choice of effective catalytic systems, and optimization of the reactant ratio with the aim to obtain high-purity products in high yields.

EXPERIMENTAL

Methyl methacrylate (MMA) met GOST (State Standard) 20370–74, and fractions of synthetic fatty alcohols, TU (Technical Specifications) 38.107119–85. As catalysts we tested potassium carbonate (GOST 4421–76, pure grade), sodium carbonate (GOST 83–79, pure grade), dibutyltin dicaprylate (TU 6-09-1150–76), sodium methylate (prepared in the laboratory), sodium borohydride (TU 1-92-162–90), and sodium phosphate (GOST 9337–79). The inhibiting system consisted of *p*-methoxyphenol (*p*-MOP) (TU 6-09-1248–78) and Ionol (TU 3810 1459–75). The ester interchange follows the scheme



I–IV **V–VIII**

where R = C_8H_{17}–$C_{10}H_{21}$ (**I**, **V**), $C_{12}H_{25}$–$C_{14}H_{29}$ (**II**, **VI**), $C_{12}H_{25}$–$C_{18}H_{37}$ (**III**, **VII**), and $C_{16}H_{33}$–$C_{20}H_{41}$ (**IV**, **VIII**).

A chromatographic analysis was performed with a Tsvet-500 chromatograph equipped with a flame-ionization detector and a 2-m packed glass column; stationary phase polyethylene glycol adipate, column temperature 150±5°C, vaporizer temperature 290°C, carrier gas N_2, flow rate 30 ml min^{-1}.

The IR spectra were recorded on a Specord M80 spectrophotometer in the range 4000–400 cm^{-1} from thin films of the substances pressed between KBr plates.

The ester interchange of MMA with alcohols **I**–**IV** was performed in a four-necked vessel equipped with a power-driven stirrer thermometer, bubbler for feeding dry air, and heated distillation column with a total condenser and a receiver for taking off the MMA–methanol azeotrope formed in the course of the synthesis.

The reaction mixture was heated to 110°C and kept for 1 h, after which the mixture was brought to boiling (120°C), the distillation column heater was switched on, and the MMA–methanol azeotrope distilling at 65–78°C was taken off. After the distillation of the azeotrope ceased, the reaction was stopped, the vessel was cooled, the catalyst was separated, and the excess MMA was removed.

The conversion of the starting alcohol was evaluated by gas–liquid chromatography and acetylation [12].

To choose an effective catalytic system for ester interchange of MMA with fractions of synthetic higher alcohols **I**–**IV**, we tested a series of ester interchange catalysts differing in catalytic activity [8, 13] and reactivity toward the starting compounds.

To avoid undesirable polymerization in the course of the synthesis and isolation of the desired product, we added a system of inhibitors *p*-MOP + Ionol (0.1 and 0.03 wt % relative to the sum of the reactants, respectively) and performed the reaction with continuous air bubbling through the reaction mixture.

We found (Fig. 1a) that sodium methylate and sodium borohydride are effective catalytic systems and provide the highest yield of alkyl methacrylate **V** (96% in 8 h). However, use of these catalysts requires thorough drying of MMA, and it is difficult to separate the suspended catalyst from the reaction mixture. To remove trace amounts of the catalyst completely, twofold washing with water followed by drying is required. A similar pattern (necessary washing with water) is observed with dibutyltin dicaprylate, although the yield (96%) and the rate of formation of alkyl methacrylate with this catalyst are also acceptable.

Of particular interest in this context are heterogeneous base catalysts which are insoluble in the reaction mixture and can be readily separated after the reaction completion. Among the three catalysts meeting these requirements, potassium carbonate appeared to be the most active: Alcohol **I** was completely exhausted in 15 h, and the ester yield was 97%. The desired product was readily separated from potassium carbonate by filtration. One more advantage of potassium carbonate over sodium phosphate and sodium carbonate was that it did not appreciably lose its activity in repeated runs (Fig. 1b), whereas the other two catalysts, when reused, did not provide the required conversion. Potassium carbonate was reused without additional washing or heat treatment.

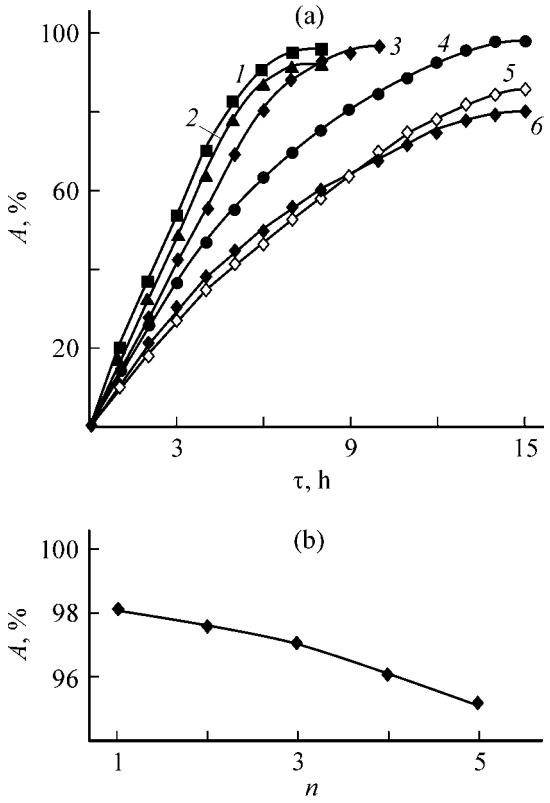


Fig. 1. Yield of alkyl methacrylate **V** *A* (a) vs. time τ with various catalysts and (b) vs. the number *n* of runs performed with potassium carbonate. Molar ratio MMA : alcohol **I** = 2 : 1, catalyst concentration 1%. (a) Catalyst: (*1*) sodium methylate, (*2*) sodium borohydride, (*3*) dibutyltin dicaprylate, (*4*) potassium carbonate, (*5*) sodium carbonate, and (*6*) sodium phosphate.

In ester interchange of MMA with longer-chain fractions of alcohols **II**–**IV**, the catalytic activity of potassium carbonate is of particular importance, because specifically in this case there are problems with separation of the desired esters from the high-boiling starting alcohols.

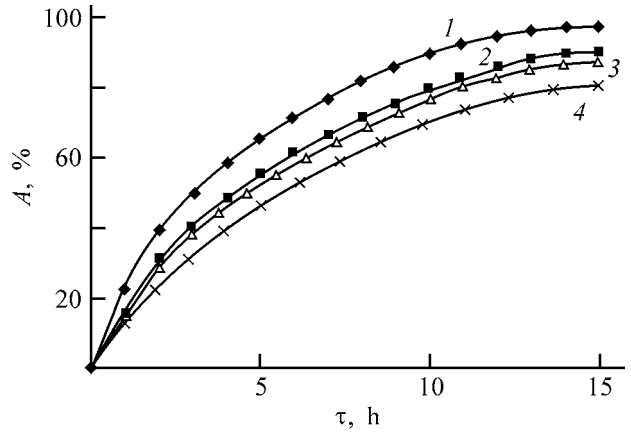


Fig. 2. Yield *A* of alkyl methacrylates **V**–**VIII** vs. time τ. Ratio MMA : alcohol **I**–**IV** = 2 : 1, catalyst (potassium carbonate) concentration 1%. Monomer: (*1*) **V**, (*2*) **VI**, (*3*) **VII**, and (*4*) **VIII**.

Experiments on the ester interchange of MMA with alcohols of fractions **II**–**IV** showed (Fig. 2) that, at the initial molar ratio MMA : alcohol = 2 : 1, and presence of 1% catalyst, the reaction decelerated with an increase in the length of alkyl chains in alcohols, and the yield of monomer **VIII** was as low as 80% (cf. 97% for **V**).

To raise the conversion of long-chain alcohols **II**–**IV**, we performed the ester interchange in the presence of 3 and 5% potassium carbonate; however, increased amounts of the catalyst did not provide increased yield of the long-chain alkyl methacrylates.

To attain the maximal exhaustion of higher alcohols, we studied how the yield of esters **VI**–**VIII** is influenced by the ratio of the starting components, MMA : alcohol (Table 1).

We found that, at the component ratio increased to 3 : 1 and 5 : 1, long-chain alkyl methacrylates **VI**–**VIII** can be prepared in acceptable yields, 91–95%.

It should be noted that, after the completion of ester interchange, excess MMA was removed at 50°C and a pressure of 30 mm Hg. The distilled MMA was reused in the synthesis of alkyl methacrylates, which ensured a virtually quantitative exhaustion of MMA.

The refining of the synthesized alkyl methacrylates to remove unchanged alcohols or traces of MMA was performed on a rotary-film evaporator at a jacket temperature of 135–150°C and residual pressure of 20 mm Hg. The properties of the higher alkyl methacrylates obtained are listed in Table 2.

Monomers **V**–**VII** are weakly colored or colorless transparent liquids with a characteristic ester odor. Alkyl methacrylate **VIII** is a wide solid waxy substance without odor.

The structures of the higher alkyl methacrylates synthesized were confirmed by the IR spectra. The spectra are similar and are characterized by the following absorption bands (cm^{-1}): ~1726 (C=O); 1150–

Table 1. Yield of alkyl methacrylates **VI**–**VIII** at various MMA : alcohol ratios (synthesis time 15 h)

Ester	Starting substance, mol		Ester yield, %	Ester	Starting substance, mol		Ester yield, %	Ester	Starting substance, mol		Ester yield, %
	MMA	fraction of higher fatty alcohols			MMA	fraction of higher fatty alcohols			MMA	fraction of higher fatty alcohols	
VI		**II**:		**VII**		**III**:		**VIII**		**IV**:	
	2.5	1	94		3	1	94		4	1	91
	3	1	95		3.5	1	95		5	1	93

Table 2. Properties of alkyl methacrylates obtained

Ester	Monomer	Main substance content, %	Kinematic viscosity at 20°C, cSt	d_4^{20}	n_D^{20}
V	Alkyl(C_8H_{17}–$C_{10}H_{21}$) methacrylate	98.3	4.7	0.8783	1.4410
VI	Alkyl($C_{12}H_{25}$–$C_{14}H_{29}$) methacrylate	98.0	5.1	0.8771	1.4458
VII	Alkyl($C_{12}H_{25}$–$C_{18}H_{37}$) methacrylate	97.4	6.5	0.8796	1.4475
VIII	Alkyl($C_{16}H_{33}$–$C_{20}H_{41}$) methacrylate	95.0	Melting point 32°C		

1350 (C–O in the C–O–C fragment of methacrylates); ~1644 (C=C); 724 [rocking vibrations of $(CH_2)_n$ fragments, where $n \geq 4$].

The higher alkyl methacrylates **V**–**VIII** synthesized were used in free-radical polymerization without additional purification.

CONCLUSION

A procedure was developed for preparing higher alkyl methacrylates by ester interchange of methyl methacrylate with fractions of higher fatty alcohols in the presence of a catalyst, potassium carbonate. The ester interchange rate decreases with an increase in the length of the alkyl radical.

REFERENCES

1. *Copolymerization*, Ham, G.E., Ed., New York: Interscience, 1964.
2. Wang Bivgli and Shi Zhizhong, *Jingxi Huagond*, 1998, vol. 15, pp. 79–82.
3. Krupnova, N.G., Likhterov, V.R., Fomin, V.A., et al., Abstracts of Papers, *Mezhdunarodnaya nauchno-tekhnicheskaya konferentsiya "Polimery-2002"* (Int. Scientific and Technical Conf. "Polymers-2002"), Yaroslavl, December 2–5, 2002, p. 33.
4. *Topliva, smazochnye materialy, tekhnicheskie zhidkosti: Spravochnik* (Fuels, Lubricants, and Technical Fluids: Handbook), Shkol'nikov, V.M., Ed., Moscow: Tekhinform, 1999.
5. RF Patent 2154091.
6. Czechoslovak Patent 259632.
7. JPN Int. Patent Appl. 9712010.
8. JPN Int. Patent Appl. 63–5055.
9. RF Patent 2102402.
10. French Int. Patent Appl. 2849857.
11. Becker, H., Berger, W., Domschke, G., et al., *Organikum. Organisch-chemisches Grundpraktikum*, Berlin: Wissenschaften, 1976.
12. *Preparativnaya organicheskaya khimiya* (Preparative Organic Chemistry), Vul'fson, N.S., Ed., Moscow: GKhI, 1959.
13. German Int. Patent Appl. 10026644.

ISSN 1070-4272, Russian Journal of Applied Chemistry, 2006, Vol. 79, No. 12, pp. 1994–1997. © Pleiades Publishing, Inc., 2006.
Original Russian Text © V.P. Fadeeva, O.N. Nikulicheva, V.N. Kobrina, 2006, published in Zhurnal Prikladnoi Khimii, 2006, Vol. 79, No. 12, pp. 2018–2021.

ORGANIC SYNTHESIS AND INDUSTRIAL ORGANIC CHEMISTRY

Separation of Pyrimidine Derivatives by Reversed-Phase High-Performance Liquid Chromatography

V. P. Fadeeva, O. N. Nikulicheva, and V. N. Kobrina

Vorozhtsov Institute of Organic Chemistry, Siberian Division, Russian Academy of Sciences, Novosibirsk, Russia
EkoNova Institute of Chromatography, Private Company, Novosibirsk, Russia

Received August 10, 2006

Abstract—Chromatographic behavior and separation conditions of pyrimidine derivatives were studied by high-performance liquid chromatography using a reversed-phase column and a multiwave UV detector.

DOI: 10.1134/S1070427206120172

Pyrimidine derivatives are of both scientific and practical interest. Functionalized pyrimidines exhibit chelating, photochromic, and biologically active properties. These compounds are used in preparation of heat-resistant polymers. They are contained in many biologically significant compounds and in antitumor and antiviral drugs [1].

Reversed-phase high-performance liquid chromatography (RF HPLC) is widely used for analysis of pyrimidines and their derivatives. Since these compounds are weak organic bases, they are analyzed and separated on alkyl silica gel columns, using organic buffer solutions as eluents [2, 3].

Most of published studies concern development of the sorbents and mobile phases for analysis of specific pyrimidine derivatives used in medicine, biology, and food industry [4–10].

In this study, to develop a procedure for identifying pyrimidine derivatives with different substituents in positions **2**, **4**, and **6**, we examined chromatographic separation of these compounds by RFHPLC with a multiwave UV detector.

EXPERIMNETAL

We studied the following compounds: 2,4-bis(*p*-aminophenyl)pyrimidine, 2-amino-4-(*p*-nitrophenyl)py-

Table 1. Parameters* of chromatographic separation of pyrimidine derivatives

Compound no.	Pyrimidine	*N*, TP	*t*, min (±0.003)	*k*', (± 0.001)	α, (± 0.001)	R_s
1	2,4-Bis(*p*-aminophenyl)pyrimidine**	7935	7.43	3.95	1.07	1.62 ± 0.06
2	2-Amino-4-(*p*-nitrophenyl)pyrimidine	9049	7.93	4.29	1.15	4.06 ± 0.15
3	2-Trichloromethyl-4,6-dimethylpyrimidine	14995	9.15	5.10	1.05	1.40 ± 0.08
4	2,4-Bis(*p*-aminophenyl)-6-phenylpyrimidine	14564	9.57	5.38	1.05	1.50 ± 0.08
5	2-Methyl-4-phenylpyrimido[4,5-β]indole	10368	10.08	5.69	1.25	6.30 ± 0.24
6	2,4-Bis-(*p*-bromophenyl)pyrimidine	10812	12.47	7.31	1.25	0.00

* *N* (TP) is the number of theoretical plates; *t*, retention time of the component; *k*', reduced capacity factor, α, selectivity; and R_s, resolution.

** Structural formulas of compounds **1**–**6**:

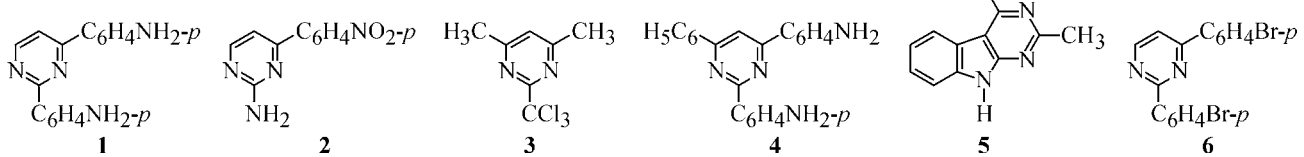


Table 2. Resolution of pyrimidine peaks obtained with different elution systems

System	Peak resolution R_s						
	1 → 2*	**2 → 3**	**4 → 5**	**1 → 4**	**3 → 4**	**1 → 3**	**3 → 5**
A	1.35	4.65	**0.87****	>4	3.12	>4	>4
B	1.17	>4	>4	>4	>4	>4	1.60
C	**0.96**	3.0	1.69	>4	1.46	>4	>4
D	**0.70**	2.46	**0.75**	>4	1.07	>4	~2
E	1.65	>4	1.37	>4	>4	>4	>4
F	>4	>4	>4	1.80	>4	>4	1.38
G	~4	>4	>4	**0.99**	>4	>4	1.96
H	1.69	>4	2.64	>4	0	>4	2.64
I	>4	>4	>4	1.57	>4	>4	3.68
K	>4	>4	>4	1.85	>4	>4	5.15
L	2.92	2.92	2.23	>4	>4	**0**	>4
M	**0**	>4	~2	1.36	**0.56**	~2	6.38
N	1.76	4.20	1.58	>4	1.59	>4	>4

* Numumbering of the component peaks is similar to that in Table 1.

** The resolution factors of incompletely resolved and unresolved peaks are printed bold.

Table 3. Composition of the elution systems

System	Eluent	
	A	**B**
A	Methanol–acetate buffer, 20 : 80	Methanol
B	Methanol–phosphate buffer, 0.01 M NaCl	″
C	Methanol–acetate buffer, 70 : 30	″
D	Methanol–phosphate buffer, 30 : 20	″
E	Methanol–phosphate buffer, 0.01 M NaCl–0.001 M tetrabutylammonium bromide	″
F	0.05 M phosphoric acid	″
G	0.1% trifluoroacetic acid	″
H	0.2 M lithium perchlorate in 0.005 M perchloric acid	″
I	0.05 M phosphoric acvid	Acetonitrile
K	0.1% trifluoroacetic acid	″
L	0.2 M lithium perchlorate in 0.005 M perchloric acid	″
M	Water	″
N	″	Methanol

rimidine, 2-trichloromethyl-4,6-dimethylpyrimidine, 2,4-bis(*p*-aminophenyl)-6-phenylpyrimidine, 2-methyl-4-phenylpyrimido[4,5-β]indole, and 2,4-bis-(*p*-bromophenyl)pyrimidine. The structures of these compounds are listed in Table 1. Compounds **1**, **4**, and **6** (Table 1) were used as monomers for preparing high-strength heat-resistant polymers [11–13]. Derivatives of pyrido[4,5]indole (Table 1, compound **5**) exhibit various kinds of biological activity [14, 15].

The pyrimidine derivatives were separated on a Milikhrom A-02 chromatograph (EkaNova Institute of Chromatography, Novosibirsk) equipped with a multiwave UV detector and a 2 × 75-mm steel column packed with Prontosil 120-5-C18 AQ reversed-phase sorbent (Bischoff Chromatography, Germany).

The elution was performed in the gradient mode by changing the acetonitrile or methanol content from 30 to 100% within 7 and 8 min and in the isocratic mode using 100% organic solvent. The eluent flow rate v was 100 μl min^{-1}; sample volume V = 4.0 μl; pyrimidine concentration 1 mg ml^{-1}; column temperature T = 35°C; maximal pressure 5.0 MPa; λ = 210 nm.

The results of a chromatographic separation of a mixture of six pyrimidines using different elution systems (Table 3) including published systems are presented in Table 2. The mixture was successfully separated using a half of the solvent systems examined

Table 4. Spectral ratios

Pyrimidine derivative no.	Ratio of absorption of pyrimidine derivative at indicated wavelength to absorption at 210 nm					
	240	250	270	300	320	330
1	0.469 ± 0.002	0.199 ± 0.001	0.364 ± 0.001	1.306 ± 0.003	1.641 ± 0.005	1.621 ± 0.005
2	0.485 ± 0.001	0.552 ± 0.002	0.698 ± 0.001	0.464 ± 0.002	0.424 ± 0.004	0.435 ± 0.002
3	0.524 ± 0.002	0.516 ± 0.002	0.054 ± 0.002	0.004 ± 0.001	0.004 ± 0.001	0.003 ± 0.002
4	0.615 ± 0.003	0.586 ± 0.003	0.604 ± 0.006	1.021 ± 0.010	1.224 ± 0.010	1.134 ± 0.009
5	0.605 ± 0.001	0.746 ± 0.017	0.428 ± 0.008	0.333 ± 0.004	0.236 ± 0.002	0.146 ± 0.001
6	0.334 ± 0.004	0.647 ± 0.017	1.438 ± 0.046	0.428 ± 0.010	0.074 ± 0.003	0.014 ± 0.004

Table 5. Detection limit of pyrimidines (sample volume, 5 μl)

Pyrimidine derivative no.	λ_{max}, nm	Detection limit, μg	Pyrimidine derivative no.	λ_{max}, nm	Detection limit, μg
1	210	0.010	**4**	210	0.020
2	210	0.016	**5**	250	0.010
3	210	0.020	**6**	270	0.030

(B, E, F, I, K, and N). With the other systems, the separation was incomplete within the optimal period of time. To separate a mixture of pyrimidine derivatives with the multiwave detection and the gradient elution mode, we used an efficient and simple gradient elution system N (methanol–water), which has not been applied previously to pyrimidine derivatives.

Pyrimidines were detected at 210, 240, 250, 270, 300, 320, and 330 nm. Multiwave detection of the chromatograms allows calculation of the so-called "spectral ratios," i.e., ratios of the optical density at a wavelength examined to that at a reference wavelength (210 nm in our case). This parameter is independent of the sample concentration, is well reproducible, and allows identification of compounds in mixtures without references (Table 4). The UV spectra of the components recorded in a wide spectrum range at stopped eluent flow (Fig. 1) can also be used to identify these compounds in mixtures in the absence of references.

The chromatographic parameters are more conveniently calculated using the chromatogram plotted as total absorption of the component at all the wavelengths examined vs. time (Fig. 2). To optimize

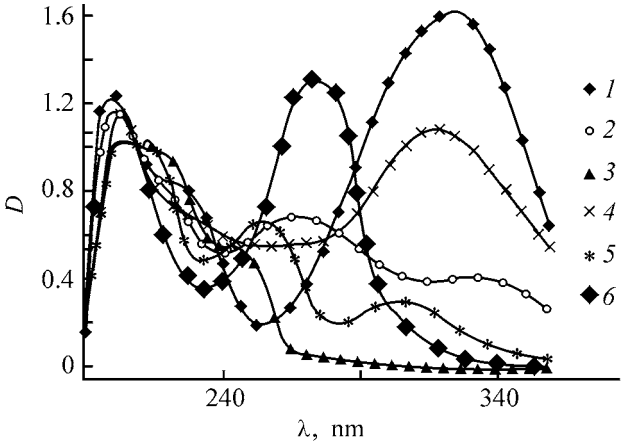


Fig. 1. UV spectra of substituted pyrimidines. (*D*) Optical density and (λ) wavelength. *Numbers at the curves* correspond to the pyrimidine derivative numbers in Table 1; the same for Fig. 2.

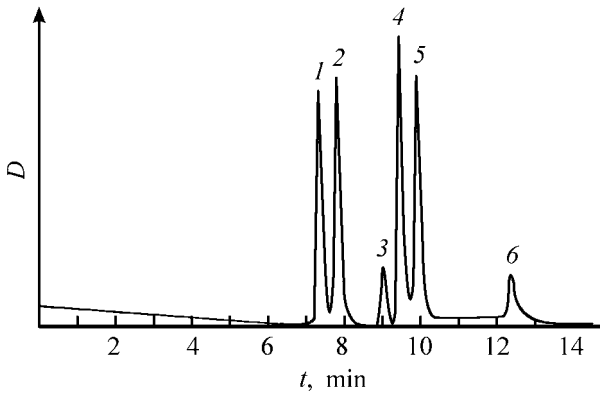


Fig. 2. Chromatrogram of a pyrimidine mixture (system N). Gradient of methanol in water is 30–100% in 7 min; isocratic conditions: 100 % methanol for 8 min; sample volume 4 μl; temperature 35°C (*D*) Total optical density of the component at all wavelengths and (*t*) time.

the separation conditions, we calculated the reduced capacity factor k', and the selectivity of separation α and resolution R_s of the adjacent peaks of the components (Table 1).

We determined the minimal detectable concentrations of the pyrimidines (Table 5). The detection limit of the pyrimidines at the indicated wavelength under the optimal conditions is 0.01–0.03 mg ml^{-1}.

CONCLUSIONS

(1) The chromatographic parameters [reduced capacity factor (k'), selectivity of separation (α), and resolution R_s of adjacent peaks of the components] of the pyrimidine derivatives were determined.

(2) The detection limits of the components at 210, 250, and 270 nm are 0.01–0.03 mg ml^{-1}.

ACKNOWLEDGMENTS

The authors are grateful to V.P. Borovikov for placing the pyrimidine derivatives at our disposal.

REFERENCES

1. Nametkin, S.S., *Geterotsyklicheskie soedineniya* (Heterocyclic Compounds) Moscow: Nauka, 1981, pp. 259–263.
2. Kharitonova, A.G., Bulanova, A.V., Osyanin, V.A., and Larionov, O.G., *Sorbts. Khromatogr. Prots.*, 2005, vol. 5, no. 3, pp. 289–295.
3. Shatts, V.D. and Brivkale, L.A., *Zh. Fiz. Khim.*, 1990, vol. 64, no. 9, pp. 2460–2466.
4. Kazhoka, Kh.A. and Shatts, V.D., *Khim.-Farm. Zh.*, 1989, vol. 23, no. 12, pp. 1516–1519.
5. Galushko, S.V., Shishkina, I.P., and Pilipenko, A.G., *Zh. Anal. Khim.*, 1989, vol. 44, no. 6, pp. 1094–1099.
6. Galushko, S.V., Shishkina, I.P., and Pilipenko, A.G., *Zh. Anal. Khim.*, 1989, vol. 44, no. 5, pp. 923–927.
7. Ghet, A.M., Chiavari, G., and Evgenidis, J., *Talanta*, 1986, vol. 33, no. 5, pp. 379–384.
8. Galushko, S.V., *Talanta*, 1989, vol. 36, no. 10, pp. 1017–1020.
9. Caruso, U., Minniti, G., and Romano, C., Abstracts of Papers, *HPLC 95: 19 Int. Symp. On Column Liquid Chromatography and Related Techniques, Innsbruck, May 28–June 2*, 1995, vol. 2, p. 193.
10. Lugari, M.T., Maggiali, C.A., and Mangia, A., *J. Chromatogr.*, 1983, vol. 281, pp. 304–308.
11. Mamaev, V.P., Borovik, V.P., Koton, M.M, et al., *Vysokomol. Soedin., Ser. B*, 1983, vol. 25, pp. 102–106.
12. Borovik, V.P., Baram, S.G., Kozlova, E.Yu., and Mamaev, V.P., *Izv. Sib. Otd. Akad. Nauk SSSR, Ser. Khim.*, 1985, no. 5, pp. 97–99.
13. Mognonov, D.V., Borovik, V.P., Radnaeva, L.D., et al., *Sib. Khim. Zh.*, 1991, no. 4, pp. 99–101.
14. Borovik, V.P., Ivanovskaya, L.Yu., and Mamaev, V.P., *Izv. Sib. Otd. Akad. Nauk SSSR, Ser. Khim.*, 1997, issue 6, no. 14, pp. 110–114.
15. Borovik, V.P., and Shkurko, O.P., *Izv. Ross. Akad. Nauk, Ser. Khim.*, 2002, no. 11, pp. 1974–1977.
16. Schoenmakers, P.J., *Optimization of Chromatographic Selectivity. A Guide to Method Development*, Amsterdam: Elsevier, 1986.

ISSN 1070-4272, Russian Journal of Applied Chemistry, 2006, Vol. 79, No. 12, pp. 1998–2006. © Pleiades Publishing, Inc., 2006.
Original Russian Text © A.V. Kalinin, A.P. Voznyakovskii, 2006, published in Zhurnal Prikladnoi Khimii, 2006, Vol. 79, No. 12, pp. 2022–2030.

MACROMOLECULAR CHEMISTRY AND POLYMERIC MATERIALS

Inverse Gas Chromatographic Study of Supramolecular Organization in Microheterogeneous Systems for the Example of Polyblock Copolymers

A. V. Kalinin and A. P. Voznyakovskii

Institute of Macromolecular Compounds, Russian Academy of Sciences, St. Petersburg, Russia
Lebedev Research Institute of Synthetic Rubber, St. Petersburg, Russia

Received July 14, 2006

Abstract—The potentialities of inverse gas chromatography for studying microheterogeneous polymer systems are analyzed. For the first time this method is applied to examination of the microstructure of multiblock copolymers obtained by condensation. A procedure for evaluation of the partial contribution of the dissolution to the total retention volume is suggested.

DOI: 10.1134/S1070427206120184

The steadily increasing environmental pollution hazard and the necessity for green technologies stimulate polymeric materials science to develop new generations of materials with considerably enhanced performance characteristics. The limited spectrum of available monomers and the low possibility of emergence of novel ones make it clear that new generations of polymeric materials are to be based on development of new 3*D* structures and composites. By a polymeric composite material is meant that consisting of at least two phases with a distinctly pronounced interface. In fact, a composite material is a polymeric matrix with incorporated particles of inorganic or organic filler. The occurrence of a filler in the bulk of a polymer results in the formation of interfacial layers, making the supramolecular structure remarkably more complex. In turn, the supramolecular structure of polymeric materials controls to considerable extent their physicochemical and mechanical properties.

The development of novel materials requires relatively simple methods for characterization of a small amount of a material with respect to its supramolecular organization.

In recent decades, the X-ray diffraction, dielectric, mass spectrometric, and, in particular, sorption methods used for characterization of the polymer structure have been considerably improved. Among the advantages of the sorption method are sufficiently high informativeness and the simplicity of the hardware implementation. At the same time, the establishment of an equilibrium in most of polymer–solvent systems takes a long time. In this respect, the dynamic version of the sorption method, i.e., inverse gas chromatography (IGC) is rather convenient and also allows examination of fine aspects of the supramolecular organization in polymers.

The use of IGC for characterization of homopolymers is well known and does not present any significant problems. In studying di- and triblock polymers, the contribution of the dissolution can be roughly estimated from data on the sorption characteristics of the homopolymer constituting the flexible block of the macromolecule. However, in microheterogeneous systems, the resultant sorption is a superposition of partial contributions of various (generally different) mechanisms of sorption of the molecular sample on each of the existing phases, interfacial layers, and on the dispersion medium [1]. In this case, it should be taken into account that the covalent bonds between the blocks prevent complete phase separation, so that the dispersion medium does not fully correspond to the individual phase of the flexible block.

Brown and Guillet have demonstrated [2] for a polymer of complex structure that the total retained volume can be correctly estimated using additive equation (1):

$$V_g = V_{g1} + V_{g2} + \ldots + V_{gn}, \quad (1)$$

where V_{g1}, V_{g2}, …, V_{gn} are the retention volumes of each of the phases of the polymer.

The simplest case is the presence of two phases in the bulk of the polymer. If both phases are in the viscoelastic state, the retention mechanism in each of them will involve the dissolution of the mobile phase in the polymer mass. If one of the phases occurs below its glass transition or crystallization temperature, the corresponding retention mechanism is associated with surface sorption. Then, for a block copolymer of the AB or ABA type, consisting of two phases, one of these (A) is in the viscoelastic state, and the other (B), in the glassy or crystalline state, the retention volume can be written as:

$$V_g = k_{S(A)}\omega_A + k_{D(B)}A_B, \quad (2)$$

where $k_{S(A)}$ is the volume sorption coefficient of phase A; ω_A, weight of phase A; $k_{D(B)}$, surface adsorption coefficient of phase B; and A_B, surface area of the domains formed by phase B.

It follows from Eq. (2) that the adsorption retention volume is influenced not by the weight fraction of the dispersed phase, but only by the surface area of its particles. Therefore, if a blend of homopolymers A and B were used instead of the block copolymer with the same A/B ratio, the second term whould become negligible, since the dispersed particles are too large in size [3]. Brown and Guillet have demonstrated [2] that, for polymers in which both the above-mentioned retention mechanisms act simultaneously, the concepts of the volume and adsorption retention volumes can be introduced:

$$\ln V_{gA} = \ln \omega_A + \ln k_{S(A),0} - (\Delta H_{solv}/RT), \quad (3)$$

$$\ln V_{gB} = \ln A_B + \ln k_{D(B),0} - (\Delta H_{ads}/RT), \quad (4)$$

where ΔH_{solv} and ΔH_{ads} are the enthalpies of solvation and adsorption, respectively.

It has been demonstrated [2, 4] that the simultaneous action of two retention mechanisms in a polymer is reflected in that the retention diagram is no longer linear, which makes it impossible to calculate the thermodynamic parameters of the sorption in terms of the commonly accepted model. For the first time this phenomenon was described for homopolymers over an extremely narrow temperature range (3–5°C) corresponding to glass transition or crystallization [2]. In the subsequent years, it was reported that this phenomenon is widely spread among di- and triblock copolymers [5–7]. A similar effect on the shape of the retention curve has also been observed when the aggregates of an inorganic filler were sufficiently small ($<5 \times 10^{-6}$ m) [8–11].

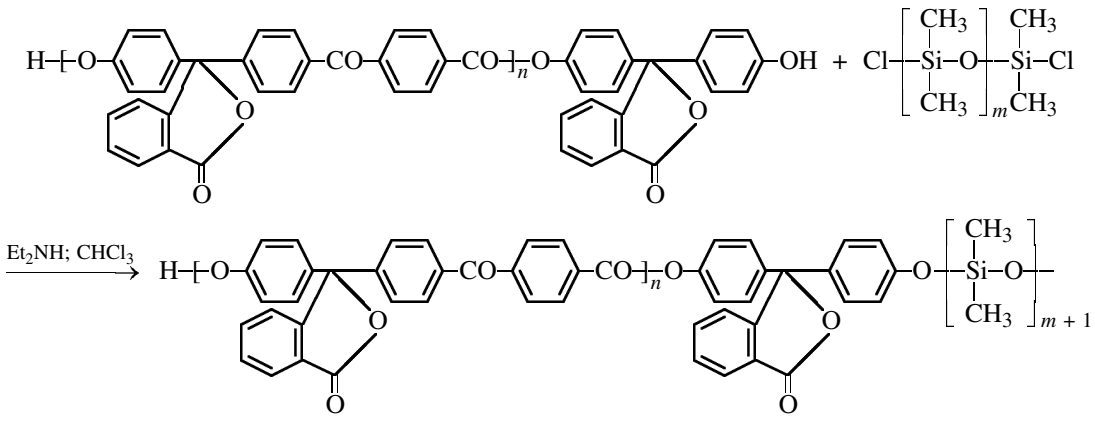
Schlick and Levy [12] were the first who demonstrated that properties of copolymers can be strongly affected not only by the chemical structure of the blocks, but also by their size and number in the macromolecule [this was shown for the example of isoprene/styrene copolymers of fixes molecular weight, but with different numbers of blocks (from two to nine) and, accordingly, with their different lengths]. From the modern standpoint, this phenomenon can be attributed to a decrease in the size of the rigid block nanodomains and also to the fact that the supramolecular structure of the polymer becomes more complex on passing from diblock to polyblock copolymers. It follows from Eqs. (2)–(4) that a change of the macrochain structure in this direction should generally result in a more intricate shape of the retention curve (as superposition of several linear functions). However, we have found no published IGC studies of the supramolecular structure of polyblock copolymers.

Therefore, we examined in this study the potentialities of IGC for studying the supramolecular structure of polymers on the basis of such parameters of sorption of low-molecular-weight substances as the excess partial molar enthalpy and entropy.

To determine the thermodynamic parameters of sorption, it is necessary to estimate separately the contribution from dissolution of the sorbate in the dispersion medium. It has been demonstrated previously [13] that, for polymers of a complex supramolecular structure, the contribution of absorption of low-molecular-weight substances by the polymers increases with temperature, while the contribution of adsorption tends to zero. Therefore, it may be suggested that, at high temperatures, the adsorption term is negligible, and the tangent to the retention curve is, in fact, the plot of $\ln V_{gA}$ vs. $1/T$. Then, using the iteration procedure described in [14, 15], we can accurately estimate the partial contributions of dissolution and adsorption to the total retention.

EXPERIMENTAL

In the experiments, we used poly(dimethylsiloxane) (PDMS) as a reference sample and three specially synthesized samples of copolymers of PDMS and poly(phenolphthalein terephthalate) (PPT) with rigid to flexible block ratios of 1 : 4.5 (sample no. 1), 1 : 10.5 (sample no. 2), and 1 : 21.5 (sample no. 3). Block copolymers of PPT and PDMS were synthesized by condensation of oligomeric phenolphthalein terephthalate with bis(ethylamine)-substituted siloxane oligomers:



Generally, we used the procedure described in [16], which was slightly modified with allowance for available chemicals.

The molecular weight of all the three samples was determined by gel filtration chromatography to be about 150000, and that of the PDMS sample, at least 200000.

The chromatographic experiments were carried out on the installation designed on the basis of an LKhM-8MD chromatograph (Fig. 1). The carrier gas (He),

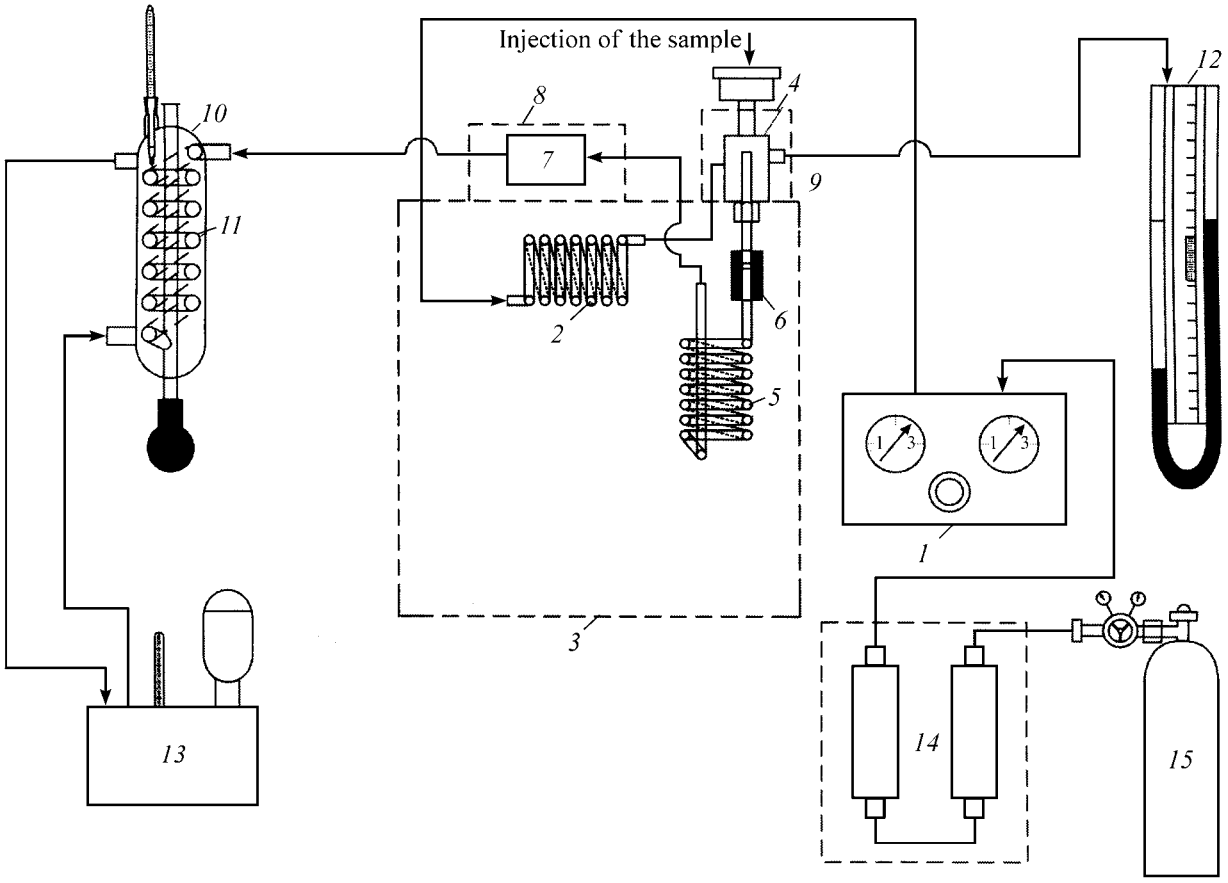


Fig. 1. Schematic of the experimental setup: (*1*) gas preparation unit, (*2*) heat exchanger, (*3*) chromatographic oven, (*4*) sample injection block, (*5*) chromatographic column, (*6*) connector, (*7*) thermal conductivity detector, (*8*) detector oven, (*9*) injection block oven, (*10*) foam flow meter, (*11*) heat exchanger of the foam flow meter, (*12*) mercury gage, (*13*) liquid thermostat, (*14*) gas dewatering unit, and (*15*) high-pressure cylinder with the carrier gas.

purified by passing through a set of NaX zeolite filters, was fed into the gas preparation unit (*1*), which allowed control over the carrier gas flow to within 0.5%. This unit was a PPR-1 unit from the set of components for a Tsvet-100 chromatograph. Then the carrier gas was heated to the working temperature of the column, using the spiral copper heat exchanger *2* arranged inside the chromatographic oven *3*, and was fed into the sample injection block *4*, to heat it to the working temperature. In the experiments, we used spiral glass columns 1.5 m long with an inner diameter of 4 mm (diameter of the spiral was 65 mm). The oven was temperature-controlled to within 0.05% using a Pt resistance sensor mounted directly in the column zone.

The gas flow rate at the column outlet was measured with a temperature-controlled foam flow meter. Before measurement, the carrier gas was heated to the standard temperature of 30°C in the spiral heat exchanger mounted in the same temperature-controlled space. The pressure of the carrier gas at the column inlet was measured by a mercury gage to within 0.5 mm Hg. The samples (vapor mixtures with air, collected from over the surface of the corresponding liquid) were injected into the column using a microsyringe.

Aa a support for the stationary phase served Chromaton N-AW-DMCS with a particle size of 0.315–0.400 mm. The support was dried to remove water adsorbed on the particle surface by heating to 300°C at 1–2 mm Hg in a long-necked round-bottom flask connected to a vacuum pump through a trap placed in a Dewar bottle with liquid nitrogen. The process was stopped when the ice formation ceased.

Double-reprecipitated polymer, pretreated to remove volatiles, was applied onto the solid support. A packing for the columns was prepared by removal of the solvent from a coarse suspension of the solid support in the polymer solution with continuous gentle stirring.

The specific retention volumes were estimated by Eq. (5) [17]:

$$V_g^0 = (t_R F/g) J_3^2 (P_{input}/P_{output}), \quad (5)$$

where t_R is the corrected retention time $t_R = t - t_0$; t, retention time corresponding to the peak maximum; t_0, dead point; and F, flow rate;

$$F = \{[F_T(P_f - P_W)]/P_0\}(273.2/T_f), \quad (6)$$

where F_t is the flow rate at the flow-meter temperature T_f; P_f, pressure in the flow meter; P_W, saturated vapor pressure of water at the flow-meter temperature; P_0, atmospheric pressure; g, amount of the polymer in the column; and J_3^2, carrier gas compressibility factor:

$$J_3^2 = (3/2)\{[(P_{input}/P_{output})^2 - 1] \times [(P_{input}/P_{output})^3 - 1]\}, \quad (7)$$

where P_{input} and P_{output} are the carrier-gas pressure at the column inlet and outlet, respectively.

The t_R value necessary to calculate V_g^0 by Eq. (5) was calculated as the average of 5–6 replicate measurements. The error of determination of V_g^0, determined by the standard procedure [11], was within 1%.

To analyze data obtained for the investigated set of polymers, it is necessary to have a possibility to calculate V_g^0 at fixed temperatures (it is convenient to select temperatures divisible by 10°C). This task can be solved most reliably by deriving an equation for V_g^0 as a function of temperature. For this purpose, we performed statistical processing of the V_g^0 dataset obtained over the range 20–120°C. An approximating equation was selected taking into account that, in general case, the retention curve is fitted by Eq. (8):

$$\partial \ln V_g^0/\partial\, 1/T = -\Delta H_{cond}/R - \Delta \bar{H}_1^{E\infty}/R + [\partial \ln f_1^{\infty}/\partial\, 1/T)], \quad (8)$$

where ΔH_{cond} is the standard enthalpy of condensation of a mole of the pure sorbate from the state of ideal gas into the liquid state at the temperature T; $\Delta H_1^{E\infty}$, excess enthalpy of mixing in the sorbate–polymer system; and f_1^{∞}, fugacity coefficient of the sorbate at infinite dilution in the carrier gas.

Taking into account that all the three terms on the right-hand side of Eq. (8) are temperature-dependent, the retention curve plotted in the coordinates $\ln V_g^0$–$1/T$ will be strictly linear (particularly, over a wide temperature range) only in the case of mutual compensation of the temperature dependences of these terms [18]. It is clear that, generally, the retention diagrams can deviate from linearity to a greater or lesser extent. Therefore, as a fitting equation we used the relation we suggested in [19]:

$$\ln V_g^0 = A \ln T + B \ln T + C(1/T) + D. \quad (9)$$

This equation allows minimization of the approximation error in calculating V_g^0. The dataset obtained for each sorbate included 30–35 points, which, taking into account the number of replicate runs for each

point, gives at least 150 degrees of freedom, allowing reduction of the error of determination of V_g^0 to below 0.5%.

Based on Eq. (5), we can writte the expression for the relative error of V_g^0 as

$$\Delta V_g^0/V_g^0 = \Delta t/t + \Delta F/F + f(P)\Delta P/P + \Delta g/g. \quad (10)$$

Since the column temperature can be measured to within 0.1°C, and the flow rate, to within 0.5°C, the total error of the first three terms in Eq. (11) does not exceed 1%. The main contribution to the error of determination of V_g^0 is provided by the uncertainty of determination of the amount of the polymer in the column [9]. In this study we used an ADV-200 analytical balance (weighing error ±1 mg). Since the weight of the solid support in the column ranged from 2 to 10 g, and the weight of the supported polymer was 5–15% relative to the support, the error of determination can be accepted to be below 1%.

The corrected retention time was determined from t_0 and t, which were measured using a modified ITs-26 integrator to within 0.05 cm.

A weighed portion of the packing was triply washed with large volumes of the solvent, placed in a muffle, and heated at 800°C for several hours. The amount of the polymer removed was estimated taking into account the weight loss in calcination by the initial inert support, and then was recalculated to 1 g of packing.

For the investigated polyblock copolymers of PPT and PDMS, we examined the factors influencing the retention volume: gas flow rate, thickness of the polymeric film, and sample weight. It was demonstrated that, on changing the flow rate from 15 to 90 ml min^{-1} and the amount of the polymer in the column from 5 to 15 wt % relative to the weight of the solid support, the retention volume remained unchanged to within the experimental error, suggesting that the equilibrium chromatography condition was met in our experiments and also that the contribution of adsorption at the gas–polymer and polymer–support interfaces can be neglected.

To characterize the activity coefficients of polymers, the mass activity coefficient $\Omega_1^\infty = a_1/w_1$ is used [20]. We estimated Ω_1^∞ as

$$\ln \Omega_1^\infty = \frac{273.15R}{V_g^0 P_1 M_1} - \frac{P_1^0}{RT}(B_{11} - V_1), \quad (11)$$

where V_g^0 is the specific retention volume of the sorbate; P_1, V_1, and M_1 are the saturated vapor pressure, molar volume, and molecular weight of the sorbate, respectively; B_{11} is the second virial coefficient of the sorbate; and R, gas constant.

The excess thermodynamic functions related to Ω_1^∞ by the well-known expression:

$$\Delta\bar{H}_1^{E\infty} = RT^2\partial(\ln\Omega_1^\infty)/\partial(T), \quad (12)$$

$$\Delta\bar{S}_1^{E\infty} = (R/T)\,\partial(\ln\Omega_1^\infty)/\partial(T) - R\ln\Omega_1^\infty, \quad (13)$$

where $\Delta\bar{H}_1^{E\infty}$ and $\Delta\bar{S}_1^{E\infty}$ are excess partial molar enthalpy and entropy, respectively.

The enthalpy of solution of a low-molecular-weight substance in a polymer can be estimated from the temperature dependence of the retention volume:

$$-\Delta H_s/RT^2 = \partial(\ln V_g^0)/\partial T. \quad (14)$$

We believe that the choice of the approximating equations for calculation of thermodynamic functions of mixing (12) and (13) requires some comments. In estimating $\Delta\bar{H}_1^{E\infty}$, its independence from temperature is generally assumed ($\Delta C_{s\,1}^{E\infty} = 0$). In this case, $\Delta\bar{H}_1^{E\infty}$ is determined from the slope of the linear dependence $\ln\Omega_1^\infty$–$1/T$. Note that, in this case, the temperature interval should not exceed 30–50°C [21]. In most cases, the least-squares method provides a high accuracy in calculating the slope. However, it should be taken into account that, in the system polymer–"good" solvent, the slope of the dependence $\ln\Omega_1^\infty$–$1/T$ frequently only slightly differs from zero, which can lead to a considerable (100% and more) error in determination of the slope [22], and, accordingly, to a considerable error of determination of $\Delta\bar{H}_1^{E\infty}$. Therefore, linear approximation of the dependence $\ln\Omega_1^\infty$–$1/T$ is of little use for precise estimation of $\Delta\bar{H}_1^{E\infty}$ even if the condition $\Delta C_{s\,1}^{E\infty} = 0$ is sutisfied.

In a more rigorous approach, it is assumed that $\Delta C_{s\,1}^{E\infty} = \text{const}$ (const ≠ 0). In this case, the temperature dependence of $\Delta\bar{H}_1^{E\infty}$ should be taken into account, but this dependence can be extrapolated by a linear function. Previously it has been demonstrated [23, 24] that, in calculating the activity coefficients in the above approximation, the best suited extrapolating function is as follows:

$$\ln\Omega_1 = C\ln T + D/T + E, \quad (15)$$

where C, D, and E are constants.

According to Eqs. (13) and (14), the corresponding relationships for $\Delta\bar{H}_1^{E\infty}$ and $\Delta\bar{S}_1^{E\infty}$ are written as

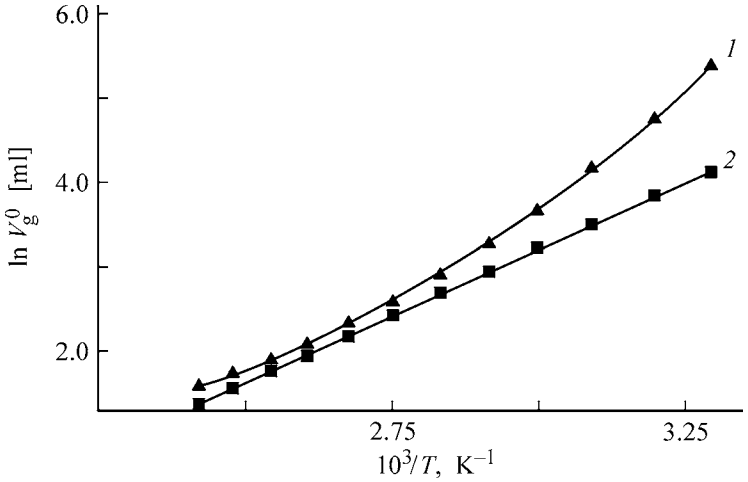


Fig. 2. Retention curves of *n*-pentane on (*1*) PDMS/PPT copolymer and (*2*) homo-PDMS. (V_g^0) Retention volume and (T) temperature.

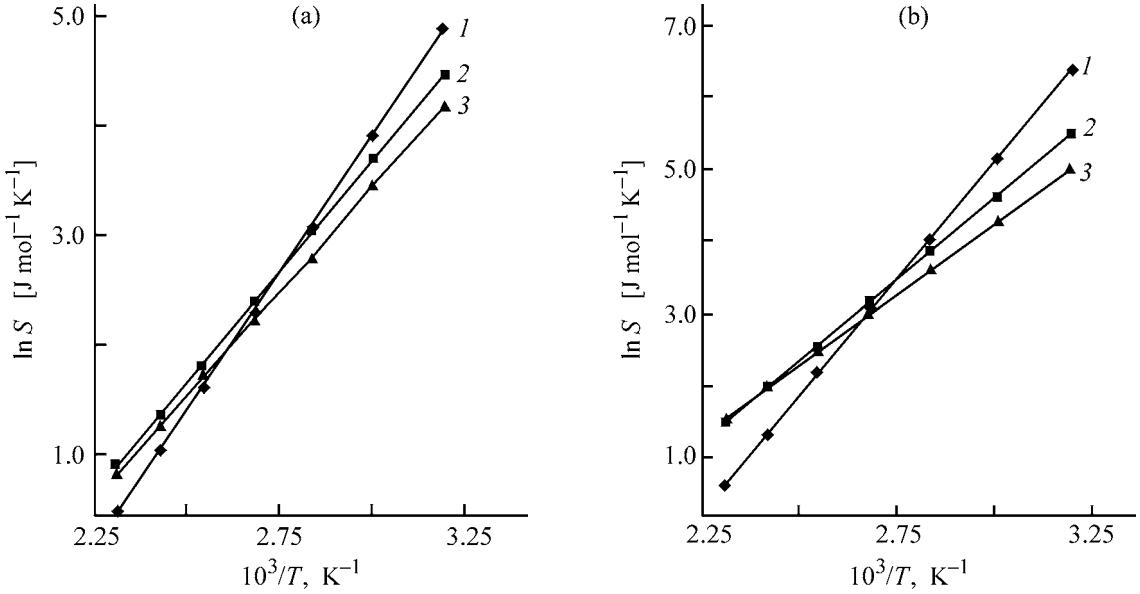


Fig. 3. ln$S$ vs. 1/T for (a) *n*-pentane and (b) *n*-hexane on three block copolymers: (*1*) PPTDMS-1, (*2*) PPTDMS-2, and (*3*) PPTDMS-3.

$$\Delta\bar{H}_1^{E\infty} = RD - RTC, \quad (16)$$

$$\Delta\bar{S}_1^{\infty} = -R(C + E) - RC\ln T. \quad (17)$$

Coefficients C, D, and E can be derived from Eq. (15) using the statistical methods. With at least 30 points in the dataset, the error of determination of the coefficients was generally within 0.5%. In this case, $\Delta\bar{H}_1^{E\infty}$ can be estimated to within 10%. It should be pointed out also that calculation by Eqs. (16) and (17) provides closer insight into the relationship between the excess thermodynamic functions and the polymer structure. In this case, the excess functions can be estimated at a fixed (standard) temperature, whereas in the linear approximation, the calculated $\Delta\bar{H}_1^{E\infty}$ depends on the selected temperature range, thus considerably impairing the validity of the comparative analysis.

As expected, the retention diagrams of various sorbates on the stationary phase composed of PDMS/PPT copolymer are nonlinear (Fig. 2), in contrast to those on homopolymeric supports. The contribution of the dissolution S, extracted using the method of successive approximations, is a linear function of the reciprocal temperature (Figs. 3a, 3b). It should be pointed out that, among the three investigated samples, the slope of the plot of ln S vs. 1/T is maximal for

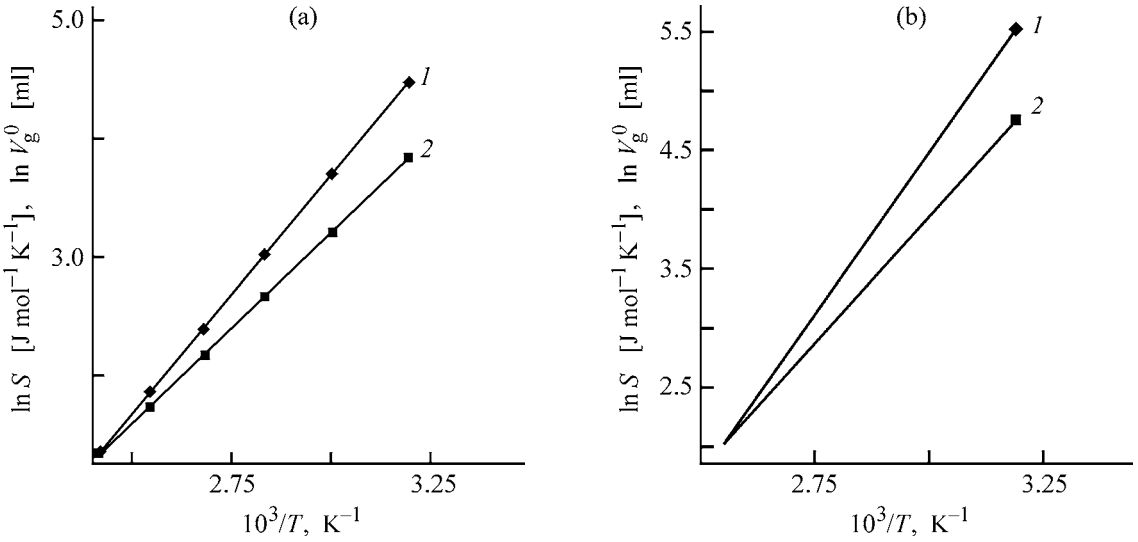


Fig. 4. ln S vs. $1/T$ for (a) *n*-pentane and (b) *n*-hexane on PPTDMS-2 (*1*) and ln V_g^0 vs. $1/T$ on PDMS as the pure flexible-block phase (*2*).

the polymer with the highest fraction of rigid blocks, and the most gently sloping plot is observed for the polymer with the lowest fraction of the terephthalate blocks, suggesting that, in polyblock copolymers, complete phase separation does not occur, in contrast to di- and triblock copolymers. Not all the rigid-chain parts of the molecules can be incorporated into nanodomains, and a considerable fraction of them remains in the bulk of the dispersion medium, having a significant effect on its properties. It is the presence of a large amount of such rigid-chain fragments "loosening" the dispersion medium that provides the emergence of free-volume elements, which, in turn, may remarkably change its sorption characteristics. To test this hypothesis, we compared lnS of a sorbate on the copolymers investigated with the retention diagram of the same sorbate on straight PDMS (Figs. 4a, 4b). If the dispersion medium of the block copolymer consisted of pure PDMS, these two plots would be coincident. However, as can be clearly seen from Fig. 4, this is not the case. For both the examples, the slope of the plot of ln S vs. $1/T$ is considerably higher than that of ln V_g^0 vs. $1/T$, and the values of ln S obtained for the copolymer over the temperature range 30–140°C are higher than those for PDMS.

We used the calculated S values to calculated by the above algorithm, the mass activity coefficient, an important characteristic parameter of the system polymer–low-molecular-weight solvent, and then excess partial molar enthalpy and entropy.

Previously, we have demonstrated [25] that the excess partial molar enthalpy is a resultant of all the intermolecular interactions in the system polymer–low-molecular-weight substance at a nearly infinite dilution. It can be written as the following sum:

$$\Delta H_1^{E\infty} + \Delta H_{BREAK} + \Delta H_{HOLE} + \Delta H_{DISP} + \Delta H_{SP}, \quad (18)$$

where ΔH_{BREAK} is the enthalpy of rupture of the bond between the solute molecules; ΔH_{HOLE}, enthalpy of cavity formation in pure solvent, i.e., in the polymer in our case; ΔH_{DISP}, enthalpy of nonspecific interaction; and ΔH_{SP}, enthalpy of specific interaction.

To calculate the excess functions of mixing in the system polymer–low-molecular-weight substance, we derived the equations for the temperature dependences of Ω_1^∞. The mass activity coefficients calculated for the temperature range 30–120°C at a step of 10°C are given in Table 1, and the estimated $\Delta\bar{H}_1^{E\infty}$, in Table 2.

The $\Delta\bar{H}_1^{E\infty}$ values obtained for the solutions of PDMS/PPT block copolymers appeared to be fairly high in the absolute value and negative in sign. This is quite expectable, knowing that *n*-alkanes are good solvents for PDMS forming a continuous phase of this block copolymer. In the case of the polymer with a rigid-to-flexible block ratio of 1 : 4.5, the dependence of the enthalpy of solution on the number of carbon atoms in the sorbate demonstrates a maximum for hexane. It may be suggested that, in such a microstructure of the polymer chain, a considerable amount of nanoscopic intraassociate cavities occur, whose size is close to that of the hexane molecule. In this case, the partial characteristic ΔH_{HOLE} is reduced, which

Table 1. Activity coefficients of certain *n*-alkanes in systems with the investigated polymers*

T °C	$\Omega_1^\infty \pm 2\%$											
	pentane	hexane	heptane	pentane	hexane	heptane	octane	pentane	hexane	pentane	hexane	heptane
	PDMS			PTPDMS-1				PTPDMS-2		PTPDMS-3		
30	6	6.28	6.75	1.72	0.87	1.3	1.77	2.87	2.63	3.93	4.53	4.67
40	6.06	6.15	6.47	2.1	1.17	1.57	2.01	3.17	2.87	4.23	4.64	4.72
50	6.15	6.08	6.27	2.54	1.55	1.9	2.27	3.5	3.13	4.56	4.77	4.8
60	6.27	6.04	6.12	3.06	2.05	2.28	2.58	3.85	3.42	4.92	4.93	4.91
70	6.42	6.04	6.02	3.66	2.66	2.72	2.92	4.25	3.74	5.31	5.12	5.05
80	6.59	6.07	5.96	4.36	3.44	3.24	3.3	4.68	4.08	5.73	5.32	5.2
90	6.79	6.13	5.93	5.16	4.39	3.83	3.73	5.15	4.46	6.2	5.55	5.39
100	7.02	6.211	5.94	6.09	5.56	4.52	4.22	5.66	4.87	6.7	5.8	5.6
110	7.27	6.32	5.98	7.14	6.99	5.31	4.76	6.22	5.32	7.24	6.08	5.83
120	7.54	6.45	6.04	8.35	8.72	6.22	5.37	6.83	5.81	7.82	6.38	6.08

* (PTPDMS) Copolymer built by the phenolphthalein terephthalate (**I**) and PDMS blocks (**II**). **I** : **II** ratio: PTPDMS-1 1 : 4.5, PTPDMS-2 1 : 10.5, and PTPDMS-3 1 : 21.5.

Table 2. Excess partial molar enthalpy $\Delta\bar{H}_1^{E\infty}$ and entropy of mixing $\Delta\bar{S}_1^{E\infty}$ for polymers with various chain microstructures

Sorbate	$-\Delta\bar{H}_1^{E\infty}$, kJ mol^{-1}	$-\Delta\bar{S}_1^{E\infty}$, J mol^{-1} K^{-1}	$-\Delta\bar{H}_1^{E\infty}$, kJ mol^{-1}	$-\Delta\bar{S}_1^{E\infty}$, J mol^{-1} K^{-1}	$-\Delta\bar{H}_1^{E\infty}$, kJ mol^{-1}	$-\Delta\bar{S}_1^{E\infty}$, J mol^{-1} K^{-1}	$-\Delta\bar{H}_1^{E\infty}$, kJ mol^{-1}	$-\Delta\bar{S}_1^{E\infty}$, J mol^{-1} K^{-1}
	PDMS		PTPDMS-1		PTPDMS-2		PTPDMS-3	
n-Pentane	2 ± 0.2	540 ± 50	17 ± 2	500 ± 50	9 ± 0.9	525 ± 50	7.0 ± 0.7	532 ± 50
n-Hexane	–0.3 ± 0.03	590 ± 60	24 ± 2	122 ± 12	8 ± 0.8	564 ± 60	3.2 ± 0.3	576 ± 60
n-Heptane	–1.9 ± 0.2	650 ± 70	16 ± 2	600 ± 60	–	–	2.3 ± 0.2	640 ± 60
n-Octane	–	–	11 ± 1	705 ± 70	–	–	–	–

gives rise to a minimum in the dependence of $\Delta\bar{H}_1^{E\infty}$ on the number of carbon atoms in the sorbate molecule.

In the Flory–Hugging thermodynamics, the partial molar entropy of alkanes is written as

$$\Delta\bar{S}_1^{E\infty} = R[\ln m - (m - 1)/m], \qquad (19)$$

where m is the ratio of the rigid-core volumes of a polymer and a low-molecular-weight component [26].

The limitations of Eq. (19) are the lack of intermolecular interactions and the constancy of the free volume in the course of mixing. Under these conditions, Eq. (19) predicts the decrease in $\Delta\bar{S}_1^{E\infty}$ with increasing molar volume of *n*-alkane.

The dependence of $\Delta\bar{S}_1^{E\infty}$, calculated by Eq. (19), on the number of carbon atoms in the sorbate molecule has a maximum at $N = 6$ (hexane).

It should be pointed out here that, for elastomers, Eq. (19) is not generally valid [27]. Conversely, they are characterized by the independence of $\Delta\bar{S}_1^{E\infty}$ from the molar volume of alkane. The occurrence of the minimum in $\Delta\bar{S}_1^{E\infty}$ in the case of hexane can be attributed to the sorption mechanism involving the insertion of the hexane molecules into intraassociate cavities (free-volume elements) of the elastomer, like that in sorption on associated liquids [27, 28].

CONCLUSIONS

(1) Inverse gas chromatography shows promise as a method for studying fine (nanoscopic) organization of block copolymers.

(2) An algorithm is suggested for calculating the partial contribution of dissolution for the cases of the dual mechanism of retention on polyblock copolymers.

(3) The partial molar enthalpy and entropy are calculated for three different compositions of the copolymers built by the phenolphthalein terephthalate and poly(dimethylsiloxane) blocks.

(4) The abnormally high $\Delta\overline{H}_1^{E\infty}$ obtained for the copolymers, compared to poly(dimethylsiloxane) (flexible-block phase), and small differences in $\Delta\overline{S}_1^{E\infty}$ suggest the presence of a considerable amount of free-volume elements in the supramolecular structure of the polymers investigated, which makes them promising materials for, e.g., selective gas-permeable membranes.

REFERENCES

1. Brown, J.-M. and Guillet, J.E., *Adv. Polym. Sci.*, 1976, vol. 21, pp. 108–145.
2. Brown, J.-M. and Guillet, J.E., *Macromolecules*, 1976, vol. 9, no. 4, pp. 617–621.
3. *Polymer Blends*, Paul, D.R. and Newman, S., Eds, New York: Academic, 1978.
4. Courval, G.J., *Macromolecules*, 1975, vol. 8, no. 3, pp. 328–331.
5. Bousmmina, M., Lavoie, A., and Riedl, B., *Macromolecules*, 2002, vol. 35, no. 16, pp. 6274–6283.
6. Ito, K., Usami, N., and Jamashita, Y., *Macromolecules*, 1980, vol. 13, no. 2, pp. 216–221.
7. Raspopova, E.N. and Irzhak, V.I., *Vysokomol. Soedin., Ser. A*, 1987, vol. 9, no. 10, pp. 2138–2142.
8. Wang, M.J., Tu, H., Murphy, L.J., and Mahmud, K., *Rubber Chem. Technol.*, 2000, vol. 74, pp. 666–667.
9. Kachal'nikov, A.Yu. and Voznyakovskii, A.P., Abstracts of Papers, *Fiziko-khimicheskie osnovy novei-shikh tekhnologii 21 veka* (Physicochemical Principles of the 21st Century State-of-the-art Technologies), Moscow: Granitsa, 2005, vol. 1, part. 1, p. 322.
10. Kachal'nikov, A.Yu. and Voznyakovskii, A.P., Abstracts of Papers, *Khimiya vysokoorganizovannykh veshchestv i nauchnye osnovy nanotekhnologii* (Chemistry of Highly Organized Substances and Scientific Background for Nanotechnology), St. Petersburg (Russia), June 28–July 2, 2004, pp. 198–199.
11. Voznyakovskii, A.P., Neverovskaya, A.Yu., and Krivoruchko, E.M., *Vopr. Khim. Khim. Tekhnol.*, 2004, no. 5, pp. 96–101.
12. Schlick, S. and Levy, M., *J. Phys. Chem.*, 1960, vol. 64, no. 7, pp. 883–886.
13. Kiselev, A.V., Poshkus, D.P., and Yashin, Ya.I., *Molekulyarnye osnovy adsorbtsionnoi khromatografii* (Molecular Principles of Adsorption Chromatography), Moscow: Khimiya, 1986.
14. Nosach, V.V., *Reshenie zadach approksimatsii s pomoshch'yu personal'nykh komp'yuterov* (Solution of Optimization Problems Using Personal Computers), Moscow: MIKAP, 1994.
15. Bunday, B.D., *Optimization Methods in Pascal*, London: Edward Arnold, 1987.
16. Grigoryan, G.V., Polyether–Polysiloxane Block Copolymers, *Cand. Sci. Dissertation*, Leningrad, 1982.
17. Vigdergauz, M.S., *Raschety v gazovoi khromatografii* (Calculations in Gas Chromatography), Moscow: Khimiya, 1978.
18. Nesterov, A.E., *Obrashchennaya gazovaya khromatografiya polimerov* (Inverse Gas Chromatography of Polymers), Kiev: Naukova Dumka, 1988.
19. Voznyakovskii, A.P. and Genkin, A.N., *Vysokomol. Soedin., Ser. A*, 1988, vol. 30, no. 11, pp. 2319–2322.
20. Genkin, A.N., Petrova, N.A., and Evstigneeva, T.V., *Vysokomol. Soedin., Ser. A*, 1981, vol. 23, no. 2, pp. 329–2336.
21. Kiselev, A.V., *Mezhmolekulyarnye vzaimodeistviya v adsorbtsii i khromatografii* (Intermolecular Interactions in Adsorption and Chromatography), Moscow: Vysshaya Shkola, 1986, p. 310.
22. Eremin, E.N., *Osnovy khimicheskoi termodinamiki* (Basic Chemical Thermodynamics), Moscow: Vysshaya Shkola, 1978.
23. Dontsov, A.A., *Protsessy strukturirovaniya elastomerov* (Structuring in Elastomers), Moscow: Khimiya, 1978.
24. Vigdergauz, M.S., *Usp. Gaz. Khromatogr.*, 1978, issue 5, pp. 18–32.
25. Genkin, A.N., Voznyakovskii, A.P., and Krivoruchko, E.M., *Zh. Fiz. Khim.*, 1998, vol. 72, no. 7, pp. 1303–1308.
26. Belousov, V.P. and Morachevskii, A.G., *Teploty smesheniya zhidrostei: Spravochnik* (Enthalpies of Mixing of Liquids: A Handbook), Leningrad: Khimiya, 1970.
27. Nesterov, A.E., *Obrashchennaya gazovaya khromatografiya polimerov* (Inverse Gas Chromatography of Polymers), Kiev: Naukova Dumka, 1988.
28. Voznyakovskii, A.P., *Vysokomol. Soedin., Ser. A*, 2003, vol. 45, no. 2, pp. 262–271.
29. Prigogine, I.R., *The Molecular Theory of Solutions*, Amsterdam: North-Holland, 1957.

ISSN 1070-4272, Russian Journal of Applied Chemistry, 2006, Vol. 79, No. 12, pp. 2007–2012. © Pleiades Publishing, Inc., 2006.
Original Russian Text © A.M. Bochek, I.L. Shevchuk, L.M. Kalyuzhnaya, 2006, published in Zhurnal Prikladnoi Khimii, 2006, Vol. 79, No. 12, pp. 2031–2036.

MACROMOLECULAR CHEMISTRY AND POLYMERIC MATERIALS

Properties of Aqueous Solutions of Methyl Cellulose–Polyvinyl Alcohol Blends

A. M. Bochek, I. L. Shevchuk, and L. M. Kalyuzhnaya

Institute of Macromolecular Compounds, Russian Academy of Sciences, St. Petersburg, Russia

Received June 9, 2006

Abstract—Rheological properties of dilute and moderately concentrated aqueous solutions of methyl cellulose–polyvinyl alcohol blends, as well as the conditions of gelation in these solutions were studied. The compatibility of the polymers was examined by the solvent vapor sorption method; the range of the compositions corresponding to thermodynamic compatibility of methyl cellulose and polyvinyl alcohol was identified.

DOI: 10.1134/S1070427206120196

Recently there has been increased interest in self-associated polymer systems based on environmentally safe and biodegradable natural polymers. As is known, a number of cellulose compounds form physically thermoreversible gels in aqueous solutions. These compounds include methyl cellulose (MC), hydroxypropyl cellulose (HPC), hydroxypropyl methyl cellulose (HPMC), and methyl ethyl cellulose (MEC). These cellulose ethers are widely used as gel-forming agents, thickeners, stabilizers, and emulsifiers in food industry [1]. Among the cellulose compounds mentioned, the most widely used is MC.

The gelation temperature of aqueous solutions of MC is affected by many factors: polymer concentration and degree of substitution and uniformity of distribution of the substituents in anhydroglucoside units and along the macrochain [2–5]. Substituents of a different nature, introduced into the MC macromolecule, affect the solubility of mixed cellulose ethers, the rheological properties of solutions, their associative structural organization, and the gelation and phase segregation conditions in these solutions [6–11]. The rheological properties of MC solutions and conditions of gelation in them, as well as the physicomechanical properties of the film obtained from solutions, can be also varied by introducing another water-soluble polymer into solutions [12–14].

Aqueous solutions of MC (systems with lower critical solution temperature, LCST) form physically thermoreversible gels under heating [15–18], whereas solutions of polyvinyl alcohol (PVA) (systems with upper critical solution temperature, UCST) form gels under cooling [19–22]. Examination of blends of these two kinds of polymers in a common solvent is of both scientific and practical interest.

In this study, we examined the rheological properties of dilute and moderately concentrated solutions of MC–PVA blends and the conditions of gelation in them, as well as the thermodynamic compatibility of the polymers in the solid state, depending on the polymer blend composition.

EXPERIMENTAL

As initial materials served MC-100 commercial cellulose with the degree of substitution of 1.62, M_η = 147 000, and two PVA samples, PVAI with M_η = 17 500 and degree of hydrolysis of 98% and PVAII with M_η = 58 000 and degree of hydrolysis of 98%. Distilled water served as the solvent.

The 3% aqueous MC and PVA solutions, prepared in advance, were mixed in the necessary proportions. Dilution of the 3% solutions yielded 0.15–0.20% solutions, which were examined viscometrically.

An aqueous solution of MC was prepared by polymer swelling in hot water at 80–90°C, followed by dissolution under cooling to 5–10°C with stirring for 6 h. The PVA solutions were prepared at 80°C, stirred for 3 h, and then cooled to room temperature. The resulting solutions were filtered under pressure and then deaerated for 1 h. The solutions of the two polymers were mixed in the necessary proportions and stirred for 4 h.

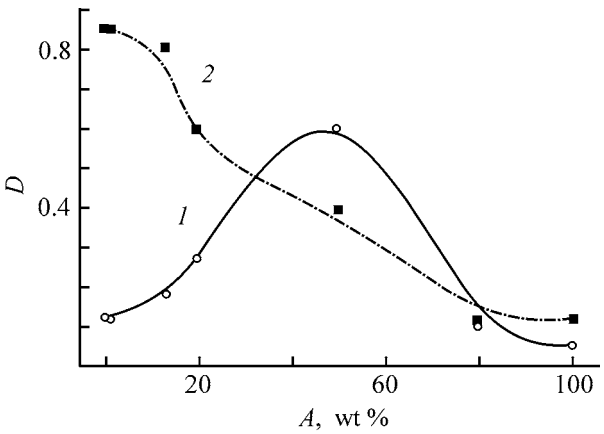


Fig. 1. Optical density D in relation to the composition of the 3% solutions of the blends at (*1*) 20 and (*2*) 60°C. (*A*) PVAI concentration; the same for Figs. 2–4.

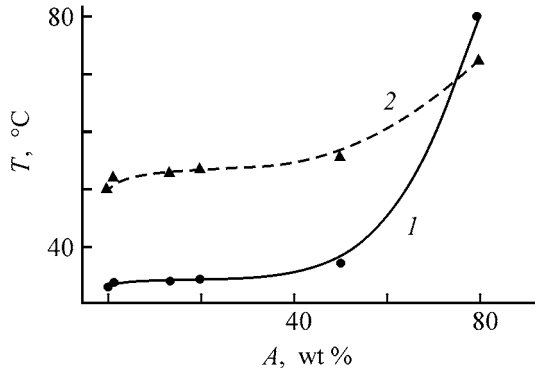


Fig. 2. (*1*) T_{gel} and (*2*) T_{cloud} (9 s) in relation to the composition of the 3% solutions of the blends.

Films were prepared from the aqueous solutions of the polymer blends by casting the solution through a laboratory draw plate with controlled slit onto Teflon plates at 20°C, followed by drying at 30°C. The films were detached from the support after 1 day.

The gelation conditions in the solutions were monitored by variation of the viscosity of the solutions and also photometrically. The gelation onset temperature T_{gel} in the 3% solutions, depending on the composition, was determined with a Hoeppler viscometer according to the procedure from [6]. The phase segregation (cloud) point T_{cloud} in the 0.2% solutions was determined with a KFK-2 photocolorimeter in a temperature-controlled cell (at λ = 670 nm) at a light transmission of 50% by the procedure from [3, 6, 9].

The viscosity characteristics of the dilute (0.15 and 0.20%) solutions were measured on an Ubbelohde capillary viscometer at 20°C. The rheological properties of the concentrated solutions were examined on a Rheotest 2.1 rotary viscometer with a cylinder–cylinder working unit in the shear stress range 3–600 Pa at 20–40°C.

As is known, cellulose and its compounds are in most cases only partially compatible with other polymers in blends [23]. To elucidate the compatibility of MC with PVA in the moderately concentrated solutions, we examined the optical properties of these blends (Fig. 1). We measured the optical density of the solutions of the MC–PVAI blends. It is seen that, upon addition of the PVAI solution to the MC solution at 20°C, the optical density of the blends increases. The maximal optical density is observed for solutions of the polymer blends at 50 wt % PVAI. On the whole, the optical densities of the solutions of the blends substantially exceeds those of the MC and PVAI solutions at the polyvinyl alcohol content in the blend from 20 to 80%. The higher optical densities of the solutions of the blends in this range of the PVAI concentrations suggest phase segregation in the systems. Upon heating an aqueous solution of MC to 60°C, gelation occurs; as a result, the solution becomes turbid, and the optical density of the solution sharply increases [4, 5, 15, 16]. A decrease in the optical density of the solutions of the blends at 60°C with increasing PVA proportion may be due to a decrease in the proportion of the polymer, responsible for formation of the gel under heating, i.e., of MC.

It would be expected that a change in the MC concentration in the solutions of the blends, phase segregation in solutions, and interaction between the macromolecules of the different kinds of polymers should modify the gelation conditions in the systems of interest. Therefore, we determined T_{gel} and T_{cloud} in the solutions examined (Fig. 2). It is believed that, if interactions between the MC and PVA macromolecules dominate over the MC–MC and PVA–PVA interactions, the heat resistance of the MC macrochains in water is enhanced because of an increase in the solubility of PVA in water with temperature. It should be noted that a decrease in the MC concentration in solutions always causes T_{gel} and T_{cloud} to increase [3].

It is seen that introduction of up to 50.0 wt % PVAI into the blends does not substantially modify the gelation conditions in the solutions, which indirectly confirms the interaction between the macromolecules of the different kinds of the polymers. Substantial increases in T_{gel} and T_{cloud} are observed for blends with over 50.0 wt % PVAI. Such a change in the gelation conditions can be due to a decrease in the propor-

tion of the gelating polymer, MC. At the PCA content above 80.0 wt %, no gelation is observed in the solutions.

To evaluate the compatibility of MC and PVA, we used the solvent vapor sorption method [24]. The films prepared by the above-described procedure were vacuum-dried to constant weight. The residual content of the solvent was no greater than 0.02%. The water vapor sorption by the films was measured at 20°C in a vacuum setup with a McBain quartz spring balance (spring sensitivity 0.5–0.7 μg m^{-1}, accuracy within 0.01%) at the saturated solvent vapor pressure.

The polymer–solvent interaction parameter ζ_1 for MC, PVA, and their blends was calculated from the sorption data by the Flory–Huggins equation [25]:

$$\ln a_1 = \ln(P_1/P_1^0) = \ln(1 - \varphi_2) + \varphi_2 + \zeta_1\varphi_2^2, \quad (1)$$

where a_1 is the solvent vapor activity, and P_1/P_1^0, relative pressure of the solvent vapor. The experiments were performed at the saturated solvent vapor pressure, i.e., at $a_1 = P_1/P_1^0 = 1$, which suggests $\ln a_1 = 0$. The volume proportion of the polymer in the swollen film was calculated by expression (2):

$$\varphi_3 = \frac{1}{1 + (d_2/d_1)Q}, \quad (2)$$

where d_1 is the solvent density; d_2, polymer density; and Q, amount of the solvent sorbed (grams of solvent per gram of dry polymer). The density of the samples was determined by hydrostatic weighing in heptane.

The polymer–polymer interaction parameter was calculated from the sorption data by the Patterson relationship [26]:

$$\zeta_{23} = (\zeta_{12}\varphi_a + \zeta_{13}\varphi_b - \zeta_{1(23)})/\varphi_a\varphi_b, \quad (3)$$

where ζ_{12}, ζ_{13}, and $\zeta_{1(23)}$ are the Flory–Huggins parameters of interaction with water of individual polymers MC and PVA and their blends, respectively, and φ_a and φ_b, volume proportions of the polymers in the blend, respectively. For blends of compatible polymers, $\zeta_{23} < 0$ [27]. Therefore, any positive ζ_{23} suggests the incompatibility of polymers.

Figure 3 shows that, in the MC–PVAI blends with a PVA content of up to 15.0 wt %, the polymers are compatible, i.e., $\varphi_{23} < 0$. At a higher content of PVA, the polymers in the solid state are incompatible.

The pattern of variation of the viscosity for the dilute solutions of the polymer blends suggests possible interaction of the macromolecules of different kinds

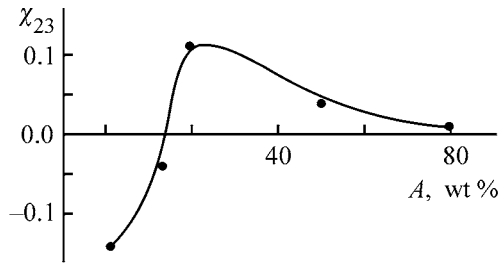


Fig. 3. Polymer–polymer interaction parameter 23 vs. the PVAI content *A*.

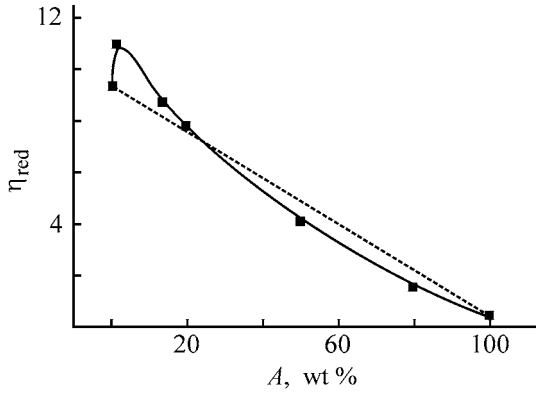


Fig. 4. Reduced viscosity $\eta_{red} = \eta_{sp}/C$ of the 0.20% solutions of the MC–PVAI blends vs. the PVAI content *A* at 20°C. *Dashed line*: calculated additive values.

of polymers in solution [7, 28, 29]. In dilute solutions (Fig. 4) with up to 30.0 wt % PVAI in the blend, the viscosity of 0.20% solutions exceeds the additive value. The viscosities of the solutions of the blends with over 30.0 wt % PVAI are lower than the additive values. The fact that the viscosities of the blends of the dilute solutions exceed the additive values suggests that intermolecular interactions between the macromolecules of different kinds of the polymers dominate in solution. This is responsible for the formation of structures whose hydrodynamic volume exceeds the weighted-average hydrodynamic volume of the two components taken separately. The fact that the reduced viscosities of the solutions of the blends (with over 30.0% PVAI) are lower than the additive value can be due both to compaction of the macromolecules of the polymers if they are incompatible and to formation of mixed complexes whose hydrodynamic volume is smaller than those of either polymer. Figure 4 shows that, in our case, a decrease in the reduced viscosity is due to incompatibility of the polymers. It should be noted that, with increasing molecular weight of PVA, the range of the composition of the blends within which MC and PVA are compatible tends to narrow. This is consistent with the published data on the thermodynamic compati-

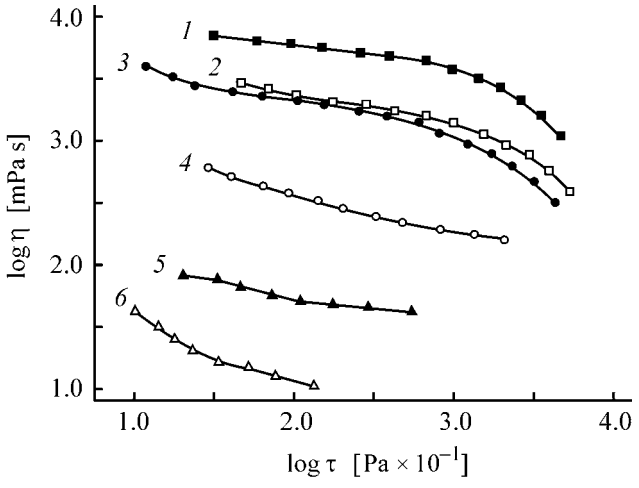


Fig. 5. Flow curves for 3% solutions of (*1*) MC, (*2–5*) MC–PVA blends containing (*2*) 1.4, (*3*) 20, (*4*) 50, and (*5*) 80% PVA, and (*6*) PVA at 20°C. (η) Viscosity and (τ) shear stress.

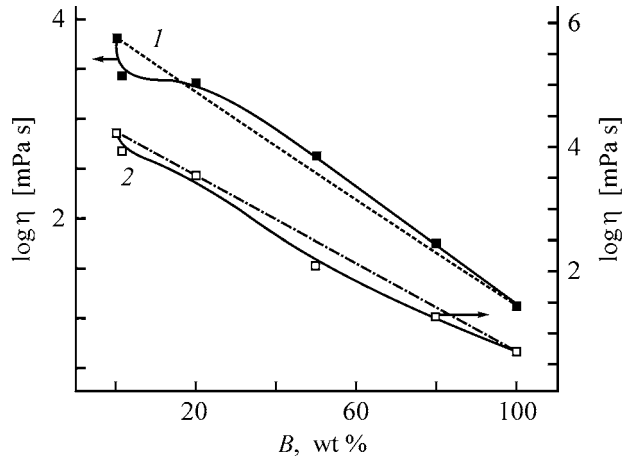


Fig. 6. Viscosity of the 3% solutions of the MC–PVAII mixtures in relation to the composition at (*1*) 20 and (*2*) 40°C. (η) Viscosity and (*B*) PVAII content.

bility of polymers in relation to their molecular weight [25]. In the case of PVAII with a higher molecular weight, the reduced viscosity exceeds the additive value for the blends with up to 8.0 wt % PVAII only.

The intermolecular interactions in moderately concentrated solutions were analyzed by examination of the rheological properties of the 3% solutions of MC–PVAI and MC–PVAII blends at 20–40°C. The temperature of 40°C exceeds the T_{gel} of the MC solution (Fig. 2), which makes it suitable for elucidating the influence of gelation of MC on the viscosity of the solutions of polymer blends.

Figure 5 presents as an example the flow curves for the solutions of the MC–PVAII blends at 20°C. The flow curves for the solutions of MC, PVA, and their blends are partial flow curves of non-Newtonian fluids. The structural viscosity branch for the MC solution becomes prominent at shear stresses over $\log \tau = 2.8$ (630 Pa × 10^{-1}). On the flow curve of the PVAII solution, the structural viscosity branch is less prominent in the shear stress range of interest because of the substantially lower molecular weight of PVA compared to MC. Variation of the viscosity with the shear stress is typical of structured polymer systems. Similar flow curves are also observed for the MC–PVAI solutions.

Figure 6 shows the viscosity of the MC–PVAII blends in relation to the composition at 20 and 40°C. For convenience, these dependences were plotted on different scales, which prevented their overlapping.

At 20°C, the viscosity–composition dependence for moderately concentrated solutions of MC–PVA blends is opposite to that for the dilute solutions at the same temperature (Fig. 4). Such a trend is typical of the viscosity of semirigid chain polymers due to changing thermodynamic affinity of the polymer for the solvent. The worsening of the solvent quality is responsible for the contraction of the macromolecules of the cellulose compounds and reduction of the viscosity of dilute solutions. At the same time, the degree of aggregation of the solvated macromolecules in concentrated solutions increases due to enhancement of intermolecular interactions, which is responsible for an increase in viscosity [25].

The viscosity of concentrated solutions of the polymer blends is affected by many factors. In blends of polymer solutions, new hydrogen bond systems can be formed, stronger than those in solutions of MC and PVA taken separately, as can be seen from Fig. 3 (the range of the compositions in which MC and PVA are thermodynamically compatible). It should be noted that the thermodynamic quality of the solvent (water) with respect to MC can change upon addition of a different polymer, PVA, to the MC solution. Also, under phase segregation in solution, the mechanism of flow of the heterogeneous blend will differ from that of the homogeneous solution. The viscosity will be affected by the shape, number, and stability (strength) of the microparticles of the disperse phase, in a solution of a different phase, matrix. The viscosity can be both higher and lower than the additive value.

Presumably, addition of PVA to an MC solution (up to 20 wt %) at 20°C destroys the system of intermolecular hydrogen bonds between the solvated

macromolecules of the cellulose ether, which causes the viscosity of the solutions to decrease over the PVA concentration range of interest. Further increase in the PVA proportion in the blend causes the viscosity to increase due to phase segregation in solutions (the polymers are incompatible).

The temperature dependences of the viscosities of the solutions of the blends (20–35°C) were used for calculating the heat of activation of viscous flow of solutions E_a. For the MC and PVAII solutions, E_a was estimated at 28.0 and 27.0 kJ mol^{-1}, respectively. In the solutions of the blends with the PVAII content of up to 30.0 wt %, the heats of activation are lower than the additive values, while at the PVAII content in the blends over 30.0 wt %, the heat of activation of the viscous flow of the solutions reaches 40.0 kJ mol^{-1}. Such a deviation of the E_a parameters from the additive values, depending on the PVA content in the blends, suggests a major change in the strength of the structure of the solutions due to changes in the fluctuation network of hydrogen bonds between the solvated macromolecules of the two polymers and phase segregation in the blends of certain composition.

At temperatures above T_{gel} of the MC solution (40°C), the viscosity of the solutions of the blends is lower than the additive value throughout the composition range examined (Fig. 6, curve *2*). With increasing temperatures, two opposite processes occur in the solutions of the blends. On the one hand, gelation in the MC solutions is accompanied by phase segregation and an increase in viscosity [15, 16, 30, 31]. On the other hand, the increase in temperature causes the viscosity of the PVA solution to decrease because of the improvement of the solvent quality with respect to the polymer of interest and an increase in the energy of thermal motion of the macromolecules. Presumably, at 40°C the viscosity of the solutions of the blends is more strongly affected by the latter factor: Solvated PVA macromolecules hinder formation of gel throughout the solution body and act as a "lubricant" between the nucleation sites of the MC macromolecules. As a result, the viscosity becomes lower than the additive values.

Thus, by varying the amount of the polymer (in particular, PVA) introduced into an aqueous solution of MC, it is possible to modify the rheological properties of solutions and conditions of gelation in them, as well as to prepare mixed film materials in which the polymers can be both compatible and incompatible.

CONCLUSIONS

(1) The viscosities of dilute and concentrated solutions of blends of methyl cellulose and polyvinyl alcohol differ from the additive values, which suggests a change in the conformations of the macromolecules of the polymers in blends and structural rearrangement of the solutions.

(2) The polymers are thermodynamically compatible in blends with up to 15.0 wt % polyvinyl alcohol.

(3) In solutions of the blends with over 50.0 wt % polyvinyl alcohol, the gelation-onset and phase-segregation temperatures substantially increase.

REFERENCES

1. Petropavlovskii, G.A., *Gidrofil'nye chastichno zameshchennye efiry tsellyulozy i ikh modifikatsiya putem khimicheskogo sshivaniya* (Hydrophilic Partially Substituted Cellulose Ethers and Their Modification by Chemical Cross-Linking), Leningrad: Nauka, 1988.
2. Petropavlovskii, G.A., Krunchak, M.M., and Vasil'eva, G.G., *Cellulose Chem. Technol.*, 1972, vol. 6, no. 2, pp. 135–144.
3. Sarkar, N., *J. Appl. Polym. Sci.*, 1979, vol. 24, no. 4, pp. 1073–1079.
4. Kato, T., Yokoyama, M., and Takabashi, A., *Colloid Polym. Sci.*, 1978, vol. 256, no. 1, pp. 15–21.
5. Takahashi, S.-I., Fujimoto, T., Miyamoto, T., and Inagaki, H., *J. Polym. Sci., Part A: Polym. Chem.*, 1987, vol. 25, no. 4, pp. 987–984.
6. Bochek, A.M., Petropavlovskii, G.A., Kutsenko, L.I., and Karetnikova, E.B., *Zh. Prikl. Khim.*, 2000, vol. 73, no. 1, pp. 152–155.
7. Kutsenko, L.I., Petropavlovskii, G.A., Karetnikova, E.B., et al., *Zh. Prikl. Khim.*, 2000, vol. 73, no. 4, pp. 652–656.
8. Petropavlovsky, G.A., Bochek, A.M., Kutsenko, L.I., et al., *Cellulose Chem. Technol.*, 2000, vol. 34, nos. 1–2, pp. 63–70.
9. Bochek, A.M., Nud'ga, L.A., Petrova, V.A., and Petropavlovskii, G.A., *Zh. Prilk. Khim.*, 2000, vol. 73, no. 2, pp. 304–308.
10. Kalinina, N.A., Bochek, A.M., Silinskaya, I.G., et al., *Zh. Prikl., Khim.*, 2001, vol. 74, no. 9, pp. 1522–1525.
11. Kalinina, N.A., Silinskaya, I.G., Bochek, A.M., et al., *Vysokomol. Soedin., Ser. A*, 2004, vol. 46, no. 2, pp. 314–315.
12. Kustenko, L.I., Ivanova, N.P., Karetnikova, E.B., et al., *Zh. Prikl. Khim.*, 2002, vol. 75, no. 2, pp. 314–318.
13. Kutsenko, L.I., Karetnikova, E.B., Bochek, A.M., and Kalyuzhnaya, L.M., *Zh. Prikl, Khim.*, 2003, vol. 76, no. 10, pp. 1720–1724.

14. Kutsenko, L.I., Bochek, A.M., and Karetnikova, E.B., in *Materialy 10-oi Vserossiiskoi. nauchno-tekhnicheskoi konferentsii "Efiry tsellyulozy i krakhmala: sintez, svoistva, primenenie"* (10th Russian Scientific and Technical Conf. "Cellulose and Starch Ethers and Esters: Synthesis, Properties, and Application"), Suzdal, May 5–8, 2003, pp. 162–165.
15. Bochek, A.A. and Petropavlovskii, G.A., *Cell. Chem. Technol.*, 1995, vol. 29, no. 5, pp. 567–574.
16. Bochek, A.M., Petropavlovskii, G.A., and Kallistov, O.V., *Zh. Prikl. Khim.*, 1996, vol. 69, no. 8, pp. 1363–1368.
17. Kalyuzhnaya, L.M., Bochek, A.M., Petropavlovskii, G.A., and Frenkel, S.Ya., *Zh. Prikl. Khim.*, 2000, vol. 73, no. 9, pp. 1525–1530.
18. Bochek, A.M., Zabivalova, N.M., Lavrent'ev, V.K., et al., *Zh. Prikl. Khim.*, 2001, vol. 74, no. 8, pp. 1322–1327.
19. Takahashi, A. and Hiramitsu, S., *Polym. J.*, 1974, vol. 6, no. 2, pp. 103–107.
20. Briscoe, B., Luckham, P., and Zhu, S., *Polymer*, 2000, vol. 41, pp. 3851–3860.
21. Hohg, P.-D., Chou, C.-M., and He, C.-H., *Polymer*, 2001, vol. 42, pp. 6105–6112.
22. Ricciardi, R., Auriemma, F., De Rosa, C., and Laupretre, F., *Macromolecules*, 2004, vol. 37, no. 5, pp. 1921–1927.
23. *Polymer Blends*, Paul, D.R. and Newman, S., Eds., New York: Academic, 1978. vol. 1.
24. *Eksperimental'nye metody v adsorbtsii i molekulyarnoi khromatografii* (Experimental Methods in Adsorption and Molecular Chromatography), Kiselev, A.V. and Dantsig, V.P., Eds., Moscow: Mosk. Gos. Univ., 1973.
25. Tager, A.A., *Fiziko-khimiya polimerov* (Physical Chemistry of Polymers), Moscow: Khimiya, 1978.
26. Su, C.S. and Patterson, D., *Macromolecules*, 1974, vol. 10, pp. 708–712.
27. Scott, R.L., *J. Polym. Sci.*, 1952, vol. 9, pp. 423–432.
28. Staikos, G. and Bokias, G., *Makromol. Chem.*, 1991, vol. 192, pp. 2649–2657.
29. Budtova, T.V., Bel'nikevich, N.G., Belyaev, V.M., et al., *Vysokomol. Soedin., Ser. B*, 1991, vol. 33, no. 7, pp. 520–524.
30. Kobayashi, K., Huang, Ch.-I., and Lodge, T., *Macromolecules*, 1999, vol. 32, no. 21, pp. 7070–7077.
31. Desbrieres, J., Hirrien, M., and Ross-Murphy, S.B., *Polymer*, 2000, vol. 41, no. 1, pp. 2451–2461.

ISSN 1070-4272, Russian Journal of Applied Chemistry, 2006, Vol. 79, No. 12, pp. 2013–2015. © Pleiades Publishing, Inc., 2006.
Original Russian Text © L.M. Trufakina, 2006, published in Zhurnal Prikladnoi Khimii, 2006, Vol. 79, No. 12, pp. 2037–2039.

MACROMOLECULAR CHEMISTRY AND POLYMERIC MATERIALS

Viscoelasticity and Surface Properties of Blends of Aqueous Solutions of Polyvinyl Alcohol and Carboxymethyl Cellulose

L. M. Trufakina

Institute of Petroleum Chemistry, Siberian Division, Russian Academy of Sciences, Tomsk, Russia

Received January 24, 2006

Abstract—Rheological properties of aqueous solutions of carboxymethyl cellulose, polyvinyl alcohol, and of their blends prepared under various conditions (temperature, concentration, time) were studied by viscometry and of ball indenter penetration.

DOI: 10.1134/S1070427206120202

Complexation of a polymer with another polymer or with a low-molecular-weight compound is of great practical interest [1–3] since this modification changes the physical properties of the polymer without chemical synthesis.

Among blends of water-soluble polymers, gels of polyacrylamide [4], polyacrylic acid and cellulose ethers and esters [5], polysaccharide and polyvinyl alcohol [6], etc. have been studied in detail.

The conditions of formation of polymer complexes, their rheological and surface properties, and the kinetics of formation and degradation of the complexes are required for their successful application.

At present the rheological approach is widely used as the most powerful tool to estimate the kinetics of formation of physical networks in polymer blends.

The aim of this study was to examine the variation of the rheological and surface properties of polymer complexes with time. The results of this study can be used to assess the possibility of storage and estimate the storage temperature and the shelf life of these composites.

The polymer complexes were prepared from water-soluble flexible-chain polyvinyl alcohol (PVA) and rigid-chain carboxymethyl cellulose (CMC).

EXPERIMENTAL

The molecular weight M of PVA in distilled water at 20°C, calculated by the equation $[\eta] = 5.6 \times 10^{-4} M^{0.67}$ [7], is 2.2×10^5. The molecular weight of CMC in 0.1 N NaCl, calculated by the equation $[\eta] = 7.3 \times 10^{-3} M^{0.99}$, is 3.67×10^5.

The dynamic viscosity of the polymer solutions was measured on Rheotest-2 rotary viscometer with a cylinder-cylinder working unit at shear rates of 1.5 to 1312 s^{-1}. The viscosity and shear stress of aqueous solutions of the polymers are listed in the table. The critical concentrations c_{cr} of the crossovers of PVA and CMC are 5 and 6%, respectively.

The polymer blends were prepared by the procedures described in our previous study [8]. The viscosity and the shear stress of the polymer complexes were measured on a rheoviscometer with a cone-plate working unit at shear rates of 0.56 to 4860 s^{-1}.

When solutions with the polymer concentrations close to the critical values (4–8 wt %) were used, the properties of the polymer blend substantially changed.

The structure formation rate in the PVA-CMC system was estimated, as influenced by the concentration,

Dynamic viscosity and shear stress of aqueous solutions of CMC and PVA at T = 20°C

c_{CMC}, wt %	η, Pa s	τ, Pa	c_{PVA}, wt %	η, Pa s	τ, Pa
4	0.175	28.45	4	0.14	22.76
5	0.561	91.04	5	0.21	34.14
6	0.597	96.73	6	0.31	51.21
7	0.667	108.1	7	0.42	68.28
8	0.772	125.1	8	0.56	91.04

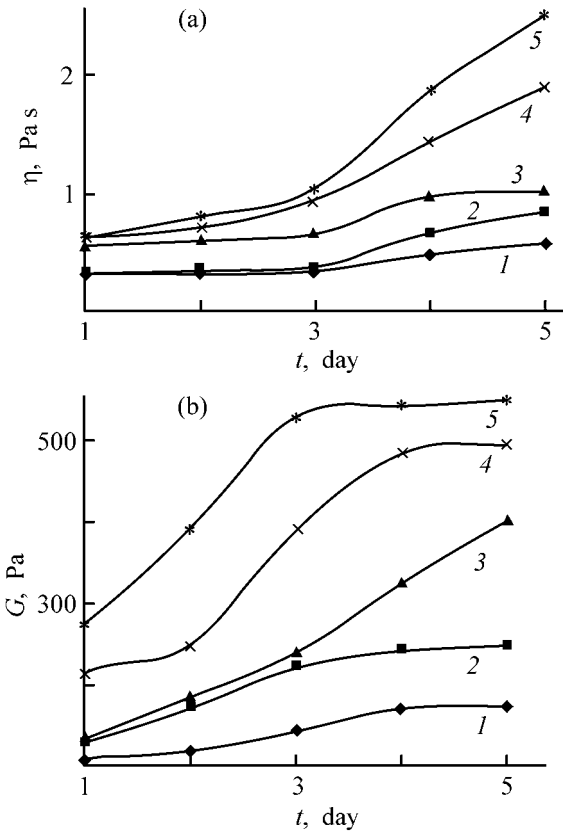


Fig. 1. (a) Dynamic viscosity η and elastic modulus G of polymer complexes vs. the time t of structuring at (a) 80°C and (b) 20°C. Initial concentration of polymers, wt %: (*1*) 4, (*2*) 5, (*3*) 6, (*4*) 7, and (*5*) 8; The same for Fig. 3.

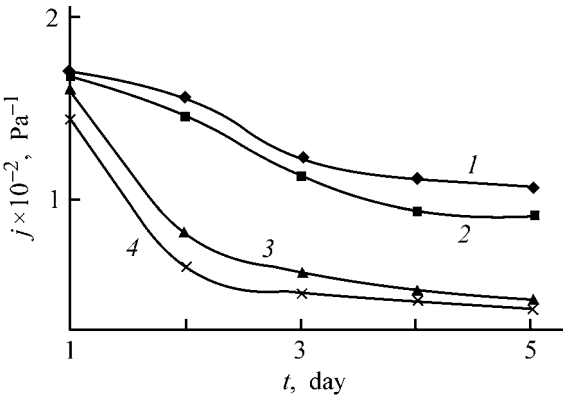


Fig. 2. Creep J of polymer complexes vs. time t of structuring at (*1*) 20, (*2*) 40, (*3*) 60, and (*4*) 80°C. Initial concentration of the polymers 5 wt %

time, and temperature, using the results of the rheological study. The dependence of the dynamic viscosity at T = 80°C on the gelation time at concentrations of the initial polymers in the range 4–8 % is shown in Fig. 1a. The increase in the viscosity suggests association of the molecules in the first reaction steps. The monotonic growth of the viscosity is also due to an increase in the total concentration of the initial polymers. At polymer concentrations higher than c_{cr}, an additional physical network is formed between themacromolecules. Under more rigorous conditions, i.e., at high polymer concentrations and low temperatures, the blend becomes more viscous due both to formation of additional hydrogen bonds between hydroxy groups of PVA molecules and to intramolecular cross-linking. On cooling from 80°C to 20°C, the viscosity increases from 2.5–3.0 to 6.0 Pa s. The complex is additionally stabilized by hydrophobic interactions promoted by hydrogen bonds [9].

The elastic modulus is the measure of the resistance of a material to deformation under the action of an external stress. This parameter can be measured by the method of ball indenter penetration [4, 10, 11]. The indenter radius was R = 7 mm. The cylindrical gel samples were 40 mm in diameter (D) and 40 mm in height (H). The elastic modulus was calculated by the equation

$$G = 3F/16h^{3/2}R^{1/2},$$

where F is the force acting on the indenter (N), and h is the penetration depth (mm) of a ball indenter of radius R (mm) into the flat sample surface.

The elastic modulus is related to the cross-link density, i.e., to the degree of system structuring. We studied the dependence of the elastic modulus of the gels on the concentration, temperature, and time.

The time dependence of the elastic modulus of the gels formed at 20°C is shown in Fig. 1b.

The gels can be conditionally divided into high-modulus (G > 500 Pa) and low-modulus (G < 500 Pa) gels [11]. The high-modulus gels are formed at the PVA concentration of 7–8%, which is higher than the cross-over concentration, and on cooling. In all cases, the elastic modulus increases during 4–5 days owing to formation of a cross-linked structure. The increase in the elastic modulus of the gels with G < 500 Pa is insignificant. These gels are stable.

The dependences of the creep of polymer complexes formed at the initial polymer concentration in the solution of 5% on the time of structuring at T = 20–80°C are shown in Fig. 2. The relaxation properties of the sample decrease with increasing temperature at a constant stress. The curves level-off with increasing structuring time.

The viscoelastic properties of an adhesive are important when a high-viscous polymer forms adhesive

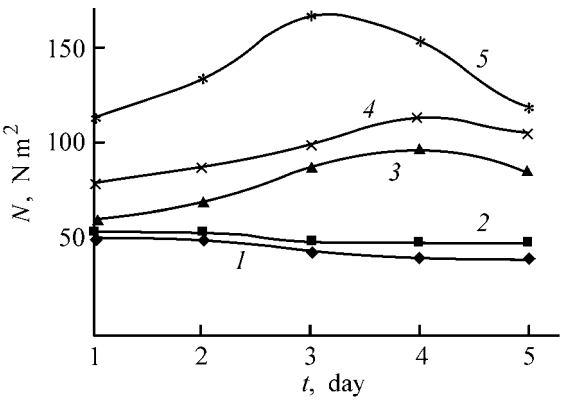


Fig. 3. Work of adhesion N of polymer complexes vs. time t of structuring at 20°C.

joints with the substrate surface [12, 13]. The rheological processes in the bulk of the polymer in the course of formation of adhesive joints have been extensively studied [9, 14]. The adhesive strength was evaluated by the work of detachment of a St.3 plate from the polymer complex under the action of an external force [13]:

$$W = W_{break}/S,$$

where S is the area of contact of the adhesive with the substrate (m^2), and W_{break} is the detachment adhesion ($N\ m^{-1}$).

To determine the features of formation of the surface of polymer blends with different structures and mechanical properties, we studied the influence of time, temperature, and concentration on these properties. The dependence of the work of adhesion of the polymer complexes on the reaction time is shown in Fig. 3. It is seen that the concentration of the initial solutions of the polymers affects this dependence. The time at which the curves level-off corresponds to completion of the surface formation. At the 7–8% concentration of the polymers in the initial solution, the surface layer is formed faster owing to the formation of supramolecular structures interfering with the work of adhesion. The adhesion mechanism of the detachment confirms the formation of hydrogen bonds decreasing the free volume and increasing the cohesion energy.

CONCLUSIONS

(1) The dynamic viscosity of aqueous solutions of polyvinyl alcohol, carboxymethyl cellulose, and their complexes was measured. The crossover concentration of polymers was determined.

(2) The elastic modulus of the polymer blends was determined in relation to concentration, temperature, and gelation time.

(3) The work of adhesion of the polymer complexes was studied by the method of detachment of a St.3 plate.

(4) The viscosity and the elastic modulus increase and the formation of the surface of polymer compositions accelerates with increasing total concentration of the initial monomers and with decreasing temperature.

REFERENCES

1. *Polymer Blends*, Paul, D.R. and Newman, S., Eds., New York: Academic, 1978, Vol. 1.
2. Bekturov, E.A. and Bimendina, L.A., *Interpolimernye kompleksy* (Interpolymer Complexes), Alma-Ata: Nauka, 1977.
3. Plate, N.F., Litmanovich, A.D., and Kudryavtsev, Ya.V., *Vysokomol. Soedin., Ser. A*, 2004, vol. 46, no. 11, pp. 1834–1874.
4. Lopatin, V.V., Askadskii, A.A., Vasil'ev, V.G., and Kurskaya, E.A., *Vysokomolek. Soedin., Ser. A*, 2004, vol. 46, no. 7, pp. 1217–1224.
5. Nikolaeva, O.V., Budtova, T.V., Kalyuzhnaya, L.M., et al., *Vysokomolek. Soedin., Ser. A*, 1999, vol. 41, no. 7, pp. 1176–1182.
6. Rashidova, S.Sh., Voropaeva, I.L., Mukhamedzhanova, M.Yu., et al., *Zh. Prikl. Khim.*, 2002, vol. 75, no. 7, pp. 1159–1163.
7. *Entsiklopediya polimerov* (Encyclopedia of Polymers), Prokhorov, A.M., Ed., Moscow: Khimiya, 1972, vol. 2, p. 1082.
8. Trufakina, L.M. and Kudeshova, E.G., *Inzh.-Fiz. Zh.*, 2003, vol. 76, no. 3, pp. 55–58.
9. Fel'dshtein, M.M., *Vysokomolek. Soedin., Ser. A*, 2004, vol. 46, no. 11, pp. 1905–1938.
10. Nielsen, L.E., *Mechanical Properties of Polymers and Composites*, New York: Marcel Dekker, 1974.
11. Medvedeva, V.V., Myasnikova L.I., Semchikov, Yu.D., and Rogovina, L.Z., *Vysokomolek. Soedin., Ser. B*, 1998, vol. 40, no. 3, pp. 492–497.
12. Zimon, A.D., *Adgeziya plenok i pokrytii* (Adhesion of Films and Coatings), Moscow: Khimiya, 1977.
13. Berlin, A.A. and Basin, V.E., *Osnovy adgezii polimerov* (Main Principles of Polymer Adhesion), Moscow: Khimiya, 1974.
14. Summ, B.D., in *Materialy 22-ro simpoziuma poreologii* (Proc. 22th Symp. on Rheology), Valdai, June 21–26, 2004.

ISSN 1070-4272, Russian Journal of Applied Chemistry, 2006, Vol. 79, No. 12, pp. 2016–2021. © Pleiades Publishing, Inc., 2006.
Original Russian Text © A.V. Tokarev, N.V. Sirotinkin, 2006, published in Zhurnal Prikladnoi Khimii, 2006, Vol. 79, No. 12, pp. 2040–2045.

MACROMOLECULAR CHEMISTRY AND POLYMERIC MATERIALS

A Study of Swelling of Polyurethane Wastes with the Aim of Regeneration

A. V. Tokarev and N. V. Sirotinkin

St. Petersburg State Technological Institute, St. Petersburg, Russia

Received March 10, 2006

Abstract—The optimum time of swelling (required for weakening of the intermolecular interaction) of polyurethanes of various compositions in a series of organic plasticizers was determined. The deterioration of the physicomechanical characteristics with plasticization allows a decrease in the expenses for secondary recovery of wastes formed in polyurethane production.

DOI: 10.1134/S1070427206120214

In the last decades, polyurethane compositions have found increased application in all branches of industry. As predicted, the Russian market of polyurethanes (PUs) can reach 210 thousand tons in 2007. The production of polyurethane materials on an increasingly large scale requires a search for efficient procedures for utilization or breakdown of these wastes.

At present, the main procedures for PU reprocessing are mechanical grinding with subsequent use of the resulting crumb as a filler for various composite materials, physical or physicomechanical treatment, and chemical reprocessing.

Mechanical degradation is the most acceptable procedure for utilization of PU foams, since their degradation requires lower power expenditure in comparison with the degradation of monolithic PUs [1, 2]. In addition, grinding of wastes formed in production of thermoplastic block PUs is very difficult because of their high elasticity at elevated temperatures: energy is mostly transformed into heat and only an insignificant part of energy is expended for degradation.

Physical methods, such as die casting, pressing, and extrusion, are suitable for reprocessing of thermoplastic linear or weakly cross-linked polyurethane systems [3, 4] and are inapplicable in the case of thermosetting plastics. Additional use of high temperatures can result in uncontrolled degradation of cross-linked PU to be recovered, which is reflected on the quality of the final product.

A huge number of foreign and Russian inventions are devoted to thermochemical degradation based on the reaction of PUs with hydroxyl- and amino-containing compounds, which can be regenerated to the initial components [5–7]. The drawbacks of this procedure are the high process temperature and formation of polyols nonuniform in molecular weight, which hampers their subsequent use.

One of the successful procedures for utilization of polyurethane wastes is plasticization, which partly destroys the structure and makes it possible to obtain secondary product, e.g., crumb, with high operation characteristics at minimal power and economic expenses; however, sorption of low-molecular-weight liquids or their vapor results in a decrease in the ultimate strength and elasticity of swollen PUs. The procedure used for processing of wastes formed in production of soles, multicellular PUs of ester nature [8], is based on a similar effect of polar plasticizers of the dimethylformamide type.

Previously [9], plasticizers of this type have been studied as agents promoting thermal degradation. Granulated wastes were dissolved in boiling DMF in the presence of amines and organotin compounds (degradation catalysts) and were added to hydroxy components. The resulting liquid and paste-like products were used as polyol substitutes (20%) in production of PU.

Finely divided polyurethane reclaim was prepared by dissolution of PU-elastomer foams in DMF at 90°C and subsequent precipitation of the polymer into methanol [10] or treatment of wastes preliminary degraded by heating with a mixture of methylene chloride (80%) and DMF (20%) [11].

Table 1. Composition of the polyurethane elastomers studied

Component	Content of components, wt %						
	PU-1	PU-2	PU-3	PU-4	PU-5	PU-6	PU-7
Polyoxytetramethylene glycol, MW 1000	63.06	63.06	–	65.76	–	70.19	61.16
Polyoxypropylene glycol, MW 1000	–	–	63.06	–	–	–	–
Polyethylene butylene glycol adipate P-6 BA, MW 2000	–	–	–	–	72.66	–	–
2,4-Toluylene diisocyanate	21.60	–	–	18.90	12.00	24.04	20.95
Toluylene diisocyanate T-80*	–	21.60	21.60	–	–	–	–
Methylenebis-*o*-chloroaniline (Diamet Kh)	15.34	15.34	15.34	15.34	15.34	–	–
Diamin-304**	–	–	–	–	–	–	17.88
Butanediol-1,4	–	–	–	–	–	5.77	–

* The product is an isomeric mixture of 2,4-toluylene diisocyanate (80%) and 2,6-toluylene diisocyanate (20%).

** The product is an eutectic mixture of Diamet Kh and 3,3'-dichloro-4,4'-diaminotriphenylmethane in the molar ratio of 1 : 1.

Table 2. Characteristics of the samples studied

Characteristic	PU-1	PU-2	PU-3	PU-4	PU-5	PU-6	PU-7
Isocyanate index, %	6.0	6.0	6.0	4.2	3.2	6.0	6.0
Density, kg m^{-3}	1140	1150	1155	1130	1170	1024	1180
Shore hardness A, arb. units	95	95	92	90	70	50	75
Nominal stress, MPa, at elongation:							
100 %	16.8	16.0	13.1	9.2	1.92	1.4	4.9
300 %	30.8	45.0	19.8	21.6	15.1	4.3	14.7
Nominal tensile strength, MPa	42.0	50.0	25.1	27.4	25.2	9.65	32.0
Relative elongation at break, %	320	310	380	380	500	670	300

It should be noted that the features of swelling of polymers, among them polyurethanes, in organic solvents have been widely covered in the classic [12, 13] and recent [14, 15] publications.

The reaction of oligoether microheterogeneous segmented polyurethanes with plasticizing agents remain inadequately studied. In this study, we examined this problem with the aim to develop an efficient procedure for secondary processing of castable PUs of varied chemical nature and to estimate their working capacity in corrosive media.

EXPERIMENTAL

The subjects of the study were polyurethanes widely used in various branches of technology [16] and prepared by the prepolymer procedure. The composition and characteristics of the synthesized samples are listed in Tables 1 and 2, respectively.

The preliminary choice of plasticizers is complicated by the structural features of the polymers in hand, in particular, by the presence of segments with different polarities in polyurethane chains and their ability to form hydrogen bonds of two types: between NH group and carbonyl of the urethane bond or between the NH group and the –C–O–C– group of the soft block. With increasing microphase separation, the first type of interaction predominates; as a result, the number of bonded carbonyl groups increases [17]. This results in the appearance of a strong physical network, along with the chemical network, in macromolecules. The nodes of this network are hard urethane–urea domains. Depending on their nature, solvents affect this network differently.

The capacity of hard chain fragments of polyurethanes for self-association has a significant effect on the resistance to the action of corrosive media [18]. Nonpolar solvents partly destroy hydrogen bonds in PU due to the fact that molecules of these liquids screen soft blocks in the polymer chain. As a result, the fraction of NH groups bound with hydrogen bonds in PU gradually decreases with increasing solvent

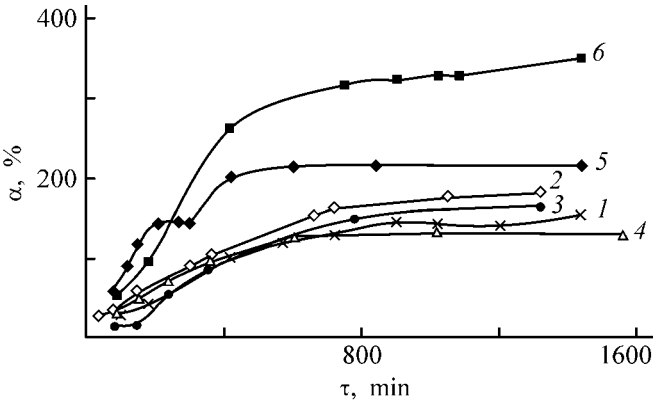


Fig. 1. Kinetic curves of swelling of the samples in DMF and DMSO. (α) Weight degree of swelling and (τ) time; the same for Figs. 2 and 3. DMF: (*1*) PU-1, (*2*) PU-2, (*4*) PU-4, (*5*) PU-5; and (*6*) PU-6; DMSO: (*3*) PU-2.

concentration. Highly polar aprotic liquids react with the NH group of PU through their proton-acceptor groups (C=O or S=O), entering into competitive interaction with carbonyl of its urethane group and dissolving both soft and partially hard blocks of segmented PU [15, 19].

Accordingly, we used in studying the swelling of polymers the following compounds of various classes as solvents: *N*,*N*-dimethylformamide (DMF), dimethyl sulfoxide (DMSO), toluene, cyclohexanone, tetrahydrofuran (THF), and dioctyl phthalate (DOP). All the solvents were of analytically pure grade and were purified by distillation.

To compare the results, we used the samples cut from plates 0.2 ± 0.02 cm thick with the same volume and shape. In all the runs, the temperature was kept at the level of 15 ± 0.2°C. Swelling was carried out in glassware. The samples were immersed completely in the liquid, so that, in the suspended state, they did not touch one another and the vessel bottom and walls. The tests involved determination of the sample weight before and after swelling. The weight degree of swelling α (%) was calculated by the formula $\alpha = (G_1 - G_0) \times 100/G_0$, where G_0 and G_1 are the sample weights before and after swelling (g). Before weighing a swollen sample after the prescribed period of time, the excess liquid was removed from the sample surface with filter paper.

The results of swelling of the polyurethanes studied in aprotic solvents are presented in Fig. 1. It is seen that, compared to DMSO (curve *3*), DMF (curve *2*) exerts a more pronounced plasticizing effect on the polar PU-2 phase. There are data [18] suggesting that the higher the fraction of the symmetric isomer in the composition of the diisocyanate (in the series TDI 100 < TDI 80/20 < TDI 65/35), the stronger the tendency to form stable associates and the higher the resistance of the polymers to corrosion media. However, it is seen from Fig. 1 that this trend is not observed with aprotic plasticizers. For example, the degree of swelling of PU-1 in DMF is lower than that of PU-2 (curves *1* and *2*, respectively).

Data of X-ray, spectral, and electron-microscopic analyses confirm that segmented polyurethanes, among them the materials studied, contain spatially segregated flexible (oligoether units) and hard (fragments involving diisocyanates) segments. The hard block provides strong intermolecular interaction in the chain, comparable to the chemical cross-linking and responsible for the high strength of the polymer; the flexible block is characterized by fairly weak intermolecular interaction and is responsible for elasticity. The rigid blocks are linked with each other by nonionic bonds to form 3*D* domains regularly arranged in the continuous phase (matrix) of the elastic block. Therefore, these polyurethanes can be regarded as two-phase systems in which dispersed particles, domains, are arranged in the amorphous dispersion medium, the elastic part of the polymer [13, 18, 20].

The characteristics of segmented PUs are governed by the content of the hard phase, nature of the elastic phase, and molecular weights of the blocks contained in the polymer. The larger the difference in the polarity of hard and elastic blocks of PU, the lower their thermodynamic compatibility and the higher the "purity" of phases [16]. The polarity of flexible blocks based on esters is higher than that of blocks built from oligoethers. At the same time, the content of the hard phase dispersed in the elastic phase in polyurethanes of ester nature is low in comparison with polyurethanes based on polyethers. Therefore, swelling of PU-5 (Fig. 1, curve *5*) in an aprotic solvent, starting with the flexible phase, proceeds more intensively than that of PU-1 (curve *1*). Since both phases of PU-1 are close in ability to resist to external stresses, the kinetic curve of swelling is monotonic. In the case of PU-5, the process is two-stage: the portion of curve *5* in the range 3–5 h is a conditional transition area from the process occurring in the soft phase, where the spatial network is fairly weak, to plasticization of not numerous, but strongly cross-linked hard segments.

The PU-6 sample synthesized in the presence of the chain extender 1,4-butanediol has an amorphous structure and considerably surpasses highly segregated PU-1 (Fig. 1, curves *6*, *1*) in the degree of swelling

in DMF. The same difference has been noted previously in comparison of swelling processes of these and other polyurethanes in toluene [21]. The PUs that virtually do not contain the hard microphase are characterized by the network of interchain hydrogen bonds outside domains of hard blocks, tending to degrade in toluene. It was confirmed that, as a result of this degradation, the fraction of free NH groups in the elastomer increases and associates of NH groups with the π-electron system of the aromatic ring of the solvent are formed. A similar mechanism is also possible in treatment of polyurethanes with aprotic compounds.

The fundamental distinction between PU-1 and PU-4 is that the isocyanate indices of the prepolymers used for curing. Apparently, the higher the content of isocyanate groups in the polymer, the larger the volume of urethane-urea self-associates localized in the domains of hard blocks. Thus, in PU-1 (Fig. 1, curve *1*) the conditions of formation of strength characteristics are better in the initial stage, which retards its swelling in comparison with PU-4 (Fig. 1, curve *4*). However, the kinetic curve of swelling of PU-4 with lower concentration of urethane groups flattens out after 12 h, whereas the absorption of the plasticizing agent with the hard phase of PU-1 continues.

Low-polarity liquids like toluene do not significantly affect hard domains and are not able to destroy segregations of hard blocks. This fact accounts for the rather low characteristics of equilibrium swelling (Fig. 2). The PU-1 and PU-3 samples cured with Diamet Kh have denser chemical network than PU-7 cross-linked with branched Diamin 304: steric hindrances appearing in the reaction of branched amines with the reactive terminal groups of the prepolymer hamper formation of an ordered developed spatial structure of the material, which leads to their better swelling (Fig. 2, curve *3*). Polyurethanes based on Diamet Kh are characterized by better physicomechanical characteristics and, hence, lower degree of swelling (Fig. 2, curves *1*, *2*), which is in good agreement with the data previously obtained for other models [22].

In polyether-urethane-urea PU-3 based on polypropylene oxide flexible blocks, the degree of microphase separation is lower and the amount of hard blocks dissolved in the flexible phase is higher in comparison with PU-1, whose flexible phase is less polar. With increasing polarity of flexible blocks and, as result, increasing volume of the polar phase, interchain interactions in the polymer matrix are broken under the action of low-polar toluene to a greater extent [as seen from a comparison of curves *1* and *3* (Fig. 2)], similarly to aprotic liquids.

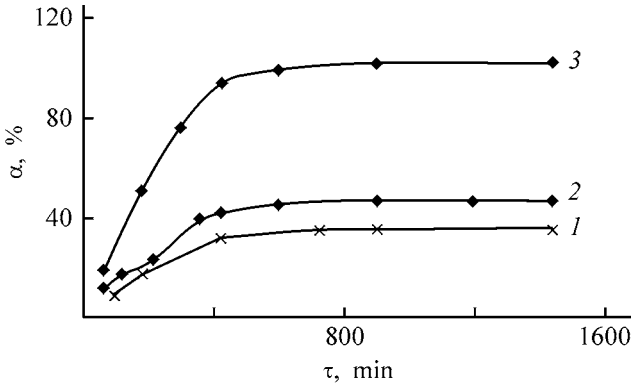


Fig. 2. Kinetics curve of swelling of polyurethanes in toluene. (*1*) PU-1, (*2*) PU-3, and (*3*) PU-7.

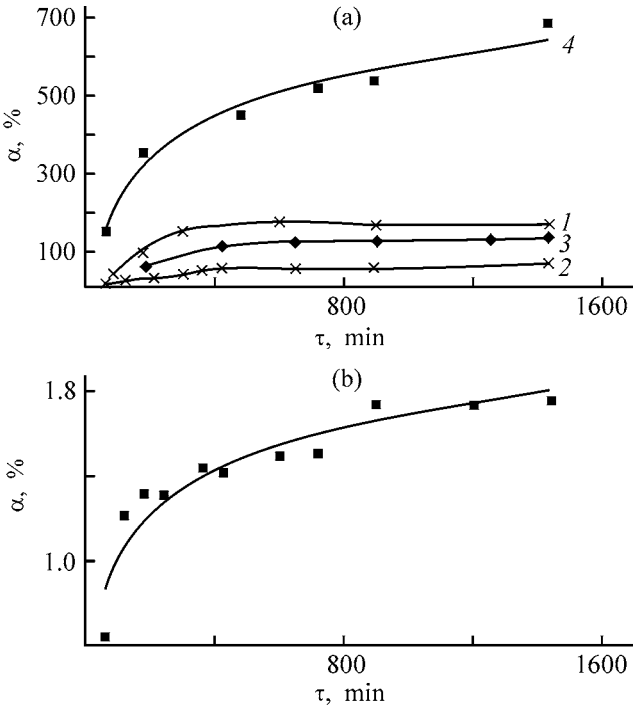


Fig. 3. Kinetic curves of swelling of (a) polyurethanes in THF and cyclohexanone and (b) PU-1 in DOP. (a) THF: (*1*) PU-1, (*3*) PU-3, (*4*) PU-5; cyclohexanone: (*2*) PU-1.

In swelling of polyglycol adipate urethanes in THF, stable complexes involving urethane group are formed [13]; cyclohexanone is also able to specifically interact with these substances, with an irreversible alteration of the structure.

The results of the action of monomeric THF on the samples containing the product of addition polymerization of this compound are shown in Fig. 3a.

Comparison of the results obtained with the data for the aprotic plasticizer (Fig. 1) shows that THF is

Table 3. Kinetic parameters of swelling of PU-1

Plasticizer	α	*A*	*C*
THF	120.5	0.24	45.47
DMF	87.0	0.17	14.86
Cyclohexanone	37.5	0.05	19.28
Toluene	22.5	0.04	8.90
DOP	1.3	0.12×10^{-2}	0.94

a stronger plasticizer with respect to PU-1 and PU-6. This is due to the fact that, structurally similar THF molecules split the chains of polyurethanes based on polytetrahydrofuran with lower energy consumption. The oligoether component of PU-3 is polyoxypropylene glycol, and hence PU-3 has a lower affinity for THF and better swells in DMF.

As can be seen from Fig. 3b, dioctyl phthalate does not exert any significant influence on self-associates of urea groups. It ruptures hydrogen bonds in the flexible phase of PU-1, leaving unchanged the physical network whose nodes are the domains of hard blocks, similarly to polyurethanes of the ester nature [8, 14].

Summarizing the data of Figs. 1–3b concerning the action of plasticizers of various chemical structures, we can conclude that the intensity of swelling decreases in the order tetrahydrofuran > dimethylformamide > cyclohexanone > toluene > dioctyl phthalate. Table 3 lists the degrees of swelling of PU-1 in the above solvents after 10 h of contact and the kinetic parameters of swelling, evaluated for the same time interval of the curves by the equation

$$Y = Ax + C.$$

Here *A* is the slope of the straight line of the swelling kinetics to the τ axis, characterizing the process rate, and *C* is the intercept on the τ axis by the straight line.

The results obtained quantitatively confirm the above conclusions about the level of the plasticizing activity of compounds of varied nature with respect to polyurethanes based on THF. It should be noted that dioctyl phthalate, which is hardly useful as plasticizing agent for PU-1, can find application in recovery of wastes. It is known that addition of plasticizers of the butyl benzyl phthalate [23] and also dibutyl phthalate or dioctyl phthalate type [24] to a mixture of thermoplastic and cross-linked milled microcellular PU has a positive effect.

CONCLUSIONS

(1) The difference in the degree of swelling of the oligotetrahydrofuran polyurethanes considered can reach two orders of magnitude, depending on plasticizer used.

(2) As a plasticizer, monomeric tetrahydrofuran is more active than dimethylformamide and dimethyl sulfoxide with respect to polyoxytetramethylene glycol urethanes and is less active in contact with polyurethane elastomers based on oligoglycol adipates and oligooxypropylene glycols.

(3) In regeneration of wastes of polyurethanes based on oligoethers, it is appropriate to use in the initial stage of regeneration plasticization to save energy and intensify the process.

REFERENCES

1. RF Patent 2158246.
2. Gorban', T.V., Zhuravlev, V.A., Onorina, L.E., et al., *Plast. Massy*, 2001, no. 4, pp. 39–41.
3. Matveev, K.S., Soltovets, G.N., and Burkin, A.N., *Plast. Massy*, 2002, no. 10, pp. 46–47.
4. UK Patent 1551274.
5. Bakirova, I.N., Valuev, V.I., Demchenko, I.G., and Zenitova, L.A., *Vysokomol. Soedin., Ser. A*, 2002, vol. 44, no. 6, pp. 987–995.
6. FRG Patent 19917932.
7. Elchueva, A.D., Nazipov, M.M., and Tabachkov, A.A., *Kauchuk Rezina*, 2001, no. 5, pp. 12–14.
8. RF Patent 2069675.
9. FRG Inventor's Certificate. *Verfahren zum Aufschließen von granulierten Polyurethanabfallen*.
10. GDR Patent 262237.
11. Polish Patent 133527.
12. Tager, A.A., *Fizikokhimiya polimerov* (Physical Chemistry of Polymers), Moscow: Khimiya, 1968.
13. Kercha, Yu.Yu., Lipatov, Yu.S., and Sergeeva, L.M., *Struktura i svoistva poliuretanov* (Structure and Properties of Polyurethanes), Kiev: Naukova Dumka, 1970.
14. Tereshatova, E.N., Tereshatov, V.V., and Makarova, M.A., Abstracts of Papers, *Vserossiiskaya nauchno-prakticheskaya konferentsiya "Aerokosmicheskaya tekhnika i vysokie tekhnologii-2002"* (Int. Scientific and Practical Conf. "Aerospace Technique and High Technologies 2002"), Perm: Ural'sk. Otd. Ross. Akad. Nauk, 2002.
15. Tereshatov, V.V., Makarova, M.A., and Tereshatova, E.N., *Vysokomol. Soedin., Ser. A*, 2004, vol. 46, no. 12, pp. 2019–2027.

16. Lyubartovich, S.A., Morozov, Yu.L., and Tret'yakov, O.B., *Reaktsionnoe formovanie poliuretanov* (Reactive Extrusion of Polyurethanes), Moscow: Khimiya, 1990.
17. Razumovskii, L.P., Iordanskii, A.L., Zolotova, E.V., and Trezvova, A.V., *Vysokomol. Soedin., Ser. A*, 1991, vol. 33, no. 15, pp. 989–995.
18. Sharipova, A.G., Zenitova, L.A., and Bazhenova, L.N., *Plast. Massy*, 2001, no. 5, pp. 13–16.
19. Tereshatov, V.V. and Senichev, V.Yu., *Vysokomol. Soedin., Ser. A*, 1995, vol. 37, no. 11, pp. 1888–1895.
20. Moiseev, V.V., *Termoelastoplasty* (Thermoplastic Elastomers), Moscow: Khimiya, 1985.
21. Tereshatov, V.V., Tereshatova, E.N., and Volkova, E.R., *Vysokomol. Soedin., Ser. A*, 1995, vol. 37, no. 11, pp. 1881–1887.
22. Sharipova, A.G., Zenitova, L.A., and Bazhenova, L.N., *Kauchuk Rezina*, 2001, no. 13, pp. 3–5.
23. US Patent 5 908 894.
24. RF Patent 2 168 523.

ISSN 1070-4272, Russian Journal of Applied Chemistry, 2006, Vol. 79, No. 12, pp. 2022–2024. © Pleiades Publishing, Inc., 2006.
Original Russian Text © V.Z. Maslosh, N.P. Golovnenko, O.V. Maslosh, N.F. Tyupalo, 2006, published in Zhurnal Prikladnoi Khimii, 2006, Vol. 79, No. 12, pp. 2046–2048.

MACROMOLECULAR CHEMISTRY AND POLYMERIC MATERIALS

A Zero-Discharge Procedure for Production of Urea–Formaldehyde Resins

V. Z. Maslosh, N. P. Golovnenko, O. V. Maslosh, and N. F. Tyupalo

Severodonetsk Technological Institute, Dal' East-Ukrainian National University, Ministry of Education and Science of Ukraine, Severodonetsk, Lugansk oblast, Ukraine

Received August 2, 2006; in final form, May 2006

Abstract—A zero-discharge procedure was suggested for preparing urea–formaldehyde resins by polycondensation of urea, formaldehyde, and dimethylolurea at variable pH, with urea added continuously or in a single portion.

DOI: 10.1134/S1070427206120226

Urea–formaldehyde resins (UFRs), used as a binder in production of woodchip boards, wood fiberboards, and plywood are large-volume commercial products; the features of their preparation are fairly well understood [1]. The raw materials for their production, urea (U) and formaldehyde (F), are cheap and commercially available in large quantities. A specific feature of the production of all the commercial UFR brands is the use of 37% Formalin, which gives rise to large amounts of waste, so-called tar for water. Their amount in various UFR brands is 300–400 kg per ton, with the free F content ranging from 2.5 to 8.0 wt %. Various methods for their treatment or reprocessing have been described in the literature [2], but these processes require additional expenditure and equipment.

Our goal was to develop a zero-discharge procedure for UFR production. Published solutions to this problem involve using, instead of F, difficultly available and relatively expensive paraform or U precondensate (solution in U methylol derivatives in F) [3]. We examined the possibility of preparing UFR by joint polycondensation of U, F, and dimethylolurea (DMU).

EXPERIMENTAL

Dimethylolurea was prepared by condensation of U with F according to [4]. Urea–formaldehyde resins were synthesized as follows. A 500-ml glass flask was charged with 45 ml of water and 162 g (2 mol) of 37% F; pH 8.0–8.5 was adjusted by adding a NaOH solution, and 120 g (2 mol) of DMU was added (step I). After DMU dissolved completely, the mixture was heated to 60–70°C and kept at this temperature for 1 h; then 120 g (2.0 mol) of U was added (continuously over a period of 1–1.5 h in one series of experiments and in a single portion in another series). Then the mixture was heated to 94–98°C and kept at this temperature for 1 h. The mixture was acidified to pH 4.0– 4.5 by adding ammonium chloride and stirred for 0.5 h, after which a NaOH solution was added to pH 8.5–9.5, and the mixture was kept until the refractive index n reached a value of 1.4520–1.4560.

In industry, UFR is produced by polycondensation of F with U (molar ratio 1.33 : 1) at 94–98°C and variable pH. In the first step of the polycondensation, the concentration of F is relatively high, 23.8 wt % (Fig. 1, curve *1*), and its reaction with U yields methylol derivatives of U; in the process, the methylol groups (MGs) are accumulated and the F concentra-

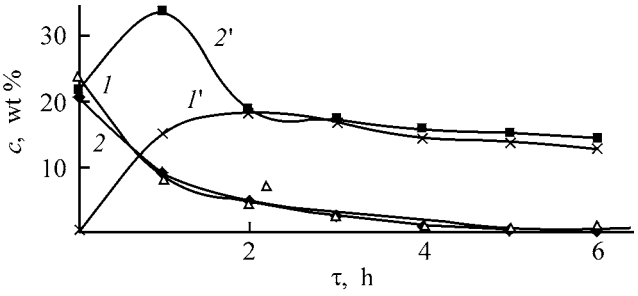


Fig. 1. Content c of (*1*, *2*) formaldehyde and (*1'*, *2'*) methylol groups vs. time τ of polycondensation of F with U. UFR: (*1*) commercial and (*2*) synthesized.

tion decreases (Fig. 1, curves *1*, *1'*). The reaction mixture mainly consists of mono- and dimethylolurea.

In preparation of UFR from DMU, the initial reaction mixture contains F and DMU, with a relatively high content of U and MGs: 21.1 and 21.85 wt %, respectively. The reaction of F with DMU is accompanied by accumulation of MGs and a decrease in the F concentration. The MG content reaches 33.6 wt % (Fig. 1, curves *2*, *2'*). In this case, the reaction mixture essentially differs in composition from the mixture formed in the industrial synthesis of UFR.

The qualitative composition of the reaction mixture was determined by ^{13}C NMR spectroscopy. The spectra were measured on a Varian-200 pulse spectrometer in D_2O–DMSO-d_6 (1 : 3) at 20°C. The analysis conditions and procedure of signal assignment were the same as in [5]. The ^{13}C NMR spectrum of the reaction mixture is shown in Fig. 2.

The ^{13}C NMR spectrum of the mixture formed in the reaction of F with DMU in 60 min (step I) contains, along with the peaks of disubstituted urea derivatives (nos. 8, 9), methylenemethoxy groups at the tertiary nitrogen atom (no. 7), and methylol and methylene ether groups mainly at the secondary nitrogen atom (nos. 4, 5), also new peaks of methylenemethoxy groups at tertiary and secondary nitrogen atoms (nos. 13, 3) (Fig. 2).

The spectrum shows that both linear and linear-branched products are formed in step I in alkaline solution. Methylol derivatives formed at the tertiary nitrogen atom are relatively unstable and occur in equilibrium with F.

As can be seen, the initial reaction mixture in step I of base condensation of U with F differs essentially from that in the reaction of DMU with F, but the quality parameters of the resulting UFRs are similar (see table).

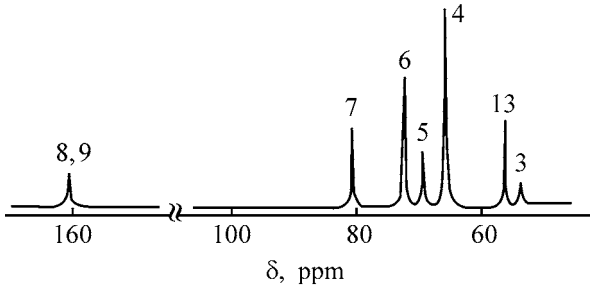


Fig. 2. ^{13}C NMR spectrum of the reaction mixture after the dissolution of DMU in formaldehyde. (δ) Chemical shift; the same for Fig. 3. Peak nos.: 8, 9, disubstituted ureas; 7, methylenemethoxy groups at the tertiary nirogen atom; 4, 5, methylol and methylene ether groups at the secondary nitrogen atom; 6, methylol groups at the tertiary nitrogen atom; and 13, 3, methylenemethoxy groups at the tertiary and secondary nitrogen atoms.

All the quality parameters of UFR samples synthesized from DMU meet the existing requirements, and the content of free F does not exceed 0.06 wt %, which is considerably lower, compared to the commercial UFR. However, the resins prepared from DMU essentially differ in fragment composition from the UFR prepared from F and U. Figure 3 shows the ^{13}C NMR spectra of the synthesized and commercial UFR samples. It is seen that all the samples contain methylene groups in the middle chain of the macromolecule (peak no. 1), methylene groups at the nitrogen atom bound to methylene ether groups (no. 5), methylol groups at the primary nitrogen atom (no. 4), methylene ether fragments (no. 7), and methylene groups in urea fragments with a free amino group (no. 9). In addition, commercial UFR contains methylene groups at the tertiary nitrogen atom (no. 2), methylene groups at the nitrogen atom with the oxy-

Quality praameters of commercial and synthesized UFR samples

Parameter	UFR		
	commercial	sample	
		no. 1 (U added continuously)	no. 2 (U added in one portion)
Weight fraction of dry residue, %	64–68	65.6	66.2
Free U content, wt %	Up to 0.15	0	0.06
Viscosity (outflow time from VZ-4 device), s	50–80	65–72	65–72
pH	7.5–8.5	8.2	8.2
Gelation time at 100°C, s	50–70	66.5	68
Miscibility with water (volume ratio)	1 : (2–10)	1 : 8	1 : 8
Refractive index	1.452–1.46	1.458	1.456

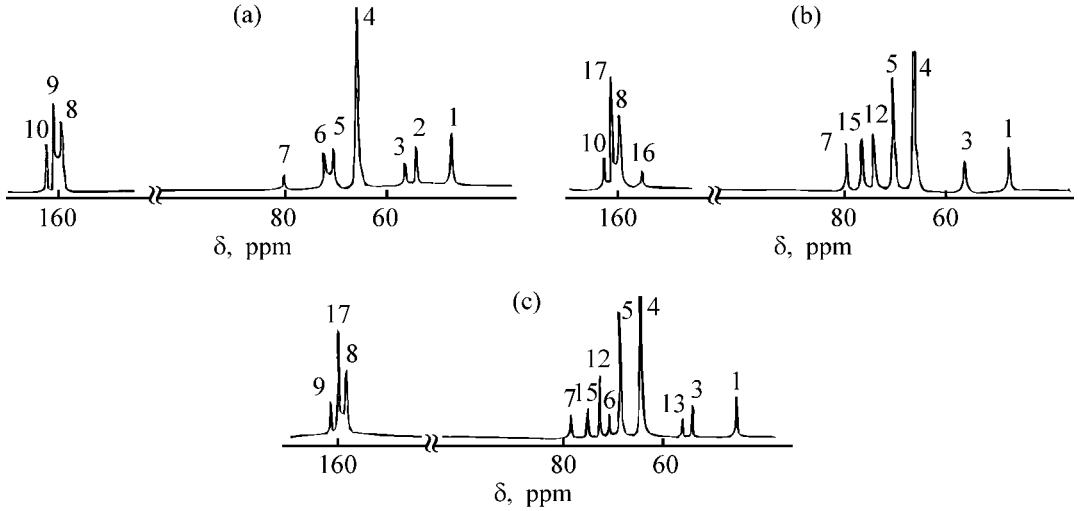


Fig. 3. ^{13}C NMR spectra of urea–formaldehyde resins. UFR: (a) commercial and (b, c) synthesized with urea added continuously and in a single portion, respectively. Peak nos.: 1, methylene groups in the middle chain of the macromolecule; 2, methylene groups at the tertiary nitrogen atom; 3, methylene groups at the nitrogen atom with the oxymethylene group; 4, methylene groups at the primary nitrogen atom; 5, methylene ether groups at the nitrogen atoms bound to the methylene group; 6, methylol groups at the tertiary nitrogen atom; 7, methylene ether fragments; 8, 9, 10, free urea and terminal amino groups; 12, 13, methylenemethoxy groups at secondary and tertiary nitrogen atoms; 15, DMU tetraethers; 16, uronic rings; and 17, trisubstituted amino groups of urea.

methylene group (no. 3), methylol groups at the tertiary nitrogen atom (no. 6), and free U (no. 10).

In contrast to the commercial UFR, urea–formaldehyde resin prepared from DMU with continuous addition of urea contains methylenemethoxy groups at the secondary and tertiary nitrogen atoms (peak nos. 12, 13), uronic rings (no. 16), and DMU tetraethers (no. 15). Urea–formaldehyde resin prepared from DMU with addition of U in a single portion differs from UFR prepared with continuous addition of U in that it contains small amounts of U (peak no. 10) and trisubstituted amino groups of urea (no. 17). These data suggest that UFR prepared from DMU has a more branched structure with a higher content of ether fragments, compared to commercial UFR. The ether fragments are responsible for the longer gelation time of the resins synthesized, compared to the commercial sample (see table), in view of the fact that the UFR stability is enhanced by etherification with alcohols [6].

CONCLUSION

Use of dimethylolurea as the starting compound allows preparation of urea–formaldehyde resins meeting the requirements of the existing standards and having a more branched structure, with the formation of tar water avoided.

REFERENCES

1. Wirpsza, Z. and Brzezinski, J., *Aminoplasty*, Warsaw: Naukowo-Techniczne, 1970.
2. Maslosh, O.V., Kotova, V.V., Galstyan, G.A., and Maslosh, D.V., *Khim. Prom–st. Ukr.*, 2004, no. 3, pp. 17–20.
3. Makhlai, V.N. and Afanas'ev, S.V., *Vvedenie v khimiyu karbamidoformal'degidnogo kontsentrata* (Introduction to the Chemistry of Urea–Formaldehyde Concentrate), Togliatti: Politekh. Inst., 2001.
4. De Jong, J.J. and De Jong, J., *Recl. Trav. Chim. Pays-Bas*, 1952, vol. 7, pp. 890–892.
5. Slonim, I.Ya. and Urman, Ya.G., *YaMR spektry geterotsepnykh polimerov* (NMR Spectra of Heterochain Polymers), Moscow Khimiya, 1983.
6. Kurta, S.A., Fedorchenko, S.V., and Khaber, M.V., *Vopr. Khim. Khim. Tekhnol.*, 2002, no. 3, pp. 77–80.

ISSN 1070-4272, Russian Journal of Applied Chemistry, 2006, Vol. 79, No. 12, pp. 2025–2027. © Pleiades Publishing, Inc., 2006.
Original Russian Text © L.P. Firsova, 2006, published in Zhurnal Prikladnoi Khimii, 2006, Vol. 79, No. 12, pp. 2049–2051.

BRIEF COMMUNICATIONS

Effect of Urea on the Phase Composition and Strength of Phosphogypsum Grains

L. P. Firsova

Lomonosov State University, Moscow, Russia

Received December 8, 2003; in final form, October 2006

Abstract—The effect of urea addition on the composition and strength of grains produced by pelletization of wet phosphogypsum and its subsequent drying was studied experimentally.

DOI: 10.1134/S1070427206120238

Phosphogypsum is a waste formed in manufacture of phosphoric acid in sulfuric acid processing of natural phosphorites. It is used as a secondary raw material for soil development in agriculture. The continued work on utilization of phosphogypsum in agriculture is aimed at its modification and primarily on its enrichment with bioactive micro- and macroadditives necessary for plant nutrition, including microelements (Mn, Cu, Zn, Mo, Co, B, and I), and also at granulation. It has been shown, however, that introduction of some microelements, e.g., boron in the form of boric acid, enriches the chemical composition of grains based on phosphogypsum, but strongly impairs their strength [1–4]. In this study, we examined the effect of urea additives, which enrich the composition of granules with biologically important nitrogen, on the strength properties of phosphogypsum grains.

EXPERIMENTAL

To prepare the grains, we used a phosphogypsum powder mostly composed of calcium sulfate hemihydrate formed in sulfuric acid decomposition of phosphorus-containing raw materials at Voskresensk chemical fertilizer plant. To stabilize the powder composition and, first of all, to prevent the transformation of calcium sulfate hemihydrate to the corresponding dihydrate, we successively washed the powder with a hot saturated $CaSO_4 \cdot 2H_2O$ solution and with acetone. The presence of 6.5–7.0% crystallization water in the stabilized powder indicates that it contains only a minor amount of calcium sulfate dihydrate. The porosity of the powder was about 65%. The hemihydrate $CaSO_4 \cdot 0.5H_2O$ formed 1–30-μm-long hexagonal prisms combined in druses of size 10–250 μm.

Before the beginning of granulation, the hemihydrate powder was wetted with distilled water or with aqueous solutions of urea (60–80%). Water-soluble compounds of bioactive microelements, which contained 0.1–5% boron, zinc, manganese, and molybdenum, were introduced into a part of the wetting solutions (the initial amount of these elements in the industrial phosphogypsum waste did not exceed 0.1%). The powder and a wetting solution were mixed for 1–3 min and then the wet stock was pelletized in a plate-type granulator. The l : s ratio in wetted phosphogypsum was varied within the range 0.2–0.5. For each wetting solution, we visually selected, based on the results granulation, the optimal l : s ratio, which allowed us to obtain spherical grains of diameter 1–5 mm in high yield at prescribed granulation modes. For example, the stock humidity of 27–30% was found to be the optimal for wetting solutions containing minor amounts of ammonium molybdate and zinc or manganese sulfate.

The pellets formed in granulation were dried in air at room temperature and a part of them were transferred from the granulator plate into desiccators, where they were preliminarily, before drying, kept in humid air for grain "maturation" accompanied by strengthening of the grains. During the maturation and drying, the static strength of the grains, p (kg cm^{-2}), was determined with an extensometer from the uniaxial force required for their destruction. Preliminarily, the 4–5 mm fraction was selected from the whole amount of grains of a given composition by sieving. The strength was found as an average of parallel measurements for 15–20 grains of this size and the same composition. As another characteristic of the grain strength, we

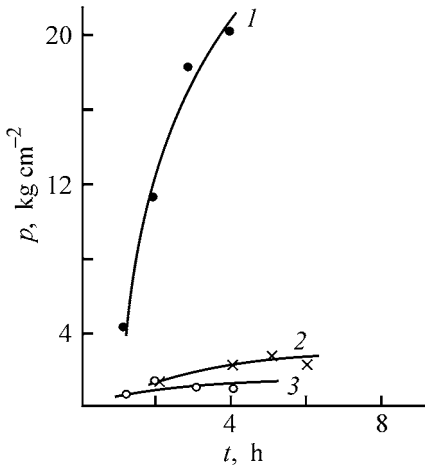


Fig. 1. Strength p of grains vs. drying time t. The grains were produced from a stock wetted with solutions of (*1*) 0.2% $MnSO_4$ and 60% urea, (*2*) 1.5% $MnSO_4$ (after maturation), and (*3*) 2% H_3BO_3 (after maturation).

determined the mass fraction of dust with a particle diameter less than 0.05 mm, which was formed in abrasion of a portion of grains in the rotating plate of the granulator.

The results obtained in determining the strength parameters of grains are presented in Fig. 1 and in the table. The phase composition of the powder formed in grain abrasion was determined by X-ray phase analysis on an ARL X-TRA (USA–Switzerland) diffractometer with a semiconductor detector. The X-ray patterns obtained for samples with and without urea are shown in Figs. 2a and 2b.

It follows from the data in Fig. 1 and the table that, in the absence of urea, some admixtures, e.g., boric acid, strongly reduce the grain strength. Introduction of urea into a wetting solution promotes strengthening of grains, including those containing zinc or manganese sulfates and ammonium molybdate.

Grain strength p in relation to the composition of a wetting solution*

Concentration of solution components, wt %		p, kg cm^{-2}	Fraction of dust, wt %
urea	microelement compounds		
0	$1.5MnSO_4$	6	1 ± 0.5
0	$1.5H_3BO_3$	1.5	3 ± 1
60	$0.4(NH_4)_2MoO_4$	20	0.8 ± 0.2
60	$0.2\mu nSO_4$	17	0.8 ± 0.2
80	$1.5ZnSO_4$	17	0.7 ± 0.2

* The strength parameters of "ripened" air-dry grains are given.

As shown previously [5, 6], recrystallization and topochemical transformation of calcium sulfate hemihydrate to dihydrate occur in wetted phosphogypsum grains. As a result of these processes, a rigid network responsible for the grain strength is formed mainly from dihydrate crystals. The redistribution of water among its hygroscopic and crystal states in the bulk of grains was confirmed by direct experiments.

The kinetics of strength gain by wetted grains, including those formed upon introduction of compounds of bioactive microelements, agrees with the variation of the fraction of crystal water and with the corresponding extent of transformation of calcium sulfate hemihydrate to the dihydrate [1–4]. When interpreting the fact that the grain strength increases under the action of urea additives in wetting solutions, we considered several hypotheses, e.g., that of formation of the $CaSO_4 \cdot 4Co(NH_2)_2$ crystalline phase. The results of our X-ray phase analysis confirm another assumption, according to which mostly anhydrous calcium sulfate is formed in the grains in the presence of urea.

Crystalline anhydrous $CaSO_4$ has a considerably higher density and hardness, compared with hydrated forms of calcium sulfate. Anhydrous $CaSO_4$, dihydrate, and hemihydrate have densities of 2900, 2600, and 2300 kg cm^{-3}, respectively. The hardness (on the mineralogical scale) is 3.5 for the anhydrite (anhydrous $CaSO_4$), 1.5 for gypsum (dihydrate $CaSO_4 \cdot 2H_2O$), and <1.5 for the hemihydrate ($CaSO_4 \cdot 0.5H_2O$). The X-ray patterns (Fig. 2a) of the powders obtained from air-dry urea-containing grains show a single main peak corresponding to the anhydrous form of $CaSO_4$. Grains formed in the absence of urea (Fig. 2b) contain hydrated forms $CaSO_4 \cdot xH_2O$, along with the anhydrite. The fractions of these forms are governed by the conditions of maturation and drying of the grains.

To elucidate the mechanism of urea action on the phase transformations in grains, additional studies of the processes of recrystallization and topochemical transitions between crystalline forms of calcium sulfate are necessary. Probably, urea changes the nucleation conditions. Being incorporated into the coordination sphere of calcium ions, urea forms complexes of the type of the known $CaSO_4 \cdot 4CO(NH_2)_2$, precludes formation of dihydrate nuclei, and promotes formation of anhydrite nuclei, including those on the sur-

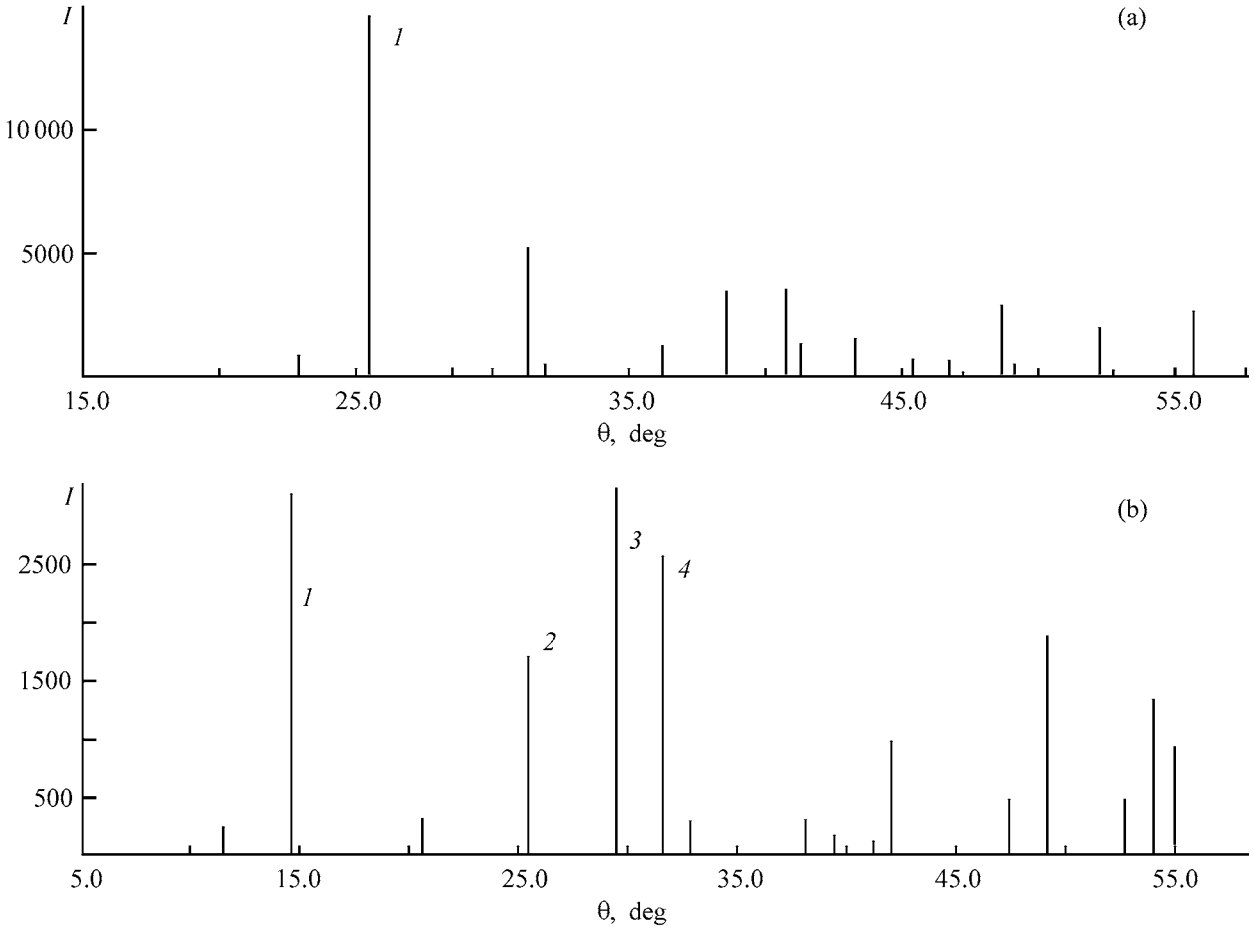


Fig. 2. X-ray patterns of phosphogypsum grains wetted with (a) urea solution and (b) solution free of urea. (*I*) Intensity and (θ) diffraction angle. (a) (*1*) peak of anhydrite. (b) (*2*) peak of anhydrite; (*1*, *3*, and *4*) peaks of $CaSO_4 \cdot xH_2O$ hydrates.

face of the existing hemihydrate crystals, which are then transformed to anhydrite crystals via a topochemical process.

CONCLUSION

It was shown experimentally that the static strength of phosphogypsum-based grains increases if urea is added to solutions used to wet phosphogypsum before granulation. In this case, the abradability (dusting) of the grains decreases. If urea is present in the wetting solutions, the grains are mostly constituted by anhydrite crystals.

REFERENCES

1. Firsova, L.P., *Vestn. Mosk. Univ.*, Khimiya, 2003, vol. 44, no. 5, pp. 352–355.
2. Firsova, L.P., *Zh. Prikl. Khim.*, 2003, vol. 76, no. 3, pp. 353–355.
3. Firsova, L.P., *Zh. Prikl. Khim.*, 2004, vol. 77, no. 2, pp. 179–183.
4. Firsova, L.P., *Vestn. Mosk. Univ., Khimiya*, 2004, vol. 45, no. 3, pp. 204–207.
5. Melikhov, I.V., Rudin, V.N., and Vorob'eva, L.J., *Mendeleev Commun.*, 1991, vol. 1, pp. 33–34.
6. Melikhov, I.V., Rudin, V.N., and Vorob'eva, L.J., *Neorg. Mater.*, 1988, vol. 24, no. 3, pp. 448–452.

ISSN 1070-4272, Russian Journal of Applied Chemistry, 2006, Vol. 79, No. 12, pp. 2028–2029. © Pleiades Publishing, Inc., 2006.
Original Russian Text © B.V. Patrov, 2006, published in Zhurnal Prikladnoi Khimii, 2006, Vol. 79, No. 12, pp. 2052–2053.

BRIEF COMMUNICATIONS

Activity of Components of Melts of Binary Systems with a Common Anion

B. V. Patrov

St. Petersburg State Polytechnic University, St. Petersburg, Russia

Received September 28, 2006

Abstract—The model of regular solutions and the data on the enthalpy of mixing for binary systems with a common anion were used to calculate the activities of the components of the systems LiF–KF, NaI–CsI, NaCl–RbCl, and NaCl–$SrCl_2$.

DOI: 10.1134/S107042720612024X

Calculations of the activities of components of mutual melts from data on the surface tension have been described earlier [1]. It has been shown that activities found from surface tension data for the systems LiF–NaCl and LiF–KCl coincide with the activities calculated after Fellner [2].

In terms of the regular solution model [3], the activity coefficients of components of binary systems can be represented as

$$\ln \gamma_1 = \frac{A}{RT} x_2^2, \quad (1)$$

$$\ln \gamma_2 = \frac{A}{RT} x_1^2, \quad (2)$$

where A is the interaction parameter and x_1 and x_2 are the mole fractions of the components.

It is known that the component activities are related to the activity coefficient and the mole fraction:

$$a_1 = \gamma_1 x_1, \quad (3)$$

$$a_3 = \gamma_2 x_2, \quad (4)$$

Further we obtain

$$\ln a_1 = \ln x_1 + \frac{A}{RT} x_2^2, \quad (5)$$

$$\ln a_2 = \ln x_2 + \frac{A}{RT} x_1^2. \quad (6)$$

We express the interaction parameter A in these equations in terms of the molar enthalpy of mixing of components, ΔH^{M} (J mol^{-1}):

$$A = \frac{\Delta H^{\mathrm{M}}}{x_1 x_2}. \quad (7)$$

Experimental data on the surface tension are described by Burylev's equation for regular solutions [4]:

$$\sigma = \sigma_1 x_1 + \sigma_2 x_2 + C x_1 x_2, \quad (8)$$

here σ_1, σ_2 and x_1, x_2 are the surface tensions and mole fractions of the components of the binary systems; C is the constant of Burylev's equation.

The structural and energy variations in the systems with a common anion are more significant than those in systems with a common cation. Therefore, we studied the binary systems LiF–KF, NaI–CsI, NaCl–RbCl, and NaCl–$SrCl_2$ with a common anion. For these systems, there are experimental data on the surface tension [5, 6] and enthalpy of mixing [7], they have simple phase diagrams with an eutectic [8].

The average values of the constant C in Burylev's equation and of the interaction parameter A for the systems under study are as follows:

System	T, K	$-C$, mJ m^{-2}	$-A$, J mol^{-1}
LiF–KF	1171	91.47	19580
NaI–CsI	1013	17.25	5710
NaCl–RbCl	1083	21.09	3390
NaCl–$SrCl_2$	1167	33.34	4085

Enthalpy of mixing and the activities of the components of the systems under study

x_1	$-\Delta H^M$, J mol^{-1}	γ_1	a_1	γ_2	a_2	x_1	$-\Delta H^M$, J mol^{-1}	γ_1	a_1	γ_2	a_2
LiF(1)–KF(2), 1171 K						NaCl(1)–RbCl(2), 1083 K					
0.1	1550	0.1960	0.0196	0.9801	0.8821	0.1	293	0.7370	0.0737	0.9962	0.8966
0.2	2900	0.2759	0.0552	0.9227	0.7382	0.2	526	0.7858	0.1572	0.9850	0.7880
0.3	3960	0.3731	0.1119	0.8344	0.5841	0.3	698	0.8315	0.2494	0.9667	0.6767
0.4	4680	0.4846	0.1939	0.7247	0.4348	0.4	805	0.8732	0.3493	0.9415	0.5649
0.5	5000	0.6047	0.3023	0.6047	0.3023	0.5	847	0.9101	0.4551	0.9101	0.4551
0.6	4890	0.7247	0.4348	0.4846	0.1939	0.6	821	0.9415	0.5649	0.8732	0.3493
0.7	4330	0.8344	0.5841	0.3731	0.1119	0.7	726	0.9667	0.6767	0.8315	0.2494
0.8	3320	0.9227	0.7382	0.2759	0.0552	0.8	558	0.9850	0.7880	0.7858	0.1572
0.9	1870	0.9801	0.8821	0.1960	0.0196	0.9	317	0.9962	0.8966	0.7370	0.0737
NaI(1)–CsI(2), 1013 K						NaCl(1)–$SrCl_2$(2), 1167 K					
0.1	530	0.5773	0.0577	0.9932	0.8939	0.1	280	0.7105	0.0711	0.9956	0.8962
0.2	940	0.6478	0.1296	0.9732	0.7786	0.2	510	0.7635	0.1527	0.9835	0.7867
0.3	1220	0.7172	0.2152	0.9408	0.6585	0.3	710	0.8135	0.2441	0.9626	0.6760
0.4	1390	0.7833	0.3133	0.8972	0.5383	0.4	860	0.8590	0.3436	0.9846	0.5607
0.5	1430	0.8440	0.4220	0.8440	0.4220	0.5	970	0.9006	0.4503	0.9006	0.4503
0.6	1360	0.8972	0.5383	0.7833	0.3133	0.6	1010	0.9846	0.5607	0.8590	0.3436
0.7	1180	0.9408	0.6585	0.7172	0.2152	0.7	970	0.9626	0.6760	0.8135	0.2441
0.8	890	0.9732	0.7786	0.6478	0.1296	0.8	820	0.9835	0.7867	0.7635	0.1527
0.9	490	0.9932	0.8939	0.5773	0.0577	0.9	510	0.9956	0.8962	0.7105	0.0711

A comparison of the experimental values of the surface tension and those calculated by Burylev's equation demonstrated that the discrepancy does not exceed the measurement error (2%). Therefore, the melts under study are regular solutions, and Eqs. (1)–(7) are applicable to these melts. The calculated activities of the melt components are listed in the table.

CONCLUSIONS

1. It was shown that the common-anion salt melts under study are regular solutions.

2. It was demonstrated that, in the regular solution model, the activity coefficients of components of binary systems can be determined in terms of the interaction parameter, which can be found using experimental values of the enthalpy of mixing of the components.

3. The activities of the components of the binary systems with a common anion were calculated from the data on the surface tension and the enthalpy of mixing.

REFERENCES

1. Patrov, B.V., *Zh. Prikl. Khim.*, 1998, vol. 71, no. 3, pp. 507–508.
2. Fellner, P., *Chem. Zvesti*, 1983, vol. 37, pp. 603–607.
3. Hildebrand, J.H., *Solubility of Non-Electrolytes*, New York: Reinhold, 1936, 2nd ed.
4. Burylev, B.P. and Vasil'ev, V.V., *Fizicheskaya khimiya poverkhnostnykh yavlenii v rasplavakh* (Physical Chemistry of Surface Phenomena in Melts), Kiev: Naukova Dumka, 1971, pp. 144–149.
5. Patrov, B.V. and Ostal'tseva, R.G., *Elektrokhimiya rasplavlennykh solei i metallov* (Electrochemistry of Molten Salts and Metals), Leningrad: Leningr. Politekhn. Inst., 1976, no. 348, pp. 63–65.
6. Stepanov, V.P., *Mezhfaznye yavleniya v ionnykh solevykh rasplavakh* (Interphase Phenomena in Ionic Salt Melts), Yekaterinburg: Nauka, 1993.
7. Markov, B.F., Volkov, S.V., Prisyazhnyi, V.D., et al., *Termodinamicheskie svoistva rasplavov solevykh sistem* (Thermodynamic Properties of Melts of Salt Systems), Kiev: Naukova Dumka, 1985.
8. Posypaiko, V.I. and Alekseeva, E.A., *Diagrammy plavkosti solevykh sistem. Ch. 1, 2. Dvoinye sistemy s obshchim anionom* (Fusibility Diagrams of Salt Systems, parts 1 and 2, Binary Systems with a Common Anion), Moscow: Metallurgiya, 1977.

ISSN 1070-4272, Russian Journal of Applied Chemistry, 2006, Vol. 79, No. 12, pp. 2030–2032. © Pleiades Publishing, Inc., 2006.
Original Russian Text © D.S. Kireev, I.N. Beloglazov, S.Z. El'-Salim, 2006, published in Zhurnal Prikladnoi Khimii, 2006, Vol. 79, No. 12, pp. 2054–2056.

BRIEF COMMUNICATIONS

A Method for Monitoring the Composition of Suspensions

D. S. Kireev, I. N. Beloglazov, and S. Z. El'-Salim

St. Petersburg Mining Institute (Technical University), St. Petersburg, Russia

Received October 18, 2006

Abstract—The concentrations of particulates in dispersion media, as well as of true solutions, were analyzed by ratiometric method. The error in determination of the concentrations was estimated for the ratiometric, as well as for the conventional procedure based on the calibration connection equations.

DOI: 10.1134/S1070427206120251

Application of photometric methods entails certain technical difficulties associated with industrial (line) implementation of simple systems for analytical control over processes. The stability of the connection equations is governed by the stability and degree of monochromaticity of the light sources, by the adequacy of the set of calibration samples to the real process, and by the degree of contamination of the measuring part of the analytical system.

One of the promising ways for development of commercial photometric analyzers consists in implementation of the ratiometric principle with fixed difference of the optical bases and possible variation of the light wavelength.

Let us consider the transformation of the basic light absorption law for true solutions in the case of two optical bases and coordinated analytical signals. For light with a wavelength λ, passed through cells with different optical path lengths, we have from the light extinction law

$$I_1 = kI_0 \exp(-\varepsilon_1 L_1 c),\ I_2 = kI_0 \exp(-\varepsilon_2 L_2 c), \quad (1)$$

where I_0, I_1, and I_2 are the incident light intensity and the analytical signals on the photodetectors, respectively; ε_1 and ε_2, molecular extinction coefficients, $1\ g^{-1}\ cm^{-1}$; L_1 and L_2, optical path lengths of the cells, cm; c, concentration of the solutions, $g\ l^{-1}$; and k, optical transparency coefficient of the cells [1, 2].

For KU-13 quartz glass, the degree of contamination of the cells can be taken identical for all the optical channels with a high degree of accuracy. Then Eq. (1) can be transformed into

$$\ln(I_1/I_2) = c(\varepsilon_2 L_2 - \varepsilon_1 L_1). \quad (2)$$

From Eq. (2), c can be easily determined:

$$c = \frac{\ln(I_1/I_2)}{\varepsilon_2 L_2 - \varepsilon_1 L_1}. \quad (3)$$

For a fixed wavelength λ, $\varepsilon_1 = \varepsilon_2$, and Eq. (3) takes the form

$$c = \frac{1}{\varepsilon}\frac{\ln(I_1/I_2)}{L_2 - L_1}. \quad (4)$$

The mass extinction coefficient for an absorption line is a constant unaffected by the solution concentration and the optical path length of the cell. Passing to optical densities we rewrite Eq. (4) as

$$c = \frac{1}{\varepsilon}\frac{D_1 - D_2}{L_1 - L_2} = \frac{1}{\varepsilon}\frac{\Delta D}{\Delta L}, \quad (5)$$

where ΔD is the difference of the optical densities in the cells used, and ΔL, difference of the optical path lengths of these cells.

Thus, a knowledge of the mass extinction coefficient makes unnecessary calibration against a set of reference solutions, the more so as the difference of the optical path lengths of two cells is determined with a high accuracy, and the only contribution to the error in determination of c in Eq. (5) comes from the inaccuracy in measurement of the optical densities.

We tested the validity of Eq. (5) with solutions of copper and nickel sulfates, cobalt chloride, and colored iron complexes with thiocyanate; the optical path length of the cells was 5, 3, 2, and 1 cm. Using

Table 1. Comparison of the calibration connection equations with ratiomertic calculations

c, g l^{-1}	Relative error, %, for elements							
	method of calibration using a set of reference samples				ratiometric calculation			
10^{-4}–10^{-3}	2.3	2.56	1.89	1.25	3.14	2.89	3.11	2.45
10^{-3}–10^{-2}	2.56	3.01	2.01	1.14	2.95	2.46	2.99	3.05
10^{-2}–10^{-1}	3.25	3.11	2.47	1.78	2.12	3.47	2.16	3.01
10^{-1}–1	1.56	1.48	1.24	1.01	2.07	2.11	2.09	2.12
1–10	1.48	1.35	1.12	1.02	2.11	2.14	1.89	1.96
10–100	2.56	3.87	1.89	1.45	0.99	1.06	2.03	1.05

Table 2. Comparison of the mass absorption coefficients for Cu, Ni, Co, and Fe, calculated by the ratiometric method, with the tabulated data [3]

Element	λ, nm	Calculated coefficient ε, l g^{-1} cm^{-1}, for indicated optical path lengths of the cells						ε, l g^{-1} cm^{-1} [3]
		5–1	5–2	5–3	3–2	3–1	2–1	
Cu	680	0.126	0.123	0.131	0.135	0.139	0.14	0.13
Ni	405	0.89	0.98	0.89	1.02	0.95	1.03	0.9
Co	525	0.124	0.119	0.13	0.135	0.132	0.14	0.125
Fe	430	0.447	0.435	0.462	0.425	0.435	0.421	0.45

model solutions (Table 1), we determined the relative errors in determination of the concentrations by calibration connection equations and by Eq. (5). Equation (5) yielded an expression for the mass extinction coefficient

$$\varepsilon = \frac{1}{c}\frac{\Delta D}{\Delta L}. \qquad (6)$$

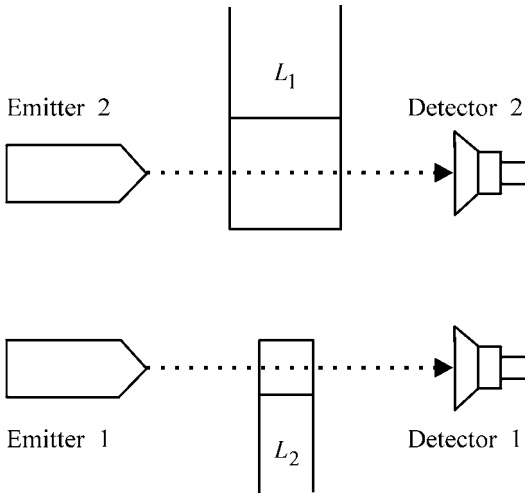
We compared the mass absorption coefficients ε obtained for various optical path lengths with the tabulated data for the working wavelengths (Table 2) [3].

Tables 1 and 2 suggest that the results of calculations by the ratiometric method well agree with those obtained by the conventional procedure of photometric measurements for colored solutions. The mass absorption coefficient calculated by formula (6) is identical to the tabulated value to within 7%. Hence, the error in calculation of the concentrations cannot be larger than 5%. Also, Table 2 suggests that, with increasing difference in the optical path lengths, the mass absorption coefficient calculated by the ratiometric method tends to the tabulated value.

Thus, the ratiometric scheme of photometric analysis of colored solutions is suitable for calculation of the concentrations and determination of the mass absorption coefficient of a complex mixture by Eq. (6).

The ratiometric scheme was implemented with a multibeam photometric correlator for in-line measurements. An original optical scheme (variation of two optical channels) allows implementation of the ratiometric method for flows under laboratory and industrial conditions.

With two optical cells and four independent optical spectral channels, it is possible to divide the flow under study and carry out measurements in two cells with different thicknesses at two wavelengths. The figure shows the schematic diagram of the ratiometric measurements for two cells and two wavelengths. Two cells with optical path lengths L_1 and L_2 are exposed



Ratiometric optical scheme.

to light sent by matched emitters. The photodetectors are linked by negative feedback for setting a common zero level. The power supply of the emitters has a common point for correction of the emitter–detector optopairs by the scheme suggested in [4]. The initial signal is measured with water passed through the cells. This allows estimation of the degree of contamination of the working surfaces of the cells. The output signals come to logarithmic amplifiers having a coordinated correction of the amplification coefficient. The amplified signal is the logarithm of the voltage proportional to the intensity of passed light, i.e., corresponds to the optical density. Hence, Eq. (5) can be written in terms of the amplifier output voltages:

$$c = \frac{1}{\varepsilon}\frac{\Delta D}{\Delta L} = a\frac{\Delta U}{\varepsilon}\frac{1}{\Delta L}, \qquad (7)$$

where a is the voltage scale coefficient.

CONCLUSION

The ratiometric method is suitable for analyzing the concentration of particulates in dispersion media, as well as of true solutions, and affords more efficient monitoring of processes in chemical and metallurgical industries without unnecessary sophistication of the analytical system.

REFERENCES

1. Budnikov, G.K., Maistrenko, V.N., and Vyaselev, M.R., *Osnovy sovremennogo elektrokhimicheskogo analiza* (Fundamentals of Modern Electrochemical Analysis), Moscow: Mir, Binom LZ, 2003.
2. Shifrin, K.S., *Teoreticheskie i prikladnye problemy rasseyaniya sveta* (Theoretical and Applied Problems of Light Scattering), Minsk: Nauka i Tekhnika, 1971, pp. 228–244.
3. Lur'e, Yu.Yu., *Spravochnik po analiticheskoi khimii* (Reference Book on Analytical Chemistry), Moscow: Khimiya, 1971.
4. Gulyaev, P.Yu., Es'kov, A.V., Korotkikh, V.M., and Romanov, V.A., *Datchiki elektricheskikh i neelektricheskikh velichin "Datchik-95": Doklady Vtoroi mezhdunarodnoi konferentsii* (Sensors of Electric and Nonelectric Parameters "Sensor-95": Proc. Second Int. Conf.), Barnaul: Altaisk. Gos. Tekhn. Univ. im. I.P. Polzunova, 1995, pp. 174–177.

ISSN 1070-4272, Russian Journal of Applied Chemistry, 2006, Vol. 79, No. 12, pp. 2033–2034. © Pleiades Publishing, Inc., 2006.
Original Russian Text © I.M. Osadchenko, A.P. Tomilov, 2006, published in Zhurnal Prikladnoi Khimii, 2006, Vol. 79, No. 12, pp. 2057–2058.

BRIEF COMMUNICATIONS

Oscillopolarographic Reduction of White Phosphorus

I. M. Osadchenko and A. P. Tomilov

Volgograd Research and Technological Institute of Meat and Milk Cattle Breeding and Processing of Cattle Products, Russian Academy of Agricultural Science, Volgograd, Russia

Received October 3, 2006

Abstract—Reduction of white phosphorus in ethanol solutions on a dropping mercury electrode was studied by oscillopolarography. The effect of the type of electrolyte and potential sweep rate on the peak potential was demonstrated.

DOI: 10.1134/S1070427206120263

Use of solutions of white phosphorus has been reported [1], and, therefore, data on its redox properties are of interest.

We have noted previously [2–4] that alcohol solutions of white phosphorus are polarographically active and their polarographic waves are suitable for analytical purposes. Because polarographic studies of white phosphorus solutions are scarce, we continued our studies to elucidate the influence exerted by some process parameters, including the nature of electrolyte and potential sweep rate, on the peak potential of the oscillopolarographic curve of phosphorus.

White phosphorus was obtained by purification of a technical-grade yellow phosphorus by the known procedure: melting and subsequent treatment with 3.5% solutions of $K_2Cr_2O_7$ and H_2SO_4 [5]. The constants of the purified phosphorus (density at 20°C and melting point) were in agreement with published data (1.8 g cm^{-3} and 44°C). The method of the phosphorus preparation was changed for the sake of convenience. It was prepared in the form of cylindrical grains 3 mm in diameter and 3–5 mm long, instead of spheres [6]. For this purpose, melted phosphorus was collected into a heated pipette and charged in a glass pipe (inner diameter 3 mm) with a bottom stopper, filled with distilled water and submerged in a water bath. In the process, water was discharged from the pipe, with a 4–5-mm layer remaining. The pipe with phosphorus was cooled with a cold water to room temperature (22–23°C), and the crystallization of phosphorus was confirmed by touching its surface with a solid object. After that, the phosphorus mass was squeezed-out with a glass rod into a vessel with water, cut into 3–5-mm pieces, and stored under a layer of distilled water.

Ethanol to be used as solvent was distilled and the supporting electrolytes were of analytically pure and chemically pure grades. The polarographic measurements were performed on an O2-TsLA oscillopolarograph. The capillary used had the following characteristics: m = 0.89 mg s^{-1}, τ = 8.0 s at a mercury column height of 225 mm. The potential was measured relative to this mercury at 23 ± 1°C. The potential of this mercury (0.02 V) was measured experimentally relative to a saturated calomel electrode. Oxygen was removed from the solution by bubbling of nitrogen for 10 min. When determining the reduction current, account was taken of the current in the supporting electrolyte.

A weighed portion of white phosphorus was washed with ethanol and ether, dried in a flow of nitrogen, and transferred into a vessel (flask) for weighing and dissolution.

It has been demonstrated previously [2] that white phosphorus gives in oscillopolarograms a polarographic wave with a peak potential of –1.88 V (relative to the mercury bottom) on the background of a 0.1 M ethanol solution of LiCl (at a phosphorus concentration of 10×10^{-4} g-at l^{-1}) at a potential sweep rate of 1 V s^{-1}. A set of measurements related the nature and concentration of the supporting electrolyte to the peak potential:

Electrolyte, M	Potential, V	Electrolyte, M	Potential, V
0.05 LiCl	–1.98	0.1 $(C_2H_5)_4NI$	–1.54
0.1 LiCl	–1.88	0.1 NH_4Cl	–1.65
0.5 LiCl	–1.83	0.1 NH_4NO_3	–1.73
0.1 NH_4Cl	–1.65	0.1 NH_4CNS	–1.53
		0.1 NH_4CH_3COO	–1.80

As can be seen from these data, the nature of electrolyte strongly affects the reduction potential of white phosphorus. The reduction of white phosphorus is facilitated to the greatest extent if we use ammonium rhodanide (the least negative peak potential) as the supporting electrolyte. In our opinion, this is due to the higher adsorption of this salt on the cathode. The effect of the potential sweep rate on the peak potential is insignificant: 0.5 V s^{-1} –1.85 V, 1.0 V s^{-1} –1.88 V, and 2.0 V s^{-1} –1.92 V.

CONCLUSIONS

(1) A study of the oscillopolarographic reduction of white phosphorus in supporting electrolytes of varied nature in ethanol solutions demonstrated that the reduction of white phosphorus is facilitated to the greatest extent if ammonium rhodanide (the least negative peak potential of –1.53) is used as the supporting electrolyte.

(2) It was shown that the effect of the potential sweep rate on the peak reduction potential of white phosphorus is insignificant.

REFERENCES

1. White, D.A. and Dolan, M.J., *J. Electrochem. Soc.*, 1977, vol. 124, no. 8, pp. 1175–1177.
2. Tomilov, A.P. and Osadchenko, I.M., *Zh. Anal. Khim.*, 1966, vol. 21, pp. 1498–1499.
3. Tomilov, A.P., Brago, I.N., and Osadchenko, I.M., *Elektrokhimiya*, 1968, vol. 4, pp. 1153–1156.
4. Osadchenko, I.M., *Elektrokhimiya fosforsoderzhashchikh soedinenii* (Electrochemistry of Phosphorus-containing Compounds) Volgograd: Volgograd. Gos. Univ., 2001.
5. Karyakin, Yu.V. and Angelov, I.M., *Chistye khimicheskie reaktivy* (Pure Chemicals), Moscow: Goskhimizdat, 1955.
6. *Handbook of Preparative Inorganic Chemistry*, Brauer, G., Ed., New York: Academic, 1963.

ISSN 1070-4272, Russian Journal of Applied Chemistry, 2006, Vol. 79, No. 12, pp. 2035–2036. © Pleiades Publishing, Inc., 2006.
Original Russian Text © I.M. Osadchenko, A.P. Tomilov, 2006, published in Zhurnal Prikladnoi Khimii, 2006, Vol. 79, No. 12, pp. 2059–2060.

BRIEF COMMUNICATIONS

Electrochemical Methoxylation of Anethole on a Graphite Anode

I. M. Osadchenko and A. P. Tomilov

Volgograd Research and Technological Institute of Meat-and-Milk Cattle Breeding and Animal Product Processing, Russian Academy of Agricultural Sciences, Volgograd, Russia

Received October 3, 2006

Abstract—A procedure is suggested for electrochemical methoxylation of anethole in an electrolyzer with a graphite cathode and potassium *p*-toluenesulfonate in methanol as supporting electrolyte; a mixture of two products is formed in the process.

DOI: 10.1134/S1070427206120275

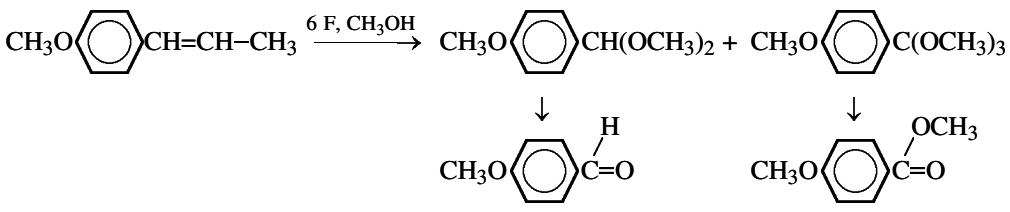
Electrochemical alkoxylation of organic compounds on platinum, carbon, and graphite anodes has been reported [1]. The source of the methoxylating agent was methanol, acting as a solvent for both the organic substance and the electrolyte. Alcoholic solutions of alkalis and alcoholates were recommended for electrochemical alkoxylation of hydrocarbons, tertiary amines, and ethers. The alkoxylation pathway is strongly influenced by the concentration of the organic substrate [1]. If dimerization occurs concurrently with alkoxylation, the contribution of the former process, as a rule, increases with the concentration of the organic substrate.

The methoxylation of aryl-substituted unsaturated hydrocarbons, styrene and its derivatives, has been studied in detail; it was shown that electrochemical methoxylation of styrene gives dimethoxyphenylethane in 30% yield [1]. Anodic methoxylation of anethole (1-methoxy-4-propenylphenol) is of interest as a route to anisaldehyde (aubepine) diacetal, which can be readily converted by hydrolysis into the free aldehyde, a valuable fragrance compound and an intermediate for organic synthesis. Methoxylation of alkenylarenes, including anethole, in a methanolic solution of potassium or sodium trifluoroacetate in a diaphragmless electrolyzer with graphite electrodes was reported in [2]. However, the electrolyses may be complicated by anodic decomposition of trifluoroacetate.

The goal of this study is to simplify this process and extend its potentialities.

Previously [3] we have demonstrated the possibility in principle of electrochemical methoxylation of anethole at 55–65°C on a graphite anode in methanol, with potassium *p*-toluenesulfonate as supporting electrolyte. An advantage of this system is that the salt crystallizes and precipitates on cooling, and it can be readily separated by filtration. The filtrate is treated with 10% sulfuric acid and extracted with toluene; the extract is washed with a sodium carbonate solution and vacuum-distilled. In the process, anethole is gradually added to the electrolyte, because at low concentrations its oxidative dimerization is suppressed.

We examined the influence exerted on the methoxylation by the temperature, current density, amount of electricity, and electrolyte concentration. The best results were obtained under the following conditions: 55–65°C, anodic current density 0.02–0.05 A cm^{-2}, amount of electricity 5.5–6 F per mole of anethole, 3–5% supporting electrolyte concentration, and up to 0.4 M concentration of anethole in the electrolyte. Anisaldehyde and methyl *p*-methoxybenzoate were obtained in yields of up to 70 and 25%, respectively. The electrochemical methoxylation and hydrolysis follow the scheme



It should be noted that methyl *p*-methoxybenzoate (anisic acid methyl ester) is used as a stabilizer for fragrance compounds. As a target product we obtained a mixture of anisaldehyde and methyl *p*-methoxybenzoate. Their boiling points are close (248 and 256°C, respectively [4]), making difficult their separation by distillation.

EXPERIMENTAL

Anethole, toluene, and potassium *p*-toluenesulfonate were reagent-grade. The electrolyzer was a cylindrical glass vessel with a temperature-control jacket. Current leads and tubes for the stirrer, addition of anethole, and removal of the gas were fixed on the lid. The electrolyzer was charged with a mixture of 150 g of methanol and 3.5 g of potassium *p*-toluenesulfonate; the mixture was stirred at 55–65°C until the salt dissolved completely, and the electrolysis was performed at a current density of 0.03 A cm^{-2} (3 A current) with gradual addition of anethole (15 g in total; the running concentration did not exceed 0.4 M). The electricity was passed in an amount of 6 F per mole of anethole. After the electrolysis completion, the solution was cooled to ensure complete precipitation of the salt, the salt was separated, and the filtrate was evaporated to remove methanol, treated with 15 ml of 10% H_2SO_4, and extracted with toluene (3×20 ml). The toluene extract was washed with an aqueous solution of sodium carbonate and then distilled; toluene was distilled off at atmospheric pressure and vapor temperature of up to 110°C, and the target product, at reduced pressure (8–9 mm Hg) and vapor temperature of 120–125°C. An oily liquid (14 g) with a pleasant hawthorn odor was obtained; according to the chromatographic analysis, it contained 69% anisaldehyde and 25% methyl *p*-methoxybenzoate (total yield based on anethole 94%). The product can be used as a component of odorants, cosmetics, and aromatic food essences [5], and also as a component of agricultural chemicals for rodent and pest control [6, 7]. Anisaldehyde can be isolated from the product via bisulfite derivative. The product components were identified by gas chromatography (comparison of the retention times with those of the authentic samples).

CONCLUSION

The procedure developed for electrochemical methoxylation of anethole in methanol on a graphite anode with potassium *p*-toluenesulfonate as supporting electrolyte, yields a mixture of two valuable products, anisaldehyde and methyl *p*-methoxybenzoate and allows simplification of the process and extension of its potentialities.

REFERENCES

1. Tomilov, A.P., Fioshin, M.Ya., and Smirnov, V.A., *Elektrokhimicheskii sintez organicheskikh veshchestv* (Electrochemical Synthesis of Organic Compounds), Leningrad: Khimiya, 1976.
2. Ogibin, Yu.N., Ilovaiskii, A.I., and Nikishin, G.I., Abstracts of Papers, *Novosti elektrokhimii organicheskikh soedinenii: XII Vsesoyuznoe soveshchanie EKhOS-90* (News in Electrochemistry of Organic Compounds: XII All-Union Meet. ECOC-90), Moscow, 1990, p. 50.
3. Osadchenko, I.M. and Tomilov, A.P., Abstracts of Papers, *Novosti elektrokhimii organicheskikh soedinenii: XIV soveshchanie po elektrokhimii organicheskikh soedinenii* (News in Electrochemistry of Organic Compounds: XIV Meet. on Electrochemistry of Organic Compounds), Novocherkassk, 1998, p. 97.
4. *Spravochnik khimika* (Chemist's Handbook), Nikol'skii, B.P., Ed., Moscow: Goskhimizdat, 1963, vol. 2.
5. Shulov, L.M. and Kheifits, L.A., *Dushistye veshchestva i poluprodukty parfyumerno-kosmeticheskogo proizvodstva: Spravochnik* (Fragrant Compounds and Intermediates in Production of Perfumes and Cosmetics), Moscow: Agropromizdat, 1990.
6. JPN Patent 30720.
7. JPN Patent Appl. 62-298546.

ISSN 1070-4272, Russian Journal of Applied Chemistry, 2006, Vol. 79, No. 12, pp. 2037–2038. © Pleiades Publishing, Inc., 2006.
Original Russian Text © E.V. Pyatnitsyna, M.M. El'chaninov, A.P. Savost'yanov, 2006, published in Zhurnal Prikladnoi Khimii, 2006, Vol. 79, No. 12, pp. 2061–2062.

BRIEF COMMUNICATIONS

Electrolytic Reduction of 2-Butyne-1,4-diol as a Route to *trans*-2-Butene-1,4-diol

E. V. Pyatnitsyna, M. M. El'chaninov, and A. P. Savost'yanov

South-Russian State Technical University (Novocherkassk Polytechnic Institute), Novocherkassk, Rostov oblast, Russia

Received December 21, 2005; in final form, September 2006

Abstract—The effect of the cathode material on the electrochemical transformations of 2-butyne-1,4-diol at atmospheric pressure was studied by chromatographic analysis. The optimal parameters of the selective synthesis of *trans*-2-butene-1,4-diol were determined.

DOI: 10.1134/S1070427206120287

Among the starting compounds for preparing polyurethanes [1], detergents, alkyd resins [2], Endosulfan insecticide, plasticizers, and drugs [3], compounds containing the required functional groups are of particular importance. Among such compounds is 2-butene-1,4-diol (BED) whose synthesis by catalytic hydrogenation of 2-butyne-1,4-diol (BYD) yields a ~90 : 10 mixture of *cis* and *trans* isomers.

With the aim to examine the effect of the *trans* isomer on the properties of SKU-90 urethane rubber, we developed in this study a procedure for regioselective synthesis of *trans*-BED.

EXPERIMENTAL

Previously *trans*-BED has been prepared from divinyl via dihalo derivatives [4, 5] and diacetoxy-2-butene [6, 7]. The drawbacks of these methods are multistep procedure, presence of isomers, and lacrimogenic properties of the intermediate dihalobutenes. Another pathway involves chemical reduction of BYD in a nitrogen atmosphere with chromium(II) sulfate [8]. However, such steps of this procedure as intermediate reduction of chromium(III) sulfate with zinc dust in a nitrogen atmosphere, followed by filtration (also in an inert atmosphere), prevent commercial implementation of the process.

To simplify the synthesis of the target product, we attempted electrochemical reduction of BYD in the presence of $CrSO_4$ on stationary solid cathodes. In this case, the reduction of $Cr_2(SO_4)_3$ to $CrSO_4$ with hydrogen liberated at the cathode occurs in aqueous solution at atmospheric pressure:

$$2Cr^{3+} + H_2^0 \longrightarrow 2Cr^{2+} + 2H^+,$$

$$HOH_2C{-}C{\equiv}C{-}CH_2OH \xrightarrow{2H^+,\ 2e} \begin{matrix} H & & CH_2OH \\ & \diagdown\!\!=\!\!\diagup & \\ HOH_2C & & H \end{matrix}$$

To evaluate the qualitative and quantitative characteristics of the BYD transformation, we examined the effect of the cathode material on the electrolytic reduction. The electrolysis conditions were as follows: catholyte temperature 20–60°C, pH 2–3, cathodic current density 0.02 A cm^{-2}, BYD concentration 1.16 M, and cromium(III) sulfate concentration 0.2 M. The amount of electricity passed was 300% of that reqiured theoretically for complete conversion of BYD into *trans*-BED.

The electrolytic reduction of BYD occurs on all the electrodes examined, but only on lead cathodes the BED yield based on BYD is reasonably high (see table), 60–70%, with 98–99% selectivity with respect to the desired product and 97–98% isomeric purity. Electrolysis on porous stainless steel provides high selectivity with respect to the desired product, but its yield based on BYD is lower. With copper, nickel,

Effect of cathode material on electrolytic reduction of BED

Cathode material	BYD conversion	BED yield based on BYD	Selectivity with respect to *trans*-BED
	%		
Smooth Cr18Ni10Ti steel	66.8	12.2	13.5
Copper	90.0	32.5	33.7
Porous Cr18Ni10Ti steel	62.5	42.5	100.0
Nickel	31.5	17.3	18.1
Lead	99.2	66.1	98.8
Zinc	72.6	15.5	23.7
Iron	64.0	17.3	18.0

zinc, and iron cathodes, both the product yield and the selectivity of the cathodic reduction were low (see table).

For the electrochemical synthesis we used a cell in the form of a cylindrical glass vessel (serving as a cathode chamber) with a temperature-control jacket. The vessel lid had opening for the anode chamber, thermometer, current lead to the cathode, and stirrer. The cathode and anode compartments were separated by a porous tubular diaphragm with a blind bottom. The anode was platinum, the anolyte was 15% sulfuric acid, and the catholyte was purified BYD in 0.2 M chromium(III) sulfate.

To purify BYD, a commercial solution of BYD was boiled with activated charcoal to remove tars. The resulting solution was evaporated in a vacuum, and BYD was crystallized from a mixture of ethyl acetate with methylene chloride.

The initial and final reaction products were analyzed with a Tsvet-104 chromatograph under the following conditions: column length 2.0 m, inside diameter 3 mm; carrier gas nitrogen; column temperature 60–200°C; support Chromaton Super 0.16–0.20 mm; stationary phase polyethylene glycol 15000. For better separation of *cis*- and *trans*-BED, the samples were acetylated by the procedure described in [9].

The reaction product was isolated as follows. After the disappearance of the initial BYD from the chromatogram, the contents of the cathode chamber were neutralized with a concentrated ammonia solution to pH 8–9, after which the precipitate of chromium(III) hydroxide was filtered off on a Büchner funnel. Water was distilled off from the filtrate in a water-jet-pump vacuum under heating on a water bath. The residue was distilled in a vacuum (10 mm Hg), and the fraction boiling at 125–127°C was collected. The yield of *trans*-BED was about 66%. The isomeric purity of the product exceeded 98%.

CONCLUSIONS

(1) Electrolytic reduction of butyne-1,4-diol on a lead cathode is a stable process at 20–60°C and cathodic current density of 10–90 A dm^{-2}.

(2) The lowest amount of the passed electricity ensuring complete reduction of butyne-1,4-diol is 2.5 A h per gram of the starting compound; the current efficiency by 2-butene-1,4-diol is 53%.

(3) Freshly prepared $Cr_2(SO_4)_3$ solution can be used repeatedly without a decrease in the yield of *trans*-2-butene-1,4-diol.

REFERENCES

1. Sokol'skii, D.V., Pak, A.M., and Ten, E.I., in *Doklady IV Vsesoyuznoi konferentsii po khimii atsetilena* (Proc. IV All-Union Conf. on Acetylene Chemistry), Alma-Ata: Inst. Khim. Nauk Akad. Nauk Kaz. SSR, 1972, vol. 3, pp. 254–259.
2. FRG Patent 2412341.
3. Mel'nikov, N.N., *Khimiya i tekhnologiya pestitsidov* (Chemistry and Technology of Pesticides), Moscow: Khimiya, 1974.
4. Stepanov, N.A., Ovchinnikova, T.F., Kryukov, S.I., et al., in *Osnovnoi organicheskii sintez i neftekhimiya: Mezhvuzovskii sbornik nauchnykh trudov* (Basic Organic Synthesis and Petroleum Chemistry: Intercollegiate Coll. of Scientific Works), Yaroslavl: Yaroslav. Politekh. Inst., 1975, issue 4, pp. 39–43.
5. JPN Patent 51–18927.
6. JPN Patent 12333.
7. JPN Patent 56–18584.
8. Castro, C.E., *J. Am. Chem. Soc.*, 1961, vol. 83, pp. 3262–3267.
9. Dorofeenko, T.N., Zhdanov, Yu.A., Dumenko, V.I., et al., *Khlornaya kislota i ee soedineniya v organicheskom sinteze* (Perchloric Acid and Its Compounds in Organic Synthesis), Rostov-on-Don: Rostov. Gos. Univ., 1965.

ISSN 1070-4272, Russian Journal of Applied Chemistry, 2006, Vol. 79, No. 12, pp. 2039–2040. © Pleiades Publishing, Inc., 2006.
Original Russian Text © R.I. Yurchenko, T.N. Pilipenko, M.A. Yurchenko, T.I. Krivovyaz, 2006, published in Zhurnal Prikladnoi Khimii, 2006, Vol. 79, No. 12, pp. 2063–2064.

BRIEF COMMUNICATIONS

Protective Effect of 1-Benzyl-2-R-Pyridinium Halides in Steel Acid Corrosion

R. I. Yurchenko, T. N. Pilipenko, M. A. Yurchenko, and T. I. Krivovyaz

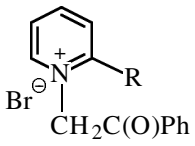
Kievskii Politekhnicheskii Institut National Technical University of Ukraine, Kiev, Ukraine

Received September 4, 2006

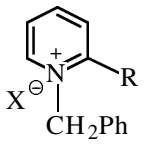
Abstract—The inhibiting effect of 1-benzoyl-2-R-pyridinium halides on the acid corrosion of steel was studied and compared with that of 1-phenacylmethyl-2-R-pyridinium halides.

DOI: 10.1134/S1070427206120299

Previously, using a fairly large data set, we have considered the correlation between the nature of substituent R in 1-phenacylmethyl-2-R-pyridinium bromides (**I**) and their protective properties in steel acid corrosion [1–3]. The coefficients of corrosion inhibition for these compounds range from 10 to 40 at room temperature and may reach almost 900 at 60°C [2]. We assumed that the major factor responsible for the corrosion inhibition may be adsorption of the carbonyl group of the phenacyl fragment and probably of substituents in the pyridinium ring. In order to confirm the decisive role of the carbonyl groups of **I** at elevated temperatures and to clarify the role of R, we studied protective properties of 1-benzyl-2-R-pyridinium halides (**II**, **II**') in the steel acid corrosion and compared them with the properties of 1-phenacylmethyl-2-R-pyridinium bromides (**I**) with the same R:



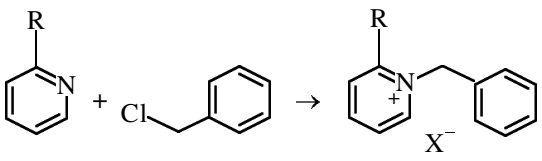
I



II, II'

where X = Cl (**II**), Br (**II**')

By alkylation of the corresponding pyridine derivatives with benzyl chloride, we synthesized 1-benzyl-R-pyridinium chlorides (**II**, X = Cl). The subsequent treatment with an alcoholic solution of KBr yielded **II**'



where X = Cl (**II**), R = H (**a**), NH_2 (**b**), NHCOCH=CHPh (**c**), NHCO-furyl-2 (**d**), NHCOAd-1 (**e**), NHCSNHPh (**f**); X = Br (**II**'), R = CH_3 (**a**) and NH_2 (**b**).

EXPERIMENTAL

Corrosion tests were performed by the conventional procedure [1] with samples of 08 KP steel with a working surface area of 14×10^{-4} m^2. The samples were kept in 3 M H_2SO_4 at 20°C for 24 h and at 60°C for 2 h. The efficiency of steel protection with substances synthesized at their concentration of 1×10^{-2} M was evaluated by the inhibition coefficient γ and degree of protection *Z*.

We found that, at 20°C, benzylpyridinium bromides (**II'a**, **II'b**) and the corresponding 1-phenacylmethylpyridinium bromides (**Ia**, **Ib**) differ only slightly in γ, but this difference becomes more substantial with increasing temperature. At 60°C, γ is 209 and 200 for **Ia** and **Ib** and 25.19 and 32.81 for **II'a** and **II'b**, respectively (Table 1).

A comparison of the inhibiting effects of 1-benzyl-2-R-pyridinium chlorides, bromides, and the corresponding phenacylmethylpyridinium bromides **I** showed that, at room temperature, replacement of chloride with bromide, variation of the substituent R in the 2-position of the pyridine ring, and passing from 1-benzyl-2-R-pyridinium bromides to phenacylmethylpyridinium bromides do not substantially change the protective properties of the pyridinium salts (Table 2). For example, the inhibition coefficient γ varies within the range of 6 units for compounds **II** and **II**',

Table 1. Inhibition coefficient γ and degree of protection *Z* of 08 KP steel corrosion in 3 M H_2SO_4 in the presence of 1×10^{-2} M 1-phenacylmethylpyridinium bromides (**Ia**, **Ib**) and 1-benzylpyridinium bromides (**II'a**, **II'b**)

Compound	20°C		40°C		60°C		80°C	
	γ	*Z*, %	γ	*Z*, %	γ	*Z*, %	γ	*Z*, %
Ia [1]	15.51	93.55	18.73	94.66	209.11	99.52	150.44	99.33
II'a	12.80	92.19	15.23	93.43	25.19	96.03	19.53	94.88
Ib [1]	23.70	95.78	29.02	96.55	200.32	99.50	144.60	99.30
II'b	19.19	95.04	21.40	95.32	32.81	96.95	26.22	96.19

Table 2. Protective properties of 1-benzyl-2-R-pyridinium chlorides and the corresponding 1-phenacylmethyl-2-R-pyridinium bromides (1×10^{-2} M) for 08 KP steel in 3 M H_2SO_4

R	γ at indicated temperature °C		R	γ at indicated temperature °C	
	20	60		20	60
H	10.98* 11.30 [1]	23.00 221.20 [1]	NHCO-Furyl-2	18.36 24.30 [2]	38.33 317.15 [2]
NH_2	17.31 23.70 [1]	28.75 200.32 [1]	NHCOAd-1	17.28 26.60 [2]	51.11 432.45 [2]
NHCOCH=CHPh	23.68 32.10 [2]	33.79 365.90 [2]	NHCSNHPh	19.15 29.17 [3]	49.29 634.30 [3]

* Numerator, data for 1-benzyl-2-R-pyridinium chlorides; denominator, data for 1-phenacylmethyl-2-R-pyridinium bromides.

13 units at variation of substituent R in the series of pyridinium chlorides **IIa**–**IIf**, and 21 units for the corresponding compounds **I**. At 60°C, higher values of γ are observed for **II** and **II'**: 29–33 upon replacement of the anion (with the order of variation on replacing the anion remaining the same) and 23–51 in variation of R in the series of benzylpyridinium chlorides (**IIa**–**IIf**). The difference between the inhibiting effects of phenacylmethyl- and benzylpyridinium halides becomes especially pronounced. For compound **II'b**, i.e., it is a factor of 8 (by 167 units) lower than that for the corresponding 1-phenacylmethyl-2-aminopyridiniun bromide (**Ib**).

Thus, the data obtained confirm that high protecting effect of 1-phenacylmethylpyridinium bromides at 60°C is largely caused by carbonyl-containing groups at the nitrogen atom. Substituents R that can participate in adsorption of pyridinium salt on the steel surface also produce a noticeable, but weaker effect.

CONCLUSIONS

(1) A comparative study of the influence of 1-phenacylmethyl- and 1-benzylpyridinium halides on the steel acid corrosion showed the key role of the carbonyl group of 1-phenacylmethylpyridinium bromides in the inhibiting effect of these compounds at elevated temperatures.

(2) Functional groups of the pyridine ring are directly involved in adsorption on the metal surface and enhance the protective effect of the compounds studied.

REFERENCES

1. Yurchenko, R.I., Pogrebova, I.S., Pilipenko, T.N., and Kras'ko, E.M., *Zh. Prikl. Khim.*, 2003, vol. 76, no. 11, pp. 1814–1818.
2. Yurchenko, R.I., Pogrebova, I.S., Pilipenko, T.N., and Shubina, T.E., *Zh. Prikl. Khim.*, 2004, vol. 77, no. 7, pp. 1132–1135.
3. Yurchenko, R.I., Pogrebova, I.S., Pilipenko, T.N., and Shubina, T.E., *Zh. Prikl. Khim.*, 2006, vol. 79, no. 12, pp. 1969–1972.

ISSN 1070-4272, Russian Journal of Applied Chemistry, 2006, Vol. 79, No. 12, pp. 2041–2042. © Pleiades Publishing, Inc., 2006.
Original Russian Text © Yu.P. Perelygin, D.Yu. Chistyakov, 2006, published in Zhurnal Prikladnoi Khimii, 2006, Vol. 79, No. 12, p. 2065.

BRIEF COMMUNICATIONS

Boric Acid

Yu. P. Perelygin and D. Yu. Chistyakov

Penza State University, Penza, Russia

Received September 12, 2006

Abstract—pH ranges of existence of boric acid and its ionic species $H_2BO_3^-$, HBO_3^{2-}, BO_3^{3-}, and $B(OH)_4^-$ in aqueous solutions are calculated using Mathcad software package.

DOI: 10.1134/S1070427206120305

Boric acid is widely used in electroplating [1], analytical chemistry [2], medicine [3], and other branches of industry [4].

Boric acid is a tribasic acid [4, 5]. The first-, second-, and third-step dissociation constants are as follows [4]:

$$K_1 = \frac{[H^+]\,[H_2BO_3^-]}{[H_3BO_3]} = 5.8 \times 10^{-10},$$

$$K_2 = \frac{[H^+]\,[HBO_3^{2-}]}{[H_2BO_3^-]} = 4 \times 10^{-13},$$

$$K_3 = \frac{[H^+]\,[BO_3^{3-}]}{[HBO_3^{3-}]} = 4 \times 10^{-14}.$$

The acid properties of boric acid in aqueous solutions are caused by the liberation of protons by reaction (1) [3, 4]:

$$H_3BO_3 + H_2O \rightleftarrows [B(OH)_4^-] + H^+. \quad (1)$$

The equilibrium constant of this reaction has been reported [3] to be

$$K_4 = \frac{[H^+][B(OH)_4^-]}{[H_3BO_3]} = 7.3 \times 10^{-10}.$$

As seen, data characterizing the dissociation of boric acid are rather contradictory, which initiated this study.

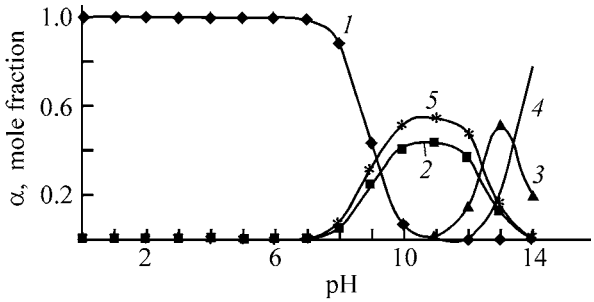
The above equations and the material balance equation

$$[H_3BO_3] + [H_2BO_3^-] + [HBO_3^{2-}] + [BO_3^{3-}] + [B(OH)_4^-] = c \quad (2)$$

(boric acid concentration c was taken to be 0.1 M) were simultaneously solved using Mathcad software package at pH varied from 0 to 14 at a step of 1 pH unit (see figure). The results show that reaction (1) and the first step of dissociation of boric acid simultaneously occur in the pH range 7–14.

In a human body, pH of biological fluids does not exceed 8 [3]. In this case, it follows from our calculations that the acid–base properties of boric acid are due to the simultaneously occurring first-step dissociation and reaction (1) [at pH ≤8, fractions of $H_2BO_3^-$ and $B(OH)_4^-$ are below 0.06].

Boric acid exists as H_3BO_3 in the nickel-plating electrolyte (pH 4.5–5.5 [1]), and as H_3BO_3 and also as $H_2BO_3^-$ and $B(OH)_4^-$ species in buffer solutions at pH from 8.2 to 10 [2].



Calculated concentrations of boric acid and its ionic species, α, vs. pH: (*1*) H_3BO_3, (*2*) $H_2BO_3^-$, (*3*) HBO_3^{2-}, (*4*) BO_3^{3-}, and (*5*) $B(OH)_4^-$.

REFERENCES

1. *Gal'vanotekhnika: Spravochnik* (Electroplating: A Handbook), Ginberg, A.M., Ivanov, A.F., and Kravchenko, L.M., Eds., Moscow: Metallurgiya, 1987.
2. Lur'e, Yu.Yu., *Spravochnik po analiticheskoi khimii* (A Handbook of Analytical Chemistry), Moscow: Khimiya, 1965.
3. Ershov, Yu.A., Popkov, V.A., Berlyand, A.S., et al., *Obshchaya khimiya: Biofizicheskaya khimiya: Khimiya biogennykh elementov: Uchebnik dlya meditsinskikh spetsial'nykh vuzov* (General Chemistry: Biophysical Chemistry: Chemistry of Biogenic Elements: A Handbook for Higher Medical Schools), Ershov, Yu.A., Ed., Moscow: Vysshaya Skola, 1993.
4. *Khimicheskaya entsiklopediya* (Chemical Encyclopedia), Knunyants, I.L., Ed., Moscow: Sovetskaya Entsiklopediya, 1988, vol. 1.
5. Glinka, N.L., *Obshchaya khimiya: Uchebnoe posobie dlya vuzov* (General Chemistry: A Handbook for Higher Schools), Ermakov, A.I., Ed., Moscow: Integral, 2003.

ISSN 1070-4272, Russian Journal of Applied Chemistry, 2006, Vol. 79, No. 12, pp. 2043–2045. © Pleiades Publishing, Inc., 2006.
Original Russian Text © Editorial Board, 2006, published in Zhurnal Prikladnoi Khimii, 2006, Vol. 79, No. 12, pp. 2066–2068.

Academician Mikhail Grigor'evich Voronkov

DOI: 10.1134/S1070427206120317

On December, 6, 2006, Academician Mikhail Grigor'evich Voronkov is 85. He is the oldest active author of *Zhurnal Prikladnoi Khimii* (Russian Journal of Applied Chemistry). His first paper appeared in *Zhurnal Prikladnoi Khimii* 55 years ago (1951, 24, 93–94). Since that time, he has published 117 papers in the journal.

Academician Voronkov is an outstanding Russian scientist, well-known in the world. He heads one of Russia's leading scientific schools, which is concerned with basic research in the field of chemistry of organic derivatives of tetracoordinated hypo- and hypervalent silicon, germanium, and tin; and halogen-substituted thiols, hemdithiols, thioketones, and thiiranes containing the S–C–C–X group (X = F, Cl, Br, I). The success of these studies is favored by the broad and encyclopedic scientific knowledge of Voronkov and by his fantastic working capacity.

According to the site www.scientific.ru/whoiswho, he occupies now the first place among all Russian chemists-scientists in citation in the world's scientific literature (data of 1986–2004). His name is included in the reference book Leading Scientists of the World, published by the International Biographic Centre of Cambridge in 2006.

Voronkov is a member of a number of foreign academies and scientific societies, honorary professor of two foreign universities, and member of the editorial boards of four foreign chemical journals and *Russian Zhurnal Prikladnoi Khimii*.

Among Voronkov's achievements as a scientist is the formation of numerous areas of research in organoelement chemistry.

Particularly well-known in the USSR and abroad is his basic research in the field of chemistry, physical chemistry, biology and pharmacology of silatranes, germatranes, and their analogues (established by him), and other compounds of hypervalent silicon (draconoids, derivatives of lactams, amides, azoles, hydrazides of carboxylic acids, etc.). For his studies in the field of chemistry of organic derivatives of pentacoordinated silicon, Voronkov was awarded a State Prize of the Russian Federation in 1997. His studies



in the chemistry of silatranes and germatranes, commenced in 1962, generated interest among world's scientists in mid-1970s and have been carried in many countries (USA, Germany, France, Japan, Hungary, Poland, China, Israel, Mongolia, and others) since that time.

In recent years, Voronkov's attention was attracted by organosilicon compounds containing Si–F bonds and especially those of the intracomplex type. In particular, an original reaction of protolysis of the Si–C bond in phenylfluorosilane and new transformations of tetrafluorosilane have been studied. These reactions initiated an extensive study of silatrane analogues, quasi-silatranes.

He also paid a considerable attention to *Q*-hydrometallatranes exhibiting a high biological activity.

Methods for low-temperature generation of compounds of hypovalent (tricoordinated) silicon, silanones, have been developed under Voronkov's supervision. The generation of silanones formed the basis of his theory of formation and destruction of siloxane structures.

He was the first to carry out, in the middle of the last century, fundamental studies of heterolytic reactions of splitting of the Si–O–Si group by widely diverse reagents, which demonstrated that this group is substantially more reactive than the C–O–C group.

A prominent place in his studies was occupied by organic derivatives of elements belonging to the silicon subgroup, germanium and tin. Intracomplex organic compounds of pentacoordinated germanium, 1-organylgermatranes, were for the first time synthesized under Voronkov's supervision and their physicochemical properties and biological activity have been studied. A valuable contribution to organotin chemistry was made by studies of Voronkov's school, devoted to compounds containing a stanthiane bond (S–N), derivatives of hypervalent tin, homolytic reactions of addition to alkenylstannanes, and possible use of organotin compounds in organic synthesis.

At the very beginning of his scientific activities, Voronkov was attracted by reactions of organic compounds with elementary sulfur. One of these reactions (that of sulfur with arylhalogenalkanes and -alkenes) was named for him. In the 1960s–1970s, he developed a new area in organic chemistry of sulfur: high-temperature reactions of thiyl radicals.

In recent years, difficultly accessible classes of organic compounds of sulfur: sulfur-containing macroheterocycles, thioaldehydes and thioketones, α-halogen-thioketones, α-halogen-hemdithiols, dithiirane derivatives, condensed heterocyclic systems, 1,2-dithiolene-3-thiones, etc. have become objects of studies supervised by Voronkov.

Together with making a fundamental contribution to theoretical and synthetic chemistry, Voronkov's studies have resulted in the development of numerous practically valuable materials and technological processes (organosilicon coatings for various purposes, new materials for microelectronics, polysiloxane sorbents, ion-exchangers and complexites, additives to lubricant oils, aqueous quenching medium, medicinals of a new generation, original means of chemicalization of agriculture, etc.).

The first biologically active organic compounds of hypervalent silicon, silatrane, have found application in medicine and agriculture (these data are summarized in a book by Voronkov and V.P. Baryshok *Silatrany v medtsine i sel'skom khozyaistve* (Silatranes in Medicine and Agriculture) (2005).

Successful studies carried out by the large research team headed by Voronkov in the field of bioorganosilicon chemistry yielded organosilicon compounds exerting adaptogenic, carcinostatic, sedative, immunomodulating, immunodepressing, growth-controlling, and other kinds of influence on living organisms. A number of original medicinals having no analogues in the world's medicine (Ferakril, Argakril, Atsizol, Trekrezan, Silokast, Silimin, Kobazol, etc.) have been created under Mikhail Grigor'evich's supervision. Also, polymeric biocide coatings protecting various materials (metals, optical glass, wood, paper, etc.) from biocorrosion and biogrowth have been developed on the basis of biologically active organosilicon monomers.

In the late 1970s, an additional new original area of research in chemistry of organic derivatives of silicon, carbofunctional polyorganyl sesquioxanes, which are effective sorbents, ion-exchangers, and complexites, was opened-up under Voronkov's supervision. A number of these compounds have been introduced into analytical practice for high-precision and high-sensitivity determination of noble and rare metals in ores and minerals. These compounds have also been used in cigarette filters for deep purification of tobacco smoke to remove toxic and carcinogenic elements, deep purification of industrial wastewater and solid wastes to remove highly toxic elements, sorption filters, methods for recovery of precious metals from industrial waste, etc.

Foundations of the following new research areas have been laid under Voronkov's supervision:

(1) Polyfunctional organoelement silicon compounds, precursors of thin-film structures for modern technology of production of articles for micro- and optoelectronics and of special and superhard coatings;

(2) Polyunsaturated macrolinear and macrocyclic silicanes, promising precursors of silicon carbide fibers and ceramics.

All the above-mentioned Voronkov's studies are extensively cited in domestic and international literature. The importance of the research conducted by his scientific school is also indicated by the fact that virtually all of its pioneering scientific areas in the field of organosilicon chemistry have found followers among scientists both in our country and abroad.

During 64 years of scientific activities, Voronkov published 52 monographs (15 of these published in translation in the United States, Great Britain, Germany, Japan, Israel, Romania, Poland). These publications include fundamental monographs *Siloksanovaya svyaz'* (Siloxane Bond), *Electronnoe stroenie organicheskikh soedinenii kremniya, germaniya i olova* (Electronic Structure of Organic Compounds of Sili-

con, Germany, and Tin), a capital three-volume work *Geterosiloksany* (Heterosiloxanes), all published in Russian and English, and also a monograph *Kremnii i Zhizn'* (Silicon and Living), which proclaimed the birth of a new area of silicon chemistry, bioorganosilicon chemistry, 149 reviews and chapters in books, and about 2780 scientific articles. Under his supervision, 131 candidate dissertations were prepared and defended, 33 of his pupils became doctors of science.

All the studies supervised by Voronkov are being carried out in close cooperation with research institutes, higher school institutions, and specialized plants and organizations of our country, as well as with scientists from former CIS and other countries. Most of these studies are being carried out in the framework of creative, integration, and international projects and contracts. In recent years, research of this kind has been conducted in the framework of INTAS international project on chemistry of compounds of hypervalent silicon and of the integration project with the Institute of Inorganic Chemistry, Siberian Division, Russian Academy of Sciences (Novosibirsk); Institute of Chemical Kinetics and Combustion, Siberian Division, Russian Academy of Sciences (Novosibirsk); and Institute of Silicate Chemistry, Russian Academy of Sciences (St. Petersburg). These studies are devoted to multifunctional organoelement silicon compounds as syntones and reagents for microelectronic technologies. The biological activity of organoelement compounds is studied in cooperation with medical institutes: Military Medical Academy, 1st Central Military Medical Institute, Ministry of Defense of the Russian Federation (St. Petersburg), State Hematological Center, Russian Academy of Medical Sciences (Moscow), Institute of Traumatology and Orthopedics, Siberian Division, Russian Academy of Medical Sciences, and Institute of Reconstructive and Regenerating Surgery, Eastern-Siberian Scientific Center, Siberian Division, Russian Academy of Medical Sciences (Irkutsk), Institute of Clinical Immunology, Russian Academy of Medical Sciences (Novosibirsk), Siberian Institute of Physiology and Biology of Plants, Siberian Division, Russian Academy of Sciences (Irkutsk), and others. This integration enables exhaustive solution of numerous problems of theory and application of practically valuable organosilicon and other heteroatomic compounds created under Voronkov's supervision.

For his studies in the field of organic derivatives of silicon and their practical use, Voronkov was awarded a State Prize of the Russian Federation (1997), State Prize of the Ukrainian SSR (1981), Prize of the Council of Ministers of the USSR (1991), title of an Honorary Chemist of the USSR (1983), Nesmeyanov Prize of the Russian Academy of Sciences (2003), Kosta medal (2006) instituted by the Russian Chemical Society, Moscow State University, and InterBioScreen international foundation. For his contribution to the development of science and industry of Eastern Siberia, Voronkov was made an honorary citizen of Irkutsk oblast (2002).

For his scientific achievements and military service during the Great Patriotic War, Voronkov was awarded Order of Merit for the Fatherland (4th class), Order of Great Patriotic War (2nd class), Order of Red Banner of Labor, Order of People's Friendship, and 20 medals.

Despite his extreme old age and full loss of sight (in the last 25 years), Voronkov continues his active scientific activities and heads a large team of scientists in two institutes of the Russian Academy of Sciences: Irkutsk Institute of Chemistry, Siberian Division, and Institute of Silicate Chemistry.

Editorial Board and Editorial staff
of Zhurnal Prikladnoi Khimii

ISSN 1070-4272, Russian Journal of Applied Chemistry, 2006, Vol. 79, No. 12, pp. 2046–2047. © Pleiades Publishing, Inc., 2006.
Original Russian Text © A.G. Morachevskii, N.A. Smirnova, A.A. Belyustin, I.S. Ivanovskaya, 2006, published in Zhurnal Prikladnoi Khimii, 2006, Vol. 79, No. 12, pp. 2069–2070.

OBITUARY

In Commemoration of Mikhail Mikhailovich Shul'ts

DOI: 10.1134/S1070427206120329

Mikhail Mikhailovich Shul'ts, Academician of the Russian Academy of Sciences, Hero of Socialist Labor, and known scientist in the field of physical chemistry, thermodynamics, chemistry and electrochemistry of glass, and membrane electrochemistry, passed away on October 9, 2006.

Shul'ts headed one of the best known Russian chemical schools. Forty-five scientists defended candidate dissertations prepared under his supervision. Six persons, members of his school, became doctors, and one of these was elected a corresponding member of the Academy of Sciences.

Shul'ts entered the chemical faculty of Leningrad State University in 1937, volunteered to the field forces with the advent of the Great Patriotic War, demobilized in 1944, and graduated from the faculty in 1947 to become a postgraduate student. Boris Petrovich Nikol'skii, an outstanding scientist and, later, an academician, was his supervisor. Shul'ts became the principal continuer of Nikol'skii's research work.

Shul'ts spent most of his life and conducted a major part of his studies at St. Petersburg (Leningrad) State University, where he successively worked as an assistant, docent, professor of the chair of glass electrochemistry at the Research Institute of Chemistry, professor of the chair of physical chemistry, and, in recent years, professor of the chair of thermodynamics and kinetics. In 1967–1972, he was dean of the chemical faculty. In 2006, he was elected honorary professor of St. Petersburg State University.

The main scientific achievements of Shul'ts at the University are associated with studies of the electrode properties of glasses and with the solution of a wide variety of theoretical and practical problems of ionometry, and especially pH-metry. Shul'ts suggested a rigorous proof of the metallic functions of the glass electrode and elucidated the mechanism of ion transport in membranes of varied nature. A set of glasses for pH-metry, glasses with metallic electrode functions, and glass redox electrodes were developed



under his supervision. The results of his studies in this area are exceedingly widely used in numerous branches of industry, agriculture, medicine, and scientific research.

Another important area of research conducted by Shul'ts at the University consisted in that he studied, together with professor A.V. Stronkin, fundamental problems of the thermodynamic theory of heterogeneous systems. Here, particular emphasis should be placed on the fact that the Le Chatelier–Brown principle was refined, thermodynamic laws of phase and chemical transformations in closed systems were established, and methods for analysis of complex systems forming solid solutions were developed.

After having passed to Grebenshchikov Institute of Silicate Chemistry (1972), Academy of Sciences of the USSR, to become director of this institute (till 1998), Shul'ts continued intensive scientific activities, remaining a professor at the chemical faculty of St. Petersburg State University, in already the third area of research, studies of the structure and thermodynamic properties of glasses and oxide melts. He

created and efficiently supervised the activities of a leading scientific school "Thermodynamics and Chemical Structure of Glasses and Oxide Melts."

Shul'ts's was twice awarded State Prizes of the USSR (for the theory of the glass electrode in 1973, and for studies of the ion transport in biological and model membranes in 1986), two times received the First University Prize, and was awarded the Mendeleev Prize of the St. Petersburg Government and Grebenshchikov Prize of the Russian Academy of Sciences.

His intensive research work was combined with pedagogical activities: Shul'ts delivered a general course of lectures on physical chemistry and special courses at the University, and minor special courses at the Technological University. At St. Petersburg State University and at the Institute of Silicate Chemistry, he supervised the work of postgraduate students and consulted doctoral candidates. The list of his research works comprises more than 500 items, including monographs, textbooks, and subject collections of works, edited by him.

The life and creative activities of Shul'ts are represented most completely in two brochures from the series Bibliografiya uchenykh RAN (Bibliography of Scientists Working at the Russian Academy of Sciences).[1]

Numerous pupils, comrades, friends, and colleagues of Shul'ts grieve over the loss of teacher, supervisor, and friend. His works will be in demand for many years to come.

A.G. Morachevskii, N.A. Smirnova, A.A. Belyustin, and I.S. Ivanovskaya

---

[1] Mikhail Mikhailovich Shul'ts. *Materialy po bibliografii uchenykh SSSR, Seriya Khimicheskikh Nauk* (Mikhail Mikhailovich Shul'ts, Materials on the Bibliography of Scientists of the USSR, Chemical Sciences Series), Moscow: Nauka, 1989, issue 83. Mikhail Mikhailovich Shul'ts. *Materialy po bibliografii uchenykh SSSR, Seriya Khimicheskikh Nauk* (Mikhail Mikhailovich Shul'ts, Materials on the Bibliography of Scientists of the USSR, Chemical Sciences Series), Moscow: Nauka, 2004, issue 108.

ISSN 1070-4272, Russian Journal of Applied Chemistry, 2006, Vol. 79, No. 12, pp. 2048–2049. © Pleiades Publishing, Inc., 2006.
Original Russian Text © Editorial Board, 2006, published in Zhurnal Prikladnoi Khimii, 2006, Vol. 79, No. 12, pp. 2071–2072.

OBITUARY

In Commemoration of Vladimir Aleksandrovich Proskuryakov

DOI: 10.1134/S1070427206120330

Vladimir Aleksandrovich Proskuryakov, a known scientist, doctor of technical science, corresponding member of the Russian Academy of Education, professor of St. Petersburg State Technological Institute (Technical University), passed away on October 30, 2006.

All Proskuryakov's scientific and pedagogical activities had been associated with the development of science in the field of processing on natural fuels (shale, oil, coal) and with training of engineering and scientific cadre both in our country and abroad.

Proskuryakov was born on June 21, 1919, in Petrograd. In 1937, he entered the Lensovet Technological Institute in Leningrad. In 1941, he volunteered for military service to go to the frontline and served in the field force until the end of the war. He was severely wounded at Nevskii pyatachok bridge-head. In 1946, he continued his studies at the Lensovet Technological Institute and, having graduated from the institute in 1947, remained there as a postgraduate student. After defending his candidate dissertation in 1951, he was assigned to work as a lecturer at the chair of organic chemistry.

In 1959, Proskuryakov was elected head of the chair of pyrogenetic processes and held this position during 30 years. Owing to his organizational talent and to a clear target vision, Proskuryakov managed to transform a minor chair into a leading group of pedagogues and scientists and created a new specialty of basic organic and petrochemical synthesis. In 1964, the chair was officially named the chair of technology of petro- and coal-chemical industries.

Proskuryakov paid a considerable attention to training of scientific cadre: in 1967, the degree of doctor of technical science was conferred on him on the basis of a series of his works. In the 1970s–1980s, the chair had up to 30 postgraduate students. Ten lecturers and research workers of the chair defended their doctoral dissertations.

In 1965, Proskuryakov was appointed pro-rector of education, and in 1975, he became rector of the Institute. During this period of time, he worked hard to improve the education level at the institute, to supply the institute with modern equipment and computers, and to open-up new promising specialties. Thanks to his high scientific and pedagogical authority, Proskuryakov was elected a corresponding member of the Russian Academy of Education in 1974. He headed during 15 years the Leningrad department of Znanie (Knowledge) Society, was the chairman of the Council of rectors of Leningrad, and served as an expert and member of presidium of the Higher Attestation Commission.



During many years, Proskuryakov headed the Scientific council of the Technological Institute, was the chairman of the specialized council for conferment of doctoral degrees, actively worked in the methodological council of the institute and its scientific-technological commission, and was deputy Editor-in-chief of *Zhurnal Prikladnoi Khimii* (*Russian Journal of Applied Chemistry*) and a member of the editorial boards of the journals *Khimiya Tverdogo Topliva* (*Chemistry of Solid Fuel*) and *Goryuchie Slantsy* (*Oil Shale, Academy of Sciences of Estonia*).

Proskuryakov was a pioneer in the field of shale dressing and chemical utilization of the organic component of shale: kerogen. The technology he developed was used by the shale-dressing shop at Slantsy plant.

A prominent contribution to science and technology was made by the laboratory of chemistry and technology of processing of Kansk-Achinsk coal, headed by Proskuryakov.

Rather fruitful was the series of Proskuryakov's studies of oxidation of peat, shale, hydrocarbons, and heteroatomic components of oil. He performed original works devoted to purification of water to remove oil and oil products. These studies are well known to specialists in our country and abroad.

The results of Proskuryakov's scientific activities in the field of chemical processing of combustible fossils were reported in more than 500 scientific publications, including four monographs. He received more than 100 Inventor's certificates and patents. The textbook *Khimiya nefti i gasa* (Chemistry of Oil and Natural Gas) ran into three editions and was translated into French, Spanish, and Arabic.

For his meritorious pedagogical, scientific, administrative, and military services, Proskuryakov was awarded six orders and numerous medals of the USSR, and also orders of the Korean Peoples Democratic Republic, Czechoslovakia, and Bulgaria.

Proskuryakov was elected honorary doctor of Mersenburg and Vesprem technical universities.

He was a prominent scientist and excellent man. The memory of Vladimir Aleksandrovich Proskuryakov will be forever preserved in the hearts of his numerous colleagues, pupils, and all those who knew him.

The scientific and technological community grieves over the death of Vladimir Aleksandrovich Proskuryakov. He was a well-wishing and sympathetic person and excellent family man. He came in due time to help anybody, from a student to a professor. His activities earned well-deserved deep respect of students, postgraduate students, lecturers, and graduates of the Institute.

The Editorial board and the editorial staff of our journal present their deep condolences to relatives and friends of Vladimir Aleksandrovich Proskuryakov

ISSN 1070-4272, Russian Journal of Applied Chemistry, 2006, Vol. 79, No. 12, pp. 2050–2051. © Pleiades Publishing, Inc., 2006.
Original Russian Text © A.G. Morachevskii, I.N. Beloglazov, 2006, published in Zhurnal Prikladnoi Khimii, 2006, Vol. 79, No. 12, pp. 2073–2074.

BOOK REVIEWS

Tarasov, A.V., Besser, A.D., and Mal'tsev, V.I., *Metallurgicheskaya pererabotka vtorichnogo tsinkovogo syr'ya* (Metallurgical Processing of Secondary Zinc Raw Materials), Tarasov, A.V., Ed.,

Moscow: Gintsvetmet, 2004, 219 pp.

DOI: 10.1134/S1070427206120342

At present, processing of secondary raw materials is an important source for manufacture of a number of nonferrous metals, including lead and zinc. The annual world's consumption of zinc is about 10 million tons and zinc is among nonferrous metals that are in the highest demand by many branches of industry. The structure of zinc consumption in economically developed countries is rather stable, about 48% of the metal manufactured is consumed for anticorrosive coatings for steel and iron rolled products, and about 34%, for manufacture of zinc-based construction and cast alloys (brasses, alloys for precise casting). Thus, zinc plating and manufacture of alloys consume most part of zinc. Various technological schemes for utilization of zinc-containing materials have been developed and are used in a number of countries. These technologies provide a rather high recovery of zinc and accompanying components to give commercial products.

A.V. Tarasov's monograph considers in detail, for the first time in the domestic scientific-technological literature, the problem of processing of secondary zinc-containing materials. The book comprises a preface, introduction, ten chapters, conclusion, and bibliographic list for the whole monograph. In a brief preface (p. 5), the authors note the necessity for creating in Russia a new branch of industry for manufacture of zinc from secondary raw materials. The introduction (pp. 6–10) considers specific applications of zinc in the industry and ways of accumulation of secondary zinc-containing raw materials and notes the economical and ecological advantages of manufacture of secondary zinc, compared with its production from ores.

The first chapter (pp. 11–20) analyzes the present-day state of manufacture and use of zinc in the world. According to the International Lead and Zinc Study Group (ILZSG), the world's production of zinc steadily increased during the last ten years: from 7123 thousand tons in 1994 to 9849 thousand tons in 2003. A considerable increase was observed during this period of time in the Peoples' Republic of China, and the manufacture of zinc also increased in a number of other countries (Australia, Kazakhstan, Mexico, and Russia). According to the prognosis by ILZSG, the use of zinc for coating of steel rolled products and construction articles will grow in the first decade of the XXI century in machine-building and construction industries, which will stimulate further rise in consumption of zinc. In some countries, a considerable amount of zinc is used in manufacture of dry power cells. The second chapter (pp. 20–40) is completely devoted to characterization of secondary raw materials. These are mostly composed of wastes formed in manufacture of commercial products from zinc or zinc-containing materials and consumers' wastes, which are widely diverse and allow different degrees of zinc recovery.

The third chapter (pp. 41–53) summarizes the evidence concerning processing of steel with low content of zinc. Preparation of waste zinc-plated steel for utilization and various ways to recover zinc from wastes (dezincing) are considered. The fourth chapter (pp. 54–119) considers methods for processing of dusts from electric-arc furnaces (EAF), in which zinc-plated steels are remelted. In most countries, EAF dusts are regarded as harmful wastes and should be either processed or stabilized (converted into a glassy state) and then buried. The already used or promising technological schemes for dust processing (content of zinc in the starting dust of up to 18%) are described. These techniques include both pyrometallurgical and hydrometallurgical methods. There is good reason to believe that the EAF dusts could become the most important source of secondary zinc in the near future.

The fifth chapter (pp. 122–138) discusses processing of wastes with high content of zinc and low content of iron. Wastes of this kind are characteristic of plants using zinc as a material in the technological cycle of manufacture of commercial products. The recycling of such a secondary raw material is eco-

nomically feasible. The sixth chapter (pp. 139–152) is devoted to utilization of zinc-containing wastes in nonferrous metallurgy and chemical industry. In the seventh chapter (pp. 153–167), the authors discuss the possibility of joint processing of zinc concentrates produced from ores and secondary zinc-containing materials.

The very small eighth chapter (pp. 168–172) contains evidence concerning the liquation and liquation-chemical refining of raw zinc and the distillation and rectification techniques as finishing methods for metal purification. The ninth chapter (pp. 173–194) is devoted to processing of a specific type of secondary zinc-containing materials, dry power cells. In Asian countries, up to 60% of the whole amount of consumed zinc goes to manufacture of dry power cells (~11% in Europe and ~19% in the United States). The tenth chapter (pp. 195–199) discusses the ecological and social aspects of processing of secondary zinc-containing raw materials. In accordance with the classification in force in the Russian Federation, zinc and its compounds belong, as regards the toxicological effect on humans, to moderately hazardous substances (III class of hazard). In the conclusion (pp. 200–206), the authors present reference data on the output capacities of plants for manufacture of zinc from ores and secondary raw materials in various regions and countries. Three countries, China, Canada, and Japan, give 34% of the whole amount of zinc manufactured in the world. Particularly productive are the facilities for manufacture of primary zinc in China.

The bibliographic list (pp. 207–219) contains 196 references, of which 75% are references to foreign publications of the last decade. Many of these publications are hardly accessible to a wide audience of readers. On the whole, the monograph by Tarasov and co-authors has a descriptive nature, the authors virtually do not comment the material presented and give no assessments or recommendations. Nevertheless, the informational and educational value of the book is very high. The monograph is of indubitable interest; it can be of use for a wide audience of specialists and also can be recommended as a textbook in training of engineers-metallurgists of the corresponding specialization.

A. G. Morachevskii and I. N. Beloglazov